

VOICES AND SILENCES

NARRATIVES OF GIRMITIYAS AND JAHAJIS FROM FIJI AND THE CARIBBEAN

Anjali Singh

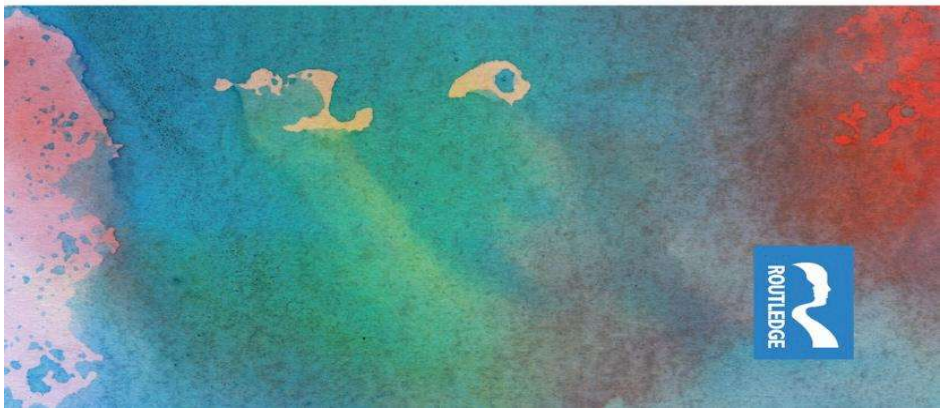

First published 2023
by Routledge
4 Park Square, Milton Park, Abingdon, Oxon OX14 4RN

and by Routledge
605 Third Avenue, New York, NY 10017

Routledge is an imprint of the Taylor & Francis Group, an informa business

© 2023 Anjali Singh and Manohar Publishers

The right of Anjali Singh to be identified as author of this work has been asserted in accordance with sections 77 and 78 of the Copyright, Designs and Patents Act 1988.

All rights reserved. No part of this book may be reprinted or reproduced or utilised in any form or by any electronic, mechanical, or other means, now known or hereafter invented, including photocopying and recording, or in any information storage or retrieval system, without permission in writing from the publishers.

Trademark notice: Product or corporate names may be trademarks or registered trademarks, and are used only for identification and explanation without intent to infringe.

Print edition not for sale in South Asia (India, Sri Lanka, Nepal, Bangladesh, Pakistan or Bhutan)

British Library Cataloguing-in-Publication Data
A catalogue record for this book is available from the British Library

Library of Congress Cataloging-in-Publication Data
A catalog record for this book has been requested

ISBN: 978-1-032-37704-9 (hbk)
ISBN: 978-1-032-37707-0 (pbk)
ISBN: 978-1-003-34149-9 (ebk)

DOI: 10.4324/9781003341499

Typeset in Adobe Garamond 11/13
by Digital Print Hut, Delhi 110002



MANOHAR

Contents

Acknowledgements 7

Preface 9

1. Cartographies of Indenture: Historical Overview 15

2. The *Girmitiyas* of Fiji: A Forgotten Generation 42

3. The *Jahajis:* Indentured Indians in the Caribbean 86

4. The Aesthetics of Narrative: Poetics of Indenture 133

5. Emerging from Indenture/ship: Evolving Being and Belonging 174

Bibliography 199

Index 211

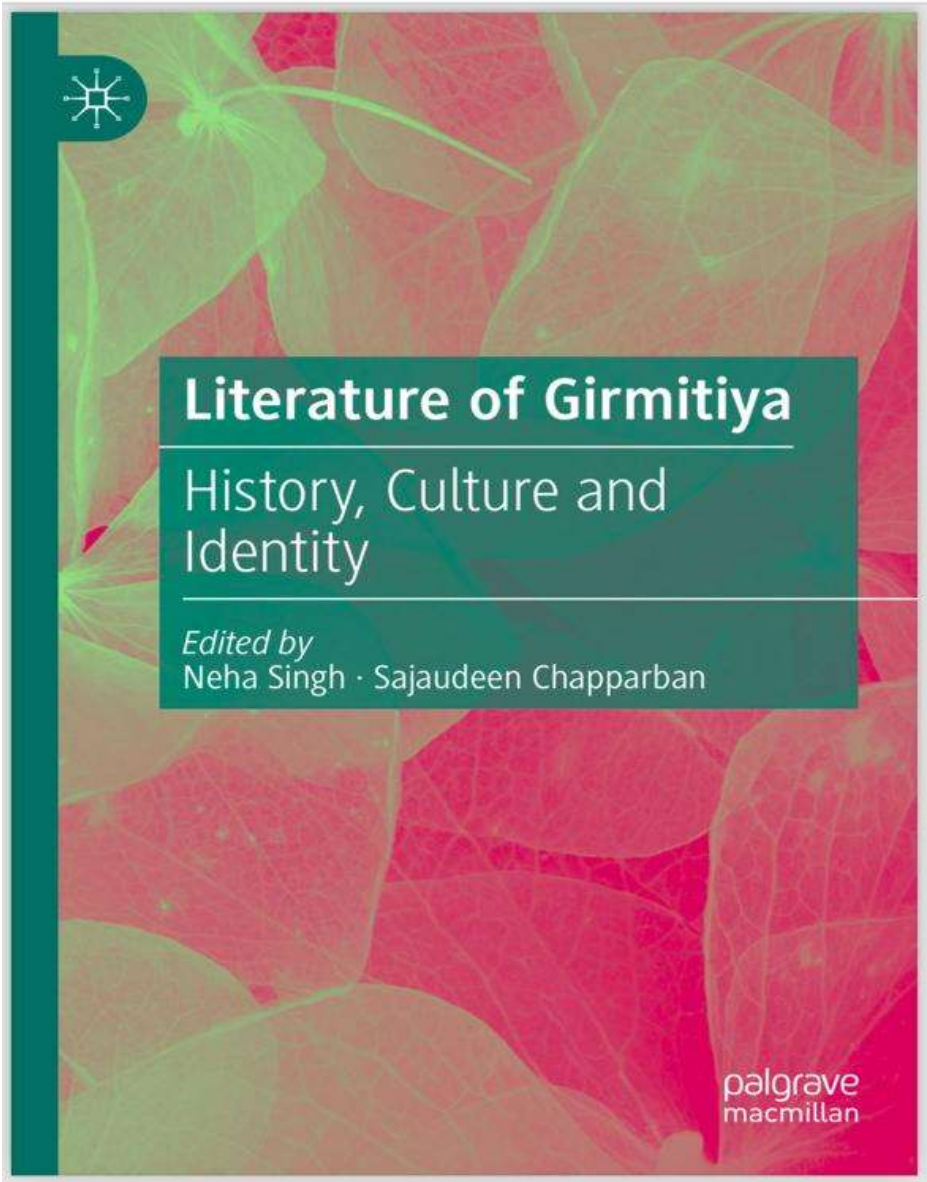
Literature of Girmitiya
History, Culture and Identity
Edited by
Neha Singh · Sajaudeen Chapparban
palgrave
macmillan

Editors
Neha Singh
Department of Languages, Literatures and Cultural Studies, School of Humanities and Social Sciences
Manipal University Jaipur
Rajasthan, India

Sajaudeen Chapparban
Centre for Diaspora Studies
Central University of Gujarat
Gandhinagar, India

ISBN 978-981-19-4620-2 ISBN 978-981-19-4621-9 (eBook)
https://doi.org/10.1007/978-981-19-4621-9

© The Editor(s) (if applicable) and The Author(s), under exclusive license to Springer Nature Singapore Pte Ltd. 2023
This work is subject to copyright. All rights are solely and exclusively licensed by the Publisher, whether the whole or part of the material is concerned, specifically the rights of translation, reprinting, reuse of illustrations, recitation, broadcasting, reproduction on microfilms or in any other physical way, and transmission or information storage and retrieval, electronic adaptation, computer software, or by similar or dissimilar methodology now known or hereafter developed.
The use of general descriptive names, registered names, trademarks, service marks, etc. in this publication does not imply, even in the absence of a specific statement, that such names are exempt from the relevant protective laws and regulations and therefore free for general use.
The publisher, the authors, and the editors are safe to assume that the advice and information in this book are believed to be true and accurate at the date of publication. Neither the publisher nor the authors or the editors give a warranty, expressed or implied, with respect to the material contained herein or for any errors or omissions that may have been made. The publisher remains neutral with regard to jurisdictional claims in published maps and institutional affiliations.

This Palgrave Macmillan imprint is published by the registered company Springer Nature Singapore Pte Ltd.
The registered company address is: 152 Beach Road, #21-01/04 Gateway East, Singapore 189721, Singapore

Contents

1 **Literature of Girmitiya: History, Culture, and Identity** 1
Neha Singh and Sajaudeen Chapparban

Part I Language, Literature, and Identity

2 **Language, Literature and Cultural Identity: A Narrative from the Malaysian Tamil Diaspora** 23
M. Mahalingam

3 **Poetics of the Crossing: Rerouting Identity in Indian Indenture** 43
Anjali Singh

4 **Unutterable Sufferings of Girmitiyas in Amitav Ghosh's *Sea of Poppies*** 59
Pulkita Anand

5 **A Critical Reflection on Imperialism, Nostalgia and Traumatic Experiences in Totaram Sanadhya's *My Twenty-One Years in the Fiji Islands*** 73
Rabindra Kumar Verma

Netritva 4.0

Leadership in the Era of Connection and Collaboration

Editors:

Prabhat Pankaj • Lokesh Vijayvargy • Prerna Jain

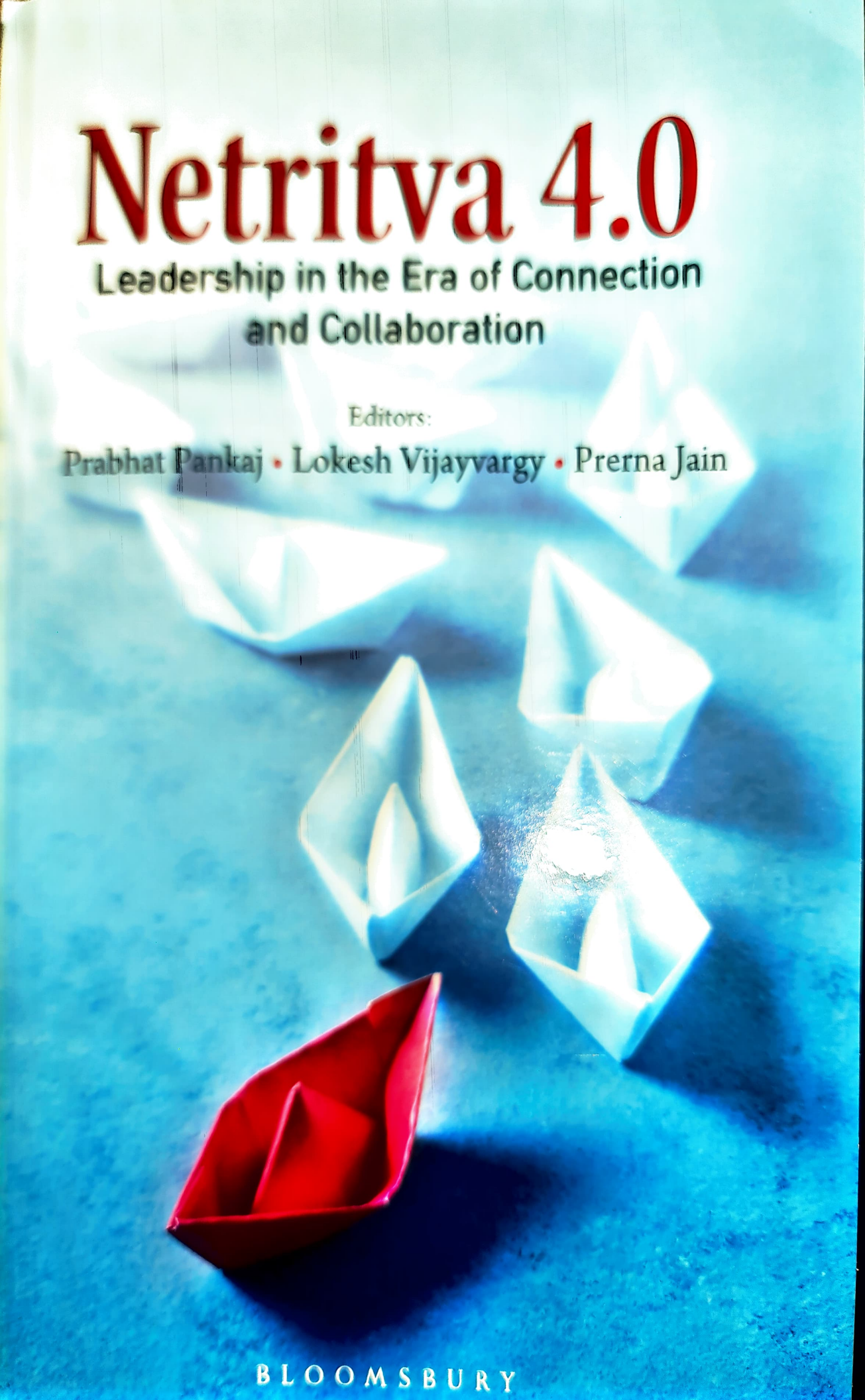

BLOOMSBURY

BLOOMSBURY INDIA
Bloomsbury Publishing India Pvt. Ltd
Second Floor, LSC Building No. 4, DDA Complex,
Pocket C – 6 & 7, Vasant Kunj,
New Delhi 110070

BLOOMSBURY, BLOOMSBURY PRIME and the Diana logo are trademarks of Bloomsbury Publishing Plc

First published in India 2023
This edition published 2023

Copyright © Jaipuria Institute of Management, Jaipur, 2023

Prabhat Pankaj et al. have asserted their right under the Indian Copyright Act to be identified as the editor of this work

All rights reserved. No part of this publication may be reproduced or transmitted in any form or by any means, electronic or mechanical, including photocopying, recording or any information storage or retrieval system, without the prior permission in writing from the publishers

The book is solely the responsibility of the editor and the publisher has had no role in creation of the content and does not have responsibility for anything defamatory or libellous or objectionable.

Bloomsbury Publishing Plc does not have any control over, or responsibility for, any third-party websites referred to or in this book. All internets addresses given in this book were correct at the time of going to press. The author and publisher regret any inconvenience caused if addresses have changed or sites have ceased to exist, but can accept no responsibility for any such changes

ISBN: 978-93-5640-279-9
2 4 6 8 10 9 7 5 3 1

Typeset by Fortune Graphics, Naraina, New Delhi
Printed and bound in India by Replika Press Pvt. Ltd

To find out more about our authors and books, visit www.bloomsbury.com and sign up for our newsletters

13. Transformation of Technical and Management Leadership for Enterprise Success
Manoj Kumar Singhal

14. Leadership through Industry 4.0
Bhanu Pratap Singh Tanwar, Akshat Sharma and Lokesh Vijayvargy 124

15. Recreational Facilities at the Workplace Affect Employee Well-being through Nurturing Support and Bonding
Harold Andrew Patrick, Ujjal Mukherjee, Jacqueline Kareem and Nepoleon Prabakaran 130

16. The Future Work Trend of the Hybrid Model among IT Employees and its Challenges
B. Vidya Sri and S. Vasantha 134

17. Finance 4.0 and Leaders of Tomorrow
Vinay Khandelwal, Aditya Tiwari and Aishwarya Parihar 153

18. Impact of Hybrid Model of Work on Employee Performance with a Moderating Effect of Managerial Support
S. Anisha Estherita and S. Vasantha 162

19. A Case Study on the Impact of Citizen Perceived Service Quality Experience in E-Government Services between Citizen Satisfaction and Citizen Loyalty
D. Vimala and S. Vasantha 167

20. Tribals are the Backbone of India: A Review on the Next Generation of Sustainability Leaders
Neetu Mishra and Anil Vashisht 178

21. Examining the Impact of Tourism on Happiness and Subjective Well-being: A Review
Trapati Narwaria and Deepali Soni 186

22. Effect of Income and Age Groups on Happiness and Life Satisfaction
Rashmi Singh and Arpan Chawla 197

23. Quality of Work Life and its Impact on Job Performance and Job Satisfaction
Damyanti Sodha and Narender Singh Bhati 211

24. Dynamic Corporate Scenario: Role of 4.0 Leadership Style
Durga Narayan Sharma 219

25. A Review of Job Embeddedness Literature in the Hospitality Industry and Recommendations for Future Research
Megha Bumrah 232

239



Healthy Aging For A Healthy Planet

Edited by

Dr. Pooja Varma | Dr. Pooja Rai | Dr. Alka Ranjan

Bharti Publications

HEALTHY AGING FOR A HEALTHY PLANET

Editors

Dr. Pooja Varma

Dr. Pooja Rai

Dr. Alka Ranjan

Bharti Publications

New Delhi- 110002 (INDIA)

Copyright © Editors

Title: Healthy Aging for a Healthy Planet

Editors: Dr. Pooja Varma | Dr. Pooja Rai | Dr. Alka Ranjan

All rights reserved. No part of this publication may be reproduced or transmitted, in any form or by any means, without permission. Any person who does any unauthorised act in relation to this publication may be liable to criminal prosecution and civil claims for damages.

First Published, 2022

ISBN: 978-93-94779-67-9

Published by :

Bharti Publications

4819/24, 2nd Floor, Mathur Lane

Ansari Road, Darya Ganj, New Delhi-110002

Phone: 011-23247537

Mobile : +91-989-989-7381

E-mail : bhartipublications@gmail.com

info@bharatipublications.com

Website : www.bhartipublications.com

Printed in India, by: Sagar Color Scan, Delhi

Disclaimer: The views expressed in the book are of the authors and not of the publisher and author. Authors themselves are responsible for any kind of Plagiarism found in the book and any related issues found with the book.

ACKNOWLEDGMENTS

The editors wish to sincerely thank all those who have helped to bring the present venture to a successful completion. They would like to especially acknowledge the important role played by Dr. Asha Rajiv, Director, School of Sciences and IQAC, Jain (Deemed to be University), Bangalore for her relentless support and acceptance of the present book publication and Dr. Pooja Varma, co-editor of this Book, working as a Head of the Department, Assistant Professor, Psychology, Jain (Deemed to be University) for taking the publication at the departmental level.

The editors also thank diligent departmental faculty Ms. Pallavi P., Ms. Manasa Raman and Dr. Sukriti Banda, Assistant Professor, Department of Psychology, Jain (Deemed to be University) for looking after the international conference work on Healthy Ageing in collaboration with NIMHANS, Bangalore in March 2022 efficiently.

The editors would like to record their special appreciation and gratitude for the honourable Vice chancellor of Jain (Deemed to be University), Dr. Raj Singh and his team for his cooperation in taking time out of his busy schedule and contribute towards the Foreword of this book which highlights the importance of healthy ageing from all perspectives in our lives, be it physically, socially, psychologically and cognitively. In addition it brings the attention of the readers towards key content and potent researches covered in the book.

Editors

FOREWORD

The world today, inhabited by more than a billion aged people, is currently witnessing fast rise in proportions of aged people. Projections claim that by 2050 nearly one in five people in developing countries will be over the age of 60. Longer life expectancy, though heartening, this new reality seems impregnated with a host of pressing challenges in view of its failure to guarantee an experience of healthy ageing. This is especially so for those dwelling in the low and middle income countries due to the fact that lack of basic resources and amenities often deprive large numbers of them of a meaningful and dignified life. The COVID-19 pandemic has further exposed glaring disconnects in policies, systems and services. As this global demographic transition remains one of the foremost medical, social and economic concerns of the day, one that impinges upon almost every aspect of society including demographic structure, the phenomenon of 'healthy' ageing is catching the attention of researchers, policy-makers and health professionals alike. Successful or active ageing refutes the stigmatized understanding of age as a mere pathological process and the associated lurking fear that ageing leads to an inevitable decline in the quality of life. Instead it hinges on the non-judgmental concerns relating to physical-mental wellness and cognitive capabilities of aged adults along with their active engagement with life. It is believed that the reduced probability of diseases and debilities will help contain health and social care costs associated with later life. Driven by the growing need to preserve health and vitality and preserve sound lifestyle choices among the older populace, the social policy responses world over seek to foster healthy ageing by largely focusing on the following critical areas of action: social connectedness, nutritious diet and physical activity.

The United Nations Decade of Healthy Ageing (2021–2030) offers a robust platform for concerted decade-long global action on healthy ageing. The initiative intends enhancement of possibilities of engagement with elderly people besides enabling them to realize their potentials, participation and autonomy in a healthy, protective and age-inclusive environment. Resonating with the spirit of UN SDGs, WHO had come forward with its Global Strategy and Action Plan for Ageing and Health for 2016–2020 and its continuation with the WHO programme The Decade of Healthy Ageing 2020–2030. In its ongoing support towards advancement of functional ability and well-being in older age WHO has prioritized country planning and action, research promotion and collection of global data on healthy ageing, aligning health-care systems to the needs of older people, ensuring human resources necessary for long-term integrated care, undertaking a global campaign to combat ageism, and enhancing global network for age-friendly cities and communities.

I am delighted that this publication is on its way to a timely fruition. The critical issue of healthy ageing is multidimensional, influenced heavily by the society and the environment we live in particularly, the people and relationships in our lives together with the attitudes and values we and others around us hold. Successful ageing, therefore, calls for perceptual change among differentiated sets of stakeholders on either side of the spectrum. Set against the backdrop of post pandemic "new" normal the volume contains a rich collection of empirical essays which I am sure will contribute towards a sensitive and nuanced understanding of the phenomenon of ageing from diverse perspectives from an inter-disciplinary approach. The articles reflect a range of rich discussions on value of social support, unconditional self-acceptance and compassion, disciplined spiritual practices, soul-consciousness, emotional intelligence, inner resilience and mindfulness in combating depressive disorder and loneliness syndromes. Contributors candidly spell out simple aerobic exercises, self-care activities and personal hygiene habits for nurturing higher self-esteem, physiological wellness and psychological fitness. The book also has dedicated chapters that elaborate on effective Ayurveda-inspired techniques and smart ICT enablement mechanisms to cope with ageing in the modern world.

Developing holistic and insightful understanding of the problem of 'ageing' is a work in progress and a collective endeavour. The book opens up broader avenues for engagement with our personal journeys of acceptance and adaptations to ageing process both within and without. And, the pieces therein rest on the hope for seizure of these opportunities at its best.

Dr. Raj Singh

Vice Chancellor,

Jain (Deemed to be University), Bangalore

CONTENTS

	Acknowledgments	***iii***
	Foreword	***iv-v***
1.	**A Roof Over the Head: A Gender Specific Correlation Study** Himanshi Singh & Dr. Hema Kumari Mehar	**1-11**
2.	**Attitude Towards Elderly Among Mental Health Professionals** Aaliya Sultana R, Arlene Fernandes & Dr Sukriti Banda	**12-21**
3.	**Relationship Between Self-Compassion and Psychological Wellbeing among Geriatric Population in India** Aditi Dubey & Aparajita Chakraborty	**22-28**
4.	**Psychological Distress among Elderly Naga Cancer Patients in Relation with Hope and Social Support** Sashirenla Mollier	**29-33**
5.	**Diabetes and the Elderly in the Post-Pandemic World** Pavithra Parthasarathy & Dr. Pooja Varma	**34-38**
6.	**A Positive Psychology-Based Intervention Model (C. A. R. E) for Pain Catastrophizing and Well-being among the Elderly during the pandemic: A Randomized Control Trial** Sudha. R & S. Gayatridevi.	**39-47**
7.	**Unconditional Self-Acceptance and Psychological Well-Being among Older Adults** Priyanga A & Dhivyadharshini G	**48-51**
8.	**Correlation between Affectivity and Coping Strategies when directly Exposed to COVID-19** Dolly Rawat & Mansi Agarwal Riya Iyer	**52-57**
9.	**Resilience and Mindfulness: Concomitants of Perceived Wellbeing of Elderly** Ms. Madhuri Vaidya & Prof. Urmi Nanda Biswas	**58-67**

10. Narrative Analysis of Adaptive Coping in Older Couples in Times of COVID-19 **68-80**
Meenakshi Menon

11. Existential Psychotherapy as an Effective Intervention for Psychological Issues in Older Females in India **81-87**
Purnima Gupta

12. Ayurveda for Healthy Ageing **88-95**
R. Vasumathi

13. Relationship Between Functional Digital Skills and Anxiety in Geriatric Population During the COVID-19 Pandemic **96-104**
Samreen K. Ahuja & Dr. Ganesh Kumar .J

14. Understanding Implications of Comorbidity of Major Depressive Disorder and Conversion Disorder/Functional Neurological Symptom Disorder: A Case Study with the Elderly **105-113**
Shraddha J Kamble & Dr. Pooja Rai

15. Emotional Intelligence in People with Elderly **114-118**
Sowmya B R & Dr. Pooja Rai

1 A Roof Over the Head: A Gender Specific Correlation Study

Himanshi Singh* &
Dr. Hema Kumari Mehar**

Abstract

Background: Aging is a progressive physiological changes in an organism that lead to senescence, or a decline of biological functions and of the organism's ability to adapt to metabolic stress. A roof over the head is a critical need of the elder who are destitute, sick and abandoned by family and those uprooted by disasters. The rapid urbanization of communities and nuclearization of families adds to the old age-related difficulties leading to many elderly shifting to Old age homes (OAH) safety and care. Female elderly faces many difficulties in daily life whether they are living in an Old age home or with family. The living environment along with the adjustment, coping and Quality of Life (QoL) are the main focus of this study.

Aim: To assess and compare the relationship of Quality of Life (QoL), Coping, and Adjustment among female elderly living in old age homes and within a family setup.

Methods and Materials: Forty Elderly female living in Old age homes, and forty female elderly living in the family from the community. They were assessed using WHO QoL Scale-BREF (Hindi version) Global Adjustment scale (GAS) and the ways of coping scale.

Result and Conclusion: Findings of this study indicated that female elderly living in old age homes had a better quality of life, coping, and adjustment in comparison to female elderly living within the family setup. It is not possible to conclude if the Old age homes is better than the community for female elderly. However, there is a need to replicate the study as these can have some influence on policy making for female elderly.

Keywords: Aging, Coping, QoL, Mental health

* PhD Scholar, Department of Psychology, MLSU, Udaipur

** Assistant Professor, Department of Psychology, MLSU, Udaipur

Introduction

Old age is a challenging period of human life and is associated with many health-related psychological, social, and economic difficulties. Nowadays, Older adults (OA) are highly vulnerable in society (Devi & Roopa, 2013). Their vulnerability increases with age, particularly for females. The elderly female suffer from emotional alienation while living with their son/daughter and grandchildren. Urbanization has caused a drastic change in the socio-economic scenario of the country, leaving the younger generation with no time to interact with the elderly in the family. It is weakening Indian society's traditional bonds between grandchildren and grandmothers thereby making older people more vulnerable due to lack of employment, financial insecurity, ill health and social neglect (Amonkar et al., 2018). The traditional concept of family in India to provide support to the OA is changing with the disintegration of joint families. In past many studies have reported better QOL of the elderly in the family setup as compared to OAH (Roby & Sullivan, 2000). However, with changing social scenario this aspect needs a review.

Elderly female face age-related discrimination, and abuse due to a lack of awareness about their rights and the support system. A typical Indian woman being dependent on others for social, financial, emotional needs is, vulnerable and soft target of wrongdoers. They are forced to lead a life full of distress due to lack of social protection and poverty. Their financial needs are a major concern with the increased life span of elderly female (Neale et al, 1996). Though financial abuse is hard to define, it is reported to be widely prevalent among elderly female. Financial exploitation is the most frequent form of perpetrator-related elder abuse in the US (Jackson, 2017; Sandhu & Arora, 2003).

QoL is widely recognized as an important concept and measure of outcomes in health care, and the concept is emerging more and more often also in connection with long term care. Amonkar et al. (2018) reported higher satisfaction and quality life among elders living in institutional settings than non-institutional settings. Significant differences between the institutional and non-institutional elderly men and women in the area of physical, psychological, level of independence, social relationship, and environment domains of QoL

Adjustment processes in old age are difficult because of the declining physical and mental abilities. Dubey et al. (2011) reported most of the women in OAH were staying there unwillingly. The primary reasons stated for decision to stay in OAH were not having anyone to take care of them at home and not willing to stay with married daughters as per social norms.

Elderly female living in families had a positive attitude towards old age but simultaneously felt it to be a period of dependency. There is yet a lack of consensus about the attitude of the younger generation with their duties towards their older generation is being eroded - and has led to the rapid increase in their institutionalization (Koul, 2015; Singh et al., 2014).

However, there is no consensus about if the family or OAH is a better place to live for the elderly. Kotwal & Prabhakar (2009) found that some of the physical and behavioural symptoms reported by the inmates of OAH are tearfulness and sadness, irritability, social isolation, sleep deprivation, exacerbation of pre-existing pains, and the pains caused by the increase in muscular tension, loss

of appetite, difficulty in sleep, loss of sexual activity, and the loss of interest in daily activities that produce pleasure. Sethi et al. (2013) found that OA who live with family faced more health problems compared to those living with families. Kalavar & Jamuna (2011) reported emotional difficulties of women in OAH. They felt more closeness to their daughters than sons wile staying in OAH However, many felt well away from family in OAH. Thus there is a complex interplay of the social and psychological attributes determine the satisfaction of the Elderly female with living arrangement.

There are lots of gaps in the knowledge regarding the status of elderly female concerning their adjustment, coping, QoL living in families, and OAH. Geriatric health is an upcoming discipline in India. The knowledge is required given the rapidly changing social structure and upcoming need of OAH. The knowledge can be helpful in better designing the psycho-social environment in the OAH for better QOL of elderly female. Hence, we preferred to carry out this study.

Method

Aim: To assess and compare the QoL, coping, and adjustment between elderly female living in OAH and within a family setup.

Methods and Materials: A cross-descriptive research design method was adopted for the study. The study was conducted on OAH and Elderly females residing in families at Rohtak, Haryana. Forty elderly females from authorised OAH and 40 Elderly female from family were selected for this study. Two areas of Rohtak namely, Ram Gopal Colony and Meham were identified for sampling elderly females living in the family. Purposive sampling using the following inclusion and exclusion criteria was followed for collecting the sample. The participants were informed that their participation is purely voluntary and they may withdraw from the study at any stage. They were also assured of confidentiality about the personal information, A written informed consent was taken before enrolling the participants in the study.

Inclusion criteria: The female subjects were considered for inclusion if they were

1. age range between 60-80 years
2. educated up to 5th standard
3. living with family members
4. living in OAH between 2- 5 years (for subjects from OAH)

Exclusion criteria:

1. History of major physical/ psychiatric illness or neurological illness.

Tools:

Socio-Demographic Data Sheet:

It is a semi-structured, self-prepared performa especially drafted for this study. It contains information about socio-demographic variables like age, religion, education, marital status, and domicile.

QoL Scale (WHOQoL-BREF, Hindi version (Saxena et al., 1998)

The Hindi version WHOQoL-BREF Scale was used to assess QoL. This is a short version of the WHOQoL-100 questionnaire contains only 26 items. It can assess QoL in the domains of physical health, psychological health, social relationships, and environment. Higher scores correspond to better QoL. This scale has been widely used for QoL research in India.

Global Adjustment Scale (GAS) (Vohra, 2012)

The adult form of Global Adjustment Scale was used to assess adjustment is valid for subjects aged 20 years and above. The adult form tries to obtain information from the individual regarding Family relationships, Health, Social environment, Emotion, Occupation, Sex-related behaviour, higher scores mean lower adjustment.

Ways of Coping Questionnaire (Lazarus & Folkman, 1988)

It assesses thoughts and actions individual uses to cope with the stressful encounters of everyday living. Ways of Coping Questionnaire has 66 items measuring confronting coping, distancing, self-controlling, seeking social support, accepting responsibility, escape-avoidance, painful problem solving, and positive reappraisal on a 4-point Likert Scale.

Procedure: The subjects were assessed in a single session. The session with each subject lasted for approximately 60-80 minutes.

Bivariate statistical analysis was carried out. Student's t-test and chi-squared test were used for continuous and categorical data respectively.

RESULTS

Table-1

Socio-Demographic Variables between Elderly Females Living in OAH and with Family Setup

Variable		Group		Df	t/x^2
		Old age home	Family		
Age in years (*Mean±SD*)		68.90±6.92	68.37±7.71	79	0.27 NS*
Religion	Hindu	20(50%)	24(60%)	2	1.63 NS*
	Christian	12(30%)	10(25%)		
	Other	08(20%)	06(15%)		
Category	GEN	24(60%)	22(55%)	3	1.27NS
	OBC	6(15%)	6(15%)		
	SC	4(10)	4(10%)		
	ST	6(15%)	8(20%)		
Marital Status	Married	18(45%)	16(40%)	2	1.34NS
	Widowed	6(15%)	4(10%)		
	Other	16(40%)	20(50%)		

Education	Below Metric	24(60%)	26(65%)	2	2.13NS
	Metric	4(10%)	4(10%)		
	Above Metric	12(30%)	10(25%)		
Residence	Rural	18(45%)	16(40%)	1	1.12NS
	Urban	22(55%)	24(60%)		
Family	Nuclear	24(60%)	20(50%)	1	1.28NS
	Joint	16(40%)	20(50%)		

**NS= Not Significant*

Table 1 shows the socio-demographic variable between Elderly females living in an OAH and within a family setup. In socio-demographic variables, there were no significant differences between both groups.

Table -2

Comparison of QoL between Elderly Females Living in OAH and within Family Setup.

Variable	Group		*t*
	OAH (*N*=40) Mean ± *SD*	**Family setup (*N*=40) Mean ± *SD***	
Physical Health	24.85±3.34	18.22±5.014	6.82**
Psychological Health	24.65±4.38	17.67±3.23	8.09**
Social Health	3.05 ±0.87	2.27±1.06	3.56**
Environmental Health	25.50 ± 3.48	19.62±4.96	6.12**
Total QoL	78.05±4.88	57.80±8.52	10.62**

**=significant at 0.05 Level*

***=significant at 0.01 Level*

Table 2 shows the mean scores and comparison of QoL (domain wise) between Elderly females living in OAH and within the family setup. Significant group difference was found in term of social health and environmental health between elderly females living in OAH and within a family setup. It shows that the mean score of social health of elderly females living with the family was better than the elderly females living in OAH. There were significant differences in scores on all domains. Elderly females living with the family were having better social health than those living in OAH. The mean score of environmental health between Elderly females livings in OAH was better than the elderly females living with family. Its indicate that Elderly females living in OAH were better in environmental health than the elderly females living with family. The mean score of QoL between elderly females living in OAH were better than the elderly females living with family. In the physical health domain, the finding suggested that the mean score of persons who live with family was lower than persons who live in OAH.

Table- 3

Comparison of Global Adjustment between Elderly Females Living in OAH and Family Setup

Variable	B		t
	OAH (*N*=40) Mean ± *SD*	Family (*N*=40) Mean ± *SD*	
Emotional Adjustment	14.90±3.90	23.50±6.21	7.41**
Health Adjustment	16.65±6.72	25.17±8.99	4.80**
Social Adjustment	15.95 ±5.63	25.30±7.82	6.13**
Total Adjustment	47.50±9.92	73.97 ±10.48	7.35**

***=significant at 0.05 Level*

Table shows the comparison of Global adjustment (domain wise) between the groups of elderly females living in OAH and within a family setup. Significant group difference were found in terms of health adjustment, social adjustment, and total adjustment between elderly females living in OAH and within a family setup. Elderly females living with family faced more emotional problems. That's the result they faced more emotional problems in comparison to elderly females. Who lived in an OAH.

Table-4

Comparison of Coping and its Domains Among Elderly Females Living in OAH and within Family Setup:

Variable	Group		*t*
	OAH (*N*=40) Mean ± *SD*	Family (*N*=40) Mean ± *SD*	
Confrontive	9.60±=1.79	7.42±2.76	4.18**
Distancing	9.30±1.75	6.90±2.64	4.77**
Self-Controlling	11.80 ±1.18	7.40±2.75	7.06**
Seeking Social Support	7.65 ±2.13	8.52±3.22	1.43
Accepting	7.26 ±1.35	5.67±2.05	4.04**
Escape Avoidance	8.60±3.22	6.72±2.96	2.70*
Plan full Problem Solving	9.25±2.32	7.75±2.67	2.67**
Positive re-appraisal	10.00±2.69	8.60±3.41	2.03
Coping	54.55±6.99	44.67±10.83	4.84**

***=significant at 0.01 Level*

Table 4 shows the mean score and comparison of coping scores (domain wise) between elderly females living in an OAH and within a family setup. Significant group differences were found in term of distancing, seeking social support, escape avoidance, positive re-appraisal, and total coping.

The mean scores for the elderly females in OAH were significantly higher for all coping domains except for domains of 'seeking social support' and 'positive reappraisal'.

Discussion

India is going through a rapid population change due to industrialization and urbanization of the communities. Consequently, the OA are generally left alone to take care of themselves. The situation is particularly tougher for elderly females due to the feminization of the elderly population and more dependency needs of women (Pande, 2020). Therefore, we aimed to assess the QoL, global adjustment and coping among elderly females living in OAH in comparison to counterparts residing in the community.

We didn't found any difference in the sociodemographic characteristics of the women living in family and OAH in this study (Table-1). However, those the living in OAH reported better QoL on all measures of WHOQoL-BREF than those living with family (table-2). As this comparison is not addressed in many studies, we can simply speculate the reasons. The elderly females living with family is likely to face more emotional problems (Brock & Lawrence, 2011; Geo, 2019). This can be troublesome especially if she is the only representative of her elderly age group. Emotional isolation due to younger people not interacting sufficiently may add to her problems, she might also not be able to confide thereby having no vent to her distress. Further, asymmetrical power dynamics are already being perceived as stressful for the spouses (Mehra et al., 2005; Rayirala, 2016). Though the both the groups didn't had any difference in the marital status (Table-1)Though both the groups didn't have any difference in the marital status (Table 1), even then the same may hold for married women in our study. On the other hand, a person living in an OAH with equal relationships with the same age can share her feelings. The study by Mehra (2005) lend support to our findings and reported that females in OAH had better physical health as well as the psychological health of people living in OAH than people lived with the family. They reported stressful family relationships and lack of family care precipitates poor psychological well-being in the family. However, due to small sample of the current study limits the power of study, we would prefer to deal with our findings conservatively despite good support from literature. The other reasons for not attempting to generalise the findings is that many other studies have reported contrary findings too. A study revealed that elderly females who were living alone had a higher level of financial strain, more depressive symptoms and low level of life satisfaction (Chou & Chi, 2000; Dutta, 1989; Top, 2015). Study has shown that elderly females living in community faced many psychological problems. Social health was good for those respondents who were living in the family because of interactions with many people in the family and visiting relatives, neighbours, religious places etc. In OAH social deprivation, negligence, a sense of isolation and poor social health may reduce the subjective social worth of the individual (Jamwal, 2016; Varma, 2010). Poor social health in OAH can be seen because of reduced religious activities and interaction

with community people. They also noticed good environmental health in OAH .This can be attributed to the fact that the management of any authorised OAH has essential responsibilities for maintaining housing, sanitation, electricity, water (Dey, 2012; Lee, 2020; Whitelock & Ensaff, 2018). The QoL women living in OAH were better than those who were living with family. We feel that the environmental attributes may be playing a role in it. Besides that no family burden, having a peer group, and regular cultural activities may also be contributing to it. People often engage the whole day in these types of activities. Goswami and Deshmukh (2018) conducted a study on OAH and rural community people and found that people living in an OAH had higher QoL than people living in a rural community. Dubey et al. (2011) also reported better QoL in institutional settings for the elderly people. However, it was found that poor QoL, more loneliness, and psychological distress can be seen among the inmates of institutions than those living with families in urban areas of Jammu.

We also aimed to study the social adjustment between the groups of FAO living in OAH and within a family setup. The global adjustment scale was used for this purpose. The Table 3 depicts that the elderly females living in the OAH had better adjustment on all domains. The reasons again are speculative as not many studies have touched this aspect of life in OAH. The elderly females living with family faced more emotional problems people living in an OAH had higher QoL than people living in a rural community most of the day when younger members of the family are either at schools or work place during day. This also restricts their movement outside the home due to their physical and psychological dependencies. The findings of Dubey et al. (2011) ruled that people living in OAH had better emotional adjustment than elderly living with a family member also supported this study. The health adjustment was significantly better for those respondents who were living in OAH primarily because of the availability of doctors on the panel to look after their health as a minimum standard is required for an old age home. Otherwise, the elderly are likely to take their health casually (Akbar et al., 2014). In developed countries sufficient resources are available to the elderly living alone and they can manage themselves. However, this is not the situation in the developing countries (Gupta & Kohli, 2011; Kulkarni, 2009). The OAH facilities in that way may be superior than those available to the community residents. We can say this due to the fact that as per minimum requirement guidelines from the department of social welfare, the OAH besides having facilities like food, care, recreation; they must have a visiting doctor to look after the health of inmates. Availability of these essential services facilities should lead to better physical and psychological health.

In current study the elderly females in the OAH had better social QoL and social adjustment (Tables 2 & 3) than those living in community. The reasons can be manifold. Most of the times the elderly deciding to stay in OAH in India find this as the last feasible option for their survival. They generally face multiple socially adverse events compelling them to decide for staying in old age home. Kulkarni et al. (2009) had found a better social adjustment of those respondents living in family than those in old age home. O'Donnell et al. (2008) however reported low social worth, feeling of social deprivation, negligence, a sense of isolation, and poor adjustment among the inmates of old age home. Thus there appears to be discordance between the scientific observations

and media or public opinion. In the family, people certainly participate in many social occasions related to their relatives, neighbours, and community. In our culture, any visitor to the family generally interacts with the elderly persons as a token of regard. But in OAH, the inmates get little chance to attend a social gathering. In old age home, people live with the same age group so they share their feeling with each other easily. They are self-dependent to take decision about themselves. However with urbanisation of communities such trends are not as frequent as in past at any time. Thus, in coming times the social health of FAO in families may decline. Many other studies also supported this study as Singh et al. (2014) found older adults had a poor adjustment in the community.

As evident from table 4 the elderly females residing in OAH had better coping ability in comparison to the family set up. Sandhu and Arora (2003) also reported that seeking social support for coping is more used by a person living in an OAH in comparison to people living in the family. However, the analysis in the current study was not designed to find the predominant ways of coping by the FAO. In OAH, people live alone so they try to take help from different sources including inmates. Choi et al. (2012) reported that persons living in an OAH used full problem solving coping. In OAH people need to manage all alone unlike those living in family who can get help from other members. Somewhat opposite to it Heydari-Fard et al. (2014) reported that OA used positive re-appraisal coping to reduce their stress particularly in the OAH. They hypothesised that the OA live alone in OAH so they try more to cope with the situation emotionally. They further stated those living in OAH tend to take help from others in the OAH thus using social support coping more often. But many times the OA living in the family get all help from family members so they did not do an effort for any work thus having poor coping abilities in case of distress. Scientific studies are yet needed to verify this speculation.

To conclude we found better QoL, coping and adjustment among the FAO residing in the OAH as compared to their community counterparts. These findings though coming from a cross-sectional study with a restricted sample do suggest a need for educating younger generations about aging and their role in keeping the elders healthy and active. Supporting them physically, socially, and environmentally is equally important. Keeping in view poorer coping, adjustment and QoL in the community dwelling OA mental health professionals, researchers and policy makers need to play equal roles for the OA in community and OAH for preventive, therapeutic and rehabilitative health services. The findings are difficult to generalise due to small sample, non-probability sampling technique and involvement of only one OAH. However, these factors seem to provide need base and direction for further research and policy in relation to the well-being of elderly females.

We recommend that larger sample with probability based sampling covering diverse geographic areas should be selected to study the psychosocial aspects of elderly females so that the findings can be generalised and used for policy making.

REFERENCES

Akbar, S., Tiwari, S. C., Tripathi, R. K., Kumar, A., & Pandey, N. M. (2014). Reasons for living of elderly to in old age homes: An exploratory study. *International Journal of Indian Psychology*, *2*(1). https://doi.org/10.25215/0201.029

Amonkar, P., Mankar, M. J., Thatkar, P., Sawardekar, P., Goel, R., & Anjenaya, S. (2018). A comparative study of health status and quality of life of elderly people living in old age homes and within family setup in Raigad District, Maharashtra. *Indian journal of community medicine: official publication of Indian Association of Preventive & Social Medicine*, *43*(1), 10. 10-13. https://doi.org/10.4103/ijcm.IJCM_301_16

Brock, R. L., & Lawrence, E. (2011). Marriage as a risk factor for internalizing disorders: clarifying scope and specificity. *Journal of consulting and clinical psychology*, *79*(5), 577. 577 - 589.

Choi, N. G., Hegel, M. T., Sirrianni, L., Marinucci, M. L., & Bruce, M. L. (2012). Passive coping response to depressive symptoms among low-income homebound older adults: Does it affect depression severity and treatment outcome? *Behaviour research and therapy*, *50*(11), 668-674.

Chou, K. L., & Chi, I. (2000). Comparison between elderly Chinese living alone and those living with others. *Journal of Gerontological Social Work*, *33*(4), 51-66.

Devi, L., & Roopa, K. S. (2013). Quality of life of elderly men and women in institutional and non-institutional settings in urban Bangalore district. *Research Journal of Family, Community and Consumer Sciences*, 1(13), 7-13.

Dey, S., Nambiar, D., Josyula, L. K., Sheikh, K. & Reddy, K. S. (2012). Health of the elderly in India: Challenges of access and affordability. In J. Smith & Majumdar, M. (Eds.), Aging in Asia: Findings from New and Emerging Data Initiatives (pp. 371-386). The National Academic Press.

Dubey, A., Bhasin, S., Gupta, N., & Sharma, N. (2011). A study of elderly living in old age home and within family set-up in Jammu. *Studies on Home and Community Science*, *5*(2), 93-98.

Dutta, E. (1989). Growing old in young India. *Sunday Review, The Times of India*, *17*.

Geo, J., Krishnan, J. B., Benjamin, M., & Kallivayalil, R. A. (2019). First episode depression in women-a study of clinical characteristics through the female reproductive stages in a rural tertiary care center in Kerala. *Kerala Journal of Psychiatry*, *32*(1), 39-45.

Goswami, S., & Deshmukh, P. R. (2018). How "elderly staying alone" cope up with their age and deteriorating health: A qualitative exploration from rural Wardha, Central India. *Indian Journal of Palliative Care*, *24*(4), 465.

Gupta, A., & Kohli, S. (2011). Adjustment patterns and anxiety in community-dwelling elderly: Exploring the gender differences. *Journal of mental Health and Human Behavior*, *16*(1), 29-32.

Heydari-Fard, J., Bagheri-Nesami, M., Shirvani, M. A., & Mohammadpour, R. A. (2014). Association between quality of life and religious coping in older people. *Nursing older people*, 26(3), 24-29.

Jackson, S. L. (2017). Senate Special Committee on Aging Hearings and GAO Reports. *Elder Abuse*, 595-613.

Jamwal, N. (2016). Psychosocial Consequences among Elderly Living In Institutional and Non-Institutional Settings. *The International Journal of Indian Psychology*, *4*(1), 25-31.

Kalavar, J. M., & Jamuna, D. (2011). Aging of Indian women in India: The experience of older women in formal care homes. *Journal of women & aging*, *23*(3), 203-215.

Kotwal, N., & Prabhakar, B. (2009). Physical needs and adjustments made by the elderly. *Studies on Home and Community Science*, *3*(2), 115-221.

Koul, P., Shekhar, C., & Kour, T. Old age and adjustment: Gender differences in Institutionalized non-Institutionalized elderly. *Volume*, *2*, 31-33.

Kulkarni, J., Bharati, V., & Rekhade, N. (2009). Adjustmental problems of old persons. *Shodh, Samiksha aur Mulyankan,* II (9-10), 9-10.

Lazarus R, Folkman S. (1988). Manual for Ways of Coping Questionnaire. *Palo Alto*, CA, 12–40. Folkman, S. & Lazarus, R. S. (1988). Manual for the ways of coping questionnaire. Consulting Psychologists Press.

Lee, J. M. G., Chan, C. Q. H., Low, W. C., Lee, K. H., & Low, L. L. (2020). Health-seeking behaviour of the elderly living alone in an urbanised low-income community in Singapore. Singapore Medical Journal, 61(5), 260-265.

Litwin, H., & Shiovitz-Ezra, S. (2006). The association between activity and wellbeing in later life: what really matters?. *Ageing & Society*, *26*(2), 225-242.

Mehra, H. D., Kasar, N., Waykar, V., & Dhadphale, M. (2005). Evaluation of quality of life, functional and socio-demographic status of residents of old age home. *Ind Psychiatry J*, *14*(1-2), 32-4.

Neale, A. V., Hwalek, M. A., Goodrich, C. S., & Quinn, K. M. (1996). The Illinois elder abuse system: Program description and administrative findings. *The Gerontologist*, *36*(4), 502-511.

O'Donnell, K., Badrick, E., Kumari, M., & Steptoe, A. (2008). Psychological coping styles and cortisol over the day in healthy older adults. *Psychoneuroendocrinology*, *33*(5), 601-611.

Pande, R. (2020). The forgotten widows of Vrindavan in India. In *Religion and Theology: Breakthroughs in Research and Practice* (pp. 61-77). IGI Global.

Rayirala, A., Nallapaneni, N. R., Bhogaraju, A., & Mandadi, G. D. (2016). A cross sectional comparative study assessing the quality of life in elderly living in old age homes and community and association of various factors with QOL. *Journal of Psychiatry*, *2*(1), 48-53.

Roby, J. L., & Sullivan, R. (2000). Adult protection service laws: A comparison of state statutes from definition to case closure. *Journal of Elder Abuse & Neglect*, *12*(3-4), 17-51.

Sandhu, J., & Arora, T. (2003). Institutionalized elderly in Punjab: a sociological study of an old age home. *Help Age India Research and Development Journal*, *9*(3), 24-28.

Saxena, S., Chandiramani, K., & Bhargava, R. (1998). WHOQOL-Hindi: A questionnaire for assessing quality of life in health care settings in India. *National Medical Journal of India*, *11*, 160-165.

Sethi, V., Verma, V., & Singh, U. (2013). Impact of ageing on depression and activities of daily livings in normal elderly subjects living in old age homes and communities of Kanpur, UP. *International Journal of Medical Research & Health Sciences*, *2*(2), 243-249.

Singh, S., Raut, N. B., Subramanyam, A. A., Kamath, R., Pinto, C., & Shanker, S. (2014). Perception of old age and self: A comparative study of elderly females living in community and in old age home. *Journal of Geriatric Mental Health,* 1(1), 32 – 37.

Top, M., & Dikmetaş, E. (2015). Quality of life and attitudes to ageing in T urkish older adults at old people's homes. *Health Expectations*, *18*(2), 288-300.

Varma, G. R., Kusuma, Y. S., & Babu, B. V. (2010). Health-related quality of life of elderly living in the rural community and homes for the elderly in a district of India. *Zeitschrift für Gerontologie und Geriatrie*, *43*(4), 259-263.

Vohra S. (2012). Global Adjustment Scale. Prasad Psycho Corporation.

Whitelock, E., & Ensaff, H. (2018). On your own: Older adults' food choice and dietary habits. Nutrients, 10 (4), 413.

2 Attitude Towards Elderly Among Mental Health Professionals

Aaliya Sultana R*, Arlene Fernandes & Dr Sukriti Banda*****

Abstract

An attitude represents a combination of sentiments, beliefs, and behaviours that one has toward a given object, person, thing, or event. Attitudes endure, but they may also change. Ageism is described as any stereotypes, prejudices and discrimination based on their age. There is considerable evidence that there is some extent of ageism present among mental health professionals and this impacts the manner in which services are offered. In order to achieve these objectives, the researchers conducted a study to determine the attitudes of mental health practitioners toward the elderly. The research included 80 mental health practitioners. The variables were measured using a standardized questionnaire namely Kogan's attitude towards old people scale (Kogan, 1961). The study adopted an exploratory research design. t-test analysis was used for statistical computation of the results and testing their significance. The result concluded from the study showed that there is a significant difference in attitude among mental health professionals with respect to living with/without the elderly.

Keywords: Mental health professionals, Ageism, Elderly, Attitude

Attitude Towards Elderly Among Mental Health Professionals

In their influential book, The Psychology of Attitudes, Eagly and Chaiken (1993, p. 1) define an attitude as 'a psychological tendency that is expressed by evaluating a particular entity with some degree of favour or disfavor'. Entailing in this definition is the notion that detailing an attitude includes the outflow of an evaluative judgment about an object. At the end of the day, deciding on an attitude involves making a decision about whether you like or dislike something, whether you

* Research scholar, Jain (Deemed-to-be-University), Bangalore

** Research scholar, Jain (Deemed-to-be-University), Bangalore

*** Assistant Professor, Jain (Deemed-to-be-University), Bangalore

like or disagree with something, or whether you favour or disfavour a certain problem, object, or person.

"Ageism—defined here as social stigma related to old age or older people (Widrick & Raskin, 2010)". It has been shown that ageism is connected with a shortage of mental health resources accessible to elderly adults (Bartels & Naslund, 2013) and that when unfavourable views regarding ageing are internalised by older adults, serious implications to health and well-being may result (Levy, 2009). The public understanding of the elderly is largely influenced based on their family involvement, leading to behavioural changes and attitudes toward the elderly (Cilingiroglu & Demirel 2004; Akdemir et al., 2007). Society's attitude towards advanced age is extraordinarily impacted by certain qualities including the person's age, previous encounters, social convictions, values, and instructive foundation (Akdemir et al., 2007).

Many variables, including older people's attitudes about mental health care and ageism, are theorised to contribute to elderly people's under-utilization of mental health services (Lagana & Shanks, 2002). According to Lagana and Shanks (2002), there seems to be a general propensity among the present elder generation, as well as the general community, to regard psychological issues as a natural part of the ageing process.Since the early 1960s, there has been documented evidence of professional bias or therapists' inability to connect with older clients. This trend is likely to continue to have a negative influence on therapists' work with older clients in the future (Kastenbaum, 1964). (Danzinger & Welfel, 2000; James & Haley, 1995; Meeks, 1990; Woolfe & Biggs, 1997; Zivian, Larsen et al., 1992).

Misguided judgments regarding ageing and negative attitudes of that populace may impede behaviour towards more older adults, correspondence, and the quality and viability of services provided (Gething et al., 2004). For a reasonable public advancement plan and fruitful execution, nations need to decide how their general public, especially the mental health professionals, see advanced age and the assumptions about the elderly.

Research Problem

The number and percentage of India's elderly are increasing, and programmes designed to assure the comfort and safety of this part of the population should rise in tandem, according to the Ministry of Statistics and Programme Implementation's 'Elderly In India 2021' study. According to the estimate, India would have 138 million senior citizens in 2021, with 67 million males and 71 million women. In 2021, the population census showed an increase of nearly 34 million elderly people compared to the 2011 census. By 2031, it is anticipated that this number would have increased by 56 million (Nahata, 2021). With an increasing population of elderly individuals, there will undoubtedly be a greater need for mental health care. Despite this danger, statistics indicate that mental health professionals are undeserving the elderly (Tomko & Munley, 2013). As many as 63% of older persons with mental problems are not receiving the treatments they need, while just 3% of older adults report visiting a mental health professional, according to the American Psychological Association (2003).

Rationale for the Study

The phenomenon of ageism, shown in the forms of age discrimination and age stereotypes, is believed to be a domain-specific phenomenon (Voss et al., 2018). Ageism in health care and long-term care has been extensively studied (Wyman et al., 2011 & Buttigieg et al, 2018). There has been little emphasis on ageism in the mental health profession. Despite this, a number of research conducted over the past three decades have indicated that mental health professionals have unfavourable opinions of elderly persons in general (Bodner et al., 2018). As a result, mental health professionals' views about the elderly should be taken into consideration and whether living with/without the elderly has an impact on the attitudes of mental health professionals

Review of Literature

From the 1950s to the present, an extensive study on attitudes toward the elderly has shed light on the status, development, and impacts on attitudes toward the elderly. This section discusses mental health professionals' views about the elderly.

Chonody et al. (2014) investigate students', academic teaching staff's, and practitioners' comfort levels while spending time with older persons. The purpose of this study was to establish if terror management theory helped predict fear of being around older adults. They also looked at ageism, interaction with older persons, and established demographic characteristics linked with attitudes toward older adults. The findings revealed that dread of ageing, positive ageism, negative ageism, engagement with older individuals, and sex were all key indicators of comfort when interacting with older adults. Educational initiatives addressing common misconceptions about ageing and older individuals may lead to increased comfort when interacting with older adults.

In order to obtain a better knowledge of the characteristics that impact future psychologists' interest in working with older clients, Koder and Helmes (2008) investigated predictors of student intention of working with older clients. A study of 431 postgraduate psychology students in Australia was assessed training, contact, and attitude factors with respect to the elderly. The strongest predictor of interest was having or expecting to undertake a placement in an aged care facility, with the confidence in dealing with the elderly and favourably anticipating old age being attitude characteristics connected to higher interest. According to hierarchical regression analysis, the amount or quality of interaction with older persons, as well as formal education via ageing-related courses, failed to predict interest. The implications for future psychologist training emphasise the necessity of meaningful therapeutic interactions with elderly clients above mere teaching.

Specifically, the research conducted by LEE et al. (2003), which is presented here, aims to investigate this problem among the future generation of clinical psychologists: those who are presently enrolled in graduate school. The responses to questionnaires provided to 25 clinical psychology training programmes in the United Kingdom comprised 371 trainees. The trainees were asked, among other things, why it could be difficult to recruit to the older adult speciality and how recruiting can be improved. According to the findings, many trainees think that clinical psychology, despite many recent breakthroughs, has less to offer older people than other age

groups, despite many recent advances. The comments demonstrate ageism as well as a dread of ageing and death. The most common suggestions for improving recruitment into the older adult clinical psychology specialization were better placements and training, better promotion by clinical psychologists practising in this speciality, and better support, terms, and conditions.

Research Gap

The existing literature shows that there is an unfavourable aptitude among mental health professionals towards the elderly. However, there is a dearth of studies when it comes to inspecting the component of living with or without the elderly. Therefore, keeping this variable as a significant factor this study aims to explore the attitudes of mental health professionals towards the elderly.

Research Question

Is there a significant difference in attitudes of mental health professionals toward the elderly?

Methodology

Aim

To study the attitudes of mental health professionals toward the elderly.

Specific Objective

To study the difference in attitudes of mental health professionals toward the elderly among those living with/without the elderly.

Hypothesis

H_1: There is a significant difference in attitudes of mental health professionals toward the elderly among those living with/without the elderly.

Research Design

An exploratory research approach was used for the investigation.

Variables

Grouping Variables

Living with/without elderly

Test Variable

Attitudes of mental health professionals

Operational Definitions

Elderly

Individuals who are 65 years or older are commonly referred to as 'elderly' since they have completed a natural process that has been measured chronologically (Orimo et al., 2006).

Mental Health Professionals

Mental health professionals are specialists in providing treatment, rehabilitation or support to people with a mental illness or disability (National Standards for Mental Health Services, 2010).

Attitude

Attitude is an acquired tendency to persistently respond positively or negatively to a certain event (Fishbein & Ajzen, 1975).

Sample

Description

The sample consisted of psychologists, counselling and clinical psychologists identified as practitioners within the age range of 25 to 40 years

Sample Size

The sample consisted of 80 mental health professionals, 42 living with the elderly and 38 living without the elderly were included the study

Sample Method

Snowball and Purposive sampling methods were used in this research.

Inclusion and Exclusion Criteria

Individuals having a minimum of one year of experience as a practitioner in the fields of psychology, counselling, and clinical were included in the research. Individuals pursuing their undergraduate and postgraduate in the field of psychology were excluded.

Tools for Data Collection

Consent Form

The use of an informed consent form ensured that the participants were participating voluntarily in the study. The information obtained was only for the objective of academic or research endeavours.

Socio-Demographic Sheet

A socio-demographic data sheet was constructed to obtain information about the participants, including name/initials, age, gender, urban/rural, educational qualifications, years of experience in the mental health field, living with/without old, marital status, and employment.

Kogan's Attitude Towards Old People Scale

The Kogan Attitude Towards Old People Scale is a 34-item self-report questionnaire designed to assess attitudes toward older adults in a variety of settings (Kogan,1961). Seventeen questions are framed negatively, whereas seventeen are phrased favourably, forming the Older Adult Positive and Older Adult Negative subscales. The response options are given utilizing a 6-point added Likert-type scale (1 = strongly disagree, 6 = strongly agree), with a score of 4 given on the occasion a respondent neglected to address an inquiry. Higher ratings suggest that people have an

unfavourable view of the elderly. Researchers have shown a high degree of test-retest reliability. Cronbach's alpha was found to be .81.

Procedure for Data Collection

Mental health professionals residing in Bangalore and Chennai were approached for data collection through Google form. Prior to participating in the study, the researcher obtained informed consent from the individuals. The Kogan attitude toward elderly scale was used to obtain data from participants (Kogan, 1961). The instructions for filling out the form were provided to the participants and the responses were obtained.

Procedure for Data Analysis

The collected responses were scored and interpreted in accordance with the established criteria. The outcomes of the test were tabulated and evaluated using a statistical tool for social sciences (SPSS) (SPSS- 21 Version). Descriptive statistical measures, such as measures of central tendency, variability, skewness, and kurtosis, were used to analyse the data set. As the current study aimed to explore the attitudes of mental health professionals towards the elderly, t-test analysis was used for statistical computation of the results and testing their significance

Ethical Consideration

A consent form was filled out by every participant in the study. The participants were assured of confidentiality. The participants were given the right to withdraw if they were not willing to continue as mentioned in the consent form. The data was exclusively used for academic reasons.

Results & Analysis

Descriptive Statistics

The present section attempts to analyse the descriptive statistics to determine measures of central tendency (Mean), standard deviation and measures of skewness and kurtosis of the Participant's attitudes toward the elderly

Table 4.1

Results of the Descriptive Statistical Analysis of the Variables of the Study

Dependent Variable	*N*	*Mean*	*SD*	Skewness	Kurtosis
Attitude Towards Elderly	80	135.74	31.029	-.386	-.120

From the above table, it can be inferred that the mean score of the attitude towards the elderly was found to be 134.74 with an SD of 31.029. The skewness and kurtosis were -.386 and -.120 respectively, which clearly indicates that the measures of skewness and kurtosis were identified between the range of -1.96 and +1.96., hence the distribution of data is normal.

Inferential Statistics

The present section attempts to analyse the significant difference in attitudes of mental health professionals with respect to living with/without the elderly

Table 4.2

Results of the Independent Sample t-test

Test Variable	Living with/without Elderly	*N*	*Mean*	*SD*	*t*	*df*	*Sig.*
Attitude Towards Elderly	Living with Elderly	42	154.88	20.973	7. 609	78	.000
	Living without Elderly	38	114.58	26.317			

For the research sample (N=80), the mental health professionals living with the elderly (M=154.88, SD=20.973, n=42) has obtained a higher score on the attitude towards elderly than mental health professionals living without elderly (M=114.58, SD= 26.317, n= 38) and was significant at 0.01 level. Therefore, p<0.001, hence the alternative hypothesis that there is a significant difference in attitudes of mental health professionals with respect to living with/without the elderly has been accepted.

Discussion

The aim of the study is to study the attitudes of mental health professionals towards the elderly. The hypothesis stated that there is a significant difference in attitudes of mental health professionals with respect to living with/without the elderly. *t*-test analysis was used for statistical computation of the results and testing their significance. The results obtained indicated that there is a significant difference in attitudes of mental health professionals with respect to living with/without the elderly. Thus, the formation of attitudes, with the role of family and living circumstances has a substantial impact on the development of these attitudes towards the elderly among mental health professionals. It can also be inferred from the evidence that mental health therapists continue to be less prepared to engage with and provide therapy to older persons than younger adults, have typically unfavourable attitudes about older adults as psychiatric patients, and lack appropriate professional understanding of the geriatric population. Additionally, internalised ageism has an effect on older patients' relationships with the mental health care system and might lead to an unwillingness to seek mental health care services (Bodner et al., 2018). The study has scope for further research with respect to its sample size and also the inclusion of other demographic details.

Limitations and Directions for Future Research

Mental health is one of the contemporary topics that is widely discussed and every individual should have equal access to the same. Professionals working in this field have an important role to play in order to spread this awareness. Therefore, it becomes essential that these professionals have an unbiased attitude towards the entire population. According to research conducted over the past

30 years worldwide, many mental health professionals are unwilling to engage with older adults, have misconceptions about the efficacy of geriatric psychotherapy, and lack professional expertise in the geriatric population (Bodner et al., 2018). Keeping this as a basis, this study explored the attitudes of mental health professionals toward the elderly population and the results obtained helped determine whether living with/without the elderly is influential in shaping these attitudes. However, the study also has a few limitations which will broaden the scope of further research for this study. The sample recruited for this study was minimal in nature and therefore the aspect of generality of the results remains as a limitation to the study. Also, many of the demographic details and environmental factors which play a crucial role in the development of attitudes were not taken into consideration. Larger sample sizes with equal representation from various Indian states could be recruited for future studies. To acquire qualitative data to validate the conclusions of the research, interviews may be done with mental health experts. These interviews can also be used to investigate the many variables that influence their attitudes about the elderly. On the other hand, from the various research evidence, it can be taken into consideration that mental health professionals should be encouraged to seek training programmes for dealing with the elderly. The validity of mental health diagnostic criteria and accessible assessment tools requires more research. Improved cooperation and exchange of information among health professionals in the area of gerontology may result in improved evaluation and treatment capacities in serving the elderly.

Conclusion

The aim of the study was to study the attitudes of mental health professionals towards the elderly. The hypothesis stated that there is a significant difference in attitudes of mental health professionals with respect to living with/without the elderly. t-test analysis was used for statistical computation of the results and testing their significance. The results obtained indicated that there is a significant difference in attitudes of mental health professionals with respect to living with/without the elderly. However, there are certain limitations with respect to the sample recruited and the inclusion of other demographic variables which will further act as directions for future research in this area.

References

Akdemir, N., Çinar, F. İ., & Görgülü, Ü. (2007). Perception of ageing and ageism. *Turkish Journal of Geriatrics,* 10(4), 215-222.

American Psychological Association. (2003a). *Mental health care and older adults: Facts and policy recommendations.* Retrieved March 02, 2022, from http://www.apa.org/ ppo/issues/oldermhfact03 .html

Bartels, S. J., & Naslund, J. A. (2013). The underside of the silver tsunami—Older adults and mental health care. *The New England Journal of Medicine, 368*, 493–496. doi:10.1056/NEJMp1211456

Bodner, E., Palgi, Y., & Wyman, M. F. (2018). Ageism in mental health assessment and treatment of older adults. *International Perspectives on Aging*, 241–262. https://doi.org/10.1007/978-3-319-73820-8_15

Bohner, G., & Dickel, N. (2013). *Attitudes and Attitude Change*. University of Bielefeld.

Briñol, P., Petty, R. E., & Stavraki, M. (2019). *Structure and function of attitudes.* In M. Hogg (Ed.), Oxford Encyclopedia of Social Psychology.

Buttigieg, S. C., Ilinca, S., de Sao Jose, J. M., & Larsson, A. T. (2018). Researching ageism in health-care and long term care. *International Perspectives on Aging*, 493–515. https://doi.org/10.1007/978-3-319-73820-8_29

Chonody, J. M., Webb, S. N., Ranzijn, R., & Bryan, J. (2014). Working with older adults: Predictors of attitudes towards ageing in psychology and Social Work students, faculty, and Practitioners. *Australian Psychologist*, *49*(6), 374–383. https://doi.org/10.1111/ap.12056

Çilingiroğlu, N., & Demirel, S. (2004). Aging and ageism. *Turkish Journal of Geriatrics*, *7*(4), 225-230.

Danzinger, P. R., Welfel, E. R. (2000). Age, gender and health bias in counselors: An empirical analysis. *Journal of Mental Health Counseling, 22*(2), 135-149.

Eagly, A. H., & Chaiken, S. (1993). *The psychology of attitudes*. Harcourt brace Jovanovich college publishers.

Hewstone, M., Stroebe, W., & Jonas, K. (2011). *Introduction to social psychology: A European perspective*. Blackwell Publishing.

James, J. W. & Haley, W. E. (1995). Age and health bias in practicing clinical psychologists. *Psychology and Aging, 10*(4), 610-616.

Kane, R., & Kane, R. (2005). Ageism in healthcare and long-term care. *Generations*, *29*(3), 49-54.

Kastenbaum, R. (1964). The reluctant therapist. In R. Kastenbaum (Ed.), *New thoughts on old age* (pp. 139-145). New York: Springer.

Koder, D.-A., & Helmes, E. (2008). Predictors of interest in working with older adults: A survey of postgraduate trainee psychologists. *Gerontology & Geriatrics Education*, *29*(2), 158–171. https://doi.org/10.1080/02701960802223233

Kogan, N. (1961). Attitudes toward old people: The development of a scale and an examination of correlates. *The Journal of Abnormal and Social Psychology*, *62*(1), 44–54. https://doi.org/10.1037/h0048053

Lagana, L. & Shanks, S. (2002). Mutual biases underlying the problematic relationship between older adults and mental health providers: Any solution in sight? *International Journal of Aging and Human Development, 55*(3), 271-295.

Lee, K. Volans, P. Jane., & Gregory, Nicola (2003). Trainee clinical psychologists' views on recruitment to work with older people. *Ageing and Society*, *23*(1), 83–97. https://doi.org/10.1017/s0144686x02001009

Levy, B. (2009). Stereotype embodiment: A psychosocial approach to aging. *Current Directions in Psychological Science, 18,* 332–336. doi:10.1111/j.14678721.2009.01662.x

Lyons, A., Alba, B., Heywood, W., Fileborn, B., Minichiello, V., Barrett, C., ... & Dow, B. (2018). Experiences of ageism and the mental health of older adults. *Aging & mental health*, *22*(11), 1456-1464.

Meeks, S. (1990). Age bias in the diagnostic decision-making behavior of clinicians. *Professional Psychology: Research and Practice, 21*(4), 279-284.

Nahata, P. (2021, August 14). *In charts: How India is ageing*. BloombergQuint. Retrieved March 2, 2022, from https://www.bloombergquint.com/business/in-charts-how-india-is-ageing

Orimo H, Ito H, Suzuki T, Araki A, Hosoi T, Sawabe M. Reviewing the definition of "elderly" *Geriatrics & gerontology international.* 2006;6(3):149–158. doi:10.1111/j.1447-0594.2006.00341.x.

Tomko, J. K., & Munley, P. H. (2013). Predicting counselling psychologists attitudes and clinical judgments with respect to older adults. *Aging & Mental Health*, *17*(2), 233–241. https://doi.org/10.1080/13607863.2012.715141

Wells, Y., Foreman, P., Gething, L., & Petralia, W. (2004). Nurses' attitudes toward aging and older adults. *Journal of Gerontological Nursing*, *30*(9), 5-9.

Widrick, R. M., & Raskin, J. D. (2010). Age-related stigma and the golden section hypothesis. *Aging & Mental Health, 14*, 375–385. doi:10.1080/13607860903167846

Woolfe, R. & Biggs, S. (1997). Counselling older adults: Issues and awareness. *Counselling Psychology Quarterly, 10*(2), 189-194.

Wyman, M. F., Gum, A., & Arean, P. A. (2011). Psychotherapy with older adults. In M. E. Agronin & G. J. Maletta (Eds.), *Principles and practice of geriatric psychiatry* (pp. 177–203). Philadelphia: Lippincott Williams & Wilkins.

Voss, P., Bodner, E., & Rothermund, K. (2018). Ageism: The relationship between age stereotypes and age discrimination. *International Perspectives on Aging*, 11–31. https://doi.org/10.1007/978-3-319-73820-8_2

Zivian, M. T., Larsen, W., Knox, V. J., Gekoski, W. L. & Hatchette, V. (1992). Psychotherapy for the elderly: Psychotherapists' preferences. *Psychotherapy, 29*(4), 668-674.

3 Relationship Between Self-Compassion and Psychological Wellbeing among Geriatric Population in India

Aditi Dubey* &
Aparajita Chakraborty **

Abstract

In the last few decades, advancement in the field of medical sciences and technology has changed our understanding of the process of aging. Studies suggest increased life expectancy as more individuals are entering into a ripe and active old age. There are multiple interpersonal and intrapersonal factors behind it, one could be self-compassion. Self-compassion (SC) is a construct to describe healthy self-to-self relation, which involves a non-judgmental attitude toward one's pain, inadequacies, and failures, along with the perception that these are part of the greater human experience. It encompasses three fundamental components: (1) self-kindness (2) common humanity and (3) mindfulness. There are growing studies indicating the role of self-compassion in a wide range of desirable psychological outcomes, at inter and intrapersonal levels, especially among adolescents. However, very few studies have been done on the geriatric population. In this regard, the present study investigated the relationships between self-compassion and psychological well-being among 65 old adults (Mean age 67 yrs) using Self-Compassion Scale for Adults Short form and the Psychological Wellbeing Scale (Ryff 18 items). Results indicated that self-compassion is and a few of its components are positively correlated with psychological well-being and few of its components indicate its wider role and application in this population as well and it also throws light on the probable usage of self-compassion-based psychotherapies among this population.

Keywords: Self- Compassion, Psychological wellbeing, Geriatric, Mindfulness

* M. Phil Trainee, Amity Institute of Behavioural Health and Allied Sciences, Amity University, Kolkata Campus

** Assistant Professor, Amity Institute of Behavioural Health and Allied Sciences, Amity University, Kolkata Campus

Introduction

The 14th Dalai Lama, known as Gyalwa Rinpoche said, "We can never obtain peace in the outer world until we make peace with ourselves".

With the advent of technology, exponential industrial growth, development of advanced medicine health care facilities, enhanced lifestyle, healthy nutrition, and exercise there has been an increase in life expectancy of human beings because there are modern equipment and assistant services readily available for the old people. However, studies have found that during late adulthood, many factors like impairment due to declining in health, being widowed, having a low religious commitment are linked to lower self-esteem (Giarrusso and Bengston, 2007) and consequently affect immunity (Walston et al. 2009) putting them at risk of physical illness(Bauer, Jeckel and Luz, 2009). Hence, it is necessary to explore the protective factors that can play a pivotal role in the conceptualization of cases, understanding the goals of psychotherapy, and eventually enhance the overall well-being and quality of life of the elderly. In this regard, a construct called Self-compassion can be introduced. Derived from ancient Buddhist concept, it is a "healthy self-to self-relation", comprising of three core components, namely self-kindness (exhibiting warmth and kindness towards oneself as opposed to harsh criticism); Common humanity (it stands for universality and unavoidability of basic human emotions like pain and suffering) and Mindfulness (Paying attention to the emotions at present without being overly attached to it)(Neff, 2003; Hollis-Walker and Colosimo, 2011). Self Compassion turned out to be a health-promoting behavior as many studies found its link with enhanced optimism, adaptive coping, emotional intelligence, and health benefits as well. (Neff, 2003). A study by Ashley and Mark (2013) on 121 participants with a mean age of 76 years predicted the effect of self-compassion on the positive response towards aging. It is also associated with well-being in later stages of life (Allen et al. 2012). There are studies suggesting a mediating role of self-compassion between adult attachment style and well-being. (Moreira et al., 2016; Neff & Faso, 2015). Psychological well-being or Eudamonic Well-being is a concept developed by Ryff (1989) which describes the optimal functioning of a human being with respect to developmental, personal, and humanistic tradition, thereby focusing on the fulfillment of human potential. (Keyes et al. 2002). Ryffs' model of psychological well-being is based on life-span development and comprises 6 components namely: Self-acceptance, Autonomy, Purpose in life, Environmental mastery, Personal growth, and Positive relation with others. (Homan, 2016). Interestingly, a study by Bendre (2020) on the Indian population found that older adult women were more self-compassionate with better well-being than middle-aged women. As psychological well-being emphasizes the pursuance of human potential, its associated factors are needed to explore as well such as self-compassion.

However, there are very few studies on the Indian population to explore the relationship between self-compassion and psychological well-being. Therefore, the study aims to explore the relationship, if any, between self-compassion and psychological well-being in the geriatric population.

Objective

To explore the relationship between self-compassion and psychological well-being among older adults.

Hypothesis

1. *Ho*: There is no significant relationship between self-compassion and psychological well-being among the geriatric population.
2. *Ho*: There exists no significant relationship between Self-compassion and Self-Acceptance among the geriatric population.
3. *Ho*: There exists no significant relationship between Self-compassion and Autonomy among the geriatric population.
4. *Ho*: There exists no significant relationship between Self-compassion and Purpose in Life among geriatric population.
5. *Ho*: There exists no significant relationship between Self-compassion and Environmental Mastery among the geriatric population.
6. *Ho*: There exists no significant relationship between Self-compassion and Personal Growth among the geriatric population.
7. *Ho*: There exists no significant relationship between Self-compassion and Positive relations with others among the geriatric population.

Methodology

It is a correlational, cross-sectional, non-experimental, and quantitative study with the objective to assess the relationship between self-compassion and psychological well-being among the geriatric population, in India

Participants

65 older adults (45 males and 20 females), of Indian nationality, aged 60 yrs and above, of both sexes, participated in the study, who self-reported to have no current psychopathology or history of psychiatric illness. Data was collected through an online platform with the snowball method.

Measures

1. Self-Compassion Scale Short form of 12 items was employed to assess the self-compassion, developed by Raes et al. (2011) on a 5 point Likert scale ("almost never" to "almost always"). Items were reversed and scored accordingly. This scale has good internal consistency (Raes et al., 2011) and a near-perfect correlation with the original scale (Neff, 2003)
2. Psychological Well-Being was measured by the Psychological well-being scale of Ryff et al. (2010) with 18 items. It comprises 6 domains namely Self-acceptance, Autonomy, Purpose in life, Environmental mastery, Personal growth, and Positive relation with others and was measured on a 7 point Likert scale.

   In the present study, the reliability of these scales were 0.79 and 0.75 respectively with subscales ranging between 0.54 to 0.79.

Results

Table 1

Demographic Details of the Participants

Domain	*Mean*	*SD*
Age	67 yrs	4.7

Table 2

Indicating Correlation between Scores of Self-compassion and Psychological Well-being

Variable	*N*	1	2
Self-Compassion	65	-----	
Psychological well-being	65	.448**	-----

***p < 0.001*

Table 3

Indicating Correlation between Scores of Self-compassion and Subdomains of Psychological Well-being (Autonomy, Environmental Mastery, Purpose in Life, Positive relations with others, Personal Growth and Self-Acceptance)

Variables	N	1	2	3	4	5	6	6
1. Self Compassion	65	---						
2. Psychological well-being – Autonomy	65	.300*	---					
3. Psychological well-being – Environmental Mastery	65	.238	.103	---				
4. Psychological well-being – Personal Growth	65	.244	.332**	.136	---			
5. Psychological well-being – Positive relations with others	65	.309*	.297*	.011	.366**	---		
6. Psychological well-being – Purpose in Life	65	.130	.144	-.440**	.343*	.290*	---	
7. Psychological well-being – self-acceptance	65	.358**	.358**	.150	.501**	.307*	.319*	---

** p < 0.05*

*** p < 0.001*

DISCUSSION

The data was found to be normally distributed as the scores had significant value on Kolmogrov-Smirnov's test(0.200) and Shapiro-Wilk value (0.25) was > 0.005, hence parametric statistics were used. To assess the relationship between these two variables (Self-Compassion and Psychological Well-being), Karl Pearson's correlation was used.

From Table 1, which is describing the demographic details of the participants, it can be inferred that 654 older adults (454 males and 20 females) participated in the study with a mean age of 67 years. Their age range is between 61 and 82 years where 57.8% of the participant's hem reported having any form of physical illness at present such as diabetes (42.9%), heart conditions(17.1%), or others (40%).

From table 2, it can be inferred that there exists a moderate strength of positive correlation (r = 0.448) between the scores of self-compassion and psychological well-being, which is significant at 0.001 level of significance. Hence it can be indicated that an increase in self-compassion will enhance psychological well-being as well. This finding is consistent with the findings of a study by Allen et al., (2012) and Homan (2016), indicating a significant relationship between self-compassion and Eudamonic or psychological well-being. Hence first alternate hypothesis is accepted indicating that there exists a significant relationship between Self-compassion and psychological wellbeing among geriatric population, in India. nstead of being resentful towards the process of ageing, a self-compassionate outlook enables adaptive coping with the aid of kindness, care,deep understanding shared human experience and with objective perspective on negative feelings and emotions (Neff, 2003) Autonomy can be understood as a state of setting and following one's own rule, (Evans, 1983) but the process of ageing has detrimental effects in the latter stage of life. Hence, self-compassion can be one important factor associated with autonomy, as it helps in acceoting the senescence, as a feeling of common experience, universal and inevitable in nature.

From table 3, it can be inferred that self-compassion has a weak but positive correlation with Autonomy among the geriatric population (r=0.300) significant at 0.05 level. As a healthy and functional being, auntonmy plays a crucial role during the process of aging (Perrig-Chiello et al. 2006) Hence, instead of being resentful towards the process of ageing, a self-compassionate outlook enables adaptive coping with the aid of kindness, care,deep understanding shared human experience and with objective perspective on negative feelings and emotions (Neff, 2003) Autonomy can be understood as a state of setting and following one's own rule, (Evans, 1983) but the process of ageing has detrimental effects in the latter stage of life. Hence, self-compassion can be one important factor associated with autonomy, as it helps in acceoting the senescence, as a feeling of common experience, universal and inevitable in nature.

There is a weak positive correlation between self-compassion and positive relations with others (r = .309) which is significant at 0.05 level. As understood by Socioemotional selective theory (Laura Carstensen, 2008), that in due course of time, the older adults become selective about their social network therby giving emphasis to emotional satisfaction from rewarding relationship to enhance positive experiences; Self-compassion can be associated with it as it has interpersonal benefits

like altruism, empathy and social connectedness (Neff et al. 2007; Welp and Brown (2014))

There exists a positive correlation of moderate strength between self-compassion and self-acceptance, siginifcant at 0.001 level. (r = .358) Self compassion comprises of Self-kindness as one if its core elements, which lays emphasis on treating oneself with warmth and care amidst adverse situation. Therefore, it has a relationship with self-acceptance, because they are closely related. Studies found that treating oneself with forgiveness after acceptance will enhance interpersonal relations (Homan, 2016)

Rest subscales of Psychological well-being that is Environmental mastery, personal growth, and purpose in life had positive correlation with self-compassion but not at a significant level. Study by Kim et al (2010) found association between self-compassion and self-appraisal that were associated with growth outcomes.

From the current study, self-compassion was found to be related with psycholigical well-being and few of its domain, among the older adults. Therefore future studies can focus on the effect of these varaibles and on ways of enhancing self-compassion . There are amny studies that show beneficial effect of self-compassion on the eudamonic well- being and promote overall psychological functioing. (Leary et al. 2007; Albertson et al. 2014; Baker and McNulty 2011;) Lastly, psyhotherapies can emphasis on this construct in establishing the goal for treatment to enhance mental health and well-being.

Conclusion

The process of aging has its own challenges to be met. There are extensive researches trying to explore and find protective factors to enhance and facilitate a better experience for the senile. Here, Self-compassion can play a crucial role as it was found to be positvely correlated with psychological well-being and few of its domains like autonomy, positive relations with others and self-acceptance, in the current study. Therefore, more studies can explore its role in therapies to promote well-being among the older adults.

References

Allen, B. A., Goldwasser, E. R., & Leary, M. R. (2012). Self-Compassion and Well-being among Older adults. Self Identity, 11(4), 428 – 453. https://doi.org/10.1080/15298868.2011.595082

Allen, B. A., & Leary, M. R. (2014). Self-compassionate response to aging. Gerontologist, 54(2), 190 - 200. https://doi.org/10.1093/geront/gns204

Bendre, V. M. (2020). Self-compassion, wellbeing and collective family efficacy of women: An intergenerational study. Journal of Psychosocial Research,15(2),629–637.

Ryff, C. D., Almeida, D. M., Ayanian, J. S., Carr, D. S., Cleary, P. D., Coe, C., … Williams, D. (2010). *National Survey of Midlife Development in the United States (MIDUS II), 2004-2006: Documentation of psychosocial constructs and composite variables in MIDUS II Project 1.* Ann Arbor, MI: Inter-university Consortium for Political and Social Research.

Ryff, C. D., & Keyes, C. L. M. (1995). The structure of psychological well-being revisited. *Journal of Personality and Social Psychology*, *69*(4), 719–727.

Raes, F., Pommier, E., Neff, K. D., & Van Gucht, D. (2011). Construction and factorial validation of a short form of the Self-Compassion Scale. Clinical Psychology & Psychotherapy, 18, 250-255.

Ding, N., & Xu, Z. (2021). Attachment, self-esteem, and subjective well-being among people in China aged 50 and over: The role of self-compassion. Social Behavior and Personality: An international journal, 49(5), e10160

Evans, J. G. (1984). Prevention of age-associated loss of autonomy: epidemiological approaches. *Journal of chronic diseases*, *37*(5), 353-363.

Giarrusso, R., Feng, D., & Bengtson, V. L. (2005). The intergenerational-stake phenomenon over 20 years. In M. Silverstein & K. W. Schaie (Eds.), Annual review of gerontology and geriatrics, 2004: Focus on intergenerational relations across time and place (pp. 55–76). Springer Publishing Co.

Walston, J. D., Amy M. M., Caroline N., Leslie A. L., Dani M. F., Nir B., Elad Z., Ludmila P., Pui K., Steve R. C., Charles K., Andrea LaCroix, Russell P. T., Gil A., Ethan M. L., Alex P. R. (2009). Inflammation and stress-related candidate genes, plasma interleukin-6 levels, and longevity in older adults. Experimental Gerontology, 44(5), 350-355.

ISSN 0531-5565,

Kumari, V. (2014). Problems and challenges faced by urban working women in India. [Unpublished Masters' Dissertation]. Department of Humanities and Social Sciences, National Institute of Technology, Odisha.

Lachman, M. E., Ro¨cke, C., Rosnick, C., and Ryff, C. D. (2008). Realism and illusion in Americans' temporal views of their life satisfaction: Age differences in reconstructing the past and anticipating the future. Association for Psychological Science, 19(9), 889-897.

Lifshitz, R., Nimrod, G. and Bachner, Y. G. (2019). Spirituality and wellbeing in later life: a multidimensional approach. Aging & Mental Health, 23, 984-991.

Merz, E., Schuengel, C., & Schulze, H. (2009). Intergenerational relations across 4 years: Well-being is affected by quality, not by support exchange. The Gerontologist, 49 (4), 536-548.

Neff, K. (2017). Self-Compassion and Psychological Wellbeing. In E. Seppälä, E. Simon-Thomas, S. Brown, M. Caroline, C. Cameron & J. Doty Ed.), Oxford Handbook of Compassion Science (pp 1-42). Oxford University Press.

Neff, K. (2011). Self-Compassion: The Proven Power of Being Kind to Yourself. Harper Collins.

Neff, K. D. (2003a). The development and validation of a scale to measure self-compassion. Self and Identity, 2, 223-250.

Phillips, W. J. and Ferguson, S. J. (2013). Self-Compassion: A resource for positive aging. Journal of Gerontology, 68(4), 529-539.

Shin, N. Y., and Lim, Y. - J. (2019). Contribution of self-compassion to positive mental health among Korean university students. International Journal of Psychology, 54(6), 800 – 806. https//doi.org/10.1002/ijop.12527

Perrig-Chiello, P., Perrig, W. J., Uebelbacher, A., & Stähelin, H. B. (2006). Impact of physical and psychological resources on functional autonomy in old age. *Psychology, health & medicine*, *11*(4), 470-482.

4 Psychological Distress among Elderly Naga Cancer Patients in Relation with Hope and Social Support

Sashirenla Mollier*

Abstract

Objective: The study was conducted to determine the prevalence of psychological distress among elderly Naga cancer patients and find its relationship with Hope and Social support.

Methods: The study followed purposive sampling method which included 48 elderly Naga cancer patients presently undergoing treatment in various hospitals across Nagaland. Data were collected using Herth Hope Index (HHI) for assessing the levels of hope, Berlin Social Support Scale (BSSS) and DASS-21 (Depression, Anxiety and Stress scale-21) to assess the levels of depression, anxiety and stress. The data was analysed by using SPSS-v21.

Results: Out of the 48 cancer patients, there were 36 males and 12 females. Among the total, it was seen that 45%, 60% and 66% of the patients were having some levels of depression, anxiety and stress respectively, while the others were found to be normal. Pearson Product Moment Correlation revealed that there was significant negative correlation between hope and psychological distress i.e., depression (r= -.644, p< .001), anxiety (r= -.498, p< .001) and stress (r= -.479, p< .001) of elderly Naga cancer patients. On the other hand, the study showed no significant correlation between social support and psychological distress of elderly Naga cancer patients (p<.01).

Conclusion: Psychological distress is found to be prevalent among elderly cancer patients. The findings of the study highlight the need for psychological care in the treatment of elderly cancer patients.

Keywords: Cancer, Psychological distress, Hope, Social support, Elderly

* Research Scholar, Psychology department, Nagaland University

Introduction

Cancer is life threatening, fear, despair and dejection associated, and its diagnosis is perceived by many to be their death sentence. It is a disease causing a biological disturbance where there is no organ in the human body in which cancer cannot develop. It is reported in study done by Given & Given (2009) that approximately 60% of cancer incident and 70% of cancer mortality occurs among adults aged 65 and older. This shows that cancer affects the elderly people greatly as much as it affects the younger ones. Coupled with the burden of being aged and weary among the elderly, the symptoms of cancer will much affect physically as well as emotionally and psychologically adding more despair to one's life. It is important that psychological distress particularly depression, anxiety and stress be considered a necessity for patients to undergo screening as it remains to be a strong contributor in interfering with the patients' health promotion.

Nagaland is reported to have enormous growth of cancer patients and today it has become like a trend among the Nagas on being diagnosed with this disease. When observed, the older generation in general tend to have very light concern in undergoing regular medical check-ups or in particular lack knowledge about cancer. This could be a reason why illnesses such as cancer remain undiagnosed and untreated among the older people. Additionally, we might also find that many people live within a limited budget provision hampering one to go ahead for treatment. Due to these possible reasons, high prevalence rate of cancer is seen among the elderly Nagas where many are diagnosed only in late stage, resulting in high rate of morbidity and mortality. It should also be understood that with increasing severity of the illness, psychological disorders on the other hand also ushers wherein, a patients' quality of life is likely to worsen. Thus along with treating the disease, mental health should also be considered important. The present study thus felt the need to find out the levels of psychological distress such as depression, anxiety and stress among elderly Nagas afflicted with cancer and how hope and perceived social support as a positive aspect is helping one to cope with the illness.

Objectives

1. To find out the prevalence of psychological distress among elderly Naga cancer patients.
2. To find out the correlation between Hope and psychological distress levels of elderly Naga cancer patients.
3. To find out the correlation between Perceived Social Support and psychological distress levels of elderly Naga cancer patients.

Methodology

Sampling technique: The study was conducted by following purposive sampling method which is a non-probability sampling method in which a researcher selects the respondents according to his/her convenience that is based on the typicality of the cases to be included in the sample.

Sampling size: It included 48 elderly Naga cancer patients presently undergoing treatment in various hospitals which has provisions specifically for treating cancer patients across Nagaland. Besides, data were also collected from patients who were being monitored at home. These were

patients availing treatment from outside the State of Nagaland or those who visit hospital only on a basis of monthly regular treatment. The study excluded patients who were admitted in Intensive Care Unit (ICU) at the time of data collection and those who exhibit symptoms of mental disorders. Data were collected between the years 2021.

Tools used: Data were collected using DASS-21 (Depression, Anxiety and Stress scale-21) to assess the levels of depression, anxiety and stress, Herth Hope Index (HHI) for assessing the levels of hope and Berlin Social Support Scale (BSSS) to assess the levels of social support. The data was analysed by using SPSS-v21. Mean, standard deviation, Pearson product correlation was used to analyze the data.

Results

Out of the 48 elderly Naga cancer patients, there were 36 males and 12 females. Among the total, it was found that 45%, 60% and 66% of the patients were having some levels of depression, anxiety and stress respectively, while the others were found to be normal. The following Figures (Figuresno.1, 2 and 3) show the severity levels of depression, anxiety and stress precisely according to DASS-21 scale.

Figure 1

Showing severity of depression among elderly Naga cancer patients.

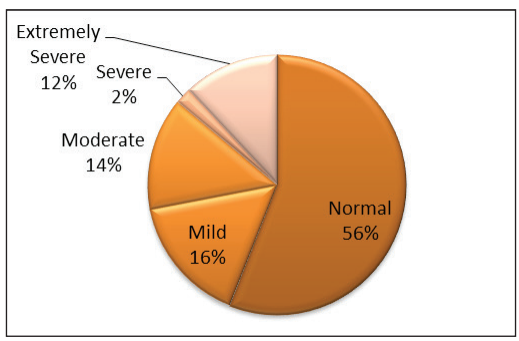

Figure 2:

Showing severity of anxiety among elderly Naga cancer patients.

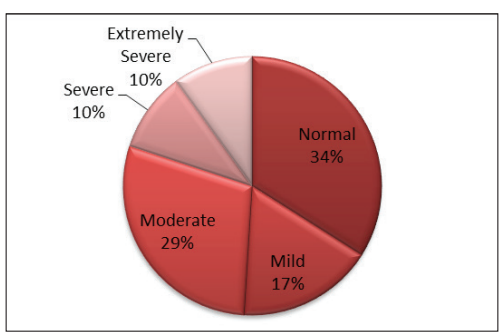

Figure 3:

Showing severity of stress among elderly Naga cancer patients.

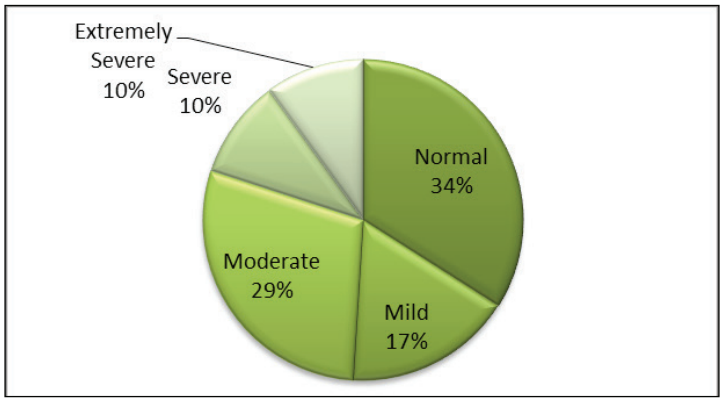

To evaluate the correlation between hope and psychological distress, Pearson Product Correlation was used which revealed that there is significant negative correlation between hope and psychological distress depression (r= -.644, p< .001), anxiety (r= -.498, p< .001) and stress (r= -.479, p< .001) of elderly Naga cancer patients. This shows that an increase in hope leads to decrease in depression among elderly Naga cancer patients. Table 1 shows mean, standard deviation and correlation between hope and psychological distress among elderly Naga cancer patients.

Table 1

Mean, Standard Deviation and Correlation between Hope and Depression Among Naga Cancer Patients.

Psychological Distress	*Mean*	*SD*	*r*
Depression among cancer patients	2.02	1.39	-.644
Anxiety among cancer patients	2.29	1.38	-.498
Stress among cancer patients	2.48	1.33	-.479

*p< .001

To evaluate the correlation between perceived social support and psychological distress, Pearson Product Correlation was used which revealed that there is no significant correlation between social support and psychological distress of elderly Naga cancer patients (p<.01).

Discussion

Palliative care to elderly people with cancer includes Palliative care to elderly people with cancer includes several issues. It will include the treatment to win over cancer, dealing to overcome psychological distresses which usually come as a package with cancer diagnosis and along with

the general old age care. The findings of the present study showed that there is prevalence of psychological distress namely, depression, anxiety and stress with 45%, 60% and 66% respectively while the others were found to be normal. Similar finding was reported by study done by Hong el al. (2015) which shows that psychological distress is exhibited among elderly cancer patients to some degree. Study done by Jahanara (2007) reports that hope is positively related to psychological well-being and negatively correlated to psychological problems. The result of the present study is consistent with this finding which shows that hope and psychological distress are negatively correlated. This could be so because hope is regarded as a feeling that allows one to sustain belief in dire circumstances. Perceived social support which is considered as an individual feeling of being valued, cared and loved by others showed no significant correlation between social support and psychological distress of elderly Naga cancer patients ($p<.01$).

Conclusion

The findings of the study highlight the need for psychological care in the treatment of elderly cancer patients through various ways such as giving frequent counselling and also providing support by professionals, caregivers, families and friends. It is important to note that psychological distress is common among elderly cancer patients and can greatly affect them in various ways. The result also suggests that hope and perceived social support may be considered an important dimension in reducing psychological distress and its symptoms.

References

Given, B., & Given, C. (2009). Older adults and cancer treatment. *PMC* https://doi.org/10.1002/cncr.23939

Hong, J., Zhang, W., Song, Y., Xie, L., & Wang, W. (2015). Psychological distress in elderly cancer patients. *International Journal of nursing sciences. 2*(1), 23-27. https://doi.org/10.1016/j.ijnss.2015.02.006

Jahanara M. (2017). Optimism, hope and mental health: Optimism, hope, psychological well being and psychological distress among students, university of Pune, India. International *Journal of Psychological and Behavioral Sciences. 11* (8), 452-455. https://doi.org/10.5281/zenodo.1131553

5 Diabetes and the Elderly in the Post-Pandemic World

Pavithra Parthasarathy* &
Dr. Pooja Varma**

Abstract

This paper aims to discuss the impact of COVID-19 on the management of diabetes in the elderly. The initial days of the pandemic focused on identifying treatments and controlling the spread of COVID-19. Individuals with pre-existing chronic conditions, like diabetes and those older than 60 years, were a high-risk population and to experience more severe symptoms of the disease. COVID-19 has led to the development of the new normal. This population has dealt with changes both physically and mentally. Apart from problems relating to diabetes, social isolation, dependence on technology, lack of access to health care and medication, lifestyle changes, loss of family/ friends to COVID, changes in the economic conditions in the family are some of the issues addressed in this paper. On the psychological aspect, dealing with the stress due to COVID, anxiety, depression, fears, contamination, social isolation, lack of social support, emotional outbursts, helplessness , and sleep issues are common symptoms that directly impacted lifestyle therefore on their diabetes management. While the development of psychological issues is on the rise, lack of awareness and the stigma attached to seeking help adds as an additional cause of concern among patients with diabetes. This paper highlights the key issues of elderly diabetic individuals in the post-pandemic world.

Keywords: COVID-19, Elderly, Diabetes, Lifestyle management, Post-pandemic world

Introduction

Diabetes mellitus is a complex chronic disease that occurs when the pancreas does not produce enough insulin or the body cannot use its insulin. In 1985, 30 million people suffered from diabetes, 537 million in 2021 and it is estimated to affect about 783 million by 2045. (Abdi et

* Research Scholar,Jain (Deemed-to-be University), Bangalore

** HOD, Department of Psychology, Jain (Deemed-to-be University), Bangalore

al., 2020, International Diabetes Federation , 2021). In 2021, about 74.2 million Indians were diagnosed with diabetes. ("Down to Earth", 2021). While diabetes was considered to affect the "wealthy Western" nations, it has become a major cause for concern among the low and middle-income countries affecting even the younger age groups (Pradeepa & Vishwanathan, 2021) Physical inactivity, imbalanced diet and abdominal obesity are important risk factors for the development of type 2 Diabetes mellitus (T2DM). Despite the obvious magnitude of the problem, only around 50-75% of Indians showed an awareness of the condition (Deepa et al., 2014). The macrovascular (strokes, peripheral vascular diseases and coronary artery disease) and microvascular (neuropathy, nephropathy and retinopathy) complications further add to the woes of people with diabetes (Misra et al., 2014). The key factors that play a role in diabetes management include food insecurities, homelessness, literacy, language barriers, psychological factors like cognitive dysfunctions, personality factors, health literacy and health behaviours.

The spread of COVID-19 began in December 2019 with a catastrophic growth by 2020. The World Health Organisation declared it as a state of a pandemic in March 2020(Cucinotta & Vanelli, 2020). The first case in India was declared in January 2020(Andrews et al., 2020). With the spread of the pandemic, the government initiated social distancing and travel restrictions. In a short period, a complete lockdown was announced in India. People were asked to stay indoors and avoid contact with the outside world. The government arranged for the essentials to be available in all areas, to avoid crowding and the spread of COVID.

The psychological impact of COVID is far worse than the medical impact. Society as a whole experienced panic, anxiety, fear, emotional outbursts, stigma and mass hysteria(Banerjee, 2020). People with chronic health conditions like diabetes and the elderly were especially vulnerable to these symptoms. American Diabetes Association has identified that the presence of diabetes increases the severity and complications of symptoms of COVID (American Diabetes Association, 2020). Along with the risk posed due to chronic illness, psychological symptoms can accelerate, leading to the development of psychiatric/psychological disorders. The strain of psychological illness in turn will worsen the experience of symptoms. Post- COVID/post-pandemic refers to the time after the third wave of COVID. This paper aims to understand the psychological issues in the post COVID world, in the elderly patients of diabetes in India.

The objective of this paper is to identify the common problems faced by elderly patients with diabetes in the post-pandemic world.

Methods

Secondary data were accessed on PubMed and Google Scholar for studies between 2020- 2022 Feb:

- Elderly diabetes self-care
- Elderly diabetes self-management

- Elderly diabetes self-management education
- Elderly diabetes self-management India
- While all studies included contained patients of diabetes, there were limited information specific to self-management behaviours in the elderly population.

Key findings

The initial search for diabetes self-management during COVID-19 identified many challenges faced by individuals with diabetes. No studies specifically targeted the elderly population. This article compares and contrasts the effects of covid faced by elderly patients with diabetes.

Studies during the pandemic suggested that contracting covid lead to increased blood sugar levels. (ADA, 2020) This finding suggests that covid has a direct impact on blood sugar levels. Individuals with pre-existing diabetes were more vulnerable to serious symptoms of covid. The risk increases with age and therefore it is important to address the issues faced by elderly patients with diabetes. Diet, physical activity, medications and monitoring – the key factors in diabetes self-management are discussed in comparison with the initial pandemic period.

The first and second waves of covid had a strong impact on the lifestyle of people with diabetes. Lack of contact with the external world led to increased emotional experiences, loneliness, frustration and boredom (Banerjee et al., 2020). Increased access to information regarding no of positive cases, number of deaths and local containment zones lead to increased fear and anxiety. This circular relationship of boredom, information overload, lack of motivation and a sense of helplessness caused erratic changes in sugar levels. Among older adults, the magnitude of such problems increased multifold. Digital solutions lead to increased reliance on technology, which has been an added burden for the elderly due to the digital divide.

1. **Diet:** Initial lockdown period led to major changes in eating patterns. While the pandemic has fuelled unhealthy food practices, some positive changes were also noticed. Studies indicated increased food quantities and food groups among patients with diabetes. Lack of availability of diabetic diet, increased access to unhealthy food, erratic meal timings, increased quantity of food, snacking, increased food cravings, changes in sleep patterns, loss of appetite, no socialising, comfort eating are some common changes noticed during the lockdown period. Kishimoto et al. (2021) and Ruiz-Roso et al. (2020) state that it involved potential health consequences, especially on patients with Type 2 Diabetes Mellitus (T2DM).

   Among the older adults, mixed results were obtained on eating patterns and diet quality. Older adults were able to maintain dietary patterns better than the younger population but increased sugary foods and increased snacking led to worsened glucose levels. (Nicklett et al., 2021).

2. **Physical activity:** Lockdowns and travel restrictions have had a huge impact on the physical activity level among older adults. Unhealthy nutritional needs along with increased sedentary behaviours have resulted in erratic blood glucose levels.(Grabowski et al., 2021) Disruption of daily life activities along with lack of physical space created problems in reaching the optimal level of physical activity. From regular exercise, cessation of all forms of physical movement

caused increased weight gain and problems associated with weight management. Physical activity not just helps in blood sugar control but also in the prevention of complications and building immunity.

The elderly population specifically faced greater problems in managing their physical activity regimes. Inability to go out, fear of covid along with the need to maintain their sugar levels and overall health acted as an additional stressor.

3. **Medications and monitoring:** Access to medications took a major turn during covid. Inability to visit doctors, non-availability of doctors, lack of transportation and restrictions led to changing trends in diabetes management. Monitoring of glucose levels and other testing parameters were not available. This led to more wait time for testing and delayed results. Monitoring day to day changes in the sugar levels along with the other changes in diet and physical activities caused increasing stress levels. With a lack of boundaries between work and personal life, monitoring was not considered a priority.

   Among the three main factors in diabetes management, diet and physical activity seemed to have more impact in comparison with medications and monitoring. Changes in the financial conditions of the household, the loss of family members and friends resulted in a change in mindset. Now, after the end of the third wave, a new normal has set in. While elderly diabetes patients had an initial difficulty managing the changes, learning newer coping mechanisms along with the added advantage of having social support from family and friends, has led to better management of blood sugar levels. The use of technology like home monitoring kits, apps to manage diet, physical activity, sleep trackers, step trackers which narrow the digital divide have become a boon in the post covid world. Initial studies indicated that older adults had better emotional regulation and resilience, the long-term effect especially among elderly diabetics needs to be studied (Vahia et al., 2020).

Conclusion

The post-pandemic period has resulted in a better understanding of diabetes management among the elderly. Lockdown resulted in making healthier food choices. Understanding the role of nutrition along with a need to stay healthy promoted the development of healthy behaviours. While restrictions lead to innovation in managing physical activity, online yoga, Zumba classes, devices to track activity levels have assisted in the improvement of healthy behaviours. As with any major event, COVID-19 initially lead to many complications and problems. With time, individuals have learnt to cope and even improve living conditions.

References

Abdi, A., Jalilian, M., Sarbarzeh, P. A., & Vlaisavljevic, Z. (2020). Diabetes and COVID-19: A systematic review on the current evidences. *Diabetes Research and Clinical Practice*, *166*, 108347. https://doi.org/10.1016/J.DIABRES.2020.108347

American Diabetes Association. (2020). *Frequently Asked Questions: COVID-19 and Diabetes | ADA*. American Diabetes Association. https://www.diabetes.org/coronavirus-COVID-19/how-coronavirus-impacts-people-with-diabetes

Andrews, M. A., Areekal, B., Rajesh, K., Krishnan, J., Suryakala, R., Krishnan, B., Muraly, C., & Santhosh, P. (2020). First confirmed case of COVID-19 infection in India: A case report. *Indian Journal of Medical Research*, *151*(5), 490–492. https://doi.org/10.4103/IJMR.IJMR_2131_20

As told to Parliament : Diabetes prevalence to grow almost 70% by 2045. (2021, December 6). *Down to Earth*. https://www.downtoearth.org.in/news/agriculture/as-told-to-parliament-december-3-2021-diabetes-prevalence-to-grow-almost-70-by-2045-80537.

Banerjee, D. (2020). The COVID-19 outbreak: Crucial role the psychiatrists can play. *Asian Journal of Psychiatry*, *50,* 102014. https://doi.org/10.1016/J.AJP.2020.102014

Banerjee, M., Chakraborty, S., & Pal, R. (2020). Diabetes self-management amid COVID-19 pandemic. *Diabetes and Metabolic Syndrome: Clinical Research and Reviews*, *14*(4), 351–354. https://doi.org/10.1016/j.dsx.2020.04.013

Cucinotta, D., & Vanelli, M. (2020). WHO Declares COVID-19 a Pandemic. *Acta Bio-Medica : Atenei Parmensis*, *91*(1), 157–160. https://doi.org/10.23750/ABM.V91I1.9397

Deepa M, Bhansali A, Anjana RM, et al. (2014). Knowledge and awareness of diabetes in urban and rural India: the Indian Council of Medical Research India Diabetes Study (Phase I): Indian Council of Medical Research India Diabetes 4. *Indian journal of endocrinology and metabolism*, *18*(3), 379-385. https://doi.org/10.4103/2230-8210.131191

Grabowski, D., Overgaard, M., Meldgaard, J., Johansen, L. B., & Willaing, I. (2021). Disrupted Self-Management and Adaption to New Diabetes Routines: A Qualitative Study of How People with Diabetes Managed Their Illness during the COVID-19 Lockdown. *Diabetology 2021, 2*(1), 1–15. https://doi.org/10.3390/DIABETOLOGY2010001

International Diabetes Federation. IDF Diabetes Atlas, 10th ed. Brussels, Belgium: International Diabetes Federation; 2021. https://www.diabetesatlas.org

Kishimoto, M., Ishikawa, T., & Odawara, M. (2021). Behavioral changes in patients with diabetes during the COVID-19 pandemic. *Diabetology International*, *12*(2), 241. https://doi.org/10.1007/S13340-020-00467-1

Misra, A., Ramchandran, A., Jayawardena, R., Shrivastava, U., Snehalatha, C. (2014) Diabetes in South Asians. *Diabetes Medicine, 31*(10):1153-62. https://doi.org/10.1111/dme.12540

Nicklett, E. J., Johnson, K. E., Troy, L. M., Vartak, M., & Reiter, A. (2021). Food Access, Diet Quality, and Nutritional Status of Older Adults During COVID-19: A Scoping Review. *Frontiers in Public Health*, *9*, 1943. https://doi.org/10.3389/FPUBH.2021.763994/BIBTEX

Pradeepa, R., & Mohan, V. (2021). Epidemiology of type 2 diabetes in India. *Indian journal of ophthalmology*, *69*(11), 2932–2938. https://doi.org/10.4103/ijo.IJO_1627_21

Ruiz-Roso, M. B., Knott-Torcal, C., Matilla-Escalante, D. C., Garcimartín, A., Sampedro-Nuñez, M. A., Dávalos, A., & Marazuela, M. (2020). COVID-19 Lockdown and Changes of the Dietary Pattern and Physical Activity Habits in a Cohort of Patients with Type 2 Diabetes Mellitus. *Nutrients*, *12*(8), 1–16. https://doi.org/10.3390/NU12082327

Vahia, I. V., Jeste, D. V., & Reynolds, C. F. (2020). Older Adults and the Mental Health Effects of COVID-19. *JAMA*, *324*(22), 2253–2254. https://doi.org/10.1001/JAMA.2020.21753

6 A Positive Psychology-Based Intervention Model (C. A. R. E) for Pain Catastrophizing and Well-being among the Elderly during the pandemic: A Randomized Control Trial

Sudha. R* & S. Gayatridevi. **

Abstract

Ageing is a natural process in life. Ageing brings with it experience, wisdom, courage, knowledge and on the flip side pain, illness and loss. This may bring psychological ill-being and stress. Positive Psychology postulates that the absence of "Negative", that is the absence of disease, does not ensure Well-being. Applying this construct, an intervention model was constructed and named "The C. A. R. E intervention Model". C. A. R. E is an acronym that can be expanded as follows:

C: stands for Compassion and Self-Compassion

A: stands for Achieving a Purpose in Life

R: stands for Relationship Building

E: stands for Enhancing Positive Emotions

The C. A. R. E intervention consisted of activities and exercises designed to develop compassion and self-compassion, achieve a sense of purpose in life, build relationships and enhance positive emotions.

The sample of 68 elderly persons both male and female who were COVID survivors was selected through purposive sampling. They were then randomly assigned into an experimental group and a waitlist control group of 34 elders in each group. They were assessed initially using the Pain Catastrophization Scale (Sullivan, 1995), and the WHO Well Being Scale (WHO, 1998).

* Ph. D Research Scholar, Department of Psychology, Avinashilingam Institute for Home Science and Higher Education for Women, Coimbatore

** Professor and Head, Department of Psychology, Avinashilingam Institute for Home Science and Higher Education for Women, Coimbatore

The C. A. R. E intervention was then administered over the duration of 28 sessions, four days a week for the experimental group. The assessments were repeated after the intervention. Results indicated that the C. A. R. E intervention was successful in reducing the severity of the pain and also improving the Well-being of the elders in the experimental group.

Keywords: Pain Catastrophization, Well-being, Positive Psychology, Intervention

Introduction

Old age is a period of life that brings physical ailments, pains and aches and many other issues. By the time people reach the age of 60 or 65, many of them become insecure due to loss of employment due to retirement, leading to economic dependence on their children. When this is combined with physical ailments, fatigue and exhaustion over reduced functionality, and a sense of insecurity, the problems multiply and tends to have an effect on the well-being of the elderly. An additional burden may be emotional and psychological troubles caused by family issues or illness or the loss of a spouse. All these varied issues lead to a lack of a feeling of wellness or stress, anxiety, depression and various other psychological issues. Such an influx of negativity calls for building positive thoughts and emotions to cope and strengthen their well-being. Aches and pains are a coming problem in ageing. Many times such pains are combined with worrying or rumination about the pain. This combined onslaught causes pain catastrophization. Catastrophization can be defined as, "an exaggerated negative mental set brought to bear during actual or anticipated painful experience" (Sullivan et al., 2001). This explanatory style (how one interprets and explains events to oneself) of an individual yield a clear idea of an individual's worry about the pain, accompanied by feelings of helplessness experienced or the magnification of the sensation of pain, which all leads to catastrophization of the pain. As the elderly face the pain, their mental health deteriorates and they start thinking and worrying about the pain, which in turn, intensifies the pain.

Positive Psychology is a relatively new branch of psychology founded by Martin Seligman and his colleagues. This branch of psychology postulates that the absence of negative does not ensure positive well-being. Well-being needs to be built by ensuring "Flourishing", that is, a state of mind characterised by positive emotional and social functioning. This state of flourishing that equates to a very high form of well-being can be created by deliberately focusing on constructing and maintaining positive thoughts and emotions. This paper attempts to create one such positive psychology-based intervention model to alleviate the pain catastrophization among the elderly and hence build their well-being. Applying this construct, an intervention model was constructed and named "The C. A. R. E intervention Model". C. A. R. E is an acronym that can be expanded as follows:

C: stands for Compassion and Self-Compassion

A: stands for Achieving a Purpose in Life

R: stands for Relationship Building

E: stands for Enhancing Positive Emotions

The C. A. R. E intervention consisted of activities and exercises designed to develop compassion and self-compassion, achieve a sense of purpose in life, build relationships and enhance positive emotions.

A brief review of available literature was conducted by the researchers in order to better understand the constructs taken up for study. In a study on the effect of positive psychology-based intervention modules in elderly participants, Bar-Tur (2021) developed a Mental Fitness programme and found it effective for the well being of the elderly. In a review on the effectiveness of positive psychology interventions for positive ageing, Marks (2021) reported that such interventions have the maximum effect when they are given in the residences of the elderly. It was also reported that such positive psychology applications are a cost-effective and promising means to ensure health promotion ventures for the elderly. These positive psychology interventions help to reduce the negative psychological complications associated with ageing such as depression and loneliness. Verhiel et al. (2019) in a study of the efficacy of positive psychology intervention for pain intensity and physical limitations among the elderly, reported that among all the positive psychology constructs, satisfaction with life and mindfulness played important roles. Also, skill-based interventions focusing on building mindfulness was found very effective in reducing pain intensity.

In a study on the response to the COVID crisis, Scheibe et al (2021) found that the response of the aged population was better as they used the time of crisis for personal growth. This was manifested by the better resilience scores of the older participants compared to the younger participants. An earlier study by Rowe and Kahn (2017) also reported that interventions enhance the successful ageing process as the concept of ageing is multidimensional involving physical, social and psychological domains. Reker and Wong (2012) reported that psychosocial adaptation among the elderly can be better achieved by enhancing the concept of the personal meaning of life. This concept of personal meaning is said to comprise a global meaning that is generalized and a situational meaning of life that is dynamic and changes as per situational demands. In a comparative study of self-reported well being, it was reported by Hillman (2015) that the ages 82 to 85 could have the maximum well being if they are given targeted practices to develop their character strengths and virtues. Sudha and Gayatridevi (2021) in a positive psychology-based intervention study on COVID survivors found that intervention based on compassion, achieving a purpose in life, relationship building and enhancing positive emotions are effective in reducing negative psychological complications such as depression and loneliness.

Based on the above review of literature it can be inferred that the elderly are a population that is highly vulnerable due to their physical, psychological and social decline. Positive psychology focuses on enhancing positive constructs such as happiness, optimism, hope and compassion will have an effect on a satisfied, and contented ageing process.

Method

The study on "A Positive Psychology-Based Intervention Model (C. A. R. E) for Pain Catastrophizing and Well-being among the Elderly during the pandemic: A Randomized Control Trial" was conducted with the objectives of identifying the correlation between pain catastrophization

(levels of rumination, magnification and helplessness) and well-being among the elderly and understanding the efficacy of the C. A. R. E intervention using a randomized control trial. The hypotheses framed for the study were as follows:

Ho There is no significant relationship between rumination, magnification, helplessness and well-being among the elderly

Ho There is no significant difference in the Pre-test and Post-test phases of the experimental group in the levels of rumination, magnification, helplessness and well being among the elderly

Ho There is no significant difference in the levels of rumination, magnification, helplessness and well-being of the elderly between the experimental group and the waitlist control group.

The sample consisted of 68 elderly persons both male and female who were COVID survivors selected through purposive sampling. They were then randomly assigned into an experimental group and a waitlist control group of 34 elders in each group. They were assessed initially using the:

1. The Pain Catastrophizing Scale (PCS) (Sullivan, 1995) consists of 13 items with a five-point scale and three subscales namely, rumination, magnification and helplessness. Reliability established through Cronbach alpha values is 0.87 and validity are established through construct validity. (Sullivan, 1995)
2. WHO Well Being Scale (WHO-5, 1998) consisting of 5 items measuring the well-being of an individual.

C. A. R. E Intervention Module

It includes Relaxation Exercises such as Counted Breathing, Deep Breathing, Breathing from the Stomach, and Jacobson's Progressive Muscle Relaxation (for a period of 30 to 40 minutes every day in the morning)

The C. A. R. E intervention with a sample of the activities used in the intervention is given below:

On day one, the focus of the activities was on developing Compassion. This activity required the participant to choose a kind task (Donate money/time/clothing, smile and wish someone when they least expect it, show concern to someone, give your time and pleasantness to someone from your family).

Day two consisted of activities striving to build Optimism. The participant is asked to deliberately consider an adverse event that has happened to them in the past 15 days and look at the advantages/positives deliberately hidden behind the negative emotion associated. (Examples given to the participants). They are then required to write down a thought opposed to the negative thinking associated with the adverse event.

Day three comprised of helping to build Resilience. Here, the participant must think of a stressful situation weighing them down. They are asked to write it down in detail. Also, to write down ways in which they believe they can challenge themself and bounce back from the negativity. They are asked to imagine that the stressful event is a cloud spreading over them. They are then required to break through the barrier and build on thoughts focusing on building the strength to bounce back.

Similarly, each day comprises activities to build one particular positive psychology construct. The constructs included were creating a sense of purpose, building good relationships, constructing one positive emotion of their choice, developing self-compassion, understanding and practising gratitude even for small things in life, exploring their strengths through an activity, building hope and happiness, spreading smiles, and overcoming obstacles in the path to positivity.

The sample comprised of 68 elderly persons both male and female who were COVID survivors were selected through purposive sampling. They were then randomly assigned into an experimental group and a wait-list control group of 34 elders in each group. They were assessed initially using the Pain Catastrophization Scale (Sullivan, 1995), and the WHO Well Being Scale (WHO, 1998). The C. A. R. E intervention was then administered over the duration of 28 sessions, four days a week for the experimental group. The assessments were repeated after the intervention.

Results

The data collected was analysed using the SPSS statistic version 21. Initially, the descriptive statistics were analysed.

Table 1

Mean and Standard Deviation for Rumination, Magnification, Helplessness and Well-being among the Elderly

Variables	*Mean*	*SD*	*N*
Rumination	14.71	1.67	68
Magnification	11.16	1.02	68
Helplessness	22.35	1.65	68
Well-being	35.46	11.66	68

Table 1 shows the mean and standard deviation of the variables taken up for study. The Shapiro-Wilk test of Normality was conducted to ascertain if the sample was normally distributed. The Pearson's Product Moment Correlation was computed to understand the relationship between variables.

Table 2

Correlation between Pain Catastrophization and Well-being

Variables	*N*	1	2
1. Pain Catastrophization	68	---	
2. Well-being	68	-0.25*	---

** $p < 0.05$*

Table 2 indicates that there is a significant negative correlation between pain catastrophization and well-being among the elderly. It can be interpreted that as pain catastrophization increases, the well-being decreases and vice versa. Hence, the Hypotheses, "There is no significant relationship between rumination, magnification, helplessness and well-being among the elderly" is rejected.

Paired samples t-test was conducted to understand any significant differences between the pre-test and post-test phase scores of rumination, magnification, helplessness and well-being levels of the experimental group and the control group.

Table 3

Paired Samples t-test of Rumination, Magnification, Helplessness and Well-being in the Pre-test and Post-test Phases of the C.A. R. E Intervention for Experimental Group

Pairs Variables		*Mean*	*N*	*SD*	*t*
Pair 1	Rumination pre-test Experimental Group	14.53	34	1.745	18.42**
	Rumination post-test Experimental Group	5.76	34	2.001	
Pair 2	Magnification pre-test Experimental Group	11.18	34	.999	29.09**
	Magnification post-test Experimental Group	4.32	34	1.273	
Pair 3	Helplessness pre-test Experimental Group	22.21	34	1.737	20.05**
	Helplessness post-test Experimental Group	7.53	34	3.277	
Pair 4	Well-being pre-test Experimental Group	36.03	34	12.951	9.74**
	Well-being post-test Experimental Group	64.91	34	16.101	

$^{**}p < 0.01$

Table 3 indicates that there is a significant difference between the pre-test and post-test phase scores of rumination, magnification, helplessness and well-being levels of the experimental group. The mean levels of the rumination, magnification and helplessness levels have reduced in the post-intervention phase, while the mean of the well-being levels increases in the post-intervention phase. This indicates that the C. A. R. E intervention is very effective in reducing the rumination, magnification and helplessness concepts of pain catastrophization. Also, at the same time, the C. A. R. E intervention is very effective in improving the well-being levels of the elderly.

Hence, the hypothesis, "There is no significant difference in the Pre-test and Post-test phases of the experimental group in the levels of rumination, magnification, helplessness and well being among the elderly" is rejected.

Table 4

Paired Samples t-test of Rumination, Magnification, Helplessness and Well-being in the Pre-test and post-test Phases for Waitlist Control Group

Pairs Variables		*Mean*	*N*	*SD*	*t*
Pair 1	Rumination pre-test Waitlist Control Group	14.88	34	1.591	1.47_{NS}
	Rumination post-test Waitlist Control Group	15.18	34	1.218	
Pair 2	Magnification pre-test Waitlist Control Group	11.15	34	1.048	0.52_{NS}
	Magnification post-test Waitlist Control Group	11.24	34	.987	
Pair 3	Helplessness pre-test Waitlist Control Group	22.50	34	1.562	1.29_{NS}
	Helplessness post-test Waitlist Control Group	22.88	34	1.200	
Pair 4	Well-being pre-test Waitlist Control Group	34.88	34	10.365	0.15_{NS}
	Well-being post-test Waitlist Control Group	34.97	34	9.183	

NS= Not significant

Table 4 indicates that there is no significant difference between the pre-test and post-test phase scores of rumination, magnification, helplessness and well-being levels of the waitlist control group. Independent samples t-test was conducted to understand any significant differences between the experimental and waitlist control group in the post-intervention phase.

Table 5

Independent Samples t-test of Rumination, Magnification, Helplessness and Well-being in the Post-test Phases between the Experimental Group and Waitlist Control Group

Variables	*Groups*	*Mean*	*SD*	*t*
	Experimental Group	5.76	2.001	23.43^{**}
Rumination	Waitlist Control Group	15.18	1.218	
Magnification	Experimental Group	4.32	1.273	25.03^{**}
	Waitlist Control Group	11.24	.987	
Helplessness	Experimental Group	7.53	3.277	25.64^{**}
	Waitlist Control Group	22.88	1.200	
Well-being	Experimental Group	64.91	16.101	9.42^{**}
	Waitlist Control Group	34.97	9.183	

$^{**}p < 0.01$

Table 5 shows that there is a significant difference between the post-intervention scores of rumination, magnification, helplessness and well-being between the experimental group and the waitlist control group. This indicates that the C. A. R. E Intervention is very effective in reducing the rumination, magnification, and helplessness concepts of the pain catastrophization and at the

same time also effective in improving the well-being levels of the experimental group. No such change is evident in the waitlist control group.

Hence the hypothesis, "There is no significant difference in the levels of rumination, magnification, helplessness and well-being of the elderly between the experimental group and the waitlist control group" is rejected.

Discussion

The results section above clearly indicates that the C. A. R. E intervention module is very effective in reducing the pain catastrophization levels and helps in building well-being among the elderly. Pain among the elderly is a common feature. Physical pain often manifests itself in various psychological aspects such as stress and anxiety, depression or also simply catastrophization of the pain due to high levels of worry about the pain and its intensity. Such catastrophization often has a detrimental effect on the well-being of the elderly. Positive psychology is a branch of study that focuses on building positive emotions in an effort to reduce the negative psychological effects. The C. A. R. E intervention is one such effective module that is a simple to use, time effective and user friendly intervention that helps build positive emotions, hope, savoring, gratitude, compassion, a sense of achievement of a purpose in life among many other positive psychological constructs. Similar findings were reported by a study where positive psychology interventions of gratitude and kindness building activities were given to elderly participants (above 50 years old) who suffered from arthritis. These interventions were very effective in reducing the pain intensity and also in reducing the psychological contributors to pain in the participants. (Hausmann et al. 2018).

The present study is a randomized control trial that compares the effect of the aforesaid intervention model among a randomized experimental and waitlist control group. This trial effectively establishes the validity of the intervention module taken up for study. There are a few limitations to this study as it uses a limited number of participants and tests only limited psychological issues of the elderly. Further studies using the same intervention can look to overcome these limitations.

Conclusions

The study on "A Positive Psychology-Based Intervention Model (C. A. R. E) for Pain Catastrophizing and Well-being among the Elderly during the pandemic: A Randomized Control Trial" yields the following conclusions:

- There is a significant negative relationship between pain catastrophization and well-being among the elderly. As the pain catastrophization levels increase, the well-being decreases.
- The C. A. R. E intervention module is effective in reducing pain catastrophization and increasing the well-being among the elderly as validated by the randomized control trial conducted.

The above conducted randomized control trial effectively paves the path for the C. A. R. E intervention module to be used for the reduction of negative psychological concepts and enhancing positive emotions and well-being of human beings.

References

Bar-Tur L. (2021). Fostering Well-Being in the Elderly: Translating Theories on Positive Aging to Practical Approaches. *Frontiers in medicine*, *8*, 517226. https://doi.org/10.3389/fmed.2021.517226

Hillman, J. (2015) The Oak Tree and the U-Bend Age, Well-Being, and the Experience of Me'ness What is it that persists and endures? In Greenstein, M & Holland, J (2015) Lighter as We Go, Virtues, Character Strengths, and Aging. Oxford University Press.

Hausmann, L., Youk, A., Kwoh, C. K., Gallagher, R. M., Weiner, D. K., Vina, E. R., Obrosky, D. S., Mauro, G. T., McInnes, S., & Ibrahim, S. A. (2018). Effect of a Positive Psychological Intervention on Pain and Functional Difficulty Among Adults With Osteoarthritis: A Randomized Clinical Trial. *JAMA network open*, *1*(5), e182533. https://doi.org/10.1001/jamanetworkopen.2018.2533

Marks, R. (2021). Ageing and Positive Psychology. Journal of Aging Research and Healthcare, 4(1), 43-54. https://doi.org/10.14302/issn.2474-7785.jarh-21-3979

Reker, G. T., & Wong, P. T. P. (2012). Personal meaning in life and psychosocial adaptation in the later years. In P. T. P. Wong (Ed.), The human quest for meaning: Theories, research, and applications (2nd ed., pp. 433-456). Routledge.

Rowe, J. W., & Kahn, R. L. (1997). Successful aging. *The Gerontologist*, *37*(4), 433–440. https://doi.org/10.1093/geront/37.4.433

Scheibe, S., De Bloom, J., & Modderman, T. (2022). Resilience during Crisis and the Role of Age: Involuntary Telework during the COVID-19 Pandemic. *International journal of environmental research and public health*, *19*(3), 1762. https://doi.org/10.3390/ijerph19031762

Sudha, R., & Gayatridevi, S. (2021) Abstracts of Award-Winning Posters, 19th International Forum on Mood and Anxiety Disorders, Virtual Edition, July 22–24, 2021. Neuropsychobiology, 80 – 82. https:// doi.org/10.1159/000519078

Sullivan M.J. L., Bishop, S., & Pivik, J. (1995). The Pain Catastrophizing Scale: Development and Validation. Psychological Assessment ,7, 524-532.

Verhiel, S., Greenberg, J., Zale, E. L., Chen, N. C., Ring, D. C., & Vranceanu, A. M. (2019). What Role Does Positive Psychology Play in Understanding Pain Intensity and Disability Among Patients with Hand and Upper Extremity Conditions?. *Clinical orthopaedics and related research*, *477*(8), 1769–1776. https://doi.org/10.1097/CORR.0000000000000694

World Health Organization. Regional Office for Europe. (1998). Wellbeing measures in primary health care/ the DepCare Project: report on a WHO meeting: Stockholm, Sweden, 12–13 February 1998. World Health Organization. Regional Office for Europe. https://apps.who.int/iris/handle/10665/349766

7 Unconditional Self-Acceptance and Psychological Well-Being among Older Adults

Priyanga A* &
Dhivyadharshini G**

Abstract

Even though there are many factors that affects a person's psychological well being, accepting oneself as he/she is helps the individual to attain a higher psychological wellbeing in life. Accepting oneself as they are may become difficult for people as they grow older mostly depended on others, to live without their spouse and so on. Being unconditionally self accepted helps people to achieve hope, and to satisfy their own desires. Self acceptance plays a vital role in Rational Emotive Behavioral Therapy (REBT), it is not often measured in experimental manner. The current study examines how unconditional self acceptance affect psychological well being in older adults. The participants completed the Unconditional Self Acceptance Questionnaire (USAQ) by Chamberlain & Haaga, 2001, 20 items and the Ryff Psychological Well Being Scale (RPWB) 18 items. The data were collected from one hundred and thirty (130) Older adults by random sampling method. The study reveals that there is a relationship between unconditional self acceptance and psychological well being among older adults.

Keywords: Unconditional self acceptance, Psychological well being, Older adults

The unconditional self acceptance in an individual is concerned with the acceptance of one's own self without concerning other people love, respect, and approval (Hill, Hall, Appleton, & Kozub, 2008). The term unconditional self acceptance referred to things which we accept without any demand even it may be right or wrong. Self acceptance is an individual's satisfaction about himself or herself and is considered important for good mental health (Rogers, 1951; Scott, 1968). Self acceptance is a subjective measure and it may differ from individual characteristics termed as "Unique value" (English and English 1958; Jersild, 1960). This unconditional self acceptance must be noticed among older adults, where they feel inferior about their physical and the mental

* B.Sc., Psychology, Department of Psychology, Theivanai Ammal College for Women
** B.Sc., Psychology, Department of Psychology, Theivanai Ammal College for Women

abilities. The thoughts of the older adults focus on the weakness of themselves. Psychological well-being of an individual tends to be affected with the level of unconditional self acceptance of an individual. The need for the self acceptance among the elderly people is must to maintain their psychological well-being. The decrease in the psychological well-being will surely affect the person's emotional and physical well-being. In the most of the cases, the older adults will always have a conflict in accepting things as it is, where they might have any inconvenience in accepting the things. Self acceptance plays a major role in the psychological well-being because once the individual starts to accept things they will no more suffer for any reason. The unconditional self acceptance makes a positive attitude towards facing problems, especially in older adults. The unconditional self acceptance is even after having any weakness and deficiencies. Self acceptance is said to be more realistic in nature where the positive and negative concepts are taken into count.

Unconditional self acceptance

The Unconditional self acceptance is the condition which the individual accepts himself or herself in spite of having any weakness. Unconditional self acceptance includes oneself without any concern about others love, respect, and approval. Unconditional Self Acceptance is one of the determinable factors of Well-being. This makes an individual a positive approach to their life. The unconditional self acceptance is said to be more influential in all aspects of human life, especially in older age people. When the older adults develop conditional self acceptance there they may suffer from the issues of love, care and support lacking given from others. The regardless acceptance of the one's self is most important for older adults

Psychological well-being

Well being depends on both the individual and the environment, during childhood and adolescents. The psychological well-being of an individual is determined by many factors, but when it comes to older adults certain variables that affect the psychological well-being of an individual in the late age. Well being specifically relates to happiness, life satisfaction and positive affect. Psychological well being is a diverse multidimensional concept which develops through a combination of emotional regulation personality characteristics, and identity and life experience. Psychological well-being is the subjective measure the individual feelings and thoughts are valid in assessing the psychological well-being. It can be affected by many factors, social factors will mainly affect the psychological state of an individual it includes things such as what they see, what they do, where they live. All these factors influence the person's psychological well-being of older people.

Methodology

In the present study, samples from older adults in and around, Villupuram were taken

Participants, Procedure and Data collection

In this study one hundred and twenty older adults were taken taken in to count. The purpose of the study is to find the correlation between unconditional self acceptance and psychological well-being among older adults. The response for the study was collected randomly in older people in and around Villupuram, Tamilnadu.

Demographics and its measures

In the present study the participants are asked to provide the demographics information through self-reporting as part of the different questionnaire.

The unconditional self acceptance scale has 19 items with 7 point Likert scale range from 1 (almost always unture) to 7 (almost always true). The item total correlations ranged from .40 to .72

The tool used to measure psychological well-being among elderly people was Ryff's Psychological well-being scale developed by Ryff and Keyes 1995. The scale consists of 18 items rated on 7 point Likert scale ranging from 1 (strongly disagree) to 5 (strongly agree). The score range of 18-126. Some questions have been reverse scored and scores represents the high and low level of psychological well-being

Statistical analyses

In the present study used the Pearson correlation coefficient to analyze the association between the scores. The statistical significance level was set at 0.05. The statistical packages used for the present study were SPSS version 26. Our independent variable was unconditional self acceptance, while psychological well-being was the dependent variable.

Results

In the present study the correlation analysis for unconditional self-acceptance and psychological well-being helps to identify the relationship between the variables.

Table 1

Correlation Statistics for Unconditional Self-acceptance and Psychological well-being

Variables	1	2
1. **Psychological wellbeing**	---	**0.206***
2. **Unconditional Self Acceptance**		

* $p < 0.05$

Discussion

In the present study table 1 shows the correlation between unconditional self acceptance and psychological well-being. A significant positive relationship was observed between the two variables stating that, as psychological well-being increases, there is an increase in unconditional self-acceptance. A number of studies have been carried out by various researchers that exhibit an inverse relationship between loneliness and psychological well-being. People who accept themselves as they are, have higher psychological wellbeing.

Conclusion

The present study examined the unconditional self acceptance and psychological well-being among older adults. The Elderly people who have good self acceptance possess good psychological

well being. The present study has revealed that when a person has higher unconditional self acceptance, then he also possess a higher amount of psychological well being. Therefore this study finds that self acceptance enhances a person's psychological well being.

Limitations

The present study shows only the correlation between unconditional self acceptance and Psychological wellbeing. But the demographics were not taken into account only the correlation study was conducted. The sample size that was taken was in a smaller size. In future to make the study much valid samples can be taken in a larger amount.

References

Bingöl, Y. B. & Batik, M. V. (2018). Unconditional self- acceptance and Perfectionistic Cognitions as Predictors of Psychological Well-Being. Journal of Education and Training Studies, 7(1), 67 - 75. https://doi.org/10.11114/jets.v7i1.3712

Vasile, C. (2013). An evaluation of self-acceptance in adults. Procedia – Social and Behavioral Sciences, 78, 605 – 609. https://doi.org/10.1016/j.sbspro.2013.04.360

Gómez-López, M.,Viejo, C., & Ortega-Ruiz, R. (2019). Psychological Well-Being During Adolescence: Stability and Association with Romantic Relationships. Frontiers in Psychology, 10:1772. https://doi.org/10.3389/fpsyg.2019.01772

De-Juanas, A., Romero, T. B., & Goig, R. (2020). The Relationship Between Psychological Well-Being and Autonomy in Young People According to Age. Frontiers in Psychology, 11: 559976. https://doi.org/10.3389/fpsyg.2020.559976

Ingersoll-Dayton, B., & Saengtienchai, C., & Kespichayawattana, J. & Aungsuroch, Y. (2001). Psychological well-being Asian style: The perspective of Thai elders. Journal of Cross- Cultural Gerontology, 16 (3), 283 – 302. https://doi.org/10.1023/A:1011984017317

ÇARDAK, M. (2013). Psychological well-being and internet addiction among university students. Turkish Online Journal of Educational Technology, 12(3), 134-141.

Akın, A. (2009). The effect of rational emotive behavioural therapy based group counselling to the psychological well-being and self-compassion (Unpublished doctoral thesis), Sakarya University.

Godin, J. (2010). The effect of the enneagram on psychological well-being and unconditional self-acceptance of young adults (unpublished doctoral dissertation). Family and Consumer Sciences Education, Iowa State University.

Roothman, B., Kirsten, D. K., & Wissing, M. P. (2003). Gender differences in aspects of psychological well-being. South African Journal of Psychology, 33(4), 212-218. https://doi.org/10.1177/008124630303300403

Telef, B. B. (2013). The adaptation of psychological well-being into Turkish: A validity and reliability study. Hacettepe University Journal of Education, 28(3), 374-384.

8 Correlation between Affectivity and Coping Strategies when directly Exposed to COVID-19

Dolly Rawat* &
Mansi Agarwal Riya Iyer**

Abstract

This study is conducted during a global medical crisis called COVID-19 pandemic. The pandemic was due to COVID-19 disease which was highly infectious and contagious respiratory disease by coronavirus. This study is aiming to understand the correlation between affectivity of an individual and how it affects coping mechanisms in an individual when directly exposed to the disease COVID-19. With this data we will be able to guide and spread awareness about the impact which affectivity makes under a crisis. The population selected for this study is the middle adulthood which ranges from the age 50-65 years old serving in public and were directly exposed to the corona virus. The PANAS scale and the Brief Cope Scoring were used for the purpose of data collection. Pearson Product Moment Correlation was used for the statistical analysis of the data. The findings indicate that this age group is more effectively helpful with their presence during the crisis showing higher percentage of the sample experiencing positive affect during the crisis scenario. The results also indicate positive correlation of 0.515 between Positive Affectivity and Adaptive Coping strategies which is significant at the level of 0.01. This concludes that the middle aged adults are more likely to have active and effective coping strategies encouraging volunteers amongst them for crises and their advices for action based problem focused issues.

Keywords: Pandemic, COVID-19 disease, Affectivity, Coping mechanism, Middle Aged group

The COVID-19 (Coronavirus Disease 2019) pandemic is a crisis affecting almost all the countries in the world. All the countries have tried to incorporate strategies that will help in curbing the spread of disease (Wilder-Smith & Freedman, 2020). The strategies majorly used by the countries are social isolation, which further challenges the coping capacities of an individual. Older adults was believed to be on higher risk of commuting the disease and were specifically instructed to follow social distancing (Promislow, 2020). The study focused in understanding how they coped

* Department of Psychology, Vishwakarma University, Pune, Maharashtra

in this kind of situation. At the same time it is argued that older people have more life experience as compared to the younger adults. Throughout their life experiences, they have faced personal challenges which built up their coping mechanisms (Lind et al., 2021).Younger adults are more future-oriented whereas older adults are more past oriented. This past orientation gives the older adults access to integrate all the experiences, challenges and positive coping into an acceptable whole (Webster et al., 2014). The older adults are found to have positive reminiscence style allowing remembering negative situation and how it was dealt during those situations and also remember the positive situations helping to boost their current mood(Cappeliez et al., 2008).

The positive affect amongst the older adults also further helped them in using adaptive coping strategies which further enhanced more positive affect amongst the older adults (Vahia et al., 2020). Adverse psychosocial outcomes are the result of using maladaptive coping such as escape the feeling or using avoidant strategies (Ben-Zur, 2009). A lot of researches have also found that individuals who have higher level of pandemic uncertainty were more prone to use maladaptive coping strategies (Rettie & Daniels, 2021).

Affect and Coping shows reciprocal relationship where Positive affect predisposes an individual to see stressful situation as challenging, gain learning experiences and opportunities, whereas coping process used by an individual for dealing with stressful situation leads to generate positive affect and sustaining it for longer time (Khosla, 2006) . Coping has always been studied with negative impact in stressful situation. There is a need to study positive outcomes along with coping, as positive affect also impacts coping of an individual. If utilized meaning based coping processes, it supports in enhancing positive affect during the chronic stress (Folkman & Moskowitz, 2000). Broaden-and-build theory of positive emotion was used to understand the connection of flow and affect. Flow was found to be positively correlated with positive affect and negatively correlated with negative affect. It has been predicted that an individual who uses Adaptive coping shows higher level of flow and vice versa can be found with maladaptive coping (Sophie & Giovanni, 2013).

In a research to investigate the effect of positive affect and its relationship with problem focused coping, it was found that more use of problem focused coping, and emotion focused coping along with positive affect predicted lower levels of HbA. It was also noted that Positive affect proceeded as a moderator in the use of problem focused coping strategies (Tsenkova et al., 2008). In one of the longitudinal study, it was found that people usually experiencing positive affect succeeded in showing them as stronger without frailty. This findings paved the way to positive psychology as a protective factor against physical and functional decline (Ostir et al., 2004). A study showed evidence of biological and psychological health connection with positive affect. At the biological level, individual reporting positive affect shown to be lower cortisoloutput, as well as its association with other biological markers. At the psychological level, positive affect leads to increase in social activities building social connections amongst the people. This social connection leads a person to perceive social support, have optimistic attitude and use more adaptive coping resources. Positive affect will help a person to be resilient. Aresilient person will be able to bounce in the case of adverse physical and psychological health(Steptoe et al., 2009). Positive affect and negative affect

usually co-occurs during stressful situation. Co-occurrence of positive affect may have beneficial consequences. It is also reported that positive affect interventions are easy, practicable, acceptable and effective in outcome(Moskowitz, 2011).

During COVID-19, the situation all around the world went into lockdown and social isolation. A study was done to see how elderly people cope during this situation. The findings indicated that positive refocusing and social connectedness had positive effect whereas negative emotions such as intolerance, uncertainty and loneliness affected mental health. Further it was also seen that the maladaptive strategies lead to intolerance, uncertainty, fear and loneliness whereas adaptive strategies lead to building social support from friends and positive reframing (Lábadi et al., 2022). Another study conducted during COVID-19 indicated that Positive Religious Coping predicts Positive Affect and at the same time someone with Negative Religious Coping will develop Negative Affect. Further it was also seen that the Positive affect is positively correlated with Life satisfaction (Habib et al., 2020). Another study compared the coping and positive affect between younger adults and older adults. It was found that older age could deal the scenario of COVID-19 with less concern about developing COVID-19. They showed better well-being, greater association of the situation with positive events or outcome, and ability to cope with the stressors in the environment. On the other hand, younger and middle-aged adults found it difficult to deal the COVID-19 scenario. There were more interpersonal conflicts and higher number of daily stressors in their life. (Klaiber et al., 2021).

Method

Participants

32 participants with age ranging from 50 to 65 years old were selected as the participants for this research. Random Sampling method was used for collecting the data. The data was collected with the help of Google form as well as by visiting to places following COVID norms.

Instruments

1. Brief COPE by Carver (1997) is a shorter version of the COPE. This test consists of 28-items in a form of self-report. An individual can complete the questionnaire by self-using a 4 point likert scale. The 4 point ranges from 1 = I haven't been doing this at all; 2 = I've been doing this a little bit; 3 = I've been doing this a medium amount; 4 = I've been doing this a lot. The Brief COPE measures 14 theoretically identified coping responses. Each of these 14 subscales comprises of 2 items. Every item under the particular subscale is calculated for the total scores on each of the scales. These 14 subscales are categorized into Maladaptive and Adaptive Coping. Higher score son a specific coping style indicate more use of that particular coping strategy.
2. The PANAS scale by Watson, Clark and Tellengen (1988) is a brief scale consisting of one word items i.e. the list of emotions. It is very easy to administer on any age group. This test is used for the assessment of Positive and Negative Affect. The total item scale in PANAS is 20 items with further division of 10 positive affect markers and 10 negative affect markers describing different feelings and emotions. All the items are rated on a scale ranging from

1= very slightly or not at all, to 5= extremely. Total scores are calculated by summing up the respective 10 items under positive affect and summing up 10 items under negative affect. The scores for both the domain ranges from 10 to 50. An individual scoring high on positive affect indicate a person using more of a positive affect and vice-versa. Similarly an individual scoring high on negative affect indicate more use of a negative affect and vice-versa.

Research Design

The study is a correlational study between Affectivity and Coping strategies by using Pearson Product Moment Correlation

Results and Interpretation

After the data collection process, the scoring and analysis was done. Parametric model was used for the purpose of data analysis. The results are displayed below:

The Descriptive statistics were done by calculating Mean, Standard deviation of Positive Affect, Adaptive Coping and Maladaptive Coping as shown in Table 1

Table 1

Descriptive Statistics: Mean and Standard Deviation of Positive Affect, Adaptive Coping and Maladaptive Coping

Variables	*Mean*	*SD*	*N*
Positive Affect	34.31	7.11	32
Adaptive Coping	43.53	6.20	32
Maladaptive Coping	20.94	4.28	32

Pearson product moment correlation was calculated to find the relationship between Positive Affect, Adaptive Coping and Maladaptive Coping. The correlation analysis is shown in Table 2

Table 2:

Inferential Statistics: Correlation between Positive Affect, Adaptive Coping and Maladaptive Coping

Variables	1	2	3
1. Positive Affect	---		
2. Adaptive Coping	.515**	--	
3. Maladaptive Coping	-0.120	-0.053	---

*** p< .01*

As shown in the table, it was reported that Positive Affect is positively correlated with Adaptive Coping (r =.51) and Positive Affect is negatively correlated with Maladaptive Coping with a very low correlation value (r = -.12).

Discussion

The current study gives emphasis on Positive affect developing Adaptive Coping strategies among the older adults population. Many studies reported their findings of older adults using more positive affect and its association to the use of Adaptive Coping strategies. The current study specifically focused older adult population who was directly exposed to COVID-19disease. The previous studies also supported the relationship between Positive Affect and Adaptive coping strategies. Labadi et al., (2002) stated that maladaptive strategies lead tointolerance, uncertainty, fear and loneliness whereas adaptive strategies lead to building social support from friends and positive reframing. Habib et al., (2002) stated that during COVID-19

Positive Religious Coping predicts Positive Affect and at the same time someone with Negative Religious Coping will develop Negative Affect Klaiber et al., (2021) stated that older age could deal the scenario of COVID-19 with less concern about developing COVID-19. They showed better well-being, greater association of the situation with positive events or outcome, and ability to cope with the stressors in the environment. On the other hand, younger and middle-aged adults found it difficult to deal the COVID-19 scenario. There were more interpersonal conflicts and higher number of daily stressors in their life.

Older adults are more likely to have active and effective coping strategies. They have more past experiences, more coping strategies tried and tested, and more social contacts, etc. encouraging volunteers amongst them for crises and their advices for action based problem focused issues. They are the important source of resources to access during the times of crisis. Their services and volunteer role should be encouraged and motivate participating for the betterment of the country and the world.

Conclusion

Positive Affect is found to be positively correlated with Adaptive Coping strategies amongst the middle aged adults especially the one exposed to COVID-19.

References

Ben-Zur, H. (2009). Coping styles and affect. *International Journal of Stress Management*,

16(2), 87–101. https://doi.org/10.1037/a0015731

Cappeliez, P., Guindon, M., & Robitaille, A. (2008). Functions of reminiscence and emotionalregulation among older adults. *Journal of Aging Studies*, *22*(3), 266–272.https://doi.org/10.1016/j.jaging.2007.06.003

Folkman, S., & Moskowitz, J. T. (2000). Positive affect and the other side of coping. American Psychologist, 55(6), 647–654. https://doi.org/10.1037/0003-066X.55.6.647

Psycnet.Apa. https://psycnet.apa.org/doiLanding?doi=10.1037%2F0003-066X.55.6.647

Habib, H. A., Hussain, S., & Habib, N. A. (2020). Religious Coping as a Predictor of Positive Affect and Life Sa is faction during Epidemic Conditions of COVID-19. Sir Syed Journal of Education & Social Research, 3(3), 42–48. https://doi.org/10.36902/sjesr-vol3-iss3-2020(42-48)

Khosla, M. (2006). Positive Affect and Coping with Stress. Journal of the Indian Academy of Applied Psychology, 32(3), 185 -192.

Klaiber, P., Wen, J. H., DeLongis, A., & Sin, N. L. (2021). The Ups and Downs of Daily LifeDuring COVID-19: Age Differences in Affect, Stress, and Positive Events. *The Journalsof Gerontology: Series B*, *76*(2), e30–e37. https://doi.org/10.1093/geronb/gbaa096

Lábadi, B., Arató, N., Budai, T., Inhóf, O., Stecina, D. T., Sík, A., & Zsidó, A. N. (2022).

Psychological well-being and coping strategies of elderly people during the COVID-19 pandemic in Hungary. *Aging & Mental Health*, *26*(3), 570–577.https://doi.org/10.1080/13607863.2021.1902469

Lind, M., Bluck, S., & McAdams, D. P. (2021). More Vulnerable? The Life Story Approach Highlights Older People's Potential for Strength During the Pandemic. *The Journals of Gerontology: Series B*, *76*(2), e45–e48. https://doi.org/10.1093/geronb/gbaa105

Moskowitz, J. T. (2011). Coping interventions and the regulation of positive affect. In S. Folkman (Ed.), The Oxford handbook of stress, health, and coping (pp. 407–427). Oxford University Press.

Ostir, G. V., Ottenbacher, K. J., & Markides, K. S. (2004). Onset of Frailty in Older Adults and the Protective Role of Positive Affect. *Psychology and Aging*, *19*(3), 402–408.https://doi.org/10.1037/0882-7974.19.3.402

Promislow, D. E. L. (2020). A Geroscience Perspective on COVID-19 Mortality. *The Journals of Gerontology: Series A*, *75*(9), e30–e33. https://doi.org/10.1093/gerona/glaa094

Rettie, H., & Daniels, J. (2021). Coping and tolerance of uncertainty: Predictors and mediators ofmental health during the COVID-19 pandemic. *American Psychologist*, *76*(3), 427–437.https://doi.org/10.1037/amp0000710

Sophie, T., & Giovanni, M. (2013). *EBSCOhost | 90572549 | Flow as a Function of Affect andCoping in the Workplace.*https://web.s.ebscohost.com/abstract?direct=true&profile=ehost&scope=site&authtype=crawler&jrnl=1541745X&AN=90572549&h=Q3oH1YLHsBQwJ3vkzXk1ypK0ykQJOb3pd9Y8uiMydBBB7CHVspCDl7fu%2fZixQPnlbr9Ar7k%2bYHEqr%2fV4OmvvEw%3d

Steptoe, A., Dockray, S., & Wardle, J. (2009). Positive Affect and Psychobiological ProcessesRelevant to Health. *Journal of Personality*, *77*(6), 1747–1776.https://doi.org/10.1111/j.1467-6494.2009.00599.x

Tobert, S., & Moneta, G. B. (2013). Flow as a function of affect and coping in the workplace. Individual Differences Research, 11(3), 102–113.

Tsenkova, V. K., Dienberg Love, G., Singer, B. H., & Ryff, C. D. (2008). Coping and positiveaffect predict longitudinal change in glycosylated hemoglobin. *Health Psychology*, *27*(2,Suppl), S163–S171. https://doi.org/10.1037/0278-6133.27.2(Suppl.).S163

Vahia, I. V., Jeste, D. V., & Reynolds, C. F., III. (2020). Older Adults and the Mental HealthEffects of COVID-19. *JAMA*, *324*(22), 2253–2254.https://doi.org/10.1001/jama.2020.21753

Webster, J. D., Bohlmeijer, E. T., & Westerhof, G. J. (2014). Time to flourish: The relationship of temporal perspective to well-being and wisdom across adulthood. *Aging & Mental Health*, *18*(8), 1046–1056. https://doi.org/10.1080/13607863.2014.908458

Wilder-Smith, A., & Freedman, D. O. (2020). Isolation, quarantine, social distancing and community containment: Pivotal role for old-style public health measures in the novel coronavirus (2019-nCoV) outbreak. *Journal of Travel Medicine*, *27*(2), taaa020.https://doi.org/10.1093/jtm/taaa020

9 Resilience and Mindfulness: Concomitants of Perceived Wellbeing of Elderly

Ms. Madhuri Vaidya* &
Prof. Urmi Nanda Biswas**

Abstract

An increasing evidence suggests resilience and mindfulness contribute to wellbeing which canpromote healthy ageing. In the context of collectivist culture, family and social support play acrucial role in the resilience and mindfulness in elderly's life. Living arrangements which include the place of stay, type of family and the interpersonal relationships within the family significantly influence the psyche and the ageing process in the elderly, manifesting into their perceived wellbeing. The present research aims to find out whether resilience and mind fulness contribute to perceived wellbeing among elderly and whether living arrangements make adifference in the resilience, mindfulness and perceived wellbeing of the elderly in the Indian context. The study was carried out on 103 institutionalized and 349 non- institutionalized male and female elderly between 60 and 75 years from Mumbai and Pune city. The hypotheses, 'Resilience and mindfulness have significant effect on perceived wellbeing among elderly' and 'The institutionalized and non- institutionalized elderly will not differ in resilience,mindfulness and perceived wellbeing' and 'There will be no significant difference between males and female elderly in their resilience, mindfulness, and perceived wellbeing' were tested by using multiple regression and independent sample t test. The hypotheses were partially supported by the findings in the study; however, living arrangements were proved to be important determinant of resilience, mindfulness, and perceived wellbeing among the elderly. The implications of the research will contribute to policymaking towards healthy ageing in the Indian context.

Keywords: Resilience, Mindfulness, Perceived Wellbeing and Elderly

* Research scholar, Dept. of Psychology, Faculty of Education and Psychology, The M S University of Baroda, Vadodara, Gujarat,

** Professor, Dept. of Psychology, Faculty of Education and Psychology, The M S University of Baroda, Vadodara, Gujarat

Introduction

The United Nations has outlined 'health and wellbeing for all' as one of the Sustainable Development Goals to build a more prosperous and secure world. The attainment of this goal will indeed navigate the process of healthy ageing to a large extent. Addressing mental health issues of elderly is one of the primary concerns to ensure healthy ageing.

Wellbeing is one of the trajectories that takes an individual towards healthy ageing (Franco et al., 2009). Healthy ageing and wellbeing are bi-directionally related. Positive ageing perceptions benefits wellbeing; however, wellbeing is one of the major contributors of healthy ageing (Cramm & Nieboer, 2018). Natural dysregulation of immune functioning in the elderly when they experience adversities on emotional and social level, challenge their coping in the context of chronic stress. Ageing interacting with stress strengthens the risk of various chronic diseases, if not mortality (Gouin, et al., 2008; Kiecolt-Glaser, 2001).

Resilience allows to develop ability to cope with the life stressors or challenges effectively. As the possibility of such experiences in various domains of life of the elderly is very high,resilience can be considered a life skill. Resilience changes the perception of illness in the adversities helps the elderly to meet challenges successfully and maintain wellbeing among them (Connor & Davidson, 2003).

Accepting every experience as it comes is considered to be a key to wellbeing in older adults;as lack of acceptance leads to despair and reduced wellbeing(Ranzijn & Luszcz, 2011).Mindfulness is non-judgmental observation of every phenomenon, which not only regulates behaviour but allows effective coping with the grieving process among elderly promoting wellbeing. One of the effective strategies needed to withstand increasingly complex and demanding world is developing life skills such as mindfulness and resilience. Mindfulness –Based Stress Reduction and mindfulness meditation are proved to be effective techniques to develop mindfulness (Kabat – Zinn, 2013).

In Indian context although the family acts as a major defense particularly in the life of elderly when he/she faces the adversity, the support available in the family does not necessarily confirm their wellbeing (Rajan & Kumar, 2003). The institutionalised elderly may enjoy social life but may be deprived of intimacy in relationships, possibly leading to loneliness and other mental health issues (Sandhyarani & Rao, 2014).

Rationale

As the population ageing is a mark of development for a nation, addressing mental health issues becomes a necessity to ensure their wellbeing. With increasing longevity and reducing fertility, independent and healthy ageing is looked upon globally. Although social and economic challenges of the elderly are aimed to be met by the policymakers, it is essential for every common man to extend the help by protecting their rights leading to healthy ageing. The past literature in the field has suggested resilience and mind fulness predict perceived wellbeing. Resilience within an individual helps develop qualities such as equanimity, perseverance, self-reliance which enhance the potential of maintaining positive adaptation in the face of adversities. Mindfulness provides powerful route for getting oneself unstuck and take charge of one's life. Implications of this

research will be useful for creating awareness about the role of such psychological constructs in healthy ageing to build a healthy society.

Objectives

1. To understand the relationship between resilience, mindfulness, and perceived well being among elderly.
2. To study the effect of resilience and mindfulness on perceived wellbeing among elderly.
3. To examine whether institutionalised elderly differ in resilience, mindfulness, and perceived wellbeing from non- institutionalised elderly.
4. To study whether there are any gender differences in resilience, mindfulness, and perceived wellbeing of the elderly.

Hypotheses

The following hypotheses are constructed based on the literature review and the above objectives -

H1. Resilience and mindfulness will significantly predict perceived wellbeing of elderly.

H0. There will be no significant difference between institutionalised and non- institutionalised elderly in their mindfulness, resilience and perceived wellbeing.

H0. There will be no significant difference between males and female elderly in their resilience,mindfulness, and perceived wellbeing.

Design

It is a survey research with correlational design.

Variables

Predictor Variables: Resilience, Mindfulness

Outcome Variable: Perceived wellbeing

Sample

The areas of Municipality of Mumbai Metropolitan and Pune city were identified.The sample comprised of 452 elderly in the age range of 60 to 70 years, randomly chosen with convenient sampling technique from selected areas of Mumbai and Pune city. Amongst them 349 male and female elderly were non-institutionalised and 103 male and female elderly were from different institutions / homes for the senior citizens in Mumbai and Pune city. Elderly without any major psychopathological problems and locomotive disability were the inclusion criteria used in the study.

Tool description

The data were collected through the standardized psychometric tools, such as -

Connor-Davidson Resilience Scale-

CD-RISC is a measure of Resilience developed by Connor and Davidson (2003) which comprises of 25 items. Each item is rated on a five-point scale (0-4), with higher scores reflecting greater

resilience. The factor analysis of the scale yielded five factors, such as Personal competence, Trust in one's instincts, Positive aspects of change & secure relationships, Control and Spiritual influences. The scale homogeneity with Cronbach alphafor the full scale is 0.89 and 0.80, 0.75, 0.74 and 0.69 for the factors 1 through 4 respectively. Test-Retest reliability was found to be 0.87. The scale proves to have a good Construct and Predictive validity, particularly on Asian population. It also distinguishes between those with greater and lesser resilience. The Cronbach alpha was found to be 0.75 for the present sample.

FFMQ-15: 15-item Five-Facet Mindfulness Questionnaire developed by Baer et al. (2008), a short form of the 39-item FFMQ self-reported measure of dispositional Mindfulness. It includes the same five facets as the long form: Observing, Describing, Acting with Awareness,Non-Judging of inner experience, and Non-Reactivity to inner experience. The test consists of 15 items on five different dimensions developed on a five-point Likert scale. Each Facet is being measured by 3 items. Gu et al. (2016) found adequate internal consistency and high convergent validity. The Cronbach alpha was found to be 0.74 for the present sample.

Subjective Well-being Inventory is a 40-item measure of feelings of well-being/ill-being asperceived by an individual in different aspects of life constructed by Nagpal & Sell in 1992. Eleven factorial dimensions of life are measured on 3-point Likert scale. The factor analysis ofthe scale showed stability in content of factors and time. The scale has 0.79 test-retest reliability with inter-rater reliability and inter-scores reliability. The scale has 0.86 validity. The Cronbach alpha was found to be 0.74 for the present sample.

Procedure

The researchers gave basic outline of the study, and an informed consent was obtained from the participant. After establishing rapport, the researchers collected demographic information with the help of a prepared questionnaire. Prevalence of any disease was noted down, if at all,with its nature, duration, frequency and intensity. The tests were administered with 10 minutes interval to avoid fatigue effect in the participant. Then the data were compiled and analysed with appropriate statistical measures.

Results and Discussion

Table 1

Prediction of Perceived Wellbeing by Resilience and Mindfulness Among Elderly

	Perceived wellbeing		
	B	**Beta**	**t**
Mindfulness	0.57	0.36	7.39**
Resilience	0.25 z	0.30	6.50**
F	136.81**		
R	0.69		
R^2	0.44		
Adjusted R^2	0.43		

**p<.01

The findings from the Table 3 of multiple regression analysis reveal that resilience, and mindfulness to be the significant predictors of perceived wellbeing among elderly. Resilience and mindfulness together cause 43% variance; none the less, each one of them is an independent predictor of the perceived wellbeing among elderly.

Resilience is a capacity to maintain or regain wellbeing during or post adversity (Whitson et al., 2016). The past research suggests that older adults are capable of developing high resilience despite the demographic factors such as socioeconomic background or poor health and benefit with lowered depression, longevity, successful ageing (MacLeod et al., 2016). Resilience has promising effects on building health and wellbeing in later years of life, particularly among the community dwellers (Lau et al., 2018).

Mindfulness is a central element in health and human services. Perceived wellbeing is enhanced through therapeutic recreation exercise of mindfulness meditation technique. It helps the individual to live more creative and meaningful life by reducing unnecessary suffering and enhanced emotional regulation (Seligman et al., 2004; Carruthers & Hood,2011). Mindfulness is effective in nurturing one's mental health and thus, enhance wellbeing (Rybak, 2013). In case of older adults facing adversity in terms of natural disasters, mindfulness helps in developing adequate psychological resources, coping styles and maintain wellbeing(Aliche & Onyishi, 2019). Mindfulness shows magical effects in rehabilitative therapy in the form of cognitive and affective benefits, significantly preventing the decline in attentional control due to ageing (Fountain-Zaragoza & Prakash, 2017), improves visuospatial attention restraining alliedage-related cognitive impairment and promotes wellbeing leading to healthy ageing (Malinowski et al., 2017).

The findings support the hypothesis 'Resilience and mindfulness and will significantly predict perceived wellbeing of elderly'.

Table 2

The Mean Differences in Resilience, Mindfulness, and Perceived Wellbeing Among Institutionalised and Non-institutionalised Young Elderly

	Institutionalised elderly (n1=103)		**Non- Institutionalised elderly (n2=349)**		**t value**
	Mean	**SD**	**Mean**	**SD**	
Mindfulness	50.86	12.23	53.43	8.66	2.38*
Resilience	64.10	21.89	69.45	17.36	2.58*
Perceived wellbeing	84.40	19.44	93.69	13.34	5.55**

*p<.05; **p<.01

The figures in Table 2 show significant difference in resilience, mindfulness, and perceived wellbeing among elderly staying at home and / institution. The non-institutionalised elderly are more mindful, resilient and thus perceive significantly higher wellbeing than the institutionalised elderly.

Although the elderly living with the spouse and children do not necessarily share a healthy relationship with their children and find them dependable (Rajan & Kumar, 2003); when the elderly are forced to be institutionalised, they feel severely socially disconnected and that affects their overall wellbeing (Sandhyarani & Rao, 2014).

In the context of collectivist cultures, living arrangements or a place of stay plays importantrole in the elderly's life, considering the family as a major social support. With reference to social exchange theory applied to ageing process, other than age and gender, contextual factors such as retirement, relocation, loss of spouse influence wellbeing, particularly among those older adults with limitations on physical mobility and independence. Living in the institution after a certain age influences the development of social exchange, as it demands adaptation on multiple levels. Positive social exchange provides tangible/intangible support and protection from stress. Companionship, presence of a spouse, children and close friends is one such support which adds to the wellbeing in later years (Wan & Antonucci, 2016).

In a longitudinal study on institutionalized and non-institutionalized adults, positive effects of both providing and receiving support on positive affect are observed only for then on institutionalized older adults (Kroemeke & Gruszczynska, 2016). Mindfulness is found to be low in the elderly from old age homes than living with the family; and mindfulness training is effective in mitigating depression amongst them (Verma & Kumar, 2019). It supports the findings of the present research and reject the hypothesis 'There will be no significant difference between institutionalised and non- institutionalised elderly in their mindfulness,resilience and perceived wellbeing'.

Older population is vulnerable to chronic illnesses, chronic respiratory problems and neurocognitive disorders like Alzheimer's disease leading to various psychological symptoms,while moderate level of clinical depression and anxiety are found to be more common(Yohannes et al., 2000; Geiger et al., 2016). Approximately 10% of institutionalised older adults suffer from anxiety disorders, majorly Generalised Anxiety Disorder in later years of life(Beekman et al., 1998; Bryant et al., 2008). Mindfulness shows significant effect of lowering depression and anxiety (Moore, 2016; Geiger et al., 2016), alleviating loneliness and promoting life satisfaction and wellbeing among older adults (Pandya, 2019).

More than 50% of the elderly sample from an old age home showed low level of resilience as againststaying with the family(Britto et al., 2020). Resilience is an effective mediating variable in a study of effect of family life on the quality of life of the Chinese older adults indicates the role of living arrangement on the resilience of elderly(Lu et al., 2017). The type of family and the family members indeed have a role to play in building resilience in individual across the life(Singh & Gupta, 2011). The findings of an explanatory study on Korean elderly revealed family support as a significant predictor of resilience other than monthly income and standard of living(Lee & Choi, 2021).

Table 3

The Mean Differences in Resilience, Mindfulness, and Perceived Wellbeing among elderly males and females

	Male (n=201)		Female (n=251)		t value
	Mean	**SD**	**Mean**	**SD**	
Mindfulness	53.55	9.98	52.29	9.33	1.38
Resilience	71.35	18.55	65.73	18.28	3.23**
Perceived wellbeing	93.42	16.36	90.10	14.50	2.29*

**p<.05, **p<.001*

The above figures show 55% of the sample are female elderly, who significantly differ from the male elderly in resilience and perceived wellbeing. The male elderly tend to perceive more wellbeing in life as well as more resilient; however, there are not gender differences seen in mind fulness.

Various demographical factors such as age, gender, and physical activity significant influence resilience among the older adults; males are found to be more resilient and physical activity is a significant mediator variable (Martínez-Moreno et al., 2020). The findings are supporting the present research. Although the culture shapes certain trends with reference to resilience and other behavioural characteristics, the results are in favour of male elderly (Fergus et al., 2020).Trauma shows its impact on individual, familial and community level. In a study done by Sambu & Mhongo (2019) on traumatised older adults, older males were found to be more resilient, who benefitted from the intervention strategies to overcome the traumatic experiences. However, contradictory findings are found by Lakomý et al. (2020), where the older women are more resilient, partly explaining the 'gender paradox'.

Women tend to live longer but with number of functional limitations, which affect manycriteria of subjective wellbeing (Carmel, 2019); reflecting in the self-reported health measures(Boerma, 2016), weaker 'will to live' and less desire to prolong life by being dependent on medication than men (Carmel, 2001). Self-acceptance, autonomy, purpose in life,environmental mastery and more importantly self-esteem and social support are the precursors of subjective wellbeing which promote successful ageing, which are found significantly higher among male old adults than females (Matud et al., 2020).

Gender differences and perceived wellbeing has been discussed ever since Wilson (1967) proposed that 'one's happiness is not related to sex'; however, the past research focuses on the 'definition' of 'perceived/ subjective wellbeing'.When the perceived wellbeing comprises of positive affect, negative affect and life satisfaction,it is imperative to comment on the gender differences with respect to these three components separately. Shmotkin (1990) claims marginal gender differences in subjective wellbeing,confirming the findings of Larsen and Stock et al. (Batz & Tay, 2018). The findings in the present study support these researches; however partially

rejecting the hypothesis 'There will be no significant difference between males and female elderly in their resilience, mindfulness,and perceived wellbeing'.

Conclusion

The present study establishes direct positive relationship between resilience mindfulness, and perceived wellbeing among elderly which implies that mindful and resilient elderly are more satisfied with their life and experience more positive emotions and less negative emotions. The research also shows a significant gender difference only in resilience and perceived wellbeing and not in mindfulness of the elderly. The findings also reveal the importance of place of stay/ the living arrangements in resilience mindfulness, and perceived wellbeing of the elderly. The elderly living with the family are significantly more resilient, mindful, experience more positive emotions, less negative emotions and overall satisfied with the life than elderly living in the institution.

Implications

The present research confirms the importance of mental health and wellbeing in healthy ageing. The findings are useful in understanding the dynamics of wellbeing among old people. The role of resilience and mindfulness in perceived wellbeing of the elderly is highlighted. It shows a need to create an awareness of enhancing the same to build a healthy society; keeping in mind the interventions are cost-effective and thus can be practiced by the elderly across the sociodemographic variables. Institutions for the elderly is recognized as a need of an hour;however, perception towards the same needs to be made positive and healthy. At the same time,these institutions should be architecture and designed to be more and more elderly-friendly. An inclusive approach towards the elderly to be necessarily practiced at societal and national level,considering psychological concomitants of healthy ageing.

References

Aliche, J. & Onyishi, I.(2019).The mediating effect of positive reappraisal. Published online, 2019. https://www.tandfonline.com/doi/full/10.1080/13607863.2019.1602592

Batz, C., & Tay, L. (2018). Gender differences in subjective well-being. In E. Diener, S.Oishi, & L. Tay (Eds.), *Handbook of well-being*. Salt Lake City, UT: DEF Publishers. DOI:nobascholar.com

Beekman AT, Bremmer MA, Deeg DJ, van Balkom AJ, Smit JH, de Beurs E, van Dyck R,van Tilburg W.(1998). Anxiety disorders in later life: a report from the Longitudinal AgingStudy Amsterdam. *Int J Geriatr Psychiatry.13*(10):717-26. doi:10.1002/(sici)1099- 1166(1998100)13:10<717::aid-gps857>3.0.co;2-m. PMID: 9818308.

Boerma, T., Hosseinpoor, A. R., Verdes, E., & Chatterji, S. (2016). A global assessment ofthe gender gap in self-reported health with survey data from 59 countries. *BMC publichealth*, *16*, 675. https://doi.org/10.1186/s12889-016-3352-y

Britto, J, John, S. & Selvaraj, B. (2020). Quality of life and resilience of institutionalizedsenior citizens. *Global Journal for Research Analysis,9*(5). DOI :10.36106/gjra

Bryant, C., Jackson, H.& Ames, D. (2008). The prevalence of anxiety in older adults:Methodological issue and a review of the literature. *Journal of Affective Disorders* 109, 233–250. doi:10.1016/j.jad.2007.11.008

Carmel S. (2001). The will to live: Gender differences among elderly persons. *Soc Sci Med. 52*(6):949-58. doi: 10.1016/s0277-9536(00)00198-2.

Carmel S. (2019). Health and well-being in late life: Gender differences worldwide. *Frontier sin medicine*, *6*, 218. https://doi.org/10.3389/fmed.2019.00218

Carruthers C. & Hood, C.(2011) Mindfulness and Well-Being: Implications for TR Practice. *Therapeutic Recreation Journal, XLV* (3), 171-189

Connor, K. & Davidson, J.(2003). Development of a new resilience scale: the Connor-Davidson Resilience Scale (CD-RISC). *Depression and anxiety 18*:76–82.DOI. 10.1002/da.10113

Cramm, J.M., Nieboer, A.P. (2018). Aging perceptions matter for the well-being of elderly

Turkish migrants, especially among the chronically ill. *BMC Geriatrics,*18, 229.https://doi.org/10.1186/s12877-018-0902-4

Fergus, D., Chen, Y., Chuang, Y., Ma, A. & Chuang, K. (2020). Gender differences inresilience among older Taiwanese adults. 10.21203/rs.3.rs-133704/v1.

Fountain-Zaragoza, S., & Prakash, R. S. (2017). Mindfulness Training for Healthy Aging: Impact on Attention, Well-Being, and Inflammation. *Frontiers in aging neuroscience*, *9*, 11.https://doi.org/10.3389/fnagi.2017.00011

Francoa,O., Karnik, K., Osbornea, G.,Ordovas, J.,Catt , M & Oudera a, F.(2009). Changing course in ageing research: The Healthy Ageing Phenotype. *Maturitas, 63*,13-19.doi:10.1016/j.maturitas.2009.02.00

Geiger, P. J., Boggero, I. A., Brake, C. A., Caldera, C. A., Combs, H. L., Peters, J. R., & Baer, R. A. (2016). Mindfulness-Based Interventions for Older Adults: A Review of the Effects on Physical and Emotional Well-being. *Mindfulness*, *7*(2), 296–307. https://doi.org/10.1007/s12671-015-0444-1

Gupta, L. & Singh, R. (2011). Impact of family type on Resilience. *Indian journal of positive Psychology. 2*. 17-20.

Gouin, J. P., Hantsoo, L., & Kiecolt-Glaser, J. K. (2008). Immune dysregulation and chronicstress among older adults: a review. *Neuroimmunomodulation*, *15*(4-6), 251–259. https://doi.org/10.1159/000156468

Kiecolt-Glaser, J. K., & Glaser, R. (2001). Stress and immunity: Age enhances therisks. *Current Directions in Psychological Science*, *10*(1), 18-21. https://doi.10.1.1.1078.3317

Kroemeke, A., & Gruszczynska, E. (2016). Well-Being and Institutional Care in Older

Adults: Cross-Sectional and Time Effects of Provided and Received Support. *PloS one*, *11*(8), e0161328. https://doi.org/10.1371/journal.pone.0161328

Lakomý, Martin & Petrová Kafková, Marcela. (2017). Resilience as a Factor of Longevityand Gender Differences in Its Effects. *Czech Sociological Review*. 53. 369. 10.13060/00380288.2017.53.3.336.

Lau S., Guerra RO, Barbosa JFdS, et al. (2018).Impact of resilience on health in older adults: a cross sectional analysis from the International Mobility in Aging Study (IMIAS). *BMJOpen* 2018;8:e023779. doi:10.1136/ bmjopen-2018-023779

Lu C, Yuan L, Lin W, Zhou Y, Pan S. (2017). Depression and resilience mediates the effectof family function on quality of life of the elderly. *Archives of Gerontology andGeriatrics,71*:34-42. doi:10.1016/j.archger.2017.02.011.

Lee,S. & Choi, Y.(2021). Factors influencing family support and resilience in the elderly. R*eview of International Geographical Education,11*(8),515-526. Doi: 10.48047/rigeo.11.08.48

MacLeod, S.,Musich, S.,Hawkins, K., Alsgaard, K.,.&Wicker,E.(2016). The impact ofresilience among older adults. *Geriatric nursing, 37*(4),266-272 https://doi.org/10.1016/j.gerinurse.2016.02.014

Malinowski P, Moore AW, Mead BR, Gruber T. Mindful Aging: The effects of regular briefmindfulness practice on electrophysiological markers of cognitive and affective processing inolder adults. *Mindfulness,8*(1):78-94. doi:10.1007/s12671-015-0482-8.

Martínez-Moreno, A., Ibáñez-Pérez, R. J., Cavas-García, F., & Cano-Noguera, F. (2020).Older adults' gender, age and physical activity effects on anxiety, optimism, resilience andengagement. *International Journal of Environmental Research and Public Health*, *17*(20), 7561. https://doi.org/10.3390/ijerph17207561

Matud, M., Bethencourt, J., Ibáñez, I., & Fortes, D. (2020). Gender and psychological well-being in older adults. *International Psychogeriatrics, 32*(11), 1293-1302.doi:10.1017/S1041610220000824

Moore, R. C., Depp, C. A., Wetherell, J. L., & Lenze, E. J. (2016). Ecological momentaryassessment versus standard assessment instruments for measuring mindfulness, depressedmood, and anxiety among older adults. *Journal of psychiatric research*, *75*, 116–123.https://doi.org/10.1016/j.jpsychires.2016.01.011

Okun M. &Stock, W.(1987).Correlates and Components of Subjective Well-Being Amongthe Elderly. *The Journal of Applied Gerontology, 6*(1), 95-112

Pandya,S.(2019) Meditation program mitigates loneliness and promotes wellbeing, lifesatisfaction and contentment among retired older adults: a two-year follow-up study in four South Asian cities. Published online: 22 Nov 2019. 286-298. https://www.tandfonline.com/doi/full/10.1080/13607863.2019.1691143

Rajan, S. & Kumar,S.(2003). Living arrangements among Indian elderly: New evidence from national family health survey. *Economic and Political Weekly, 38*(1), 75-80. DOI:10.2307/4413048

Ranzijn, R. & Luszcz, M.(2011). Acceptance: A key to wellbeing in older adults? *Australian Psychologist,34* (2),94-98. https://doi.org/10.1080/00050069908257435

Rybak ,C.(2013). Nurturing positive mental health: Mindfulness for wellbeing in counselling. *Int J Adv Counselling* 35, 110–119. https://doi.org/10.1007/s10447-012-9171-7

Sambu, L. & Mhongo,S.(2019). Age and gender in relation to resilience after the experienceof trauma among Internally Displaced Persons (IDPS) in Kiambaa village, Eldoret East Sub-County, Kenya. *Journal of Psychology and Behavioral Science, 7*(1), 31-40. DOI: 10.15640/jpbs.v7n1a4

Sandhyarani Rao (2014) Elderly in the institutional care –A case study. *International Journal of Current Research,6*(9),8525-8527.

Seligman, M., Parks, A.& Steen, T. (2004). A balanced psychology and a full life. *The Royal Society*,1379–1381. doi.10.1098/rstb.2004.1513

Shmotkin, D. (1990). Subjective Well-Being as a Function of Age and Gender: AMultivariate Look for Differentiated Trends. *Social Indicators Research*, *23*(3), 201–230. http://www.jstor.org/stable/27520842

Verma, Udai & Kumar, Arun. (2019). Study of mindfulness and depression in old age people. *Environment Conservation Journal. 20*. 93-96. DOI.10.36953/ECJ.2019.SE02018.

Wan, W.& Antonucci, T. (2016) Social Exchange Theory and Aging. Encyclopedia ofGeropsychology. DOI: https://doi.org/10.1007/978-981-287-080-3_285-1. Retrieved fromhttps://www.researchgate.net/publication/303791167_

Whitson, H., Wei Duan-Porter, Schmader, K., Morey, M., Cohen, H.& Colón-Emeric,C.(2016). Physical resilience in older adults: Systematic review and development of anemerging construct. *The Journals of Gerontology: Series A*, *71*(4), 489-495.https://doi.org/10.1093/gerona/glv202

Yohannes AM, Baldwin RC, Connolly MJ.(2000). Depression and anxiety in elderlyoutpatients with chronic obstructive pulmonary disease: Prevalence, and validation of theBASDEC screening questionnaire. *Int J Geriatr Psychiatry,15*(12):1090-6.doi:10.1002/1099-1166(200012)15:12<1090::aid-gps249>3.0.co;2-l. PMID: 11180464.

10 Narrative Analysis of Adaptive Coping in Older Couples in times of COVID-19

Meenakshi Menon*

Abstract

A strengths-based lens to the process of ageing is yet to be extensively explored and studying this is vital in today's age where the proportion of the elderly is on the rise. The present study explored the strengths-based narratives of elderly couples living in isolation (empty nest) in India, in the context of the COVID-19 pandemic. In-depth qualitative narrative inquiry and analysis were used to understand the lived experiences of older couples in terms of the developmental tasks faced by them and the adaptive coping strategies employed to deal with these tasks. The study also looked to determine whether the partner's interactions with each other have an influence on the coping strategies employed by them. The emerging themes within and across the couple's life narratives pointed out to their reflections of current developmental tasks, challenges, and strengths. Current challenges in retired life were navigated through positive reframing, continued engagement in work and activities and mutual interaction. The COVID-19 pandemic and the intersectional domains of isolation associated with it had an impact on their wellbeing. The participants reported changes in routine and psychological effects arising from situations surrounding the pandemic. Emerging coping strategies, role of community and technology and shared meaning making aided in their adaptation and adjustment. This study highlights the need for a more humane, sensitive, and nuanced approach to discerning older couples functioning. Exploring these narratives in the context of India allows for a better understanding of the experiences faced by older couples in the country.

Keywords: Ageing, COVID-19, Coping, Wellbeing

* Psychotherapist and Researcher at Kaha Mind, Bangalore MA Applied Psychology, TISS Mumbai

Ageing as a construct under the critical gerontology lens not only impacts the individual but the social organization as a whole. The COVID-19 pandemic has brought about a mental health crisis in this population. As consequent lockdowns brought about a restraint in movement and travel, the activities of older adults had been constrained, further aggravating mental health challenges during the COVID-19 pandemic.

Ageing in the Modern World

According to the 'Population Projections for India and States 2011-2036' report, the proportion of older persons in the country is projected to rise from 8.4% to 14.9% by 2036. Inadequate social support, lack of adequate infrastructure, economic dependency, accessibility to healthcare is some of the important determinants of the overall quality of life of this population.

There has been a shift in the family system with the emergence of nuclear family systems in the past decades. The proportion of elderly staying alone or with a spouse has seen a stark increase from 9% in 1992 to 18.7% in 2006. This exposes the elderly population to financial, emotional, and physical difficulties.

The imperative now lies on exploring models of ageing that are sustainable, healthy, allowing the geriatric population to remain an integral part of society and enjoy a good quality of life. These initiatives must have a strong analytical understanding of the demographic factors and processes of this population, along with being pertinent to the challenges and realities of our country, rather than adopting a 'one size fits all' perspective.

Migration of Adult Children and Health of Elderly

Some of the consistent findings on research into migration of children and health of left-behind parents points out to lower levels of physical and mental functioning in the left-behind population. An elaborate review by Thapa et al (2018) found that older adults who were living by themselves had higher depressive symptoms, lower cognitive abilities, lower life satisfaction, and overall poorer psychological health. Migration has led to lower happiness and a higher probability of loneliness in older parents (Scheffel & Zhang., 2018).

COVID-19 and the Elderly

Older adults are more vulnerable and at a higher risk for developing mental health issues like stress, anxiety, and depression during the pandemic. Difficulty in accessing regular medication and routine health care along with social isolation and lack of access to technology can worsen pre-existing medical conditions in the geriatric population. These factors could result in fear of contracting the virus, panic attacks, anxiety about death, and dying or uncertainty about the future. (Banerjee, 2020).

With reduced social networks, lack of face-to-face interaction with their friends or family, this population has been experiencing depression and generalized anxiety disorders (Armitage & Nellums., 2020; Brooke & Jackson., 2020).

The changes in health-related behaviours, relationships, work, socialization, and travel as a result of the pandemic are likely to last long after the pandemic has run its course (Scott, 2020).

A study by Verhage et al. (2021) points to older adults viewing the pandemic as being ungraspable with disruptions in their daily and social lives. There is a sense of loss and lack of purpose despite keeping themselves engaged. Coping with this involved measure to decrease infection risk as a means to gain control along with applying emotion and problem focused strategies.

There is a call for brief evidence-based interventions with a focus on prevention to be explored and implemented in centres like residential complexes, nursing centres and community spaces for the elderly or through virtual mediums for those with access to technology. Developing social support systems and cognitive skills helps enable the geriatric population to experience a sense of belongingness, enhances mental wellbeing and improves social affiliation during a crisis like COVID-19 that can be an isolating experience (Mukhtar, 2020).

With reference to the way in which the elderly describes the COVID-19 pandemic, there was a gentle proposition that the situation is temporary, with regard to the coping strategies employed by this population. Considering the population's vulnerability to contracting the COVID-19 virus as well as the associated secondary physical and mental health effects of the pandemic, there is a need to have more manageable and age- responsible measures along with associated policy making and reforms directed towards the elderly.

Method

Rationale

This study is focused on the adaptive coping employed by 'left-behind' older couples in the context of the COVID-19 pandemic. This study looks to use a strengths-based approach to understand the way in which older couples respond to the developmental tasks arising from their current developmental tasks with regard to their family life cycle stage keeping in mind the contextual factor i.e., COVID-19.

- Integrating strengths-based perspective with a systemic framework.
- Isolation as an Intersectionality.
- Unfolding of the Life Story of the couple.
- Policies and Reform.

Objectives

The objectives of the study are:

- To understand the intersectional domains of isolation, and its associated challenges arising from their current developmental stage and the COVID-19 Pandemic.
- To explore the influence of the life narrative in the couple's reflections of the current developmental tasks, challenges and strengths.
- To understand their strengths in the context of the couple's shared narratives.

Research Design

A narrative inquiry using semi-structured interviews was used for this study. It allows researchers to analyse not only meanings and motives but also how people structure the flow of experience to make sense of events and actions in their lives.

Sample and Participant Profile

Four older couples were interviewed for this study. Purposive and snowball sampling was used in this study to select participants. The criteria for inclusion were: Older couples (aged 55-75 years) belonging to a middle or higher middle socioeconomic background, residing alone whose children have moved to towns/cities for education/work and visit them occasionally but the elderly couple are on their own most of the time.

Table 1

Demographic Details of the Participants

Name* (Female/Male)	Age	Birthplace	Years together	Number of children	Age of the children
Laya/Vignesh	68/75	Palakkad, Kerala/ Palakkad, Kerala	50	2	49, 47
Uma/Prakash	63/70	Chennai, Tamil Nadu/ Kolkata, West Bengal	35	2	29, 27
Asha/ Sachin	59/66	Talacherry, Kerala/ Kozhikode, Kerala	36	2	34, 27
Indira/ Sanjay	66/75	Palakkad, Kerala/ Ponnani, Kerala	45	2	44, 40

**All names of the participants have been changed to protect their confidentiality*

Method of Data Collection

The mode of the interviews were video and audio calls using an unstructured interview guide. The broad domains of inquiry included- initial life experiences, marriage, empty nest, developmental tasks, challenges as well as adaptation/adjustment in the context of COVID-19 and mutual/ interactional experiences of the couple. The language in which the interviews were conducted was English. All the interviews were recorded.

Data Analysis

The first process of data analysis was the transcription of the taped interviews. Two levels of data analysis were conducted, the first involving restorying each narrative and identifying the emerging themes in them. The second level involved identifying the common themes and categories emerging across the four stories or narratives. The thematic analysis was conducted in order to identify patterns of meaning across the raw data that helps provide an answer to the research question that is posed.

As the stories told by the four couples that were interviewed were in a nonlinear manner, moved back and forth between the past, present and future, with limited chronology, by re-storying them, a sequential link was brought about among the ideas. Clandinin and Connelly's (2000) three dimensional space approach was used for the restorying process.

In this particular study the interactional processes between the couple were explored, also taking into consideration the dialogic process between the researcher and the partners. The current as well as past stories and experiences of the couple members were looked into. The contexts in which these stories occurred, such as their home or workplace or neighbourhood are described. After the re-storying process of each couple's narrative, the themes arising from them were detailed for each of the four couple's narratives. The context of Covid served as the primary anchor in the dialogue between researcher and participants. The context of COVID-19 also brought out unique interplay of relationship dynamics in the current scenario which were otherwise hidden from view in their life narratives.

Reflexivity: The Data Collection Process and Experiences

In qualitative research, the researcher is the major instrument in data collection and analysis (Shenton, 2004). In the current study, the researcher's ideas and interests fuelled research in this topic, along with experiences and perceptions of interviewing the four couples for the study.

Due to the age and the generational gap with the participants, the researcher was very respectful of language used during the interviews. Relational terms were used to refer to the participants as it was more culturally appropriate in this space.

Results: Across Narrative Analysis

The overarching themes across the following developmental stages- childhood, marriage, child-rearing, empty nest, retirement will be highlighted. The contextual factor of COVID-19 and the emerging themes and subthemes are delved into.

Childhood

Family Background

The couple's family backgrounds had an influential role to play in the ideas, values, and morals that they built for themselves, and carried throughout their lives, spilling over into their relational spheres.

Marriage

Type of Alliance

All the four couples that were interviewed described having an arranged marriage, that was decided by their respective families. Their similar cultural and regional affinities had a strong role to play in the match.

Interpersonal Relationship

The connections, associations, and affiliations among the partners varied across the four stories. While Vignesh is more strong-headed and absolute regarding the ideas he holds, Laya is more open to change. The couple has some similar ideas on family bonding and independence of their children and emphasizes the importance that their social relationships have in their lives. Uma and Prakash have different approaches towards responding to stressful situations. Uma emphasizes the importance of open communication and is comfortable in expressing her emotions and thoughts to Prakash, whom she describes as her *"rock*". Prakash is more reserved with his emotions and doesn't express that easily. Asha is fierce in her opinions and viewpoints and put her foot down more when she wants her way. Sachin was more easy-going in nature. Sanjay and Indira continue to grow and learn from their mutual experiences, accepting change wholeheartedly.

Child rearing

Shaping Children's Future

The four couples that were interviewed had different approaches to childrearing and parenting. However, there is a commonly agreed need to shape the futures of their children and prepare them to face the outside world. There are strongly held views on the importance of quality education and a successful job, and to empower and safeguard their children through fostering their dreams and providing them the opportunity to grow.

Empty nest

Impact of Empty Nest

All the four couples interviewed express the period of empty nest as being difficult. While they were mentally prepared for their children to move out, it still seemed sudden and difficult to process. The interviewees have accepted and made meaning of these experiences in their own unique ways. They want their children to lead independent lives, with no compulsions on their children to stay back and take up the role of caretakers.

Retirement

Challenges in Retired Life

The interviewees express that retirement brought with it challenges regarding financial security, losing perks of the job, and managing the extra time available. There exists a feeling of being unwanted and forgotten, and a lack of sense of purpose. Caring for one's own aged parents brought with it its own set of challenges and difficulties.

Level of Engagement/ Activity

All four couples interviewed are continually engaging in work and activities post retirement to keep themselves occupied and physically and mentally healthy. This includes engaging in part time work, being a part of social groups and pursuing interests in nature, arts and travel. Interviewees

have also taken up childhood art forms again during this time. The partners engage together in shared interests and passions, with one of the couple's stating that they volunteer together at an NGO and enjoy traveling to offbeat locations together.

COVID-19: Impact

Changes in Routine. For Laya and Vignesh there has been an inability to travel to meet friends and family and be a part of family functions. Their children have been unable to meet them as well due to the social distancing norms in place. Due to the lack of house help, Laya has been taking over extra household chores which she says is tiresome. Uma and Prakash's plans to travel to meet their daughter had to be cancelled. The shutting down of the amenities in the apartment resulted in their activities and engagements discontinued. Asha had to stop teaching due to the closure of colleges, and this inability to tread outside was difficult for her. There was an excessive workload due to the lack of house help. For Indira and Sanjay their yearly trips to meet their children and their families, as well as their relatives, were cancelled. They stopped going on their routine walks, and also stopped meeting friends.

Psychological Impact. While Vignesh states that while at present he does not experience any challenges, he is wary about the sustained impacts on his mental health if the pandemic continues to rage on. Laya experiences fear and worry over her family's wellbeing. For Uma, the pandemic brought with it anxiety and panic attacks. As cases began being reported closer to home, there was contagion fear for the couple. The job security and wellbeing of their children was also a cause for concern. For Asha, the pandemic has been making her feel panicky, anxious, and frustrated. The inability to break the monotony and the changing circumstances have made her feel uncertain about the future. There is loneliness and strain from the added workload around the house and panic arising from the news about the pandemic. She describes the situation as "*depressing and harassing*". There is worry over her daughter's mental health. For Indira and Sanjay, the pandemic has brought with it uncertainty and fear over their health and that of their loved ones. Watching others suffer through this has been disconcerting. There is immense sadness over losing loved ones and a feeling of "*helplessness*" over the inability to go for a condolence visit. Their increased vulnerability due to their age brings fear of being dependent. Indira is also concerned about the effect that the pandemic can have on the education sector as a whole.

COVID-19: Adjustment/ Adaptation

Emerging Coping Strategies. All the couples interviewed have been following government guidelines, avoiding social gatherings, and taking all the precautionary measures. Health is an important aspect for all of them. Laya and Vignesh have changed some of their food habits with a focus on eating healthier meals, and have been keeping themselves fit by practicing yoga. Uma and Prakash have begun taking more nutrient-rich foods. Yoga and physical activities help them keep a better frame of mind. Asha and Sachin have been avoiding ordering food from outside, and have also reduced consuming unhealthy food. Indira and Sanjay keep themselves fit through yoga and consuming balanced meals.

Laya and Vignesh as well as Asha and Sachin have been avoiding misinformation from the media by following only government channels for information. Asha has been trying not to pass on

disturbing news to others. Uma has cut down her news intake and urges her husband to do the same due to the flurry of disturbing news that added to her distress.

Laya has been taking up most of the household chores. She has been connecting with friends and resuming her activities online. Uma has been reading self-help books, chanting, and meditating to keep herself centred. She has been relying on social support through her friends, and family. Prakash's analytical approach helps her balance her emotions when she experiences anxiety. Prakash has been volunteering for social causes during this time. Asha and Sachin have taken up reading and watching movies together. Both Asha and Indira mention that their husbands have begun helping them with household chores during this period. Through keeping in touch with friends and family and taking up activities like reading, Indira and Sanjay have been coping with the isolation brought about by the pandemic. The balanced approach to stress between the couple and the unexpected visit from their son and family helped them navigate some of the loneliness and stress during this period.

Role of Community. From maintaining precautionary measures to helping vulnerable populations residing in the area, the neighbourhood or communities in which the couples live have been facilitating their adaptive response to the pandemic. The communities have helped them gain a sense of safety and security, derive feelings of positivity and resilience and help them feel more in control of their surroundings.

Technology. The four couples interviewed are adapting to virtual platforms to stay in touch with their friends and family. Their activities like yoga, dance and music have shifted online. There is a reliance on online mediums to order essentials, stay connected with social groups and family. that they are a part of through technology. They are also educating themselves to use technology in order to not feel "*left behind*".

Meaning-making. Across the four narratives, the interviewees state that universality of COVID-19 has helped place the focus now on positive thought, willpower, and mental fortitude. There is a comparison with others who are facing tougher times due to COVID-19, which brings about a feeling of gratitude and privilege. The interviewees are taking precautionary measures, helping each other cope and deriving comfort in knowing the entire world was going through the same situation.

Discussion

The present study delved into the lived experiences of "left behind" older couples in the current context of COVID-19 through a life story approach. While each couple's narratives had their unique themes and subthemes, there were certain overarching themes identified across the four narratives.

Influence of the Life Narrative in the Couple's Reflections of the Current Developmental Tasks, Challenges, and Strengths

The participants have described how their mutual interactions have played a role in their response to stress over the course of their marriages, and how they impact their coping in the context of the pandemic. The partner's complementary response styles to adversity have helped them feel centred and aided in their overall coping. Open communication was stated as the key to a strong relationship.

The participants expressed that with time they were able to navigate their differences in their relationships, and in the present day have a more linear way of approaching their lives. There has been a shared meaning-making which has helped them accept and adapt to the developmental stage of an empty nest. There is an emphasis on their agency and independence from their children which is seen across the four narratives. Adler (2012) found that the themes of agency or sense of control and communion, or good relationships in life correlate with better wellbeing.

The participants state how the relationships provided them the space to grow, how it changed their worldviews for the better, and provided them with the support to navigate their careers and passions. Through shared interests, couples have been pursuing their passions during the current developmental stage and resuming activities that they left midway in their earlier stages of life.

Navigating the Intersectional Domains of Isolation on Mental and Physical Health

The social isolation during the pandemic added to the pre-existing isolation of older couples as a result of their developmental stage. There was a general sense of apprehension over the sustained impacts of the pandemic if it rages on over several months. These views are similar to those expressed by the older adults studied by Hamm et al (2020), who are concerned about the long-term physical and financial wellbeing due to the prolonged effects of the pandemic.

This physical isolation combined with the influx of negative news reports added to the worry and fear over their wellbeing and that of their loved ones. Couples reported experiencing panic and anxiety surrounding the situation. The uncertainty surrounding the COVID-19 protocols, impacts of the virus, and vulnerability of their age group to the virus added to the existing worry. Social disconnection predicted higher perceived isolation, depressive and anxiety symptoms in older adults (Sartini et al., 2020).

Navigating this isolation through the use of technology to connect with loved ones, avail resources and stay active was identified across the four narratives. They navigated grief, worry, and fear by confiding in their friends and family and deriving positives from others as well as their surroundings.

The community or neighbourhood in which the couples reside has played a significant role in helping them navigate the *"new normal"*. From helping them procure necessities to ensuring their safety and security, the community has helped alleviate some of the worry and fear associated with these times.

Staying active through physical and mental exercise was an emergent theme across the narratives. Physical exercise plays a role in delaying immunity dysfunction, promoting immune system regulation, and thus could prevent the risk of acquiring COVID-19 infection and reduce the complications of recommended self-isolation in older adults and elderly individuals (Abdelbasset, 2020).

Conclusion

The study delved into the various developmental tasks associated with old age and with the current pandemic as well as the adaptive coping mechanisms employed by the couples to respond

to them. It not only threw light into the experience faced by this population but is a step towards future research employing a strengths-based perspective to study the geriatric population.

Limitations of the Study

This study was conducted on a small population of older couples, and as in all qualitative studies, these stories are in no way representative of the larger population of the elderly. Triangulation was not included in the research design. Furthermore, all the participants of this study are fairly educated belonging to the middle or higher socioeconomic category. Therefore, the results are limited and may not reflect the experiences of older couples belonging to varied socioeconomic statuses.

As the participants were elderly, the duration of the interviews was maintained according to their comfort. Since all the four couples had such rich and detailed relational stories, it would have required much longer interviews or multiple interviews in order to understand the countless experiences across their lives.

In qualitative research, the researcher's subjectivity is unavoidable and my personal biases and assumptions could have possibly influenced the findings of the study.

Implications of the Study

This study contributes to the limited body of research focused on the geriatric population from a strengths-based lens in India. The population has been increasingly facing isolation which has magnified in the light of the current COVID-19 pandemic. While online technology could be used to provide a sense of belonging through social support networks, due to the disparity in access and digital literacy, interventions could be in the form of simple telephone contact. Community outreach programs that provide peer support or contact with healthcare professionals involving more frequent telephone interaction could be facilitated.

Through focusing on the strengths of the elderly, policies and reform can be focused on empowering and assisting this group in overcoming the challenges that are a part of their developmental stage and influenced by the current contextual factor, COVID-19.

Future Considerations

A majority of the literature available on loneliness, ageing, and COVID-19 is from the standpoint of western countries. Further research needs to be focused on the impact of the added loneliness associated with the COVID-19 pandemic in the long run for older adults residing in the Indian subcontinent.

Mental health practitioners must recognize the importance of employing nonpharmacological approaches towards enhancing resilience, and coping, and reducing loneliness in older adults. This could include using cognitive behavioural therapies, promoting compassion training, greater connectedness, and physical activity.

References

Abdelbasset, W. K. (2020). Stay home: Role of physical exercise training in elderly individuals' ability to face the COVID-19 infection. *Journal of Immunology Research*, *2020*, 1-5. https://doi.org/10.1155/2020/8375096

Adler, J. M. (2012). Living into the story: Agency and coherence in a longitudinal study of narrative identity development and mental health over the course of psychotherapy. *Journal of Personality and Social Psychology*, *102*(2), 367-389. https://doi.org/10.1037/a0025289

Agewell digital literacy program for older persons –. (2020). Agewell Foundation. https://www.agewellfoundation.org/?page_id=5768

Armitage, R., & Nellums, L. B. (2020). COVID-19 and the consequences of isolating the elderly. *The Lancet Public Health*, *5*(5), e256. https://doi.org/10.1016/s2468-2667(20)30061-x

B Mane, A. (2016). Ageing in India: Some social challenges to elderly care. *Journal of Gerontology & Geriatric Research*, *05*(02). https://doi.org/10.4172/2167-7182.1000e136

Banerjee, D. (2020). The impact of covid-19 pandemic on elderly mental health. *International Journal of Geriatric Psychiatry*, *35*(12), 1466-1467. https://doi.org/10.1002/gps.5320

Banerjee, D., D'Cruz, M., & Sathyanarayana Rao, T. (2020). Coronavirus disease 2019 and the elderly: Focus on psychosocial well-being, agism, and abuse prevention – An advocacy review. *Journal of Geriatric Mental Health*, *7*(1), 4. https://doi.org/10.4103/jgmh.jgmh_16_20

Braun, V., & Clarke, V. (2013). *Successful qualitative research: A practical guide for beginners*. SAGE.

Brooke, J., & Jackson, D. (2020). Older people and COVID-19: Isolation, risk and ageism. *Journal of Clinical Nursing*, *29*(13-14), 2044-2046. https://doi.org/10.1111/jocn.15274

Brookover, B. C. (2013). Gary Kenyon, Ernst Bohlmeijer, and William L. Randall (2011).Storying later life: Issues, investigations, and interventions in narrative gerontology. *Journal of Women & Aging*, *25*(2), 201-203. https://doi.org/10.1080/08952841.2013.760375

Cavanaugh, J. C., & Blanchard-Fields, F. (2010). *Adult development and aging*. Nelson Education.

Clandinin, D. J., & Connelly, F. M. (1999). *Narrative inquiry: Experience and story in qualitative research*. Jossey-Bass.

COVID-19: A gender lens. (2020, March). UNFPA - United Nations Population Fund. https://www.unfpa.org/resources/COVID-19-gender-lens

Creswell, J. W. (2005). *Educational research: Planning, conducting, and evaluating quantitative and qualitative research*. Prentice Hall.

Czarniawska, B. (2004). *Narratives in social science research*. SAGE.

Datta, P. (2011). Population projection of EAG states of India: Vision until 2051. *SSRN Electronic Journal*. https://doi.org/10.2139/ssrn.1861769

D'cruz, M., & Banerjee, D. (2020). 'An invisible human rights crisis': The marginalization of older adults during the COVID-19 pandemic – An advocacy review. *Psychiatry Research*, *292*, 113369. https://doi.org/10.1016/j.psychres.2020.113369

Gerst-Emerson, K., & Jayawardhana, J. (2015). Loneliness as a public health issue: The impact of loneliness on health care utilization among older adults. *American Journal of Public Health*, *105*(5), 1013-1019. https://doi.org/10.2105/ajph.2014.302427

Giridhar, G., Sathyanarayana, K. M., James, K. S., Alam, M., & Kumar, S. (2014). *Population ageing in India*. Cambridge University Press.

Hamm, M. E., Brown, P. J., Karp, J. F., Lenard, E., Cameron, F., Dawdani, A., Lavretsky, H., Miller, J. P., Mulsant, B. H., Pham, V. T., Reynolds, C. F., Roose, S. P., & Lenze, E. J. (2020). Experiences of American older adults with pre-existing depression during the beginnings of the COVID-19 pandemic: A Multicity, mixed-methods study. *The American Journal of Geriatric Psychiatry*, *28*(9), 924-932. https://doi.org/10.1016/j.jagp.2020.06.013

Havighurst, R. J. (1961). Successful Aging1. *The Gerontologist*, *1*(1), 8-13. https://doi.org/10.1093/geront/1.1.8

Havighurst, R. J. (1980). Life-span developmental psychology and education. *Educational Researcher*, *9*(10), 3-8. https://doi.org/10.3102/0013189x009010003

Healey, J. (2011). Gary Kenyon, Ernst Bohlmeijer and William L. Randall (EDS), storying later life: Issues, investigations, and interventions in narrative gerontology, Oxford University press, New York, 2011, 424 pp., hbk £32.50, ISBN 13: 978 0 19 539795 6. *Ageing and Society*, *32*(1), 169-170. https://doi.org/10.1017/s0144686x11000882

Klaiber, P., Wen, J. H., DeLongis, A., & Sin, N. L. (2020). The UPS and downs of daily life during COVID-19: Age differences in affect, stress, and positive events. *The Journals of Gerontology: Series B*, *76*(2), e30-e37. https://doi.org/10.1093/geronb/gbaa096

Lazarus, R. S., & Folkman, S. (1984). *Stress, appraisal, and coping*. Springer Publishing Company.

Mount, S. D., & Moas, S. (2015). Re-purposing the "Empty nest". *Journal of Family Psychotherapy*, *26*(3), 247-252. https://doi.org/10.1080/08975353.2015.1067536

Mukhtar, S. (2020). Mental health and emotional impact of COVID-19: Applying health belief model for medical staff to general public of Pakistan. *Brain, Behavior, and Immunity*, *87*, 28-29. https://doi.org/10.1016/j.bbi.2020.04.012

Mukhtar, S. (2020). Mental health and psychosocial aspects of coronavirus outbreak in Pakistan: Psychological intervention for public mental health crisis. *Asian Journal of Psychiatry*, *51*, 102069. https://doi.org/10.1016/j.ajp.2020.102069

Munnichs, J. M. (1984). Erik H. Erikson, the life cycle completed, a review. Norton, New York/London, 1982, 108 P., $10.95, ISBN 0 393 01622 6. *Ageing and Society*, *4*(3), 375-377. https://doi.org/10.1017/s0144686x00010965

Newman, B. M., & Newman, P. R. (2017). Development through life: A psychosocial approach. Cengage Learning.

Not found. (2020, March 31). The New York Times - Breaking News, US News, World News and Videos. https://www.nytimes.com/2020/03/31/us/coronavirus-covid-triage-rationingventilators

Older people and COVID-19. (2020). WHO | World Health Organization. https://www.who.int/teams/social-determinants-of-health/demographic-change-and-healthy-ageing/COVID-19

Pasupathi, M., Weeks, T., & Rice, C. (2006). Reflecting on life. *Journal of Language and Social Psychology*, *25*(3), 244-263. https://doi.org/10.1177/0261927x06289425

Pearman, A., Hughes, M. L., Smith, E. L., & Neupert, S. D. (2020). Age differences in risk and resilience factors in COVID-19-Related stress. *The Journals of Gerontology: Series B*, *76*(2), e38-e44. https://doi.org/10.1093/geronb/gbaa120

Ribeiro, M. D., Borges, M. D., Araújo, T. C., & Souza, M. C. (2017). Coping strategies used by the elderly regarding aging and death: An integrative review. *Revista Brasileira de Geriatria e Gerontologia*, *20*(6), 869-877. https://doi.org/10.1590/1981-22562017020.170083

Santini, Z. I., Jose, P. E., York Cornwell, E., Koyanagi, A., Nielsen, L., Hinrichsen, C., Meilstrup, C., Madsen, K. R., & Koushede, V. (2020). Social disconnectedness, perceived isolation, and symptoms of depression and anxiety among older Americans (NSHAP): A longitudinal mediation analysis. *The Lancet Public Health*, *5*(1), e62-e70. https://doi.org/10.1016/s2468-2667(19)30230-0

Scheffel, J., & Zhang, Y. (2018). How does internal migration affect the emotional health of elderly parents left-behind? *Journal of Population Economics*, *32*(3), 953-980. https://doi.org/10.1007/s00148-018-0715-y

Scott, A. (2020, April 22). *How aging societies should respond to pandemics*. Project Syndicate. https://www.project-syndicate.org/commentary/how-aging-societies-should-respond-to-pandemics-by-andrew-scott-2020-04?barrier=accesspaylog

Sepúlveda-Loyola, W., Rodríguez-Sánchez, I., Pérez-Rodríguez, P., Ganz, F., Torralba, R., Oliveira, D. V., & Rodríguez-Mañas, L. (2020). Impact of social isolation due to COVID-19 on health in older people: Mental and physical effects and recommendations. The journal of Nutrition, Health & Aging. https://doi.org/10.1007/s12603-020-1469-2

Thapa, D. K., Visentin, D., Kornhaber, R., & Cleary, M. (2018). Migration of adult children and mental health of older parents 'left behind': An integrative review. *PLOS ONE*, *13*(10), e0205665. https://doi.org/10.1371/journal.pone.0205665

Tomás, J. M., Sancho, P., Melendez, J. C., & Mayordomo, T. (2012). Resilience and coping as predictors of general well-being in the elderly: A structural equation modeling approach. *Aging & Mental Health*, *16*(3), 317-326. https://doi.org/10.1080/13607863.2011.615737

Tovel, H., & Carmel, S. (2013). Maintaining successful aging: The role of coping patterns and resources. *Journal of Happiness Studies*, *15*(2), 255-270. https://doi.org/10.1007/s10902-013-9420-4

Van Tilburg, T. G., Steinmetz, S., Stolte, E., Van der Roest, H., & De Vries, D. H. (2020). Loneliness and mental health during the COVID-19 pandemic: A study among Dutch older adults. *The Journals of Gerontology: Series B*. https://doi.org/10.1093/geronb/gbaa111

Verhage, M., Thielman, L., De Kock, L., & Lindenberg, J. (2021). Coping of older adults in times of COVID-19: Considerations of temporality among Dutch older adults. *The Journals of Gerontology: Series B*. https://doi.org/10.1093/geronb/gbab008

Williams, N. (2010). Public health and aging, maximizing function and well-being. *Occupational Medicine*, *60*(7), 580-580. https://doi.org/10.1093/occmed/kqq103

Zadworna-Cieślak, M., & Ogińska-Bulik, N. (2019). Satisfaction with life in old age – the role of developmental tasks attainment and resiliency. *Przegląd Badań Edukacyjnych*, *1*(28), 23. https://doi.org/10.12775/pbe.2019.002

11 Existential Psychotherapy as an Effective Intervention for Psychological Issues in Older Females in India

Purnima Gupta*

Abstract

Can existential psychotherapy be the answer to the issues faced by the older women in India? A look at the concerns faced by the older women who have reached to the other side of their mid-lives and the question finds its answer. A careful observation of the older women in India leads to the understanding that most of these women feel a sense of emptiness. Most of their concerns are related to their self-worth or the nature of their existence during their old age. Approaching the end or culmination is never smooth for an individual. It calls for tremendous rationality, objectivity, and resilience on one's part to be able to take stock of one's life and stay hopeful despite all that has been passed. The growing age catches up with one's psychological, emotional, and physical abilities and leaves the individual with a gaping sense of worthlessness, depression, anxiety, or some other mental health issues. The problem gets aggravated in a patriarchal society like India where women usually struggle to express their valid needs and expectations. Patriarchal atmosphere leads to intense suppression in women and the impact of which becomes visible in their older years. Such women struggle with mental health issues, psychosomatic illnesses, and emotional disturbance in their lives after middle age.

As an intervention approach for the mental health challenges of Indian older women, counselling and psychotherapy have been proven effective. Out of all the available frameworks of psychotherapy, the paper is an attempt to explore existential psychotherapy as a choice of intervention for older women. The paper also explores the nature of issues experienced by older women in India.

Keywords: Older women, Existential psychotherapy, Geriatric mental health, Geriatric counselling, depression, Anxiety in older women

* Assistant Professor (Psychology), Karnavati University, Gandhinagar, Gujarat

Introduction

Middle age years begin from 45th year of life and then go till the retirement year. Middle age is usually considered a period of substantial physical, emotional and psychological changes in an individual's life. It also is understood through detailed research that women experience significant changes beginning from the onset of their menopause making the middle years a cumbersome period for them. One of the biggest challenges during the middle age years is an unintentional visit to one's past choices and decisions. As women start moving towards their old age, they uncontrollably start experiencing the urge to take stock of their years gone by. Much of their lives in the past are governed by the norms put in place through social and cultural traditions. Their persona is a representation of their adherence to social and cultural norms. But once the middle age hits, women find themselves being rendered out of demand. They are no longer sought after by their spouse and children or other family members. Most of these women find themselves experiencing a state of worthlessness, a gaping void or vacuum and a future that appears bleak. The feeling is common to almost every woman, yet the solution is far from being approached. Many women also experience psychosomatic chronic illnesses as an expression of their inner struggle, whereas some even fail to recognize and seek appropriate interventions for the same owing to their social, cultural, and demographic limitations.

During the past 2 decades, there is a rise in the number of women approaching counsellors or psychotherapists to seek help for their psychological and physical health issues. The realization of not having lived as their true self gnaws at them as they realize that their time draws closer. While all the psychotherapies prove to be effective in supporting the women in their journey of self-exploration/individuation, this paper lays emphasis upon existential technique as a tool of psychological intervention. Existential theory propounds that the task of individuation or achieving one's true potential is easy to be attained if the individual has a purpose/ meaning for one's life. This purpose is akin to being true to one's inner conviction to the life and living with an awareness of the ultimate truths about the same. The purpose acts as a ground beneath one's feet and helps the individual move beyond the everyday drudgeries of life. The existential model of psychotherapy supports the individual in excavating his core personality through various layers of conditioning and facing the subjective truth in the form of a purpose that is sacred to an individual's existence.

The existential exploration is not about analysing the everyday challenges of an individual life rather it is about an honest encounter with what it is (Frankl, 1963). It is proposed through this paper that when applied as an approach to support the middle-aged women in exploring and accepting their true self, existential model/approach can be an effective pathway.

Living and existence sound similar but they are different from each other in the way they explain an individual's pattern of life. Living is more about being fully involved in all the matters and situations of life whereas existence is more about adapting oneself to ensure smooth, non-frictional sailing from birth to death. Some philosophers may argue that existence is deeper in meaning whereas living is just going about your routine. As a researcher with a deep interest in exploring the human existence and its various facets, I look at existence as a term that carries personal value while living is more about attributing a common value to each life and certain parameters. Following my own

personal definition of existence, I am trying to explore the existence of women in India pertaining to their middle age situations and conditions. A lot has been written, researched and documented about various problems and solutions revolving around mid-life challenges for women though, yet this research paper is my sincere attempt towards all that the women contribute in their various roles so that people like me grow up to do something substantial/ follow our dreams.

My understanding of the nature of problems faced by women in their Middle Ages comes from my own observation of my surroundings and thus, forming the basis of my argument and research. Seeing women in their Middle Ages has often ignited extreme rage and helplessness, in those who possess the capacity to feel. This research paper is attempted to put my everyday observations of middle-aged women and their woes into a perspective that can lead us become more empathetic towards the existential challenges faced by the aging women in India. I also have suggested a solution in the light of existential psychotherapy, as it addresses the issues in their entirety and provides long-term solutions.

Method

This research paper is a result of literature review method after an intensive reading and reflection of the available literature and texts in the field of existential theory. The papers reviewed for the paper include both original work and review literature. Books written by the founders of existential theory were also referred for further reflections along with the available information in the form of articles and research papers on internet.

Indian Women and the Mid-life Crisis

Women in Indian culture have long been entrusted with the responsibility of nurturing and caring for their family members. There are set paths and traditions that slowly mould young girls into the future nurturers. By the time, they reach their middle age, their sense of identity majorly relies upon the relationship they share with their spouse, children, and other family members. But the scene changes with growing age and especially when the middle years of life come knocking. Middle age for Indian women is a period of transition in many ways. This specific period not only brings significant physiological changes but also demands women to adapt themselves to a life with fewer responsibilities and more time with oneself. A sense of loneliness and worthlessness also dawns upon women as their children begin to establish their own life and identity different than their parents. It is in these times that women begin to feel unworthy, unloved, and abandoned by their family members. Their social space also paints a bleak picture for them as they realize the limited existence of their social transactions. Amidst all physiological, psychological, and social transitions, the middle age transition brings a lot of challenges for women in terms of their self-worth, identity, and purpose (Sharifi et al., 2014). With new insights pouring in, women experience a need to express their concerns and be their authentic self. The stifled expressions and earlier suppressed emotions throw them into a situation where their physical health goes downhill. An outbreak of psychosomatic symptoms in the form of chronic disorders such as rheumatoid arthritis, diabetes, hypertension, knee problems, cardiac problems become synonymous to middle age years (Ahmed, 2017). Many of these problems leave these women questioning their future as they

look at a dependent life. A dual challenge in terms of changing relationship dynamics and health issues owing to ageing pushes the women to look deeply into one's inner life and face the truth. A deep sense of worthlessness and emptiness plagues the mind of these women, pushing them into a vicious cycle of self-pity and sadness. Anxiety, depression, and other such mental health disturbances appear very common in the women around their middle age years. Conventional methods of intervention rarely provide any permanent relief aggravating the whole feeling of being rendered with no hope for their future. At the bottom of such hopelessness, lies the fear of being mortal or not being in use as a human being. This feeling is the onset of what is addressed as "existential dread" or "existential anxiety" by the existential philosophers and psychologists (May, 1977). The theory of existential intervention strongly proposes that any attempt to cure the presenting symptoms (physical or psychological) must address the underlying core of one's fearfulness or disappointment with the meaninglessness or absurd nature of the existence.

Existential Approach

The discovery of one's true self has been considered the highest goal of an individual's life and almost every culture and religion encourage its followers to walk towards their true expression of the self. Since the beginning of psychotherapy as an intervention/ solution to an individual's inner struggles, has also proposed "knowing oneself" as an effective approach to the struggles. Carl Rogers, an American Psychologist, and the founder of Client-centered Therapy wrote about the concept of "Real Self" and Ideal self (Rogers, 1961). He mentioned that the more is the gap between what a human being IS and what the human being idealizes to BE, the more challenges a human being will have in his life. The authentic expression of a human being is what brings more authenticity to the expression of an individual and the same is needed for the maintenance and restoration of balance between one's physical and psychological entities/ expression.

Another important mention in terms of existential challenges is proposed by the Austrian Psychiatrist and the founder of Logotherapy Dr. Viktor Frankl- a holocaust survivor. Dr. Frankl came up with this theory that the lack of meaning for one's life is what gives rise to anxiety, feelings of worthlessness and other similar mid-life challenges (Frankl V, 1969). He proposed that finding a purpose for one's life is what keeps the individual involved with the life and motivates the individual to face the challenges with all his might and not give up easily.

Around 1970s, Dr, Irvin Yalom also proposed his theory of what an existential crisis looks alike. According to Dr. Yalom, death, isolation, meaninglessness, and freedom are the four given conditions of human life. These 4 key areas are what determines the intensity of an existential crisis for everyone.

Rollo May was one of the earliest psychotherapists in 1950s who brought the existential movement to America and said that the root cause of all the neurotic conditions is the anxiety that one experiences regarding one's own death.

All the existential concerns point out at the sense of despair, alienation, worthlessness and lack of any direction or orientation experienced by an individual. Sometimes, the presence of a chronic illness or economic challenges pushes an individual into a crisis whereas, for most of the people, the existential crisis knocks at the door when the middle age comes calling.

During the therapeutic interactions, the focus area for existential approach is the "ultimate concern about one's disappearance or mortality", which, is believed to be the chief cause of all the presenting forms of anxiety in an individual.

One's relationship with oneself is sacred to the successful implementation of existential psychotherapy. This relationship is sacred than any other relationship the individual may be having with other human individuals and with his surroundings. This existential relationship reaches far beyond the conventional take on what it means to be oneself. It is believed that coming to terms with one's past or accepting the tumultuous past that one has had will bring ultimate peace to one's present and future. The existential approach offers a different perspective and urges the individual to explore his relationship with the "ultimate givens" of life (Yalom, 1986). The approach doesn't discard the past as unimportant but proposes that the individual answer to the fundamental questions of "what it means to be born as a human" and the conditions that surround the human existence, lies in facing it all. The existential approach has been through certain makeovers in terms of what all needs to be included in the approach as a therapeutic technique. However, the essence has largely remained unchanged.

Discussion

Effective Intervention of Mid-life Crisis through Existential Psychotherapy

Living and existence sound similar but they are different from each other in the way they explain an individual's pattern of life. Living is more about being fully involved in all the matters and situations of life whereas existence is more about adapting oneself to ensure smooth, non-frictional sailing from birth to death. Some philosophers may argue that existence is deeper in meaning whereas living is just going about your routine. As a researcher with a deep interest in exploring the human existence and its various facets, I look at existence as a term that carries personal value while living is more about attributing a common value to each life. Following my own personal definition of existence, I feel compelled to propose the use of existential psychotherapy as an influential approach by mental health practitioners to support the women, particularly those in their mid-life years, in overcoming their existential woes.

Application of existential technique demands that the therapist has a deeper, clearer understanding of the nature and intensity of existential issues. Helping a client see through her anxieties and other physical as well as psychological symptoms is more than just trying to gauge the spectrum of the issue. The client is gently nudged by an existential therapist to recognize the core concern i.e., the fear of being rendered useless or the realization of having left with a limited period to accomplish the tasks/ goals set by oneself. The whole exercise of being present to one's dreadful yet faint recognition of the limitations that exist in various areas of one's life, requires tremendous patience and above all, wisdom. The therapist must be well-versed with the experience of existential challenges and the various symptoms in an individual's behaviour that signal the presence of such an existential angst.

It is imperative to note here that the deeper one dives into one's unconscious fear of death, the more one is faced by a truth about one's being just an ordinary individual with skills, talents, and

abilities common to the entire human race. The identification of one not being special is akin to facing a mirror that reflects the truth of what one is. The day-to-day failures in various actions and behaviours are nothing but a reminder of humans being ordinary. Our failures and miseries and disappointments are a stark realization of the fact that essentially, we are not in control of anything, rather we are controlled by the life.

Existential therapy is a technique to explore all such universal yet largely ignored and forgotten truths of a human life form. The gradual uncovering of all the unconscious psychological defences ignites intense fear and dread in an individual leaving him vulnerable to the ever-present challenges around. The fact that the death anxiety is the main reason beneath all the psychological and psychosomatic symptoms is a huge discovery around mental well-being. Clinical investigations done in this area have been revealing startling facts about death anxiety being the root cause of all anxieties.

It can be suggested here that women going though their mid-life crisis can be encouraged to find a solution for their issues through existential psychotherapy and overcome their existential challenges as suggested by Viktor Frankl. According to Frankl, a human being can lead a meaningful existence by dedicating herself for a cause that she believes in, an involved relationship with another human being and adopting resilience in the face of adversities. The purpose always is personal to an individual and can neither be adopted nor can it be taught. A thorough investigation into one's inner world paves the way for a woman to come out in her full glory and grow into an individuated expression of human form.

The identification of one's underlying fear of one's disappearance from the world and later, accepting one's mortality with grace and gratitude is what brings life a full circle.

Limitations and Directions for future research

The paper is written as a conceptual paper but the limited availability of writings from an eastern perspective was felt all along. The theory, its applications and the case studies all are documented from a western cultural approach, and this offers an opportunity to explore the theory from a cross-cultural perspective. Also, there is a strong recommendation to document the case studies in a detailed manner to substantiate the future research in the area of existential psychotherapy as an effective intervention technique.

Conclusion

It is concluded that the existential method can fill the gap between middle age problems experienced by Indian Women and the intervention methods used to address them. Existential method guides and supports the women in facing their true self and shed behind their external persona (developed because of socio-cultural conditioning). The techniques of existential therapy proposed by Viktor Frankl and Irvin Yalom pave the way forward to holistic well-being for women going through their mid-life crisis. A thorough exploration and later, acceptance of one's inner world is essential to find an authentic expression of oneself.

References

Vos, J., Roberts, R., & Davies, J. (2019). Mental health in crisis. Sage.

Chang, G. (2020). Mental health. Religion, Migration, and Existential Wellbeing*, 157-167.*

Karki, P. (2019). A critical evaluation of theories and practices in existential psychotherapy. *International Journal of Science and Research*, 8,1, 681-683.

Deuzen, E.V. (2010) *The framework for existential psychotherapy, Existential Counselling and Psychotherapy in Practice*, Sage Publications.

Yalom, I. (1980). *Existential Psychotherapy*, Harper Collins Publishers.

May, R.; Yalom, I. (1995) *Existential Therapy, Current Psychotherapies*, Cengage Learning.

Fromm, E. (1941). *Escape from freedom. New York:* Rinehart.

May, R. (1999). *Freedom and destiny. WW* Norton & Company.

Wong, P. T. P (2004). Editorial: Existential psychology for the 21st century. *International Journal of Existential Psychology and Psychotherapy*, 1, 1–2.

Frankl, V. E. (1986). *The doctor and the soul: From psychotherapy to logotherapy*. Vintage.

Frankl, V. (1963). *Man's search for meaning: An introduction to logotherapy.* New York: Pocket Books.

Frankl, V. (1964). *The Will to Meaning: Foundations and Applications of Logotherapy*. Penguin Books USA Inc.

Marino, G. (1952). *The Existentialist's Survival Guide: How to live authentically in an inauthentic age*. Harper Collins

May, R. (1977). *The Meaning of Anxiety*. The Ronald Press Company.

12 Ayurveda for Healthy Ageing

R. Vasumathi*

Abstract

Humans have always been looking for techniques that help delay the ageing process. With the rapid advancements in the medical field, extending an individual's lifetime through various medications is now possible Geriatrics is a separate branch in Ayurveda called as "Jara Chikitsa" which deals with prevention and cure of problems and diseases related to old age. This branch deals with the all the physical, mental and emotional ailment that develops in Vridhopacharaneeyam" (Old age)

This research paper helps to understand the steps behind ageing healthily and happily through the various techniques in Ayurveda. Etymologically the word Ayurveda is associated with a prolonged healthy life. Ayurveda advocates healthy body through a healthy mind. It clearly mentions that if there is a disturbance in the body or mind then ailment or disease becomes prevalent. Diseases manifest mainly due to the imbalance of the tridoshas or humors present inside the body. This system believes that treatment methods are different for each individual and understand the uniqueness of an individual's immune system. Ayurveda helps an individual age naturally by combining body, mind and spirit. The methods followed in Ayurveda are not just medicines or pills to stay healthy. It is a complete holistic process offering various methods and steps to age graciously, live longer and align with the environment and nature.

Keywords: Ayurveda, Healthy Ageing, Vridhopacharaneeyam, Jara chikitsa

* M.phil Trainee, Amity Institute of Behavioural Health and Allied Sciences, Amity University, Kolkata Campus

** Assistant Professor, Amity Institute of Behavioural Health and Allied Sciences, Amity University, Kolkata Campus

Introduction

Ayurveda is the mother of all healing systems. From its eight principal branches, geriatrics explains the ways and methods of healthy ageing. Ayurveda helps lead our daily life in harmony with nature and its laws. This ancient wisdom of science aims to prevent diseases or disorders and heal disorders or diseases from the sick person.

The Ayurveda system is a holistic healing system to its truest sense (Lad, 1999). In the human body, Ayurveda advocates the balance of three vital energies or dosha's, Vata, Pitta and Kapha, to help maintain good health and a healthy mind. If the human mind constantly interacts with nature, the body and mind will self-heal or stay in their best health.

Ayurveda means "the Veda or science of longevity". It is a part of Atharvana Veda. Ayurveda advocates diet, lifestyle, relaxation, rejuvenation, cleansing, kashayams, choornams and medicinal herbs. It also gives an insight into lifestyle choices (*Dinacharya*), which helps one stay healthy or unhealthy based on their choices.

Each individual has their own or unique body properties based on the composition and balance of the three doshas. Unlike modern medicine, Ayurveda prescribes medicines based on every individual body nature and composition. It considers the external environment's influence, like seasonal changes, and the changes in our emotions, diet, and lifestyle before prescribing any medications. In order to remain healthy, both our internal and external conditions should be in harmony.

If the inner doshas are unbalanced, then various ailments develop. The imbalance of *Kapha* leads to cold and cold-related sicknesses. *Vata* imbalance leads to constipation, indigestion, gastritis, arthritis and gastric based issues. Imbalance in *pitta* dosha leads to indigestion, heartburn, rashes, diarrhoea, rash and other indigestion issues. We need to balance, juggle and adjust these three doshas accordingly not to disturb our bodily or mental equilibrium as we age. To achieve this, Ayurveda shows the path and methods to age healthily.

Ayurveda makes each individual responsible for their own life as it helps the individual attain or reach the purpose of his/her life, the final salvation or spiritual liberation. This can be achieved only through good health and healthy living.

Health issues crop up when the lifestyle of the individual is not good. Stressful work, marital issues, relationship problems, and other pressures from the environment cause imbalances in the three doshas, which leads to disease or ill health.

Ageing or *Jara*, as Ayurveda defines is a natural, inevitable phenomenon like thirst and hunger. The three doshas are prominent at various stages of life. *Kapha* dominates during childhood, whereas *Pitta and Vata* dominate during middle and older.

Composition of the body according to Ayurveda

According to Ayurveda, the human body is made up of the three humors (*Pitta, Vata and Kapha*), five essential elements (Earth, Water, Fire, Air and Space), seven tissues (*Mansa, Asthi, Rasa, Meda, Shukra, Raktha and Majja*) along with the excretory products (urine, sweat and faeces). Balance in these above compositions in different proportions is unique to each human body. The

development and the balance of these compositions depend on the nutrition one absorbs from the food, which is made of the five essential elements mentioned above. The different permutations and combinations of the five essential elements lead to the humors present in the human body, which is different for each human being. When the balance or equilibrium of the doshas are lost due to internal and external reasons like erratic lifestyle, seasonal changes, dietary issues, and so on, it gives rise to disease or chronic illness, which can be cured through *Panchakarma or Rasayana treatments*. Through these treatments, Ayurveda mainly restores the balance of the humors in the body. A healthy body leads to a healthy mind. Ayurveda prescribes medications and treatments based on the illness individually rather than generic medication to all with the same illness.

Ashtanga of Ayurveda

Eight limbs or branches of Ayurveda are known as Ashtanga Ayurveda. The eight branches are exclusive or specialised uniquely. The eight angas or ashtanga are prevalent from the olden days, which shows that Ayurveda is an advanced branch of holistic medical practice.

Kaya Cikitsa (Internal Medicine): This is also like general medicine, and it helps to maintain or restore the metabolism in the body by correcting the imbalance created by Agni (*Kaya*) – the digestive fire in the body. It also deals with treating general illnesses like cough, fever, loose stools, etc.

Vrushya Cikitsa (Fertility): This branch deals with fertility and reproductive issues and helps to get good offspring. It also improves virility and sexual prowess through proper medication and therapies.

Bala Cikitsa (Paediatrics): As the name suggests, this branch deals with health and illness related to children.

Urdhwanga Cikitsa (ENT): This branch deals with the diseases that affect the parts of the body, which are above the neck, like eyes, ears, mouth, teeth, throat, nose and head.

Jara Cikitsa (Health and Longevity): This branch is mainly for longevity, good health, graceful ageing and improving the complexion, memory and immunity. It mainly deals with preventing, managing, and treating old age issues with the help of various herbs and therapies.

Damshtra Cikitsa (Toxicology): This branch deals with the study and treatment of poisoning from animals, plants, various poisons, minerals, metals, and toxic elements from all types of pollution.

Shalya Cikitsa (Surgery): This is mainly about surgical procedures like pre-operative, post-operative, anaesthesia and sutures. This branch is the treatment for diseases like tumours, fractures, plastic surgery, and many other surgical treatments.

Graha Cikitsa (Psychiatry): This deals with psychological disorders and mental health issues.

Methodology

Aims and Objectives:

The aim and objective of this study is to understand, re-assess, discuss and elaborate on health-related problems of ageing and ageing naturally with the help of Ayurveda.

Materials and Methods:

This article is based on ayurvedic textbooks like Charaka Samhita and other books that advocate the benefits of Ayurveda for healthy living and healthy ageing. This article has also referred to various websites which explain ayurvedic concepts in detail.

Geriatrics in Ayurveda (Jara or Rasayana Cikitsa):

According to Charaka, Ageing or Jara is a natural but inevitable process that is degenerative. The deteriorating changes in the body happen during the final span of life, which is called *Vriddhavastha* (Charaka Samhitha). The energy principals or doshas dominate each phase of the human life span, divided into three phases known as *Vaya* in Ayurveda. *Kapha* dominates during *Balavastha* (childhood, 0 – 16 years), *Pitta in Madhyavastha* (Youth, 16-60/70 years) and *Vata in Vriddhavastha (Jara,* Old age, 70 years and above). When these doshas are disturbed or imbalanced due to wrong nutrition choices, senses and lifestyle, it leads to early ageing and deteriorating health. Balancing these doshas bring about good health and will delay the ageing process smoother.

During *Vriddhavasatha*, due to *Vata dosha*, there will be decaying of the physical body like wrinkling the skin, greying of hair and impairments in mental and cognitive functions. When *Vata dosha* is dominant, it leads to indigestion and does not provide the required nourishment to carry the metabolic activities due to the change in the Agni, which is called *Vishamagni* (Chakrapani). Agni plays a significant role in the ageing process as the Agni (fire) helps digest food and convert the food into its nutrients.

Ageing, as per Charaka, can be classified into two types: timely ageing *(Kala Jara)* and untimely ageing *(Akala Jara)*. Timely ageing is ageing at the appropriate age of 70 years (Charaka Samhita), whereas untimely ageing happens due to the aggravation of *Kapha and Pitta* doshas during young age. Various reasons like lifestyle issues, diet, sleep and so on are the reasons for this untimely ageing.

Jaravadhana Poshana

Modern medicine speaks a lot about the aetiology of ageing and how to prevent early ageing and to age healthily. It mentions the ageing process as a slow, continuous and insidious destruction in the structure and metabolic activities of the human being after attaining sexual maturity. However, in Ayurveda, a separate branch is dedicated to *Jaravadhana Poshana* (Healthy Aging). The natural ageing process is uniquely different for each person (Brahmanand et al., 1999).

Preventive health care is the chief aim of Ayurveda. The chief perspective of Ayurveda is to delay natural ageing (*Kala-Jara*) and prevent Premature ageing (*Akala-Jara*). From its extensive methods, Ayurveda advocates *kaashayams, Dinacharya (*daily regimen*), Panchakarma techniques (*removing toxins from the body*),* palliation and pacification *(shamanam),* wholesome diet *(Hitakara and Matravata ahara), therapies and Rasayana* care to combat premature ageing and help in healthy ageing.

Prevention of premature ageing and Healthy Aging

Ayurveda guides for preventing premature ageing and help for healthy ageing. The process of ageing rests with the correct diet and lifestyle. Untimely ageing can be prevented through following the regular routines mentioned in Ayurveda.

Regular routines

Dinacharya (Daily Regime)

Ayurveda highlights the importance of cleaning the senses, namely *Jnana* (Wisdom – five sensory organs), *Karma* (Action – five motor organs) and *Manas*, which help the soul to discover the secret of healing. Dinacharya helps to keep these five senses and mind clean. *Mahatriphala ghritam, Anjana, trataka and Netra bhasti* for eye treatment*, Karnapurana* for ears*, Nasya, Jalneti and Neti pot* for nose*,* oil pulling*, Gandusha* for mouth and *Abhyanga and Shiro Abhyanga* for body and head all helps to balance the doshas and thereby to delay untimely ageing. Excretion or removal of unwanted or toxic materials from the body is also considered an essential daily ritual in Ayurveda. It suggests removing the waste from the body as soon as possible in the morning. The domination of the doshas determines the quantity, quality and frequency of the bowel movements (Bhattacharya. B, 2011). The *purisha pariksha and muthra pariksha,* in Ayurveda*,* explain the observation of the faeces and urine in detail.

Ratricharya (Night Routines)

Ayurveda advocates good sleep for healthy ageing as sleeplessness or insomnia can lead to many chronic illnesses and cognitive impairments. It recommends ending the day with meditation, gratitude and conscious recalling of the day for peaceful *Nidra yoga*. Charaka Samhita advocates understanding and following the circadian rhythm through simple ayurvedic principles to increase longevity and age healthily**.**

Ritucharya (Seasonal Routines)

Being a system of natural medicine, Ayurveda helps to understand the seasonal changes and their effects on the bodily doshas and indriyas. Thus, maintaining a seasonal regime is essential as it aids in healthy ageing and living in harmony with the environment and the surroundings.

Vyayam (Exercise)

"*Laghavam-karmasamarthyam-dipto-agnirmedasah:-ksaya:1*

Vibhaktaghanagatratvam-vyayamadupajayate" – Ashtanga Hrdayam – Sutra-sthana;; Chaper 2, Sloka 11

"This sloka explains that the practice of physical exercise renders the body light and efficient in activities, improves digestive power, decreases obesity, and renders finely chiselled contours and consistency in body structure". (Dr. Bhattacharya. B, 2015). Thus regular gentle exercising helps balance all three doshas and increases neuroplasticity and memory.

Diet and Nutrition

Every organ works in conjunction with the biological clock and the doshic clock. Diet is explained in great detail in Ayurveda. Ayurveda books like Charaka Samhitha, Ashtanga Hridhaya, and Susrutha Samhita have detailed diet and nutrition. They explain daily diets, seasonal diets, incompatible foods, food that creates balance to the tridoshas and diet that needs to be taken at various stages in human life. Food is divided into three types *Sathvik food, Rajasic food and tamasik*

*food***,** as they have a close relationship with the three *Gunas and tridoshas***.** *Sathvik* food is light and easily digestible is usually recommended during the *Vriddhavasatha*. *Rajasic* foods are hot and spicy and increase agitation, hate, anger and temptation in the minds. *Tamasic* food leads to a lazy, lethargic and dull mind.

Good nutrition helps to improve the *Ojas* (immunity), *Varna* (Complexion) and *Bala* (Strength). The importance is given to the ideal diet that will protect the *Jatharagni*(digestive fire), prevents *Ama* (toxic, foul-smelling undigested food particles), and increase *Dhatwagni*. When the *Jatharagni and Dhatwagni* are regulated, it significantly impacts healthy ageing. A well balanced *Sattvik* diet should include carbohydrates (*Shastik and Shali rice*), Grams (*Mudga*), rock salt (*Saindhava*), *Amlaki, Gritham* (ghee), *Madhuram*(honey), fruits, milk products, nuts and minimum fats. (Chowdhury et al., 2014)

Rejuvenation and Rasayana Therapies

Ayurvedic *rasayanams* bring longevity and renewal to the cells as they give strength, vitality, and longevity, strengthen the tone, increase energy and build immunity (Lad. V, 1999). *Panchakarma purification* also helps rejuvenate, detoxify, and rebuild worn-out cells and tissues, thereby curing chronic and degenerative disorders. It also helps in healthy ageing and avoiding premature ageing through the circulation of blood and helps in preventing persistent ailments as well. Charaka identified a specialized rasayana medicine called Vayasthapana which is list of ten drug which helps to increase life span and decrease untimely ageing (Wajpeyi, S.M., 2017). *Nithya Rasayanas* (Daily rasayanas) like *Chyawanprash, Triphala and Amruth* boosts the immune system if taken regularly.

Abhyanga

Doing regular *abhyanga* or oil massage with warm oil will help maintain good health and restore the balance of tridoshas, enhancing healthy ageing and longevity.

Yoga, Pranayama and Meditation

Ayurveda recommends yoga practices as it increases the flexibility of the joints and aids in digestion and sound sleep. Yoga also helps ease menopause-related transitions, and ayurvedic herbs and therapies—meditation and *Pranayam*a help to harmonise the body, mind and soul. Meditation helps in fighting modern-day illnesses like stress, depression and anxiety. Ayurveda recommends meditation every morning or before sleeping to relax the nerves and be healthy. *Prana* means life, and the art of breathing is taught through Pranayama, which bridges the balance of the body and mind and consciousness. "*Ayurveda says that breathing is the physical part of thinking and thinking is the psychological part of breathing*" (Lad, 1999). One can lead a happy, blissful, and healthy life by controlling one's breath.

Dharma and Sadvritta:

The dharma explained through Vedas, *Sanadhana Dharma,* understands and explains the nature of laws through various scriptures and textbooks. It refers to the eternal dharma and follows the way of truth and cosmic order, which has neither beginning nor end nor limits or boundaries. (Bhattachary. B, 2011). Ayurveda follows the philosophy of *Sanadhana Dharma* with a view of

aligning the prevention and curing properties with nature. It advocates being honest and speaking the truth, and understanding the subtle messages the body communicates. Ayurveda approves that the physical urges should be expressed, whereas the mental urges should be subdued. This m*anasika vegas,* or the expression of these mental urges, leads to seven deadly sins mentioned in the *Sanadhana Dharma* due to the lack of control of the mind. To overcome this, Ayurveda advocates being sensitive to the environment, being in touch with nature, and understanding and loving oneself and others unconditionally.

Discussion

Ageing is considered a disease, and it is tried best to avoid or delay it. Ayurveda is a medical science that recommends measures to prevent premature ageing, slow down the ageing process, manage this period by palliative treatment, and treat *Vriddhavastha* as prescribed in the Ayurvedic texts. *Vriddhavastha*, according to Ayurveda, is identified as a natural process of change that happens inside the body, which can be intervened with healthy lifestyles and proper routines. Untimely ageing (*Akala Jara)* or unhealthy ageing can be avoided with the help of nutritional diets, rasayana therapies, following regular routines like *dinacharya, rathricharya and ritucharya,* meditation and yoga. When a person follows the principles of Ayurveda through simple home remedies, and with the help of proper ayurvedic practitioners, ageing naturally (*Kala Jara)* and healthily is still possible. With the current age, man has lost his connection with nature, and the interpersonal relationship has gone for a toss. There are few superfoods like *Ashwagandha, amla, Guduchi, ginseng, Basil, turmeric, methi seeds, guggul, fennel seeds and sesame seeds* to help in anti-ageing and avoid the physical and mental changes accompanied during the ageing process. (Wajpeyi, 2017).

Conclusion

Right from the age of Mahabharata, stories to delay or stop ageing (*Story of King Yayadi*) had been present to exhibit the human's desire to conquer the concept of ageing. Modern medical science, with its advancement, has increased the longevity of humans, but when it comes to the question of ageing healthily and ageing at the right time, only Ayurveda has the key to the solution. Ayurveda helps prevent and manage old age-related issues and illnesses as it is a holistic ancient medicinal science. When a person chooses to follow ayurvedic principles and techniques from his *Madhyavastha* (late adolescent or early adult stages), he can avoid premature ageing (Akala Jara) and age naturally and healthily. Thus Ayurveda helps prevent and decrease the harshness of old age disorders and age gracefully.

References

Acharya, T. Y. (2009). Agniveshakrita Charaka Samhita Chakrapani Commentary. *Chikitsasthan26/77, Varanasi, Chaukhambha Sanskrita Sansthan.*

Vaidya, A.B., Vaidya, R.A. (1997). Ancient insights and modern discoveries in the process of aging--an overview. *Indian J Med Sci*. 51(10):349-63. PMID: 9567510.

Agnives, C.R. (2008). *Rejuvenation therapy (Jarra chikitsa) – Ayurvedic perspective. Geriatric Care. A textbook of Geriatrics and Gerontology*. 1st Edn. K-49, Green park, New Delhi.

Bhattachrya. B (2015). *Everyday Ayurveda.* Penguin Random House India.

Lad. V (1999). *The Complete book of ayurvedic home remedies – A comprehensive guide to the ancient healing of India.* Piatkus Book, London.

Devi, D., Srivastava, R., & Dwivedi, B. K. (2010). A critical review of concept of aging in Ayurveda. *Ayu*, 31(4), 516.

Patnaik, N. (2015). Role of Brahmi and Ashwagandha in Anti-Aging. *Journal of Biosciences and Medicines.* 102-104.

Raghuraman, Y.S., & Manasa. (2018, June 06). Easy Ayurveda. *Astanga Ayruveda – The Eight Branches of Ayurveda Blog.* https://www.easyayurveda.com/2018/06/06/ashtanga-ayurveda-branches/amp/

Rao, R.V. (2018). Ayurveda and the science of aging. *J Ayurveda Integr Med*. 225-232. doi: 10.1016/j.jaim.2017.10.002.

Sastri, K.N., Caturvedi , G.N. (2001). *Charaka. Charaka Samhita (Vidyotini Hindi Commentary)*, (1st ed). Shareerasthana, Caukhambha Bharati Academy, Varanasi.

Sharma O.P (2008). *Geriatric Care, A textbook of Geriatrics and Gerontology* (3rd ed). Viva Books Private Ltd., 4737/23, Ansari road, Daryaganj, New Delhi,

Srikanthamurthy. K.R (2008). *Sushruta. Susruta samhita,Vol-I (* 1st ed). Chaukhamba orientalia, Varanasi

Vivek. A. (2013). An Ayurvedic insight towards Aging with its preventive measures. *Int. J. Res. Ayurveda Pharm*. 31-33.

Wajpeyi, S.M. (2017). Healthy aging through Ayurveda: A review. *Int. J. Res. Ayurveda Pharm.* 93-97. http://dx.doi.org/10.7897/2277-4343.083176

Zahid. (2016, March 08). National Health Portal. *Jaravastha Poshana Blog* https://www.nhp.gov.in/Jaravastha-Poshana-(Geriatric-Nutrition)_mtl

13 Relationship Between Functional Digital Skills and Anxiety in Geriatric Population During the COVID-19 Pandemic

Samreen K. Ahuja*
Dr. Ganesh Kumar .J**

Abstract

Since its onset, the COVID-19 pandemic has made a widespread impact on the lives of people across the world. While recurrent lockdowns and protracted restrictions may have helped reduce the spread of the virus, the adverse effects on the economy, the reduced access to healthcare facilities and the strict quarantine protocols have negatively affected the physical, psychological and social health of people and raised anxiety to unprecedented levels. To mitigate this anxiety, Information & Communication Technology (ICT) has been used to provide digital solutions for many day-to-day activities which cannot be performed physically. This has forced people to adopt new technologies to carry out routine tasks and counter loneliness and social isolation caused by restrictions. However, elderly people, who have been affected the most by both the pandemic as well as the associated confinement, are also the most ill-equipped to make use of ICT because of lack of access and the necessary skills. Thus, the COVID-19 pandemic has left a large majority of the elderly suffering from high levels of anxiety as they do not have the Functional Digital Skills (FDS) to use the digital alternatives put in place to help them. The objective of the present research was to analyse the relationship between the level FDS and the level of anxiety in geriatric population during the COVID-19 pandemic. The levels of FDS and anxiety were assessed in elderly adults visiting COVID-19 vaccination centres based on questionnaires filled by them. Statistical analysis revealed a moderate degree of negative correlation between the levels of FDS and the levels of anxiety.

Keywords: COVID-19, Pandemic, Digital divide, Digital skills, Elderly

* B.Sc Honours 2nd year, Department of Psychology, Christ University, Bangalore.

** Assistant Professor, Department of Psychology, Christ University, Bangalore

Introduction

COVID-19 pandemic has afflicted close to 400 million throughout the world, with nearly 6 million succumbing to the disease (World Health Organization, 2020). The restrictive measures like the suspension of non-essential activities, restrictions on gatherings and lockdowns forcing people, especially those over 60 years, to remain indoors to check the spread of the disease have in turn created a whole set of problems not directly related to the virus itself. While the threat of infection is producing fear and anxiety in the minds of people, closure of workplaces, interruption of exercise schedules, and extended quarantines are adding to the anxiety and posing a threat to the physical and mental health of people already under stress. Studies have documented depression, stress and anxiety as the psychological effects of the pandemic and the lockdowns (Cao et al., 2020; Rajkumar, 2020).

Cumulative data shows that approximately 74% of the deaths due to COVID-19 occur in the age group of 65 years and above (National Center for Health Statistics, 2020). Because the elderly are more vulnerable, restrictive measures have been stricter for them. This implies that the elderly are likely more affected by the restrictions as well (Armitage & Nellums, 2020). While social isolation negatively affects individuals of all ages, it affects older people much more (Jaarsveld, 2020). Social isolation often leads to loneliness and depression in elderly adults.

To mitigate the challenges posed by the restrictive measures alternatives digital mechanisms have been put in place to carry out essential activities (Jaarsveld, 2020). Online banking and shopping have enabled people to carry on their day-to-day activities without stepping out of their homes. Digital technology has enabled people to socialize with family and friends virtually to counter the negative effects of extended isolation and loneliness. Online education has helped to keep student education on track. Telemedicine has made physical and mental healthcare available online.

The elderly too have been forced to adopt new Information and Communication Technologies (ICT) to carry out their routine tasks and to counter loneliness and social isolation caused by the lockdowns. While ICT may have alleviated the negative impacts of the pandemic in the younger population to some extent, the situation in the geriatric population is different. The elderly often are less affluent with limited access to the digital technologies, may have co-morbidities and are usually quite aloof from digital services (Nair et al., 2020). Even when digital services are available, it is not easy for the elderly to adopt them for want of necessary skills Fisher, 2000).

Aims

This study aimed to examine the relationship between the level FDS and the level of anxiety in the geriatric population during the COVID-19 pandemic. We hypothesized that the elderly adults with lower levels of FDS tend to have higher levels of anxiety during the on-going pandemic.

Theoretical Background

The digital divide refers to the disparity in access to new technology which exists between different groups of people (Jaarsveld, 2020). In addition to the divide based on uneven material access to technology, it exists on three more levels - based on uneven motivation to use technology, uneven

distribution of technological skills and uneven ability to make use of technology (Jaarsveld, 2020). In the elderly population it may exist at all the four levels. The elderly not only have less access to technology, but also have less digital skills and motivation so that they end up making limited use of technology. The reasons for this are the changes that are present at the physical, emotional and social level (Iancu & Iancu, 2017). Vision, speech, and hearing may diminish with age. With advancing age in adults, responses to stimuli become slower and time taken to learn new skills increases. This potentially decreases the ability of elderly to adopt new technology (Nair et al., 2020). At the social level, there may be a decrease in income and isolation. These changes may lead to emotional issues like loneliness and anxiety of becoming dependent on others (Iancu & Iancu, 2017).

The COVID-19 pandemic has changed the way people use technology. The elderly, who lack Functional Digital Skills (FDS), are likely more susceptible to the negative psychological effects of the pandemic and social isolation. This underlines the need to bridge the digital divide in the elderly population, in order to mitigate the negative effects on this vulnerable section of the society (Jaarsveld, 2020).

Review of literature

Yang et al. (2020) identified elderly as being more vulnerable to the effect of the COVID-19 pandemic on mental being in view of the high incidence of pre-existing symptoms of depression in older adults and inadequate access to mental health services available to them (Yang et al., 2020). Armitage R and Nellums LB noted that social isolation makes the elderly more vulnerable to depression and anxiety (Armitage & Nellums, 2020). However, a cross-sectional study conducted by Das et al on psychological health in the elderly during the COVID-19 pandemic found lower levels of anxiety and depression in the geriatric population. They concluded that this may be due to the support of family members and the greater resilience among the older adults (Das et al., 2021).

Jaarsveld (2020) described how technology has been adapted to provide digital alternatives for performing day-to-day tasks no longer possible in the physical mode and for countering loneliness due to social isolation. Lima et al. (2020) underlined the need to use telemedicine for mental health care during the pandemic.

Friemel (2016) drew attention to the 'grey divide', among elderly (Friemel, 2016). Nair et al. (2020) observed that in India only about 47% of the mobile phone users use smartphones, while 53% are still on feature phones (Nair et al., 2020). A study by Lam et al. (2020) showed that about 40% of the elderly population lacked the skills to effectively use telemedicine Niehaves and Plattfaut (2010) highlighted the fact that a significant segment of the elderly population is largely excluded from the benefits of internet usage Dijk (2006) elaborated (2006) elaborated the reasons for this as lack of access, motivation and skills and infrequent usage Martínez-Alcalá CI et al. (2021) while noting that COVID-19 has forced older adults to adopt digital technologies, underlined that Digital Literacy is essential for all those left out of the digital transformation.

To our knowledge, no quantitative study to date has examined the relationship between the level FDS and the level of anxiety in the elderly population during the COVID-19 pandemic.

Method

The study was conducted using a quantitative research approach with non-experimental survey design.

Sampling

The data was collected through a questionnaire using purposive sampling technique from elderly subjects visiting 3 randomly selected COVID-19 vaccination centres in New Delhi. The data was collected over 15 days from 30 January, 2022 to 13 February, 2022.

Inclusion criteria

Elderly people aged over 65 years and agreeing to participate in the study

Exclusion criteria

Persons with past history any psychiatric disorder were excluded from the study.

Age

75% of the respondents were between 65 and 74 yr., 22% between 75 and 84 years and 3% were 85 years old or more.

Gender

62% of the respondents were males and 38% were females.

Education

32% of the respondents had education up to the undergraduate level, 20% till secondary school level, 14% till high school level, 12% till postgraduate level, 8% till primary level, 2% till doctorate level and 12% had had no formal education.

Procedure

Participants were explained about the background and the objectives of the study. They were also assured about the confidentiality of their data and informed consent was obtained.

Questionnaire

The questionnaire consisted of 29 questions. Q1 – 3 were general questions. Q4-6 pertained to demographic data. Q 7-9 assessed digital resources available (internet access, type of digital device available). Q 10 - 22 were designed to assess Functional Digital Skills (FDS). Q 23 – 29 were the 7 questions of GAD-7 screening tool (20).

To assess the digital skills of the participants we devised a simplified Functional Digital Skills Scale adapted from 'Digital Skills Questionnaire' developed by AAL Association (Active and Assisted

Living Programme, 2017). It assessed the participants for 13 FDS required to carry out day-to-day activities digitally – making voice call, sending message using a messaging service, making video call, searching for information online, reading emails, sending emails, filling online forms, interacting digitally with government departments, using mobile / internet banking, shopping online, using Telemedicine, playing music, videos or games on a digital device and downloading apps to a digital device. It is based on questions that are easy to understand and therefore, it is easy to administer to older adults. For each 'Yes' answer pertaining to these skills a score of 1 was awarded. A score of 0 was awarded if the answer was 'No' or 'I do not understand what you mean by that'. The total number of 'Yes' answers gave the Functional Digital Skills Score (FDSS).

The anxiety levels were assessed using the well-validated Generalized Anxiety Disorder Scale (GAD-7) (Spitzer et al., 2006). The GAD-7 comprises seven questions based on seven core symptoms of anxiety. Respondents record their symptoms based on a 4-item Likert rating scale ranging from 0 (not at all) to 3 (almost every day), such that the total score ranges from 0 to 21.

Results

A total of 105 subjects were requested to fill the questionnaire. Four of them refused to participate in the study. One participant was excluded on account of being under treatment for depression, leaving a final sample of 100 participants.

Statistical analysis

The collected data were analyzed using SPSS version 21.0. Mann–Whitney U–and Chi-Square tests were used to explore the significance of associations of internet access and smart device ownership with the anxiety levels. A p value of <0.05 was considered to be statistically significant. To assess the relationship between FDSS and levels of anxiety, we applied Spearman's coefficient of correlation.

Levels of anxiety

On GAD-7 Scale, scores of more than 10, indicating moderate to severe anxiety were present in 28% of subjects.

Table 1: Shows the Detailed Levels of Anxiety Among Respondents

Number of subjects with different anxiety levels (n = 100)		
Anxiety Level	**Number**	**Percentage**
Minimal	56	56
Mild	16	16
Moderate	14	14
Severe	14	14

Of the 100 subjects, 30 (30%) had no symptoms of anxiety, whereas subjects with mild, moderate, and severe anxiety were 16%, 14%, and 14%, respectively.

Digital Access

8% of the respondents did not have any phone, 26% had only a feature phone and 66% had a smartphone or other smart device. Statistically significant correlation was found between not owning a smart device and presence of GAD (GAD-7 score ≥ 10) (p=.012) (Table 2). Those without a smartphone device showed a 2.6 times greater chance of having GAD than those who with.

18% of the respondents did not have internet access. Statistically significant correlation was found between not having internet access and presence of GAD (p=0.016) (Table 2).They showed a 2.5 times greater chance of having Generalized Anxiety Disorder than those who had internet access.

Table 2

Association of Access to Technology and Anxiety (GAD-7 Score > 10)

Variable	Frequency (%)	Mean	Std. Deviation	Mann-Whitney Test (Sig.)	Pearson Chi-Square Test		
					Value	*df*	*P*
Smart Device Access							
Yes	66	4.73	5.264	0.012*	9.282	1	0.002*
No	34	9.47	8.240				
Internet Access							
Yes	82	5.49	6.270	0.016*	8.268	1	0.00⁴*
No	18	10.22	7.788				

*N =100, p = two-tailed p-value, *Significant (p<0.05)*

FDSS

The average Functional Digital Skills Score was 4.96 on a scale of 0-13. There was a moderate statistically significant inverse correlation between FDSS and GAD-7 score (r= -0.341, p=0.001) (Table 3). Participants, who were less proficient in Functional Digital Skills, displayed higher levels of anxiety.

Table 3

Correlation Analysis between FDS and Anxiety

Stressor	Anxiety level	
	r	p
Functional Digital Skills Level	-0.341	0.001

*r =Correlation coefficient, p = two-tailed p-value, *Significant at 0.05 level*

Discussion

The present study explored the relationship between the levels of Functional Digital Skills possessed by the elderly for carrying out day-to-day activities and their anxiety levels during the COVID-19 pandemic.

In a study on anxiety and depression in older adults due to COVID-19 pandemic in Chandigarh the percentage of elderly with anxiety was 8.7% (Armitage & Nellums, 2020). In another study on the effects of COVID-19 lockdown on the psychosocial health of elderly population in Kerala, 37.9% of the elderly showed significant anxiety symptoms (Balasundaram et al., 2020). In our study 28% of the elderly showed moderate to severe levels of anxiety, which correlates well with other studies.

Among the study participants, 34% either did not have a smartphone or other digital device. 19% did not have access to the internet. Univariate analysis showed that those who did not have access to a smart device had 2.6 higher the risk of having GAD, while for those who did not have access to the internet the risk was 2.5 times higher. There was found to be moderate negative correlation between the levels of FDS and the levels of anxiety. This is quite understandable as people with low levels of FDS or lack of access to digital resources cannot make full use of the digital solutions available to interact with family and friends digitally, to seek medical and psychological support virtually or to perform on digital platforms day-to-day activities like banking or shopping, which may not be possible physically during lockdowns, which adds to their anxiety.

While there have been many studies documenting the low levels of digital literacy among the elderly (Agewell Foundation, 2017; National Academies Press, 2000) and high levels of anxiety among elders during the COVID-19 pandemic (Balasundaram et al., 2020; Ho et al., 2020), few quantitative studies has been conducted so far to establish a statistical correlation between the levels of digital skills and of anxiety in the elderly during the pandemic. Our hypothesis posited that the elderly adults with lower levels of Functional Digital Skills tend to have higher levels of anxiety during the on-going pandemic. The results of this study corroborated this. Hence our hypothesis was proved.

While this study reiterates that digital literacy among the elderly is a necessity during the pandemic, it will continue to be in the future as well. Government agencies, NGOs and businesses must get together to ensure that elderly have access to affordable devices and connectivity and elderly friendly software and hardware. Family members and volunteers must support the elderly through training and hand holding to enable them to handle digital technology independently.

Limitations and Directions for Future Research

The study has some limitations like the small sample size, which reduces the statistical power. Although in this study the Functional Digital Skills Scale was used to assess the digital skills for the sake of its simplicity and easy comprehension by the elderly, it has not been validated. The Functional Digital Skills Score is only indicative and may not provide absolute digital skills values, but we believe it represents functional indication of the competencies of the elderly required for carrying out day-to-day activities digitally. Apart from digital skills, other factors affecting the level of anxiety like the presence of comorbidities, family support, economic status etc. were not

studied in the current research. Further studies with larger sample sizes and including the above factors may be needed in the future to conclusively establish the relationship between Functional Digital Skills and anxiety in the elderly even after the current pandemic is over.

Conclusion

Lower levels of functional digitals skills are moderately correlated with higher levels of anxiety in elderly adults during the COVID-19 pandemic. Not owning a smart digital device and lack of internet access are significantly associated with GAD in the elderly during the on-going pandemic. Bridging the digital divide among the elderly is the need of the hour.

References

Armitage, R., & Nellums, L. B. (2020). COVID-19 and the consequences of isolating the elderly. *The Lancet Public Health, 5*(5). https://doi.org/10.1016/s2468-2667(20)30061-x

Balasundaram, P., Libu, G. K., George, C., & Chandy, A. J. (2020). Study on the effect of COVID-19 lockdown on health care and psychosocial aspects of elderly in Kerala State. *Journal of the Indian Academy of Geriatrics, 16*(3), 101. https://doi.org/10.4103/jiag.jiag_3_20

Das, S., Arun, P., Rohilla, R., Parashar, K., & Roy, A. (2021). Anxiety and depression in the elderly due to COVID-19 pandemic: A pilot study. *Middle East Current Psychiatry, 28*(1). https://doi.org/10.1186/s43045-021-00145-1

Centers for Disease Control and Prevention. (2022, July 6). COVID-19 provisional counts - weekly updates by select demographic and geographic characteristics. *Centers for Disease Control and Prevention*. Retrieved July 13, 2022, from https://www.cdc.gov/nchs/nvss/vsrr/covid_weekly/index.htm

Changing Needs & Rights of older people in India a review - un. (n.d.). Retrieved July 13, 2022, from https://social.un.org/ageing-working-group/documents/eighth/Inputs%20NGOs/ChangingNeeds_Rights.pdf

Friemel, T. N. (2014). The digital divide has grown old: Determinants of a digital divide among seniors. New *New Media & Society, 18*(2), 313–331. https://doi.org/10.1177/1461444814538648

Ho, F. K., Petermann-Rocha, F., Gray, S. R., Jani, B. D., Katikireddi, S. V., Niedzwiedz, C. L., Foster, H., Hastie, C. E., Mackay, D. F., Gill, J. M. R., O'Donnell, C., Welsh, P., Mair, F., Sattar, N., Celis-Morales, C. A., & Pell, J. P. (2020). Is older age associated with COVID-19 mortality in the absence of other risk factors? General population cohort study of 470,034 participants. *PLOS ONE, 15*(11), e0241824. https://doi.org/10.1371/journal.pone.0241824

Iancu, I., & Iancu, B. (2017). Elderly in the Digital Era. Theoretical Perspectives on Assistive Technologies. *Technologies, 5*(3), 60. https://doi.org/10.3390/technologies5030060

Lam, K., Lu, A. D., Shi, Y., & Covinsky, K. E. (2020). Assessing Telemedicine Unreadiness Among Older Adults in the United States During the COVID-19 Pandemic. *JAMA Internal Medicine, 180*(10). https://doi.org/10.1001/jamainternmed.2020.2671

Lima, C. K. T., Carvalho, P. M. de M., Lima, I. de A. A. S., Nunes, J. V. A. de O., Saraiva, J. S., de Souza, R. I., da Silva, C. G. L., & Neto, M. L. R. (2020). The emotional impact of Coronavirus 2019-nCoV (new Coronavirus disease). *Psychiatry Research, 287*, 112915. https://doi.org/10.1016/j.psychres.2020.112915

Martínez-Alcalá, C. I., Rosales-Lagarde, A., Pérez-Pérez, Y. M., Lopez-Noguerola, J. S., Bautista-Díaz, M. L., & Agis-Juarez, R. A. (2021). The Effects of COVID-19 on the Digital Literacy of the Elderly: Norms for Digital Inclusion. *Frontiers in Education, 6*. https://doi.org/10.3389/feduc.2021.716025

Martins Van Jaarsveld, G. (2020). The Effects of COVID-19 Among the Elderly Population: A Case for Closing the Digital Divide. *Frontiers in Psychiatry, 11*. https://doi.org/10.3389/fpsyt.2020.577427

Nair, I., Mahesh, J., Mariam, S., Ms, A., Anitha, K., Corresponding, J., & Lakshmi, M. (2020). The awareness and the usage of digital devices among senior citizens-A study with special reference to Kerala in India. *International Journal of Humanities and Social Science Invention. 9* (7), 28-34. https://doi.org/10.35629/7722-0907022834

National Research Council (US) Committee on Future Directions for Cognitive Research on Aging, Stern, P. C., & Carstensen, L. L. (2018). Cognitive Aging and Adaptive Technologies. Nih.gov; National Academies Press (US). https://www.ncbi.nlm.nih.gov/books/NBK44840/

Niehaves, B., & Plattfaut, R. (2010, August). What is the issue with internet acceptance among elderly citizens? Theory development and policy recommendations for inclusive E-government. *In International Conference on Electronic Government* (pp. 275-288). Springer, Berlin, Heidelberg.

Rajkumar, R. P. (2020). COVID-19 and mental health: A review of the existing literature. *Asian Journal of*

Psychiatry, 52(102066), 102066. https://doi.org/10.1016/j.ajp.2020.102066

Rajkumar, R. P. (2020). COVID-19 and mental health: A review of the existing literature. Asian Journal of

Psychiatry, 52(102066), 102066. https://doi.org/10.1016/j.ajp.2020.102066

Rajkumar, R. P. (2020). COVID-19 and mental health: A review of the existing literature. *Asian Journal of Psychiatry, 52*(102066), 102066. https://doi.org/10.1016/j.ajp.2020.102066van Dijk, J. A. G. M. (2006). Digital divide research, achievements and shortcomings. Poetics, 34(4-5), 221–235. https://doi.org/10.1016/j.poetic.2006.05.004

Van Dijk, J. A. (2006). Digital divide research, achievements and shortcomings. Poetics, 34(4-5), 221-235.

World Health Organization. (2020). Who coronavirus disease (COVID-19) Dashboard: World Health organization, 2020. *WHO Coronavirus Disease (COVID-19) Dashboard.*

Yang, Y., Li, W., Zhang, Q., Zhang, L., Cheung, T., & Xiang, Y.-T. (2020). Mental Health Services for older adults in China during the COVID-19 Outbreak. *The Lancet Psychiatry, 7(4). https://doi.org/10.1016/s2215-0366(20)30079-1*

14 Understanding Implications of Comorbidity of Major Depressive Disorder and Conversion Disorder/Functional Neurological Symptom Disorder: A Case Study with the Elderly

Shraddha J Kamble* & Dr. Pooja Rai**

Abstract

Major Depressive Disorder is a common mood disorder which leads to a wide range of emotional and physical problems as well as reducing an individual's ability to perform tasks. At times, symptoms of depression can become so severe that they impact person's life to the point where they commit suicide or attempt suicide. The most prevalent psychological comorbidities with depression are anxiety disorder, personality disorders, Obsessive Compulsive disorder, somatic symptom disorder and functional neurological symptom disorder. The purpose of the study is to understand the implications of comorbidity of major depression disorder in elderly. In the present case study of 65y/o female who has complaints of feelings of sadness, loss of interest in household work, difficulty in sleep, loss of appetite and she also has suicidal ideations, along with the complaint of feeling tingling sensations in hand and neck with constant headache. Patient also had a complaint of left side body ache. The single-subject case study design was used. The detailed case history was explored and a mental status examination was administered on the patient to make an accurate diagnosis. Patient is under the impression of major depression disorder with conversion disorder/functional neurological disorder. In order to relieve the symptoms, treatment plans utilized for the patient are psychopharmacology and psychotherapy.

Keywords: *Major Depressive Disorder, Conversion Disorder, Comorbidity, Symptoms, Diagnosis, Elderly*

* Department of Psychology, Jain Deemed-to-be University, Bangalore

** Assistant Professor, Department of Psychology, Jain Deemed-to-be University, Bangalore

Introduction

Major Depressive Disorder (MDD) is known as a common mood disorder and a significant mental disease that has an adverse effect on an individual's way of thinking, feeling and behavior. It can result in a wide range of emotional and physical difficulties as well as reducing one's capability to operate at work or home settings. Females are found more prone towards depression than males. There are other types of depression namely Disruptive Mood Dysregulation Disorder (DMDD), Major Depressive Disorder (MDD), Bipolar and related Disorders, Persistent Depressive Disorder (Dysthymia), Premenstrual Dysphoric disorder (PMDD), Depression related to another medical condition, Substance/Medicine Induced Depression Disorder, Other specified Depressive Disorder and Unspecified Depressive Disorder (American Psychiatric Association, 2013). Sad mood, difficulty concentrating and making decisions, anxiety, loss of sleep, fatigue and suicidal ideations are the most common symptoms of Major Depressive Disorder.

The Greek physician Hippocrates, the father of modern medicine suggested a theory in 4th century BC that human emotions mainly had physiological foundation and differences were due specifically to fluctuations in bodily fluids called "humors". And these humors were called yellow bile, black bile, phlegm, and blood. In Greek dialect, the meaning of the term "Melancholy" is black bile. Hippocrates theory of melancholy proposed that imbalance between these bodily fluids lead to emotional disturbances. He classified mental illnesses in three different categories that mainly encompasses mania, melancholia(depression) and phrenitis (brain fever). It's from this perception of melancholia that our current view of depression ultimately evolved. Subsequently, Greek philosopher and physician Galen expanded upon the Hippocrates theory by pointing out that personality types resulted from an excess of one of these four fluids.

During the late 19th century, a Prominent German psychiatrist named "Emil Kraepelin'' made a significant contribution to the understanding of mental illnesses using natural scientific notions. Kraepelin introduced a binary approach toward mental illness, he separated depression into two distinct forms: dementia praecox and manic depression. He pointed out that 'dementia praecox' is an organic disease caused by anatomical or toxic processes. Whereas, he believed "manic depression" as an episodic condition which does not result in long-term brain damage (Ebert, A., & Bär, K. J., 2010). The two primary classification manuals, the International Classification of Diseases (WHO) and the American Psychological Association's DSM-Classification, have relied on Kraepelin's concept until now. (K Haddad et al., 2008) Later, Sigmund Freud, the father of psychoanalysis, elaborated his view stating that depression is a result of an individual's retaliation towards an event of a loss, where the individual attributes the lost object as a way of belonging to it.

Today, the diagnosis of Major Depressive Disorder is conducted on the basis of International Statistical Classification of Diseases and Health Related Problems (ICD-10 depression criteria) and Diagnostic and Statistical Manual of Mental Disorders fifth Edition Classification system (DSM-V). Fatigue, impaired concentration, weight gain/loss, low mood, sleeplessness, loss of interest, feelings of worthlessness, psychomotor agitation, and recurring thoughts of death or suicidal ideation are all diagnostic criteria for major depressive disorder, according to the DSM-V

system. Five or more symptoms out of nine should be present for a diagnosis of Major depressive disorder (MDD). Whereas, in the ICD-10 system core symptoms include depressed mood or persistent sadness, lack of pleasure or interest, lack of energy or experiencing fatigue. And out of ten symptoms, at least 4 or more symptoms are required for making diagnosis and formulating treatment (Ijaz & Saqeeda, 2018).

Functional Neurological symptom disorder (FND), which is also known as conversion disorder, is defined as a mental illness characterized by symptoms and signs impacting voluntary motor or sensory functions which cannot be explained by any neurological or medical condition. The Father of Psychoanalysis, Sigmund Freud, Suggested the term 'Conversion' stating that the development of certain symptoms is not explainable by bodily causes that reflect unconscious conflicts. The process of substitution of Somatic Symptoms for a repressed belief is called Conversion. He also believed that FND is a conversion disorder as he thought it has been a mental illness that is converted into a neurological disease. Conversion symptoms include paralysis, blindness, Psychogenic nonepileptic seizures, difficulty in walking, hallucinating, tingling sensations, numbness, loss of senses, chronic pain, headache/migraine (Ali et al., 2015).

The belief of hysteria to conversion are often traced back to 5th and 4th centuries before the Christian era (BCE), when the Father of Medicine, Hippocrates, elucidates hysteria as a condition in which a dehydrated womb wanders around the body looking for humidity. The uterus pressing on other organs, he said, would then develop the symptoms. Furthermore, in the 17th century, Rene Descartes posited mind-body dualism, in which the mind and body are two distinct entities that cannot coexist. This led to the establishment of a reductionist medical model with a dualistic perspective on symptom management. Whereas, in the 19th century, the emerging theories focused on the association of the central nervous system with hysterical symptoms. Psychodynamic theories also played a role because of Freud's description of symptom formation, in which converted bodily complaints are the result of unconscious conflict and effective motive. Thus, psychodynamic theory helped the study of hysteria and prepared the way for the concept of conversion symptoms. (Ali et al., 2015)

Individuals with Functional Neurological Symptom Disorder have a pathophysiological etiology in which their brain is unable to send and receive signals effectively. Interference in the lobe functioning and emotional processing is seen. Brain functions like memory, concentration, cognition and the processing of sensations can all be impaired. Psychogenic nonepileptic seizures and functional movement disorder are the two main types of Functional Neurological Symptom Disorder.

Diagnostic and Statistical Manual of Mental Disorders, fifth edition classifies Functional Neurological Symptom disorder (FNSD)/ Conversion disorder is categorized under the Somatic Symptom and related Disorders. According to the DSM-V, Functional neurological Symptom Disorder/Conversion Disorder is marked by having at least one symptom of altered voluntary motor or sensory function, no organic cause (neurological condition, substance use or physical disease) should be present which may explain the symptoms and lastly, symptoms are resulting in crucial distress in one's important areas of functioning such as social, occupational, personal (Boeckle, Liegl, Jank, et al., 2016).

Various research studies have revealed that panic, anxiety and depression disorders are the most commonly occurring co-morbidity disorder with conversion disorder (Khan, 2005). One of the research study results indicated that patients with conversion disorder presented symptoms of anxiety and depression as well. And patients who were diagnosed with Conversion Disorder, they were needed to be managed for symptoms of depression as well as anxiety for better end result (Kazan-Kizilkurt, MertAkgul, Izci, 2018). One of the studies revealed that a patient with Conversion disorder and Major depressive Disorder comorbidity benefited from pharmacotherapy and Psychodrama techniques and utilizing these two therapeutic approaches helped in the effectiveness of the treatment. It is seen that there is less emphasizes on a holistic formulation of treatment plan for managing symptoms of Conversion disorder as well as Major depressive Disorder. Therefore, the present study aims to understand implications of comorbidity of major depression disorder and conversion disorder: A case study with the elderly.

Methodology

Research design

Single case study design was used in this research

Sample

In current study, 65 y/o married female, came to visit the Psychiatric Out Patient Department (OPD). Patient A has studied till standard 7th and she belongs from a lower-middle class background. Patient is Hindu by religion and she resides in Mumbai, Maharashtra.

Materials

Case history and Mental status examination was administered on the patient. And DSM-V was used for diagnosing the patient.

Procedure

Initially, rapport was established with patient A. Patient's data was collected by administering case history and mental status examination to make an accurate diagnosis. Patient A was debriefed about the present study's objective, potential risks and harms and right to withdraw. Informed consent was taken place. Also, she was notified that her detailed responses and data will be kept anonymous and confidential including patient's decision to withdraw from the study at any period of time.

Results

In the present study, a 65 y/o female came to visit the Psychiatric Out Patient Department (OPD) with depression symptoms. She had complaints of feelings of sadness, loss of interest in household work, insomnia, loss of appetite and recurrent thoughts of death along with the other physical complaints of tingling sensations in hand and head with constant headache. She also stated that her left body aches. She was experiencing these symptoms from the last 5-6months.

History of presenting illness

Patient informant states that she feels tensed about her sons and that they won't take care of her. Patient's sons left her and started living as a nuclear family in the year 2019. Also, she has a feeling that everyone will betray her and leave her alone. Patient A states that she is not able to sleep as she always worries about her children. And she doesn't like doing anything and is unable to feel pleasure in usual activities. Informant also confirms that she took 20 tablets of diabetes medication so that she can die.

Past medical or Psychiatric History

H/O hypotension and diabetes

N/H/O psychiatric illness

Family history

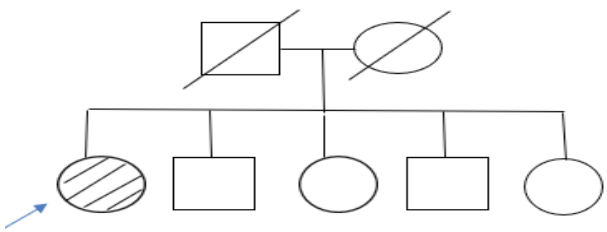

N/H/O any psychiatric illness in family

Personal History

Childhood- patient was a normal delivery child with no complications. All developmental milestones were achieved.

Occupational History- Patient studied till seventh standard and she is a homemaker

Psychosocial History- Patient is happily married and she is an outgoing person.

Sexual history: Menses Stopped 15 years ago

Mental Status Examination

Attitude and General Appearance: Patient is constantly falling down her head on the table. Patient is not cooperative. Patient seems irritable, seductive and apathetic

Mood: SAD, hopeless, depressed, anhedonia, fearful and suicidal

Affect: Anxious

Speech: Loud, High pitch, incoherent

Thought: Suicidal

Perception: intact

Orientation: Oriented to Place, Time and Person

Intelligence: Below average

Judgment: Intact

Insight: grade III (patient was aware about her being sick but she was blaming it on external factors)

Diagnostic approach

Patient A was experiencing symptoms of Conversion Disorder as well as Major depressive disorder. According to the DSM-V, patient A has the symptoms of Major Depressive Disorder (MDD) and Conversion disorder. She was experiencing feeling of sadness, difficulty in sleeping, loss of appetite, diminished interest or pleasure in her daily activity, and passive suicidal ideations. The symptoms have caused significant distress in her social functioning. Her symptoms aren't caused by a substance's physiological effects or by any other medical disorders. Also, she fulfilled the criteria for Conversion Disorder/Functional Neurological Symptom Disorder, as she was having somatic complaints which affected her sensory and motor functions. She was experiencing somatic complaints such as tingling sensations in her hands and head, left-side body ache and recurrent headache as it was seen that patient A was constantly falling her head on table during case study and MSE taking. Therefore, the patient was under the impression of Major Depressive Disorder and Conversion Disorder/Functional Neurological Symptom Disorder (FNSD).

Treatment approach

Considering, patient's provisional diagnosis comprised of two mental illness, a holistic treatment approach will help in managing patient's A complex symptoms and dysfunctions. Psychopharmacological approach for treatment can be used for patient A's condition. Whereas, there are various Non-psychopharmacological approaches that can be utilizes for the treatment of patient A.

Psychodynamic treatment: Hypnosis and free association therapy techniques can be used to understand repressed thoughts or emotions that resulted in the mental disorder. Patient A's unconscious unresolved conflicts which contributed to current condition of conversion symptoms (Left-side body ache, headache, tingling sensations) can be understood utilizing psychodynamic therapies.

Other Psychotherapies: Cognitive behavioral therapy helps in understanding, modifying and restructuring of irrational thoughts or beliefs. In the present case study, patient A feels that everyone is going to leave her and she will be alone, CBT can be helpful in identifying her cognitive distortions and maladaptive behaviors, and replacing these emotions, thoughts and behavior with rational thoughts and behavioral. Also, CBT is effective for major depressive disorder as well as conversion disorder. Family therapy, group therapy and dialectical behavioral therapy can also aid in effective management and treatment of mental disorders.

Complementary and Alternative treatments: Complementary and Alternative treatments emphasize on individual as a whole and various aspects altogether such as physical, emotional, social and spiritual. And these treatments are designed to support the natural innate healing functions of the human body. It includes Yoga, Mindfulness, Naturopathy, Ayurveda, Nutrition therapy, homeopathy, relaxation techniques, reiki, acupuncture and Expressive Art therapies etc.

Discussion

Patient was experiencing key symptoms of depression according to the diagnostic criteria. In the present study the patient was suffering from insomnia, lack of interest/pleasure, sadness, recurrent thoughts of death and loss of appetite. Patient was experiencing other symptoms like tingling sensations in hand and head, left-side body ache and recurrent headache. Patient's informant stated that she worries about her sons and now that they have left her and she has started leaving alone, the patient feels and fears betrayal. Patient feels that everyone will leave her and she will be left alone. Informant also claims that she ate 20 diabetes tablets at once so that she can die. Her informant also stated that she is not able to do her daily household work. Patient was experiencing a lack of energy and drive to care for herself and engaged in less physical activities.

In the Case history, the patient reported that there is no presence of any medical or psychological illness in her family. She has a history of Blood Pressure and diabetes. There is no history of OCD and mania/hypomania. Patient's menses stopped around 15-16 years ago.

Patient was constantly falling on her head on the table and she wasn't cooperative while conducting case history and MSE. On the Mental Status Examination, her general appearance and attitude was conscious, communicative, apathetic, seductive. As the patient has studied till standard 7th, her intelligence has been found below average. She had passive suicidal ideations. Patient's Judgment and perception is intact. Whereas, her level of insight is graded III. she had passive suicidal thoughts. She presented combined signs and symptoms of Conversion disorder/FNSD and Major depressive Disorder. Patient A, was given a provisional diagnosis of MDD and Conversion Disorder/ Functional Neurological Symptom Disorder as she met required diagnostic criteria's for both mental disorders. She was experiencing feeling of sadness, difficulty in sleeping, loss of appetite, diminished interest or pleasure in her daily activity, and passive suicidal ideations. And her symptoms have caused significant distress in her social functioning. Also, symptoms weren't produced or caused by any substance's physiological effects or by any other medical disorders. She had few somatic complaints such as tingling sensations in hand and head, left-side body ache and recurrent headache which indicated symptoms of Conversion Disorder/ Functional Neurological Symptom Disorder.

The formulation of treatment plan for patient A included psychopharmacological approach to manage her physiological dysfunctions. Though, her provisional diagnosis included two mental disorder that are Major depressive disorder and Conversion disorder. So, incorporation of Non-Psychopharmacological treatment along with Psychopharmacological treatment would help in managing her complex symptoms. Non-Psychopharmacological treatment involves Various Psychotherapies which emphasizes on identifying maladaptive behaviors, cognitive distortion's, irrational belief, interpersonal conflicts and coping patterns which are adversely contributing to the presenting illness such as Cognitive Behavioral therapy, Family therapy, Dialectical Behavioral Therapy, Psychodynamic therapy and Group therapy. One of the research studies revealed that family/marital/couple therapy and counselling, psychoeducation, exercising problem solving therapy, guided self-help, and behavioral activation treatments, acupuncture, computerized Cognitive behavioral therapy are the treatment elements are the treatments which has adequate level of evidence-based options for managing depression (Dirmaier, J., 2012). Also, there are

Complementary and Alternative interventions/therapies which can aid patient A in coping with the side effects of the medications, relieving her conversion symptoms of headache and left body ache, managing her stress and symptoms using various relaxation techniques (Biofeedback, Guided-Imagery, meditation), building a positive outlook towards life, regulating emotions in a better way, increasing general health and well-being.

Results of a research study indicated that yoga-based intervention can be one of the treatments utilized under Non-psychopharmacological approach in patients with Somatoform disorders (Sutar, R., Desai, G., Varambally, S., & Gangadhar, B. N., 2016). Yoga can be helpful in managing conversion symptoms of Tingling sensations in hands and head, headache and Left-body ache in the case of patient A. There are various Complementary and Alternative interventions comprises of Mindfulness, Yoga, Ayurveda, Acupuncture, Reiki, Naturopathy, Homeopathy and Expressive Art expressive. Holistic approach of treatments for patient A can aid in improving and promoting healthy behaviors alongside managing the physiological symptoms of existing disorders using psychopharmacological medicines.

Conclusion

This study emphasized on understanding implications of comorbidity of Major Depressive Disorder and Conversion Disorder/Functional Neurological Symptom Disorder in elderly. It is found that patient A was given a provisional diagnosis of Major Depressive Disorder and she needs to be managed for Conversion Disorder and Major Depressive Disorder symptoms appropriately utilizing psychopharmacological and Non-psychopharmacological treatment approach. Psychopharmacological approach will assist in managing the physiological symptoms of depression and Conversion Disorder/Functional Neurological Symptom Disorder. Whereas, Non-psychopharmacological approach will aid in cultivating Adaptive behavior, managing the side effects of the medicines, Positive attitude and coping styles, reducing pain both psychological and physiological, and overall psychological well-being of patient A.

References

Ali, S., Jabeen, S., Pate, R. J., Shahid, M., Chinala, S., Nathani, M., & Shah, R. (2015). Conversion Disorder- Mind versus Body: A Review. *Innovations in Clinical Neuroscience*, *12*(5-6), 27–33. https://www.ncbi.nlm.nih.gov/pmc/articles/PMC4479361/

American Psychiatric Association. (2013). *Diagnostic Statistical Manual of Mental Disorders DSM-5* (5th ed., p. 309-321). American Psychiatric Association.

American Psychiatric Association. (2013). *Diagnostic Statistical Manual of Mental Disorders DSM-5* (5th ed., pp. 155- 187). American Psychiatric Association.

Boeckle, M., Liegl, G., Jank, R., Pieh, C. (2016). Neural correlates of conversion disorder: overview and meta-analysis of neuroimaging studies on motor conversion disorder. *BMC Psychiatry 16*, 195. https://doi.org/10.1186/s12888-016-0890-x

Dirmaier, J., Steinmann, M., Krattenmacher, T., Watzke, B., Barghaan, D., Koch, U., & Schulz, H. (2012). Non-pharmacological treatment of depressive disorders: a review of evidence-based treatment options. *Reviews on Recent Clinical Trials*, *7*(2), 141–149. https://doi.org/10.2174/157488712800100233

Ebert, A., & Bär, K. J. (2010). Emil Kraepelin: A pioneer of scientific understanding of psychiatry and psychopharmacology. *Indian Journal of Psychiatry*, *52*(2), 191–192. https://doi.org/10.4103/0019-5545.64591

Haddad, S. K., Reiss, D., Spotts, E. L., Ganiban, J., Lichtenstein, P., & Neiderhiser, J. M. (2008). Depression and internally directed aggression: genetic and environmental contributions. *Journal of the American Psychoanalytic Association*, *56*(2), 515–550. https://doi.org/10.1177/0003065108319727

Ijaz, I., & Sadeeqa, S. (2018). *Depression: A Case Study*. https://medwinpubllishers.com/ARTOA/ARTOA16000102.pdf

Kazan-Kizilkurt O, MertAkgul S, Izci F. (2018) An approach to conversion disorder with comorbid major depression using pharmacotherapy and psychodrama techniques: a case report. Dusunen Adam *The Journal of Psychiatry and Neurological Sciences* 2018;31:413-420. https://doi.org/10.5350/DAJPN2018310412

Khan, M. N., Ahmad, S., Arshad, N., Ullah, N., & Maqsood, N. (2005). Anxiety and depressive symptoms in patients with conversion disorder. *Journal of the College of Physicians and Surgeons--Pakistan: JCPSP*, *15*(8), 489–492. https://pubmed.ncbi.nlm.nih.gov/16202361/

Paykel E. S. (2008). Basic concepts of depression. *Dialogues in Clinical Neuroscience*, *10*(3), 279–289. https://doi.org/10.31887/DCNS.2008.10.3/espaykel

Sutar, R., Desai, G., Varambally, S., & Gangadhar, B. N. (2016). Yoga-based intervention in patients with somatoform disorders: an open label trial. *International review of psychiatry (Abingdon, England)*, *28*(3), 309–315. https://doi.org/10.1080/09540261.2016.1188785

15 Emotional Intelligence in People with Elderly

Sowmya B R* & Dr. Pooja Rai**

Abstract

Introduction : Emotional Intelligence is the competency of a person to understand, control, express, evaluate a person's own emotion and also that of the others in day to day interaction with the world around them. The development of emotions is a lifelong process which starts right from the time a baby is born till we grow old. However, it has been seen that there is an overall emotional decline in people with elderly. Thus, the objective of the present study will help understand whether the emotional quotient (EQ) or components of emotional intelligence (EI) of a person in his golden years declines or does it increase as they grow old.

Method: For this present study emotional intelligence development among the geriatric population is being reviewed using specific keywords. Out of 30 articles, 10 articles have been finalised to understand the impact of age on the development of EI.

Result: The articles for the review are studies that are based on the hypothesis that certain components of emotional intelligence increase as people age. Studies are consistent with this hypothesis and reveal the experiences people gain during their developmental stages and their interaction with other people. The paper will discuss different psychological assessments to measure emotional intelligence scales to assess the different components of emotional intelligence.

Conclusion: Emotional Intelligence and some of its components increase with age and help the elderly to deal with their and others emotions better when compared to what they were able to do during adulthood.

Keywords : Emotional Intelligence, Ageing

* Research Scholar, Department of Psychology, School of Sciences, Jain Deemed-to-be University, Bangalore

** Assistant Professor, Department of Psychology, School of Sciences, Jain Deemed-to-be University, Bangalore

Introduction

Emotional Intelligence is the competency of a person to understand, control, express, evaluate a person's own emotion and that of the others in day to day interaction with the world around us. Wanye Payne was one of the first person who coined the term EI in his doctoral thesis. This term was later used by others like Keith Beasley, Beldoch and leuner. The term was popularised by Daniel Goleman with the publication of his book titled "emotional intelligence". Emotional intelligence is based on three models – the ability model which was proposed by John Mayer and Peter Salovey, mixed model by Daniel Goleman and the trait model was by K V Petrides. Emotional intelligence is studied by two types of tests – self-report tests and ability tests. The Mayer –Salovey – Caurso emotional intelligence test (MSCEIT) is an ability based test which includes the assessment of a person's skill. This assessment usually involves responding to a situation. The emotional and social competence inventory (ESCIII) is a self assessment scale where in the person himself or someone who knows the person rates the individual under different emotional situations.

Method

In this review paper and attempt is made to understand whether emotional quotient or the components of EI increase or decrease as the person grows old .Factors such as stress ,physical aliments ,illness and mental wellness are also affected by the development of EI.

Emotional Intelligencefrom development perspective

Research pertaining to the life span perspective and many other inquries have found a positive correlation between EI and age i.e. as people age their emotional quotient or competencies also increase (Salovey & Mayer 1990, Goleman 1998, Maddocks & Sparrows 1998). Emotional intelligence is made up of many components, the research work done on emotional intelligence in relation to older people addresses these components which have also been used as variables for study. One component is the psychosocial and physical factors in the elderly and its effect on emotional intelligence (Galdonna et al. 2018). The study emphasises that physical, psychological and social health are important factors that play an important part in the growth of EI.

Emotional intelligence components increase with age. while some elements of emotional intelligence are developed by giving training. One study showed that the emotional quotient in the elderly is more compared to people of other age groups, it is an ability that is developing and most likely the higher score on the assessment is due to the accumulation of the experiences that helps them to be better adjusted or more empathetic as they grow older (Fariselli et.al. 2008). In the work place also EI plays a major role in how a person interacts with the client and this is called as emotional labour strategy which refers to the rules of expressions of the organisation which can be very different than what that person is actually feeling. The outcome of the study indicated that there was a positive relationship between age and emotional labour strategy, which also in turn had a positive effect on their well-being. Older people showed more strategy when compared to people of other ages (Sliter et.al. 2013).

Education and Emotional Intelligence

A person's educational level is also another component that has shown a positive effect on the growth of emotional intelligence as people grow older. People who had a University education had more emotional quotient score compared to people who had only primary or secondary education. People who had studied upto the primary or the secondary level fared better on other elements of emotional intelligence using the Mayer – Salovey emotional intelligence scale (Cabello et.al. 2014). Emotional maturity, emotional competency and emotional sensitivity which are components of emotional intelligence, their growth was linked to ageing. Elderly people were seen to be more competent, sensitive and mature in their expression of emotions as compare to other age groups. In a study where the sample was clustered into three age groups and continuous statistics was taken for every respondent, the age group between 35 to 60 showed higher level of emotional intelligence compare to 17 to 23 year group and 24 to 34 year group (Sharma 2017).

Mental Health and Emotional Intelligence

Subjective well-being (SWB) which includes both satisfaction in life and emotional well-being, is one of the components that was measured in relation to ageing. The outcome of the study showed a positive relationship between age and subjective well-being (Chen et.al. 2016). Old age is also the age where we can see both physical and cognitive decline. Many research works support the fact that while there is decline in the cognitive and physical area, emotional ageing seems to improve as people grow older. Results of the present study indicates that if there is a shift in the way cognitive processing of emotional situations are done and motivation of emotional components are enhanced, this may curb the decline seen in cognitive development during old age. People with low EQ sores and also who lacked in social interaction skill, were found to have lower levels mental wellness (Tafti et al. 2018). Older people have many adjustment problems like inclusion of new family members. They also go through losses like losing of the spouse. EI was found to be helpful in using problem based method of coping, which results in increase of positive mood and better adjustment psychologically. The results in the study showed that promotion of EI activities can help improve the lifestyle of elderly persons.

Life satisfaction has a positive correlation with components of EI (Mostafaei et. al. 2019). Components of EI include relationship management, being aware of social situations, managing and being aware of others' emotions as well as self. There is also a positive correlation between psychological capital (resilience, hope, optimism, self efficiency) and life satisfaction.

Social support and important component among elderly people. Good social support helps people by giving them strength to plan and to lead their life successfully. A positive relationship between AI and support social support has identified that elderly people with IQ changing circumstances of life which also helps in maximising their well-being(Elsherif et al. 2021)

Emotional Intelligence as a coping mechanism

Old age is also a phase where the body becomes weak and people develop some common diseases and disorders. Some common diseases include blood pressure, diabetes, heart problems,

paralysis etc. Disorders like Parkinson, Alzheimer's and dementia cause more problems, which in some cases can lead to institutionalisation of old people as they cannot be taken care of at home. A comparative study where the EI, SWB and cognitive style of both institutionalised and non-institutionalised people where compared to understand whether there will be any significant differences among these factors (Bhattacharya et al. 2010). Ageing successfully is related to many factors and EI is one of the main factors. Stressful events of the past were used as a variable to understand whether it has an effect on successful ageing. But the results indicated a negative correlation between ageing and stressful past events, while emotional intelligence emerged as the main factor for ageing successfully (Guirado, 2021). Emotions have been used to solve problems in a much better way as people age. Their experiences lead to increase in emotional intelligence which helps in problem-solving and studies have shown that females are much more adept add using emotions for solving problems (Atkins, 2005).

Result

The studies reviewed for this paper all agree with the hypothesis that certain components of emotional intelligence increased with age. Some of the variables include psychosocial and physical factors, accumulation of experiences and developing emotional ability, emotional strategies, the education level of a person, emotional maturity and emotional sensitivity. Subjective well-being is one very important variable that is being studied in the recent years which is linked to life satisfaction also. High EQ scores of a person helps them to cope better with diseases and many stressful events be it past or the present. Emotional intelligence and its training during the developmental stages helps in curbing cognitive decline in elders and also helps them in better decision making and problem-solving.

Conclusion

Emotional intelligence in elders as compare to its development in the earlier years has helped the elderly in understanding, controlling, expressing, evaluating one's own emotion and emotion of others.

References

Akhavan Tafti, M., & Mofradnezhad, N. (2018). The relationship of emotional intelligence and social skills with psychological well-being in the elderly. *Iranian Journal of Ageing, 13*(3), 334-345.

Atkins, P., & Stough, C. (2005). Does emotional intelligence change with age. *In Society for Research in Adult Development annual conference, Atlanta, GA.*

Bhattacharya, A., & Mukherjee, T. (2010). A Comparative Study on Cognitive Style, Subjective Well-being, Spirituality & emotional Intelligence in Institutionalised & Non-institutionalized Elderly. *Indian Journal of Positive Psychology, 1*(1-2), 61-66.

Buedo-Guirado, C., Dumitrache, C. G., & Rubio, L. (2021). 507-Stressful past events and emotional intelligence as predictors of Successful aging. International *Psychogeriatrics, 33*(S1), 59-60.

Cabello, R., Navarro, B., Latorre, J. M., & Fernández-Berrocal, P. (2014). Ability of university-level education to prevent age-related decline in emotional intelligence. *Frontiers in Aging Neuroscience, 6,* 37.

Cabello, R., Sorrel, M. A., Fernández-Pinto, I., Extremera, N., & Fernández-Berrocal, P. (2016). Age and gender differences in ability emotional intelligence in adults: A cross-sectional study. *Developmental Psychology, 52*(9), 1486.

Chen, Y., Peng, Y., & Fang, P. (2016). Emotional intelligence mediates the relationship between age and subjective well-being. *The International Journal of Aging and Human Development, 83*(2), 91-107.

Delhom, I., Gutierrez, M., Mayordomo, T., & Melendez, J. C. (2018). Does emotional intelligence predict depressed mood? A structural equation model with elderly people. *Journal of Happiness Studies, 19*(6), 1713-1726.

Elsherif, Z. A. E. G. (2021). Emotional Intelligence, Perceived Social Support and Mental Health of Institutionalized Elderly. *Tanta Scientific Nursing Journal, 20*(1), 220-243.

Fariselli, L., Ghini, M., & Freedman, J. (2008). *Age and emotional intelligence. Six Seconds: The Emotional Intelligence Network,* 1-10.

Galdona, N., Martínez-Taboada, C., Etxeberria, I., Urdaneta, E., & Aldaz, E. (2018). Positive aging: the relationship between emotional intelligence and psychological, social and physical wellbeing. *MOJ Gerontol Ger, 3*(1), 9-11.

Mayer, J. (1997). en: John D. Mayer, Peter Salovey, David R. Caruso, y Lillia Cherkasskiy. Eds. *Emotional Intelligence.* Cap, 26.

About the Editors



Dr. Pooja Varma is working currently as Head of department, Psychology and Assistant Professor of Psychology at Jain (Deemed-to-be) University. She specializes in Applied psychology (Gold Medallist) with work on Indigenous therapies, Expressive therapies, Health psychology, Developmental psychology, Clinical psychology and Counselling psychology. She has over a decade experience in teaching undergraduate and postgraduate courses in Psychology at a university level after completion of her Ph.D. in 2007. She has published more than twenty research papers in edited books, national and international journals. She has guided and taught PhD students as well as guided PG dissertations and PG diploma projects. She has conducted various workshops and guest lectures on various potent concerns and arenas of psychology. She is currently practising counselling psychologist working as a freelancer. She has organized various national and international conferences in the field. One of the successful event organized recently was an international conference on Healthy ageing with a key focus on geriatric health in collaboration with NIMHANS which was the sole reason for the conceptualization of this valuable book.



Dr. Alka Ranjan is an Assistant Professor of Psychology at Jain (Deemed-to-be) University. Her specialization is in Counselling Psychology and Public Health. She has 10 years of experience in teaching undergraduate and postgraduate courses in Psychology. She has more than 10 research papers in edited books, national and international journals. She is supervising PhD students and has guided undergraduate research projects and more than 100 master's dissertations. She has conducted various workshops, seminars and community outreach programs. She has organized 10 National and International Conferences. She is a practicing consultant psychologist and has qualified the exam for the licenced graduate professional counsellor in U.S.A. She has cross-cultural experience of working in the field of Counselling Psychology and Community Health in Singapore, U.S.A. and India.



Dr. Pooja Rai is an Assistant Professor of Psychology at Jain (Deemed-to-be) University. She specializes in Gerontology, cognitive disorders, memory, cognitive neuropsychology, neurodegenerative diseases, cognitive neurosciences, executive functions and neuropsychological assessment. She has immense experience in teaching undergraduate and postgraduate courses in subject like Clinical Psychology, Biological processes, Research Methods, Developmental psychology and so on. She has published more than 10 research papers in edited books, national and international journals in UGC, Scopus and web of sciences. She has guided and taught PhD students as well as guided PG dissertations. She has qualified UGC net and post doc fellowship in her field. She has conducted various workshops, seminars, conference, research based discussions and guest lectures on Neuropsychology and related fields.

Bharti Publications, New Delhi
Email-info@bartipublications.com | bhartipublication@gmail.com
www.bhartipublications.com

ISBN 978-93-94779-67-9

Price- Rs. 680/-



PRINCIPLES OF RESEARCH METHODOLOGY

DR. MOHD. SHAIKHUL ASHRAF, PARMAR VISHALKUMAR RAJENDRASING
DR. HEMA KUMARI MEHAR, DR. JAVAD GHALAMBOR, DR. S. KUMAR

PRINCIPLES OF
RESEARCH METHODOLOGY

EXCLUSIVE PARTNER



PARADOX
PUBLICATIONS GUIDE HOUSE
Trivandrum, Kerala
+91 8848074612 \ +91 7907367147

PRINCIPLES OF
RESEARCH METHODOLOGY

Dr. Mohd. Shaikhul Ashraf
Parmar Vishalkumar Rajendrasing
Dr. Hema Kumari Mehar
Dr. Javad Ghalambor
Dr. S. Kumar

red'shine
Publication
INDIA

PRINCIPLES OF RESEARCH METHODOLOGY

by: Dr. Mohd. Shaikhul Ashraf, Parmar Vishalkumar Rajendrasing , Dr. Hema Kumari Mehar, Dr. Javad Ghalambor, Dr. S. Kumar

■

RED'SHINE PUBLICATION PVT. LTD.

Headquarters (India): 88-90 REDMAC, Navamuvada,
Lunawada, India-389 230
Contact: +91 76988 26988
Registration no. GJ31D0000034

In Association with,

RED'MAC INTERNATIONAL PRESS & MEDIA. INC

India | Sweden | UK

■

Text © *Authors*, 2022
Cover page ©RED'SHINE Studios, Inc, 2022

■

All rights reserved. No part of this publication may be reproduced or used in any form or by any means- photographic, electronic or mechanical, including photocopying, recording, taping, or information storage and retrieval systems- without the prior written permission of the author.

■

ISBN: 978-93-954560-2-9
ISBN-10: 93-954560-2-7
DIP: 18.10.9395456027
DOI: 10.25215/9395456027
Price: ₹ 400
September, 2022 (First Edition)

■

The views expressed by the authors in their articles, reviews etc. in this book are their own. The Editor, Publisher and owner are not responsible for them. All disputes concerning the publication shall be settled in the court at Lunawada.

■

www.redshine.co.in | info@redshine.in
Printed in India | Title ID: 9395456027

PREFACE

Students in the social sciences, business, education, public health, and other relevant fields may find this book to be an excellent resource for learning about the steps involved in conducting scientific research. our lecture materials that we generated over the course of a decade of teaching the subject on Research Methods provide the foundation for this book. Students, young researchers, and professors who offer courses on research techniques make up the primary audience for this book. However, older researchers may also utilize this book as a useful and compact reference source.

The first and most crucial question that prospective readers of this book should have is, "How is it different from other text books that are now available on the market?" To be clear, there are two primary distinctions.

To begin, in contrast to other textbooks, this one is not just about "research techniques" (empirical data collecting and analysis), but also about the "research process" in its whole, from the very beginning to the very conclusion. The research technique is only one step in the whole research process, but perhaps the one that is least difficult and most regimented. The majority of textbooks provide an in-depth discussion of research methods, but they omit topics that are more difficult, less structured, and possibly more significant. These topics include theorizing and thinking like a researcher, both of which are frequently prerequisites for empirical research. In my experience, the majority of students are able to develop a reasonable level of research procedure competence, but they struggle to develop research topics that are engaging or relevant or to construct scientific ideas. In order to make up for this shortcoming, we have dedicated whole chapters to subjects like "Thinking Like a Researcher" and "Theories in Scientific Research," which are fundamental abilities for a young researcher.

Second, the book was written in a way that makes it concise and easy to carry. When we were writing the book, we made the decision to concentrate exclusively on the most important ideas and avoid

cluttering the pages with side topics or irrelevant information that would draw the attention of the readers away from the primary subject matter. The majority of classes consist of a substantial amount of assigned readings culled from the relevant academic field. Instead of burdening students with a lengthy text on top of their prescribed readings, this book is intended to supplement those readings by condensing all relevant themes in a single compact volume.

Authors

SYLLABUS

UNIT NO.	UNIT TITLE
1	**UNIT-1: INTRODUCTION TO RESEARCH METHODOLOGY** Meaning of Research - Function of Research Meaning of Research - Function of Research – Characteristics of Research – Steps involved in Research – Research in Pure and Applied Sciences - Inter Disciplinary Research. Factors which hinder Research – Significance of Research - Research and scientific methods – Research Process– Criteria of good Research – Problems encountered by Researchers – Literature review.
2	**UNIT - 2: IDENTIFICATION OF RESEARCH PROBLEM** Selecting the Research problem – Necessity of defining the problem – Goals and Criteria for identifying problems for research. Perception of Research problem – Techniques involved in defining the problem – Source of problems – Personal consideration.
3	**UNIT- 3: RESEARCH DESIGN** Formulation of Research design – Need for Research design – Features of a good design – Important concepts related to Research design. Different research designs – Basic principles of experimental designs – Computer and internet in designs.
4	**UNIT -4: STATISTICAL TECHNIQUES AND TOOLS** Introduction of statistics – Functions – Limitations – Measures of central tendency - Arithmetic mean– Median – Mode – Standard deviation – Co-efficient of variation (Discrete serious and continuous serious) – Correlation - Regression – Multiple Regression. Sampling distribution – Standard error – Concept of point and interval estimation – Level of significance – Degree of freedom – Analysis of variance – One way and two way classified data – 'F'-test.
5	**UNIT-5: INTERPRETATION AND REPORT WRITING** Meaning and Technique of interpretation – Precautions in interpretation – Significance of report writing – Different steps in writing a report – Layout of a Research report.

UNIT NO.	UNIT TITLE
	Types of report –Mechanics of writing a research report – Precautions for writing a research report – Conclusion.

CONTENTS

SR.NO.	MODULE NAME	PAGE NO.
1	INTRODUCTION TO RESEARCH METHODOLOGY	1
2	IDENTIFICATION OF RESEARCH PROBLEM	54
3	RESEARCH DESIGN	65
4	STATISTICAL TECHNIQUES AND TOOLS	84
5	INTERPRETATION AND REPORT WRITING	155
*	REFERENCE	197

UNIT I

INTRODUCTION TO RESEARCH METHODOLOGY

Meaning of Research

The Department of Education and Training in Australia offers the following explanation of what constitutes research in their country:

Research can be defined as either the production of new information or the use of data that has already been gathered in an innovative and imaginative manner for the purpose of generating new ideas, ways of thinking, and comprehensions. Either way, the goal of research is to generate new ideas, ways of thinking, and comprehensions. In another sense, research may be seen as the act of using previously gleaned knowledge in a way that is novel and creative. One possible interpretation of the term "research" is as follows: This may include putting together a summary and doing an analysis of prior research to the point where it leads to discoveries that are novel and innovative.

This definition of research is consistent with a broad concept of research and experimental development (R&D), which is comprised of creative expression initiated on a comprehensive basis to increase the stock of knowledge, including knowledge of humanity, culture, and society, and the use of this knowledge base to devise new applications. Research and experimental development (R&D) is an abbreviation that stands for research and experimental development. R&D is an acronym that stands for "research and experimental development." Another way to say "R&D" is "research and experimental development." To put it another way, research is creative work done with the purpose of adding to the body of information already available, while research and development (R&D) is creative work done with the intention of contributing to the body of knowledge already available.

This concept of research incorporates all of the subfields of research, such as fundamental research, which may be carried out for

academic or strategic objectives, applied research, and experimental development. An example of applied research would be the collecting of new information via the process of doing original research with the particular intention of working toward the achievement of a definite and quantifiable goal (including a client-driven purpose).

When doing several searches, it is necessary to conduct more searches in order to locate anything. According to one definition of the word "research," the term "research" refers to human activity that includes the application of cognitive processes in the analysis of subject matter. This is the meaning of the word "research." The primary goals of applied research are to discover, understand, and build procedures and systems for the progression of human knowledge on a wide variety of scientific disciplines pertaining to our world and the universe. Applied research also aims to advance human understanding of a wide range of topics related to the scientific study of our universe. To be of benefit to society as a whole is one of the secondary purposes of applied research. Applied research aims to: The scientific method is often used while doing research; however, this is not always the case in every instance.

The term "scientific research" refers to a more general field of endeavour that encompasses both the "discipline" of study as well as the "art form" of study. The act of obtaining new information in a way that is well-structured and consistent is what is meant by the term "learning." The definition of "research" that can be found in the Merriam-Webster Dictionary describes it as "an lengthy examination or enquiry especially by hunt for unique information in any domain of competence." A Definition of What the Term "Research" Means in Its Own Right The process of carrying out research involves defining and redefining problems, developing hypotheses or suggesting potential solutions, collecting, organising, and analysing data, drawing inferences and coming to conclusions, and, as a final step, carefully evaluating the conclusions to determine whether or not they are consistent with the developing hypothesis.

Definitions of what it means for something to be considered research M. Stephenson and D. Slesinger, writing in the Encyclopedia of Social Sciences, defined research as "the manipulation of things,

concepts, or symbols for the purpose of generalising to extend, correct, or verify knowledge, whether that knowledge aids in the development of theory or in the practise of an art." This definition describes the purpose of research as "the manipulation of things, concepts, or symbols for the purpose of generalising to extend, correct, or verify knowledge." This definition explains the steps involved in doing research. Research may also be defined as "the manipulation of things, ideas, or symbols with the objective of generalising to extend, correct, or verify knowledge," which is another way of stating the same thing. 3

"The process of doing research is one that is distinguished by a high degree of organisation as well as an approach that is methodical," This term refers to the manner in which information is structured and presented as being systematic in the sense that there is a predefined sequence of activities and actions that you are expected to follow. When doing research, there are certain steps that must at all times be followed in order to attain the highest possible level of precision in the findings that can be obtained. If this is not done, the accuracy of the findings will suffer.

The research process is a rigorous approach that helps us find new facts and information, supports us in validating the existing knowledge, and motivates us to question things that are confusing and difficult to grasp based on the material that is already accessible. If you want to be a competent manager, you need to be able to recognise solutions to difficult situations and base your judgments on the information you get from those answers. Because of this, it is vital for you to have understanding of the many different processes that are involved in the process of obtaining solutions. You may get this information by reading books or watching documentaries.

Additionally, one is able to make sense of it by considering it in terms of the following:

• Research is an endeavour that is always being pursued, both in the vast majority of academic disciplines and professional sectors. This is the case both in the United States and internationally.

• It is important to keep this in mind while doing an in-depth analysis of how our organisation operates, how we implement rules, and how we instruct individuals in the many fields in which we work.

• It is the examination of processes in a methodical manner with the aim of discovering more effective methods to carry out operations, minimising the amount of work required to reach a goal, and determining whether or not the objectives are genuine.

• In point of fact, we are always engaged in the process of doing research, whether it be in the process of acquiring items for daily use, a vehicle, an electronic commodity, or the preparation for a vacation. It makes no difference what sort of purchase is being made; this is always the case.

According to Clifford Woody, the process of doing research consists of determining and reframing questions, formulating hypotheses, collecting, organising, and analysing data, and drawing conclusions. In this section of the chapter, it is highlighted that in order for any study to be effective in accomplishing the objectives that have been established, it must be carried out in a methodical and sensible manner.

The activity known as research is described as the process of obtaining new information with the intention of determining the solutions to a problem that has been posed. The two components of the word "research" are the words "re," which means "again," and "search," which means "find." Together, these words signify that we are engaging in an activity in order to look at an element once again or that we wish to seek out some new information about something. Together, these words signify that we are researching. [Case in point:] [Case in point:] [Case in point:] [Case in point:] The term may be understood to imply any one of these things. A Front Office Executive needs to educate themselves on the facilities, timings, and important characteristics of items and services that are available at the hotel in order to become an excellent sales professional in addition to being a host. For example, a person who wants to become an excellent sales professional in addition to being a host. These may be discovered in the many things and services that the hotel provides. " Curiosity is the seed

from which all creation springs; it is the place from which all else originates. It is better to have a reasonable level of healthy scepticism rather than an excessive quantity of self-assurance on occasion. Having an excessive amount of self-assurance might be dangerous. This is due to the fact that reasonable scepticism inevitably results in questioning, and questioning inevitably results in innovation "is a well-known proverb from Hudson that, when taken into consideration in the appropriate context, makes it simple to comprehend the significance of carrying out research. [Citation needed]

Different researchers, depending on the area in which they have chosen to concentrate their efforts and the resources that are available to them at any given point in time, have comprehended and described research in their respective fields in a manner that is unmistakably unique to themselves. This is the case regardless of the field. You will find that the background knowledge and major importance of each of these definitions are equal to one another, which is one of the things that you are going to discover. The only thing that really differentiates these definitions from one another is the technique that each author utilised when doing research inside their respective unique domains. This is the only factor that makes a difference.

The findings of the research that Thyer conducted back in 2001 may be summarised as follows: "The word "research" is broken down into its component parts, which are the syllables "re" and "search." These syllables, when put together, make up the phrase. The prefix "re" may have two distinct meanings: the first one is "once more," while the second one is "over and over again." The process of searching for something might imply to investigate something in depth and attentively, to test something out and see how it works, or to do more research on something. All of these are examples of what it means to "look for" something. They combine to form a phrase that, according to the definition found on dictionary.com, refers to "an attentive, methodical, and patient study and examination in any area of knowledge, carried out with the intention of establishing facts or principles.""

According to the edition of the Merriam-Webster Dictionary that is available online, the term "research" originates from the Middle

French word "recherche," which literally means "to go about searching." The first known written reference to the term dates back to 1577, when it was first documented.

Research is defined as "an structured investigation that makes use of trustworthy scientific procedure in order to solve difficulties and produce new information that is relevant across a range of situations," according to one definition of the term.

According to Martyn Shuttleworth, who offers a comprehensive definition of research when he says, "In the fullest meaning of the term, the definition of research covers the collecting of data, information, and facts for the progress of knowledge," the term "research" refers to the process of gathering information for the purpose of furthering one's understanding of a particular subject. A thorough comprehension of what it takes to do research has been shown here. According to Creswell's definition, research is "a series of approaches used to gather and evaluate information in order to expand our knowledge of a subject or situation." This definition of research is not the only one available; nonetheless, it is the definition that is most often used. The following are the three separate stages that may be split down into it: Following the formulation of a question as the first phase, the subsequent step is the collecting of pertinent data to address the issue in question, and finally, the question itself needs to be answered.

Research also contains the characteristics that are included in the following list:

a) The investigation has been given careful consideration, and it has been organised (a formal step-by-step procedure or sequence to carry out research activity is designed to assure the accuracy of data and the validity of processes). The categorization of the data, the act of making observations, and the interpretation of those findings are the three processes that are considered to be of the utmost significance in the scientific method. The amount of formality, rigour, verifiability, and general validity of the techniques used to get the conclusions that are attained through the use of scientific processes is what determines the findings that are obtained. The findings that are obtained can be used to draw conclusions about a variety of topics.

b) The challenges that it tackles are approached in an appropriate and respectable scientific manner (the technique used ought to be able to yield repeatable findings under situations that are comparable).

c) It should provide new information that may be used in a variety of various contexts and circumstances. (The results should be of the form that they are not unique to a particular problem or a set of circumstances; rather, they should be capable of being generalised for application to problems that are related.)

d) Due to the fact that it is a creative process, it helps to contribute to the development of a greater understanding of people, as well as social and cultural challenges and economic concerns.

e) Other individuals who seek to make use of the findings in the creation of new policies or applications of the findings of a research project for the benefit of the general public should find it advantageous.

The Aims and Objectives of the Research

If you describe the kinds of essential questions that are going to be taken into consideration during your investigation in your research objectives, you may be able to discover the overarching purpose or primary focus of your investigation. This may be possible because your research objectives will help direct your investigation. You are, in effect, telling me of the things that it is required for me to explore and analyse when you provide me with a description of the goals of your research. In spite of the fact that they are only different methods of referring to the same thing, the significance of the study may also be referred to as its objectives. It discusses a broad variety of topics, some of which are listed here for your convenience:

[Question: What are the objectives of the study, and why is it necessary to carry out research in the first place?] [Answer:]

1) To discover the truth in its purest form As we are all well aware, each and every type of research has its own objective, but the fundamental goal of the research is always to discover or obtain the information from the relevant marketplaces, societies, and the amount of people who participated in the study. A researcher will either conduct an analysis of the material that they uncover or seek for

information that is real or accurate in order to give answers to our inquiries that are relevant to the situation.

2) To accomplish new ideas: This aim of the study emphasises that anybody could come up with new ideas as a consequence of the research; hence, the objective is open to different interpretations. The process of discovering specific knowledge by making effective use of observation, optimization, and experimentation is referred to as research. Research refers to this kind of work that is carried out.

These are the scientific procedures that may be used in order to either identify the information or assess it, both of which are very essential in order to figure out how to proceed with the activity.

3) To evaluate the information: The initial purpose of the study is to locate the information, and then to evaluate it in a way that is suitable or effective so that they can easily construct the research issue and also solve it. This will allow them to easily construct the research issue and also solve it. This is done in order to facilitate the easy construction of the research issue as well as the solution to it.

A researcher will analyse the content by using a broad variety of scientific approaches and methods, statistical analyses and methods, as well as a significant number of tables and graphs.

4) To put a theory to the test in the methods that follow: During this phase of the investigation, the researcher will determine the correlational and causal linkages that exist between all of the different variables (it can also be said that the hypothesis testing research studies). In order to validate the hypothesis, the following is a summary of the total number of instances that were analysed as part of this research:

(a) as an integral component of the procedure for releasing an official statement,
(b) Figuring out the right significance level to use,
(c) Figuring out how to make distribution work for you in the most effective way possible,
(d) Choosing a random sample that is representative and establishing the lowest value for which there is an acceptable threshold,

(e) The analysis of the many potential events that could take place,
(f) doing an investigation of the disparities that exist among the different probabilities.

5) To design or carry out the study: As soon as all of the information has been gathered, the researcher will develop the framework of a research design that the organisation may employ. As a consequence of this, the organisation will have the capacity to quickly explain or recognise the framework of a certain area of research. When doing research, it is important to keep in mind that there are options available for both experimental and non-experimental designs. These are the two groups that may be used for the purpose of classifying the various research designs. As soon as the fundamental structure of the research project has been established, the researcher will start applying the findings to the issue at hand and will decide which of the available options is going to be the most useful in resolving the problems that have been uncovered.

6) To have a better understanding: This objective of the research seeks to have the researcher have a much better understanding of the topic at hand while also asking what else needs to be supported before the research can be considered purposeful, or what knowledge could be gathered from a more focused investigation, or scrutiny of the findings that have already been discovered. 7) To have a better understanding: This objective of the research seeks to have the researcher have a much better understanding of the topic at hand while also asking what else needs to be This objective of the study leads to the development of a more in-depth grasp of a particular issue on the part of the researcher.

The Importance of Motivation in the Scientific Process

Every inquiry starts with a collection of concepts, which are then researched further and drawn from a wide range of different scenarios and circumstances. In addition, the purpose of research is to approach an issue in an orderly way with the idea of discovering viable solutions to that problem. Research is a procedure that entails developing an in-depth study as well as completing investigations of crucial areas in order to discover a solution to an issue. The goal of this process is to

find a way to solve the problem. This is done in the interest of locating responses to various inquiries. In general, research is a procedure that involves an approach that is methodical. Its purpose is to ensure that the information acquired is reasonable and that it is supported by qualitative information. Accuracy in the information obtained is intended to be the result of this endeavor's primary focus. The establishment of a research technique, the collection and description of data, and the procedure of reporting information to the proper parties are all included in this step of the process. Research has the potential to provide solutions that will solve problems that have been brought about as a consequence of a problem in this way, and it can do so in a way that will clarify things up.

One of the most essential occupations in the modern academic world is teaching, but other key responsibilities include doing research and publishing the findings of that study. Teaching is not the only important academic job. These three commitments are in some way or another inexorably tied to one another. Research not only provides new information but also contributes to the body of previously held knowledge while simultaneously adding to the expansion of previously held knowledge. In other words, research not only produces new information but also adds to the body of previously held knowledge. Research is not just something that must be done in order to get a degree, but it has also become something of a responsibility that must be fulfilled. When a higher education establishment demonstrates outstanding performance in the areas of research and the production of publications that are of a high grade, the status of such an establishment may be elevated. This is a fact that cannot be disputed, and it is a fact that can elevate the status of such an institution. The researcher is responsible for determining which technique of publishing is most appropriate for each and every result that is acquired and must do so for all of the results.

You should not only be a good researcher, but you should also be an amazing instructor.

Every exceptional student has their very own one-of-a-kind strategy that they follow in order to be able to carry out the

responsibilities of their profession effectively. The work that has to be done by an academic is often difficult and has to be finished by a specified date in order to be considered satisfactory. It is possible that beginners may find this goal to be challenging since the activities may seem to have no link to one another. As a consequence of this apparent lack of connection, it is possible that beginners will struggle to meet this expectation. Even if a novice is capable of completing all of the tasks that have been assigned to them, the quality of the work that they produce may not be very impressive. The purpose of all of the interviews that were carried out for the purpose of this work was to collect information from productive researchers and academics about the methods that they use to organise their careers as lecturers and researchers. This information was gathered from the interviews that were carried out. These interviews, which were carried out, were the source of the information that was acquired. In order to make things easier for you, the following paragraphs provide a condensed and simplified version of a summary of the ideas and recommendations provided by those individuals who served as role models.

The driving force behind this research:

• Take responsibility for your time management, and organise your work in a way that makes sense to you. Creating a logical plan, for instance, may make life easier to manage in terms of issues such as time management. This is one benefit of developing a logical strategy. It is possible to accomplish this objective by the use of several pieces of software, for instance Google Calendar.

• It is crucial for researchers to bear in mind that the fundamental reason for the development of their study is not money but rather a deep interest in the topic on which they are working. This is because money is not the primary motivation for developing their study. This is a very important fact to bear in mind, since it is the fundamental reason why they decided to carry out their research in the first place.

• Every researcher needs to have a high degree of self-assurance and should never give up easily, even if there comes a point in their investigation when it seems as if they have reached a dead end in their search for answers. If they keep looking, they will eventually find what

they are looking for. If, on the other hand, the researcher is really interested in expanding their own body of knowledge, then the research project will, in the end, be an endeavour that is successful.

• Researchers should never keep quiet about newly obtained information and should always be happy to share information with their colleagues | Researchers should always be eager to share knowledge with their colleagues • Researchers should never keep quiet about newly found information When working on a group project, cooperation is not only one of the most valuable assets that can be brought to the table, but it is also one of the most vital things that can be done.

• It is absolutely necessary to make sacrifices of both one's time and one's energy since there is no easy way to produce remarkable study discoveries. This is because there is no shortcut.

The Inspiration Behind the Writing

• Acquiring the abilities necessary to produce writing of an exceptional and high-quality level can only be accomplished via the accumulation of experience, and this is true for both reading and writing. Reading and writing both need experience. Learning should be something that is done on a continual basis and should be something that is done on a daily basis.

• Before beginning to write, we need to give careful thought to the purpose of the writing, since the purpose of the writing defines the scope of each individual writing project. This is why we need to pay careful consideration to the purpose of the writing. • After we have identified why we are writing this, we can then go on to the first step of the process, which is getting started. • The degree to which the author is willing to dedicate oneself entirely to the act of writing is one of the most significant elements that will define the quality of the final product. This is one of the most important aspects that will determine the quality of the finished output. A piece of work that is of a high quality will be beneficial not just to the scientific community, but also to the community as a whole in its whole. This is because the scientific community is merely one subset of the larger community.

• The reader needs to have a comprehensive understanding of what should be written, and the writer needs to have a comprehensive understanding of what should be written. In order to have a higher level of desire to finish the writing, the writer should choose tasks that have shorter deadlines, such as paper works and modules.

Beginning writers may benefit from working on a paper for a conference since it may help them enhance their general writing abilities. Working on a paper for a conference may be useful. With the help of this expertise, you will be able to develop a solid basis for your writing.

• A well-respected mentor has the ability to be an effective reviewer of the work that is produced by their mentees. This is because of the high level of credibility that the mentor has.

• In order to ensure that the clients or customers are pleased with the work that has been done, it is essential that the prescribed writing format for the project be adhered to in an exacting manner at all times. This will guarantee that there are no hiccups in the execution of the project.

• If you want to be a competent writer, you need to have a firm command of the language and the ability to interpret research data in a way that will have a huge influence on the people who are reading your work in a manner that will have a major impact on the people who are reading your work.

Plagiarism is a serious crime, thus it is imperative that authors never lift the concepts or words of others and use them in their own writing without giving proper credit. It is essential for writers to never steal the concepts or phrases of others in their work. Authors have an extra obligation to ensure that their works are fully original by implementing the appropriate safety measures. They have a duty to bring to the attention of the audience any instances in which they have taken ideas from the works of other authors and explain how they have done so.

The Value of Inspiring Others in a Learning Environment

• If you want to be a successful educator, the first and most crucial thing you need to do is develop a love for the work that you do.

This is the single most significant thing you can do to improve your teaching abilities. Work that is performed with passion will inspire the individual performing it to put up their best effort while they are working on the task at hand. It is possible to nurture interest, even if there is a lack of it, by becoming more cognizant of the responsibilities that come with being a professor. • When it comes to becoming a successful teacher, one of the most crucial talents to acquire is the ability to manage one's time efficiently. This is one of the most vital abilities to develop. Because time spent in the office is frequently devoted to other pursuits, such as meetings and lectures, lecturers should make more room in their schedules for writing in order to get the most out of the time they spend in the workplace. This will allow them to maximise the value of the time they spend there. To keep their level of competence in their respective professions at a high level and to continue to develop it, educators need to make research a mandatory part of their professional lives. This is done with the expectation that the findings of the research will result in innovations in the field of study, which will ultimately be to the advantage of the nation.

Tips to Become A Successful Academic

Teaching, doing research, publishing academic work, offering academic advice and services, and giving services to students are the five fundamental academic activities that educators and researchers are obligated to take part in. Participating in all of these different kinds of activities will be challenging, especially at the beginning of the process. However, as time goes on, there will be a significant reduction in the difficulty of effectively carrying this out.

• In order for lecturers to cultivate their competence in their respective professions, they should place a high priority on their fundamental responsibilities, which include instructing students, doing research, and writing. They will be able to better serve their pupils as a result of this. It is critical to do empirical study on novel ideas that have not been investigated to an adequate level up to this point in time. It's conceivable that ideas that have been used in the past or that are recycled might have their worth diminished as a result. Never give in to your hesitance or wait for the backing of others before starting a new

enterprise. Both of these things will only hold you back. You won't go very far with either one.

• In order for researchers to successfully complete their study, they need to be prompt and active because, if the time span is too long, other researchers who are working on similar projects will publish their findings before the researchers who are doing the original research. If the time span is too long, the researchers who are doing the original research will not be able to successfully complete their study. This is due to the fact that other academics who are working on similar topics will publish their results before the researchers who are undertaking the original study publish theirs. On the other hand, one cannot only presume that the degree of research that was carried out met the necessary criteria and proceed from there.

• Because we do not want other people to find any rationale to throw doubt on the validity of our results, the principles of research ethics need to be adhered to stringently throughout the whole of the project. This is because we do not want to compromise the integrity of the study. Because of this, it is very necessary that the guidelines for ethical conduct in research be followed.

Why should someone go through the trouble of doing research?

To provide insight into prospective courses of action, to compile evidence in support of hypotheses, and to make a substantial contribution to the expansion of knowledge in a particular area of study are the fundamental goals of research. This article demonstrates the value of research, as well as the different reasons why it is vital for all people—not just students and scientists—to engage in it. In addition to this, the essay emphasises the multiple reasons why research is necessary for everyone. To provide a more precise explanation, the main emphasis of the article is on the significance of doing research.

In spite of the fact that it would seem to be self-evident that research is essential, a substantial percentage of individuals continue to steer clear of it like the plague. On the other hand, doing research is not simply useful for individuals who aspire to study in any subject, regardless of whether or not they are members of a research institution;

rather, it is an absolute must for such individuals to carry out such research.

Why does it make a difference to do research, and why is it so important for our day-to-day lives?

- It is a tool that makes the process of education more manageable while also extending one's intellectual frontiers and increasing one's intellectual horizons.
- It is a tool that assists individuals in better comprehending challenges, while at the same time elevating general public knowledge of issues of this kind.
- The success of our company may, in part, be attributed to this component, which contributes to our overall success.
- It affords us the opportunity to debunk urban legends and strengthen our cases for why the reality is more compelling.
- It is a tool for locating possibilities, evaluating the worth of those chances, and seizing those opportunities when they become available.
- It encourages a love of reading, as well as self-confidence in writing, reading, and comprehending material, as well as the capacity to convey this knowledge with other people.
- As a direct result of this, the mental capabilities are both nourished and exercised, which is beneficial.

Research is essential for all kinds of people, whether they are students, academics, professionals, or those who are not in those professions. However, those in the academic world and students aren't the only ones that need it. It is a tool that may facilitate easier learning and help one's existing knowledge become more comprehensive. It is essential for aspiring authors as well as established writers, and it does not matter if they write offline or online; either way, it applies to both groups. It is necessary for all of them, regardless of whether or not they decide to publish their work.

By engaging in research, persons who are not experts but who place a high value on education have the chance to gain information about the world as well as skills that will aid them in surviving and improving their life in ways that will be beneficial to them. On the

other hand, in order to find an interesting subject to talk or write about, professionals and writers need to look for sources of inspiration other than their own personal experiences. This is necessary in order to discover an interesting topic to speak or write about. One of the many reasons research may be done is to find out what the general public would be interested in learning or what academics want people to understand or think about. This is only one of the many reasons research might be done. This is only one of the many different reasons why research might be carried out. As a consequence of this, doing research is a necessary step in the process of acquiring new knowledge, and the same is true when it comes to the accumulation of new information.

It is common parlance to characterise one's knowledge as a truthful assertion that is kept inside one's own head. It is a reference to the facts that are processed by the human brain and are derived through either objective insights or the results of investigations. A simple definition of it would be anything that makes reference to facts. It is possible to acquire it through a variety of different means, such as through the reading of books and articles, the observation of experts in person or on television, the observation of investigative or documentary television shows, the participation in social activities, and the performance of scientific experiments. All of these methods can be utilised to acquire it. One technique to check the validity and correctness of the information collected via research is to cross-reference one set of research results with another set of sources. This is an example of a cross-reference.

Numerous Articles and Research Studies Covering a Wide Range of Topics Concerning the Necessity of Conducting Research

David Truncellito, an associate professor of philosophy at Yale University, outlines his findings in a paper titled "Epistemology," in which he distinguishes between three separate types of knowledge (n.d.). There are three main types of knowledge, which are as follows: procedural (also known as competence or know-how), acquaintance (also known as familiarity), and propositional knowledge (description of "a fact or a state of affairs").

Brain Research UK, a medical research charity that is situated in the United Kingdom and was previously known as the Brain Research Trust, recognises the importance of research in the process of gathering new information. Brain Research UK was originally known as the Brain Research Trust. Before changing its name, Brain Research UK was known as the Brain Research Trust. Research is considered to be of utmost significance in terms of the importance of identifying effective remedies for illnesses as well as approaches that may be employed to prevent individuals from acquiring diseases in the first place. As a consequence of this, it is vital to do study in order to determine whether or not previous studies support one's beliefs and whether or not these concepts still need more evidence in order to be called knowledge.

In 2016, a group of researchers interested in the field of psychology joined together to carry out an investigation with the purpose of discovering whether or not there is a correlation between obtaining adequate sleep and being able to retrieve memories that have been stored in the past. In "The researchers came to the conclusion that "interleaving sleep between learning sessions not only cut the amount of practise needed by half but also secured much improved long-term recall." This research was presented in a publication with the title "Relearn Faster and Retain Longer: Along with Practice, Sleep Makes Perfect." This finding was stated in the study article that was published under the title "Relearn Faster and Retain Longer: Along with Practice, Sleep Makes Perfect." It is a well-known fact that getting some shut-eye after a learning session is beneficial; however, research has shown that sleeping during the time frame in which one learning session is followed by another is much more effective." This research lends credence to the theory that people are better able to retain knowledge for longer periods of time after engaging in activities that include both repetition and sleep. Specifically, the research demonstrates that people are better able to retain knowledge for longer periods of time after sleeping on it. In particular, the study shows that individuals are able to remember information for longer stretches of time once they have had time to reflect on it while they were sleeping. Their results also highlight how critically crucial sleep is to the proper functioning of a

healthy brain, which is another significant takeaway from their research.

1) A Way to Gain a Deeper Understanding of the Issues at Hand and Raise Awareness Among the General Public

Employing Research as a Tool to Acquire a Greater Comprehension of Existing Problems in Order to Better Prepare for Future Challenges

In both fictional and nonfictional episodes and films that are shown on television and in movie theatres, the use of research is a regular practise that is often seen. Oprah Winfrey, for example, would not have been able to achieve the incredible success that she has as a news anchor and presenter of a television programme if she had chosen not to do study on certain topics and famous persons. If she had done so, she would have had a much harder time breaking into the industry. She would have had a lot harder difficulty breaking into the business if she had done that. It would have made her job much more difficult.

2) Implementing Research in Order to Acquire a Deeper Understanding of People

Actors who work in the film and television industries frequently conduct interviews with real people in order to gain a more profound comprehension of the characters that they play on screen. This makes it easier for the actors to empathise with the characters they play. In order to receive an insider's perspective on what it's like to have a given character, actors have, among other things, collaborated with detectives, boxers, chemists, company owners, criminals, and instructors. This has allowed them to get this knowledge. Because of this, the performers are able to more convincingly convey the events that their characters go through. Some people will go so far as to put themselves in the position of their characters in order to have a deeper understanding of the difficulties those characters face. This could involve spending time in jail or a drug rehabilitation centre, beginning a strenuous diet or exercise routine, learning how to sail a sailboat, gaining a considerable amount of weight, or losing a significant amount of weight. Other options include learning a new skill, such as

how to drive a stick shift or learning a musical instrument. In addition to that, it can mean putting on a significant amount of weight. Many people read works of fiction, biographies, or diaries in order to get a better perspective or grasp of the tale that they have been entrusted to tell. This might be because they want to learn more about the subject matter or because they are interested in the topic. This might be due to causes in your personal life or reasons in your work life.

3) Using Research as Part of the Creative Writing Process in Order to Generate More Realistic Stories

There are a lot of movies, plays that are performed in theatres, television dramas, and videos that are put on the internet that portray narratives that are based on real-life occurrences and situations. Some examples of these types of media include: It is possible to find examples of these. When it comes to entertaining and enlightening audiences across a variety of media channels, a professional writer or content producer understands how important research is in substantiating the background of the story they are delivering. This understanding is based on the fact that they are aware of the importance of research. To put it another way, they are aware of the importance of the research that they carry out.

According to the concepts that Terry Freedman presented in "The Importance of Research for ICT Teachers" (2011), "Research may shine light on difficulties we didn't even know existed, and can raise concerns we hadn't even realised even required asking" (Research may shine light on difficulties we didn't even know existed, and can raise concerns we hadn't even realised even required asking) (The results of research may throw light on challenges that we were unaware ever existed, and it may also pose questions that we were unaware even needed to be asked.) Because of this, the vast majority of authors of both fictional and factual reports do research, since doing so enables them to develop intriguing stories and ensures that their credibility is maintained. This holds true for writers of both fictional and nonfictional works of storytelling.

4) The Contribution That Your Support Will Make Towards Our Achieving Financial Success

The Rewards That May Be Obtained If One Is Willing To Put In The Effort And Time Required For Research And Development (R&D)

It is possible that doing research will be beneficial to the corporate world. Research and development, which is often referred to as R & D at times, is a field that is an area of investment for many prosperous firms, particularly those who operate in the consumer goods or mass market item manufacturing industries. Research and development is another name for this particular subject area. In a variety of different sectors, including agriculture, the food and beverage industry, manufacturing, healthcare and pharmaceuticals, computer software, aerospace, aviation, and the energy business, the costs involved with research and development are rather high. This is because the scientific and engineering methods that are used in these sectors play a significant role in the production and advancement of the goods and services offered by these businesses.

5) Carrying Out Research Concerning the Market and Specifying Particular Marketing Goals

A firm may benefit from research in a number of other ways as well, including the maintenance of a favourable commercial image, the retention of current customers, and the acquisition of new customers via the use of targeted marketing. Research is the key to achieving all of these objectives, and it should be your first priority. The use of research in real-world settings has the potential to provide the benefits outlined above. Because marketing is a kind of communication, for it to be successful, companies need to have a large amount of information about the people who buy the products and services they provide.

This is typically accomplished through the utilisation of market research, which may involve, among other things, the review of psychological studies concerning consumption, the facilitation of focus groups, the beta testing of products with a specific subset of customers, the distribution of satisfaction surveys to existing customers, and the investigation of the primary competitors of the company. In general, this objective is reached through the utilisation of market research. In

most cases, this purpose may be accomplished by doing research on consumer preferences and preferences currently held by the market. The most successful companies, regardless of their size, are those who construct their product designs, service offerings, and marketing messages on the basis of the insights obtained by doing in-depth research. This holds true for both big and small firms. This is true irrespective of the size of the organisation.

6) Leveraging the Applications of Research to Make the Most of Your Current Position and Future Career Opportunities

It is essential for people who are seeking for work or who are interested in developing their careers to do research if they want to increase their chances of success. People may improve their chances of obtaining work by doing in-depth study, searching for open opportunities through job-posting websites, and getting in contact with recruitment organisations. These three actions can all be done online. This may make it easier for individuals to find jobs. Research offers a number of benefits, one of which is the potential to assist individuals in determining whether or not employment opportunities actually exist for them. A job seeker or travelling worker who is naive yet optimistic, but who does not conduct their homework, runs the risk of being taken advantage of by unethical headhunters, phoney employment offers, or even outright frauds. This is especially true if the person does not complete their investigation.

Job seekers have the ability to learn about the experiences that others have had with an employer that they are thinking about working for or a placement agency that they are thinking about employing thanks to websites such as Glassdoor and organisations such as the Better Business Bureau. Job seekers have the ability to learn about the experiences that others have had with an employer that they are thinking about working for or a placement agency that they are thinking about employing. Job seekers have the ability to learn about the experiences that others have had with an employer that they are considering working for or a placement agency that they are considering utilising when they read reviews on the Internet (BBB). Once they have identified an academic course or training for skills

development that is available for free or for a nominal fee, students and professionals are able to conduct additional research to determine whether or not they are qualified for particular roles, as well as to learn the requirements and application deadlines for those roles. This is possible once they have discovered an academic course or training for skills development that is offered for skills development. After they have identified a training programme or academic course that is available for skill development, the next step that can be taken is the one that is being discussed here.

7) Using Research to Its Full Potential in Order to Realize the Highest Possible Returns on Investment

In addition, members of civil society could gain advantages as a result of research in a variety of different ways. The acquisition of financial resources for the many initiatives and research endeavours that those who are interested in finding solutions to societal issues have planned should be a high priority for those who are serious about their pursuit of such solutions. However, not all funding organisations are accepting proposals throughout the entire year, and they are not all interested in discovering solutions to the same kinds of societal issues. As a consequence of this, it is of the utmost importance to conduct research in order to identify organisations whose goals are compatible with the goals of particular advocacy campaigns or initiatives to bring about social change.

8) Research That Backs Up the Theory and Method of Reflective Thinking

Reading and writing are two processes that are crucial components of the research process that you are required to finish. It is possible for an individual to maintain both their comprehension and their capacity for critical thinking with the assistance of these two literacy processes. The process of doing research is going to be a lot more challenging for you if you don't have these talents. Reading gives one access to a large store of knowledge, while writing teaches us how to express our thoughts and translate abstract ideas into concepts that others can comprehend. Reading gives one access to a great store of

information. Reading also offers one the opportunity to have access to a vast store of information. Reading broadens a person's perspective on the world and deepens their understanding of the world in which they live.

Reading and writing are necessary skills for doing research, but it is also necessary to be able to listen to people and communicate oneself verbally. It is difficult to conduct research without having all of these skills. We have the opportunity to collect information and develop study topics when we take part in activities such as conducting interviews, going to events where new information is created, and taking part in casual discussion. Reading and writing, in addition to all of these other activities, have an influence on our capacity for critical thinking that is analogous to that of the other activities. Hearing professionals talk about the job that they do might potentially help us look at problems from fresh angles and add new approaches to our toolset for acquiring information.

9) The dissemination of discoveries in order to promote a deeper level of comprehension among a wider population

Researchers, regardless of whether they are affiliated with academic institutions or not, now have the opportunity to disseminate their findings to a more extensive readership as a result of the internet's capacity to facilitate the proliferation of information and the interconnectivity of people and locations. This is because the internet has the ability to facilitate the proliferation of information and the interconnectivity of people and locations. This activity is considered by some as a method of bolstering one's ego, while others see it as a means of piqueing one's curiosity and motivating greater investigation into certain subjects or situations. Both of these interpretations are valid, depending on who is doing the viewing.

Research not only assists in the development of these fundamental life skills but also makes learning an endeavour that continues throughout one's whole life. Literacy helps increase a person's social and economic mobility as well as their level of awareness, and research contributes to the improvement of these core life skills.

10) Gives It the Emotional and Mental Stimulation, as Well as the Nutritional Support, That It Needs in Order to Thrive

Analyses of Reasoning and a Concentration on Both Physical and Mental Health

It is true that curiosity may be fatal, but it also serves to keep the intellect fresh and keeps one motivated to find answers to questions. "helps students gain critical thinking talents... valuable for any field of higher education," as stated in an article written by Todd Johnson and published by College Admission Partners (n.d.), the author outlines the various ways in which scientific research, in particular, "helps students gain critical thinking talents." The creative and logical qualities that are already there in each of us may be maintained via the stimulation of the brain through activities such as learning new things and taking part in critical thinking. It has been hypothesised that maintaining a busy mind might aid in the avoidance of some mental diseases, including Alzheimer's disease.

These Qualities are Commonly Observed in Scientific Investigations

The characteristics of a piece of research provide light on any underlying biases, assumptions, or subjective inaccuracies that may or may not be present in the study. [Case in point:] [Case in point:] [Case in point:] [Cas [Here's a good example:] The phrases are used rather often in research, and the achievement of a satisfactory conclusion to any study is dependant on the amount of accuracy shown by the terms. To summarise them, consider the following:

- Generalized
- Controlled
- Exhaustive
- Empirical
- Being Organized
- Reliability
- The ability to evaluate and verify the outcomes of the analysis.
- Considers the existence of the hypothesis.
- Skilled in deductive reasoning and precise expression

• A sense of veracity
• Critical

1) In general, the researcher would normally divide the population that has been identified into smaller samples. The particulars of this procedure will depend on the resources that are available at the time that the study is being carried out. Given that it is commonly accepted that this specific sample is an accurate representative of the target population, the conclusions that are formed from it should be applicable to and indicative of the target population as a whole. The diagnostic information that is gathered from the study of these samples needs to produce a credible estimate of the percentage of the entire population that adheres to a particular ideology, views, stigmatisation, driving force, etc. This estimate needs to be derived from the information that is collected during the diagnostic process. This estimate has to be produced from the data that has been examined, which has been acquired via study. For instance, if a researcher wanted to understand the occupancy statistics and patterns of small hotels and resorts in a particular city, they would first have to divide the city into zones, and then they would investigate selected properties. This would be necessary in order for the researcher to gain the necessary information (East, West, North, South and Central). For the sake of classification and selection for the study, it's probable that he would also classify the residences into groups according to the quantity of rooms that are in each one. This will ensure that the findings are true representations of the whole city.

2) Controlled: The concept of control suggests that, in order to investigate the possibility of a causal link existing between two variables (factors), you should design the experiment in such a manner as to reduce the influence of any other factors that may be relevant to the investigation. This is because the idea of control suggests that in order to investigate the possibility of a causal link existing between two variables (factors), you should design the experiment in such a manner as to investigate the There are some variables that are taken into consideration to be controlling factors, and there are also other

variables that may be taken into consideration to be the likely repercussions of controlling factors.

Experiments that take place in a controlled environment, like a laboratory, such as those in the pure sciences like chemistry, can be managed; however, no study that tackles social issues can be managed. Studies of locations, for instance, are unable to be controlled because they take into account aspects such as location, climate, accessibility, seasonality, and other such aspects. On the other hand, research into the impact of standard operating procedures in a hotel applied to a particular service can be controlled.

3) Comprehensive: Using utmost care is required in order to ensure that the approaches used to discover answers to questions are appropriate, germane, and reasonable. This may be accomplished by being thorough. Once again, the degree of rigour varies greatly between the physical sciences and the social sciences, as well as across the several subfields that fall under the umbrella of the social sciences.

4) The empirical method requires that the techniques that are used be evaluated to ensure that they are accurate, and the progression from one step to the next must be logically consistent. This indicates that any conclusions drawn are based upon solid evidence gained from information that was gathered through experiences or observations that were carried out in real life. Specifically, this indicates that the information was gathered through experiences or observations that were carried out in real life.

When it is indicated that a piece of study contains an empirical component, this indicates that it was carried out in line with rigorous scientific procedures and processes. It is much simpler to demonstrate that a piece of study is legitimate from a scientific perspective if it is quantitative rather than qualitative. When doing qualitative research, it is quite simple to let one's own prejudices and biases get in the way.

5) Methodical: The plan or procedure that is being developed in order to carry out an inquiry has to be thoroughly planned in order to ensure that the utilization of the available resources is maximized. The expected outcomes will never be achieved by following procedures that are either random or poorly designed. In order to achieve the desired outcome, it is necessary to carry out the acts in the sequence that makes

the most logical sense. As an example, the meal cannot begin with dessert being served first at a restaurant that is appropriate for a five-star hotel. Instead, it has to start with either the appetizer or the soup course, whichever comes first.

6) Reliability: The degree to which one may depend on the results of a measurement, calculation, or specification to be accurate is referred to as the reliability of the results. One may describe this in terms of a percentage.

Despite the fact that it might be difficult to measure anything accurately, there is presently machinery that can assess the reliability of a research.

The results of several iterations of an experiment, test, measurement method, study, research equipment, instrument, or methodology need to be consistent with one another. The degree to which this is true is what is meant when we talk about repeatability. The reliability of a piece of research is measured by its ability to be replicated with the same group of participants, using the same procedures, and yet arriving at the same conclusions each time.

7) Validity and Verifiability: Validity is the degree to which an idea, conclusion, or measurement is well-founded and likely corresponds correctly to the real world. Verifiability is the degree to which an idea, conclusion, or measurement can be independently verified. The verifiability of an idea, conclusion, or measurement refers to the extent to which it is possible to test the concept, conclusion, or measurement. It is possible to trace the etymology of the word "valid" back to the Latin word validus, which may be translated as "strong." In no way can this be construed as implying that something is completely guaranteed or that there are conditions that cannot be avoided. The degree to which a measuring instrument (such as a test used in education, for example) really measures the item that it claims to measure is considered to be an indication of the tool's validity. The viability of an argument may be evaluated based on the significance that should be attached to different types of evidence. In the context of academic inquiry, the word "validity" relates to the extent to which it is possible for us to ascertain whether certain study findings, statements, or assumptions are true or false. The phrase "validation" refers to the

correctness of a measurement, regardless of whether or not it measures what it is intended to measure. Validation measures the accuracy of a measurement. In addition to this, it investigates the ways in which research might be used to the process of seeking answers to questions raised by a number of different scenarios. This gives a clear and focused direction for the work that is being put into the study. The findings of a study should be able to be independently confirmed, not only by the investigator who was responsible for carrying out the investigation, but also by any other individual who is interested in carrying out a similar investigation using the same procedures and in conditions that are comparable to those that were utilized in the initial investigation.

8) Incorporates a Hypothesis: The creation of a hypothesis ought to always act as the first phase of any research endeavour. On the basis of the little evidence that is currently available, a hypothesis or an explanation is formed as a starting point for future research. This hypothesis or explanation is a guess or a recommended explanation. An educated prediction regarding the relationship between two or more variables is an example of what is meant by the meaning of the term "hypothesis." This definition accurately conveys the core meaning of the term "hypothesis." To put this another way, a hypothesis is a theory or idea on which one starts to build their work before the idea is really put into practice via research. It is a question that serves as the basis, which is then referred to as the hypothesis; this hypothesis may or may not draw a logical conclusion. The question that serves as the foundation is called the hypothesis. When the research is done, the hypothesis can be proved to be wrong, flawed, or unjustified since it was not established on any evidence.

One possible definition for the term "hypothesis" is "an educated and well-informed guess or explanation for a particular issue." As part of the research process, the hypothesis needs to be put to the test. After that, the results of the tests have to be analyzed in connection to the hypothesis and the reality in which you find yourself. When a researcher formulates a hypothesis, they are, in effect, drawing out a road map for themselves to follow over the course of the research endeavour. It provides the researcher with information regarding the

factors that are significant to investigate, as well as how those factors may be related to one another or how they may be caused by a manipulation that is introduced by the researcher. In addition, it provides information regarding how those factors may be caused by a manipulation that is introduced by the researcher (such as a programme, treatment, or change in the environment). By using this map as a tool to assist in understanding the data that the researcher has gathered, the researcher will be able to arrive at sound conclusions on the results of the study.

9) Analytical and accurate: The focus of a research project should not only be on what is happening, but also on how and why a certain event or process draws specific conclusions. This should not be confused with just "what is happening." If any of the data collected is worthless, either because it does not offer the intended conclusions or because it cannot be used in later research or applications, then the purpose of the study will be rendered moot and the study would have been a failure. As a consequence of this, the data that is acquired has to be precise while also being acceptable in order for it to be straightforward to analyze.

The degree to which the myriad of research procedures, equipment, and tools are related to one another is another aspect of accuracy. Accuracy also takes into account whether or not the research instruments and processes were selected in the most optimal way possible and whether or not they are appropriate for the research topic. Accuracy also takes into account whether or not the research topic is appropriate for the research instruments and processes.

It is very essential to the accomplishment of a research endeavour that the appropriate tools for data collection be chosen.

In contrast to being asked to provide feedback verbally, requesting written feedback from customers, such as with a Guest Comments Card in hotels or a Feedback Collection Card in dining establishments, provides customers with the opportunity to provide candid feedback regarding the quality of the services they received. This feedback can be used to make improvements to the customer experience.

10) Credibility: This is the tenth and last criterion, and it relates to the degree to which a study's results may be viewed as being trustworthy. Credibility measures how much a study's findings can be trusted. Research conducted using the most trustworthy methods and with the most trustworthy sources of information is the only way to provide a 100% assurance of this result. The reliability of research that is predicated on secondary data is severely compromised due to the fact that the data may have been manipulated or skewed by earlier researchers in order to conform to the findings of those researchers. As a direct consequence of this, research based on secondary data is not trustworthy. These documents could have been misplaced or erased totally. It is not difficult to collect secondary data by relying on information published in public domains; but, doing so brings with it a large element of risk. Studies that are carried out on the basis of primary data are always more credible and trustworthy than studies that are based on secondary data. This is because primary data are collected directly from the source of interest. It is feasible to use some secondary data in the event that the main source cannot be accessible; nevertheless, it is not prudent to base an inquiry solely on secondary data when it is viable to acquire primary data. Because of this, the research's credibility is diminished. If the researcher uses genuine references in the research, then the credibility of the study will increase. On the other side, the credibility of the study will decrease if fraudulent references are used in the research.

11) It is important to do an in-depth and critical analysis of the procedures and methods that were used in the course of a research inquiry. The process that will be used to carry out the study has to be entirely trustworthy and free of any possible issues that might arise. The approach that was decided to take and the actions that were taken needed to be able to withstand careful inspection in order to be successful.

Standards for Acceptable Research

Every day, fresh information is gained in a variety of academic subjects, and the fruition of fruitful academic research is the source of all of this new information. According to the National Science

Foundation, the amount of research conducted worldwide in only the fields of science and engineering has increased at an annual pace of around 4 percent over the last decade. Each year, there are more scientific and technical conference papers and journal articles that have been published thanks to the quality of the research that is being conducted.

The process of doing research for an academic paper entails more than merely deciding on a subject, gathering data, and interpreting it. Research has to fulfil a number of prerequisites before it can be deemed credible. By providing a list of the requirements for such research, the purpose of this article is to provide a response to the question "What are the features of excellent research?" It is my hope that this advice would be of use to researchers in ensuring the quality of their work.

Research has become an important tool for us to use in our efforts to better understand the state of affairs in the globe. It is predicated on the belief that the universe is a cosmic system, the events of which are governed by forces and interactions that can be articulated in the form of rules and fundamentals, and that these systems can be described as having causes. The implicit belief that the universe is a cosmic system is what underpins the Big Bang theory. As a kind of a hunting licence, the knowledge that nature imposes these limitations on us gives us the green light to search for strategies that will allow us to exercise control over our environment.

However, the research methods that are now available to us are not nearly as good as they might be. In the course of humanity's drawn-out march toward civilisation, it has taken it thus long to uncover only three key means for getting closer to the truth: authority, logic, and controlled observation. These approaches are as follows: Up until around 300 years ago, the majority of investigations into uncovering the truth focused significantly on the application of reason and showing respect to those in authority positions. Since that time, academics have placed a greater emphasis on carefully controlled observation that is supported by the reasoning of mathematics.

However, many of the natural phenomena that we are interested in examining do not lend themselves readily to any combination of the

three research methodologies that are currently being used. This is something that we are working to address. There are certain aspects of the reality for which there is no authority anywhere in the world, just inadequate methods of mathematical reasoning, and no procedures of controlled observation that are known to exist. It is true that the growth of research procedures and their subsequent refinement are gradually widening the field of inquiry. This is due to the fact that both of these processes are occurring simultaneously. On the other hand, the closer we get to exposing some part of the truth, the more broad the realm of the unknown seems to become. This is because the truth is not static. Due to the limitations discussed above, research very rarely enlightens us with all there is to know about a subject. The revelation of anything that initially appears to be the truth about the nature of some aspect of the process of learning almost always reveals itself to be merely a rough approximation of the reality at a later point in time. This is because the nature of the learning process is inherently unpredictable. When a new instructional method is established, it usually always turns out, after more research, that although it first seems to have universal application, in reality, it only has limited utility. This is the case despite the fact that it initially seems to have universal applicability. Because of this, it seems more advisable to interpret the findings of the research as a method of approaching the truth rather than as a means of revealing the absolute truth. This is because there is no such thing as an absolute truth.

When compared to the results of other studies, the quality of a particular piece of research will be able to assess how closely its findings fit the reality. Due to the fact that the quality of research efforts might vary quite a bit, a problem of major significance is the question of how much trust can be placed in the appropriate manner in the findings of a particular study. The primary purpose of this essay is to present a handful of criteria that are founded in common sense and have the potential to assist practical schoolmen in distinguishing between research that deserves a fair amount of faith and research whose conclusions should only be accepted with misgivings. This will be accomplished by comparing and contrasting the two types of research.

1) A research problem that is clearly defined: It is essential that the purpose of the study, in addition to the nature of the problem that is being investigated, be specified in as few words as possible while still maintaining as much clarity as is practically possible. This is one of the most important aspects of the research problem.

You should include an analysis of the problem into its most basic components, as well as its scope and constraints, as well as full descriptions of the meanings of all terminology that are necessary to the study, in the description of the research issue that you will be doing. If the researcher does not accomplish this in a suitable manner, there is a possibility that the readers will have valid reasons to question whether or not the researcher has a sufficient comprehension of the issue to devise an effective strategy for addressing it. In other words, if the researcher does not accomplish this in a suitable manner, the readers will have valid reasons to question whether or not the researcher has a sufficient comprehension of the issue

In order for the results of the study to be reproduced by another researcher, the methods for carrying out the research should be described in as much detail as possible.

2) A keen eye for detail: Research reports ought to describe the sources of data and the methods that were used to gather them in a manner that is honest and open, with the exception of circumstances in which secrecy is required to protect the national interest. In such circumstances, the information should be withheld. Due to the omission of essential methodological components, it is either difficult or impossible to assess the authenticity and trustworthiness of the data, which, in turn, damages the reader's confidence in the research for reasons that are completely acceptable.

3) A thoroughly designed research design is required in order to give results that are as objective as is humanly possible. The methodological framework for the study has to be properly constructed in order to accomplish this.

When there is a requirement to collect a sample from a population, the report should include information related to the degree to which the sample is representative of the population. In other words, it should show how closely the sample matches the characteristics of

the population. When there is more trustworthy material available, either from documentary sources or from direct observation, using a questionnaire as a research tool is not the proper choice. It is necessary for bibliographic searches to be conducted in the most thorough and comprehensive way that is technically possible. In experiments, controls have to be designed such that they are appropriate for the task at hand. After the event in issue, direct observations need to be put into writing as soon as it is humanly possible to do so. When selecting and recording data, there should be attempts made to mitigate the impact of personal bias to the greatest extent feasible.

4) Report any and all flaws in the research: The researcher is obligated to explain any faults with the methodological design in an honest and straightforward way, as well as analyse the influence such flaws have on the outcomes of the study.

There aren't very many methods of doing research that are completely foolproof. There is a potential that some of the defects may not considerably damage the validity and trustworthiness of the data, but others may make the data utterly untrustworthy. It is possible that some of the problems may not significantly influence the authenticity and trustworthiness of the data. An experienced researcher should be vigilant to the consequences of flawed design, and the researcher's competence in interpreting the data should provide him with a basis for appraising the relevance of these effects. [Case in point:] [Case in point:] [Case in point:] [Case in point:] [

5) An analysis of the data that is sufficiently competent: The study of the data has to be comprehensive enough to demonstrate the importance of the information, and the methods of analysis that are used need to be appropriate.

The amount of success that was obtained in achieving these criteria is often a reliable measure of the level of expertise held by the researcher. [Case in point:] [Case in point:] The author, who has over twenty years of experience supervising the research projects of graduate students, has arrived at the conclusion that the most challenging aspect of research for a novice researcher is the appropriate analysis of the data. This conclusion was reached after the author had come to the conclusion that the most challenging aspect of research for

a novice researcher was the proper analysis of the data. It is essential to do exhaustive tests to ensure that the data are of a high quality and can be relied upon. It is essential that the data be organised in a fashion that makes it simpler for the researcher to come at conclusions that are pertinent to the topic at hand. When making use of statistical methods, it is essential to take into account the possibility of making a mistake and to apply the standards for deciding whether or not a result is statistically significant.

6) Limiting Your Conclusions: It is important to limit one's conclusions to only those that are adequately supported by the findings of the study and to only those for which the data provide a sufficient foundation. It is also important to limit one's conclusions to only those that are adequately supported by the findings of the study.

Researchers are often tempted to incorporate personal experiences that were not subject to the circumstances under which the study data were gathered in order to expand the bases of inductions. This is done in an effort to extend the bases of inductions. This has the effect of making the research less objective, which in turn reduces the amount of faith that can be put in the findings. Equally unfavourable is the all-too-common practise of drawing conclusions from research carried out on a small sample and then extending those findings to the wider community as a whole. This is a practise that has a negative impact on both the community and the researchers. Researchers who are knowledgeable have pointed out in detail the conditions that must be met for their findings to be considered credible. In the event that this is not carried out, there is a fair foundation for a reduced level of confidence in the results.

If the researcher is well-established in the field and has a sterling reputation for honesty and fair play, then the results of the study will naturally carry more weight. If, in other words, the researcher is honest.

7) An experienced researcher is a plus: This criterion would possibly be one of the best bases for judging the degree of confidence a piece of research warrants if it were possible for the reader of a research report to obtain sufficient information about the researcher. This criterion would be a plus if it were possible for the reader of a research report to obtain sufficient information about the researcher. To put it another way,

whether the reader was able to get an adequate amount of knowledge about the researcher. As a result of this, the research report has to be accompanied with considerably further information about the qualifications of the researcher than is often the case.

Research Done in Universities

Every day, new knowledge is obtained in a wide range of academic fields, and the culmination of successful academic research is the source of all of this latest information. The National Science Foundation estimates that during the last decade, the quantity of research carried out in only the domains of science and engineering throughout the globe has expanded at an annual rate of around 4 percent. Because of the high quality of the research that is being carried out, there are ever more journal articles and conference papers in the fields of science and technology that are being published each year.

The process of doing research for an academic paper requires more steps than just settling on a topic, amassing relevant data, and providing an analysis of that material. Before a body of research can be considered reliable, it must first satisfy a number of necessary conditions. The objective of this article is to offer a solution to the question "What are the characteristics of good research?" by presenting a list of the needs for such study. It is my sincere wish that the researchers would find the following recommendations helpful in improving the quality of their work.

Characteristics of Reliable Research

1. A solid research subject is essential for doing successful research since it serves as the basis for the following:

Developing a research topic that is not only relevant to the problem at hand but also intriguing is one of the most important steps in doing productive research. In their work that was released in 2010, Farrugia and co-authors claimed that the process of developing a research subject is the phase that is the most important in the process of carrying out a research project.

An outstanding research question outlines, in excruciatingly minute particulars, just what it is that the researcher hopes to learn

about the topic at hand and defines the limits of the investigation's purview. Those doing research have the ability to ensure that they stay on track for the whole of their project by formulating a robust research question from the very beginning of their work. The research question, in the great majority of cases, has some type of effect onto the remaining acts that a researcher takes while performing their study in order to gather data for their investigation. On the other hand, developing a framework for a study issue is often more easier in principle than it is in practise. Because of this, several models like the FINER and PICO criteria have been established to guide researchers through the process of generating legitimate research questions. These models were developed as a consequence of the fact that researchers needed assistance in developing valid research questions. According to the criteria list, an effective research topic should include the following characteristics:

The letter "F" stands for "feasible."
The letter "I" stands for "interesting."
"Innovative" is what the letter "N" stands for.
The letter "E" stands for "ethical."
The letter "R" stands for "relevant."

2. Reliable research is always conducted in accordance with a planned and approved research methodology:

One of the most significant aspects that determines not only the overall quality of a study but also the degree of success it achieves is the methodology of research that was conducted for the study. The selection of a reliable research methodology is one of the most important steps in ensuring that researchers will be able to successfully collect relevant data and carry out the appropriate processes for data analysis.

The phrase "research methodology" refers to the systematic procedures or tactics that a researcher uses in order to ensure that his study provides accurate and trustworthy conclusions. This word was coined by the American Sociological Association (ASA). When classifying research methodologies, the most popular categories that

are utilized are quantitative research, qualitative research, and mixed-methods research.

The methodology known as qualitative research involves the collecting and examination of non-numerical data, such as language, with the goal of gaining insight into the beliefs, experiences, and behaviours of the people who are taking part in the study. The term "qualitative research methodology" refers to a range of approaches, some examples of which include interviews, focus groups, and case studies.

Quantitative research methods focus on uncovering patterns, investigating relationships, and developing hypotheses via the collection and analysis of numerical data. At the core of these methods is the collection and evaluation of numerical data. When conducting out quantitative research, some of the techniques that are available to choose from for the purpose of data collecting include surveys, experiments, and systematic observation.

Methodologies that combine qualitative and quantitative techniques are known as mixed methods. Mixed methods are used in research. Combining qualitative and quantitative research methods "permits a more thorough and synergistic exploitation of data than do separate quantitative and qualitative data collecting and analysis." This statement was made in reference to the fact that the combined method "permits a more thorough and synergistic exploitation of data."

Researchers need to take a number of different variables into account in order to pick the research technique that is the most suited for the topic that they are working on. The questions and objectives of the study, in the vast majority of cases, have a significant bearing on the choice of the research approach that will prove to be the most fruitful. In addition, it is essential for researchers to take into account the methods that are currently being used by other researchers in their specific field of study. For instance, recent study has shown that mixed-method research is gaining popularity in the area of health sciences. [Citation needed] [Citation needed] [Further citation is required] In their 2019 article titled "Mixed methods and survey research in family medicine and community health," which was published in the journal Family Medicine and Community Health,

Cresswell and Hirose observed how surveys were used in combination with focus groups on resident physicians' communication and collaboration competencies. The article was titled "Mixed methods and survey research in family medicine and community health." Therefore, in order to assess the competence of the IP physicians to offer feedback to paediatric residents while they were completing their rotation, the authors of the study by Sonnenberg et al. used an explanatory sequential mixed methods design. In the first part of this investigation, the researchers compared the communication styles of IP supervisors and physician supervisors. They also used survey research to determine whether or not the collaborative training objectives had been achieved.... After finishing the first phase of their study, the researchers went on to the second part of their project, which consisted of conducting follow-up qualitative focus groups in order to get a deeper contextual understanding of the factors that influenced the process of assessment.

3. Good research takes into account previous investigations that have been carried out on the topic in question:

To do excellent research, one must, in addition to leading to the collection of fresh material, become acquainted with the work that others have done on the same topic. When you read academic publications and other works that are connected to the topic that interests you, you may gain a sense of what previous research has been done on the topic and how your own research fits in with the findings of the previous research. This can help you determine how your own research fits in with the findings of the previous research. Investigating the results of studies that were conducted in the past may also be a useful way to ensure that you are not duplicating work that has previously been completed. The corpus of literature that is relevant to the topic at hand may also provide information about potential obstacles and difficulties that researchers could face in the course of their inquiries.

The majority of academic research projects, such as theses and dissertations, contain a literature review because of how vital it is to analyse research that is relevant to the topic that is being investigated.

This is the case because of how crucial it is to evaluate previous research. The aim of a literature review is to provide readers a full understanding of the topic at hand by describing and providing an unbiased evaluation of the academic papers, books, and other sources that are relevant to a certain field of study (Bloomsburg University of Pennsylvania, n.d.). According to the most recent version of The STM Report, which is an annual publication put out by the International Association of Scientific, Technical, and Medical Publishers, there were approximately 33,100 active academic peer-reviewed English-language journals as of the middle of 2018. This information was gleaned from the publication. The yearly article output of these publications is close to three million, and the annual growth rate of their circulation is around four percent (Johnson et al., 2018). It is quite improbable, in light of these figures, that researchers will have difficulty discovering published material that is pertinent to the topic of their investigation.

4. Reliable research makes use of data that is relevant and factual in addition to proper procedures for data analysis:

One of the most important characteristics to look for in a research study is whether or not it deals with empirical data, since this is a hint that the study is of high quality. Information that was obtained by the researchers themselves by techniques such as observation, experience, or experimentation is an example of the kind of data that is referred to be empirical (Bradford, 2017). This is an incredibly crucial component of doing high-quality research since empirical data is often seen as being proof that is both objective and unbiased.

The gathering of empirical data is just the first step in doing quality research; in order to produce findings that are of any value, the data collected first need to be processed in the proper manner. The kind of data that was collected is the primary factor that decides which method of data analysis should be used to the information. When analysing quantitative data, for instance, one of two types of statistics—descriptive statistics or inferential statistics—is often used (Humans of Data, 2018). Researchers may develop figures with the use of these statistics that summarise variables, find patterns, and make

predictions using the data. On the other side, the analysis of qualitative data comprises discovering patterns and themes within the textual data and offering an interpretation of those results. This is done in conjunction with presenting a summary of the findings. When dealing with qualitative data, it is common practise to use several forms of analysis, including content analysis, narrative analysis, and theme analysis (Warren, 2020)

In order to offer a response to the question raised by your research project, you may put these methods of analysis to work in order to examine either quantitative or qualitative data.

5. Reliable research should not only be able to be generalized but should also be reflective of the whole:

One of the factors for determining whether or not research is of high quality is whether or not it is representative. The potential of a sample to act as a stand-in for a larger population is what is meant by "representativeness" when used in the context of scientific investigation. This suggests that the characteristics of the individuals who are being investigated (the subjects) closely match those of the population that the research seeks to analyze.

Utilizing population sampling is, in the vast majority of cases, the most effective method for ensuring representativeness in research (Economic Research and Social Council, n.d.). Researchers have the ability to guarantee that their findings can be extrapolated to the larger population represented by the sample they establish if they use appropriate methodologies to create a representative sample. This allows the researchers to guarantee that their findings can be extrapolated to the larger population.

6. Good research is guided by sound reasoning, which acts as a compass:

One of the distinguishing characteristics that sets this endeavour aside from others is the use of logic across the board during the whole of the research procedure. For instance, utilizing logic may help researchers define what kind of data they require in order to answer the question that they are exploring for their study. This is something that

they are doing for their investigation. When researchers are guided by logic throughout the whole course of the study, it significantly improves their capacity to identify logical fallacies and inconsistencies in the claims and conclusions they draw from the data.

In addition to their possible applications, the logical processes of induction and deduction may also be of significant benefit in the process of doing research. Logic is beneficial to researchers since it makes it easier for them to draw believable conclusions from their findings. According to the results of the study, inductive reasoning may be used in the process of developing generalizations and hypotheses, as well as in the search for patterns that emerge from the data. In the meanwhile, the application of deductive reasoning may be of assistance to researchers in the process of gathering empirical information, which may subsequently be used to support or reject hypotheses or concepts.

In addition to these applications of logic, logical thinking may also make subsequent research more understandable. This is of utmost importance when the study is going to be used in the context of decision-making, which is why it is so crucial (Mehran University of Engineering and Technology, n.d.).

7. A good research project should be relevant to the larger world:

It is said that a piece of research has what's known as "external validity" if it can have its findings or conclusions put into practice in the real world (Glen, 2015). If the findings of your study can be generalized to apply to a wider range of circumstances or extrapolated to cover a broader range of circumstances, then your research is said to have high external validity.

When determining the extent to which their work has external validity, researchers need to take into account both the demographic validity and the ecological validity of their findings (Bhandari, 2021b). If the findings of a piece of study can be generalized from the sample to the larger population, then the population validity of that research is considered to be strong. In the meanwhile, you may achieve ecological validity if you are able to link the findings of your study to situations and environments that exist in the real world. This will demonstrate that your findings are applicable to the real world. Since acquiring

knowledge that can be used in a variety of settings is almost always the purpose of scientific research, ensuring that one's findings have external validity is a vital component of doing high-quality research.

8. Quality research should be able to be reproduced and should be subject to close examination:

Reproducibility, transparency, and the ability to be duplicated are three of the characteristics of research that are considered to be among the most important. The replicability of a research study determines whether or not the findings of that study can be independently verified by other researchers. This is one of the most important aspects of a research project. The ability of the findings of a study to be replicated by other researchers is one factor that might contribute to the study's credibility with the general public (Understanding Health Research, 2020).

Another defining characteristic of high-quality research is its ability to be reproduced. Although the terms "replicability" and "reproducibility" are sometimes used interchangeably, a piece of research can only be considered repeatable if the researchers who carried it out were able to arrive at the same conclusions each time they used the same data and analytical procedures. This is the only criterion that determines whether or not a study is repeatable. The ability of a research study to be reproduced and repeated, in addition to the study's results, may give proof of the study's general validity and trustworthiness.

Either the study has to be completely open and honest with its methods and findings, or it needs to be made readily available to other scientists so that it may be replicated. When research is written up or presented, it has to be done so in a way that provides comprehensive information on how the data was gathered and analyzed, as well as how the findings were formed (Baskin, 2015). As a result of this, the vast majority of scientific articles include in-depth descriptions of the research process to which they are relevant.

Different Kinds of Research

When conducting studies, researchers have access to a wide variety of methods, which are collectively referred to as "types of study." According on the goals, schedules, and motivations behind the study that is being carried out, several methods of research are more suited for certain types of investigations than others. The first thing that has to be done when planning research is determining what you want to look into and what you want to learn from it. You might, for instance, just be interested in acquiring additional information about a subject, or you might be interested in attempting to understand how a new policy would impact lower-level workers at your organization. Either way, there are a few reasons why you might have an interest in either of these things.

There are many industries and types of enterprises that might benefit from the use of various types of research studies, including the following:

- The academic fields that are associated with the scientific method, including chemistry, biology, and others
- Branches and departments of the state that are administered by the state
- For reasons pertaining to education
- Business necessity

The following is a list of 19 different types of research that you should consider when establishing your research methodology:

1) Qualitative investigation:

In qualitative research, nonnumerical data like opinions and books are employed instead of numerical data. Qualitative data examples include:

- Conversations in small groups
- Surveys
- Commentary from those who took part
- Observations
- Interviews

It is common practise for companies to do qualitative research to learn the opinions and reactions of customers. To receive feedback on a new advertisement before it is released to the general public, a marketing organisation, for instance, would first show it to a focus group. In order to make decisions, the company gathers information that is not quantifiable, such as the perspectives of people who participate in focus groups.

2) Quantitative investigation:

In quantitative research, examples of numerical data such as statistics and measures include things like measurements and statistics. For example, a car manufacturer may look at the number of red cars sold in comparison to the number of white sedans sold. The research derives results based on actual data (sales figures for red and white autos) (sales numbers for red and white automobiles).

3) Fundamental Research:

The purpose of fundamental research, often referred to as basic research, is to aid academics in gaining a greater understanding of certain occurrences that occur in the world; this kind of study investigates how things function. Your understanding of scientific concepts and explanations will perhaps improve as a result of participating in this research. For the purpose of doing fundamental research, a corporation may, for instance, investigate the impact that varying product placements have on product sales. This study is knowledge-based and provides data at the same time.

4) Research that can be put to use:

The purpose of applied research is to find solutions to existing problems or give responses to existing worries. The purpose of the research is to produce knowledge that can be put to use that is both relevant and pertinent. For instance, a study on how to increase the amount of student engagement in the classroom may be an example of applied research. This research looks at potential solutions to a particular problem, as well as the issue itself.

Both basic and applied research are considered to be the two primary types of research. The nature of most research may be

categorised as either fundamental or applied, according on the questions it seeks to answer.

5) Longitudinal studies:

A longitudinal research follows the same group of people through time but makes no adjustments to any of the other variables. For instance, a researcher may explore whether or if and how the level of satisfaction experienced by employees who have been employed by the same company for one, three, and five years changes over time.

6) A study using a cross-sectional design:

A cross-sectional study is one that takes a snapshot of a population or sub-population at a specific point in time. Researchers often choose participants based on shared characteristics like as age, gender, or wealth, and then analyse the similarities and differences that exist within each group as well as across the groups. A larger population is often represented by the group in discussions. Researchers investigate individuals in a manner similar to that of longitudinal research, in which factors are not altered.

For instance, a company may look at the sales tactics used by the top 10 percent of its salespeople and compare them to the tactics used by the worst 10 percent of its salespeople. This may be of assistance to the company in gaining knowledge regarding the sales strategies that are most effective and those that are least effective.

7) Research using a combination of methods:

Research that is mixed draws from both qualitative and quantitative sources for its findings. Take into consideration the OEM tracking sales of sedans. The company may also request that clients take out a survey after buying a red or white vehicle, in which they will be asked how much the colour impacted their decision as well as other open-ended questions.

Investigative research number eight:

When doing exploratory research, one considers not just what is already known about a topic but also what new information there may

be. It is more likely to give a general grasp of a subject as a springboard for additional research than to provide specific answers to queries that have been posed. Exploratory research is often conducted on subjects and phenomena that are not well recognised.

Take into consideration what is now known about the efficacy of maternity and paternity leave programmes that last for a whole year. For the sake of this research, it may be necessary to compile all relevant information and provide it in a format that was not previously available but is now. Your inquiry could turn up certain knowledge holes, which would make more investigation in the future necessary.

9) An inquiry on the field:

Research in the field is done "on site," which means it takes place wherever the participants or subjects are. For this kind of research, on-location observation and data collection are both required. For instance, a manufacturing business may hire an environmental engineering firm to evaluate the air quality inside the facility to ensure that it satisfies all of the standards for health and safety. In order to collect samples, the scientists would go to the factory.

10) An inquiry in the laboratory:

The controlled atmosphere of a laboratory is where research is carried out, as opposed to being carried out in the wild. A strict commitment to the established limits, such as the removal of variables or the criteria for scheduling, is often required for the study. Laboratory research might include things like conducting experiments in the pharmaceutical and chemical industries.

11) A comparative investigation:

A comparative research attempts to determine the degrees to which two individuals, subjects, or organizations share and differ from one another. When an owner, for instance, reviews the documents pertaining to new hire training, they might notice that new employees receive a significant portion of the same training both during orientation and their initial training with their respective departments.

To afford more time for department-specific training, the owner may chose to bundle all similar training into orientation papers.

12) The research of possible causes:

The objective of causal research, which is often referred to as explanatory study, is to establish relationships of cause and effect between different variables. The purpose of this research is to identify the degree to which one variable may impact another one. Research on causes is essential for evaluating existing processes and procedures, determining whether or not changes should be made, and determining how those changes should be implemented.

For instance, a company could compare employee retention rates before and after implementing a work-from-home policy after the first six months of employment in order to determine whether or not the policy improves employee retention. This comparison would take place after the company had offered employees the opportunity to work from home.

13) Investigative method known as induction:

The objective of inductive research, often referred to as theory-building research, is to collect data that may be used as a contributing factor in the formulation of a new hypothesis on a certain process or event. This kind of research examines data and trends, then puts up a variety of hypotheses to explain the findings. The scope of an inductive investigation expands as it moves from the specific to the general.

Inductive research is often used in the process of theory generation, and it frequently results in the need for more study, such as deductive research, in order to investigate prospective concepts.

Researchers may discover, for instance, that the year 12 multinational companies introduced in-house carbon emissions controls, worldwide emissions declined. This may be a correlation that they find interesting. The researchers may postulate that if multinational corporations implement in-house emissions controls, worldwide emissions may be considerably cut.

The progression of inductive research is from the general to the specific, while the progression of deductive research is from the

general to the specific. Researchers first construct a hypothesis, then put that hypothesis to the test by conducting experiments or making observations.

Take, for instance, the example of global business emissions standards that was presented earlier. In order to test this theory in a manner that is consistent with logic, one should do research that compares the levels of global emissions both before and after the implementation of emissions limitations by multinational firms.

14) The inquiry will be fixed:

Fixed research comprises experiment methods that are defined in advance, such as how often testing will occur, where testing will place, how many persons will be tested, and the types of subjects that will be tested on. The study relies on specific circumstances and strict adherence to predetermined methods in order to reduce the amount of variation. Research that is fixed in its nature is typically more reliable and reproducible than research that is flexible.

The term "experiment" is frequently used interchangeably with "fixed research." A researcher, for instance, might investigate the impact that altering labels has on the opinions that consumers have regarding a particular brand of sports drink. Aside from the label, the researcher has to make an effort to control any and all other elements that could have an impact on how the participants evaluate the beverage. At the same time, participants are given the same beverage but with a different label, and they are then tasked with filling out a questionnaire assessing the flavour as well as their overall thoughts. The validity of the research is heavily dependent on the timing of each beverage as well as the questionnaires that came after it.

15) Research That Is Adaptable:

During the course of a flexible research study, the procedures may be subject to change. There are many different kinds of flexible research, including the following:

Case studies are detailed examinations and observations of a single person, group of people, or issue. In the field of anthropology, ethnography refers to the practise of doing in-depth research and

observations on a certain population. Investigations based on the grounded theory aim to construct ideas by painstakingly gathering and analysing evidence from a variety of sources.

16) Research involving participants in active participation:

Action research is the process of investigating your actions, assessing their effectiveness in accomplishing the desired purpose, and deciding on a course of action based on your results based on the findings from your action research. Action research is often applied in educational settings to assist educators and administrators in conducting self-evaluations and making necessary adjustments to lesson plans.

For instance, a teacher may compile information on the methods they use to instruct fifth-grade mathematics. At the end of the first school quarter, the teacher could discover that only one-third of the students displayed competent performance in the topics they were studying. As a direct result of this, the instructor of the fifth-grade mathematics class implements new tactics during the second quarter of the school year.

17) An examination of the policy:

The purpose of policy research is to either investigate the effects of pre-existing policies enacted by the government or by social institutions, or to foresee the potential implications of new policies in terms of how they will affect the distribution of available resources. Researchers that focus on policy are often employed by government entities and do the following types of research:

- An evaluation of the costs and benefits
- Carry out an examination of the cost-benefit ratio.
- Evaluation of the programme
- Analysis of requirements
- Investigation into classification

In classification research, individual components of a group are isolated and placed into larger groups or subgroups based on their

shared characteristics. For instance, biologists investigate animals and classify them according to shared characteristics like the following:

- Segmentation of the body
- Habitat classification
- Methods and means of procreation
- Diet

18) A comparative investigation:

A comparative research attempts to determine the degrees to which two individuals, subjects, or organizations share and differ from one another. When an owner, for instance, reviews the documentation pertaining to new hire training, they could observe that new employees get a significant portion of the same training both during orientation and their first training with their respective departments. Consolidating all similar training into orientation papers may be a choice that the owner makes in order to free up more time for training that is specialized to certain departments.

19) The study of the causes:

The objective of causal research, which is often referred to as explanatory study, is to establish relationships of cause and effect between different variables. The purpose of this research is to identify the degree to which one variable may impact another one. Research on causes is essential for evaluating existing processes and procedures, determining whether or not changes should be made, and determining how those changes should be implemented.

For instance, a company could compare employee retention rates before and after implementing a work-from-home policy after the first six months of employment in order to determine whether or not the policy improves employee retention. This comparison would take place after the company had offered employees the opportunity to work from home.

20) Inductive investigation:

The objective of inductive research, often referred to as theory-building research, is to collect data that may be used as a contributing

factor in the formulation of a new hypothesis on a certain process or event. This kind of research examines data and trends, then puts up a variety of hypotheses to explain the findings. The scope of an inductive investigation expands as it moves from the specific to the general.

Inductive research is often used in the process of theory generation, and it frequently results in the need for more study, such as deductive research, in order to investigate prospective concepts.

Researchers may discover, for instance, that the year 12 multinational companies introduced in-house carbon emissions controls, worldwide emissions declined. This may be a correlation that they find interesting. The researchers may form the hypothesis that if multinational corporations implement emissions regulations inside their own facilities, there would be a significant drop in worldwide emissions.

The progression of inductive research is from the general to the specific, while the progression of deductive research is from the general to the specific. Researchers first construct a hypothesis, then put that hypothesis to the test by conducting experiments or making observations.

Take, for instance, the example of global business emissions standards that was presented earlier. In order to test this theory in a manner that is consistent with logic, one should do research that compares the levels of global emissions both before and after the implementation of emissions limitations by multinational firms.

UNIT 2

IDENTIFICATION OF RESEARCH PROBLEM

The exploration of scientific questions has several aims, two of the most important of which are broadening people's perspectives and shedding light on the truth. Participation in research, which leads to the development of theory, is an absolute need for academics if they are to realise this goal.

Both forecasting the future and comprehending it are essential components of theory, and the two tasks typically and always go hand in hand with one another. Predicting and understanding the future go hand in hand with one another. To be able to make a forecast, one must first know and comprehend why the variables act in the manner in which they do. Theories provide an explanation as to why the variables behave in a certain manner. A cohesive set of general assertions that are used as guiding principles in order to explain the apparent links of particular observable events is the definition of a theory. Theories may be found in many different fields of study. A theory is defined as a set of broad assumptions about a subject. The development of hypotheses and the subsequent testing and refinement of those hypotheses is carried out via a sequence of steps that make up the scientific method.

Concepts serve as the foundation for the method in which scientists approach their job as well as the way in which they think. Creating concepts is the first step that has to be taken for people to be able to think about and express abstract thoughts. In order to provide specialised explanations of occurrences that cannot be directly seen, the scientific community makes use of ideas that are on a higher level. On the level of the conceptual and the construct, concepts and constructs are employed, whilst on the level of the empirical, variables are utilised. In the course of carrying out research in a scientific field, a great number of hypotheses are developed and then put to the test via the use of inductive and deductive reasoning, in addition to reflective thinking. In the scientific community, research is conducted in

accordance with a methodical approach that conforms to a standardised procedure that integrates induction, deduction, observation, and the testing of hypotheses into a sequence of actions that include reflective thinking. The approach in question is often referred to as the scientific method.

Individuals have varied ways of assessing situations owing to the fact that they have diverse perspectives on the world and have been conditioned in various ways by the environment that affects them; as a direct consequence of this, the kinds of questions that people ask also vary. Investigating potential solutions to issues via the use of scientific methodology is one possible approach to issue resolution. It will be to the benefit of the researchers to have a better understanding of the link between scientific research and research in general when they are developing the study.

SCIENTIFIC METHOD

There is a possibility that throughout the course of time, the definition of "science" will grow increasingly explicit. It makes an effort to describe the circumstance in a manner that is true to life, which it successfully achieves. In the end, it is a strategy for the generation of new knowledge, and this strategy may take the form of an organisation or a system. But ultimately, it is a strategy. The scientific method is one of the many things that have been generated as a result of the system.

The vast majority of people are aware that science may be segmented into two separate subfields, which are known as hard science and soft science respectively. Hard science encompasses both biological and physical sciences (human science). The questions that are asked by science play a substantial part in figuring out the approaches and methods that are used to scholarly inquiry, as well as the tools and resources that are made use of. In the world of academia, one of the most common strategies for achieving the objective of achieving new levels of knowledge is to use what is known as a scientific approach. Research conducted in the area of business is considered to be scientific since it adopts a method that is objective when evaluating the processes and linkages that are inherent to the

world of business. Included in this section is research conducted on a wide range of topics, including those pertaining to education, information and communication technology, and others.

To arrive at generalisations that can be believed and that are backed by data, as well as to establish the relationships that exist between the various variables, are the major aims of the scientific method. When scientists have a complete understanding of the relationships between phenomena, they will be able to comprehend a phenomenon in terms of the patterns of connections, they will be able to make predictions about the phenomenon, and they will be able to discover the causal linkages that exist between the phenomena. When scientists have a complete understanding of the relationships between phenomena, they will be able to comprehend a phenomenon in terms of the patterns of connections. The scientific method is absolutely necessary for reliable scientific practise, and reliable scientific practise may be recognised by searching for the following characteristics in the practise:

(a) It is empirical, which means that its validity is determined by how closely it corresponds to the world as it really exists;
(b) it is repeatable or objective, which shows that the perspective of the researcher is independent of the findings and that other researchers who did the study would obtain the same results;
(c) it is analytical, which means that it dissects and explains empirical data in accordance with the procedure outlined by the scientific method;
(d) it is theory driven, which means that it is based on a body of knowledge that has already been established; and
(e) it makes sense, which suggests that it is necessary to underline the fact that the degree of control over confounding factors is what differentiates rigorous research from other types of scientific inquiry that are not as rigorous. For instance, in the world of business, there are a great deal of circumstances that are outside the control of managers. As a consequence of this, there is a need for some kind of middle ground to be found between the strict criteria of science and the practical issues of running a business in the real world. It is required for

there to be some kind of agreement established that fulfils both the interests of people involved in business and the wants of those engaged in research. This is because it is necessary for there to be some kind of agreement created.

Even if this will result in errors, the research should still proceed with the creation of the information as long as the researcher advises the decisionmaker of the constraints, and the results are qualified based on how the restrictions were dealt with. Even if this will result in mistakes, the research should still proceed with the creation of the information. An excellent scientific investigation will also adhere to the concept of parsimony, which states that it is preferable to find a solution that does not involve an excessive amount of complexity. This concept asserts that it is better to discover a solution that does not involve an excessive amount of complexity. When doing research, it is essential to keep an understanding that is as basic as is reasonably feasible while simultaneously ensuring that any questions that are raised may be answered in a way that is to the researcher's satisfaction.

TRADITIONAL SOURCES OF KNOWLEDGE

The acquisition of new information and the expansion of one's existing knowledge are two goals that may be achieved by using any one of a myriad of different approaches and procedures. The knowledge that is gained through traditional sources is not obtained by scientific techniques; as a result, it is likely that this information is erroneous. The following is a list of typical examples of places where one may get information:

a) Relying Too Heavily on One's Sense Perceptions

It is feasible to acquire information and knowledge by depending on what is publicly known and what is consistent logically. [Citation needed] [Citation needed] This is one possible approach. Even while having common sense may be helpful in day-to-day life, if it isn't put to good use, it might leave one's thinking open to logical fallacies. This is especially true if common sense isn't analysed critically. As a consequence of the fact that these ideas are employed at various periods, many people may not be aware of the fact that common sense

includes views that are in direct contrast to one another. This is because these ideas are utilised at different times. One of the places where common sense may be found is in tradition; this kind of information may be useful, and it may even be genuine, but it also may include mistakes, disinformation, and contradictions. It is quite likely that the prejudice originates not just from thinking but also from disparities in society and culture. Recognizing the reality that one is lacking in particular areas of common sense knowledge is one way to reduce the likelihood of making judgments that aren't in one's best interests. This is accomplished by the use of the phrase "acknowledging one's lack of common sense knowledge."

In order to close this information gap, one must first generate the appropriate sort of information, and then one must rigorously assess knowledge that is considered to be common sense in order to identify the root cause of the problem. Both the establishment of experiments for the purpose of conducting systematic testing and the ongoing collection of data in order to investigate the recurrence of an event are viable options for determining the underlying factor (or factors) that are responsible for a phenomenon. Continuing to collect data in order to investigate the recurrence of an event is an important step in the process of determining the underlying factor (or factors) that are responsible for Systematic testing may be carried out by monitoring the outcomes of several repetitions of the event and recording the findings. As a direct and immediate result of this, recent developments in scientific knowledge are integrated into scientific

In the context of the scientific community, what traits are necessary for valid research?

In this part of the self-test, rather than depending just on one's own common sense, the need of doing research is emphasised. The gathering of the right sort of information could be accomplished by conducting an investigation that is extensive and meticulous.

(b) Personal Experience

When something happens to you, you not only have the opportunity to feel it, but you also have the chance to experience it, and in the end, you come to the realisation that it is true. When something

happens to you, you have the opportunity to feel it, experience it, and come to the conclusion that it is true. The phrase "seeing is believing" relates to one of the most powerful sources of information, which is the individual's own firsthand experience. Direct experience is one of the most strong forms of knowledge. On the other side, a person's very own experiences have the potential to steer them in the wrong direction. What may seem to be true might, on closer inspection, be the result of a little lapse in judgement on the part of the individual or a warping of their point of view. The human species has a high propensity for error and is susceptible to being duped by many illusions. They may put their faith in what they see or experience, despite the fact that such data may be rife with inaccuracies, and this may be to their detriment. Even if they are aware of the danger of making such mistakes, it is possible for this to still occur. My own personal experiences have shown me how important it is to steer clear of making these four critical errors in judgement:

I When people come across evidence that backs up what they believe, they have a propensity to presume that this evidence can also be applied to a wide variety of other scenarios as well. This is because most people prefer to believe what they see rather than question it. Because people have little or no knowledge about a wide variety of other people, topics, and circumstances, it may seem fair to them to draw generalisations based on the information that they do have access to.

(ii) An example of selective observation is when individuals pay more attention to certain other individuals or events than they do to others in order to draw conclusions about a larger population or phenomenon. This is done in order to draw conclusions about the phenomenon. People are more sensitive to characteristics that support their beliefs; as a consequence, their attention is directed more intently to aspects of the reality that match to their preconceived concepts. People are more sensitive to qualities that support their views. [The chain of causation] People pay more attention to qualities that provide credence to the perspectives they hold.

(iii) Untimely closure: This error often occurs in combination with some of the other two flaws, and it serves to reinforce both of

those flaws. This mistake is one that should be avoided at any and all costs. When someone reaches the opinion that they have already learned all there is to learn about a topic and that it is no longer essential for them to listen, seek information, or ask questions on that topic, they have attained a premature closure. When someone have an erroneous sense that they have all the answers to a topic, it's possible for this to happen to them.

(iv) The halo effect is a phenomenon that may manifest itself in a wide variety of distinct ways. It is the tendency of people to make an excessive amount of conclusions based on what they believe to be particularly advantageous or prestigious, and it is referred to as the inference bias.

PHILOSOPHY OF SCIENTIFIC RESEARCH

The two major pillars that support the structure of the scientific method are logical reasoning and the careful observation of events that occur in the actual world. In order for a scientific explanation to be regarded genuine, it has to not only make sense (be logical), but also fit in with what we can see and experience. The reality that we see may be validated via the use of observation and the amassing of data through the collecting of measurements of what can be observed in the world. Both are crucial elements of the scientific method, each of which is connected to one of the three fundamental pillars that serve as the foundation for the scientific community:

On the basis of this provisional theory, it is feasible to draw further hypotheses and predictions with the intention of doing more study or testing. Continued investigation or testing will be carried out until the hypotheses and guidelines that were developed have been perfected to the extent that they can realise their full potential. At this point, any rules or ideas that have been honed to a more refined form are only educated assumptions. Adjustments will need to be made in the event that it is discovered that a new observation does not readily fit into an existing body of knowledge, or if it is shown that the theories or laws are erroneous. The process will continue to repeat itself in a cycle that never reaches its conclusion whenever new information is gained as a direct consequence of fresh observations.

DEDUCTIVE AND INDUCTIVE MODELS

The application of theoretical frameworks to issues that occur in the actual world is essential to the conduct of research and would not be feasible without it. A clear declaration of a theory may or may not be included in the process of organising a research endeavour; nonetheless, ties to theories will be exposed openly throughout the presentation of data and the conclusion.

(a) Model The method through which basic rules are formed from specific evidence is referred to as the inductive reasoning paradigm. The process of deriving anything begins with the particular and then moves on to the general; it begins with the gathering of specific data and ends with the recognition of a pattern that implies there is some sense of consistency among all of the provided events. The process of deriving anything through induction begins with the particular and moves on to the general.

(b) a model that is constructed via the use of the method of deduction The logical paradigm in which precise expectations of hypotheses are derived from general principles begins with a pattern that can be logically or theoretically predicted and then moves on to observations that test whether or not the anticipated pattern actually happens. The next step in the process is observations that test whether or not the anticipated pattern actually happens. starts with a pattern that can be expected logically or theoretically and then moves on to observations that test whether or not the anticipated pattern really occurred. proceeds from the general to the specific by beginning with a pattern that can be predicted logically or theoretically. A pre-existing theory is used as a jumping off point in the deductive process, which is used to determine what sort of hypothesis should be tested. After that, the hypothesis is tested utilising data gleaned from the field as the main source of information in an attempt to disprove it via an empirical investigation. Following the completion of the data analysis, the hypothesis is contrasted with the results to determine whether or not the latter provide confidence to the former's precision. In the case that the facts do not support the hypothesis, then it is required to reject the hypothesis since it is not grounded. This is because the hypothesis is not supported by any evidence. If the results are consistent with the

anticipated outcomes, then the hypothesis may be said to be valid. [Clarification needed] As a direct result of this, theories are altered so that they are compatible with the facts that have been uncovered.

An observation is collated within the context of the inductive model in order to aid the construction of an initial notion, which eventually adds to a deeper grasp of a phenomena. This is done in order to further one's understanding of the phenomenon. After that, the method is used to the process of developing more relevant research questions, which, after that step has been finished, will be helpful for the process of gathering data in the future.

The findings are analysed to determine whether or not the primary premise was correct. [Further citation is required] The idea that has been shown to be effective serves as the basis for the construction of the new theory, which is created on top of it. Following that, the original hypothesis is analysed by considering it in light of an existing theory. If it can be proven that an existing hypothesis is reinforced or confirmed by a new theory, then the present hypothesis is said to have been verified or strengthened, depending on which of the two outcomes was achieved. In the case that the comparison shows any inconsistencies, the hypothesis that is currently accepted will be altered in order to take into account the new information that has been discovered.

LINKS BETWEEN THEORY AND RESEARCH

Concepts, definitions, and hypotheses that are systematically related with one another, in addition to those that are put to use in order to explain and anticipate occurrences, are regarded to be the essential parts of a theory (facts). It is a logical justification for making the observation, and it relates to a particular aspect of the activities that a person partakes in. On the basis of theories, every function is carried out since theories are broad claims about variables and the relationships between them. This is because theories make comprehensive statements concerning a variety of factors. After that point, judgments and projections of future occurrences are generated from the inferences that were taken from these overarching generalisations. In the realm of

academic study, theory has the potential to be useful in accomplishing a wide variety of goals, including the following:

It helps to reduce the scope of the facts that need to be studied and makes it possible to study any subject using a broad variety of methods. a. It cuts down on the quantity of facts that need independent investigation. b. It's feasible that a theory will be able to steer us in the direction of the procedures that are most likely to yield the highest relevance;

(b) it has the potential to provide the researcher with a framework that may be used to apply to the acquired data in order to meaningfully categorise the information;
(c) It may include a synopsis of the information that is currently known to them about a certain item.
(e) It assists with the prediction of future facts that may be revealed, and (d) it draws attention to patterns that are not immediately apparent.

A problematic circumstance uncovered by the study on marketing

Challenges posed by marketing research are used by organisations and enterprises in order to ascertain the amount of risk that is associated with the launch of a new product or service. They do not want to make an investment in expanding a product line if analysis shows that there is a low probability of the line becoming profitable. It is useful to do marketing research that is both well-designed and well-executed in order to aid in making judgements about the product or service, especially if the study is conducted online. This makes it easier to determine the likes and preferences of customers as well as the interests of customers.

Contacting a faculty member or research worker who has a larger degree of competence is a beneficial practise, despite the fact that research subjects should not be assigned, nor should they be suggested and allotted by a guide. One of the most important things that the research guide does is help the student clarify his thoughts. It also helps the student gain a sense of focus and construct a manageable problem from one that may be too vague and too difficult.

This is one of the most important goals that the research guide is trying to accomplish. A Glance at the Previous Investigations

• A literature review is a comprehensive compilation of the information obtained from published and unpublished sources of data in a specific field that is of interest to the researcher. the information may be found in the particular area that is of interest to the researcher.
• A "literature review" is a systematic, transparent, and repeatable strategy for identifying, evaluating, and interpreting the existing corpus of recorded materials. This kind of approach is known as a "review of the available literature." The goal of this review is to

i) Get some background information on the subject of the research.
ii) Identify ideas and linkages associated with it, and propose hypotheses that are amenable to inquiry.
iii) Determine the approach, study design, methodologies, and procedures that are suitable for the analysis.
iv) Determine the data sources that have been utilised by other researchers
vi) Obtain an understanding of how other people have organised their reports for review purpose ii) Learn some background information about the subject of the research.
vii) Determine the ideas and connections that are associated with it, as well as the works of literature that will be investigated and the rationale for the study.

UNIT 3
RESEARCH DESIGN

It includes an outline of what the researcher will do from writing the hypothesis and its operational implications to the final analysis of data. A research design is the conceptual structure within which research is conducted. It constitutes the blueprint for the collection, measurement, and analysis of data. Components that Make Up a Research Plan A plan is what's known as the research design, and it outlines the many information sources and kinds that are pertinent to the study challenge. It is a plan that outlines the methodology that will be used in the process of data collection and analysis. In addition to that, it incorporates the cost and time budgets.

Steps/stages in developing a research design

The phases in the design of the research are as follows:

1. **The definition of the problem and its parameters**: This is the first phase, and it begins with the definition of the problem. Following an analysis of the relevant literature and a comprehension of the current circumstance, a potential area of the issue has been identified. The study's goals and objectives are being developed. This is the beginning of any research project, which will determine how additional study will go.
2. **Developing a framework for the research design -** The research framework is developed based on the goals of the study and the nature of the variables. It specifies the action plan for collecting data and doing analysis.
3. **Sample design -** The next step is the design and selection of samples. At this point in the process, the researcher is responsible for determining whether a census or sample study is to be carried out, as well as the sampling procedures that will be used.
4. **The gathering of data-** It is important to predetermine the sources and procedures that will be used to collect data in order to prevent collecting data that is not relevant and wasting time.

In order to attain reliability and validity, the techniques, sources, and instruments used to gather data should be chosen using a scientific approach. It is important to identify both the main and secondary sources of data.

5. **Analysis of the data-** Once the data gathering has been finished, the data will be sorted and organized appropriately to make further analysis easier. After the data has been obtained, it is next subjected to editing, coding, and decoding. Different approaches to analysis are used for qualitative and quantitative data, depending on the characteristics of the data being analyzed.
6. **Writing a report -** A report that is inclined towards research is a reflection of the research activity that was done. The value of a research study may be improved by reporting that is straightforward, unambiguous, and objective. Reports are beneficial to future research, because they broaden the scope of the study field. In order to make the report easier to interpret, several aids, such as tables, charts, and diagrams, have been included. It is important to use effective language and present it in an organized manner in order to successfully combine the different components of the report.

Overview of types of research design

The manner in which research inquiry is carried out and the degree to which problems are formulated may be used as the foundation for a general classification of research designs. Researchers are required to use any sort of research design that is appropriate given the objective of the study, the nature of the variables being studied, knowledge of the research topic, and the availability of information.

There are two primary categories that may be used to broadly categorize research designs.

1. The design of exploratory research
2. The design of conclusive research

The research design is considered by some specialists to be:

1. the exploratory research design
2. A convincing plan for the research

a. Research layout that is descriptive

b. The design of a causal research study or an experimental research study

1. The Exploratory Research Design is the Most Fundamental Investigation Design It is the most fundamental research design since it is the means through which appropriate extra information about the research are gathered. The design acts as a compass to guide the subsequent research process.

2. Conclusive research design — The researcher will use conclusive research if the goal of the investigation is to reach any conclusion about the research topic. The primary purpose of using this research strategy is to establish a causal link or to test a hypothesis in order to arrive at a conclusion. Either a descriptive or a causal design may be used. It is important to highlight that a descriptive research design is used when the objective of the study is to provide a description of the studied phenomenon. ➔ If the goal of the conclusive study is to investigate the link between causes and effects, then the researcher would choose for the causal research design, which is also commonly referred to as the experimental design.

a. Descriptive Research Design: This is the stage at which the researcher attempts to describe the search phenomenon and is more explicit and clear about the research topic. It mostly employs quantitative data. A more systematic, formal, and well defined approach is used in descriptive design. When opposed to an exploratory design, it sets a certain result and has a more narrowed focus.

b. Causal research design — A researcher would employ a causal design when they wish to investigate the cause-and-effect connection between different variables. The researcher is interested not only in establishing a link, but also in examining the degree of the association, measuring it, and attempting to explain the variety in the results. It is more structured, stiff, and less flexible than before. Some industry professionals refer to the methodology of causal research as experimental research design.

Aspects to be considered before selecting research design

Before settling on a specific research design, researchers should do a thorough analysis of the study scenario. This will ensure that the research design chosen is appropriate and offers the most advantageous alternative course of action at each step of the research. Before settling on a particular design, it is important to give some thought to the elements listed below.

1. Knowledge of the research issue: The researcher's level of familiarity with the study topic, as well as the amount of material that is at his or her disposal, is a guiding element in choosing a design. When there is insufficient information about the study topic and the need for more investigation, an exploratory design is appropriate. On the other hand, if a researcher already has all of the knowledge that is essential about the study topic, then he might use the descriptive design.

2. Clarity of goals: Descriptive design is appropriate if the research objectives are known, clear, and there is no need to rework on the objectives of the research. In this case, there is no need to rework on the objectives of the research. The exploratory design is the one that should be used when there is a lack of clarity on the research goals, as well as when further deskwork or preparatory research is necessary to establish the objectives.

3. Hypothesis: If the research hypotheses are well established and presented without any ambiguity, then the researcher is free to choose either a causal or descriptive design, depending on the needs of the investigation. An exploratory design is appropriate when the aims of the study are unclear and it is necessary to define the hypothesis.

4. The requirement for Accuracy: If the researcher is interested in achieving a high degree of accuracy in their study, then it is recommended that they use either descriptive or causal research methods. Exploratory design, despite the fact that it gives accuracy, is based more on qualitative aspects, and it is not possible to obtain a high degree of precision.

5. The nature of the variable and the type of variable: Knowledge about the research variable, nature of the variable, and type of variable also plays a role in the decision-making process regarding

research design. Exploratory design is appropriate when the variables being studied are qualitative and when it is difficult to quantify them. If the researcher is familiar with the characteristics of the study variables and their relationships, and if the characteristics of the study variables are quantitative in nature, then a descriptive or causal design is acceptable. In addition to the aforementioned considerations, the choice of study design is also affected by the amount of time and money required to carry out the research, the level of risk involved, and other variables.

RESEARCH DESIGN FOR DESCRIPTIVE RESEARCH

Research studies that are considered to be descriptive are those that focus on characterizing the features of a specific person or of a group. In such studies, the design has to be stiff and not flexible, and it needs to concentrate attention on the following:

1. Establishing the purpose of the research (what the investigation will focus on, and why will it be carried out) The first thing that has to be done in order to make sure that the information gathered for a descriptive research is meaningful is to make sure that the goals are specified with appropriate accuracy.

2. Planning the procedures for the collection of data - (which strategies for amassing data will be utilized?) - This step is followed by the decision-making process of choosing the procedures via which the data are to be gathered. It is necessary to develop methods for the collection of the information. The researcher has access to a variety of methodologies, including observation, questionnaires, interviews, and the review of records, amongst others, and may choose to use one or more of these approaches in their investigation. During the process of creating the processes for collecting data, suitable precautions against bias and dependability must be provided.

3. Choosing the specimen - (how much of the material will be required?) The majority of descriptive studies include the researcher collecting samples from the population under study, who then intends to draw conclusions about the population based on the findings of the sample. It is important to approach the challenge of sample design in such a way that it is possible for the samples to provide correct

information while requiring a minimal amount of work from the researcher.

4. The process of data collection (where can the necessary data be located, and to what time period should the data be related?)

5. Putting the data through processing and analyzing- It is necessary to put the data that was obtained through processing and analyzing. This involves activities such as tabulating the data, doing several statistical calculations, and coding the interview responses, observations, and other relevant information.

6. Reporting the results- This job involves conveying the findings to others, and the researcher is responsible for doing so in an effective way. The structure of the report has to be carefully designed in advance in order to ensure that all aspects relevant to the research study may be presented in an organized manner that is clear and concise.

RESEARCH DESIGN FOR ANALYTICAL RESEARCH

Research that employs analytical processes and methods is known as analytical study. This kind of research focuses on quantitative data. It is possible that it will consist of a set of mathematical models or statistical approaches that may be applied to numerical data. Therefore, another name for it is the statistical method. The purpose of the analytical investigation is to put hypotheses to the test as well as to identify and understand connections. It places an emphasis on doing in-depth data analysis and investigating correlations from a variety of perspectives by include as many relevant variables as is practically practicable in the analysis plan. This strategy has widespread use in the corporate world as well as other areas where quantitative numerical data is created. It is used for determining the values of variables, contrasting different groups, and investigating the associations between different elements. Data may be gathered from either primary or secondary sources. Either one is acceptable. Analytical studies are distinguished by stringent standards for measurement and analysis, and their designs are often intended to be approximations of the experimental designs of other types of research.

RESEARCH DESIGN FOR EMPIRICAL RESEARCH

Empirical research is limited to using either experience or observation as its primary sources of data. Database research that arrives to results that can be validated by observation or experiment is an example of this kind of study. Research of this kind might also be referred to as experimental research. When conducting this kind of investigation, it is essential to collect first-hand data directly from the relevant institutions, as well as to take active steps toward producing the material that is being sought for. When doing this kind of study, the researcher is required to first come up with a working hypothesis or a best estimate on the likely outcomes. After that, he sets out to collect enough evidence (data) to either support or refute his theory. After that, he devises experimental designs that he believes will influence the individuals or the materials that are of interest in order to elicit the information that he is looking for. In this kind of research, the experimenter retains control over the variables that are being investigated, and he or she purposefully alters one of the variables in order to investigate the impact of the change.

RESEARCH DESIGN FOR EXPERIMENTAL RESEARCH

The experimental research designs serve as blueprints for carrying out the tests in a manner that is consistent with a certain framework. The following is a list of the main categories of experimental designs:

- Pre experimental design
- True experimental design
- Statistical design

1. Pre experimental design-Pre-experimental designs are frequently referred to as informal designs. Manipulation is another word for this.

2. Randomization The term "randomization" refers to the process of assigning participants to a treatment in an experiment in a way that is completely at random.

3. Control: In the context of performing an experiment, a control is a component that does not undergo any changes and is not influenced in any way by the other variables.

The two primary types of genuine experimental designs are the

1) Pre-test control groups and the

2) Post-test with control group designs.

1. In the Pre-test control groups, test units are distributed randomly to both the experimental and test groups at the same time. Only the members of the experimental group get therapy, and the dependent variable is evaluated both before and after it has been administered. The dependent variable is evaluated both before and after the experiment for the control group, but they do not receive any treatment.

2. Post-test solely with control groups (after just with the group serving as a control) - In this design, a preliminary test is not carried out. In this stage of the study process, the researcher will choose two groups at random to serve as the experimental group and the control group. After therapy has been administered to the experimental group, the dependent variable is assessed for the first time. The simultaneously dependent variable for the control group that did not receive treatment is assessed.

Qualities of a good research design:

1. A solid research design should be focused on the research topic and aligned with the study goals.
2. There can be no hint of partiality.
3. It has to be flexible enough to accommodate change and practical.
4. The criteria of validity, reliability, correctness, adequacy, economy, and efficiency should guide its development.
5. It need to be based on scientific principles, so that judgments on options at each step may be rationally defended.
6. It ought to strive toward a method that is both cost-effective and does not compromise the quality of the study.
7. It need to take into consideration the time frame in which the investigation is to be finished.
8. It should guide the methods for the gathering of data and the analysis of data.

Delimiting a Problem

All the elements required to answer the research question must be clearly addressed as part of the delimitation of the research topic.

The researcher should provide more details regarding the topic of the study than just the title while performing the study. The subject should be sufficiently narrow to make the research process easier. The researcher must provide a subject, a problem with a solution, a question with a reason, a general aim, the particular objectives, and the research's constraints. A delimitation is necessary to structure the whole procedure. The goal of defining the research topic is to determine the precise population to be investigated, the amount of time required to study the population, and the physical location where the research will be conducted.

The research question has to include reference of the three aforementioned components. It is crucial to note that certain issues do not need the three delimitation factors and will not have an impact on the inquiry.It should be emphasized that the problem's definition and the investigation's restrictions do not relate to the same thing. It often causes confusion for many individuals.

How should the research issue be defined?

Other factors, such as those listed above, should be taken into account after choosing the subject you intend to research. However, the three factors important to the definition of the research issue will be the main emphasis of this section.

In contrast to the title and goals, which must adhere to predetermined rules, there is no rule that specifies how to phrase the delimitations of the research topic. Making a specified subject the study object is the sole need for this component of the investigation.

It's crucial to remember that the researcher must justify his decision to explore the delimitations he selected as well as the reasons he didn't choose any other ones. The delimitations listed below are those that a researcher must take into account.

Geographical encirclement

The geographical or spatial delimitation entails confining the subject's examination to a certain location, whether it a particular

nation, state, city, or parish. This will enable the population to be examined to be deduced.

Population limit definition

The population to be used as the research's subject must be chosen once the study area has been identified. You may describe the population's age and gender in this section, as well as the total number of participants, or you can identify the institution or business that will handle the population function by name.

However, it may be further circumscribed if you wish to examine the population of an organization or business, designating the precise segment of the population to be investigated. A particular degree and area might be chosen, for instance, if you are an educational institution in addition to specifying the name of the institution. By doing so, it would openly and concurrently describe the geographical delimitation.

Timing restrictions

The length of time required to do the study will be determined depending on the topic. Given that this might be about events or phenomena that have previously occurred or are now occurring, it is crucial to be aware of the topic of study's scope.

Continuing with the example of population delimitation, if the researcher's population of choice is an educational institution, then the researcher needs to specify whether the study will be based on an entire elective year and which year it will be based on, or whether it will only be based on a given period of time.

Why is it being done?

Regardless of the topic being investigated, an inquiry has the potential to include significant points and societies as objects of study. The establishment of delimitations will assist in keeping the study at the centre of attention.

In order for the researcher to concentrate on the most important facets of the investigation, the delimitations are drafted so that they may serve as a kind of guide for him or her to follow. In a similar vein,

delimitations act as a map to direct readers in the direction of the sort of study that they will read.

Why even bother?

It is possible to have the misconception that the answers to the queries "what" and "why" will be the same; nevertheless, this is not the case. The question that has to be answered is "why is the delimitation of the research issue made?" is inextricably bound up with the question of why. On the other hand, they are not comparable.

The question "what for?" responds to the definite emphasis that the study will have, as was described earlier in the sentence. On the other hand, the delimitation is established, which is why it is necessary for you to establish a centre point. To put it in another way, to erect impassable barriers from which the investigator will be unable to escape.

These barriers are meant to, in a way, restrict the object of study that is being conducted. If there were no such obstacles, the amount of data that could be collected would be so enormous that the conclusion could not be written. It is necessary to begin by providing definitions of both the delimitations and the constraints of the research topic before we can proceed to determining the distinction between the two.

As was just discussed, the delimitations are used to determine the boundaries of the area that will be the focus of the research. This is done in order to provide a starting point and a conclusion for the gathering of data, and as a result, to acquire a topic that may be explored with more specificity. On the other hand, the constraints of the research might be seen as the study's flaws. These are all the aspects of the inquiry over which the researcher has no influence or over which it is impossible to make accurate predictions before they take place.

Nevertheless, the investigator has the ability to exploit the constraints that are readily apparent to their advantage. The researcher will be able to devise a strategy to address them once they have this information.

However, if these constraints do not permit the progress of research, then it is time for the researcher to shift the emphasis of the

study. Before beginning the process of research, these should be taken into consideration. Therefore, it is possible to assert that the most significant distinction between delimitations and limits is that the former are within the control of the researcher, but the latter are outside of the researcher's ability to exercise control.

Evaluation Research

What exactly is evaluations research ?

Evaluation study is a frequent kind of research design that comprises carrying out a systematic assessment of the worth of resources devoted to a project or specified aim. This type of research is often referred to as programme evaluation. It often makes use of several approaches from the field of social research in order to collect and examine relevant data about organisational procedures and outputs.

Evaluation research, which falls under the category of applied research, is often related with real-life situations that take place inside organisational environments. This indicates that in order to arrive at objective research results that will be beneficial to stakeholders, the researcher will need to harness standard workplace qualities such as interpersonal skills and the ability to play well on a team.

Research on Evaluation: Traits and Characteristics

1) Environment of Research: Evaluation research is carried out in the "real world," or more specifically, inside the framework of an organization.

   The primary aim of research in the field of evaluation is not the study of the process itself but rather the measurement of the results produced by the process.

   The findings of study have shown that evaluation research is used by businesses for the purpose of making strategic decisions.

2) Aim of the Research: The purpose of a programme evaluation is to establish whether or not a certain method has produced the anticipated outcome (s). The results of this kind of study serve to safeguard the interests of the organization's many stakeholders. It often occupies a position bridging the gap between fundamental and applied research. Research on evaluation is conducted in a

manner that is both comprehensive and ongoing. Rather to focusing on descriptions, it concentrates on the operations that are being performed. Process of Study This research design makes use of both qualitative and quantitative research approaches in order to collect pertinent data on a product or action-based plan. Among these approaches are observations, experiments, and questionnaires.

Different Kinds of Research on Evaluations

From "appreciative inquiry" to "connoisseurship" to "transformative assessment," the forty-two various evaluation techniques and models are covered in detail in Mathison's (2004) Encyclopedia of Evaluation. The following are examples of common sorts of research that are evaluated:

Evaluation in a Formative Sense

Before beginning a project, it is common practise to do a formative assessment, also known as a baseline survey. This kind of research entails determining the requirements of the users or the target market. Evaluation research always begins with formative evaluation since this sort of assessment establishes the overall tone of the organization's project and gives valuable information that can be used in subsequent forms of evaluation.

Evaluation at the Halfway Point

Assessing how far a project has progressed and judging whether or not it is in accordance with the goals and objectives that were established are both components of a mid-term review. Midterm reviews serve two purposes: they enable the company to assess whether or not a change or modification of the implementation strategy is required, and they act as a tracking mechanism for the project.

Summative Evaluation

This kind of assessment is carried out immediately after a project has been brought to a successful conclusion, and it is also known as an end-term evaluation or project-completion evaluation. In this stage of

the research process, the researcher analyses the value and outputs of the programme in relation to the outcomes that were anticipated. The organization is able to determine the level of success that a project achieved by conducting a summative assessment. These kinds of findings may be communicated to various stakeholders, target audiences, and potential investors.

Outcome Evaluation

Due to the fact that it assesses how a project, programme, or product impacts its end users, outcome assessment focuses largely on the intended recipients of the information. This sort of assessment examines the results of the project from the perspective of the audience that was intended to benefit from it. Changes such as greater work efficiency, improved knowledge, and acquired skills are often measured during this type of evaluation.

The Appreciative Inquiry Approach

An method to assessment study known as appreciative inquiry focuses on strategies that are effective in creating results. It is premised on the assumption that an organisation will develop in whichever direction its stakeholders give main attention to, so that if all of the attention were focused on issues, it would be simple to discover them. This view underpins the concept of stakeholder engagement.

When conducting appreciative inquiry, the research identifies the factors directly responsible for the positive results realized in the course of a project, analyses the reasons for these results, and then intensifies the utilization of these factors. Appreciative inquiry is a form of action research that focuses on finding and analyzing patterns of success.

Methodologies of Research and Evaluation

There are four primary approaches to research in the field of evaluation: the output measurement, the input measurement, the effect evaluation, and the service quality evaluation.

The measurement of output and performance

Evaluation study often makes use of a technique known as output measurement, which is designed to demonstrate the outcomes of an endeavour carried out by an organization. To put it another way, performance assessment takes into consideration the outcomes that were brought about by the application of resources to a certain endeavour or organizational procedure.

It is not enough for an organization to spend resources in a project; they must also be able to monitor the amount to which these resources have given outcomes. Performance assessment is where this tracking and tracking ability comes in. With the help of output measurement, businesses are able to focus their attention not only on the process itself, but also on how successful it is and what kind of impact it has.

User happiness, organizational capacity, market penetration, and facility usage are some more important factors that are considered while evaluating a company's success. Organizations need to determine the characteristics that are pertinent to the process at hand, as well as the industry in which they operate and the target markets, before they can conduct out performance assessment.

Variables in terms of their operationalization

When presenting a topic, a researcher has to make certain that it is neither presented in words that are so broad as to render it incomprehensible nor detailed in a manner that is so restricted as to render it meaningless and inconsequential.

In this way, the most important step is to explain the elements that are involved in the problem and characterize them in terms of the significance that they have in terms of their context. To illustrate this point, let's say that you made an announcement that you want to conduct research on the "Impact of Television on the Success of Learners in Course One of the Master of Arts in Distance Education that is offered by the Indira Gandhi National Open University." As an illustration, let's say that the Indira Gandhi National Open University is located in India. This is a fairly general phrase that explains in a very fundamental way what it is that you want to achieve in the future.

Having said that, it is necessary to characterize the problem with an exceptionally high level of specificity.

In order to do this, the first thing that needs to be done is to describe the variables that are a part of the issue and define them in terms of their operational meaning.

The terms "efficacy" and "performance" are the ones that are up for grabs in this predicament. It is important to keep in mind that the meanings of these idioms extend beyond those given in dictionaries. For instance, "creating the intended impact" is one of the definitions of "effectiveness" included in dictionaries. The interpretation presented here is insufficient for the purposes of study. It is essential that you be specific about the indicator of effectiveness that you want to use or the activities that you intend to do in order to quantify the existence or absence of the phenomena that is signified by the word "effectiveness." In a similar manner, you need to define the second variable, which is "performance," also in terms of the actions or procedures that will be used to quantify it later on. You can decide that for the sake of this research, "efficacy" refers to the degree to which Diploma students improved their results on a standardized achievement exam that was administered during Course One. It's possible that when we talk about "performance," we're referring to how well we did on the accomplishment exam for Course One.

The issue should be described in such a manner that it demonstrates a link between at least two of the variables. This is an important point to keep in mind. It should not entail any philosophical concerns, value questions, or questions of judgement that can't be resolved by scientific research.

Is it possible, for instance, that pupils' performance levels may be improved by increasing their exposure to television?

Research cannot provide answers to concerns of this kind about worth. In a similar vein, the question "what is there in television education that increase performances" is a philosophical subject that cannot be investigated in a straightforward manner.

Examination and Analysis of the Issue

Before beginning the investigation, it would be beneficial for you to pose a number of questions to yourself. The questions ought to be useful in evaluating the situation on several criteria, which will be discussed later. Before beginning the study, yes has to be given as a response to each and every one of these questions.

Which questions are the most important for us to ask?

i) Is the issue amenable to investigation?

There are certain issues that can't be resolved satisfactorily by the use of research for any reason. Always, the connection that exists between two or more variables that can be identified and quantified is the primary focus of an issue that may be investigated via research. It should be possible to describe the issue in the form of viable research questions that are capable of being addressed experimentally.

ii) Is this a recent occurrence?

There is no use in doing more research into a topic that has already been thoroughly examined by a number of previous scholars. It is vital to evaluate the literature that is accessible in the subject in question very thoroughly in order to prevent duplication of efforts like these. The issue at hand shouldn't be chosen until after you have shown without a reasonable doubt that it is, in fact, an uncharted territory that has never been thoroughly researched and solved. However, it is essential to keep in mind that a researcher is permitted to relaunch a study if he or she intends to validate the study's results or to eventually expand the authenticity of the study's findings in a framework that is vastly different from the one in which the study was initially conducted. This is something that a researcher can do in order to validate or extend the validity of the study's findings.

iii) Is the nature of the issue important?

The challenge should be designed in such a way that it has a good chance of filling in the blanks in the existing body of knowledge, of shedding light on some of the inconsistencies that were found in the earlier research, or of providing assistance in the presentation of the

evidence that are already known. This may be accomplished in a few different ways. The findings or outcomes of an investigation should serve as the foundation for either a theory, broad generalizations, or guiding principles. In addition, they should either give rise to new questions that may be investigated further or have some practical applications that might be of service.

iv) Is it possible for the specific researcher to tackle the problem?

It is possible for a research topic to be researchable, substantial, or innovative; nonetheless, it may still not be viable due to the following considerations:

a. Competencies in research: The issue at hand should pertain to a field in which the researcher has the necessary expertise and qualifications. It is vital for him or her to have the abilities, skills, and knowledge that may be required in order to design and manage the instruments for data collection, as well as evaluate the data that is accessible for analysis. The researcher should also possess the necessary understanding of the research design, qualitative and quantitative methodologies of data analysis, and other such skills that may be required in order to carry out the study all the way through to its conclusion. In addition, the researcher should possess the required understanding of research design, qualitative and quantitative methodologies of data analysis, and other such skills.

b. Interest and zeal: The researcher need to have an authentic interest in, and a healthy amount of zeal for, the subject that he or she plans to investigate in the course of the study.

c. Financial concerns and the problem's feasibility: The issue should be viable from a financial standpoint. It is the responsibility of the researcher to determine whether or not they have the financial and/or time resources required to carry out the study. Every project has some kind of expense associated with it, and this is especially true for DE initiatives that need students to be located in different locations. When considering feasibility, cost is an essential component. It is essential to determine the potential costs of the project as well as the financial resources that are available. Depending on the answer to this

question, it will become clear whether or not the project can be carried out.

d. Administrative considerations: In addition to personal limitations, financial limitations, and time constraints, the researcher needs to take into account the type of data, equipment, specialized personnel, and administrative facilities that are required in order to successfully complete the study. It is important for him/her to determine whether or not they will be able to get the assistance of a variety of administrative agencies in order to gather a variety of data kinds.

e. Time: The successful completion of a project is a competition against the passage of time. The great majority of you, if not most of you, are already engaged in more than one activity at the same time, whether it be at your place of employment, in your personal life, or within your social circles. It is essential to make an accurate estimate of the amount of time necessary to finish a research. In addition to the evaluation of the whole time, it is vital to determine which season of the year is most relevant to the investigation based on its purpose. For example, if you want to research the instructional transactions that take place during personal contact programmes, you will need to schedule your project in such a way that it allows you to really watch a number of sessions that take place during personal contact programmes.

UNIT 4
STATISTICAL TECHNIQUES AND TOOLS

Data collection is the systematic acquisition of information, such as observations or measurements. Collecting data allows you to gain first-hand facts as well as unique insights into the topic you are researching. This is true regardless of whether you are doing research for academic, governmental, or commercial purposes.

Although the methods and objectives of data collection may differ from field to field, the data collection process itself is, for the most part, similar. Before you begin data collection, there are a few considerations you must make:

The objective of the inquiry is to:

- The information categories that will be collected.
- The methods and activities you will use to collect, store, and analyse the data.

Follow these four steps to collect data that is of good quality and relevant to your intended use.

1) You must first establish the aim of your studies.

Before you can begin the process of data collection, you must have a crystal-clear understanding of what you want to achieve. You may begin by developing a problem statement that answers the following questions: what is the practical or scientific issue you intend to tackle, and why is it significant?

Create one or more research questions that precisely identify the information you want to get as the last stage. It is conceivable that you may need to collect quantitative or qualitative data to answer your research questions:

Quantitative information is often given in the form of numbers and graphs and is analysed using statistical methods.

Words are employed to represent qualitative data, which is subsequently analysed and classified for statistical analytic purposes.

If you want to test a hypothesis, gain an exact measurement of anything, or get large-scale statistical insights, you need collect quantitative data. Collecting qualitative data is advantageous if your goals are to test theories, interpret occurrences, or get a better understanding of a certain situation. If you have several objectives to achieve, you may choose a mixed-methods technique that collects both types of data.

Numerous instances of qualitative and quantitative research objectives

- You are doing research on how direct supervisors are seen by their direct subordinates inside a large organisation.
- Your major purpose is to determine if there are substantial differences in the opinions of managers from diverse divisions and office locations.
- Your second purpose is to obtain meaningful feedback from employees in order to examine fresh methods for enhancing managers' effectiveness.
- You conclude that a mixed-methods approach is the optimal technique for collecting quantitative and qualitative data.

2) Select the method through which you will collect data.

Determine the most suitable technique for your inquiry depending on the information you want to collect.

In experimental research, the application of quantitative methods predominates.

Among the qualitative research methods are interviews, focus groups, and ethnographies.

Archival research, questionnaires, observations, and secondary data collecting may all be classified as either quantitative or qualitative.

Consider carefully the strategy you will use to obtain the data that will get you closer to answering the research questions.

1) Plan out the procedures for data collection.

2) When you have decided the technique or approaches you will use, the following step is to explain how you will implement

these ideas. How will you guarantee that the observations or measurements you make of the variables of interest using the procedures you've created are accurate?

For example, if you are conducting surveys or interviews, you must choose the structure of the questions. If you want to perform an experiment, you must determine how the experiment will be constructed.

Operationalization

There are times when variables can be evaluated directly. If you ask employees for their dates of birth, for instance, you can simply determine the average age of your staff. On the other side, you will often be interested in acquiring knowledge on more abstract concepts or intangible aspects.

Operationalization is the process of converting abstract intellectual notions into observable and measurable facts. Converting the conceptual definition of what you want to investigate into the operational description of what you will measure is a critical step in defining how you will collect data.

Sampling

It may be necessary to develop a sampling strategy in order to gather data in a systematic way. Determining a population, or the broader group from which you aim to draw conclusions, and a sample, or the smaller group from which you will collect data, are both required phases in this procedure.

Your sampling technique will have a significant impact on how you recruit participants or collect data for your project. When selecting a sampling strategy, you will need to examine a number of different parameters, such as the intended sample size, the accessibility of the sample, and the length of the data collection.

Standardizing procedures

If several researchers are working on your project, you should create a detailed guide to standardize data collection procedures.

To guarantee that each member of your research team gathers data in a uniform way, you will need to provide them with comprehensive, step-by-step instructions. This may be achieved, for example, by running tests under identical settings and using objective criteria to record and classify findings.

This not only helps to ensure the integrity of your data, but you can also use it to recreate the whole study in the future.

Developing a data management plan

Before beginning the process of data collection, you should also have a strategy for storing and organizing the data you gather.

If you are going to gather data from people, you will almost likely need to anonymize and secure the data so that no sensitive information becomes public (e.g. names or identity numbers).

If you are collecting data through interviews or other techniques involving the use of pencil and paper, you will need to undertake transcriptions or data entry in a thorough way in order to minimize the possibility of distortion.

Having an organizational structure that regularly makes backups is one technique to prevent the loss of data.

4) Acquire the Required Information

At this stage, you are finally able to use the approaches you have chosen in order to measure or observe the variables of interest.

Following are some best practices that should be followed to ensure that high-quality data are collected in a systematic manner

Ensure that you record any essential information as soon as you have it. Consider, for example, if laboratory equipment is recalibrated throughout experimental study.

Check the manually entered data for errors twice.

If you collect quantitative data, you will be able to assess its reliability and validity, giving you a sense of the quality of your data.

What precisely does "Data Collection" mean?

Data collection is a thorough process including the collecting and evaluation of specific data in order to offer answers to applicable

questions and evaluate the consequences. It emphasises learning all there is to know about a certain topic or subject area. The objective of data collection is to test a hypothesis in an attempt to explain a phenomenon in the future.

The testing of a hypothesis eliminates the need for assumptions while simultaneously creating a claim supported by logic.

There are several objectives for which data collectors acquire information, each with its own possible outcomes. The primary purpose of data collecting, on the other hand, is to enable the researcher to predict future possibilities and trends with more accuracy.

Primary and secondary data are the two most prevalent types of information that humans may obtain. The first kind of information is collected by a researcher from first-hand sources, whereas the second type is collected by a non-user third party.

The Various Data Collection Methods

Before delving into the intricacies of the various data collection methods, let's first create some context. It is essential to remember that the process of data collecting may be divided into two distinct categories: primary data collection and secondary data collection.

The acquisition of primary data

Primary data collection is the acquisition of unprocessed data at the source. This is what primary data collecting entails. It is the process of assembling the main data collected by a researcher for a specific research project. It may be further subdivided into quantitative data collection techniques and qualitative research approaches.

Research Method Based on Qualitative Data

The qualitative research approaches of data collection do not require the collection of numerical data or the need to infer via the use of mathematical calculations; rather, it is based on qualitative characteristics such as the researcher's experience or emotion. Such an approach may, for instance, consist of an open-ended questionnaire.

Method of Measurement

Quantitative techniques include the use of numbers and need a mathematical derivation of the findings for comprehension. In order to get data that can be calculated statistically, it is possible to conduct research using a questionnaire with solely closed-ended questions. In addition, correlation and regression approaches, as well as the mean, mode, and median.

Information Obtained from Secondary Sources

On the other hand, secondary data collection refers to the gathering of data from sources other than the original user. This kind of data collecting is known as second-hand data acquisition. Data mining is the process of collecting data that already exists, whether in the form of previously published books, journals, or online portals. It is also far less expensive and easier to collect than other methods.

The nature, scope, and location of your research, as well as its aims and objectives, should inform your judgement about whether primary or secondary data collection is more suitable.

The relevance of data accumulation

There are several reasons at play, especially for a researcher in terms of data collection. Explaining them in detail, the following are some of the reasons why:

Investigate Integrity and Objectivity

One of the most significant reasons for collecting data, whether qualitative or quantitative, is to ensure that the integrity of the research topic is maintained.

Reduce the likelihood of making errors.

When appropriate data collection processes are used, the likelihood of errors that are consistent with the results is decreased.

Making a Call or Selection

It is crucial to collect trustworthy data so that the researcher does not make conclusions without enough knowledge in order to reduce the possibility of decision-making errors.

Spend both less money and time.

The researcher may save time and money by gathering data that would ordinarily be required but would be squandered without a deeper understanding of the topic or issue.

To meet a need for a novel idea, a novel approach, or cutting-edge innovation, it is necessary to develop a novel concept, a novel approach, or cutting-edge innovation.

It is crucial to collect data as evidence to support these statements in order to prove that a change in the norm or the introduction of new information that will be accepted by the majority of people is necessary.

What precisely is a data collection tool?

The phrase "data gathering tools" refers to the many devices and equipment used for data collection. Computer-assisted interviewing systems and paper questionnaires are examples of data collecting instruments. Case Studies, Checklists, Interviews, and, on occasion, Observation, as well as Surveys and Questionnaires, are examples of data collection techniques.

Due to the fact that research may be conducted in a number of ways and for a range of purposes, it is necessary to choose the data collection equipment. The objective of data collection is to collect credible evidence for the purpose of performing an analysis, which will then result in the formulation of credible and convincing answers to the addressed issues.

The seven most successful methodologies and devices for data collection in academic, opinion, or product research are listed below.

The seven most successful methods for gathering data for academic, opinion-based, or product research are listed below. The nature of each, as well as its advantages and disadvantages, are also examined in detail. This section will provide you with the most up-to-date information available on the approach best suitable for your research.

INTERVIEW

An interview is a face-to-face conversation between two persons whose main aim is to collect relevant data for a research purpose. The

interview may take place in person, through telephone, or via video conference. There are many various interview types, with organised, semi-structured, and unstructured dialogues being the most prevalent. Each of these forms is distinct from the others in some way.

Utilize this template for an interview consent form to allow an interviewee to provide you permission to utilize interview data for the purposes of conducting an investigational research.

Structured Interviews are, in their most basic form, a spoken questionnaire administered to the respondent. In terms of depth, it is often completed quickly and does not go behind the surface. It is strongly suggested if you place a premium on quickness and effectiveness, but it lacks depth and intricacy.

In the case of semi-structured interviews, there are a few key questions designed to cover the breadth of the topic under investigation. This provides the researcher with a little more freedom to examine the subject matter.

Unstructured Interviews are a kind of in-depth interview that allows the researcher to acquire information on a wide range of subjects while remaining focused on the research issue. This strategy offers a lot of advantages, one of which is that it allows researchers to combine structure and flexibility in their work, despite the fact that it requires much more time.

Pros

Specific information and facts
Freedom and flexibility in practise
Accurate data.

Cons

Time-consuming
Gathering is a pricey endeavour.

What are the most effective data gathering tools while doing interviews?

Using interviews, you may collect data in a simple and effective way by using the following techniques:

Sound Recording Equipment A device that can record sound onto a disc, tape, or film is known as an audio recorder. Audio information has the ability to meet the needs of a varied range of persons and may act as an alternative to conventional data collection techniques.

Digital Camera

One of the advantages of a digital camera is that it allows the user to transmit captured images to a display screen anytime this capability is necessary.

Camcorder

Frequently, a camcorder is used while conducting interviews for data collecting. It combines a video camera and an audio recorder into a single, user-friendly gadget. The material provided is qualitative in nature, and respondents were given the option to reply to all of the questions posed. If you need to record sensitive material during an interview but also need to protect your subject's privacy, a camcorder may not be the most appropriate instrument to employ.

Do you need to collect qualitative information or create a specific report and want to conduct an interview? Before utilising interview data for research or a report, you must first get the interviewee's permission using our online interview consent form template. Formplus Builder is the most effective tool for building online permission forms, even if you lack coding knowledge. Among other premium features, it includes electronic signatures, upload fields, and form security.

QUESTIONNAIRES

A data collecting instrument is a series of questions and prompts provided to someone in order to elicit a response. This procedure is known as data collecting. The objective of questionnaires is to collect information from group members.

It is crucial to clarify that a questionnaire is not the same as a survey; rather, it is a part of the latter. A questionnaire is only one of

the several data collection methods that may be used during a survey, which is a process that gathers data using a variety of methods.

A questionnaire normally consists of three separate types of questions. They are known as open-ended, scale, and fixed-alternative questions. With each inquiry adapted to the kind and scope of the investigation being done.

Pros

Can be distributed to a large number of individuals at an acceptable cost.
This study may be compared and contrasted with previous studies to measure change.
Easy to imagine and comprehend.
Questionnaires deliver actionable data.
The respondent's name will remain confidential.
Utilizing questionnaires permits comprehensive coverage of a topic.
Costs a reasonable amount overall.

Cons

It is likely that respondents will not provide truthful responses because they become bored halfway through the poll.
Questionnaires can't produce qualitative data.
It is conceivable that certain inquiries will not be answered.
There is a chance that responders have anything to conceal.
Not all issues are amenable to easy analysis.

Paper Questionnaire

A paper questionnaire is a data collection tool consisting of a sequence of questions and/or prompts designed to elicit responses from respondents. This data may then be put into a database. Despite the fact that their major purpose is statistical analysis of the findings, they may also be used to gather data.

REPORTING

Data reporting refers to the process of gathering and submitting information for further inquiry. Since faulty data reporting may lead to

misinformed decision making, reliable data reporting is the most crucial aspect of data reporting.

Pros
Decision-making that is based on information.

Cons
Self-reported replies are not guaranteed to be accurate.
There is a chance that bias affected the results.
It is likely that responders are too ashamed to disclose all of the requested data.
Inaccurate reports will lead to ill-informed decisions.

Which Data Collection Instruments Are the Most Effective for Report Generation?

Reporting tools enable you to extract data and display it in the form of charts, tables, and other visualizations so that users may discover relevant information. You could get the information you need for your report from non-governmental organization (NGO) reports, newspapers, online articles, or medical records.

The Reports of Non-Governmental Organizations

The reports provided by non-governmental organisations (NGOs) provide an in-depth and detailed account of the organization's activity, addressing themes such as business and human rights. The content of these articles relates especially to research and may serve as a suitable academic basis for the collecting of data. NGOs focus their efforts on coordinated development projects that advance a certain cause.

Newspapers Not only are newspaper statistics relatively easy to collect, but they are also sometimes the only continuously available source of event information. Even though there is a problem with bias in the data released in newspapers, it remains an effective tool for gathering information for reporting.

Content Discovered on Websites

Reading Internet articles in order to extract and utilise the information offered there is another type of data collection. The collection of information from web publications is a more efficient and less expensive way. There may be inherent biases in the data collection process, and there may be concerns regarding the confidentiality and security of the data obtained using this method. These are two of the most major disadvantages of using this technique of data reporting.

Hospital Care records

In the health care business, several governmental and commercial data gathering methods are deployed. Health surveys, administrative enrollment and billing information, and medical records are included in these systems. Numerous institutions, including hospitals, CHCs, doctors, and health insurance, employ these systems. The offered material is succinct, impartial, and accurate; nonetheless, it must have been obtained via legal routes, since medical information is subject to the strictest rules.

EXISTING DATA

During this stage, new investigative questions are offered in lieu of or in addition to the questions posed during the first phase of data collecting. It involves combining measurement into a research or inquiry. This is illustrated by retrieving data from a repository.

Pros

The degree of precision is rather high.
Information that is easily accessible.

Cons

Evaluation concerns must be addressed.
Understanding is not simple to gain.

Which Data Collection Tools Are the Most Efficient for Existing Data?

The phrase "existing data" refers to the process of acquiring information from pre-existing sources in order to address research

questions that are distinct from those for which the data were originally collected. Among the available tools for acquiring existing data are:

Unlike newspapers and magazines, which are published for a wide public, research journals are produced for a particular academic or technical audience. A journal is a scientific publication that contains articles written by researchers, academics, and other informed persons.

Surveys are a type of data collection involving the collection of information from a subset of a community in order to extrapolate the results to a larger population. Surveys may be used for a variety of purposes, and their implementation can take a variety of forms, depending on the desired outcomes.

OBSERVATION

Observation is a kind of data collection that includes acquiring information about a phenomenological event via direct experience. The nature of the observation might be conducted in one of four ways: as a complete observer, an observer who also participates in the activity, a participant who also observes it, or a participant who fulfils both roles. This method provides a crucial basis for the creation of a hypothesis.

Pros

Easy to use and administer.
It is possible to get a better degree of accuracy with the results.
It is an internationally recognized standard.
It addresses the issue of respondents' reluctance to submit a report by overcoming their resistance.
There are instances when it is permissible to do so.

Cons

Certain events are not visible in their normal condition.
It cannot be relied upon in any manner.
Bias may arise.
It incurs a substantial expense to handle.
It is impossible to forecast its truthfulness with precision.

Which observational data gathering methods are the most efficient?

Observation refers to the process of actively acquiring knowledge from first-hand sources. Using different sorts of scientific equipment to collect data and record observations is another type of observation. The following are the most effective observational tools:

The use of checklists, which are state-specific criteria, enables users to access information and make decisions on what they should know in relation to the outcomes. They give a systematic approach to the collecting of data on certain behaviours, knowledge, and skills.

Direct observation, a method for gathering evaluative data, is under the field of observational research and studies. The evaluator examines the subject in his or her normal environment without altering that environment.

FOCUS GROUPS

This method of data collecting stresses qualitative research more than quantitative research, which is defined by the collection of numerical data. It is considered the primary kind of information for data based on the feelings and perceptions of respondents. This research comprises asking open-ended questions to a group of people, often between six and 10 individuals, in order to collect feedback.

Pros

In most instances, the gathered information is highly precise.

This strategy leads in substantial cost reductions as compared with individual interviews.

It is a reflection of the efficiency and speed with which results are delivered.

Cons

Insufficient depth in addressing the core issues of a subject.

The risk of prejudice remains.

Interviewer certification is necessary.

The researcher has relatively little control over the ultimate outcome.

A small number of strong voices may quickly overwhelm the others.

Challenges inherent in establishing an inclusive group.

What are the most efficient data collection methods for focus groups?

A focus group is an approach for gathering data in which members are carefully observed and the conversation is structured according to a set of predefined questions. The purpose of the meeting is to learn as much as possible about how the participants would respond to the questions. The following are the most successful focus group tools:

One group watches the responses of the other group to the questions posed by the moderator. After hearing what the other group has to say, the attentive group is in a better position to encourage more discussion and may reach different conclusions than the first group.

In the "dueling-moderator" style, two moderators take turns playing the role of "devil's advocate." The primary benefit of using duelling moderators for a focus group is that it facilitates the generation of new ideas by exposing members to new ways of thinking and diverse perspectives.

COMBINATION RESEARCH

This strategy for acquiring information employs creative methods to stimulate more participation from individuals and groups. In addition to relying on focus groups and interviews to collect qualitative data, this strategy also includes interviews. This technique is crucial when dealing with sensitive subjects.

Pros

Encourage responses from participants.

It enables people to develop stronger bonds with one another.

The respondents' ability to maintain a level of anonymity increases their participation.

Consequently, the received information is of greater quality.

Cons

It is the most costly of the top seven alternatives.

It is the most time-consuming option.

What are the most efficient methods for data collection while doing combination research?

Combination Research is a methodology that combines two or more data collection techniques, such as interviews in addition to questionnaires or semi-structured telephone interviews and focus groups. Examples of such techniques include: The following are the most effective research techniques for combination studies:

Internet-based interviews and the completion of questionnaires are the two modalities that comprise the online survey. There is an internet-based questionnaire that may be completed by the target population. It is fast, efficient, and effective simultaneously. Especially given the quantitative nature of the required data collection.

The two approaches that comprise this dual-moderation strategy are focus group conversations and structured surveys. While two moderators supervise the proceedings, structured questioners give direction for the direction of the research. While one person ensures that the session with the focus group runs well, the other ensures that all of the questions requested are answered. Almost often, focus groups with two moderators result in a more productive session, which increases the quantity of information collected from the experience.

Here Are Seven Tips to Help You Create the Most Effective Surveys for Data Collection:

Specify the objective of your survey. Once the aim of your survey has been determined, it will be simpler to determine which questions should be prioritized. For instance, if there is a clear explanation for why something is happening, there should also be a clear goal that can be achieved. Example: "The goal of this survey is to have a deeper understanding of why workers are leaving an organization."

Employ questions that are not open-ended but rather explicitly expressed. You should avoid open-ended questions and avoid guiding the respondent towards the answer you believe they should provide. If feasible, provide a range of replies along with choice alternatives and star ratings.

The survey findings should have a favourable and promising outlook. A more visually beautiful survey will encourage more individuals to participate and offer comments.

Assure Respondents of the Security of Their Data Because you want your respondents to feel comfortable providing you with their personal information, it is crucial that you reassure them that their data will be safe. It is your obligation to advise respondents that the information they provide will be kept strictly confidential and used only for research reasons.

Ensure that your survey can be completed in record speed; ideally, users should be able to complete a normal survey in less than one hundred seconds. It is essential to remember that responders are providing you with a favour by offering feedback. They should not be subjected to excessive pressure. Keep your comments brief and direct to the point.

Conduct a test survey and examine a preview of it before distributing it to the individuals who are expected to respond. Create a test version and email it to a few persons for their input. On the basis of the replies to your survey, you will be able to make conclusions and determine whether or not it is ready for prime time.

Include a prize in the survey to give users something to look forward to when the survey is completed. Give your respondents something to anticipate upon completion of the survey. Imagine it as a cent for every pound of flesh they sacrificed throughout their battle. This may provide the motivation they need to complete the survey instead of quitting up halfway through.

An Explanation of the Sampling Method in Detail

It is critical that we carefully consider each individual before inviting them to take part in our research and become a member of our sample group. The way in which we choose our participants will determine the size of the population to which our results may be applied, and this will rely on the approach that we adopt (random sampling).

INTRODUCTION TO THE TERMS "POPULATION" AND "SAMPLE" IN RESEARCH

The term "sample" refers to a smaller representative of a larger group or aggregate that has been selected from among all of the individuals that make up that larger group. To phrase it another way, the sample provides a representation that is indicative of the total as a whole.

This more all-encompassing entity is referred to as "the people" and "the universe" in common parlance. This expression is used in a broader sense in the field of study; it refers to a well-defined group that may include humans, items, human qualities, or even the behaviour of insentient things, such as the roll of a dice or the flip of a coin. Additionally, it may refer to a well-defined group that may include humans, items, human qualities, or even the behaviour of insentient things. The behaviour in question may be seen by rolling a dice or flipping a coin, for example.

It is not possible to conduct research that involves each individual member of a population and arrive at a conclusion that can be trusted based on the evidence gathered from that group since doing so would be impractical. In addition, the numbers of populations are often so large that the study of all the units would not only be expensive, but it would also be challenging, time-consuming, and tiresome. This is because it would be necessary to do the research in a very meticulous manner. For example, IGNOU's undergraduate programme now has more than fifty thousand students registered in it. For the aim of our research, it is impossible for us to acquire information on the studying habits of all of these students.

Because of this, in order for a researcher to carry out the survey, they will need to choose a sample from the whole population that is representative of the whole. The process in issue is known as sampling, and its name describes what it does.

It is crucial that the sample correctly represents the characteristics of the population as a whole if we are going to make inferences about the features of the population based on a sample. These conclusions will be based on the sample. In addition to this, it necessitates the selection of a "representative proportion" of the whole

population. In the population, it's conceivable that there are only a set number of persons or units. There are certain contexts in which it is appropriate to speak to the population as "infinite," such as when discussing the varying degrees of atmospheric pressure that may be found in various parts of the atmosphere. Because of this, it is essential to establish a detailed description of a population so that there is no room for ambiguity about the question of whether or not a certain unit is a part of the population. This will ensure that there is no room for confusion. In this case, the researcher would be at a loss to decide which units need to be taken into account when picking a sample since there is no clear pattern to follow. For instance, one of our goals is to reach a degree of knowledge about the methods of education that are used by students who are enrolled in programmes that are offered via distance learning. It is hard to establish who the population is since we are not given any information on which university or universities need to be included in this poll. It is difficult to tell who the population is in this situation since the population is not stated in the proper way. When everything is said and done, there are over nine distinct methods for choosing from among the one hundred educational institutions in India that provide remote learning, not to include the thirteen open universities that are run by the government. As a direct result of this, in order to provide an appropriate description of it, we need to define the group as, for example, students who are enrolled in the undergraduate programme offered by the IGNOU.

The second factor that goes into determining the degree to which a sample is archetypical of the whole population is the determination of the "sampling frame," which is the listing of all the units of the population under distinct headings. This is done so that the sample can be more accurately representative of the whole population. In the study that was just presented, there is the possibility for a wide range of sample frames, which may include male and female students, employed and unemployed students, and students from other backgrounds as well. Before selecting a sample, the sampling frame has to be established, at which time it need to already be exhaustive, accurate, and current.

Thirdly, the examination of a sample need to be conducted in a manner that is unbiased and impartial. It ought should offer all the information there is to know about the people from whom it was taken, if we lived in a perfect world, and it should. According to the induction principle, which indicates that one should go from the particular to the general, this sort of sample would be deemed to be within the margin of error for random sampling. This is because the induction principle implies that one should travel from the specific to the general. This gets us to the results, which are next discussed in terms of "probability."

A sample should not only be accurate in portraying the population as a whole, but it should also be large enough to ensure that its features remain consistent. It is necessary to fulfil both of these prerequisites. Then, what precisely is the most appropriate measurement for the size of a sample? A sufficient sample is one that includes sufficient numbers of instances to assure that the results may be believed. In other words, a sufficient sample is one that meets the criteria for "sufficient." If the characteristics of the population being researched are fairly constant, then a small representative sample will suffice. On the other hand, in order to have an accurate representation of the population as a whole, it is necessary to have a sample size that is far larger than is typical. Therefore, the process for determining the sample size differs based on the sort of characteristics that are being investigated as well as the distribution of those qualities throughout the population. This is because the sample size is used to represent the whole population. In addition, the appropriateness of a sample will be determined not only by the method that was used to generate the sample, but also by our understanding of the population from which the sample was drawn. This is because the sample will only be representative of the population from which it was drawn. For example, if we try to find out the study habits of undergraduate students at Lady Irwin College in Delhi, the population will obviously be more similar to one another than the population of undergraduate students at IGNOU in terms of socio-economic status, employment of students, or study hours available. This is because the population of undergraduate students at Lady Irwin College in Delhi is much smaller than the population of undergraduate students at IGNOU. This is due to the fact

that IGNOU has a more diversified community of students enrolled in its undergraduate programmes. However, it is vital to be aware that even if the sample is of appropriate size, this does not necessarily ensure that the results will be correct. This is something that has to be taken into consideration.

METHODS OF SAMPLING

When attempting to arrive at credible results or conclusions, one of the most crucial considerations to take into account is the method that was used to choose the sample that was used in the study. This topic was brought up in the most recent segment of this conversation. In light of this fact, we are going to move on to a discussion of the various methods of sampling that are accessible in this section here. When it comes to a rough classification, the many different sampling techniques may be broken down into the following two categories:

i) Probability Sampling
ii) Non-probability Sampling

Probability Sampling

When employing probability sampling, the selection of units to sample from a population is done so in a way that is completely random. To put it another way, the researcher does not have any influence over the selection of units to sample; rather, the procedure is carried out in such a way that each unit in the population has an equal chance of being included in the final results. This is because the procedure is carried out in such a manner as to ensure that each unit in the population has an equal chance of being sampled. In the case of something like a lottery, for example, every single individual has the same chance of being selected. The following are some of the properties of a probability sample:

I the selection of units to be included in the sample is made in one or more steps of the sampling procedure that is automated;

ii) the analysis of the sample uses weights that are appropriate in light of the probabilities; and
iii) each individual in the population has a certain chance of being included in the sample that is taken.

The process of conducting probability sampling may be carried out in a number of different ways, and each of these ways has a distinct collection of benefits and drawbacks that are exclusive to that method. An overview of these subjects is provided in the following abbreviated form:

A simple or unrestricted method of sampling is preferred for random sampling.

An example of simple random sampling would be the selection of a sample from a finite population via the use of a procedure in which every unit in the population has an equal chance of being picked [see to item I above]; this would be an example of selecting a sample from a population. In point of fact, you may easily produce a random sample by going through the following steps in the following order:

i) Please provide an explanation of what you mean by "population."
ii) Make a list of all of the units that comprise the population, and number each unit starting with one and going up to n.
iii) Determine the size of the sample, also known as the number of units that will be included in the sample. iv) Compute the standard deviation of the sample.
iv) Choose the units that are going to be included in the sample by either making use of the "lottery approach" or the "random number tables."

For instance, if there are n units in the population, you could use the lottery method to choose a sample at random by making use of a set of n tickets, each of which would have a number from 1 to n printed on it. The numbers on the tickets would be in ascending order, starting with 1 and going all the way up to n. After giving the tickets a thorough shake, the sample of the needed size is selected by selecting the required number of tickets from the shuffled stack. For this example,

let's suppose that the required size is x. It will be determined that the units that have serial numbers that are printed on these tickets are the ones that have been chosen. The success of this tactic is reliant on the assumption that the tickets are jumbled together in such a manner that the population may be seen as being grouped in a way that is completely at random. Before selecting one hundred people at random from the whole population of one hundred thousand undergraduate students at IGNOU, you would write the roll numbers of all of the students on little pieces of paper in a similar fashion.

First, the chits should be mixed together, and then the roll numbers for the five hundred should be chosen.

When drawing a sample from a simple random pool, the most efficient method is to use a table containing random integers as the generator.

These tables, which include random numbers, have been created and are available. The same goes for Yates and Fisher (1967). After having first allotted consecutive numbers to the different units of population, the researcher then moves on to the next step of reading consecutive numbers from the table of random numbers, which may begin at any place. The researcher has the option of reading the successive numbers in whatever orientation they want, including horizontally, vertically, or diagonally. If the number that is read out agrees with the number that is displayed on one of the unit cards, then that unit will be used as the sample. If the numbers do not coincide, then the sample will not be taken from that unit.

The approach known as systematic sampling technique

Through the use of systematic sampling, one is able to produce a distribution of the sample that is more uniform throughout the population list, which eventually results in improved accuracy. The following steps are included as part of the process:

I Create a list of the population units based on some kind of order, such as alphabetical, seniority, street number, house number, or any other similar criteria that you believe to be acceptable.

ii) Figure out the proper sample percentage, such as fifty percent out of one thousand, as well as the number of the Kth unit. For example: [K=N/n= 1000/50 = 20].

iii) Choose one thing from the list for every Kth unit, starting with a number chosen at random between 1 and K, and making sure to include both numbers in the range. In the preceding example, if the number that was chosen at random was 4, the sample would include the fourth, twenty-fourth, forty-fourth, sixty-fourth, and eighty-fourth units of each series that went all the way up to the nine hundred and eighty-fourth unit.

This strategy results in a sample that is on par with that of a plain random sample, and it is a great deal less difficult to put into action. A researcher who is interested in studying the average telephone bill of an area in his or her city could select every fourth telephone holder at random from the telephone directory and find out what their annual telephone bills are. This would allow the researcher to study the average telephone bill of the area. This would make it possible for the researcher to investigate the typical monthly telephone bill of a certain neighbourhood in his or her city. The structure of the population units is not randomised, which is one of the reasons why this method has several drawbacks, which are outlined in more detail below.

i) Periodic effects

It is not at all unusual to come across populations that have a periodic tendency that might be more or less distinct. A few examples of periodic trends or cyclic fluctuations in a given population include the number of students present at a residential university library that is open seven days a week, sales at a store over the course of twelve months in a year, and the flow of road traffic past a particular traffic point on a road over the course of twenty-four hours. All of these examples take place over the course of one year. Under these types of conditions, a systematic sample may not precisely represent the population or might not be beneficial all the time. Alternatively, it could not be useful at all.

ii) Trend

One further drawback of systematic sampling is that very often, "n" is not an essential multiple of "k," which is a factor that has to be taken into account. This is a problem that needs to be taken into consideration. As a consequence of this, the sample will include an unpredictable number of units that are drawn from the same restricted population. Take into consideration the following possibility: A researcher is interested in selecting 20 of the most experienced counsellors from a pool of 100 who are ranked according to the number of years they have been practicing. To begin, the person determines the size of the gap by taking the number that is generated by dividing 100 by 20, which is 5, and using that value. Let's imagine that he or she picks the number 4 at random from the range of 1 to 5 for the first number in the sequence. After that, he or she selects a name every fifth time beginning at 9 and continuing through 14, 19, and so on until he or she has drawn the required number of names, which is 20. If this individual uses the number 2 as their starting point, then another illustration would use the digits 2,7,12,.... Each counsellor's seniority in the second sample is lower than the seniority of his or her counterpart in the first sample. This is because the first sample contains more experienced counsellors. The mean and average of these two samples would be significantly different from one another if we were to compare them based on seniority and the other factors that are associated with it. When starting from a number of different locations, one may be able to gather a large number of samples in this manner; but, there will be greater variation among them.

Calculations that are carried out using samples of this kind are unable to provide insight into the factors that contribute to variability because the 'periodic effects' and 'trend' of the population in question contribute disproportionately to the increase in the samples' overall degree of variation.

The most important advantages of utilizing a technique of systematic sampling are as follows:

a) The calculations are less complicated, and

b) It has a lower overall cost compared to other methods, such as random sampling.

Stratified random sampling is a kind of sampling method.

There are a few different scenarios in which the population that requires a sample cannot be assumed to be uniform. As a consequence of this, rather of selecting people from the overall population at random, the main population is divided into a number of sub-populations that are referred to collectively as strata. One or more of these features are shared by each of these strata, making them all comparable to one another (s). After that, a method known as random selection is used to pick certain aspects of the sample from inside each stratum. Therefore, the sample is representative of each and every strata in its entirety. Because the population is first stratified into its sub-populations before the selection is performed, this method of sampling is referred to as stratified random sampling. This is due to the fact that the condition of random selection is satisfied by the selection that is made inside the strata.

The process of stratified sampling consists of the phases that are outlined in the following list:

I Determining the appropriate stratification characteristics, which may include gender, age, geographical location, the kind of education acquired, and a variety of other factors as well.

ii) The procedure of subdividing the whole population into smaller groups by utilising the stratification criteria as a map to direct the process.

iii) Providing specific information on the individual units that are included in the listing for each distinct subpopulation.

iv) Using a suitable random selection technique to pick the needed number of units from each sub-population in order to finish the selection process. v) Using the units that were chosen in step iv.

v) Combining the samples from the subsamples into a single, bigger sample that will serve as the principal one.

Because of this, the degree to which a sample is representative of the population as a whole may be improved via the use of stratification, which contributes an additional component to the control process. On the other hand, the efficiency of the stratified random sample is dependent on the distribution of the sample size over all of the strata. This is because the strata are divided up into subgroups. There are three

unique ways of allocation that may be used within the context of stratified random sampling, which are as follows:

1. Equal Allocation

When taking a sample of this kind, each stratum provides the same number of items to the total collection as the other strata. As a result, if there are three distinct strata, one third of the sample will be selected from each of the distinct strata. This form of allocation is carried out when there is a balance of population between the strata that are being considered.

2. Proportional Allocation

In this kind of sample, the contribution that each stratum makes to the overall number of samples is proportional to the size of that stratum's share of the population as a whole. When a stratum is larger, it is able to contribute a higher number of people to the sample because of this fact. The level of the sample fraction is held steady at the same value.

3. The Distribution That Is the Most Effective

In optimal allocation, the contributions of each stratum to the sample are calculated in such a way that they are proportionate to the artefact of the strata population sizes and the amount of variation in the dependent variable that exists within each stratum. This ensures that the sample is representative of the population as a whole. The strata that are either larger in size or have a higher degree of variability will provide a greater proportion of the total to the sample. Because precise calculations of the population variability of the dependent variable are seldom available before the sample is selected, the optimal allocation is rarely applied. This is because the optimum allocation needs exact predictions of the population variability of the dependent variable. Because of this need, precise estimates of the amount of variation that exists within the population of the dependent variable are almost never accessible.

When there are no easily available lists of the units or people who make up the population, it is useful to use a stratified random sample because it provides more accurate results. In addition to this, it is useful since the conclusions that it gives are more accurate than those that can be obtained from only random sampling. For instance, in the process of selecting a sample of undergraduate students from the Open University in your country, the researcher may decide that the entire population of undergraduate students should be broken down into males and females, north, east, south, and west regions of the country, and should then be employed in government, private, and autonomous institutions in the country. This decision may be made while the researcher is in the process of selecting a sample of undergraduate students from the Open University in your country. All of them will be their own individual layers or strata. The researchers may choose a sample size ranging from 50 to 15 children from each demographic category. There are several circumstances in which stratification is not possible before the data are gathered.

It's likely that the researcher won't be able to tell to which stratum a unit belongs until after they've finished the survey and analysed the results. Personal characteristics, such as age, gender, social standing, educational level, and so on and so forth, are all examples of such elements that may be used to stratify populations. In situations such as this one, the method includes first acquiring a random sample of the required size, and then secondly classifying the units into a number of distinct strata once the sample has been categorised. The method is highly efficient provided that the sample is large enough, that is, provided that there are more than 20 people in each stratum.

Cluster-based methods for collecting samples

Cluster sampling is utilized in situations in which the population that is being studied is infinite, there is no list of units of population, the geographic distribution of units is dispersed, or when sampling of individual units would be inconvenient for a number of different administrative reasons. It involves segmenting the population into groups or clusters with the purpose of using those groups as the

primary sample units for the data. Following that, a decision is made on which of the clusters are going to be included in the sample. As a result, the sample unit for cluster sampling is the cluster itself, as opposed to an individual member of the population or an item from the population as a whole.

For the purpose of selecting a sample of middle school teachers in a state, for example, you could enlist all middle schools rather than teachers teaching in middle schools and then randomly select ten percent of the middle schools as clusters. Another option would be to select all teachers teaching in middle schools. You would then be able to pick certain middle school teachers as candidates for the sample. After then, the persons who make up the sample might be selected at random from among the educators working at the selected schools, or the sample can be made up of any and all of the educators working at those schools.

A "cluster" may be described as any geographical location in which we find a continuous group of individuals who have characteristics that are similar to one another (members of a population). There are many other kinds of settings that have the potential to be categorized as clusters, including classrooms, schools, hospitals, and study centres. Cluster sampling is an efficient method to utilize, especially in circumstances in which the cost of measuring a unit is comparatively cheap in relation to the cost of travelling to it.

Multi-stage sampling

In order to conduct research with more depth, it is common practise for large-scale surveys to employ many phases of sampling. It's feasible that the researcher may need to take samples in two, three, or even four separate phases.

For the purpose of gathering information from respondents located in various parts of the country, for example, postal questionnaires are often used as the main technique of data collection. It is conceivable for incomplete questionnaires to establish a bias, which would make it difficult to obtain a sample that is representative. This is true despite the fact that the technique is cost-effective. In order to remove this bias, it is necessary to use a sampling method that

consists of two stages. A second sample is gathered from the individuals who did not respond. This sample is selected at random by personal contact with the individuals. By carrying out this action, the dependability of the data obtained from the first sample may be removed from the list of items that need to be validated. In a similar vein, if a researcher is interested in conducting a survey of counsellors located around the nation, he or she may pick a sample consisting of five states, each of which may represent a distinct region: the north, the south, the west, and the centre of the country. A comprehensive database of all of the districts in these five states may be prepared, and then a random sample of thirty to forty districts can be chosen from among them. It is possible to build, using this information, an inventory of all of the study centres that are situated in the different districts. After then, a random selection is made to provide a representative sample of somewhere between 300 and 400 distinct research centres. In addition, counsellors who volunteer to take part in the research are chosen at random from a pool of between 1500 and 2000 individuals. It is also possible to produce a multi-stage sample by randomly picking first the state governments, then the district governments, then the study centres, and finally the individual counsellors. Because of the use of multi-stage sampling, the burden that is imposed on respondents is lessened, expenses are kept to a minimum, time is saved, and an accurate representation of the sub-sample is produced more rapidly and successfully. On the other hand, one should only think about using this strategy if it seems to be difficult to choose a simple random sample.

The correlation between the sample size and the likelihood of an event.
Methods for the Collection of Samples
The Resources That Are At Your Disposal For Research

When the units vary in size, it is desirable to choose a sample in such a way that the probability of selection of units is related to its size. This is the best way to ensure that there is a balanced distribution of results. When attempting to achieve a true and accurate depiction of the people, this is of the utmost importance. One learning centre has a total population of two hundred pupils, whereas another only has one hundred students enrolled. This is only one example. When it comes

time to choose a sample, the first research centre will have access to double the number of individuals that the second research centre will have available to them.

This particular kind of sample is referred to as a PPS sample, which is an acronym that stands for probability proportion to size sample.

Implementation of Computers Into the Procedure of Sample Selection

There are a lot of websites that you may visit, each one of which will provide you with random numbers for your own personal usage.

To provide one example, the website www.randomizer.org may be navigated and used in a very straightforward manner. You will be required to submit answers to a variety of questions the first time you use this website. These questions include the following: how many sets of random numbers are to be formed; how many numbers are to be produced for each set; number range; and so on.

A broad number of software programmes are equipped with the capability to pick samples at random from their respective databases. One example of this sort of software is the Statistical Program for Social Sciences (SPSS) for Windows 15.0 (SPSS, Inc., 2006), which was developed by SPSS. SPSS provides users with two distinct choices when it comes to determining the size of the random sample to be taken:

a. To an exact degree; b. Approximately As its name suggests, precisely calls for an exact or specific quantity, such as 600 out of 2000 Class IX students being indicated. The second option, on the other hand, gives the user the freedom to choose the sampling fraction, which is also sometimes referred to as the ratio of sample size to population size. For instance, one may select thirty percent of all of the students who are now enrolled in Class IX.

There is a wealth of software available on the market today that, in addition to a simple random sample, enables the selection of a random sample based on a more intricate set of criteria than is possible with a plain random sample. You are allowed to use any programme so long as you adhere to the instructions that are outlined in the user manual that comes packaged with the software.

Non-probability Sampling

The term "non-probability sampling," which is also known as "non random sampling," refers to the sampling techniques that do not include any aspect of random sampling at any point in the selection process of the samples. Another name for this technique is "sampling without probability," which is a synonym for "non random sampling." The phrase "non probability sampling" is also used to refer to the same procedure since it is impossible to calculate the likelihood that each individual member of the population will be picked for the sample. This is why the word "probability sampling" is used. When selecting samples for this assignment, the researcher will do so according to his or her own judgement. The availability of the units, the personal experience of the researcher, and the simplicity with which the researcher may carry out a survey are the guiding components in non-probability sampling. Non-probability samples are the sort of samples that are referred to as "non-probability" samples because it is not possible to calculate the chance that any one particular member of the population will be selected for the sample. Depending on the approach that was used, nonprobability samples may be divided into one of three categories: incidental samples, quota samples, and deliberate samples. Each of these subcategories has its own unique set of characteristics. The following is an explanation, although a shortened one, of these various samples:

Incidental sample

The word "incidental sample" is used to refer to samples that have been obtained owing to the easy availability of units. It is also known as a "accidental sample" or a "convenient sample." Other names for this kind of sample are "convenient sample" or "accidental sample." The phrases "convenient sample" and "accidental sample" are concepts that are related. An investigator working for the IGNOU who is conducting a research project on the perceptions that distance students have regarding MDE has the option to conduct interviews with learners who are currently enrolled in the MDE programme and who happen to visit the university for one reason or another. This choice can be made during the course of the research project. These pupils can be reached

without much effort and fulfil all of the criteria that have been established for the study. Nevertheless, despite the fact that they have a predetermined population, there has not been any genuine randomization conducted. This is one of the problems with the research. As a consequence of this, any attempt to arrive at a generalised conclusion under the sorts of circumstances described above will result in wrong assumptions and interpretations. The key advantages of using this approach are the ease with which testing can be performed, the comprehensiveness of the data that is provided, and the convenience with which units can be obtained. Other benefits include the following:

Quota sample

A quota sample is a sort of non-probability sample that is used in the conduct of survey research more often than any other non-probability sample type. This kind of sample is used in situations in which it is physically impossible to list each and every member of the population of interest. It entails the selection of sample units within each stratum on the basis of the judgement of the researcher rather than on the basis of a calculable probability of the individual units being included in the sample. This is in contrast to the probabilistic sampling method, which selects sample units on the basis of the probability that they will be included in the sample. To be more specific, it entails selecting sample units in the way as follows: Imagine that there is a need to conduct a survey covering the whole nation using a quota sampling approach.

In order to carry out quota sampling, the first thing that has to be done is to split the population into several strata based on geographical characteristics such as rural vs urban regions, administrative districts, and so on. This will allow for a more accurate representation of the population. The next thing that has to be done is to figure out how many individuals will be selected from each category of the population. When it comes to the first phases of the sampling process, quota sampling operates in a way that is analogous to stratified sampling. On the other hand, in contrast to probability sampling, it does not always begin with a method for random selection from the beginning of the

process. This is due to the fact that it functions differently. The most basic difference between probability sampling and quota sampling is found in the methods' respective approaches to the selection of the final sample units. The majority of the time, the quota is determined by looking at the percentages of the different groups.

Imagine for a second that there is a researcher who is interested in investigating the viewpoints that university instructors have on the topic of distance learning. First of all, he or she may categorize the instructors at the establishment according to their gender, and then after that, he or she might further categorize them as professors, readers, and lecturers. It is possible that at some point in the future, he or she will make the decision to establish quotas for each of these groups. In this way, the quota sample would include the use of strata; but, selection within the strata would not be carried out in a manner that was entirely random. The information was gathered from the individuals who were easiest to contact and most readily accessible. Those individuals that are harder to communicate with therefore have a less proportion of their voices heard.

Using quota sampling provides a variety of advantages, some of which are that it is more practical, less expensive, and suited to scenarios in which there are missing or incomplete sample frames. Another advantage is that it is suitable for circumstances in which there are missing or incomplete sample frames.

Purposive sample

In certain circles, the term "judgement sample" is used interchangeably with "purposive sample." The reason why this specific form of sample was chosen to represent the whole population is because there are solid reasons for the opinion that it is representative of that group as a whole. The researcher will choose a sample for the study based on his or her prior experience dealing with the group that will be sampled. This will be done to ensure that the results of the study are accurate. For the purpose of conducting research on "gifted" children, for instance, the researcher would, on the basis of his or her prior experience, select particular individuals who have demonstrated exceptionally high levels of achievement in school while excluding all

other students from the sample. This would be done in order to ensure that the results of the study are accurate.

A purposive sample is different from a convenience sample in that, instead of choosing individuals based on their availability at the time of the study, the researcher draws on their previous expertise and experiences to establish the selection criteria for the sample. This is in contrast to a convenience sample, which chooses individuals based on their availability at the time of the study. When talking about purposive samples and arguing for the validity of such samples, the stated criteria serve as the basis that these conversations are based on. In qualitative research, the majority of the sampling is done on purpose. This is due to the fact that the primary emphasis is not placed on individuals who necessarily reflect some larger population, but rather on people who may give rich material for an in-depth study on the specific issue and setting. It is more critical that the participants be able to offer the information that is required than that the sample be as representative as possible.

Purposive sampling is a technique that may be used in qualitative research, and it encompasses around sixteen different kinds of specific approaches that can be utilized in qualitative research. The following are a few instances of such things: selection at random from a pool of candidates for a specific purpose One has the option of picking the required number of persons from among the subjects who were selected purposively when the size of the purposive sample is more than what they are able to work with. The technique in issue is called "random purposive sampling," and its name describes exactly what it does. For example, if the researcher had chosen twenty prospective participants for the study on purpose but could only interview 10 people, they would choose ten subjects at random from the pool of twenty potential participants.

The practice of selecting a limited number of persons who are then charged with discovering other individuals who they feel would make ideal participants for an inquiry is referred to as "snowball sampling." This practice is referred to by the phrase "snowball sampling." When conducting interviews with members of a population, for example, you may ask those being questioned to suggest other

people who might be able to be contacted for additional information or viewpoints about the topic at hand. You may also ask those being questioned to suggest other people who might be able to be contacted for additional information or viewpoints about the topic at hand. After that, you conduct interviews with these new individuals and continue in the same fashion until the information gets saturated, at which point you are unable to obtain any fresh viewpoints from the new persons you have interviewed. For example, a researcher wishes to analyse the opinions of distance learners on the quality of Swayam programmes, but they can only find five people who listen to these programmes. She asks these students if they have any other information that they can share with her.

They give her with a number of other references, and those references in turn create more links of their own. She is able to communicate with a sizeable number of people who are learning Swayam as a result of these ways.

When we do not have access to a sufficient number of people who have the characteristics we are looking for, such as in a situation when possible participants are scattered or not found in clusters, for such populations that are not well delimited nor well enumerated, for example the homeless, snowball sampling is the most useful method. Snowball sampling is also useful when we do not have access to a sufficient number of people who have the characteristics we are looking for.

The technique has the drawback of not providing an accurate image of the genuine distribution of viewpoints within the population that is being researched, which is a disadvantage. People have a tendency to propose people with whom they are acquainted and who share their values; as a consequence, communities of interest that cater to a certain niche are often ignored in favour of those that are bigger and more prominent. You might try asking people to nominate persons who have the same ideas as them as well as those who have the opposite viewpoint as them as a way to make up for this. This might be one option to rectify the imbalance in the situation. An alternate tactic is to start the snowball chain with not just one but many different

people, maybe coming from a range of different social groups. This is an example of an alternative use of the phrase "snowball effect."

Intensity sampling is the process of selecting cases that are rich in information, manifest the phenomenon intensely, and allow for the study of different levels of a research topic without selecting cases that are extreme or deviant. In other words, intensity sampling excludes selecting cases that are extreme or deviant. Examples of intensity sampling include distance tutors who have either extensive or limited experience, excellent or subpar students, students who score above or below the average, and experienced or inexperienced distance tutors. When doing intensity sampling, it is necessary to have both prior information and make an effort to explore the area in order to be able to uncover examples of high intensity. One of the many methods of sampling that may be used in conjunction with many other procedures is known as intensity sampling. For instance, one may collect fifty samples and then, for the purpose of conducting a more in-depth analysis, choose a smaller set of really severe situations.

The practice of selecting people who are considerably similar to one another in terms of their experiences, attitudes, or perspectives is referred to as homogenous sampling. This makes it more simpler to collect and analyze data, while also lowering the amount of variation that occurs. For instance, rather than focusing on enrolling as many students as possible in all of the many professional programmes that can be completed online, the school may decide to focus on only one programme at a time, such as the B.Ed. programme by itself. This allows the school to better cater to the needs of its students.

The use of stratified purposive sampling elucidates the characteristics of certain subgroups of interest and makes it simpler to compare the many different groupings.

In criteria sampling, a criterion is first set, and then all of the examples that satisfy that criterion or have some feature are picked. This process begins with the selection of the cases that have the criterion. For instance, all of the distance instructors with ten years of experience might be sampled, as well as all of the distant learners who fell out of the formal system but finished the programme via the distance mode of instruction. Both groups of individuals may be

surveyed. This particular method of sampling delivers the greatest possible standard of quality control and assurance.

Extreme and deviant case sampling is a method that involves learning from highly unusual manifestations of the subject of interest. Some examples of this method include learning from exceptional triumphs or substantial failures. Learning from previous situations' illustrative cases is the focus of this strategy.

When the sample size that needs to be picked is relatively small and the researcher wishes to gain an understanding of the features of the population in a short amount of time, non-probability samples are often regarded as being more convenient than probability samples. This is because non-probability samples can be selected at random, whereas probability samples require the researcher to select each member of the sample at random. In circumstances such as these, the primary objective of the researcher is to get insight into the problem at hand by selecting just those individuals who are capable of providing the greatest quantity of information on the problem.

The use of non-probability sampling methods is associated with the following list of inherent restrictions, which can be found in the following order:

i) There is not yet a statistical theory that has been developed to quantify the dependability of data obtained through purposeful or other non-random sampling methods. The reason for this is that it is not possible to select samples of this kind at random. Because of this, there is no reason to put any trust in the data that were acquired from such samples, and one cannot generalise the conclusions to the whole population as a result of their findings.

ii) The use of selective sampling based on convenience has an influence not only on the variation between groups but also on the variation within each group. This is because the convenience of the sampling method is taken into account. In addition, there is no statistical method that can be utilized to determine how much of a margin of error is associated with sampling.

iii) There are times when such samples are based on an obsolete frame that does not cover the population in a manner that is deemed acceptable.

The Process of Choosing Which Sampling Method to Employ

A lot of criteria that are unique to the current project being worked on are taken into consideration in order to make a decision on the method of sampling to use. These include concerns regarding the definition of population, the availability of information regarding the structure of the population, the parameters to be estimated, the objectives of the analysis including the required degree of precision, and the availability of financial and other resources. In addition, there are concerns regarding the availability of information regarding the structure of the population. In addition to this, there are issues with the parameters that need to be approximated. Because of this, selecting a sample for the operation of any kind of research study has to be done with extreme caution.

Those characteristics that make an outstanding illustration

It is important for a decent sample to have the characteristics of I Representativeness and (ii) Adequacy. The characteristics of a good sample are as outlined above.

It is very essential for the information gained from the sample to be "representative" of the population as a whole for it to be possible to generalise the findings of the sample to the whole population. The term "representative sample" refers to an ideal "miniature" or "replica" of the population from which it was selected. This "miniature" or "replica" may be thought of as an exact representation of the population. This is what is intended when the phrase is used. To put it another way, the average of the characteristics of the components that make up the sample is the same as or very near to the average of the qualities that make up the population. This is the case because the sample is representative of the population.

A good sample should also be "adequate," which means it should be of sufficient size to establish faith in the stability of the attributes it has. This is one of the criteria for determining whether or not a sample is adequate. When determining whether or not a sample satisfies the requirements for an acceptable one, one of the factors that is considered is whether or not it has a sufficient number of examples. Because of this, determining the size of the sample in advance is something that

has to be done as soon as possible. Both the nature of the traits that are being analysed and the manner in which they are distributed have an effect on the fluctuations that are seen. It is possible to point out that the findings will not necessarily be accurate even if the representativeness and adequateness of the sample are satisfactory. The techniques of data collection and sampling both need to be properly selected and implemented in order to attain a higher degree of accuracy in the conclusions drawn about the population and the generalizations that are drawn from those conclusions.

Certain study data are qualitative in character. Qualitative data include information on the attitudes, opinions, or behaviours of workers, customers, sales people, and others. In research conducted in the fields of psychology and sociology, the words "attitude" and "opinion" have often been distinguished from one another. The difference between an opinion and an attitude that is often made is that an opinion is a verbalization of an attitude, while an attitude is seen as a tendency to behave in a specific manner. As a result, the assertion made by a respondent that he favours watching television shows in colour as opposed to black-and-white would be considered an opinion that expresses one facet of the respondent's attitude toward colour television. Evaluation of attitudes is necessary for determining things like as motivation, commitment, level of satisfaction, and the efficacy of leadership, among other things. In order to accurately assess this qualitative data, measuring scales are required.

Different kinds of measurement scales that might be found in research

Research employs nominal, ordinal, interval, and ratio scales of measurement, each of which is a distinct kind of measuring system. The kind of scale and degree of measurement are both defined by the rules that are employed to assign numbers to things. The following provides a concise explanation of each scaling type:

The nominal scale is the most straightforward approach to the measuring of quantities. A variable that is assessed using a nominal scale is one that can be separated into two or more categories. For instance, gender may be classed as either male or female, and the response to the question of whether or not a family has an iPhone can

be either "yes" or "no." It is nothing more than a sorting procedure in which all of the persons, units, or responses may be put in either one of two groups (i.e. the categories are exhaustive). One of the most important aspects of a nominal scale is that each person is distinct from one another in terms of the variable being measured, and that the categories can be differentiated from one another (i.e. the categories are mutually exclusive). This aspect of categorization is essential to the operation of each and every scale of measurement. Nominal scales that only have two categories, such as female and male, agree and disagree, aware and oblivious, yes and no, are considered to be dichotomous scales and are considered to be unique. Due the numerical labels for the two scale categories may be considered as if they are of interval scale value, dichotomous nominal scales are relevant to researchers. This is because of the importance of interval scale value.

Ordinal Scales: Ordinal scales have all of the features that a nominal scale has, but in addition, categories may be ordered along a continuum, in terms of a particular criteria. Ordinal scales have all of the properties that nominal scales have. On an ordinal scale with three categories labelled A, B, and C, one could be able to argue, for instance, that A is greater than B, and one might also say that B is greater than C. If numerals are assigned to the categories of an ordinal scale, those numerals serve only as ranks for ordering observations from least to most in terms of the characteristic that was measured. They do not indicate the distance between scales that organise observations in terms of categories such as high, medium, and low or strongly agree, agree, not sure, disagree, and strongly disagree. If numerals are assigned to ordinal scale categories, those numerals serve only as ranks for ordering observations from least to most in terms of the characteristic that was measured

Interval Scales: Interval scales combine all of the qualities of nominal and ordinal scales, in addition to indicating the distance or interval between the categories. Interval scales are a hybrid of nominal and ordinal scales. Not only is it possible to assert in a formal sense that A is higher than B and that B is higher than C, but one can also state that (A-B)=(B-C) or that (A-C)=(A-B)+ (B-C). Age, income, and investment portfolios are all good examples of interval scales. On the

other hand, a scale is said to be interval if there is no absolute zero point. It may be located anywhere along a continuum; for example, a person's age can be anywhere from 20 to 60 years old; it does not necessarily have to begin at 0 years old. The ratio comparison, which states that A is twice that of B or such, is invalidated by this.

The ratio scale is a subtype of the interval scale that varies from other interval scales in that it features a real zero point, which is a point at which the quality being measured is assumed to be missing. This point distinguishes the ratio scale from other interval scales. Some examples of ratio scales include length, weight, income, and other expenses as well as other metrics. In each, the thought of having no income, weight, or anything else is present. As a general rule, ratio scales and interval scales are not differentiated from one another, and both names are used interchangeably. This is due to the fact that ratio scales are a more precise form of interval scales.

The four different kinds of scales that have been discussed so far each have their own particular way of measuring things. Nominal and ordinal scales have the characteristic of having a fixed number of distinct categories to which points are allotted. Therefore, the only possible values for a variable like the number of households who possess a BMW or iPhone are zero, one, two, three, and so on. Due to the fact that the units are integers and cannot be divided, it cannot have values such as 1.5 or 2.5. However, interval and ratio scales are able to accept any value between two integers since the variables in these scales are continuous. For instance, given any two ages, regardless of how close they are to one another, it is feasible to discover a third that falls somewhere in between. Interval and ratio scales are preferable than normal and ordinal scales, and their analysis may make use of a wide variety of statistical methods. Normal and ordinal scales are not as flexible as interval and ratio scales. The many statistical tools and measurement scales used in research are connected in the sense that there is typically a correlation between the mathematical assumptions behind each statistical instrument and the assumptions underlying each measurement scale. Always make sure that the instruments you're using correspond to the scale of measurement of the variables you're working

with, and make sure that the technique you're using indicates a greater scale measurement than the variable really permits.

Sources of error in measurement

Measurement Errors in the Scientific Research Methodology

In a perfect research study, the measurements of errors in measurement would be clear and unambiguous. This purpose, on the other hand, is not always accomplished in its full. As a result, the researcher has to have an understanding of the factors that contribute to measurement inaccuracy. The following are some of the potential factors that contribute to measurement errors.

Responder: Sometimes the respondent could be hesitant to voice strong negative sentiments, or it's conceivable that he might have very little information but might not accept his ignorance. It's also possible that he might have very little knowledge but might not admit his ignorance. Because of all of this hesitation, the interview will probably consist of a lot of "guesses." The capacity of the responder to react precisely and completely may be hindered by fleeting circumstances such as exhaustion, boredom, or worry, amongst others.

The characteristics that are present in the situation might also make it difficult to get accurate measurements. Any circumstance that makes the interview more difficult will likely have a negative impact on the relationship between the interviewer and the responder. For example, if there is another person there, that person may influence the replies either by taking part in the conversation or just by being there. It is possible that the responder may be hesitant to convey certain thoughts if he believes that his anonymity is not guaranteed.

The interviewer has the ability to skew replies by changing the phrasing of questions or switching their sequence. His demeanour, mannerisms, and appearance might either promote or discourage certain responses from responders. The results might have been skewed due to careless mechanical processing. Inaccurate coding, improper tabulation, and/or incorrect statistical computations are additional potential sources of error, especially during the stage of the process when data analysis is being performed.

Instrument: An inaccurate reading may be obtained due to a malfunction in the measuring instrument. A number of factors, including, but not limited to, the use of difficult words that are beyond the comprehension of the respondent, ambiguous meanings, poor printing, insufficient space for responses, response choice omissions, and so on, all contribute to the defective nature of the measuring instrument, which can lead to measurement errors. Another form of instrument flaw is one that results in an inadequate sample of the whole set of things that are of concern.

The researcher has to be aware that accurate measurement is contingent on properly resolving all of the issues that have been outlined above. In order to prevent the final findings from being tainted throughout any way, it is imperative that he makes every effort to eradicate, nullify, or otherwise deal with any and all potential errors in the process.

Measures of central Tendency and Measures of dispersion

What exactly is meant by "Central Tendency"?

A descriptive overview of a dataset that is represented by a single number that represents the centre of the data distribution is referred to as the central tendency. In descriptive statistics, the central tendency of a dataset is one of the subfields, along with the variability (dispersion) of the data.

One of the most fundamental and fundamentally important ideas in statistics is the central tendency. Even while it does not give information on the specific values that are included in the dataset, it does provide a complete overview of the dataset as a whole.

Calculations of the Mean and Variance

In most cases, the following metrics may be used to provide an accurate description of a dataset's central tendency:

A dataset's mean, also known as its average, is calculated by taking the sum of all the values in the dataset and dividing it by the total number of values.

The value that is in the centre of a collection of numbers that are ordered from lowest to highest (from the smallest value to the largest

value). When a dataset has an even number of values, the median of the dataset is determined by taking the mean of the two values that are in the centre of the dataset.

The mode of a dataset is defined by the value that appears the most often. Some datasets could have more than one mode, while others might not have any mode at all. This depends on the specifics of the dataset.

Even though the aforementioned measures are the ones that are used to identify central tendency the most often, there are a few others, such as the geometric mean, the harmonic mean, the midrange, and the geometric median. These are not the only measures available, however.

The characteristics of a dataset should be taken into consideration before deciding on a central tendency measure to use. For example, the sole central tendency measure that can be used with categorical data is called the mode, although the median is most useful when working with ordinal data.

In the case of quantitative data, the mean is often thought to be the most accurate indicator of the central tendency; however, this is not always the case. It's possible, for instance, that the mean won't function very well with quantitative datasets that include values that are either exceedingly high or extremely low. It's possible that the extreme numbers will skew the mean. As a result, you may think about taking further actions.

You may calculate the measures of central tendency by using a formula or looking up the definition. In addition, one may recognize them via the use of a frequency distribution graph. It is important to take note that the mean, the median, and the mode are all positioned in the same place on the graph when the data follows a normal distribution.

Suppose you are given a data series. Someone has asked you to discuss some fascinating information about this data series. How can you do so? You may state that you are able to tell about the distribution of these data by finding the mean, the median, or the mode of this data series. But is it the only option you have available to you? Is there no other method for us to learn about the focus of the observation except looking at the key tendencies? In this part, we will get further

knowledge about the data by becoming familiar with another measurement. The measure of dispersion is what we are going to learn about in this section.

What exactly is the dispersion?

The 'distribution' of things over a vast area is what we mean when we talk about dispersion. In statistics, the term "dispersion" refers to the extent to which numerical data are scattered or compressed around an average value. In other words, dispersion measures how close numerical data are to the average. The scattering of data is what it boils down to, in a nutshell. There will always be a large quantity of data that is either densely packed or widely scattered. Information with a large range of values, such as 0, 30, 60, 90, and 120. With little data clustered closely together as 1, 2, 2, 3, 3, 4,...

Understanding Dispersion

The degree to which a collection of data is scattered is referred to as its "dispersion." The dispersion measure is always a non-negative real number that begins at zero when all of the data is the same and climbs as the number of different data points increases. Dispersion metrics are what determine whether or not the dispersed data have a homogeneous or heterogeneous distribution. Additionally, it refers to the ways in which the data vary from one another.

Dispersion Quantification and Measures

The metric known as dispersion illustrates the scatterings that are present in the data, as its name indicates. It offers a clear picture about the distribution of the data and reveals how different the data are from one another in terms of variation. The measure of dispersion reveals whether or not the observations are distributed in a manner that is homogenous or heterogenous.

Imagine that you have four datasets of the same size, and that the mean of all of them is the same number—call let's it m. In any scenario, the total number of observations will amount to the same value. The measure of central tendency is not providing an accurate

and comprehensive picture of the distribution of the data for the four sets that have been provided.

If we learn about the distances that the observations have from one another both inside and across the datasets, is it possible that this will provide us some insight into the distribution? The primary goal of the dispersion measure is to provide insight into the manner in which the data are dispersed. It illustrates the degree to which the data deviate from their mean value.

Measures of dispersion have certain characteristics.
A rigorous definition has to be established for a dispersion measure.
It ought to be straightforward to compute and comprehend.
Not much influenced by the shifting patterns of observations
Given all that has been seen
Measures of Dispersion Are Divided Into Several Categories
The following kind of measurements make up the dispersion:
I An absolute measure of dispersion that takes into account:
The dispersion of the observations is expressed by the metrics in terms of distances, such as the range and the quartile deviation.
A measure that describes differences in terms of the average of deviations from observations, such as the mean deviation and the standard deviation, is called a measure.

(ii) A relative measurement of dispersion that takes into account:

When comparing the distributions of two or more data sets, as well as when doing unit-free comparisons, we look at the dispersion using a relative measure. The coefficient of range, the coefficient of mean deviation, the coefficient of quartile deviation, the coefficient of variation, and the coefficient of standard deviation are the names given to these statistical measures.

Different Types of Dispersion Measurements

The observations and varieties of central tendency measurements that are used both have a continuous influence on the dispersion. These are some examples of measures that may be used to disperse:

Range
Variation away from the middle point
The standard error of the mean
The standard error of the mean
Range

The term "range" refers to the disparity in value that exists between the lowest and highest points in each series. The range gives us a decent sense of how scattered the data is, but in order to determine the dispersion of data based on central tendency measurements, we need additional measures of variability. A range is the most frequent kind of dispersion measurement, and it is also the most straightforward to comprehend. It is the gap between the two most extreme observations in the data collection. If the maximum and minimum values of X are the two most extreme observations, then...

Range = X max – X min
The Value of the Range
It is the most straightforward method for determining dispersion.
It is simple to compute.
Simple and easy to grasp
Unaffected by a shift in the point of origin
Demerits of Range

It is based on two quite different kinds of observations. Therefore, allow yourself to be influenced by changes.
Dispersion cannot be accurately measured based on range alone.
Dependent on change of scale
Quartile Deviation

The quartiles split a data collection into quarters. The first quartile, abbreviated as Q1, is the number that falls exactly in the centre of the data set, between the lowest number and the median. The median of the data set is located in the second quartile, often known as Q2. The number that falls in the third quartile, also known as Q3, is the one that is in the halfway between the median and the highest number.

Quartile deviation or semi-inter-quartile deviation is
$Q = ½ \times (Q3 – Q1)$
Considerations Regarding the Quartile Deviation

All of the limitations of Range are addressed by its departure from the quartile.

It utilises 50% of the available info.
Unaffected by a shift in the point of origin

The most accurate representation of the open-end classification's dispersion

The Positive Aspects of the Quartile Deviation
It disregards fifty percent of the available data.
Depending on the degree of the shift in scale
A measure of dispersion that cannot be relied upon
Variation from the Mean

The arithmetic mean of the absolute departures of the observations from a measure of central tendency is what is meant by the term "mean deviation." If the set of observations is comprised of x1, x2,..., xn, then the mean deviation of x from the average A (mean, median, or mode) is calculated as

The standard deviation of the mean, A, is equal to 1 n I xi minus A].
It is computed as follows for a frequency that is grouped:
The mean value of the departure from the average A is equal to 1N I fi $|xi – A|]. , N = \sum fi$

Here, the median value of the ith class interval, denoted by xi, as well as its frequency, denoted by fi, are shown.

The Value of the Standard Deviation
Given all that has been seen
It provides a minimal value when the deviations from the median are taken into consideration.

Unaffected by a shift in the point of origin

The Positive Aspects of Standard Error

Not readily digestible by the average person

The computation of it is not simple and takes a lot of time.

Depending on the degree to which the scale is altered

Lack of understanding of the negative sign leads to the creation of artificiality and renders further mathematical treatment pointless.

The standard deviation of values

The positive square root of the arithmetic mean of the squares of the deviations of the provided values from their arithmetic mean is the formula for what statisticians refer to as a standard deviation. It is represented by the Greek letter sigma, which may be written as. A different name for this concept is root mean square deviation. The expression for the standard deviation is:

$$\sigma = [(\Sigma i\ (yi - \bar{y})/n]\ ½ = [(\Sigma\ I\ yi\ 2/n) - \bar{y}\ 2]\ ½$$

It may be shown that, with a clustered frequency distribution,

$$\sigma = [(\Sigma i\ fi\ (yi - \bar{y})/N]\ ½ = [(\Sigma i\ fi\ yi\ 2/n) - \bar{y}\ 2]\ ½$$

The variance is equal to the square root of the standard deviation. In addition to that, it is a measurement of dispersion.

$$\sigma\ 2 = [(\Sigma i\ (yi - \bar{y})\ /\ n]\ ½ = [(\Sigma i\ yi\ 2/n) - \bar{y}\ 2]$$

It may be shown that, with a clustered frequency distribution,

$$\sigma\ 2 = [(\Sigma i\ fi\ (yi - \bar{y})/N]\ ½ = [(\Sigma\ I\ fi\ xi\ 2/n) - \bar{y}\ 2].$$

If we choose any other random number, let's say A, as the new mean, the standard deviation will be transformed into the root mean deviation.

The Combined Series in its Variant Form

If 1 and 2 are two standard deviations, then n1 and n2 are the sizes of the two series, and 1 and 2 are the means of each series. The standard deviation of the two series of sizes, n1 and n2, is calculated as follows:

$\sigma 2 = (1/ n1 + n2) \div [n1 (\sigma 1\ 2 + d1\ 2) + n2 (\sigma 2\ 2 + d2\ 2)]$

where, $d1 = \bar{y}\ 1 - \bar{y}$, $d2 = \bar{y}\ 2 - \bar{y}$, and $\bar{y} = (n1\ \bar{y}\ 1 + n2\ \bar{y}\ 2) \div (n1 + n2)$.

The Values Behind the Standard Deviation

By quadrupling the deviations, one may get around the disadvantage of disregarding signals in mean deviations.

Appropriate for further mathematical investigation.

The one least impacted by the inherent variability of the observations

If all of the observations remain the same across time, the standard deviation will equal zero.

Unaffected by a shift in the point of origin

The positive aspects of deviating from the norm

It is not simple to compute.

Difficult to comprehend for the average person

Depending on the degree to which the scale is altered

The value of the dispersion coefficient

Whenever we wish to make a comparison between the two series, despite the fact that their averages are quite different from one another. In addition, instances in which the unit of measurement varies. In addition to calculating the dispersion measure, we need to also compute the coefficients of dispersion. The coefficients of dispersion, abbreviated as C.D., are calculated using a variety of metrics of dispersion.

Based on Range = (X max – X min)⁄(X max + X min).

The coefficient of variation, based on the quartile deviation, is calculated as (Q3 – Q1) (Q3 + Q1).

Calculated based on the mean deviation, which is defined as the standard deviation divided by the average.

The formula for calculating standard deviation is as follows:

Variational Coefficient of Error

The coefficient of variation equals the coefficient of dispersion multiplied by 100. It is calculated using the standard deviation (C.V.).

C.V. = 100 (Standard Deviation / Mean) = (/) 100

Example Formulation Regarding the Measurement of Dispersion

The values of the findings for both Company A and Company B are included in the following table, which can be found below.

	Company A	Company B
Number of employees	900	1000
Average daily wage	Rs. 250	Rs. 220
Variance in the distribution of wages	100	144

Which of the companies has a higher total payroll expense?

Perform the necessary calculations to determine the coefficients of variation for both of the businesses.

Determine the daily average salary as well as the standard deviation of the wage distribution for all of the workers that work for both companies A and B combined.

Solution:

Regarding Company A

The number of workers is equal to 900, and the average hourly salary is equal to Rs. 250.

We are aware that the formula for calculating the average daily salary is total wages divided by the total number of workers.

Alternatively, Total Wages = Total Employees Times Average Daily Wage = 900 Times 250 = Rs. 225,000... (i)

Regarding Company B

The number of workers is equal to n2 = 1000, and the average hourly salary is equal to 2 = Rs. 220.

Therefore, Total Wages equals Total Employees times the Average Daily Wage, which is 1000 times 220, which equals Rs. 220000... (ii)

When we look at I and (ii), we see that Company A has a higher total payroll expense.

Regarding Company A

The standard deviation of the pay distribution is 12 times 100.

The coefficient of variation of wages is equal to one hundred times the standard deviation of the pay distribution divided by the average daily salary.

Or, C.V. A = $100 \times \sqrt{100/250} = 100 \times 10/250 = 4$ … (i)

Regarding Company B

The standard deviation of the pay distribution is - 22 times 144.

C.V. B = $100 \times \sqrt{144/220} = 100 \times 12/220 = 5.45$ … (ii)

When we look at I and (ii), we see that Company B has a larger degree of variability.

When Companies A and B are considered together

When both firms are considered combined, the average daily pay are as follows:

$\bar{\bar{y}} = (n_1 \bar{y}_1 + n_2 \bar{y}_2)/(n_1 + n_2) = (900 \times 250 + 1000 \times 220) \div (900 + 1000) = 445000/1900 = \text{Rs. } 234.21$

The combined variance, $\sigma^2 = (1/n_1 + n_2) \div [n_1 (\sigma_1^2 + d_1^2) + n_2 (\sigma_2^2 + d_2^2)]$

Here, $d_1 = \bar{y}_1 - \bar{\bar{y}} = 250 - 234.21 = 15.79$, $d_2 = \bar{y}_2 - \bar{y} = 220 - 234.21 = -14.21$.

Hence, $\sigma^2 = [900 \times (100 + 15.79^2) + 1000 \times (144 + -14.21^2)]/(900 + 1000)$

or, $\sigma^2 = (314391.69 + 345924.10)/1900 = 347.53$.

Graphical representation of Data

The display of facts and information may also be done via the use of graphical representations, in addition to diagrams. The presentation of time series and frequency distributions is often done via the use of graphs. In this piece, we will discuss the graphical display of data and information, including its advantages and disadvantages, as well as the many formats it may take.

Building a Graph from Scratch

The graphical representation of facts and information provides a fast and straightforward method for comprehending the characteristics

and making comparisons. Additionally, it is a useful analytical tool, and a graph may assist us in locating the mode, median, and other important values.

We are able to determine the location of a point on a plane by using two lines that are perpendicular to one another: the X-axis, which is the horizontal line, and the Y-axis (the vertical line). The Origin is located at the spot where these two paths meet.

We are able to determine the location of a point by using the distance that it is from both of these axes. For instance, if a point P is located 3 units away from the Y-axis and 5 units away from the X-axis, then the following information may be used to determine its location:

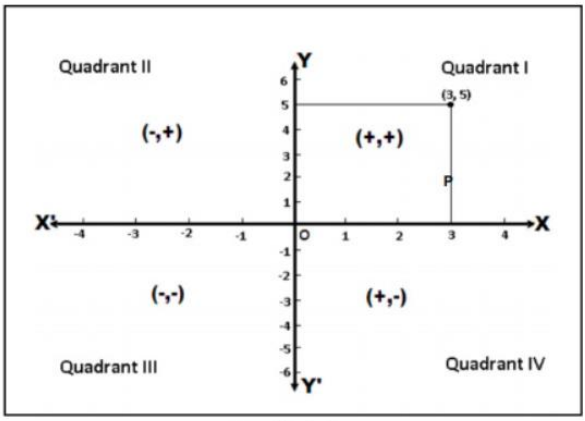

Graphical Plane

Several things to keep in mind:

We take a measurement along the X-axis to determine how far away the point is from the Y-axis. In a similar manner, we determine how far the point is from the X-axis by measuring its distance along the Y-axis. As a result, in order to measure three units away from the Y-axis, we must travel three units along the X-axis, and the same logic applies to the opposite coordinate.

After that, we will draw lines that are perpendicular to these two spots.

The location of the point P is determined by the intersection of the perpendiculars at this point.

The notation for it is as follows: (3, 5) or (abscissa, ordinate). They constitute the coordinates of the point P when taken together.

The word "Quadrant" refers to each of the four sections of the aircraft.

Additionally, we are able to plot unique points for each unique combination of value.

Standard Operating Procedures for the Visual Representation of Data and Information

There are certain recommendations to follow in order to create a graphical representation of facts and information that is both appealing and useful. The following describe each of these:

Appropriate Title - It is imperative that you provide the graph with an appropriate title that unmistakably communicates the nature of the material that you will be presenting using the graph.

Below the title, you should provide the unit of measurement in a way that is easy to understand.

Select an Appropriate Scale It is important that you select an appropriate scale so that you can accurately portray all of the data.

Index: Include a short index that describes the various colours and shades, lines and patterns that you have used in the graph. This should be done at the end of the graph. In addition, a scale of interpretation should be included for improved comprehension.

Data Sources Whenever it is feasible to do so, include a list of the information's origins at the very bottom of the graph.

Keep It Simple - When creating a graph, you should aim to create something that even a person who has had no prior experience in the fields of statistics or mathematics can comprehend.

A graph is a handy visual tool that may be used to convey facts and statistics in an organised fashion. As a result, you are obligated to maintain its tidiness and attractiveness. Pick the proper dimensions, the right text, and the right lines, colours, dashes, and other elements.

The Positive Aspects of Graphs

The data is presented in a form that is much simpler to comprehend thanks to the graph.

In contrast to tables, it enables us to show statistical information in a format that is visually appealing. At a glance, users are able to comprehend the primary characteristics, patterns, and variations included within the data.

Time may be saved with a graph.

The user is given the ability to compare data pertaining to two distinct time periods or geographical areas.

A viewer does not need to have any previous understanding of mathematics or statistics in order to comprehend the information shown in a graph.

Finding the numbers that represent the mode, median, and mean of the data may be accomplished with the use of a graph.

It may be helpful for making predictions, as well as when interpolating and extrapolating data.

Constraints imposed by a Graph

A graph does not display information with total precision.

It just illustrates a small number of carefully chosen aspects of the data.

We are unable to utilise a graph as evidence to support our claim.

A graph is not an acceptable replacement for tables.

In most cases, it might be challenging for non-experts to comprehend and make sense of a graph.

In most cases, a graph will display an implausible trend in the data, but the real values will remain obscure.

Different kinds of graphs

There are two distinct kinds of graphs: graphs depicting a time series diagrams showing the distribution of frequencies

Time Series Graphs

A graph known as a "histogram" or a "time series graph" is one that illustrates the value of a variable over the course of a number of distinct points in time. In a graph depicting a time series, time is the

most significant variable, and the variable is connected to time in some way. It is helpful in understanding and analysing the changes that occur in the variable at various points in time. These graphs are used by a lot of statisticians and businesspeople since they are simple to grasp and also because they present complicated information in an easy-to-understand way.

In addition, the user does not need to have any specific technical abilities in order to design a time series graph. The building of a time series graph consists of a number of important phases, which are as follows:

Place the passing of time along the axis labelled "X," and the value of the variable along the axis labelled "Y."

The Y-value should begin at zero, and you should think of an appropriate scale that will let you show all of the data in the space that is available to you.

Create a graph of the variable's values while connecting the various points with a straight line.

It is possible to plot numerous variables using a variety of lines.

Line Graph

You may make a summary of how two different pieces of information are connected to one another and how they fluctuate with one another by using a line graph.

Advantages

You can compare numerous continuous data-sets simply

From the line on the graph, you may deduce the data during the interim period.

Disadvantages

Only continuous data may be utilised with this method.

Utilization of a fictitious base line

In a graph, the Origin is often the point at which the vertical line begins. However, in some circumstances, a fabricated Base Line will

be used in order to get a more accurate depiction of the data. There are two instances in which you should make use of a fictitious Base Line:

In order to emphasise the relatively little changes that occur in the time series,

In order to make the most efficient use of the area

Net Balance Graph

If you need to demonstrate the net balance of income and expenditures, revenue and expenses, imports and exports, or anything else along those lines, you will need to utilise a graph that shows the net balance. You may utilise a variety of hues or tones to differentiate between good and negative aspects.

Graphs Showing the Distribution of Frequencies

Let's have a look at the many forms of graphs that represent frequency distributions.

Histogram

A graph of a clustered frequency distribution is referred to as a histogram. The class intervals are shown along the X-axis of a histogram, and the relative frequencies of each class are plotted along the Y-axis. In addition to this, we draw a rectangle on each class interval, with the height of the rectangle being proportional to the frequency density of the class.

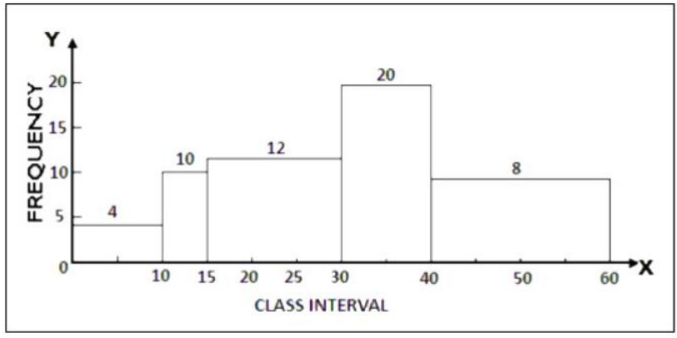

Histograms as well as Frequency Polygons

On a graph, another means of displaying a frequency distribution is by the use of a frequency polygon or a histograph. To create a

frequency polygon, you start by drawing a histogram. Then, you take the midpoints of the top widths of the rectangles that are adjacent to each other and unite them with straight lines.

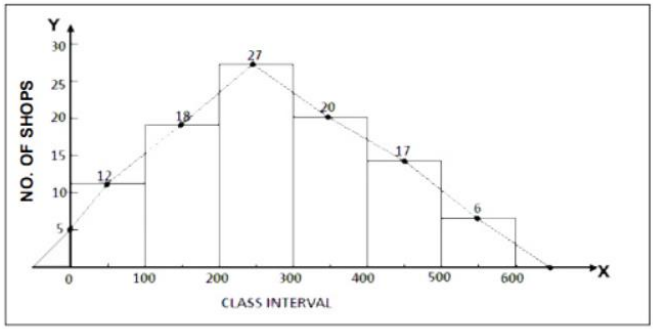

FREQUENCY POLYGON

Diagram Showing the Frequency Curve

A Frequency Curve is the name given to the figure that is produced when the verticals of a polygon are connected by means of a smooth curve. As the total number of observations grows, we will need more classes to handle the workload. As a result, the breadth of each class becomes narrower. In this kind of situation, the variable has a greater likelihood of becoming continuous, and the frequency polygon will begin to take on the form of a frequency curve.

The Cumulative Frequency Curve, Also Known as the Ogive

The graphical depiction of a cumulative frequency distribution is called an Ogive, often known as a cumulative frequency curve. Ogives may be divided into two categories: "less than ogives" and "more than ogives" due to the fact that the kind of cumulative frequency can either be "less than" or "greater than."

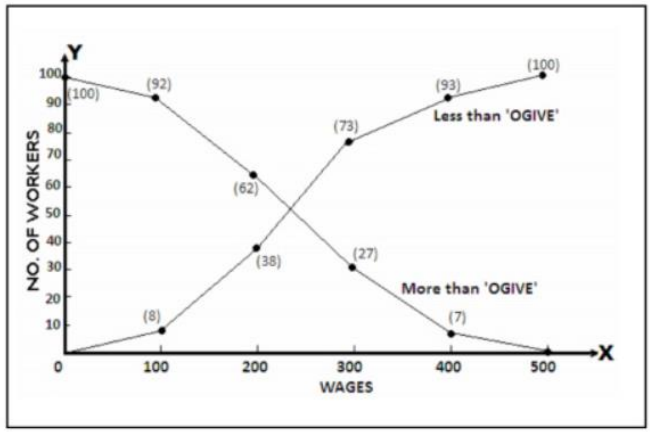

Scatter Diagram

The nature of the connection that exists between the variables may be determined with the use of a dot chart or a scatter diagram. If there is a large amount of dispersion between the plotted points, then there is less of a correlation between the two variables.

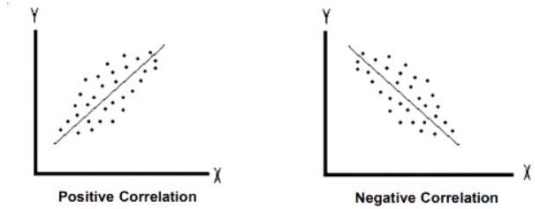

Illustrations of Inferential Statistics

Because it is possible to form conclusions about the population even while the entire data have not been collected, inferential statistics is a particularly helpful and cost-effective method of statistical analysis. The following is a list of some instances of inferential statistics:

Assume that the average grades of one hundred students from a certain nation have been determined. Inferential statistics allow for an approximation of the mean marks earned by students throughout the nation based on the information provided in the sample.

Imagine that a coach at a college wants to find out how many average cartwheels sophomores at his school can do in a row without pausing. A random selection of students will be questioned about their ability to do cartwheels, and then the average will be determined. This information will be used using inferential statistics to draw a conclusion on the average number of cartwheels that sophomores are capable of doing.

Statistics based on inference vs statistics based on description

Both descriptive and inferential statistics are used in the process of describing data and drawing conclusions about the population based on samples taken from the population. The differences between inferential statistics and descriptive statistics are compared and contrasted in the table that follows.

When working with inferential statistics, the goal is to arrive at conclusions that go beyond what can be drawn from the immediate data alone. For instance, we make use of inferential statistics to make an educated guess about what the general population would believe based on the sample data. Alternately, we may use inferential statistics to make judgements about the possibility that a difference between groups that was seen is a reliable one or one that could have occurred by chance in this research. Therefore, we use inferential statistics to draw conclusions about more general circumstances based on our data and descriptive statistics to simply explain what's going on in our data. Inferential statistics are used to draw conclusions about more general conditions based on our data.

In this section, I will focus on inferential statistics that may be helpful in the design of experimental and quasi-experimental research as well as in the assessment of the outcomes of programmes. When you wish to compare the average performance of two groups on a single measure to determine whether or not there is a difference, you may apply what is perhaps the most straightforward kind of inferential test. You could be interested in finding out whether there is a difference in the math test scores of eighth-grade boys and girls, or if there is a difference in the end measure between a programme group and a control group. When you want to compare the average performance of

two groups, you should think about using the t-test to look for differences between the groups whenever you do this.

The Broad Linear Model is a general family of statistical models that is responsible for producing the majority of the most important inferential statistics. This encompasses the t-test, the Analysis of Variance (ANOVA), the Analysis of Covariance (ANCOVA), regression analysis, and a great deal of the multivariate techniques like as factor analysis, multidimensional scaling, cluster analysis, discriminant function analysis, and so on. In light of the significance of the General Linear Model, it is recommended that every social researcher who takes their job seriously familiarise themselves with the GLM's methodology. The description of the General Linear Model presented here is quite fundamental, and it only takes into account the most fundamental model, which is the straight-line model. On the other hand, it will acquaint you with the concept of a linear model and help you prepare for the more complicated studies that will be discussed further on.

The concept of a "dummy" variable is one that should be familiar to everyone who is interested in learning how to compare different groups. The term does not imply that we are making use of variables that are not very intelligent or, even worse, that the analyst who makes use of them is a "dummy"! These variables could be better understood if they were referred to as "proxy" variables. A dummy variable is just a variable that employs discrete integers, generally 0 and 1, to represent various groups in your research. These numbers may be either positive or negative. The use of dummy variables is a straightforward concept that paves the way for the execution of quite complex operations. For example, if I include a straightforward dummy variable in my model, I may model two distinct lines—one for each treatment group—using only a single equation. Check out the section on dummy variables to have a better understanding of how this works.

A comparison of the programme group and the non-program group on the outcome variable or variables is one of the most essential studies that can be performed when evaluating the results of a programme. The study design that we adopt will determine how we go about doing this. Experimental and quasi-experimental designs are the

two primary categories that make up the broad category of research designs. The analyses of each are provided individually because of the differences between them.

Experimental Analysis

The straightforward randomised experiment with merely a posttest for two groups is often evaluated using either the one-way ANOVA or the basic t-test. The Analysis of Variance (ANOVA) Model is often used in order to conduct the analysis of the factorial experimental designs. Randomized Block Designs make use of a subtype of the ANOVA blocking model known as the "dummy-coded variable method" to represent the different sections of the study. It should come as no surprise that the Analysis of Covariance statistical model is the one used in the Analysis of Covariance Experimental Design.

Quasi-Experimental Analysis

The experimental designs and the quasi-experimental designs both vary in that the quasi-experimental designs do not employ random assignment to allocate units (such as individuals) to the different programme groups. Analysis of these designs is often made much more difficult by the absence of a random assignment component. For instance, in order to conduct an analysis using the Nonequivalent Groups Design (NEGD), we have to use a model that is often known as a Reliability-Corrected Analysis of Covariance and alter the pretest scores so that they account for the possibility of measurement error. When using the Regression-Discontinuity Design, we need to be particularly wary of curvilinearity and the possibility of model misspecification. As a consequence of this, we have a tendency to apply a conservative analytical technique that is based on polynomial regression. This strategy begins by overfitting the probable true function, and then reduces the model depending on the outcomes of the process. The Regression Point Displacement Design only incorporates a single treatment unit within its structure. Nevertheless, the conventional ANCOVA model is used as a foundation for conducting the analysis of the RPD design.

When you've looked at all of these different analytical models, you'll find that they all belong to the same family—the General Linear Model—and that this will become clear to you. If you have a good knowledge of that model, you will be well on your way to being familiar with the complexities of data analysis in the context of applied and social research.

Statistics that rely on inferences

When comparing the differences that exist between the treatment groups, inferential statistics are often used. Inferential statistics are used to compare the treatment groups and to draw generalisations about the wider population of participants. These statistics are derived from measurements taken from a sample of the people who participated in the experiment.

There is a wide variety of inferential statistics, each of which is suitable for a particular study design and the features of a sample in a particular context. In order for researchers to determine the appropriate statistical test for their experiment, they need review the various books that are available on experimental design and statistics. On the other hand, the vast majority of inferential statistics are predicated on the idea that the value of a test statistic is derived by applying a specific formula to the data. This number, in conjunction with the degrees of freedom, a measurement linked to the sample size, and the rejection criteria, are used in the process of determining whether or not there are differences between the treatment groups. The greater the size of the sample that is being analysed, the greater the likelihood that a statistic will suggest that there are differences between the treatment groups. Therefore, the more people that are included in the sample, the more convincing the statistic is regarded to be.

Almost every kind of inferential statistic relies on an essential assumption in the background. It is expected that each replication inside a condition may be considered independent. That is to say, it is believed that any value inside a condition is unrelated to any other value within the sample. Researchers that study animal behaviour often face a variety of obstacles because they work under the notion that animals are independent.

Statistics that allow for inferences to be drawn about a situation or event are called inferential statistics. In this manner, it is fundamentally different from descriptive statistics, which only report the data that has been really measured. It gives you the ability to make inferences based on extrapolations, which is a key distinction between the two. Let us return to our earlier example of a party. It has been said that comparison data indicate that the parties that your buddy Sophia throws are quite successful (e.g., the average number of attendees and the median duration of her parties are greater than those of other parties). Your following queries can revolve on the reasons behind her gatherings' overwhelming popularity. Is it the alcoholic beverages she provides, the food she serves, the size of her social network, the prestige of her job, the number of men or women she knows, her physical attractiveness, the number of men or women she knows, her number of friends, the size of her residence, the location, or some combination of these factors? You may find that inferential statistics are helpful in responding to these issues. The fact that parties with lower attendance levels had, on average, less beverages offered would lead one to believe that the drinks provided by your friend Sophia are likely the critical component. In order to come to any conclusions, the disparities between her events and other parties, in terms of attendance and the kind of beverages provided, would need to be substantial enough.

It is important to keep in mind that inferential statistics almost always imply, but are unable to definitively establish, an explanation or a cause-and-effect link. The term inferential originates from the verb "infer." According to the American Heritage Dictionary, to infer is to draw a conclusion or make a judgement based on premises or evidence, but not to prove anything. Statistics that are used in an inferential manner are those that examine a subset of a larger population in order to derive conclusions about the larger population as a whole. Estimation, or making educated guesses about the characteristics of a population based on a sample of that population, and hypothesis testing are two of the most common components of inferential statistics (i.e., finding evidence for or against an explanation or theory).

The study of statistics involves describing and analysing variables. In Chapter 4, we go further into discussions on measurements and variables. A measurable quality or aspect of anything that may take on a variety of values is referred to as a variable. A variable may either be quantitative, such as height, or categorical, such as gender (e.g., eye color). Variables may either be independent, in which case the value they adopt is not influenced by any other variables, or reliant on the values of other variables (the value it assumes is pre-determined by other variables). Variables are neither necessarily independent or dependent. An independent variable in one statistical model may be dependent on another. Imagine, for the sake of this illustration, that we had a statistical model to utilise in determining what causes heart disease. The risk factors for heart disease would be independent variables. These risk factors include the number of cigarettes smoked per day, beverages consumed per day, and cholesterol level. A dependent value would be considered to be the existence of heart disease. The existence of heart disease is affected by the many risk factor factors.

Statistical approaches may either study one variable at a time (also known as univariate analysis) or several variables simultaneously and all at once (also known as multivariate analysis) (i.e., multivariate analysis). Analysis of bivariates involves looking at two variables at the same time. A straightforward investigation of the mortality rates of various nations is an example of a univariate study. [Case in point] An investigation of the connection between drunkenness and premature death is a good illustration of a bivariate study.

Testing a statistical hypothesis may lead to errors of two types: type I and type II.

A quantitative strategy for determining whether or not the null hypothesis (H0) should be rejected is made available by inferential statistics. In an inferential test, there are only two potential right outcomes since H0 must either be true or false; the first is the proper rejection of H0 when it is false, and the second is the correct retention of H0 when it is true. As a result, there are two distinct kinds of mistakes that might take place, which have been designated as Type I

errors and Type II errors respectively. When H0 is wrongly rejected, this is referred to as a type I error. This is what is known in the industry as a false positive. When H0 is allowed to stand despite the knowledge that it cannot be true, this is a type II mistake. A false negative is the conventional name for this kind of inaccuracy. When it comes to repeatability, having a solid understanding of the likelihood of committing type I or type II errors is very necessary. This likelihood is dependent on the design and execution of the experiment, as well as the size of the sample, which once again emphasises the need of power analysis.

Comparison of Inductive and Transductive Inference, as well as Sample and Population Statistics

The field of statistics known as inferential statistics is concerned with drawing conclusions about populations by analysing samples. How can we make inferences about the whole collection of instances, taking into account other particular cases that are part of the complete set, if we only have knowledge about a portion of the examples? When drawing conclusions based on the principles of evidence, sample statistics are used. Our research leads us to believe that matching and similarity-based judgments are supported by population statistics. That is, if one has sample statistics, then the inferential issue to solve is how to interpret those statistics as evidence, and this difficulty arises only if one has sample statistics. If one has population data, the inferential difficulty becomes determining the degree of fit between the two groups. Psychologists are quite knowledgeable when it comes to inferential statistics and the interpretation of evidence: In general, the findings of our investigations allow us to make inferences about populations based on samples. We very seldom, if ever, have information on every single member of the population. What are some examples of conclusions that may be drawn from population statistics? Thankfully, there is a description of population-statistical inferences, as well as a name for this kind of inference: Transductive.

The phrase "transductive inference" was coined by Piaget and is common parlance in the field of developmental psychology (1959). Piaget called the preoperational mode of reasoning that connects specific cases without any general rule or underlying mechanism "transductive," and he used this term to describe that mode. It is reasonable to assume a causal connection between two events just because they occurred close together. The lights went out after a honk from an automobile horn; the horn was the source of the darkness. The conclusion is drawn from a specific occurrence (the honking) to another occurrence (the darkness), but there is no suggestion of a general process. To clarify, how exactly may blaring horns bring about darkness? How might this relationship be maintained on a larger scale? It would seem that Piaget's transductive inference is a kind of sympathetic magic's "principle of connection" (Frazer, 1894; events perceived together are taken to be causally related). A Humean or associative view of causality and causal inference both share this concept as one of its distinguishing features: The simple act of seeing a connection between two things constitutes a causal link. When someone first connects horns with darkness, they will begin to anticipate the presence of the former given the latter. Therefore, it would seem that known associative learning and similarity-based induction underlie the process of transductive reasoning (horn = darkness). Perhaps Piaget was trying to illustrate some specific qualities of young children's similarity-based inferences (for example, "one-trial" connections), but the basic process of inference is something most people are already acquainted with. In particular, it is not quite obvious how Piaget's transductive reasoning handles the issue that conclusions based on similarity depend on population statistics. On the other hand, there is an alternative theory of transductive reasoning that does.

Vladimir Vapnik is credited as being the one who first brought the term "transductive inference" into the literatures of machine learning and statistical learning theory, seemingly independently of Piaget (1998). Vapnik also uses the term "transductive" to refer to conclusions drawn from specific instances based on those same specific examples. Transductive inferences, on the other hand, are,

according to Vapnik, a kind of simplifying assumption and a technique of handling difficult learning challenges. According to Vapnik's argument, statistical inference—the kind that uses evidence and is considered standard—is an effort to answer a more general issue. How is it possible for a learner to derive a rule or pattern from their previous experience with a collection of instances that can then be applied to new examples? The fact that there is an unlimited number of possible fresh instances is the most important aspect of evidentiary inference. The idea behind transductive reasoning is that it is possible to draw just a limited number of conclusions from a given set of data. For instance, an inspector may run into the challenge of determining which of a batch of one hundred widgets are flawed (see Fig. 1.1). In most cases, finding a solution to the issue with a specific batch will be a great deal less difficult than finding a solution to the challenge of recognising faulty widgets in general. According to Vapnik, the method of transductive inference is the practise of confining one's emphasis to the particular instances that the learner will actually come into contact with. In order to access Piaget's transductive inference, please click here. If the child's conclusion that horns produce darkness is limited to the specific scenario in which it was witnessed, then the issue looks to be less severe: The problem arises only when it is extrapolated outside its own context. In a similar vein, the connection between sample statistics and population statistics becomes clearer. In (traditional, evidential) statistical inference, the sample size is equal to one hundred widgets. The goal of this activity for the student is to construct a representation of the class or population of widgets using this sample. The population for the purpose of transductive inference is the one hundred widgets. The learner's mission is to acquire and use statistical knowledge in order to formulate hypotheses on this population.

The connection between evidential-sample inferences and transductive-population inferences may be better understood with the assistance of an example. Consider the one hundred different widgets. Imagine that an inspector has gone over all 100 of them and found the following issues: There are a total of 100 widgets, 10 of which are black and 90 of which are white. Furthermore, five of the black widgets are broken, while nine of the white are broken. These are statistics that

describe the population. Inferences need to be drawn from these descriptive data, which presents a problem for the inspector. Transductive inferences and evidential inferences, or what we have been referring to as "ordinary statistical inferences," are the two types of inferences that we differentiate here. The inspector may be asked to make either kind. The statistics that were observed are examples of population statistics if the inference is about the hundred widgets. Take, for instance, the scenario in which the inspector is presented with one of the widgets and informed that it is white. The inspector is certain that there won't be any problems since just ten percent of the white widgets had defects in the past. This is an example of an inductive inference, which may be characterised by the fact that its validity cannot be established with certainty: The judgement is likely to be correct given the inspector's previous work, but it is not absolutely definite. However, this is an example of a certain kind of inductive inference known as a transductive inference. The difficulty that the inspector is facing is not too complicated. After determining that the descriptive statistic p(defective|white) equals 0.1, there is, in reality, very little work left to be done. Because the descriptive statistic was computed on the basis of the instances that the inspector is using as a basis for his conclusions, the inspector may confidently use the descriptive statistic as a guide for his inferences. The inspector is only providing a description of the population; he or she is not drawing any conclusions at all from this information. It doesn't seem like much of a leap in inductive reasoning to go from "nine of these ninety white widgets are defective" to "one of these white widgets has a ten percent chance of being defective" to "a white widget chosen at random is probably not defective." This progression goes from "nine of these ninety white widgets are defective" to "one of these white widgets has a ten percent chance of being defective." To put it another way, after the inspector has solved the descriptive issue (what percentage of the 100 widgets are faulty or white?), the inferential challenge, which is to make a prediction about a widget that was randomly chosen, is simple.

When it comes to drawing conclusions about a widget that was not included in the "training" set, Widget 101 presents the inspector with a more challenging challenge. In this scenario, the descriptive

statistics (such as the value p(defective|white) = 0.1) are characteristics of a sample, and the inspector is tasked with calculating inferential statistics in order to formulate predictions. In this scenario, the inspector has to think about the evidentiary connection between his sample (which consists of one hundred widgets) and the whole population (from which the new widget was drawn). Is there a bias in the sample? One particular challenge of evidentiary inference is the identification and correction of any sample bias that may exist. This particular inferential difficulty is what differentiates evidential inference from its counterpart, transductive inference. When drawing a transductive inference to one of the 100 original widgets, the sample bias does not important.

Take, for example, the challenge of determining what colour a gadget that has been deemed faulty will be. If the faulty widget was one of the 100, then it is easy to make a forecast about its colour: it is most likely white. White was the most common colour for the 14 faulty widgets that were found. If the faulty widget is a brand new one, like widget 101, the forecast is cloudier. The majority of the original 100 widgets were white in colour. Is it representative of the widgets in the general population, or is it due to a bias in the sample? It is impossible for the inspector to draw conclusions about the whole population based on the results of his sample alone unless he is aware of the connection that exists between the two. To make a transductive inference, however, it is not necessary to determine that connection or find a solution to this inferential difficulty. There is no evidence of sample bias if the one hundred widgets are used to represent the population. In this sense, transductive inference may be used in the same manner as inductive inference, namely as a form of simplifying assumption. Inductive reasoning is called transductive reasoning when the relationship between the sample and the population is neglected and the statistics from the sample are handled as if they were population data. The difficulty of transductive reasoning is restricted to the process of constructing effective descriptions (characterizing the patterns in the available data).

UNIT 5
INTERPRETATION AND REPORT WRITING

RESEARCH REPORTS: DEFINITION

After doing structured research, often in the form of surveys or qualitative approaches, researchers and statisticians would compile recorded data known as research reports after completing analysis on the information they have gleaned from the study.

Reports often cover a wide variety of subject areas, but their primary purpose is to provide information on one specific subject area to a relatively specific subset of the population as its target audience. The fundamental objective of research reports is to communicate significant findings from a study to marketers so that they may incorporate those findings into the formulation of new tactics. Those in authority need to be informed of certain occurrences, facts, and other information based on incidents, and the most effective method of communication is the production of research reports. In an ideal research report, the material that is provided is exceedingly accurate, and the report also has a crystal clear aim and conclusion. In order for these reports to be useful in conveying information to readers, the format they are presented in should be clear and organised.

In most cases, a research report is believed to be a truthful witness of all the effort that was done to acquire specifics of study. A research report is a dependable source that recounts information about a research that was completed.

The following are the many parts that make up a research report:

1. Summary
2. Background/Introduction
3. Methods That Were Put Into Practice
4. The Outcomes Determined by the Analysis
5. Deliberation

6. Conclusion

The researcher is responsible for completing the task of drawing conclusions after completing the process of gathering and evaluating the data, followed by the task of producing the report. It is essential that this step be carried out with extreme caution; otherwise, erroneous inferences may be formed, and the whole point of doing research may be rendered moot. The researcher will not be able to reveal the linkages and processes that lie behind his results unless he or she engages in the process of interpretation. Throughout the case of studies that test hypotheses, the researcher may come to generalisations if the assumptions are tested and sustained several times in the course of the study. In the event that the researcher did not have a hypothesis to begin with, however, he or she would attempt to explain the data using some theory. This might sometimes result in new questions, which would then lead to more research. All

This analytic information and the resultant inference (or inferences) might very well be conveyed to the consumers of research findings, ideally in the form of a research report. Consumers of research results could be people, groups of persons, or public or private organisations.

MEANING OF INTERPRETATION

After conducting an investigation that is analytical or experimental, the next step is to perform the work of interpretation, which entails deducing meaning from the data that have been gathered. In point of fact, it is an investigation of the potential ramifications of the results of study. The undertaking of interpretation may be broken down into two primary components:

I the process of attempting to maintain continuity in research by tying the findings of one study to those of another, and

(ii) The formulation of a few conceptual frameworks for explanation. "Interpretation, in a sense, is concerned with connections within the data that were obtained, somewhat overlapping with analysis. In addition to the findings of the study itself, interpretation also takes into account the findings of other studies, as well as theories and hypotheses.

(iii) Therefore, interpretation is the tool that allows for a better understanding of the aspects that seem to explain what the researcher has seen over the course of the study, and it also gives a theoretical conception that may serve as a guide for additional inquiries.

The significance of interpretation lies in the fact that it is via accurate interpretation that the results of research may be put to beneficial and practical use. Because of the following reasons, it is now being regarded as a fundamental part of the research process:

The researcher will not have a complete understanding of the abstract principle that lies underneath his results until he or she has interpreted those findings. Because of this, he is able to connect up his results with those of other studies that have the same abstract concept, and as a result, he is able to make predictions about the events that will take place in the real world. In the future, these hypotheses may be put to the test via new research. In this manner, we can ensure that there is no break in the flow of research.

(ii) The process of interpretation leads to the formulation of explanatory ideas, which may be used as a map to direct the conduct of subsequent research projects; it also paves the way for new pathways of intellectual exploration and piques one's curiosity to learn more.

(iii) Only by interpretation can the researcher better realise why his results are what they are, and only through interpretation can the researcher help others understand the true relevance of his study findings.

(iv) The interpretation of the findings of an exploratory research study often leads in hypotheses for experimental research, and as such, interpretation is engaged in the shift from exploratory research to experimental research. Because an exploratory research does not begin with a predetermined hypothesis, the results of such a study are required to be interpreted in a way that does not assume anything.

METHODS AND PRACTICES OF INTERPRETATION

The process of interpretation is not a simple one; rather, it is one that calls for a significant amount of expertise and dexterity on the side of the researcher. Interpretation is a skill that can only be acquired through years of experience and repeated practise. In order to

successfully complete the process of interpretation, the researcher may on occasion decide to seek the advice of specialists. In many cases, the following procedures are involved in the method of interpretation:

The researcher is obligated to provide reasonable explanations of the relations that he has discovered, as well as to interpret the lines of relationship in terms of the underlying processes. Furthermore, the researcher is required to make an effort to discover the thread of uniformity that lies beneath the surface layer of his diverse research findings. In point of fact, this method is the methodology that should be used when generalising, and it is also how ideas should be constructed.

(ii) If any extraneous information was gathered during the course of the research study, it must be taken into account when interpreting the findings of the research study as a whole because it has the potential to become an essential component in better comprehending the issue that is being considered.

(iii) Before going into final interpretation, it is preferable to seek the advice of someone who has insight into the topic in question, as well as someone who is forthright and honest, and will not be bashful in calling attention to gaps and inconsistencies in logical arguments. A consultation of this kind will lead to the accurate interpretation of the data, which will, in turn, increase the value of the findings of the study.

(iv) In order to prevent making incorrect generalisations, the researcher must not proceed with the work of interpretation until all pertinent aspects impacting the situation have been taken into consideration. It is essential that he take his time when analysing the data since there is a good chance that the conclusions, which at first glance seem to be correct, are really not at all accurate.

THE ELEMENTS THAT COMPRISE INTERPRETATION AND WRITTEN REPORTS

There is a possibility that the particulars of a research report may change in accordance with the objectives of the study, but the report's primary elements will always be the same. The manner in which the market researcher gathers information also has an impact on the writing style used in reports. The following are the seven primary elements that make up an effective research report:

• Research Report Summary: An full aim as well as an overview of the research is to be contained in a summary that is the length of a couple of paragraphs. Under the section titled "Report Summary," a concise explanation is provided for each of the several aspects that make up the study. It ought to be captivating enough to draw attention to all of the important aspects of the report.

• Research Introduction: Every time a researcher writes a report, they do it with the end aim of accomplishing one or more specific objectives. In the beginning, he or she may discuss the responses that are relevant to this objective and formulate a thesis statement that will be included to aim toward answering it in depth. In this part of the document, you need to provide a solution to an essential question: "What is the present state of the goal?" If the organisation was able to determine that the aim had been accomplished after the research was carried out, or if they are still in the process of accomplishing it, this information should be included in the introductory section of the research report.

• The Research Methodology Chapter is the Most Important Part of the Report since It Contains All the Important Information. Readers are able to not only obtain knowledge about the subject at hand but also evaluate the level of quality presented in the material, and the study can also be validated by other market researchers. As a result, this part has to include a significant amount of information, with a detailed discussion of every facet of the study. It is necessary for the information to be given in a chronological sequence in accordance with its value and priority. In the event that the researchers gleaned any knowledge from previously developed methods, references should be included.

• Research Results: This area of the results will consist of a brief summary of the findings, as well as calculations that were carried out in order to accomplish the objective. In most cases, the discussion section of the report is where the exposition comes after the data analysis has been completed.

• Research Discussion: In this part, the findings are examined in extreme depth, and a comparison study of publications that may possibly exist in the same subject is also provided. Any irregularity that

was discovered while doing the study will be discussed in the section under "Discussion." In the process of putting up reports on their study, researchers will need to demonstrate how their findings will be useful in everyday life and connect the dots between theory and practise.

• References to the Research and a Conclusion: Conclude all of the results from the research while also citing each and every author, publication, or content item from which references were gathered.

One of the goals of doing research is to add new information to the store of previously accumulated knowledge. As a result of this, while you are carrying out research, you are required to record both your procedures and your results in a research report.

With the help of a research report, it is simple to summarise the results of your comprehensive study as well as any holes that call for more examination. When you are faced with the need of doing research, having the skills necessary to compile a comprehensive research report will be of great assistance to you.

What exactly is included in a Research Report?

A well-written report on research is a document that summarises the procedures, facts, and results of an inquiry that was carried out in a methodical manner. It is a significant document that provides a first-hand description of the research process and is often regarded as an impartial and accurate source of information. This makes the document very valuable.

A research report may be seen in many different ways as a summary of the research process that eloquently emphasises the results, suggestions, and other significant facts. Reading a research report that has been thoughtfully prepared should provide you with all of the knowledge that you need about the fundamental aspects of the investigation method.

Components that Make Up a Research Report

How exactly can one identify a study report when they come across one? The following are a few of the fundamental characteristics that constitute a research report:

It is an in-depth discussion of the procedures involved in the study as well as the conclusions, and it often include tables and figures.

It is written in a language that is considered to be formal.

In most cases, the author uses the third person while writing a research report.

It is educational and based on knowledge that can be verified through first-hand experience.

It follows a conventional format with headers, sections, and bullet points throughout.

It always offers suggestions for things that might be done in the future.

Different Varieties of Research Reports

The type of the study as well as the audience that was targeted are taken into consideration when classifying the research report.

The Makeup of the Investigation

Research Report Based on Qualitative Methods

The sort of report that is prepared for qualitative research is known as this. It provides an overview of the techniques, operations, and conclusions of a qualitative approach of systematic study. An chance to use one's knowledge and enhance one's abilities in the design and execution of qualitative research projects may be obtained via the use of a qualitative research report in the field of educational research.

The type of a qualitative research report is often one that is descriptive. Therefore, in addition to providing specifics on the methodology used in the study, you are required to also compose a story that is illustrative of the material.

Research Report Based on Quantitative Methods

The form of research report known as a quantitative research report is one that is composed specifically for quantitative research. Quantitative research is a sort of systematic study that, in an effort to discover answers to research questions, pays attention to numerical or statistical values. This style of research is also known as empirical research.

The researcher gives quantitative data in this kind of research report to support the study method and the results. In contrast to a qualitative research report, which focuses mostly on description, a quantitative research report utilises numbers; in other words, its primary focus is on numerical information.

Target Audience

Additionally, the audience that the research report is intended for might lend the document either a technical or popular tone. If you are dealing with a broad audience, you will need to provide a research report that is accessible to the general public. On the other hand, if you are dealing with an expert audience, you will need to submit a technical study.

Report on the Results of Technical Research

After doing research that is specific to an industry, you should provide a comprehensive document known as a technical research report. This report is very specialised since it offers information for a technical audience, which consists of people who have an above-average level of understanding in the area of study that it covers.

It is required of a researcher to offer precise information on the study process in a technical research report, including statistical analysis and sampling procedures. In addition, the way language is used is quite specialised, and it is full with jargon.

Research reports in the fields of law and medicine are two good examples of technical research reports.

The Most Famous Research Report

A research report that is written for a broad audience, or for persons who may not necessarily have any prior understanding in the area of study, is said to have widespread appeal. A well-known research report often strives to make the material it compiles available to everyone and everyone.

The fact that it is written in very easy-to-understand English makes it quite straightforward to comprehend both the results and the

suggestions. Newspaper articles and magazine articles both offer material that may be considered examples of popular research reports.

The Value of Conducting a Research Report

Knowledge Transfer: As was said before, one of the main purposes of doing research is to make a contribution to the existing body of knowledge, and the research report is the vehicle via which this contribution may be delivered. A research report is a useful tool for efficiently communicating the results of an in-depth inquiry to anybody and everyone who is interested in the topic.

Identification of Knowledge Gaps: If you have a study report, you will be able to identify areas of knowledge that need more investigation. A study report will detail the work that has been completed while also making hints about additional topics that need further in-depth inquiry.

In the field of market research, a research report may assist you in gaining a general understanding of the demands and nuances of the industry.

A research report gives you the opportunity to convey facts in a way that is clear and succinct.

It is both time-efficient and practical since you do not have to spend time explaining the conclusions of your research work in person in a research report. You may quickly distribute the report to stakeholders through email, and they can see it at their convenience.

Writing a Research Report: A Step-by-Step Guide

Writing a research report requires attention to many specifics; thus, being aware with the many criteria will be of great assistance to you in developing the perfect research report. A research report is often divided up into various parts, which enables material to be presented in a manner that is both clear and organised.

The Outline of a Research Report, Along with an Example

Title

This is the title of the in-depth inquiry that you are doing. A research report need to have a title that is clear and succinct, pointing to the study's goals, objectives, and conclusions.

Listing of Contents (Table of)

This acts similarly to a compass in that it assists readers in navigating their way through the study report.

Abstract

An overview is what an abstract is, and it emphasises all of the main components of the study, such as the methodology of the research, the data gathering procedure, and the conclusions of the research. Consider an abstract to be a condensed version of your research report that highlights the most important facts in a straightforward manner.

An abstract is normally between 100 and 150 words long and gets right to the point. An abstract is always short. The arrangement known as the "5 Ws and 1 H," which consists of "What, Where, Why, When, Who, and How," should serve as the primary emphasis of your research abstract.

Introduction

In this section, the researcher will discuss the goals and objectives of the systematic inquiry, as well as the issue that the researcher will attempt to address using the results of the systematic investigation. When you are writing the opening to the report, it is also very important to state whether or not the goals of the study were accomplished or whether or not further work is required.

The researcher explains the relevance of the systematic inquiry as well as the research topic that they are attempting to solve in the opening portion of the paper. Additionally, it is required of the researcher to provide an explanation of any jargons or terminology that are included in the study.

Literature Review

A written examination of the information that already exists in the topic of research is called a "literature review." In a nutshell, this is the part of the paper in which you provide an overview and analysis of the many research works that are pertinent to your systematic examination.

It emphasises current research information as well as areas that need future exploration and fills in gaps in knowledge that your research has aimed to cover. You may start dropping hints about your research hypothesis and the prospective ramifications it might have for the current body of knowledge in your area of study at this point in the process.

A Discussion of the Results of the Investigation

This is a comprehensive breakdown of the study procedure, including everything from the methodology to the research subjects and samples. In this section, you will be asked to offer comprehensive information about the research method, including the protocols for collecting data and conducting analysis.

You will need to offer information on the surveys, questionnaires, and other quantitative data collecting techniques that you employed in your study if you are writing a report on quantitative research. It is required of you, as the author of a qualitative research report, to explain the qualitative data collecting techniques utilised in your study. These methods may include interviews and focus groups.

Findings

You are tasked with presenting the findings of the systematic study in this portion of the report.

Discussion

This part provides a more in-depth explanation of the conclusions of the study that was discussed before. Here, you are expected to present a justification for each outcome and show whether the results are in line with your hypotheses or if other research studies have come up with similar results. In addition, you are expected to show whether or not other research studies have come up with similar results.

Conclusions

The following is a synopsis of all of the material that is included in the report. In addition to this, it discusses the relevance of the whole research.

References as well as further material

In this part, you will find a list of all of the main and secondary sources that were used for the study.

Guidelines for the Construction of a Research Report

Define the Environment in Which the Report Will Be Read

If you define the context of your research report, it will be easier for you to write a document that is both thorough and succinct. This is similar to what can be accomplished while writing an essay. Because of this, you need to make an outline before you begin writing in order to ensure that you do not leave anything out.

Define your Audience

It is crucial to write with your audience in mind since this will affect the tone of the report you are writing. When writing for a wide range of people, it's important to deliver the material in a way that's easy to understand and familiar to them. You would need to make use of technical and field-specific phrases if you were writing for a more specialist readership.

Include Notable Observations in Your Report

The purpose of presenting a research report is to provide a condensed version of the findings that you obtained after doing an in-depth inquiry. You should leave out any material that isn't related to your report and focus instead on showcasing the most crucial results and facts.

Include Illustrations

Illustrations and other visual representations of your data have to be included in your study report in some capacity. Your methodical inquiry is given more credibility when accompanied with graphs, pie charts, and other pertinent pictures.

Find the Appropriate Name for It

A good title for a research report should be succinct, specific, and include keywords from the study's subject matter. It should convey

a clear concept of your systematic study so that readers can comprehend the complete emphasis of your research from the title. This will ensure that your research is successful.

Examine the Report for Any Errors.

Make sure that you verify all of the facts by giving the document a second glance before you release it into the public domain. You should also have the report checked by another person if at all possible, and you should also put it through some kind of editing and proofreading programme.

A Guide to the Data Collection Process for Your Report

Comprehend the Nature of the Issue

When you are writing your research report, you should keep in the back of your mind that every piece of research is aimed at finding a solution to a certain issue or group of problems. If you had a better understanding of the issue, you would be better able to sort through the data you have and include just the most relevant information in your report.

Be aware of the goals that your report aims to accomplish.

This is somewhat related to the argument that was made before since, in some way, the aims of your systematic study are entwined with the goal of the research report that you are writing. If you can determine the main aim of producing a research paper, it will be much easier for you to locate the necessary material and present it in the appropriate manner.

Identify your audience

When it comes to the collecting of data for a research report, having a solid understanding of your intended audience is quite necessary. If the research report that you are writing is going to be intended for an organisation, then you should offer information that is unique to the industry, or demonstrate how the results of the study are important to the job that the firm undertakes.

Create Surveys/Questionnaires

A research technique known as a survey is comprised of a series of questions that are posed to a select population in order to collect information from those individuals. Quantitative or qualitative approaches are both acceptable here.

The questions that make up a survey are often organised in a certain way, and the process of collecting responses might either take place online or in person. On the other hand, an online survey is a more efficient technique of research data gathering than other methods since it allows you to save time and obtain information with more convenience.

Precautions for writing a research report

The efficient transmission of research results to the readers of the report is the primary objective of a research report, which serves as a channel of communication between the findings of the study provided by the researcher on the one hand and the readers of the report on the other.

Therefore, while putting up the study report, the researcher need to take in mind the following safety precautions:

1. The length of the report should indeed be kept in mind of the fact that it should cover the topic in depth, but it should also be kept in mind that it should be brief enough to sustain the attention of readers.
2. The report shouldn't be boring in any way. It should be designed in such a way that it keeps one interested.
3. The report must to have the qualities of being straightforward and staying away from ambiguity.
4. The readers of the report are primarily interested in getting a rapid understanding of the important results, and the report should give a prompt availability of the findings with the aid of charts, graphs, and statistical tables.
5. The information that is included in the report needs to have been carefully considered with the end goal of the research issue in mind.

6. It is important to avoid making any grammatical errors, and the report should be written in a manner that is in complete compliance with the guidelines for the writing of a report. Writing, including the use of quotes and footnotes, as well as the application of appropriate punctuation and the utilisation of abbreviations in the footnotes, etc.
7. The preparation of a research report need to begin with a logical appraisal of the situation.
8. The report has to highlight the policy implication related to the issue that is being considered, and it needs to assist us in making predictions about the future.
9. The report need to include an appendix with all of the relevant technical information.
10. Prior to writing the report, you should compile a bibliography listing all of the different sources of information that were used in the research project.
11. In addition to that, a decent report need to include an index of the authors and topics covered. It need to be included as an appendix at the very end of the report.
12. The report must to have an appealing format and be nice and clean, regardless of whether it is typed or printed.
13. Calculated confidence bounds need to be provided in the report as well, along with the numerous restrictions that the researcher encountered while doing his study. These should also be included in the report.
14. A excellent report has to additionally explain the purpose of the research, the nature of the issue, the methodology and analytical techniques that were used, and so on. The report need to begin with some kind of introduction that covers all of these topics.

Therefore, after outlining all of the aspects associated with the process of interpreting and writing reports, we should always bear in mind the fact that the process of writing a report is an art that can only be acquired by extensive practise and previous experience.

On the basis of a public readiness to confer the status of property, ideas, innovations, and creative expressions have been

identified as being within the purview of intellectual property rights (IPR), which is an abbreviation for intellectual property rights. IPR offer certain exclusive rights to the inventors or creators of that property, in order to enable them to reap financial advantages from their creative efforts or reputation. These rights allow the inventors or creators to profit from their creative efforts or reputation. There are many different kinds of legal safeguards for intellectual property, such as patents, copyrights, trademarks, and so on. A patent is a kind of recognition that is granted for an invention that meets the requirements of being globally unique, being non-obvious, and having an industrial use. IPR is a requirement for improved invention or creativity protection, including better identification, planning, marketing, and representation of the innovation or creativity. Depending on the area of expertise that it focuses on, each sector of the economy need to have its own IP policies, management style, strategies, and so on. The intellectual property rights strategy used by the pharmaceutical business is now undergoing significant change and will need improved concentration and strategy moving forward.

What exactly is the commercialization process?

The process through which a newly developed product or service is made available to consumers all over the world is known as commercialization. The process of going to market is done in stages, beginning with the launch of the product and continuing through large manufacturing and widespread use of it. It takes into consideration the manufacturing, distribution, marketing, sales, and customer support that are essential for a business to achieve commercial success. Commercialization is a business tactic that necessitates the development of a marketing plan, the determination of how the product will be provided to the market, and the anticipation of potential obstacles to the company's success. Gain a better understanding of the commercialization approach used by Pitt Ventures.

Advantages of Entering the Commercial Market

The commercialization of research results in the creation of new products and services that can be utilised to address some of life's most

pressing issues. These products and services can also be used to make incremental improvements to the quality of life for consumers and the effectiveness of business operations across a wide variety of domains.

Societal Benefit

The innovations that emerge from university research have the potential to have the greatest impact when they are put into the hands of those who stand to gain the most from them. These innovations can have an effect not only in the realm of healthcare but also in the realms of the environment, wellness, physical fitness, education, and industrial applications. In general, the University of Pittsburgh's focus on social benefit is the primary motivation driving its efforts to commercialise innovative technologies.

Expanding of the Economy

Bringing inventions to consumers via the process of commercialization results in economic benefits as well. Commercialization results in the generating of new money as well as the creation of new jobs locally, regionally, and potentially all over the world. This may be accomplished via the licencing of technology to other businesses or by the formation of new startup enterprises.

Partnerships with Local Businesses

The process of commercialization creates an opening for collaboration with members of related industries, financial backers, and other companies. These agreements may bring in new sources of financing that the university might use to further their research. Quite often, the university is able to provide more research and development resources to industrial partners, who in turn act as a conduit for disseminating findings to the general public. In addition, the university has the ability to produce cash, which may then be put back into research, used to pay expenses associated with commercialization, and funded to pursue entrepreneurial endeavours.

Both in terms of Recruitment and Retention

Positive publicity and increased knowledge of the University's research, inventions, and entrepreneurial culture are both outcomes of

successfully commercialising breakthroughs and bringing them to market. These achievements and the resulting publicity have the potential to aid in retaining and recruiting professors and students, in addition to new commercial and research partners.

Entrepreneurship

Both the teachers and the staff have the opportunity to interact with members of the local business community if the institution places an emphasis on entrepreneurialism and commercialization. This interaction may be useful in a variety of ways. When academics and industry work together, beneficial outcomes such as better understanding of the business sector, possibilities for career growth, and improved investor relations may emerge.

Commercialization may take many forms, such as selling a licence to an existing business or an entrepreneur to use their technology, or it might include starting a whole new business from the bottom up. Get more information about the several ways your idea may be brought to market.

The cornerstones of copyright law are novelty and permanence.

Works That Aren't Copies

When a human author alone creates a work and that work has at least some degree of originality, we refer to that work as original. Independent invention is shorthand for the act of coming up with something on one's own, without resorting to imitation. The United States Supreme Court has said that in order for a piece of work to be considered creative, it must have at least a "spark" and "modicum" of originality. There are certain things, however, that are not creative, including titles, names, brief phrases, and slogans; well-known symbols or designs; simple changes of typographic ornamentation, writing, or colouring; and simply enumeration of components or contents. Always bear in mind that the only thing that may be protected by copyright is expression; not ideas, procedures, techniques, systems, processes, concepts, or discoveries.

Work That Is Fixed

A piece of work is considered to be fixed when it has been recorded (either by the author themselves or with the author's permission) in a medium that is sufficiently long-lasting so that it may be observed, reproduced, or conveyed for more than a brief period of time. For instance, a work is considered finished after it has been written down or recorded.

A royalty is simply a regular payment that is given by the user of an asset to the asset's owner or the person who created the item in exchange for the usage of the asset. To put it another way, the person who created the asset, whether it is a mine, a patent, a book, an artistic production, etc.

The Trade-Related Aspects of Intellectual Property Rights (TRIPS) agreement protects the majority of different types of intellectual property, including copyright, patents, geographical indications, trademarks, industrial designs, trade secrets, and exclusive rights over new plant varieties. On January 1, 1995, TRIPS was officially put into effect.

Generally speaking, when people talk about academic publication, they mean the publishing of research findings. To put it another way, it refers to the findings that were presented in a written format by researchers who used scientific theories and procedures to acquire new information in their respective fields of study and then published their findings.

Journal articles, research reports, conference papers, and books are the typical forms of publishing, and previous research is used as a point of departure while also being critically explored and expanded further. The authors of these publications always cite the sources upon which they build their own arguments. This is an important aspect because it allows potential readers to look up the sources in question and determine not only whether or not the authors have correctly understood them, but also whether or not they have the opportunity to form their own opinion.

The vast majority of scientific articles are created in accordance with a format that is referred to as

IMRAD. The phrase is a representation of the first letters of the terms "Introduction," "Materials and Methods," "Results," and "Discussion." It provides an example of a pattern or structure rather than a comprehensive list of headings or components of research papers; the portions of a document that are not included are the following: the title, the authors, the keywords, the abstract, the conclusions, and the references. Additionally, some papers consist of an Acknowledgements section as well as an Appendix section. The Introduction explains the scope and objective of the study in light of current knowledge on the subject; the Materials and Methods section describes how the study was conducted; the Results section reports what was found in the study; and the Discussion section explains the meaning and significance of the results and provides suggestions for future directions of research. [Citation needed] The Introduction explains the scope and objective of the study in light of current knowledge on the subject. It is required that the paper be prepared in accordance with the directions given to authors by the Journal.

It is essential to bear in mind that there is neither a standard nor a consistent style that all journals adhere to. This is one of the most crucial things to keep in mind. Each publication publishes articles in its own unique format, yet all of them adhere to a standard set of Instructions to Authors (or other word combinations to mean the same thing).

You should FOLLOW THE JOURNAL'S INSTRUCTIONS TO AUTHORS once you have chosen a journal to which you wish to submit your manuscript. These instructions can typically be found in each volume of the journal (keep in mind that a volume may contain several numbers, and there could be multiple volumes in a year), or they can be easily accessed from the website of the journal. It is possible that some authors are not completely persuaded by the rationale behind some of these recommendations; nonetheless, it is a waste of time to dispute with the journal or complain about the directions that it provides. It is important to keep in mind that writers have the option of publishing their articles in any one of many different journals. The majority of scientific articles are written in accordance with a standardised structure known as IMRAD. These four letters

represent the initial letters of the phrases Introduction, Materials and Methods, Results, and Discussion, respectively. These do not constitute a comprehensive list of the headings or components that are included in research papers; the following are absent: title, authors, keywords, abstract, conclusions, and references. In addition, some papers have an acknowledgements section as well as an appendix (Appendices). In certain cases, some parts may be represented and/or augmented by others; for example, "Theory" may be used in place of "Materials and Methods." In addition, the Results and Discussion sections have been combined into a single section, and the word "Conclusions" has been added as the last component of the Discussion section. There has been a recent shift toward giving just the most significant components of the article and publishing any extra or "less important" aspects as "Supplemental Materials" on the website of the journal. This practise has becoming more common. Review articles often make use of alternative headings rather than IMRAD headings, and they do not include the section titled "Results and Discussion." More than the individual words that are included by the acronym, the term IMRAD refers to a pattern or arrangement. Since the American National Standards Institute (ANSI) chose to use this phrase as the norm both in 1972 and again in 1979 (ANSI 1979), the majority of research journals have opted to use it.

One of the characteristics of sound scientific inquiry is known as reproducibility, which refers to the capacity of separate researchers to reproduce an experiment or test and come up with the same or comparable findings. The ability to reproduce study results provides scientists with proof that the findings are objective and dependable and were not the product of chance or prejudice. Irreproducibility, on the other hand, may point to issues with any one of the stages of the research process, including but not limited to the experimental design, the variability of biological materials (such as cells, tissues, or animal or human subjects), the quality or integrity of the data, the statistical analysis, or the study description. In spite of the fact that researchers have been aware of the significance of reproducibility for quite some time, the issue has only recently become a pressing concern. This is due to the fact that scientists and the general public are becoming more

aware of the fact that the results of many studies that are published in journals that are peer-reviewed cannot be reproduced.

Plagiarism occurs when someone presents the work or ideas of another person as their own, either with or without the other person's consent, by incorporating the work or ideas into their own work without giving proper acknowledgment. This definition encompasses all of the content that has been published or that has not been published, regardless of whether it is in the form of a manuscript, a printed book, or an electronic file.

RESEARCH ETHICS

Objectives in the field of ethical research

1. The protection of human participants is the primary and overarching aim of this project.
2. The second goal is to make certain that research is carried out in such a manner that it is beneficial to the interests of people, organizations, and/or society as a whole.
3. The third and final goal is to investigate particular research projects and activities to determine whether or not they adhere to ethical standards. This will include looking at concerns such as the management of risks, the preservation of confidentiality, and the procedure of informed consent.

The term "research ethics" refers to the practice of applying basic ethical principles to a wide range of issues that arise in the context of scientific study.

The practice of applying basic ethical concepts to contemporary issues like as

1. The planning and execution of research including the use of animals and/or humans as test subjects
2. Multiple facets of the controversy in the academic community, including scientific misconducts (such as fraud, fabrication of data and plagiarism),
3. "blowing the whistle," also known as disclosing misconduct inside an institution to the general public or to individuals in

positions of responsibility; regulation of research, etc. The field of scientific research is the one in which the notion of research ethics has progressed the greatest.

4. The research that is conducted in the social sciences raises a unique set of challenges in comparison to the research that is conducted in the medical field.

Trust is the cornerstone upon which the enterprise of scientific investigation is constructed. Scientists have faith that the findings published by other researchers are accurate. People have faith that researchers are making genuine efforts to explain the world in a way that is objective and truthful, and that these efforts will be reflected in the findings of their studies. However, this trust will only continue to exist for as long as the scientific community makes a concerted effort to both model and pass on the principles that are associated with ethical behavior in the scientific community.

When doing research, there are a great deal of moral dilemmas that need to be carefully considered. Sociologists need to be conscious that it is their job to gain the true consent and interests of everyone who is participating in the research. This is a responsibility that they cannot shirk. They are not permitted to put any of the information they have obtained to improper use, and they are expected to maintain a certain level of moral duty toward the participants. Participants in the research have a moral obligation to have their rights, as well as their confidentiality and sensitivity, safeguarded. It is necessary to maintain the secrecy of those individuals who took part in the observation, as well as to protect their identity and privacy. According to what is stated in the BSA for Sociology, all of these ethical standards have to be honored, unless there are other reasons that are more compelling to do so, such as any behavior that is unlawful or terroristic.

The vast majority of people learn their understanding of ethical principles either at home, in schools, in religious institutions such as temples and churches, or in some other kind of social setting. Even though the majority of people get their sense of what is good and bad while they are young, moral development takes occur throughout the course of a person's whole life, and humans go through a number of

stages of growth as they become older. Given how prevalent ethical norms are, one might be excused for assuming them to be nothing more than common sense due to their widespread application. If, on the other hand, morality were nothing more than common sense, then it raises the question as to why our society is riddled with so many controversies and difficulties related to ethics.

Although everyone admits the presence of some universal ethical standards, different individuals interpret, apply, and strike a balance between these rules in accordance with their own set of values and their own experiences in life. One explanation that appears to make sense for these conflicts is that although everyone acknowledges the existence of certain universal ethical norms, these norms are interpreted differently by various people.

On the other hand, ethical standards have a tendency to be less formal and more comprehensive than legal laws, which are employed to control behaviour in the majority of nations. Legal regulations are utilised to govern most countries. Even while laws are employed in the majority of civilizations to enforce universally agreed moral standards, and even though ethical and legal concepts include many of the same ideas, it is very important to bear in mind that law and ethics are not the same thing. It is conceivable for the same action to be considered morally commendable in one setting yet immorally unacceptable in another. In addition, by using ethical ideas and concepts, we are able to analyse, evaluate, propose, or interpret laws. In point of fact, throughout the course of the 20th century, a number of proponents of social change encouraged members of society to break the law in order to voice their opposition to laws that they viewed as being immoral or unfair. They did this in order to express their disapproval of these laws. Through the use of nonviolent civil disobedience, one is able to express a political position in a way that is appropriate from a moral standpoint.

One further way to define the word "ethics" focuses on academic disciplines that explore standards of conduct, such as philosophy, theology, law, psychology, or sociology. This is an additional method to defining the word "ethics." This is another possible interpretation of the word "ethics." A "medical ethicist," for instance, is a person who examines the ethical concepts that underlie the practise of medicine.

[Further citation is required] An additional meaning of the word "ethics" is "a technique, process, or point of view for deciding how one should behave and for studying challenging circumstances and themes," and this is one way to characterise ethics. For instance, while thinking about a difficult subject like global warming, one might approach the problem from a variety of different angles, such as economic, ecological, political, or ethical, depending on which perspective they pick. An environmental ethicist may explore the ethical values and principles that are at stake in various policies related to global warming. This is in contrast to the work of an economist, who would analyse the benefits and drawbacks of various policies related to global warming.

There are numerous various areas of study, institutions, and professions, and each of them has its own set of behavioural expectations that are suited to the specific aims and goals it seeks to achieve. These standards not only help participants in the field plan their actions and activities, but they also contribute to the growth of public trust in the field as a whole. In professions such as medicine, law, engineering, and business, for instance, one is expected to conduct oneself in accordance with a set of ethical guidelines. People who participate in scientific research or any other kind of intellectual or creative activity are held to the ethical standards that apply to them because these standards support the purposes or goals of study. These standards also apply to people who engage in any other kind of intellectual or creative activity. The study of these norms is the primary subject of research ethics, a discipline of applied ethics that is explicitly devoted to the topic.

The importance of doing research in accordance with ethical standards may be attributed to a number of different factors. To begin, standards advance the goals of research, such as acquiring information, uncovering the truth, and staying away from making mistakes. For instance, laws that make it illegal to fabricate, distort, or otherwise misrepresent research findings help spread the truth and prevent people from making mistakes. Second, ethical standards promote the values that are essential to collaborative work, such as trust, accountability, mutual respect, and fairness. This is important for two reasons. First,

research frequently involves a significant amount of cooperation and coordination between a large number of different people working in a variety of different fields and institutions. For instance, many of the ethical conventions in research, such as criteria for authorship, copyright and patenting regulations, data sharing policies, and confidentiality restrictions in peer review, are all geared to preserve intellectual property interests while also fostering cooperation. The majority of researchers want to be recognized for their work, and they do not want their ideas to be taken by another person or shared too soon. Third, many of the ethical standards guarantee that researchers may be held responsible to the general public by helping to ensure that they follow the rules. For example, government laws on research misconduct, conflicts of interest, the protection of human subjects, animal care and usage, and so on are required in order to guarantee that researchers who are supported financially by the public may be held responsible to that public. In the fourth place, ethical standards in research contribute to the development of public support for research. It has been shown that individuals are more willing to provide financial support for a study project if they have faith in the reliability and objectivity of the research. In conclusion, many of the standards that govern research also promote a wide range of other essential moral and social values. These include social responsibility, human rights, and animal care, as well as compliance with the law, health and safety. Research that violates ethical standards may cause severe damage to the human and animal subjects, as well as the students and the general public. For instance, if a researcher fabricates data during a clinical trial, it may cause patients harm or even death. Additionally, if a researcher does not adhere to the regulations and guidelines relating to radiation or biological safety, it may put his own health and safety, as well as the health and safety of staff and students, in jeopardy.

CODES AND POLICIES FOR RESEARCH ETHICS

It should not come as a surprise that many different professional organisations, government agencies, and institutions have developed particular codes, norms, and policies pertaining to research ethics given the significance of ethics for the conduct of research. The National

Institutes of Health (NIH), the National Science Foundation (NSF), the Food and Drug Administration (FDA), the Environmental Protection Agency (EPA), and the Department of Agriculture (USDA) are just some of the federal agencies that have ethics guidelines for researchers who receive funding from their organizations. Other important policies regarding research ethics include the Uniform Requirements for Manuscripts Submitted to Biomedical Journals, which was developed by the International Committee of Medical Journal Editors; the Chemist's Code of Conduct, which was developed by the American Chemical Society; the Code of Ethics, which was developed by the American Society for Clinical Laboratory Science; the Ethical Principles of Psychologists, which was developed by the American Psychological Association; the Statements on Ethics and Professional Responsibility, which was developed by the American Anthropolog (World Medical Association).

The following is an approximate and broad outline of certain ethical principles that are addressed by several codes:

1. Honesty It is essential that all scientific communications be conducted in an honest manner. Report the data, the findings, the methodology and the processes, and the publishing status with complete honesty. Do not manufacture, falsify, or distort data. Do not fool your coworkers, the organizations that award funding, or the general public.
2. Objectivity: Make it a priority to eliminate any potential for subjectivity in the experimental design, data processing, data interpretation, peer review, personnel choices, grant writing, expert testimony, and any other areas of research where objectivity is anticipated or needed. It is important to steer clear of or reduce instances of self-deception. Disclosing personal or financial interests that might potentially have an impact on research is required.
3. Integrity is keeping your word and honoring the deals you make; acting honestly; and working hard to maintain coherence between your thoughts and deeds.
4. Attention to Detail Steer clear of casual mistakes and laziness, and take the time to thoroughly and analytically assess both your own

work and that of your colleagues. Maintain thorough records of all aspects of the research process, including data collecting, study design, and any communication with organizations or publications.

5. Transparency: Share information, including outcomes, ideas, and resources. Maintain an open mind when it comes to constructive criticism and novel ideas.
6. Show veneration for various types of knowledgeable property, including copyrights, patents, and other forms of IP. Do not utilize any data, methodology, or findings that have not been published without first obtaining permission. It is important to give credit where it is due. It is important to properly thank and credit everyone who has contributed to the study. Never plagiarize.
7. Maintain confidentiality in all communications, including those that are submitted for publication, such as papers or grants, as well as documents pertaining to personnel, trade or military secrets, and patient data.
8. Responsible Publication: Publish in order to improve research and scholarship, and not simply your own career, rather than only publishing in order to advance your own career. Publication that is both wasteful and redundant should be avoided.
9. Responsible Mentoring: Offer assistance to students in the areas of education, mentoring, and advising. Foster their well-being and respect their autonomy by giving them decision-making power.
10. Respect for one's coworkers It is important to respect one's coworkers and to treat them decently.
11. Take Responsibility for Your Community: Through study, education of the general public, and advocacy, you should work to improve your community while also minimizing any negative effects it may have.
12. Non-Discrimination It is important to refrain from acting unfairly against coworkers or pupils on the basis of their gender, colour, ethnicity, or any other factor that is unrelated to their ability or honesty in the scientific field. This encompasses not just racial discrimination but but ethnic prejudice and gender discrimination as well.

13. Competence You should continue your education and pursuit of knowledge throughout your whole life in order to sustain and further increase your own level of professional competence and skill. In addition to this, you need to take measures to increase general scientific knowledge and expertise.
14. Compliance with the Law: Be aware of and abide by all applicable laws, as well as rules established by institutions and the government.
15. Treatment of Animals Researchers are obligated to show appropriate respect and compassion for the animals they use in their experiments. Experiments on animals should not be performed if they are unneeded or poorly conceived.
16. Protection of Human Subjects When conducting research on human subjects, researchers should make an effort to minimize potential risks and harms while simultaneously maximizing potential benefits; they should also respect human dignity, privacy, and autonomy; they should take extra precautions when working with vulnerable populations; and they should make an effort to distribute the benefits and burdens of research in an equitable manner.
17. There are a great number of additional actions that do not fit the definition of "misconduct," but which are nevertheless recognized as unethical by the majority of researchers. The following are examples of what are referred to be "additional departures" from appropriate research practices:

- Submitting the identical article to many publications without informing the appropriate journal editors.
- Sending the identical work to many journals without informing the editors of the other journals
- Keeping a collaborator in the dark about your plans to apply for a patent in order to establish yourself as the sole creator of the invention;
- Listing a colleague as an author on a paper in exchange for a favor, despite the fact that the colleague did not make a significant

contribution to the work, even if the colleague was included on the manuscript as an author.

- Sharing with your coworkers information that is deemed secret from a piece of writing that you are examining for a journal
- Eliminating data from a collection that contains outliers without first articulating the rationale for doing so in a paper
- Employing an unsuitable method of statistical analysis in order to bolster the relevance of your previous study.
- Skipping the step of having your work reviewed by peers and instead revealing the findings of your study at a press conference, without providing your colleagues with sufficient information so that they can evaluate your work.
- Carrying out a review of the published research without giving credit to the efforts of other researchers in the area or previous work that is pertinent to the topic at hand
- Exaggerating claims made in a grant application in order to give the impression to committee members that the work being proposed would have a substantial impact on the industry as a whole
- Lying on a resume or application for a job; this includes embellishing the facts.
- Comparing the completion times of two graduate students working on the identical research topic in order to determine who can finish it more quickly.
- Subjecting graduate or post-doctoral students to excessive workloads, ignoring their needs, or using them inappropriately
- Failing to maintain accurate records of the research
- Failing to keep research data for a length of time that is considered to be acceptable
- Using insulting language and making personal attacks in your assessment of the author's submission
- Promising a pupil a higher score for sexual favors
- Using a slur that is deemed to be racist in a scientific setting
- Deviating significantly from the study protocol that has been authorized by your institution's Animal Care and Use Committee or Institutional Review Board for Human Subjects Research

without informing either of those committees or boards of those major deviations.

- Failing to disclose a potentially harmful occurrence during a human study trial
- Misuse of animals in scientific research
- Violating the biosafety regulations of your school in a way that puts children and employees at risk of exposure to biological hazards
- Refusing to study a submitted work before rejecting it as unsuitable for publication
- Undermining the efforts of another individual
- Larceny of items such as supplies, literature, or information
- Conducting an experiment in such a way that the outcome can be predicted.
- Copying confidential information, documents, or computer programs without authorization
- Making a conscious decision to exaggerate the therapeutic relevance of a new medicine in order to maximize one's potential financial gain

The vast majority of scientists would consider these practices unethical, and some of them could even be breaking the law. The majority of these would also contravene various codes of professional ethics or standards established by the organization.

Fostering Responsible Behavior in Scientific Research

Many of you are probably curious about the reasoning for the need that you get training in research ethics. It's possible that you think you have a strong moral compass and understand what constitutes good and bad behavior. You would never knowingly create false data, plagiarize, or otherwise fake information. In point of fact, you could think that the vast majority of your coworkers have very high ethical standards and that there is no ethical dilemma in research.

Relax if this is how you're feeling. You are not being accused of operating in an unethical manner by anybody. In point of fact, the best data that we have demonstrates that unethical behavior in research is a

very uncommon occurrence, despite the fact that different estimates indicate a significant amount of variance. It has been estimated that the rate of misconduct ranges from as low as 0.01% of researchers per year to as high as 1% of researchers per year, and this estimate is based on proven occurrences of misconduct in research that was supported by the federal government (based on self-reports of delinquency on unidentified surveys).

It is obvious that having more data on this subject would be beneficial, but there is currently no evidence to suggest that the scientific community has become unethical. However, regardless of how seldom it occurs, unethical behavior in research may still have a significant influence on the field. Consider an example with the issue of crime: it does not take very many homicides or rapes in a town for the community's feeling of trust to deteriorate, and for dread and paranoia to spread across the community. The same may be said about the three crimes in science that are considered to be the gravest: fabrication, falsification, and plagiarism. On the other hand, the majority of crimes that are done in the field of science are probably not on the same level as rape or murder; rather, they are morally important transgressions that the government labels as "deviations." In addition, there are other instances in the realm of research that provide actual ethical conundrums.

Will becoming trained and educated in research ethics help lessen the amount of misbehavior that takes place in the scientific community? It is too soon to know at this point. The response to this question is going to be somewhat determined by how well one knows the factors that lead to inappropriate behavior. There are two primary schools of thought about the reasons why researchers engage in unethical behavior. The "bad apple" idea asserts that the vast majority of scientists adhere to strict ethical standards. Misconduct in the scientific community can only be committed by researchers who are morally corrupt, monetarily desperate, or mentally ill. In addition, only an idiot would engage in unethical behavior in the scientific community due to the fact that the peer review system and the self-correcting processes would ultimately uncover those who attempt to trick the system. In any event, it may be argued that taking a class on

research ethics won't have much of an effect on those who are "bad apples." According to the "stressful" or "imperfect" environment theory, misconduct occurs because various institutional pressures, incentives, and constraints encourage people to commit misconduct. These institutional pressures, incentives, and constraints include things like the pursuit of profit or fame, career ambitions, the pressure to publish or obtain grants or contracts, and inadequate supervision of students and trainees as well as inadequate oversight of researchers. In addition, proponents of the stressed environment hypothesis highlight the fact that the peer review mechanism used in the scientific community is far from ideal and that it is quite simple to game the system. It is very uncommon for erroneous or fraudulent research to be published in the public record for years before being discovered. A course in research ethics is likely to help people get a better understanding of the stresses that are associated with research environments, make people more sensitive to ethical concerns, and improve ethical judgment and decision making. This is true to the extent that research environments are an important factor in misconduct.

People who are morally weak, uninformed, or insensitive are probably more likely to engage in unethical behavior when they are put in stressful or flawed circumstances. Environmental factors likely have a role in unethical behavior as well. A course in research ethics is helpful in helping to avoid departures from norms, even if it does not prevent misconduct; this is the case even if the training does not prevent misconduct. It is possible that the majority of the deviations that take place in research are due to the fact that researchers either just do not know or have never given some of the ethical principles of study considerable attention. For instance, certain unethical authoring practices are presumably the result of years of tradition within the academic community, which, until relatively recently, was not called into serious question until now. What could possibly be wrong with it if the director of a laboratory is included as an author on each and every publication that is produced in that laboratory, even if he does not make a meaningful contribution to the work? One may make the case that this is the standard practice in the industry. What exactly is

wrong with the practice of a pharmaceutical corporation having its medical personnel "author" articles that were really written by ghostwriters? These days, ghost writers contribute to the writing of a wide variety of publications; if the use of ghostwriters is acceptable in other contexts, why not research?

The existence of conflicts of interest in research is another example of an area where there may be some ignorance or mistaken traditions. A researcher can believe that a "regular" or "traditional" financial arrangement, such as receiving stock or a consulting fee from a drug firm that finances her study, does not create any significant ethical difficulties since they are considered to be "normal" or "traditional." Or, it's possible that a university administrator doesn't see a problem with accepting a large gift from a pharmaceutical company that comes with conditions attached to it. Perhaps a physician feels that it is quite acceptable to earn a finder's fee of three hundred dollars for sending patients to participate in a clinical trial.

If "deviations" from ethical behaviour in research are caused by ignorance or a failure to critically reflect on harmful traditions, then completing a course in research ethics may assist lower the occurrence of major "deviations" by increasing the researcher's grasp of ethics and by sensitising him or her to the problems. This may be accomplished by improving the researcher's understanding of ethics and by sensitising the researcher to the difficulties. This is due to the fact that the researcher's comprehension of ethics will improve as a result of taking the course, and that the researcher's awareness of the concerns will also rise as a result of taking the course.

Last but not least, training in research ethics should be able to assist researchers in resolving ethical conundrums by acquainting them with significant ideas, techniques, principles, and methodologies that may be of value in the process of finding solutions to these conundrums. In point of fact, the problems have reached such a critical state that the NIH and the NSF have required that research ethics education be provided to graduate students.

RESEARCH ANIMAL (often abbreviated as RA)

The use of animals in scientific study is very important. Researchers put them to use in a number of contexts, including the evaluation of novel medications, the instruction of medical students, and the testing of new surgical methods on experimental individuals. Animal research is typically the required first step towards research involving novel medical treatments and medications meant for human use. As a result, research with animals is essential to biomedical research and must be conducted in order to advance the field.

Concerning the use of animals as study subjects, there are a great number of organizations and people that are committed to ensuring their protection and safety. There are some groups that are working toward the goal of doing away with the use of animals in scientific research. Others believe that doing research on animals is an unfortunate but essential step toward advancing medical knowledge, but they are committed to reducing the amount of needless suffering, pain, and substandard facility conditions that animal subjects are exposed to.

Reviewing research initiatives that include the use of animals is necessary to ensure the protection of animals. These evaluation systems analyze both the hazards and the potential advantages of doing research on animals. This may be problematic for project reviewers and frequently causes for passionate discussions and disagreements regarding the proper use of animal subjects, especially given the animal subjects normally suffer all the dangers while human people enjoy all the advantages. Whether or not animals feel pain in the same manner that people do, whether or not animals experience agony to the same degree that humans do, and whether or not these notions should even play into the discussion at all are all topics that are being discussed and debated.

The government has enacted laws concerning the use of animals in teaching, testing, and research in order to guarantee that research using animals is carried out in an ethical and responsible manner. These regulations also address the care of animals.

Institutions of higher learning and scientific research often make use of a wide variety of animals for a variety of objectives. Others are

investigated within the context of their native environments. There is a huge amount of variety in both the ends to which they are put and the effects that their usage has on the animals themselves. In each and every scenario, it is very necessary that the particular animal be handled in a kind and compassionate way.

Regulation and Administrative Norms

Research and teaching that include the use of animals are only permitted under certain circumstances, including the following:

- To acquire and establish important knowledge that is vital to the comprehension of humans and/or animals;
- For the purpose of preserving and/or enhancing the health and well-being of humans and/or animals;
- To enhance either the management of animals or the production of meat;
- To acquire and compile substantial data that is pertinent to the comprehension, preservation, or enhancement of the natural environment; or
- In order to accomplish the goals set for the educational experience.

Projects that require the use of animals cannot be carried out unless it has first been assessed whether or not they are ethical to do so. This conclusion is obtained by evaluating the potential instructional or scientific value of the research with the effect that it is likely to have on the wellbeing of the animals.

For each and every activity involving animals, researchers and educators are obligated to provide an Animal Ethics Committee with a written proposal. This proposal has to take into account the predicted value of the information that will be obtained, the reason for the project, as well as the ethical and animal welfare considerations taking into mind the 3RS - replacement, reduction, and refinement - as defined in the Australian Code of Practice for the Care and Use of Animals for Scientific Purposes.

In the state of South Australia, adhering to the Australian Code of Practice for the Care and Use of Animals for Scientific Purposes, often known as "the Code," is both required by law and considered to

be obligatory behavior. Infractions of the Code are subject to the penalties that are outlined in the Animal Welfare Act of 1985. The Code was created with the intention of ensuring that the ethical and humane treatment of animals in research and education is maintained at all times. The investigators, instructors, institutions, Animal Ethics Committees (AECs), and all other individuals who are responsible for the care and use of animals for scientific reasons should look to the guiding principles that are outlined in the Code for direction.

The Code emphasises the responsibilities of researchers, educators, and institutions that use living creatures to ensure that animal use is appropriate, that animals' welfare is always taken into account, that alternatives to animal testing are developed, that the number of creatures used is minimised, and that procedures are refined to confirm that animals do not experience pain or distress.

Replacement, reduction, and refinement are the three R's to keep in mind.

The tenets of this view are enshrined in the code of practice for the care and use of animals for scientific purposes.

1. Substitution: Methods that can fully or partly substitute the use of animals in scientific research should be actively required out and implemented whenever and wherever this is feasible.

2. Each study shall utilize no more than the minimal number of animals essential to assure the validity of the scientific and statistical findings. It is unacceptable to put into practice the principle of tumbling the number of animals used if doing so would result in more individual animals being subjected to pain and suffering. Scientific and educational activities involving the use of animals may not be repeated unless needed for the objective or design of the activity. The least amount of animals necessary to accomplish the learning goals must be used in instruction activities, and this number cannot be increased above what is necessary. It is important to prevent the overproduction of animals produced for scientific objectives in order to reduce the number of healthy animals that must be sacrificed.

3. Clarification: In order for animals to be used for scientific purposes, it is necessary to take into consideration their behavioral and

genetic traits, as well as their nutritional, microbial, and overall health conditions. The design and management of animal housing should take into account the particular requirements of individual species. In situations in which this cannot be done because of the requirements of the project, special consideration is required. Transport, housing, feeding, watering, handling, and use of animals should all be carried out in accordance with the requirements unique to each species.

When providing care for the animals, the primary concern must be for the animals' well-being, and the care given should be based on both the animals' behavioral and their biological requirements. It is unethical to remove wild animals from their natural habitats unless they have been bred.

Projects should be developed to prevent both pain and discomfort in animals. In the event that this cannot be accomplished, any discomfort or anguish must be kept to a minimum. Because it is difficult to determine whether or not an animal is experiencing pain or suffering, researchers and educators are required to operate on the assumption that animals go through these sensations in a way comparable to that of people, unless there is evidence to the contrary. This premise must serve as the foundation for all choices pertaining to the well-being of the animals. It is imperative that any animal exhibiting indicators of pain or distress that were not anticipated in the proposal receives early relief from that pain or distress. The relief of this kind of suffering or grief has to take priority over the completion of the project. In the event that this cannot be accomplished, the animal must be put down as soon as possible.

Activities in the fields of science and education that have the potential to cause pain or distress of a kind or degree for which anesthesia would typically be used in medical or veterinary practice must be carried out utilizing anesthesia that is suitable for both the species and the procedure in question. There must be provision made for pain management that is suitable for the animal in question, the procedure in question, and the circumstances. The use of local or general anesthetics, analgesics, or tranquilizing agents must be suitable for the species in question, and at the very least, it should be comparable to how these medications are currently employed in the

field of human or veterinary medicine. In the event that it is determined that the aim of the project precludes the use of anesthetic or analgesic agents to alleviate pain, the planned endpoint of the project must be as early as is practically possible in order to prevent or reduce the amount of pain or distress experienced by the animals. It is not permissible to employ neuromuscular blocking medications in the absence of proper general anesthesia, with the exception of animals in whom all sensory awareness has been removed. If such agents are used, it is essential to monitor the paralyzed animals in a continuous or frequent manner to ensure that the level of anesthesia is sufficient to prevent the animals from experiencing any pain or distress. Avoiding death as a destination whenever it's at all feasible is a necessary. Scientific and educational activities involving the use of animals shall be of minimal duration commensurate with the aims of the project.

CONCERNING ETHICAL PROBLEMS Involved in Agricultural Research

1. Sustainability: Ethical conundrums occur when solutions to issues in the short term are prioritized above those in the long term. In order for institutions to be able to solve long-term challenges, they need a different form of reinforcement than they would normally get. When particular sectors, segments, social classes, or seasons are favored over others when picking issues, finding them, fixing them, or distributing the answers discovered, an ethical challenge might also develop. Concerns that cut across different species and sectors also have an impact on the long-term viability of the results. Not all of the local customs and traditions need to be preserved. Sustainability requires an understanding of both continuity and discontinuity in equal measure (that is innovations or fundamental change in values).

2. Analysis of the ecological health system Scientists not only engage in a process of trade-off but also exercise a form of value judgement when they are aware of the elements that contribute to the environmental system's but continue to produce technologies that undermine it. It might be unethical and fiscally irresponsible to place the burden of short-term compromises on people who would feel their effects over a longer time frame. If the potential or actual long-term

consequences of using a certain chemical input are recognised, but that input is nonetheless used, the eco system will suffer. Applying or not applying the precautionary principle, transferring technologies to countries that might or might not have the ability to analyze the repercussions of their use, and allowing the use of chemicals that are censored in developed countries are all examples of situations that require making value judgments.

3. Acceptance: Not everyone's worries are of equal weight in any given circumstance. Michael Lipton once pointed out the inherent biases that exist in favour of intriguing pests rather than the ones that are pertinent to the topic. When problems exist for millennia without being addressed, it must say something about the values of the society as a whole that such problems don't pose a moral dilemma or make people feel uneasy. The stove, used by millions of women every day, is a great illustration of this point. Transplanting paddy while keeping one's feet submerged is another activity that may cause fungal infections and other health issues, as does carrying water pots on one's head for long distances or carrying grass or twigs on one's head on the slopes of hills by women.

4. Responsibility It is uncommon for researchers to communicate their conclusions to the individuals who provided them with the data they collected. In addition to that Quite often, they do not even bother to calibrate their criteria of relevant or not so relevant research by include the consumers of research in the calibration process. Another situation that gives rise to an ethical conundrum is when a huge multinational firm informs the customers who buy its chemical inputs about a desired resource use technique that is common in the west but is not common in developing nations. It is necessary for the community of companies to have its own code of conduct that prohibits behavior of this kind.

5. The development of capabilities: Any community that must contend with the risk and uncertainty that is inherent in the management of agricultural resources must learn to develop the capabilities not only to predict but also to solve issues that may arise in the future. Therefore, the education and training of young brains becomes an extremely crucial factor in determining the ability to deal

with rising issues in the future. An ethical decision has been made when it is determined that the educational system does or does not include content or pedagogical means that make a potential leader aware of the challenges facing their organization. Values are already communicated when particular crops and/or other agricultural products are depicted in the school curriculum as being purposely inferior on cultural grounds rather than on nutritional grounds or other scientific reasons. This occurs more often than the reverse. A lack of periodic review of the skills that are being developed to address such concerns as externality, diversity, inter sectoral linkages, etc., invariably involves making trade-offs about what should be told to young people and what should be left up to them to learn on their own.

6. The specificity of the location It is common knowledge that the agroecological environment in regions that are rainfed is significantly more diverse. In addition to the technical challenges, developing technologies that would only spread within a limited area presents institutions with a unique set of problems to solve. Incentives for organizations are often offered, and their value is proportional to the spread or prospective reach of a solution. If a technology is addressing problems of small community, it may not invoke a significant encouragement or incentive. As a consequence of this, either the issues in question are not addressed or the individuals who do solve them are pushed to the margins of society. In either situation ethical judgements have to be made by the decision makers. When the research infrastructure, allocation of human resources, and research priorities are weighted more heavily toward communities and regions that have a greater abundance of resources, the ethics of ignoring the communities and regions that are bypassed need to be made clear. It is possible that judgments have been made when hand tools are given less attention than technologies that require a lot of energy.

7. An imbalance between the rights and duties of knowledge holders Neither established nor emerging nations' agricultural research councils have ever mandated that the imbalance of power between formal and informal sectors' knowledge holders be rectified. Those who take part in community-based research projects are seldom thanked, rarely shown the results to which they contributed data, and

almost never offered a cut of the profits made from applying or commercializing the insights their respondents or they themselves gave.

8. Empowerment of informal innovators and holders of information It should come as no surprise that inventiveness may be found in both formal and informal settings. There is no reason why a farmer or an artisan couldn't come up with a novel and inventive solution to a problem in the same way that scientists can. It is quite clear that there is a widespread prejudice towards innovations in the informal sector. The inability of the organized sector of agricultural research and technology to listen to and learn from informal innovators not only deprives the organized sector of ideas from the periphery but also stops it from being motivated by the ideals of many of the grassroots innovators.

The moral choices that must be made in such situations inevitably have an effect on the effectiveness, equality, and excellence of resource and institutional management, as well as the environmental repercussions.

REFERENCES

1. Argenti, P.A. 2003. Corporate communication. Boston: McGraw-Hill Irwin.
2. Argyris, C., Putnam, R. & Smith, D. 1985. Action science: Concepts, methods, and skills for research intervention. San Francisco: Jossey-Bass.
3. Babbie, E. 1992. The practice of social research. Belmont: Wadsworth.
4. Bartlett, C.A. & Ghoshal, S. 1998. Transnational management: Text, cases and readings in cross-border management. Chicago: Irwin.
5. Belasco, J.A. & Stayer, R.C. 1993. Flight of the buffalo. New York: Warner Books.
6. Belsch, G.E. & Belsch, M.A. 1995. Introduction to advertising and promotion: An integrated marketing communications approach. Chicago: Irwin.
7. Bennett, P.D. 1995. Dictionary of marketing terms. Chicago: American Marketing Association.
8. Bennis, W. 1997. 'Becoming a leader of leaders'. (In Gibson, R. ed. Rethinking the future. London: Nicholas Brealy.)
9. Cornelissen, J.P. 2000. 'Theoretical concept of management fashion? Examining the significance of IMC'. Journal of Advertising Research, 40(5):7-16.
10. Einwiller, S. & Will, M. 2002. 'Towards an integrated approach to corporate branding – an empirical study'. Corporate Communications: An International Journal, 7(2):100-109.
11. Bagalkoti, V. T., & Hosamani, S. C. (2014). Mapping of the Indian Research Productivity of Biochemistry and Molecular Biology: A Scientometric Analysis. Journal of Advances in Library and Information Science, 3(3), 249-256.
12. Chaman, S., Dharani, K., & Biradar, B. (2018). Assessment of Chemical Science Research Output Using Scientometric Indicators. Asian Journal of Chemistry and Pharmaceutical Sciences, 2(2), 1-16.

13. Chaman, S., Dharani, K., & Biradar, B. (2018). Medicine research in India: A Scientometrics Assessment of publications during 2009 - 2018. Library Philoshphy and Practice, 1-17.25.12.2018. form https://digitalcommons.unl.edu/libphilprac/2186/
14. Chaman, S., Dharani, K., & Biradar, B. (2017). Mapping of Indian biomedicine research: a scientometric analysis of research output during 2012 – 2016. International Journal of Current Advanced Research, 6(7), 4688-4691.
15. Emmer, A. (2018). Geographies and scientometrics of research on natural hazards. Geosciences, 8(10), 382.
16. Hood, W., & Wilson, C. (2001). The literature of bibliometrics, scientometrics, and informetrics. Scientometrics, 52(2), 291-314.
17. Jin, Y., Li, X., Campbell, I., & Ji, S. (2017). Visualizing the hotspots and emerging trends of 3D printing through scientometrics. Rapid Prototyping Journal, 24 (5), 801-812.
18. Laengle, S., Merigó, J.M., Miranda, J., Słowiński, R., Bomze, I., Borgonovo, E., & Teunter, R. (2017). Forty years of the European Journal of Operational Research: A bibliometric overview. European Journal of Operational Research, 262(3), 803–816.
19. McGrath, W. E. (1996). The unit of analysis (objects of study) in bibliometrics and scientometrics. Scientometrics, 35(2), 257-264.
20. Merigó, J.M., & Yang, J.B. (2017). A bibliometric analysis of operations research and management science. Omega, 73, 37-48.
21. Merigó, J.M., Blanco-Mesa, F., Gil-Lafuente A.M., & Yager, R.R. (2017). Thirty years of the International Journal of Intelligent Systems: A bibliometric review. International Journal of Intelligent Systems, 32(5), 526-554.
22. Noruzi, A., & Abdekhoda, M. (2014). Scientometric analysis of Iraqi-Kurdistan universities' scientific productivity. The Electronic Library, 32(6), 770-785.

ABOUT THE AUTHORS



Dr. Mohd. Shaikhul Ashraf, Assistant Professor, Department of Botany, HKM Govt. Degree College Bandipora Kashmir, obtained his M.Sc., M.Phil. and Ph.D. from the Aligarh Muslim University, Aligarh. He has also done B.Ed. from the University of Kashmir, Srinagar and M .A. in English from IGNOU, New Delhi. The area of his Research is Plant Pathology and Nematology. He is teaching Botany in various Degree Colleges of Kashmir since 2009. He has published 23 research papers in reputed journals and co- authored five books. He is recipient of several awards and life member of several Scientific and Educational Societies.



Parmar Vishalkumar Rajendrasing
(M.Sc, M.Ed)
Reacher Scholar
Shri Govind Guru University, Godhara (Gujarat)



Dr. Hema Kumari Mehar, Assistant Professor, Ph.D, NET, SLET, Clinical Psychologist. She is assistant Professor in Psychology at UCSSH, Mohanlal Sukhadia University, Udaipur (Raj). She is Master Hypnotist & Practitioner of Self Hypnosis and completed clinical hypnotherapist level –III from California Hypnosis Institute , California USA in 2015. She has presented more than 35 research papers at national and international level and also published more than 12 Research Papers.



Dr. Javad Ghalambor is currently Assistant Professor in the School of Business at Acharya Institute of Management & Sciences (AIMS), Bangalore. He obtained his MBA and a doctorate in Finance from University of Mysore. His areas of interest are quantitative analysis, including statistical analysis, and finance. Besides, he serves as Manager of Research Centre at AIMS.



Dr. S. Kumar working as a Assistant Professor (Teaching Assistant), Department of Disaster Management (Ph.D. in Economics), Alagappa University, Karaikudi, Tamilnadu. He has received the Research Fellowship Bharat Ratna Dr. M.G. Ramachandran Centenary research Fellowship for persuing his Ph.D Research at Manonmaniam Sundaranar University, Tirunelveli. He has experience in teaching 1 year & Research in 3 years. He has published more than 30 articles in reputed journals; more than 30 papers presented in conferences & published 4 patents. He received Best Paper Award, Research Scholar Excellence Award (ICWA), Kalai Rathna Award and Best Assistant Professor Award.

₹ 400/- eBook

ISBN 978-93-954560-2-9

red'shine PUBLICATION INDIA

RED'SHINE PUBLICATION PVT. LTD.
88-90 REDMAC, Navamuvada,
Lunawada, Gujarat-389230
Website: www.redshine.co.in
Email: info@redshine.in
Helpline: 0-76988 26988

exclusive partner | Paradox PUBLICATIONS GUIDE HOUSE +91 88 18074612 \ +91 7907 367117

EDITED BOOK FOR
SOCIAL SCIENCE, COMMERCE AND LAW

About the Author



Dr. Kundan Kumar, done the Schooling from St. Michael's High School, Patna, Pursued B.Com (Hons.) in Accounts Vanijya Mahavidyalya, Patna University, Patna, and M.Com. from Patna University, Patna, MBA (Finance) from Lalit Narayan Institute of Economic Development and Social Change, Patna with distinction in 9 papers. Ph.D in Commerce from Patna University, Patna. Qualified UGC NET In Management conducted by UGC and Commerce conducted by NTA. Dr. Kundan worked in two multinational Companies for 6 Years as Senior Finance Executive and presently giving Professional Consultancy to various departments of Govt. of Bihar as well as visiting Faculty in various colleges. He has written 15 research papers out of which 8 are published in UGC approved Journals and 7 in refereed Journals published national and international level. He is author of A Collectively Edited Book in Fields of Law, Politics, and Economics and FINANCIAL MANAGEMENT AND COST ANALYSIS. He also attended Numbers of Nationals and Internationals Seminars, Conferences and workshops related to Management, Commerce and Economics. Dr. Kundan is also Lifetime member of Indian Economic Association as well as Indian Commerce Association.



Ashi is a highly accomplished scholar, holding a B.A. in English Honors from Delhi University, an M.A. in English from the same institution, and a Ph.D. in English from Shri Venkateshwara University. Her academic journey is distinguished by a series of impactful research publications that delve into the realm of Queer studies. Notable contributions include "Understanding Queer: Analysis of Queer Writings in Indian Literature" and "Indian Cinema's Queer Gaze: Portrayal of LGBTQIA+ Narrative on Screen," both published in the International Journal of Research in Social Sciences in January 2021 and May 2021, respectively. Ashi's scholarly pursuits extend to socio-cultural contexts, as evidenced by her work "Exploring Adolescent Sexuality in A Socio-Cultural Context: Abha Dawesar's Babyji" in Shodh Disha (January-March 2022 Volume), and her exploration of mythology and queerness in the works of Devdutt Pattanaik published in the International Journal of Research in Economics and Social Sciences in September 2022. Her recent research on the "Fortrayal of Lesbian Narrative on Indian Screen" in the International Journal of Research in Social Sciences (August 2023) further underscores her commitment to diverse perspectives. Ashi has actively participated in prominent conferences and seminars, such as NCMESS-2017, ICHD-2022 (International Conference), and the National Conference hosted by Shri Venkateshwara University in 2022, showcasing her engagement in academic discourse at both national and international levels.

₹725/-

ISBN 978-93-91771-54-6

Crescent

CRESCENT PUBLISHING CORPORATION
4806/24, Mathur Lane, Ansari Road, Darya Ganj,
New Delhi - 110002
Mob.: 9711991838, 9999021668, Phone: 011-23244131
e-mail : crescentbook@gmail.com
Website : www.crescentpublishingcorp.weebly.com

EDITED BOOK FOR
SOCIAL SCIENCE, COMMERCE AND LAW

Dr. Kundan Kumar
Ashi



EDITED BOOK FOR
SOCIAL SCIENCE, COMMERCE AND LAW

Dr. Kundan Kumar
Ashi



Edited Book for
Social Science, Commerce and Law

Kundan Kumar

CRESCENT
PUBLISHING CORPORATION

Edited Book for Social Science, Commerce and Law

© Reserved

First Published: 2023

ISBN 978-93-91771-95-9

All rights reserved. No part of this publication may be reproduced, stored in a retrieval system, or transmitted in any form or by any means, electronic, mechanical or photocopying or otherwise, without prior permission in writing from the authors/publisher.

Published by:

CRESCENT PUBLISHING CORPORATION

4806/24, Mathur Lane,
Ansari Road, Darya Ganj,
New Delhi - 110 002
Ph.: 011 - 23244131
Mob.: + 91 - 9711991838, 9999021668
E-mail: crescentbook@gmail.com
Website: www.crescentpublishingcorp.weebly.com

Printed at:
Roshan Offset Printers
Delhi

PRINTED IN INDIA

Contents

1. Issues Faced by Transgenders in India
   Ashi 1
2. How Contemporary Teaching Methods Affect the Learning Process
   Dr. Munmun Sharma 13
3. Evolution of the Tragic Hero in Shakespearean Drama
   Dr. Anupa Sharma 26
4. Privatisation of the Public Sector Enterprises
   Nirmala. R 37
5. The Foreign Policies of India And The United States: A Comparative Study
   Dr. Fakhrul Alom 45
6. An Examination of Factor that Influence Individual Investment Decision
   Dr. Kundan Kumar 55
7. Questionnaire
   Renu Bala 67
8. Investment Straegies and Stock Market Analysis
   Dr Monika Jaroli 88
10. A Comparative Study of Teacher Cybercrime Awareness
    Suman kumar 99
11. A Comparative Study of Folk Drama forms of Rajasthan and Maharashtra with Reference to Raga
    Dr Shiva Vyas 110
12. Parents and Teachers Monitor Cyberbullying
    Anindita Mazumder 123

About the Authors



Prof. Shurveer S. Bhanawat has been working as a Professor and Head, Department of Accountancy and Business Statistics, Mohanlal Sukhadia University, Udaipur. Sixty eight research articles have been published. He was awarded by ICAI international research award in 2021 and 2022.



Dr. Avinash Panwar is currently working as Associate Professor, Department of Comp. Sc., Course Director, Informatics and Computational Sciences Programme, Nodal Officer College of Engineering and Architecture & Director, Computer Center at Mohanlal Sukhadia University, Udaipur.



Dr. Shilpa Vardia has been working as an Assistant Professor in the Department of Accountancy and Business Statistics, Mohanlal Sukhadia University, Udaipur. She is the convener of the Master of Finance and Control and Post-Graduation Diploma in Taxation Programme. She has contributed thirty-four research papers and also received ICAI International Research award in 2020.



Dr. Shilpa Lodha is Assistant Professor at Department of Accountancy and Statistics, Mohanlal Sukhadia University, Udaipur (Raj). Her more than 25 research papers have been published in journals of national and international repute. She is Convener of B. Com. Honours.



Dr. Asha Sharma is Assistant Professor in the Department of Accountancy and Business Statistics at Mohanlal Sukhadia University, Udaipur. She is the convener of Bachelor of Vocation and Master of Vocation (Accounting, taxation, and auditing). She has contributed more than 85 research papers.



Dr. Parul Dashora is an Assistant Professor in Department of Accountancy and Business Statistics, Mohanlal Sukhadia University, Udaipur, [RAJ]. She is also Convener of Certification Programmes of the department. She also has two patents to her credit.



Pushpraj Meena is an Assistant Professor in Department of Accountancy and Business Statistics, University College of Commerce and Management Studies at Mohanlal Sukhadia University, Udaipur (Rajasthan). He has 6 years of experience in practical field of Accounting, Auditing and Taxation.

Published by
Weser Books, No. 79737
Äussere Weberstr. 57
02763 Zittau, Germany
Email: weserbooks@gmail.com

ISBN 9783964925503
9 783964 925503
Price - € 18

BLOCOUNTING

A Futuristic Approach

Prof. Shurveer S. Bhanawat

Dr. Avinash Panwar
Dr. Shilpa Vardia
Dr. Shilpa Lodha
Dr. Asha Sharma
Dr. Parul Dashora
Pushpraj Meena



Weser Books

वर्तमान पाठ्यक्रम एवं प्रतिबल

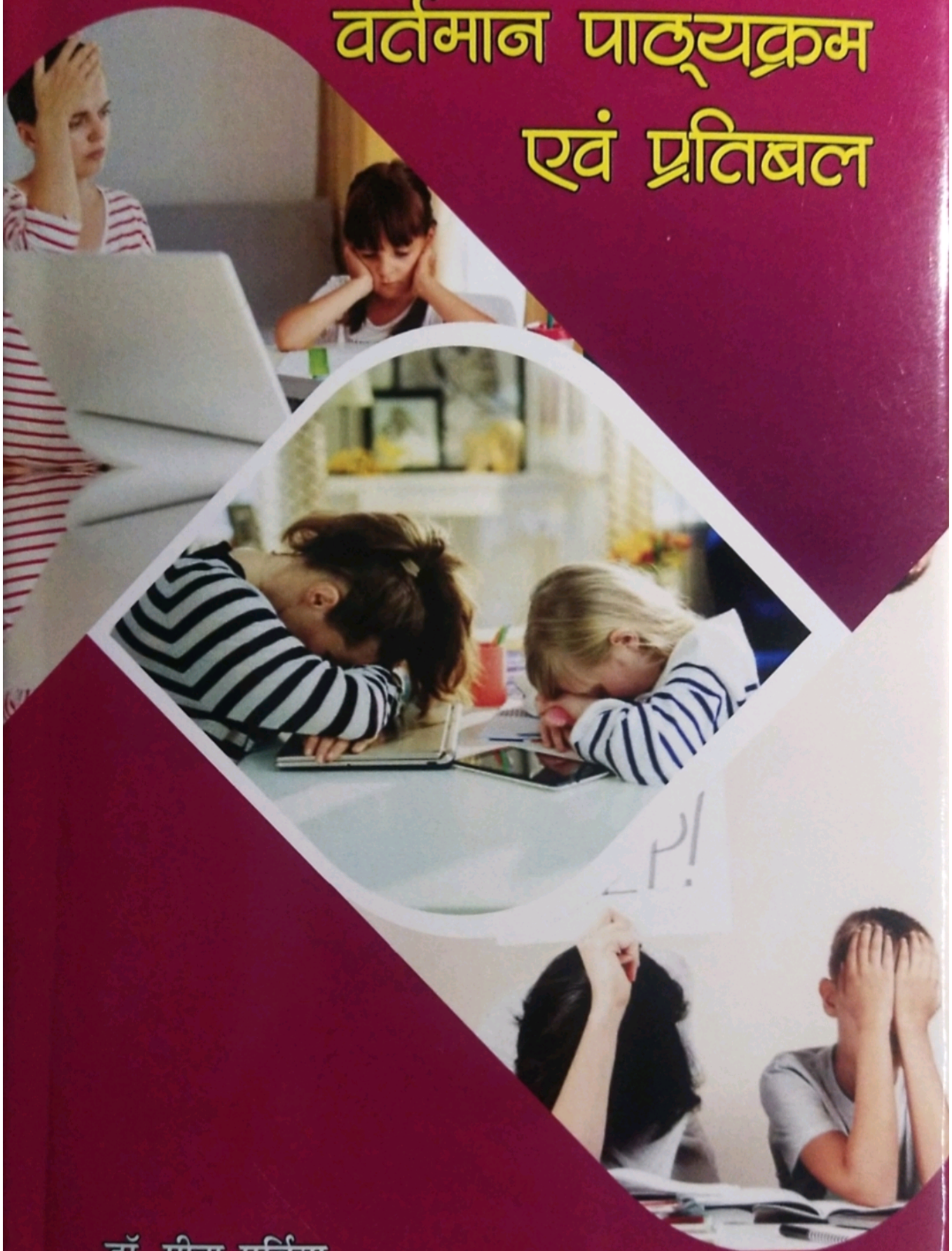

डॉ. मीना पूर्बिया

HIMANSHU Publications

वर्तमान पाठ्यक्रम एवं प्रतिबल

डॉ. मीना पूर्बिया
UGC NET (Geography & Education)

हिमांशु पब्लिकेशन्स
उदयपुर □ नई दिल्ली

मुद्रणाधिकार ©

इस पुस्तक के किसी भी अंश की किसी भी रूप में प्रतिकृति करना या किसी भी साधन-इलेक्ट्रॉनिक, मैकेनिकल या अन्य प्रकार, फोटोकॉपी, रिकॉर्डिंग या सूचना संचयन और पुनः प्राप्ति पद्धति द्वारा प्रसारित करना लेखिका/प्रकाशक की लिखित अनुमति के बिना मना है।



हिमांशु पब्लिकेशन्स

464, हिरण मगरी, सेक्टर 11, उदयपुर 313 002 (राज.), फोन: 0294-2421087
4379/4-B, प्रकाश हाऊस, अंसारी रोड़, दरियागंज, नई दिल्ली-2, मोबाईल: 96109-73739
Web : *himanshupublications.com;* email : *himanshupublications@gmail.com*

ISBN : 978-93-94954-77-9
संस्करण : 2023
मूल्य : ₹ 495.00

Distributor
ARYAS PUBLISHERS DISTRIBUTORS (P) LTD.
2-D, Hazareshwar Colony, Near Court Choraha, Udaipur (Raj.) - 313 001; Phone : 0294-2526160
E-mail : apdpl.2012@gmail.com

Printed at : R.K. Offset Process, Delhi

पुस्तक परिचय

आज इस प्रतियोगी युग में हर एक की महत्वाकांक्षाओं को पूरा करना संभव नहीं है। विद्यालय का वातावरण, अध्यापक और माता-पिता की उच्चाकांक्षाएं, विस्तृत पाठ्यक्रम एवं बस्ते के बढ़ते बोझ से विद्यार्थी एवं अभिभावक कई प्रकार की चिंताओं और कुंठाओं से ग्रस्त होने लगता है, जो उसके प्रतिबल को उत्पन्न करता है। इस प्रतिबल का उन पर शारीरिक, भावनात्मक एवं सामाजिक प्रभाव पड़ता है। उपरोक्त सभी बातों पर गौर किया जाए तो वर्तमान पाठ्यक्रम का विद्यार्थियों एवं अभिभावकों पर प्रतिबल सामने आता है। अतः इस विषय पर यह पुस्तक आपके हाथों में प्रस्तुत करते हुए अत्यंत प्रसन्नता हो रही है कि यह हमारा ध्यान इस ओर ले जाने में सहायक होगी। इस पुस्तक में प्राथमिक विद्यालय में पढ़ने वाले विद्यार्थियों एवं उनके अभिभावकों को अपना उत्तरदाता बनाया व प्रतिबल का अध्ययन आरंभ किया, परिणाम आपके समक्ष हैं।

लेखिका परिचय

डॉ. मीना पूर्बिया (B.A., M.A. Geography, B.Ed., M.Ed., NET Geography & NET Education, Ph.D. Education, TET, REET) ने विद्यालय शिक्षा जिला चित्तौड़गढ़ एवं महाविद्यालय शिक्षण उदयपुर शहर में पूर्ण किया। प्राथमिक विद्यालय शिक्षण से कैरियर की शुरुआत करके आपने अकादमिक रुचि के साथ अपना अध्ययन एवं अध्यापन निरंतर जारी रखा। आपने भूगोल एवं शिक्षा स्नातकोत्तर के बाद भूगोल एवं शिक्षा दोनों में नेट उत्तीर्ण किया। आपने अपने साथियों के साथ 'बी.एड. पाठ्यचर्या का संपोषित विकास हेतु शिक्षा विषयक विश्लेषण' विषय पर सीटीई के प्रोजेक्ट पर भी कार्य पूर्ण किया। आपने 'जनजातीय विद्यार्थी की शैक्षिक उपलब्धि पर निर्मितवादी उपागम आधारित अधिगम पैकेज की प्रभावशीलता का अध्ययन' विषय में डॉक्टरेट की उपाधि प्राप्त की। अब तक चार शोध पत्रों का प्रकाशन विभिन्न पत्र-पत्रिकाओं में किया जा चुका है। साथ ही कई राष्ट्रीय एवं अंतर्राष्ट्रीय विषयों पर वर्कशॉप, सेमिनार तथा वेबीनार में भी आपने अपनी भागीदारी सुनिश्चित की है। दो वर्षों के विद्यालय में अध्यापन के बाद पिछले 11 वर्षों से विभिन्न शिक्षक प्रशिक्षण महाविद्यालय में व्याख्याता के पद पर कार्य करने का अनुभव प्राप्त कर वर्तमान में भी अपनी सेवाएं निरंतर दे रही हैं।

₹ 495.00
ISBN : 978-93-94954-77-9

हिमांशु पब्लिकेशन्स
HIMANSHU Publications

464, हिरण मगरी, सेक्टर 11, उदयपुर 313 002 (राज.), फोन: 0294-2421087
4379/4-B, प्रकाश हाऊस, अंसारी रोड, दरियागंज, नई दिल्ली-2, मोबाईल: +91-96109-73739
Web : himanshupublications.com; email : himanshupublications@gmail.com

The book is about analyzing the financial performance of banks. First Chapter deals with the concept, Importance, significance aspects of banks, and the Banking system. It describes Introduction to the banking industry, Evolution of the banking sector in India, the basic concept behind construction of banks in India, and also deals with the phases of Indian Banking namely: Pre-Nationalization Era, Nationalization Stages, and Post-Liberalization Stages. The second chapter deals with the source of information for the financial performance appraisal of public and private sector banks. and the Journals, Research material, Articles, Reviews for the research work. The aim of the book is to study the impact of various external and internal factors on Financial Performance and to access the level of Financial Performance with reference to stakeholders. The fourth chapter is related to the Research Methodology used for the analysis of data Fifth Chapter deals with the hypothesis testing of the research work and analysis of data through the Kruskal- Wallis Test. The sixth chapter is concerned with the finding and conclusion.

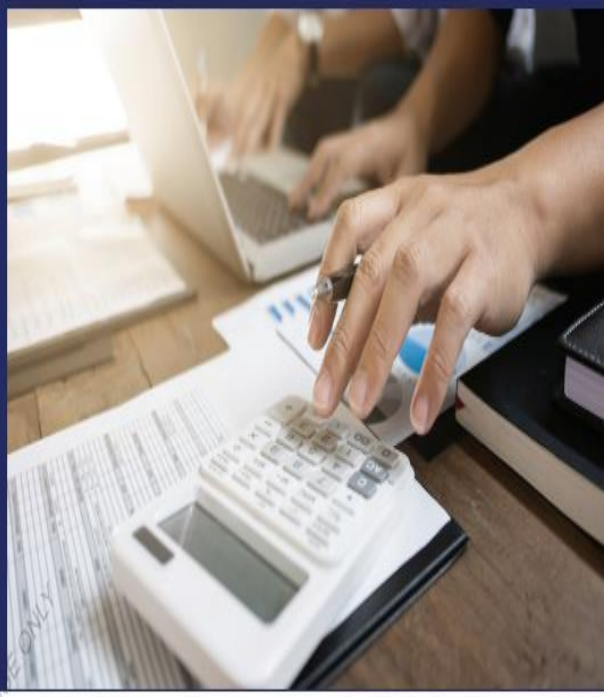

FOR AUTHOR USE ONLY

Asha Sharma
Sonia Chabra

An Analysis of Financial Performance of Scheduled Commercial Banks

In India

Dr. Asha Sharma, is Assistant Professor, Department of Accountancy and statistics at Mohanlal Sukhadia University, Udaipur. Dr. Sharma has a teaching experience of twenty years. She has contributed more than seventy research papers.
Ms. Sonia Chabra is a research scholar of JNV University, Jodhpur.

Tourism has gained importance on account of its economic impacts on the host destination. It provides for support to local economy and provides for ample of employment opportunities as well as helps the region to develop and grow. Tourism nowadays has emerged as a major industry that has economic impacts that are favorable to the host. Efforts are being made to make the industry sounder so as to increase the economic benefits from the same.

The concept of the book is to discover the social or societal effects of tourism industry. It is aimed to find out the social benefit as well as social cost bearded by the host destination, society.

This book concluded that tourism impacts the society in various ways, it has social benefits as well there are social costs being bared up by the society. Tourism has risen as one of the major service industry providing for employment their by improving economy of the state. Tourism has both impacts negative as well as positive of which the latter supersede the ill effects.

The primary objective of this research is to review the cost incurred and social, economic, cultural and overall benefits as enjoyed by the society on account of tourism.



FOR AUTHOR USE

Dr Asha Sharma, is Assistant Professor in department of Accountancy and Business Statistics at Mohanlal Sukhadia University, Udaipur. Dr Sharma has teaching experience of twenty years. She has contributed 75 research papers to reputed international and national journals.
Ms Raksha Bishnoi is research scholar of Jai Narain Vyas University, Jodhpur.

9 786204 733937

Asha Sharma
Raksha Bishnoi

SOCIAL COST BENEFIT ANALYSIS

A STUDY OF TOURISM INDUSTRY IN RAJASTHAN

LAP LAMBERT Academic Publishing

Asha Sharma, Raksha Bishnoi

Photochemistry and Photophysics of Coordination Compounds

Fundamentals and Applications



Rakshit Ameta, Avinash Kumar Rai,
Jayesh P. Bhatt, Shipra Bhardwaj
and Suresh C. Ameta

Photochemistry and Photophysics of Coordination Compounds

Fundamentals and Applications

This page intentionally left blank

Photochemistry and Photophysics of Coordination Compounds

Fundamentals and Applications

Rakshit Ameta
Department of Chemistry, Faculty of Science, J.R.N. Rajasthan Vidyapeeth, Udaipur, Rajasthan, India

Avinash Kumar Rai
Department of Chemistry, PAHER University, Udaipur, Rajasthan, India

Jayesh P. Bhatt
Department of Chemistry, PAHER University, Udaipur, Rajasthan, India

Shipra Bhardwaj
Department of Chemistry, Govt. Meera Girls College, Udaipur, Rajasthan, India

Suresh C. Ameta
Department of Chemistry, PAHER University, Udaipur, Rajasthan, India



ELSEVIER

Elsevier
Radarweg 29, PO Box 211, 1000 AE Amsterdam, Netherlands
The Boulevard, Langford Lane, Kidlington, Oxford OX5 1GB, United Kingdom
50 Hampshire Street, 5th Floor, Cambridge, MA 02139, United States

Copyright © 2023 Elsevier Inc. All rights reserved.

No part of this publication may be reproduced or transmitted in any form or by any means, electronic or mechanical, including photocopying, recording, or any information storage and retrieval system, without permission in writing from the publisher. Details on how to seek permission, further information about the Publisher's permissions policies and our arrangements with organizations such as the Copyright Clearance Center and the Copyright Licensing Agency, can be found at our website: www.elsevier.com/permissions.

This book and the individual contributions contained in it are protected under copyright by the Publisher (other than as may be noted herein).

Notices

Knowledge and best practice in this field are constantly changing. As new research and experience broaden our understanding, changes in research methods, professional practices, or medical treatment may become necessary.

Practitioners and researchers must always rely on their own experience and knowledge in evaluating and using any information, methods, compounds, or experiments described herein. In using such information or methods they should be mindful of their own safety and the safety of others, including parties for whom they have a professional responsibility.

To the fullest extent of the law, neither the Publisher nor the authors, contributors, or editors, assume any liability for any injury and/or damage to persons or property as a matter of products liability, negligence or otherwise, or from any use or operation of any methods, products, instructions, or ideas contained in the material herein.

ISBN: 978-0-12-824493-7

For information on all Elsevier publications visit our website at https://www.elsevier.com/books-and-journals

Publisher: Susan Dennis
Acquisitions Editor: Charles Bath
Editorial Project Manager: Kathrine Esten
Production Project Manager: R. Vijay Bharath
Cover Designer: Greg Harris

Typeset by TNQ Technologies



Dedication

Dedicated to Mrs. Anita Ameta
Who had been a source of inspiration
throughout writing this book



This page intentionally left blank

Contents

List of contributors xiii

1. Introduction

Suresh C. Ameta

1.1 Introduction 1
1.1.1 d-d transitions 2
1.2 Deactivation processes 2
1.2.1 Photophyscial deactivation processes 3
1.2.2 Photochemical deactivation processes 4
1.3 Effect of solvent polarity on charge transfer spectra 9
References 13

2. Basic concepts

Rameshwar Ameta

2.1 Introduction 15
2.2 Photochemical aspects 22
2.3 Photoluminescence in coordination compounds 30
2.4 Photochemical processes 34
2.4.1 Photosubstitution reactions 34
2.4.2 Photorearrangement reactions 37
2.4.3 Photoredox reactions 40
2.5 Applications 41
2.5.1 Photochromism 41
2.5.2 Chemical actinometers 42
2.5.3 Release of CO/NO 44
2.5.4 Photoredox catalysis 46
2.5.5 Photochemiluminescence in ruthenium complexes 47
2.5.6 Coordination compounds as triplet quenchers 48
2.5.7 Coordination compounds as sensors 49
2.5.8 Photocatalysis 49
2.5.9 Nano-scale devices and machines 51
References 52

3. Coordination compounds of titanium, zirconium and hafnium

Neetu Shorgar, Priyanka Jhalora, Khushbu Sharma and Shubang Vyas

3.1 Introduction 55
3.2 Coordination compounds of titanium 55
3.3 Coordination compounds of zirconium 61
3.4 Coordination compounds of hafnium 67
References 70

4. Coordination compounds of vanadium, niobium and tantalum

Chetna Ameta, Dharmendra, Yogeshwari Vyas and Purnima Chaubisa

4.1 Introduction 75
4.2 Coordination compounds of vanadium 76
4.3 Coordination compounds of niobium 82
4.4 Coordination compounds of tantalum 85
References 88

5. Coordination compounds of chromium, molybdenum and tungtsen

Saroj Lohar, Dushyant Kumar Prajapati, Jeevan Kunwar Chouhan, Ankita Vijay and Shipra Bhardwaj

5.1 Introduction 91
5.2 Coordination compounds of chromium 92
5.3 Coordination compounds of molybdenum 100
5.4 Coordination compounds of tungsten 106
References 109

6. Coordination compounds of manganese, technetium and rhenium

Monika Jangid, Jayesh P. Bhatt, Mamta Ahuja, Shubang Vyas and Avinash Kumar Rai

6.1 Introduction 115
6.2 Coordination compounds of manganese 115
6.3 Coordination compounds of technetium 123
6.4 Coordination compounds of rehenium 125
References 131

7. Coordination compounds of iron, ruthenium and osmium

Liju Raju and E. Rajkumar

7.1 Introduction 135
7.2 Coordination compounds of iron 136
7.2.1 Electronic structures and photophysics of iron complexes 136
7.2.2 Photochemistry of iron complexes 144
7.3 Coordination compounds of ruthenium 147
7.3.1 Photophysics of $[Ru(NN)_3]^{2+}$ complexes 147
7.4 Coordination compounds of osmium complexes 178
7.4.1 Photoactive oxidation states of osmium complexes 178
7.4.2 Near IR phosphorescent osmium complexes 184
7.4.3 Photophysics of osmium complexes on surfaces 186
7.4.4 Photosensitizers for photodynamic therapy 187
7.4.5 Photochemistry and applications of osmium complexes 188
7.5 Summary 193
References 193

8. Complexes of cobalt, rhodium and iridium

Simran Sharma, Priya Sahni, Rahat Gupta, Anindya Roy and Amlan K. Pal

8.1 Introduction 205
8.2 Luminescent Co(II/III) complexes 206
8.2.1 Photophysical properties of polyhetrocyclic and polypyridyl Co(II/III) complexes 206
8.2.2 Photoredox catalysis of Co(III)-guanidyl complexes 213
8.2.3 Metal-ion sensing by Co(II) complexes 217
8.3 Luminescent Rh(0/I/II/III) complexes 220
8.3.1 Rh(II/III) complexes of acetylacetonato, polypyridylamine, thiolato and macrocyclic ligands 220
8.3.2 Metal-ion sensing by Rh(III) complexes 228
8.3.3 Application of Rh(III) complexes in OLED devices 228
8.4 Luminescent Ir(II/III) complexes 232
8.4.1 Photophysical properties of polypyridyl Ir(III) complexes and their applications in solid-state lighting (OLED and LEC) devices 232
8.4.2 Application of Ir(III) complexes in photoredox catalysis 241
8.4.3 Application of Ir(III) complexes in biological sensing of metal-ion 246
8.5 Conclusion 248
Acknowledgments 248
References 249

9. Coordination compounds of nickel, palladium, and platinum

Athanasios Zarkadoulas and Christiana A. Mitsopoulou

9.1 Introduction 255
9.2 Ligand field photophysics and photochemistry 256
9.2.1 Nickel complexes 256
9.2.2 Palladium and platinum complexes 258
9.3 Charge-transfer photochemistry 259
9.3.1 Diimine and dipyrrin complexes 259
9.4 Bis-dithiolene and diimine-dithiolene complexes 266
9.5 Salen-type complexes 271
9.5.1 Other complexes 276
9.6 Conclusion 286
References 286

10. Coordination complexes of copper, silver and gold

Gustavo A. Álvarez and Esteban Mejía

10.1 Introduction 293
10.2 General considerations 295
10.3 Homoleptic Cu(I) coordination compounds 299
10.4 Heteroleptic Cu(I) coordination compounds 306
10.4.1 Phenanthroline complexes 310
10.4.2 Complexes with pyridyl-type ligands 311
10.4.3 Complexes with N^O, N^P and S^P ligands 312
10.4.4 Complexes with carbene ligands 313
10.4.5 Miscellaneous Cu(I) coordination compounds 316
10.5 The entatic principle and its implication on the photophysical properties of Cu(I) complexes 317
10.6 Silver complexes 322
10.6.1 Homoleptic Ag(I) coordination compounds 322
10.6.2 Heteroleptic Ag(I) coordination compounds 324
10.7 Gold complexes 327
10.7.1 Au(I) coordination compounds 327
10.7.2 Au(III) coordination compounds 330
10.8 Conclusion 332
References 333

11. Coordination compounds of lanthanides

Jean-Claude G. Bünzli

11.1 The elements and their coordination chemistry 341
11.1.1 Lanthanides and rare earths 341
11.1.2 Electronic configuration and oxidation numbers 342
11.1.3 Coordination chemistry 343
11.2 Lanthanide luminescence 345

11.2.1 Energy levels 345
11.2.2 Electronic transitions 349
11.2.3 Sensitization of lanthanide luminescence 358
11.2.4 Quantitative aspects of energy transfer processes 361
11.3 Designing highly luminescent chelates 367
11.3.1 Principles 367
11.3.2 Optimizing energy transfer 367
11.3.3 Minimizing non-radiative deactivation processes 369
11.3.4 Examples of efficient sensitizing systems 376
11.4 Luminescent lanthanide chelates at work 380
11.5 Conclusion 384
References 384

12. Future prospects

Rakshit Ameta

12.1 Introduction 391
12.2 Solar cells 391
12.3 Photochromism 392
12.4 Photodynamic therapy (PDT) 393
12.5 Actinometry 394
12.6 Hydrogen as fuel of future 395
12.7 Reduction of carbon dioxide 396
12.8 Others 398
References 399

Index 403

This page intentionally left blank

List of contributors

Mamta Ahuja, Department of Chemistry, Government Meera Girls College, Udaipur, Rajasthan, India

Gustavo A. Álvarez, Leibniz Institute for Catalysis (LIKAT), Rostock, Germany

Chetna Ameta, Department of Chemistry, Mohanlal Sukhadia University, Udaipur, Rajasthan, India

Rakshit Ameta, Department of Chemistry, J.R.N. Rajasthan Vidyapeeth (Deemed to be University), Udaipur, Rajasthan, India

Rameshwar Ameta, Department of Chemistry, PAHER University, Udaipur, Rajasthan, India

Suresh C. Ameta, Department of Chemistry, PAHER University, Udaipur, Rajasthan, India

Shipra Bhardwaj, Department of Chemistry, Government Meera Girls College, Udaipur, Rajasthan, India

Jayesh P. Bhatt, Department of Chemistry, PAHER University, Udaipur, Rajasthan, India

Jean-Claude G. Bünzli, Institute of Chemical Sciences & Engineering, Swiss Federal Institute of Technology, Lausanne (EPFL), Switzerland and Department of Chemistry, Baptist University, Hong Kong S.A.R., People's Republic of China

Purnima Chaubisa, Department of Chemistry, Mohanlal Sukhadia University, Udaipur, Rajasthan, India

Jeevan Kunwar Chouhan, Department of Chemistry, Government Meera Girls College, Udaipur, Rajasthan, India

Dharmendra, Department of Chemistry, Mohanlal Sukhadia University, Udaipur, Rajasthan, India

Rahat Gupta, Department of Chemistry, Indian Institute of Technology, Jammu, Jammu and Kashmir, India

Monika Jangid, Department of Chemistry, PAHER University, Udaipur, Rajasthan, India

Priyanka Jhalora, Department of Chemistry, PAHER University, Udaipur, Rajasthan, India

Saroj Lohar, Department of Chemistry, Government Meera Girls College, Udaipur, Rajasthan, India

Esteban Mejía, Leibniz Institute for Catalysis (LIKAT), Rostock, Germany

Christiana A. Mitsopoulou, Inorganic Chemistry Laboratory, Department of Chemistry, National and Kapodistrian University of Athens, Athens, Greece

Amlan K. Pal, Department of Chemistry, Indian Institute of Technology, Jammu, Jammu and Kashmir, India

Dushyant Kumar Prajapati, Department of Chemistry, Government Meera Girls College, Udaipur, Rajasthan, India

Avinash Kumar Rai, Department of Chemistry, PAHER University, Udaipur, Rajasthan, India

E. Rajkumar, Department of Chemistry, Madras Christian College, Affiliated to University of Madras, Chennai, Tamil Nadu, India

Liju Raju, Department of Chemistry, Madras Christian College, Affiliated to University of Madras, Chennai, Tamil Nadu, India

Anindya Roy, Department of Chemistry, Indian Institute of Technology, Jammu, Jammu and Kashmir, India

Priya Sahni, Department of Chemistry, Indian Institute of Technology, Jammu, Jammu and Kashmir, India

Simran Sharma, Department of Chemistry, Indian Institute of Technology, Jammu, Jammu and Kashmir, India

Khushbu Sharma, Department of Chemistry, B. N. University, Udaipur, Rajasthan, India

Neetu Shorgar, Department of Chemistry, PAHER University, Udaipur, Rajasthan, India

Ankita Vijay, Department of Chemistry, Government Meera Girls College, Udaipur, Rajasthan, India

Yogeshwari Vyas, Department of Chemistry, Mohanlal Sukhadia University, Udaipur, Rajasthan, India

Shubang Vyas, Department of Chemistry, PAHER University, Udaipur, Rajasthan, India

Athanasios Zarkadoulas, Inorganic Chemistry Laboratory, Department of Chemistry, National and Kapodistrian University of Athens, Athens, Greece

Chapter 1

Introduction

Suresh C. Ameta
Department of Chemistry, PAHER University, Udaipur, Rajasthan, India

1.1 Introduction

Photochemistry is well defined as chemistry of excited state of molecules. Excited state has a different electronic state than that of ground state and therefore, it will show a different behavior. The metal complexes are known to have photosensitivity for a long time. The field of photochemistry and photophysics of coordination compound is not new but monumental work of Balzani and Carassitti (1970) gave it a momentum. This field has been excellently reviewed and presented in the form of some reviews, books and proceeding (Adamson et al., 1968; Balzani and Moggi, 1990; Sýkora and Šima, 1990; Horváth and Stevenson, 1993; Kirgan et al., 2007; Balzani and Campagna, 2010; Roundhill, 2013; Chen and Browne, 2018; Glaser and Wenger, 2020; Mensah et al., 2021).

For an effective electronic transition, there must be some interaction between the two: (i) Electric dipole of the molecule and (ii) Electric field vector of the light.

Here, light is absorbed by some species and the probability of absorption is expressed by the Beer–Lambert's law, a well established equation relating various factors.

$$A = \epsilon\, cl = \log \frac{I0}{I} \tag{1.1}$$

Where A = Absorbance (earlier known as optical density), ϵ = Molar extinction coefficient, e = Concentration of substance, l = Path length, I_0 = Intensity of incident light and I = Intensity of transmitted light. A number of electronic transitions are possible in case of coordination compounds and most frequently transitions are:

- d-d transitions and
- Charge transfer (CT) transitions

Photochemistry and Photophysics of Coordination Compounds. https://doi.org/10.1016/B978-0-12-824493-7.00010-1
Copyright © 2023 Elsevier Inc. All rights reserved.

1.1.1 d-d transitions

The d-d transitions gives weak absorption bands and due to these transitions, most of the d-block metal complexes display colors in solution with low intensity; however, vacant (d^0) and filled orbitals (d^{10}) are exceptions to it. Presence of such low intensity of colors indicates that probability of d-d transition is low.

The color in solutions of these transition metal complexes depends on three factors.

- Metal,
- Oxidation state of that metal, and
- Number of d-electrons (metal)

For example, iron (II) complexes are normally green in color, while iron (III) complexes are either brown/orange in color.

1.1.1.1 The laporte selection rule

The probability of undergoing d-d transitions are decided by the Laporte selection rule. These are as follows

- Laporte selection rule: $\Delta l = +1$
- If there is a change in parity (s $\rightarrow$ p and p $\rightarrow$ d), then these are Laporte allowed transitions.
- If there is no change in parity (p $\rightarrow$ p and d $\rightarrow$ d), then these are Laporte forbidden transitions.

1.2 Deactivation processes

The electronically excited states of coordination compounds (ML^*) can be deactivated in different pathways. Some of them are:

- ML + Heat
- Energy transfer; $ML + Q^*$
- Physical quenching; ML + Q + Heat
- Ionization; $ML^+ + e^-$
- Chemical reaction products of ML
- Chemical reaction products of ML and Q
- ML + hv (Luminesceene)
- Radiationless transfer

The quantum yield of any particular primary process gives the efficiency of total process (Fig. 1.1).

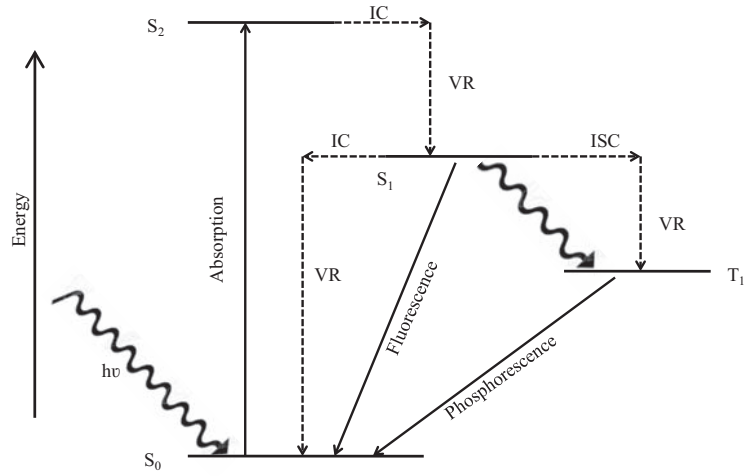

FIG. 1.1 Jablonski diagram.

$$\varphi = \frac{\text{Number of molecules undergoing that process}}{\text{Number of photons absorbed by reactant}} \tag{1.2}$$

Now the excited state can undergo various deactivation pathways:

(i) Photophysical deactivation processes, and

(ii) Photochemical deactivation processes

1.2.1 Photophyscial deactivation processes

First of all, a light of suitable wavelength/frequency is absorbed by some species, which is excited to higher singlet states (S_1, S_2, …) from ground state (S_0). Then there are many possibilities:

This species reverts back to its original ground state with a radiative process and it is called fluorescence. The wavelength of these radiations are same as that of absorbed and it is a rapid process and gives fluorescence immediately. Fluroscence stops, as soon as source of light is removed.

- This excited species (if in higher state like S_2) may undergo internal conversion (IC) to vibrationally excited state of lower excited state S_1, which relaxes in its ground state through vibrational relaxation (VR) by releasing heat.
- If the excited state is S_1, then it can undergo intersystem crossing (ISC) to vibrationally excited state of T_1 (triplet state), which relaxes through vibrational relaxation liberating heat.

- This triplet state T_1 can undergo radiative process, known as phosphorescence. The wavelength of this process is more than the wavelength of light absorbed and it continues even after removing the source of light as it is a slow process.

1.2.2 Photochemical deactivation processes

Excited states have different molecular structures and thermodynamic properties than the ground state. Such as excited state may make use of its excess energy and undergo reactions, which are not normally possible with the ground state molecules. The process of excitation can be associated with some angular and radial distortions, which may promote cleavage of bond.

- **Photoredox addition and elimination processes**

The redox properties of the excited state are different than the ground state. The activated complex may undergo photoredox elimination along with addition reactions. In such cases, a change is there in the oxidation state of the central metal ion accompanied by a change in the coordination number of the complexes. Generally, the obtained products are transient species, which may undergo further secondary (thermal) reactions to give the final products. Photoaddition reactions are normally attributed to an increase in the Lewis acidity of the metal upon excitation.

$$[PtCl_2(bpy)_2] \xrightarrow[Cl^-]{h\nu} [PtCl_4(bpy)_2]$$

Here, oxidation state of platinum(II) is increased to platinum(IV) and the coordination number of the complex is increased from four to six.

- **Intramolecular redox processes**

Redox processes are also possible through an intramolecular pathway, where an electron is exchanged (formally) between a coordinated ligand and the central metal atom. The primary products (reduced metal center and an oxidized ligand), are very reactive and as a result, they may undergo secondary thermal reactions.

$$[CuCl_4]^{2-} \xrightarrow{h\nu} [CuCl_3]^{2-} + {}^{\bullet}Cl$$

$${}^{\bullet}Cl + {}^{\bullet}Cl \xrightarrow{h\nu} Cl_2$$

Here, copper is present in Cu(II) state in the complex $[CuCl_4]^{2-}$, which will be reduced to Cu(I) state in $[CuCl_3]^{2-}$, and chlorine radicals are generated, which as dimerize to yield chlorine.

- **Photochemical isomerization reactions**

Different types of isomerization reactions are there such as optical isomerization, geometrical isomerization, transformations between linkage isomers, tautomerizations, etc. These processes are normally mediated by transients species, which are formed via inner-sphere redox pathways.

$$[Co(NH_3)_5(NO_2)]^{2+} \xrightarrow{hv} [Co(NH_3)_5(ONO)]^{2+}$$

Here, the NO_2 ligand changes its linkage from N (NO_2) to O (ONO)

- **Photosubstitution reactions**

Photosubstitution reactions involve exchange of ligands between the primary and secondary coordination spheres, where oxidation state of the metal ions and its coordination number are retained.

$$[Co(CN)_6]^{n-} + H_2O \xrightarrow{hv} [Co(CN)_5(H_2O)]^{2-} + CN^-$$

$$[Co(CN)_5X]^{n-} + SCN^- \xrightarrow{hv} [Co(CN)_5(SCN)]^{3-} + [Co(CN)_5(NCS)]^{3-}$$

Most common photosubstitution reaction is aquation, where some ligand is being replaced by water in aqueous solutions.

$$[Cr(NH_3)_6]^{3+} + H_2O \xrightarrow{hv} [Cr(NH_3)_5(H_2O)]^{3+} + NH_3$$

$$[Fe(CN)_5NO]^{2-} + H_2O \xrightarrow[H_2O]{hv} [Fe(CN)_5(H_2O)]^{3-} + NO^+$$

- **Photorecemization reactions**

Some complexes may undergo change in its optical isomer from d- to l- or l- to d- in presence of light. In some cases, the reaction is reversible and the product is a racemic mixture of d- and l-forms of the complex.

$$d - [Cr(L-L)_3]^{3+} \overset{nv}{\rightleftarrows} l - [Cr(L-L)_3]^{3+}$$

Tris-complexes of chromium (III) can usually be separated into d- and or l-isomers as these are kinetically inert, but in presence of light, they undergo racemization reactions, as the photochemical reaction is reversible. Here, two probable mechanisms are possible:

(i). 'Twist' mechanism, where a pseudo−rotation causes racemization without affecting the coordination sphere of the central metal ion, and

(ii). 'Bond rupture' mechanism, when a bond is broken and racemization is there, before or during bond is formed again.

- **Photoanation reactions**

In such reactions, a neutral ligand is replaced by an anionic ligand.

$$[Cr(H_2O)]^{3+} + CI^- \xrightarrow{hv} [Cr(H_2O)Cl]^{2+} + H_2O$$

When an aqueous solution of Cr(III) was exposed to light in presence of some anionic ligand such as Cl^-, SCN^-, etc., then a water molecule is replaced by this anionic ligand.

Mehta et al. (2003) made use of photoaquation followed by photoanation reaction of sodium nitroprusside, where first water replaces nitrosylium ligand (a cationic ligand) and then this water is substituted by some sulfur containing ligands. The formation of new complex can be monitored spectrophotometrically and this thio-ligand can be estimated quantitatively.

- **Photochemical isomerization reactions**

Some complex may also undergo isomerization reaction in presence of light from its cis-to transform or vise-versa. Here, cis-form of chromium complex is converted to its transform in presence of light; however, it is also accomplained by some photoanation reaction.

When the complex cis-$[CoCl_2(en)_2]^+$ is irradiated in methanol solution, then the charge transfer band resulted in isomerization to trans-$[CoCl_2(en)_2]^+$ form.

$$\text{cis} - [CoCl_2(en)_2]^+ \overset{hv}{\rightleftarrows} \text{trans} - [Co\,Cl_2(en)_2]^+$$

One of the example of photoinduced linkage isomerization is of cobalt(III) ammine complexes, where exchange of ligand SCN^-- NCS- takes place. It is generally there, when one of the ligands is ambidentate (NCS^-/SCN^- to NO^{2-}/ONO^-).

$$[Co(NH_3)_5SCN]^+ \xrightarrow{hv} [Co(NH_3)_5NCS]^+$$

Such photoisomerization reactions are proposed to proceed through a pathway, where thermally equilibrated excited state is formed on irradiation. This excited state dissociates in the radical pair. For the thiocyanate complex as the photoisomerization reaction of $[Co(NH_3)_5SCN]^{2+}$ to $[Co(NH_3)_5NCS]^{2+}$ does not present in photoisomer to $[Co(NH_3)_5SCN]^{2+}$

$$[Co(NH_3)_5X]^{2+\cdot} \xrightarrow{hv} Co(NH_3)_5{}^{2+}\_\_\_\_X^{\cdot}$$

1.2.2.1 Charge transfer bands

Here, question arises that if color is dependent only on d-d transitions, then why some transition metal complexes are intensely colored in solution? In

such cases, there is some change in electron distribution between the metal and the ligand in transition metal complexes giving rise to charge transfer (CT) bands. CT absorptions in the UV/Vis region are intense. The high intensity of the color ($\mathcal{E} > 50{,}000$ L mol^{-1} cm^{-1} or greater) is attributed to high probability of such transitions. It is the case, when these transition are allowed, but as d-d transitions are forbidden, low intensity of color is there. Here, transition are forbidden by selection rule and hence, it resulted in weak absorptions ($\mathcal{E} > 20$ L mol^{-1} cm^{-1}) (Brisdon, 1998).

The CT bands can be easily identified, as these are:

- Very intense with a large extinction coefficient (ε),
- Normally broad, and
- Very strong absorptions even with dilute solutions.

Charge transfer bands of transition metal complexes are due to shift of charge density between molecular orbitals (MOs), which are predominantly metal or ligand in character.

There are generally four types of charge transfer bands such as:

- Ligand-to-metal charge transfer (LMCT),
- Metal-to-ligand charge transfer (MLCT)
- Ligand-to-ligand charge transfer (LLCT), and
- Intraligand charge-transfer (ILCT)
- **Ligand-to-metal charge transfer (LMCT) bands**

Ligands possess bonding (σ and π), antibonding (σ*, π*), and nonbonding (n) molecular orbitals. If the molecular orbitals of any ligand are full, then there is a possibility of charge transfer from the molecular orbitals of ligand to metal d-orbitals (either empty or partially filled). If the transfer is there from the molecular orbital with ligand-like character to the metal-like one, then such transition is called a ligand-to-metal charge-transfer (LMCT).

The absorptions that arise from in this process are called ligand-to-metal charge-transfer bands (LMCT). These LMCT transitions give intense bands, although forbidden d-d transitions may be there, but with weak absorptions. Any such charge transfer from ligand-to-metal resulted in the reduction of the metal (lower oxidation state of the metal). There is grater probability of LMCT transitions, if coordination compounds have π-acceptor ligands. Such LMCT is presented in Fig. 1.2, taking A case of octahedral complex, where metal has d^6 configuration and ligand has filled d-orbital.

Example of these type of complexes include $[Cr(NH_3)_6]^{3+}$, $[Cr(Cl)(NH_3)_5]^{2+}$, etc. An intermediate is formed in the reaction between $[Co(CN)_5]^{3-}$ and $[Fe(CN)_6]^{3-}$, where one cyanide ligand formed a bridge between these two complexes and electron transfer is there

$$[Fe\ (CN)_5{-}C{\equiv}N{-}CO(CN)_5]$$

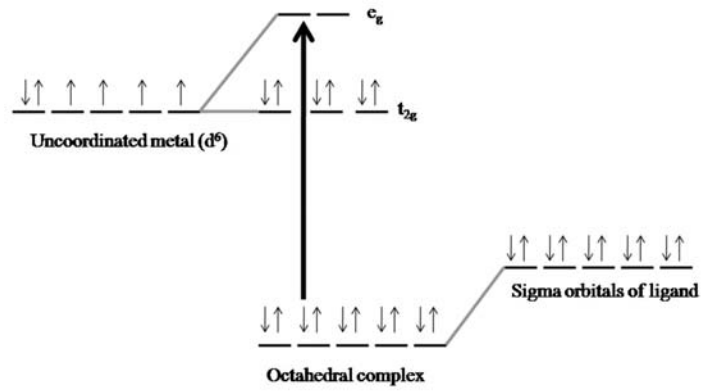

FIG. 1.2 Ligand-to-metal charge transfer (LMCT) in octahedral complex (d^6 state).

- **Metal-to-Ligand Charge Transfer (MLCT) Bands**

On the contrary, if a metal is present in its lower oxidation state (electron rich in nature) and there are low-lying empty orbitals in the ligand; then also there may be a transition, but it is in the reverse direction i.e. metal-to-ligand and therefore, these are called metal-to-ligand charge transfer (MLCT) transitions. Electrons present in the metal orbitals are excited to ligand π^* orbitals on absorption of light. Such metal-to-ligand charge transfer may occur resulting in intense bands. Here also, some forbidden d−d transitions may also be there, but with weak intensity. These MLCT transitions resulted in an increase in oxidation state of the metal as electrons are transferred to ligand. Such MLCT transfer is represented in octahedral complex, where metal has d^5 configuration and vacant π^* orbitals are there in ligand (Fig. 1.3).

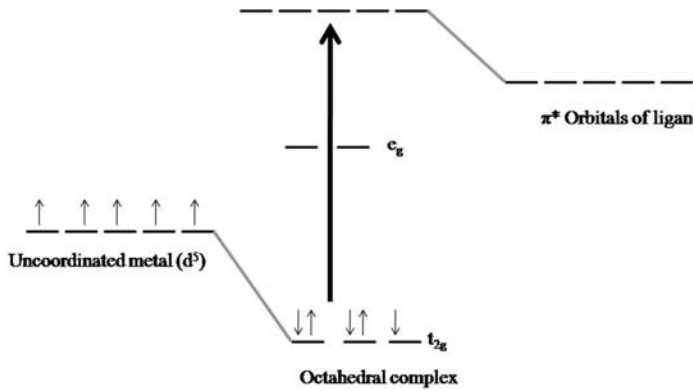

FIG. 1.3 Metal-to-ligand charge transfer (MLCT) in octahedral complex (d^5 state).

In Cu(I) complex of 2,9-dimethyl-1,10-phenanthroline, the copper ion changes its oxidation state as Cu(II) through metal-to-ligand charge transfer upon absorption of light (Iwamura et al., 2007). Complexes with ligands having empty orbitals prefer to undergo MLCT transfer and ligands in this category include CN^-, carbon monoxide, SCN^-, pyrazine, pyridine, bipyridine, o-phenanthroline, dithiolene, dithiocarbamate, etc. Some example of complexes showing MLCT transition are $[Fe(CO)_3(bipy)]$, $[W(CO)_4(phen)]$ $[Ru(bipy)_3]$,$^{2+}$ etc.

- **Ligand-to-ligand charge transfer (LLCT) bands**

Ligand-to-ligand charge transfer (LLCT) is defined as an electronic transition of a metal complex that corresponds to excitation populating an electronic state in which considerable electron transfer between two ligands has occurred.

If a reducing and an oxidizing ligand both are present in same coordination compounds, then there is possibility of low-energy LLCT transitions. Vogler and Kunkely (2007) has reviewed such relationship between zwitterions and metal complexes with low-energies LLCT transitions. Here, the zwitterions can also serve as ligands. Han et al. (2007) prepared a series of platinum(II) terpyridyl alkynyl complexes and observed a lowest-energy absorption corresponding to a ligand-to-ligand charge-transfer transition from the acetylide to the terpyridyl ligand. Intraligand charge-transfer (ILCT) transition is also there in complex from the π orbital of the 4′-phenyl group to the π^* orbital of the terpyridyl.

- **Intraligand charge-transfer (ILCT) bands**

It a ligand itself has a chromophore, then there is also a possibility of an absorption band, when an electron is transferred from one part of ligand to its other part, and it is called an intraligand band charge transfer (ILCT).

Larsen et al. (2014) reported the synthesis of donor—acceptor ligands 11-(4-diphenylaminophenyl)dipyrido[3,2-a:2′,3′-c]phenazine (dppz-$PhNPh_2$) and 11-(4-dimethylaminophenyl)dipyrido[3,2-a:2′,3′-c]phenazine (dppz-$PhNMe_2$), and their rhenium complexes $[Re(CO)_3X]$ (where $X = Cl^-$, py, 4-dimethylaminopyridine (dmap)^2). It was reported that optical properties of the ligands and complexes were dominated by intraligand charge-transfer transitions from the amine to the dppz moieties. These ligands show strong emission in organic solvents, which are consistent with the ILCT character exhibiting strong solvatochromic behavior (Fig. 1.4).

1.3 Effect of solvent polarity on charge transfer spectra

The charge transfer spectrum is affected by polarity of solvents, if the complex is an ion pair. As the position of the charge transfer band is considered as a transition energy and therefore, it depends on the solvating ability of the

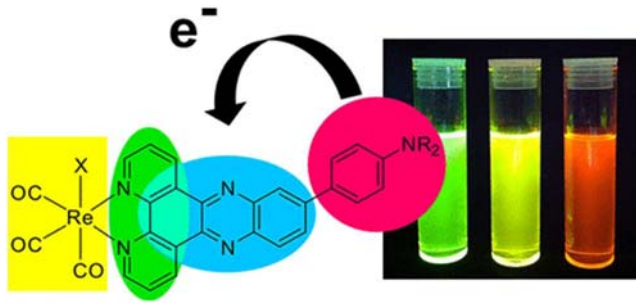

FIG. 1.4 Change of color through intraligand energy transfer. *Adapted from Larsen, C.B., van der Salm, H., Clark, C.A., Elliott, A.B., Fraser, M.G., Horvath, R., et al., 2014. Intraligand charge-transfer excited states in Re(I) complexes with donor-substituted dipyridophenazine ligands. Inorg. Chem. 53 (3), 1339−1354. With permission.*

solvent. It was observed that if the solvent of high solvating ability is there, then there is a shift to lower wavelength (higher frequency) in the position of charge transfer bands.

The dipole moments of solvent molecules (polar) are aligned perpendicularly or maximally with the dipoles of ground or excited state. An interaction will be there, if the ground or excited state is polar, which will lower the energy of the ground or excited state through solvation. The effect of solvent polarity on charge transfer spectra can be understood by following examples.

In total, there are four possibilities and these are:

- **Ground state and excited state; both are neutral**

When the ground and the excited state are both neutral in nature, then no shift will be observed in wavelength. In that case, no change is there. A polar solvent is not able to align its dipole with either ground or excited state, if these are neutral.

- **Ground state is neutral, but excited state is polar**

In some cases, if the ground state is neutral, but excited state is polar, then the solvent will interact only with the excited state. The solvent will align its dipole with the excited state and as a result, its energy is lowered through solvation. Such type of interaction will lower the energy of the polar excited state and as a consequence, wavelength is increased and energy (frequency) is decreased (Fig. 1.5).

- **The ground state and excited state; both are polar**

If the ground state is polar, then the polar solvent will align its dipole moment with the ground state. As a result, maximum interaction will be there and energy of the ground state will be lowered (higher wavelength, and lower frequency or energy). On the other hand, dipole moment of the excited state

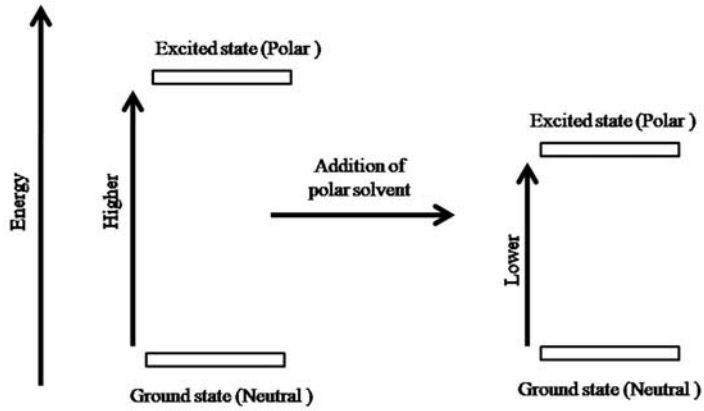

FIG. 1.5 The ground state is neutral, but excited state is polar.

would be perpendicular to the dipole moment of the ground state, because of alignment of dipole moment of polar solvent with the ground state. Such an interaction will increase the energy of the polar excited state (lower wavelength, and higher frequency or energy) (Fig. 1.6).

- **The ground state is polar, but the excited state is neutral**

If the ground state is polar in nature, then polar solvent will align its dipole moment with the ground state. In this case, maximum interaction will be there and the energy of the ground state will be lowered (higher wavelength, and lower frequency or energy). If the excited state is neutral in nature, then no change in energy will be there. A polar solvent will not be able to align its dipole with a neutral excited state. As a result, an increase in energy will be

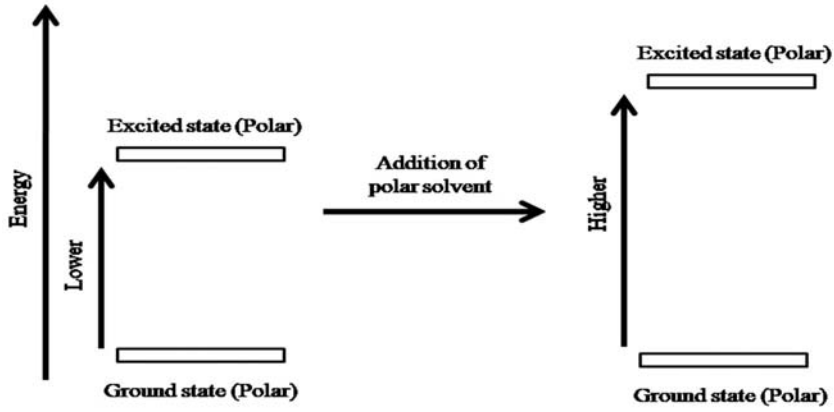

FIG. 1.6 Ground and excited states; both are polar.

observed, because the ground state is lower in energy (lower wavelength, and higher frequency or energy) (Fig. 1.7.).

There are various applications of photochemistry and photophysics of coordination compounds. These include the use of coordination complexes in:

- Solar cells, particularly dye-sensitized solar cells, where these have been used as photosensitizer,
- Actinometry, where these have been used for determining photon flux,
- Photosensors to detect the presence of some specific material in minute quantities,
- Photogeneration of hydrogen from photospliting of water as hydrogen has been predicted as the fuel of future,
- Photoreduction of carbon dioxide to some useful synthetic fuels using these compounds as photocatalysts or photosensitizers even upto the primary stage of mimicking photosynthesis (Artificial photosynthesis), and putting a check an ever increasing amount of carbon dioxide in atmosphere (control of global warming).
- Photochromic devices, where a complex will change its color in presence of light and reverts back to the original color on removing the source of light, and
- Use in photodynamic therapy (PDT) or photochemotherapy (PCT) for treatment of some diseases including dreadful disease like cancer.

Some more applications of photochemistry of coordination compound will emerge in further decades.

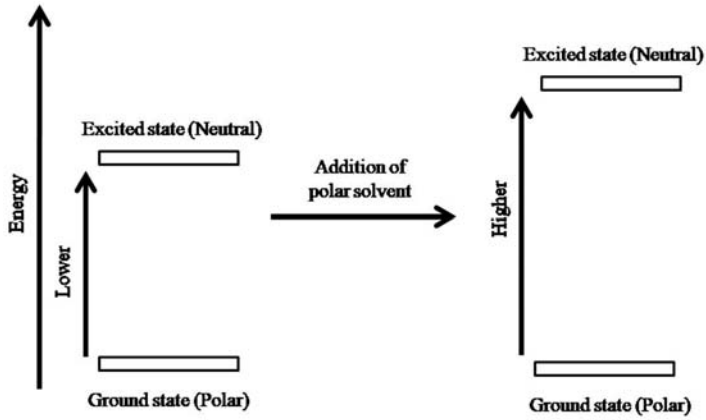

FIG. 1.7 Ground state is polar, but excited states is neutral.

References

Adamson, A.W., Waltz, W.L., Zinato, E., Watts, D.W., Fleischauer, P.D., Lindholm, R.D., 1968. Photochemistry of transition-metal coordination compounds. Chem. Rev. 68 (5), 541−585.

Balzani, V., Campagna, S. (Eds.), 2010. Photochemistry and Photophysics of Coordination Compounds I: 280, Topics in Current Chemistry. Springer, Berlin.

Balzani, V., Moggi, L., 1990. Photochemistry of coordination compounds: a glance at past, present, and future. Coord. Chem. Rev. 97, 313−326.

Balzani, V., Carassiti, V., 1970. Photochemistry of Coordination Compounds. Academic Press, London.

Brisdon, A.K., 1998. UV-visible Spectroscopy. Inorganic Spectroscopic Methods, Oxford: Oxford UP, pp. 70−73.

Chen, J., Browne, W.R., 2018. Photochemistry of iron complexes. Coord. Chem. Rev. 374, 15−35.

Glaser, F., Wenger, O.S., 2020. Recent progress in the development of transition-metal based photoredox catalysts. Coord. Chem. Rev. 405. https://doi.org/10.1016/j.ccr.2019.213129.

Han, X., Wu, L.Z., Si, G., Pan, J., Yang, Q.Z., Zhang, L.P., et al., 2007. Switching between ligand-to-ligand charge-transfer, intraligand charge-transfer, and metal-to-ligand charge-transfer excited states in platinum (II) terpyridyl acetylide complexes induced by pH change and metal ions. Chem.−A European J. 13 (4), 1231−1239.

Horváth, O., Stevenson, K.L., 1993. Charge Transfer Photochemistry of Coordination Compounds. Wiley-VCH, New York.

Iwamura, M., Takeuchi, S., Tahara, T., 2007. Real-time observation of the photoinduced structural change of bis (2, 9-dimethyl-1, 10-phenanthroline) copper (I) by femtosecond fluorescence spectroscopy: a realistic potential curve of the Jahn−Teller distortion. J. Am. Chem. Soc. 129 (16), 5248−5256.

Kirgan, R.A., Sullivan, B.P., Rillema, D.P., 2007. Photochemistry and photophysics of coordination compounds: rhenium, 281. Top. Curr. Chem. 45−100.

Larsen, C.B., van der Salm, H., Clark, C.A., Elliott, A.B., Fraser, M.G., Horvath, R., et al., 2014. Intraligand charge-transfer excited states in Re(I) complexes with donor-substituted dipyridophenazine ligands. Inorg. Chem. 53 (3), 1339−1354.

Mehta, M.R., Vyas, P.J., Vardia, J., Ameta, S.C., 2003. Ligand exchange reactions of sodium nitroprusside in the presence of sulphate ion under photochemical conditions. Indian J. Chem. A. 42 (7), 1671−1673.

Mensah, A., Shao, J.J., Ni, J.L., Li, G.J., Wang, F.M., Chen, L.Z., 2021. Recent progress in luminescent Cu(I) halide complexes: a mini-review. Front. Chem. 9. https://doi.org/10.3389/fchem.2021.816363.

Roundhill, D.M., 2013. Photochemistry and Photophysics of Metal Complexes. Springer Science and Business Media, Berlin.

Sýkora, J., Šima, J., 1990. Photochemistry of coordination compounds. Coord. Chem. Rev. 107, 1−212.

Vogler, A., Kunkely, H., 2007. Ligand-to-ligand and intraligand charge transfer and their relation to charge transfer interactions in organic zwitterions. Coord. Chem. Rev. 251 (3−4), 577−583.

This page intentionally left blank

Chapter 2

Basic concepts

Rameshwar Ameta
Department of Chemistry, PAHER University, Udaipur, Rajasthan, India

2.1 Introduction

The photochemistry and photophysics of coordination compounds has been excellently presented by Balzani and Carassitti (1970). Then onwards it has progressed rapidly and this field has been reviewed by several workers from time to time (Balzani and Moggi, 1990; Horváth and Stevenson, 1993; Kirgan et al., 2007; Balzani and Campagna, 2010; Roundhill, 2013; Ford, 2016; Chen and Browne, 2018; Glaser and Wenger, 2020).

The main difference between organic and coordination compounds (metal complexes) lies in their ground state electron configuration. In most of cases, ground state electronic configuration of organic compounds is a closed shell type, and the ground state is a singlet state (S_0). When light is absorbed and an electron is promoted from lower energy (Highest occupied molecular orbital, HOMO) to higher energy (Lowest unoccupied molecular orbital, LUMO) molecular orbitals, singlet and triplet states both are formed in pairs (S_1 T_1), (S_2 T_2), etc. Every triplet state is of lower energy than its corresponding singlet state and it is due to less electron−electron repulsion, when electrons have parallel spins. Hence, in organics, the lower excited state is commonly a triplet state (T_1). But, when metal complexes are taken, the situation is very much different. In many of the cases, the ground state has degeneracy of orbitals and some orbitals are not completely filled and therefore, the ground state has multiplicity higher than one (in accordance with Hund's rule). Another difference observed is the presence of heavy atoms, which are not present in organic molecules, but in complexes, presence of such metal atoms may cause considerable amount of spin−orbit coupling (particularly for metals of second and third transition series). It has been observed that in such cases, spin−forbidden absorption bands are having the same intensities as that of the absorption bonds obtained for spin−allowed transitions. This has been found particularly in platinum complexes. The efficiency of intersystem crossing (ISC) i.e., $S_1 \rightarrow T_1$ for complexes having S_0 ground state is close to 100% and fluorescence quantum yield reaches almost zero.

Photochemistry and Photophysics of Coordination Compounds. https://doi.org/10.1016/B978-0-12-824493-7.00014-9
Copyright © 2023 Elsevier Inc. All rights reserved.

Also, the rate constants of phosphorescence ($T_1 \rightarrow S_0$) and ISC ($S_1 \rightarrow T_1$) for organic compounds are very less than the rate constant of these processes in complexes. This can be seen that the varying extent of spin−orbital coupling causes longer life time to lowest spin−forbidden excited state (1 s) as compared to the life time of lower spin−forbidden excited state of $[Ru(bpy)_3]^{2+}$ (microseconds).

In last 6 decades or so, the field of photochemistry and photophysics of coordination compounds has gone through many steps with increase in complications. The photophysical behavior of simple complexes of simple ligands (ammonia, cyanide, etc.) were investigated in photosubstitution and phototredox decomposition reactions. Earlier studies were also focused on the use of metal complexes in biomolecular process i.e., energy and electron transfer. The Jablonski diagram was the solely guiding about various processes, which was successful in explaining the photochemical and photophysical nature of organic compounds, but there is much difference in the Jablonski diagram for the organic compounds and the coordination compounds. The main reason is the significant difference in the involvement of ligands and metal orbitals. Photodecomposition of organic compounds in singlet states was found quite common but sufficiently good number of coordination compounds were found to be stable toward photodecomposition; however, these are capable of undergoing excited state redox processes, which can be used to convert light energy into chemical energy.

It was also observed that the rate constants for a large number of complexes are inconsistent in the modern theories of kinetics. The field of photo-induced reactions of coordination compounds has reached to a stage now that if supramolecular chemistry and photochemistry are considered, then the constructed systems can easily perform the photo-induced processes. In present scenario, the photoredox reactions of metal complexes are used as essential parts for fabrication of molecular machines, which gets power and other molecular functional devices (light signaling processes) employing bottom-up approach. If one looks at the history of photochemistry, then its first mention was the effect of light on silver chloride and photography (John and Field,1963). It was then followed by sensitivity of metal complexes, particularly $[(Fe(CN)_6)]^{4-}$toward light was observed (Balzani et al., 2008) gradually with the development of the concepts of light absorption and quantum yield, chemical actinometer were developed using Fe^{3+} and UO_2^{2+} complexes.

Later on, quantitative investigation on the photochemical behavior of $[Fe(CN)_6]^{4-}$ and Co(III) amine complexes in aqueous solution provided insight about the mechanism of photochemical reactions involved. At that time, no theoretical framework was available, which can explain the absorption spectra and nature of the excited states of the coordination compounds. Due to this drawback of non-availability of theoretical bases, the mechanism of the photoreaction and luminescence in complexes could not be interpreted. But later on with the development of change transfer (CT) bands in the

absorption spectra of these complexes resulted into the explanation of absorption spectrum of the complexes (Orgel, 1954). After this development the photochemistry of coordination compounds has reached to a state of modern science, but much of the work published was on the Cr(III) complexes and their luminescence. Then scientists focused an Co(III) complexes due to the observation that in these complexes, photochemical behavior changes with the wavelength of light used for excitation.

In late sixties, enormous progress of photochemical and luminescence studies an organic compound was there. Large number of publications in the field of photochemical reactions of organic compounds has put forward some basic photochemical concepts, which were immediately utilized for coordination compounds also. Thereafter, 1965 onwards, the photochemical and photophysical behavior of any species either an organic compound or a charged metal complex can be interpreted on the basis of energy level diagrams, selection rules, electronic configuration and their electronic spectra.

It is necessary to understand various photophysical and photochemical pathways and for this, Jablonski diagram was proposed (Fig. 2.1).

Where S_0 is the singlet ground state and S_1 and T_1 are the lowest singlet and triplet excited states, respectively. Straight arrows are used to indicate radiative transition (photons) and wavy arrows are used to indicate the non-radiative transitions (not involving photons). By using Jablonski diagram, one can explain the mechanism of photochemical reaction. Now a days, the explanation is given in terms of different potential energy surfaces (PESs), which are acquired by a molecule after excitation of light. Different PESs are related to different electronic states, which typically change their electronic character and can cross PESs in different ways.

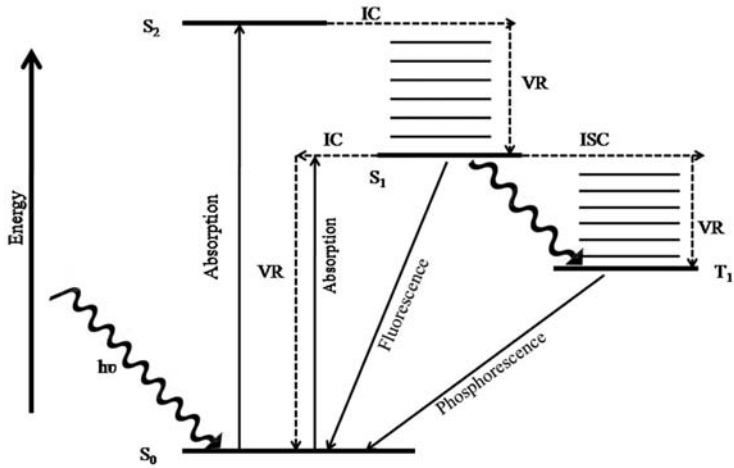

FIG. 2.1 Jablonski diagram.

After the absorption of light, the molecule reaches to an electronic excited state and by this process, a wave packet is generated, which progressed with the time. This is due to the fact that the forces, which are operating on the excited state of the molecule are different from the ground state. In order words, the position of minima of this wave in ground and excited states are different. This motion of molecule from ground to excited state by absorption of photon (hυ) will direct the molecule to be in different geometry in the excited state, than that in the ground state. On the basis of the nature and surface potential of the excited state, the wave packet may be relaxed to a new minimum; thereby, providing long-lived excited state, which finally decays to the ground state via fluorescence (Fl); or continues moving to the other regions of the potential energy surfaces.

There is another possibility also that wave packet may reach to the crossing points after surpassing same potential energy barrier; and hence, the so called non-adiabatic population transfer to other surfaces may occur. In these cases, Born-Oppenhiener approximation is broken down and electric and nuclear motions are coupled. This will push a radioationless process to return to the reactant or a new molecule is formed as a photochemical product. Internal conversion (IC) is a process, in which radiationless transition of molecule takes place between the states of same multiplicity (i.e., S_1 and S_0) and these processes are mediated by crossing points, which are called conical intersections as there is double conical surface around the degeneracy point. This discovery that IC process in mediated by conical intersections, which are ubiquitously present in chemistry and in biology, can also be said as breakthrough in the development of modern theoretical photochemistry.

The intersystem crossing process is mediated by crossing points between states of different multiplicities (i.e., S_1 and T_1), if there is almost no spin-orbit coupling (SOC). It is well known that SOC is highly dependent on the electronic wave function of the two states as well as the nuclear change of atoms, and therefore, the probability of ISC process will be high in those molecules, which contain heavy atoms as compared to pure organic compounds. However, ISC is also possible in molecules with only light atoms. ISC will produce a long-lived state (triplet), which finally goes to ground state via radiative (which is called phosphorescence) or non-radiative transitions or as an alternate, some photochemical transformations take place in this state (triplet) to give rise to the products.

It has been observed that there are many systems, which have additional states, more than two multiplicates or other processes affecting the life time of excited states. It is to be noted that understanding of excited state and its chemistry can be predicted, if knowledge about PESs is sufficiently strong enough. However, PESs processes function of large dimensions in polyatomic molecules and make them difficult to characterize. This type of general computational approaches, namely static and dynamic approaches have been developed to know about PESs. Static approach is well established geometry

optimization method (i.e., minima, transition states, crossing points), which are related to get relaxation routes. The main drawback of this approach is that there may be missing of important geometrics and therefore, the relaxation mechanism will be overlooked. Also, this approach does not give information about time scales and so it can not indicate that which routes are most important and it does not show the quantum yield (ϕ) of the photochemical relation? Complementary to it, there is another approach (dynamic approach), the progress, or the evolution of the coupled nuclear and electrons is directly stimulated. This is also called non-radiative molecular dynamics simulations. This approach is also capable of finding directly the critical geometries, which were really formed by the systems after excitation like a sort of molecular movie. This approach also gives information about time scales, so that the quantum yield can be obtained.

Although the concepts discussed here are simple in the approach, but these methods are greatly hampered by the multidimensional nature of potential energy surfaces and electronic complexity of the system. Also, dynamic simulations cannot be carried out beyond picoseconds and therefore, it puts a limit, above which time scale, the approach cannot be used. So in practice, many problems of balancing computational cost, and accuracy, time scale limitations and dimensionality process various approximation and therefore, for better understanding of the photophysical and photochemical concepts of coordination compounds, one has to return back to the Jablonski diagram for organic molecules.

Molecular systems are many electron systems. Approximate electronic wave functions can be written for molecule in the form of multiplication of one electron wave functions. Each of these function contains two parts i.e., orbital and spin parts. The orbital part of the many electron system defines the electronic configuration. Molecular photochemistry of organic compounds can be also better understood using molecular orbital energy level diagrams and electronic transitions can be expressed from highest occupied molecular orbital (HOMO) to lowest unoccupied molecular orbital (LUMO) and by this transition, the excited state and ground state electronic configuration of the molecule can be expressed. For example in case of formaldehyde, the $n \rightarrow \pi^*$ and $\pi \rightarrow \pi^*$ leads to the electronic configuration $(\pi)^2\,(n)^0\,(\pi^*)^0$ and $(\pi)^0\,(n)^2\,(\pi^*)^0$ excited state configuration. In approximation, every state associated with a specific electronic configuration is considered to be the sum of the energies of the occupied molecular orbitals. To obtain more appropriate description of the energy states of the molecule: (i) Spin functions should be linked to orbital functions and (ii) Interelectronic repulsion must be considered as it was neglected in all earlier discussions. These (i) and (ii) aspects are closely associated with each other and the importance of these points lies in the result that splitting of an electronic configuration into various states can occur. For examples in case of formaldehyde, when spin and electronic repulsion were incorporated, it resulted into the splitting of excited electronic configuration

into a pair of triplet and singlet states. Singlet states are always of higher energy as $e^- - e^-$ repulsion is higher for paired electrons. It has also been observed that the state, which arises due to π - π^* configuration splits more (singlet-triplet splitting) as compared to the state, which arise due to n - π^* configuration.

This effect of splitting of electronic configuration into singlet-triplet states is due to the dependence of the electron-electron repulsion on the quantity of the overlapping of MOs containing the two electrons. The electronic states can also be designated by symmetry species of the point group to which the molecule belongs. For example, in case of formaldehyde (HCHO), which belongs to $C_{2\upsilon}$ symmetry point group, A_1, A_2, etc. can be assigned. The $^1S_0$ state belongs to A_1 symmetry species, where the left superscript denotes the spin multiplicity (which can be calculated by 2 S + 1, where S in total spin of the system under consideration) and it multiplicity can be calculated by adding one into the number of unpaired electrons.

Hence, in case of coordination compound, the old Jablonski diagram will be very less effective to describe various photophysical and photochemical processes involved after absorption of light by metal complexes, but the pathways after absorption may be understood by constructing MOs energy level diagrams and incorporating the spin-spin interaction and $e^- - e^-$ repulsion. The splitting of electronic configuration of the complexes can be viewed as similar to the general lines discussed earlier for organic molecules.

The excited state configuration of the octahedral complex can be obtained by promotion of an electron from occupied MOs to vacant MOs. The various MOs are designated according to their greater contribution of AOs, which means (a) Strongly bonding, predominantly ligand centered σ_L π orbitals, (b) Bonding predominating ligand, (c) Essential non-bonding metal centered π_M orbitals of t_{2g} symmetry, (d) Antibonding, predominating metal centered σ_n^* orbitals of e.g., symmetry (e) Antibonding, predominantly ligand centered π_L^* orbitals, and (f) Strongly antibonding, predominantly metal centered σ_M^* orbitals.

In octahedral complexes of metal ions with d^n, the ground state electronic configuration has completely filled orbitals of the type (a) and (b), whereas n electrons occupy the orbitals of the type (c) and (d). The following electronic transition are expected for octahedral complexes:

(i) Metal-centered transition (MC) form orbitals of type: (c) → (d),
(ii) Ligand-centered transition (LC) from the orbitals of type: (b) → (e),
(iii) Ligand-to-metal change transfer (LMCT) transitions in orbitals of the type: (b) → (d), and
(iv) Metal-to-ligand change transfer (MLCT) transition from the orbitals of the type: (c) → (e)

The order of the relative energies of the excited electronic configuration depends upon the nature of metal and ligands, which can be predicted from the

knowledge of chemistry. When first row transition metals are taken, it is expected that low energy metal centered transition may occur in these cases, while low energy LMCT transitions are predicted, when at least one of the ligand is easy to oxidize and the metal is easy to reduce. However, the low energy MLCT transition are expected in the complexes, in which metal is easy to oxidize and ligand is easy to reduce and low energy LC (ligand centered) transition are expected for aromatic ligands with extended π and π^* orbitals.

In case of coordination compounds, the splitting of electronic configuration into states is more simple as compared to organic compounds as coordination compounds possess high symmetry (i.e., degenerate MOs) and ground configuration (i.e., partially occupied HOMO).

Therefore, in case of coordination compounds, the Jablonski diagram will be more complex and specific as compared to organics. The following points are to be seen:

(i) Another state than singlet and triplet state can appear, but the lowest one will be that state., which has highest multiplicity for each electronic configuration,
(ii) Ground state possesses highest spin multiplicity. Excited states can occur that belong to the same electronic configuration of the ground state and
(iii) A single electronic configuration can give rise to more than one pair of states of different multiplicity.

Therefore, in general discussion of molecular photochemisty, generic Jablonski diagram based on singlet and triplet states will be used.

After the absorption of light, the excited state formed may decay intramolecularly. Theoretically, the transitions between states of same multiplicities and transition between states of different multiplicities are spin allowed and spin-forbidden, respectively. So, in the UV visible spectrum, the molecule shows an absorption based corresponding to $S_o \rightarrow S_n$ transitions.

Metal complexes are generally having high degree of symmetry, and therefore, selection rules based on symmetry also play an important role in determining the intensity of the absorption bands. However, the spin conservation condition is relaxed, when a heavy atom (the metal) is present.

As the excited states are unstable and they can decay not only through dissociation or iomerization (intramolecular reaction), but also very often through intramolecular radiative and non-radiative relaxations also. The electronically exited molecule in upper spin allowed excited states normally acquires fast and 100% efficient radiationless (shown by wavy arrow) deactivation (IC) to the lowest spin-allowed excited state (S_1). Other than intramolecular photochemical processes, the excited state in S_1 has three process (first order) to exercise for its deactivation:

(i) Non-radiative decay to ground state, $S_1 \rightarrow S_0$ (IC) Rate constant (k_{IC})
(ii) Radiactive deactivation $S_1 \rightarrow S_0$ Rate constant (k_{Fl})

(iii) Intersystem crossing (ISC) to the lowest triplet state (T_1) rate constant (k_{ISC}) and after reaching T_1, it can undergo deactivation through non-radiative intersystem crossing (k'_{ISC}) or radiative (phosphorescence, k_{Ph}) decay to S_0. In case of metal complexes, the usually forbidden process, namely intersystem crossing (ISC) and phosphorescence processes became faster due to presence of heavy atom (metal itself). The lifetime (τ) of an excited state is the time needed to reduce the exited state concentration and it is given by the reciprocal of the summation of the deactivation rate constants. It can be expressed as:

$$\tau(s_1) = \frac{1}{k_{IC} + k_{F1} + k_{ISC}} \tag{2.1}$$

$$\tau(T_1) = \frac{1}{k'_{ISC} + k_{Phosp.}} \tag{2.2}$$

The lifetimes of the lowest spin allowed and spin forbidden excited states τ (S_1) and τ (T_1) are approximately 10^{-9}–10^{-7} and 10^{-3} –10 degrees, respectively for organics, but for metal complexes, these lifetimes are even more shorter. The lifetime of the lowest spin forbidden excited state of naphthalene is about 2 s, while that of $[Ru(bpy)_3]^{2+}$ is about 1 μs (as Ru ion is a heavy atom).

The fluorescence and phosphorescence quantum yields (Φ) are known for various metal complexes and these can be expressed as:

$$\Phi_{Fe} = \frac{K_{F1}}{k_{IC} + k_{F1} + k_{ISC}} \tag{2.3}$$

$$\Phi_{phosp.} = \frac{K_{Phosp.} \times k_{ISC}}{\left(k'_{ISC} + k_{Phosp.}\right) \times \left(k_{IC} + k_{F1} + k_{ISC}\right)} \tag{2.4}$$

The knowledge of lifetimes of excited state and quantum yields of fluorescence and phosphorescence are helpful in understanding the mechanism of various photochemical reactions of coordination compounds.

2.2 Photochemical aspects

In the early half of seventies, a number of publications appeared about the bimolecular processes involving metal complexes, where main focus was on the ligand substitution reactions, photoredox decompositions and photoionoization reactions. However, biomolecular processes were not investigated at any level. This situation drastically changed, when researchers started working on limitations of coordination compounds and the discovery that the lowest excited state of the various complexes of Cr(III), Ru(II), Os(II), etc. showed a sufficiently longer lifetime in fluid solution, so that these are able to

participate as a reactant in biomolecular reactions. More advantageous is the fact that Ru(II) and Os(II) bipyridyl type complexes can undergo reversible redox reactions; in ground as well as excited states and, therefore, they were used as reactants and also as a mediator in light induced and light generating electron transfer processes. The photochemical transformations for solving various energy problems have attracted the attention of scientific community and much work was carried out after the energy crisis in the early 1970s. The particular interest was focused on water splitting and it was understood that $[Ru(bpy)_3]^{2+}$ and related coordination compounds can function as photocatalysts for such a process.

The main revolution in the field of photochemistry of coordination compounds was observed in the period 1975−85. The properties of a molecule (compound) in excited state is quite different from properties in ground state. Because of high energy content, an excited state is both; a stronger reducing species as well as a strong oxidizing species than the corresponding ground state. Therefore, redox potential of the excited and ground states played an important role to understand the use of photoexcited species for various applications. It can be shown from kinetics that excited states ($>10^{-9}$s) may possess a chance to be involved in encounters with other solute molecules. Generally, only the lowest excited state fulfill this condition in metal complexes with longer lifetime and therefore, the coordination compounds in their lowest photoexcited states have number of interesting properties, which can be used in harnessing solar energy, photosplitting of water, photoreduction of CO_2 (the main culprit of the global warming), etc.

Introduction of superamolecular photochemistry added another photochemical aspect, which gained a lot of attraction in late 1980s. This field is an interdisciplinary subject in nature in true sense and it is based on concepts like molecular recognition, organization, and self-assembly. In supramolecular chemistry, focus is changed from molecular photochemistry of metal complexes to molecular assemblies or multicomponent systems. Various light powered devices and molecular machines can be designed using supramolecular photochemistry. Here, preorganization is very important because that favors energy and electron-transfer processes.

The chemical reactivity of the transition metal complexes can be understood on the basis of the d-electron configuration of central atom. The kinetic inertness of $(t_{2g})^6$ octahedral complexes is attributed to the rearrangement of the ground state of octahedral structure to any transition state will certainly require a large activation energy.

But, the reactivity in the excited state will be different due to change in the electron distribution (as compared to ground state). It can be seen that in the MO energy level diagram for an octahedral complex that in $\pi\ (t_{2g}) \rightarrow \sigma_{M*}\ (e_g)$ transition in octahedral complexes, the charge distribution between metal and ligand remains almost unchanged due to metal−centered (MC) character of these transitions. Therefore, the ground state is generally stable toward

intramolecular redox processes (homolytic cleavage of M−L bonds), and the MC excited state tends to remain stable toward redox decomposition of the complexes. The σ_{M*} (e.g.,) orbitals are greatly σ−antibonding, and hence, presence of any electron in these σ* orbitals will make some M−L bonds weak, which will facilitate a ligand substitution reaction. The entering of new ligand in facilitated by the presence of empty π_M (t_{2g}) orbital for bond formation.

In case of charge transfer excited state, which are produced by the transition from MOs basically localized on the ligand to localized on the metal (LMCT, ligand−to−metal charge transfer). These transitions create a radical distribution of the electronic charge between central metal and ligands, which will cause change in the oxidation state of metal (or oxidation of ligand and reduction of metal). Therefore, CT excited state will tend to produce intramolecular redox processes, resulting in the reduction of the ligand and oxidation of metal or vice versa. It can be seen that due a CT process, the oxidation state of metal changes and consequently an inert complexes may become labile and as a result, the complex may undergo decomposition. It can be observed that LMCT transition in Co(III) complex changed it to Co(II) complex, which will become kinetically labile due to the presence of an electron in the σ_{M*} (e.g.,) orbital and therefore, it is assumed thar all legands will leave the coordinate shape, whether or not their involvement is there in CT transition? It is to be emphasized that MLCT transition increases the positive charge on the metal, which will facilitate a nucleophilic attack by outer ligands. The CT transition may also affect the acid strength of the complexes having protic ligands (NH_3, H_2O, etc).

Intermolecular CT transitions undergo redox process, which give a reduced form of a complex and if it is not stable, it will decompose. However, any redox process to take place actually, it depends on the intrinsic properties of the ion pair and environment. In the same way, charge−transfer−to−solvent transition (CTTS) may result into an oxidized form of the complex and a solvated electron.

When an electron transition takes place between two MOs, the ligand centered (LC) or intraligand excited states are formed, which are almost localized on the ligand. Since, there are many varieties of ligands, the reactivity of LC excited state cannot be predicted with certainity. However, as a first approximation, neither the charge transfer distribution between metal and ligand is changed nor the bonding structure of the complexes due to LC transition. But due to change in the electronic structure of the ligand, change in various important parameters will be there such as its donor and acceptor properties, dipole moment, acid strength, equilibrium geometry, etc. These changes may affect the stability of the complexes.

Till now, the conceptual framework for the photochemical and photophysics processes of complexes have been discussed, but there cannot be any rule formulation for the photoreactivity i.e., which type of photoreaction will

occur, because the nature of the electrically excited states is yet to be fully understood? As mentioned earlier, the excited states directly formed by irradiation can undergo radiationless deactivation processes before getting a chance for reaction and therefore, the lower excited states may be produced, which are different in nature from the original state, e.g., an excited state of MC can be formed by deactivation of CT state. It is clear that the type of reaction (redox, substitution, etc.) depends on the nature of the excited state, in which the reaction is taking place. When ligand substitution and redox reaction are taking place, one cannot be certain that these reactions are the results of the CT or ligand filled nature of the excited state. In reality, the photophysics and photochemical behavior of the complex is caused by a complicated adjustment between inherent chemical reactions, radiative and nonradiative deactivation processes of the electronic states.

In case of solution photochemistry of complex ions, the pertinent question arises that which particular excited state is formed? The answer can be given on the basis of MO energy level diagram of the complex and one can develop qualitative view of expected reaction pathways. Earlier, mechanism of the photochemical reaction were largely proposed on the basis of reaction products and quantum yield of the reaction; thus, making a comparison of their data with electronic and spectroscopic properties, but with the advent of density functional theory (DFT) and laser flash photolysis, the scenario of knowing the mechanism of the photochemical reaction of complexes has drastically changed.

In short, the conceptual basis of photophysical and photochemical processes of complexes can be understood on illustrating one-electron transition for assigning absorption bands and excited states (mononuclear complexes). The d-orbital splits due to mixing with σ−donor and π−donor & accepter orbitals of the ligand. So, the characteristic absorption bands correspond to the excitation between these split d−orbitals (with partially filled d−orbital). These d−d ligand field (LF) transition involve MOs, which are mainly metal in character and therefore, the resulting excited states are often called metal centered excited states (MC*). In complex having center of symmetry, LF bands are Laporte forbidden and have very low value of molar extraction coefficient. However, metal-to-ligand charge transfer (MLCT) and lignd-to-metal charge transfer (LMCT) bands process higher intensity due to change in the dipole moments between ground and excited states. The one-electron transition in octahedral mononuclear complexes is shown in Fig. 2.2.

Where, IL = Intraligand or ligand centered transition,

MLCT = Metal-to-ligand charge transfer,

LMCT = Lignd-to-metal charge transfer, and.

LF = Ligand filled transition.

The IL transitions are actually intraligand or ligand centric transition represented by $\pi_L \rightarrow \pi*_L$ excitation. So these one electron transitions provide a convenient framework to understand the nature of the excited states formed;

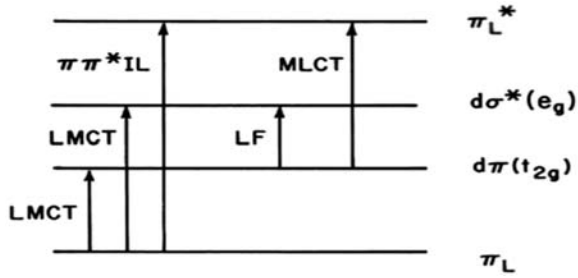

FIG. 2.2 One-electron transition in octahedral mononuclear complexes. *Adapted from Ford, P.C., 2016. From curiosity to applications. A personal perspective on inorganic photochemistry. Chem. Sci. 7 (5), 2964–2986. With permission.*

however, theoretical calculation has predicted more mixing of the excited state characters than what is depicted? In case of $[Ru(NH_3)_5(py\text{-}x)]^{2+}$, where (py-x is substituted pyridine), and other related complexes, such as $[Ru(NH_3)_5(pz)]^{2+}$ (where pz = pyrazine), the strong absorption band in visible region was attributed to MLCT transition, which is allowed singlet to singlet transition. But in UV region, the absorption band corresponding to a transition ($\pi_L \rightarrow \pi*_L$) is IL in nature. S_o, the question arises that at what point one would expect to obtain the LF absorption for these low spin d^6? The absorption spectrum of $[Ru(NH_3)_6]^{2+}$ can be taken as an empirical model, in which the spectrum does not include any π-unsaturated ligands. The electronic spectrum of this complex showed two absorption bands; one at 390 nm ($\varepsilon = 35\ M^{-1}cm^{-1}$) and other at 275 nm ($\varepsilon = 640\ M^{-1}cm^{-1}$) as predicted by group theory ($^1A_{1g} \rightarrow {}^1T_{1g}$) and ($^1A_{1g} \rightarrow {}^1T_{2g}$) respectively. Here, the higher intensity of the band at 275 nm is due to mixing of a charge transfer-to-solvent transition (CTTS). In $[Ru(NH_3)_5(py\text{-}x)]^{2+}$ ions, the analogous LF bands are expected at comparable energies for the $[Ru(NH_3)_5(py\text{-}x)]^{2+}$ ions, but they are enveloped by much strong MLCT bonds.

The photoreaction and their mechanism are also proposed on the basis of quantum yield (Φ), which indicates that the efficiency of the photochemical reaction may have higher values as almost equal to units or in many reactions, Φ is very small. The key points here is the denominator in the definition of Φ as:

$$\Phi = \frac{\text{Number of molecules taking part in the photochemical reaction}}{\text{Number of quanta of light absorved}} \tag{2.5}$$

As the photochemical reaction is possible only, when light is absorbed, the denominator in this expression of Φ is main factor for generating either high or low value of Φ. Kinetics of the photochemical reaction is an important aspect in the sense that delivering a drug at a proper targeted

biological organs, the overall rate of the photochemical reaction has the significant importance.

The rate of photochemical reaction is expressed as:

$$\text{Rate} = \Phi \times I_a, \tag{2.6}$$

where I_a is the intensity of the light absorbed (in unit of "Einstein" per unit time) and Φ is the quantum yield (1 E = 1 mol of photons). A solution containing only one photoreactant, which absorbs incident light, $I_a = I_0 (1-10^{-Abs})$ (where absorbance (A) = εCl), where ε is the molar extension coefficient (L mol^{-1} cm^{-1}), C is the concentration of the photoreactant and "l" is the pathlength of the cell (cm). In such processes, there will be no unimolecular rate constant. When photolysis of $[Ru(NH_3)_5(py)]^{2+}$ is continuously carried out at 405 mm under light irradiation at ambient temperature, the photosubstitution reaction takes place and the quantum yields for pyridine and ammonia substitutions (Φ_{py} and Φ_{NH3}) were found to be 0.045 and 0.063, respectively. This wavelength is close to λ_{max} of the spin−allowed MLCT band (407 mm) and therefore, it can be said that majority of the absorbed photons resulted into MLCT excitation.

The understanding of nature of excited state can give insight of the type of photochemical reaction. But sometimes, correct conclusion could not be drawn. The behavior expected for MLCT excitation was not found in the case of photosubstitution reaction having an oxidized metal center and reduced pyridine $[Ru^{III}(py)]^{2+}$, but it is known that Ru(III) complexes are not thermally very labile. In the opposite situation, the MC excited state, in which an electron is promoted from a non-bonding or even π−bonding MO to σ* relative to the metal−ligand bond will appear as the precursor for the ligand photosubstitution. If this is true, then the hexaammine complex $[Ru(NH_3)]^{2+}$ is relatively labile toward photodissociation of NH_3 ($\Phi_{NH3} = 0.27$ at $\lambda = 405$ mm). Such conclusions are drawn on the assumption that the mechanism for excited state ligand labilization is mainly dissociative in nature. It was confirmed that for $[Ru(NH_3)_5(py)]^{2+}$, the ^{3}MC excited state is almost dissociative in character.

This discussion leads to propose that the excitation state responsible for the photosubstitution reaction was the outcome of the fast internal conversion (IC)/Inter System Crossing (ISC) from MLCT states, which are populated by excitation to MC excited states (these states are not observed spectroscopically) (Fig. 2.3).

This observation that the photolabilization of aqueous solution of $[Ru(NH_3)_5(py)]^{2+}$ does not depend mainly on the wavelength of excitation indicates that the lowest energy excited state (LEES) are responsible for these photosubstitution reactions. In this framework, another conclusion can be drawn that the ligand substituents can be used to tune the excited state energies, where the ^{3}MLCT is the LEES. In that case, considerable decrease in the photolability will be observed.

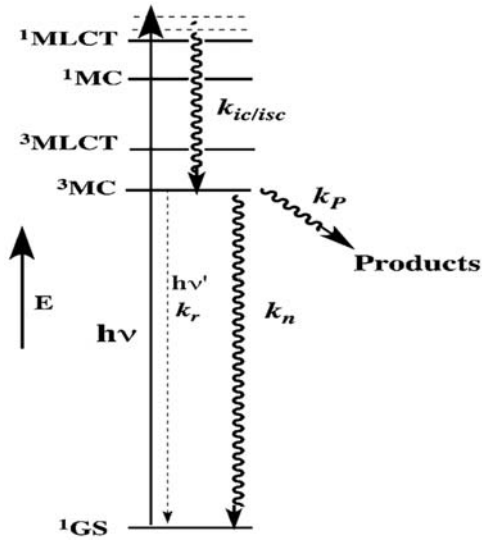

FIG. 2.3 Proposed ES diagram to explain photoaquation of aq. $Ru(NH_3)_5(py)^{2+}$ upon irradiation of MLCT bands. k_P is the rate constant for reactions to photoproducts. K_{ic}/i_{sc}, k_n and k_r are rate constants for internal conversion/intersystem crossing to a lowest energy metal centered excited state, nonradiative deactivation to the ground state ^{1}GS and radiative deactivation (emission), respectively. *Adapted from Ford, P.C., 2016. From curiosity to applications. A personal perspective on inorganic photochemistry. Chem. Sci. 7 (5), 2964–2986. With permission.*

Thus, the tuning of excited state can be shown by study of photoreaction of a series of $[Ru(NH_3)_5(py{-}X)]^{2+}$ complexes. It was observed that electron withdrawing substituents, which give red shift ($\lambda_{max} > 470$ nm), resulted into dramatically less photolability than those with substitution, which gives less value of λ_{max} (blue shift).

The tuning of MLCT/MC states by using various substituents is being used with many systems including those based on the Ru(II) polypyridyl complexes are of interest from solar energy conversion point of view. Similarly, Ir(III) phenylpyridyl complexes have been employed for orange light exciting diodes (OLED) application. The kinetics of excited state is much complex due to many states formation and deactivation processes involved. The kinetics becomes more complicated, when more than one excited state is involved for the chemical or photoluminescence property. The reaction kinetics envisaged form Jablonski diagram can guess that the excited state of lowest energy lies on the potential surface with very well defined minima. This is called bound excited state. There exists an energy boundary greater than k_BT (where k_B is the Boltzmann constant) for the bound excited state to decay along any pertinent reaction coordinate (Fig. 2.4).

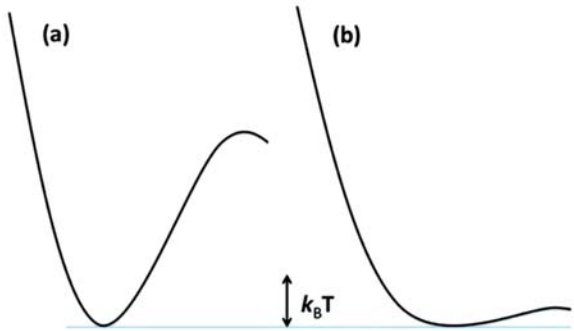

FIG. 2.4 Potential surfaces for (A) a bound excited state where the barrier is $>k_BT$ and (B) a dissociative ES where the barrier is $<k_BT$. Since k_BT is temperature dependent, if any barrier is present, an ES that is dissociative at a high T, may behave as a bound state at low T. *Adapted from Ford, P.C., 2016. From curiosity to applications. A personal perspective on inorganic photochemistry. Chem. Sci. 7 (5), 2964–2986. With permission.*

There are two possibilities:

- A bound exicted state having barrier greater than k_BT, and
- A dissociative exicted state having barrier less than k_BT.

Here, it is clear that k_BT is dependent on temperature, the excited state may exhibit a bound state at low temperature because at any barrier, the excited state at higher temperature will be dissociative in nature.

If the barrier is less than k_BT, the possibility of having a dissociative state is there. In this situation, they will have shorter lifetimes and their kinetics cannot be treated by classical kinetic methods.

The quantitative photochemical studies of ammine complex of Rh(III) revealed that the kinetics and mechanism of ligand photossubstitution reaction involves metal centered (MC*) excited states: These are d^6 complexes and metal system with this electron configuration (d^6) has found application in dye–sensitizerd solar cells (DSSCs) and organic light emitting diodes (OLEDs). Therefore, metal centered excited states are also important, even when the initial excitation is of MLCT nature. It can be seen that in Rh(III) ammine complexes, the absorption spectra is mainly due to the spin allowed LF bands ($^1A_1 \rightarrow {}^1T_2$, $^1A_1 \rightarrow {}^1T_1$ for the octahedral complex $[Rh(NH_3)_6]^{3+}$) whereas, the emission spectra exhibited the character of lowest energy triplet metal centered excited state (^{3}MC*) in aqueous solution.

Studies on the photosubstitution reactions and lumininiscent behavior of $[Rh(NH_3)_6]^{3+}$ revealed that these reactions and luminescence are independent of excitation wavelength, which indicated that initial LF excitation to ^{1}MC* states was followed by efficient IC/ISC to give lowest energy ^{3}MC* state

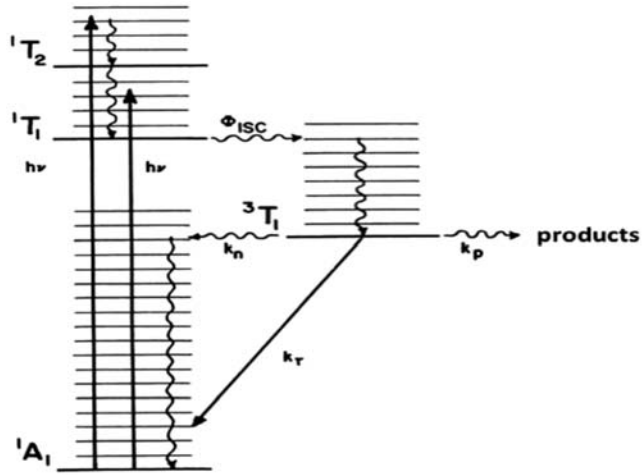

FIG. 2.5 Excited state diagram of MC states in $[Rh(NH_3)_6]^{3+}$. *Adapted from Ford, P.C., 2016. From curiosity to applications. A personal perspective on inorganic photochemistry. Chem. Sci. 7 (5), 2964–2986. With permission.*

($^3T_1$). This $^3T_1$ is mainly responsible for the photoreaction or emission (Fig. 2.5).

Therefore, the photochemical reaction and emission quantum yield can be treated in terms of rate constants of excited states.

2.3 Photoluminescence in coordination compounds

Rare earth ions like Eu^{3+}, Sm^{3+}, Gd^{3+}, Tb^{3+}, etc. form complexes with bidentate ligands, and there occurs emission due to transition within the metal energy levels, though they are Laporte forbidden. The energy levels become populated by intramolecular energy transfer in the complex, when ligand absorbs the radiation. The fluorescence and phosphorescence from ligand moiety can be observed, if the emission state of metal lies higher than the lowest triplet state of ligand moiety. The uranyl ion (UO_2^{2+}) is also highly luminescent.

The emission properties are observed in transition metal complexes with d^3 (Cr^{3+}, Co^{3+}) and d^6 (Ru^{2+}, Rh^{3+}, Os^{2+} and Ir^{3+}) configurations. In these cases, the nature of emissive transition is d-d transition and dominance of spin-forbidden phosphorescence in seen. The fluorescence efficiency is low due to spacing and coupling of lowest excited vibration levels with the ground state vibrational levels.

In these cases, fluorescence was found to show broad band (and large Stoke's shift) indicating the distortion in the geometry of excited states. Phosphorescence is identified with very small Stoke's shift and at low

temperature in glassy solution, the vibration structure is resolved. The phosphoroscence is due to the transition assigned as $^2E_g \rightarrow {}^4A_{2g}$, which coresponds to $T_1 \rightarrow S_0$ in Jablonski diagram. In these complex compounds, non-radiative internal conversion (IC) processes are relatively more prominent than the non-radiative ISC processes. Therefore, the spin-orbit coupling is not the sole deciding factor for the loss of luminescence. Therefore, if there are low-lying d-d states, then there will be absence of luminescence as in the complex having configuration d^1, d^7, d^8, d^9 and for most of the d^6 complexes.

If one focus on the emissive transitions in transition metal complexes, then these transition generally obey Kasha's rule and generated from the lowest excited state i.e., triplet (π, π^*) or triplet (d, π^*) state, and triplet (d-d) states. The emissive transition of the type of $^3(\pi, \pi^*)$ is observed in $[Rh(phen)_3](ClO_4)_3$. The ^{3}(d, π^*) transition was there is $[Ru(dpy)_3]Cl_2$ and ^{3}(d-d) transition in case of solid $[RhCl_2\ (phen)_2]Cl$. A weak fluorescence form Cr(III) complex was also observed occasionally. A very good luminescence was observed in $K_3[Co(CN)_6]$. It has also been proposed that in some cases, $^3(\pi, \pi^*)$ and ^{3}(d, π^*) states are formed from delocalized orbitals and ^{3}(d-d) state is formed from localized orbitals. It has been observed that the increase in the shift of the emission of chelate complexes in comparison to the free ligand is associated with the increase in the participation of d-orbitals in the emissive transition. A decrease in the lifetime of the chelate complex may also be attributed to the increase in d-character in molecular orbital. This gives a reasonable explanation for the behavior of metal complexes as quencher of excited state of π-electrons in organic compounds. In Rusy laser, the emissions from Cr^{3+} is the basis of functioning as laser.

Recent progress in exhibiting luminescence by metal complexes with photochromic units like azobenzene, spiropyrane and diarylethene, which undergo reversible photoisomerization between two isomers on irradiation with proper wavelength is very interesting. The emerging electronic and photonic devices have seen a progress due to investigations in the area of photoresponsive molecules and their light irradiation characters, which modulate certain physics and chemical properties. If the metal complex contains some photochromic units as ligands, then these ligands act as photoresponsive unit and such complexes are found suitable for advanced photonic applications such as photoswitching, photomemory, electronic conductors, electrochemical response, magnetic interaction, etc. These advanced properties are due to their high sustainability, resolution, contracts and quick response time in luminescence technology.

Luminescence−switching properties of metal complexes having photochromic units as ligand are due to characteristics electronic transitions, which are classified as:

- The $\pi-\pi^*$ transition of the ligand,
- MLCT and LMCT transitions in transition metal complexes, and
- f-f transition in lanthanide complexes

Therefore, the knowledge and understanding of their transitions will be useful in luminescence intensity modulation for applications in smart molecular switches. These advanced photonic applications will provide avenues for synthesizing such new different metal complexes, which will be also useful in devices with photonic memory and photosensing properties.

Traditionally, the inorganic photochemistry and photophysics was dominated by rare earth and costly metals, but now complexes of low cost and abundant metals have also shown their potential to photoemit or fluorescence. The first row transition metal complexes have also shown their unexpected reactivity and photoluminescence behavior due to increase in the understanding of the nature of excited states.

After the great progress in the conceptual understanding of excited states, a broad range of elements in various oxidation states show the photoluminescence behavior. The complexes of vanadium, chromium, manganese, iron, cobalt, nickel, copper, etc. now show luminescence properties, which were not known earlier in detail. In 3d-series metal, the ligand field is poor as compared to 4d- and 5d- complexes, due to poor spatial overlap of metal d-orbitals with ligand orbitals. Therefore, the complexes having partially filled 3d-orbitals produce very many metal centered excited states with very less spacing between them and also less space with ground state. This situation is somewhat precious, because it will allow a series (cascading) of non-radiative processes from MC state to the other and ultimately back to the ground state. However, in some cases, the situation of metal-ligand bond is much different (from ground state) in some MC state as in the case of promotion of d-electrons from non-bonding to antibonding orbitals. In such situations, the excited states are called distorted and this can be seen in the shift of the potential well along a certain nuclear coordinate (e.g., M−L bond distance). Therefore, the efficiency of the crossing barrier from one potential well into next lower is very less and this will cause rapid non−radiative processes to occur, whereas in 4d- and 5d-complexes, the spacing between MC states and also between MC and ground state is large, so the lowest MC state can be luminescent and photoactive because the efficiency of non−radiative processes is less, when the excitation energy is released through more number of vibrational levels.

High energy MC states open the door for formation of fundamentally different excited states at lower energies (keeping the spacing with ground state large enough). This is the case, when electron density shifts from metal to ligand or from ligand to metal. The most important state, which govern the photochemical and photophysical properties is the lowest excited state; that is MLCT or LMCT states. In these charge transfer states, redox properties are very much different from the ground state, making them to involve in photoredox chemistry with organics or to act like dyes in inorganic semiconductor

solar cells. Ligand-to-ligand charge transfer (LLCT), in which the electron density shifts from one ligand to another ligand, can also be useful to exhibit luminescent properties. This is totally different from what is called intraligand (IL) excitation, in which the electron density is redistributed within the π− conjugation framework of the ligand.

Contrary to the organics, the fast ISC processes in many metal complexes from excited singlet to lower lying triplet excited states are due to greater spin−orbit coupling. This phenomena has significance with regard to photoreactivity (which could not be observed from singlet state) and the triplet excited state being more stable (higher lifetime) produced an improved kinetic reactivity. Also, the photo-induced electron transfer from triplet states will result into primary photoproduct, which undergoes less charge recombination. This will increase the quantum yield of the photoredox reaction. Various applications highlight the important role played by metal complexes like luminophores in organic light emitting diodes (OLEDs), and light emitting electrochemical cells (LEECs), photocatalysis in synthetic photochemistry and artificial photosynthesis, harnessing the solar energy in dye−sensitized solar cell (DSSCs), etc. Therefore, search for newer photoactive complexes of low cost and abundantly available metals will bring many laurels to this field of photochemistry.

Emissions of Cu(I) and Cr(III) complexes in solution phase at room temperature have been known earlier. The progress in key concepts and lifetime of excited state has motivated the scientists to synthesize complexes with exceptional illumination properties. Complexes of cobalt and nickel have also attracted the attention of inorganic chemists for this purpose. The most abundant transition element iron has become a point of interest for chemists, while manganese and vanadium complexes have exhibited luminescence in solution at room temperature. This has revolutionized the present field. When a compound exhibited emissions in solution at room temperature, this indicates that the lifetime of excited state are sufficiently more from diffusion controlled biomolecular reactions and therefore, such compounds become suitable for photochemical applications, which are very advanced in nature as compared to simple lighting.

The important complexes in the term of photoactivity are there, in which the metal is directly involved in shaping the photochemical and photophysical properties. Complexes, in which IL excitation plays a prominent role, will have different mechanism for luminescence. Therefore, LLCT, MLCT, LMCT and MC excited states are more relevant for $3d^n$ configuration ($n = 2-10$). Examples of base metal complexes showing luminescence are as follows: $3\ d^{10}$ (Cu(I) complexes as LLCT emission), $3\ d^6$ (Mn(I) and Cr(0) complexes) and $3\ d^8$ (Ni(II) complexes, as MLCT emission), $3\ d^0$ (Sc(III)), $3\ d^3$ (Mn(IV)), $3\ d^5$ (Fe(III)) and $3\ d^6$ (Co(III)) complexes as LMCT emission, $3\ d^2$ (V(III)), $3\ d^3$ (Cr(III), Mn(IV)) and $3\ d^6$ (Co(III)) complexes as MC emission have been reported.

A drastic change was observed, when two-coordinated Cu(I) complexes, (which are LLCT luminophores as well as LMCT emitters), got change in the direction of charge transfer (Wegeberg and Wenger, 2021). Change in the direction of charge transfer (i.e., from MLCT to LMCT) has resulted into the use of these complexes in dye-sensitized solar cells; however, for luminescence properties of LMCT or LLCT emitters are very competitive with MLCT luminphores. This is especially true for lower Cu(I) LLCT emitters. This shows a paradigm shift in the conceptual framework of metal complexes.

Therefore, traditionally the photoemissions was due to MLCT and MC transitions, but in addition in this, LMCT and LLCT transition also resulted into the emission for complexes of 3d- and other elements. Also, molecular complexes of abundant main group elements have attracted chemists to act as luminophores and give an insight to control the non-radiative pathways.

2.4 Photochemical processes

As it is known that in metal complexes, non-radiative activation of low lying energy states is fast and therefore, the photochemical reactions from these states must possess zero activation energy. In case of transition metal complexes; both $^4T_{2g}$ and ^2E_g are photoactive states but these may take different pathways. There are three fundamental photochemical reactions for coordination compounds. These are:

(i) Photosubstitution,
(ii) Photorearrangement, and
(iii) Photoredox reactions.

2.4.1 Photosubstitution reactions

This is further divided into three categories i.e., aquation, anation or ligand exchange reactions.

- **Photoaquation reactions**: The general equation for photoaquation reaction can be represented as:

$$[Cr(III)L_6] + H_2O \xrightarrow{hv} [Cr(III)L_5(H_2O)] + L$$

In this reaction, M−L bond is heterolytically cleaved. In some specific Cr(III) complexes of O_h symmetry, such aquation reactions are efficiently observed, when $^4T_{2g}$ states lies sufficiently above the ^2E_g state. If the energy difference between these two states decreases, the efficiency of the aquation reaction also decreases. This is observed for $[Cr(NH_3)_6]^{3+}$ on successive aquation. The labileness of ligand NH_3 and H_2O become reversed in the

thermal and photochemical reactions. The two aquation modes for $[Cr(NH_3)_6(NCS)]^{3+}$ in 0.1 H_2SO_4 are

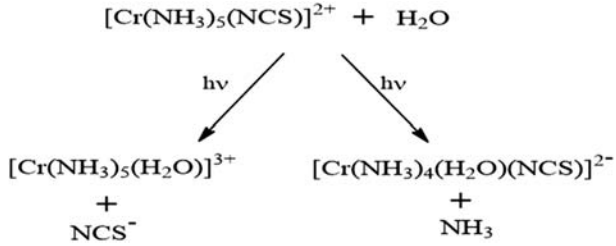

Here, both $^4T_{2g}$ and ^2Eg states are photochemically active and the ratio of $\Phi_{NH3}/\Phi_{\overline{NCS}}$ depends upon the wavelength.

This photoaquation reaction can also be obtained through photosensitization by a mechanism known as energy transfer from biacetyl and acridinium ion in the same solvent. When biacetyl is used as a sensitizer, phosphoresence was quenched, but fluorescence remained unaffected. No degradation of biacetyl and release of NH_3 was observed. The ratio $\Phi_{NH3}/\Phi_{\overline{NCS}}$ was found to be greater than 100. When acridinium ion was used a sensitizer, fluorescence was quenched, NH_3 and NCS both were released (though NH_3 was predominant). The release of NCS^- was less in presence of O_2 and hence, the triplet state of the sensitizer was involved. The Φ_{NH3}/Φ_{NCS} was found to be 33 for $^4T_{2g}$ states and eight for ^2E_g state. These observations clearly indicated the release of NH_3 from $^4T_{2g}$ and NCS from ^2E_g states.

These reactions were found useful in the synthesis of coordination compounds. The photoaquation of $K[Cr(NH_3)_2(SCN)_4]$ and $[Cr(Urea)_6]Cl_3$ can be employed as efficient actinometers in the range of 316−750 nm. The photochemical reaction for $[Co(CN)_6]^{3-}$ is

$$[Co(CN)_6]^{3-} + H_2O \xrightarrow{h\nu} [Co(CN)_5(H_2O)]^{2-} + CN^-$$

This reaction takes place without any complication and its quantum yield is also higher ($\Phi = 0.31$).

- hν **Photoanation reaction**: Such reactions are common in Cr(III) complexes, and these can be represented as-

$$[Cr(H_2O)_6]^{3+} + NCS^- \xrightarrow{h\nu} [Cr(H_2O)_5(CNS)]^{2+} + H_2O$$

$$[Cr(H_2O)_6]^{3+} + Cl^- \xrightarrow{h\nu} [Cr(H_2O)_5(C1)]^{2+} + H_2O$$

Such reactions play a vital role in the synthesis of new coordination compounds using solution phase reactions.

- hv **Ligand exchange reactions**: When carbonyl metal complexes $[M(CO)_6L]$ was irradiated with light in presence of excess L, the substituted complex is produced.

$$[M_0(CO)_6] + L \xrightarrow{hv} [M_0(CO)_5L] + CO$$

Where L may be NH_3, $(C_2H_5)NH_2$, $(CH_3)_2NH$, $(CH_3)_3N$, $(C_2H_5)_3N$ or other amines. The pentacarbonyl complex formed here may undergo further substitution reaction. In case of $[Fe(CN)_6]^{4-}$, the photosubstitution of dipyridyl ligand takes place as:

$$[Fe(CN)_6]^{4-} + dpy \xrightarrow{hv} [Fe(CN)_4(dpy)]^{2-} + 2\ CN^-$$

When mix ligands are involved, the photoreactivity can be predicted by considering the strength of ligand fields. In case of a complex of O_h symmetry, the axis which possess weakest average field (estimated from the position of its respective ligands in the spectrochemical series) will be labilized. If the labilized axis has two different ligands, then the ligand having greater field strength will be replaced first as in the case of $[Cr(NH_3)_5Cl]^{2+}$.

The $NH_3-Cr-Cl$ is a labilized axis and not the $NH_3-Cr-NH_3$. So, the strong ligand NH_3 will be replaced preferentially along $NH_3-Cr-Cl$ axis; however, prediction may deviate, when steric and solvation effects are present. If the symmetry of the complex is lowered, then the position of states also changed and due to this, the nature of reaction also changes.

Photosubstitution reaction of Ru(II) imine complexes are good examples of use of these complexes in the field of photobiology and photodynamic therapy. The mechanism of the photosubstitution reaction of these Ru(II) complexes can be understood using the simple Jablonski diagram.

The photoreactivity of Ru(II) complexes is affected with MLCT transition in visible region due to absorption. These complexes contain one or more diimine ligands (bpy = 2,2′- bipyridine, phen = 1,10-phenenanthrine, etc). and one or more ligands, which can be easily labilized in the excited state. Here, three states of ^{3}MLCT are split. The largest wavelength absorption in the visible region corresponds to MLCT transition. After excitation by ISC, triplet ^{3}MLCT state is formed (very fast of the order of femto seconds i.e., 10^{-15} s) with almost unit efficiency. Relaxation of the triplet state to the ground state is in the range of nanoseconds and includes internal conversion, resulting into triplet ligand field state (^{3}LF). Recent advances in this field have provided more insight into the energetics of MLCT and LF states, because these two important states are involved in the photosubstitution reactions. So, more understanding about the nature of these states will further the research in the

development of newer complexes acting as therapeutic agents. In case of bidentate ligand, Ru(II) complex also involves new ^{3}MC states (which are involved in the formation of trans−photoproduct).

2.4.2 Photorearrangement reactions

These are classified into four categories:

(i) Geometrical isomerization,
(ii) Photoracemization,
(iii) Linkage isomerization, and
(iv) Ligand rearrangement (or Ligand exchange reaction).

- **Geometrical isomerization**

hv The cis−trans isomerization occurs through the ligand field transition (Scandola et al., 1967)

$$\text{Cis}-\text{bis(glycinato)} \quad \text{Pt(II)} \xrightarrow{\text{hv}} \text{trans}-\text{isomer}$$

But,

$$\text{trans} \xrightarrow{\times} \text{cis}$$

This kind of photochemical process involved intramolecular twist mode without bond cleavage. The triplet state formed with pseudo−tetrahedral geometry is the intermediate in this reaction. This process is photochemically allowed but thermally forbidden on the basis of symmetry rules (Richardson et al., 1971).

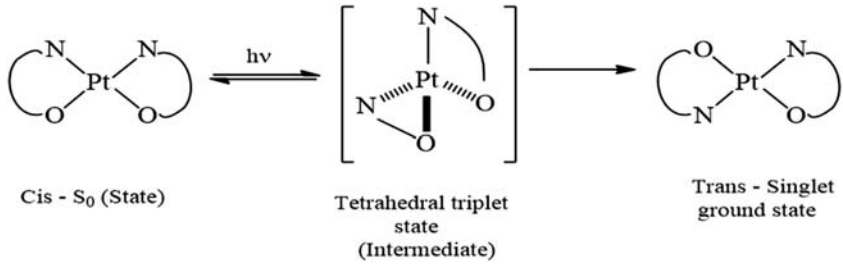

- **Photoracemization**

Ligand field transition may also result into the racemization in case of trisoxalatochromium (III) (Richardson et al., 1971).

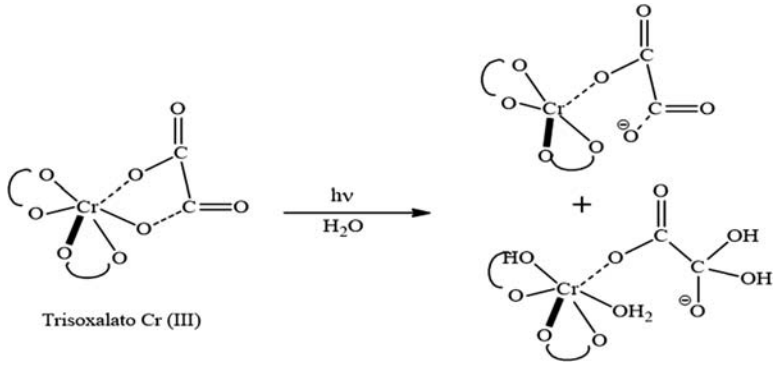

The racemic mixture can be separated and this photoreactivity has scope in synthesizing those stereoselective and enantioselective (chiral) coordination compounds, which could not be synthesized by other thermal reactions. This reaction also exhibit deuterium isotope effect.

- **Linkage photoisomerization**

Linkage isomerism in coordination compounds is very fascinating aspect of synthetic coordination chemistry. In this isomerism, only the mode of the attachment of an ambidentate ligand to the metal ion is changed. Various ambidenttate ligands like NO_2^-, SCN^-, $S_2O_{3^{2-}}$, CN^-, $SeCN^-$, SO_3^{2-}, etc. have shown this type of isomerism.

$$[Co(NH_3)_5(NO_2)]^{2+} \xrightarrow{hv(solid)} [(NH_3)_5 - Co(ONO)]^{2+}$$

The nitro−nitrito photoisomerization takes place in solution using an intra molecular mode, which involves the homolytic cleavage of $Co-NO_2$ bond and then two fragments are joined back with altered attachment (as Co−ONO). This complex shows CT and LMCT characters at 239 and 325 nm and a ligand field transition at 458 nm.

$$[Co(NH_3)_5.(NO_2)]^{2+} \xrightarrow[\text{in 0.1 N } HCLO_4]{\text{CT and LF}} [Co(NH_3)_5.NO_2]^{2+}$$

Isomerisation Reaction → $[Co(NH_3)_5(ONO)]^{2+}$

Redox Reaction → $Co^{2+} + 5\,NH_3 + NO_2$

The nitrosyl linkage isomers (metatable states) in solid state are useful for optical data storage. This kind of isomerism finds application in

photoswitching. Photoisomerization of ruthenium bis sulfoxide molecular photoswitch $[Ru(bpy)_2(bpSO)]^{2+}$ takes place in gas phase. When irradiated in gaseous phase, there is direct switching of the S,S−isomer to O,O−isomer by absorption of single photon, but in solution phase, stepwise isomerization occurs with each sulfoxide ligand switching turn by turn. This change in the dynamics of isomerization may be due to fast vibrational quenching, which suppresses isomerization in solution. The spectra of this photoisomerization reveals two bands: One corresponding to ligand centered (S,O−isomer) (π, π^*) transition and other is MLCT band (S,S−isomer).

- **Ligand rearrangements**

The photochemical exchange of ligand is also a very attractive synthetic methodology for preparing new coordination compounds. In case of cobalt complexes, this is represented as

$$[Co(CN)_5(NO)]^3 + {}^*CN^- \xrightarrow{hv} [Co(CN^*)_5(NO)]^{3-} + CN^-$$

These reactions are very significant in biologically processes, where the release of biological active species is concerned. The process of chemotherapy using photoactivation involves the light−induced cleavage of chemical bond that releases biological active fragment. Therefore, complexes having such tendency are called photoactivated chemotherapeutic complexes. Ru(II) complexes have been investigated in much detail and still lie at the forefront of researches in photochemistry. The excited states, which involve various types of reactions exhibited by Ru(II) complex, are MLCT and MC types. These are main responsible excited states for their photophysical and photochemical properties. The photorelease of monodentate and bidentate ligands in these complexes give new hypothesis for mechanism of the ligand exchange reactions. The release of bidentate ligand involves new ^{3}MC states of flattened geometry. Therefore, the interaction of MLCT and MC excited states play a key role for both; the photophysics (i.e., photoluminescence, electron or energy transfer) and photochemical (photoisomerization, photorelease, etc) properties. Here, in case of Ru(II) complex, the release of monodentate ligand takes place through the excited triplet state (^{3}MLCT) and the release of bidentate ligand takes place by involvement of the triplet excited state called ^{3}MC state (having flattened geometry). The ^{3}MC states are mainly involved in the formation of trans−product. Such distorted ^{3}MC state formation is a common feature for Ru(II) complex such as $[Ru(bpy)_3]^{2+}$ and also for other complexes, where such ^{3}MC flattened states were identified. One important aspect of these ^{3}MC state is their accessibility form ^{3}MLCT state along with the minimum energy paths, which connect these two (^{3}MC and ^{3}MLCT) and relative reach toward minimum energy crossing points to singlet ground state surface of both; the reactant and photoproduct. The population of intermediate

states along the photoinduced release of bidentate ligand to give final photoproduct.

In further steps, there will be preferential relaxation modes by excited states as not all, but certain specific ^{3}MC state resulted into release of ligand. The knowledge and understanding of the interplay between ^{3}MLCT and ^{3}MC state will provide a predictive tool for synthetic coordination chemists to control and fine tune the photochemical behavior with the purpose to influence selective ^{3}MC population to obtain efficient photo-release of ligand.

2.4.3 Photoredox reactions

Photoredox reactions take place via two modes and these are intermolecular and intramolecular reactions. In solution, the photoredox process may be intermolecular, when the complex reacts with another species present in the solution but when the reaction takes place between the central atom and one of its ligand, then it is called intramolecular redox reaction.

When a complex is irradiated, the central metal ion become strongly oxidizing in nature due to ligand field transition (d−d transition). It will result in intramolecular reduction of the central metal ion.

$$2[\mathrm{Fe(III)(C_2O_4)_3}]^{3-} \xrightarrow{\mathrm{hv}} 2[\mathrm{Fe(C_2O_4)_2}]^{2-} + 2\ \mathrm{CO_2}$$
$$[\mathrm{Co(III)(NH_3)_5I}]^{2+} \xrightarrow{\mathrm{hv}} \mathrm{Co(II)} + 5\ \mathrm{NH_3} + \mathrm{I}$$

The ferrioxalate is a good actinometer, which works in the UV and visible region up to 400 nm. The actinometer functions through redox photoreaction. In some low-valence hydrated cations such transition may result into photooxidation

$$\mathrm{Fe(II).H_2O} \xrightarrow{\mathrm{hv}} \mathrm{Fe(III)} + {}^{-}\mathrm{OH} + \mathrm{H}$$

Also, the

$$[\mathrm{Fe(thionine)}]^{2+} \underset{\text{dark}}{\xrightarrow{\mathrm{hv}}} \mathrm{Fe}^{3+} + \mathrm{Semithionine}$$

This reaction reverts back in dark. These reversible photoredox reactions are useful in the conversion of light energy into the electricity (solar cells). The irradiation of the complexes at LMCT band will be conducive for photoreduction

$$[\mathrm{ML_n}]^{Z+} \xrightarrow{\mathrm{hv}} \mathrm{M}^{(Z-1)} + (\mathrm{n}-1)\mathrm{L} + \mathrm{Oxidation\ \ product\ \ of\ \ L}$$

Here, the M−L bond will be homolytically cleaved due to excitation. Such photoreactivity is not found in the ligand field bands (d-d transition) and if redox reaction takes place under such excitation, it is likely to hide a low lying reactive CT band under its envelope. It is not essential in such reactions that ligand should decompose, but if the central metal ion forms a stable complex

with one lower (or higher) oxidation state, then the stable product (complex) formation is due to intramolecular redox reaction.

$$[IrCl_6]^{2-} \xrightarrow[H_2O]{h\nu} [IrCl_5(H_2O)]^{2-} + Cl^-$$

In case of intermolecular photoredox reaction, the light induced electron transfer takes place between a complex and any other species available in the solution. In this case, an oxidized or reduced form of the complex is produced.

$$[ML_n]^{z+} + X \xrightarrow{h\nu} ML_n{}^{(z+1)} + X^-$$
$$[ML_n]^{z+} + Y \xrightarrow{h\nu} ML_n{}^{(z-1)} + Y^+$$

If the new complex formed is unstable, then decomposition reaction was observed

$$[Co(NH_3)_6]^{3+} + I^- \xrightarrow{h\nu} [Co(NH_3)_6]^{2+} + I$$
$$[Mo(CN)_8]^{3-} + H_2O \xrightarrow{h\nu} [Mo(CN)_8]^{4+} + H^+ + OH$$

Here, no decomposition takes place in the reaction of molybdenum complex. The excitation is there in ligand field band region. When the newly formed complex is stable, an electron may be ejected and hydrated electron is obtained (e^-_{aq}) as

$$[Fe(CN)_6]^4 + H_2O \xrightarrow{h\nu} [Fe(CN)_6]^{3.} + e^- aq$$

This corresponds to the type charge transfer—to—solvent (CTTS) transition. Photoejection of electron can also take place, if LMCT band increase the charge density toward the periphery of the complex.

2.5 Applications

2.5.1 Photochromism

The phenomenon of photochromism is shown by systems, in which photochemical reaction is complemented by a reverse thermal reaction and as a result, the change in color was observed, and this color appeared again in dark. The reaction of a photochromism can be represented as:

$$A \overset{h\upsilon_1 k_1}{\rightleftarrows} B$$

A photostationary state may exists here, where the photochemical (and thermal) reaction is balanced by reverse thermal reaction.

Various coordination systems were found to show photochromism. When 0.01 M $[Cr(CN)_6]^{3-}$ with 0.1 M cyanide ion was irradiated, a photostationery state involving mainly $[Cr(OH)_3(H_2O)_3]$ was formed and in the reverse reaction, mainly $[Cr(CN)_4(H_2O)_2]^-$ is formed in dark.

Similarly, $[Co(CN)_5I]^{3-}$ in concentrated iodide solution will show photochromism and gives $[Co(CN)_5(H_2O)]^{2-}$,which reverts back in dark. Such sequence also occurs in $[Cr(H_2O)_5(NCS)]^{2+}$. There may be cases, when k_{-1} (backward reaction rate constant) is very large than k_1 (forward reaction rate constant), then photostationary state will lie at far left of the equilibrium and therefore, photolysis will not be there. Such labile complexes may also be said as non-photosensitive material (of course incorrectly). The chelate formed by the ligand dithiazine, HD_z^-, is likely to exhibit photochromism. This was found true in the complexes, $Hg(HDz)_2$ and $Pd(HDz)_2$. The mercury complex is square planar and its structure is (Adamson, 1969).

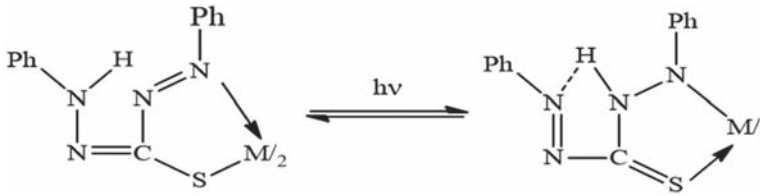

Yellow orange in colour Blue in colour

(Where, $M = Hg^{2+}$, Pd^{2+}, etc.)

The photosensitivity of the system involves the absorption band due to absorption center in chelate ring. These chelate complexes are generally very much colored but do not seem to be photosensitive (as in the case of β-diketonate complexes). There are examples of complexes showing photochromism for which ΔG were determined from the entropy terms. The search is still on for systems having higher ΔH, as in the case of redox cycles of the type, such as

$$A \xrightarrow{h\nu} A^+ + e^-$$

Oxidized from $\xrightarrow{h\nu}$ Reduced form

This type of photochemical cell can form, if reaction of A^+ with reductant is slow. Such systems are normally not found, but system in which A is $[Fe(CN)_6]^{4-}$ and oxidized form is a redox dye (methylene blue) have shown such type of a photoredox cycling.

2.5.2 Chemical actinometers

A chemical actinometer or dosimeter is a chemical system (fluid, gas, solid or in microheterogeneous environment) that undergoes a light-induced reaction (at a certain wavelength, λ) for which the quantum yield (Φ) is accurately known. An actinometer is a chemical system (substance) or physical device

(thermistors, thermopiles, bolometer and photovoltaic cell) by which one can measure the intensity of light (UV and visible range). In photochemistry, the quantum yield (Φ) of the photochemical reaction is determined using the value of light intensity absorbed by the photoactive substance in the reaction. The Φ in expressed as

$$\Phi = \frac{\text{Number of molecules decomposed or formed per second per unit volume}}{\text{Number of quanta absorbed per second per unit volume}} \tag{2.7}$$

$$\Phi = \frac{\text{Rate of reaction}}{\text{Intensity of light absorbed}} \tag{2.8}$$

$$\Phi = \frac{-\frac{dc}{dt} \text{ or } +\frac{dx}{dt}}{I_0 \times \text{Fraction of light absorbed}} \tag{2.9}$$

Therefore, a simple method for standardization of a light source can be selection of a suitable photochemical reaction, where quantum yield is already known. In this method, the light absorption must remain constant during exposure. In the above expression, I_0 is the intensity of induced light and the fraction of light absorbed can be determined in a separate experiment. When quantum yield, Φ is known and extent of decomposition is also known, the intensity of incident radiation can be calculated in the unit of Einstein per unit volume per unit second. There are various photochemical reactions, which are being used as chemical actinometoes. They are only useful in a particular range of wavelengths. The following chemical actinometers for different ranges are suitable:

- **Ferrioxalate actinometer**

A solution of a potassium ferrioxalate $K_3[Fe(C_2O_4)_3]$ in 0.1 M H_2SO_4 is irradiated with oxygen free solution in 250−500 nm range of wavelength, which resulted into the formation of free Fe^{2+} ions. There ferrous ions can be analyzed spectroscopically by adding 1,10−phenanthroline to the final solution. The oxalate complex of the reduced Fe^{2+} ions does not absorb the incident radiation, but the precursor oxalate complex of Fe (III) ions has good absorption in this range. Such actinometer has an added advantage that quantum yield is almost independent of the environment effects, such as concentration of reactant and product, intensity of the incident light, and temperature of the solution.

- **Uranyl oxalate actinometer**

This actinometer is useful in the range 208−435 nm with average quantum yield of 0.5. Here, uranyl ion (UO_2^{2+}) acts as a photosensitizer for the decomposition of oxalate and therefore, the light absorption remained

constant. A prolonged exposure is needed for final oxalate titration with permanganate. This actinometer is relatively less reactive in comparison to ferrioxalate actinometer. It is also insensitive to incident light and temperature, but the photochemical reaction does not have a simple stoichiometry. The products formed are the U^{4+} ion, CO and CO_2. Now, it is not commonly in use practically.

$$H_2C_2O_4 \xrightarrow{h\nu} H_2O + CO_2 + CO$$

- **Malachite green leucocyanide (MGL) actinometer**

This is a useful actinometer in the range 220−300 nm, where it absorbs strongly. When malachite green was irradiated in slightly acidified ethanol, it is converted to ionized form (MG^+), which absorbs strongly at 662 nm. The quantum yield for its production is 0.91 for the given range.

- **Reinecke's salt actinometer**

This is a good chemical actinometer, which worked well in the range 316−735 nm, and therefore, it is useful in visible range. Reinecke's salt is ammonium salt $(NH_4)_3[Cr(NH_3)_2(NCS)]$. First, it is converted to its potassium salt and then it is used. Its ligand field band extend from 400 to 735 nm. When its aqueous solution is irradiated, the aquation of the complex takes place and thiocyanate ions are released. Quantum yield can be determined in terms of moles of a thiocyanate ion released per Einstein of light absorbed. The concentration of the actinometer should be kept such that 99% of incident light is absorbed. The pH is adjusted between 5.3 and 5.5. The quantum yield for this reaction is 0.27−0.34 for visible region.

Other complexes like hexakis(urea) chromium(III) chloride $[Cr(urea)_6]Cl_3$ and Co(III) of ammine complexes are also in use for actinometry experiments.

2.5.3 Release of CO/NO

One interesting use of photochemistry of complex can be observed in the Cr(III) complex of nitric oxide (NO). Nitric oxide plays very significant role in cardiovascular regulatory processes. The researchers are interested to develop method for controlled release of these molecules (small molecular bio-regulators like NO and CO) at targeted sites. Therefore, successful photo-uncaging and the mechanism of transport of these molecules to the targeted site requires the knowledge of fundamental photochemistry and photophysics of such molecules (NO, CO, etc). This aspect is illustrated by synthesizing metal complexes, which act as photoactivated CO or NO releasing moieties. Such complexes have a proper stability, non−toxic precursor, ability to activate NO or CO release using longer wavelengths excitation (particularly near

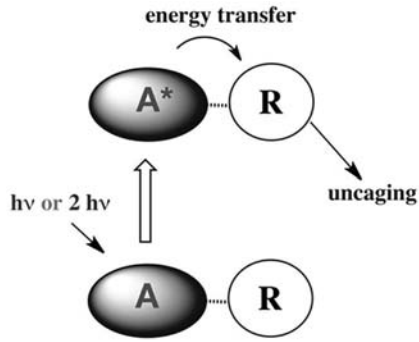

FIG. 2.6 Release of NO/CO. *Adapted from Ford, P.C., 2016. From curiosity to applications. A personal perspective on inorganic photochemistry. Chem. Sci. 7 (5), 2964–2986. With permission.*

infrared) and the tracking mechanism to locate these species in organisms. Photoluminescence (PL) is good imaging tool for tracking NO or CO (Fig. 2.6).

Here, A is the antenna molecule and R is the precursor of small molecule bioregulators (CO/NO) that is uncaged, if R is photosensitized. All the desired qualities were found in Cr(III)–O–nitro complex i.e., trans–[Cr(cydam)NO_2]$^+$ (this complex is abbreviated as CrONO and cylam is 1,4,8,11–tetraazacyclotetradecane). This is stable and non-toxic in nature also. The photoproduct in this case is NO. In the photochemistry of CrONO, the complex undergoes photodissociation of CrO–NO to give NO and Cr(IV)(O) species. This occurs from the lowest energy ^{2}MC state of the Cr(III) center. The main problem associated with CrONO to be used as photoreleaser of NO is that its longer wavelength absorption are LF bands with very low absorptivity (ε) and this complex contains center of symmetry. Therefore, the transition for the LF absorption is Laporte–forbidden. So, the rate of NO generation will be relatively slow, if the concentration of CrONO and light intensity are not high. This point was handled by attaching many organic chromophores to the CrONO type platform to serve as antenna to increase the absorption of light, and accordingly, the production of NO. Here, the anthracene molecule acts as (pentdant) antenna, which collects light and transfer the energy to CrONO and photosensitize the process of NO release from it.

Such new constructions exhibited antenna effect, but the absorption is not extended to visible light required for biological systems. Therefore, quantum dots (QDs) were used as photosensitizers as the absorption and emission of quantum dots can be tuned by varying the size of the nanoparticles (diameter). This idea worked well and using water soluble CdSe/ZnS core shell QDs and adding CrONO salts to such nanoparticles (3–8 mm core diameter) resulted into quenching of the quantum dot photoluminescence (QDPL) centered at 370 nm with increasing CrONO concentration.

In such situation, more NO were photogenerated than from solution containing only CrONO. Therefore, PL quenching and photosensitized product of NO are due to transfer of energy from the excited QDs to CrONO. But, the structure CrONO/QDs assemblies are not likely to be stable in physiological fluid, so there is a need of another protocol to be established, where CrONO and other such biomaterials are to be attached to the surface of QDs through a covalent bond. Therefore, more investigations in this area will be able to identify the excited state mainly responsible for particular photochemical reaction. The quantum yield, chemically and spectroscopic properties of product will help in identifying the excited state involved and these information are used to tune the excited state to direct the resulting photoreaction in a desired direction.

2.5.4 Photoredox catalysis

At this juncture, it is to be highlighted that greener organic synthetic routes have been established using a new concept known as "photoredox catalysis", which found a wide range of applications in the field of carbon dioxide reduction, splitting of water, design of new materials for solar cells and organic synthesis. This platform of photoredox catalysis uses mainly metal polypyridyl complexes and organic dyes to facilitate the conversion of light energy into chemical energy under very mild conditions. When light is allowed to fall on these molecules, excited molecules will be involved in single electron transfer (SET) with organic (and organometallic) substrates giving free access to open-shell reactive species. When visible light is used, where general organics don't absorb, the selective excitation of the photoredox catalyst will take place. The excited species can act as both; a strong oxidant and a strong reductant, simultaneously, which provides a unique environment for organic synthesis. This new type of photoredox catalysis provided avenues for the development of various novel synthetic methodology. At present, the field of photoredox catalysis has attracted large number of synthetic chemists as a strong strategy for activation of molecules.

This approach is based on the ability of the complexes and dye molecules to convert light energy into chemical energy by engaging SET with organic reactant, by which reactive intermediates are produced. This kind of approach gives a new type of reaction mechanism, where importance is given to multicatalytic strategies making it possible to obtain the formation of C−C, C−N, or C−S bonds. The important strategies to obtain the desired product stems form the ability of the photoredox catalyst to effectively convert light into chemical energy. Also, if ligand backbone on metal polypyridyl photoredox catalyst can be modified, then the redox properties of the complex can be fine tuned to access any desired product.

The mechanism of such photoredox catalysis can be understood by the formation of triplet excited state of the complex by energy transfer. Inspite of

rapid progress in this field, it is still in its infancy. The recent developments of dual photoredox catalytic platforms have produced novel activation mode, which direct the synthetic routes toward very highly regio- and enantio−selective products. These catalytic platforms are very useful in pharmaceutical industries in combination with flow technology to scale up the synthesis. In case of Pschorr reaction, it was found that the reaction could be catalyzed by $[Ru(bpy)_3]Cl_2$ producing phenanthrene in quantitative yields. This reaction was found to give higher quantum efficiency, when the photoredox catalyst was used as compared to direct photolysis of reacting mixture. The mechanism of photoredox catalysis can be represented as Fig. 2.7.

The catalyst used in these photoredox catalysis functions like a photoredox sensitizer or photoelectron transfer catalyst. Ruthenium complex acts like this. An electron in one of the photocatalyst metal centered t_{2g} orbitals is excited to a ligand centered π^* orbital in photoredox catalyst $[Ru(bpy)_3]^{2+}$ upon irradiation with light. This is the MLCT type transition and it will produce a species, where metal is effectively oxidized to Ru(III) and a single electron reduction takes place for ligand moiety. The initially occupied singlet MLCT state adopts rapid ISC to give lowest energy triplet MLCT state. This long lived triplet state is responsible for single electron transfer. The longer lifetime is due to spin−forbidden transition to singlet ground state. These are represented in Fig. 2.8.

2.5.5 Photochemiluminescence in ruthenium complexes

In some complexes of ruthenium (III), [Ru(III)−2,2′−bipyridyl−5−methyl−1,10−phenetherene] and in some other complexes also, the

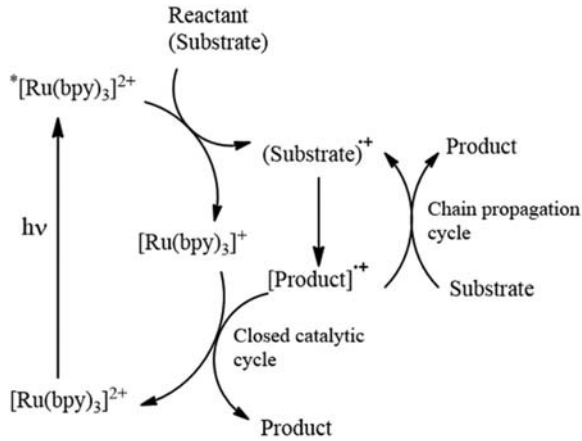

FIG. 2.7 Mechanism of photoredox catalysis using $[Ru(bpy)_3]^{2+}$. *Adapted from Prier, C.K., Rankic, D.A., MacMillan, D. W., 2013. Visible light photoredox catalysis with transition metal complexes: applications in organic synthesis. Chem. Rev. 113 (7), 5322−5363. With permission.*

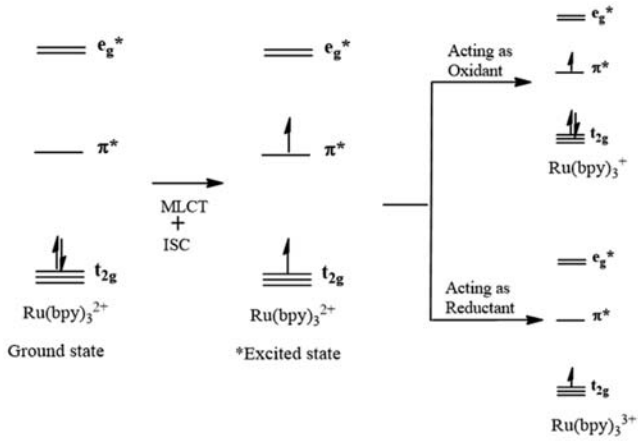

FIG. 2.8 $[Ru(bpy)_3]^{2+}$ as an oxidant and a reductant. *Adapted from Prier, C.K., Rankic, D.A., MacMillan, D. W., 2013. Visible light photoredox catalysis with transition metal complexes: applications in organic synthesis. Chem. Rev. 113 (7), 5322−5363. With permission.*

electrically excited states are obtained, when these complexes are allowed to reach with OH ions. Due to exothermic nature of this reaction, sufficient thermal energy is released, which excites the Ru(III) complex. When the excited state releaxes through radiative emission of the electronic energy, the phenomena of chemiluminescence is obtained. The general reaction for this chemiluminescence can be represented as

$$[ML_x]^{(n+1)+} + e^- (\text{from reductant}) \xrightarrow{h\nu} [ML_x]^{n+} + h\upsilon$$

Photochemiluminescence method is useful in the determination of antioxidant activities of carotenoids and antioxidant capacities of various fruit products, nutraceuticals and other dieting supplements.

A photosensitizer (S) on excitation by light gives two types of radicals: One is a photosensitizer cation (S^{*+}) and second is the superoxide anion radical ($O_2^{\bullet -}$). The free radicals are identified using chemiluminescence reagent (which functions as photosensitizer) and using oxygen radical detector. As the concentration of antioxidant increases, the intensity of chemiluminescence decreases.

2.5.6 Coordination compounds as triplet quenchers

Metallocenes function as very good quenchers of triplet excited state having energies between 177 and 280 kJ mol^{-1}. The rates of quenching process is nearly equal to the rate of diffusion controlled process. Metallocenes are also good sensitizers for cis−trans isomerization. Good examples of triplet state quenchers are ferrocene, $Fe^{III}(acac)_3$ and tris(dipivaloylnethanate) iron(III),

$Fe^{III}(dpm)_3$,etc. These coordination compounds quench the triplet states through the mechanism of electronic energy transfer. There exists high degree of correlation between the energy levels of these quenchers and plots of energy of triplet state v/s quenching rate constant. In all these complexes, ligand field excitation states are involved in quenching of triplet state and not the MLCT, LMCT or IL states. Therefore, understanding of triplet energy transfer to produce ligand field excitation in coordination compounds and the nature of triplet energy state of organic compounds will give an insight to these quenching mechanisms.

2.5.7 Coordination compounds as sensors

It has been reported that coordination compounds can be used as sensors for detection of highly toxic ion, CN^-, which is very necessary to maintain a greener environment and protect human health. The CN^- ion acts as ligand in coordination chemistry and its extreme toxicity causes concern also. So the facile and sensitive detection of such hazardous material CN^- ion is necessary. It can coordinate with some proper metals and form complexes and this coordination property of CN^- is harnessed in its detection. It also attacks the central metal ion and fluorescence may be produced. Therefore, coordination compounds can function as sensor for the detection of CN^- ions. It has attracted the attention due to the facile synthesis, clear & multianalyte detection and low detection limit.

The CN^- ions are detected by Cu(II) complexes; however, other metal complexes can also function as sensors. So, design and synthesis of coordination compounds, which can show luminescence on coordination and therefore, these can detect other species acting as sensor. The photophysical properties of the transition metal complexes has also attracted the attention for their possible use as sensors. The lifetime methods are more advantageous for detection than intensity measurement methods, because lifetime is independent of source variation, photobleaching of the material to be detected and change in efficiency of the optical system. The use of luminescent transition metal complexes as sensors has been reported with the structural effects on pH response.

Ru(II) complexes showed luminescence from MLCT transition. In the study of such complexes, environmental and structural features affect the luminescence of the sensor. The most general environmental factor is the presence of oxygen, which can quench the excited state, and reduce the intensity and lifetime; both.

2.5.8 Photocatalysis

There is an urgent need to respond the environmental and energy crisis for the development of green and renewable energy. Photocatalysis is the emerging

technology to address both these important issues. Photocatalysis is the process, in which catalyst (semiconductor) absorbs photon and as a result, electrons in valence band are excited to the conduction band and holes are created in the valence band of the photocatalysts. This is called formation of generation of excitons ($e-h^+$ pair), and therefore, reduction and oxidation reactions are initiated. One of the major goals of the photocatalysis is to harness solar energy to drive the reaction with high efficiency and large scale production. The field of photocatalysis has attracted the attention of scientists all over the globe due to its immense potential and wide range of applications starting from the development of first artificial photosynthetic system, water splitting, energy conversion, CO_2 reduction, organic synthesis, wastewater treatment, optoelectronic devices and nanomaterial science. Photocatalysis is categorized in two types; heterogeneous and homogeneous photocatalysis.

Heterogeneous photocatalysis is widely used due to easy separation of catalyst from the reaction mixture, applicability in chemical industries and stable photoactivity of the catalyst making them recyclable. However, homogeneous photocatalysis has also attracted great deal of attention due to their higher activity; selectivity and tunable light absorption. Therefore, if the advantages of both; homogeneous and heterogeneous photocatalysis can be combined, then more output is expected and for that the coordination chemistry can act as the bridge between them. The coordination compounds have been used in photocatalytic processes to engineer catalytically active sites tuning the band gap of photocatalysts (to bring it in visible region to harness solar energy), charge transfer kinetics and checking the phenomena of recombination of charge carriers, etc.

The photocatalysis can be graphically represented as (Fig. 2.9).

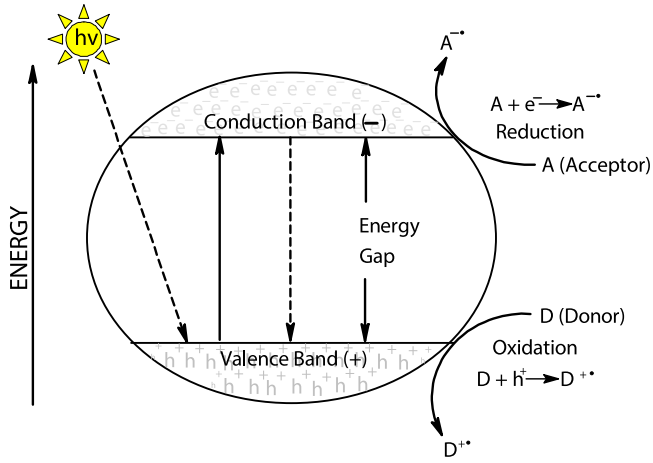

FIG. 2.9 Mechanism of photocatalysis.

Using photochemistry of coordination compounds, homogeneous photocatalyst has seen a vast increase in its horizon and the benefits of homogeneous photocatalysis are utilized in upgrading the heterogeneous catalysis. The demerits of heterogeneous photocatalysis is mainly less absorption of light due to wide band gaps, insufficient charge separation & transport, and lack of effective catalytic sites on the surface of semiconductor, but in homogeneous photocatalysis, ideal light harvesting centers and catalytic active sites are present. The Ru complex−g−C_3N_4 hybrid photocatalysts have been used for photocatalytic reduction of CO_2. The Ru(II) and Re(I) complexes have been widely investigated as photocatalyst for CO_2 reduction.

The use of metal complexes as photocatalysts for polymerization in presence of visible light has also been reported. When the complexes are excited by visible light, MLCT transition is there and therefore, these complexes easily adopt both; oxidation and reduction quenching modes, which can be utilized for synthetic organic reactions. The photophysical properties of these complexes can be tuned for the desired purpose by modifying the ligand scaffolds. Among the transition metals, first row transition metals particularly, copper complexes have attracted special attention for their use as photocatalysts; however, the copper−based photocatalysts are generally less efficient due to limited luminescence lifetime than Ru and Ir complexes, but copper complexes have been successfully used for organic transformations.

The photocatalysts using metal complexes consist of much diverse reactions induced by light as compared to organics. In organic photochemistry, there are only three states: S_0, S_1 and T_1 in general, but the photochemistry of transition metal complexes in quite different from the organic compounds in term of formation of more number of excited states with different multiplicities. So depending on the wavelength of irradiation, different kinds of electrically excited states are observed. This will cause population of excited states of varied reactivity. This situation provides good opportunity to tune the photochemical reactivity for switching over other various reaction pathways such as electron transfer due to population of diverse CT state substitution, disassociation, rearrangement reactions (due to excited LF states) and ligand centered conversion (due to population of IL$*$ states), etc. The electronic excitation by light can be used to generate coordinatively unsaturated species, complexes with altered oxidation number, free ligands and ligand redox products. Almost all such species are very reactive and found place to be utilized for photocatalytic reactions. Therefore, photocatalysis using transition metal complexes has gained applicable status in the research fields.

2.5.9 Nano-scale devices and machines

The field of photochemistry of coordination compounds had a very long journey in its progress and development of conceptual framework and its use in a wide range of applications. Starting from photography and light sensitivity

of metal complexes, it has now reached to construction of nano-scale devices and machines. This progress is spectacular due to expanded horizons of photoreactivity of coordination compounds. In earlier work, photosubstitution and photoredox reactions using simple inorganic ligands, quantum yields and life time studies, use of these complexes in biomolecular processes, energy and electron transfer were the main focus of investigations but with the advent of supramolecular chemistry, the photochemistry of coordination compounds has led to the design and construction of new systems, which can perform various light induced functions. In this area, luminescent and/or photoredox reactive metal complexes are in use as necessary components to construct the molecular devices and machines using bottom-up approach. In the light−powdered nanoscale devices, molecular wires based on coordination compounds containing polypiridine metal complexes as donor and acceptor units have been investigated. The excited state of $[Ru(bpy)_3]^{2+}$ acts as energy donor or redox reagent in many systems. In molecular wires, the photoinduced electron and energy transfer over long distances have been investigated. Similarly, molecular switches, in which energy transfer is very efficient due to favorable position of MLCT excited state of the complex and other bridging moiety. Molecular antennas for harnessing light energy using coordination compounds are also a fascinating area. Antenna systems are being used by nature also in photosynthetic process, where the light energy is converted to chemical energy. The collection of light energy by antenna may be used for increasing in signal intensity for luminescence and sensors. Supramolecules play a key role in the antenna effect.

Light powered nanoscale machines have also been investigated using coordination compounds metal complexes like dethreading or rethreading of pseudorotaxanes, shuttling processes in rotaxanes, ring switching process in catenanes, etc. and these are of much significance for their applications in opto−electronics and data information technology.

The research filed of photochemistry of coordination compounds is mainly based on intramolecular photochemical reactions to identify the photostable luminescent compounds and their utility in energy/electron transfer. Incorporating these coordination compounds in supramolecular systems and use of coordination compounds is an essential part of the bottom up approach to construct light powered nanoscale devices and machines. The $[Ru(bpy)_3]^{2+}$ complex has been very largely investigated in this regard. Looking to the spectacular progress of this field, the community of coordination chemists can hope to design and construct new families of coordination compounds for the furtherance of nanoscience and nanotechnology in near future.

References

Adamson, A.W., 1969. Photochemistry of transition metal coordination compounds. Pure Appl. Chem. 20 (1), 25−52.

Balzani, V., Campagna, S. (Eds.), 2010. Photochemistry and Photophysics of Coordination Compounds I: 280, Topics in Current Chemistry. Springer, Berlin.

Balzani, V., Bergamini, G., Ceroni, P., 2008. From the photochemistry of coordination compounds to light-powered nanoscale devices and machines. Coord. Chem. Rev. 252 (23−24), 2456−2469.

Balzani, V., Moggi, L., 1990. Photochemistry of coordination compounds: a glance at past, present, and future. Coord. Chem. Rev. 97, 313−326.

Balzani, V., Carassiti, V., 1970. Photochemistry of Coordination Compounds. Academic Press, London.

Chen, J., Browne, W.R., 2018. Photochemistry of iron complexes. Coord. Chem. Rev. 374, 15−35.

Ford, P.C., 2016. From curiosity to applications. A personal perspective on inorganic photochemistry. Chem. Sci. 7 (5), 2964−2986.

Glaser, F., Wenger, O.S., 2020. Recent progress in the development of transition-metal based photoredox catalysts. Coord. Chem. Rev. 405. https://doi.org/10.1016/j.ccr.2019.213129.

Horváth, O., Stevenson, K.L., 1993. Charge Transfer Photochemistry of Coordination Compounds. Wiley-VCH, New York.

John, D.H.O., Field, G.T.J., 1963. A Text Book of Photographic Chemistry. Chapman and Hall Ltd., London, p. 29.

Kirgan, R.A., Sullivan, B.P., Rillema, D.P., 2007. Photochemistry and photophysics of coordination compounds: rhenium, 281. Top. Curr. Chem. 45−100.

Orgel, L.E., 1954. Charge-transfer spectra and some related phenomena. Q. Rev. Chem. Soc. 8 (4), 422−450.

Prier, C.K., Rankic, D.A., MacMillan, D.W., 2013. Visible light photoredox catalysis with transition metal complexes: applications in organic synthesis. Chem. Rev. 113 (7), 5322−5363.

Richardson, F.S., Shillady, D.D., Waldrop, A., 1971. A theoretical study of cis-trans photoisomerization in the bis (glycinato) platinum (II) complex. Inorg. Chim. Acta. 5, 279−289.

Roundhill, D.M., 2013. Photochemistry and Photophysics of Metal Complexes. Springer Science & Business Media, Berlin.

Scandola, F., Traverso, O., Balzani, V., Zucchini, G.L., Carassiti, V., 1967. The role of the excited-state geometry in the photochemical isomerization of bis (glycinato) platinum (II). Inorg. Chim. Acta. 1, 76−80.

Wegeberg, C., Wenger, O.S., 2021. Luminescent first-row transition metal complexes. JACS Au 1 (11), 1860−1876.

This page intentionally left blank

Chapter 3

Coordination compounds of titanium, zirconium and hafnium

Neetu Shorgar[1], **Priyanka Jhalora**[1], **Khushbu Sharma**[2] **and Shubang Vyas**[1]

[1]*Department of Chemistry, PAHER University, Udaipur, Rajasthan, India;* [2]*Department of Chemistry, B. N. University, Udaipur, Rajasthan, India*

3.1 Introduction

Group 4 elements titanium (Ti), zirconium (Zr), and hafnium (Hf) have outermost electronic configuration as $(n-1)d^2\ ns^2$ and these exist mostly in +4 oxidation state. They form coordination compounds in this state. Some of these complexes exhibited luminescent behavior mostly due to metal-to-ligand charge transfer. There is a great potential in such complexes for their use as photosensitizer, sensor, solar cells, imaging microscopy, light emitting diodes, and photocatalytic generation of hydrogen from water and also in degradation of wastewater containing different organic contaminants. There is also scope for use of these complexes in photodynamic therapy, particularly hafnium complexes.

3.2 Coordination compounds of titanium

Titanium is a chemical element with the symbol Ti and atomic number 22. It belongs to group 4 and its electronic configuration is [Ar] 3 d^2 $4s^2$. It is found in nature as an oxide, which can be reduced to produce a lustrous transition metal with a silver color, high strength, and low density. This element is also resistant to corrosion in sea water, aqua regia, and chlorine. Titanium is the ninth-most abundant element in Earth's crust about 0.63% by mass and the seventh-most abundant metal. The common minerals of titanium are anatase, rutile, brookite, perovskite, ilmenite, and titanite (sphene). Titanium was discovered in 1791 by an amateur geologist Reverend William Gregor. He found a black magnetic sand, which was a mixture of titanium and iron. Titanium has high strength-to-weight ratio. It is a strong metal (metallic-white in color) with low density, very ductile and lustrous.

Photochemistry and Photophysics of Coordination Compounds. https://doi.org/10.1016/B978-0-12-824493-7.00006-X
Copyright © 2023 Elsevier Inc. All rights reserved.

Its +4 oxidation state is quite common but compounds in the +3 oxidation state are also sufficient in number. Generally, titanium has an octahedral geometry in its complexes, with tetrahedral ($TiCl_4$) is an exception.

The photochemistry of $TpTiCl_3$ and Tp^*TiCl_3 (where Tp = hydrotris(pyrazol-1-yl)borate) and Tp* = hydrotris(3,5-dimethylpyrazol-1-yl)borate) was studied by Gazzi et al. (2005) in tetrahydrofuran. It was observed that reactive decay of excited states produced either $HBpz_3^{\bullet}$ (or $HBpz_3^{\bullet *}$) and metal center Ti(III) radicals through homolytic cleavage of Tp → Ti (Tp* → Ti) bond.

The synthesis, photophysical properties and fluorescence quenching of four octa-substituted oxotitanium phthalocyanines were reported by Tau and Nyokong (2006). These are- 2,3,9,10,16,17,23,24-octaphenylthiophthalocyaninato titanium(IV) oxide, 2,3,9,10,16,17,23,24-octaphenoxyphthalocyaninato titanium(IV) oxide, 2,3,9,10,16,17,23,24-{octakis[(4-benzyloxy)phenoxy]phthalocyaninato}titanium(IV) oxide and 2,3,9,10,16,17,23,24-[octakis(4-t-butylphenoxyphthalocyaninato)]titanium(IV) oxide. It was reported that moderate fluorescence quantum yields (0.14−0.19) and lifetimes were there. It was also revealed that good triplet quantum yields were obtained, while triplet lifetimes (40−100 μs) were quite short.

Atilla et al. (2007) reported synthesis, photophysical and photochemical properties of tetra- and chlorotetrapoly (oxyethylene)-substituted oxotitanium(IV) phthalocyanines. These complexes were found to be monomeric in nature in solution. It was revealed that photophysical and photochemical properties of these phthalocyanine complexes may be very useful for photodynamic therapy applications. These complexes have potential as photosensitizer (in type II mechanism) of singlet oxygen, where quantum yields (Φ_Δ), were in the range 0.72 and 0.78.

The aryloxy and arylthio tetrasubstituted oxotitanium(IV) phthalocyanine complexes were used by Tau and Nyokong (2007) for the oxidation of 1-hexene in dichloromethane as photocatalyst. It was observed that 1,2-epoxy hexane and 1-hexen-3-ol were found to be the major and minor products, respectively. The photooxidation followed two reaction pathways: (i) Singlet oxygen (Type II) and (ii) Radical (Type I) reaction. Oxidation of 1-hexene also depends on singlet oxygen quantum yields and photostabilities of the phthalocyanines.

The photophysical and photosensitizing properties of two octacationic oxotitanium phthalocyanines (TiOPcs) (bearing pyridiniomethyl or cholinyl substituents) were reported by Kuznetsova et al. (2009). Both these compounds were found monomeric in water with high quantum yields of singlet oxygen formation ($\Phi_\Delta = 0.4-0.5$) and fluorescence ($\Phi_F = 0.17-0.19$). It was found that aqueous TiOPc solutions and produced hydroxyl radicals under illumination, which may be due to photocleavage of water molecules. Photobleaching of TiOPcs was also observed on irradiation of TiOPc solutions and its quantum yield in water was found to be about 1×10^{-4}. It was revealed that both; OH and $^1O_2$ may be responsible for the bactericidal effects of TiOPcs.

Erdoğmuş et al. (2010) reported syntheses of peripherally tetra-, non-peripherally tetra and peripherally octa-3,4-(methylendioxy)-phenoxy substituted oxo-titanium(IV) phthalocyanine complexes. It was found that all these oxo-titanium(IV) phthalocyanine complexes were soluble in organic solvents. They also investigated photophysical and photochemical properties of oxo-titanium(IV) phthalocyanine complexes in DMSO as well as toluene. The effects of the position of the substituents on the phthalocyanine skeleton and solvents (DMSO and toluene) were also observed on photophysical and photochemical parameters of the oxo-titanium(IV) phthalocyanine complexes.

Hu and Tao (2011) developed an optical fiber sensor technique for determining trace amount of H_2O_2 in aqueous solutions. They used a titanium(IV) oxyacetylacetonate doped Nafion coating on the surface of a bent optical fiber probe as a transducer. Here, trace amount of H_2O_2 in an aqueous solution diffused into the polymer coating reacted with the sensing agent. The product obtained absorbs light (wavelength 360 nm). It was revealed that this sensor reversibly responses to trace H_2O_2 in water with detection limit (3σ) as 7.4×10^{-8} mol H_2O_2 L^{-1}. It was interesting to note that this fiber-optic sensor does not have interference from electromagnetic field making it useful in proton exchange membrane for fuel cells. Although high-valence Ti(IV)-based metallocalixarene coordination cages (linked by oriented ancillary ligands) are not known and therefore, tunable calixarene-based coordination cages of Ti(IV) with a framework formula $[Ti_{12}(O^iPr)_{12}(TBC[4])_6L_6]$ were assembled from six pyridinedicarboxylic ligands and six $\{Ti_2(O^iPr)_2(TBC[4])\}^{2+}$ nodes. These as-prepared $\{Ti_{12}L_6\}$ cage displayed strong photocatalytic activity for H_2 evolution.

Chauke et al. (2011) reported the synthesis of 2,(3) (peripheral) and 1,(4) (non-peripheral) (2-mercaptopyridine) phthalocyanine complexes of titanium(IV) oxide. They studied photocatalytic oxidation of cyclohexene in the presence of gold nanoparticles (AuNPs). It was observed that singlet oxygen quantum yield values were increased in the presence of AuNPs for these complexes and percentage conversion was 27% and 20%, respectively. Cyclohexene oxide, 2-cyclohexen-1-ol, 2-cyclohexene-1-one and 1, 2-cyclohexanediol were obtained as the products.

Liu et al. (2016a) reported a new cadmium doped titanium−oxo complex with a $\{Cd_2Ti_4\}$ cluster core, which was stabilized by tert-butylacetic acid ligands. It was observed that this new 75 heterometallic cluster is a semiconductor, which has a bandgap of 3.39 eV. It also exhibited good photocatalytic activity and stability for evolution of hydrogen. It was claimed that transition metal doped polyoxotitanium compounds have a potential for the development of efficient water splitting photocatalysts.

He et al. (2018) prepared palladium-directed self-assembly of multi-porphyrin array ultrathin films on substrate surfaces. They used sodium tetrachloropalladate (Na_2PdCl_4) as a connector and oxo[5,10,15,20-tetra(4-pyridyl)porphyrinato] titanium(IV) complex [TiO(TPyP)] as a linker. It was

reported that Soret absorption band of TiOTPyP was red shifted by 6 nm, when the Pd-TiOTPyP multilayer-modified quartz substrate was immersed in an aqueous solution of hydrogen peroxide. This shift may be due to the formation of TiO_2TPyP monoperoxo complex. It was revealed that immobilized Pd-TiOTPyP multilayers act as light-harvesting units for generation of photocurrent and photochromism of viologens, which has strong stability, recyclability, and reproducibility. It was also found that photocurrent density was enhanced in electrolyte solutions, which contain electron donors (triethanolamine), or electron acceptors (viologens). They also investigated photoinduced reduction (photochromism) of viologens using EDTA as the electron donors and Pd-TiOTPyP multilayers as light sensitizers.

Hydrothermal syntheses is normally used in the area of polyoxometalates and metal organic frameworks, but hydrothermal synthesis of crystalline titanium(IV) complexes is an exciting challenge, because of high reactivity and spontaneous hydrolysis of titanium(IV) ions, which leads to rapid precipitation of oxide rather crystalline compounds. Dong et al. (2018) reported an effective route to synthesize crystalline titanium(IV) complexes and three titanium(IV) compounds were isolated in the presence of organic amines. It is intresting to note that organic amines played an important role in the synthesis and introduction of chromophores increased the visible light harvesting.

Janek et al. (2018) synthesized titanium oxo-clusters composed of $\{Ti_4O_2\}$ and $\{Ti_6O_6\}$ cores by from the direct reaction of $Ti(O^iBu)_4$ and 4-aminobenzoic acid (HABZ) in different molar ratios (4:1, 2:1, and 1:1) at room temperature. The complex $[Ti_4O_2(O^iBu)_{10}(ABZ)_2]$ 0.7^iBuOH $0.5C_7H_8$ was isolated from the reaction mixture having molar ration (4:1); however, slow evaporation of in situ alcohol; however, led to the formation of complex $[Ti_4O_2(O^iBu)_{10}(ABZ)_2]$. The formation of other two complexes $[Ti_4O_2(O^i\text{-}Bu)_{10}(ABZ)_2]$ and $[Ti_6O_6(O^iBu)_6(ABZ)_6]$ was separated by 2:1, and 1:1 mother liquor, respectively. The photocatalytic activity of these composite foils produced by dispersion of second complex in the polystyrene matrix was evaluated by the photodegradation of the methylene blue in presence of UV light irradiation.

The first Ti_8L_{12} cube was assembled by Zhu et al. (2018a) that could further encapsulate an $[Ti(H_2O)_6]$ species. It was observed that host−guest hydrogen-bonding interactions in $[Ti(H_2O)_6]@Ti_8L_{12}$ resulted in different behavior in photophysical properties, luminescent bands, redshifted absorption, longer excited-state lifetime, and larger photocurrents. Titanium-based coordination cages are interesting species for both; photophysical and supramolecular chemistry. The $[Ti(H_2O)_6]@Ti_8L_{12}$ complex is stable in both; as well as solution and solid states, the photodynamics of both; free as well as $[Ti(H_2O)_6]$ guest encapsulated Ti_8L_{12} cube was confirmed.

Zhu et al. (2018b) reported the synthesis of two salicylate-stabilized polyoxo-titanium clusters (PTCs) with as well as without fluorine. These are $H_2[Ti_{13}(\mu_3\text{-}O)_7(\mu_2\text{-}O)_4(Sal\text{-}F)_9(O^iPr)_{14}]$ (PTC-95), (where $H_2Sal\text{-}F = 5\text{-flu}$

orosalicylic acid) and $H_2[Ti_{14}(\mu_3\text{-}O)_8(\mu_2\text{-}O)_4(Sal)_8(O^iPr)_{18}]\cdot HO^iPr$ (PTC-96), (where H_2Sal = salicylic acid). It was indicated that PTC-95 had a compact structure, which is made up of a quadrangular prism with an appended linear Ti_3 cluster and two additional Ti atoms, while PTC-96 has an arch bridge-shaped structure, which is linked by two Ti_4 $(\mu_3\text{-}O)_2$ and two $Ti_3(\mu_3\text{-}O)$ clusters. It was also revealed that these clusters exhibited diverse photocurrent response properties and photocatalytic activities toward dye degradation.

Janek et al. (2019) synthesized titanium(IV) oxo-complexes (TOCs) of the general formula $[Ti_3O(O^iPr)_8(OOCR')_2]$ (where $R' = -C_{13}H_9$, -*p*-PhCl, -*m*-$PhNO_2$, and $-C_4H_7$). They used different carboxylate ligands for changing optical band gaps of the as-prepared microcrystals. It was reported that dispersion of TOCs in the poly(methyl methacrylate) matrix (PMMA) resulted in polymer/TOCs composites, which can be applied for estimation of photocatalytic activity of as-synthesized trinuclear Ti(IV) oxo-complexes. Photocatalytic degradation of methylene blue was used as the model system in prescence of UV irradiation.

The synthesis of two new polyoxo−titanium cluster complexes with thiacalix[4]arene ligands was reported by Wang et al. (2020). It was revealed that there were two distinctly different conformations of core-protecting ligands, i.e., 1,2-alternate and cone in the tetranuclear Ti4 and the hexanuclear Ti6 complexes. Such ligand−cluster core coordination not only extended absorption edge of these complexes in visible-light region but it also increased their stability in the photocatalytic process for evolution of hydrogen. It was also indicated that calixarene conformation significantly affected the visible-light photocatalytic performances of such clusters. It was revealed that incorporation of S and suitable titanium coordination geometry may be responsible for the photocatalytic activities.

It is known that construction of three-dimensional (3D) covalent organic frameworks (COFs) is an exciting challenge due to the limited types of organic building blocks. Lu et al. (2021) prepared a 3D anionic titanium-based COF (Ti−COF-1) with an edge-transitive (6, 4)-connected soc topology with octahedral Ti^{IV} complex as the building unit. It was reported that Ti−COF-1 exhibited superior stability, high crystallinity, and large specific surface area (1000.4 $m^2\ g^{-1}$). It was revealed that this COF has a broad absorption band with band gap of 1.86 eV, and it exhibited high photocatalytic activity toward Meerwein addition reactions.

Kubiak et al. (2021) produced composite materials by the dispersion of titanium(IV)-oxo complexes (TOCs) in poly(ε-caprolactone) (PCL) matrix with the $[Ti_4O_2(O^iBu)_{10}(O_2CR')_2]$ (where $R' = PhNH_2$ and $C_{13}H_9$) by direct reaction of titanium(IV) isobutoxide with 9-fluorenecarboxylic acid or 4-aminobenzoic acid. As a result, the composites PCL + *n*TOCs ($n = 5$ and 20 wt.%) was produced. It was revealed that as-prepared PCL + TOCs composites, exhibited higher photocatalytic activity in the visible range.

Lebedkin et al. (2021) investigated optical properties of four trinuclear chalcogenolato bridged metal complexes $[Ag_2Ti(SPh)_6(PPh_3)_2]$, $[Na(thf)_3]_2[Ti(SPh)_6]$, $[Cu_2Ti(SePh)_6(PPh_3)_2]$, and $[Ag_2Ti(SePh)_6(PPh_3)_2]$. All of these complexes displayed efficient near-infrared luminescence at ~880−1200 nm at low temperatures in the solid state. It is quite intense in case of $[Cu_2Ti(EPh)_6(PPh_3)_2]$, (E = S, Se) at ambient temperature and exhibited PL quantum yields of 9.5% and 4.8% at $\lambda_{PL} = 1090$ and 1240 nm, respectively. It was reported that lowest-energy electronic transitions in these complexes is due to their high localization on the metal and chalcogen atoms, with almost negligible contributions of the external ligand groups.

Mou et al. (2021) synthesized tartrate-stabilized titanium−oxo clusters with sulfonate chromophore ligands, $Ti_4(C_4H_2O_6)(AS)_2(O^iPr)_{10}$ and $Ti_4(C_4H_2O_6)(ATS)_2(O^iPr)_{10}$ (where $C_4H_2O_6$ = tartrate, AS = aniline-2-sulfonate, and ATS = 4-aminotoluene-3-sulfonate). It was indicated that these crystals are a class of small TOCs, which contain only four titanium atoms in the asymmetric unit, and formed a centrosymmetric planar square $\{Ti_4\}$ core. This core was chelated by a bridging hexadentate tartrate ligand in *trans*-orientation. These TOCs have band gaps of 3.16 and 2.95 eV, respectively. Their photocurrent response and the photocatalytic activity for degrading methylene blue was also examined.

The d^0 complexes with ligand-to-metal charge-transfer (LMCT) excited states represent a new series of photocatalysts. London et al. (2021) studied photochemistry and photophysics of d^0 titanocenes, $Cp_2Ti(C_2R)_2$, [where C_2R = ethynylphenyl (C_2Ph), 4-ethynyldimethylaniline (C_2DMA), or 4-ethynyltriphenylamine (C_2TPA)]. It was found that two aryl rings in $Cp_2Ti(C_2DMA)_2$ are nearly face-to-face in the solid state, while these are mutually perpendicular in $Cp_2Ti(C_2Ph)_2$. All these three complexes are highly emissive at 77 K, but they undergo photodecomposition at room temperature on irradiation into their lowest-energy absorption bands. They found that emission wavelengths and photodecomposition quantum yields of these complexes are: $Cp_2Ti(C_2Ph)_2$, (575 nm and 0.65), $Cp_2Ti(C_2TPA)_2$, (642 nm and 0.42), and $Cp_2Ti(C_2DMA)_2$ (672 nm and 0.25). It was reported that computational data are in favor of emission from a ^{3}LMCT state, which is indicated by compression of the C−Ti−C bond angle as evident from ^{3}LMCT state, which is consistent with the known products of photodecomposition.

Wang et al. (2021) synthesized three lanthanide-doped titanium−oxo clusters (Ln-TOCs): $[Ti_4La(\mu_3\text{-}O)_3(O^iPr)_2(C_6H_5COO)_{11}]\cdot 3CH_3CN$, $[Ti_4Eu_2(\mu_3\text{-}O)_4(acac)_2(C_6H_5COO)_{13}]$, (where acac = acetylacetonate), and $[Ti_7Ce(\mu_2\text{-}O)_2(\mu_3\text{-}O)_5(O^iPr)_2(C_6H_5COO)_{15}]\cdot CH_3CN$. It was reported that these Ln−TOCs displayed strong UV-light absorption with extended visible light absorption, may be due to doping of lanthanides and benzoates. The Ln doped clusters exhibited good photocurrent responses. Particularly, third cluster showed highest photocurrent intensity, because of Ce(IV)/Ce(III) redox reaction.

London et al. (2022) synthesized nine titanocene complexes, $Cp_2Ti(C_2Ar)_2 \cdot MX$ (where Ar = phenyl, dimethylaniline, triphenylamine; and MX = CuCl, CuBr, or AgCl). It was reported that MX coordinates to alkyne tweezers and CuX coordination has more structural impact than AgCl. All these complexes are brightly emissive at 77 K (emission max between 575 and 767 nm), but with coordination of MX, the emission was redshifted. It was observed that parent complexes photodecomposed at room-temperature solution with quantum yields, Φ_{rxn}, ranging between 0.25 and 0.99. A clear trend was there that the emission energy increases with increase in Φ_{rxn}.

Śmigiel et al. (2022) synthesized oxo complex $[Ti_4O_2(O^iBu)_{10}(asp)_2] \cdot H_2O$ by reaction of titanium(IV) isobutoxide and acetylsalicylic acid (Hasp) in 4:1 M ratio. They also studied photocatalytic activity of as-synthesized complex using composite foils produced by the dispersion of micrograins, as the inorganic blocks, in a polycaprolactone (PCL) matrix. It was observed that on absorption maximum wavelength shifted to 425−450 nm on introduction of micrograins to the PCL matrix. This composite samples exhibited good activity toward photodecolorization of methylene blue in prescence of visible light.

3.3 Coordination compounds of zirconium

Precious stones containing zirconium, such as hyacinth and zircon, have been used as decorations since ancient times. Zirconium was recognized as an element by Martin Heinrich Klaproth (1789), and Jacob Berzelius (1824), was able to produce zirconium as an amorphous black powder. This element was given its name by Persian word 'zargon', which means gold-like. Zirconium is belongs to group 4 and its electronic configuration is [Kr] 4 d^2 $5s^2$. In general, zirconium compounds are colorless and diamagnetic in nature with the oxidation state as +4; of course, a few. Zr(III) compounds are known, but Zr(II) is very rare. Zirconium forms a wide range of coordination complexes.

Loukova and Smirnov (2000) reported long-lived ligand-to-metal charge transfer (LMCT) excited states based on zirconium and hafnium complexes using $Cp_2Zr(IV)Cl_2$ and $Cp_2Hf(IV)Cl_2$. The lifetime of these complexes was of the order of 2000 and 300 μs, respectively. The phosphorescence spectra, quantum yields and lifetimes in these metallocenes $Cp_2M(IV)Cl_2$ was discussed in light of the nature of the metal (Ti, Zr or Hf)−ligand π-bonding character.

Kunkely and Voglev (2004) reported a complex ethylenebis(indenyl)zirconium(IV) binolate (where = binol (1,1′-binaphthyl-2,2′-diol) exhibited lowest-energy ππ* binolate intraligand (IL) excited state with absorption peak at $\lambda_{max} = 348$ nm. It was also revealed that this IL triplet undergoes an emission at $\lambda_{max} = 490$ nm.

Gerasymchuk et al. (2005) incorporated Zr(IV) and Hf(IV) phthalocyanines with gallate as axial ligand coordinated to the central metal atom of

phthalocyanine in silica gels via sol−gel process. They used tetraethyl orthosilicate (TEOS) as a precursor. It was reported that as-obtained mixed inorganic−organic composites were homogeneous and transparent. An intensive fluorescence emission (700−725 nm) was observed upon long-wavelength excitation and much larger Stokes shift (about 45 nm) in the Q region, suggesting that Zr(IV) and Hf(IV) phthalocyanines could be used as photosensitizers in the photodynamic therapy.

The luminescent properties of mixed-ligand complexes of zirconium(IV) and hafnium(IV) phthalocyaninates with 4-benzoyl-3-methyl-1-phenyl-2-pyrazolin-5-one were investigated by Tret'yakova et al. (2006) in different organic solvents. They have determined quantum yields of fluorescence lifetimes of the excited states, and the molar extinction coefficients for these complexes.

Zirconium(IV) and hafnium(IV) phthalocyanines were synthesized with various carboxylic acids as out-planed ligands using an interaction between di(chloro)zirconium(IV)- or hafnium(IV)-phthalocyanines and carboxylic acids (Tret'yakova et al., 2007). They have indicated coordination of two acid fragments in a *cis*-geometry about the central atom of the macrocycle. These compounds were found non-aggregated in the organic solvents. They have also evaluated fluorescence quantum yields (Φ_F) and natural lifetimes (τ) of zirconium phthalocyanine complexes in toluene and DMSO.

Some zirconium(IV) and hafnium(IV) phthalocyanines were also prepared by Tomachynski et al. (2008) with various β-dicarbonyl ligands through direct interaction between di(chloro)zirconium(IV) or hafnium(IV) phthalocyanines and free β-diketones 4-benzoyl-3-methyl-1-phenyl-2-pyrazolin-5-one. Fluorescence quantum yields (Φ_F) and natural life times (τ) of zirconium phthalocyanine complexes were also determined in different solvents such as DMSO, toluene, and THF.

Kathirgamanathan et al. (2011) synthesized two new phases of zirconium tetrakis(8-hydroxyquinolinolate) (Zrq_4). It was observed that these two phases have remarkable differences in their performance in organic light emitting devices. It was revealed that α-Zrq_4 has lower operating voltage, longer lifetime and higher efficiencies as compared to β-Zrq_4 in organic light emitting devices.

It was reported by Loukova et al. (2012) that spectral-luminescent properties (phosphorescent) of organometallic complexes of Ti, Zr, and Hf with aromatic ligands are due to ligand-to-metal charge transfer (LMCT) states. It was revealed that there was a linear dependence of the phosphorescent characteristics of zirconocene on nature of coordinative (inner- and outersphere) interactions of the phosphorescent metal complex with media molecules and molecular structure of organic media.

Radivojevic et al. (2012) evaluated Zr(IV) and Hf(IV) complexes of 5,10,15,20-tetraphenylporphyrin (TPP) and metallophthalocyanine (Pc) as dyes for the dye-sensitized solar cells. It was observed that Zr(IV)

phthalocyanine dye performed better in DSSCs, as compared to Zr(IV) porphyrin with an overall efficiency of ~1.0% while Hf(IV) complexes were found to be less efficient. It was found that photophysical properties of these complexes in solution are responsible for energetically favorable injection of electrons into the conduction band of TiO_2 nanoparticles, as well as good band gap match with I_3^-/I^-pair in ionic liquid, 1-butyl-3-methyl imidazolium iodide. It was reported that a combination of TPP (blue absorbing) with the Pc complexes (red absorbing) can enhance absorbance of solar light in the DSSCs.

Shahroosvand et al. (2012) synthesized zirconium complexes using a mixture of zirconium nitrate, potassium thiocyanate, 1,2,4,5-benzene tetracarboxylic acid (H_4btec), and 1,10-phenanthroline (phen). It was reported that photoluminescence emission of seven zirconium complexes exhibited two series of peaks: (i) Sharp and intense bands from 300 to 500 nm and (ii) Broadened with less intensity from 650 to 750 nm. The PVK:PBD blend was used as a host for doping of zirconium compounds and ratio of zirconium complexes were modified by 8 wt.% in PVK:PBD(100:40).

Pritchard et al. (2013) prepared zirconium and hafnium metallocene dihalides based on simple polyphenyl cyclopentadienes. These were found to be stable at room-temperature and can act as lumophores with large Stokes shifts, emitting from states with sufficient LMCT character. It was also indicated that these species have a potential as lumophores for fluorescence cell-imaging microscopy.

Shahroosvand et al. (2013) synthesized eight new zirconium complexes using 1,2,4,5-benzenetetracarboxylic acid (H_4btec), 1,10-phenanthroline (phen) and 4,7-diphenyl−1,10-phenanthroline (Bphen), as ligands. They used these as light emitting material in fabricated organic light emitting diodes (OLEDs). A yellow−green photoluminescence (PL) emission was observed with a red shift compared to the PVK:PBD blend. It was reported that devices with Zr complexes (ITO/PEDOT:PSS/PVK:PBD/zirconium complex/Al) emitted a yellow−red light.

Some zirconium-carboxylate metallocavitands were prepared by Iden et al. (2014) $[(CpZr)_3(\mu\text{-}\kappa_2,O',O''CR)_3(\mu_3\text{-}O)(\mu_2\text{-}OH)_3]Cl$ (where Cp = cyclopentadienyl; R = C_5H_4N, C_6H_7N, $C_{18}H_{14}N$ and $C_{18}H_{12}N$) with moderate to high yields (40%−83%). The carboxylic acids was treated with Cp_2ZrCl_2 at room temperature for this purpose. It was reported that two complexes exhibited efficient photoluminescence properties in solution with a peak at 464 and 422 nm and quantum yields as 87% and 65% in solution, respectively.

Guo et al. (2015) reported a broad-band direct white-light emission, which was originated from a single-phased and single-doped phosphor luminescent mesoporous zirconium oxy-hydroxy acetate−persulfate complex and Eu^{3+}-doped complex. It was also observed that amorphous complexes exhibited the photoluminescence and color properties. It was interesting to note that a white-light emission is from the single-phased and single-doped phosphors, which

were prepared via low-cost chemical approach. The pristine complex has been used as a precursor of environmentally benign catalysts in the esterification of lauric acid with methanol and in n-hexane isomerization.

Bestgen et al. (2016) synthesized phosphine-functionalized zirconocene derivatives as metalloligands. The reactivity and photoluminescent properties of methylzirconocene phosphines were also investigated. It was reported that some of the compounds show bright emission with quantum yields of up to 19% even at room temperature on excitation at 350 nm.

Zhang et al. (2016) synthesized titanium and zirconium complexes using two 2,6-bis(pyrrolyl)pyridine ligands. It was reported that neutral complexes Ti(^{Me}PDP)$_2$ and Zr(^{Me}PDP)$_2$ (where ^{Me}PDP = 2,6-bis(5-methyl-3-phenyl-1H-pyrrol-2-yl)pyridine) exhibited intense ligand-to-metal charge-transfer (LMCT) bands in the visible range. They undergo reversible redox reactions under highly reducing conditions. It was also observed that Zr(^{Me}PDP)$_2$ is photoluminescent in nature and its excited state can be quenched even by mild reducing agents to generate a powerful electron transfer reagent. It can enhance dehalogenation reactions, reduction of olefins (electron-poor) and the reductive coupling of benzyl bromide via photoredox catalysis (Fig. 3.1). It was also claimed by them that the earth-abundant metal complex like Zr(^{Me}PDP)$_2$ can be used an alternative to costly metal photosensitizer such as $[Ru(bpy)_3]^{2+}$.

Zhang et al. (2018) prepared these compounds have long-lived excited states on exposure to visible light, which resulted in phosphorescent emission with relatively higher lifetimes (microsecond range) and luminescence quantum yields of 3% and 18% for Zr(HCNN)$_2$, and Zr(MeCNN)$_2$, respectively in benzene solution at room temperature. It was revealed that IL transitions with

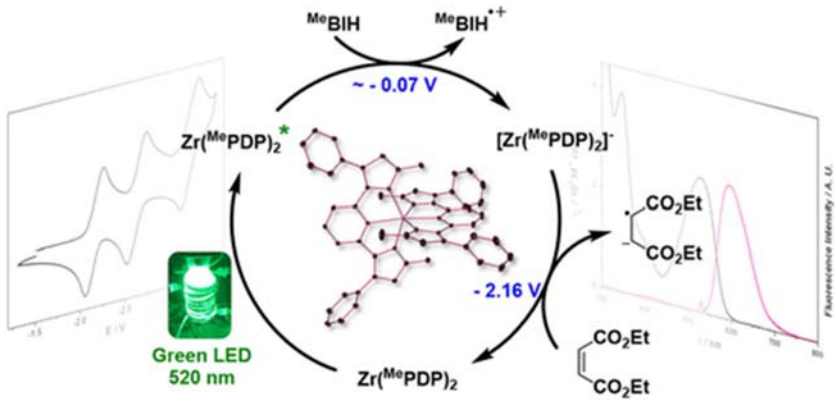

FIG. 3.1 Use of zirconium complexes in reduction of olefins. *Adapted from Zhang, Y., Petersen, J.L., Milsmann, C., 2016. A luminescent zirconium (IV) complex as a molecular photosensitizer for visible light photoredox catalysis. J. Amer. Chem. Soc. 138 (40), 13115−13118. With Permission.*

significant LMCT character of 20%−30% was there. The photochemical reactivity of $Zr(MeCNN)_2$ is photoinduced outersphere electron transfer, which enabled it in photoredox catalysis, while $Zr(HCNN)_2$ undergoes C−C reductive elimination upon photoexcitation with mild oxidants resulting in the formation of $Zr(DPDP)X_2$ (where X = Br or SBn) complexes (Fig. 3.2). It was attributed to the absene of methyl group adjacent to Zr−C bond.

Low et al. (2018) synthesized and investigated the reactivity of Zr complexes supported by a 9,10-anthracenediyl-linked bisphenoxide ligand (L). It was reported that $Zr^{IV}LBn_2$ undergoes photolytic reduction with formation of bibenzyl and $Zr^{IV}L(THF)_3$, which displayed a two-electron reduced anthracene moiety. It was reported that leveraging ligand-stored reducing equivalents promoted the oxidative coupling of internal and terminal alkynes both to zirconacyclopentadiene complexes, which suggested that anthracene can be used as a redox reservoir reversibly.

Some new heteroleptic zirconium and hafnium complexes were synthesized by Kuhlmann et al. (2018a). Different substituted phenoxy benzoxazoles (where HL1 = 2-(2′-hydroxyphenyl)benzoxazole, HL2 = 2-(2′-hydroxynaphthyl)benzoxa-zole, and HL3 = 2-(2′-hydroxy-3′,5′-di-tert-butylphenyl) benzoxazole) were used as ligands along with chloride in these complexes. Their crystals showed distorted octahedral or capped trigonal prismatic coordination spheres. It was reported that a fluorescence was there from short-lived excited state and emission maxima was observed in the blue region.

Sun et al. (2018) synthesized a porous and visible light responsive zirconium metal−organic framework ($[Zr_6O_4(OH)_4(L)_6]\cdot 8DMF$ (Zr-SDCA-NH_2). They used a conjugated amine-functionalized dicarboxylic ligand (where H_2L = 2,2′-diamino-4,4′-stilbenedicarboxylic acid; H_2SDCA-NH_2). It was reported that Zr-SDCA-NH_2 exhibited visible-light activity for CO_2 reduction, when used as a photocatalyst. The formate formation rate of 96.2 μmol h^{-1} $mmol^{-1}_{MOF}$ could be achieved, which is higher than other

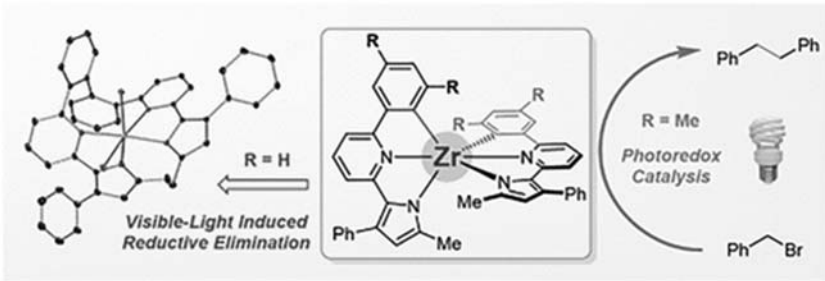

FIG. 3.2 Visible-light induced reductive elimination and photoredox catalysis by zirconium complexes. *Adapted from Zhang, Y., Petersen, J.L., Milsmann, C., 2018 Photochemical C−C bond formation in luminescent zirconium complexes with CNN pincer ligands. Organometallics 37 (23), 4488−4499. With Permission.*

reported amine-functionalized Zr-MOFs. It was indicated that Zr_6 oxo-cluster contributed to the CO_2 photoreduction through the LMCT process and the organic ligand; both.

The extreme ultraviolet (EUV) photochemistry of metal oxoclusters based on Ti, Zr, and Hf with methacrylate ligands (Mc) and their sensitivity as resist materials was compared by Castellanos et al. (2018). The decarboxylation was observed upon EUV exposure in all these cases; however, higher sensitivity was reported for the Hf-based material as compared to Zr-based analogue. It was indicated that there was not a major loss of organic shell and high degree of aggregation of the naked inorganic cores, which are very much are required for this type of molecular thin film so that these can operate as a resist material.

Tahershamsi et al. (2019) synthesized two complexes of bis(amino-benzoato) zirconium(IV) phthalocyanine and their graphite oxide-based composites. These complexes generated reactive oxygen species (ROS) in presence of light. The photoactivity of as-prepared materials was compared for their potential in biomedical applications, such as photosensitizers in photo-dynamic therapy.

Zhang et al. (2019) synthesized luminescent seven-coordinated zirconium and hafnium complexes with three mono-anionic 2,2′-pyridylpyrrolide ligands and a chloride. A hybrid of ligand-to-metal charge transfer (LMCT)/ligand-to-ligand charge transfer (LLCT) was considered responsible for visible light absorption band. It was observed that complexes $(^{Me}PMP^{Me})_3MCl$ (where M = Zr, Hf, and $^{Me}PMP^{Me}$ = 3,5-dimethyl-2-(2-pyridyl)pyrrolide) were found emissive at room temperature in solution upon irradiation with visible light. It was due to a combination of fluorescence and phosphorescence, which are having excited state lifetimes in the low to sub-ns and μs timescale, respectively.

Salojärvi et al. (2020) synthesized some soluble and intensely near-IR-absorbing complexes of transition metal (where metal = Ti, Zr, V, and Ni). They used redox non-innocent *N*,*N*′-bis(3,5-di-tertbutyl-2-hydroxy-phenyl) −1,2-phenylenediamine (H_4L) as a ligand precursor. Two organic molecules were coordinated to the metal center as tri- or tetradentate ligands in these complexes ($[Ti\ (L^{ox})_2]$, $[Zr\ (L^{ox})_2]$, $[V(L^{sq1})(HL^{ox})]$ and $[Ni(HL^{ox})_2]$. These complexes were thermally stable. All compounds strongly absorb in the near-IR region.

Zhang et al. (2020a) prepared seven bis(pyridinedipyrrolide)zirconium complexes $Zr(^{R}{}_1PDP^{R}{}_2)_2$, (where $[^{R}{}_1PDP^{R}{}_2]^{2-}$ is the doubly deprotonated form of [2,6-bis(5-R_1-3-R_2-1*H*-pyrrol-2-yl)pyridine]). It was reported that all these complexes exhibited significant long emission lifetimes (τ = 190−576 μs) and high quantum efficiencies (Φ_{PL} = 0.10−0.38) under visible light in benzene. It was observed that substituents on the pyrrolide rings had significant effects on the electrochemical properties and photoluminescence of these compounds. It was revealed that R_2 substituents (where R_2 = H, Me, Ph, or C_6F_5) had only limited effects on the absorption as well as emission profiles of the complexes but it allowed tuning of the ground- and excited-state redox

potentials, while R_1 substituents (where $R_1 = H$, Me, Ph, or 2,4,6-Me_3Ph) influenced both; optical and electrochemical properties. The photoredox catalytic dehalogenation of aryl iodides and chlorides with $Zr(^{Me}PDP^{Me})_2$, showed a potential of $Zr(PDP)_2$ as-photosensitizer to enhance difficult reductive transformations upon excitation with green light and that too under mild conditions.

Zhang et al. (2020b) reported an air- and moisture-stable, visible light-absorbing Zr(IV) photosensitizer, Zr(MesPDPPh)2,(where $[^{Mes}PDP^{Ph}]^{2-}$ is the doubly deprotonated form of [2,6-bis(5-(2,4,6-trimethylphenyl)-3-phenyl-1*H*-pyrrol-2-yl)pyridine]). It was observed that this molecule has a long-lived triplet LMCT excited state ($\tau = 350$ μs) with highly efficient photoluminescence emission ($\Phi = 0.45$). This was attributed to thermally activated delayed fluorescence from the higher-lying singlet configuration with significant LMCT contributions. It was revealed that Zr(MesPDPPh)2 can be used in many photoredox catalytic processes and triplet energy transfer. This work provides a blueprint for development of photosensitizer in future with early transition metals and excited states with significant LMCT contributions.

Dunlop et al. (2021) prepared some metallocene complexes of cationic group 4 with pendant imine and pyridine donor groups as stable crystalline $[B(C_6F_5)_4]^-$ salts. These were obtained by: (i) Protonation of the intramolecularly bound ketimide moiety in neutral complexes $[(\eta^5\text{-}C_5Me_5)\{\eta^5\text{-}C_5H_4CMe_2CMe_2C(R)=N\text{-}\kappa N\}MCl]$ (where M = Ti, Zr, Hf and R = *t*-Bu, Ph) by $PhNMe_2H^+[B(C_6F_5)_4]^-$ to give $[(\eta^5\text{-}C_5Me_5)\{\eta^5\text{-}C_5H_4CMe_2CMe_2C(R)=NH\text{-}\kappa N\}MCl]^+[B(C_6F_5)_4]^-$ or (ii) Chloride ligand abstraction from the complexes $[(\eta^5\text{-}C_5Me_5)(\eta^5\text{-}C_5H_4CMe_2CH_2C_5H_4N)MCl_2]$ (where M = Ti, and Zr) by $Li[B(C_6F_5)_4]\cdot 2.5Et_2O$ to give $[(\eta^5\text{-}C_5Me_5)(\eta^5\text{-}C_5H_4CMe_2CH_2C_5H_4N\text{-}\kappa N)MCl]^+[B(C_6F_5)_4]^-$. It was observed that these cationic complexes of Zr and Hf, exhibited enhanced luminescenceas as compared to the corresponding neutral species. It was predominantly from triplet ligand-to-metal (^{3}LMCT) excited states with quantum yields up to 58% and lifetimes up to 62 μs in the solid state (Fig. 3.3).

3.4 Coordination compounds of hafnium

Hafnium is a chemical element with the symbol Hf and atomic number 72. Hafnium belongs to group 4 and its electronic configuration is [Xe] $4f^{14}$ 5 d^2 $6s^2$. It is lustrous, silvery gray, and tetravalent transition metal. It resembles chemically with zirconium and it is found in many zirconium minerals. Although, its existence was predicted by Dmitri Mendeleev in 1869, but it was identified in 1923 by Dirk Coster and George de Hevesy. Hafnium is named after Hafnia, which is a Latin name for Copenhagen. It is used in electrodes and filaments. Some superalloys are prepared for special applications, which contain hafnium along with niobium, titanium, or tungsten. It is corrosion-resistant also.

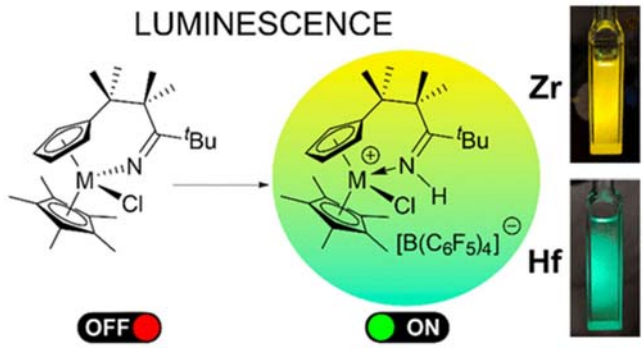

FIG. 3.3 Enhanced luminicence of cationic complex of Zr and Hf using LMCT as compared to there neutral species. *Adapted from Dunlop, D., Vecera, M., Gyepes, R., Kubat, P., Lang, K., Horacek, M., et al., 2021. Luminescent cationic group 4 metallocene complexes stabilized by pendant N-donor groups. Inorg. Chem. 60 (10), 7315−7328. With Permission.*

Yam et al. (1998) synthesized a series of luminescent hafnium thiolate complexes $(\eta5\text{-}C_5Me_5)_2Hf(SR)_2$ (where R = nBu, C_6H_5, C_6H_4OMe-p, C_6H_4tBu-p) by the reaction of $(\eta5\text{-}C_5Me_5)_2HfCl_2$ with LiSR. It was observed that these complexes exhibited rich luminescence behavior. Gong and Zhou (2007) prepared $OHf(\eta2\text{-}O_2)(\eta2\text{-}O_3)$, as a side-on bonded oxo−superoxo hafnium ozonide complex. This complex has two possibilities on visible light irradiation (532 nm) (i) rearranges photochemically to a more stable $Hf(\eta2\text{-}O_2)_3$ isomer, i.e. a side-on bonded di-superoxo hafnium peroxide complex, (ii) Reacts with dioxygen to form an unprecedented homoleptic tetra-superoxo hafnium complex: $Hf(\eta2\text{-}O_2)_4$. It was found that these oxygen-rich complexes are photoreversible in nature, which means formation of $Hf(\eta2\text{-}O_2)_3$ and $Hf(\eta2\text{-}O_2)_4$ was accompanied by demise of $OHf(\eta2\text{-}O_2)(\eta2\text{-}O_3)$ in prescence of visible light (532 nm) irradiation and vice versa with UV light (266 nm) irradiation.

Chernii et al. (2012) synthesized some phthalocyanine complexes of zirconium (IV) and hafnium (IV) containing dibenzoylmethane groups as out-of-plane ligands As-prepared compounds (ZrN_4O_4 and HfN_4O_4) were isomorphous in nature and their central atoms exhibited square-antiprism coordination geometry, with four nitrogen atoms from the phthalocyanine macrocycle and four oxygen atoms from the two bidentate dibenzoylmethane ligands. There is a high ability of this complex to self-associate in the gas phase. The spectral-luminescent properties of these compounds in different solvents were studied and fluorescence quantum yields of these complexes were determined in toluene and DMSO.

As nanoscale metal organic frameworks (NMOFs) have potential in biomedicine due to their structural/chemical diversities, and high molecular loading capacities. Liu et al. (2016b) reported NMOF composed by hafnium

(Hf^{4+}) and tetrakis (4-carboxyphenyl) porphyrin (TCPP). In as-prepared Hf-TCPP NMOFs, TCPP acts as photosensitizer in photodynamic therapy (PDT), while Hf^{4+} could serve as a radio-sensitizer to enhance radiotherapy (RT). It was observed that NMOFs with polyethylene glycol (PEG) coating exhibited efficient tumor homing upon intravenous injection, and therefore, could be used for in vivo combined RT & PDT, with a remarkable anti-tumor effect. It was interesting to observe that Hf-TCPP NMOFs show efficient clearance from the body of mouse after use; thus, minimizing their possible long-term toxicity. These multifunctional NMOFs can be used as biodegradable carrier-free system, where both; metal ions as well as organic ligands are completely utilized to exert their therapeutic functions.

The Ti-, Zr-, and Hf-phthalocyanines were synthesized by Starukhin et al. (2017), which contain chloride ions or dibenzoylmethanate fragments coordinated to macrocycle in out-of-plane positions. It was observed that an efficient intersystem crossing was there for Hf-phthalocyanine, which leads to very weak fluorescence with lifetimes to <1 ns. It was intresting to note that variation in the nature of central metals from heavy Hf(IV) atom was also changed with lighter atoms: Ti(IV), and Zr(IV) lead to an increasing fluorescence lifetimes and maximum value of 6.6 ns was observed for Mg-phthalocyanine. The values of fluorescence quantum yield was raised from 1% for Hf-phthalocyanine to 56% for Mg-phthalocyanine on such a change. This type of heavy atom effect has impact on photophysical parameters of metallocomplexes containing phthalocyanines as compared to influence of attachment out-of-plane ligands.

Kuhlmann et al. (2018b) synthesized a series of 10 heteroleptic and homoleptic mononuclear Zr(IV) and Hf(IV) complexes with different substituted phenoxy-benzoxazole ligands. It was found that molecular structures were octahedral or tetragonal-antiprismatic coordination motifs at the metal atom and crystal packing patterns was dependent on the substitution of the ligands. It was revealed that all these 10 complexes exhibited a ligand-centered fluorescence with emission maxima in the blue region.

Lamač et al. (2022) reported cationic metallocene complexes, containing with pendant N-donor moieties. These complex exhibited enhanced luminescence in the solid-state, which, may be due to their triplet states with luminescence quantum yields, ΦL, (approximately 0.52), not reported so far for this class of compounds. It was suggested that these complexes can be used as an efficient singlet oxygen photosensitizers. They also evaluated photogeneration of $O_2(^1\Delta_g)$ by Ti, Zr and Hf metallocenes in dichloromethane solution. It was reported that cationic Zr and Hf metallocenes stabilized by N-donor imine and pyridine moieties on excitation by UV A light, exhibited green, yellow or orange luminescence from long-lived ^{3}LMCT excited states (with ΦL $\sim$0.02−0.40 in argon-saturated solutions) and efficient O2(1Δg) production (ΦΔ $\sim$0.29−0.77 in air-saturated solutions).

References

Atilla, D., Durmuş, M., Yılmaz, Ö., Gürek, A.G., Ahsen, V., Nyokong, T., 2007. Synthesis, photophysical and photochemical properties of poly (oxyethylene)-substituted phthalocyaninato oxotitanium (IV) complexes. Eur. J. Org Chem. https://doi.org/10.1002/ejic.200700057, 2007.

Bestgen, S., Schoo, C., Zovko, C., Köppe, R., Kelly, R.P., Lebedkin, S., et al., 2016. Early−late heterometallic complexes of gold and zirconium: photoluminescence and reactivity. Chem. Eur. J. 22 (21), 7115−7126.

Castellanos, S., Wu, L., Baljozovic, M., Portale, G., Kazazis, D., Vockenhuber, M., et al., 2018. Ti, Zr, and Hf-based molecular hybrid materials as EUV photoresists. SPIE Advan. Lithog. 58−69. https://doi.org/10.1117/12.2297167. San Jose, California, US.

Chauke, V.P., Arslanoglu, Y., Nyokong, T., 2011. Synthesis and photophysical behaviour of tantalum and titanium phthalocyanines in the presence of gold nanoparticles: photocatalysis towards the oxidation of cyclohexene. J. Photochem. Photobiol., A: Chem 221 (1), 38−46.

Chernii, V.Y., Bon, V.V., Tretyakova, I.N., Severinovskaya, O.V., Volkov, S.V., 2012. Novel zirconium (IV) and hafnium (IV) phthalocyanines with dibenzoylmethane as out-of-plane ligand: synthesis, X-ray structure and fluorescent properties. Dyes Pigments 94 (2), 187−194.

Dong, G.L., Wang, L., Fang, W.H., Zhang, L., 2018. Hydrothermal synthesis, structures and visible light harvest of three titanium complexes. Inorg. Chem. Commun. 93, 61−64.

Dunlop, D., Vecera, M., Gyepes, R., Kubat, P., Lang, K., Horacek, M., et al., 2021. Luminescent cationic group 4 metallocene complexes stabilized by pendant N-donor groups. Inorg. Chem. 60 (10), 7315−7328.

Erdoğmuş, A., Durmuş, M., Uğur, A.L., Avciata, O., Avciata, U., Nyokong, T., 2010. Synthesis, photophysics, photochemistry and fluorescence quenching studies on highly soluble substituted oxo-titanium (IV) phthalocyanine complexes. Synth. Met. 160 (17−18), 1868−1876.

Gazzi, R., Perazzolo, F., Sostero, S., Ferrari, A., Traverso, O., 2005. Photochemistry of tris (pyrazolyl) borate titanium (IV) complexes. J. O. C. 690 (8), 2071−2077.

Gerasymchuk, Y., Chernii, V.Y., Tomachynski, L.A., Legendziewicz, J., 2005. Spectroscopic characterization of zirconium (IV) and hafnium (IV) gallate phthalocyanines in monolithic silica gels obtained by sol−gel method. Opt. Mater. 27 (9), 1484−1494.

Gong, Y., Zhou, M., 2007. Formation and characterization of the oxygen-rich hafnium dioxygen complexes: OHf ($\eta2$-O_2)($\eta2$-O_3), Hf ($\eta2$-O_2)$_3$, and Hf ($\eta2$-O_2)$_4$. J. Phys. Chem. A 111 (37), 8973−8979.

Guo, G.Y., Chen, Y.L., Xu, S., 2015. A luminescent mesoporous zirconium complex and it as a precursor of environmentally benign catalysts. Microporous Mesoporous Mater. 213, 100−107.

He, W.L., Fang, F., Ma, D.M., Chen, M., Qian, D.J., Liu, M., 2018. Palladium-directed self-assembly of multi-titanium (IV)-porphyrin arrays on the substrate surface as sensitive ultrathin films for hydrogen peroxide sensing, photocurrent generation, and photochromism of viologen. Appl. Surf. Sci. 427, 1003−1010.

Hu, X., Tao, S., 2011. An optical fiber H_2O_2−sensing probe using a titanium (IV) oxyacetylacetonate immobilized Nafion coating on an bent optical fiber probe. IEEE Sensor. J. 11 (9), 2032−2036.

Iden, H., Bi, W., Morin, J.F., Fontaine, F.G., 2014. Zirconium (IV) metallocavitands as blue-emitting materials. Inorg. Chem. 53 (6), 2883−2891.

Janek, M., Muzioł, T.M., Piszczek, P., 2018. The structure and photocatalytic activity of the tetranuclear titanium (IV) oxo-complex with 4-aminobenzoate ligands. Polyhedron 141, 110−117.

Janek, M., Muzioł, T.M., Piszczek, P., 2019. Trinuclear oxo-titanium clusters: synthesis, structure, and photocatalytic activity. Materials 12 (19). https://doi.org/10.3390/ma12193195.

Kathirgamanathan, P., Surendrakumar, S., Antipan-Lara, J., Ravichandran, S., Reddy, V.R., Ganeshamurugan, S., et al., 2011. Discovery of two new phases of zirconium tetrakis (8-hydroxyquinolinolate): synthesis, crystal structure and their electron transporting characteristics in organic light emitting diodes (OLEDs). J. Mater. Chem. 21 (6), 1762−1771.

Kubiak, B., Radtke, A., Topolski, A., Wrzeszcz, G., Golińska, P., Kaszkowiak, E., et al., 2021. The composites of pcl and tetranuclear titanium (IV)-oxo complexes as materials exhibiting the photocatalytic and the antimicrobial activity. Int. J. Mol. Sci. 22 (13). https://doi.org/10.3390/ijms22137021.

Kuhlmann, L., Methling, R., Simon, J., Neumann, B., Stammler, H.G., Strassert, C.A., et al., 2018a. Fluorescent heteroleptic zirconium and hafnium complexes. Z. Anorg. Allg. Chem. 644 (18), 1091−1095.

Kuhlmann, L., Methling, R., Simon, J., Neumann, B., Stammler, H.G., Strassert, C.A., et al., 2018b. Fluorescent phenoxy benzoxazole complexes of zirconium and hafnium: synthesis, structure and photo-physical behaviour. Dalton Trans. 47 (32), 11245−11252.

Kunkely, H., Vogler, A., 2004. Optical properties of ethylenebis (indenyl) zirconium (IV) binolate with binol= 1, 1′-binaphthyl-2, 2′-diol. Binolate intraligand phosphorescence under ambient conditions. Inorg. Chem. Commun. 7 (1), 35−37.

Kuznetsova, N., Makarov, D., Yuzhakova, O., Strizhakov, A., Roumbal, Y., Ulanova, L., et al., 2009. Photophysical properties and photodynamic activity of octacationic oxotitaniumiv phthalocyanines. Photochem. Photobiol. Sci. 8 (12), 1724−1733.

Lamač, M., Dunlop, D., Lang, K., Kubát, P., 2022. Group 4 metallocene derivatives as a new class of singlet oxygen photosensitizers. J. Photochem. Photobiol., A: Chem. 424. https://doi.org/10.1016/j.jphotochem.2021.113619.

Lebedkin, S., Weigend, F., Eichhofer, A., 2021. Near-infrared luminescence in trinuclear mixed-metal chalcogenolate complexes of the types $[M_2Ti\ (EPh)_6\ (PPh_3)_2]$(M= Cu, Ag; E= S, Se) and $[Na\ (thf)_3]_2\ [Ti\ (SPh)_6]$. Inorg. Chem. 60 (12), 8936−8945.

Liu, J.X., Zeng, X.C., Zhang, L., Zhang, J., 2016a. A new cadmium-doped titanium−oxo cluster with stable photocatalytic H_2 evolution properties. Dalton Trans. 45 (11), 4501−4503.

Liu, J., Yang, Y., Zhu, W., Yi, X., Dong, Z., Xu, X., et al., 2016b. Nanoscale metal− organic frameworks for combined photodynamic & radiation therapy in cancer treatment. Biomaterials 97, 1−9.

London, H.C., Whittemore, T.J., Gale, A.G., McMillen, C.D., Pritchett, D.Y., Myers, A.R., et al., 2021. Ligand-to-metal charge-transfer photophysics and photochemistry of emissive d^0 titanocenes: a spectroscopic and computational investigation. Inorg. Chem. 60 (18), 14399−14409.

London, H.C., Pritchett, D.Y., Pienkos, J.A., McMillen, C.D., Whittemore, T.J., Bready, C.J., et al., 2022. Photochemistry and photophysics of charge-transfer excited states in Emissive d^{10}/d^0 heterobimetallic titanocene tweezer complexes. Inorg. Chem. 61. https://doi.org/10.1021/acs.inorgchem.2c01746.

Loukova, G.V., Smirnov, V.A., 2000. Phosphorescent ligand-to-metal charge-transfer excited states in the group IVB metallocene triad. Chem. Phys. Lett. 329 (5−6), 437−442.

Loukova, G.V., Vasiliev, V.P., Smirnov, V.A., Mel'nichuk, E.E., 2012. Photonics of metallocene complexes based on metals of the titanium subgroup. Nanotechnol. Russia 7 (5), 288−297.

Low, C.H., Rosenberg, J.N., Lopez, M.A., Agapie, T., 2018. Oxidative coupling with Zr (IV) supported by a noninnocent anthracene-based ligand: application to the catalytic cotrimerization of alkynes and nitriles to pyrimidines. J. Am. Chem. Soc. 140 (38), 11906−11910.

Lu, H.S., Han, W.K., Yan, X., Chen, C.J., Niu, T., Gu, Z.G., 2021. A 3D anionic metal covalent organic framework with soc topology built from an octahedral Ti (IV) complex for photocatalytic reactions. Angew. Chem. Int. Ed. 60 (33), 17881−17886.

Mou, W.Y., Xie, B., Li, X.L., Lai, C., Li, T., Chen, L., et al., 2021. Tartrate-stabilized titanium−oxo clusters containing sulfonate chromophore ligands: synthesis, crystal structures and photochemical properties. New J. Chem. 45 (24), 10930−10939.

Pritchard, V.E., Thorp-Greenwood, F.L., Balasingham, R.G., Williams, C.F., Kariuki, B.M., Platts, J.A., et al., 2013. Simple polyphenyl zirconium and hafnium metallocene room-temperature lumophores for cell imaging. Organometallics 32 (12), 3566−3569.

Radivojevic, I., Bazzan, G., Burton-Pye, B.P., Ithisuphalap, K., Saleh, R., Durstock, M.F., 2012. Zirconium (IV) and hafnium (IV) porphyrin and phthalocyanine complexes as new dyes for solar cell devices. J. Phys. Chem. C 116 (30), 15867−15877.

Salojärvi, E., Peuronen, A., Lahtinen, M., Huhtinen, H., Vlasenko, L.S., Lastusaari, M., et al., 2020. Series of near-IR-absorbing transition metal complexes with redox active ligands. Molecules 25 (11). https://doi.org/10.3390/molecules25112531.

Shahroosvand, H., Nasouti, F., Mohajerani, E., Khabbazi, A., 2012. Synthesis, characterization and optical properties of novel N donor ligands-chelated zirconium (IV) complexes. Opt. Mater. 35 (1), 79−84.

Shahroosvand, H., Nasouti, F., Mohajerani, E., Khabbazi, A., 2013. Red−yellow electroluminescence, yellow−green photoluminescence of novel N, O donor ligands−chelated zirconium (IV) complexes. J. Lumin. 135, 339−344.

Śmigiel, J., Muzioł, T., Piszczek, P., Radtke, A., 2022. Titanium (IV) oxo-complex with acetylsalicylic acid ligand and its polymer composites: synthesis, structure, spectroscopic characterization, and photocatalytic activity. Materials 15 (13). https://doi.org/10.3390/ma15134408.

Starukhin, A., Gorski, A., Knyukshto, V., Kijak, M., Tretyakova, I., Dovbii, Y., et al., 2017. Photophysical features of phthalocyanines metallocomplexes with out-of-plane ligands. Univer. J. Phys. Appl. 11 (4), 109.

Sun, M., Yan, S., Sun, Y., Yang, X., Guo, Z., Du, J., et al., 2018. Enhancement of visible-light-driven CO_2 reduction performance using an amine-functionalized zirconium metal−organic framework. Dalton Trans. 47 (3), 909−915.

Tahershamsi, L., Gerasymchuk, Y., Wedzynska, A., Ptak, M., Tretyakova, I., Lukowiak, A., 2019. Synthesis, spectroscopic characterization and photoactivity of Zr (IV) phthalocyanines functionalized with aminobenzoic acids and their GO-based composites. J. Carbon Res. 6 (1). https://doi.org/10.3390/c6010001.

Tau, P., Nyokong, T., 2006. Synthesis and photophysical properties of octa-substituted phthalocyaninato oxotitanium (IV) derivatives. J. Porphyr. Phthalocyan. 10 (08), 1040−1048.

Tau, P., Nyokong, T., 2007. Comparative photocatalytic efficiency of oxotitanium (IV) phthalocyanines for the oxidation of 1-hexene. J. Mol. Catal. Chem. 273 (1−2), 149−155.

Tomachynski, L.A., Tretyakova, I.N., Chernii, V.Y., Volkov, S.V., Kowalska, M., Legendziewicz, J., et al., 2008. Synthesis and spectral properties of Zr (IV) and Hf (IV) phthalocyanines with β-diketonates as axial ligands. Inorg. Chim. Acta. 361 (9−10), 2569−2581.

Tret'yakova, I.N., Chernii, V.Y., Tomachinskaya, L.A., Volkov, S.V., 2006. Physicochemical properties of novel mixed-ligand complexes of zirconium and hafnium bis (4-benzoyl-3-methyl-1-phenyl-2-pyrazolin-5-onato) phthalocyaninates. Theor. Exp. Chem. 42 (3), 175−180.

Tret'yakova, I.N., Chernii, V.Y., Tomachynski, L.A., Volkov, S.V., 2007. Synthesis and luminescent properties of new zirconium (IV) and hafnium (IV) phthalocyanines with various carbonic acids as out-planed ligands. Dyes Pigments 75 (1), 67–72.

Wang, X., Yu, Y., Wang, Z., Zheng, J., Bi, Y., Zheng, Z., 2020. Thiacalix [4] arene-protected titanium–oxo clusters: influence of ligand conformation and Ti–S coordination on the visible-light photocatalytic hydrogen production. Inorg. Chem. 59 (10), 7150–7157.

Wang, C., Zhang, J., Zhu, X., 2021. Synthesis of lanthanide-doped titanium-oxo clusters for efficient photocurrent responses. J. Solid State Chem. 304. https://doi.org/10.1016/j.jssc.2021.122586.

Yam, V.W.W., Qi, G.Z., Cheung, K.K., 1998. Synthesis, emission, and molecular orbital studies of luminescent hafnium thiolate complexes. Crystal structures of (η5-C_5Me_5) 2Hf $(SR)_2$ (R= nBu, C_6H_5, C_6H_4OMe-p). Organometallics 17 (25), 5448–5453.

Zhang, Y., Petersen, J.L., Milsmann, C., 2016. A luminescent zirconium (IV) complex as a molecular photosensitizer for visible light photoredox catalysis. J. Am. Chem. Soc. 138 (40), 13115–13118.

Zhang, Y., Petersen, J.L., Milsmann, C., 2018. Photochemical C–C bond formation in luminescent zirconium complexes with CNN pincer ligands. Organometallics 37 (23), 4488–4499.

Zhang, Y., Akhmedov, N.G., Petersen, J.L., Milsmann, C., 2019. Photoluminescence of seven-coordinate zirconium and hafnium complexes with 2, 2′-pyridylpyrrolide ligands. Chem. Eur. J. 25 (12), 3042–3052.

Zhang, Y., Leary, D.C., Belldina, A.M., Petersen, J.L., Milsmann, C., 2020a. Effects of ligand substitution on the optical and electrochemical properties of (pyridinedipyrrolide) zirconium photosensitizers. Inorg. Chem. 59 (20), 14716–14730.

Zhang, Y., Lee, T.S., Favale, J.M., Leary, D.C., Petersen, J.L., Scholes, G.D., et al., 2020b. Delayed fluorescence from a zirconium photosensitizer with ligand-to-metal charge-transfer excited states. Nat. Chem. 12 (4), 345–352.

Zhu, B.C., Fang, W.H., Wang, J., Du, Y., Zhou, T., Wu, K., 2018a. Host–guest and photophysical behavior of Ti_8L_{12} cube with encapsulated [Ti $(H_2O)_6$] species. Chem. Eur. J. 24 (54), 14358–14362.

Zhu, B.C., Fang, W.H., Emayavaramban, P., Zhang, L., Zhang, J., 2018b. Structures and photophysical performances of (fluoro) salicylate stabilized polyoxo-titanium clusters. Cryst. Eng. Comm. 20 (39), 5964–5968.

This page intentionally left blank

Chapter 4

Coordination compounds of vanadium, niobium and tantalum

Chetna Ameta, Dharmendra, Yogeshwari Vyas and Purnima Chaubisa
Department of Chemistry, Mohanlal Sukhadia University, Udaipur, Rajasthan, India

4.1 Introduction

Group 5 element, vanadium, niobium, and tantalum form a series of complexes with different ligands. These complexes exhibited different photophysical and photochemical behaviors apart from normal properties. Some of their complexes also show metal-to-ligand-charge transfer (MLCT). These complexes find various applications in photosplitting of water, photodynamic therapy, and photodegradation of organic pollutants. There are good future prospects of these complexes in years to come.

The creation of Jablonski diagrams for metal complexes is almost similar to that of organic molecules (Adamson et al., 1968). According to the predominant atomic orbital contributions, different MOs can be simply classified as follows:

(i) Predominantly ligand centered σ_L orbitals (strongly bonding)
(ii) Predominantly ligand-centered π_L orbitals (bonding)
(iii) Metal-centered π_M orbitals of t_{2g} symmetry (essentially nonbonding)
(iv) Predominantly metal-centered σ_M* orbitals of e_g symmetry (antibonding)
(v) Predominantly ligand-centered π_L* orbitals (antibonding) and
(vi) Predominantly metal-centered σ_M* orbitals (strongly antibonding).

The orbitals of types (i) and (ii) are filled in the ground state electronic configuration of an octahedral complex of d^n metal ion, while n electrons occupied the orbitals of (iii) and (iv) types. Excited electronic state configurations can be obtained from the ground electronic state configuration by promoting an electron from occupied MO to vacant MO in case of organic

Photochemistry and Photophysics of Coordination Compounds. https://doi.org/10.1016/B978-0-12-824493-7.00007-1
Copyright © 2023 Elsevier Inc. All rights reserved.

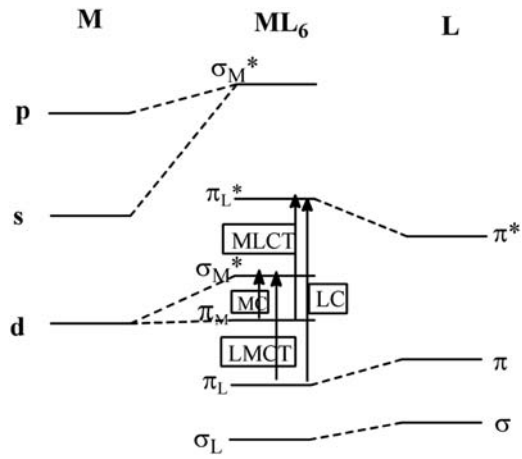

FIGURE. 4.1 Molecular orbital diagram for an octahedral complex of a transition metal.

compounds. These electronic transitions are expected to occur at low energy (Fig. 4.1):

- Metal-centered (MC) transitions from orbitals of type (iii) to orbitals of (iv) type,
- Ligand centered (LC) transitions from orbital of (ii) to (v) type,
- Ligand-to-metal charge-transfer (LMCT) transitions from (ii) to (iv) type, and
- Metal-to-ligand charge-transfer (MLCT) transitions, from (iii) to (v) type.

The relative order of energy of the resultant excited electronic configurations is affected by the type of metal and ligands. These are:

- Low-energy metal-centered transitions are there in case of metals in the first transition series (3d series).
- Low-energy ligand-to-metal charge-transfer transitions are there, when the metal can be easily reduced and at least one ligand is easily oxidized and
- Low-energy metal-to-ligand charge-transfer transitions are there, when reverse conditions are there i.e., when a ligand is easily reduced and metal is easy to oxidized.
- Low-energy ligand-centered transitions can also expected.

As coordination compounds have high symmetry and open-shell ground configurations, and therefore, transition is simpler as compared to organic molecules (partially occupied HOMOs) (Calvert et al., 1966; Balzani et al., 2007).

4.2 Coordination compounds of vanadium

Vanadium (V) was discovered in the form of vanadinite ($Pb_5(VO_4)_3Cl$) in 1801. Vanadium was given the name "panchromium" at that time because its

salts were found in a wide range of colors. This chemical element was discovered in the form of oxide. It was named as "vanadium" after Vanadis, which is a goddess in Norse mythology. Vanadium is a member of first-row transition metal (3d metals). It belongs to group 5 and its atomic number is 23, which has electronic configuration as [Ar] $3d^3 4s^2$. Vanadium is fifth (0.019%) in all transitional metals and 20 second in all elements in the Earth's crust. It is a transition metal with various oxidation states from +II to +V.

Vanadium complexes exist in all oxidation states starting from +I to +V that suggests that vanadium (II) (d^3) may undergo some photochemical redox processes. If photooxidation of vanadium (II) is followed by a second thermal electron transfer, it formed vanadium (IV), and the entire two-electron-transfer process is initiated photochemically. Shah and Maverick (1986) observed the photochemistry of vanadium(II) complexes of 2,2′-bipyridine and 1,10-phenanthroline. The lowest energy excited states in such vanadium systems are most probably either quartet MLCT states or $^2E/^2T_1$. Electrode potentials for these $V(NN)_3^{3+/2+}$ couples were found to be approximately 0.09 and 0.13V, where NN is bpy and phen, respectively. It was revealed that when the lowest energy electronic absorption band of $V(phen)_3^{2+}$ ($\lambda_{max} = 640$ nm) was irradiated in the presence of different electron acceptors, then there is one-electron oxidation leading to the formation of $(phen)_2V(\mu\text{-}OH)_2V(phen)_2^{4+}$. The $V(NN)_3^{2+}$ complexes followed similar photoredox mechanisms. The first step is oxidative quenching of $V(NN)_3^{2+}$ excited state, which is followed by hydrolysis and dimerization during the process of photooxidation process. They reported that reactions using methyl viologen (MV^{2+}) and Eu^{3+} followed the pathway:

$$V(phen)_3^{2+}\ (^4A_2) \xrightarrow[<35\ ps]{hv} V(phen)_3^{2+*}\ (2E \text{ or } MLCT)$$

$$V(phen)_3^{2+*} + A \longrightarrow V(phen)_3^{3+} + A^-$$

$$2V(phen)_3^{3+} + 2H_2O \longrightarrow (phen)_2V^{III}(\mu\text{-}OH)_2V^{III}(phen)_2^{4+} + 2phen + 2H^+$$

The three glycine-peroxo complexes of vanadium-(V), $NH_4[VO(O_2)_2GlyH]\cdot H_2O$, $K[VO(O_2)_2\text{-}GlyH]\cdot H_2O$ and $[V_2O_2(O_2)_3(GlyH)_2(H_2O)_2]$ have been synthesized by Bhattacharjee et al. (1990) from the reaction of V_2O_5 with hydrogen peroxide and glycine (GlyH) at different pH. It was reported that when glycine is in its zwitterionic form, it is coordinated to the V(V) center in a monodentate fashion through its carboxylic oxygen, and the peroxides are there as terminal bidentate ones in first two complexes, but one of the peroxide ligands is present as a μ-peroxo group in third complex. It was revealed that an aqueous solution of second complexexhibited peroxo-V(V) LMCT bands at 328 and in the 200−190 nm region, while third complex has only one broad LMCT band at 310−330 nm.

Sun et al. (2012) synthesized three new oxovanadium(IV) complexes with Hypocrellin B (HB), as a bridging ligand (where phen = 1,10-phenanthroline, tmp = 3,4,7,8-tetramethyl-1,10-phenanthroline and dpq = dipyrido[3,2-f:2′3′-h]quinoxaline) as terminal ligands. It was found that VO^{2+}-HB complexes exhibited higher water solubility, binding affinity toward dsDNA, absorptivity in the phototherapeutic window, and singlet oxygen quantum yield as compared to HB; thus, enhanced DNA photocleavage activity.

Holder et al. (2013) synthesized mixed-metal binuclear ruthenium(II)−vanadium(IV) complexes, and used them as potential photodynamic therapeutic agents for melanoma cell growth inhibition. They reported that complex, $[Ru(pbt)_2(phen_2DTT)](PF_6)_2 \cdot 1.5H_2O$ (where phen$_2$DTT = 1,4-bis(1,10-phenanthrolin-5-ylsulfanyl)butane-2,3-diol and pbt = 2-(2′-pyridyl) benzothiazole), [VO(sal-L-tryp)(H_2O)] (where sal-L-tryp = *N*-salicylidene-L-tryptophanate) afforded $[Ru(pbt)_2(phen_2DTT)VO(sal\text{-}L\text{-}tryp)](PF_6)_2 \cdot 5H_2O$; while [VO(sal-L-tryp)($H_2O$)] was treated with $[Ru(pbt)_2(tpphz)](PF_6)_2 \cdot 3H_2O$ (where tpphz = tetrapyrido[3,2-*a*:2′,3′-*c*:3″,2″-*h*:2‴,3‴-*j*]phenazine) to from $[Ru(pbt)_2(tpphz)VO(sal\text{-}L\text{-}tryp)](PF_6)_2 \cdot 6H_2O$. They carried out in vitro cell toxicity studies (with the 3-(4,5-dimethylthiazol-2-yl)-2,5-diphenyltetrazolium bromide (MTT) colorimetric assay) *in* dark and light with sodium diaqua-4,4′,4″,4‴ tetrasulfophthalocyanine cobaltate(II) ($Na_4[Co(tspc)(H_2O)_2]$), $[VO(sal\text{-}L\text{-}tryp)(phen)] \cdot H_2O$. The anti-cancer property of the chloride salts of finally produced complexes was found to be further enhanced, when treated cells were exposed to light, while no such observation was there on non-cancerous skin fibroblast cells. There is a great potential for using such mixed-metal binuclear ruthenium(II)−vanadium(IV) complexes to fight skin cancer.

Apostolopoulou et al. (2015) reported a DSSC using an electrolyte based on square pyramidal oxidovanadium(IV/V) complexes (Fig. 4.2). This oxidovanadium(IV) complex $(Ph_4P)_2[V^{IV}O(hybeb)]$ was combined with its oxidized analogue $(Ph_4P)[V^{V}O(hybeb)]$ {where $hybeb^{4-}$ = diamidodiphenolate ligand [1-(2-hydroxybenzamido)-2-(2-pyridinecarboxamido)benzenato}and applied as a redox couple in the electrolyte of DSSCs. They applied these complexes as a new redox mediator in DSSCs, with the Ru-based sensitizer N719 absorbed on a TiO_2 semiconducting film. They observed maximum energy conversion efficiencies of 2% at simulated solar light (AM 1.5; 1000 W m^{-2}) with an open circuit voltage (V_{oc}) of 660 mV, a short-circuit current (Jsc) of 5.2 mA cm^{-2} with a fill factor of 0.58 were achieved.

Gazi et al. (2015) observed that base metal vanadium photocatalysts can harvest visible light to carry out chemoselective C−C bond cleavage of lignin model compounds. Lignin is a major aromatic constituent of non-food biomass, which is inexpensive, and accessible source of fine chemical feedstocks such as phenols and aryl ethers. They have also reported that a new C−C activation reaction with high conversions under mild conditions. Visible light was used in the presence of earth-abundant vanadium oxo catalysts under

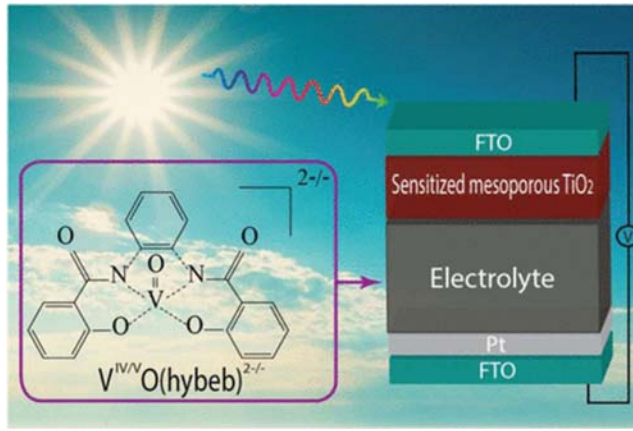

FIGURE. 4.2 Dye-sensitized solar cell involving vanadium complex. *Adapted from Apostolopoulou, A., Vlasiou, M., Tziouris, P.A., Tsiafoulis, C., Tsipis, A.C., Rehder, D., et al., 2015. Oxidovanadium (IV/V) complexes as new redox mediators in dye-sensitized solar cells: a combined experimental and theoretical study. Inorg. Chem. 54 (8), 3979–3988, with permission.*

ambient conditions. It was suggested that this is a unique pathway involving a photogenerated T_1 state during the C–C bond cleavage reaction. It is a sustainable approach to harvest sunlight for an unusual, and selective bond activation, which has potential for application in biomass valorization and organic transformations.

Sanasam et al. (2020) prepared four oxidovanadium (IV) complexes of 1H-imidazo[4,5-f][1,10]phenanthroline analogs with the general formula $[VO(L)_2](acac)_2$. They also evaluated their in vitro photodynamic activity. They reported that 1-(pyren-2-yl)-1H-imidazo[4,5-f][1,10]phenanthroline oxidovanadium(IV) complex exhibited remarkable photocytotoxicity in HaCaT cells. The IC_{50} of this complex was 8.2 μM under visible light (400–700 nm), but it was found to be less toxic in dark (IC_{50} ~70 μM). Its photophysical studies indicated that the lowest triplet excited states of this complex was long-lived and facilitated effective intersystem crossing, which resulted in the efficient generation of $^1O_2$ with good quantum yields (0.49).

Luminescence at room temperature from Earth-abundant metal ions in solution is a quite challenging as no Earth-abundant first-row transition metal complexes displayed emission (more than >1000 nm). Dorn et al. (2020) reported a vanadium(III) complex *mer*-$[V(ddpd)_2][PF_6]_3$, which exhibited phosphorescence around 1100 nm (in valeronitrile glass at 77 K) as well as at room temperature (in acetonitrile) with quantum yield 1.8×10^{-4}% (where ddpd = *N*,*N*′-dimethyl-*N*,*N*′-dipyridine-2-ylpyridine-2,6-diamine) (Fig. 4.3). This *mer*-$[V(ddpd)_2][PF_6]_3$ also revealed strong blue fluorescence with 2% quantum yield in acetonitrile at room temperature.

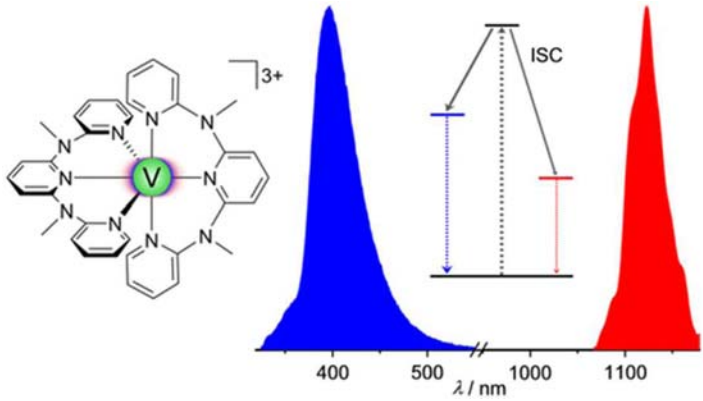

FIGURE. 4.3 Phosphorescence in *mer*-$[V(ddpd)_2][PF_6]_3$. *Adapted from Dorn, M., Kalmbach, J., Boden, P., Päpcke, A., Gómez, S., Förster, C., et al., 2020. A vanadium (III) complex with blue and NIR-II spin-flip luminescence in solution. J. Am. Chem. Soc. 142 (17), 7947−7955, with permission.*

Fomenko et al. (2021) prepared and investigated photochemistry of the binuclear heterometallic complex $[Ru(NO)(NO_2)_2(\mu\text{-}NO_2)(\mu{-}CH_3COO)(\mu\text{-}O)VO(dbbpy)]\cdot CH_3CN$ (where bdbbpy = 4,4′-di-tert-butyl-2,2′-bipyridyl). It was reported that acetonitrile solution of the complex undergoes an NO photo-release reaction on irradiation at 445 nm. It was observed that light excitation induces the charge transfer from NO_2 and dbbpy ligands to the antibonding orbitals of ON−Ru−O−V chain, and as a result, NO release is there. It was found that quantum yield of the Ru−NO photo-cleavage is 0.57 ± 0.05%. This complex represents a bifunctional platform, which can release nitric oxide in solution and reversibly switch the NO ligand coordination in the solid state. It was also found that the presence of vanadium strongly influences the photochemical properties of ruthenium nitrosyl in both; solid phase and solution.

Four new ternary oxovanadium(IV) complexes, $[VO(L)(B^{1\text{-}4})](acac)$ (where L = (E)-2-(2-hydroxybenzylideneamino)-5-guanidinopentanoic acid (Argininesalisylidene), 1H-imidazo-[4,5-f][1,10]-phenanthroline, 2-phenyl-1H-imidazo [4,5-f][1,10] phenanthroline, 2-(naphthalen-1-yl)-1H-imidazo [4,5-f][1,10] phenanthroline and (1-(pyren-2-yl)-1H-imidazo[4,5-f][1,10] phenanthroline) were synthesized by Sanasam et al. (2021). They also studied photocytotoxicity in A549 cell in dark and visible light (400−700 nm, 10 J cm^{-2}). They investigated that photochemistry of these four complexes is related to the generation of singlet oxygen ($^1O_2$). The degree of photocytotoxicity of the complexes was related to their ability in photo-activated $^1O_2$ generation. It was observed that four complex exhibited remarkable photocytotoxicity in A549 cells with its photo index (PI) ∼ 16 in visible light (400−700 nm, 10 J cm^{-2}) (IC_{50}, 3.81 μM), while complexes were almost less-toxic in dark (IC_{50}, 59.7 μM). A remarkable photocytotoxic efficacy of these

oxovanadium(IV) complexes can be promising photochemotherapeutic agents in place of porphyrin-based PDT agents.

Heller et al. (2021) observed photochemistry of hydrated vanadium ions (positively charged), $V^{+}(H_2O)_n$, where n = 1 to 41. It was found that there were electronic excitations related to the V^{+} core in clusters with up to 12 water molecules. There were strong 3d−4p transitions, which is redshifted, when vanadium is solvated more and it reaches a saturated initial solvation shell with 4 coordinated water molecules, which produced; $[HVOH(H_2O)_{n-1}]^{+}$. The structure and change of oxidation state of vanadium was from +I to +III, which started, where n is around 9. They observed that internal conversion (IC) and intersystem crossover (ISC) were shown as photochemical relaxation processes in this $V^{+}(H_2O)$ system (Fig. 4.4), leading to decomposition in low-lying triplet or quintet states. It was interesting to note that photons in different ranges behaved in different manner such as low photon energies (yellow, <1.5 eV) prevented fragmentation, while increased excitation energies (green, ~2 eV) allowed water loss. The more energy (blue, ~2.4 eV) allowed water splitting in the triplet manifold and it is also possible to eliminate hydrogen molecules with transition state (TS), hydrogen radical loss and water removal are become increasingly significant with increasing photon energy (purple, ~3.8 eV).

Zhang et al. (2021) investigated photochemical activation of C−H bonds by vanadium(V)−dioxo and vanadium(V)−oxo−peroxo diimine complexes. Organic substrates were selected with C−H bond having dissociation free energy between 70 and 97 kcal mol^{-1}. Compounds having weaker C−H bonds are earily oxidized and that too, in minutes, which otherwise takes days for

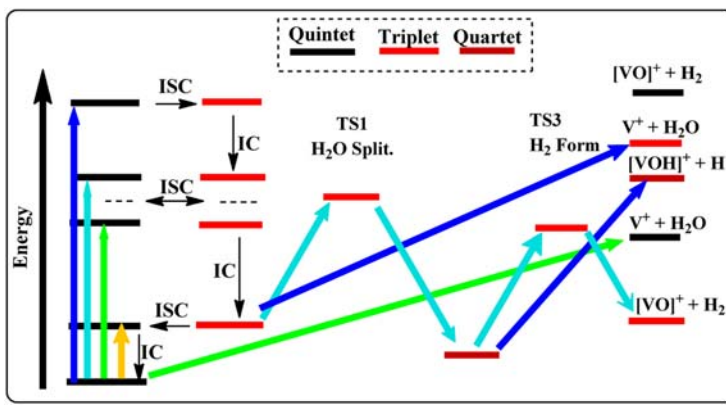

FIGURE. 4.4 Some photochemical relaxation processes in the $V^{+}(H_2O)$ system. *Adapted from Heller, J., Pascher, T.F., Muß, D., van der Linde, C., Beyer, M.K., Ončák, M., 2021. Photochemistry and UV/vis spectroscopy of hydrated vanadium cations, V+(H2O)n, n = 1−41, a model system for photochemical hydrogen evolution. Phys. Chem. Chem. Phys. 23 (39), 22251−22262, with permission.*

thermal oxidation by these complexes. It was observed that dioxygen was necessary for substrate consumption, suggesting that these electronically excited V complexes are radical reaction initiators through H-atom abstraction from the organic substrate.

Jose et al. (2022) synthesized vanadium complex anchored reduced graphene oxide (rGO-VO) by coordination interaction with phenyl azo salicylaldehyde (PAS) coupled trimethoxy silyl propanamine (TMSPA). They also studied physicochemical properties of rGO-VO. The photocatalytic studies of this anchored rGO-VO and $VO(acac)_2$ was also investigated for its use in methylene blue degradation, which indicated that methylene blue was degraded fast (about 64.2%) in 100 min under visible light irradiation in presence of anchored rGO-VO as compared to $VO(acac)_2$.

Psoriasis is a chronic inflammatory skin disease that can significantly impact the quality of human life. Various drug treatments are available; however, due to their long-term severe side effects, the usage of these drugs is limited. Photodynamic therapy (PDT) has been clinically approved for skin diseases due to its non-invasive nature. Lin et al. (2022) presented NNO-tridentate vanadium(IV) complexes, which has been used in PDT for anti-inflammatory effects in an imiquimod-induced psoriasis-like skin disease mouse model. They synthesized vanadium(IV) complexes using the NNO-tridentate ligand with a benzo[*i*]dipyrido[3,2-*a*;2′,3′-*c*]phenazine (dppn) moiety. It was found that photocytotoxicity of these vanadium(IV) complexes was low in dark, but fourth complex exhibited remarkable photocytotoxicity under blue light irradiation. It was suggested that [VO(*t*-butylL)(dppn)] could be a promising candidate for the treatment of psoriasis both; in vitro and in vivo.

4.3 Coordination compounds of niobium

Niobium is a shiny and silvery metal. It has an atomic number of 41 and belongs to group 5 with electron configuration $[Kr]4d^45s^1$. The oxidation state of niobium varies from +II to +IV. It is relatively soft and flexible, when very pure but impurities make it harder. Niobium is also used in alloys including stainless steel, and used in jet engines, rockets, oil rigs, and oil gas pipelines, prosthetics and implant devices, such as pacemakers.

Foust et al. (1982) reported the photolysis of $Nb(\eta^5\text{-}C_5H_5)_2H_3$ in C_6D_6 with H/D interchange with benzene. The photolysis of toluene solution of $Nb(\eta^5\text{-}C_5H_5)_2H_3$ in the presence of ligands formed $Nb(\eta^5\text{-}C_5H_5)_2(H)L$, where ligand is CO, and PEt. It was also revealed that the $Nb(\eta^5\text{-}C_5H_5)_2(H)CO$ complexes react photochemically with H, or PEt ligands and as a result, $Nb(\eta^5\text{-}C_5H_5)_2H_3$ and $Nb(\eta^5\text{-}C_5H_5)_2(H)PEt_3$ are produced, respectively. These reactions supported the participation of $Nb(\eta^5\text{-}C_5H_5)_2H$ as an intermediate from $Nb(\eta^5\text{-}C_5H_5)_2H_3$ and $Nb(\eta^5\text{-}C_5H_5)_2(H)CO$.

$$NbCp_2H_3 \xrightarrow{hv,\ Ar} NbCp_2H + H_2$$

$$NbCp_2(H)CO \xrightarrow{hv,\ Ar} NbCp_2H + CO$$

Clark (1984) investigated the photochemistry of some niobium complexes, $NbCp_2(X)(CO)$ (where $Cp = \eta^5\text{-}C_5H_5$, and $X = H$, Cl, CH_3, and C_6H_5) on irradiation in the presence of neutral ligands. It was observed that irradiation of $NbCp_2H(C_2H_4)$ in the presence of H_2, C_2H_4, PMe_2Ph, $P(OMe)_3$, and PPh_3 resulted in addition of a hydrogen ligand into the coordinated ethylene, but then substitution of ethylene was the main path in the existence of CO. The photochemistry of $NbCp_2H_3$ was studied and it was reported that chemistry of this trihydride is further complex in nature and it has numerous reactions.

$$NbCp_2H_3 + L \xrightarrow{h\nu} NbCp_2H(L) + H_2$$

A series of bimetallic compounds were obtained, when the trihydride of niobium was photolyzed using metal carbonyls. All of which cover the $NbCp_2(CO)$ part;

$$NbCp_2H_3 + NbCp(CO)_4 \xrightarrow{h\nu} NbCp_2CO(u\text{-}H)NbCp(CO)_3$$

$$NbCp_2H_3 + MnCp(CO)_3 \xrightarrow{h\nu} NbCp_2CO(u\text{-}H)MnCp(CO)_2$$

$$NbCp_2H_3 + M(CO)_3 \xrightarrow{h\nu} NbCp_2CO(u\text{-}H)M(CO)_5 \quad (M=Cr, Mo, W)$$

$$NbCp_2H_3 + Mn_2(CO)_{10} \xrightarrow{h\nu} [(NbCp_2CO)_2(u\text{-}H)]^+Mn(CO)_5^-$$

Baynham et al. (1985) carried out photolysis of $Nb(\eta^5\text{-}C_5H_5)_2H_3$ in nitrogen and argon atmospheres, which produces 16 electron complex $Nb(\eta^5\text{-}C_5H_5)_2H$. It was earlier assumed to be an intermediate in the catalytic initiation of aryl C—H bonds. It was reported that complexes were produced through photolysis of $Nb(\eta^5\text{-}C_5H_5)_2(H)CO$, self-possessed by minor quantities of the 17 electron $Nb(\eta^5\text{-}C_5H_5)_2CO$. It was also revealed that $Nb(\eta^5\text{-}C_5H_5)_2H_3$ was transformed to $Nb(\eta^5\text{-}C_5H_5)_2(H)CO$ in the CO medium while an advance reaction of $Nb(\eta^5\text{-}C_5H_5)_2(H)CO$ produces $Nb(\eta^5\text{-}C_5H_5)_2CO$ and some dicarbonyl products.

Cao et al. (2015) introduced niobium complex into atom transfer radical polymerization (ATRP) system and used as recyclable photocatalyst. Here, niobium complex acted as photocatalyst, which could be activated by the photoredox reaction in presence of visible light using ethyl 2-

bromoisobutyrate (EBiB) as initiator. It was reported that well-defined polymers with controlled molecular weight and narrow polydispersity index (PDI) (Mw/Mn = 1.16−1.30) were obtained on controlling feed ratio of photocatalyst to EBiB. It was also observed that the polymerization was highly responsive to light exposure and initiation and therefore, polymerization can be controlled on or off at ease. Apart from it, the photocatalyst can be recycled and reused again to initiate the polymerization for number of times without any significant loss of efficiency.

Rogachev et al. (2015) carried out some substitution reactions of binuclear niobium cluster anion $[Nb_2S_4(NCS)_8]^{4-}$ with different pyridine-based diimine ligands. The monosubstituted complexes $[Nb_2S_4(NCS)_6L]^{2-}$ were obtained on using 2,2′-bipyridine (bipy) and its derivatives but mono- and disubstituted complexes, $[Nb_2S_4(NCS)_6L]^{2-}$ and $[Nb_2S_4(NCS)_4L_2]$ have been obtained using 1,10-phenanthroline and 2-(2-pyridyl)benzimidazole (Hpbz), respectively. They diffused TiO_2 nanoparticles with $(Et_4N)_2[Nb_2S_4(NCS)_6(bipy)]$, which exhibited moderate photocatalytic activity in generation of hydrogen from water in the presence of Na_2S/Na_2SO_3 as a sacrificial electron donor. It was also reported that complexes with bipyridine ligands can function as broad-band optical limiters.

Camp et al. (2016) reported the synthesis and photo-reactivity of d^0 niobium imidoazido complexes supported by β-diketiminate ligands. Nitrides were formed through a photo-assisted intramolecular rearrangement, and it provides a new approach for formation of metal nitrides that does not require low-valent metal centers and it was claimed that it is a rare example, where the metal-imido moiety in complexes belonging to group 5 participates in reactivity.

Filippou el al. (2017) reported that photodecarbonylation of $[(\eta^5\text{-}C_5H_5)Nb(CO)_4]$ in the presence of $Ge(Ar^{Mes})Cl$ afforded a red-orange chlorogermylidene complex $[\eta^5\text{-}C_5H_5(CO)_3Nb = Ge(Ar^{Mes})Cl])$, (where Ar^{Mes} = 2,6-mesitylphenyl). They prepared $[(\eta^5\text{-}C_5H_5)(CO)_4]$ by a modified method and irradiated it in tetrahydrofuran with a high-power blue light LED yielding $Ge(Ar^{Mes})Cl$. It was observed that a relatively selective decarbonylation was there to chlorogermylidene $[\eta^5\text{-}C_5H_5(CO)_3Nb = Ge(Ar^{Mes})Cl]$ complex, in the form of red-orange crystals.

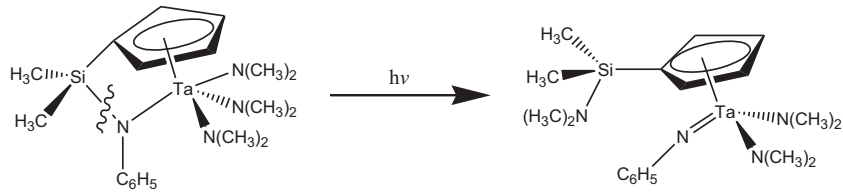

Shmakova et al. (2018) added 2-aminopyridine (2-NH_2-py), 2,2′-bipyridine (Bpy), and 1,10-phenanthroline (phen) in aqueous solutions of (NH_4)

$[NbO(C_2O_4)_2(H_2O)_2]\cdot 3H_2O$ (Nb-Ox) to produce tris-oxalato complexes such as $(BpyH_2)(BpyH)[NbO(C_2O_4)_3]\cdot 2H_2O$, $(2\text{-}NH_2\text{-}pyH)_3$ $[NbO(C_2O_4)_3]\cdot 2H_2O$ and $(phenH)_3[NbO(C_2O_4)_3]\cdot 3H_2O$, respectively. It was reported that complex $(BpyH_2)(BpyH)[NbO(C_2O_4)_3]\cdot 2H_2O$ showed strong blue photocoloration in daylight irradiation. The mechanism of this reaction is light absorption through $BpyH_2^{+\bullet}$ followed by energy transmission to $[NbO\ (C_2O_4)_3]^{3-}$, and electron transmission from the excited anion posterior to the cation fabricating blue cation radical $BpyH_2^{+}$. Here, oxalate ligands generated very reducing anion radical $CO_2^{-\bullet}$, which spreads such blue paramagnetic centers. Therefore, there is a great potential in these niobium oxalates in photochemical procedures such as photocatalysis.

Motorina et al. (2019) studied reactions of pyridine with (5,10,15,20-(tetra-4-tert-butylphenyl)porphinato)trichloroniobium(V) $(Nb(Cl)_3TtBuPP)$ and H+-bonded $Nb(Cl)_3TtBuPP$ $(Nb(Cl)_3TtBuPP\cdots H^+\cdots Cl^-)$ in toluene. It was reported demonstrated that $Nb(Cl)_3TtBuPP$ and $Nb(Cl)_3TtBuPP\cdots H^+\cdots Cl^-$ can be used as optical and fluorescent chemosensors of volatile organic compounds (VOCs) and nitrogenous bases-building blocks of food components, pharmaceuticals, and environmental pollutants. It was found that stability constant of the complex with pyridine $K = (1.99 \pm 0.3) \times 104\ L^2\ mol^{-2}$ and $(2.8 \pm 0.5) \times 10^2\ L\ mol^{-1}$, relative optical response $A = 0.91$ and 0.35, detection limit of pyridine 1.74×10^{-3} and $4.05 \times 10^{-4}\ mol^{-1}\ L$, respectively. These are applicable for use in the design of dye-sensitized solar cells (DSSCs).

Two new dodeca-niobate materials were synthesized by Zhang et al. (2020) via hydrothermal method and these are $K_3[Nb_2O_2][H_7SiNb_{12}O_{40}]\cdot 16H_2O$ $[Cu(en)_2]_9[(VNb_{12}V_{1.69}Nb_{0.31}O_{42}en_{0.31})_2]\cdot 20.69H_2O$ (where en = ethylenediamine). It was revealed that first compound had a bridging layer structure model and K plays a great role in its three-dimensional structure. On the other hand, second was capped Keggin POM with organic ligand chelating the capping atom. Their activity for photocatalytic hydrogen evolution and epoxidation of styrene has been evaluated. It was found that first was also a good photocatalyst to degrade rhodamine B.

4.4 Coordination compounds of tantalum

Tantalum belongs to group 5 and its atomic number is 73. Tantalum has filled 4f orbitals and 6s orbitals but 5d orbitals has only 3 electrons having electronic configuration as $4f^{14}5d^36s^2$. Its normal oxidation state is +V, but at extreme conditions of pressure and temperature, it can have a +II oxidation state. It is chemically stable, and is only attacked by strong alkalis and acids. It is corrosion-resistant, since it adsorbed O_2 and forms a passivating layer of Ta_2O_5. Tantalum is a suitable material for capacitors. Tantalum has several uses in electronics, medical fields, superalloys, capacitors, ballistics, chemical

processing. Tantalum is also used in making surgical sutures and prosthetic devices.

Herrmann and Baratta (1996) reported that niobium(V) amides [(η^5-C_5H_4)$-Si(CH_3)_2$-NR]Nb[$N(CH_3)_2]_3$ (where R = C_6H_5) having chelate like C, N-Ligands with 45% inaccessible product from the N-functionalized cyclopentadiene $C_5H_5-Si(CH_3)_2$-NHR and homoleptic amides M[$N(CH_3)_2]_5$ with binary amine subtraction. It was revealed that niobium derivatives exhibited an unparalleled photo-incited readjustment at room temperature, which afforded imido complexes [(η^5-C_5H_4)$-Si(CH_3)_2-N(CH_3)_2$]Nb(=NR)[$N(CH_3)_2]_2$ as a product 60% yield due to Si−N bond cleavage. Such Si−N bond cleavage in niobium complex, tris(dimethyl amido) [η^1:η^5-{(N-phenylamido)dimethyl-silyl} cyclopentadienyl]niobium(V) is there form bis (dimethylamido)(N-phenylimido)[η^5-{(dimethyl-amido)(dimethyl-silyl)} cyclopentadienyl] niobium(V) in presence of visible light in solution as well as in the solid-state.

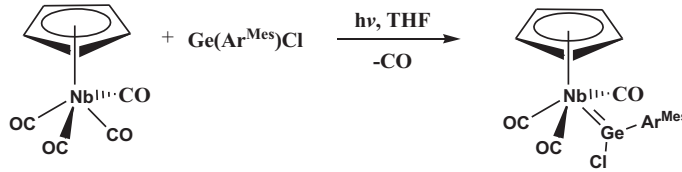

A series of η^5-pentamethylcyclopentadienyl tantalum(V) complexes have been prepared by Tonzetich et al. (2003). Their electronic and emission spectra were also examined. Compounds of the form Cp*TaX_4 (where X = Cl, Br, or OC_6F_5) and Cp*$TaCl_2X_2$ (where X = OC_6Cl_5, or 2,6-$OC_6H_3Cl_2$) have been found to luminesce at 77 K in frozen glasses. The shifts in luminescence maxima with ligand variation lead to the conclusion that the emissive state is a ligand-to-metal charge transfer, in which the highest occupied orbital is based on the donor atom of one of the monodentate ligands and the lowest unoccupied orbital is Ta-based.

Tonks and Bercaw (2010) synthesized two complexes of tantalum (dme) $TaCl_3(NNPh_2)$ and (dme)$NbCl_3(NNPh_2)$ (where dme = 1,2-dimethoxyethane) from MCl_5 and diphenylhydrazine via a Lewis-acid assisted dehydrohalogenation reaction. It was reported that first complex was monomeric in nature and it contains a κ^1-bound hydrazido(2-) moiety, but its corresponding imido derivatives is dark blue because of LMCT, which has been lowered in energy as a result of an $N_\alpha-N_\beta$ antibonding interaction that raises the level of highest occupied molecular orbital (HOMO). It was also observed that reaction of first complex with different neutral, mono- and dianionic ligands generated the corresponding ligated complexes retaining the κ^1-bound [Ta−$NNPh_2$] moiety.

Chauke et al. (2011) synthesized the tantalum (III) hydroxide complex and reported its photochemical application in the oxidation of cyclohexene to various products (cyclohexanol, cyclohexanediol, and cyclohexane oxide)

using it with the gold nanoparticles (Au NPs). The selectivity of products is in the order:

For tantalum (III) hydroxide complexes:

1,2-Cyclohexanediol (24.5%) > Cyclohexene oxide (12.3%) > 2-Cyclohexene-1-ol (11.6%) > 2-Cyclohexene-1-one (9.7%)

For tantalum (III) hydroxide complexes Au NPs:

1,2-Cyclohexanediol (17.6%) > Cyclohexene oxide (12.9%) > 2-Cyclohexene-1-ol (8.6%) > 2-Cyclohexene-1-one (7.2%)

Some brightly colored terminal hydrazido(2−) (dme)$MCl_3(NNR_2)$ complexes (where dme = 1,2-dimethoxyethane; M = Nb, Ta; and R = alkyl, aryl) have been synthesized by Tonks et al. (2012) (Fig. 4.5). It was observed that perturbation of the electronic environment of the β (NR_2) nitrogen affected the energy of the lowest-energy charge-transfer (CT) transition in these complexes. It was revealed that increasing the energy of the Nβ lone pair resulted in a decrease in the ligand-to-metal charge transfer (LMCT) energy, except for electron-rich niobium dialkylhydrazides. It was revealed that photophysical properties of these complexes had a potential redox noninnocence of hydrazido ligands, which could lead to ligand- and/or metal-based redox chemistry.

A simple and inexpensive method was reported by Ramos et al. (2015) for synthesis of a new series of β-diketonate-tantalum complexes. They used $[TaF_7]^{2-}$ solution (as the precursor of tantalum), thenoyltrifluoroacetone (TTA), hexafluoroacetylacetone (HFA), and benzoyltrifluoroacetylacetone (BFA) in basic medium. The pH was maintained using urea in the reaction medium. It was revealed that these complexes (in the solid state and in solution) upon irradiation with UV light at room temperature exhibited blue emission, and it may be due to heavy atom effect. It was suggested that these β-diketonate complexes have a great potential for application as optical ethanol, humidity sensors and materials for the development of luminescent devices.



FIGURE. 4.5 Some colored complexes of tantalum. *Adapted from Tonks, I.A., Durrell, A.C., Gray, H.B., Bercaw, J.E., 2012. Groups 5 and 6 terminal hydrazido (2−) complexes: Nβ substituent effects on ligand-to-metal charge-transfer energies and oxidation states. J. Am. Chem. Soc. 134 (17), 7301−7304, with permission.*

Zhao et al. (2018) prepared tantalum phosphate, trideca-sodium distrontium ditantalum nona-phosphate, $Na_{13}Sr_2Ta_2(PO_4)_9$, using the high-temperature flux method. It was revealed that it is an insulator with band gap of 4.78 eV, which makes it suitable as a luminescent host matrix. A series of solid solutions, i.e., $Na_{13}Sr_2Ta_2(PO_4)_9$:xDy^{3+} (where x = 0.01, 0.02, 0.04, 0.06, 0.08, 0.1, 0.12 and 0.14), were prepared and their photoluminescence properties were studied. It was reported that these emit two typical emissions of the Dy^{3+} ion, i.e., the $^4F_{9/2} \rightarrow {}^6H_{15/2}$ transition (476 nm) and the $^4F_{9/2} \rightarrow {}^6H_{13/2}$ transition (570 nm) under 350 nm light excitation.

Hao et al. (2022) used tantulum ureate (pre-catalyst), for photocatalytic hydroaminoalkylation of unactivated alkene with unprotected amine at room temperature. A unique reactivity were observed, when $Ta(CH_2SiMe_3)_3Cl_2$ and ureate ligand were combined with saturated cyclic backbone. They evaluated Ta photocatalytic hydroaminoalkylation (β-alkylation of amine) with an idea of finding the scope of substrate. It was suggested that both; similarities as well as differences were observed in reaction mechanism with Ta catalyzed hydroaminoalkyaltion under thermo-conditions.

Hernández et al. (2022) developed a single-step synthesis of $\{Ta_6Br^i_{12}\}$ @GO (GO = graphene oxide) nanohybrids by immobilizing $[\{Ta_6Br^i_{12}\}Br^a_2(H_2O)^a_4]\cdot 4H_2O$ (i = inner and a = apical positions of the Ta_6 octahedron) on GO nanosheets. They took advantage of an easy ligand exchange of the apical cluster ligands with the oxygen functionalities of GO. It was observed that hybrid formation enhanced the yield of H_2 from photocatalytic splitting of water as compared to their precursors and that two without using precious metals. This increase was attributed to the optimal cluster loading onto the GO support and its crucial role in the electron transfer from Ta_6 clusters into GO sheets; thereby, suppressing the charge recombination. Thus, octahedral tantalum clusters have a potential to develop new and environmentally friendly photocatalysts for generation of H_2 from water.

References

Adamson, A.W., Waltz, W.L., Zinato, E., Watts, D.W., Fleischauer, P.D., Lindholm, R.D., 1968. Photochemistry of transition-metal coordination compounds. Chem. Rev. 68 (5), 541−585.

Apostolopoulou, A., Vlasiou, M., Tziouris, P.A., Tsiafoulis, C., Tsipis, A.C., Rehder, D., et al., 2015. Oxidovanadium (IV/V) complexes as new redox mediators in dye-sensitized solar cells: a combined experimental and theoretical study. Inorg. Chem. 54 (8), 3979−3988.

Balzani, V., Bergamini, G., Campagna, S., Puntoriero, F., 2007. Photochemistry and photophysics of coordination compounds: overview and general concepts. Photochem. Photophys. Coord. Comp. I. https://doi.org/10.1007/128_2007_132.

Baynham, R.F., Chetwynd-Talbot, J., Grebenik, P., Perutz, R.N., Powell, M.H., 1985. Photochemistry of M (η5-C5H5)2 (H) CO and M (η5-C5H5)2 H3 (M= Nb, Ta) in low-temperature matrices. J. Organomet. Chem. 284 (2), 229−242.

Bhattacharjee, M., Chaudhuri, M.K., Islam, N.S., Paul, P.C., 1990. Synthesis, characterisation and physicochemical properties of peroxo-vanadium (V) complexes with glycine as the hetero-ligand. Inorg. Chim. Acta. 169 (1), 97−100.

Calvert, J.G., Pitts Jr., J.N., 1996. Photochemistry. J. Wiley, and Sons. Inc., New York.

Camp, C., Grant, L.N., Bergman, R.G., Arnold, J., 2016. Photo-activation of d0 niobium imido azides: en route to nitrido complexes. Chem. Commun. 52 (32), 5538−5541.

Cao, Y., Xu, Y., Zhang, J., Yang, D., Liu, J., 2015. Well-controlled atom transfer radical polymerizations of acrylates using recyclable niobium complex nanoparticle as photocatalyst under visible light irradiation. Polymer 61, 198−203.

Chauke, V.P., Arslanoglu, Y., Nyokong, T., 2011. Synthesis and photophysical behaviour of tantalum and titanium phthalocyanines in the presence of gold nanoparticles: photocatalysis towards the oxidation of cyclohexene. J. Photochem. Photobiol., A: Chem. 221 (1), 38−46.

Clark, R.J., 1984. Photochemistry and Electronic Structure of Some Niobocene Derivatives. ProQuest LLC, p. 8415455.

Dorn, M., Kalmbach, J., Boden, P., Päpcke, A., Gómez, S., Förster, C., et al., 2020. A vanadium (III) complex with blue and NIR-II spin-flip luminescence in solution. J. Am. Chem. Soc. 142 (17), 7947−7955.

Filippou, A.C., Hoffmann, D., Schnakenburg, G., 2017. Triple bonds of niobium with silicon, germaniun and tin: the tetrylidyne complexes [(k3-tmps)(CO)2Nb ≡ E−R](E = Si, Ge, Sn; tmps = MeSi (CH2PMe2)3; R = aryl). Chem. Sci. 8. https://doi.org/10.1039/c7sc02708g.

Fomenko, I.S., Mikhailov, A.A., Vorobyev, V., Kuratieva, N.V., Kostin, G.A., Schaniel, D., 2021. Solution and solid-state light-induced transformations in heterometallic vanadium-ruthenium nitrosyl complex. J. Photochem. Photobiol., A: Chem. 407. https://doi.org/10.1016/j.jphotochem.2020.113044.

Foust, D.F., Rogers, R.D., Rausch, M.D., Atwood, J.L., 1982. Photoinduced reactions of (. eta. 5-C5H5)2MH3 and (. eta. 5-C5H5)2M (CO) H (M= Nb, Ta) and the molecular structure of (. eta. 5-C5H5)2Ta (CO) H. J. Am. Chem. Soc. 104 (21), 5646−5650.

Gazi, S., Ng, W.K.H., Ganguly, R., Moeljadi, A.M.P., Hirao, H., et al., 2015. Selective photocatalytic C−C bond cleavage under ambient conditions with earth abundant vanadium complexes. Chem. Sci. 6 (12), 7130−7142.

Hao, H., Manßen, M., Schafer, L., 2022. Tantalum ureate complexes for photocatalytic hydroaminoalkylation. Catalyst. https://doi.org/10.26434/chemrxiv-2022-vcn22.

Heller, J., Pascher, T.F., Muß, D., van der Linde, C., Beyer, M.K., Ončák, M., 2021. Photochemistry and UV/vis spectroscopy of hydrated vanadium cations, V+(H2O)n, n=1−41, a model system for photochemical hydrogen evolution. Phys. Chem. Chem. Phys. 23 (39), 22251−22262.

Hernández, J.S., Shamshurin, M., Puche, M., Sokolov, M.N., Feliz, M., 2022. Nanostructured hybrids based on tantalum bromide octahedral clusters and graphene oxide for photocatalytic hydrogen evolution. Nanomaterials 12 (20), 3647.

Herrmann, W.A., Baratta, W., 1996. First amido-functionalized niobium and tantalum complexes of the ansa-structural type: synthesis and photochemical Si−N bond cleavage. J. Organomet. Chem. 506 (1−2), 357−361.

Holder, A.A., Taylor, P., Magnusen, A.R., Moffett, E.T., Meyer, K., Hong, Y., et al., 2013. Preliminary anti-cancer photodynamic therapeutic in vitro studies with mixed-metal binuclear ruthenium (II)−vanadium (IV) complexes. Dalton Trans. 42 (33), 11881−11899.

Jose, J., Balakrishnan, S.P., 2022. Synthesis, structural characterization, electrochemical and photocatalytic properties of vanadium complex anchored on reduced graphene oxide. Inorg. Nano-Metal Chem. 52 (6), 881−889.

Lin, R.K., Venkatesan, P., Yeh, C.H., Chien, C.M., Lin, T.S., Lin, C.C., et al., 2022. Effective topical treatments using innovative NNO-tridentate vanadium (IV) complexes-mediated photodynamic therapy in a psoriasis-like mouse model. J. Mater. Chem. B 10 (25), 4759−4770.

Motorina, E.V., Lomova, T.N., Mozhzhukhina, E.G., Gruzdev, M.S., 2019. New molecular chemosensors based on niobium (V) 5, 10, 15, 20-(Tetra-4-tert-butylphenyl) porphine for detection of VOCs. Russ. J. Inorg. Chem. 64 (12), 1538−1547.

Ramos, A.P., dos Reis, D.C., Pereira, R.R., Dias, L.G., Gonçalves, R.R., 2015. Synthesis and spectroscopic properties of luminescent tantalum (v)-β-diketonate complexes and their use as optical sensors and the preparation of nanostructured Ta2O5. Dalton Trans. 44 (8), 3829−3836.

Rogachev, A.V., Gushchin, A.L., Abramov, P.A., Kozlova, E.A., Vicent, C., Piryazev, D., et al., 2015. Binuclear sulfide niobium clusters coordinated by diimine ligands: synthesis, structure, photocatalytic activity and optical limiting properties. Eur. J. Inorg. Chem. 2015 (17), 2865−2874.

Sanasam, B., Raza, M.K., Musib, D., Pal, M., Pal, M., Roy, M., 2020. Photodynamic applications of new imidazo [4, 5-f][1, 10] phenanthroline oxidovanadium (IV) complexes: synthesis, photochemical, and cytotoxic evaluation. Chem. Select 5 (44), 13824−13830.

Sanasam, B., Raza, M.K., Musib, D., Roy, M., 2021. Photochemical and photocytotoxic evaluation of new oxovanadium (IV) complexes in photodynamic application. J. Chem. Sci. 133 (2), 1−14.

Shah, S.S., Maverick, A.W., 1986. Photophysics and photochemistry of 2, 2′-bipyridine and 1, 10-phenanthroline complexes of vanadium (II). Inorg. Chem. 25 (11), 1867−1871.

Shmakova, A.A., Glebov, M.E., Korolev, V.V., Stass, D.V., Benassi, E., Abramov, P.A., et al., 2018. Photochromism in oxalatoniobates. Dalton Trans. 47, 2247−2255.

Sun, Y., Zheng, Y., Lei, W.H., Zhou, Q.X., Hou, Y.J., Zhang, B.W., et al., 2012. Oxovanadium (IV) based hypocrellin B complexes with enhanced photodynamic activity. Dalton Trans. 41 (2), 651−657.

Tonks, I.A., Bercaw, J.E., 2010. (dme) MCl3 (NNPh2)(dme = dimethoxyethane; M= Nb, Ta): a versatile synthon for [Ta = NNPh2] hydrazido (2-) complexes. Inorg. Chem. 49 (10), 4648−4656.

Tonks, I.A., Durrell, A.C., Gray, H.B., Bercaw, J.E., 2012. Groups 5 and 6 terminal hydrazido (2−) complexes: Nβ substituent effects on ligand-to-metal charge-transfer energies and oxidation states. J. Am. Chem. Soc. 134 (17), 7301−7304.

Tonzetich, Z.J., Eisenberg, R., 2003. Luminescent η5-pentamethylcyclopentadienyl tantalum (V) complexes: synthesis, characterization, and emission spectroscopy. Inorg. Chim. Acta 345, 340−344.

Zhang, R., Zhou, W., Warren, J.J., 2021. Photo-initiated oxidation of C−H bonds by diimine complexes of vanadium (v). Chem. Commun. 57 (33), 4007−4010.

Zhang, T.T., Lin, P.H., Yu, G.Y., Zhang, X., Cui, X.B., 2020. Syntheses, characterization and properties of two new dodeca-niobates presenting unprecedented features. Dalton Trans. 49 (19), 6495−6503.

Zhao, J., Zhao, D., Xue, Y.L., Zhong, Q., Zhang, S.R., Liu, B.Z., 2018. Novel tantalum phosphate Na13Sr2Ta2 (PO4)9: synthesis, crystal structure, DFT calculations and Dy3+-activated fluorescence performance. Acta Crystallogr. C: Struct. Chem. 74 (9), 1045−1052.

Chapter 5

Coordination compounds of chromium, molybdenum and tungtsen

Saroj Lohar, Dushyant Kumar Prajapati, Jeevan Kunwar Chouhan, Ankita Vijay and Shipra Bhardwaj
Department of Chemistry, Government Meera Girls College, Udaipur, Rajasthan, India

5.1 Introduction

Coordination compounds or complexes are substances, in which a central metal ion is surrounded by nonmetal atoms or group of atoms, known as ligands. These are joined by coordinate bonds. Coordination compounds were known from the beginning of modern chemistry. The complex ion chain theory was proposed, where the ammonia molecules compensate the charge of the ion by forming chains of $[(NH_3)_x]^{x+}$ ions. Here, x is the coordination number of the metal ion. This ammonia chain was compared to hydrocarbon chain of $(CH_2)_x$. Some commonly known coordination compounds are vitamin B_{12}, hemoglobin, chlorophyll, etc.

Werner's theory is the most accepted theory to explain the bonding in coordination compounds. Alfred Werner proposed this theory in 1893. According to this theory, "if the ions were to form a chain, this would occur outside the coordination sphere" while the ions that bound directly to the metal would do so within the coordination sphere. Since then, a number of coordination complexes have been synthesized, analyzed and applied in various fields. The synthesis of $Cr(CO)_6$ involved treatment of Cr(III) salts with carbon monoxide at high pressure using phenyl magnesium bromides as reductant (Andre and Antoine, 1927; Owen et al., 1950). Chromium(II) acetylacetonate, $Cr(acac)_2$ is air-sensitive, yellow solid and the Cr center is square planar (Cotton et al., 1977) Chromium (III) acetylacetonate was also prepared by the reaction of chromium(III) oxide with acetylacetone. This is a purplish coordination compound and it is used in NMR spectroscopy as a relaxation agent (Fernelius et al., 2007). Ligand field analysis of the double excited states in Cr(III) tris chelated complexes was also carried out (Ceulemans et al., 1987).

Photochemistry and Photophysics of Coordination Compounds. https://doi.org/10.1016/B978-0-12-824493-7.00001-0
Copyright © 2023 Elsevier Inc. All rights reserved.

Excited state behavior as a probe of ground state ion pair interaction in chromium (III) polypyridyl complexes was presented by Hoffman and Serphone (1987). Structure, reactivity, photochemical and photophysical properties of Cr(III) complexes were also studied extensively in last 2 decades of last century (Ditze and Wesgestion, 1985; Endicott et al., 1986, 1987). The mechanisms of photochemical reactions involving transition metal complexes were studied extensively (Oskam et al., 1987).

The luminescence in transition metal complexes at room temperature in solution on excitation by visible light was paid more attention. Such species have low energy excited states and may be used in preparation of some chemicals because they allow the utilization of optical energy. Bis-donor ligand-substituted tungsten arylcarbyne complexes $[(W{=}CAryl)X(CO)_2L_2]$ (where X = halide, L = donor ligand) has been established as a new class of luminescent organometallic species. The photoemission from tungsten alkylidyne complexes in fluid solution was also studied (Bocarsly et al., 1985). Several tungsten phenylcarbyne complexes of the type $[(WCPh)X(CO)_2L_2]$ have been found to show luminescent behavior at room temperature in fluid phase on excitation with visible radiations (Bocarsly et al., 1987). The synthesis and characterization of some Cr(0), Mo(0) and W(0) carbonyl complexes containing chelating P, N and N, N ligands (2-(2′-pyridyl)-4,6-diphenylphosphinine and 2-(2′-pyridyl)-4,6-diphenylpyridine) was carried out by Krom et al. (2015). Significant changes in these properties of complex on replacing nitrogen atoms by phosphorous atoms are due to electronic differences between the heteroatoms. An attempt was made by Van Atta et al. (2000) to synthesize some $ML(CO)_4$ (where M = Cr, Mo, W; and L = en, bipy, dppm, dppe) complexes in presence of microwaves, resulting in the reduction of reaction times and an increase in yields over conventional syntheses. They also observed reduction in reaction time of about 5−500 folds.

Coordination compounds find a wide range of applications in chemistry, biology as well as medical sciences. These are found as a component in protein, enzymes, vitamin B_{12}, hemoglobin, chlorophyll, dyes, pigments, and as catalysts in preparing organic substances. They can do it due to presence of inner and outer coordination sphere and therefore, two types of reactions are possible simultaneously. Chelation therapy involves chelating agents to trap toxic metal agents, such as arsenic, mercury, and lead, by converting them to a chemically inert form that can be excreted without further interaction with the body.

5.2 Coordination compounds of chromium

Nicolas-Louis Vauquelin, a French chemist, discovered chromium in 1797. This metal was separated, and given the name chromium, because of its pigmented compounds. Small levels of chromium are responsible for different colors in some gems like ruby, emerald, serpentine, etc. This element has the

atomic number 24 and its symbol its Cr. It belongs to group 6. It is tough and brittle. The trivalent and hexavalent species of Cr are stable forms; however, there are some other valence states, which are unstable and transient in biological systems.

Structure, reactivity, photochemical and photophysical properties of Cr(III) complexes were also studied extensively in last 2 decades of last century (Kirk, 1981; Kane-Maguire et al., 1985; Ditze and Wasgestion 1985; Endicott et al., 1986, 1987). Photochemical oxidative substitution of $Cr(CO)_6$ with o-quinones (o-chloranil, 3,5-di-tert-butyl-l,2-benzoquinone) was investigated by two methods stationary as well as flash photolysis in aromatic hydrocarbon solvents (Vlcek, 1986). It was found that photogenerated $Cr(CO)_5$ species was coordinatively unsaturated and it undergoes a rapid oxidative addition of the o-quinone molecule. There was a strong labilization of Cr−CO bonds and CO-free Cr(III) complex [Cr(o-semiquinone)$_3$] was formed.

Indelli and Scandola (1993) synthesized cyano-bridged trinuclear complex [Ru(CN),[Cr(cyclam)(CN)*]$_2$. It was observed that its absorption spectrum was dominated by an intense Ru(I1)−Cr(II1) charge transfer (intervalence transfer) band. Efficient (q = 1) population was there of the Cr(II1)-centered doublet state by excitation into this band giving rise to a characteristic phosphorescent emission. It was reported that efficiency of this unusual process is dependent on the peculiar energetics of the system (activationless crossing between [-Ru(III)−Cr(II)] and [-Ru(11)-*Cr(III)], strongly "inverted" situation between [-Ru(III)−Cr(II)] and [-Ru(11)-Cr(III)]). The electronic states of this dyad system were interconverted ion this sequence ground state-charge-transfer state-locally excited state-ground state is just reverse of normally observed sequence in photoinduced electron transfer.

Delio and Ford (2000) investigated photoreactions of coordinated nitrite ion and reversible nitric oxide labilization from a chromium(III) complex [trans-Cr(cyclam)$(ONO)_2]^+$. It was suggested that such complexes can be used as photochemical source. They observed that there is potential of using such nitrite ion complexes as the photochemical source delivery nitric oxide to biological targets. They also reported photoreactions of the chromium(III) complex, trans-Cr(cyclam)$(ONO)_2^+$ (where cyclam = 1,4,8,11 tetraazacyclotetradecane) to give nitric oxide and Cr(IV) complex, which then changes Cr(V) complexes in the presence of molecular oxygen.

Shaw and Langford (2000) observed the wavelength dependence of photoinduced electron transfer and photosubstitution of $Cr(CNPh)_6$, which has low-lying MLCT states. It was observed that photosubstitution quantum yields increases with increasing excitation energy while photoinduced electron transfer quantum yields decrease with increasing excitation energy. At the lowest excitation energy used (532 nm, or 18 800 cm^{-1}) it was indicated that quantum yields for both these process; electron transfer and photosubstitution

reached same maximum value (0.29). It was also revealed picosecond time-resolved absorption spectra at 355 and 532 nm show two features:

- A bleach signal, which was centered at 400 nm, and an excited state absorption (ESA) in the 600 nm region.
- The ESA signal was found to be much weaker for 532 nm excitation than for 355 nm excitations.

The bleach and ESA decay exponentially with the same lifetime of 23 μs following a 355 nm flash. The $Cr(CNPh)_6$ exhibited two photochemical mechanisms: (i) A simple charge neutral dissociation and at high excitation energy, and (ii) Phenylisocyanide radical anion dissociates in a radical pair at low energy. This pair was considered responsible for the electron transfer reactivity and substitution, as well as complicated nanosecond kinetics. The primary processes for both these reactions take less than 20 ps.

Some new heteroleptic tris(polypyridyl)chromium(III) complexes, $[Cr(phen)_2L]^{3+}$ (L = substituted phenanthrolines or bipyridines), have been prepared by Isaacs et al. (2006). It was reported that both; ground state potentials and lifetime decays were found sensitive to structure of ligand and the nature of the solvent; of course, ligands 5-amino-1,10-phenanthroline (aphen) and 2,2′-bipyrimidine (bpm) are exceptions. It was also observed that addition of electron-donating groups in the ligand shifted the redox potentials to more negative side as compared to parent compound, $[Cr(phen)_3]^{3+}$. The longest lifetime ($\tau = 273$ μs) was observed in case of $[Cr(phen)_2(dip)]^{3+}$, (where dip = 4,7-diphenylphenanthroline) in air-free aqueous solutions.

Ford (2008) reported that electrostatic assemblies are formed between $Cr(L)(ONO)^{2+}$ cations and anionic surface of water-soluble core/shell quantum dots (CdSe/ZnS) and via an ion-pairing mechanism. It was observed that photoexcition of such modified QDs enhanced NO generation and these nanomaterials may have promising applications such as photochemical drugs.

Kushch et al. (2009) derived photochromic paramagnet from polyoxometalate $[Cr(OH)_6Mo_6O_{18}]^{3-}$ and ruthenium mononitrosyl complex $[RuNO(en)_2Cl]^{2+}$. As−prepared bifunctional material $[RuNO(en)_2Cl]_3[Cr(OH)_6Mo_6O_{18}]_2 \cdot 17H_2O$ (where en = ethylenediamine), was observed to have photochromic as well as paramagnetic molecular blocks.

Pokhrel and Nagaraja (2009) investigated photogalvanic behavior of $[Cr_2O_2S_2(1\text{-Pipdtc})_2(H_2O)_2]$ in a Honda cell using pure DMF and its mixture with water. They could obtain maximum potential and current as 200 mV and 18 μA, respectively in DMF. It was also found that this system was reversible, when the irradiated solution was aerated immediately, but when the solution was kept in dark for 12 h and then aerated system was found to be irreversible in nature.

Dethlefsen et al. (2009) prepared nitrosyl complex $[Cr(dmso)_5(NO)](PF_6)_2$ (where dmso = dimethyl sulfoxide) by the solvolysis of $[Cr(NCCH_3)_5(NO)](PF_6)_2$ in neat DMSO. It was observed that continuous photolysis of this

complex with $\lambda = 365-580$ nm light released NO with quantum yield, Φ (0.034−0.108 mol E^{-1}). A deoxygenated CH_3CN solution of $[Cr(NCCH_3)_5(NO)](PF_6)_2$ in the presence of excess of $[Fe(S_2CNEt_2)_2]$ resulted in a transfer of NO to the iron center on irradiation.

The chromium (III) nitrito complex trans-$Cr(cyclam)(ONO)^{2+}$ is a very promising photochemical precursor for nitric oxide delivery to physiological targets (Ostrowski et al., 2010). It was reported that visible wavelength excitation of this complex in solution containing thiol reductant such as the biological antioxidant glutathione (GSH) leads to permanent reaction even under anaerobic conditions, resulting in high quantum yield NO release. The nitric oxide formed under such conditions is sufficient, even at μM concentrations using a low-intensity light source, to activate the enzyme soluble guanylyl cyclase (sGC). It was also observed that photolysis of complex in the nM concentration range with a portable blue LED leads to vasorelaxation of porcine coronary arterial rings, a process which was attributed to the NO activation of sGC (Fig. 5.1).

Toneatto et al. (2010) investigated the ability of $[Cr(phen)_2(dppz)]^{3+}$ (where dppz = dipyridophenazine, and phen = 1,10-phenanthroline) associate with DNA and its use as photocleavage reagent for photodynamic therapy (PDT) was described. The dppz is a planar bidentate ligand having extended π system and it binds strongly to double strand oligonucleotides (ds-oligo) and plasmid DNA. Their intrinsic DNA binding constants was found to be $3.9 \pm 0.3 \times 10^5$ and $1.1 \pm 0.1 \times 10^5$ M, respectively. It was indicated that $[Cr(phen)_2(dppz)]^{3+}$ bound non-covalently to DNA, promoting the photocleavage of plasmid DNA under 457 nm exposure. The role of the excited state of $[Cr(phen)_2(dppz)]^{3+}$ was confirmed for damaging the DNA structure. It was reported that a combination of DNA, $[Cr(phen)_2(dppz)]^{3+}$ and light was



FIGURE. 5.1 Vasorelaxation via NO activation of sGC. *Adapted from Ostrowski, A.D., Deakin, S.J., Azhar, B., Miller, T.W., Franco, N., Cherney, M.M., et al., 2010. Nitric oxide photogeneration from trans-Cr (cyclam)(ONO)$^{2+}$ in a reducing environment. Activation of soluble guanylyl cyclase and arterial vasorelaxation. J. Med. Chem. 53 (2), 715−722. With Permission.*

necessary to induce such damage. The *Escherichia coli* may also be photoinactivated by irradiation in the presence of this complex. Thus, it was considered that $[Cr(phen)_2(dppz)]^{3+}$complex is a promising candidate for photocleavage of DNA with possible applications in photodynamic therapy.

Hagiwara et al. (2013) reported that photocatalytic water splitting activities of GaN:ZnO modified with tetraphenylporphyrinato-chromium(III) chloride (Cr-TPPCl) can enhance its photocatalytic activity. It can be used without decomposition in the photocatalytic splitting of water for 24 h. It was also revealed that photoluminescence intensity of GaN:ZnO was decreased by it with modification with Cr-TPPCl and also loading of NiO and RhOX cocatalysts. It was suggested that artificial photosynthetic water splitting could be achieved on GaN:ZnO photocatalyst (modified with various porphyrins) in presence of visible light. It was reported that apparent quantum efficiency of the dye-modified GaN:ZnO photocatalyst was 2.73% at 410 nm (RhOX (0.1 wt%), NiO (0.1 wt%)/Dye (0.5 wt%)/IrO_2(0.1 wt%)−GaN:ZnO).

The photophysics and photochemistry of $[(CO)_5CrC(OMe)Me]$ were investigated by McMohan et al. (2015). They could provide an unambiguous evidence for the photochemical formation of a long-lived, 18-electron metallaketene species, which was found to be capable of acting as synthetically useful intermediate. It was revealed that an intermediate metallacyclopropanone singlet excited state of Cr complex was detected with a lifetime of less than 100 ps.

DMSO > DMF > AC

Barbour et al. (2017) prepared some chromium(III) bis-arylterpyridyl complexes containing intraligand charge-transfer (ILCT) excited states. It was reported that these ILCT bands are tunable under UV and visible radiation by incorporating electron-donating and electron-withdrawing groups on the aryl ring. It was observed that absorption of $Cr(4'$-(4-methoxyphenyl)-2,2′:6′,2″-terpyridine)$]_2^{3+}$ was stronger in the visible region ($\varepsilon = 11{,}900$ and 5090 M^{-1} cm^{-1} at 450 and 500 nm) as compared to parent complex $[Cr(tpy)_2]^{3+}$ (where tpy = 2,2′:6′,2″-terpyridine) ($\varepsilon = 2160$ and 170 M^{-1} cm^{-1} at 450 and 500 nm), respectively.

Büldt et al. (2017) reported that meta-terphenyl unit substituted with an isocyanide group its two terminal aryls afforded a bidentate chelating ligand $(CNtBuAr_3NC)_3$. This ligand was found to stabilize chromium in its zerovalent oxidation state. The homoleptic $Cr(CNtBuAr_3NC)_3$ complex exhibited luminescence in solution at room temperature, with excited-state lifetime (2.2 ns) and as a result, it can find applicationas as earth-abundant sensitizer in dye-sensitized solar cells. The Cr(0) complex is a very strong photoreductant, because of its excited-state oxidation potential.

The synthesis and photophysical properties of an acidic, luminescent chromium(III) complex, $[Cr(H_2tpda)_2]^{3+}$ (where H_2tpda = 2,6-bis(2-pyridylamino)pyridine) was reported by Otto et al. (2018). It was observed that excitation of as-prepared complex at 442 and 782 nm resulted in strong

long-lived NIR luminescence in water and in acetonitrile, respectively. It was interesting to observe that deprotonation of the NH groups of this complex with a non-nucleophilic Schwesinger base in CH_3CN switched off the luminescence, while re-protonation with $HClO_4$ restores its emissive properties. Although its pK_a value of $\mathbf{2}^{\mathbf{3+}}$ in water was 8.8, even then deprotonation was not found reversible in the presence of hydroxide ions.

Huang et al. (2019) developed hydrophobic silicone loaded photoNORM polymer disks (PDs), which is photoactivated nitric oxide-releasing moiety (oxygen satble). The pohotoNORM is a new O-nitrito chromium(III) complex trans-[Cr(PetA)$(ONO)_2$](BF_4) (where PetA = 5,14-dimethyl-7,12-diphenyl-1,4,8,11-tetraaza-cyclotetradecane). They tried different silicone polymers with this photoNORM. It was observed that there is photouncaging of nitric oxide with 451 nm light from these systems. It was indicated that such ensembles can be used as implants providing a potential strategy for in vivo uncaging of NO at specific physiological targets triggered by tissue-transmitting NIR excitation.

Jiménez et al. (2019) prepared chiral resolution of a kinetically inert molecular ruby $[Cr(dqp)_2]^{3+}$ (where dqp = 2,6-di(quinolin-8-yl)pyridine), which displayed strong dual light emission at room temperature. It was reported that wrapped arrangement of this dqp chelating ligands around the Cr(III) provided a helical conformations (nonplanar), which leads to the diastereoselective assembly of chiral bis-tridentate monometallic Cr(III)-helix. It was revealed that circularly polarized luminescence (CPL) spectra had two polarized emission bands within the NIR region, which were attributed to characteristic metal-centered spin-flip $Cr(^2E \rightarrow {}^4A_2)$ and $Cr(^2T_1 \rightarrow {}^4A_2)$. A long excited-state lifetime of 1.2 ms with high quantum yield (5.2%) was observed in water at room temperature. Thus, $[Cr(dqp)_2]^{3+}$ can act an ideal sensitizer for the fabrication of enantiopure luminescent supramolecular energy-converting devices, which will open up new avenues for construction of polarized photonic devices and NIR-CPL materials using chiral Cr(III) chromophores based on earth-abundant metals.

Photochemical transformations of paramagnetic chromium(I) 1,3 bis(diphenylphosphino), $[Cr(CO)_4(Ph_2PCH_2CH_2CH_2PPh_2)]^+$ (where dppp = $Ph_2PCH_2CH_2CH_2PPh_2$) complex was studied in dichloromethane under by UV radiations (Luckham et al., 2019). It was observed that this complex $[Cr(CO)_4(dppp)]^+$ was transformed into trans-$[Cr(CO)_2(dppp)_2]^+$. It was also revealed that an intermediate isomer-$[Cr(CO)_3(\kappa^1\text{-dppp})(\kappa^2\text{-dppp})]^+$ complex was formed at low temperature (77−120 K) in presence of UV irradiation, which is photochemically transformed into trans-$[Cr(CO)_2(dppp)_2]^+$. This type of photoinduced reaction was found to be concentration-dependent, leading to a distribution of the three complexes ($[Cr(CO)_4(dppp)]^+$, trans-$[Cr(CO)_2(dppp)_2]^+$) and mer-$[Cr(CO)_3(\kappa^1\text{-dppp})(\kappa\ ^2\text{-dppp})]^+$.

The effects of an inversion center and ligand non-innocence was observed by Treiling et al. (2019) to tune the luminescence and photochemistry of excited state of $[CrN_6]$ chromophore $[Cr(tpe)_2]^{3+}$ (where tpe = 1,1,1-tris(pyrid-2-yl)ethane). The $[Cr(tpe)_2]^{3+}$ exhibited the longest luminescence lifetime ($\tau = 4500$ μs) for polypyridyl chromium(III) complex with a very high luminescence quantum yield ($\Phi = 8.2\%$) at room temperature. The tpe ligands were redox non-innocent in $[Cr(tpe)_2]^{3+}$. It was revealed that excited state redox potential and lifetime of this complex surpassed the classical photosensitizer $[Ru(bpy)_3]^{2+}$ (where bpy = 2,2′-bipyridine).

The photochemical functionalization of 2D and layered gray arsenic with chromium hexacarbonyl was studied by Sturala et al. (2019). They carried out covalent functionalization and exfoliation of arsenic rhombohedral under ultraviolet light irradiation in presence of chromium hexacarbonyl. Here, arsenic atoms were found to act as ligands on the central chromium. This modification can find applications in different fields such as sensors, electronics, energy devices, etc.

Two new chromium and manganese bimetallic nanoclusters, $[Cr_{8-x}Mn_x(OH)_{8-x}(H_2O)_x(OOCC_6H_5)_{16}, \quad x = 1.11]$ and $[Cr_4Mn_4O_4(OOCC_6H_5)_{12}\cdot 3CH_3CN\cdot H_2O]$, have been synthesized by Zhang et al. (2019) in a one-pot solvothermal reaction under visible irradiation. First cluster can produce an increased photocurrent and exhibited significant visible-light-driven photocatalytic activity for H_2 evolution in aqueous system. It also exhibited ultrahigh stability in both; acid and base aqueous solutions, making it an excellent synthon for preparing functional materials.

An ultrafast photochemistry of the $[Cr(NCS)_6]^{3-}$ complex was studied by Khvorost et al. (2020) upon excitation to the $^4T_2$ ligand field (LF) state in N,N-dimethylformamide (DMF) and dimethyl sulfoxide (DMSO). It was observed that vibrational relaxation occurs in 1−5 ps. It was also revealed that this $[Cr(NCS)_6]^{3-}$ complex in the 2E state also underwent intersystem crossing to the ground state in 85 ± 5 and 65 ± 5 ns in DMF and DMSO, respectively but only a small amount undergoes irreversible photochemical decomposition in case of electronically excited state. It was found that $[Cr(NCS)_6]^{3-}$ complex released single or double isothiocyanate ions followed by its photolysis in DMSO by the coordination of the solvent molecules.

Anzani et al. (2020) investigated the effect of magnetic field on phosphorescence lifetime, emission spectrum, and quenching of tris (1,10 phenantroline) chromium (III) complex by phenols. Changes in the emission spectrum and lifetime of the ($^2T/^2E$) states of $[Cr(phen)_3]^{3+}$ were observed in presence of an external magnetic field. It was observed that emission spectrum showed changes in their phosphorescent states (^2E and $^2T_1$ doublets); (split and shift), with enhanced emission of a band corresponding to the $^2T_1 \rightarrow {}^4A_{1g}$ transition located at 700 nm and decrease in intensity of the band located at 730 nm corresponding to $^2E \rightarrow {}^4A_{1g}$ transition. The phosphorescent lifetime for both these emission states was found to be about ∼70 μs in aerated

aqueous solutions at ambient temperature and a decrease was observed with increasing applied external magnetic field.

Wegeberg et al. (2021) reported that chromium(0) with chelating diisocyanide ligands exhibited very weak MLCT emission (in solution) at room temperature. The luminescence quantum yield of chromium(0) isocyanide complex was enhanced by almost double with a significant increase in the MLCT lifetime also. The pyrene units in the diisocyanide ligand backbone gives an enlarged π-conjugation system and strongly delocalized MLCT state, where nonradiative relaxation was less dominant although a redshift of the emission was there. Here, pyrene moiety is coupled electronically to chromium(0) complex core in the excited state, but this is not the case in the ground state. It was reported that luminescence lifetimes and quantum yields for this pyrenyl-decorated chromium(0) complex exhibited bell-shaped dependence on polarity of solvent, which indicated two counteracting effects governing the MLCT deactivation. These two effects were predominant in deactivation through:

- Direct nonradiative relaxation to the ground state following the energy gap in more polar solvents, and
- Energetically nearby lying metal-centered state in apolar solvents.

A highly luminescent spin-flip emitter with a quantum chemically predicted blue-shifted luminescence was reported by Reichenauer et al. (2021). It was observed that spin-flip emission band of the chromium complex $[Cr(bpmp)_2]^{3+}$ (where bpmp = 2,6-bis(2-pyridylmethyl)pyridine) shifted to higher energy from 780 to 709 nm. The photoluminescence quantum yields was increased to 20%, and a long excited state lifetimes (ms) could be achieved at room temperature in acidic D_2O solution. The photophysical and ground state properties (lifetime, quantum yield, redox potential, and acid/base) of as-prepared spin-flip complex incorporating an earth-abundant metal surpassed $[Ru(\alpha\text{-diimine})_3]^{2+}$ charge transfer complexes, (commonly employed in optical sensing and photoredox catalysis), which indicates a bright future of these molecular ruby analogs.

Bapsita et al. (2021) reported the participation of the excited states of $[Cr(TMP)_2dppz]^{3+}$ (where TMP = 3,4,7,8-tetramethyl-1,10-phenanthroline; and dppz = dipyrido[3,2-a:2′,3′-c]phenazine) in photoreactions of DNA. It was observed that interactions of its enantiomers with natural DNA or with oligodeoxynucleotides with varying AT content (0%−100%) resulted in quenching of its emission. It was revealed that relatively long-lived dppz-centered states was found there in the region between 350 and 400 nm after excitation; thus, yielding emissive metal-centered state. It has promising application in the field of photocatalysis and phototherapeutics.

Hou et al. (2021) prepared two hetero-binuclear complexes $[Cr(L)Cl(\mu_1\text{-}OAc)Ln(\mu_2\text{-}OAc)Cl(H_2O)]$ (Ln = Eu or Tb) by self-assembling of $Ln(OAc)_3 \cdot 6H_2O$ with the chromium(III)-complex precursor $[Cr(L)Cl(H_2O)]$,

which was formed from oxidation and coordination reactions of $CrCl_2$ and the Salen-type Schiff-base ligand N,N′-bis(3-methoxy-salicylidene)cyclohexane-1,2-diamine. It was attributed to effective Eu^{3+}-to-Cr^{3+} energy transfer. The [Cr(L)Cl(μ_1-OAc)Eu(μ_2-OAc)Cl(H_2O)] exhibited the highly improved Cr^{3+}-characteristic near-infrared (NIR) phosphorescence as compared to its terbium counterpart [Cr(L)Cl(μ_1-OAc)Tb(μ_2-OAc)Cl(H_2O)] or Cr(III)-complex precursor [Cr(L)Cl(H_2O)].

Boden et al. (2021) used high-level spectroscopic methods on highly luminescent chromium(III) complex $[Cr(ddpd)_2](BF_4)_3$ (where ddpd = N,N′-dimethyl-N,N′-dipyridine-2-ylpyridine-2,6-diamine), which was two near-IR emissive doublet states with of the order of lifetimes microseconds. A remarkable rise in the integrated emission intensity by more than 3 times was observed at <10 K.

Lee et al. (2021) synthesized a new ligand (1,10-phenanthrolin-5-amine, N-(2-fluorenylmethylene)) and formed UV activable photoCORMs with the $M(1)(CO)_4$ (M = Cr, Mo, and W. These compounds contain four COs bonded to the metal center with distorted octahedral geometry, and these CO can be released on UV light (365 nm). It was observed that chromium compound displayed the shortest half-life and shortest CO-releasing rate. These compounds exhibited potent cytotoxicity against two human colorectal cancer cell lines (HT-29 and HCT 116) and with strong photo-induced cytotoxicity and high selectivity.

Nassar and Ali (2021) synthesized four binuclear complexes $[Cr_2(CO)_2L_2]$, $[Mo_2O_4(L)_2]$ (2), and $[W_2O_4(L)_2]$ (3) $[Mo_2O_5(CO)L]$. H_2O from the reaction of $[M(CO)_6]$ (M = Cr, Mo and W) with 6,6'-(([1,1′-biphenyl]-4,4′ diylbis(azaneylylidene)) bis(methaneylylidene)) bis(2,4-dichlorophenol) (H2L) in THF. It was reported that magnetic measurements indicated diamagnetic properties for molybdenum and tungsten complexes, but paramagnetic character for chromium complex. It was revealed that H2L was coordinated as tetradentate ligand via two imine nitrogen and two deprotonated phenolic oxygen atoms. It was also observed that Schiff base ligand (H2L) and its complexes exhibited fluorescence properties and can serve potentially as photoactive materials.

5.3 Coordination compounds of molybdenum

Molybdenum was discovered by Carl Welhelm Scheele, a Swedish Chemist in 1778. It was found in a mineral known as molybdenite (MoS_2) and at that time, it was confused as a lead compound. Molybdenum was isolated later in 1781 by Peter Jacob Hjelm. Presently, molybdenum is mostly obtained from molybdenite, powellite ($CaMoO_4$) and wulfenite ($PbMoO_4$). Molybdenum is an element with given atomic number 42 and its symbol is Mo. It is placed in group 6 and period 5. Molybdenum does not occur as free metal on Earth; however, it is present in various oxidation states in form of different minerals.

It forms compounds in various oxidation states starting from II to VI. It is a silvery-white metal, which is ductile and highly resistant to corrosion.

The photochemical studies were reported for a series of M(CO),L complexes (where M = Cr, Mo, or W and L = 2,2′-bipyridine, 1.10-phenanthroline, or a derivative diimine ligand) by Manuta and Lees (1986). They observed low-energy LF and intense metal-to-ligand charge-transfer (MLCT) transitions in these complexes. It was observed that energy positions of the MLCT transitions were found to be extremely sensitive to solvent medium and the nature of ligand substituent. The photoreaction efficiencies depends on wavelength of irradiation; e.g., W(CO)(bpy) in benzene; LF excitation at X = 395 nm yields $\phi = 1.2 \times 10^{-5}$, whereas MLCT excitation at X = 514 nm yields $\phi = 5.4$ X. It was revealed that LF state was responsible for the photochemistry in these $M(CO)_4L$ complexes. The photoefficiencies following MLCT excitation (514 nm) were found to be slightly temperature-dependent, which indicated that the MLCT state is intrinsically photoactive or some another excited state is close in energy.

Szymańska-Buzar et al. (1995) reported that photochemical reactions in low-temperature matrix X (where X = Ar or CH_4) doped with molybdenum hexacarbonyl and an alkyne (HC≡CH, MeC≡CH, or MeC≡CMe) afforded corresponding alkyne complex of molybdenum pentacarbonyl, [(η^2-RC≡CR') $Mo(CO)_5$], [X … $Mo(CO)_5$] and CO. They also investigated photochemical interconversion of these three species [$Mo(CO)_6$], [X … $Mo(CO)_5$] and[(η^2-RC≡CR')$Mo(CO)_5$]. It was observed that a further irradiation ($\lambda = 313$ nm) caused the pentacarbonyl complexes to release one CO with the formation of tetracarbonyl species, while there was photoejection of CO at $\lambda = 369$ nm and formation of [(η^2-RC≡CR')$Mo(CO)_4$] (R,R′ = H,H or Me,Me).

The photochemistry of (η^6-arene)$Mo(CO)_3$ compounds (where arene = benzene, mesitylene, hexamethylbenzene, *or p*-xylene) was investigated by Breheny et al. (1998) using laser flash photolysis, matrix isolation and time-resolved infrared spectroscopy (TRIR). It was reported that the efficiency for photochemical expulsion of CO from (η^6-mesitylene)$Mo(CO)_3$ was dependent on wavelength of irradiation, which was found to be different from behavior of analogous (η^6-arene)$Cr(CO)_3$.

Fui et al. (2013) observed that mononuclear molybdenum complex with the general formula [MoTp*(NO)I(X)] (where Tp* = tris(3,5-dimethylpyrazolyl) hidroborate and X = 1,4-bis(pyridin-4-ylethynyl)benzene) exhibited properties of a photosensitizer in photoelectrochemical cell. It was observed that photoelectrochemical properties of TiO_2 photoelectrode sensitized by [MoTp*(NO)I(X)] gave positive photoinduced current as compared to unsensitize TiO_2photoelectrode.

Mark-Lee et al. (2013) reported that molybdenum dithiolene complexes [MoTp*(NO)(L)] (where Tp* = tris(3,5-dimethylpyrazolyl)hydroborate and L = toluene-3,4-dithiolate, 1,2-benzenedithiolate, or 3,6-dichloro-1,2-benzenedithiolate) exhibited the desired chemical and physical properties

as photosensitizer in a photoelectrochemical cell. It was revealed that all the three complexes had an energy band gap in the range of 1.45−1.48 eV, which falls in visible light region. It was reported that [MoTp*(NO)(L3)]-doped TiO_2 photoanode showed an enhanced photoinduced current as compared to undoped TiO_2 photoanode. It was also revealed that Cl atoms on the dithiolene group was responsible for a better interaction between TiO_2 photocatalyst and the photosensitizer molecule using halogen atom-induced chemical bonding.

A homoleptic Mo^0 complex with bidentate isocyanide ligands was reported by Büldt et al. (2016), which exhibited metal-to-ligand charge transfer (MLCT) luminescence with lifetimes and quantum yields almost similar to $Ru(bpy)_3^{2+}$(where bpy = 2,2′-bipyridine). It was observed that this Mo^0 complex is very strong photoreductant and it could reduce acetophenone. They revealed that this complex has a potential for its use in photoredox catalysis in rearrangement of acyl cyclopropane to a 2,3-dihydrofuran whereas strongly reducing Ir(2-phenylpyridine)$_3$ photosensitizer also cannot catalyze it because of highly negative reduction potential. They opened new avenues for use of Mo^0 complexes with chelating isocyanides with long-lived MLCT excited states that can find applications in photoredox chemistry.

Kirakci et al. (2014) synthesized two octahedral molybdenum cluster compounds $Na_2[Mo_6I_8(N_3)_6]$ and $Na_2[Mo_6I_8(NCS)_6]$ and studied their luminescent properties and biological activity. Most of the molybdenum clusters have low solubility in water and undergo hydrolysis along with sedimentation, aggregation and diminishing luminescence as well as singlet oxygen-sensitizing properties. These as-prepared compounds behaved in a different manner. They are soluble in water and also show red luminescence, which is quenched by molecular oxygen to produce singlet oxygen ($^1\Delta_g$) with high quantum yields. It was also reported that these $[Mo_6I_8(N_3)_6]^{2-}$ and $[Mo_6I_8(NCS)_6]^{2-}$complexes gradually hydrolyze but they do not form sedimentation, aggregation and there are luminescence properties also. Apart from it, quantum yields of singlet oxygen also remained unaffected.

Luo et al. (2016) prepared two polymolybdate-based complexes $(H_2L1)_2(Mo_4O_{13})$ and $(L2)_2(HL2)_2(Mo_8O_{25})\cdot 7H_2O$ (where L1 = 4-(5-((2H-1,2,4-triazol-3-yl)-2H-1,2,4-triazol-3-yl)pyridine) and L2 = 5-[4-(1 Himidazol-1-yl)-phenyl]-2H-tetrazole) via hydrothermal method. It was found that in first complex, one-dimensional (1D) $[Mo^V_4Mo^{VI}_4O_{26}]_\infty^{8-}$ chain was constructed by vertice-sharing of $\{MoO_6\}$ octahedra, while uncoordinated protonated $[H_2L1]^{2+}$ species are linked with different $[Mo_8O_{26}]_\infty^{8-}$ chains via supramolecular forces. In second complex $[Mo_8O_{25}]^{2-}$ moieties are linked by the μ_3-$[HL2]^+$ and μ_2-L2 ligands into 1D chain, which possesses more narrow band gap than first complex showing stronger photocurrent response as compared to first complex under the visible light (650 nm > λ > 350 nm). It was observed that the electroconductivity of the complex/graphene composite material in case of first complex on addition of graphene was much improved.

It exhibited much improved electrocatalytic activity for the evolution of H_2 reaction (HER) as compared to second one.

Martínez et al. (2016) investigated photo-assisted oxygen transfer to cyclohexene, 1-octene and cyclooctene. They used molecular oxygen as a primary oxidant using dichloro-dioxo-(4,4′-dicarboxylato-2,2′-bipyridine) molybdenum (VI) complex grafted on the surface of mesoporous TiO_2. It was observed that porosity of the support titania, as well as the amount and dispersion of the covalently anchored dioxo Mo(VI) complex strongly influenced the photocatalytic properties. It was reported that new hybrid Mo(VI) derivatized mesoporous TiO_2catalyst was found to be efficient in the photo-assisted oxygen transfer to different alkenes. The high stability of such catalyst was also confirmed by recycling studies.

Two complexes of molybdenum have been synthesized by Mitra and Sarkar (2016): $[NBu_4][MoO(bpy)(mnt)(SePh)]\cdot CH_2Cl_2$ and $[NBu_4][MoO(phen)(mnt)(SePh)]\cdot CH_2Cl_2$ (where bpy = 2,2′-bipyridine, phen = 1,10-phenanthroline, and mnt = maleonitriledithiolate ion). These were stabilized by aromatic diimine. These complexes generated superoxide radical under aerobic conditions is presence of sunlight (or tungsten lamp) in solution associated with the formation of paramagnetic Mo(V) species because of single electron transfer from the Mo(IV) complex to oxygen. The presence of Mo(V) under photo-irradiation was ascertained by EPR spectroscopy while generated superoxide radical was confirmed by nitrobluetetrazoleum (NBT) chloride test giving blue diformazan. The emission lifetime of phosphorescence of both these complexes was 6−8 μs.

Cheplakova et al. (2017) used nanosized mesoporous metal−organic framework MIL-101 (Matérial Institut Lavoisier) as nanocarrier for photoactive hexamolybdenum cluster compounds. They investigated hexamolybdenum cluster complexes for their possible use in biological and medical applications like singlet oxygen generation, luminescence, cytotoxicity, cellular uptake behavior, etc. It was also revealed that as-prepared materials were then used in living cells because of their low toxicity values. It was found that cluster supported on MIL-101 exhibited in vivo phototoxicity

A Schiff (Mo) based complex was prepared by Bian et al. (2018) supported on GO surface. Then it was combined with graphitic carbon nitride (g-C_3N_4) polymer (Mo-GO/g-C_3N_4) so that it becomes photoactive. The photocatalytic activity of as-prepared nanocomposite was evaluated under simulated sunlight (AM 1.5) for epoxidation of different olefin substrates. It was also revealed that both; metal active centers and GO can efficiently enhance electron transfer; thus, improving its catalytic performance.

Fogeron et al. (2018) synthesized two dithiolenes with a pyrazine ring fused with a pyran ring, which mimicked molybdopterin (MPT) present in the active site of formate dehydrogenases (FDHs). It was revealed that one mimicks MPT in the dihydropyrazine form while the other mimicks MPT in tetrahydropyrazine form, which is the more biologically relevant. Both these

complexes were duly characterized. The as-prepared $MoO(dithiolene)_2$ complexes catalyze the photoreduction of CO_2, where formic acid was obtained as the major product, and carbon monoxide with turnover number 100 in about 8 h.

Herr et al. (2019) reported that tris(diisocyanide)molybdenum(0) complexes have long-lived ^{3}MLCT (metal-to-ligand charge transfer) excited states. It was observed that complex of Mo was better as compared to $[Ru(2,2'\text{-bipyridine})_3]^{2+}$ with quantum yield (0.20), luminescence excited state lifetimes (microseconds) could be achieved at room temperature in solution. It was also revealed that such excited Mo(0) complexes are capable of inducing chemical reactions, which required precious metal-based photosensitizers. It was revealed that a robust Mo(0) complex exhibited stable photoluminescence and it was found to be photoactive on continuous irradiation for more than 2 months. It was indicated that Mo(0) complexes with diisocyanide chelate ligands, form a new family of luminophores, photosensitizers, which can be used as an alternate costly metal-based 4 d^6 and 5 d^6 complexes and to non-emissive Fe(II) compounds. Thus, it can be used for in lighting, sensing, and catalysis.

Ma et al. (2019) covalently decorated some molybdenum(VI/V) POM-based self-constructed complexes $[Mo^{VI}_{12}O_{24}(\mu_2\text{-}O)_{12}(trz)_6(H_2O)_6] \cdot 6Hma \cdot 18H_2O$, $[Mo^{VI}_{7}O_{14}(\mu_2\text{-}O)_8(trz)_5(H_2O)] \cdot 7Hma \cdot 5H_2O$, $Na_3[Mo^{V}_{6}O_6(\mu_2\text{-}O)_9(Htrz)_3(trz)_3] \cdot 7.5H_2O$ and $[Mo^{V}_{8}O_8(\mu_2\text{-}O)_{12}(Htrz)_8] \cdot 30H_2O$ (Where Htrz = 1*H*-1,2,3-triazole, ma = methylamine) with tri-coordinated deprotonated/protonated 1,2,3-triazoles. The channels were observed in first complex with an inner diameter of 7.5 Å, while a tunnel with inner diameter of 4.1 Å composed of stacking molecules was there in other complex. It is occupied by free disordered methylamines, showing selective adsorption of O_2 and CO_2 at 25°C. The last two complexes are fine adsorption materials with diversified pores for CH_4 and CO_2 under low pressure, while first two complexes exhibited reversible photoresponsive thermochromism. The photo-/thermoresponse properties of these as-prepared complexes offer a new pathway for the self-constructions of one-off hybrid materials having good properties of both; MOFs and POMs.

Two complexes mono-dithiolene complexes $[Mo(CO)_2(dt)(dppe)]$ and $[W(CO)_2(dt)(dppe)]$ [where dt = cyclohex-1-ene-1,2-dithiol; 5,6-dihydro-2*H*-pyran-3,4-dithiol and dppe = 1,2-bis(diphenylphosphino)ethane)] were synthesized by Elvers et al. (2019) by a photochemical procedure. It was reported that the typical basic deprotection of the dithiolene ligand precursor was replaced by a light-induced opening of the 1,2-dithiole-2-one moiety. Advantages of this method are; cleaner transformations, higher yields and the possibility to monitor the reaction progress continuously and precisely. It was revealed that the light induced pericyclic reaction of the protection group releases CO with formation of a 1,2-dithione, which can oxidize an electron rich metal precursor because of its non-innocent character.

A carbon monoxide-releasing material (CORMA) has been prepared by Silva et al. (2021). They incorporated molybdenum hexacarbonyl in a hafnium-based metal-organic framework (MOF) with the UiO-66 architecture. They adsorbed $Mo(CO)_6$ from solution to afford supported materials having 6.0−6.6 wt% Mo. It was revealed that both crystallinity and morphology of the porous host was not affected by the loading. They can behave as CORMAs and transfer CO to heme proteins, They used the standard myoglobin (Mb) assay method to test these materials. It was observed that encapsulated hexacarbonyl molecules in Mo(6.0)/UiO-66(Hf) liberated CO, when photoactivate with low-power UV light (365 nm) leading to a maximum amount of 0.26 mmol CO released per g of material, while it was found stable in dark.

Ultrafast photochemistry of molybdenum carbonyl-nitrosyl complex with a triazacyclononaneco ligand was studied by Gessner et al. (2021). They observed that transition metal complexes capable of releasing small-molecule messengers (carbon monoxide and nitric oxide) upon photoactivation can be used as an effective tools. It was reported that photodissociation of one CO ligand on UV excitation was there, but release of NO was not observed under similar conditions.

De la Torre et al. (2022) incorporated an ionic assembly of the hexanuclear molybdenum cluster compound $(Bu_4N)_2[Mo_6I_8(CH_3CO_2)_6]$ in amino-decorated mesoporous silica nanoparticles (MCM-41) affording molybdenum-based hybrid photosensitizer (1@MCM-41). As-prepared photoactive material had high porosity because of intrinsic high specific surface area of MCM-41 nanoparticles (989 $m^2\ g^{-1}$), and it provided a good dispersion of the hexamolybdenum clusters on the nanoparticles surface. It was reported that this hybrid photosensitizer can generate singlet oxygen efficiently, and it gave photooxygenation reaction of 9,10-anthracenediyl-bis (methylene)dimalonic acid (ABDA) in water. It was also revealed that a good activity of as-prepared hybrid photosensitizer was there in presence of LED light (15.6 mW/cm^{-2}) against human cervical cancer (HeLa) cells. It was observed that it reduced the viability up to 70% after 20 min irradiation, while there was low cytotoxicity in the darkness.

Quiñonez et al. (2022) reported selective oxygen atom transfer to α-pinene, β-pinene, camphene and (R)-limonene by dioxo-Mo(VI) Ln complex (where Ln = 2-aminothiazole-4-carboxylic acid) anchored on TiO_2 nanotubes (TiO_2-NT). Here, O_2 was used as an oxidant under UV light at ambient conditions. It was observed that the molecular oxygen reoxidizes the reduced (Mo(IV)═O) unit in the darkness, forming an intermediate oxo-peroxo-Mo. It was also revealed that catalyst under UV radiation transfers two oxygen atoms to the olefin and α-pinene was found to be the most reactive monoterpene.

The synthesis of chromium, molybdenum, tungsten, manganese, and iron complexes bearing N-heterocyclic carbene and carbonyl supporting ligands have been reported by Tang et al. (2022). The general formula of these complexes is $[ML(CO)_3X]$ or $[ML(CO)_3]$ (where X = CO or Br and

L = 1-phenyl-3-(2-pyridyl)imidazolin-2-ylidene). They studied photophysical properties of these complexes and revealed that there is decarbonylation, whenever these complexes were exposed to ultraviolet light. Here, CO ligand is replaced with a labile acetonitrile (solvent) molecule. The potential utility and applications of these complexes as visible-light-mediated photoredox catalysts and their capability to facilitate some photoinduced reactions was investigated through reductive or oxidative functionalization of organic molecules.

5.4 Coordination compounds of tungsten

Spanish chemists Juan José and Fausto Elhuyar made the discovery of tungsten in 1783, when they were dealing with samples of the mineral wolframite. The name "tungsten" is accepted from the old Swedish term for heavy stone. The element tungsten has an atomic number of 74 and its symbol is W. It belongs to group 6 (d^6). It exhibited oxidation states from II to VI.

The luminescence lifetimes have been determined by Rawlins et al. (1990) for W(CO)5(4-CNpy) and W(CO),(pip) complexes (where 4-CNpy = 4-cyanopyridine and pip = piperidine). It was reported that $W(CO)_5$,(4-CNpy) is a multiple-state emitter, which displayed dual emission bands and emitting levels are assigned to metal to ligand charge-transfer (MLCT) excited states with predominantly triplet character. It was also revealed that two MLCT emitting levels established a thermal equilibrium in solution, while the two radiative MLCT excited states are there in frozen glass, which are no longer thermally equilibrated. Luminescence spectra and lifetimes were also observed from $W(CO)_5$(pip) at low temperatures, and it was concluded that is a LF state with predominantly triplet character is responsible for emitting level. It was indicated that LF levels are populated on near-UV light excitation, and they can undergo efficient radiationless deactivation, which includes conversion to the emitting 'MLCT excited-state manifolds.

Ali and Kaur (1991) ligand field excitation of octacyano complexes of molybdenum(IV) and tungsten(IV) produced $[M(CN)_7OH]^{4-}$ and a free cyanide ion. This complex reacts with 1,2,3-indane-trione-hydrate in 1:1 stoichiometry. The rate constants and quantum yields were found to be maximum at pH 8.0. It was also revealed that rate of reaction and quantum yield increases with increase in the concentration of ligand, but decreases with $[M(CN)_8]^{4-}$ concentration. It was also indicated that quantum yields are higher for molybdenum complex as compared to tungsten complex due to shorter lifetime of the excited state species. This was attributed to physical deactivation, which is more rapid in the heavier element because was attributed to enhanced spin-orbit coupling. The molecular-orbital-induced splitting was also larger in $[W(CN)_8]^{4-}$ than in $[Mo(CN)_8]^{4-}$resulting in greater bond strength for tungsten.

Schoch et al. (1996) studied photophysics of some tungsten and molybdenum arylcarbyne complexes $Cp(CO)\{P(OMe)_3\}M{\vdots}C{-}Ar$ (where M = W, Ar = phenyl; o-tolyl; and, M = W, Ar = 2-naphthyl). It was indicated that the lowest excited state of these arylcarbyne complexes is based on a d(M) → π*(M⋮C−Ar) configuration and they displayed a weak, mid-visible absorption band attributed to the d → π* transition. Out of these, the tungsten complexes exhibited red luminescence with a lifetime in the 100−200 ns range. It was also revealed that arylcarbyne complexes had a strong transient absorption with a maximum in the 400−450 nm.

El-Medani et al. (2005) reported that sunlight irradiation of $[M(CO)_6]$, (where M = Cr, Mo and W) with N-salicylidene-2-hydroxyaniline (shaH2) or bis-(salicylaldehyde) phenylenediimine (salphenH2) in tetrahydrofuran afforded complexes with molecular formula $[Cr(shaH2)_3]$, $[MoO_2(shaH2)_2]$, & $[W_2O_5(shaH)_2]$ and oxo complexes [CrO(salphenH2)], $[Mo_2O_6(salphenH2)_2]$, and $[W_2O_6(salphenH2)]$. It was revealed that visible bands are due to ligand-to-metal or metal-to-ligand charge transfer.

Rimmer et al. (2010) reported a photoactivated carbon monoxide releasing moiety (photoCORM), $[W(CO)_5(TPPTS)]^{3-}$, which is air-stable and water-soluble tungsten(0) carbonyl complex of trianionic ligand tris(sulphonatophenyl)phosphine. It was reported that aqueous buffer solution of this complex had high quantum yield release of a single CO on near-UV photolysis. It was also observed that additional CO was slowly released from the $[W(CO)_4(H_2O)(TPPTS)]^{3-}$ photoproduct in aerated media due to autoxidation of tungsten center. It was revealed that first complex can serve as a carbon monoxide releasing moiety in primary photochemical reaction as well as in the secondary reactions of initially formed photoproduct.

Arifin et al. (2013) investigated optical and photoelectrochemical properties of TiO_2 thin film electrode doped with a new variation of ruthenium−(4,4′dimethyl-2,2′-bipyridine)−isothiocyanato−tungsten[bis-(phenyl-1,2-ethilenodithiolenic)] bimetallic complex (BM). Physical adsorption process was to immobilize the BM on the TiO_2 thin film. They used N3 commercial dye used as a dopant for the TiO_2 films. It was found that light absorption of the TiO_2 thin film doped with BM was better as compared to TiO_2 doped with the N3 commercial dye. It was reported that photocurrent of TiO_2 doped with the BM electrode was more as compared to TiO_2 doped with the N3 dye in the initial stage of illumination, but its performance was slowed down after a while. It was claimed that optical properties of as-prepared BM has potential application as dye sensitizer in a photoelctrochemical (PEC) cell.

Koutsouri and Mitsopoulou (2016) observed homogeneous photocatalytic hydrogen evolution using prismatic symmetric tris−dithiolene complexes of tungsten as reductive catalysts. These are $[W(S_2C_2(Ph)_2)_3]$ and its monoanion $[W(S_2C_2(Ph)_2)_3]$. It was reported that photocatalytic system consisting of $[ReBr(CO)_3(bpy)]$ triethanolamine and acetic acid as photosensitizer

sacrificial electron donor and proton source, respectively. Although the activity of this photocatalytic system was lower (TON = 18), but it indicated that the homoleptic tris-dithiolene complexes can be used as proton reductive catalysts and its monoanion form was found to be more active.

Yeung et al. (2017) reported synthesis and applications of two series of air-stable luminescent tungsten(VI) complexes. It was observed that these tungsten(VI) complexes show phosphorescence in the solid state and also in solutions with emission quantum yields (up to 22%) in thin film (5% in mCP) at room temperature. It was also indicated that a complex with 5,7-diphenyl-8-hydroxyquinolinate ligand displayed fluorescence (blue−green) and phosphorescence (red) with comparable intensity, which could be used for ratiometric luminescent sensing. It was also found that solution-processed organic light-emitting diodes based on one of the complex showed a stable yellow emission with an external quantum efficiency (EQE) and luminance up to 4.79% and 1400, cd m^{-2}, respectively. They also applied these tungsten(VI) complexes in light-induced aerobic oxidation reactions.

Huckaba et al. (2018) synthesized (pyridyl)-N-heterocyclic carbene tungsten tetracarbonyl complex, [W(pyNHC)$(CO)_4$]. It was then used as a pre-catalyst for photocatalytic generation of hydrogen. It was reported that in situ generated catalyst [W(pyNHC)$(CO)_3$] for production of H_2 in the presence of triflic acid, decamethylferrocene and visible-light without using any photosensitizer. A turnover number (TON) of more than 17 was observed in 3 h for the production of hydrogen with this system, which is better as compared to homogeneous photocatalyst using visible light (4 TON) reported earlier.

Peschel et al. (2019) synthesized four tungsten alkyne complexes coordinated by the bio-inspired S,N-donor ligand 2-(4′,4′-dimethyloxazoline-2′-yl) thiophenolate (S-Phoz). Earlier, a reaction of the respective alkyne with the bis-carbonyl precursor [$W(CO)_2$(S-Phoz)$_2$] was used for preparing such complexes [W(CO)(C_2R_2)(S-Phoz)$_2$] (where R = H, Me, and Ph). It was reported that oxidation with pyridine-N-oxide gave W-oxo species [$WO(C_2R_2)$(S-Phoz)$_2$], which were found to release alkyne upon light irradiation affording this five-coordinated complex [WO(S-Phoz)$_2$].

Fajardo et al. (2019) carried out base-promoted homolytic aromatic substitution of 1-(2-iodobenzyl)-pyrrole in deuterated benzene catalyzed by W$(CNAr)_6$ (where CNAr = arylisocyanide) photoreductants. It was observed that moderate to high efficiencies has a correlation with W$(CNAr)_6$ excited-state reduction potentials on one-photon excitation (445 nm) with 10 mol % loading of the most powerful photoreductants W$(CNDipp)_6$ and W$(CNDipp\text{-}PhOMe_3)_6$ (where $CNDippPhOMe_3$ = 4-(3,4,5-trimethoxyphenyl)-2,6-diisopropylphenylisocyanide), which afforded almost complete conversion. It was found that photocatalysis can be driven with femtosecond-pulsed excitation (810 nm) using two-photon absorption (TPA) cross sections of W$(CNAr)_6$ complexes. The photocatalysis for one- and two-photon excitation both was terminated by the formation of seven-coordinate [$W_{I2}(CNAr)_5$]

complex. It was also reported that $W(CNDipp)_6$ can be regenerated again by chemical reduction of $W_{I2}(CNDipp)_5$with excess ligand present in solution.

Wang et al. (2021) reported phenomenon in coordination-promoted photoluminescence (CPPL) of organometallic complex, tBu(ONO). Here, ligand is tBu(ONO) and metal is tungsten. A weak photoluminescence of ligand tBu(ONO) was attributed to destroyed planarity because of configuration twisting in the excited state. But, coordination bond formed between tBu(ONO) and the metal tungsten in this complex changes the two twisted parts of tBu(ONO) into an almost planar configuration. It was reported that excited state configuration many have some configurational changes but the coplanarity of tBu(ONO)−W has not been distrubed. As a result, photoluminescence of tBu(ONO)−W is enhanced as compared to ligand tBu(ONO). It was revealed that coordination effect between the ligand and the metal inhibited the configuration twisting of ligands; thus, promoting light emission. It was also found that the emission peaks of tBu(ONO)−W are due to the relaxation of ILCT and LMCT states. Such a photoluminescence performance based on regulation of metal-ligand coordination bonds provided a newer strategy for designing high-performance luminescent materials.

Barth et al. (2022) observed $W(CNDipp)_6$ catalyzed photochemical cyclization of 1-(2-iodobenzyl)-pyrrole (IBP) and 1-(2-bromobenzyl)-pyrrole (BBP) to 5H-pyrrolo[2,1-a]isoindol catalyzed in 1,2-difluorobenzene (DFB). It was observed that 78% of IBP (50 mM) was converted to product after 1 h (16 turnovers) on irradiating $W(CNDipp)_6$ (5 mol %) in DFB solution at 445 nm. A fast photoinduced disappearance of $W(CNDipp)_6$was found on adding tetra-n-butyl ammonium hexafluorophosphate (TBAPF6) (0.2 M) to the DFB solution, but it did not inhibit photochemical cyclization of IBP, which indicated that IBP cyclization could also be driven by a nonluminescent photocatalyst.

The photochemical properties of complexes of chromium, molybdenum and tungsten are quite interesting involving different transitions and therefore, they can find some interesting applications in the field of sensors, electronics, energy devices, photodynamic therapy, release of NO and CO, etc., but much more is to be done before such applications come really into practice. Some more future applications will be available in near future.

References

Ali, S.I., Kaur, H., 1991. Photocatalytic system: kinetics and mechanism of the photoreactions of octacyano complexes of molybdenum (IV) and tungsten (IV) with 1, 2, 3-indane-trione-hydrate. J. Photochem. Photobiol., A: Chem 61 (2), 183−190.

Andre, J., Antoine, C., 1927. Chromium carbonyl. Bull. Soc. Chim. France 41, 1041.

Anzani, A.F., Bazán, C.M., García, P.F., Paci, M.A.B., Argüello, G.A., 2020. Magnetic field effect on the photochemistry of chromium complex. J. Photochem. Photobiol., A: Chem. 398. https://doi.org/10.1016/j.jphotochem.2020.112516.

Arifin, K., Daud, W.R.W., Kassim, M.B., 2013. Optical and photoelectrochemical properties of a TiO_2 thin film doped with a ruthenium−tungsten bimetallic complex. Ceram. Int. 39 (3), 2699−2707.

Baptista, F.A., Krizsan, D., Stitch, M., Sazanovich, I.V., Clark, I.P., Towrie, M., et al., 2021. Adenine radical cation formation by a ligand-centered excited state of an intercalated chromium polypyridyl complex leads to enhanced DNA photo-oxidation. J. Am. Chem. Soc. 143 (36), 14766−14779.

Barbour, J.C., Kim, A.J., deVries, E., Shaner, S.E., Lovaasen, B.M., 2017. Chromium (III) bisarylterpyridyl complexes with enhanced visible absorption via incorporation of intraligand charge-transfer transitions. Inorg. Chem. 56 (14), 8212−8222.

Barth, A.T., Morales, M., Winkler, J.R., Gray, H.B., 2022. Photoredox catalysis mediated by tungsten (0) arylisocyanides in 1, 2-difluorobenzene. Inorg. Chem. 61 (19), 7251−7255.

Bian, G., Jiang, P., Wang, F., Shen, Y., Jiang, K., Liu, L., et al., 2018. Light driven epoxidation of olefins using a graphene oxide/g C_3 N_4 supported Mo (salen) complex. New J. Chem. 42 (1), 85−90.

Bocarsly, A.B., Randy, E., Cameron, H.D.R., McDermott, G.A., Wolff, C.R., Mayr, A., 1985. Photoemission from tungsten alkylidyne complexes in fluid solution. Inorg. Chem. 24 (24), 3976−3978.

Bocarsly, A.B., Cameron, R.E., Mayr, A., McDermott, G.A., 1987. Photophysics and photochemistry of tungsten carbyne complexes. In: Photochemistry and Photophysics of Coordination Compounds. Springer, Berlin, Heidelberg, pp. 213−216.

Boden, P., Di Martino-Fumo, P., Niedner-Schatteburg, G., Seidel, W., Heinze, K., Gerhards, M., 2021. Transient FTIR spectroscopy after one-and two-colour excitation on a highly luminescent chromium (III) complex. Phys. Chem. Chem. Phys. 23 (25), 13808−13818.

Breheny, C.J., Kelly, J.M., Long, C., O'Keeffe, S., Pryce, M.T., Russell, G., et al., 1998. Photochemistry of (η6-arene)$Mo(CO)_3$ and the role of alkane solvents in modifying the reactions of coordinatively unsaturated metal carbonyl fragments. Organometallics 17 (17), 3690−3695.

Büldt, L.A., Guo, X., Prescimone, A., Wenger, O.S., 2016. A molybdenum (0) isocyanideanalogue of Ru (2, 2′-Bipyridine)$^{2+}_3$: a strong reductant for photoredox catalysis. Angew. Chem. Int. Ed. 55 (37), 11247−11250.

Büldt, L.A., Wenger, O.S., 2017. Chromium (0), molybdenum (0), and tungsten (0) isocyanide complexes as luminophores and photosensitizers with long-lived excited states. Angew. Chem. Int. Ed. 56 (21), 5676−5682.

Ceulemans, A., Bongaerts, N., Vanquickenborne, L.G., 1987. Orbital description of the emitting doublet states in quadrate and trigonal chromium (III) complexes. Inorg. Chem. 26 (10), 1566−1573.

Cheplakova, A.M., Solovieva, A.O., Pozmogova, T.N., Vorotnikov, Y.A., Brylev, K.A., Vorotnikova, N.A., et al., 2017. Nanosized mesoporous metal−organic framework MIL-101 as a nanocarrier for photoactive hexamolybdenum cluster compounds. J. Inorg. Biochem. 166. https://doi.org/10.1016/j.jinorgbio.2016.11.014.

Cotton, F.A., Rice, C.E., Rice, G.W., 1977. The crystal and molecular structures of Bis(2,4-pentanedionato)chromium. Inorg. Chim. Acta. 24, 231−234.

De la Torre, C., Gavara, R., García-Fernández, A., Mikhaylov, M., Sokolov, M.N., Miravet, J.F., Galindo, F., 2022. Enhancement of photoactivity and cellular uptake of $(Bu_4N)_2$ $[Mo_6I_8(CH_3COO)_6]$ complex by loading on porous MCM-41 support. Photodynamic studies as an anticancer agent. Biomater. Adv. 140. https://doi.org/10.1016/j.bioadv.2022.213057.

DeLeo, M.A., Ford, P.C., 2000. Photoreactions of coordinated nitrite ion. Reversible nitric oxide labilization from the chromium(III) complex [trans-Cr(cyclam)$(ONO)_2]^+$. Coord. Chem. Rev. 208 (1), 47–59.

Dethlefsen, J.W., Døssing, A., Kadziola, A., 2009. Crystal structure, optical, magnetic, and photochemical properties of the complex pentakis (dimethyl sulfoxide) nitrosylchromium (2+) hexafluorophosphate. Inorg. Chim. Acta. 362 (5), 1585–1590.

Ditze, A., Wasgestion, F., 1985. Photophysics of bis(l,4,7-triazacyclononane) chromium III. J. Phys. Chem. 89, 426–428.

El-Medani, S.M., Ali, O.A., Ramadan, R.M., 2005. Photochemical reactions of group 6 metal carbonyls with N-salicylidene-2-hydroxyaniline and bis-(salicylaldehyde) phenylenediimine. J. Mol. Struct. 738 (1–3), 171–177.

Elvers, B.J., Schulzke, C., Fischer, C., 2019. Photochemical unmasking of 1, 3-dithiol-2-ones: an alternative route to heterolepticdithiolene complexes from low-valent molybdenum and tungsten precursors. Eur. J. Inorg. Chem. 2019 (23), 2796–2805.

Endicott, J.F., Lessard, R.B., Lei, Y., Ryu, C.K., Tamilarasan, R., 1986. Manipulation of doublet excited state lifetimes in chromium(III) complexes. In: Lever, A.P.B. (Ed.), Excited States and Reactive Intermediates. ACS Symp. Ser. No. 307. Am. Chem. Soc., Washington DC, p. 85.

Endicott, J.F., Ramasami, T., Tamilarasan, R., Lessard, R.B., Ryu, C.K., Brubaker, G.R., 1987. Structure and reactivity of metalcentered transition metal excited states. Coord. Chem. Rev. 77. https://doi.org/10.1016/0010-8545(87)85032-4.

Fajardo Jr., J., Barth, A.T., Morales, M., Takase, M.K., Winkler, J.R., et al., 2019. Photoredox catalysis mediated by tungsten (0) arylisocyanides. J. Am. Chem. Soc. 143 (46), 19389–19398.

Fernelius, W.C., Blanch, J.E., 2007. Chromium(III) acetylacetonate. Inorg. Synth. 5, 130–131.

Fogeron, T., Retailleau, P., Chamoreau, L.M., Li, Y., Fontecave, M., 2018. Pyranopterin related dithiolene molybdenum complexes as homogeneous catalysts for CO_2 photoreduction. Angew. Chem. Int. Ed. 57 (52), 17033–17037.

Ford, P.C., 2008. Polychromophoric metal complexes for generating the bioregulatory agent nitric oxide by single-and two-photon excitation. Acc. Chem. Res. 41 (2), 190–200.

Fui, M.L.W., Pui, L.K., Heng, L.Y., Kassim, M.B., 2013. Molybdenum complex as potential photosensitiser for direct water splitting. Int. Mater. Sci. Forum. 756, 231–237.

Gessner, N., Back, A.K., Knorr, J., Nagel, C., Marquetand, P., Schatzschneider, U., et al., 2021. Ultrafast photochemistry of a molybdenum carbonyl-nitrosyl complex with a tri-azacyclononanecoligand. Phys. Chem. 23, 24187–24199.

Hagiwara, H., Nagatomo, M., Seto, C., Ida, S., Ishihara, T., 2013. Dye-modification effects on water splitting activity of GaN: ZnO photocatalyst. J. Photochem. Photobiol., A: Chem 272, 41–48.

Herr, P., Glaser, F., Buldt, L.A., Larsen, C.B., Wenger, O.S., 2019. Long-lived, strongly emissive, and highly reducing excited states in Mo (0) complexes with chelating isocyanides. J. Am. Chem. Soc. 141 (36), 14394–14402.

Hoffman, M.Z., Serpone, N., 1987. Excited state behavior as a probe of ground-state ion-pair interactions in chromium (III)-Polypyridyl complexes. In: Photochemistry and Photophysics of Coordination Compounds. Springer, Berlin, Heidelberg, pp. 43–47.

Hou, S., Guo, Y., Zhang, Y., Wang, B., Li, W., Liu, J., et al., 2021. Eu^{3+}-to-Cr^{3+} energy transfer for the improved Cr^{3+}-characteristic near-infrared (NIR) phosphorescence in the Cr (III)-Eu (III)-Salen complex. Inorg. Chem. Commun. 132. https://doi.org/10.1016/j.inoche.2021.108811.

Huang, P.J., Garcia, J.V., Fenwick, A., Wu, G., Ford, P.C., 2019. Nitric oxide uncaging from a hydrophobic chromium (III) photoNORM: visible and near-infrared photochemistry in biocompatible polymer disks. ACS Omega 4 (5), 9181−9187.

Huckaba, A.J., Shirley, H., Lamb, R.W., Guertin, S., Autry, S., Cheema, H., et al., 2018. A mononuclear tungsten photocatalyst for H_2 production. ACS Catal. 8 (6), 4838−4847.

Indelli, M.T., Scandola, F., 1993. Excited-state charge recombination in a ruthenium (II)-chromium (III) polynuclear complex. J. Phys. Chem. 97 (13), 3328−3332.

Isaacs, M., Sykes, A.G., Ronco, S., 2006. Synthesis, characterization and photophysical properties of mixed ligand tris (polypyridyl) chromium (III) complexes,$[Cr(phen)_2L]^{3+}$. Inorg. Chim. Acta. 359 (12), 3847−3854.

Jiménez, J.R., Doistau, B., Cruz, C.M., Besnard, C., Cuerva, J.M., Campana, A.G., 2019. Chiral molecular ruby $[Cr\ (dqp)_2]^{3+}$ with long-lived circularly polarized luminescence. J. Am. Chem. Soc. 141 (33), 13244−13252.

Kane-Maguire, N.A.P., Wallace, K.C., Miller, D.B., 1985. Synthesis, characterization, and photobehavior of cis- and trans-diammine (l,4,8,ll-erraazacyclotetradecane)chromium(III) and some related compounds. Inorg. Chem. 24, 597−605.

Khvorost, T.A., Beliaev, L.Y., Potalueva, E., Laptenkova, A.V., Selyutin, A.A., Bogachev, N.A., Mereshchenko, A.S., 2020. Ultrafast photochemistry of the $[Cr(NCS)_6]^{3-}$complex in dimethyl sulfoxide and dimethylformamide upon excitation into ligand-field electronic state. J. Phys. Chem. B 124 (18), 3724−3733.

Kirakci, K., Kubát, P., Kučeráková, M., Šícha, V., Gbelcová, H., Lovecká, P., et al., 2014. Water-soluble octahedral molybdenum cluster compounds $Na_2[Mo_6I_8\ (N_3)_6]$ and $Na_2[Mo_6I_8\ (NCS)_6]$: syntheses, luminescence, and in vitro studies. Inorg. Chim. Acta. 441, 42−49.

Kirk, A., 1981. Chromium (III) photochemistry and photophysics. Coord. Chem. Rev. 39 (1−2), 225−263.

Koutsouri, E., Mitsopoulou, C.A., 2016. Photocatalytic hydrogen evolution by tris-dithiolene tungsten complexes. Open Chem 14 (1), 393−403.

Krom, I., Lutz, M., Müller, C., 2015. 2-(2′-Pyridyl)-4,6-diphenylphosphinine versus 2-(2′-pyridyl)-4,6-diphenylpyridine: synthesis and characterization of novel Cr0, Mo0 and W0 carbonyl complexes containing chelating P,N and N,N ligands. Dalton Trans. 22. https://doi.org/10.1039/C5DT01261A.

Kushch, L.A., Emel'yanov, V.A., Golhen, S., Cador, O., Schaniel, D., Woike, T., et al., 2009. The photochromic paramagnet derived from polyoxometalate $[Cr(OH)_6Mo_6O_{18}]^{3-}$ and ruthenium mononitrosyl complex $[RuNO\ (en)_2Cl]^{2+}$. Inorg. Chim. Acta. 362 (7), 2279−2282.

Lee, S.X., Tan, C.H., Mah, W.L., Wong, R.C.S., Cheow, Y.L., Sim, K.S., 2021. Synthesis of group 6 (chromium, molybdenum, and tungsten) photoCORMs as potential antimicrobial and anticancer agents. Inorg. Chim. Acta. 525. https://doi.org/10.1016/j.ica.2021.120491.

Luckham, S.L.J., Folli, A., Platts, J.A., Richards, E., Murphy, D.M., 2019. Unravelling the photochemical transformations of chromium(I) 1,3 bis(diphenylphosphino), $[Cr(CO)_4(dppp)]^{l+}$, by EPR spectroscopy. Organometallics 38 (12), 2523−2529.

Luo, H.Q., Zhang, P., Yang, Y.X., Gong, Y., Lin, J.H., 2016. Two polymolybdate-based complexes and their graphene composites with visible-light photo-responses. RSC Adv. 6 (100), 97890−97898.

Ma, J.S., Lin, L.Y., Chen, Y.S., 2019. Facile solid-state synthesis for producing molybdenum and tungsten co-doped monoclinic $BiVO_4$ as the photocatalyst for photoelectrochemical water oxidation. Int. J. Hydrogen Energy 44 (16), 7905−7914.

Manuta, D.M., Lees, A.J., 1986. Emission and photochemistry of $M(CO)_4$ (diimine)(M= chromium, molybdenum, tungsten) complexes in room-temperature solution. Inorg. Chem. 25 (9), 1354−1359.

Mark-Lee, W.F., Ng, K.H., Minggu, L.J., Umar, A.A., Kassim, M.B., 2013. A molybdenum dithiolene complex as a potential photosensitiser for photoelectrochemical cells. Int. J. Hydrogen Energy 38 (22), 9578−9584.

Martínez, H., Cáceres, M.F., Martínez, F., Páez-Mozo, E.A., Valange, S., Castellanos, N.J., Arzoumanian, H., 2016. Photo-epoxidation of cyclohexene, cyclooctene and 1-octene with molecular oxygen catalyzed by dichlorodioxo-(4, 4′-dicarboxylato-2, 2′-bipyridine) molybdenum (VI) grafted on mesoporous TiO_2. J. Mol. Catal. Chem. 423, 248−255.

McMahon, S., Amirjalayer, S., Buma, W.J., Halpin, Y., Long, C., Rooney, A.D., et al., 2015. An investigation into the photochemistry of, and the electrochemically induced CO-loss from, $[(CO)_5MC(OMe)Me]$(M = Cr or W) using low-temperature matrix isolation, picosecond infrared spectroscopy, cyclic voltammetry, and time-dependent density functional theory. Dalton Trans. 44, 15424−15434.

Mitra, J., Sarkar, S., 2016. Photoinduced electron transfer from the oxo−Mo IV selenolato complex to oxygen. J. Chem. 40 (1), 626−633.

Nassar, D.A., Ali, O.A., 2021. Structural Characterization, thermal studies, fluorescence and optical properties of metal carbonyl derivatives of N_2O_2 Schiff Base. J. Sci. Res. 38, 164−186.

Oskam, A., Andréa, R.R., Stufkens, D.J., Vuurman, M.A., 1987. Identification of H_2-, D_2-, N_2-Bonded Intermediates in the $Cr(CO)_6$ Photocatalyzed Hydrogenation Reactions. Springer, Berlin, Heidelberg, pp. 243−246. Photochem. Photophys. Coord. Comp.

Ostrowski, A.D., Deakin, S.J., Azhar, B., Miller, T.W., Franco, N., Cherney, M.M., et al., 2010. Nitric oxide photogeneration from trans-Cr (cyclam)$(ONO)^{2+}$ in a reducing environment. Activation of soluble guanylyl cyclase and arterial vasorelaxation. J. Med. Chem. 53 (2), 715−722.

Otto, S., Förster, C., Wang, C., Resch-Genger, U., Heinze, K., 2018. A strongly luminescent chromium (III) complex acid. Chem. Eur J. 24 (48), 12555−12563.

Owen, B.B., English, J., Cassidy, H.G., Dundon, C.V., 1950. Chromium hexacarbonyl. Inorg. Synth. 3, 156−160.

Peschel, L.M., Vidovič, C., Belaj, F., Neshchadin, D., Mösch-Zanetti, N.C., 2019. Activation and photoinduced release of alkynes on a biomimetic tungsten center: the photochemical behavior of the W− S-phoz system. Chem. Eur J. 25 (15), 3893−3902.

Pokhrel, S., Nagaraja, K.S., 2009. Photogalvanicbehaviour of $[Cr_2O_2S_2$ (1-Pipdtc) 2 $(H_2O)_2]$ in aqueous DMF. Sol. Energy Mater. Sol. Cells 93 (2), 244−248.

Quiñonez, H., Amaya, Á.A., Paez-Mozo, E.A., Martinez Ortega, F., 2022. Aminothiazole ligand-type dioxo-mo (VI) complex anchored on TiO_2 nanotubes for selective oxidation of monoterpenes with light and O_2. Top. Catal. 65 (9), 1088−1101.

Rawlins, K.A., Lees, A.J., Adamson, A.W., 1990. Photophysical studies of tungsten carbonyl W $(CO)_5L$ complexes. Multiple-state luminescence of W $(CO)_5$(4-cyanopyridine) in fluid and glassy solutions. Inorg. Chem. 29 (19), 3866−3871.

Reichenauer, F., Wang, C., Forster, C., Boden, P., Ugur, N., Báez-Cruz, R., et al., 2021. Strongly red-emissive molecular ruby $[Cr\ (bpmp)_2]^{3+}$surpasses $[Ru\ (bpy)_3]^{2+}$. J. Am. Chem. Soc. 143 (30), 11843−11855.

Rimmer, R.D., Richter, H., Ford, P.C., 2010. A photochemical precursor for carbon monoxide release in aerated aqueous media. Inorg. Chem. 49 (3), 1180−1185.

Schoch, T.K., Main, A.D., Burton, R.D., Lucia, L.A., Robinson, E.A., Schanze, K.S., et al., 1996. Photophysics of tungsten and molybdenum arylcarbyne complexes. Observation of the lowest excited state by laser flash photolysis. Inorg. Chem. 35 (26), 7769−7775.

Shaw, L.E., Langford, C.H., 2000. Wavelength-dependent photochemistry in Cr (cnph)$_6$: a study of photosubstitution and photoinduced electron transfer using time-resolved spectroscopy. Inorg. Chem. 39 (3), 541−546.

Silva, A.F., Calhau, I.B., Gomes, A.C., Valente, A.A., Gonçalves, I.S., Pillinger, M., 2021. A hafnium-based metal-organic framework for the entrapment of molybdenum hexacarbonyl and the light-responsive release of the gasotransmitter carbon monoxide. Mater. Sci. Eng. C 124. https://doi.org/10.1016/j.msec.2021.112053.

Sturala, J., Sofer, Z., Pumera, M., 2019. Coordination chemistry of 2D and layered gray arsenic: photochemical functionalization with chromium hexacarbonyl. NPG Asia Mater. 11. https://doi.org/10.1038/s41427-019-0142-x.

Szymańska-Buzar, T., Downs, A.J., Greene, T.M., Marshall, A.S., 1995. Matrix-isolation studies of alkyne complexes in the photochemical reactions of Mo(CO)$_6$ with alkynes. J. Organomet. Chem. 495, 149−161.

Tang, M., Cameron, L., Poland, E.M., Yu, L.J., Moggach, S.A., Fuller, R.O., Bissember, A.C., 2022. Photoactive metal carbonyl complexes bearing n-heterocyclic carbene ligands: synthesis, characterization, and viability as photoredox catalysts. Inorg. Chem. 61 (4), 1888−1898.

Toneatto, J., Boero, R.A., Lorenzatti, G., Cabanillas, A.M., Argüello, G.A., 2010. New insights in the DNA-[Cr (phen)$_2$(dppz)]$^{3+}$ binding and photocleavage properties by the complex with an intercalating ligand. J. Inorg. Biochem. 104 (7), 697−703.

Treiling, S., Wang, C., Förster, C., Reichenauer, F., Kalmbach, J., Boden, P., et al., 2019. Luminescence and light-driven energy and electron transfer from an exceptionally long-lived excited state of a non-innocent chromium (III) complex. Angew. Chem. Int. Ed. 58 (50), 18075−18085.

Van Atta, S.L., Duclos, B.A., Green, D.B., 2000. Microwave-assisted synthesis of Group 6 (Cr, Mo, W) zerovalent organometallic carbonyl compounds. Organometallics 19 (12), 2397−2399.

Vlcek, A., 1986. Redox reactivity of photogeneratedpentacarbonylchromium species: formation of [Cr(III)(o-semiquinone)$_3$] complexes. Inorg. Chem. 25, 522−526.

Wang, Y., Guo, Y., Liang, Y., Pan, Y., Shi, Y., Wang, Y., et al., 2021. Coordination-promoted photoluminescence induced by configuration twisting regulation. J. Lumin. 231, 117783.

Wegeberg, C., Häussinger, D., Wenger, O.S., 2021. Pyrene-decoration of a chromium (0) tris (diisocyanide) enhances excited state delocalization: a strategy to improve the photoluminescence of 3d^6 metal complexes. J. Am. Chem. Soc. 143 (38), 15800−15811.

Yeung, K.T., To, W.P., Sun, C., Cheng, G., Ma, C., Tong, G.S.M., et al., 2017. Luminescent tungsten (VI) complexes: photophysics and applicability to organic light-emitting diodes and photocatalysis. Angew. Chem. 129 (1), 139−143.

Zhang, J., Zhang, J., Liu, X., Xu, T., Liu, S., Hou, X., et al., 2019. Hyperstable chromium (III)/manganese (II) bimetallic wheel clusters with visible photoactivity. Dalton Trans. 48 (28), 10669−10675.

Chapter 6

Coordination compounds of manganese, technetium and rhenium

Monika Jangid[1], Jayesh P. Bhatt[1], Mamta Ahuja[2], Shubang Vyas[1] and Avinash Kumar Rai[1]

[1]*Department of Chemistry, PAHER University, Udaipur, Rajasthan, India;* [2]*Department of Chemistry, Government Meera Girls College, Udaipur, Rajasthan, India*

6.1 Introduction

It is known that precious metal complexes with valence electron configuration d^n normally exhibit luminescent metal-to-ligand charge transfer (MLCT) excited states and they can find numerous applications in the field of lighting, solar cells, sensing, and synthetic photochemistry. A lot of attention has been received by iron(II) as a possible Earth-abundant alternative to these precious metal, but till date no iron(II) complex has been reported to exhibit MLCT emission on continuous-wave excitation. The manganese(I) has also electron configuration similar to iron(II), but till now, it has been overlooked in the search for low cost MLCT luminophores. Photochemical and photophysical properties of coordination compounds make them useful in varied fields such as imaging, sensing, catalysis, photodynamic therapy, etc. Group 7 contains elements manganese, technetium and rhenium. Out of these, photochemical behavior of technetium has not been much explored because of its radioactive nature. Its complexes are also not much stable for study; however, coordination compounds of manganese and rhenium have found numerous applications.

6.2 Coordination compounds of manganese

Johann Heinrich Pott (1740) reported a new element as manganese. He was able to prepare potassium permanganate, which is one of the strongest oxidizing agents known. The name manganese was carried from two routes: (i) from the Latin "magnes", meaning magnet, or (ii) from the black magnesium oxide, "magnesia nigra". Black ore of manganese, pyrolusite (manganese

Photochemistry and Photophysics of Coordination Compounds. https://doi.org/10.1016/B978-0-12-824493-7.00003-4
Copyright © 2023 Elsevier Inc. All rights reserved.

dioxide, MnO_2) was used by cave painters of the Lascaux region of France around 30000 years ago. Now, it is used by glass makers for removal of pale greenish tint of natural glass.

- Manganese is a hard, brittle and silvery metal. It is mainly used in alloys, such as steel (1% manganese).
- To increase its strength, workability and resistance to wear.
- Manganese steel contains about 13% manganese. It is extremely strong and therefore, it is used for safes, railway tracks, prison bars and rifle barrels.
- Drinks cans are resistant to corrosion as these are made of an alloy of aluminum with 1.5% manganese.
- Manganese is the fifth most abundant metal in the crust of Earth.
- Nodules of manganese are found on the floor of the oceans containing approx. 24% manganese; of course with smaller amounts of other elements.
- The enzyme responsible for converting water molecules to oxygen during photosynthesis contains four atoms of manganese.
- The average human body contains about 12 mg of manganese. It is also essential for utilization of vitamin B_1. About 4 mg of manganese is required and it is supplied from nuts, bran, wholegrain cereals, parsley, and tea. The bones grow spongier and break more easily with deficiency of manganese.
- Its atomic number is 25 and its electron configuration is [Ar] 3 d^5 $4s^2$, and it belongs to group 7.
- Its exist in various oxidation state as +7, +6, +5, +4, +3, +2, 0 and sometimes −1 also.

Kokkes et al. (1985) reported photolysis of several complexes $(CO)_5MM'(CO)$, (a-diimine) (where M, M′ = Mn, Re) in 2-MeTHF at temperatures in the range 133−230 K. It was observed that homolysis of the metal-metal bond occurred for the complexes with M = Mn and M′ = Mn, Re above 200 K, but the main products of the reaction were [M(CO),]- and [M′(CO), (a-diimine)(2-MeTHF)]* (if M = Mn, Re and M′ = Mn) at temperatures below 200 K. The ions were not formed by direct heterolysis of the metal-metal bond but through thermal disproportionation of a photosubstituted product $(CO)_5MM'(CO_2)$ (a-diimine)(2-Me-THF). It was revealed that corresponding $(CO)_5MnRe(CO)_3$(a-diimine) ones (where M = Mn, Re and M′ = Mn) did not show photosubstitution of CO but breaking of a metal-nitrogen bond on photolysis at temperature 133 K. It was also proposed that the primary photoprocess at lower temperatures is bond breaking is and it is followed by release of CO (where M′ = Mn).

Stufkens et al. (1991) revealed that photochemistry of irradiation of $(CO)_5MnMn(CO)_3$(α-diimine) complex, where $Mn(CO)_5$ and $Mn(CO)_3$(α-diimine) radicals were formed, which undergo radical coupling and electron transfer (chain) reactions. A relationship has been proposed for halide

complexes $XMn(CO)_3(\alpha\text{-diimine})$ (where X = Cl, Br, and I), which undergo homolysis of Mn-X bond on irradiation. It was also reported that $(CO)_5MnMn(CO)_3(\alpha\text{-diimine})$ and $XMn(CO)_3(\alpha\text{-diimine})$ exhibited similarity in their photochemical behavior as both of them formed the dimeric species $Mn_2(CO)_6(\alpha\text{-diimine})_2$ upon irradiation into their lowest-energy absorption band.

The fac-Mn(Cl) (CO_3) (H-DAB) has low-energy Mn−3d to 1,4-diaza-1,3-butadiene (H-DAB) π^* metal-to-ligand charge transfer (MLCT) excited states, which are not Mn−CO dissociative by their electronic nature (Rosa et al., 1996). It was also reported that loss of an equatorial CO ligand upon MLCT excitation can be explained by a radiationless transition from the MLCT states to this ground state. The complex will undergo a strong rearrangement (structural) upon equatorial CO dissociation, where chloride shifts to an equatorial open site. This rearrangement explained the formation of mer-$Mn(Cl)(CO)_3(\alpha\text{-diimine})$ complexes on back-reaction of their CO-loss product with CO. The equatorial CO dissociation is quite different from the normal photochemical dissociation from the dissociative ligand-field state or through crossing of the photoactive excited state by this ligand-field state. On the other hand, axial CO dissociation, which does not occur ordinarily and it does not give rise to rearrangement (structural), but predicted to produce the fac-complex upon back-reaction with CO.

Carlos and Neumann (2000) reported photoreactions resulting from metal-to-ligand charge transfer (MLCT) excitation of the manganese(I) tricarbonyl complexesfac-$[Mn(CO)_3(phen)(Im)](SO_3CF_3)$ and fac-$[Mn(CO)_3(phen)(Im\text{-}CH_3)](SO_3CF_3)$ in different solvents at a wide range of wavelengths. The reaction product was found to be corresponding mer-$[Mn(CO)_3(phen)(Im\text{-}L)]^+$ isomer. The high quantum yields ($\sim$0.66 mol E^{-1}) indicated primary photoprocesses from ligand-field states. It was also reported that these complexes were luminescent even at room temperature and this emitting state can be tuned from an MLCT emission to intra-ligand (IL) fluorescence with variation in polarity of solvent and wavelength of excitation.

Carlos et al. (2004) observed photochemical and photophysical preparation of a series of fac-$[Mn(CO)_3(phen)(Im\text{-}R)](SO_3CF_3)$ complexes (where phen = 1,10-phenanthroline and Im = imidazole). It was reported that intra-ligand and metal-to-ligand charge transfer (MLCT) transitions were observed in the electronic absorption spectra of these complexes, which depends on nature of the ligand substituents. It was revealed that the emission spectra show an MLCT to highly structured π-π^* emission at room temperature on going from R = H, CH_3, C_6H_5, to Metro, (where metro = 2-methyl-5-nitroimidazole). The trend in photophysical and photochemical properties in the emission spectra was found to be same with the changes in the electron-donating or electron-withdrawing power of the substituent on the imidazole ligand. It was revealed that MLCT irradiation of the complexes with R = H, CH_3 resulted in formation of mer-$[Mn(CO)_3(phen)(Im\text{-}R)]^+$ isomers, while

complexes with the imidazole ligand substituted by C_6H_5 or metro release the Im-R ligand forming stereoretentive fac-$[Mn(CO)_3(phen)(S)]^+$ complexes.

Doux et al. (2005) prepared fac-$[Mn(SPS)(CO)_3]$ by reacting $[Mn(CO)_5Br]$ with lithium salt of the anionic SPS pincer ligand composed of a central hypervalent λ^4-phosphinine ring bearing two ortho-positioned diphenylphosphine sulfide side arms. It was reported that this isomer can be converted photochemically to mer-$[Mn(SPS)(CO)_3]$, with a very high quantum yield (0.80 ± 0.05) (Fig. 6.1). It was observed that both these isomers exhibited but luminescence from a low-lying ^{3}IL (SPS-based) excited state, but light emission of fac-$[Mn(SPS)(CO)_3]$ was quenched by the efficient photoisomerization, may be due to a low-lying Mn−CO dissociative excited state.

Three acylhydrazidate-containing complexes $[Zn(N_2H_4)(dphkh)]\cdot H_2O$ (where, dphkh = 4,4′-diphthalhydrazidatoketone hydrazone), $[Zn(npth)_2]$ (npth = naphthalhydrazidate) and $[Mn(mpdh)_2(H_2O)_2]\cdot 2H_2O$, were prepared by Wang et al. (2013a) via hydrothermal in situ acylation of N_2H_4 with aromatic polycarboxylic acids. It was reported that first compound is a layered Zn^{2+} coordination polymer with a mixed ligand of hydrazine and dphkh. Second compound is a unique example of a npth-extended coordination polymer, which exhibited a double-chain structure. It was revealed by solid-state photoluminescence analysis that first compounds exhibited strong luminescence with the maximum at 490 nm.

Bikas et al. (2014) prepared mixed-metal dicyanoargentate-bridged coordination polymers of Ag(I)−Mn(II). It was reported that coordination polymer 2D-$[Mn(\mu\text{-}L^1)(Cl)(\mu\text{-}NCAgCN)Mn_{0.5}(CH_3OH)]_n$, 1D-$\{[Mn(L^2)(Cl)(\mu\text{-}NCAgCN)Mn_{0.5}(CH_3OH)]CH_3OH\}_n$ and $[Mn(L^3)(Cl)(\mu\text{-}NCAgCN)Mn_{0.5}(CH_3OH)]_n$ were produced by reaction of manganese(II) chloride and potassium dicyanoargentate(I) with (X)(pyridin-2-ylmethylene)isonicotinohydrazide ligands (where HL^1 X = Ph, HL^2 X = Me, HL^3 X = H in good yields. Variable temperature magnetic

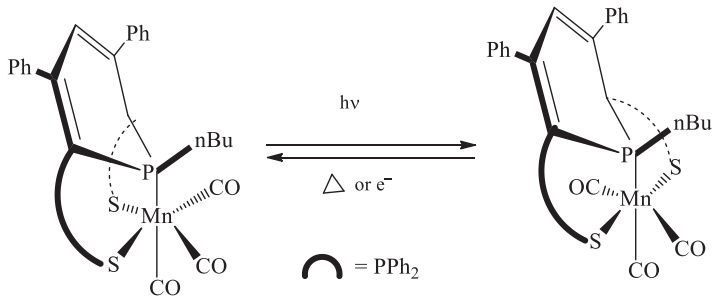

FIGURE. 6.1 A reversible change in fac-$[Mn(SPS)(CO)_3]$ complex. *Adapted from Doux, M., Mézailles, N., Ricard, L., Le Floch, P., Vaz, P. D., Calhorda, M.J., et al., 2005. Syntheses, X-ray structures, photochemistry, redox properties, and dft calculations of interconvertible f ac-and m er-[Mn (SPS)(CO)$_3$] isomers containing a flexible SPS-based pincer ligand. Inorg. Chem 44 (25), 9213−9224. With Permission.*

susceptibility measurements showed that despite the long distance among the high spin Mn(II) ions [10.4676(12) and 10.522(1) Å, respectively], weak antiferromagnetic coupling takes place through the long NC—Ag—CN bridge. Their photoluminescence behavior was also studied. The first compound exhibited a broad emission centered around 450 nm with two excitation maxima at 270 and 310 nm.

Fodor et al. (2016) reported that Mn(III) porphyrins are weakly emissive, but the fluorescence displayed by Mn(III) complexes with the cationic $TMPyP^{2+}$ ligand (where H_2TMPyP^{4+} = 5,10,15,20-tetrakis(1-methylpyridinium-4-yl) porphyrin) as well as its other alkyl derivatives (where alkyl = hexyl and dodecyl) were strong enough. It was also observed that elongation of the alkyl chain increased both; quantum yield as well as lifetime of the emission for the Mn(III) porphyrins. It was revealed that these cationic metalloporphyrins were used in a photocatalytic system with triethanolamine (TEOA) and methylviologen (MV^{2+}) as a sacrificial electron donor and acceptor, respectively. The outer-sphere photoinduced reduction of the metal center was there through quenching of the triplet excited state of these metalloporphyrins by TEOA. It was observed that there manganese(II) porphyrins were photoactive and an electron was transformed to MV^{2+} upon irradiation; thus, regenerating the starting complex. It was reported that as the alkyl substituents was increased, the quantum yield of the formation of methylviologen radical ($MV^{\bullet+}$) was also increased, but there was a considerable decrease in the durability of the photocatalyst. It was also found that anionic micelles totally hindered the photoinduced generation of Mn(II) porphyrins, but cationic micelles increased the efficiency of the accumulation of $MV^{\bullet+}$ significantly.

Reade et al. (2017) investigated the photochemical behavior of two metal-organic frameworks (MOFs) (single crystals) $\{Li_2(DMF)_2$ [(2,2′-bipy-5,5′-dicarboxylate)$Re(CO)_3Cl]\}_n$ (RELI) or $\{Li_2(DMF)_2$[(2,2′-bipy-5,5′-dicarboxylate)$Mn(CO)_3Br]\}_n$ (MNLI) reaction. These were prepared by the reaction of Re(2,2′-bipy-5,5′-dicarboxylic acid)$(CO)_3Cl$ or Mn(2,2′-bipy-5,5′-dicarboxylic acid)$(CO)_3Br$ with LiCl or LiBr, respectively, produces single crystals of. It was revealed that rhenium-containing MOF (RELI) exhibited luminescence and the excited state behavior is quite close in behavior of unsubstituted [Re(bipy)$(CO)_3Cl$], rather than a related MOF, where Li(I) cations are replaced by Mn(II) cations. It was also revealed that MNLI formed a dicarbonyl species, which rapidly recombined upon excitation with the dissociated CO, similar to photoejected CO not escaping the MOF channels.

Wei et al. (2018) prepared two novel tetrahedral manganese(II) complexes; (N-methylpiperidinium)$MnCl_4$ and (N-methylpyrrolidinium)$MnCl_4$. These complexes exhibited distinct fluorescence characteristics through organic cation modulation. The first complex showed prominent green luminescence with a high quantum yield (79.37%) while second complex emitted unusual red emission at 611 nm.

Wu et al. (2018) reported that reactions of $MnBr_2$ and ethane-1,2-diylbis(diphenylphosphine oxide) ($dppeO_2$) in dichloromethane−methanol solutions gave colorless crystals; $[MnBr_2(dppeO_2)]_n$, $[MnBr_2(dppeO_2)(DMF)]_n$, $[Mn(dppeO_2)_3][MnBr_4]$, and $Mn_2Br_4(dppeO_2)_2$, which depend on the conditions of crystallization. First two compounds displayed one-dimensional chain structures, which is composed of Mn(II) ions linked by bridging $dppeO_2$ with tetrahedral or trigonal-bipyramidal geometry, while the last one exhibited a cyclic dinuclear structure with two Mn(II) centers bridged by double $dppeO_2$ to have tetrahedral geometry. The third compound consisted of octahedrally coordinated cation $[Mn(dppeO_2)_3]^{2+}$ and tetrahedrally arranged anion $[MnBr_4]^{2-}$. It was found that first and last complexes were crystalline and these are highly luminescent with green emission bands centered (510 nm) on exposure of first complex to N,N-dimethylformamide vapor, while third compound showed intense orange luminescence (594 nm). A green emission (510 nm) was converted to red luminescence (630 nm), which was attributed to the formation of DMF-coordinated compound with a trigonal-bipyramidal ligand field (Fig. 6.2). It was also revealed that red-emitting 1a compound could be reverted to the original green-emitting 1 form with a tetrahedral ligand field upon heating at 160°C, and this reversible conversion could be repeated many times.

A new 3-position substituted imidazo[1,2-a]pyridine ligand, (E)-4-(3-(2-chloroimidazo[1,2-a]pyridin-3-yl)acryloyl)benzoic acid (HL) was synthesized by Li et al. (2018). Two new coordination polymers, $[ML_2(H_2O)]_n$

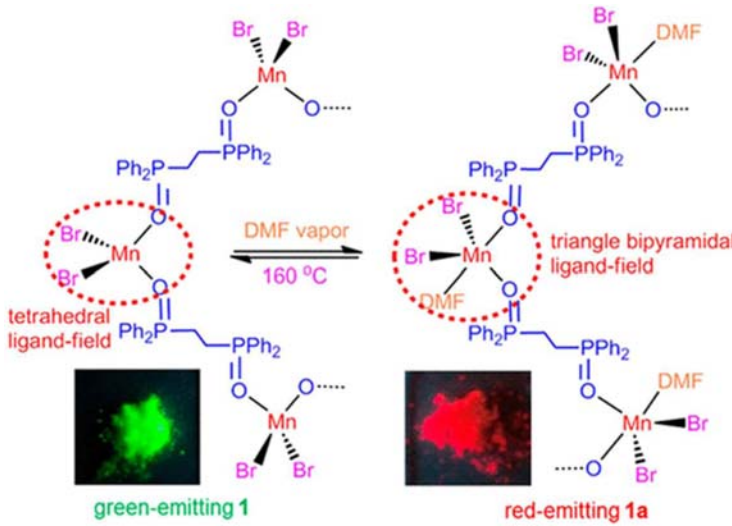

FIGURE. 6.2 Conversion of green emission to red-emission. *Adapted from Wu, Y., Zhang, X., Xu, L.J., Yang, M., Chen, Z. N., 2018. Luminescent vapochromism due to a change of the ligand field in a one-dimensional manganese (II) coordination polymer. Inorg. Chem. 57 (15), 9175−9181. With Permission.*

(M = Zn, and Cd) and one discrete complex, $MnL_2(H_2O)_4$, were synthesized using this ligand under the solvothermal conditions. Among these, first two coordination compounds are isostructural and show one-dimensional chain structures. The third complex was assembled into a dimer structure via supramolecular interactions. They also investigated photoluminescent properties of HL ligand and these coordination compounds.

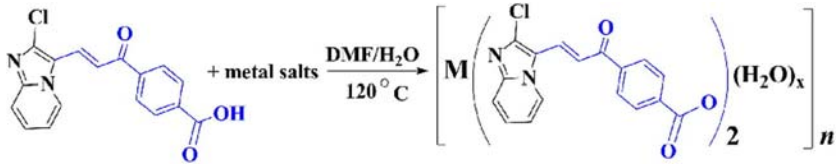

Yue et al. (2019) synthesized eight new coordination compounds by incorporating a semi-rigid ether-based unsymmetrical tetracarboxylic acid (where H_4detc = 2,3,3′,4′-diphenyl ether tetracarboxylic acid) with various ancillary dipyridyl ligands (where phen = 1,10-phenanthroline, bipy = 4,4′-bipyridine, bpea = 1,2-bis(4-pyridyl)ethane, and bpee = 1,2-bis(4-pyridyl) ethylene), via hydrothermally technique. It was reported that $[Mn(H_2detc)(phen)_2]\cdot H_2O$ is a supramolecular networks built from binuclear structures.

Bortoluzzi et al. (2020) prepared manganese(II) tetrahedral complexes having general formula $[MnX_2L_2]$ (where X = Cl, Br, I; and L = 1,3-dimethyl-2-phenyl-1,3-diazaphospholidine-2-oxide). It was reported that these three species are quite luminescent in the green region, when excited with UV light. It was also observed that luminescence lifetimes strongly depend on coordinated halide. It was also revealed that photoluminescence was improved with this rigid 1,3-diazaphospholidine-2-oxide moiety as compared to phenylphosphonic diamide Mn(II) derivatives.

Manganese tricarbonyl complexes have a potential as catalysts for reduction of CO_2, but these complexes are normally photosensitive and are decomposed rapidly in presence of visible light. Henke et al. (2020) reported photochemical studies probe the initial steps of light-driven speciation for $Mn(CO)_3(^{R}bpy)Br$ complexes bearing a range of 4,4′-disubstituted 2,2′-bipyridyl ligands (where R = ^{t}Bu, H, CF_3, and NO_2). It was found that $Mn(CO)_3(^{NO}{}_2bpy)Br$ complex is unique in nature in all these compounds, which has a long-lived excited state and it does not undergo CO release or subsequent solvent coordination. It was also revealed that kinetics of photolysis and solvent coordination for light-sensitive complexes depend on electronic properties of the disubstituted bipyridyl ligand. It was indicated that metal-to-ligand charge-transfer (MLCT) and dissociative ligand-field (d−d) excited states both play a role in the ultrafast photochemistry (Fig. 6.3). It was also suggested that more robust catalysts could be prepared by designing



FIGURE. 6.3 Effect of substitution on MLCT and CO ligand loss in Mn complexes. *Adapted from Henke, W.C., Otolski, C.J., Moore, W.N., Elles, C.G., Blakemore, J.D., 2020. Ultrafast spectroscopy of [Mn (CO)$_3$] complexes: tuning the kinetics of light-driven CO release and solvent binding. Inorg. Chem. 59 (4), 2178–2187. With Permission.*

complexes, which avoid crossing between the excited states that drive photochemical loss of CO.

Herr et al. (2021) reported that isocyanide chelate ligands can form air-stable manganese(I) complexes, which exhibited MLCT luminescence in solution at room temperature. It was reported that these complexes can be used as photosensitizers for energy- and electron-transfer reactions and also promote the photoisomerization of trans-stilbene. It was revealed that electron transfer photoreactivity was from the emissive MLCT state, while the triplet energy transfer photoreactivity was due a ligand-centered $^3\pi-\pi^*$ state.

A cadmium coordination polymer assembled with aminopyrazine (ampyz) and acetate (AcO) is a high-efficiency material, which is able to convert ultraviolet radiation into blue light (with internal and external photoluminescence quantum yields of about 80%). Lemes et al. (2021) prepared a blue-light-emitter by just replacing the toxic cadmium element for Mn^{2+} and an isostructural Mn^{2+}coordination polymer was obtained. It was revealed that low-frequency radiative decay occurred before the target luminescence, which reduced much of its blue-light-emission efficiency not exceeding 3%.

Bortoluzzi et al. (2021a) synthesized tetrahedral Mn(II) bromo- and iodo-complexes with phosphoramidate and phosphonate ligands. They could prepare these mononuclear complexes, $[MnX_2L_2]$ by using monodentate ligands, $O{=}P(OPh)_2(NMe_2)$ and $O{=}P(OPh)_2Ph$. The bidentate resorcinol derivative $1,3\text{-}O{=}P(NMe_2)O{-}C_6H_4{-}O(NMe_2)_2P{=}O$ behaved as a bridging ligand, and afforded dinuclear complex by reaction of coordination polymer with MnX_2

salts, in the case of X = Br and I, respectively. It was reported that all these compounds showed green photoluminescence of Mn(II) in a tetrahedral environment, while complexes with $O{=}P(OPh)_2(NMe_2)$ in the coordination sphere displayed high photoluminescence quantum yields.

Bortoluzzi et al. (2021b) synthesized manganese(II) halide complexes using ligand, N,N,N′,N'-tetramethyl-P-naphtalen-2-ylphosphonic diamide from anhydrous MnX_2 salts (where X = Cl, Br, and I). It was revealed that slightly distorted tetrahedral geometry of the coordination sphere was there. The photoluminescence spectra exhibited superimposition of a green emission, related to the $^4T_1(^4G) \rightarrow {}^6A_1(^6S)$ transition of Mn(II), along with a band in the red range. It was found that emission spectra of the isolated products not only depend on nature of the halide, but also upon the excitation wavelength in case of X = Br.

Merzlyakova et al. (2021) prepared six crown-ether coordination compounds ZnX_2(18-crown-6), EuX_2(18-crown-6) (where X = Cl, Br, and I), MnI_2(18-crown-6), Mn_3Cl_6(18-crown-6)$_2$, Mn_3I_6(18-crown-6)$_2$, and Mn_2I_4(18-crown-6) through ionic-liquid-based synthesis. Some of these compounds exhibited outstanding photoluminescence. Excellent quantum yield was observed for Mn_3I_6(18-crown-6)$_2$ (98%). It was revealed that specific structural features of Mn_2I_4(18-crown-6) with finite sensitizer−activator couples resulted in an extremely strong emission with excellent quantum yield of 100%.

6.3 Coordination compounds of technetium

Technetium was discovered by Emilio Segrè (1937). He found that technetium was present in molybdenum exposed to high energy radiation. He could separate it.

All its isotopes are radioactive in nature and there is about 1 mg of technetium in a tonne of uranium (after nuclear fussion). The name has been derived from the Greek term "tekhnetos", which means artificial.

- It is a radioactive (silvery) metal not found naturally. Technetium-99 m (metastable) emits gamma-rays and therefore, it is used for medical diagnostic studies.
- Although technetium is an excellent corrosion inhibitor for steel, but its use is limited because it is radioactive.
- Its atomic Number is 43 and electronic configuration is [Kr] 4 d^5 $5s^2$. It belongs to group 7 and its common oxidation state is +7. Its different isotopes are ^{97}Tc (H.L. 4.2×10^6 y), ^{98}Tc (H.L. 6.6×10^6 y), and ^{99}Tc (H.L. 2.13×10^6 y)

Ikeda et al. (2012) synthesized six-coordinate distorted octahedral tetracyanidonitridorhenium(V) and -technetium(V) complexes having a volatile organic compound (VOC) coordinated at the trans position of a nitrido ligand,

$(PPh_4)_2[MN(CN)_4L]$ (where M = Re, L = MeOH, EtOH, acetone, or MeCN; and M = Tc, L = MeOH), and five-coordinate square-pyramidal tetracyanidonitrido complexes without an axial ligand, $(PPh_4)_2[MN(CN)_4]$ (where M = Re or Tc). All these complexes displayed photoluminescence at room temperature in the solid state. It was reported that there was a reversible luminescence switching between six- and five-coordinate rhenium(V) complexes. Luminescence changes were there from the five-coordinate technetium(V) complexes in MeOH vapor in the solid state, but no vapochromic luminescence was exhibited from the five- and six-coordinate complexes in an acetone vapor.

Ikeda et al. (2013) synthesized six-coordinate tetracyanidonitridorhenium(V) and -technetium(V) complexes with axial N-heteroaromatic ligands, $(PPh_4)_2[MN(CN)_4L]$ [where M = Re, L = 4-(dimethylamino)pyridine (dmap), 3,5-lutidine (lut), 4-picoline (pic), 4-phenylpyridine (ppy), pyridine (py), 3-benzoylpyridine (3bzpy), 4,4′-bipyridine (bpy), pyrazine (pz), 4-cyanopyridine (cpy), or 4-benzoylpyridine (4bzpy); where M = Tc, L = dmap, lut, pic, py, pz, or cpy]. These complexes displayed photoluminescence at room temperature in the crystalline phase. It was found that emission maximum wavelengths (λ_{em}) of the rhenium complexes with dmap, lut, pic, ppy, or py ligands were almost similar to each another with high emission quantum yield (Φ_{em}): $\lambda_{em} = 539-545$ nm, $\Phi_{em} = 0.39-0.93$, and emission lifetime (τ_{em}) = 10−45 μs at 296 K. The emissive excited state was characterized as $^3[(d_{xy})^1(d_{\pi^*})^1]$ ($d_{\pi^*} = d_{xz}, d_{yz}$). On the contrary, the emission maximum wavelength of the rhenium complex with 3bzpy, bpy, pz, cpy, or 4bzpy ligands was significantly dependent on the nature of the axial ligand in the crystalline phase: $\lambda_{em} = 564-669$ nm, $\Phi_{em} \leq 0.01-0.36$, and $\tau_{em} = 0.03-13.3$ μs at 296 K. That emissive excited state of the rhenium complex with bpy, pz, cpy, or 4bzpy ligands can be assigned to metal-to-N-heteroaromatic ligand charge-transfer (MLCT)-type emission with a spin-triplet type. It was observed that change in the excited-state characteristics of rhenium complexes by the N-heteroaromatic ligand is due to stabilization of π* orbital of the N- heteroaromatic ligand to a lower energy level than the d_{π^*} orbitals.

Chatterjee et al. (2013) investigated ligand-to-metal charge transfer (LMCT) excited state luminescence of $[Tc(dmpe)_3]^{2+}$ (where dmpe = 1,2-bis-(dimethylphosphino)ethane) in solution at room temperature and it was compared with its Re analogue. It was interesting to note that both $[M(dmpe)_3]^{2+*}$ (where M = Re, or Tc) species have very large excited-state potentials (ESPs) as oxidants, the highest among any coordination complex of a transition metal. It was revealed that this potential was available using a photon of visible light (calculated for M = Tc; $E^{\circ\prime *} = +2.48$ V vs. SCE; $\lambda_{max} = 585$ nm). It was also revealed that lowest energy transition in both the technetium and rhenium complexes were doublet−doublet process involving predominantly LMCT (dmpe-to-metal) character. Quenching was also observed for the excited states of both these rhenium and technetium

complexes due to highly oxidizing excited state potentials. Benzene and toluene both are oxidized by these Re and Tc systems.

6.4 Coordination compounds of rehenium

The element rehenium was discovered by Noddack, Tacke and Berg in (1925), it was named after the river Rhine in Europe. It is a stable metal. Its atomic number is 75 and it belongs to group 7. It exhibits a wide variety of oxidation states ranging from −1 to +7. It is used as a catalyst and it is added to high-temperature superalloys used in making jet engine parts.

Kunkely and Vogler (2000) reported that complex $Re^{VII}O_3$(oxinate) (where oxine = 8-quinolinol or 8-hydroxyquinoline) exhibited a green fluorescence at $\lambda_{max} = 511$ nm with $\varphi = 0.012$ along with a very weak red phosphorescence at $\lambda_{max} = 645$ nm. It was revealed that both these emissions originated from the lowest-energy $\pi\pi^*$ intraligand state of the oxinate ligand and heavy atom effect transmitted to the π-electron system of the ligand oxinate was very weak due to d^0 electron configuration and the higher oxidation state of rhenium.

Striplin and Crosby (2001) investigated electronic states of three complexes with the generic formula Re(I)Cl$(CO)_3$(s-phen) (where s-phen = 4,7-dimethyl-1,10-phenanthroline, 5,6-dimethyl-1,10-phenanthroline, and 3,4,7, 8-tetramethyl-1,10-phenanthroline). It was observed that methyl substitution leads to composite phosphorescence bands, which arise from ^{3}MLCT and $^3\pi\pi^*$ terms that are being separated by Franck−Condon (FC) barriers. They also defined some criteria for the occurrence of FC barriers and slow rates of radiationless transitions between terms arising from disparate electronic configurations.

Yam et al. (2003) synthesized a series of luminescent mixed-metal acetylide complexes, $[Cu_3(\mu{-}LL)_3\{\ \mu_3{-}\eta^1{-}C{\equiv}CC_6H_2R_2C{\equiv}C{-}\ p{-}Re(NN)(CO)_3\}_2]^+$ (where LL = dppm, ^{n}PrPNP; NN = bpy, ^{t}Bu$_2$bpy where R = H, Me) and $[M_3(\mu{-}LL)_3\{\ \mu_3{-}\eta^1{-}C{\equiv}CC{\equiv}C{-}Re(NN)(CO)_3\}_2]^+$ (where M = Cu, Ag and; LL = dppm, dppa; NN = bpy, Me$_2$bpy, ^{t}Bu$_2$bpy). They reported that all of them exhibited strong photoluminescence and assigned their low-energy emission as derived from states of ^{3}MLCT [d(Re)→*(NN)] character.

Zuo et al. (2003) reported that reactions of $Re(CO)_5X$ (where X = Cl, Br) with 7-amino-2,4-dimethyl-1,8-naphthyridine (H_2L^1) and 7-[2-(6-chloropyridyl)amino]-2,4-dimethyl-1,8-naphthyridine (HL^2) in the presence of t-BuOK produced η^1-naphthyridylcarbamoyl complex $[Re(CO)_4(HL^1CO)]$ and the naphthyridylamido complex $[Re(CO)_4(L^2)]$, respectively. It was revealed that first complex displayed a weak emission at 453 nm in an EtOH/MeOH (1:4, v/v) glassy solution at 77 K while second complex exhibited an intense (quantum yield: 0.22 in CH_2Cl_2) and long-lived emission (46 μs in CH_2Cl_2), (solvent-sensitive λ_{max}), in degassed solutions at room temperature.

Wenger et al. (2004) synthesized [Re(diimine)$(CO)_3$(dpe)](PF_6) (where dpe = 1,2-di(4-pyridyl)ethylene) compounds. It was reported that cis-dpe complexes exhibited yellow luminescence on UV excitation, whereas the trans-dpe counterparts are nonluminescent. It was observed that luminescence quantum yields of the cis-dpe complexes were found to be strongly dependent on diimine ligand. Trans-dpe complexes induces trans → cis dpe-ligand isomerization on irradiation (350 nm) with quantum yields (0.2), and this process also leads to on-switching of yellow luminescence. A steady state (approximately 70% cis- and 30% trans-dpe complexes) was reached after long 350-nm irradiation. On the other hand, a reverse cis → trans photoisomerization reaction was also induced on irradiating the cis-dpe complexes at 250 nm, which switches off the yellow luminescence (Fig. 6.4). The photodecomposition of the $[Re(diimine)(CO)_3(dpe)]^+$ complexes efficiently complete with photoisomerization on 250 nm excitation.

Wolcan et al. (2006) investigated photochemical properties of $\{(vpy\text{-}[Re(CO)_3(2,2'\text{-}bpy)])_m(vpy\text{-}[Re(CO)_3(phen)])_n(vpy)_p\}(CF_3SO_3)_{m+n}\}$ (where vpy = 4-vinylpyridine, m = 131, n = 131 or m = 200, n = 150, and m + n + P = 600) in solution phase. It was revealed that luminescence spectrum is similar to the emission spectrum of $\{(vpy\text{-}[Re(CO)_3(phen)])_{200}(vpy)_{400}\}(CF_3SO_3)_{200}$. The quenching of the luminescence by various quenchers was also observed and redox reactions of the MLCT excited states with the quenchers were considered responsible for quenching of luminescence. When Cu(II) and Fe(III)EDTA complexes were used as quenchers, a static quenching resulted. On the other hand, dynamic quenching was observed, where $Fe(CN)_6^{4-}$ or 2,2′,2″-triethanolamine, (TEOA) was used. They discussed photochemical and photophysical properties of the mixed-pendant polymers in terms of arrays of MLCT excited states, whose energies were determined by the diverse environments of the Re(I) chromophores. The upper-energy MLCT excited states conversions (with and without

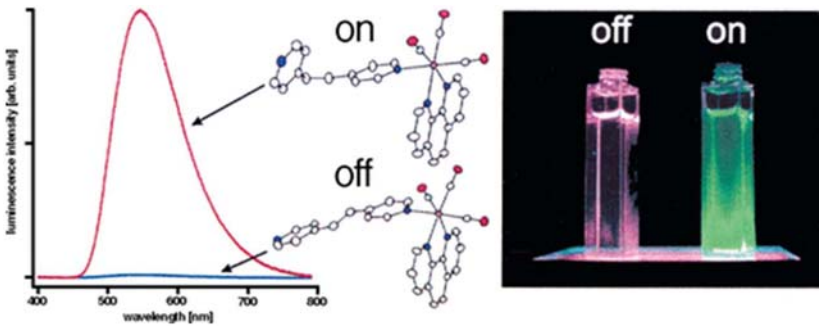

FIGURE. 6.4 Reversible cis-to trans-photoisomerization (on-off system). *Adapted from Wenger, O.S., Henling, L.M., Day, M.W., Winkler, J.R., Gray, H.B., 2004. Photoswitchable luminescence of rhenium (I) tricarbonyl diimines. Inorg. Chem. 43 (6), 2043–2048. With Permission.*

radiation) to the ground state and lower-energy MLCT excited states and excited state to the ground state could explain the experimental results.

Polo et al. (2006) reported photochemistry and photophysics of thefac-$[Re(CO)_3(NN)(L)]^+$ complexes, (where NN = polypyridyl ligands and L = stilbene-like ligands) in acetonitrile solution and in poly(methyl methacrylate) (PMMA) polymer film. These complexes diplayed trans-to-cis photoassisted isomerization of the coordinated stilbene-like ligand on irradiation. The better luminescence properties of the photoproduct, fac-$[Re(CO)_3(NN)(cis\text{-}L)]^+$ was attributed to the change of the lowest lying excited state from ^{3}IL to ^{3}MLCT. It was also revealed that emission maxima of these complexes displayed hypsochromic shifts with the increase in the medium rigidity and this change was discussed on the basis of luminescence rigidochromic effect.

Lee et al. (2007) prepared series of diarylethene-containing 1-aryl-substituted 2-(2-pyridyl)imidazole (**L**) ligands. Further reactions of 2-(2-pyridyl)imidazole ligands with $Re(CO)_5Cl$ afforded $[Re(CO)_3(\mathbf{L})Cl]$ under reflux conditions. It was also reported that open forms of the ligands showed an intense absorption band at about 320 nm corresponding to $\pi \rightarrow \pi^*$ and $n \rightarrow \pi^*$ transitions of the 1-aryl-2-(2-pyridyl)imidazole moiety, with mixing of $\pi \rightarrow \pi^*$ and $n \rightarrow \pi^*$ transitions of the thiophene moieties. It was also revealed that rhenium(I) complexes displayed IL absorption bands around 352 nm with additional MLCT $[d\pi(Re) \rightarrow \pi^*(\mathbf{L})]$ transitions at about 425 nm. The rhenium(I) complexes exhibited three new absorption bands at 288−290, 475−480, and 712−713 nm upon excitation into either the IL or MLCT bands. This shift was attributed to the planarization of the four heterocyclic rings relative to the open forms.

Mauro et al. (2009) prepared a series of neutral, dinuclear, luminescent rhenium(I) complexes, which can be suitable as phosphorescent organic light emitting devices (OLEDs). These compounds $[Re_2(\mu\text{-}Cl)_2(CO)_6(\mu\text{-}1,2\text{-}diazine)]$ contain diazines bearing alkyl groups either in one or both the β positions. Their electrochemical and photophysical properties were investigated. It was observed that complexes show intense green/yellow emissions in toluene solution and some of the complexes exhibited high emission quantum yields ($\varphi = 0.18-0.22$ for derivatives with disubstituted diazines) in the solid state. A strong blue shift of the emission was observed with an increase in the lifetime values. The highest-performing emitting complex, having cyclopentapyridazine ligand, was tested in a polymer-based light-emitting device with poly(9-vinylcarbazole) as matrix, and also in a device obtained by vacuum sublimation of the complex in 2,7-bis(diphenylphosphine oxide)-9-(9-phenylcarbazol-3-yl)-9-phenylfluorene (PCF) matrix.

Schneider et al. (2011) investigated photochemistry and photophysics of the cationic molecular dyad, ($[Re(CO)_3(Pic)Bpy\text{-}PdTPP][PF_6]$) 5-{4-[rhenium(I)tricarbonylpicoline-4-methyl-2,2′-bipyridine-4′-carboxyamidyl] phenyl}-10,15,20-triphenylporphyrinatopalladium(II). It was reported

that a steady-state photoexcitation ($\lambda_{ex} = 520$ nm) of $[Re(CO)_3(Pic)Bpy\text{-}PdTPP][PF_6]$ in dimethylformamide (DMF) resulted in substitution of Pic by bromide at the Re(I)Bpy core. It was also revealed that when $[Re(CO)_3(Pic)Bpy\text{-}PdTPP][PF_6]$ was used as a photocatalyst for the reduction of CO_2 to CO in DMF/NEt_3 solution with $\lambda_{ex} > 420$ nm, two turnovers (TNs) CO were formed after 4 h (Fig. 6.5). In case of a two-component mixture of PdTPP sensitizer and mononuclear $[Re(CO)_3(Pic)Bpy][PF_6]$ catalyst, TNs CO were formed. It was revealed that only CO was formed after a slight induction period along with photoreduction of the sensitizer to a Pd(II) chlorin species. Palladium(II) meso-tetraphenylchlorin (a hydrogenated porphyrin analogue of PdTPP) was also synthesized and it can be substituted for PdTPP in the two-component system with $[Re(CO)_3(Pic)Bpy][PF_6]$, which gives 9 TNs for CO formation.

An overview of synthesis and properties of luminescent dinuclear tricarbonyl rhenium(I) complexes, $[Re_2(\mu\text{-}X)_2(CO)_6(\mu\text{-}1,2\text{-diazine})]$ (where X = halide, hydride, alkoxide, and thiolate) has been presented by Panigati et al. (2012). Their electrochemical and photophysical properties in solution were studied. It was reported that photoluminescent quantum yields (Φ) up to 0.53 have been obtained in fluid solution for dichloro complexes having diazines bearing alkyl groups in both the β positions. These properties, along with good processability and high stability, permitted the use of some of these complexes as a phosphorescent dopant in OLEDs.

Six Re(I) complexes$ReL^nnn(CO)_33Cl$ (n = 1−6) were synthesized by Wang et al. (2013b) using different ligands (where 2,2′:6′,2″-terpyridine ligands (**L1**), five terpyridine derivatives, namely 4′-carbazol-9-yl-2,2′:6′,2″-terpyridine (**L2**), 4′-diphenylamino-2,2′:6′,2″-terpyridine (**L3**), 4′-bis(4-tert-butylphenyl)amino-2,2′:6′,2″-terpyridine (**L4**), 4′-[naphthalen-1-yl-(phenyl) amino]-2,2′:6′,2″-terpyridine (**L5**), 4′-[naphthalen-2-yl(phenyl)amino]-2,2′:6′,

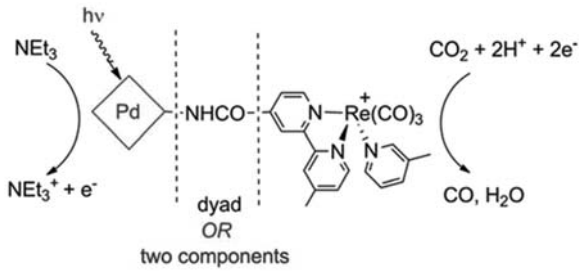

FIGURE. 6.5 The porphyrin photoreduction products during steady-state photolysis of $[Re(CO)_3(Pic)Bpy\text{-}PdTPP][PF_6]$ saturated with CO_2. *Adapted from Schneider, J., Vuong, K.Q., Calladine, J.A., Sun, X.Z., Whitwood, A.C., George, M.W., et al., 2011. Photochemistry and photophysics of a Pd (II) metalloporphyrin: Re (I) tricarbonyl bipyridine molecular dyad and its activity toward the photoreduction of CO_2 to CO. Inorg. Chem. 50 (23), 11877−11889. With Permission.*

2″-terpyridine (**L6**). It was reported that luminescence spectra of ReL2$(CO)_3$3Cl−ReL5$(CO)_3$3Cl, in CH_2Cl_2 solution at room temperature displayed strong dπ (Re) → π* (diimine) MLCT character (λ_{max} ∼ 600 nm) a small red shift relative to ReL1$(CO)_3$3Cl. It was also revealed that, the introduction of electron-donating moieties on the terpyridine unit decreases the triplet levels of the ligands at low temperature (77 K rigid matrix); thus, leading to a reduction of the energy gap between d and π* orbitals. It was found that all the complexes show an even stronger emission and a blue spectral shift (λ_{max} ∼ 550 nm) in the solid state on MLCT excitation as-compared to those obtained in solution.

Octahedral d^6 low-spin Re(I) tricarbonyl complexes are important due to their biological stability, low toxicity, long luminescence lifetimes, and large Stokes shifts. Bertrand et al. (2014) reported the bimodal IR and luminescence imaging of a Re(I) tricarbonyl complex with ligand 4-(2-pyridyl)-1,2,3-triazole (Pyta) as ligand in cells. Although Re(I) tricarbonyl complexes have certain interesting photophysical properties, which allowed for their detection in cells, but a drawback is also there like very low luminescence quantum yield in aqueous medium. They developed Re(I) tricarbonyl complexes using different ancillary ligands. It was reported that complexes with benzothiadiazole−triazole ligands displayed luminescent quantum yields in acetonitrile and can be used as luminescent metal complexes in organic media. A series of complexes was also prepared with bidentate 1-(2-quinolinyl)-1,2,3-triazole (Taquin) and 1-(2-pyridyl)-1,2,3-triazole (Tapy) ligands with different 4-substituted alkyl side chains. Their photophysical properties were also studied in acetonitrile and in mixture H_2O/DMSO (98/2). It was observed that Tapy complexes bearing long alkyl chains exhibited an enhancement of their luminescent properties relative to the parent Pyta complex. It was also revealed that MDA-displayed a strong increase in the luminescence signal in MB231 breast cancer cells incubated with the Tapy complex substituted with a C12 alkyl chain.

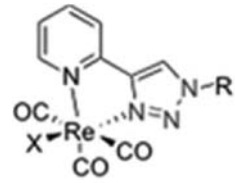

Re-Pyta

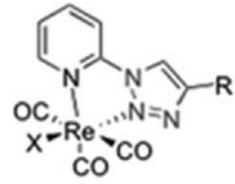

Re-Tapy

Adams et al. (2015) demonstrated ligand-to-metal charge transfer state (LMCT) of $[(dmpe)_3Re]^{2+}$ (where dmpe = 1,2-bis(dimethylphosphino) ethane) to be a potent oxidant ($E^0(Re^{2+}*/Re^+ = 2.61$ V vs. standard calomel electrode). This complex was earlier prepared by nontrivial routes with low yields, and in optimizing the ground state and emission energy properties of complexes of the type $[(PP)_3Re]^{2+}$ only little could be achieved through phosphine achieved modification. Improved syntheses of Re(I) tris-homoleptic diphosphine complexes $[(PP)_3Re]^+$ (where PP = 1,2-bis(dimethylphosphino)ethane (dmpe), bis(diphenylphosphino)methane (dppm), 1,2-bis(diethylphosphino)ethane (depe), bis(dimethylphosphino) methane (dmpm), $Me_2PCH_2PPh_2$, 1,3-bis(dimethylphosphino)propane (dmpp), or 1,2-bis(dimethyl-phosphino)benzene (dmpb)) was achieved by single-pot reactions making use of reducing potential of the phosphines, when treated with Re (V) oxo-complexes in 1,2-dichlorobenzene at 160−180°C. It was observed that single-electron chemical oxidation of $[(PP)_3Re]^+$ afforded luminescent Re^{II} analogs and $[(PP)_3Re]^{2+}$ complexes in good yields using Ph_3C^+, Cp_2Fe^+, or $(4\text{-}BrC_6H_4)_3N^+$ $B(C_6F_5)_4^-$ salts. It was revealed that redox and luminescence behavior of these complexes indicated that the luminescence is from a ligand P(σ)-to-metal (Re(dπ)) charge transfer (^{2}LMCT) state for all the complexes. It was also reported that structured luminescence (at 77 K) was considered due to relaxation of the ^{2}LMCT state into two spin−orbit coupled states; the ground state and a state $\sim 3000\ cm^{-1}$ above the ground state.

Lee et al. (2017) reported that most of the rhenium (I) tricarbonyl polypyridine complexes has diverse photochemical and photophysical properties through the coordination of functionalized ligands. The typical photophysical properties of the complexes (large Stokes shifts, high photostability and long emission lifetimes) allow them to act as attractive candidates for optical imaging. Isostructural relationship between rhenium and technetium-99m, rhenium(I) tricarbonyl complexes and characteristic infrared absorption bands have been studied as multimodal imaging reagents for vibrational and radioimaging. It was also revealed that facile photosensitizing properties and the three carbon monoxide (CO) ligands make rhenium(I) tricarbonyl complexes promising candidates for photodynamic therapy reagents and photoactivatable CO-releasing molecules, respectively, for treatment of cancer.

Mamud et al. (2021) synthesized a series of rhenium(I) polypyridyl compounds having photoisomerizable nitrones as ligands and investigated their photochemical and photophysical behaviors. These complexes resulted in Z → E due to the photosensitized isomerization of the coordinated ligand on irradiation and it was also confirmed. It was observed that photoisomerization quantum yields depend on the nature of the nitrone substituent, which changes the energy of the $^3IL_{Z\text{-}NitX}$ excited state (populated by photosensitization). It was also reported that ^{3}MLCT becomes the lowest-lying excited state in the E-product, which resulted in an enhancement in emission intensity. It was

suggested that such changes in spectroscopic properties of the Z or E coordinated nitrones has a potential to be used in molecular devices such as photosensors.

References

Adams, J.J., Arulsamy, N., Sullivan, B.P., Roddick, D.M., Neuberger, A., Schmehl, R.H., 2015. Homoleptic tris-diphosphine Re (I) and Re (II) complexes and Re (II) photophysics and photochemistry. Inorg. Chem. 54 (23), 11136−11149.

Bertrand, H.C., Clède, S., Guillot, R., Lambert, F., Policar, C., 2014. Luminescence modulations of rhenium tricarbonyl complexes induced by structural variations. Inorg. Chem. 53 (12), 6204−6223.

Bikas, R., Hosseini-Monfared, H., Vasylyeva, V., Sanchiz, J., Alonso, J., Barandiaran, J.M., et al., 2014. Heteronuclear, mixed-metal Ag (I)−Mn (II) coordination polymers with bridging N-pyridinylisonicotinohydrazide ligands: synthesis, crystal structures, magnetic and photoluminescence properties. Dalton Trans. 43 (31), 11925−11935.

Bortoluzzi, M., Castro, J., Di Vera, A., Palù, A., Ferraro, V., 2021a. Manganese (II) bromo-and iodo-complexes with phosphoramidate and phosphonate ligands: synthesis, characterization and photoluminescence. J. Chem. 45 (29), 12871−12878.

Bortoluzzi, M., Castro, J., Gobbo, A., Ferraro, V., Pietrobon, L., Antoniutti, S., 2020. Tetrahedral photoluminescent manganese (II) halide complexes with 1, 3-dimethyl-2-phenyl-1, 3-diazaphospholidine-2-oxide as a ligand. J. Chem. 44 (2), 571−579.

Bortoluzzi, M., Ferraro, V., Castro, J., 2021b. Synthesis and photoluminescence of manganese (II) naphtylphosphonic diamide complexes. Dalton Trans. 50 (9), 3132−3136.

Carlos, R.M., Neumann, M.G., 2000. Photochemical and photophysical properties of [Mn(imidazole)$(CO)_3$(phen)](SO_3CF_3) complexes. J. Photochem. Photobiol., A: Chem. 131 (1−3), 67−73.

Carlos, R.M., Neto, B.S.L., Neumann, M.G., 2004. The effects of the substitution on the lmidazole ligand on the photochemical properties of fac [Mn $(CO)_3$(phen)(lmidazole)](SO_3CF_3) complexes. Photochem. Photobiol. 80 (2), 203−208.

Chatterjee, S., Del Negro, A.S., Smith, F.N., Wang, Z., Hightower, S.E., Sullivan, B.P., et al., 2013. Photophysics and luminescence spectroelectrochemistry of [Tc (dmpe) 3]$^{+/2+}$(dmpe = 1, 2-bis (dimethylphosphino) ethane). J. Phys. Chem. A 117 (48), 12749−12758.

Doux, M., Mézailles, N., Ricard, L., Le Floch, P., Vaz, P.D., Calhorda, M.J., et al., 2005. Syntheses, X-ray structures, photochemistry, redox properties, and dft calculations of interconvertible f ac-and m er-[Mn (SPS)$(CO)_3$] isomers containing a flexible SPS-based pincer ligand. Inorg. Chem. 44 (25), 9213−9224.

Fodor, M.A., Horváth, O., Fodor, L., Vazdar, K., Grampp, G., Wankmüller, A., 2016. Photophysical and photochemical properties of manganese complexes with cationic porphyrin ligands: effects of alkyl substituents and micellar environment. J. Photochem. Photobiol., A: Chem. 328, 233−239.

Henke, W.C., Otolski, C.J., Moore, W.N., Elles, C.G., Blakemore, J.D., 2020. Ultrafast spectroscopy of [Mn $(CO)_3$] complexes: tuning the kinetics of light-driven CO release and solvent binding. Inorg. Chem. 59 (4), 2178−2187.

Herr, P., Kerzig, C., Larsen, C.B., Häussinger, D., Wenger, O.S., 2021. Manganese (I) complexes with metal-to-ligand charge transfer luminescence and photoreactivity. Nat. Chem. 13 (10), 956−962.

Ikeda, H., Ito, A., Sakuda, E., Kitamura, N., Takayama, T., Sekine, T., et al., 2013. Excited-state characteristics of tetracyanidonitridorhenium (V) and-technetium (V) complexes with N-heteroaromatic ligands. Inorg. Chem. 52 (11), 6319−6327.

Ikeda, H., Yoshimura, T., Ito, A., Sakuda, E., Kitamura, N., Takayama, T., et al., 2012. Photoluminescence switching with changes in the coordination number and coordinating volatile organic compounds in tetracyanidonitridorhenium (V) and-technetium (V) complexes. Inorg. Chem. 51 (22), 12065−12074.

Kokkes, M.W., Stufkens, D.J., Oskam, A., 1985. Photochemistry of metal-metal-bonded complexes. 1. MLCT photolysis of $(CO)_5MM'(CO)_3$ (. alpha.-diimine)(M, M′ = Mn, Re) in 2-MeTHF between 133 and 230 K. Inorg. Chem. 24 (19), 2934−2942.

Kunkely, H., Vogler, A., 2000. Photoluminescence of 8-quinolinolato (trioxo) rhenium (VII). Inorg. Chem. Commun. 3 (11), 645−647.

Lee, L.C.C., Leung, K.K., Lo, K.K.W., 2017. Recent development of luminescent rhenium (I) tricarbonyl polypyridine complexes as cellular imaging reagents, anticancer drugs, and antibacterial agents. Dalton Trans. 46 (47), 16357−16380.

Lee, P.H.M., Ko, C.C., Zhu, N., Yam, V.W.W., 2007. Metal coordination-assisted near-infrared photochromic behavior: a large perturbation on absorption wavelength properties of N, N-donor ligands containing diarylethene derivatives by coordination to the rhenium (I) metal center. J. Am. Chem. Soc. 129 (19), 6058−6059.

Lemes, M.A., do Nascimento Neto, J.A., Guimarães, F.F., Maia, L.J.Q., de Santana, R.C., et al., 2021. Isostructural coordination chains assembled with aminopyrazine: decreasing photoluminescence yield by Cd (II) replacement for Mn (II). J. Mol. Struct. 1236. https://doi.org/10.1016/j.molstruc.2021.130352.

Li, B., Ni, L.S., Yong, G.P., 2018. Three new coordination compounds based on a new 3-position substituted imidazo [1, 2-a] pyridine ligand: syntheses, crystal structures and photoluminescent properties. Polyhedron 154, 21−26.

Mamud, J.F., Biazolla, G., Marques, C.S., Cerchiaro, G., de Queiroz, T.B., Keppler, A.F., et al., 2021. Z to E light-activated isomerization of α-pyridyl-N-arylnitrone ligands sensitized by rhenium (I) polypyridyl complexes. Inorg. Chim. Acta. 514. https://doi.org/10.1016/j.ica.2020.120009.

Mauro, M., Procopio, E.Q., Sun, Y., Chien, C.H., Donghi, D., Panigati, M., et al., 2009. Highly emitting neutral dinuclear rhenium complexes as phosphorescent dopants for electroluminescent devices. Adv. Funct. Mater. 19 (16), 2607−2614.

Merzlyakova, E., Wolf, S., Lebedkin, S., Bayarjargal, L., Neumeier, B.L., Bartenbach, D., et al., 2021. 18-Crown-6 coordinated metal halides with bright luminescence and nonlinear optical effects. J. Am. Chem. Soc. 143 (2), 798−804.

Panigati, M., Mauro, M., Donghi, D., Mercandelli, P., Mussini, P., De Cola, L., et al., 2021. Luminescent dinuclear rhenium (I) complexes containing bridging 1, 2-diazine ligands: photophysical properties and application. Coord. Chem. Rev. 256 (15−16), 1621−1643.

Polo, A.S., Itokazu, M.K., Frin, K.M., de Toledo Patrocínio, A.O., Iha, N.Y.M., 2006. Light driven trans-to-cis isomerization of stilbene-like ligands in fac-[Re $(CO)_3$ (NN) (trans-L)]$^+$ and luminescence of their photoproducts. Coord. Chem. Rev. 250, 1669−1680.

Reade, T.J., Murphy, T.S., Calladine, J.A., Horvath, R., Clark, I.P., Greetham, G.M., et al., 2017. Photochemistry of framework-supported M (diimine)$(CO)_3$X complexes in three-dimensional lithium carboxylate metal−organic frameworks: monitoring the effect of framework cations. Phil. Trans. Royal Soc. A: Math. Phys. Eng. Sci. 375 (2084). https://doi.org/10.1098/rsta.2016.0033.

Rosa, A., Ricciardi, G., Baerends, E.J., Stufkens, D.J., 1996. Metal-to-ligand charge transfer (MLCT) photochemistry of fac-Mn (Cl)$(CO)_3$ (H-DAB): a density functional study. J. Phys. Chem. 100 (38), 15346−15357.

Schneider, J., Vuong, K.Q., Calladine, J.A., Sun, X.Z., Whitwood, A.C., George, M.W., et al., 2011. Photochemistry and photophysics of a Pd (II) metalloporphyrin: Re (I) tricarbonyl bipyridine molecular dyad and its activity toward the photoreduction of CO_2 to CO. Inorg. Chem. 50 (23), 11877−11889.

Striplin, D.R., Crosby, G.A., 2001. Photophysical investigations of rhenium(I) $Cl(CO)_3$ (phenanthroline) complexes. Coord. Chem. Rev. 211 (1), 163−175.

Stufkens, D.J., Van der Graaf, T., Stor, G.J., Oskam, A., 1991. The photochemistry of (CO) 5MnMn $(CO)_3$ (α-diimine) and XMn (CO_3)(α-diimine)(X = halide) complexes. Coord. Chem. Rev. 111, 331−336.

Wang, D., Xu, Q.L., Zhang, S., Li, H.Y., Wang, C.C., Li, T.Y., et al., 2013b. Synthesis and photoluminescence properties of rhenium (I) complexes based on 2, 2′: 6′, 2″-terpyridine derivatives with hole-transporting units. Dalton Trans. 42 (8), 2716−2723.

Wang, Y.N., Bai, F.Q., Yu, J.H., Xu, J.Q., 2013a. Synthesis, structural characterization and photoluminescence property of three Zn^{2+}/Mn^{2+}-acylhydrazidate complexes and two acylhydrazide molecules. Dalton Trans. 42 (47), 16547−16555.

Wei, Y.L., Jing, J., Shi, C., Ye, H.Y., Wang, Z.X., Zhang, Y., 2018. High quantum yield and unusual photoluminescence behaviour in tetrahedral manganese (II) based on hybrid compounds. Inorg. Chem. Front. 5 (10), 2615−2619.

Wenger, O.S., Henling, L.M., Day, M.W., Winkler, J.R., Gray, H.B., 2004. Photoswitchable luminescence of rhenium (I) tricarbonyl diimines. Inorg. Chem. 43 (6), 2043−2048.

Wolcan, E., Feliz, M.R., Alessandrini, J.L., Ferraudi, G., 2006. Aggregation in nanobundles and the effect of diverse environments on the solution-phase photochemistry and photophysics of−Re $(CO)_3L^+$ (L= 1,10-phenanthroline,2,2′-bipyridine) pendants bonded to poly (4-vinylpyridine). Inorg. Chem. 45 (17), 6666−6677.

Wu, Y., Zhang, X., Xu, L.J., Yang, M., Chen, Z.N., 2018. Luminescent vapochromism due to a change of the ligand field in a one-dimensional manganese (II) coordination polymer. Inorg. Chem. 57 (15), 9175−9181.

Yam, V.W.W., Lo, W.Y., Lam, C.H., Fung, W.K.M., Wong, K.M.C., Lau, V.C.Y., et al., 2003. Synthesis and luminescence behaviour of mixed-metal rhenium (I)−copper (I) and−silver (I) alkynyl complexes. Coord. Chem. Rev. 245 (1−2), 39−47.

Yue, Q., Wang, Y.Y., Hu, X.L., Guo, W.X., Gao, E.Q., 2019. Eight coordination compounds assembled from unexplored semi-rigid ether-based unsymmetrical tetracarboxylate and various dipyridyl ligands: structural variation, magnetic and photoluminescence properties. Cryst. Eng. Comm. 21 (44), 6719−6732.

Zuo, J.L., Fu, W.F., Che, C.M., Cheung, K.K., 2003. Synthesis, crystal structure, and photoluminescent properties of a tetracarbonyl (naphthyridylcarbamoyl) rhenium (I) complex and a highly emissive tetracarbonyl (naphthyridylamido) rhenium (I) complex. Eur. J. Inorg. Chem. 2003 (2), 255−262.

This page intentionally left blank

Chapter 7

Coordination compounds of iron, ruthenium and osmium

Liju Raju and E. Rajkumar
Department of Chemistry, Madras Christian College, Affiliated to University of Madras, Chennai, Tamil Nadu, India

7.1 Introduction

Earth-abundant transition metal complexes have gained increasing attention in the recent decade, offering the attractive potential to build sustainable large-scale molecular-based technologies in the fields of solar energy conversion, photocatalysis, and biological applications (Roundhill, 2013; Balzani et al., 1996; Kalyanasundaram et al., 1982, 1991; Lindh et al., 2020; Pashaei et al., 2016; Hagfeldt et al., 2010; Campagna et al., 2007; Xue et al., 2015; Cauwenbergh and Das, 2021; Lakowicz, 2013; Zhang and Huang, 2018; Wehlin et al., 2020; Bouché et al., 2020; Glazer, 2017; Monro et al., 2018; Li and Chen, 2020; Banerjee, 2021). Transition metal complexes, particularly Fe, Ru, and Os metal complexes have a wide range of coordination numbers, oxidation states, and geometries (Roundhill et al., 2013; Balzani et al., 1996; Kalyanasundaram et al., 1982, 1991). Coordination compounds of d^6 transition metals are being developed to provide favorable photoredox properties that rival or exceed the photophysical and photochemical properties of the existing compounds of transition metals. The fundamental understanding of the ground and the excited state dynamics of metal complexes is important for the construction of molecular architecture for their appropriate applications such as the construction of dye-sensitized solar cells, light-harvesting antennas, molecular probes, molecular machines, luminescence sensors, catalysis, and biological applications. There are several review articles and book chapters, where the photochemistry and photochemistry of Fe, Ru, and Osmium complexes are discussed (Roundhill et al., 2013; Balzani et al., 1996; Kalyanasundaram et al., 1982, 1991; Liu et al., 2016; Omar et al., 2018; Juris et al., 1988). This book chapter focuses on the recent development and different approaches adopted in fine-tuning of photophysical and photochemical properties of polypyridine and related

Photochemistry and Photophysics of Coordination Compounds. https://doi.org/10.1016/B978-0-12-824493-7.00008-3
Copyright © 2023 Elsevier Inc. All rights reserved.

complexes of Fe, Ru, and Os complexes over the last decade. Few representative transition metal complexes were presented that have strong absorption in the visible region and the long-lived triplet states. Applications of these complexes are also briefly discussed in the fields of photodynamic therapy (PDT), dye-sensitized solar cells (DSSC), and photocatalysis (hydrogen generation, water oxidation, and CO_2 reduction), etc.

7.2 Coordination compounds of iron

The abundant transition metal elements all belong to the first-row transition metals, with iron being the most abundant transition metal in the Earth's crust. The coordination compounds based on iron are particularly intriguing. Since iron is a bio-essential element and its complexes are well known as candidates for photometallodrugs in cancer therapy, specifically by DNA cleavage and photocytotoxicity (Bouché et al., 2020). Further, photocatalytic reactions using iron complexes are receiving attention for the conversion and/or oxidation of organic substrates, dye-sensitized solar cells, photoelectrochemical cells and solar energy conversion. The well-documented photochemical reactions are the photo-induced decarboxylation reaction and photo-assisted Fenton reaction, both of which find their importance in the fields of environmental, materials and biological sciences (Yang et al., 2021; Lin and Lin, 2021). Unlike ruthenium and osmium complexes, the photophysics and photochemical properties of iron polypyridyl complexes and other related complexes are less explored, due to their exceptionally short (sub-picosecond) charge-transfer excited-state lifetime (Auböck and Chergui, 2015). The understanding of excited dynamics is essential for the light driven applications ranging from solar energy conversion, photoredox, photoelectrochemical, photocatalysis and chemical synthesis. The recent advances in the photophysics and photochemistry of coordination compounds of iron-polypyridyl complexes and related complexes will be discussed in the following sections.

7.2.1 Electronic structures and photophysics of iron complexes

The chemistry of iron is influenced by the range of accessible spin states, which includes low, intermediate, and high-spin iron complexes. Although iron complexes are known to exist in a variety of oxidation states ranging from 0 to +6, photoactivity has been reported mainly for the Fe^{2+} and Fe^{3+} states. The photochemistry of iron complexes is side-lined by photophysics and photochemistry of ruthenium and osmium complexes. In Fe(II)-complexes, the ligand field is much weaker than in Ru(II), this is because the distribution of the six 3d electrons in iron is closer to the nucleus than that of the 4d electrons in ruthenium (Wenger, 2019). Therefore, the metal-centered (MC) excited state ($^3T_{1g}$ and $^5T_{2g}$) falls below the triplet metal to ligand charge transfer (^{3}MLCT) state in Fe^{2+}, and three other MC states, namely ($^3T_{2g}$, $^1T_{1g}$, $^1T_{2g}$)

are energetically close. In this situation, the triplet MLCT state is deactivated within a period of ca. 50 fs, followed by vibrational relaxation on a timescale of a few ps (McCusker, 2014). The $^5T_{2g}$ state although being non-luminescent, yet it is fairly long-lived (ca. 650 ps), and this has been exploited in photochemical contexts, but it would be much more desirable to obtain a long-lived luminescent MLCT state resembling to that of Ru^{2+}. To date, this has not yet been achieved with iron. Fig. 7.1 depicts the Tanabe−Sugano diagram for the d^6 electron configuration of the simplified potential energy diagram with the key electronic states in $[Fe(bpy)_3]^{2+}$complex.

The weaker split in the ligand field (first-row transition element), which limits the photoactivity of iron complexes, causes a rapid deactivation of charge-transfer states via low-energy metal-centered states. Many attempts have been made to produce iron complexes that make them effective in light-based applications. The strategies include the following.

- Development of highly symmetric ligands field,
- Employing push-pull ligand sets,
- By creating highly strained complexes that give rise to ^{5}MLCT states
- By employing strong sigma donating N-heterocycliccarbene (NHC) ligands or by using cyclometalled ligands, which are both; σ and π donors and
- By the use of mesoionic carbenes as combined σ-donor, π - acceptor ligands.

Chelating ligands enhances the symmetry in complexes, allowing coordination of Fe^{2+} with bond angles (180 degrees between N−Fe−N) as close as possible for ideal octahedral geometry. This ensures maximum overlapping between the ligand and metal-based orbitals. This phenomenon was demonstrated by McCusker (2014) using a tridentate ligand with three pyridine binding motifs linked by carbonyl groups, resulting in a complex with an ideal octahedral geometry with a biting angle of 178.3 degrees between N−Fe−N. The inclusion of the electron-withdrawing carbonyl group aided energetically, favoring the stabilization of the lowest π* orbital of the tridentate chelating ligand. The Fe(II)-complex exhibits an excited state lifetime of 280 ps in acetonitrile at room temperature. The ligand field is so strong that the $^3T_{1g}$ state is lower than $^5T_{2g}$ state, which can lead to faster excited state decay for two main reasons.

(i) Electronic coupling between $^3T_{1g}$ and $^1A_{1g}$ is likely to be stronger than that between $^5T_{2g}$ and $^1A_{1g}$ because of the smaller change in net spin, and
(ii) Reorganization energy associated with the transition from $_3T_{1g}$ to $_1A_{1g}$ is smaller, because it involves the relaxation of a single e.g., electron to a t_{2g} orbital, while the transition from $_5T_{2g}$ to $_1A_{1g}$ involves the relaxation of two electrons from antibonding e.g., to formally non-bonding t_{2g} orbitals (Jamula et al., 2014).

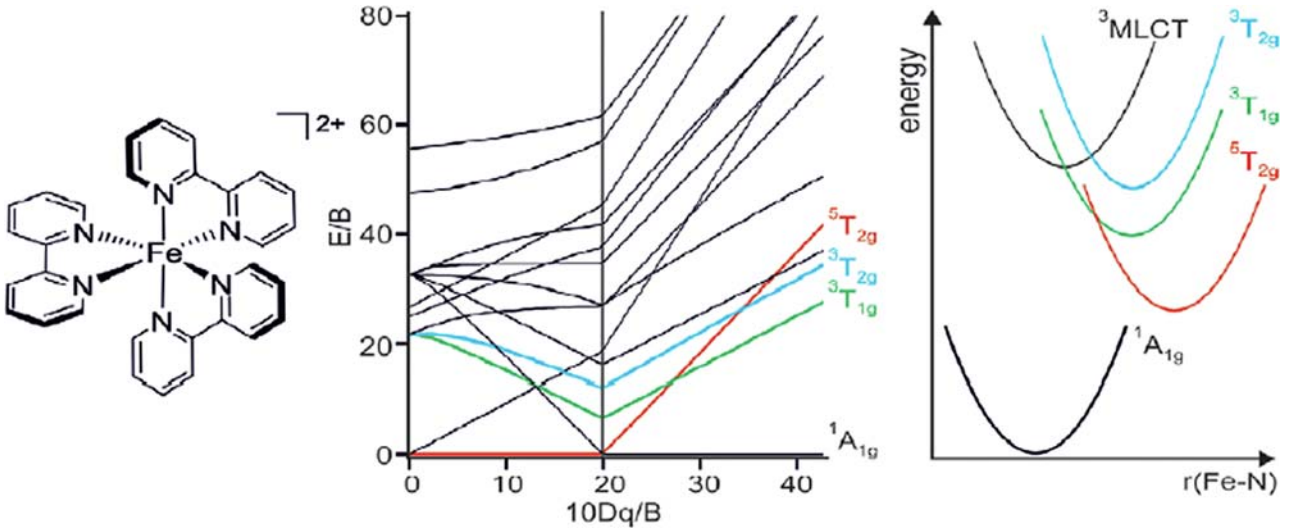

FIG. 7.1 Molecular structure of $[Fe(bpy)_3]^{2+}$; Tanabe−Sugano diagram for the d^6 electron configuration and simplified potential energy diagram with the key electronic states in $[Fe(bpy)_3]^{2+}$. *Adapted from Wenger, O.S., 2019. Is iron the new ruthenium? Chem. Eur J. 25 (24), 6043−6052. With permission.*

The push-pull ligand system developed by Mengel et al. (2015) was based on the combination of both, electron withdrawing ligand, 2,6-bis(2-carboxypyridyl)pyridine (dcpp), and electron-rich ligand *N*,*N*′-dimethyl-*N*,*N*′-dipyridine-2-yl-pyridine-2,6-diamine (ddpd) which are capable of forming tridentate chelates of the type $[Fe(dcpp)(ddpd)]^{2+}$. The push-pull combination of these ligands lowers the $^{1/3}$MLCT manifold of Fe^{2+} complexes, while at the same time raising the $^{3}T_{1g}$ and $^{5}T_{2g}$ states through increased metal-ligand orbital overlap enabled by the favorable bite angles of these two particular ligands. $[Fe(dcpp)(ddpd)]^{2+}$ exhibits a low-lying absorption band centered at 585 and 559 nm corresponding to the mixed MLCT and ligand-to-ligand charge transfer (LLCT) character (ddpd → dcpp), respectively. Interpreted this method of producing luminescence by the ligand dcpp, inducing a ligand field strength near or may be beyond the $^{5}T_{2g}/^{3}T_{1g}$ crossing point (Jamula et al., 2014). Push-pull complexes with Fe(II) have been particularly promising with ligand-to-ligand charge transfer (LLCT) states (instead of MLCT).

Another technique for improving the photophysical characteristics of Fe(II)-complexes was to access the ^{5}MLCT state via strained low spin Fe(II)-complexes. (Fatur et al., 2017; Shepard et al., 2016) were demonstrated this concept using homoleptic Fe(II)-complexes with halogenated terpyridine ((2,2′; 6′,2″-terpyridine) -tpy) ligands at the 6- and 6″-positions. The chloro and bromo substituted ligands based complexes exhibit a weaker ligand field compared to the parent complex $[Fe(tpy)]^{2+}$, due to the repulsion experienced between the tpy ligands because of the bulky halogen atoms. As a result of this repulsive interaction, the $^{5}T_{2g}$ state becomes the ground state, as expected for a weak ligand field. This strained arrangement makes it possible to excite the complex into a spin allowed $^{5}T_{2g} \rightarrow {}^{5}$MLCT transition followed by the decay from ^{5}MLCT state (or ^{7}MLCT arising due to intersystem crossing). The important observation from the $^{5/7}$MLCT lifetime of the 6,6′-halogenated-terpyridine-Fe(II)-complexes, increases from 14.0 to 16.0 and 17.4 ps along the F^{-}, Cl^{-} and Br^{-} series of complexes in acetonitrile at room temperature.

A complementary approach to enhancing the ligand field strength is to destabilize the e_g orbitals (hence, raising the ^{3}MC states' energies) with strongly σ-donating ligands such as N-heterocyclic carbenes (NHC) (Chábera et al., 2021). This strategy has resulted in an increase in ^{3}MLCT lifetime to a few tens of picoseconds in some iron(II)-complexes. This very promising approach has been well-reviewed (Lindh et al., 2020; Duchanois et al., 2018) and several different research groups have made an important contributions in recent times. Liu et al. (2013) reported a ^{3}MLCT life time of 9 ps (in acetonitrile, at room temperature (RT)) for a homoleptic complex with the tetradentate 2,6-bis(imidazole-2-ylidene)pyridine ligand, which was the longest known ^{3}MLCT lifetime for Fe(II)-complexes. The NHC ligands are known to exhibit a strong σ-donation; however, it is important to note that their π-acceptor properties are limited, that is why the pyridine unit is included to

accommodate the MLCT-excited state electron. Unfortunately, the ^{3}MLCT energy is not raised to the level of $[Fe(tpy)_2]^{2+}$complex due to its π-acceptor abilities, and this was counteracted to some extent by increasing the π-conjugation by replacing imidazolylidene by benzimidazolylidene subunits (Fig. 7.2A) offering a ^{3}MLCT life time of 16 ps as reported by Liu et al. (2016). The strong σ-donation provided by NHC ligands is possible by heteroleptic complexes maintaining a lower ^{3}MLCT (Duchanois et al., 2014). Such heteroleptic complexes of iron are as shown in Fig. 7.4.

Many research groups had envisioned the idea of using cyclometalating chelate ligands to construct photoactive iron(II)-complexes through computational studies (Tang et al., 2020). Using cyclometalating chelate ligands (Fig. 7.4), MLCT states can be stabilized owing to their π donating character, leading to a red shift in their absorption bands (Fig. 7.3D) (Dixon et al., 2015).

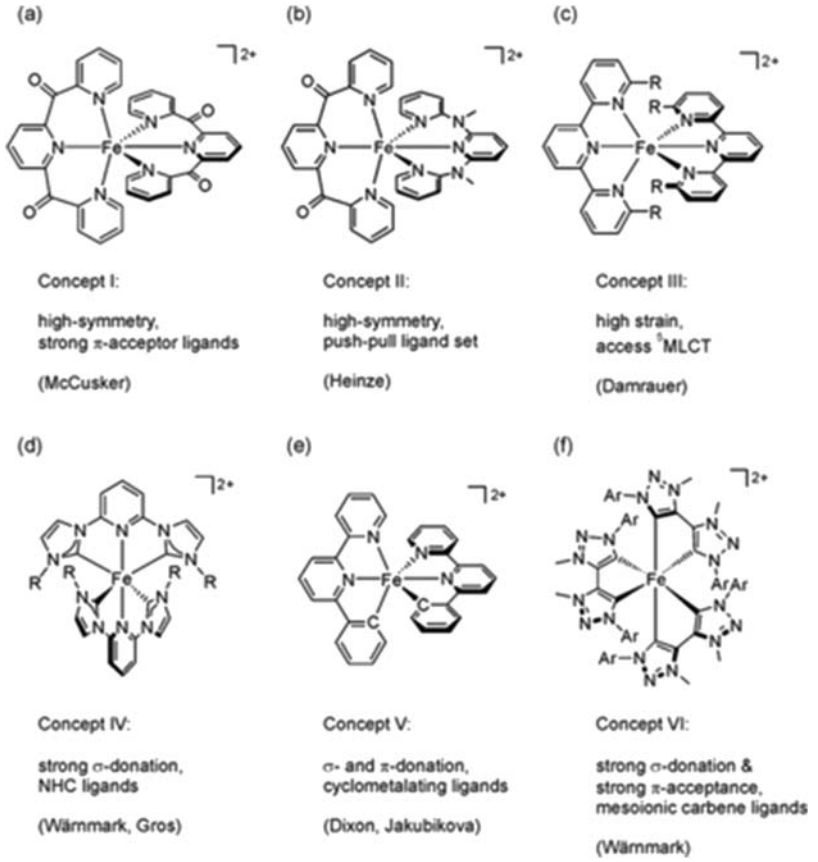

FIG. 7.2 Key strategies and concepts for obtaining Fe^{II} complexes with long-lived MLCT states, along with exemplary molecular structures. *Adapted from Wenger, O.S., 2019. Is iron the new ruthenium? Chem. Eur J. 25 (24), 6043−6052. With permission.*

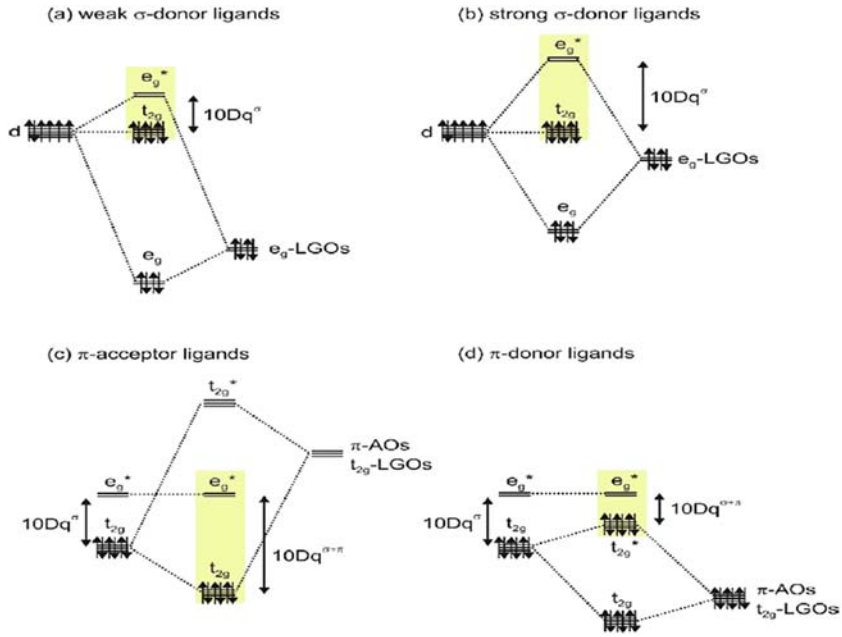

FIG. 7.3 Ligand field effects depending on the type of bonding interactions between metal d orbitals and ligand group orbitals (LGOs) or atomic orbitals (AO). *Adapted from Wenger, O.S., 2019. Is iron the new ruthenium? Chem. Eur J. 25 (24), 6043−6052. With permission.*

The ^{3}MC states are less influenced by cyclometalation, which implies that the destabilization of the e_g, orbitals by σ donation (Fig. 7.3B) is of similar magnitude to that of the destabilization of the t_{2g} orbitals by π donation. However, the ^{3}MC state is destabilized only, if the ligating carbon atoms are on one of the peripheral rings of the tridentate ligand, whereas if they are on the

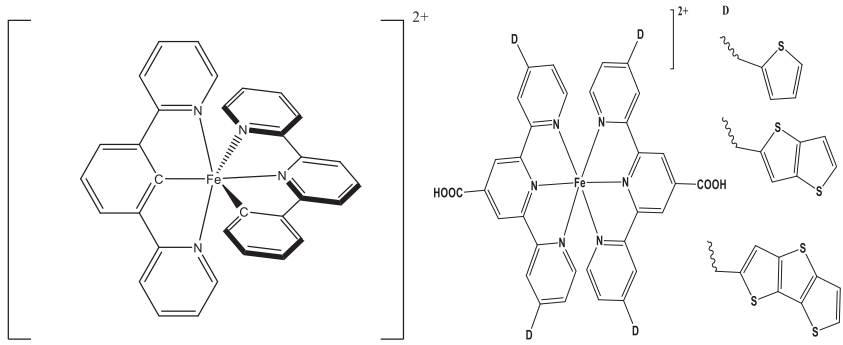

FIG. 7.4 Fe(N^C^N) (N^N^C) and complexes with π-donating ligands.

central ring, an undesirable stabilization of ^{3}MC is observed. The complexes shown in Figs. 7.2E and 7.4 are therefore identified as particularly favorable with regard to avoiding the population of the ^{3}MC state out of the ^{3}MLCT state. Depending upon the position and number of aryl groups, cyclometalation could increase the energy gap between the $^1A_1$ and ^{5}T states by the tuning of energy $\sim 8-20$ kcal mol^{-1} (Mukherjee et al., 2015). Based on all these observations, it can be predicted that cyclometalation has the potential to slow down the relaxation from the $^{1/3}$MLCT states into the ^{3}MC and ^{5}MC states. On the basis of computational studies, it is possible to identify the efficient ligands that would offer an energetically lower ^{3}MLCT compared to the ^{3}MC states. For example, a strong σ-donating acetylide based systems, in addition to the NHC chelates offered promising results (Dixon et al., 2016). Similarly, incorporation of furan thiophene, and selenophenes moieties in *tpy* unit (Fig. 7.4) greatly enhance the optical properties of the complexes (Mukherjee et al., 2017). These systems were found to have occupied π orbitals that were perfectly aligned with the t_{2g} orbitals on the iron(II), resulting in a stronger metal-ligand π interactions and an increase in the HOMO energy level. If *tpy* unit was substituted with donor groups containing extended π conjugations, for example dithienothiophene, thienothiophene, further stabilization of the ligand π orbitals can be achieved which results in a ligand-centered HOMO leading to an effect termed as HOMO inversion (Mukherjee et al., 2017).

The combined effect of having strong σ donating and π accepting ligands is another approach to tune the photophysics of Fe^{2+} complexes. Mesoionic carbene-based ligands offer this feature of being strong σ donating and π accepting character. Liu et al. (2015) developed a mesoionic carbene ligand. The heteroleptic $[Fe(btz)_2(bpy)]^{2+}$complexes displayed ^{3}MLCT lifetime of 13 ps, which was 100 times longer than $[Fe(bpy)_3]^{2+}$complexes. Fe(II)/(III) complex with mesoionic carbene ligand (btz) are presented in Fig. 7.5.

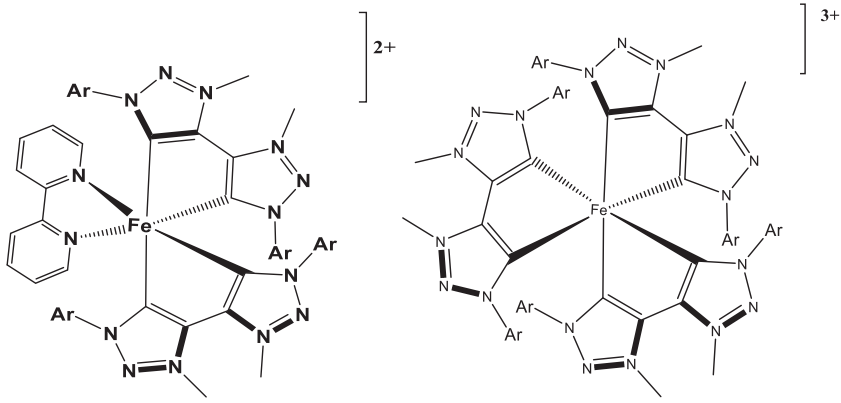

FIG. 7.5 Fe(II)/(III) complex with mesoioniccarbene ligand (btz).

The photophysical properties of the low spin d^5 Fe(III)-complex is even more spectacular than those of the Fe(II)-complexes. Chábera et al. (2017) recently reported that a low-spin Fe(III)-complex with a relatively long-lived (~100 ps) ^{2}LMCT state attained at room temperature using a strong σ-donor and π-acceptor NHC ligand. Even though the life time is short, it is promising and sufficient enough to participate in photochemical processes together with the spin allowed radiative decay to the ground state. The absorption spectra of both the oxidation states (Fe^{3+} and Fe^{2+}) feature very similar bands in the ultraviolet region, (307 nm). That are assigned to ligand-centered π-π* transitions irrespective of metal oxidation state. The visible absorption spectrum of the Fe^{3+} state features a weaker band at 384 nm (with shoulders at 400 and 420 nm), 528, and 558 nm. These low-energy absorption bands of Fe^{3+} are ascribed to LMCT transitions from the Fe(III) ground state, similar to those observed in $[Fe(CN)_6]^{3-}$ (Fig. 7.6). Excitation by any of these absorption bands resulted in readily detectable ^{2}LMCT photoemission with a quantum yield of 3×10^{-4} in CH_3CN at room temperature.

The recent advances on photoactive iron complexes can be condensed into two main strategies.

(i) Use of chelating ligands that facilitate strong metal coordination with high symmetry, as close to the ideal octahedral geometry to maximize the overlapping between metal and ligand orbitals (Darari et al., 2020), and

(ii) Use of ligands that combine strong σ-donor and π-acceptor characteristics to create strong ligand fields, in which non-radiative decay of MC states

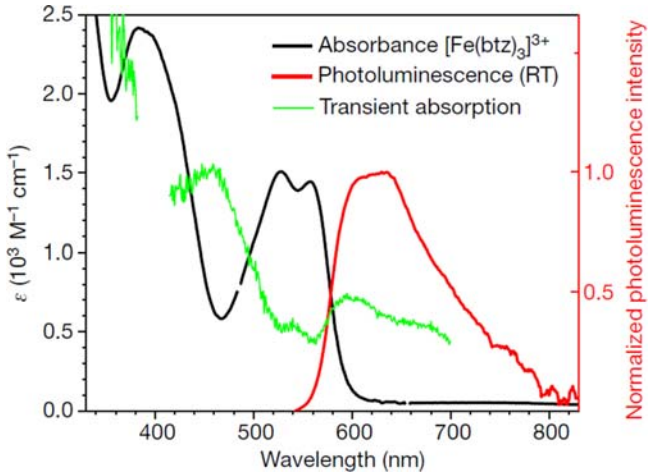

FIG. 7.6 Steady-state absorption and emission spectra of $[Fe(btz)_3](PF_6)_3$ in CH_3CN atroom temperature (RT). *Adapted from Chábera, P., Liu, Y., Prakash, O., Thyrhaug, E., El Nahhas, A., Honarfar, A., et al., 2017. A low-spin Fe (III) complex with 100-ps ligand-to-metal charge transfer photoluminescence. Nature 543 (7647), 695–699. With permission.*

are shifted to high energies. Fe(III)-systems have also gained attraction in inorganic photophysics. The photophysical and photochemical properties of recently reported Fe^{3+}complex with an anionic scorpionate tris(NHC) ligand are very similar to that of the prototype ruthenium(II)tris-bipyridine complex in several aspects, and they appear to be even better in terms of photostability (Kjaer et al., 2019). Furthermore, heteroleptic Fe(III)-complexes could be interesting systems for fine tuning of HOMO and LUMO energies.

7.2.2 Photochemistry of iron complexes

Iron complexes are known to exhibit a wide range of photo-induced reactions, which include photo-induced electron/energy transfers, photo-induced ligand degradation, photo-induced cleavage of bonds, photo-induced release of small molecules, and photocatalysis reactions, etc. There are several articles available in the literature based on iron photochemistry, and hence, we have discussed representative examples on a few photochemical processes involving iron complexes (Lindh et al., 2020; Chen and Browne, 2018).

The earliest report on the photochemistry of iron complexes was in Fenton type reactions. The Fenton reagent is a combination of $H_2O_2/Fe^{3+/2+}$, which is typically used as a by-product to generate reactive oxygen species (ROS) with water. This is used in waste water treatment and antimicrobial treatment processes (Gonçalves et al., 2020; Costa et al., 2020). The production of ROS is initiated under irradiation (($\lambda > 580$ nm) by the rapid generation of $Fe^{3+/2+}$ through photoreduction of the Fenton reagent. The photoreduction of Fe(II) ion by hydrogen peroxide to Fe(III) ion can occur in the radiation range of 280−550 nm. A general mechanism can be depicted as:

$$Fe^{2+} + H_2O_2 \rightarrow Fe^{3+} + HO^{\bullet} + OH^{-} \quad (7.1)$$

$$Fe^{3+} + H_2O_2 \rightarrow Fe^{2+} + HOO^{\bullet} + H^{+} \quad (7.2)$$

$$Fe(OH)^{2+}\ h\nu \rightarrow Fe^{2+} + HO^{\bullet} \quad (7.3)$$

The drawback of this type of Fenton reaction is the need to maintain an acidic pH that helps in generating photoactive Fe-complexes and to avoid the formation of Fe(OH) precipitates (Zhang and Zhou, 2019). Thus, carboxylate ligands based Fe-complexes were investigated to achieve (Zhang et al., 2019; Vilar et al., 2017).

(i) Formation of strong and steady complexes between iron in an aqueous medium,

(ii) Formation of more photo-active species with the largest production of $^{\bullet}OH$ radicals, thereby resulting in a higher quantum efficiency compared to the conventional photo-Fenton reactions, and

(iii) Reactions that can occur at near-neutral pH (Lumbaque et al., 2019). Seibert et al. (2017) reported the use of Fe(III)-carboxylate complexes for photo-Fenton type degradation of landfill leachate.

The best results were obtained with the photo-reactor operating at pH of 6.0, 100 mg Fe(III) per liter of EDTA (Ethylenediamine tetraacetic acid); consuming 275 mM H_2O_2 and demanding about 8 kJ_{UV} L^{-1}, resulting in total discoloration and 80% reduction of the landfill leachates. Solar Fenton reaction, which employ siron(III)-ethylendiamine-N′,N′-disuccinic acid (EDDS) for inactivation of pathogen in ground water was reported by García-Fernández et al. (2019). A suitable candidate for the development of iron chelated soluble complexes, ethylendiamine-N′,N′-disuccinate acid (EDDS) is environmentally acceptable, biodegradable and operates closely to neutral pH.

Reduction of water and CO_2 can be affected photocatalytically by iron complexes. Though ruthenium and osmium complexes have displayed outstanding performance as photosensitizers, many iron complexes are seen to be reported to act as photosensitizers. Iron polypyridyl complexes exhibit a very strong absorption in the visible-light region but suffer from very rapid deactivation of the photocatalytically active $^{1/3}$MLCT states into inactive MC states. This behavior is different for the other members of the iron family as they have a large energy gap between the $^{1/3}$MLCT and MC states sufficient enough to have a longer lifetime (Liu et al., 2016). However, the photophysical properties of iron complexes can be finely-tuned by their coordinating ligands, based on various concepts explained in earlier sections; thereby, increasing their applicability in photochemical processes. One such effective technique to achieve the expected photophysical properties of Fe-complexes is to use N-heterocyclic carbene ligand (NHC) with the polypyridyl system. Iron-NHC complexes are envisioned to exhibit potential photochemical properties from the intensive physicochemical and computational analyses (Harlang et al., 2015). Bauer et al. (2017), Zimmer et al. (2017) reported (NHC) complexes of iron as photosensitizers for the photo-induced water reduction (Fig. 7.7). They first demonstrated that Fe^{2+}—NHC complexes can be used as noble metal-free transition-metal complex as photosensitizer for a light-driven water reduction process.

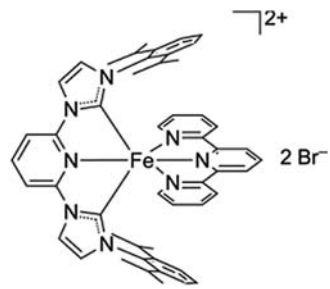

FIG. 7.7 Fe:NHC complex, photosensitizer for water reduction. *Adapted from Bauer et al., 2017, Eur. J. Inorg. Chem. 2017 (11), 1504—1509. With permission.*

The combined effect of both; tpy and NHC ligand in heteroleptic Fe(II) complexes would offer optimized photochemical properties for photocatalytic proton reduction (Zimmer et al., 2018). The tpy would help to have intense absorption in the visible region and bis-NHC ligand stabilizes the photoactive MLCT states and ensures photostability of the complexes (Duchanois et al., 2014). The resulting complex offered the advantages of high stability and low price compared to conventional Ru/Os/Ir-based photosensitizers. Iron-based coordination compounds have recently been employed as photosensitizers for reducing CO_2 (Rao et al., 2018). A simple terpyridineiron(III)-complex was used as an organic thermally activated delayed fluorescence (TADF) photosensitizers for carbon dioxide reduction (Wang et al., 2020).

A significant enhancement of CO production with 99.3% selectivity in the presence of water was observed. The turn over number (TON) was determined to be 2250 and turn over frequency (TOF) was 60 min^{-1}. The proposed mechanism of the photo catalytic reaction is shown in Fig. 7.8.

Because of their capacity to penetrate deeper tissue, metal complexes that can be triggered by red light (biological window) are extremely important as phototherapeutic sensitizers (Tang et al., 2020). Iron based complexes have also proved to be efficient photosensitizer in photodynamic therapy and used

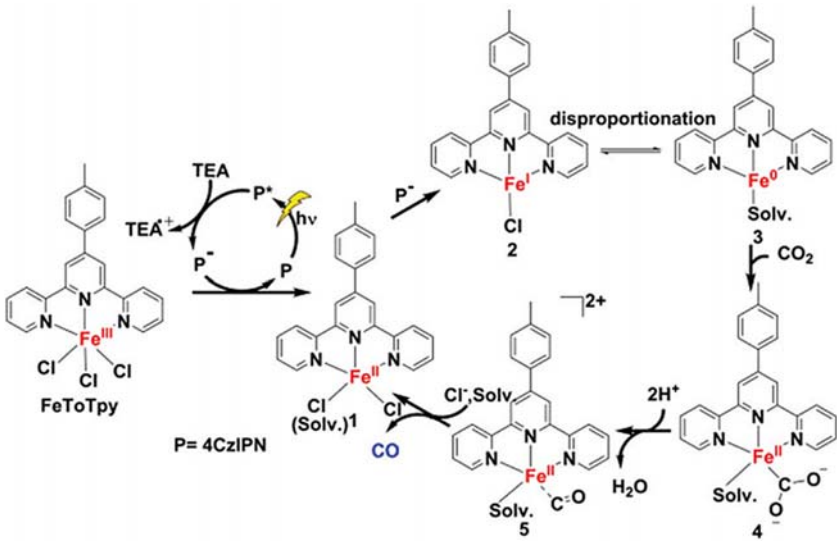

FIG. 7.8 Proposed mechanism for photocatalytic CO_2 reduction. *Adapted from Wang, Y., Gao, X.W., Li, J., Chao, D., 2020. Merging an organic TADF photosensitizer and a simple terpyridine−Fe (III) complex for photocatalytic CO_2 reduction. Chem. Commun. 56 (81), 12170−12173. With permission.*

as photochemotherapeutic agents (Tabrizi, 2018; Karges et al., 2019; Karges and Gasser, 2020; Sahoo et al., 2021). Sahoo et al. (2021) reported a Fe(III)-curcumin complexes appended with biotin for targeted PDT. The visible light triggered cytotoxicity was studied in HeLa, HepG2 and MCF-7 cell lines. The photodynamic effect was observed between 400 and 700 nm excitation. The complexes displayed their ability to act as targeted photochemotherapeutic drugs.

As an alternative for other transition metals in sustainability, eco-friendly as well as industrial uses, the fundamental photophysical, photochemical and applications of iron-based coordination compounds are increasing rapidly. However, in order to employ iron as a PS effectively, one must fine tune its photophysical features such as long-lived excited state, red light absorption by carefully selecting their ligand system, which can be useable for efficient PS for light driven applications.

7.3 Coordination compounds of ruthenium

Ruthenium(II)-complexes are of great interest for researchers due to their rich photochemistry and photophysical properties. Ruthenium complexes are extensively used for the construction of dye- sensitized solar cells, light harvesting antennas, molecular probes, molecular machines, luminescence sensors, catalysis and biological applications (Roundhill, 2013; Balzani et al., 1996; Kalyanasundaram, 1982, 1991; Lindh et al., 2020; Campagna et al., 2007). This interest is due to unique photophysical properties such as luminescence at RT, long excited state life time, moderate quantum yield, spectroscopically distinctive redox states, ability to undergo electron and energy transfer processes and fine tuning of electronic properties and chemical stability. Here, a recent development and different approaches adopted in fine tuning the photophysical and photochemical properties of Ru(II)-complexes over the last decade have been discussed.

7.3.1 Photophysics of $[Ru(NN)_3]^{2+}$ complexes

The photophysical and photochemical properties of $[Ru(NN)_3]^{2+}$ (NN- polypyridine ligands) complexes can be tailored to a greater extent by introducing electron-donating and electron-withdrawing groups into the 2,2′-bipyridine (bpy), 1,10-phenanthroline (phen) and additional nitrogen atoms into the pyridine ring; thus, it offers greater tenability (Ashford et al., 2014). Furthermore, the extensive synthetic chemistry available allows for systematic modification of their photophysical properties, and the addition of anchoring groups that allow immobilisation on a variety of surfaces, including semiconductors, polymers, and other materials, leads to a diverse set of applications (Roundhill, 2013; Balzani et al., 1996; Kalyanasundaram, 1982, 1991; Juris et al., 1988).

7.3.1.1 Absorption spectra of $[Ru(NN)_3]^{2+}$ complexes

The d^6, Ru(II) system and the polypyridyl ligands forms six coordination "Oh" geometry, where the ligands possess σ donor orbitals localized on the nitrogen atoms and π donor and π^* acceptor orbitals essentially delocalized on aromatic rings. $[Ru(bpy)_3]^{2+}$ and its analogs complexes have an octahedral geometry of D_3 symmetry. A simplified molecular orbital diagram along with the absorption spectrum of $[Ru(bpy)_3]^{2+}$ is shown in Fig. 7.9.

The different types of transitions between molecular orbitals in the complex correspond to several absorption bands in the visible region absorption spectrum of the complex. The observation of absorption bands in the visible region is due to the photoexcitation of $[Ru(NN)_3]^{2+}$. These bands are usually assigned to metal-to-ligand-charge-transfer (MLCT) transitions, in which an electron is promoted from a Ru-based molecular orbital (π_M), belonging to the filled metal t_{2g} shell, to the empty π^* orbitals of the bipyridine ligands (π^*_L) (Frank-Condon singlet metal-to-ligand charge transfer ^{1}MLCT state) and localization of the electron on one of the bipyridine ligands, while promotion of an electron from π_M to σ^*_M orbitals leads to metal-centered (MC) excited states. The ligand-centered (LC) excited states can be obtained by promoting an electron from the π_L ligand orbital to π^*_L ligand orbital.

Modern inorganic photochemistry focuses on the interplay of metal-to-ligand charge transfer (MLCT) and metal-centered (MC) excited state of

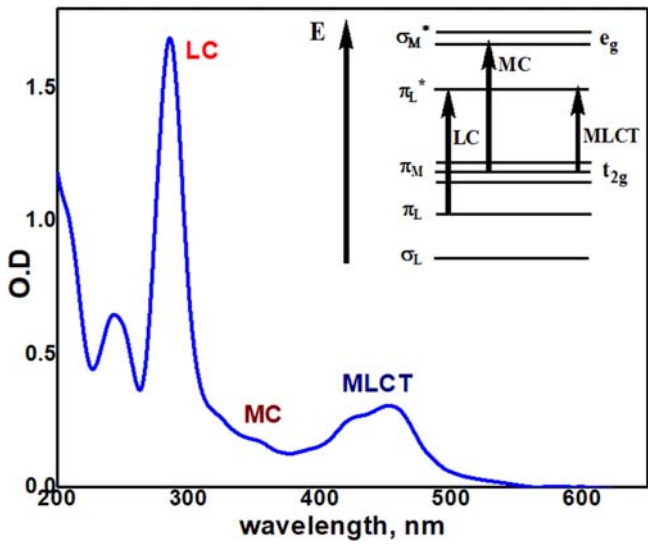

FIG. 7.9 Absorption spectrum of $[Ru(bpy)_3]^{2+}$ in acetonitrile (Inset shows the molecular orbital diagram). *Adapted from Feng, L., Wang, Y., 2018. A key factor dominating the competition between photolysis and photoracemization of* $[Ru(bpy)_3]^{2+}$ *and* $[Ru(phen)_3]^{2+}$ *complexes. Inorg. Chem. 57 (15), 8994−9001. With permission.*

Ru(II)-complexes and their derivatives. Both of these two states play important role in the photophysical properties such as photoluminescence, photoinduced electron and energy transfer processes and photochemical properties such as photo-isomerization, and photo-release properties of these metal complexes for their applications in the fields of solar energy conversion, photocatalysis, sensor, imaging and photodynamic therapy etc (Feng and Wang, 2018; Soupart et al., 2020; Brabec and Kasparkova, 2018). The multiple deactivation pathway of $*[Ru(NN)_3]^{2+}$ are depicted in Fig. 7.10. According to picosecond time resolved spectral studies, the MLCT states become essentially localized onto one ligand extremely rapidly, even when the ligands are identical, as in $[Ru(bpy)_3]^{2+}$. Dongare et al. (2017) comprehend various experimental techniques to analyze the electronic structure of the excited MLCT state and whether the excited state ($dp^5\pi^{*1}$) may be localised on one ligand $[Ru^{III}(bpy)_2(bpy^{-\bullet})]^{2+*}$or delocalized over all three ligand $[Ru^{III}(bpy^{-\bullet 1/3})_3]^{2+*}$. The derived electronic structural model originated from various time scale spectroscopic techniques from initial light absorption by $[Ru(bpy)_3]^{2+}$ and related MLCT excited state to final excited state equilibration, and the given sequence is GS → ^{1}MLCT → ^{3}MLCT → Vibrational relaxation → Solvent relaxation.

In less than 300 fs, ^{1}MLCT state undergoes rapid intersystem crossing (ISC) to a long-lived triplet excited state (^{3}MLCT) (Damrauer et al., 1997; Cannizzo et al., 2006; Wallin et al., 2005; Dietzek et al., 2006; Alary et al., 2007; Henry et al., 2008; Harriman and Izzet, 2007; and Kim et al., 2020). Dietzek et al. (2006) established that the two distinctive time scales have been discovered by using femtosecond four-wave mixing of the relaxation processes leading to a thermalized ^{3}MLCT state in the complex, $[Ru(tbbpy)_3]^{2+}$ (tbbpy = 4,4′-di-*tert*-butyl-2,2′-bipyridine). An ultrafast process, which is attributed to intersystem crossing, takes place within 200 fs by rapidly depopulating the initially photoexcited ^{1}MLCT state, followed by a second process on a picosecond time scale, assigned to vibrational cooling within the

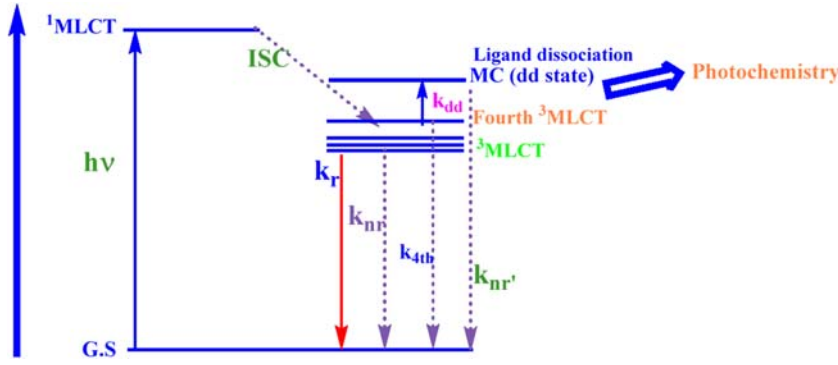

FIG. 7.10 Various deactivation pathways of $*[Ru(NN)_3]^{2+}$.

^{3}MLCT state. Henry et al. (2008) investigated the early picosecond time scale of excited state dynamics of $[Ru(NN)_3]^{2+}$ complexes by picosecond Kerr-gated time resolved resonance Raman (ps-TR^3) spectroscopy. From these results, the observation that the thermally equilibrated excited (THEXI) state is not fully evolved on the femtosecond timescale, as previously suggested, but the changes in the vibrational spectra are seen up to some 10 ps. The ^{3}MLCT state comprises manifold of four MLCT states that spans a narrow energy range. The three lowest-energy triplet states can be separated only at low temperature, the energy spacing being less than 200 cm^{-1}, and they can be approximated to a single entity at RT (Horvath and Gordon, 2010; Chang et al., 2012; Zigler et al., 2016). The fourth ^{3}MLCT state lies $\sim$400−1000 cm^{-1} above this ensemble and its existence is indicated from a variety of kinetic, emission polarization and temperature dependent emission studies (Wallin et al., 2005; Bhasikuttan et al., 2002; Shaw et al., 2004; Myrick et al., 1987; Ito and Meyer, 2012). Molecular orbital calculations led to the conclusion that the fourth MLCT state possesses more singlet character than the low energy triplet, and temperature dependent studies confirmed that this species decays faster than the ensemble.

The direct observation of the vibrational band at 1599 cm^{-1} in time resolved infrared spectroscopy under photoexcitation of $[Ru(bpy)_3]^{2+}$complex at different experimental conditions confirms the observation of a short-term population of ^{3}MC state ($\sim$23 ps) during the relaxation to the bottom of the ^{3}MLCT state (Mukuta et al., 2016; Sun et al., 2013). The localization of the electron on one bpy ligand changes the ground state D_3 symmetry to a C_2 symmetry in the ^{3}MLCT state. The interplay between electronic and geometric changes is of prime importance in elementary charge-transfer processes. Static and time-resolved resonance Raman studies have been carried out on $[Ru(bpy)_3]^{2+}$ to measure the structural changes in the ^{3}MLCT state, but these were mainly concentrated on the bond changes within bpy^- ligand. Bressler and Chergui (2004) and Gawelda et al. (2006) reported the picosecond time resolved XANES (X-ray Near-Edge Absoption Structure) and EXAFS (Extended X-ray Absorption Fine Structure) study of both; ground and excited state $[Ru(bpy)_3]^{2+}$ complexes in aqueous medium is attempted. From these studies, a Ru−N bond contraction by $\sim$0.03Å in the excited state compared to the ground state has been proposed. This weak bond contraction is due to dominant electrostatic and polarization interaction between the oxidized Ru atom and the neutral & reduced bpy ligands and by steric effects due to straining of the latter.

Because of the spin forbidden ($T_1 \rightarrow S_0$) transition, ^{3}MLCT excited state is long lived and commonly used for photoinduced electron or energy transfer processes. The molar absorption coefficient of the complex depends on the overlapping of HOMO and LUMO molecular orbitals and its usually partially allowed ($S_0 \rightarrow {}^1$MLCT) transition. The partially allowed transitions that determine the molar absorptivity of the complexes, where there is a partial

overlapping of HOMO and LUMO molecular orbitals. The intersystem crossings (ISC) ($S_1 \rightarrow T_1$) and ($T_1 \rightarrow S_0$) is dramatically enhanced by the process called spin orbit coupling (SOC), which is induced by the heavy atom effect. When there is a greater spin orbit coupling, the T_1 state has a shorter life time. In addition, the photoexcited state have a stronger redox property than its ground state, which is useful for constructing photocatalysts, where electron relay plays a key role (Kim et al., 2020).

7.3.1.2 Emission properties

The emission of ^{3}MLCT ($*[Ru(bpy)_3]^{2+}$) state exhibited a measured life time of about 900 ns in acetonitrile. This is long enough for the excited state to efficiently transfer its energy to another molecule (quencher) either by energy or electron transfer. In the absence of a quencher, the excited state undergoes deactivation through both non-radiative and radiative decay pathways with an emission quantum yield of 0.062 (in acetonitrile). $[Ru(NN)_3]^{2+}$ complexes are highly luminescent and the λ_{max}^{em} is in the range of 600−700 nm. The excitation of any one of its absorption bands, it emits a single emission band with maximum wavelength at 602 nm (in H_2O). The emission properties of ruthenium(II)-polypyridyl complexes can provide much information about the lowest excited state (Lakowicz, 2013). It exhibits a fairly long lived emission with moderate intensity in degassed aqueous solutions ($\tau = 0.6$ μs; $\Phi = 0.042$). With a quantum yield of 0.4 and life time of 5 μs at 77 K, the emission spectrum of $[Ru(NN)_3]^{2+}$ complex exhibits some vibrational structure.

The highest energy peak in the steady state emission spectrum at 77 K can be used to estimate the excited state energy. The excited state energy is depends on the electron donating and accepting substituents on the ligands and the delocalization effect in the ligands. The excited state energy can be tuned by the appropriate choice of the substituents. Emission properties of Ru(II)-complexes, such as intensity, life time, quantum yield and energy position are strongly influenced by the medium (Roundhill, 2013; Balzani et al., 1996; Kalyanasundaram, 1982, 1991; Mareeswaran et al., 2014; Rajkumar et al., 2014; Sangiliapillai et al., 2016; Swarnalatha et al., 2011). The introduction of electron withdrawing groups lowers the ^{3}MLCT level; thereby, shifts the emission maximum to the longer wavelength region.

7.3.1.3 Excited state life time

The photoexcited molecule, the time allowed for a reaction to occur is of the order of the lifetime of the particular excited state or less, when the reaction step must compete with other photophysical processes. The excited state lifetime (τ_r) of a molecule is related to the rate of radiative and nonradiative processes, through Eq. (7.4).

$$1 / \tau_r = k_r + k_{nr} + k_{4th} \exp(-\Delta G_{4th} / k_B T) + k_{dd} \exp(-\Delta G_{dd} / k_B T) \quad (7.4)$$

where k_r and k_{nr} are the radiative and nonradiative rate constants for the deactivation of ^{3}MLCT state and k_{4th} and k_{dd} represent the sum of radiative and nonradiative decay rate constants for the depopulation of the corresponding state. According to the energy gap law, the nonradiative decay rate constant, k_{nr}, is influenced by the energy gap between the ground state and the ^{3}MLCT state. The rate of non-radiative decay increases as the energy difference between the ground state and the ^{3}MLCT state decreases, and the life time of the excited state decreases. The excited state lifetime values of $[Ru(NN)_3]^{2+}$ are highly sensitive to the nature of the substituents in the 2,2′-bipyridine and 1,10-pheanthroline ligands and solvent system used. The influence of the nature of the ligand and medium on the τ values can be explained in terms of energy level diagram shown in Fig. 7.2.

7.3.1.4 Quantum yield

The emission quantum yield (Φ) measures the efficiency by which the absorption of photon leads to the production of excited state molecules. The emission quantum yield is related to the rate of radiative (k_r) and nonradiative (k_{nr}) decays of excited states through Eq. (7.5).

$$\Phi_{em} = k_r \tau = k_r / (k_r + k_{nr} + k_{4th} + k_{dd}) \quad (7.5)$$

In Eq. (7.5), τ is the excited state life time of $[Ru(NN)_3]^{2+}$. The quantum yield of $[Ru(bpy)_3]^{2+}$ is 0.062 in acetonitrile. According to the energy gap law, the rate of nonradiative decay is related to the emission energy by Eq. (7.6).

$$k_{nr} \; \alpha \; e^{-CE_{em}} \quad (7.6)$$

where E_{em} is the energy in cm^{-1} at the maximum wavelength. Nonradiative deactivation of excited states takes place via two routes. One is from the lowest excited state (^{3}MLCT), which decays to the ground state directly. The other is via the high-lying ligand field (^{3}LF) state, which undergoes fast nonradiative decay to the ground state or ligand dissociation. This fast nonradiative decay is responsible for the low quantum yield. It also depends on the intersystem crossing of ^{3}MLCT state to the ^{3}LF state. The quantum yield and life time was found to decrease with increase in temperature (Hagfeldt et al., 2010).

7.3.1.5 Excited state redox properties

All molecular excited states are potential redox reagents since the absorption of light leads to excitation of electron to a high energy level, where it is more weakly bound and at the same time, an electron hole in the low energy level. Hence, excited state species can be a better oxidant as well as a better reductant than the corresponding ground state and it is represented in Eq. (7.7).

$$[Ru^{II}(bpy)_3]^{2+} \rightarrow [Ru^{III}(bpy)_2(bpy)^-]^{2+} \quad (7.7)$$

The excited state redox potentials are obtained from the redox potentials of the corresponding ground state and the spectroscopic excited state energy. The excited state redox potentials are given to a first approximation by the following Eqs. (7.8) and (7.9).

$$E^{+}_{(D/*D)} = E^{+}_{(D/D)} - E_{0\text{-}0} \tag{7.8}$$

$$E_{(*A/A-)} = E^{-}_{(A/A)} + E_{0\text{-}0} \tag{7.9}$$

Here $E_{(D+/D)}$ and $E_{(A/A-)}$ are the ground state and $E_{(D+/*D)}$ and $E_{(*A/A-)}$ are the excited state oxidation and reduction potentials of $[Ru(NN)_3]^{2+}$, respectively and $E_{0\text{-}0}$ is the zero, zero excitation energy of the complex. Oxidation of $[Ru(NN)_3]^{2+}$ complexes usually involves the removal of the electron from a metal orbital ($d\pi_M$) and reduction involves addition of electron to the ligand.

The oxidation potential is affected by the nature of the ligands because the amount of electric charge localized on the metal (the tendency to lose an electron) is governed by σ and π donor properties of the ligands. For the ligands of same series, the presence of electron withdrawing groups increases the oxidation potential while the opposite occurs for electron donating substituents. Reduction usually takes place on the ligand. So the ground state reduction potential of $[Ru(NN)_3]^{2+}$ will be related to the reduction potential of the free ligand. However, the ability of a coordinated ligand to accept an electron also depends on the amount of charge transferred to the metal or received from the metal via σ and π bonding by the other ligands. In addition, the changes in the reduction potential of the ground state do not cause an equal change in the reduction potential of the excited state because the energy of the MLCT level decreases as the ligand becomes easier to be reduced. So the main factor, which governs the excited state redox potentials of $[Ru(NN)_3]^{2+}$, is the change in the structure of the ligands. In mixed ligand complexes, the electron is located on the ligand with the larger reduction potential value.

7.3.1.6 Photophysical properties of Ru(II)-complexes

The research interest focuses on to achieve lower energy absorption with a significant emission and a long-lived excited state. One strategy to achieve this is to reduce the HOMO-LUMO energy gap, which would result in a red shift in the absorption and emission signature of the complexes. Though this strategy may not alter the molar extinction coefficient significantly, (Cerfontaine et al., 2020) demonstrated that trinuclear Ru(II)-polypyridyl complexes with tritopicbridging ligands connecting between 4,4′ and 5,5′ positions of the bipyridine moiety between para and meta position of the central as well as peripheral bipyridine moieties (Fig. 7.11), exhibiting lower energy π^* acceptor orbitals that induces a red shift of MLCT absorption bands and photoluminescence. The absorption and normalized steady state emission spectra are shown in Fig. 7.11. In addition to the expected peaks, a broadening of

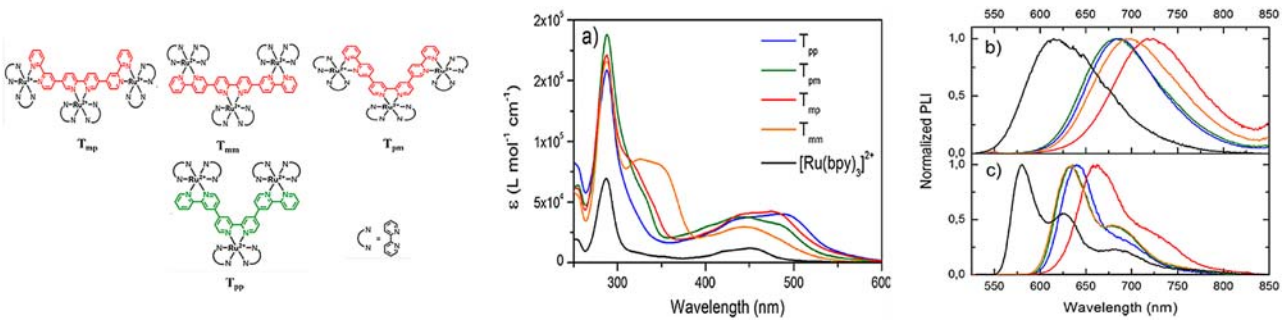

FIG. 7.11 The ortho/para/meta substituted bypyridine group on to the bipyridine core at their 4,4′ and 5,5′ positions and the trinuclear Ru(II) complexes and UV−visible absorption spectra for the complexes in acetonitrile at 293 K (A). Normalized steady-state photoluminescence spectra of the complexes in acetonitrile solution at 293 K; (B) and in butyronitrile rigid matrix at 77 K and (C). *Adapted from Cerfontaine, S., Troian-Gautier, L., Duez, Q., Cornil, J.R.M., Gerbaux, P., Elias, B., 2020. MLCT excited-state behavior of trinuclear ruthenium (II) 2, 2′-bipyridine complexes. Inorg. Chem. 60 (1), 366−379. With permission.*

ligand-centered transition around 290 nm was observed and became more prominent as the number of linearly arranged bipyridine moieties increased ($T_{mm} > T_{mp} > T_{pm} > T_{pp}$). Complex, T_{mm} exhibited an additional peak around 336 nm and having low energy peak at 445 nm, whereas other studied complexes exhibited two peaks around 450 and 480 nm. All these transitions are assigned to ^{1}MLCT transitions and have high molar absorption coefficients than parent complex, $[Ru(bpy)_3]^{2+}$. The spectral correlation was further supported by cyclic voltammetry.

At both 77 and 293 K, the emission spectrum of all the four complexes exhibits a strong photoluminescence (PL) peak with single exponential life time. Though there are two types of metal centers, i.e., peripheral and central Ru(II), the single exponential life time indicated that the photoemission originated from only one type of Ru(II), this was due to the energy transfer associated between the two types of metal ceneters. The bathochromic shift in the PL suggests that the energy transfer is taking place from the peripheral metal centers to the core metal center. At 77 K, the corresponding photoluminescence life times and quantum yields followed in the order $T_{pp} > T_{pm} > T_{mm} > T_{mp}$. These complexes exhibit a decrease in life time and quantum yield with increase in temperature. An increase in the molecular hierarchy is one way of tuning the photophysics of Ru(II)-polypyridyl complexes, such as polymetallic and other supramolecular architectures. Metallodendrimers are one of the categories. It could be one of three types: Metal core, metal at the periphery, or metal as connectors on a dendrimeric ligand (Vögtle et al., 1999; Vonlanthen et al., 2016). Ru(II)-based polynuclear complexes, dendrimers and hetero-metallic complexes, etc have been developed and their photophysical properties have been explored (Mishra et al., 2013; El-Batal et al., 2013; Anandkumar et al., 2017; Zhang et al., 2020).

The substitution on the ancillary unit on the polypyridyl core has strong influence on the photophysical properties of Ru(II)-complexes. In a study conducted by Shalan et al. (2017), correlating the effect of *para* substitutionson ruthenium(II)-polypyridine complex to their photophysical properties was investigated. A series of ruthenium(II)-complexes, containing electron donating and withdrawing groups of the type $[Ru(4,4'\text{-}X_2bpy)_2(phenA)]^{2+}$, (where X (*para* substituted) = Cl, H, *t*-Bu, Me OPhe, OMe, or NMe_2, bpy = 2,2′-bipyridine, and phenA = 5-acetamido-1,10-phenanthroline) were prepared and their photophysical properties were also investigated. Further, these complexes were evaluated for their photocatalytic activity. The quantum yield and life time of the complexes containing electron withdrawing group on the 4,4′-disubstituted-2,2′-bipyridine ligand have higher values than the electron donating NMe_2 group. In addition, the photocatalytic activity of the complexes exhibited a three fold enhancement in initial reaction rate, when substituent was changed from Cl to *t*-Bu. However, the reaction rates of the catalytic system decrease thereafter with the more electron donating groups introduced in the ligand, which suggests that it followed

different reaction pathway. Furthermore, the introduction of anionic donors, like carbanionic or N-containing aromatic units, into ruthenium(II) coordination sphere is another proven strategy to increase the HOMO level in the system. This method was successfully demonstrated by O'regan and Gratzel (1991) on highly efficient dye- sensitized solar cells (DSSC).

In recent years, Ru(II)-complexes incorporating boron have been reported. Because of the presence of vacant p-orbital on the boron atom in the triarylborane molecule, it exhibits synergetic interactions between MLCT of a transition metal complex and intramolecular CT interaction between π orbitals of the aryl group. Nakagawa et al. (2015, 2017) developed a series of Ru(II)-complexes bearing (dimesityl)borylduryletheynyl (DBDE) moiety in the 4,4′- and 5,5′position of the 2,2′-bipyridine and 1,10-phenathaline ligands (Fig. 7.12). The molar extinction coefficient at $\lambda_{abs}{}^{max}$ of the complex increases with increasing n value i.e., number of DBDE groups in the periphery units. Furthermore, the complex ($n = 3$) exhibited an intense absorption ($\varepsilon_{MLCT} = 5.6 \times 10^4\ M^{-1}\ cm^{-1}$) at 488 nm for $n = 3$ and emission quantum yield of 0.43, which was very high compared to the other Ru(II)-analogs. It was attributed that S_1-T_1 splitting of energy ($\Delta E_{ST} = E_{abs} - E_{em}$) and the mixing of excited singlet-triplet state favors larger radiative transition (k_r).

A long lived temperature dependent emission from Ru(II) system having and arylboron unit was demonstrated. The tris(1,10-phenanthroline)ruthenium(II) complexes $[Ru(phen)_3]^{2+}$ bearing a (dimesityl)borylduryletheynyl (DBDE) charge-transfer (CT) unit at the four or five position of one of the three phenanthroline core as shown in Fig. 7.13 (Sakuda et al., 2011).

In comparison to $[Ru(phen)_3]^{2+}$complex ($\tau = 0.42\ \mu s$), Ru(II)-complexes bearing a (dimesityl)borylduryletheynyl (DBDE) moiety exhibited a long lived emission life time around 12 μs. Ru(II)-polypyridyl systems have been known to exhibit a decrease in emission life time upon elevation of temperature, owing to thermal deactivation from the emissive ^{3}MLCT* to the non-emissive dd* excited triplet state followed by a fast nonradiative decay from ^{3}dd* to the ground state. However, boron incorporated ruthenium(II)-complexes exhibited an unusual temperature independent emission life time over a long range of temperatures, 10.7 μs (280 K)−9.8 μs (330 K). This unique photophysical characteristic was attributed to the involvement of the CT interaction between the vacant p-orbital of the boron atom and π orbital of the aryl group in DBDE ligand, which results in the stabilization of ^{3}MLCT energy with respect to the ^{3}dd energy. It leads to the restriction of thermal activation from ^{3}MLCT to ^{3}dd, and as a result, the long-lived temperature independent emission was observed. They have reported a dual emission from the complex at low temperature (Sakuda et al., 2015).

It was shown that the Ru(II)-DBDE complex possesses spatially-isolated excited ^{3}MLCT states namely T1 and T2, in close proximity in energy (270−290 cm^{-1} estimated at 77 K) and the two excited triplet states exhibited individual emissions below 220 K independently. The T1 state possesses both

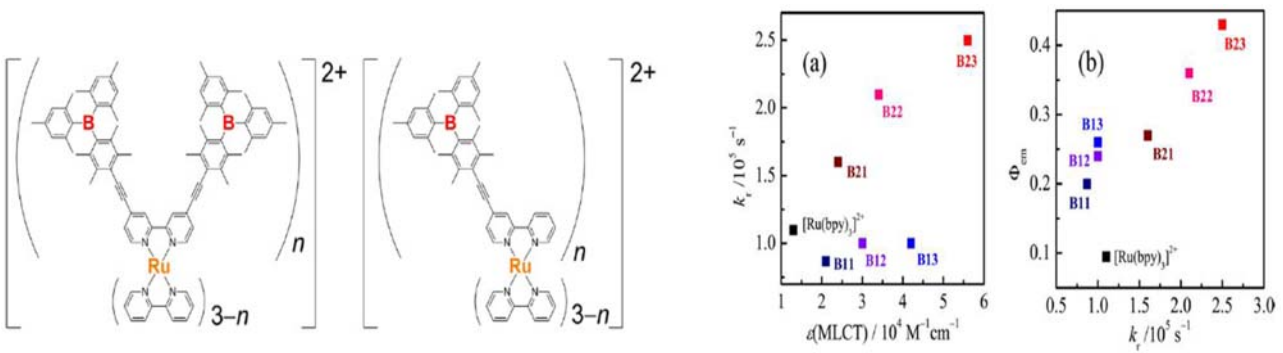

FIG. 7.12 Ru(II) complexes having a triarylborane-appended 2,2′-bipyridine (bpy) ligand. Relationships between (A) kr and ε(MLCT) and (B) Φemand kr for RuBbpys and $[Ru(bpy)_3]^{2+}$ in CH_3CN at 298 K. *Adapted from Nakagawa, A., Sakuda, E., Ito, A., Kitamura, N., 2015. Remarkably intense emission from ruthenium (II) complexes with multiple borane centers. Inorg. Chem. 54 (21), 10287−10295. With permission.*

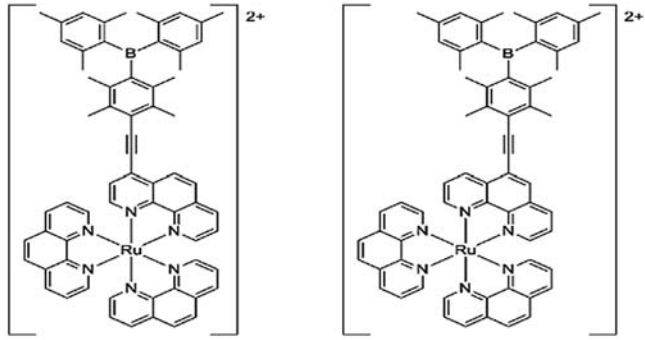

FIG. 7.13 Tris(1,10-phenanthroline)ruthenium(II) complexes $[Ru(phen)_3]^{2+}$ bearing a (dimesityl)boryldurylethynyl (DBDE). *Adapted from Sakuda, E., Ando, Y., Ito, A., Kitamura, N., 2011. Long-lived and temperature-independent emission from a novel ruthenium (II) complex having an arylborane charge-transfer unit. Inorg. Chem. 50 (5), 1603−1613. With permission.*

MLCT/LC characters, while T2 state was predominantly MLCT character. The T2 MLCT excited state of the complex exhibit a longer emission life time around 27 μs and became non-emissive above the glass-to-fluid transition temperature of $T_g \approx 220$ K due to strong solvation around the MLCT excited states and subsequent fast non-radiative relaxation to the ground states, while the T1 MLCT/LC excited states exhibit a lifetime around 13 μs irrespective of temperature T: 77−320 K (Fig. 7.14).

In another approach, the photophysical properties of ruthenium complexes have been finely tuned by introducing organic radical as ancillary group onto the bipyridine core. Ito et al. (2017) prepared a novel ruthenium(II) complex containing, 1,5-dimethyl-6-oxoverdazyl group, a stable radical as a substituent (Fig. 7.15) and explored the photophysical properties.

Owing to the presence of free radical, it has been reported that the intersystem crossing ISC in such complexes have been highly accelerated. Since such high acceleration of singlet-triplet transitions are achievable in organic derivatives, containing π-radicals, and metal complexes, hybrid metal-complex-π-radicals becomes ideal choice for development of novel photoactive systems. In comparison with parent complex $[Ru(bpy)_3]^{2+}$, MLCT absorption peak was enhanced and shifted to the lower energy region. The enhancement of MLCT intensity and low energy absorption of the radical complexes can be explained by the electron withdrawing nature of the organic radical moiety, which resulted in lowering the energy π^* orbital of the bipyridine group and enhanced in transition dipole moment. The presence of long-lived emissions in the complex was associated with the reduction of non-radiative deactivation by the ^{3}MLCT level via the ^{3}dd* state, where a large activation energy is associated with the $^3\text{MLCT} \rightarrow {}^3\text{dd}^*$ transition. The co-existence of low-energy/high intense absorption in the UV−visible region and long-lived excited state obtained for the radical complexes are valuable features for their applications as photosensitizers.

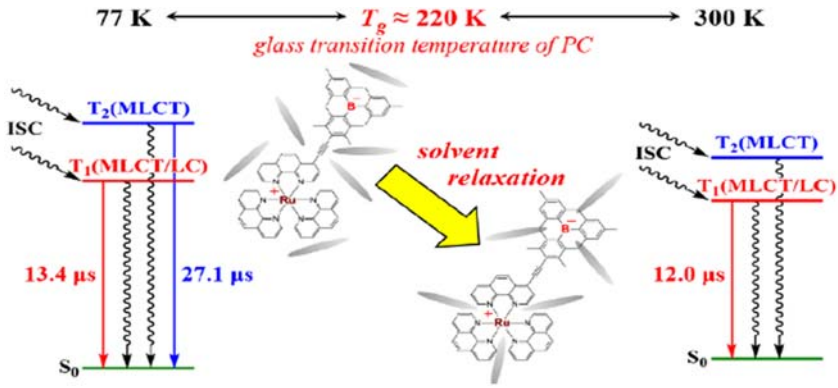

FIG. 7.14 Energy diagram of the excited triplet states of $[RuBE]^{2+}$. *Adapted from Sakuda, E., Matsumoto, C., Ando, Y., Ito, A., Mochida, K., Nakagawa, A., Kitamura, N., 2015. Dual emissions from ruthenium (II) complexes having 4-Arylethynyl-1, 10-phenanthroline at low temperature. Inorg. Chem. 54 (7), 3245−3252. With permission.*

Dong et al. (2014) reported that the improvement of optical properties of heteroleptic Ru(II)-polypyridyl complexes can be achieved by incorporating electron donating ancillary ligands. This was established by DFT/TDDFT tools. Density functional theory calculation were done on three previously reported Ru(II)-complexes (El-Shafei et al., 2012), where the experimental data revealed that these novel complexes are red-shifted and have stronger molar absorptivity over the visible range of the solar spectrum extending into the near IR region, with a lower ionization potential (i.e., upshift of the HOMO level) and a reduced HOMO−LUMO energy gap, while preserving the correct band alignment intact. The theoretical calculation showed that inclusion of electron donating conjugated ligands enriches the population of the occupied frontier molecular levels, decreases the ionization potential and the

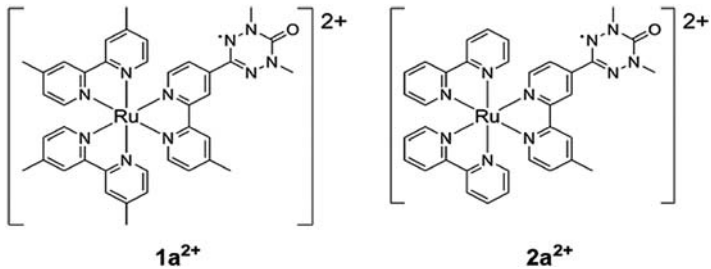

$1a^{2+}$ $2a^{2+}$

FIG. 7.15 Ruthenium(II) complexes having a 4,4′-monosubstituted-2,2-bipyridine (bpy) derivative which possesses a 1,5-dimethyl-6-oxoverdazyl radical group. *Adapted from Ito, A., Kobayashi, N., Teki, Y., 2017. Low-energy and long-lived emission from polypyridyl ruthenium (II) complexes having a stable-radical substituent. Inorg. Chem. 56 (7), 3794−3808. With permission.*

HOMO−LUMO energy gap. This helps to improve the performance of the sensitizer by reducing the hole-regeneration loss.

Schlotthauer et al. (2017) developed a series of new cyclometalated Ru(II)-complexes bearing tridendate 2,6-di(quinolin-8-yl)pyridine ligands (Fig. 7.16) and their photophysical properties were evaluated.

The primary motive behind the selection of cyclometalated complexes is that the triplet excited state is dominated by (^{3}MLCT) metal to ligand charge transfer character with some admixing of the cyclometalating donor (Motley et al., 2017). The organic subunits (donating/accepting) contribute to the charge separation in HOMO/LUMO levels, leading to charge separation in the excited state. Deactivation of excited state by both radiative and non-radiative influences the spectral properties, life time and energy/electron transfers process and is controlled by strong σ donors or an improved octahedral geometry, which can be achieved by cyclometalated systems (Zhang et al., 2019).

The optical properties of luminescent ruthenium complexes are strongly affected by changes in the polarity and rigidity of their environments. The nature of solvent has a very important significance in photophysical properties of Ru(II)-complex system. A study was carried out by Schneider et al. (2018), which demonstrated an unusually short-lived solvent-dependent excited state in a Ru(II) complex induced by low-lying triplet metal centered MC states.

A ruthenium complex with a half-sandwich geometry [(p-cymene)Ru(Cl)(curcuminoid)] was synthesized and its solvent dependent photophysical properties was investigated (Fig. 7.17). The study revealed a weak and short-lived emission from the initially populated singlet MLCT state and exhibited solvent dependent photo-induced dynamics, where the secondarily populated ^{3}MC state was found to be stabilized by non polar solvents. There is a direct decay from ^{1}MLCT to the ground state in dichloromethane, and in acetonitrile medium, whereas ^{3}MLCT state character was accessible through high polar solvent (DMSO) with a significantly longer ground-state recovery. The presence of the characteristic triplet MC states can be accounted by considering the half-sandwich structure as highly distorted octahedral geometry.

The microenvironment, changes in solvent, viscosity and change in medium from homogeneous to heterogeneous have a significant impact on the photophysics and photochemistry of ruthenium(II)-polypyridine complexes $[Ru(NN)_3]^{2+}$ (NN = 2,2′-bipyridine and its derivatives). The $[Ru(NN)_3]^{2+}$ complexes have been extensively used as probes in micellar media and their photophysical properties vary enormously with the nature of the surfactant and concentration (Sangiliapillai et al., 2016). The photophysical properties of amphiphilic ruthenium(II)-complexes in the presence of micelles (anionic(SDS), cationic (CTAB) and neutral (Triton-X100) have been investigated (Rajkumar et al., 2014) (Fig. 7.18).

There are two possible interactions between the complex and the micelles and these are electrostatic attraction or repulsion and hydrophobic interaction.

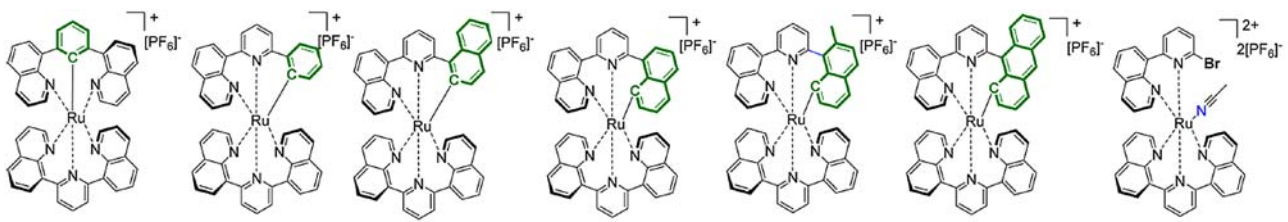

FIG. 7.16 Ruthenium complexes featuring central cyclometalation, peripheral cyclometalation with five-memberedchelates or six-membered chelates. *Adapted from Schlotthauer, T., Parada, G. A., Gorls, H., Ott, S., Jager, M., Schubert, U.S., 2017. Asymmetric cyclometalated RuII polypyridyl-type complexes with π-extended carbanionic donor sets. Inorg. Chem. 56 (14), 7720−7730. With permisssion.*

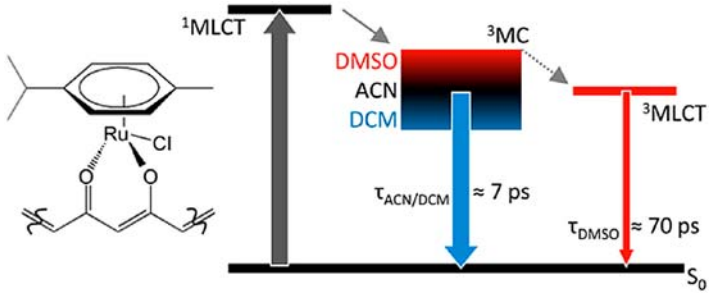

FIG. 7.17 Ruthenium complex with a half-sandwich geometry ([(p-cymene)Ru(Cl) (curcuminoid)]) exhibiting solvent dependent excited state dynamics. *Adapted from Schneider, K.R., Traber, P., Reichardt, C., Weiss, H., Kupfer, S., Gorls, H., et al., 2018. Unusually short-lived solvent-dependent excited state in a half-sandwich Ru (II) complex induced by low-lying 3MC states. J. Phys. Chem. A 122 (6), 1550−1559. With permission.*

In cationic micelles, the luminescence intensity and lifetime increases with increase in [CTAB], which confirms that the electrostatic repulsion is overcome by the hydrophobic interactions between the ligands and cationic surfactant. These binding interactions stabilize the ^{3}MLCT state compared with d-d state in micelles. In the case of anionic micelles, electrostatic interaction between the cationic complexand anionic micelle is predominant, whereas cationic and neutral micelle, hydrophobic interactions play important role in the binding of cationic complexes with micelles. The increase of quantum yield in the presence of micelle was attributed to the decrease in therate of non-radiative decay from excited sate. It has been demonstrated that micellization has a significant effect on relaxation to ground state via the d-d state with k_{dd} values reduced by $\sim$50%.

7.3.1.7 Excited state reactions of ruthenium(II)-complexes

Electron transfer reactions play an important role in the biological systems such as photosynthesis, respiration, and metabolic processes. Understanding the mechanisms of these highly efficient electron transfer processes that take place in biological system is very important that would help us to develop artificial photosynthesis, development of new diagnostic and therapeutic protocols, etc. Ru(II)-complexes are well known systems, which are used to for mimicking these studies. Many Ru(II) based complexes are developed as model compounds that exhibit photoinduced electron transfer systems. The ^{3}MLCT states of $[Ru(NN)_3]^{2+}$ complexes are sufficiently long-lived to undergo bimolecular collisions with other molecules (quenchers) present in the solution (either oxidative or reductive quenching process). During this process, the excited states are rapidly deactivated. The excited-state quenching process can proceed either by energy transfer or electron transfer. The two main factors that determine the rate of electron transfer (ET) between two molecules are the

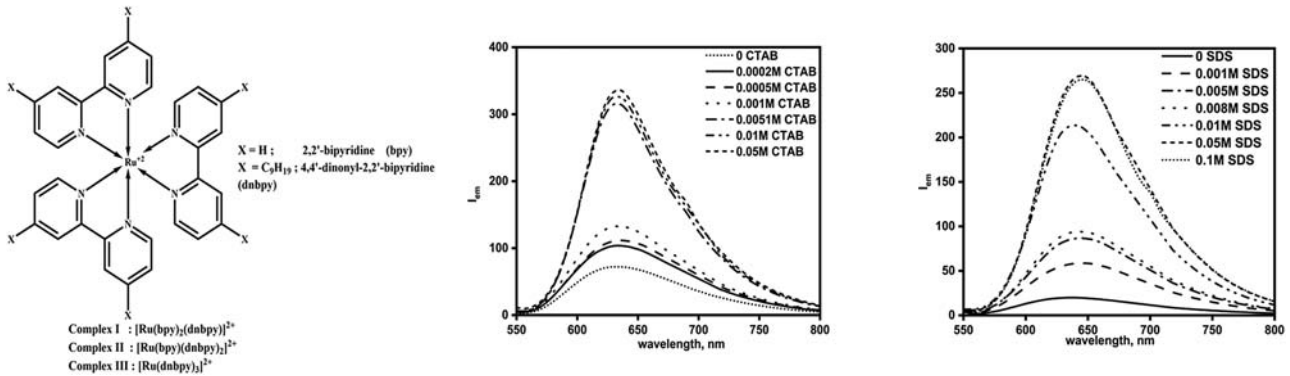

FIG. 7.18 The structure of the $[Ru(NN)_3]^{2+}$ complexes used in the study and the emission spectra of $[Ru(bpy)_2(dnbpy)]^{2+}$ (II) in the presence of cationic micelles, CTAB, and anionic micelles, SDS at different concentrations. *Adapted from Rajkumar, E., Mareeswaran, P.M., Rajagopal, S., 2014a. Photophysical properties of amphiphilic ruthenium (II) complexes in micelles. Photochem. Photobiol. Sci. 13 (9), 1261−1269. With permission.*

extent of the vibrational trapping of electron exchange's by medium and intramolecular vibration.

$$*[Ru(NN)_3]^{2+} + Q \longrightarrow [Ru(NN)_3]^{3+} + Q- \quad (7.10)$$

$$*[Ru(NN)_3]^{2+} + Q \longrightarrow [Ru(NN)_3]^{+} + Q+ \quad (7.11)$$

$$*[Ru(NN)_3]^{2+} + Q \longrightarrow [Ru(NN)_3]^{2+} + Q* \quad (7.12)$$

In Eq. (7.10), the metal complex upon excitation undergoes reduction and it is known as reductive quenching, while Eq. (7.11), represents the oxidative quenching reactions. The complex in the excited state can transfer the excess energy to the acceptor molecule (Eq. 7.12).

The photoinduced electron transfer reactions of the Ru(II)-complexes with different quenchers have been studied (Rajkumar et al., 2011, 2014; Sangiliapillai et al., 2016; Swarnalatha et al., 2011). For example, the photoluminescence quenching of Ru(II)-complexes with quinones can be explained by the oxidative quenching mechanism (Rajkumar et al., 2014). The structure of Ru(II)-complexes and quinones are shown in Figs. 7.19 and 7.20 and the bimolecular quenching rate constant are tabulated in Table 7.1.

The value of quenching rate constant k_q is sensitive to the reduction potential of quinones. It is apparent from the data in Table 7.1 that quinones with higher reduction potentials exhibited higher quenching rate constants, a trend that is indicative of electron transfer quenching. The electron transfer nature of the quenching of $*[Ru(NN)_3]^{2+}$ with phenolate ions and quinone radical has already been established from laser flash photolysis study and the spectrum of phenoxyl radical is already reported (Rajkumar et al., 2011, 2014; Sangiliapillai et al., 2016; Swarnalatha et al., 2011).

According to this scheme, the excited state donor ($*Ru^{II}$) and the ground state acceptor (quinone) molecules diffuse together to form an encounter complex ($*Ru^{II} \ldots Q$). This encounter complex then undergoes a reorganization to reach the transition state, where ET takes place from the donor to the acceptor to give an ion-pair species, ($Ru^{III} \ldots Q^{-}\cdot$), the successor complex. The parameters k_{12} and k_{21} are the diffusion-controlled rate constants for the formation and dissociation of the encounter complex ($*Ru^{II} \ldots Q$), respectively. The k_{23} and k_{32} are the forward and reverse ET rate constants. Apart from the back electron transfer to form the precursor complex (k_{32}), the ion-pair state, ($Ru^{III} \ldots Q^{-}\cdot$) can form the separated species $Ru^{III} \ldots Q^{-}$ (k_{sep}) and undergoes back electron transfer to form the reactants in the ground state (k_{34}).

7.3.1.8 Ruthenium (II) complexes in photodynamic therapy

Photodynamic therapy (PDT) is a globally approved, and non-invasive treatment protocol for various types of cancer, bacterial, fungal, & viral infections, and skin diseases, which induces cell death upon light activation (Mari et al.,

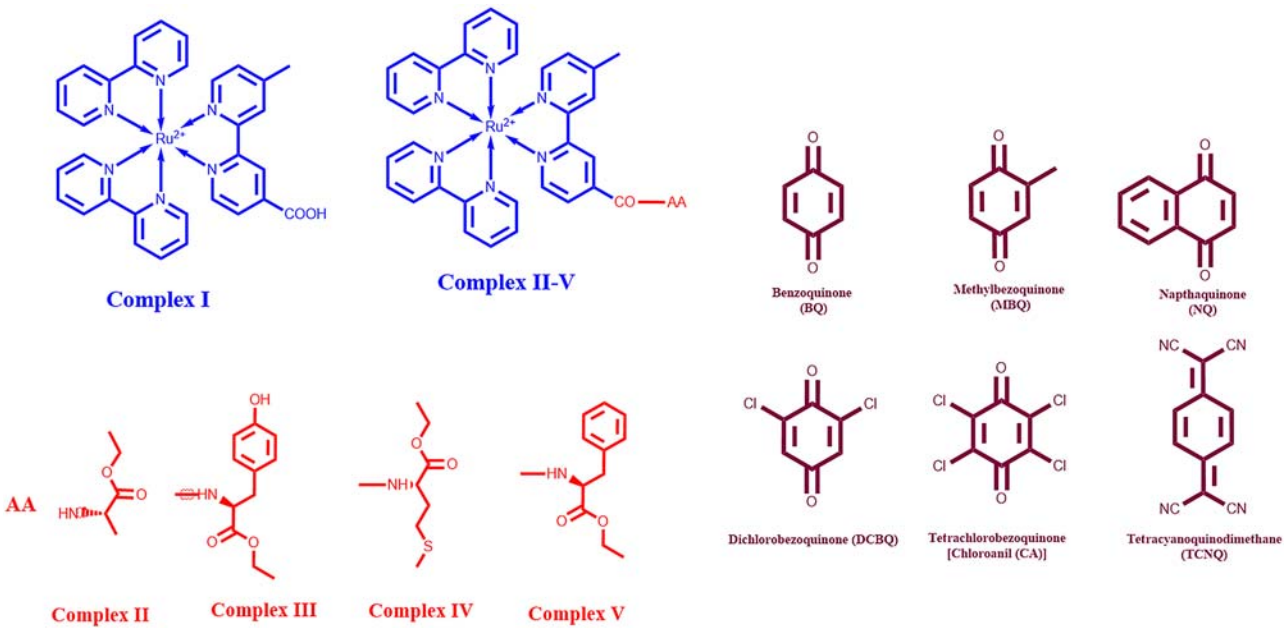

FIG. 7.19 Structure of Ru(II)-complexes and quinones used in the study. *Adapted from Rajkumar, E., Kalayar, S., Paulpandian, M.M., Seenivasan, R., 2014b. Photoinduced electron transfer reactions of ruthenium (II)-Complexes containing Amino acid with quinones. J. Fluoresc. 24 (3), 875–884. With permission.*

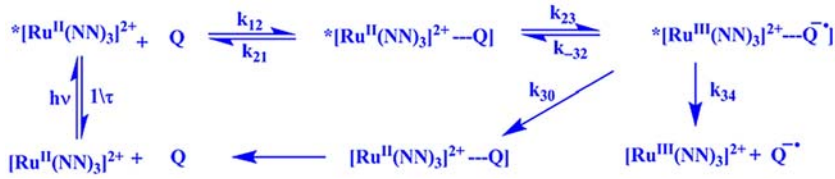

FIG. 7.20 Mechanism for the oxidative quenching of $*[Ru(NN)_3]^{2+}$ with quinines. *Adapted from Rajkumar, E., Kalayar, S., Paulpandian, M.M., Seenivasan, R., 2014b. Photoinduced electron transfer reactions of ruthenium (II)-Complexes containing Amino acid with quinones. J. Fluoresc. 24 (3), 875–884. With permission.*

2015; Liu et al., 2018; Shum et al., 2019). The PDT consists of basically three components, light, photosensitizer (PS) and molecular oxygen. PDT takes place in two steps.

The mechanism of PDT action is shown in Fig. 7.21. First, a patient is administered with non-toxic PS followed by irradiation of PS at a specific wavelength. The PS absorbs light and reached to excited singlet state S_1, which is unstable. From this state, PS can undergo the intersystem crossing (ISC) process to reach the more stable excited triplet state T_1. After reaching T_1 state, apart from normal deactivation modes, it may influence the biological environment through two different pathways known as Types I and II (Heinemann et al., 2017).

In Type I pathway, an electron or proton is transferred either from/to PS or to/from the biological environment to create a radical anion and its corresponding cation. The generated reactive oxygen species (ROS), induces cell death. Alternatively, via type II pathway, the excited PS transfers its energy to the proximal molecular oxygen to produce short lived highly reactive singlet oxygen which triggers cell death. The most widely adapted pathway is the Type II route (Plaetzer et al., 2009).

The main challenge in PDT is development of PS, that is non-toxic, and it must be able to excite in the optical biological window, i.e., 600–900 nm, since photochemically accessing the PS at a deeply buried spot would be a challenge (Fig. 7.22). The majority of the PS developed so far has several disadvantages: (i) tedious synthesis, (ii) poor water solubility, (iii) poor absorption in biological window, (iv) photobleaching (v) target selectivity and (vi) poor clearance from the body. Due to their excellent photophysical properties and water solubility, absorption in the NIR region (He et al., 2021; Qiao et al., 2021), and target selectivity (e.g., DNA targeting probes) (Shao et al., 2021), Ru(II)-complexes have proved to be preferential PS, which can be finely-tuned by chemically to overcome all the above stated challenges (Li and Chen, 2020; Shen et al., 2021). Clinically approved Ru(II)-complexes used as a photosensitizers in PDT to treat skin diseases, cancer, infections, etc (Banerjee, 2021; Mari et al., 2015).

TABLE 7.1 Bimolecular quenching rate constants, k_q, for the oxidative quenching of $*[Ru(NN)_3]^{2+}$ complexes by quinones in CH_3CN at 298 K.

Quencher	E^0red, V	k_q, $M^{-1}s^{-1}$				
		I	II	III	IV	V
TCNQ	−0.18	2.0×10^{10}	1.5×10^{10}	1.0×10^{10}	2.1×10^{10}	2.0×10^{10}
CA	−0.34	1.1×10^{10}	8.6×10^{9}	9.0×10^{9}	1.7×10^{10}	1.5×10^{10}
DCBQ	−0.45	1.0×10^{10}	8.2×10^{9}	9.1×10^{9}	1.3×10^{10}	9.9×10^{9}
BQ	−0.86	6.2×10^{9}	7.9×10^{9}	8.0×10^{9}	9.9×10^{9}	1.4×10^{10}
MBQ	−0.91	1.6×10^{9}	2.4×10^{9}	4.3×10^{9}	3.1×10^{9}	2.0×10^{9}
NQ	−1.02	4.1×10^{9}	3.8×10^{9}	4.4×10^{9}	4.1×10^{9}	4.9×10^{9}

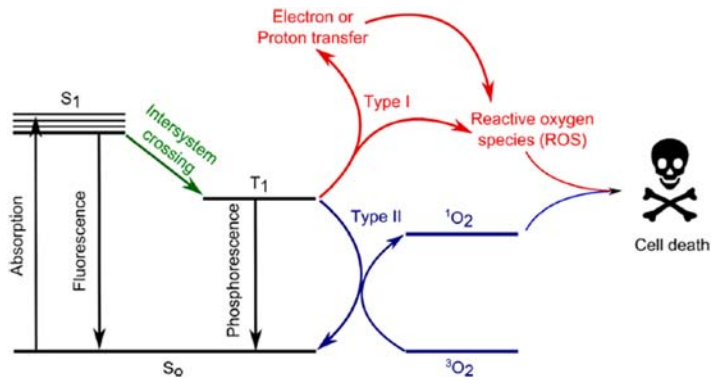

FIG. 7.21 The schematic representation of mechanism of photodynamic therapeutic activity. *Adapted from Heinemann, F., Karges, J., Gasser, G., 2017. Critical overview of the use of Ru (II) polypyridyl complexes as photosensitizers in one-photon and two-photon photodynamic therapy. Acc. Chem. Res. 50 (11), 2727−2736. With permission.*

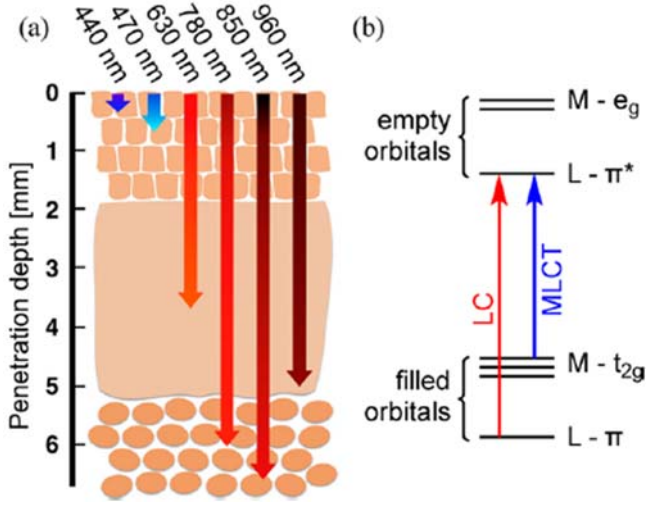

FIG. 7.22 (A) light penetration depth into skin. The optical biological window between 600 and 900 nm is mainly limited by hemoglobin and melanin absorbing at the lower end and water and fat at the upper end, and (B) simplified MO scheme of the frontier orbitals for octahedral d^6 complexes like $[Ru(bpy)_3]^{2+}$. *Adapted from Heinemann, F., Karges, J., Gasser, G., 2017. Critical overview of the use of Ru (II) polypyridyl complexes as photosensitizers in one-photon and two-photon photodynamic therapy. Acc. Chem. Res. 50 (11), 2727−2736. With permission.*

Recently (He et al., 2021), developed a red-light-responsive Ru(II)-complex photosensitizer for lysosome localization photodynamic therapy. Ru-complex photosensitizer [Ru(terpy) (Cl-7-IVQ)I]$^+$ (terpy = 2,2′:6′,2′-terpyridine, Cl7-IVQ = 5-chloro7-(2-(1,3,3-trimethyl-3H-indol-1-ium-2-yl)- vinyl)quinolin-8-

olate) (Ru−I) using large-conjugated indolinepyridobenzopyrans as the ligand was synthesized (Fig. 7.23). The activation of the photosensitizers was achieved using 660 nm red light. Ru(II)-complexes was quickly internalized into cancer cells and seen to get accumulated in lysosome. Under irradiation, the complex drastically suppressed the cancer cells.

7.3.1.9 Ru(II)-complexes in dye- sensitized solar cell (DSSC) applications

The role of Ru(II)-center is similar as in the case of PDT. They act as dyes to sensitize the semiconductor component in the solar cell (Pashaei et al., 2016). A typical dye sensitized solar cell consists of a mesoporous layer of a semiconductor TiO_2 nanoparticles, with a dye anchored onto it, which acts a sensitizer to harvest light photons and convert them to an electric current. A redox mediator commonly used in DSSC is iodide/triiodide (I^-/I_3^-) couple, and a counter electrode (CE). The working principle of DSSC is depicted in Fig. 7.24. The sensitizer dye is the most fundamental and important component that governs the performance of the DSSCs. Among various types of photosensitizers, ruthenium-based dyes are widely used due to their suitable ground- and excited state potentials and broad MLCT absorption bands. An effective sensitizer plays an important role of facilitating a favorable electron injection into the conduction band (CB) of a semiconductor (Hagfeldt et al., 2010).

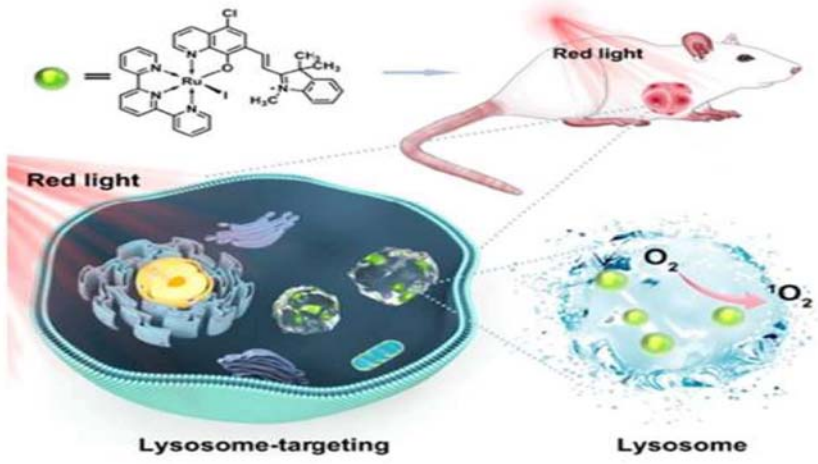

FIG. 7.23 Schematic illustration of the PDT effect toward a tumor-bearing mouse model using Ru(II) with red light irradiation. *Adapted from He, G., Xu, N., Ge, H., Lu, Y., Wang, R., Wang, H., et al., 2021. Red-Light-Responsive Ru complex photosensitizer for lysosome localization photodynamic therapy. ACS Appl. Mater. Inter. 13 (17), 19572−19580. With permission.*

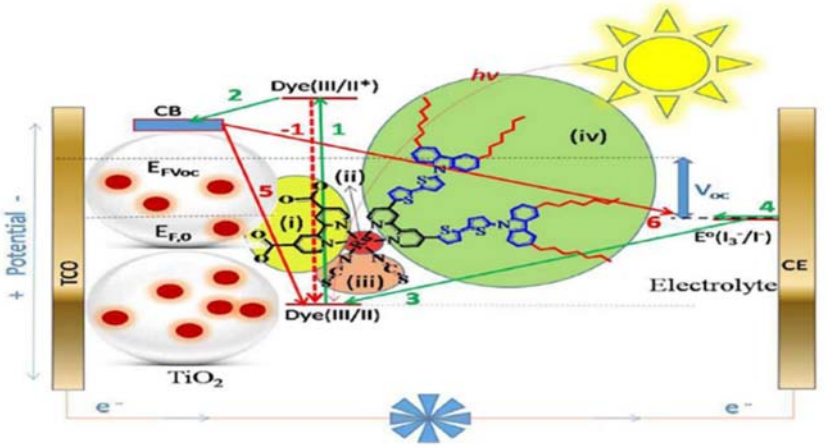

FIG. 7.24 Schematic representation of working principle of dye- sensitized solar cells (DSSCs). *Adapted from Pashaei, B., Shahroosvand, H., Graetzel, M., Nazeeruddin, M.K., 2016. Influence of ancillary ligands in dye-sensitized solar cells. Chem. Rev. 116 (16), 9485−9564. With permission.*

An ideal photosensitizer for the DSSC must fulfill the following conditions.

(i) It should have panchromatic absorption in the solar spectrum i.e., visible to near IR region,
(ii) Sufficiently high molar extinction coefficient
(iii) Efficient electron injection from the lowest unoccupied molecular orbital to the conduction band before the deactivation of the sensitizer from the excited state, and
(iv) Thermal and chemical stability in the ground and oxidized states.

Ru(II) complexes have exhibited strong candidature as sensitizers due to their remarkable photophysical properties with a power conversion efficiency around 11%. The rational modification of ligand is one way of improving the efficiency of Ru(II)-complexes as photosensitizers. The modifications include incorporation of aliphatic, aromatic or both moieties on the pyridyl core. Recently, Pashaei et al. (2016), accounting the possible novel and rapidly expanding families of chelating ancillary ligands bearing 2,2′-bipyridyl, 1,10-phenanthroline, dipyridylamine, carbene, pyridyl-benzimidazole, pyridyl-azolate, and other miscellaneous aromatic ligands that show a potentially enhanced performance and stability of DSSCs.

7.3.1.10 Ru(II)-complexes as sensors and for imaging applications

Owing to remarkable photophysical property of Ru(II)-complexes, these were much used as probes for sensor and imaging of biological and environmental

systems in last few decades (Shum et al., 2019; Patra et al., 2019). Sensor and imaging based on absorbance and luminescence is highly desirable due to their very high sensitivity i.e., detection of analyte in nano level or ppm level concentrations could be achieved, with the use of very low concentration of probes. The selectivity and sensitivity of the probes are designed by selecting appropriate peripheral functional groups placed on the ligand architecture (Kumar et al., 2021). The responses of the probe can be either turn off or turn on their luminescence, shift in absorbance and emission wavelength upon interaction with analyte molecule. These responses are generated by various processes such as quenching of luminescence (energy/electron transfers), association and proton transfer between the probe and analytes. Few recently developed Ru(II)-based sensors and their detection of analytes are tabulated in Table 7.2.

7.3.1.11 Photocatalysis of ruthenium(II)-complexes

The photophysical features of Ru(II)-complexes have opened up new possibilities for using them as catalyst in light driven chemical reactions like water oxidation, hydrogen generation, carbon dioxide reduction, etc. In order to meet the global energy demand, artificial systems were developed to mimic the natural photosystems and other processes. There are three key components required to perform water oxidation; light photosensitizer (PS), water oxidation catalyst (WOC) and a sacrificial electron acceptor. A typical mechanism of water oxidation is shown in Fig. 7.25, where A is the sacrificial electron acceptor such as $S_2O_8^{2-}$ or $Co^{III}(NH_3)_5Cl$, Ru_p is the PS usually $[Ru(bpy)_3]^{2+}$and Ru_c is the WOC. The stability of catalyst in aqueous medium, turn over frequency (TOF), turn over number (TON) and low catalytic overpotential are crucial factors for the complex to act as a efficient WOC in water splitting reactions (Xue et al., 2015).

A number of high-valent metal complexes of the first *d* block series as well as heavier transition metals have been reported to show catalytic activity for the oxidation of water to produce molecular oxygen. Among the transition metal complexes, ruthenium-complexes have shown very high activity toward water oxidation. Several ruthenium based WOC successfully prepared and few of them are shown in Fig. 7.26. The efficiency of the catalyst has strong influence on the nature of ligand around the ruthenium center in the complexes.

Patel et al. (2017) reported the influence of electron withdrawing pyridyl substituted terpyridine ligand-based Ru-complexes on the rate of generation of oxygen by chemical and photochemical methods. The $[Ru(tpy)(bpy)(OH_2)]^{2+}$, $[Ru(2\text{-py-tpy})(bpy)(OH_2)](PF_6)_2$, $[Ru(3\text{-py-tpy})(bpy)(OH_2)](PF_6)_2$ and $[Ru(4\text{-pytpy})(bpy)(OH_2)](PF_6)_2$ (bpy = 2,2′-bipyridine; tpy = 2,2′,6,2″-terpyridine) complexes were prepared and their photocatalytic water oxidation properties were evaluated. The free nitrogen on the pyridine ring gets protonated at pH 1, and acts as an electron withdrawing group. The electron withdrawing ability of

TABLE 7.2 Selected examples of ruthenium complexes based probes.

Complex	Analyte	Remarks	References
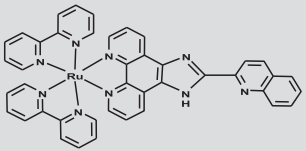	Cu^{2+}		Kumar et al. (2020)
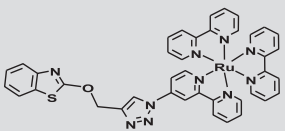	H_2PO_4/ $H_2P_2O_{7^{2-}}$	Fluorescence enhancement by C−H anion interaction	Ramachandran and Anandan (2020)
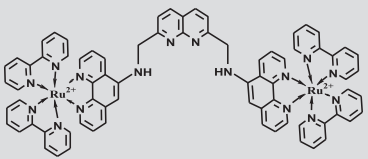	Fe/Cu	Fluorescence quenching	He et al. (2019)
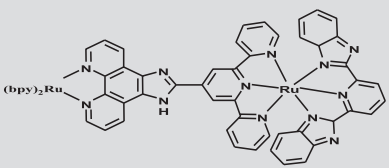	H^+ or pH	Fluorescence Turn on	Meng et al. (2017)

	Oxygen level in cells	Dual emission oxygen dependent fluorescence and oxygen dependent phosphorescence	Hara et al. (2015)
	F^-	Colorimetric detection	Jose et al. (2007)

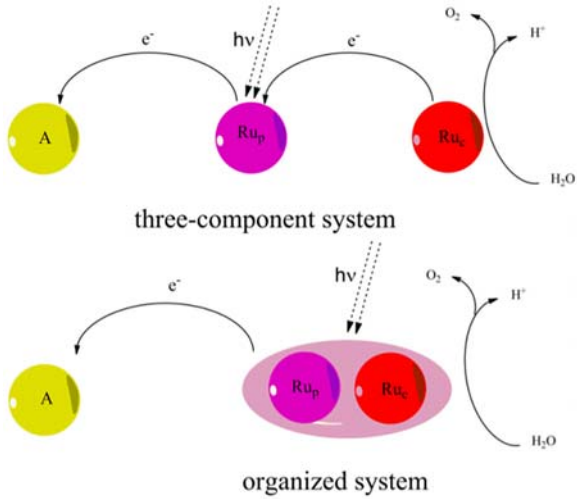

FIG. 7.25 Illustration of the mechanism of water oxidation catalysis. *Adapted from Xue, L.X., Meng, T.T., Yang, W., Wang, K.Z., 2015. Recent advances in ruthenium complex-based light-driven water oxidation catalysts. J. Photochem. Photobiol. B Biol. 152, 95–105. With permission.*

the pyridine in ortho− and para−position is comparatively less with respect to 3-py-tpy ligand, due to the distribution of partial positive charge on the nitrogen and carbon atoms of the pyridine ring and acts as better catalyst in chemical and photochemical water oxidation reactions. Designing of catalyst with heteronuclear systems is another strategy to enhance water oxidation process. Aratani et al. (2017) developed a dual function photocatalyst based on cyano-bridged heteronuclear metal complexes of the type, $(M^{2+}[Ru^{2+}(CN)_4(bpy)]$; where $M^{2+} = Ni^{2+}$, Fe^{2+} and Mn^{2+} for water oxidation. Here, the catalyst acts as both; photosensitizer and photocatalyst. These catalysts integrate both visible-light activated photosensitizer and catalytic units for photocatalytic reduction of O_2 to H_2O_2 and for oxidation of H_2O.

The $Ni[Ru(CN)_4(bpy)]$ complex exhibit a high efficient photocatalytic water oxidation catalyst than other complexes and the proposed mechanism is shown in Fig. 7.27.

Hydrogen evolution reaction is also an important process that utilizes Ru(II)-complexes. The natural hydrogen production process suggested a viable method of collecting, converting, and storing energy via photocatalytic reduction of water. The photocatalytic hydrogen reduction systems consist of a PS that absorbs light and transfers an electron from excited state to the catalyst, wherein water is reduced to H_2. A sacrificial electron donor or reducing agent is needed to restore the PS. A photocatalytic hydrogen evolution reaction driven by red light was demonstrated using a ruthenium quaterpyridine complexes (Fig. 7.28), which having extensive π conjugation (Rousset et al., 2017).

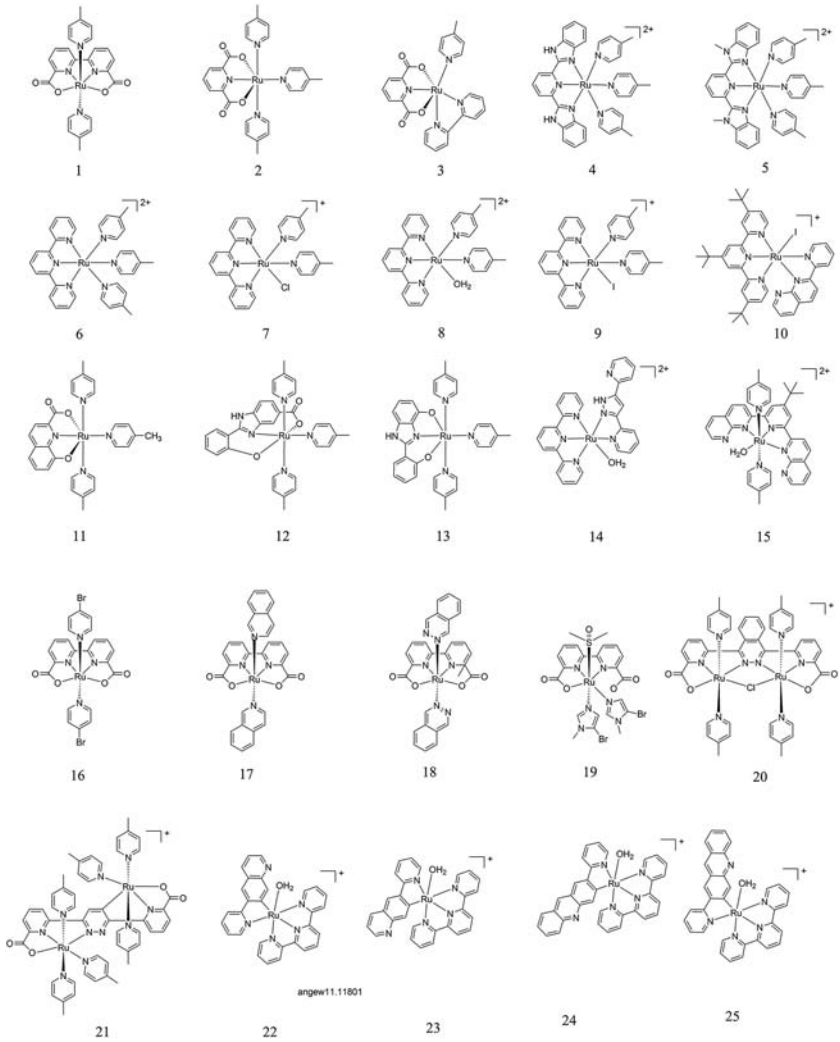

FIG. 7.26 Structures of the ruthenium complex-based WOCs. *Adapted from Xue, L.X., Meng, T.T., Yang, W., Wang, K.Z., 2015. Recent advances in ruthenium complex-based light-driven water oxidation catalysts. J. Photochem. Photobiol. B Biol. 152, 95−105. With permission.*

The average twist angle between the 4-pyridyl moiety and the bipyridine core is 30 degrees in the solid-state, which allowed an inter-annular delocalisation in the ground state and excited state. In the thermally-equilibrated triplet MLCT state, extended π-system of fully planar 4-pyridyl groups give rise to high quantum yields and excited life time of ruthenium quaterpyridine complex, $[Ru(qpy)_3]^{2+}$ (Φ = 23; lifetime = 1780 ns) as compared to

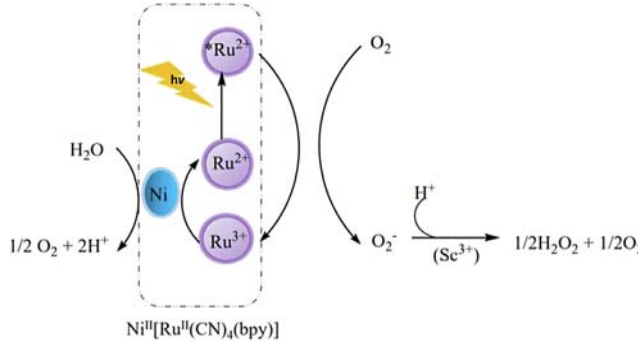

FIG. 7.27 Catalytic cycle of visible-light driven water oxidation by O_2 with $Ni[Ru(CN)_4(bpy)]$ complex. *Adapted from Aratani, Y., Suenobu, T., Ohkubo, K., Yamada, Y., Fukuzumi, S., 2017. Dual function photocatalysis of cyano-bridged heteronuclear metal complexes for water oxidation and two-electron reduction of dioxygen to produce hydrogen peroxide as a solar fuel. Chem. Commun. 53 (24), 3473–3476. With permission.*

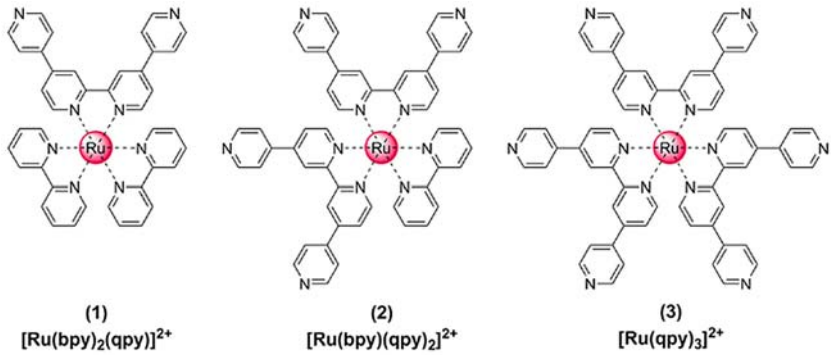

FIG. 7.28 Ruthenium(II) quaterpyridine based photosensitizers for hydrogen production. *Adapted from Rousset, E., Ciofini, I., Marvaud, V., Hanan, G.S., 2017. Facile one-pot synthesis of ruthenium (II) quaterpyridine-based photosensitizers for photocatalyzed hydrogen production. Inorg. Chem. 56 (16), 9515–9524. With permission.*

$[Ru(bpy)_3]^{2+}$. A maximum turn over frequency (TOF) of 650 mmol $mol_{PS}{}^{-1}min^{-1}$, was observed for qpy complex, whereas the TOF of bpy complex was only about 30 mmol $mol_{PS}{}^{-1}min^{-1}$, when excited by red light with wavelength of 630 nm. The efficiency of the $[Ru(qpy)_3]^{2+}$ complex is due to the possible spatial interactions with the photocatalyst through the nitrogen heteroatoms in the pendant pyridines, when compared to the phenyl analogs.

Multinuclear ruthenium complexes are another class of PS used for photocatalytic hydrogen evolution, Veikko et al. (2013) synthesized mononuclear and dinuclear ruthenium(II)-complexes and evaluated their hydrogen evolution efficiency Fig. 7.29.

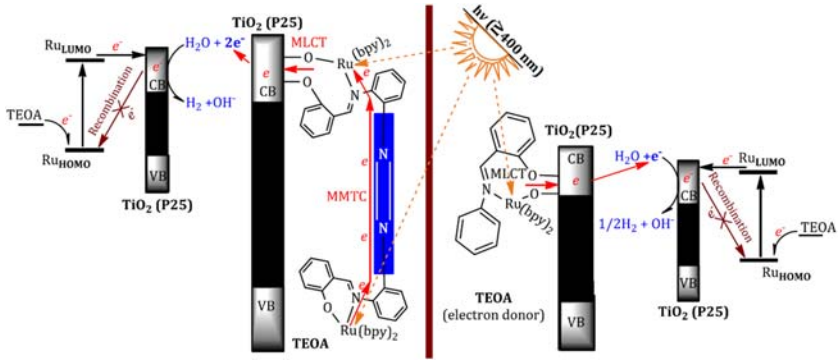

FIG. 7.29 Photoinduced electron transfer cycle of Ru(II)-complex and the mechanism of hydrogen generation. *Adapted from Veikko, U., Zhang, X., Peng, T., Cai, P., Cheng, G., 2013. The synthesis and characterization of dinuclear ruthenium sensitizers and their applications in photocatalytic hydrogen production. Spectrochim. Acta Mol. Biomol. Spectrosc. 105, 539–544. With permission.*

It was found that the dinuclear system was superior in catalytic efficiency over the mononuclear system. This is attributed to the "antenna effect", where additional charge transfer mechanism through metal-to-metal charge transfer (MMCT) takes place than mononuclear complex. The sensitizer is linked to TiO_2 via flexible oxygen bridges and hydrogen bonds, which spontaneously changes the coordination based on the circumstances of the ground state and oxidation state of ruthenium unit. It is evident that the performance of the catalysis is based on both; anchoring ligands and antenna effect. Heterometallic multinuclear systems are also reported as highly efficient PS for photocatalytic hydrogen evolution. Das et al. (2017) developed supramolecular assemblies of the type $[Ru(dceb)_2(\mu\text{-bisbpy})MCl_2](PF_6)_2$ and $[Ru(bpy)_2(\mu\text{-bisbpy})MCl_2](PF_6)_2$ (where M = Pd or Pt, dceb = diethyl-2,2′-bipyridine-4,4′-dicarboxylate, bpy = 2,2′-bipyridine and bisbpy = 2,2′:5′,5″:2″,2‴-quaterpyridine). The photocatalytic investigations of these complexes were dependent on the nature of the peripheral ligand, the catalytic center, and the amount of water present in the photocatalytic mixtures.

Recently, several researchers have reported the photocatalytic reduction of CO_2 using Ru(II)-complexes (Cauwenbergh and Das, 2021). Hawecker et al. (1985) reported for the first time the photocatalytic reduction of carbon dioxide to formate using $[Ru(bpy)_3]Cl_2$, when triethanolamine was used as a sacrificial oxidant. The catalytic process is strongly influenced by the nature of ligands around the catalytic metal center and PS, solvent, and the interaction between the catalyst and the PS (separated or linked).

Yoshitomi et al. (2015) have done pioneering work on photocatalytic carbon dioxide reduction using Ru(II)-semiconductor hybrid system. A hybrid material consisting of perovskiteoxynitride semiconductor and binuclear

ruthenium complex as photocatalyst was developed that produced formic acid via CO_2 reduction. The mechanism of CO_2 reduction is depicted in Fig. 7.30.

Use of visible-light-absorbing semiconductor and metal complex have attracted attention as efficient photocatalysts for CO_2 reduction with high selectivity in products. They developed a defect fluorite-type Ln−Ta oxynitrides $LnTaO_xN_y$ (Ln = Nd, Sm, Gd, Tb, Dy and Ho) and examined it as a semiconductor component in a hybrid photocatalyst system combined with silver nanoparticles as promoter and binuclear ruthenium(II)-system. $TbTaO_xN_y$ gave the highest efficiency for CO_2 reduction under visible light ($\lambda > 400$ nm), with a turn over number of 18 and high selectivity to formate above 99%. The physicochemical analysis shows that the presence of high crystalline structure and highly negative conduction band potential of $LnTaO_xN_y$ contributed to the higher activity of the hybrid photocatalyst.

Supramolecular assembly is another method for improving the photocatalytic efficacy of the systems. Fabry et al. (2020) developed a Ru(II)−Mn(I) supramolecular photocatalyst consisting of a redox photosensitizer, catalyst, and the bridging ligand for CO_2 reduction (Fig. 7.31). The supramolecular assembly constituted 1:1 ratio between the PS and catalyst units, which showed higher activity for HCOOH formation in comparison to the corresponding mixed system of mononuclear complexes.

In summary, Ru(II)-complexes are versatile systems, which can be fine-tuned on need to need basis. It is clear that the photophysics and photochemistry of ruthenium complexes can be tailor made by strategic designing its coordinating ligands. Ruthenium(II)-complexes have exhibited their potential in a large spectral window ranging from UV-Vis-near IR, opening wide scope of utility, in the field of photodynamic therapy, solar cells, and photocatalysis, etc.

7.4 Coordination compounds of osmium complexes

The photophysics of osmium complexes are similar to that of ruthenium complexes. The photophysics of osmium complexes are well exploited in the field of OLED, phosphorescent materials, photodynamic therapy, imaging, and diagnosis, etc. Fine tuning of the ligands and chemical architecture around the osmium metal core can results in near IR and far visible probes for various applications in the biological window.

7.4.1 Photoactive oxidation states of osmium complexes

Osmium complexes are reported to be photoactive in four oxidation states, which are Os(II), Os(III), Os(IV) and Os(VI). The most commonly observed oxidation state is 2+ oxidation state. The photophysics of the parent complex of this series, $[Os(bpy)_3]^{2+}$ (bpy = 2,2′-bipyridine) has been thoroughly investigated Yersin et al. (1990). It was established that the emissive state in

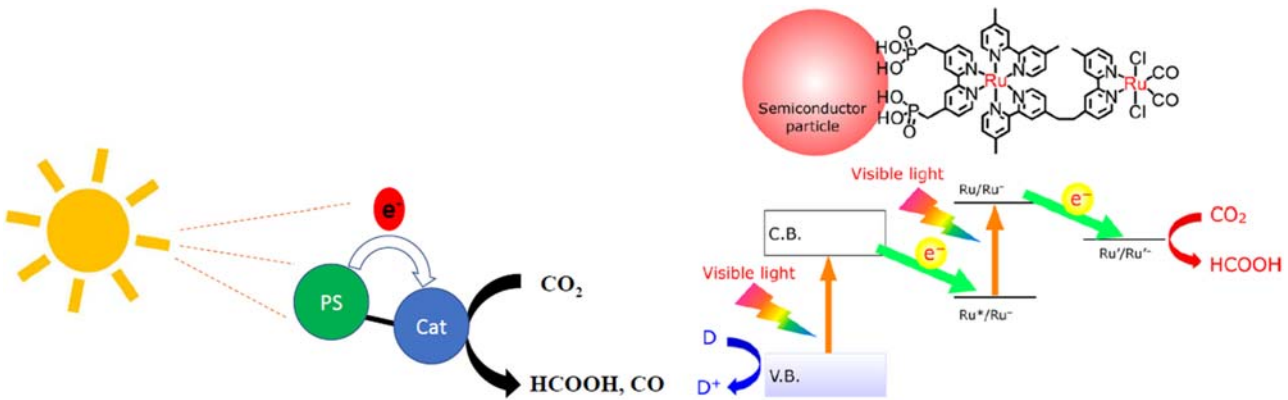

FIG. 7.30 Mechanism of photocatalytic conversion of carbon dioxide to formats. Z-scheme of CO_2 reduction under visible light using a hybrid that consists of a semiconductor and a binuclear Ru(II)-complex. *Adapted from Yoshitomi, F., Sekizawa, K., Maeda, K., Ishitani, O., 2015. Selective formic acid production via CO_2 reduction with visible light using a hybrid of a perovskite tantalum oxynitride and a binuclear ruthenium (II) complex. ACS Appl. Mater. Interfaces 7 (23), 13092−13097. With permission.*

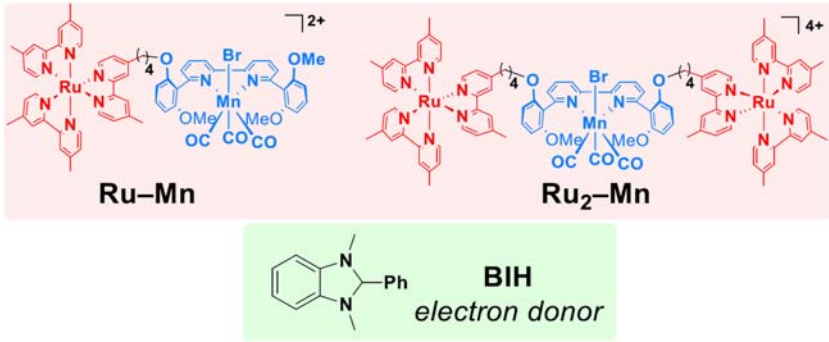

FIG. 7.31 Supramolecular photocatalysts for CO_2 reduction, constituting of redox photosensitizer, catalyst, and bridging ligand. *Adapted from Fabry, D.C., Koizumi, H., Ghosh, D., Yamazaki, Y., Takeda, H., Tamaki, Y., et al., 2020. A Ru(II)−Mn(I) supramolecular photocatalyst for CO_2 reduction. Organometallics 39 (9), 1511−1518. With permission.*

Os(II) complexes arises due to metal to ligand charge transfer (MLCT). The position of these states depends on the ligand field strength (Δ) of the heavy metal. Osmium(II)-complexes have larger Δ values than Ru(II)-complexes with the same ligand field. This raises the energy of the non-emissive d−d states, which reduces thermal deactivation of the MLCT states. As a result, Os(II)-complexes have greater photostability compared to Ru(II)-complexes. However, considering the differences in oxidation potentials and larger spin-orbit coupling, Os(II)-complexes generally have lower emission energies and shorter excited-state life times than Ru(II)- analogs. These disadvantages were addressed in a recent study by Zammit et al. (2012) by substituting one or more polypyridyl type ligands with stronger π −acceptor moiety, such as diphosphine or diarsine, ligands.

Ito et al. (2014) studied the effect of rigid medium such as poly(ethylene glycol)dimethacrylate monoliths on the photophysical properties of series of Os(II)-polypyridyl complexes. Higher energy emissions from the metal-to-ligand charge transfer (MLCT) excited states of a series of polypyridyl Os(II)-complexes were observed at the solution to film transition. It is due to the frozen (rigid) nature of the film and the inhibition in the local medium dielectric to respond to the change in charge distribution induced by the photoexcitation. This led to an increase in emission energies in the film, longer excited-state life times and enhanced emission quantum yields, consistent with the energy gap law. Apart from the mononuclear Os(II)-complexes, one would also bring remarkable photophysical features by incorporating multi metal polynuclear complexes. With regard to metal-metal interactions in mixed valence states of the intramolecular electron or energy transfer process, the polynuclear heteroleptic complexes have displayed superior photophysical properties compared to mononuclear complexes. Boonyavong et al. (2014)

prepared an unsymmetrical dinuclear ruthenium osmium 2,2′-bipyridine complexes and studied their photoinduced electron transfer reactions.

The incorporation of anionic ligands into the cationic transition-metal complex systems is a workable strategy to develop neutral emissive materials. Chu et al. (2014) developed a new class of neutral bis(isocyanoborato) bis(bipyridyl) Os(II)-complexes with the general formula of $[Os(N{-}N)_2(CNBR_3)_2]$ (N−N = bpy, 4,4-Me_2bpy; R = C_6F_5,C_6H_5), Unlike the mostly reported neutral bis(bipyridyl)Os(II) complexes (Fig. 7.32), which are very weak or non-emissive, these isocyanoborato complexes exhibited an intense orange to red luminescence with maxima in the range of 610−660 nm with a luminescent quantum yield up to 0.09 at RT. The emission profile of the complexes were very sensitive to the change of the electronic properties of the borane, which is in accordance with the π-accepting ability of the isocyanoborate ligands, $CNB(C_6F_5)_3 > CNB(C_6H_5)_3$. This is due to the variation of energy level of the dπ(Os) orbital, resulting from the Os−$CNBR_3$ interaction.

Os(III)-complexes were used as oxidants in analysis of oxidizable analytes by photoluminescence followed by electron transfer (PFET) based detection methods (Jung et al., 2006). To date, $[Ru(bpy)_3]^{3+/2+}$ and $[Os(bpy)_3]^{3+/2+}$ were used in PFET applications as oxidants for the quantitative determination of proteins, small organic molecules, and other biomolecules. The $[Os(bpy)_3]^{3+}$ was found to be a more superior PFET reagent than $[Ru(bpy)_3]^{3+}$owing to its fast electron-transfer exchange rate and greater stability in 3+ oxidation state. The detection strategy is based on reduction of oxidant by chromatographic eluent to generate a measurable luminescence signal. Patel et al. (2014) demonstrated that tetramethyl-1,10-phenanthroline osmium(III) complex in neutral pH displayed a photoluminescence followed by electron-transfer, which was exploited in the detection of acetaminophen in urine and pharmaceutical formulations (Fig. 7.33).

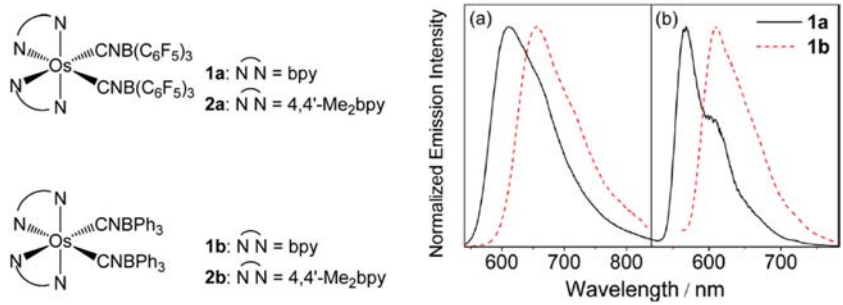

FIG. 7.32 $Os(N{-}N)_2(CNBR_3)_2]$ complexes and overlaid emission spectra of 1a−1b in (A) CH_2Cl_2 solution at room temperature and (B) glassy medium at 77 K. *Adapted from Chu, W.K., Yiu, S.M., Ko, C.C., 2014. Neutral luminescent Bis (bipyridyl) osmium (II) complexes with improved phosphorescent properties. Organometallics 33 (23), 6771−6777. With permission.*

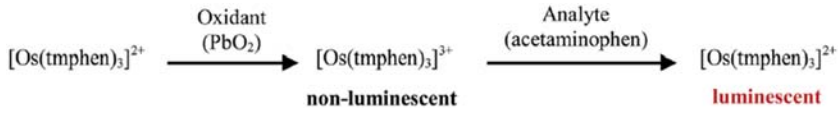

FIG. 7.33 Generalized pathway for the production of Os(III) specie and subsequent regeneration of the emitting specie, $[Os(tmphen)_3]^{2+}$. *Adapted from Patel, M., Varnum, S., Gandla, D., Zdilla, M., Martoff, C., 2014. Stable tetramethyl-1, 10-phenanthroline osmium (III) complex in neutral pH as a photoluminescence-following electron-transfer reagent for the detection of acetaminophen in urine and pharmaceutical formulations. Anal. Methods 6 (15), 5818–5829. With permission.*

The photophysics of d^2 metal complex system is very important in the design of photooxidants. The d^2 metal complexes coordinated to heteroatoms are capable of forming multiple bonds such as oxygen and nitrogen usually having a long-lived and high energy $(d_{xy})^1(d\pi^*)^1$ ($d_{\pi^*} = d_{xz}$, d_{yz}) excited states, which makes them suitable for photocatalysis or photo-induced atom transfer processes (Li et al., 1992; Che et al., 1987). Osmium(IV)-complexes may offer a great deal of flexibility for color tuning, in addition to being more difficult to oxidize than osmium(II) derivatives. Furthermore, OLEDs utilizing Os(IV)-based emitters should be more immune from the formation of an exciplex in the device (Chou and Chi, 2006). Osmium(IV)-based phosphors are exhibiting promising potential application, and their development is certainly challenging. However, emissive Os(IV)-complexes have received little attention, due the fact that they are difficult to prepare several of their geometrical structures are close in energy. The facile exchange of structural form between them allowed the dynamic quenching of the phosphorescence. As a result, emissive Os(IV)-complexes reported up to now are characterized by their low stability and quantum efficiency lower than 0.06. Hence, it is highly demanding to overcome to major challenges; increasing the stability of Os(IV) complexes and the quantum yield of their emissions (Crespo et al., 2012; Eguillor et al., 2015).

Pincer ligands are excellent candidates to stabilize osmium(IV) species with a pentagonal-bipyramidal structure, since this makes two consecutive angles close to 72 degrees, creating an ideal L−M−L angle in the equatorial plane of the bipyramidal structure and fluxional relaxations processes can be restricted (Choi et al., 2011; Benito-Garagorri and Kirchner, 2008). Alabau et al. (2017) reported the preparation of phosphorescent osmium(IV)-complexes with 2-phenyl-6-(1H-pyrazol-3-yl)pyridine and its functionalized derivatives as dianionic and monoanionic N,N,C and C,N,C-pincer ligands, respectively (Fig. 7.34). Osmium(IV)-complexes containing these pincer ligands are phosphorescent emitters in the green to red region with quantum yields (∼0.45−0.5) that are unusually high compared to the previously reported osmium(IV)-complexes with narrow emissions. This is a consequence of the rigidity imposed by the pincer ligand, which reduces both; the energy dissipation by means of dynamic processes and the difference between the excited-state and ground-state structures.

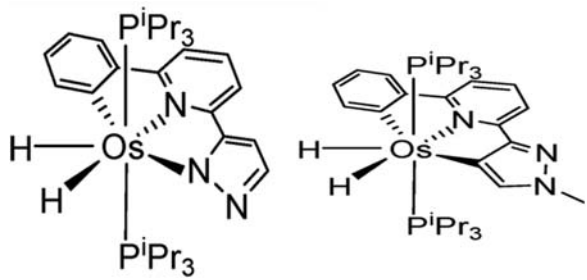

FIG. 7.34 Osmium complexes containing N,N,C and C,N,C-pincer ligands. *Adapted from Alabau, R.G., Esteruelas, M.A., Olivan, M., Onate, E., 2017. Preparation of phosphorescent Osmium (IV) complexes with N, N′, C-and C, N, C′-pincer ligands. Organometallics 36 (9), 1848–1859. With permission.*

The d^2 Os(VI)-complexes are known to be luminescent. Che et al. (1989) reported the synthesis, photophysical and photochemical properties of Os(VI)-centric nitrido and imido complexes. The distorted octahedral complex $[Ph_4As]_2[\ Os^{VI}(CN)_5N]$ showed intense photoluminescence at 550 nm on excitation at 300–400 nm at room temperature. The emission mainly originated from metal-centered ligand-field $^3[(d_{xy})^1(d_{\pi^*})^1]$ excited states.

Luo et al. (2020) developed a series of Os(VI) complexes of the type $[Os^{VI}(N)\ (NO_2\text{-L})\ (CN)_3]^-$ [HNO_2-L = 2-(2-hydroxy-5-nitrophenyl)benzoxazole] with varying substitution on the bidentate ligand L. All the prepared Os(VI)-complexes exhibited a distorted octahedral geometry, with one nitrido ligand being located at the axial site trans-to the phenolate O donor while maintaining the three CN ligands in *mer* configuration (Fig. 7.35). The series

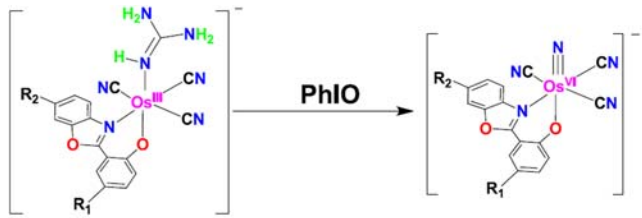

R_1 = H, R_2 = H (1); R_1 = Me, R_2 = H (2);
R_1 = MeO, R_2 = H (3); R_1 = Cl, R_2 = H (4);
R_1 = F, R_2 = H (5); R_1 = CH_3OOC, R_2 = H (6);
R_1 = CF_3, R_2 = H (7); R_1 = NO_2, R_2 = H (8);
R_1 = NO_2, R_2 = Me (9); R_1 = NO_2, R_2 = Cl (10);

FIG. 7.35 Osmium(VI)-nitrido complexes. *Adapted from Luo, L.J., Su, Q.Q., Cheng, S.C., Xiang, J., Man, W.L., Shu, W.M., et al., 2020. Tunable luminescent properties of tricyanoosmium nitrido complexes bearing a chelating O^ N ligand. Inorg. Chem. 59 (7), 4406–4413. With permission.*

of complexes exhibited a strong luminescence both in the solution and in solid state. The luminescence of these nitrido complexes are attributed to the ^{3}LML'CT [π(N^O)$\rightarrow$dπ*(Os$\equiv$N)] phosphorescence emissions. Introduction of strong electron-withdrawing groups such as NO_2, CH_3COO and CF_3, weakens the π-donor properties of the phenolate moiety, which effectively increases the relative contribution of LMLCT in their emissive states resulting in a significant enhancement of LMLCT luminescence.

7.4.2 Near IR phosphorescent osmium complexes

Phosphorescent materials have been designed, and explored because of their wide range of applications (Evans et al., 2006) such as phosphor materials in organic light emitting diodes (OLED), biological probes for theranostics (Monro et al., 2018; Liu et al., 2018), signaling, imaging, and wound healing, etc. The near IR wavelength is considered to be the biological window, as it could penetrate deep through the skin, and tissues. Development of novel phosphorescent probes is the focus of researchers owing to their numerous applications. Some strategies for NIR emission comprise, the use of the donor-acceptor organic dyes, semiconductor quantum dots, conjugated oligomers, and coordination complexes, etc. Os(II)-complexes are well known for their phosphorescent photophysical characteristics. Their structural design can be finely tuned to exhibit panchromatic emission. Though there are several reports on the Os(II)-based panchromatic emitters in the literature, this discussion focus mainly on near IR/far visible phosphorescent Os(II)-complexes (Glazer, 2017). Lee et al. (2009) have done pioneering work on the development of Os(II)-phosphors. A series of new neutral Os(II)-complexes with highly conjugated isoquiniolinyltriazolate chelate was prepared to obtain phosphors that emit at longer wavelength region. Unlike, the Pt(II)-based red emitters, the Os(II)-counterparts use their lower energy MLCT contribution to further red shift the emission, whereas the former uses the intermolecular π-π stacking interaction to lower the emission gap due to the square planar geometry, but in the case of Os(II)-phosphors, the π-π stacking is not realised because of their octahedral configuration. [Os(ibtz)$_2$(PPhMe$_2$)$_2$](5-(1-isoquinolyl)-3-tert-butyl-1,2,4-triazole $-$ibtz) showed an absorption at 468 nm assigned to the spin-allowed $^1\pi\pi$* transition mainly associated with the chromophoric ligand isoquinolyl-triazolate. The next absorption band was observed at 522 nm assignable to a spin allowed ^{1}MLCT transition, and broadened absorption band at the longer wavelength can reasonably be ascribed to a mixed state involving both; spin-orbit coupling enhanced $^3\pi\pi$* and ^{3}MLCT transitions. The T_1-S_0 transition (phosphorescence) occurred at 805 nm, which possess contribution from both spin-forbidden π-π* and MLCT characters. The maximum external quantum efficiency obtained was 1.5%.

Chen et al. (2010) reported the use polypyridyl ligand architectures in achieving highly efficient energy/electron transfers for the development of

solid state near IR phosphorescent Os(II) complexes. Insertion of appropriate conjugated π bridges between these complexes, resulted in rod-like donor-sensitizer-acceptor molecular assemblies, which facilitates an efficient energy/electron transfer process. The typical approach takes up the advantage of the substituent effects for tuning the energy gap between ^{3}MLCT and ^{3}MC states, which involves the insertion of judiciously selected heterocyclic substituents to the pyridyl chelates (Fig. 7.36). Further, an increase of the ligand bite angle was attempted to make the complex adopt a less distorted octahedral arrangement so that the increased ligand field strength and reduced non-radiative decay can be achieved.

The charge neutral Os(II)-complex [Os(fpbpyk)$_2$] [fpbpyk = [5-(trifluoromethyl)pyrazol-3-yl](2,2′-bipyrid-6-yl) ketone] was prepared by the treatment of osmium(III) trichloridetrihydrate with 2 equivalents of the terdentate chelate fpbpykH. The resulting complex was non-luminescent in solution (CH_2Cl_2 or MeOH) at room temperature, but exhibited near IR phosphorescence at 994 nm in solid state at RT.

Near IR phosphors is not restricted to OLED applications only, but they play a vital role in biological science as sensors, for imaging and therapeutics. Zhang et al. (2017) developed a novel Os(II)-NIR phosphorescent probe for lysosomes tracking and photodynamic therapy. The complex showed MLCT absorption at 488 and 683 nm, and exhibiting NIR emission centered between 700 and 850 nm. Due to strong spin-orbit coupling induced by heavy Os(II), the spin-forbidden ^{3}MLCT absorption bands were seen in the NIR region. Smitten et al. (2020) reported the trizole based Os(II)-complexes that displayed strong red/near-IR luminescence. The phosphorescence emission was well exploited in the photodynamic antimicrobial activity against *saureus* and super high resolution cellular imaging. The prepared complexes $[Os(N^\wedge N)_3]^{2+}$ (N^N = 1-benzyl-4-(pyrid-2-yl)-1,2,3-triazole (**I**); 1-benzyl-4-(pyrimidin-2-yl)-1,2,3-triazole (**II**), and 1-benzyl-4-(pyrazin-2-yl)-1,2,3-triazole (**III**) displayed a prominent spin-forbidden ground state to triplet metal-to-ligand charge transfer state absorption bands enabling excitation as low as 600 nm for *fac/mer*-complex (**III**) and an emission in the deep-red/near-IR regions was observed for the aqueous solution of the complexes. Cellular uptake studies within MRSA cells showed antimicrobial activity with greater toxicity for the meridional isomers in each case, with *mer*-(**I**) exhibiting the greatest potency.

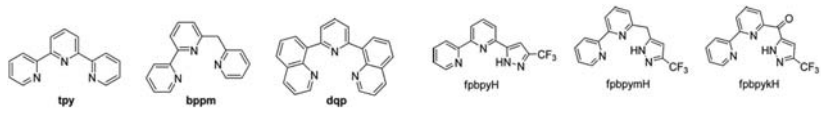

FIG. 7.36 Polypyridyl chelating ligands with conjugated π bridges. *Adapted from Chen, J.L., Chi, Y., Chen, K., Cheng, Y.M., Chung, M.W., Yu, Y.C., et al., 2010. New series of ruthenium (II) and osmium (II) complexes showing solid-state phosphorescence in far-visible and near-infrared. Inorg. Chem. 49 (3), 823−832. With permission.*

Super-resolution imaging experiments demonstrated the binding of *mer*- and *fac*-(**I**) to bacterial DNA with high Pearson's colocalisation coefficients (up to 0.95 using DAPI). The phototoxicity studies revealed that the complexes exhibited a higher antimicrobial activity upon irradiation with light. In another study, a series of Os(II) complexes $[Os(bpy)_{3-n}(pytz)_n][PF_6]_2$ (bpy = 2,2-bipyridyl, pytz = 1-benzyl-4-(pyrid-2-yl)-1,2,3-triazole, with n = 0, 1, 2, and 3) were prepared and optoelectrically characterized. These complexes exhibited a strong red phosphorescence (Omar et al., 2018). The pyridyltriazole complexes exhibited phosphorescence in the biologically transparent red to near-IR region of the spectrum in aqueous solution or in acetonitrile solution through low energy excitation into spin-forbidden direct ^{3}MLCT bands. The homoleptic tris(pyridyltriazole) complex (with n = 4) was brightly emissive ($\lambda_{em} = 614$ nm) and undergoes cellular uptake in two cancer cell lines with likely lysosomal and endosomal localization.

7.4.3 Photophysics of osmium complexes on surfaces

The interfacial electron-transfer dynamics in the construction of these solar cells is an area of intense research. Sensitization of TiO_2 electrodes with molecular chromophores form the basis of efficient solar energy conversion in regenerative photoelectrochemical cells, where the anchoring of chromophores onto the semiconductors was achieved by connecting them covalently on to the semiconductor surfaces (Asbury et al., 2001). Ru/Os-polypyridyl complexes have been used extensively by various researchers as the prospective photosensitizer molecule for the development of dye-sensitized solar cell (DSSC). Owing to their lower energy absorption in the visible region, the Os(II)-polypyridyl complexes may be more suitable for this purpose as there, they may offer a lower-energy absorption band and a lower $M^{II/III}$ oxidation potential was also obtained; thereby, an improved performance in photoelectrochemical energy conversion can be achieved (Kalyanasundaram, 1991). Further, the large spin-orbit coupling effectively promotes an intersystem crossing from singlet excited states to lower triplet emitting states (Ramakrishna et al., 2001). Verma et al. (2008) demonstrated the interfacial electron-transfer dynamics on TiO_2 and ZrO_2 semiconductor nanoparticle surface sensitized by novel catechol derivatives of Os(II)-polypyridyl complexes (Fig. 7.37). This group previously established that the deprotonated catecholate moiety binds strongly to TiO_2 through the formation of a five-member chelate ring.

Both these complexes exhibit two strong MLCT absorption bands in the visible region that are ascribed to the ^{1}MLCT (spin allowed) and ^{3}MLCT (spin forbidden) transitions and with an emission maximum around 650−700 nm. The optical absorption studies revealed that both these complexes form charge transfer (CT) complexes with TiO_2 and ZrO_2 (higher band gap) nanoparticles. Photoinduced electron injection takes place from the Os(II)-complexes to the

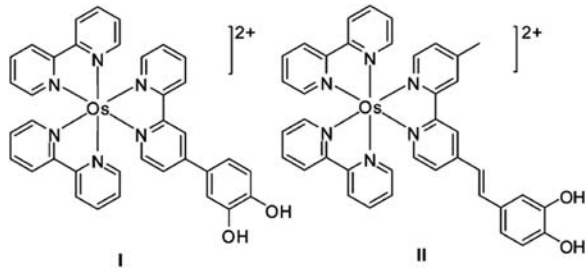

FIG. 7.37 Novel catechol derivatives of Os(II)-polypyridyl complexes. *Adapted from Verma, S., Kar, P., Das, A., Palit, D.K., Ghosh, H.N., 2008. Interfacial electron-transfer dynamics on TiO_2 and ZrO_2 nanoparticle surface sensitized by new catechol derivatives of Os (II)-polypyridyl complexes: Monitoring by charge-transfer emission. J. Phys. Chem. C 112 (8), 2918–2926. With permission.*

conduction band of TiO_2 and surface states of ZrO_2 nanoparticles following excitation of the respective Os(II) catecholic complexes. The ligands were strategically designed to ensure an efficient anchoring on the semiconductor surface and to achieve highly efficient interfacial electron transfer also for solar cell applications.

7.4.4 Photosensitizers for photodynamic therapy

The efficiency of PDT system relies on the photosensitizer and their photophysical properties. The highly reactive oxygen species (ROS) such as singlet oxygen ($^1O_2$) and free radicals, induced oxidative damage on biomolecules, enhance lipid peroxidation, and disrupt the tumor microenvironment; thereby, resulting in cellular oxidative injury, induce mutations, necrosis, and/or apoptosis, etc. There are many reports on development of novel efficient photostable Os(II)-complexes for the PDT. Zhang and Huang (2018) explored the efficacy of three osmium terpyridiyl complexes as photosensitizes, exhibiting obvious metal-to-ligand charge transfer (MLCT) with absorption at 476, 481 and 492 nm as well as a weak singlet ground state to triplet metal to ligand charge transfer absorption band centered in the NIR region (650–775 nm). These complexes exhibit dual emissions in both; visible and NIR regions with the maximum wavelengths around 583/702, 588/709, and 583/719 nm, respectively with a life time around 90–120 ns (Wehlin et al., 2020). Recently, Roque et al. (2020) demonstrated Os(II)-oligothienyl complexes as a hypoxia-active photosensitizer for PDT. A series of Os(II)-oligothienyl polypyridyl complexes were prepared as shown in Fig. 7.38.

The absorption and emission spectra of the Os(II)-complex is shown in Fig. 7.39. The spectra put forward three important features: (i) Pair of absorption bands between 400 and 500 nm and a much broader and weaker band extending beyond 700 nm, which is due to the Os(dπ)→ LL(π^*) MLCT transitions for LL = bpy and dmb, with the lower-energy transition being

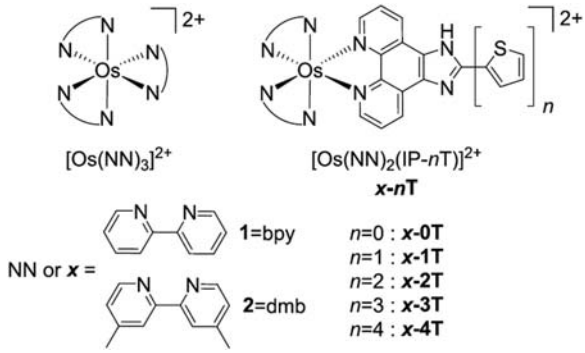

FIG. 7.38 A series of Os(II)-oligothienyl polypyridyl complexes. *Adapted from Roque III, J.A., Barrett, P.C., Cole, H.D., Lifshits, L.M., Bradner, E., Shi, G., 2020. Os(II)-Oligothienyl complexes as a hypoxia-active photosensitizer class for photodynamic therapy. Inorg. Chem. 59 (22), 16341−16360. With permission.*

associated with a formally spin-forbidden absorption to the triplet state, (ii) An intense peak around 290 nm correspond to the intra ligand (IL) ($^1\pi\pi^*$) transition localized on the ancillary LL (bpy/dmb) ligands and were also largely unaffected by the presence of imidazo[4,5-f][1,10]-phenanthroline-oligothiophene ligands, and (iii) A peak that appeared in the 300−500 nm window, only for complexes with thiophene units. This peak increases its intensity and decreases in energy as the number of conjugated thiophene rings increases and therefore, assigned to the thienyl-localized IL ($^1\pi\pi^*$) transition of the IP-nT ligand, which is ^{1}ILCT for $n \geq 2$.

These complexes exhibit an emission profile with $^{em}\lambda_{max}$ between 745 and 770 nm for the bpy series and between 768 and 774 nm for the dmb series. The spectra were broad, featureless, shifting to slightly red shifted with the increase in degree of conjugation. The excitation maxima did not vary significantly within or between families ($\sim$470 nm) and were the same as observed previously for phenanthroline-based Os(II)-complexes. This indicates that the emission arises predominantly from the ^{3}MLCT state. The oligothiophene complexes 1−4T and 2−4T had singlet oxygen quantum yields of 70% and 56%, respectively, which were related to their microsecond ^{3}ILCT life times. It was concluded that a ^{3}ILCT of sufficiently low energy relative to the ^{3}MLCT state, which is an essential condition for the effective singlet oxygen sensitization. The dominant and highly photosensitizing ^{3}ILCT state in 1−4T and 2−4T was responsible for the activity against SK-MEL-28 cancerous cells under both; normoxic and hypoxic conditions.

7.4.5 Photochemistry and applications of osmium complexes

Osmium complexes have been designed as photocatalyst for organic conversion like amines to imines, carbonates to formaldehyde, etc. and in photoredox

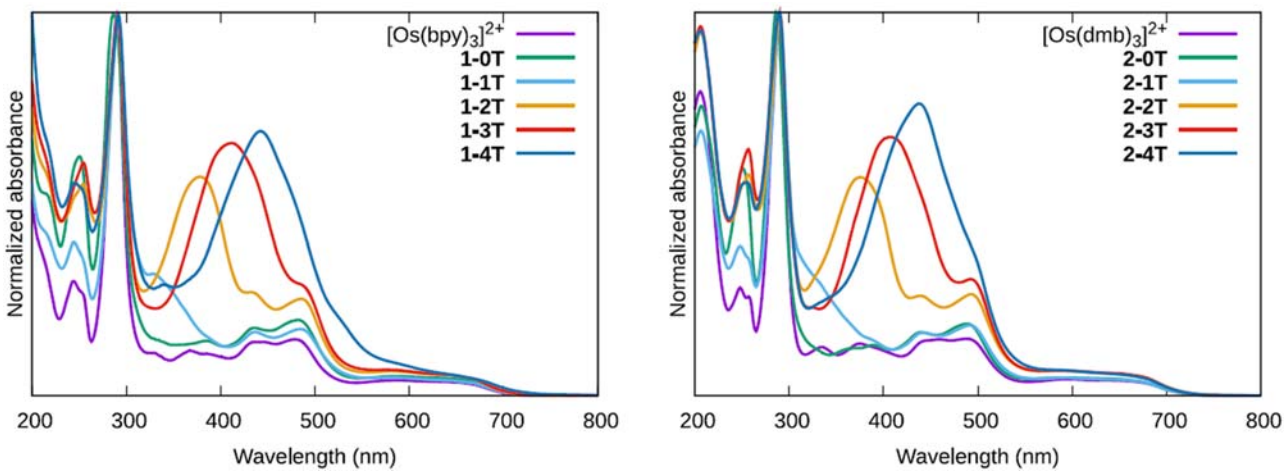

FIG. 7.39 Normalized absorption and emission spectra of Os(II)-oligothienyl polypyridyl complexes. *Adapted from Roque III, J.A., Barrett, P.C., Cole, H.D., Lifshits, L.M., Bradner, E., Shi, G., 2020. Os (II) Oligothienyl complexes as a hypoxia-active photosensitizer class for photodynamic therapy. Inorg. Chem. 59 (22), 16341−16360. With permission.*

reaction such as photocatalytic generation of hydrogen, and hydrohalic acid splitting, etc. Li et al. (2016) developed triazole based Os(II)-complexes for light driven anaerobic oxidation of amines to imines, the complexes $[Os(fptz)_2(PPhMe_2)_2]$ (where, fptzH = 3-trifluoromethyl-5-pyridyl-1,2,4-triazole), $[Os(fptz)_2(CO)\ (L1)]$ (where, L1 = PPh_3; or = pyridine) have been used successfully as photocatalyst for the oxidation of amine to imine by using molecular oxygen as green oxidant. The photocatalytic activity of the $[Os(fptz)_2(PPhMe_2)_2]$ was much higher than that of the other reported Os(II)-complexes. This enhanced activity can be attributed to its ability to produce singlet oxygen, which was responsible for the oxidation of amine to imine. This activity was due to strong absorption of visible light at 410 nm and weak absorption bands centered around 460 and 550 nm and the long-lived triplet state of $[Os(fptz)_2(PPhMe_2)_2]$. The emission band was around 643 nm originating from the ^{3}MLCT [Os(dπ) → fptz (π*)] excited state. This result was confirmed by DFT/TD-DFT calculations.

Miyake al. (2009) prepared a series of Os(II)-complexes and used for photocatalytic production of dihydrogen. This group developed diphosphine ligand bearing Os(II) bis(terpyridyl) complexes for light harvesting in the production of dihydrogen (Fig. 7.40).

The Os(II)-terpyridyl complex with diphosphine moiety was synthesized and combined with $[RhCl(CO)_2]_2$ to form a dinuclear Os−Rh complex (Fig. 7.41). These complexes exhibit two similar visible absorption bands around 483 and 655 nm, which were due to the ^{1}MLCT and ^{3}MLCT, respectively. The emission maximum of the Os−Rh complex was observed around 727 nm. The complex was found to be an effective photocatalyst for the production of dihydrogen and, a plausible mechanism was proposed (Fig. 7.42). The Os−Rh complex A is photoexcited at above 380 nm, the quenching of A* at the coordinated rhodium center and by sodium ascorbate (NaHA) proceeds smoothly to cause one electron reduction of the rhodium center via intramolecular electron transfer, followed by sequential second electron reduction of the rhodium center to form the reduced rhodium species B. Reaction of B with a proton generates the rhodium hydride species C, which turns into dihydrogen and the rhodium species A by protonolysis. Vogler (2016) reported the photochemistry of osmium complex $[Os(bipy)_2(CO_3)]$ and phororeduction of carbonate to formaldehyde. The complex undergoes a photoredox reaction to form $[Os(VI)\ (bipy)_2(O)_2]^{2+}$ and formaldehyde.

In recent times, although water splitting with hydrogen generation has attracted much attention, yet another promising focus is on hydrohalic acid (HX) splitting, Wehlin et al. (2020) used osmium-complexes for photocatalytic splitting of hydrohalic acid. Two osmium(II)- photocatalysts bearing a dicationic 4,4′-bis-(trimethylaminomethyl)-2,2′-bipyridine (tmam) ligand and 2,2′-bipyridine $[Os(bpy)_2(tmam)]^{4+}$ or 4,4′−$(CF_3)_2$−2,2′-bipyridine $[Os((CF_3)_2bpy)_2(tmam)]^{4+}$ ancillary ligands were prepared and used for HX splitting.

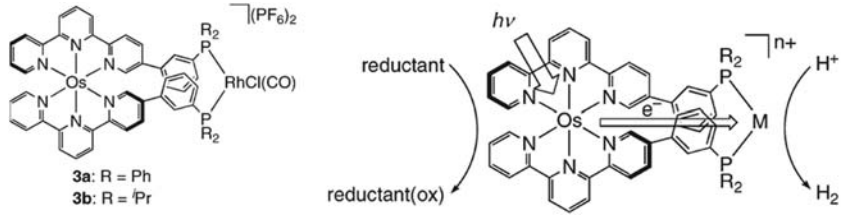

FIG. 7.40 Design of diphosphine ligands bearing$Os(tpy)_22^+$ as a light-harvesting unit. *Adapted from Miyake, Y., Nakajima, K., Sasaki, K., Saito, R., Nakanishi, H., Nishibayashi, Y., 2009. Design and synthesis of diphosphine ligands bearing an osmium (II) bis (terpyridyl) moiety as a light-harvesting unit: application to photocatalytic production of dihydrogen. Organometallics 28 (17), 5240–5243. With permission.*

Fig. 7.42 represents the absorption and emission properties of osmium complexes. Visible light excitation of both complexes exhibited a photo-luminescence (PL) centered at 815 and 775 nm for Os-bpyand Os-CF_3, respectively. The electron withdrawing nature of the trifluromethyl moiety resulted in a 40 nm hypsochromic shift in the emission maximum compared to unsubstituted Os-bpy complex. The photocatalyst $[Os(bpy)_2(tmam)]^{4+}$was found to be inefficient in iodide oxidation. In contrast, visible light excitation of $[Os((CF_3)_2bpy)_2(tmam)]^{4+}$ led to rapid iodide oxidation ($k_q = 2.8 \times 10^{11}\ M^{-1}\ s^{-1}$). The data revealed that Os(II)-photocatalysts can be finely tuned for its application in HX splitting.

Osmium complexes offer a wide range utility in the field of OLEDs, solar energy, diagnosis, therapeutic, and light driven organic reactions. The choice of osmium complexes over other analogs is due to their remarkable photo-physical properties, which can be tuned strategically by designing the ligands, and its chemical architecture.

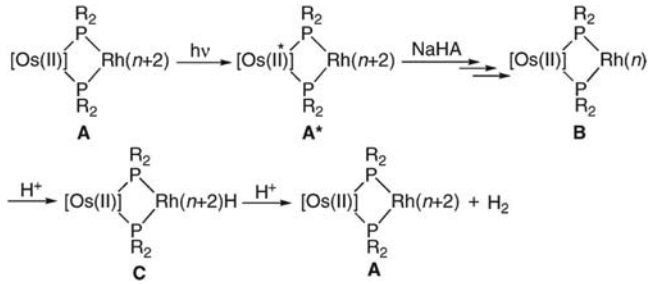

FIG. 7.41 Plausible mechanism of photocatalytic production of dihydrogen. *Adapted from Miyake, Y., Nakajima, K., Sasaki, K., Saito, R., Nakanishi, H., Nishibayashi, Y., 2009. Design and synthesis of diphosphine ligands bearing an osmium (II) bis (terpyridyl) moiety as a light-harvesting unit: application to photocatalytic production of dihydrogen. Organometallics 28 (17), 5240–5243. With permission.*

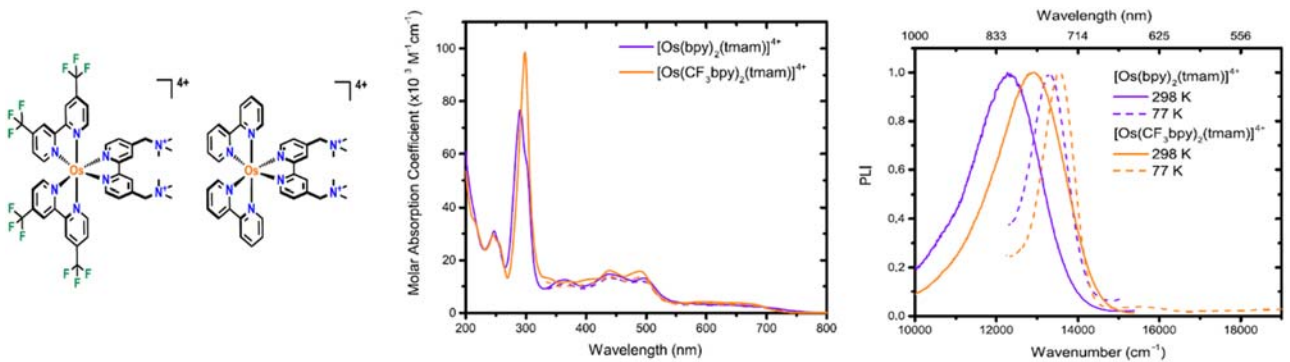

FIG. 7.42 Absorption and photoluminescence spectra of Os(II) photocatalysts for HI splitting bearing the di-cationic 4,4′-bis(trimethylaminomethyl)-2,2′-bipyridine ligand. *Adapted from Wehlin, S.A., Troian-Gautier, L., Maurer, A.B., Brennaman, M.K., Meyer, G.J., 2020. Photophysical characterization of new osmium (II) photocatalysts for hydrohalic acid splitting. J. Chem. Phys., 2020 153 (5), https://10.1063/5.0014269. With permission.*

7.5 Summary

In summary, the recent development of the photophysics and photochemistry of coordination of compounds of Fe, Ru, and Os complexes demonstrated that there is excellent visible light absorption and long-lived excited state with efficient intersystem crossing process. The understanding of the photophysical properties of transition metal complexes, in particular, the role of excited states, provides insight into the design of transition metal complexes for the application in photodynamic therapy, solar energy conversion and photocatalysis. The development of sustainable, eco-friendly, and industrially useful transition metal complexes will be promising in the future.

References

Alabau, R.G., Esteruelas, M.A., Olivan, M., Onate, E., 2017. Preparation of phosphorescent Osmium (IV) complexes with N, N′, C-and C, N, C′-pincer ligands. Organometallics 36 (9), 1848–1859.

Alary, F., Heully, J.-L., Bijeire, L., Vicendo, P., 2007. Is the 3MLCT the only photoreactive state of polypyridyl complexes? Inorg. Chem. 46 (8), 3154–3165.

Anandkumar, D., Ganesan, S., Rajakumar, P., Maruthamuthu, P., 2017. Synthesis, photophysical and electrochemical properties and DSSC applications of triphenylamine chalcone dendrimers via click chemistry. New J. Chem. 41 (19), 11238–11249.

Aratani, Y., Suenobu, T., Ohkubo, K., Yamada, Y., Fukuzumi, S., 2017. Dual function photocatalysis of cyano-bridged heteronuclear metal complexes for water oxidation and two-electron reduction of dioxygen to produce hydrogen peroxide as a solar fuel. Chem. Commun. 53 (24), 3473–3476.

Asbury, J.B., Hao, E., Wang, Y., Ghosh, H.N., Lian, T., 2001. Ultrafast electron transfer dynamics from molecular adsorbates to semiconductor nanocrystalline thin films. J. Phys. Chem. B 105 (20), 4545–4557.

Ashford, D.L., Glasson, C.R., Norris, M.R., Concepcion, J.J., Keinan, S., Brennaman, M.K., et al., 2014. Controlling ground and excited state properties through ligand changes in ruthenium polypyridyl complexes. Inorg. Chem. 53 (11), 5637–5646.

Auböck, G., Chergui, M., 2015. Sub-50-fs photoinduced spin crossover in [Fe (bpy) 3]$^{2+}$. Nat. Chem. 7 (8), 629–633.

Balzani, V., Juris, A., Venturi, M., Campagna, S., Serroni, S., 1996. Luminescent and redox-active polynuclear transition metal complexes. Chem. Rev. 96 (2), 759–834.

Banerjee, S., 2021. Polypyridyl ruthenium (II) complexes with red-shifted absorption: new Promises in photodynamic therapy. Chembiochem 22, 2407.

Bauer, et al., 2017. Eur. J. Inorg. Chem. 2017 (11), 1504–1509.

Benito-Garagorri, D., Kirchner, K., 2008. Modularly designed transition metal PNP and PCP pincer complexes based on aminophosphines: synthesis and catalytic applications. Acc. Chem. Res. 41 (2), 201–213.

Bhasikuttan, A.C., Suzuki, M., Nakashima, S., Okada, T., 2002. Ultrafast fluorescence detection in Tris (2, 2 ‘-bipyridine) ruthenium (II) complex in solution: relaxation dynamics involving higher excited states. J. Am. Chem. Soc. 124 (28), 8398–8405.

Boonyavong, N., Suwanruji, P., Hannongbua, S., Li, F., Sun, L., Karpkird, T.M., 2014. Synthesis, electrochemistry and photo-induced electron transfer of unsymmetrical dinuclear ruthenium osmium 2, 2′-bipyridine complexes. J. Photochem. Photobiol., A: Chem 287, 40–48.

Bouché, M., Hognon, C., Grandemange, S., Monari, A., Gros, P.C., 2020. Recent advances in iron-complexes as drug candidates for cancer therapy: reactivity, mechanism of action and metabolites. Dalton Trans. 49 (33), 11451−11466.

Brabec, V., Kasparkova, J., 2018. Ruthenium coordination compounds of biological and biomedical significance. DNA binding agents. Coord. Chem. Rev. 376, 75−94.

Bressler, C., Chergui, M., 2004. Ultrafast X-ray absorption spectroscopy. Chem. Rev. 104 (4), 1781−1812.

Campagna, S., Puntoriero, F., Nastasi, F., Bergamini, G., Balzani, V., 2007. Photochemistry and photophysics of coordination compounds: ruthenium. Photochem. Photophys. Coord. Comp. I 280, 117−214.

Cannizzo, A., van Mourik, F., Gawelda, W., Zgrablic, G., Bressler, C., Chergui, M., 2006. Broadband femtosecond fluorescence spectroscopy of [Ru (bpy) 3]$^{2+}$. Angew. Chem. 118 (19), 3246−3248.

Cauwenbergh, R., Das, S., 2021. Photochemical reduction of carbon dioxide to formic acid. Green Chem. 23 (7), 2553−2574.

Cerfontaine, S., Troian-Gautier, L., Duez, Q., Cornil, J.R.M., Gerbaux, P., Elias, B., 2020. MLCT excited-state behavior of trinuclear ruthenium (II) 2, 2′-bipyridine complexes. Inorg. Chem. 60 (1), 366−379.

Chábera, P., Liu, Y., Prakash, O., Thyrhaug, E., El Nahhas, A., Honarfar, A., et al., 2017. A low-spin Fe (III) complex with 100-ps ligand-to-metal charge transfer photoluminescence. Nature 543 (7647), 695−699.

Chábera, P., Lindh, L., Rosemann, N.W., Prakash, O., Uhlig, J., Yartsev, A., et al., 2021. Photofunctionality of iron (III) N-heterocyclic carbenes and related d5 transition metal complexes. Coord. Chem. Rev. 426, 213517.

Chang, J., Fedro, A., Veenendaal, V.M., 2012. Ultrafast X-ray spectroscopy as a probe of nonequilibrium dynamics in ruthenium complexes. Chem. Phys. 407, 65−70.

Che, C.-M., Yam, V.W.-W., Cho, K.-C., Gray, H.B., 1987. Metal−oxo photo-oxidants. Photochemistry and photophysics of trans-[Os VI (tmc)(O) 2] 2+(tmc= 1, 4, 8, 11-tetramethyl-1, 4, 8, 11-tetra-azacyclotetradecane) and trans-[Os VI (CN) 4 (O) 2] 2. J. Chem. Soc., Chem. Comm. 12, 948−949.

Che, C.-M., Lam, M.H.-W., Mak, T.C., 1989. Metal nitrido and imido photo-oxidants. Photophysics and photochemistry of nitrido and imido complexes of osmium (VI) and X-ray crystal structure of [Ph 4 As] 2 [Os VI (CN) 5 N]. J. Chem. Soc., Chem. Comm. (20), 1529−1531.

Chen, J., Browne, W.R., 2018. Photochemistry of iron complexes. Coord. Chem. Rev. 374, 15−35. https://doi.org/10.1016/j.ccr.2018.06.008.

Chen, J.-L., Chi, Y., Chen, K., Cheng, Y.-M., Chung, M.-W., Yu, Y.-C., et al., 2010. New series of ruthenium (II) and osmium (II) complexes showing solid-state phosphorescence in far-visible and near-infrared. Inorg. Chem. 49 (3), 823−832.

Choi, J., MacArthur, A.H.R., Brookhart, M., Goldman, A.S., 2011. Dehydrogenation and related reactions catalyzed by iridium pincer complexes. Chem. Rev. 111 (3), 1761−1779.

Chou, P.T., Chi, Y., 2006. Osmium-and ruthenium-based phosphorescent materials: design, photophysics, and utilization in OLED fabrication. Eur. J. Inorg. Chem. 2006 (17), 3319−3332.

Chu, W.-K., Yiu, S.-M., Ko, C.-C., 2014. Neutral luminescent Bis (bipyridyl) osmium (II) complexes with improved phosphorescent properties. Organometallics 33 (23), 6771−6777.

Costa, E.P., Roccamante, M., Amorim, C.C., Oller, I., Pérez, J.A.S., Malato, S., 2020. New trend on open solar photoreactors to treat micropollutants by photo-Fenton at circumneutral pH: increasing optical pathway. Chem. Eng. J. 385, 123982.

Crespo, O., Eguillor, B., Esteruelas, M.A., Fernández, I., García-Raboso, J., Gómez-Gallego, M., et al., 2012. Synthesis and characterisation of [6]-azaosmahelicenes: the first d 4-heterometallahelicenes. Chem. Comm. 48 (43), 5328–5330.

Damrauer, N.H., Cerullo, G., Yeh, A., Boussie, T.R., Shank, C.V., McCusker, J.K., 1997. Femtosecond dynamics of excited-state evolution in [Ru (bpy) 3]$^{2+}$. Science 275 (5296), 54–57.

Darari, M., Francés-Monerris, A., Marekha, B., Doudouh, A., Wenger, E., Monari, A., et al., 2020. Towards iron (II) complexes with octahedral geometry: synthesis, structure and photophysical properties. Molecules 25 (24). https://doi.org/10.3390/molecules25245991.

Das, N., Bindra, G.S., Paul, A., Vos, J.G., Schulz, M., Pryce, M.T., 2017. Enhancing photocatalytic hydrogen generation: the impact of the peripheral ligands in Ru/Pd and Ru/Pt complexes. Chem. Eur J. 23 (22), 5330–5337.

Dietzek, B., Akimov, D., Kiefer, W., Rau, S., Popp, J., Schmitt, M., 2006. Excited-state dynamics of Ru (tbbpy) 32+ investigated by femtosecond time-resolved four-wave mixing. Laser Phys. Lett. 4 (2). https://doi.org/10.1002/lapl.200610086.

Dixon, I.M., Alary, F., Boggio-Pasqua, M., Heully, J.-L., 2015. Reversing the relative 3 MLCT–3 MC order in Fe (ii) complexes using cyclometallating ligands: a computational study aiming at luminescent Fe (ii) complexes. Dalton Trans. 44 (30), 13498–13503.

Dixon, I.M., Boissard, G., Whyte, H., Alary, F., Heully, J.-L., 2016. Computational estimate of the photophysical capabilities of four series of organometallic iron (II) complexes. Inorg. Chem. 55 (11), 5089–5091.

Dong, R., Calzolari, A., Di Felice, R., El-Shafei, A., Hussain, M., Nardelli, B.M., 2014. Optical enhancement in heteroleptic Ru (II) polypyridyl complexes using electron-donor ancillary ligands. J. Phys. Chem. C 118 (17), 8747–8755.

Dongare, P., Myron, B.D., Wang, L., Thompson, D.W., Meyer, T.J., 2017. [Ru (bpy) 3]$^{2+*}$ revisited. Is it localized or delocalized? How does it decay? Coord. Chem. Rev. 345, 86–107.

Duchanois, T., Etienne, T., Beley, M., Assfeld, X., Perpète, E.A., Monari, A., Gros, P.C., 2014. Heteroleptic pyridyl-carbene iron complexes with tuneable electronic properties. Eur. J. Inorg. Chem. 2014 (23), 3747–3753.

Duchanois, T., Liu, L., Pastore, M., Monari, A., Cebrián, C., Trolez, Y., et al., 2018. NHC-based iron sensitizers for DSSCs. Inorganics 6 (2). https://doi.org/10.3390/inorganics6020063.

Eguillor, B., Esteruelas, M.A., Fernández, I., Gómez-Gallego, M., Lledós, A., Martín-Ortiz, M., et al., 2015. Azole assisted C–H bond activation promoted by an osmium-polyhydride: discerning between N and NH. Organometallics 34 (10), 1898–1910.

El-Batal, H., Guo, K., Li, X., Wesdemiotis, C., Moorefield, C.N., Newkome, G.R., 2013. Perylene-based bis-, tetrakis-, and hexakis (terpyridine) ligands and their ruthenium (II)–Bis (terpyridine) complexes: synthesis and photophysical properties. Eur. J. Org. Chem. 2013 (18), 3640–3644.

El-Shafei, A., Hussain, M., Atiq, A., Islam, A., Han, L., 2012. A novel carbazole-based dye outperformed the benchmark dye N719 for high efficiency dye-sensitized solar cells (DSSCs). J. Mater. Chem. 22 (45), 24048–24056.

Evans, R.C., Douglas, P., Winscom, C.J., 2006. Coordination complexes exhibiting room-temperature phosphorescence: evaluation of their suitability as triplet emitters in organic light emitting diodes. Coord. Chem. Rev. 250 (15–16), 2093–2126.

Fabry, D.C., Koizumi, H., Ghosh, D., Yamazaki, Y., Takeda, H., Tamaki, Y., et al., 2020. A Ru (II) –Mn (I) supramolecular photocatalyst for CO2 reduction. Organometallics 39 (9), 1511–1518.

Fatur, S.M., Shepard, S.G., Higgins, R.F., Shores, M.P., Damrauer, N.H., 2017. A synthetically tunable system to control MLCT excited-state lifetimes and spin states in iron (II) polypyridines. J. Am. Chem. Soc. 139 (12), 4493−4505.

Feng, L., Wang, Y., 2018. A key factor dominating the competition between photolysis and photoracemization of [Ru (bipy) 3]$^{2+}$ and [Ru (phen) 3]$^{2+}$ complexes. Inorg. Chem. 57 (15), 8994−9001.

García-Fernández, I., Miralles-Cuevas, S., Oller, I., Malato, S., Fernández-Ibáñez, P., Polo-López, M.I., 2019. Inactivation of E. coli and E. faecalis by solar photo-fenton with EDDS complex at neutral pH in municipal wastewater effluents. J. Hazard Mater. 372, 85−93.

Gawelda, W., Johnson, M., de Groot, F.M., Abela, R., Bressler, C., Chergui, M., 2006. Electronic and molecular structure of photoexcited [RuII (bpy) 3] $^{2+}$ probed by picosecond X-ray absorption spectroscopy. J. Am. Chem. Soc. 128 (15), 5001−5009.

Glazer, E.C., 2017. Panchromatic osmium complexes for photodynamic therapy: solutions to existing problems and new questions. Photochem. Photobiol. 93 (5), 1326−1328.

Gonçalves, B.R., Guimarães, R.O., Batista, L.L., Ueira-Vieira, C., Starling, M.C.V., Trovó, A.G., 2020. Reducing toxicity and antimicrobial activity of a pesticide mixture via photo-fenton in different aqueous matrices using iron complexes. Sci. Total Environ. 740. https://doi.org/10.1016/j.scitotenv.2020.140152.

Hagfeldt, A., Boschloo, G., Sun, L., Kloo, L., Pettersson, H., 2010. Dye-sensitized solar cells. Chem. Rev. 110 (11), 6595−6663.

Hara, D., Komatsu, H., Son, A., Nishimoto, S.-I., Tanabe, K., 2015. Water-soluble phosphorescent ruthenium complex with a fluorescent coumarin unit for ratiometric sensing of oxygen levels in living cells. Bioconjug. Chem. 26 (4), 645−649.

Harlang, T.C., Liu, Y., Gordivska, O., Fredin, L.A., Ponseca, C.S., Huang, P., et al., 2015. Iron sensitizer converts light to electrons with 92% yield. Nat. Chem. 7 (11), 883−889.

Harriman, A., Izzet, G., 2007. Direct observation of the fourth MLCT triplet state in ruthenium (ii) tris (2, 2′-bipyridine). Phys. Chem. Chem. Phys. 9 (8), 944−948.

Hawecker, J., Lehn, J.-M., Ziessel, R., 1985. Photochemical reduction of carbon dioxide to formate mediated by ruthenium bipyridine complexes as homogeneous catalysts. J. Chem. Soc., Chem. Comm. 2, 56−58.

He, C., Yu, S., Ma, S., Liu, Z., Yao, L., Cheng, F., Liu, P., 2019. A novel ruthenium (II) polypyridyl complex bearing 1, 8-Naphthyridine as a high selectivity and sensitivity fluorescent chemosensor for Cu^{2+} and Fe^{3+} ions. Molecules 24 (22). https://doi.org/10.3390/molecules24224032.

He, G., Xu, N., Ge, H., Lu, Y., Wang, R., Wang, H., et al., 2021. Red-Light-Responsive Ru complex photosensitizer for lysosome localization photodynamic therapy. ACS Appl. Mater. Inter. 13 (17), 19572−19580.

Heinemann, F., Karges, J., Gasser, G., 2017. Critical overview of the use of Ru (II) polypyridyl complexes as photosensitizers in one-photon and two-photon photodynamic therapy. Acc. Chem. Res. 50 (11), 2727−2736.

Henry, W., Coates, C.G., Brady, C., Ronayne, K.L., Matousek, P., Towrie, M., et al., 2008. The early picosecond photophysics of Ru (II) polypyridyl complexes: a tale of two timescales. J. Phys. Chem. A 112 (20), 4537−4544.

Horvath, R., Gordon, K.C., 2010. Understanding excited-state structure in metal polypyridyl complexes using resonance Raman excitation profiles, time-resolved resonance Raman spectroscopy and density functional theory. Coord. Chem. Rev. 254 (21−22), 2505−2518.

Ito, A., Meyer, T.J., 2012. The Golden Rule. Application for fun and profit in electron transfer, energy transfer, and excited-state decay. Phys. Chem. Chem. Phys. 14 (40), 13731−13745.

Ito, A., Knight, T.E., Stewart, D.J., Brennaman, M.K., Meyer, T.J., 2014. Rigid medium effects on photophysical properties of MLCT excited states of polypyridyl Os (II) complexes in polymerized poly (ethylene glycol) dimethacrylate monoliths. J. Phys. Chem. A 118 (45), 10326−10332.

Ito, A., Kobayashi, N., Teki, Y., 2017. Low-energy and long-lived emission from polypyridyl ruthenium (II) complexes having a stable-radical substituent. Inorg. Chem. 56 (7), 3794−3808.

Jamula, L.L., Brown, A.M., Guo, D., McCusker, J.K., 2014. Synthesis and characterization of a high-symmetry ferrous polypyridyl complex: approaching the 5T2/3T1 crossing point for FeII. Inorg. Chem. 53 (1), 15−17.

Jose, D.A., Kar, P., Koley, D., Ganguly, B., Thiel, W., Ghosh, H.N., Das, A., 2007. Phenol-and catechol-based ruthenium (II) polypyridyl complexes as colorimetric sensors for fluoride ions. Inorg. Chem. 46 (14), 5576−5584.

Jung, M.C., Munro, N., Shi, G., Michael, A.C., Weber, S.G., 2006. Use of tris (2, 2 '-bipyridine) osmium as a photoluminescence-following electron-transfer reagent for postcolumn detection in capillary high-performance liquid chromatography. Anal. Chem. 78 (6), 1761−1768.

Juris, A., Balzani, V., Barigelletti, F., Campagna, S., Belser, P.l., Von Zelewsky, A.V., 1988. Ru (II) polypyridine complexes: photophysics, photochemistry, eletrochemistry, and chemiluminescence. Coord. Chem. Rev. 84, 85−277.

Kalyanasundaram, K., 1982. Photophysics, photochemistry and solar energy conversion with tris (bipyridyl) ruthenium (II) and its analogues. Coord. Chem. Rev. 46, 159−244.

Kalyanasundaram, K. (Ed.), 1991. Photochemistry of Polypyridine and Porphyrin Complexes. Academic Press, London.

Karges, J., Gasser, G., 2020. Synthesis, characterisation and biological evaluation of π-extended Fe (II) bipyridine complexes as potential photosensitizers for photodynamic therapy. Inorganica Chim. Acta 499. https://doi.org/10.1016/j.ica.2019.119196.

Karges, J., Goldner, P., Gasser, G., 2019. Synthesis, characterization, and biological evaluation of red-absorbing Fe (II) polypyridine complexes. Inorganics 7 (1), 4.

Kim, J., Kang, D.-g., Kim, S.K., Joo, T., 2020. Role of coherent nuclear motion in the ultrafast intersystem crossing of ruthenium complexes. Phys. Chem. Chem. Phys. 22 (44), 25811−25818.

Kjaer, K.S., Kaul, N., Prakash, O., Chábera, P., Rosemann, N.W., Honarfar, A., et al., 2019. Luminescence and reactivity of a charge-transfer excited iron complex with nanosecond lifetime. Science 363 (6424), 249−253.

Kumar, P., Kumar, S., 2020. Copper ion luminescence on/off sensing by a quinoline-appended ruthenium (II)-polypyridyl complex in aqueous media. J. Mol. Struc. 1202. https://doi.org/10.1016/j.molstruc.2019.127242.

Kumar, S., Singh, S., Kumar, A., Kumar, P., 2021. Recognition, mechanistic investigation and applications for the detection of biorelevant Cu^{2+}/Fe^{2+}/Fe^{3+} ions by ruthenium (ii)-polypyridyl based fluorescent sensors. Dalton Trans. 50 (8), 2705−2721.

Lakowicz, J.R. (Ed.), 2013. Principles of Fluorescence Spectroscopy. Springer science & business media, London.

Lee, T.C., Hung, J.Y., Chi, Y., Cheng, Y.M., Lee, G.H., Chou, P.T., et al., 2009. Rational design of charge-neutral, near-infrared-emitting osmium (II) complexes and OLED fabrication. Adv. Funct. Mater. 19 (16), 2639−2647.

Li, J., Chen, T., 2020. Transition metal complexes as photosensitizers for integrated cancer theranostic applications. Coord. Chem. Rev. 418. https://doi.org/10.1016/j.ccr.2020.213355.

Li, C.-K., Che, C.-M., Tong, W.-F., Tang, W.-T., Wong, K.-Y., Lai, T.-F., 1992. Synthesis, structure, reactivity and electrochemistry of cis-dioxoruthenium-(VI) and-(V) complexes containing N, N, N′, N′, 3, 6-hexamethyl-3, 6-diazaoctane-1, 8-diamine. J. Chem. Soc., Dalton Trans. 13, 2109–2116.

Li, Y.-H., Liu, X.-L., Yu, Z.-T., Li, Z.-S., Yan, S.-C., Chen, G.-H., Zou, Z.-G., 2016. Osmium (ii) complexes for light-driven aerobic oxidation of amines to imines. Dalton Trans. 45 (31), 12400–12408.

Lin, H.H.-H., Lin, A.Y.-C., 2021. Solar photo-Fenton oxidation of cytostatic drugs via Fe (III)-EDDS at circumneutral pH in an aqueous environment. J. Water Process Eng. 41. https://doi.org/10.1016/j.jwpe.2021.102066.

Lindh, L., Chábera, P., Rosemann, N.W., Uhlig, J., Wärnmark, K., Yartsev, A., et al., 2020. Photophysics and photochemistry of iron carbene complexes for solar energy conversion and photocatalysis. Catalysts 10 (3). https://doi.org/10.3390/catal10030315.

Liu, Y., Harlang, T., Canton, S.E., Chábera, P., Suárez-Alcántara, K., Fleckhaus, A., et al., 2013. Towards longer-lived metal-to-ligand charge transfer states of iron (II) complexes: an N-heterocyclic carbene approach. Chem. Commun. 49 (57), 6412–6414.

Liu, Y., Kjær, K.S., Fredin, L.A., Chábera, P., Harlang, T., Canton, S.E., et al., 2015. A heteroleptic ferrous complex with mesoionic bis (1, 2, 3-triazol-5-ylidene) ligands: taming the MLCT excited state of iron (II). Chem. Eur J. 21 (9), 2628–2639.

Liu, L., Duchanois, T., Etienne, T., Monari, A., Beley, M., Assfeld, X., et al., 2016. A new record excited state 3 MLCT lifetime for metalorganic iron (II) complexes. Phys. Chem. Chem. Phys. 18 (18), 12550–12556.

Liu, Y., Persson, P., Sundstrom, V., Warnmark, K., 2016. Fe N-heterocyclic carbene complexes as promising photosensitizers. Acc. Chem. Res. 49 (8), 1477–1485.

Liu, J., Zhang, C., Rees, T.W., Ke, L., Ji, L., Chao, H., 2018. Harnessing ruthenium (II) as photodynamic agents: encouraging advances in cancer therapy. Coord. Chem. Rev. 363, 17–28.

Lumbaque, E.C., Araújo, D.S., Klein, T.M., Tiburtius, E.R.L., Argüello, J., Sirtori, C., 2019. Solar photo-Fenton-like process at neutral pH: Fe (III)-EDDS complex formation and optimization of experimental conditions for degradation of pharmaceuticals. Catal. Today 328, 259–266, 2019.

Luo, L.-J., Su, Q.-Q., Cheng, S.-C., Xiang, J., Man, W.-L., Shu, W.-M., et al., 2020. Tunable luminescent properties of tricyanoosmium nitrido complexes bearing a chelating Oˆ N ligand. Inorg. Chem. 59 (7), 4406–4413.

Mareeswaran, P.M., Rajkumar, E., Sathish, V., Rajagopal, S., 2014. Electron transfer reactions of ruthenium (II)–bipyridine complexes carrying tyrosine moiety with quinones. Luminescence 29 (7), 754–761.

Mari, C., Pierroz, V., Ferrari, S., Gasser, G., 2015. Combination of Ru (II) complexes and light: new frontiers in cancer therapy. Chem. Sci. 6 (5), 2660–2686.

McCusker, J.K., 2014. Enlightened state. Nat. Phys. 10 (7), 476–477.

Meng, T.-T., Wang, H., Zheng, Z.-B., Wang, K.-Z., 2017. pH-switchable "Off–On–Off" near-infrared luminescence based on a dinuclear ruthenium (II) complex. Inorg. Chem. 56 (9), 4775–4779.

Mengel, A.K., Förster, C., Breivogel, A., Mack, K., Ochsmann, J.R., Laquai, F., et al., 2015. A heteroleptic push–pull substituted iron (II) Bis (tridentate) complex with low-energy charge-transfer states. Chem. Eur J. 21 (2), 704–714.

Mishra, A., Mena-Osteritz, E., Bäuerle, P., 2013. Synthesis, photophysical and electrochemical characterization of terpyridine-functionalized dendritic oligothiophenes and their Ru (II) complexes. Beilstein J. Org. Chem. 9 (1), 866–876.

Miyake, Y., Nakajima, K., Sasaki, K., Saito, R., Nakanishi, H., Nishibayashi, Y., 2009. Design and synthesis of diphosphine ligands bearing an osmium (II) bis (terpyridyl) moiety as a light-harvesting unit: application to photocatalytic production of dihydrogen. Organometallics 28 (17), 5240–5243.

Monro, S., Colón, K.L., Yin, H., Roque III, J., Konda, P., Gujar, S., et al., 2018. Transition metal complexes and photodynamic therapy from a tumor-centered approach: challenges, opportunities, and highlights from the development of TLD1433. Chem. Rev. 119 (2), 797–828.

Motley, T.C., Troian-Gautier, L., Brennaman, M.K., Meyer, G.J., 2017. Excited-state decay pathways of tris (bidentate) cyclometalated ruthenium (II) compounds. Inorg. Chem. 56 (21), 13579–13592.

Mukherjee, S., Bowman, D.N., Jakubikova, E., 2015. Cyclometalated Fe (II) complexes as sensitizers in dye-sensitized solar cells. Inorg. Chem. 54 (2), 560–569.

Mukherjee, S., Torres, D.E., Jakubikova, E., 2017. HOMO inversion as a strategy for improving the light-absorption properties of Fe (II) chromophores. Chem. Sci. 8 (12), 8115–8126.

Mukuta, T., Tanaka, S.I., Inagaki, A., Koshihara, S.Y., Onda, K., 2016. Direct observation of the triplet metal-centered state in [Ru (bpy) 3]$^{2+}$ using time-resolved infrared spectroscopy. Chem. Select 1 (11), 2802–2807.

Myrick, M., Blakley, R., DeArmond, M., 1987. Time-resolved photoselection of [Ru (bpy) 3]$^{2+}$-exciton hopping in the excited state. J. Am. Chem. Soc. 109 (9), 2841–2842.

Nakagawa, A., Sakuda, E., Ito, A., Kitamura, N., 2015. Remarkably intense emission from ruthenium (II) complexes with multiple borane centers. Inorg. Chem. 54 (21), 10287–10295.

Nakagawa, A., Ito, A., Sakuda, E., Fujii, S., Kitamura, N., 2017. Bright and long-lived emission from a starburst-type arylborane-appended polypyridyl ruthenium(II) complex. Eur. J. Inorg. Chem. 2017 (32), 3794–3798.

Omar, S.A., Scattergood, P.A., McKenzie, L.K., Jones, C., Patmore, N.J., Meijer, A.J., et al., 2018. Photophysical and cellular imaging studies of brightly luminescent osmium (II) pyridyl-triazole complexes. Inorg. Chem. 7 (21), 13201–13212.

O'regan, B., Grätzel, M., 1991. A low-cost, high-efficiency solar cell based on dye-sensitized colloidal TiO_2 films. Nature 353 (6346), 737–740.

Pashaei, B., Shahroosvand, H., Graetzel, M., Nazeeruddin, M.K., 2016. Influence of ancillary ligands in dye-sensitized solar cells. Chem. Rev. 116 (16), 9485–9564.

Patel, M., Varnum, S., Gandla, D., Zdilla, M., Martoff, C., 2014. Stable tetramethyl-1, 10-phenanthroline osmium (III) complex in neutral pH as a photoluminescence-following electron-transfer reagent for the detection of acetaminophen in urine and pharmaceutical formulations. Anal. Meth. 6 (15), 5818–5829.

Patel, J., Majee, K., Ahmad, E., Das, B., Padhi, S.K., 2017. Effect of pyridyl substitution on chemical and photochemical water oxidation by [Ru (terpyridine)(bipyridine)(OH2)]$^{2+}$ scaffolds. Eur. J. Inorg. Chem. 2017 (1), 160–171.

Patra, G.K., Ghorai, A., Manna, A.K., 2019. Ru (II)-polypyridyl complexes as potential sensing agents for cations and anions. Recent Adv. Anal. Tech. 3, 263–291.

Plaetzer, K., Krammer, B., Berlanda, J., Berr, F., Kiesslich, T., 2009. Photophysics and photochemistry of photodynamic therapy: fundamental aspects. Lasers Med. Sci. 24 (2), 259–268.

Qiao, L., Liu, J., Han, Y., Wei, F., Liao, X., Zhang, C., et al., 2021. Rational design of a lysosome-targeting and near-infrared absorbing Ru (ii)–BODIPY conjugate for photodynamic therapy. Chem. Comm. 57 (14), 1790–1793.

Rajkumar, M., Bhuvaneswari, J., Velayudham, M., Rajkumar, E., Rajagopal, S., 2011. Photoluminescence electron-transfer quenching of rhenium (I) complexes with organic sulfides. J. Fluores. 21 (4), 1729−1737.

Rajkumar, E., Mareeswaran, P.M., Rajagopal, S., 2014a. Photophysical properties of amphiphilic ruthenium (II) complexes in micelles. Photochem. Photobiol. Sci. 13 (9), 1261−1269.

Rajkumar, E., Kalayar, S., Paulpandian, M.M., Seenivasan, R., 2014b. Photoinduced electron transfer reactions of ruthenium (II)-Complexes containing Amino acid with quinones. J. Fluoresc. 24 (3), 875−884.

Ramachandran, M., Anandan, S., 2020. Triazole appending ruthenium (ii) polypyridine complex for selective sensing of phosphate anions through C−H−anion interaction and copper (ii) ions via cancer cells. New J. Chem. 44 (16), 6186−6196.

Ramakrishna, G., Ghosh, H.N., Singh, A.K., Palit, D.K., Mittal, J.P., 2001. Dynamics of back-electron transfer processes of strongly coupled triphenyl methane dyes adsorbed on TiO_2 nanoparticle surface as studied by fast and ultrafast visible spectroscopy. J. Phys. Chem. B 105 (51), 12786−12796.

Rao, H., Bonin, J., Robert, M., 2018. Toward visible-light photochemical CO_2-to-CH_4 conversion in aqueous solutions using sensitized molecular catalysis. J. Phys. Chem. C 122 (25), 13834−13839.

Roque III, J.A., Barrett, P.C., Cole, H.D., Lifshits, L.M., Bradner, E., Shi, G., 2020. Os (II) Oligothienyl complexes as a hypoxia-active photosensitizer class for photodynamic therapy. Inorg. Chem. 59 (22), 16341−16360.

Roundhill, D.M. (Ed.), 2013. Photochemistry and Photophysics of Metal Complexes. Springer science & business media, London.

Rousset, E., Ciofini, I., Marvaud, V., Hanan, G.S., 2017. Facile one-pot synthesis of ruthenium (II) quaterpyridine-based photosensitizers for photocatalyzed hydrogen production. Inorg. Chem. 56 (16), 9515−9524.

Sahoo, S., Raghavan, A., Kumar, A., Nandi, D., Chakravarty, A.R., 2021. Biotin-appended iron (III) complexes of curcumin for targeted photo-chemotherapy. Eur. J. Inorg. Chem. 2021 (17), 1640−1650.

Sakuda, E., Ando, Y., Ito, A., Kitamura, N., 2011. Long-lived and temperature-independent emission from a novel ruthenium (II) complex having an arylborane charge-transfer unit. Inorg. Chem. 50 (5), 1603−1613.

Sakuda, E., Matsumoto, C., Ando, Y., Ito, A., Mochida, K., Nakagawa, A., Kitamura, N., 2015. Dual emissions from ruthenium (II) complexes having 4-Arylethynyl-1, 10-phenanthroline at low temperature. Inorg. Chem. 54 (7), 3245−3252.

Sangiliapillai, R., Arumugam, R., Eswaran, R., Seenivasan, R., 2016. Micellar effect on the photophysics of heteroleptic ruthenium (II)−phenanthrolinedisulfonato complexes. Luminescence 31 (1), 30−37.

Schlotthauer, T., Parada, G.A., Gorls, H., Ott, S., Jager, M., Schubert, U.S., 2017. Asymmetric cyclometalated RuII polypyridyl-type complexes with π-extended carbanionic donor sets. Inorg. Chem. 56 (14), 7720−7730.

Schneider, K.R., Traber, P., Reichardt, C., Weiss, H., Kupfer, S., Gorls, H., et al., 2018. Unusually short-lived solvent-dependent excited state in a half-sandwich Ru (II) complex induced by low-lying 3MC states. J. Phys. Chem. A 122 (6), 1550−1559.

Seibert, D., Diel, T., Welter, J.B., De Souza, A.L., Modenes, A.N., Espinoza-Quinones, F.R., et al., 2017. Performance of photo-Fenton process mediated by Fe (III)-carboxylate complexes applied to degradation of landfill leachate. J. Environ. Chem. Eng. 5 (5), 4462−4470.

Shalan, H., Colbert, A., Nguyen, T.T., Kato, M., Cheruzel, L., 2017. Correlating the para-substituent effects on Ru (II)-polypyridine photophysical properties and on the corresponding hybrid P450 BM3 enzymes photocatalytic activity. Inorg. Chem. 56 (11), 6558−6564.

Shao, J., Yan, Z.-Y., Tang, M., Huang, C.-H., Sheng, Z.-G., Chen, J., et al., 2021. Potent oxidation of DNA by Ru (II) tri (polypyridyl) complexes under visible light irradiation via a singlet oxygen-mediated mechanism. Inorg. Chem. Front. 8, 3421−3432.

Shaw, G.B., Styers-Barnett, D.J., Gannon, E.Z., Granger, J.C., Papanikolas, J.M., 2004. Interligand electron transfer dynamics in [Os (bpy) 3]$^{2+}$: exploring the excited state potential surfaces with femtosecond spectroscopy. J. Phys. Chem. A 108 (23), 4998−5006.

Shen, J., Rees, T.W., Ji, L., Chao, H., 2021. Recent advances in ruthenium (II) and iridium (III) complexes containing nanosystems for cancer treatment and bioimaging. Coord. Chem. Rev. 443. https://doi.org/10.1016/j.ccr.2021.214016.

Shepard, S.G., Fatur, S.M., Rappé, A.K., Damrauer, N.H., 2016. Highly strained iron (II) polypyridines: exploiting the quintet manifold to extend the lifetime of MLCT excited states. J. Am. Chem. Soc. 138 (9), 2949−2952.

Shum, J., Leung, P.K.K., Lo, K.K.W., 2019. Luminescent ruthenium (ii) polypyridine complexes for a wide variety of biomolecular and cellular applications. Inorg. Chem. 58 (4), 2231−2247.

Smitten, K.L., Scattergood, P.A., Kiker, C., Thomas, J.A., Elliott, P.I., 2020. Triazole-based osmium (ii) complexes displaying red/near-IR luminescence: antimicrobial activity and super-resolution imaging. Chem. Sci. 11 (33), 8928−8935.

Soupart, A., Alary, F., Heully, J.-L., Elliott, P.I., Dixon, I.M., 2020. Theoretical study of the full photosolvolysis mechanism of [Ru (bpy) 3]$^{2+}$: providing a general mechanistic roadmap for the photochemistry of [Ru (N^ N) 3]$^{2+}$-Type complexes toward both cis and trans photoproducts. Inorg. Chem. 59 (20), 14679−14695.

Sun, Q., Mosquera-Vazquez, S., Lawson Daku, L.V.M., Guénée, L., Goodwin, H.A., Vauthey, E., et al., 2013. Experimental evidence of ultrafast quenching of the 3MLCT luminescence in ruthenium (II) tris-bipyridyl complexes via a 3dd state. J. Am. Chem. Soc. 135 (37), 13660−13663.

Swarnalatha, K., Rajkumar, E., Rajagopal, S., Ramaraj, R., Banu, I.S., Ramamurthy, P., 2011. Proton coupled electron transfer reaction of phenols with excited state ruthenium (II)−polypyridyl complexes. J. Phys. Org. Chem. 24 (1), 14−21.

Tabrizi, L., 2018. Novel cyclometalated Fe (II) complex with NCN pincer and BODIPY-appended 4'-ethynyl-2, 2′: 6′, 2″-terpyridine as mitochondria-targeted photodynamic anticancer agents. Appl. Organomet. Chem. 32 (3). https://doi.org/10.1002/aoc.4161.

Tang, Z., Chang, X.-Y., Wan, Q., Wang, J., Ma, C., Law, K.-C., 2020. Bis (tridentate) iron (II) complexes with a cyclometalating unit: photophysical property enhancement with combinatorial strong ligand field effect. Organometallics 39 (15), 2791−2802.

Veikko, U., Zhang, X., Peng, T., Cai, P., Cheng, G., 2013. The synthesis and characterization of dinuclear ruthenium sensitizers and their applications in photocatalytic hydrogen production. Spectrochim. Acta Mol. Biomol. Spectrosc. 105, 539−544.

Verma, S., Kar, P., Das, A., Palit, D.K., Ghosh, H.N., 2008. Interfacial electron-transfer dynamics on TiO_2 and ZrO_2 nanoparticle surface sensitized by new catechol derivatives of Os (II)-polypyridyl complexes: monitoring by charge-transfer emission. J. Phys. Chem. C 112 (8), 2918−2926.

Vilar, V.J., Nogueira, A.A., Souza, B.M., Dezotti, M.W., Boaventura, R.A., 2017. Ferrioxalate complexes as strategy to drive a photo-FENTON reaction at mild pH conditions: a case study on levofloxacin oxidation. J. Photochem. Photobiol., A: Chem 345, 109−123.

Vogler, A., 2016. Photochemistry of Os (bipy) 2 (CO3). Photoreduction of carbonate to formaldehyde. Inorg. Chem. Comm. 70, 175–176.

Vögtle, F., Plevoets, M., Nieger, M., Azzellini, G.C., Credi, A., De Cola, L., et al., 1999. Dendrimers with a photoactive and redox-active [Ru (bpy) 3]$^{2+}$-type core: photophysical properties, electrochemical behavior, and excited-state electron-transfer reactions. J. Am. Chem. Soc. 121 (26), 6290–6298.

Vonlanthen, M., Cevallos-Vallejo, A., Aguilar-Ortíz, E., Ruiu, A., Porcu, P., Rivera, E., 2016. Synthesis, characterization and photophysical studies of novel pyrene labeled ruthenium (II) trisbipyridine complex cored dendrimers. Polymer 99, 13–20.

Wallin, S., Davidsson, J., Modin, J., Hammarström, L., 2005. Femtosecond transient absorption anisotropy study on [Ru (bpy) 3]$^{2+}$ and [Ru (bpy)(py) 4]$^{2+}$. Ultrafast interligand randomization of the MLCT state. J. Phys. Chem. A 109 (21), 4697–4704.

Wang, Y., Gao, X.-W., Li, J., Chao, D., 2020. Merging an organic TADF photosensitizer and a simple terpyridine–Fe (III) complex for photocatalytic CO_2 reduction. Chem. Commun. 56 (81), 12170–12173.

Wehlin, S.A., Troian-Gautier, L., Maurer, A.B., Brennaman, M.K., Meyer, G.J., 2020. Photophysical characterization of new osmium (II) photocatalysts for hydrohalic acid splitting. J. Chem. Phys. 153 (5). https://doi.org/10.1063/5.0014269.

Wenger, O.S., 2019. Is iron the new ruthenium? Chem. Eur J. 25 (24), 6043–6052.

Xue, L.-X., Meng, T.-T., Yang, W., Wang, K.-Z., 2015. Recent advances in ruthenium complex-based light-driven water oxidation catalysts. J. Photochem. Photobiol. B Biol. 152, 95–105.

Yang, L., Xiang, Y., Jia, F., Xia, L., Gao, C., Wu, X., et al., 2021. Photo-thermal synergy for boosting photo-Fenton activity with rGO-$ZnFe_2O_4$: novel photo-activation process and mechanism toward environment remediation. Appl. Catal., B 292. https://doi.org/10.1016/j.apcatb.2021.120198.

Yersin, H., Huber, P., Braun, D., 1990. Highly resolved emission of tris (2, 2'-bipyridine-d8) osmium (2+). J. Phys. Chem. 94 (9), 3560–3564.

Yoshitomi, F., Sekizawa, K., Maeda, K., Ishitani, O., 2015. Selective formic acid production via CO_2 reduction with visible light using a hybrid of a perovskite tantalum oxynitride and a binuclear ruthenium (II) complex. ACS Appl. Mater. Interface. 7 (23), 13092–13097.

Zammit, E.M., Barbante, G.J., Carlson, B., Doeven, E.H., Barnett, N.W., Hogan, C.F., et al., 2012. Chemiluminescence from osmium (II) complexes with phenanthroline, diphosphine and diarsine ligands. Analyst 137 (12), 2766–2769.

Zhang, P., Huang, H., 2018. Future potential of osmium complexes as anticancer drug candidates, photosensitizers and organelle-targeted probes. Dalton Trans. 47 (42), 14841–14854.

Zhang, Y., Zhou, M., 2019. A critical review of the application of chelating agents to enable fenton and fenton-like reactions at high pH values. J. Hazard Mater. 362, 436–450.

Zhang, P., Wang, Y., Qiu, K., Zhao, Z., Hu, R., He, C., et al., 2017. A NIR phosphorescent osmium (II) complex as a lysosome tracking reagent and photodynamic therapeutic agent. Chem. Commun. 53 (91), 12341–12344.

Zhang, J., Song, H., Liu, Y., Wang, L., Li, D., Liu, C., 2019. Remarkable enhancement of a photochemical fenton-like system (UV-A/Fe (II)/PMS) at near-neutral pH and low Fe (II)/peroxymonosulfate ratio by three alpha hydroxy acids: mechanisms and influencing factors. Sep. Purif. Technol. 224, 142–151.

Zhang, X.Z., Cheng, C.C., Chih, Y.R., Lin, Y.-T., Chen, H.-Y., Chen, Y.J., et al., 2019. Low-temperature spectra and density functional theory modeling of Ru (II)-Bipyridine complexes with cyclometalated ancillary ligands: the excited state spin–orbit coupling origin of variations in emission efficiencies. J. Phys. Chem. A 123 (44), 9431–9449.

Zhang, X., Hou, Y., Xiao, X., Chen, X., Hu, M., Geng, X., 2020. Recent development of the transition metal complexes showing strong absorption of visible light and long-lived triplet excited state: from molecular structure design to photophysical properties and applications. Coordin. Chem. Rev. 417. https://doi.org/10.1016/j.ccr.2020.213371.

Zigler, D.F., Morseth, Z.A., Wang, L., Ashford, D.L., Brennaman, M.K., Grumstrup, E.M., et al., 2016. Disentangling the physical processes responsible for the kinetic complexity in interfacial electron transfer of excited Ru (II) polypyridyl dyes on TiO_2. J. Am. Chem. Soc. 138 (13), 4426−4438.

Zimmer, P., Müller, P., Burkhardt, L., Schepper, R., Neuba, A., Steube, J., et al., 2017. N-Heterocyclic carbene complexes of iron as photosensitizers for light-induced water reduction. Eur. J. Inorg. Chem. 2017 (11), 1504−1509.

Zimmer, P., Burkhardt, L., Friedrich, A., Steube, J., Neuba, A., Schepper, R., et al., 2018. The connection between NHC ligand count and photophysical properties in Fe (II) photosensitizers: an experimental study. Inorg. Chem. 57 (1), 360−373.

This page intentionally left blank

Chapter 8

Complexes of cobalt, rhodium and iridium

Simran Sharma, Priya Sahni, Rahat Gupta, Anindya Roy and Amlan K. Pal

Department of Chemistry, Indian Institute of Technology Jammu, Jammu and Kashmir, India

8.1 Introduction

Group 9 of the periodic table constitutes transition elements cobalt ($^{58}Co_{27}$), rhodium ($^{103}Rh_{45}$) and iridium ($^{192}Ir_{77}$) exhibiting the most common oxidation states of +2 and +3 and having nine valence electrons with a general electronic configuration of $(n-1)d^74s^2$. The elements of this group are hard, shiny and silvery-white in appearance. In the earth's crust cobalt accounts for 25 ppm only and is the least abundant metal in the first row of the transition elements, whereas the abundance of rhodium and iridium are even daunting with a value of 0.0001−0.001 ppm only (Lide, 2004). In the early decades, only a handful number of reports were available for the photochemistry of these elements but recently the literature has seen tremendous growth in the research area of the photochemistry and photophysics of group 9 complexes, in particular complexes of 3d transition-metals (Hefffern et al., 2013). In general, group 9 elements find a diverse set of applications, e.g., cobalt shows a wide range of applications in lithium-ion batteries, alloys, catalysts, etc (Yang et al., 2013). Vitamin B_{12} is the only organometallic complex in nature comprising Co(II) (Schrauzer, 1968). Rhodium shows applications in ornamental decorations, electronics, as nuclear fuels and also in the glass industry. Rhodium is also used as a catalyst, one of the common examples is Wilkinson's catalyst $[Rh(Cl)(PPh_3)_3]$, used for the hydrogenation of the unsaturated olefins (Perea-Buceta et al., 2015). Iridium displays its applications in different sectors of industrial and medicinal chemistries (Ho et al., 2020). Iridium is also used as a catalyst, the well-known example is Vaska's complex (Matheau-Raven et al., 2020). Another example is the Cativa process, which involves the use of an iridium complex for the carbonylation of methanol (Sunley and Watson, 2000). In this chapter, published works on the synthesis, photochemistry and photophysics of group 9 (Co, Rh, Ir) complexes that appeared

Photochemistry and Photophysics of Coordination Compounds. https://doi.org/10.1016/B978-0-12-824493-7.00004-6
Copyright © 2023 Elsevier Inc. All rights reserved.

over the past few decades have been reviewed. Applications in the fields of photoredox catalysis, metal-sensing, solid-state lighting devices (OLEDs and LECs) of group 9 complexes have also been discussed. The discussions of the photophysical properties of the group 9 complexes will be considered by tuning the these properties of the complexes behaving as phosphorescence emitters. In this respect, some commonly used ligands in the synthesis of group 9 complexes are shown in Fig. 8.1.

The splitting of d-orbitals in the Co, Rh and Ir metal ions in an octahedral ligand field is shown in Fig. 8.2A. The complexes show different natures of the origin of luminescence, e.g., ^{3}MLCT, ^{3}LMCT, ^{3}ILCT and ^{3}LC. In general, MLCT is the metal-to-ligand charge transfer transition that takes place from the molecular orbital (M O). Of the metal to the ligand orbital whereas LMCT is the ligand-to-metalcharge transfer, i.e., transfer of electrons from the M O of ligand to the metal (Verhoeven, 1996). MC and LC states are originated from the metal-centered d $\rightarrow$ d transitions and $\pi \rightarrow \pi^*$ and/or n $\rightarrow \pi^*$ ligand centered transitions, respectively. LLCT corresponds to the transfer of an electron from one ligand to other within the complex (Fig. 8.2B and C). The origin of transition depends on the spatial distributions of the outershell orbitals of the group 9 elements. The 3d(Co), 4d(Rh) and 5d(Ir) orbitals have different spatial extensions; the effect of destabilization and splitting is minimum for the 3d orbital in an octahedral ligand field. The amount of ligand field splitting (Δ_{oct}) depends on the field strength exerted by the ligands, as arranged in the spectrochemical series (Ryutaro, 1938). In an octahedral field, Δ_{oct} is small for Co(II), because of which the lowest-excited state for Co(II)-polypyridyl complexes mostly show non-emissive nature but in association with specially designed ligands, these complexes show ^{3}LMCT, ^{3}MLCT and ^{3}ILCT nature too. In Rh(II)-polypyridyl complexes, as the Rh(II) 4d orbitals display intermediate values of Δ_{oct} of Co(II) and Ir(II), the MC levels show some contribution in the deactivation of the MLCT levels, which are normally emissive at 2.10−2.88 eV. On the another hand, for Ir(III)-polypyridyl complexes, the values of Δ_{oct} are very large due to which ^{3}MC levels are high in energy that they do not usually affect the emissive ^{3}LC and ^{3}MLCT states (2.10−3.00 eV) (Balzani and Campagna, 2007).

8.2 Luminescent Co(II/III) complexes

8.2.1 Photophysical properties of polyhetrocyclic and polypyridyl Co(II/III) complexes

The first luminescent Co(III) complex, $K_3[Co(CN)_6]$, **(1)**, was reported by Porter and Mingardi (1966). A broad and structureless emission band centered at 704 nm was observed for $K_3[Co(CN)_6]$ with a fullwidth at halfmaximum (FWHM) of $\sim$2000 cm^{-1}. This band was assigned as $^3T_{1g} \rightarrow {}^1A_{1g}$(Oh) phosphorescence based on band position and lifetime ($\tau_{PL} = 10^{-3}$ s). Later,

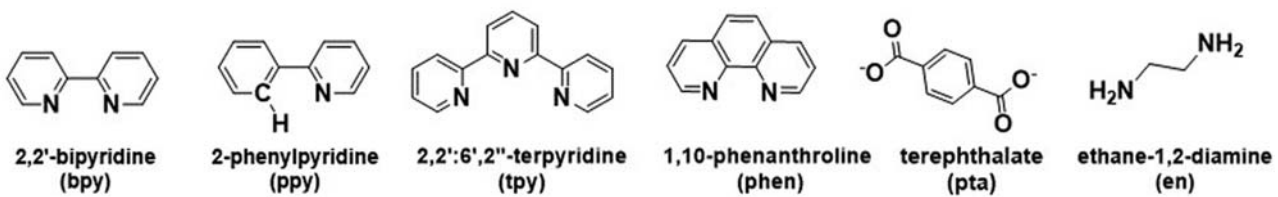

FIG. 8.1 Benchmark ligands used in the synthesis of the complexes of group 9 elements.

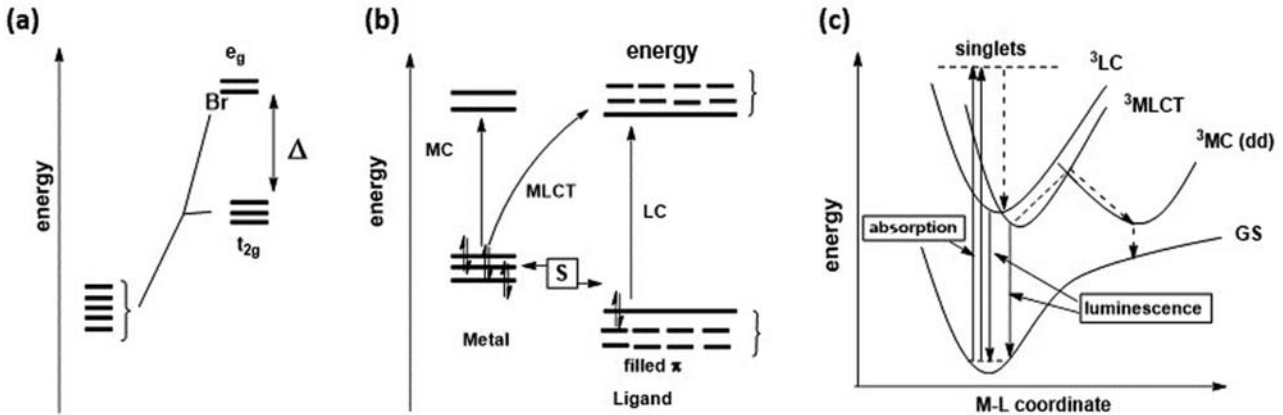

FIG. 8.2 (A) d-orbitals splitting in an octahedral field; (B) the orbital description of MC, MLCT and LC transitions; (S = EWG, resulting in stabilization or destabilization) and (C) electronic transitions involving MC, MLCT and LC excited states (MC states are not emissive).

Zuloaga and Kasha (1968) reported another example of luminescent Co(III) complex, *trans*-$Na_5[Co(CN)_4(SO_3)_2]$, **(2)**. This complex exhibited a broad and structureless luminescence spectrum centered at 699 -nm at 77 K and the luminescence was assigned as $^3T_{1g} \rightarrow {}^1A_{1g}$(Oh) phosphorescence. Yusuke (1979) also reported some examples of luminescent Co(III) complexes, namely, *cis*-$K_3Na_2[Co(CN)_4(SO_3)_2]$, **(3)**, $M_3[Co(CN)_6]$, **(4)**, (M = K **(4A)**, Rb **(4B)**, Cs **(4C)**) and *trans*-$Na_5[Co(CN)_4(SO_3)_2]$, **(2)**. Luminescence spectrum of *cis*-$K_3Na_2[Co(CN)_4(SO_3)_2]$, **(3)**, at 20 K, exhibited a broad and structureless band at 757 nm and a FWHM of 2000 cm^{-1} when excited at 365 nm. Luminescence spectra of $M_3[Co(CN)_6]$, **(4)**, (M = K, Rb, Cs) excited at 313 nm measured on a single crystal at 20 and 77 K, exhibited a peak position of 704−709 nm. The FWHM was found to be about 2600 cm^{-1} for $K_3[Co(CN)]_6$. Luminescence spectrum of *trans*-$Na_5[Co(CN)_4(SO_3)_2]$, **(2)**, excited at 365 nm exhibited a broad and structureless band at 704 nm with FWHM about 2300 cm^{-1}, which was found to be close to the observation of Zuloaga and Kasha (1968). Muto et al. (1979) synthesized a novel Co(II) complex, $Co(koj)_2 \cdot H_2O$, **(5)**, (Hkoj = kojic acid, 5-hydroxy-2-(hydroxymethyl)-4*H*-pyran-4-one) by adding the $Co(OH)_3$ to a kojic acid suspension, in which the kojate ions were found to be coordinated to the metal as bidentate ligands. It exhibited a green luminescence at 500 nm in aqueous, acidic solutions and even in the solid-state upon excitation at 365 nm.

Zhang et al. (2002) reported two Co(III)-polypyridyl complexes, $[Co(phen)_2HPIP]^{3+}$, **(6)**, (HPIP = 2-(2-hydroxyphenyl)imidazo[4,5-f][1,10] phenanthroline, phen = 1,10-phenanthroline) and $[Co(phen)_2HNAIP]^{3+}$, **(7)**, (HNAIP = 2-(2-hydroxy-l-naphthyl)imidazo[4,5-f][1,10]phenanthroline) to study the effect of intramolecular hydrogen bond on the DNA-binding and photocleavage properties of polypyridyl Co(III) complexes. The complexes were synthesized by refluxing *cis*-$[Co(phen)_2Cl_2]Cl \cdot 3H_2O$ and HPIP or HNAIP in EtOH in good yields of 72%−78%. The luminescence nature of these complexes **(6)** and **(7)** was used in the detection of CT DNA, where both the complexes exhibited enhancement in luminescence intensity ~350 nm in aqueous buffer (20 μM [Co], 5 mM Tris, 50 mM NaCl, pH 7.2, λ_{irr} = 300 nm) at 298 K. The effect was found to be more pronounced for complex **(6)** as this intercalated into the hydrophobic environment of the DNA helix and thus, the collision and energy dissipation with the environmental water and oxygen was found to be lower. Thus, complex **(6)** displayed stronger binding affinity whereas **(7)** exhibited partial intercalation.

A three-dimensional polymeric cobalt compound $[Co(DCNT)(H_2O)]_n$, **(8)**, (H_2DCNT = 2,4-bis(4-carboxyphenylamino)-6-diethylamino-1,3,5-triazine) was synthesized by Wei and Wu (2007) by the hydrothermal reactions of $Co(NO_3)_2 \cdot 6H_2O$ and H_2DCNT. In the polymer, each $[DCNT]^{2-}$ possessed three coordination sites, one nitrogen atom in the triazine ring coordinating to Co(II) and two carboxylates adopting μ_2-bridging mode, which made the infinite Co(II) chains array uniform and even towards the crystallographic

c-axis. The emission spectrum exhibited a maximum peak at 410 nm and a shoulder peak at 374 nm. The peak at 374 and 410 nm was assigned to ^{3}ILCT (triplet intraligand charge transfer) and ^{3}LMCT (triplet ligand-to-metal charge transfer), respectively. The ^{3}ILCT resembled the ligand-centered transitions observed in the ligand H_2DCNT and the triazine ring, one nitrogen atom coordinated to Co(II), which favored the ^{3}LMCT from the diethylamino donor group along the aromatic triazine ring to Co(II).

Anbalagan and Ganeshraja (2013) explored the luminescent complexes as *cis*-$[Co^{III}(en)_2(RNH_2)Cl]Cl_2$, **(9)**, with R = Hex^n **(9A)**, Pen^n **(9B)**, Bui **(9C)**, Bu^n **(9D)**, Pr^n **(9E)**, Et **(9F)**, Me **(9G)** and Bz^n **(9H)** complexes exhibiting ferromagnetism. The complexes displayed emission, $\lambda_{em} \sim 411$ nm upon excitation at 360 nm, with associated excited-state lifetime (τ_{PL}) values of $\tau_1 = 3.9-3.1$, $\tau_2 = 12.3-9.5$, $\tau_3 = 0.7-0.9$ ns in fluid solutions (water and mixture of water:^{i}PrOH (70:30, w/w)) and the emission was attributed to the ^{3}LMCT transition. Despite different geometries and ligand environments, the excitation spectra of these complexes closely resembled the peak profiles. The d → d absorption features of these complexes at 362−366 nm were assigned to spin-allowed $^1A_1 \rightarrow {}^1T_{2g}$ transition, mixed with some extent of ^{3}LMCT [π^*(N) → dπ(Co)]. Thus, it was suggested that the emissions were an admixture of ^{3}LMCT + ^{3}LC transitions. The emission intensities of the complexes followed the order:

(9A) > **(9B)** > **(9C)** > **(9D)** > **(9E)** > **(9F)** > **(9G)** due to the higher electron donation of the hexyl group compared to that of the methyl group. The multi-exponential decay was explained on the basis of (i) different electronic coupling strengths existing in the complexes due to the varied electron donations of the coordinating ligands and (ii) fast and slow components due to the thermally equilibrated emitting states. The enhancement of lifetime from **(9A)** ($\tau_2 = 9.5$ ns) to **(9G)** ($\tau_2 = 12.3$ ns) may be attributed to (i) accumulation of higher negative charge in complex **(9A)** compared to that in **(9G)**, leading to destabilization of the emitting (d → d) + LMCT state, (ii) lower HOMO-LUMO gap in **(9A)** compared to that in **(9G)** due to the e^- delocalization in the long C_6 alkyl chain and (iii) pronounced radiationless decay in **(9A)** due to the vibrational coupling of the long C_6 alkyl chain (Xue et al., 2010). On the other hand, hydrophobicity, the rigidity of the coordination environment and the hydrogen bond donor/acceptor abilities of the solvent molecules may also alter the emissive behavior.

Two novel Co(III) complexes $[Co(phen)_2(bbenzimH_2)](ClO_4)_3$, **(10)** and $[Co(bpy)_2(bbenzimH_2)](ClO_4)_3$, **(11)**, (bbenzim$H_2$ = bibenzimidazole and bpy = 2,2′-bipyridine) were synthesized (Indumathy et al., 2014). The complexes **(10)** and **(11)** were synthesized by refluxing the precursor complex $[Co(phen)_2Cl_2]Cl$ or $[Co(bpy)_2Cl_2]Cl$ and $[Ag(bbenzimH_2)]NO_3$ in methanol with good yields of ∼ 87%. Complex **(11)** exhibited an emission band at 402 nm, upon excitation at 280 nm. Anion sensing studies of the complex **(11)** with different biologically important anions like F^-, Br^-, I^-, ClO_4^-, OH^-,

OAc^- were carried out using various methods such as fluorescence spectroscopy. The addition of Br^- and ClO_4^- anions caused a slight decrease in the intensity of the emission spectra of the complex **(11)**. The emission intensity of complex **(11)** was completely quenched on the addition of tetrabutylammonium (TBA) salts of F^-, I^-, OH^- and OAc^-. The complete quenching for F^-, OH^- and OAc^- was due to the hydrogen bonding ability and high basicity of these anions, whereas for I^-, which lacks in both these properties, the quenching of fluorescence was tentatively assigned to the heavy atom effect *via* formation of a charge-transfer complex (Watkins, 1974). Similar effects were reported for TBAI salt and metal iodides in carbazole-based conjugated co-polymers and benzimidazole-based tripodal receptors (Vetrichelvan et al., 2006; Lee et al., 2011).

Li et al. (2015) investigated three coordination polymers of cobalt, e.g.,$\{[Co(4pmntd)_2(CF_3SO_3)(H_2O)]\cdot(CF_3SO_3)\cdot(C_2H_5OH)\cdot 0.5(CHCl_3)\cdot H_2O\}_n$, **(12)**, $\{[Co(4\text{-}pmntd)(H_2O)_4]\cdot(NO_3)_2\cdot H_2O\}_n$, **(13)** and $\{[Co(4pmntd)(pta)(CH_3OH)_2]\cdot 2(CHCl_3)\}_n$, **(14)**, (4-pmntd = *N,N′*-bis(4-pyridylmethyl)-naphthalene diimide; pta = terephthalate). The polymers were synthesized by the reactions of 4-pmntd with $Co(CF_3SO_3)_2\cdot 4H_2O$, $Co(NO_3)_2\cdot 6H_2O$ and Co(pta) to yield **(12)**, **(13)** and **(14)**, respectively, in poor yields of 11%−25%. The emission spectra of complexes **(12−14)**, $\lambda_{em} = 420$ nm upon excitation at 320 nm resembled that of the free 4-pmntd ligand, excluding peak positions and the emission intensity. The emission intensity of complex **(13)** increased gradually upon the addition of two equivalents of acetate into the DMF solution of complex **(13)**, whereas, anions like F^-, Cl^-, Br^-, I^-, N^{3-}, SCN^- and Ox^{2-} (Ox^{2-} = oxalate^{2-}) led to a decrease in the emission intensity. The variation was speculated to occur due to the coordinating nature of the OAc^- anions to the Co(II) ion in **(13)**. This coordination was further supported by M06L/DZP level calculations as well as polarizable continuum models in DMF solution that indicated the easy dissociation of the monodentate pyridine substituted ligands.

A novel dicubane Co(III)/Co(II) complex for applications in optoelectronics, namely $[Co^{II}_2Co^{III}_2(HPN)_4(H_2O)_2(CH_3COO)_2]\cdot 4H_2O$, **(15)**, ($H_2HPN$ = [1-(3-hydroxypropyliminomethyl)naphthalene-2-ol) was synthesized by Coban et al. (2018). Complex **(15)** was synthesized by mixing the hot alcoholic solutions of $Co(CH_3COO)_2\cdot 4H_2O$ and the ligand in a good yield of 75%. The complex was characterized by elemental analysis, FT-IR, solid-state UV-vis absorption spectroscopy and single-crystal X-ray diffraction (XRD). The XRD studies showed a cationic tetrameric arrangement consisting of a defected dicubane core with two missing vertexes. Each cobalt ion has a distorted octahedral geometry with six-coordinations. At room temperature (RT), the free ligand H_2HPN displayed a strong blue emission band at $\lambda_{em} = 482$ nm ($\lambda_{exc} = 349$ nm) which was tentatively assigned to the $n \rightarrow \pi$ or $\pi \rightarrow \pi^*$ electronic transitions (^{3}ILCT), while complex **(15)** exhibited two emission bands at $\lambda_{em} = 469$

and 682 nm, respectively ($\lambda_{exc} = 349$ nm) (Kocak et al., 2017; Oylumluoglu et al., 2017). The enhancement of luminescence in complex **(15)** was tentatively attributed to the chelation of the ligand to the metal center, which enhanced the "rigidity" of the ligand and reduced the energy loss *via* a radiationless pathway (Oylumluoglu et al., 2017; Feng et al., 2015). The emissions of the complex were tentatively assigned to the $n \rightarrow \pi$ or $\pi \rightarrow \pi^*$ type intraligand fluorescence as similar emission was also observed for the free ligand H_2HPN.

Two emissive Co(II) complexes **(16)** and **(17)** with redox-active anthraquinone-type ligand, 2-(2-pyridyl)-1*H*-anthra[1,2-*d*]imidazole-6,11-dione (abbreviated as PyAnIm) were also reported (Shiga et al., 2018). The ligand PyAnIm adopted tridentate and bidentate chelating modes to give rise to the complexes $[Co^{II}(PyAnIm)_2].n(solv.)$, **(16)** and $[Co^{III}(PyAnIm)_3]$, **(17)**, respectively. Trimethylamine and PyAnIm in acetonitrile were added in the solution of $Co(BF_4)_2 \cdot 6H_2O$ to synthesize **(16)** and **(17)**. The stirring was done for 5 min and L-ascorbic acid in methanol was added to it. The resulting solution was filtered and allowed to stand, yielding dark brown blocks of **(16)** in a poor yield of 14%. If **(16)** was left to stand for several days, it resulted in yielding red crystals of **(17)** in a very poor yield of 0.02%. The ligand PyAnIm exhibited a ^{1}ILCT absorption at 395 nm and a broad ^{3}ILCT fluorescence at 519 nm with a quantum yield of 0.95%. Complex **(16)** exhibited a weaker emission at ~ 510 nm while **(17)** displayed a stronger emission at ~ 560 nm. The weak emission of **(16)** was tentatively due to the paramagnetic quenching of the unpaired e^- from the Co(II) center and the effect of dissociation equilibrium of the complex. On the contrary, the bathochromic shift of the emission band of **(17)** relative to that of **(16)** was caused by the decrease in LUMO energy, which was affected by the charge and acidity of the coordinated metal ion.

Özbek et al. (2019) synthesized a Co(II) complex, $[Co^{II}(3\text{-fba})_2(na)_2(H_2O)_2]$, **(18)**, (where 3-fba = 3-fluorobenzoate and na = pyridine-3-carboxamide or nicotinamide) with a yield of 67% by mixing a solution of sodium 3-fluorobenzoate in water to a mixture containing $CoSO_4 \cdot 7H_2O$ and pyridine-3-carboxamide in water. Complex **(18)** was characterized by the single-crystal XRD studies that revealed the distorted octahedral geometry of the metal ion with an N_2O_4 bonding set of atoms around the metal center. The Co-O and Co-N bond lengths lie in the range of 2.07−2.17 Å and the bond angles around the Co(II) cation lie in the range of 88 to 180 degrees. The UV-vis absorption spectrum of complex **(18)** in DMSO exhibited a sharp band at 365 nm and a shoulder at 501 nm, which were tentatively assigned to a mixture of $n \rightarrow \sigma^*$, $n \rightarrow \pi^*$ and $\pi \rightarrow \pi^*$ transitions and a singlet ligand-to-metal charge transfer (^{1}LMCT) transition, respectively. The HOMO-LUMO band gap – was found to be 3.50 eV. The fluorescence emission spectrum of complex **(18)** displayed a peak at 370 nm, albeit with a weak emission intensity and a shoulder at 465 nm in DMSO solution. The peaks were assigned

as ligand-centered emissions due to the difference in electron density in the ligands.

Sathiyakumar et al. (2020) explored two novel Co(II) complexes, [Co(2-PYMC)$(NO_3)(H_2O)_2]\cdot NO_3$, **(19)**, (where, 2-PYMC = methyl-2-(pyridine-2-yl-methylene)hydrazinecarboxylate) and [Co(2-PYEC)$(NO_3)(H_2O)_2]\cdot NO_3$, **(20)**, (2-PYEC = ethyl-2-(pyridine-2-yl-methylene)hydrazinecarboxylate) by using a solvent-free mechano-chemical method. Equimolar mixtures of $Co(NO_3)_2\cdot 6H_2O$ and 2-PYMC or 2-PYEC by mechanochemical mixing afforded the complexes **(19)** and **(20)** in good yields (73%−82%). These complexes were characterized by elemental analysis, single-crystal XRD, UV-vis, IR and photoluminescence measurements. In the UV-vis absorption spectroscopy, the cobalt complexes exhibited λ_{max} values at 540 and 535 nm for **(19)** and **(20)**, respectively, which were tentatively assigned to a $^4T_{1g}(F) \rightarrow {}^4T_{1g}(P)$ transition (Newkome et al., 1984). The broad shoulder at 350 nm was tentatively assigned to either a charge transfer or a d → d transition (Ivanovic-Burmazovic and Jelkovic, 2004). The emission spectra of the free ligands were recorded in the solid-state ($\lambda_{exc} = 300$ nm) at RT. The ligand, 2-PYMC exhibited two intense bands at 348 and 351 nm whereas, four peaks at 355, 401, 457 and 527 nm were observed for 2-PYEC. The complex **(19)** exhibited multiple emission peaks between 430 and 450 nm upon excitation at 280 nm, whereas **(20)** showed a broad emission with $\lambda_{em} = 428$ nm.

Recently, four mononuclear luminescent Co(II)-Schiff base complexes with substituted hydrazinoquinoline Schiff bases, Ar-2-(salicylidene hydrazino)quinoline, [Ar = 4-methyl **(21)**, Ar = 4,6-dimethyl **(22)**, Ar = 4-methyl-6-chloro **(23)**, Ar = 4-methyl-6-methoxy **(24)**] were reported by Priyadarshini and Selvi (2021). The ligands were synthesized by simple condensation of hydrazones with salicylaldehyde in a 1:1 M ratio. An equimolar mixture of the ligands to an ethanolic solution of $CoCl_2\cdot 6H_2O$ afforded the complexes **(21−24)** with 50%−80% yield. The complexes were characterized by various analytical techniques, e.g., UV-vis, IR, NMR and TGA. The Co(II) ion was found to occupy a distorted octahedral geometry with the ligands coordinating through NˆNˆO tridentate fashion. In the emission study complexes **(21−24)** exhibited blue luminescence at 435−465 nm in MeCN. The complex **(23)** exhibited high luminescence intensity; the blue-shifted emission ($\lambda_{em} = 435$ nm) of this complex was due to the presence of electron-withdrawing substituents, which led to a stronger interaction with the metal center in the excited state. The sharp and intense nature of the luminescence peak of **(23)** was concluded to be originated from ^{3}MLCT transitions.

8.2.2 Photoredox catalysis of Co(III)-guanidyl complexes

Two rare examples of photoactive Co(III) complexes, $[Co(dgpy)_2][(BF_4)_3]$, **(25)** and $[Co(dgpz)_2][(BF_4)_3]$, **(26)**, (dgpy = diguanidylpyridine and dgpz = diguanidylpyrazine) were also reported exhibiting deep blue luminescence at RT

(Fig. 8.3). These complexes were found to be attractive alternatives to the traditional photocatalysts based on Ru(II) and Ir(II) (Pal et al., 2018b). The electron-rich ligands e.g., dgpy and dgpz capable of forming six-membered chelate rings and containing a strongly σ-donating hpp moiety (hpp = 1,3,4,6,7,8-hexahydropyrimido[1,2-a]pyrimidine, also abbreviated as guanidyl here) were used to synthesize the complexes **(25)** and **(26)** (Fig. 8.3) (Pal et al., 2014; Pal and Hanan, 2014). The reactions of dgpy and dgpz with $[Co(OH_2)_6][(BF_4)_2]$ in 2.2:1 stoichiometry afforded the complexes $[Co(dgpy)_2][(BF_4)_3]$, **(25)** and $[Co(dgpz)_2][(BF_4)_3]$, **(26)** in 52%−61% yields. Complexes **(25)** and **(26)** exhibited an irreversible oxidation at 1.75 and 1.98 V *vs* SCE, with associated quasi-reversible reductions at −0.58 ($E_{LUMO} = -2.51$ eV) and −0.39 ($E_{LUMO} = -2.73$ eV) *vs* SCE, respectively. The oxidation process was based on the electron rich ligand systems for both the complexes whereas for complexes **(25)** and **(26)**, the reductions were assigned to be based on the Co(III) ion and the Co(III) + pyrazine moieties, respectively, as suggested by the DFT calculations. The higher energy calculated for the HOMO of **(25)** ($E_{HOMO} = -6.49$ eV) compared to that of **(26)** ($E_{HOMO} = -6.75$ eV) confirmed the relative electron-poor nature of dgpz as compared to dgpy. The UV-visible absorption spectra of **(25)** and **(26)** displayed ligand-centered (LC) $\pi \rightarrow \pi^*$ transitions around 220−330 nm in MeCN solutions. The low-energy bands of **(25)** and **(26)** appearing at $\lambda_{abs} = 345-402$ nm were assigned as a mixture of ligand-to-metal and ligand-to-ligand charge transfer transitions (^{1}LMCT + ^{1}LLCT). Complexes **(25)** and **(26)** in degassed MeCN exhibited emission maxima at 440 and 412 nm, respectively. The photoluminescence quantum yields (Φ_{PL}) were found to be 0.70% and 0.40% for **(25)** and **(26)**, respectively, in degassed MeCN at RT, while in aerated MeCN the Φ_{PL} values of **(25)** and **(26)** were reduced to 0.40% and 0.12%, respectively. Complex **(25)** displayed monoexponential emission decay with an associated excited-state lifetime (τ_{PL}) of 5.07 ns in degassed MeCN at RT, whereas **(26)** exhibited a biexponential decay of 3.21 and 8.69 ns (Fig. 8.3). In comparison to an isoelectronic Fe^{II}−NHC (NHC = *N*-heterocyclic carbene) complex ($E_{T1} = 1240$ nm, $\tau_{PL} = 528$ ps) the τ_{PL} values of **(25)** and **(26)** were found to be about 950 times higher, presumably due to the very low energy of the triplet state in the iron complex (Chábera et al., 2018). The excited-state oxidation (E_{Ox}*) and reduction potentials (E_{Red}*) were calculated as −1.26 and −1.15 V for **(25)** and −2.26 and 2.75 V for **(26)** *vs* SCE. These complexes showed significantly higher E_{Red}* values compared to the $[Ru(bpy)_3]^{2+}$ (E_{Red}* = 0.77 V), $[Ir(dF(CF_3)ppy)_2(dtbubpy)]^+$, (dF-($CF_3$)ppy = 2-(2,4-difluorophenyl)-5-(trifluoromethyl) pyridinato-C^2,N′) (E_{Red}* = 0.89 V), $[Cr(Ph_2phen)_3]^{3+}$, (Ph_2phen = 4,7-diphenyl-1,10-phenanthroline) (E_{Red}* = 1.40 V), triphenylpyrylium (E_{Red}* = 2.30 V) and mesityl diaminoacridinium (E_{Red}* = 1.25 V) and were reported to be the strongest photo-oxidant to-date (Pal et al., 2018b).

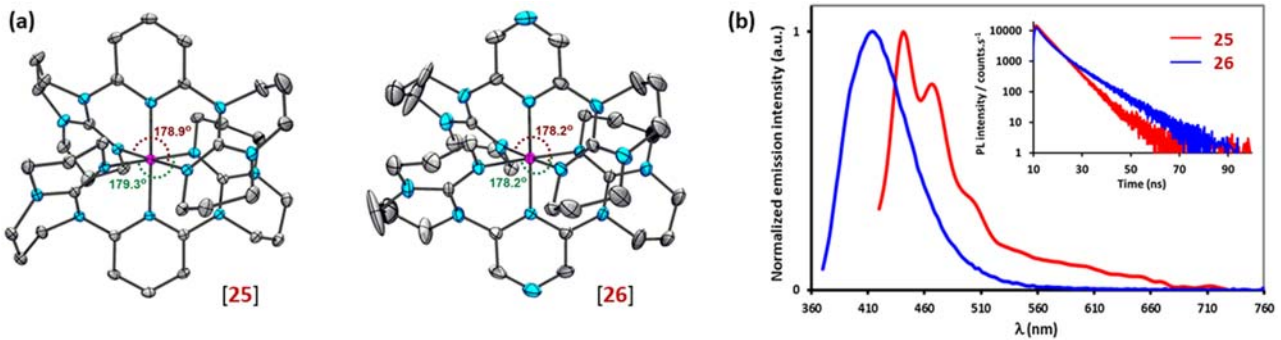

FIG. 8.3 (A) X-ray structures of **(25)** and **(26)** exhibiting the N^Co^N bite angles and (B) emission and excited-state lifetime decay (inset) profiles of complexes **(25)** and **(26)**. *Adapted from Pal, A.K., Krotkus, S., Fontani, M., Mackenzie, C.F.R., Cordes, D.B., Slawin, A.M.Z., et al., 2018. High-efficiency deep-blue-emitting organic light-emitting diodes based on iridium(III) carbene complexes. Adv. Mater. 30 (50), https://10.1002/adma.201804231. With Permission.*

The favorable excited-state redox properties of **(25)** and **(26)** helped in exploring the field of photochemical regioselective mono(trifluoromethylation) of polycyclic aromatic hydrocarbons (PAHs), e.g., pyrene, perylene, coronene and 9,10-diphenyanthracene using **(25)** and **(26)** as photocatalysts under mild reaction condition (CF_3SO_2Cl as the trifluoromethylating agent, irradiation at 420 nm, RT, 20 h) as compared to the reported traditional method of trifluoromethylation (CF_3I as the trifluoromethylating agent, 360°C, flame sealed ampule under high pressure) (Fig. 8.4). Due to the mild reaction photocatalytic condition, the reactions progressed to form selectively the mono(trifluoromethylation) PAHs in good yields (42%−58%) as opposed to multi(trifluoromethylation) PAHs (yield < 3%) prepared by the traditional method.

A possible reaction mechanism, using pyrene as the substrate and **(26)** as the photoredox catalyst (PRC) is depicted in (Fig. 8.4). The PAHs were themselves photoactive and can act as photosensitizers. Firstly, through energy transfer from the excited state of the photocatalyst, the excitation of pyrene occured to its triplet state **1**. The excited pyrene, **1**, underwent an oxidative quenching *via* a single electron transfer (SET) event with the trifluoromethylating agent, CF_3SO_2Cl to produce a pyrenyl radical cation **2** and $CF_3SO_2Cl^-$. This process was driven by the difference in the reduction potentials of **1** and CF_3SO_2Cl. The soformed $CF_3SO_2Cl^-$ produced a CF_3 radical **3** by the liberation of SO_2 gas. The electron-deficient CF_3 radical was then well-suited to add to the most electron-rich position of pyrene in a regioselective fashion to form a CF_3-pyrenyl radical, **4**. The resultant CF_3-pyrenyl radical, **4**, then under goes a second SET event with the excited photocatalyst,

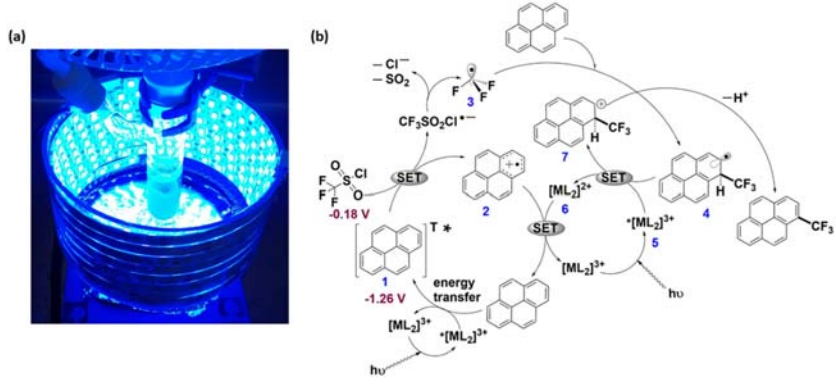

FIG. 8.4 (A) A photocatalytic trifluoromethylation reaction under experimental set-up and (B) mechanism of the trifluoromethylation of PAH using **(25)** and **(26)** as photocatalysts. *Adapted from Pal, A.K., Li, C., Hanan, G.S., Zysman-Colman, E., 2018. Blue-emissive cobalt(III) complexes and their use in the photocatalytic trifluoromethylation of polycyclic aromatic hydrocarbons. Angew. Chem. Int. Ed. 57 (27), 8027−8031. With Permission.*

5 (abbreviated as $*[ML_2]^{3+}$, where M = Co and L = dgpy/dgpz) to produce the reduced photocatalyst $[ML_2]^{2+}$, **6** and CF_3-pyrenyl cation, **7**. The formation of **6** was supported by in-situ reaction monitoring by UV-vis spectroscopy with the evolution of the band at 291 nm, which is a signature of $[ML_2]^{2+}$. A third SET event closed the two photocatalytic events, where **2** was reduced to pyrene and **6** was oxidized to $[ML_2]^{3+}$. Finally, deprotonation of **7** with K_2HPO_4 as the base afforded the desired CF_3-pyrene. As compared to another photoredox catalyst, $[Ir(dF(CF_3)ppy)_2(bpy)]PF_6$, reaction kinetics for mono(-trifluoromethylation) of pyrene using complex **(26)** was found to be slower, albeit resulted in a cleaner conversion of the product with high regioselectivity.

8.2.3 Metal-ion sensing by Co(II) complexes

Recently Liu et al. (2020) reported, five multi-functional luminescent coordination polymers (LCPs), $[Co_2(PNA)_2(PDA)_2]\cdot H_2O$, **(27)**, $[Co(PNA)(TPD)(H_2O)_2]\cdot 8H_2O$, **(28)**, $[Co(PNA)(1,3\text{-}BDC)]\cdot 2H_2O$, **(29)**, $[Co(PNA)(MIP)]\cdot H_2O$, **(30)** and $[Co_3(PNA)_3(HIPA)_3]$, **(31)**, [H_2PDA = 1,3-phenylenediacetic acid, H_2TPD = 2,5-thiophenedicarboxylic acid, 1,3-H_2BDC = 1,3-benzenedicarboxylic acid, H_2MIP = 5-methylisophthalic acid, H_2HIPA = 5-hydroxyisophthalic acid and PNA = [N,N′-bis(4-methylenepyridin-4-yl)-1,4-naphthalene dicarboxamide]. Polymers **(27−31)** were synthesized by a solution of $CoCl_2\cdot 6H_2O$, PNA and respective ligands in a mixture of water-NaOH in a poor yield of 14%−18%. The ligand PNA showed a $\pi \rightarrow \pi^*$ based fluorescence at 367 nm upon excitation at 250 nm in the solid-state. Upon similar excitation, the fluorescence of the LCPs was observed at 348−380 nm in the solid-state, which were attributed to the intraligand $\pi \rightarrow \pi^*$ and $n \rightarrow \pi^*$ transitions. The difference in fluorescence intensities among the LCPs may be attributed to the difference in the respective ligand structures. The luminescent LCP **(27−29)** exhibited the property of sensing of metal cations (M = Na^+, K^+, Ba^{2+}, Zn^{2+}, Co^{2+}, Ni^{2+}, Mg^{2+}, Sr^{2+}, Sm^{3+}, Nd^{3+} and Fe^{3+} at a concentration of 10^{-2} M (Fig. 8.5). It was observed that among different cations, the increase in the $[Fe^{3+}]$ dramatically quenched the fluorescence of the LCPs, with a detection limit of $5.3-9.1 \times 10^{-4}$ and a Stern-Volmer quenching constant (K_{SV}) value of 2670−4789. The fluorescence quenching effect could be due to the donor-acceptor electron transfer effect of Fe^{3+} ions with PNA containing functional spacers. Similarly, toxic anions, such as $Cr_2O_7^{2-}$, CrO_4^{2-} and MnO_4^- significantly quenched the fluorescence of the LCPs **(27−29)** with maximum detection limits of 6.3×10^{-4} (for LCP **28**), 7.2×10^{-4} (for LCP **27**) and 6.5×10^{-4} (for LCP **29**) (Fig. 8.5). The luminescent LCP **(27)** was used as the potential fluorescent sensor of Bovine Serum Albumin (BSA) that exhibited a strong fluorescence peak at 350 nm (λ_{exc} = 280 nm) due to the presence of tryptophan, tyrosine and phenylalanine residues in BSA. It was observed that on increasing the concentration of LCP **(27)**, the emission intensities of BSA

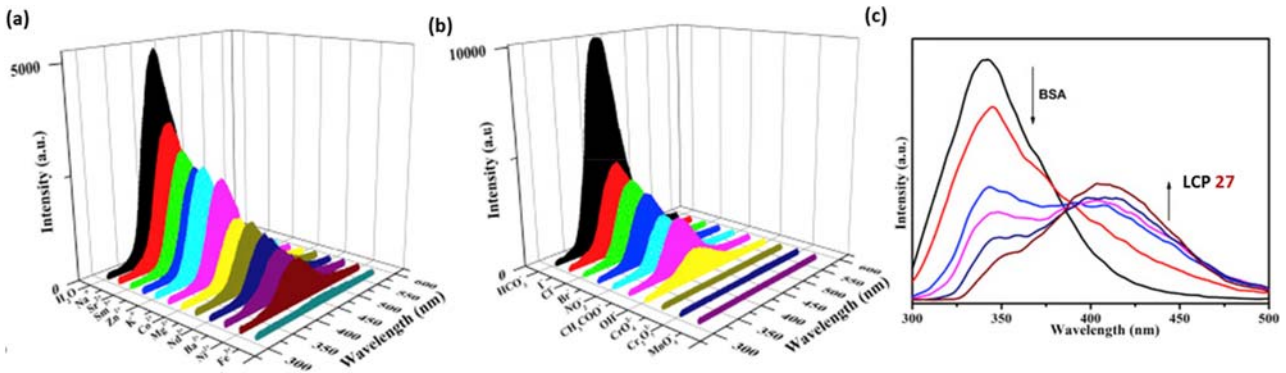

FIG. 8.5 (A) Fluorescence emission intensities of M^{n+}@LCP **(27)**, (B) fluorescence emission intensities of LCP **(27)** in different anion solution and (C) fluorescence spectra of BSA@LCP **(27)**. *Adapted from Liu, G.C., Li, Y., Chi, J., Xu, N., Wang, X.L., Lin, H.Y., et al., 2020. Multi-functional fluorescent responses of cobalt complexes derived from functionalized amide-bridged ligand. Dyes Pigm., 174, https://10.1016/j.dyepig.2019.108064. With Permission.*

and corresponding LCP **(27)** gradually decreased and increased, respectively, due to the supramolecular hydrogen bonding interaction between the LCP **(27)** and BSA. Similarly, as the concentration of LCP **(27)** increased from 0 to 40 μL, the τ_{PL} value of BSA decreased from 6.07 to 5.91 ns.

A hydrothermally synthesized novel $\{[Co(SBzIm)_2(npht)]\cdot H_2O\}_n$, **(32)**, [$H_2$npht = 5-nitrophthalic acid, SBzIm = 1,4-bis(thiabendazol-1-ylmethyl) benzene)] complex was investigated by Shi et al. (2020). A mixture of $Co(OAc)_2\cdot 4H_2O$, SBzIm, H_2npht, NaOH and distilled water were mixed and heated for 72 h at 140°C to afford **(32)** in 34% yield. The SBzIm exhibited an emission peak at 297 nm (λ_{exc} = 276 nm) in the solid-state, due to the ligand-based $\pi \rightarrow \pi^*$ transitions. The complex **(32)** exhibited a red-shifted emission peak at 376 nm (λ_{exc} = 298 nm), which was tentatively assigned to the ^{3}ILCT transitions. The emission of complex **(32)** exhibited solvatochromic effects in different solvents, e.g., ethylene glycol (EG), *N,N′*-DMF, MeCN, *n*-butanol, MeOH, EtOH, dichloromethane, *p*-xylene and acetone. Among these solvents, EG showed 97.8% fluorescence quenching of **(32)** and the calculated K_{SV} and the detection limit values were found to be 4.8×10^2 M and 2.5 mM, respectively. The complex **(32)** exhibited the property of sensing of metal cations, M = K^+, Na^+, Pb^{2+}, Cd^{2+}, Zn^{2+}, Cu^{2+}, Co^{2+}, Sr^{2+}, Mg^{2+}, Ca^{2+}, Fe^{3+}, Sm^{3+}, La^{3+}, Eu^{3+} or Cr^{3+}, at a concentration of 5×10^{-4} M. It was observed that among different cations, the increase in the concentration of Cu(II) from 0 to 0.50 mM displayed the increase in fluorescence quenching of **(32)**, leading to almost disappearance of the emission of **(32)** at the maximum [Cu(II)]. The K_{SV} and the detection limit of Cu(II) using complex **(32)** were found to be 1.4×10^3 M and 1.0 μM, respectively. Su et al. (2020) also reported a hydrothermally synthesized novel 2D Co(II) organic framework, $\{[Co_2(ImPh)(hfpd)(H_2O)]\cdot 1.75H_2O\}_n$, **(33)**, ($H_4$hfpd = 4,4′-(hexafluoroisopropylidene)diphthalic acid, ImPh = 4,4′-bis(imidazole-1-yl)-biphenyl) for the reorganization and quantification of highly carcinogenic acetylacetone (acac) and mercury (Hg(II)) ion. A mixture of $Co(SO_4)_2$, H_4hfpd, ImPh and NaOH in a 2:1:1 metal:H_4hfpd:ImPh ratio was heated in water at 140°C for 3 days in a Teflon lined steel container to afford the complex in a 51% yield. Complex **(33)** was crystallized in a triclinic space group in which the asymmetric unit **(33)** had two Co(II) centers, one $[hfpd]^{4-}$ ligand, one ImPh ligand and one coordinated water molecule. The six-coordinated Co1(II) and four-coordinated Co2(II) surrounded by O and N atoms displayed distorted octahedral $\{CoNO_5\}$ and distorted trigonal-pyramidal $\{CoNO_3\}$ coordination geometries, respectively. The ligand ImPh exhibited an emission peak at 407 nm in the solid-state, which can be attributed to $\pi \rightarrow \pi^*$ or $n \rightarrow \pi^*$ based transitions within the ligand ImPh. Complex **(33)** exhibited luminescence at 356 nm (λ_{exc} = 294 nm) which was tentatively assigned to intraligand or ^{3}LLCT transition. Luminescence of **(33)** in different solvents, such as EG, MeOH, EtOH, n-butanol, acac, *N,N′*-dimethyl acetamide, DMSO, MeCN, etc. revealed that the luminescence in

acac was almost completely quenched with a quenching efficiency ($Q = (1-I/I_0) \times 100\%$, where I_0 and I are the luminescence intensities without adding and adding acac, respectively) ~99.46% (Fig. 8.6A). Anti-interference experiments suggested that the luminous intensity of **(33)** in presence of acac and other organic solvents showed no significant difference, hence complex **(33)** was found to be a very selective sensor for the detection of acac (Fig. 8.6B). The calculated values of K_{SV} and the detection limit of acac were found to be 1915 M^{-1} and 14 μM, respectively. Complex **(33)** exhibited the property of sensing of metal cations ($M = Na^+$, K^+, Mg^{2+}, Sr^{2+}, Ba^{2+}, La^{3+}, Sm^{3+}, Eu^{3+}, Tb^{3+}, Fe^{3+}, Co^{2+}, Ni^{2+}, Cu^{2+}, Ag^+, Zn^{2+}, Cd^{2+} and Hg^{2+}) (Fig. 8.6C). It was observed that among different cations, the increase in the $[Hg^{2+}]$ dramatically quenched the luminescence of **(33)**; the calculated value of Stern-Volmer constant K_{SV} was 6497 M^{-1} with an associated detection limit of 4 μM (Fig. 8.6D).

8.3 Luminescent Rh(0/I/II/III) complexes

8.3.1 Rh(II/III) complexes of acetylacetonato, polypyridylamine, thiolato and macrocyclic ligands

DeArmond and Hillis (1968) studied the luminescence properties of Rh(III) complexes, e.g., $[Rh(acac)_3]$, **(34)**, $[Rh(tfacac)_3]$, **(35)**, $[Rh(hfacacac)_3]$, **(36)** with various β-diketone chelates (where tfaca = trifluoracetylacetone and hfacacac = hexafluoroacetylacetone). These complexes **(34–36)** exhibited emission maxima and FWHM in the ranges 413–419 nm and 2100–3600 cm^{-1}, respectively. The nature of the emission was attributed as $\pi \rightarrow \pi^*$ triplet to singlet ($T \rightarrow S_o$) transition. The excited-state lifetime (τ_{PL}) of these complexes ranges from 310 to 390 ms. The calculated lowest singlet-triplet energy for these ligand systems was 2.30–2.70 eV, which supported the emission of the $Rh(acac)_3$ complexes. Later, Carstens and Crosby (1970) observed the photoluminescence of some Rh(III) complex ions $[Rh(bpy)_3]^{3+}$, **(37)** and $[Rh(phen)_3]^{3+}$, **(38)**. These complexes were synthesized by adding the 2,2′-bpy or 1,10-phen ligand to a refluxing aqueous-ethanol solution of rhodium(III) chloride in ~70–90% yield (McKenzie and Plowman, 1970). In emission spectra, complexes **(37)** and **(38)** at 77 K exhibited long-lived $\pi \rightarrow \pi^*$ phosphorescence which was similar to that observed from the free ligand (Halper and DeArmond, 1974). Complex **(37)** is also known to exhibit a ^{3}IL excited state. Hillis and DeArmond (1971a) studied the emission properties of Rh(III) complexes $[Rh(bpy)_3]Cl_3$, **(37)**, $[Rh(phen)_3]Cl_3$, **(38)** and $[Rh(en)_3]Cl_3$, **(39)** with nitrogen donor ligands (where en = ethylenediamine). The complex **(39)** was synthesized by adding an excess of ethylenediamine to a warm alcoholic solution of rhodium trichloride trihydrate (Gillard et al., 1965). In emission spectrum, complexes **(37–39)** at 77 K varied from 450 to 588 nm and

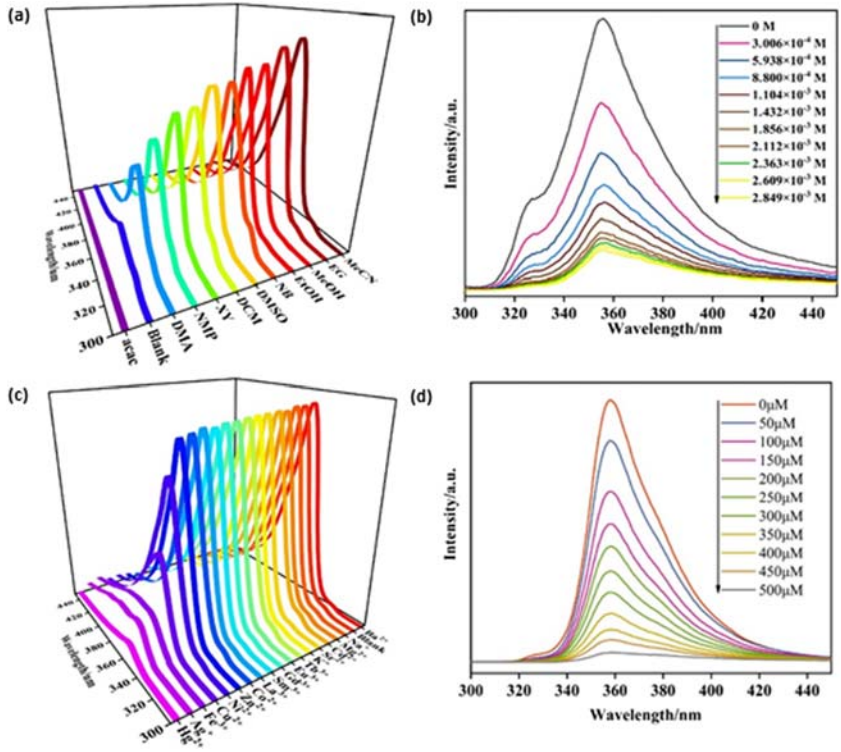

FIG. 8.6 (A) Luminescent intensities for **(33)** dispersed in aqueous solution upon dropping different organics; (B) emission spectra of **(33)** dispersed in aqueous solutions with different concentrations of acac at RT; (C) luminescent intensities of **(33)** immersed in EtOH with various metal ions and (D) emission spectra of **(33)** in EtOH suspension with different concentrations of [Hg^{2+}] ions. *Adapted from Su, Y.Q., Qu, Y.H., Fu, L., Cui, G.H., 2020. An unprecedented binodal (4,6)-connected Co(II) MOF as dual-responsive luminescent sensor for detection of acetylacetone and Hg^{2+} ions. Inorg. Chem. Commun., 118, https://10.1016/j.inoche.2020.108013. With Permission.*

lifetimes (τ_{PL}) 0.02 **(39)**, 2.20 **(37)** and 47−48.4 **(38)** ms (Hillis and DeArmond, 1971a,b; Kalyanasundram et al., 1992). The Φ_{PL} values at 77 K were found to be 29%, 90% and 0.09% for **(37)**, **(38)** and **(39)**, respectively, upon excitation at 313 nm (Hillis and DeArmond, 1971a). Kalyanasundaram et al. (1992) further studied complexes **(37)** and **(38)**, where they reported that emission maxima were obtained at 454 and 579 nm with associated τ_{PL} values of <15 and 220 ns, respectively, at 293 K in acetonitrile. Complexes **(38)** and **(39)** exhibited structured emission principally at 483 nm with shoulders at 450, 510 and 553 nm in EtOH:MeOH (4:1 v/v) at 77 K. These emissions were tentatively attributed to the ligand-centered (^{3}LC) $\pi \rightarrow \pi^*$ or metal-centered (^{3}MC) d → d transitions, where, the ^{3}MC emission was the dominant feature at 77 K, but the LC emission was enhanced relative to the MC luminescence

in fluid solutions. The lifetimes of the complexes were found to be 30−40 times shorter than those of the respective free ligands.

Geoffroy et al. (1974) synthesized two Rh(I) phosphine complexes, e.g., [Rh(2-phos-ene)$_2$]Cl, **(40)** and [Rh(2-phos)$_2$]Cl, **(41)**, (2-phos-ene = *cis*-l,2-bis(diphenylphosphino)ethylene and 2-phos = 1,2-bis(diphenylphosphino) ethane). These complexes were synthesized adopting the method of Vaska and Catone (1966) by mixing a benzene solution of the reactants, ligands and [Rh(CO)Cl(PPh$_3$)$_2$] at 25°C, followed by decarbonylation in a 10:1 mixture of toluene:1-propanol at 100°C. Complex **(40)** exhibited luminescence at 606 nm in the solid-state at RT with associated FWHM of 2880 cm^{-1} and τ_{PL} value of 22.3 μs. The complexes **(40)** and **(41)** in EPA solution [5:5:2 (v/v/v) ethyl ether:isopentane:ethyl alcohol) at 77 K exhibited λ_{em} at 584 and 613 nm, with FWHM of 2890 and 2120 cm^{-1}, respectively. The τ_{PL} and Φ_{PL}values of complexes **(40)** and **(41)** at 77 K were found to be 20.8 μs, 27.5 μs and 75%, 5.2%, respectively (Geoffroy et al., 1974).

Two *tris*(dithioketone) complexes of Rh(III), e.g., [Rh(SacSac)$_3$], **(42)** and [Rh(SSBB)$_3$], **(43)**, (where SacSac = dithioacetylacetone and SSBB = dithiodibenzoylmethane) were synthesized by Merrill and DeArmond (1979). Complex **(42)** was synthesized following the procedure developed by Heath and Martin (1969) in a yield of 3%. Complex **(43)** was synthesized by adding an aqueous solution of $RhCl_3$ into a suspended ethanolic solution of $NaBH_4$ and 3,5-diphenyl-1,2-dithiolium chloride. The resulting mixture was refluxed for 2 h to afford the complex **(43)** in 35% yield. The emission spectra of **(42)** and **(43)** are broad, asymmetric and overlap substantially with the absorption spectra. The differences between the energy of the emission maximum and the energies of the intensities at one-half of the emission maximum were found to be 960 and 1250 cm^{-1} for the blue side and red side, respectively, in complex **(42)**. Thus, the emission spectra of complexes **(42)** and **(43)** could each be represented by the sum of two Gaussian functions. Without the Gaussian deconvolution, complexes **(42)** and **(43)** exhibited luminescence at ∼ 794 and ∼ 833 nm, respectively, in ETA at 77 K with associated FWHM of 2210 and 2150 cm^{-1}. The Gaussian fit values of complex **(42)** were found to be 12,750, 12,000 cm^{-1} with associated FWHM at 1710 and 2570 cm^{-1}, respectively. Similarly, the Gaussian fit values of complex **(43)** were found to be 12,230 and 11,590 cm^{-1} for luminescence with associated FWHM of 1580 and 2300 cm^{-1}, respectively. The fitting of two Gaussian components was found to be consistent with the two-exponential fit of the excited-state lifetime decay-curve data. Complexes **(42)** (λ_{exc} = 764 nm) and **(43)** (λ_{exc} = 801 nm) exhibited τ_{PL} values of 10.9 and 3.8 μs (short component) and 30.8 and 63.6 μs (long component) in methylcyclohexane. The two-Gaussian fit, multiple lifetimes and polarization spectra indicated that the emission occurred from two different states. The half-width of the broader band from the two-Gaussian fits suggested the assignment of this band as ^{3}(d-d) → $^1A_1$, while from the

charge transfer-to-metal visible absorption band position and the solvent dependence of the emission, the other band was assigned as $^3(\pi\text{-}d^*) \rightarrow {}^1A_1$.

A new series of Rh(I) complexes $[Rh(CO)_2(mnt)]^-$, **(44)**, $[Rh(CO)(PPh_3)(mnt)]^-$, **(45)** and $[Rh(P(OPh)_3)_2(mnt)]^-$, **(46)**, (mnt = maleonitriledithiolate) was reported by Johnson et al. (1983). The complexes were synthesized by mixing sodium maleonitriledithiolate and respective tetrabutylammonium rhodium salt in (1:1 v/v) acetone:ethanol for several hours until the product was formed as a brown precipitate. The solid-state luminescence spectra of complexes **(44–46)** at 77 K exhibited emission values at 609, 619 and 603 nm and associated τ_{PL}values of 238, 99 and 281 μs, respectively, in EPA. The τ_{PL}values for the Rh complexes were found to belong as expected for the spin-forbidden transition based on their high spin-orbit coupling constants. The emission spectra of all the complexes were tentatively assigned to (i) the mnt-based intraligand (IL) $\pi \rightarrow \pi^*$ state, (ii) MLCT state involving mnt and (iii) LMCT state involving mnt. The solid-state emissions were highly structured with a major vibrational progression value of 1400 cm^{-1}.

The luminescence properties of a series of red-emissive Rh(III)-amine complexes were investigated by Sexton et al. (1984). Only a few of these, e.g., $[Rh(NH_3)_5Cl](ClO_4)_2$, **(47)**, *trans*-$[Rh(NH_3)_4Cl_2]Cl\cdot H_2O$, **(48)**, *trans*-$[Rh(NH_3)_4(H_2O)Cl](ClO_4)_2$, **(49)**, *trans*-$[Rh(NH_3)_4(OH)Cl]$, **(50)** are mentioned here. In general, the intensities of emission followed the order:

$$Rh(NH_3)_5X_2^+ >> \textit{trans}\text{-}Rh(NH_3)_4X_2^+ > \textit{cis}\text{-}Rh(NH_3)_4X_2^+ > \textit{trans}\text{-}Rh(NH_3)_4(OH)X^+ > \textit{cis}\text{-}Rh(NH_3)_4(OH)X^+ > \textit{cis}\text{-and } \textit{trans}\text{-}Rh(NH_3)_4(H_2O)X^{2+}.$$

Bromo compounds were generally brighter emitters than the homologous chloro complexes. No emission was found for the dihydroxo complexes, *cis*- and *trans*-$Rh(NH_3)_4(OH)_2^+$. For the series of $Rh(NH_3)_4XY^{n+}$ complexes, (X = either $C1^-$ or Br^-), the λ_{em}, values at 77 K followed the order:

$$Y = NH_3 > \textit{cis}\text{- or } \textit{trans}\text{-OH} > \textit{trans}\text{-X} > \textit{cis}\text{-X} \sim H_2O.$$

A similar situation was observed with the $\lambda_{0\text{-}0}$ values, which followed the apparent order:

$$Y = NH_3 > OH > \textit{cis}\text{- or } \textit{trans}\text{-X} \sim H_2O.$$

At both 77 and 298 K, the complexes exhibited a broad Gaussian distribution of luminescence. Complexes **(47–50)** at 77 K in 4:1 (v/v) MeOH:water glasses exhibited ligand field red-phosphorescence at 666, 763, 775 and 699 nm with associated FWHM at 0.28, 0.25, 0.29 and 0.27 μm^{-1}, respectively. Photoexcitation of the haloamminerhodium(III) complexes at 298 K aqueous solution led to two emission components, a very fast (picosecond) decay, which was attributed to fluorescence from incompletely relaxed LF singlets and as lower (nanosecond) decay, which was attributed to the phosphorescence from a thermally relaxed lowest energy triplet LF state. The

lifetime of complexes at 77 K was found to be longer (in μs) compared to those in aqueous conditions at 298 K (in ns). The quantum yields for emission were found to be in the range $10^{-7} < \Phi_{PL} < 10^{-6}$. Later, Frink et al. (1988) synthesized some interesting NIR emissive Rh(III)-terpyridyl complexes, e.g., $[Rh(tpy)_2]^+$, **(51)**, $[Rh(tpy)(bpy)(py)]^{3+}$, **(52)** and $[Rh(tpy)(bpy)C1]^{2+}$, **(53)**, (bpy = 2,2′-bipyridine; py = pyridine, tpy = 2,2′:6′,2″-terpyridine). Complex **(51)** was synthesized by the reaction of tpy with $Rh(tpy)Cl_3$ Haris and McKenzie (1963). Complex **(52)** was synthesized by refluxing a mixture of $[Rh(tpy)(bpy)Cl](ClO_4)_3 \cdot 3H_2O]$, pyridine and ethanol for 10 h. Ether was added in excess to the cooling solution leading to the formation of complex **(52)**. Complex **(53)** was synthesized by refluxing $Rh(tpy)Cl_3$ and bpy in a mixture of dimethylformamide and ethanol for 6 h. The mixture was cooled and filtered, and then ether was added to the filtrate to yield the desired product. Emission spectra for complexes **(51)**, **(52)** and **(53)** at 77 K, when measured in EtOH:MeOH (4:1, v/v) glasses exhibited λ_{em} at 735, 730 and 763 nm and τ_{PL} values of 8.0, 16.5 and 9.3 μs, respectively. The Φ_{PL} values at 77 K were found to be 9%, 8% and 10% for **(51)**, **(52)** and **(53)**, respectively. In aqueous solutions at 298 K, τ_{PL}values for **(51)** and **(52)** at 10^{-3} M were found to be three orders of magnitude lower than those at 77 K, with values of 14.2 and 14.9 ns, respectively, and emission intensities were found to be very weak. The emission spectra at both the temperatures displayed broad Gaussian-shaped bands resulting from the lowest energy excited ^{3}LF state.

Rh(III) complexes with mixed-chelates, namely $[Rh(ppy)_2bpy]^+$, (ppyH = phenylpyridine), **(54)**, $[Rh(ppy)_2en]^+$, **(55)** and $[Rh(thpy)_2bpy]^+$, (thpyH = thienylpyridine), **(56)** were also studied Colombo et al. (1990). At low-temperature in the visible part of the spectrum, luminescence spectra of Rh(III) complexes with π-accepting ligands in glassy matrices are characterized by a structured band. At 6 K, luminescence spectrum of complex **(54)** in nitrile glass having a range of 454−625 nm exhibited the wide luminescence lines from 100 to 200 cm^{-1} when excited at 337 nm. The complex **(54)** was earlier reported to be emissive also at 454 nm both at 222 and 77 K with a structured profile (Maestri et al., 1987). The τ_{PL} values were measured to be < 0.05 μs and 0.17 ms, respectively, at 222 and 77 K. The width was inhomogeneously arising from the broad distribution of sites in the glass. The LLN (LLN = Luminescence Line Narrowing) spectra of $[Rh(ppy)_2bpy]^+$, **(54)**, $[Rh(ppy)_2en]^+$, **(55)** and $[Rh(thpy)_2bpy]^+$, **(56)** in a nitrile glass or in Plexi glass was investigated. It was observed that substitution of bpy by en in **(54)** had almost no effect on the sharp-line pattern of the complex. Therefore, following the previous study, it was concluded that the ppy^- ligand was involved in the lowest energy excited state of **(53)** which, in addition, was further confirmed by the spectrum obtained by substituting the ligand ppy^- with $thpy^-$ (Maestri et al., 1987). Further to understand the nature of the first excited state, an extended-Hückel calculation on model complexes **(54)** and **(55)** were performed. The lowest energy unoccupied orbital turned out to be a

bpy-based orbital from the calculations. The lowest energy excited states in both these complexes were assigned to $\pi \rightarrow \pi^*$ on the cyclometalated ligand. The LLN experiments showed that the cyclometalated ligand were involved in the first excited state and not bpy. In a later report by Kunkely and Vogler (2000), the blue-green photoluminescence ($\lambda_{em} = 460$, 490 nm, $\Phi_{PL} = 0.006$) of $[Rh(ppy)_2(CN)_2]^{2-}$, **(57)**, (ppy = 2-phenylpyridinato-C^2,N') was attributed to be ^{3}LC in character. Due to the presence of higher LF strength in complex **(57)**, it showed brighter luminescence at RT than the other previously reported Rh(III)-ppy analogs.

Dulebohn et al. (1990) explored the luminescence properties of dirhodium $Rh_2(0,0)$, $Rh_2(0,II)$ and $Rh_2(II,II)$ fluorophosphine complexes, e.g., $[Rh_2(dfpma)_3(PF_3)_2]$, **(58)**, $[Rh_2(dfpma)_3Cl_2(PF_3)_2]$, **(59)**, $[Rh_2(dfpma)_3Cl_4]$, **(60)**, respectively, (where dfpma = $CH_3N(PF_2)_2$ = bis(difluorophosphino) methylamine). Complex **(58)** was synthesized by mixing $CH_3N(PF_2)_2$ and DCM solution of $[RhCl(PF_3)_2]_2$. The change in the color of solution was accompanied by the liberation of PF_3. Then the $Co(C_5H_5)_2$ was added. The mixture was stirred for 10 min under PF_3 and the addition of hexane led to the precipitation of cobaltocene, which was filtered out to afford the complex in 32% yield. Complex **(59)** was synthesized by mixing benzene solution of $[RhCl(PF_3)_2]_2$ and $CH_3N(PF_2)_2$ with a yield of 25%. Complex **(60)** was synthesized in the same way as **(58)**, where unlike **(58)**, the PF_3^- anion was exchanged with Cl^- by the addition of $Cl_2IC_6H_5$ to give 59% yield **(60)**. In a different study, kadis et al. (1996) synthesized structurally similar two more complexes, $[Rh_2^{(0,II)}(dfpma)_3Br_2(\eta^1\text{-dfpma})]$, **(61)** and $[Rh_2^{(II,II)}(dfpma)_3Br_4]$, **(62)** which were synthesized by refluxing $CH_3N(PF_2)_2$ and benzene solutions of $[RhBr(PF_3)_2]_2$ for 9 and 3.5 h, respectively. Br_2 was added to synthesize **(62)**. The vibrationally featureless emission spectra of complexes **(58–60)** in crystalline form at 77 K, exhibited λ_{em} at 840, 780 and 820 nm with associated τ_{PL} values of 53, 79 and 287 μs, respectively. The red-emissions in these complexes were attributed to $^3(d\pi^* \rightarrow d\sigma^*)$ phosphorescence. The intensities of the emissions monotonically decreased with increasing temperature and the FWHM of emission bands exhibited a substantial temperature sensitivity, increasing by more than 1500 cm^{-1} from 10 K to the highest temperatures at which emission can be detected. The lack of luminescence in solution at temperatures equivalent to those at which the crystalline solids demonstrated the importance of medium rigidity as a crucial controlling factor of $d\sigma^*$ luminescence. It was indicated that with the two-electron mixed-valence $Rh_2(0,II)$ complex as a benchmark, the preparation of its multielectron $Rh_2(0,0)$ and $Rh_2(II,II)$ counterparts could be achieved such that a long-lived emissive $d\sigma^*$ excited state can be preserved. Conversion of the octahedral Rh(II) center of **(59)** to the trigonal-bipyramidal Rh(0) center of **(58)** stabilized a formally highly energetic level that could accommodate the addition of two electrons to the metal core. In this manner, the overall electronic structure necessary for $d\sigma^*$ luminescence was preserved. Complexes **(58–62)** also

exhibited $^3(d\pi^* \rightarrow d\sigma^*)$ based phosphorescence maxima ranging from 760 to 850 nm in dichloromethane at 77 K with associated τ_{PL} values of 74, 270, 190, 300 and 79 μs, respectively, in the amorphous solid state.

Kalyanasundaram et al. (1992) studied the luminescence properties of Rh(III)-polypyridyl complexes of the type, $[Rh(dpp)_2C1_2]^+$, **(63)**, $[Rh(bpy)_2(dpp)]^{3+}$, **(64)** and $[Rh(dpp)_2(bpy)]^{3+}$, **(65)**, (dpp = 2,3-bis(2-pyridyl)pyrazine). Complex **(63)** was synthesized by refluxing $RhC1_3 \cdot 3H_2O$ and the ligand dpp in an ethanol:water (2:1 v/v) mixture whereas complexes **(64)** and **(65)** were synthesized by refluxing $RhC1_3 \cdot xH_2O$ and ligand bpy/dpp, in DMF. At 293 K, complex **(63)** in acetonitrile showed a very weak emission for which the τ_{PL} was calculated to be 90 ns by transient absorption method. Both complexes **(64)** and **(65)** in acetonitrile at 293 K exhibited λ_{em} at 450 nm with τ_{PL}values of 390 and 800 ns, respectively. These transitions were tentatively assigned as an admixture of primarily $\pi \rightarrow \pi^*$ transitions with a minor contribution from d $\rightarrow$ d transitions. At 77 K, in EtOH:MeOH (4:l v/v), complexes **(64)** and **(65)** exhibited λ_{em} principally at 484 and 477 nm, respectively, with shoulders ranging from 445 to 543 nm. These emissions were attributed due to $\pi \rightarrow \pi^*$ based transitions. The τ_{PL} of complexes **(64)** and **(65)** were found to be 2.25 and 2.05 ms at 77 K. Complexes **(63)**, **(64)** and **(65)** also exhibited a very weak secondary emission in the range of 704−758 nm with associated τ_{PL}values of $\sim$19.6−24 μs in the same solvent mixture at 77 K. These emissions were attributed to d $\rightarrow$ d transitions.

Rh(III) complexes were also reported with some tetrazamacrocyclic ligands, e.g., *trans*-[Rh([14]aneN$_4$)(CN)$_2$]C1O$_4$, **(66)**, *trans*-[Rh([15]aneN$_4$)(CN)$_2$]C1O$_4$, **(67)**, *trans*-[Rh([14]pyaneN$_4$)(CN)$_2$](C1O$_4$)$_3$, **(68)**, (McClure and Ford, 1992). Complexes **(66−68)** were synthesized by refluxing the aqueous solution of *trans*-dichloro([14]aneN$_4$)rhodium(III) chloride, *trans*-dichloro([15]aneN$_4$)rhodium(III)chloride or *trans*-dichloro([14]pyaneN$_4$)-rhodium(III) perchlorate and NaCN for about 4−24 h. The anion was metathesized by ClO_4^- by the addition of an aliquot of aqueous $NaClO_4$ to afford the complex with in a yield of 45%−53%. Complexes **(66)** and **(67)** exhibited broad and unstructured strong spin-forbidden emissions from the lowest energy ^{3}LF states at 468 and 570 nm, respectively, in an aqueous acidic solution (pH = 4, $HClO_4$) with associated τ_{PL}values of 8.1 and 0.74 μs. The Φ_{PL} values at 296 K in aqueous solution for the perchlorate salts of **(66)** and **(67)** were found to be 0.25 and 0.018. The broad, unstructured emission spectra of complexes from **(65−67)** at 77 K in MeOH:H_2O (4:1 v/v) glasses exhibited λ_{em} at 472, 529, 610 nm with associated FWHM at 4400, 3900 and 3400 cm^{-1}, respectively. The τ_{PL} values of **(65−67)** were found to be 286, 56 and 15.4 μs, respectively at 77 K. The 0 $\rightarrow$ 0 transition energies were found to be 26,900, 23,900 and 20,700 cm^{-1}, respectively, from the 77 K experiments.

An interesting cyclometalated Rh(III) complex $[Rh(ppy)_2(dpt\text{-}NH_2)]PF_6$, **(68)**, (dpt-NH$_2$ = 4-amino-3,5-bis(2-pyridyl)-4*H*-1,2,4-triazole) was

synthesized by Calogero et al. (1995). Complex **(68)** was synthesized by adding a dichloromethane solution of $[Rh(ppy)_2C1]_2$ to a refluxing dichloromethane solution of dpt-NH_2. After the anion metathesis with PF_6^-, the product was obtained in a good yield of 87%. Complex **(68)** exhibited highly structured luminescence with λ_{em} at 458 nm at 77 K in rigid matrices, with 4:1 MeOH:EtOH (v/v), which was attributed to the metal-perturbed, triplet ppy-centered (^{3}LC) excited state with mono-exponential τ_{PL} value of 160 μs. This assignment was confirmed by the lack of RT luminescence of **(68)**, as the ^{3}LC states were effectively deactivated by the thermal population to upper-lying ^{3}MC levels, which finally got deactivated by fast radiationless transitions to the ground state. The structured luminescence spectra do not vary with the excitation wavelength and exhibited a vibrational progression of about 1300 cm^{-1}. In comparison to the previously reported $[Rh(ppy)_2(bpy)]^+$, **(54)**, ($\lambda_{em} = 454$ nm, $\tau_{PL} = 170$ μs at 77 K in 4:1 MeOH:EtOH (v/v)), complex **(68)** showed emission from a ppy-centered orbital mixed with an upper-lying CT level (Colombo et al., 1990). Since the dpt-NH_2 is a slightly better donor group than bpy and could move the Rh $\rightarrow$ ppy CT level to lower energy, it could decrease the energy gap between ^{3}LC and ^{3}MLCT states, promoting a better mixing and leading to a shortened lifetime. Complex **(68)** displayed irreversible oxidation peaks at +1.51 V and reduction peaks at −1.90 V *vs* SCE, attributed to the removal and addition of an electron from a metal-ligand (C^-) σ-bonding orbital and the dpt-NH_2 ligand, respectively.

Two interesting optically active cyclometalated Rh(III) complexes, Δ[Rh(thpy4,5p(R,R)py)$_2$TAP]Cl, **(69)** and Δ[Rh(phpy4,5p(R,R)py)$_2$TAP]Cl, **(70)**, (where TAP = 1,4,5,8-tetraazaphenanthrene; thpy4,5p(R,R)py = (8R,10R)-2-(2′-thienyl)-4,5-pinenopyridine and phpy4,5p(R,R)py = (8R,10R)-2-(2′-phenyl)-4,5-pinenopyridine) were reported (Ghizdavu et al., 2003). Complexes **(69)** and **(70)** were synthesized with a yield of 76%−85% by refluxing a solution of $\Delta\Delta$[Rh(thpy4,5p(R,R)py)$_2$(μ-Cl)]$_2$/$\Delta\Delta$[Rh-(phpy4,5p(R,R)py)$_2$(μ-Cl)]$_2$ and TAP in CH_2Cl_2 for $\sim$2 h under N_2 in dark. Complexes **(69)** and **(70)** exhibited broad and structureless ^{3}CT based (from thpy/phpy $\rightarrow$ TAP) red to near-infrared emission (λ_{em} and $\tau_{PL} = 720$ nm and 11 ns (for **69**) and 647 nm and 152 ns (for **70**)) at 298 K in acetonitrile. The complexes **(69)** and **(70)** exhibited broad-structured and structureless luminescence centered at 526 and 553 nm with associated τ_{PL} values of 5.8 ± 0.5 (a shorter component present couldn't be determined precisely) and 9 μs, respectively, at 77 K in EtOH:MeOH (4:l(v/v)) matrix. The nature of the emissions of **(69)** at 77 K was ascribed as a mixture of ^{3}CT (from thpy to TAP) and $^3LC_{\pi\text{-}\pi^*}$ (centered on thpy), while the same for **(70)** was due to ^{3}CT emission (from phpy to TAP) only. This is due to three probable reasons as suggested by TD-DFT calculations (a) energy differences among the first four triplets were larger in **(70)** than in **(69)** such that the nonradiative transitions from T_4 to T_3, T_2 and T_1 was favored for the former, (b) the radiationless

decays from T_4 to T_3 and T_2 to T_1 was found to be favored in **(70)** as compared to **(69)** as T_4 andT_3 have the same orbital parentage as well as T_2 and T_1 in **(70)**, which was not the case for the corresponding pairs of triplets (T_4-T_3 and T_2-T_1) in **(69)** and (c) although in both these complexes; the decay concerned a transition from an LC state to a CT state (CT from the orthometalated to the TAP ligand). The LC state was localized on the TAP in complex **(70)** whereas, the LC state was localized on the orthometalated ligand in **(69)**. Thus, a different electron transfer process was implied for the transition $^3LC_{\pi\text{-}\pi^*}(T_3) \rightarrow CT(T_2)$ in the complexes.

8.3.2 Metal-ion sensing by Rh(III) complexes

Luminescent Rh(III) complex, e.g., $[Rh(L)(ppy)_2]PF_6$, **(71)**, (L = (E)-3′,6′-bis(ethylamino)-2′,7′-dimethyl-2-((pyridin-2-ylmethylene)amino)spiro[isoindoline-1,9′-xanthen]-3-one) has also been employed for cation sensing application (Wang et al., 2015). Complex **(71)** displayed emission at 548 nm in MeCN at RT, which was suggested to be derived from the triplet excited state of intraligand (^{3}IL) [$\pi \rightarrow \pi^*$(NˆC)] transition, mixed with the metal-to-ligand charge transfer (^{3}MLCT) [dπ(Rh) $\rightarrow \pi^*$(NˆC)] character. The probability of mixing this emission with the characteristic rhodamine 6G emission due to the occurrence of ring-opening was not ruled out. Complex **(71)** exhibited sensing behavior to $[Hg]^{2+}$ by inducing the ring-opening of the rhodamine derivative with an emerging absorption band at 530 nm (Fig. 8.7). The log K_s value of 4.04 for $[Hg]^{2+}$ ion binding was estimated from the satisfactory result of the theoretical fit of the 1:1 stoichiometric binding mode with a detection limit of 4×10^{-7} M.

8.3.3 Application of Rh(III) complexes in OLED devices

An extensive and interesting work on OLEDs was reported by Wei et al. (2019), where they synthesized a series of luminescent cyclometalated Rh(III) complexes $[Rh(dpqx)_2(acac)]$, **(72)**, $[Rh(dpqx)_2(hfacac)]$, **(73)**, $[Rh(dpqx)_2(Ph_2\text{-acac})]$, **(74)**, (where, dpqx = 2,3-diphenylquinoxaline, Ph_2-acac = 1,3-diphenylpropane-1,3-dione) in which the luminescence quenching problem from the lowest-lying d-d state was overcome by the incorporation of a strong σ-donor cyclometalating ligand with lower-lying IL state (Fig. 8.8A). The complexes **(72–74)** were synthesized with a yield of 69%–81% by cleaving the dinulcear precursor $[Rh(dpqx)_2Cl]_2$ in MeOH–CH_2Cl_2 mixture with sodium-2,4-pentanedionate/hfacac/Ph_2-acac, respectively, in the presence of nitrogen atmosphere for 8 h. Complexes **(72–74)** displayed ^{3}ILCT based (from phenyl moiety to quinoxaline unit of the dpqx ligand) bright ($\Phi_{PL} = 0.11\%-0.98\%$) orange-red phosphorescence ($\lambda_{em} = 598-612$ nm, $\tau_{PL} = 0.79-1.64$ μs) in dichloromethane mixed with ^{3}MLCT [dπ(Rh) $\rightarrow \pi^*$(dpqx)] photoluminescence at 298 K. The observation of a reduction in τ_{PL}

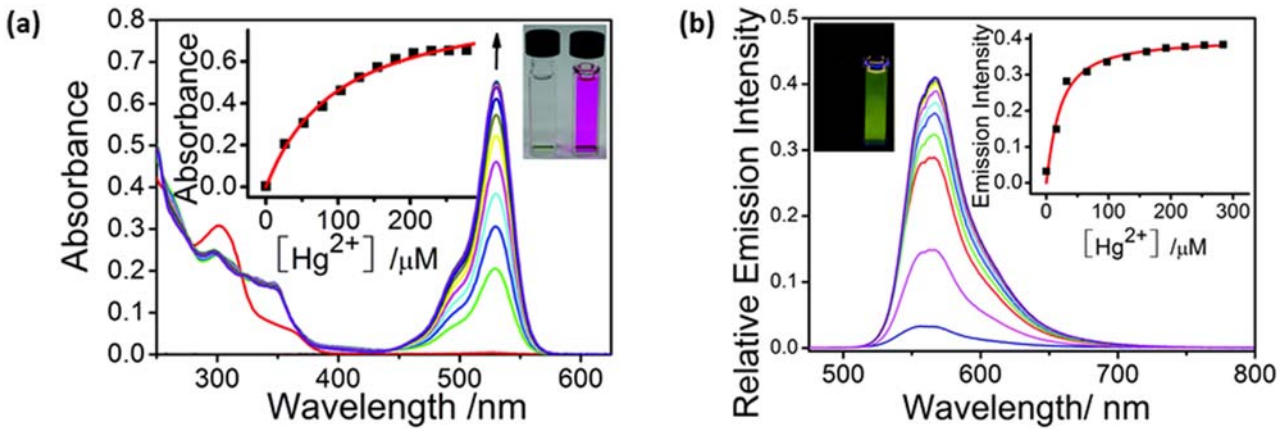

FIG. 8.7 (A) Changes in electronic absorption spectra of **(71)** in MeCN ([C] = 11.8 μM) at 298 K upon addition of varying concentrations of $[Hg]^{2+}$. Insets show the photograph of color changes and the plot of the absorbance at 530 nm as a function of the concentration of $[Hg]^{2+}$ with a theoretical fit and (B) changes in emission spectra of **(71)** in MeCN ([C] = 11.8 μM) at 298 K upon addition of varying concentrations of $[Hg]^{2+}$. Insets show the photograph of emission enhancement and the plots of the emission intensity at 560 nm as a function of the concentration of $[Hg]^{2+}$ with a theoretical fit. *Adapted from Wang, C., Lam, H.C., Zhu, N., Wong, K.M.C., 2015. Introduction of luminescent rhenium(I), ruthenium(II), iridium(III) and rhodium(III) systems into rhodamine-tethered ligands for the construction of bichromophoric chemosensors. Dalton Trans. 44 (34), 15250−15263. With Permission.*

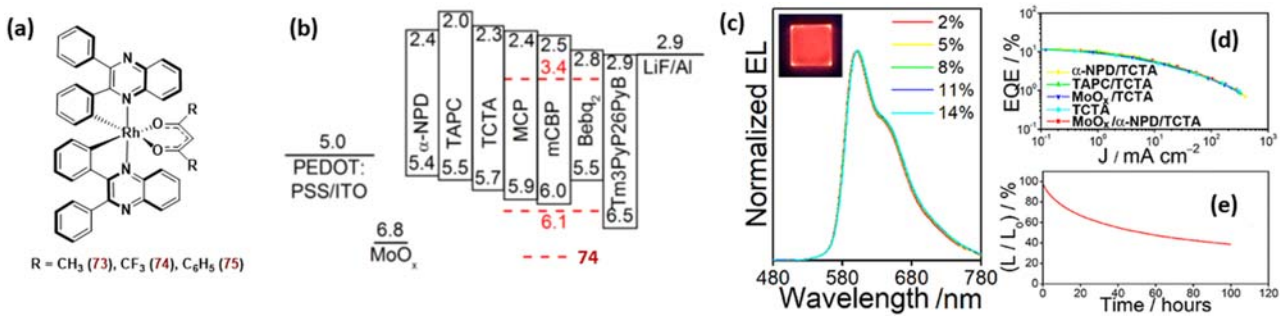

FIG. 8.8 (A) Molecular structures of complexes **(72−74)**, (B) energy-level diagram of vacuum-deposited OLED, (C) electroluminescence spectra with different dopant concentrations (inset - photo of thin-film PL of **(74)** under UV irradiation), (D) EQEs with different hole-transporting layers and (E) the operational lifetime of the vacuum-deposited OLED was made with 5 v/v% of **(74)**. *Adapted from Wei, F., Lai, S.L., Zhao, S., Ng, M., Chan, M.Y., Yam, V.W.W., et al., 2019. Ligand mediated luminescence enhancement in cyclometalated rhodium(III) complexes and their applications in efficient organic light-emitting devices. J. Am. Chem. Soc. 141 (32), 12863−12871. With permission.*

values **(72)**, 0.08 μs; **(73)**, 0.65 μs; **(74)**, 0.22 μs in oxygenated compared to those in degassed solutions proved the triplet nature of the emissions in these complexes. The acac ligand influenced the dπ(Rh) orbital and the occurrence of very similar luminescence energy of **(72−74)** comprising of acac ligands with various substituents, [CH_3 **(72)**; CF_3 **(73)**; C_6H_5 **(74)**], showed the similar nature of phosphorescence in all the three complexes. Complexes **(72−74)** in doped *N,N*-dicarbazolyl-3,5-benzene (MCP) thin films exhibited intense ($\Phi_{PL} = 44\%-65\%$) orange-red phosphorescence ($\lambda_{em} = 597-603$ nm, $\tau_{PL} = 23-32$ μs). No observable luminescence quenching, as well as shift in luminescence peak maxima = were found in **(72−74)** upon increasing the doping concentration from 2 to 10 wt%, which indicated that no triplet-triplet annihilation and π-π interaction between the molecules at high doping concentration occurred. Complexes **(72−74)** were used for fabricating a solution-processed organic light emitting device (OLED). The solution-processed device possessed a structure of indium-tin-oxide (ITO)/poly(-ethylenedioxythiophene):poly(styrene sulfonic acid) (PEDOT:PSS) (40 nm)/ emissive layer (30 nm)/tris(2,4,6-trimethyl-3-(pyridine-3-yl)phenyl)borane (3TPyMB) (5 nm)/1,3,5-tri[(3-pyridyl)-phen-3-yl]benzene (TmPyPB) (40 nm)/LiF (1 nm)/Al (100 nm) with the emissive layer formed by spin-coating a solution of Rh(III):MCP in dichloromethane. The average current and external quantum efficiencies (C.E. and EQE) were found to be 5.0 cd/A and 3.2% with the optimized device (C.E. = 9.4 cd/A and EQE = 6.4%) made with 8 wt% of **(73)**, with CIE (x = 0.62, y = 0.38). Complex **(74)** was further used for vacuum-deposited OLED with a structure of ITO/molybdenum oxide (MoOx; 2 nm)/di-[4-(N,N-di-*p*-tolyl-amino)-phenyl]cyclohexane (TAPC) (40 nm)/4,4′,4″-tris(carbazol-9-yl)triphenylamine (TCTA)(5 nm)/x% rhodium(III):MCP (20 nm)/1,3,5-tris(6-(3-(pyridin-3-yl)phenyl)pyridine-2-yl)benzene (Tm3PyP26PyB) (50 nm)/LiF (1 nm)/Al (150 nm) (x = 2, 5, 8, 11 and 14 v/v%) (Fig. 8.8B and C). The maximum current efficiency of 9.9 cd/A and EQE of 7.0% were achieved for the 5 v/v% doped device. The device efficiency could be improved to 11.9 cd/A and 8.1%, when 3,3′-di(9*H*-carbazol-9-yl)biphenyl (mCBP) was used as the host. The current efficiencies and EQEs could be significantly boosted up to ~ 17.5 cd/A and ~ 12.2%, respectively, by either removing the hole-injecting MoOx or using a hole-transporting material (HTM) with lower hole mobility, i.e., *N,N′*-bis(naphthalene-1-yl)-*N,N′*-bis(phenyl)-2,2′-dimethyl-benzidine (α-NPD) or TCTA (Fig. 8.8D). The reduced hole-transport can result in a better balance in the hole and electron currents in the emissive layer and thus improved efficiency of device. Impressively, the device exhibited an operational half-lifetime (i.e., the time required for the luminance to drop to 50% of its initial value) ~ 946 h at 1000 cd/m^2 and over 3000 h at 100 cd/m^2 (Fig. 8.8E).

8.4 Luminescent Ir(II/III) complexes

8.4.1 Photophysical properties of polypyridyl Ir(III) complexes and their applications in solid-state lighting (OLED and LEC) devices

Flynn and Demas (1974) reported that a prototype Ir(III) complex $[Ir(bpy)_3]^{3+}$, **(75)**, synthesized by boiling a mixture of $K_3IrCl_6 \cdot 3H_2O$, $K_2S_2O_8$, $KHSO_4$ and 2,2′-bpy in water at 220−300°C. This complex exhibited blue-green emission ($\lambda_{em} = 440$ nm) with an associated τ_{PL}value of 2.4 μs in MeOH at 294 K (Demas et al., 1975). The complex exhibited $\pi \rightarrow \pi^*$ ligand based phosphorescence at 446 nm with τ_{PL} value of 80 μs at 77 K in MeOH−EtOH glass (Kahl et al., 1979). A triply ortho-metalated ppy complex [*fac*-$Ir(ppy)_3]^{3+}$, **(76)**, was synthesized with 45% yield upon refluxing $Ir(acac)_3$ and Hppy in degassed glycerol under nitrogen for 10 h at ~ 200°C (Dedeian et al., 1991). The complex **(76)** exhibited unstructured emission ($\lambda_{em} = 492$ nm) with associated τ_{PL} and Φ_{PL}values of 4.2 μs and 0.40 in 2-MeTHF at 298 K. The emission was attributed to the admixture of (^{3}LC + ^{3}MLCT) transitions (Tamayo et al., 2003). The complex **(76)** exhibited ^{3}MLCT based emission at 494 nm with an associated τ_{PL} of 5 μs and a Φ_{PL}value of 40 ± 10% in EtOH-MeOH glass at 77 K (in degassed toluene) Dedeian et al. (1991); King et al. (1985). Later, Tamayo et al. (2003) synthesized [*mer*-$Ir(ppy)_3]^{3+}$, **(77)**, by refluxing $[(ppy)_2IrCl]_2$, ppy and K_2CO_3 under an inert atmosphere in glycerol for 20−24 h at 140−150°C in a high yield of 75%. The complex **(77)** exhibited ^{3}MLCT based structured emission at 512 and 493 nm, respectively, with associated τ_{PL} and Φ_{PL} values of 0.15 μs (at 298 K), 4.2 μs (at 77 K) and ~ 4% (at 298 K), respectively. The lower quantum efficiencies of meridional than the facial complexes were due to the strong influence of the *trans* phenyl in the meridional isomers. Baldo et al. (1999) further used the complex **(76)** for the fabrication of vacuum-deposited OLED device (CIE x = 0.27, y = 0.63, Fig. 8.9A). The device displayed peak EQE and power efficiencies of 8.0% (28 cd/A) and 31 lm/W, respectively, due to a shorter triplet lifetime and reasonable photoluminescent efficiency. At an employed voltage of 4.3 V with 6% of **(76)** in 4,4′-bis(*N*-carbazolyl)-1,1′-biphenyl (CBP), the luminance reached at 100 cd/m^2 with EQE and power efficiencies (P.E.s) as 7.5% (at 26 cd/A) and 19 lm/W, respectively. High internal efficiency was observed due to the effective transmission of both; singlet and triplet excited states in the host CBP to $Ir(ppy)_3$, associated with a short phosphorescent decay of $Ir(ppy)_3$ (< 1 μs) that reduced the saturation of the phosphor at high drive currents, affording a peak luminance of 100,000 cd/m^2.

Lanansky et al. (2001) reported the synthesis and photophysical studies of cyclometalated Ir(III) complexes such as $[(ppy)_2Ir(acac)]$, **(78)**, $[(bt)_2Ir(acac)]$, **(79)** and $[(btp)_2Ir(acac)]$, **(80)**, [bt = 2-phenylbenzothiozolato-C^2,N'), btp = 2-(2′-benzothienyl)-pyridinato- C^3,N')]. The complexes were synthesized with a

yield of 75%–90% by refluxing chloro-bridged Ir(III)-dimer, $C\hat{}N_2Ir(\mu\text{-}Cl)_2IrC\hat{}N_2$($C\hat{}N$ = ppy, bt, btp), acac and Na_2CO_3 in an inert atmosphere in 2-ethoxyethanol for 12–15 h. Complexes **(78–80)** in 2-MeTHF exhibited unstructured ^{3}MLCT and structured $^3(\pi\text{-}\pi^*)$ C^N based luminescence centered at 516, 557, 612 nm (τ_{PL} and Φ_{PL} = 1.6 μs and 34% **(78)**, 1.8 μs and 26% **(79)**, 5.8 μs and 21% **(80)**) at 298 K. The OLEDs structure used for the complexes **(78–80)** (7 wt% in CBP) was the same as was formerly established for *fac*-Ir(*ppy*)$_3$-based OLEDs (Fig. 8.9B) (Baldo et al., 1999). The OLEDs with very similar current-voltage characteristic displayed green **(78)**, (CIE x = 0.31, y = 0.64), yellow **(79)**, (CIE x = 0.51, y = 0.49) and red electroluminescence **(80)**, CIE (x = 0.68, y = 0.33). The OLEDs based on **(78)**, **(79)** and **(80)** showed the EQEs of 12.3% (at 0.01 mA/cm^2), 9.7% (at 1 mA/cm^2) and 6.6% (at 1 mA/cm^2) with associated P.E.s of 38, 11 and 2.2 lm/W, respectively. These high efficiencies were due to efficient trapping and radiative relaxation of the singlet and triplet excitons formed in the electroluminescent process. The complex **(78)** was further studied with various doping concentrations to afford a change in the EQE, e.g., on lowering the concentration of **(78)** from 7% to 4% in CBP, the EQE increased from 9.5% to 11.9% whereas on increasing the concentration to 100%, the efficiency dropped to 1.5%, due to enhanced self-quenching in the neat film of **(78)** (Fig. 8.9C). The performances of OLEDs (EQEs, P.E.s, etc.) of **(78–80)** were found to be in the same trend as the photoluminescence quantum efficiencies of **(78–80)**.

Archetype ionic transition-metal complexes (iTMCs) [Ir(ppy)$_2$(bpy)]PF$_6$, **(81)** and [Ir(ppy$_)_2$(phen)]PF$_6$, **(82)** used by Costa et al. (2009) as the primary active components in light-emitting electrochemical cells (LECs). The complexes **(81)** and **(82)** were synthesized by the traditional way of cleaving the chloro-bridged Ir(III) dimer in presence of an ancillary ligand. These complexes **(81)** and **(82)** exhibited an admixture of ^{3}MLCT + ^{3}LLCT based unstructured emissions at 585 nm (τ_{PL} = 0.43 μs, Φ_{PL} = 14%) and 530 nm (τ_{PL} = 1.29 μs, Φ_{PL} = 17%), respectively, in deaerated MeCN at 298 K. The iTMCs exhibited similar nature of emission, as described earlier, at 590 nm (Φ_{PL} = 66%) (for **81**) and 578 nm (Φ_{PL} = 71%) (for **82**) with 5 wt% doped film in poly(methylmethacrylate) (PMMA). The higher observed Φ_{PL} value of iTMC **(82)** compared to that of **(81)** was due to the lower degree of non-radiative deactivation through the closely lying ^{3}MC state to the emitting state in the later. The iTMCs **(81)** and **(82)** were used as the single active components in double-layer LECs. The LECs fabricated possessed a structure of indium-tin-oxide (ITO)/poly(3,4-ethylenedioxythiophene):polystyrene sulfonate (PEDOT:PSS) (100 nm)/Ir-iTMCs (80 nm)/Al (80 nm). At an applied voltage of 3 V, The LEC using complex **(81)** showed a high luminance (219 cd/m^2) with a higher stability (t = 668 h, total photon flux = 6.61 J, EQE (neat film) = 2.1%, CIE x = 0.5078, y = 0.4859) with turn-on time much lower (t_{ON} = 70.2 h) than the device comprising of **(82)** (t_{ON} = 160 h, luminance = 40 cd/m^2, t = 567 h, total photon flux = 2.42 J, EQE (neat film) =

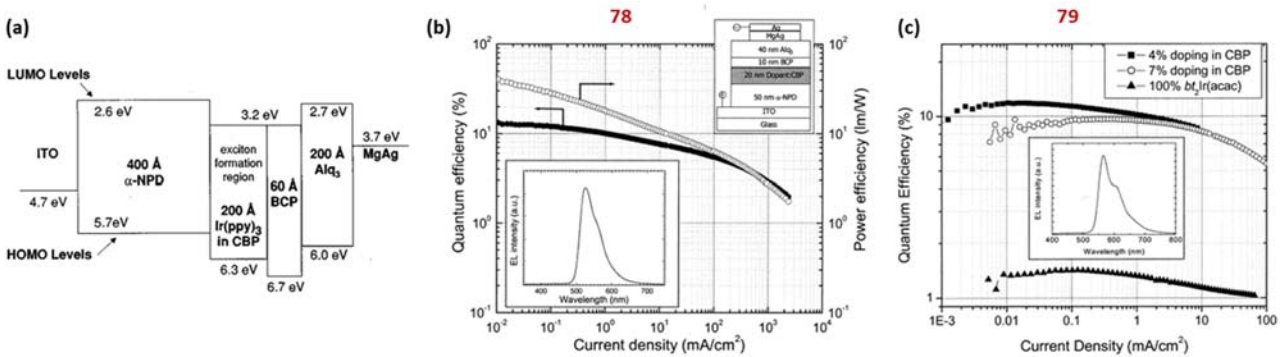

FIG. 8.9 (A) Energy-level diagram of vacuum-deposited OLED of complex **(77)** and (B) EQE and P.E. of vacuum-deposited OLED of complex **(78)** (the inset at the top and bottom shows the energy level structure OLEDs of **(78–80)** and PL spectra of complex **(79)**, respectively) and (C) EQE and P.E.s ofvacuum-deposited OLEDs of complex **(79)** with different doping concentration (the inset shows the PL spectra of complex **(79)**. *(A) Adapted from Baldo, M.A., Lamansky, S., Burrows, P.E., Thompson, M.E., Forrest, S.R., 1999. Very high-efficiency green organic light-emitting devices based on electrophosphorescence. Appl. Phys. Lett. 75 (1), 4–6. With Permission. (C) Adapted from Lamansky, S., Djurovich, P., Murphy, D., Abdel-Razzaq, F., Lee, H.E., Adachi, C. et al., 2001. Highly phosphorescent bis-cyclometalated iridium complexes: synthesis, photophysical characterization and use in organic light emitting diodes. J. Am. Chem. Soc. 123 (18), 4304–4312, With permission.*

1.5, CIE x = 0.5174, y = 0.4824) which indicated that device having complex **(81)** had better performance. This poor performance of **(82)** as compared to **(81)** was the result of closely lying triplet states T_1 and T_2 ($\Delta E_{T1\text{-}T2} = 0.23$ eV) in **(82)** owing to the near degeneracy of the LUMO and LUMO + 1 located on the phen ligand whereas in **(81)** lowest triplet states were well separated and emission took place from T_1 independently of the medium. This fact also resulted in the red-shift of the EL maximum by 48 nm compared to the PL maximum of iTMC **(82)**, whereas the PL and EL maxima of iTMC **(81)** appeared at similar energies. The performance of the devices dramatically improved when small amounts of ionic liquid (IL = 1-butyl-3-methylimidazolium hexafluorophosphate) were added to the Ir-iTMC; the turn-on time improved drastically (from hours to minutes) and the device current and power efficiencies increased by almost one order of magnitude. However, the improvement of the turn-on time was accompanied by a decrease in the stability of the device from 700 h to a few hours ($t_{ON} = 7.2$ h, luminance = 334 cd/m^2, $t_{1/2} = 69$ h, EQE = 3.0% for **(81)** and $t_{ON} = 6.4$ h, luminance = 63 cd/m^2, $t_{1/2} = 73$ h, EQE = 2.1% for **(82)**; $t_{1/2}$ is the time from voltage turn-on to the time where the luminance is half of the maximum value).

Blue phosphorescent OLEDs with tris-cyclometalated iridium complex [*fac*-Ir(mpim)$_3$], (where mpim = mesityl-2-phenyl-1H-imidazole) doped in different hosts, e.g., 2,6-bis(3-(carbazol-9-yl)phenyl)pyridine (26DCzPPy) and TCTA were also reported (Udagawa et al., 2014). The photo luminescent quantum efficiency (Φ_{PL}) of solid-state films comprising TCTA/10 wt% *fac*-Ir(mpim)$_3$ **(83)** and 26DCzPPy/10 wt% *fac*-Ir(mpim)$_3$, **(84)** were found to be 61% **(83)** and 62% **(84)**, the films exhibiting single exponential decay with $\tau_{PL} = 1.50$ (for **83**) and $\tau_{PL} = 1.55$ μs (for **84**). Two different host materials, e.g., 26DCzPPy or TCTA were used in the devices. These blue OLEDs (CIE x = 0.18, y = 0.41) possessed a common structure as ITO (90 nm)/1,4,5,8,9,11-hexaazatriphenylenehexacarbonitrile (HATCN) (5 nm)/TAPC (35 nm)/10 wt% *fac*-Ir(mpim)$_3$-doped host (10 nm)/Tm4PyPB (50 nm)/liq (2 nm)/Al (80 nm). With an extremely low operating voltage of 3.06 V at 100 cd/m^2, a TCTA-based OLED exhibited P.E. = 51.7 lm/W, C.E. = 50.3 cd/A and EQE = 22.8%. With lower driving voltage, TCTA (5 nm)/10wt% *fac*-Ir(mpim)$_3$-doped TCTA (5 nm) device displayed higher P.E., EQE and much higher current density due to a lower hole-injection barrier from TAPC to TCTA. At a driving voltage of 3.22 at 100 cd/m^2, the 26DCzPPy-based OLED showed highest performance with P.E. = 71.9 lm/W, C.E. = 73.6 cd/A and EQE = 33.2% due to the hole trapping property of [*fac*-Ir(mpim)$_3$]. A combination of two hosts, TCTA/26DCzPPy in another device was used, which had two advantages for which it reduced the driving voltage as (i) TCTA can enhance the hole injection from TAPC and (ii) 26DCzPPy can promote the electron injection from Tm4PyPB. The TCTA/26DCzPPy-based OLED showed P.E. = 72.5 lm/W, C.E. = 67.4 cd/A and EQE = 30.7% at 100 cd/m^2,

with an extremely low driving voltage of 2.92 V. Since the blue device with Tm4PyPB didn't show both high EQE of 30% and high P.E. over 70 lm/W and therefore, in a new blue device, ETL was changed from Tm4PyPB to B_3PyPB. The device showed P.E. = 75.6 L m/W, C.E. = 73.2 cd/A, EQE = 29.6% without any light-outcoupling enhancement at a driving voltage of 3.04 V at 100 cd/m^2.

Sajjad et al. (2016) synthesized interesting blue-green cationic Ir(III) complexes $[Ir(ppy)_2(Me\text{-}gpy)]PF_6$, **(85)**, $[Ir(dFppy)_2(CF_3\text{-}gpy)]PF_6$, **86**, $[Ir(dFppy)_2(Me\text{-}gpy)]PF_6$, **(87)**, (where Me-gpy = 2,3,4,6,7,8-Hexahydro-1-(5-methylpyridin-2-yl)-pyrimido[1,2-a]pyrimidine and CF_3-gpy = 1-(5-(trifluoromethyl)pyridin-2-yl)-2,3,4,6,7,8-hexahydro-pyrimido-[1,2-a]pyrimidine, dFppy = 2-(4,6-diflurophenyl)pyrdinato). The complexes were synthesized by heating the suspension of degassed mixture of $[Ir(C^{\wedge}N)_2Cl]_2$ and the gpy-CF_3/gpy-Me ligand in DCM:MeOH (1:1, v/v) in 71−81%. Complexes **(85−87)** in MeCN in a degassed solution exhibited ^{3}LC and ^{3}CT based emissions centered at 510 nm ($\tau_{PL} = 1.90\ \mu s$, $\Phi_{PL} = 50.8 \pm 4.0\%$ for **85**), 462 nm ($\tau_{PL} = 0.11$ and 0.98 μs, $\Phi_{PL} = 1.7 \pm 0.2\%$ for **86**), 470 nm ($\tau_{PL} = 2.60\ \mu s$, $\Phi_{PL} = 65.6 \pm 5.0\%$ for **87**). The 2 wt% **(85)** in PMMA thin film showed Φ_{PL} of 65.9% and 72.4% in air and vacuum, respectively, at 300 K. Complexes **(85−87)** fabricated as solution-processed OLEDs comprised of structure ITO/PEDOT:PSS (30 nm)/PVK (30 nm)/mCP:OXD7 (2,2′-(1,2-phenylene)bis[5-(4-*tert*-butylphenyl)-1,3,4-oxadiazole]: **(85−87)** (75:20:5wt%) (30 nm)/B_3PYMPM (60 nm)/Ca (20 nm)/Al (100 nm). EL spectra of **(85−87)** are similar to their PL spectra but these were red-shifted and displayed different relative intensities of the vibronic peaks. The OLEDs at 100 cd/m^2 showed the EQEs and C.E. of 6.3%, 20.8 cd/A (CIE x = 0.29, y = 0.58 for **85**), 2.3%, 6.2 cd/A (CIE x = 0.26, y = 0.47 for **87**) and 2.8%, 7.1 cd/A (CIE x = 0.22, y = 0.43 for **86**) with associated P.E.s of 8.7, 1.9 and 1.6 lm/W, respectively. Complex **(87)** showed the best performing OLED with low turn-on voltage ($V_{ON} = 5.8$) based on the use of cationic iridium complexes as emissive layer attributed to the shallower HOMO enabling more effective hole injection, which explained the low-turn on voltage and enhanced device efficiency and charge balance. Subsequently, the same group synthesized another four cationic Ir(III) complexes $[Ir(2\text{-}TFMePpy)_2(dtBubpy)]PF_6$, **(88)**, $[Ir(2\text{-}TFMyPy)_2(dtBubpy)]PF_6$, **(89)**, $[Ir(2\text{-}TFMtPpy)_2(dtBubpy)]PF_6$, **(90)**, $[Ir(2\text{-}TFMsPpy)_2(dtBubpy)]PF_6$, **(91)**, (where2-TFMePpy = 2-(4-(trifluoromethyl) phenyl)-pyridine, 2-TFMyPpy = 2-(4-(trifluoromethoxy)phenyl)pyridine, 2-TFMtPpy = 2-(4-((trifluoromethyl)thio)phenyl)pyridine, 2-TFMsPpy = 2-(4-((trifluoromethyl)sulfonyl)phenyl)pyridine) in high yields of 70%−86% (Pal et al., 2016). At RT ($\lambda_{exc} = 360$ nm) complexes **(88−91)** in degassed MeCN displayed mixed structured/unstructured ^{3}LC + (^{3}MLCT/^{3}LLCT) structured transition centered at 484 nm ($\tau_{PL} = 1.79\ \mu s$, $\Phi_{PL} = 45\%$ for **88**), 527 nm ($\tau_{PL} = 1.14\ \mu s$, $\Phi_{PL} = 50\%$ for **89**), 491 nm ($\tau_{PL} = 3.31\ \mu s$, $\Phi_{PL} = 66\%$ for **90**) and 515 nm ($\tau_{PL} = 4.28\ \mu s$, $\Phi_{PL} = 55\%$ for **91**). Complex **(91)** with the

strongest electron withdrawing (EWG) group $-SO_2CF_3$ exhibited red-shifted emission whereas complex with $-CF_3$ displayed the most blue-shifted emission. The thin film PL of complexes (**88**−**91**) showed the similar trend as observed for the solution photoluminescence. Single layer LECs were fabricated with a general structure ITO/PEDOT:PSS/[Bmim][PF_6]:emitter (4:1 M ratio)/Al with complexes (**88**−**91**) acting as the emitters (Bmim = 1-butyl-3-methylimidazolium hexafluorophosphate). All the EL maxima were found to be red-shifted with respect to the thin film maxima though the position of shoulder in complexes (**88**) and (**90**) remained at the same energy. The red-shift of the EL and thin-film PL maxima in solution was found to be due to the aggregation in the solid state. The operating voltage of LECs (**88**−**90**) at 50 A/m^2 displayed sky-blue to green (CIE x = 0.37−0.45, y ∼ 0.54) and reached a steady-state value at 2.80−3.00 V, demonstrating no charge injection barrier. At current density of 100 A/m^2, the LECs displayed EQE = 3.0%, C.E. = 9.8 Cd/A, luminance = 987 Cd/m^2 (for **88**), EQE = 2.3%, C.E. = 7.3 Cd/A, luminance = 726 Cd/m^2 (for **89**), EQE = 1.1%, C.E. = 3.5 Cd/A, luminance = 350 Cd/m^2 (for **90**). Complex (**91**) with an irreversible reduction potential only achieved a very low level of luminance (32 Cd/m^2). In the subsequent year, Pal et al. (2017) also reported red-to-NIR cationic Ir(III) complexes, [Ir(ppy)$_2$(Btz)]PF_6, (**92**) and [Ir(ppy)$_2$(Bbtz)]PF_6, (**93**), (Btz = 2,2′-bithiazole, Bbtz = 2,2′-Bibenzo[d]thiazole) in excellent yield (91%−95%) and used them in red-to-NIR LECs. In degassed MeCN at 298 K, complexes (**92**) and (**93**) exhibited featureless ^{3}CT emission at 658 nm ($\tau_{PL} = 0.08$ μs, $\Phi_{PL} = 1.72\%$ for **92**) and 744 nm ($\tau_{PL} = 0.044$ μs, $\Phi_{PL} = 0.35\%$ for **93**). At an excitation value of 320 nm, the thin films of complexes (**92**) and (**93**) mixed with [Bmim][PF_6] exhibited featureless ^{3}CT emission at 658 nm ($\tau_{PL} = 257$ ns, $\Phi_{PL} = 14\%$ for **92**) and 707 nm ($\tau_{PL} = 117$ ns, $\Phi_{PL} = 5\%$ for **94**). The LECs of complexes (**92**) and (**93**) possessed a structure of ITO/PEDOT:PSS/Ir-iTMCs:[Bmim][PF_6] (4:1 molar ratio)/Al LEC based device of complexes (**92**) and (**93**) exhibited EL at 661 and 705 nm, respectively. The efficiency of LEC-(**92**) was more strongly affected by increased in the current density. LEC-(**92**) showed an EQE of 0.23% ($t_{1/2} = 0.24$ h) and 0.13% ($t_{1/2} = 0.15$ h) and LEC-(**93**) showed an EQE of 0.37% ($t_{1/2} = 80$ h) and 0.33% ($t_{1/2} > 80$ h) at current densities of 400 and 800 A/m^2, respectively. The higher $t_{1/2}$ value for LEC-(**93**) in comparison to the same of LEC-(**92**) was assigned to the presence of the annulated benzenes in the ancillary ligand.

Ir(III) complexes were also synthesized with *N*-heterocyclic carbene such as [*fac*-Ir(pmp)$_3$], (**94**) and [*mer*-Ir(pmp)$_3$], (**95**), (where pmp = *N*-Phenyl-*N*-methyl-pyridoimidazol-2-yl) (Lee et al., 2016). This unique work dealt with Ir−NHC complexes, which can act as both: a deep blue emissive layer (EML) as well as efficient hole-conducting electron blocking layer (EBL). The complexes showed ^{3}LC/^{3}MLCT based broad emission at 418 nm ($\tau_{PL} = 1.2 \pm 0.1$ μs, $\Phi_{PL} = 76 \pm 5\%$ (for **94**)) and at 465 nm

($\tau_{PL} = 0.8 \pm 0.1$ μs, $\Phi_{PL} = 78 \pm 5\%$ (for **95**)) in deaerated 2-MeTHF at 295 K. The PL spectrum of **(95)** was found to be broader and red-shifted compared to that of **(94)** due to stabilized excited states of **(95)**. Complexes **(94)** and **(95)** were used in fabricating two Phosphorescent Organic Light-Emitting Diodes (PHOLEDs) (Fig. 8.10A and B). The electron blocking layer (EBL) consisted of **(94)** (when **94** was also used in EML) and [*fac*-Ir(pmb)$_3$] (when **95** was also used in EML) (pmb = *N*-Phenyl-*N*-methyl-benzimidazol-2-yl), which had either equal or shallower LUMO energies than that of the host, as well as equal or larger triplet energy levels than the dopants ($E_T = 2.90$ eV). This empowered effective hole injection into the hole-conducting dopants through blocking electrons transported by the host. At a 20 vol% doping concentration near the EBL/EML interface, it enabled hole injection and transport, which decreased gradually at the EML/HBL interface at 8 vol% dopant concentrations. At 10 mA cm^{-2}, complex **(94)** based PHOLED showed EQE = 9.0 ± 0.1 (at 1000 cd/m^2), luminance = 7800 ± 400 cd/m^2 (at $J_{1/2}$), CIE x = 0.16, y = 0.09 whereas **(95)** based PHOLED showed EQE = 13.3 ± 0.1 (at 1000 cd/m^2), luminance = $22{,}000 \pm 1000$ cd/m^2 (at $J_{1/2}$), CIE x = 0.16, y = 0.15 (Fig. 8.10C). The difference in EQE values was assigned to (i) different degrees of aggregation-induced quenching, which in turn were induced due to their different static dipole moments (17.2 D for **(94)** and 10.8 D for **(95)** and (ii) lower absorptivity of **(95)** leading to the higher fraction of host quenching. Later, Pal et al. (2018a) reported two deep blue-emitting homoleptic Ir(III) complexes *mer*-Ir(3-TFpIm)$_3$, **(96)** and *mer*-Ir(4-TFpIm)$_3$, **(97)**, (where (3/4-TFpIm)$_3$ = 3-methyl-1-(3/4-(trifluoromethyl)phenyl)-1*H*-3λ^4-imidazole). Complexes **(96)** and **(97)** exhibited admixture of ^{3}LC + ^{3}MLCT based deep blue structured emission at 424 nm ($\tau_{PL} = 280$ μs (65%), 1816 μs (35%), $\Phi_{PL} = 25\%$ (for **96**)) and λ_{em} at 427 nm ($\tau_{PL} = 698$ μs (48%), 1820 μs (52%), $\Phi_{PL} = 72\%$ (for **97**)) in deaerated CH_2Cl_2 at 298 K. Complexes **(96)** and **(97)** also showed structured emission at 409 nm ($\tau_{PL} = 2167$ μs, $\Phi_{PL} = 13.7\%$ (N_2), 13.5% (air) (for **96**)) and λ_{em} at 428 nm ($\tau_{PL} = 3993$ μs, $\Phi_{PL} = 46.6\%$ (N_2), 38.6% (air) (for **97**)) in 10 wt% doped PMMA film. Complexes **(96)** and **(97)** were used in fabricating vacuum-deposited OLEDs where **(97)** was used as the emitter and **(96)** was used as the EBL due to its high triplet energy ($E_T = 3.19$ eV at 77 K) and shallow LUMO level. The high emission energy of **(97)** restricted the choice of the host material. Apart from three OLED devices (devices I-III) reported in this work that included different HTL, exciton blocking layers, the best OLED performance came from minimum possible interlayered-device, device IV, (TAPC as HTL, **(96)** as EBL, 10 wt% **(97)** in DPEPO as EML and TPBi as ETL (DPEPO = (Bis [2-(diphenylphosphino) phenyl] ether oxide), TPBi = 1,3,5-tris(1-phenyl-1H-benzimidazol-2-yl)benzene). DPEPO was used because of its wide band gap and high triplet energy, which was higher than the triplet energy of **(97)** ($E_T = 3.31$ eV). On comparing the emission spectra of **(97)** in DPEPO with

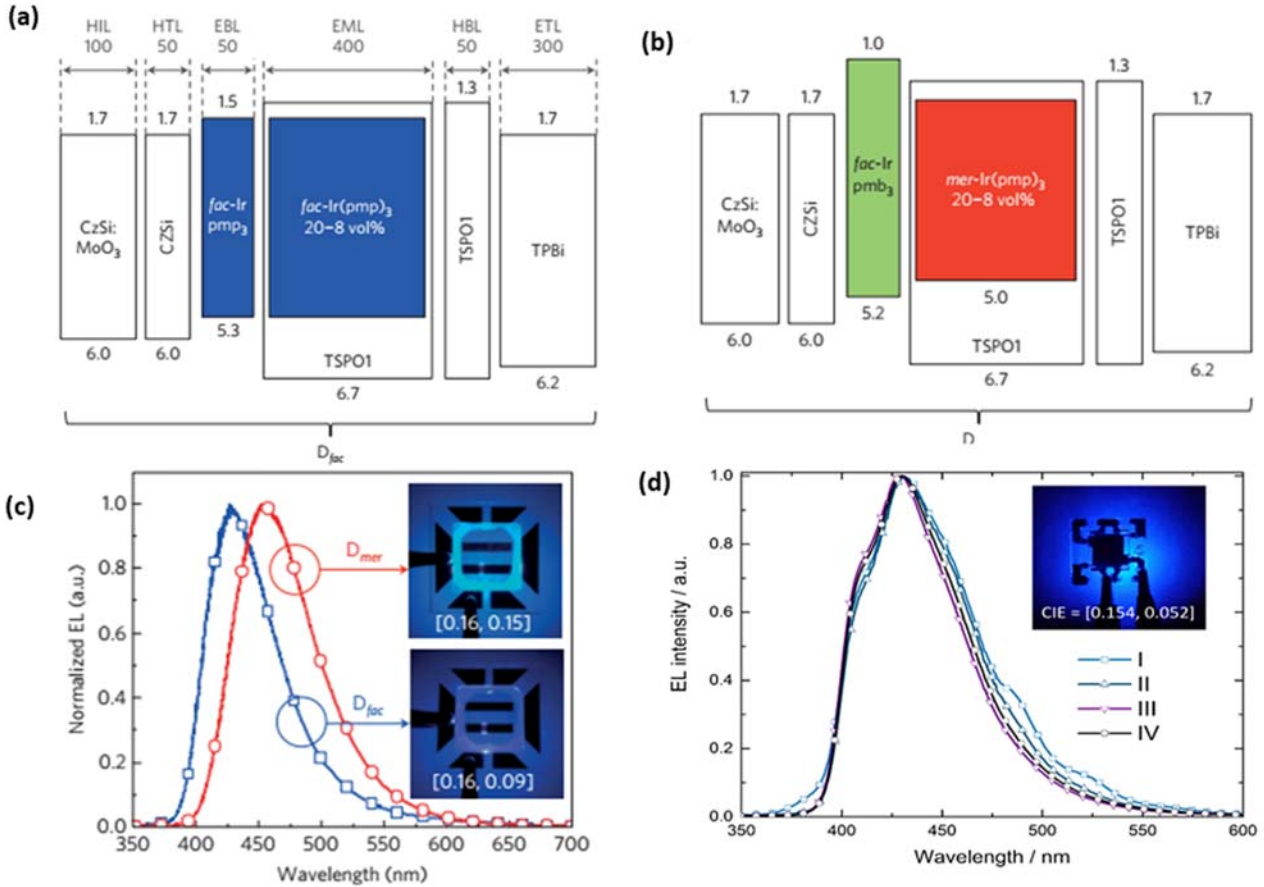

HIL = hole injecting layer, HTL = hole transporting layer, EBL = electron blocking layer, EML = emissive layer, HBL = hole blocking layer, ETL = electron transporting layer CzSi = 9-(4-*tert*-butylphenyl)-3,6-bis(triphenylsilyl)-9H-carbazole, TSPO1 = diphenyl-4-triphenylsilylphenylphosphine oxide, TPBi = 1,3,5-tris(1-phenyl-1H-benimidazole-2-yl)benzene.

emission spectra observed in thin films, it was found that in DPEPO, emission was narrower and had lower Φ_{PL}, which was assigned to the different polarity of the surrounding host medium and guest-host interactions that affect the nature of the excited state. These devices exhibited electroluminescence at 430−431 nm with associated FWHM = 62−68 nm, EQE from 7.2% to 13.4%, P.E. = 2.80−3.95 and CIE x = 0.151−0.156, y = 0.052−0.077 (Fig. 8.10D). Device IV displayed the bluest and best performance with max EQE and P.E. values at 13.4% and 3.50 lm/W, respectively, whereas at 100 cd/m^2 this device showed EQE and P.E. values at 12.5% and 2.98 lm/W, respectively. Optical anisotropy of the DPEPO:**97** film was studied with variable spectroscopic ellipsometryto optimize the device performance and to evaluate the emitter arrangement. A value of S (order parameter) of −0.26 was found, which corresponded to the fact that a majority of transition dipole moments were lying horizontal to the substrate plane.

Tokito et al. (2003) reported the fabrication of OLEDs of an interesting Ir(III) complex, bis[(4,6-di-fluorophenyl)-pyridinato-C^2,N']picolinate iridium(III), **(98)**, also commercially known as FIrpic. The complex was synthesized by the heterolytic cleavage of FIr_2Cl_2 with picolinic acid (Fig. 8.11A) (Yen et al., 2005). The OLED devices of complex **(98)** with CBP (E_T = 2.6 eV at 77 K) and 4,4′-bis(9-carbazolyl)2,2′-dimethyl-phenyl (CDBP) (E_T = 3.0 eV at 77 K) as host materials were fabricated as ITO (200 nm)/PEDOT:PSS (40 nm)/α-NPD (30 nm)/(CDBP or CBP):FIrpic (40 nm, 3%)/bis(2-methyl-8-quinolinato)-4-phenylphenolatealuminum(III) (BAlq) (30 nm)/LiF (1 nm)/Al (150 nm). The OLED of complex **(98)** with CDBP as host material showed an EQE = 10.4% (at 20.5 cd/A), P.E. = 10.5 lm/W and C.E. = 20.4 cd/A which was found to be greater than the CBP based OLED device having EQE = 5.1% (Fig. 8.11B). In both; CBP and CDBP based OLEDs, EQE decreased at a high current density, which was assigned to triplet-triplet annihilation. The high efficiency in the CDBP based device was due to the alignments of the triplet energies of the organic materials comprised in the devices. As CDBP has E_T = 3.00 eV, which was higher than the E_T of FIrpic (2.70 eV) and therefore, the transfer of triplet energy from FIrpic to CDBP was

FIG. 8.10 Device structures and their frontier orbital energies for (A) energy level diagram of PHOLED based on (A) **(94)** and (B) **(95)**, (C) EL spectra of **(94)** and **(95)** at >14 vol% doping in TSPO1 at a current density of 10 mA/cm^2 (inset shows a photograph of 2 mm^2 packaged PHOLEDs) and (D) EL spectra of OLED devices I-IV inset shows the photograph of the PHOLED emission with the CIE color coordinates of device IV. *(A-C) Adapted from Lee, J., Chen, H.F., Batagoda, T., Coburn, C., Djurovich, P.I., Thompson, M.E., et al., 2018. Deep blue phosphorescent organic light-emitting diodes with very high brightness and efficiency. Nat. Mater. 15, 92−98. With permission; (D) Adapted from Pal, A.K., Krotkus, S., Fontani, M., Mackenzie, C.F.R., Cordes, D.B., Slawin, A.M.Z., et al., 2018. High-efficiency deep-blue-emitting organic light-emitting diodes based on iridium(III) carbene complexes. Adv. Mater. 30 (50), https://10.1002/adma.201804231. With Permission.*

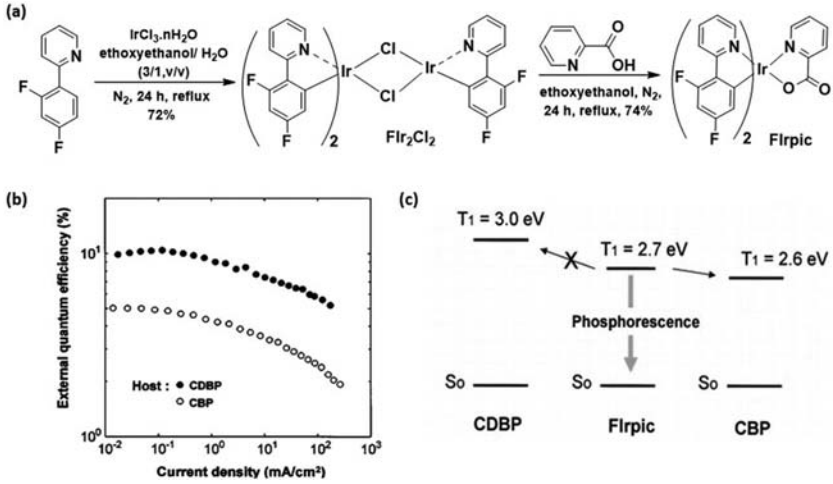

FIG. 8.11 (A) Synthesis of FIrpic, (B) EQE *vs* current density for OLEDs with CBP and CDBP as host materials and (C) E_T alignment of FIrpic, CBP and CDBP. *Adapted from Tokito, S., Iijima, T., Suzuri, Y., Kita, H., Tsuzuki, T., Sato, F., 2003. Confinement of triplet energy on phosphorescent molecules for highly-efficientorganic blue-light-emitting devices. Appl. Phys. Lett. 83 (3), 569–571. With Permission.*

suppressed and energy-restricted on the FIrpic, which led to high phosphorescence from FIrpic triplet in the device (Fig. 8.11C). Yeh et al. (2005) reported two OLED devices with new host materials, e.g., 1,3-bis(9-carbazolyl) benzene (mCP) and 3,5-bis(9-carbazolyl)tetraphenylsilane (SimCP). The OLED comprised of structure as ITO/*N*,*N*′-di(naphthalene-1-yl)-*N*,*N*′-diphenylbenzidine (NPB) (30 nm)/SimCP:dopant (30 nm, 7%)/2,2′,2″-(1,3,5-phenylene)tris(1-phenyl-1*H*-benzimidazole) (TPBI) (30 nm)/LiF/Al. Although having the same E_T value of 2.9 eV, the SimCP based OLED showed a better EQE of 14.4% as compared to that of mCP based OLED (EQE = 12.3%) with a P.E. = 11.9 lm/W. This fact was attributed to the rigidity of the triphenylsilyl structural moiety that brought more balanced electron and hole combination in the host matrix of the SimCP or by alleviating the T_1-T_1 annihilation, concluding that the host material played an important role for the EQE of the OLEDs.

8.4.2 Application of Ir(III) complexes in photoredox catalysis

Ir(III) complex, $[Ir(ppy)_2(dtbbpy)]PF_6$, (dtbbpy = 4,4′-di-tert-butyl-2,2′-bipyridine), **(99)**, was used for the oxidative coupling of nitroalkanes and tertiary *N*-arylamines *via* visible-light photoredox catalysis by Condie et al. (2010). A variety of *N*-aryltetrahydroisoquinolines was subjected to the optimized conditions by aza-Henry reaction with 1 mol% of **(99)** and visible light

that showed high yields of the coupling products in 92–96% (Fig. 8.12A–Entries 1–3). The light and PRC were found to be the basic requirements for the reaction to give the desired yield of the product. When the reaction was conducted in the dark, the substrate did not display any conversion (Fig. 8.12A–Entry 1-substrate 3). In the absence of catalyst, the substrate took 180 h for the 83% conversion of the reaction (Fig. 8.12A–Entry 1-substrate 4). The non-benzylic amine afforded the desired coupling in a moderate yield of 27% (Fig. 8.12A–Entry 2). The use of a less volatile nitro compound, $PhCH_2NO_2$ in DMF, in the presence of **(99)** resulted in the full conversion of the substrate (Fig. 8.12A–Entry 3). After degassing, the same reaction took 72 h with the attenuated rate for the clean formation of the product. The use of this less volatile nitro compound provided evidence for the proposed mechanism as shown (Fig. 8.12B). Upon excitation, the Ir(III)* reductively quenched the amine to give rise to radical iminium cation. The so generated powerful reducing agent Ir(II) [Ir(III)/Ir(II) = −1.51 V *vs* SCE] reduced oxygen to produce an oxygen radical anion, which in turn abstracted a hydrogen atom from the trialkylammonium radical cation to form the iminium ion. This ion reacted with the nitroalkane to afford the desired product. Nguyen et al. (2011) reported an Ir(III) complex, $[Ir\{dF(CF_3)ppy\}_2(dtbbpy)]PF_6$, **(100)**, for the intermolecular Atom Transfer Radical Addition (ATRA) to olefins. The reaction of tosylated allylamine and diethyl 2-bromomalonate (DBM) in DMF in the presence of **(100)** for 24 h resulted in the first intermolecular ATRA in a 17% yield. Optimization of the reaction with LiBr as an additive and H_2O as a co-solvent led to an increase in the yield from 45% to 67%. Later, the reaction was performed with BOC-protected (BOC = *tert*-Butyloxycarbonyl protecting group) allylamine and 5-hexen-1-ol, which afforded more consumption of the substrate and resulted in a high yield of the product up to 99%. The light and PRC were found to be the basic requirements for the reaction to give the desired yield of the product, e.g., using substrate 5-hexen-1-ol, no reaction took place without the presence of light and PRC. The atom transfer of various functional groups including free alcohols, silyloxyethers, benzylethers, alkylbromides, esters, enones, carbamates and aromatic rings were well tolerated with optimized conditions. The achievement of the intermolecular atom transfer with DBM encouraged the investigation of the other compounds comprising of activated C-X bonds (Fig. 8.12C– Entries 1–2). It was found that hexene did not undergo coupling with DBM but it resulted in effectual ATRA with ethyl bromodifluoroacetate (Fig. 8.12C–Entry 2). The dehydroiodination of the atom transfer products with CF_3I, comprehended by subjecting the ATRA product to diazabicycloundecene (DBU) in toluene, resulted in the formation of the trifluoromethylalkene (Fig. 8.12C– Entry 3). In addition, 1,1-cyclopropane diesters were generated in an excellent yield (Fig. 8.12C – Entry 4). It was concluded that only 0.01 mol% of **(100)** was required for the 97% yield that resulted from the coupling reaction of DBM with 5-hexen-1-ol. In the mechanism, upon excitation, oxidative quenching of

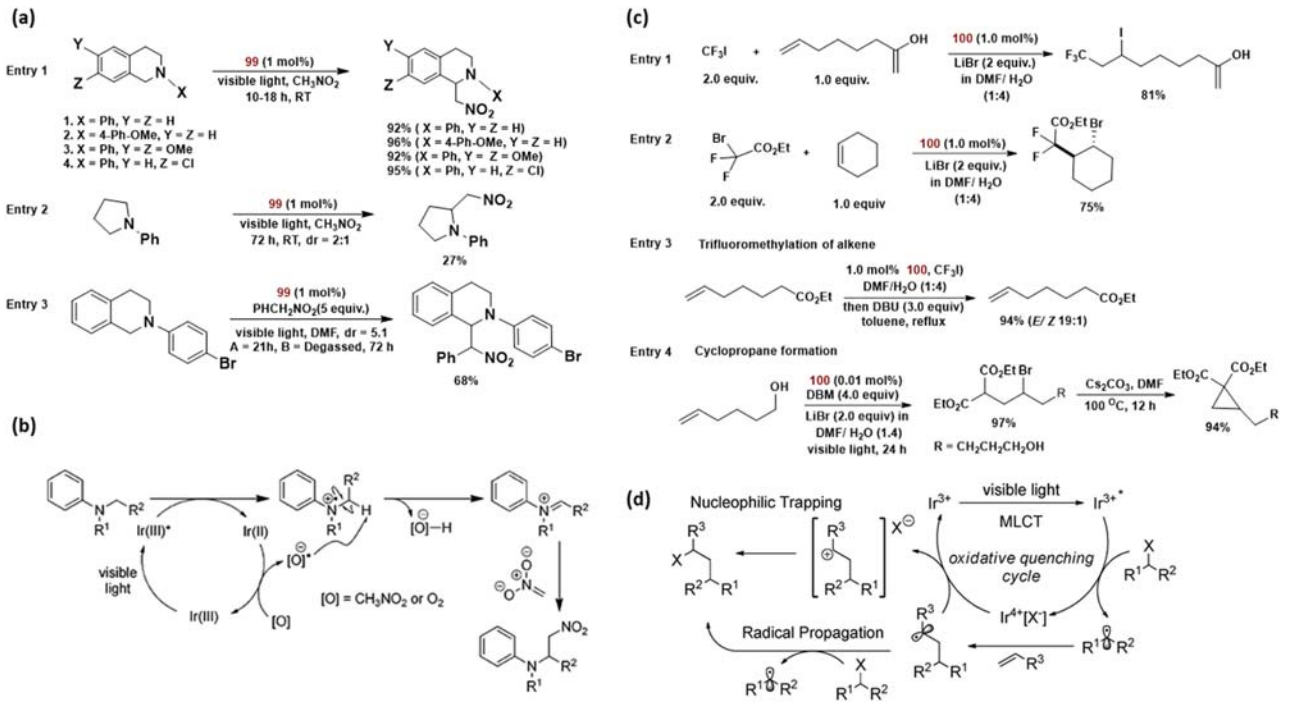

FIG. 8.12 (A) Examples of oxidative aza-Henry reactions using PRC, (B) mechanism of iminium ion generation using photoredox catalysis, (C) examples of ATRA reactions using PRC and, (D) proposed mechanism of an ATRA reaction. *(B) Adapted from Condie, A.G., González-Gómez, J.C., Stephenson, C.R.J., 2010. Visible-Light photoredox catalysis: aza-Henry reactions via C−H functionalization. J. Am. Chem. Soc. 132 (5), 1464−1465. With Permission; (D) Adapted from Nguyen, J.D., Tucker, J.W., Konieczynska, M.D., Stephenson, C.R.J., 2011. Intermolecular atom transfer radical addition to olefins mediated by oxidative quenching of photoredox catalysts. J. Am. Chem. Soc. 133 (12), 4160−4163. With Permission.*

the visible-light-induced Ir(III)* by the haloalkane and α-halocarbonyl took place, which generated an electrophile radical along with the Ir(IV) complex, with halide as the counter ion (Fig. 8.12D). The halide then resulted in the addition to the olefin. The ATRA product can be generated by two potential pathways. First, the oxidation of the alkyl radical (0.47 V *vs* SCE) by Ir(IV) generated the carbocation pre-associated with the halide, which in turn combined with the halide to afford the final product selectively.

MacMillan et al. (2011) investigated photoredox catalyzed C−H arylation reactions of cyclicbenzylic amines using Ir(III) complex, [*fac*-Ir(ppy)$_3$], **(76)**. The reaction of *N*,*N*-alkyl/cyclic amine and 1,4-dicyanobenzene (DCB) with **(76)** as a photoredox catalyst afforded α-arylamines in good yields (Schemes 8.1−8.3 in Fig. 8.13A). Substrates like five-membered pyrrolidine, six-membered piperidine, morpholine, *N*-BOC-piperazine and seven-membered azepane rings with DCB resulted in a high yield (91%−98%) of C−H arylated products. The variation of the R substituents with methyl, halogen and naphthyl groups in *N*-R substituted amines showed a high yield of 81%−93% (Scheme 8.1 in Fig. 8.13A). The non-aryl protecting group, e.g., dimethoxybutane (DMB) also showed a high yield of the C−H arylated product in 78% with > 20:1 regiomeric ratio (r:r) (product b in Scheme 8.1 in Fig. 8.13A). The medicinally important cyclic amine structures, e.g., protected indoline was also subjected for C−H arylation reaction, which showed a distinct preference for the arylation at the ring position as opposed to the acyclic benzylic site (product C in Scheme 8.1 in Fig. 8.13A). The scope of the variation of substituents in the aryl rings in the α-aminearylation was also studied. Benzonitriles substituted with esters, amides, phosphonate esters, electron-deficient tetrazoles and heterocycles were found to be suitable substrates for the C−H arylation reaction (Scheme 8.2A−C in Fig. 8.13A). In addition, a chloride ion in a five-membered heteroaromatic moiety can function equivalently to CN^- as a leaving group (product d in Scheme 8.2 in Fig. 8.13A). This empowered the arylation of amines with chloro-substituted caffeine, benzoxazole and *N*-BOC benzimidazole. Pharmaceutical agents, such as linezolid (antibiotic) went direct heteroarylation with 2-chlorobenzoxazole in a yield of 58% (Scheme 8.3 in Fig. 8.13A). This result established the scope of drug molecules to participate in the C−H functionalization reaction. For the mechanism, upon excitation, the powerful reductant Ir(III)* [$E_{1/2ox} = -1.73$ V *vs* SCE] reduced the 1,4-DCB [$E_{1/2red} = -1.61$ V *vs* SCE] to produce a dicyanoarene radical anion. The resulting strong oxidant $Ir^{IV}(ppy)_3$ [$E_{1/2red} = +0.77$ V *vs* SCE] underwent SET with the amine generating an amine-radical cation and $Ir^{III}(ppy)_3$ (Fig. 8.13B). The C−H bonds adjacent to the nitrogen atom in the amine-radical cation were found to be weakened by 40 kcal mol^{-1} and underwent deprotonation by NaOAc to give an α-amino radical. Then, a radical-radical coupling reaction between the dicyanoarene radical anion and the α-amino radical followed by the elimination of CN^- afforded the aromatized benzylic amine product.

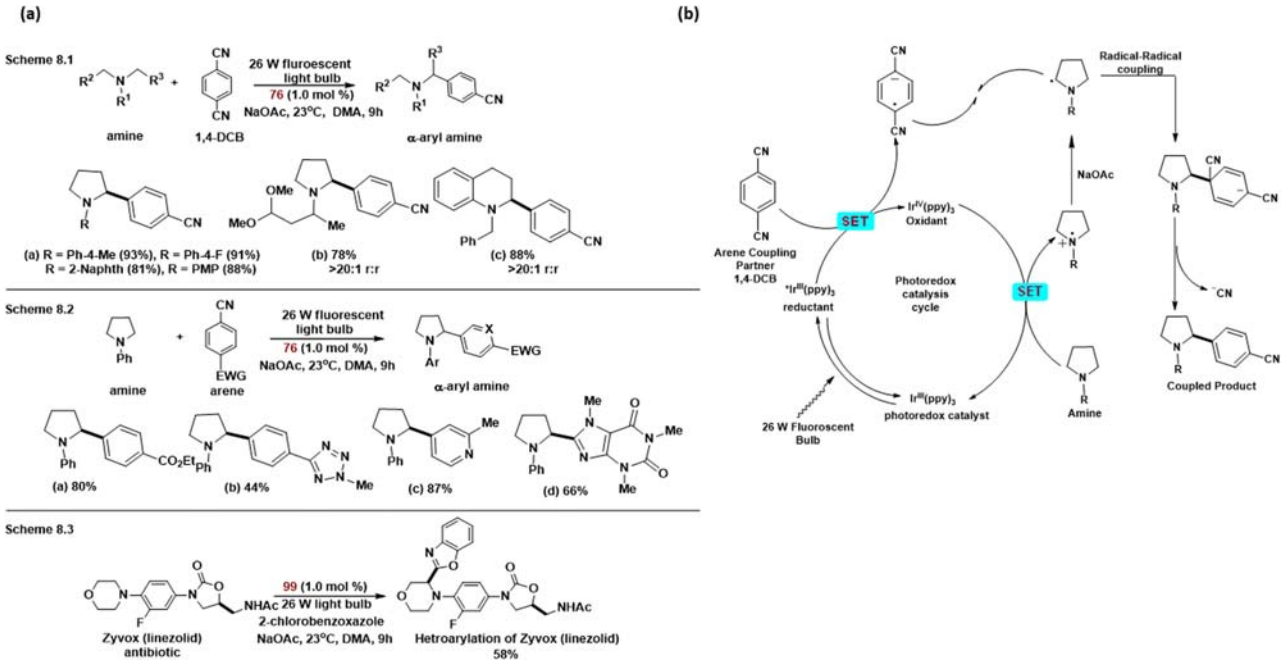

FIG. 8.13 (A) Schemes 8.1−8.3. Photoredox C−H arylation reactions with cyclic and acyclic amines and (B) proposed mechanism for C−H arylation reactions.

8.4.3 Application of Ir(III) complexes in biological sensing of metal-ion

Ir(III) complexes have also been used for biological sensing of the photophysically inactive Zn(II), as ZIrdfppy, **(101)**, ZIrdCF_3, **(102)** and ZIrfppy, **(103)**, (where dfppy = 2-(2,4-Diflourophenyl)pyridine, dCF_3 = 2,4-Bis(trifluoromethyl)phenyl]pyridine, fppy = 2-(4-fluorophenyl)pyridine) (Fig. 8.14A) (You et al., 2014). The complexes **(101−103)** showed ^{3}MLCT emission as the parent complexes without the chelated Zn(II) ion at 499−548 nm; however, the Φ_{PL} values of **(101−103)** were in the range of 0.14−3.0% in degassed MeCN at RT. The complexes were judiciously designed with a Zn(II) receptor, di-2-picolylamine (DPA) at the *para* position of the phen ligand through a methylene linker to sense the Zn(II) ions. In this dyad structure, the photoexcitation of the ^{3}MLCT transition promoted the photoinduced electron transfer (PeT) from DPA to the photoexcited iridium species, effectively suppressing the ^{3}MLCT emission of the Ir(III) complex and lowering the Φ_{PL} values of **(101−103)** compared to those of the parent analogous complexes without the pendant $-CH_2-$ bridged DPA group (Φ_{PL} = 11−23%). The binding of Zn(II) to the DPA reduced the electron-donating ability of the later to the Ir(III) complex, which resulted in the restoration of the phosphorescent ^{3}MLCT emission of the Ir(III) species, i.e., phosphorescence was turned on. To confirm the PeT from DPA, an experiment was conducted, in which tri-2-picolylamine (TPA) was used instead of DPA as the electron donor. TPA affected the phosphorescence decay of the Irdfppy, Irfppy and IrdCF_3 parent complexes of Ir(III) and the bimolecular rate constants for PeT (k_{PeT}) from TPA to the Ir(III) complexes were found to be in the range of (6.0−7.5) × 10^6 $M^{-1}s^{-1}$. The phosphorescence turn-on ratios were quantified by the dynamic range [DR = Φ_{PL} (Zn^{2+})/Φ_{PL} (Zn^{2+}-free)] values as 31 (for **102**), 12 (for **102**) and 2.9 (for **103**). An additional mechanism for the phosphorescence turn-on response of zinc-ion probes was proposed from the femtosecond laser flash photolysis study. The Ir(III) analog of complex **(101)** without the pendant $-CH_2-$ bridged DPA group showed transient absorption bands at 540 and 1100 nm due to the phen radical anion ($phen^{\bullet -}$), signifying the generation of the ^{3}MLCT transition state involving the phen ligand ($ML_{N^{\wedge}N}CT$), which hypsochromically shifted to 530 and 1000 nm for ZIrdfppy (Fig. 8.14B). This showed a different origin for the charge-transfer state as DPA can be more easily oxidized than the Ir(III) center (1.28 *vs* 1.56 V *vs* SCE) and this transient absorption of $phen^{\bullet -}$ of zinc-free ZIrdfppy was attributed to charge transfer from DPA. Thus, an $IL_{N^{\wedge}N}CT$; i.e., DPA → phen charge transfer took place (Fig. 8.14C), resulting in weak phosphoresce in ZIrdfppy as also observed in the lowering in Φ_{PL} values. Complexes

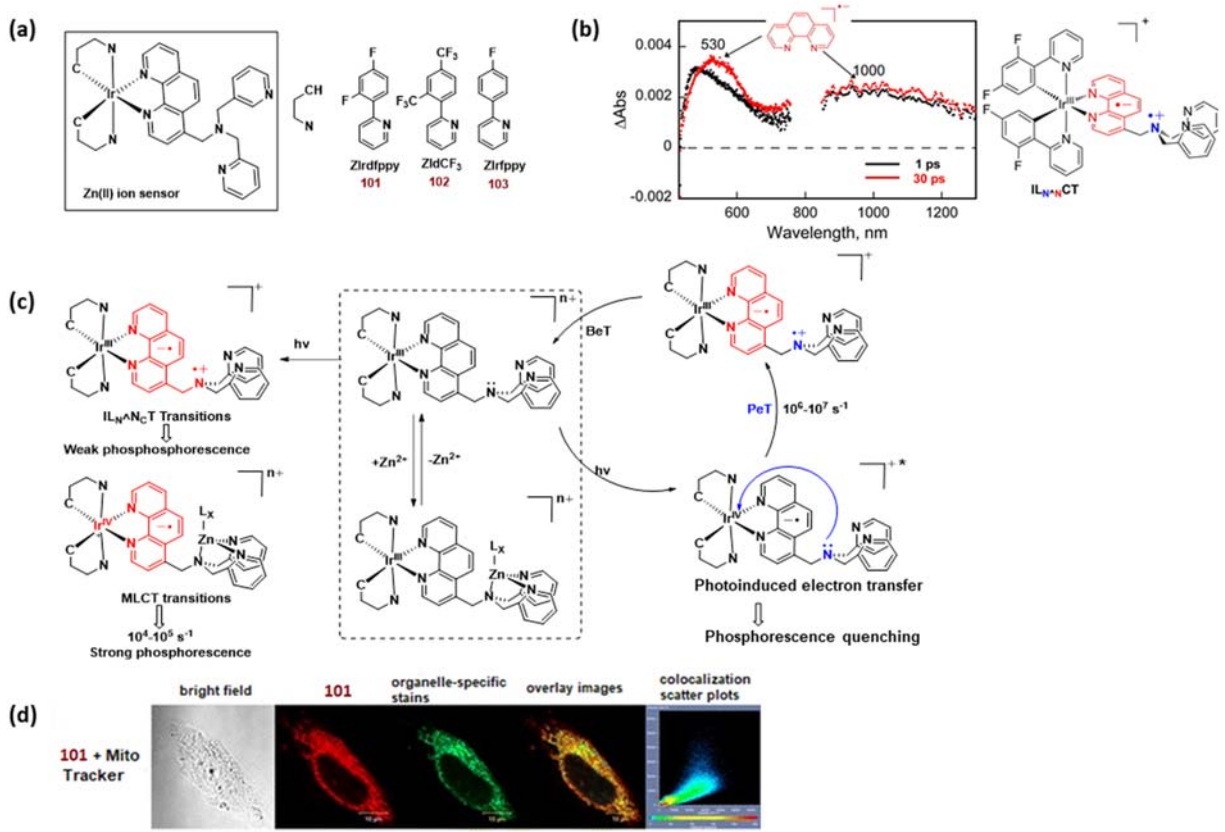

FIG. 8.14 (A) Structure of phosphorescent sensors of Zn(II), (B) femtotransient absorption spectra of zinc-freeform of 0.30 mM **(101)** measured at 1 ps (black curves) and 30 ps (red (gray in print version) curves) delay after photoexcitation at 420 nm, (C) proposed photophysical mechanism for phosphorescence signaling and (D) mitochondrial localization of ZIrdfppy in HeLa cells, 10 μM **(101)** (10 min incubation at 37°C; $\lambda_{exc} = 405$ nm; $\lambda_{em} = 406-550$ nm) and 500 nM MitoTracker deep red FM (45 min incubation at 37 °C; $\lambda_{exc} = 633$ nm; $\lambda_{em} = 637-758$ nm). *Adapted from You, Y., Cho, S., Nam, W., 2014. Cyclometalated iridium(III) complexes for phosphorescence sensing of biological metal ions. Inorg. Chem. 53 (4),1804−1815. With Permission.*

(101−103) were found to be cell-permeable once added to the culture media and were found to be confined on the HeLa cells. At 310 K, media containing 5−10 μM of **(101)** eagerly entered live HeLa cells and showed the lower phosphorescence intensity due to DPA → phen $IL_{N^{\wedge}N}$ CT. The colocalization experiments with organelle-specific stains, e.g., MitoTracker Deep Red FM, discovered the localization of **(101)** within the mitochondria of the HeLa cells (Fig. 8.14D). The confocal laser scanning microscopy images of live A549 cells preincubated with 5 μM of **(101)** initially exhibited weak phosphorescence, but the successive addition of the zinc ionophore, $ZnCl_2$/NaPT (PT = 2-pyridinethiol-1-oxide), turned on the phosphorescence. A stronger Zn(II) chelator, *N,N,N′,N′*-tetrakis(2-picolyl)ethylenediamine (TPEN), restored the lower phosphorescence intensity; thus, indicating the re-occurrence of $IL_{N^{\wedge}N}$CT; i.e., free DPA → phen charge transfer. Such monitoring of the cellular flux of Zn(II) suggested effective sensing of zinc-ion-rich specimens, e.g., hippocampus.

8.5 Conclusion

In this chapter, the synthesis, photophysics and photochemistry of complexes of group 9 (Co, Rh, Ir) elements have been presented. The impact of various ligands like polypyridyl, carbene, thiazole, quinoxaline and phenanthrene, tuning the excited-state photophysics of the complexes of this group (Co, Rh, Ir) have been discussed. It was concluded that Co(II/III) complexes mostly show ^{3}LLCT, ^{3}LMCT transitions, Rh(III) exhibit ^{3}MLCT and $^3(\pi\text{-}\pi)^*$ whereas Ir(III) complexes mostly display transitions from the $^3(\pi\text{-}\pi)^*$, ^{3}LLCT and ^{3}MLCT states. It can be seen that in the last few years, numerous works have been done and the development of group 9 complexes in biological sensors, photoredox catalyst, OLED/PhOLED and LEC has come a long way with many more brilliant examples being established. Although abundant work has been achieved on Ir(III)-OLEDs with good EQE values and photoredox catalysis, extensive research is still needed on Co(III)-based photoredox catalysts and Rh(III)-based OLEDs to achieve champion PRCs, useful in organic and medicinal chemistries in particular and to increase the performance and stability of the solid-state lighting device to achieve commercial applications, respectively.

Acknowledgments

AKP thanks the Science and Engineering Research Board (SERB) for a start-up research grant (SRG/2020/000080) and the Indian Institute of Technology Jammu (SGT-100028). SS thanks to the University Grant Commission for a Junior Research Fellowship (Certificate No. DEC19C00758). RG thanks the Council of Scientific and Industrial Research for a Junior Research Fellowship (Certificate No. Nov/06/2020(i)EU-V).

References

Anbalagan, K., Ganeshraja, A.S., 2013. Electron-rich ligand modified, ferromagnetic luminescent cis-[CoIII(en)$_2$(RNH$_2$)Cl]Cl$_2$ complexes and their electrochemical reduction behavior. Inorg. Chem. Commun. 37, 59–65.

Baldo, M.A., Lamansky, S., Burrows, P.E., Thompson, M.E., Forrest, S.R., 1999. Very high-efficiency green organic light-emitting devices based on electrophosphorescence. Appl. Phys. Lett. 75 (1), 4–6.

Balzani, V., Campagna, S., 2007. Photochemistry and Photophysics of Coordination Compounds II. Springer, Berlin, pp. 117–214.

Calogero, G., Giuffrida, G., Serroni, S., Ricevuto, V., Campagna, S., 1995. Absorption spectra, luminescence properties, and electrochemical behavior of cyclometalated iridium(III) and rhodium(III) complexes with a bis(pyridyl)triazole ligand. Inorg. Chem. 34 (3), 541–545.

Carstens, D.H.W., Crosby, G.A., 1970. Luminescence from complexes of rhodium(III). J. Mol. Spectrosc. 34 (1), 113–135.

Chábera, P., Kjaer, K.S., Prakash, O., Honarfar, A., Liu, Y., Fredin, L.A., et al., 2018. FeII Hexa N-Heterocyclic carbene complex with a 528 ps metal-to-ligand charge-transfer excited-state lifetime. J. Phys. Chem. Lett. 9 (3), 459–463.

Coban, M.B., Gungor, E., Kara, H., Baisch, U., Acar, Y., 2018. New Mixed valence defect dicubane cobalt(II)/cobalt(III) complex: synthesis, crystal structure, photoluminescence and magnetic properties. J. Mol. Struct. 1154, 579–586.

Colombo, M., Zilian, A., Guedel, H., 1990. Luminescence line narrowing, a highly specific probe of excited state properties in rhodium(III) mixed chelate complexes. J. Am. Chem. Soc. 112, 4581–4582.

Condie, A.G., González-Gómez, J.C., Stephenson, C.R.J., 2010. Visible-Light photoredox catalysis: aza-Henry reactions via C–H functionalization. J. Am. Chem. Soc. 132 (5), 1464–1465.

Costa, R., Ortí, E., Bolink, H., Graber, S., Schaffner, S., Neuburger, M., Housecroft, C., Constable, E., 2009. Archetype cationic iridium complexes and their use in solid-state light-emitting electrochemical cells. Adv. Funct. Mater. 19, 3456–3463.

DeArmond, M.K., H, J.E., 1968. Phosphorescence of transition-metal chelates. J. Chem. Phys. 49, 466.

Dedeian, K., Djurovich, P.I., Garces, F.O., Carlson, G., Watts, R.J., 1991. A new synthetic route to the preparation of a series of strong photoreducing agents: fac-tris-ortho-metalated complexes of iridium(III) with substituted 2-phenylpyridines. Inorg. Chem. 30 (8), 1685–1687.

Demas, J.N., Harris, E.W., Flynn, C.M., Diemente, D., 1975. Luminescent osmium(II) and iridium(III) complexes as photosensitizers. J. Am. Chem. Soc. 97 (13), 3838–3839.

Dulebohn, J.I., Ward, D.L., Nocera, D.G., 1990. Synthetic design of a multielectron series of homologous dirhodium fluorophosphines possessing an emissive dσ* excited state. J. Am. Chem. Soc. 112 (8), 2969–2977.

Feng, X., Feng, Y.-Q., Chen, J.J., Ng, S.-W., Wang, L.-Y., Guo, J.-Z., 2015. Reticular three-dimensional 3d–4f frameworks constructed through substituted imidazole-dicarboxylate: syntheses, luminescence and magnetic properties study. Dalton Trans. 44 (2), 804–816.

Flynn, C.M., Demas, J.N., 1974. Synthesis and luminescence of the tris(2,2'-bipyridine)Iridium(III) ion. J. Am. Chem. Soc. 96 (6), 1959–1960.

Frink, M.E., Sprouse, S.D., Goodwin, H.A., Watts, R.J., Ford, P.C., 1988. Synthesis and excited-state properties of rhodium(III) terpyridine complexes. Inorg. Chem. 27 (7), 1283–1286.

Geoffroy, G.L., Wrighton, M.S., Hammond, G.S., Gray, H.B., 1974. Electronic absorption and emission spectral studies of square-planar rhodium(I) and iridium(I) complexes. evidence for a charge-transfer emitting state. J. Am. Chem. Soc. 96 (10), 3105−3108.

Ghizdavu, L., Lentzen, O., Schumm, S., Brodkorb, A., Moucheron, C., Kirsch-De Mesmaeker, A., 2003. Synthesis and characterization of optically active and racemic forms of cyclometalated Rh(III) complexes. An Experimental and Theoretical Emission Study. Inorg. Chem. 42 (6), 1935−1944.

Gillard, R.D., Osborn, J.A., Wilkinson, G., 1965. Catalytic approaches to complex compounds of rhodium(III). J. Chem. Soc. 1951−1965, 353.

Halper, W., DeArmond, M.K., 1974. Phosphorescence decay of 2,2′-dipyridyl, 1,10-phenanthroline and their tris and bis complexes with rhodium(III) at low temperatures. Chem. Phys. Lett. 24 (1), 114−116.

Harris, C.M., McKenzie, E.D., 1963. The preparation and colour of tris-2,2′-bipyridyl- and bis-2,2′,2″-terpyridylrhodium(III) salts. J. Inorg. Nucl. Chem. 25 (2), 171−174.

Heath, G.A., Martin, R.L., 1969. Synthesis and properties of tris(dithioacetylacetonato)-complexes of cobalt(III), rhodium(III), and iridium(III). J. Chem. Soc. Chem. Commun. (17), 951−952.

Heffern, M.C., Yamamoto, N., Holbrook, R.J., Eckermann, A.L., Meade, T.J., 2013. Cobalt derivatives as promising therapeutic agents. Curr. Opin. Chem. Biol. 17 (2), 189−196.

Hillis, J.E., Dearmond, M.K., 1971a. Luminescence of transition metal d6 chelates. J. Chem. Phys. 54, 2247−2253.

Hillis, J.E., DeArmond, M.K., 1971b. Nonradiative processes in transition metal complexes: luminescence data for Rh (III) and Ir (III) complexes. J. Lumin. 4 (4), 273−290.

Ho, P.-Y., Ho, C.-L., Wong, W.-Y., 2020. Recent advances of iridium(III) metallophosphors for health-related applications. Coord. Chem. Rev. 413, 213267.

Indumathy, R., Parameswaran, P.S., Aiswarya, C.V., Nair, B.U., 2014. Bibenzimidazole containing mixed ligand cobalt(III) complex as a selective receptor for iodide. Polyhedron 75, 22−29.

Ivanović-Burmazović, I., Jelković, K., 2004. Transition metal complexes with bis(hydrazone) ligands of 2,6-diacetylpyridine. In: van Eldik, R. (Ed.), Hepta-coordination of 3d Metals. Adv. Inorg. Chem., 55. Academic Press, Cambridge, pp. 315−360.

Johnson, C.E., Eisenberg, R., Evans, T.R., Burberry, M.S., 1983. Luminescent iridium(I), rhodium(I), and platinum(II) dithiolate complexes. J. Am. Chem. Soc. 105 (7), 1795−1802.

Kadis, J., Shin, Y.-g. K., Dulebohn, J.I., Ward, D.L., Nocera, D.G., 1996. Molecular structures and photophysical properties of dirhodium fluorophosphine complexes. Inorg. Chem. 35 (4), 811−817.

Kahl, J.L., Hanck, K., DeArmond, K., 1979. Preparation and identification of iridium bipyridine and phenanthroline complexes. J. Inorg. Nucl. Chem. 41 (4), 495−502.

Kalyanasundaram, K., Graetzel, M., Nazeeruddin, M.K., 1992. Excited-state interactions in ligand-bridged chromophore-quenchercomplexes containing rhodium(III) and ruthenium(II) polypyridyl units. J. Phys. Chem. 96 (14), 5865−5872.

King, K.A., Spellane, P.J., Watts, R.J., 1985. Excited-state properties of a triply ortho-metalated iridium(III) complex. J. Am. Chem. Soc. 107 (5), 1431−1432.

Kocak, C., Oylumluoglu, G., Donmez, A., Coban, M.B., Erkarslan, U., Aygun, M., et al., 2017. Crystal structure and photoluminescence properties of a new monomeric copper(II) complex: bis(3-{[(3-hydroxypropyl)imino]methyl}-4-nitrophenolato-[kappa]3O,N,O')copper(II). Acta Cryst. C 73 (5), 414−419.

Kunkely, H., Vogler, A., 2000. Photoluminescence of [RhIII(phpy)2(CN)2]−(phpy−=ortho-metalated 2-phenylpyridine anion). Chem. Phys. Lett. 319 (5), 486−488.

Lamansky, S., Djurovich, P., Murphy, D., Abdel-Razzaq, F., Lee, H.-E., Adachi, C., et al., 2001. Highly phosphorescent bis-cyclometalated iridium complexes: synthesis, photophysical characterization, and use in organic light emitting diodes. J. Am. Chem. Soc. 123 (18), 4304−4312.

Lee, D.Y., Singh, N., Kim, M.J., Jang, D.O., 2011. Chromogenic and fluorescent recognition of iodide with a benzimidazole-based tripodal receptor. Org. Lett. 13 (12), 3024−3027.

Lee, J., Chen, H.F., Batagoda, T., Coburn, C., Djurovich, P.I., Thompson, M.E., et al., 2016. Deep blue phosphorescent organic light-emitting diodes with very high brightness and efficiency. Nat. Mater. 15, 92−98.

Li, G.-B., Liao, Z.-H., Pan, R.-K., Liu, J.-M., Liu, S.-G., Zhang, Z., 2015. Synthesis, fluorescence, and sorption properties of cobalt coordination polymers of the N,N′-bis(4-pyridylmethyl) naphthalene diimide ligand. Transit. Met. Chem. 40 (6), 691−697.

Lide, D.R., 2004. CRC Handbook of Chemistry and Physics, Boca Raton.

Liu, G.C., Li, Y., Chi, J., Xu, N., Wang, X.L., Lin, H.Y., et al., 2020. Multi-functional fluorescent responses of cobalt complexes derived from functionalized amide-bridged ligand. Dyes Pigm 174. https://doi.org/10.1016/j.dyepig.2019.108064.

MacMillan, W.C.D., McNally, A., Christopher, K.P., 2011. Discovery of an a-amino C−H arylation reaction using the strategy of accelerated serendipity. Science 334 (6059), 1114−1117.

Maestri, M., Sandrini, D., Balzani, V., Maeder, U., Von Zelewsky, A., 1987. Absorption spectra, electrochemical behavior, luminescence spectra, and excited-state lifetimes of mixed-ligand ortho-metalated rhodium(III) complexes. Inorg. Chem. 26 (8), 1323−1327.

Matheau-Raven, D., Gabriel, P., Leitch, J.A., Almehmadi, Y.A., Yamazaki, K., Dixon, D.J., 2020. Catalytic reductive functionalization of tertiary amides using vaska's complex: synthesis of complex tertiary amine building blocks and natural products. ACS Catal. 10 (15), 8880−8897.

McClure, L.J., Ford, P.C., 1992. Ligand macrocycle effects on the photophysical properties of rhodium(III) complexes: a detailed investigation of cis- and trans-dicyano(1,4,8,11-tetraazacyclotetradecane) rhodium(III) and related species. J. Phys. Chem. 96 (16), 6640−6650.

McKenzie, E.D., Plowman, R.A., 1970. Rhodium(III) compounds with 1,10-phenanthroline and 2,2′-bipyridyl. J. Inorg. Nucl. Chem. 32 (1), 199−212.

Merrill, J.T., DeArmond, M.K., 1979. Multiple emission from sulfur complexes of rhodium(III) and iridium(III). J. Am. Chem. Soc. 101 (8), 2045−2055.

Mingardi, M., Porter, G.B., 1966. Phosphorescence of $K_3Co(CN)_6$. J. Chem. Phys. 44 (11), 4354. -4354.

Muto, M., Yokota, S., Yamamoto, Y., Nakahara, M., Mori, W., 1979. Synthesis and luminescence spectra of the cobalt (II) complex with kojate. Chem. Lett. 8 (6), 689−692.

Newkome, G.R., Gupta, V.K., Fronczek, F.R., Pappalardo, S., 1984. Multidentate ligands containing 2,2′-Bipyridine and/or pyridine moieties: structural aspects of their octahedral and pentagonal-bipyramidal complexes. Inorg. Chem. 23 (16), 2400−2408.

Nguyen, J.D., Tucker, J.W., Konieczynska, M.D., Stephenson, C.R.J., 2011. Intermolecular atom transfer radical addition to olefins mediated by oxidative quenching of photoredox catalysts. J. Am. Chem. Soc. 133 (12), 4160−4163.

Oylumluoglu, G., Coban, M.B., Kocak, C., Aygun, M., Kara, H., 2017. 2-and 1-D coordination polymers of Dy(III) and Ho(III) with near infrared and visible luminescence by efficient charge-transfer antenna ligand. J. Mol. Struct. 1146, 356−364.

Özbek, F.E., Sertçelik, M., Yüksek, M., Küçüköz, B., Elmali, A., Sahin, E., 2019. Two new potential optical materials: Co(II) and Ni(II) 3-fluorobenzoate complexes with pyridine-3-Carboxamide. J. Coord. Chem. 72 (5−7), 786−795.

Pal, A.K., Hanan, G.S., 2014. Design, synthesis and excited-state properties of mononuclear Ru(II) complexes of tridentate heterocyclic ligands. Chem. Soc. Rev. 43 (17), 6184−6197.

Pal, A.K., Zaccheroni, N., Campagna, S., Hanan, G.S., 2014. Near infra-red emission from a mer-Ru(II) complex: consequences of strong σ-donation from a neutral, flexible ligand with dual binding modes. Commun. Chem. 50 (52), 6846−6849.

Pal, A.K., Cordes, D.B., Slawin, A.M.Z., Momblona, C., Orti, E., Samuel, I.D.W., et al., 2016. Synthesis, properties, and light-emitting electrochemical cell (LEEC) device fabrication of cationic Ir(III) complexes bearing electron-withdrawing groups on the cyclometallating ligands. Inorg. Chem. 55 (20), 10361−10376.

Pal, A.K., Cordes, D.B., Slawin, A.M.Z., Momblona, C., Pertegás, A., Ortí, E., Bolink, H.J., Zysman-Colman, E., 2017. Simple design to achieve red-to-near-infrared emissive cationic Ir(III) emitters and their use in light emitting electrochemical cells. RSC Adv. 7 (51), 31833−31837.

Pal, A.K., Krotkus, S., Fontani, M., Mackenzie, C.F.R., Cordes, D.B., Slawin, A.M.Z., et al., 2018. High-efficiency deep-blue-emitting organic light-emitting diodes based on iridium(III) carbene complexes. Adv. Mater. 30 (50). https://doi.org/10.1002/adma.201804231.

Pal, A.K., Li, C., Hanan, G.S., Zysman-Colman, E., 2018. Blue-emissive cobalt(III) complexes and their use in the photocatalytic trifluoromethylation of polycyclic aromatic hydrocarbons. Angew. Chem. Int. Ed. 57 (27), 8027−8031.

Perea-Buceta, J.E., Fernández, I., Heikkinen, S., Axenov, K., King, A.W.T., Niemi, T., et al., 2015. Diverting hydrogenations with wilkinson's catalyst towards highly reactive rhodium(I) species. Angew. Chem. Int. Ed. 54 (48), 14321−14325.

Ryutaro, T., 1938. Absorption spectra of co-ordination compounds. I. Bull. Chem. Soc. Jpn. 13, 388−400.

Sajjad, M.T., Sharma, N., Pal, A.K., Hasan, K., Xie, G., Kölln, L.S., et al., 2016. Controlling the emission efficiency of blue-green iridium(III) phosphorescent emitters and applications in solution-processed organic light-emitting diodes. J. Mater. Chem. C 4 (38), 8939−8946.

Sathiyakumar, S., Selvam, P., Antharjanam, S., Hakkim, F.L., Srinivasan, K., Harrison, W.T.A., 2020. Mechano-chemical syntheses of new cobalt(II) complexes of alkyl 2-(pyridine-2yl-methylene) hydrazinecarboxylates: crystal structures, spectroscopic and photoluminescence properties. J. Mol. Struct. 1205. https://doi.org/10.1016/j.molstruc.2019.127666.

Sathya Priyadarshini, G., Selvi, G., 2021. Luminescence cobalt (II) complexes: synthesis, characterization, photophysical and DFT study. Mater. Today Proc. 40, S19−S27.

Schrauzer, G.N., 1968. Organocobalt chemistry of vitamin B12 model compounds (Cobaloximes). Acc. Chem. Res. 1 (4), 97−103.

Sexton, D.A., Skibsted, L.H., Magde, D., Ford, P.C., 1984. Ligand effects on the excited-state dynamics of rhodium(III) complexes, photoluminescence properties of the tetraammine complexes Rh(NH3)4XYn+, and their relationship to photoreactivity. Inorg. Chem. 23 (26), 4533−4538.

Shi, Y.-S., Hao, Z.-C., Han, C., Cui, G.-H., 2020. Synthesis, crystal structures, and luminescence sensing properties of two metal complexes containing bis(thiabendazole) moieties. J. Mol. Struct. 1201. https://doi.org/10.1016/j.molstruc.2019.127218.

Shiga, T., Kumamaru, R., Newton, G.N., Oshio, H., 2018. Cobalt complexes with redox-active anthraquinone-type ligands. Dalton Trans. 47 (23), 7804−7811.

Su, Y.-Q., Qu, Y.-H., Fu, L., Cui, G.-H., 2020. An unprecedented binodal (4,6)-connected Co(II) MOF as dual-responsive luminescent sensor for detection of acetylacetone and Hg^{2+} ions. Inorg. Chem. Commun. 118. https://doi.org/10.1016/j.inoche.2020.108013.

Sunley, G.J., Watson, D.J., 2000. High productivity methanol carbonylation catalysis using iridium: the Cativa™ process for the manufacture of acetic acid. Catal. Today 58 (4), 293–307.

Tamayo, A.B., Alleyne, B.D., Djurovich, P.I., Lamansky, S., Tsyba, I., Ho, N.N., et al., 2003. Synthesis and characterization of facial and meridional tris-cyclometalated iridium(III) complexes. J. Am. Chem. Soc. 125 (24), 7377–7387.

Tokito, S., Iijima, T., Suzuri, Y., Kita, H., Tsuzuki, T., Sato, F., 2003. Confinement of triplet energy on phosphorescent molecules for highly-efficientorganic blue-light-emitting devices. Appl. Phys. Lett. 83 (3), 569–571.

Udagawa, K., Sasabe, H., Cai, C., Kido, J., 2014. Low-driving-voltage blue phosphorescent organic light-emitting devices with external quantum efficiency of 30. Adv. Mater. 26 (29), 5062–5066.

Vaska, L., Catone, D.L., 1966. A New series of four-, five-, and six-coordinated iridium complexes. J. Am. Chem. Soc. 88 (22), 5324–5325.

Verhoeven, J.W., 1996. Glossary of terms used in photochemistry. Pure Appl. Chem. 68, 2223–2286.

Vetrichelvan, M., Nagarajan, R., Valiyaveettil, S., 2006. Carbazole-containing conjugated co-polymers as colorimetric/fluorimetric sensor for iodide anion. Macromolecules 39 (24), 8303–8310.

Wang, C., Lam, H.-C., Zhu, N., Wong, K.M.-C., 2015. Introduction of luminescent rhenium(I), ruthenium(II), iridium(III) and rhodium(III) systems into rhodamine-tethered ligands for the construction of bichromophoric chemosensors. Dalton Trans. 44 (34), 15250–15263.

Watkins, A.R., 1974. Short-lived intermediates formed by the interaction between electronically excited molecules and inorganic ions. J. Phys. Chem. 78 (19), 1885–1890.

Wei, Y., Wu, K., Broer, R., Zhuang, B., Yu, Y., 2007. A Polymeric cobalt compound [Co(DCN-T)(H2O)]n with novel topology: synthesis, structure, luminescence, and magnetic property. Inorg. Chem. Commun. 10 (8), 910–913.

Wei, F., Lai, S.-L., Zhao, S., Ng, M., Chan, M.-Y., Yam, V.W.-W., et al., 2019. Ligand mediated luminescence enhancement in cyclometalated rhodium(III) complexes and their applications in efficient organic light-emitting devices. J. Am. Chem. Soc. 141 (32), 12863–12871.

Xue, Y.L., Wu, P., Liu, Y., Zhang, X., Lin, L., Jiang, Q., 2010. Highly efficient near-ir photo-luminescence of Er^{3+} immobilized in mesoporous SBA-15. Nanoscale Res. Lett. 5 (12). https://doi.org/10.1007/s11671-010-9732-9.

Yang, D., Zhu, J., Rui, X., Tan, H., Cai, R., Hoster, H.E., et al., 2013. Synthesis of cobalt phosphides and their application as anodes for lithium ion batteries. ACS Appl. Mater. Interfaces 5 (3), 1093–1099.

Yeh, S.-J., Wu, M.-F., Chen, C.-T., Song, Y.-H., Chi, Y., Ho, M.-H., et al., 2005. New dopant and host materials for blue-light-emitting phosphorescent organic electroluminescent devices. Adv. Mater. 17 (3), 285–289.

You, Y., Cho, S., Nam, W., 2014. Cyclometalated iridium(III) complexes for phosphorescence sensing of biological metal ions. Inorg. Chem. 53 (4), 1804–1815.

Yusuke, Y., 1979. Luminescence spectra of cobalt(III) cyano complexes. Bull. Chem. Soc. Jpn. 52 (1), 84–89.

Zhang, Q.-L., Liu, J.-G., Liu, J.-Z., Li, H., Yang, Y., Xu, H., et al., 2002. Effect of intramolecular hydrogen-bond on the DNA-binding and photocleavage properties of polypyridyl cobalt(III) complexes. Inorg. Chim. Acta. 339, 34–40.

Zuloaga, F., Kasha, M., 1968. Luminescence spectra of transition metal complexes. Photochem. Photobiol. 7 (6), 549–555.

This page intentionally left blank

Chapter 9

Coordination compounds of nickel, palladium, and platinum

Athanasios Zarkadoulas and Christiana A. Mitsopoulou
Inorganic Chemistry Laboratory, Department of Chemistry, National and Kapodistrian University of Athens, Athens, Greece

9.1 Introduction

Group 10 compounds of nickel, palladium, and platinum have been used as paradigms over the years of evolution of inorganic chemistry, from early stages of chemical kinetics that employed Pt(II) compounds for the mechanistic studies of square planar complexes and factors that govern these processes (Basolo and Pearson, 1962, 1967). As inorganic chemistry evolved and more properties of metal complexes came into light, it became clear that photophysical process and subsequent photochemical reactions are interwoven with the bonding and electronic properties of metal and ligands, especially for group 10 ions, which differ remarkably. Thus, going down the group from nickel to platinum, several marked differences occur, which have an effect on photophysical properties. First of all, one can mention geometry preferences; nickel can adopt octahedral, tetrahedral, square planar, square pyramidal, and trigonal bipyramidal conformations. On the other hand palladium and platinum, are mostly found under square planar or octahedral geometries. From a traditional point of view, i.e., ligand field theory, it becomes immediately apparent that as the ligands approach the metal ion, they impose a different field symmetry and thus, cause a rearrangement of metal orbitals in terms of energy. As theoretical chemistry and calculations became more sophisticated, it was found that mixing of metal and ligand orbitals give rise to molecular orbitals that now explain electronic transitions and any molecular changes that might take place as a consequence. This evolution will become evident in the progress of this chapter, where initially ligand field photophysics is reported, from a historical but also pedagogical point of view, laying the basics for group 10 metal complexes. Then it proceeds with important classes of

Photochemistry and Photophysics of Coordination Compounds. https://doi.org/10.1016/B978-0-12-824493-7.00009-5
Copyright © 2023 Elsevier Inc. All rights reserved.

complexes and very recent examples from the literature, where one can discern trends and strategies toward the preparation of photoactive group 10 complexes.

9.2 Ligand field photophysics and photochemistry

9.2.1 Nickel complexes

Nickel, the first element of group 10 under study, adopts various oxidation states and geometries in transition metal complexes. The most notable is $_{28}$Ni(II): [Ar]3d^8, giving rise to 45 microstates which can be reduced to the following free ion terms: $^1S + {}^1D + {}^1G + {}^3P + {}^3F$. Using group theory, one can apply the method used to derive the splitting of various types of orbitals under a specific environment to obtain the splitting of each free ion term in the desired environment imposed by the ligands. Thus, the S term will split in $^1A_{1g}$ (O_h), $^1A_1$ (T_d), or $^1A_{1g}$ (D_{4h}) states. The terms listed here are of g symmetry, since we only work with metal d-orbitals which are centrosymmetric in a field with an inversion center (Cotton, 1990).

In order to construct an energy diagram, one must take into consideration the two extremes, i.e., splitting due to weak- or strong-field ligands. Starting with the simplest, weak-field approximation, finding the matrix elements of the secular determinant under the action of the ligand field potential operator is required. Since exact calculations are beyond our scope at this point, we can readily use that the S term is not affected and P term does not split; a D term splits to T and E terms, F term splits into two T and A terms, while the G term splits to A, an E, and two T terms (Fig. 9.1), in the same way that the corresponding orbital wavefunctions undergo splitting under O_h and T_d symmetries.

For other geometries, as symmetry becomes lower, e.g., in square planar complexes belonging to group D_{4h}, just one parameter Δ (as we had Δ_o or Δ_t for O_h and T_d, respectively) is not enough to describe the energy differences between states. Group theory operations for a square planar Ni(II) complex belonging to the D_{4h} group split the aforementioned free-ion terms in 19 states, so it comes down to the relative energies between states in each complex to properly put them in energy order. The same is valid for other broken symmetries, for example, when Jahn-Teller distortions are present for other d^n configurations.

Of course, in spectra of Ni(II) compounds, not all possible transitions are experimentally observed, since selection rules make some of the transitions forbidden. In this spirit, Orgel diagrams (Fig. 9.2) are also valuable for calculation of spectral parameters for high-spin compounds under a weak field, taking into consideration the two relevant F and P terms for a tetrahedral or octahedral environment (Orgel, 1955). Notice that the non-crossing and spin conservation rules are observed.

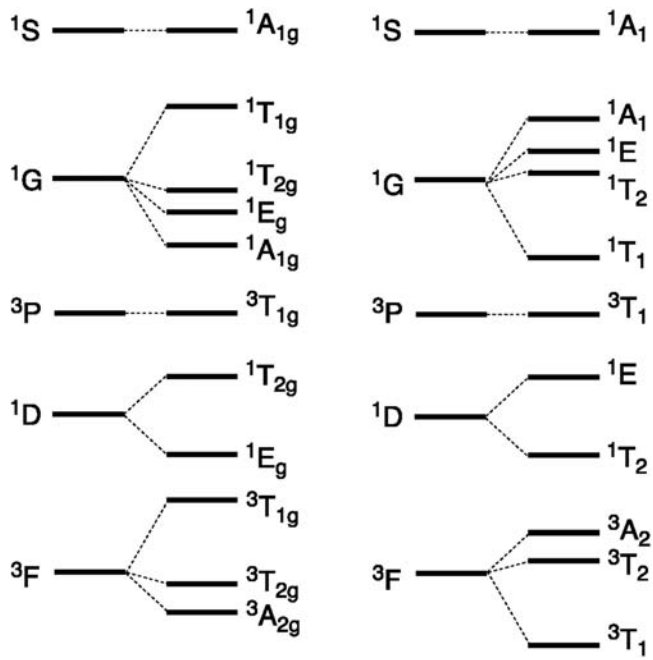

FIGURE. 9.1 Term splitting for Ni(II): $[Ar]3d^8$ in octahedral (O_h, *left*) and tetrahedral (T_d, *right*) environments under the influence of a weak field.

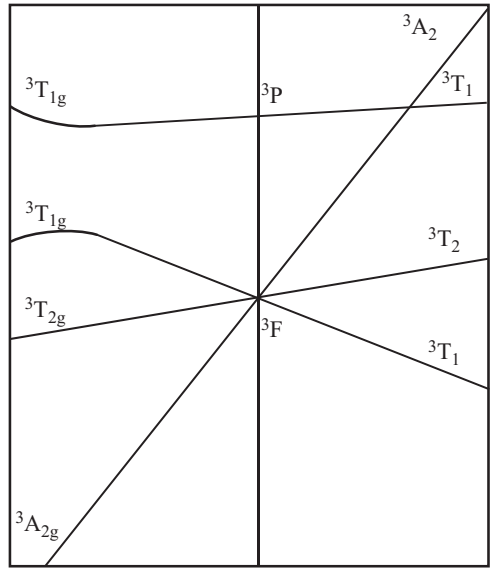

FIGURE. 9.2 Orgel diagram for a Ni(II): $[Ar]3d^8$ ion in O_h (*left*) or T_d (*right*) field.

TABLE 9.1 Band positions and assignments for transitions observed at $[NiL_n]^{2+}$ complexes in aqueous solutions.

L	$^3A_{2g} \rightarrow {}^3T_{2g}$	$^3A_{2g} \rightarrow {}^3T_{1g}$ (F)	$^3A_{2g} \rightarrow {}^3T_{1g}$ (P)
H_2O	8500 (1180)	13,500 (740)	25,300 (395)
NH_3	10,750 (930)	17,500 (571)	28,200 (355)
Ethylenediamine	11,200 (890)	18,350 (545)	29,000 (345)
1,10-Phenanthroline	11,550 (865)	12,700 (788)	-

In this case, calculation of $10D_q$ (Δ_o or Δ_t) and nephelauxetic parameter β can be derived from spectral data and the Racah parameter B for the free ion (Figgis and Hitchman, 1999)

For hexacoordinate complexes of the type $[NiL_6]^{2+}$, band positions are summarized in Table 9.1.

As expected by the spectrochemical series, the increasing π-accepting nature of ligands induces a blue shift in each band and in the case of 1,10-phenanthroline, the high-energy transition is lost in the ligand-based, charge-transfer transitions observed in the UV region of the spectrum. A typical splitting in the middle band may occur for weak field ligands, which is attributed to mixing with ^1E_g (^1D) first singlet excited state.

For a typical Ni(II), $3d^8$ complex, a square planar configuration is preferred due to orbital stabilization, leaving the antibonding $3d(x^2-y^2)$ orbital vacant. As a typical example, the diamagnetic yellow $[Ni(CN)_4]^{2-}$exhibits two bands at ~18,000 and ~23,000 cm^{-1} (Oppenheim et al., 2019). Using single-crystal absorption data, theoretical calculations, and taking into consideration the significant π-back bonding of nickel ion to cyanide, the correct orbital series for the aforementioned square planar complex was found to be:

$$d(xy) < d(xz) < d(yz) < d(z^2) < p(z) < d(x^2-y^2) < p(x), p(y)$$

Thus, the following assignments were made: the transition found at 18,154 cm^{-1} (551 nm) as $^3B_{1g} \leftarrow {}^1A_{1g}$ ($b_{1g} \leftarrow a_{1g}$) and the band at 23,844 cm^{-1}(420 nm) $^3E_g \leftarrow {}^1A_{1g}$ ($e_g \leftarrow b_{1g}$). Other bands at 35,220 cm^{-1} (284 nm) and 37,590 cm^{-1} (266 nm) were assigned as 3d to 4p transitions. However, this orbital order has been disputed in another work (Deeth, 2020). Earlier work regarding irradiation of an aqueous solution of this complex ion at 254, 313, and 365 nm did not report any chemical change after irradiation (Moggi et al., 1966).

9.2.2 Palladium and platinum complexes

Contrary to Ni(II) complexes, the majority of palladium and platinum complexes prefer square planar geometry, based on the stabilization of the occupied d metal orbitals and destabilization of unoccupied $d(x^2-y^2)$ orbital. Ligand field

splitting (Δ) generally increases in the second and third row transition metals and spin-orbit coupling becomes more prominent as the atoms become heavier, with consequences on geometry, kinetic stability, and electronic properties. In fact, d-d transitions in square complexes of palladium and platinum lead to population of antibonding orbitals that eventually lead to distortions in the excited state and subsequent photochemical reactivity. These complexes are typically not luminescent in solution due to non-radiative decay pathways, but may exhibit emission in the solid state or low temperature, where distortions are minimized, or, typically for square planar Pt compounds in the solid state, stacking along the z-axis involving $d(z^2)$ interactions can lead to interesting photophysical properties (Li et al., 2016 and references therein)

It is instructive to examine the series $[MX_4]^{2-}$, where M = Ni, Pd, Pt and X = halogenide. In the case of Ni(II), the field induced by halides is not strong enough to lead to a square planar conformation and typically $[NiX_4]^{2-}$ complexes possess a tetrahedral conformation to achieve the minimum stereochemical and electronic repulsions between ligands. Pd(II) and Pt(II) analogs, on the other hand, are essentially square planar. Complex ion $[PtCl_4]^{2-}$ displays ligand field bands at 330, 400, and 475 nm and an LMCT band at 254 nm (Xian etg al., 2021). Irradiation with LED lamps of different wavelengths leads to stepwise hydrolysis of the platinum complex to yield aquo complexes; irradiation at the LMCT band leads to faster hydrolysis, indicating that the same reactive state is reached regardless of the irradiation wavelength (Fig. 9.3).

Tetrachloropalladate exhibits a same pattern (Drew Tait et al., 1991) i.e., an LMCT absorption at 280 nm and d-d-transition at 474 nm appear, which upon UV irradiation leads to the formation of Pd nanoparticles, following aquation and reduction reactions (Kundu et al., 2010).

9.3 Charge-transfer photochemistry

9.3.1 Diimine and dipyrrin complexes

A plethora of group 10 complexes can form stable, chelate complexes with multidentate ligands, many of which exhibit interesting photophysical properties. Diimine complexes analogous to the very versatile and scrutinized $[Ru(bpy)_3]^{2+}$ chromophore are of interest. In this spirit, the nickel analog, $[Ni(bpy)_3]^{2+}$ will be examined here. Spectroscopic studies of this compound in aqueous solution showed ligand field-based bands in the visible region and two bands in the ultraviolet region (296 and 308 nm) (Sadhiya Banu et al., 2011). Laser flash photolysis revealed transients involving ligand-centered events, leading to generation of ligand-centered radicals. Continuous photolysis led to decomposition of the complex. Since Ni(II) possesses a $t_{2g}^6 e_g^{*2}$ electron configuration, the ligand-centered electronic excitation of the complex involves increased electron density at the antibonding $d(x^2-y^2)$ and $d(z^2)$ orbitals. This induces elongation of Ni−N bonds, which in turn explain the decomposition of the complex (Fig. 9.4).

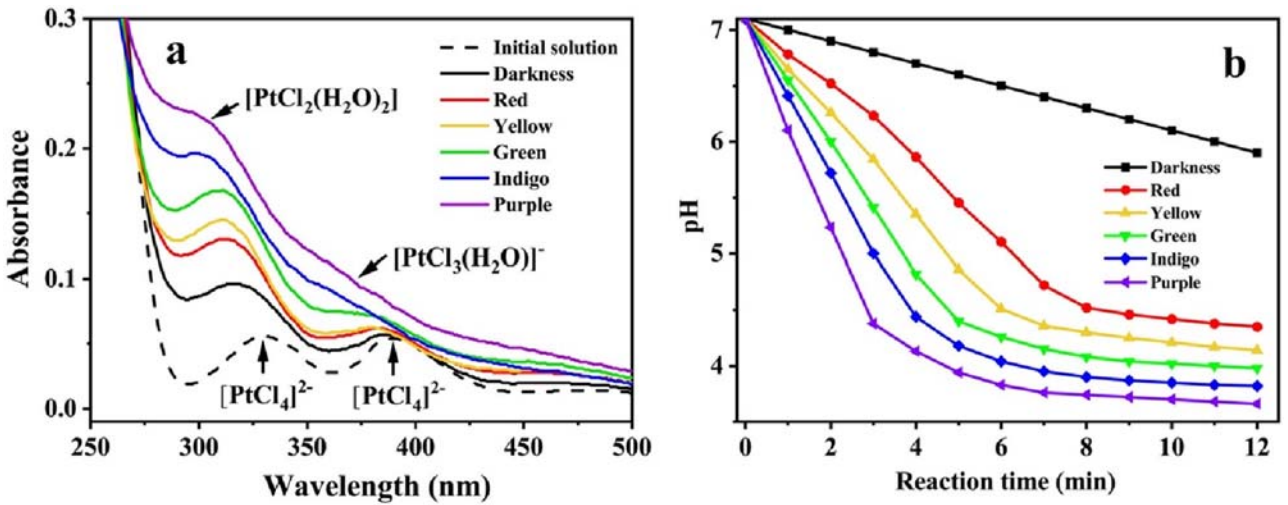

FIGURE. 9.3 Irradiation of an aqueous solution of $[PtCl_4]^{2-}$. *Adapted from Xian, L., Su, B.-Q., Feng, Y.-X., Xi, B., Duan, Z.-Y., 2021. The photochemical effects of visible light on $K_2[PtCl_4]$ hydrolysis and the synthesis of Pt nano catalysts. Inorg. Nano-Met. Chem. 51, 882–888, with permission.*

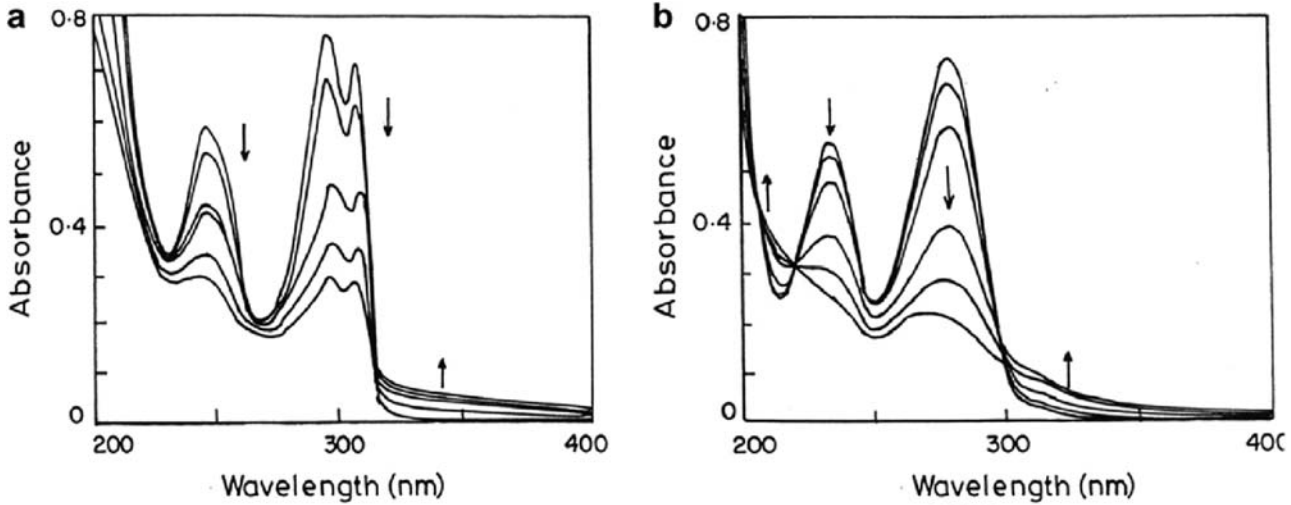

FIGURE. 9.4 Change in the absorbance during irradiation of $[Ni(bpy)_3]^{2+}$ aqueous solution (excitation at 254 nm). *Adapted from Sadhiya Banu, I., Prakash, H., Natarajan, P., 2011. Laser flash photolysis studies of tris(2,2′-bipyridine)nickel(II) ion in aqueous solution. Inorg. Chim. Acta 372, 429–435, with permission.*

Pd(II) and Pt(II) form mainly neutral complexes of the type $[M(bpy)X_2]$, where M = Pd or Pt and X = monodentate anionic ligand. Complexes containing 4,4′-dimethyl-2,2′-bipyridine (dmbpy) of the type $[Pd(dmbpy)X_2]$ ($X = Cl^-$, I^-, N_3^-, NO_2^-) (Scheme 9.1) exhibit a low-energy MLCT transition around 370 nm and several ILCT bands at the ultraviolet region (Anbalagan, 2003). The assignment for the charge-transfer transition involves an HOMO-LUMO transition between a $d(x^2\text{-}y^2)$-based HOMO to a $\pi^*_{diimine}$-based LUMO. These complexes can successfully sensitize the formation of singlet oxygen ($^1O_2$) in solution. The properties of $[Pt(diimine)X_2]$, Pt-acetylide, and Pt-terdentate complexes have been excellently reviewed by Williams et al. (2007).

Nickel diimine complexes have recently attracted attention due to their utilization in photoredox coupling reactions in sustainable organic transformations. Apart from traditional catalytic protocols that use traceless directing groups of earth abundant 3d metals (Greene et al., 2012; Han et al., 2018; Takahashi et al., 2020; Zarkadoulas et al., 2021), the versatility, user-friendliness, and sustainability of photocatalytic reactions is gaining more and more interest. Chlorine photoelimination from mononuclear, well-defined Ni(III) complexes bearing 1,2-bis(diphenylphosphino)ethane (dppe) and chloride ligands (Scheme 9.2) was achieved with visible light (Hwang et al., 2015) and was attributed to excitation to an LMCT transition at 450 nm (Fig. 9.5). Later, several other complexes have been studied in terms of their photosensitized or direct irradiation photochemistry (Wenger, 2021 and references therein).

Briefly, photochemical dissociation/homolysis of several organometallic square planar complexes occurs after excitation of a ^{3}MLCT state, which then relaxes to metal-centered d-d states, with a concomitant tetrahedral configuration facilitating bond scission/homolysis. This property of Ni complexes in various oxidation states is still under exploration with impressive results in sustainable organic transformations with low cost, first-row transition metals. More detailed studies and scope of catalytic reactions can be found in recent review articles (Tian et al., 2020; Cagan et al., 2020; Kariofillis and Doyle, 2021; Mantry et al., 2021; Till et al., 2021; Campbell et al., 2021; Stevenson et al., 2021; Hu et al., 2021).

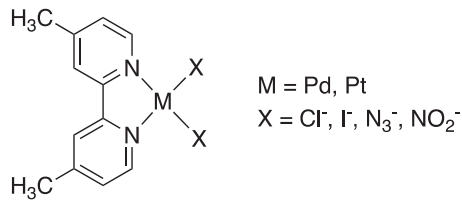

SCHEME 9.1 Pd(II) and Pt(II) diimine complexes.

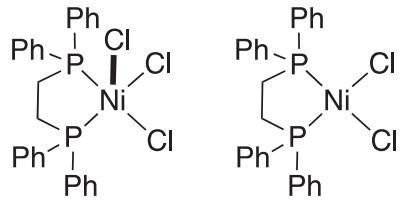

SCHEME 9.2 Chlorine elimination from $[Ni^{III}(dppe)Cl_3]$ complex to afford $[Ni^{II}(dppe)Cl_2]$ by irradiation with visible light.

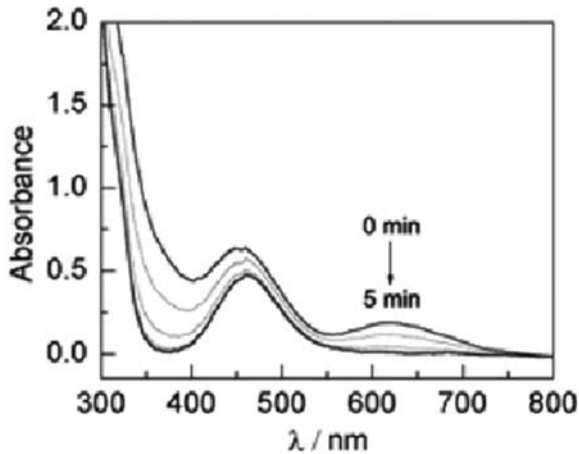

FIGURE. 9.5 Photolysis of an acetonitrile solution of $[Ni^{III}(dppe)Cl_3]$ ($\lambda > 430$ nm). *Adapted from Hwang, S.J., Powers, D.C., Maher, A.G., Anderson, B.L., Hadt, R.G., Zheng, S.-L., et al., 2015. Trap-free halogen photoelimination from mononuclear Ni(III) complexes. J. Am. Chem. Soc. 137, 6472−6475, with permission.*

Another important, established class of ligands is dipyrrin ligands (Wood and Thompson, 2007; Singh et al., 2020; Baudron et al., 2020). They can accommodate a variety of transition metal ions, support different geometries, and exhibit tunable properties based on steric and electronic factors. Ni(II) dipyrrinato complexes (Scheme 9.3) possess a distorted tetrahedral geometry around Ni(II) ion and exhibit a prevailing absorption band at ∼470 nm in solution. DFT calculations showed that both; HOMO and LUMO are localized on the ligands giving rise to LLCT transitions (Wang et al., 2015; Xue et al., 2017). Although this class of nickel compounds is relatively new and their photophysical study has not been performed in detail yet, heteroleptic Ni-dipyrrinate complexes were found non-emissive at room temperature (Toyoda et al., 2015). Despite their lack of photophysical properties, they have been employed as photosensitizers in photodynamic cancer therapy with negligible toxicity against cancer cells due to poor $^1O_2$ production (Karges et al., 2020) (Fig. 9.6).

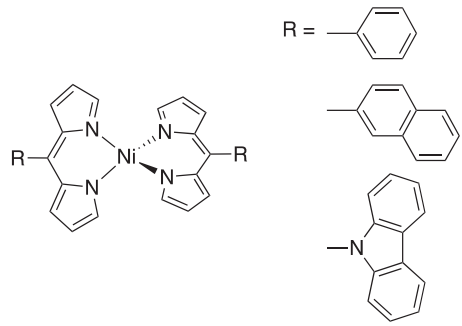

SCHEME 9.3 Ni(II) dipyrrin complexes.

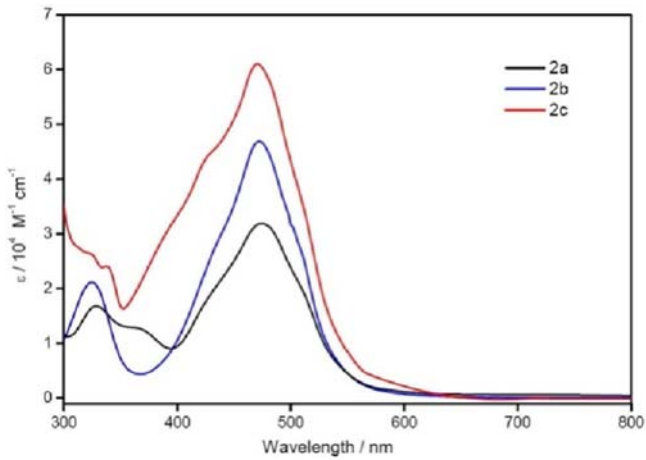

FIGURE. 9.6 UV-Vis absorption spectra of Ni(II) dipyrrin complexes in CH_2Cl_2. *Black trace*: R = phenyl, *blue* (dark gray in print version) *trace*: R = naphthyl, *red* (light gray in print version) *trace*: R = carbazole. (For interpretation of the references to colour in this figure legend, the reader is referred to the web version of this article.) *Adapted from Xue, Z., Dong, Y., Ma, J., Wang, Y., Zhu, W., 2017. Synthesis, characterization and electrochemistry of dipyrrinato nickel(II) complexes with different aromatic rings to meso-position. Polyhedron 127, 287–292, with permission.*

With palladium, the situation is slightly different; Pd(II) dipyrrin complexes (Scheme 9.4) adopt a slightly distorted square planar geometry (Mathew et al., 2020), and exhibit weak fluorescence in solution at room temperature, with lifetimes of ∼3 ns at 573 nm. This difference occurs due to the presence of Pd, which, as a heavy atom, facilitates ISC without phosphorescence, based on short lifetimes found (Fig. 9.7).

Imposing a structural rigidity on a Pd(II) phenyl-substituted dipyrrin complex (Scheme 9.5) (Riese et al., 2018) revealed that the flexible or rigid nature of the ligand framework affects its photophysical properties; thus, while

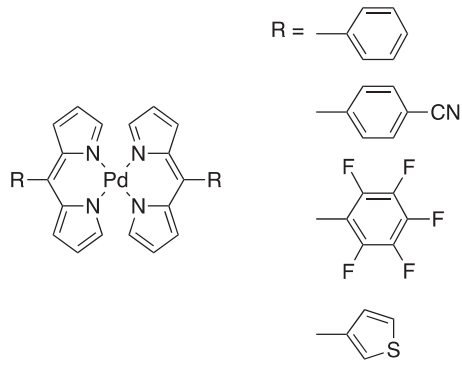

SCHEME 9.4 Pd(II) dipyrrin complexes.

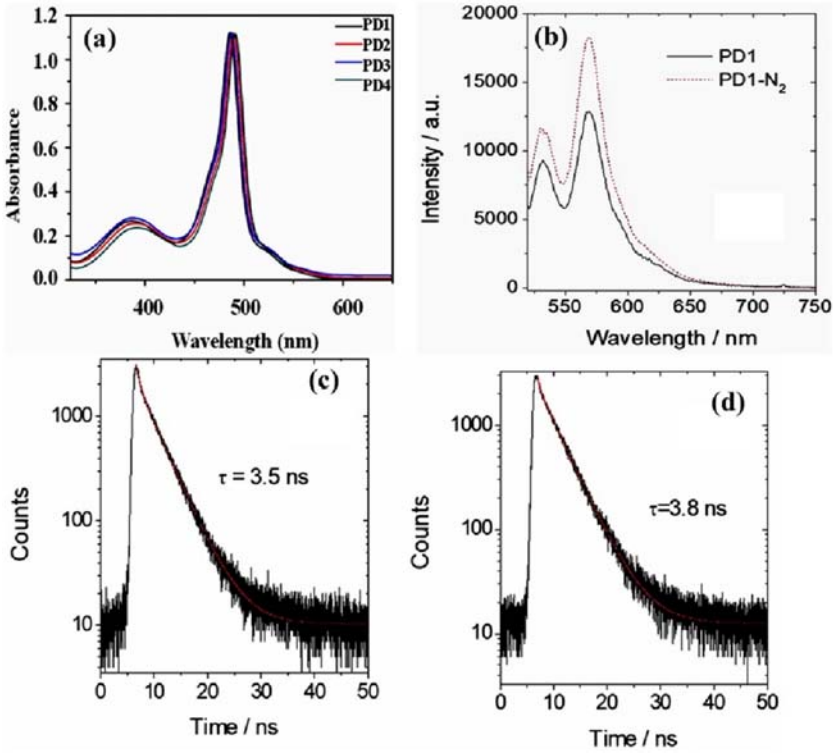

FIGURE. 9.7 (A) UV-Vis absorption spectra of Pd(II) dipyrrin complexes in $CHCl_3$. (B) Emission spectra of $-C_6F_5$ complex in acetonitrile ($\lambda_{exc.} = 510$ nm). (C, D) Delayed fluorescence for the same compound in air (C) and under N_2 (D) ($\lambda_{em.} = 573$ nm). *Adapted from Mathew, D., Hu, Y., Zhao, J., Arunkumar, C., Sujatha, S., 2020. Synthesis, structure, photophysical properties and evaluation of in vitro cytotoxic activity of homoleptic dipyrrin based palladium complexes. Polyhedron 190. https://doi.org/10.1016/j.poly.2020.114794, with permission.*

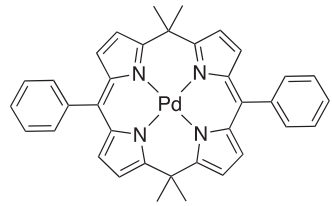

SCHEME 9.5 Rigid dipyrrin Pd(II) complex.

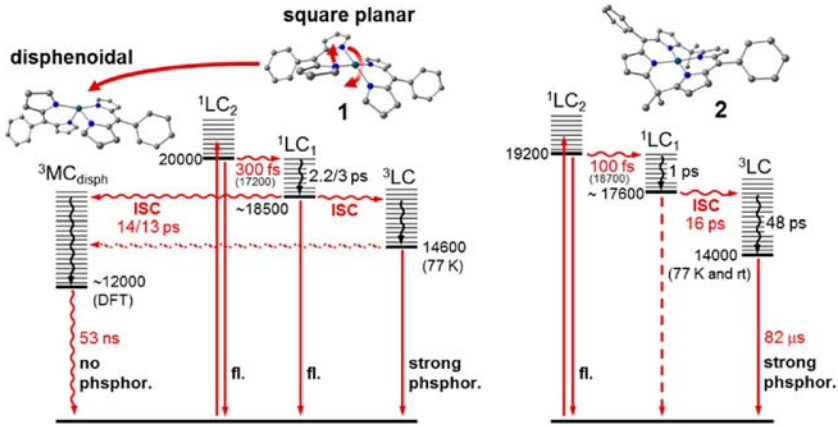

FIGURE. 9.8 State diagrams for flexible and rigid Pd(II) dipyrrin complexes. *Adapted from Riese, S., Holzapfel, M., Schmiedel, A., Gert, I., Schmidt, D., Würthner, F., et al., 2018. Photo-induced dynamics of bis-dipyrrinato-palladium(II) and porphodimethenato-palladium(II) complexes: governing near infrared phosphorescence by structural restriction. Inorg. Chem. 57, 12480−12488, with permission.*

both complexes undergo LC transitions that lead, via ISC, to low-lying triplet states ($\tau = 13$ ps), in the case of the more flexible analog (Scheme 9.4), structural reorganization leads to a non-emissive ^{3}MC state with absence of emission in solution at room temperature (Fig. 9.8).

9.4 Bis-dithiolene and diimine-dithiolene complexes

These complexes comprise a large family of group 10 complexes. The term "dithiolene" or "dithiolate" many times is used interchangeably but actually refers to different resonance forms of the ligand (Scheme 9.6)

The soft base nature of S-donor atoms coordinates with group 10 ions that act as soft Lewis acids to yield a great variety of metal complexes that can stabilize various oxidation states. In fact, the dithiolene ligand framework is classified among other ligands in the large group of "non-innocent ligands",

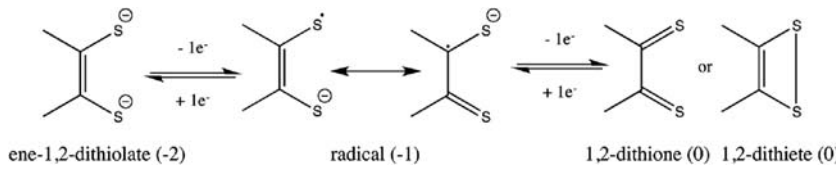

SCHEME 9.6 Charge localization, resonance forms and nomenclature for a bis-1,2-dithiolene ligand. *Adapted from Zarkadoulas, A., Field, M.J., Papatriantafyllopoulou, C., Fize, J., Artero, V., Mitsopoulou, C.A., 2015. Experimental and theoretical insight into electrocatalytic hydrogen evolution with nickel bis (aryldithiolene) complexes as catalysts. Inorg. Chem. 55, 432−444, with permission.*

i.e., ligands that render difficult the precise determination of the oxidation state of the metal ion (Eisenberg and Gray, 2011).

Metal bis-dithiolene complexes can be divided in several sub-categories; compounds of the type $[M(bdt)_2]^{n-}$, where bdt = Benzene-1,2-dithiolate and similar aromatic dithiolene ligands, $[M(sdt)_2]^{n-}$, sdt = *Z*-Stilbene-1,2-dithiolate, and bis-heteroleptic dithiolene complexes (Scheme 9.7).

In the first category, each member of series $[M(bdt)_2]^{-}$ (M = Ni, Pd, Pt) is most stable in the monoanionic form but it can be found in the dianionic state as well. They exhibit very intense absorption bands at the nIR region of the spectrum (~900 nm), with molar absorptivity values reaching several thousands. These transitions are of CT character, with different contribution of either metal or ligand HOMO toward a ligand-based LUMO (Cummings and Eisenberg, 2004). Bis-dithiolene d^8 complexes are not usually emissive, although when the heavy Pt is present, longer excited state lifetimes can be observed. Their intense absorption band has been used in sensory applications and dye-sensitization of TiO_2 (Islam et al., 2001; Linfoot et al., 2011; Ghosh and Schulzke, 2016; Jeon et al., 2017).

Heteroleptic [M(diimine)(dithiolate)] complexes (M = Ni, Pd, Pt) exhibit different photooxidation products, depending on the metal (Scheme 9.8) (Zhang et al., 1996; Connick and Gray, 1997). In the dark no reaction was observed for this series of complexes. Using Fukui functions and DFT-TDDFT theoretical calculations, the reactive centers of these complexes can be identified and different sulfur nucleophilicities can be explained (Cocker and

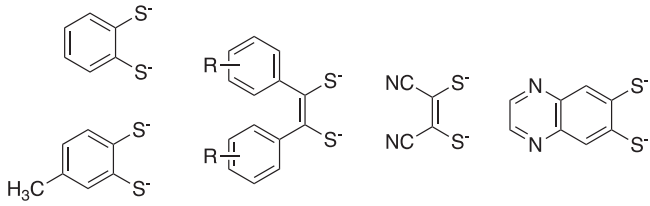

SCHEME 9.7 Various dithiolene ligands.

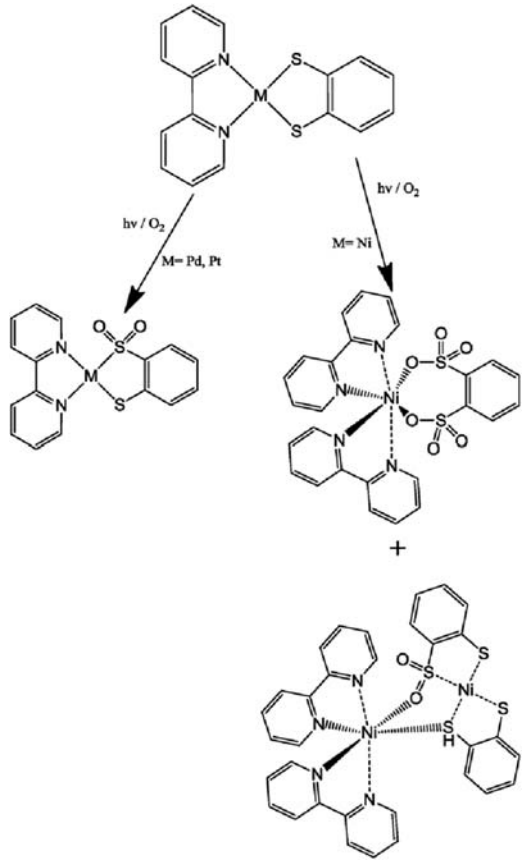

SCHEME 9.8 Photochemical oxidation products of [M(diimine)(dithiolene)] complexes. *Adapted from Mitsopoulou, C.A., 2010. Identifying of charge-transfer transitions and reactive centers in M(diimine)(dithiolate) complexes by DFT techniques. Coord. Chem. Rev. 254, 1448–1456, with permission.*

Bachman, 2001; Makedonas and Mitsopoulou, 2006; Mitsopoulou, 2010). Since the electronic structure of these complexes involves a mixed-dithiolene-metal HOMO and a diimine LUMO, the different reaction patterns are attributed to the different contribution of each metal in the bonding scheme.

The high nucleophilic nature of sulfur donor atoms has been exploited for both electrocatalytic and photocatalytic hydrogen evolution from acidic media (Zarkadoulas et al., 2012, 2017; Letko et al., 2014). Catalytic activity is not always observed by dithiolene complexes themselves and a photosensitizer may be required. Existing examples of other dithiolene complexes that split water without added photosensitizer may provide insight, combined with the energetics and details of hydrogen evolution mechanism followed by nickel complexes (Humphry-Baker, 1998).

A series of nickel bis-dithiolene complexes has been investigated for the photocatalytic hydrogen evolution reaction from acidic organic media (acetic acid in DMF) in combination with triethanolamine as a sacrificial electron donor, with rhenium(I) diimine of the type [Re(diimine)$(CO)_3$X] complexes as photosensitizers (Koutsouri et al., 2019) (Scheme 9.9).

The different structure of each catalyst has an effect on photocatalytic activity; interestingly, different organic substituents on the organic ligand framework affect the formal charges on sulfur atoms in the NiS_4 core. This has also been shown by similar complexes under electrocatalytic conditions along with DFT studies (Zarkadoulas et al., 2015) that demonstrated how each redox equivalent is stored on the NiS_4 core, indicating how important the second coordination sphere is for this class of catalysts. The proposed catalytic cycle involves the following steps:

The monoanionic catalyst is reduced to the dianionic state, after reductive quenching of the excited photosensitizer. Subsequent protonation at sulfur and further reduction yields a highly reactive, protonated intermediate that can be protonated a second time to yield dihydrogen and the monoanionic catalyst (Drosou et al., 2020). The limiting factor in this case was the dissociating paths followed by the rhenium photosensitizer. The different activity of each catalyst, along with the catalytic superiority of asymmetric and heteroleptic complexes raised questions regarding the possible participation of nickel ion in the catalytic cycle.

Further study of this catalyst class revealed the nature of catalytic cycle upon interfering with the delocalization of electron density on the NiS_4 core (Zarkadoulas et al., 2018; Drosou et al., 2021). Thus, selectively alkylating

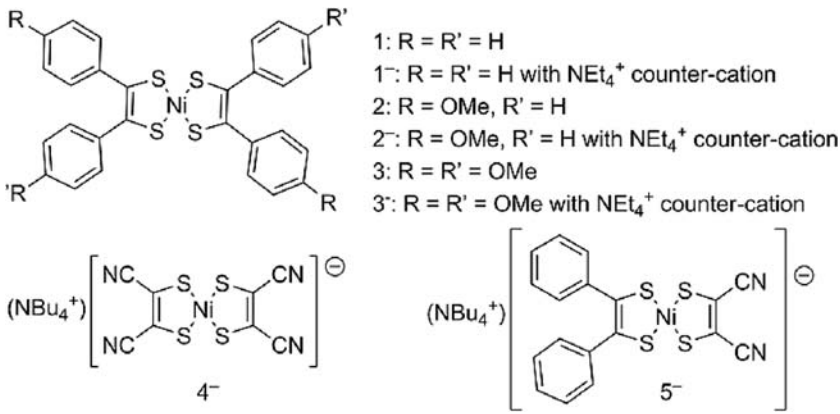

SCHEME 9.9 $[Ni(dithiolene)_2]^-$ catalysts for the photocatalytic hydrogen evolution reaction. *Adapted from Koutsouri, E., Zarkadoulas, A., Kefalidi, C., Papatriantafyllopoulou, C., Mitsopoulou, C.A., 2019. Establishing structure–activity relationships in photocatalytic systems by using nickel bis(dithiolene) complexes as proton reduction catalysts. Eur. J. Inorg. Chem. 2019, 4908–4919, with permission.*

two adjacent sulfur atoms by creating a $-CH_2CH_2CH_2-$ alkyl bridge, directs protonation toward the non-alkylated, more nucleophilic sulfur atoms. Electrochemistry and theoretical studies indicated a structural distortion accompanying the reductions in this case, in contrast with the non-alkylated counterparts. Then, subsequent reduction and protonation can take place on the now reduced, Ni(I) ion.

For these catalysts, detailed DFT studies confirm that an increased metal basicity is observed in the case of alkylated nickel bis-dithiolene complexes. Alkylation imposes a specific, more localized, electronic structure on the NiS_4 core, rendering coordinated sulfur atoms capable of acting as internal proton relays that transfer protons to the metal, facilitating protonation of a nickel-hydride species. Similar work for related ligand frameworks has been reported (Das et al., 2015; Drosou et al., 2021; Kamatsos et al., 2021a,b).

Dithiolene complexes also find interesting applications in medicinal chemistry. An initial report can be found on [Pt(pq)(bdt)] (pq = 2-(2′-Pyridyl) quinoxaline, bdt = benzene-1,2-dithiolate) complex (Mitsopoulou et al., 2008) and its interaction with CT-DNA both in the dark and after illumination. More recent studies focus on the use of bis-dithiolene complexes for theranostic applications (Camerel and Fourmigué, 2020). In this context, nickel bis-dithiolene complexes bearing bulky groups (Scheme 9.10) have been prepared (Mebrouk et al., 2015, 2017; Ciancone et al., 2018, 2019; Park et al., 2020; Chen et al., 2021). These organic groups allow incorporation in nanocarriers that, upon nIR irradiation, can be photothermally active and release

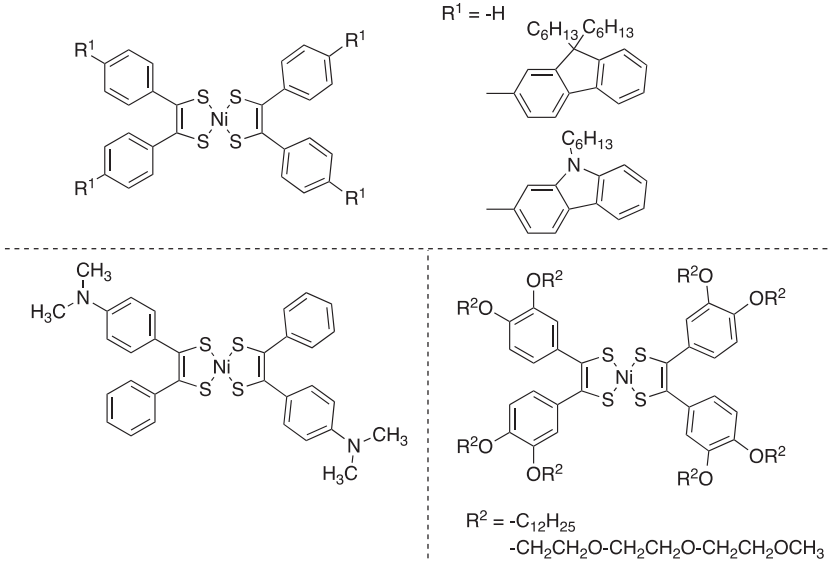

SCHEME 9.10 Structures of [Ni(dithiolene)$_2$] complexes used for theranostic applications.

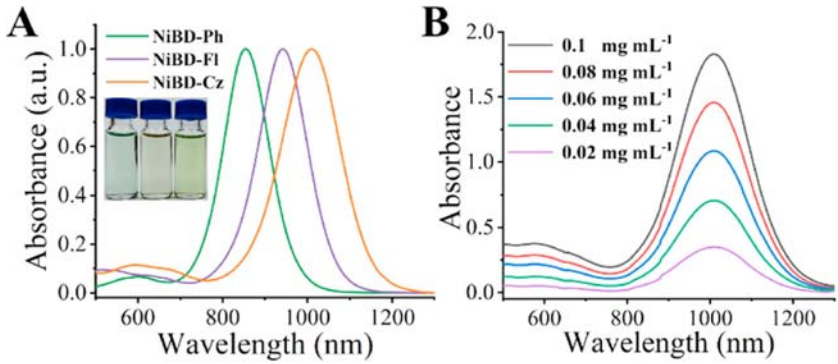

FIGURE. 9.9 (A) (Normalized) UV-Vis absorption spectra of phenyl-, fluorenyl-, and carbazoyl-bis-dithiolene complexes in THF and (B) Spectrum of carbazoyl-complex at different concentrations. *Adapted from Chen, K., Fang, W., Zhang, Q., Jiang, X., Chen, Y., Xu, W., et al., 2021. Tunable NIR absorption property of a dithiolene nickel complex: a promising NIR-II absorption material for photothermal therapy. ACS Appl. Bio Mater. 4, 4406–4412, with permission.*

encapsulated drugs on specific sites. Compared to other release agents, bis-dithiolene complexes do not produce singlet oxygen upon irradiation, require low power laser intensity, and are effective in low concentrations. Additionally, typically for this class of compounds, nIR absorption can be finely tuned by altering the ligand framework, with absorption maxima spanning 900–1700 nm (Fig. 9.9).

9.5 Salen-type complexes

Salen complexes of the type shown in Scheme 9.11 and related Schiff base complexes have long been studied for their catalytic properties (Cozzi, 2004).

In terms of group 10 salen complexes and their photochemistry, nickel complexes have been reported in early 2000s (de Castro et al., 2002), where several Ni(II) complexes with different peripheral substitutions were reported. They exhibit absorption in the range of 255–415 nm involving LLCT and MLCT transitions, and they are emissive after excitation at the MLCT band at 425 nm, with observed $\lambda_{em.} = 580$ nm and quantum yields reaching 0.08 for fluorescence. Stern-Volmer analysis for O_2 quenching rate constants were found in the order of $>10^9\ M^{-1}\ s^{-1}$ (Fig. 9.10 and Scheme 9.12).

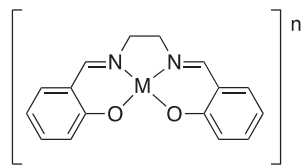

SCHEME 9.11 [M(salen)] complex.

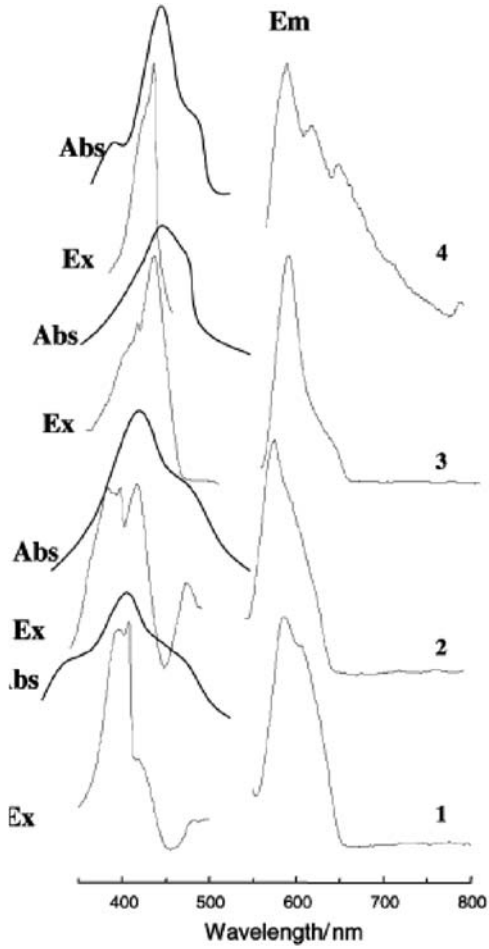

FIGURE. 9.10 UV-Vis absorption, emission ($\lambda_{exc.} = 425$ nm), and excitation ($\lambda_{em.} = 580$ nm) spectra of [Ni(salen)] complexes. *Adapted from de Castro, B., Ferreira, R., Freire, C., García, H., Palomares, E.J., Sabater, M.J., 2002. Photochemistry of nickel salen based complexes and relevance to catalysis. New J. Chem. 26, 405–410, with permission.*

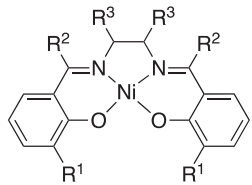

$R^1 = R^2 = R^3 = -H$
$R^1 = R^2 = -H$, $R^3 = -(CH_3)_4-$
$R^1 = R^3 = -H$, $R^2 = -CH_3$
$R^1 = -OCH_3$, $R^2 = R^3 = -H$

SCHEME 9.12 [Ni(salen)] complexes with various substitution.

Photophysical study revealed an initial metal-to-ligand electron transfer from d_{Ni} orbitals to π^*_{salen} orbitals, yielding an excited state with charge separation. Deactivation from this state accounts for the emission observed, while intersystem crossing to the triplet state results in a short-lived (μs) transient detected by flash photolysis. Substitution on the salen ring did not have an effect on the pathway but affected the excited state lifetimes.

Related complexes [Pd(salen)] and [Pt(salen)] are reported to be non-emissive and slightly emissive ($\phi = 0.19$). Based on theoretical calculations (Tong et al., 2014), for the case of Pd this is attributed to the population of a d-orbital excited state after excitation, and a subsequent fast, non-radiative decay occurring before ISC, preventing any emission (Scheme 9.13).

In this type of Pd complexes, σ_{Pd} d-orbitals are positioned higher than π^*_{salen} orbitals. Since σ symmetry d-orbitals of Pd are difficult to influence, peripheral modification of the salphen ligand that leads to lowering of π^* orbitals is a way to prepare emissive Pd(II) salen-type complexes. Indeed, introduction of -COOMe groups led to complexes with weak triplet emissions and short lifetimes ($\tau < 0.2$ μs, $\phi = 1.7 \times 10^{-4}$).

The case with [Pt(salen)] is quite different; although the bonding scheme is similar to the Pd analog, the metal contribution in this case is larger, giving rise to singlet MLCT/IL excited states. Combined with the lower energy of σ_{Pt} d-orbitals, the MC d-excited state is lifted above the singlet excited states. Then, excitation at 390 nm can lead to population of either MLCT or IL singlet excited states with triplet states in proximity that allow efficient ISC and observation of phosphorescence.

The intrinsic photophysical properties of Pt-salen complexes have found applications in the development of luminescent probes for G-quadruplex DNA (Wu et al., 2009), bearing similarities to $[Pt(terpy)]^+$ complexes that have been used for the same purpose (Scheme 9.14).

Several Pt complexes with varying substitution patterns on either the backbone or the periphery of Schiff base ligand were prepared and their photophysical study revealed ILCT bands at ~390 nm and MMLCT and LLCT bands in the visible region (400−500 nm). A slight negative solvatochromic effect indicative of a polar ground state was also reported. Emission lifetimes of several μs were observed around 600 nm.

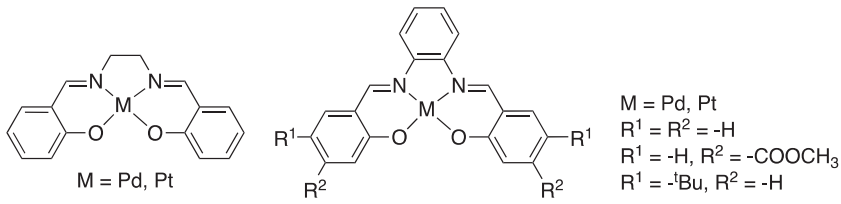

SCHEME 9.13 [M(salen)] and [M(salphen)] complexes.

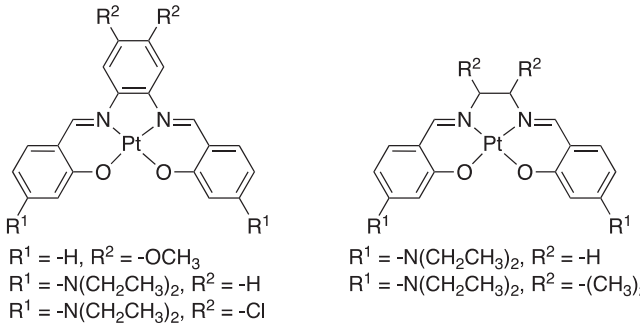

SCHEME 9.14 [Pt(salphen)] and [Pt(salen)] complexes studied as probes for G-quadruplex DNA.

After initial reports on platinum salen-type complexes, various complexes that have been prepared exhibit interesting optical properties and possible applications in mechanochromic crystalline materials. In one case, a series of bis-salen type group 10 metal complexes has been prepared (Scheme 9.15) (Achira et al., 2016).

The complexes display similar features between the mono- and binuclear counterparts in each case, i.e., ILCT bands in the UV region and wide multiple bands in the region 400−500 nm. In the case of Pt(II), emission and excitation spectra of the mononuclear and binuclear complexes are similar, indicating no significant interaction between the two moieties. Solid state absorption spectra for both Ni(II) and both Pd(II) complexes were similar to thin-films prepared in this study, but in the case of binuclear Pd(II) complex, the spectrum was more finely structured, owing to fixed crystal conformations of the molecules. However, the single-crystal spectra of Pt(II) complexes exhibited different behavior compared to the thin films, with an extra absorption band observed at 520 nm. A similar band observed for the Ni(II) complexes was attributed to d-

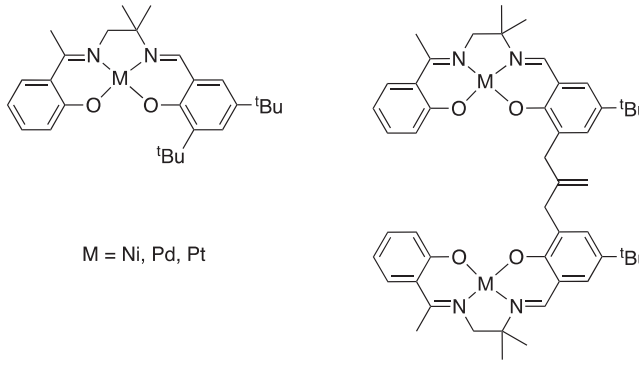

SCHEME 9.15 Mononuclear and binuclear salen complexes of group 10 metals.

d transitions. Crystal crushing and smearing experiments revealed different optical properties for the Pt(II) complexes under mechanical stress, more pronounced in the case of the binuclear Pt(II) complex, attributed to the semi-rigidity imposed by the organic linker. In a similar case of a rigid, binuclear Pt-salen type complex, the fused organic linker between ligands of the two Pt-moieties leads to probable mixing of $^3MLCT_{Pt}$ and $^3\pi$-π*states that result in emission 700−800 nm (Houjou et al., 2017).

Due to aforementioned interesting properties of salen and salen-type group 10 complexes, peripheral modification of ligand framework led to the preparation of boron dipyrromethene (BODIPY) and anthracene substituted compounds shown in Scheme 9.16 (Razi et al., 2018; Chen et al., 2020).

Selective excitation of BODIPY moiety (490 nm) led to Förster energy transfer to Pt(II) moiety in a 6.7 ps time interval, followed by a fast ISC and triplet-triplet back-transfer to BODIPY. The triplet state had ∼30 times longer lifetime compared to the Pt compound without BODIPY moiety and was studied in terms of triplet-triplet annihilation (TTA) upconversion with a quantum yield of 10% and a large anti-Stokes shift (Razi et al., 2018) (Fig. 9.11).

On the other hand, the anthryl moiety on a similar platinum backbone induces interesting photophysical properties. The Pt(II) complexes exhibit small Stokes shifts, indicating low energy losses during ISC, rendering them useful triplet photosensitizers. Phosphorescence of the Pt-moiety with quantum yields of ∼11% is quenched in the case of complexes bearing anthracene moiety, giving rise to phosphorescence with $\Phi = 4\%$. Transient absorption spectroscopy indicates both triplet anthracene and ^{3}MLCT states, increasing the excited state lifetime of anthryl-complexes compared to phenyl-complex. These complexes have also been used for TTA upconversion, with quantum yield up to 15% (Fig. 9.12).

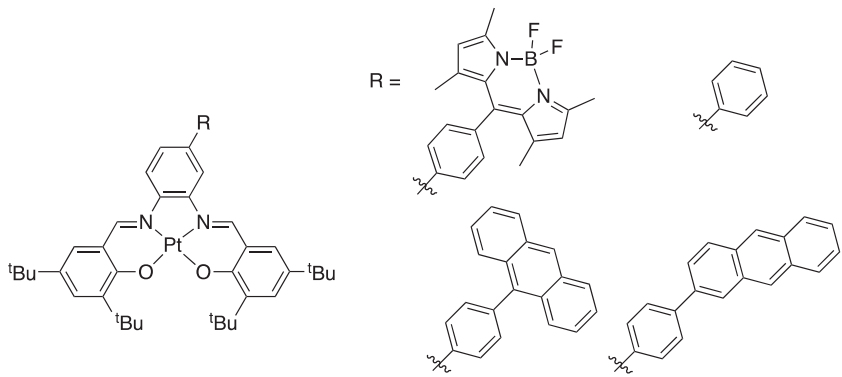

SCHEME 9.16 Chromophore appended [Pt(salen)] complexes.

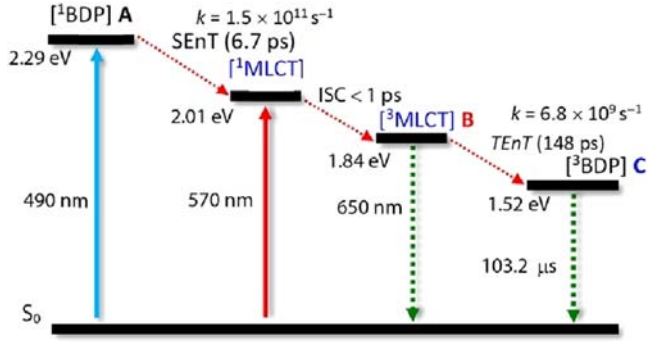

FIGURE. 9.11 Photophysical processes of BODIPY-[Pt(salen)] complex upon excitation at 490 and 570 nm. *Adapted from Razi, S.S., Koo, Y.H., Kim, W., Yang, W., Wang, Z., Gobeze, H., et al., 2018. Ping-Pong energy transfer in a boron dipyrromethane containing Pt(II)−Schiff base complex: synthesis, photophysical studies, and anti-Stokes shift increase in triplet−triplet annihilation upconversion. Inorg. Chem. 57, 4877−4890, with permission.*

9.5.1 Other complexes

Since interest in luminescent, first-row transition metals has risen over the last years (Wegeberg and Wenger, 2021), mostly several nickel complexes with various ligand frameworks will be mentioned here, with some recent examples of palladium and platinum complexes as well.

Three cyclometalated Ni(II) complexes of the type NˆCˆN and NˆCˆNˆO (Scheme 9.17) have been scrutinized in terms of photophysical properties; the compound bearing the carbazoyl group exhibits room temperature luminescence with a triplet excited state at low temperatures (Wong et al., 2020). The complexes exhibit intense absorption bands at $\lambda < 350$ nm, attributed to ILCT transitions, and MLCT or mixed LLCT/MLCT transitions in the region of 350−500 nm (Fig. 9.13).

The carbazoyl-substituted complex exhibits a broad, structureless emission band with a maximum at 600 nm, which shows vibronic structure at 77 K, along with intense emission intensity in solids and glass matrices.

Due to the square planar geometry of the rigid, tetradentate complex of Scheme 9.17, Ni−Ni interactions occur and cause aggregation. This becomes evident in concentration-dependent UV-vis spectra, where a new band rises at 480 nm, which is attributed to formed aggregates.

A nickel(II) complex bearing a non-innocent ligand, incorporating both an oxime and pyridyl moiety (Scheme 9.18) (Pramanik et al., 2017) exhibits broad absorption bands in the 400−650 nm region, attributed to ligand-based, charge transfer transitions. Excitation at either absorption maximum leads to broad luminescence around 410 nm, with quantum yields of ∼6%.

As a substitute to different 3d transition metals complexes that exhibit spin-crossover properties, nickel complexes bearing phenazine ligands display

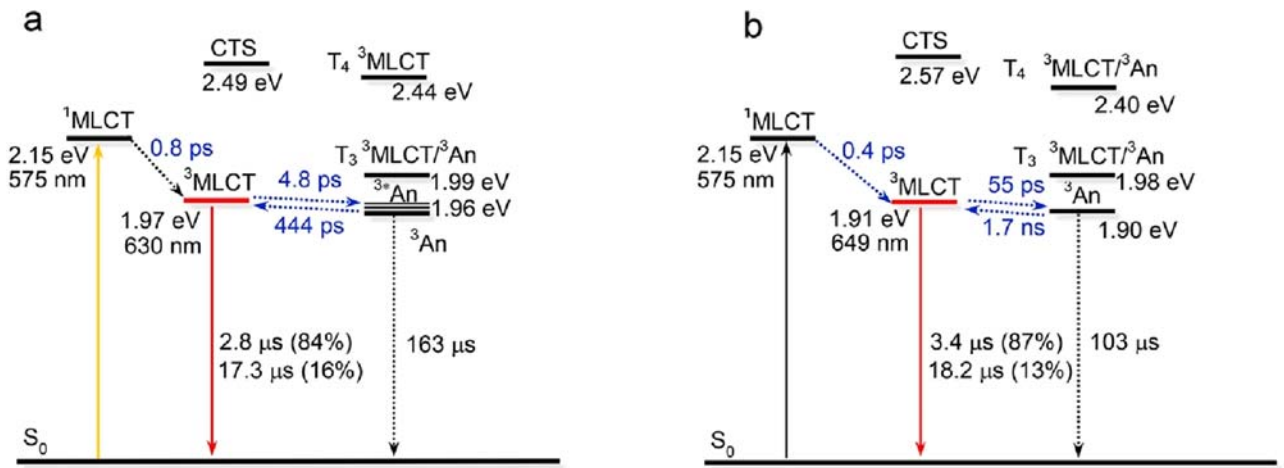

FIGURE. 9.12 Photophysical processes of (A) 9-anthryl- and (B) 2-anthryl-[Pt(salen)] complex. *Adapted from Chen, K., Hussain, M., Razi, S.S., Hou, Y., Yildiz, E.A., Zhao, J., et al., 2020. Anthryl-appended platinum(II) schiff base complexes: exceptionally small Stokes shift, triplet excited states equilibrium, and application in triplet−triplet-annihilation upconversion. Inorg. Chem. 59, 14731−14745, with permission.*

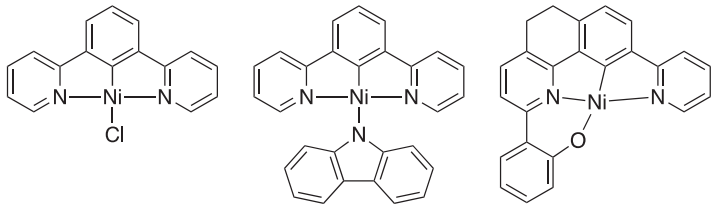

SCHEME 9.17 Emissive Ni(II) complexes.

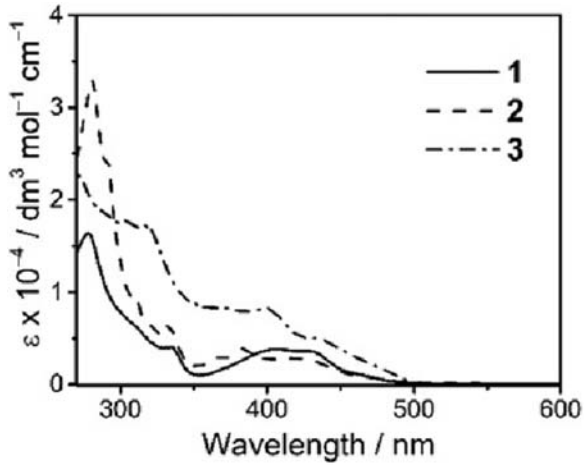

FIGURE. 9.13 UV-Vis absorption spectra of (N^C^N) (*solid trace*), carbazoyl- (*dashed trace*), tetradentate-nickel complex (*dotted trace*). *Adapted from Wong, Y.-S., Tang, M.-C., Ng, M., Yam, V.W.-W., 2020. Toward the design of phosphorescent emitters of cyclometalated earth-abundant nickel(II) and their supramolecular study. J. Am. Chem. Soc. 142, 7638−7646, with permission.*

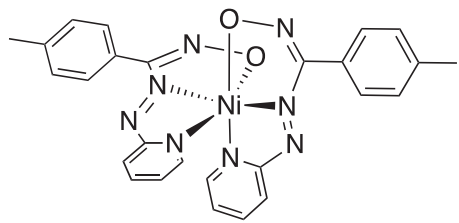

SCHEME 9.18 Ni(II) pyridyl-azooximate complex.

coordination-induced spin state switch (CISSS) (Kurz et al., 2021). The ability of the compounds to undergo conformation changes, which in Ni(II) complexes are accompanied by coordination geometry (square planar diamagnetic to square pyramidal or octahedral paramagnetic), can be monitored by fluorescence spectroscopy.

The complexes exhibit intense absorption bands near 420 nm, with high molar absorptivity values ($\sim$40,000 M^{-1} cm^{-1}) in chloroform. The complex with $-CF_3$ groups is non emissive, contrary to the other compounds which emit at 476 nm, when excited at 385 nm. TD-DFT studies revealed both HOMO and LUMO to be of phenazine nature and charge transfer transitions from the NiN_2O_2 moiety to the phenazine, rendering the transitions MLCT. The opposite is observed for the $-CF_3$ substituted compound, where the transition is inverted and is assigned to be LMCT in nature. Quite long fluorescence lifetimes were observed for the complex $R^1 = -COOCH_2CH_3$, $R^2 = -CH_3$(1 ns) and the emission lifetime extends to 1.8 ns at lower temperatures.

Recording absorption spectra at different pyridine/chloroform ratios drastically change, when pyridine:complex ratio is 30,000:1. At even higher ratios, two bands appear at 370 and 510 nm, which are indicative of the formation of five- and six-coordinate species that resulted from CISSS. Remarkably, the fluorescence quenching by Lewis bases was reported to occur in the singlet state of the excited chromophore (Fig. 9.14).

In the same spirit of preparing planar Ni(II) complexes with intriguing photophysical properties, multifunctional nickel complexes with three functionalities have been prepared (Scheme 9.20) (Alrefai et al., 2021). Although these complexes are not emissive, significant conclusions can be drawn regarding the design of multifunctional Ni(II) chromophores.

In each Ni(II) complex, the aromatic ring system becomes extended, going from phenanthroline to dipyridophenazine and tetrahydrodipyridophenazine, with increasing delocalization, and this has a small effect on the charge transfer absorptions. However, different ligands coordinated on Ni(II) modulate the absorption in the visible region, spanning from 350 to 750 nm.

By design, the π-extended ligands affect the LUMO, and the coordinated co-ligand R-E, along with Ni(II) contribution, is responsible for modulation of the HOMO. The remaining moiety, i.e., the pendant aryl arm, actually modifies the energy of (occupied) donor and (unoccupied) acceptor frontier molecular orbitals. The subtle balance of these three contributing factors leads to the observed situation: when an excited state is populated due to Ni-donor-to-π-system charge transfer transition, nonradiative decay takes place due to

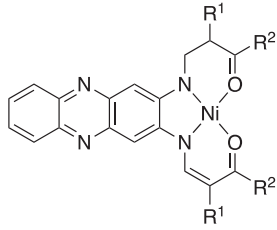

R^1 = -$COOCH_2CH_3$, R^2 = -CH_3
R^1 = -$COOCH_3$, R^2 = -CH_3
R^1 = -$COCH_3$, R^2 = -CH_3
R^1 = -$COOCH_2CH_3$, R^2 = -CF_3

SCHEME 9.19 Ni(II) complex exhibiting coordination-induced spin state switch.

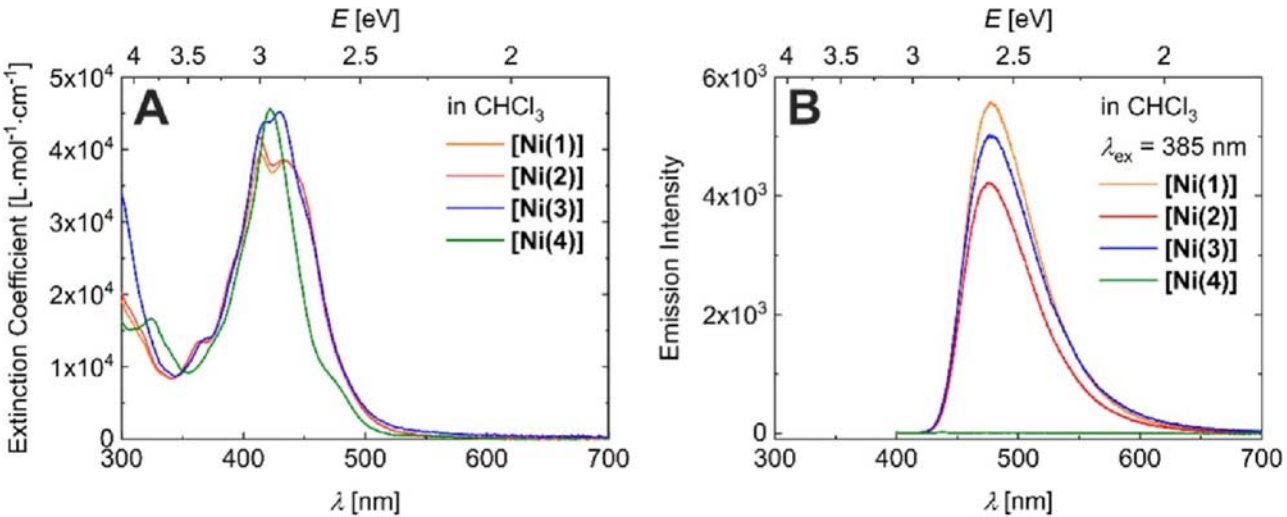

FIGURE. 9.14 (A) UV−Vis absorption spectra of Ni(II) complexes of Scheme 9.19 measured in $CHCl_3$. (B) Emission spectra of the aforementioned complexes in $CHCl_3$ ($\lambda_{exc.} = 385$ nm). *Adapted from Kurz, H., Schötz, K., Papadopoulos, I., Heinemann, F.W., Maid, H., Guldi, D.M., 2021. A fluorescence-detected coordination-induced spin state switch. J. Am. Chem. Soc. 143, 3466−3480, with permission.*

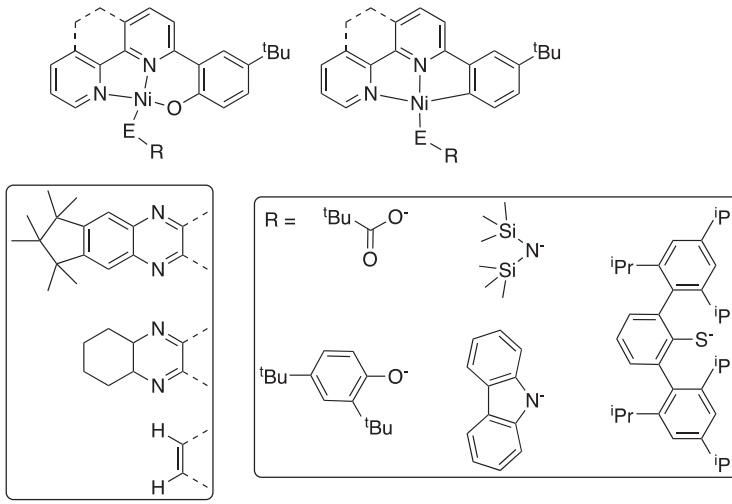

SCHEME 9.20 Structures of multifunctional Ni(II) complexes.

conformational rotations, which adds a Ni(III) character to the excited state. The presence of phenolate oxygen stabilizes the HOMO and contributes more to its orbital character, when compared with the C-coordinated aryl ring.

In the field of Pd(II) complexes, recently progress has been made in emissive isocyanide complexes (Wan et al., 2018).

These complexes display intermolecular interactions that give rise to emissive ^{3}MMLCT excited states in various aggregation states. Bands below 400 nm are attributed to ILCT or mixed IL-MLCT transitions, and interestingly, changes in solvent system induced aggregation with the concomitant emergence of a new band at 439 or 389 nm, depending on the complex. Detailed photophysical study revealed that the pincer complexes display emission based on either singlet or triplet MMLCT excited states at room temperature that is influenced by the formation of aggregates in various extents. In fact, the HOMO-LUMO gap is modulated by the degree of aggregation (Fig. 9.15).

In this context, several macrocyclic complexes of Pd(II) and Pt(II) encompassed by a modified porphyrinoid core, have been reported as fluorescent but not phosphorescent in the nIR region (Scheme 9.22) (Yao et al., 2019).

The absorption spectra of Pd(II) and Pt(II) complexes display intense bands at 300−400 nm and broad bands at 500−600 nm, and upon excitation at 500 nm display intense emission at ∼600 nm in the case of −CN substituted complexes and a weak emission at 550−800 nm for the electron donating groups $-NMe_2$ and −OMe (Fig. 9.16).

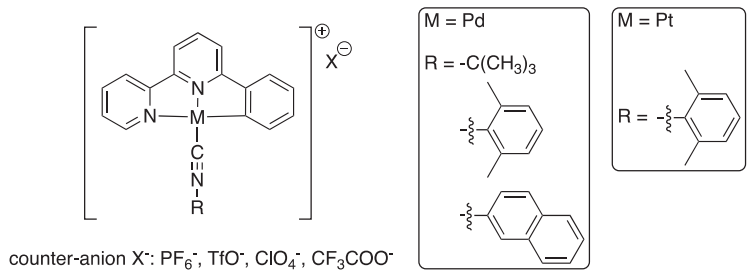

SCHEME 9.21 Pd(II) and Pt(II) emissive isocyanide pincer complexes.

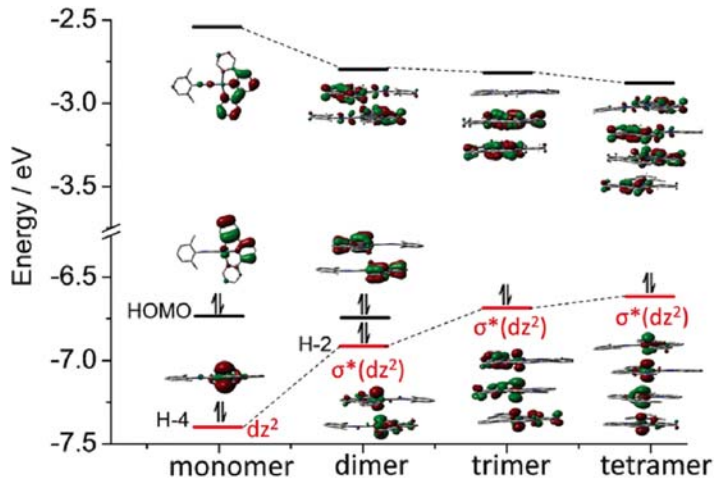

FIGURE. 9.15 Calculated molecular orbitals for 2,6-dimethyl-phenyl Pd(II) isocyanide complex of Scheme 9.21 in its different aggregate forms and subsequent d(z^2) orbital energy level. *Adapted from Wan, Q., To, W.-P., Yang, C., Che, C.-M., 2018. The metal–metal-to-ligand charge transfer excited state and supramolecular polymerization of luminescent pincer PdII–isocyanide complexes. Angew. Chem. Int. Ed. 57, 3089–3093, with permission.*

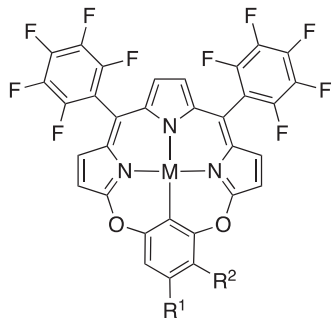

M = Pd, Pt, $R^1 = R^2 = -H$
M = Pd, $R^1 = -N(CH_3)_2$, $R^2 = -H$
M = Pd, $R^1 = -CN$, $R^2 = -H$
M = Pd, Pt, $R^1 = -H$, $R^2 = -OCH_3$
M = Pd, Pt, $R^1 = -H$, $R^2 = -CN$

SCHEME 9.22 Pd(II) and Pt(II) macrocyclic complexes.

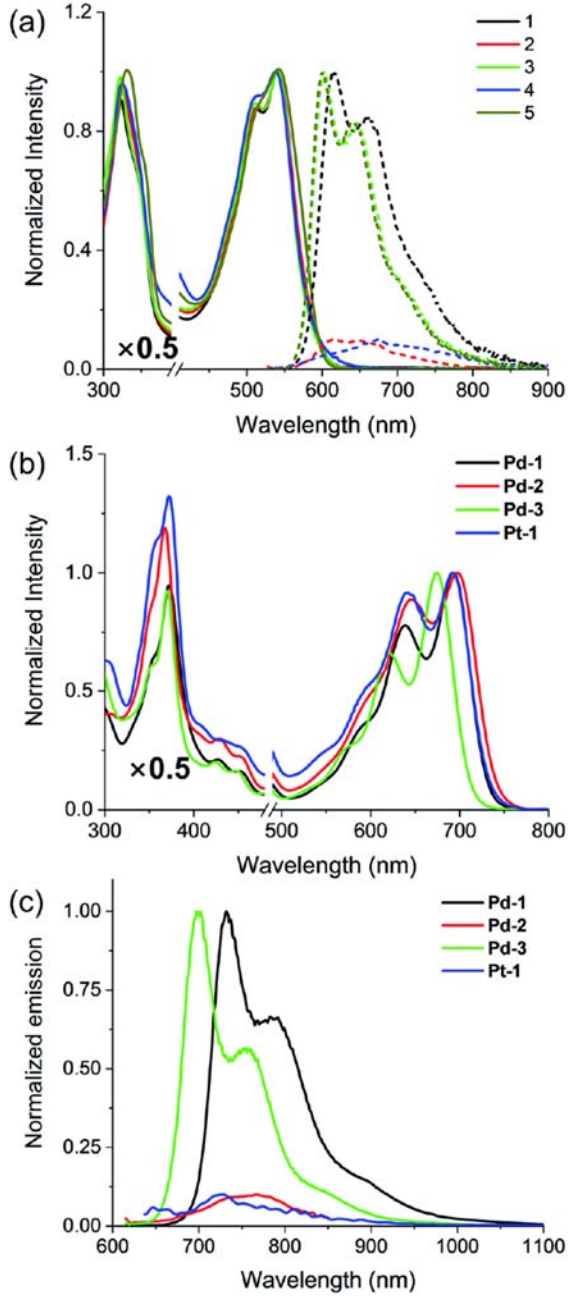

FIGURE. 9.16 (A) UV-Vis absorption and emission spectra of free ligands in CH_2Cl_2. (B) UV-Vis absorption spectra and (C) emission spectra of Pd(II) complexes with $R^1 = R^2 = -H$ (*black trace*), $R^1 = -N(CH_3)_2$, $R^2 = -H$ (*red trace*), $R^1 = -CN$, $R^2 = -H$ (*green trace*). *Blue trace:* Pt-compound with $R_1 = R_2 = -H$. *Adapted from Yao, Y., Hou, C.-L., Yang, Z.-S., Ran, G., Kang, L., Li, C., 2019. Unusual near infrared (NIR) fluorescent palladium(II) macrocyclic complexes containing M−C bonds with bioimaging capability. Chem. Sci. 10, 10170−10178, with permission.*

Upon complexation of either Pd(II) or Pt(II), a bathochromic shift is observed for absorption and emission spectra of free ligands, pointing to small differences in both; ground and excited states. The Pd(II) complexes exhibit strong nIR fluorescence, but contrary to structurally similar Pd(II) porphyrins, no phosphorescence is observed. Time-dependent spectroscopy and TD-DFT studies of both Pd and Pt complexes with $R^1 = R^2 = -H$ suggest that triplet state is not populated, owing to a small spin-orbit coupling effect that occurs due to large energy gaps and molecular orbitals mainly of ligand character. These photophysical properties can have applications in bio-imaging applications, since the dimethylamino-substituted complex can act as a pH probe in HeLa cells.

As rigid structures have proved beneficial for enhancing emission from group 10 complexes, another report deals with tetradentate Pd(II) and Pt(II) complexes with long-lived excited states (Maisuls et al., 2021) (Scheme 9.23).

The complexes display absorption bands in dichloromethane solution at 235−300 nm (^{1}LC) and exhibit several bands in the region 350−450 nm. The latter are assigned to transitions into ligand centered and low-lying MLCT states (Fig. 9.17).

The Pt(II) complexes exhibit emission at 508 and 544 nm, with a slight shift in the case of fluorinated compound, where emission maxima are found at 489 and 524 nm. The emission profile is similar for the Pd(II) complexes ($\lambda_{em.} = 481$ and 473 nm). At room temperature, non-radiative decay pathways are accessible via metal-centered orbitals for the Pd(II) complexes, making them non-emissive at this temperature, since $\Phi_{lum.} < 2\%$ for Pd(II) compounds even under Ar ($\Phi_{lum.} = 27$ and 36% for Pt(II) complexes with −H and −F ligands, respectively). Based on DFT calculations and spectroscopy at different temperatures, it was concluded that the emission spectra of Pd(II) complexes can be attributed to dimers with ligand-centered and excimer character. Also, the Pt(II) complexes possess a more pronounced MLCT character than the Pd(II) analogs, but the structural confinement favors all complexes in terms of avoiding non-radiative deactivation pathways. The

SCHEME 9.23 Tetradentate Pd(II) and Pt(II) complexes.

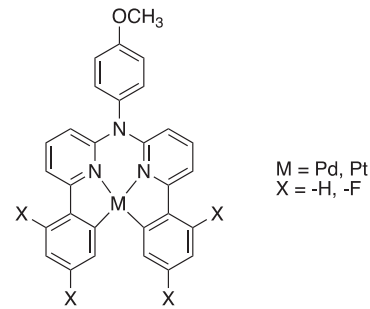

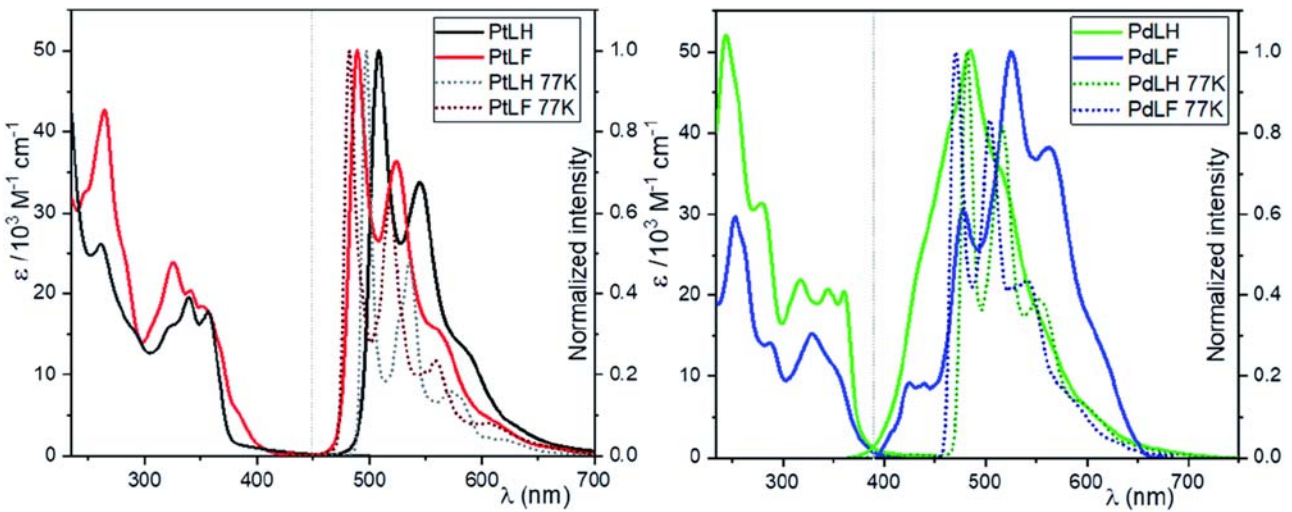

FIGURE. 9.17 UV-Vis absorption spectra and normalized emission spectra of complexes found in Scheme 9.23. *Black trace*: M = Pt, X = −H, *red* (gray in print version) *trace*: M = Pt, X = −F, *green* (light black in print version) *trace*: M = Pd, X = −H, *blue* (dark gray in print version) *trace*: M = Pd, X = −F. *Solid lines*: CH_2Cl_2 at room temperature, *dotted lines*: glass matrix at 77 K $\lambda_{exc.} = 350$ nm. (For interpretation of the references to colour in this figure legend, the reader is referred to the web version of this article.) *Adapted from Maisuls, I., Wang, C., Gutierrez Suburu, M.E., Wilde, S., Daniliuc, C.-G., Brünink, D., et al., 2021. Ligand-controlled and nanoconfinement-boosted luminescence employing Pt(II) and Pd(II) complexes: from color-tunable aggregation-enhanced dual emitters towards self-referenced oxygen reporters. Chem. Sci. 12, 3270−3281, with permission.*

monomeric fluorinated Pt(II) complex can act as a triplet oxygen sensor, since both its luminescence lifetime and intensity are affected by the presence of $^3O_2$ in its dual emission profile, i.e., monomer emission at 490 nm and insensitive ^{3}MMLCT luminescence found at 635 nm.

9.6 Conclusion

This chapter has sought to present and highlight recent advances in photophysics and photochemistry of group 10 metal complexes, with a focus on nickel complexes, in the spirit of employing earth abundant, low cost, metal ions for fulfilling interesting (photo)chemical reactions. The main factors governing emission from group 10 metal complexes are now apparent and are even more under scrutiny for the case of nickel, where much progress has been made very recently. One of the factors that affect photophysical and photochemical properties is geometry in terms of rigidity and flexibility, and fine tuning of steric factors combined with careful choice of electronic properties modulators via ligand design. As structure—properties become more clarified, one can prepare multifunctional complexes with applications in sustainable catalysis for chemical transformations, solar fuels utilization and hydrogen evolution, materials chemistry, and medicinal or theranostic applications.

References

Achira, H., Hoga, Y., Yoshikawa, I., Mutai, T., Matsumura, K., Houjou, H., 2016. Effects of a semiflexible linker on the mechanochromic photoluminescence of bis(Pt-salen) complex. Polyhedron 113, 123−131.

Alrefai, R., Hörner, G., Schubert, H., Berkefeld, A., 2021. Broadly versus Barely variable complex chromophores of planar nickel(II) from κ3-N,N′,C and κ3-N,N′,O donor platforms. Organometallics 40, 1163−1177.

Anbalagan, V., 2003. Photochemical behavior of platinum(II) and palladium(II) complexes of 4,4′-dimethyl-2,2′-bipyridine. J. Coord. Chem. 56, 161−172.

Basolo, F., Pearson, R.G., 1967. Mechanisms of Inorganic Reactions: A Study of Metal Complexes in Solution. Wiley, New York.

Basolo, F., Pearson, R.G., 1962. The trans effect in metal complexes. Prog. Inorg. Chem. 4, 381−453.

Baudron, S.A., 2020. Dipyrrin based metal complexes: reactivity and catalysis. Dalton Trans. 49, 6161−6175.

Cagan, D.A., Stroscio, G.D., Cusumano, A.Q., Hadt, R.G., 2020. Multireference description of nickel−aryl homolytic bond dissociation processes in photoredox catalysis. J. Phys. Chem. A 124, 9915−9922.

Camerel, F., Fourmigué, M., 2020. (Photo)thermal stimulation of functional dithiolene complexes in soft matter. Eur. J. Inorg. Chem. 2020, 508−522.

Campbell, M.W., Yuan, M., Polites, V.C., Gutierrez, O., Molander, G.A., 2021. Photochemical C−H activation enables nickel-catalyzed olefin dicarbofunctionalization. J. Am. Chem. Soc. 143, 3901−3910.

Chen, K., Fang, W., Zhang, Q., Jiang, X., Chen, Y., Xu, W., et al., 2021. Tunable NIR Absorption property of a dithiolene nickel complex: a promising NIR-II absorption material for photothermal therapy. ACS Appl. Bio Mater. 4, 4406−4412.

Chen, K., Hussain, M., Razi, S.S., Hou, Y., Yildiz, E.A., Zhao, J., et al., 2020. Anthryl-appended platinum(II) Schiff base complexes: exceptionally small Stokes shift, triplet excited states equilibrium, and application in triplet−triplet-annihilation upconversion. Inorg. Chem. 59, 14731−14745.

Ciancone, M., Mebrouk, K., Bellec, N., Le Goff-Gaillard, C., Arlot-Bonnemains, Y., Benvegnu, T., et al., 2018. Biocompatible nanoparticles containing hydrophobic nickel-bis(dithiolene) complexes for NIR-mediated doxorubicin release and photothermal therapy. J. Mater. Chem. B. 6, 1744−1753.

Ciancone, M., Bellec, N., Cammas-Marion, S., Dolet, A., Vray, D., Varray, F., et al., 2019. Liposomes containing nickel−bis(dithiolene) complexes for photothermal theranostics. Langmuir 35, 15121−15130.

Cocker, T.M., Bachman, R.E., 2001. Photochemical and chemical oxidation of α-diimine−dithiolene metal complexes: insight into the role of the metal atom. Inorg. Chem. 40, 1550−1556.

Connick, W.B., Gray, H.B., 1997. Photooxidation of platinum(II) diimine dithiolates. J. Am. Chem. Soc. 119, 11620−11627.

Cotton, F.A., 1990. Chemical Applications of Group Theory. John Wiley & Sons.

Cozzi, P.G., 2004. Metal−Salen Schiff base complexes in catalysis: practical aspects. Chem. Soc. Rev. 33, 410−421.

Cummings, S.D., Eisenberg, R., 2004. Luminescence and photochemistry of metal dithiolene complexes. In: Stiefel, E.I. (Ed.), Progress in Inorganic Chemistry. John Wiley & Sons, Inc., Hoboken, NJ, USA, pp. 315−367.

Das, A., Han, Z., Brennessel, W.W., Holland, P.L., Eisenberg, R., 2015. Nickel complexes for robust light-driven and electrocatalytic hydrogen production from water. ACS Catal. 5, 1397−1406.

de Castro, B., Ferreira, R., Freire, C., García, H., Palomares, E.J., Sabater, M.J., 2002. Photochemistry of nickel salen based complexes and relevance to catalysis. New J. Chem. 26, 405−410.

Deeth, R.J., 2020. d-orbital energy levels in planar $[MIIF4]^{2-}$, $[MII(NH_3)_4]^{2+}$ and $[MII(CN)_4]^{2-}$ complexes: the nature of M−L π bonding and the implications for ligand field theory. Dalton Trans. 49, 9641−9650.

Drew Tait, C., Janecky, D.R., Rogers, P.S.Z., 1991. Speciation of aqueous palladium(II) chloride solutions using optical spectroscopies. Geochem. Cosmochim. Acta 55, 1253−1264.

Drosou, M., Kamatsos, F., Mitsopoulou, C.A., 2020. Recent advances in the mechanisms of the hydrogen evolution reaction by non-innocent sulfur-coordinating metal complexes. Inorg. Chem. Front. 7, 37−71.

Drosou, M., Zarkadoulas, A., Bethanis, K., Mitsopoulou, C.A., 2021. Structural modifications on nickel dithiolene complexes lead to increased metal participation in the electrocatalytic hydrogen evolution mechanism. Null 74 (2021), 1425−1442.

Eisenberg, R., Gray, H.B., 2011. Noninnocence in metal complexes: a dithiolene dawn. Inorg. Chem. 50, 9741−9751.

Figgis, B.N., Hitchman, M.A., 1999. Ligand Field Theory and its Applications. Wiley.

Ghosh, A.C., Schulzke, C., 2016. Selectively detecting Hg^{2+}—a "mercury quick test" with bis-(coumarin−dithiolene) niccolate. Inorg. Chim. Acta 445, 149−154.

Greene, M.A., Yonova, I.M., Williams, F.J., Jarvo, E.R., 2012. Traceless directing group for stereospecific nickel-catalyzed alkyl−alkyl cross-coupling reactions. Org. Lett. 14, 4293−4296.

Han, Y.-L., Zhao, B.-Y., Jiang, K.-Y., Yan, H.-M., Zhang, Z.-X., Yang, W.-J., et al., 2018. Mechanistic insights into the Ni-catalyzed reductive carboxylation of C−O bonds in aromatic esters with CO_2: understanding remarkable ligand and traceless-directing-group effects. Chem. Asian J. 13, 1570−1581.

Houjou, H., Hoga, Y., Ma, Y.-L., Achira, H., Yoshikawa, I., Mutai, T., Matsumura, K., 2017. Dinuclear fused salen complexes of group-10 metals: peculiarity of the crystal structure and near-infrared luminescence of a bis(Pt-salen) complex. Inorg. Chim. Acta 461, 27−34.

Hu, Y.-Z., Ye, Z.-P., Xia, P.-J., Song, D., Li, X.-J., Liu, Z.-L., et al., 2021. Visible-light-driven, photocatalyst-free cascade to access 3-cyanoalkyl coumarins from ortho-hydroxycinnamic esters. J. Org. Chem. 86, 4245−4253.

Humphry-Baker, R., Mitsopoulou, C.A., Katakis, D., Vrachnou, E., 1998. Photophysical study of the decomposition of water using visible light and tungsten tris(dithiolenes) as photosensitizers-catalysts. J. Photochem. Photobiol., A 114, 137−144.

Hwang, S.J., Powers, D.C., Maher, A.G., Anderson, B.L., Hadt, R.G., Zheng, S.-L., et al., 2015. Trap-free halogen photoelimination from mononuclear Ni(III) complexes. J. Am. Chem. Soc. 137, 6472−6475.

Islam, A., Sugihara, H., Hara, K., Singh, L.P., Katoh, R., Yanagida, M., et al., 2001. Dye sensitization of nanocrystalline titanium dioxide with square planar platinum(II) diimine dithiolate complexes. Inorg. Chem. 40, 5371−5380.

Jeon, S., Suh, W., Noh, D.-Y., 2017. Anion-dependent Hg^{2+}-sensing of colorimetric (dppe) Pt(dmit) chemosensor (dppe: 1,2-bis(diphenylphosphino)ethane; dmit: 1,3-dithiole-2-thione-4,5-dithiolate). Inorg. Chem. Commun. 81, 43−46.

Kamatsos, F., Bethanis, K., Mitsopoulou, C.A., 2021. Synthesis of novel heteroleptic oxothiolate Ni(II) complexes and evaluation of their catalytic activity for hydrogen evolution. Catalysts 11. https://doi.org/10.3390/catal11030401.

Kamatsos, F., Drosou, M., Mitsopoulou, C.A., 2021. Heteroleptic thiolate diamine nickel complexes: noble-free-metal catalysts in electrocatalytic and light-driven hydrogen evolution reaction. Int. J. Hydrogen Energy 46, 19705−19716.

Karges, J., Blacque, O., Gasser, G., 2020. Metal dipyrrin complexes as potential photosensitizers for photodynamic therapy. Inorg. Chim. Acta 505. https://doi.org/10.1016/j.ica.2020.119482.

Kariofillis, S.K., Doyle, A.G., 2021. Synthetic and mechanistic implications of chlorine photoelimination in nickel/photoredox C(sp3)−H cross-coupling. Acc. Chem. Res. 54, 988−1000.

Koutsouri, E., Zarkadoulas, A., Kefalidi, C., Papatriantafyllopoulou, C., Mitsopoulou, C.A., 2019. Establishing structure−activity relationships in photocatalytic systems by using nickel bis(-dithiolene) complexes as proton reduction catalysts. Eur. J. Inorg. Chem. 2019, 4908−4919.

Kundu, S., Huitink, D., Liang, H., 2010. Formation of electrically conductive palladium nanowires on polymer scaffolds by photochemical approach. Colloids Surf. A Physicochem. Eng. 360, 129−136.

Kurz, H., Schötz, K., Papadopoulos, I., Heinemann, F.W., Maid, H., Guldi, D.M., 2021. A fluorescence-detected coordination-induced spin state switch. J. Am. Chem. Soc. 143, 3466−3480.

Letko, C.S., Panetier, J.A., Head-Gordon, M., Tilley, T.D., 2014. Mechanism of the electrocatalytic reduction of protons with diaryldithiolene cobalt complexes. J. Am. Chem. Soc. 136, 9364−9376.

Li, K., Ming Tong, G.S., Wan, Q., Cheng, G., Tong, W.-Y., Ang, W.-H., et al., 2016. Highly phosphorescent platinum(II) emitters: photophysics, materials and biological applications. Chem. Sci. 7, 1653−1673.

Linfoot, C.L., Richardson, P., McCall, K.L., Durrant, J.R., Morandeira, A., Robertson, N., 2011. A nickel-complex sensitiser for dye-sensitised solar cells. Sol. Energy 85, 1195−1203.

Maisuls, I., Wang, C., Gutierrez Suburu, M.E., Wilde, S., Daniliuc, C.-G., Brünink, D., et al., 2021. Ligand-controlled and nanoconfinement-boosted luminescence employing Pt(II) and Pd(II) complexes: from color-tunable aggregation-enhanced dual emitters towards self-referenced oxygen reporters. Chem. Sci. 12, 3270−3281.

Makedonas, C., Mitsopoulou, C.A., 2006. An investigation of the reactivity of [(diimine)(dithiolato)M] complexes using the Fukui functions concept. Eur. J. Inorg. Chem. 2006, 590−598.

Mantry, L., Maayuri, R., Kumar, V., Gandeepan, P., 2021. Photoredox catalysis in nickel-catalyzed C−H functionalization. Beilstein J. Org. Chem. 17, 2209−2259.

Mathew, D., Hu, Y., Zhao, J., Arunkumar, C., Sujatha, S., 2020. Synthesis, structure, photophysical properties and evaluation of in vitro cytotoxic activity of homoleptic dipyrrin based palladium complexes. Polyhedron 190. https://doi.org/10.1016/j.poly.2020.114794.

Mebrouk, K., Chotard, F., Goff-Gaillard, C.L., Arlot-Bonnemains, Y., Fourmigué, M., Camerel, F., 2015. Water-soluble nickel-bis(dithiolene) complexes as photothermal agents. Chem. Commun. 51, 5268−5270.

Mebrouk, K., Ciancone, M., Vives, T., Cammas-Marion, S., Benvegnu, T., Le Goff-Gaillard, C., et al., 2017. Fine and clean photothermally controlled NIR drug delivery from biocompatible nickel-bis(dithiolene)-containing liposomes. ChemMedChem 12, 1753−1758.

Mitsopoulou, C.A., 2010. Identifying of charge-transfer transitions and reactive centers in M(diimine)(dithiolate) complexes by DFT techniques. Coord. Chem. Rev. 254, 1448−1456.

Mitsopoulou, C.A., Dagas, C.E., Makedonas, C., 2008. Characterization and DNA interaction of the Pt(II)(pq)(bdt) complex: a theoretical and experimental research. Inorg. Chim. Acta 361, 1973−1982.

Moggi, L., Bolletta, F., Balzani, V., Scandola, F., 1966. Photochemistry of co-ordination compounds—XV: cyanide complexes. J. Inorg. Nucl. Chem. 28, 2589−2597.

Oppenheim, J.J., McNicholas, B.J., Miller, J., Gray, H.B., 2019. Electronic structure of tetracyanonickelate(II). Inorg. Chem. 58, 15202−15206.

Orgel, L.E., 1955. Spectra of transition-metal complexes. J. Chem. Phys. 23, 1004−1014.

Park, B., Lee, K.M., Park, S., Yun, M., Choi, H.-J., Kim, J., et al., 2020. Deep tissue photoacoustic imaging of nickel(II) dithiolene-containing polymeric nanoparticles in the second near-infrared window. Theranostics 10, 2509−2521.

Pramanik, S., Dutta, S., Roy, S., Dinda, S., Ghorui, T., Kumar Mitra, A., et al., 2017. Luminescent closed shell nickel(II) pyridyl-azo-oximates and the open shell anion radical congener: molecular and electronic structure, ligand redox behaviour and biological activity. New J. Chem. 41 (2017), 4157−4164.

Razi, S.S., Koo, Y.H., Kim, W., Yang, W., Wang, Z., Gobeze, H., et al., 2018. Ping-pong energy transfer in a boron dipyrromethane containing Pt(II)−Schiff base complex: synthesis, photophysical studies, and anti-Stokes shift increase in triplet−triplet annihilation upconversion. Inorg. Chem. 57, 4877−4890.

Riese, S., Holzapfel, M., Schmiedel, A., Gert, I., Schmidt, D., Würthner, F., et al., 2018. Photoinduced dynamics of bis-dipyrrinato-palladium(II) and porphodimethenato-palladium(II) complexes: governing near infrared phosphorescence by structural restriction. Inorg. Chem. 57, 12480−12488.

Sadhiya Banu, I., Prakash, H., Natarajan, P., 2011. Laser flash photolysis studies of tris(2,2′-bipyridine)nickel(II) ion in aqueous solution. Inorg. Chim. Acta 372, 429–435.

Shikha Singh, R., Prasad Paitandi, R., Kumar Gupta, R., Shankar Pandey, D., 2020. Recent developments in metal dipyrrin complexes: design, synthesis, and applications. Coord. Chem. Rev. 414. https://doi.org/10.1016/j.ccr.2020.213269.

Stevenson, B.G., Spielvogel, E.H., Loiaconi, E.A., Wambua, V.M., Nakhamiyayev, R.V., Swierk, J.R., 2021. Mechanistic investigations of an α-aminoarylation photoredox reaction. J. Am. Chem. Soc. 143, 8878–8885.

Takahashi, Y., Tsuji, H., Kawatsura, M., 2020. Nickel-catalyzed transformation of alkene-tethered oxime ethers to nitriles by a traceless directing group strategy. J. Org. Chem. 85, 2654–2665.

Tian, Y.-M., Guo, X.-N., Krummenacher, I., Wu, Z., Nitsch, J., Braunschweig, H., et al., 2020. Visible-light-induced Ni-catalyzed radical borylation of chloroarenes. J. Am. Chem. Soc. 142, 18231–18242.

Till, N.A., Oh, S., MacMillan, D.W.C., Bird, M.J., 2021. The application of pulse radiolysis to the study of Ni(I) intermediates in Ni-catalyzed cross-coupling reactions. J. Am. Chem. Soc. 143, 9332–9337.

Tong, G.S.M., Chow, P.K., To, W.-P., Kwok, W.-M., Che, C.-M., 2014. A theoretical investigation into the luminescent properties of d8-transition-metal complexes with tetradentate Schiff base ligands. Chem. Eur. J. 20, 6433–6443.

Toyoda, R., Tsuchiya, M., Sakamoto, R., Matsuoka, R., Wu, K.-H., Hattori, Y., et al., 2015. Heteroleptic bis(dipyrrinato)copper(ii) and nickel(ii) complexes. Dalton Trans. 44, 15103–15106.

Wan, Q., To, W.-P., Yang, C., Che, C.-M., 2018. The metal–metal-to-ligand charge transfer excited state and supramolecular polymerization of luminescent pincer PdII–isocyanide complexes. Angew. Chem. Int. Ed. 57, 3089–3093.

Wang, Y., Xue, Z., Dong, Y., Zhu, W., 2015. Synthesis and electrochemistry of meso-substitutes dipyrromethene nickel (II) complexes. Polyhedron 102, 578–582.

Wegeberg, C., Wenger, O.S., 2021. Luminescent first-row transition metal complexes. JACS Au 1, 1860–1876.

Wenger, O.S., 2021. Photoactive nickel complexes in cross-coupling catalysis. Chem. Eur. J. 27, 2270–2278.

Williams, J.A.G., 2007. Photochemistry and photophysics of coordination compounds: platinum. In: Balzani, V., Campagna, S. (Eds.), Photochemistry and Photophysics of Coordination Compounds II. Springer Berlin Heidelberg, Berlin, Heidelberg, pp. 205–268.

Wong, Y.-S., Tang, M.-C., Ng, M., Yam, V.W.-W., 2020. Toward the design of phosphorescent emitters of cyclometalated earth-abundant nickel(II) and their supramolecular study. J. Am. Chem. Soc. 142, 7638–7646.

Wood, T.E., Thompson, A., 2007. Advances in the chemistry of dipyrrins and their complexes. Chem. Rev. 107, 1831–1861.

Wu, P., Ma, D.-L., Leung, C.-H., Yan, S.-C., Zhu, N., Abagyan, R., Che, C.-M., 2009. Stabilization of G-quadruplex DNA with platinum(II) Schiff base complexes: luminescent probe and down-regulation of c-myc oncogene expression. Chem. Eur. J. 15, 13008–13021.

Xian, L., Su, B.-Q., Feng, Y.-X., Xi, B., Duan, Z.-Y., 2021. The photochemical effects of visible light on $K_2[PtCl_4]$ hydrolysis and the synthesis of Pt nano catalysts. Inorg. Nano-Met. Chem. 51, 882–888.

Xue, Z., Dong, Y., Ma, J., wang, Y., Zhu, W., 2017. Synthesis, characterization and electrochemistry of dipyrrinato nickel(II) complexes with different aromatic rings to meso-position. Polyhedron 127, 287–292.

Yao, Y., Hou, C.-L., Yang, Z.-S., Ran, G., Kang, L., Li, C., 2019. Unusual near infrared (NIR) fluorescent palladium(II) macrocyclic complexes containing M−C bonds with bioimaging capability. Chem. Sci. 10, 10170−10178.

Zarkadoulas, A., Field, M.J., Artero, V., Mitsopoulou, C.A., 2017. Proton-reduction reaction catalyzed by homoleptic nickel−bis-1,2-dithiolate complexes: experimental and theoretical mechanistic investigations. ChemCatChem 9, 2308−2317.

Zarkadoulas, A., Field, M.J., Papatriantafyllopoulou, C., Fize, J., Artero, V., Mitsopoulou, C.A., 2015. Experimental and theoretical insight into electrocatalytic hydrogen evolution with nickel bis (aryldithiolene) complexes as catalysts. Inorg. Chem. 55, 432−444.

Zarkadoulas, A., Koutsouri, E., Mitsopoulou, C.A., 2012. A perspective on solar energy conversion and water photosplitting by dithiolene complexes. Coord. Chem. Rev. 256, 2424−2434.

Zarkadoulas, A., Koutsouri, E., Semidalas, E., Psycharis, V., Raptopoulou, C.P., Mitsopoulou, C.A., 2018. Photocatalytic hydrogen production with alkylated nickel bis-dithiolene complexes. Polyhedron 152, 138−146.

Zarkadoulas, A., Zgouleta, I., Tzouras, N.V., Vougioukalakis, G.C., 2021. Traceless directing groups in sustainable metal-catalyzed C−H activation. Catalysts 11. https://doi.org/10.3390/catal11050554.

Zhang, Y., Ley, K.D., Schanze, K.S., 1996. Photooxidation of diimine dithiolate platinium(II) complexes induced by charge transfer to diimine excitation. Inorg. Chem. 7102−7110.

This page intentionally left blank

Chapter 10

Coordination complexes of copper, silver and gold

Gustavo A. Álvarez and Esteban Mejía
Leibniz Institute for Catalysis (LIKAT), Rostock, Germany

10.1 Introduction

Copper, silver and gold, the three non-radioactive members of the 11th group in the periodic table, have played a protagonist role in the history of mankind. This is not only because its importance in the early days of metallurgy (as they were most certainly the first metals known to man), but also as the embodiment of power and the basis of money. Hence, these have been traditionally known as "Coinage metals".

The photosensitivity of certain metal salts is a phenomenon known since the early days of chemistry. Perhaps the first rigorous scientific investigations on the "Combustible principle in light" were carried out by the Pomeranian chemist Carl Wilhelm Scheele around 1768-1770 (Lennartson, 2017) In his famous treatise *ChemischeAbhandlung von der Luft und dem Feuer,* Scheele (1777) described the detection and isolation of (metallic) silver black from silver carbonate and silver chloride samples previously exposed to sunlight. Moreover, Scheele also observed that when light was divided into its different colors by a prism and shown over a piece of paper treated with silver chloride, it was the violet portion of the spectrum, which had the most destructive effect on the silver salt. This observation, unbeknownst to Scheele, was the first photochemical experiment and the laying ground of the field of photography (Eaton, 1965; Belloni, 1997). By the beginning of the 21st century, the photographic film industry was responsible for about one-third of the world's silver consumption (Mak et al., 2005).

Away from their applications in photography, during the last decades, the most exciting developments in the field of photoactive metal compounds have been driven by their success in several "green" and sustainable applications including: solar energy conversion devices, i.e., photovoltaics and dye-sensitized solar cells (DSSSCs) (Cahen et al., 2001; Gratzel, 2003; Yum et al., 2008; Gratzel, 2009; Kalyanasundaram and Gratzel, 2009; Bella et al., 2015), light sources like organic light-emitting diodes (OLEDS) (Bergmann

Photochemistry and Photophysics of Coordination Compounds. https://doi.org/10.1016/B978-0-12-824493-7.00002-2
Copyright © 2023 Elsevier Inc. All rights reserved.

et al., 2016; Yersin et al., 2017; Lian et al., 2019; Hong et al., 2021), and, importantly, as photocatalysts and photosensitizers in a myriad of chemical reactions (Zeitler, 2009; Narayanam, 2011; Xuan and Xiao, 2012; Prier et al., 2013; Yoon et al., 2010; Schultz and Yoon, 2014; Marzo et al., 2018; Chen et al., 2016; Bryden and Zysman-Colman, 2021). This is especially true for metal complexes of d^{10} metals, i.e., monovalent copper, silver and gold, which display a rich photoredox chemistry, producing highly reducing (and oxidizing) excited states upon visible light absorption. The high reactivity of these species has been exploited in various fields of applied sciences. These include photocatalysis for organic synthesis and energy conversion technologies (Reiser, 2016; Paria and Reiser, 2014; Witzel et al., 2021; Hopkinson and Dix, 2019; Sandoval-Pauker et al., 2021; Hossain and Bhattacharyya, 2019; Nicholls and Bissember, 2019; Huang et al., 2002), in which copper complexes play an increasingly important role, and in medicine (Langdon-Jones and Pope, 2014; Yam et al., 1994; García Calavia, 2018; Sherwani et al., 2015), where particularly gold nanoparticles and composites have been actively used in the development of photodynamic therapeutic agents and antitumor drugs.

The historical developments that lead the field to its current status and provided the theoretical basis for its understanding will be left out of this account, as there are uncountable excellent text books, chapter and reviews available covering this matter (Yersin and Vogler, 1987; Bitterwolf, 2006; Balzani et al., 2007; Maldotti, 2009; Daniel, 2011, 2015). In here, without aiming to be encyclopaedical, we will discuss the most representative examples from in the last decade (2010−20) an overview of the scientific trends and societal necessities have been provided that have inspired these endeavors.

To simplify the structure of this chapter and to avoid unnecessary repetition, explanations of the photophysical principles and theories that govern the photochemistry of complexes of the 11th periodic group have been only given in detail for copper complexes, as these are by far the most abundant, more thoroughly investigated and those with the widest application palette. Despite the myriad of reported Ag(I) complexes, their photophysical and photochemical studies are relatively scare, compared to the over abundant data available for their Cu(I) congeners. This is chiefly due to the inherent thermal instability and light sensitivity of many silver compounds, thus hampering their preparation and manipulation under ambient conditions. Thus, due to the comparatively scarcity of data, silver complexes have been left out of this overview. A similar picture appears for gold complexes, whose photophysical studies are chiefly focused on multimetalic species and clusters. In this review, focus is on monometallic molecular complexes, since the photophysics and photochemistry of polynuclear and multimetallic species, as well as clusters, has been reviewed extensively elsewhere (Wing-Wah Yam and Kam-Wing Lo, 1999; Tong et al., 2009; Yam et al., 2015; Ravotto and Ceroni, 2017; Lei et al., 2017; Seifert et al., 2020; Zheng et al., 2020). Photoactive polymers, extended self-assembled materials, and plasmon-active

surfaces, from which gold materials have a significant share, are also left out of the scope of this chapter.

10.2 General considerations

Among those coordination compounds, whose photophysical and photochemical properties have been most thoroughly studied, those made from noble metals like ruthenium and iridium occupy the most prominent places. In most cases, such complexes work very well on the intended applications, displaying high photophysical and photochemical performance as well as good stability. However, due to the scarcity and the subsequent high prices of those metals, their widespread use is limited. To bypass such issues, it was proposed that using more abundant, first transition row metals with the adequate set of ligands, the orbital energies and thus, the redox properties of these complexes could be tailored to resemble, or even surpass, the performance of their noble congeners. From these endeavors, it became quickly apparent that from the studied 3d metals, copper was the best suited for the task, thanks to its d^{10} character, facile monoelectronic redox chemistry and stability of its complexes in different available oxidation states (mainly +1 and +2). Thus, to review the development and the last advances in the photophysics and photochemistry of copper coordination compounds, it is necessary to point out the most important properties of these compounds.

Arguably, the most important property is the nature of the metal center, i.e., its (formal) oxidation state. As briefly mentioned above, copper complexes can be found in various oxidation states, namely 0, +1, +2 and, although still debated, +3 (DiMucci et al., 2019). At the lower end of the scale, copper complexes in the zero-oxidation state are thermodynamically stable species that tend to aggregate into clusters and larger macro-structures. At the opposite end of the scale, compounds with +3 oxidation state provide an example of very unstable species (kinetically and thermodynamically), given that extracting a third electron from copper implies leaving the 3d subshell with two orbitals half occupied in a high spin configuration and, as a consequence, Cu(III) species only appear in "exotic" compounds or as postulated reactive intermediates in chemical reactions that cannot be isolated. Thus, their presence is in most of the cases only hypothesized and barely demonstrated. For this very reasons, the photochemistry of Cu(0) and Cu(III) is by no means representative for this metal, and thus, has been left out of this compilation.

On the contrary, Cu(I) and Cu(II) tend to form well defined and more stable coordination compounds in both; solid state and solution. In this regard, Cu(I) coordination compounds are the most studied for photochemical and photophysical behavior both. The reason is that Cu(I) possesses a full 3 d^{10} sub-shell and does not perform metal centered (MC) electronic transitions, being thus the most common transitions metal-to-ligand charge transfer (MLCT) in nature. The photophysical properties of Cu(II) coordination compounds have

been less studied than for Cu(I) complexes, since the former can perform, among other, MC transitions, being prone to easy deactivation of its short-lived excited states through non-radiative process. Nevertheless, several examples of photochemical process including Cu(II) complexes have been reported (Conry, 2005; Lipshutz and Pfeiffer, 2005).

The next parameter to consider is type of ligands at the copper coordination sphere as well as their coordination geometry around the metal center. In the first place, it is known that in the absorption process, the electronic transition HOMO-LUMO needs to fulfill some symmetry parameters to be optimal. Then, the geometry of the complex is of paramount importance and knowing the possible alternatives is advantageous. Hence, as will be discussed in the following subsections, from the historical point of view, the research on photoactive copper complexes can be divided in four periods. First, it was noticed that some copper compounds in both the oxidation states +1 and +2 could carry out some chemical reactions driven by light. However, as the reaction intermediates had only short lifetimes, their structural characterization remained elusive in most of the cases. The second stadium is marked by the discovery of the emissive properties of homoleptic phenanthroline complexes $[Cu(N\hat{}N)_2]^+$, yielding high photoluminescence and quantum yields as well as significantly longer lifetimes. The third epoch comprises was the rise of heteroleptic phenanthroline-diphosphino complexes $[Cu(N\hat{}N)\ (P\hat{}P)]^+$, which overcome some geometry relaxations in the excited state and further extension in the lifetime of luminescent species was reached. The fourth period has been developing during the last decade and it has been marked by the introduction of carbene type ligands, leading to linear or planar complexes or polydentate ligands, pincer-type, and anthocyanin, leading to planar geometries. Furthermore, in the last few years, the combination of both; transient spectroscopy technics and computational chemistry (mainly DFT and TDDFT methods) has gained importance in the characterization of both, ground- and excited-state structure dynamics, supporting the experimental results and allowing to perform a more proper assessment of the different photophysical events, leading to a deeper understanding of these phenomena.

The following subsections are dealing with the photophysical and photochemical properties of different complexes as a function of the oxidation state of the metal, starting with a discussion about Cu(I), which has been the most studied oxidation state, focusing in its homoleptic and heteroleptic complexes, concluding the section with some examples of another type of complexes (miscellaneous).

In the 1970s decade, the photochemistry of Cu(I) systems was subject of increasing interest, especially of those complexes exhibiting photoredox activity. Notably, the group of McMillin (1977), along with their research on blue Cu proteins, discovered a light-induced redox reaction of the homoleptic complex (2,9-dimethyl-1,10-phenanthroline)copper(I),$[Cu(dmp)_2]^+$. Following these pioneering works, this group started the systematic

characterization of the electronic transitions and the emissive character of homoleptic and heteroleptic Cu(I) complexes (Buckner and McMillin, 1978). However, as will be seen in the next section, the research in heteroleptic diamine-diphosphine remained comparatively neglected until early 2000s, when parallel developments in the chemistry of organophosphorus compounds allowed the preparation of new bidentate ligands with high steric demand and large bite-angles thus; giving access to novel diphosphine ligand scaffolds.

As previously mentioned, the efficient non-radiative deactivation of the MLCT states via low lying MC states observed in most transition metal complexes is preclude their application in photochemical processes (Ravotto and Ceroni, 2017; Liu et al., 2018; Förster and Heinze, 2020). However, this problem is circumvented by Cu(I) complexes, where the metal center possesses a 3 d^{10} closed-shell configuration in the ^{1}GS, then the non-radiative deactivation via MC states is absent (Mara et al., 2015; Liu et al., 2018; Förster and Heinze, 2020). In this case, the symmetrical electronic charge distribution in a d^{10} configuration favors a (pseudo)tetrahedral geometry in the GS, and the degree of distortion from the ideal tetrahedral geometry depends on both; the electronic and steric properties of the ligands attached to the metallic center (Armaroli et al., 2007; Lu et al., 2018).

A graphical representation of the most relevant electronic and energetic transitions suffered by a Cu(I) complex upon photon absorption is given in the Jablonski diagram in Fig. 10.1. First, a Frank-Condon (FC) ^{1}MLCT

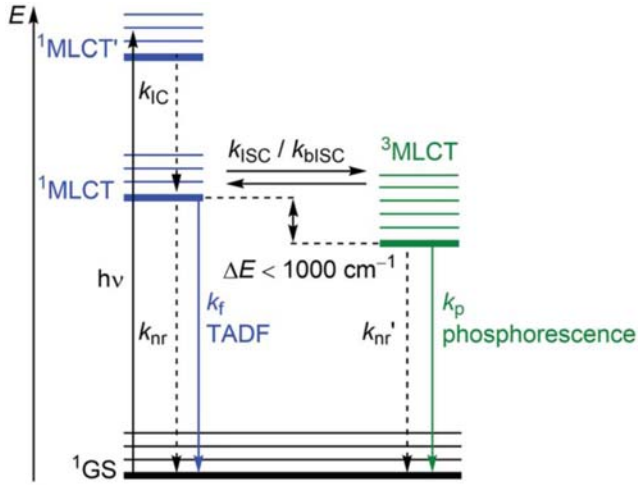

FIG. 10.1 Jablonski diagram illustrating the different photophysical process occurring in a homoleptic Cu(I) complex upon absorption of a photon. *Adapted from Förster, C., Heinze, K., 2020. Photophysics and photochemistry with Earth-abundant metals — fundamentals and concepts. Chem. Soc. Rev. 49, 1057–1070. With Permission.*

vibrationally excited state is formed through a spin and symmetry allowed absorption. In this process, the Cu(I) atom is formally oxidized, yielding a formal Cu(II) excited species, along with a radical anion delocalized in one of the ligands. In the new excited species, the metal center possesses a d^9 electronic configuration and the promotion of the electron from the 3d orbital of the metal to the π^* orbital of the ligand induces a change in the dipolar moment of the molecule driven by the more unsymmetrically distributed electronic density, generating a second order Jahn-Teller distortion, in a process referred as flattening distortion (Liu et al., 2018). As consequence, the minimal energy geometry of the excited state is not (pseudo)tetrahedral but (distorted) square planar, as it is well known for closed-shell Cu(II) complexes.

After its formation, the Cu(II) excited species tends to undergo vibrational relaxation, followed by an internal crossing (IC) to get a more flattened ^{1}MLCT structure. Depending on the energy gap between the latter and the GS, the ^{1}MLCT has two deactivation pathways, either non-radiative, or radiative (luminescent). The former is favored by small energy gaps, due to large vibrational overlaps and by dissimilar geometries of the ^{1}MLCT and the ^{1}GS states, i.e., highly distorted excited state, due to the vibronic coupling (strong coupling limit) (Förster and Heinze, 2020). In the case of luminescent deactivation, an allowed transition from ^{1}MLCT to ^{1}GS produces a photon emission (fluorescence). However, molecules with optimal spin-orbit coupling (SOC) carry out an efficient and spin forbidden inter-system crossing (ISC) to produce a lower energy-lying and long-lived ^{3}MLCT with a subsequent radiative relaxation to the ^{1}GS (phosphorescence), which in general, in absence of coordinating solvents or ligands, is faster than non-radiative deactivations pathways at low temperatures. On the other hand, when the energy difference between the ^{1}MLCT and the ^{3}MLCT states is small and enough thermal energy is available, the long-lived ^{3}MLCT state can enable back-ISC (bISC), leading to a Boltzmann distribution for the emissive $^{1/3}$MLCT state population. As fluorescence is a spin-allowed process, a thermally activated delayed fluorescence (TADF) is more efficient than phosphorescence at high temperatures (Lu et al., 2018; Förster and Heinze, 2020).

All the afore-mentioned process are unimolecular in nature, since many of them (especially the fastest ones including flattening distortion and ISC) are not directly affected by the dynamics of their surroundings (Mara et al., 2015; Iwamura et al., 2015). Moreover, it must be pointed out that some photophysical and photochemical properties, as well as the deactivation pathways are highly influenced by the chemical nature and physical state of the media where, the excited species are generated. The photoluminescent properties of Cu(I) complexes have been studied in different environments and media, including microcrystalline solids, solutions in different coordinating (acetonitrile, THF, methanol, etc.) or non-coordinating solvents (DCM, toluene, chloroform, etc.), both in liquid or solid phase (i.e., at 77 K), as well as in polymeric films. This information has been collected in different reviews

(Lu et al., 2018; Zhang et al., 2018; Forero Cortés, 2021; Sandoval-Pauker et al., 2021) and book chapters (Elie et al., 2017; Mani and Subramaniyan, 2019). Comparison of properties like quantum yields or lifetime of excited species suggests that the luminescent performance increases along with the aggregation state. This phenomenon is known as aggregation induced phosphorescence (AIP), referring to a compound that is non-emissive as an isolated entity in solution but emissive in the aggregated form, or aggregation induced phosphorescence enhancement (AIPE), for a compound that is weakly emissive as moiety and more emissive as an aggregate. In the case of mononuclear Cu(I) complexes, aggregation causes a rigidification both; in the ground- and in the excited states. Then, trapped chromophores in a crystalline or amorphous structure leads to a reduction of molecular motions with respect to the individual molecules in solution. The structural rigidity limits vibration or rotation of appended subunits and hinders structural distortion of the equilibrium geometry of the phosphorescent excited states. Both of these factors lead to a decrease of the rate of non-radiative processes, which deactivate the phosphorescent excited state, resulting in an increase of phosphorescence quantum yield (Ravotto and Ceroni, 2017). However, in solution, without considerable steric constrains, upon light absorption, flattening distortions of the excited complex take place due to the preferred square planar geometry of the *Cu(II) in the ^{3}MLCT state. Thus, the flattened complex enables an extra coordination site at the metal center, where a bimolecular quenching process with a Lewis base (or ligand) could take place. This process is called exciplex formation. Here, the long lived ^{3}MLCT intermediate can accept an additional axial ligand acquiring a square pyramidal geometry (exciplex). Then, as the formed species lowers the energy of the triplet state, the luminescent pathway is inhibited and the exciplex relaxes to the ^{1}GS preferentially through non-radiative processes (energy gap law) (Ravotto and Ceroni, 2017; Förster and Heinze, 2020).

10.3 Homoleptic Cu(I) coordination compounds

Since McMillin et al. (1977) reported for the first time the remarkable photophysical properties of homoleptic Cu(I) coordination compounds, these systems have been widely studied, both practically and theoretically. An overview of the myriad of reports on this section has been not been provided here, mainly because it has been extensively reviewed elsewhere (Armaroli et al., 2007; Lavie-Cambot, 2008; Mara et al., 2015; Sandoval-Pauker, 2021). However, an up-to-date discussion, taking in account the new trends and findings in the area is lacking in the literature. For instance, in the recent years, stepping away from phenanthrolines, new different kind of ligands have been found to exhibit photoluminescent properties. Importantly, hundreds of new homoleptic coordination compounds have been described based on diimines ($[Cu(N\hat{}N)_2]^{+}$), as well as new 1,10-phenantrolines, 2,2-bipyridines,

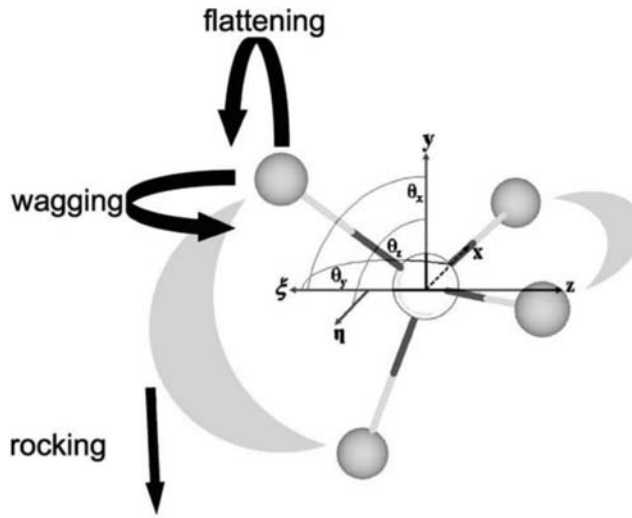

FIG. 10.2 Representation of the ξ_{CD} parameter used to describe the deviation from the ideal tetrahedral geometry in $[Cu(N\hat{}N)_2]^+$ complexes. *Adapted from Armaroli, N., Accorsi, G., Cardinali, F., Listorti, A., 2007. Photochemistry and photophysics of coordination compounds: copper, in: Balzani, V., Campagna, S. (Eds.) Photochemistry and Photophysics of Coordination Compounds I, Springer Berlin Heidelberg, Berlin, Heidelberg, 69–115. With permission.*

bisindazol, or biphosphines ($[Cu(PP)_2]^+$), and more recently, ligands of the type $[Cu(NP)_2]^+$ like phosphinooxazoline or phosphaalkene.

Before providing specific examples, highlight the most important photophysical features of these compounds are highlighted, since their study has paved the way to optimization of photoluminescent performance of other systems by systematic modifications in the ligand architecture throughout chemical synthesis and subsequent structure-activity evaluation.

The ground state geometry of homoleptic Cu(I) complexes with phenanthroline ligands can be described by its ξ_{CD} parameter (Fig. 10.2). This parameter quantifies the distortion from the ideal tetrahedral geometry, and it has been shown (by X-ray crystallography) to be dependent on the substituting groups at the positions two and nine of the phenanthroline scaffold (Armaroli et al., 2007; Lavie-Cambot, 2008).

Regardless of the substituents, the nature of the electronic transitions remains the same when systematic variations in the ligands are performed (Mara et al., 2015). Therefore, the ultraviolet (UV) absorption spectra of these complexes are dominated by LC transitions of the phenanthroline moieties ($50\,000 < \varepsilon < 60\,000\,M^{-1}$). Another common feature are the bands lying in the visible (VIS) region, which are much weaker than those in the UV ($\varepsilon < 10\,000\,M^{-1}$), being assigned to MLCT electronic transitions (Fig. 10.3). Those bands are the sum of three different electronic transitions labeled as band I, II, and II (Armaroli etr al., 2007; Lu et al., 2018).

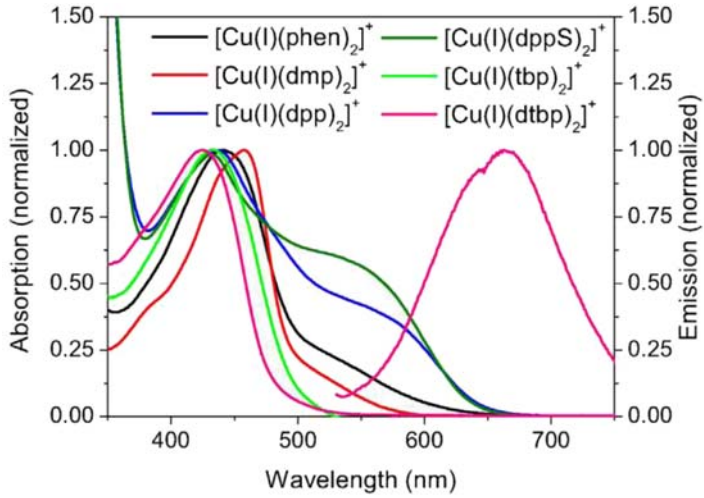

FIG. 10.3 Example of the absorption and emission spectra features of $[Cu(N^{\wedge}N)_2]^+$type complexes. *Adapted from Mara, M.W., Fransted, K.A., Chen, L.X., 2015. Interplays of excited state structures and dynamics in copper(I) diimine complexes: implications and perspectives. Coord. Chem. Rev. 282–283, 2–18. With Permission.*

The main electronic transitions in $[Cu(N^{\wedge}N)_2]^+$complexes as well as their accompanying structural distortions are pictorially represented in Fig. 10.4. A photon absorption matching the MLCT bands leads to an electronic transition from the GA (S_0) to the FC state S_2 (instead of S_1) due to the general transition forbiddance. Besides, upon excitation into the high-lying FC ^{1}MLCT states, minor $^3MLCT_{flattened}$ state can be generated via ISC directly to triplet states bypassing the S_1 state, where the absence of flattening distortion enables large SOC and thus allows fast ISC (on a sub-picosecond timescale) (Zhang et al., 2018). Otherwise, the S_2 state relaxes to S_1 via IC (non-radiative decay) after around 45 fs. This process depends on the steric congestion around the metal center. If there are bulky groups in the ligand surrounding the metal center, S_1 would relax directly to the lowest triplet state ^{3}MLCT through ISC. If that is not the case, the S_1 state will suffer from a flattening in geometry within a timescale of approximately 660 fs, reaching a flattened $^1MLCT_{flat}$ state and then decaying to the $^3MLCT_{flat}$ state with a higher rate constant of $<$10 ps, followed by an emission process of around 50 ns from the triplet excited state to the ground state. In addition, the degree of distortion of the ^{1}MLCT state is vital for the rate constant of ISC since the SOC is controlled by orbital overlap between the copper ion and the chelating ligands (Lu et al., 2018). This later tends to decrease as the molecule flattens due to the symmetry change from D_{2d} (which has strongly coupled spin-orbital wavefunction overlap) to D_2, where the stabilized molecular orbitals (MOs) have reduced spin-orbital wavefunction overlap. Consequently, the ISC time constant, whose value is fundamental for the

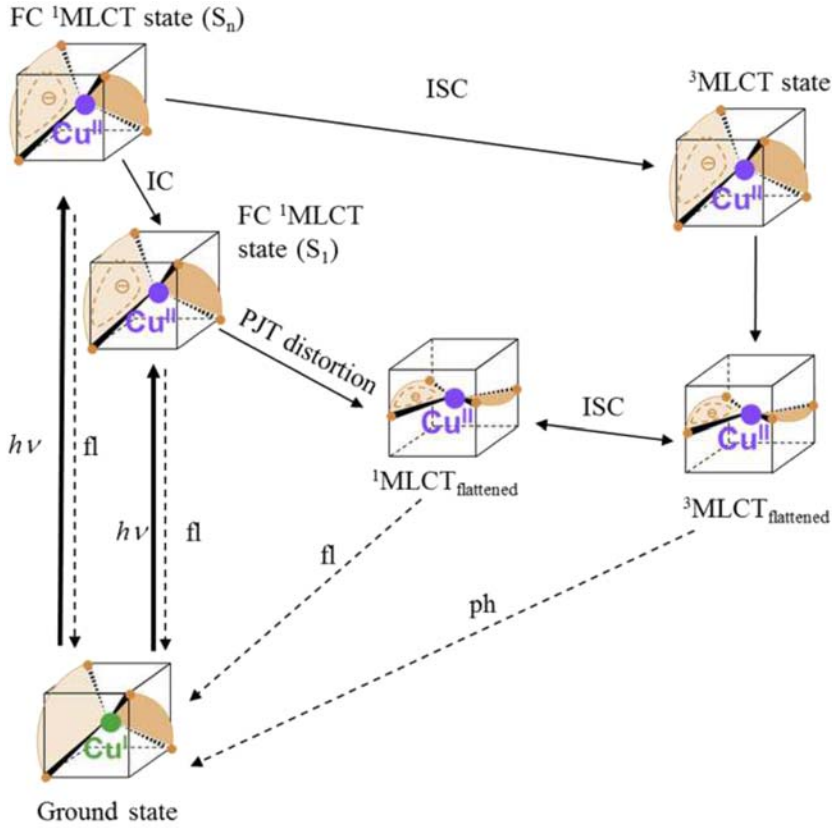

FIG. 10.4 General geometrical changes of Cu(I) complexes upon excitation into MLCT absorption bands. Radiative transitions (fluorescence (fl) and phosphorescence (ph)) are shown as *dashed lines* and non-radiative transitions as thin *solid lines*. *Adapted from Zhang, Y., Schulz, M., Waechtler, M., Karnahl, M., Dietzek, B., 2018. Heteroleptic diimine-diphosphine Cu(I) complexes as an alternative towards noble-metal based photosensitizers: design strategies, photophysical properties and perspective applications. Coord. Chem. Rev. 356, 127−146. With Permission.*

formation of the luminescent long-lived ^{3}MLCT, is a function of the angle between the two phenanthroline planes (Mara et al., 2015).

In summary, the overall dynamics of the MLCT state for several Cu(I) diimine complexes can be described within three time scales: (i) < 1 ps, corresponding to the Jahn-Teller distortion, or flattening, which is absent when the structural change is severely hindered, (ii) 320 ps, assigned to ISC, which is a function of the excited state geometry and increases as the flattening becomes more significant, and (iii) 1 ns to a few s, corresponding to ^{3}MLCT decay, which is determined by the direct interactions of Cu center and solvent, and depends on accessibility of solvent molecules to the metal center (Mara et al., 2015).

Among the non-emissive events, the flattening distortion, driven by the change in the formal oxidation state of the copper center (from Cu(I) to Cu(II)) is one of fundamental relevance. It has been demonstrated by light-initiated time-resolved X-ray absorption spectroscopy (LITR-XAS) that pentacoordinate exciplex formation leads to the deactivation of the excited state through non-radiative pathways. As consequence, it appears reasonable that steric factors are more important that electronic factors for reaching radiative long-lived deactivation (Armaroli et al., 2007; Mara et al., 2015). In this sense, the addition of groups to the phenanthroline ligandsat the 2,9 positions results inmuch longer excited-state lifetimes, as such substitutions help the ligand to shield the metal center by blocking the access to solvent molecules. Furthermore, it should be noticed that even though substitutions at the 2,9- positions are imperative for observing efficient luminescence, substitutions at other positions still have an effect on it. This result is interesting regarding Jahn-Teller flattening distortion, given that it can only be avoided, when extreme structural constrains are present (Mara et al., 2015) (Fig. 10.5).

Most of the structures of N-donor ligands, including phenanthrolines, recently reported for the preparation of homoleptic Cu(I) complexes are summarized in Fig. 10.6. These examples have been chosen to highlight structural diversity of the available ligands and the endless possibilities they

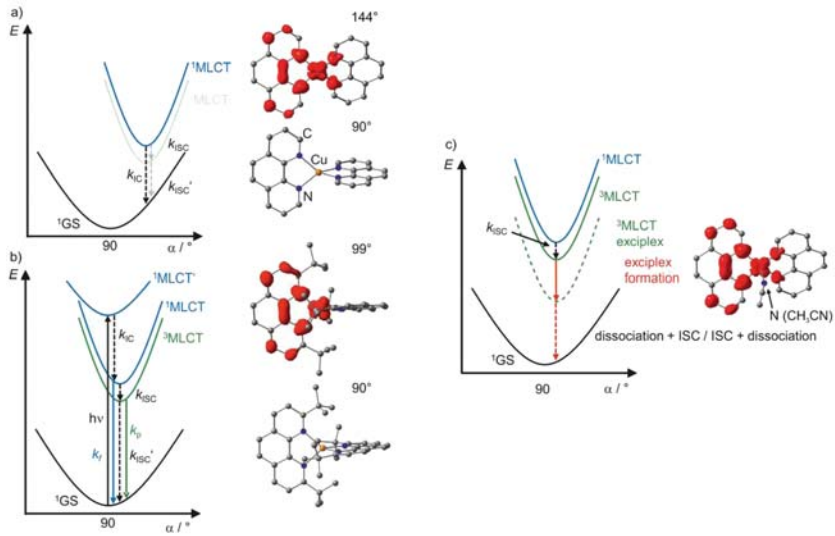

FIG. 10.5 Schematic potential energy surface diagrams of $[Cu(phen^{R2})_2]+$ complexes with relevant electronic states and photophysical processes of (A) $[Cu(phen)2]^+$, (B) $[Cu(phen^{tBu2})_2]^+$ and (C) exciplex formation exemplified by the acetonitrile adduct of $[Cu(phen)_2]^+$. *Adapted from Förster, C., Heinze, K., 2020. Photophysics and photochemistry with Earth-abundant metals — fundamentals and concepts. Chem. Soc. Rev. 49, 1057—1070. With Permission.*

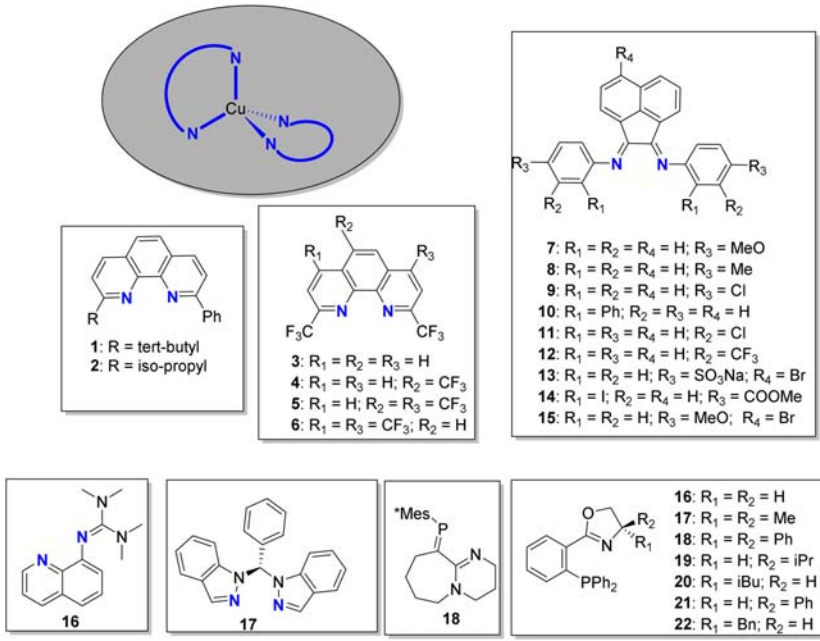

FIG. 10.6 Ligands used recently for the preparation of homoleptic Cu(I) complexes.

offer for the tuning of the photophysical performance of homoleptic complexes.

In an interesting example (Gimeno et al., 2020), prepared homoleptic complexes with asymmetrically substituted phenanthrolines (**1**−**2**), having an alkyl group at the 9-position (providing steric encumbrance to rise the excited state energy), and a phenyl group at the 2-position (allowing intramolecular π-stacking). Assessment of their excited-state properties indicated a relatively lower luminescence performance (compared with symmetrically substituted analogs), while an enhanced photo-oxidating power was observed.

Another interesting study showed by Livshits et al. (2020) the effect of trifluoromethylation at the 2- and 9-positions, as well as at other positions of the phenanthroline scaffold (**3**−**6**). In this case, they supported their results with DFT calculations and concluded that trifluoromethylation at the 2- and 9-positions of the phenanthroline changes the potential energy surface to favor interplanar angles of $\theta \sim 90$ degrees between both ligands by inhibiting the pseudo-Jahn-Teller distortions. The latter allowed to enhance the luminesce performance of the complex compared to the dmp complex. However, the phenanthroline were also susceptible to electronic effects caused by additional substitutions with trifluoromethyl groups, which decreases the luminesce performance, as the electron withdrawing nature of this groups affects the ability of the ligand to coordinate the metal center.

Apart from phenantrolines, other kinds of bidentate ligands have been used recently to obtain homoleptic compounds of Cu(I), and their photophysical properties have been assessed. In 2013, a family homoleptic complexes based on bis(aryl)acenaphthenequinonediimine (BIAN) (**7**−**12**) was synthesized by Papanikolaou et al. (2013), and their photophysical behavior has been analyzed (Papanikolaou et al., 2013; Ng et al., 2018). These complexes present some expected features like a distorted tetrahedral geometry, but also some remarkable and unexpected properties like a rhombically-distorted scare planar geometry, panchromatic light absorption (extending to the NIR region), and fast ISC from the ^{1}MLCT to the ^{3}MLCT (Kee et al., 2016; Ng et al., 2018). However, their luminescence is limited by the presence of low-energy lying ^{3}ILCT states, which decay to the ground state through non-radiative pathways (Papanikolaou et al., 2013). However, those kinds of complexes can also display emission properties from both ^{3}ILCT and ^{3}MLCT although the lifetime of the latter is very small comparted with their phenanthroline counterparts (Ng et al., 2018).

A new homoleptic complex based on a bis(indazol-1-yl)methane ligand (**17**) was prepared by Ferraro et al. (2020) displaying absorption for wavelengths below 410 nm and luminescence in the solid state. According to them, the observed luminescence was related to the population of triplet states like ^{3}MLCT and ^{3}LLCT. However, the complex presented low photoluminescence quantum yield due to non-radiative decay that seems to be related to the distortion of the coordination sphere toward square planar geometry.

Some examples of homoleptic copper complexes based in NP-type ligands have been reported recently. In the first case, a rare example of an emissive phosphaalkene (**18**) copper complex was reported by Clausing et al. (2020). Though the complex resulted weakly emissive, they used theoretical and spectroscopic studies to support an acceptor character of the ligand, whose complex displayed absorption in the UV-VIS region with LLCT and MLCT transitions. However, the lifetime of the excited state was about 9 ns upon irradiating into the MLCT band as consequence of a complex dynamic behavior of the compound in solution as indicated by NMR studies. Another example of luminescent Cu(I) homoleptic complexes with an NP-type ligand was also reported by Giereth et al. (2020). They synthetized a series of phosphinooxazasoline (phox) ligands (**16**−**22**), which could be obtained in a two-step procedure. These complexes resulted emissive in the solid state but only slightly emissive in solution. Moreover, supported by TD-DFT calculations and time resolved emission spectroscopy, the emission was assigned to a ^{3}MLCT excited state. Interestingly, the luminescent properties of the complexes appeared to be related to the chirality of the ligand. However, the MLCT states underwent a strong flattening distortion, which could not be avoided by changing the size or number of the substituents.

Despite of being recently known, the photocatalytic activity of homoleptic Cu(I) complexes has been widely reviewed during the last 10 years (Paria and

Reiser, 2014; Hossain et al., 2019; Nicholls and Bissember, 2019; Zhong et al., 2020; Sandoval-Pauker et al., 2021). Due to their unique photo-redox properties, these compounds have been used as photocatalysts or photosensitizers in different atom-transfer radical addition reactions (ATRA) (Pirtsch et al., 2012; Bagal et al., 2015; Ng et al., 2018; Nicholls et al., 2019), allylations (Pirtsch et al., 2012), coupling of carbazoles with alkyl iodides (Bissember et al., 2013), and others (Sandoval-Pauker, 2021).

10.4 Heteroleptic Cu(I) coordination compounds

The systematic study of Cu(I) heteroleptic complexes started in the same place as for their homoleptic McMillin et al. (1977) who fi congeners. It was also McMillin et al. (1977) who first reported the interesting luminescent properties of Cu(I) heteroleptic complex like [Cu[(N^N) $(PPh_3)_2$]. However, these studies were hampered by the coordination dynamics of these compounds in solution, having a strong tendency to undergo ligand redistribution reactions, which affected its luminescent performance (Forero Cortés et al., 2021). More than 2 decades later, the interest around heteroleptic diimne-diphosphine Cu complexes was reborn, when Cuttell et al. (2002) reported [Cu(N^N) (POP)] complexes with unprecedented excited-state lifetimes. From there on, numerous publications have reported the photophysical properties of different types of heteroleptic Cu complexes including [Cu(N^N) (N^N)'], [Cu(N^N) (P^P)], [Cu(N^P)L_n] and [Cu(N^O)L_n], and more recently [Cu(NHC)L_n] (NHC: N-Heterocyclic Carbenes).

In this account, before discussing the photophysical properties of some of those complexes, the important characteristics of heteroleptic Cu complexes have been discussed, especially those that set them apart from their homoleptic relatives.

The introduction of chelating diphosphine ligands allowed the improvement of photophysical and electrochemical properties of Cu complexes due to their tunable steric and electronic properties. This improvement has its origin in the three-dimensional arrangement (distorted tetrahedron) of the substituents around the P atoms, which (in contrast with diimide ligands) provides additional steric shielding to the metal center. Moreover, chelating diphosphines with wide natural bite angles can stabilize the tetrahedral geometry of the copper center, and at the same time, it can destabilize the square planar coordination environment. Furthermore, the σ-Lewis base character of the P atom (lone pair donation), along with its π-acceptor ability through π-back-bonding, makediphosphinesastounding coordination partners to Cu(I). As a consequence, [Cu(N^N) (P^P)] complexes display a distorted tetrahedral geometry in the GS, with a dihedral angle (DHA) defined by the N−Cu−N and P−Cu−P planes. It ranges from 78 to 89 degrees in the solid state, depending on the interaction of the ligands (e.g., π -stacking) and their steric hindrance, and with average Cu−N and Cu−P bond distances around 2.1 and 2.2 Å,

respectively. However, although stable heteroleptic complexes are predominantly obtained from [Cu(NˆN) (PˆP)] without sterically demanding substituents, heteroleptic complexes involving sterically crowded diimine ligands (commonly substituted at the 2,9-positions) are usually only stable in the solid state. Upon dissolution, a dynamic ligand exchange reaction takes place, resulting in the formation of homoleptic $[Cu(N\^N)_2]^+$ and $[Cu(P\^P)_2]^+$ species. This dynamic depends on the coordinating ability of the solvent, although its impact on the dissociating process has not been yet fully understood (Zhang et al., 2018; Forero Cortés et al., 2021) (Fig. 10.7).

Regarding their UV-vis absorption features, analogous to those observed for $[Cu(N\^N)_2]^+$ complexes, [Cu(NˆN) (PˆP)] complexes display intense high energy absorption bands in the UV region. In order to understand those absorption features from the electronic point of view, TDDFT calculations have been performed. According to these, the HOMO and HOMO+1 of $[Cu(N\^N)(P\^P)]^+$ complexes generally have a strong Cu-d and diphosphine ligand character with a small contribution from the diiminenitrogens. The LUMO and LUMO+1 are essentially the p orbitals delocalized over the diimine ligand with only minor (<10%) contributions from the copper atom and the

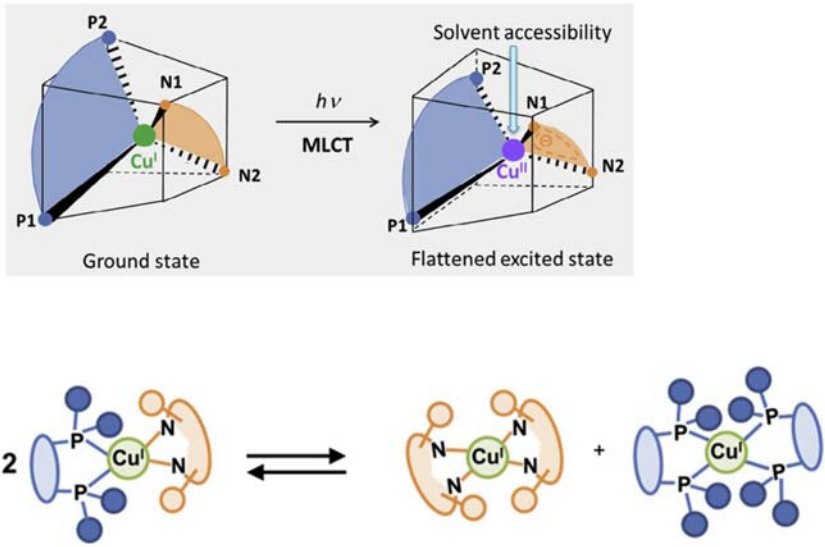

FIG. 10.7 Top: general geometries of heterolepticdiimine−diphosphine Cu(I) complexes in the ground state and flattened MLCT excited state. Botom: schematic representation of a possible ligand exchange reaction of heteroleptic $[Cu(N\^N)(P\^P)]^+$ complexes forming homoleptic species in solution. *Adapted from Zhang, Y., Schulz, M., Waechtler, M., Karnahl, M., Dietzek, B., 2018. Heteroleptic diimine-diphosphine Cu(I) complexes as an alternative towards noble-metal based photosensitizers: design strategies, photophysical properties and perspective applications. Coord. Chem. Rev. 356, 127−146. With Permission.*

diphosphine ligand. Therefore, the energetically lowest electronic transitions in $[Cu(N^{\wedge}N)\ (P^{\wedge}P)]^{+}$ exhibit a mixed MTCT, LLCT and ILCT character. However, the exact contribution of each orbital to the lowest electronic transition varies among individual systems. Moreover, calculation of the relative contribution to the frontier orbitals of complexes of the type$[Cu(I)\ (N^{\wedge}N)\ (DPEPhos)]^{+}$, showed that the contribution of Cu(I) to HOMOs is larger in complexes with bulky substituents in the vicinity of the copper center as well as in complexes bearing the DPEphos moiety. Moreover, the introduction of a diphosphine ligand decreases the energy levels of the corresponding orbitals (such as HOMOs) by virtue of its ability to accept electron density from the copper center, which results in an increased HOMO-LUMO gap and blue-shifted absorption bands.

Nevertheless, the strategy of increasing the transition dipole strength via tuning the π-conjugated system of the ligands, where the LUMO is localized has been effective to increase the molar extinction coefficient and to red-shift the absorption profile of the $[Cu(N^{\wedge}N)\ (P^{\wedge}P)]^{+}$ complexes (Zhang et al., 2018). However, it is worth to mention that the introduction of a chelating diphosphine ligand by itself is not enough to obtain luminescent complexes and the conjugated (aromatic) diimine donor is mandatory, since the use of aliphatic diiminies hampers the stabilization of the ^{3}MLCT state, as a result of the large structural relaxation during excitation (Yoshida et al., 2020).

In general, the excited dynamics of heteroleptic Cu(I) complexes differs from than that of their homoleptic counterparts (Fig. 10.8). Regarding their geometry, the change in the DHA for $[Cu(N^{\wedge}N)\ (P^{\wedge}P)]^{+}$ complexes is less pronounced than in the corresponding $[Cu(N^{\wedge}N)_2]^{+}$ complexes. In the latter, the change in the DHA (defined by the planes of the ligands) is more than 20 degrees, going from around 90 degrees in the GS to 58/67 degrees in the $^{1}MLCT_{flattened}$, while in the former, it could be as small as 12 degrees, depending on the bulkiness of the diphosphine ligand. Given the structure dependence of $^{1}MLCT_{flattened}$-^{3}MLCT transition on ISC, theoretical studies have reported that the rate of ISC increases as the structure of both states is more similar. As singlet-triplet splitting $E_{(S1-T1)}$ between those two states, is relatively small for most of the $[Cu(N^{\wedge}N)\ (P^{\wedge}P)]^{+}$ complexes, owing to the spatially separated frontier orbitals involved in these states; thus, a small exchange interaction integral. The thermal activated back-ISC has a higher probability to occur at higher temperature and luminescence can be observed as TADF, whose associated lifetime is shorter than that of phosphorescence at high temperatures. Furthermore, sterically congested $[Cu(N^{\wedge}N)\ (P^{\wedge}P)]^{+}$ complexes are efficient in suppressing the accessibility of the Cu center toward solvent molecules, avoiding the quenching decay. This results in strong and long-lived emissions, even in coordinating solvents (Zhang et al., 2018).

In addition, these complexes can be excited to a ^{1}ILCT state, followed by an ISC into the ^{3}ILCT. In such cases, the deactivation to the ground state

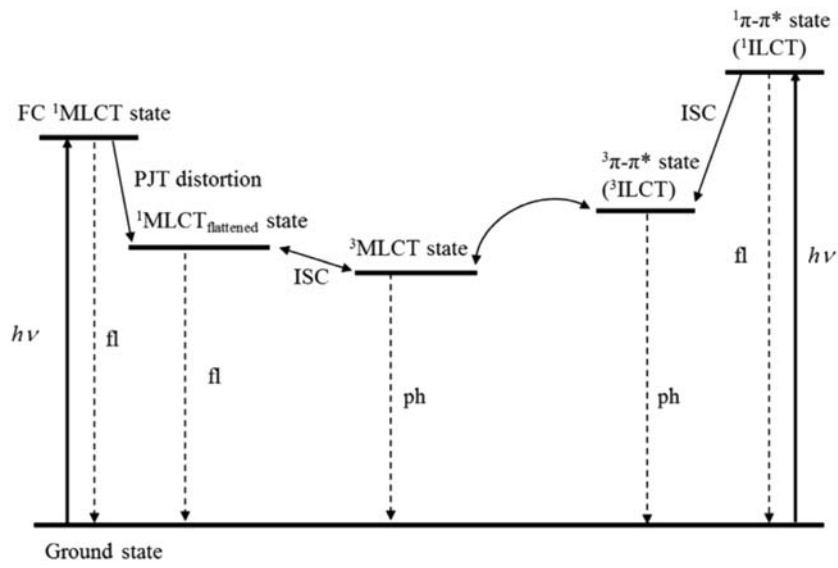

FIG. 10.8 Simplified photoinduced energetic transitions generally observed for heteroleptic Cu(I) complexes. *Adapted from Zhang, Y., Schulz, M., Waechtler, M., Karnahl, M., Dietzek, B., 2018. Heteroleptic diimine-diphosphine Cu(I) complexes as an alternative towards noble-metal based photosensitizers: design strategies, photophysical properties and perspective applications. Coord. Chem. Rev. 356, 127–146. With Permission.*

occurs through both; radiative and non-radiative decay pathways. Excitation into the ILCT states for $[Cu(N^{\wedge}N)\ (P^{\wedge}P)]^+$ complexes can be achieved with high-energy photons. It should be noted that the energy splitting between ^{1}ILCT and ^{3}ILCT states is greater than that of the corresponding MLCT states (Fig. 10.8), which is due to the bigger spatial overlap of the involved frontier orbitals in ILCT states and thus, greater exchange interaction integral. However, this ^{3}ILCT emission tends to vanish at higher temperature due to the thermally activated interconversion between ^{3}ILCT and ^{3}MLCT states (Zhang et al., 2018).

In order to illustrate the concepts described so far, some examples extracted from the recent scientific literature will be discussed in the next subsections. These have been arbitrarily segregated into different groups depending on their ligand scaffolds: phenanthroline complexes, complexes with pyridyl-type ligands, complexes with N,P and N,O ligands and complexes with carbene ligands. This account is not exhaustive regarding the photophysical data of the complexes, which has been judiciously collected in several reviews and book chapters, nor give the overview of all the structures reported with luminescent properties, since it has been collected somewhere else as well. Instead, this section highlights some interesting examples reported in the last decade and discuss them in the light of conceptual and theoretical

knowledge about heteroleptic Cu(I), softening the transition, when switching between experimental and theoretical results.

10.4.1 Phenanthroline complexes

In 2012, the excited-state structure of cation (**23**) (Fig. 10.9) in their crystalline [BF_4] salt was determined by single-pulse time resolved synchrotron experiments with the modified polychromatic Laue method at both 180 and 90 K by Makal et al. (2012). In this study, they have pointed out that unexpectedly, in the crystalline form, the flattening distortion of this unsubstituted phenanthroline complex was very similar to the distortion experienced, when the ligand dmp is used instead. This predominant effect of the crystalline environment, clearly illustrates the fact that molecules in the solid state have different physical properties from those (isolated) in solution and that their properties heavily depend on the specific molecular environment. Nishikawa et al. (2015) reported the synthesis of new Cu(I) complexes bearing diop and dmpp or dmp ligands (**24** and **25**). The complex bearing the dmpp ligand (**24**) displayed a high quantum yield (0.38) and a long lifetime (26 μs). The latter is consequence of a positive effect coming from a small non-radiative decay rate of the excited states by introducing the diop ligand and phenyl groups at

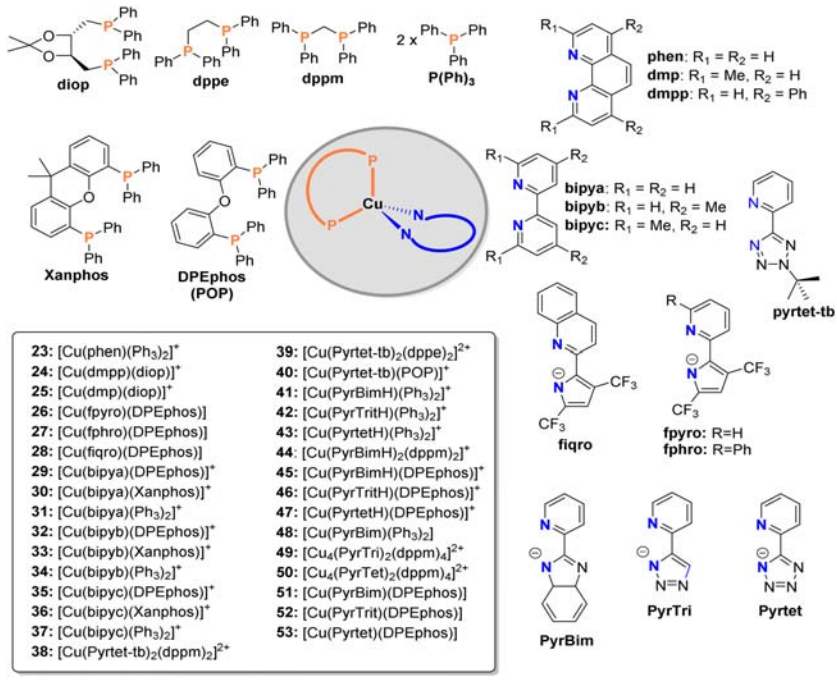

FIG. 10.9 Ligands used recently in the preparation of heteroleptic [Cu(N^N) (P^P)] complexes.

positions four and seven of the phenanthroline. Furthermore, TD-DFT studies indicated that the observed luminescence was consequence of MLCT and LLCT transitions where the π^* orbital of the phenanthroline is the acceptor.

10.4.2 Complexes with pyridyl-type ligands

Several complexes of different coinage metals using functionalized 2-pyridyl pyrrolide and DPEphos as coligand (**26**−**28**) have been reported, all with good emission quantum yield and lifetime above 20 μs. Hsu et al. (2011) found by using TD-DFT calculations that, in the lowest-lying electronic transition, the Cu(I) complexes show an appreciable metal d contribution, i.e., an MLCT transition, which allowed these complexes to exhibit a substantially larger rate of ISC and phosphorescence radiative decay rate constants than their Ag^I and Au^I counterparts. The latter, provided a proof that the direct involvement of the d orbital in the lowest-lying electronic transition plays a major role in inducing SOC.

The Cu(I) complexes based on mono- and di-phosphine ligands (DPEphos, Xanphos and PPh_3) and 2,2′-bipyridyl derivatives (**29**−**37**) were prepared by Andrés-Tomé et al. (2012). All the reported complexes displayed characteristic MLCT transitions and luminescence in the solid stated. However, the combination of rigid di-phosphine ligand and steric hindered bypridyl ligand substituted at the 6 and 6′ positions was necessary to attain luminescence in solution.

Examples of heteroleptic complexes using tetrazolyl pyridine ligands with chelating diphosphines including dppm, dppe and POP (**38**−**40**) were developed by Femoni et al. (2013). They showed by NMR an X-ray crystallography that while using dppm and dppe as ligands, bimetallic complexes were obtained. Regarding the luminescent properties, all the prepared compounds were poorly or non-luminescent in DCM solution at room temperature, but exhibited high quantum yields and emission lifetimes up to 22 μs in a KBr matrix at room temperature.

The coordination chemistry and the photophysical properties of a series of copper(I) complexes (**41**−**53**) with N^N ligands with a varying number of coordinating N-atoms like pyridine-benzimidazole, -triazole and -tetrazole, or their deprotonated analogs with PPh_3 or bidentate phosphines like dppm and DPEPhos were systematically studied. It was found that mononuclear cationic species are obtained with DPEPhos and PPh_3, but to obtain neutral complexes, the right combination of pyridine-amide and phosphine ligand must be chosen. The photophysical characterization of the substances had to be performed in the solid state because of the lack of stability or luminescence of some of them in solution. For the mononuclear complexes, DTF calculations suggested that the luminescent behavior of the cationic species is due to MLCT, but in the case of neutral complexes, there is also an additional ILCT input, suggesting that electronic effects of the pyridine-amide ligands play a major role in the

character of the luminescent transition. Therefore, the coordination chemistry, oxidation stability and emission properties of the neutral complexes are strongly controlled by the electronic effects of the pyridine-amide ligands, whereas in the cationic complexes mainly steric effects play a role in the coordination chemistry (Bergmann et al., 2018).

10.4.3 Complexes with NˆO, NˆP and SˆP ligands

Heteroleptic Cu(I) complexes using different diphenyl(2-pyridylmethyl) phosphane oxide ligands with both; PPh_3 and DPEphos as auxiliary ligand (**54**–**59**) were reported by Sun et al. (2010) (Fig. 10.10). They presented an example of heteroleptic luminescent complexes with a coordinating oxygen, where the complex containing PPh^3, displayed better performance than the one with the chelate DPEphos. Hight quantum efficiencies were reached as well as lifetimes over 1 μs were shown in solution. Moreover, the presence of MLCT transitions were demonstrated by electronic absorption and DFT calculations.

Osawa et al. (2013) reported a series of complexes of d^{10} coinage metals containing the monoanionic bidentate ligand diphenylphosphinobenzenethiolate, along with 1,2-bis(diphenylphosphino)benzene as ancillary ligand (**60**). Particularly, the copper complex displayed a distorted tetrahedral geometry with a DHA of 86.44 degrees, and green luminescence in the solid state (as well as in 2-MeTHF) at 77 and 293 K, with only a small red shift at higher temperature. The luminesce at room temperature was ascribed to TADF, as the quantum yield and the lifetime increased as the temperature was decreased. Furthermore, by using TD-DFT calculations, they assigned the luminescence to S → π* and π → π* (LLCT) transitions, and their contributions to the S_1

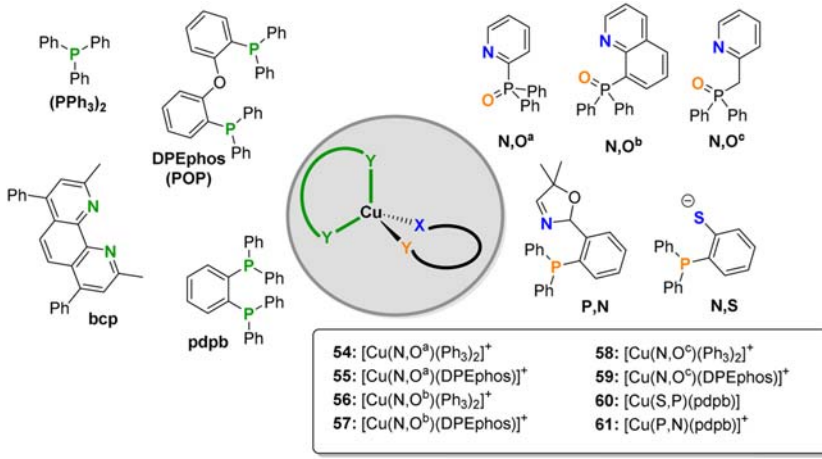

FIG. 10.10 Examples of heteroleptic complexes with bidentate NˆO, NˆP and SˆP ligands.

state were calculated to be 59% and 27%, respectively, while the contribution from MLCT transitions was only 4.6%. Hence, the thiolate ligand with electron-donating character reduced the contribution of metal orbitals to the HOMO of the complex, decreasing the MLCT character of their excited states. As a result, the origin of the TADF was an LLCT transition.

Giereth et al. (2017) reported the preparation of an heteroleptic complex using one of their phox ligands as well as bcp as ancillary ligand (**61**). They found that the heteroleptic complex displays improved absorption properties compared to the homoleptic phox complex, highlighting the importance of the diamine in the absorptivity of Cu(I) complexes. The latter conclusion was supported by TD-DFT calculations, where it was found that the LUMO and LUMO+1 MOs are mainly located at the bcp scaffold. Furthermore, the heteroleptic phox complex leads to an increase in absorptivity and a bathochromic shift of the main MLCT absorption compared to the heteroleptic reference complex $[Cu(bcp)(xant)]^{+}$.

10.4.4 Complexes with carbene ligands

An alternative strategy to avoid the flattening distortion in the excited state of Cu(I) emmiters has been the preparation of tricoordinated, trigonal planar complexes (Fig. 10.11), moving away from the "classical" tetracoordinated, tetrahedral geometries. The first example was presented by Krylova et al. (2010),who synthesized and characterized two different complexes bearing a monodentate N-heterocyclic carbene (NHC) ligand, 1,3-bis(2,6-diisopropylphenyl)imidazole-2-ylidene with an neutral phenanthroline (phem) or a negatively charged pyridyl-benzimidazole (pybim) as bidentate counterpart (**62** and **63**), obtaining a cationic and neutral complex, respectively (Fig. 10.12). They displayed phosphorescence in both; the solution and solid media, suggesting that solvent coordination is not the main quenching mechanism in liquid phase, and that molecular distortions may be the main quenching mechanism in solution.

In further investigations, the same group reported a series of luminescent [Cu(NHC) (N^N)] complexes, where the NHC ligand is principally involved in the excited state, demonstrating a wide range emission color tunability through modification of the carbene moiety. In addition, di(2-pyridyl)dimethylborate was used as ancillary ligand (**64**–**66**), being the first examples of luminescent heteroleptic Cu(I) complexes using a pyrazolyl-borate ligand. In the absorption spectra, the lower energy bands, which were not observed in absorption spectra of the precursors, were assigned to charge transfer (CT) transitions involving the NHC ligands.

It was also found that the modification of the carbene ligand allows the emission color to be tuned over 200 nm, from blue to orange-red, while retaining high emission efficiencies. However, even though these complexes displayed luminescence at room temperature in the solid state, their emission

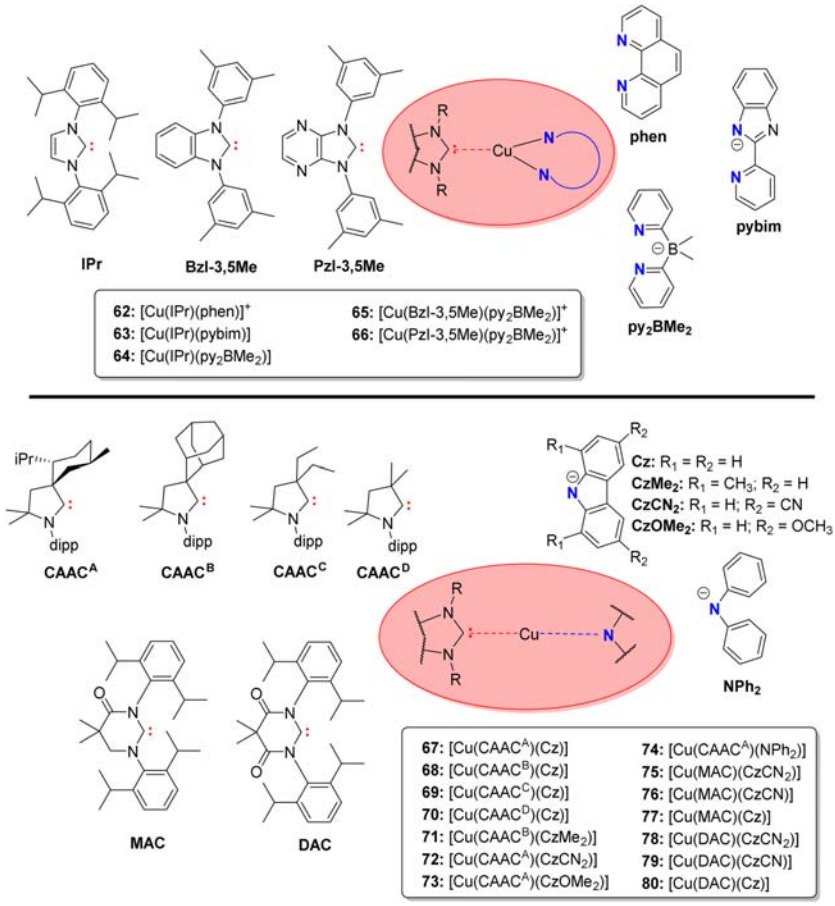

FIG. 10.11 Examples of heteroleptic Cu(I) complexes using N-heterociclyc carbene type ligands.

efficiencies in fluid solution were substantially lower. Furthermore, modest increase in emission lifetimes upon cooling were inconsistent with processes typically associated with TADF, suggesting instead that the emission arises from a state that is principally triplet in character. Finally, DFT and TD-DFT calculations suggested that the lowest-lying transition can be ascribed as (M + L)LCT admixed with intra-ligand $\pi \rightarrow \pi^*$ (of the pyrazolyl-borate ligand) (ILCT) character, whereas for the other complexes the transition is mainly metal-ligand to NHC ligand charge transfer ((M + L)LCT) (Krylova et al., 2014).

Hamze et al. (2019a) reported the synthesis and characterization of two series of linear heterolepticlinear biscoordinated Cu(I) complexes using common amides (N-carbazoyl) with different carbene ligands (Fig. 10.11).

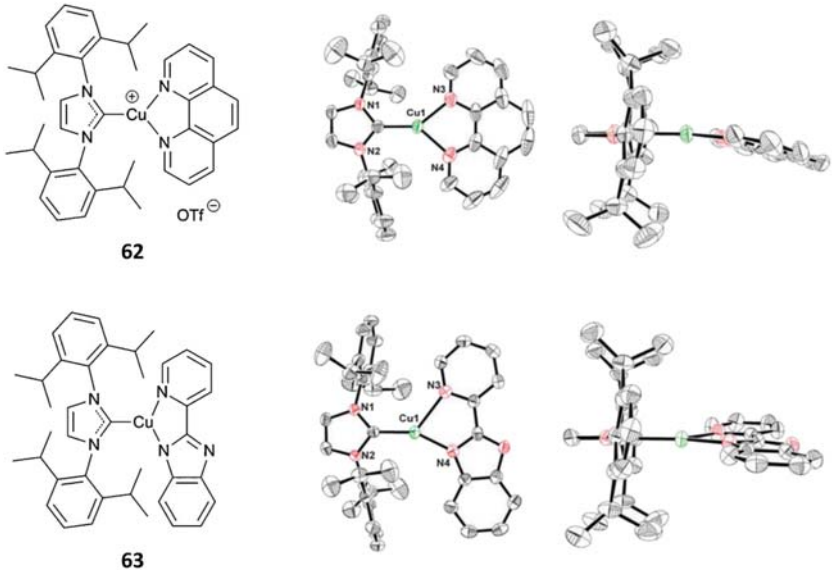

FIG. 10.12 Structural representation (left) and crystalline structures (rigth) of two planar Cu(I) complexes bearing an NHC ligand (IPr) with an neutral phenanthroline (phen) (**62**)or a negatively charged pyridyl-benzimidazole (pybim) (**63**). *Adapted from Krylova, V.A., Djurovich, P.I., Conley, B.L., Haiges, R., Whited, M.T., Williams, T.J. et al., 2014. Control of emission colour with N-heterocyclic carbene (NHC) ligands in phosphorescent three-coordinate Cu(i) complexes. Chem. Commun. 50, 7176−7179. With Permission.*

The first series made use of different cyclic (alkyl) (amino)carbene (**CAAC**) ligands with substituted cabazoyl ligands (**67−74**) as accompanying ligand. The second series of complexes consisted of monoamido-aminocarbene (**MAC**) and diamidocarbene (**DAC**) ligands with substituted cabazolyl moieties (**75−80**) as ancillary ligand (Shi et al., 2019). The complexes presented high luminescence efficiency in both; fluid and rigid media and short lifetimes. The main source of absorption and emission in the visible spectrum were strongly allowed amide-to-carbene ICT. The coplanarity of the two ligands demonstrated to be fundamental for the high performance of the luminesce wherein the metal d orbitals act as a weak electronic bridge between the parallel donor (N_{amide} $2p_z$) and acceptor ($C_{carbene}$ $2p_z$) orbitals; thereby, illustrating the potential for long-range p interaction. Furthermore, it was found that changing the metal center to obtain isoelectronic complexes does not change in a significative way neither the geometry, nor the electrochemical properties. However, photophysical properties like the CT bands in the absorption spectra and the emission lifetimes are affected (Hamze et al., 2019b). It was also postulated that the emission observed for those complexes is not by TADF but it is better described as thermally enhanced luminescence, where both the lower-energy and higher-energy states are highly emissive, albeit with

the lower state having a much longer radiative lifetime. Additionally, for the mentioned complexes, the luminesce is fully governed neither by the ISC rates between T_1 and S_1, nor by k_{fl} and k_{ph} from the respective S_1 and T_1 states, but by $\Delta E_{S1\text{-}T1}$ instead (Hamze et al., 2019a, b; Shi et al., 2019).

Importantly, like in the case of homoleptic complexes, the photocatalytic activity of heteroleptic Cu(I) complexes has been widely exploited and has been the subject of several reviews during the last 10 years (Paria and Reiser, 2014; Hossain et al., 2019; Nicholls and Bissember, 2019; Zhong et al., 2020; Sandoval-Pauker et al., 2021; Forero Cortés et al., 2021). Due to their remarkable photo-redox properties, long excited-state lifetimes and thigh stability, these compounds have been used as photosensitizers or photocatalysts in several transformations including ATRA reactions (Knorn et al., 2015) C−N cross-couplings (Kainz et al., 2016), pinacol-type couplings (Caron et al., 2019), reductions of aryl and alkyl halides, cyclization of aryl and alkyl iodides and arylation of (hetero)-arenes with aryl halides (Michelet et al., 2017), among others (Sandoval-Pauker et al., 2021). Remarkably, heteroleptic Cu(I) complexes have been also used (with relative success) in energy- and sustainability-relevant applications like water (proton) (Lennartson, 2017; Chen et al., 2017; Heberle et al., 2017; Giereth et al., 2019), and CO_2reductions (Gracia et al., 2020).

10.4.5 Miscellaneous Cu(I) coordination compounds

In addition to the already discussed structures containing one or two bidentate ligands in tetrahedral, planar or linear arrangements around the copper center, other kind of complexes with different ligand architectures have been also reported as photoactive. Among those examples, the most relevant include π-diborene complexes, several tridentate ligands, phthalocyanine and porphyrin.

A series of highly luminescent π-diborene complex of coinage metals were prepared by Bissinger et al. (2015),who obtained fluorescence quantum yields up to 100% in solution by suppression of phosphorescence (**81**, Fig. 10.13). Based on DFT and TD-DFT calculations, they supported this observation in the fact that metal atoms participate in a low degree in the excited states, resulting in a weakly active SOC leading to a low efficient ISC.

The luminescence properties of amine-bis(N-heterocyclic carbene) copper(I) and silver(I) complexes in solution and solid state were recently studied by (**82**, Fig. 10.13). The X-ray analysis of the complexes yielded a mononuclear structure with the three coordinating sites of the ligand attached to the metal center in the case of copper. Moreover, the absorption spectra of the complexes displayed three bands, associated with different type of transitions, and both these complexes were emissive in both; solution and the solid state. Finally, DFT/TD-DFT analysis suggested that the low-energy absorption and the emission properties were associated with a combination of both; MLCT

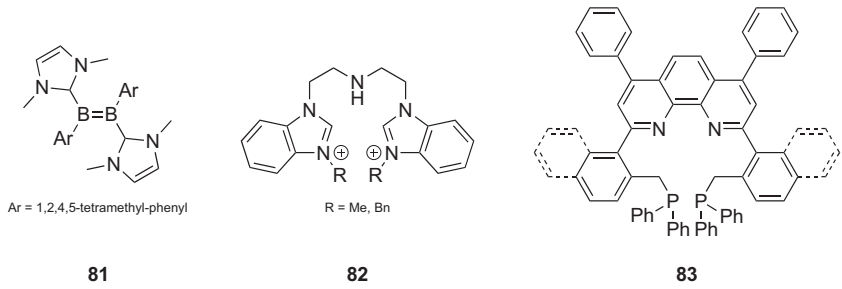

FIG. 10.13 Alternative ligands used for the preparation of luminescent complexes of copper and silver.

and LC from the metal atom and the amine, respectively, to the bis(N-heterocyclic carbene) moiety.

Chen et al. (2020) reported the preparation of two luminescent Cu(I) complexes with different tetradentate PNNP ligands, resembling an heteroleptic complex with a phenanthroline and a biphosphine (**83**, Fig. 10.13). In the six-step reaction, they managed to couple phosphines in 2- and 9-positions of the phenanthroline both; obtaining afterward copper(I) complexes with a distorted tetrahedral geometry around the metal center, as testified by X-ray crystallography. Although the ligands were also luminescent, the complexes presented a red shift compared to the "classic" $[Cu(P\hat{}P)\ (N\hat{}N)]^{+n}$ complexes. DFT/TD-DFT calculations revealed that complexes with this tetradentate ligands have a broader MLCT transition.

One example of the photochemical activity of Cu(I) complexes with tridentate ligands was recently reported (Fig. 10.14). In that work, Ahn et al. (2017) designed and synthesized a new copper-based photoredox catalyst, bearing a tridentate carbazolide/bisphosphine ligand, whose Cu(I) complex displayed photoluminescence. The complex was envisaged to yield the selective mono-alkyation of primary carbamates by unactivated secondary alkyl halides induced by irradiation under mild conditions. A key observation to reach this objective was that 2-bromo-4-phenylbutane quenches the luminescence of the excited state of copper complex. The mechanistic studies supported a pathway, where the photoredox catalyst generates an alkyl radical and a Cu(II) intermediate.

10.5 The entatic principle and its implication on the photophysical properties of Cu(I) complexes

As discussed previously, the geometry of Cu(I) complexes plays a fundamental role in their photophysical and photochemical properties. In this sense, a cumulative synthetic effort has been done to unravel the physical principles behind the luminescent behavior of these complexes. Nevertheless, the ability

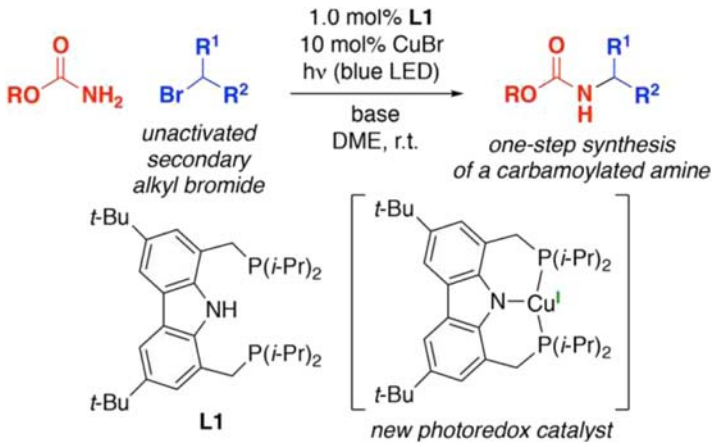

FIG. 10.14 Selective photocatalyzed mono-alkyation of primary carbamates by unactivated secondary alkyl halides using Cu(I) complexeswith chelating ligands. *Adapted from Ahn, J.M., Peters, J.C., Fu, G.C., 2017. Design of a photoredox catalyst that enables the direct synthesis of carbamate-protected primary amines via photoinduced, copper-catalyzed N-Alkylation reactions of unactivated secondary halides. J. Am. Chem. Soc. 139, 18101−18106. With Permission.*

to predict complex photoactivity based on structural parameters is still limited, and sometimes seems to be contradictory, when the same principles are applied to the different known coordination arrangements. For instance, from the available observations, it can be generalized, that controlling steric factors is more important that the electronic ones, as attested by complexes containing phenanthroline ligands, whose substituents at the 2,9-positions are fundamental to attain luminescence. However, it is still not possible to predict to which extent, this trend can be applied. Conversely, when considering heteroleptic complexes, the bite angle of the bisphosphine ligand and rigidity that this chelate confers to the complex seems to be the most important parameter.

In both cases, steric congestion, avoiding both deviation from the ideal tetrahedral geometry in the GS, and flattening distortion in the excited state, yields the best emission performance, regarding quantum yield and excited state lifetime. This behavior has been attributed to the inhibition of non-radiative deactivation pathways through exciplex formation. In this sense, the experimental data points out to a causal relationship: "The higher is the steric congestion around the copper center, the larger will be the lifetime of the excited species". This logical assumption is not absolute and has the limitations as discussed previously, then its applicability is surrogated to an specific context, mainly where complexes of the type $Cu[(N\^N)_2]^{n+}$ or $[Cu(P\^P)(N\^N)]^{n+}$ are used.

However, deepening in what steric congestion means for absorption-deactivation processes, one can arrive to the following conclusion: As copper changes from Cu(I) to Cu(II) after excitation by photon absorption, not

only its formal oxidation state changes, but also its preferred coordination geometry, yielding to an atomic reorganization from the Frank-Condon state to a more stable configuration (flattening distortion). Thus, if this process takes place at the limit, where both geometries are infinitely similar (due to steric congestion), then such reorganization would be avoided, and no energy will be invested there. As a consequence, at this point, the process would not find any restriction and its kinetics would be optimized according to the alternative pathways that demand a change in the geometry. This appears to be the same "reasoning" that evolution does in living systems according to Vallee and Williams (1968), who postulated that "*In all enzymes, the active site is constrained by the surrounding protein matrix to adopt a geometry similar to that anticipated for the corresponding transition state geometry of an unconstrained system. As a result, the reorganizational energy required to reach the transition state would be minimized and the reaction kinetics would be maximized and redox-active metalloenzymes with iron and copper at the active sites should represent prime examples of this entatic (constrained) state*" (Rorabacher, 2004). This principle is based on a pre-organization of the ligand sphere by a constrained geometry, which depends weakly on the oxidation state of the copper cation. Although pre-organization imposes an "energized" structure at the metal center, the metal is endowed with an activated geometric and electronic structure that can finely tune the complex for a specific function (Kohler et al., 2017; Dicke et al., 2018; Stroscio et al., 2019). Therefore, although not straightforward, an extension of this *entatic* principle could be done to understand the photophysical process in Cu complexes. This has been applied to the understanding electron transfer processes in Cu metalo-enzymes (where a transition state can be drawn), given that, in principle, an MLCT is rationalized as an intramolecular charge transference, where a transition state is not formed, but transient species instead.

Kohler et al. (2017) were the first to postulate that an *entatic* state was involved in a photophysical process. They found a linear correlation between the experimental GS redox potentials and τ_3. Afterward, they noticed a linear correlation between calculated GS-^{3}MLCT gap and the experimental E°s. Such correlation is maintained, when the calculated E°s or the $\ln(\tau_3)$ were used instead. They proposed that the ligand architectures of their synthesized complexes can be utilized to apply *entatic* state concepts to tune the ground state redox potential (E°) and thus, excited state lifetimes (τ_3). Furthermore, given the reorganization energies, they estimated the entatic energy contribution to the ground state for the 2,9-phenanthroline substitution by making use of the total inner sphere reorganization energies across their ligand set compared to one of the $Cu(phen)_2$ complex. Their estimated *entatic* was around 6−7 kcal mol^{-1}, which is similar to ground state *entatic* energies estimated for Cu enzymes.

A more thorough demonstration that the *entatic* principle could be extended to photophysical processes in Cu complexes was reported by Dicke

et al. (2018) In their work, a multi-method approach that featured time-resolved UV/Vis, infrared and X-ray absorption and optical emission spectroscopy was used to study a homoleptic biscoordinated guanidine-quinoline (**16**) copper complex with geometric restrains that allowed only small structural changes after photoexcitation. This led to very fast structural dynamics since all the involved states were structurally similar, owing to the pre-organization of the ligands around the metal. Although dynamics of the excited state were similar to those reported for phenanthroline complexes, including ^{3}MLCT and exciplex formation, they showed that the *entatic* principle is also applicable for spin-state control (Fig. 10.15). The reaction path from the Franck−Condon S_1 state over $S_{1,relax}$ into T_1 benefits from the *entatic* state principle because both extremes of the reaction coordinate (1 and 2 in their ground states) are structurally similar. The large amount of covalency of the guanidine−Cu bond and the structural constraint lower the degree of potential "flattening" of $S_{1,relax}$ and T_1 (an implication of the *entatic* state) and led to the rotation of the corresponding orbital required for efficient SOC.

Following this approach, Strocio et al. (2019) reported a combined experimental and computational methodology to quantify *entatic* contributions to photophysical process. Their approach is also based on the observation that

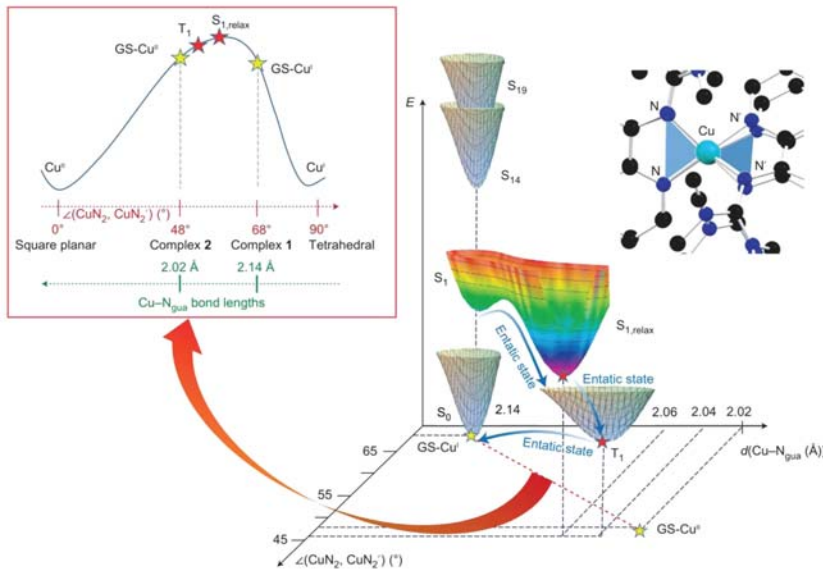

FIG. 10.15 Visualization of the "entatic" coordinates for the optical excitation of a homoleptic Cu(I) complex with ligand **16**. One axix illustrates thedihedral angle between the chelate planes and the other axis depicts the Cu−N_{gua} bond length. *Adapted from Dicke, B., Hoffmann, A., Stanek, J., Rampp, M.S., Grimm-Lebsanft, B., Biebl, F., et al., 2018. Transferring the entatic-state principle to copper photochemistry. Nat. Chem. 10, 355−362. With Permission.*

the natural logarithm of the ^{3}MLCT excited state lifetime ($\ln(\tau_3)$) for a range of Cu(I) bis-phen complexes correlate linearly with redox potentials (experimental and calculated), ground state inner sphere reorganization energies, excited state relaxation energies, and energy gaps (Fig. 10.16). Interestingly, most of the experimental data were subtracted from the scientific literature. In the first place, to determine the effect of the solvent in the same parameter, they compared the results obtained in the gas phase with those using the conductor-like polarized continuum model. Furthermore, they found a difference between the experimental and the calculated E°, which is attributed to the interactions between the oxidized state and some combination of solvent, electrode surface and counter ion that are not accounted by using continuum solvation calculation. The latter can affect the correlation between E° and $\ln(\tau_3)$ and thus, the quantification of *entatic* contributions. To avoid these differential oxidation-state interactions, the effects of the interaction with a weakly coordinating ligand (H_2O) were included in the calculations. Moreover, given that in addition to steric factors, the difference in electron-donating/withdrawing ability of the 2,9-substitutions in the phen ligands can affect the parameters mentioned before, the authors successfully decomposed steric and electronic contributions by using "H-capped" versions of the 2,9-substituents, which involves replacing the 2,9-group with H atom and keeping the geometry completely unperturbed otherwise.

In general, a linear correlation between $\ln(\tau_3)$ and the other parameters mentioned above was found, for 1 and 4 orders of magnitude changes in τ_3. As an illustrative example, looking at reorganization energies in 2,9-alkyl substituted phenanthrolines, a linear correlation between $\ln(\tau_3)$ and λ_i was

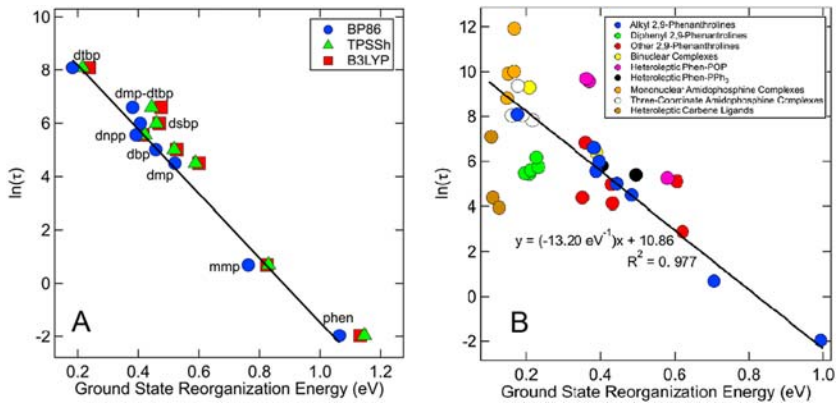

FIG. 10.16 Correlations between ln(τ)'s and ground state reorganization energies for (A) 2,9-disubstited phenanthrolines using different theory levels and (B) different classes of Cu(I) complexes. *Adapted from Stroscio, G.D., Ribson, R.D., Hadt, R.G., 2019. Quantifying entatic states in photophysical processes: applications to copper photosensitizers. Inorg. Chem. 58, 16800−16817. With permission.*

observed using different bases for the calculations (Fig. 10.16A). The model provides *entatic* contributions for one and four order of magnitude changes in τ of 4.3 ± 0.6 and 17.3 ± 2.2 kcal^{-1} mol, respectively, when differential oxidation-state contributions are not considered and 5.4 ± 0.5 and 21.7 ± 2.0 kcal^{-1} mol, when they are, indicating a small effect of them in the correlation. *Entatic* contributions provided by H-capped ligands (4.4 ± 0.7 and 17.7 ± 3.0 kcal^{-1} mol) were similar to those obtained from uncapped structures, indicating that the *entatic* contributions estimated using λ_i are largely due to sterics and further suggested that these play a more significant role in excited state lifetimes than electronic contributions. Finally, *entatic* contributions estimated using CPCM solvation approaches (15.7 ± 2.4 and 17.3 ± 2.2 kcal^{-1} mol), were similar to those in the gas phase, supporting that λ_i reflects geometric and steric contributions rather than solvation and electronic effects.

This analysis could be extended to other kind of Cu complexes (Fig. 10.16B). For instance, when heteroleptic $[Cu(phen)(POP)]^+$ were used, the linear correlation is maintained but the complexes display higher λ_i. As the changes in the dihedral angle are similar to those of 2,9-akyl substituted complexes, this effect seems to be due the increase in the covalent nature of Cu−P bonds relative to the Cu−N. On the other hand, in the case of linear complexes featuring an N-heterocyclic carbene and carbazolyl ligands (Fig. 10.16B), the observed reduction in the reorganization energy was not attributed to *entatic* contributions because of ILCT nature of the excited state and the small Cu contribution to it.

10.6 Silver complexes

10.6.1 Homoleptic Ag(I) coordination compounds

As show cased in the previous sections, the photophysics of tetrahedral Cu(I) complexes has been thoroughly studied, especially for homoleptic bisimine complexes (see Section 3.1). Comparatively, studies of analogous Ag(I) complexes of tetrahedral geometry are still very scarce. Pioneering reports on this topic were presented by Osawa and Hoshino (2008), who prepared the homoleptic complex with diphosphine ligands: $[Ag(dppb)_2]PF_6$ (Fig. 10.17) and investigated its excited-state properties.

Interestingly, the phosphorescence of this complex is strongly dependent on the matrix and conditions. It emits in the blue range ($\lambda max = 456$ nm) in a degassed 2-methyltetrahydrofurane solution at 77 K, while it emits orange color ($\lambda max = 670$ nm) at room temperature. Moreover, it displays blue emission, when embedded in polymethylmethacrylate films. Assuming that these emissions occur from an MLCT state, it was explained by evoking a flattening distortion from the tetrahedral ground state, leading to a red shift in the emission at room temperature since the flattened structure is more stable

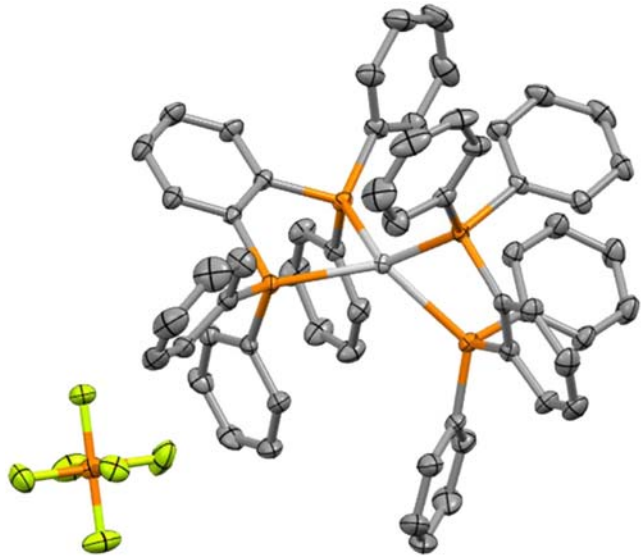

FIG. 10.17 Single-crystal X-ray structure of the $Ag(dppb)_2]PF_6$(CCDC 698226). Thermal ellipsoids are presented at 50% probability. *Adapted from Osawa, M., Hoshino, M., 2008. Photochemistry and photophysics of the tetrahedral silver(I) complex with diphosphine ligands: [Ag(dppb)2]PF6 (dppb = 1, 2-bis[diphenylphosphino]benzene). Chem. Commun. 47, 6384–6386. With Permission.*

than the tetrahedral in the excited MLCT state. This structural change was hampered in the solid phase, either in the frozen solvent at 77 K, or in the polymeric films, resulting in emissions from the tetrahedral state instead (Fig. 10.18).

Further investigations by Kaeser et al. (2014) on homoleptic Silver(I) bisphosphine complexes (along with their Cu(I) and Au(I) congeners) showed that complexes of the wide bite-angle POP (Fig. 10.10) displayed a distorted tetrahedral AgP_4 coordination geometry, in strong contrast with analogous copper and gold complexes, where only one POP ligand behaves as chelate, being the second coordinated through only one P donor in a trigonal geometry. Contrary to its dppb analog, the emission is attributed to a triplet MLCT state, where POP complexes display ligand-centered triplet excited states.

Virtually all Cu(I) and Ag(I) emitters possess some sort of distorted tetrahedral geometry in their ground state and their corresponding triplet MLCT states show some degree of square-planar flattening. Interestingly, there were no reports upto before 2019 describing square-planar d^{10}-emiters. Thus, it was not known that what would happen to planar Ag(I) complexes upon excitation, or if they would be luminescent. In an interesting report, Artem'ev et al. (2019) described for the first time the emission properties of Ag(I) complexes with a square-planar geometry. They answered these

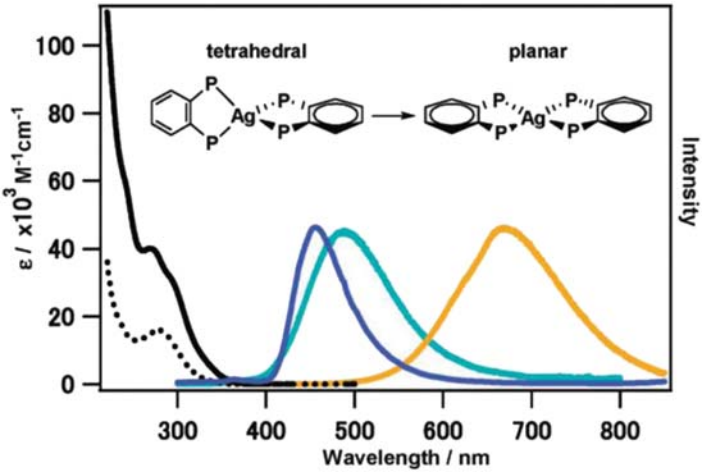

FIG. 10.18 Absorption spectra of ligand dppb (*dashed line*) and silver complex $Ag(dppb)_2]PF_6$ (*solid line*) in2-methyltetrahydrofurane and emission spectra ($\lambda_{exc} = 266$ nm) of the complex in polymethylmethacrylate film (light blue) and in 2-methyltetrahydrofurane (orange at 293 K, blue at 77 K). The inset shows the proposed flattening distortion upon light irradiation. The phenyl-groups on each ligand were omitted for clarity. *Adapted from Osawa, M., Hoshino, M., 2008. Photochemistry and photophysics of the tetrahedral silver(I) complex with diphosphine ligands: [Ag(dppb)2]PF6 (dppb = 1, 2-bis[diphenylphosphino]benzene). Chem. Commun. 47, 6384−6386. With Permission.*

questions by preparing and analyzing such Ag(I) square-planar complexes, reacting the ligand tris(2-pyridyl)phosphine oxide (Py_3PO) with different Ag(I) salts (Fig. 10.19).

From the three complexes prepared by these authors (**84**-**86**), only **84** and **85** were thoroughly characterized, as co-crystals of **86** readily decomposed during the measurements. Both complexes display yellow emission at 300 K, with an interesting thermochromic behavior, turning the emission red-orange at 77 K. The novel Ag(I) square planar complexes showed very short phosphorescence lifetimes (compared to their tetrahedral congeners) of only 5−6 μs at 77 K. Theoretical calculation suggest that the S_1 state has ^{1}MLCT nature; thus being responsible for the fluorescence. Interestingly, the S_1 state readily relax via spin-forbidden inter-system crossing (ISC) to the T_1 state, due to the small energy gap (46 meV) resulting from the structural similarity between these states. After the fast ISC, radiative deactivation in the microsecond scale results in phosphorescence emission. The thermochromic effect has not been clearly rationalized.

10.6.2 Heteroleptic Ag(I) coordination compounds

Just as in the case of homoleptic Ag(I) complexes, most of the reported accompanying ligands are chelating phosphines, heterocyclic nitrogen donors

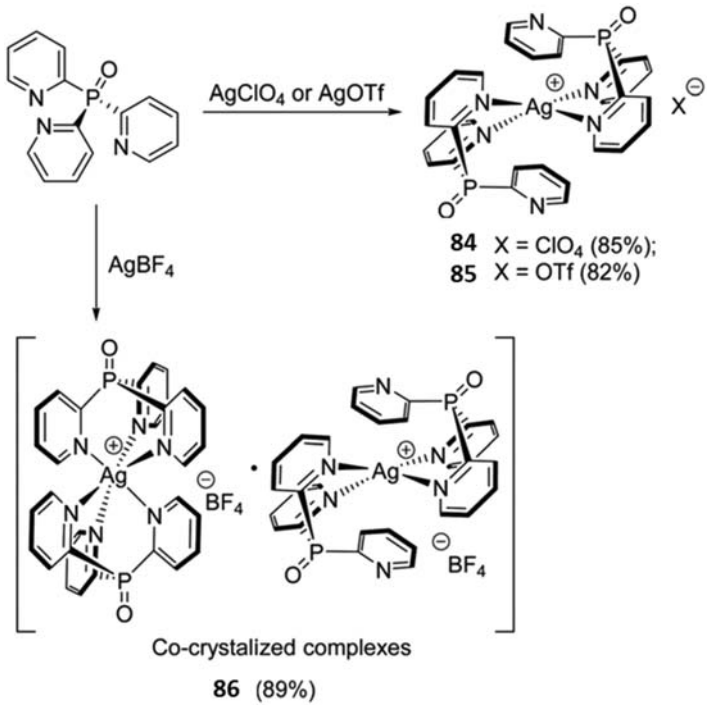

FIG. 10.19 First preparation of luminescent Ag(I) square-planar complexes. *Adapted from Artem'ev, A.V., Ryzhikov, M.R., Berezin, A.S., Kolesnikov, I.E., Samsonenko, D.G., Bagryanskaya, I.Y., 2019. Photoluminescence of Ag(I) complexes with a square-planar coordination geometry: the first observation. Inorg. Chem. Front. 6, 2855–2864. With Permission.*

and combinations thereof. Among the few reports dealing with these types of complexes, the studies by Igawa et al. (2012) dealing with heteroleptic diphosphine emitters are noteworthy. They prepared the homoleptic complex $[Ag(L)_2]PF_6$ (**87**), and the heteroleptic complexes $[Ag(L)(L_{Me})]BF_4$ (Fig. 10.20, **88**)and $[Ag(L)\text{-}(L_{Et})]BF_4$(L = 1,2-bis(diphenylphosphino)benzene (**89**) (L = dppb, L_{Me} = 1,2-bis[bis(2-methylphenyl)phosphino]benzene, L_{Et} = 1,2-bis[bis(2-ethylphenyl)phosphino]benzene)and studied their photophysical properties at room temperature.

These complexes include dppb-derived ligands containing alkyl substituents at the ortho positions of the peripheral phenyl groups, resulting in congested, rigid environments around the metal center. The homoleptic complex **87** displays strong blue luminescence in degassed 2-methyltetrahydrofurane solution at 77 K, while it weakly emits in the orange region ($\lambda max = 670$ nm) at room temperature. This large red shift is indicative of a large geometry change upon excitation, due to flattening distortion from the pseudotetrahedral ground state. Conversely, heteroleptic

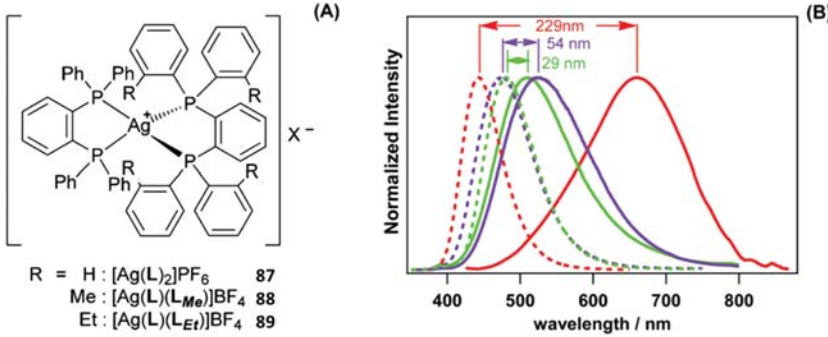

FIG. 10.20 Homoleptic and heterolepticdiphosphine Ag(I) complexes reported by Osawa and co-workers (A) and corrected emission spectra ($\lambda_{exc} = 300$ nm) of complexes **87**(red [light gray in print version]), **88** (purple [dark black in print version]), and **89** (green [light gray in print version]) in degassed 2-methyltetrahydrofurane solution at 77 K (*dashed lines*) and 293 K (*solid lines*) (B). *Adapted Igawa, S., Hashimoto, M., Kawata, I., Hoshino, M., Osawa, M., 2012. Photoluminescence properties, molecular structures, and theoretical study of heteroleptic silver(I) complexes containing diphosphine ligands. Inorg. Chem. 51, 5805−5813. With Permission.*

complexes **88** and **89**, display a bright green phosphorescence with only slight shifts at 77 K, of 54 and 29 nm, respectively. This green phosphorescence is attributed to a mixture of σ - π * and π - π* transitions, as theoretical studies. Moreover, with the help of time-dependent DFT calculations, they have confirmed that the steric congestion caused by the alkyl substituents in the ligands effectively prevents the flattening of the tetrahedral geometry upon light absorption. The introduction of interligand steric interactions is a general approach to improve the luminescence of d^{10} emitters, both in the solid state as well as in solution.

Another interesting series of heteroleptic complexes was reported by Hsu et al. (2011) using the chelating biphosphine POP and functionalized 2-pyridyl pyrrolide (**90** and **91**, Fig. 10.21). They studied the nature of their emissive states as well as the structure-photophysics relationships compared to their Cu(I) analogs (**26**−**28**). They concluded that, compared to their lighter copper congeners, the metal center possess a higher oxidation potential due to the low-lying d orbital, resulting in insignificant contributions of MLCT in their lowest singlet and triplet excited states. Thus, in these heteroleptic Ag(I) complexes, both S_1 and T_1 states have mainly a ligand-centered ππ* character. Hence, upon light absorption, since the S_1 state is dominated by the ππ* contributions, there is not a marked geometry deviation from its ground-state tetrahedral structure. This was confirmed experimentally by the very small emission shift observed for these complexes, when recorded at 77 K and at room temperature (Fig. 10.21). This is in strong contrast with other tetrahedral Ag(I) emitters, as those described at the beginning of this section, where the flattening distortion upon excitation is imminent. This apparent discrepancy only provides another example of the critical role played by the ligand

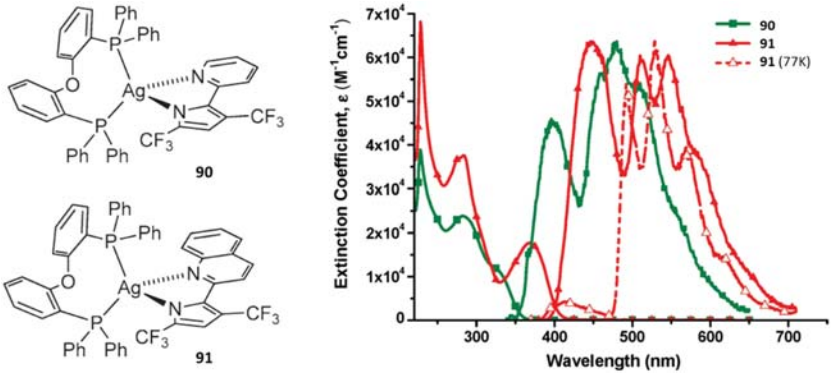

FIG. 10.21 Heteroleptic Ag(I) complexes bearing POP chelates and pyridyl/pyrrolide ligands and their absorption and normalized emission spectra in CH_2Cl_2 solution at RT 77 K. *Adapted from Hsu, C.W., Lin, C.C., Chung, M.W., Chi, Y., Lee, G.H., Chou, P.T., et al., 2011. Systematic investigation of the metal-structure–photophysics relationship of emissive d10-complexes of group 11 elements: the prospect of application in organic light emitting devices. J. Am. Chem. Soc. 133, 12085–12099. With Permission.*

architectures on determining the photophysical properties of luminescent metal complexes.

Another impressive example of fine-tuning of the photophysical properties of heteroleptic Ag(I) complexes by varying the interligand steric interactions was provided by Shafikov et al. (2017). They designed a series of complexes containing the chelating biphosphane P_2-nCB (bis(diphenylphosphine)-nido-carborane) and different phenanthroline derivatives with different substituent at their 2,9-positions (**92–94**, Fig. 10.22).

The strongly donating P_2-nCB ligand is necessary to provide contribution of d orbitals (of the metal) to the HOMO and HOMO-1 molecular orbitals, being these located at the "phosphine side" of the complex. Thus, with the LUMO and LUMO +1 orbitals centered at the phenanthroline moiety, it is possible to have S_1 and T_1 states with a charge-transfer character (in contrast to other complexes discuses earlier in this section), which is prerequisite to an efficient TADF.

The different substituents at the phenanthroline scaffold have an electronic effect, influencing the radiative decay of the S_1 state, while, at the same time, increase the rigidity of the pseudotetrahedral geometry, minimizing the non-radiative relaxation. This results in boosting the photoluminescence quantum yield (Φ_{PL}) up to 100% for the most sterically congested complex (**94**).

10.7 Gold complexes

10.7.1 Au(I) coordination compounds

Along the series of d^1 degree complexes, those of Au(I) show the highest propensity to be coordinatively unsaturated, favoring aggregation through

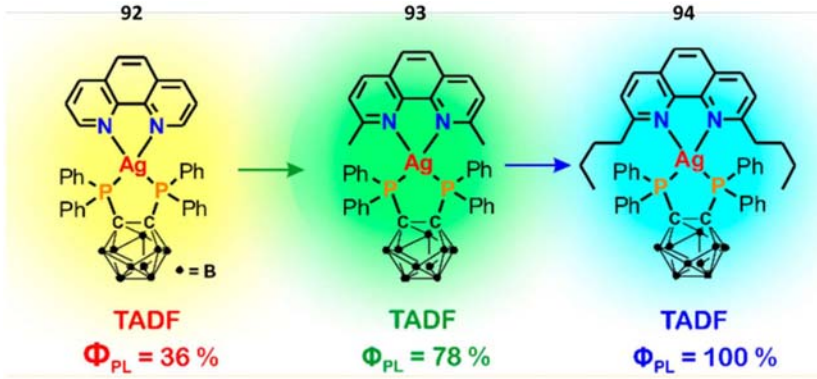

FIG. 10.22 Heteroleptic complexes with highly efficient thermally activated delayed fluorescence (TADF). *Adapted from Shafikov, M.Z., Suleymanova, A.F., Czerwieniec, R., Yersin, H., 2017. Thermally activated delayed fluorescence from Ag(I) complexes: a route to 100% quantum yield at unprecedentedly short decay time. Inorg. Chem. 56, 13274−13285. With Permission.*

metallophilic interactions. This phenomenon results in new excited states for the aggregates, different to the "original" ligand-centered or charge transfer in the monometallic species (Lei et al., 2017; Seifert et al., 2020; Schmidbaur and Raubenheimer, 2020). In spite of this tendency, there are various fairly stable monometallic Au(I) complexes prepared using rigid chelating ligands, especially biphosphines and terpyridines. Pioneering reports of Kaeser et al. (2014) described the preparation of Au(I) homoleptic complexes of biphosphine ligands dppb (**95**) and POP (**96**), adopting the former expected pseudotetrahedralgeometry (like its copper and silver analogs), while the later displays a trigonal coordination geometry, probably due to the smaller van der Waals radio of the Au(I) cation, resulting in a more difficult "accommodation" of the two POP ligands, which have a wider bite-angle than dppb (Fig. 10.23).

Both complexes (**95**) and (**96**) have exited estates resulting from transitions of a non-bonding electron at the phosphorous atom to an antibonding π^* orbital at the phenyl substituents at the same atom. Importantly, the steric congestion provided by the diphosphine ligands is fundamental to guarantee the stability of these complexes in solution and retain its luminescence.

In a similar report, Hsu et al. (2011) compared the structural and photophysical properties of heterolepticd[10] complexes bearing phosphine and pyridyl/pyrrolide ligands, finding that, while Cu(I) and Ag(I) complexes display MP_4 distorted tetrahedral geometries, all Au(I) derivatives display essentially linear arrangements, with P−Au−N angles from 163.4 to 174.1 degrees, as exemplified by the complex complex Au(PPh3) (fphro) (fphro = 3,5-bis(trifluoromethyl)-2- (6′-phenyl-2′-pyridyl) pyrrolide) (**97**) in (Fig. 10.24). The lower-lying S_1 state of these type of Au(I) complexes possess $\pi\pi^*$ ligand-centered character and hence, it is not expected to undergo structural

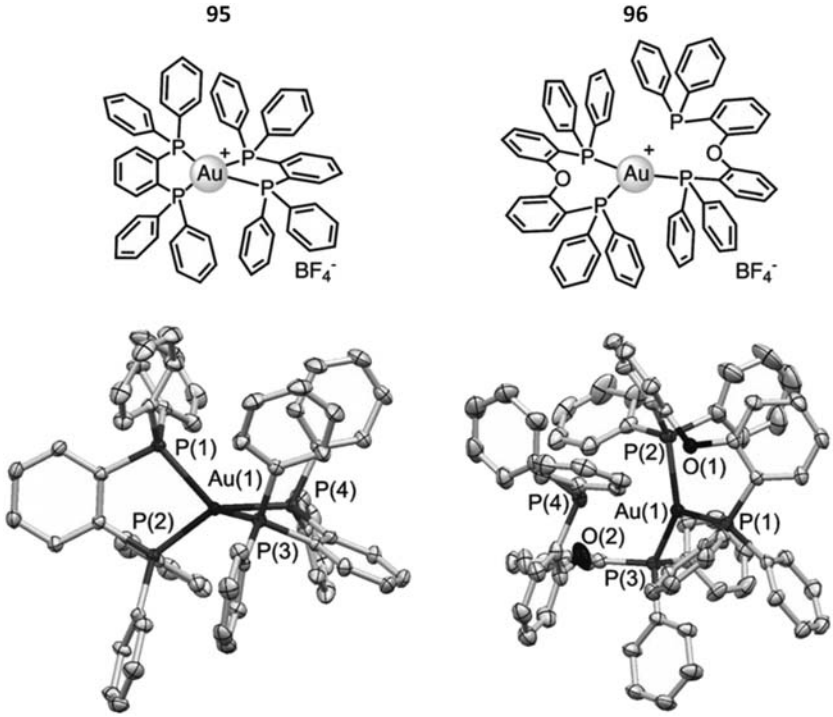

FIG. 10.23 Homoleptic Au(I) complexes of biphosphineligandsdppb (**95**) and POP (**96**). The X-ray structure of the corresponding cations is presented with thermal ellipsoids at the 50% probabilitylevel. *Adapted from Kaeser, A., Moudam, O., Accorsi, G., Séguy, I., Navarro, J., Belbakra, A., et al., 2014. Homoleptic copper(I), silver(I), and gold(I) bisphosphine complexes. Eur. J. Inorg. Chem. 2014, 1345−1355. With Permission.*

distortions upon excitation (Fig. 10.24). This was confirmed experimentally by the observation of very similar emission wavelengths for these complexes at room temperature and at 77 K. Interestingly, all the prepared complexes were monomeric, with no hints of intermetallic interactions.

An important class of linear luminescent Au(I) complexes are organometallic compounds with the general backbone C−Au-E (E = N or P), being carbon ligands normally fluorinated aryl moieties, alkynyl rests or N-heterocyclic carbenes (Fig. 10.25) Langdon-Jones and Pope (2014). The simple complex [Au(C_6F_5) (η^1-terpy)] (**98**) exhibits green luminescence in the solid state at 77 K, with a lifetime of the excite state in the nanosecond range, suggesting a fluorescent emission from an LMCT state. In solution (in acetonitrile) at room temperature, this complex undergoes a dissociative equilibrium, releasing its terpyridine ligand.

Recently, Hamze et al. (2019a,b) reported the systematic study of the photophysical properties of linear d^{10} complexes containing an amide donor

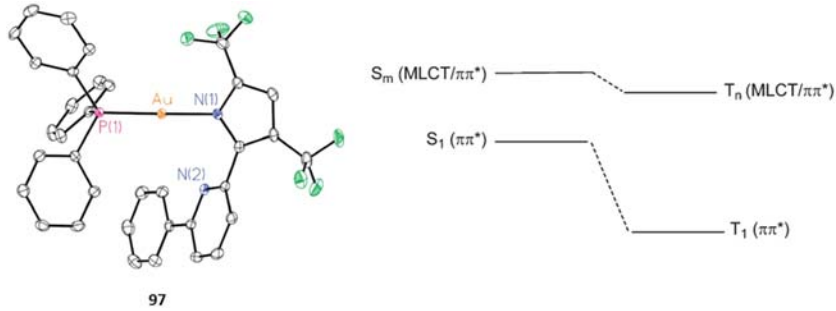

97

FIG. 10.24 Left: X-ray structure of Au(I)complex **97**. Thermal ellipsoids are presented at the 30% probability level. Right: schematic correlation of the corresponding lower-lying S and T levels (m and n are integer number higher or equal to 2). *Adapted from Hsu, C.W., Lin, C.C., Chung, M.W., Chi, Y., Lee, G.H., Chou, P.T., et al., 2011. Systematic investigation of the metal-structure−photophysics relationship of emissive d10-complexes of group 11 elements: the prospect of application in organic light emitting devices. J. Am. Chem. Soc. 133, 12085−12099. With Permission.*

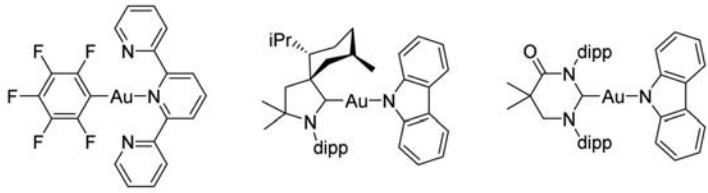

98 99 100

FIG. 10.25 Some examples or emissive linear Au(I) organometallic complexes.

(N-carbazoyl) and two different carbene ligands. They observed that Cu, Ag and Au complexes (**99** and **100**) have nearly the same structure, with C-M-N bond angles close to 180 degrees. Interestingly, the luminescence of these linear complexes does not have the same nature as in other emissive metal complexes where the metal center is a redox active donor in the ground state, and the emissive states are generally of MLCT character. In this case, the metal center is "redox innocent" and behaves only as a channel to modulate the electron transfer between the two redox active C- and N-ligands.

10.7.2 Au(III) coordination compounds

Comparedto their isoelectronic Pt(II) congeners, there are relatively few reports of luminescent Au(III) complexes, mainly due to their orbital situation. Au(III) compounds have low-lying $5d_{x^2-y^2}$ anti-bonding orbitals, with once populated, can easily undergo non-radiative decay to the singlet ground state. Thus, to achieve long-living emissive excited states, the energy of these

orbitals needs to be increased over the one of potentially emissive IL or MLCT states (Wing-Wah Yam and Chung-Chin Cheng, 2007; To et al., 2013). A common strategy to raise the energy of *d-d* ligand field states is the introduction of good σ-donating ligands, as the metal center is rendered more electron-rich. Following this method, pioneering reports for the preparation and characterization of a series of cyclometallated Au(III) chlorides **101** and **102**, containing chelating CNN ligands (Fig. 10.26) have been described (Chan et al., 1994; Liu et al., 1995). These square-planar complexes were emissive both in the solid state (at 77 K) and in liquid solutions at room temperature with excited-state lifetimes in the microsecond range. Interestingly, the high excited state reduction potential of **101** ($E^{\circ *}(Au^{III/II}) = 2.2$ V versus NHE) was exploited for the photooxidation of 1,4-dimethoxy benzene under visible light in THF (Chan et al., 1994). Moreover, complex **102** showed a high binding to calf-thymus DNA, effectively quenching and blue-shifting the complex emission by intercalation (Liu et al., 1995).

Au et al. (2009) reported the first introduction of N-heterocyclic carbene (NHC) ligands to Au(III) complexes (**103**), capitalizing on the high stability and good electron-donating features of these popular ligand class. These complexes displayed vibronic-structured emissions spectra, which was attributed to intraligand ππ* states. Even though the nature of the accompanying NHC ligands did not affect their photophysical properties, its presence was fundamental to achieve enhanced luminescence (Au et al., 2009). Similar compounds including an extended conjugation on the chelate (**104**) were later reported by Che et al. (Fig. 10.27) (To et al., 2012). Compared to the Yam complexes (**103**), Che's emitters (**104**) possess higher emission quantum yields, and much higher triplet excited state lifetimes. These improvements are attributed to the rigidity of the extended p-system at the cyclometallated ligand, resulting in a much lower structural distortion upon excitation. With the new set of enhanced photophysical properties, these complexes (**104**), were able to serve as photocatalysts for the dehydrogenation of secondary amines, as well as for the cyanation of isoquinolines under aerobic conditions.

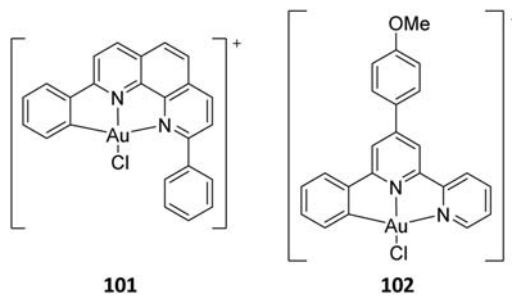

101 **102**

FIG. 10.26 Structure of the cation of cyclometallated Au(III) chlorides.

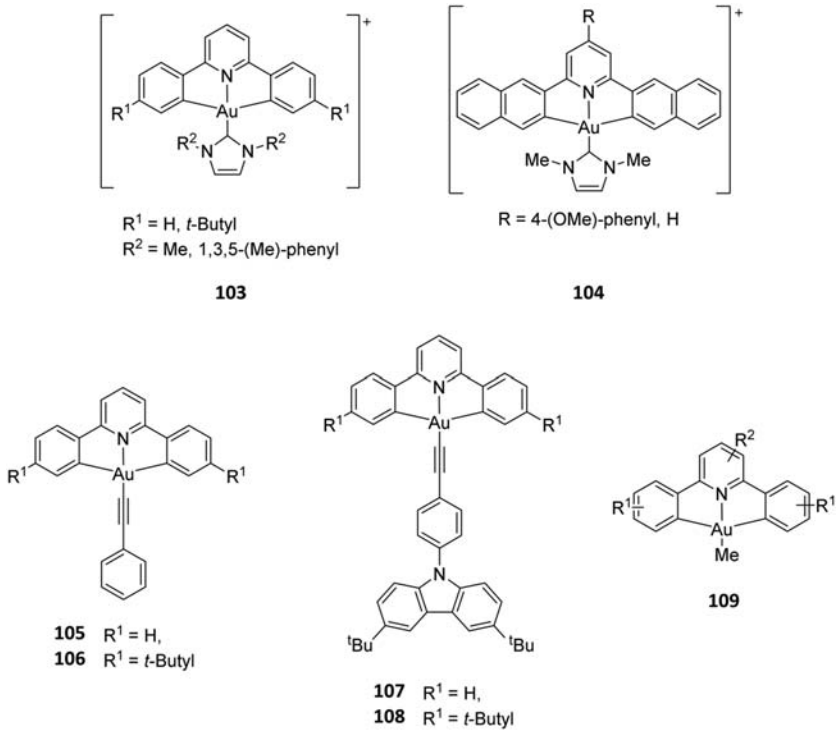

FIG. 10.27 Organometallic Au(III) complexes featuring cyclometallated ligands.

The potential of Au(III) as photocatalysts/photosensitizer was further exploited by Yu et al. (2016) reported the successful use of neutral bis-cyclometallated Au(III) complexes bearing akynyl ligands as light-harvesting materials in the production of hydrogen from water. The system used complexes **105**−**108** (Fig. 10.27) as sensitizers and cobalt or rhodium-based proton-reduction catalysts, with triethanolamine as sacrificial reductant. The high quantum yields (up to 13.7%) and turn-over numbers (up to 1441.5) are analogous to other popular ruthenium and iridium photosensitizers. An increase in emission quantum yields and lifetimes (up to 40%) was observed, when the alkynyl ligand is replaced by an alkyl moiety (i.e., methyl, **109**). Thanks to the absence of low-lying π-orbitals, along with their strong electron-donor capabilities. These features avoid the population of LLCT and LMCT states and result in highly emissive, long-lived ^{3}IL state instead (To et al., 2017).

10.8 Conclusion

The struggles and challenges posed to mankind by the turn of the century, including growing energetic demands, depletion of natural resources,

pollution, etc. have led us to the search for alternative technologies to tackle these problems in a low cost and sustainable manner. Thus, mimicking the way nature harnesses energy from the Sun to fuel the thrive of life on Earth seems to be a reasonable starting point. To achieve this goal, it is necessary to understand the complex mechanisms behind light absorption and emission in metal complexes to apply these insights in the design of novel photoactive complexes amenable to the multiple applications related to the aforementioned tasks: solar energy conversion and storage, CO_2 valorization, water sanitation, sustainable chemical synthesis, etc. For this purpose, base metals are the most desirable candidates for this endeavor, alas, not all of them are suitable, considering the necessary stabilities, redox potentials and absorption properties. Copper stands out as (arguably) the most versatile contestant, as quickly noticed by many researches and thoroughly attested by a myriad of publications on the photophysical properties of copper compounds and their uses. This field, however, is far for exhausted, as every day new analytical tools are developed, calculation power is increasing, and ligand architectures are developed, assuring more exciting insights and applications of the photophysics and photochemistry of copper complexes for the years to come.

References

Ahn, J.M., Peters, J.C., Fu, G.C., 2017. Design of a photoredox catalyst that enables the direct synthesis of carbamate-protected primary amines via photoinduced, copper-catalyzed N-Alkylation reactions of unactivated secondary halides. J. Am. Chem. Soc. 139, 18101−18106.

Andrés-Tomé, I., Fyson, J., Baiao Dias, F., Monkman, A.P., Iacobellis, G., Coppo, P., 2012. Copper(I) complexes with bipyridyl and phosphine ligands: a systematic study. Dalton Trans. 41, 8669−8674.

Armaroli, N., Accorsi, G., Cardinali, F., Listorti, A., 2007. Photochemistry and photophysics of coordination compounds: copper. In: Balzani, V., Campagna, S. (Eds.), Photochemistry and Photophysics of Coordination Compounds I. Springer Berlin Heidelberg, Berlin, Heidelberg, pp. 69−115.

Artem'ev, A.V., Ryzhikov, M.R., Berezin, A.S., Kolesnikov, I.E., Samsonenko, D.G., Bagryanskaya, I.Y., 2019. Photoluminescence of Ag(I) complexes with a square-planar coordination geometry: the first observation. Inorg. Chem. Front. 6, 2855−2864.

Au, V.K.-M., Wong, K.M.-C., Zhu, N., Yam, V.W.-W., 2009. Luminescent cyclometalated N-heterocyclic carbene-containing organogold(III) complexes: synthesis, characterization, electrochemistry, and photophysical studies. J. Am. Chem. Soc. 131, 9076−9085.

Bagal, D.B., Kachkovskyi, G., Knorn, M., Rawner, T., Bhanage, B.M., Reiser, O., 2015. Trifluoromethylchlorosulfonylation of alkenes: evidence for an inner-sphere mechanism by a copper phenanthroline photoredox catalyst. Angew. Chem. Int. Ed. 54, 6999−7002.

Balzani, V., Bergamini, G., Campagna, S., Puntoriero, F., 2007. Photochemistry and photophysics of coordination compounds: overview and general concepts. Top. Curr. Chem. 280, 1−36.

Bella, F., Gerbaldi, C., Barolo, C., Gratzel, M., 2015. Aqueous dye-sensitized solar cells. Chem. Soc. Rev. 44, 3431−3473.

Belloni, J., 1997. Photocatalytic aspects of silver photography. In: Homogeneous Photocatalysis. John Wiley & Sons Ltd., pp. 169−219

Bergmann, L., Zink, D.M., Baumann, T., Volz, D., Brase, S., Brase, S., 2016. Metal-organic and organic TADF-materials: status, challenges and characterization. Top. Curr. Chem. 374, 201–239.

Bergmann, L., Braun, C., Nieger, M., Bräse, S., 2018. The coordination- and photochemistry of copper(i) complexes: variation of N^N ligands from imidazole to tetrazole. Dalton Trans. 47, 608–621.

Bissember, A.C., Lundgren, R.J., Creutz, S.E., Peters, J.C., Fu, G.C., 2013. Transition-metal-catalyzed alkylations of amines with alkyl halides: photoinduced. copper-catalyzed couplings of carbazoles. Angew. Chem. Int. Ed. 52, 5129–5133.

Bissinger, P., Steffen, A., Vargas, A., Dewhurst, R.D., Damme, A., Braunschweig, H., 2015. Unexpected luminescence behavior of coinage metal π-diborene complexes. Angew. Chem. Int. Ed. 54, 4362–4366.

Bitterwolf, T., 2006. Photochemistry of transition metal complexes. In: Encyclopedia of Inorganic and Bioinorganic Chemistry. John Wiley & Sons Ltd., Hoboken, New Jersey.

Bryden, M.A., Zysman-Colman, E., 2021. Organic thermally activated delayed fluorescence (TADF) compounds used in photocatalysis. Chem. Soc. Rev. 50, 7587–7680.

Buckner, M.T., McMillin, D.R., 1978. Photoluminescence from copper(I) complexes with low-lying metal-to-ligand charge transfer excited states. J. Chem. Soc., Chem. Commun. 759–761.

Cahen, D., Gratzel, M., Guillemoles, J.F., Hodes, G., 2001. Dye-sensitized solar cells: principles of operation. In: Electrochemistry of Nanomaterials. Wiley-VCH Verlag GmbH, pp. 201–228.

Caron, A., Morin, É., Collins, S.K., 2019. Bifunctional copper-based photocatalyst for reductive pinacol-type couplings. ACS Catal. 9, 9458–9464.

Chan, C.-W., Wong, W.-T., Che, C.-M., 1994. Gold(III) photooxidants. Photophysical, photochemical properties, and crystal structure of a luminescent cyclometalated gold(III) complex of 2,9-diphenyl-1,10-phenanthroline. Inorg. Chem. 33, 1266–1272.

Chen, J., Cen, J., Xu, X., Li, X., 2016. The application of heterogeneous visible light photocatalysts in organic synthesis. Catal. Sci. Technol. 6, 349–362.

Chen, N.-Y., Xia, L.-M., Lennox, A.J.J., Sun, Y.-Y., Chen, H., Jin, H.-M., et al., 2017. Structure-activated copper photosensitisers for photocatalytic water reduction. Chem. Eur J. 23, 3631–3636.

Chen, H., Xu, L.-X., Yan, L.-J., Liu, X.-F., Xu, D.-D., Yu, X.-C., et al., 2020. Mononuclear copper(I) complexes based on phenanthroline derivatives P^N^N^P tetradentate ligands: syntheses, crystal structure, photochemical properties. Dyes. Pigm. 173. https://doi.org/10.1016/j.dyepig.2019.108000.

Clausing, S.T., Morales Salazar, D., Orthaber, A., 2020. Preparation, photo- and electrochemical studies of a homoleptic imine-phosphaalkene Cu(I) complex. Inorg. Chim. Acta. 513. https://doi.org/10.1016/j.ica.2020.119958.

Conry, R.R., 2005. Copper: inorganic and coordination chemistry. In: Encyclopedia of Inorganic Chemistry. John Wiley & Sons Ltd., Hoboken, New Jersey.

Cuttell, D.G., Kuang, S.-M., Fanwick, P.E., McMillin, D.R., Walton, R.A., 2002. Simple Cu(I) complexes with unprecedented excited-state lifetimes. J. Am. Chem. Soc. 124, 6–7.

Daniel, C., 2011. Photochemistry of transition metal complexes: theory. In: Encyclopedia of Inorganic and Bioinorganic Chemistry. John Wiley & Sons Ltd., Hoboken, New Jersey, pp. 1–15.

Daniel, C., 2015. Photochemistry and photophysics of transition metal complexes: quantum chemistry. Coord. Chem. Rev. 282–283, 19–32.

Dicke, B., Hoffmann, A., Stanek, J., Rampp, M.S., Grimm-Lebsanft, B., Biebl, F., et al., 2018. Transferring the entatic-state principle to copper photochemistry. Nat. Chem. 10, 355–362.

DiMucci, I.M., Lukens, J.T., Chatterjee, S., Carsch, K.M., Titus, C.J., Lee, S.J., et al., 2019. The myth of d8 copper(III). J. Am. Chem. Soc. 141, 18508−18520.

Eaton, G.T., 1965. Photographic Chemistry for Black-And-White and Color Photography, second ed. Morgan & Morgan Inc., New York.

Elie, M., Gaillard, S., Renaud, J.-L., 2017. Luminescent cationic copper(I) complexes: synthesis, photophysical properties and application in light-emitting electrochemical cells. In: Costa, R.D. (Ed.), Light-Emitting Electrochemical Cells: Concepts, Advances and Challenges. Springer, Cham, Berlin, Heidelberg, pp. 287−327.

Femoni, C., Muzzioli, S., Palazzi, A., Stagni, S., Zacchini, S., Monti, F., et al., 2013. New tetrazole-based Cu(i) homo- and heteroleptic complexes with various P^P ligands: synthesis, characterization, redox and photophysical properties. Dalton Trans. 42, 997−1010.

Ferraro, V., Bortoluzzi, M., Castro, J., Vomiero, A., You, S., 2020. Luminescent Cu(I) complex with bis(indazol-1-yl)phenylmethane as chelating ligand. Inorg. Chem. Commun. 116. https://doi.org/10.1016/j.inoche.2020.107894.

Forero Cortés, P.A., Marx, M., Trose, M., Beller, M., 2021. Heteroleptic copper complexes with nitrogen and phosphorus ligands in photocatalysis: overview and perspectives. Chem Catal. 1, 298−338.

Förster, C., Heinze, K., 2020. Photophysics and photochemistry with Earth-abundant metals − fundamentals and concepts. Chem. Soc. Rev. 49, 1057−1070.

García Calavia, P., Bruce, G., Pérez-García, L., Russell, D.A., 2018. Photosensitiser-gold nanoparticle conjugates for photodynamic therapy of cancer. Photochem. Photobiol. Sci. 17, 1534−1552.

Giereth, R., Frey, W., Junge, H., Tschierlei, S., Karnahl, M., 2017. Copper photosensitizers containing P^N ligands and their influence on photoactivity and stability. Chem. Eur J. 23, 17432−17437.

Giereth, R., Reim, I., Frey, W., Junge, H., Tschierlei, S., Karnahl, M., 2019. Remarkably long-lived excited states of copper photosensitizers containing an extended π-system based on an anthracene moiety. Sustain. Energy Fuel. 3, 692−700.

Giereth, R., Mengele, A.K., Frey, W., Kloss, M., Steffen, A., Karnahl, M., et al., 2020. Copper(I) phosphinooxazoline complexes: impact of the ligand substitution and steric demand on the electrochemical and photophysical properties. Chem. Eur J. 26, 2675−2684.

Gimeno, L., Blart, E., Rebilly, J.-N., Coupeau, M., Allain, M., Roisnel, T., et al., 2020. Non-symmetrical sterically challenged phenanthroline ligands and their homoleptic copper(I) complexes with improved excited-state properties. Chem.Eur. J. 26, 11887−11899.

Gracia, L.-L., Luci, L., Bruschi, C., Sambri, L., Weis, P., Fuhr, O., et al., 2020. New Photosensitizers based on heteroleptic CuI complexes and CO_2 photocatalytic reduction with [NiII(-cyclam)]Cl_2. Chem. Eur J. 26, 9929−9937.

Gratzel, M., 2003. Dye-sensitized solar cells. J. Photochem. Photobiol., C 4, 145−153.

Gratzel, M., 2009. Recent advances in sensitized mesoscopic solar cells. Acc. Chem. Res. 42, 1788−1798.

Hamze, R., Peltier, J.L., Sylvinson, D., Jung, M., Cardenas, J., Haiges, R., et al., 2019a. Eliminating nonradiative decay in Cu(I) emitters: >99% quantum efficiency and microsecond lifetime. Science 363, 601−606.

Hamze, R., Shi, S., Kapper, S.C., Muthiah Ravinson, D.S., Estergreen, L., Jung, M.-C., et al., 2019b. Quick-Silver from a systematic study of highly luminescent, two-coordinate, d10 coinage metal complexes. J. Am. Chem. Soc. 141, 8616−8626.

Heberle, M., Tschierlei, S., Rockstroh, N., Ringenberg, M., Frey, W., Junge, H., et al., 2017. Heteroleptic copper photosensitizers: why an extended π-system does not automatically lead to enhanced hydrogen production. Chem. Eur J. 23, 312−319.

Hong, G., Gan, X., Leonhardt, C., Zhang, Z., Seibert, J., Busch, J., et al., 2021. A brief history of OLEDs-emitter development and industry milestones. Adv. Mater. 33. https://doi.org/10.1002/adma.202005630.

Hopkinson, M.N., Dix, S., 2019. Gold in photocatalysis. In: König, B. (Ed.), Photocatalysis in Organic Synthesis. Georg Thieme Verlag, Stuttgart, p. 297.

Hossain, A., Bhattacharyya, A., Reiser, O., 2019. Copper's rapid ascent in visible-light photoredox catalysis. Science 364. https://doi.org/10.1126/science.aav97.

Hsu, C.-W., Lin, C.-C., Chung, M.-W., Chi, Y., Lee, G.-H., Chou, P.-T., et al., 2011. Systematic investigation of the metal-structure−photophysics relationship of emissive d10-complexes of group 11 elements: the prospect of application in organic light emitting devices. J. Am. Chem. Soc. 133, 12085−12099.

Huang, B., Hu, M., Toste, F.D., 2002. Homogeneous gold redox chemistry: organometallics, catalysis, and beyond. Trend. Chem. 2, 707−720.

Igawa, S., Hashimoto, M., Kawata, I., Hoshino, M., Osawa, M., 2012. Photoluminescence properties, molecular structures, and theoretical study of heteroleptic silver(I) complexes containing diphosphine ligands. Inorg. Chem. 51, 5805−5813.

Iwamura, M., Takeuchi, S., Tahara, T., 2015. Ultrafast excited-state dynamics of copper(I) complexes. Acc. Chem. Res. 48, 782−791.

Kaeser, A., Moudam, O., Accorsi, G., Séguy, I., Navarro, J., Belbakra, A., et al., 2014. Homoleptic copper(I), silver(I), and gold(I) bisphosphine complexes. Eur. J. Inorg. Chem. 2014, 1345−1355.

Kainz, Q.M., Matier, C.D., Bartoszewicz, A., Zultanski, S.L., Peters, J.C., Fu, G.C., 2016. Asymmetric copper-catalyzed C-N cross-couplings induced by visible light. Science 351, 681−684.

Kalyanasundaram, K., Gratzel, M., 2009. Efficient dye-sensitized solar cells for direct conversion of sunlight to electricity. Mat. Matt. 4, 88−91.

Kee, J.W., Ng, Y.Y., Kulkarni, S.A., Muduli, S.K., Xu, K., et al., 2016. Development of bis(arylimino)acenaphthene (BIAN) copper complexes as visible light harvesters for potential photovoltaic applications. Inorg. Chem. Front. 3, 651−662.

Knorn, M., Rawner, T., Czerwieniec, R., Reiser, O., 2015. [Copper(phenanthroline)(bisisonitrile)]+-complexes for the visible-light-mediated atom transfer radical addition and allylation reactions. ACS Catal. 5, 5186−5193.

Kohler, L., Hadt, R.G., Hayes, D., Chen, L.X., Mulfort, K.L., 2017. Synthesis, structure, and excited state kinetics of heteroleptic Cu(I) complexes with a new sterically demanding phenanthroline ligand. Dalton Trans. 46, 13088−13100.

Krylova, V.A., Djurovich, P.I., Whited, M.T., Thompson, M.E., 2010. Synthesis and characterization of phosphorescent three-coordinate Cu(i)−NHC complexes. Chem. Commun. 46, 6696−6698.

Krylova, V.A., Djurovich, P.I., Conley, B.L., Haiges, R., Whited, M.T., Williams, T.J., et al., 2014. Control of emission colour with N-heterocyclic carbene (NHC) ligands in phosphorescent three-coordinate Cu(i) complexes. Chem. Commun. 50, 7176−7179.

Langdon-Jones, E.E., Pope, S.J.A., 2014. Recent developments in gold (i) coordination chemistry: luminescence properties and bioimaging opportunities. Chem. Commun. 50, 10343−10354.

Lavie-Cambot, A., Cantuel, M., Leydet, Y., Jonusauskas, G., Bassani, D.M., McClenaghan, N.D., 2008. Improving the photophysical properties of copper(I) bis(phenanthroline) complexes. Coord. Chem. Rev. 252, 2572−2584.

Lei, Z., Zhang, J.-Y., Guan, Z.-J., Wang, Q.-M., 2017. Intensely luminescent gold (I) phosphinopyridyl clusters: visualization of unsupported aurophilic interactions in solution. Chem. Commun. 53, 10902−10905.

Lennartson, A., 2017. The Chemical Works of Carl Wilhelm Scheele, first ed. Springer International Publishing.

Lian, H., Shen, J., Guo, H., Cheng, X., Dong, Q., Yang, J., et al., 2019. Recent advances in the optimization of organic light-emitting diodes with metal-containing nanomaterials. Chem. Rec. 19, 1753−1767.

Lipshutz, B.H., Pfeiffer, S.S., 2005. Copper: organometallic chemistry. In: Encyclopedia of Inorganic Chemistry. John Wiley & Sons Ltd., Hoboken, New Jersey.

Liu, H.-Q., Cheung, T.-C., Peng, S.-M., Che, C.-M., 1995. Novel luminescent cyclometaiated and terpyridine gold(III) complexes and DNA binding studies. J. Chem. Soc. Chem. Commun. 1787−1788 (1995).

Liu, Y., Yiu, S.-C., Ho, C.-L., Wong, W.-Y., 2018. Recent advances in copper complexes for electrical/light energy conversion. Coord. Chem. Rev. 375, 514−557.

Livshits, M.Y., Reeves, B.J., DeWeerd, N.J., Strauss, S.H., Boltalina, O.V., Rack, J.J., 2020. Trifluoromethylated phenanthroline ligands reduce excited-state distortion in homoleptic copper(I) complexes. Inorg. Chem. 59, 2781−2790.

Lu, T., Wang, J.-Y., Shi, L.-X., Chen, Z.-N., Chen, X.-T., Xue, Z.-L., 2018. Synthesis, structures and luminescence properties of amine-bis(N-heterocyclic carbene) copper(I) and silver(I) complexes. Dalton Trans. 47, 6742−6753.

Mak, T.C.W., Zhao, X.-L., 2005. Silver: inorganic & coordination chemistry. In: Encyclopedia of Inorganic Chemistry. John Wiley & Sons Ltd.

Makal, A., Benedict, J., Trzop, E., Sokolow, J., Fournier, B., Chen, Y., et al., 2012. Restricted Photochemistry in the molecular solid state: structural changes on photoexcitation of Cu(I) phenanthroline metal-to-ligand charge transfer (MLCT) complexes by time-resolved diffraction. J. Phys. Chem. A. 116, 3359−3365.

Maldotti, A., 2009. Photochemistry and photophysics of transition-metal complexes. Photochem 37, 240−299.

Mani, G., Subramaniyan, V., 2019. Homoleptic and Heteroleptic copper(I) Complexes Bearing Diimine-Diphosphine Ligands. Elsevier B.V., p. 237

Mara, M.W., Fransted, K.A., Chen, L.X., 2015. Interplays of excited state structures and dynamics in copper(I) diimine complexes: implications and perspectives. Coord. Chem. Rev. 282−283, 2−18.

Marzo, L., Pagire, S.K., Reiser, O., Koenig, B., 2018. Visible-light photocatalysis: does it make a difference in organic synthesis? Angew. Chem. Int. Ed. 57, 10034−10072.

McMillin, D.R., Buckner, M.T., Ahn, B.T., 1977. A light-induced redox reaction of bis(2,9-dimethyl-1,10-phenanthroline)copper(I). Inorg. Chem. 16, 943−945.

Michelet, B., Deldaele, C., Kajouj, S., Moucheron, C., Evano, G., 2017. A general copper catalyst for photoredox transformations of organic halides. Org. Lett. 19, 3576−3579.

Narayanam, J.M., Stephenson, C.R., 2011. Visible light photoredox catalysis: applications in organic synthesis. Chem. Soc. Rev. 40, 102−113.

Ng, Y.Y., Tan, L.J., Ng, S.M., Chai, Y.T., Ganguly, R., Du, Y., et al., 2018. Spectroscopic characterization and mechanistic studies on visible light photoredox carbon−carbon bond

formation by bis(arylimino)acenaphthene copper photosensitizers. ACS Catal. 8, 11277−11286.

Nicholls, T.P., Bissember, A.C., 2019. Developments in visible-light-mediated copper photocatalysis. Tetrahedron Lett. 60. https://doi.org/10.1016/j.tetlet.2019.06.042.

Nicholls, T.P., Caporale, C., Massi, M., Gardiner, M.G., Bissember, A.C., 2019. Synthesis and characterisation of homoleptic 2,9-diaryl-1,10-phenanthroline copper(I) complexes: influencing selectivity in photoredox-catalysed atom-transfer radical addition reactions. Dalton Trans. 48, 7290−7301.

Nishikawa, M., Sawamura, S., Haraguchi, A., Morikubo, J., Takao, K., Tsubomura, T., 2015. Highly emissive copper(i) complexes bearing diimine and bis(diphenylphosphinomethyl)-2,2-dimethyl-1,3-dioxolane. Dalton Trans. 44, 411−418.

Osawa, M., Hoshino, M., 2008. Photochemistry and photophysics of the tetrahedral silver(I) complex with diphosphine ligands: [Ag(dppb)2]PF6 (dppb = 1, 2-bis[diphenylphosphino] benzene). Chem. Commun. 47, 6384−6386.

Osawa, M., Kawata, I., Ishii, R., Igawa, S., Hashimoto, M., Hoshino, M., 2013. Application of neutral d10 coinage metal complexes with an anionic bidentate ligand in delayed fluorescence-type organic light-emitting diodes. J. Mater. Chem. C 1, 4375−4383.

Papanikolaou, P., Akrivos, P.D., Czapik, A., Wicher, B., Gdaniec, M., Tkachenko, N., 2013. Homoleptic bis(aryl)acenaphthenequinonediimine-CuI complexes - synthesis and characterization of a family of compounds with improved light-gathering characteristics. Eur. J. Inorg. Chem. 2013, 2418−2431.

Paria, S., Reiser, O., 2014. Copper in photocatalysis. Chem. Cat. Chem. 6, 2477−2483.

Pirtsch, M., Paria, S., Matsuno, T., Isobe, H., Reiser, O., 2012. [Cu(dap)$_2$Cl] as an efficient visible-light-driven photoredox catalyst in carbon−carbon bond-forming reactions. Chem. Eur J. 18, 7336−7340.

Prier, C.K., Rankic, D.A., MacMillan, D.W., 2013. Visible light photoredox catalysis with transition metal complexes: applications in organic synthesis. Chem. Rev. 113, 5322−5363.

Ravotto, L., Ceroni, P., 2017. Aggregation induced phosphorescence of metal complexes: from principles to applications. Coord. Chem. Rev. 346, 62−76.

Reiser, O., 2016. Shining light on copper: unique opportunities for visible-light-catalyzed atom transfer radical addition reactions and related processes. Acc. Chem. Res. 49, 1990−1996.

Rorabacher, D.B., 2004. Electron transfer by copper centers. Chem. Rev. 104, 651−697.

Sandoval-Pauker, C., Molina-Aguirre, G., Pinter, B., 2021. Status report on copper (I) complexes in photoredox catalysis; photophysical and electrochemical properties and future prospects. Polyhedron 199. https://doi.org/10.1016/j.poly.2021.115105.

Scheele, C.W., 1977. Chemische Abhandlung von der Luft und dem Feuer, Magn. Swederus. Upsala and Leipzig.

Schmidbaur, H., Raubenheimer, H.G., 2020. Excimer and exciplex formation in gold(I) complexes preconditioned by aurophilic interactions. Angew. Chem. Int. Ed. 59, 14748−14771.

Schultz, D.M., Yoon, T.P., 2014. Solar synthesis: prospects in visible light photocatalysis. Science 343. https://doi.org/10.1126/science.1239176.

Seifert, T.P., Naina, V.R., Feuerstein, T.J., Knöfel, N.D., Roesky, P.W., 2020. Molecular gold strings: aurophilicity, luminescence and structure−property correlations. Nanoscale 12, 20065−20088.

Shafikov, M.Z., Suleymanova, A.F., Czerwieniec, R., Yersin, H., 2017. Thermally activated delayed fluorescence from Ag(I) complexes: a route to 100% quantum yield at unprecedentedly short decay time. Inorg. Chem. 56, 13274−13285.

Sherwani, M.A., Tufail, S., Khan, A.A., Owais, M., 2015. Gold nanoparticle-photosensitizer conjugate based photodynamic inactivation of biofilm producing cells: potential for treatment of c. albicans infection in BALB/c Mice. PLoS One 10. https://doi.org/10.1371/journal.pone.0131684.

Shi, S., Jung, M.C., Coburn, C., Tadle, A., Sylvinson, M.R.,D., Djurovich, P.I., et al., 2019. Highly efficient photo- and electroluminescence from two-coordinate Cu(I) complexes featuring nonconventional N-heterocyclic carbenes. J. Am. Chem. Soc. 141, 3576−3588.

Stroscio, G.D., Ribson, R.D., Hadt, R.G., 2019. Quantifying entatic states in photophysical processes: applications to copper photosensitizers. Inorg. Chem. 58, 16800−16817.

Sun, W., Zhang, Q., Qin, L., Cheng, Y., Xie, Z., Lu, C., Wang, L., 2010. Phosphorescent cuprous complexes with N,O ligands − synthesis, photoluminescence, and electroluminescence. Eur. J. Inorg. Chem. 2010, 4009−4017.

To, W.-P., Tong, G.S.-M., Lu, W., Ma, C., Liu, J., Chow, A.L.-F., et al., 2012. Luminescent organogold(III) complexes with long-lived triplet excited states for light-induced oxidative C-H bond functionalization and hydrogen production. Angew. Chem. Int. Ed. 51, 2654−2657.

To, W.-P., Zou, T., Sun, R.W.-Y., Che, C.-M., 2013. Light-induced catalytic and cytotoxic properties of phosphorescent transition metal compounds with a d^8 electronic configuration. Philos. Trans. Royal Soc. A. 371. https://doi.org/10.1098/rsta.2012.0126.

To, W.-P., Tong, G.S.M., Cheung, C.-W., Yang, C., Zhou, D., Che, C.-M., 2017. Luminescent cyclometalated gold(III) alkyl complexes: photophysical and photochemical properties. Inorg. Chem. 56, 5046−5059.

Tong, G.S.M., Kui, S.C.F., Chao, H.-Y., Zhu, N., Che, C.-M., 2009. The 3[ndσ*(n+1)pσ] emissions of linear silver(I) and gold(I) chains with bridging phosphine ligands. Chem. Eur J. 15, 10777−10789.

Vallee, B.L., Williams, R.J., 1968. Metalloenzymes: the entatic nature of their active sites. Proc. Natl. Acad. Sci. U. S. A. 59, 498−505.

Wing-Wah Yam, V., Chung-Chin Cheng, E., 2007. Photochemistry and photophysics of coordination compounds: gold. In: Balzani, V., Campagna, S. (Eds.), Photochemistry and Photophysics of Coordination Compounds II. Springer Berlin Heidelberg, Berlin, Heidelberg, pp. 269−309.

Wing-Wah Yam, V., Kam-Wing Lo, K., 1999. Luminescent polynuclear d10 metal complexes. Chem. Soc. Rev. 28, 323−334.

Witzel, S., Hashmi, A.S.K., Xie, J., 2021. Light in gold catalysis. Chem. Rev. 121 (14), 8868−8925.

Xuan, J., Xiao, W.J., 2012. Visible-light photoredox catalysis. Angew. Chem. Int. Ed. 51, 6828−6838.

Yam, V.W.-W., Choi, S.W.-K., Lo, K.K.-W., Dung, W.-F., Kong, R.Y.-C., 1994. Photolytic cleavage of DNA by $[Au3(dmmp)2]^{3+}$. J. Chem. Soc., Chem. Commun. 20, 2379−2380.

Yam, V.W.-W., Au, V.K.-M., Leung, S.Y.-L., 2015. Light-emitting self-assembled materials based on d^8 and d10 transition metal complexes. Chem. Rev. 115, 7589−7728.

Yersin, H., Vogler, A. (Eds.), 1987. Photochemistry and Photophysics of Coordination Compounds. Springer, Berlin, Heidelberg.

Yersin, H., Czerwieniec, R., Shafikov, M.Z., Suleymanova, A.F., Shafikov, M.Z., Suleymanova, A.F., 2017. TADF material design: photophysical background and case studies focusing on Cu(I) and Ag(I) complexes. Chem. Phys. Chem. 18, 3508−3535.

Yoon, T.P., Ischay, M.A., Du, J., 2010. Visible light photocatalysis as a greener approach to photochemical synthesis. Nat. Chem. 2, 527−532.

Yoshida, M., Yanagida, S., Saito, D., Kobayashi, A., Kato, M., 2020. Aromatic versus aliphatic α-diimine ligands in heteroleptic copper(I) emitters: photophysical and electrochemical properties. Anal. Sci. 36, 67−73.

Yu, Z.-T., Liu, X.-L., Yuan, Y.-J., Li, Y.-H., Chen, G.-H., Zou, Z.-G., 2016. Evaluation of bis-cyclometalated alkynylgold(III) sensitizers for water photo reduction to hydrogen. Dalton Trans. 45, 17223−17232.

Yum, J.-H., Chen, P., Gratzel, M., Nazeruddin, M.K., 2008. Recent developments in solid-state dye-sensitized solar cells. Chem. Sus. Chem. 1, 699−707.

Zeitler, K., 2009. Photoredox catalysis with visible light. Angew. Chem. Int. Ed. 48, 9785−9789.

Zhang, Y., Schulz, M., Waechtler, M., Karnahl, M., Dietzek, B., 2018. Heteroleptic diimine-diphosphine Cu(I) complexes as an alternative towards noble-metal based photosensitizers: design strategies, photophysical properties and perspective applications. Coord. Chem. Rev. 356, 127−146.

Zheng, J., Lu, Z., Wu, K., Ning, G.-H., Li, D., 2020. Coinage-metal-based cyclic trinuclear complexes with metal−metal interactions: theories to experiments and structures to functions. Chem. Rev. 120, 9675−9742.

Zhong, M., Pannecoucke, X., Jubault, P., Poisson, T., 2020. Recent advances in photocatalyzed reactions using well-defined copper(I) complexes. Beilstein J. Org. Chem. 16, 451−481.

Chapter 11

Coordination compounds of lanthanides

Jean-Claude G. Bünzli
Institute of Chemical Sciences & Engineering, Swiss Federal Institute of Technology, Lausanne (EPFL), Switzerland and Department of Chemistry, Baptist University, Hong Kong S.A.R., People's Republic of China

11.1 The elements and their coordination chemistry

11.1.1 Lanthanides and rare earths (Bünzli and McGill, 2000)

Lanthanides (Ln) are a series of 15 metallic elements with atomic numbers 57 (La) to 71 (Lu) belonging to the group of rare earth elements (RE = Sc, Y, Ln). According to IUPAC nomenclature rules, they should be named "lanthanoids" but "lanthanides" (corresponding in principle to Ce−Lu) is still the most used designation for these silvery metallic elements and their compounds. Another name for lanthanides is 4f-elements since the series Ce−Lu corresponds to the progressive filling of the 4f orbitals. In the short form of the periodic table of elements, La is positioned in column 3 (Sc, Y, La, Ac) with Ce−Lu listed separately below for the sake of saving space. In the long form of the periodic table, Ln elements (group 3) are inserted between Ba (56, group 2) and Hf (72, group 4) with Sc, Y, and Lu forming a column to the left of Ti, Zr, and Hf (Fig. 11.1). This arrangement agrees better with the electronic and chemical properties of the corresponding elements.

The denomination "rare earths" is a bit abusive, since the abundance of some RE elements is larger than several other technological metals, such as silver or indium, and comparable to that of lead, for instance. The least abundant rare earth is radioactive promethium that is only found as traces in some uranium ores; the natural abundances of the other 4f elements in the earth crust span a large range, from 0.5 ppm for lutetium to 60 ppm for the most abundant, cerium. The term "rare earths" stems from the fact that while the RE content in specific minerals is relatively large (35−75 wt%), these minerals are rather dispersed into the rocks or sands, in which they are found. In addition, each RE mineral contains several elements, sometimes even the entire RE series, which necessitates lengthy separation processes. Resources

Photochemistry and Photophysics of Coordination Compounds. https://doi.org/10.1016/B978-0-12-824493-7.00011-3
Copyright © 2023 Elsevier Inc. All rights reserved.

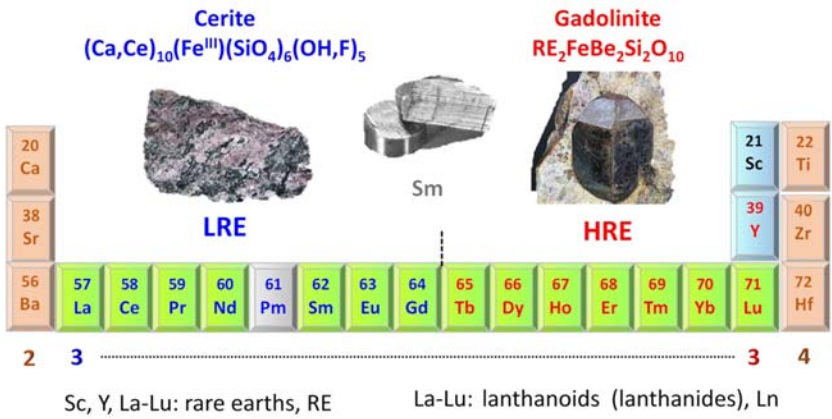

FIG. 11.1 Position of the rare earths and lanthanides in the long form of the periodic table. LRE stands for lighter rare earths and HRE for heavier rare earths. Inserts show two historically important minerals containing LRE (cerite) and HRE (gadolinite) as well as the silvery aspect of metallic samarium.

are found in many places around the world in Europe, Asia, Australia, North and South Americas. Remarkably, the total production of RE represents only a tiny fraction of all the metals produced worldwide, about 0.01%. In 2020, 243,000 tons of equivalent RE oxides were officially produced, of which about 58% was by China. Presently known rare earth reserves are large enough to cover more than 400 years of production at the current rate of extraction. Recycling is not yet substantial (a few % only), but will gain momentum, particularly for magnets which represent 20%−30% of the used RE tonnage. The main applications of rare earths are in catalysis, magnets, polishing powders and optical materials. As a matter of fact, rare-earth elements are presently providing irreplaceable functionalities in a wealth of daily-usage and high-technology items. Although essential elements, they often enter in minute quantities in a given commodity, e.g., about 200 mg in a smart phone.

11.1.2 Electronic configuration and oxidation numbers (Bünzli, 2020)

The most stable oxidation number of lanthanides is +3, with electronic configurations $[Xe]4f^n$ ($n = 0-14$), but oxidation number +2 exists for all lanthanides as well (except for radioactive and short-lived Pm), at least under the form of organometallic complexes. In the latter, two different electronic configurations have been evidenced, $[Xe]4f^n$ (Nd, Sm, Eu, Dy, Tm, Yb) and $[Xe]4f^{n-1}5\,d^1$ (La, Pr, Gd, Ho, Er, Lu) while Ce and Tb are borderline between the two configurations (MacDonald et al., 2013). In addition, cerium has also a quite stable +4 oxidation state with configuration [Xe] while this state is far

less reachable for the other ions except, until recently, in some praseodymium and terbium inorganic compounds; indeed, coordination chemistry of Pr^{IV} and Tb^{IV} is now starting to develop and might open unexpected perspectives in lanthanide chemistry and photophysics (Gompa et al., 2020).

A major feature of lanthanides is the shielding of the 4f orbitals by the $5s^25p^6$ subshells, which confers them an inner rather than a valence character. This, in turn, determines their unique chemical, magnetic and optical properties that are at the heart of so many practical applications. Indeed, lanthanide compounds have gradually become indispensable functional materials in a wealth of devices, ranging from cracking catalysts to high coercivity magnets and luminescent optical bioprobes. In this chapter, focus is put on the design and optimization of lanthanide luminescent coordination compounds.

11.1.3 Coordination chemistry (Bünzli, 2014)

Compared to d-transition elements, the coordination chemistry of RE elements had a slow start. Indeed these elements were long considered as minor by inorganic chemists. In water, their main oxidation number is +3 for the entire series and the shielding of the 4f subshell leads to similar chemical properties so that until the 1970s their coordination chemistry was thought to be uninteresting. But soon after, major developments in biosciences, namely the advent of Gd^{III}-based contrast agents for magnetic resonance imaging (MRI) and of chelates for time-resolved luminescent immunoassays considerably overturned this opinion. The advent of macrocyclic and supramolecular chemistry, as well as single molecule magnets, considerably contributed to increased interest for rare-earth chelates.

Several key factors govern RE coordination chemistry, particularly when considering $4f^n$ trivalent ions.

11.1.3.1 The ionic radius

The ions are large with radii of the order 100−120 pm that decrease more or less monotonically along the series, a consequence of increasing electronic density. This leads to the well-known "lanthanide contraction" but the overall contraction from La^{III} to Lu^{III} is only about 18 pm. Nevertheless, when ligands have small denticity, a coordination number change can occur along the series, usually around the middle of it.

11.1.3.2 The nature of the Ln-ligand chemical bond

Given the shielding of the $4f^n$ configuration, the chemical bonds are either ionic or of ion-dipole nature. Covalency is very small, usually in the range 3% −5% only. As a consequence, these bonds are non-directional and variable coordination numbers, ranging between 3 and 12 in the solid state, and coordination environments can be achieved by judicious choice of the ligands.

The types of complexes formed are commonly uniform along the series and their stability usually increases gradually with increasing atomic numbers; this is at clear variance with transition metal complexes, where covalent forces and ligand-field stabilization energies cause significant variations. In RE compounds, ligand-field splitting is the order of 100–500 cm^{-1} (1.2–6 kJ mol^{-1}) while it reaches 15′000 to 25′000 cm^{-1} (180–300 kJ mol^{-1}) for d-transition metal ions.

11.1.3.3 Hydration and chelate effect

The bonds between water and RE^{III} ions are very stable so that when complexing these ions in water the enthalpy change resulting from the replacement of H_2O with a ligand is often positive; as a consequence, complexes have to be entropy stabilized. In other terms, stable complexes usually require multidentate ligands (chelating agents), as illustrated by the stability constants of 1:1 complexes with acetates going up from $\log K \sim 2$ for simple acetate (denticity 2) to $\log K \sim 15–20$ for ethylenediaminetetraacetate ($edta^{4-}$, denticity 6). To avoid water competition, complexes with weak donors are preferentially synthesized in aprotic solvents.

11.1.3.4 Lability

Ligand exchange kinetics is very rapid with small-denticity ligands. For instance, water exchange rate is around $10^8–10^9$ s^{-1}. This leads to mixtures of differently coordinated complexes in solution and overall fractional coordination numbers. In water, the coordination number varies from 9 for La^{III} to 8 for Lu^{III}, with most of the change occurring in the middle of the series. The exchange rate strongly decreases with polydentate ligands: for an aminopolycarboxylate such as $[Lu(dtpa)]^{-2}$, k_{ex} is on the order of $\sim 10^{-1}$ s^{-1} ($dtpa^{5-}$ is diethylenetriaminepentaacetate, denticity 8), and it decreases further to $\sim 10^{-4}$ s^{-1} for the macrocyclic complex $[Lu(dota)]^-$ ($dota^{4-}$ is 1,4,7,10-tetraazacyclododecane-1,4,7,10-tetraacetate, denticity 8).

The coordination chemistry of RE^{III} ions is therefore subtle with steric effect having a predominant role so that these ions can be accommodated in many different environments. They preferentially bind to hard donor atoms, typically oxygen atoms or to the more polarizable nitrogen atoms. Classical ligands are carboxylates, aminopolycarboxylates, β-diketonates, and Schiff bases. Macrocyclic ligands such as crown ethers, aza-crown ethers, cryptands, calixarenes, porphyrins, or phthalocyanines have produced a wealth of quite stable and useful compounds in which the RE ions are encapsulated (Bünzli, 2003). As an extension to these classes of ligands, small macrocycles, e.g., tetraazacyclododecane (cyclen) or triazacyclononane, fitted with coordinating pendant arms have been extensively used to synthesise both stable and inert complexes. Moreover, self-assembly of carefully tailored ligands with RE ions allows the chemists to program specific functions into polynuclear

supramolecular structures such as helicates or polyhedral cages (Piguet and Bünzli, 2010). Finally, more extended structures are found in functional coordination polymers, in which the unique chemical, luminescent, and magnetic properties of RE ions can be exploited for various purposes.

11.2 Lanthanide luminescence (Bünzli and Eliseeva, 2011; Bünzli, 2015)

11.2.1 Energy levels

The electronic configuration of most lanthanide ions, $4f^n$, is usually well separated from the first excited configuration, $4f^{n-1}5\,d^1$, but, depending on the ion, the latter configuration can nevertheless play a role and lead to interesting spectroscopic applications. These two configurations generate an amazing number of electronic levels. Indeed, there are 7 f-orbitals and 5 d-orbitals so that there exist numerous ways of associating the n valence electrons with these orbitals, taking their spin into account. Each of these ways corresponds to a *microstate* $|\,(m_l\ m_s)_1\ (m_l\ m_s)_2\ \ldots.(m_l\ m_s)_n >$ where m_l values are the projections of the angular momentum of the electron ($\ell = 2$ and 3 for d- and f-orbitals, respectively) and m_s values are the projection of the spin moment ($s = \pm\ ^1/_2$); the number of microstates is called the *degeneracy* (or *multiplicity*) of the configuration. The degeneracy of a homogeneous configuration (e.g., $4f^n$) can be calculated from the following equation:

$$D_{4f^n} = \frac{(4\ell + 2)!}{n!(4\ell + 2 - n)!} = \frac{14!}{n!(14 - n)!} \tag{11.1}$$

A simple procedure for determining the various electronic levels is as follows (Fig. 11.2, top): (i) Interelectronic repulsion splits the configuration into *spectroscopic terms* $^{(2S\ +\ 1)}\Gamma$ defined by two quantum numbers, S (total spin momentum) and L (total angular momentum); $S = {}^1/_2$ times the number of unpaired electrons and Γ is a letter corresponding to L = 0 (S), 1 (P), 2 (D), 3 (F), 4 (G), 5 (H), and so on The quantities (2S + 1) and (2L + 1) are the spin and angular degeneracies, respectively, the overall degeneracy of a term being (2S + 1) × (2L + 1). (ii) Each term is then split by the spin-orbit interaction; Russel-Saunders scheme is commonly used for the sake of simplicity although the intermediate coupling scheme is more accurate for lanthanides. This interaction results in *spectroscopic levels* defined by an additional quantum number J (total angular momentum). The levels are denoted $^{(2S+1)}\Gamma_J$, with J = L + S, L + S −1, …. down to L - S and the degeneracy of each level is (2J + 1). (iii) Finally, each ^SL_J level is further split by the electric field generated by the surrounding ligands (*ligand-field splitting*, LF); the number of LF (or Stark) *sub-levels* depends on the symmetry around the lanthanide ion and the sub-levels are labeled according to their irreducible representations in group theory. An example is given for $Eu^{III}(4f^6)$ in an octahedral environment

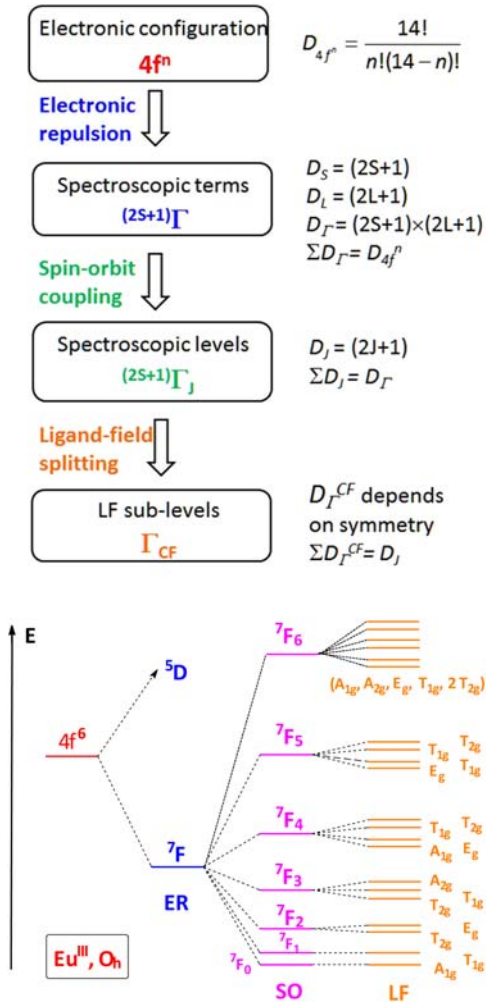

FIG. 11.2 (Top) flow chart for the determination of electronic sublevels of a $4f^n$ electronic configuration; *D* is the degeneracy (number of microstates). (Bottom) schematic representation of the splitting of the $Eu^{III}(4f^6)$ electronic configuration due to electron repulsion (ER, blue [dark black in print version]), spin-orbit coupling (SO green [light gray in print version]) and ligand field (LF orange [light black in print version]). Levels are not drawn to scale; approximate experimental energy differences are 2×10^4 cm^{-1} for ^5D-^7F, 5×10^3 cm^{-1} for $^7F_6$—$^7F_0$, and 3-5 $\times 10^2$ cm^{-1} for LF splitting.

in Fig. 11.2 (bottom) while the numbers of LF sub-levels for different point groups of symmetry versus the value of the J-quantum number are listed in Table 11.1. LF effects in lanthanide ions can be rationalized in terms of LF parameters, the number of which depends on symmetry (Görller-Walrand and Binnemans, 1996).

TABLE 11.1 Number of ligand-field sub-levels versus the value of quantum number J and the point group of symmetry.

		Integer J								
Symmetry	**Site symmetry**	**0**	**1**	**2**	**3**	**4**	**5**	**6**	**7**	**8**
Cubic	T, T_d, T_h, O, O_h	1	1	2	3	4	4	6	6	7
Hexagonal	C_{3h}, D_{3h}, C_6, C_{6h}, C_{6v}, D_6, D_{6h}	1	2	3	5	6	7	9	10	11
Trigonal	C_3, S_6, C_{3v}, D_3, D_{3d}									
Tetragonal	C_4, S_4, C_{4h}, C_{4v}, D_4, D_{2d}, D_{4h}	1	2	4	5	7	8	10	11	13
Low	C_1, C_S, C_2, C_{2h}, C_{2v}, D_2, D_{2h}	1	3	5	7	9	11	13	15	17
Symmetry	Site symmetry	Half-integer J								
		1/2	3/2	5/2	7/2	9/2	11/2	13/2	15/2	17/2
Cubic	T, T_d, T_h, O, O_h	1	1	2	3	3	4	5	6	6
All others[a]	(see above)	1	2	3	4	5	6	7	8	9

[a] *All LF sub-levels are doubly degenerate (Kramer's doublets); this degeneracy can only be lifted in a magnetic field.*

For instance, Ce^{III} has only 2 spectroscopic levels, $^2F_{5/2}$ (ground state) and $^2F_{7/2}$ (excited state), and each split into a maximum of 3 and 4 sublevels, respectively, but Eu^{III} features 119 spectroscopic terms and 295 spectroscopic levels that in total can generate up to 3003 ligand-field sub-levels in a non-symmetric C_1 environment. Altogether the number of electronic levels for the Ce−Yb series is 16,384 for the $4f^n$ configurations and 180,199 for the $4f^{n-1}5\,d^1$ configurations. The two configurations only overlap substantially above 50,000 cm^{-1} ($\lambda < 200$ nm) (Fig. 11.3). This ladder-like structure of electronic levels makes lanthanide ions beautifully adequate for many photonic applications, including wavelength converting materials.

Finally, the ground spectroscopic SLJ level is readily determined using Hund's rules in sequence; it corresponds to:

Rule 1 The largest spin multiplicity.
Rule 2 The largest orbital multiplicity.
Rule 3 If $n < (2\ell + 1)$, $J = J_{min}$; if $n > (2\ell + 1)$, $J = J_{max}$; if $n = (2\ell + 1)$, $J = S$.

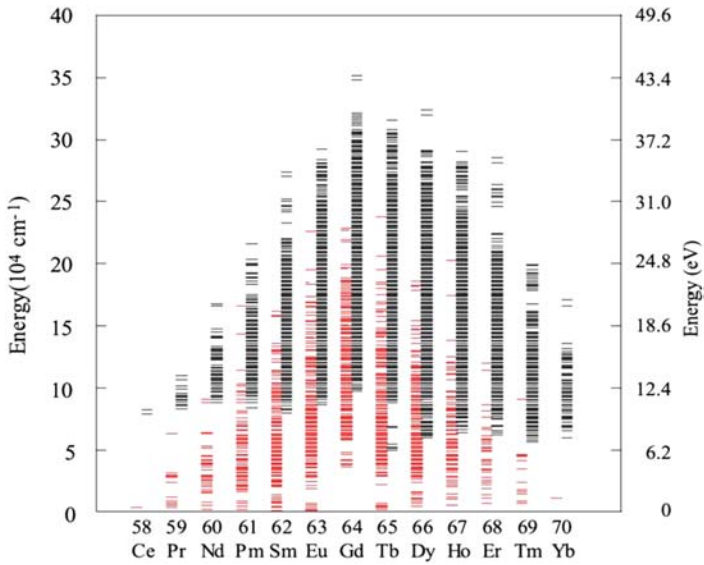

FIG. 11.3 Calculated energy diagram for all $4f^n$ (left, red [dark black in print version]) and $4f^{n-1}5\,d^1$ (right, black) electronic configurations of trivalent lanthanide ions. Ligand-field splitting is not taken into account. Note that for the right scale, 1 eV corresponds to 8066 cm^{-1}. *Adapted from Ogasawara, K., Watanabe, S., Toyoshima, H., Brik, M.G., 2007. First-principles calculations of 4f-4f5d transition spectra, in: Gschneidner Jr., K.A., Bünzli, J.C.G., and Pecharsky, V.K., Handbook on the Physics and Chemistry of Rare Earths, Elsevier Science B.V., Amsterdam, vol. 37, Ch. 231, pp.1−59.*

As examples, $Eu^{III}(4f^6)$ has ground state $^7F_0$ ($S = 3$, $L = 3$, $J = 0$) and $Tb^{III}(4f^8)^7$ has F_6 ($S = 3$, $L = 3$, $J = 6$), while Gd^{III} ground state corresponds to $^8S_{7/2}$. There is a relationship between the configurations $4f^n$ and $4f^{14-n}$ in that they have the same S and L quantum numbers, but the SO multiplet is regular for $4f^n$ with energy of the levels increasing with increasing J while it is inverted for $4f^{14-n}$ the energy of the levels increasing with decreasing J number.

11.2.2 Electronic transitions

Electronic transitions correspond to the rearrangement of electrons in the electronic configuration upon absorption or emission of light. Any rearrangement (i.e., transition) is not allowed. Transitions must obey *selection rules* that depend on the mechanism of absorption/emission. Since light is comprised of two perpendicularly oscillating electric and magnetic fields, each of them interact with corresponding dipoles in the electronic configuration leading to electric (ED) or magnetic (MD) dipole transitions.

The probability that a given transition occurs is defined by its *oscillator strength*. This is a positive dimensionless quantity ≤ 1 representing the ratio between the quantum mechanical transition rate and the classical absorption/emission rate of a single electron oscillating with the same frequency as the transition. Alternatively, the *dipole strength* can be used; for ED transitions, it is proportional to the square of the electric dipole and its unit is D^2cm^2 (D is the debye unit). Roughly speaking ED transitions are 10^2- to 10^3-fold more intense than MD transitions. More complex interactions such as quadrupolar ones also promote transitions, but their efficiency is much smaller ($\sim 10^4$ smaller than MD transitions) so that they are rarely observed or reported with an acceptable level of confidence.

11.2.2.1 Selection rules

Selection rules have been derived for pure electronic functions. In their hierarchy, the first one to be taken into account is the parity (or Laporte's) rule stating that an ED transition cannot occur between two levels of same parity. This obviously makes ED f-f transitions forbidden (similarly to ED d-d transitions). However, under the influence of the ligand field, of vibrations, and of the J-mixing, wave functions with opposite parity mix with the f-orbitals; therefore partially relaxing the selection rules derived for pure electronic functions. The corresponding transitions are called *forced ED transitions* (fED). Some of the fED transitions are particularly sensitive to minute changes in the Ln^{III} environment; they are labeled as *hypersensitive transitions* and are very useful to investigate changes in the coordination

sphere of the metal ion and/or in analytical chemistry. Anyhow, the oscillator strengths of the forced ED transitions remain small, with corresponding molar absorption coefficients not exceeding $12-15\ M^{-1}cm^{-1}$ (except for some hypersensitive transitions), and more usually in the range $0.1-1\ M^{-1}cm^{-1}$. On the other hand, MD f-f transitions are allowed by Laporte's rule; but they are quite weak. Depending on the symmetry, they can nonetheless have oscillator strengths on the same order of magnitude than forbidden ED transitions, so that both are commonly observed in f-f absorption and emission spectra. There are however few purely MD transitions, $Eu^{III}(^5D_0 \leftrightarrow {}^7F_1)$ being a typical example, and many transitions have a mixed ED/MD character making detailed interpretation of spectra sometimes difficult.

The second rule deals with the spin that should be kept constant during the transition ($\Delta S = 0$); it is valid for both ED and MD transitions. Other rules are concerned with changes in angular momentum (ΔL) and total momentum (ΔJ). Finally, the selection rules governing transitions between LF sublevels are more involved in that they depend on the symmetry around the emitting ion; they can be worked out using group-theoretical considerations. Selection rules are summarized in Table 11.2 along with the ground electronic configuration of the $4f^n$ ions and the numbers of electronic (^SL_J) levels and LF sublevels in C_1 symmetry.

Selection rules are the same for absorption and emission transitions.

11.2.2.2 Types of transitions

The following transitions can be observed in lanthanide-containing compounds. They are of vastly different intensities and often overlap with ligand-centered transitions.

- **Allowed interconfigurational $4f^n \leftrightarrow 4f^{n-1}5d^1$ transitions**

The promotion of a 4f electron into the 5d sub-shell is parity allowed. However the spin rule has to be taken into consideration so that only spin-allowed $4f^n \leftrightarrow 4f^{n-1}5\ d^1$ transitions have sizable intensity. The energy of these transitions depends largely on the metal environment since the 5d orbitals are external and interact directly with the ligand orbitals. As a consequence, they are also broader. The 4f-5d transitions have usually high energies (Fig. 11.4) so that only those of Ce^{III}, Pr^{III}, Sm^{II}, Eu^{II}, and Tb^{III} are commonly observed. It is noteworthy that in coordination compounds, they are often obscured by transitions involving ligands. The absorption spectrum of the $[Ce(H_2O)_9]^{3+}$ aqua ion is displayed in Fig. 11.5 along with the ligand-field splitting of both the $4f^1(^2F_{5/2}, {}^2F_{7/2})$ and $5\ d^1(^2D_{3/2}, {}^2D_{5/2})$ electronic configurations in D_{3h} symmetry. The absorption coefficients are of the order $10^2-10^3\ M^{-1}cm^{-1}$ owing to the allowed nature of the transitions both with respect

TABLE 11.2 (Left) Numbers of f-electrons (n), $^{S}L_J$ levels (N_{SLJ}), and ligand-field sublevels (N_{CF}) in C_1 symmetry, as well as ground electronic levels $^{(2S+1)}\Gamma_J$ for trivalent lanthanide ions; (right) selection rules for d-f and f-f transitions.

Ln^{III}	n	N_{SLJ}	$^{(2S+1)}\Gamma_J$	N_{CF}[a]	Main selection rules	
La	0	1	$^1S_0$	1	All transitions	
Ce	1	2	$^2F_{5/2}$	14	Laporte	$\Delta\ell \neq 0$
Pr	2	13	$^3H_4$	91	Spin	$\Delta S = 0$
Nd	3	41	$^4I_{9/2}$	364	**Electric dipole**	
Pm	4	107	$^5I_4$	1001	d-f transition	$\lvert\Delta L\rvert \leq 1$, $\lvert\Delta J\rvert \leq 1$
Sm	5	198	$^6H_{5/2}$	2002	f-f transition	$\lvert\Delta L\rvert \leq 6$, $\lvert\Delta J\rvert \leq 6$ 2, 4, 6, if L (or L′) or J (or J′) = 0 0-0 forbidden
Eu	6	295	$^7F_0$	3003		
Gd	7	327	$^8S_{7/2}$	3432		
Tb	8	295	$^7F_6$	3003	**Magnetic dipole**	
Dy	9	198	$^6H_{15/2}$	2002	f-f transition	$\lvert\Delta L\rvert = 0$, $\lvert\Delta J\rvert = 0, \pm 1$
Ho	10	107	$^5I_8$	1001	**Symmetry**	$\Gamma_{op} \in \Gamma_i \times \Gamma_f$ where Γs are group-theoretical irreducible representations of the operator and of the initial and final wavefunctions
Er	11	41	$^4I_{15/2}$	364		
Tm	12	13	$^3H_6$	91		
Yb	13	2	$^2F_{7/2}$	14		
Lu	14	1	$^1S_0$	1		

[a]*For $J = 1/2$ integer, there are $N_{CF}/2 = J + 1/2$ doubly degenerate sub-levels (Kramer's doublet) that can only be split by magnetic fields.*

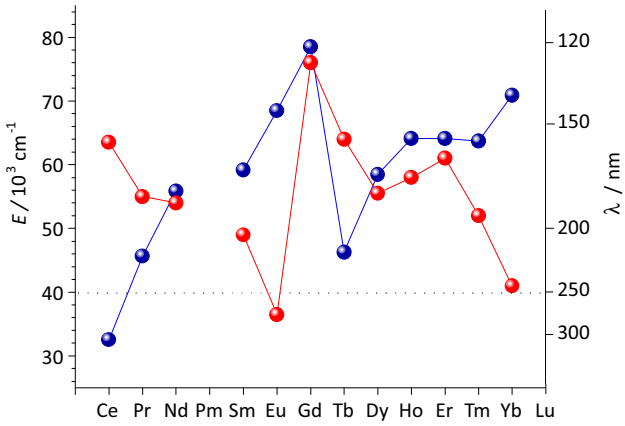

FIG. 11.4 Experimental energies of the first spin-allowed f → d transitions of Ln^{III} ions doped in CaF_2 (blue balls [dark black in print version]) and calculated energies of the O(2p)-to-Ln^{III} charge transfers (red balls [light gray in print version]). Note that in other matrix/complexes, ligand-field effects can extend the energy of the d-f transitions down toward the visible range (especially for Ce^{III}, Pr^{III}, and Tb^{III}). *Data from Dorenbos, P., 2000. The 4f to 4f5d transitions of the trivalent lanthanides in halogenides and chalcogenides. J. Lumin. 91, 91–106; Kano, T., 1999. Principal phosphor materials and their optical properties: luminescence centers of rare-earth ions, in: Shionoya, S., Yen, W.M. (Eds), Phosphor Handbook, CRC Press Inc., Boca Raton, 1999, vol. 3 (3), 177–200.*

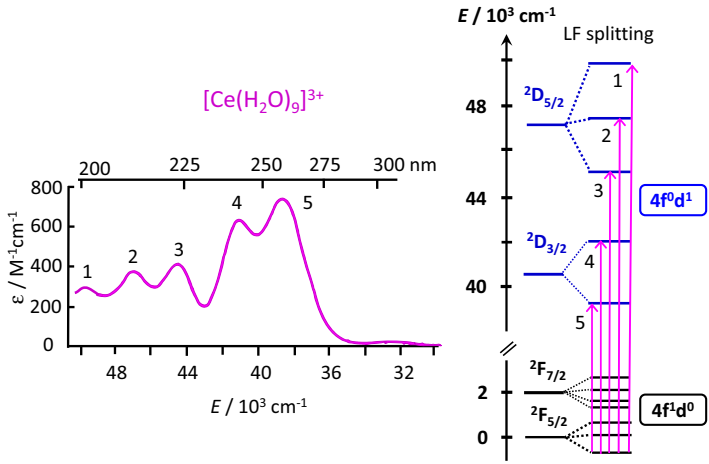

FIG. 11.5 Absorption spectrum of the Ce^{III} aqua ion with its interpretation in terms of $4f^1/5\,d^1$ electronic configurations. *Redrawn from Jørgensen, C.K., Brinen, J.S., 1963. Far UV absorption spectra of cerium(III) and europium(III) aqua ions. Mol. Phys. 6, 629–631.*

to Laporte's and spin rules. The ligand-field splittings of the $^2D_{3/2}$ and $^2D_{5/2}$ levels are approximately 3000 and 5500 cm^{-1}, respectively. Depending on the matrix or coordination compound into which Ce^{III} is inserted, its d-f emission can be tuned from about 290 to 500 nm because of large ligand-field effects on

the 5 d^1 excited configuration. The d-f emission of divalent lanthanide ions such as Eu^{II} or Sm^{II} can be even tuned into the red or the beginning of the near infrared and are useful in the design of light-emitting diodes (LEDs) (Qin et al., 2017).

- **Charge-transfer transitions**
  Charge transfer transitions are essential in sensitizing the luminescence of lanthanide-containing inorganic phosphors, but they can be totally detrimental in other instances, quenching light emission completely if the overlap with 4f-states is large (see Section 3.2). Three main types of charge transfer transitions may be present.
- **Ligand-to-metal charge transfers (LMCT):** During the process, an electron is transferred from the surrounding to the metal ion. As for the 4f-5d transitions, the corresponding energies are usually large, so that the transitions are often observed in the UV spectral range. The lowest energies occur for the easily reducible ions, namely Sm^{III}, Eu^{III}, Tm^{III}, and Yb^{III} as shown in Fig. 11.4 that displays calculated $2p(O) \rightarrow Ln$ transitions. Note that in this particular case, the transition is in principle forbidden since 2p and 4f orbitals have the same parity. The LMCT energies depend largely on the Ln^{III} surroundings and in complexes, covalent contributions to the bonding by organic ligands considerably lowers them, down to the range 18−25 000 cm^{-1} for Eu^{III}. In addition, the energy can be modulated by substitution at the coordinating ligands. Mixing of LMCT and 4f states leads to enhanced forced electric dipole f-f transitions. As an example, in the dinuclear complex with *p-t*-butyl-calix[8]arene H_8L, $[Eu_2(H_2L)(DMF)_5]$, such a state is located at 400 nm ($\varepsilon = 720\ M^{-1}cm^{-1}$) and the corresponding absorption band extends up to about 600 nm; as a consequence of the LMCT/4f-orbitals mixing, the very weak and highly forbidden $Eu^{III}(^5D_0 \leftarrow {}^7F_0)$ absorption band is enhanced by a factor ~5000, reaching $\varepsilon = 5\ M^{-1}cm^{-1}$, compared to $\varepsilon = 10^{-3}\ M^{-1}cm^{-1}$ for the aqua ion (Bünzli et al., 1993); this phenomenon is called *intensity stealing*.
- **Metal-to-ligand charge transfers (MLCT):** Commonly observed with d-transition metal ions, MLCT are very rarely identified in spectra of lanthanide complexes since +4 oxidation states are difficult to stabilize, except for Ce^{III}, which is easily oxidized into Ce^{IV}. The new chemistry of Pr^{IV} and Tb^{IV} that is presently developing might reveal more of these transitions (Rice et al., 2019; Gompa, 2020; Willauer et al., 2020).
- **Ligand-centered charge transfers:** If the ligand has polarized electronic distribution (e.g., in so-called push-pull ligands), then charge transfer can occur internally. The states are referred to as intraligand CTs (ILCTs) or intramolecular CTs (ICTs); sometimes more precision is added to point to the origin of the polarization, such as twisted intraligand CT (TICT). Such states are ideal for sensitizing lanthanide luminescence in view of their

large absorption and, often, of their relatively low energy; moreover substituent modification enables easy tuning of the ILCT energy.

In some heterometallic nd-4f polynuclear molecular edifices, singlet or triplet MLCT, LMCT, or MMCT (metal-to-metal CT) states linked to the d-transition metal may also act as convenient donors for transferring energy on the Ln excited states.

- **Intraconfigurational f↔f transitions**

Owing to the screening of the f-orbitals, these transitions are quite sharp with fwhh (full width at half height) usually in the range $0.1-30\ cm^{-1}$ only. Another consequence is their extremely small Stokes' shifts (energy difference between absorption and emission maxima), reaching only a few cm^{-1}. Their intensity is faint with oscillator strengths in the range of $10^{-4}-10^{-5}$ for spin-allowed fED transitions and $10^{-5}-10^{-6}$ for spin-allowed MD transitions. Spin-forbidden transitions are about 10−100 times less intense. Oscillator strengths of vibronic transitions, often associated with fED transitions, are in the range $10^{-7}-10^{-10}$ while those for electric quadrupole transitions are $\sim 10^{-10}$. As a comparison, the oscillator strengths of allowed f-d transitions range between 10^{-2} and almost 1.

Some characteristic features of f↔f transitions are exemplified in Fig. 11.6A and C along with an example of d-f emission spectrum for comparison (Fig. 11.6B). The tris(dipicolinate) complex $Cs_3[Eu(dpa)_3]$ in water has narrow absorption bands and small molar absorption coefficients ($<5\ M^{-1}cm^{-1}$), typical of an f-f spectrum. The emission spectrum of the neutral dinuclear helicate $[Eu_2L_3]$ in solid state at low temperature shows well resolved ligand-field splitting of the SLJ levels and points to how this splitting can be used to determine the symmetry of the coordination environment of the emitting ion; here, it is close to D_3 (refer to Table 11.1 for the number of expected components for each value of J) as indicated by the small splitting of the $^5D_0 \rightarrow {}^7F_1$ transition into two main components; since the E component is further split, this means that there is a deviation from D_3. Analysis of the transition to $^7F_2$ is more difficult because it contains some weak vibronic components. Note that the intensity of this fED transition is the same as that of the allowed MD transition to $^7F_1$. The d-f emission spectrum of the YAG:Ce^{III} (YAG is for yttrium aluminum garnet $Y_3Al_5O_{12}$) yellow phosphor is shown for comparison in (b); the broad band has fwhh $\sim$100 nm and features a maximum at 530 nm and a shoulder around 565 nm; referring to Fig. 11.5 (right), the labels of these two components would be $^2D_{3/2}$(lowest LF sublevel) $\rightarrow {}^2F_{5/2}$ and $^2F_{7/2}$, respectively.

11.2.2.3 Modeling the intensity of f-f transitions

Historically, the forbidden nature of lanthanide ED transitions made their intensity difficult to understand until 1953 when two researchers, Judd (1962)

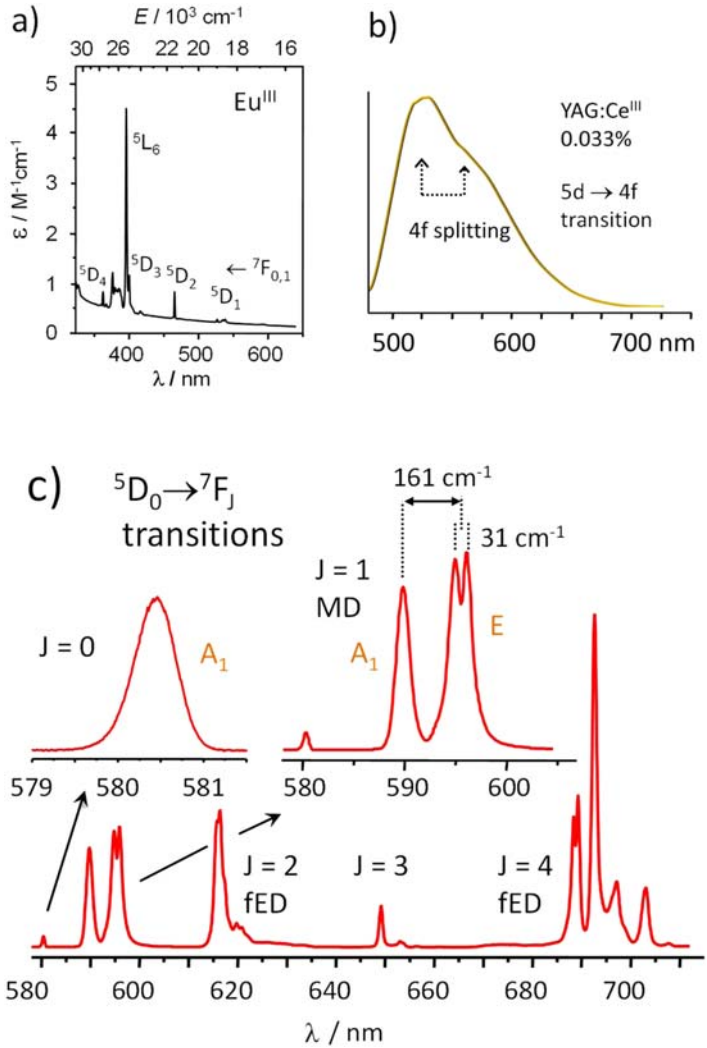

FIG. 11.6 (A) Absorption spectrum of $Cs_3[Eu(dpa)_3]$ 1.8×10^{-2} M in Tris-HCl 0.1 M (pH 7.4) at room temperature; refer to Fig. 11.2 (bottom) for the SLJ level labeling. (B) Emission spectrum of the yellow [light black in print version] phosphor used in first-generation LEDs, YAG:Ce^{III} (0.033%), in the solid state at room temperature. (C) Emission spectrum of a neutral helicate $[Eu_2L_3]$ in water/glycerol (90/10) at 10 K; orange letters are the irreducible representations of the LF-sublevels in D_3 symmetry. *Adapted from (A) Aebischer, A., Gumy, F., Bünzli, J.C.G., 2009. Intrinsic quantum yields and radiative lifetimes of lanthanide Tris(dipicolinates). Phys. Chem. Chem. Phys. 11, 1346−1353. With Permission; (B) Adapted from Bünzli, J.C.G., 2019. Lanthanide photonics: shaping the nanoworld. Trends Chem. 1, 751−762. With Permission; (C) Adapted from Bünzli, J.C.G., Chauvin, A.S., Vandevyver, C.D.B., Song, B., Comby, S., 2008. Lanthanide bimetallic helicates for in vitro imaging and sensing. An. N. Y. Acad. Sci. 1130, 97−105. With Permission.*

and Ofelt (1962), independently proposed the same theory, now known as Judd-Ofelt (JO) theory. The model has been established within the frame of the ligand-field concept and it provides a simple scheme for reproducing the intensities of f-f absorption spectra by use of three phenomenological parameters labeled Ω_2, Ω_4, and Ω_6. Spin-orbit coupling is treated by means of the intermediate coupling scheme but the model only takes into account the $4f^n$ electronic configuration, that is, inter-configurational $4f^n$-$4f^{n-1}5d^1$ interaction is neglected. It is further assumed that all LF sublevels within the ground level are equally populated, which is only true for non-degenerate electronic levels such as $Eu^{III}(^7F_0)$. Finally, the model is constructed for optically isotropic materials; it is therefore not valid for uniaxial or biaxial crystals, but, of course, holds for solutions. These hypotheses explain why sometimes JO theory does not perfectly reproduce the observed spectral intensities for some Ln^{III} ions. An outline is given below, but for more details, please refer to (Görller-Walrand and Binnemans, 1998; Bünzli, 2003; Walsh et al., 2006).

The dipole strength in esu^2cm^2 ($=10^{36}$ $debye^2$) of a fED f-f transition between an initial state $|\Psi_J\rangle$, characterized by a quantum number J, and a final state $|\Psi'_{J'}\rangle$ with quantum number J′is given by:

$$D_{ED} = e^2 \cdot \sum_{\lambda=2,4,6} \Omega_\lambda \cdot \left|\langle \Psi \| U^\lambda \| \Psi' \rangle\right|^2 \tag{11.2}$$

in which e is the electric charge of the electron, wavefunctions ψ and ψ' are full intermediate-coupled functions $f^n[SLJ]$, U^λ are components of the irreducible tensor of the ED operator, Ω_λ are the phenomenological Judd-Ofelt parameters, expressed in cm^2, and $\lambda = 2, 4, 6$. The bracketed expressions in Eq. (11.2) are dimensionless doubly-reduced matrix elements that are in principle insensitive to the metal-ion environment; they are tabulated.

JO parameters are adjustable and they are evaluated from the experimental dipole strength, in esu^2cm^2, calculated from the normalized absorption spectrum $\varepsilon\left(\widetilde{\nu}\right)$:

$$D_{exp} = \frac{10^{-36}}{108.9 \cdot \widetilde{\nu}_{mean} \cdot X_A} \cdot \left((2J+1) \cdot \frac{9n}{(n^2+2)^2}\right) \cdot \int \varepsilon\left(\widetilde{\nu}\right) d\widetilde{\nu} \tag{11.3}$$

with X_A being the fractional population of the initial state, $(2J + 1)$ is the degeneracy of the initial state and the expression involving the refractive index n is known as Lorentz's local-field correction while $\widetilde{\nu}_{mean}$, the barycentre of the transition, is given by:

$$\widetilde{\nu}_{mean} = \frac{\int \widetilde{\nu} \cdot \varepsilon\left(\widetilde{\nu}\right) d\widetilde{\nu}}{\int \varepsilon\left(\widetilde{\nu}\right) d\widetilde{\nu}} \tag{11.4}$$

It is worth noting that the oscillator strength is related to the dipole strength by the following equation:

$$P_{exp} = \frac{\widetilde{\nu}_{mean}}{2.127 \times 10^{-30}} D_{exp} = 4.32 \times 10^{-9} \cdot \int \varepsilon\left(\widetilde{\nu}\right) d\widetilde{\nu} \qquad (11.5)$$

The phenomenological JO parameters are determined from a fit of Eq. (11.2) to the experimental values defined by Eq. (11.3), using tabulated matrix elements. In the case of Eu^{III} the procedure is simpler since Ω_2, Ω_4, and Ω_6 can be directly extracted from the dipole strength of the $^5D_2 \leftarrow {}^7F_0$, $^5D_4 \leftarrow {}^7F_0$, and $^5L_6 \leftarrow {}^7F_0$ transitions, respectively. Indeed, all squared reduced matrix elements (Eq. 11.2) are zero for fED transitions originating from $^5D_0$ (or $^7F_0$) except for those involving the levels $^{(2S+1)}\Gamma_\lambda$ with $\lambda = 2, 4, 6$ and $\Gamma = D, F$ and for which the corresponding U^λ is non-zero. For instance, the parameters corresponding to the spectrum showed in Fig. 11.6A are $\Omega_2 = 10.3$, $\Omega_4 = 5.59$, and $\Omega_6 = 9.16$ in units of $10^{-20}\,cm^2$. The parameter Ω_2 is related to the polarizability (or covalency) of the Ln-ligand bonds. The JO parameters can also be calculated from excitation spectra, reflectance spectra and, for Sm^{III}, Eu^{III}, Tb^{III}, and Dy^{III} from emission spectra (Zhang et al., 2018). Extensive tabulations of JO parameters can be also found (Görller-Walrand and Binnemans, 1998).

An application, open-source, software for calculating the JO intensity parameters for Eu^{III} is now available under the name of JOES (Ciric et al., 2019). The program has a large database of refractive indices, which is crucial for calculating the spontaneous emission coefficient of the $Eu^{III}(^5D_0 \rightarrow {}^7F_1)$ MD transition used as internal reference for estimating the JO parameters.

11.2.2.4 Emission probability and radiative lifetime

The emission probability is given by Einstein's rates of spontaneous emission A (or k_{rad}) from an initial state $|\Psi_J\rangle$ to a final state $|\Psi\prime_{J\prime}\rangle$:

$$A(\Psi_J, \Psi\prime_{J\prime}) = k_{rad} = \frac{1}{\tau_{rad}} = \frac{64\pi^4\left(\widetilde{\nu}_{mean}\right)^3}{3h(2J+1)}\left[\frac{n(n^2+2)^2}{9} D_{ED} + n^3 D_{MD}\right] \qquad (11.6)$$

where τ_{rad} is the radiative lifetime of the emitting level, i.e., the lifetime in absence of non-radiative de-activation processes; h is Planck's constant (6.626×10^{-34}Js), D_{ED} is given by Eq. (11.2) and D_{MD} by Eq. (11.7), where c is the light velocity in vacuo and m_e the electron mass:

$$D_{MD} = \left(\frac{e \cdot h}{4 \cdot \pi \cdot m_e \cdot c}\right)^2 \cdot |\langle \Psi || L + 2S || \Psi\prime \rangle|^2 \qquad (11.7)$$

The radiative lifetime can therefore be extracted from the spectral intensity, that is from Eqs.(11.2), (11.6), and (11.7). Except in few cases, this calculation

is not trivial and large errors may occur, including those pertaining to the hypotheses made within Judd-Ofelt theory. Moreover, it is noteworthy that the local field correction is not the same for absorption and emission.

When the absorption spectrum corresponding to an emission spectrum is measurable, which may be the case when the luminescence transitions terminate onto the ground level, the radiative lifetime can be simply calculated from the following equation where N_A is Avogadro's number (6.023 … $\times 10^{23}$):

$$\frac{1}{\tau_{rad}} = 2303 \times \frac{8\pi c n^2 \tilde{\nu}^2 (2J+1)}{N_A (2J'+1)} \int \varepsilon\left(\tilde{\nu}\right) d\tilde{\nu} \tag{11.8}$$

In the special case of Eu^{III} for which one transition ($^5D_0 \rightarrow {}^7F_1$) has pure magnetic origin, a convenient, simplified equation can be derived (Werts et al., 2002), where $A_{MD,0}$ is the $^5D_0 \rightarrow {}^7F_1$ emission probability in vacuo and is equal to 14.65 s^{-1}, and I_{tot} and I_{MD} are integrated intensities of the entire emission spectrum and of the MD transition, respectively:

$$A(\Psi_J, \Psi\prime_{J\prime}) = \frac{1}{\tau_{rad}} = A_{MD,0} \cdot n^3 \left(\frac{I_{tot}}{I_{MD}}\right) \tag{11.9}$$

It is important to realize that the radiative lifetime depends on the refractive index, on the chemical environment of the emitting ion (bond polarizability), and on the specific emitting level. Another remark is that all the equations above are derived under specific hypotheses so that some deviations with experimental values may occur; on the other hand, it has been demonstrated that Eq. (11.8) yields a correct value of τ_{rad} is the case of Eu^{III} tris(dipicolinate) (Aebischer et al., 2009).

- **Vibronic transitions**

As indicated by their name, these transitions originate from mixing between 4f-orbitals and vibrational levels. They are mainly associated with fED transitions and have the same selection rules. Their intensity is about 10−100 times less than MD transitions and varies largely with temperature. This provides a mean of identifying them, which is crucial for not confusing them with LF transitions. Both Stokes and anti-Stokes vibronic transitions may be seen (Fig. 11.7).

11.2.3 Sensitization of lanthanide luminescence

The luminosity of a luminescent compound is characterized by its brightness B, the product of the molar absorption coefficient ε at the excitation wavelength by the quantum yield Q (Wong et al., 2020):

$$B = \varepsilon(\lambda_{exc}) \times Q \tag{11.10}$$

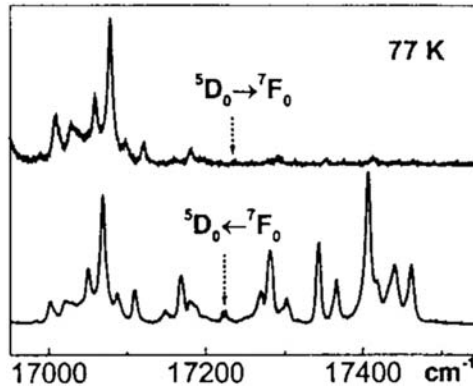

FIG. 11.7 Vibronic transitions associated with the $^5D_0 \rightarrow {}^7F_0$ and $^5D_0 \leftarrow {}^7F_0$ transitions in $NaCs_s[Eu(NO_2)_6]$ at 77 K. *Adapted from Bünzli, J.C.G., Petoud, S., Moret, E., 1999. Luminescent properties of the hexakis(nitrito)europate(III) ion, $[Eu(NO_2)_6]^{3-}$. Spectrosc. Lett. 32, 155–163. With permission.*

In the case of lanthanides, this brightness is seriously limited by the small molar absorption coefficients of f-f transitions. Fortunately, a major finding was made by Weissman (1942) who discovered that lanthanide luminescence can be triggered in molecular complexes by excitation into the ligand levels, followed by energy transfer onto the metal ion. Initial studies involved Eu^{III} β-diketonates, salicylates, phenolates, benzoates, and complexes with aldehydes. A mechanism for this *luminescence sensitization* (or *antenna effect*, Fig. 11.8) has been postulated in which the long-lived triplet state of the ligands is the principal donor state (Kleinerman, 1968). Its energy is not always easy to determine, especially if the ligand-to-Ln^{III} energy transfer is efficient. For this reason the 0-phonon component of the phosphorescent band of the Gd^{III} complex at low temperature (<77 K) is most often taken as the value to be considered. It was however soon recognized, based on the analysis of 600 Ln^{III} chelates, that the singlet state of the ligand may also play an important role in the energy transfer (Kleinerman, 1969), depending on the systems implied, particularly on the nature of the Ln^{III} ion, a fact now well established (Aquino et al., 2021).

In order to evaluate the efficiency of the sensitization process, one needs two quantum yields: Overall quantum yield Q_{ovl} obtained upon excitation into the ligand levels and the intrinsic quantum yield Q_{int} obtained by direct excitation into the f-f transitions. The sensitization efficiency is then given by (note that $Q_{int} \geq Q_{ovl}$, always!):

$$\eta_{sens} = \frac{Q_{ovl}}{Q_{int}} = Q_{ovl}\frac{\tau_{rad}}{\tau_{obs}} \tag{11.12}$$

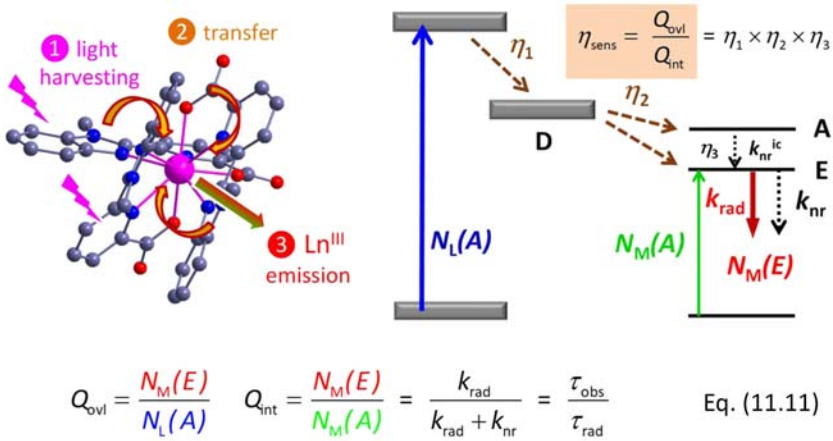

FIG. 11.8 (Left) lanthanide luminescence sensitization through the antenna effect: ① absorption by ligand, ② transfer onto Ln^{III}, and ③ Ln^{III} emission. (Right) simplistic modeling of the phenomenon: $N_X(A)$ are the numbers of photons absorbed by the ligand (X = L) or the metal ion (X = M) and $N_M(E)$ are the numbers of photons emitted; k_{rad} is the radiative rate constant, k_{nr} is the sum of non-radiative rate constants, k_{nr}^{ic} is the rate constant of internal conversion, η are efficiencies, D is the donor state, A the acceptor state and E the emissive state. Overall (Q_{ovl}) and intrinsic (Q_{int}) quantum yields are defined at the bottom (τ_{obs} is the observed lifetime of the emitting state).

An example of such an analysis is shown in Fig. 11.9 for 9-coordinate Eu^{III} complexes with pyridine-benzimidazole derivatives (Shavaleev et al., 2009a,b). The structure of all complexes has been determined by X-ray methods and the nature of their bonding analyzed by bond-valence theory. As expected from the similar coordination N_6O_3 environment, the radiative lifetime is rather constant over the series (3.9−4.6 ms) and so is the observed lifetime (∼2.5−3.0 ms), pointing to similar deactivation processes. With these data, the intrinsic quantum yield varies within narrow limits (0.53−0.67; note that uncertainty is of the order ±12%). The overall quantum yield shows somewhat larger variation (0.53−0.71, uncertainty ±10%). Except for complex 3, the sensitization efficiency is very large (0.82−1, uncertainty ±22%), pointing to very efficiency energy transfer. Therefore, if higher overall quantum yields would be needed, one would have to further minimize non-radiative deactivations. Finally, the brightness of the reported complexes is high: for complexes four to eight, for which Q_{ovl} has also be determined in CH_2Cl_2 solutions, molar absorption coefficients are in the range $5.1-6.0 \times 10^4\ M^{-1}cm^{-1}$ and Q_{ovl} are between 0.51 and 0.52, yielding brightness values in the range $2.7-3.1 \times 10^4\ M^{-1}cm^{-1}$.

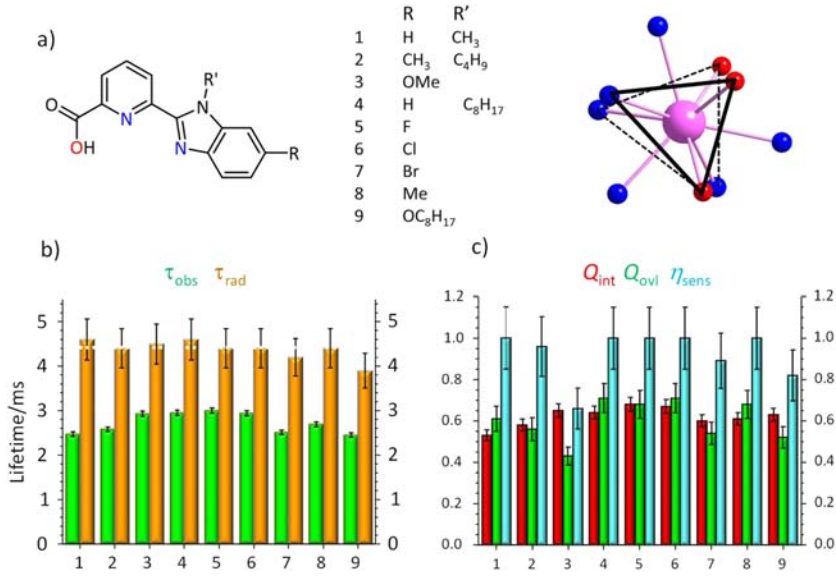

FIG. 11.9 (A) Ligand formulae for the 9-coordinate [EuL_3] neutral complexes with a sketch of the coordination polyhedron. (B) Observed and radiative lifetimes, and (C) intrinsic, overall quantum yields and sensitization efficiencies. Solid state data at room temperature from. *Adapted from Shavaleev, N.M., Eliseeva, S.V., Scopelliti, R., Bünzli, J.C.G., 2009a. Designing simple tridentate ligands for highly luminescent europium complexes. Chem. Eur J. 15, 10790–10802. With Permission.*

11.2.4 Quantitative aspects of energy transfer processes

11.2.4.1 Simplistic model

As described above, the first mechanistic explanation of the antenna effect was the triplet pathway. Energy transfer depends on the orbital overlap between the donor (D) and acceptor (A) states, on the D-A distance and on the energy difference between the two states. In a simplistic, empirical approach scientists have tried to rationalize the quantum yields of Ln^{III} chelates (mainly Ln = Eu, Tb) by looking at the energy difference between the 0-phonon component of the triplet state, E^T_0, and the Ln^{III} emitting level. Although some correlations were obtained, one has to stress here that this can only be working, when comparing chelates with similar chemical environments or, rather, with chemical environments causing similar non-radiative deactivations. This is the case for the Eu^{III} tetrakis β-diketonates thoroughly studied by Sato and Wada (Fig. 11.10A). From this study, it can be concluded that an "ideal" energy gap would be around 2500 cm^{-1} for energy transfer on $Eu^{III}(^5D_0)$; they also

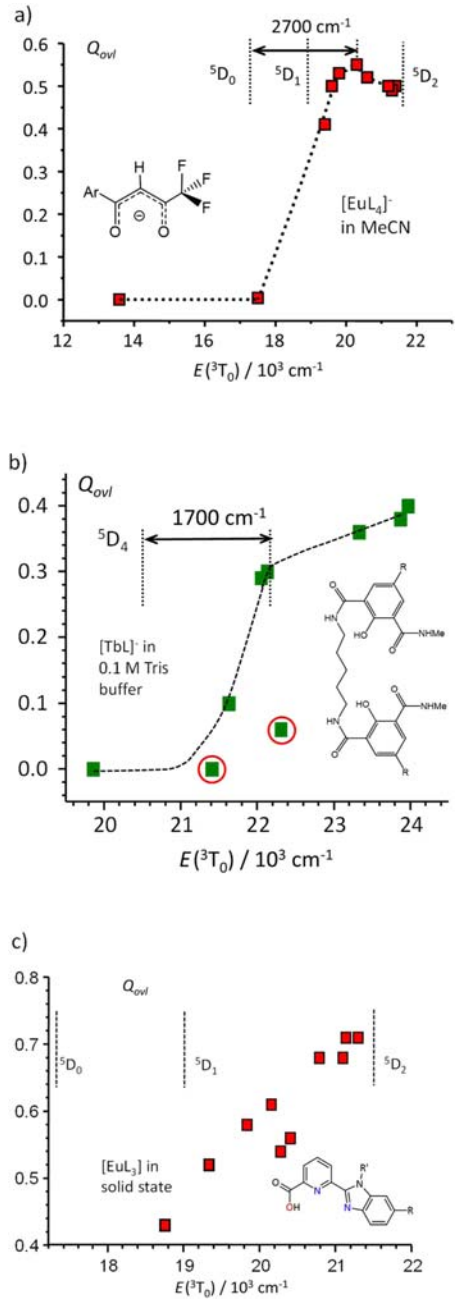

FIG. 11.10 Overall quantum yields versus the triplet state energy for (A) Eu^{III} tetrakis β-diketonates, (B) Tb^{III} chelates with 2-hydroxy-isophthalamides, and (C) Eu^{III} complexes with benzimidazole-pyridine derivatives. *Drawn from data based on Sato, S., Wada, M., 1970. Relations between intramolecular energy transfer efficiencies and triplet state energies in rare earths β-diketonates. Bull. Chem. Soc. Jpn. 43, 1955–1962; Shavaleev, N.M., Eliseeva, S.V., Scopelliti, R., Bünzli, J.C.G., 2009a. Designing simple tridentate ligands for highly luminescent europium complexes. Chem. Eur J. 15, 10790–10802; Shavaleev, N.M., Scopelliti, R., Gumy, F., Bunzli, J.C.G., 2009b. Surprisingly bright near-infrared luminescence and short radiative lifetimes of ytterbium in hetero-binuclear Yb-Na chelates. Inorg. Chem. 48, 7937–7946.*

established that a sizable portion of the excitation is funneled through the $^5D_1$ level, up to 99%, if $E^T{}_0$ becomes resonant with that level. Internal conversion then populates the $^5D_0$ level. Similar correlations have been worked out for Tb^{III} (Sato and Wada, 1970; Samuel et al., 2009) with about the same conclusion regarding the energy gap (Fig. 11.10B), i.e., quantum yields become larger than 30% when the energy gap is $>$ 1700-2000 cm^{-1}; however, two data points (red [dark black in print version]-circled) deviate from the correlation in Fig. 11.10B, probably because of the presence of ILCT in the ligands. For the compounds shown in Fig. 11.9, Q_{ovl} becomes >50% when the energy gap is >2000 cm^{-1} but then the quantum yield increases almost linearly with the energy of the triplet state (Fig. 11.10C). These examples point to the fragility of the energy gap rule especially that another point to consider is that charge-transfer states can relay energy when they are positioned between the singlet and triplet states (Puntus et al., 2008).

Moreover, when the coordination environment of the Ln^{III} ion is changing, the energy gap correlation does not work anymore: for instance, replacing one ligand by water molecules in a $[Ln(L_3)]$ complex to yield $[Ln(L_2)(H_2O)_3]$ will not influence the triplet energy of the ligand but the quantum yield will see a large decrease due to the quenching of Ln^{III} luminescence by the water molecules.

Accordingly, the energy gap rule should be used with great precaution and only considered as being a first simplistic approach. Not only does it fail to account for varying non-radiative deactivation processes but, equally importantly, it only considers one energy transfer path, one donor state, one acceptor state and, finally, it is rather silent on the exact mechanism considered while it is known that several mechanisms may potentially contribute to the transfer. In addition, the distinction between triplet, singlet, and charge transfer states is not always clear-cut as some of these states may mix.

11.2.4.2 Quantitative models and calculation packages

- **The LUMPAC program**

Quantum mechanical calculations are difficult to carry out for 4f-containing chelates. This may be the reason, why a workable model for the antenna effect had to wait the beginning of this century (de Sá et al., 2000). This model has been then constantly improved and an open-access software package designed for the Windows operating system (LUMPAC) (Dutra et al., 2014). The procedure has essentially been applied to Eu^{III} chelates, but it also works for other ions such as Sm^{III} (Gonçalves e Silva et al., 2002) and Tb^{III}. Many examples of such modeling have been published that are often in line with the triplet path of energy transfer but also point sometimes to the contribution of the singlet state and to the importance of the dipole-quadrupole mechanism. It is not the purpose of this chapter to give a detailed account of the model; however the readers are being directed to recent reviews (Neto et al.

2019a,b). The various steps of the LUMPAC procedure has been simply outlined and one example has been discussed. These steps are.

- Optimization of the ligand geometry using the Austin 1 procedure (AM1) or other more performing calculations like parametric models PM3, PM6, or PM7, all working within the frame of the Neglect of Differential Diatomic Overlap (NDDO) scheme.
- Optimization of the complex geometry using the Sparkle model within the Molecular Orbital Package (MOPAC) program, i.e., a central Coulomb potential with the Ln^{III} ion replaced with a +3e point charge and coupled with one of the AM1 or PMx procedures. Recent improvement uses the RM1 model for the Ln^{III} (Ln = Eu, Gd, Tb) ions: the {[Xe] $4f^n$} electronic configuration is described by the effective core potential with the RM1 core charge of the lanthanide set as $+3e$. The semi-empirical basis set used is composed of 5d, 6s, and 6p orbitals, for a total of 9 orbitals. With this model, Ln-X (X = C, N, O, S, Cl, Br) bond lengths can be predicted within ±0.06 Å (Dutra et al., 2014).
- Calculation of the ligand excited states and transition probabilities with Zerner's Intermediate Neglect of Differential Overlap (ZINDO) program.
- Calculation of the JO intensity parameters from the emission spectrum of Ln^{III} with the simple overlap model (SOM) for the odd-component of the ligand-field and the dynamic coupling mechanism for the contributions of ligand polarizability. Covalency effects are not considered explicitly and the calculation is limited to two parameters only, Ω_2 and Ω_4.
- Laying out a kinetic model of energy transfer taking into account the relevant ligand and Ln^{III} states (chosen by considering their respective energy and potential overlap), back transfer, as well as several mechanisms: Dipole-dipole (Förster), dipole-2^{λ}-multipole, and spin exchange (Dexter). Calculations have shown that dipole-quadrupole transfers may contribute substantially to the overall process, especially for ED forbidden transitions. Selection rules have also to be considered (Tanner et al., 2018): $|J - J'| < \lambda \leq |J + J'|$ for dipole-dipole and dipole-multipole transfer ($\lambda = 2$, 4, 6) and $|J - J'| = 0 \pm 1$ for exchange transfer; 0-0 transfers are excluded. These rules hold for pure orbitals and J-mixing can relax them, fortunately. In the case of Eu^{III}, direct excitation of $^5D_0$ from $^7F_0$ is forbidden by Laporte, ΔS, ΔL (however MD allowed), and ΔJ selection rules, but J-mixing, that can be estimated by the intensity ratio between $^5D_0 \rightarrow {}^7F_0$ and $^5D_0 \rightarrow {}^7F_2$ transitions effectively makes transfer to $^5D_0$ possible. Moreover, the $^5D_0 \leftarrow {}^7F_1$, $^5D_1 \leftarrow {}^7F_0$, and $^5D_1 \leftarrow {}^7F_1$ transitions are partially MD allowed (Table 11.3); the population of $^7F_1$ at room temperature is about 25%−30% so that this level is a important actor in the transfer process; it then rapidly relaxes to $^5D_0$.
- Solving the kinetic equations under steady state approximation and with Runge-Kutta method with adaptive integration steps. Finally, the quantum

TABLE 11.3 Selection rules for some $Eu^{III}(^5D_{J'} \leftarrow {}^7F_J)$ transitions of interest in the sensitization of this ion. Symmetry selection rules depend on the point group of symmetry and are not displayed.

Transition	Parity		Spin		ΔL		ΔJ			
							Transition		Energy transfer	
	ED	MD	ED	MD	ED	MD	ED	MD	$2\text{-}2^{\lambda}$ pole	Exchange
$^5D_0 \leftarrow {}^7F_0$	X	√	X	X	X	X	X	X	X	X
$^5D_0 \leftarrow {}^7F_1$	X	√	X	X	X	X	X	√	X	√
$^5D_1 \leftarrow {}^7F_0$	X	√	X	X	X	X	X	√	X	√
$^5D_1 \leftarrow {}^7F_1$	X	√	X	X	X	X	X	√	√	√

yield can be determined from the calculated rate constants. Most of the calculated Q_{ovl} values are within ±10%−20% of the experimental data (themselves subject to an estimated similar experimental uncertainty (Ishida and Bünzli, 2016).

An example of such a calculation is shown in Fig. 11.11 for a dimeric Eu^{III} tetrakis(β-diketonate). The chosen model takes into account 3 levels for the ligand and 4 for the Eu^{III} ion. Internal conversion rate constants (10^6 s^{-1}) are estimated as well as fluorescence and phosphorescence rates of the ligand (based on experimental determinations for similar ligands). The calculated triplet state energy (20,030 cm^{-1}) is in good agreement with the experimentally determined one (21,320 cm^{-1}). The following conclusions can be drawn from the resulting rate constants: (i) Energy transfer from the singlet state contributes less than 0.01% to the total transfer, and therefore, the sample fit within the classical $S_0 \rightarrow S_1 \rightarrow T_1 \rightarrow {}^5D_{1,0}$ scheme; (ii) given the arguments developed above, it may be surprising that direct transfer to $^5D_0$ accounts for 56% of the overall transfer, overcoming transfer to $^5D_1$ (44%); this is partly due to much faster back transfer from $^5D_1$ (6.9×10^8 s^{-1}) compared with $^5D_0$ (1.8×10^5 s^{-1}) while the forward transfer rates are quite comparable; and (iii) Calculated quantum yield compares very well with the experimentally determined one, validating this semi-empirical procedure.

11.2.4.3 The JOYSpectra platform

In 2021, a free-of-charge web platform, termed JOYSpectra, has been proposed for online calculations of spectroscopic properties of lanthanide-based

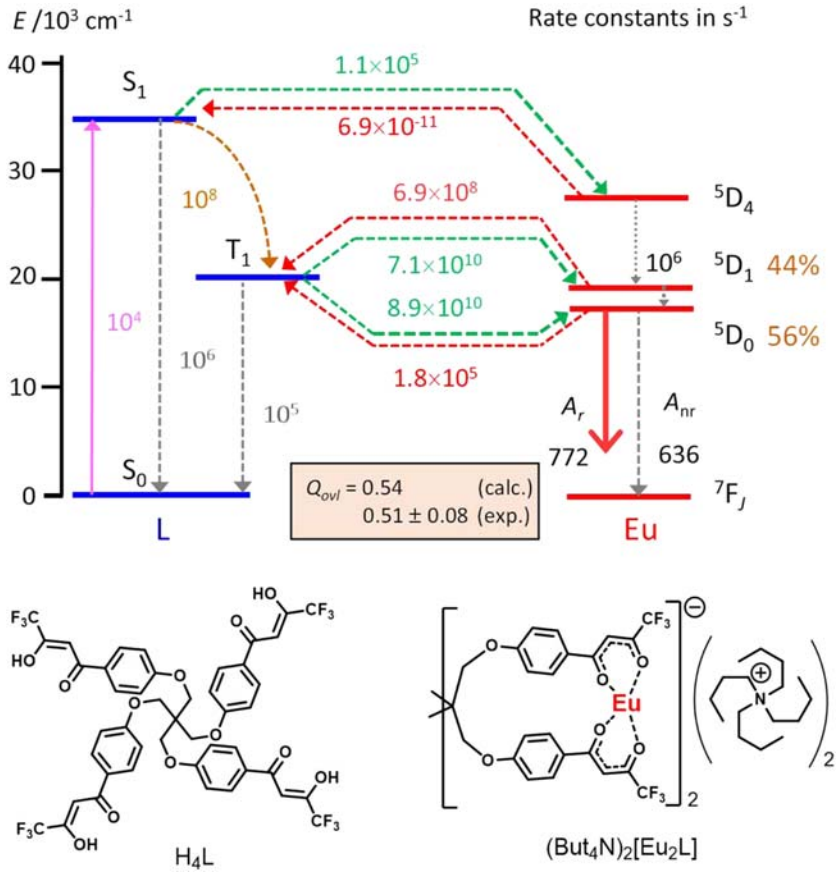

FIG. 11.11 Modeling of energy transfer processes in the Eu^{III} tetrakis(β-diketonate) dimeric complex $(But_4N)_2[Eu_2L]$ in solid state using the Sparkle/AM1 procedure (LUMPAC program). A_r and A_{nr} are the radiative and non-radiative rates, respectively. *Adapted from Biju, S., Freire, R.O., Eom, Y.K., Scopelliti, R., Bünzli, J.C.G., Kim, H.K., 2014. A Eu(III) tetrakis(β-diketonate) dimeric complex: photophysical properties, structural elucidation by sparkle/AM1 calculations, and doping into PMMA films and nanowires. Inorg. Chem. 53, 8407−8417. With Permission.*

compounds. It calculates and analyses the JO intensity parameters and evaluates intramolecular energy transfer rates from excited donor states up to 310 transitions involving 12 Ln^{III} ions (Moura et al., 2021). On the other hand, it does not calculate or optimize the geometry of the complexes that has consequently to be input, either under the form of Cartesian coordinates or as output of programs such as Gaussian, Orca, or MOPAC. The package is illustrated by convincing calculation of the energy transfers in and quantum yields for $[Ln(tta)_3(H_2O)_2]$ (tta is thenoyl-trifluoro-acetylacetonate; Ln = Eu, Tb).

11.3 Designing highly luminescent chelates (Bünzli, 2015)

11.3.1 Principles

The principles governing the design of highly luminescent lanthanide chelates are very simple to spell out: one has to maximize light absorption by the ligands, maximize energy transfer and minimize non-radiative de-activation processes. Additionally, one wants to try decreasing the radiative lifetime, in order to increase the intrinsic quantum yield, which can be done during the synthetic step by implementing polarizable Ln-ligand bonds or post-synthetically by incorporating the luminescent chelate into a matrix with large refractive index. In order to be successful, these optimizations can only be achieved taking into account the specific properties of each emitting ion and of their surroundings.

11.3.2 Optimizing energy transfer

This step is fairly well mastered for visible-emitting ions, particularly for Eu^{III} and Tb^{III}. In principle, ligands containing an extended aromatic π-system are favored since they feature relatively low-lying excited states. On one hand, one needs to elaborate a stable molecular construction with strong Ln-ligand bonds that are as polarizable as possible and make sure that the distance between the localisation of the electronic density of the donor orbital and the metal ion is as short as possible. There are basically two strategies. In the first one (Fig. 11.12, top), chromophores are appended to a spectroscopically silent chelate framework, here triazacyclononane is an example. Energy transfer from the chromophores induces Ln^{III} emission provided the aromatic system is positioned as close as possible from the metal ion and is orientated correctly. The overall quantum yield of the displayed Eu^{III} chelate amounts to 0.35 in water at pH 6.5 (Neil et al., 2014). Such a strategy favors dipole-dipole (Förster) energy transfer that has $1/r_{DA}^6$ distance dependence.

In the second strategy, the chromophore is incorporated into the ligand with the advantage of reducing the distance between the donor state and the Ln^{III} ion. Energy transfer through exchange (Dexter) mechanism is favored; since the distance dependence is in $e^{-r_{DA}}$, this mechanism is highly efficient for short distances, $r_{DA} < 5$ to 8 Å although in case of extended π-conjugation in the ligand, this can be expanded to about 20 Å (Lazarides et al., 2008). In the example depicted in Fig. 11.12 (bottom), the $Tb^{III}L_3$ complex exhibits a quantum yield of 0.66 in the solid state (Wartenberg et al., 2013).

The energy of the ligand donor state(s) should of course match reasonably well the Ln^{III} excited states, taking into account an adequate gap in order to minimize back energy transfer (see Section 11.2.4). Fig. 11.13 exemplifies the problem in the case the donor state is an MLCT state. The theoretical modeling is made for an initial $Q_{ovl} = 0.5$, for triplet and singlet state energies

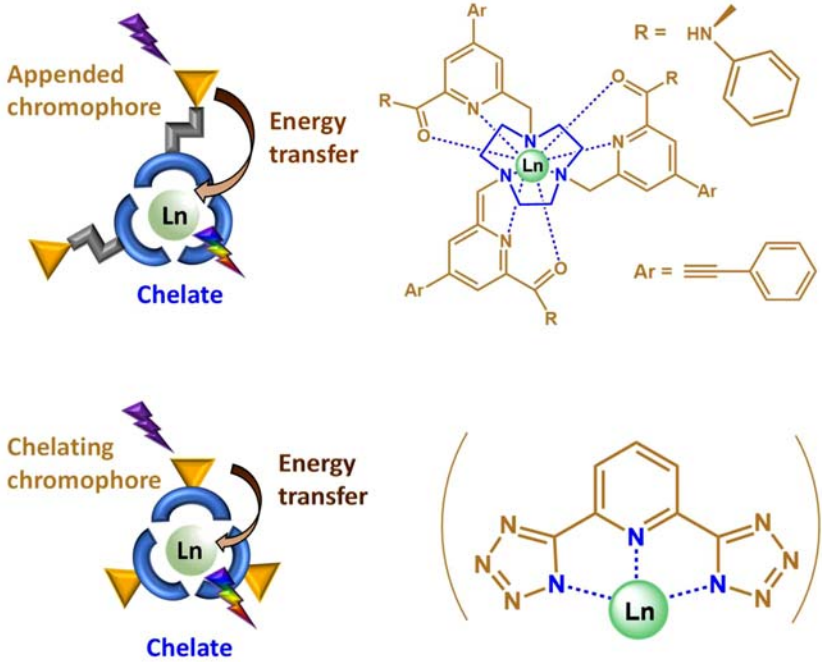

FIG. 11.12 Strategies for the synthesis of efficient antenna ligands. (Top) appended chromophore. (Bottom) chromophore incorporated into the ligand. *Adapted from Neil, E.R., Funk, A.M., Yufit, D.S., Parker, D., 2014. Synthesis, stereocontrol and structural studies of highly luminescent chiral tris-amidepyridyl-triazacyclononane lanthanide complexes. Dalton Trans. 43, 5490–5504. With permission; Adapted from Wartenberg, N., Raccurt, O., Bourgeat-Lami, E., Imbert, D., Mazzanti, M., 2013. Multicolour optical coding from a series of luminescent lanthanide complexes with a unique antenna. Chem. Eur J. 19, 3477–3482. With Permission.*

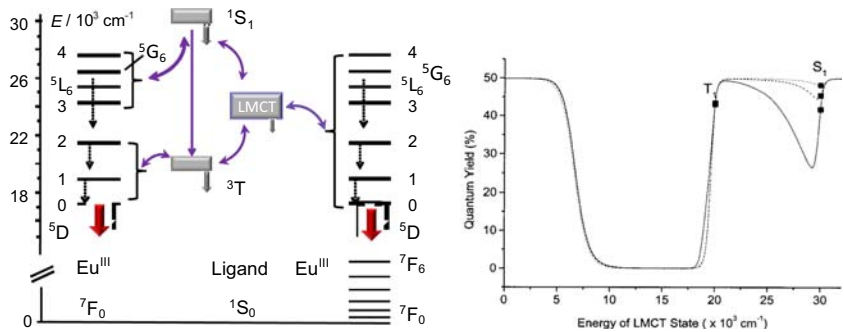

FIG. 11.13 (Left) energy level scheme taken into account for modeling the influence of LMCT on the Eu^{III} quantum yield. (Right) results of the calculations for 3 values of the overlap integral between LMCT and ligand π orbitals: 0.01 (*solid line*), 0.05 (*dashed line*), and 0.10 (*dotted line*). *Adapted from Faustino, W.M., Malta, O.L., de Sá, G.F., 2005. Intramolecular energy transfer through charge transfer state in lanthanide compounds: a theoretical approach. J. Chem. Phys. 122, doi.10.1063/1.1830452. With Permission.*

set to 20,000 and 30,000 cm^{-1}, respectively, and it takes into account LMCT interactions with both 4f-orbitals and the $^1\pi$ and $^3\pi$ orbitals of the ligand. The magnitude of $Q_{ovl}(Eu^{III})$ is calculated for three values of the overlap between the LMCT and the π molecular orbitals, 0.01, 0.05, and 0.10. When the energy of the MLCT is between 8000 and 17,000 cm^{-1}, the quantum yield drops to almost nil. It then sharply increases up to 20,000 cm^{-1} and then decreases again up to the energy of the singlet state for finally regaining its initial value (Faustino et al., 2005). Experiments corroborating these variations are described in the literature, for instance for non-fluorinated and fluorinated β-diketonates (Zhuravlev et al., 2018).

11.3.3 Minimizing non-radiative deactivation processes

11.3.3.1 Photoelectron transfers (PET)

There are several non-radiative deactivation channels but the most important are temperature-dependent electronic and vibrational quenching. In the first one, termed *photo-induced electron transfer* (PET), an electron is transferred either from the ligand to the metal ion or from the metal ion to the ligand. The first alternative is more common and leads to switching the corresponding Ln^{III} luminescence off. This essentially happens for easily reduced ions. Many documented examples stem from Eu^{III} with the ligand reducing it to Eu^{II}; the condition for PET to occur is that the excited state energy of the ligand must be larger than the energy required for reducing the metal ion. Another way of looking into the competition between luminescence and PET is to consider the lowest oxidation potential for an antenna for which PET will not be possible for a given excited state. These redox potentials are plotted in Fig. 11.14 (top) for two excitation wavelengths, 280 and 330 nm. It is clear from this graph that PET is likely feasible for Eu^{III} and Yb^{III} for most organic ligands. Another, unexpected result is that even for ions like Sm^{III}, Tm^{III}, Dy^{III}, and, possibly, Nd^{III}, PET should be considered in the interpretation of their luminescence spectra. An example of the detrimental influence of PET process is shown in Fig. 11.14 (bottom). $[Eu(DPPOT)_3]^{3+}$ was found to have a very small quantum yield of 1% so that a detailed time-resolved photophysical study was undertaken to unravel its origin and it became evident that the culprit was the PET process that reduces Eu^{III} into Eu^{II}, switching off the trivalent ion luminescence (Ha-Thi et al., 2010).

The on/off (or off/on) switching of luminescence by PET is a convenient tool for analytical applications. Different analytical strategies take advantage of PET, including some in which the metal ion is not directly implied but its complexation modifies the energies of the excited states of the ligand with the consequence of, usually, switching the PET process off. For a comprehensive description, the reader is referred to the review by Kovacs and Borbas (2018). Regarding Yb^{III}, it is noteworthy that PET is involved in one mechanism proposed for sensitizing its luminescence by ligands having

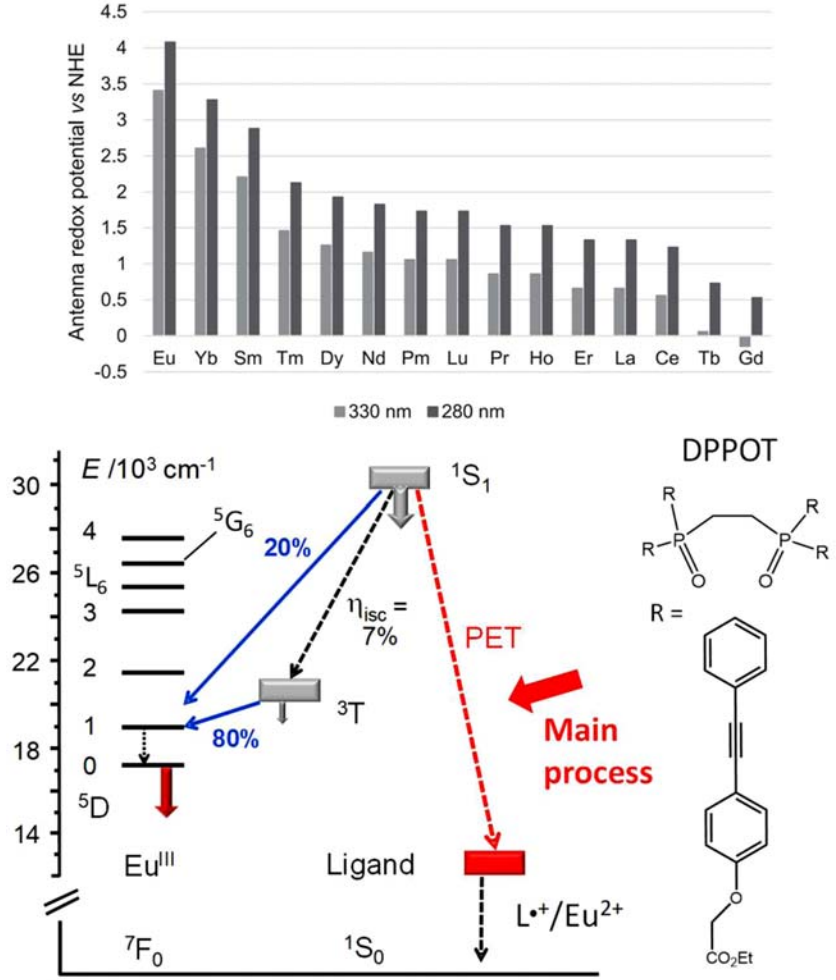

FIG. 11.14 (Top) antenna redox potentials below which PET to Ln^{III} ions is unfavorable for 280 and 330 nm excitation. (Bottom) Luminescence PET quenching of $Eu(NO_3)_3(DPPOT)_3$. *Adapted from Kovacs, D., Borbas, K.E., 2018. The role of photoinduced electron transfer in the quenching of sensitized europium emission. Coord. Chem. Rev. 364, doi.10.1016/j.ccr.2018.03.004. With Permission; Adapted from Ha-Thi, M.H., Delaire, J.A., Michelet, V., Leray, I., 2010. Sensitized emission of luminescent lanthanide complexes based on a phosphane oxide derivative. J. Phys. Chem., A 114, 3264−3269. With Permission.*

energetic excited states, that is when the energy gap is unreasonably large for efficient energy transfer to occur. In a first step, the ligand excited state transfers one electron onto $Yb^{III}(^2F_{7/2})$ reducing it to an excited divalent form $(Yb^{II})^*$; in a subsequent step, $(Yb^{II})^*$ transfers this electron back and

becomes excited $Yb^{III}(^2F_{5/2})$; then this species de-excites by emitting its characteristic NIR light at 980 nm.

11.3.3.2 Vibrational quenching

A major quenching channel is provided by vibrations in the surroundings of the emitting ion, a fact that has been recognized as early as the 1960s. For instance, Kropp and Windsor (1963) noticed that the luminescence intensity of lanthanide salts is enhanced in heavy water compared with regular water. They also pointed out that the enhancement is dependent on the energy gap between the emitting level and the highest-lying sub-level of the ground state, $\Delta E_{e\text{-}g}$. For instance, enhancement factors for chlorides were measured to be ~20, 8, and 1 for Eu^{III}, Tb^{III}, and Gd^{III}, respectively. That no enhancement was recorded for Gd^{III} was interpreted on the basis of its large gap, 32,100 cm^{-1} as compared with 14,800 and 12,300 cm^{-1} for Tb^{III} and Eu^{III}, respectively.

The rate constant for non-radiative deactivation by vibrations and their combinations/overtones depends on the energy of the vibration, $\hbar\omega$, the energy gap $\Delta E_{e\text{-}g}$, the distance between the oscillator and the emitting ion, and the temperature. The dependence with respect to the energies can be written as:

$$k_{nr} = C_1 \times e^{-C_2\left(\Delta E_{e-g}/\hbar\omega\right)} \tag{11.13}$$

in which C_1 and C_2 are empirically fitted parameters characteristic of a given system. The energy gaps for the luminescent Ln^{III} ions are reported in Fig. 11.15. The non-radiative deactivation will be more efficient if a small number of phonons are needed to bridge the gap. For instance, quenching $Tb^{III}(^5D_4)$ emission will require 4 O−H vibrations (or, more correctly, the fourth overtone of the O−H oscillator) while only about 3 are needed for de-activating $Eu^{III}(^5D_0)$, and therefore, the latter is more quenched than Tb^{III}. As a rule of thumb, an efficient luminescent molecular edifice should not have vibrations larger than 1/6th of the energy gap:

$$\hbar\omega_{max} < \frac{\Delta E_{e-g}}{6} \tag{11.14}$$

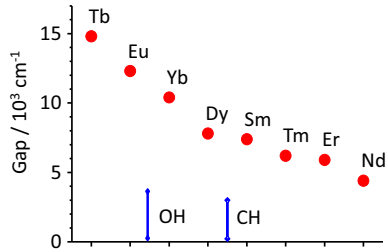

FIG. 11.15 Energy gaps $\Delta E_{e\text{-}g}$ in cm^{-1} for some lanthanide ions and energies of OH and CH vibrations.

This is relatively easy to realize for visible-emitting Ln^{III} ions in an inorganic environment, but much more difficult for NIR-emitting ions and for molecular complexes with organic ligands.

The simple "energy-gap law" treatment works well in many cases, particularly when considering Ln^{III} ions in solid inorganic matrices. It is however more problematic, when trying to interpret NIR luminescence of Ln^{III} molecular complexes. Indeed, it is based on several not always valid hypotheses: first, anharmonic and not harmonic oscillators should be considered, then the spectral overlap between the normalized emission spectrum $I_{em}\left(\widetilde{\nu}\right)$ and the vibrational spectrum $\varepsilon_{vib}\left(\widetilde{\nu}\right)$ plays an important role and should be incorporated into the model and, finally, several vibrations can be simultaneously active. Therefore, a more involved model was proposed, the *inductive-resonant mechanism* considering that the quenching is analogous to a dipole-dipole energy transfer with distance dependence in r^6. The non-radiative deactivation rate constant is then given by Eq. (11.15) (Doffek et al., 2012):

$$k_{nr} = \frac{161.9 \cdot k_r \cdot \kappa^2}{\pi^2 \cdot n^4 \cdot N_A \cdot r_{DA}^6} \times SOI \tag{11.15}$$

in which k_r is the rate of radiative deactivation in the absence of any non-radiative deactivation, κ is a factor depending on the relative orientation of the transition dipole moment of the donor (the Ln^{III} ion) and the acceptor (the quenching oscillator), n is the refractive index, N_A Avogadro's number and r_{DA} the distance between the Ln^{III} and the oscillator. Finally, the spectral overlap integral SOI is given by (Eq. 11.16)

$$SOI = \int I_{em}\left(\widetilde{\nu}\right) \cdot \varepsilon_{vib}\left(\widetilde{\nu}\right) \cdot \widetilde{\nu}^{-4} d\widetilde{\nu} \tag{11.16}$$

This model could explain quantitatively, why deuteration of a Pr^{III} cryptate leads to less emission intensity from the $^1D_2$ level whereas the contrary was expected. The reason is that the third harmonic of the C-D vibration overlaps better with the $^1D_2 \rightarrow {}^1G_4$ transition than the second harmonic of the C−H vibration, resulting in a larger SOI, as shown in Fig. 11.16.

11.3.3.3 Winning strategies for avoiding vibrational quenching in NIR emission (Hernandez and Gillin, 2015)

As can be inferred from the previous section, deuteration of the ligands and, when appropriate, of the solvent, will, in general, considerably minimize vibrational quenching. Deuteration of ligands or complexes can be simply achieved by exchange reaction with deuterated solvents and is therefore easy to achieve. When a complex contains coordinated water molecules that are replaced with D_2O, the effect is usually large for an ion such as Eu^{III} and

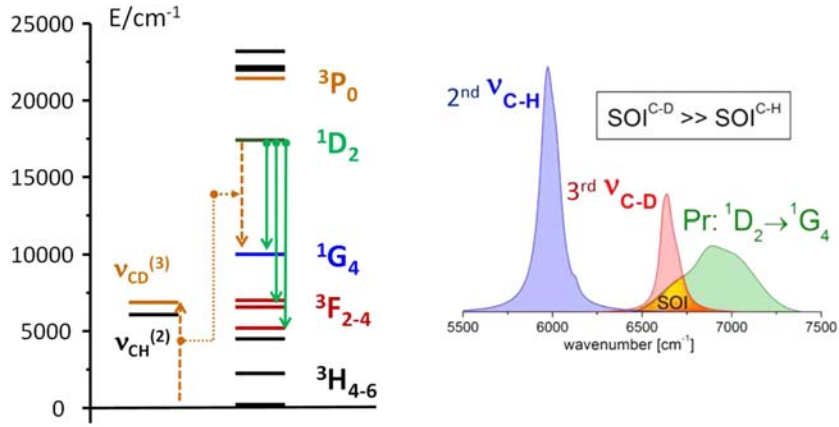

FIG. 11.16 (Left) energy diagram for the Pr^{III} cryptate with (bpy.bpy.bpy) showing quenching of $^1D_2$ by the third harmonic of the C-D vibration. (Right) spectral overlap integrals of the second C−H harmonic and third C-D harmonic. *Adapted from Doffek, C., Alzakhem, N., Bischof, C., Wahsner, J., Güden-Silber, T., Lügger, J., Platas-Iglesias, C., Seitz, M., 2012. Understanding the quenching effects of aromatic C−H- and C−D-oscillators in near-IR lanthanoid luminescence. J. Am. Chem. Soc. 134 16413−16423. With permisson.*

moderate for Tb^{III}. However for NIR-emitting ions such as Nd^{III}, Er^{III}, or Yb^{III}, this may not be always sufficient. For instance, after deuteration of [Nd(hfa)$(H_2O)_2$] to yield [Nd(hfa-D)$_3$(D_2O)$_2$], where hfa^- is hexafluoroacetylacetonate, vibrational non-radiative deactivations remain important and the overall quantum yield is still very low, e.g., 0.004 in acetone-d_6; replacement of the D_2O molecules with DMSO-d_6 increases Q_{ovl} about 3-fold, but its value is still uninterestingly small, at 0.011 (Hasegawa et al., 1996). Not only are O−H vibrations heavily quenching NIR luminescence but, also, N−H and C−H vibrations, ubiquitous in organic ligands. It has been calculated that in Cs[Er(hfa)$_4$], the rate constant for luminescence deactivation by one C−H vibration, k_{CH}, is equal to 91 ms^{-1} so that a single C−H oscillator located at 20 Å of an emitting Er^{III} ion quenches half its emission! A summary of some k_{XH} rate constants is given in Table 11.4.

Another strategy has been proposed: halogenation instead of deuteration, or, sometimes, a combination of both. One advantage of halogenation, more particularly chlorination and bromination is the heavy atom effect of the halogen that, in addition to minimizing vibrational quenching, promotes triplet population via intersystem crossing. Despite this, fluorination remains the most common way of switching off non-radiative deactivations in molecular NIR-emitting complexes (Hernandez, 2015). It has several effects due to the strong withdrawing properties of the fluorine atoms. This makes more difficult for the ligand to bind the metal ions but, on the other hand, it also allows more orbital mixing with concomitant reduction of the radiative lifetime, and hence,

TABLE 11.4 Selected rate constants for the quenching of Nd^{III}, Er^{III}, and Yb^{III} luminescence by C−H and C-D oscillators.

Complex	Oscillator	Distance/Å	k_{CX}/ms^{-1}
$Cs[Nd(hfa)_4$	C−H	4.7	600
[Nd(bpy.bpy.bpy)]	CH_2(eq)	3.6	73
	CH_2(ax)	4.4	22
	CH(aryl)	5.5	3.9
$Cs[Er(hfa)_4]$	C−H	4.7	91
	C-D	4.7	2.4
$[Yb(dota)]^-$	C−H(ring)	3.7	11
	NCH_2CO	n.a.	13
[Yb(bpy.bpy.bpy.)]	CH_2(eq)	3.5	12.8
	CH_2(ax)	4.2	11.0
	CH_2(aryl)	5.4	4.3

$Dota^{4-}$ is 1,4,7,10-tetraazacyclododecane-1,4,7,10 tetraacetate and (bpy.bpy.bpy) is a cryptand based on three bipyridine units.
Adapted from Bünzli, J.C.G., 2015. On the design of highly luminescent lanthanide complexes. Coord. Chem. Rev. 293, 19-−7. With permission.

increasing the emission efficiency (Ye et al., 2013). Another drawback of some fluorinated ligands, even if they present reasonable complexing properties and enhancement of f-f oscillator strengths, is their insufficient antenna effect or the fact that they have to be excited in the UV. For instance, the ligand tpip (Scheme 11.1) yields [Ln(tpip)$_3$] complexes with lifetimes of 2.7 (Nd^{III}), 6.5 (Er^{III}), and 53 (Yb^{III}) µs in dry MeCN (Bassett et al., 2005). Fluorinating the ligand results in lengthening these lifetimes to 46, 316, and 582 µs in solid state, respectively (Glover et al., 2007). The corresponding intrinsic quantum yields for the Er^{III} complexes calculated with $\tau_{rad} = 8$ ms, are 0.05% and 1.8% in solid state (Mancino et al., 2005). The problem is the excitation wavelength of 266 nm. To overcome this drawback, an interesting strategy has been proposed by Ye et al. (2014): Introduction of an additional chromophore separated from the chemical environment of the emitting Ln^{III} ion, $[Zn(F\text{-}TBZ)_2]_2$, that can be excited at 368 nm. A waveguide has been fabricated comprising a 2-µm film of $[Zn(F\text{-}TBZ)_2]_2$ doped at 30% [Er(F-tpip)$_3$] and deposited onto a 0.7-µm SiO_2 layer on a silicon substrate. Amplification performances are good and the device can easily be integrated with other components.

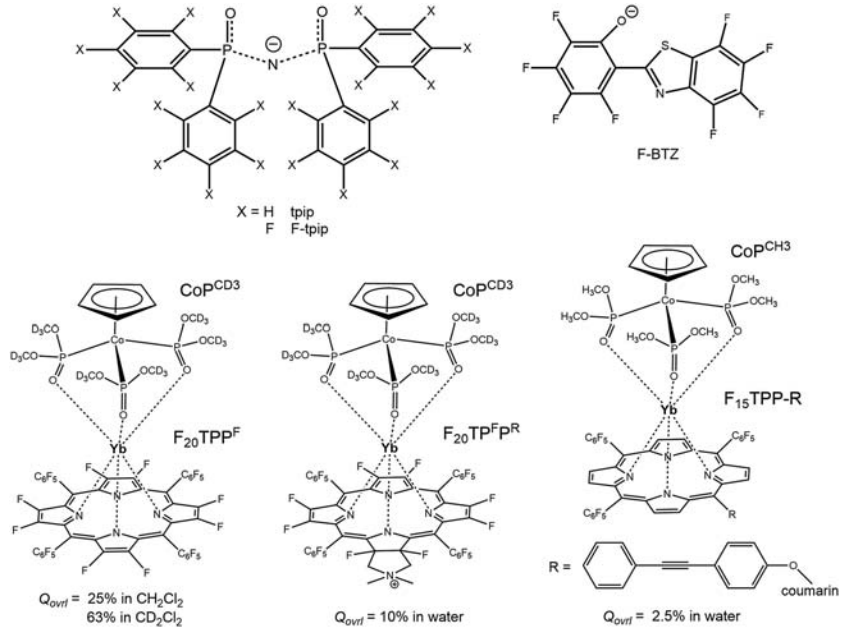

SCHEME 11.1 Chemical formulae of tpip, F-tpip, and of the Yb^{III} monoporphyrinates with large quantum yield.

Another successful move was to replace oxygen with sulfur in $[Ln(XC_6F_5)_3(DME)_2]$ (Ln = Nd, Er, Tm), where DME is 1,2-dimethoxyethane and $(XC_6F_5)^-$ pentafluoro phenolate (X = O) or perfluoro benzenethiolate (X = S). The luminescence efficiency, calculated from the lifetimes (i.e., corresponding to Q_{int}) increases from 2% to 9% for Nd^{III} and from 19% to 75% for Er^{III}; the effect is far less pronounced for Tm^{III} for which the efficiency of the $^3H_4 \rightarrow {}^3F_4$ emission remains almost constant (from 1.9% to 2.0%) (Norton et al., 2009).

A remarkable improvement in the quantum yield of Yb^{III} complexes has recently been achieved. Despite a relatively large $^2F_{5/2}$-$^2F_{7/2}$ energy gap of $\sim$10,500 cm^{-1}, quantum yields of Yb^{III} chelates were long confined in the range 1%–4% (Shavaleev et al., 2009a,b). Well in line with this statement, the Yb^{III} tetrakis(pentafluorophenyl)porphyrinate capped with Kläui's ligand, [Yb(F_{20}TPP) (CoP^{CH3})], has an overall quantum yield of 2.4% in methylene chloride (Hu et al., 2017), an already large improvement over the non-fluorinated complex that presents no Yb^{III} emission. Fluorinating the β-positions of the macrocycle increases the quantum yield to 5.1% for [Yb($F_{20}TPP^F$) (CoP^{CH3})]. Further drastic improvement comes from the deuteration of Kläui's ligand with the quantum yield reaching 25% for [Yb($F_{20}TPP^F$) (CoP^{CD3})]

(Scheme 11.1) in CH_2Cl_2 and 63% in CD_2Cl_2 while the lifetime increases from 49 to 285 μs in CH_2Cl_2 and from 54 to 714 μs in CD_2Cl_2. The influence of the β-substituents is also quite dramatic and can be deciphered by comparing the overall quantum yields for [Yb($F_{20}TPP^X$) (CoP^{CD3})] which increase from 3.9% (X = H) to 15% (X = D) and 25% (X = F), respectively. On the other hand, the hydrogen atoms of the phenyl substituents have less effect, the overall quantum yield of [Yb(TPP^F) (CoP^{CD3})] remaining high at 20%, with a lifetime at 197 μs. Therefore, combined complete fluorination of the macrocycle and partial deuteration of the tripodal ligand improves the quantum yield by one order of magnitude! Interestingly, the ligand can be modified for rendering the complex water-soluble by fusing a dimethylpyrrolidinium group into it: the quantum yield of [Yb($F_{20}TP^FP^R$) (CoP^{CD3})] amounts to 10% in water and 23% in DMSO (Ning et al., 2018), representing a large improvement with respect to the best Q_{ovl} obtained so far in water for an Yb^{III} monoporphyrinate with F_{15}TPP-R linked to coumarin (Scheme 11.1), 2.5% (Zhang et al., 2011).

11.3.4 Examples of efficient sensitizing systems

The design of highly luminescent compounds must meet several requirements, which may be different depending on the emission spectral range and on the end use of the material. Brightness is of course a crucial parameter and molecular designers will attempt to optimize both η_{sens} and Q_{int} as described above by finding the antenna most suitable for the targeted Ln^{III} ion and by tailoring a rigid coordination environment, devoid of high-energy vibrations as much as possible. In addition, dedicated needs are required for specific applications. For instance, luminescent materials for light-emitting diodes, solar energy conversion, telecommunications, or luminescent coatings should display high thermal stability and easy processing, while luminescent bioprobes should be thermodynamically stable and kinetically inert in live biological environment and, at the same time, they should be non-cytotoxic. Finally, solubility may also be an important issue. The subject is vast and out of the scope of this chapter so that in the following, only a few examples of efficient antenna chromophores for selected Ln^{III} ions are given to help the reader figuring out where the field stands presently (Table 11.5, Scheme 11.2). Data reported in Table 11.4 are overall quantum yields only. In the literature intrinsic quantum yields derived either from lifetime measurements, or measured by direct f-f excitation are often reported, as well as partial quantum yields, especially for NIR-emitting ions. It is noteworthy that for a given compound, the quantum yield is often smaller in solution compared to solid state, unless unwanted interactions (e.g., excimer formation, or concentration quenching) occur in this state.

As one can gather from the data listed in Table 11.4, presently, quantum yields between 80 and almost 100% are common for Eu^{III} and Tb^{III} chelates.

TABLE 11.5 Quantum yield data for selected Ln^{III} coordination compounds. Ligand formulae are given in Scheme 11.2.

Complex	State	λ_{ex}/nm	Q_{ovl}/%	τ_{obs}/μs	E_{T1}/cm^{-1}	Other Ln ions sensitized	References
[Pr(hfa) (bipy)$_2$]	CHCl3		1.5[a]	11	22,900	Tb, Dy, Tm	Ahmed and Iftikhar (2014)
[PrGa$_8$(shi)$_8$(OH)$_4$]	Solid	340	0.03	0.1	22,620	Nd–Yb[b]	Salerno et al. (2020)
[Nd(Pyr$_2$POAc)$_3$(thf)]	DMSO	355	1.9	n.a.	13 −14000[c]	Yb	Deng et al. (2018)
[Nd(tcbx)$_3$(NO$_3$)$_3$]	CH$_3$CN	304	0.19	3.5	23,100	Eu, Er, Yb	Johnson et al. (2020)
[SmGa$_8$(shi)$_8$(OH)$_4$] Na·6H$_2$O	Solid	340	10.4[d]	151	22,620	Pr–Yb[b]	Salerno et al. (2020)
[(La:Sm 4%) (dcpa)$_3$(H$_2$O)] ∞	Solid	303	9.2	380	24,700	Eu	Pointel et al. (2020)
[Eu(F-benz) (bpy)]	Solid	347	90	1450	n.a.	n.a.	Kalyakina et al. (2018)
[Eu(DPPOP)$_3$	Solid	270	81	2400	27,780	Tb, Dy, Sm	Wei et al. (2020)
[Tb(DPPOP)$_3$	Solid	270	97	1900	27,780	Eu, Dy, Sm	Wei et al. (2020)
[Tb(py$_2$-triaz)$_2$(NO$_3$)$_3$]	Solid	330	97	1040	23,130	Sm,Eu,Dy	Gusev et al. (2019)
[Dy(pybenz-triaz)$_2$(NO$_3$)$_3$]	Solid	330	24	16	24,175	Sm,Eu,Tb	Gusev et al. (2019)
[Dy(cum)$_3$(H$_2$O) (ROH)]	EtOH	340	22	22	24,570	Sm,Eu,Tb	Guzmán-Méndez et al. (2018)
[Zn(py) (valnap)Er(NO$_3$)$_3$]	Solid	340	0.03	3.56	n.a.	Nd, Yb	Linden-Leibeszeit (2020)

Continued

TABLE 11.5 Quantum yield data for selected Ln^{III} coordination compounds. Ligand formulae are given in Scheme 11.2.—cont'd

Complex	State	λ_{ex}/ nm	Q_{ovl}/ %	τ_{obs}/ μs	E_{T1}/cm^{-1}	Other Ln ions sensitized	References
$[Er(tcbx)_3(NO_3)_3]$[e]	CH_3CN	305	0.01	n.a.	23,100	Nd, Eu, Yb	Johnson et al. (2020)
$[Tm(hfa)_3(bipy)]$	$CHCl_3$	340	0.78	2.6	22,500	Pr, Tb, Dy	Ahmed and Iftikhar (2014)
$[Tm(TPPO\text{-}Et\text{-}O)_3]$	Solid	350	0.50	14	22,800	Eu, Tb, Dy, Yb	Shuvaev et al. (2014)
$[Yb(Pyr_2POAc)_3(thf)]$[f]	DMSO	355	12.8	n.a.	13 −14000[c]	Nd	Johnson et al. (2020)
$[Yb(Ga_4shi_4)]_2(iph)_4]$	DMF	320	8.6	51	22,385	n.a	Lutter et al. (2020)

[a] *Visible range only.*
[b] *Except Pm, Gd.*
[c] *Excimer.*
[d] *visible range only; 83% in CD_3OD.*
[e] *See also Section 11.3.3.3.*
[f] *For larger Q_{ovl} (up to 63%) see Section 11.3.3.3.*

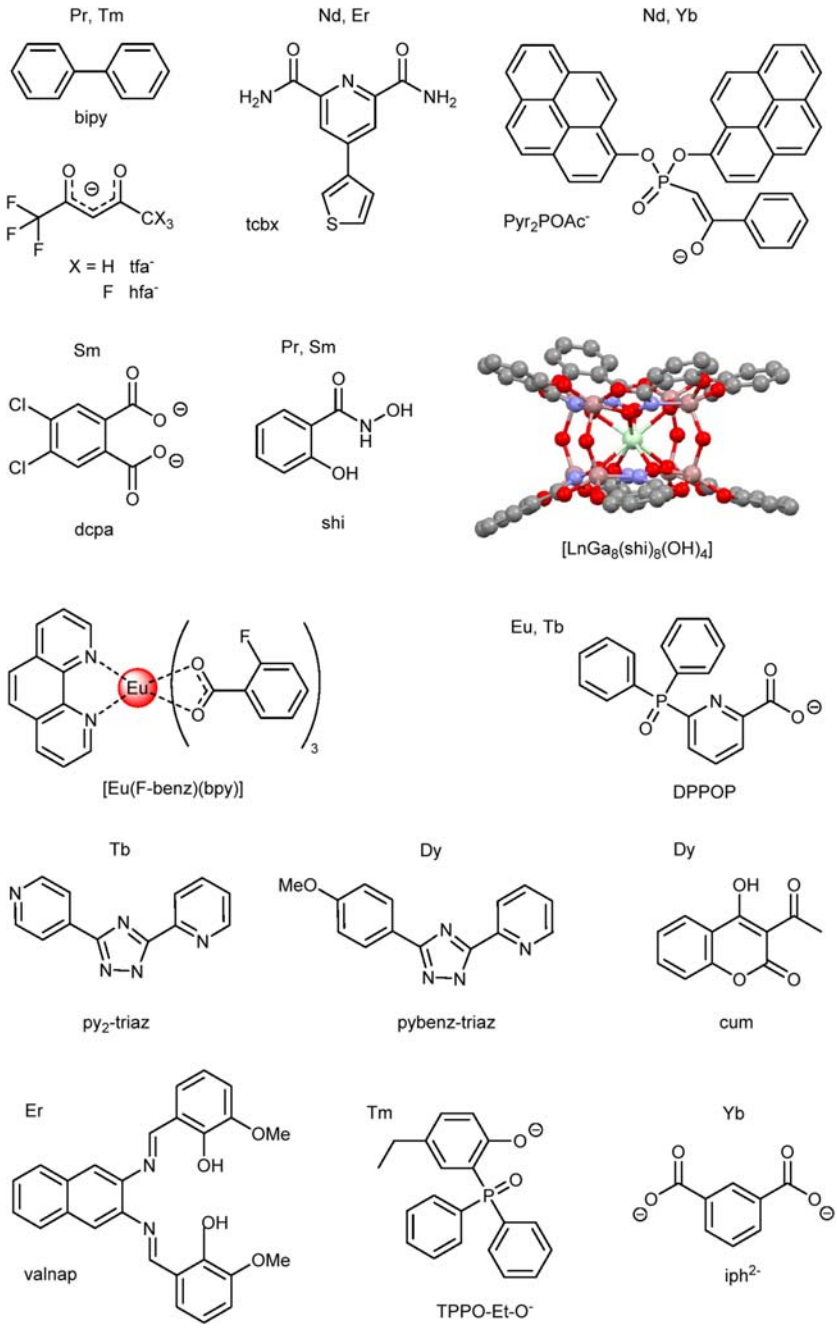

SCHEME 11.2 Formulae of the ligands and complexes mentioned in Table 11.4. Ln labels refer to the lanthanides coordinated by the displayed ligand.

This figure decreases to about 10%−25% for Dy^{III} and Yb^{III} complexes in the solid state or in non-deuterated solvents. With deuterated solvents, Q_{ovl} of Yb^{III} porphyrinates and porpholactonates can be much higher, in the range 50%−60%. Until now no Sm^{III} complex has been reported with Q_{ovl} much larger than 10%. Pr^{III} and Nd^{III} chelates have quantum yields of 1%−2% only and Tm^{III} chelates have difficulty in reaching 1%. This is apparently also true for Er^{III}, except for the systems developed for telecommunications mentioned above and for which long lifetimes have been reported (Peng et al., 2017), foreshadowing quantum yields of a few percent.

Considering the amazing advances made during the past decade, particularly for Yb^{III} complexes, one may be reasonably optimistic that in near future, similar efforts will contribute to considerably better the emissive properties of the complexes with, presently, poorly emitting Ln^{III} ions. However, each Ln^{III} ion will preferably have to be considered for its own properties. Indeed, literature survey shows that there are few ligands able to sensitize several different lanthanide ions or when they do, the sensitization is efficient only for a few of them (Zhang and Petoud, 2008; Salerno et al., 2020).

11.4 Luminescent lanthanide chelates at work

Luminescent lanthanide chelates are at the heart of numerous applications (Bünzli and Eliseeva, 2013), particularly in the field of biology and medicine (Bünzli, 2014). Here only a flavor of them is given with three noteworthy applications.

Circularly polarized luminescence (CPL) occurs, when a luminophore is chiral. Since in nature most biological molecules are chiral, CPL is an extremely valuable tool for exploring their primary and secondary structures. Among CPL luminophores, it happens that chiral lanthanide complexes present a high dissymmetry factor g_{lum} (particularly when emission arises from the $Eu^{III}(^5D_0 \rightarrow {}^7F_1)$ transition):

$$g_{lum} = 2\frac{(I_L - I_R)}{(I_L + I_R)} \tag{11.17}$$

where I is equal to the emitted light intensity and L and R represent left and right, respectively. For instance, Frawley et al. (2016) have recently demonstrated that triazacyclononane complexes $[EuL^1]$ and $[EuL^2]$ (Fig. 11.16, top) can be used for time-gated contrast imaging. The complexes have reasonably large Q_{ovl}, around 50%, and τ_{obs} around 1.2 ms enables easy time-resolved (TR) experiments. Dissymmetry factors for $[EuL^2]$ are between +0.15 and −0.32, depending on the transition. A commercial time-resolved epifluorescence microscope has been modified in order to separate left- and right-handed luminescence emitted by enantiopure Λ- and Δ-[EuL] by means of a quarter-wave plate and a linear polarizer; the right channel detects right

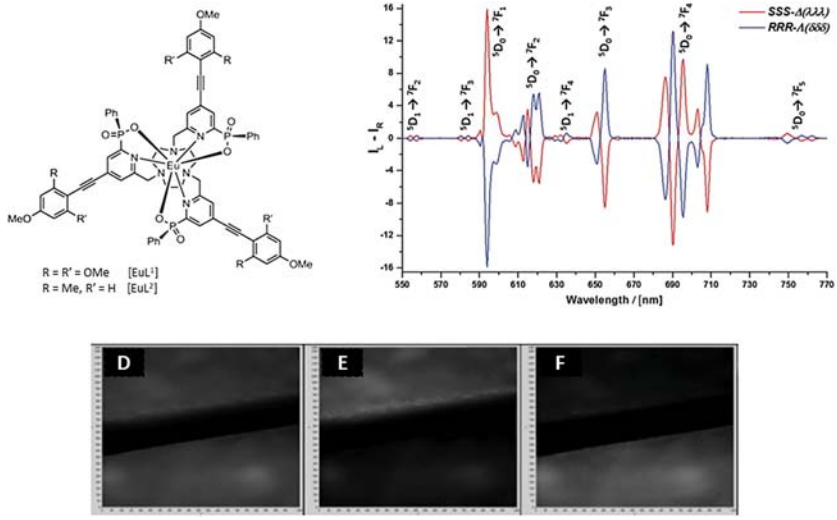

FIG. 11.17 (Top) formulae of Eu^{III} complexes, whose chiral enantiomers display CPL; the CPL spectra of Δ- and Λ-[EuL^2] are displayed on the right. (Bottom) time resolved images of (top) Λ-[EuL^2] and (bottom) Δ-[EuL^2]: D without chiro-optical selection, E right circularly polarized channel, F left circularly polarized channel. *Adapted from Frawley, A.T., Pal, R., Parker, D., 2016. Very bright, enantiopure europium(III) complexes allow time-gated chiral contrast imaging. Chem. Commun. 52, 13349–13352.*

circularly polarised light and the left channel left circularly polarized light. The obtained contrast is evident from Fig. 11.17 (bottom) that could easily be taken advantage of in biosciences and, also, in security tagging.

Creatine kinase (CK) is an important cardiac biomarker that is often used in the clinical diagnosis of acute myocardial infarction. It is therefore desirable to have an efficient assay enabling its quantification at ultralow levels. A bioassay relying on an Eu^{III} metal-organic framework (MOF) with $Q_{ovl} = 48\%$ meets this requirement with CK activity detected down to about 1 U/L (Li et al., 2019). Nanoparticles (NPs) of the corresponding MOF were synthesized from 1,1′:4′,1″:4″,1‴-quaterphenyl-3,3‴,5,5‴-tetracarboxylic acid (H_4QPTCA), europium acetate and oleic acid. When adenosine triphosphate (ATP) is added to a solution of $[Eu(QPTCA)]_\infty$ its intense red emission is quenched, probably because of a PET from ATP to the ligand. On the other hand, adenosine diphosphate (ADP) has a less important quenching effect. This observation and the fact that CK catalyzes the transformation of ATP into ADP while simultaneously converting creatine (Cr) into phosphocreatine (CrP) are the basis of the bioassay described in Fig. 11.18. The analytical reagent is prepared by mixing Eu-QPTCA NPs with creatine and ATP in a solution buffered at pH 9.0. The assay is conducted on human serum samples deposited in a 96-well microplate to which the reagent is added. The Eu^{III}

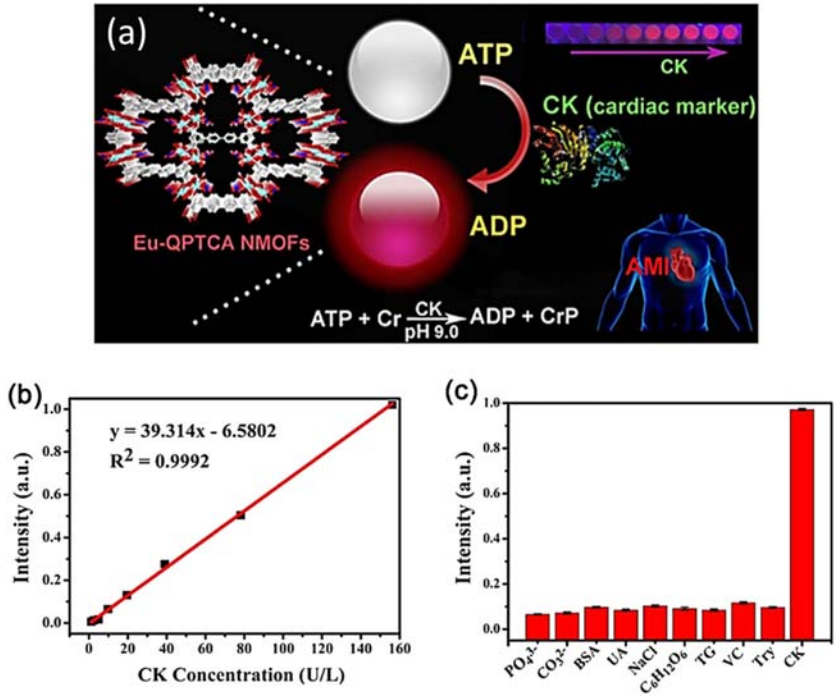

FIG. 11.18 (A) Principle of a bioassay based on an Eu^{III} MOF with $QPTCA^{4-}$. (B) Linear relationship between Eu^{III} emission intensity and the concentration of creatine kinase. (C) Selectivity of the assay with respect to several other analytes. *Adapted from Li, X., Zhou, S., Lu, S., Tu, D., Zheng, W., Liu, Y., et al., 2019. Lanthanide metal-organic framework nanoprobes for the in vitro detection of cardiac disease markers. ACS Appl. Mater. Interf. 11, 43989–43995.*

luminescence is detected in TR mode (delay 0.2 ms) after suitable incubation time. The linear range of the assay is between 1.2 and 156 U/L. The validity of the assay was tested on 100 human serum samples for which CK concentrations between about 40 and 165 U/L were determined by both; the present assay and conventional one; the correlation is very good, with an R^2-factor equal to 0.98.

The Epstein–Barr virus (EBV) belongs to the γ herpes virus family. It infects about 90% of the world population causing latent infection in most cases. The virus replicates in oral epithelium but infects B lymphocytes; it persists in the memory B-cell pool and the host remains asymptomatic with a life-long latent infection. EBV is associated with several distinct human tumors, Burkitt's lymphoma, Hodgkin's disease, B-cell lymphoproliferative syndromes, plasmablastic lymphoma and primary effusion lymphoma. EBV is also linked to non B-cell tumors including T/NK cell lymphomas, nasopharyngeal, and gastric carcinomas; furthermore, it is the causal agent for infectious mononucleosis.

During a latent infection, only a few EBV genes are expressed; latent membrane protein 1 (LMP1) is one of these genes and is the major transforming protein of EBV. With its localization in the cell membrane, LMP1 emerges as an attractive therapeutic agent in EBV-associated malignancies. LMP1 contains a cytoplasmic N-terminus, six trans-membrane domains labeled TM1-6, and a cytoplasmic C-terminus. It works by mimicking the cell surface receptor CD40 to prevent apoptosis of infected B-lymphocytes and drive their proliferation. Several cellular signaling pathways are activated, including those of the nuclear factor NF-κB. The Tm domain TM1 is critical for clustering the LMP1 monomers and therefore, activating them. In particular, the amino acid sequence $FWLY_{38\text{-}41}$ of TM1 plays an essential role in NF-κB activation.

Therefore, the peptide P19 (Pra-KAhx-K-LDLALK-FWLY-K-IVMSDKW-K-RrRK) was designed to mimic the key amino acid sequence $FWLY_{38\text{-}41}$ and for inactivating the NF-κB signal transduction (Chau et al., 2021). This peptide was appended onto lanthanide probes based on a derivatised macrocyclic dota receptor (Fig. 11.19). The EuP19 and YbP19 probes are

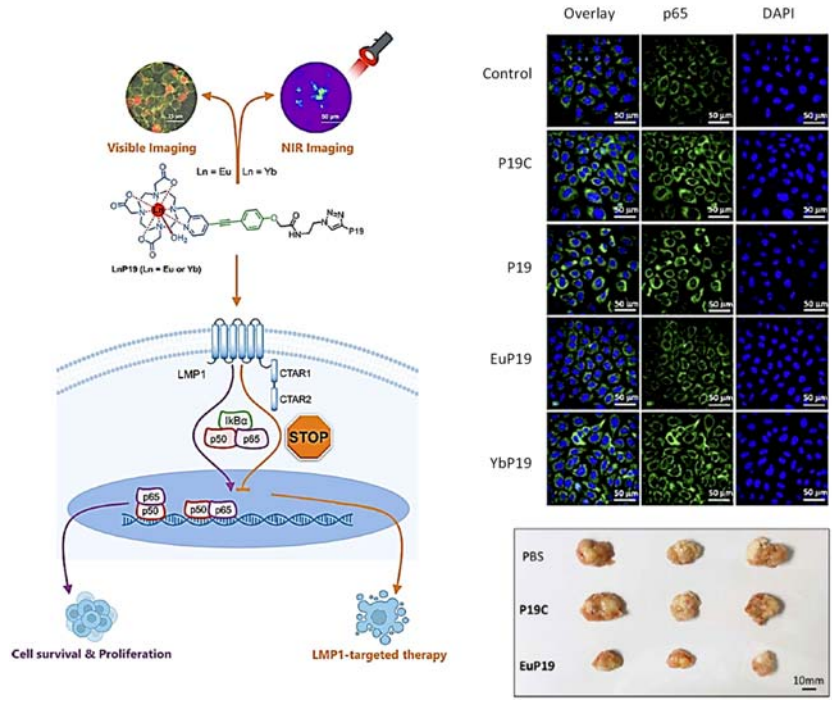

FIG. 11.19 (Left) principle of cancerous cell proliferation inhibition imaging by the LnP19 probes (Ln = Eu, Yb), (Right) imaging ability of the probes (HeLa cells) and tumor inhibition in three groups of LCL3-xenograft mice. *Adapted from Chau, H.F., Wu, Y., Fok, W.Y., Thor, W., Cho, W.C.S., Ma, P.A., et al., 2021. Lanthanide-based peptide-directed visible/near-infrared imaging and inhibition of LMP1. JACS Au, 1, doi 10.1021/jacsau.1c00187. With permission.*

designed for visible and NIR imaging, respectively, while both interact with the TM1 region of LMP1 and inhibit cancer growth. A modified peptide interacting with TM2, and therefore unable to interrupt the oligomerization of LMP1 was also synthesized as control. The in vitro imaging capability of the LnP19 probes are shown for HeLa cells and their prevention of tumor growth on xenograft mice is exemplified in Fig. 11.18. These probes exhibit high cytotoxicity toward LMP1-expressing cells and will contribute to therapeutic advances in Epstein−Barr related cancers.

11.5 Conclusion

This short overview on the luminescence of lanthanide coordination compounds points to its importance in several high-technology applications, particularly in the field of biomedicine. The design of such compounds is intricate and we have tried to draw the attention of the reader on several aspects that are not always reported correctly in the literature, in which oversimplified models are often applied without discrimination. Generalized conclusions cannot be easily drawn and each case has to be considered with its own peculiarities and constraints. Much remains to be done in this 80-year old field and the new tools at disposal of the researchers, such as efficient synthetic methods (e.g., click chemistry) and modeling platforms for assessing energy transfer processes, for instance, should stimulate originality and incite young scientists to have a try!

References

Aebischer, A., Gumy, F., Bünzli, J.-C.G., 2009. Intrinsic quantum yields and radiative lifetimes of lanthanide Tris(dipicolinates). Phys. Chem. Chem. Phys. 11, 1346−1353.

Ahmed, Z., Iftikhar, K., 2014. Efficient photoluminescent complexes of 400-1800 nm wavelength emitting lanthanides containing organic sensitizers for optoelectronic devices. RSC Adv. 4, 63696−63711.

Aquino, L.E.D.N., Barbosa, G.A., Ramos, J.d.L., Giese, O.K., Santana, F.S., Hughes, D.L., et al., 2021. Seven-coordinate Tb^{3+} complexes with 90% quantum yields: high-performance examples of combined singlet- and triplet-to-Tb^{3+} energy-transfer pathways. Inorg. Chem. 60, 892−907.

Bassett, A.P., Van Deun, R., Nockemann, P., Glover, P.B., Kariuki, B.M., Van Hecke, K., et al., 2005. Long-lived near-infrared luminescent lanthanide complexes of imidodiphosphinate "shell" ligands. Inorg. Chem. 44 (18), 6140−6142.

Biju, S., Freire, R.O., Eom, Y.K., Scopelliti, R., Bünzli, J.-C.G., Kim, H.K., 2014. A Eu(III) tetrakis(β-diketonate) dimeric complex: photophysical properties, structural elucidation by sparkle/AM1 calculations, and doping into PMMA films and nanowires. Inorg. Chem. 53, 8407−8417.

Bünzli, J.-C.G., Eliseeva, S.V., 2011. Basics of lanthanide photophysics. In: Wolfbeis, O.S., Hof, M. (Eds.), Springer Series on Fluorescence. Lanthanide Luminescence: Photophysical, Analytical and Biological Aspects, vol. 7. Springer Verlag, Berlin, pp. 1−45.

Bünzli, J.-C.G., Eliseeva, S.V., 2013. Photophysics of lanthanoid coordination compounds. In: Yam, V.W.-W. (Ed.), Comprehensive Inorganic Chemistry II, vol. 8. Elsevier B.V., Amsterdam, pp. 339–398.

Bünzli, J.C.G., Froidevaux, P., Harrowfield, J.M., 1993. Photophysical properties of lanthanide dinuclear complexes with p-tert-Butylcalix[8]arene. Inorg. Chem. 32, 3306–3311.

Bünzli, J.C.G., McGill, I., 2000. Rare earth elements. Ullmann's Encycl. Ind. Chem. 1–53. https://doi.org/10.1002/14356007.a22_607.pub2.

Bünzli, J.-C.G., Petoud, S., Moret, E., 1999. Luminescent properties of the hexakis(nitrito)europate(III) ion, $[Eu(NO_2)_6]^{3-}$. Spectrosc. Lett. 32, 155–163.

Bünzli, J.-C.G., Chauvin, A.-S., Vandevyver, C.D.B., Song, B., Comby, S., 2008. Lanthanide bimetallic helicates for *in vitro* imaging and sensing. An. N. Y. Acad. Sci. 1130, 97–105.

Bünzli, J.C.G., 2003. Macrocyclic complexes. In: Sastri, V.S., Bünzli, J.-C.G., Rao, V.R., Rayudu, G.V.S., Perumareddi, J.R. (Eds.), Modern Aspects of Rare Earths and Complexes, 4B. Elsevier Science B.V., Amsterdam, pp. 303–375.

Bünzli, J.C.G., 2014. Lanthanide coordination chemistry: from old concepts to coordination polymers. J. Coord. Chem. 67, 3706–3733.

Bünzli, J.-C.G., 2014. Luminescence bioimaging with lanthanide complexes. In: de Bettencourt-Dias, A. (Ed.), Luminescence in Lanthanide Coordination Compounds and Nanomaterials. Wiley-Blackwell, Oxford, pp. 125–197. Ch. 4.

Bünzli, J.-C.G., 2015. On the design of highly luminescent lanthanide complexes. Coord. Chem. Rev. 293, 19–47.

Bünzli, J.-C.G., 2019. Lanthanide photonics: shaping the nanoworld. Trend. Chem. 1, 751–762.

Bünzli, J.C.G., 2020. Coordination chemistry. In: Pöttgen, R. (Ed.), Rare Earth Chemistry. De Gruyter, Berlin & Boston, pp. 185–200. Ch. 2.6.

Chau, H.F., Wu, Y., Fok, W.Y., Thor, W., Cho, W.C.S., Ma, P.A., et al., 2021. Lanthanide-based peptide-directed visible/near-infrared imaging and inhibition of LMP1. JACS Au. 1. https://doi.org/10.1021/jacsau.1c00187-.

Ciric, A., Stojadinovic, S., Sekulic, M., Dramicanin, M.D., 2019. JOES: an application software for Judd-Ofelt analysis from Eu^{3+} emission spectra. J. Lumin. 205, 351–356.

De Sa, G.F., Malta, O.L., de Mello Donegá, C., Simas, A.M., Longo, R.L., Santa-Cruz, P.A., et al., 2000. Spectroscopic properties and design of highly luminescent lanthanide coordination complexes. Coord. Chem. Rev. 196, 165–195.

Deng, M., Schley, N.D., Ung, G., 2018. Solvent-dependent sensitization of ytterbium and neodymium via an intramolecular excimer. Inorg. Chem. 57, 15399–15405.

Doffek, C., Alzakhem, N., Bischof, C., Wahsner, J., Güden-Silber, T., Lügger, J., Platas-Iglesias, C., Seitz, M., 2012. Understanding the quenching effects of aromatic C–H- and C–D-oscillators in near-IR lanthanoid luminescence. J. Am. Chem. Soc. 134, 16413–16423.

Dorenbos, P., 2000. The 4f to 4f5d transitions of the trivalent lanthanides in halogenides and chalcogenides. J. Lumin. 91, 91–106.

Dutra, J.D.L., Bispo, T.D., Freire, R.O., 2014. LUMPAC lanthanide luminescence software: efficient and user friendly. J. Comput. Chem. 35, 772–775.

Faustino, W.M., Malta, O.L., de Sá, G.F., 2005. Intramolecular energy transfer through charge transfer state in lanthanide compounds: a theoretical approach. J. Chem. Phys. 122. https://doi.org/10.1063/1.1830452.

Frawley, A.T., Pal, R., Parker, D., 2016. Very bright, enantiopure europium(III) complexes allow time-gated chiral contrast imaging. Chem. Commun. 52, 13349–13352.

Glover, P.B., Bassett, A.P., Nockemann, P., Kariuki, B.M., Van Deun, R., Pikramenou, Z., 2007. Fully fluorinated imidodiphosphinate shells for visible-and NIR-emitting lanthanides: hitherto unexpected effects of sensitizer fluorination on lanthanide emission properties. Chem.−A Eur. J. 13 (22), 6308−6320.

Gompa, T.P., Ramanathan, A., Rice, N.T., La Pierre, H.S., 2020. The chemical and physical properties of tetravalent lanthanides: Pr, Nd, Tb, and Dy. Dalton Trans. 49, 15945−15987.

Gonçalves e Silva, F.R., Malta, O.L., Reinhard, C., Güdel, H.U., Piguet, C., Moser, J.E., et al., 2002. Visible and near-infrared luminescence of lanthanide-containing dimetallic triple-stranded helicates: energy transfer mechanisms in the Sm(III) and Yb(III) molecular edifices. J. Phys. Chem. A. 106, 1670−1677.

Görller-Walrand, C., Binnemans, K., 1996. Rationalization of crystal field parameterization. In: Gschneidner Jr., K.A., Eyring, L. (Eds.), Handbook on the Physics and Chemistry of Rare Earths, vol. 23. Elsevier Science B.V., Amsterdam, pp. 121−283. Ch.155.

Görller-Walrand, C., Binnemans, K., 1998. Spectral intensities of f-f transitions. In: Gschneidner Jr., K.A., Eyring, L. (Eds.), Handbook on the Physics and Chemistry of Rare Earths, vol. 25. Elsevier Science B.V., Amsterdam, pp. 101−264.

Gusev, A., Shul'gin, V., Braga, E., Zamnius, E., Lyubomirskiy, N., Kryukova, M., et al., 2019. Strong enhancement of ionic luminescence Dy(III), Tb(III), Eu(III) and Sm(III) by pyridyl-triazoles. J. Lumin. 2123, 315−321.

Guzman-Mendez, O., Gonzalez, F., Bernes, S., Flores-Alamo, M., Ordonez-Hernandez, J., Garcia-Ortega, H., et al., 2018. Coumarin derivative directly coordinated to lanthanides acts as an excellent antenna for UV−Vis and Near-IR emission. Inorg. Chem. 57, 908−911.

Hasegawa, Y., Kimura, Y., Murakoshi, K., Wada, Y., Kim, J.-H., Nakashima, N., et al., 1996. Enhanced emission of deuterated tris(hexafluoroacetylacetonato)neodymium(III) complex in solution by suppression of radiationless transition via vibrational excitation. J. Phys. Chem. 100, 10201−10205.

Ha-Thi, M.H., Delaire, J.A., Michelet, V., Leray, I., 2010. Sensitized emission of luminescent lanthanide complexes based on a phosphane oxide derivative. J. Phys. Chem., A 114, 3264−3269.

Hernandez, I., Gillin, W.P., 2015. Organic chromophores-based sensitization of NIR-emitting lanthanides: toward highly efficient halogenated environments. In: Bünzli, J.-C.G., Pecharsky, V.K. (Eds.), Handbook on the Physics and Chemistry of Rare Earths, vol. 47. Elsevier Science B.V., Amsterdam, pp. 1−100. Ch. 269.

Hu, J.Y., Ning, Y., Meng, Y.S., Zhang, J., Wu, Z.Y., Gao, S., Zhang, J.L., 2017. Highly near-IR emissive ytterbium(III) complexes with unprecedented quantum yields. Chem. Sci. 8, 2702−2709.

Ishida, H., Bünzli, J.-C.G., Beeby, A., 2016. Guidelines for measurement of luminescence spectra and quantum yields of inorganic compounds, metal complexes, and materials. Pure Appl. Chem. 88, 701−711.

Johnson, K.R., Gracia-Nava, M.A., de Bettencourt-Dias, A., 2020. Thiophene-derivatized pyridine-biscarboxamide as a sensitizer for Ln^{III} luminescence and $^1O_2$ generation. J. Lumin. 224. https://doi.org/10.1016/j.jlumin.2020.117309.

Jørgensen, C.K., Brinen, J.S., 1963. Far UV absorption spectra of cerium(III) and europium(III) aqua ions. Mol. Phys. 6, 629−631.

Judd, B.R., 1962. Optical absorption intensities of rare earth ions. Phys. Rev. 127, 750−761.

Kalyakina, A.S., Utochnikova, V.V., Zimmer, M., Dietrich, F., Kaczmarek, A.M., Van Deun, R., et al., 2018. Remarkable high efficiency of red emitters using Eu(iii) ternary complexes. Chem. Commun. 54, 5221−5224.

Kano, T., 1999. Principal phosphor materials and their optical properties: luminescence centers of rare-earth ions. In: Shionoya, S., Yen, W.M. (Eds.), Phosphor Handbook, vol. 3. CRC Press Inc, Boca Raton, pp. 177−200.

Kleinerman, M., 1968. Choi Sang-Il, Exciton-migration processes in crystalline lanthanide chelates I. Triplet exciton migration in lanthanide chelates of 1,10- phenanthroline. J. Chem. Phys. 49, 3901−3908.

Kleinerman, M., 1969. Energy migration in lanthanide chelates. J. Chem. Phys. 51, 2370−2381.

Kovacs, D., Borbas, K.E., 2018. The role of photoinduced electron transfer in the quenching of sensitized europium emission. Coord. Chem. Rev. 364. https://doi.org/10.1016/j.ccr.2018.03.004.

Kropp, J.L., Windsor, M.W., 1963. Enhancement of fluorescence yield of rare earth ions by heavy water. J. Chem. Phys. 39, 2769−2770.

Lazarides, T., Sykes, D., Faulkner, S., Barbieri, A., Ward, M.D., 2008. On the mechanism of d-f energy transfer in Ru-II/Ln(III) and Os-II/Ln(III) dyads: dexter-type energy transfer over a distance of 20 angstrom. Chem. Eur J. 14, 9389−9399.

Li, X., Zhou, S., Lu, S., Tu, D., Zheng, W., Liu, Y., et al., 2019. Lanthanide metal-organic framework nanoprobes for the in vitro detection of cardiac disease markers. ACS Appl. Mater. Interf. 11, 43989−43995.

Linden-Leibeszeit, J.B.S., Eliseeva, S.V., Chaudhary, N., Zeller, M., Petoud, S., Trivedi, E.R., 2020. Near-infrared emitting heterobimetallic Zn-4f schiff base complexes with visible excitation wavelength. Eur. J. Inorg. Chem. 2020, 75−78.

Lutter, J.C., Eliseeva, S.V., Collet, G., Martinić, I., Kampf, J.W., Schneider, B.L., et al., 2020. Iodinated metallacrowns: toward combined bimodal near-infrared and X-ray contrast imaging agents. Chem. Eur J. 26, 1274−1277.

MacDonald, M.R., Bates, J.E., Ziller, J.W., Furche, F., Evans, W.J., 2013. Evans, completing the series of +2 ions for the lanthanide elements: synthesis of molecular complexes of Pr^{2+}, Gd^{2+}, Tb^{2+}, and Lu^{2+}. J. Am. Chem. Soc. 135, 9857−9868.

Mancino, G., Ferguson, A.J., Beeby, A., Long, N.J., Jones, T.S., 2005. Dramatic increases in the lifetime of the Er^{3+} ion in a molecular complex using a perfluorinated imidodiphosphinate sensitizing ligand. J. Am. Chem. Soc. 127 (2), 524−525.

Moura Jr., R.T., Neto, A.N.C., Aguiar, E.C., Santos- Jr., C.V., de Lima, E.M., Faustino, W.M., et al., 2021. JOYSpectra: a web platform for luminescence of lanthanides. Opt. Mater. X 11. https://doi.org/10.1016/j.omx.2021.100080.

Neil, E.R., Funk, A.M., Yufit, D.S., Parker, D., 2014. Synthesis, stereocontrol and structural studies of highly luminescent chiral tris-amidepyridyl-triazacyclononane lanthanide complexes. Dalton Trans. 43, 5490−5504.

Neto, A.N., Moura, R.T., Malta, O.L., 2019a. On the mechanisms of non-radiative energy transfer between lanthanide ions: centrosymmetric systems. J. Lumin. 210, 342−347.

Neto, A.N.C., Teotonio, E.E., de Sá, G.F., Brito, H.F., Legendziewicz, J., Carlos, L.D., et al., 2019b. Modeling intramolecular energy transfer in lanthanide chelates: a critical review and recent advances. In: Bünzli, J.-C.G., Pecharsky, V.K. (Eds.), Handbook on the Physics and Chemistry of Rare Earths, Including Actinides, vol. 56. Elsevier B.V., Amsterdam, pp. 55−162. Ch. 310.

Ning, Y., Tang, J., Liu, Y.W., Jing, J., Sun, Y., Zhang, J.L., 2018. Highly luminescent, biocompatible ytterbium (III) complexes as near-infrared fluorophores for living cell imaging. Chem. Sci. 9, 3742−3753.

Norton, K., Kumar, G.A., Dilks, J.L., Emge, T.J., Riman, R.E., Brik, M.G., et al., 2009. Lanthanide compounds with fluorinated aryloxide ligands: near-infrared emission from Nd, Tm, and Er. Inorg. Chem. 48, 3573−3580.

Ofelt, G.S., 1962. Intensities of crystal spectra of rare earth ions. J. Chem. Phys. 37, 511–520.

Ogasawara, K., Watanabe, S., Toyoshima, H., Brik, M.G., 2007. First-principles calculations of 4f-4f5d transition spectra. In: Gschneidner Jr., K.A., Bünzli, J.-C.G., Pecharsky, V.K. (Eds.), Handbook on the Physics and Chemistry of Rare Earths, vol. 37. Elsevier Science B.V., Amsterdam, pp. 1–59. Ch. 231.

Peng, Y., Hu, J.X., Lu, H., Wilson, R.M., Motevalli, M., Hernández, I., et al., 2017. Functionalisation of ligands through click chemistry: long-lived NIR emission from organic Er(III) complexes with a perfluorinated core and a hydrogen-containing shell. RSC Adv. 7, 128–131.

Piguet, C., Bünzli, J.C.G., 2010. Self-assembled lanthanide helicates: from basic thermodynamics to applications. In: Gschneidner Jr., K.A., Bünzli, J.-C.G., Pecharsky, V.K. (Eds.), Handbook on the Physics and Chemistry of Rare Earths, vol. 40. Elsevier Science, B.V., Amsterdam, pp. 301–553. Ch. 247.

Pointel, Y., Suffren, Y., Daiguebonne, C., Le Natur, F., Freslon, S., Calvez, G., 2020. Rational design of dual IR and visible highly luminescent light-lanthanides-based coordination polymers. Inorg. Chem. 59, 10673–10687.

Puntus, L.N., Lyssenko, K.A., Antipin, M.Y., Bünzli, J.-C.G., 2008. Role of inner- and outer-sphere bonding in the sensitization of Eu(III) luminescence deciphered by combined analysis of experimental electron density distribution function and photophysical data. Inorg. Chem. 47, 11095–11107.

Qin, X., Liu, X., Huang, W., Bettinelli, M., Liu, X., 2017. Lanthanide-activated phosphors based on 4f-5d optical transitions: theoretical and experimental aspects. Chem. Rev. 117, 4488–4527.

Rice, N.T., Popov, I.A., Russo, D.R., Bacsa, J., Batista, E.R., Yang, P., 2019. Design, isolation, and spectroscopic analysis of a tetravalent terbium complex. J. Am. Chem. Soc. 141, 13222–13233.

Salerno, E.V., Eliseeva, S.V., Schneider, B.L., Kampf, J.W., Petoud, S., 2020. Visible, near-infrared, and dual-range luminescence spanning the 4f series sensitized by a gallium(III)/lanthanide(III) metallacrown structure. J. Phys. Chem. A. 124, 10550–10564.

Samuel, A.P.S., Xu, J., Raymond, K.N., 2009. Predicting efficient antenna ligands for Tb(III) emission. Inorg. Chem. 48, 687–698.

Sato, S., Wada, M., 1970. Relations between intramolecular energy transfer efficiencies and triplet state energies in rare earths β-diketonates. Bull. Chem. Soc. Jpn. 43, 1955–1962.

Shavaleev, N.M., Eliseeva, S.V., Scopelliti, R., Bünzli, J.C.G., 2009a. Designing simple tridentate ligands for highly luminescent europium complexes. Chem. Eur J. 15, 10790–10802.

Shavaleev, N.M., Scopelliti, R., Gumy, F., Bunzli, J.C.G., 2009b. Surprisingly bright near-infrared luminescence and short radiative lifetimes of ytterbium in hetero-binuclear Yb-Na chelates. Inorg. Chem. 48, 7937–7946.

Shuvaev, S., Utochnikova, V., Marciniak, Ł., Freidzon, A., Sinev, I., Van Deun, R., et al., 2014. Lanthanide complexes with aromatic o-phosphorylated ligands: synthesis, structure elucidation and photophysical properties. Dalton Trans. 43, 3121–3136.

Tanner, P.A., Zhou, L., Duan, C., Wong, K.-L., 2018. Misconceptions in electronic energy transfer: bridging the gap between chemistry and physics. Chem. Soc. Rev. 47, 5234–5265.

Walsh, B.M., 2006. Judd ofelt theory: principles and practices. In: Di Bartolo, B., Forte, O. (Eds.), Advances in Spectroscopy for Lasers and Sensing. Springer Verlag, Berlin, pp. 403–433.

Wartenberg, N., Raccurt, O., Bourgeat-Lami, E., Imbert, D., Mazzanti, M., 2013. Multicolour optical coding from a series of luminescent lanthanide complexes with a unique antenna. Chem. Eur J. 19, 3477–3482.

Wei, C., Sun, B., Zhao, Z., Cai, Z., Liu, J., Tan, Y., et al., 2020. A family of highly emissive lanthanide complexes constructed with 6-(diphenylphosphoryl)picolinate. Inorg. Chem. 59, 8800−8808.

Weissman, S.I., 1942. Intramolecular energy transfer. The luminescence of complexes of europium (β-diketonate complexes). J. Chem. Phys. 10, 214−217.

Werts, M.H.V., Jukes, R.T.F., Verhoeven, J.W., 2002. The emission spectrum and the radiative lifetime of Eu^{3+} in luminescent lanthanide complexes. Phys. Chem. Chem. Phys. 4, 1542−1548.

Willauer, A.R., Palumbo, C.T., Fadaei-Tirani, F., Zivkovic, I., Douair, I., Maron, L., et al., 2020. Accessing the +IV oxidation state in molecular complexes of praseodymium. J. Am. Chem. Soc. 142, 5538−5542.

Wong, K.-L., Bünzli, J.-C.G., Tanner, P.A., 2020. Quantum yield and brightness. J. Lumin. 224. https://doi.org/10.1016/j.jlumin.2020.117256.

Ye, H.Q., Peng, Y., Li, Z., Wang, C.C., Zheng, Y.X., Motevalli, M., et al., 2013. Effect of fluorination on the radiative properties of Er^{3+} organic complexes: an opto-structural correlation study. J. Phys. Chem. C 117 (45), 23970−23975.

Ye, H.Q., Li, Z., Peng, Y., Wang, C.C., Li, T.Y., Zheng, Y.X., 2014. Organo-erbium systems for optical amplification at telecommunications wavelengths. Nat. Mater. 13, 382−386.

Zhang, J., Petoud, S., 2008. Azulene-moiety-based ligand for the efficient Sensitization of four near-infrared luminescent lanthanide cations: Nd^{3+}, Er^{3+}, Tm^{3+}, and Yb^{3+}. Chem. Eur J. 14, 1264−1272.

Zhang, T., Zhu, X., Cheng, C.C., Kwok, W.M., Tam, H.L., Hao, J., 2011. Water-soluble mitochondria-specific ytterbium complex with impressive NIR emission. J. Am. Chem. Soc. 133, 20120−20122.

Zhang, Y., Chen, B., Xu, S., Li, X., Zhang, J., Sun, J., et al., 2018. A universal approach for calculating the Judd-Ofelt parameters of RE^{3+} in powdered phosphors and its application for the β-NaYF4:Er^{3+}/Yb^{3+} phosphor derived from auto-combustion-assisted fluoridation. Phys. Chem. Chem. Phys. 20, 15876−15883.

Zhuravlev, K.P., Tsaryuk, V.I., Kudryashova, V.A., 2018. Photoluminescence of europium and terbium trifluoroacetylacetonates. Participation of LMCT state in processes of the energy transfer to Eu^{3+} ion. J. Fluor. Chem. 212, 137−143.

This page intentionally left blank

Chapter 12

Future prospects

Rakshit Ameta
Department of Chemistry, J.R.N. Rajasthan Vidyapeeth (Deemed to be University), Udaipur, Rajasthan, India

12.1 Introduction

Photochemistry deals with the chemistry of excited states and as such, it includes some interesting reactions, which are not available in chemistry of ground state species. This change in their properties like optical, magnetic, thermal, electrical, electronic, etc. will find numerous applications. Some of them are switching behavior, photochromism, photodynamic therapy & sensors in biomedical fields, solar cells like dye-sensitized solar cells, photochemical reduction of carbon dioxide, etc. All such possibilities have been discussed in brief in this chapter.

12.2 Solar cells

Initial works on DSSCs were mainly focused on the coordination compounds of ruthenium only, but these are highly expensive and hazardous in nature to environment as well as human health, both. Nazeeruddin et al. (1993) could achieve an effieciency of 10.3% using Ru (II) complex as sensitizer. Such materials are still in use inspite of these disadvantages. Coordination compounds of copper can be used in DSSCs as dyes as well as redox mediators in liquid electrolytes along with hole-transporting materials because of their available electronic energy levels. Some zinc, iron and cobalt coordination compounds have also been reported to exhibit potential for DSSC applications. Colombo et al. (2017) reviewed the role of copper complexes in dye-sensitized solar cells as redox mediators.

The Ni(II)-chlorophyll complex was used as a sensitizer for increasing efficiency of solar cells (DSSCs) such as short-circuit current (3.00 mA cm^{-2}), open circuit voltage (0.15 V) and the efficiency (0.20%) (Darmokoesoemo et al., 2017). Cebeci et al. (2021) used ruthenium (II) complex with catechol and boronic acid as anchoring group in dye-sensitized solar cell.

Dye-sensitized solar cells are novel type of solar cells, which has lower toxicity on using coordination transition metal compounds alongwith high

Photochemistry and Photophysics of Coordination Compounds. https://doi.org/10.1016/B978-0-12-824493-7.00005-8
Copyright © 2023 Elsevier Inc. All rights reserved.

power conversion efficiency. It was pointed by Pawlus and Jarosz (2022) that there should be more stress on complex containing Cu, as it can act as both; dyes as well as redox mediators, though coordination compounds of other transition metals can also been commonly used.

12.3 Photochromism

Photochromism is defined as reversible transformation of a chemical species (it may also be called as photoswitching) between two forms by absorbing electromagnetic radiations (photoisomerization), where two forms have different absorption spectra (Irie, 2000; Durr and Bouas-Laurent, 2003). Simply, photochromism has been described as a reversible change of color upon exposure to light.

Mastuda et al. (2004) observed that complexes composed of 1,2-bis(2-methyl5-(4-pyridyl)-3-thienyl) perfluorocyclopentene (bidentate ligand) and 1-(2-methyl-5-phenyl-3-thienyl)-2-(2-methyl-5-(4-pyridyl)-3-thienyl) perfluor ocyclopentene (monodentate ligand) of Zn(II), Mn(II), and Cu(II) undergo reversible photochromic reactions on irradiation with UV and visible lights, alternatively. Chan et al. (2011) studied photochromic behavior of some cyclometalated platinum (II) complexes. These complexes exhibited drastic color changes on photoexcitation due to reversible photochromic behavior. Such a behavior was attributed to the substituents on the pyridyl ring and on extent of π-conjugation of the ligand. Chowdhury et al. (2018) observed photochromic behavior of coordinated 1-alkyl-2- (arylazo) imidazole in silver complex due to light induced trans-to-cis isomerization around a bond.

The effect of molecular packing on photochromic performance was studied by Liu et al. (2021). Three secondary building linkers were introduced into the bipyridinium-based complexes and it was observed that these complexes display photochromic behavior due to photo-induced electron transfer process on UV exposure. Xu et al. (2018) reported photochromic behavior in poly-oxometalate (POM)-based diarylethene (DAE) coordination complex. This complex self-organizes and adopted a molecular dumb-bell structure, which is a prerequisite for the photocyclization reaction. Such an assembly can be found to be switchable between two states in presence of visible light.

Wang et al. (2021) synthesized two new crystalline inorganic-organic hybrid compounds as: $\{[Cd(PCV)_{0.5}(BDC)_{0.5}(H_2O)]\cdot 3H_2O\}_n$ and $\{[Zn(PCV)_{0.5}(BDC)_{0.5}]\cdot 3H_2O\}_n$ solvothermally using viologen analog 1-(4-carboxyphenyl)-4,4′-bipyridinium (PCV) and 1,4-benzenedicarboxylate (BDC^{2-}) ligands. It was reported that both these compounds exhibited photochromism with dramatic decrease of photoluminescence upon irradiation. It was also revealed that powdered sample of zinc complex can deposit easily on paper, when it was diffused into ethanol solution. It was suggested that it may have potential application as an inkless and erasable print medium.

12.4 Photodynamic therapy (PDT)

Photodynamic therapy (PDT) has been developed, where there is possibility of using coordination compounds as photosensitizer, which can first absorb the light and generate some reactive oxygen species (ROS). These complexes can be used as such or in combination with some polymers, non-tubules, metal organic framework (MOFs), etc. It was observed that any interaction between deoxyribosenucleic acid (DNA) and such photosensitizer (coordination compound) may play an important role in development of some new effective anticancer drugs. McKenzie et al. (2019) have excellently reviewed the field of use of coordination compound in photodynamic theory. They have reported that use of coordination compounds in photodynamic theory to develop newer anticancer drugs, as these can have relatively much stronger impact on.

(i) Phototoxic index (PI),
(ii) Amount of ROS generated, and
(iii) Quantum emission efficiency.

The major cases of deaths worldwide are caused by cancer, but in many of the cases, it remained undignosed. Raab (1900) introduced use of photosensitizers in photodynamic therapy (PDT) and his work has increased interest of scientists and medical practitioners all over the globe for treatment of cancer. PDT in specific and it does not damage healthy cells as compared to other method used in treatments of cancer.

Near-IR-emitting and/or efficiently photodynamic water-soluble complexes may hold great application potentials in photodynamic therapy and/or photo detection agents for cancers, but this field has been poorly explored. Zhang et al. (2019) reported solvatochromism, calf thymus DNA binding, and singlet oxygen generation properties of ruthenium(II) complex of visible light $[Ru(bpy)_2(dtdpq)](ClO_4)_2$ **(Ru1)** and a new homoleptic complex of near-IR-emitting $[Ru(dtdpq)_3](ClO_4)_2$ **(Ru2)** (bpy = 2,2′-bipyridine, dtdpq = 2,3-bis(thiophen-2-yl)pyrazino[2,3-f][1,10]phenanothroline) in water. They also discussed DNA photocleavage, singlet oxygen generation in HeLa cells, cellular uptake/localization, and in vitro photodynamic therapy for cancer cells of water-soluble **Ru1**. It was observed that **Ru1** has a potential in photodynamic cancer therapy and as mitochondrial imaging agents while **Ru2** can also find application provided its water solubility can be further improved.

Transition metal complexes are quite interesting for their possible applications as photosensitizers in photodynamic therapy and, photochemotherapy (PCT) (Monro et al., 2018). As Ru(II) polypyridyl complexes have emerged as potential candidates for applications in PDT and PCT; both. They have discussed the principles involved in the development of TLD1433, the first Ru(II)-based photosensitizer for PDT, which has reached to a state of human clinical trial. They have also summarized the future trends and exsiting challenges to use PDT into mainstream of cancer therapy. A photosensitizer

TLD-1433 was found quite successful against non-muscle invasive urinary bladder cancer, which was not responsive to contemporary anticancer therapies (Kaspler et al., 2020).

Geraldes et al. (2021) reported that Mn(III) porphyrins have a great potential as MRI contrast agents, which is Gd-free. It is all due to the fact that the cation and the ligand both have some interesting properties. The redox properties of the Mn(III)-ion can be used for the generation of reactive oxygen species, while porphyrin ligand allowed these complexes to have higher affinity for tumor tissues.

Chemotherapy is used for the treatment of cancer. It is a systemic treatment and therefore, in such treatments, all cells in the body of patient are exposed to cytotoxic effects. On the other hand, photodynamic therapy utilizes same reactive oxygen species such as cytotoxic singlet oxygen ($^1O_2$) to induce cell death in cancer cells, so that PDT is a potential localized method (which can treat several types of cancers by making use of inorganic complexes as photosensitizing agents) (Smith et al., 2022).

Presently, platinum (Pt)-based drug, cisplatin, is still used for chemotherapy in treatment of cancer. As transition metal complexes have unique photochemical and photophysical properties, these can find application in photodynamic therapy as well as photoactivated chemotherapy (PCT), as the photobiological activity is based on energy transfer and electron transfer processes, which makes use of these properties. Different transition metal complexes of Ru(II), Rh(III), Pt(IV), Os(II), Ir(III) copper (0 or I), etc. are either being used in diagnosis and therapy of malignant tumors or are under clinical trial. There is a wide scope for designing, synthesizing and using coordination compound of different metal ions for diagnosis and treatment of cancerous cells of various types. Time is not far off, when some effective solution will be searched out for treatment of this dreadful diseases using transition metal complexes.

12.5 Actinometry

An actinometer is a physical device or chemical system, which determines the number of photons in a beam of light integrally or per unit time. It is also called a dosimeter (Kuhn et al., 2004). It was reported by Allmand and Webb (1929a; 1929b) that potassium ferrioxalate actinometer [$K_3Fe(C_2O_4)_3$] was much more sensitive and convenient as compared to uranyl oxalate actinometer. Uranyl oxalate was used as chemical actinometer because accurate quantum yield determination was made for the photolytic destruction of oxalic acid in the uranyl oxalate aqueous system by Forbes and Heidt (1934). The use of iodide as a chemical actinometer using iodate as an electron scavanger was reported by Rahn (1993, 1997). Goldstein and Rabani (2008) determined the quantum yield of the ferrioxalate and iodide−iodate actinometers using a xenon lamp.

Reinecke's salt has also been used as an actinometer, but it has certain disadvantages.

- Experiments should be carried out in dark,
- Reaction medium is temperature sensitive, and
- Toxic reactant is used such as perchloric acid.

Reinecke's salt still remained an affordable actinometer, particular, when implementation is required at pilot- or industrial -scale photoreactors.

Some other actinometers were reported from time to time by various workers (Heller and Langan, 1981; Brauer et al., 1983; Pitre et al., 2015; Roibu et al., 2018).

12.6 Hydrogen as fuel of future

World is facing the problem of energy shortage. The conventional fuels are on the border line of exhaustion and it has been predicted that fuels will reach almost an end within next two or 3 decades such as coal, petrol, diesel, kerosene, etc. Therefore, it is an urgent requirement of the society to develop some alternate sources of energy, which can fulfill our energy demand for future also. Here, hydrogen enters the scene as hydrogen has high energy storage capability and it can produce electricity, when burnt in fuel cells. Hydrogen can be generated by splitting of water in presence of light. Three-fourth of the world is covered by water, so that at present, there is no shortage of source of hydrogen (water). On burning hydrogen, water is again produced and hence, it is a cyclic process. Therefore, hydrogen is advocated as the fuel of future.

Du et al. (2008) used platinum(II) bi- and terpyridyl chloro complexes [Pt(dcbpy)Cl_2 and [Pt(ttpy)Cl]$^+$], [dcbpy = 4,4′-dicarboxyl-2,2′-bipyridine and ttpy = 4-tolyl-2,2′:6′,2″-terpyridine] for photocatalytic production of hydrogen from water. They used methanol or triethanolamine (TEOA) as sacrificial electron donors, and titanium dioxide as an electron relay. It was observed that good sizable amounts of H_2 could be achieved on UV exposure. It was also suggested that the these complexes are simply acting as precursors to platinum colloids that act as the H_2 generating catalyst.

Zarkadoulas et al. (2012) reviewed use of dithiolene complexes as photocatalysts for the photosplitting of water. As these photocatalysts are not much stable in homogeneous solutions and therefore, heterogeneous approach can be applied by anchoring these catalysts on semiconductor or they can be deposited on an electrode in electrocatalytic cell. Such dithiolene complexes composed of some abundantly available and inexpensive metals can replace most expensive platinum for generation of hydrogen.

Lv et al. (2016) reported the synthesis of four Fe bis(benzenedithiolate) complexes. These complexes exhibited catalytic activity for generation of hydrogen, when water-soluble CdSe QDs and ascorbic acid were used as

photosensitizer and sacrificial electron donor, respectively under visible light (520 nm). It was also revealed that the highest activity was exhibited by the complex with the most electron-donating dithiolene ligand.

Inoue et al. (2017) synthesized three Schiff-base-type nickel(II) complexes and corresponding noninnocent-type complexes. They also evaluated their catalytic ability for the photoproduction of hydrogen from water. It was revealed that Schiff-base-type complex with chlorine atoms and noninnocent-type complex with methyl groups on the pendant phenyl rings exhibited higher activity with turnover numbers of four hundread or more. Kadassery et al. (2017) used $[Mn(CO)_3(\mu 3{-}OH)]_4$ tetramer to produce CO, H_2 and hydrogen peroxide (products) in photosplitting of water. It may develop some new strategies for water-splitting reactions using organomanganese complexes.

Some organometallic compounds based on iridium(III) and metal complexes have exhibited some interesting features (Tritton et al., 2022) such as:

- Wide range of versatile chemical structures,
- Unique photophysical properties, and
- Photocatalytic capabilities.

They have also discussed design and evaluation of these compounds as photocatalysts/photosensitizers for production of hydrogen, photocatalytically and suggested some guidelines for design of more efficient and robust photocatalytic systems in future.

Panagiotakis et al. (2019) studied the behavior of a thiosemicarbazone-nickel (II) complex (NiTSC-OMe) as a molecular catalyst for photo-induced production of hydrogen. They used three photosesnsitizers $[ZnTMePy]PCl_4$, $[Ir(ppy)_2(bpy)]PF_6$, and $[Ru(bpy)_3]Cl_2$. It was reported that the system was found to be most efficient, when NiTSC-OMe and $[Ir(ppy)_2(bpy)]PF_6$ were used as catalyst and chromophore, respectively.

12.7 Reduction of carbon dioxide

The global warming and scarcity of energy resources is an existing challenge for scientists all over world. A search is therefore necessary for some alternate strategy to combat against these rapid and ever increasing problems. The conversion of CO_2 into useful synthetic fuels or chemicals through photocatalytic process is an eco-friendly and economical strategy just to achieve a sustainable energy supply. The carbon dioxide can be reduced to variety of products such as HCOOH, HCHO, CO, CH_3OH, CH_4, C_2H_4, C_2H_5OH, etc. Although kinetic barrier increases with the increase of electrons and protons, the reduction of CO_2 to formaldehyde/methanol/methane/ethane is still more difficult as compared to formic acid or CO.

Developing photocatalytic systems for CO_2 reduction will provide useful and energy-rich compounds and would be one of the most important focuses in the field of “artificial photosynthesis” and “solar fuels”. Such studies have

been conducted in the past 3 decades from the perspective of basic science and for solving the problem of shortage and dependence on fossil resources. Yamazaki et al. (2015) reviewed the photocatalytic reduction of carbon dioxide using some metal complexes as photocatalyst and/or photosensitizer.

They discussed the photocatalytic abilities of these three categories.

- Multicomponent systems having photosensitizer and photocatalyst,
- Supramolecular photocatalysts comprising a multinuclear complex, and
- Hybrid systems with metal-complex photocatalysts and inorganic materials.

Fujita (1999) reported the use of transition-metal complexes $Ru(bpy)_2(CO)Xn+$ (bpy = 2,2′-bipyridine, X = CO, Cl, H, etc.), and $CoHMD^{2+}$ (HMD = 5,7,7,12,14,14-hexamethyl-1,4,8,11-tetraazacyclotetradeca-4,11-diene) for photochemical reduction of carbon dioxide.

Liu et al. (2020) reviewed the use of complexes of non-noble metals (Ni, Co, Cu, Fe, and Mn) as molecular catalysts for photochemical CO_2 reduction. It was opined that modification in structure of ligand can also be effective in improving the catalytic performance of complexes (Fig. 12.1).

Obermeier et al. (2021) reported light-driven CO_2 reduction using [Cu(xant)(bcp)]+, (xant = xantphos, bcp = bathocuproine) or $Ir(dFppy)_3$ [dFppy = 2-(4,6-difluorophenyl)pyridine] as photosensitizer. They used triethylamine (TEA) as sacrificial electron donor. The 3d metal catalysts have either dptacn (dipicolyl-triazacyclononane, LN3) or dpdatcn (dipicolyl-diazathiocyclononane, LN2S) as ligands with central metal ion as Fe^{3+}, Co^{3+} or Ni^{2+}. It was suggested that nature of ligand, metal center and composition of solvent influences the selectivity in product formation, meaning that it can be solely H_2 or CO or a mixture of both. The ratio between these two products can be controlled by the right choice of reaction conditions.

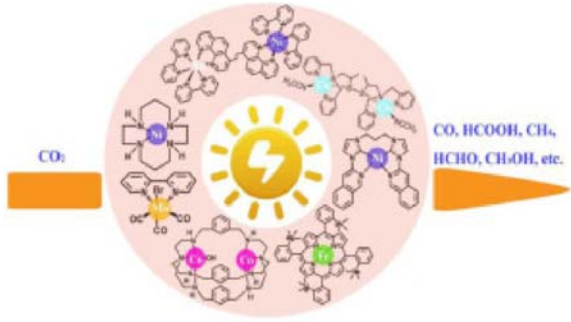

FIGURE. 12.1 Photochemical reduction of carbon dioxide. *Adapted from Liu, D.C., Zhong, D.C., Lu, T.B., 2020. Non-noble metal-based molecular complexes for CO_2 reduction: from the ligand design perspective. EnergyChem 2 (3). doi:10.1016/j.enchem.2020.100034. With permission.*

Kumagai et al. (2022) developed various stable, highly efficient, and selective photocatalytic systems for reduction of CO_2. They used transition metal complexes as photosensitizers as well as catalysts. A mixed system containing ring-shaped Re(I) trinuclear complex (photosensitizer) and fac-[Re(bpy)$(CO)_3\{OC_2H_4N(C_2H_4OH)_2\}$] (catalyst) was used, which selectively photocatalyzed reduction of CO_2 to CO with 82% quantum yield and a high turnover number (600). Not only this, other earth abundant ions, such as Fe(II), Cu(I), and Mn(I) can also be used as central metal cations. When Cu(I) dinuclear complex was taken as a photosensitizer and fac-Mn(bpy)$(CO)_3Br$ as a catalyst, then the total formation quantum yield of CO and HCOOH was 57% and TON was more than 1300.

12.8 Others

A number of complexes exhibited stability toward photodecomposition, but they can undergo excited state redox processes, finding applications in interconversion of chemical energy and light. A combination of photochemistry with supramolecular chemistry can help in designing and fabrication of some multicomponent systems, capable of performing light induced functions. Such photoreactive or luminescent metal complexes can be used in different molecular devices and machines, which can process light signals and molecular machines (Balzani et al., 2008).

As some complexes are photosensitive, they undergo photoaquation reaction, where one of the ligand is replaced by water. Then this water can be exchanged by some other anionic ligand. Sodium nitroprusside contains cyanide ligand, which cannot be easily replaced by other ligands. Sodium nitroprusside has been investigated in this context, where CN^- can be replaced and metabisulphite entered the coordination sphere developing a blue colored complex. It was reported that the amount of ligand can also be estimated spectrometrically within desired limits (Mehta et al., 2003).

Different valence isomers are generated by metal-to-metal charge transfer with markedly different electronic configurations. In particular, because of this transfer, the spin states of single-metal sites and their coupling interactions will also change the symmetry in charge distribution. As a result, significant changes are there, in both; magnetic as well as electric properties of material. Not only this, MMCT affects bond length and absorption spectra, and therefore, some thermal expansion and photochromic behavior can be observed. Such materials having MMCT are potential candidates for switchable multifunctional devices with synergistic responses. Meng et al. (2018) reviewed use of MMCT units as actuators for tuning electric, magnetic, thermal expansion, and photochromic properties and they have also discussed existing challenges and future aspects of this field.

Molecular transition metal ligand complexes are emerging as promising systems in materials science as with different oxidation states coordination

numbers and geometries, and metal d electron configurations, they can undergo electronic transitions. Metal-to-ligand charge-transfer transitions provide them interesting rich redox properties as well as robustness. The properties can be tuned by appropriate selection of strong π-acceptor ligands and low-valence metal centers. They have light-harvesting properties and applications in photocatalysis, and as such, these transition metal complexes can be used as useful materials in phosphorescent organic light-emitting diodes as well as resistive memory devices (Yan et al., 2020).

The photochemistry and photophysics of coordination compounds of actinide ions (An^{n+}) and actinyl ions (AnO_2^{n+}) have been nicely reviewed by Natrajan (2012), almost a decade back. Mostly photochemistry of uranyl(VI) ion has been studied extensively, but photochemistry of other actinides remained less explored, may be due to instability of these ions as most of the actinide elements are undergo radioactive disintrigration. As such, photochemistry of complexes of actinides is not fully understood and it needs further progress in this direction.

References

Allmand, A.J., Webb, W.W., 1929a. The photolysis of potassium ferrioxalate solutions. Part I. Experimental. J. Chem. Soc. 1929, 1518–1531.

Allmand, A.J., Webb, W.W., 1929b. The photolysis of potassium ferrioxalate solutions. Part II. Discussion. . J. Chem. Soc. 1929, 1531–1537.

Balzani, V., Bergamini, G., Ceroni, P., 2008. From the photochemistry of coordination compounds to light-powered nanoscale devices and machines. Coord. Chem. Rev. 252 (23–24), 2456–2469.

Brauer, H.D., Schmidt, R., Gauglitz, G., Hubig, S., 1983. Chemical actinometry in the visible (475–610 nm) BY meso–diphenylhelianthrene. Photochem. Photobiol. 37 (6), 595–598.

Cebeci, C., Arslan, B.S., Güzel, E., Nebioğlu, M., Sişman, İ., Erden, İ., 2021. 4, 5-Diazafluorene ligands and their ruthenium (II) complexes with boronic acid and catechol anchoring groups: design, synthesis and dye-sensitized solar cell applications. J. Coord. Chem. 74 (9–10), 1366–1381.

Chan, J.C.H., Lam, W.H., Wong, H.L., Zhu, N., Wong, W.T., Yam, V.W.W., 2011. Diarylethene-containing cyclometalated platinum (II) complexes: tunable photochromism via metal coordination and rational ligand design. J. Am. Chem. Soc. 133 (32), 12690–12705.

Chowdhury, B., Naskar, K., Mallick, D., Sarkar, K.K., Sen, C., Sinha, C., 2018. Photochromism of {bis (diphenylphosphino) methane} (1-alkyl-2-(arylazo) imidazole) silver hexaflurophosphate complexes. Inorg. Chim. Acta. 483, 87–92.

Colombo, A., Dragonetti, C., Roberto, D., Fagnani, F., 2017. Copper complexes as alternative redox mediators in dye-sensitized solar cells. Molecules 26 (1). https://doi.org/10.3390/molecules26010194.

Darmokoesoemo, H., Fidyayanti, A.R., Setyawati, H., Kusuma, H.S., 2017. Synthesis of complex compounds Ni (II)-chlorophyll as dye sensitizer in dye sensitizer solar cell (DSSC). Korean Chem. Eng. Res. 55 (1), 19–26.

Du, P., Schneider, J., Li, F., Zhao, W., Patel, U., Castellano, F.N., Eisenberg, R., 2008. Bi-and terpyridyl platinum (II) chloro complexes: molecular catalysts for the photogeneration of

hydrogen from water or simply precursors for colloidal platinum? J. Am. Chem. Soc. 130 (15), 5056−5058.

Durr, H., Bouas-Laurent, H. (Eds.), 2003. Photochromism: Molecules and Systems. Elsevier, Amsterdam.

Forbes, G.S., Heidt, L.J., 1934. Optimum composition of uranyl oxalate solutions for actinometry. J. Am. Chem. Soc. 56 (11), 2363−2365.

Fujita, E., 1999. Photochemical carbon dioxide reduction with metal complexes. Coord. Chem. Rev. 185, 373−384.

Geraldes, C.F., Castro, M.M.C., Peters, J.A., 2021. Mn (III) porphyrins as potential MRI contrast agents for diagnosis and MRI-guided therapy. Coord. Chem. Rev. 445. https://doi.org/10.1016/j.ccr.2021.214069.

Goldstein, S., Rabani, J., 2008. The ferrioxalate and iodide-iodate actinometers in the UV region. J. Photochem. Photobiol. A: Chem. 193, 50−55.

Heller, H.G., Langan, J.R., 1981. Photochromic heterocyclic fulgides. Part 3. The use of (E)-α-(2, 5-dimethyl-3-furylethylidene) (isopropylidene) succinic anhydride as a simple convenient chemical actinometer. J. Chem. Soc. 2 (2), 341−343.

Inoue, S., Mitsuhashi, M., Ono, T., Yan, Y.N., Kataoka, Y., Handa, M., Kawamoto, T., 2017. Photo- and electrocatalytic hydrogen production using valence isomers of N2S2-type nickel complexes. Inorg. Chem. 56 (20), 12129−12138.

Irie, M., 2000. Photochromism: memories and switches − introduction. Chem. Rev. 100 (5), 1683−1684.

Kadassery, K.J., Dey, S.K., Cannella, A.F., Surendhran, R., Lacy, D.C., 2017. Photochemical water-splitting with organomanganese complexes. Inorg. Chem. 56 (16), 9954−9965.

Kaspler, P., Mandel, A., Dumoulin-White, R., Roufaiel, M., 2020. Anticancer photodynamic therapy using ruthenium (II) and Os (II)-based complexes as photosensitizers. In: Tumor Progression and Metastasis. IntechOpen, London.

Khun, H.J., Braslavsky, S.E., Schmidt, R., 2004. Chemical actinometry (IUPAC technical report). Pure Appl. Chem. 76 (12), 2105−2146.

Kumagai, H., Tamaki, Y., Ishitani, O., 2022. Photocatalytic systems for CO_2 reduction: metal-complex photocatalysts and their hybrids with photofunctional solid materials. Acc. Chem. Res. 55 (7), 978−990.

Liu, D.C., Zhong, D.C., Lu, T.B., 2020. Non-noble metal-based molecular complexes for CO_2 reduction: from the ligand design perspective. EnergyChem 2 (3). https://doi.org/10.1016/j.enchem.2020.100034.

Liu, J., Lu, Y., Liu, N., 2021. The influence of secondary building linkers on the photochromism of bipyridinium-based complexes. Inorg. Chem. Commun. 132. https://doi.org/10.1016/j.inoche.2021.108783.

Lv, H., Ruberu, T.P.A., Fleischauer, V.E., Brennessel, W.W., Neidig, M.L., Eisenberg, R., 2016. Catalytic light-driven generation of hydrogen from water by iron dithiolene complexes. J. Am. Chem. Soc. 138 (36), 11654−11663.

Matsuda, K., Takayama, K., Irie, M., 2004. Photochromism of metal complexes composed of diarylethene ligands and Zn (II), Mn (II), and Cu (II) hexafluoroacetylacetonates. Inorg. Chem. 43 (2), 482−489.

McKenzie, L.K., Bryant, H.E., Weinstein, J.A., 2019. Transition metal complexes as photo-sensitisers in one-and two-photon photodynamic therapy. Coord. Chem. Rev. 379, 2−29.

Mehta, M.R., Prajapati, V., Ameta, S.C., 2003. Photochemical ligand exchange reactions of sodium nitroprusside: use of metabisulphite ions. Asian J. Chem. 15 (1), 279−286.

Meng, Y.S., Sato, O., Liu, T., 2018. Manipulating metal-to-metal charge transfer for materials with switchable functionality. Angew. Chem. Int. Ed. 57 (38), 12216−12226.

Monro, S., Colon, K.L., Yin, H., Roque III, J., Konda, P., Gujar, S., McFarland, S.A., 2018. Transition metal complexes and photodynamic therapy from a tumor-centered approach: challenges, opportunities, and highlights from the development of TLD1433. Chem. Rev. 119 (2), 797−828.

Natrajan, L.S., 2012. Developments in the photophysics and photochemistry of actinide ions and their coordination compounds. Coord. Chem. Rev. 256 (15−16), 1583−1603.

Nazeeruddin, M.K., Kay, A., Rodicio, I., Humphry-Baker, R., Müller, E., Liska, P., et al., 1993. Conversion of light to electricity by cis-X2bis (2, 2′-bipyridyl-4, 4′-dicarboxylate) ruthenium (II) charge-transfer sensitizers (X = Cl^-, Br^-, I^-, CN^-, and SCN^-) on nanocrystalline titanium dioxide electrodes. J. Am. Chem. Soc. 115 (14), 6382−6390.

Obermeier, M., Beckmann, F., Schaer, R.S., Wenger, O.S., Schwalbe, M., 2021. Sensitized photocatalytic CO_2 reduction with earth abundant 3d metal complexes possessing dipicolyltriazacyclononane derivatives. Front. Chem. 812. https://doi.org/10.3389/fchem.2021.751716.

Panagiotakis, S., Landrou, G., Nikolaou, V., Putri, A., Hardré, R., Massin, J., et al., 2019. Efficient light-driven hydrogen evolution using a thiosemicarbazone-nickel (II) complex. Front. Chem. 7. https://doi.org/10.3389/fchem.2019.00405.

Pawlus, K., Jarosz, T., 2022. Transition metal coordination compounds as novel materials for dye-sensitized solar cells. Appl. Sci. 12 (7). https://doi.org/10.3390/app12073442.

Pitre, S.P., McTiernan, C.D., Vine, W., DiPucchio, R., Grenier, M., Scaiano, J.C., 2015. Visible-light actinometry and intermittent illumination as convenient tools to study Ru (bpy) $3Cl_2$ mediated photoredox transformations. Sci. Rep. 5 (1). https://doi.org/10.1038/srep16397.

Raab, O., 1900. Über die Wirkung fluorescierender Stoffe auf Infusoria. Z. Biol. 39, 524−546.

Rahn, R.O., 1993. Use of potassium iodide as a chemical actinometer. Photochem. Photobiol. 58 (6), 874−880.

Rahn, R.O., 1997. Potassium iodide as a chemical actinometer for 254 nm radiation: use of iodate as an electron scavenger. Photochem. Photobiol. 66 (4), 450−455.

Roibu, A., Fransen, S., Leblebici, M.E., Meir, G., Van Gerven, T., Kuhn, S., 2018. An accessible visible-light actinometer for the determination of photon flux and optical pathlength in flow photo microreactors. Sci. Rep. 8 (1). https://doi.org/10.1038/s41598-018-23735-2.

Smith, C.B., Days, L.C., Alajroush, D.R., Faye, K., Khodour, Y., Beebe, S.J., Holder, A.A., 2022. Photodynamic therapy of inorganic complexes for the treatment of cancer. Photochem. Photobiol. 98 (1), 17−41.

Tritton, D.N., Tang, F.K., Bodedla, G.B., Lee, F.W., Kwan, C.S., Leung, K.C.F., et al., 2022. Development and advancement of iridium (III)-based complexes for photocatalytic hydrogen evolution. Coord. Chem. Rev. 459. https://doi.org/10.1016/j.ccr.2021.214390.

Wang, P.H., Yu, C.M., Wang, M.S., Guo, G.C., 2021. Viologen-based photochromic coordination compounds for inkless and erasable prints. Dye. Pigment. 185. https://doi.org/10.1016/j.dyepig.2020.108888.

Xu, J., Volfova, H., Mulder, R.J., Goerigk, L., Bryant, G., Riedle, E., et al., 2018. Visible-light-driven "on"/"off" photochromism of a polyoxometalate diarylethene coordination complex. J. Am. Chem. Soc. 140 (33), 10482−10487.

Yam, V.W.W., Chan, A.K.W., Hong, E.Y.H., 2020. Charge-transfer processes in metal complexes enable luminescence and memory functions. Nature Rev. Chem. 4 (10), 528−541.

Yamazaki, Y., Takeda, H., Ishitani, O., 2015. Photocatalytic reduction of CO_2 using metal complexes. J. Photochem. Photobiol. C Photochem. Rev. 25, 106−137.

Zarkadoulas, A., Koutsouri, E., Mitsopoulou, C.A., 2012. A perspective on solar energy conversion and water photosplitting by dithiolene complexes. Coord. Chem. Rev. 256 (21−22), 2424−2434.

Zhang, S.Q., Meng, T.T., Li, J., Hong, F., Liu, J., Wang, Y., et al., 2019. Near-IR/visible-emitting thiophenyl-based Ru (II) complexes: efficient photodynamic therapy, cellular uptake, and DNA binding. Inorg. Chem. 58 (20), 14244−14259.

Index

Note: 'Page numbers followed by "*f*" indicate figures and "*t*" indicate tables.'

A

Acetylacetonato, 220−228
Actinometry, 12, 394−395
Aggregation induced phosphorescence enhancement (AIPE), 298−299
Aminopyrazine (ampyz), 122
Anti-interference experiments, 219−220
Archetype ionic transition-metal complexes (iTMCs), 233−235
Aryloxy, 56
Arylthio tetrasubstituted oxotitanium(IV) phthalocyanine complexes, 56
Atom-transfer radical addition reactions (ATRA), 305−306
Au(I) coordination compounds, 327−330, 328f−330f
Au(III) coordination compounds, 330−332, 331f−332f

B

1,2-bis(diphenylphosphino)benzene, 312−313
Bis-dithiolene and diimine-dithiolene complexes, 266−271
Bis(indazol-1-yl)methane ligand, 305
Born-Oppenhiener approximation, 18
Boron dipyrromethene (BODIPY), 275
Bromo compounds, 223

C

Cadmium doped titanium-oxo complex, 57
Carbazoyl-substituted complex, 276
Carbene ligands complexes, 313−316, 314f−315f
Carbon dioxide, reduction of, 396−398, 397f
C-coordinated aryl ring, 279−281
Charge transfer bands, 6−9
Charge-transfer photochemistry, 259−266
  diimine and dipyrrin complexes, 259−266, 260f−261f
Charge transfer spectra, solvent polarity on, 9−12, 10f
Charge transfer-to-solvent transition (CTTS), 24−26
Charge-transfer transitions, 353
Chelating diphosphine ligands, 306−307
Chelating ligands, 137
Chemical actinometers, 42−44
Chemotherapy, 394
Chromium
  heteroleptic tris(polypyridyl) chromium(III) complexes, 94
  intraligand charge-transfer (ILCT), 96
  Nicolas-Louis Vauquelin, 92−93
  photochemical functionalization, 98
  photodynamic therapy (PDT), 95−96
Cisplatin, 394
Cobalt/rhodium-based proton-reduction catalysts, 332
Co(III)-guanidyl complexes, photoredox catalysis of, 213−217, 215f−216f
Coinage metals, 293
CO/NO, release of, 44−46, 45f
Conventional fuels, 395
Coordination-induced spin state switch (CISSS), 276−278
Coordination-promoted photoluminescence (CPPL), 109
Covalent organic frameworks (COFs), 59
CTTS. *See* Charge transfer-to-solvent transition (CTTS)
Cyano-bridged trinuclear complex, 93
Cyclic (alkyl) (amino)carbene (CAAC), 314−316
Cyclometalated Ir(III) complexes, 232−233
Cyclometalated Rh(III) complex, 226−228
Cyclometalation, 141−142

D

d-d transitions, 2
  laporte selection rule, 2
Deactivation processes, 2−9, 3f

Deactivation processes (*Continued*)
photochemical deactivation processes, 4–9
photophyscial deactivation processes, 3–4
Density functional theory (DFT), 25
Deoxyribosenucleic acid (DNA), 393
Designing highly luminescent chelates, 367–380
optimizing energy transfer, 367–369, 368f
principles, 367
Diamidocarbene (DAC), 314–316
Dichloromethane solution, 284
Dihedral angle (DHA), 306–307
Diimine
complexes, 259
dipyrrin complexes, 259–266, 260f–261f
Dimesitylborylduryllethynyl (DBDE), 156
Di-2-picolylamine (DPA), 246–248
Distorted tetrahedral geometry, 312–313
Dithiolene complexes, 270–271
Dodeca-niobate materials, 85
DSSC. *See* Dye-sensitized solar cell (DSSC)
Dye-sensitized solar cell (DSSC), 169–170, 169f–170f, 293–294, 391–392

E

Efficient sensitizing systems, examples of, 376–380, 377t–378t
Electronic coupling, 137
Electronic transitions, 349–358
Electron transfer (ET), 162–164
Elements and coordination chemistry, 341–345
coordination chemistry, 343–345
electronic configuration, 342–343
hydration and chelate effect, 344
ionic radius, 343
lability, 344–345
lanthanides and rare earths, 341–342, 342f
Ln-ligand chemical bond, 343–344
oxidation numbers, 342–343, 342f
Elimination processes, 4
Emission
probability and radiative lifetime, 357–358
properties, 151
Energy levels, 345–349, 346f, 347t
Energy transfer processes, quantitative aspects of, 361–366
calculation packages, 363–365
JOYSpectra platform, 365–366, 366f
LUMPAC program, 363
quantitative models, 363–365
simplistic model, 361–363, 362f
Epstein–Barr virus (EBV), 382
Ethylenediamine tetraacetic acid (EDTA), 145
Excited state life time, 151–152
Excited-state potentials (ESPs), 124–125
Excited state redox properties, 152–153
External quantum efficiency (EQE), 108
Extreme ultraviolet (EUV), 66

F

Favorable excited-state redox properties, 216
Ferrioxalate actinometer, 43
f↔f transitions, modeling the intensity of, 354–357
Franck–Condon (FC) barriers, 125
Fukui functions, 267–268

G

Glycine-peroxo complexes of vanadium, 77
Gold complexes
Au(I) coordination compounds, 327–330, 328f–330f
Au(III) coordination compounds, 330–332, 331f–332f

H

Hafnium, coordination compounds of, 67–69
Haloamminerhodium(III) complexes, 223–224
Heteroleptic Ag(I) coordination compounds, 324–327, 325f–327f
Heteroleptic Cu(I) coordination compounds, 306–317, 307f, 309f
carbene ligands complexes, 313–316, 314f–315f
miscellaneous Cu(I) coordination compounds, 316–317, 317f
N^O, N^P and S^P ligands, 312–313, 312f
phenanthroline complexes, 310–311, 310f
pyridyl-type ligands, complexes with, 311–312
Heteroleptic [M(diimine)(dithiolate)] complexes, 267–268
Heteroleptic tris(polypyridyl)chromium(III) complexes, 94
Heteroleptic zirconium and hafnium complexes, 65
Highest occupied molecular orbital (HOMO), 15, 19–20
Hole-transporting material (HTM), 228–231

Homogeneous photocatalytic hydrogen, 107–108
Homoleptic Ag(I) coordination compounds, 322–324, 324f
Hund's rule, 15
Hydrated vanadium ions, 81
Hydrogen
  evolution reaction, 174
  as fuel of future, 395–396
Hydrohalic acid, 190
Hydrothermally synthesized novel, 219–220
Hydrothermal syntheses, 58

I

Interconfigurational transitions, 350, 351t, 352f
Internal conversion (IC), 18, 27
Intersystem crossing (ISC), 15, 22, 27, 149–150, 298
Intraconfigurational f↔f transitions, 354
Intraligand charge-transfer (ILCT), 9, 96
Intramolecular redox processes, 4
Iron, coordination compounds of
  electronic structures and photophysics, 136–144, 138f, 140f–143f
  photochemistry of, 144–147, 146f

J

Jablonski diagram, 16–17, 17f, 21
JOYSpectra platform, 365–366, 366f

L

Lanthanides
  designing highly luminescent chelates, 367–380
    optimizing energy transfer, 367–369, 368f
    principles, 367
  efficient sensitizing systems, examples of, 376–380, 377t–378t
  elements and coordination chemistry, 341–345
    coordination chemistry, 343–345
    electronic configuration, 342–343
    hydration and chelate effect, 344
    ionic radius, 343
    lability, 344–345
    lanthanides and rare earths, 341–342, 342f
    Ln-ligand chemical bond, 343–344
    oxidation numbers, 342–343, 342f
  emission probability and radiative lifetime, 357–358
  energy transfer processes, quantitative aspects of, 361–366
    calculation packages, 363–365
    JOYSpectra platform, 365–366, 366f
    LUMPAC program, 363
    quantitative models, 363–365
    simplistic model, 361–363, 362f
  Epstein–Barr virus (EBV), 382
  f↔f transitions, modeling the intensity of, 354–357
  lanthanide luminescence, sensitization of, 358–360, 359f–361f
  luminescence, 345–366
    electronic transitions, 349–358
    energy levels, 345–349, 346f, 347t
    selection rules, 349–350
  luminescence, sensitization of, 358–360, 359f–361f
  luminescent lanthanide chelates at work, 380–384, 381f
  minimizing non-radiative deactivation processes, 369–376
    NIR emission, 372–376, 373f, 374t
    photoelectron transfers (PET), 369–371, 370f
    vibrational quenching, 371–372, 371f
  transitions, 350–354
    charge-transfer transitions, 353
    interconfigurational transitions, 350, 351t, 352f
    intraconfigurational f↔f transitions, 354
    ligand-centered charge transfers, 353–354
    ligand-to-metal charge transfers (LMCT), 353
    metal-to-ligand charge transfers (MLCT), 353
  vibronic transitions, 358
Laporte selection rule, 2
Ligand-centered charge transfers, 353–354
Ligand field analysis, 91–92
Ligand field photophysics and photochemistry
  bis-dithiolene and diimine-dithiolene complexes, 266–271
  carbazoyl-substituted complex, 276
  C-coordinated aryl ring, 279–281
  charge-transfer photochemistry, 259–266

Ligand field photophysics and photochemistry (*Continued*)
diimine and dipyrrin complexes, 259–266, 260f–261f
coordination-induced spin state switch (CISSS), 276–278
dichloromethane solution, 284
nickel complexes, 256–258, 257f, 258t
other complexes, 276–286
palladium and platinum complexes, 258–259
photophysical processes, 277f
salen-type complexes, 271–286, 272f, 276f
UV-Vis absorption, 278f
Ligand rearrangements, 39
Ligand-to-ligand charge transfer (LLCT) bands, 9
Ligand-to-metal charge transfer (LMCT), 7, 60, 62, 64
Light-initiated time-resolved X-ray absorption spectroscopy (LITR-XAS), 303
Linkage photoisomerization, 38
Lowest energy excited state (LEES), 27
Lowest unoccupied molecular orbital (LUMO), 15, 19–20
Luminescence, 79, 345–366
electronic transitions, 349–358
energy levels, 345–349, 346f, 347t
selection rules, 349–350
Luminescent Co(II/III) complexes
Co(III)-guanidyl complexes, photoredox catalysis of, 213–217, 215f–216f
metal-ion sensing by Co(II) complexes, 217–220, 218f
polyhetrocyclic and polypyridyl Co(II/III) complexes, photophysical properties of, 206–213
Luminescent coordination polymers (LCPs), 217–219
Luminescent Ir(II/III) complexes
metal-ion, biological sensing of, 246–248, 247f
photoredox catalysis, 241–244, 243f, 245f
polypyridyl Ir(III) complexes, photophysical properties of, 232–241
solid-state lighting, 232–241, 234f, 240f–241f
Luminescent lanthanide chelates at work, 380–384, 381f
Luminescent Rh(0/I/II/III) complexes
acetylacetonato, 220–228
metal-ion sensing by Rh(III) complexes, 228
OLED devices, Rh(III) complexes in, 228–231, 229f–230f
polypyridylamine, 220–228
thiolato and macrocyclic ligands, 220–228, 221f
LUMPAC program, 363

M

Malachite green leucocyanide (MGL) actinometer, 44
Manganese, 115–123, 118f, 120f, 122f
tricarbonyl complexes, 121–122
Mesoionic carbene ligand, 142
Metal bis-dithiolene complexes, 267
Metal centered (MC) electronic transitions, 295–296
Metal complexes, 21
Metal-ion sensing, 246–248, 247f
biological sensing of, 246–248, 247f
Co(II) complexes, 217–220, 218f
Rh(III) complexes, 228
Metal organic framework (MOFs), 393
Metal-to-ligand charge transfer (MLCT), 8, 8f, 75, 101, 115, 121–122, 353
Metal-to-metal charge transfer (MMCT), 177, 398
Minimizing non-radiative deactivation processes, 369–376
Miscellaneous Cu(I) coordination compounds, 316–317, 317f
Mixed-metal dicyanoargentate-bridged coordination polymers, 118–119
Molecular systems, 19–20
Molecular transition metal ligand complexes, 398–399
Molybdenum, 100–106
Monoamido-aminocarbene (MAC), 314–316
Mono- and binuclear counterparts, 274–275
Monoanionic catalyst, 269
Monometallic molecular complexes, 294–295
Mononuclear molybdenum complex, 101
Multinuclear ruthenium complexes, 176
Multiporphyrin array ultrathin films, 57–58

N

Nano-scale devices and machines, 51–52
N-donor ligands, 303–304

Near IR phosphorescent osmium complexes, 184−186, 185f
N-heterocycliccarbene (NHC), 139−140, 145, 313, 331
Nickel bis-dithiolene complexes, 269
Nickel complexes, 256−258, 257f
Nickel diimine complexes, 262
Nicolas-Louis Vauquelin, 92−93
Niobium complexes, coordination compounds of
  atom transfer radical polymerization (ATRP), 83−84
  bimetallic compounds, 83
  dodeca-niobate materials, 85
  photochemistry of, 83
  polydispersity index (PDI), 83−84
  pyridine, 85
NIR emission, 372−376, 373f, 374t
Nitrides, 84
N^O, N^P and S^P ligands, 312−313, 312f

O

Octahedral molybdenum cluster compounds, 102
OLED. *See* Organic light emitting device (OLED)
Organic and coordination compounds, 15
Organic light emitting device (OLED), 29, 63, 127, 182, 184, 228−231, 293−294
  Rh(III) complexes in, 228−231, 229f−230f
Osmium complexes, coordination compounds of
  near IR phosphorescent osmium complexes, 184−186, 185f
  photoactive oxidation states of, 178−184, 179f−183f
  photochemistry and applications of, 188−191, 189f, 191f−192f
  photodynamic therapy, photosensitizers for, 187−188, 188f
  photophysics of, 186−187, 187f

P

Palladium and platinum complexes, 258−259
Palladium-directed self-assembly, 57−58
Pd(II) phenyl-substituted dipyrrin complex, 264−266
PDT. *See* Photodynamic therapy (PDT)
Phenantrolines, 305, 310−311, 310f
Phenyl azo salicylaldehyde (PAS), 82
Phosphine-functionalized zirconocene, 64
Photoactivated carbon monoxide releasing moiety (photoCORM), 107
Photoactivated chemotherapy (PCT), 394
Photoactive iron complexes, 143−144
Photoactive oxidation states of, 178−184, 179f−183f
Photoanation reactions, 6
Photocatalysis, 49−51, 50f
Photocatalysts, photosensitizer, 332
Photochemical deactivation processes, 4−9
  charge transfer bands, 6−9
  elimination processes, 4
  intraligand charge-transfer (ILCT) bands, 9
  intramolecular redox processes, 4
  ligand-to-ligand charge transfer (LLCT) bands, 9
  ligand-to-metal charge transfer (LMCT) bands, 7
  metal-to-ligand charge transfer (MLCT) Bands, 8, 8f
  photoanation reactions, 6
  photochemical isomerization reactions, 5−6
  photorecemization reactions, 5
  photoredox addition, 4
  photosubstitution reactions, 5
Photochemical dissociation/homolysis, 262
Photochemical functionalization, 98
Photochemical isomerization reactions, 5−6
Photochemical process
  applications, 41−52
  charge transfer-to-solvent transition (CTTS), 25−26
  charge−transfer-to-solvent transition (CTTS), 24
  chemical actinometers, 42−44
  CO/NO, release of, 44−46, 45f
  coordination compounds, photoluminescence in, 30−34
  definition, 34−41
  density functional theory (DFT), 25
  ferrioxalate actinometer, 43
  internal conversion (IC), 27
  Inter System Crossing (ISC), 27
  lowest energy excited state (LEES), 27
  malachite green leucocyanide (MGL) actinometer, 44
  nano-scale devices and machines, 51−52
  orange light exciting diodes (OLED), 28
  organic light emitting diodes (OLEDs), 29
  photocatalysis, 49−51, 50f

Photochemical process (*Continued*)
photochromism, 41−42
photorearrangement reactions, 37−40
ligand rearrangements, 39
linkage photoisomerization, 38
photoracemization, 37
photoredox
catalysis, 46−47, 48f
reactions, 40−41
photosubstitution reactions, 34−37
ligand exchange reactions, 36
photoanation reaction, 35
photoaquation reactions, 34, 37−40
Reinecke's salt actinometer, 44
ruthenium complexes,
photochemiluminescence in, 47−48
sensors, coordination compounds as, 49
superamolecular photochemistry, 23
triplet quenchers, coordination compounds as, 48−49
uranyl oxalate actinometer, 43
Photochemistry, 188−191, 189f, 191f−192f
charge transfer spectra, solvent polarity on, 9−12, 10f
d-d transitions, 2
laporte selection rule, 2
deactivation processes, 2−9, 3f
photochemical deactivation processes, 4−9
photophyscial deactivation processes, 3−4
excited state, 10
ground state, 10
photochemotherapy (PCT), 12
photodynamic therapy (PDT), 12
solar cells, 12
Photochemotherapy (PCT), 12
Photochromism, 41−42, 392
Photodynamic therapy (PDT), 12, 95−96, 164−169, 165f, 167t, 168f, 393−394
photosensitizers for, 187−188, 188f
Photoelctrochemical (PEC) cell., 107
Photoelectron transfers (PET), 369−371, 370f
Photogeneration of hydrogen, 12
Photoinduced electron transfer reactions, 162−164
Photo-induced reactions, 16
Photoluminescence, 30−34
Photoluminescence (PL), 155
Photoluminescence followed by electron transfer (PFET), 181
Photoluminescence quantum, 327
Photophyscial deactivation processes, 3−4
Photophysical processes, 277f
Photophysical properties of CU(I) complexes
entatic principle and implication, 317−322, 318f, 320f−321f
Photoracemization, 37
Photorearrangement reactions, 37−40
ligand rearrangements, 39
linkage photoisomerization, 38
photoracemization, 37
Photorecemization reactions, 5
Photoredox addition, 4
Photoredox catalysis, 46−47, 48f, 241−244, 243f, 245f
Photoredox catalyst (PRC), 216−217
Photoredox reactions, 40−41
Photoreduction of carbon dioxide, 12
Photosensitizer (PS), 164−166
Photosensors, 12
Photosubstitution reactions, 5, 34−37
ligand exchange reactions, 36
photoanation reaction, 35
photoaquation reactions, 34, 37−40
Pincer ligands, 182
Platinum (Pt)-based drug, 394
Polycaprolactone (PCL) matrix., 61
Polyhetrocyclic and polypyridyl Co(II/III) complexes, photophysical properties of, 206−213
Polyoxo-titanium cluster complexes, 59
Polypyridylamine, 220−228
Polypyridyl Ir(III) complexes, photophysical properties of, 232−241
Polypyridyl ligand architectures, 184−185
Potential energy surfaces (PESs), 17−19
Psoriasis, 82
Push-pull ligand system, 139
Pyridyltriazole complexes, 185−186
Pyridyl-type ligands, complexes with, 311−312

Q

Quantum yield, 152

R

Reactive oxygen species (ROS), 144, 166, 187
Reduced graphene oxide (rGO-VO), 82
Rehenium, 125−131, 126f, 128f
Reinecke's salt actinometer, 44

Ruthenium complexes,
photochemiluminescence in, 47–48
Ruthenium, coordination compounds of
dye-sensitized solar cell (DSSC), 169–170, 169f–170f
excited state reactions of, 162–164, 163f
photocatalysis of, 171–178
photodynamic therapy (PDT), 164–169, 165f, 167t, 168f
photophysical properties of, 153–162, 157f, 159f, 161f–162f
photophysics of, 147–178
absorption spectra of, 148–151, 148f–149f
emission properties, 151
excited state life time, 151–152
excited state redox properties, 152–153
quantum yield, 152
selected examples of, 172t–173t, 174f–177f
sensors and for imaging applications, 170–171

S

Salen-type complexes, 271–286, 272f, 276f
Salicylate-stabilized polyoxo-titanium clusters, 58–59
Schiff-base-type nickel(II) complexes, 396
S-donor atoms coordinates, 266–267
Selection rules, 349–350
Sensors, coordination compounds as, 49
Silver complexes
heteroleptic Ag(I) coordination compounds, 324–327, 325f–327f
homoleptic Ag(I) coordination compounds, 322–324, 324f
Single-crystal absorption data, 258
Single electron transfer (SET), 216–217
Sodium ascorbate (NaHA), 190
Sodium nitroprusside, 398
Solar cells, 12, 391–392
Solid-state lighting, 232–241, 234f, 240f–241f
Spin-orbit coupling (SOC), 18, 298
Superamolecular
photochemistry, 23
Supramolecular
assembly, 178

T

Tantalum, coordination compounds of, 85–88, 87f
Technetium, 123–125
Tert-butylacetic acid ligands, 57
Tetrachloropalladate, 259
Tetraethyl orthosilicate (TEOS), 61–62
Tetrazamacrocyclic ligands, 226
Thermally activated delayed fluorescence (TADF), 146, 298
Thermally equilibrated excited (THEXI), 149–150
Thiolato and macrocyclic ligands, 220–228, 221f
Three-dimensional polymeric cobalt compound, 209–210
Titanium, coordination compounds of, 55–61
Titanium(IV) oxo-complexes (TOCs), 59
Transition metal complexes, luminescence in, 92
Transitions, 350–354
charge-transfer transitions, 353
interconfigurational transitions, 350, 351t, 352f
intraconfigurational f↔f transitions, 354
ligand-centered charge transfers, 353–354
ligand-to-metal charge transfers (LMCT), 353
metal-to-ligand charge transfers (MLCT), 353
Triethanolamine (TEOA), 119, 395
Trimethoxy silyl propanamine (TMSPA), 82
Triplet quenchers, coordination compounds as, 48–49
Triplet-triplet annihilation (TTA), 275
Tungsten, 106–109
Two octacationic oxotitanium phthalocyanines (TiOPcs), 56

U

Uranyl oxalate, 394
actinometer, 43
UV-Vis absorption, 278f

V

Vanadium, coordination compounds of, 76–82, 79f–81f
C–H bonds, 81–82
DSSC, 78
electrode potentials, 77
internal conversion (IC), 81

Vanadium, coordination compounds of (*Continued*)
intersystem crossover (ISC), 81
oxovanadium, 78
panchromium, 76–77
phenyl azo salicylaldehyde (PAS), 82
psoriasis, 82
trimethoxy silyl propanamine (TMSPA), 82
Vibrational quenching, 371–372, 371f
Vibronic transitions, 358
Visible-light-absorbing semiconductor, 178
Volatile organic compound (VOC), 85, 123–124

W

Water oxidation catalyst (WOC), 171
Werner's theory, 91–92

X

X-ray
absorption and optical emission, 319–320
crystallography, 311

Z

Zirconium, 61–67, 64f–65f

Photochemistry and Photophysics of Coordination Compounds

Fundamentals and Applications

Rakshit Ameta, Avinash Kumar Rai, Jayesh P. Bhatt, Shipra Bhardwaj and Suresh C. Ameta

A structured guide to the photochemical and photophysical properties of coordination compounds for a wide range of applications.

Coordination complexes offer a huge range of interesting properties, and understanding the differing photochemical and photophysical characteristics of complexes with different metal centers, will allow researchers to understand behaviors, compare available options, and make the best selection for their specific needs. *Photochemistry and Photophysics of Coordination Compounds* provides a systematic overview of the photochemical and photophysical properties of coordination compounds with different metal cores.

Beginning with a clear introduction to the fundamentals of both, photochemistry and coordination chemistry, the book goes on to outline the photochemical and photophysical properties of a large range of coordination compounds, clustering metal cores together in chapters according to their periodic table group, ranging across transition metals, lanthanides, and actinides. In addition to outlining their properties, each chapter discusses the synthesis, current applications, and future potential of coordination compounds in each group.

Drawing on the experience of a global team of experts, *Photochemistry and Photophysics of Coordination Compounds* is an authoritative guide for all those interested in understanding and harnessing the photochemical properties and potential applications of coordination complexes for their own work.

Key Features

- Introduces the fundamentals of both: photochemistry and coordination compounds
- Supports learning through carefully structured content, with chapters uniquely arranged by group of periodic table
- Bridges the knowledge gap between theory and practice by presenting application examples in each chapter

ELSEVIER

ACADEMIC PRESS
An imprint of Elsevier
elsevier.com/books-and-journals

ISBN 978-0-12-824493-7

Quantum Dots

Fundamentals, Synthesis and Applications



Edited by
Rakshit Ameta
Jayesh P. Bhatt
Suresh C. Ameta

ELSEVIER

Quantum Dots

Fundamentals, Synthesis and Applications

This page intentionally left blank

Quantum Dots

Fundamentals, Synthesis and Applications

Edited by

Rakshit Ameta

Jayesh P. Bhatt

Suresh C. Ameta



ELSEVIER

Elsevier
Radarweg 29, PO Box 211, 1000 AE Amsterdam, Netherlands
The Boulevard, Langford Lane, Kidlington, Oxford OX5 1GB, United Kingdom
50 Hampshire Street, 5th Floor, Cambridge, MA 02139, United States

Copyright © 2023 Elsevier Inc. All rights reserved.

No part of this publication may be reproduced or transmitted in any form or by any means, electronic or mechanical, including photocopying, recording, or any information storage and retrieval system, without permission in writing from the publisher. Details on how to seek permission, further information about the Publisher's permissions policies and our arrangements with organizations such as the Copyright Clearance Center and the Copyright Licensing Agency, can be found at our website: www.elsevier.com/permissions.

This book and the individual contributions contained in it are protected under copyright by the Publisher (other than as may be noted herein).

Notices

Knowledge and best practice in this field are constantly changing. As new research and experience broaden our understanding, changes in research methods, professional practices, or medical treatment may become necessary.

Practitioners and researchers must always rely on their own experience and knowledge in evaluating and using any information, methods, compounds, or experiments described herein. In using such information or methods they should be mindful of their own safety and the safety of others, including parties for whom they have a professional responsibility.

To the fullest extent of the law, neither the Publisher nor the authors, contributors, or editors, assume any liability for any injury and/or damage to persons or property as a matter of products liability, negligence or otherwise, or from any use or operation of any methods, products, instructions, or ideas contained in the material herein.

ISBN: 978-0-12-824153-0

For Information on all Elsevier publications
visit our website at https://www.elsevier.com/books-and-journals

Publisher: Susan Dennis
Acquisitions Editor: Charles Bath
Editorial Project Manager: Ali Afzal-Khan
Production Project Manager: Bharatwaj Varatharajan
Cover Designer: Mark Rogers

Typeset by MPS Limited, Chennai, India



Dedication

Dedicated to Mrs. Anita Ameta
who had been a vital force behind us to complete
this project



This page intentionally left blank

Contents

List of contributors xiii
About the editors xv
Preface xvii

1. Introduction 1
Suresh C. Ameta

1.1 Introduction 1
1.1.1 Advantages 2
1.1.2 Disadvantages 3
1.2 Unique features of quantum dots 3
1.2.1 High surface-to-volume ratio 3
1.2.2 Surface plasmon resonance 3
1.2.3 Quantum confinement effect 4
1.3 Classification of quantum dots 4
1.3.1 Core-type quantum dots 4
1.3.2 Core–shell quantum dots 5
1.3.3 Alloyed quantum dots 5
1.4 Synthesis of quantum dots 8
1.4.1 Top-down approach 8
1.4.2 Bottom-up approach 9
1.4.3 Methods of synthesis 9
1.5 Applications of quantum dots 9
1.5.1 Solar cells 10
1.5.2 Sensors 11
1.5.3 Light emitting diodes 11
1.5.4 Photocatalysis 11
1.5.5 Hydrogen generation 12
1.5.6 Biomedicals 12
1.6 Conclusion 13
References 13

2. Hydrothermal synthesis of quantum dots 15
Jayesh P. Bhatt and Neha Godha

2.1 Introduction 15
2.1.1 Advantages 17

2.1.2 Disadvantages 17
2.2 Metal-based quantum dots 17
2.2.1 Metal oxide quantum dots 17
2.2.2 Metal sulfide quantum dots 19
2.2.3 Others 21
2.3 Nonmetal-based quantum dots 21
2.3.1 Carbon-based quantum dots 21
2.3.2 Graphene-based quantum dots 26
2.4 Recent developments 28
2.5 Conclusion 29
References 29

3. Sol–gel synthesis of quantum dots 35
Avinash K. Rai and Kanchan K. Jat

3.1 Introduction 35
3.1.1 Advantages 37
3.1.2 Disadvantages 37
3.2 Synthesis of quantum dots 37
3.2.1 Oxides 37
3.2.2 Sulfides 44
3.2.3 Carbon-based quantum dots 46
3.2.4 Graphene based 47
3.3 Others 47
3.4 Conclusion 48
References 48

4. Laser ablation synthesis of quantum dots 53
Neetu Shorgar, Indu Bhati and Priyanka Jhalora

4.1 Introduction 53
4.2 Laser ablation 53
4.2.1 Advantages 54
4.2.2 Disadvantages 55
4.3 Metal-based quantum dots 55
4.3.1 Metals 55
4.3.2 Metal oxides 56
4.3.3 Metal sulfides 59
4.3.4 Metal selenides 62
4.4 Nonmetal-based quantum dots 63
4.4.1 Carbon-based quantum dots 63
4.4.2 Graphene-based quantum dots 64
4.5 Others 65
4.6 Recent developments 68
4.7 Conclusion 69
References 69

5. Coprecipitation synthesis of quantum dots 77
Monika Jangid and Seema Kothari

5.1 Introduction 77
5.1.1 Advantages 77
5.1.2 Disadvantages 78
5.2 Classification of coprecipitation 78
5.3 Synthesis of quantum dots 79
5.3.1 Metal oxide quantum dots 79
5.3.2 Metal sulfides 80
5.3.3 Metal selenide quantum dots 83
5.3.4 Carbon-based 84
5.3.5 Graphene-based 85
5.3.6 Others 87
5.4 Conclusion 87
References 88

6. Biogenic synthesis of quantum dots 93
Meghavi Gupta, Inderjeet Yadav and Abhilasha Jain

6.1 Introduction 93
6.1.1 Advantages 94
6.1.2 Disadvantages 94
6.2 Plants 94
6.3 Bacteria 98
6.4 Fungi 103
6.5 Others 107
6.6 Conclusion 108
References 108

7. Microwave-assisted synthesis of quantum dots 115
Chetna Ameta, Yogeshwari Vyas, Priyanka Chundawat and Dharmendra

7.1 Introduction 115
7.1.1 Advantages 116
7.1.2 Disadvantages 117
7.2 Synthesis of core-type quantum dots 117
7.2.1 Oxide quantum dots 118
7.2.2 Sulfide quantum dots 122
7.2.3 Selenide quantum dots 126
7.2.4 Telluride quantum dots 127
7.2.5 Other quantum dots 129
7.3 Synthesis of core–shell quantum dots 130
7.3.1 Type I CS quantum dots 131
7.3.2 Inverse type I CS quantum dots 131
7.3.3 Type II CS quantum dots 132

7.3.4 Inverse Type II CS quantum dots 132
7.3.5 Core–shell–shell quantum dots 132
7.4 Synthesis of alloyed quantum dots 133
7.5 Carbon and graphene quantum dots 135
7.6 Recent developments 135
7.7 Conclusion 136
References 136

8. Sonochemical synthesis of quantum dots 147
Garima Ameta and Seema Kothari

8.1 Introduction 147
8.1.1 Advantages 148
8.1.2 Disadvantage 149
8.2 Instrumentation 149
8.3 Synthesis of quantum dots 149
8.3.1 Metals 149
8.3.2 Metal oxides 151
8.3.3 Metal sulfides 153
8.3.4 Selenides 157
8.3.5 Tellurides 158
8.3.6 Carbon-based quantum dots 159
8.3.7 Others 162
8.4 Conclusion 163
References 163

9. Application of quantum dots in photocatalysis 169
Shubang Vyas, Rameshwar Ameta and Rakshit Ameta

9.1 Introduction 169
9.2 Quantum dots 170
9.3 Wastewater treatment 171
9.3.1 Dyes 173
9.3.2 Drugs 181
9.3.3 Pesticides 185
9.3.4 Phenol 186
9.4 Reduction of carbon dioxide 188
9.5 Hydrogen production 189
9.6 Other applications 192
9.7 Recent developments 192
9.8 Conclusion 194
References 194

10. Application of quantum dots in light-emitting diodes 205
Anca Armăşelu and Monika Jangid

10.1 Introduction 205

10.2 Display and lighting 206
10.2.1 White light-emitting diodes 207
10.2.2 Blue light-emitting diodes 213
10.2.3 Red light-emitting diodes 217
10.2.4 Green light-emitting diodes 219
10.2.5 Orange light-emitting diodes 222
10.2.6 Yellow light-emitting diodes 223
10.2.7 Other light-emitting diodes 223
10.3 Night vision 224
10.4 Data communication 225
10.5 Agriculture and horticulture 226
10.6 Antimicrobial technology 228
10.7 Recent developments 229
10.8 Conclusion 231
References 231

11. Application of quantum dots in biomedical and biotechnological fields 245
Anca Armăşelu and Priyanka Jhalora

11.1 Introduction 245
11.2 Biolabeling and bioimaging 246
11.3 Targeted drug delivery 248
11.4 Sensing 254
11.4.1 Photoluminescence sensors 255
11.4.2 Chemiluminescence sensors 257
11.4.3 Electroluminescence sensors 259
11.5 Others 261
11.6 Toxicity of quantum dots 264
11.7 Conclusion 267
References 267

12. Application of quantum dots in solar cells 277
Shwetharani R, Chandan Hunsur Ravikumar, M.S. Jyothi and R. Geetha Balakrishna

12.1 Introduction 277
12.1.1 Basic structure of quantum dot sensitized solar cells 278
12.1.2 Working principle of quantum dot sensitized solar cells 280
12.2 Properties of quantum dots 281
12.2.1 Energy gap tuning 281
12.2.2 Multiple exciton generation 283
12.3 Synthesis of quantum dots 286
12.3.1 Chalcogenide quantum dots 286
12.3.2 Perovskite quantum dots 289

12.4 Quantum dot sensitized solar cells 292
12.4.1 Perovskite quantum dots-based quantum dot sensitized solar cells 294
12.4.2 Other quantum dots-based quantum dot sensitized solar cells 297
12.5 Recent developments 300
12.6 Conclusion 300
References 302

13. Application of quantum dots in sensors 313
Neelam Kunwar, Hetal Zala and Kushnuma Parveen

13.1 Introduction 313
13.2 Sensors 314
13.2.1 Chemical sensors 314
13.2.2 Biosensors 324
13.2.3 Humidity sensors 326
13.2.4 Temperature sensors 327
13.3 Recent developments 329
13.4 Conclusion 331
References 331

14. Application of quantum dots in photosplitting of water 339
Luma M. Ahmed, Thaqeef M. Jawad, Hamad H. Kadium and Jayesh P. Bhatt

14.1 Introduction 339
14.2 Hydrogen production 340
14.2.1 Basic principle of overall water splitting 341
14.2.2 Photoelectrochemical cells 346
14.3 Metal-based quantum dots 347
14.3.1 Metals 347
14.3.2 Oxides 348
14.3.3 Metal sulfides 350
14.3.4 Others 354
14.4 Carbon and graphene-based quantum dots 355
14.5 Conclusion 358
References 359

Index 369

List of contributors

Luma M. Ahmed Department of Chemistry, College of Science, University of Kerbala, Karbala, Iraq

Chetna Ameta Department of Chemistry, M. L. S. University Udaipur, Rajasthan, India

Garima Ameta Department of Chemistry, M. L. S. University, Udaipur, Rajasthan, India

Rakshit Ameta Department of Chemistry, J. R. N. Rajasthan Vidhyapeeth (Deemed to be University), Udaipur, Rajasthan, India

Rameshwar Ameta Department of Chemistry, PAHER University, Udaipur, Rajasthan, India

Suresh C. Ameta Department of Chemistry, PAHER University, Udaipur, Rajasthan, India

Anca Armăşelu Department of Electrical Engineering and Applied Physics, Faculty of Electrical Engineering and Computer Science, Transilvania University of Brasov, Brasov, Romania

R. Geetha Balakrishna Centre for Nano and Material Sciences, Jain University, Bengaluru, Karnataka, India

Indu Bhati Maribyrnong, VIC, Australia

Jayesh P. Bhatt Department of Chemistry, PAHER University, Udaipur, Rajasthan, India

Priyanka Chundawat Department of Chemistry, M. L. S. University Udaipur, Rajasthan, India

Dharmendra Department of Chemistry, M. L. S. University Udaipur, Rajasthan, India

Neha Godha Department of Chemistry, PAHER University, Udaipur, Rajasthan, India

Meghavi Gupta Department of Chemistry, PAHER University, Udaipur, Rajasthan, India

Chandan Hunsur Ravikumar Centre for Nano and Material Sciences, Jain University, Bengaluru, Karnataka, India; Pilot Plant Development and Training Institute, King Mongkut's University of Technology Thonburi, Thakam, Bangkok, Thailand

Abhilasha Jain Department of Chemistry, St. Xavier's College, Mumbai, Maharashtra, India

Monika Jangid Department of Chemistry, PAHER University, Udaipur, Rajasthan, India

Kanchan K. Jat Department of Chemistry, M. L. S. University Udaipur, Rajasthan, India

Thaqeef M. Jawad Department of Chemistry, College of Science, University of Kerbala, Karbala, Iraq

Priyanka Jhalora Department of Chemistry, PAHER University, Udaipur, Rajasthan, India

M.S. Jyothi Department of Chemistry, AMC Engineering College, Bengaluru, Karnataka, India

Hamad H. Kadium Department of Chemistry, College of Science, University of Kerbala, Karbala, Iraq

Seema Kothari Department of Chemistry, PAHER University, Udaipur, Rajasthan, India

Neelam Kunwar Department of Chemistry, PAHER University, Udaipur, Rajasthan, India

Kushnuma Parveen Khamis Mushayt, Ahad Rafaidah, Kingdom of Saudi Arabia

Shwetharani R Centre for Nano and Material Sciences, Jain University, Bengaluru, Karnataka, India

Avinash K. Rai Department of Chemistry, PAHER University Udaipur, Rajasthan, India

Neetu Shorgar Department of Chemistry, PAHER University, Udaipur, Rajasthan, India

Shubang Vyas Department of Chemistry, PAHER University, Udaipur, Rajasthan, India

Yogeshwari Vyas Department of Chemistry, M. L. S. University Udaipur, Rajasthan, India

Inderjeet Yadav Department of Applied Sciences, University of Technology and Applied Sciences, Alkhuwair, Muscat, Sultanate of Oman

Hetal Zala 1197-1, Uchigashimacho, A-101, Gunma, Ota-Shi, Japan

About the editors

Dr. Rakshit Ameta has a thoroughly first class career, securing first position in his MSc. and was awarded a Gold Medal. He was also given the Fateh Singh Award from Maharana Mewar Foundation, Udaipur for his meritorious performance. After completion of his PhD, he served in Hindustan Zinc Limited, Vedanta Group for 1 year. He has served in M.L. Sukhadia University, Udaipur; University of Kota, Kota, PAHER University, Udaipur, and presently is at J.R.N. Rajasthan Vidyapeeth (Deemed to be University) Udaipur. Under his supervision 12 PhD students have been awarded PhDs on various aspects of Green Chemistry. He has around 140 research publications to his credit in journals of national and international repute. He has a patent to his credit as well. He is a reviewer of around 50 international journals. Dr. Rakshit has successfully organized many National Conferences at University of Kota, Kora; PAHER University, Udaipur; and J.R.N. Rajasthan Vidyapeeth, Udaipur. He has delivered Invited lectures and chaired sessions in 20 national conferences in different parts of the country. Dr. Rakshit has served as a council member (2011−13 and 2020−22) and associate editor, Physical Chemistry Section (2014−16), scientist-in-charge in the Industrial and Applied Chemistry Section (2014−2016) of the Indian Chemical Society, Kolkata, and executive council member (2012−14) and Zonal Secretary (2016−18) of Indian Council of Chemists, Agra. He had been a recipient of the Dr. U.C. Pant Memorial Award, Indian Chemical Society, Kolkata. He has written six books published by Taylor & Francis, UK; Academic Press, Elsevier; Apple Academic Press, and a number of chapters in books by these publishers and also Nova Publishers; Trans-Tech Publications, Springer, etc. His main research focus is on photochemistry, green chemistry, microwave-assisted reactions, environmental chemistry, wastewater treatment, nanochemistry, solar cells, bioactive & conducting polymers.

Dr. Jayesh P. Bhatt received his MSc. from RSTM Nagpur University in 2011. He was awarded his PhD in the year 2019 from PAHER University, Udaipur. Since 2019 he has been working as an assistant professor in the Department of Chemistry, PAHER University, Udaipur. He has done research in the field of nanomaterials, particularly quantum dots, wastewater treatment, etc. Dr. Jayesh has published 11 research articles in journals of

national and international repute and contributed 12 chapters. Currently four PhD students are working under his supervision. He has been honored with the Young Scientist Award at an international conference in 2018, Best Poster Presentation in 2019, Best Oral Presentation in 2020, and Senior Scientist Award for Best Oral Presentation in an international conference (2021).

Prof. Suresh C. Ameta obtained his master's degree from the University of Udaipur and was awarded a gold medal in 1970. He obtained his PhD degree from Vikram University in 1980. He has served as professor and head, Department of Chemistry, North Gujarat University Patan (1994) and M.L. Sukhadia University, Udaipur (2002−05) and head, Department of Polymer Science (2005−08). He also served as dean, P.G. Studies for a period of 4 years (2004−08) in M.L. Sukhadia University, Udaipur and dean, Faculty of Science, PAHER University (2011−18). Now, he is serving as professor of eminence (distinguished professor), Faculty of Science, PAHER University, Udaipur. Prof. Ameta has around 50 years of experience of teaching and research. He has successfully guided 108 students through their PhDs. Prof. Ameta has occupied the prestigious position of President, Indian Chemical Society, Kolkata (2000−01) and is now a lifelong advisor. He was awarded a number of prizes during his career, including the National prize twice for writing chemistry books in Hindi, Prof. M.N. Desai Award, Prof. W.U. Malik Award, Scientist of the Year Award, National Teacher Award, Prof. G.V. Bakore Award, and above all, Life Time Achievement Awards from the Indian Chemical Society (2011), Kolkata, Indian Council of Chemists, Agra (2015) and Association of Chemistry Teachers, Mumbai (2018). Dr. Ameta has more than 400 research papers and 36 books to his credit. He has contributed chapters in books published by Trans-Tech, Switzerland; Nova Science; Taylor & Francis; Elsevier; Springer; and Apple Academic Press. He has 12 books to his credit, including Green Chemistry, Microwave Assisted Organic Synthesis, Solar Energy Conversion and Storage, Group Theory, Photocatalysis, Storage, Advanced Oxidation Processes for Waste Water Treatment, Sonochemistry, etc. The Indian Chemical Society, Kolkata published a special issue of the Journal of Indian Chemical Society on his 60th birthday in 2008 and also instituted a National Prize in his honor as the Prof. Suresh C. Ameta Award to be given to a Senior Scientist of the country from 2003 onwards.

Preface

Nanomaterials have revolutionized many research areas due to their unique optical, electronic, and other properties. Quantum dots have lower dimensions (2−10 nm) in the nanometric range. These quantum dots have a high surface area-to-volume ratio, a quantum confinement effect, and surface Plasmon resonance. As such they have great potential for applications in different fields. The present book is divided into three parts. First, it deals with the basics or fundamentals of quantum dots, while the second part is devoted to various methods of synthesizing quantum dots, including hydrothermal, sol−gel, laser ablation, coprecipitation, biogenic, microwave-assisted, and sonochemical. The third part of the present book is devoted to the possible applications of quantum dots in these areas, such as photocatalysis, solar cells, light-emitting diodes, sensors, photosplitting of water, targeted drug delivery, cancer therapy, etc. The time is not far off when quantum dots will find a firm footing, and they will be considered a miracle particle in the years to come.

Rakshit Ameta
Jayesh P. Bhatt
Suresh C. Ameta

This page intentionally left blank

Chapter 1

Introduction

Suresh C. Ameta
Department of Chemistry, PAHER University, Udaipur, Rajasthan, India

1.1 Introduction

The materials in the nanorange (1−100 nm) are termed as nanomaterials. There are some nanostructured materials with size in the 2−10 nm range, such nanomaterials are called quantum dots. The name quantum dot was given because it is a tiny speck of matter (2−10 nm), which is very small, just like a single point or dot. In other words, it is considered zero-dimensional. The particles inside the quantum dot that carry electricity (electrons and holes) are trapped (constrained) and have well-defined energy levels, following the laws of quantum theory just like individual atoms. There are a few dozen to hundreds or a few thousand atoms. Although these quantum dots are nanocrystals, they behave more like individual atoms; therefore, they have been nicknamed artificial atoms also.

Quantum dots have quantized energy levels. On excitation an electron in the quantum dot jumps to a higher energy level. When this excited electron returns to a lower level, the quantum dot emits a photon of light with the same energy as was originally absorbed. The color of the emitted light depends on the energy levels and it varies from one quantum dot to another. The energy levels of quantum dots are governed by their size and not the substance from which it was made. The quantum dots and their application have been excellently reviewed by different researchers (e.g., Jamieson et al., 2007; Jacak et al., 2013; Michler, 2003; Wu et al., 2019; Molaei, 2019; Divsar, 2020; Nair et al., 2020; Abd Rani et al., 2020; Vyas et al., 2021).

A small quantum dot has a longer bandgap, and hence it requires more energy to excite its electron. As the frequency of emitted light is proportional to the energy, smaller quantum dots emit radiation of higher energy or frequency, that is, shorter wavelengths, while larger quantum dots have closely spaced energy levels and emit photons of lower energy or frequency, that is, longer wavelengths. It means that as the size of quantum dots increases, the quantum dot will emit photons with lower energy or frequency and higher wavelength and vice versa. This is presented in Fig. 1.1.

Quantum Dots. DOI: https://doi.org/10.1016/B978-0-12-824153-0.00001-X
© 2023 Elsevier Inc. All rights reserved.

When the size of the quantum dot is greater (diameter 5−6 nm), then it will emit radiation of larger wavelengths with orange or red colors. On the other hand, if the size of quantum dot is smaller (diameter 2−3 nm), then it will emit radiation of shorter wavelengths with blue and green colors. But the actual color depends on the exact size and composition of the quantum dots. Accordingly, a change in color can be observed as the particle size of quantum dots varies. This is clearly visible in Fig. 1.2.

1.1.1 Advantages

These are some advantages of quantum dots and these are:

- High quantum yield
- High photostability
- Symmetric and narrow peak of emission

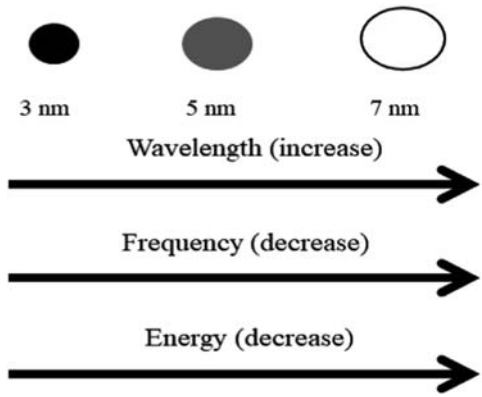

FIGURE 1.1 Relationship between size of quantum dots, energy or frequency of emitted light, and wavelength of radiation.

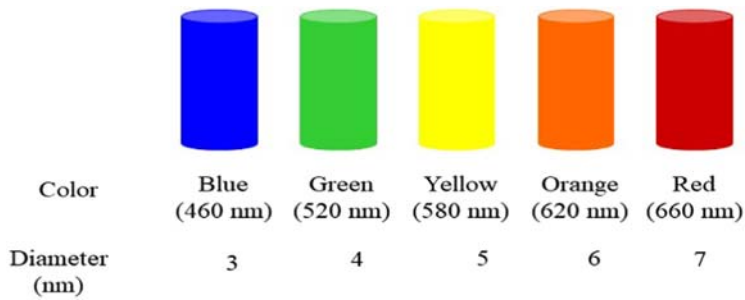

FIGURE 1.2 Change in color with size of quantum dots.

- Longer lifetime
- Possibility to control emission by changing the size and structure of quantum dots
- Brightness
- Resistance to photobleaching as compared to organic fluorophores
- Required small amount of energy for excitation (blue or UV radiation)

1.1.2 Disadvantages

Apart from the advantages, there are some disadvantages of quantum dots such as:

- High toxicity, when used in vivo
- Decline of fluorescence exponentially
- Blinking of quantum dots makes them invisible sometimes
- Quantum yield deterioration
- Extended lifetime may create a problem when rapid degradation is required

1.2 Unique features of quantum dots

Various properties of nanomaterials or quantum dots change as their size is changed. At this stage, the percentage of atoms available at the surface of a semiconducting material becomes quite significant. There are three main factors that are considered responsible for some unique properties in nanomaterials as well as quantum dots, which are significantly or totally different from their counterpart micro-, macro-, or bulk materials. These are:

1.2.1 High surface-to-volume ratio

As the size of the particle approaches a few nm, the surface area-to-volume ratio and surface-to-bulk atom ratio both increase dramatically. Depending on the composition and structure of the material used to produce nanoparticles or quantum dots, properties like absorption or emission wavelength, solubility, transparency, color, catalytic behavior, conductivity, melting point, etc. are changed only by variation in the size of the particle. It leads to some interesting behaviors of quantum dots.

1.2.2 Surface plasmon resonance

Surface plasmon resonance (SPR) is the collective oscillation of valence electrons in a solid stimulated by incident light. Such a resonance condition is established whenever the frequency of light photons matches the natural frequency of oscillating surface electrons against the restoring force of the positive nuclei. This SPR in nanometric structures is termed as localized

SPR (LSPR). LSPRs are collective oscillations of electron charge in metallic nanoparticles or quantum dots that are excited by light. Solutions containing nanoparticles or quantum dots of metals (gold, silver, etc.) are colored due to the SPR of the particles. Some properties like conductivity, dispersible nature, catalytic behavior, optical properties, etc. change with different surface properties of the particle.

1.2.3 Quantum confinement effect

The quantum confinement effect can be observed once the diameter of any material reaches the same magnitude as the de Broglie wavelength of an electron wave function. When materials are so small, their electronic and optical properties deviate substantially from those of bulk materials. Here, energy levels are not continuous but are quantized, that is, discrete, and therefore these materials in the range of nanosize or the size of quantum dots exhibit the quantum confinement effect.

1.3 Classification of quantum dots

Quantum dots are classified mainly into three types and these are:

- core-type quantum dots,
- core−shell quantum dots (CSQDs), and
- alloyed quantum dots.

1.3.1 Core-type quantum dots

These quantum dots can be single component materials, which have uniform internal compositions. The properties of these core-type nanocrystals such as photo- and electroluminescence can be fine-tuned just by simply changing the crystallite size. The examples of core-type quantum dots are chalcogenides (sulfides, selenides, or tellurides) of metals like cadmium, zinc, or lead (Fig. 1.3).

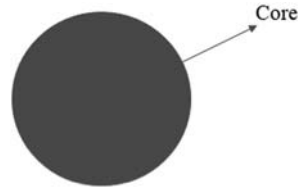

FIGURE 1.3 Core-type quantum dots.

1.3.2 Core–shell quantum dots

The luminescent properties of quantum dots are due to recombination of electron–hole pairs (excitons) through radiative pathways. The decay of an exciton can also occur via nonradiative methods, which reduces the fluorescence quantum yield. One of the possible methods to improve efficiency and brightness of these nanocrystals is to grow a shell of a semiconducting material with higher bandgap around it. Such particles, where small regions of one material are embedded in another with a wider bandgap, are termed CSQDs or core–shell semiconducting nanocrystals (Fig. 1.4). If the order is reversed, then they are called reverse type quantum dots, where a shell is inside the core structure (Fig. 1.5). Coating of quantum dots with some shells improves the quantum yield just by passivizing nonradiative recombination sites. This also makes them more robust to processing conditions, so that they can find use in various applications. CSQDs are classified into two types:

- Core–shell type-I quantum dots (Figs. 1.6 and 1.7)
- Core–shell type-II quantum dots (Figs. 1.8 and 1.9)

1.3.3 Alloyed quantum dots

Although electronic and optical properties of a quantum dot can be tuned by just changing its crystallite size, even then some problems are faced in many applications wherever there are some restrictions on size. Properties of

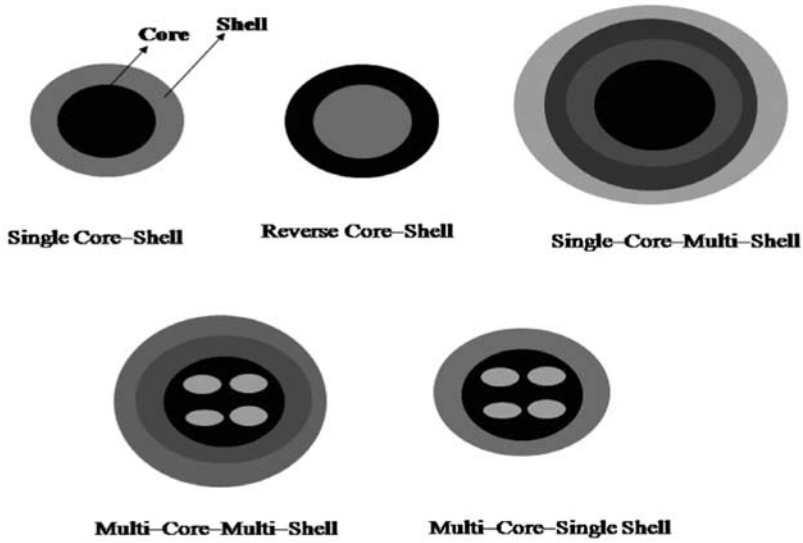

FIGURE 1.4 Core–shell type quantum dots with various arrangements of core–shell.

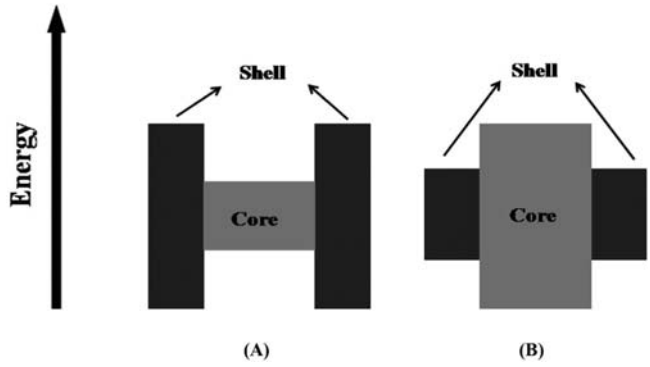

FIGURE 1.5 Core−shell type−I: (A) normal, and (B) reversed quantum dots.

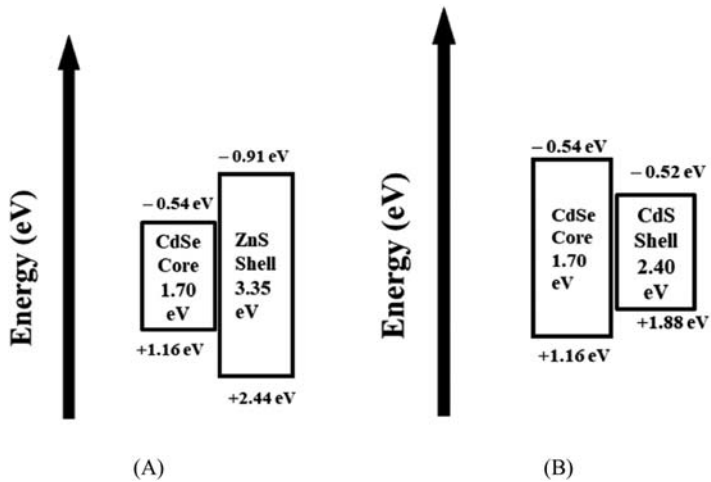

FIGURE 1.6 Energy diagram of core−shell type−I: (A) normal and (B) reversed quantum dots.

quantum dots having multicomponents can be tuned without any change in crystallite size. Such multicomponent systems are called alloyed quantum dots (homogeneous and gradient internal structures) and it is possible to tune their electronic and optical properties by changing their internal structure and composition. These alloyed quantum dots are fabricated by alloying any two semiconductors with different bandgaps (Fig. 1.9). These quantum dots show some interesting properties, which are sometimes very different from the properties of their original bulk counterparts or parent semiconductors. They can be homogeneous in nature or with a particular zone rich in a specific element.

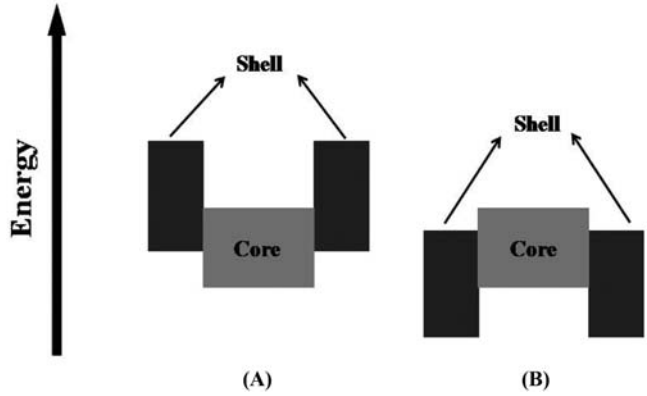

FIGURE 1.7 Core–shell type–II quantum dots. (A) Both the bands (conduction and valence) of shell are higher than core and (B) Both the bands of shell are lower than the core.

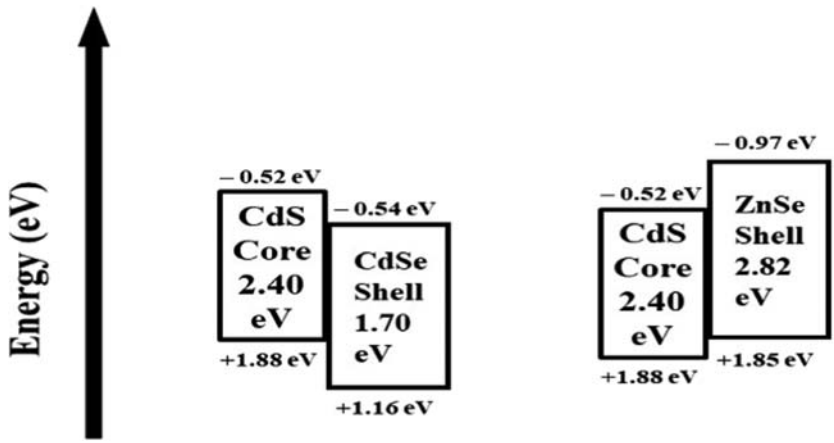

FIGURE 1.8 Energy diagram of core–shell type–II quantum dots.

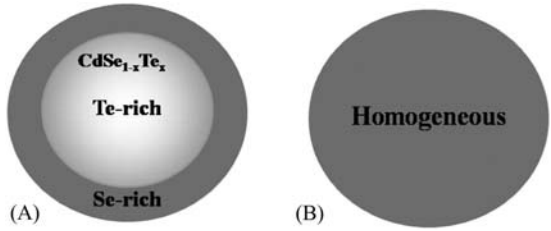

FIGURE 1.9 (A) Specific element (Te- or Se-) rich alloyed quantum dots, and (B) homogeneous alloyed quantum dots.

1.4 Synthesis of quantum dots

A number of routes have been developed for the synthesis of QDs with controlled size, shape, structure, and dimensionality, but generally used techniques are categorized into two approaches:

- top-down approach; and
- bottom-up approach.

New physical properties and applications of nanomaterials are only possible when nanostructured materials are made available with the desired size, shape, morphology, crystal structure, and chemical composition.

1.4.1 Top-down approach

The top-down approach involves breaking the bulk material into nanosized structures or particles. This approach is based on physical methods (Fig. 1.10). These are nothing but an extension of those methods, which are used for producing micro-sized particles. Top-down approaches are relatively simpler as they depend either on the removal/division of the bulk material or on miniaturization of any bulk process of fabrication to produce the nano-desired structures. But there is a problem with this approach, that is, the surface structure prepared is imperfect in nature. Nanostructured materials prepared by this approach are not smooth and have structural defects on the surface and also contain a number of impurities. Examples of such top-down techniques are high-energy wet ball milling, laser ablation, electron beam lithography, liquid phase exfoliation, atomic force manipulation, gas-phase condensation, and aerosol spray.

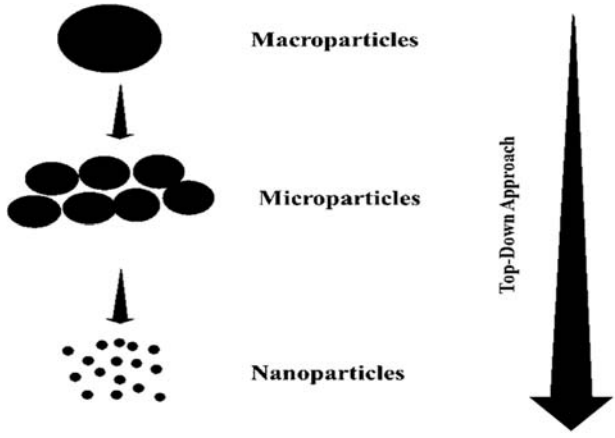

FIGURE 1.10 Top-down approach.

1.4.2 Bottom-up approach

Another approach for this purpose is the bottom-up approach (Fig. 1.11). These are mostly chemical-based methods. These are economical also. This approach builds up a material starting from the bottom, that is, atom-by-atom, molecule-by-molecule, cluster-by cluster, etc. Some of the examples are sol−gel synthesis, hydrothermal synthesis, electrodeposition, organometallic chemical route, reverse-micelle route, colloidal precipitation, and template-assisted sol−gel.

1.4.3 Methods of synthesis

Different methods are available for the synthesis of quantum dots. These are:

- Hydrothermal method
- Sol−gel method
- Laser ablation method
- Coprecipitation method
- Biogenic method
- Microwave-assisted method
- Sonochemical method

1.5 Applications of quantum dots

Although there are numerous applications of quantum dots covering a wide range, the main applications include:

- Solar cells
- Biolabeling
- Bioimaging

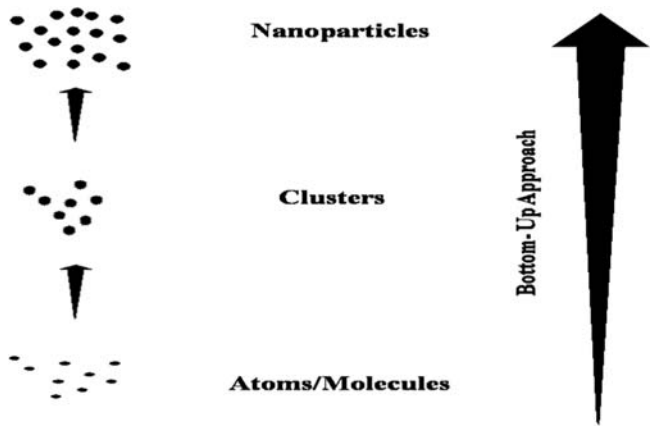

FIGURE 1.11 Bottom-up approach.

- Cancer therapy
- Chemical and biosensors
- Microscopy
- Lasers
- Inkjet printing
- Spin coating
- Photosplitting of water to generate hydrogen
- Light-emitting diodes
- Wastewater treatment using photocatalysts
- Photothermal and photodynamic therapy
- Targeted drug delivery,

This list is not complete and many more new applications will emerge in years to come. Some major applications of quantum dots are depicted in Fig. 1.12.

1.5.1 Solar cells

The world is facing a scarcity of energy resources, as the conventional fuels are either exhausted or reaching an end within the coming few decades. Therefore, there is an urgent demand to search for or to develop some new alternate resources, which are likely to fulfill the demand of the society in forthcoming years. Many attempts have been made in this direction, where sunlight has been used as the source of energy to generate electrical energy.

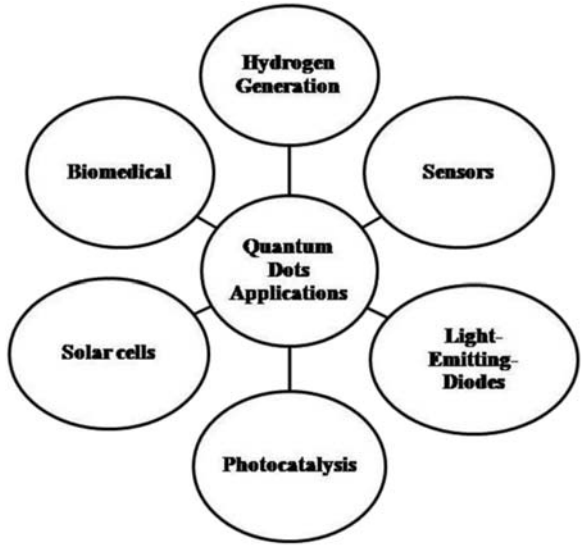

FIGURE 1.12 Different major applications of quantum dots.

It is very important to find some low-cost materials for the conversion and storage of solar energy with good conservation efficiency and long-term storage. Various solar cells are available, such as photovoltaic cells, photogalvanic cells, dye-sensitized solar cells, etc. Nanomaterials are already in use in solar cells, but now quantum dots are also being utilized in some solar cells to increase the efficiency of these cells and prolong their lifetime. Quantum dots sensitized solar cells have become a topic of interest these days, because of some unique properties of quantum dots. The use of pervoskites has also added a new dimension to the field of solar cells.

1.5.2 Sensors

Sensing a particular material or conditions has become a field of general interest in society. There is a long history for developing different and active sensors that can sense the presence of harmful chemicals; but now the presence of nanomaterials or quantum dots has added newer dimensions to the field of sensors. Sensing a specific chemical at ppm or sometimes even at ppb level has become possible by the use of quantum dots, for example, alcohol, ammonia, pesticides, carbon dioxide, nitrogen peroxide, hydrogen sulfide, liquefied petroleum gas (LPG) commonly used drugs (antibiotics, antiseptic, antiinflammatories, antipyretics, etc.), etc. Apart from this, these quantum dots also sense any small variation in the surroundings or environment (chemical and biological) and these can be used for measuring the temperature and humidity of a particular room or area.

1.5.3 Light emitting diodes

Whenever current flows in a semiconductor, electrons and holes recombine. As a result, energy is released in the form of photons. Thus the semiconductor becomes a light source and it is called a light-emitting diode light. Quantum dots are used in fabricating such light-emitting diodes. They can give a variety of colors: green, blue, red, orange, yellow, etc. apart from white. This color depends on the bandgap of that semiconductor, that is, corresponding to the energy of photons. Normally, electrical energy is first converted into heat then into light, but light-emitting diodes convert electrical energy directly into light so that no or negligible electricity is wasted in the form of heat. LEDs find application in a number of areas such as display and lighting (different colors), night vision (security cameras), data communication, agriculture and horticulture (plant growth and improved crop production), antimicrobial properties, etc.

1.5.4 Photocatalysis

Photocatalysis has a beauty in that it can provide the oxidizing as well reducing environment simultaneously in the same vessel, which is not otherwise

possible with any oxidant or a reductant, which gives only one kind of environment. Instead, the oxidant and reductant will react (if both are present there) with each other rather than attacking a particular molecule or entity. It can generate a very strong oxidizing species, hydroxyl radicals in the majority of cases, which are quite effective in degrading the organic pollutants to less harmful or almost harmless end products. Thus the use of quantum dots in photocatalytic degradation can be useful in the complete mineralization of water and air contaminants like dyes, pharmaceuticals, pesticides, nitro and chloro compounds, endocrine-disrupting chemicals, phenols, carbon dioxide, carbon monoxide, nitrogen dioxide, etc. Not only this, quantum dots are now utilized in the photoreduction of carbon dioxide to some useful chemicals, which can be used as synthetic fuels such as methanol or methane. This will solve the problem of the energy crisis on one hand and decrease the amount of carbon dioxide in the atmosphere; thus placing a control on the ever increasing global warming.

1.5.5 Hydrogen generation

The shortage of natural energy resources is becoming a burning problem in the world these days and it is likely to increase exponentially in the coming future. The requirement for energy is regularly increasing and it will be very difficult to depend for a long time on the natural fuels such as wood, coal, kerosene, diesel, petrol, natural gas, or LPG, and therefore there is a pressing demand that some alternative should be developed that can fulfill the demand for energy from society in coming decades. Here, hydrogen enters the scene, It has a high energy storage capacity and can be used as an alternative fuel. It has been predicted to be the fuel of the future. It is presently produced by the consumption of electricity, which is a costly affair. It has been advocated that hydrogen should be generated by the splitting of water photocatalytically in the presence of a light source, and the most preferred one is sunlight, as it freely available at present and it is inexhaustible also. It can be utilized as a source of energy for the future at relatively low cost. The source of hydrogen is water, which is abundantly available, covering almost three-fourths of the Earth, and the final product of its combustion is water again, which is harmless Now, quantum dots are being used in photocatalytic splitting of water to produce hydrogen with relatively high efficiency.

1.5.6 Biomedicals

Quantum dots have great potential for application in the biomedical and biotechnology fields because of their smaller size and other unique properties. They can pass the blood−brain barrier and also can cross the cell boundaries in some cases. These can be used for the diagnosis of a particular disease at earlier stages and hence help in timely treatment. Quantum dots are also

used in targeted drug delivery so that a drug can be supplied to a specific organ or location and as a result, the healthy cells or other parts are not affected adversely. This will increase the efficacy of that drug. They have a bright future in combating dreadful diseases like cancer. They are also effectively utilized in biolabeling and bioimaging processes.

1.6 Conclusion

Quantum dots have certain unique features, such as large surface area-to-volume ratio, quantum confinement effect, and SPR. These make quantum dots quite interesting for possible application in a variety of fields. They are used as photocatalysts for degradation or the removal of a variety of environmental pollutants to smaller fragments, which are almost harmless, reduction of carbon dioxide curbing the ever increasing global warming, photosplitting of water generating hydrogen (the fuel of future), light emitting diodes (display, lighting, plant growth, improved crop production, night vision, antimicrobial activities), biolabeling, bioimaging, targeted drug delivery, solar cells, cancer therapy, sensing a particular compound in very low concentrations (ppm or even sometimes ppb also), etc. Quantum dots will find many more useful applications in the years to come.

References

Abd Rani, U., Ng, L.Y., Ng, C.Y., Mahmoudi, E., 2020. A review of carbon quantum dots and their applications in wastewater treatment. Adv. Colloid Interface Sci. 278. Available from: https://doi.org/10.1016/j.cis.2020.102124.

Divsar, F. (Ed.), 2020. Quantum Dots: Fundamental and Applications. IntechOpen, London.

Jacak, L., Hawrylak, P., Wojs, A., 2013. Quantum Dots. Springer Science & Business Media, Berlin/Heidelberg.

Jamieson, T., Bakhshi, R., Petrova, D., Pocock, R., Imani, M., Seifalian, A.M., 2007. Biological applications of quantum dots. Biomaterials 28 (31), 4717–4732.

Michler, P., 2003. Single Quantum Dots: Fundamentals, Applications and New Concepts. Springer Science & Business Media, Berlin/Heidelberg.

Molaei, M.J., 2019. A review on nanostructured carbon quantum dots and their applications in biotechnology, sensors, and chemiluminescence. Talanta 196, 456–478.

Nair, A., Haponiuk, J.T., Thomas, S., Gopi, S., 2020. Natural carbon-based quantum dots and their applications in drug delivery: a review. Biomed. Pharmacother. 132. Available from: https://doi.org/10.1016/j.biopha.2020.110834.

Vyas, Y., Chundawat, P., Dharmendra, D., Punjabi, P.B., Ameta, C., 2021. Review on hydrogen production photocatalytically using carbon quantum dots: future fuel. Int. J. Hydrog. Energy 46 (75), 37208–37241.

Wu, H.L., Li, X.B., Tung, C.H., Wu, L.Z., 2019. Semiconductor quantum dots: an emerging candidate for CO_2 photoreduction. Adv. Mater. 31 (36). Available from: https://doi.org/10.1002/adma.201900709.

This page intentionally left blank

Chapter 2

Hydrothermal synthesis of quantum dots

Jayesh P. Bhatt and Neha Godha
Department of Chemistry, PAHER University, Udaipur, Rajasthan, India

2.1 Introduction

The term "hydro" means water and "thermal" means heat. This word was first used by the British geologist Sir Roderick Murchison (1841). The action of water at high temperature and pressure has been considered responsible for changes in the Earth's crust, and it leads to the formation of various minerals and rocks. The first report on hydrothermal synthesis was of tiny quartz crystals by freshly precipitated silicic acid (Schafthaul, 1845). Now this term refers to any heterogeneous reaction that is carried out in the presence of aqueous solvents under high temperature and pressure conditions. Artificial diamond was also synthesized by Hannay (1880) using the hydrothermal method and Moissan (1893) also claimed to synthesize artificial diamond.

It is interesting to note that the hydrothermal method keeps a good control on composition and porosity. It is known that materials having high vapor pressure near this melting point normally form nanoparticles (NPs) by this method only. The solvothermal method is almost similar to the hydrothermal method but the only difference is in the wetting liquid, which is usually an organic solvent in place of water. The hydrothermal technique is used in a variety of fields, like chemistry, material science, biology, etc.

The hydrothermal conditions (high pressure and temperature) require a reaction vessel for crystal growth, which is called an autoclave. As some highly corrosive salts are used in the hydrothermal method to synthesize inorganic materials for a longer period reaction time, an autoclave must be able to sustain these highly corrosive materials at high pressure and temperature. The corrosion resistance is the most important property required in the material of the autoclave. Such corrosion-resistant

Quantum Dots. DOI: https://doi.org/10.1016/B978-0-12-824153-0.00002-1
© 2023 Elsevier Inc. All rights reserved.

materials include the following materials such as high-strength alloys, stainless steel, iron, titanium, nickel, and cobalt-based alloys. An autoclave is also coated inside with a non-reactive material to avoid corrosion; the most suitable material is Teflon (tetrafluoroethylene). As the Teflon has a larger coefficient of thermal expansion compared with the material enclosed within the liner, the coating of Teflon will expand and contract much more on heating and cooling than the reacting materials present inside the autoclave.

A good hydrothermal autoclave should have the following properties:

- It is inert to acids, bases, and oxidizing agents.
- It should be easy to assemble and dissemble.
- It should have a sufficient length to obtain a desired temperature gradient.
- It should be leakproof at desired temperature and pressure.
- It should bear high pressure and temperature for a longer duration of time.
- Reaction can be carried out under mild hydrothermal conditions of temperature less than 300°C and pressure 250 bars.

Parts of the Teflon-coated autoclave are presented in Fig. 2.1.

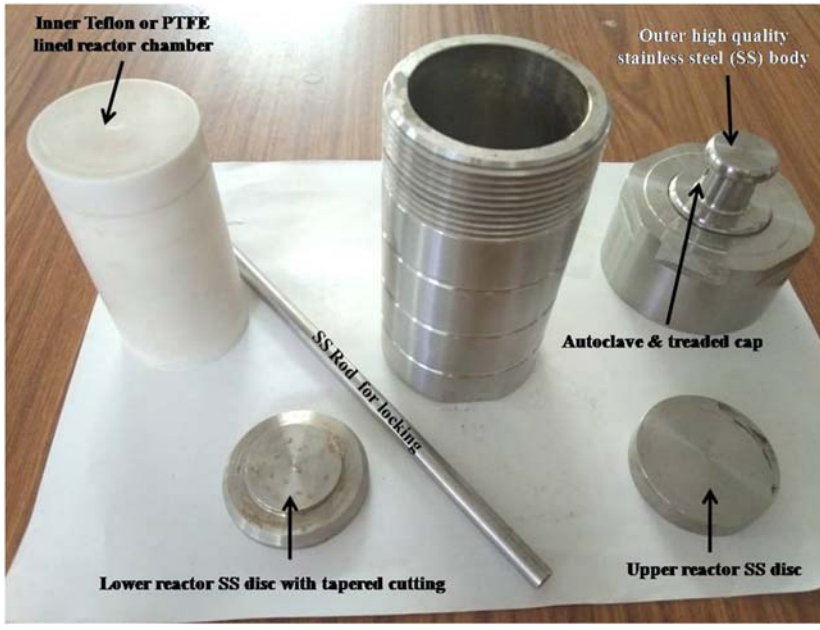

FIGURE 2.1 Teflon-lined autoclave reactor.

2.1.1 Advantages

The following are the advantages of hydrothermal synthesis:

- This method has the ability to create crystallize phases, particularly those that are not stable at the melting point.
- The material having high vapor pressure near its melting point can also be grown by this method.
- This method is suitable for the growth of large and good-quality crystals with a control on their composition.
- Relative cost is lower for this method compared with others.
- The hydrothermal method is more eco-friendly (green) than other methods of synthesis.
- It requires low temperatures, which avoids the problems encountered with high-temperature processes.
- It regulates the uniformity of nucleation, rate growth, aging, etc., which affect morphology, size, and aggregation. Various particle sizes and morphologies can be obtained with the hydrothermal method.
- Materials prepared by this method exhibit differences in point defects as compared with high-temperature synthesis. There are no Schottky defects in tungstates of Ca, Ba, and Sr prepared by this method, which are normally present in these compounds prepared at high temperatures.
- This method can be used in combination with other methods such as microwave, ultrasound, mechanochemistry, electrochemical, etc.

2.1.2 Disadvantages

- One of the major disadvantages of this method is that it needs expensive autoclaves.
- It is not possible to observe the crystal growing inside a steel tube.
- Now autoclaves made of thick-walled glass are used up to 300°C and 10 bar.
- The greatest disadvantages of Teflon lining is that beyond 300°C, it cannot be used because Teflon dissociates, which affects the pH of neutral solutions. This coating tends to get torn and generally must be replaced after experiments.

2.2 Metal-based quantum dots

2.2.1 Metal oxide quantum dots

A simple hydrothermal approach was used by Zhu et al. (2006) for synthesis of SnO_2 quantum dots. Here, hydrazine hydrate was used as the mineralizer and not the commonly used NaOH. The diameters of the SnO_2 NPs were determined to be in the range of 2.3−3.1 nm. A blueshift was observed of

0.28 eV and the bandgap of as-prepared SnO_2 QDs was found to be 3.88 eV. A biomolecule-assisted hydrothermal route was used by Wu et al. (2009) for generating SnO_2 QDs (diameters 10 nm). These were used for photocatalytic degradation of rhodamine B in a basic medium, where its degradation reached almost 100% within 150 min.

Wei et al. (2010) made use of WO_{3-x} QDs (nonstoichiometric) in combination with silver nanowires (Ag NWs) and reported that the incident photon-to-electron conversion efficiency (IPCE) can be increased by 8.5% and dye degradation improved by 40% with the sample $WO_{2.72}$ QD@Ag NW composite.

Perera et al. (2012) prepared TiO_2 nanotube (TNT)/reduced graphene oxide (rGO) composites using an alkaline hydrothermal process. They could achieve this by decorating graphene oxide (GO) layers on TiO_2 NPs. The TiO_2 NPs were found to be small in diameter ($\sim$9 nm). As-prepared composites were used for the photodegradation of malachite green. It was observed that composite with 10% rGO showed the highest photocatalytic activity, which was almost three times higher than pure TNTs.

The Mg-doped VO_2 NPs were synthesized by Zhou et al. (2013) via a hydrothermal method. It was reported that optical bandgap changed from 2.0 eV for pure VO_2 to 2.4 eV on 3.8% Mg doping. Yao et al. (2017) fabricated $CoFe_2O_4$ quantum dots/N-doped graphene ($CoFe_2O_4$ QDs/N-G) composites using the hydrothermal process followed by calcination at high temperatures. It was observed that NPs were homogeneously anchored on the surfaces of graphene sheets and the size of $CoFe_2O_4$ QDs was within 4−12 nm. It was reported that as-obtained $CoFe_2O_4$ QDs/N-G can be used as anode material for lithium-ion batteries (LIBs) with an initial discharge capacity of 1616 mAh g^{-1} maintaining a reversible capacity of 1223 mAh g^{-1} even after 90 cycles at a current of 100 mA g^{-1}.

Ma et al. (2017) observed the effects of N doping on the deposition of $ZnCo_2O_4$ QDs on rGO nanosheets. It was reported that as-prepared $ZnCo_2O_4$ QDs decorated on nitrogen-doped graphene (NG) were 4.3 ± 0.9 nm in diameter and were well-dispersed on the surface. It was indicated that as-obtained $ZnCo_2O_4$/NG hybrids can be used as a battery-type electrode for a hybrid supercapacitor and can deliver high specific capacity, outstanding rate capability, and excellent cycle performance of 301.8 C g^{-1} at 1 A g^{-1}, 84.5% remaining at 30 A g^{-1} and 89.1% after 5000 cycles, respectively.

Min et al. (2017) used a one-step hydrothermal route for preparing GQDs coupled with TiO_2 in the form of composite (TiO_2/GQDs) photocatalysts. They used 1,3,6-trinitropyrene (TNP) as the precursor of GQDs. Here, GQDs act as a photosensitizer as well as an excellent electron acceptor and this composite exhibited a seven times higher evolution rate of H_2. A highly efficient ternary photocatalytic nanocomposite, $ZnFe_2O_4/TiO_2$/CDs, was synthesized by Lu et al. (2018) through a hydrothermal method. This composite was used in the decomposition of rhodamine B. It was also revealed that it

retained its photocatalytic efficiency even after four cycles. A wide range of transition metal-doped TiO_2 (metal/TiO_2) (where M = Co, Ag, Cu, Au, Cr, Ni, Fe, Pt, Pd, and Zn) was prepared by Wu et al. (2018) combining the hydrothermal synthesis with air-thermal treatment. It was observed that 0.5 mol.%-Cu/TiO_2 NFs exhibited the highest photocatalytic activity in the production of hydrogen (208 $\mu mol^{-1}\ h^{-1}$).

SnO_2 QDs/TiO_2 NPs composite was prepared by Jat et al. (2019) via a hydrothermal method. They used stannic chloride (hydrate) as a precursor for SnO_2 quantum dots. It was observed that the photocatalytic activity of the composite was more than titania nanopowder for the degradation of fast green. The effects of various parameters like pH, the concentration of dye, amount of catalyst, and light intensity on the rate of degradation was also studied. It can be a promising method for wastewater treatment. A simple hydrothermal route was reported by Liu et al. (2019a,b) for the synthesis of tungsten oxide quantum dots (WO_{3-x} QDs). They used ammonium tungstate hydrate as a precursor and polyvinyl pyrrolidone. It was reported that this material is photochromic in nature and changes color in the presence of UV or sunlight.

2.2.2 Metal sulfide quantum dots

Zhao et al. (2009) selected thiol ligand, N-acetyl-l-cysteine as a stabilizer for the synthesis of high-quality NIR-emitting CdTe/CdS QDs by an hydrothermal route. It was reported that as-prepared NIR-emitting CdTe/CdS QDs exhibited high photoluminescence quantum yields (45% − 62%) and good photostability. It was also suggested that as-prepared QDs can be used for bioimaging as they have biological compatibility and excellent water solubility. Liu et al. (2012) synthesized water-soluble high-quality ternary $CuInS_2$ quantum dots via hydrothermal synthesis. They used mercaptopropionic acid (MPA) as the stabilizer. It was observed that it can be used to label liver cancer cells. It was also revealed that as-synthesized near-infrared (NIR) $CuInS_2$ QDs have excellent photostability.

The CdSeS quantum dots with diameter of 4.5 nm were prepared by Santra and Kamat (2013), which were highly luminescent. They observed maximum power conversion efficiencies of 3.2% and 3.0% in two- and three-layered tandem quantum dots solar cells, respectively. Liu et al. (2013) synthesized water-soluble $CuInS_2$ ternary quantum dots in aqueous solution, which was capped by MPA. The $CuInS_2$ QDs were covalently linked to 3-aminophenylboronic acid molecules to get functionalized $CuInS_2$ QDs (F-$CuInS_2$ QDs). These QDs were found to be reactive toward vicinal diols in alkaline solution to form five- or six- member cyclic esters.

Water-soluble Mn^{2+}-doped ZnS nanocrystals were synthesized by Zhang et al. (2014). These were surface capped with polyethylene glycol (PEG-ZnS:Mn^{2+}) in aqueous solution. It was reported that the size of particles had

an average diameter of 3 nm with a zinc blende structure. It was also revealed that as-obtained nanocrystals were water soluble and biocompatible. Han et al. (2014) prepared a ternary CdS/ZnO/graphene composite by loading ZnO and CdS NPs in graphene nanosheets using a one-step hydrothermal method. It was reported that as-prepared CdS/ZnO/graphene composite exhibited enhanced photocatalytic activity as compared to pure ZnO and CdS. It was attributed to the light absorption, efficient charge separation, and durability of the composite.

Uniform MoS_2 quantum dots were synthesized by Ren et al. (2015) via a hydrothermal route. It was reported that the as-prepared material has a monolayer thickness with an average size of 3.6 nm. A facile hydrothermal route has been also used by Wang and Ni (2014) for the synthesis of photoluminescent MoS_2 quantum dots. They used sodium molybdate and cysteine as precursors. As-prepared MoS_2 QDs were used to construct a sensor for the detection of 2,4,6-trinitrophenol (TNP) in a wide range of concentration from 0.099 to 36.5 μM with a high detection limit (95 nM). It was reported that this sensor can be applied for the detection of TNP in real samples.

Monolayer MoS_2 quantum dots with lateral size (3 nm) were prepared by Qiao et al. (2015). It was observed that the lateral size of the nanosheets decreases on increasing the number of exfoliations. It was reported that monolayer MoS_2 QDs exhibited higher hydrogen evolution reaction (HER) catalytic activities. Uniformly dispersed ZnS quantum dots (<10 nm) on graphene nanosheets were synthesized by Zhang et al. (2018) via a hydrothermal method. It was reported that as-prepared ZnS/graphene composites can be used as a dual anode for both LIB and sodium-ion batteries with excellent performance.

The Ag_2S/ Bi_4/Ti_3O_{12} heterojunction composite was prepared by Zhao et al. (2019). The Ag_2S quantum dots were assembled onto the surface of $Bi_4Ti_3O_{12}$ nanosheets. Its photocatalytic performance was evaluated for photocatalytic degradation of rhodamine B in aqueous solution under simulated sunlight. It was found that 15 wt.% Ag_2S $Bi_4Ti_3O_{12}$ composite exhibited the highest photocatalytic activity, which was about 2.8 and 4.0 times higher than that of pure $Bi_4Ti_3O_{12}$ and Ag_2S, respectively. This enhanced activity was explained on the basis of Z-scheme electron transfer from $Bi_4Ti_3O_{12}$ (conduction band) to Ag_2S (valence band).

Zeng et al. (2019) synthesized flower-like $MoS_2/Ag_2S/Ag$ nanocomposites. It was reported that as-prepared $MoS_2/Ag_2S/Ag$ nanocomposites can be used as photocatalysts for the photodegradation of tetracycline hydrochloride and Congo red and also for the disinfection of *P. aeruginosa*. It was verified that the electron transport path is a Z-scheme system. A one-step hydrothermal approach was reported by Li et al. (2019) to synthesize water-dispersed MoS_2 quantum dots. These QDs have an ultrasmall size of ~ 3.3 nm. These were loaded on CdS nanorods and then they exhibited an enhanced HER under visible light ($\lambda > 420$ nm) (131.7 mmol h^{-1} g^{-1}), which is about 65-fold the rate of pure CdS (2.0 mmol h^{-1} g^{-1}).

2.2.3 Others

A simple hydrothermal method was developed by Wang and Han (2010) for the synthesis of water-soluble, and NIR-emitting type core−shell CdTe/CdSe quantum dots. They used $CdCl_2$ and Na_2SeO_3 and thiol-capped CdTe QDs as core templates for this purpose. It was revealed that as-prepared CdTe/CdSe QDs showed excellent photostability, good monodispersity, and hardened lattice structure which has a great potential for different biological applications.

A high-performance supercapacitor cathode electrode was developed by Xia et al. (2015). It was composed of well-dispersed $MnCO_3$ quantum dots ($\sim$1.2 nm) decorated on nickel hydrogen carbonate−manganese carbonate ($Ni(HCO_3)_2$−$MnCO_3$). It was reported that as-prepared $MnCO_3$ QDs/NiH−Mn−CO_3 composites exhibited superior supercapacitive performance, which makes them potential cathode materials to be used in high energy density asymmetric supercapacitors.

2.3 Nonmetal-based quantum dots

2.3.1 Carbon-based quantum dots

Yu et al. (2012) prepared ZnO/carbon quantum dots (ZnO/CQDs) nanocomposites by hydrothermal reaction. It was reported that as-obtained photocatalyst can be used for the degradation of toxic gas (methanol and benzene) under visible light exhibiting higher photocatalytic activity (80%, 24 h) as compared to N-doped TiO_2 and ZnO NPs. A simple one-step hydrothermal method was developed by Guo et al. (2013) for the synthesis of highly fluorescent carbon NPs (F-CNPs). It was reported that these F-CNPs exhibited excellent probe ability for the detection of mercury ions in aqueous solution with good sensitivity and selectivity.

Yu et al. (2014a,b) prepared CQDs/TiO_2 nanosheet composites by a simple low-temperature process. The photocatalytic activity of this composite was observed for the degradation of rhodamine B in the presence of visible light irradiation. CQDs modified TiO_2P25 composites (CQDs/P25) were prepared by Yu et al. (2014a,b) via hydrothermal reaction. This composite exhibited enhanced photocatalytic H_2 evolution in the presence of visible light and UV without using any noble metal cocatalyst. Here, CQDs played dual roles for improving photocatalytic activity as they act as an electron reservoir as well as for efficient separation of the electron−hole pairs.

Zhang and Chen (2014) used a hydrothermal route to prepare highly luminescent nitrogen-doped CQDs (NCQDs). They used folic acid as the source of both carbon and nitrogen. It was reported that as-prepared NCQDs have an average size of 4.5 ± 1.0 nm. It was reported that an effective quenching effect of Hg^{2+} ions was achieved, and NCQDs can detect Hg^{2+} ions with a detection limit of 0.23 μM. This type of ions sensor was

successfully applied for the determination of Hg^{2+} in real samples such as tapwater and lake water. A facile method to synthesize stable CDs was reported by Wang et al. (2015) via hydrothermal treatment using glucose in the presence of glutathione. It was reported that as-prepared CDs can be used as pH sensors. Wei et al. (2016) prepared a series of carbon dots (CDs)/$NiCo_2O_4$ composites, It was observed that these samples have good electrical conductivities and exhibited high specific capacitances, cycling stabilities, and superior rate performance. It was revealed that this hybrid supercapacitor exhibited a high energy density up to 62.0 Wh kg^{-1}.

Martins et al. (2016) prepared a new composite of TiO_2 (P25) and N-doped CQDs (P25/NCQD) via a hydrothermal method. It was then used as a catalyst for the photooxidation of NO in the presence of UV and visible light. It was reported that as-prepared P25/NCQD composite exhibited NO conversion (27.0%), which was almost 2.7 times that of P25 (10%). It was also revealed that photodegradation of methylene blue was increased from 68% to 91% on UV irradiation.

Qian et al. (2016) incorporated CQDs with Bi_2WO_6. Then these were used for photocatalytic removal of gaseous volatile organic compounds in the presence of sunlight. It was revealed that CQDs/ Bi_2WO_6 exhibited higher photocatalytic oxidation in degrading toluene and acetone under both UV and visible light.

Wu et al. (2017) synthesized NCQDs by a hydrothermal method. They used microcrystalline cellulose as a source of carbon and ethylenediamine as a nitrogen dopant. It was reported that as-obtained NCQDs particles were spherical with an average diameter of 3.2 nm. When these NCQDs were used as a fluorescent probe for the detection of Fe^{3+} via fluorescent quenching, then they could achieve high sensitivity and selectivity with a limit of detection of 0.21 nM.

A ternary composite of GO/CD/polypyrrole (GO/CDs/PPy) was prepared by Zhang et al. (2017) and then used as an electrode active material for supercapacitors. It was reported that CDs sandwiched between PPy and GO film layer can promote electron transportation in such composites and as a result, charge transfer resistance of the electrode and internal resistance are reduced. It was interesting to note that it retained excellent cycle stability even after 5000 cycles. Liu et al. (2017) monitored the effect of arginine (Arg) on the growth of gold NPs/CQDs (Au/CQDs) composite. Ethylene glycol was used as the reducing as well as stabilizing agent for the preparation of CQDs. The arginine can be detected with a low detection limit of 37 nM using this nanocomposite based on the color change.

A three-dimensional (3D) ternary graphene-CQDs/g-C_3N_4 nanosheet (GA-CQDs/CNN) aerogel was synthesized by He et al. (2018) via a hydrothermal method. It was reported that this ternary photocatalyst could improve the absorption of visible light as well as promote separation of charges. It was observed that methyl orange can be removed up to 91.1% using

GA-CQDs/CNN-24%, which was about 7.6 times more than that with bulk g-C_3N_4 (BCN).

Zhao et al. (2018) synthesized nitrogen-doped CQDs via a hydrothermal method. They used polyacrylamide as both the carbon and nitrogen source. It was reported that as-prepared NCQDs could be used as effective probes for selective and sensitive detection of dopamine with a detection limit of 0.05 μM in the concentration range of 0.1−200 μM. The proposed method was also applied for determination of dopamine in urine samples. Wang et al. (2018) reported a novel ternary photocatalyst, which comprised single atom-dispersed silver and CQDs coloaded with ultrathin g-C_3N_4 (SDAg-CQDs/UCN). It was then used for photocatalytic degradation of naproxen, which involved hydroxylation, decarboxylation, and opening of the naphthalene ring.

Liu et al. (2019a,b) prepared nitrogen and boron codoped CQDs (NB-CQDS) via a one-pot hydrothermal treatment. They used citric acid, borax, and *p*-phenylenediamine for this purpose as the source of carbon, boron, and nitrogen, respectively. It was revealed that NB-CQDs were almost monodispersed with an average particle diameter of 3.53 nm. A sensor was designed using NB-CQDs for the determination of acetone and dopamine with a limit of detection of 0.54 μM and 11 nM, respectively. Aziz et al. (2019) prepared CQDs using branched polyethyleneimine to modify these dots. It was observed that fluorescence of CDs could be efficiently quenched by mercuric ions in aqueous solution. It was revealed that this probe can be used for the detection of Hg^{2+} ions in the concentration range from 20 to 800 nM with a detection limit of 10.0 nM. It provides a simple, selective, and sensitive fluorescence probe for Hg^{2+}.

Wang et al. (2019) used biomass of cyanobacteria as a carbon source for synthesizing fluorescent and water-soluble CQDs via a hydrothermal method. It was reported that as-synthesized CQDs were found to be monodispersed with an average diameter of 2.48 nm. It was observed that as-prepared CQDs exhibited high photostability with no photobleaching, even if kept for a longer time under UV irradiation. One advantage of such CQDs is that they could illuminate the complete cell and differentiate the cytoplasm from nucleus. It was also proposed that biomass of cyanobacteria can be used to fabricate CQDs on a large scale.

Water-soluble highly green fluorescent CQDs were prepared by Dhandapani et al. (2020) via hydrothermal carbonization of cost-effective wastes of fish. It was reported that the as-synthesized sample exhibited photoluminescence with high green emission 406 at the excitation of 330 nm. The UV−Vis spectra showed the presence of two major peaks at 266 and 371, due to $\pi \rightarrow \pi^*$ and $n \rightarrow \pi^*$ transition, respectively. It was revealed that as-prepared CQDs are spherical in shape with size $\sim 6 \pm 1$ nm. It was suggested that as-synthesized CQDs may be used for water treatment and energy application.

Guo and Zhao (2020) synthesized blue emissive NCQDs via the hydrothermal treatment with a high quantum yield as high as 84.79%. They used diethylenetriamine and citric acid as a source of nitrogen and carbon, respectively. It was reported that as-prepared NCQDs exhibited good photostability, and excellent stability in high-salt conditions. It was revealed that as-prepared NCQDs can be used as potential probes for detecting ellagic acid selectively in a concentration range of 0.01−50 μM on the basis of the inner filter effect. It was suggested that there is good biocompatibility of the NCQDs, which indicates that it has a great potential for application in biomedical fields.

Khan et al. (2020) synthesized nitrogen and sulfur codoped water-soluble CQDs (NS-CQDs) via a hydrothermal route. They used L-lysine and thiourea for this purpose. It was reported that as-obtained NS-CQDs have a high quantum yield of 53.19 % with a blue fluorescence on excitation UV light (365 nm). It was revealed that NS-CQDs were spherical in shape with sizes in the range 5−8 nm (average diameter 6.86 nm). It was observed that NS-CQDs can act as a fluorescent probe for the sensitive and selective detection of picric acid in aqueous solution in the concentration range of 1−10 μM with a limit of detection as 0.24 μM. It was reported that these NS-CQDs fluorescent probes can be used to measure the concentration of picric acid in a real water sample of tapwater.

Wei et al. (2020) synthesized boron and nitrogen codoped CQDs (BNCQDs) via a microwave-assisted hydrothermal method. They used boric acid and o-phenylenediamine as the sources of boron, carbon, and nitrogen. It was reported that as-prepared BNCQDs exhibited high QY (13.79%), good biocompatibility, fluorescent stability, and low toxicity, which are necessary requirements for a cell imaging agent. It was revealed that accumulation was increased with an extension of incubation time with HeLa cells, and it was observed that BNCQDs imaging is suitable for cell morphology (Fig. 2.2).

Li et al. (2020) obtained two types of CQDs via a hydrothermal method. These CQDs had luminous peaks at 480 (blue CDs) and 525 nm (green quantum dots). These two QDs were used for the detection of Hg^{2+} ions. It was

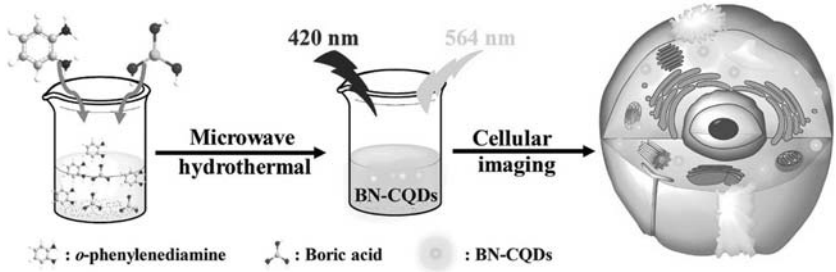

FIGURE 2.2 Synthesis of B, N-doped carbon quantum dots and their use in cellular imaging. *Adapted from Wei, Y., Chen, L., Wang, J., Liu, X., Yang, Y., Yu, S., 2020. Rapid synthesis of BN co-doped yellow emissive carbon quantum dots for cellular imaging. Optical Mater. 100. https://doi.org/10.1016/j.optmat.2019.109647. With Permission.*

observed that mixed CDs could detect Hg^{2+} ions in the range of 0−1.0 μM with a low detection limit of 0.05 μM.

Shahba and Sabet (2020) synthesized highly photoluminescence carbon nanofibers/CQDs using pine fruit via a ball milling-assisted hydrothermal method. It was revealed that the as-obtained product was composed of carbon nanofibers and very tiny nitrogen-doped CDs with a high photoluminescence intensity. The photocatalytic activity of as-prepared material was investigated by degradation of six different dyes (methyl orange, erichrome black T, acid blue, eosin Y, methylene blue, and methyl). It was also reported that it can adsorb Cd^{2+} and Pb^{2+} ions from the water with almost 100% efficiency.

Wang et al. (2020) prepared biomass CQDs via a hydrothermal process. They used four biomass wastes as a source of carbon (magnolia flower, orange peel, paulownia leaves and ginkgo biloba leaves). The as-prepared biomass CQDs exhibited homogeneous particle size, optical properties, stability, and superior water solubility. A quenching effect on fluorescence was observed on the addition of Fe^{3+} ions into CQDs solution. It was reported that as-prepared CQDs have a sensitive response to Fe^{3+} ions and these ions can be measured in the concentration range of 0.2 − 100 μM with the limit of detection of 0.073 μM (Fig. 2.3).

Sharma et al. (2020) synthesized fluorescent CQDs via a hydrothermal approach using red cabbage (rc). It was reported that as-synthesized rcCQDs were having an average size of 3 nm with blue fluorescence and quantum yield of 8.3%. It was interesting to note that rcCQDs exhibited strong antioxidant activities of 56%, 61%, and 91% against hydroxyl,2,2-diphenyl-1-picrylhydrazyl, and potassium permanganate radicals, respectively, which was almost comparable with that of L-ascorbic acid (standard antioxidant). A superior biocompatibility and negligible cytotoxicity of as-synthesized rcCQDs on SH-SY5Y neuroblastoma cells was there as evident from Cell Counting Kit−8 assay. These rcCQDs were also used as a fluorescent probe for biolabeling of *Staphylococcus aureus* and *Escherichia coli*. These rcCQDs can also be utilized as a fluorescent ink, and may found to be suitable for varnish and paints.

Chaudhary et al. (2020) synthesized highly fluorescent NS-CQDs via hydrothermal process. They used banana (*Musa acuminata*) juice as the source of carbon. It was revealed that NS-CQDs were spherical shaped with an average size of 1.27 nm, but with poor crystallinity. The proposed method

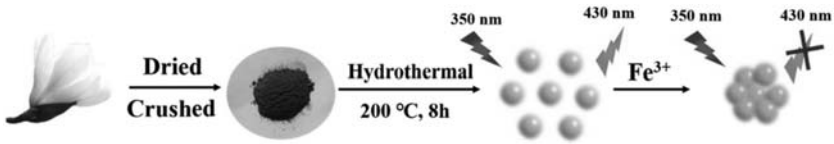

FIGURE 2.3 Preparation of quantum dots from biomass waste and detection of ferric ions. *Adapted from Wang, C., Shi, H., Yang, M., Yan, Y., Liu, E., Ji, Z., et al., 2020. Facile synthesis of novel carbon quantum dots from biomass waste for highly sensitive detection of iron ions. Mater. Res. Bull. 124, https://doi.org/10.1016/j.materresbull.2019.110730. With Permission.*

offers higher quantum yield (32%) compared to samples prepared from other natural sources. It was reported that as-synthesized NS-CQDs can be utilized as a fluorescent probe for the detection of Cu(II) in the concentration range of 1−800 μg mL^{-1} with the LOD of 0.3 μg mL^{-1} in the water sample.

2.3.2 Graphene-based quantum dots

Shen et al. (2012) prepared graphene quantum dots (GQDs) by a one-pot hydrothermal reaction. They used polyethylene glycol (PEG) and small GO sheet as the starting materials. It was reported that as-prepared GQDs-PEG exhibited luminescence properties. Tang et al. (2012) prepared crystalline GQDs that were water soluble. Glucose was used as the source of carbon. As-prepared QDs have an average diameter as small as 1.65 nm. A microwave-assisted hydrothermal method was used for this purpose. It was revealed that as-prepared GQDs can convert blue light into white light, when these GQDs were coated onto a blue light-emitting diode.

Wang et al. (2014) synthesized stable blue fluorescent GQDs via a hydrothermal method. The fluorescence of reoxidized grapheme oxide was quenched by Cu(II) in water. It can be used as a fluorescence sensor for the detection of cupric ions with high selectivity and sensitivity as compared to other metal ions in concentration range of 0−15 μM with a detection limit of 0.226 μM.

Qu et al. (2014) synthesized a series of GQDs via a hydrothermal process. They used citric acid as a carbon precursor and formed an N-free GQD graphite framework. It was reported that N-doped GQDs were prepared using urea. It was reported that the pyrrolic N was transformed to graphite N under these conditions. It was reported that the highest photoluminescence quantum yield PL QY (94%) of N-doped GQDs could be achieved using ethylenediamine as an N source.

Wu et al. (2014) reported the preparation of dicyandiamide (DCD) N-doped high quantum yield GQDs via a hydrothermal method. They used citric acid as the source of carbon. It was observed that N-doping of GQDs can promote a photoluminescence quantum yield (36.5%). It was also revealed that as-obtained N-doped GQDs were pH-sensitive, photostable, and had low toxicity, and therefore can be used as a pH sensor in a wide range from real water to intracellular contents. Ju and Chen (2014) prepared nitrogen-doped GQDs via hydrothermal treatment, a simple and low-cost approach. They used hydrazine as the source of nitrogen. Due to the selective coordination to Fe^{3+}, as-prepared N-GQDs can be used for selective detection of Fe(III) ions in aqueous solution as well as real water samples with a detection limit of 90 nM.

Fei et al. (2014) synthesized GQDs from anthracite coal, and then self-assembly on graphene by hydrothermal treatment. They observed the formation of hybrid nanoplatelets which were then codoped with nitrogen and boron. It was reported that as-prepared composite exhibited excellent oxygen

reduction reaction (ORR) electrocatalysis with higher activity as compared to commercial Pt/C in alkaline media. Lee et al. (2015) synthesized graphene-decorated V_2O_5 nanobelts (GVNBs) via a hydrothermal method. The GVNBs composite with (VO/GO = 3:1) exhibited excellent specific capacitance as compared to other composites and pure materials. This composite also showed excellent cyclic stability and retention of capacitance (82%) even after 5000 cycles.

Permatasari et al. (2016) synthesized GQDs containing N atoms via a hydrothermal method. They used urea and citric acid as the starting materials. It was revealed that as-prepared GQDs were spherical in shape with an average diameter of 2.17 nm. Fan et al. (2017) functionalized covalently arylamine-based polyazomethine with functionalized GO quantum dots (TPAPAM-GOQDs). It was prepared by an amidation reaction to design a ternary memory device with a configuration of gold/TPAPAM-GOQDs/indium tin oxide. It was claimed that this memory device could enhance the memory capacity of a device from the conventional 2^n to 3^n as compared to binary memory devices.

The composites of N, S codoped GQDs (N, S-GQDs)-rGO-TiO_2 nanotubes (TiO_2NT) were prepared by Tian et al. (2017) via alkaline hydrothermal reaction. It was reported that as-prepared N, S-GQDs/10%rGO/TNT composite exhibited the highest photodegradation efficiency for the degradation of methyl orange, which was 1.8 times and 16.3 times more than 10% rGO + TNT and pure TNT, respectively.

Yao et al. (2018) prepared in situ sulfur-doped GQDs via a hydrothermal method, which were decorated with CNPs to give (S-GQDs/CNPs) hybrid. It was reported that S-GQDs were decorated on CNPs by $\pi-\pi$ stacking. In this case, the advantages of both GQDs as well as CNPs are combined, which will facilitate the electron transfer between S-GQDs and CNPs. It was indicated that the layer by layer modified method in the S-GQDs/CNPs hybrid can inhibit the two-electron pathway and cause a four-electron pathway for ORR rate. It was revealed that the as-prepared S-GQDs/CNPs hybrid exhibited a better methanol tolerance along with long-term durability as compared to commercial 20% Pt/C.

A ternary nanocomposite of high fluorescent polyaniline (PANI)/2-acrylamido-2-methylpropanesulfonic acid (AMPSA) capped silver NPs/GO quantum dots (PANI/Ag (AMPSA)/GO QDs) was synthesized by Shokry et al. (2019) via in situ oxidative polymerization of aniline in the presence of Ag (AMPSA) NPs and GO QDs. The Ag(AMPSA) NPs and GO QDs were prepared by reduction by silver nitrate and carbonization of glucose methods, respectively.

GQDs were synthesized by Hoang et al. (2020) from GO via a microwave-assisted hydrothermal method. This proposed method requires a relatively shorter time (10 min.) as compared to conventional hydrothermal routes. It was reported that as-prepared NPs have a diameter of about

2–8 nm. There was a blue emission on exposure to UV irradiation. It was observed that as-synthesized GQDs can be utilized as a hole transport layer in organic solar cells and quantum efficiency of the cell was increased. It was revealed that on mixing P3HT:PCBM polymer and GQDs, potential difference was reduced at the interfaces of the two materials. It was observed that the overall efficiency of the cell was enhanced by 1.43%, which was about a 44% increase compared to pristine cells (0.99%).

2.4 Recent developments

Although hydrothermal synthesis has been used for a long time with good results, there are some recent developments in this direction. Some of these advancements are summarized in Table 2.1.

TABLE 2.1 Synthesis of quantum dots by hydrothermal route.

Source	Application	References
Carbon quantum dots	Fluorescent (emission range 280–420 nm), a highly sensitive and selective probes for detection of Fe^{3+} ions	Latief et al. (2021)
Fingernails carbon quantum dots (FNCQDs/g-C_3N_4)	Cu^{2+} sensing and photodegradation of 2,4-dichlorophenol	Tai et al. (2021)
Carbon quantum dots	Detection of formaldehyde	Amer et al. (2021)
Carbon quantum dots	Detection of Fe^{3+} ions	Raja and Sundaramurthy (2021)
Carbon quantum dots	Bioimaging	Li et al. (2021)
Carbon quantum dots	In vivo bioimaging	Atchudan et al. (2021)
Carbon quantum dots	Sensitivity and detection of highly toxic chromium(VI) ions	Baragau et al. (2021a,b)
N-doped carbon quantum dots	Ion detection and cell imaging	Shen et al. (2021)
Carbon quantum dots	Oil recovery	Baragau et al. (2021a,b)
Carbon quantum dots/ silver nanoparticles	Determination of losartan potassium (pure form and pharmaceutical formulations)	Abdoon and Atawy (2021)

2.5 Conclusion

Various nanomaterials or quantum dots can be easily prepared by the hydrothermal approach. This method has the advantages of a good control on the size of the particle and their morphology. It requires relatively low temperatures, thus avoiding the problems encountered with high-temperature processes. The materials having high vapor pressure near their melting points can also be synthesized using this technique. Apart from this, the hydrothermal method can also be used in combination with some other approaches, such as microwave-assisted, ultrasound-assisted, etc., to give good yields of the desired products with high purity.

References

Abdoon, F.M., Atawy, H.M., 2021. Prospective of microwave-assisted and hydrothermal synthesis of carbon quantum dots/silver nanoparticles for spectrophotometric determination of losartan potassium in pure form and pharmaceutical formulations. Mater. Today: Proc. 42, 2141–2149.

Amer, W.A., Rehab, A.F., Abdelghafar, M.E., Torad, N.L., Atlam, A.S., Ayad, M.M., 2021. Green synthesis of carbon quantum dots from purslane leaves for the detection of formaldehyde using quartz crystal microbalance. Carbon 179, 159–171.

Atchudan, R., Edison, T.N.J.I., Shanmugam, M., Perumal, S., Somanathan, T., Lee, Y.R., 2021. Sustainable synthesis of carbon quantum dots from banana peel waste using hydrothermal process for in vivo bioimaging. Phys. E Low. Dimens. Syst. Nanostruct. 126. Available from: https://doi.org/10.1016/j.physe.2020.114417.

Aziz, K.H.H., Omer, K.M., Hamarawf, R.F., 2019. Lowering the detection limit towards nanomolar mercury ion detection via surface modification of N-doped carbon quantum dots. N. J. Chem. 43 (22), 8677–8683.

Baragau, I.A., Lu, Z., Power, N.P., Morgan, D.J., Bowen, J., Diaz, P., et al., 2021a. Continuous hydrothermal flow synthesis of S-functionalised carbon quantum dots for enhanced oil recovery. Chem. Eng. J. 405. Available from: https://doi.org/10.1016/j.cej.2020.126631.

Baragau, I.A., Power, N.P., Morgan, D.J., Lobo, R.A., Roberts, C.S., Titirici, M.M., et al., 2021b. Efficient continuous hydrothermal flow synthesis of carbon quantum dots from a targeted biomass precursor for on–off metal ions nanosensing. ACS Sustain. Chem. Eng. 9 (6), 2559–2569.

Chaudhary, N., Gupta, P.K., Eremin, S., Solanki, P.R., 2020. One-step green approach to synthesize highly fluorescent carbon quantum dots from banana juice for selective detection of copper ions. J. Environ. Chem. Eng. 8 (3). Available from: https://doi.org/10.1016/j.jece.2020.103720.

Dhandapani, E., Duraisamy, N., Periasamy, P., 2020. Highly green fluorescent carbon quantum dots synthesis via hydrothermal method from fish scale. Mater. Today: Proc. 26. Available from: https://doi.org/10.1016/j.matpr.2021.04.396.

Fan, F., Zhang, B., Cao, Y., Yang, X., Gu, J., Chen, Y., 2017. Conjugated polymer covalently modified graphene oxide quantum dots for ternary electronic memory devices. Nanoscale 9 (30), 10610–10618.

Fei, H., Ye, R., Ye, G., Gong, Y., Peng, Z., Fan, X., 2014. Boron-and nitrogen-doped graphene quantum dots/graphene hybrid nanoplatelets as efficient electrocatalysts for oxygen reduction. ACS Nano 8 (10), 10837–10843.

Guo, Y., Zhao, W., 2020. Hydrothermal synthesis of highly fluorescent nitrogen-doped carbon quantum dots with good biocompatibility and the application for sensing ellagic acid. Spectrochim. Acta Part. A: Mol. Biomol. Spectrosc. 240. Available from: https://doi.org/10.1016/j.saa.2020.118580.

Guo, Y., Wang, Z., Shao, H., Jiang, X., 2013. Hydrothermal synthesis of highly fluorescent carbon nanoparticles from sodium citrate and their use for the detection of mercury ions in an aqueous solution. Carbon 52, 583–589.

Han, W., Ren, L., Qi, X., Liu, Y., Wei, X., Huang, Z., et al., 2014. Synthesis of CdS/ZnO/graphene composite with high-efficiency photoelectrochemical activities under solar radiation. Appl. Surf. Sci. 299, 12–18.

Hannay, J.B., 1880. On the artificial formation of the diamond. Proc. R. Soc. Lond. 30 (200–205), 188–189.

He, H., Huang, L., Zhong, Z., Tan, S., 2018. Constructing three-dimensional porous graphene-carbon quantum dots/g-C_3N_4 nanosheet aerogel metal-free photocatalyst with enhanced photocatalytic activity. Appl. Surf. Sci. 441, 285–294.

Hoang, T.T., Pham, H.P., Tran, Q.T., 2020. A facile microwave-assisted hydrothermal synthesis of graphene quantum dots for organic solar cell efficiency improvement. J. Nanomater. 2020. Available from: https://doi.org/10.1155/2020/3207909.

Jat, K.K., Bhatt, J., Ameta, S.C., 2019. Photodegradation of fast green by using SnO_2 quantum dots/TiO_2 nanoparticles composite. J. Appl. Chem. 8 (1), 139–145.

Ju, J., Chen, W., 2014. Synthesis of highly fluorescent nitrogen-doped graphene quantum dots for sensitive, label-free detection of Fe(III) in aqueous media. Biosens. Bioelectron. 58, 219–225.

Khan, Z.M., Saifi, S., Aslam, Z., Khan, S.A., Zulfequar, M., 2020. A facile one step hydrothermal synthesis of carbon quantum dots for label-free fluorescence sensing approach to detect picric acid in aqueous solution. J. Photochem. Photobiol. A: Chem. 388. Available from: https://doi.org/10.1016/j.jphotochem.2019.112201.

Latief, U., ul Islam, S., Khan, Z.M., Khan, M.S., 2021. A facile green synthesis of functionalized carbon quantum dots as fluorescent probes for a highly selective and sensitive detection of Fe^{3+} ions. Spectrochim. Acta Part. A: Mol. Biomol. Spectrosc. 262. Available from: https://doi.org/10.1016/j.saa.2021.120132.

Lee, M., Balasingam, S.K., Jeong, H.Y., Hong, W.G., Kim, B.H., Jun, Y., 2015. One-step hydrothermal synthesis of graphene decorated V_2O_5 nanobelts for enhanced electrochemical energy storage. Sci. Rep. 5. Available from: https://doi.org/10.1038/srep08151.

Li, X., Lv, X., Li, N., Wu, J., Zheng, Y.Z., Tao, X., 2019. One-step hydrothermal synthesis of high-percentage 1T-phase MoS_2 quantum dots for remarkably enhanced visible-light-driven photocatalytic H_2 evolution. Appl. Catal. B., Environ. 243, 76–85.

Li, D.Y., Wang, S.P., Azad, F., Su, S.C., 2020. Single-step synthesis of polychromatic carbon quantum dots for macroscopic detection of Hg^{2+}. Ecotoxicol. Environ. Safe. 190. Available from: https://doi.org/10.1016/j.ecoenv.2019.110141.

Li, Z., Wang, Q., Zhou, Z., Zhao, S., Zhong, S., Xu, L., et al., 2021. Green synthesis of carbon quantum dots from corn stalk shell by hydrothermal approach in near-critical water and applications in detecting and bioimaging. Microchem. J. 166. Available from: https://doi.org/10.1016/j.microc.2021.106250.

Liu, S., Zhang, H., Qiao, Y., Su, X., 2012. One-pot synthesis of ternary $CuInS_2$ quantum dots with near-infrared fluorescence in aqueous solution. RSC Adv. 2 (3), 819–825.

Liu, S., Shi, F., Zhao, X., Chen, L., Su, X., 2013. 3-Aminophenyl boronic acid-functionalized $CuInS_2$ quantum dots as a near-infrared fluorescence probe for the determination of dopamine. Biosens. Bioelectron. 47, 379–384.

Liu, T., Li, N., Dong, J.X., Zhang, Y., Fan, Y.Z., Lin, S.M., et al., 2017. A colorimetric and fluorometric dual-signal sensor for arginine detection by inhibiting the growth of gold nanoparticles/carbon quantum dots composite. Biosens. Bioelectron. 87, 772–778.

Liu, Q., Hu, C., Wang, X., 2019a. Hydrothermal synthesis of oxygen-deficiency tungsten oxide quantum dots with excellent photochromic reversibility. Appl. Surf. Sci. 480, 404–409.

Liu, Y., Li, W., Wu, P., Ma, C., Wu, X., Xu, M., 2019b. Hydrothermal synthesis of nitrogen and boron co-doped carbon quantum dots for application in acetone and dopamine sensors and multicolor cellular imaging. Sens. Actuators B Chem. 281, 34–43.

Lu, Y., Feng, Y., Wang, F., Zou, X., Chen, Z.F., Chen, P., et al., 2018. Facile hydrothermal synthesis of carbon dots (CDs) doped $ZnFe_2O_4/TiO_2$ hybrid materials with high photocatalytic activity. J. Photochem. Photobiol. A: Chem. 353, 10–18.

Ma, X., Zhang, P., Zhao, Y., Liu, Y., Li, J., Zhou, J.Y., et al., 2017. Role of N doping on the electrochemical performances of $ZnCo_2O_4$ quantum dots/reduced graphene oxide composite nanosheets. Chem. Eng. J. 327, 1000–1010.

Martins, N.C., Angelo, J., Girão, A.V., Trindade, T., Andrade, L., Mendes, A., 2016. N-doped carbon quantum dots/TiO_2 composite with improved photocatalytic activity. Appl. Catal. Environ. 193, 67–74.

Min, S., Hou, J., Lei, Y., Ma, X., Lu, G., 2017. Facile one-step hydrothermal synthesis toward strongly coupled TiO_2/graphene quantum dots photocatalysts for efficient hydrogen evolution. Appl. Surf. Sci. 396, 1375–1382.

Moissan, H. 1893. Le diamant: Conférence faite à la Société des amis de la science le 17 mai [The diamond: Lecture to the Society of Friends of Science 17 May 1893] (in French). Europeana (accessed 27.06.12).

Murchison, R.I., 1841. First sketch of some of the principal results of a second geological survey of Russia. Phil. Mag. J. Sci. 3 (19), 417–422.

Perera, S.D., Mariano, R.G., Vu, K., Nour, N., Seitz, O., Chabal, Y., et al., 2012. Hydrothermal synthesis of graphene-TiO_2 nanotube composites with enhanced photocatalytic activity. ACS Catal. 2 (6), 949–956.

Permatasari, F.A., Aimon, A.H., Iskandar, F., Ogi, T., Okuyama, K., 2016. Role of C-N configurations in the photoluminescence of graphene quantum dots synthesized by a hydrothermal route. Sci. Rep. 6. Available from: https://doi.org/10.1038/srep21042.

Qian, X., Yue, D., Tian, Z., Reng, M., Zhu, Y., Kan, M., et al., 2016. Carbon quantum dots decorated Bi_2WO_6 nanocomposite with enhanced photocatalytic oxidation activity for VOCs. Appl. Catal. B: Environ. 193, 16–21.

Qiao, W., Yan, S., Song, X., Zhang, X., Sun, Y., Chen, X., 2015. Monolayer MoS_2 quantum dots as catalysts for efficient hydrogen evolution. RSC Adv. 5 (118), 97696–97701.

Qu, D., Zheng, M., Zhang, L., Zhao, H., Xie, Z., Jing, X., et al., 2014. Formation mechanism and optimization of highly luminescent N-doped graphene quantum dots. Sci. Rep. 4 (1). Available from: https://doi.org/10.1038/srep05294.

Raja, D., Sundaramurthy, D., 2021. Facile synthesis of fluorescent carbon quantum dots from Betel leafs (Piper betle) for Fe^{3+} sensing. Mater. Today: Proc. 34, 488–492.

Ren, X., Pang, L., Zhang, Y., Ren, X., Fan, H., Liu, S.F., 2015. One-step hydrothermal synthesis of monolayer MoS_2 quantum dots for highly efficient electrocatalytic hydrogen evolution. J. Mater. Chem. A 3 (20), 10693–10697.

Santra, P.K., Kamat, P.V., 2013. Tandem-layered quantum dot solar cells: tuning the photovoltaic response with luminescent ternary cadmium chalcogenides. J. Am. Chem. Soc. 135 (2), 877–885.

Schafthaul, K.F.E., 1845. Gelehrte Anzeigen Bayer. Akad. 20, 557–593.

Shahba, H., Sabet, M., 2020. Two-step and green synthesis of highly fluorescent carbon quantum dots and carbon nanofibers from pine fruit. J. Fluoresc. 30 (4), 927–938.

Sharma, N., Das, G.S., Yun, K., 2020. Green synthesis of multipurpose carbon quantum dots from red cabbage and estimation of their antioxidant potential and bio-labeling activity. Appl. Microbiol. Biotechnol. 104 (16), 7187–7200.

Shen, J., Zhu, Y., Yang, X., Zong, J., Zhang, J., Li, C., 2012. One-pot hydrothermal synthesis of graphene quantum dots surface-passivated by polyethylene glycol and their photoelectric conversion under near-infrared light. N. J. Chem. 36 (1), 97–101.

Shen, T.Y., Jia, P.Y., Chen, D.S., Wang, L.N., 2021. Hydrothermal synthesis of N-doped carbon quantum dots and their application in ion-detection and cell-imaging. Spectrochim. Acta Part. A: Mol. Biomol. Spectrosc. 248. Available from: https://doi.org/10.1016/j.saa.2020.119282.

Shokry, A., Khalil, M.M.A., Ibrahim, H., Soliman, M., Ebrahim, S., 2019. Highly luminescent ternary nanocomposite of polyaniline, silver nanoparticles and graphene oxide quantum dots. Sci. Rep. 9 (1). Available from: https://doi.org/10.1038/s41598-019-53584-6.

Tai, J.Y., Leong, K.H., Saravanan, P., Tan, S.T., Chong, W.C., Sim, L.C., 2021. Facile green synthesis of fingernails derived carbon quantum dots for Cu^{2+} sensing and photodegradation of 2, 4-dichlorophenol. J. Environ. Chem. Eng. 9 (1). Available from: https://doi.org/10.1016/j.jece.2020.104622.

Tang, L., Ji, R., Cao, X., Lin, J., Jiang, H., Li, X., et al., 2012. Deep ultraviolet photoluminescence of water-soluble self-passivated graphene quantum dots. ACS Nano 6 (6), 5102–5511.

Tian, H., Shen, K., Hu, X., Qiao, L., Zheng, W.N., 2017. S co-doped graphene quantum dots-graphene-TiO_2 nanotubes composite with enhanced photocatalytic activity. J. Alloy. Compd. 691, 369–377.

Wang, J., Han, H., 2010. Hydrothermal synthesis of high-quality type-II CdTe/CdSe quantum dots with near-infrared fluorescence. J. Colloid Interface Sci. 351 (1), 83–87.

Wang, Y., Ni, Y., 2014. Molybdenum disulfide quantum dots as a photoluminescence sensing platform for 2,4,6-trinitrophenol detection. Anal. Chem. 86 (15), 7463–7470.

Wang, F., Gu, Z., Lei, W., Wang, W., Xia, X., Hao, Q., 2014. Graphene quantum dots as a fluorescent sensing platform for highly efficient detection of copper (II) ions. Sens. Actuators B: Chem. 190, 516–522.

Wang, C., Xu, Z., Cheng, H., Lin, H., Humphrey, M.G., Zhang, C., 2015. A hydrothermal route to water-stable luminescent carbon dots as nanosensors for pH and temperature. Carbon 82, 87–95.

Wang, F., Wang, Y., Feng, Y., Zeng, Y., Xie, Z., Zhang, Q., 2018. Novel ternary photocatalyst of single atom-dispersed silver and carbon quantum dots co-loaded with ultrathin g-C_3N_4 for broad-spectrum photocatalytic degradation of naproxen. Appl. Catal. B: Environ. 221, 510–520.

Wang, X., Yang, P., Feng, Q., Meng, T., Wei, J., Xu, C., et al., 2019. Green preparation of fluorescent carbon quantum dots from cyanobacteria for biological imaging. Polymers 11 (4). Available from: https://doi.org/10.3390/polym11040616t.

Wang, C., Shi, H., Yang, M., Yan, Y., Liu, E., Ji, Z., et al., 2020. Facile synthesis of novel carbon quantum dots from biomass waste for highly sensitive detection of iron ions. Mater. Res. Bull. 124. Available from: https://doi.org/10.1016/j.materresbull.2019.110730.

Wei, W., Yao, Y., Zhao, Q., Xu, Z., Wang, Q., Zhang, Z., et al., 2010. Oxygen defect-induced localized surface plasmon resonance at the WO_{3-x} quantum dot/silver nanowire interface: SERS and photocatalysis. Nanoscale 11 (12), 5535–5547.

Wei, J.S., Ding, H., Zhang, P., Song, Y.F., Chen, J., Wang, Y.G., et al., 2016. Carbon dots/$NiCo_2O_4$ nanocomposites with various morphologies for high performance supercapacitors. Small 12 (43), 5927–5934.

Wei, Y., Chen, L., Wang, J., Liu, X., Yang, Y., Yu, S., 2020. Rapid synthesis of BN co-doped yellow emissive carbon quantum dots for cellular imaging. Opt. Mater. 100. Available from: https://doi.org/10.1016/j.optmat.2019.109647.

Wu, S., Cao, H., Yin, S., Liu, X., Zhang, X., 2009. Amino acid-assisted hydrothermal synthesis and photocatalysis of SnO_2 nanocrystals. J. Phy. Chem. C. 113 (41), 17893–17898.

Wu, Z.L., Gao, M.X., Wang, T.T., Wan, X.Y., Zheng, L.L., Huang, C.Z., 2014. A general quantitative pH sensor developed with dicyandiamide N-doped high quantum yield graphene quantum dots. Nanoscale 6 (7), 3868–3874.

Wu, P., Li, W., Wu, Q., Liu, Y., Liu, S., 2017. Hydrothermal synthesis of nitrogen-doped carbon quantum dots from microcrystalline cellulose for the detection of Fe^{3+} ions in an acidic environment. RSC Adv. 7 (70), 44144–44153.

Wu, M.C., Wu, P.Y., Lin, T.H., Lin, T.F., 2018. Photocatalytic performance of Cu-doped TiO_2 nanofibers treated by the hydrothermal synthesis and air-thermal treatment. Appl. Surf. Sci. 430, 390–398.

Xia, Q.X., Hui, K.S., Hui, K.N., Kim, S.D., Lim, J.H., Choi, S.Y., 2015. Facile synthesis of manganese carbonate quantum dots/Ni $(HCO_3)_2$–$MnCO_3$ composites as advanced cathode materials for high energy density asymmetric supercapacitors. J. Mater. Chem. 3 (44), 22102–22117.

Yao, L., Deng, H., Huang, Q.A., Su, Q., Du, X., Du, G., 2017. Facile synthesis of $CoFe_2O_4$ quantum dots/N-doped graphene composite with enhanced lithium-storage performance. J. Alloy. Compd. 693, 929–935.

Yao, Y., Guo, Y., Du, W., Tong, X., Zhang, X., 2018. In situ synthesis of sulfur-doped graphene quantum dots decorated carbon nanoparticles hybrid as metal-free electrocatalyst for oxygen reduction reaction. J. Mater. Sci.: Mater. Electron. 29 (20), 17695–17705.

Yu, H., Zhang, H., Huang, H., Liu, Y., Li, H., Ming, H., et al., 2012. ZnO/carbon quantum dots nanocomposites: one-step fabrication and superior photocatalytic ability for toxic gas degradation under visible light at room temperature. N. J. Chem. 36 (4), 1031–1035.

Yu, X., Liu, J., Yu, Y., Zuo, S., Li, B., 2014a. Preparation and visible light photocatalytic activity of carbon quantum dots/TiO_2 nanosheet composites. Carbon 68, 718–724.

Yu, H., Zhao, Y., Zhou, C., Shang, L., Peng, Y., Cao, Y., et al., 2014b. Carbon quantum dots/TiO_2 composites for efficient photocatalytic hydrogen evolution. J. Mater. Chem. 2 (10), 3344–3351.

Zeng, Y., Guo, N., Li, H., Wang, Q., Xu, X., Yu, Y., et al., 2019. Construction of flower-like MoS_2/Ag_2S/Ag Z-scheme photocatalysts with enhanced visible-light photocatalytic activity for water purification. Sci. Total. Environ. 659, 20–32.

Zhang, R., Chen, W., 2014. Nitrogen-doped carbon quantum dots: facile synthesis and application as a "turn-off" fluorescent probe for detection of Hg^{2+} ions. Biosens. Bioelectron. 55, 83–90.

Zhang, Y., Jiang, D., He, Z., Yu, Y., Zhang, H., Jiang, Z., 2014. Hydrothermal synthesis of PEG-capped ZnS:Mn^{2+} quantum dots nanocomposites. Chem. Res. Chin. Univ. 30 (1), 176–180.

Zhang, X., Wang, J., Liu, J., Wu, J., Chen, H., Bi, H., 2017. Design and preparation of a ternary composite of graphene oxide/carbon dots/polypyrrole for supercapacitor application: importance and unique role of carbon dots. Carbon 115, 134–146.

Zhang, R., Wang, Y., Jia, M., Xu, J., Pan, E., 2018. One-pot hydrothermal synthesis of ZnS quantum dots/graphene hybrids as a dual anode for sodium ion and lithium ion batteries. Appl. Surf. Sci. 437, 375–383.

Zhao, D., He, Z., Chan, W.H., Choi, M.M., 2009. Synthesis and characterization of high-quality water-soluble near-infrared-emitting CdTe/CdS quantum dots capped by N-acetyl-L-cysteine via hydrothermal method. J. Phys. Chem. C. 113 (4), 1293–1300.

Zhao, C., Jiao, Y., Hua, J., Yang, J., Yang, Y., 2018. Hydrothermal synthesis of nitrogen-doped carbon quantum dots as fluorescent probes for the detection of dopamine. J. Fluoresc. 28 (1), 269–276.

Zhao, X., Yang, H., Li, R., Cui, Z., Liu, X., 2019. Synthesis of heterojunction photocatalysts composed of Ag_2S quantum dots combined with Bi_4Ti_3 O_{12} nanosheets for the degradation of dyes. Environ. Sci. Res. 26 (6), 5524–5538.

Zhou, J., Gao, Y., Liu, X., Chen, Z., Dai, L., Cao, C., 2013. Mg-doped VO_2 nanoparticles: hydrothermal synthesis, enhanced visible transmittance and decreased metal–insulator transition temperature. Phys. Chem. Chem. Phys. 15 (20), 7505–7511.

Zhu, H., Yang, D., Yu, G., Zhang, H., Yao, K., 2006. A simple hydrothermal route for synthesizing SnO_2 quantum dots. Nanotechnology 17 (9). Available from: https://doi.org/10.1088/0957-4484/17/9/052.

Chapter 3

Sol–gel synthesis of quantum dots

Avinash K. Rai[1] **and Kanchan K. Jat**[2]
[1]*Department of Chemistry, PAHER University Udaipur, Rajasthan, India,* [2]*Department of Chemistry, M. L. S. University Udaipur, Rajasthan, India*

3.1 Introduction

The sol–gel process is a new approach to the preparation of nanomaterials. A sol is a stable dispersion of colloidal particles or polymers in a solvent. It allows a better control in the synthesis of solids. It is a wet-chemical technique used for the preparation of both glassy as well as ceramic materials. The sol–gel process is based on hydrolysis and polycondensation reactions. During this process, first the sol (or solution) is evolved, which gradually proceeds to the formation of a gel-like network containing both a liquid phase and a solid phase. The basic structure (morphology) of the solid phase can have a wide range, starting from discrete colloidal particles to chain-like polymer networks. Synthesis using a sol–gel approach is used in the preparation of ceramic materials such as metal oxides, nitrides, and carbides. It results in the formation of a sol, which turns into a gel after a series of chemical reactions and/or mild thermal treatments. It is finally calcined to obtain the desired product.

- The basic idea behind sol–gel synthesis is to first dissolve the compound in a liquid and then bring it back as a solid; of course in a controlled manner.
- This technique provides facile preparation of compounds by mixing sols of different compounds.
- It avoids problems encountered in coprecipitation methods and gives smaller particles.

Sol–gel is a method for preparing metal oxide glasses, ceramics, etc. First, a chemical precursor or their mixtures are hydrolyzed, forming a solution state, which is converted to a gel state and then it is dehydrated to a ceramic or glass (Fig. 3.1).

Quantum Dots. DOI: https://doi.org/10.1016/B978-0-12-824153-0.00003-3
© 2023 Elsevier Inc. All rights reserved.

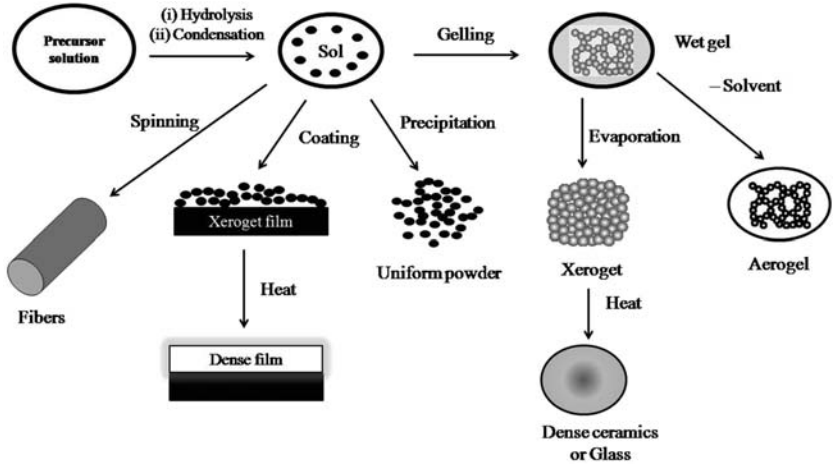

FIGURE 3.1 Different steps involved in sol–gel and related processes.

This technology can be used to prepare thin films, fibers, microspheres, fine powders, etc. It can be used to obtain catalysts, protective coatings, piezoelectric devices, lenses, wave-guides, superconductors, high-strength ceramics, insulating materials, nanoparticles (quantum dots also) etc.

Basically, it involves three steps:

- firstly, partial hydrolysis of metal alkoxides to form reactive monomers;
- condensation of as-prepared monomers to form colloid-like oligomers, known as sol formation; and
- additional hydrolysis leading to polymerization and cross-linking for a gel formation (three-dimensional matrix).

The various steps involved in sol–gel process are:

1. hydrolysis and condensation of compounds (sol formation);
2. gelation (sol–gel transformation);
3. aging; and
4. drying.

In the first step, a sol is formed, which is a stable dispersion of colloidal particles (it may be crystalline or amorphous) or polymers in a solvent. Then gel is formed by a three-dimensional (3D) continuous network, which contains a liquid phase, or by polymer chains. Some agglomerates of colloidal particles are there while the particles have some polymeric aggregates of subcolloidal particles in a polymer gel.

During this process, the solvent is trapped inside the gel as viscosity rapidly increases. Its structure may change considerably with time, depending on temperature, solvent, and pH. The liquid phase still contains agglomerates

and sol particles, which react there and condense on drying of the gel. Originally, the gel is flexible, but on condensation, it becomes more viscous. This will squeeze out the liquid present in the interior of the gel, and shrink it until there is a flexibility in the gel.

3.1.1 Advantages

The following are the advantages of this process:

- It provides a better control of the structure, such as particle size and porosity.
- It provides possibility of incorporating nanosized materials.
- It can ensures an excellent adhesion between top layers and substrate by forming thin coating.
- Relatively high purity is retained.
- It provides a good control on composition.
- It can be carried out at a relatively low temperature.
- There is no need for special or expensive equipment.

3.1.2 Disadvantages

There are some disadvantages of this process also and these are:

- There is long processing time.
- Organic solvents are used, some of which may be toxic.

3.2 Synthesis of quantum dots

3.2.1 Oxides

Lin et al. (2005) synthesized ZnO quantum dots via a simple sol–gel method. It was reported that the average size of these quantum dots can be tailored by variation of the concentration of the precursor of zinc. Size-dependent blueshifts of photoluminescence and absorption spectra revealed the quantum confinement effect. The ZnSe quantum dots were embedded in SiO_2 thin films by Jiang et al. (2004) via a sol–gel process. They used Zn $(Ac)_2 \cdot H_2O$ and H_2SeO_4 as the source of zinc and selenium, respectively. It was indicated that the size of the crystallite was increased with the concentration of selenium.

Li and Qu (2007) prepared CdTe quantum dots-derived composite with silica spheres coated with 5,11,17,23-tetra-*tert*-butyl-25,27-diethoxy-26,28-dihydroxycalix[4]arene (C[4]/SiO_2/CdTe) via a sol − gel approach. It was observed that FL intensity was increased linearly with increasing methomyl (pesticide) concentration (0.1 − 50 μM) with a limit of detection of 0.08 μM. On the other hand, it was negligible as compared to other pesticides, such as

parathion-methyl, fenamithion, acetamiprid, and optunal. Bera et al. (2008) reported synthesis and spectroscopic characterization of sol−gel derived zinc oxide quantum dots of 3−8 nm size. The quantum dots exhibited a broad and strong visible emission peak centered near 520 nm with a quantum efficiency of approximately 5%.

Zhang et al. (2010a) synthesized ZnO quantum dots via a sol − gel route. They used a zinc − oleate complex as a precursor. It was reported that as-obtained ZnO QDs had diameters in the range of 2.2 − 7.8 nm. It was revealed that ionized oxygen vacancies are responsible for the origin and intensity of the visible emission of ZnO QDs, while the visible emission peak position of ZnO QDs is decided by the following two factors:

- size; and
- transition of holes from the valence band to preexisting deep donor energy level.

The ZnO quantum dots were synthesized using the same precursors (Zhang et al., 2010b). It was reported that as-obtained ZnO QDs hexagonal had a wurtzite structure with particle size diameter of 8.9 nm. It was revealed that there is a redshift excitation. It was also observed that visible emission also shifted to the green luminescence band from yellow on increasing the annealing temperature.

Yu et al. (2010) synthesized Eu^{3+}-doped glass ceramics embedded ZnO quantum dots via a sol−gel method. It was revealed that ZnO QDs obtained were in the range of 3−6 nm. It was reported that these glass ceramics had a high transparency in the visible−infrared range, which may be due to the much smaller size of the ZnO QDs as compared to the wavelength of the visible light. CdTe quantum dots-doped TiO_2 photocatalysts were synthesized by Li et al. (2010) via a facile sol−gel method at room temperature. The photocatalytic activities of the as-prepared sample were investigated for the degradation of malachite green. It was found that the sample doped with 0.06 wt.% CdTe QDs exhibited the highest photocatalytic activity.

Chen et al. (2011) also synthesized ZnO quantum dots by a sol−gel method. These QDs exhibited a strong blue emission. It has been reported that ZnO QDs had an average diameter of 16.0−32.2 nm. It was observed that a higher reaction temperature and longer reaction time resulted in larger average size for QDs. It was revealed that a reduction in photoluminescence and increase of the size of ZnO QDs were similar for annealing in nitrogen, vacuum, and air.

Zinc oxide quantum dots with blue emission were synthesized by Han et al. (2012) via a sol−gel method. It was interesting to note that the blue emission was neither due to quantum confinement nor intermediate products. It was achieved only in the presence of Li^+ cations and hydroxide ions. It was revealed that an excess of OH^- ions is responsible for the formation of interstitial oxygen defects, while Li^+ ions can stabilize these defects by

substituting Zn atoms causing a blueshift of the blue emission. The Cd-doped ZnO quantum dots were prepared by Zhang et al. (2012) through a sol−gel method. The effect of Cd concentration and mass ratio of trioctylphosphine oxide (TOPO)/octadecylamine (ODA) on structural and luminescent properties of QDs was also evaluated. It was reported that Cd-doped ZnO QDs are 3−6 nm in diameter. It was observed that QD particle size was found to be reduced on increasing the Cd content. It was revealed that UV and fluorescence spectra both were blueshifted. The best optical performance was achieved when the TOPO/ODA mass ratio was kept 1:2.

The lanthanum-doped ZnO quantum dots were synthesized by Sun et al. (2012) via a modified sol−gel method. It was reported that La-doped quantum dots exhibited enhanced luminescent properties and their quantum yield was 77.9%. Then they prepared anticounterfeiting inks by incorporating these La-doped ZnO QDs into the transparent oil. The sol−gel method was applied by Korala et al. (2013) to fabricate thin films of CdSe and core(shell) CdSe(ZnS) QDs. It was reported that more than twofold enhancement in photocurrent could be achieved with an increase in photovoltage due to passivation of surface defects via overcoating with a thin ZnS shell. As a result as-prepared QD thin films are considered suitable for a wide range of optoelectronic applications.

Ge et al. (2013) fabricated a composite of TiO_2 films with CdTe quantum dots. Different CdTe QDs (green-, yellow-, and red-emitting) were obtained, when thioglycolic acid was used as a capping agent. It was revealed that red-emitting CdTe QDs exhibited a small blueshift of 1 nm, while green-emitting QDs showed a blueshift of 7 nm. A nonhydrolytic sol−gel combustion method was used by Leelavathi et al. (2013) for synthesis of nanocomposites of PbO quantum dots on anatase TiO_2. It was indicated that the photocatalytic activity of quantum dot dispersed TiO_2 was higher than that of TiO_2 and much higher as compared to commercial Degussa P-25.

Zinc oxide quantum dots were synthesized by Kumar et al. (2014) via a simple sol−gel method. They used zinc acetate dehydrate, sodium hydroxide, and methanol as starting materials. A good crystallinity was observed in these QDs with average crystallite sizes $\sim$14 nm. It was suggested that as-synthesized ZnO QDs can be used as the electrode material for dye-sensitized solar cells. Li et al. (2014) synthesized Pr^{3+}-doped semiconductor ZnO quantum dots via a sol−gel method. It was reported that as-obtained ZnO QDs were spherical in shape and the diameter was around 5 nm. It was revealed that emission peaks of aged ZnO QDs exhibited a redshift due to the increasing size of the QDs.

Zhong et al. (2014) synthesized $CuGaS_2$ quantum dots, which were embedded in sodium borosilicate glass matrix by combining two processes: sol−gel and heat treatment in H_2S gas. It was observed that as-obtained $CuGaS_2$ quantum dots had a spherical shape and were uniformly distributed with sizes ranging from 5−25 nm. The formation of stable colloids

containing surface-modified ZnO QDs was reported by Moghaddam et al. (2015) via a sol−gel process in an ultrasonic bath. They used 3-aminopropyltriethoxysilane (APTES) as a capping agent. Alcoholic solutions of zinc acetate and potassium hydroxide were used as the reactants. The formation of nanocrystals of ZnO QDs with average size of ∼3 nm was confirmed. It was suggested that the as-prepared ZnO QDs were found to be suitable for optical and optoelectronic applications.

Liu et al. (2015) synthesized ZnO quantum dots by a sol−gel method. They used (methanol, ethanol, or hexanol) as solvents. It was indicated that as-prepared ZnO QDs were having good dispersion and their size ranged from 3.3−7.7 nm, which could be controlled by variation of the solvents. It was revealed that ZnO QDs exhibited visible emissions ranging from green to orange. Bajaj and Omanwar (2015) synthesized α-Al_2O_3 quantum dots by the stearic acid sol−gel synthesis. The as-prepared sample exhibited good UV absorption and blue emission at 254 and 403 nm, respectively. Gnanasekaran et al. (2015) synthesized TiO_2 quantum dots by the sol−gel method. It was reported that TiO_2 QDs have a pure anatase phase with a tetragonal structure. The photocatalytic activity of TiO_2 QDs have been evaluated for the degradation of methylene blue and methyl orange under UV light irradiation.

The synthesis of TiO_2 quantum dots has been reported by Sood et al. (2015) via a simple sol−gel, template-free method. They also evaluated catalytic behavior of as-synthesized quantum dots by photocatalytic degradation of Indigo carmine dye in the presence of UV light. Chen et al. (2016) synthesized TiO_2 and carbon quantum dots-doped TiO_2 nanocomposite (CQDs/TiO_2 nanocomposite) by a sol−gel approach. They evaluated the photocatalytic activity of TiO_2 and CQDs/TiO_2 composite for the degradation of rhodamine B and cefradine. It was observed that the photocatalytic activity of CQDs/TiO_2 was higher compared to TiO_2.

Miao et al. (2016) prepared visible light responsive carbon quantum dots embedded in mesoporous TiO_2 materials via a sol−gel process. The photocatalytic performance of as-prepared CQDs/meso-Ti-450 was investigated for the degradation of methylene blue. It was revealed that 5% CQDs/meso-Ti-450 can remove almost complete (98%) methylene blue, whereas commercial P25 can remove only 10% of the dye. The TiO_2 (mesoporous) with different concentration of CdS quantum dots was successfully fabricated by Zhou et al. (2017) via a sol−gel method. The photocatalytic activity of the as-prepared CdS/TiO_2 samples was evaluated for the degradation of methyl orange, and it followed the order:

$$2\%\ \mathrm{CdS/TiO_2} > 4\%\ \mathrm{CdS/TiO_2} > 8\%\ \mathrm{CdS/TiO_2} > \text{pure}\ \mathrm{TiO_2} > 1\%\ \mathrm{CdS/TiO_2}.$$

The 2% CdS/TiO_2 has also been used for the degradation of methylthionine chloride, malachite green, rhodamine B, and bisphenol A.

Soumya et al. (2018) synthesized Sn and Ag-doped ZnO quantum dots via a microwave-assisted sol−gel strategy. They used 3-aminopropyl trimethoxy silane as a capping agent. Then these ZQDs were dispersed in methyl methacrylate monomer and polymerized in situ to obtain PMMA/ZQDs. It was indicated that as-prepared doped ZQDs/PMMA hybrid coatings exhibited blue emission under UV light. It was revealed that undoped PMMA/ZQDs hybrid coatings showed only <14% NIR reflectance, which was enhanced by 30% and 23% on doping with Ag and Sn in PMMA/ZQDs hybrids, respectively. It was concluded that these ZQDs doped with Sn and Ag ions on treatment with dye and inorganic coactivators, can find applications in photochromic and UV/NIR shielding solar-control interface coatings.

Ye (2018) used a sol−gel method for the synthesis of stable ZnO QDs. They also observed the effects of reactants concentration, reaction time, and material ratio on particle sizes and defects structures of ZnO. The highest photoluminescence quantum yield (40%) with green emission was observed under UV light excitation (359 nm). Garcia et al. (2019) synthesized TiO_2 quantum dots by sol−gel process. They used ionic liquid (1-*n*-butyl-3-methylimidazolium tetrafluoroborate) as the stabilizing agent. An adhesive resin was formulated by mixing these QDs with methacrylate monomers. As-prepared adhesive resins were evaluated for antibacterial activity, cytotoxicity, polymerization behavior, fracture pattern, degree of conversion, and microtensile bond strength. It was reported that 26 wt.% of $BMI.BF_4$. TiO_2 QDs/$BMI.BF_4$ had a minimum size range of 1.19−7.11 nm, and an average size of 3.54 ± 1.08 nm.

A sol−gel reflux condensation route was developed by Javed et al. (2019) to produce TiO_2 QDs. They used titanium tetraisopropoxide as the precursor, which was first hydrolyzed and followed by reflux condensation for 24 h. It was revealed that as-prepared QDs were spherical in shape with an average crystallite size of 5−7 nm. The energy bandgap of TiO_2 QDs was found to be $\sim$3.76 eV. A series of ZnO quantum dots were prepared by Sowik et al. (2019) modified with rare-earth metals through a sol−gel approach. They selected Eu, Er, Tb, Yb, Ho, and La to modify ZnO QDs. It was observed that as-prepared modified ZnO QDs can degrade phenol in aqueous phase. The order of photocatalytic activity among all these as-obtained nanomaterials followed the order:

$$\mathrm{ZnO/0.09\ mm\_Er} > \mathrm{ZnO/0.18\ mm\_Eu} > \mathrm{ZnO/0.09\ mm\_La} > \mathrm{ZnO/0.27\ mm\_Er} > \mathrm{ZnO/0.18\ mm\_Tb} > \mathrm{pristine\ ZnO\ QDs}.$$

The ZnO and Au textured ZnO-based quantum dot thin film was fabricated by Dey and Sarkar (2020) and used as sensors. The as-fabricated sensor had an operating temperature of 35°C and it could be used for detecting a minute fraction vapors of different alcohols such as methanol, ethanol, propanol, and butanol. An annealing treatment at 350°C temperature was

imposed to improve the response of as-prepared sensors. Mohamed et al. (2020) synthesized three samples of ZnO quantum dots using a modified sol−gel method. It was reported that the average crystallite size, bandgap energy, and active surface area were 7.1 nm, 3.49 eV, and 150.1 $m^2\ g^{-1}$) for a sample prepared at 27°C. The other two samples prepared at 500°C and 900°C had an average particle size of 9.8 and 13.5 nm, respectively. It was observed that the photocatalytic performance decreases as the crystallite size increases in the case of degradation of methyl orange. It was revealed that the as-prepared samples could be recycled eight times.

Zou et al. (2020) prepared water-soluble ZnO quantum dots modified with (3-aminopropyl)triethoxysilane (APTES) by a simple sol−gel method. They displayed strong yellow-green fluorescence. It was observed that the emission from as-prepared NH_2−ZnO QDs was quenched in the presence of Cu^{2+} ions. They designed a fluorescent probe based on an as-prepared sample of NH_2−ZnO QDs for the detection of Cu^{2+} in water with a limit of detection of 1.72 nM. This fluorescent probe had also been applied in drinking water samples. Haghani et al. (2020) also prepared ZnO-QDs using a sol−gel method and then fabricated an optical sensor based on these QDs for the determination of chlorogenic acid (CGA). Tetraethoxysilane and 3-aminopropyltriethoxysilane were used as a cross-linker and functional monomer, respectively, to prepare the molecularly imprinted polymer (MIP). As-prepared ZnO-QDs MIP composite was used to measure CGA in the range of 0.2−5.3 $\mu g\ mL^{-1}$ with a limit of detection of 0.06 $\mu g\ mL^{-1}$. This sensor was also used to measure the concentration of CGA in human plasma samples.

Wang et al. (2020) prepared graphene oxide/WO_3 quantum dots/TiO_2 (GOWT) composite. These GOWT films were prepared by using this GOWT composite powder and $Al(H_2PO_4)_3$ as adhesive and low-cost gauze as substrates. As-prepared GOWT film was used for removal of rhodamine B. It was observed that the degradation rate of rhodamine B was around 2.6 times than GO/TiO_2 films in the presence of UV light. It was proposed that GOWT films can find potential application in sewage treatment without causing any further contamination. Song et al. (2020) used an efficient method to improve the stability of $MAPbBr_3$ QDs by encapsulating them in ZrO_2 sol. It was observed that this three-dimensional network ZrO_2 colloid formed a coating on the surface of $MAPbBr_3$ QDs, which protected these QDs from acid, base, and ultraviolet light. It was revealed that the photoluminescence intensity of as-prepared nanocomposites could retain 95% of its initial value even after 4.5 h in a basic environment and 90% in an acid environment after 10 h.

Schmitz et al. (2020) prepared colloidal ethanolic dispersions of zinc oxide (undoped) and ZnO particles doped with magnesium (II) (ZnO:Mg) via a sol−gel method. The particle sizes of these QDs were found to be 4.26 and 3.65 nm, respectively. As-prepared QDs were then used as nanofillers to obtain zein-based nanocomposite films, which displayed homogeneity, good

visual appearance, and transparency. These thin films have an extended UV-blocking range in the absorbance spectra as compared to those of pure zein. It was observed that ZnO NPs, loaded into zein films exhibited 96.5 ± 4.9% inhibition of growth of *S. aureus*. It was suggested that as-prepared nanocomposites could be used for the development of food packaging and UV protective films.

The ZnS QDs/gelatin nanocomposites were prepared by Guo et al. (2020) using green one-pot method. The method shows advantages such as being an environment friendly strategy, with mild conditions, no need for organic solvents, and simple posttreatment. Here, gelatin acted as the green capping agent apart from being main component in the QDs/gelatin nanocomposites. The presence of gelatin provides the composite with a thermoresponsive sol−gel transition property. As-prepared composite with this property can find potential uses in imaging, fluorescence labeling, and controlled release.

The Fe_3O_4 quantum dots decorated silica (FS) adsorbent were prepared by Rakibuddin and Kim (2020) via a sol−gel method. The formation of Fe_3O_4 quantum dots (organically modified silica surface) with an average size of 3−4 nm was confirmed. One of the samples showed the best arsenic removal efficiency (38.2 mg g^{-1}), which was higher than Fe_3O_4 and silica particles. As-Fe_3O_4 and silica both are environmentally sustainable, therefore this composite could be a potential candidate for the removal of arsenic. Vasiljevic et al. (2020) synthesized iron titanate (Fe_2TiO_5) nanoparticles via a modified sol−gel method followed by calcination. The bandgap of as-prepared iron tantalate was around 2.16 eV. Its photocatalytic activity was evaluated for degradation of methylene blue in the presence of natural sunlight.

Wang and Li (2021) prepared ZnO quantum dots (ZQ) and Ag/ZQ nanocomposites with different percentages of Ag loadings via a sol−gel method. It was observed that the as-fabricated sample of nanocomposite (Ag content of 11 wt.%) exhibited excellent photocatalytic activity for degradation of methylene blue in the presence of Ag11/ZQ, when Ag content was kept at 11%. Xu et al. (2021) prepared CeO_2 QDs through a sol−gel method using a recursor of $Ce(NO_3)_3 \cdot 6H_2O$ as the source of cerium. Then they developed a fluorescence probe based on these CeO_2 quantum dots and used it for highly selective and ultrasensitive direct determination of 4-nitrophenol (4-NP). It was reported that the concentration of 4-NP can be determined in the range of 0.005−75.00 μM with a limit of detection of 1.50 nM. It was also revealed that as-prepared CeO_2 QDs could be applied in the determination of 4-NP in real water samples.

Li et al. (2021) developed ZnO quantum dots using a sol−gel method. They also evaluated the antibacterial activities of ZnO QDs against *Staphylococcus aureus*, *Escherichia coli*, and *Salmonella pullorum*. It was found that the particle size of ZnO QDs was in the range of 3−6 nm. It was reported that as-prepared ZnO QDs inhibited the growth of *S. aureus*,

E. coli, and *S. pullorum* by 94.75 ± 2.28%, 87.06 ± 0.98%, and 85.55 ± 1.15%, respectively. These QDs also reduced the mortality of chicks infected with *S. pullorum* effectively via regulating the balance of the intestinal flora, protecting intestine and liver.

The mesoporous graphene quantum dots-doped TiO_2 (TiO_2-GQD) nanocomposites were prepared by Zhao et al. (2021) through a sol−gel method under ultrasonic radiation. As-prepared TiO_2-GQD nanocomposites exhibited superior performance for sunlight absorption, and photocathodic protection. It was revealed that they can protect the active metal as well as reduce the corrosion rate. It was suggested that TiO_2-GQD nanocomposites could be used in marine engineering for marine corrosion protection in the future.

Zhang et al. (2021) synthesized ZnO QDs using a hydrolysis−condensation reaction. The effect of alkali bases (LiOH, NaOH, and KOH) as well as the ratio of Zn^{2+}:OH^- was investigated on the properties of as-synthesized ZnO QDs and it was observed that the particle size of ZnO QDs prepared in the presence of LiOH and NaOH was smaller as compared to that prepared with KOH. It was reported that ZnO QDs prepared with ratio of Zn^{2+}: LiOH = 1:1 exhibited the best dispersibility and fluorescence performance.

3.2.2 Sulfides

Yamane et al. (1992) prepared CdS dispersed in soda-borosilicate glasses using by the sol−gel process. They used cadmium acetate, tetramethoxysilane, sodium acetate, and triethylborate. The gel formed was exposed to H_2S at 120°C. It was observed that glass containing about 10 wt.% CdS crystallites (4−7 nm in diameter) was obtained by sintering at 590°C. Hayakawa et al. (2000) prepared rare-earth ions and semiconductor nanocrystals using Eu^{3+} doped silica gel with adsorbed cadmium sulfide particles via a sol−gel technique. It was proposed that surface-trapped electrons on CdS particles excited 4 f electrons (nonradiatively) in Eu^{3+} ions via an energy transfer process.

The CdS/ZnO quantum dots were prepared by Wang et al. (2011) via a sol−gel method. They used triethanolamine as a capping agent. The bandgaps for different ratios of CdS/ZnO (1:9, 1:1, and 9:1) were found to be 4.13, 3.93, and 3.11 eV, respectively. The size of as-obtained QDs was found to be in the range of 5−10 nm; of course with some agglomerated particles. Yang et al. (2018) prepared ZnS nanoparticles on nitrogen and sulfur codoped carbon nanosheets (ZnS@NSC) via a sol−gel synthesis. It was reported that nanosheets and ultrafine carbon shells together constituted an N, S codoped carbon framework, providing abundant active sites for sodium storage along with enhanced electrical conductivity. It was revealed that ZnS@NSC could achieve excellent cycling stability (73.6% capacity retention after 380 cycles at 0.5 A g^{-1}) and reversible capacity of 734 mAh g^{-1} at 0.5 A g^{-1}.

The ZnS/CdS/γ-TaON composite was prepared by An et al. (2019) via nitridation of Ta_2O_5 and deposition of CdS and ZnS quantum dots. It was revealed that CdS and ZnS quantum dots (3−8 nm diameter) were uniformly dispersed on the surface of γ-TaON. It was revealed that under optimized condition, H_2 evolution rate of ZnS/CdS/γ-TaON composite was 839.6 $\mu mol\ h^{-1}\ g^{-1}$, which is about 14 times higher than that of CdS/γ-TaON and 47 times higher than Pt loaded γ-TaON sample. Rakibuddin et al. (2020) prepared different MoS_2 morphologies (bulk, flake, and quantum dots) that were then fabricated onto indium tin oxide using the sol−gel method. The MoS_2 bulk, flake, and quantum dots were used as electrochromic anodic layers, and WO_3 as a cathodic layer to fabricate MoS_2/WO_3-based electrochromic devices. It was reported that as-fabricated MoS_2/WO_3 ECDs exhibited high optical contrasts (59%−75%) at 1.5−0 V and 700 nm. It was suggested that solution-processed MoS_2/WO_3-based ECDs can find an application in the processing of flexible and optical devices. Cadmium sulfide nanostructures were prepared by Sonker et al. (2020) using sol−gel method. Then CdS thin films of different thickness were prepared. They used an as-fabricated sample for gas sensing measurements for detecting 20 ppm NO_2 gas.

A phosphorescent probe of type SiO_2-Mn:ZnSQDS-MIP was synthesized by Chen et al. (2020) using MIP as a polymer coating via a sol−gel method. They used thioglycolic acid (TGA)-modified QDs, cephalexin, 3-aminopropyltriethoxysilane and tetraethoxysilane as luminescent materials, template, functional monomer, and cross-linking agent, respectively. It was revealed that cephalexin can be determined in 2.5−50 $\mu g\ L^{-1}$ concentration range with a limit of detection of 0.81 $\mu g\ L^{-1}$. The as-fabricated nanoprobe was applied for determination of cephalexin in (spiked) raw milk and milk powder. Sankar et al. (2020) synthesized Ni-doped CdS nanoparticles with 0.5%, 1.0%, 1.5%, and 2.0% via the sol−gel method. The average crystalline size of the particles was found to range from 8.70 to 9.93 nm. The SEM images indicated combination of metal oxide cubes and rod-like structures with 12−35 nm unequal grain size with excellent crystallinity quality. It was revealed that the bandgap energy decreases from 2.36 to 2.29 eV on increasing the percentage of Ni. Photocatalytic degradation of methylene blue and methyl orange was also carried out and it was found that 94% methyl orange can be degraded in 75 min.

Rempel et al. (2020) synthesized a complex sandwich catalyst, which was based on nanotubular TiO_2 and colloidal cadmium sulfide via a sol−gel method. They investigated the photocatalytic activity of this catalyst for oxidation of acetone in the gas phase under visible light and UV irradiation. Ajibade and Oluwalana (2021) prepared ODA-capped ZnS quantum dots from a bis(morpholinyldithiocarbamato)Zn(II) complex. It was confirmed that an hexagonal wurtzite crystalline phase of ZnS was present in the sample with particle sizes of about 1−3 nm. It was reported that the as-prepared ZnS can be used as photocatalysts for degrading brilliant green, rhodamine B, and their binary mixture. It was revealed that the highest photocatalytic

degradation efficiency of 94% was obtained with a sample with a low photoluminescence intensity. It was also found that ZnS quantum dots can be reused five times without any significant loss in degradation efficiency.

Zaidi and Azam (2021) synthesized zinc sulfide quantum dots using the sol−gel method. They used zinc nitrate and sodium sulfide as the source of zinc and sulfur, respectively. The particle size of as-prepared QDs was found to be 1.74 nm. The antimicrobial activity of these QDs was studied against *Pseudomonas aeruginosa*, where they exhibited good bactericidal activity. Perovskite-sensitized solar cell is an effective hybrid organic−inorganic solar cell device. Sonker et al. (2021) synthesized CdS quantum dots via the sol−gel approach. It was found that the maximum grain diameter was about ~4 nm. It was observed that as-fabricated CdS QD-based dye-sensitized solar cell and PSSC exhibited a maximum power conversion efficiency (η) of 0.5% and 1.8% at 1 Sun condition, which was improved by approximately 72% as compared to the reference cell.

3.2.3 Carbon-based quantum dots

Ke et al. (2017) prepared carbon quantum dots-modified TiO_2 photocatalysts via the sol−gel method. The photocatalytic performance of the as-prepared composite was the degradation of methylene blue in the presence of visible light irradiation and it was observed that the degradation efficiency of methylene blue was high (90%) within 2 h, which is almost 3.6 times higher than compared to TiO_2.

Ensafi et al. (2018) anchored MIP on the surface of GQDss using the sol−gel method. It was used for highly sensitive and selective determination of *p*-nitroaniline (*p*-NA) in the range of 0−15.0 μM. This was also applied to real samples of water and fish with satisfactory results. Molecularly imprinted silica was prepared via the sol−gel method by Yang et al. (2020). They used fipronil as the template, tetraethoxysilane as cross-linker, and 3-aminopropyltriethoxysilane as a functional monomer in the presence of carbon quantum dots. It was reported that blue fluorescence of the CQD@MIS, was quenched in the presence of fipronil, a commonly used insecticide. These QDs can detect fipronil in the range of 0.70 pM to 47 μM with the limit of detection being 19 pM. This method was applied for the determination of fipronil in real samples such as milk, spiked eggs, and tap water.

Yu et al. (2021) developed a composite of carbon nitride quantum dots in situ-doped TiO_2 inverse opal (TiO_2 IO) via the sol−gel method. It was reported that the as-prepared photocatalyst exhibited excellent photocatalytic degradation of toluene and 93% of toluene can be degraded into harmless products such as CO_2 and H_2O under simulated sunlight irradiation. On the other hand, only 37% of toluene was found to degrade in the presence of commercial P25. They also used this composite for the degradation of phenol and rhodamine B. Vyas et al. (2022) synthesized water-soluble, green incandescent CQDs at high yield by carbonization of water hyacinth (*Eichhornia crassipes*) weed. They

fabricated copper sulfide nanoparticles and composite CQDs@CuS. This composite was used for the photocatalytic degradation of brilliant green dye.

3.2.4 Graphene based

A fluorescent sensor was prepared by Zhang et al. (2020) based on water-soluble nitrogen-doped GQDs (N-GQDs), which were coupled with MIPs via a simple sol−gel method. It was then used for detection of tetracycline, an antibiotic. It was revealed that this method can be used in detecting the presence of tetracycline in animal-derived food.

Nickel-cobaltite/GQDs ($NiCo_2O_4$/GQDs) composites were prepared by Kharangarh et al. (2021). It was observed that the as-prepared sample exhibited improved electrical conductivity and can function as electrode materials with higher energy density compared to $NiCo_2O_4$ and GQDs. The observed specific capacitance for the fabricated composite was found to be 481.4 Fg^{-1} at 0.35 Ag^{-1}. It was higher than that of GQDs ($C_{sp} \sim 45.6\ Fg^{-1}$). It was proposed that the as-fabricated composites could be used as superior electrode materials in supercapacitors due to their unique characteristics.

Qiu et al. (2021) prepared cadmium sulfide quantum dots/dodecahedral phosphotungstic acid potassium $K_3PW_{12}O_{40}$ (KPW)/oxygen-doped mesoporous graphite carbon nitride (meso-g-C_3N_4) nanosheets with tandem heterojunctions. It was reported that the photocatalytic production rate of hydrogen formation and photocatalytic removal rate of Cr^{6+} over CdS/KPW/meso-g-C_3N_4 were found to be higher than with KPW and CdS/KPW.

3.3 Others

The CdSe quantum dots sensitized TiO_2 photocatalysts were synthesized by Shi et al. (2014) via the sol−gel method. The photocatalytic performance of as-prepared material was enhanced in the degradation of methylene blue. It was revealed that the catalysts doped with 0.05% CdSe QDs exhibited the highest activity, and the degradation efficiency of methylene blue could reach up to 99.2% within 3 h.

A solvothermal-assisted sol−gel method was reported by Anupama et al. (2021) to synthesize Se quantum dots. It was revealed that Se quantum dots having average size 3−8 nm were obtained with a trigonal crystal structure. It was found that as-prepared selenium quantum dots could work as ideal candidates for inner filter effect-based sensing of curcumin. Liu et al. (2022) synthesized the MIP@CdTe QDs through a simple sol−gel method. They used 3-aminopropyltriethoxysilane and tetraethoxysilane as functional monomer and cross-linker, respectively. These were then used for the determination of ciprofloxacin in the range of 0.5−24 μM with the limit of detection being 0.23 μM. This probe was also applied for the determination of this antibiotic in seawater samples with recoveries ranging between 98% and 110%.

3.4 Conclusion

The sol−gel process can provide nanoparticles of controlled sized and porosity along with purity. It avoids the problems of the coprecipitation method. Quantum dots of metals and metal chalcogenides, carbon, graphene, etc. can be easily prepared using this process. There is a wide scope for preparing quantum dots of different materials using this method.

References

Ajibade, P.A., Oluwalana, A.E., 2021. Photocatalytic degradation of single and binary mixture of brilliant green and rhodamine B dyes by zinc sulfide quantum dots. Molecules 26 (24). Available from: https://doi.org/10.3390/molecules26247686.

An, L., Han, X., Li, Y., Hou, C., Wang, H., Zhang, Q., 2019. ZnS−CdS−TaON nanocomposites with enhanced stability and photocatalytic hydrogen evolution activity. J. Sol−gel Sci. Technol. 91 (1), 82−91.

Anupama, K., Paul, T., Ann Mary, K.A., 2021. Solid-state fluorescent selenium quantum dots by a solvothermal-assisted sol−gel route for curcumin sensing. ACS Omega 6 (33), 21525−21533.

Bajaj, N.S., Omanwar, S.K., 2015. Low-temperature stearic acid sol−gel synthesis of α-Al_2O_3 quantum dots and its optical properties. J. Sol−gel Sci. Technol. 75 (1). Available from: https://doi.org/10.1007/s10971-015-3667-7.

Bera, D., Qian, L., Sabui, S., Santra, S., Holloway, P.H., 2008. Photoluminescence of ZnO quantum dots produced by a sol−gel process. Opt. Mater. 30 (8), 1233−1239.

Chen, J., Shu, J., Anqi, Z., Juyuan, H., Yan, Z., Chen, J., 2016. Synthesis of carbon quantum dots/TiO_2 nanocomposite for photo-degradation of rhodamine B and cefradine. Diam. Relat. Mater. 70, 137−144.

Chen, S., Li, Y., Wu, S., Jiang, X., Yang, H., Su, X., et al., 2020. A phosphorescent probe for cephalexin consisting of mesoporous thioglycolic acid-modified Mn: ZnS quantum dots coated with a molecularly imprinted polymer. Microchim. Acta. 187 (1). Available from: https://doi.org/10.1007/s00604-019-4038-9.

Chen, Z., Li, X.X., Du, G., Chen, N., Suen, A.Y., 2011. A sol−gel method for preparing ZnO quantum dots with strong blue emission. J. Lumin. 131 (10), 2072−2077.

Dey, A., Sarkar, S.K., 2020. Room temperature ZnO and Au-ZnO quantum dots thin film gas sensor fabrication for detecting of volatile organic compound gases. IEEE Sens. J. 20 (21), 12602−12609.

Ensafi, A.A., Nasr-Esfahani, P., Rezaei, B., 2018. Synthesis of molecularly imprinted polymer on carbon quantum dots as an optical sensor for selective fluorescent determination of promethazine hydrochloride. Sens. Actuators B: Chem. 257, 889−896.

Garcia, I.M., Souza, V.S., Hellriegel, C., Scholten, J.D., Collares, F.M., 2019. Ionic liquid−stabilized titania quantum dots applied in adhesive resin. J. Dental Res. 98 (6), 682−688.

Ge, L., Liu, N., Yang, P., Cheng, X., 2013. Composite TiO_2 film with quantum dots fabricated through a sol−gel process. J. Nanosci. Nanotechnol. 13 (4), 2943−2947.

Gnanasekaran, L., Hemamalini, R., Ravichandran, K., 2015. Synthesis and characterization of TiO_2 quantum dots for photocatalytic application. J. Saudi Chem. Soc. 19 (5), 589−594.

Guo, C., Cao, K., Zhang, Z., Xiong, Y., Chen, Y., Wang, Y., 2020. ZnS quantum dots/gelatin nanocomposites with a thermo-responsive sol−gel transition property produced by a facile and green one-pot method. ACS Sustain. Chem. Eng. 8 (11), 4346−4352.

Haghani, S.K., Ensafi, A.A., Kazemifard, N., Rezaei, B., 2020. Development of a selective and sensitive chlorogenic acid fluorimetric sensor using molecularly imprinted polymer ZnO quantum dots. IEEE Sens. J. 20 (11), 5691−5697.

Han, L.L., Cui, L., Wang, W.H., Wang, J.L., Du, X.W., 2012. On the origin of blue emission from ZnO quantum dots synthesized by a sol−gel route. Semicond. Sci. Technol. 27 (6). Available from: https://doi.org/10.1088/0268-1242/27/6/065020.

Hayakawa, T., Selvan, S., Nogami, M., 2000. Energy transfer between Eu^{3+} ions and CdS quantum dots in sol−gel derived CdS/SiO_2: Eu^{3+} gel. J. Sol−gel Sci. Technol. 19 (1), 779−783.

Javed, S., Islam, M., Mujahid, M., 2019. Synthesis and characterization of TiO_2 quantum dots by sol gel reflux condensation method. Ceram. Int. 45 (2), 2676−2679.

Jiang, H., Yao, X., Che, J., Wang, M., Kong, F., 2004. Preparation of ZnSe quantum dots embedded in SiO_2 thin films by sol−gel process. Ceram. Int. 30 (7), 1685−1689.

Ke, J., Li, X., Zhao, Q., Liu, B., Liu, S., Wang, S., 2017. Up conversion carbon quantum dots as visible light responsive component for efficient enhancement of photocatalytic performance. J. Colloid Interface. Sci. 496, 425−433.

Kharangarh, P.R., Ravindra, N.M., Rawal, R., Singh, A., Gupta, V., 2021. Graphene quantum dots decorated on spinel nickel cobaltite nanocomposites for boosting supercapacitor electrode material performance. J. Alloy. Comp. 876. Available from: https://doi.org/10.1016/j.jallcom.2021.159990.

Korala, L., Wang, Z., Liu, Y., Maldonado, S., Brock, S.L., 2013. Uniform thin films of CdSe and CdSe (ZnS) core (shell) quantum dots by sol−gel assembly: enabling photoelectrochemical characterization and electronic applications. ACS Nano 7 (2), 1215−1223.

Kumar, S., Singh, F., Kapoor, A., 2014. Synthesis and characterization of nano-crystalline ZnO quantum dots via sol−gel route for dye-sensitized solar cells. Int. J. Recent. Trends Electr. Electron. Engg 4 (1), 25−29.

Leelavathi, A., Mukherjee, B., Nethravathi, C., Kundu, S., Dhivya, M., Ravishankar, N., et al., 2013. Highly photoactive heterostructures of PbO quantum dots on TiO_2. RSC Adv. 3 (43), 20970−20977.

Li, H., Qu, F., 2007. Synthesis of CdTe quantum dots in sol−gel-derived composite silica spheres coated with calix [4] arene as luminescent probes for pesticides. Chem. Mater. 19 (17), 4148−4154.

Li, Y.S., Jiang, F.L., Xiao, Q., Li, R., Li, K., Zhang, M.F., et al., 2010. Enhanced photocatalytic activities of TiO2 nanocomposites doped with water-soluble mercapto-capped CdTe quantum dots. Appl. Cataly. B: Environ. 101 (1−2), 118−129.

Li, H., Luo, K., Xia, M., Wang, P.W., 2014. Synthesis and optical properties of Pr^{3+}−doped ZnO quantum dots. J. Non-Crystal. Solids 383, 176−180.

Li, Y., Xie, S., Xu, D., Shu, G., Wang, X., 2021. Antibacterial activity of ZnO quantum dots and its protective effects of chicks infected with *Salmonella pullorum*. Nanotechnology 32 (50). Available from: https://doi.org/10.1088/1361-6528/ac2846.

Liu, X., Xing, X., Li, Y., Chen, N., Djerdj, I., Wang, Y., 2015. Controllable synthesis and change of emission color from green to orange of ZnO quantum dots using different solvents. N. J. Chem. 39 (4), 2881−2888.

Lin, K.F., Cheng, H.M., Hsu, H.C., Lin, L.J., Hsieh, W.F., 2005. Band gap variation of size-controlled ZnO quantum dots synthesized by sol−gel method. Chem. Phys. Lett. 409 (4−6), 208−211.

Liu, Y.H., Tan, L.J., Wang, K.P., Wang, J.T., 2022. Rapid detection of ciprofloxacin in seawater based on CdTe quantum dots coated with molecularly imprinted polymers. Int. J. Mod. Phys. B . Available from: https://doi.org/10.1142/S0217979222400124.

Miao, R., Luo, Z., Zhong, W., Chen, S.Y., Jiang, T., Dutta, B., et al., 2016. Mesoporous TiO_2 modified with carbon quantum dots as a high-performance visible light photocatalyst. Appl. Cataly. B: Environ. 189, 26–38.

Moghaddam, E., Youzbashi, A.A., Kazemzadeh, A., Eshraghi, M.J., 2015. Preparation of surface-modified ZnO quantum dots through an ultrasound assisted sol–gel process. Appl. Surf. Sci. 346, 111–114.

Mohamed, W.A., Ibrahem, I.A., El-Sayed, A.M., Galal, H.R., Handal, H., Mousa, H.A., et al., 2020. Zinc oxide quantum dots for textile dyes and real industrial wastewater treatment: solar photocatalytic activity, photoluminescence properties and recycling process. Adv. Powder Technol. 31 (6), 2555–2565.

Qiu, Y., Xing, Z., Guo, M., Zhao, T., Wang, Y., Chen, P., et al., 2021. Cadmium sulfide quantum dots/dodecahedral polyoxometalates/oxygen-doped mesoporous graphite carbon nitride with Z-scheme and type-II as tandem heterojunctions for boosting visible-light-driven photocatalytic performance. J. Colloid Interface Sci. 582, 752–763.

Rakibuddin, M., Kim, H., 2020. Sol–gel derived Fe_3O_4 quantum dot decorated silica composites for effective removal of arsenic (III) from water. Mater. Chem. Phys. 240. Available from: https://doi.org/10.1016/j.matchemphys.2019.122245.

Rakibuddin, M., Shinde, M.A., Kim, H., 2020. Facile sol–gel fabrication of MoS_2 bulk, flake and quantum dot for electrochromic device and their enhanced performance with WO_3. Electrochim. Acta 349. Available from: https://doi.org/10.1016/j.electacta.2020.136403.

Rempel, A.A., Kuznetsova, Y.V., Dorosheva, I.B., Valeeva, A.A., Weinstein, I.A., Kozlova, E. A., et al., 2020. High photocatalytic activity under visible light of sandwich structures based on anodic TiO_2/CdS nanoparticles/Sol–gel TiO_2. Top. Catal. 63 (1), 130–138.

Sankar, M., Jothibas, M., Muthuvel, A., Rajeshwari, A., Jeyakumar, S.J., 2020. Structural, optical and photocatalytic degradation of organic dyes by sol gel prepared Ni doped CdS nanoparticles. Surf. Interfaces 21. Available from: https://doi.org/10.1016/j.surfin.2020.100775.

Schmitz, F., de Albuquerque, M.B.S., Alberton, M.D., Riegel-Vidotti, I.C., Zimmermann, L.M., 2020. Zein films with ZnO and ZnO: Mg quantum dots as functional nanofillers: new nanocomposites for food package with UV-blocker and antimicrobial properties. Poly. Test. 91. Available from: https://doi.org/10.1016/j.polymertesting.2020.106709.

Shi, Y., Ke, J., Zhao, Q.D., Li, X.Y., Zheng, N., Xue, F.H., 2014. Synthesis of CdSe quantum-dots-sensitized TiO_2 nanocomposites with visible-light photocatalytic activity. Adv. Mater. Res. 924. Available from: https://doi.org/10.4028/http://www.scientific.net/AMR.924.3.

Song, T., Feng, X., Ju, H., Fang, T., Zhu, F., Liu, W., et al., 2020. Enhancing acid, base and UV light resistance of halide perovskite $CH_3NH_3PbBr_3$ quantum dots by encapsulation with ZrO_2 sol. J. Alloy. Compd. 816. Available from: https://doi.org/10.1016/j.jallcom.2019.152558.

Sonker, R.K., Yadav, B.C., Gupta, V., Tomar, M., 2020. Synthesis of CdS nanoparticle by sol–gel method as low temperature NO_2 sensor. Mater. Chem. Phys. 239. Available from: https://doi.org/10.1016/j.matchemphys.2019.121975.

Sonker, R.K., Shastri, R., Johari, R., 2021. Superficial synthesis of CdS quantum dots for an efficient perovskite-sensitized solar cell. Energy Fuels 35 (9), 8430–8435.

Sood, S., Kumar, S., Umar, A., Kaur, A., Mehta, S.K., Kansal, S.K., 2015. TiO_2 quantum dots for the photocatalytic degradation of indigo carmine dye. J. Alloy. Comp. 650, 193–198.

Soumya, S., Sheemol, V.N., Amba, P., Mohamed, A.P., Ananthakumar, S., 2018. Sn and Ag doped ZnO quantum dots with PMMA by in situ polymerization for UV/IR protective, photochromic multifunctional hybrid coatings. Sol. Energy Mater. Sol. Cell 174, 554–565.

Sowik, J., Miodyńska, M., Bajorowicz, B., Mikolajczyk, A., Lisowski, W., Klimczuk, T., et al., 2019. Optical and photocatalytic properties of rare earth metal-modified ZnO quantum dots. Appl. Surf. Sci. 464, 651–663.

Sun, L.W., Shi, H.Q., Li, W.N., Xiao, H.M., Fu, S.Y., Cao, X.Z., et al., 2012. Lanthanum-doped ZnO quantum dots with greatly enhanced fluorescent quantum yield. J. Mater. Chem. 22 (17), 8221–8227.

Vasiljevic, Z.Z., Dojcinovic, M.P., Vujancevic, J.D., Jankovic-Castvan, I., Ognjanovic, M., Tadic, N.B., et al., 2020. Photocatalytic degradation of methylene blue under natural sunlight using iron titanate nanoparticles prepared by a modified sol–gel method. R. Soc. Open. Sci. 7 (9). Available from: https://doi.org/10.1098/rsos.200708.

Vyas, Y., Chundawat, P., Dharmendra, D., Jain, A., Punjabi, P.B., Ameta, C., 2022. Biosynthesis and characterization of carbon quantum DOTS@ CuS composite using water hyacinth leaves and its usage in photocatalytic dilapidation of Brilliant Green dye. Mater. Chem. Phys. 281. Available from: https://doi.org/10.1016/j.matchemphys.2022.125921.

Wang, X., Li, J., 2021. Sol–gel fabrication of Ag-Coated ZnO quantum dots nanocomposites with excellent photocatalytic activity. Opt. Mater. 118. Available from: https://doi.org/10.1016/j.optmat.2021.111235.

Wang, Y., Lin, F., Gu, X.L., 2011. Load and resistance factors for progressive collapse resistance design of reinforced concrete building structures. Adv. Mater. Res. 255, 338–344.

Wang, C., Luo, S., Liu, C., Chen, C., 2020. W_{O3} quantum dots enhanced the photocatalytic performances of graphene oxide/Ti_{O2} films under flowing dye solution. Inorg. Chem. Commun. 115. Available from: https://doi.org/10.1016/j.inoche.2020.107875.

Xu, H., Wang, H., Lu, Y., Zeng, Y., Yang, Y., Zhang, Z., et al., 2021. Ce_{O2} quantum dots for highly selective and ultrasensitive fluorescence detection of 4-nitrophenol via the fluorescence resonance energy transfer mechanism. Spectrochim. Acta Part. A: Mol. Biomol. Spectrosc. 262. Available from: https://doi.org/10.1016/j.saa.2021.120115.

Yamane, M., Takada, T., Mackenzie, J.D., Li, C.Y., 1992. Preparation of quantum dots by the sol–gel process. Sol–gel Opt. II 1758, 577–586.

Yang, K., Guo, Q., Li, H., Hao, X., Ma, Y., Yang, M., et al., 2018. Highly efficient sol–gel synthesis for ZnS@ N, S co-doped carbon nanosheets with embedded heterostructure for sodium ion batteries. J. Power Sources 402, 340–344.

Yang, C., Wang, L., Zhang, Z., Chen, Y., Deng, Q., Wang, S., 2020. Fluorometric determination of fipronil by integrating the advantages of molecularly imprinted silica and carbon quantum dots. Microchim. Acta 187 (1). Available from: https://doi.org/10.1007/s00604-019-4005-5.

Ye, Y., 2018. Photoluminescence property adjustment of ZnO quantum dots synthesized via sol–gel method. J. Mater. Sci.: Mater. Electron. 29 (6), 4967–4974.

Yu, Y., Chen, D., Huang, P., Lin, H., Wang, Y., 2010. Structure and luminescence of Eu^{3+} doped glass ceramics embedding ZnO quantum dots. Ceram. Int. 36 (3), 1091–1094.

Yu, J., Caravaca, A., Guillard, C., Vernoux, P., Zhou, L., Wang, L., et al., 2021. Carbon nitride quantum dots modified TiO_2 inverse opal photonic crystal for solving indoor vocs pollution. Catalysts 11 (4). Available from: https://doi.org/10.3390/catal11040464.

Zaidi, R., Azam, A., 2021. Investigation of structural, optical and antibacterial properties of zinc sulphide quantum dots prepared by sol–gel method. In: AIP Conference Proc. 2369, 1, doi: org/10.1063/5.0060815.

Zhang, L., Yin, L., Wang, C., Lun, N., Qi, Y., Xiang, D., 2010a. Origin of visible photoluminescence of ZnO quantum dots: defect-dependent and size-dependent. J. Phys. Chem. C. 114 (21), 9651–9658.

Zhang, X., Hou, S., Mao, H., Wang, J., Zhu, Z., 2010b. Influence of annealing temperature on the photoluminescence properties of ZnO quantum dots. Appl. Surf. Sci. 256 (12), 3862–3865.

Zhang, J., Zhao, S.Q., Zhang, K., Zhou, J.Q., Cai, Y.F., 2012. A study of photoluminescence properties and performance improvement of Cd-doped ZnO quantum dots prepared by the sol–gel method. Nanoscale Res. Lett. 7 (405). Available from: https://doi.org/10.1186/1556-276X-7-405.

Zhang, L., Wang, J., Fang, G., Deng, J., Wang, S., 2020. A molecularly imprinted polymer capped nitrogen-doped graphene quantum dots system for sensitive determination of tetracycline in animal-derived food. ChemistrySelect 5 (2), 839–846.

Zhang, X., Luo, S., Wu, X., Feng, M., Li, Y., Han, H., et al., 2021. Effect of alkali bases on the synthesis of ZnO quantum dots. Open. Chem. 19 (1), 377–384.

Zhao, Z., Li, H., Huang, L., Tan, Y., Liu, F., Li, W., 2021. Preparation of graphene quantum dots-doped TiO_2 nanocomposites via a sol–gel method for photocathodic protection. Mol. Cryst. Liq. Cryst. 2021. Available from: https://doi.org/10.1080/15421406.2021.1966873.

Zhong, J., Zhao, H., Zhang, C., Ma, X., Pei, L., Liang, X., et al., 2014. Sol–gel synthesis and optical properties of $CuGaS_2$ quantum dots embedded in sodium borosilicate glass. J. Alloy. Comp. 610, 392–398.

Zhou, P., Xie, Y., Fang, J., Ling, Y., Yu, C., Liu, X., et al., 2017. CdS quantum dots confined in mesoporous TiO_2 with exceptional photocatalytic performance for degradation of organic pollutants. Chemosphere 178. Available from: https://doi.org/10.1016/j.chemosphere.2017.03.024.

Zou, T., Xing, X., Yang, Y., Wang, Z., Wang, Z., Zhao, R., et al., 2020. Water-soluble ZnO quantum dots modified by (3-aminopropyl) triethoxysilane: the promising fluorescent probe for the selective detection of Cu^{2+} ion in drinking water. J. Alloy. Comp. 825. Available from: https://doi.org/10.1016/j.jallcom.2020.153904.

Chapter 4

Laser ablation synthesis of quantum dots

Neetu Shorgar[1], **Indu Bhati**[2] **and Priyanka Jhalora**[1]
[1]*Department of Chemistry, PAHER University, Udaipur, Rajasthan, India,* [2]*Maribyrnong, VIC, Australia*

4.1 Introduction

LASER or Laser is light amplification by the stimulated emission of radiation. The first laser was built by Maiman (1960) based on theoretical work by Schawlow and Townes (1958). A laser differs from other light sources in the context that it emits coherent light. Its spatial coherence allows it to be focused on a tight spot, which is utilized in laser lithography and cutting. It also allows this laser beam to stay narrow even over great distances (collimation), which finds applications in laser lidar and pointers. Lasers can have temporal coherence also, which can be used to produce a broad spectrum with ultrashort pulses of light but their duration is short enough to be in the order of femtoseconds (10^{-15} s).

Lasers find applications in laser printers, optical disk drives, barcode scanners, fiber-optics, DNA sequencing instruments, lighting displays, laser surgery, photolithography, free-space optical communication, cutting and welding materials, skin treatments, as well as military and law enforcement devices for marking targets and measuring range and speed. The semiconductor lasers (blue to near-UV) have been used in place of light-emitting diodes (LEDs) as a white light source. Such laser devices are used in some car headlights.

4.2 Laser ablation

Laser ablation (LA) is a complex process. The laser will penetrate the surface of the sample and that depends on its wavelength as well as the refractive index of the target material used. A high electric field is generated due to laser irradiation that is enough to remove electrons from the bulk of the sample. These free electrons then collide with the atoms of the sample,

Quantum Dots. DOI: https://doi.org/10.1016/B978-0-12-824153-0.00004-5
© 2023 Elsevier Inc. All rights reserved.

transferring their energies. As a result, the target surface is heated, followed by vaporization, plasma formation, nucleation, and agglomeration, resulting in raw patio and/or quantum dots (Fig. 4.1).

The field of LA has been excellently reviewed by various researchers (Kim et al., 2017; Farshbaf et al., 2018; Ravi Kumar et al., 2019).

Mansoureh and Parisa (2018) observed that purity is a very important factor when metal nanoparticles (NPs) are to be applied in biological and medical fields. It is therefore, necessary to prepare metal NPs or quantum dots with the desired shape and size distribution.

4.2.1 Advantages

There are the following advantages in using the LA method:

- It is a simple and versatile method.
- It is relatively low-cost method except the cost of the instrument.
- It is a green approach.
- It does not require toxic chemicals or reagents.
- It provides high production rates.
- It provides good control of particle size.
- It provides particles with good monodispersity.

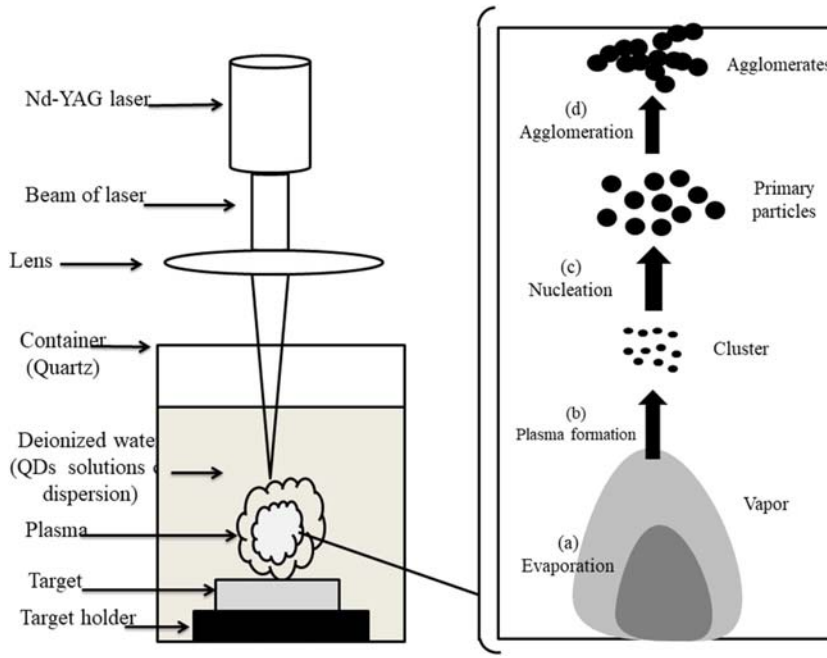

FIGURE 4.1 Laser ablation method for synthesis of quantum dots.

4.2.2 Disadvantages

The LA method has certain disadvantage also and these are:

- It has a slow rate of production of NPs.
- The consumption of energy is high.
- The cost of laser equipment is high.
- Ablation efficiency decreases on using laser for a longer period within a session.

4.3 Metal-based quantum dots

4.3.1 Metals

Silver NPs were produced by Pyatenko et al. (2004) on irradiating Ag target with a laser beam in pure water. They reported that these are very small spherical particles with size in the range of 2−5 nm.

Besner et al. (2005) obtained colloidal gold NPs using femtosecond LA of a gold plate in aqueous solutions. This method makes it possible to functionalize nanomaterial by an appropriate capping ligand. They were able to control the reactivity of as- prepared gold particles and their size by using polymers such as polyethylene glycol and dextran. The size of these NPs was found to be 5 nm, as evident from TEM images. It was also observed that long-term stability of gold particles was improved significantly on adding capping agents. A photoluminescence (PL) signal was also obtained in the violet−blue spectral range. It was revealed that as-functionalized NPs can find potential application in bioimaging and biosensing.

LA synthesis in solution (LASiS) has emerged as a new technique for synthesizing noble metal NPs (NM NPs). It is a "green" method, which does not require additional stabilizing molecules. However, presently LASiS has certain limitations in controlling the size of NM NPs, which can be overcome in the future. Amendola and Meneghetti (2009) reviewed the overview of LASiS.

Monodispersed spherical bismuth (Bi) NPs with diameters of 5−20 nm were synthesized by Verma et al. (2013) using a liquid pulsed LA method. It was reported that ablation time and surfactant ($C_{12}H_{25}NaO_4S$) both played a crucial role in the size of the NPs and their optical properties. It was proposed that such QDs can find potential applications in hypothermia treatment. Malviya and Chattopadhyay (2014) synthesized Ag−Cu alloy NPs through a LA technique under an aqueous medium in four different compositions. The observations were carried out on NPs with core−shell structure of two different sizes: ∼5 and ∼20 nm.

Kőrösi et al. (2016) synthesized ligand-free Ag NPs with particle size of 3 and 20 nm by application of picosecond LA. It was observed that a laser processing system allowed a high control on particle sizes. The effect of size

on the antibacterial activity of these as- synthesized Ag NPs was tested against *Escherichia coli* and *Staphylococcus aureus*. Li and Chen (2016) developed a new strategy for synthesizing stable and monodispersed silver quantum dots by laser fragmentation of bulk Ag in aqueous medium. They used polysorbate 80 as both a dispersing and stabilizing agent. It was revealed that surfactant played an important role in determining the size of these Ag nanostructures. The Ag QDs have excellent photostability of ~500 h and enhanced PL at 510 nm.

Ryabchikov et al. (2016) ablated a gold target using laser radiation (femtosecond) in aqueous solutions of initially prepared Si NPs. It was observed that Au-based spherical colloids were obtained with an average size in the range of 5−10 nm. It was proposed that as-prepared nanostructures can find various applications in the field of catalysis, biomedicine, and photovoltaics. Boltaev et al. (2018) observed that there is a correlation between efficient third harmonic generation in the plasmas and strong nonlinear optical response of silver NPs due to plasmon resonance. It was reported that nonlinear absorption coefficient of Ag NPs (8 nm) was high enough (3×10^{-5} cm W^{-1}) at the wavelength of 1064 nm.

Sadrolhosseini et al. (2019) fabricated gold NPs in the graphene quantum dots (GQDs) solution via LA. The particle size was controlled by changing ablation time from 5 to 25 min. A peak at 319.8 nm was attributed to GQDs. It was observed that particle size was in the range of 11.74−28.29 nm, which was found to decrease with increasing ablation time. Gold NPs in a carbon quantum dots (CQDs) solution were also prepared (Sadrolhosseini et al., 2020) using a LA method. It was observed that the variation in the photoluminescent peak in the presence of the gold NPs was higher compared to pure CQDs. It can be used for the detection of pyrene with a limit of detection of 1 ppm.

4.3.2 Metal oxides

Murali (2001) prepared indium oxide (IO) NPs via a reactive LA method. An average particle size of these particles was found to be 6.6 nm, as evident from XRD and TEM data. These laser ablated samples exhibited a blueshift of 110 meV compared to bulk material. Ajimsha et al. (2007) fabricated luminescent, transparent, and biocompatible ZnO quantum dots in three solvents (water, methanol, and ethanol) using a liquid-phase pulsed LA method. They did not use any surfactant. It was confirmed that crystalline ZnO quantum dots were found to have a uniform size distribution of 7 nm. As-prepared highly luminescent nontoxic ZnO quantum dots could find applications in the field of biomedicine as florescent probes.

A pulsed laser emitting UV radiations was used by Gondal et al. (2009) for the synthesis of nanostructured ZnO and ZnO_2. For the synthesis of NPs of ZnO_2, a highly pure metallic plate of Zn target was kept under repeated

laser irradiation in the presence of H_2O_2 as an oxidizing agent. It was reported that size, optical properties, and morphology of as-synthesized ZnO and ZnO_2 by this method were influenced by postannealing conditions. It was revealed that ZnO_2 was completely converted to ZnO by annealing ZnO_2 for 8 h at 200°C. It was reported that the size of ZnO changes from 5 to 19 nm raising the annealing temperature from 200°C to 600°C. Optical properties as well as bandgap of nano-ZnO were also changed.

Suzuki et al. (2009) used pulsed LA to prepare quantum dots of zinc oxide using differential mobility analyzer (DMA). Initially, irregularly shaped ZnO particles were obtained, but when annealing temperature was increased, then they are transformed into spherical QDs. It was observed that ZnO QDs obtained by this method were crystallized (single crystallites) with a wurtzite structure. The ZnO QDs with average size in the range of 4.8−8.1 nm could be easily prepared by reducing the specified sizes of DMA.

Zheng et al. (2010) prepared ultrafine Y_2O_3:Pr, Yb NPs using femtosecond pulsed LA. It was reported that these spherical particles have a size of about 10 nm (diameter) with a narrow size distribution. As-prepared NPs exhibited significantly improved upconversion intensity as compared to NPs, which were prepared by the sol−gel method.

Zeng et al. (2011) synthesized ZnO quantum dots through laser irradiation of hollow nanospheres of ZnO in liquid medium. It was reported that as-synthesized QDs have diameters ranging between 1 and 8 nm, exhibiting a quantum size effect, which can be tuned by variation of parameters of the laser irradiation process. It was observed that the main PL emission bands evolved are from blue to green, finally reaching ultraviolet peaks. These as-fabricated QDs can show optical and optoelectronic applications.

Eita et al. (2012) fabricated thin UV-blocking films of poly(methyl methacrylate) (PMMA) and ZnO quantum dots via spin-coating. It was revealed that an average thickness of bilayer before heating was 9.5 nm, which reduces to 8.6 nm after heating at 100°C for 1 h. It was also observed that surface roughness was 3.6 and 8.4 nm for one and ten bilayer films, respectively, as evident from atomic force microscopy. The absorption of UV radiation increases with increasing number of bilayers, but transmission was damped at wavelength <375 nm. It was reported that thin films had a high transparency in the visible region. The single layer of PMMA/ZnO QDs thin films was found to be hydrophobic in nature.

Singh and Gopal (2012) used nanosecond (ns) pulsed LA of zinc rod, which was placed on the bottom of a glass vessel containing methanol. As a result, a colloidal solution of drop-shaped zinc oxide quantum dots and their self-assembly into different dendritic nanostructures were obtained. It was observed that average length, width, and aspect ratio of these as-prepared drop-shaped zinc oxide quantum dots were found to be 6 ± 2.4 nm, 3.5 ± 1.4 nm, and 1.69 ± 0.4 nm, respectively. Its PL spectrum exhibited emission peaks in UV, violet, blue, and green spectral regions.

The SnO_2 quantum dots were synthesized by Singh et al. (2012) using LA in liquid. The diameter of the SnO_2 NPs was found in the range of 1−5 nm as evident from HRTEM images. As-prepared SnO_2 QDs exhibited tetragonal crystalline structure. Their PL spectrum showed green and blue emission peaks at 540 nm and 445 nm, respectively. It was proposed that these QDs have great potential for use in biosensors, optoelectronics, etc. Patel et al. (2013) synthesized SnO_2-QDs ($\sim$ 1−5 nm) by LA technique in liquid. Then these QDs were electrophoretically deposited onto the surface of indium tin oxide (ITO)-coated glass electrodes. Then ssDNA/SnO_2-QDs/ITO bioelectrodes were fabricated and these bioelectrodes have been used for DNA hybridization.

Drmosh et al. (2019) fabricated ZnO NPs by decomposing zinc peroxide (ZnO_2) quantum dots, which were synthesized by LA of microstructured Zn powder in 3% H_2O_2. Then rGO/ZnO nanocomposite was prepared from them via pulsed LA in liquid (PLAL). The surface of the rGO/ZnO hybrid was decorated with a Pt thin film so as to get a ternary rGO/ZnO/Pt hybrid nanocomposite. It was observed that this Pt-loaded rGO/ZnO gas sensor (thickness of 2 nm) exhibited selectivity and excellent response for sensing a low concentration of hydrogen. This nanocomposite was found to be 10 and five times better than pure ZnO, and rGO/ZnO nanocomposite, respectively. It was proposed that rGO/ZnO/Pt hybrid nanocomposite is a potential promising candidate for fabricating high-performance gas sensors for H_2.

Mitra et al. (2019) prepared highly crystalline p-type manganese oxide (MnO) wide bandgap semiconductor quantum dots via femtosecond-LA in liquid. This p-type MnO QD material could find applications in the industrial production of high-performance solution-processed deep UV optoelectronics on a large scale. Mostafa et al. (2019) synthesized tungsten oxide QDs with pulsed laser−assisted ablation. They used tungsten (tablet) as a target in liquid media. This method is a green chemical method as it uses only tungsten tablet and water for preparing tungsten oxide without impurities. It was confirmed by morphological analysis that the as-prepared tungsten oxide NPs were quantum dots with average diameter of about 5 nm. They used these as-prepared samples as the catalyst for the degradation of 4-nitrophenol.

Mwafy et al. (2019) prepared zinc oxide NPs using CQD solution through a LA technique. It was observed that ZnO-NPs in the CQD solution were formed with capping of the ZnO NPs (spherical) by a functional group of the CQD. As-prepared ZnO-NPs in the CQD solution had a particle size in the range of 7.5−14.03 nm. These prepared samples were used in the detection of lead and mercury ions in aqueous solution and it was found that a PL peak shift was greater in the presence of mercury ions compared to lead ions.

Kateshiya et al. (2020) developed a facile synthetic route for preparing highly blue fluorescent tyrosine-coated molybdenum oxide quantum dots (Tyr-MoO_3 QDs). They used tyrosine as a surface ligand for the functionalizing MoO_3 QDs.

It was revealed that as-prepared Tyr-MoO_3 QDs could act as a sensor for sensitive as well as rapid identification of imidacloprid via fluorescence quenching mechanism. The as-developed probe was also applied for detection of imidacloprid in real samples.

Wang et al. (2021) synthesized multifunctional ZnO, which was decorated on Fe hierarchical nanostructures using LA technique. They decorated ZnO quantum dots on Fe nanowires, ZnO nanospindles cluster on Fe core and flocky Fe@ZnO core−shell nanospheres (Fe@ZnO CSNSs). As-synthesized Fe@ZnO CSNSs were then used for the photocatalytic degradation of rhodamine B. It was reported that photocatalytic removal of rhodamine B was about 94.1% in the presence of natural light irradiation for 20 min.

4.3.3 Metal sulfides

Formation of quantum dots of ZnSe and CdS was reported under ablation of bulk semiconductors in a liquid environment (ethanol, diethyleneglycol, etc.) by Anikin et al. (2002). It was confirmed that these quantum dots are crystalline in nature with an average size of ∼10−20 nm. Lalayan (2005) prepared colloidal quantum dots of GaAs and CdS semiconductors through LA in the liquid media. The large blueshift of the PL was evaluated, and it was connected to size effects. Luminescence spectra at the wavelength 405 nm (CdS) and 420 nm (GaAs) indicated that sizes of QDs were in the range 2−3 nm.

Zheng et al. (2008) synthesized Cu-doped ZnS (ZnS:Cu) quantum dots in deionized water using femtosecond LA of a bulk (ZnS:Cu) target. It was reported that these quantum dots exhibited good water solubility and colloidal stability. An average size of as-prepared quantum dots varied in the range of 2.1−4.0 nm on changing the laser fluence. It resulted in a redshift of the emission peak.

Ka et al. (2011) synthesized lead sulfide (PbS) NPs layers onto different substrates at room temperature using pulsed laser deposition (PLD). It was reported that average size of these NPs can be controlled by changing the number of LA pulses. A blueshift in PL was observed from 1420 to 880 nm. As-prepared PbS NPs had a diameter of 8.5 nm, which was decreased to 2.5 nm, which confirmed the quantum size effect. Khan and BiBi (2014) synthesized densely packed CdS NPs using ns-pulsed LA. The average size of these NPs was found to be in the range of 5−10 nm. An energy bandgap of around 3.03 eV was attributed to band-to-band transition in CdS.

Ka et al. (2012) used the pulsed LA technique for direct synthesis of single-walled carbon nanotube/PbS-quantum dot (SWCNT/PbS-QD) nanohybrids (NHs). This not only permitted control on the size of the PbS-QDs but also made it possible for integration of these SWCNT/PbS-QD NHs into photoconductive devices with a strong photoresponse. Ka et al. (2014) used a PLD technique for fabricating NH heterojunctions (NH-HJs) solar cells.

They decorated TiO_2 nanorods (TiO_2-NRs) on PbS quantum dots (PbS-QDs). They could achieve NH-HJs-based PV devices with high power conversion efficiency (PCE) (4.85%). It was interesting to note that the PCE of these devices was found to be quite stable for several months in the presence of air. It was also reported that the addition of SWCNTs onto the TiO_2-NRs before decorating them by PbS-QDs further enhanced PCE to 5.3%, which may be due to more light absorption and improved charge collection by SWCNTs.

Darwish et al. (2015) synthesized size-tunable (5−12 nm) cadmium sulfide (nano II−VI semiconductor) with different shapes, such as rod, sphere, rope, etc., using a pulsed laser in liquid environment method. It was confirmed that the NPs are crystalline. These nanomaterials can find application in biosensing and photonics. Gondal et al. (2015) prepared TiO_2/ZnO/CdS QDs using a PLAL technique. Here, ZnO reduces the electron−hole recombination in the TiO_2 while CdS will increase the light harvesting efficiency of TiO_2. The morphology of the composite quantum dots was observed by high-resolution TEM indicating that the size of the composite ranges between 10 and 40 nm. Such a composite can be used for energy harvesting using sunlight.

Baldovi et al. (2016) synthesized MoS_2 quantum dots in colloidal suspensions by LA of commercial MoS_2 in acetonitrile. It was found that there was a lateral size distribution from 5 to 20 nm, as evident from HRTEM images. It was also revealed that these MoS_2 QDs were constituted by 3−6 MoS_2 layers (1.8−4 nm thickness). It was predicted that its photocatalytic activity may be enhanced for H_2 generation in the presence of UV−Vis irradiation using methanol as a sacrificial electron donor. Ka et al. (2016) decorated SWCNTs with PbS quantum dots by the PLD method. As a result, SWCNTs/PbS-QDs NHs were formed. It was found that the number of pulses controlled the average size of PbS-QDs as well as their coverage on the SWCNTs surface. The photoconductive devices were fabricated from these NHs exhibiting an enhanced photoresponse, which was dependent on size of PbS-QDs. The diameter of PbS-QDs was found to be 6.5 nm and bandgap was calculated as 0.86 eV.

The CdS quantum dots with a narrow size distribution were synthesized by Mendonça and de Azevedo (2016) having emission range of 400−700 nm. These were very stable, water-dispersible, and bright. They used a combination of LA technique and thioglycerol, which acted as a catalyst for the hydrolysis of thiosulfate as well as a stabilizing agent. The decomposition of thiosulfate catalyzed by thioglycerol produced S^{2-} ions, which interacted with Cd^{2+} ions to form CdS quantum dots. It was observed that the particle size of monodispersed CDs QDs was about 2.75 nm. As-prepared QDs exhibited bright PL in the yellow-orange region.

Li et al. (2017) fabricated monolayer MoS_2 QDs. They used temporally shaped femtosecond LA of bulk MoS_2 in water. It was revealed that

as-prepared MoS_2 QDs exhibited the highest electrocatalytic activity for the generation of hydrogen evolution reactions (HER) because of the high specific surface area, excellent electrical conductivity, and abundant active edge sites. Caigas et al. (2018) used pulsed LA technology for doping of WS_2 quantum dots with diethylenetriamine (DETA). As-prepared DETA-doped 2H-WS_2 QDs were found to have an average size of $\sim$6 nm. It was interesting to note that PL in WS_2 QDs was enhanced by 74-fold on DETA doping. A dopant-dependent negative photoconductivity was also observed for WS_2 QDs, which may be due to light-induced desorbing of water (oxygen) molecules on the surface.

Ou et al. (2018) reported an ultrafast LA method for the synthesis of MoS_2 quantum dots. It was also revealed that as-prepared QDs exhibited stability and high activity in the electrocatalytic HER. This was attributed to defective structure, very large surface area, high conductivity, and abundance of active sites. As-prepared QDs could be used in sensing, optics, conversion technologies, and energy storage. Sunitha et al. (2018) prepared MoS_2 QDs by pulsed LA from bulk MoS_2 pellets in deionized water. A hexagonal structure of as-prepared MoS_2 pellet was confirmed by XRD and Raman spectra. The mean particle size of these MoS_2 QDs was found to be in the range of 2−30 nm. Kuriakose et al. (2019) synthesized Au-CdS core−shell structure via a laser-assisted method. A gold core was obtained with 8.8 nm average particle size, which was surrounded by a shell coating of CdS (5.8 nm; average diameter). They observed that the rate of photodegradation of methylene blue was more in the presence of Au/CdS core shell as compared to only CdS.

Nguyen et al. (2019a) developed a simple and green route to synthesize highly photoluminescent MoS_2/WS_2 QDs using LA (femtosecond) of raw MoS_2/WS_2 powders. It was reported that as-prepared MoS_2/WS_2 QDs exhibited excellent photostability and intense PL in the blue region with a PLQY of 22.5%. An intense fluorescent emission was attributed to the presence of abundant surface functional groups, such as C−O, CO, and C−N, which can introduce new surface-state emission centers efficiently. Xu et al. (2019) reported a facile method for the synthesis of molybdenum disulfide QDs and tungsten disulfide QDs using LA (femtosecond) and sonication-assisted liquid exfoliation. Average size of these quantum dots was determined to be 3.7 and 2.1 nm, respectively. These MoS_2 and WS_2 QDs exhibited bright blue−green luminescence in the presence of UV irradiation, which may be due to the abundance of functional groups on their surfaces.

An et al. (2020) attempted different methods to produce MoS_2 QDs, such as substrate growth, exfoliation, and colloidal synthesis. MoS_2 QDs with a size of 10 nm were obtained. The resistive switching devices were fabricated using as-prepared MoS_2 QD samples. These devices exhibited a stable unipolar resistive switching behavior without any electroforming process. Soheyli et al. (2020) prepared multicomponent In-based QDs in aqueous phase. They could also tune absorption and PL emission spectra of these

QDs by changing composition of QDs such as Ag-In-S/ZnS, Zn-Ag-In-S/ZnS, and Cu-Ag-In-S/ZnS core/shell QDs. They could produce intense emission by colloidal QDs with amber, green, and red colors. According to them, there is a potential in AgInS-based/ZnS QDs to be used as theranostic agents for treatment and imaging of cancer.

Zhao et al. (2020) designed and fabricated near-infrared fluorescence. When these amorphous Ag_2S QDs were doped by Cu, then a redshift of nontoxic amorphous $Ag_{2-x}Cu_xS$ quantum dots was observed, which improved photothermal conversion efficiency to 44.0%. This may be attributed to the generation of intragap states introduced on Cu doping. It was also revealed that as-prepared amorphous $Ag_{2-x}Cu_xS$ QDs exhibited high long-term biocompatibility also. The MoS_2 quantum dots were synthesized by Pradhan et al. (2021) via pulsed LA assisted photoexfoliation of solid MoS_2 target in distilled water. The average sizes of these MoS_2 quantum dots were $\sim$4, 2.9, and 6.1 nm, when ablation durations were 5, 10, and 20 min, respectively at a fixed laser energy of 40 mJ. The quantum dots resulted in luminescence in the visible region. The as-synthesized MoS_2 quantum dots (colloidal solution) in distilled water exhibited a redshift from excitation wavelength-dependent luminescence, which shifted to longer wavelength by varying excitation wavelength from 290 to 390 nm. It was observed that MoS_2 quantum dots exhibited higher rate of generating hydrogen.

4.3.4 Metal selenides

Singh et al. (2010) could achieve selenium QDs (with 2.74 $\pm$ 2.32 nm diameter) on laser irradiation for 15 min. It was reported that almost 3.75 $\pm$ 0.15 nm size is the quantum confinement limit for QDs of selenium. It was observed that surface defect density of these QDs increases, and defect/electron trap level energy decreases with the time of laser irradiation. CdSe quantum dots were prepared by Horoz et al. (2012) by LA in water. It was reported that as-synthesized CdSe QDs (wurtzite crystal structure) were having average particle size of around 5 nm. These QDs can be attached to ZnO nanowires, so that they can find applications in QD-sensitized nanowire solar cells.

Yang et al. (2017) proposed a femtosecond LA in microfluidics approach, which is free from toxic chemicals. ZnSe quantum dots were found to be in the range of 4−6 nm using hyperbranched polyethyleneimine as functional and structural coated layer; both. An aqueous nanosized micelles consisting of these quantum dots exhibited emission of bright green light. These quantum dots have a great potential for biomedical imaging. Je et al. (2018) synthesized PbSe QDs via PLIL method. It was found that as-prepared sample in PVP solution resulted in the formation of PbSe QDs rock salt crystalline with size of about 6.83 nm. The particle size of PbSe QDs was found to be dependent on wavelength and power of the laser as well as type and concentration of the surfactants.

Balati et al. (2019) synthesized $MoSe_2$ nanosheets, inorganic fullerene-like (IF) $MoSe_2$ and MoO_3 quantum dots using PLAL method. It was then followed by a microwave treatment of bulk-$MoSe_2$ powders. It was interesting to note that two successive microwave steps changed orientation of $MoSe_2$ crystal from horizontal to vertical.

AlGhamdi et al. (2020) reported dye sensitized solar cells, where a TiO_2 photoanode was cosensitized by organic dye N719 and CdSe quantum dots. The photovoltaic performance of this cell (cosensitized with an optimum concentration of CdSe-QDs) was found to be better than that cell, where photoanode was sensitized by N719 dye. It was observed that photovoltaic conversion efficiency of this cell cosensitized by CdSe-QDs (1 mg/15 mL of ethanol) and N719 dye was 7.09%, which was almost 37% rise in photovoltaic efficiency, as compared to the cell, which is sensitized by the N719 dye only.

Omran et al. (2021) prepared cadmium selenide quantum dots using clean-LA in ethanol. It was reported that as-prepared CdSe QDs has a cubic crystal structure with average particle size of 4 nm. These QDs can find application in dye-sensitized solar cells with higher conversion efficiency.

4.4 Nonmetal-based quantum dots

4.4.1 Carbon-based quantum dots

Yu et al. (2014) prepared CQDs/TiO_2 nanosheet (TNS) composites via a simple low-temperature process. It was indicated that TNS were combined well with CQDs via surface carbon−oxygen groups. The photocatalytic activity of this composite was investigated for degradation of rhodamine B in presence of visible light, which was more as compared with CQDs/P25 composites and TNS only.

Nguyen et al. (2016) prepared carbon nanodots (C-dots) using femtosecond LA of graphite powders. Here, they used polyethylene glycol (PEG200N) solution and different concentrations of graphite. The photoluminescent quantum yield of as-prepared C-dots was significantly increased on decreasing the graphite concentration, reaching up to 21%. These C-dots could be used as an efficient fluorescent nanosensor probes for selective and sensitive detection of Fe^{3+} ions because of their high PL.

Synthesis of fluorescent carbon dots-like nanostructures (CNDs) was reported by Reyes et al. (2016) via LA of a carbon solid target in liquid. It was reported that size of close-spherical amorphous CNDs ranged between 5 and 20 nm. An efficient light emission due to excitation at 3.54 eV was observed with the PL intensity, which was centered at 3.23 eV. It was possible to tune the emission wavelength of the CNDs from the near-UV to the green region by adjusting ablation time as well as by modification of ablation and excitation laser wavelength.

Nguyen et al. (2019b) prepared C-dots with broad emissions via femtosecond LA in ethylenediamine solution. The C-dots were found suitable for a broad range of applications, including optical down-conversion devices, bioimaging, and biosensors by selecting different excitation wavelengths without changing their structures. As-prepared C-dots exhibited broad PL from blue to green regions. It was reported that abundant of functional groups created were on the surface of C-dots such as C-N, C-H, and C-O.

Ren et al. (2019) fabricated N-doped micropore CQDs (NM-CQDs) from biomass using a pulsed LA method with a high quantum yield and dual-wavelength PL emission. They observed two coexisting indigo−blue PL emissions in these QODs. The fluorescence lifetime and quantum yield of as-obtained NM-CQDs were as high as 6.56 ns and 32.4%, respectively. It was reported that these NM-CQDs are quite suitable for cellular staining images due to stable and strong PL emission. This high fluorescence of NM-CQDs can find a great potential in engineering and biomedical imaging.

Cui et al. (2020) fabricated CQDs through ultrafast dual beam pulsed LA using low-cost carbon cloth. As-prepared CQDs were homogeneous and the quantum yield of emission was around 35.4%. These QDs exhibited a good stability and excellent performance for anti-jamming, so that these were found suitable for cell bioimaging.

It is difficult to introduce S into the carbon framework of GQDs as its size is much larger than that of C atoms, as-compared to B and N. Kang et al. (2020) reported a one-step and simple method for synthesizing sulfur-doped GQDs (S-GQDs) using PLAL process. It was observed that these S-GQDs exhibited an increased fluorescence quantum yields from 0.8 to 3.89% and excellent photostability. This method of preparing S-GQDs will open up new avenues for their potential applications.

4.4.2 Graphene-based quantum dots

Russo et al. (2014) developed a method for mass production of porous graphene (PG) and GQDs. They used femtosecond LA of highly oriented pyrolytic graphite for this purpose. It was observed that PG layers float at the water−air interface, and on the contrary, GQDs were found dispersed in the solution. It was confirmed that GQDs have dimensions in the range of 2−5 nm. They explained the formation of these materials on the basis of mechanisms, which involved coal gasification and water breakdown.

Habiba et al. (2015) fabricated GQDs (Ag-GQDs) decorated nanocomposites of silver NPs using pulsed laser. Then these nanocomposites were PEGylated, increasing their solubility in aqueous solutions and biocompatibility. The size of GQDs was in the range of 1.6−4 nm. The antibacterial activity of as-synthesized Ag-GQDs was evaluated and compared against Gram-negative (*Pseudomonas aeruginosa*) and Gram-positive bacteria (*S. aureus*) and it was found high as compared to and that of GQDs and

commercial silver NPs (Ag-NPs). It was reported that cell viability was maintained at 100% for normal mammalian cells, which were incubated with Ag-GQDs. As-prepared Ag-GQDs have potential applications in self-sterile textiles, antibacterial coatings, and personal care products.

Narasimhan et al. (2017) synthesized high-quality water-soluble GQDs using a ns pulsed laser and used these GQDs as fluorescent imaging agent. Their emission properties were attributed to the functional groups such as hydroxyl and carboxyl groups on the surface or edges. A deep red fluorescence was observed from the implanted region.

Santiago et al. (2017) synthesized N-doped GQDs using pulsed LA with diethylenetriamine (DETA). As-synthesized N-doped GQDs had an average size of about 3.4 nm and its atomic ratio (N/C) was 26%. It was reported that N-doped GQDs emitted PL with a factor 66 as compared to pristine GQDs. GQDs were synthesized by Calabro et al. (2018) via chemical oxidation of carbon nanoonions (nCNOs) followed by pulsed LA of these nCNOs to give CO-GQDS. Average diameter of these CO-GQDs was found to be 4.1 nm.

Novoa-De León et al. (2019) synthesized nitrogen-doped GQDs (N-GQDs) using PLAL. They ablated graphite target in dimethylformamide (solvent and nitrogen source, both). It was observed that these N-GQDs consists of a graphitic core with particle size of about 3 nm as well as oxygen and nitrogen functionalities. They used as-prepared N-GQDs dispersion for selective detection of ascorbic acid via a signal-on and signal-off system. These N-GQDs could also be used as PL sensor for metal ions.

4.5 Others

Goodwin et al. (1997) synthesized nanocrystalline GaN via reactive LA of gallium metal in nitrogen atmosphere. It was observed that these crystallites were as small as 2 nm (diameter). It was revealed by size-selective PL and PL excitation spectroscopy that there is a continuous range of blueshifted emissions and absorptions as compared to bulk value for gallium nitride.

Wu et al. (2005) synthesized semiconducting nanocrystals using picosecond pulsed LA. The crystalline nanometer-sized Si particles with average sizes ranging between 1−5 nm exhibited strong quantum confinement effects. Raman spectra confirmed the crystalline nature of these NPs, which showed significant shifts due to confinement. It was revealed that these quantum dots are promising candidates for solar cells.

Yoon et al. (2005) fabricated amorphous GaN quantum dots (a-GaN QDs) at room temperature using a LA technique and densified GaN target. An average particle size of as-prepared a-GaN QDs was found to be 7.9 nm. It was revealed that PL and absorption spectra exhibited a strong emission band centered at 3.9 eV, which was slightly shifted (0.5 eV), that is, a blueshift from the bandgap energy of the GaN crystal. This shift confirmed the

quantum confinement effect. Almeida et al. (2009) reported a LA route for synthesis of thiol capped CdTe colloidal quantum dots. They opined that these NPs were compatible for silica capping, which indicated that they could find application as fluorescent markers.

Qin et al. (2011) carried out Cu doping of ZnO quantum dots by LA of Zn/Cu composite targets immersed in PVP aqueous solution. Firstly, Zn/Cu core−shell particles were synthesized by a galvanic replacement reaction, followed by LA. It was reported that a large amount of Cu-doped ZnO QDs could be produced with ultrafine size, high stability, and good dispersibility. They also controlled dopant concentration (1.8%−4.8%) by just changing the atomic content of Cu in Zn/Cu composite targets. Zakharko et al. (2011) reported synthesis of luminescent SiC quantum dots using LA in pure deionized water. A higher colloidal stability was present for these laser-produced NPs. Long-term stability of colloidal solutions (as-prepared SiC quantum dots) is due to surface charges related to carboxylate anions. It was observed that emission from the Se QDs is centered at 2.75 eV and it does not depend on the laser power used for ablation.

Bagga et al. (2013) reported the synthesis of protein-functionalized luminescent silicon NPs using infrared ultrafast LA. They used silicon in an aqueous solution of *S. aureus* protein A for this purpose. Quantum dots of protein A-capped silicon (8 nm) were obtained with blue−green photoemissions. The biological functionality of these QDs was also studied by them. It was revealed that these Si-based bionanostructures bind IgG selectively in the cells, and therefore, these quantum dots may be suitable for biological applications, such as biomarkers for in vivo applications such as cell labeling, cell staining, and controlled drug delivery.

Gongalsky et al. (2016) reported a secondary toxicity problem of solution of brightly luminescent water-dispersible Si-based QDs using laser-assisted synthesis. These QDs do not exhibit any sign of toxicity; rather they show excellent cellular uptake and biodegradability making them an ideal candidate for bioimaging applications. Rodio et al. (2016) prepared amine-terminated, ultrasmall silicon NPs (Si NPs) in one step by introducing organosilane in Si NPs colloidal solution, which was prepared by ultrafast LA. It was confirmed that the successfully functionalized Si NPs was leading to 5 nm Si dots covered by a thick layer aminopropyltriethoxysilane. Such particles can find some biomedical applications such as biolabels, clinical setting, vector delivery, and contrast agents.

Rasouli et al. (2017) reported that the efficiency of photovoltaic solar cells can be increased by luminescent Si NPs. Sub Si NPs (10 nm) were synthesized using a pulsed LA technique. As-prepared ultrasmall Si NPs show PL characteristics at 517 and 425 nm upon excitation by UV light. The polycrystalline commercial solar cells are coated with these luminescent Si NPs giving an efficiency of about 10%.

Ren et al. (2018) synthesized black phosphorus quantum dots (BPQDs) using pulsed LA. They used isopropyl ether as a solvent. It was reported that QDs have average diameter of about 6 nm and also a height of about 1.1 nm. It was revealed that the PL quantum yield of as-prepared sample was about 20.7 %, which was almost three times higher than that of BPQDs prepared by some other means, for example, ultrasonic exfoliation (about 7.2 %). A stable and blue−violet emission was observed with BPQDs. Apart from it, BPQDs are also utilized in bioimaging in HeLa cells, with excellent biocompatibility. It was also revealed that as-obtained BPQDs have promising potential for biomedical applications, such as bioimaging, biolabeling, and drug delivery.

Most of the methods for synthesis of boron nitride quantum dots (BNQDs) are either complex or time-consuming. Xu et al. (2019) synthesized few-layer BNQDs by liquid-phase ultrashort laser pulse ablation and ultrasonic-assisted exfoliation methods. It was revealed that as-prepared BNQDs have an average size of about 2.1 nm. These BNQDs exhibited bright luminescence emission in the presence of UV light due to abundant surface functional groups. Anjana et al. (2020) prepared Er, Yb-codoped fluorapatite NPs using liquid-phase pulsed LA. A transparent colloidal solution had NPs sizes in the range of 2−4 nm. It was claimed that as-synthesized NPs dispersed in water are biocompatible and can find applications for cell imaging.

Morozova et al. (2020) focused on the possible use of silicon quantum dots ranging from 1 to 10 nm for LED. These QDs have a great potential as optoelectronic devices and fluorescent biomarking agents as they can exhibit blue and red fluorescence. Their biocompatibility compared to conventional toxic group II−VI and III−V metal-based quantum dots makes their practical utilization even more attractive to prevent environmental pollution and harm to living organisms. Sergeev et al. (2020) observed that coupling of HgTe QDs with lattice plasmons decreases the influence of nonradiative decay losses and IR absorption bands of dodecanethiol, which was used as a ligand on the QDs. It was reported that the ease of chemical synthesis and processing of HgTe QDs along with scalability of the direct laser fabrication of nanoantennas with tailored plasmonic responses helps in designing IR-range devices for different applications such as detectors, emitters, sensors, and security systems.

It is bit difficult to tune the PL properties of BNQDs and obtain these QDs with intense and desired PL emission. Recently, Nguyen et al. (2021) proposed a method to synthesize and functionalize BN QDs using femtosecond LA in an organic solution with tunable PL from ultraviolet to green region. It is all due to carbene zigzag edges, which are formed on the surface of BNQDs resulting in effective emission. There is a redshift in colors by increasing the content of carboxyl group on the carbene zigzag edges.

Soliman et al. (2021) synthesized stainless steel grade 304 QDs through LA in water. These were then used in the treatment of laryngeal carcinoma in vitro, without using any external laser source or magnet for hyperthermia. It was revealed that valence of chromium is +3 in these QDs and these show a resonance fluorescence property in the NIR band. It was observed that a dilute solution of QDs, on addition to cell culture medium, suppressed VEGF gene expression and cell proliferation; both of which indicated the death of cancer cells. The +3 valence of Cr and lower percentage of QDs exclude any possibility of QDs toxicity. The most plausible mechanism for death of cancer cells is due to heat shock of NIR resonance fluorescence of QDs.

4.6 Recent developments

LA is a fast-growing technique for the preparation of quantum dots. Some recent advances in this direction are shown in Table 4.1.

TABLE 4.1 Preparation of quantum dots by laser ablation.

Quantum dots	Application	References
Graphene	2D Material defect engineering	Li et al. (2021)
Graphene	Fluorescent probe for detection of Fe^{3+} ions	Shen et al. (2021)
Graphene	Detection of Fe^{+3} (500 nM to 50 μM)	Kang et al. (2022)
Carbon quantum dots	Alleviating amyloid-β mediated neurotoxicity	Li et al. (2022)
Antimony materials with perovskite quantum dots	To protect human eyes and optical equipment from high-power laser damage	Liang et al. (2022)
CQD@$LaPO_4$:Eu^{3+}	Bioimaging of plant cells and as ink for security	Raikwar (2022)
CuO NPs-CNPs	Antimicrobial and antiproliferative activities against breast cancer cell lines, MCF-7	Mohammed et al. (2022)
PVA/CMC/MoO_3NPs	Enhanced optical and electrical characterization of polymeric films	Asnag et al. (2022)
Graphitic carbon quantum dot	Catalytic dehydrogenation and carbonization	Chen et al. (2022)

4.7 Conclusion

Various metals and metal chalcogenides quantum dots can be easily prepared by the LA method. It is equally effective in the preparation of carbon and GQDs. These quantum dots have a very high degree of purity as no chemical is added from outside and a target is exposed to the laser. This method of synthesis is welcome because it provides high-purity quantum dots and in a shorter time; however, the high cost of the equipment is still a concern. This method of synthesis will surpass all other methods in the forthcoming decades.

References

Ajimsha, R.S., Anoop, G., Aravind, A., Jayaraj, M.K., 2007. Luminescence from surfactant-free ZnO quantum dots prepared by laser ablation in liquid. Electrochem. Solid. State Lett. 11 (2). Available from: https://doi.org/10.1149/1.2820767.

AlGhamdi, J.M., AlOmar, S., Gondal, M.A., Moqbel, R., Dastageer, M.A., 2020. Enhanced efficiency of dye co-sensitized solar cells based on pulsed-laser-synthesized cadmium-selenide quantum dots. Sol. Energy 209, 108–117.

Almeida, D.B., Rodriguez, E., Moreira, R.S., Agouram, S., Barbosa, L.C., Jimenez, E., et al., 2009. Laser ablation synthesis route of CdTe colloidal quantum dots for biological applications. In: European Conference on Biomedical Optics. Opt. Soc. Am. Available from: https://doi.org/10.1364/ecbo.2009.7371_0f.

Amendola, V., Meneghetti, M., 2009. Laser ablation synthesis in solution and size manipulation of noble metal nanoparticles. Phys. Chem. Chem. Phys. 11 (20), 3805–3821.

An, S.J., Park, D.Y., Lee, C., Bang, S., Nguyen, D.A., Kim, S.H., et al., 2020. Facile preparation of molybdenum disulfide quantum dots using a femtosecond laser. Appl. Surf. Sci. 511. Available from: https://doi.org/10.1016/j.apsusc.2020.145507.

Anikin, K.V., Melnik, N.N., Simakin, A.V., Shafeev, G.A., Voronov, V.V., Vitukhnovsky, A.G., 2002. Formation of ZnSe and CdS quantum dots via laser ablation in liquids. Chem. Phys. Lett. 366 (3-4), 357–360.

Anjana, R., Krishnapriya, T.K., Jayaraj, M.K., 2020. Clean synthesis of Er, Yb doped fluorapatite upconversion luminescent nanoparticles through liquid phase pulsed laser ablation. Opt. Laser Technol. 131. Available from: https://doi.org/10.1016/j.optlastec.2020.106452.

Asnag, G.M., Awwad, N.S., Ibrahium, H.A., Moustapha, M.E., Alqahtani, M.S., Menazea, A.A., 2022. One-Pot pulsed laser ablation route assisted molybdenum trioxide nano-belts doped in PVA/CMC blend for the optical and electrical properties enhancement. J. Inorg. Organometal. Poly. Mater. . Available from: https://doi.org/10.1007/s10904-022-02257-5.

Bagga, K., Barchanski, A., Intartaglia, R., Dante, S., Marotta, R., Diaspro, A., et al., 2013. Laser-assisted synthesis of *Staphylococcus aureus* protein-capped silicon quantum dots as bio-functional nanoprobes. Laser Phys. Lett. 10 (6). Available from: https://doi.org/10.1088/1612-2011/10/6/065603.

Balati, A., Bazilio, A., Shahriar, A., Nash, K., Shipley, H.J., 2019. Simultaneous formation of ultra-thin MoSe2 nanosheets, inorganic fullerene-like $MoSe_2$ and MoO_3 quantum dots using fast and ecofriendly pulsed laser ablation in liquid followed by microwave treatment. Mater. Sci. Semicond. Process. 99, 68–77.

Baldovi, H.G., Latorre-Sánchez, M., Esteve-Adell, I., Khan, A., Asiri, A.M., Kosa, S.A., 2016. Generation of MoS_2 quantum dots by laser ablation of MoS_2 particles in suspension and their photocatalytic activity for H_2 generation. J. Nanopart. Res. 18 (8). Available from: https://doi.org/10.1007/s11051-016-3540-9.

Besner, S., Kabashin, A.V., Meunier, M., Winnik, F.M., 2005. Fabrication of functionalized gold nanoparticles by femtosecond laser ablation in aqueous solutions of biopolymers. Int. Soc. Opt. Photonics 5969. Available from: https://doi.org/10.1117/12.628885.

Boltaev, G.S., Ganeev, R.A., Krishnendu, P.S., Maurya, S.K., Redkin, P.V., Rao, K.S., et al., 2018. Strong third-order optical nonlinearities of Ag nanoparticles synthesized by laser ablation of bulk silver in water and air. Appl. Phys. A. 124 (11). Available from: https://doi.org/10.1007/s00339-018-2195-z.

Caigas, S.P., Cheng, M.C., Lin, T.N., Santiago, S.R.M.S., Yuan, C.T., Yang, C.C., et al., 2018. P-type doping of WS2 quantum dots via pulsed laser ablation. ACS Photonics 5 (12), 4828−4837.

Calabro, R.L., Yang, D.S., Kim, D.Y., 2018. Liquid-phase laser ablation synthesis of graphene quantum dots from carbon nano-onions: comparison with chemical oxidation. J. Coll. Interf. Sci. 527, 132−140.

Chen, H.R., Meng, W.M., Wang, R.Y., Chen, F.L., Li, T., Wang, D.D., et al., 2022. Engineering highly graphitic carbon quantum dots by catalytic dehydrogenation and carbonization of Ti_3C_2Tx-MXene wrapped polystyrene spheres. Carbon 190. Available from: https://doi.org/10.1016/j.carbon.2022.01.028.

Cui, L., Ren, X., Wang, J., Sun, M., 2020. Synthesis of homogeneous carbon quantum dots by ultrafast dual-beam pulsed laser ablation for bioimaging. Mater. Today Nano 12. Available from: https://doi.org/10.1016/j.mtnano.2020.100091.

Darwish, A.M., Eisa, W.H., Shabaka, A.A., Talaat, M.H., 2015. Synthesis of nano-cadmium sulfide by pulsed laser ablation in liquid environment. Spectrosc. Lett. 48 (9), 638−645.

Drmosh, Q.A., Yamani, Z.H., Hendi, A.H., Gondal, M.A., Moqbel, R.A., Saleh, T.A., et al., 2019. A novel approach to fabricating a ternary rGO/ZnO/Pt system for high-performance hydrogen sensor at low operating temperatures. Appl. Surf. Sci. 464, 616−626.

Eita, M., Wagberg, L., Muhammed, M., 2012. Spin-assisted multilayers of poly (methyl methacrylate) and zinc oxide quantum dots for ultraviolet-blocking applications. ACS Appl. Mater. Interf. 4 (6), 2920−2925.

Farshbaf, M., Davaran, S., Rahimi, F., Annabi, N., Salehi, R., Akbarzadeh, A., 2018. Carbon quantum dots: recent progresses on synthesis, surface modification and applications. Artif. Cell Nanomed. Biotechnol. 46 (7), 1331−1348.

Gondal, M.A., Drmosh, Q.A., Yamani, Z.H., Saleh, T.A., 2009. Synthesis of ZnO_2 nanoparticles by laser ablation in liquid and their annealing transformation into ZnO nanoparticles. Appl. Surf. Sci. 256 (1), 298−304.

Gondal, M.A., Ilyas, A.M., Fasasi, T.A., Dastageer, M.A., Seddigi, Z.S., Qahtan, T.F., et al., 2015. Synthesis of green TiO_2/ZnO/CdS hybrid nano-catalyst for efficient light harvesting using an elegant pulsed laser ablation in liquids method. Appl. Surf. Sci. 357, 2217−2222.

Gongalsky, M.B., Osminkina, L.A., Pereira, A., Manankov, A.A., Fedorenko, A.A., Vasiliev, A. N., et al., 2016. Laser-synthesized oxide-passivated bright Si quantum dots for bioimaging. Sci. Rep. 6 (1). Available from: https://doi.org/10.1038/srep24732.

Goodwin, T.J., Leppert, V.J., Risbud, S.H., Kennedy, I.M., Lee, H.W., 1997. Synthesis of gallium nitride quantum dots through reactive laser ablation. Appl. Phys. Lett. 70 (23), 3122−3124.

Habiba, K., Bracho-Rincon, D.P., Gonzalez-Feliciano, J.A., Villalobos-Santos, J.C., Makarov, V. I., Ortiz, D., et al., 2015. Synergistic antibacterial activity of PEGylated silver−graphene quantum dots nanocomposites. Appl. Mater. Today 1 (2), 80−87.

Horoz, S., Lu, L., Dai, Q., Chen, J., Yakami, B., Pikal, J.M., et al., 2012. CdSe quantum dots synthesized by laser ablation in water and their photovoltaic applications. Appl. Phys. Lett. 101 (22). Available from: https://doi.org/10.1063/1.4768706.

Je, M., Jung, H.J., Koutavarapu, R., Lee, S.J., Lee, S.H., Kim, S.K., et al., 2018. Pulsed laser irradiation synthesis of lead selenide quantum dots from lead and selenium salts in various surfactants. Mater. Chem. Phys. 217, 427−436.

Ka, I., Ma, D., El Khakani, M.A., 2011. Tailoring the photoluminescence of PbS-nanoparticles layers deposited by means of the pulsed laser ablation technique. J. Nanopart. Res. 13 (6), 2269−2274.

Ka, I., Le Borgne, V., Ma, D., El Khakani, M.A., 2012. Pulsed laser ablation based direct synthesis of single-wall carbon nanotube/PbS quantum dot nanohybrids exhibiting strong, spectrally wide and fast photoresponse. Adv. Mater. 24 (47), 6289−6294.

Ka, I., Gonfa, B., Le Borgne, V., Ma, D., El Khakani, M.A., 2014. Pulsed laser ablation based synthesis of PbS-quantum dots-decorated one-dimensional nanostructures and their direct integration into highly efficient nanohybrid heterojunction-based solar cells. Adv. Funct. Mater. 24, 4042−4050.

Ka, I., Le Borgne, V., Fujisawa, K., Hayashi, T., Kim, Y.A., Endo, M., et al., 2016. Multiple exciton generation induced enhancement of the photoresponse of pulsed-laser-ablation synthesized single-wall-carbon-nanotube/PbS-quantum-dots nanohybrids. Sci. Rep. 6 (1). Available from: https://doi.org/10.1038/srep20083.

Kang, S., Jeong, Y.K., Jung, K.H., Son, Y., Kim, W.R., Ryu, J.H., et al., 2020. One-step synthesis of sulfur-incorporated graphene quantum dots using pulsed laser ablation for enhancing optical properties. Opt. Exp. 28 (15), 21659−21667.

Kang, S., Han, H., Lee, K., Kim, K.M., 2022. Ultrasensitive detection of Fe^{3+} ions using functionalized graphene quantum dots fabricated by a one-step pulsed laser ablation process. ACS Omega 7, 2074−2081.

Kateshiya, M.R., Malek, N.I., Kailasa, S.K., 2020. Facile synthesis of highly blue fluorescent tyrosine coated molybdenum oxide quantum dots for the detection of imidacloprid pesticide. J. Mol. Liq. 319. Available from: https://doi.org/10.1016/j.molliq.2020.114329.

Khan, T., BiBi, T., 2014. Application of NS pulsed laser ablation for dense CdS nanoparticles deposition in argon atmosphere. Sop. Trans. Appl. Phys. 1 (2), 48−54.

Kim, M., Osone, S., Kim, T., Higashi, H., Seto, T., 2017. Synthesis of nanoparticles by laser ablation: a review. KONA Powder Part. J. 34 (2014), 80−90.

Kőrösi, L., Rodio, M., Dömötör, D., Kovács, T., Papp, S., Diaspro, A., et al., 2016. Ultrasmall, ligand-free Ag nanoparticles with high antibacterial activity prepared by pulsed laser ablation in liquid. J. Chem. 2016. Available from: https://doi.org/10.1155/2016/4143560.

Kuriakose, A.C., Nampoori, V.P.N., Thomas, S., 2019. Facile synthesis of Au/CdS core-shell nanocomposites using laser ablation technique. Mater. Sci. Semicond. Process. 101, 124−130.

Lalayan, A.A., 2005. Formation of colloidal GaAs and CdS quantum dots by laser ablation in liquid media. Appl. Surf. Sci. 248 (1-4), 209−212.

Li, S., Chen, M., 2016. Convenient synthesis of stable silver quantum dots with enhanced photoluminescence emission by laser fragmentation. Chin. Phys. B 25 (4). Available from: https://doi.org/10.1088/1674-1056/25/4/046103.

Li, B., Jiang, L., Li, X., Ran, P., Zuo, P., Wang, A., et al., 2017. Preparation of monolayer MoS_2 quantum dots using temporally shaped femtosecond laser ablation of bulk MoS_2 targets in water. Sci. Rep. 7 (1). Available from: https://doi.org/10.1038/s41598-017-10632-3.

Li, X., Li, X., Jiang, L., Zuo, P., Zhao, Y., Wang, S., et al., 2021. Preparation of twin graphene quantum dots through the electric-field-assisted femtosecond laser ablation of graphene dispersions. Carbon 185, 384–394.

Li, H., Zhang, Y., Ding, J., Wu, T., Cai, S., Zhang, W., et al., 2022. Synthesis of carbon quantum dots for application of alleviating amyloid-β mediated neurotoxicity. Colloids Surf. B: Biointerfaces . Available from: https://doi.org/10.1016/j.colsurfb.2022.112373.

Liang, L., Shen, W., Wang, J., Ma, T., Chen, J., 2022. Nonlinear absorption of $CsPbBr_3$/antimonene blend materials prepared by laser ablation in liquid. Opt. Mater. 123. Available from: https://doi.org/10.1016/j.optmat.2021.111901.

Maiman, T., 1960. Stimulated optical radiation in ruby. Nature 187, 493–494.

Malviya, K.D., Chattopadhyay, K., 2014. Synthesis and mechanism of composition and size dependent morphology selection in nanoparticles of Ag–Cu alloys processed by laser ablation under liquid medium. J. Phys. Chem. C. 118 (24), 13228–13237.

Mansoureh, G., Parisa, V., 2018. Synthesis of metal nanoparticles using laser ablation technique. Emerging Applications of Nanoparticles and Architecture Nanostructures. Elsevier, Amsterdam, pp. 575–596.

Mendonça, L.T., de Azevedo, W.M., 2016. A fast bottom-up route for preparing CdS quantum dots using laser ablation in a liquid environment. J. Luminescen. 171, 79–84.

Mitra, S., Pak, Y., Alaal, N., Hedhili, M.N., Almalawi, D.R., Alwadai, N., et al., 2019. Novel P-Type wide bandgap manganese oxide quantum dots operating at deep uv range for optoelectronic devices. Adv. Opt. Mater. 7 (21). Available from: https://doi.org/10.1002/adom.201900801.

Mohammed, S.A., Khashan, K.S., Jabir, M.S., Abdulameer, F.A., Sulaiman, G.M., Al-Omar, M. S., et al., 2022. Copper oxide nanoparticle-decorated carbon nanoparticle composite colloidal preparation through laser ablation for antimicrobial and antiproliferative actions against breast cancer cell line, MCF-7. BioMed. Res. Int. 2022. Available from: https://doi.org/10.1155/2022/9863616.

Morozova, S., Alikina, M., Vinogradov, A., Pagliaro, M., 2020. Silicon quantum dots: synthesis, encapsulation, and application in light-emitting diodes. Front. Chem. 8. Available from: https://doi.org/10.3389/fchem.2020.00191.

Mostafa, A.M., Yousef, S.A., Eisa, W.H., Ewaida, M.A., Al-Ashkar, E.A., 2019. WO_3 quantum dot: synthesis, characterization and catalytic activity. J. Mol. Struct. 1185, 351–356.

Murali, A.K., 2001. Laser Ablation Synthesis of Indium Oxide Quantum Dots and a Kinetic Study of the Oxide to Nitride Conversion (Ph.D. thesis). University of California, Davis.

Mwafy, E.A., Hasanin, M.S., Mostafa, A.M., 2019. Cadmium oxide/TEMPO-oxidized cellulose nanocomposites produced by pulsed laser ablation in liquid environment: synthesis, characterization, and antimicrobial activity. Opt. Laser Technol. 120. Available from: https://doi.org/10.1016/j.optlastec.2019.105744.

Narasimhan, A.K., Santra, T.S., Rao, M.R., Krishnamurthi, G., 2017. Oxygenated graphene quantum dots (GQDs) synthesized using laser ablation for long-term real-time tracking and imaging. RSC Adv. 7 (85), 53822–53829.

Nguyen, V., Yan, L., Si, J., Hou, X., 2016. Femtosecond laser-assisted synthesis of highly photoluminescent carbon nanodots for Fe^{3+} detection with high sensitivity and selectivity. Opt. Mater. Exp. 6 (2), 312–320.

Nguyen, V., Dong, Q., Yan, L., Zhao, N., Le, P.H., 2019a. Facile synthesis of photoluminescent MoS_2 and WS_2 quantum dots with strong surface-state emission. J. Lumin. 214. Available from: https://doi.org/10.1016/j.jlumin.2019.116554.

Nguyen, V., Yan, L., Si, J., 2019b August. Synthesis of broad photoluminescence carbon nanodots by femtosecond laser ablation in liquid. In: 2016 IEEE 16th International Conference on Nanotechnology (IEEE-NANO). IEEE, pp. 901–903.

Nguyen, V., Yan, L., Zhao, N., Van Canh, N., Hang, N.T.N., Le, P.H., 2021. Tuning photoluminescence of boron nitride quantum dots via surface functionalization by femtosecond laser ablation. J. Mol. Struc. Available from: https://doi.org/10.1016/j.molstruc.2021.130922.

Novoa-De León, I.C., Johny, J., Vázquez-Rodríguez, S., García-Gómez, N., Carranza-Bernal, S., Mendivil, I., et al., 2019. Tuning the luminescence of nitrogen-doped graphene quantum dots synthesized by pulsed laser ablation in liquid and their use as a selective photoluminescence on–off–on probe for ascorbic acid detection. Carbon 150, 455–464.

Omran, Z.H., Salman, O.N., Ali, A.K., 2021. Preparation CdSe quantum dots using laser ablation technique for dye-sensitized solar cell. Int. J. Nanoelectron. Mater. 14 (1), 61–70.

Ou, G., Fan, P., Ke, X., Xu, Y., Huang, K., Wei, H., et al., 2018. Defective molybdenum sulfide quantum dots as highly active hydrogen evolution electrocatalysts. Nano Res. 11 (2), 751–761.

Patel, M.K., Singh, J., Singh, M.K., Agrawal, V.V., Ansari, S.G., Malhotra, B.D., 2013. Tin oxide quantum dot based DNA sensor for pathogen detection. J. Nanosc. Nanotechnol. 13 (3), 1671–1678.

Pradhan, G., Dey, P.P., Khare, A., Sharma, A.K., 2021. Synthesis and size modulation of MoS_2 quantum dots by pulsed laser ablation in liquid for viable hydrogen generation. J. Appl. Phys. 129 (2). Available from: https://doi.org/10.1063/5.0022833.

Pyatenko, A., Shimokawa, K., Yamaguchi, M., Nishimura, O., Suzuki, M., 2004. Synthesis of silver nanoparticles by laser ablation in pure water. Appl. Phys. A. 79 (4-6), 803–806.

Qin, W.J., Sun, J., Yang, J., Du, X.W., 2011. Control of Cu-doping and optical properties of ZnO quantum dots by laser ablation of composite targets. Mater. Chem. Phys. 130 (1-2), 425–430.

Raikwar, V.R., 2022. Synthesis and study of carbon quantum dots (CQDs) for enhancement of luminescence intensity of CQD@$LaPO_4$: Eu^{3+} nanocomposite. Mater. Chem. Phys. 275. Available from: https://doi.org/10.1016/j.matchemphys.2021.125277.

Rasouli, H.R., Ghobadi, A., Ghobadi, T.U., Ates, H., Topalli, K., Okyay, A.K., 2017. Nanosecond pulsed laser ablated sub-10 nm silicon nanoparticles for improving photovoltaic conversion efficiency of commercial solar cells. J. Opt. 19 (10). Available from: https://doi.org/10.1088/2040-8986/aa84dd.

Ravi Kumar, S., Lies, B., Zhang, X., Lyu, H., Qin, H., 2019. Laser ablation of polymers: a review. Polym. Int. 68 (8), 1391–1401.

Ren, X., Zhang, F., Zhang, X., 2018. Synthesis of black phosphorus quantum dots with high quantum yield by pulsed laser ablation for cell bioimaging. Chem. Asian J. 13 (14), 1842–1846.

Ren, X., Zhang, F., Guo, B., Gao, N., Zhang, X., 2019. Synthesis of N-doped micropore carbon quantum dots with high quantum yield and dual-wavelength photoluminescence emission from biomass for cellular imaging. Nanomater 9 (4). Available from: https://doi.org/10.3390/nano9040495.

Reyes, D., Camacho, M., Camacho, M., Mayorga, M., Weathers, D., Salamo, G., et al., 2016. Laser ablated carbon nanodots for light emission. Nanoscale Res. Lett. 11 (1), 1–11.

Rodio, M., Brescia, R., Diaspro, A., Intartaglia, R., 2016. Direct surface modification of ligand-free silicon quantum dots prepared by femtosecond laser ablation in deionized water. J. Coll. Interf. Sci. 465, 242–248.

Russo, P., Hu, A., Compagnini, G., Duley, W.W., Zhou, N.Y., 2014. Femtosecond laser ablation of highly oriented pyrolytic graphite: a green route for large-scale production of porous graphene and graphene quantum dots. Nanoscale 6 (4), 2381–2389.

Ryabchikov, Y.V., Popov, A.A., Sentis, M., Timoshenko, V.Y., Kabashin, A.V., 2016. March. Structural properties of gold-silicon nanohybrids formed by femtosecond laser ablation in water at different fluences. Synth. Photonics Nanoscale Mater. XIII 9737, 54–59.

Sadrolhosseini, A.R., Rashid, S.A., Shafie, S., Nezakati, H., 2019. Laser ablation synthesis of gold nanoparticle to enhance the fluorescence properties of graphene quantum dots. J. Laser Appl. 31 (2). Available from: https://doi.org/10.2351/1.5046062.

Sadrolhosseini, A.R., Krishnan, G., Safie, S., Beygisangchin, M., Rashid, S.A., Harun, S.W., 2020. Enhancement of the fluorescence property of carbon quantum dots based on laser ablated gold nanoparticles to evaluate pyrene. Opt. Mater. Exp. 10 (9), 2227–2241.

Santiago, S.R.M., Lin, T.N., Chang, C.H., Wong, Y.A., Lin, C.A.J., Yuan, C.T., et al., 2017. Synthesis of N-doped graphene quantum dots by pulsed laser ablation with diethylenetriamine (DETA) and their photoluminescence. Phys. Chem. Chem. Phys. 19 (33), 22395–22400.

Schawlow, A.L., Townes, C.H., 1958. Infrared and optical masers. Phys. Rev. 112 (6), 1940–1949.

Sergeev, A.A., Pavlov, D.V., Kuchmizhak, A.A., Lapine, M.V., Yiu, W.K., Dong, Y., et al., 2020. Tailoring spontaneous infrared emission of HgTe quantum dots with laser-printed plasmonic arrays. Light. Sci. Appl. 9 (1). Available from: https://doi.org/10.1038/s41377-020-0247-6.

Shen, L., Zhou, S., Huang, F., Zhou, H., Zhang, H., Wang, S., et al., 2021. Nitrogen-doped graphene quantum dots synthesized by femtosecond laser ablation in liquid from laser induced graphene. Nanotechnol. 33 (11). Available from: https://doi.org/10.1088/1361-6528/ac4069.

Singh, S.C., Gopal, R., 2012. Drop shaped zinc oxide quantum dots and their self-assembly into dendritic nanostructures: liquid assisted pulsed laser ablation and characterizations. Appl. Surf. Sci. 258 (7), 2211–2218.

Singh, S.C., Mishra, S.K., Srivastava, R.K., Gopal, R., 2010. Optical properties of selenium quantum dots produced with laser irradiation of water suspended Se nanoparticles. J. Phys. Chem. C. 114 (41), 17374–17384.

Singh, M.K., Mathpal, M.C., Agarwal, A., 2012. Optical properties of SnO_2 quantum dots synthesized by laser ablation in liquid. Chem. Phys. Lett. 536, 87–91.

Soheyli, E., Ghaemi, B., Sahraei, R., Sabzevari, Z., Kharrazi, S., Amani, A., 2020. Colloidal synthesis of tunably luminescent AgInS-based/ZnS core/shell quantum dots as biocompatible nano-probe for high-contrast fluorescence bioimaging. Mater. Sci. Eng. C. 111. Available from: https://doi.org/10.1016/j.msec.2020.110807.

Soliman, W., Yamani, R.N., Sabry, D., Mostafa, A., 2021. Stainless steel quantum dots and its resonance fluorescence impact as new therapeutic agents for Laryngeal carcinoma treatment: in vitro study. Opt. Laser Technol. 142. Available from: https://doi.org/10.1016/j.optlastec.2021.107263.

Sunitha, A.P., Hajara, P., Shaji, M., Jayaraj, M.K., Saji, K.J., 2018. Luminescent MoS_2 quantum dots with reverse saturable absorption prepared by pulsed laser ablation. J. Lumin. 203, 313–321.

Suzuki, K., Inoguchi, M., Kageyama, K., Takagi, H., Sakabe, Y., 2009. Well-crystallized zinc oxide quantum dots with narrow size distribution. J. Nanopart. Res. 11 (6), 1349–1360.

Verma, R.K., Kumar, K., Rai, S.B., 2013. Near infrared induced optical heating in laser ablated Bi quantum dots. J. Coll. Inter. Sci. 390 (1), 11–16.

Wang, X., Zhu, C., Jin, L., Lin, K., Shao, Y., Yang, J., et al., 2021. Rational synthesis of ZnO decorated Fe hierarchical nanostructures for enhanced photocatalytic performance by long-pulse-width laser ablation of binary alloys target. J. Alloy. Comp. 868. Available from: https://doi.org/10.1016/j.jallcom.2021.159171.

Wu, M.H., Mu, R., Ueda, A., Henderson, D.O., Vlahovic, B., 2005. Production of silicon quantum dots for photovoltaic applications by picosecond pulsed laser ablation. Mater. Sci. Eng. B. 116 (3), 273–277.

Xu, Y., Yan, L., Si, J., Zhao, N., 2019. Femtosecond laser-assisted fabrication of fluorescent boron nitride quantum dots. In: 2019 IEEE International Conference on Manipulation, Manufacturing and Measurement on the Nanoscale (3M-NANO). IEEE, pp. 7–10, Available from: https://doi.org/10.1109/3M-NANO46308.2019.8947381.

Yang, C., Feng, G., Dai, S., Wang, S., Li, G., Zhang, H., et al., 2017. Femtosecond pulsed laser ablation in microfluidics for synthesis of photoluminescent ZnSe quantum dots. Appl. Surf. Sci. 414, 205–211.

Yoon, J.W., Shim, S.H., Shim, K.B., Koshizaki, N., Kwon, Y.S., 2005. Quantum confinement effect of amorphous GaN quantum dots prepared by pulsed-laser ablation. Jpn. J. Appl. Phys. 44 (1S). Available from: https://doi.org/10.1143/JJAP.44.788.

Yu, X., Liu, J., Yu, Y., Zuo, S., Li, B., 2014. Preparation and visible light photocatalytic activity of carbon quantum dots/TiO2 nanosheet composites. Carbon 68, 718–724.

Zakharko, Y., Rioux, D., Patskovsky, S., Lysenko, V., Marty, O., Bluet, J.M., et al., 2011. Direct synthesis of luminescent SiC quantum dots in water by laser ablation. Phys. Status Solidi RRL. 5 (8), 292–294.

Zeng, H., Yang, S., Cai, W., 2011. Reshaping formation and luminescence evolution of ZnO quantum dots by laser-induced fragmentation in liquid. J. Phys. Chem. C. 115 (12), 5038–5043.

Zhao, Y., Song, M., Yang, X., Yang, J., Du, C., Wang, G., et al., 2020. Amorphous Ag_2-xCuxS quantum dots: "all-in-one" theranostic nanomedicines for near-infrared fluorescence/photoacoustics dual-modal-imaging-guided photothermal therapy. Chem. Eng. J. 399. Available from: https://doi.org/10.1016/j.cej.2020.125777.

Zheng, J., Zheng, Z., Gong, W., Hu, X., Gao, W., Ren, X., et al., 2008. Stable, small, and water-soluble Cu-doped ZnS quantum dots prepared via femtosecond laser ablation. Chem. Phys. Lett. 465 (4–6), 275–278.

Zheng, C.B., Xia, Y.Q., Qin, F., Yu, Y., Miao, J.P., Zhang, Z.G., et al., 2010. Femtosecond pulsed laser induced synthesis of ultrafine Y_2O_3: Pr, Yb nanoparticles with improved upconversion efficiency. Chem. Phys. Lett. 496 (4–6), 316–320.

This page intentionally left blank

Chapter 5

Coprecipitation synthesis of quantum dots

Monika Jangid and Seema Kothari
Department of Chemistry, PAHER University, Udaipur, Rajasthan, India

5.1 Introduction

The coprecipitation method is used to prepare uniform compositions in homogeneous solution of two or more ions through precipitation reaction. It is an important method for the synthesis of some materials containing two or more elements. What is the difference between the precipitation and coprecipitation? The process of precipitation is the settling down of some insoluble particles from a homogeneous solution. This insoluble compound forms precipitates. Whereas coprecipitation is a process, where normally soluble compounds are thrown out of solution in the form of a precipitate. The coprecipitation is most commonly used for synthesis of nanoparticles and quantum dots (QDs). Different operational parameters like material, pH, concentration of the initial solutions, reaction temperature and time play important roles in getting nanoparticles or QDs with the desired shapes and sizes.

It is a simple, economical, and industrially viable technique that is normally used for the synthesis of important oxide materials. The various steps involved in this process are shown schematically in the flow chart in Fig. 5.1. It is possible to prepare flowable powders using this process without any additional agglomeration steps. One can tailor such a process to obtain nano- or microsized particles by adjusting the pH, temperature, solvents, and the precipitating agent.

5.1.1 Advantages

1. It is a most useful method for controlling the sizes of nanoparticles.
2. It is commonly used in the biomedical applications, because it is easy to apply and almost harmless.

Quantum Dots. DOI: https://doi.org/10.1016/B978-0-12-824153-0.00005-7
© 2023 Elsevier Inc. All rights reserved.

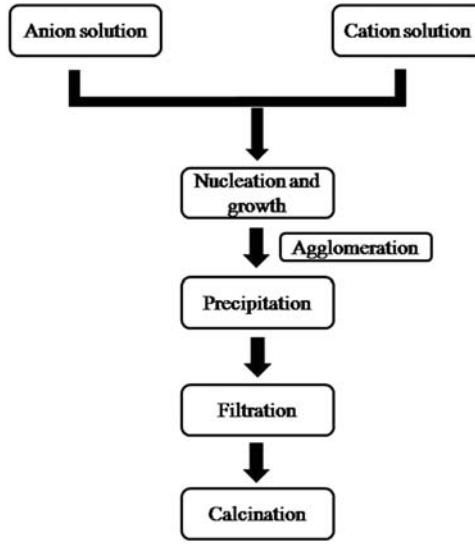

FIGURE 5.1 Flow chart of coprecipitation method.

3. In this method, nanoparticles are prepared from aqueous salt solutions, just by adding a base under an inert atmosphere at room temperature as well as at high temperatures.
4. It can be carried out at lower reaction temperature and with shorter reaction time.

5.1.2 Disadvantages

1. In this process, there in a problem because some undesired impurities may also coprecipitate with the analyte.
2. Distribution of shape of nanoparticles may be uncontrollable and size may be irregular.
3. The products are generally insoluble because of the high supersaturation condition, which is necessary to induce precipitation.
4. Salts may have similar solubilities.
5. It is often difficult to have material of high purity and accurate stoichiometry.
6. It is not cost effective in some cases.
7. One of the troubles with this method of synthesis of nanoparticles is the tendency of particles to agglomerate.

5.2 Classification of coprecipitation

Mainly, there are four types of coprecipitation:

1. surface adsorption;
2. mixed−crystal formation;
3. occulation; and
4. mechanical entrapment.

Out of these four, surface adsorption and mixed-crystal formation are equilibrium processes, while occulation and mechanical entrapment are due to the kinetics of crystal growth.

1. *Surface adsorption*: It is a common method of coprecipitation. Here, a significant contamination of precipitates occurs with large specific surface areas (coagulated colloids). Coagulation of a colloid does not decrease the amount of adsorption significantly. Therefore, the overall effect of surface adsorption is carrying down of an otherwise soluble compound as a surface contaminant.
2. *Mixed−crystal formation*: In this type of coprecipitation, one of the ions in the crystal lattice of a solid is replaced by an ion of another element. The extent of mixed-crystal contamination obeys the law of mass action and increases as the ratio of contaminant to analyte concentration increases.
3. *Occulation entrapment*: When a crystal is growing rapidly during precipitation formation, foreign ions in the counter ion layer may become trapped or occluded within the growing crystal. Occlusion is a type of coprecipitation, in which a compound is trapped within a pocket formed during rapid crystal growth.
4. *Mechanical entrapment*: Mechanical entrapment occurs when crystals lie close together during growth. Occlusion and mechanical entrapment are confined to crystalline precipitate. Both are at a minimum when the rate of precipitation formation is low.

5.3 Synthesis of quantum dots

5.3.1 Metal oxide quantum dots

Jbara et al. (2017) used the coprecipitation technique to synthesize gamma-Al_2O_3 (γ-Al_2O_3) nanopowders. As-prepared alumina nanopowders have particle diameter from 6−24 nm, as evident from XRD. Almost all particles were spherical in shape, but some particles acquired more regular hexagonal shapes on increasing annealing temperature, maybe due to agglomeration of nanoparticles. Zhao et al. (2018) synthesized graphene oxide/Mg-doped ZnO/tungsten oxide QDs composites via the coprecipitation method. It was reported that this composite exhibited photocatalytic activity that was almost 6.58 times higher than that of the composite without tungsten oxide. Transition-metal (Cr, Mn, Fe, Co, and Ni)- doped SnO_2 QDs were synthesized by Sharma et al. (2020) using the coprecipitation method. These QDs were capped by polyvinyl pyrrolidone. The size of as-synthesized particles was found to be 2.5 nm.

Sarkar et al. (2020) synthesized carbon-quantum-dot-embedded iron oxide nanoparticles (CQD@Fe_3O_4 NPs). The Fe_3O_4 NPs and CQD@Fe_3O_4 NPs were synthesized by the wet chemical coprecipitation method. A nearly spherical structure with an average size of about 7 nm was obtained for Fe_3O_4, while CQDs were around 2 nm in size in CQD@Fe_3O_4 NPs as evident from HRTEM. Hernandez et al. (2020) synthesized Fe_3O_4 MNPs modified with three different amino acids (AA): L-tryptophan, l-phenylalanine, and l-tyrosine via the coprecipitation method without using a spacer agent. This nanocomposite has high stability and good dispersibility in water and can be used in various biomedical and environmental applications.

Ragupathi et al. (2021) used the coprecipitation method for the synthesis of ZnO QDs and MPS organosilane modified ZnO@MPS. It was observed that as-prepared ZnO QDs and ZnO@MPS exhibited size reduction, better dispersion, and lower aggregation as compared to ZnO QDs. They also studied the antibacterial activities of these against *Staphylococcus aureus*, *Escherichia coli*, *Klebsiella pneumoniae*, and *Enterococcus faecalis*, and observed that ZnO@MPS QDs exhibited significant zones of inhibition, which may be due to smaller particle size.

Masmali et al. (2022) used ZnO and $ZnFe_2O_4$ as working electrodes in the QDs sensitized solar cells (QDSSCs). It was observed that $ZnFe_2O_4$ can enhance light absorption and its bandgap is 2.12 eV. They synthesized ZnO and $ZnFe_2O_4$ nanoparticles via coprecipitation. As-prepared mesoporous thin films of ZnO and $ZnFe_2O_4$ were sensitized with Ag_2S and CdS and then used as photoanodes in QDSSCs. It was revealed that Ag_2S sensitized photoanodes exhibited higher charge carrier resistance, shorter electron lifetime, and low fill factor as compared to CdS-based photoanodes.

Niu et al. (2022) prepared Cu_2O/SnO_2 QDs/ZnO arrays pn junction via a continuous sputtering−hydrothermal−coprecipitation method. It was reported that the as-prepared transparent photovoltaic device exhibited high transmittance ($\sim$80%) and photovoltaic enhancement ($\sim 1.5 \times 10^{-3}$ folds) (PCE = 1.03%), It was attributed to SnO_2 QDs, which have appropriate Fermi level increasing the charge carrier concentration/mobility, but high transparency was balanced.

5.3.2 Metal sulfides

Cadmium sulfide QDs were synthesized by Mishra et al. (2011) via a coprecipitation method. X-ray diffraction revealed that cubical zinc blend structure was present in CdS nanoparticles. It was found that CdS QDs are of 2−5 nm in size as evident from TEM data. A blue shift of 0.48 eV UV−V is absorption data was observed that compared to bulk CdS. Rahdar et al. (2012) synthesized ZnS:Cr nanoparticles by the coprecipitation method. It was possible to prepare different sized ZnS:Cr nanoparticles using this simple chemical method using different molar concentration of doping agent. They observed

that mean crystallite size of these particles ranged between 1.5 and 2.45 nm, which depended on the molar concentration of the doping agent.

Giribabu et al. (2012) synthesized $Cd_1 - _xMg_xS$ nanoparticles by the coprecipitation method. It was revealed that the structural phase transition is present from cubic to hexagonal and there is an increase in the average size of the nanoparticles (range 1.4−2.8 nm) on increasing content of Mg. The ZnS QDs along with their Be^{2+} and Mg^{2+} derivatives ($Zn_{1-x}Be_xS$ and $Zn_{1-x}Mg_xS$) were prepared by Iqbal and Iqbal (2013) via the coprecipitation route. The synthesized QDs are stable for a period of up to 7 months. It was found that particles were having cubic closed packed structure with an average particle size of 2−3 nm. It was proposed that these QDs may find applications in light-emitting diodes, sensors, coatings, and phosphor.

Zinc sulfide QDs (pure and doped with Fe^{3+}) were prepared by Shamsipur and Rajabi (2014) via a chemical coprecipitation method. The effect of different operational parameters on the decolorization of methyl violet, such as pH, initial dye concentration, dopant content, dosage of nanophotocatalyst, and UV irradiation time, were studied. It was observed that doping of ZnS QDs with Fe^{3+} enhanced its efficiency, as evident from the increased rate of dye removal. Rofouei et al. (2015) synthesized ultrasmall glycine dithiocarbamate (GDTC)-functionalized manganese doped ZnS (GDTC-Mn:ZnS) QDs via the coprecipitation method. It was then used as a sensor for cerous ions in concentration range of 2.0×10^{-6} to 3.2×10^{-5} mol L^{-1}, with a detection limit of 2.29×10^{-7} mol.L^{-1}. Tyagi et al. (2014) synthesized size tunable cadmium sulfide QDs via wet chemical coprecipitation method at pH 9 and 10.5 and different temperatures, that is, 35°C, 50°C, and 65°C. They used cadmium chloride and thiourea as precursors, while ammonium hydroxide was used as a precipitating agent and mercaptoethanol as a surfactant.

Elavarthi et al. (2016) synthesized undoped and Cr-doped CdS nanoparticles via the coprecipitation method. The average particle size was found to be 4−5 nm. Yadav et al. (2016) prepared copper-doped $Cd_1 - _xZn_xS$ QDs using a chemical coprecipitation method. The Cu-doped QDs have an hexagonal structure with average crystallite size in the range 2−12 nm. Sakthivel and Muthukumaran (2016) synthesized $Zn_{0.98} - _xCu_xMn_{0.02}S$ QDs (Cu and Mn codoped) with different copper concentrations (where $x = 0$, 0.02, 0.04) through a coprecipitation technique. The $Zn_{0.98}Mn_{0.02}S$ was in the cubic phase, which gives a mixture of cubic as well as hexagonal phases on Cu-doping. The bandgap was found to range between 3.3 and 3.93 eV on Mn and Cu codoping. These codoped zinc sulfide QDs can find use in optoelectronic devices. Youngjin and Jongsung (2016) prepared silica nanospheres containing magnetic particles. Then CdSe/ZnS QDs were functionalized and incorporated into these silica nanospheres. It was reported that fluorescence from as-prepared QDs was quenched and this magnetic silica−QD−DNA probe can be used to detect a particular DNA.

The $Zn_{0.98-x}Ni_xMn_{0.02}S$ QDs were synthesized by Sakthivel and Muthukumaran (2017) via a coprecipitation method. They reported that the average crystallite size was 1.3−1.8 nm. A red shift was observed in absorption and intensity was increased on increasing concentration of Ni. The bandgap of as-prepared samples ranged between 3.56 and 3.93 eV. As-prepared material can be used in optoelectronic devices and also as a buffer material in solar cells. Zinc sulfide QDs and transition metal-doped ZnS nanocrystals were prepared by Jabeen et al. (2017) by a coprecipitation method.

Zhang et al. (2017) synthesized hybrid rGO/$CoFe_2O_4$/ZnS nanocomposites via a combination of hydrothermal and coprecipitation route. It was reported that ZnS QDs and $CoFe_2O_4$ nanoparticles had an average diameter of 3−8 and 10−20 nm, respectively, and these were anchored on graphene sheets. It was proposed that the as-prepared nanocomposites have a potential for use in stealth camouflage techniques.

Kaur et al. (2017) synthesized ZnS QDs via a coprecipitation technique. They used sodium dodecyl sulfate as a stabilizing agent. They used these ZnS QDs as a photocatalyst for degrading brilliant green under sunlight. They could achieve about 88% degradation of brilliant green.

Desai et al. (2018) synthesized PVP-coated ZnS nanoparticles doped with transition metals by a wet chemical coprecipitation method. The average particle size of these PVP−ZnS nanoparticles was around 2.6 nm. Cobalt-alloyed ZnS QDs were synthesized by Horoz (2018) via a coprecipitation method. It was found that Cobalt-alloyed ZnS QDs had a cubic structure with size 2.71 nm, which is little bit smaller than the size of pure ZnS QDs (2.72 nm). It was revealed that there was a blueshift compared to pure ZnS QDs.

Ashokkumar and Boopathyraja (2018) prepared $Zn_{1-x}Mg_xS$ QDs by a coprecipitation method. It was observed that Mg dopant did not affect the cubic blende structure of ZnS QDs. The average crystallite size increases from ∼1.7−2 nm at initial doping of Mg (20%). It was revealed that the bandgap of the QD was decreased at initial doping of Mg due to the quantum confinement effect but at a higher doping level the bandgap was found to be increased. Sakthivel and Muthukumaran (2018) prepared Cobalt-alloyed (0%−4%) $Zn_{0.98}Mn_{0.02}S$ QDs by a coprecipitation method. It was found that the average crystallite size of the particles was around 3 nm. It was reported that average crystallite size of as-prepared QDs was ∼3 nm. Rafiq et al. (2019) prepared ZnS QDs via the coprecipitation method. They used 2-mercaptoethanol as a capping agent. An average crystallite size of ZnS QDs was found to be 4.2 nm. These uncapped ZnS QD were used for photocatalytic degradation of methylene blue.

Mansur et al. (2019) prepared fluorescent ternary and quaternary QD nanostructures based on $AgInS_2$ core and ZnS shell. These QDs were stabilized with carboxymethyl cellulose polymer ligand. They prepared colloidal $AgInS_2$ QDs by a coprecipitation process. Sizes of $AgInS_2$ and $AgInS_2$/ZnS

QDs range were in the of 8.5 ± 2.4 nm and 3.2 ± 1.1 nm under acidic or alkaline media, respectively. Yu et al. (2019) used chitosan (CS) as a biomacromolecule model and surface ligands to synthesize CuS QDs via the coprecipitation method. These CuS-CS QDs were conjugated with folic acid (FA). It was reported that the size of CuS-CS-FA QDs was around 4 nm. It was revealed that CuS-CS-FA QD can be effectively targeted and accumulated in the tumor reaching the peak dose in 1 h, when CuS-CS-FA QDs dispersion was injected (intravenously) into the tumor-bearing mice.

Devadoss et al. (2019) synthesized Zn, Cr codoped CdS QDs via a coprecipitation method. They carried out this synthesis at room temperature without using any capping agent. It was observed that samples have cubic structures, which remained unaffected by the presence of Cr, but the crystallite size was found to be reduced in the order of ~2 nm. The presence of Cr was considered responsible for a blueshift. The ZnS QD (Mg, Mn codoped) were synthesized by Sakthivel et al. (2019) using a coprecipitation method. The particle size in the range of ~2 nm. A redshift was observed with an increase in Mg doping concentration, which will reduce the bandgap.

Meng et al. (2020) synthesized cadmium sulfide QDs through the coprecipitation method. It was observed that there was a blue shift of 0.48 eV compared to that of bulk CdS. The particles size of CdS QDs was found to be 3.665 nm. Abha et al. (2020) synthesized Mn:ZnS/BSA QDs by a chemical coprecipitation method. It was reported that Mn:ZnS/BSA QDs can serve as an effective sensor platform for dopamine. The luminescence of Mn:ZnS/BSA QDs was found to decrease linearly with increasing concentration of dopamine in the range from 6.6 to 50.6 nM.

Ibraheema et al. (2020) synthesized the ability to tune the paramagnetic effect of Co-doped CdSQDs, which were prepared by a coprecipitation route with varied Co^{2+} concentrations. It was reported that the highest possible paramagnetic effect in the CdS semiconducting matrix exhibited bandgap in the visible range (2.76 eV). Sharma et al. (2021) prepared polyvinlypyrrolidone (PVP) capped CuS QDs ($Cu_1 - _xTM_xS$) via the chemical coprecipitation route. They also doped these QDs with some magnetic transition metals (TM = Fe, Cr and Co).

5.3.3 Metal selenide quantum dots

CdSe QDs were synthesized by Verma et al. (2016) via the chemical coprecipitation method. It was revealed that the cubic phase of the crystalline CdSe transformed to stable hexagonal phase at 317°C and the average particle size of these QDs ranged between (3−5 nm).

Lewis et al. (2016) synthesized semiconducting heterostructures composed of cadmium selenide QDs attached onto the surfaces of Eu-doped and Pr-doped $CaTiO_3$. It was observed that 2.7-nm diameter ligand-functionalized CdSe QDs were attached to $CaTiO_3$-based spherical assemblies. Ag_2Se QDs were prepared

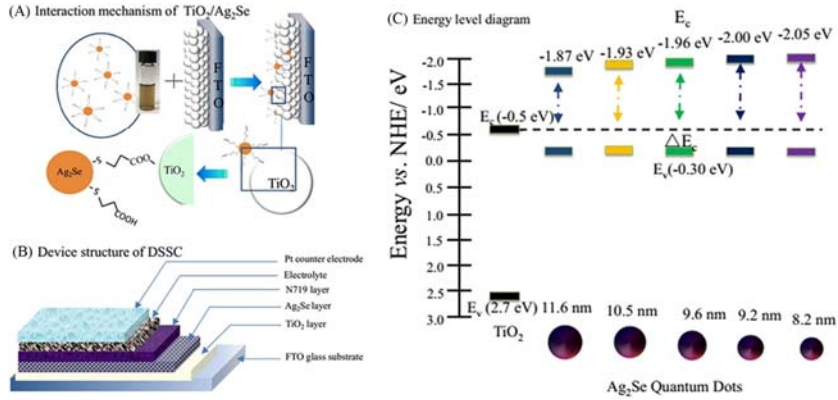

FIGURE 5.2 Dye sensitized solar cells using Ag_2Se quantum dots. *Adapted from Zhang, Z., Yang, Y., Gao, J., Xiao, S., Zhou, C., Pan, D., et al., 2018. Highly efficient Ag_2Se quantum dots blocking layer for solid-state dye-sensitized solar cells: size effects on device performances. Mater. Today Energy 7, 27–36 with permission.*

by Zhang et al. (2018) using a coprecipitation method and then used in solid-state dye-sensitized solar cells (Fig. 5.2). It was revealed that monodispersed Ag_2Se QDs had average sizes ranging between 8.2–11.6 nm. The highest power conversion efficiency of Ag_2Se QDs (9.6 nm)-based solar cells was reported to be 5.89%.

5.3.4 Carbon-based

A graphene QDs and CoNiAl-layered double-hydroxide composite was synthesized by Samuei et al. (2017) through a coprecipitation method. They fabricated a modified carbon paste electrode containing this nanocomposite that was used as a nonenzymatic sensor for determination of glucose. It was reported that the as-prepared sensor offered high reproducibility, fast response time, good electrocatalytic properties, and stability. It was revealed that the as-constructed sensor exhibited sensitivity in a wide range of concentrations of glucose (0.01–14.0 mM) with a limit of detection of 6 μM.

It was revealed that the $NiFe_2O_4$/GQD sample exhibited the highest catalytic activity and completed the reduction in a minute to afford p-aminophenol. The catalysts displayed good stability, can be recovered using a magnetic field, and can be recycled for six experiments with a conversion percentage of >95%.

Sharma et al. (2018) prepared iron nanoparticles, Fe@carbon QDs, and Fe/Ag@carbon QDs nanocomposites by a simple coprecipitation/reduction method. The photocatalytic activity of Fe, Fe@CQDs, and Fe/Ag@CQDs was evaluated for the removal of fast green dye. The catalytic nature of as-synthesized materials was also investigated for the esterification of acetic

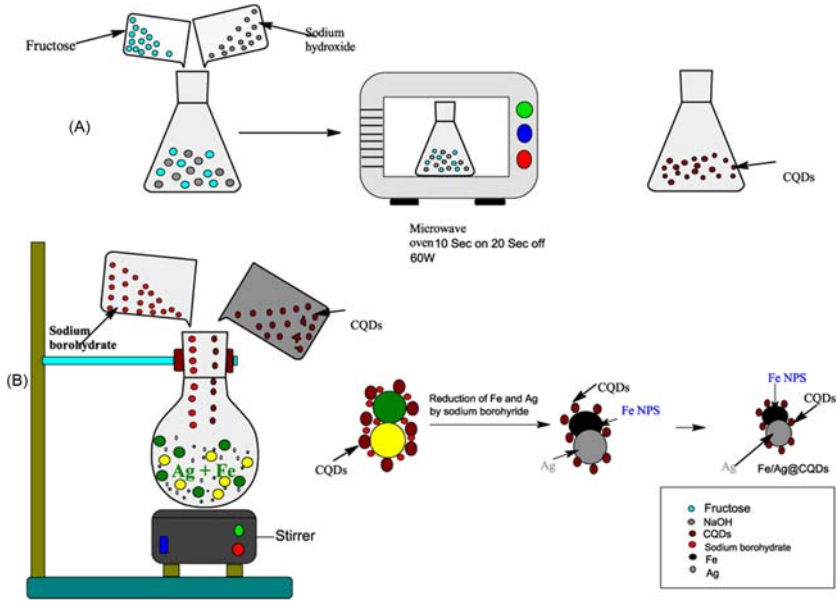

FIGURE 5.3 Use of iron-based quantum dots and nanocomposites for degradation, oxidation, and esterification. *Adapted from Sharma, G., Kumar, A., Naushad, M., Kumar, A., Ala'a, H., Dhiman, P., et al., 2018. Photoremediation of toxic dye from aqueous environment using monometallic and bimetallic quantum dots based nanocomposites. J. Clean. Product. 172, 2919–2930 with permission.*

acid and oxidation of benzyl alcohol (Fig. 5.3). It was reported that oxidation of benzyl alcohol with H_2O_2 with Fe NPs gave the highest yield (87%), while esterification of acetic acid with different alcohols (ethyl, isopropyl and butyl) showed that butyl alcohol gave a maximum yield of 82%, 80%, and 84% with Fe NPs, Fe@CQDs, and Fe/Ag@CQDs, respectively.

Lin et al. (2019) anchored nitrogen-doped carbon QDs (NCDs) and graphitic carbon nitride QDs (CNQDs) on the surface of $BiVO_4$ microspheres to fabricate $BiVO_4$/CNQDs/NCDs composite via the coprecipitation method. It was reported that as-synthesized $BiVO_4$/CNQDs/NCDs exhibited an excellent photocatalytic activity for the degradation of rhodamine B as well as tetracycline under UV illumination as compared to pure $BiVO_4$, $BiVO_4$/CNQDs, and $BiVO_4$/NCDs (Fig. 5.4).

5.3.5 Graphene-based

Wu et al. (2014) prepared composites of GQDs and Fe_3O_4 nanoparticles (GQDs/Fe_3O_4) via a coprecipitation method. It was reported that as-prepared GQDs/Fe_3O_4 composites exhibited a better stability and reusability as compared to natural peroxidases. This GQDs/Fe_3O_4 composite was also used as

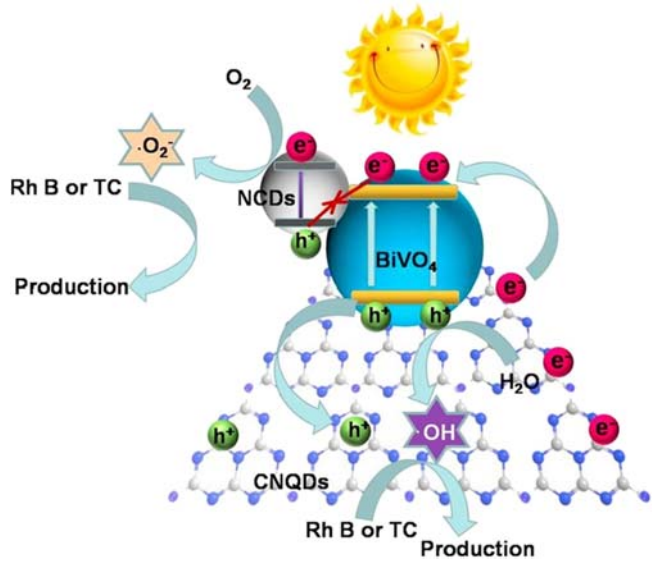

FIGURE 5.4 Use of $BiVO_4$/CNQDs/NCDs composite for degradation of rhodamine B and tetracycline. *Adapted from Lin, X., Liu, C., Wang, J., Yang, S., Shi, J., Hong, Y., 2019. Graphitic carbon nitride quantum dots and nitrogen-doped carbon quantum dots co-decorated with $BiVO_4$ microspheres: a ternary heterostructure photocatalyst for water purification. Sep. Purif. Technol. 226, 117–127, 2019, with permission.*

a catalyst for the removal of phenolic compounds (nine in all). It showed better or sometimes comparable removal efficiencies for phenolic compounds as compared to native horseradish peroxidase.

Ramachandran et al. (2018) developed a method for the synthesis of graphene QDs/cobalt ferrite nanocomposite. They synthesized graphene QDs using citric acid, which was followed by coprecipitation of cobalt ferrite nanoparticles on these graphene QDs. It was reported that as-synthesized nanocomposite exhibited good superparamagnetic properties and fluorescence, which are useful in biomedical applications.

Naghshbandi et al. (2018) synthesized graphene QDs and metal ferrites (MFe_2O_4; where, M = Ni, Co) nanocomposites via a coprecipitation method. They used these nanocomposites as catalysts in the reduction of p-nitrophenol. It was reported that the $NiFe_2O_4$/GQD composite exhibited the optimum catalytic activity and the reduction of p-nitrophenol was completed within 1 min. It was revealed that these catalysts can be separated by a magnetic field using an external magnet. They also show good stability and these can be reused for six cycles retaining activity of around 95%.

The catalytic activity of as-prepared nanocomposites and metal ferities for the reduction of p-nitrophenol was found to follow the order:

$$NiFe_2O_4/GQD > CoFe_2O_4/GQD > NiFe_2O_4 > CoFe_2O_4.$$

Zhao et al. (2021) synthesized graphitic carbon nitride QDs by incorporating the unique organic functional group of barbituric acid into the framework of the carbon nitride structure by supramolecular preorganization. Then three CNQDs were introduced onto basic zinc carbonate (BZC) surface via the coprecipitation method. It was reported that the as-prepared CNQDs/BZC composite exhibited a higher degradation efficiency of tetracycline, which was about 2.4 times higher than that of ZnO. It was revealed that $^{\bullet}O_2^-$ and $^{\bullet}OH$ radicals played major roles in degradation due to the suitable bandgap.

Hsieh et al. (2022) introduced N-GQDs in rGO, which efficiently facilitates the photocatalytic activity of composite. It was reported that an ultrahigh removal ratio ($\sim$100%) and improved rate constant could be achieved with this GQD/ZnO catalyst (1.74 more as compared to pristine ZnO). It was revealed that the presence of N-GQDs increased the absorption in the visible light region and photoinduced charge carrier, and as a result photocatalytic activity was increased. It was observed that as-prepared GQD/ZnO composite can be used as a photocatalyst for degrading metronidazole in the presence of UV−light irradiation.

5.3.6 Others

Lan et al. (2014) prepared hybrid nanocomposites of Zn-Cr layered double hydroxide (ZnCr-LDH) and graphene through a coprecipitation method. It was reported that ZnCr-LDH nanoplatelets had a diameter $\sim$6 nm and these were well dispersed on the graphene surface. These hybrid ZnCr-LDH/graphene nanocomposites were used for the photocatalytic degradation of rhodamine B, which has a higher rate as compared to ZnCr-LDH.

Bahadori et al. (2021) used a coprecipitation-assisted solvothermal method to synthesize covalent organic frameworks (COFs) QDs, which were modified with biochar. It was found that as-synthesized COFs QD nanostructures have an average size of about 3.68 nm. These nanocomposite structures were then utilized for decolorizing methyl blue, methyl orange, and methyl red.

5.4 Conclusion

Various QDs (metals, metal oxides, metal sulfides, carbon, and graphene-based materials) can be synthesized successfully using the coprecipitation approach. It is an eco-friendly and relatively low-cost approach to synthesize nanomaterials. It can also be used to prepare larger amounts of QDs on an industrial scale. As-synthesized QDs have great potential for application in varied fields of interest such as bioimaging, sensors, solar cells, water splitting, and light-emitting diodes.

References

Abha, K., Sumithra, I.S., Suji, S., Anjana, R.R., Anjali Devi, J.S., Nebu, J., et al., 2020. Dopamine-induced photoluminescence quenching of bovine serum albumin−capped manganese-doped zinc sulphide quantum dots. Anal. Bioanal. Chem. 412, 5671−5681.

Ashokkumar, M., Boopathyraja, A., 2018. Structural and optical properties of Mg doped ZnS quantum dots and biological applications. Superlattices Microstruct. 113, 236−243.

Bahadori, A., Ranjbar, M., Asadipour, A., Kalantari-Khandani, S., 2021. Covalent organic frameworks (COFs) quantum dots as supramolecular cages modified with biochar as nanobio photocatalyst for degradation of organic dyes. J. Mater. Sci.: Mater. Electron. 32 (18), 23018−23029.

Desai, N. V., Shaikh, I. A., Rawal, K. G., Shah, D.V. 2018. Synthesis, structural and optical properties of PVP coated transition metal doped ZnS nanoparticles. AIP Conf. Proceed., 1953 (1), 030149.

Devadoss, I., Sakthivel, P., Muthukumaran, S., Sudhakar, N., 2019. Enhanced blue-light emission on $Cd_{0.9-x}Zn_{0.1}Cr_xS$ ($0 \leq x \leq 0.05$) quantum dots. Ceram. Int. 45 (3), 3833−3838.

Elavarthi, P., Kumar, A.A., Murali, G., Reddy, D.A., Gunasekhar, K.R., 2016. Room temperature ferromagnetism and white light emissive CdS: Cr nanoparticles synthesized by chemical coprecipitation method. J. Alloy Compd. 656, 510−517.

Giribabu, G., Murali, G., Reddy, D.A., Vijayalakshmi, R.P., Rao, M., 2012. Effect of Mg doping on the structural and optical properties of CdS nanoparticles synthesized by co-precipitation Method. J. Nano Electron. Phys. 4 (4). Available from: http://essuir.sumdu.edu.ua/handle/123456789/30285.

Hernandez, I.P., Velazquez, E.R., Meda, M.A., Galindo, J.T.E., Delgado, F.P., Guizar, A.T., et al., 2020. Magnetic nanocomposite with fluorescence enhancement effect based on amino acid coated-Fe_3O_4 functionalized with quantum dots. Mater. Chem. Phys. 25 (1). Available from: https://doi.org/10.1016/j.matchemphys.2020.123082.

Horoz, S., 2018. Synthesis of cobalt-alloyed ZnS quantum dots and investigation of their characteristics. Mater. Technol. 52 (5), 555−559.

Hsieh, M.L., Juang, R.S., Gandomi, Y.A., Fu, C.C., Hsieh, C.T., Liu, W.R., 2022. Synthesis and characterization of high-performance ZnO/graphene quantum dot composites for photocatalytic degradation of metronidazole. J. Taiwan. Inst. Chem. Eng. 131. Available from: https://doi.org/10.1016/j.jtice.2021.104180.

Ibraheema, F., Mahdy, M.A., Ortega, J.E., Rogero, C., Mahdy, I.A., El-Sayed, A., 2020. Tuning paramagnetic effect of Co-doped CdS diluted magnetic semiconductor quantum dots. J. Alloy Compd. 835. Available from: https://doi.org/10.1016/j.jallcom.2020.155196.

Iqbal, M.J., Iqbal, S., 2013. Synthesis of stable and highly luminescent beryllium and magnesium doped ZnS quantum dots suitable for design of photonic and sensor material. J. Lumin. 134, 739−746.

Jabeen, U., Adhikari, T., Shah, S.M., Pathak, D., Nunzi, J.M., 2017. Synthesis, characterization and photovoltaic performance of Mn-doped ZnS quantum dots-P3HT hybrid bulk heterojunction solar cells. Opt. Mater. 73, 754−762.

Jbara, A.S., Othaman, Z., Ati, A.A., Saeed, M.A., 2017. Characterization of γ-Al_2O_3 nanopowders synthesized by coprecipitation method. Mater. Chem. Phys. 188, 24−29.

Kaur, S., Sharma, S., Umar, A., Singh, S., Mehta, S.K., Kansal, S.K., 2017. Solar light driven enhanced photocatalytic degradation of brilliant green dye based on ZnS quantum dots. Superlattices Microstruct. 103, 365−375.

Lan, M., Fan, G., Yang, L., Li, F., 2014. Significantly enhanced visible-light-induced photocatalytic performance of hybrid Zn−Cr layered double hydroxide/graphene nanocomposite and the mechanism study. Ind. Eng. Chem. Res. 53 (33), 12943−12952.

Lewis, C.S., Liu, H., Han, J., Wang, L., Yue, S., Brennan, N.A., et al., 2016. Probing charge transfer in a novel class of luminescent perovskite-based heterostructures composed of quantum dots bound to RE-activated $CaTiO_3$ phosphors. Nanoscale 8 (4), 2129−2142.

Lin, X., Liu, C., Wang, J., Yang, S., Shi, J., Hong, Y., 2019. Graphitic carbon nitride quantum dots and nitrogen-doped carbon quantum dots co-decorated with $BiVO_4$ microspheres: a ternary heterostructure photocatalyst for water purification. Sep. Purif. Technol. 226, 117−127.

Mansur, A.A., Mansur, H.S., Tabare, C., Paiva, A., Capanema, N.S., 2019. Eco-friendly $AgInS_2$/ZnS quantum dot nanohybrids with tunable luminescent properties modulated by pH-sensitive biopolymer for potential solar energy harvesting applications. J. Mater. Sci. Mater. Electron. 30 (18), 16702−16717.

Masmali, N.A., Osman, Z., Arof, A.K., 2022. Comparison between silver sulfide and cadmium sulfide quantum dots in ZnO and ZnO/$ZnFe_2O_4$ photoanode of quantum dots sensitized solar cells. Ionics 28, 2007−2020.

Meng, X., Zhang, C., Dong, C., Sun, W., Ji, D., Ding, Y., 2020. Carbon quantum dots assisted strategy to synthesize Co@NC for boosting photocatalytic hydrogen evolution performance of CdS. Chem. Eng. J. 389. Available from: https://doi.org/10.1016/j.cej.2020.124432.

Mishra, S.K., Srivastava, R.K., Prakash, S.G., Yadav, R.S., Panday, A.C., 2011. Structural, photoconductivity and photoluminescence characterization of cadmium sulfide quantum dots prepared by a coprecipitation method. Electron. Mater. Lett. 7 (1), 31−38.

Naghshbandi, Z., Arsalani, N., Zakerhamidi, M.S., Geckeler, K.E., 2018. A novel synthesis of magnetic and photoluminescent graphene quantum dots/MFe_2O_4 (M = Ni, Co) nanocomposites for catalytic application. Appl. Surf. Sci. 443, 484−491.

Niu, J., Pan, J., Fu, W., Xiao, G., Fu, Y., Cao, J., et al., 2022. The photovoltaic enhancement of Cu_2O/SnO_2 quantum dots/ZnO arrays transparent pn junction device via carrier injection and potential transition of SnO_2 QDs. J. Materi. Sci.: Materi. Electron. 33 (9), 7300−7311.

Rafiq, A., Imran, M., Ikram, M., Naz, M., Aqeel, M., Majeed, H., et al., 2019. Photocatalytic and catalytic degradation of organic dye by uncapped and capped ZnS quantum dots. Mater. Res. Express 6 (5). Available from: https://doi.org/10.1088/2053-1591/aaff8e.

Ragupathi, H., Choe, Y., Arockiaraj, A., 2021. Preferential killing of bacterial cells by surface-modified organosilane-treated ZnO quantum dots synthesized through a coprecipitation method. N. J. Chem. 45 (29), 12986−12995.

Rahdar, A., Asnaasahri Eivari1, H., Sarhaddi, R., 2012. Study of structural and optical properties of ZnS:Cr nanoparticles synthesized by coprecipitation method. Indian J. Sci. Technol. 5 (1), 1855−1858.

Ramachandran, S., Sathishkumar, M., Kothurkar, N.K., Senthilkumar, R. 2018. Synthesis and characterization of graphene quantum dots/cobalt ferrite nanocomposite. In IOP Conf. Ser.: Mater. Sci. Eng. 310 (1). Available from: https://doi.org/10.1088/1757-899X/310/1/012139.

Rofouei, M.K., Tajarrod, N., Masteri-Farahani, M., Zadmard, R., 2015. A new fluorescence sensor for Cerium (III) ion using glycine dithiocarbamate capped manganese doped ZnS quantum dots. J. Fluoresc. 25 (6), 1855−1866.

Sakthivel, P., Muthukumaran, S., 2016. Crystallographic, structural and band gap tailoring of $Zn_{0.98}Mn_{0.02}S$ quantum dots Co-doped with Cu by co-precipitation method. J. Inorg. Organometal. Poly. Mater. 26 (3), 563−571.

Sakthivel, P., Muthukumaran, S., 2017. Investigation of Ni influence on structural and band gap tuning of $Zn_{0.98}Mn_{0.02}S$ quantum dots by coprecipitation method. J. Mater. Sci.: Mater. Electron. 28 (11), 8309–8315.

Sakthivel, P., Muthukumaran, S., 2018. Influence of Co^{2+} on electrical and optical behavior of Mn^{2+}–doped ZnS quantum dots. Opt. Laser Technol. 103, 109–117.

Sakthivel, P., Venkatesan, G.P., Subramaniam, K., Muthukrishnan, P., 2019. Structural, optical, photoluminescence and electrochemical behaviors of Mg, Mn dual-doped ZnS quantum dots. J. Mater. Sci.: Mater. Electron. 30 (13), 11984–11993.

Samuei, S., Fakkar, J., Rezvani, Z., Shomali, A., Habibi, B., 2017. Synthesis and characterization of graphene quantum dots/CoNiAl-layered double-hydroxide nanocomposite: application as a glucose sensor. Anal. Biochem. 521, 31–39.

Sarkar, T., Dhiman, T.K., Sajwan, R.K., Sri, S., Solanki, P.R., 2020. Studies on carbon-quantum-dot-embedded iron oxide nanoparticles and their electrochemical response. Nanotechnology 31 (35). Available from: https://doi.org/10.1088/1361-6528/ab925e.

Shamsipur, M., Rajabi, H.R., 2014. Study of photocatalytic activity of ZnS quantum dots as efficient nanoparticles for removal of methyl violet: effect of ferric ion doping. Spectrochim. Acta A Mol. Biomol. Spectrosc. 122, 260–267.

Sharma, G., Kumar, A., Naushad, M., Kumar, A., Ala'a, H., Dhiman, P., et al., 2018. Photoremediation of toxic dye from aqueous environment using monometallic and bimetallic quantum dots based nanocomposites. J. Clean. Product. 172, 2919–2930.

Sharma, L.K., Choubey, R.K., Mukherjee, S., 2020. Spin-flop in transition-metal-doped SnO_2 quantum dots. Mater. Chem. Phys. 254. Available from: https://doi.org/10.1016/j.matchemphys.2020.123537.

Sharma, L.K., Kar, M., Choubey, R.K., Mukherjee, S., 2021. Low field magnetic interactions in the transition metals doped CuS quantum dots. Chem. Phys. Lett. 780. Available from: https://doi.org/10.1016/j.cplett.2021.138902.

Tyagi, C., Sharma, A., Kurchania, R., 2014. Synthesis of CdS quantum dots using wet chemical coprecipitation method. J. Non-Oxide Glasses 6 (2), 23–26.

Verma, M., Patidar, D., Sharma, K.B., Saxena, N.S., 2016. Phase transformations and thermal stability of CdSe quantum dots: cubic to hexagonal. J. Inorg. Organometal. Poly. Mater. 26 (1), 75–80.

Wu, X., Zhang, Y., Han, T., Wu, H., Guo, S., Zhang, J., 2014. Composite of graphene quantum dots and Fe_3O_4 nanoparticles: peroxidase activity and application in phenolic compound removal. RSC Adv. 4, 3299–3305.

Yadav, I., Ahlawat, D.S., Ahlawat, R., 2016. Cu-doped $Cd_{1-x}Zn_xS$ alloy: synthesis and structural investigations. Appl. Phys. A 122 (3). Available from: https://doi.org/10.1007/s00339-016-9745-z.

Youngjin, D., Jongsung, K., 2016. The preparation of magnetic silica nanospheres and incorporation of CdSe/ZnS quantum dots-DNA Probe. J. Nanosci. Nanotechnol. 16 (3), 2488–2491.

Yu, W., Yu, N., Wang, Z., Li, X., Song, C., Jiang, R., et al., 2019. Chitosan-mediated green synthesis and folic-acid modification of CuS quantum dots for photoacoustic imaging guided photothermal therapy of tumor. J. Colloid Interface Sci. 555, 480–488.

Zhang, N., Huang, Y., Zong, M., Ding, X., Li, S., Wang, M., 2017. Synthesis of ZnS quantum dots and $CoFe_2O_4$ nanoparticles co-loaded with graphene nanosheets as an efficient broad band EM wave absorber. Chem. Eng. J. 308, 214–221.

Zhang, Z., Yang, Y., Gao, J., Xiao, S., Zhou, C., Pan, D., et al., 2018. Highly efficient Ag_2Se quantum dots blocking layer for solid-state dye-sensitized solar cells: size effects on device performances. Mater. Today Energy 7, 27–36.

Zhao, H., Fang, Q., Chen, C., Chao, Z., Tsang, Y., Wu, Y., 2018. WO_3 quantum dots decorated GO/Mg-doped ZnO composites for enhanced photocatalytic activity under nature sunlight. Appl. Organomet. Chem. 32 (9). Available from: https://doi.org/10.1002/aoc.4449.

Zhao, P., Jin, B., Zhang, Q., Peng, R., 2021. Fabrication and photocatalytic activity of graphitic-C_3N_4 quantum dots-decorated basic zinc carbonate prepared by a co-precipitation method. Phys. Chem. Chem. Phys. 23 (36), 20329–20339.

This page intentionally left blank

Chapter 6

Biogenic synthesis of quantum dots

Meghavi Gupta[1], **Inderjeet Yadav**[2] **and Abhilasha Jain**[3]
[1]*Department of Chemistry, PAHER University, Udaipur, Rajasthan, India,* [2]*Department of Applied Sciences, University of Technology and Applied Sciences, Alkhuwair, Muscat, Sultanate of Oman,* [3]*Department of Chemistry, St. Xavier's College, Mumbai, Maharashtra, India*

6.1 Introduction

The synthesis of designer solid state materials by living organisms is an emerging field of research. As there is a growing trend in biomedical applications of quantum dots, biosynthesized nanomaterials are attracting the attention of researchers these days due to their biocompatible, low-energy consumption, economic, and tunable characteristics.

Zero-dimensional semiconductor quantum dots (<10 nm) have received great attention because of their potential use in biomedical applications (diagnosis and therapy), where larger nanoparticles (>10 nm) were not found to be suitable.

Biosynthesis of quantum dots is an alternate green method for the production of quantum dots with superior properties, such as tunable size, emission spectra, and a longer fluorescence lifetime. Biosynthesis of quantum dots offers other several advantages over other existing conventional chemical synthesis routes, such as low cost, eco-friendliness, and no need for any further modification of the products. Controlled monodispersity, chemical compositions, desired morphologies, and particle size could be achieved with the biosynthesis method.

However, still manipulation and control of biosynthesis of QDs remain slightly difficult because of the lack of knowledge of the mechanisms necessary for the biosynthesis or the effect of the biosynthesizing organisms is still insufficient.

Synthesis of QDs can be carried out using plants (*Avena sativa*, *Azadirachta indica*, *Alovera*, *Mangifera indica*, etc.) fungi (*Fusarium oxysporum*, *Phanerochaete chrysosporium*, *Pleurotus ostreatus*, etc.), bacteria (*Escherichia coli, Pseudomonas, Staphylococcus aureus, Acidithiobacillus*

Quantum Dots. DOI: https://doi.org/10.1016/B978-0-12-824153-0.00006-9
© 2023 Elsevier Inc. All rights reserved.

genus, etc.), and enzymes. There are many more plants, bacteria, enzymes, fungi, etc., which are still unexplored although they have a great potential for preparing quantum dots.

6.1.1 Advantages

1. It is a green chemical route.
2. It is relatively less time consuming.
3. Ambient conditions are required, and not harsh conditions.
4. It is based on natural materials such as plant extracts, enzymes, bacteria, fungi, etc.

6.1.2 Disadvantages

1. It is based on plants, which means a limited source.
2. It may cause additional problems, particularly when bacteria and fungi are used, unless carried out under control.
3. Difficult to control the size of nanocrystal.

6.2 Plants

Wang et al. (2005) prepared ZnS semiconductor nanoparticles in situ in chitosan film. It was revealed that the chitosan template was monodispersed and passivated. The average size was found to be 3.4 nm. Rosano-Ortega et al. (2006) synthesized Mn nanoparticles in the range of 1−4 nm using water hyacinth. It was reported that the as-obtained particles have a well controlled size. It was also revealed that small clusters in the range of 1−2 nm were generated, when the pH was kept at 5. It was also found that smallest aggregates with polyhedron shapes were stable in nature.

Wang et al. (2009) synthesized water-soluble biocompatible and monodispersed CdS, ZnS, and CdSe quantum dots using natural chitosan derivatives as stabilizers. It was revealed that nanoparticles with average size of 3−5 nm were obtained. It was found that the photoluminescence of QDs was enhanced and surface defects were passivated. It was found that the size of particles and photoluminescence intensity can be controlled by varying the concentration of precursor ions and stabilizer, refluxing the time and molar ratio of metal ions with sulfide. The resulting biopolymer/QDs composite can be potentially applied as a biosensor or fluorescence tags in biological systems. An efficient and green method for plant-based biosynthesis of CdS quantum dots has been reported by Borovaya et al. (2014). They used hairy root culture of *Linaria maroccana* L. for this purpose. The *Linaria* root extract was incubated with sodium sulfide and cadmium sulfate to give stable luminescent CdS nanocrystals. It was revealed that as-obtained QDs were spherical in shape with a size ranging from 5 to 7 nm. The wurtzite

crystalline structure of as-synthesized CdSQDs was confirmed by electron diffraction.

Bhattacharjee and Ahmaruzzaman (2015) synthesized SnO_2 QDs by a green biological route using sugar cane juice. It was predicated that biomolecules present in sugar cane juice act as both capping agent and complexing agent. It was observed that spherical SnO_2 quantum dots were obtained with particle size ranging between ~2.5 and 4.5 nm. It was revealed that a blue-shift in the bandgap energy was there with decreasing particle size. As-synthesized SnO_2 QDs were then used for photocatalytic degradation of methylene blue and rose Bengal under direct sunlight. The catalytic activity of these biosynthesized QDs was also evaluated for reduction of p-nitrophenol to p-aminophenol in the presence of sodium borohydride in water. It was revealed that 99.5% of p-nitrophenol was reduced in these conditions within 1 h.

Ouyang and Sun (2016) used wheat endosperm cells in the biosynthesis of Ag_2S QDs. The delivered precursors of QDs into cultured wheat endosperm cells provided Ag_2S QDs in an aging process under the effect of endogenous glutathione in the cells. It was observed that these intracellularly synthesized near-infrared (NIR) fluorescent QDs were highly photostable and can be used for bioimaging. The biosynthesis of HgTe quantum dots has been reported by Green et al. (2016) in a living plant via a mutual antagonistic reaction. It was observed that when *Allium fistulosum* was exposed to mercury and tellurium salts, it afforded crystalline HgTe quantum dots (nonpassivated) under ambient conditions. These QDs exhibited emission in the near-infrared spectral region, which is the suitable range for finding applications in solar energy conversion and telecommunications.

The hairy roots of tomato (*Solanum lycopersicum*) and also fission yeast (*Schizosaccharomyces pombe*) were used by Al-Shalabi and Doran (2016) for biological synthesis of CdS quantum dots. It was observed that the growth rate with hairy roots was much slower compared with yeast, so they can be utilized for large-scale production. It was revealed that CdS crystallites obtained with yeast were smaller in size (2−6 nm diameters) as compared to QDs obtained using the roots (4−10 nm diameters). Borovaya et al. (2016) prepared water-soluble CdS quantum dots. They used bright yellow-2 (BY-2) cell suspension culture for this purpose, which acted as both stabilizing and capping agent. It was indicated that CdS QDs were crystalline and spherical in shape, ranging from 3 to 7 nm (diameter). It was revealed that as-synthesized CdS QDs were almost nontoxic in low concentrations using *Nicotiana tabacum* protoplasts as a model.

A simple and eco-friendly method for biosynthesis of luminescent ZnO quantum dots (well dispersed) was reported by Kaviya et al. (2017) using pomegranate peel extract. The use of this method avoided the use of strong commercial stabilizing agents, higher temperature, pH conditions, and inert atmosphere. It was revealed the as-obtained ZnO QDs had an average size

distribution around 4 nm. These ZnO QDs were water soluble and found to be stable for almost 1 year. As the emission from ZnO QDs was quenched on adding Cr^{3+} ions, the presence of these ions can be detected up to 2 nM in aqueous solution. Silva et al. (2017) biosynthesized Ag quantum particles using *Eichhornia crassipes* biomass. It was reported that the shape, size, structure, and composition of QDs were dependent on the amounts of hydrolyzable tannins in this plant. It was revealed that the amounts of hydrolyzable tannins were highest in the leaves of this plant. These QDs were found to be nearly spherical in shape; however, these were mostly polyhedral. It was observed that leaf biomass could produce quantum dots with sizes <10 nm and these were mostly AgO, and not Ag.

Begum and Ahmaruzzaman (2018) used microwave heating for the biosynthesis of SnO_2 quantum dots using *Parkia speciosa* Hassk pods extract. As-synthesized SnO_2 QDs were then used as a photocatalyst for the degradation of acid yellow 23 (a food dye) in aqueous solution in the presence of UV254 light. It was reported that biosynthesized SnO_2 QDs could degrade acid yellow 23 with photocatalytic efficiency (98%) in 24 min. It was claimed that these SnO_2 QDs can be reused for up to five consecutive cycles without losing efficiency and stability. Shivaji et al. (2018) developed a green biogenic synthesis for preparing CdS QDs using tea leaf extract (*Camellia sinensis*). It was found that the particle size of QDs was in the range of 2−5 nm. They also investigated the biological activity of these CdS QDs and it was observed that they exhibited cytotoxicity toward A549 cancer cells. This activity was also compared with a standard drug, cisplatin, with comparable results.

An efficient and green approach was reported by Alvand et al. (2019) for synthesis of cadmium telluride quantum dots. They used an aqueous extract of fruits of *Ficus johannis* plant. Two extraction methods were used for extraction: (1) microwave-assisted extraction (MWAE) and (2) ultrasonic-assisted extraction (USAE). These plant extracts were used as natural stabilizing precursors for synthesizing CdTe QDs. The average particle size of as-prepared QDs was calculated as 1.2 nm. It was indicated that these CdTe QDs have negligible genotoxicity and toxicity impacts. Fatimah et al. (2020) biosynthesized SnO_2 quantum dots using flower extract of Aparajitha (*Clitoria ternatea*) as a reducing agent. This flower extract contains flavonoids as well as flavanols, which can reduce Sn^{2+} precursors into Sn° NPs, which are then oxidized to SnO_2 QDs (4−10 nm). A blueshift was observed in the wavelength of biosynthesized SnO_2 QDs. These QDs were there used for photocatalytic degradation of rhoadamine blue under UV irradiation.

Biosynthesis of CdS QDs has been reported by Gholami et al. (2020) using aqueous extracts of regenerated hairy roots of *Rhaphanus sativus* L. It was observed that as-obtained particles were spherical in shape with size ranging between 2 and 7 nm. It was also reported that these CdS QDs exhibited more apoptosis effect on MCF-7 breast cancer cells as compared to

AGS gastric cancer cell lines. Kandasamy et al. (2020) reported the synthesis of CdS quantum dots using fruit sap of *Opuntia ficus indica* (as green template). It was revealed that QDs were spherical in shape.

A green chemical route for the synthesis of copper quantum dots has been developed by Rani et al. (2020) using leaf extract of *M. indica* (L.). They used copper sulfate as the source of copper. It was proposed that a polyphenolic compound (mangiferin) in leaf extract of *M. indica* may act as a capping, reducing, and stabilizing agent during the preparation of Cu QDs. As-obtained Cu QDs were stable and spherical in shape with size ranging from 4−7 nm. It was reported that these Cu QDs can degrade methylene blue and possess higher antimicrobial activity and scavenging activity of free radical.

Zaman et al. (2020) reported the biogenic synthesis of cupric oxide nanoparticles using leaf and fruit extracts of *Tamarindus indica* L. These extracts acted as capping and reducing agents. It was observed that CuO quantum dots of size 5−10 nm could be obtained using fruit extract, but larger particles (50−100 nm) were obtained on using leaf extract. The photocatalytic activity of as-synthesized QDs was evaluated for the degradation of rhodamine B under UV−Vis light illumination. It was reported that QDs obtained with leaf extract could degrade 65% of rhodamine B in 2 h, while quantum dots prepared using fruit extract degraded 77% of the dye. These QDs exhibited an excellent photostability and in vitro antimicrobial activity against bacterial strains *S. typhi*, *E. coli*, and *L. acidophilus*.

Das and Dhar (2020) reported a method for the synthesis of tin dioxide quantum dots. They used the shoots of *C. sinensis* as a stabilizer and reducing agent. It was observed that as-prepared tin dioxide quantum dots had a flake-like morphology and were crystalline with an average size of 4.3 nm. As-obtained SnO_2 quantum dots were then used for photocatalytic degradation of thiamethoxam. They could achieve 57% degradation within 45 min.

The extracts of medicinal plants such as *Bryophyllum pinnatum*, *Mentha arvensis*, and *Dalbergia sissoo* were used by Kumar et al. (2021) to prepare Ag NPs by reducing silver nitrate. Then, Ag NP-conjugated L-cysteine-capped ZnS:Mn quantum dots were also fabricated, which exhibited antimicrobial activity against *E. coli* and *S. aureus*. This work may provide new avenues for synthesizing plasmonic NPs using nontoxic material to be used as detectors and biosensors.

The synthesis of CdS quantum dots was carried out by Tudu et al. (2021) using *Ocimum sanctum* (Tulsi) leaf extract. It was reported that the phytochemicals of Tulsi leaf extract played an important role in controlling particle size and morphology. The average crystallite size of these biosynthesized QDs was found to be in the range of 3.6−3.0 nm It is interesting to note that the bandgap of the capped CdS QDs increases with increasing extract concentration, but on the contrary particle size decreases.

Pugazhenthiran et al. (2021) prepared monodispersed silver quantum dots via a green synthesis method. They used sweet lime (*Citrus limetta*) peel

extract for this biosynthesis. It was reported that face-centered-cubic Ag QDs with size (<5 nm) were obtained. The presence of carbohydrate and citrate were considered responsible for the formation of small Ag QDs with good stability. It was also indicated that as-synthesized Ag QDs were able to cause the death of cancer cells (71%) even at a low concentration (100 $\mu g\ mL^{-1}$).

Raja and Sundaramurthy (2021) used betel leaves (piper betle) for green synthesis of fluorescent carbon quantum dots. They reported that as-prepared carbon dots were selective in the detection of Fe^{3+} ions in aqueous medium. They have detected successfully the presence of ferric ions even in the presence of interfering metal ions such as Ca^{2+}, Mg^{2+}, Cu^{2+}, Ag^{+}, Fe^{2+}, Hg^{2+}, Cd^{2+}, Fe^{3+}, and Pb^{2+} at the same concentrations. It was reported that it was possible to detect Fe^{3+} ions in the concentration range of 50−150 nM with high sensitivity.

6.3 Bacteria

A facile route for the synthesis of cadmium sulfide nanoparticles has been reported by Bai et al. (2009) using the photosynthetic bacteria *Rhodopseudomonas palustris*. It was observed that the cadmium sulfate solution incubated with *R. palustris* biomass changed its color to yellow after 2 days. As-obtained CdS nanoparticles had an average size of 8.01 ± 0.25 nm with uniform distribution, as evident from by TEM images. A bacterial synthesis for cadmium telluride quantum dots with tunable fluorescence emission has been reported by Bao et al. (2010a) using *E. coli*. It was observed that these QDs exhibited size-tunable optical properties with fluorescence emission at 488−551 nm. It was revealed that these biosynthesized QDs have great potential in a wide range of biolabeling and bioimaging applications.

Mi et al. (2011) prepared CdS quantum dots using genetically engineered *E. coli* by introducing foreign genes encoding a CdS binding peptide. They prepared CdS QDs through two methods: lysis, and freezing−thawing of cells. It was claimed that biologically synthesized CdS QDs may be more biocompatible probes in bioimaging and biolabeling. Suresh et al. (2011) reported an efficient synthesis of extracellular silver sulfide nanoparticles using the metal-reducing bacterium *Shewanella oneidensis*. It was observed that particles were homogeneously shaped, monodispersed, and produced with high yield (85%). It was also revealed that as-prepared particles were a spherical shape with a mean diameter of 9 ± 3.5 nm. As-fabricated QDs particles are biocompatible and dispersible. They have an excellent potential for application in electronic devices, optical imaging, and solar cells.

Jiang et al. (2012) prepared cadmium sulfide quantum dots via in situ crosslinked chitosan hydrogel films. It was confirmed that crosslinked chitosan hydrogel films provided a confined matrix for CdS QDs growth. As-prepared CdS QDs/chitosan composite films slow photocatalytic activity for

degradation of methyl orange solution in the presence of visible light. Luminescent CdSe quantum dots were synthesized by Fellowes et al. (2013). They used bacterially derived selenide (Se^{2-}) as the precursor. Biogenic Se^{2-} was produced by the reduction of Se(IV) by *Veillonella atypica*. It was reported that biological Se^{2-} formed smaller and narrower size distributed QDs as compared to borohydride-reduced Se(IV) under similar conditions.

Kominkova et al. (2014) evaluated the effect of CdTe quantum dots on *Collembolans*, the earthworm *Eisenia fetida*, and *E. coli*. They also studied the effect of biosynthesis of QDs in *E. fetida* and *E. coli*. It was revealed that biosynthesis in earthworms can be a protective mechanism of its own; while it is probably a by-product of protective mechanisms in *E. coli*. Yan et al. (2014) proposed a green and efficient biosynthesis method for preparing CdSe QDs using *E. coli* cells as biological matrix. These QDs were fluorescence-tunable and biocompatible. It was observed that there was a surface protein capping layer outside QDs, as evident from FT-IR data. It was suggested that as-prepared quantum dots may prove to be an excellent fluorescent marker for broad bioimaging and biolabeling.

Gallardo et al. (2014) isolated oxidative stress-resistant bacteria (*Pseudomonas* spp.) from Antarctica and then used them for biosynthesis of CdS QDs at 15°C. It was reported that there was a change in fluorescence color (green to red), which was found to be time dependent. Yang et al. (2015) engineered a bacterial strain for biosynthesis of CdS quantum dots. It was reported that extracellular and water-soluble CdS quantum dots were obtained on using this strain at ambient pressure and temperatures with low-cost precursors. The biosynthesis of α- and β- forms of ZnS quantum dots was developed by Yue et al. (2016) using *Clostridiaceae* sp. They used different concentrations of hydroxypropyl starch as dispersant in this process. It was indicated that as-obtained α-ZnS quantum dots had a wurtzite structure with a low dose of hydroxypropyl starch, while β-ZnS quantum dots were prepared with a sphalerite structure with a high dose. It was also revealed that β-ZnS quantum dots exhibited a redshift as compared to α-ZnS quantum dots.

Fluorescent *Bacillus subtilis* cells were developed as probes for imaging applications and to explore behaviorial interaction between *B. subtilis* and *S. aureus*. A controlled biosynthesis of CdSe quantum dots was developed by Yan et al. (2016) using living *B. subtilis* cells. It was reported that *B. subtilis* cells inhibit the growth of nearby *S. aureus* cells. Such inhibition was affected by both growth stage as well as amount of surrounding *B. subtilis* cells.

Ulloa et al. (2016) reported the biosynthesis of cadmium sulfide QDs using acidophilic bacteria *Acidithiobacillus genus*. These CdS QDs were obtained when *Acidithiobacillus thiooxidans*, *A. ferrooxidans*, and *A. caldus* cells were exposed to sublethal cadmium concentrations in the presence of glutathione and cysteine. It was revealed that fluorescence of cadmium-exposed cells moves from green to red with time of incubation. It was

reported that an average size of 6 and 10 nm was found to show green and red QDs, respectively.

Yan et al. (2017) reported a green biosynthesis of cadmium sulfide quantum dots. Here, *E. coli* was selected as a biomatrix. It was revealed that these CdS quantum dots emitted a blue−green fluorescence under UV excitation. It was indicated that the antibiotic resistance of *E. coli* had a slight decrease when CdS quantum dots were prepared at mild temperature. Kominkova et al. (2017) obtained CdTe QDs by the extracellular biosynthesis by *E. coli*. These CdTeQDs were also prepared by microwave-assisted synthesis. The toxicity of as-obtained QDs was tested using three cell lines, Human Prostate Cancer cells (PC-3), Human Foreskin Fibroblast (HFF), and Breast Cancer cells (MCF-7), and it was observed that the toxicity of biosynthesized QDs to the PC-3 cell lines was almost 35% lower as compared to QDs prepared by the microwave technique.

Qi et al. (2017) used a low-cost hydroxypropyl starch (HPS) to assist sulfate-reducing bacteria (SRB) in the synthesis of ZnS QDs. It was indicated that HPS enhanced the growth of SRB and reduction of sulfate ions into sulfide, which blocked the interaction between sulfide and zinc ions to control the nucleation as well as growth of ZnS QDs. It was observed that average crystal size of as-prepared ZnS QDs decreases from 5.95 to 3.34 nm on increasing the concentration of HPS. There was a blueshift in the absorption peak, which may be due to the quantum confinement effect. The color of photoluminescence spectrum was found to be changed from red to yellow, which is evidence of tunable PL of ZnS QDs. The production of CdS QDs was reported by Ulloa et al. (2018) by acidophilic bacteria, of the *Acidithiobacillus* genus. It was observed that the addition of inorganic phosphate to *A. thiooxidans* ATCC 19703 cultures favored the biosynthesis of CdS QDs in the acidic range (pH 3.5). It was also indicated that phosphate contributes to the biosynthesis of CdS QDs by influencing uptake and tolerance to cadmium.

Yan et al. (2018) produced high-quality CdSe QDs in *Bacillus amyloliquefaciens*. This process has the benefits of short reaction time, high yield, mild synthetic conditions, and good reproducibility. Then as-obtained CdSe QDs were used as a probe for detecting copper(II) ions in blood plasma. It was observed that the protein envelope on the QD surface does not permit interference by others due to selective permeability of the bacterial cell membrane. It was revealed that copper ions in human blood plasma samples could be accurately determined in the range (15.6−18.5 $\mu mol\ L^{-1}$), which is almost similar to results obtained with atomic absorption spectroscopy. Biosynthesis of CdS quantum dots sensitized nanorod arrays of ZnO was reported by Yang et al. (2018). These ZnO nanorod arrays were prepared on FTO using a simple galvanic-cell-based approach. Therefore, these were introduced silanized by (3-aminopropyl)triethoxysilane (APTES) with amino groups, so that Cd^{2+} can be introduced. As-synthesized CdS/ZnO heterostructure was used as photoelectrochemical (PEC)

sensing platform, which exhibited detection sensitivity of 32 CFV m L^{-1} for sulfate-reducing bacteria (SRB). This work can help in the detection of physiological messenger molecules such as hydrogen sulfide.

The role of volatile sulfur compounds was investigated by Gallardo-Benavente et al. (2019) in the biosynthesis of CdS QDs using Antarctic strain *Pseudomonas fragi* GC01. They used different sulfur sources such as sulfite, sulfide, sulfate, thiosulfate, cysteine, and methionine. Intracellular biosynthesis was therefore all sulfur sources except acetylcysteine (Cys) and methionine (Met), where extracellular biosynthesis was there. It was observed that as-synthesized CdSQDs were in the range of 2−16 nm (size). The importance of methane thiol (MeSH) was also confirmed in the biosynthesis of QD. An extracellular biosynthesis of ZnS QDs has been reported by Qi et al. (2019) via a molecular mediation mechanism, which was due to mixed SRB. It was observed that particle size of biogenic ZnS QDs was found to be 6.5 nm. This molecular mediation mechanism was triggered by the peculiar extracellular proteins (Eps) for the higher yield of biosynthesized ZnS QDs. Some other metal sulfide QDs were also prepared, such as CuS, PbS, and CdS.

Bruna et al. (2019) reported biological synthesis of CdS QDs using by polyextremophile halophilic bacteria *Halobacillus* sp. DS2, which was isolated from Uyuni Salt Flat (Bolivia), Atacama salt Flat (Chile), and the Dead Sea (Israel). As-prepared QDs were hexagonal in shape and monodispersed with size ranging between 2 and 5 nm. Abou-Assy et al. (2019) synthesized CdSe QDs using *Providencia vermicola* BGRW. These bacteria had the ability to resist many metals such as silver, cadmium, copper, zinc, nickel, lead, bismuth, and cobalt. It was revealed that biosynthesized CdSe QDs were cubic in shape with a size range of 2−4 nm.

The formation of CdS_xSe_{1-x} QDs has been reported by Tian et al. (2019). These QDs have quantum yield (5.2%) and size of 2.0 ± 0.4 nm. As-prepared QDs (without extra modification) were then used for bioimaging of cancer cells and tumor tissue of mice.

Qi et al. (2019) reported extracellular biosynthesis of ZnS QDs with high yield. As-prepared biogenic ZnS QDs had an average crystallite size of 6.5 nm with better uniformity and greater PL activity than obtained by a chemical route. They have fabricated other QDs such as PbS, CuS, and CdS through this method.

Anthony et al. (2020) synthesized fluorescent carbon quantum dots by nitric acid treatment. They used rice-biryani (processed white rice waste) as a precursor of carbon. As-prepared CQDs were modified further by a two-step process:

1. preparation of reduced-state CQDs (r-CQDs) using borohydride as reductant; and
2. rigidifying with a tripeptide such as glutathione (r-CQDs-GS).

It was observed that QY was enhanced from 5.46% for bare CQDs to 41% for (r-CQDs-GS). As-prepared r-CQDs-GS had an average particle size in the range of $2-5$ nm. It was reported that about 90% cell viability and normal morphology was retained even after treated with r-CQDs-GS concentrations up to $100\,\mu g\,mL^{-1}$. It was reported that r-CQDs-GS could find applications in in vitro/in vivo bioimaging.

Öcal et al. (2020) achieved intracellular preparation of PbS QDs using *Pseudomonas aeruginosa* ATCC 27853. It was revealed that these intracellular biosynthesized PbS QDs had a particle size in the range of 3.47−11.45 nm. As-synthesized PbS QDs showed antibacterial activity against *E. coli*, *Proteus mirabilis*, *Micrococcus luteus*, and *Bacillus cereus*. Órdenes-Aenishanslins et al. (2020) synthesized CdS, Ag_2S, and CdSAg nanocrystals with size less than 15 nm. As-produced CdSAg ternary QDs exhibited high stability, fluorescence, and good quantum yield (36.13%). They could also produce soluble Ag_2S nanoparticles without any traces of Cd. All these three biosynthesized QDs were used as photosensitizers, where CdSAg QDs exhibited the best photovoltaic performance. It was revealed that these nanoparticles are formed in the extracellular space of bacterial cells exposed to cysteine and cadmium chloride.

Sulfate-reducing bacteria are present in anaerobic granular sludge and convert sulfate into sulfide. Jacob et al. (2020) coupled sulfate reduction with precipitation of zinc in ZnS quantum dots. It was reported that biogenic ZnS QDs had an average particle size of 5−7 nm. They determined the bandgap energy of as-synthesized ZnS QDs to be 3.84 eV. These QDs can be used as an effective photocatalyst for the photo-assisted decolorization of Congo red. Ashengroph et al. (2020) developed a method for the biosynthesis of cadmium sulfide quantum dots using a strain of *Pseudomonas chlororaphis*. It was reported that spherical CdS QDs were produced with an average size of 6.7 ± 2.4 nm.

The biosynthetic ternary ZnCdS QDs were prepared by Qi et al. (2021a) by sulfate-reducing bacteria. It was reported that these ternary ZnCdS QDs were monodispersed, spherical in shape, with an average crystallite size as 6.12 nm. The bandgap energy of these QDs were determined to be 2.35−2.72 eV. ZnCdS QDs exhibited remarkable photocatalytic activity for hydrogen evolution ($3.752\,mmol\,h^{-1}\,g^{-1}$) under visible light without using any noble metal cocatalysts. An extracellular biosynthesis of ternary $Zn_xCd_{1-x}S$ QDs has been reported by Qi et al. (2021b) using sulfate-reducing bacteria. It was revealed that these QDs with size of 3.50−4.64 nm could be achieved within half an hour. It was reported that these biogenic QDs exhibited high stability in gastric acid and excellent biocompatibility and biosafety, so that these can enter growing HeLa cells.

Carrasco et al. (2021) analyzed the ability of Antarctic lithobiontic bacterium *Pedobacter* sp. UYP1 in the synthesis of cadmium sulfide quantum dots. Yellow−green and orange−red fluorescent emissions were observed

after 20 and 80 min of synthesis in the presence of UV light, respectively. It was revealed that QDs were obtained with size of 3.07 nm, which were then used as photosensitizers in solar cells. As-fabricated solar cells displayed $V_{oc} = 162$ mV, $J_{sc} = 0.0110$ mA cm^{-2}, and conversion efficiency up to 0.0016%. An anaerobic approach was developed by Xu et al. (2021a) for the biosynthesis of CdS quantum dots (cubic phase and hexagonal phase) using *S. oneidensis* Mr-1. It was reported that as-synthesized hexagonal CdS QDs exhibited high photocatalytic hydrogen evolution (21 mmol g^{-1}CdS h^{-1}).

6.4 Fungi

It was reported by Ahmad et al. (2005) that the synthesis of gold nanoparticles can be controlled in the presence of the fungus *Trichothecium* sp. It was observed that as-prepared gold nanoparticles were spherical, rod-like, and triangular shaped. The synthesis of highly luminescent CdSe quantum dots were reported by Kumar et al. (2007) at room temperature. They used *F. oxysporum*, a fungus incubated with a mixture of $SeCl_4$ and $CdCl_2$. A controllable synthesis of CdSe quantum dots has been reported by Cui et al. (2009) using living yeast cells as a biosynthesizer. These CdSe QDs can be synthesized at 30°C instead of at 300°C, as required in other methods. Apart from this, a control over photoluminescence could be achieved also.

A simple and efficient biosynthesis was reported by Bao et al. (2010b) to prepare biocompatible cadmium telluride quantum dots using yeast cells. It was revealed that as-prepared CdTe QDs are formed via extracellular growth and then an endocytosis pathway. These CdTe QDs are protein-capped with good crystallinity and uniform size (2−3.6 nm). As-prepared QDs are highly soluble in water and exhibit good biocompatibility. The fluorescent biocompatible CdTe QDs can find use in biolabeling and bioimaging applications.

The live yeast cell were used for biosynthesis of CdSe quantum dots by Wang et al. (2010). They prepared seleniumized yeast cells before loading. It was also reported that the on-chip biosynthesis required only 0.5×10^{-4} M concentration of cadmium chloride and only 4−5 h incubation time to obtain the optimum yield of CdSe quantum dots.

Saa et al. (2010) generated CdS quantum dots by enzymatic products. This provided an analytical assay to detect the enzymatic activity of alkaline phosphatase and acetylcholine esterase. The rate of decomposition of sodium thiosulfate to give hydrogen sulfide increases in the presence of thiocholine, which is produced by acetylthiocholine after hydrolysis by acetylcholine esterase. This H_2S in the presence of cadmium sulfate yields CdS quantum dots. This assay was also applied to detect acetylcholine esterase inhibitors.

The cadmium sulfide quantum dots were biosynthesized by Huang et al. (2012) using *Saccharomyces cerevisiae* yeast. It was reported that as-prepared CdS QDs emit blue−green fluorescence under UV light.

Syed and Ahmad (2013) reported fungal-mediated synthesis of CdTe quantum dots using the fungus *F. oxysporum*. They used cadmium chloride and tellurium chloride as the precursor of Cd and Te, respectively. It was observed that these CdTe QDs are highly fluorescent and exhibited antibacterial activity against Gram-positive as well as Gram-negative bacteria. A mechanism-oriented strategy was reported by Li et al. (2013) for controlling the biosynthesis of CdSe quantum dots (fluorescent) through metabolic engineering in yeast cells. It was reported that the glutathione metabolic pathway controlled the intracellular formation of CdSe QDs. It was revealed that yeast cells were homogeneously transformed into efficient cell-factories at the single-cell level, which provides a way to direct the cellular metabolism toward formation of CdSe QDs.

Chen et al. (2014) developed a method for extracellular microbial synthesis of CdSQDs. They used white rot fungus *P. chrysosporium*. This fungus was incubated with a solution of cadmium nitrate tetrahydrate, which turned yellow after 12 h, which indicated that CdSQDs are formed. These QDs exhibited a blue fluorescence (458 nm). The average particle size was calculated to be 2.56 nm with uniform size and good crystallinity. It was revealed that secretion of proteins and cysteine was found to play a dominant role in the stabilization and formation of CdS QDs. Borovaya et al. (2015) reported a reproducible, efficient, and eco−friendly biosynthesis of CdSQDs using mycelium of basidiomycete fungus *P. ostreatus*. The CdSQDs were synthesized using sodium sulfide and cadmium sulfate by incubating *P. ostreatus* mycelium. It was reported that as-prepared quantum dots were spherical in shape ranging between 4 to 5 nm size.

The cadmium selenium quantum dots were synthesized by Wu et al. (2015) using *S. cerevisiae* (ATCC9763). They used sodium selenide and cadmium chloride as the source of selenium and cadmium, respectively. It was reported that the biosynthesized CdSe QDs exhibited much lower cytotoxicity as compared to that obtained with hydrothermally synthesized thioglycolic acid (TGA)-capped CdSe. An efficient method for biosynthesis of CdTe and CdS has been reported by Mareeswari et al. (2016) using fungus *Rhizopus stolonifer*. It was observed that suspension of as-prepared quantum dots exhibited greenish-blue and purple luminescence. It was indicated that these quantum dots are biocompatible in nature. A good contrast in imaging was observed, when these quantum dots were incorporated in human breast adenocarcinoma Michigan Cancer Foundation-7 cell lines.

Polycrystalline ZnS quantum dots were synthesized by Uddandarao (2016) from an endophytic fungus *Aspergillus flavus*. It was revealed that they formed a spherical shape. *A. flavus* was isolated from a medicinal plant *Nothapodytes foetida*. It was proposed that quantum dots synthesized from this fungus may exhibit a great potential in medical and environmental applications. The CdSe QDs were synthesized by Yamaguchi et al. (2016) using *F. oxysporum*. It was reported that CdSe quantum dots were obtained from

the mycelial cells of *F. oxysporum*. It was also revealed that superoxide is accumulated, which may play an important role in reducing Se^{4+} to Se^{2-}; thus, inhibiting the aggregation of CdSe to form nanoparticles.

Jacob et al. (2017) reported the biosynthesis of PbSe QD using marine *Aspergillus terreus*. It was observed that an increase in the total protein content was present in the reaction mixture after biosynthesis. The involvement of metallothioneins (metal binding peptides) and other antioxidant enzymes was confirmed, and it may play an important role in biosynthesis of PbSe QDs. Brooks and Lefebvre (2017) synthesized CdSe quantum dots in the cytoplasm on treating *S. cerevisiae* sequentially with sodium selenite and cadmium chloride. As-prepared CdSe QDs exhibited a yellow fluorescence (540 nm). The presence of glutathione contributed to this biosynthetic process as it inhibited when it was applied after selenite treatment but before the addition of cadmium. It was revealed that by optimizing each aspect the production of CdSe QDs was increased 70% in this case.

Sandoval-Cárdenas et al. (2017) used a sulfur toxic waste, which was recovered after hydrodesulfurization of Mexican oil's sour acid gases. They synthesized cadmium sulfide quantum dots (hydrophilic) via a green method using a fungus, *F. oxysporum*. The mycelia of *F. oxysporum f.* sp. *lycopersici* were incubated with cadmium nitrate (1 mM) and sulfur waste (1% w/v) for 24 h, and then filtered to provide a yellow solution of cadmium sulfide quantum dots. As-obtained CdS QDs were biocompatible, hydrophilic, and stable in nature. It was also revealed that CdS QDs had a wurtzite crystalline structure with size of 6.116 ± 2.111 nm (diameter).

The cadmium selenide QDs were prepared by Tian et al. (2017) in vivo using *Candida utilis* WSH02−08. It was observed that fluorescence properties of these QDs can be turned using different precursor concentrations. It was found that as-synthesized QDs with longer photostable life time and high fluorescence intensity could be obtained by keeping Cd content higher than Se. It was suggested that such synthesized QDs can find application in live-cell imaging without any further modification. A white rot fungus *Trametes versicolor* was used by Qin et al. (2018) for biosynthesis of cadmium sulfide quantum dots. As-obtained cadmium sulfide quantum dots were found to be biocompatible and stable and therefore could have great potential in biological and biomedical applications.

Biosynthesis of CdSe QDs was reported by Shao et al. (2018) using *S. cerevisiae*. The selenocysteine was considered (SeCys) as the primary precursor of selenium in the intracellular biosynthesis of these QDs. It was revealed that the selenomethionine (SeMet)-to-SeCys pathway regulated biosynthesis of CdSe QD. The biosynthesis of ZnS QDs was reported by Jacob et al. (2019a) using the fungus *Aspergillus* sp. It was observed that as-prepared QDs were spherical and crystalline with a mean diameter of 6.3 nm. These ZnS QDs can find numerous applications in the fields of photocatalysis, medical imaging, and biosensing.

Jacob et al. (2019b) biosynthesized ZnS quantum dots from Zn-tolerant *Penicillium* sp. They also revealed that spherical particles of ZnS QDs were obtained with an average diameter of 11.08 nm. As-prepared biogenic ZnS were used for the photodegradation of methylene blue and this degradation efficiency was increased on increasing ZnS nanocatalyst/dye ratio reaching an equilibrium within six hours. These ZnS nanohybrids can find practical utility in the removal of different pollutants released from paper, textile, and dyeing industries. The carbon quantum dots were doped with nitrogen and sulfur (N,S-CDs) by Shi et al. (2019) using fungus fibers. It was reported that N,S-CDs exhibited excellent stability with high quantum yield as well as being water soluble with activity as quenching-based detection and cellular imaging of cancer cells. These QDs can be used as fluorescent probe for efficient, sensitive, and selective probe determination of tetracyclines the linear range of 0.5 to 47.6 μM, with a limit of detection of 15.6 nM. They also prepared test papers using N,S-CDs, which could detect tetracyclines present in aquiculture wastewater in lesser time.

Cao et al. (2020) biosynthesized CdSe QDs using a yeast *Rhodotorula mucilaginosa* PA-1 under aerobic conditions. It was reported that concentration of cadmium ions decides synthesis of CdSeQDs and not the selenium ions. It was found that bio-synthesized CdSe QDs had a narrow size distribution in the range of 3.2 ± 0.4 nm. These QDs exhibited excellent photocatalytic activity in degradation of malachite green in presence of ultraviolet and visible light. The photocatalytic degradation efficiency of malachite green under ultraviolet light was 86.5% after, while it was 94.28% under visible light. A green system was developed by Xu et al. (2020) for the biosynthesis of CdS_xSe_{1-x} QDs by *Phomopsis* sp. XP-8. The QDs were shown to have a CdS0.75Se0.25@oligopeptide transporter structure. It was observed that these QDs were monodispersed with a uniform spherical shape with diameter as 3.22 ± 0.07 nm. These QDs are water soluble and exhibited excellent fluorescence. It was revealed that they can be used as a sensor for detecting chloramphenicol (CAP) in the range of 3.13 to 500 $\mu g\ L^{-1}$ with a limit of detection of 0.89 $\mu g\ L^{-1}$. The detection method was highly selective for CAP with minimal interference from other antibiotics and it was also used successfully to detect CAP in milk samples.

A biosynthesis method to synthesize Ag_2Se QDs was developed by Liu et al. (2021) using *S. cerevisiae*. It was reported that nanoparticles obtained by extracellular purification had a uniform size of 3.9 ± 0.6 nm. These Ag_2Se QDs had good biocompatibility, maybe due to capping by protein. It was observed that the as-synthesized Ag_2Se QDs had lower toxicity and these could be used for in vivo imaging.

Xu et al. (2021a,b) developed a method to biosynthesize $Cd_{0.5}Zn_{0.5}S$ quantum dots using filamentous fungus *Phomopsis* sp. XP-8. It was reported that heterogeneous catalyst functionalized composite mycelium pellets (CMP) exhibited an enhanced visible light degradation activity. The catalytic

activity was also improved as biosorption capacity of CMP increased the contact rate between organic dyes and catalysts. This CMP has high mechanical strength and is easy to separate and recycle; thus the problems of recovery after use and secondary pollution of the environment were avoided.

6.5 Others

Ascencio et al. (2006) obtained small metallic nanoparticles of neodymium via biosynthesis. They could obtain particles of 1−8 nm depending on pH conditions. It was also revealed that smaller clusters were obtained at pH 5, but nanorods were formed at pH 10. Yu et al. (2006) synthesized water-soluble CdSe-ZnS (core-shell) QDs. The g-aminobutyric acid (GABA), an inhibitory transmitter in the central nervous system of mammals, was then bioconjugated to these QDs in the presence of N-hydroxysuccinimide (NHS) and 1-ethyl-3-(3)-dimethylaminopropyl carbodiimide (EDC) to make a fluorescence probe. They could detect GABA binding sites on protoplast membrane of both pollen as well as somatic cells using.

One-pot synthesis of neoglycoconjugates with a reactive thiol group was reported by Babu et al. (2007). Their functionalization with carbohydrates can provide high solubility and stabilization of CdSe − ZnS quantum dots. They used melibiose, lactose, and maltotriose to obtain three different sizes of quantum dots. These sugar-QDs were found to be very selective in the detection of lictin. Huilan et al. (2008) developed a bioinspired technique to synthesize hybrid nanocomposites. It consisted of well-dispersed CdS quantum dots on silk fibroin fibers (SFF). It was observed that biomaterial SFF acts as both a supporting substrate and functional sites for in situ generation of CdSQD. As-prepared CdSQDs/SFF nanocomposites can be used as novel luminescent, photoelectron transfer devices and in photocatalysis.

Manzoor et al. (2009) reported the synthesis of luminescent quantum dots, which were conjugated with a cancer-targeting ligand, folic acid (FA). Doped QDs were prepared by a simple aqueous method at room temperature. It was observed that these QDs are monodispersed with an average size ∼4 nm. The dopants selected were Al^{3+}, Cu^{2+}, Mn^{2+}, and F^{-} and color tunability could be achieved ranging from blue (480 nm) to red (622 nm). It was claimed that nontoxic, Hg-, Pb-, Cd-, Te-, and Se-free luminescent QDs can be used for targeted cancer imaging.

Dong et al. (2009) used l-glutathione (GSH) as a stabilizer for the preparation of CdTe quantum dots in aqueous solution. It was reported that as-prepared QDs were linked to prostate-specific antigen (PSA) for indirect labeling of fixed prostate cancer cells. It was indicated that as-prepared QD-based probes were fluorescent markers and exhibited excellent photostability and spectral properties. These were found to be much better than organic dyes in target detection. It was also suggested that the l-glutathione capped

CdTe had low cytotoxicity as these QDs did not show a detectable effect on cell growth after culturing for three days.

Stürzenbaum et al. (2013) showed that an earthworm's metal detoxification pathway can be used to produce cadmium telluride (CdTe) quantum dots. It was observed that these QDs are water soluble and luminescent in green region. They exposed standard wild-type *Lumbricus rubellus* earthworms to soil that was spiked with cadmium chloride and Na_2TeO_3 salts for 11 days. They isolated luminescent quantum dots from chloragogenous tissues surrounding the gut of the earthworm and used them in live-cell imaging.

Tan et al. (2013) reported that near-infrared fluorescent silver sulfide quantum dots can be synthesized in hepatoma carcinoma cells (HepG2) cancer cells, which is intracellular synthesis. Silver sulfide quantum dots were synthesized by delivering quantum dot precursors into cultured HepG2 cells and these can be used for cell imaging. Zhang et al. (2020) developed CdSe/CdS QDs and used these as a fluorescence sensor for Hg^{2+} detection with high sensitivity in the range of 0.25−100 nM with a limit of detection of 0.01 nM. The as-fabricated sensor exhibited a high selectivity for Hg^{2+} detection of mercuric ion even in the presence of other metal ions and it gave satisfactory results in the case of some samples such as tap water, river water, and landfill.

6.6 Conclusion

Various chemical and physical methods for the synthesis of quantum dots have their own demerits. The majority of them are not green in nature. Biosynthesis methods have certain advantages, such as they are clean, nontoxic, and eco-friendly in nature. In this technique, no hazardous chemicals or reagents are required and harsh conditions are avoided. It is interesting that several nanoparticles (quantum dots) can be easily biosynthesized, which is sometimes not possible by the conventional chemical synthesis. The field of biogenic synthesis is a fairly new and exciting area of research and it has a great potential for further development.

References

Abou-Assy, R.S., El-Deeb, B.A., Al-Talhi, A.D., Mostafa, N.Y., 2019. Biosynthesis of cadmium selenide quantum dots by *Providencia vermicola*. Afr. J. Microbiol. Res. 13 (6), 106−121.

Ahmad, A., Senapati, S., Khan, M.I., Kumar, R., Sastry, M., 2005. Extra-/intracellular biosynthesis of gold nanoparticles by an alkalotolerant fungus, *Trichothecium* sp. J. Biomed. Nanotechnol. 1 (1), 47−53.

Al-Shalabi, Z., Doran, P.M., 2016. Biosynthesis of fluorescent CdS nanocrystals with semiconductor properties: comparison of microbial and plant production systems. J. Biotechnol. 223, 13−23.

Alvand, Z.M., Rajabi, H.R., Mirzaei, A., Masoumiasl, A., Sadatfaraji, H., 2019. Rapid and green synthesis of cadmium telluride quantum dots with low toxicity based on a plant-mediated approach after microwave and ultrasonic assisted extraction: synthesis, characterization, biological potentials and comparison study. Mater. Sci. Eng.: C 98, 535–544.

Anthony, A.M., Murugan, R., Subramanian, R., Selvarangan, G.K., Pandurangan, P., Dhanasekaran, A., et al., 2020. Ultra-radiant photoluminescence of glutathione rigidified reduced carbon quantum dots (r-CQDs) derived from ice-biryani for in vitro and in vivo bioimaging applications. Colloids Surf. A: Physicochem. Eng. Asp. 586. Available from: https://doi.org/10.1016/j.colsurfa.2019.124266.

Ascencio, J.A., Canizal, G., Medina-Flores, A., Bejar, L., Tavera, L., Matamoros, H., et al., 2006. Neodymium nanoparticles: biosynthesis and structural analysis. J. Nanosci. Nanotechnol. 6 (4), 1044–1049.

Ashengroph, M., Khaledi, A., Bolbanabad, E.M., 2020. Extracellular biosynthesis of cadmium sulphide quantum dot using cell-free extract of *Pseudomonas chlororaphis* CHR05 and its antibacterial activity. Process. Biochem. 89, 63–70.

Babu, P., Sinha, S., Surolia, A., 2007. Sugar–quantum dot conjugates for a selective and sensitive detection of lectins. Bioconjug. Chem. 18 (1), 146–151.

Bai, H.J., Zhang, Z.M., Guo, Y., Yang, G.E., 2009. Biosynthesis of cadmium sulfide nanoparticles by photosynthetic bacteria *Rhodopseudomonas palustris*. Colloids Surf. B: Biointerf. 70 (1), 142–146.

Bao, H., Hao, N., Yang, Y., Zhao, D., 2010a. Biosynthesis of biocompatible cadmium telluride quantum dots using yeast cells. Nano Res. 3 (7), 481–489.

Bao, H., Lu, Z., Cui, X., Qiao, Y., Guo, J., Anderson, J.M., et al., 2010b. Extracellular microbial synthesis of biocompatible CdTe quantum dots. Acta Biomater. 6 (9), 3534–3541.

Begum, S., Ahmaruzzaman, M., 2018. Green synthesis of SnO2 quantum dots using Parkia speciosa Hassk pods extract for the evaluation of anti-oxidant and photocatalytic properties. J. Photochem. Photobiol. B: Biol. 184, 44–53.

Bhattacharjee, A., Ahmaruzzaman, M., 2015. Photocatalytic-degradation and reduction of organic compounds using SnO2 quantum dots (via a green route) under direct sunlight. RSC Adv. 5 (81), 66122–66133.

Borovaya, M.N., Naumenko, A.P., Matvieieva, N.A., Blume, Y.B., Yemets, A.I., 2014. Biosynthesis of luminescent CdS quantum dots using plant hairy root culture. Nanoscale Res. Lett. 9 (1). Available from: https://doi.org/10.1186/1556-276X-9-686.

Borovaya, M., Pirko, Y., Krupodorova, T., Naumenko, A., Blume, Y., Yemets, A., 2015. Biosynthesis of cadmium sulphide quantum dots by using *Pleurotus ostreatus* (Jacq.) P. Kumm. Biotechnol. Biotechnol. Equip. 29 (6), 1156–1163.

Borovaya, M.N., Burlaka, O.M., Naumenko, A.P., Blume, Y.B., Yemets, A.I., 2016. Extracellular synthesis of luminescent CdS quantum dots using plant cell culture. Nanoscale Res. Lett. 11 (1). Available from: https://doi.org/10.1186/s11671-016-1314-z.

Brooks, J., Lefebvre, D.D., 2017. Optimization of conditions for cadmium selenide quantum dot biosynthesis in *Saccharomyces cerevisiae*. Appl. Microbiol. Biotechnol. 101 (7), 2735–2745.

Bruna, N., Collao, B., Tello, A., Caravantes, P., Díaz-Silva, N., Monrás, J.P., et al., 2019. Synthesis of salt-stable fluorescent nanoparticles (quantum dots) by polyextremophile halophilic bacteria. Sci. Rep. 9 (1). Available from: https://doi.org/10.1038/s41598-018-38330-8.

Cao, K., Chen, M.M., Chang, F.Y., Cheng, Y.Y., Tian, L.J., Li, F., et al., 2020. The biosynthesis of cadmium selenide quantum dots by *Rhodotorula mucilaginosa* PA-1 for photocatalysis. Biochem. Eng. J. 156. Available from: https://doi.org/10.1016/j.bej.2020.107497.

Carrasco, V., Amarelle, V., Lagos-Moraga, S., Quezada, C.P., Espinoza-González, R., Faccio, R., et al., 2021. Production of cadmium sulfide quantum dots by the lithobiontic Antarctic strain *Pedobacter* sp. UYP1 and their application as photosensitizer in solar cells. Microb. Cell Factories 20 (1). Available from: https://doi.org/10.1186/s12934-021-01531-4.

Chen, G., Yi, B., Zeng, G., Niu, Q., Yan, M., Chen, A., et al., 2014. Facile green extracellular biosynthesis of CdS quantum dots by white rot fungus *Phanerochaete chrysosporium*. Colloids Surf. B: Biointerfaces 117, 199–205.

Cui, R., Liu, H.H., Xie, H.Y., Zhang, Z.L., Yang, Y.R., Pang, D.W., et al., 2009. Living yeast cells as a controllable biosynthesizer for fluorescent quantum dots. Adv. Funct. Mater. 19 (15), 2359–2364.

Das, J., Dhar, S.S., 2020. Synthesis of SnO2 quantum dots mediated by *Camellia sinensis* shoots for degradation of thiamethoxam. Toxicol. Environ. Chem. 102 (1–4), 186–196.

Dong, W., Guo, L., Wang, M., Xu, S., 2009. CdTe QDs-based prostate-specific antigen probe for human prostate cancer cell imaging. J. Lumin. 129 (9), 926–930.

Fatimah, I., Sahroni, I., Muraza, O., Doong, R.A., 2020. One-pot biosynthesis of SnO2 quantum dots mediated by Clitoriaternatea flower extract for photocatalytic degradation of rhodamine B. J. Environ. Chem. Eng. 8 (4). Available from: https://doi.org/10.1016/j.jece.2020.103879.

Fellowes, J.W., Pattrick, R.A.D., Lloyd, J.R., Charnock, J.M., Coker, V.S., Mosselmans, J.F.W., et al., 2013. Ex situ formation of metal selenide quantum dots using bacterially derived selenide precursors. Nanotechnology 24 (14). Available from: https://doi.org/10.1088/0957-4484/24/14/145603.

Gallardo, C., Monrás, J.P., Plaza, D.O., Collao, B., Saona, L.A., Durán-Toro, V., et al., 2014. Low-temperature biosynthesis of fluorescent semiconductor nanoparticles (CdS) by oxidative stress resistant Antarctic bacteria. J. Biotechnol. 187, 108–115.

Gallardo-Benavente, C., Carrión, O., Todd, J.D., Pieretti, J.C., Seabra, A.B., Durán, N., et al., 2019. Biosynthesis of CdS quantum dots mediated by volatile sulfur compounds released by Antarctic *Pseudomonas fragi*. Front. Microbiol. 10. Available from: https://doi.org/10.3389/fmicb.2019.01866.

Gholami, Z., Dadmehr, M., Jelodar, N.B., Hosseini, M., Parizi, A.P., 2020. One-pot biosynthesis of CdS quantum dots through in vitro regeneration of hairy roots of *Rhaphanus sativus* L. and their apoptosis effect on MCF-7 and AGS cancerous human cell lines. Mater. Res. Express 7 (1). Available from: https://doi.org/10.1088/2053-1591/ab66ea.

Green, M., Haigh, S.J., Lewis, E.A., Sandiford, L., Burkitt-Gray, M., Fleck, R., et al., 2016. The biosynthesis of infrared-emitting quantum dots in allium fistulosum. Sci. Rep. 6 (1). Available from: https://doi.org/10.1038/srep20480.

Huang, H., He, M., Wang, W., Liu, J., Mi, C., Xu, S., 2012. Biosynthesis of CdS quantum dots in *Saccharomyces cerevisiae* and spectroscopic characterization. Spectrosc. Spectr. Anal. 32 (4), 1090–1093.

Huilan, S., Jie, H., Qun, D., Di, Z., Qixin, G., 2008. In situ synthesis and photoluminescence of QD-CdS on silk fibroin fibers at room temperature. Nanotechnology (Print.) 19. Available from: https://doi.org/10.1088/0957-4484/19/02/025601.

Jacob, J.M., Sharma, S., Balakrishnan, R.M., 2017. Exploring the fungal protein cadre in the biosynthesis of PbSe quantum dots. J. Hazard. Mater. 324, 54–61.

Jacob, J.M., Rajan, R., Tom, T.C., Kumar, V.S., Kurup, G.G., Shanmuganathan, R., et al., 2019a. Biogenic design of ZnS quantum dots-insights into their in-vitro cytotoxicity, photocatalysis and biosensing properties. Ceram. Int. 45 (18), 24193–24201.

Jacob, J.M., Rajan, R., Aji, M., Kurup, G.G., Pugazhendhi, A., 2019b. Bio-inspired ZnS quantum dots as efficient photo catalysts for the degradation of methylene blue in aqueous phase. Ceram. Int. 45 (4), 4857–4862.

Jacob, J.M., Sinharoy, A., Lens, P.N., 2020. Photocatalytic degradation of congo red by zinc sulfide quantum dots produced by anaerobic granular sludge. Environ. Technol. 41. Available from: https://doi.org/10.1080/09593330.2020.1856940.

Jiang, R., Zhu, H., Yao, J., Fu, Y., Guan, Y., 2012. Chitosan hydrogel films as a template for mild biosynthesis of CdS quantum dots with highly efficient photocatalytic activity. Appl. Surf. Sci. 258 (8), 3513–3518.

Kandasamy, K., Venkatesh, M., Khadar, Y.S., Rajasingh, P., 2020. One-pot green synthesis of CdS quantum dots using *Opuntia ficus*-indica fruit sap. Mater. Today: Proc. 26, 3503–3506.

Kaviya, S., Kabila, S., Jayasree, K.V., 2017. Room temperature biosynthesis of greatly stable fluorescent ZnO quantum dots for the selective detection of Cr3 + ions. Mater. Res. Bullet. 95, 163–168.

Kominkova, M., Michalek, P., Moulick, A., Nemcova, B., Zitka, O., Kopel, P., et al., 2014. Biosynthesis of quantum dots (CdTe) and its effect on *Eisenia fetida* and *Escherichia coli*. Chromatographia 77 (21), 1441–1449.

Kominkova, M., Milosavljevic, V., Vitek, P., Polanska, H., Cihalova, K., Dostalova, S., et al., 2017. Comparative study on toxicity of extracellularly biosynthesized and laboratory synthesized CdTe quantum dots. J. Biotechnol. 241, 193–200.

Kumar, S.A., Ansary, A.A., Ahmad, A., Khan, M.I., 2007. Extracellular biosynthesis of CdSe quantum dots by the fungus, *Fusarium oxysporum*. J. Biomed. Nanotechnol. 3, 190–194.

Kumar, S., Taneja, S., Banyal, S., Singhal, M., Kumar, V., Sahare, S., et al., 2021. Biosynthesised silver nanoparticle-conjugated l-cysteine ceiled Mn: ZnS quantum dots for eco-friendly biosensor and antimicrobial applications. J. Electron. Mater. 50 (7), 3986–3995.

Li, Y., Cui, R., Zhang, P., Chen, B.B., Tian, Z.Q., Li, L., et al., 2013. Mechanism-oriented controllability of intracellular quantum dots formation: the role of glutathione metabolic pathway. ACS Nano 7 (3), 2240–2248.

Liu, J., Zheng, D., Zhong, L., Gong, A., Wu, S., Xie, Z., 2021. Biosynthesis of biocompatibility Ag_2Se quantum dots in Saccharomyces cerevisiae and its application. Biochem. Biophys. Res. Commun. 544, 60–64.

Manzoor, K., Johny, S., Thomas, D., Setua, S., Menon, D., Nair, S., 2009. Bio-conjugated luminescent quantum dots of doped ZnS: a cyto-friendly system for targeted cancer imaging. Nanotechnology 20 (6). Available from: https://doi.org/10.1088/0957-4484/20/6/065102.

Mareeswari, P., Brijitta, J., Etti, S.H., Meganathan, C., Kaliaraj, G.S., 2016. Rhizopus stolonifer mediated biosynthesis of biocompatible cadmium chalcogenide quantum dots. Enzyme Microb. Technol. 95, 225–229.

Mi, C., Wang, Y., Zhang, J., Huang, H., Xu, L., Wang, S., et al., 2011. Biosynthesis and characterization of CdS quantum dots in genetically engineered *Escherichia coli*. J. Biotechnol. 153 (3–4), 125–132.

Öcal, N., Ceylan, A., Duman, F., 2020. Intracellular biosynthesis of PbS quantum dots using Pseudomonas aeruginosa ATCC 27853: evaluation of antibacterial effects and DNA cleavage activities. World J. Microbiol. Biotechnol. 36 (10). Available from: https://doi.org/10.1007/s11274-020-02917-z.

Órdenes-Aenishanslins, N., Anziani-Ostuni, G., Monrás, J.P., Tello, A., Bravo, D., Toro-Ascuy, D., et al., 2020. Bacterial synthesis of ternary CdSAg quantum dots through cation exchange: tuning the composition and properties of biological nanoparticles for bioimaging

and photovoltaic applications. Microorganisms 8 (5). Available from: https://doi.org/10.3390/microorganisms8050631.

Ouyang, W., Sun, J., 2016. Biosynthesis of silver sulfide quantum dots in wheat endosperm cells. Mater. Lett. 164, 397–400.

Pugazhenthiran, N., Murugesan, S., Muneeswaran, T., Suresh, S., Kandasamy, M., Valdés, H., et al., 2021. Biocidal activity of citrus limetta peel extract mediated green synthesized silver quantum dots against MCF-7 cancer cells and pathogenic bacteria. J. Environ. Chem. Eng. 9 (2). Available from: https://doi.org/10.1016/j.jece.2021.105089.

Qi, S., Zhang, M., Guo, X., Yue, L., Wang, J., Shao, Z., et al., 2017. Controlled extracellular biosynthesis of ZnS quantum dots by sulphate reduction bacteria in the presence of hydroxypropyl starch as a mediator. J. Nanopart. Res. 19 (6), 1–13. Available from: https://doi.org/10.1007/s11051-017-3899-2.

Qi, S., Yang, S., Chen, J., Niu, T., Yang, Y., Xin, B., 2019. High-yield extracellular biosynthesis of ZnS quantum dots through a unique molecular mediation mechanism by the peculiar extracellular proteins secreted by a mixed sulfate reducing bacteria. ACS Appl. Mater. Interfaces 11 (11), 10442–10451.

Qi, S., Miao, Y., Chen, J., Chu, H., Tian, B., Wu, B., et al., 2021a. Controlled biosynthesis of ZnCdS quantum dots with visible-light-driven photocatalytic hydrogen production activity. Nanomaterials 11 (6). Available from: https://doi.org/10.3390/nano11061357.

Qi, S., Chen, J., Bai, X., Miao, Y., Yang, S., Qian, C., et al., 2021b. Quick extracellular biosynthesis of low-cadmium ZnxCd1 − xS quantum dots with full-visible-region tuneable high fluorescence and its application potential assessment in cell imaging. RSC Adv. 11 (35), 21813–21823.

Qin, Z., Yue, Q., Liang, Y., Zhang, J., Zhou, L., Hidalgo, O.B., et al., 2018. Extracellular biosynthesis of biocompatible cadmium sulfide quantum dots using *Trametes versicolor*. J. Biotechnol. 284, 52–56.

Raja, D., Sundaramurthy, D., 2021. Facile synthesis of fluorescent carbon quantum dots from Betel leafs (Piper betle) for Fe3 + sensing. Mater. Today: Proc. 34, 488–492.

Rani, H., Singh, S.P., Yadav, T.P., Khan, M.S., Ansari, M.I., Singh, A.K., 2020. In-vitro catalytic, antimicrobial and antioxidant activities of bioengineered copper quantum dots using *Mangifera indica* (L.) leaf extract. Mater. Chem. Phys. 239. Available from: https://doi.org/10.1016/j.matchemphys.2019.122052.

Rosano-Ortega, G., Schabes-Retchkiman, P., Zorrilla, C., Liu, H.B., Canizal, G., Avila-Pérez, P., et al., 2006. Synthesis and characterization of Mn quantum dots by bioreduction with water hyacinth. J. Nanosci. Nanotechnol. 6 (1), 151–156.

Saa, L., Virel, A., Sanchez-Lopez, J., Pavlov, V., 2010. Analytical applications of enzymatic growth of quantum dots. Chem.–A Eur. J. 16 (21), 6187–6192.

Sandoval-Cárdenas, I., Gómez-Ramírez, M., Rojas-Avelizapa, N.G., 2017. Use of a sulfur waste for biosynthesis of cadmium sulfide quantum dots with *Fusarium oxysporum* f. sp. lycopersici. Mater. Sci. Semicond. Process. 63, 33–39.

Shao, M., Zhang, R., Wang, C., Hu, B., Pang, D., Xie, Z., 2018. Living cell synthesis of CdSe quantum dots: manipulation based on the transformation mechanism of intracellular Se-precursors. Nano Res. 11 (5), 2498–2511.

Shi, C., Qi, H., Ma, R., Sun, Z., Xiao, L., Wei, G., et al., 2019. N, S-self-doped carbon quantum dots from fungus fibers for sensing tetracyclines and for bioimaging cancer cells. Mater. Sci. Eng. C. 105. Available from: https://doi.org/10.1016/j.msec.2019.110132.

Shivaji, K., Mani, S., Ponmurugan, P., De Castro, C.S., Lloyd Davies, M., Balasubramanian, M. G., et al., 2018. Green-synthesis-derived CdS quantum dots using tea leaf extract:

antimicrobial, bioimaging, and therapeutic applications in lung cancer cells. ACS Appl. Nano Mater. 1 (4), 1683–1693.

Silva, A., Martínez-Gallegos, S., Rosano-Ortega, G., Schabes-Retchkiman, P., Vega-Lebrún, C., Albiter, V., 2017. Nanotoxicity for *E. Coli* and characterization of silver quantum dots produced by biosynthesis with *Eichhornia crassipes*. J. Nanostruct. 7 (1). Available from: https://doi.org/10.22052/JNS.2017.01.001.

Stürzenbaum, S.R., Höckner, M., Panneerselvam, A., Levitt, J., Bouillard, J.S., Taniguchi, S., et al., 2013. Biosynthesis of luminescent quantum dots in an earthworm. Nat. Nanotechnol. 8 (1), 57–60.

Suresh, A.K., Doktycz, M.J., Wang, W., Moon, J.W., Gu, B., Meyer III, H.M., et al., 2011. Monodispersed biocompatible silver sulfide nanoparticles: facile extracellular biosynthesis using the γ-proteobacterium, *Shewanellaoneidensis*. Acta Biomater. 7 (12), 4253–4258.

Syed, A., Ahmad, A., 2013. Extracellular biosynthesis of CdTe quantum dots by the fungus *Fusarium oxysporum* and their anti-bacterial activity. Spectrochim. Acta Part. A: Mol. Biomol, Spectrosc. 106, 41–47.

Tan, L., Wan, A., Li, H., 2013. Synthesis of near-infrared quantum dots in cultured cancer cells. ACS Appl. Mater. Interf. 6 (1), 18–23.

Tian, L.J., Zhou, N.Q., Liu, X.W., Liu, J.H., Zhang, X., Huang, H., et al., 2017. A sustainable biogenic route to synthesize quantum dots with tunable fluorescence properties for live cell imaging. Biochem. Eng. J. 124, 130–137.

Tian, L.J., Min, Y., Li, W.W., Chen, J.J., Zhou, N.Q., Zhu, T.T., et al., 2019. Substrate metabolism-driven assembly of high-quality CdSxSe1−x quantum dots in *Escherichia coli*: molecular mechanisms and bioimaging application. ACS Nano 13 (5), 5841–5851.

Tudu, S.C., Zubko, M., Kusz, J., Bhattacharjee, A., 2021. Structural, optical and dielectric studies of wurtzite-type CdS quantum dots green synthesised using *Ocimum sanctum* (Tulsi) leaf extract. Adv. Nat. Sci.: Nanosci. Nanotechnol. 12 (3). Available from: https://doi.org/10.1088/2043-6262/ac2732.

Uddandarao, P., 2016. ZnS semiconductor quantum dots production by an endophytic fungus *Aspergillus flavus*. Mater. Sci. Eng. B 207, 26–32.

Ulloa, G., Collao, B., Araneda, M., Escobar, B., Álvarez, S., Bravo, D., et al., 2016. Use of acidophilic bacteria of the genus Acidithiobacillus to biosynthesize CdS fluorescent nanoparticles (quantum dots) with high tolerance to acidic pH. Enzyme Microb. Technol. 95, 217–224.

Ulloa, G., Quezada, C.P., Araneda, M., Escobar, B., Fuentes, E., Álvarez, S.A., et al., 2018. Phosphate favors the biosynthesis of CdS quantum dots in *Acidithiobacillus thiooxidans* ATCC 19703 by improving metal uptake and tolerance. Front. Microbiol. 9. Available from: https://doi.org/10.3389/fmicb.2018.00234.

Wang, X., Du, Y., Ding, S., Fan, L., Shi, X., Wang, Q., et al., 2005. Large two-photon absorbance of chitosan–ZnS quantum dots nanocomposite film. Phys. E: Low-Dimens. Syst. Nanostruct. 30 (1–2), 96–100.

Wang, X., Li, Y., Du, Y., 2009. Novel water-soluble chitosan derivatives/quantum dots nanocomposite: synthesis, characterization and photoluminescence properties. J. Nanosci. Nanotechnol. 9 (12), 6866–6875.

Wang, L., Zhang, Z. L., Cui, R., Liu, H. H., Li, J., Liu, S. L., et al., 2010. Dynamic tracking of single cell synthesis of cdse quantum dots with a microflufidic device. In: Proceedings of the Fourteenth International Conference on Miniaturized Systems for Chemistry and Life Sciences, pp. 1868–1870.

Wu, S.M., Su, Y., Liang, R.R., Ai, X.X., Qian, J., Wang, C., et al., 2015. Crucial factors in biosynthesis of fluorescent CdSe quantum dots in *Saccharomyces cerevisiae*. RSC Adv. 5 (96), 79184–79191.

Xu, X., Yang, Y., Jin, H., Pang, B., Yang, R., Yan, L., et al., 2020. Fungal in situ assembly gives novel properties to CdSxSe1−x quantum dots for sensitive label-free detection of chloramphenicol. ACS Sustain. Chem. Eng. 8 (17), 6806–6814.

Xu, L.X., Wang, Y.Z., Zhou, D., Chen, M.Y., Yang, X.J., Ye, X.M., et al., 2021a. Bio-metabolism-driven crystalline-engineering of CdS quantum dots for highly active photocatalytic H2 evolution. ChemistrySelect 6 (15), 3702–3706.

Xu, X., Yang, Y., Jin, H., Pang, B., Jiang, C., Shao, D., et al., 2021b. Filamentous fungal in situ biosynthesis of heterogeneous Au/Cd0.5Zn0.5S nano-photocatalyst: a macroscopic assembly strategy for preparing composite mycelial pellets with visible light degradation ability. J. Hazard. Mater. 406. Available from: https://doi.org/10.1016/j.jhazmat.2020.124797.

Yamaguchi, T., Tsuruda, Y., Furukawa, T., Negishi, L., Imura, Y., Sakuda, S., et al., 2016. Synthesis of CdSe quantum dots using *Fusarium oxysporum*. Mater 9 (10). Available from: https://doi.org/10.3390/ma9100855.

Yan, Z., Qian, J., Gu, Y., Su, Y., Ai, X., Wu, S., 2014. Green biosynthesis of biocompatible CdSe quantum dots in living *Escherichia coli* cells. Mater. Res. Express 1 (1). Available from: https://doi.org/10.1088/2053-1591/1/1/015401.

Yan, Z.Y., Ai, X.X., Su, Y.L., Liu, X.Y., Shan, X.H., Wu, S.M., 2016. Intracellular biosynthesis of fluorescent CdSe quantum dots in *Bacillus subtilis*: a strategy to construct signaling bacterial probes for visually detecting interaction between *Bacillus subtilis* and *Staphylococcus aureus*. Microsc. Microanal. 22 (1), 13–21.

Yan, Z.Y., Du, Q.Q., Qian, J., Wan, D.Y., Wu, S.M., 2017. Eco-friendly intracellular biosynthesis of CdS quantum dots without changing *Escherichia coli*'s antibiotic resistance. Enzyme Microb. Technol. 96, 96–102.

Yan, Z.Y., Yao, C.X., Wan, D.Y., Wang, L.L., Du, Q.Q., Li, Z.Q., et al., 2018. A sensitive and simple method for detecting Cu2 + in plasma using fluorescent *Bacillus amyloliquefaciens* containing intracellularly biosynthesized CdSe quantum dots. Enzyme Microb. Technol. 119, 37–44.

Yang, Z., Lu, L., Berard, V.F., He, Q., Kiely, C.J., Berger, B.W., et al., 2015. Biomanufacturing of CdS quantum dots. Green. Chem. 17 (7), 3775–3782.

Yang, Z., Wang, Y., Zhang, D., 2018. A novel signal-on photoelectrochemical sensing platform based on biosynthesis of CdS quantum dots sensitizing ZnO nanorod arrays. Sens. Actuators B: Chem. 261, 515–521.

Yu, G., Liang, J., He, Z., Sun, M., 2006. Quantum dot-mediated detection of γ-aminobutyric acid binding sites on the surface of living pollen protoplasts in tobacco. Chem. Biol. 13 (7), 723–731.

Yue, L., Qi, S., Wang, J., Cai, J., Xin, B., 2016. Controllable biosynthesis and characterization of α-ZnS and β-ZnS quantum dots: comparing their optical properties. Mater. Sci. Semicond. Process. 56, 115–118.

Zaman, M.B., Poolla, R., Singh, P., Gudipati, T., 2020. Biogenic synthesis of CuO nanoparticles using *Tamarindus indica* L. and a study of their photocatalytic and antibacterial activity. Environ. Nanotechnol. Monitor. Manage. 14. Available from: https://doi.org/10.1016/j.enmm.2020.100346.

Zhang, Y., Xiao, J.Y., Zhu, Y., Tian, L.J., Wang, W.K., Zhu, T.T., et al., 2020. Fluorescence sensor based on biosynthetic CdSe/CdS quantum dots and liposome carrier signal amplification for mercury detection. Anal. Chem. 92 (5), 3990–3997.

Chapter 7

Microwave-assisted synthesis of quantum dots

Chetna Ameta, Yogeshwari Vyas, Priyanka Chundawat and Dharmendra
Department of Chemistry, M. L. S. University Udaipur, Rajasthan, India

7.1 Introduction

Quantum dot (QD) materials have huge potential for the expansion of novel analytical approaches because of their tiny nanosizes, typically <10 nm for various specific applications (Kumar et al., 2018). Over the last few decades, QDs of different materials have attracted increasing attention in various research fields, for example, as fluorescent biological labels, solar cells, and optoelectronic transistor components, as they have unique size-tunable electronic and optical properties (Kim and Yoon, 2014). Carbon-based QDs, for example, graphene QDs (GQDs), carbon QDs (CQDs), and several types of semiconducting QDs have potential in planning and tuning fluorescent probes (Lim et al., 2015). The zero-dimensional (0D) GQDs generated using top-down methods like electrochemical synthesis, chemical ablation from graphene, oxygen plasma treatment, etc. display a dynamic area of superior interest (Wang et al., 2015a,b). The semiconducting QDs, particularly cadmium telluride (CdTe), cadmium selenide (CdSe), and cadmium sulfide (CdS), have been investigated extensively due to their fluorescent properties in the near-infrared, infrared, and observable spectra (Rodrigues et al., 2017). Lee et al. (2004) reported the production and analysis of size-sensitive and outstanding selective QD structures. Several methods have been employed for synthesizing QD structures using various chemicals; although other synthesis techniques are time-consuming and require costly equipment. Consequently, there is a necessity for a quick, sensitive, simple, and selective process for large-scale production of all types of QDs.

Research is focused on precise experiments for less time-consuming, facile, and fast synthetic methods without losing any heat into the surroundings. Microwave (MW)-aided synthesis provides a facile and fast approach, since it has an alternate energy source and it is exploited widely due to its power of control on volumetric and inner heating of constituents (Agranovich et al., 2017).

Quantum Dots. DOI: https://doi.org/10.1016/B978-0-12-824153-0.00007-0
© 2023 Elsevier Inc. All rights reserved.

Recently, more attraction has been paid to MW-assisted generation of inorganic/organic nanostructured materials in different media (gaseous and liquid) and future studies are significant. MWs are largely employed in the synthesis of QD materials, since the interaction is strong with MW rays generating uniform heating and higher heating rates. Thus MW synthesis of metal oxides supported on graphene sheets (Kumar et al., 2014), metal oxide NPs (nanoparticles), and nanostructured carbon materials (Zhang and Liu, 2012) has been studied. Apart from (3D) carbon hybrid metal such as oxide-held graphene and CNTs, activated carbons and carbon nanocapsules were also synthesized (Hu et al., 2012). The MW-assisted path is a quite promising, clean, economic, and low-temperature synthetic route with huge potential. One of the ultimate and notable advantages is that it yields a specific shape and size of QD that depends on the experimental parameters. These MW-assisted synthesized QDs are useful for current and developing technologies and may play a noteworthy role in numerous research areas.

The basic use of MW technology is in the field of transmission of energy or telecommunication by electromagnetic waves. MWs are electromagnetic radiation, ranging between infrared radiation and radiofrequencies. These have frequencies between 300 GHz (1 mm) and 0.3 GHz (1 m). The irradiation technique for rapid heating is based on the principle that materials absorb electromagnetic energy and convert it into heat. The electromagnetic energy transferred from MWs to the irradiated material is believed to occur either through relaxation or resonance. Only contracted frequency windows located at 0.915 and 2.54 GHz are appropriate for MW heating purposes. The MW entails coordinated perpendicular oscillations of magnetic and electric fields. These MW rays are absorbed by materials causing heating, which is known as dielectric heating. This heating is not the same as in the case of conventional form of heating, since energy is transferred in the form of radiation at the surface in MW heating, whereas thermal energy is transported to the material's bulk through conduction.

MW heating is a quick and simple process which is why it is widely employed nowadays in academia and industries for the synthesis of several kinds of QDs. This process results in speedy and even heating (volumetric). Thus, MW is an essential tool in all branches of green synthesis approaches since the time of its origin (Giguere et al., 1986). A wide range of QDs can be synthesized for industrial uses by putting extra efforts into MW-aided synthesis.

7.1.1 Advantages

The MW-assisted production of QDs has numerous advantages compared to conventional routes. The major benefit is the molecular interaction of reagents with an electromagnetic field without direct contact. This method is safe, eco-friendly, with energy proficiency and selectivity, and provides high

yield in a shorter time. All such advantages of MW-assisted synthesis are shown in Fig. 7.1.

7.1.2 Disadvantages

Apart from the many advantages of MW-assisted synthesis, there are some disadvantages or limitations associated with its use in organic synthesis.

1. There is lesser penetration depth in some cases.
2. Metallic substrates or metallic reagents cannot be used for synthesis.
3. Only polar solvents are used, which can interact with the MW.
4. Heating reactions above boiling point of the solvent can generate high pressure, which may cause an explosion.
5. In some cases, the yields are not reproducible because of uneven heating, particularly while using a domestic MW oven.

7.2 Synthesis of core-type quantum dots

Core-type QDs are made up of a single material, basically a metallic chalcogenide like CdTe, CdS, CdSe, PbS, SnO_2, etc. The existing oil-bath heating techniques transfer heat internally from the source (heat), while radiowaves in MW-mediated heating exactly pierce the wall of the vessel to excite polar units like alcohol, water, and fatty acids. Polar molecules absorb this radiation and transform it directly into nuclear motion to convert it into heat. The complete procedure is different from ordinary oil-bath heating since the heat is generated via a native domain by exciting molecules/atoms rather than

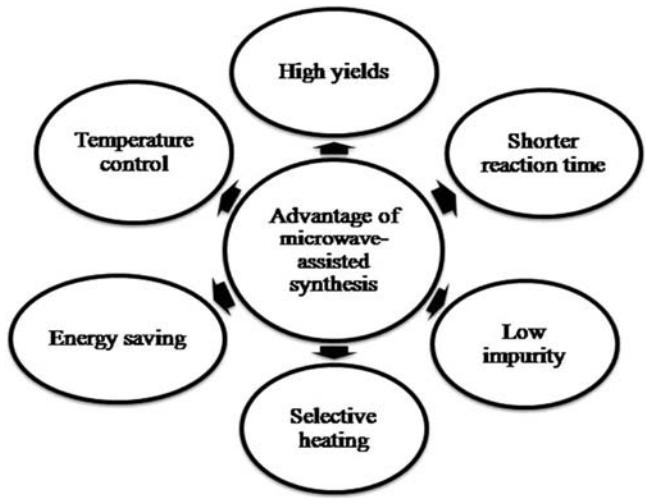

FIGURE 7.1 Advantages of microwave-assisted synthesis.

conduction. Hence, there is no need to drift heat internally by conduction, since all particles are excited simultaneously in the MW field. The use of MW heating in accelerating chemical reactions has fascinated the scientific world extensively in the last few decades. The reducing time of the reaction is not only its merit but it has improved controllability, allowed larger production yields, greener reactions, and reproducibility.

7.2.1 Oxide quantum dots

7.2.1.1 SnO_2 quantum dots

Semiconductor QDs such as tin oxide are attractive materials because of their unique physical and optical properties (Han et al., 2010; Bajorowicz et al., 2018). Tin oxide (SnO_2) has a broad bandgap of 3.6 eV at room temperature. It is a pure n-type semiconductor oxide and it has been widely used in gas sensors, dye-sensitized solar cells (DSSCs), photocatalysts, lithium-ion batteries, and transparent electrodes (Shi and Lin, 2010; Wang et al., 2011a; Wang et al., 2012; Song et al., 2013). Various methods are available for the production of tin oxide such as wet chemical method, laser ablation routes, and MW irradiation technique (Pang et al., 2001; Xiao et al., 2010; Wang et al., 2012, Singh et al., 2012). But most of them require the use of toxic poisonous compounds, critical reaction conditions, and long periods of time. Therefore, there is a challenge for the synthesis of SnO_2 QDs in a fast facile, greener way on an industrial scale. Among several approaches, MW heating has several advantages including better control over the size, lesser reaction time, and even nucleation of precipitates in suspension. Several research teams have utilized MW technique for synthesizing SnO_2 QDs (Xiao et al., 2010; Liu et al., 2013; Bhattacharjee and Ahmaruzzaman, 2015; Begum et al., 2016; Zhu et al., 2016).

Liu et al. (2013) fabricated SnO_2 QDs using MW-irradiation in 10 min. at 150°C with (150 W). These QDs were then used for photocatalytic degradation of methylene blue. The $SnCl_4$ was used as a source of tin. It was revealed that QDs were having particle size of about 3−5 nm. A green synthetic technique was developed for preparation of SnO_2 QDs using MW irradiation. Amino acids (aspartic, glutamic, L-lysine, serine) were used by them. (Bhattacharjee and Ahmaruzzaman, 2015; Begum et al., 2016).

Bhattacharjee and Ahmaruzzaman (2015) obtained globular SnO_2 QDs, when aspartic or glutamic acid (amino acids) and stannous chloride were used as starting materials. It was revealed that diameter of SnO_2 was found to be 1.6 and 2.6 nm for glutamic and aspartic acid, respectively. As-produced QDs were used as an efficient photocatalyst in degradation of two dyes; eosin Y and rose Bengal in presence of solar isolation.

Begum et al. (2016) prepared SnO_2 QDs using L-lysine monohydrate, and sodium dodecyl sulfate (surfactant) under MW exposure. They used these QDs in degradation of humic acid. Then the reaction solution was

given MW treatment. It was revealed that sizes of SnO_2 QDs obtained was 2.3 nm. They used these QDs for degredation of humic acid on solar exposure for 3 h. Begum and Ahmaruzzaman (2018) used *Parkia speciosa* Hassk pods extract in a green economical and less time-consuming process for synthesizing SnO_2 QDs in presence of MW irradiation. As-produced QDs were then used in photodegradation of acid yellow 23. It was reported that QDs also have scavenging activity. It was revealed that average crystallite size of as-obtained SnO_2 QDs was found in the range of 1.5−1.9 nm.

Tin oxide QDs have been prepared by Zhu et al. (2016) using a MW-assisted method. It was reported that SnO_2 QDs (organic component-wrapped) can be synthesized with size 2−4 nm in only 30 s. If these SnO_2 QDs can be obtained by annealing the organic component-wrapped SnO_2 QDs in air at 400°C in 4 h, then QDs with good crystallinity and bigger size (5−10 nm) could be obtained. As-prepared QDs exhibited an excellent sensitivity toward vapors of ethanol as a sensor.

Zhu et al. (2016) reported MW-aided preparation of SnO_2 QDs. They used a mixture of $SnCl_4$, oleic acid (OA), C_2H_5OH, oleylamine (OLA), and H_2O and exposed it to MW (200 W) for different time intervals (0.5−20 min). It was revealed that QDs with diameter of 2−4 nm could be obtained on 0.5 min exposure, but on increasing time to 20 min, QDs are obtained with a larger size of 8−20 nm. Xiao et al. (2010) prepared highly crystalline QDs of SnO_2 under MW irradiation. This involved dissolving $Sn(OtBu)_4$ and 1-butyl-3-methylimidazolium tetrafluoroborate (desiccated) in an inert atmosphere of argon and 1 min exposure to MW irradiation. As-obtained SnO_2 QDs were spherical, monodispersed, and crystalline in nature with size of 4.27 ± 0.67 nm.

A synthetic route was reported by Parthibavarman et al. (2019) for pure and Ag-doped SnO_2 QDs under MW irradiation. It was revealed by TEM images that average particle size of QDs increases on Ag doping. A smaller bandgap (3.54−3.09 eV) was observed on Ag doping. The photocatalytic degradation of rhodamine B and methylene blue was observed in with as-obtained catalyst. A maximum efficiency (97.5%) for degradation of rhodamine B could be achieved in the presence of visible light irradiation. As-obtained Ag−SnO_2 QDs catalyst can be reused and these are stable after even seven cycles.

Mohanta and Ahmaruzzaman (2020) used *Allamanda cathartica* leaf extract for synthesis of SnO_2 QDs. They boiled chopped leaves in water and stannous chloride solution was added dropwise under continuous sonication. On addition of carbon nanoflakes and sonication, a greyish solution was obtained. This solution was exposed to MWs. As-obtained SnO_2 QDs were then used for the removal of bisphenol A.

7.2.1.2 Co_3O_4 quantum dots

Uniform Co_3O_4 octahedrons were obtained by Zhang et al. (2012a,b) via a MW method. Here, various carbon materials were used, which not only acted

as a secondary heater, but also as an agent for directing morphology. A weak ferromagnetic property was found in octahedral Co_3O_4 as-obtained carbon nanotubes using MW.

Zhou et al. (2014) synthesized Co_3O_4 QDs/graphene composites via a MW irradiation method. The crystals of Co_3O_4 were found to be in the size of 3−8 nm. These composites exhibited a high rate capability as well as enhanced cycling performance on use as anode materials for Li-ion batteries. In addition, the well-dispersed Co_3O_4 nanodots and the synergetic effect between graphene nanosheets (conductive and flexible) also gave a better electrochemical performance due to reducing the diffusion pathway of lithium ions and the high surface area.

7.2.1.3 ZnO quantum dots

Lu et al. (2011) synthesized ZnO QDs using zinc sulfate heptahydrate as a precursor. They mixed a Zn precursor with GO. They utilized NaOH for precipitation, where a chocolatey−black suspension was obtained. It was then placed in a MW for half an hour at 150°C. The as-prepared product was filtered and dried at 70°C for a day. This composite was utilized for electrochemical superconductors, and it was proved that ZnO QDs exhibited enhanced activity as compared to GO only.

The Ag and Sn-doped ZnO QDs (ZQDs) were synthesized by Soumya et al. (2018) via a MW-assisted sol−gel method. They used 3-aminopropyl trimethoxy silane as a capping agent. As-obtained ZQDs were then dispersed in methyl methacrylate (MMA) monomer to obtain polymethyl methacrylate (PMMA)/ZQDs. It was observed that doped PMMA/ZQDs hybrid coatings exhibited a blue emission in the presence of UV light. A photochromic dye (spiropyran) was introduced in the doped PMMA/ZQDs hybrids and it displayed photochromic behavior with a red emission. This hybrid can be used in solar radiation control active interface layers.

Rangel-Mendez et al. (2018) reported solvothermal synthesis of C-doped ZnO and TiO_2 hybrid materials under MW irradiation. Titanium isopropoxide, saccharose, and zinc acetate were used as sources of Ti, Zn, and C, respectively. There was a redshift in bandgap of these semiconductors. The TiO_2-C and ZnO-C was obtained (3.02 and 3.13 eV), which was attributed to C-doping effect. It was indicated that these present materials can find application as photoelectrodes for QD-sensitized solar cells (QSSCs).

The nanocomplex was prepared of ZnO QDs by a MW-assisted reaction in the presence of avobenzone (Av) (Asok et al., 2018). It was reported that ZnO QDs can catalyze the formation of highly photostable surface enolate species via an aldol condensation reaction. It was observed that molar absorptivity and photostability was extended beyond the UV-A filtering range, and therefore it can provide a visible emission color matching human skin.

7.2.1.4 WO_3 quantum dots

Le Houx et al. (2009) carried out the synthesis of WO_3 QDs by both MW and conventional heating and compared the results. It was reported that particles obtained with MW-heating were more suitable compared to conventional heating or routine preparation. There have greater specific surfaces and particle size, ranging between 5 and 30 nm.

Wang et al. (2015a,b) fabricated tungsten oxide QDs using a one-pot MW-assisted method. It was reported that as-obtained WO_3 QDs have a size ranging from 2 to 3 nm. These WO_3 QDs exhibited significant photonic/thermal stabilities. It was interesting to note that a colorless aqueous suspension of WO_3 QDs turned blue in the presence of sunlight in 10 s indicating its photochromic behavior. This type of behavior was attributed to surface oxygen vacancies as well as exposed reactive sites of ultrafine WO_3 QDs.

7.2.1.5 SiO_2 quantum dots

Mao et al. (2014) prepared N-acetyl-L-cysteine-stabilized CdTe/CdS@ZnS−SiO_2 QDs red-luminescent under MW irradiation. The Stober method was used for coating silica on CdTe/CdS QDs. The as-compared QDs exhibited high photoluminescence (PL), low biotoxicity, and superoptical stability. They utilized the QDs in a low-power surface-mounted and a high-power device.

7.2.1.6 CeO_2 quantum dots

Lehnen et al. (2014) prepared CeO_2 QDs via MW-solvothermal synthesis of N-methylpyrrolidone. The synthesis procedure involves a MW reactor at 50 W at 150°C and 1.5 bar for 5−15 min. It was observed that crystallinity of CeO_2 QDs was improved, when reaction time was kept at 15 min. The product was collected after centrifugation and purification. The average size of CeO_2 QDs was found to be 4.3 nm. He et al. (2017) synthesized CeO_2 QDs using a MW-assisted method. A mixture of OLA and cerium (III) nitrate hexahydrate was first heated for half an hour at 80°C under vacuum and then placed in a MW oven at 180°C. These QDs were cooled down and washed and were then kept dispersed in tetrahydrofuran and stored at −20°C.

Soren et al. (2015) fabricated CeO_2 QDs via MW-assisted synthesis. In MW-hydrothermal synthesis, autoclave cerric ammonium nitrate and NaOH were used in the ratio (1:6) with water and pH was adjusted to 10 and exposed to MW irradiation, while in MW solvothermal synthesis, cerric ammonium nitrate and 1,4-butanediol were used and pH was maintained at 6. This mixture was then exposed to MW rays for 20 min. It was revealed that MW-mediated solvothermal method could yield less agglomerated and smaller size QDs (5−10 nm), whereas larger NPs size (15−20 nm) was produced on using the MW-mediated hydrothermal technique.

7.2.1.7 TiO_2 quantum dots

Alves et al. (2018) reported the synthesis of graphene-TiO_2 QDs via the MW-oleothermal method. They mixed OLA, graphene oxide (GO), OA, 98% titanium propoxide, and Triton-X under magnetic stirring at ambient conditions, which was followed by the oleothermal method and sonicated for 15 min in the presence of MW radiation. It was observed that the diameter of synthesized QDs was found to be around 3 nm.

7.2.1.8 MoO_2 quantum dots

Cao et al. (2020) fabricated phosphorus and nitrogen codoped MoOx QDs (N,P-MoOx QDs) using MW-assisted method. The $H_3P(Mo_3O_{10})_4.xH_2O$, glutathione (GSH), and ultrapure water were mixed, stirred, and sonicated for 5 min. The mixture was placed under MW radiation in an autoclave for 8 min after adding ammonium solution.

7.2.1.9 CuO quantum dots

The CuO QDs were prepared by Bekru et al. (2021) using the MW-assisted modified method. They used copper acetate as the source of copper extract of leaves of *Cordia africana* Lam. Then, the mixture was irradiated by MWs (1000 W) for 9 min. A brown precipitate of CuO QDs was obtained and thius were utilized in the reduction of 4-nitrophenols. Felix et al. (2015) also synthesized CuO QDs using a MW-assisted method. An average size of CuO QDs was found to be about 4 nm. As-prepared CuO QDs exhibited high sensitivity for electrochemical sensing as compared to their microcounterparts.

7.2.2 Sulfide quantum dots

7.2.2.1 CdS quantum dots

Alehdaghi et al. (2020) obtained CdS QDs and examined the consequence of gamma radiation on their chemical and physical properties. These QDs were prepared in less than 10 min under MW radiation. They studied the PL and transmittance characteristics of CdS QDs. The size of CdS QDs was confirmed as 3−4 nm from TEM analysis. It was revealed that degradation of PL of QDs was found to be inversely dependent on concentration. The redshift was found to be more with a lower size of QDs. It was claimed that as-prepared CdS QDs may be promising material for use as a gamma dosimeter.

Zheng et al. (2010) synthesized mesoporous CdS QDs via a simple and cost-effective method (in situ conditions). They used OA. A soft template for MW treatment was used instead of sintering, because the mesostructure is destructed under this condition. It was observed that on adding Na_2S, the color of the gel changed to yellow. It was revealed that both these samples of CdS QDs (naturally evaporated and MW irradiated) had a size of 3−4 nm.

Fregnaux et al. (2013) made a comparative study of CdS formation via single-source precursor methodology (SSPM) and MW synthetic route (MWSR). The average particle size of QDs ranged between 4.5−5.2 and 2.8−4.5 nm when prepared with MWSR and SSPM techniques, respectively. It was observed that CdS QDs prepared by MWSR had a cubic structure, while SSPM afforded QDs with hexagonal structure. It was also concluded that there is better optical quality in MWSR-grown QDs. It was revealed that a stable behavior of QDs was due to the absence of S vacancies when treated in air.

Alehdaghi et al. (2014) synthesized CdS QDS by dissolving both in S as well as Cd precursor deionized water, followed by the addition of TGA. It turned into a milky solution, which was made transparent by adding ammonia. This solution was then exposed to MWs for various time intervals to afford QDs of different sizes. Liu et al. (2014) synthesized CdS QDs using the MW-assisted chemical bath deposition technique. They utilized thiourea and cadmium nitrate as precursor solutions. Then TiO_2 film was introduced containing a precursor solution, and it was placed under MW exposure for 20 min. The crystal size of as-obtained QDs was found to be 5 nm.

Butova et al. (2017) prepared CdS QDs via a MW hydrothermal method in 5 min. They stabilized these QDs with 4,4'-bipyridine and dioctyl sodium sulfosuccinate. They also investigated the impact of different capping mediators on particle shape, size distribution, and properties. They used cadmium nitrate as precursors. It was revealed that Cds QDs were about 5 nm in size. It was revealed that smaller particle size was obtained when 4, 4'- bipyridine was used as a stabilizer.

The CdS QDs were also prepared by Radzi et al. (2020). They used a mixture of solutions of $C_{10}H_{17}N_3O_6S$ (GSH), and $CdCl_2$, and added Na_2S to these drop wise. This mixture was heated at 150°C in a MW reactor for 1 min only. It was revealed that the average diameter of CdsQDs produced was found to be 5.8 ± 0.3 nm. These QDs were embedded into PVA (polyvinyl alcohol) (matrix film) and were used in an absorber in Q-switches.

7.2.2.2 ZnS quantum dots

ZnS is a significant type of II-VI semiconductor QD because of its luminous properties. ZnS crystals are in two phases: hexagonal phase (wurtzite form) and cubic phase (zinc blende, sphalerite). The bandgap of ZnS falls in the range of 3.68−3.80 eV. It was observed that the cubic phase of ZnS is more stable at lower temperatures, but at higher temperatures it transforms to its wurtzite phase. MW-irradiation is an efficient and eco-friendly method as it provides high-purity particles, a greater yield of QDs, requires a simple reaction medium, has a lesser reaction time, and is an economically visible route. Here, capping agents may play an important role in enhancing the properties of QDs, such as luminescent nature, stability, and morphology, which prevents their agglomeration.

Ayodhya and Veerabhadram (2018) prepared ZnS QDs (undoped and doped) under MW irradiation. They used Rh^{3+}, Pd^{2+}, and Zr^{2+} as dopant materials. The precursor solutions (zinc acetate and sodium sulfide) were prepared in water. The white colored ZnS was obtained on MW irradiation (1000 W) on exposure of a mixture of precursor solutions for 10 min. Undoped and doped ZnS QDs were prepared in the absence and presence of dopant. The structure of ZnS QDs was cubic and the size of these as-prepared QDs ranged between 2 and 10 nm. It was observed that both these ZnS QDs exhibited superior fluorescence quenching with the cysteine molecules and these can be used as an efficient fluorescent material for quenching and binding practices.

Mathew et al. (2010) fabricated folic acid (FA) conjugated carboxymethyl chitosan (CMC), which was coordinated to Mn-doped ZnS QD (FA−CMC−ZnS:Mn) nanoparticles. The zinc acetate, manganese sulfate, and sodium sulfide were used as precursors of zinc, manganese, and sulfur, respectively. A white colloid was obtained, which was treated under MW irradiation for 1 min. These as-obtained QDs were utilized for monitoring, targeting drug delivery, and imaging of breast cancer cells.

Shahid et al. (2012) reported MW-assisted fabrication of ZnS QDs (wurtzite). The size of as-obtained QDs was 3 nm. Saravanan et al. (2012) made a comparison between MW and conventional techniques for preparation of ZnS QDs. They used sodium sulfide and zinc acetate as the source of sulfur and zinc, respectively. It was revealed that the size of QDs prepared using the MW method was very small (diameter $\sim$3 nm). It was revealed that these QDs were almost 30 times smaller than those produced by the conventional method. The bandgap of bulk ZnS was 3.67 eV, which was found to increase to 3.9 eV on MW treatment.

Zhu et al. (2014) synthesized Mn-ZnS QDs via MW-assisted technique. Zinc nitrate and manganese chloride were selected as the source of zinc and manganese, respectively. A solution of sodium sulfide was added to sodium palmitate solution. The mixture was kept under MW irradiation (260 W) for 35 min. It was revealed that the average particle size of Mn−ZnS QDs was found to be 4.2 nm as evident from HRTEM images.

He et al. (2019) reported a facile method of producing copper-doped ZnS QDs (ZnS:Cu QDs) using MW irradiation. They used 3-mercaptopropionic acid as a source of sulfide as well as a stabilizer. The copper sulfate and zinc acetate were used as precursor of copper and zinc, respectively. It was observed that the size of QDs increased very little from 4.1 to 4.7 nm on increasing the time from 10 min to 2 h. As-prepared ZnS:Cu QDs were utilized in the lighting device. It was interesting to note that as the time of exposure was increased, the emission color of ZnS:Cu QDs changed from blue → green → yellow → orange−red.

Shaheen et al. (2020) synthesized zinc sulfide QDs by MW route. They found 1-dodecyl-3-ethylimidazolium bromide, surface active ionic liquid

suitable as a capping agent because of its amphiphilic nature, superior aggregation property, and eco-friendly behavior. As-obtained QDs were found to be thermally stable with a size of 3.03 nm (diameter). They also reported their application as a sensor for ascorbic acid. The fluorescence property of QDs was attributed to high sensitivity, low cost, and ease.

7.2.2.3 PbS quantum dots

He et al. (2012) prepared PbS QDs. They used lead chloride and thioacetamide as the source of lead and sulfur, respectively, and 3-mercaptopropionic acid as a stabilizer. The reaction mixture was exposed to MW irradiation (960 W) only for 40 s. As-obtained PbS QDs solution was light gray-green in color and the particle size of PbS QDs was 5 nm in diameter.

Liu et al. (2019) embedded $Pb(DMDC)_2$ with PbS QDs by reducing dimethyl dithiocarbamate (DMDC) in ethanol. It was further treated by MW and ultrasonic−irradiation (200 W). The color of the solution was finally changed from colorless to black, which indicates the formation of PbS QDs.

Molaei et al. (2020) prepared PbS QDs in water using LG as a stabilizer and for distribution in the blood transmission. They mixed lead acetate and LG before the treatment by MW irradiation for 30 s after addition of sodium sulfide.

7.2.2.4 CuS quantum dots

Nethravathi et al. (2019) utilized MW irradiation in the synthesis of CuS QDs. They used sonication before MW exposure. They used copper hydroxydodecylsulfate and thiourea as a precursor of copper and sulfur, respectively. The resulting mixture was treated with MW (800 W) for 5 min. Black colored CuS QDs were obtained. These QDs were used for photocatalytic degradation of methylene blue, methyl orange, and 4-chlorophenol in sunlight. They were separated via centrifugation and purified by washing and then dried.

CuS QDs were synthesized by Chaudhary et al. (2014) in very high yield in MWs in 2 min. The particle size of as-obtained QDs was in the range of 2−3 nm. These CuS QDs were used as a catalyst in Biginelli reaction under solvent-free conditions affording dihydropyrimidinones in excellent yields. This catalyst can be recovered and reused for a number of cycles. Malankowska et al. (2020) obtained CuS_2 QDs under MW irradiation. The size of CuS_2 QDs was found to be 2−3 nm. The efficiency of CuS_2 QDs and QDs-sensitized TiO_2 composites was evaluated in the degradation of toluene under LED irradiation.

7.2.2.5 AgS quantum dots

Mir et al. (2018a) prepared silver indium sulfide (AIS@ZnS) core−shell QDs via a MW-assisted method. They used a stabilizer GSH. The appearance of a

golden color indicates the formation of silver−indium sulfide QDs. An average diameter of core and core−shell nanocrystals diameter was found to be 2.5−3.25 nm, with corresponding bandgap and yield of 2.3−3.1 and 2.4−3.5 eV and 26% and 49%, respectively. The core−shell QDs display color-tunable production in the noticeable region (500−600 nm) by varying the Ag:In molar ratio.

Mirahmadi et al. (2020) synthesized Ag_2S and Ag_2S@ZnS QDs via a MW method. These as-prepared Ag_2S and Ag_2S@ZnS QDs were used as cosensitizers in the fabrication of QDs solar cells (QDSCs), where an enhancement of cell efficiency (3%) and short current density (12.5 mA cm^{-2}) could be achieved.

7.2.3 Selenide quantum dots

7.2.3.1 CdSe quantum dots

Attempts were made to produce CdSe QDs (Peng and Peng, 2001; Li et al., 2003). Here, organic phosphine and cadmium oxide/organometallic precursors were utilized as ligand and crude material in a temperature range of 250°C−350°C. As-produced CdSe NPs were found to be soluble only in nonpolar solvents unless some surface modification is made. It has been observed that PL of CdSe QD was reduced, if any surface alteration is being made since it is hypersensitive to the surface characteristics (Nazzal et al., 2003). So, it is necessary to develop a directly water-soluble production route. The commercial preparation of CdSe has its own limitations, such as the use of poisonous organic phosphines, elevated temperature, and costs linked with oxygen-free equipment. Therefore, there is a necessity for a pathway that is greener, with harmless chemicals, lower temperatures, and fast reaction method. The CdSe QDs can be utilized in photovoltaic biomedical engineering lasers and solar drive cells (Peng, 2002; Pradhan and Peng, 2007). The MW-assisted heating method is easy as well as there is swift control of the reaction.

Wang et al. (2004) were able to produce fairly stable CdSe NPs utilizing MW heating of 1,1-dimethylselenourea and cadmium perchlorate (in the presence of citrate). They used MW (900 W) for preparation of CdSe QDs. Zhu et al. (2009) reported MW-assisted synthesis of CdSe QDs. They used OA as a nonphosphine ligand. Cadmium oxide and diesel were mixed with OA, followed by the addition of selenium powder in diesel and glycerol. This mixture was exposed to MW (170 W) for 2 min.

A rapid MW-assisted process was developed by Zhang et al. (2012a,b) to produce protein-conjugated CdSe QDs. They used ribonuclease A (RNase A) as a template for the generation of CdSe clusters. These clusters were found to be less toxic and exhibited excellent stability. The MW exposure was required for 5 min. It was revealed that the shape of QDs was regular

spherical with an average size of 5 nm. Moghaddam et al. (2012) reported a one-pot protocol for the synthesis of monodispersed colloidal CdSe QDs with the help of MW radiation. Here, 1-octadecene (ODE) played a dual role of a solvent and reducing agent. They observed that CdSe QDs can be fabricated with different sources of cadmium, where their particle sizes ranged between 0.5 and 4 nm.

Xuan et al. (2013) prepared CdSe QDs via MW-assisted synthesis for use in white light-emitting diodes with outstanding color rendering features. It was reported that size and optical properties of these QDs can be modified by changing the MW power growth temperature as well as reaction interval and molar ratio of Cd^{2+} with Se. It was revealed that as-produced QDs exhibited spherical shapes with a diameter of 4.8 nm.

CdSe QDs were prepared by Mehrjoo et al. (2017) using the MW-assisted method. They used TGA as a capping agent and $CdSO_4$ and Na_2SeO_3 as precursors. The MW (720 W) was used for 90 s for their synthesis. It was reported that as-produced CdSe QDs were found to be 5 nm in size. Then, these QDs were used for the degradation of methyl orange.

Abolghasemi et al. (2019) also used an MW-assisted method for the production of CdSe QDs. They used CdO and Se powder as precursors. It was observed that the particle size of CdSe QDs varied in the range of 5−7 nm. It was indicated that as-prepared QDs can be used in solar cells (as a sensitizer) with an efficiency of 3.57%.

7.2.4 Telluride quantum dots

7.2.4.1 ZnTe quantum dots

Alvand et al. (2019) synthesized zinc telluride QDs (ZnTe QDs) using the aqueous extract of *Ficus johannis*. Ultrasonic as well as MW techniques were applied for the preparation of plant extracts, which can be utilized as stabilizing precursors during the synthesis of ZnTe QDs. The nanoparticles of ZnTe QDs had an average size of 8 nm. It was reported that as-prepared QDs produced antimicrobial, antifungal, and antioxidant properties.

A series of $Zn_{1-x}Pm_xTe$ QDs was synthesized by Al-Harthi et al. (2021) via 4,4-bis-*N*-1-naphyl-*N*-phenylaminobiphenyl through MW-assisted method. These QDs showed remarkable optoelectronic properties. It was observed that the bandgap of ZnTe QDs was reduced from 3.06 to 2.8 eV in the presence of promethium ions and particle size was increased from 1.4 to 4.3 nm. The inclusion of promethium ions in these QDs ions was found to be responsible for tuning the color of QDs in the visible region. It was suggested that as-prepared $Zn_{1-x}Pm_xTe$ QDs can find potential application in photovoltaic devices.

Du et al. (2012) developed a MW-assisted method for synthesis of GSH-capped $Zn_{1-x}Cd_xTe$ alloyed QDs. They used Na_2TeO_3 as a source

of tellurium. The photoluminescent quantum yield of as-synthesized alloyed QDs could reach up to 90%. As-prepared $Zn_{1-x}Cd_xTe$ alloyed QDs have a potential as biological fluorescent labels in different biological applications.

Zhan et al. (2013) prepared CdSe QDs covered by double-shells of CdZnS and CdS using a one-pot MW-assisted route. It was reported that as-prepared CdSe/CdS/CdZnS core−shell−shell (CSS) QDs exhibited high crystallinity and high-fluorescence quantum yield of 90%. As-obtained QDs also displayed stability toward light, acid, and oxidation. These CSS particles have an average size of QDs around 3.2 nm. It was revealed that as-prepared QDs can find a potential for fluorescent QDs-based biological applications.

Kim and Kim (2016) synthesized CdZnTe QDs using MW irradiation in aqueous solution. They used 3-mercaptopropionic acid as a stabilizer. Zinc nitrate, cadmium nitrate, and NaHTe were used as precursors of Zn, Cd, and Te, respectively. It was reported that absorbance spectra and PL of these QDs exhibited a redshift.

7.2.4.2 CdTe quantum dots

CdTe has found varied applications like sensors, photovoltaic devices, bioimaging, and biolabeling because of its higher quantum efficiency. These are synthesized via aqueous and nonaqueous methods such as thermal breakdown, solvothermal, MW, and sonochemical treatment routes. MW irradiation has several advantages over other methods.

He et al. (2006) synthesized CdTe QDs with a MW-assisted method. They used NaHTe and $CdCl_2$ as precursors solutions of Te and Cd respectively. The 3-mercaptopropionic acid was utilized as a stabilizer. Kanwal et al. (2010) also used this method with slight modifications. Here, mercaptosuccinic acid was used as a stabilizer. It was observed that dimensions of CdTe QDs can be changed by simply changing the time intervals of heating. It was also revealed by Wang et al. (2008) that production of CdTe QDs with mercap to succinic acid as a stabilizer consumed less time and as-obtained QDs exhibited durable PL with high quantum yield.

Kominkova et al. (2017) prepared CdTe QDs by MW treatment. They used Na_2TeO_3 as the precursor of tellurium. The reaction mixture was heated under MW (300 W) for 10 min. Molaei et al. (2015) also prepared CdTe QDs. They used $CdSO_4$ and NaHTe as the precursor of Cd and Te, respectively. Here, TGA was used as a capping agent. In the final stage, a yellow-orange solution was obtained, which was placed under MW (720 W) for various time periods. The diameter of as-obtained CdTe QDs was found to be 2.5 nm.

Singh et al. (2017) fabricated CdTe QDs using $CdCl_2$ and TeO_2 as the precursor of Cd and Te, respectively. The MPA was also mixed in this solution in 100 mL milli-Q water. Then this mixture was exposed to MW irradiation

(300 W). It was observed that spherical QDs were obtained in a cubic structure and an average diameter of 2.5 nm was evident from XRD and TEM analysis. A redshift was also found with a change in particle size on increasing the time of exposure. These as-fabricated CdTe QDs were then used in latent fingerprinting and it was claimed that only a few seconds were needed to detect fingermarks under UV treatment.

Singh et al. (2017) used the one-step MW irradiation method for the synthesis of capped CdTe QDs. They used 3-mercaptopropionic acid as capping agent. The TeO_2 was used as the source of tellurium in place of commonly used Te powder, Na_2TeO_3, or Al_2TeO_3. The average particle size of the QDs was found in the range of 2−3 nm. These capped CdTe QDs can be used for latent fingerprinting.

MW irradiation route was developed by Duan et al. (2009) for the synthesis of CdTe QDs. The 3-mercaptopropionic acid was used as stabilizer. It was revealed that as-obtained CdTe QDs could be used as fluorescent probes for detect ion of mercuric ions in aqueous solution with a detection limit of 2.7×10^{-9} mol L^{-1}.

Ribeiro et al. (2017) reported a MW-assisted synthesis of CdTe QDs. They used three different ligands (2-mercaptoethanesulfonate, 3-mercaptopropionic acid, and L-GSH reduced) as capping agents. They could achieve CdTe QDs with quantum yield of ∼60%. A simple synthesis of CdTe QDs has been reported by Chen et al. (2015a) under MW irradiation. They used GSH as a modifier. It was revealed that as-prepared CdTe/CdS QDs were more dispersible and exhibited higher fluorescence intensity.

Dong and Ren (2012) developed a MW-assisted method for synthesis of CdTe QDs. They used long-chain thiols-mercaptoundecanoic acid (MUA) as surface ligand. It was revealed that as-obtained MUA-coated CdTe QDs were having have good stability, small diameter, long lifetime, and high luminescence. It was also revealed that these MUA-coated QDs could be used for HeLa cell imaging.

A MW-assisted synthesis of water-soluble cadmium telluride QDs was reported by Alibolandi et al. (2014). They used sodium tellurite and cadmium chloride as the source of Te and Cd, respectively. The mercaptosuccinic acid was used as a capping agent, CdTe nanocrystals with different colors ranging from blue to orange were obtained in less than one hour. It was revealed that qualified AS1411-aptamer-conjugated QDs exhibited that these can be used as excellent nanoprobes for targeting of cancer and molecular imaging. Bichpuria and Oudhia (2016) prepared GSH capped CdTe QDs (GSH-CdTe QDs) using a MW assisted wet chemical method. It was observed that high loss tangents and high boiling point were effective in controlling the size dispersion of QDs in MW-assisted synthesis.

7.2.5 Other quantum dots

A MW-assisted synthesis of silver indium sulfide (AIS) and AgInS@ZnS (AIS@ZnS) core−shell QDs was reported by Mir et al. (2018b). They used

GSH as a stabilizing agent. An average particle size of 2.5 and 3.25 nm was obtained for core and core−shell nanocrystals with bandgap as 2.3−3.1 and 2.4−3.5 eV, respectively. It was revealed that AIS@ZnS particles can easily penetrate the cells. It was suggested that as-obtained QDs have the potential to be used as antifungal and photodynamic agents as well as in high contrast cell imaging.

Fitzmorris et al. (2015) synthesized $CuInS_2$ QD cores using a MW-assisted reaction. It was indicated that the $CuInS_2$/ZnS (core/shell) QDs were ~98% ZnS, while In and Cu were present in lower concentrations. It was reported that PL stability was improved with ZnS shell and PL down conversion efficiency of ~65% was there on using a blue LED source.

Hong et al. (2015) synthesized $CuInS_2$/ZnS (core/shell) QDs via one-pot MW irradiation. It was observed that as-prepared QDs exhibited emission ranging from the red to NIR. The as-prepared CIS/ZnS QDs not only possess a high PLQY (56%) but also exhibit a large Stokes shift. It was revealed that these QDs can convert near UV and blue light in the Si solar cell with lower sensitivity to red and NIR light, where these solar cell has relatively higher sensitivity. Especially when they were first embedded into a PMMA transparent matrix to form a composite film as a luminescent downshifting layer for Si solar cell, the photoelectric conversion efficiency of the cell shows a marked enhancement by spectral downshifting as compared to the bare glass substrate, and the maximum achieved is 16.21%.

A green MW-assisted synthesis of $CuInS_2$ (CIS) and $CuInS_2$@ZnS core−shell QDs (CIS@ZnS) was reported by Mir et al. (2018b). They also used GSH as a stabilizer. The average particle size of CIS and CIS@ZnS was found to be 2.9 and 3.5 nm, respectively. It was observed that core−shell QDs exhibited better binding with lysozyme as compared to core structures.

Yang et al. (2012) synthesized Cu-doped ternary ZnCdS QDs (ZnCdS:Cu QDs) using a MW-assisted method in aqueous solution. They prepared samples at different Cd concentrations. These ternary QDs were found to be dispersible in water solution. It was observed that their PL peak was red-shifted and quantum yield of these QDs could reach as high as 12% depending on the doping concentration of Cu. It was concluded that as-fabricated ZnCdS:Cu ternary QDs may find application in fields such as bioimaging, sensing, and light-emitting diodes.

7.3 Synthesis of core−shell quantum dots

Core−shell QDs (CSQDs) have a solid core that is encapsulated within a second QDs material with an upper bandgap. Such hybrid particles have an enhanced quantum yield over QDs of single material. The II−VI compounds are useful for many purposes such as sensors, solar cells, probes, LEDs, photocatalysts, etc. QDs have a very high surface-to-volume ratio (around 80%) of atoms. They can provide various interesting properties. The CdSe

QDs have been exclusively investigated, which can be further improved by having a shell of ZnS as its bandgap is high compared to CdSe. The CSQDs can be categorized depending on the position of conduction and valence bands in the semiconductor materials. If the core has a larger bandgap as compared to the shell, then these are known as type I or conversely (inverse type I). On the other hand, if the conduction band or valence band of the core is placed within the bandgap of the shell, then these are classified as type II, CS QDs.

7.3.1 Type I CS quantum dots

Ziegler et al. (2007) used a green method to synthesize a ZnS shell over a CdSe core using MW irradiation. The proximity of core and shell was examined by the thiophenol test. Formation of the shell was started by MW exposure (within 30 s at 800 W). The mixture was then stirred for a minute and exposed to MWs (600 W).

Duran et al. (2014) reported a rapid method for the synthesis of water-soluble CdSe/ZnS QDs using MW technique. They used L-cysteine, cysteamine, and 3-MPA as thiol ligands. It was found that CdSe core was covered by ZnS shell. This method also increased the crystallinity of ZnS (shell).

Molaei et al. (2016) prepared CdSe/CdS CSQDs by an MW-assisted method in a single pot. They used two methods: MW irradiation (720 W) and chemical reaction (between NaHSe, $CdSO_4$, and TGA as capping ligand). It was observed that a CdS shell was developed on the CdSe. The formation of CdSe/CdS core−shell QDs is given as:

$$\mathbf{CdSO_4} + \mathrm{TGA} \xrightarrow[\mathbf{MW}]{\mathbf{NaHSe}} \mathbf{CdSeQDs}$$

$$\mathrm{CdSeQDs} + \mathbf{CdSO_4} \xrightarrow[\mathbf{MW}]{\mathbf{Na_2S_2O_3}} \mathrm{CdSe/CdS}\ \ \mathbf{CS\ \ QDs}$$

7.3.2 Inverse type I CS quantum dots

Shen et al. (2012) reported MW-assisted fabrication of highly luminescent cadmium selenide tellurium@zinc sulfide-silicon dioxide (CdSeTe@ZnS-SiO_2) QDs, which are helpful in detecting Cu(II) ions. These QDs were prepared with ZnS-like clusters, which were incorporated into the shell of SiO_2 in the presence of MW irradiation. The Zn^{2+} and GSH were utilized as precursors for ZnS. An average diameter of CdSeTe QDs was found to be 3.9 nm. It was reported that as-prepared CSS QDs have high luminescence and water solubility.

Ma et al. (2013) utilized a MW irradiation oven for the synthesis of GSH-capped ZnSe/ZnS core−shell QDs. Zinc acetate and KHSe were used as the source of zinc and selenium, respectively. The GSH was utilized as a capping agent. The molar ratio of Zn:GSH:KHSe was kept as 1:1.6:0.1 for better results.

Ebrahimi and Souri (2020) synthesized ZnSe:Cu@ZnS core−shell QDs using a MW-assisted colloidal method. It required 6 min of exposure to MW irradiation. It involves ZnSe and ZnSe:Cu semiconducting NCs in aqueous medium. The thioglycolic acid was used as a capping agent so that no agglomeration occurred. The NaHSe was prepared by reaction of Se with $NaBH_4$.

7.3.3 Type II CS quantum dots

Sai and Kong (2011) synthesized crystalline, water-soluble CS QDs (CdTe/CdSe QDs) via a MW technique. These are type II QDs. The solution of cadmium chloride (N_2-saturated) and NaHTe in the presence of MPA was exposed to MW irradiation for core formation (CdTe) for 2 min. It was reported that as-prepared QDs were monodispersed with a crystalline nature and size of 2 nm.

The MW-assisted technique was used by Chen et al. (2015b) to synthesize GSH conjugated CdTe (core)/CdSe (shell) QDs (CS QDs). The core QDs was prepared using cadmium chloride and MPA solutions. They used NaHTe solution as a source of Te. The resultant solution was exposed to MW irradiation for 2 min. The NaHSe solution was used as a precursor for selenium. Then, a solution of CdTe core QDs was added and exposed to MW for 20 min.

7.3.4 Inverse Type II CS quantum dots

Ren et al. (2013) produced PbS/CdS CS QDs via MW-assisted cation interchange method. A mixture of CdO, 1-ODE, and OA was heated in an oil bath until color disappeared. Then PbS QDs were injected using a syringe and the resultant solution was heated under MW (300 W) irradiation. It was observed that CS QDs were monodispersed with QY of 57%, which was almost 1.4 times more in the case of MW-assisted preparation as compared to the oil bath method.

7.3.5 Core−shell−shell quantum dots

The CSS (CdTe/CdS/ZnS) QDs were synthesized by He et al. (2008) under MW irradiation. As-prepared CSS QDs may be found useful as fluorescent probes in biological applications as these have good spectral properties, good biocompatibility, aqueous dispersibility, and excellent photostability (Fig. 7.2).

Wang et al. (2013) synthesized CdTe/CdS/ZnS QDs under MW irradiation for 10 min. The average particle size of CdTe/CdS/ZnS QDs was found to be >8 nm. It was reported that as-prepared CdTe/CdS/ZnS CSS QDs showed a maximum emission wavelength of 780 nm. Their synthesis is diagrammatically presented in Fig. 7.3.

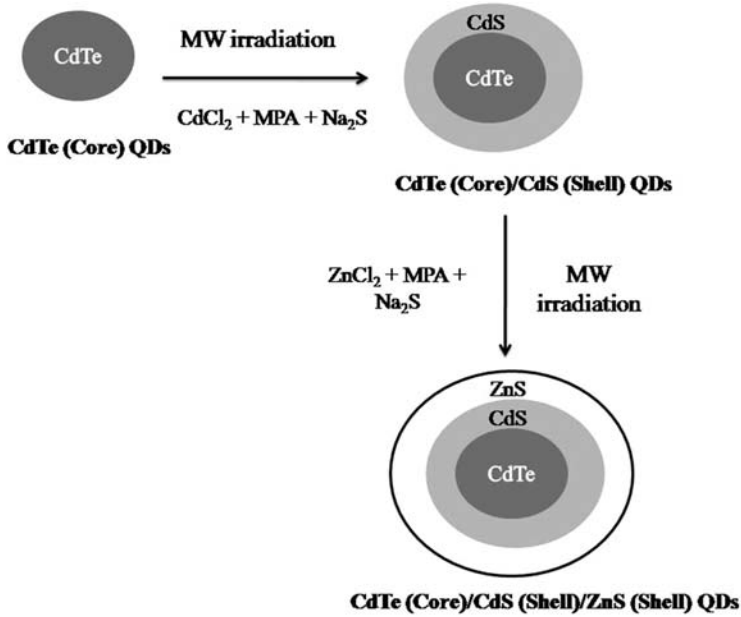

FIGURE 7.2 Microwave-assisted preparation of CdTe (core)/CdS (shell-I)/ZnS (shell-II) QDs.

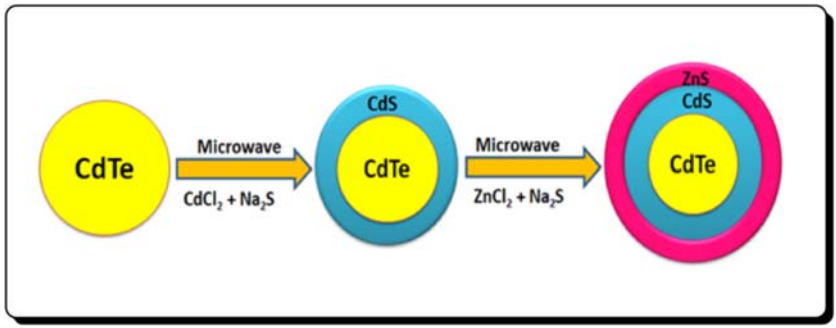

FIGURE 7.3 Microwave-assisted production of water-dispersed CdTe/CdS/ZnS core−shell−shell quantum dots. *Adapted Wang et al., 2013. Biomaterials 34 (37), 9509−9518. With Permission.*

7.4 Synthesis of alloyed quantum dots

These include multiple materials, but in the same combination. Therefore, combinations of two diverse semiconductors with unlike bandgaps may introduce some unique properties to the dots.

ZnSe QDs are interesting as these have the potential to be used in solar cells, diodes, scintillators, etc. (Abd Elhamid et al., 2018). Huang and Han (2010) have developed a simple plan for preparing GSH-capped ZnSe QDs

under MW irradiation. The Na_2SeO_3 was used as a source of Se. The GSH, zinc nitrate, Na_2SeO_3, and surplus $NaBH_4$ were mixed and exposed to MWs treatment (300 W) for 1 h. It was revealed that as-prepared ZnSe QDs had cubic shapes and ZnS spherical shapes with diameters in the range of 2−3 nm.

Qian et al. (2005) developed a seed-mediated technique for the synthesis of alloyed QDs (CdSe−CdS) under MW irradiation in aqueous phase. They prepared CdSe seeds by a reaction between Cd^{2+} and NaHSe. The MPA was used as a source of sulfide ions followed by MW exposure (1000 W). It was observed that the black-colored solution turned to white after 3 h. The NaHSe was prepared by $NaBH_4$ and Se powder. Again, the resultant solution was irradiated with MWs at for 5 min^{-1} h. It was reported that the size of alloyed QDs was 28 nm with QY of 25%.

Yang et al. (2013) synthesized CdSe-TeS alloyed QDs in aqueous solution using MW radiation. They used $CdCl_2$, NaHTe, and NaHSe as sources of Cd, Te, and Se, respectively. The MPA served as a source of sulfur and acted as a stabilizer also. These alloyed QDs could achieve 57.7% QY and are used in cancer imaging.

A simple MW treatment procedure for the preparation of $CdSe_xTe_{1-x}$−CdS QDs was reported by Luo et al. (2014). They carried out this MW-assisted method in two steps:

1. CdS shell ($CdSe_xTe_{1-x}$-CdS-I) was prepared by 3-mercaptopropionic acid capped $CdSe_xTe_{1-x}$ QDs.
2. CdS layer formation on the $CdSe_xTe_{1-x}$ core.

It was revealed that the XRD data supported the formation of alloyed QDs and the size of QDs was found to be 3.2 nm. These QDs were used in QSSCs.

Al-Hazmi et al. (2020) prepared nanocrystalline $Zn_{1-x}Pa_xTe$ ($0 \leq x \leq 0.09$) QDs using poly[(9,9-bis(3′-(N,Ndimethylamino)propyl)-2,7-fluorene)-alt-2,7-(9,9-dioctylfluorene)] via a MW-assisted method. They used a solution of poly[(9,9-bis(3′-(N,N-dimethylamino)propyl)-2,7-fluorene)-alt-2,7-(9,9-dioctylfluorene)], OLA, and 1-ODE, zinc acetate, trioctylphosphine telluride, and a sufficient amount of protactinium chloride. The resultant solution was irradiated with MWs (1200 W) for 2 h. They could obtain crystalline and monodispersed $Zn_{1-x}Pa_xTe$ QDs with a size ranging between 3 and 8 nm and very good QY up to 95%.

Mubiayi et al. (2020) synthesized $CuInGaSe_2$ QDs using MW exposure. Equal quantities and concentration of tri-n-octylphosphine (TOP) capped copper, gallium, and indium chloride in solvent OLA were mixed and MW (500 W) exposure was given for 10 min. Then TOPSe was injected and it was irradiated again with MW (600 W) for 10 min. It was observed that as-obtained QDs were pyramidal in shape with a crystalline nature and had

an average diameter of 10 nm. It was reported that films of as-prepared QDs can be applied as a counter electrode in DSSCs.

7.5 Carbon and graphene quantum dots

Graphite and GO are normally used for the preparation of GQDs. Several workers have used these precursors with different methods, but the MW technique was found to be better for this purpose. Li et al. (2012) synthesized greenish-yellow and blue GQDs (g-GQDs and b-GQDs). They did not utilize a stabilizer in this method. It was reported that PL QY of b-GQDs and gGQDs was found to be 22.9% and 11.7%, respectively. Their average diameter of QDs was found to be in the range of 2−7 nm.

The GQDs were also synthesized by Chen et al. (2012) using a MW-hydrothermal method. They used GO as the precursor of GQDs in the presence of nitric and sulfuric acids and exposed them to MWs (200°C) for 5 min. The size of as-prepared QDs was in the range of 2−5 nm. The MW-assisted hydrothermal method was also used by Chen et al. (2013) for the synthesis of pyrrole-ring functionalized GQDs (p-GQDs). They used the similar MW conditions here. It was reported that the final solution was pink and particle size ranged between 2 and 6 nm.

Shin et al. (2014) prepared GQDs directly from graphite powder in large amounts under MW irradiation (600 W) for 1 h. An average particle size of GQDs was found to be below 8 nm only. Carbon black, lamp black, and candle soot were used by Wang et al. (2011b) for the generation of CQDs.

Alves et al. (2018) synthesized grapheme TiO_2-QDs via nanoemulsification. They used different precursors of carbon (GO, Triton-X, n-heptane, OLA, OA) and titanium propoxide as precursors of TiO_2. The MW exposure (300 W) was given to get QDs of globular shape with 3.3 nm.

Li et al. (2018) prepared S, N-carbon QDs under MW irradiation for 7 min. They used thiourea as the source of dopant (S, N). Later, they used as-prepared QDs for the reduction of carbon dioxide. Jusuf et al. (2018) made use of eggshell for preparing CQDs under MW irradiation (560 W) for 2 min CQDs and used these QDs in the degradation of pollutants. It was reported that as-prepared CQDs were 3.88 nm in diameter. Yang et al. (2018) used xylan and ammonium hydroxide as a carbon-precursor and source of dopant (N) to prepare fabricate nitrogen-doped CQDs under an MW approach (200 W) for 10 min. A change in color of the solution was observed from dull yellow to brown.

7.6 Recent developments

There has been rapid progress in the field of MW-assisted synthesis of different QDs and their varied applications in last few decades. Some recent advances are summarized in Table 7.1.

TABLE 7.1 Synthesis of quantum dots under microwave irradiation.

Quantum dots	Size (nm)	Applications	References
CdTe	2.6–3.5	Ratiometric fluorescence sensor	Amiri and Hosseini (2020)
$CuInGaSe_2$	10	Ultrasonic spray system	Mubiayi et al. (2020)
SnO_2	1–1.5	Planar perovskite solar cells	Xu et al. (2021)
Graphene	3.78	Photocatalytic degradation of dyes	Van Tam et al. (2019)
Boron and nitrogen-rich graphitic	2	Fluorescence of photosynthetic pigments	Budak et al. (2020)
Graphitic carbon nitride	<10	Photocatalytic removal of heavy metals	Shorie et al. (2019)
Sulfur dots	3.58–4.00	Photoluminescence	Hu et al. (2020)
Niobium pentoxide	4	Photocatalytical processes	Nakagomi et al. (2019)
Carbon quantum dots	2	Photocatalytic degradation of synthetic dyes.	Zhang et al. (2020)
Nitrogen doped carbon	4.5	Fluorescence detection	Du et al. (2019)
Fe–BiOBr–N	12.93–8.43	Photocatalytic properties	Lopez-Velazquez et al. (2021)

7.7 Conclusion

This chapter highlights the generation of QDs by MW-assisted synthesis. These QDs have found various applications in varied fields such as sensors, LED, photocatalyst, solar cells, biomedicals (drug target delivery, cancer therapy, biolabeling, bioimaging, etc.). One can control/modify the parameter of QDs. This technique has many other advantages over conventional methods. The MW process has also been used in combination with solvothermal, ultrasound, and hydrothermal methods for a better yield and within a limited time, that is, within minutes or sometimes even in seconds. The use of MW technique has great potential in providing uniform and homogeneous QDs and it will prove to be an asset in the years to come.

References

Abd Elhamid, A.M., Aboulfotouh, A.M., Hafez, M.A., Azzouz, I.M., 2018. Structural effect of Ni-Cu catalysts for graphene growth by pulsed laser deposition. Thin Solid. Films 653, 93–100.

Abolghasemi, R., Rasuli, R., Alizadeh, M., 2019. Microwave-assisted growth of high-quality CdSe quantum dots and its application as a sensitizer in photovoltaic cells. Mater. Today Commun. 22. Available from: https://doi.org/10.1016/j.mtcomm.2019.100827.

Agranovich, I.P.B., Katz, G., Bezman, D., Feldman, Y., 2017. Microwave dielectric spectroscopy study of water dynamics in normal and contaminated raw bovine milk. Colloids Surf. B 154, 391–396.

Alehdaghi, H., Marandi, M., Molaei, M., Irajizad, A., Taghavinia, N., 2014. Facile synthesis of gradient alloyed $Zn_xCd_{1-x}S$ nanocrystals using a microwave-assisted method. J. Alloy Comp. 586, 380–384.

Alehdaghi, H., Assar, E., Azadegan, B., Baedi, J., Mowlavi, A.A., 2020. Investigation of optical and structural properties of aqueous CdS quantum dots under gamma irradiation. Radiat. Phys. Chem. 166. Available from: https://doi.org/10.1016/j.radphyschem.2019.108476.

Al-Harthi, A.M., Al-Marzouki, F., Elsayed, W., 2021. Development of highly luminescent and color-tunable $Zn_{1-x}Pm_xTe$ QDs synthesized using 4, 4-bis-N-1-naphyl-N-phenylaminobiphenyl assisted microwave technique for solar cell applications. Optik 227. Available from: https://doi.org/10.1016/j.ijleo.2020.166031.

Al-Hazmi, F., Al-Ghamdi, A.A., Alshehrei, A., Alsayed, W., 2020. Synthesis, optical and luminescence behavior of $Zn_{1-x}Pa_xTe$ ($0 \leq x \leq 0.09$) ceramics prepared via poly[(9,9-bis(3′-(N, N-dimethylamino)propyl)-2,7-fluorene)-alt-2,7-(9,9-dioctylfluorene)] assisted microwave approach. Optik 202. Available from: https://doi.org/10.1016/j.ijleo.2019.163703.

Alibolandi, M., Abnous, K., Ramezani, M., Hosseinkhani, H., Hadizadeh, F., 2014. Synthesis of AS1411-aptamer-conjugated CdTe quantum dots with high fluorescence strength for probe labelingtumor cells. J. Fluoresc. 24 (5), 1519–1529.

Alvand, Z.M., Rajabi, H.R., Mirzaei, A., Masoumiasl, A., Sadatfaraji, H., 2019. Rapid and green synthesis of cadmium telluride quantum dots with low toxicity based on a plant-mediated approach after microwave and ultrasonic assisted extraction: synthesis, characterization, biological potentials and comparison study. Mater. Sci. Eng. C. 98, 535–544.

Alves, A.K., Frantz, A.C.S., Berutti, F.A., 2018. Microwave-assisted oleothermal synthesis of graphene-TiO_2 quantum dots for photoelectrochemical oxygen evolution reaction. FlatChem. 12, 26–34. Available from: https://doi.org/10.1016/j.flatc.2018.12.001.

Amiri, N.S., Hosseini, M.R.M., 2020. Application of ratiometric fluorescence sensor-based microwave-assisted synthesized CdTe quantum dots and mesoporous structured epitope-imprinted polymers for highly efficient determination of tyrosine phosphopeptide. Ana. Methods 12 (1), 63–72.

Asok, A., Deshlahra, P., Ramachandran, A.M., Kulkarni, A.R., 2018. Multifunctional photostable nanocomplex of ZnO quantum dots and avobenzone via the promotion of enolate tautomer. Glob. Chall. 2 (11). Available from: https://doi.org/10.1002/gch2.201800025.

Ayodhya, D., Veerabhadram, G., 2018. Microwave-assisted synthesis, characterization and photoluminescence interaction studies of undoped, Zr^{2+}, Rh^{3+} and Pd^{2+} doped ZnS quantum dots. Mater. Discov. 12. Available from: https://doi.org/10.1016/j.md.2018.08.001.

Bajorowicz, B., Kobylanski, M.P., Go ła˛biewska, A., Nadolna, J., ZaleskaMedynska, A., Malankowska, A., 2018. Quantum dot-decorated semiconductor micro- and nanoparticles: a review of their synthesis, characterization and application in photocatalysis. Adv. Colloid Interface Sci. 256, 352–372.

Begum, S., Ahmaruzzaman, M., 2018. Green synthesis of SnO_2 quantum dots using Parkia speciosa Hassk pods extract for the evaluation of anti-oxidant and photocatalytic properties. J. Photochem. Photobiol. B: Biol. 184, 44–53.

Begum, S., Devi, T.B., Ahmaruzzaman, M., 2016. Surfactant mediated facile fabrication of SnO_2 quantum dots and their degradation behavior of humic acid. Mater. Lett. 185, 123–126.

Bekru, A.G., Zelekew, O.A., Andoshe, D.M., Sabir, F.K., Eswaramoorthy, R., 2021. Microwave-assisted synthesis of CuO Nanoparticles using cordiaafricana lam. leaf extract for 4-nitrophenol reduction. J. Nanotechnol. 2021. Available from: https://doi.org/10.1155/2021/5581621.

Bhattacharjee, A., Ahmaruzzaman, M., 2015. A novel and green process for the production of tin oxide quantum dots and its application as a photocatalyst for the degradation of dyes from aqueous phase. J. Colloid Interface Sci. 448, 130–139.

Bichpuria, P., Oudhia, A., 2016. Effective size control through solvents in microwave aided synthesis of GSH-CdTe quantum dots. IOSR J. Appl. Phy. 8 (4). Available from: https://doi.org/10.9790/4861-0804010105.

Budak, E., Aykut, S., Paşaoğlu, M.E., Ünlü, C., 2020. Microwave assisted synthesis of boron and nitrogen rich graphitic quantum dots to enhance fluorescence of photosynthetic pigments. Mater. Today Communi. 24. Available from: https://doi.org/10.1016/j.mtcomm.2020.100975.

Butova, V.V., Budnyk, A.P., Lastovina, T.A., Kravtsova, A.N., Soldatov, A.V., 2017. Rapid microwave synthesis of CdS quantum dots stabilized with 4,4' -bipyridine and dioctyl sodium sulfosuccinate. Mendeleev Commun. 27 (3), 313–314.

Cao, H., Tang, M., Wang, X., Shi, W., 2020. Facile and rapid synthesis of color-tunable molybdenum oxide quantum dots as a versatile probe for fluorescence imaging and environmental monitoring. Analyst 145. Available from: https://doi.org/10.1039/d0an01510e.

Chaudhary, G.R., Bansal, P., Mehta, S.K., 2014. Recyclable CuS quantum dots as heterogeneous catalyst for Biginelli reaction under solvent free conditions. Chem. Eng. J. 243, 217–224.

Chen, S., Liu, J.W., Chen, M.L., Chen, X.W., Wang, J.H., 2012. Unusual emission transformation of graphene quantum dots induced by self-assembled aggregation. Chem. Commun. 48, 7637–7639.

Chen, S., Hai, X., Xia, C., Chen, X.W., Wang, J.H., 2013. Preparation of excitationindependent photoluminescent graphene quantum dots with visible-light excitation/emission for cell imaging. Chem. Eur. J. 19, 15918–15923.

Chen, X., Li, L., Lai, Y., Yan, J., Tang, Y., Wang, X., 2015a. Microwave-assisted synthesis of glutathione-capped CdTe/CdSe near-infrared quantum dots for cell imaging. Int. J. Mol. Sci. 16, 11500–11508.

Chen, J., Xiao, A., Zhang, Z., Yu, Y., Yan, Z., 2015b. The synthesis and modification of CdTe/CdS core shell quantum dots. Spectrochim. Acta Part. A: Mole. Biomole. Spectrosc. 151, 506–509.

Dong, C., Ren, J., 2012. Water-soluble mercaptoundecanoic acid (MUA)-coated CdTe quantum dots: one-step microwave synthesis, characterization and cancer cell imaging. Luminescence 27 (3), 199–203.

Du, J., Li, X., Wang, S., Wu, Y., Hao, X., Xu, C., et al., 2012. Microwave-assisted synthesis of highly luminescent glutathione-capped Zn 1 − x Cd x Te alloyed quantum dots with excellent biocompatibility. J. Mater. Chem. 22 (22), 11390–11395.

Du, F., Cheng, Z., Lai, Z., Ruan, G., Zhao, C., 2019. Red-emissive nitrogen doped carbon quantum dots for highly selective and sensitive fluorescence detection of the alachlor herbicide in soil samples. N. J. Chem. 43 (47), 18695–18701.

Duan, J., Song, L., Zhan, J., 2009. One-pot synthesis of highly luminescent CdTe quantum dots by microwave irradiation reduction and their Hg^{2+}-sensitive properties. Nano Res. 2 (1), 61–68.

Duran, G.M., Plata, M.R., Zougagh, M., Contento, A.M., Ríos, A., 2014. Microwave-assisted synthesis of water soluble thiol capped CdSe/ZnS quantum dots and its interaction with sulfonylurea herbicides. J. Colloid Interface Sci. 428, 235–241.

Ebrahimi, S., Souri, D., 2020. Green synthesis and optical properties of ZnSe:Cu@ZnS core/shell nanocrystals fabricated by new photochemical microwave-assisted colloidal method. J. Alloy. Comp. 840. Available from: https://doi.org/10.1016/j.jallcom.2020.155712.

Felix, S., Chakkravarthy, R.B.P., Grace, A.N. 2015. Microwave assisted synthesis of copper oxide and its application in electrochemical sensing. IOP Conf. Ser.: Mater. Sci. Eng., 73, doi: 10.1088/1757-899x/73/1/012115.

Fitzmorris, R.C., Oleksak, R.P., Zhou, Z., Mangum, B.D., Kurtin, J.N., Herman, G.S., 2015. Structural and optical characterization of $CuInS_2$ quantum dots synthesized by microwave-assisted continuous flow methods. J. Nanopart. Res. 17 (7). Available from: https://doi.org/10.1007/s11051-015-3123-1.

Fregnaux, M., Dalmasso, S., Durand, P., Zhang, Y., Gaumet, J.-J., Laurenti, J.-P., 2013. Fast-grown CdS quantum dots: single-source precursor approach vs microwave route. Mater. Chem. Phys. 142 (1), 52–60.

Giguere, R.J., Bray, T.L., Duncan, S.M., Majetich, G., 1986. Application of commercial microwave ovens to organic synthesis. Tetrahedron Lett. 27, 4945–4948.

Han, H., Francesco, G.D., Maye, M.M., 2010. Size control and photophysical properties of quantum dots prepared via a novel tunable hydrothermal route. J. Phys. Chem. C. 114 (45), 19270–19277.

He, Y., Lu, H.-T., Sai, L.-M., Lai, W.-Y., Fan, Q.-L., Wang, L.-H., et al., 2006. Synthesis of CdTe nanocrystals through program process of microwave irradiation. J. Phys. Chem. B. 110 (27), 13352–13356.

He, Y., Lu, H.T., Sai, L.M., Su, Y.Y., Hu, M., Fan, C.H., et al., 2008. Microwave synthesis of water-dispersed CdTe/CdS/ZnS core-shell-shell quantum dots with excellent photostability and biocompatibility. Adv. Mater. 20 (18), 3416–3421.

He, X., Demchenko, I.N., Stolte, W.C., van Buuren, A., Liang, H., 2012. Synthesis and transformation of Zn-doped PbS quantum dots. J. Phys. Chem. C. 116 (41), 22001–22008.

He, J., Zhou, L., Liu, J., Yang, L., Zou, L., Xiang, J., et al., 2017. Modulation of surface structure and catalytic properties of cerium oxide nanoparticles by thermal and microwave synthesis techniques. App. Surf. Sci. 402, 469–477.

He, L., Yang, L., Liu, B., Zhang, J., Zhang, C., Liu, S., et al., 2019. One-pot synthesis of color-tunable copper doped zinc sulfide quantum dots for solid-state lighting devices. J. Alloy. Comp. 787, 537–542.

Hong, M., Xuan, T., Liu, J., Jiang, Z., Chen, Y., Chen, X., et al., 2015. Air-exposing microwave-assisted synthesis of $CuInS_2$/ZnS quantum dots for silicon solar cells with enhanced photovoltaic performance. RSC Adv. 5 (124), 102682–102688.

Hu, H., Zhao, Z., Zhou, Q., Gogotsi, Y., Qiu, J., 2012. The role of microwave absorption on formation of graphene from graphite oxide. Carbon 50, 3267–3273.

Hu, Z., Dai, H., Wei, X., Su, D., Wei, C., Chen, Y., et al., 2020. 49.25% efficient cyan emissive sulfur dots via a microwave-assisted route. RSC Adv. 10 (29), 17266–17269.

Huang, L., Han, H., 2010. One-step synthesis of water-soluble ZnSe quantum dots via microwave irradiation. Mater. Lett. 64, 1099–1101.

Jusuf, B.N., Sambudi, N.S., Isnaeni, Samsuri, S., 2018. Microwave-assisted synthesis of carbon dots from eggshell membrane ashes by using sodium hydroxide and their usage for degradation of methylene blue. J. Environ. Chem. Eng. 6, 7426–7433.

Kanwal, S., Traore, Z., Zhao, C., Su, X., 2010. Enhancement effect of CdTe quantum dots–IgG bioconjugates on chemiluminescence of luminol–H_2O_2 system. J. Luminescence. 130 (10), 1901–1906.

Kim, D., Kim, J., 2016. Synthesis of CdZnTe quantum dots in the aqueous phase by microwave irradiation. J. Nanosci. Nanotechnol. 16 (8), 8411−8414.

Kim, H.S., Yoon, K.B., 2014. Preparation and characterization of CdS and PbS quantum dots in zeolite Y and their applications for nonlinear optical materials and solar cell. Coord. Chem. Rev. 263, 239−256.

Kominkova, M., Milosavljevic, V., Vitek, P., Polanska, H., Cihalova, K., Dostalova, S., et al., 2017. Comparative study on toxicity of extracellularly biosynthesized and laboratory synthesized CdTe quantum dots. J. Biotech. 241, 193−200.

Kumar, R., Kim, H.-J., Park, S., Srivastava, A., Oh, I.-K., 2014. Graphene-wrapped and cobalt oxide-intercalated hybrid for extremely durable super-capacitor with ultrahigh energy and power densities. Carbon 79, 192−202.

Kumar, R., Joanni, E., Singh, R.K., Singh, D.P., Moshkalev, S.A., 2018. Recent advances in the synthesis and modification of carbon-based 2D materials for application in energy conversion and storage. Prog. Energy Combust. Sci. 67, 115−157.

Le Houx, N., Pourroy, G., Camerel, F., Comet, M., Spitzer, D., 2009. WO_3 nanoparticles in the 5 − 30 nm range by solvothermal synthesis under microwave or resistive heating. J. Phys. Chem. C. 114 (1), 155−161.

Lee, J., Yang, C.S., Chang, C.T., Liu, J., Chou, W.C., Lai, C.M., et al., 2004. Analysis of size distributions of type II ZnTe/ZnSe quantum dots. Phys. Status Solidi. 241, 3532−3543.

Lehnen, T., Schläfer, J., Mathur, S., 2014. Rapid microwave synthesis of CeO_2 quantum dots. Z. Anorg. Allg. Chem. 640 (5), 819−825.

Li, J.J., Wang, Y.A., Guo, W., Keay, J.C., Mishima, T.D., Johnson, M.B., et al., 2003. Large-scale synthesis of nearly monodisperse CdSe/CdS core/shell nanocrystals using air-stable reagents via successive ion layer adsorption and reaction. J. Am. Chem. Soc. 125 (41), 12567−12575.

Li, L.L., Ji, J., Fei, R., Wang, C.Z., Lu, Q., Zhang, J.R., et al., 2012. A facile microwave avenue to electrochemiluminescenttwo-color graphene quantum dots. Adv. Funct. Mater. 22, 2971−2979.

Li, M., Wang, M., Zhu, L., Li, Y., Yan, Z., Shen, Z., et al., 2018. Facile microwave assisted synthesis of N-rich carbon quantum dots/dual-phase TiO_2heterostructured nanocomposites with high activity in CO_2 photoreduction. Appl.Catal. B: Environ. 231, 269−276.

Lim, S.Y., Shen, W., Gao, Z., 2015. Carbon quantum dots and their applications. Chem. Soc. Rev. 44, 362−381.

Liu, X., Pan, L., Chen, T., Li, J., Yu, K., Sun, Z., et al., 2013. Visible light photocatalytic degradation of methylene blue by SnO_2 quantum dots prepared via microwave-assisted method. Catal. Sci. Technol. 3, 1805−1809.

Liu, X., Pan, L., Lv, T., Sun, Z., 2014. CdS sensitized TiO_2 film for photocatalytic reduction of Cr (VI) by microwave-assisted chemical bath deposition method. J. Alloy. Comp. 583, 390−395.

Liu, A., Jin, H., Li, J., Chen, L., Zheng, H., Mao, X., et al., 2019. One-step facile synthesis of PbS quantum dots/Pb $(DMDC)_2$ hybrids and their application as a low-cost SERS substrate. J. Raman Spectrosc. 50, 1445−1451.

Lopez-Velazquez, K., Guzman-Mar, J.L., Hernández-Ramírez, A., Gonzalez-Juarez, E., Villanueva-Rodriguez, M., 2021. Synthesis of Fe−BiOBr−N by microwave-assisted solvothermal method: characterization and evaluation of its photocatalytic properties. Mater. Sci. Semiconduc. Process. 123, 105499.

Lu, T., Pan, L., Li, H., Zhu, G., Lv, T., Liu, X., et al., 2011. Microwave-assisted synthesis of graphene−ZnO nanocomposite for electrochemical supercapacitors. J. Alloy. Compds 509 (18), 5488−5492.

Luo, J., Wei, H., Li, F., Huang, Q., Li, D., Luo, Y., et al., 2014. Microwave assisted aqueous synthesis of core-shell $CdSe_xTe_{1-x}$-CdS quantum dots for high performance sensitized solar cells. Chem. Commun. 50, 3464–3466.

Ma, R., Zhou, P.-J., Zhan, H.-J., Chen, C., He, Y.-N., 2013. Optimization of microwave-assisted synthesis of high-quality ZnSe/ZnS core/shell quantum dots using response surface methodology. Opt. Commun. 291, 476–481.

Malankowska, A., Kulesza, D., Sowik, J., Cavdar, O., Klimczuk, T., Trykowski, G., et al., 2020. The effect of $AgInS_2$, SnS, CuS_2, Bi_2S_3 quantum dots on the surface properties and photocatalytic activity of QDs-sensitized TiO_2 composite. Catalysts 10 (4), 403.

Mao, L.-H., Zhang, Q.-H., Zhang, Y., Wang, C.-F., Chen, S., 2014. Construction of highly luminescent CdTe/CdS@ZnS−SiO_2 quantum dots as conversion materials toward excellent color-rendering white-light-emitting diodes. Ind. Eng. Chem. Res. 53 (43), 16763–16770.

Mathew, M.E., Mohan, J.C., Manzoor, K., Nair, S.V., Tamura, H., et al., 2010. Folate conjugated carboxymethyl chitosan–manganese doped zinc sulphide nanoparticles for targeted drug delivery and imaging of cancer cells. Carbohydr.Polym. 80 (2), 442–448.

Mehrjoo, M., Molaei, M., Karimipour, M., 2017. A novel process for synthesis of CdSe/ZnS core-shell QDs and their application for the methyl orange (MO) degradation. Mater. Chem. Phys. 201, 165–169.

Mir, I.A., Radhakrishanan, V.S., Rawat, K., Prasad, T., Bohidar, H.B., 2018a. Bandgap tunable AgInS based quantum dots for high contrast cell imaging with enhanced photodynamic and antifungal applications. Sci. Rep. 8 (1). Available from: https://doi.org/10.1038/s41598-018-27246-y.

Mir, I.A., Das, K., Akhter, T., Ranjan, R., Patel, R., Bohidar, H.B., 2018b. Eco-friendly synthesis of $CuInS_2$ and $CuInS_2$@ZnS quantum dots and their effect on enzyme activity of lysozyme. RSC Adv. 8 (53), 30589–30599.

Mirahmadi, F.S., Marandi, M., Karimipour, M., Molaei, M., 2020. Microwave activated synthesis of Ag_2S and Ag_2S@ ZnS nanocrystals and their application in well-performing quantum dot sensitized solar cells. Sol. Energy 202, 155–163.

Moghaddam, M.M., Baghbanzadeh, M., Keilbach, A., Kappe, C.O., 2012. Microwave assisted synthesis of CdSe quantum dots: can the electromagnetic field influence the formation and quality of the resulting nanocrystals? Nanoscale. 4, 7435–7442.

Mohanta, D., Ahmaruzzaman, M., 2020. Biogenic synthesis of SnO_2 quantum dots encapsulated carbon nanoflakes: an efficient integrated photocatalytic adsorbent for the removal of bisphenol A from aqueous solution. J. Alloy. Compd. 828. Available from: https://doi.org/10.1016/j.jallcom.2020.154093.

Molaei, M., Hasheminejad, H., Karimipour, M., 2015. Synthesizing and investigating photoluminescence properties of CdTe and CdTe@CdS core-shell quantum dots (QDs): a new and simple microwave activated approach for growth of CdS shell around CdTe core. Electron. Mater. Lett. 11 (1), 7–12.

Molaei, M., Bardsiri, F.S., Bahador, A.R., Karimipour, M., 2016. One-pot microwave assisted approach for synthesis of CdSe/CdS core-shell quantum dots (QDs) and investigating optical properties. Mod. Phys. Lett. B. 30. Available from: https://doi.org/10.1142/S0217984916500743.

Molaei, M., Karimipour, M., Abbasi, S., Khanzadeh, M., Dehghanipour, M., 2020. PbS and PbS/CdS quantum dots: synthesized by photochemical approach, structural, linear and nonlinear response properties, and optical limiting. J. Mater. Res. 35, 401–409.

Mubiayi, K.P., Neto, D.M.G., Morais, A., Nogueira, H.P., de Almeida Santos, T.E., Mazon, T., et al., 2020. Microwave assisted synthesis of $CuInGaSe_2$ quantum dots and spray deposition

of their composites with graphene oxide derivatives. Mater. Chem. Phys. 242. Available from: https://doi.org/10.1016/j.matchemphys.2019.122449.

Nakagomi, F., Cerruti, S.E., de Freitas, M.R., Neto, E.S.F., de Andrade, F.V., Siqueira, G.O., 2019. Niobium pentoxide produced by a novel method microwave assisted combustion synthesis. Chem. Phys. Lett. 729, 37–41.

Nazzal, A.Y., Qu, L., Peng, X., Xiao, M., 2003. Photoactivated CdSe nanocrystals as nanosensors for gases. Nano Lett. 3, 819–822.

Nethravathi, C., Rajamathi, J.T., Rajamathi, M., 2019. Microwave-assisted synthesis of porous aggregates of CuS nanoparticles for sunlight photocatalysis. ACS Omega 4 (3), 4825–4831.

Pang, G., Chen, S., Koltypin, Y., Zaban, A., Feng, S., Gedanken, A., 2001. Controlling the particle size of calcined SnO_2 nanocrystals. Nano Lett. 1 (12), 723–726.

Parthibavarman, M., Sathishkumar, S., Jayashree, M., BoopathiRaja, R., 2019. Microwave assisted synthesis of pure and Ag doped SnO_2 quantum dots as novel platform for high photocatalytic activity performance. J. Clust. Sci. 30 (2), 351–363.

Peng, X., 2002. Green chemical approaches toward high-quality semiconductor nanocrystals. Chem. Eur. J. 8 (2), 334–339.

Peng, Z.A., Peng, X., 2001. Formation of high-quality CdTe, CdSe, and CdS nanocrystals using CdO as precursor. J. Am. Chem. Soc. 123, 183–184.

Pradhan, N., Peng, X., 2007. Efficient and color-tunable Mn-doped ZnSe nanocrystal emitters: control of optical performance via greener synthetic chemistry. J. Am. Chem. Soc. 129 (11), 3339–3347.

Qian, H., Li, L., Ren, J., 2005. One-step and rapid synthesis of high quality alloyed quantum dots (CdSe–CdS) in aqueous phase by microwave irradiation with controllable temperature. Mater. Res. Bull 40 (10), 1726–1736.

Radzi, N.M., Latif, A.A., Ismail, M.F., Liew, J.Y.C., Wang, E., Lee, H.K., et al., 2020. Q-switched fiber laser based on CdS quantum dots as a saturable absorber. Results Phys. 16. Available from: https://doi.org/10.1016/j.rinp.2020.103123.

Rangel-Mendez, J.R., Matos, J., Cházaro-Ruiz, L.F., González-Castillo, A.C., Barrios-Yáñez, G., 2018. Microwave-assisted synthesis of C-doped TiO_2 and ZnO hybrid nanostructured materials as quantum-dots sensitized solar cells. Appl. Surf. Sci. 434, 744–755.

Ren, F., Zhao, H., Vetrone, F., Ma, D., 2013. Microwave-assisted cation exchange toward synthesis of near-infrared emitting PbS/CdS core/shell quantum dots with significantly improved quantum yields through a uniform growth path. Nanoscale 05 (17), 7800–7804.

Ribeiro, D.S., de Souza, G.C., Melo, A., Soares, J.X., Rodrigues, S.S.M., Araújo, A.N., et al., 2017. Synthesis of distinctly thiol-capped CdTe quantum dots under microwave heating: multivariate optimization and characterization. J. Mater. Sci. 52 (6), 3208–3224.

Rodrigues, S.S.M., Ribeiro, D.S.M., Soares, J.X., Passos, M.L.C., Saraiva, M.L.M.F.S., Santos, J.L.M., 2017. Application of nanocrystalline CdTe quantum dots in chemical analysis: implementation of chemo-sensing schemes based on analytetriggered photoluminescence modulation. Coord. Chem. Rev. 330, 127–143.

Sai, L.-M., Kong, X.Y., 2011. Microwave-assisted synthesis of water-dispersed CdTe/CdSe core/shell type II quantum dots. Nanoscale Res. Lett. 6. Available from: https://doi.org/10.1186/1556-276X-6-399.

Saravanan, R.S.S., Pukazhselvan, D., Mahadevan, C.K., 2012. Studies on the synthesis of cubic ZnS quantum dots, capping and optical–electrical characteristics. J. Alloy. Comp. 517, 139–148.

Shaheen, A., Arif, R., Sharma, D., Singh, T., 2020. Microwave-mediated synthesis of surface-active ionic liquid-capped ZnS quantum dots: morphological studies and their applicability

for fluorometric sensing of ascorbic acid. Appl. Phys. A. 126 (10). Available from: https://doi.org/10.1007/s00339-020-03968-7.

Shahid, R., Toprak, M.S., Muhammed, M., 2012. Microwave-assisted low temperature synthesis of wurtzite ZnS quantum dots. J. Solid. State Chem. 187, 130–133.

Shen, Y., Li, L., Lu, Q., Ji, J., Fei, R., Zhang, J., et al., 2012. Microwave-assisted synthesis of highly luminescent CdSeTe@ZnS-SiO_2 quantum dots and their application in the detection of Cu(II). Chem. Commun. 48, 2222–2224.

Shi, L., Lin, H., 2010. Facile fabrication and optical property of hollow SnO_2 spheres and their application in water treatment. Langmuir 26 (24). Available from: https://doi.org/10.1021/la103769d.

Shin, Y., Lee, J., Yang, J., Park, J., Lee, K., Kim, S., et al., 2014. Mass production of graphene quantum dots by one-pot synthesis directly from graphite in high yield. Small 10, 866–870.

Shorie, M., Kaur, H., Chadha, G., Singh, K., Sabherwal, P., 2019. Graphitic carbon nitride QDs impregnated biocompatible agarose cartridge for removal of heavy metals from contaminated water samples. J. Hazard. Mater. 367, 629–638.

Singh, M.K., Mathpal, M.C., Agarwal, A., 2012. Optical properties of SnO_2 quantum dots synthesized by laser ablation in liquid. Chem. Phys. Lett. 536, 87–91.

Singh, S., Sabri, Y.M., Jampaiah, D., Selvakannan, P.R., Nafady, A., Kandjani, A.E., et al., 2017. Easy, one-step synthesis of CdTe quantum dots via microwave irradiation for fingerprinting application. Mater. Res. Bullet. 90, 260–265.

Song, H., Lee, K.-H., Jeong, H., Um, S.H., Han, G.-S., Jung, H.S., et al., 2013. A simple self-assembly route to single crystalline SnO_2 nanorod growth by oriented attachment for dye sensitized solar cells. Nanoscale. 5, 1188–1194.

Soren, S., Jena, S.R., Samanta, L., Parhi, P., 2015. Antioxidant potential and toxicity study of the cerium oxide nanoparticles synthesized by microwave-mediated synthesis. App. Biochem. Biotechnol. 177 (1), 148–161.

Soumya, S., Sheemol, V.N., Amba, P., Mohamed, A.P., Ananthakumar, S., 2018. Sn and Ag doped ZnO quantum dots with PMMA by in situ polymerization for UV/IR protective, photochromic multifunctional hybrid coatings. Sol. Energy Mater. Sol. Cell 174, 554–565.

Van Tam, T., Altahtamouni, T.M., Le Minh, V., Ha, H.K.P., Chung, N.T.K., Van Thuan, D., 2019. One-pot microwave-assisted green synthesis of amine-functionalized graphene quantum dots for high visible light photocatalytic application. C R Chim. 22 (11–12), 822–828.

Wang, Y., Tang, Z., Correa-Duarte, M.A., Pastoriza-Santos, I., Giersig, M., Kotov, N.A., et al., 2004. Mechanism of strong luminescence photoactivation of citrate-stabilized water-soluble nanoparticles with CdSe cores. J. Phys. Chem. B. 108, 15461–15469.

Wang, C., Ma, Q., Su, X., 2008. Synthesis of CdTe nanocrystals with mercaptosuccinic acid as stabilizer. J. Nanosci. Nanotechnol. 8 (9), 4408–4414.

Wang, H., Liang, Q., Wang, W., An, Y., Li, J., Guo, L., 2011a. Preparation of flower-like SnO_2 nanostructures and their applications in gas-sensing and lithium storage. Cryst. Growth Des. 11 (7), 2942–2947.

Wang, Q., Zheng, H., Long, Y., Zhang, L., Gao, M., Bai, W., 2011b. Microwavehydrothermal synthesis of fluorescent carbon dots from graphite oxide. Carbon. 49, 3134–3140.

Wang, H.E., Xi, L.J., Ma, R.G., Lu, Z.G., Chung, C.Y., Bello, I., et al., 2012. Microwave-assisted hydrothermal synthesis of porous SnO_2 nanotubes and their lithiumion storage properties. J. Solid. State Chem. 190, 104–110.

Wang, J., Lu, Y., Peng, F., Zhong, Y., Zhou, Y., Jiang, X., et al., 2013. Photostable water-dispersible NIR-emitting CdTe/CdS/ZnS core–shell–shell quantum dots for high-resolution tumor targeting. Biomaterials 34 (37), 9509–9518.

Wang, S., Kershaw, S.V., Li, G., Leung, M.K., 2015a. The self-assembly synthesis of tungsten oxide quantum dots with enhanced optical properties. J. Mater. Chem. C. 3 (14), 3280−3285.

Wang, H., Yuan, X., Zeng, G., Wu, Y., Liu, Y., Jiang, Q., et al., 2015b. Three dimensional graphene-based materials: synthesis and applications from energy storage and conversion to electrochemical sensor and environmental remediation. Adv. Colloid Interface Sci. 221, 41−59.

Xiao, L., Shen, H., von Hagen, R., Pan, J., Belkoura, L., Mathur, S., 2010. Microwave assisted fast and facile synthesis of SnO_2 quantum dots and their printing applications. Chem. Commun. 46, 6509−6511.

Xu, Z., Jiang, Y., Li, Z., Chen, C., Kong, X., Chen, Y., et al., 2021. Rapid microwave-assisted synthesis of SnO_2 quantum dots for efficient planar perovskite solar cells. ACS Appl. Energy Mater. 4 (2), 1887−1893.

Xuan, T., Wang, X., Zhu, G., Li, H., Pan, L., Sun, Z., 2013. One-step microwave-assisted synthesis of water soluble CdSe quantum dots for white light-emitting diodes with excellent color rendering. J. Alloy. Comp. 558, 105−108.

Yang, Y., Liang, S., Yu, X., Wang, Q., 2012. Microwave synthesis of Cu-doped ternary ZnCdS quantum dots with composition-controllable photoluminescence. Wuhan. Univ. J. Nat. Sci. 17 (3), 217−222.

Yang, F., Xu, Z., Wang, J., Zan, F., Dong, C., Ren, J., 2013. Microwave-assisted aqueous synthesis of new quaternary-alloyed CdSeTeS quantum dots; and their bioapplications in targeted imaging of cancer cells. Luminescence. 28, 392−400.

Yang, P., Zhu, Z., Chen, M., Chen, W., Zhou, X., 2018. Microwave-assisted synthesis of xylan-derived carbon quantum dots for tetracycline sensing. Opt. Mater. 85, 329−336.

Zhan, H., Zhou, P., Pan, K., He, T., He, X., Zhou, C., et al., 2013. One-pot aqueous-phase synthesis of ultra-small CdSe/CdS/CdZnS core−shell−shell quantum dots with high-luminescent efficiency and good stability. J. Nanopart. Res. 15 (6). Available from: https://doi.org/10.1007/s11051-013-1680-8.

Zhang, X., Liu, Z., 2012. Recent advances in microwave initiated synthesis of nanocarbon materials. Nanoscale. 4, 707−714.

Zhang, T., Jin, J., Yang, C., Peng, H., Lai, L., Han, J., et al., 2012a. Microwave synthesis CdSe quantum dot clusters via ribonuclease A protein. Micro Nano Lett. 7 (12), 1289−1291.

Zhang, P., Hu, G.X., Bao, S.J., Guo, J., Lei, C., Cai, C.J., et al., 2012b. One step microwave synthesis and magnetic properties of Co_3O_4 octahedrons. Mater. Lett. 83, 195−197.

Zhang, H., Wang, H., Wang, Y., Xin, B., 2020. Controlled synthesis and photocatalytic performance of biocompatible uniform carbon quantum dots with microwave absorption capacity. Appl. Surf. Sci. 512. Available from: https://doi.org/10.1016/j.apsusc.2020.145751.

Zheng, X., Weng, J., Hu, B., 2010. Microwave-assisted synthesis of mesoporous CdS quantum dots modified by oleic acid. Mater. Sci.Semicond. Process. 13 (3), 217−220. Available from: https://doi.org/10.1016/j.mssp.2010.10.012.

Zhou, X., Shi, J., Liu, Y., Su, Q., Zhang, J., Du, G., 2014. Microwave irradiation synthesis of Co_3O_4 quantum dots/graphene composite as anode materials for Li-ion battery. Electrochim. Acta 143, 175−179.

Zhu, M.-Q., Gu, Z., Fan, J.-B., Xu, X.-B., Cui, J., Liu, J.-H., et al., 2009. Microwave-mediated nonaqueous synthesis of quantum dots at moderate temperature. Langmuir 25 (17), 10189−10194.

Zhu, D., Li, W., Wen, H.-M., Chen, Q., Ma, L., Hu, Y., 2014. Microwave-assisted aqueous synthesis of Mn-doped ZnS quantum dots and their room-temperature phosphorescence detection of indapamide. Anal. Methods 6 (18), 7489−7495.

Zhu, L., Wang, M., Kwan Lam, T., Zhang, C., Du, H., Li, B., et al., 2016. Fast microwave-assisted synthesis of gas-sensing SnO_2 quantum dots with high sensitivity. Sensor. Actuator. B Chem. 236, 646–653.

Ziegler, J., Merkulov, A., Grabolle, M., Resch-Genger, U., Nann, T., 2007. High-quality ZnS shells for CdSe nanoparticles: rapid microwave synthesis. Langmuir 23, 7751–7759.

This page intentionally left blank

Chapter 8

Sonochemical synthesis of quantum dots

Garima Ameta[1] **and Seema Kothari**[2]
[1]*Department of Chemistry, M. L. S. University, Udaipur, Rajasthan, India,* [2]*Department of Chemistry, PAHER University, Udaipur, Rajasthan, India*

8.1 Introduction

Sound frequencies beyond the upper audible limit of human hearing are normally categorized as ultrasound. The frequency range of ultrasound that has been used sonochemistry is 16−3000 kHz. Ultrasonic irradiation has been widely used in chemical synthesis and it has become an interesting field of research. When an ultrasonic wave passes through a liquid medium, than a large number of microbubbles are formed, they grow, and finally collapse in a very short time, which is of the order of a few microseconds. This is called ultrasonic cavitation (Fig. 8.1).

Extremely high pressures and temperatures are generated during the process of acoustic cavitation, which initiates a number of chemical and physical effects, such as microjetting, shock waves, shear forces, microstreaming, and generation of different radicals. Sonochemistry finds a variety of applications such as drug encapsulation and delivery, food science, electrochemistry, material engineering, synthesis of nanoparticles, etc.

Bang and Suslick (2010) have reviewed the application of ultrasound in the synthesis of nanostructured materials. Sonochemical approach can provide control morphology over size. Cavitation-induced sonochemistry with the temperature and pressures provides hot spots inside the bubbles of the order of ∼5000 K, and ∼1000 bar, respectively. These extraordinary conditions permit the synthesis of a wide range of nanostructured materials, particularly quantum dots.

The field of sonochemistry has been excellently delivered by various workers over time (Einhorn et al., 1989; Pestman et al., 1994; Mason, 1999; Suslick and Flannigan, 2008; Ameta et al., 2018).

The high energy and pressure for chemical reaction is generated by collapsing bubbles. This can be divided into three regions (Fig. 8.2):

Quantum Dots. DOI: https://doi.org/10.1016/B978-0-12-824153-0.00008-2
© 2023 Elsevier Inc. All rights reserved.

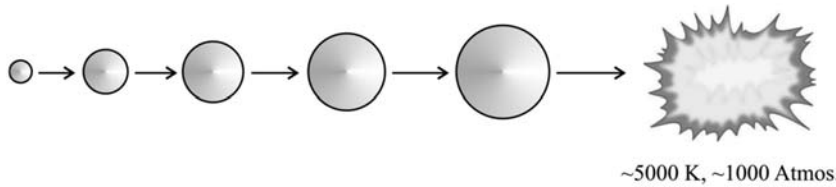

FIGURE 8.1 Growth and implosion of a bubble. *Adapted from Ameta et al., Sonochemistry: An Emerging Green Technology, Apple Academic Press, New Jersey, 2018, with permission.*

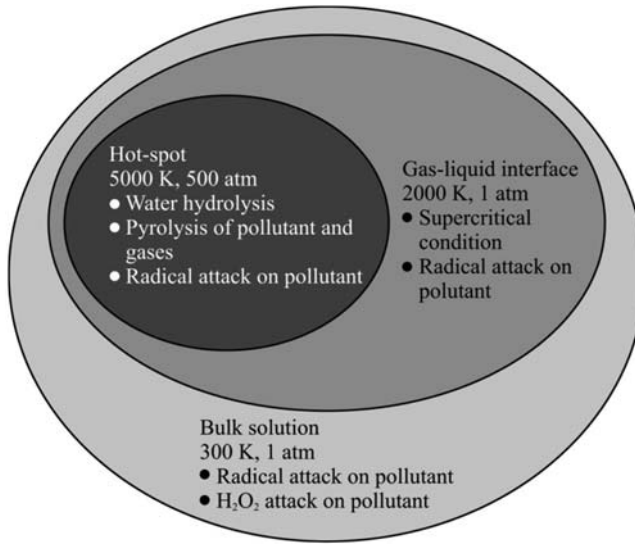

FIGURE 8.2 Reaction zone in cavitation process (Chowdhury and Viraraghavan, 2009). *Adapted from Chowdhury, P.; Viraraghavan, T. Sonochemical degradation of chlorinated organic compounds, phenolic compounds and organic dyes—a review. Sci. Total. Environ., 2009, 407 (8), 2474—2492. With permission.*

1. First region is a hot spot region or thermolytic center, which has a quite high temperature of 5000 K and a high pressure of 500 atm during the collapse of a bubble or cavitation.
2. Second region is a interfacial region between the bulk liquid cavitation bubble.
3. Third region is a bulk region. Here, temperature is almost equal to room temperature due to process of adiabatic cavitation.

8.1.1 Advantages

There are some advantages of using the sonochemical route for the synthesis of quantum dots. These include:

1. It improves the reaction rate.
2. It involves high energies and pressures in a short time.
3. No additives are required.
4. It reduces the number of reaction steps.
5. It provides uniform size distribution, higher surface area, with improved phase purity.
6. It is a solvent-free synthesis producing less waste.

8.1.2 Disadvantage

The sonochemical method has a disadvantage as:

1. It affords relatively low yield of the product.

8.2 Instrumentation

Various sources are used for generating ultrasound.

1. The first ultrasound transducer was developed by Galton (1883), now known as Galton's whistle (Fig. 8.3A). It is a brass tube and a jet of gas is passed through an orifice into a resonating cavity.
2. Liquid whistle is also used for this purpose (Fig. 8.3B). Cavitation is generated in this transducer through motion of a liquid in place of gas.
3. Piezoelectric transducers are also used for generation of ultrasound (Fig. 8.3C). A transducer is based on electrical and mechanical vibrations via piezoelectric effect. There are many materials that have a range of piezoelectric effects. Some examples of natural materials are quartz, topaz. tourmaline, belemnite, etc., while synthetic materials are bismuth ferrite, lithium tantalite, $Ba_2Na\ Nb_5\ O_5$, $Pb_2KNb_5O_{15}$, etc.
4. Cup horn (Fig. 8.3D). It is a high intensity ultrasonic bath. In this transducer, indirect sonication technology is involved. This cup horn sonication is effective, where the liquid sample is higher in volume.

8.3 Synthesis of quantum dots

8.3.1 Metals

Liu et al. (2011) prepared highly fluorescent and water-soluble gold nanoclusters (AuNCs) and Au@AgNCs emitting near-infrared via a sonochemical approach. It was reported that yellow emission was observed from Au@AgNCs. It was revealed that as-prepared Au NCs could be successfully applied in the determination of copper ions in a wider of range of concentration with a lower of limit NCs. A facile and fast sonochemical route was proposed by Wang et al. (2017) to synthesize fluorescent AgNCs. They used glutathione (GSH) and hydrazine hydrate, respectively, as capping and reducing agent. It was revealed that

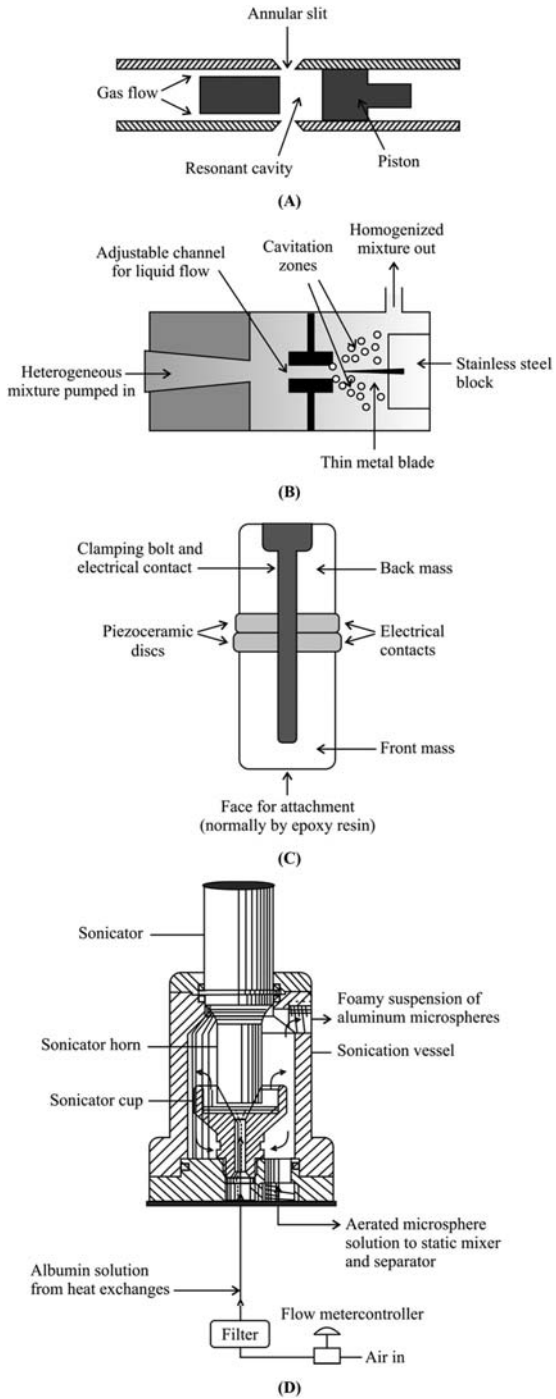

FIGURE 8.3 Various sources for ultrasound generation: (A) Galton whistle; (B) liquid whistle; (C) piezoelectric transducer; and (D) cup horn. *Adapted from Ameta et al., Sonochemistry: An Emerging Green Technology, Apple Academic Press, New Jersey, 2018, With Permission.*

AgNCs waweres formed quickly within 15 min in the presence of ultrasonic waves. As-prepared QDs show red fluorescence and good dispersion in aqueous solution. The size of AgNCs was found to be small enough ($\sim$2 nm). Use of GSH as protecting agent on the surface of these AgNCs provides high, photo-, and pH-stability. They designed a stable Ag nanoclusters-based nanosensor for detection of Pb^{2+} ions with high sensitivity and selectivity. The as-fabricated nanosensor can also be used as a probe for monitoring Pb^{2+} ions in living cells. It was proposed that these stable and fluorescent AgNCs can find potential applications for sensing and biolabeling.

Mallikarjuna et al. (2021) fabricated g-C_3N_4 and Ag-g-C_3N_4 composite structures by the ultrasonication method. It was reported that the silver quantum dots anchored to g-C_3N_4 structures may show better photocatalytic activities for dye degradation, H_2 production, and antimicrobial activity in the presence of visible-light. As-prepared Ag/g-C_3N_4 composite (Ag loading of 0.02 mole) exhibited optimum photoactivity for production of H_2 (335.40 $\mu molg^{-1}h^{-1}$), which is much better than other Ag loaded g-C_3N_4 composites. These synthesized Ag/g-C_3N_4 nanoparticles also show potential antimicrobial activity and inhibition zones were found comparable to that of an antibiotic chloramphenicol. Calderón-Jiménez et al. (2022) reported a sonochemical synthesis of silver nanoparticles in aqueous suspension. These Ag NPs were found to be quasi-spherical in shape and highly stable. The particle size of as-prepared sample was found to be 8.1 $\pm$ 2.4 nm with narrow dispersion of the size distribution. The bandgap of these Ag NPs was 2.795 $\pm$ 0.002 eV. A high stability of the optical properties of these Ag NPs were found at 10 h (short term) and 24 weeks.

8.3.2 Metal oxides

Sedghi et al. (2010) prepared SnO_2 QDs by sonication-assisted precipitation. It was reported that they can be used as a low temperature sensor for detecting CO as well as methane. There was a good of selectivity to CO in the presence of methane below 375°C using this sensor. The average particle size of SnO_2 QDs was found to be 3−4 nm and their sensing properties were compared with the nanoparticles prepared by conventional sol−gel method. It was observed that bandgap measurements of as-prepared sample indicated a 2.1 eV blueshift. Majumdar and Devi (2010) synthesized SnO_2 nanoparticles at room temperature by a sonication-assisted precipitation method. It was reported that 3 h sonication was found to produce nanoparticles with size below 10 nm. It was found that a gradual increase of the sonication time gradually decreases the particle size with interesting morphology and increased surface area. It was also observed that as-synthesized powders exhibited a direct influence by the sonication time on the sensing properties of butane. A maximum response of 98.88% was reported toward butane (5000 ppm) at 450°C along with a fast recovery time.

A sonochemical approach was developed by Islam et al. (2011) for large-scale synthesis of iron oxide magnetic nanoparticles (Fe_3O_4 NPs) using inexpensive and nontoxic metal salts as reactants. It was revealed that as-prepared nanoparticles had average particle size around 11 nm and these were almost spherical in shape. It was also proved that these particles were super paramagnetic with magnetization values of 80 emu g^{-1}. Chlorine-doped titanium dioxide (anatase) nanocrystallites were prepared by Wang et al. (2012) through sonicating sodium chloride solution of tetraisopropyl titanate in water/ethanol at 70°C. The presence of dopant (chloride) was confirmed and it was found that Cl is incorporated into TiO_2. It was reported that as-prepared samples were used in the photodegradation of butyl benzyl phthalate (BBP) in aqueous condition in the presence of visible light irradiation. It was reported that photodegradation of BBP could reach to 92% in 4 h.

N-doped TiO_2 nanocrystals were synthesized by Jia et al. (2014) via a sonochemical route. The urea, titanium tetrachloride, and aqueous ammonia were used as starting materials. It was revealed that as-synthesized nanocrystals had size of 10 nm. It was reported that the adsorption band edge of N-doped TiO_2 samples exhibited redshift to the visible region compared to TiO_2. The photocatalytic activity of as-prepared photocatalyst was observed for degradation of rhodamine B under visible light. It was revealed that the use of an optimal amount of urea enhanced the photocatalytic activity of TiO_2 due to its mesoporous structure and incorporation of nitrogen as a dopant.

Yang et al. (2016a) synthesized ZnO quantum dots using an ultrasonic microreactor. It was observed that flow rate, ultrasonic power, and temperature affected type and quantity of defects in ZnO quantum dots, and size of ZnO quantum dots can also be controlled by variation of these conditions. It was reported that the size of ZnO quantum dots decreased on increasing flow rate but quantum yields first increased and then decreased. The size of ZnO quantum dots was found to decrease first, and then increased on increasing ultrasonic power while the quantum yields kept on increasing. Moreover, the quantum yields of ZnO QDs synthesized by ultrasonic microreactor could reach 64.7%, which is higher than those synthesized only under ultrasonic radiation or only by microreactor.

The ZnO quantum dots were synthesized by Yang et al. (2016b) using an ultrasonic-assisted sol−gel method. It was reported that ultrasonic exposure time and temperature both affected type and amount of defects in as-prepared ZnO quantum dots. Total defects of ZnO quantum dots were found to decrease with the increasing ultrasonic time and temperature. The optical defects changed from oxygen interstitial defects to oxygen vacancy and then zinc interstitial defects. These were again transformed back to oxygen interstitial defects. It was observed that the sizes of ZnO quantum dots first decreased on increasing ultrasonic temperature and time and then increased.

Moghaddam et al. (2017) prepared two samples of ZnO quantum dots by sonochemical as well as conventional methods. It was indicated that the quantum dots prepared under ultrasonic waves had smaller size and also a narrow size distribution. It was observed that phase purity of nanocrystals could be obtained on using ultrasonic waves as there is complete conversion of precursors into ZnO, and as a result as-prepared ZnO can find application in optoelectronics.

8.3.3 Metal sulfides

The histidine functionalized CdS quantum dots were synthesized by Yadav et al. (2010) via a sonochemical method. It was revealed that as-prepared CdS QDs are well-defined with almost spherical shape. The X-ray diffraction pattern indicates the formation of cubic phase QDs. The confinement of histidine functionalized CdS QDs was confirmed. The photoluminescence property of CdS/histidine QDs was found to be better than that of CdS QDs. These as-functionalized QDs can find potential applications in the biological fields. Estandarte et al. (2011) synthesized ionic liquid-capped cadmium sulfide QDs in PET fibers as photocatatyst. Its photocatalytic activity was evaluated in the photodegradation of methylene blue. These CdS QDs and PET-CdS QDs nanocomposites were synthesized via a sonochemical route using an ionic liquid, 1-octyi-3-methylimidazolium lauryl sulfate ([OMIM]LS). They used PET fibers prepared from waste bottles and used these as matrix for preparation of the PET-CdS QDs nanocomposite. It was revealed that PET-CdS QDs nanocomposite has the highest bandgap energy (2.79 eV), which is suitable for absorption in the visible range. The CdS QDs and PET-CdS QDs nanocomposites were used as photocatalyst for photodegradation of methylene blue under visible light and degradation efficiency was 53.64 and 77.96%, respectively, which was much better than uncatalyzed degradation (19.57%).

Semiconductor nanoparticles of CdS have been prepared by Entezari and Ghows (2011) in microemulsion (O/W) under ultrasound irradiation. The effect of some operational parameters was observed, such as intensity of ultrasound, sonication time, temperature, and oil fraction. It was observed that as-prepared QDs had about 2 nm size with a hexagonal phase and this size can also be tuned. It was postulated that the collapse of bubbles generates high temperature and a number of nucleation sites, thus leading to uniform spherical particles with small size. It was revealed that the bandgap of as-prepared CdS NPs decreases with increasing sonication time. Goharshadi et al. (2012) developed a sonochemical method to prepare zinc sulfide nanoparticles with extremely small size (about 1 nm in diameter). They used a set of ionic liquids, which are based on the bis(trifluoromethylsulfonyl)imide anion and different 1-alkyl-3-methyl-imidazolium cations. This method provides wide bandgap ZnS nanocrystals, which can find application in different photonic devices.

A template-free chemical and sonochemical method was developed by Pejova and Bineva (2013) to prepare 3D assemblies of indium(III) sulfide quantum dots. This method allowed the deposition of cubic α-In2S3 nanocrystals (close packed) in thin film because of heterogeneous sonochemical effects. The average crystal radius of QD was reduced from 2.5 to 2.0 nm on sonication by continuous high-intensity ultrasound. It was observed that these values increased to 4.1 nm by postdeposition annealing treatment. It was reported that bandgap energy value (2.85 eV) was blueshifted (2.00 eV). It was revealed that Bohr's excitonic radius lies in the range of 2.5−4.1 nm.

Zhao et al. (2013) synthesized gamma-cyclodextrin-folate (gamma-CD/FA) inclusion-coated CdSe/ZnS quantum dots by a sonochemical method. It was observed that these gamma-CD/FA-coated CdSe/ZnS QDs were monodispersed and have smaller size, but with longer fluorescence lifetime and higher quantum yield. The cytotoxicity of gamma-CD/FA-coated CdSe/ZnS QDs was found to be lower and they could more effectively enter cancer cells. It is the smaller size of QDs (4−5 nm diameters) that allowed them to easily enter the cell and be removed through kidneys. These QDs are more suitable for some biomedical applications like bioprobes and bioimaging.

Das and Wai (2014) synthesized lead sulfide quantum dots. They used 1,2-benzenedimethanethiol, sodium sulfide, and lead nitrate solutions in ethanol under ultrasound irradiation. As-prepared PbS quantum dots had sizes of 2.7 and 3.6 nm in diameter. A simple one-pot method for synthesis of SWNT−PbS nanoparticle composite was also developed just by addition of single-walled carbon nanotubes (SWCNT) to the system under ultrasonic irradiation. This allowed the attachment of PbS nanoparticles to the SWCNTs' surface via π−π stacking. Kim et al. (2015) synthesized CdS quantum dots (QDs)/mesoporous TiO_2 (mp-TiO_2) by a sonochemical successive ionic layer adsorption and reaction (SC-SILAR) process. It was found that there is less growth time and larger absorbance of CdS QDs along with a uniform penetration into mp-TiO_2 films in the case of the SC-SILAR process as compared to the SILAR process. As-prepared CdS QDs/mp-TiO_2 was used to fabricate photoanode. This was used in quantum dot-sensitized solar cells (QDSCs) and these cells exhibited high efficiency.

Palanisamy et al. (2015) developed a continuous flow sonochemical reactor, which can produce metastable cadmium sulfide nanoplatelets. It was observed that continuous sonochemical synthesis was found to give high aspect ratio for hexagonal platelets of CdS with cubic crystal structures with thicknesses below 10 nm. It was revealed that uniformity in particle size was much better, when the continuous sonochemical process was used as compared to conventional synthesis processes and batch sonochemical process.

Xu et al. (2015) synthesized uniform molybdenum disulfide/tungsten disulfide quantum dots by the combination of solvothermal and sonication treatment. They used bulk MoS_2/WS_2 reactants at a mild temperature. It was observed that monolayer thickness had an average size of 3 nm. It was

reported that a highly exfoliated and defect-rich structure provides these quantum dots with enough active sites for catalyzing the hydrogen evolution reaction (HER) with long-term durability. These as-prepared particles had good cell permeability, strong fluorescence, and low cytotoxicity, which make them quite promising and biocompatible probes for imaging.

Sonochemical method for the synthesis of zinc sulfide quantum dots has been developed by Panda et al. (2016). They used a single precursor Zn ion and sulfur containing complex. It was indicated that the prepared complexes decomposed to form zinc sulfide quantum dots under high intensity ultrasound irradiation. It was revealed that as-obtained ZnS quantum dots had an 8.2 nm diameter with a cubic structure. The bandgap of these ZnS QDs was also calculated and was found to be 3.73 eV. The Cu and Mn-doped glutathione (GSH)−ZnS polypeptide quantum dots were prepared by Shi et al. (2016) via microwave-assisted sonochemical approach. The glutathione acted as a source of sulfide as well as a dispersant and reducing agent to form polypeptide QDs. It was indicated that the size of the polypeptides QDs was 2−3 nm. It was also reported that the doping of Cu and Mn could decrease the bandgap of GSH−ZnS from 3.67 to 2.86 eV. It was observed that photoelectrochemical (PEC) properties of GSH−ZnS were also enhanced due to the doping of Mn and Cu with excellent chemical stability.

ZnS quantum dots and ZnS:graphene QDs were synthesized by Jindal and Giripunje (2016) via a sonochemical method. It was reported that the average size of ZnS and ZnS:graphene QDs was 3.7 and 8.4 nm, respectively. The bandgap of ZnS:graphene QDs was calculated as 4.9 eV. An increase in current density from 2.44 to 98.4 $\mu A\ cm^{-1}$ was observed with lower turn on voltage from 0.40 to 0.12 V in the active layer as compared to pristine ZnS QDs. Such an enhancement in current density in these ZnS:graphene QDs indicated a great potential for such an active layer in photovoltaic devices. Kapatel et al. (2017) reported the synthesis of tungsten disulfide quantum dots, which were highly stable. They used sodium chloride, sodium hydroxide, lithium hydroxide, and ammonium hydroxide-assisted sonochemical exfoliation of bulk WS_2 powder in N-methyl-2-pyrrolidone for 2 h. It was observed that as-prepared WS_2 quantum dots (few-to-monolayer) have a size of 3 ± 0.5 nm. It was also revealed that better yield of WS_2 quantum dots was obtained in N-methyl-2-pyrrolidone. The as-obtained WS_2 quantum dots exhibited a blueshift with a bandgap of 2.7 eV.

Tin sulfide quantum dots were synthesized by Cheraghizade et al. (2017) via a sonochemical method. They kept sonication time as 10, 15, and 20 min. It was reported that SnS and Sn_2S_3 (orthorhombic phase) and Sn_2S_3 (hexagonal phase) was there in as-prepared QDs. The particle size of tin sulfide QDs was smaller than other QDs, when sonication time was kept at 20 min. It was revealed that smaller spherical shaped particles were obtained on increasing sonication time. The solar cell devices manufactured using tin sulfide QDs exhibited a better performance with the samples prepared with

more sonication time. It was concluded that sonication time is the key factor affecting the synthesis of Sn_2S_3 QDs. Not only this, it will also affect photocatalytic, optical, electrical, and photovoltaic conversion.

Kadeer et al. (2018) synthesized CdS quantum dots/Bi_2WO_6 three-dimensional (3D) heterojunction photocatalyst by ultrasonic method. These composites were found to be active for the degradation of rhodamine B and tetracycline hydrochloride under visible light irradiation and also for the reduction of Cr(VI) in aqueous solution. As-prepared CdS QDs/Bi_2WO_6 heterojunctions exhibited a significantly enhanced photocatalytic activity in all these cases as-compared with samples of CdS and Bi_2WO_6. The highest photocatalytic efficiency for degradation of rhodamine B was 94.5% with 3% CdS QDs/Bi_2WO_6 heterojunction in 30 min, which was about 6 and 1.5 times higher than that with those of pure Bi_2WO_6 and CdS QDs respectively. This enhancement was attributed to the synergetic effect between CdS QDs and Bi_2WO_6, including fast transfer of charge carriers between CdS QDs and Bi_2WO_6 and an efficient electron−hole separation.

Rajabi et al. (2018) developed a sono-assisted chemical precipitation method for synthesizing zinc sulfide quantum dots at room temperature. Then ZnS QDs doped with some transition metal ions (Ag, Mn and Cu) were also prepared using l-cysteine as the capping agent. It was revealed that the time required for a complete synthesis in the presence of ultrasonic irradiations was less than other conventional chemical methods. It takes hardly 15 min at a temperature of 40°C. The bandgap of colloidal ZnS QDs was found to be larger than 3.68 eV. The average particle size of these QDs was less than 5 nm. These were then used for driving the photocatalytic process for degradation of Victoria blue R. It was reported that the maximum removal of this dye (>95%) could be achieved under optimum conditions: pH 10.5, amount of QDs 3 mg, and time 30 min under UV irradiation. It was also revealed that these QDs can be reused six further times, without any significant loss in their photocatalytic properties.

A chemical precipitation method was used by Karimi et al. (2019) for thesynthesis of zinc sulfide quantum dots under the ultrasonic radiation, which was water based and fast also. They used two capping agents, l-cysteine and 2-mercaptoethanol, for this purpose. It was indicated that as-synthesized QDs were cubic in structure with a size less than 10 nm. These ZnS QDs were then used as photocatalysts for the degradation of crystalline violet under UV light. It was revealed that as-synthesized QDs can be reused five times without any significant decrease in their photocatalytic activities.

The cadmium sulfide QDs-sensitized mesoporous-TiO_2 (mp-TiO_2) photoanodes were fabricated by Kim et al. (2019) using the sonochemical successive ionic layer adsorption and reaction (SC-SILAR) methods to achieve highly efficient quantum dots (QDs)-sensitized solar cells. It was reported that the SC-SILAR method took a shorter time for synthesis of CdS QDs as

compared to the conventional SILAR method. It was suggested that the cavitation energy of microbubbles formed in the SC-SILAR method provided an additional energy for the synthesis of CdS QDs. Kandasamy et al. (2022) synthesized cadmium sulfide quantum dots through a green sonochemical method. They used *Delonix elata* leaves water extract as a capping as well as stabilizing agent. It was reported that the corrosion inhibition performance of as-prepared CdS QDs was studied in 3.5% NaCl, 1 M HCl, and 6 M KOH. It was observed that corrosion of zinc plate was reduced when the plates were coated with CdS QDs and these aqueous electrolytes, particularly with 3.5% NaCl.

Goharshadi et al. (2013) synthesized zinc sulfide nanoparticles under ultrasonic irradiation. They did not use any surfactant in this method under high temperature treatment. It was reported that the average particle size of as-prepared ZnS QDs was found to be 2 nm. The photocatalytic activity of ZnS quantum dots was evaluated for the degradation of reactive black 5 under UV light irradiation. It was revealed that about 95% of dye was removed within 10 min when using 0.2 g ZnS at a neutral pH.

8.3.4 Selenides

Three-dimensional (3D) assemblies of CdSe quantum dots (zinc blende structure) were synthesized by Pejova (2013) by two routes: (1) colloidal chemical and (2) sonochemical. A decreasing trend was observed on postdeposition thermal annealing treatment, with increasing average crystal size. Mousavi-Kamazani et al. (2016) synthesized $NiSe_2$ quantum dots from the reaction of selenium tetrachloride with pomegranate marc peels (PMP) dyes and Ni as a nickel precursor in the presence of potassium borohydride through a sonochemical-assisted method. They used PMP because it has several dyes (proanthocyanidins) and flavonoids and ions that can easily extract these from PMP.

Tavakolian and Tashkhourian (2018) prepared cadmium selenide quantum dots capped with reduced graphene oxide and then modified with thioglycolic acid in only 5 min under sonication. They used a solution of cadmium(II) nitrate, graphene oxide, thioglycolic acid, and selenium powder with $NaBH_4$ for this purpose. The glassy carbon electrode (GCE) was modified with as-prepared nanocomposite and used for the determination of ascorbic acid (AA), dopamine (DA), and uric acid (UA) simultaneously. The detection limit was found to be 0.11, 66 and 0.12 μM for DA, AA and UA, respectively. This electrode was also successfully applied for determination of these compounds in spiked urine samples. Kastilani et al. (2019) reported the sonochemical synthesis of CdSe quantum dots in single-liquid bulk phase as well as emulsion-based system. They used cadmium oleate and trioctylphosphine selenide as precursors. It was observed that synthesis of QDs was found to be slow in the case of a single-phase liquid system (1-octadecene)

but it was quite enhanced in a dispersed system (emulsions of 1-octadecene in ethylene glycol). It was also observed that the single-phase solvent system produced ultrasmall QDs exhibiting white-light emission (broad band), while the emulsion system produced well-defined magic-size clusters (MSCs) with high photoluminescence quantum yield (34%).

An ultrasound-assisted method was used by Zare and Tashkhourian (2020) for synthesis of L- and D-cysteine-capped CdSe quantum dots at room temperature. It was observed that as-prepared QDs were in the range of 5−7 nm diameters. These capped QDs exhibited green fluorescence, which was quenched differently by D- and L-tryptophen in a high selective manner, so that they can be used for their recognition with negligible interference by other species. It was reported that detection limits for the recognition of L- and D-tryptophen are 4.2 and 4.7 nm, respectively. However, it was 4.4 and 4.8 nm in the presence of other enantiomers. Tb-doped CdSe nanoparticles were synthesized by Hanifehpour et al. (2021) with variable Tb^{3+} content via a sonochemical route. The sonophotocatalytic activities of the as-prepared sample were evaluated for the photodegradation of reactive black 5. It was reported that the sonophotocatalytic process could degrade 85.25% of the dye, which was much more compared to individual sono- (22%) and photocatalytic degradation (8%) processes. It was observed that photodegradation was inhibited in the presence of benzoquinone and ammonium oxalate. Superoxide radicals and photogenerated holes were detected as the main oxidative species.

8.3.5 Tellurides

Luminescent CdTe quantum dots were produced in an aqueous medium by Menezes et al. (2011) within a few minutes using ultrasound irradiation. It was reported that as-produced QDs exhibited a strong quantum confinement effect and only one fluorescence band was present. These nanoparticles were monodispersed. It was revealed that the morphology of QDs can be better controlled and surface defects are also reduced by the use of ultrasound. The colloidal cadmium telluride quantum dots have been synthesized by Hwang et al. (2011) via one-pot sonochemical reaction. They used multibubble sonoluminescence (MBSL) conditions for this work. The tellurium powder and cadmium chloride with hexadecylamine and trioctylphosphine/trioctylphosphineoxide (TOP/TOPO) (dispersants) were sonicated in toluene (solvent) using ultrasound (20 kHz) at 60°C for 5−40 min. It was reported that a very wide size range of CdTe particles (2−30 μm), could be obtained by just controlling sonicating and thermal heating conditions. It was observed that as-prepared CdTe QDs exhibited different colors, ranging from pale yellow to dark brown, and they showed photoluminescence properties mainly due to the quantum confinement effect. The bandgap of these CdTe particles was found to be 1.53 eV.

Chen et al. (2012) prepared highly fluorescent and water-soluble CdTe quantum dots. They used β-cyclodextrin (β-CD) as surface-coating agents. This

involved a substitution reaction at the C-6 position of mono-6-deoxy-6-(p-tolylsulfonyl)-cyclodextrin (6-tso-β-CD) by the $-NH_2$ of (3-aminopropyl)triethoxysilane-coated CdTe QDs to afford APTES/ CdTe QDs under mild conditions. It was proved that the CdTe QDs were effectively modified by β-CD. The quantum yields of CdTe QDs, APTES/CdTe QDs, and β-CD/APTES/CdTe QDs in water were about 17%, 12%, and 9%, respectively. It was reported that β-CD/APTES/CdTe QDs could recognize molecules of p,p′-DDT and o,p′-DDT.

Shi et al. (2014) developed a fast one-pot method for synthesis of CdTe quantum dots in aqueous solution using a sonoelectrochemical route without the protection of N. It was indicated that the water-soluble CdTe QDs with high photoluminescence qualities can be synthesized without the preparation of precursor and N protection. The PL emission wavelength and quantum yield can be controlled by variation of some operational parameters. It was suggested that QDs prepared by this method have a great potential for application in the fields of sensors, photocatalysis, and solar cells. The cadmium telluride quantum dots were synthesized by Yoo et al. (2017) under ultrasonic irradiation. It was observed that bandgap reduces with the growth of CdTe quantum dots on increasing time of synthesis. There was a redshift in wavelength range (510 ~ 610 nm) on increasing the ratio of Te and cubic zinc blende structure was observed. The size of CdTe quantum dots was found to be about 2.5 nm and these were uniformly dispersed, when the time of synthesis was 210 min.

8.3.6 Carbon-based quantum dots

Li et al. (2011) synthesized monodispersed water-soluble fluorescent carbon nanoparticles. They used glucose as the source of carbon by a one-step alkali or acid-assisted ultrasonic treatment. It was reported that particle surfaces were quite rich in hydroxyl groups so as to provide a high hydrophilic nature. These could emit bright and colorful photoluminescence covering a broad range starting from visible to near infrared (NIR). It was also revealed that these particles had an excellent upconversion fluorescent properties also.

Bavireddi and Kikkeri (2012) synthesized highly fluorescent water-soluble glycoquantum dots through a sonochemical method. It was based on specific host−guest interactions between trioctylphosphine oxide (TOPO) surfactant and β-cyclodextrin (β-CD) on quantum dots. It was indicated that these QDs (β-CD modified) provided good cell viability of human hepatocellular carcinoma cell line (HepG2) cells. It was also revealed that β-CDgal-capped QDs can have a preferential binding with HepG2 cells and therefore could be a promising candidate for some biomedical applications.

Composite architectures consisting of graphitic carbon nitride quantum dots/bismuth phosphate were synthesized by Li et al. (2014). Then as-synthesized composite was used as a visible light-induced photocatalyst for photodegradation of methyl orange with appreciable efficiency.

A one-step sonochemical preparation of carbon dots (C-dots) doped with Ga atom (Ga@C-dots) have been reported by Kumar et al. (2015). This synthesis was carried out with molten Ga, and polyethylene glycol (PEG-400) as the reaction medium for 30−120 min under sonication. It was revealed that as-produced Ga@C-dots in PEG supernatant had an average diameter of 5 ± 2 nm. The fluorescence emission of Ga@C-dots was used as a probe and compared with pristine C-dots.

Kumar et al. (2016a,b) also used a sonochemical approach for the formation of C-dots using ultrasonic irradiation. They sonicated a two-phase mixture to yield Sn@C-dots and achieved Sn nanoparticles decorated by Sn@C-dots (Sn@C-dots@Sn). They directly deposited as-synthesized Sn@C-dots@Sn nanoparticles on the copper foil (current collector) and used them as a promising anode for Li-ion batteries. It was revealed that high lithiation and delithiation properties were present in Sn@C-dots@Sn nanoparticles with enhanced rate capabilities and high coulombic efficiency due to the conducting carbon dot network on the tin nanoparticles minimizing pulverization effects. They also reported a one-step synthesis of carbon dots (Kumar et al., 2016a,b) via sonication of polyethylene glycol (PEG-400) for 0.5−3 h. They also observed the effect of the different operational parameters on the size and the fluorescence of the C-dots such as temperature, amplitude, and sonication. The average diameter of the C-dots was found to be in between 2 and 9 nm; of course, it depends on the conditions of preparation. The highest quantum yield of emissions was found to be $\sim$16%. High fluorescence properties of C-dots can find applications in bioimaging and solar cells.

Sajjadi et al. (2017) prepared cadmium selenide/graphene quantum dots (CdSe/g-QDs) nanocatalyst via a three-step sonochemical−hydrothermal process. It was observed that they have a small bandgap and large specific surface area. It was also observed that the sonocatalytic activity of as-synthesized CdSe/g-QDs was enhanced in the degradation of methylene blue as compared to pure CdSe nanoparticles. It was reported that the degradation efficiency of methylene blue could reach 99% in 90 min under ultrasonic irradiation in the presence of CdSe/g QDs. It was revealed that degradation efficiency increased on the addition of $K_2S_2O_8$ and H_2O_2 as enhancers, while the presence of carbonate, sulfate, and chloride had an adverse effect. It was also indicated that the CdSe/g-QDs sonocatalyst can be reused for up to five successive runs.

The graphene/Ag_3PO_4 quantum dot (rGO/Ag_3PO_4 QD) composite was synthesized by Reheman et al. (2018) via photoultrasonic-assisted reduction method. It was confirmed that as-obtained Ag_3PO_4 QDs were of the size of 1−4 nm and these were dispersed uniformly on rGO nanosheets. The photocatalytic activity of as-synthesized rGO/Ag_3PO_4 QD composites was evaluated for the decomposition of methylene blue. It was found that the best results were obtained when the ratio W_{rGO}:$W_{composite}$ was kept at 2.3%. This composite could degrade 97.5% of methylene blue within 5 min. It was

indicated that enhanced photocatalytic activities and stabilities were due to a synergistic effect between rGO and Ag_3PO_4 QDs with a high specific surface area. It was suggested that these rGO/Ag_3PO_4 QDs photocatalysts can find a great potential in water splitting and sewage treatment. Kumar et al. (2019) used sonochemistry to develop a one-pot synthesis of carbon dots, and metal-doped CDs M@CDs (where M = Zn, Ag, Ga, and Au). The size of these CDs was found to range between 2 and 10 nm. The highest quantum yield of fluorescence emission was measured as ~16%. It was revealed that M@CDs can be used for imaging and neuronal interactions. They also have potential selective affinity, photostability, and biocompatibility. As-prepared M@CD nanocomposites were biocompatible, as well as photostable, so that these can be used for different multifunctional biomedical applications.

Lu and Zhou (2019) prepared fluorescent carbon quantum dots via a sonochemical approach. As-prepared QDs were low cost with high efficiency. They prepared nitrogen-doped CQDs (NCQDs) by ultrasonic treatment of dopamine in dimethylformamide for 8 h. It was reported that as-obtained NCQDs had high water dispersibility as well as stability, within a range of pH and ionic strength, and exhibited bright and stable fluorescence, high photostability, and low cytotoxicity. The fluorescence of CQDs can be quenched by Fe ions in the range of 0−50 μm in both water as well as in the interior of cancer cells. The limit of detection was found to be 38 nm. It was also proposed that the QDs can serve as a nanothermometer to sense temperature both in water as well as in cells.

A template-free sonochemical synthesis of α-Bi_2O_3/C-dots was reported by Sharma et al. (2019). It was confirmed that α-Bi_2O_3 in the nanocomposite was present in monoclinic phase and crystallite size with 28.75 nm. The bandgap of as-prepared nanocomposite was determined to be 2.49 eV. This photocatalyst was used for photocatalytic degradation of 86% of indigo carmine dye under visible light. It was reported that dye was degraded in 2 h as compared to pure α-Bi_2O_3, which only degraded 57%. The Bi_2O_3/C-dots could also achieve about 79% degradation of levofloxacin within 2 h. It was revealed that hydroxyl radicals and electrons played major roles in the photocatalytic degradation of indigo carmine, as evident from scavenger studies.

Yuan et al. (2019) reported a sonochemistry-assisted synthesis of hybrid black/red phosphorus quantum dots (BP/RPQDs). As-prepared quantum dots have small sizes, tunable bandgaps, and high absorption coefficients. They can find application in dye-sensitized solar cells (DSSCs). It was observed that as-prepared hybrid BP/RPQDs exhibited high light-response over a wide range of wavelength (ultra-violet to visible and even near-infrared region) along with longer recombination lifetime of photo generated carriers. It was revealed that DSSCs with BP/RPQDs and BP/RPQDs-N719 cosensitizer could achieve efficiencies of 0.12% and 8.02%, respectively as compared to 7.60% for N719-only solar cell.

Kaimal et al. (2022a) synthesized graphene quantum dots (GQDs) via ultrasonication and fabricated a glassy carbon electrode embedded on

amine-functionalized silica nanoparticles (Si NPs). It was reported that as-developed electrode exhibited a good response to glutathione (most abundant antioxidant in the majority of cells and tissues) with a wide linear range (0.5−7 μm) and a low detection limit of 0.5 μm with high sensitivity. It was revealed that reproducibility, outstanding selectivity, and long-term stability of these as-prepared QDs can find application in real sample analysis even in the presence of interferences.

Kaimal et al. (2022b) prepared gold-loaded boron-doped graphene quantum dots (Au@B-GQDs) interface using the ultrasound-aided reduction method. A sensor was constructed by depositing these as-prepared Au@B-GQDs (thin layer) on a glassy carbon (GC) electrode and they were used for electrochemical studies. These as-obtained QDs have good reproducibility, long-lasting stability, prominent selectivity, and repeatability. It was reported that as-fabricated Au@B-GQDs/GC electrodes can be used as simple and effective sensing platforms for the detection of guanine and adenine in neutral media.

8.3.7 Others

Pejova et al. (2011) studied transport properties of sonochemically synthesized three-dimensional (3D) assemblies of $AgBiS_2$ quantum dots (thin films). The bandgap energy was determined as ∼1.18 eV, which was found to be higher than the optical bandgap of a bulk semiconductor. It may be attributed to 3D confinement effects on the charge carrier motions within individual QDs. Panda et al. (2017) prepared $AgInS_2$ (silver indium sulfide) quantum dots with size ∼1.4 nm by a sonochemical method in 5 min. They used dodecylamine as a capping agent. The bandgap of as-prepared $AgInS_2$ QDs was found to be about 2.15 eV.

Pejova et al. (2020) synthesized quantum nanocrystals of $CuInS_2$ (cubic modification) by a sonochemical route. It was reported that average particle size, size distribution and degree of structural disorder of these $CuInS_2$ can be controlled by adjusting reactor content and exposure to ultrasonic irradiation. It was revealed that bandgap of as-prepared material can also be tuned. As-prepared material can find application in materials in optoelectronics and solar cells based on inorganic semiconductor systems. Zhang et al. (2020) fabricated AgCl quantum dots via ultrasonic method. The average size of AgCl QDs was found to be 2.5 nm. It was reported that as-prepared AgCl QDs exhibited an excellent photocatalytic activity for degradation of rhodamine B and tetracycline under visible light irradiation. It was also revealed that degradation rate of rhodamine B and tetracycline could reach up to 96.6 and 72.2%, respectively in 20 min, which was much higher with AgCl nanoparticles (23 nm) and AgCl nanospheres (114 nm).

Ramalingam et al. (2021) deposited silver quantum dots particles and nanoparticles of magnetite on nanotubes of bismuth in situ doped manganese oxide (Bi-MnOx). It was reported that Ag QDs particles with very fine size

and Fe_3O_4 nanoparticles were incorporated into the Bi-MnOx polymer composite through high power ultrasonication deposition method. It was reported that nanoparticles of silver were spherical in shape with size ranging between 5−15 nm and these were deposited on the Bi-MnOx surfaces (porous). On the other hand, Fe_3O_4 particles (nanorods) were deposited on Bi-MnOx nanotube composite. As-prepared nanoparticle-modified Bi-MnOx composite electrode can be used as electrochemical sensor for hydrogen peroxide detector. It was also revealed that as-prepared Fe_3O_4 and Ag QDs particle-modified Bi-MnoOx nanotubes could remove more than 90% Cr (VI) within 60 min.

8.4 Conclusion

There is a wide range of available methods for synthesizing quantum dots including top-down and bottom-up approaches. Sonochemical synthesis of quantum dots has certain advantages over other conventional methods such as high purity, higher surface area, uniform size distribution, no requirement of additives, and a faster rate. However, it is associated with a disadvantage in that a relatively low yield is obtained, which can be overcome by certain modifications. Quantum dots of various metals, their chalcogenides, and some nonmetals-based QDs have been discussed with their applications. This approach can occupy a prominent position amongst other methods of synthesizing quantum dots in the coming few decades.

References

Ameta, S.C., Ameta, R., Ameta, G. (Eds.), 2018. Sonochemistry: An Emerging Green Technology. CRC Press, New Jersey.

Bang, J.H., Suslick, K.S., 2010. Applications of ultrasound to the synthesis of nanostructured materials. Adv. Mater. 22 (10), 1039−1059.

Bavireddi, H., Kikkeri, R., 2012. Glyco-β-cyclodextrin capped quantum dots: synthesis, cytotoxicity and optical detection of carbohydrate−protein interactions. Analyst 137 (21), 5123−5127.

Calderón-Jiménez, B., Montoro Bustos, A.R., Pereira Reyes, R., Paniagua, S.A., Vega-Baudrit, J.R., 2022. Novel pathway for the sonochemical synthesis of silver nanoparticles with near-spherical shape and high stability in aqueous media. Sci. Rep. 12 (1). Available from: https://doi.org/10.1038/s41598-022-04921-9.

Chen, X.F., Zhou, M., Chang, Y.P., Ren, C.L., Chen, H.L., Chen, X.G., 2012. Novel synthesis of β-cyclodextrin functionalized CdTe quantum dots as luminescent probes. Appl. Surf. Sci. 263, 491−496.

Cheraghizade, M., Jamali-Sheini, F., Yousefi, R., Niknia, F., Mahmoudian, M.R., Sookhakian, M., 2017. The effect of tin sulfide quantum dots size on photocatalytic and photovoltaic performance. Mater. Chem. Phys. 195, 187−194.

Chowdhury, P., Viraraghavan, T., 2009. Sonochemical degradation of chlorinated organic compounds, phenolic compounds and organic dyes−a review. Sci. Total Environ. 407 (8), 2474−2492.

Das, A., Wai, C.M., 2014. Ultrasound-assisted synthesis of PbS quantum dots stabilized by 1, 2-benzenedimethanethiol and attachment to single-walled carbon nanotubes. Ultrason. Sonochem. 21 (2), 892–900.

Einhorn, C., Einhorn, J., Luche, J.L., 1989. Sonochemistry-The use of ultrasonic waves in synthetic organic chemistry. Synthesis 1989 (11), 787–813.

Entezari, M.H., Ghows, N., 2011. Micro-emulsion under ultrasound facilitates the fast synthesis of quantum dots of CdS at low temperature. Ultrason. Sonochem. 18 (1), 127–134.

Estandarte, A.K., Paredes, F., Bartolome, A., Arco, S., Arellano, I.H., 2011. Synthesis, characterization and application of imidazolium ionic liquid-capped CdS quantum dots in PET fibers as a photocatalyst for the photodegradation of methylene blue. Quezon City (Philippines) .

Galton, F., 1883. Inquiries into Human Faculty and Development. McMillan, London.

Goharshadi, E.K., Sajjadi, S.H., Mehrkhah, R., Nancarrow, P., 2012. Sonochemical synthesis and measurement of optical properties of zinc sulfide quantum dots. Chem. Eng. J. 209, 113–117.

Goharshadi, E.K., Hadadian, M., Karimi, M., Azizi-Toupkanloo, H., 2013. Photocatalytic degradation of reactive black 5 azo dye by zinc sulfide quantum dots prepared by a sonochemical method. Mater. Sci. Semicond. Process. 16 (4), 1109–1116.

Hanifehpour, Y., Nozad Ashan, N., Amani-Ghadim, A.R., Joo, S.W., 2021. Sonochemical synthesis, characterization and optical properties of Tb-doped CdSe nanoparticles: Synergistic effect between photocatalysis and sonocatalysis. Nanomaterials. 11 (2), 378.

Hwang, C.H., Park, J.P., Song, M.Y., Lee, J.H., Shim, I.W., 2011. Syntheses of CdTe quantum dots and nanoparticles through simple sonochemical method under multibubble sonoluminescence conditions. Bull. Korean Chem. Soc. B 32 (7), 2207–2211.

Islam, M.N., Phong, L.V., Jeong, J.R., Kim, C., 2011. A facile route to sonochemical synthesis of magnetic iron oxide (Fe_3O_4) nanoparticles. Thin Solid. Films 519 (23), 8277–8279.

Jia, T., Fu, F., Zhao, J., Chen, J., Wang, X., Fan, Z., et al., 2014. Sonochemical synthesis, characterization, and photocatalytic activity of N-Doped TiO_2 nanocrystals with mesoporous structure. Int. J. Photoenergy 2014. Available from: https://doi.org/10.1155/2014/516806.

Jindal, S., Giripunje, S.M., 2016. Enhanced photovoltaic performance of bulk heterojunction based on ZnS quantum dots-grafted graphene. Superlattices Microstruct. 100, 683–693.

Kadeer, K., Tursun, Y., Dilinuer, T., Okitsu, K., Abulizi, A., 2018. Sonochemical preparation and photocatalytic properties of CdS QDs/Bi_2WO_6 3D heterojunction. Ceram. Int. 44 (12), 13797–13805.

Kaimal, R., Vinoth, V., Salunke, A.S., Valdés, H., Mangalaraja, R.V., Aljafari, B., et al., 2022a. Highly sensitive and selecstive detection of glutathione using ultrasonic aided synthesis of graphene quantum dots embedded over amine-functionalized silica nanoparticles. Ultrason. Sonochem. 82. Available from: https://doi.org/10.1016/j.ultsonch.2021.105868.

Kaimal, R., Mansukhlal, P.N., Aljafari, B., Anandan, S., Ashok kumar, M., 2022b. Ultrasound-aided synthesis of gold-loaded boron-doped graphene quantum dots interface towards simultaneous electrochemical determination of guanine and adenine biomolecules. Ultrason. Sonochem. 83. Available from: https://doi.org/10.1016/j.ultsonch.2022.105921.

Kandasamy, K.; Surendhiran, S.; Devi, R. C.; Khadar, Y. S.; Rajasingh, P.; Balamurugan, A. Facile and eco-friendly synthesis of CdS quantum dots for enhancing corrosion inhibition of Zn metal plate in various environments. In AIP Conference Proceedings. AIP Publishing LLC. 2022, 2385 (1), doi: 10.1063/5.0070727.

Kapatel, S., Mania, C., Sumesh, C.K., 2017. Salt assisted sonochemical exfoliation and synthesis of highly stable few-to-monolayer WS_2 quantum dots with tunable optical properties. J. Mater. Sci.: Mater. Electron. 28 (10), 7184–7189.

Karimi, F., Rajabi, H.R., Kavoshi, L., 2019. Rapid sonochemical water-based synthesis of functionalized zinc sulfide quantum dots: Study of capping agent effect on photocatalytic activity. Ultrason. Sonochem. 57, 139–146.

Kastilani, R., Bishop, B.P., Holmberg, V.C., Pozzo, L.D., 2019. On-Demand sonochemical synthesis of ultrasmall and magic-size CdSe quantum dots in single-phase and emulsion systems. Langmuir 35 (50), 16583–16592.

Kim, J.H., Kim, G.Y., Sohn, S.H., 2015. Sono-chemical successive ionic layer adsorption and reaction for the synthesis of CdS quantum dots onto mesoporous TiO_2 photoanodes. Japn. J. Appl. Phys. 54 (7). Available from: https://doi.org/10.7567/JJAP.54.070304.

Kim, J.H., Jang, T., Seo, S.R., Sohn, S.H., 2019. Properties of CdS quantum dots synthesized using sonochemical successive ionic layer adsorption and reaction method for quantum dot-sensitized solar cells. J. Phys. Chem. Solids 127, 101–106.

Kumar, V.B., Perelshtein, I., Lipovsky, A., Porat, Z.E., Gedanken, A., 2015. The sonochemical synthesis of Ga@ C-dots particles. Rsc Adv. 5 (32), 25533–25540.

Kumar, V.B., Tang, J., Lee, K.J., Pol, V.G., Gedanken, A., 2016a. In situ sonochemical synthesis of luminescent Sn@C-dots and a hybrid Sn@C-dots@Sn anode for lithium-ion batteries. RSC Adv. 6 (70), 66256–66265.

Kumar, V.B., Porat, Z.E., Gedanken, A., 2016b. Facile one-step sonochemical synthesis of ultrafine and stable fluorescent C-dots. Ultrason. Sonochem. 28, 367–375.

Kumar, V.B., Kumar, R., Gedanken, A., Shefi, O., 2019. Fluorescent metal-doped carbon dots for neuronal manipulations. Ultrason. Sonochem. 52, 205–213.

Li, H., He, X., Liu, Y., Huang, H., Lian, S., Lee, S.T., et al., 2011. One-step ultrasonic synthesis of water-soluble carbon nanoparticles with excellent photo luminescent properties. Carbon 49 (2), 605–609.

Li, Z., Li, B., Peng, S., Li, D., Yang, S., Fang, Y., 2014. Novel visible light-induced g C_3N_4 quantum dot/$BiPO_4$ nanocrystal composite photocatalysts for efficient degradation of methyl orange. RSC Adv. 4 (66), 35144–35148.

Liu, H., Zhang, X., Wu, X., Jiang, L., Burda, C., Zhu, J.J., 2011. Rapid sonochemical synthesis of highly luminescent non-toxic AuNCs and Au@AgNCs and Cu (II) sensing. Chem. Commun. 47 (14), 4237–4239.

Lu, M., Zhou, L., 2019. One-step sonochemical synthesis of versatile nitrogen-doped carbon quantum dots for sensitive detection of Fe^{2+} ions and temperature in vitro. Mater. Sci. Eng. C 101, 352–359.

Majumdar, S.; Devi, P. S. Synthesis of SnO_2 nanoparticles using ultrasonication. In AIP Conference Proceedings, American Institute of Physics. 2010, 1276 (1), doi: 10.1063/1.3504298.

Mallikarjuna, K., Vattikuti, S.V.P., Manne, R., Manjula, G., Munirathnam, K., Mallapur, S., et al., 2021. Sono-chemical synthesis of silver quantum dots immobilized on exfoliated graphitic carbon nitride nanostructures using ginseng extract for photocatalytic hydrogen evolution, dye degradation, and antimicrobial studies. Nanomaterials 11 (11). Available from: https://doi.org/10.3390/nano11112918.

Mason, T.J., 1999. Sonochemistry. Oxford University Press, New York.

Menezes, F.D., Galembeck, A., Junior, S.A., 2011. New methodology for obtaining CdTe quantum dots by using ultrasound. Ultrason. Sonochem. 18 (5), 1008–1011.

Moghaddam, E., Youzbashi, A.A., Kazemzadeh, A., 2017. Investigation of ultrasonic effect on morphology, optical and growth properties of ZnO quantum dots. J. Nano Res. 49, 10–17.

Mousavi-Kamazani, M., Salavati-Niasari, M., Goudarzi, M., Gharehbaii, A., 2016. A facile novel sonochemical-assistance synthesis of $NiSe_2$ quantum dots to improve the efficiency of dye-sensitized solar cells. J. Inorg. Organomet. Polym. Mater. 26 (1), 259–263.

Palanisamy, B., Paul, B., Chang, C.H., 2015. The synthesis of cadmium sulfide nanoplatelets using a novel continuous flow sonochemical reactor. Ultrason. Sonochem. 26, 452–460.

Panda, B.B., Sharma, B., Rana, R.K., 2016. Sonochemical synthesis and characterization of ZnS quantum dots. Adv. Sci. Eng. Med. 8 (4), 333–337.

Panda, B.B., Rana, R.K., Sharma, B., 2017. Sonochemical synthesis of $AgInS_2$ quantum dots and characterisation. J. Nano-Electron. Phys. 9. Available from: https://doi.org/10.21272/jnep.9(2)0.02002.

Pejova, B., 2013. Phonon confinement and related effects in three-dimensional assemblies of cubic cadmium selenide quantum dots synthesized by conventional chemical and sonochemical routes. J. Phys. Chem. C 117 (38), 19689–19700.

Pejova, B., Bineva, I., 2013. Sonochemically synthesized 3D assemblies of close-packed In_2S_3 quantum dots: Structure, size dependent optical and electrical properties. J. Phys. Chem. C 117 (14), 7303–7314.

Pejova, B., Nesheva, D., Aneva, Z., Petrova, A., 2011. Photoconductivity and relaxation dynamics in sonochemically synthesized assemblies of $AgBiS_2$ quantum dots. J. Phys. Chem. C 115 (1), 37–46.

Pejova, B., Sherif, E., Minde, M.W., 2020. Sonochemically synthesized quantum nanocrystals of cubic $CuInS_2$: Evidence for multifractal surface morphology, size-dependent structure, and particle size distribution. J. Phys. Chem., C 124 (37), 20240–20255.

Pestman, J.M., Engberts, J.B., de Jong, F., 1994. Sonochemistry: theory and applications. Recl. des Trav. Chimiques des Pays-Bas 113 (12), 533–542.

Rajabi, H.R., Karimi, F., Kazemdehdashti, H., Kavoshi, L., 2018. Fast sonochemically-assisted synthesis of pure and doped zinc sulfide quantum dots and their applicability in organic dye removal from aqueous media. J. Photochem. Photobiol. B: Biol. 181, 98–105.

Ramalingam, R.J., Arunachalam, P., Appaturai, J.N., Thiruchelvi, P., Al-othman, Z.A., Alanazi, A.G., et al., 2021. Facile sonochemical synthesis of nanoparticle modified Bi-MnOx and Fe_3O_4 deposited Bi-MnOx nanocomposites for sensor and pollutant degradation application. J. Alloy. Compd. 859. Available from: https://doi.org/10.1016/j.jallcom.2020.158263.

Reheman, A., Tursun, Y., Dilinuer, T., Halidan, M., Kadeer, K., Abulizi, A., 2018. Facile one-step sonochemical synthesis and photocatalytic properties of graphene/Ag_3PO_4 quantum dots composites. Nanoscale Res. Lett. 13 (1). Available from: https://doi.org/10.1186/s11671-018-2466-9.

Sajjadi, S., Khataee, A., Kamali, M., 2017. Sonocatalytic degradation of methylene blue by a novel graphene quantum dots anchored CdSe nanocatalyst. Ultrason. Sonochem. 39, 676–685.

Sedghi, S.M., Mortazavi, Y., Khodadadi, A., 2010. Low temperature CO and CH_4 dual selective gas sensor using SnO_2 quantum dots prepared by sonochemical method. Sens. Actuators B Chem. 145 (1), 7–12.

Sharma, S., Mehta, S.K., Ibhadon, A.O., Kansal, S.K., 2019. Fabrication of novel carbon quantum dots modified bismuth oxide (α-Bi_2O_3/C-dots): Material properties and catalytic applications. J. Colloid Interface Sci. 533, 227–237.

Shi, J.J., Wang, S., He, T.T., Abdel-Halim, E.S., Zhu, J.J., 2014. Sono electrochemical synthesis of water-soluble CdTe quantum dots. Ultrason. Sonochem. 21 (2), 493–498.

Shi, J.J., Gong, L., Zhang, Y.H., Yang, P., He, J., 2016. Microwave-assisted sonochemical synthesis of Cu and Mn doped GSH–ZnS polypeptide quantum dots and their enhanced photoelectrochemical properties. RSC Adv. 6 (111), 109386–109393.

Suslick, K.S., Flannigan, D.J., 2008. Inside a collapsing bubble: Sonoluminescence and the conditions during cavitation. Annu. Rev. Phys. Chem. 59 (1), 659–683.

Tavakolian, E., Tashkhourian, J., 2018. Sonication-assisted preparation of a nanocomposite consisting of reduced graphene oxide and CdSe quantum dots, and its application to simultaneous voltammetric determination of ascorbic acid, dopamine and uric acid. Microchim. Acta 185 (10). Available from: https://doi.org/10.1007/s00604-018-2988-y.

Wang, X.K., Wang, C., Jiang, W.Q., Guo, W.L., Wang, J.G., 2012. Sonochemical synthesis and characterization of Cl-doped TiO_2 and its application in the photodegradation of phthalate ester under visible light irradiation. Chem. Eng. J. 189, 288−294.

Wang, C., Wu, J., Jiang, K., Humphrey, M.G., Zhang, C., 2017. Stable Ag nanoclusters-based nano-sensors: Rapid sonochemical synthesis and detecting Pb^{2+} in living cells. Sens. Actuators B Chem. 238, 1136−1143.

Xu, S., Li, D., Wu, P., 2015. One-pot, facile, and versatile synthesis of monolayer MoS_2/WS_2 quantum dots as bioimaging probes and efficient electrocatalysts for hydrogen evolution reaction. Adv. Funct. Mater. 25 (7), 1127−1136.

Yadav, R.S., Mishra, P., Mishra, R., Kumar, M., Pandey, A.C., 2010. Histidine functionalised biocompatible CdS quantum dots synthesized by sonochemical method. J. Exp. Nanosci. 5 (4), 348−356.

Yang, W., Yang, H., Ding, W., Zhang, B., Zhang, L., Wang, L., et al., 2016a. High quantum yield ZnO quantum dots synthesizing via an ultrasonication micro reactor method. Ultrason. Sonochem. 33, 106−117.

Yang, W., Zhang, B., Ding, N., Ding, W., Wang, L., Yu, M., et al., 2016b. Fast synthesize ZnO quantum dots via ultrasonic method. Ultrason. Sonochem. 30, 103−112.

Yoo, J.Y., Kim, W.S., Park, S.A., Kim, J.G., 2017. Study on Sonochemical Synthesis and Characterization of CdTe Quatum Dot. Appl. Chem. Eng. 28 (5), 571−575.

Yuan, H., Zhao, Y., Wang, Y., Duan, J., He, B., Tang, Q., 2019. Sonochemistry-assisted black/red phosphorus hybrid quantum dots for dye-sensitized solar cells. J. Power Sources 410, 53−58.

Zare, S., Tashkhourian, J., 2020. Ultrasound-assisted synthesis of chiral cysteine-capped CdSe quantum dots for fluorometric differentiation and quantitation of tryptophan enantiomers. Microchim. Acta 187 (1). Available from: https://doi.org/10.1007/s00604-019-4046-9.

Zhang, J., Maimaitizi, H., Zhang, T., Tursun, Y., Talifu, D., Abulizi, A., 2020. Facile one-step sonochemical synthesis of AgCl quantum dots with enhanced photocatalytic activity and its size effects. Funct. Mate. Lett. 13 (06). Available from: https://doi.org/10.1142/S1793604720510364.

Zhao, M.X., Li, Y., Wang, C.J., 2013. Synthesis and bioactivity of the folate receptor targeted gamma-cyclodextrin-folate inclusion-coated CdSe/ZnS quantum dots. Yao xue xue bao = Acta Pharmaceutica Sin. 48 (4), 566−572.

This page intentionally left blank

Chapter 9

Application of quantum dots in photocatalysis

Shubang Vyas[1], **Rameshwar Ameta**[1] **and Rakshit Ameta**[2]
[1]*Department of Chemistry, PAHER University, Udaipur, Rajasthan, India,* [2]*Department of Chemistry, J. R. N. Rajasthan Vidhyapeeth (Deemed to be University), Udaipur, Rajasthan, India*

9.1 Introduction

Photocatalysis is a branch of chemistry that deals with chemical reactions taking place in the presence of light and a photocatalyst. A photocatalyst is a semiconductor that enhances the rate of reaction by its presence. Thus photocatalysis is a phenomenon, where an electron−hole pair (exciton) is generated on exposing semiconducting materials to light of suitable energy. Thus the chemical reactions that occur in the presence of a semiconductor and light are collectively termed as photocatalytic reactions. Photocatalytic reactions are mainly classified into two categories: (1) homogeneous photocatalysis, where substrate and photocatalyst both exist in the same phase; and (2) heterogeneous photocatalysis, in which substrate and photocatalyst exist in different phases.

Different dyes and some soluble coordination compounds are used as homogeneous photocatalysts, whereas different semiconducting powders are good examples of heterogeneous photocatalysts. The importance of photocatalysis lies in the fact that a photocatalyst provides both an oxidation and reduction environment simultaneously. This field has been extensively reviewed by various researchers (e.g., Fox and Dulay, 1993; Ameta et al., 1999; Chong et al., 2010; Pelaez et al., 2012; Ameta et al., 2013; Ibhadon and Fitzpatrick, 2013; Schneider et al., 2014; Ameta and Ameta, 2016; Zhang et al., 2019; Djurišić et al., 2020; Ren et al., 2021).

Photocatalysis is a main tool in dealing with some major problems of the world such as environmental pollution, wastewater treatment, water splitting for combating energy crises, self-cleaning, antifogging, biomedicals, solar cells, etc.

Thus heterogeneous photocatalysis involves a chain of oxidative and reductive reactions on the surface of the photocatalyst. The energy difference between

Quantum Dots. DOI: https://doi.org/10.1016/B978-0-12-824153-0.00009-4
© 2023 Elsevier Inc. All rights reserved.

the valence band and the conduction band is called the bandgap (Eg). When a photocatalyst is exposed to light of the desired wavelength (sufficient energy, i.e., equal to or more than bandgap), the energy of photons is absorbed by an electron (e^-) of the valence band and it is excited to the conduction band. In this process, a hole (h^+) is created in the valence band. This process leads to the formation of photoexcitation state e^- and h^+ pair. This excited electron is used for reducing an acceptor, while a hole is used for oxidation of donor molecules.

There are some advantages of photocatalysts and these are:

- The catalyst is low cost, nontoxic, and reusable.
- The only requirement for such a reaction is the presence a semiconductor and light.
- The process takes place at ambient conditions.
- The pollutants may be degraded finally to CO_2, H_2O, and other inorganic substances, that is, complete mineralization.

Water is a universal solvent and it is required for the survival of life on this planet. Water is polluted due to an increased utilization in domestic and industrial activities, which poses a special threat of contaminating surface and groundwater. In recent years, advanced oxidation processes (AOPs), particularly photocatalysis, have been applied to treat wastewater problems. This is a green method to oxidize organic contaminants with strong reactive oxidizing radical species like $^{\bullet}OH$, $HOO^{\bullet}$, $O_2^{-\bullet}$, etc. It fulfills the goals of being environmentally friendly and showing sustainable development due to the unique electronic, optical, and structural properties. The important aspect of these nanoscale materials is their large surface area-to-volume ratio and quantum confinement effects, which are necessary for catalysis.

After the discovery of quantum dots (QDs), their potential applications for chemical sensing, bioimaging, drug delivery, and photocatalysis have been tremendously developed. It is due to their excellent aqueous solubility, magnificent electron transfer, and ability to harness light to make full utilization of solar insolation. Green QDs, particularly carbon QDs (CQDs), have received considerable interest in this blooming field due to their nontoxic behavior, greater sustainability, outstanding photostability, and their natural photoluminescence properties. These CQDs also have tunable optical properties and high biocompatibility; as a result, they have a number of applications. The importance of such studies lies in designing efficient photocatalysts, surface modification, charge transfer, and development of ternary photocatalysis. These techniques will significantly increase the photocatalytic activity of semiconductors with wide bandgaps, which can be utilized for solar energy conversion.

9.2 Quantum dots

QDs are semiconductor nanoparticles that exhibit size and composition-dependent optical and electronic (optoelectronic) properties. These are ultrasmall

in terms of size, ranging between 2.0 and 10.0 nm. These can be used in wastewater treatment (removal or degradation of pollutants), hydrogen generation from water (as the fuel of future), reduction of carbon dioxide (putting a check on ever increasing amount of CO_2 in atmosphere, that is, controlling global warming), and converting solar energy into electrical energy (solar cell, drug delivering), etc.

9.3 Wastewater treatment

Industries are regularly increasing the level of manufacture of materials due to the demands of society. These materials include different drugs, dyes, pesticides, etc. These industries release their effluents into the water resources with no or negligible treatment. As a result, water is polluted. Most of the chemicals are quite toxic and some of them are even carcinogenic, and therefore there is a necessity to treat wastewater by any alternate but eco-friendly and effective method. Photocatalysis can degrade most of these pollutants through oxidation because it is one of the techniques involving AOPs (green chemical pathways).

Wahab et al. (2013) compared the photocatalytic properties of TiO_2 and ZnO QDs for oxidation and degradation of acetaldehyde in gaseous phase. It was observed that rate constant for as-prepared ZnO QDs and Degussa P-25 was 8.3×10^{-3} and 1.9×10^{-2} min., respectively about, which was about two times. Their efficiencies were 70% and 92% for Degussa P-25 and ZnO-QDs, respectively in 2 h. It was observed that as-prepared QDs were of 6−7 nm size with wurzite phase.

Quan et al. (2016) prepared quasinoble-metal graphene QDs (GQDs) deposited stannic oxide by just sintering citric acid and SnO_2 together. A redox process between GQDs and SnO_2 generated oxygen vacancy (OV) states somewhere below the conduction band of stannic oxide. These VOs will shift the optical absorption band of SnO_2 towards the visible light region. The GQDs can also effectively increase the charge separation efficiency through noble metal promoting visible light response to some extent. The best performance was exhibited by samples calcinated at 450 °C due to relatively high concentrations of VOs. This study revealed that a combination of defect modulation and noble metal deposition together increased the photocatalytic activity.

Zeng et al. (2016) reported that when graphene oxide QDs (GOQDs) are covalently bonded onto amino modified polyvinylidene fluoride (PVDF) membrane, it resulted into a new type of nanocarbon functionalized membrane with remarkable enhanced antibacterial and antibiofouling properties. An *Escherichia coli* containing water exhibited a decrease in relative flux over GOQDs modified PVDF, which was 23%, and it is significantly lower than with GO-sheet modified PVDF (62%) and pristine PVDF (86%) after 10 h of filtration. The GOQD coating layer effectively inactivated *Staphylococcus aureus* and *E. coli* cells

such that the biofilm could not form a membrane surface. As a result, antimicrobial activity and antibiofouling capability was improved as compared to GO and CNTs modified membranes. This better performance may be due to uniform dispersion and unique structure of GOQDs. A long-term stability and durability was observed in GOQDs modified membrane due to strong covalent interaction between GOQDs and PVDF.

Cheraghizade et al. (2017) synthesized tin sulfide QDs by sonication. It was indicated that SnS and Sn_2S_3 (orthorhombic phase) and SnS_2 (hexagonal phase) wer present and the particle size of these QDs was smaller than other QDs. It was observed that smaller spherical shaped particles were obtained on increasing sonication time. A greater photocatalytic activity was observed for tin sulfide QDs, which were synthesized with longer sonication time. It was reported that solar cell devices constructed using as-prepared tin sulfide QDs exhibited a better performance. This shows that the duration of sonication is an important factor that affects the synthesis process as well as the optical, electrical, photocatalytic, and photovoltaic conversion properties of these QDs.

Xu et al. (2019) fabricated CQDs-N-TiO_{2-x} nanocomposites by decorating CQDs on the Ti^{3+} and nitrogen codoped TiO_2 nanoparticles via a combination of the hydrothermal−calcination method. The formation of N/Ti^{3+} codoping levels and introduction of CQDs in the nanocomposite was also confirmed. It was observed that as-prepared CDs-N-TiO_{2-x} nanocomposite showed increased visible light absorption as well as better charge separation compared to pristine CQDs-TiO_2, TiO_2, N-doped TiO_2 (N-TiO_2), N and Ti^{3+} codoped TiO_2 (N-TiO_{2-x}). As-prepared CQDs-N-TiO_{2-x} nanocomposite exhibited an excellent performance for Cr(VI) reduction in the presence of visible light (Fig. 9.1). It was reported that there was significant increase in the reduction of Cr(VI) on addition of citric acid (hole scavenger). As-prepared CQDs-N-TiO_{2-x} nanocomposite was found to exhibit efficient photocatalytic reduction of Cr(VI) in real samples of wastewater.

There are three important factors that control recovery: draw solution (DS), forward osmosis, and membrane. Doshi and Mungray (2020) reported the synthesis of a novel DS based on CQDs via two different hydrothermal methods (autoclave, A-1; reflux, R-1). They used tulsi (*Ocimum tenuiflorum*) for this purpose. It was found that 5% CQDs prepared by R-1 with 50% glycerol DS (TCQD-G) was found to be effective in inhibiting microbial growth. It was observed that the highest water flux (5.34 LMH) could be achieved with synthetic wastewater (feed solution) using TCQD-G as a DS.

Zhang et al. (2020) studied the use of dual QDs cocatalyst for remediation of organic pollutants. H_2O_2 is considered a green oxidant. They reported that FeOOH QDs/CQDs/g-C_3N_4 composite (FCCN) showed excellent photoactivity for the degradation of oxytetracycline (OTC) under visible light irradiation. The enhanced photoactivity was due to photoexcited electron transfer, where electrons can be quickly utilized by molecular oxygen to form H_2O_2. This results in facilitating the activation of oxygen molecules.

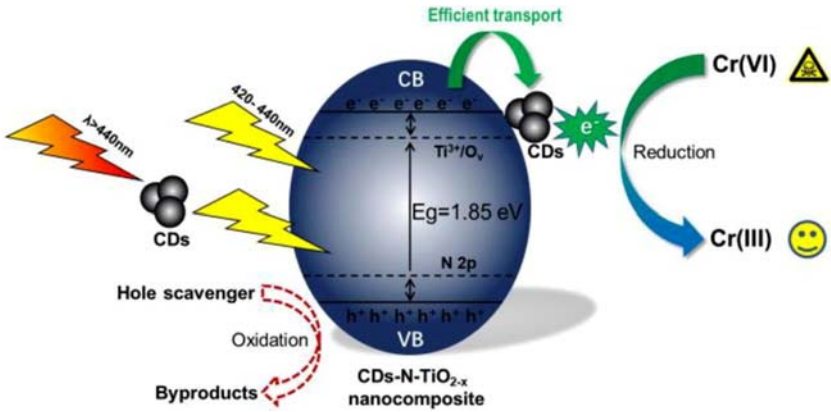

FIGURE 9.1 Photocatalytic reduction of Cr (VI). *Adapted from Xu et al., 2019. Chem. Eng. J., 357, 473–486. With Permission.*

The Fe^{3+} in FeOOH QDs was also reduced to Fe^{2+} by these photoexcited electrons, which react with H_2O_2 to produce the $^{\bullet}OH$ radicals responsible for photodegradation. As a result, surface carrier transfer efficiency (41.01%) was enhanced as compared to only g-C_3N_4 and CQDs/g-C_3N_4 photocatalyst.

9.3.1 Dyes

Different dyes are synthesized and manufactured to fulfill the demand of different color shades by the society, but these are very harmful. If these dyes are accumulated in nearby water resources, this can harm aquatic life, animal life, and human beings on consumption of this polluted water. Thus effluents containing different dyes are to be given photocatalytic treatment, before release to water bodies.

Colloidal oil-soluble Bi_2O_3 QDs were synthesized by Zhang et al. (2010). Water-soluble Bi_2O_3 QDs were produced from oil-soluble QDs through phase transfer by modifying the surface with mercaptopropionic acid. It was reported that water-soluble Bi_2O_3 QDs exhibited outstanding photocatalytic activity for the degradation of methyl orange over a wide range of pH. As-prepared Bi_2O_3 QDs maintained high degradation efficiency even after several cycles. Kusic et al. (2011) reported the use of QDs nanoparticles for treatment of colored wastewater. They used chemical processes for water treatment and disinfection (direct ozonation and direct UV photolysis) for the degradation of colored organic pollutant (reactive azo dye), in the presence of CdSe/ZnS core–shells QDs.

Chen et al. (2013) reported hybrid metal oxide QDs, where Cu_xO and Fe_xO, were anchored on TiO_2 blocks (Cu_xO/TiO_2 and Fe_xO/TiO_2). Their photocatalytic activities were examined by photocatalytic decoloration of methylene blue in the presence of visible light as well as simulated sunlight.

It was observed that these hybrid metal oxide QDs were dispersed uniformly on TiO_2 blocks and both copper and iron were present in mixed valence states (Fe^{2+} and Fe^{3+}; Cu^{+} and Cu^{2+}).

Mansur et al. (2014) reported the fabrication of nanophotocatalysts based on ZnS QDs, which were functionalized with chitosan (CHI) using a green method at room temperature. It was observed that in as-prepared ZnS/CHI nanophotocatalysts (ZnS−CHI) CHI was acting as an effective capping ligand to produce water-soluble ZnS QDs with an average size of 3.8 nm. They selected two model organic pollutants (methylene blue and methyl orange), and these were effectively degraded by ZnS/CHI under UV irradiation. It was also observed that ZnS−CHI nanoconjugates displayed blue photoluminescent behavior, when excited by UV radiation.

Muthulingam et al. (2015) prepared composites containing CQDs/nitrogen-doped ZnO (CQD/N-ZnO) via a one-step method. Three dyes were selected as model pollutants: fluorescein, methylene blue, and malachite green. It was reported that as-prepared CQD/N-ZnO photocatalyst exhibited an increased cohesiveness to degrade all these three dyes within 30−45 min in the presence of daylight. Also, it was found that the composite can be reused because of its antiphotocorrosion behavior furnished by CQDs.

Saud et al. (2015) prepared CQDs/titanium dioxide (CQDs/TiO_2) composite nanofibers through hydrothermal route. It was revealed that the photocatalytic efficiency of as-prepared composite nanofibers was found to be higher than pristine TiO_2 nanofibers for the degradation of methylene blue under visible light irradiation as well as antibacterial properties against *E. coli*. The anchored CQDs can increase light absorption as well as suppressed recombination of photogenerated electron−hole pair resulting in an increase in photocatalytic and antibacterial properties.

Vidhya et al. (2015) reported a modified green synthesis route to prepare pure and starch-capped ZnO (ZnO/starch) QDs. It was observed that a hexagonal crystal structure was present in both pure and ZnO/starch QDs, as evident from XRD data. It was reported that the particles were spherical in shape with a size of 5−10 nm. It was revealed that ZnO/starch QDs showed an increased emission behavior as compared to ZnO QDs. The photocatalytic activity of ZnO QDs was evaluated using the degradation of rhodamine B. Here, it was found that ZnO/starch QDs showed a higher decomposition of dye as compared to pure ZnO QDs.

Fan et al. (2016) synthesized GQDs and polymer-modified GQDs using a hydrothermal method. They used citric acid as a precursor of carbon. The GQDs were modified with polyethylene glycol and polyethylenimine. It was revealed that GQDs were uniform in size (2−5 nm). The photocatalytic activity of these samples was evaluated for the degradation of methylene blue. It was observed that the rate of photocatalytic degradation was found to be in the order:

$$\text{GQDs} > \text{GQDs-PEIs} > \text{GQDs-PEGs}$$

Miao et al. (2016) prepared CQDs embedded in mesoporous TiO_2 materials via a sol−gel method. It was observed that the nanoparticles were randomly packed in inverse surfactant micelles and mesopores are formed by interconnected intraparticles. The photocatalytic activity of as-prepared CQDs/meso-Ti-450 was observed in the degradation of methylene blue. It was observed that photocatalytic activity of the composite material was greatly increased due to the upconversion property and electron withdrawing property of CQDs. The highest photocatalytic activity was obtained by the sample (5% CQDs/meso-Ti-450). It was observed that almost 98% dye was removed while only 10% methylene blue can be degraded by commercial P 25.

Rajabi and Farsi (2016) studied the effect of capping agent on the photocatalytic properties of zinc sulfide QDs. They synthesized ZnS QDs by an aqueous chemical precipitation method using different capping agents (thiourea, 2-mercaptoethanol, and l-cysteine). It was observed that the optical absorption band of ZnS nanostructures also changed with capping agents. As-prepared ZnS QDs were used for photodegradation of crystal violet as a model dye in an alkaline medium with a low concentration of QDs.

Zhang et al. (2016) prepared nitrogen-doped CQDs/TiO_2 (NCQDs/TiO_2) hybrid composites. It was reported that the NCQDs were introduced onto the TiO_2 surface. The photocatalytic activity of as-prepared NCQDs/TiO_2 hybrid composites was evaluated by selecting methylene blue as the target pollutant. It was found that the photodegradation efficiency of dye over 1NCQDs/TiO_2 was about 86.9%, which was much more than pristine TiO_2 (53.8%) The increased photocatalytic activities of NCQDS/TiO_2 hybrid may be due to interfacial transfer of photogenerated charges to NCQDs from the conductive band of TiO_2; leading to effective charge separation in TiO_2.

Anh et al. (2017) fabricated N, S-codoped GQDs (N, S-GQDs) by a hydrothermal route. It can be used for selective and sensitive detection of mercury ions (Hg^{2+}) in water as well as wastewater. It was reported that as-prepared N, S-GQDs were uniform in size with an average particle size of 3.5 ± 0.5 nm. It was reported that doping of nitrogen atoms increased the quantum yield up to 41.9%, whereas sulfur atoms were responsible for better selectivity of Hg^{2+} through strong coordination interaction. It was found that the fluorescence intensity of N, S-GQDs was proportional to Hg^{2+} quenching with a limit of detection of 0.14 nM. As-prepared N, S-GQDs were used for detecting mercuric ions samples of sewage and dye wastewater.

Kumar et al. (2018) synthesized GQDs decorated ZnO nanorods heterojunctions. They evaluated photocatalytic performance of these heterojunctions for the degradation of methylene blue and also carbendazim, a fungicide in the presence of sunlight. It was observed that this heterojunction with 2 wt.% of GQD (ZGQD2) exhibited best photocatalytic degradation (about 95%) of methylene blue and carbendazim as compared to ZnO and GQD in 70 min. Higher photocatalytic activity of these ZnO-GQD heterojunctions may be due to an efficient charge carrier separation, increased light

absorption from UV to visible region, as well as high specific surface area of the ZGQD2 heterojunction.

Qu et al. (2018) prepared CQDs/$KNbO_3$ photocatalyst, via hydrothermal and mixed-calcination methods, and it was a visible light driven composite. They also evaluated the photocatalytic activity of CQDs/$KNbO_3$ composites for the degradation of crystal violet dye along with hydrogen production under visible light (Fig. 9.2). It was reported that CQDs/$KNbO_3$ composites exhibited much higher photocatalytic activity than the $KNbO_3$. This is all due to the presence of CQDs as cocatalyst on $KNbO_3$ particles surface. This formed much more active sites, which can trap electrons; thus inhibiting recombination of photogenerated electron−hole pairs. It was also observed that as-prepared CQDs/$KNbO_3$ can be used again even after four repetitive cycles.

Gao et al. (2019) synthesized CQDs via a hydrothermal method. They used waste larch wood as the raw material. The 3D Bi_2MoO_6 hollow microspheres can be prepared by a mixed solvothermal method without using any surfactants. The Bi_2MoO_6 was used as a matrix and it was doped with CQDs to get a new composite material (CQDs/Bi_2MoO_6). It was observed that methylene blue was degraded by Bi_2MoO_6 hollow microspheres in the presence of visible light. This photocatalytic performance was found to increase when these hollow microspheres were modified with CQDs.

Jat et al. (2019) investigated the photocatalytic degradation of fast green in the presence of visible light using SnO_2-TiO_2. They prepared SnO_2 QDs by a hydrothermal method using stannic chloride (hydrate) as the source of tin. This composite exhibited more photocatalytic activity than titania nanopowder for the degradation of fast green. Karimi et al. (2019) synthesized zinc sulfide QDs by chemical precipitation method under ultrasonic radiation. They used two capping agents, l-cysteine and 2-mercaptoethanol. It was

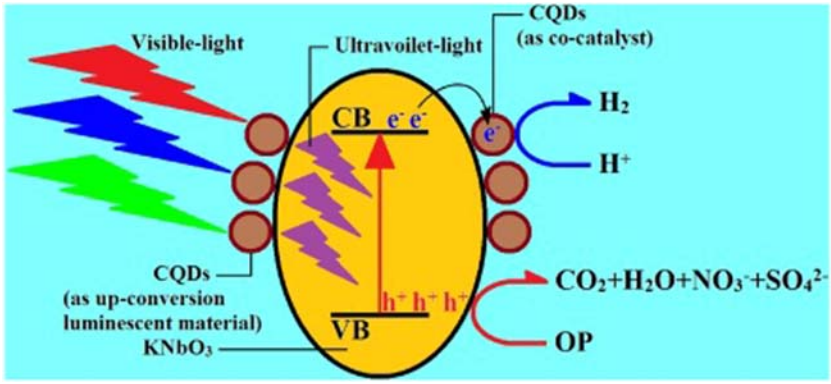

FIGURE 9.2 Photocatalytic hydrogen generation by CQDs/KN composite. *Adapted from Qu et al., 2018. Mol. Catal., 445, doi: 10.1016/j.mcat.2017.11.002. With Permission.*

observed that the as-synthesized QDs were cubic in structure with a particle size less than 10 nm. These QDs were then used for the degradation of crystal violet. It was also revealed that QDs can be reused five times without any significant loss in photocatalytic activity.

Lin et al. (2019) synthesized ternary heterostructure photocatalyst by coanchoring the NCQDs and graphitic carbon nitride QDs (CNQDs) on the surface of $BiVO_4$ microspheres. The as-synthesized $BiVO_4$/CNQDs/NCDs ternary heterostructure was found to exhibit an excellent photocatalytic activity for the degradation of rhodamine B and tetracycline in the presence of visible light as compared to pure $BiVO_4$, $BiVO_4$/NCDs, and $BiVO_4$/CNQDs. The higher photocatalytic activity in this composite may be attributed to an efficient separation and transport of photogenerated charge carriers.

Sharma et al. (2019) reported a template-free sonochemical synthesis of α-Bi_2O_3/C-dots. They used this composite for the degradation of indigo carmine and levofloxacin under visible light (Fig. 9.3). It was reported that α-Bi_2O_3 in the nanocomposite has a monoclinic phase. Its bandgap was found to be 2.49 eV. The as-prepared photocatalyst exhibited higher visible light driven photocatalytic activity for the degradation of indigo carmine (86%) than α-Bi_2O_3 (57%) and levofloxacin (79%) within 2 h. It was confirmed that hydroxyl radicals played a dominant role in the photocatalytic degradation of indigo carmine.

The plasmonic Au nanoparticle (NP)/SnO_2 quantum dot (SQD) (Au/SQD) nanocomposites were prepared by Babu et al. (2019) via a solvothermal method. The photocatalytic activity of as-prepared plasmonic Au/SQD nanocomposites was evaluated for the degradation of rhodamine B. The Au/SQD photocatalyst prepared by using tin chloride (1.0 g), exhibited better dye degradation as compared to pristine SQDs. This increased catalytic performance may be attributed to a shift of the bandgap from the UV to visible region. It was also revealed that synergistic coupling of the semiconductor and metal QDs as well as surface

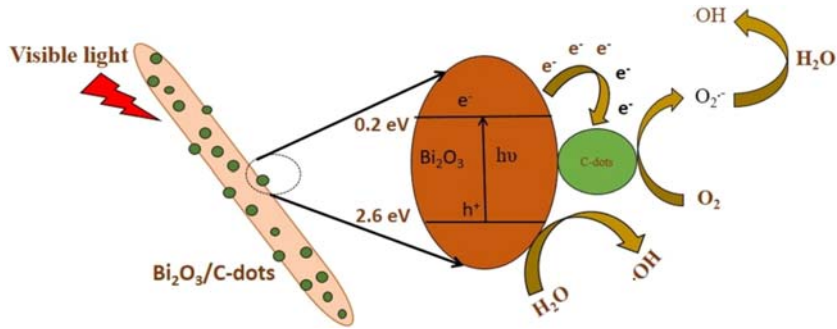

FIGURE 9.3 Photocatalytic degradation of indigo carmine and levofloxacin in the presence of α-Bi_2O_3/C-dot. *Adapted from Sharma et al., 2019. J. Colloid Interf. Sci., 533, 227–237. With Permission.*

plasmon resonance effect of Au NPs played an important role in increasing the catalytic performance.

Xu et al. (2022a) synthesized TiO_2 thin flakes modified with g-C_3N_4 QDs. It was revealed that g-C_3N_4 QDs were in the size of $\sim$10 nm. It was observed that TiO_2 nanoflakes/g-C_3N_4 QDs hybrid exhibited an excellent activity for hydrogen evolution from methanol degradation of rhodamine B (Fig. 9.4).

Jacob et al. (2020) reported the coupling of sulfate reduction with the precipitation of zinc as ZnS QDs at ambient conditions. It was observed that biogenic ZnS QDs had average sizes of 5−7 nm and their formation took 2−4 days of incubation. There was an absorption peak (<325 nm), which may be due to surface plasmon resonance of ZnS QDs and the bandgap of these biogenic ZnS QDs was found to be 3.84 eV. These QDs were successfully used as effective photocatalysts for photoassisted decolorization of Congo red.

Jamila et al. (2020a) fabricated an effective CuO/NCQDs solar photocatalyst using p-type copper oxide, which was modified with NCQDs. A leaf-like morphology for CuO was confirmed for CuO/NCQDs composites by SEM images. It was confirmed that NCQDs are well incorporated on nanoleaves of CuO. As-prepared photocatalyst was used for the degradation of methyl orange (Fig. 9.5). It was observed that this composite catalyst showed higher degradation efficiency as compared to pure CuO nanoleaves, which was attributed to an increased charge separation ability and visible light absorption.

Jamila et al. (2020b) also prepared NCQDs by modifying the surface of graphene oxide (GO) incorporated WO_3 nanosheets. It was observed that the surface of WO_3 nanosheets was modified with morphological defects so that more active sites were available there. As-synthesized ternary composites were used to degrade methyl orange photocatalytically. These ternary

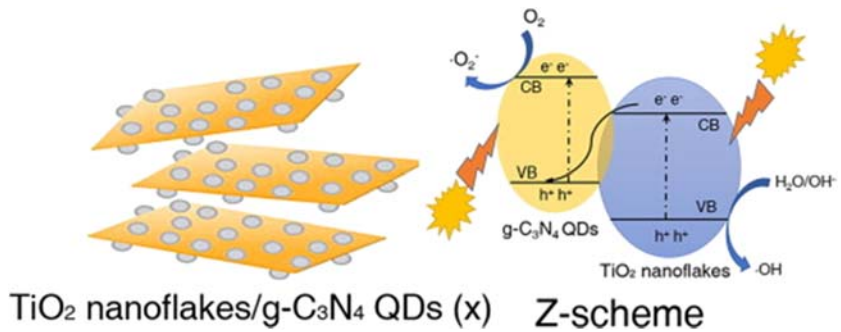

FIGURE 9.4 Use of TiO_2 nanoflakes/g-C_3N_4 for hydrogen generation along with degradation of rhodamine B. *Adapted from Xu et al., 2022a. Chem. Eng. J. 430, doi: 10.1016/j.cej.2021.132861. With Permission.*

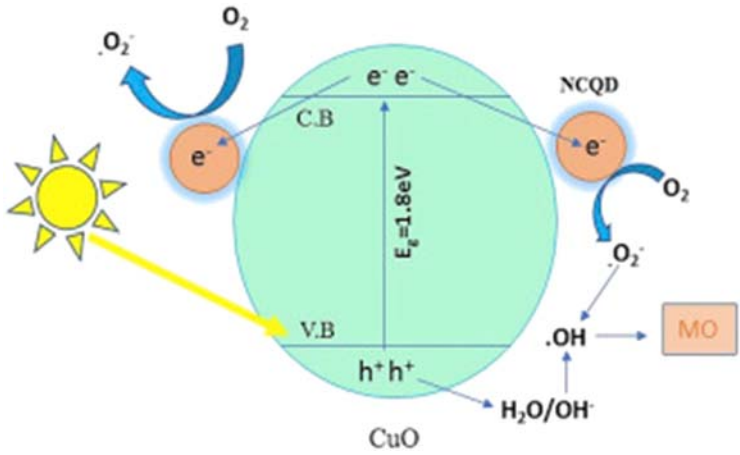

FIGURE 9.5 Photocatalytic degradation of methyl orange on CuO/NCQDs. *Adapted from Jamila et al., 2020. J. Phys. Chem. Solids 138, doi: 10.1016/j.jpcs.2019.109233. With Permission.*

composites exhibited an excellent photocatalytic activity as compared to binary and WO_3 photocatalysts.

The NCQDs were modified with defect-rich g-C_3N_4 (DCN) (NCDs/DCN) by Liu et al. (2020) using an impregnation method. As-prepared NCDs/DCN with narrow bandgap showed excellent visible light absorption and electron transfer ability, which were found useful for photocatalysis of rhodamine B degradation and simultaneous production of H_2. These NCDs/DCN expressed better efficiency in removal of different combination pollutants such as bisphenol A (BPA)/Cr(VI), ofloxacin (OFL)/Cr(VI), and ciprofloxacin (CIP)/Cr (VI) than in a single system. This is due to the synergistic effect between oxidation of organic pollutants and reduction of Cr(VI). An excellent photocatalytic H_2 generation activity and degradation of rhodamine B was there simultaneously with the evolution of H_2 (3.68 μmol h^{-1} g^{-1}) and 100% removal of dye, respectively.

Vatanpour et al. (2020) used GQDs for preparing polyvinyl chloride (PVC) blended matrix. It was then used for the removal of reactive blue 19 dye from wastewater. An improved antifouling performance was also reported by the filtration of bovine serum albumin (BSA) solution. When GQDs were added to the PVC matrix (1 wt.%), it was found that water flux reached 19.1 Lm^{-2} h^{-1}, which was around 56% higher than the unfilled membrane. It was observed that as-prepared PVC membranes have rejection of reactive blue 19 (>96%) and BSA (>98%).

Hui et al. (2021) synthesized heteroatoms-doped CQDs using rice husk as a biowaste precursor. They studied the effects of nitrogen and bismuth doping. They used ethylenediamine and bismuth nitrate pentahydrate as the source of nitrogen and bismuth, respectively. It was observed that these CQDs were spherical in shape with a size of less than 10 nm. The addition

of bismuth nitrate pentahydrate and ethylenediamine tuned the fluorescence intensity and shifted the emission to higher wavelength from the blue to green region. The activity of rice husk derived CQDs (RHCQDs) was examined by photodegradation of methylene blue as well as removal of copper (II). It was revealed that Bi-RHCQDs (5 wt.%) and N-RHCQDs (10 vol.%) exhibited the highest methylene blue degradation performance, 68.91% and 72.16%, respectively. These doped RHCQDs were also tested for removal of copper(II) with 56.23% and 33.13%, efficiency.

Sahu et al. (2021) decorated GO with SnO_2 QDs and used them for the degradation of methylene blue under visible light. It was revealed that about ~94% methylene blue was degraded using only 0.5 mg of GO-SnO_2 catalyst in 30 min. The preparation of GQDs from pyrocatechol has been reported by Mandal et al. (2021) at different pH. The photocatalytic behavior of as-synthesized GQDs was evaluated in the degradation of two dyes, methyl orange and methylene blue, in the presence of visible light irradiation.

Empty fruit bunches by-products of palm oil mill industry containing lignin were used as raw material in the fabrication of sulfur-doped CQDs (SCQDs) by Abd Rani et al. (2021) through a hydrothermal treatment. The SCQDs remained unchanged even after several hours of UV light exposure and also after storage for 8 months, which indicates the excellent stability. The average particle size of as-prepared SCQDs was found to be 2.9 nm. The photocatalytic activity of SCQDs was evaluated for the degradation of crystal violet dye under UV light, which could reach 99.7% degradation in 200 min.

The TiO_2/GQDs nanocomposite was synthesized by Niazi et al. (2021) and used for the degradation of textile dye, reactive black 5 (RB5). It was reported that almost complete (100%) degradation of 50 ppm RB5 could be achieved by TiO_2/GQDs within 30 min under sunlight irradiation. The main active species for the degradation of RB5 was confirmed as surface hydroxyl radicals based on scavenger studies.

Ahlawat et al. (2021) synthesized CQDs via a microwave-assisted method. It was reported that CQDs were small in size (about 2 nm) with spherical shapes. The photocatalytic degradation of rhodamine B was studied in the presence of CQDs and the highest degradation of 99.7% could be achieved under UV light irradiation.

Hatefi et al. (2021a,b) reported that photocatalytic activity was enhanced in electron-rich GQDs with Fe_3O_4/TiO_2 nanocomposites. They could achieve 86.08% removal efficiency of methylene blue, which was more than with TiO_2. The as-synthesized material improved photocatalytic efficiency for the degrading MB under UVA light irradiation compared with merely pure anatase TiO_2.

Two samples of zinc oxide QDs (ZQs) (S_1 and S_2) were synthesized by Mohamed et al. (2021) via a solvothermal method. The crystallite size of these samples, S_1 and S_2, was found to be 8.4 and 9.6 nm, respectively. It

was revealed that the sample S_1 exhibited the best degradation of dianix blue dye. Sharma et al. (2021) synthesized CQDs via a hydrothermal method. They used m-phenylenediamine and l-glutamic acid for this purpose. Then these were combined with nano-TiO_2 to obtain CQDs/TiO_2 composites. It was observed that CQDs/TiO_2 (CT-1) composite with 1:1 molar ratio of l-glutamic acid to TiO_2 exhibited the best degradation efficiency for methyl orange. It was revealed that sample CT-1 can degrade 70.56% of methyl orange, which was almost is 12.7 times higher than that of TiO_2.

The ZQs was synthesized by Mohamed et al. (2022) using a modified precipitation process. The crystallite size of ZQs was found to be 4.4 and 5.3 nm for the ZQ1 and ZQ2 samples, respectively. The photodegradation process of indigo carmine dye ZQ1 reached the highest synthetic levels equal to $1.718 \times 10^{-2}\ s^{-1}$. They tried it on 16 factory effluents samples, and it was observed that it can be used for 10 replication cycles after recovery in the presence of ZQs by sunlight for 2 months.

Smrithi et al. (2022) reported the green synthesis of NCQDs via a hydrothermal technique using extract of *Cucurbita pepo*. The photocatalytic activities of NCQDs were evaluated for the degradation of crystal violet under visible light. They could achieve 99.9% degradation of crystal violet in 3 h in the presence of 1 mL H_2O_2. It was revealed that a prominent role was played by $^{\bullet}OH$ radicals in this degradation.

The black phosphorus QDs (BPQDs) were prepared by Fan et al. (2022) and photocatalytic activity of BPQDs was investigated by selecting indigo carmine as a model dye. It was observed that decolorization efficiency of this dye could reach 98.22% in the presence of sunlight.

Sun et al. (2022) synthesized cerium dioxide QDs modified graphitic carbon nitride. It was reported that CeO_2QDs was dispersed homogeneously on the surface of g-C_3N_4. It was observed that as-prepared CeO_2QDs/g-C_3N_4 exhibited a higher rate for the photodegradation ($0.00985\ min^{-1}$) for rhodamine B, which was found to be that seven times higher than that with single g-C_3N_4 (Fig. 9.6).

9.3.2 Drugs

Pharmaceuticals and personal care products are required by the society and their use is increasing day by day. These are emerging as water contaminants as they can affect the quality of water adversely. This results into a potential harm to water supplies, ecosystem and human health. Photocatalysis can degrade these water pollutants into almost harmless products.

Shi et al. (2015) used CdS QDs modified nitrogen-doped TiO_2 plates (NTP) for decomposition of diclofenac (DCF). They used thiolactic acid as a linker to bind CdS QDs on NTP in situ. This composite NTP/CdS exhibited much higher photocatalytic activity for the degradation of DCF under visible light. It was observed that degradation rate was significantly increased as

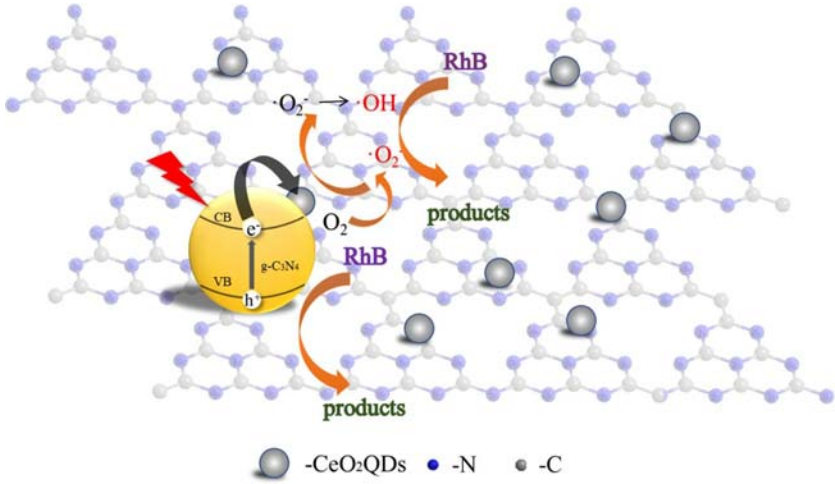

FIGURE 9.6 Photocatalytic degradation of rhodamine B on CeO_2QDs/g-C_3N_4. *Adapted from Sun et al., 2022. Appl. Surf. Sci., 576, doi: 10.1016/j.apsusc.2021.151901. With Permission.*

compared to NTP and CdS, which was about 1.95 and 2.88 times, respectively. The TiO_2 QDs were synthesized by Kaur et al. (2015) via ultrasonic-assisted hydrothermal process. They used as-prepared QDs for photocatalytic degradation of ketorolac tromethamine in the presence of sunlight. It was revealed that ~99% ketorolac tromethamine drug was photodegraded.

Ionic liquid induced strategy was used by Xia et al. (2016) for controlled synthesis of CQDs (CQDs)/BiOX (X = Br, Cl) hybrid nanosheets. They selected three different types of pollutants, such as CIP rhodamine B (RhB), and bisphenol A (BPA) to evaluate the photocatalytic activity of CQDs/BiOX composite nanosheets. The highest photocatalytic activity was observed with sample 3 wt.% CQDs/BiOBr nanosheets for the degradation of CIP, RhB, and BPA under visible light irradiation. It was revealed that are three factors are responsible for enhanced photocatalysis: Lower resistance, high visible light absorbance and high separation efficiency of photoinduced holes and electrons.

Di et al. (2017) prepared NCQDs/$BiPO_4$ composite using ionic liquid assisted solvothermal method. This N-CQDs/$BiPO_4$ exhibited an enhanced photocatalytic activity for the degradation of three antibiotics (CIP, tetracycline and enrofloxacin) under UV irradiation The main active species was found to be superoxide radicals and not hydroxyl radicals. Kaur et al. (2017) synthesized Ag_2O/TiO_2 QDs using pH-mediated precipitation method. It was revealed that as-obtained Ag_2O/TiO_2 QDs were spherical in shape with size ranging between 2−9 nm. As-synthesized composite exhibited significant photocatalytic activity for the degradation of levofloxacin under visible light than TiO_2.

A metal-free composite photocatalyst (GQDs) decorated graphitic carbon nitride nanorods (g-CNNR), was obtained by Yuan et al. (2019) via

hydrothermal technique. The GQDs/g-CNNR exhibited higher photocatalytic activity for removal of antibiotics. It was observed that photocatalytic reaction rate was 2.03 and 3.46 times higher as compared with g-CNNR and pristine graphitic carbon nitride (g-C_3N_4), respectively. It was revealed that this composite show excellent stability and reusability. It was confirmed that photoinduced holes as well as superoxide radicals are main active species in the photocatalytic degradation.

Chen et al. (2019) synthesized CQDs modified potassium titanate nanotubes (CQDs/$K_2Ti_6O_{13}$) via hydrothermal treatment. The successful deposition of CQDs on $K_2Ti_6O_{13}$ photocatalyst was evident from TEM images. The performance of CQDs/$K_2Ti_6O_{13}$ composite was evaluated by degradation of amoxicillin (AMX) under visible light (Fig. 9.7). The photocatalytic activity of CQDs/$K_2Ti_6O_{13}$ hybrid material was found to be higher as compared to neat $K_2Ti_6O_{13}$. It was confirmed that hole (h^+) and hydroxyl radical ($^{\bullet}OH$) played important roles in photocatalytic degradation of AMX.

Jiang et al. (2019) synthesized Fe_3O_4 QDs modified BiOCl/$BiVO_4$ p-n heterojunction. It was observed that 20% Fe_3O_4QDs@BiOCl/$BiVO_4$ p-n heterojunction exhibited an excellent photocatalytic activity for removal of four different broad-spectrum antibiotics in the presence of visible light. The improved photocatalytic performance for the degradation of broad-spectrum antibiotics was mainly attributed to the strong visible light absorption, effective charge carrier mobility, and large specific surface areas. As-fabricated photocatalyst was found stable even after four cycles and it can also be easily separated using an external magnetic field.

Mou et al. (2019) fabricated ultrathin two dimensional (2D) BiOCl/nitrogen-doped GQDs (BiOCl/NGQDs) composites using a hydrothermal process.

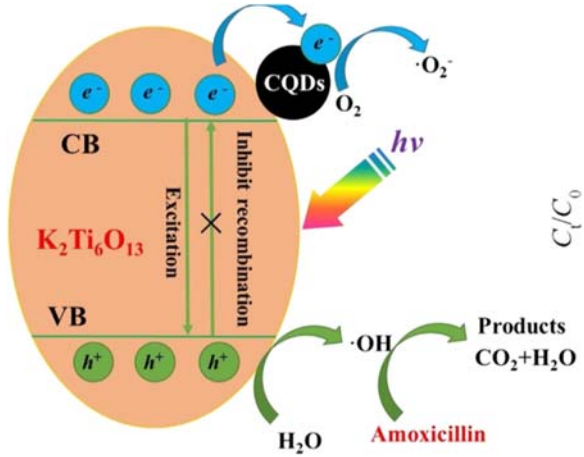

FIGURE 9.7 Photocatalytic degradation of amoxicillin by CQDs/$K_2Ti_6O_{13}$. *Adapted from Chen et al., 2019. Chin. Chem. Lett., 30(6), 1214–1218. With Permission.*

It was observed that BiOCl/NGQDs composites exhibited an increase in both adsorption and photodegradation of CIP as compared to BiOCl. The optimum degradation efficiency of CIP was 82.5% within an hour under visible light, when NGQDs was kept 6.9%, which was much better as compared to BiOCl (34.9%). It was also revealed that this removal efficiency could reach to 95.5% within 5 h.

SCQDs/hollow tubular g-C_3N_4 photocatalyst (HTCN-C) was prepared by Wang et al. (2019) via ultrasonic-assisted method. It was used as catalyst for the degradation of tetracycline (TC) as well as destruction of *E. coli*. It was reported that HTCN-C(2) exhibited an excellent performance for the degrading tetracycline degradation (rate = 0.0293 min^{-1}) and could distract 99.99% *E. coli* under visible destructed light.

Zhao et al. (2019) decorated Co_3O_4 QDs onto phosphorus-doped g-C_3N_4 nanosheets via thermal polymerization method. They used vitamin B_{12} (VB_{12}) as precursor of cobalt and phosphorus mixed with melamine. It was observed that as-prepared sample exhibited the maximum photodegradation efficiency for metronidazole (MTZ), when the sample was prepared with weight ratio of VB12 in precursors at 1%. The efficiency was almost two times better than the removal rate with pure g-C_3N_4. An inhibition was also observed by NO_3^-, Ca^{2+} and HCO_3^-, but Fe^{3+} was found to promote this photodegradation.

The synthesis of self-assembled CQDs and reduced graphene oxide layers modified S@g-C_3N_4/B@g-C_3N_4 (CRSB) (all metal free) was reported by Kumar et al. (2020a). Later, it was used as photocatalyst for the degradation of chloramphenicol (CMP) under visible light and sunlight. It was reported that 99.1% CMP was photodegraded by CRSB in the presence to visible light within 90 min. It was revealed that rate of degradation over CRSB was ten times higher than with g-C_3N_4.

Huang et al. (2020) fabricated up-converted CQDs incorporated goethite (α-FeOOH) nanohybrids (CQDs/α-FeOOH) via hydrolysis method. As-fabricated CQDs/α-FeOOH exhibited excellent degradation of tetracycline (TC), which was almost 3.7 times as compared to α-FeOOH under visible light.

Koe et al. (2020) fabricated a novel photocatalytic membrane by incorporating N,S-CQDs/TiO_2 nanocomposite on polysulfone (PSF) membrane. They used it for photodegradation of DCF in water. The N,S-CQDs/TiO_2 nanocomposites were synthesized with different loadings of N,S-CQDs on TiO_2 nanoparticles. It was observed that N,S-CQDs/TiO_2 (1.5 g) membrane exhibited the best photodegradation performance for DCF removal (62.3%) in the presence of visible light, while TiO_2 membrane showed 3.33% removal only.

Patel et al. (2020) prepared Mn-doped ZnS (Mn:ZnS) QDs through chemical precipitation method. It was observed that as-obtained Mn:ZnS QDs exhibited excellent properties for photodegradation of norfloxacin (NOFX)

in the presence of both UV light and sunlight. These QDs showed excellent stability and reusability up to four consecutive cycles. It was also concluded that these Mn:ZnS QDs could also prove to be useful as efficient as photocatalytic materials in ecological remediation and energy conversion.

Wang et al. (2021) constructed CdS−TiO_2 heterostructure using potato extract as a modifier and a stabilizer. It was revealed that as-prepared CdS−TiO_2 composite exhibited high photocatalytic degradation efficiency with the degradation rate of penicillin (88%). Liu et al. (2021) prepared CQD oxygen-rich titanium dioxide nanosheets (CQD-OTNs) via two-step hydrothermal method. As-prepared composite was used in photodegradation of tetracycline. It was reported that CQD-OTNs could increase the degradation rate of drug to 94.1% within 2 h under visible light irradiation; which was about 2.3 times higher than that with titanium dioxide nanosheets.

Singh et al. (2021) synthesized CdS and CdSe QDs. It was reported that size of the QDs can be controlled by using different mole ratio of water and surfactant. They used thioglycolic acid as capping agent prevent ratio aggregation of QDs The photocatalytic activity of as-synthesized CdSe and CdS QDs was evaluated by selecting 3-aminopyridine as a pollutant.

Wang et al. (2021) used olive leaves as the carbon source to prepare CQDs through hydrothermal treatment. These CQDs were then loaded on the surface of TiO_2 (CQDs/TiO_2 composite). The photocatalytic performance of CQDs/TiO_2 composites was evaluated in the degradation of tetracycline under visible light for 10 min. It was observed that degradation rate of 5% CQDs/TiO_2 could achieve about 81% tetracycline removal.

The silicon-doped CQD were decorated on bismuth molybdate to prepare (1.0SiCQDs/Bi_2MoO_6) nanocomposite by Kumar et al. (2022) via hydrothermal method. It was reported that about 97 and 95% of tetracycline (TC) and of CIP were degraded in 90 min on sunlight exposure.

Xu et al. (2022b) synthesized a series of 0D boron carbon nitride QDs (BCNQDs) modified 2D $Bi_4O_5I_2$ (0D/2D $Bi_4O_5I_2$/BCNQDs) composites. They used these composite for photodegradation of tetracycline (TC) and OTC. It was observed that as-prepared $Bi_4O_5I_2$/BCNQDs composite exhibited highest photocatalytic performance for the degradation of TC and OTC and it was about 4.95 and 2.17 times as compared with $Bi_4O_5I_2$, respectively.

9.3.3 Pesticides

Demand for pesticides, insecticides, weedicides, herbicides, etc. is regularly increasing due to their widespread use in agricultural practices. These are required to safeguard the food grains, foods, vegetables, etc. against any infection or wastage by pest, rodents, etc. and also harm by weeds. These pesticides will reach animals and humans through the food chain causing a number of health problems. It is therefore necessary to treat or degrade these harmful materials. Photocatalysts can play an important role in achieving this object.

Shahnazi et al. (2020) synthesized poly N-isopropylacrylamide (NIPAM) coated MWCNTs/TiO_2 nanocomposite (MWCNTs/TiO_2/TMIP). They selected pendimethalin (PM) herbicide as the target pollutant. This photocatalyst exhibited a higher activity in the degradation of PM (rate constant of 0.0438 min^{-1}) under visible light as compared to other photocatalysts.

The GQDs-ZnO nanocomposites were synthesized by Phophayu et al. (2020). They added GQDs solution into starting precursors during the precipitation. Photocatalytic activity was evaluated for the degradation of glyphosate herbicide over GQDs-ZnO nanocomposites. It was observed that as-prepared GQDs−ZnO nanocomposites exhibited an increased (23% increase) photocatalytic degradation as compared to ZnO.

Xu et al. (2021) fabricated ultrathin CoO/Bi QDs Bi_2MoO_6. It was observed that as-prepared composites exhibited an excellent photocatalytic activity for the removal of diazinon (DZN) (94.2%). They attributed this enhanced photocatalytic activity to the synergistic effect of SPR, ultrathin hollows, oxygen valencies (OVs), and the Z-scheme heterostructure, which will increase visible light absorption and also prevent the recombination of change carriers.

9.3.4 Phenol

Phenols in one or other form are essential at some stages. These also have certain adverse effects on the health of human beings, animals, and aquatic organisms. These phenols can be degraded using an eco-friendly photocatalyst route.

Vertically aligned CdTe−ZnO composite nanorods were fabricated by Liu et al. (2013) from indium tin oxide substrates (ITO). They used a layer-by-layer deposition method formation (CdTe QDs on ZnO nanorod arrays). It was observed that 75% phenol was removed from wastewater in the presence of visible light and composite and 53.2% total organic carbon removal could be achieved within 150 min.

SnO_2 QDs were synthesized by Bhattacharjee and Ahmaruzzaman (2015) via a green biological method using sugar cane juice. The biomolecules of the juice were used as complexing and capping agents and no external agents were required for this purpose. It was observed that as-prepared SnO_2 QDs were spherical in shape with a particle size of ∼3−4.5 nm. They observed a blueshift in the bandgap energy with decreasing particle size, which may be due to quantum confinement effects. The SnO_2 QDs were used for the conversion of *p*-nitrophenol to *p*-aminophenol in the presence of $NaBH_4$ in an aqueous medium. It was reported that 99.5% of *p*-nitrophenol could be reduced in the presence of SnO_2 QDs within an hour.

Kandi et al. (2017) synthesized CdS QDs sensitized self-doped Bi_2MoO_6 via a hydrothermal method. They used glucose as a reducing agent. As-synthesized catalyst was then used to degrade phenol and reduce toxic

Cr(VI) from the aqueous solution. It was reported that 47.5% and 97% degradation of phenol and reduction of Cr(VI), respectively, was obtained using 3% CdS QDs-sensitized self-doped Bi_2MoO_6 in the presence of solar light. Their photostability and reusability was also evaluated and it was observed that this catalyst can be reused for up to five cycles without any significant loss in its activity.

Bajorowicz et al. (2018) comodified CdS quantum dot-decorated $KNbO_3$ composite with Bi_2S_3 QDs by a combination of hydrothermal method with a linker-assisted adsorption route. They used starch and thioglycolic acid as capping agents. It was observed that as-prepared $KNbO_3$-based composites exhibited enhanced photocatalytic performance for the degradation of phenol in an aqueous solution under visible light. It was also reported that the highest photocatalytic performance with better stability were obtained in ternary 30% CdS−5%Bi_2S_3 quantum dot-decorated $KNbO_3$ composite. They also observed catechol, benzoquinone, hydroquinone, and 1,2,4-benzenetriol as the oxidation intermediates of phenol.

Bhatt et al. (2019a) synthesized SnO_2 QDs decorated on TiO_2 nanospheres. Later, they used these composites as photocatalyst for the degradation of 2-nitrophenol. It was found that photocatalytic activity of as-synthesized samples exhibited an efficient degradation of 2-nitrophenol as compared to pure TiO_2 nanospheres.

They also used SnO_2 QDs/TiO_2 nanospheres composite for photocatalytic degradation of picric acid (2,4,6-trinitrophenol) Bhatt et al. (2019b). It is all due to high tunability, high specific surface area, and visible light absorbing ability. It was reported that photocatalytic behavior of as-synthesized samples exhibited better activity compared to only TiO_2 nanospheres.

Hasija et al. (2019) employed a green synthesis approach using bamboo leaves (precursors) for CQDs production via a hydrothermal method. As-fabricated CQDs were then used for the construction of Z-scheme P-doped g-C_3N_4/AgI/ZnO/CQDs (PGCN) heterojunction via immobilization of AgI/ZnO/CQD on graphitic carbon nitride (g-C_3N_4). This composite was then used for the degradation of 2,4-dinitrophenol. The photocatalytic activity of this composite was attributed to electron sink behavior of CQDs. It was reported that this photocatalyst exhibited good stability and recyclability for almost ten cycles.

A solvothermal route was selected by Kumar et al. (2020b) to construct O and S codoped graphitic carbon nitride QDs (OSCNQDs), which were hybridized with Bi_2MoO_6 (BMO). They used these composites for the degradation of aqueous phenol under visible light. As-prepared OSCNQDs/BMO hybrid photocatalyst exhibited almost complete degradation of phenol (98%).

Liang et al. (2020) prepared ZnO composites, which were sensitized by CQDs. They used these composites for the photocatalytic degradation of phenol in the presence of visible light. It was reported that photocatalytic performance of as-prepared ZnO composites (sensitized by CQDs) was

almost 60% higher than that with ZnO. It was also observed that there is good stability and reusability of these composites, as there was no significant change in their activity even after 10 cycles.

9.4 Reduction of carbon dioxide

Scarcity of fossil fuel resources is increasing regularly along with more and more demand for energy in any form. Photocatalytic reduction of carbon dioxide into useful fuels (value-added chemicals) may provide a solution to both these worldwide problems, that is, the problem of the energy crisis and the ever deteriorating environmental quality. Here, photocatalysts have many added advantages. However, some photocatalytic conversion approaches for efficient, economical, and industrialized scalable are to be developed, which can utilize visible and near infrared irradiation.

Wang et al. (2011) sensitized TiO_2 catalysts with PbS QDs. It was observed that PbS QDs enhanced photoreduction rates of CO_2 with TiO_2 almost fivefold as compared to unsensitized TiO_2.

Shao et al. (2017) synthesized ZnO QDs and KNb_3O_8 nanosheets by a hydrothermal technique. They used it for the photocatalytic reduction of CO_2 to methanol. It was observed that the formation rate of pure methanol was only 1257.21 $\mu mol\ g^{-1}\ h^{-1}$, and was found to increase to 1539.77 $\mu mol\ g^{-1}\ h^{-1}$ on deposition of 2 wt.% ZnO QDs on the surface of KNb_3O_8 nanosheets.

The CQDs decorated ultrathin Bi_2WO_6 nanosheets (UBW) were used by Kong et al. (2017) for photoreduction of CO_2 under Vis−NIR irradiation. It was reported that 1CQDs/UBW (1 wt.% CQD content) exhibited higher rate of reduction under visible light irradiation, which has almost 3.1 and 9.5 times enhancement in CH_4 production over UBW and pristine Bi_2WO_6 nanoplatelets (PBW).

ZnO QDs/KNb_3O_8 nanosheets were synthesized by Shao et al. (2017) via a hydrothermal method. The photocatalytic activity of as-prepared materials was evaluated for the photoreduction of CO_2 into formaldehyde under UV light irradiation. The rate with KNb_3O_8 nanosheets was found to be 1257.21 $\mu mol\ g^{-1}\ h^{-1}$, which was increased to 1539.77 $\mu mol\ g^{-1}\ h^{-1}$ on using 2 wt.% ZnO QDs on the surface of KNb_3O_8 nanosheets.

Zubair et al. (2018) reported a photocatalyst composed of graphene-TNT (G-TNT) films and TiO_2 nanotube arrays (TNTs) sensitized with electrodeposited GQDs. It was observed that optimal G-TNT samples could promote the reduction of CO_2 to CH_4 with a rate of 1.98 ppm $cm^{-2}\ h^{-1}$.

Kumar et al. (2019) prepared a hybrid photocatalyst that consisted of a cobalt phthalocyanine tetracarboxylic acid (CoPc-COOH) complex immobilized on organic graphitic carbon nitride. They used triethylamine as a sacrificial electron donor. It was observed that 88.5 μmol (1770 $\mu mol\ g^{-1}$cat) and 59.2 μmol (1184 $\mu mol\ g^{-1}$cat) yield of methanol was obtained (6.5 μmol Co, equivalent to g-C_3N_4/CoPc-COOH) and g-C_3N_4 (50 mg).

A simple complexation−oxidation method was used by Li et al. (2020) to encapsulate CuO QDs in the pores of a metal−organic framework (MOF) of MIL-125(Ti). Then they combined it with g-C_3N_4 to develop a composite photocatalyst, g-C_3N_4/CuO@MIL-125(Ti). It was reported that the photogenerated electrons in MIL-125(Ti) and g-C_3N_4 could be easily transferred to the confined CuO QDs, resulting in enhancement of photocatalytic activity of g-C_3N_4/CuO@MIL-125(Ti) for reducing CO_2 in the presence of water. Use of this photocatalyst could afford CO, methanol, ethanol, and acetaldehyde with yields up to 180.1, 997.2, 1505.7, and 531.5 $\mu mol\ g^{-1}$, respectively.

Indium phosphide (InP) QDs and CdS nanorods were integrated by Do et al. (2020). They used CdS-InP composites for the photoreduction of CO_2 in aqueous solution, where triethanolamine was used as a sacrificial donor. It was observed that photocatalytic activity of the as-synthesized composites was better compared to that of pure CdS alone. The evolution rate of CO over composite was 216 $\mu mol\ h^{-1}\ g^{-1}$ in 3 h.

Qin et al. (2020) synthesized g-C_3N_4 photocatalyst modified by NiS_2 QDs (cocatalyst) via a hydrothermal method. It was observed that this composite exhibited higher activity and stability in the photocatalytic reduction of CO_2. They could achieve the highest evolution rate of CO (10.68 $\mu mol\ h^{-1}\ g^{-1}$) on NSQD/CN-25 catalyst, which was almost 3.88-fold higher compared to g-C_3N_4.

Wang et al. (2020) fabricated 0D/2D heterojunction of $CsPbBr_3$ QDs/Bi_2WO_6 nanosheet (CPB/BWO). Pristine $CsPbBr_3$ has a low catalytic performance due to severe charge recombination. As-prepared CPB/BWO photocatalyst could achieve excellent photocatalytic performance in photocatalytic CO_2 reduction. The total yield of CH_4/CO was 503 $\mu mol\ g^{-1}$, which was nearly 9.5 times higher than that achieved with pristine $CsPbBr_3$.

Que et al. (2021) anchored $FAPbBr_3$ QDs on Ti_3C_2 nanosheets to fabricate $FAPbBr_3$/Ti_3C_2 composite. It was observed that $FAPbBr_3$/Ti_3C_2 composite photocatalyst exhibited an excellent photocatalytic reduction of CO_2. The Ti_3C_2 nanosheet acted as an electron acceptor to promote the rapid separation of excitons and supply specific catalytic sites. It was reported that a consumption rate of 717.18 $\mu mol\ g^{-1}\ h^{-1}$ could be obtained by $FAPbBr_3$/0.2-Ti_3C_2 composite and it was almost 2.08 times the rate of the pristine $FAPbBr_3$ QDs (343.90 $\mu mol\ g^{-1}\ h^{-1}$). This photocatalyst also exhibited good stability during photocatalytic reaction.

A direct Z-scheme 0D/2D heterojunction of CuO QDs/ultrathin CoAl-LDH (CuO/CoAl-u) was prepared by Jiang et al. (2022). It was revealed that 4.5%CuO/CoAl-u heterojunction could achieve yield of CH_3OH as 283.26 $\mu mol\ g^{-1}\ h^{-1}$ by photocatalytic reduction of CO_2.

9.5 Hydrogen production

It has become almost certain that future energy demands cannot be fulfilled by fossil fuel resources because they are reaching a level of

complete exhaustion. Therefore, it is necessary to find an alternate renewable energy source. Nature is playing an indirect role in converting carbon dioxide to carbohydrate (biomass). Here, water is utilized as a reducing agent. Hydrogen can be produced by photosplitting of water in the presence of a photocatalyst and light. It has also been advocated as a fuel of the future creating no pollution, as the final product of combustion is water.

Ge et al. (2012) synthesized CdS quantum dot-coupled graphitic carbon nitride photocatalysts. It was observed that the H_2 evolution rate was 17.27 μmol h^{-1} with CdS QD content (30 wt.%) under visible light irradiation, which was about nine times higher than that with pure g-C_3N_4.

Yu et al. (2014) prepared cobalt sulfide QDs (CoS_x QDs) modified TiO_2 nanoparticles using a precipitation−deposition method. They used cobalt acetate, TiO_2, and sodium sulfide as the precursors of Co, Ti, and S, respectively. The CoS_x QDs act as an effective cocatalyst in photocatalytic H_2 production by TiO_2. It was reported that the amount of CoS_x exhibited an optimum value at about 5% (mole ratio to TiO_2), where the production rate of H_2 could reach 838 μmol h^{-1} g^{-1}, which was 35 times more than with pure TiO_2. Here, ethanol was used as a sacrificial reagent.

Kuang et al. (2016) embedded Au QDs rimous cadmium sulfide nanospheres to synthesize hybrid photocatalysts via a hydrothermal process followed by photoreduction. The rimous cadmium sulfide nanospheres had irregular fissures and a rough surface, which will greatly strengthen their adhesion and interaction with (Au) QDs. It was revealed that the highest photocatalytic activity for hydrogen generation was 601.2 μmol h^{-1} g^{-1} and it was achieved by adjusting the Au mass loading.

Lee et al. (2018) synthesized molybdenum disulfide QDs decorated bismuth sulfide photocatalyst and used them for the generation of hydrogen by photosplitting water. They could achieve the highest hydrogen yield (17.7 mmol g^{-1} h^{-1}) with 0.14MoS_2QD/Bi_2S_3, and this yield was 4.5-fold higher than undoped Bi_2S_3 in the presence of stimulated solar light. As-prepared photocatalyst could achieve a yield of hydrogen (53.6 μmol g^{-1}) in 6 h under NIR irradiation.

Pan et al. (2018) prepared thermally stable and highly dispersed TiO_2 QDs (TiO_2-QDs) in pore channels of SiO_2 foams with large pore size (14−20 nm) using in situ hydrolysis of Ti-alkoxide. It was observed that there was an anchoring effect between the pore-wall of SiO_2 foam and TiO_2-QDs, which resulted in the efficient prohibition of the change in both the TiO_2 phases (anatase to rutile) as well as aggregation of TiO_2-QDs. The crystal size was found to be less than 7 nm. These hybrid photocatalysts show higher efficiency in hydrogen evaluation with a quantum efficiency 17.8% using UV irradiation. It was reported that TiO_2-QDs/SiO_2

photocatalysts exhibited a significant H_2 evolution rate. The outstanding activity of these photocatalysts in hydrogen evolution was due to high anatase crystallinity, short electron-transfer distance, excellent stability of TiO_2-QDs, and uniform dispersity in silica foam.

Sun et al. (2018) adopted two facile synthetic routes for the synthesis of MoS_2 QDs: (1) hydrothermal process and (2) liquid exfoliation strategy. They were used as cocatalyst in photocatalytic hydrogen production under visible light. It was reported that MoS_2 QDs-L (L = liquid exfoliation method) can increase the photocatalytic hydrogen activity of CdS under visible light irradiation. The composite MoS_2 QDs-L/CdS could achieve maximum hydrogen production activity with a rate of 1032.1 $\mu mol\ h^{-1}$ using lactic acid as a sacrificial agent, which was almost 2.7 and 15.4 times more than MoS_2/CdS (383.5 $\mu mol\ h^{-1}$) and CdS (66.9 $\mu mol\ h^{-1}$), respectively.

Luo et al. (2018) fabricated CNQDs on $SnNb_2O_6$ ultrathin nanosheets via a hydrothermal method. It was reported that upconversion behavior of CNQDs in CNQDs/$SnNb_2O_6$ nanocomposites provided the ability of photocatalytic production of H_2 utilizing wavelengths >600 nm.

Yang et al. (2019) reported the development of noble-metal-free catalysts having enhanced photocatalytic activity. The cobalt sulfide QDs g-C_3N_4 nanosheets (Co_3S_4/CNNS) nanocomposites were synthesized by a two-step method, using in situ deposition. It was observed that the particle size of highly dispersed Co_3S_4 QDs was 2−4 nm. These were uniformly fixed on carbon nitride nanosheets (CNNS), which can be a good alternative to noble metals for the improvement of photocatalytic activity of CNNS. It was revealed that Co_3S_4/CNNS-900 had apparent quantum efficiency of the order of 7.85% at 400 nm. It was also observed that the H_2 evolution rate of Co_3S_4/CNNS-900 was found to be 20,536.4 $\mu mol\ g^{-1}\ h^{-1}$, which was about 555 times greater than that with CNNS. The Co_3S_4 QDs were highly dispersed on 2D CNNS, facilitating the formation of more active sites. It also shortened the migration distance of as-generated photogenerated carriers, which finally resulted in an increased photocatalytic performance.

The functionalized carbon nanotubes−titania QDs (FCNT-TQDs) were prepared by Reddy et al. (2020). The CNTs may play a dual role as cocatalyst and photosensitizer to increase light harvesting and reduce the recombination rate of charge carriers. It was observed that the maximum production rate of hydrogen could be obtained up to 54.4 $mmol\ h^{-1}g^{-1}$ by the addition of copper. This rate was 5.4 and 2.5 times higher compared to pristine TiO_2 QDs and FCNT-TQDs composite, respectively.

The nickel (atomically dispersed) in cadmium−zinc sulfide QDs (ZCS QDs) exhibited excellent and stable photocatalytic performance for splitting of water

under sunlight (Su et al., 2020). It was observed that finely tuned Ni atoms dispersed in ZCS QDs exhibited hydrogen production of 18.87 mmol g^{-1}.

Li et al. (2021) anchored small-sized TiO_2 photocatalysts onto large-sized Ti_3C_2-Mxene cocatalysts. A higher hydrogen production rate was observed to be 62.5 μmol with as-prepared photocatalyst, which was about 15.2 times higher than that with TiO_2 (4.1 μmol).

You et al. (2022) prepared (0D/2D) heterojunction nanocomposite [Ag_2S QDs (g-C_3N_4)]. The average particle size of Ag_2S QDs was around 5.8 nm. It was observed that composite (0.5 wt.% Ag_2S QDs) loading could give the highest hydrogen evolution rate of 471.1 μmol g^{-1} h^{-1}.

9.6 Other applications

Cadmium sulfide QDs sensitized mesoporous TiO_2 (photocatalysts) were prepared by Li et al. (2009). First, cadmium oxide was preplanted as crystal seeds in ordered mesoporous titanium dioxide and then CdO was converted to CdS QDs via ion-exchange. As-prepared photocatalyst exhibited an excellent photocatalytic efficiency for oxidation of NO gas in air as well as the degradation of organic compounds in an aqueous medium under visible light.

Bismuth monoxide QDs (average size of 2−5 nm) were prepared by Sun et al. (2017) and then used for the synthesis of ammonia under simulated solar light using photocatalytic reduction of nitrogen. The highest rate (1226 μmol g^{-1} h^{-1}) was achieved for ammonia synthesis without using any cocatalyst or a sacrificial agent. It is about 10^3 times higher than with the Fe-TiO_2 photocatalyst. Zhang et al. (2017) synthesized Pt QDs (2−4 nm) and deposited them on N-doped $(BiO)_2CO_3$ hierarchical superstructures via a hydrothermal method. They used H_2PtCl_6 and ammonium bismuth citrate as precursors. It was reported that as-prepared Pt/N-doped $(BiO)_2CO_3$ catalysts exhibited an enhanced visible light photocatalytic removal of NO removal.

Xie et al. (2018) prepared tin oxide GQDs (SnO_2/GQDs) composite. They used it for the photocatalytic removal of nitric oxide (NO). It was observed that this composite exhibited an enhanced activity compared to SnO_2 only. Visible light response and charge separation efficiency of this composite was increased due to the presence of GQDs in the composite. A series of SnO_2/g-C_3N_4 composites was prepared by Zou et al. (2019). They decorated SnO_2 QDs onto g-C_3N_4 sheets. It was reported that SnO_2/g-C_3N_4 had an excellent response toward visible light and higher ability to inhibit the NO_2 generation.

9.7 Recent developments

Some recent advances are shown in Table 9.1

TABLE 9.1 Some recent applications of quantum dots in photocatalysis.

Quantum dots	Method of synthesis	Application	References
g-C_3N_4 and Ag-g-C_3N_4	Ultrasonication	H_2 production, dye degradation, antimicrobial activity	Mallikarjuna et al. (2021)
SnO_2/$AgVO_3$/g-C_3N_4	Hydrothermal	H_2 production	Koyyada et al. (2021)
Ag/cellulose nanocrystal (CNC)-doped CeO_2	Coprecipitation	Degradation of methylene blue and ciprofloxacin	Ikram et al. (2021)
Covalent organic frameworks (COFs) quantum dots	Solvothermal	Degradation of methyl red, methyl orange and methyl blue	Bahadori et al. (2021)
Carbon dots	Ultrasonication	Degradation of Congo red and methylene blue.	Zaib et al. (2021)
Boron-doped CQD (BCQD)-hybridized g-C_3N_4 homojunction (CN) nanocomposite	Hydrothermal	Degradation of rhodamine B	Phang et al. (2022)
Metal-free boron nitride quantum dots (BNQDs) $BiFeO_3$	Impregnation	Degradation of tetracycline hydrochloride	Balta and Simsek (2021)
Cu-doped carbon quantum dots(CD(Cu)) modified Ni-MOL (CD (Cu)-Ni-MOL)	Hydrothermal	Degradation of Tetracycline	Li et al. (2021)
Silver vanadate quantum dots ($AgVO_3$ QDs)-doped reduced graphene oxide and graphitic carbon nitride nanocomposites modified polyvinylidene fluoride (PVDF) membrane (AgVO3/RGO/C3N4-PVDF)	Fabricated	Degradation of tetracycline, excellent antifouling activity rejection of 97.4% of *Escherichia coli*, self-cleaning capacity	Cui et al. (2022)
Zero-dimensional WO_3 quantum dots on two-dimensional ultrathin $CdIn_2S_2$		Photocatalytic reduction of CO_2	Zhang et al. (2022)

(*Continued*)

TABLE 9.1 (Continued)

Quantum dots	Method of synthesis	Application	References
Graphitic carbon nitride quantum dots coupled Zr(IV)		Photoreduction of CO_2	Sonowal et al. (2022)
Zero-dimensional (0D) Bi_3TaO_7 (BTO) quantum dots/three-dimensional (3D) onion-ring-like g-C_3N_4 (OR-CN) S-scheme heterojunction	Solvothermal	Photocatalytic evolution of H_2	Shi et al. (2022)
N-doped carbon quantum dots (NCQDs) modified CdS nanocomposite	Hydrothermal	Photocatalytic evolution of H_2	Xu et al. (2022c)

9.8 Conclusion

Photocatalysis makes use of hydroxyl radicals as oxidants; they are considered the strongest oxidants after fluorine. They can degrade the majority of organic pollutants to harmless products such as CO_2, H_2O, and inorganic ions. In other words, it leads to complete mineralization. The ever increasing amount of carbon dioxide is creating havoc in the form of melting glaciers, raising sea level, global warming, etc. which can be controlled by photocatalytic reduction of carbon dioxide to provide some value-added chemicals (synthetic fuels). Use of these fuels will return the same amount of CO_2 to the atmosphere. Thus it can be considered as a short-term loan of CO_2. Another problem of green fuel can be solved by generating hydrogen through photosplitting of water. Hydrogen has a high storage capacity and this fuel will not add any kind of pollution to the atmosphere as water is produced on burning this fuel, which is harmless. Photocatalysis will find a prominent position in solving all these problems in the years to come.

References

Abd Rani, U., Ng, L.Y., Ng, C.Y., Mahmoudi, E., Ng, Y.S., Mohammad, A.W., 2021. Sustainable production of nitrogen-doped carbon quantum dots for photocatalytic degradation of methylene blue and malachite green. J. Water Proc. Eng. 40. Available from: https://doi.org/10.1016/j.jwpe.2020.101816.

Ahlawat, A., Rana, P.S., Solanki, P.R., 2021. Studies of photocatalytic and optoelectronic properties of microwave synthesized and polyethyleneimine stabilized carbon quantum dots. Mater. Lett. 305. Available from: https://doi.org/10.1016/j.matlet.2021.130830.

Ameta, R., Ameta, S.C. (Eds.), 2016. Photocatalysis: Principles and Applications. CRC Press, Florida.

Ameta, S.C., Ameta, R., Vardia, J., Ameta, R., Ali, Z., 1999. Photocatalysis: a frontier of photochemistry. J. Indian. Chem. Soc. 76 (6), 281–287.

Ameta, R., Benjamin, S., Ameta, A., Ameta, S.C., 2013. Photocatalytic degradation of organic pollutants: a review. Mater. Sci. Forum 734, 247–272.

Anh, N.T.N., Chowdhury, A.D., Doong, R.A., 2017. Highly sensitive and selective detection of mercury ions using N, S-codoped graphene quantum dots and its paper strip based sensing application in wastewater. Sens. Actuators B: Chem. 252, 1169–1178.

Babu, B., Koutavarapu, R., Harish, V.V.N., Shim, J., Yoo, K., 2019. Novel in-situ synthesis of Au/SnO_2 quantum dots for enhanced visible-light-driven photocatalytic applications. Ceram. Int. 45 (5), 5743–5750.

Bahadori, A., Ranjbar, M., Asadipour, A., Kalantari-Khandani, S., 2021. Covalent organic frameworks (COFs) quantum dots as supramolecular cages modified with biochar as nanobio photocatalyst for degradation of organic dyes. J. Mater. Sci.: Mater. Electron. 32 (18), 23018–23029.

Bajorowicz, B., Kowalska, E., Nadolna, J., Wei, Z., Endo, M., Ohtani, B., et al., 2018. Preparation of CdS and Bi_2S_3 quantum dots co-decorated perovskite-type $KNbO_3$ ternary heterostructure with improved visible light photocatalytic activity and stability for phenol degradation. Dalton Trans. 47 (42), 15232–15245.

Balta, Z., Simsek, E.B., 2021. Uncovering the systematical charge separation effect of boron nitride quantum dots on photocatalytic performance of $BiFeO_3$ perovskite towards degradation of tetracycline antibiotic. J. Environ. Chem. Eng. 9 (6), 106567.

Bhatt, J., Jat, K.K., Rai, A.K., Ameta, R., Ameta, S.C., 2019a. Photodegradation of 2-nitrophenol, an endocrine disruptor, using TiO_2 nanospheres/SnO_2 quantum dots 2. Green Chemistry and Biodiversity. Apple Academic Press, Cambridge, pp. 1–8.

Bhatt, J., Benjamin, S., Ameta, R., Ameta, S.C., 2019b. Enhancement of photodegradation of picric acid (2, 4, 6-trinitrophenol) by fabrication of visible-light-active SnO_2 quantum dots/TiO_2 nanospheres composite. J. Appl. Chem. 8 (4), 1805–1812.

Bhattacharjee, A., Ahmaruzzaman, M., 2015. Photocatalytic-degradation and reduction of organic compounds using SnO_2 quantum dots (via a green route) under direct sunlight. RSC Adv. 5 (81), 66122–66133.

Chen, J.W., Shi, J.W., Wang, X., Ai, H.Y., Cui, H.J., Fu, M.L., 2013. Hybrid metal oxides quantum dots/TiO_2 block composites: facile synthesis and photocatalysis application. Powder Technol. 246, 108–116.

Chen, Q., Chen, L., Qi, J., Tong, Y., Lv, Y., Xu, C., 2019. Photocatalytic degradation of amoxicillin by carbon quantum dots modified $K_2Ti_6O_{13}$ nanotubes: effect of light wavelength. Chin. Chem. Lett. 30 (6), 1214–1218.

Cheraghizade, M., Jamali-Sheini, F., Yousefi, R., Niknia, F., Mahmoudian, M.R., Sookhakian, M., 2017. The effect of tin sulfide quantum dots size on photocatalytic and photovoltaic performance. Mater. Chem. Phys. 195, 187–194.

Chong, M.N., Jin, B., Chow, C.W., Saint, C., 2010. Recent developments in photocatalytic water treatment technology: a review. Water Res. 44 (10), 2997–3027.

Cui, Y., Wang, Z., Zheng, J., Li, B., Yan, Y., Meng, M., 2022. Fabrication of silver vanadate quantum dots/reduced graphene oxide/graphitic carbon nitride Z-scheme heterostructure modified polyvinylidene fluoride self-cleaning membrane for enhancing photocatalysis and mechanism insight. J. Coll. Interf. Sci. . Available from: https://doi.org/10.1016/j.jcis.2022.01.008.

Di, J., Xia, J., Chen, X., Ji, M., Yin, S., Zhang, Q., et al., 2017. Tunable oxygen activation induced by oxygen defects in nitrogen doped carbon quantum dots for sustainable boosting photocatalysis. Carbon 114, 601–607.

Djurišić, A.B., He, Y., Ng, A.M., 2020. Visible-light photocatalysts: prospects and challenges. APL. Mater. 8 (3). Available from: https://doi.org/10.1063/1.5140497.

Do, K.H., Kumar, D.P., Rangappa, A.P., Hong, Y., Reddy, D.A., Kim, T.K., 2020. Indium phosphide quantum dots integrated with cadmium sulfide nanorods for photocatalytic carbon dioxide reduction. ChemCatChem 12 (18), 4550–4557.

Doshi, K., Mungray, A.A., 2020. Bio-route synthesis of carbon quantum dots from tulsi leaves and its application as a draw solution in forward osmosis. J. Environ. Chem. Eng. 8 (5). Available from: https://doi.org/10.1016/j.jece.2020.104174.

Fan, J., Li, D., Wang, X., 2016. Effect of modified graphene quantum dots on photocatalytic degradation property. Diam. Relat. Mater. 69, 81–85.

Fan, X., Zhang, S., Guan, R., Shao, X., Jiang, S., Hu, Y., et al., 2022. Black phosphorus quantum dots as photocatalyst for dye degradation with a high efficiency and rate constant. J. Mol. Struct. 1252. Available from: https://doi.org/10.1016/j.molstruc.2021.132163.

Fox, M.A., Dulay, M.T., 1993. Heterogeneous photocatalysis. Chem. Rev. 93 (1), 341–357.

Gao, X., Ji, X., Nguyen, T.T., Gong, X., Chai, R., Guo, M., 2019. A novel composite material with wood-based carbon quantum dots modified Bi_2MoO_6 hollow microspheres. Vacuum 164, 256–264.

Ge, L., Zuo, F., Liu, J., Ma, Q., Wang, C., Sun, D., et al., 2012. Synthesis and efficient visible light photocatalytic hydrogen evolution of polymeric g-C_3N_4 coupled with CdS quantum dots. J. Phys. Chem. C. 116 (25), 13708–13714.

Hasija, V., Sudhaik, A., Raizada, P., Hosseini-Bandegharaei, A., Singh, P., 2019. Carbon quantum dots supported AgI/ZnO/phosphorus doped graphitic carbon nitride as Z-scheme photocatalyst for efficient photodegradation of 2, 4-dinitrophenol. J. Environ. Chem. Eng. 7 (4). Available from: https://doi.org/10.1016/j.jece.2019.103272.

Hatefi, R., Younesi, H., Mashinchian-Moradi, A., Nojavan, S., 2021a. A facile decoration of anatase Fe_3O_4/TiO_2 nanocomposite with graphene quantum dots: synthesis, characterization, and photocatalytic activity. Adv. Powder Technol. 32 (7), 2410–2422.

Hatefi, R., Younesi, H., Mashinchian-Moradi, A., Nojavan, S., 2021b. The efficiency of magnetic TiO2 anatase loaded by graphen quantum dots for photocatalytic degradation of imipramine from aquatic media. Environ. Sci. 20. Available from: https://doi.org/10.52547/envs.2021.1021.

Huang, S., Zhang, Q., Liu, P., Ma, S., Xie, B., Yang, K., et al., 2020. Novel up-conversion carbon quantum dots/α-FeOOH nanohybrids eliminate tetracycline and its related drug resistance in visible-light responsive fenton system. Appl. Catal. B: Environ. 263. Available from: https://doi.org/10.1016/j.apcatb.2019.118336.

Hui, K.C., Ang, W.L., Sambudi, N.S., 2021. Nitrogen and bismuth-doped rice husk-derived carbon quantum dots for dye degradation and heavy metal removal. J. Photochem. Photobiol. A: Chem. 418. Available from: https://doi.org/10.1016/j.jphotochem.2021.113411.

Ibhadon, A.O., Fitzpatrick, P., 2013. Heterogeneous photocatalysis: recent advances and applications. Catalysts 3 (1), 189–218.

Ikram, M., Hayat, S., Imran, M., Haider, A., Naz, S., Ul-Hamid, A., et al., 2021. Novel Ag/cellulose-doped CeO_2 quantum dots for efficient dye degradation and bactericidal activity with molecular docking study. Carbohydr. Polym. 269. Available from: https://doi.org/10.1016/j.carbpol.2021.118346.

Jacob, J.M., Sinharoy, A., Lens, P.N., 2020. Photocatalytic degradation of congo red by zinc sulfide quantum dots produced by anaerobic granular sludge. Environ. Technol. . Available from: https://doi.org/10.1080/09593330.2020.1856940.

Jamila, G.S., Sajjad, S., Leghari, S.A.K., Mahmood, T., 2020a. Role of nitrogen doped carbon quantum dots on CuO nano-leaves as solar induced photo catalyst. J. Phys. Chem. Solids. 138. Available from: https://doi.org/10.1016/j.jpcs.2019.109233.

Jamila, G.S., Sajjad, S., Leghari, S.A.K., Long, M., 2020b. Nitrogen doped carbon quantum dots and GO modified WO_3 nanosheets combination as an effective visible photo catalyst. J. Hazard. Mater. 82. Available from: https://doi.org/10.1016/j.jhazmat.2019.121087.

Jat, K.K., Bhatt, J., Ameta, S.C., 2019. Photodegradation of fast green by using SnO_2 quantum dots/TiO_2 nanoparticles composite. J. Appl. Chem. 8 (1), 139–145.

Jiang, R., Wu, D., Lu, G., Yan, Z., Liu, J., Zhou, R., et al., 2019. Fabrication of Fe_3O_4 quantum dots modified BiOCl/$BiVO_4$ pn heterojunction to enhance photocatalytic activity for removing broad-spectrum antibiotics under visible light. J. Taiwan. Inst. Chem. Eng. 96, 681–690.

Jiang, Y., Guo, J., Li, X., Wu, G., Mu, M., Yin, X., 2022. Direct Z-scheme 0D/2D heterojunction of CuO quantum Dots/ultrathin CoAl-LDH for boosting charge separation and photocatalytic CO_2 reduction. Sol. Energy 231, 705–715.

Kandi, D., Martha, S., Thirumurugan, A., Parida, K.M., 2017. CdS QDs-decorated self-doped γ-Bi_2MoO_6: a sustainable and versatile photocatalyst toward photoreduction of Cr (VI) and degradation of phenol. ACS Omega 2 (12), 9040–9056.

Karimi, F., Rajabi, H.R., Kavoshi, L., 2019. Rapid sonochemical water-based synthesis of functionalized zinc sulfide quantum dots: study of capping agent effect on photocatalytic activity. Ultrason. Sonochem. 57, 139–146.

Kaur, A., Umar, A., Kansal, S.K., 2015. Sunlight-driven photocatalytic degradation of non-steroidal anti-inflammatory drug based on TiO_2 quantum dots. J. Colloid Interface Sci. 459, 257–263.

Kaur, A., Salunke, D.B., Umar, A., Mehta, S.K., Sinha, A.S.K., Kansal, S.K., 2017. Visible light driven photocatalytic degradation of fluoroquinolone levofloxacin drug using Ag_2 O/TiO_2 quantum dots: a mechanistic study and degradation pathway. N. J. Chem. 41 (20), 12079–12090.

Koe, W.S., Chong, W.C., Pang, Y.L., Koo, C.H., Ebrahim, M., Mohammad, A.W., 2020. Novel nitrogen and sulphur co-doped carbon quantum dots/titanium oxide photocatalytic membrane for in-situ degradation and removal of pharmaceutical compound. J. Water Process. Eng. 33. Available from: https://doi.org/10.1016/j.jwpe.2019.101068.

Kong, X.Y., Tan, W.L., Ng, B.J., Chai, S.P., Mohamed, A.R., 2017. Harnessing Vis–NIR broad spectrum for photocatalytic CO_2 reduction over carbon quantum dots-decorated ultrathin Bi_2WO_6 nanosheets. Nano Res. 10 (5), 1720–1731.

Koyyada, G., Siva Kumar, N., Al-Ghurabi, E.H., Asif, M., Mallikarjuna, K., 2021. Enhanced solar-driven photocatalytic performance of a ternary composite of SnO_2 quantum dots// $AgVO_3$ nanoribbons//g-C_3N_4 nanosheets (0D/1D/2D) structures for hydrogen production and dye degradation. Environ. Sci. Pollut. Res. 28 (24), 31585–31595.

Kuang, P.Y., Zheng, P.X., Liu, Z.Q., Lei, J.L., Wu, H., Li, N., et al., 2016. Embedding Au quantum dots in rimous cadmium sulfide nanospheres for enhanced photocatalytic hydrogen evolution. Small. 12 (48), 6735–6744.

Kumar, G., Cilamkoti, V., Dutta, R.K., 2022. Sunlight mediated enhanced photocatalytic degradation of antibiotics in aqueous medium using silicon doped carbon quantum dots decorated Bi_2MoO_6 nanoflakes. Colloids Surf. A: Physicochem. Eng. Asp. 639. Available from: https://doi.org/10.1016/j.colsurfa.2022.128368.

Kumar, S., Dhiman, A., Sudhagar, P., Krishnan, V., 2018. ZnO-graphene quantum dots heterojunctions for natural sunlight-driven photocatalytic environmental remediation. Appl. Surf. Sci. 447, 802–815.

Kumar, A., Prajapati, P.K., Aathira, M.S., Bansiwal, A., Boukherroub, R., Jain, S.L., 2019. Highly improved photoreduction of carbon dioxide to methanol using cobalt phthalocyanine grafted to graphitic carbon nitride as photocatalyst under visible light irradiation. J. Colloid Interf. Sci. 543, 201–213.

Kumar, A., Kumari, A., Sharma, G., Du, B., Naushad, M., Stadler, F.J., 2020a. Carbon quantum dots and reduced graphene oxide modified self-assembled S@ C_3N_4/B@ C_3N_4 metal-free nano-photocatalyst for high performance degradation of chloramphenicol. J. Mol. Liq. 300. Available from: https://doi.org/10.1016/j.molliq.2019.112356.

Kumar, A., Raizada, P., Singh, P., Hosseini-Bandegharaei, A., Thakur, V.K., 2020b. Facile synthesis and extended visible light activity of oxygen and sulphur co-doped carbon nitride quantum dots modified Bi_2MoO_6 for phenol degradation. J. Photochem. Photobiol. A: Chem. 397. Available from: https://doi.org/10.1016/j.jphotochem.2020.112588.

Kusic, H., Leszczynska, D., Koprivanac, N., Peternel, I., 2011. Role of quantum dots nanoparticles in the chemical treatment of colored wastewater: catalysts or additional pollutants. J. Environ. Sci. 23 (9), 1479–1485.

Lee, W.C., Kong, X.Y., Tan, L.L., Gui, M.M., Sumathi, S., Chai, S.P., 2018. Molybdenum disulfide quantum dots decorated bismuth sulfide as a superior noble-metal-free photocatalyst for hydrogen evolution through harnessing a broad solar spectrum. Appl. Catal. B: Environ. 232, 117–123.

Li, G.S., Zhang, D.Q., Yu, J.C., 2009. A new visible-light photocatalyst: CdS quantum dots embedded mesoporous TiO_2. Environ. Sci. Technol. 43 (18), 7079–7085.

Li, N., Liu, X., Zhou, J., Chen, W., Liu, M., 2020. Encapsulating CuO quantum dots in MIL-125 (Ti) coupled with g-C_3N_4 for efficient photocatalytic CO_2 reduction. Chem. Eng. J. 399. Available from: https://doi.org/10.1016/j.cej.2020.125782.

Li, W., Zhuang, C., Li, Y., Gao, C., Jiang, W., Sun, Z., et al., 2021. Anchoring ultra-small TiO_2 quantum dots onto ultra-thin and large-sized Mxene nanosheets for highly efficient photocatalytic water splitting. Ceram. Int. 47 (15), 21769–21776.

Liang, H., Tai, X., Du, Z., Yin, Y., 2020. Enhanced photocatalytic activity of ZnO sensitized by carbon quantum dots and application in phenol wastewater. Opt. Mater. 100. Available from: https://doi.org/10.1016/j.optmat.2020.109674.

Lin, X., Liu, C., Wang, J., Yang, S., Shi, J., Hong, Y., 2019. Graphitic carbon nitride quantum dots and nitrogen-doped carbon quantum dots co-decorated with $BiVO_4$ microspheres: a ternary heterostructure photocatalyst for water purification. Sep. Purif. Technol. 226, 117–127.

Liu, D., Zheng, Z., Wang, C., Yin, Y., Liu, S., Yang, B., 2013. CdTe quantum dots encapsulated ZnO nanorods for highly efficient photoelectrochemical degradation of phenols. J. Phys. Chem. C. 117 (50), 26529–26537.

Liu, H., Liang, J., Fu, S., Li, L., Cui, J., Gao, P., 2020. N doped carbon quantum dots modified defect-rich g-C_3N_4 for enhanced photocatalytic combined pollutions degradation and hydrogen evolution. Colloids Surf. A: Physicochem. Eng. Asp. 591. Available from: https://doi.org/10.1016/j.colsurfa.2020.124552.

Liu, X., Yang, Y., Li, H., Yang, Z., Fang, Y., 2021. Visible light degradation of tetracycline using oxygen-rich titanium dioxide nanosheets decorated by carbon quantum dots. Chem. Eng. J. 408. Available from: https://doi.org/10.1016/j.cej.2020.127259.

Luo, B., Hong, Y., Li, D., Fang, Z., Jian, Y., Shi, W., 2018. Fabrication of 0D/2D carbon nitride quantum dots/$SnNb_2O_6$ ultrathin nanosheets with enhanced photocatalytic hydrogen production. ACS Sustain. Chem. Eng. 6 (11), 14332–14339.

Mallikarjuna, K., Vattikuti, S.V.P., Manne, R., Manjula, G., Munirathnam, K., Mallapur, S., et al., 2021. Sono-chemical synthesis of silver quantum dots immobilized on exfoliated

graphitic carbon nitride nanostructures using ginseng extract for photocatalytic hydrogen evolution, dye degradation, and antimicrobial studies. Nanomaterials 11 (11). Available from: https://doi.org/10.3390/nano11112918.

Mandal, P., Nath, K.K., Saha, M., 2021. Efficient blue luminescent graphene quantum dots and their photocatalytic ability under visible light. Biointerface Res. Appl. Chem. 11 (1), 8171–8178.

Mansur, A.A., Mansur, H.S., Ramanery, F.P., Oliveira, L.C., Souza, P.P., 2014. "Green" colloidal ZnS quantum dots/chitosan nano-photocatalysts for advanced oxidation processes: study of the photodegradation of organic dye pollutants. Appl. Catal. B: Environ. 158, 269–279.

Miao, R., Luo, Z., Zhong, W., Chen, S.Y., Jiang, T., Dutta, B., et al., 2016. Mesoporous TiO_2 modified with carbon quantum dots as a high-performance visible light photocatalyst. Appl. Catal. B: Environ. 189, 26–38.

Mohamed, W.A., Handal, H.T., Ibrahem, I.A., Galal, H.R., Mousa, H.A., Labib, A.A., 2021. Recycling for solar photocatalytic activity of Dianix blue dye and real industrial wastewater treatment process by zinc oxide quantum dots synthesized by solvothermal method. J. Hazard. Mater. 404. Available from: https://doi.org/10.1016/j.jhazmat.2020.123962.

Mohamed, W.A., Abd El-Gawad, H.H., Mekkey, S.D., Galal, H.R., Labib, A.A., 2022. Facile synthesis of quantum dots metal oxide for photocatalytic degradation of organic hazardous materials and factory effluents. Arab. J. Chem. 15 (2). Available from: https://doi.org/10.1016/j.arabjc.2021.103593.

Mou, Z., Zhang, H., Liu, Z., Sun, J., Zhu, M., 2019. Ultrathin BiOCl/nitrogen-doped graphene quantum dots composites with strong adsorption and effective photocatalytic activity for the degradation of antibiotic ciprofloxacin. Appl. Surf. Sci. 496. Available from: https://doi.org/10.1016/j.apsusc.2019.143655.

Muthulingam, S., Lee, I.H., Uthirakumar, P., 2015. Highly efficient degradation of dyes by carbon quantum dots/N-doped zinc oxide (CQD/N-ZnO) photocatalyst and its compatibility on three different commercial dyes under daylight. J. Colloid Interf. Sci. 455, 101–109.

Niazi, Z., Goharshadi, E.K., Mashreghi, M., Jorabchi, M.N., 2021. Highly efficient solar photocatalytic degradation of a textile dye by TiO_2/graphene quantum dots nanocomposite. Photochem. Photobiol. Sci. 20 (1), 87–99.

Pan, D., Han, Z., Miao, Y., Zhang, D., Li, G., 2018. Thermally stable TiO_2 quantum dots embedded in SiO_2 foams: characterization and photocatalytic H_2 evolution activity. Appl. Catal. B: Environ. 229, 130–138.

Patel, J., Singh, A.K., Carabineiro, S., 2020. Assessing the photocatalytic degradation of fluoroquinolone norfloxacin by Mn: ZnS quantum dots: kinetic study, degradation pathway and influencing factors. Nanomaterials. 10 (5). Available from: https://doi.org/10.3390/nano10050964.

Pelaez, M., Nolan, N.T., Pillai, S.C., Seery, M.K., Falaras, P., Kontos, A.G., et al., 2012. A review on the visible light active titanium dioxide photocatalysts for environmental applications. Appl. Catal. B: Environ. 125, 331–349.

Phang, S.J., Lee, J., Wong, V.L., Tan, L.L., Chai, S.P., 2022. Synergistic effects of the hybridization between boron-doped carbon quantum dots and n/n-type g-C_3N_4 homojunction for boosted visible-light photocatalytic activity. Environ. Sci. Pollut. Res. Available from: https://doi.org/10.1007/s11356-021-18253-0.

Phophayu, S., Pimpang, P., Wongrerkdee, S., Sujinnapram, S., Wongrerkdee, S., 2020. Modified graphene quantum dots-zinc oxide nanocomposites for photocatalytic degradation of organic dyes and commercial herbicide. J. Reinf. Plast. Compos. 39 (3–4), 81–94.

Qin, H., Guo, R.T., Liu, X.Y., Shi, X., Wang, Z.Y., Tang, J.Y., et al., 2020. 0D NiS_2 quantum dots modified 2D g-C_3N_4 for efficient photocatalytic CO_2 reduction. Colloids Surf. A: Physicochem. Eng. Asp. 600. Available from: https://doi.org/10.1016/j.colsurfa.2020.124912.

Qu, Z., Wang, J., Tang, J., Shu, X., Liu, X., Zhang, Z., et al., 2018. Carbon quantum dots/$KNbO_3$ hybrid composites with enhanced visible-light driven photocatalytic activity toward dye waste-water degradation and hydrogen production. Mol. Catal. 445. Available from: https://doi.org/10.1016/j.mcat.2017.11.002.

Quan, B., Liu, W., Liu, Y., Zheng, Y., Yang, G., Ji, G., 2016. Quasi-noble-metal graphene quantum dots deposited stannic oxide with oxygen vacancies: synthesis and enhanced photocatalytic properties. J. Colloid Interf. Sci. 481, 13–19.

Que, M., Zhao, Y., Yang, Y., Pan, L., Lei, W., Cai, W., 2021. Anchoring of formamidinium lead bromide quantum dots on Ti_3C_2 nanosheets for efficient photocatalytic reduction of CO_2. ACS Appl. Mater. Interf. 13 (5), 6180–6187.

Rajabi, H.R., Farsi, M., 2016. Study of capping agent effect on the structural, optical and photocatalytic properties of zinc sulfide quantum dots. Mater. Sci. Semicond. Proc. 48, 14–22.

Reddy, N.R., Bharagav, U., Kumari, M.M., Cheralathan, K.K., Shankar, M.V., Reddy, K.R., 2020. Highly efficient solar light-driven photocatalytic hydrogen production over Cu/FCNTs-titania quantum dots-based heterostructures. J. Environ. Manag. 254. Available from: https://doi.org/10.1016/j.jenvman.2019.109747.

Ren, G., Han, H., Wang, Y., Liu, S., Zhao, J., Meng, X., et al., 2021. Recent advances of photocatalytic application in water treatment: a review. Nanomaterials 11 (7). Available from: https://doi.org/10.3390/nano11071804.

Sahu, B.K., Juine, R.N., Sahoo, M., Kumar, R., Das, A., 2021. Interface of GO with SnO_2 quantum dots as an efficient visible-light photocatalyst. Chemosphere 276. Available from: https://doi.org/10.1016/j.chemosphere.2021.130142.

Saud, P.S., Pant, B., Alam, A.M., Ghouri, Z.K., Park, M., Kim, H.Y., 2015. Carbon quantum dots anchored TiO_2 nanofibers: effective photocatalyst for wastewater treatment. Ceram. Int. 41 (9), 11953–11959.

Schneider, J., Matsuoka, M., Takeuchi, M., Zhang, J., Horiuchi, Y., Anpo, M., et al., 2014. Understanding TiO_2 photocatalysis: mechanisms and materials. Chem. Revs. 114 (19), 9919–9986.

Shahnazi, A., Nabid, M.R., Sedghi, R., Heidari, B., 2020. A thermosensitive molecularly imprinted poly-NIPAM coated MWCNTs/TiO_2 photocatalyst for the preferential removal of pendimethalin pesticide from wastewater. J. Photochem. Photobiol. A: Chem. 402. Available from: https://doi.org/10.1016/j.jphotochem.2020.112802.

Shao, X., Xin, W., Yin, X., 2017. Hydrothermal synthesis of ZnO quantum dot/KNb_3O_8 nanosheet photocatalysts for reducing carbon dioxide to methanol. Beilstein J. Nanotech 8 (1), 2264–2270.

Sharma, S., Mehta, S.K., Ibhadon, A.O., Kansal, S.K., 2019. Fabrication of novel carbon quantum dots modified bismuth oxide (α-Bi_2O_2/C-dots): material properties and catalytic applications. J. Colloid Interf. Sci. 533, 227–237.

Sharma, K., Raizada, P., Hasija, V., Singh, P., Bajpai, A., Nguyen, V.H., et al., 2021. ZnS-based quantum dots as photocatalysts for water purification. J. Water Process. Eng. 43. Available from: https://doi.org/10.1016/j.jwpe.2021.102217.

Shi, J.W., Wang, Z., He, C., Wang, H., Chen, J.W., Fu, M.L., et al., 2015. CdS quantum dots modified N-doped titania plates for the photocatalytic mineralization of diclofenac in water under visible light irradiation. J. Mol. Catal. A: Chem. 399, 79–85.

Shi, W., Sun, W., Liu, Y., Li, X., Lin, X., Guo, F., et al., 2022. Onion-ring-like g-C_3N_4 modified with Bi_3TaO_7 quantum dots: a novel 0D/3D S-scheme heterojunction for enhanced photocatalytic hydrogen production under visible light irradiation. Renew. Energy 182, 958–968.

Singh, S., Garg, S., Saran, A.D., 2021. Photocatalytic activity of CdS and CdSe quantum dots for degradation of 3-aminopyridine. Nanotechnol. Environ. Eng. 6 (3). Available from: https://doi.org/10.1007/s41204-021-00159-4.

Smrithi, S.P., Kottam, N., Vergis, B.R., 2022. Heteroatom modified hybrid carbon quantum dots derived from cucurbita pepo for the visible light driven photocatalytic dye degradation. Top. Catal. . Available from: https://doi.org/10.1007/s11244-022-01581-x.

Sonowal, K., Nandal, N., Basyach, P., Kalita, L., Jain, S.L., Saikia, L., 2022. Photocatalytic reduction of CO_2 to methanol using Zr (IV)-based MOF composite with g-C_3N_4 quantum dots under visible light irradiation. J. CO_2 Util. 57. Available from: https://doi.org/10.1016/j.jcou.2022.101905.

Su, D.W., Ran, J., Zhuang, Z.W., Chen, C., Qiao, S.Z., Li, Y.D., 2020. Atomically dispersed Ni in cadmium-zinc sulfide quantum dots for high-performance visible-light photocatalytic hydrogen production. Sci. Adv. 6 (33). Available from: https://doi.org/10.1126/sciadv.aaz8447.

Sun, S., An, Q., Wang, W., Zhang, L., Liu, J., Goddard III, W.A., 2017. Efficient photocatalytic reduction of dinitrogen to ammonia on bismuth monoxide quantum dots. J. Mater. Chem. A 5 (1), 201–209.

Sun, J., Duan, L., Wu, Q., Yao, W., 2018. Synthesis of MoS_2 quantum dots cocatalysts and their efficient photocatalytic performance for hydrogen evolution. Chem. Eng. J. 332, 449–455.

Sun, Y., Yuan, X., Wang, Y., Zhang, W., Li, Y., Zhang, Z., et al., 2022. CeO_2 quantum dots anchored g-C_3N_4: synthesis, characterization and photocatalytic performance. Appl. Surf. Sci. 576. Available from: https://doi.org/10.1016/j.apsusc.2021.151901.

Vatanpour, V., Khadem, S.S.M., Masteri-Farahani, M., Mosleh, N., Ganjali, M.R., Badiei, A., et al., 2020. Anti-fouling and permeable polyvinyl chloride nanofiltration membranes embedded by hydrophilic graphene quantum dots for dye wastewater treatment. J. Water Process. Eng. 38. Available from: https://doi.org/10.1016/j.jwpe.2020.101652.

Vidhya, K., Saravanan, M., Bhoopathi, G., Devarajan, V.P., Subanya, S., 2015. Structural and optical characterization of pure and starch-capped ZnO quantum dots and their photocatalytic activity. Appl. Nanosci. 5 (2), 235–243.

Wahab, R., Tripathy, S.K., Shin, H.S., Mohapatra, M., Musarrat, J., Al-Khedhairy, A.A., 2013. Photocatalytic oxidation of acetaldehyde with ZnO-quantum dots. Chem. Eng. J. 226, 154–160.

Wang, C., Thompson, R.L., Ohodnicki, P., Baltrus, J., Matranga, C., 2011. Size-dependent photocatalytic reduction of CO_2 with PbS quantum dot sensitized TiO_2 heterostructured photocatalysts. J. Mater. Chem. 21 (35), 13452–13457.

Wang, J., Wang, J., Li, N., Du, X., Ma, J., He, C., et al., 2020. Direct Z-scheme 0D/2D heterojunction of $CsPbBr_3$ quantum dots/Bi2WO6 nanosheets for efficient photocatalytic CO_2 reduction. ACS Appl. Mater. Interf. 12 (28), 31477–31485.

Wang, W., Zeng, Z., Zeng, G., Zhang, C., Xiao, R., Zhou, C., et al., 2019. Sulfur doped carbon quantum dots loaded hollow tubular g-C_3N_4 as novel photocatalyst for destruction of *Escherichia coli* and tetracycline degradation under visible light. Chem. Eng. J. 378. Available from: https://doi.org/10.1016/j.cej.2019.122132.

Wang, S., Liu, D., Yu, J., Zhang, X., Zhao, P., Ren, Z., et al., 2021. Photocatalytic penicillin degradation performance and the mechanism of the fragmented TiO_2 modified by CdS quantum dots. ACS Omega 6 (28), 18178–18189.

Xia, J., Di, J., Li, H., Xu, H., Li, H., Guo, S., 2016. Ionic liquid-induced strategy for carbon quantum dots/BiOX (X = Br, Cl) hybrid nanosheets with superior visible light-driven photocatalysis. Appl. Catal. B: Environ. 181, 260–269.

Xie, Y., Yu, S., Zhong, Y., Zhang, Q., Zhou, Y., 2018. SnO_2/graphene quantum dots composited photocatalyst for efficient nitric oxide oxidation under visible light. Appl. Surf. Sci. 448, 655–661.

Xu, L., Bai, X., Guo, L., Yang, S., Jin, P., Yang, L., 2019. Facial fabrication of carbon quantum dots (CDs)-modified N-TiO_{2-x} nanocomposite for the efficient photoreduction of Cr (VI) under visible light. Chem. Eng. J. 357, 473–486.

Xu, X., Meng, L., Luo, J., Zhang, M., Wang, Y., Dai, Y., et al., 2021. Self-assembled ultrathin CoO/Bi quantum dots/defective Bi_2MoO_6 hollow Z-scheme heterojunction for visible light-driven degradation of diazinon in water matrix: intermediate toxicity and photocatalytic mechanism. Appl. Catal. B: Environ. 293. Available from: https://doi.org/10.1016/j.apcatb.2021.120231.

Xu, C., Li, D., Liu, X., Ma, R., Sakai, N., Yang, Y., et al., 2022a. Direct Z-scheme construction of g-C_3N_4 quantum dots/TiO_2 nanoflakes for efficient photocatalysis. Chem. Eng. J. 430. Available from: https://doi.org/10.1016/j.cej.2021.132861.

Xu, Z., Wang, Y., Zhuang, J., Li, Y., Jia, L., 2022b. High temperature hydrothermal etching of g-C_3N_4 for synthesis of N doped carbon quantum dots-supported CdS photocatalyst to enhance visible light driven hydrogen generation. Mol. Catal. 517. Available from: https://doi.org/10.1016/j.mcat.2021.111900.

Xu, K., Zhang, Q., Wang, C., Xu, J., Bu, Y., Liang, B., et al., 2022c. 0D boron carbon nitride quantum dots decorated 2D $Bi_4O_5I_2$ as 0D/2D efficient visible-light-driven photocatalysts for tetracyclines photodegradation. Chemosphere 289. Available from: https://doi.org/10.1016/j.chemosphere.2021.133230.

Yang, H., Yin, J., Cao, R., Sun, P., Zhang, S., Xu, X., 2019. Constructing highly dispersed 0D Co_3S_4 quantum dots/2D g-C_3N_4 nanosheets nanocomposites for excellent photocatalytic performance. Sci. Bull. 64 (20), 1510–1517.

You, Z., Yue, X., Zhang, D., Fan, J., Xiang, Q., 2022. Construction 0D/2D heterojunction by highly dispersed Ag_2S quantum dots (QDs) loaded on the g-C_3N_4 nanosheets for photocatalytic hydrogen evolution. J. Colloid Interf. Sci. 607, 662–675.

Yu, Z., Meng, J., Xiao, J., Li, Y., Li, Y., 2014. Cobalt sulfide quantum dots modified TiO_2 nanoparticles for efficient photocatalytic hydrogen evolution. Int. J. Hydrog. Energy 39 (28), 15387–15393.

Yuan, A., Lei, H., Xi, F., Liu, J., Qin, L., Chen, Z., et al., 2019. Graphene quantum dots decorated graphitic carbon nitride nanorods for photocatalytic removal of antibiotics. J. Colloid Interf. Sci. 548, 56–65.

Zaib, M., Akhtar, A., Maqsood, F., Shahzadi, T., 2021. Green synthesis of carbon dots and their application as photocatalyst in dye degradation studies. Arab. J. Sci. Eng. 46 (1), 437–446.

Zeng, Z., Yu, D., He, Z., Liu, J., Xiao, F.X., Zhang, Y., et al., 2016. Graphene oxide quantum dots covalently functionalized PVDF membrane with significantly-enhanced bactericidal and antibiofouling performances. Sci. Rep. 6 (1). Available from: https://doi.org/10.1038/srep20142.

Zhang, H., Wu, P., Li, Y., Liao, L., Fang, Z., Zhong, X., 2010. Preparation of bismuth oxide quantum dots and their photocatalytic activity in a homogeneous system. ChemCatChem 2 (9), 1115–1121.

Zhang, J., Zhang, X., Dong, S., Zhou, X., Dong, S., 2016. N-doped carbon quantum dots/TiO_2 hybrid composites with enhanced visible light driven photocatalytic activity toward dye wastewater degradation and mechanism insight. J. Photochem. Photobiol. A: Chem. 325, 104–110.

Zhang, W., Cui, W., Sun, Y., Huang, H., Wu, Z., Dong, F., 2017. Pt quantum dots deposited on N-doped $(BiO)_2$ CO_3: enhanced visible light photocatalytic NO removal and reaction pathway. Catal. Sci. Technol. 7 (6), 1324–1332.

Zhang, F., Wang, X., Liu, H., Liu, C., Wan, Y., Long, Y., et al., 2019. Recent advances and applications of semiconductor photocatalytic technology. Appl. Sci. 9 (12). Available from: https://doi.org/10.3390/app9122489.

Zhang, M., Lai, C., Li, B., Xu, F., Huang, D., Liu, S., 2020. Unravelling the role of dual quantum dots cocatalyst in 0D/2D heterojunction photocatalyst for promoting photocatalytic organic pollutant degradation. Chem. Eng. J. 396. Available from: https://doi.org/10.1016/j.cej.2020.125343.

Zhang, Z., Cao, Y., Zhang, F., Li, W., Li, Y., Yu, H., et al., 2022. Tungsten oxide quantum dots deposited onto ultrathin $CdIn_2S_4$ nanosheets for efficient S-scheme photocatalytic CO_2 reduction via cascade charge transfer. Chem. Eng. J. 428. Available from: https://doi.org/10.1016/j.cej.2021.131218.

Zhao, Z., Fan, J., Deng, X., Liu, J., 2019. One-step synthesis of phosphorus-doped g-C_3N_4/Co_3O_4 quantum dots from vitamin B_{12} with enhanced visible-light photocatalytic activity for metronidazole degradation. Chem. Eng. J. 360, 1517–1529.

Zou, Y., Xie, Y., Yu, S., Chen, L., Cui, W., Dong, F., et al., 2019. SnO_2 quantum dots anchored on g-C_3N_4 for enhanced visible-light photocatalytic removal of NO and toxic NO_2 inhibition. Appl. Surf. Sci. 496. Available from: https://doi.org/10.1016/j.apsusc.2019.143630.

Zubair, M., Kim, H., Razzaq, A., Grimes, C.A., In, S.I., 2018. Solar spectrum photocatalytic conversion of CO_2 to CH_4 utilizing TiO_2 nanotube arrays embedded with graphene quantum dots. J. CO2 Util. 26, 70–79.

This page intentionally left blank

Chapter 10

Application of quantum dots in light-emitting diodes

Anca Armăşelu[1] and Monika Jangid[2]
[1]Department of Electrical Engineering and Applied Physics, Faculty of Electrical Engineering and Computer Science, Transilvania University of Brasov, Brasov, Romania, [2]Department of Chemistry, PAHER University, Udaipur, Rajasthan, India

10.1 Introduction

Quantum dots (QDs) have been extensively investigated in the past few decades owing to their unique properties. QDs are called artificial nanocrystals possessing confinement in all three dimensions with nanometer size that can carry electrons; optical and electrical attributes of QDs can be effectively adjusted by modifying their dimensions, resulting in the emission of specific wavelengths of light (Chen et al., 2020a; Motomura et al., 2020; Singh et al., 2021a).

QDs exhibit numerous unique optical properties such as high photoluminescence (PL) quantum yield (QY), pure and saturated colors, narrow bandwidth, tunable band gap, narrow and symmetric emission, broad and strong absorption (Shirasaki et al., 2013; Pietryga et al., 2016; Bang et al., 2020; Jia et al., 2020; Huang et al., 2020a). Due to their remarkable properties, QDs have found uses in a variety of unusual categories of electronics and optoelectronic tools with potential for application in information displays, solid-state lighting (SSL), biology (Armăşelu et al., 2011a,b), and other structures (Colvin et al., 1994; Ugarte et al., 2012; Nguyen et al., 2019).

Light-emitting diodes (LEDs) reshaped the lighting and display industry and have accomplished considerable developments compared to traditional lighting sources (Zhang et al., 2021a). Exceptional luminescence and charge transport characteristics of QDs show that they are promising alternative emitting materials for the LEDs industry (Colvin et al., 1994; Mattousi et al., 1998; Coe et al., 2002; Kagan et al., 2016; Yang et al., 2019a; Huang et al., 2020b; Bang et al., 2021).

Given the requirements for high resolution and high color saturation, technologies comprising organic LEDs (OLEDs), mini-LEDs (mLEDs), micro-LEDs (μLEDs or μ-LEDs), QD LEDs (QD-LEDs, QD LEDs, or

Quantum Dots. DOI: https://doi.org/10.1016/B978-0-12-824153-0.00010-0
© 2023 Elsevier Inc. All rights reserved.

QLEDs) (Armăşelu, 2017), and laser displays have been produced to substitute liquid crystal displays (LCDs) (Ameta et al., 2019; Ye et al., 2021), μLEDs (Wu et al., 2018; Huang et al., 2019; Wong et al., 2019; Huang et al., 2020b; Bai et al., 2020; Wu et al., 2020; Biwa et al., 2021; Zhuang et al., 2021) and mLEDs (Tan et al., 2018; Huang et al., 2019, 2020b; Sun et al., 2020) and have emerged as next-generation displays providing ultrahigh luminance and long lifetimes.

Ghamsari (2017) reminded that the display industry is interested to mix QD with OLED, noting that an improvement in operation time of OLED device can be realized with the help of QDs. Luo et al. (2018) presented that electroemissive QD displays possess the capability to revolutionize the display industry in the coming years, offering not only the thinness and flexibility of OLED displays, but with the advantages of price, color, and brightness of QDs. High color purity and wide color gamut (WCG) that can be realized using QDs have drawn much attention in display applications (Jiang et al., 2018). The QD-based consumer displays such as LED TVs, tablets, and smartphones offer a reasonable power efficiency and an accessible cost, exhibiting improved competitive edge to OLED technics (Jang, 2018).

A QD display represents a device, which utilizes QDs as a component of panel construction to produce monochromatic red, green, and blue light (Sellers, 2018). They explained that photoemissive QD particles are utilized in LED-backlit LCDs, where a QD layer converts the backlight to give out pure basic colors and electroemissive QD displays constitute a model of novel display based on QD-LEDs (QLED or QD-LED). Liu et al. (2020a) reviewed the newest advances in the implementation of μ-LEDs and QDs in display technology, together with the μ-LED design and QD full-color procedure and provided some insights on the progress of favorable QD film deposition mechanisms, showing the modern uses of QD-based μ-LED displays.

LED-based communication links can be used in both open space and optical interconnect applications. The LEDs based on evolving semiconductor materials are of special importance in the progress of the next-generation data communications (Ren et al., 2021). They are examining the advancement of some LED materials, including the case of colloidal QDs for application in optical communications systems.

This chapter reviews the latest developments on applications of QDs for LEDs, focusing on some key areas such as display, lighting, data communications, agriculture, horticulture, and antimicrobial technology.

10.2 Display and lighting

QDs have a great potential in different optoelectronic applications. They have also found application in LEDs for lighting of different colors due to their tunable fluorescence emission, characteristic broad emission, and high thermal stability. These LEDs are also useful in both SSL and flat-panel

displays. Flexible information displays hold a great promise for future optoelectronic applications, but most of these are fabricated on glass substrates and only a little work has been done LEDs based on flexible substrates.

10.2.1 White light-emitting diodes

Among the optoelectronics applications, the white LED (WLED) exhibits a considerable capability in flat panel displays and SSL (Kim et al., 2016a).

Amorphous silicon QDs (*a-Si* QDs) were grown by Park et al. (2001) in a silicon nitride film via plasma-enhanced chemical vapor deposition. Four types of PL (Red, blue, green, and white) were observed from these *a-Si* QD structures just by control of size of QDs. They fabricated orange LEDs using *a-Si* QDs with average size of 2.0 nm. An external quantum efficiency of 2×10^{-3}% was obtained. It was indicated that LED using *a-Si* QDs embedded in the silicon nitride film was found to be much better than Si-based LEDs in terms of optical and electrical properties.

Park et al. (2004) obtained white light emission from a LEDs. They prepared this diode from polymer/QD nanocomposites using poly(9,9′-dihexylfluorene-2,7-divinylene-*m*-phenylenevinylene-*stat*-*p*-phenylenevinylene) (PDHFPPV) and two kinds of CdSe nanoparticles (NPs) with different particle sizes. It was observed that blue, green, and red emission from the polymer, ~3 nm, and emission from the ~7 nm CdSe, contribute jointly to white emission of the organic−inorganic hybrid device.

Song and Lee (2007a) synthesized (CdSe)ZnS QD−polymethylmethacrylate (PMMA) polymer composite. Then they fabricated QD−polymer composite films. It was observed that 28% (wt./wt.) of PMMA in MMA was desired concentration to produce a film white good quality and the solubility of QDs was also maximized. They fabricated red or green light-emitting (CdSe)ZnS QD−PMMA polymer composite film by combining the red or green light-emitting (CdSe)ZnS dots with PMMA. It was revealed that a white light-emitting device can be prepared by a combination of these green/red light-emitting QD−polymer composites with a blue light-emitting LED (excitation source). It was proposed that as-fabricated QD−polymer composites can be used in full color displays, large-area colored wall-papers, and flexible colored filters.

Jang et al. (2010) used highly luminescent multiply passivated red− and green−light−emitting QDs as color converters in InGaN blue LEDs. They could achieve external quantum efficiencies of 34% and 72%, respectively for these LEDs. As-obtained white QD-LEDs exhibited efficacy of 41 lm W^{-1} and color reproducibility of 100%. Kim et al. (2011) studied $CuInS_2$ QDs as an excellent red emitting source for WLED due to its nontoxic deep red emission. It was revealed that $CuInS_2$ QDs can be synthesized by a one-pot method. Then ZnS shells were formed on QD surfaces so as to

reduce nonradiative recombination on its surface defects. It was observed that core/shell QDs exhibited maximum PL wavelength blue shifts by about 80 nm on increasing intensity more than six times and the QY of as-prepared $CuInS_2$/ZnS QDs was 67%. The transparent and hydrophobic dispersion of QDs in polystyrene was also observed using toluene as codispersing agent. The polystyrene/QD composite was applied on blue LEDs, which exhibited luminous efficacy (LE) of 10.7 lm W^{-1}.

A large-scale synthesis of InP/ZnS core/shell nanocrystal QDs was reported by Kim et al. (2012) using a customized hybrid flow reactor. They synthesized InP cores and InP/ZnS core/shell QDs successively in the hybrid reactor in one-step process only. The flow rate of the solutions was kept typically 1 mL min^{-1} in the reactor, which is about hundred times larger than as kept in conventional microfluidic reactors. The flow rate as well as crystal growth temperature were controlled to synthesize high-quality InP/ZnS QDs. It was revealed that high-quality InP/ZnS QDs (bluish green to red) were obtained and these core/shell QDs could be incorporated into WLEDs devices to improve performance of color rendering.

Song et al. (2012) reported the synthesis of Cu−In−Ga−S (CIGS) QDs. They applied these QDs for WLED with variation of In:Ga ratios. It was found that band gap and emission energies of as-prepared CIGS QDs were higher an increasing Ga contents. It was observed that ZnS shell-capped QDs of the CIGS/ZnS core−shell emitted tunable wavelengths (520−578 nm) with an excellent PL QY of 72%−83%. They reported high LEs of 69.1−75.0 lm W^{-1}, when highly fluorescent CIGS/ZnS QDs as color converters with a blue-emitting LED were combined with efficient white QD-based LEDs. A white QD-LED was also fabricated by blending of two kinds of CIGS/ZnS QDs, which exhibited enhanced color rendering property.

A simple solution method was used by Son et al. (2012) to prepare emissive hybrid QDs, which consists of a ZnO core wrapped in a shell of single-layer graphene. Then these QDs were used to make a WLEDs with a brightness of 798 cd m^{-2}. White emission could also be achieved by combining these QDs with some other emissive materials in a multilayer LEDs.

The color rendering index (CRI) of YAG:Ce-based WLEDs is poor. The core/shell/shell CdSe/CdS/ZnS QDs were synthesized by Shen et al. (2012) and blended into nano-YAG:Ce^{3+} phosphors to improve this index. They obtained a WLED with a combination of blue LED (with the blends of nano-YAG phosphors) and orange- and red-emission QDs in the weight ratio (1:1:1). It was revealed that as-fabricated WLEDs exhibited excellent white light with luminescent efficiency of 82.5 lm W^{-1}.

Song et al. (2013) reported the synthesis of two bright noncadmium QDs of orange (583 nm)-emitting $CuInS_2$ (CIS)/ZnS and green (512 nm)-emitting InP/ZnS core/shell. These were applied for fabrication of SSL devices. It was obtained that spectral overlap between absorptions from both emissions from InGaN-based blue LED chip and QDs was excellent. There was an

efficient downconversion of blue-to-QD emission for the generation of white light by dispensing sequentially InP/ZnS QDs on top of CIS/ZnS within epoxy resin. It was revealed that white QD-LED generated a white light with high quality having a high CRI of 90 and a warm color temperature of 3803K.

Erdem and Volkan (2013) presented that on using QDs in color-conversion LEDs, it is possible to simultaneously achieve remarkable color rendition of the illuminated objects together with an excellent spectral overlap between the emission spectrum of the tool and the sensitivity of the human eye, in addition to a warm white color, unlike other standard sources such as phosphor-based LEDs. They reviewed some modern evolutions in quantum-dot-integrated WLEDs (QD-WLEDs) based on color conversion.

Kubendhiran et al. (2019) reported in a review that WLEDs are an excellent alternative to fluorescent tubes and classical light bulbs in most lighting uses because WLEDs have greater operating lifetimes and important energy savings compared to traditional incandescent light bulbs. They noticed that at the moment there are different types of QD-WLEDs that show these kinds of benefits.

Roy et al. (2014) prepared graphene QDs (GQDs) using plant leaf extracts of Fenugreek (*Trigonella foenum-graecum*) and Neem (*Azadirachta indica*) via a hydrothermal method. They did not use any passivizing, reducing agents or organic solvents. It was reported that the average sizes of the GQDs from Fenugreek (F-GQDs) and Neem (N-GQDs) were 7 and 5 nm, respectively. F-GQDs and N-GQDs exhibited high QYs of 38.9% and 41.2%, respectively. It was revealed that as-prepared GQDs can be utilized to prepare a white light converting cap based on the red-green-blue color mixing method.

The green red Zn−Cu−In−S (ZCIS) and Zn−Ag−In−S (ZAIS)core/shell-like alloyed QDs were synthesized by Yoon et al. (2015) via a hot-injection method. They obtained tunability of red ZCIS and green ZAIS QDs by choosing a high temperature multiple alloyed reaction and low temperature core growth. It was observed that the alloyed red ZCIS and green ZAIS QDs could reach PL QYs of 0.53 and 0.61, respectively was also carried out by them. Practical realization of white downconverted LEDs (DC-LEDs). They also characterized based on CRI, LE, vision & color performance and color quality scale (CQS) of white DC-LEDs incorporated with red ZCIS and green ZAIS QDs. It was reported that tricolor white DC-LED using red-emitting ZCIS core/shell-like alloyed QDs exhibited a moderate LE 31.2 lm W^{-1} with ultrahigh color qualities CRI and CQS as 97and 94, respectively.

Kang et al. (2015) synthesized cadmium-free and water soluble $AgInS_2$/ZnS core/shell QDs. These QD powders exhibited bright orange, yellow, and orange-red luminescence in presence of UV light depending upon Ag/In ratio and PL QYs could reach as high as 57, 50.5, and 52%, respectively. They

obtained warm-WLEDs by a combination of orange-emitting QDs with blue InGaN chip having LE of 39.85 lm W^{-1} and CRI of 71.

Zhang et al. (2018a) synthesized all-inorganic halide perovskite nanocrystals. They used hot-injection method and anion exchange reaction to obtain NPs in the range of 15−40 nm and whole visible light region (410−700 nm). They also constructed a WLED by stacking $CsPbBr_3$ QDs-ethyl acetate composite film and $CaSrAlN_3:Eu^{2+}$-poly (methyl methacrylate) composite film on the blue LED chip. This displayed the ideal white light. It was reported that although WLED is not stable at higher operation current, but it can smoothly work under a lower operation current. Shen et al. (2018) fabricated an efficient flexible white QLED with mixed green, red, and blue QDs as emitters. It was reported that as-prepared flexible white QLED exhibited pure white light emission with brightness of up to 3554 cd m^{-2} and current efficiency of 10.5 cd A^{-1}.

Chen et al. (2018) fabricated silica-wrapped Mn-doped $CsPbCl_3$ QDs with improved operational stability (Fig. 10.1). They hydrolyzed (3-aminopropyl) triethoxysilane for this purpose. They could achieve high PL QY (55.4%) for the $CsPbMnCl_3@SiO_2$ composite. It was reported that wrapping by silica can protect these perovskite QDs from any damage by humidity and temperature. They prepared WLED devices by mixing of green $CsPbBr_3$ QDs and orange-red $CsPbMnCl_3@SiO_2$ composites, which exhibited high LE (77.59 lm W^{-1}) and CRI (82). It was also revealed that electroluminescence spectrum showed almost no variation even after 24 h operation.

Cesium-lead-halide perovskite QDs (PQDs) have excellent superior optical and electronic properties and therefore, these are considered potential materials for various optoelectronic devices. Yang et al. (2019c) developed to hydrolysis encapsulation method by embed PQDs into mesoporous polystyrene microspheres (MPMs), which was followed by silica shell covering process. It generated luminescent PQDs/MPMs@SiO_2 hybrid microspheres with excellent stability. It was reported that as-obtained $CsPbBr_3$-PQDs/MPMs@SiO_2 hybrid microspheres show a high PL QY (84%). As-prepared hybrid microspheres exhibited good chemical/physical stability seven under harsh conditions of environments, particularly acid/alkali solution, deionized water, anion-exchange reactions, isopropanol, and heating. It was also revealed that about 48% proportion of the initial fluorescence intensity is there, even after a quite long storage period of 30 days with water. It was also observed that WLED are achieved by mixing green $CsPbBr_3$-PQDs/MPMs@SiO_2 microspheres with red commercial phosphors on a blue chip with a high power efficiency (81 lm W^{-1}) and good electroluminescence stability.

Sadeghi et al. (2019) optimized the QY of magic-sized CdSe QDs up to 22% through controlling parameters of synthesis without shelling or posttreatment. They integrated them in liquid-state on blue LED so as to prevent the efficiency drop due to host-material effect. It was revealed that

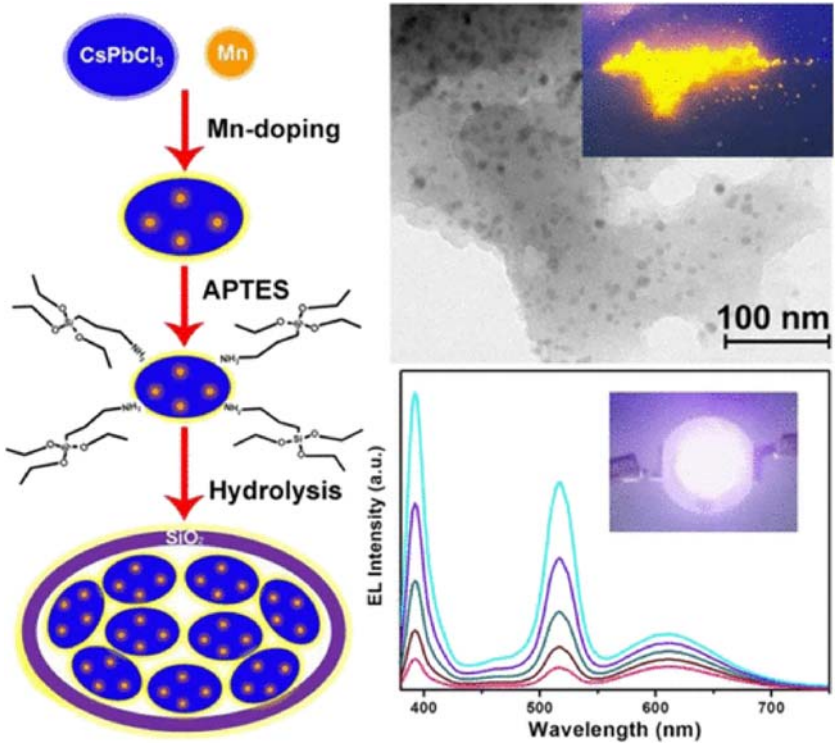

FIGURE 10.1 Fabrication of silica-wrapped Mn-doped $CsPbCl_3$ QDs for LED application. *Adapted from Chen et al., 2018. ACS Appl. Mater. Interfaces,10(50), 43978–43986. With Permission.*

as-prepared WLEDs showed color-rendering index of 89 and LE of 11.7 lmW^{-1}.

Yin et al. (2019) fabricated yellow-green emitting GQDs using low-cost as well as eco-friendly method. As-obtained GQDs were cast in UV-curable siloxane and a polymer film to obtain excellent monodispersity properties and better optical transparency through just adjusting thickness and the concentration of the color convert matrix, so as to achieve tunable color temperatures (3196K−10 870K) of the GQD-based WLEDs. Using the fluorescent polymeric matrix in WLEDs, good quality emission and gratifying stability could be obtained. It was also indicated that this technology has a great potential for applications in high-end lighting.

The synthesis of $CH_3NH_3Pb_{1-x}Mn_xI_3$ PQDs (where manganese is substituted at sites of lead) was reported by Singh et al. (2019). It was observed that these QDs exhibited strong color tunability ranging from red to orange,

when concentration of Mn^{2+} was varied from 0 to 60%. A high external PL QY (98%) was observed for unsubstituted $CH_3NH_3PbI_3$. They developed a WLED using $CH_3NH_3Pb_{1-x}Mn_xI_3$ QDs with green QDs on a blue LED chip.

Yang et al. (2019b) developed a novel package structure to prepare QD-WLEDs using dip-coating red and green QDs/polyurethane composites into TV lens and combine them with a blue LED to form white light. They demonstrated that the in-lens technique has high stability and that a 32-inch prototype LCD TV possesses a WCG of 108% under the National Television Systems Committee standard with this in-lens encapsulation construction.

Perikala and Bhardwaj (2021) reported that QD-WLEDs use diverse colors (red, blue, and green), emitting QDs to achieve white light. They communicated an open air atmosphere synthesis of highly luminescent single system white light-emitting carbon dots (CDs). It was revealed that CDs have been embedded in polydimethylsiloxane (PDSM) polymer and as-produced CD-PDMS phosphor indicated exceptional CRI $\sim$96; the maximal communicated so far with Commission Internationale de l'Eclairage coordinates (0.31, 0.33), which are very similar to pure white light. This research establishes a scaffold for the uses of CD-phosphor-based WLEDs in lighting systems.

The influence of the pore structure of SBA-15 particle was observed by Li et al. (2020) on light emission from inner adsorbed QDs and outer LEDs chips. It is was found that the particle features of a high refractive index, comparable feature size of pore structure, and lower amount of QD adsorption help with QD light extraction, demonstrating a mechanism to suppress QD light propagating through pores and thus reducing the reabsorption loss. Then they developed highly efficient QD WLEDs by wet-mixing QD/SBA-15 NPs. It was observed that as-fabricated LEDs exhibited a record LE of 206.8 lm W^{-1} for WLEDs by integration of green−red QD and green QDs color convertors with improved stability.

Chen et al. (2020b) could obtain uniform blue-green emissive GQDs and modified efficient orange-emitting GQDs (D-GQDs). These QDs were derived from fullerene under acid-free conditions. As-prepared D-GQDs exhibited excellent conversion efficiency with QY of 52.4% at an emission peak of 617 nm. These GQDs and D-GQDs were blended with a polymer; poly(vinyl alcohol) to prepare photoluminescent films (transparent) with excellent flexibility and white emission property. Hu et al. (2020) developed composite orange-red QDs (composite-QDs) by mixing red QDs (R-QDs) and CdSe/ZnS-based orange QDs (O-QDs). It was reported that optimized composite-QDs can improve the CRI of the WLED as compared to monochromatic QDs.

A simple method was developed by Rad et al. (2021) to prepare white light emissive diodes. These are based on colloidal solutions of carbon QDs (CQDs) and $CsPbI_3$ perovskite (PQDs). It was reported that a right combination generates emission across the complete visible spectrum on excitation

by UV light. It was observed that white light emission of the final films provided high and stable CRI (92%). It was also revealed that a mixture can be obtained emitting the cold, neutral, and warm white lights by changing concentration of $CsPbI_3$ QDs for indoor lighting applications. The syntheses of these materials are also low cost and scalable. The colloidal mixture of CQDs and $CsPbI_3$ PQDs shows a facile deposition for LED application, which exhibited white electroluminescence, indicating that both these QDs are stable during LED operation. It was revealed that the PL QY of as-prepared colloidal mixtures was higher (up to 75%) than single white emitters, which indicates a great potential for white emission with tunable properties.

Chen et al. (2021) used Zn doped CdS QD with ZnS shell together with green light emission phosphor. It was observed that degradation of LEDs on degradation of QDs can limit its practical applications, if used for a longer time. There was a reduction in intensity as well as a blue shift of the emitted wavelength from the white light was also observed during degradation. There were three stages of degradation and there are:

1. An enhancement state, where light intensity was increased.
2. It was followed by a rapid degradation stage, where light intensity rapidly decreases, and
3. Slower degradation stage, where the degradation rate of light intensity slows down and goes on decreasing.

The degradation of LEDs was attributed to degradation of CdS core structure, which started with oxidation of sulfur vacancy of CdS QDs by the closely available oxygen atoms. This was all due to imperfection caused in ZnS protective coating around the QDs on explosive to blue light. It was indicated that oxidation transformed CdS into CdO in the initial stage where as $CdSO_4$ is formed via some intermediate processes in final stage.

Zhang et al. (2021b) synthesized green, blue, orange-red, and yellow−green carbon QDs doped with some heteroatoms (Fig. 10.2). They showed emission peaks at 495, 435, 595, and 525 nm with high PL QY (88.9%). A WLED was fabricated with high CRI of 90.8.

10.2.2 Blue light-emitting diodes

In recent years, significant advances have been achieved in the red and green PQDs-based LEDs. However, the performances of the blue perovskite LEDs are still seriously lagging behind that of the green and red counterparts. The visualization of accurate color information using QDs has been explored for decades, and commercial products employing environment friendly materials are currently available. However, next-generation electroluminescent displays based on QDs require the development of an efficient and stable cadmium-free blue light-emitting device, which has remained a

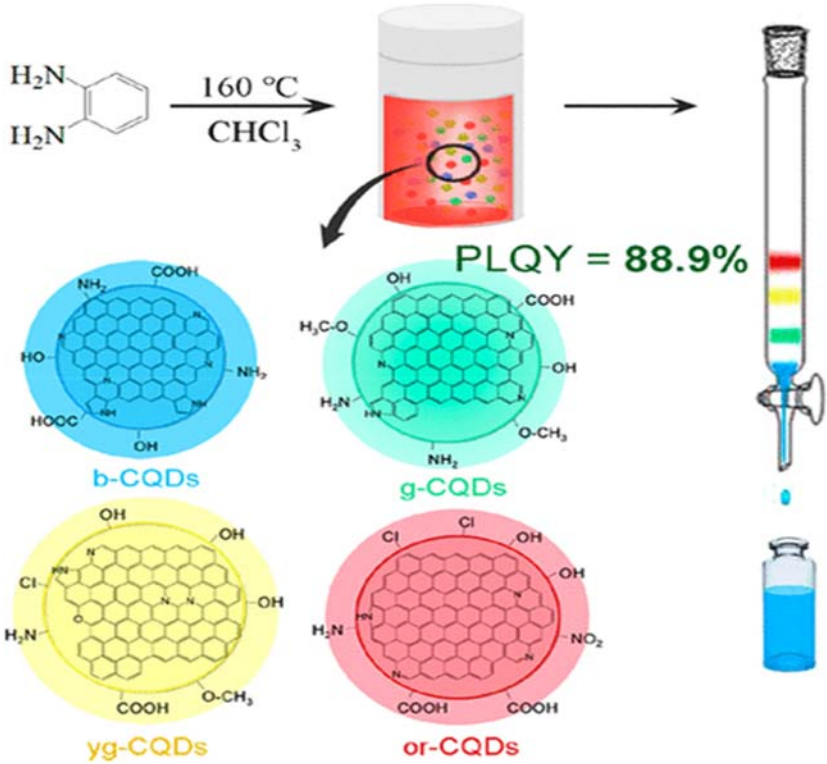

FIGURE 10.2 Synthesis of different colored carbon quantum dots doped with heteroatoms. *Adapted from Zhang et al. J. Phys. Chem. Lett.;12 (37), 8939−8946, 2021. With Permission.*

challenge because of the inferior photophysical properties of blue light-emitting materials.

Realizing of full-color quantum-dot LEDs display remains a challenge because of the poor stability of the blue quantum-dot and the immature inkjet-printing color patterning technology. For colloidal QD QD-LEDs, blue emissive device has always been inferior to green and red counterparts with respect to device efficiency, primarily because blue QDs possess inherently unfavorable energy levels relative to green and red ones, rendering hole injection to blue QDs from neighboring hole transport layer (HTL) inefficient.

Arakawa et al. (2000) have grown InGaN self-assembled QDs on a GaN epitaxial layer via atmospheric-pressure metalorganic chemical vapor deposition. The average diameter of QDs was found to be 8.4 nm. It was also observed that InGaN QDs could be formed even after 10 QD layers were stacked and as a result, the total QD density increased. Luk et al. (2012) fabricated a GQD−agar composite. As-prepared composite exhibited an

excellent optical stability, but no luminescence quenching. This composite was applied successfully as a color converting material to achieve white light emission in blue LEDs. It was reported that light conversion efficiency and LE of the WLED were 61.1% and 42.2 lm W^{-1}, respectively.

It was reported that deep-blue, high color purity electroluminescence was observed in an inverted light-emitting device using nontoxic ZnSe/ZnS core/shell QDs as the emitter (Ji et al., 2013). As-prepared device exhibited a peak at 441 nm. It was observed that current efficiency and maximum luminance could reach 0.51 cdA^{-1} and 1170 cd m^{-2}, respectively. A high performances could be achieved using a ZnO nanoparticle based electron-transporting layer, which can assist in efficient electron injection into ZnSe/ZnS QDs. It was calculated that these efficient deep-blue QD-LEDs can find application in full-color panel displays and QD-based lighting sources.

Lee et al. (2013) synthesized blue CdZnS/ZnS core/shell QDs. It was reported that as-prepared QDs exhibited high PL QY (98%), and high stability. All these solution−processed blue QD-LEDs (multilayered), consisted of HTL of poly(9-vinlycarbazole), electron transport layer of ZnO NPs, and an emissive layer of CdZnS/ZnS QDs. This as-fabricated device exhibited a maximum luminance (2624 cdm^{-2}), external quantum efficiency (7.1%), and LE of 2.2 cdA^{-1}.

Biswas et al. (2016) embedded GQDs into synthesized Amoc (*N*-anthracenemethyloxycarbonyl) capped aromatic amino acid based units. These QDs exhibited blue emission under UV irradiation at a wavelength of 365 nm. It was reported that quenching in emission spectra revealed that there are strong $\pi-\pi$ stacking interactions within Amoc-amino acids and aromatic GQDs. It was also revealed that self-healing properties and thixotropic nature of as-prepared hydrogels can be tuned by introduction of GQDs.

Bharathi et al. (2017) reported the preparation of micron-sized sheets by interconnecting GQDs (GQDs solid sheets) with intrinsic absorption and emission properties. It was observed that metal atoms interconnecting GQDs in hydrothermal growth process, induced some semiconducting behavior in these GQD solid sheets. As-prepared GQDs exhibit a 36% PL QY in the blue region (440 nm). Wang et al. (2017) synthesized highly−efficient blue CdSe/ZnS QDs with emission peak ($>$ 460 nm) with the object to protect human eyes from the harmful effect of short-wavelength light. They fabricated QLEDs based on as-prepared blue QDs and optimized ZnO NPs. It was revealed that using small-size of ZnO NPs, a maximum external quantum efficiency (19.8%) and current efficiency (14.1 cd A^{-1}) for QLEDs were observed. It was proposed that color saturation blue QLEDs have a great potential for use in next-generation full-color displays.

Yuan et al. (2017) synthesized multicolor band gap fluorescent carbon QDs (MCBF-CQDs) via a solvothermal method. The as-prepared QDs have blue to red color with high QY (75%). It was observed that maximum

luminance of as-prepared blue LEDs could reach 136 cd m^{-2}. Lin et al. (2018) synthesized blue nonblinking (> 98% "on" time) ZnCdSe/ZnS//ZnS QDs (Fig. 10.3). The absolute fluorescence QY was found to be 92% ($\lambda_{peak} = 472$ nm). It was reported that these bright nonblinking ZnCdSe/ZnS//ZnS core/shell QDs exhibited not only good tunability in the blue-cyan range (450−495 nm) but also high absolute PL quality yield, but excellent chemical and photochemical stability also.

Wang et al. (2019) synthesized four surface-modified (positively charged metal NPs) with different localized surface plasmon resonance wavelengths and then linked with red-emitting colloidal CdZnSeS/ZnS QDs (negatively charged) on the top surface of a blue-emitting InGaN/GaN quantum well (QW) LEDs. There is strong surface plasmon coupling due to short distance of NP and QD in NP-QD linkage; thus enhancing absorption and emission. A stronger QD excitation was also observed. All the factors together resulted in an increase of color conversion efficiency of the QDs.

Kim et al. (2020) reported the synthesis of ZnSe-based blue light-emitting QDs with a QY of unity. They observed that zinc chloride and hydrofluoric acid additives were found effective in increasing luminescence efficiency. It was anticipated that these efficient and stable blue QD light-emitting devices can find potential application in development of electroluminescent full-color displays.

Pan et al. (2020) developed Ni^{2+} ion-doped $CsPbCl_xBr_{3-x}$ PQDs via supersaturated recrystallization synthesis. It was simultaneously realized that the doping of various concentrations of Ni^{2+} cations modulating the Cl/Br element ratios by introducing different amounts of $NiCl_2$ solution in the reaction medium. It was reported that emission wavelength of Ni^{2+} ion-doped $CsPbCl_xBr_{3-x}$ QDs shifted from 508 to 432 nm. It was observed that blue

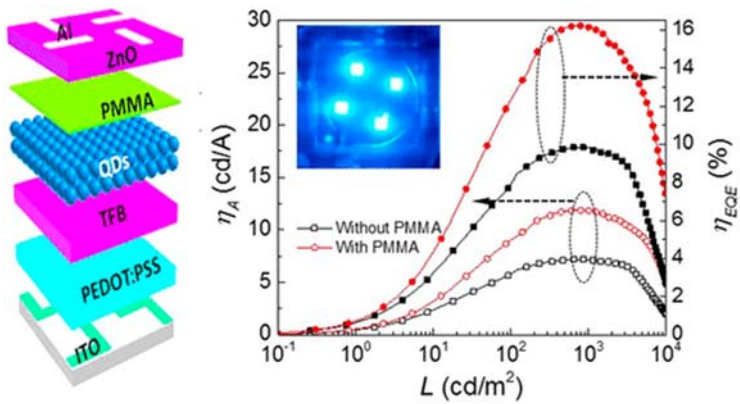

FIGURE 10.3 Luminescence efficiency of blue LEDs based on high quality nonblinking QDs. *Adapted from Lin et al., 2018. ACS Photonics, 5 (3), 939−946. With Permission.*

emission (470 nm) with PL QY 89% was achieved in 2.5% Ni^{2+} ion-doped $CsPbCl_{0.99}Br_{2.01}$ QDs, which was almost three times more than that of undoped $CsPbClBr_2$ QDs. It was revealed that external quantum efficiency of 2.4% could be achieved along with maximum luminance of 612 cd m^{-2}, which is highest amongst other blue-emitting PQD-based LED reported earlier.

Zhang et al. (2020) developed a yellow quantum-dot LED of stacking with a blue organic multifunctional tandem LED using an indium−zinc oxide intermediate connecting electrode. It was reported that as-fabricated tandem LED was full-color-tunable and it can emit green, red, and blue colors (primary color) as well as other arbitrary colors. It was revealed that this tandem LED can emit efficient white light with brightness (107000 cd m^{-2}) and maximum external quantum efficiency (26.02%). It was suggested that white light-emission and multi-functionality of full-color-tunability could find a great potential application in both solid-state lighting and full-color-display.

10.2.3 Red light-emitting diodes

Taylor et al. (2007) used a hybrid layer of poly(2-methoxy,5(2-ethylhexyloxy)-*p*-phenylene vinylene) (MEH-PPV) and CdSe QDs to convert the light emitted by electroluminescent ZnS phosphor into red light. It was revealed that emission wavelength of the display was related directly to the emission of CdSe QDs. It was observed that thin film electroluminescent displays have a potential to increase its color spectrum on integrating QDs.

Song and Lee (2007b) prepared core−shell (CdSe)ZnSe QDs by colloidal chemical synthesis and surface-passivation. They coated a core CdSe with a larger-band gap material ZnSe. As-prepared (CdSe)ZnSe QDs played a role of color conversion center (QDs nanophosphors). The red light-emitting hybrid devices were fabricated consisting of (CdSe)ZnSe QDs and a near-UV GaN LED. They also tested the possibility of using (CdSe)ZnSe QDs as red nanophosphors for UV excitation. It was indicated that (CdSe)ZnSe QDs are quite promising red nanophosphors for NUV excitation. The red LED based on these QDs and a NUV excitation source has proved to be an efficient hybrid device with good luminance.

Stouwdam and Janssen (2008) studied ZnO nanocrystals as an electron injection layer for red, green, and blue LEDs based on core−shell CdSe/ZnS QDs. The deposition of ZnO nanocrystals from isopropanol permits fabrication of multilayer QD-LEDs that include both hole and electron transport layers by simple solution processing. The ZnO nanocrystals improved electron injection in the light-emitting QD layer as evident from a decreased turn-on voltage and a reduction of emission originating from other layers than the QD layer of the LEDs.

Huang et al. (2008) fabricated a hybrid CdSe-ZnS QD (QD)-InGaN-GaN QW red LEDs. It was reported that the blue light from the InGaN QWs can be easily down converted to the red light using different blend ratios. The luminous flux and LE from the hybrid LED of 0.65 lm and 9.3 lmW^{-1} could be obtained keeping QD concentration as 40 $mg\,mL^{-1}$ of resin. It was revealed that from electroluminescence spectrum that the contribution of red light emission to the total light intensity was found to be 98%.

Cho et al. (2009) crosslinked colloidal quantum-dot layer. It can reduce charge injection barrier in a red light-emitting quantum-dot, LEDs by using a sol−gel TiO_2 layer for electron transport. It exhibited a high luminance (12,380 cd m^{-2}) and high power efficiency (2.41 lm W^{-1}). This technique may be incorporated in display device with a great promise for possible use in easy-to-fabricate, high-performance, illumination sources and large-area displays. A gold nanorod-enhanced light emission was reported by Yang et al. (2014a) in quantum-dot-doped polymer nanofibers. It was observed that there was a 67% increment in 600 nm red light emission efficiency on incorporating gold nanorods into quantum-dot-doped polymer nanofiber. The photostability was found to be increased by 100 min.

A highly efficient, ultrabright, low roll-off, inverted QD-based red light-emitting device (QLED) was reported by Dong et al. (2015). They used cesium carbonate films and solution-processed zinc oxide NPs as the hole blocking layers and electron injection, respectively. It was revealed that luminance of 165,000 Cdm^{-2} was obtained at a current density of 1000 $mAcm^{-2}$ for deep red device.

Fine tuning of emission color of Ce-doped yttrium aluminum garnet ($Y_3Al_5O_{12}:Ce^{3+}$, YAG:Ce) nanophosphor-based WLED was reported by Kim et al. (2016b). They coated CdSe/CdS/ZnS QDs onto the surface of the YAG:Ce NPs. It was observed that the luminescence spectra of the QD@YAG:Ce can be tuned by variation of QD to YAG:Ce weight ratios. Lin et al. (2016) reported highly efficient deep-red LEDs, which is based on type-II CdTe/CdSe core/shell QDs. CdTe/CdSe core/shell QDs synthesized through a green process have different PL emissions peaks at 642, 664 and 689 nm and it was observed these using three devices QDs with different PL peaks exhibited maximum external quantum efficiency of 5.24%, 5.74% and 6.19%, respectively.

Indium phosphide (InP) QDs have shown great potential as a replacement for CdSe QDs in display applications. However, the performance of InP-based QLEDs is still far behind that of the CdSe-based devices. The effects of different methods for improving the performance of InP-based QLED devices was investigated by Li et al. (2019a). They evaluated effect of magnesium doping in ZnO NPs used as an n-type electron transport layer, so as to balance charge transfer in InP-based QLED devices. It was found that ZnO band gap is broadened and its energy levels are shifted along with increase in resistivity by doping on increasing Mg content. It was revealed

that electron current density was reduced and device efficiency was improved. It was indicated that QD structures and devices in optimum conditions could prove be as current efficiencies of 11.6 cdA^{-1} to red InP QLEDs.

A highly efficient and stable red QLED was reported by Liu et al. (2020b). They used codoped lithium and magnesium along with magnesium oxide shell-coated zinc oxide nanoparticle layer (electron transport layer). It was observed that optimized QLED show a high peak EQE of (20.6%), long lifetime T_{95} of >11000 h, and low efficiency roll-off at high current.

10.2.4 Green light-emitting diodes

Steckel et al. (2006) synthesized $Cd_xZn_{1-x}Se$ alloy core nanocrystals. Then these were overcoated with $Cd_yZn_{1-y}S$ to create core−shell nanocrystals for use in QD-LED displays. It was found that these $Cd_xZn_{1-x}SeCd_yZn_{1-y}S$ core−shell nanocrystals can be used to fabricate color-saturated green−emitting QD-LEDs, which can be a potential for display applications.

Sun et al. (2007) reported green, orange, red, and yellow LEDs using CdSe core and ZnS or CdS/ZnS shell as emissive layers in the devices and it was observed that the maximum luminance was 3700, 3200, 9064, and 4470 cd m^{-2}, respectively. It was indicated that improved electroluminescent efficiency (1.1−2.8 cd A^{-1}), low turn-on voltages (3−4 V) and longer operation lifetimes of quantum-dot-based LEDs can be obtained by optimizing the thicknesses of the constituent layers of the devices. It was suggested that these QDs LEDs may be promising flat-panel displays applications.

The growth of InN, GaN, and InGaN QDs by molecular beam epitaxy (MBE) on either GaN or AlN templates was reported by Moustakas et al. (2008). InN QDs on GaN templates were found to occur without an InN wetting layer. The self-assembled GaN QDs were grown on AlN templates. It was observed that the self-assembly of InGaN QDs on GaN templates can find the applications in blue-green LEDs. It was indicated that InGaN/GaN multiple QDs (MQDs) were highly strained and at low injection, their emission is red shifted as compared to a single layer of QDs.

Park and Park (2011) fabricated LEDs with emission in the green range (540−610 nm). They grow self-assembled In-rich InGaN QDs on n-GaN via metal-organic chemical-vapor deposition. It was observed that emission wavelength of LED was red shifted from green (540 nm) to red (610 nm). This shift was attributed to an increase in the depth of potential wells of the InGaN QDs with increased roughness of the surface n-GaN layer.

Park et al. (2015) reported bright yellow−green-emitting $CuInS_2$ (CIS)-based QDs and two−band WLEDs using these QDs. They used metal−oleate precursors and 1-dodecanethiol for synthesis of yellow-green-emitting CIS QDs with CIS cores (QE = 31.7%). These CIS/ZnS/ZnS QDs exhibited a high QE (80.0%) and a peak at 559 nm, which is dominant wavelength of

blue LEDs. It was revealed that white light LEDs can be fabricated with coating of CIS/ZnS/ZnS on blue LEDs, which exhibited LE (80.3 $\mathrm{lm \cdot W^{-1}}$), CRI (73) and a high light conversion efficiency of 72.6%.

The InP/ZnS QDs were synthesized by Yang et al. (2015) via hot injection method. They used nontoxic $P(N(CH_3)_2)_3$ as precursor. It was found that triple-shell-coated InP/ZnS core−shell QDs of green, orange-red, and yellow colors could reach PL QYs as high as 0.50, 0.63, and 0.55; and FWHMs as narrow as 55, 71, and 76 nm, respectively.

Li et al. (2016) synthesized perovskite $CsPbBr_3$ QDs via hot-injection method as green phosphor for LEDs. It was reported that green light with an emission peak at 534 nm could be achieved using $CsPbBr_3$ QDs and GaN LEDs. The current-voltage characteristic of the green LED did not show any degradation as compared to GaN LEDs. It was also revealed that as-fabricated green LEDs exhibited a LE of 31.92 $\mathrm{lm\ W^{-1}}$.

Ko et al. (2017) synthesized highly efficient bright green-emitting Zn−Ag−In−S (ZAIS)/Zn−In−S (ZIS)/ZnS alloy core/inner-shell/shell QDs. They used a multistep hot injection method and zinc acetate dihydrate as precursor. It was reported that as-synthesized ZAIS/ZIS/ZnS QDs displayed a high PLQY (87%) with peak wavelength (501 nm). The green, red, and blue tripackage white DC−LEDs exhibited high LE of 72 $\mathrm{lm\ W^{-1}}$ and CRI of 95.

The heavy-metal-free InP/ZnS core/shell QDs with different fluorescence were prepared by Kuo et al. (2017) via green route. These InP/ZnS core/shell QDs exhibited maximum fluorescence at $\sim$ 530 nm and high fluorescence QY (60.1%). As-prepared multilayered InP/ZnS core/shell QD-LEDs showed highest luminance of 160 $\mathrm{cd\ m^{-2}}$ and external quantum efficiency (0.223%). It was predicted that these multilayered InP/ZnS core/shell QD-LEDs have a great potential in heavy-metal-free QD-LEDs for display applications in next generation.

The green QDs were prepared by Li et al. (2017). They used tris(mercaptomethyl)nonane (TMMN) as the capping ligand. It was observed that these TMMN-capped QDs exhibited QYs of $\sim$90% after ligand exchange with external quantum efficiency of 16.5%. The current efficiency and power efficiency of these were found to be 70.1 $\mathrm{cd\ A^{-1}}$ and 57.6 $\mathrm{l\,m\ W^{-1}}$, respectively. It was revealed that as-prepared devices exhibited high environmental stability.

It was reported by Kumar et al. (2018) that the structural and optical control of InP-based QDs can lead to high-performance LEDs. It was observed that zinc sulfide shells passivate the InP QD core and as a result, increase the QY in red and green-emitting QDs was observed by eight- and thirteen-fold, respectively. They fabricated WLEDs with LE up to 14.7 $\mathrm{lm\ W^{-1}}$ as well as color-rendering index up to 80.

QDs have high potential to fulfill the ever increasing demands for high-quality displays due to their outstanding size-tunable optical properties, high QY and reduced costs. The synthesis of efficient materials and their

integration in uniform and thin polymeric films are necessary for displays. Sadeghi et al. (2018) synthesized green− and red−emitting Cd-based QDs with QYs of 74% and 52%, respectively. These QDs were incorporated into the PDMS polymer matrix, which provide polymeric films with 123 × 68 mm for smart phone displays. It was suggested that these QD polymeric films show promising applications in smart phones.

In recent, the QY and stability of green QDs have been significantly improved. However, most of the progresses were achieved by using alloyed QDs, and the control of green emission QDs still remains challenging. Hao et al. (2019) reported synthesized thick-shell structure QDs (TSQDs) with saturated green-emission. They used tri-n-octylphosphine as both ligand as well as solvent to extract the redundant ions from the QDs surface. It was observed that as-prepared TSQDs exhibited high QY reaching up to 75% and tunable precise emission properties (532 nm).

The CdSe/ZnS core−shell QDs were synthesized by Ramalingam et al. (2019) via a chemical route. They used bioconjugated organic amino acid (L-Cysteine). The diameter of as-prepared QDs was found to be 3 nm with uniform size distribution. The optical properties QDs exhibited an absorption and emission peak at 515 and 525 nm respectively, at room temperature. It was indicated that these QDs exhibited emission in the spectral range at 516−535 nm, which is particularly find application in green LEDs.

The synthesis of heavy metal (or Cd) free QD-LEDs have been reported by Ippen et al. (2019) for all three colors. They developed heavy metal free QDs with high QY (> 95% for red and green and >80% for blue). A high efficiency was observed for these heavy metal free QD-LEDs with EQE = 16.9, 13, and 9% for red, green, and blue, respectively. The impact of shell thickness on efficiency performance of device was also evaluated.

Yang et al. (2020) reported QD films based on a poly(zinc methacrylate) coating. These alloyed CdZnSeS/ZnS QDs (QDs@PZnMA) are green−emitting with high refractive-index $BaTiO_3$ NPs. A 7.5−, 11.3−, 8.5−, and 8.6− fold increase in the absorption coefficient, scattering coefficient, optical density and green light emission QD films was observed as compared to films having identical mass percentage of pristine QDs. It was proposed that it has a potential for developing QD optical films with enhanced light emission and high scattering for flexible displays.

Zheng et al. (2020) prepared green carbon QDs (g-CQDs) with high fluorescent QY and high product yield via solvothermal method using 2,7-dihydroxynaphthalene and ethylenediamine as the carbon source and nitrogen dopant, respectively. It was revealed that the maximum product yield (70.90%) and QY (62.98%) values of g-CQDs could be achieved. They prepared WLEDs by combining these g-CQDs and blue chip.

μLEDss are considered as ideal source of light for next generation and high-speed visible light communication InGaN QDs have been proposed as the active region of (Wang et al., 2021a, b). Green InGaN QDs have an

external quantum efficiency of 18.2%, which is almost two−folds than present green μLEDss. It was indicated that InGaN QDs can provide a solution to μLEDss for display and visible light communication applications, as these are fully compatible with current LEDs industrial technology.

10.2.5 Orange light-emitting diodes

Kim et al. (2008) synthesized Mn-doped $Zn_{1-x}Cd_xS$ QDs via reverse micelle approach. It was found that band gap energy of $Zn_{1-x}Cd_xS$:Mn QDs can be tuned to a higher energy by increasing the Zn content. The average size of these QDs was calculated as 3.6 nm. A high QYs (14%−30%) was exhibited depending on the composition of the core QDs. Orange and WLEDs were fabricated using these CdS:Mn/ZnS QDs.

Nizamoglu and Demir (2009) reported Förster resonance energy transfer-enhanced color-conversion. They used colloidal semiconductor QD nanocrystals to make reddish-orange LEDs, which can find applications in ultraefficient SSL. Energy gradient hybrid structure from cyan- and orange-emitting CdSe/ZnS NCs (492 and 588 nm, respectively) can be obtained. A relative increase in quantum efficiency of 15.1% in reddish-orange full color-conversion was observed for the integrated hybrid cyan-orange NC layer.

Song and Yang (2012) reported core/shell structured QDs (CIS/ZnS) exhibited tunable emissions of yellow-orange with excellent QYs (55%−91%). A white QD-LED was fabricated using by CIS (2 h)/ZnS QD as a blue-to-yellow color converter. They also fabricated white QD-LED by blending of yellow and O-QDs so as to improve a color rendering property.

Shen et al. (2013) used solution-processed ZnO NPs as the electron injection/transport layer, bilayer structure of poly[9,9-dioctylfluorene-*co*-*N*-[4-(3-methylpropyl)]-diphenylamine] (TFB)/poly(ethylenedioxythiophene): polystyrene sulfonate (PEDOT:PSS) as the hole transport/injection layer and CdSe/CdS/ZnS core−shell QDs as the emitting layer. It was observed that highly bright orange-red and green QD-LEDs could be obtained with peak luminances and power efficiencies as $\sim 30\,000$ & $\sim 52\,000$ cd m^{-2}, and 16 & 19.7 lm W^{-1}, respectively. It was proposed that these can be commercialized for use in QD-based displays and SSLs.

Aniline GQDs (Chemically derived) were used as lumophores and LEDs exhibiting orange, green, and red electroluminescence with high color purity were fabricated by Kwon et al. (2016). They evaluated external quantum efficiency and maximum current efficiency of 1.28% and 3.47 cd A^{-1}, respectively.

The synthesis of Mn-doped cesium lead halide ($CsPbX_3$) PQDs has been reported by Zhu et al. (2017). It was observed that optical properties of as-prepared nanocrystals remained same even after several months. They fabricated red-orange LEDs by coating the composite onto ultraviolet LED chips.

This present approach may open new avenue for doping other ions in $CsPbX_3$ QDs at room temperature and developed capability in as − prepared essential material for applications in memristors and other devices.

Ren et al. (2020) proposed a facile posttreatment doping method enabling preparation of highly luminescent low-toxic $CsPbX_3$:Mn^{2+} PQDs from nonluminescent Cs_4PbX_6 PeQDs. It was reported that monodispersed $CsPbX_3$:Mn^{2+} PeQDs exhibited excellent photophysical properties such as PL QY (87%). It was revealed that variation of halide composition in Cs_4PbX_6 PeQDs or Mn doping concentration, they were able to prepare a series of $CsPbX_3$:Mn^{2+} PeQDs, which can have tunable emission. They fabricated $CsPbX_3$:Mn^{2+} Q-LED, which exhibited excellent orange light with LE of 24 lm W^{-1}.

10.2.6 Yellow light-emitting diodes

Lv et al. (2012) used InGaN/GaN multilayer QD in active regions for yellow-green LEDs. It was observed that on increasing growth temperature and switching the carrier gas (from N_2 to H_2), using improved growth parameters, a 10-layer InGaN/GaN QD LED was obtained. It was revealed that electroluminescence peak wavelength also shifted from 574 to 537 nm.

Denault et al. (2013) fabricated devices using CdSe/ZnS core/shell QDs (red-emitting) with $Y_3Al_5O_{12}$:Ce^{3+} (yellow-emitting) or $Lu_3Al_5O_{12}$:Ce^{3+} (green-emitting) and InGaN LED (blue-emitting). It was reported that devices with $Y_3Al_5O_{12}$:Ce^{3+} with QDs (590 nm) could achieve LE (57 lm W^{-1}) and CRI (81), while devices with $Lu_3Al_5O_{12}$:Ce^{3+} with QDs could achieve CRI (90) and LE (22 lm W^{-1}).

He et al. (2018) studied inorganic perovskite $CsPb(Br_xI_{1-x})_3$ QDs with QY of 50% as yellow light convertor for LEDs. It was reported that highly pure yellow LEDs were obtained, when x was kept 0.55. It gave LE (13.51 l m W^{-1}) with an emission peak at ∼570 nm. It was concluded that $CsPb(Br_xI_1 - _x)_3$ QDs are potential candidate for yellow LEDs with high purity.

Gu et al. (2021) used hydrothermal method for the preparation of nitrogen doped GQDs (N-GQDs). They used citric acid and o-phenylenediamine as precursors. It was reported that as-produced N-GQDs exhibited blue color with a QY (58%) in presence of 365 nm UV light illumination. As the concentration of N-GQDs increases, the PL exhibits an obvious red-shift from blue to yellow. A high PL QY of 28% could be with yellow luminescence is achieved under 405 nm excitation, using N-GQDs in solid state. A WLEDs device was constructed by adjusting thickness and concentration of N-GQDs in blue emitting InGaN chips.

10.2.7 Other light-emitting diodes

Qian et al. (2011) developed devices consisting of a quantum-dot emissive layer, which was sandwiched between an electron transport layer of ZnO

NPs and an organic HTL. It was reported that as-fabricated devices exhibited maximum luminance and power efficiency values of 4,200 cd m^{-2} & 0.17 lm W^{-1}, 68,000 cd m^{-2} & 8.2 lm $W^{-1}$and 31,000 cd m^{-2} and 3.8 lm W^{-1} for blue, green, and orange−red emission, respectively. It was also revealed that with the incorporation of the ZnO NPs, these devices have high environmental stability with operating lifetimes more than 250 h in low vacuum.

Jun et al. (2013) prepared a highly luminescent and photostable QD−silica monolith substance via base-catalyzed sol−gel condensation of silica. They heavily doped SM with 6-mercaptohexanol exchanged QDs up to 26 wt.% (12 vol.%) without any particle aggregation. These green and red light-emitting QD−SMs were then applied as color-converting layers on blue LEDs. It was observed that external quantum efficiency could reach up to 89% and 63% for the red and green QD−SM, respectively. A WLED made with a mixture of these green and R-QDs in the SM exhibited an efficacy of 47 lmW^{-1}.

Highly efficient tandem quantum-dot LEDs were proposed by Zhang et al. (2018b). They used an interconnecting layer (ICL) with the structure of ZnMgO/Al/HATCN/MoO_3. It was reported that as-prepared ICL exhibited efficient charge generation/injection capability, high transparency, and high robustness. The tandem QLEDs [full color (red (R)/green (G)/blue (B)] show high current efficiency and external quantum efficiency: 41.5 cdA^{-1} and 23.1%, 17.9 cdA^{-1} and 21.4%, 121.5 cdA^{-1} and 27.6% for R-QLEDs, B-QLEDs, and G-QLEDs, respectively. The EQEs of R-, G-, and B-QLEDs were more than 21%. The R-, G-, and B-QLEDs can still sustain their external quantum efficiency at 96%, 99%, and 78%, respectively. It was suggested that these full-color tandem QLEDs have long operational lifetime, high efficiency, high color purity, and low roll-off efficiency, and hence can prove to be ideal candidate for the SSL and full-color displays.

10.3 Night vision

Taking into account the requirements of different practical usages at night, LEDs are applied for infrared lighting in night vision operations comprising security cameras. It has been shown that a ring of LEDs around a video camera is a low-cost and successful kit for chroma keying in video production applications (Cabrera, 2019). Night Vision Imaging Systems (NVIS) are used in military domains such as electronic combat reconnaissance aircraft (Sabatini et al., 2016; Chen et al., 2017a).

Wu et al. (2012) examined the feasibility of using QD phosphor-based LEDs in aviation uses that solicit NVIS conformity, recommending that white QD phosphor-based LEDs can be tailored to show greater suitability with NVIS than commercial LEDs. It was expected that the QD

phosphor-based LEDs reach important goals in cockpit illumination and LED indicator lights of aviation panels.

Chen et al. (2017a) stated that LED night vision imaging detection has been applied in numerous areas. The usage of LED array as a light source possesses the advantages of reduced price and small dimension. It was revealed that utilizing the degradation model, the target image was recovered with the help of the model-based image processing algorithms and that the experimental results confirmed the efficacy of this method.

An interesting review by Zheng and Zhu (2020) emphasizes three classes of emerging near-infrared (NIR) emitting materials used in LEDs. They reported the advantages and disadvantages of these three types of materials (organic materials, inorganic QD materials, and organic−inorganic hybrid perovskite materials) used to fabricate the appropriate devices (OLEDss, QD LEDs, and perovskite LEDs), showing that NIR QLEDs possess the potential for military uses, such as night vision-readable display and iris identification systems.

Vasilopoulou et al. (2021) reported NIR LEDs based on solution-processed semiconductors, such as halide perovskites and colloidal QDs, which are suitable technological stages for night vision, surveillance, and optical communications. This research listed new developments on emissive materials synthetic methods and essential qualities that increase the performance of manufactured light-emitting devices.

10.4 Data communication

In the data communication structure, there is a requirement for higher data rates with great reliability and secure means of accessibility (Kate and Husain, 2017). The use of LEDs increases efficiency in terms of data fidelity, data rate and cost; thus permitting the progress of light fidelity (Li-Fi) technology and the Visible Light Communication (VLC) system (Kate and Husain, 2017; Yu et al., 2021). The unique properties of QDs determine their notable application in optical technologies, such as QD-LEDs that can be used as an optical transmitter in VLC (Xiao et al., 2016; Yulin et al., 2017; Choi et al., 2018; Pradhan et al., 2019; Vahabzad et al., 2019).

A new procedure has been described by Ruan et al. (2016) for the manufacture of a type of QD-WLEDs from green- and red-emitting $AgInS_2$/ZnS core/shell QDs coated on GaN LEDs. It has been mentioned that the modulation bandwidth of QD-WLEDs was much enhanced in comparison to that of YAG:Ce phosphor-based WLEDs, showing that $AgInS_2$/ZnS core/shell QDs have the potential to improve the bandwidth in VLC. The use of colloidal semiconductor QDs for light conversion of InGaN sources in VLC applications was analyzed by Leitao et al. (2017). They presented a colloidal QD/polymer composite format of color converters and reported some samples of such color converting composite that were hybridized with a μLED to create

hybrid sources for a demonstration of free-space VLC over 10 cm with data rates up to 1 Gb s^{-1}.

A microwave-assisted heating technique to manufacture multicolor QD-based phosphors in 30 s was investigated by Zhou et al. (2018) using a combination of QDs and sodium silicate aqueous solution. They indicated an application of the QD-based phosphors in VLC, noting that the bandwidth modulation reaches 42 MHz. Cao et al. (2019) developed a high bandwidth GaN-based WLED that was obtained using blue LED chip (GHz bandwidth) with a combination of CdSe/ZnS QDs. It provides an advantageous solution for the creation of high bandwidth WLEDs for VLC uses in free space. Li et al. (2019b) exhibited an interesting portable VLC system, which is suitable for indoor short-distance communication technology using CdSe/ZnS QDs as a light converter, creating a portable transmitter and receiver based on digital signal processors and observing that under a direct bias voltage of 2.70 V, the highest transmission rate is 267 Kbs^{-1}.

Recently, Singh et al. (2020) reviewed the latest advances for VLC applications based on LEDs but principally on semipolar μ-LEDs and μ-LED-based arrays with high bandwidths. It has been highlighted that a significant application of great interest for marine exploration and underwater connectivity is the use of VLC for underwater optical wireless communication, recalling the reported case of a data rate of 2 Gbps over a 3 m air-underwater channel using a single layer QD blue μ-LED (Singh et al., 2020. Wei et al., 2020a).

Li-Fi, which represents a wireless technology that is not only environment-friendly, but also low cost for the future of communication (Meshram and Meshram, 2020), demands wearable and full duplex configuration because of its important role in applications such as smart wearables and "Internet of Things" (Shan et al., 2020). They described a perovskite QD-based light-emitting/detecting bifunctional fiber built with the help of a hybrid strategy and showed that the creation of this type of fiber is promising for the manufacture of future smart wearables.

Wan et al. (2021) proposed a new plasmonic WLED using the combination of a nanohole LED (H-LED) with QDs and silver NPs (Ag NPs) together (M-LED), explaining that the improved M-LED exhibited a maximum CRI of 91.2 and a data rate of 2.21 Gbs^{-1} at a low current density of 96 Acm^{-2} (60 mA). Here, a promising scope for WLEDs in lighting and VLC applications has been discussed.

10.5 Agriculture and horticulture

In recent years, a lot of research has been carried out in the fields of horticulture and agriculture, due to the diverse successful characteristics; LED lighting systems are considered a new profitable technology for plant growth and a promising tool to improve crop production (Mitchell et al., 2012; D'Souza

et al., 2015; Hasan et al., 2017; Viršilė et al., 2017). Many studies have revealed that the monochromatic character of LEDs can help diminish the incidence of pest and diseases pressure in growing plants and that some valuable features such as energy efficiency, long lifetime, and flexibility have indicated that LEDs are more adequate for future agricultural lighting methods than conventional lighting methods (Darko et al., 2014; Gomez and Izzo, 2018; Al Murad et al., 2021; Koushik et al., 2021).

The feature, related to the fact that QD can emit specific wavelengths of light, when supplied with energy, has been exploited to shift incoming light into a certain part of spectrum that plants can most effortlessly utilize for photosynthesis (Mission, 2021). QDs technology has demonstrated some excellent benefits for the lighting sector, including the application area related to horticulture.

A new procedure has been developed by Song (2016) for the manufacture of a LED utilizing QDs as phosphor. He constructed the multiwavelength LED device to show the possibility of its application for the plant factory. It was indicated that the good use of QD can be made with the multifunction LED light source.

Zhang et al. (2019) have fabricated some exceptional WLEDs and LEDs for plant growth with the help of red-emitting $CsPb_{1-x}Ti_xI_3$QDs@glasses, showing that a series of Ti-doped $CsPbI_3$ QDs were prepared in borosilicate glass ($SiO_2-B_2O_3$-ZnO) and that the WLED was built with the help of red-emitting $CsPb_{1-x}Ti_xI_3$QDs@glasses and yellow-emitting Ce^{3+}:YAG phosphor under excitation of InGaN blue chip.

Chung et al. (2020) reported that four kinds of QD lamps (QDLs) that emit different wavelengths of light were positioned in the perilla greenhouse in Milayang (Korea) revealing that QDLs considerably increased in the perilla leaf growth in comparison with control LED lamps and that perilla leaves exposed by Q2R lamps considerably improved the contents of biologically functional constituents (chlorophyll, total flavonoid, and phenolic-acid compounds).

Choi et al. (2019) have studied the consequences of LED and QD-LED irradiation on seed germination and microbial growth, in the time of the red radish (*Raphanus sativus* L.) sprouts cultivation. It was reported that the red hypocotyl was exceptional in blue light and QD-LED light. It was revealed that when red radish seeds were germinated in the dark and cultivated for a period of 7 days as sprouts and then irradiated with QD-LED light for 24 h, the seeds furnished some superior quality red radish sprout showing a diminished level of *E. coli* contamination.

Liu et al. (2021a) investigated the luminescent spectrum of LEDs based on QD materials, which was projected depending on the photosynthetic action spectrum (PAS) of plants. For the case of the three-band QD-based LEDs (QLEDs), it was found that photosynthetic action factor (PAF) has the maximal value of 8.088 and the induced photosynthetic index (IPI) has the

maximal value of 4.012. In the case of the four-band QLEDs, the maximal value of 7.689 was calculated for PAF and the maximal value of 3.818 was determined for IPI. They showed that in the issue related to the vision features, the four-band device exhibited a maximal value of 93 for CRI and a maximal value of 2053K for the correlated color temperature (CCT). They observed that the obtained results had consistence with the simulation ones, certifying the feasibility of manufacturing growing lamps with QD materials.

Jung et al. (2021) demonstrated that the quantity of Rg1 and Rg3, the most abundant ginsenosides, which are found in ginseng sprout, increased remarkably in the root of ginseng sprouts under the QD-LED method in comparison with the LED method, indicating that the cultivation of ginseng seeds using QD-LED method can determine the progress of high-productivity products.

10.6 Antimicrobial technology

LEDs have been used to obtain air disinfection, water disinfection and purification, surface decontamination, and food preservation (Koutchma and Orlowska, 2012; Kim and Kang, 2018; Ogonowska et al., 2019; Prasad et al., 2020; Singh et al., 2021b; Kim and Kang, 2021). Ultraviolet (particularly UVC) irradiation has especially attracted tremendous attention as one of the most successful antiviral procedures (Bhardwaj et al., 2021; Memarzadeh, 2021). The UV-LEDs have shown the potential for an extensive domain of applications in sterilization, sensing, and detection (Muramoto et al., 2014; Chen et al., 2017b; Won et al., 2018; Memarzadeh, 2021).

Yang et al. (2014b) showed that high internal efficiency and high temperature stability of UV LEDs at 308 nm were obtained utilizing high density GaN/AlN QDs grown with the help of metal organic vapor phase epitaxy (MOVPE). It was observed that the value of the internal quantum efficiency was 62%.

Chen et al. (2016) communicated the enhanced excitation and directional fluorescence emission (DFE) of QD by Ag NPs using theoretical calculations, emphasizing that enhanced DFE is important for biological and medical detection processes. It has been established that a monolayer Ag NPs showed a dominant enhancement in DFE for monolayer or low concentration QDs in LED, highlighting the significance for the design and progress of high-efficiency QD LEDs.

A new solid-state-based broadband UV light source was developed by Cho et al. (2020), which could substitute arc-lamp-based uses. Taking into account that group III-nitride UV LEDs did not exhibit a broad UV spectrum region, which limits their use in areas such as medical therapy and UV spectrophotometry, they obtained different emission wavelengths in the UV

region from the GaN QDs grown on the truncated pyramid structures, which furnish a high-efficiency broadband UV spectrum.

Elgammal (2020) reported that silicon QD-based LEDs produced with the help of cyclohexasilane can affect a number of industries but in response to the COVID-19 crisis, their efficiency recommends them for public areas, where infected droplets constitute important risks for public health.

Deep ultraviolet (DUV) LEDs furnish some important benefits such as compact size, low consumption, and long lifetimes. Brault et al. (2021) presented that $Al_xGa_{1-x}N$ LEDs emitting in the UVB (230−320 nm) and UVC (below 280 nm) regions are of significant technological interest for the medical and environmental applications as alternatives to mercury-based lamps. Noticing that some improvements of their characteristics are needed, they examined the potential of $Al_yGa_{1-y}N$ QDs as DUV emitters.

10.7 Recent developments

QDs are useful in LEDs for displays, memristors, smartphones, etc. These fabricated LEDs can exhibit a variety of colors, apart from WLEDs such as blue, red, green, orange, etc. These LEDs can also find applications in data communication, night vision, agriculture, horticulture, etc. Some recent developments of QDs-based LEDs are summarized in Table 10.1.

TABLE 10.1 Recent advancement on LED application of quantum dots.

Material used	Application	References
	Display and lighting	
$CsPbBr_{3-x}Cl_x/PbBr_y$ (or $PbCl_y$) (core/shell) quantum dot	Blue light-emitting diodes, emission peak at 492−435 nm	Park et al. (2021)
Polyethylene glycol (PEG)-coated CQD clusters	Optical properties used in high-performance sensors as well as next−generation energy/biological devices; fluorescent green (540 nm) and red (620 nm)	Juang et al. (2020)
InGaN quantum dots	Green light-emitting diode (550 nm)	Wang et al. (2018)
	Night vision	
Lead-free perovskite-type material	Photoelectric effect producing a voltage that affects the silicon/IR material interface, controlling the depletion layer	Aleksandrova (2021)

(*Continued*)

TABLE 10.1 (Continued)

Material used	Application	References
Bi^{3+}-doped $Sr_3Y_2Ge_3O_{12}$ (SYGO) phosphor	Night vision signage and optical information storage	Zhou et al. (2021)
Cr^{3+}-doped $LiScGeO_4$	Night vision surveillance and short-wave infrared (SWIR) spectroscopy technology	Miao et al. (2021)
White light GaN-μLEDs employing green/red perovskite quantum dots	Color converters for visible light communication	Liu et al. (2022)
$CsPbBr_3$ quantum dots	White light-emitting diodes and visible light communication	Li et al. (2021)
	Data communication	
Micro LED based on InGaN	Displays, data communication tools, photodetectors, and sensors	Liu et al. (2021b)
WSe_2 crystals	Photonics, imaging, spectroscopy, and data communications	Ghods et al. (2022)
Single layer quantum dot	Blue μLEDs with 4-Gbps QAM-OFDM (Quadrature Amplitude Modulation Orthogonal Frequency-Division Multiplexing)	Wei et al. (2020b)
	Agriculture and horticulture	
Carbon dots@ $Mg(OH)_2$	Blue, and red LED for horticulture	Xie et al. (2021)
CRISPR/Cas9-mediated	Horticulture food crops	Wang et al. (2021a, b)
Indoor LED light	Horticulture	Appolloni et al. (2022)
Lactuca sativa L. (Cos Lettuce)	Cultivation	Jishi et al. (2022)
Mesoporous silica nanoparticle	Light harvesting	Huang et al. (2021a, b)
Luminescent nanoparticles of $Sr_{0.46}Ba_{0.50}Yb_{0.02}Er_{0.02}F_{2.04}$	Photosynthetic activity and plant growth	Yanykin et al. (2022)
	Antimicrobial technology	
Polyimine substituted zinc phthalocyanine	Antimicrobial activity	Sen and Nyokong (2021)

(*Continued*)

TABLE 10.1 (Continued)

Material used	Application	References
Graphene quantum dots	Visible light-activated antibacterial activity	Huang et al. (2021a, b)
Carbon dots	Antimicrobial photodynamic	Romero et al. (2021)
ZnO QDs	Antimicrobial	Gangadoo et al. (2021)
Carbon QDs	Antimicrobial	Ayad et al. (2021)
Nitrogen–doped graphene QDs	Antimicrobial therapy	Kuo et al. (2021)

10.8 Conclusion

LEDs are presented as an attractive option to standard light sources, being considered today's perfect lighting technology due to their high energy efficiency, low cost, and longer lifetime. QDs have produced considerable interest due to their unique properties, and are being presented as one of the promising candidates for application in LEDs. The recent trends in QDs applications for LEDs have been reviewed, including those related to the following areas of utilization: displays, lighting, data communication, agriculture, horticulture, and antimicrobial technology. There is great potential for QDs as a unique material solution that can allow the successful achievement of a broad range of applications in the field of LEDs.

References

Al Murad, M., Razi, K., Jeong, B.R., Samy, P.M.A., Muneer, S., 2021. Light emitting diodes (LEDs) as agricultural lighting: impact and its potential on improving physiology, flowering, and secondary metabolites of crops. Sustainability 13 (4). Available from: https://doi.org/10.3390/su13041985.

Aleksandrova, M., 2021. Study of lead-free perovskite and quantum dots core-shell infrared photodetector integrated with the silicon technology. Devices for Integrated Circuit (DevIC). IEEE, pp. 494–497.

Ameta, R., Jat, K.K., Bhatt, J., Ameta, S.C., 2019. Quantum dots and their applications. In: Vakhrushev, A.V., Ameta, S.C., Susanto, H., Haghi, A.K. (Eds.), Advances in Nanotechnology and the Environmental Sciences: Applications; Innovations and Visions for the Future (1sted.); Series: AAP Research Notes on Nanoscience &Nanotechnology. CRC Press/Taylor&Francis Group; Apple Academic Press, Boca Raton, p. 32. Available from: https://doi.org/10.1201/9780429425837.

Appolloni, E., Pennisi, G., Zauli, I., Carotti, L., Paucek, I., Quaini, S., et al., 2022. Beyond vegetables: effects of indoor LED light on specialized metabolite biosynthesis in medicinal and aromatic plants; edible flowers; and microgreens. J. Sci. Food Agric. 102 (2), 472–487.

Arakawa, Y., Someya, T., Tachibana, K., 2000. Progress in GaN-based nanostructures for blue light emitting quantum dot lasers and vertical cavity surface emitting lasers. IEICE Trans. Electron. 83 (4), 564–572.

Armăşelu, A., 2017. Recent developments in applications of quantum-dot based light-emitting diodes. In: Ghamsari;, M.S. (Ed.), Quantum-Dot Based Light Emitting Diodes. IntechOpen, pp. 7–23. Available from: http://doi.org/10.5772/intechopen.69177.

Armăşelu, A., Popescu, A., Apostol, I., Ardelean, I., Damian, V., Iordache, I., et al., 2011a. Passive nonspecific labeling of cyanobacteria in natural samples using quantum dots. Optoelectron. Adv. Mater. Rapid Commun. 5 (10), 1084–1090.

Armăşelu, A., Popescu, A., Damian, V., Ardeleanu, I., Apostol, D., 2011b. Fluorescence properties of quantum dots used in the study of microorganisms. J. Optoelectron. Adv. Mater. 13 (4), 439–444.

Ayad, M.F., Trabik, Y.A., Abdelrahman, M.H., Fares, N.V., Magdy, N., 2021. Potentiometric carbon quantum dots-based screen-printed arrays for nano-tracing gemifloxacin as a model fluoroquinolone implicated in antimicrobial resistance. Chemosensors 9 (1). Available from: https://doi.org/10.3390/chemosensors9010008.

Bai, J., Cai, Y., Feng, P., Fletcher, P., Zhu, C., Tian, Y., et al., 2020. Ultrasmall, ultracompact and ultrahigh efficient InGaN micro light emitting diodes (μLEDs) with narrow spectral line width. ACS Nano 14 (6), 6906–6911.

Bang, S.Y., Fan, X.B., Jung, S.M., Yang, J., Shin, D.W., Suh, Y.H., et al., 2020. Highly stable and scalable blue QD-LED via an evaporated TiO_2 thin film as an electron transport layer. Adv. Opt. Mater. 8 (21). Available from: https://doi.org/10.1002/adom.202001172.

Bang, S.Y., Suh, Y.H., Fan, X.B., Shin, D.W., Lee, S., Choi, H.W., et al., 2021. Technology progress on quantum dot light-emitting diodes for next-generation displays. Nanoscale Horiz. 6 (2), 68–77.

Bharathi, G., Nataraj, D., Premkumar, S., Sowmiya, M., Senthilkumar, K., Thangadurai, T.D., et al., 2017. Graphene quantum dot solid sheets: strong blue-light-emitting & photocurrent-producing band-gap-opened nanostructures. Sci. Rep. 7 (1). Available from: https://doi.org/10.1038/s41598-017-10534-4.

Bhardwaj, S.K., Singh, H., Deep, A., Khatri, M., Bhaumik, J., Kim, K.H., et al., 2021. UVC–based photoinactivation as an efficient tool to control the transmission of coronaviruses. Sci. Total Environ. 792. Available from: https://doi.org/10.1016/j.scitotenv.2021.148548.

Biswas, S., Rasale, D.B., Das, A.K., 2016. Blue light emitting self-healable graphene quantum dot embedded hydrogels. RSC Adv. 6 (60), 54793–54800.

Biwa, G., Aoyagi, A., Doi, M., Tomoda, K., Yasuda, A., Kadota, H., 2021. Technologies for the Crystal LED display system. J. Soc. Info. Display 29 (6), 435–445.

Brault, J., Khalfioui, M.A., Leroux, M., Matta, S., Ngo, T.-H., Zaiter, A., et al., 2021. DUV LEDs based on AlGaN quantum dots. Proc. SPIE 11686, Gallium Nitride Materials and Devices XVI, 11686OT, 11685, Available from: https://doi.org/10.1117/12.2576135.

Cabrera, R., 2019. Chapter 1: Diodes. Electronic Devices and Circuits. ED-Tech Press, London, pp. 1–102.

Cao, H., Lin, S., Ma, Z., Li, X., Li, J., Zhao, L., 2019. Color converted white light-emitting diodes with 637.6 MHz modulation bandwidth. IEEE Electron Device Lett. 40 (2), 267–270.

Chen, Z.H., He, L., Wang, Y., Gan, Z., 2016. Effects of size and distribution of silver nanoparticles on directional fluorescence emission enhancement. IEEE Photonics J. 9 (1). Available from: https://doi.org/10.1109/JPHOT.2016.2636741.

Chen, Y., Yang, L., Zeng, Z., Ren, Q., Xu, X., Zhang, Q., et al., 2017a. Degradation in LED night vision imaging and recovery algorithms. Optik. 144, 240–245.

Chen, J., Loeb, S., Kim, J.H., 2017b. LED revolution: fundamentals and prospects for UV disinfection applications. Environ. Sci.: Water Res. Technol. 3 (2), 188–202.

Chen, W., Shi, T., Du, J., Zang, Z., Yao, Z., Li, M., et al., 2018. Highly stable silica-wrapped Mn-doped $CsPbCl_3$quantum dots for bright white light-emitting devices. ACS Appl. Mater. Interfaces 10 (50), 43978–43986.

Chen, F., Lin, Q., Shen, H., Tang, A., 2020a. Blue quantum dot-based electroluminescent light emitting diodes. Mater. Chem. Front. 4, 1340–1365.

Chen, Y.X., Lu, D., Wang, G.G., Huangfu, J., Wu, Q.B., Wang, X.F., et al., 2020b. Highly efficient orange emissive graphene quantum dots prepared by acid-free method for white LEDs. ACS Sustain. Chem. Eng. 8 (17), 6657–6666.

Chen, H.C., Shabir, A., Tan, C.M., Singh, P., Lin, J.H., 2021. Degradation dynamics of quantum dots in white LED applications. Sci. Rep. 11 (1). Available from: https://doi.org/10.1038/s41598-021-02714-0.

Cho, K.S., Lee, E.K., Joo, W.J., Jang, E., Kim, T.H., Lee, S.J., et al., 2009. High-performance crosslinked colloidal quantum-dot light-emitting diodes. Nat. Photonics 3 (6), 341–345.

Cho, J.-H., Lim, S.-H., Jang, M.-H., Lee, C., Yeo, H.-S., Sim, Y.C., et al., 2020. A broadband ultraviolet light source using GaN quantum dots formed on hexagonal truncated pyramid structures. Nanoscale Adv. 2, 1449–1455.

Choi, M.K., Yamg, J., Hyeon, T., Kim, D.-H., 2018. Flexible quantum dot light-emitting diodes for next-generation displays. NPJ Flex Electron 2 (10). Available from: https://doi.org/10.1038/s41528-018-0023-3.

Choi, I.-L., Wang, L., Lee, J.H., Han, S.J., Ko, Y.-W., Kim, Y., et al., 2019. Effect of LED and QD-LED (quantum dot) treatments on production and quality of red radish (Raphanus sativus L.) sprout. Protected Horticulture and Plant Factory 28 (3), 265–272. Society for Bio-Environment Control.

Chung, S.I., Kang, M.Y., Lee, S.C., 2020. The growth and enhancement of functional ingredients for health improvement of perilla leaves using LED light source with QD application. J. Crop Sci. Biotechnol. 23, 163–169.

Coe, S., Woo, W.-K., Bawendi, M., Bulović, V., 2002. Electroluminescence from single monolayers of nanocrystals in molecular organic deveices. Nature 420 (6917), 800–803.

Colvin, V.L., Schlamp, M.C., Alivisatos, A.P., 1994. Light emitting diodes made from cadmium selenide nanocrystals and semiconducting polymer. Nature 370 (6488), 354–357.

D'Souza, C., Yuk, H.-G., Khoo, G.H., Zhou, W., 2015. Application of light-emitting diodes in food production, postharvest preservation and microbiological food safety. Compr. Rev. Food Sci. Food Saf. 14 (6), 719–740.

Darko, E., Heydarizadeh, P., Schoefs, B., Sabzalian, M.R., 2014. Photosynthesis under artificial light: the shift in primary and secondary metabolism. Phil. Trans. R. Soc. Lond. B. Biol. Sci. 369 (1640). Available from: https://doi.org/10.1098/rstb.2013.0243.

Denault, K.A., Mikhailovsky, A.A., Brinkley, S., DenBaars, S.P., Seshadri, R., 2013. Improving color rendition in solid state white lighting through the use of quantum dots. J. Mater. Chem. C 1 (7), 1461–1466.

Dong, Y., Caruge, J.M., Zhou, Z., Hamilton, C., Popovic, Z., Ho, J., et al., 2015. 20.2: ultra-bright, highly efficient, low roll-off inverted quantum-dot light emitting devices (QLEDs). SID Symp. Dig. Tech. Pap. 46 (1), 270–273.

Elgammal, R., 2020. Material advances for LED quantum dot efficiency. NASA Tech. Briefs. 44 (11), 14A–16A.

Erdem, T., Volkan, D.H., 2013. Color science of nanocrystal quantum dots for lighting and displays. Nanophotonics 2 (1), 57−81.

Gangadoo, S., Xu, C., Cozzolino, D., Latham, K., Della Gaspera, E., Chapman, J., et al., 2021. Probing nanoscale interactions of antimicrobial zinc oxide quantum dots on bacterial and fungal cell surfaces. Adv. Mater. Interfaces . Available from: https://doi.org/10.1002/admi.202101484.

Ghamsari, M.S., 2017. Quantum-dots based organic light-emitting diodes-thestate-of-the-art. In: Ghamsari, M.S. (Ed.), Quantum-Dot Based Light-Emitting Diodes. IntechOpen. Available from: http://doi.org/10.5772/intechopen.69744.

Ghods, S., Esfandiar, A., Irajizad, A., Vardast, S., 2022. Enhanced photoresponse and wavelength selectivity by SILAR-coated quantum dots on two-dimensional WSe_2crystals. ACS Omega 7 (2), 2091−2098.

Gomez, C., Izzo, L.G., 2018. Increasing efficiency of crop production with LEDs. AIMS Agric. Food 3 (2), 135−153.

Gu, B., Liu, Z., Chen, D., Gao, B., Yang, Y., Guo, Q., et al., 2021. Solid-state fluorescent nitrogen doped graphene quantum dots with yellow emission for white light-emitting diodes. Synth. Met. 277. Available from: https://doi.org/10.1016/j.synthmet.2021.116787.

Hao, J., Liu, H., Miao, J., Lu, R., Zhou, Z., Zhao, B., et al., 2019. A facile route to synthesize CdSe/ZnS thick-shell quantum dots with precisely controlled green emission properties: towards QDs based LED applications. Sci. Rep. 9 (1). Available from: https://doi.org/10.1038/s41598-019-48469-7.

Hasan, M.M., Bashir, T., Ghosh, R., Lee, S.K., Bae, H., 2017. An overview of LED's effects on the production of bioactive compounds and crop quality. Molecules (Basel, Switzerland) 22 (9). Available from: https://doi.org/10.3390/molecules22091420.

He, Y., Gong, J., Zhu, Y., Feng, X., Peng, H., Wang, W., et al., 2018. Highly pure yellow light emission of perovskite CsPb $(BrxI_{1-x})_3$quantum dots and their application for yellow light-emitting diodes. Opt. Mater. 80. Available from: https://doi.org/10.1016/j.optmat.2018.04.009.

Hu, X., Xie, Y., Geng, C., Xu, S., Bi, W., 2020. Study on the color compensation effect of composite orange-red quantum dots in WLED application. Nanoscale Res. Lett. 15 (1). Available from: https://doi.org/10.1186/s11671-020-03350-9.

Huang, C.Y., Su, Y.K., Chen, Y.C., Tsai, P.C., Wan, C.T., Li, W.L., 2008. Hybrid CdSe-ZnS quantum dot-InGaN-GaN quantum well red light-emitting diodes. IEEE Electron Device Lett. 29 (7), 711−713.

Huang, Y., Tan, G., Gou, F., Li, M.-C., Lee, S.-L., Wu, S.-T., 2019. Prospects and challenges of mini-LED and micro-LED displays. J. Soc. Inf. Disp. 27, 387−401.

Huang, Y.-M., Singh, K.J., Liu, A.-C., Lin, C.-C., Chen, Z., Wang, K., et al., 2020a. Advances in quantum-dot-based displays. Nanomaterial 10 (7). Available from: https://doi.org/10.3390/nano10071327.

Huang, Y., Hsiang, E.-L., Deng, M.Y., Wu, S.-T., 2020b. Mini-LED, micro-LED and OLED displays: present status and future perspectives. Light Sci. Appl. 9 (105). Available from: https://doi.org/10.1038/s41377-020-0341-9.

Huang, H.H., Anand, A., Lin, C.J., Lin, H.J., Lin, Y.W., Harroun, S.G., et al., 2021a. LED irradiation of halogen/nitrogen-doped polymeric graphene quantum dots triggers the photodynamic inactivation of bacteria in infected wounds. Carbon N. Y. 174, 710−722.

Huang, W.T., Su, T.Y., Chan, M.H., Tsai, J.Y., Do, Y.Y., Huang, P.L., et al., 2021b. Near-infrared nanophosphor embedded in mesoporous silica nanoparticle with high light-harvesting efficiency for dual photosystem enhancement. Angew. Chem. Int. Edi. 60 (13), 6955−6959.

Ippen, C., Guo, W., Zehnder, D., Kim, D., Manders, J., Barrera, D., et al., 2019. High efficiency heavy metal free QD-LEDs for next generation displays. J. Soci. Info. Display 27 (6), 338–346.

Jang, E., 2018. Environmentally friendly quantum dots for display applications. IEEE International Electron Devices Meeting (IEDM) . Available from: https://doi.org/10.1109/IEDM.2018.8614647.

Jang, E., Jun, S., Jang, H., Lim, J., Kim, B., Kim, Y., 2010. White-light-emitting diodes with quantum dot color converters for display backlights. Adv. Mater. 22 (28), 3076–3080.

Ji, W., Jing, P., Xu, W., Yuan, X., Wang, Y., Zhao, J., et al., 2013. High color purity ZnSe/ZnS core/shell quantum dot based blue light emitting diodes with an inverted device structure. Appl. Phy. Lett. 103 (5), 053106. Available from: https://doi.org/10.1063/1.4817086.

Jia, H., Wang, F., Tan, Z., 2020. Material and device for engineering high-performance blue quantum dot light-emitting diodes. Nanoscale 12 (25), 13186–13224.

Jiang, Y., Cho, S.-Y., Shim, M., 2018. Light-emitting diodes of colloidal quantum dots and nanorod heterostructures for future emissive displays. J. Mater. Chem. C 6, 2618–2634.

Jishi, T., Ishii, T., Shoji, K., 2022. Cultivation of cos lettuce using blue LED and quantum dot wavelength conversion sheets. Sci. Hortic. (Amsterdam) 295. Available from: https://doi.org/10.1016/j.scienta.2021.110772.

Juang, R.S., Fu, C.C., Hsieh, C.T., Gu, S., Gandomi, Y.A., Liu, S.H., 2020. Highly luminescent aggregate-induced emission from polyethylene glycol-coated carbon quantum dot clusters under blue light illumination. J. Mater. Chem. C 8 (46), 16569–16576.

Jun, S., Lee, J., Jang, E., 2013. Highly luminescent and photostable quantum dot–silica monolith and its application to light-emitting diodes. ACS Nano 7 (2), 1472–1477.

Jung, S.-M., Eom, H.-J., Lee, S.-Y., Seo, E.-H., Kim, Y.-D., Yoo, Y.-H., et al., 2021. Evaluating the contents of ginsenoside based on the growth of ginseng sprouts using QD-LED (quantum dot) plant lighting. J. Agric. Life Environ. Sci. 33 (3), 225–235.

Kagan, C.R., Lifshitz, E., Sargent, E.H., Talapin, D.V., 2016. Building devices from colloidal quantum dot. Science 353 (6302). Available from: https://doi.org/10.1126/science.aac5523.

Kang, X., Yang, Y., Wang, L., Wei, S., Pan, D., 2015. Warm white light emitting diodes with gelatin-coated $AgInS_2$/ZnS core/shell quantum dots. ACS Appl. Mater. Interfaces 7 (50), 27713–27719.

Kate, D.M., Husain, K.M.R., 2017. A real time data transmission with LED bulb using Li-Fi technology. Int. J. Sci. Technol. Eng. 3 (09), 553–556.

Kim, D.-K., Kang, D.-H., 2018. UVC LED irradiation effectively inactivates aerosolized viruses bacteria, and fungi in a chamber-type air disinfection system. Appl. Environ. Microbiol. 84 (17). Available from: https://doi.org/10.1128/AEM.00944-18.

Kim, D.-K., Kang, D.-H., 2021. Investigation of a new UVC LEDs array continuous type water disinfection system for inactivating Escherichia coli O157:H7 according to flow rate and electrical energy efficiency analysis. Food Control 119. Available from: https://doi.org/10.1016/j.foodcont.2020.107470.

Kim, J.U., Lee, M.H., Yang, H., 2008. Synthesis of $Zn_{1-x}Cd_xS$:Mn/ZnS quantum dots and their application to light-emitting diodes. Nanotechnology 19 (46). Available from: https://doi.org/10.1088/0957-4484/19/46/465605.

Kim, H., Han, J.Y., Kang, D.S., Kim, S.W., Jang, D.S., Suh, M., et al., 2011. Characteristics of $CuInS_2$/ZnS quantum dots and its application on LED. J. Crystal Growth 326 (1), 90–93.

Kim, K., Jeong, S., Woo, J.Y., Han, C.S., 2012. Successive and large-scale synthesis of InP/ZnS quantum dots in a hybrid reactor and their application to white LEDs. Nanotechnology 23 (6). Available from: https://doi.org/10.1088/0957-4484/23/6/065602.

Kim, H.H., Park, J.-S., Han, I.K., Won, S.O., Park, C., Hwang, D.K., et al., 2016a. Emissive CdTe/ZnO/GO quasi-core-shell-shell hybrid quantum dots for white light emitting diodes. Nanoscale 8 (47), 19737–19743.

Kim, M.J., Song, H.J., Cho, I.S., Jeong, S., Shin, H., Lee, S., et al., 2016b. Fine tuning of emission property of white light-emitting diodes by quantum-dot-coating on YAG: Ce nanophosphors. Appl. Surface Sci. 379, 467–473.

Kim, T., Kim, K.H., Kim, S., Choi, S.M., Jang, H., Seo, H.K., et al., 2020. Efficient and stable blue quantum dot light-emitting diode. Nature 586 (7829), 385–389.

Ko, M., Yoon, H.C., Yoo, H., Oh, J.H., Yang, H., Do, Y.R., 2017. Highly efficient green Zn–Ag–In–S/Zn–In–S/ZnS QDs by a strong exothermic reaction for down-converted green and tripackage white LEDs. Adv. Funct. Mater. 27 (4). Available from: https://doi.org/10.1002/adfm.201602638.

Koushik, P., Karthikeyan, P., Keerthi, M., Manikandan, M., 2021. Organic LED farming for self sustainability during post-COVID 19. J. Phys. Conf. Ser. 1969 (1). Available from: https://doi.org/10.1088/1742-6596/1969/1/012053.

Koutchma, T., Orlowska, M., 2012. Ultraviolet light for processing fruits and fruit products. In: Rodrigues, S., Fernandez, F.A.N. (Eds.), Advances in Fruit Processing Technologies, first ed. CRC Press/Taylor & Francis Group, Boca Raton. Available from: http://doi.org/10.1201/b12088.

Kubendhiran, S., Bao, Z., Dave, K., Liu, R.-S., 2019. Microfluidic synthesis of semiconducting colloidal quantum dots and their applications. ACS Appl. Nano Mater. 2 (4), 1773–1790.

Kumar, B.G., Sadeghi, S., Melikov, R., Aria, M.M., Jalali, H.B., Ow-Yang, C.W., et al., 2018. Structural control of InP/ZnS core/shell quantum dots enables high-quality white LEDs. Nanotechnology 29 (34). Available from: https://doi.org/10.1088/1361-6528/aac8c9.

Kuo, T.R., Hung, S.T., Lin, Y.T., Chou, T.L., Kuo, M.C., Kuo, Y.P., et al., 2017. Green synthesis of InP/ZnS core/shell quantum dots for application in heavy-metal-free light-emitting diodes. Nanoscale Res. Lett. 12 (1). Available from: https://doi.org/10.1186/s11671-017-2307-2.

Kuo, W.S., Wu, P.C., Hung, C.Y., Chang, C.Y., Wang, J.Y., Chen, P.C., et al., 2021. Nitrogen functionalities of amino-functionalized nitrogen-doped graphene quantum dots for highly efficient enhancement of antimicrobial therapy to eliminate methicillin-resistant *Staphylococcus aureus* and utilization as a contrast agent. Int. J. Mol. Sci. 22 (18). Available from: https://doi.org/10.3390/ijms22189695.

Kwon, W., Kim, Y.H., Kim, J.H., Lee, T., Do, S., Park, Y., et al., 2016. High color-purity green, orange, and red light-emitting diodes based on chemically functionalized graphene quantum dots. Sci. Rep. 6 (1). Available from: https://doi.org/10.1038/srep24205.

Lee, K.H., Lee, J.H., Song, W.S., Ko, H., Lee, C., Lee, J.H., et al., 2013. Highly efficient, color-pure, color-stable blue quantum dot light-emitting devices. ACS Nano 7 (8), 7295–7302.

Leitao, M.F., Santos, J.M.M., Guihabert, B., Watson, S., Kelly, A.E., Islim, M.S., et al., 2017. Gb/s visible light communications with colloidal quantum dot color converters. IEEE J. Sel. Topics. Quantum Electron. 23 (5). Available from: https://doi.org/10.1109/JSTQE.2017.2690833.

Li, C., Zang, Z., Chen, W., Hu, Z., Tang, X., Hu, W., et al., 2016. Highly pure green light emission of perovskite $CsPbBr_3$ quantum dots and their application for green light-emitting diodes. Opt. Express 24 (13), 15071–15078.

Li, D., Kristal, B., Wang, Y., Feng, J., Lu, Z., Yu, G., et al., 2019a. Enhanced efficiency of InP-based red quantum dot light-emitting diodes. ACS Appl. Mater. Interfaces 11 (37), 34067–34075.

Li, Z., Xue, D., Liu, D., Liu, Y., Ye, W., Zhang, Y., et al., 2019b. Portable visible light communication transmitter and receiver using core-shell CdSe/ZnS quantum dots white light-emitting diode. IET Comun. 13 (7), 873–878.

Li, Z., Hu, Y., Shen, H., Lin, Q., Wang, L., Wang, H., et al., 2017. Efficient and long-life green light-emitting diodes comprising tridentate thiol capped quantum dots. Laser Photonics Rev. 11 (1). Available from: https://doi.org/10.1002/lpor.201600227.

Li, J.S., Tang, Y., Li, Z.T., Li, J.X., Ding, X.R., Yu, B.H., et al., 2020. Toward 200 lumens per watt of quantum-dot white-light-emitting diodes by reducing reabsorption loss. ACS Nano 15 (1), 550–562.

Li, X., Cai, W., Guan, H., Zhao, S., Cao, S., Chen, C., et al., 2021. Highly stable $CsPbBr_3$ quantum dots by silica-coating and ligand modification for white light-emitting diodes and visible light communication. Chem. Eng. J. 419. Available from: https://doi.org/10.1016/j.cej.2021.129551.

Lin, Q., Song, B., Wang, H., Zhang, F., Chen, F., Wang, L., et al., 2016. High-efficiency deep-red quantum-dot light-emitting diodes with type-II CdSe/CdTe core/shell quantum dots as emissive layers. J. Mater. Chem. C 4 (30), 7223–7229.

Lin, Q., Wang, L., Li, Z., Shen, H., Guo, L., Kuang, Y., et al., 2018. Nonblinking quantum-dot-based blue light-emitting diodes with high efficiency and a balanced charge-injection process. ACS Photonics 5 (3), 939–946.

Liu, Z., Lin, C.-H., Hyun, B.-R., Sher, C.-W., Lv, Z., Luo, B., et al., 2020a. Micro-light-emitting diodes with quantum dots in display technology. Light Sci. Appl. 9 (23). Available from: https://doi.org/10.1038/s41377-020-0268-1.

Liu, D., Cao, S., Wang, S., Wang, H., Dai, W., Zou, B., et al., 2020b. Highly stable red quantum dot light-emitting diodes with long T 95 operation lifetimes. J. Phy. Chem. Lett. 11 (8), 3111–3115.

Liu, Z., Li, F., Huang, G., Wei, J., Jiang, G., Huang, Y., et al., 2021a. Spectral design of light-emitting diodes for plant photosynthesis based on quantum dots. IEEE Access 9, 156229–156238.

Liu, Z., Hyun, B.R., Sheng, Y., Lin, C.J., Changhu, M., Lin, Y., et al., 2021b. Micro-light-emitting diodes based on InGaN materials with quantum dots. Adv. Mater. Technol. . Available from: https://doi.org/10.1002/admt.2021011892101189.

Liu, X., Tao, L., Mei, S., Cui, Z., Shen, D., Sheng, Z., et al., 2022. White light GaN-μLEDs employing green/red perovskite quantum dots as color converters for visible light communication. Nanomaterial 12 (4). Available from: https://doi.org/10.3390/nano12040627.

Luk, C.M., Tang, L.B., Zhang, W.F., Yu, S.F., Teng, K.S., Lau, S.P., 2012. An efficient and stable fluorescent graphene quantum dot–agar composite as a converting material in white light emitting diodes. J. Mater. Chem. 22 (42), 22378–22381.

Luo, Z., Manders, J., Yurek, J., 2018. Your quide to television's quantum-dot future, IEEE Spectrum <https://spectrum.ieee.org/your-quide-to-televisions-quantumdot-future>.

Lv, W., Wang, L., Wang, J., Hao, Z., Luo, Y., 2012. InGaN/GaN multilayer quantum dots yellow-green light-emitting diode with optimized GaN barriers. Nanoscale Res. Lett. 7 (1). Available from: https://doi.org/10.1186/1556-276X-7-617.

Mattousi, H., Radzilowski, L.H., Dabboussi, B.O., Thomas, E.L., Bawendi, M.G., Rubner, M.F., 1998. Electroluminescence from heterostructures of poly(phenylene vinylene) and inorganic CdSe nanocrystals. J. Appl. Phys. 83 (12), 7965–7974.

Memarzadeh, F., 2021. A review of recent evidence for utilizing ultraviolet irradiation technology to disinfect both indoor air and surfaces. Appl. Biosafety 26 (1), 52–56.

Meshram, S.S., Meshram, S., 2020. Light fidelity (Li-Fi): a wireless technology. J. Biomater. Nanotechnol. 9, 7–13.

Miao, S., Liang, Y., Zhang, Y., Chen, D., Wang, X.J., 2021. Broadband Short-Wave Infrared Light-Emitting Diodes Based on Cr^{3+}–Doped $LiScGeO_4$ Phosphor. ACS Appl. Mater. Interfaces 13 (30), 36011–36019.

Mission, E.G., 2021. Recent development in agriculture based on nanomaterials. In: Singh, R.P., Singh, K.R. (Eds.), Nanomaterials in Bionanotechnology: Fundamentals and Applications, first ed. CRC Press, Boca Raton. Available from: http://doi.org/10.1201/9781003139744.

Mitchell, C.A., Both, A.-J., Bourget, C.M., Burr, J.F., Kubola, C., Lopez, R.G., et al., 2012. LEDs: the future of greenhouse lighting!. Chron. Horticult. 52, 5–13.

Motomura, G., Ogura, K., Iwasaki, Y., Nagakubo, J., Hirakawa, M., Nishihashi, T., et al., 2020. Improvement of electroluminescent characteristics in quantum dot light emitting diodes using ZnInP/ZnSe/ZnS quantum dots by mixing an electron transport material into the light-emitting layer. AIP Adv. 10. Available from: https://doi.org/10.1063/5.0010203.

Moustakas, T.D., Xu, T., Thomidis, C., Nikiforov, A.Y., Zhou, L., Smith, D.J., 2008. Growth of III-nitride quantum dots and their applications to blue-green LEDs. Phys. Status Solidi (A) 205 (11), 2560–2565.

Muramoto, Y., Kimura, M., Nouda, S., 2014. Development and future of ultraviolet light-emitting diodes: UV-LED will replace the UV lamp. Semicond. Sci. Technol. 29 (8). Available from: https://doi.org/10.1088/0268-1242/29/8/084004.

Nguyen, T.C., Can, T.T.T., Choi, W.-S., 2019. Optimization of quantum dot thin films using electrohydrodynamic jet spraying for solution-processed quantum dot light—emitting diodes. Sci. Rep. 9. Available from: https://doi.org/10.1038/s41598-019-50181-5.

Nizamoglu, S., Demir, H.V., 2009. Förster resonance energy transfer enhanced color-conversion using colloidal semiconductor quantum dots for solid state lighting. Appl. Phy. Lett. 95 (15). Available from: https://doi.org/10.1063/1.3222902.

Ogonowska, P., Woźniak, A., Pierański, M.K., Wasylew, T., Kwiek, P., Brasel, M., et al., 2019. Application and characterization of light-emitting diodes for photodynamic inactivation of bacteria. Light. Res. Technol. 51 (4), 612–624.

Pan, G., Bai, X., Xu, W., Chen, X., Zhai, Y., Zhu, J., et al., 2020. Bright blue light emission of Ni^{2+}ion-dopedCsPbCl$_x$Br$_{3-x}$perovskite quantum dots enabling efficient light-emitting devices. ACS Appl. Mater. Interfaces 12 (12), 14195–14202.

Park, I.K., Park, S.J., 2011. Green gap spectral range light-emitting diodes with self-assembled InGaN quantum dots formed by enhanced phase separation. Appl. Phys. Express 4 (4). Available from: https://doi.org/10.1143/APEX.4.042102.

Park, N.M., Kim, T.S., Park, S.J., 2001. Band gap engineering of amorphous silicon quantum dots for light-emitting diodes. Appl. Phys. Lett. 78 (17), 2575–2577.

Park, J.H., Kim, J.Y., Chin, B.D., Kim, Y.C., Kim, J.K., Park, O.O., 2004. White emission from polymer/quantum dot ternary nanocomposites by incomplete energy transfer. Nanotechnology 15 (9). Available from: https://doi.org/10.1088/0957-4484/15/9/018.

Park, S.H., Hong, A., Kim, J.H., Yang, H., Lee, K., Jang, H.S., 2015. Highly bright yellow-green-emitting $CuInS_2$ colloidal quantum dots with core/shell/shell architecture for white light-emitting diodes. ACS Appl. Mater. Interfaces 7 (12), 6764–6771.

Park, Y.R., Kim, H.H., Eom, S., Choi, W.K., Choi, H., Lee, B.R., et al., 2021. Luminance efficiency roll-off mechanism in CsPbBr$_{3-x}$Cl$_x$ mixed-halide perovskite quantum dot blue light-emitting diodes. J. Mater. Chem. C 9 (10), 3608–3619.

Perikala, M., Bhardwaj, A., 2021. Excellent color rendering index single system white light emitting carbon dots for next generation, lighting devices. Sci. Rep. 11. Available from: https://doi.org/10.1038/s41598-021-91074-w.

Pietryga, J.M., Park, Y.-S., Lim, J., Fidler, A.F., Bae, W.K., Brovelli, S., et al., 2016. Spectroscopic and device aspects of nanocrystal quantum dots. Chem. Rev. 116 (18), 10513–10622.

Pradhan, S., Di Stasio, F., Bi, Y., Gupta, S., Christodoulou, S., Stavrinadis, A., et al., 2019. High-efficiency colloidal quantum dot infrared light-emitting diodes via engineering at the supra-nanocrystalline level. Nat. Nanotechnol. 14 (1), 72–79.

Prasad, A., Du, L., Zubair, M., Subedi, S., Ullah, A., Roopesh, M.S., 2020. Applications of light-emitting diodes (LEDs) in food processing and water treatment. Food Eng. Rev. 12, 268–289.

Qian, L., Zheng, Y., Xue, J., Holloway, P.H., 2011. Stable and efficient quantum-dot light-emitting diodes based on solution-processed multilayer structures. Nat. Photonics 5 (9), 543–548.

Rad, R.R., Gualdrón-Reyes, A.F., Masi, S., Ganji, B.A., Taghavinia, N., Gené-Marimon, S., et al., 2021. Tunable carbon–$CsPbI_3$ quantum dots for white LEDs. Adv. Optical Mater. 9 (4). Available from: https://doi.org/10.1002/adom.202001508.

Ramalingam, G., Ragupathi, C., Kaviyarasu, K., Letsholathebe, D., Mohamed, S.B., Magdalane, C.M., et al., 2019. Up-scalable synthesis of size-controlled white-green emitting behavior of core/shell (CdSe/ZnS) quantum dots for LED applications. J. Nanosci. Nanotechnol. 19 (7), 4026–4032.

Ren, J., Zhou, X., Wang, Y., 2020. Water triggered interfacial synthesis of highly luminescent $CsPbX_3$: Mn^{2+} quantum dots from nonluminescent quantum dots. Nano Res. 13 (12), 3387–3395.

Ren, A., Wang, H., Zhang, W., Wu, J., Wang, Z., Penty, R.V., et al., 2021. Emerging light-emitting diodes for next-generation data communications. Nat. Electron. 4 (8), 559–572.

Romero, M.P., Alves, F., Stringasci, M.D., Buzzá, H.H., Ciol, H., Inada, N.M., et al., 2021. One-pot microwave-assisted synthesis of carbon dots and in vivo and in vitro antimicrobial photodynamic applications. Front. Microbiol. 12. Available from: https://doi.org/10.3389/fmicb.2021.662149.

Roy, P., Periasamy, A.P., Chuang, C., Liou, Y.R., Chen, Y.F., Joly, J., et al., 2014. Plant leaf-derived graphene quantum dots and applications for white LEDs. New J. Chem. 38 (10), 4946–4951.

Ruan, C., Zhang, Y., Lu, M., Ji, C., Sun, C., Chen, X., et al., 2016. White light-emitting diodes based on $AgInS_2$/ZnS quantum dots with improved bandwidth in visible light communication. Nanomater. 6 (1). Available from: https://doi.org/10.3390/nano6010013.

Sabatini, R., Richardson, M.A., Cantiello, M., Toscano, M., Fiorini, P., 2016. A novel approach to night vision imaging system development, integration and verification in military aircraft. Aerospace Sci. Technol. 31 (1), 10–23.

Sadeghi, S., Mutcu, S.E., Srivastava, S.B., Aydindogan, G., Caynak, S., Karslı, K., et al., 2018. High quality quantum dots polymeric films as color converters for smart phone display technology. Mater. Res. Exp. 6 (3). Available from: https://doi.org/10.1088/2053-1591/aaf3ef.

Sadeghi, S., KhabbazAbkenar, S., Ow-Yang, C.W., Nizamoglu, S., 2019. Efficient white LEDs using liquid-state magic-sized CdSe quantum dots. Sci. Rep. 9 (1). Available from: https://doi.org/10.1038/s41598-019-46581-2.

Sellers, N., 2018. Chapter 3: Terahertz and infrared quantum photodetectors. Handbook of Terahertz Technology. ED-Tech Press, London, pp. 100–136.

Sen, P., Nyokong, T., 2021. Promising photodynamic antimicrobial activity of polyimine substituted zinc phthalocyanine and its polycationic derivative when conjugated to nitrogen, sulfur, co-doped graphene quantum dots against *Staphylococcus aureus*. Photodiagnosis Photodyn. Ther. 34. Available from: https://doi.org/10.1016/j.pdpdt.2021.102300.

Shan, Q., Wei, C., Jiang, Y., Song, J., Zou, Y., Xu, L., et al., 2020. Perovskite light-emitting/detecting bifunctional fibres for wearable LiFi communication. Light Sci Appl. 9. Available from: https://doi.org/10.1038/s41377-020-00402-8.

Shen, C., Chu, J., Qian, F., Zou, X., Zhong, C., Li, K., et al., 2012. High color rendering index white LED based on nano-YAG: Ce^{3+} phosphor hybrid with CdSe/CdS/ZnS core/shell/shell quantum dots. J. Modern Opt. 59 (14), 1199–1203.

Shen, H., Lin, Q., Wang, H., Qian, L., Yang, Y., Titov, A., et al., 2013. Efficient and bright colloidal quantum dot light-emitting diodes via controlling the shell thickness of quantum dots. ACS Appl. Mater. Interfaces 5 (22), 12011–12016.

Shen, P., Li, X., Cao, F., Ding, X., Yang, X., 2018. Highly efficient, all-solution-processed, flexible white quantum dot light-emitting diodes. J. Mater. Chem. C 6 (36), 9642–9648.

Shirasaki, Y., Supran, G.J., Bawendi, M.G., Bulović, V., 2013. Emergence of colloidal quantum-dot light-emitting technologies. Nat. Photon. 7, 13–23.

Singh, R.K., Som, S., Dutta, S., Jain, N., Kuo, M.T., Singh, J., et al., 2019. Rapid synthesis of hybrid methylammonium lead iodide perovskite quantum dots and rich MnI_2 substitution favouring Pb-free warm white LED applications. Nanoscale Adv. 1 (8), 2999–3008.

Singh, K.J., Huang, Y.-M., Ahmed, T., Liu, A.-C., Chen, S.-W.H., Liou, F.-J., et al., 2020. Micro-LED as a promising candidate for high-speed visible light communication. Appl. Sci. 10 (20). Available from: https://doi.org/10.3390/app10207384.

Singh, K.J., Ahmed, T., Gautam, P., Sadhu, A.S., Lien, D.-H., Chen, S.C., et al., 2021a. Recent advances in two-dimensional quantum dots and their applications. Nanomaterial 11 (6). Available from: https://doi.org/10.3390/nano11061549.

Singh, H., Bhardwaj, S.K., Khatri, M., Kim, K.-H., Bhardwaj, N., 2021b. UVC radiation for food safety: an emerging technology for the microbial disinfection of food products. Chem. Eng. J. 417. Available from: https://doi.org/10.1016/j.cel.2020.128084.

Son, D.I., Kwon, B.W., Park, D.H., Seo, W.S., Yi, Y., Angadi, B., et al., 2012. Emissive ZnO–graphene quantum dots for white-light-emitting diodes. Nat. Nanotechnol. 7 (7), 465–471.

Song, J.-W., 2016. Grow light for plant factory using quantum dot LED. J. Int. Counc. Electr. Eng. 6 (1), 13–16.

Song, H., Lee, S., 2007a. Photoluminescent (CdSe) ZnS quantum dot–polymethylmethacrylate polymer composite thin films in the visible spectral range. Nanotechnology 18 (5). Available from: https://doi.org/10.1088/0957-4484/18/5/055402.

Song, H., Lee, S., 2007b. Red light emitting solid state hybrid quantum dot–near-UV GaN LED devices. Nanotechnology 18 (25). Available from: https://doi.org/10.1088/0957-4484/18/25/255202.

Song, W.S., Yang, H., 2012. Fabrication of white light-emitting diodes based on solvothermally synthesized copper indium sulfide quantum dots as color converters. Appl. Phys. Lett. 100 (18), 183104. Available from: https://doi.org/10.1063/1.4711019.

Song, W.S., Kim, J.H., Lee, J.H., Lee, H.S., Do, Y.R., Yang, H., 2012. Synthesis of color-tunable Cu–In–Ga–S solid solution quantum dots with high quantum yields for application to white light-emitting diodes. J. Mater. Chem. 22 (41), 21901–21908.

Song, W.S., Lee, S.H., Yang, H., 2013. Fabrication of warm, high CRI white LED using non-cadmium quantum dots. Opt. Mater. Express 3 (9), 1468–1473.

Steckel, J.S., Snee, P., Coe-Sullivan, S., Zimmer, J.P., Halpert, J.E., Anikeeva, P., et al., 2006. Color-saturated green-emitting QD-LEDs. Angew. Chem. Int. (Ed.) 45 (35), 5796–5799.

Stouwdam, J.W., Janssen, R.A., 2008. Red, green, and blue quantum dot LEDs with solution processable ZnO nanocrystal electron injection layers. J. Mater. Chem. 18 (16), 1889–1894.

Sun, Q., Wang, Y.A., Li, L.S., Wang, D., Zhu, T., Xu, J., et al., 2007. Bright, multicoloured light-emitting diodes based on quantum dots. Nat. Photon. 1 (12), 717–722.

Sun, Y., Fan, J., Liu, M., Zhang, L., Jiang, B., Zhang, M., et al., 2020. Highly transparent ultra-thin flexible, full-color mini-LED display with indium-gallium-zinc oxide thin-film transistor substrate. J. Soc. Inf. Disp. 28, 926–935.

Tan, G., Huang, Y., Li, M.-C., Lee, S.-L., Wu, S.-T., 2018. High dynamic range liquid crystal displays with a mini-LED backlight. Opt. Express 26 (13), 16572–16584.

Taylor, R.M., Church, K.H., Sluch, M.I., 2007. Red light emission from hybrid organic/inorganic quantum dot AC light emitting displays. Displays 28 (2), 92–96.

Ugarte, I., Castello, I., Palomares, E., Pacios, R., 2012. Quantum dots as a light indicator for emitting diodes and biological coding. In: Al-Ahmadi, A. (Ed.), Quantum Dots—A Variety of New Applications. IntechOpen. Available from: https://www.intechopen.com/chapters/34816.

Vahabzad, F., Rostami, A., Dolatyari, M., Rostami, G., Amiri, I.S., 2019. Solution-processed QD-LEDs in visible range: modulation bandwith enhancement. Phys. B 574. Available from: https://doi.org/10.1016/j.physb.2019.411667.

Vasilopoulou, M., Fakharuddin, A., Garcia de Arquer, F.P., Georgiadou, D.G., Kim, H., Gao, F., et al., 2021. Advances in solution-processed near-infrared light-emitting diodes. Nat. Photon. 15, 656–669.

Viršilė, A., Olle, M., Duchovskis, P., 2017. LED lighting in horticulture. In: Gupta, S.D. (Ed.), Light Emitting Diodes for Agriculture: Smart Lighting. Springer Nature Singapore, pp. 113–147. Available from: http://doi.org/10.1007/978-981-10-5807-3_7.

Wan, R., Li, G., Gao, X., Liu, Z., Li, J., Xiaoyan, Y., et al., 2021. Nanohole array structured GaN-based white LEDs with improved modulation bandwidth via plasmon resonance and non-radiative energy transfer. Photon. Res. 9 (7), 1213–1217.

Wang, L., Lin, J., Hu, Y., Guo, X., Lv, Y., Tang, Z., et al., 2017. Blue quantum dot light-emitting diodes with high electroluminescent efficiency. ACS Appl. Mater. Interfaces 9 (44), 38755–38760.

Wang, L., Wang, L., Yu, J., Hao, Z., Luo, Y., Sun, C., et al., 2018. Abnormal Stranski–Krastanov mode growth of green InGaN quantum dots: morphology, optical properties, and applications in light-emitting devices. ACS Appl. Mater. Interfaces 11 (1), 1228–1238.

Wang, Y.T., Liu, C.W., Chen, P.Y., Wu, R.N., Ni, C.C., Cai, C.J., et al., 2019. Color conversion efficiency enhancement of colloidal quantum dot through its linkage with synthesized metal nanoparticle on a blue light-emitting diode. Opt. Lett. 44 (23), 5691–5694.

Wang, L., Wang, L., Chen, C.J., Chen, K.C., Hao, Z., Luo, Y., et al., 2021a. Green InGaN quantum dots breaking through efficiency and bandwidth bottlenecks of micro–LEDs. Laser Photonics Rev. 15 (5). Available from: https://doi.org/10.1002/lpor.202000406.

Wang, T., Zhang, C., Zhang, H., Zhu, H., 2021b. CRISPR/Cas9-mediated gene editing revolutionizes the improvement of horticulture food crops. J. Agric. Food Chem. 69 (45), 13260–13269.

Wei, Z., Zhang, L., Wang, L., Chen, C.-J., Pepe, A., Liu, X., et al., 2020a. 2 Gbps/3 m air-underwater optical wireless communication based on a single-layer quantum dot blue micro-LED. Opt. Lett. 45 (9), 2616–2619.

Wei, Z., Zhang, L., Wang, L., Chen, C. J., Pepe, A., Liu, X., et al., 2020b. High-speed visible light communication system based on a packaged single layer quantum dot blue micro-LED with 4-Gbps QAM-OFDM. Optical Fiber Communications Conference and Exhibition, 1–3, doi: 10.1364/OFC.2020.M3I.7.

Won, W.S., Tran, L.G., Park, W.T., Kim, K.K., Shin, C.S., Kim, N., et al., 2018. UV-LEDs for disinfection and bio-sensing applications. Int. J. Precis. Eng. Manuf. 19, 1901–1915.

Wong, M.S., Nakamura, S., Den Baars, S.P., 2019. Review-progress in high performances III – nitride micro-light-emitting diodes. ECS J. Solid State Sci. Technol. 9 (1). Available from: https://doi.org/10.1149/2.0302001jss.

Wu, F., Zhang, D., Shang, S., Zhu, Y., Zhuang, S., Xu, J., 2012. Developing quantum dot phosphor-based light-emitting diodes for aviation lighting applications. J. Nanomater. 2012. Available from: https://doi.org/10.1155/2012/629157.

Wu, T., Sher, C.-W., Lin, Y., Lee, C.-F., Liang, S., Lu, Y., et al., 2018. Mini-LED and micro-LED: promising candidates for the next generation display technology. Appl. Sci. 8 (9). Available from: https://doi.org/10.3390/app8091557.

Wu, Y., Ma, J., Su, P., Zhang, L., Xia, B., 2020. Full-color realization of micro-led displays. Nanomaterials 10 (12). Available from: https://doi.org/10.3390/nano10122482.

Xiao, X., Tang, H., Zhang, T., Chen, W., Chen, W., Wu, D., et al., 2016. Improving the modulation bandwidth of LED by CdSe/ZnS quantum dots for visible light communication. Opt. Express 24 (19), 21577–21586.

Xie, Y., Geng, X., Gao, J., Shi, W., Zhou, Z., Wang, H., et al., 2021. Synthesis of carbon dots@ $Mg(OH)_2$ solid-state composites with blue, red emitting for horticultural application. J. Alloys Comp. 873. Available from: https://doi.org/10.1016/j.jallcom.2021.159663.

Yang, X., Xu, R., Bao, D., Li, B., 2014a. Gold nanorod-enhanced light emission in quantum-dot-doped polymer nanofibers. ACS Appl. Mater. Interfaces 6 (15), 11846–11850.

Yang, W., Li, J., Zhang, Y., Huang, P.K., Lu, T.-C., Kuo, H.-C., et al., 2014b. High density GaN/AlN quantum dots for deep UV LED with high quantum efficiency and temperature stability. Sci. Rep. 4. Available from: https://doi.org/10.1038/srep05166.

Yang, S.J., Oh, J.H., Kim, S., Yang, H., Do, Y.R., 2015. Realization of InP/ZnS quantum dots for green, amber and red down-converted LEDs and their color-tunable, four-package white LEDs. J. Mater. Chem. C 3 (15), 3582–3591.

Yang, Z., Gao, M., Wu, W., Yang, X., Sun, X.W., Zhang, J., et al., 2019a. Recent advances in quantum dot-based light-emitting devices: challenges and possible solutions. Mater. Today 24, 69–93.

Yang, X., Lan, X.-Y., Liu, Y.-S., Yang, H.-Y., Li, Y., Zheng, S.-W., et al., 2019b. Highly stable white light-emitting diodes based on quantum dots dispersed into the backlight lens for display backlight. IEEE Photon. J. 11 (3). Available from: https://doi.org/10.1109/JPHOT.2019.2916084.

Yang, W., Gao, F., Qiu, Y., Liu, W., Xu, H., Yang, L., et al., 2019c. $CsPbBr_3$-Quantum–dots/Polystyrene@ silica hybrid microsphere structures with significantly improved stability for white LEDs. Adv. Optical Mater. 7 (13). Available from: https://doi.org/10.1002/adom.201900546.

Yang, H., Zhou, M., Tang, H., Sun, M., Liu, P., Liu, Y., et al., 2020. Enhanced light emission of quantum dot films by scattering of poly (zinc methacrylate) coating CdZnSeS/ZnS quantum dots and high refractive index $BaTiO_3$ nanoparticles. RSC Adv. 10 (53), 31705–31710.

Yanykin, D.V., Burmistrov, D.E., Simakin, A.V., Ermakova, J.A., Gudkov, S.V., 2022. Effect of up-converting luminescent nanoparticles with increased quantum yield incorporated into the

fluoropolymer matrix on solanum lycopersicum growth. Agronomy 12 (1). Available from: https://doi.org/10.3390/agronomy12010108.

Ye, Z.T., Cheng, Y.H., Liu, K.H., Yang, K.S., 2021. Mini-LEDs with diffuse reflection cavity arrays and quantum dot film for thin, large-area, high-luminance flat light source. Nanomaterial 11 (9). Available from: https://doi.org/10.3390/nano11092395.

Yin, L., Zhou, J., Li, W., Zhang, J., Wang, L., 2019. Yellow fluorescent graphene quantum dots as a phosphor for white tunable light-emitting diodes. RSC Adv. 9 (16), 9301–9307.

Yoon, H.C., Oh, J.H., Ko, M., Yoo, H., Do, Y.R., 2015. Synthesis and characterization of green Zn–Ag–In–S and red Zn–Cu–In–S quantum dots for ultrahigh color quality of down-converted white LEDs. ACS Appl. Mater. Interfaces 7 (13), 7342–7350.

Yu, T.-C., Huang, W.-T., Lee, W.-B., Chow, C.-W., Chang, S.-W., Kuo, H.-C., 2021. Visible light communications system technology review: devices architectures and applications. Crystals 11 (9). Available from: https://doi.org/10.3390/cryst11091098.

Yuan, F., Wang, Z., Li, X., Li, Y., Tan, Z.A., Fan, L., et al., 2017. Bright multicolor bandgap fluorescent carbon quantum dots for electroluminescent light-Emitting diodes. Adv. Mater. 29 (3). Available from: https://doi.org/10.1002/adma.201604436.

Yulin, H., Weisher, C., Hsieh, D.H., Chen, X.Y., Chen, H.M.P., Chen, T.M., et al., 2017. Optical cross-talk reduction in a quantum dot-based full-color micro-light-emitting diode display by a lithographic-fabricated photoresist mold. Photon. Res. 5 (5), 411–416.

Zhang, M., Wang, M., Yang, Z., Li, J., Qiu, H., 2018a. Preparation of all-inorganic perovskite quantum dots-polymer composite for white LEDs application. J. Alloys Compd. 748, 537–545.

Zhang, H., Chen, S., Sun, X.W., 2018b. Efficient red/green/blue tandem quantum-dot light-emitting diodes with external quantum efficiency exceeding 21%. ACS Nano 12 (1), 697–704.

Zhang, Z., Shen, L., Zhang, H., Ding, L., Shao, G., Liang, X., et al., 2019. Novel red-emitting $CsPb_{1-x}Ti_xI_3$perovskite QDs@glasses with ambient stability for high efficiency white LEDs and plant growth LEDs. Chem. Eng. J. 378. Available from: https://doi.org/10.1016/j.cej.2019.122125.

Zhang, H., Su, Q., Chen, S., 2020. Quantum-dot and organic hybrid tandem light-emitting diodes with multi-functionality of full-color-tunability and white-light-emission. Nature Commun. 11 (1). Available from: https://doi.org/10.1038/s41467-020-16659-x.

Zhang, L., Sun, C., He, T., Jiang, Y., Wei, J., Huang, Y., et al., 2021a. High-performance quasi − 2D perovskite light − emitting diodes: from materials to devices. Light Sci. Appl. 10. Available from: https://doi.org/10.1038/s41377-021-00501-0.

Zhang, D., Chao, D., Yu, C., Zhu, Q., Zhou, S., Tian, L., et al., 2021b. One-step green solvothermal synthesis of full-color carbon quantum dots based on a doping strategy. J. Phys. Chem. Lett. 12 (37), 8939–8946.

Zheng, Y., Zhu, X., 2020. Recent progress in emerging near-infrared emitting materials for light-emitting diode applications. Org. Mater. 02 (04), 253–281.

Zheng, J., Xie, Y., Wei, Y., Yang, Y., Liu, X., Chen, Y., et al., 2020. An efficient synthesis and photoelectric properties of green carbon quantum dots with high fluorescent quantum yield. Nanomaterial 10 (1). Available from: https://doi.org/10.3390/nano10010082.

Zhou, D., Wang, Y., Tian, P., Jing, P., Sun, M., Chen, X., et al., 2018. Microwave-assisted heating method toward multicolor quantum dot-based phosphors with much improved luminescence. ACS Appl. Mater. Interfaces 10 (32), 27160–27170.

Zhou, Z., Wang, X., Yi, X., Ming, H., Ma, Z., Peng, M., 2021. Rechargeable and sunlight-activated $Sr_3Y_2Ge_3O_{12}$: Bi^{3+} UV–Visible-NIR persistent luminescence material for night-vision signage and optical information storage. Chem. Eng. J. 421. Available from: https://doi.org/10.1016/j.cej.2020.127820.

Zhu, J., Yang, X., Zhu, Y., Wang, Y., Cai, J., Shen, J., et al., 2017. Room-temperature synthesis of Mn-doped cesium lead halide quantum dots with high Mn substitution ratio. J. Phys. Chem. Lett. 8 (17), 4167−4171.

Zhuang, Z., Iida, D., Velazquez-Rizo, M., Ohkawa, K., 2021. 630-nm red InGaN micro-light-emitting diodes ($< 20\ \mu m \times 20\ \mu m$) exceeding 1 mW/mm2 for full-color micro-displays. Photon. Res. 9 (9), 1796−1802.

Chapter 11

Application of quantum dots in biomedical and biotechnological fields

Anca Armăşelu[1] **and Priyanka Jhalora**[2]

[1]*Department of Electrical Engineering and Applied Physics, Faculty of Electrical Engineering and Computer Science, Transilvania University of Brasov, Brasov, Romania,* [2]*Department of Chemistry, PAHER University, Udaipur, Rajasthan, India*

11.1 Introduction

Owing to their unique size-dependent features, fluorescent nanoparticles (NPs) or quantum dots (QDs) have attracted the attention of scientists all over the globe in the last few decades. There is an increasing concern in developing environment-friendly procedures to synthesize these NPs because they enhance biocompatibility and avoid the production of toxic by-products (Plaza et al., 2016).

Due to the advent of nanobiotechnology, some modern biological synthesis works of nanomaterials (NMs) have succeeded in implementing "Green chemistry" strategies, which are globally sustainable and economically viable (Abdel-Salam et al., 2020). The green revolution and scientific developments in the realm of biological sciences, agricultural biotechnology, food technology, and nanotechnology follow the route of a novel scientific perceptiveness (Palit, 2020).

Some substantial studies have explained the conception or synthesis of materials with nanoscale accuracy (Ameta and Ameta, 2016a,b) using material science, which is nanotechnology (Pandey et al., 2015; Ameta and Ameta, 2016c). These studies have described the diverse aspects of synthesis of NPs, characterization, and their crucial applications, focusing on the biogenic synthesis of NPs and their use (Ingale and Chaudhari, 2013; Bhatt et al., 2020a).

QDs have been presented as the central notion of nanoscience and nanotechnology since their inception and remain an active and intense domain of exploration in applied nanomaterial research (Damian et al., 2011; Ameta et al., 2014;

Quantum Dots. DOI: https://doi.org/10.1016/B978-0-12-824153-0.00011-2
© 2023 Elsevier Inc. All rights reserved.

Benjamin et al., 2014; Solanki et al., 2018; Ameta et al., 2019a,b; Armăşelu, 2019; Liu et al., 2020a; Ameta et al., 2020). QDs possess numerous distinctive constitutional, physicochemical, and photochemical characteristics that make them encouraging candidates in the areas of solar cells, laser, memory, light-emitting diodes (LEDs) (Armăşelu, 2017), photovoltaics, photodetectors, photocatalysts (Ameta et al., 2019c; Bhatt et al., 2019a), quantum computers (Ameta et al., 2019c), wastewater treatment (Bhatt et al., 2019b,c; Jat et al., 2019), and bioimaging applications (Ardelean et al., 2011; Armăşelu et al., 2011a,b; Damian et al., 2010).

The QDs show unique optical properties, which depend on their size, shape, and surface chemistry, and in spite of the fact that research on QDs is at a relatively early phase, their high biocompatibility and reduced cytotoxicity have already been established in vitro and in vivo, increasing the interest in this type of NM as compared to others (Perini et al., 2020).

QDs and their composites are modern and notable structures, which present unique and significant properties. Here, the basic properties of QDs, some key aspects related to the synthesis techniques of QDs, and the latest advances in the field of QDs applications in sensing, bioimaging, biolabeling, and targeted drug delivery have been presented. This work also provides some toxicological characteristics of QDs and their composites.

11.2 Biolabeling and bioimaging

Biolabeling is nothing but tracking individual cells using any material. QDs have been used for labeling of cells. It is all due to the florescence of QDs. This can pass to daughter cells upon cell division with florescence labels in such cases. These have also being used before surgery by labeling lymph nodes with florescence. Bioimaging refers to any imaging technique in the field of biomedical and biotechnology. Here, bioluminescence is used in the diagnosis of some diseases. One can visualize different infections, localizing cancer growth by creating bioimages of different internal organs and their functions.

Wolcott et al. (2006) reported a simple aqueous synthesis of silica-capped, highly fluorescent CdTe QDs. These CdTe QDs are quite useful as the emission can be tuned to the near-infrared, where tissue absorption is at the minimum. Leakage of toxic Cd^{2+} can be prevented by a silica shell. These silica shells help in increasing photostability in tris-borate-ethylenediaminetetraacetate and phosphate-buffered saline buffers. They used poly(ethylene glycol) and thiol-terminated biolinkers to functionalize silica-capped QDs to improve their biocompatibility. Conjugation specificity and bioactivity of as-synthesized thiolated QDs was confirmed by streptavidin − maleimide and biotinylated polystyrene microbeads. It was reported that these functionalized, silica-capped QDs are ideal labels, safe, robust, easily synthesized, and readily conjugated to biomolecules. They find a number of applications in biolabeling and imaging.

Li et al. (2007) synthesized aqueous CdS QDs in a direct and environment-friendly manner at room temperature. They reported the feasibility of aqueous CdS QDs as an imaging tool with *Salmonella typhimurium* cells, when 3-mercaptopropionic acid (MPA) was used as the capping molecule. The QDs exhibited stronger emission at higher pH and MPA/Cd ratio of 2. It was claimed that aqueous CdS QDs displayed a lifetime of 12 h under UV light with an excellent stability. An ease of processing and good PL properties of these aqueous CdS QDs provided a low-cost and practical approach for single-target imaging application.

Erogbogbo et al. (2008) prepared highly stable aqueous suspensions of Si QDs. It was found that the optical properties of Si nanocrystals are retained. These micelle-encapsulated Si QDs can be used for detecting pancreatic cancer cells. These silicon QDs may prove to be a significant optical probe in biomedical diagnostics.

Biologically compatible and water-soluble CdSe QDs were synthesized in aqueous medium by Liu et al. (2009) using L-cysteine as the capping agent. It was revealed that molar ratio of Se/Cd and the reaction time are deciding factors for the size distribution of CdSe/L-cysteine QDs. The fluorescence intensity of bovine serum albumin (BSA) was largely quenched with the addition of QDs, but it slightly enhanced initially and then quenched on addition of BSA to solution of QDs. They suggested that CdSe/L-cysteine QDs can be used as a probe for labeling bacterial cells and biological molecules.

Allen et al. (2010) reported the synthesis of InAs QDs with a ZnCdS shell. These can be used for biological imaging as they show stable and bright emission in the near-infrared (NIR, 700−900 nm) region. They opined that these NIR QDs can image tumor vasculature in vivo at deeper penetration depths with higher contrast than visible emitting CdSe(CdS) QDs. Tan et al. (2013) prepared nanoscaled light-triggered nitric oxide (NO) delivery consisting of chitosan (CS)-based *S*-nitrosothiols (SNO) and encapsulated silver sulfide QDs (Ag_2S QDs) and used for vehicles NIR fluorescence imaging. They used ethylenediaminetetraacetic acid (EDTA) to conjugate water-soluble Ag_2S QDs with the CS-SNO. They performed cell imaging. It was demonstrated that Ag_2S-CS-SNO nanospheres could emit observable NIR fluorescence and also release NO in living cells.

Uniform molybdenum disulfide (MoS_2)/tungsten disulfide (WS_2) QDs were prepared by Xu et al. (2015) via a combination of sonication and solvothermal treatment at a mild temperature. It was reported that as-prepared QDs have monolayer thickness (average size of about 3 nm). A good cell permeability, strong fluorescence, and low cytotoxicity make these QDs quite promising and biocompatible probes for in vitro imaging.

Justin et al. (2016) synthesized reduced graphene oxide (GO)−iron oxide QDs with photoluminescent and superparamagnetic properties. They used a green, hydrothermal method that reduced and shattered graphene nanosheets simultaneously to form QDs. A drug could be loaded onto the surface of

these QDs, with a loading ratio of drug to QD as 0.31:1. These have a potential to be used in cancer photothermal therapy. A suspension of QDs ($100\ \mu g\ mL^{-1}$) can be used for photothermal ablation of HeLa cells in vitro in presence of near infrared irradiation.

Nitrogen and phosphorus functionalized Ti_3C_2 MXene-based QDs (N,P-MQDs) were prepared via a top−bottom hydrothermal method by Guan et al. (2019). It exhibited pH resistance capacities and excellent photostability. These N,P-MQDs are highly sensitive toward Cu^{2+} ions and may be used for label-free fluorescence platform for Cu^{2+} detection. This is a low cost, sensitive, and environment-friendly method.

Xue et al. (2019) synthesized lignin hybridized CQDs (L-CQDs) via hydrothermal route. They used different molar ratios of ethanediamine and citric acid. As-obtained L-CQDs with almost spherical morphology were found to be <10 nm (diameter). It was reported that L-CQDs exhibited excitation-dependent photoluminescence (PL) behavior and maximum emission of L-CQDs exhibited a red-shift (longer wavelength) with a decrease in intensity on increasing excitation wavelengths. As-prepared L-CQDs have low good cellular biocompatibility and cytotoxicity indicating that there is a potential of these L-CQDs for bioimaging applications.

Qu et al. (2020) reported synthesis of bifunctional ibuprofen-based carbon QDs (ICQDs) via a simple one-step microwave-assisted method. As-prepared ICQDs exhibited low toxicity, high stability, good biocompatibility, and negligible cytotoxicity in water. It was reported that as-produced ICQDs had a decent imaging ability and excellent antiinflammatory effects in vivo, simultaneously. Shahid et al. (2020) reported hydrothermal synthesis of biocompatible, polyethyleneimine (PEI) surface passivated carbon dots (CDP) using mint leaves as a green source. The biolabeling potentials of nonpassivated C-dots and CDP was evaluated in the breast cancer (MCF-7) cells, when cytotoxicity was found to be concentration dependent. It was reported that C-dots synthesized from a herbal source (mint) can be used for different biolabeling applications as well as antioxidant activity.

11.3 Targeted drug delivery

Nanotechnology has the potential to develop quantitative and sensitive methods to diagnose and detect cancer. Semiconductor QDs are NPs that have intense and stable fluorescence, and these could help in the detection of various cancer biomarkers in blood assays, cancer tissue biopsies, and also as contrast agents for medical imaging. QDs are promising materials to expand to in vitro analysis, which can be extended to cellular, tissue, and whole-body multiplexed cancer biomarker imaging.

Detecting cancer at an early stage is a current challenge in the treatment of cancer. This will be supported by targeted drug delivery in and around tumors at concentrations, which decreases the growth rate of the tumors and

continues to be the primary challenge in the treatment of cancer. In most of the cases, the malignancy of tumors is only detected when it has reached an advanced stage and then chemotherapeutic drugs will be increasingly toxic to healthy cells. A targeting drug delivery system has a moiety that can recognize a tumor with a drug-loaded vesicle. Detection systems of malignant tumors involve tissue biopsy and magnetic resonance imaging (MRI), where a single system is needed that is capable of targeting drug delivery as well as imaging the delivery process, simultaneously. Here, the integration of biomaterials and semiconductor QDs can be useful for addressing these problems of cancer therapy.

Misra (2008) used biodegradable chitosan (*N*-acetyglucosamine) for targeted drug delivery to tumors and QDs noninvasive imaging. It was reported that drug-loaded chitosan-encapsulated ZnO:Mn^{2+} QDs provided a potential platform for drug delivery to targeted tumors and this delivery process was documented, simultaneously. Core−shell structured multifunctional nanocarriers (NCs) of ZnO QDs-conjugated gold NPs (Au NPs) were synthesized by Chen et al. (2013). It was indicated that camptothecin (CPT) release from these NCs was much higher at pH 7.4 than 5.3. It was reported that both NCs; and CPT-loaded NCs provided high anticancer activity against Hela cells.

Wang et al. (2013a) prepared GQDs with strongly green-PL, which were surface-passivated by polyethylene glycol (GQDs-PEG). It was observed that the PL quantum yield of as-prepared GQDs-PEG was around 18.8% with 400 nm excitation. They reported that surface-passivated PEG on GQDs can load the drug by hydrogen bonding apart from enhancing PL intensity. The GQDs-PEG have high specific surface area, which provide these higher loading capabilities (2.5 mg mg^{-1}) to carry the drug. As-fabricated GQDs-PEG were suitable for cell imaging and as drug carrier.

A novel QDs-based multifunctional nanovehicle (DOX-QD-PEG-FA) was designed for targeted drug delivery, fluorescent imaging, tracking, and cancer therapy, in which the GSH−CdTe QDs play a key role in imaging and drug delivery. The antineoplastic drug doxorubicin hydrochloride (DOX) was loaded on the GSH−CdTe QDs by Chen et al. (2014) via a condensation reaction. A PEG shell was introduced to wrap these DOX-QDs. The NPs were then decorated with folic acid (FA) to actively target particularly cancer cells and prevent the nanovehicles from being used up by normal cells allowing them to target HeLa cells that express the FA receptor. In vitro studies revealed that this multifunctional nanovehicle can deliver DOX specifically to the targeted cancer cells, and on reaching the tumor cells the FA on the DOX-QD-PEG surface increased the drug concentration so as to achieve higher curative effect. It was reported that this multifunctional DOX-QD-PEG-FA system exhibited great promise for tumor imaging, targeting, and therapy.

Wu et al. (2014) prepared dual-functional NMs consisting of QDs and an anticancer drug methotrexate (MTX). Hydrophilic $AgInS_2$/ZnS QDs were

obtained by ultrasonication by introducing the amphiphilic polymer, poly (maleic anhydride-alt-1-octadecene) (PMAO). Then MTX was covalently coupled to the surface of the $AgInS_2$/ZnS QDs by carbodiimide chemistry. It was indicated that these hydrophilic PMAO-coated $AgInS_2$/ZnS QDs exhibited negligible cytotoxicity, but $AgInS_2$/ZnS QDs conjugated with MTX were taken up effectively by human cervical (HeLa) cancer cells. It was suggested that $AgInS_2$/ZnS QDs conjugated with MTX may be a promising candidate for cancer therapeutics and diagnosis in future.

Samantara et al. (2016) developed a method to synthesize carbon QDs from Good's buffer. As-synthesized CQDs emitted a bright greenish blue colored fluorescence on exposure to UV irradiation (365 nm). This bright fluorescence of CQDs makes them useful probes for cellular imaging. More than 95% survival rate was found when H357 (human oral squamous carcinoma) and HEK293 (human embryonic kidney) cells were treated with these CQDs. The low cytotoxicity of Good's buffer-derived CQDs opens the door to biomedical applications. They easily loaded an anticancer drug DOX on as-prepared CQDs. They also explored delivery efficiency to the target cells via in vitro treatment of cancerous cells. CQDs-supported DOX exhibited a higher killing rate as compared to only DOX, which may be due to easy internalization and effective pH-triggered release inside the cells.

Rai et al. (2017) used lignosulfonate lignin as a carbon source for the synthesis of water-soluble reduced fluorescent carbon dots (r-FCDs). Then these r-FCDs were employed for bioimaging applications and as a curcumin nanocarrier. As-prepared r-FCDs were obtained under microwave irradiation after reduction with $NaBH_4$. The average diameter of r-FCDs was found to be 4.9 nm. These were water dispersible with strong photostability. It was reported that r-FCDs were efficiently taken up by cancerous cells (SW480 and A549) and illuminated the whole cell with a clear distinction between cytoplasm and nucleus. It was revealed that as-prepared r-FCDs can be used as a promising probe for diagnosis and treatment of cancer.

A novel drug delivery system was synthesized by Dong et al. (2018), which was based on arginine−glycine−aspartic acid (RGD)-conjugated GQDs. Later, it was used to load the antitumor drug, DOX for monitoring drug delivery even in the absence of external dyes. It was reported that the release of DOX was strongly pH dependent, which involves hydrogen-bonding interaction between GQDs and DOX as compared to free DOX. It was observed that DOX-GQDs-RGD conjugates exhibited substantial cytotoxicity to U251 glioma cells within a wide range of DOX concentrations. This enhancement combined with efficient nuclear delivery improved the cytotoxicity of the drug DOX on application of GQDs.

A pH responsive nanodrug delivery system was reported by Wang et al. (2018). It was based on ZnO QDs for controlled release of drugs. They introduced poly(2-(dimethylamino) ethyl methacrylate) (PDMAEMA) and zwitterionic poly(carboxybetaine methacrylate) (PCBMA) for modification of

ZnO QDs. These helped in increasing blood circulation time, water stability, and also promoted endocytosis. The DOX (anticancer drug) was successfully loaded on ZnO@P(CBMA-*co*-DMAEMA) with a 24.6% drug loading. As-prepared ZnO@P(CBMA-*co*-DMAEMA) loaded with DOX could achieve lysosomal acid degradation and release DOX after endocytosis by tumor cells, which resulted in a synergistic treatment of cancer by an anticancer effect of Zn^{2+} and DOX, both.

Flak et al. (2018) have studied the preparation of GQDs−mesoporous silica NPs (MSNs) (GQDs-MSNs) nanocomposite as an efficacious intracellular drug delivery system and as a fluorescent factor for optical imaging. GQDs-MSNs nanocomposite NPs composed of GQDs and MSNs were presented as a proficient DOX delivery agent and nontoxic nanocomposite. It has been reported that the effectiveness of prepared GQDs-MSMs nanocomposite NPs for the drug delivery and release next to the bioimaging was analyzed for the case of HeLa cancer cells using a confocal laser scanning microscope and the transmission electron microscopy imaging technique.

Qian et al. (2018) synthesized GQDs hydrothermally and then encapsulated them with supramolecular β-cyclodextrin (β-CD) as a drug delivery system. Two drugs were selected, ranibizumab (Ran) and bevacizumab (Bev), which displayed an initial burst delivery percentage of 52.2% ± 2.6% and 55.7% ± 1.6%, respectively, within the first 15 min. This release from the β-CD encapsulated GQDs reached in a sustained manner 94.2% (Ran) and 93.1% (Bev) of loaded drug molecules after an hour. The biocompatibility of these carriers was evaluated qualitatively as well as quantitatively with the mouse Fibroblast L929 cell line. It was revealed that samples are nontoxic and highly compatible to the cells with >90% cell viability after 5 days of cell culture. The observed results indicate that developed NCs were suitable for the drug delivery system in the AMD.

The fact that graphene (G) is very hydrophobic, whereas GO is decorated by oxygen−containing hydrophilic group, permits both physical and chemical binding of drugs to the surface of G/GO for drug delivery uses (Zhang et al., 2017; Tadyszak et al., 2018; Wychowaniec et al., 2018). The GQDs, which are the most proficient carbon-based nanostructures, have a notable function in biological works (Khosravanian et al., 2021). It has been observed that owing to their small dimension, GQDs present a better perspective in biomedical applications than G or GO and when compared with graphene sheets, GQDs show improved biocompatibility and low toxicity, as promising materials used for the delivery of biologically active loads into living systems (Sangam et al., 2018; Mondal et al., 2019; Fasbender et al., 2019). In recent years, many researchers have shown that GQDs are very encouraging substrates for drug delivery systems. (Li et al., 2019a; Liang et al., 2019; Wang et al., 2019b; Zhao et al., 2020; Jahdaly et al., 2021).

Thovhogi et al. (2018) investigated the use of peptide-functionalized QDs for the imaging of prohibiting (PHB)-expressing cells in vitro and in diet-induced obese rats, which could potentially be used as NCs of antiobesity

drugs, dual targeted drug delivery, and molecular imaging of adipose tissues in obese patients in real time. Abdelhamid et al. (2019) loaded a natural cytotoxic agent (sesamol) onto cadmium sulfide QDs modified chitosan (CTS) to improve its activity. It was found that sesamol-CdS@CTS was more effective against cancer cells as compared to sesamol alone. It was revealed that half maximal inhibitory concentration values (IC_{50}) of CdS@CTS, sesamol, and sesamol-CdS@CTS were 1730 ± 54, 495 ± 16.4, and 117 ± 3.2 $\mu g\ mL^{-1}$, respectively, which indicated that CdS@CTS exhibited high loading efficiency, and can be used for drug delivery.

Triple negative breast cancer (TNBC) is the most fatal type of breast cancer. No targeted chemotherapy is available for the treatment of TNBC because of the absence of progesterone receptor, estrogen receptor, and human epidermal growth factor receptor-2. Ghosh et al. (2019) developed a targeted nonviral vector, which can diagnose TNBC and deliver the gene of interest efficiently. They synthesized carbon QDs from sweet lemon peel and then conjugated it with various generation of polyamidoamine (PAMAM) dendrimers to obtain CD-PAMAM conjugates (CDPs). The RGDS peptide was then further conjugated to CDP to target $\alpha v\beta 3$ integrin. Cellular cytotoxicity, DNA complexation assay, DNase I assay, hemolysis assay, cellular uptake, and in vitro transfection supported the fact that CDP3 is a promising gene carrier system for TNBC gene therapy. The CDP3 also exhibited selective quenching of fluorescence in the presence of Cu(II) with high efficiency (93%). The Cu(II) ion concentration remains upregulated in TNBC. It was predicted that CDP3 could be a promising theranostic tool for the treatment of TNBC.

A multifunctional $(Fe_3O_4/nGO)@mSiO_2/GQDs$ drug transporter, which consists of magnetic core Fe_3O_4, microwave−absorbing nanographene oxide, fluorescent GQDs, and intermediate barrier layer (mesoporous silica), used for loading and microwave-controlled release of an etoposide (VP16) as the anticancer drug, was developed by Wang et al. (2020). The loading rate of VP16 was found to be as high as 68%, and the release rate was observed to be 87% within 280 min.

Alarfaj et al. (2020) synthesized carbon QDs conjugated zinc oxide nanocomposite and used it as highly sensitive fluorescence immunosensing solution for fast determination of CYFRA 21−1 antigen in human serum. They used a hydrothermal method to prepare these QDs using *Citrus limon* pericarp. As-prepared carbon QDs were used to synthesize carbon QDs−zinc oxide nanocomposite by the reduction and stabilization of zinc acetate. As-fabricated immunosensing system based on this nanocomposite (CQDs-ZnO) provided its potential application in rapid diagnoses of lung cancer by detecting CYFRA 21−1 in human serum.

Large doses of anticancer drugs entering cancer cell nuclei are found to be effective for killing cancer cells and increasing chemotherapeutic effectiveness. Red-emitting carbon QDs were reported by Su et al. (2020) that can not only enter into nuclei of cancer cells but also stem cells of cancer.

The DOX was loaded (30 μg mL^{-1}) on the surfaces of carbon QDs. It was observed that average cell viability of HeLa cells was decreased to only 21%, whereas it was decreased to 50% for free DOX. Thus DOX-loaded carbon QDs shows a good therapeutic effect in elimination of cancer stem cells. This has great potential for carbon quantum-dot-based anticancer drug carriers to effectively eradicate cancers.

Nasrollahi et al. (2020) encapsulated GQDs in ferritin protein nanocages to design multifunctional nanoplatforms for cancer therapy and multimodal imaging. Encapsulation of ultrasmall GQDs is expected to reduce their quick excretion from the body and increase their bioimaging efficiency. They encapsulated GQDs and iron inside the core of AfFtn-AA (it is an engineered ferritin nanocage derived from the archaeon *Archaeoglobus fulgidus*). It was achieved through an iron-mediated, self-assembly of ferritin dimers, which afforded GQD−iron complex in the ferritin nanocages, (GQDs/Fe)AA. This (GQDs/Fe)AA showed strong fluorescence at low pH values and high relaxivities in MRI. These were used as a drug nanocarrier and imaging agent. These exhibited negligible cytotoxicity on the MDA-MB-231 cells and a high loading capacity (35%) of DOX. The (GQDs/Fe)AA can find potential applications as MRI agent, drug nanocarrier, and cancer diagnosis and therapy.

Traceable and pH-responsive DDS (MoS_2-PEG-DOX) based on MoS_2 QDs (MoS_2 QDs) was fabricated by Liu et al. (2020a) by covalently grafting MoS_2 QDs with diamine-terminated oligomeric PEG. Then a fluorescent antineoplastic anthracycline drug, DOX was loaded onto it. It was found that MoS_2-PEG-DOX nanoassembly can be effectively taken up by U251 cells, and as a result, enhanced DOX release is then triggered by intracellular acid condition. It reduces or diminishes the undesired side effects derived by the incorporation of DOX into healthy cells. It was concluded that MoS_2-PEG-DOX has a potential for high treatment efficacy in future therapy with minimal side effects.

Felix et al. (2021) decorated the GQDs through carbodiimide crosslinking reaction, where the imatinib molecule, projected to obstruct tyronise kinase, was used to cure leukemia. It has been shown that the integration of the imatinib on the surface of the GQDs did not modify the morphology and the properties of the NPs and that this type of the drug nanoplatform could destroy cancer cells inducing apoptosis. Han et al. (2021) constructed CQDs-based drug delivery system (Arg-Ag@Cu). They used l-arginine as precursor with duplex metal codoping (Cu and Ag) for DOX-loading/releasing and tumor theranostics. It was observed that Ag-doping increased PL intensity while Cu^{2+} could act as an anchor resulting in adjustable size of CQD for increasing the drug loading capacity. It was revealed that the structure of Arg-Ag@Cu was disrupted due to Cu^{2+} depletion, which supported in situ DOX-releasing. It was also revealed that there were synergistic effects, which suppressed tumor progression and migration with relatively no or minimal side effects.

Liu et al. (2021) presented some GQDs functionalized with polyethyleneimime (PEI) as a new messager RNA (mRNA) delivery system demonstrating that these modified GQDs can be utilized to provide intact and functional mRNA to Huh−7 hepatocarcinoma cells at low quantities and that these functionalized GQDs can be considered as ideal delivery system. Ruzycka-Ayoush et al. (2021) used Ag−In−Zn−S QDs modified with L-cysteine, 11-mercaptoundecanoic acid, and lipoic acid decorated with FA. It was then used as a novel target drug delivery system for targeting DOX to folate receptors on adenocarcinomic human alveolar basal epithelial cells (A549).

It has been shown that GQDs are materials capable of responding to physical stimuli, such as magnetic fields, ultrasound, and light, and this fact permitted the precise control of drug release (Dai et al., 2017; Gu et al., 2019; Liu et al., 2021). Some researchers have reported that small molecule-modified GQDs could be used for simultaneous cellular drug delivery imaging, modifying GQDs with arginine−glycine−aspartic acid (RGD) (Qiu et al., 2015) and FA (Wang et al., 2014), explaining that the antitumor drug DOX-loaded RGD- or FA-modified GQDs could not only transport drugs to target cells, but supervise the cellular operation uptake of the drug in real time without using external dyes (Wang et al., 2017).

11.4 Sensing

It has been established that biotechnology, in combination with nanotechnology, provides the enhanced evolutionary biological components needed to create novel smart sensors and advanced characterization and manufacturing mechanisms to solve environmental and biological problems (Ray et al., 2009; Choi and Montemagno, 2016).

A selective chemiresistive gas sensor for detection of carbon dioxide at room temperature (~25°C) was prepared by Rathi and Pal (2020). It contains ruthenium-decorated tungsten disulfide (Ru@WS_2) QDs as the sensing material. They used a mixed solvent of lithium hydroxide and N-methyl-2-pyrrolidone (NMP) to prepare Ru-decorated WS_2 QDs from the exfoliated WS_2 nanoflakes. The gas sensors were fabricated by spraying the QDs (WS_2 QDs and Ru@WS_2 QDs) on gold interdigitated electrodes, which were then exposed to different concentrations of CO_2 gas in dry air conditions. It was reported that Ru@WS_2 QD-based sensor exhibit superior sensitivity and good selectivity to CO_2 gas as compared to WS_2 QD to isopropanol, acetone, ethanol, methanol and benzene at room temperature. This sensor showed an increase in resistance when it was exposed to CO_2 gas ranging from 500 to 5000 ppm.

Bhatt et al. (2020b) performed some excellent approaches, which present all significant aspects of QDs properties. Such unique properties have been created for successful applications, which comprise photodetectors, photovoltaic devices, photocatalysis, biosensors, chemical sensors, displays, photodynamic therapy,

laser diodes, and so on. Due to their special PL and electrochemical features, GQDs are among the most interesting carbon-based NMs used to fabricate biosensors (Xie et al., 2016).

In accordance with the technique that is applied, GQDs-based sensors can be classified into the following broad groups: PL sensors, chemiluminescence (CL) sensors, and electrochemical (ECL) sensors; these QDs-based sensors and biosensors provide a plethora of opportunities to diagnose an extensive range of diseases and improve therapeutic actions (Henna and Pramod, 2020).

Bhakat et al. (2021) developed a facile method to prepare ZnO QDs into three-dimensional superstructures through surface complexation between zinc ions and phosphate. It was reported that the addition of phosphate to ZnO QD dispersion led to growth of such parahopeite structures along with crystalline assembly of QDs in the colloidal medium. It was revealed that the as-prepared ZnO QD−phosphate crystalline assembly can be successfully applied to fabricate a gas (CO_2) sensor, which exhibited great selectivity and sensitivity toward carbon dioxide gas at room temperature.

11.4.1 Photoluminescence sensors

A new, simple and highly sensitive PL evaluation method for the activity of a protein kinase depending on the selective aggregation of the phosphorylated peptide-GQD conjugates triggered by Zr^{4+} ion coordination was proposed by Wang et al. (2013b). The developed technique has revealed some feasible uses in kinase inhibitor screening. The inhibition of CK2 phosphorylation activity by four various inhibitors was examined in human serum by analyzing the signals from samples incubated with and without any inhibitors. It was revealed that PL intensity was enhanced by improving the efficiency of the inhibitor.

Sun et al. (2013) presented various methods and some future prospects for the progress of the smart sensing platform based on GQDs, showing that GQDs, which are produced using diverse procedures, can emit PL with different colors and in these GQDs, PL is controlled by numerous parameters, such as size, shape, excitation wavelength, pH, concentration, surface oxidation degree and surface functionalization.

A precise technique for the preconcentration and the determination of GO in natural river water samples utilizing fluorescent GQDs was studied by Benitez-Martinez et al. (2014). The functioning of the presented GQDs sensor is related to the interaction between GO and GQDs via hydrophobic $\pi-\pi$ stacking of the GO with aromatic network at the GQDs surface; this fact causes a quenching effect of the fluorescence of GQDs, that was used as an investigative indicator for their quantification. The LOD was calculated to be $35\,\mu g \cdot L^{-1}$. It was reported that the precision for a $200\,\mu g \cdot L^{-1}$ concentration of GO was found to be 5.16%.

Benitez-Martinez and Valcárcel (2015) reviewed the principal analytical uses of GQDs, highlighting more details on the progress of various categories of sensors, which are used to detect metal ions, small organic molecules and biomaterials with enhanced sensitivity. They have shown that GQDs are recent materials for designing and tuning sensors (and biosensors) and they focused mostly on the presentation of some important analytical applications in the field of PL-based sensors.

Zor et al. (2015) studied the synthesis and characterization of a new multifunctional composite material, magnetic silica beads/GQDs/molecularly imprinted polypyrrole (mSGP), where mSGP is designed to capture and signal small molecules; thanks to the synergy among chemical, magnetic, and optical attributes that are connected with the molecular printing of tributyltin. It was observed that the studied multifunctional material allowed a fast and highly sensitive scaffold for small molecules detection even in complex media such as seawater without any sample treatment.

All-inorganic cesium lead halide ($CsPbBr_3$) perovskite QDs, as one kind of promising material, have attracted considerable attention in optoelectronic applications. Colloidal $CsPbBr_3$ QDs were synthesized by Chen et al. (2017a) by adjusting the reaction temperatures with tunable PL (493−531 nm). It revealed narrow emission bandwidths of 25 nm. Average diameters of the QDs were calculated and it was found that this could be adjusted from 7.1 to 12.3 nm on increasing temperature from 100°C to 180°C. They also fabricated green LEDs using $CsPbBr_3$ QDs cast on blue LED chips, which have a great potential for applications in the field of lighting technology and display.

Quaternary $Zn_xAgInSe$ QDs were synthesized by Ding et al. (2017) with different Zn/Ag ratios. These were then evaluated as temperature sensors. A correlation between different temperatures and emission intensity, luminescence energy, and full-width at half-maximum of the emission band was observed; where only a small deviation was observed from the actual temperature, indicating that $Zn_xAgInSe$ QDs can be used as temperature sensors with high sensitivity.

Duran et al. (2017) presented a modern, rapid, inexpensive, and acid treatment procedure for the synthesis of copper-modified GQDs. Then this was used for the quantification of penicillamine (PA) in pharmaceutical samples using interaction of the drug with Cu-modified GQDs (Cu−GQDs). It was reported that under the best conditions for interaction, a linear response was remarked (in the concentration range 0.10−7.50 pmol L^{-1} PA) and the viability of the recommended fluorescent sensor has been demonstrated.

The $CsPbBr_3$@Ag hybrid nanocrystals were synthesized by Ye et al. (2017). They treated $CsPbBr_3$ nanocrystals with silver halides (Cl, Br, or I) powders in hexane for this purpose. It was indicated that particle size of Ag NPs varied between 2 and 5 nm and these were nucleated randomly outside these hybrid $CsPbBr_3$ nanocrystals. An enhanced PL intensity of $CsPbBr_3$@Ag hybrid nanocrystals was observed as compared to $CsPbBr_3$ nanocrystals under the light of

400 nm, to achieve an enhanced PL. They optimized $CsPbCl_xBr_{3-x}$@Ag hybrid nanocrystals so that the effect of plasmonic resonance enhancement occupied a significantly advantageous position. It was suggested that as-constructed $CsPbBr_3$@Ag hybrid nanocrystals can find new opportunities for application in optoelectronic devices and LEDs.

Sahub et al. (2018) developed a novel real-time biosensor of GQDs-based enzymatic reaction (GQDs AChE/CHOx) for monitoring the organophosphate (PO) pesticides. It was observed that H_2O_2 created from the active enzymatic reaction of acetylcholinesterase (AChE) and choline oxidase (CHOx) allowed to react with GQDs inducing a "turn-off" PL of GQDs. The limit of detection of this biosensor was calculated to be 0.172 ppm (0.778 μM). The suggested biosensor was successfully applied for the determination of dichlorvos, utilizing a reduced price procedure via a connection with green chemistry approach.

Xu et al. (2018) produced a high PL quantum yield for transition metal carbide (2D) MXene (nitrogen-doped, N-doped Ti_3C_2) QDs. They used Ti_3C_2 and ethylenediamine as a precursor and nitrogen source, respectively. The average size of hydrothermally treated N-doped Ti_3C_2 QDs was 3.4 nm and PLQY of up to 18.7% was observed. As-prepared N-doped Ti_3C_2 QDs were then used as an ultrasensitive detector probe for iron ion (Fe^{3+}) with a limit of detection up to 100 μM. It was also reported that as-developed MXene QDs can find application in biological sensing for detection of H_2O_2 with high sensitivity. These QDs have a lot of applications such as solar cells, electronics, biomedical, optical, photocatalysis, biosensors, white light emission devices, and environmental fields.

Li et al. (2019b) introduced a stoichiometry control over both; core and shell regions of InP/ZnSe/ZnS QDs. As-obtained QDs exhibited PL quantum yield (almost approaching 1), narrow line width, monoexponential decay dynamics and nonblinking at a single-dot level. These quantum-dot LEDs (QLEDs) based on InP/ZnSe/ZnS core/shell/shell QDs are good emitters exhibiting a peak external quantum efficiency (12.2%) and a maximum brightness ($>10\ 000\ cd\ m^{-2}$), which is more than Cd/Pb-free QLEDs. It was revealed that these Cd/Pb-free QDs can prove to be outstanding optical and optoelectronic materials.

11.4.2 Chemiluminescence sensors

The L-cysteine capped CdS QDs were prepared by Hassanzadeh et al. (2017) via a hydrothermal route. It was found that as-prepared CdS QDs show a significant effect on the CL reaction of the rhodamine B (RhB)-cetyltrimethylammonium bromide (CTAB)-$KMnO_4$ system. It was also found that CL emission intensities of these QDs exhibited a change in the presence of methamphetamine (MA) (even in low quantities). It was observed that MA can remarkably increase the intensity of CL system and this improved CL intensity was found to be proportional to MA concentration in the range of

0.25−125 ng mL^{-1} with a limit of detection of 0.086 ng mL^{-1}, which was more than 20 times higher than the FL method. The as-developed CL method was used for accurate determination of MA in real samples (human urine).

The *N*-(Aminobutyl)-*N*-(ethylisoluminol)/(ABEI) functionalized GQDs (ABEI-GQDs) with outstanding CL and FL attributes were synthesized by Gao et al. (2017). They observed that as-synthesized ABEI-GQDs exhibited exceptional CL features, when reacted with H_2O_2 and wavelength−tunable FL emission with increasing excitation wavelength. They built a pesticide−sensing array for pesticide differentiation using their CL and FL properties. It was reported that new CL and FL dual-signal GQDs (ABEI−GQDs) have been developed, which could find more interesting future uses in bioassays and bioimaging.

Khataee et al. (2018) developed a modern and high CL system using the promoting effect of GQDs/bisulfite on rhodamine B(RB)−H_2O_2 CL reaction. It was reported that the existence of sodium dodecyl sulfonate (SDS) and sodium bisulfite resulted in a much improved action of GQDs. It was recalled that the International Agency for Research on Cancer and the Environmental Protection Agency estimated the cancer risk of formaldehyde (HCHO) on human and classified this compound as carcinogenic (Lobo et al., 2015; Khataee et al., 2018). This CL system, which is dependent on the oxidation of rhodamine B, has been shown to be a successful chemosensor for HCHO, noting that HCHO can decrease the developed CL system. It was found that a linear change of the CL response was achieved in HCHO concentration ranges of 0.02−5 and 5−11 μg L^{-1} with a limit of detection and quantification of 6 and 20 ng L^{-1}, respectively.

The captivating contribution of GQDs in introducing sensors is due to the fact that they can be used as a luminescent donor, energy acceptor, or amplification (catalyst) pathway for the system of CL resonance energy transfer (CRET), enhancing the sensitivity of detection (Pang et al., 2018; Chen et al., 2020). Pang et al. (2018) showed that GQDs could notably improve the CL reaction of Ce(IV) with $NaHSO_3$ using energy and electron transfer. It was observed that the CL intensity of the GQDs-Ce(IV)-$NaHSO_3$ model was inhibited by tyrosine (Tyr), which has a significant function in the metabolism and growth of human and animals. The recommended (CRET) method can be successfully used for Tyr evaluation in milk samples with a high precision.

Irani-Nezhad et al. (2019) synthesized WS_2 QDs through solvothermal method. As-obtained WS_2 QDs had a size of 1−1.5 nm with fluorescence emission depending on excitation wavelength. These WS_2 QDs show a catalytic effect in the decomposition of H_2O_2. As-prepared WS_2 QDs exhibit a mimetic effect in the H_2O_2−rhodamine B CL system. The H_2O_2 is one of the products in the enzymatic reaction of glucose, which can be easily determined using WS_2 QDs. It was reported that H_2O_2 can be detected in the concentration range (0−1000 nmol L^{-1}) with a limit of detection as 2.4 nmol L^{-1}.

Vahid et al. (2019) developed a method for the sensitive determination of cyanide ions (CN^-) in biological as well as environmental samples. They used a CRET-induced CL system for this purpose. Hydrogen peroxide−bicarbonate system was selected for CL reaction. It was reported that glutathione-stabilized CdSe QDs (CdSe QDs) increase CL intensity significantly. On the contrary, it was observed the CRET system could be prohibited and CL emission turned off by gold nanoclusters (Au NCs). On efficient dissolution of Au NCs, the CRET to CdSe QDs was restored and CL emission was turned on. It can be used as a highly sensitive and reliable measurement of cyanide ions in the concentration range of 2−225 nM, with a limit of detection of 0.46 nM.

Hallaj et al. (2020) prepared S,N-doped carbon QDs (S,N-CQDs) via a hydrothermal method. They observed effect of as-prepared CQDs on the luminol−Mn(IV) CL reaction and it was found that S,N-CQDs increased the CL intensity of this reaction about 13-fold. It was also revealed that the CL intensity of this system was drastically reduced in the presence of uric acid. They designed a probe for the detection of uric acid using the amplified CL system and it was observed that it was proportional to the logarithm of uric acid concentration in the range 0.05−1.5 μM with a detection limit of 17 nM. Thus they developed a sensitive CL method for the detection of uric acid in biological fluids.

Rasoulzadeh and Amjadi (2021) prepared highly luminescent water-soluble $AgInS_2$ QDs (AIS QDs) via a green and hydrothermal method. It was reported that $NaIO_4$ in alkaline solution elicits a remarkable CL from as-prepared QDs. It was also revealed that the addition of glutathione to this $NaIO_4$-AIS QDs system enhanced CL intensity effectively, and therefore it was used as a sensing platform for the assay of GSH. It was reported that there is a relation between GSH concentration and CL intensity, which was linear in the range (1.0×10^{-9} mol L^{-1} to 5.0×10^{-6} mol L^{-1}) with a limit of detection of 2.8×10^{-10} mol L^{-1}. They also confirmed its usefulness in the analysis of human plasma.

Yahyai et al. (2021) developed a paper-based analytical device integrated with a potent CL system to find out deltamethrin (DM), using the enhancing effect of polyphosphate (PP) on GQDs-$KMnO_4$ CL reaction. They showed that the realized multiemission CL structure was investigated for analytical applications. It was revealed that under the optimized conditions, the generated signal is reduced by increasing the DM concentration in the range of 0.3−10 μg mL^{-1} with LOD as 0.15 μg mL^{-1}. This can be presented as an advanced analytical detection technique determination for DM in food samples, for on-site screening scopes.

11.4.3 Electroluminescence sensors

A high sensitivity label-free ECL immunosensor has been constructed by Wu et al. (2016) for the detection of prostate−specific antigen (PSA) based on GQDs. They used Au/Ag-rGO as electrode material to load the amounts

of aminated GQDs and carboxyl GQDs to amplify the ECL signal. The developed methodology shows that the ECL intensity decreased linearly with the logarithm of PSA concentration and the LOD is 0.29 pg mL^{-1}. The immunosensor can be successfully utilized in disease and drug analysis.

Shan et al. (2016) proposed CdS QDs as electrochemical sensing materials for determination of ciprofloxacin (CIP). It was reported that CdS QDs-modified glassy carbon electrode (GCE) exhibited a good anodic stripping response in acidic medium, which was attributed to the release of Cd(II) ions from CdS QDs. It was observed that anodic stripping current of Cd(II) on CdS QDs/GCE was found to decrease in solution, when CIP was added, which may be due to the complexation of CIP with in situ generated Cd(II) ions. A linear relationship was obtained between the anodic stripping voltammetric response of CdS QDs/GCE and concentration of CIP in the range (1.0×10^{-7}–1.0×10^{-5} mol L^{-1}) with a limit of detection as 2.2×10^{-8} mol L^{-1}. The use of CdS QDs-modified electrode for determination of CIP was observed in biological fluids.

The black phosphorus QDs (BPQDs) were synthesized by Ding et al. (2018) and then added into the solution of ZnO nanorods to obtain BPQDs-doped ZnO NPs (BPQDs@ZnO). They used a hydrothermal route for this purpose. The doping of BPQDs resulted in the formation of cubic BPQDs@ZnO NPs. The ECL of BPQDs@ZnO was investigated under neutral conditions. They obtained a cathodic ECL signal in the presence of $K_2S_2O_8$ that is relatively stronger than for ZnO nanorods. It was observed that cytochrome c exhibited an inhibiting effect on BPQDs@ZnO ECL, which can be sensitively detected in the range of 1.0×10^{-9}–5.0×10^{-7} mol L^{-1} with a limit of detection as 9.6×10^{-10} mol L^{-1}. It was revealed that such ECL characteristic of BPQDs-based nanocomposite has a potential in biosensing application.

Jie et al. (2019) developed an innovative procedure for amplified ECL detection of DNA utilizing the magnificent ECL activity of GQDs combined with a multiple cycling amplification mechanism. They used a novel poly (diallyldimethylammonium chloride) (PDDA)-GO complex to immobilize GQDs on the electrode to improve the ECL signal. This method is based on ECL quenching of Au NPs to GQDs combined with endonuclease aided cyclic amplification scheme, which has good application perspective in biosensing research, mainly in clinical diagnoses.

Wang et al. (2019a) reported a novel highly sensitive cloth-based closed bipolar ECL (C–BP–ECL) sensor with nanostructured electrode surface. The proposed method is based on the combination of chitosan (CS), poly (diallyldimethylammonium chloride)-functioned multiwalled carbon nanotubes (PDDA-MWCNTs), and GQDs–gold NPs (GQDs–AuNPs/PDDA) on the wax/carbon ink-screen-printed cloth-based device. The combination of GQDs–AuNPs-MWCNTs/CS, C-BP-ECL, and cloth-based microfluids for the detection of highly sensitive glucose has been established for the first

time, showing that glucose concentrations in complex human serum samples can be determined with this technique.

A novel ultrasensitive ECL sensor was studied by Niu et al. (2020) that can be used to detect a common food additive (sunset yellow). They used GQDs as the luminescent factor and potassium persulfate as the coreactant, showing that the ECL signal of the GQDs changed with the inclusion of sunset yellow. It has been observed that this method provides fast screening of possibly harmful food additives and, under optimized conditions, the GQD sensor exhibits a good linearity in the detection of sunset yellow in the concentration range of 0.0025−25 μM with a LOD as 7.6 nM.

de França et al. (2021) modified graphite working electrode (5 mm diameter) with CdSe/CdS magic-sized QDs (MSQDs) to increase its sensitivity. This modified electrode was fully characterized and optimized. It was reported that the best results were obtained when MSQDs (10 μg) were deposited on the electrode surface. It was revealed that a QDs-based sensor exhibited good stability, reproducibility, and repeatability. Such an electrochemical sensor was used for detecting dopamine. The signal showed dependence in the concentration range 0.5−15 $\mu mol\ L^{-1}$ with a limit of detection of 96 $nmol\ L^{-1}$. This was also successfully used for sensing of dopamine in real samples (human blood serum) with recovery rates ranging between 95.2% and 102.6%.

11.5 Others

Shao et al. (2012) linked most the promising suicide genes (herpes simplex virus thymidine kinase, HSV-TK gene) with CdTe/CdS core/shell QDs using the EDC/NHS coupling method. It was reported that plasmid TK intracellular trafficking can be distinctly and effectively traced via monitoring QDs' luminescence for up to 4 days after transfection of QDs-TK conjugates into Hela cells. It was observed that QDs-TK conjugates have more efficient cytotoxicity on addition of GCV into Hela cells, and these QDs do not show any detectable adverse effects on the cellular processes. It was revealed that photonic NMs (QDs) can be used as a tool for monitoring TK gene delivery and anticancer activity.

Ng et al. (2013) investigated cell-based cytotoxicity of N-acetyl-cysteine (NAC) QDs and also the effect of QDs on the beta (1−40) amyloid ($A\beta_{1-40}$)-induced cytotoxicity on human neuroblastoma SH-SY5Y cells by MTT (3-(4,5-dimethylthiazol-2-yl)-2,5-diphenyltetrazolium bromide) and reactive oxidative species (ROS) assays, respectively. It was reported that the inhibition of $A\beta_{1-40}$ peptides from fibrillation using NAC−QDs had a neuroprotection effect on the neural SH-SY5Y (neuron) cells.

Shao et al. (2014) also reported a QD-based technique that revealed a method of herpes simplex virus thymidine kinase (HSV-TK) suicide gene therapy by forming a covalent linkage between the TK gene and NIR fluorescent QDs. It was interesting to note that stable QD labeling did not affect

either the biological activity of the TK gene or QDs fluorescence. They traced the intracellular behavior antitumor effect of the TK gene in vivo and in vitro. It was revealed that the TK gene was shuttled to the nucleus after 24 h treatment. A single dose of GCV administration at that time exerted a gradually increasing lethal effect for 72 h. It was proposed that this technique may be useful for cancer therapy in the future.

Weng et al. (2015) synthesized mannose-modified fluorescent carbon QDs (Man-CQDs) via a simple one-step dry heating method from solid ammonium citrate and mannose. It was reported that highly soluble Man-CQDs had average particle diameter of 3.1 ± 1.2 nm. It can be successfully applied for labeling *Escherichia coli*. The labeling efficiency of Man-CQDs can be optimized by controlling the ratio of ammonium citrate/mannose. They demonstrated that quantitative detection of the bacteria *E. coli* (450 CFU) is possible because of specific binding of the mannose units to *E. coli* in lab samples, and it can be also applied to real samples (tap water, human urine, and apple juice).

Magnesium and nitrogen codoped carbon QDs (Mg-N-CQDs) were prepared by Liu et al. (2016) via a hydrothermal method. It can be used as a fluorescent switch for selective and sensitive sensing of Hg(II) and cysteine (Cys). The fluorescence of Mg-N-CQDs aqueous solution was quenched on addition of Hg(II) and it has been attributed to the formation of a nonfluorescent complex between Mg-N-CQDs and Hg(II). But the fluorescence of these QDs aqueous solution containing Hg(II) could be recovered back in the presence of Cys in a gradual manner, as Hg(II) has stronger binding affinity toward Cys than toward Mg-N-CQDs. They designed a fluorescent probe and applied it to detect Hg(II) ions in real water samples with satisfactory results.

A green hydrothermal strategy has been devised by Bao et al. (2018) to produce water-soluble nitrogen/phosphorus (N/P) codoped CQDs using edible *Eleocharis dulcis*. As-prepared CQDs exhibited high quantum yield, remarkable excitation-dependent emission, long lifetime, and superior fluorescence stability. The N/P codoped CQDs had a wide-range capability to determine inorganic cations as fluorescence sensor. They showed remarkable selectivity and sensitivity for Fe^{3+} ions.

Kumari et al. (2018) used the residue obtained from the pyrolysis of waste polyolefins, for preparing highly green-visual fluorescent carbon QDs via a simple one-step hydrothermal approach, which consists of ultrasonic-assisted chemical oxidation. The use of as-synthesized CQDs as a fluorescent sensor for Cu^{2+} ions detection was investigated, where excellent sensitivity and selectivity were exhibited for detecting Cu^{2+} ions with a limit of detection of 6.33 nM in the detection range of $1-8.0\,\mu M$. It was also revealed that these CQDs show their use in the analysis of real water samples. Apart from this, CQDs have the potential for TNBC cells (MDA-MB 468 cells) imaging.

Xiang et al. (2018) conjugated FA onto the surface of ZnO QDs (QDs)-NH_2 via an amidation reaction. As-prepared titania nanotubes (TNTs) loaded with vancomycin (Van) are capped by these FA-functionalized ZnO (ZnO-FA) QDs. This arrangement keeps them stable in normal physiological environments, but dissolves as Zn^{2+} in the mildly acidic environment after bacterial infections. The antibacterial ratio of TNTs-Van@ZnO-FA QDs against *Staphylococcus aureus* was increased from 60.8% to 98.8%, while it only increased from 85.2% to 95.1% for TNTs-Van, when the pH of the environment was decreased from 7.4 to 5.5. It was suggested that this surface system has a promising bioplatform on Ti-based metallic implants as it prevents bacterial infection with a long-lasting effect. It is suitable for various applications like antifungal, antibacterial, antiinflammatory, antioxidant, and wound healing.

Murugan et al. (2019) developed facile, rapid and frugal approach for the synthesis of highly fluorescent carbon QDs by pyrolysis of finger millet ragi (*Eleusine coracana*) (carbon source). It was found that the size distribution was in the range of 3−8 nm. It was indicated that Cu^{2+} strongly quenched the fluorescent intensity of these CQDs as compared to other metal ions such as Mg^{2+}, Pb^{2+}, Ni^{2+}, Mn^{2+}, Hg^{2+} Al^{3+}, Ca^{2+}, and Cr^{3+}. A linear correlation was observed between quenching efficiency concentration of Cu^{2+} ions in the range from 0 to 100 μM. These CQDs were also applied in sensing of Cu^{2+} in real water samples and the limit of detection was 10 nM. It was found that Ni^{2+} and Cu^{2+} formed a very strong bonding with CQDs compared to other divalent ions. It was revealed that Cu^{2+} get adsorbed on aromatic C═C (π-bond) of CQDs preferentially while other divalent metals form σ-bond(s) with the CQDs.

An easy and economical synthesis of highly fluorescent nitrogen-rich carbon QDs (N-CQDs) was reported by Bao et al. (2019). It was observed that as-prepared N-CQDs can act as a sensor for the "turn-off" detection of Co^{2+} in the range of 0.5−3 μM with a detection limit of 0.12 μM. The fluorescence of the quenched N-CQDs was formed to reappear and get "turn-on," when GSH, AA, EDTA, and cyst were used. It was claimed that N-CQDs were also successful in detecting the trace level of Co^{2+} in vitamin B_{12} sample.

Fluorescent QDs with optical properties (such as tunable broad excitation, robust photostability high quantum output, and restricted emission spectra) are utilized as a new class of optical probe in biological and biomedical fields (Jahangir et al., 2019). Lei et al. (2019) proposed an eco-friendly synthetic procedure to prepare emission-tunable carbon QDs. The particle size of as-synthesized CQDs was found to be 2.4 nm. Significant properties of controllable emission make these QDs a potential candidate for sensor applications.

Chandra et al. (2020) developed a fast and eco-friendly one-pot hydrothermal technique for synthesizing nitrogen/sulfur-codoped fluorescent carbon QDs (NS-CQDs). They used simple precursors such as citric acid and thiosemicarbazide. The as-prepared NS-CQDs were used successfully as a

nanoprobe for detecting picric acid (PA) in different derivatives. It was also reported that this system exhibited low cytotoxicity and excellent biocompatibility in HeLa cervical cancer cells. It was reported that it can be used for the detection of PA in environmental, analytical, and pathological applications.

GQDs have low cytotoxicity and higher biocompatibility as compared to other QDs, The optical properties of QD and have the ability to cross the blood−brain barrier, and therefore GQDs can be useful in neuroscience diagnostics and therapeutics. Their smaller size, surface chemistry and ease of loading of different drugs make them potential drug delivery systems as they could travel through the bloodstream up to the brain. Perini et al. (2020) discussed the applications of GQDs in drug delivery to the central nervous system, bioimaging, and photophysical therapies.

Kateshiya et al. (2020) proposed a synthetic route for the preparation of highly blue fluorescent tyrosine coated molybdenum oxide QDs (Tyr-MoO_3 QDs). Here, tyrosine (Tyr) was used as a surface ligand to functionalize MoO_3 QDs. They obtained color changes in the solution of MoO_3 NPs, MoO_3-OH NPs and Tyr-MoO_3 QDs in presence of UV and day light. It was reported that as-prepared Tyr-MoO_3 QDs could act as a sensor for rapid and sensitive identification of imidacloprid. It was revealed that emission peak of Tyr-MoO_3 QDs at 416 nm exhibited a linear quenching on increasing concentration of imidacloprid in the range (0.045−1.00 μM). The proposed method was successfully applied for the detection of imidacloprid in real samples also.

The activities of ions are closely associated with the physiology of brain such as neural activity, intracranial cell membrane potential, and neuropathology. Therefore, monitoring the levels of ion in the brain is of utmost importance in neuroscience. A powerful tool has emerged as nanosensors for monitoring brain ion levels, cell function, neural activity, and it can also be used in the diagnosis of diseases. The advances in the design and application of these ion level nanosensors at different physiological levels have been reviewed by Wei et al. (2020).

Jlassi et al. (2021) prepared GQDs from graphitic waste. These GQDs were evaluated as resistive humidity sensors. Such resistive humidity sensors were fabricated on the prepatterned interdigital indium tin oxide electrodes with three different concentrations (2.5, 5.0, and 10 mg) of GQDs in N, N-dimethylformamide (DMF). It was observed that GQDs (10 mg mL^{-1})-based impedance sensors exhibited good sensitivity as compared to the other ratios (2.5 and 5 mg). They reported that the maximum calculated hysteresis of the GQDs-based humidity sensor was found to be around 2.2% at 30%RH while the minimum was 0.79% at 60%RH. It was revealed that response and recovery time were 15 s and 55 s, respectively.

11.6 Toxicity of quantum dots

Yan et al. (2011) investigated the potential vascular endothelial toxicity of QDs, particularly of mercaptosuccinic acid-capped CdTe QDs in vitro. They

synthesized pH stable and water-soluble CdTe QDs and their cell viability were tested. The presence of CdTe QDs ($0.1-100\ \mu g\ mL^{-1}$) decreased the cell viability of human umbilical vein endothelial cells (HUVECs), which indicated that these QDs induced significant endothelial toxicity. It was also revealed that CdTe QDs ($10\ \mu g\ mL^{-1}$) exhibited mitochondrial network fragmentation, significant oxidative stress, and disruption of mitochondrial membrane potential. It was suggested that these QDs not only impaired mitochondria but also induced endothelial apoptosis and exerted endothelial toxicity, providing strong evidence of the direct toxic effects of QDs on human vascular ECs, and indicating that exposure to QDs is a significant risk for the development of cardiovascular diseases.

Smith et al. (2012) selected primary human liver (PHL) cells and HepG2 cells as in vitro tissue culture models to observe the possible adverse effects of copolymer-coated CdSe/ZnS QDs poly(maleic anhydride-*alt*-1-tetradecene) (TOPO-PMAT copolymer CdSe/ZnS QDs) (when TOPO = tri-*n*-octylphosphine oxide) and PMAT. However, PHL cells did not take up TOPO-PMAT CdSe/ZnS QDs, but some nonparenchymal cells did, particularly Kupffer cells. No acute toxicity or morphological change was noted in these systems up to 40 nM. It was observed that cellular stress markers and proinflammatory cytokines/chemokines were increased in PHL cell cultures, which suggests that these QDs are not likely to cause acute cytotoxicity in the liver but may elicit inflammation or hepatitis.

Liu et al. (2015) evaluated cytotoxicity of four types of QD formulations (PEGylated phospholipid encapsulated CdSe/CdS/ZnS QDs (CdSe-Phos), MPA modified CdSe/CdS/ZnS QDs (CdSe-MPA), Pluronic F127 encapsulated CdTe/ZnS QDs (CdTe-F127), and PEGylated phospholipid encapsulated InP/ZnS QDs (InP-Phos)) in two different human cancer cell models (neuroblastoma (SH-SY5Y), gastric adenocarcinoma (BGC-823) cell lines).

Wang et al. (2016) reviewed the toxicity of GQDs, including raw GQDs, chemically doped GQDs, and chemically functionalized GQDs and also presented some important details related to the uptake process by cells and parameters managing the toxicity of GQDs (concentration, synthesis methods, particle size, and surface chemistry). Various issues related to the toxicity regulation of GQDs through chemical modification were discussed, exposing some important aspects about the toxicity mechanism through generation of ROS by some GQDs.

Xiao et al. (2016) studied the cytotoxicity of two types of QDs on *Chlorella pyrenoidosa* at different concentrations:

- carbon QDs (CQDs): Undoped CQDs, N-doped CQDs, N,S-doped-CQDs; and
- metal QDs (MQDs): CdS QDs, CdTe QDs, $CuInS_2$/ZnS QDs.

The Chla contents were found to be consistent to the number of algae cells, when *C. Pyrenoidosa* was treated by different concentrations of QDs.

It indicates a good dose-response relationship. The EC_{50} of undoped CQDs, N-doped CQDs, N,S-doped CQDs, CdS QDs, CdTe QDs, and $CuInS_2$/ZnS QDs was observed as 232.47, 185.83,38.56, 4.88, 0.015, and 459.5 mgL^{-1}, respectively at 96 h. They observed toxicity order as follows:

$CuInS_2$/ZnS QDs <Undoped CQDs <N-doped CQDs <N,S-doped CQDs <CdS QDs <CdTe QDs.

It was concluded that the toxicity of CQDs was relatively less as compared to MQDs, but $CuInS_2$/ZnS QDs exhibited the lowest toxicity.

The toxicity of NMs is one of the crucial challenges facing their use in biotechnology (Chen et al., 2017b). The growing biomedical domain of G-based material applications, including GQDs, raises some queries about their short- and long-term cytotoxicity (Tadyszak et al., 2018).

A comparison of the toxic effects was made by Pramanik et al. (2018) between CdSeQDs, silicon QDs, and CdSe/ZnS QDs. They selected two model bacteria: Gram-negative bacterium (*Shewanella oneidensis* Mr-1) and a Gram-positive bacterium (*Bacillus subtilis* SB 491). It was indicated that the silicon QDs not associated with the cell membranes are benign to these bacteria. On the other hand, CdSe cores exhibited significant toxicity to these bacteria while CdSe/ZnS QDs are relatively less toxic.

Deng et al. (2018) have utilized the Illumina high-throughput RNA sequencing to examine the whole-transcriptome profiling of zebrafish larvae after exposure to GQDs, identifying 2116 differentially expressed genes between GQDs exposed groups and control. Zebrafish is a preferred type of an organism for toxicity testing due to its small dimension, reduced maintenance price, and optical transparency (Grunwald and Eisen, 2002; Hill et al., 2005; Dai et al., 2014; Sonthanasamy et al., 2016; Chen et al., 2016; Tang et al., 2017; Deng et al., 2018; Liu et al., 2020b).

Little is known about the developmental disturbance in animals after GQDs exposure at some concentration values that are higher than the tolerable level (Deng et al., 2018). It has been reported that the acute inflammatory responses and detoxifying complex represent the principal GQDs-activated pathways and that GQDs can perturb the blood homeostasis via upregulating the renin−angiotensin system structure. Some results related to the molecular processes of possible bleeding risks and detoxifying operations have been reported as an effect to GQDs exposure.

Nikazar et al. (2020) pointed out that even if the latest classes of new manufactured QDs exhibit ever-better physical properties, some details related to their cytotoxicity are some major drawbacks, and in order to address the challenges of QD research it is vital to examine the type of the characteristics that make these QDs toxic. They also reviewed changes in toxicity of GQDs, when they are in association with other metal ions.

Gu et al. (2021) developed highly fluorescent Ti_3C_2 and Nb_2C MXene QDs for labeling of in vitro models cytotoxicity of the QDs to human umbilical vein endothelial cells HUVECs. It was observed that a significant

cytotoxicity was induced on exposure by 100 μg ML^{-1} Ti_3C_2 but Nb_2C QDs could not exhibit it even after 24 h. It was also revealed that Nb_2C QDs were found to be more biocompatible to HUVECs as compared to Ti_3C_2 QDs at the same mass concentrations.

The in vitro toxicity of $CuInS_2$/ZnS QDs was investigated by Xue et al. (2022) on U87 human glioma cell line. It was observed that these QDs enter the cells and are located mainly in the cytoplasm. It was reported that 1515 genes were downregulated and 220 genes were upregulated, which significantly changed gene functions, including chromosome-DNA binding, nucleosome, and chromosome assembly.

11.7 Conclusion

This chapter furnishes a complete overview of the most recent emerging advances in the research domain of QDs and QD−based composites, focusing on their applications in sensing, targeted drug delivery, cancer therapy, etc. Some size-dependent aspects, as well as the structural, morphological composition and outstanding properties of QDs are summarized. Considering that the risk and health hazard of the QDs must be eliminated prior to human exposure, some new toxicity issues of QDs are also presented. Due to their unique properties including good biocompatibility and low cytotoxicity, QDs are of great value in diverse fields and perform a major role in the progress of research in bioimaging, cancer therapy, tissue engineering, sensors, drug delivery, etc.

References

Abdelhamid, H.N., El-Bery, H.M., Metwally, A.A., Elshazly, M., Hathout, R.M., 2019. Synthesis of CdS-modified chitosan quantum dots for the drug delivery of sesamol. Carbohydr. Polym. 214, 90−99.

Abdel-Salam, M., Omran, B., Whitehead, K., Baek, K.-H., 2020. Superior properties and biomedical applications of microorganism−derived fluorescent quantum dots. Molecules 25 (19). Available from: https://doi.org/10.3390/molecules25194486.

Alarfaj, N.A., El-Tohamy, M.F., Oraby, H.F., 2020. New immunosensing-fluorescence detection of tumor marker cytokeratin-19 fragment (CYFRA 21-1) via carbon quantum dots/zinc oxide nanocomposite. Nanoscale Res. Lett. 15 (1). Available from: https://doi.org/10.1186/s11671-020-3247-9.

Allen, P.M., Liu, W., Chauhan, V.P., Lee, J., Ting, A.Y., Fukumura, D., et al., 2010. In As (ZnCdS) quantum dots optimized for biological imaging in the near-infrared. J. Am. Chem. Soc. 132 (2), 470−471.

Ameta, R., Ameta, S.C., 2016a. Binary semiconductors. In: Ameta, R., Ameta, S.C. (Eds.), Photocatalysis: Principles and Applications. CRC Press/Taylor & Francis Group; Apple Academic Press, Boca Raton.

Ameta, R., Ameta, S.C., 2016b. Metallization. In: Ameta, R., Ameta, S.C. (Eds.), Photocatalysis: Principles and Applications. CRC Press/Taylor & Francis Group; Apple Academic Press, Boca Raton.

Ameta, R., Ameta, S.C., 2016c. Ternary semiconductors. In: Ameta, R., Ameta, S.C. (Eds.), Photocatalysis: Principles and Applications. CRC Press/Taylor & Francis Group; Apple Academic Press, Boca Raton.

Ameta, K.L., Papnai, N., Ameta, R., 2014. Photocatalytic degradation of malachite green using nano-sized cerium-iron oxide. Orbital: Electron. J. Chem. 6 (1), 14−19.

Ameta, K., Trivedi, M., Bhatt, J., Soni, D., Benjamin, S., Ameta, S.C., 2019a. Antimicrobial activity of nanosized photocatalytic materials. In: Balköse, D., Ribeiro, A.C.F., Haghi, A.K., Ameta, S.C., Chakaborty, T. (Eds.), Chemical Science and Engineering Technology: Perspectives on Interdiciplinary Research. CRC Press/Taylor & Francis Group; Apple Academic Press, Boca Raton, p. 24.

Ameta, R., Kapoor, N., Pathak, B., Bhatt, J., Ameta, S.C., 2019b. Carbon nanotube composites as photocatalytic materials. In: Vakhrushev, A.V., Kodolov, V.I., Haghi, A.K., Ameta, S.C. (Eds.), Carbon Nanotubes and Nanoparticles: Current and Potential Applications Series: AAP Research Notes on Nanoscience and Nanotechnology. CRC Press/Taylor & Francis Group; Apple Academic Press, Boca Raton.

Ameta, R., Jat, K.K., Bhatt, J., Ameta, S.C., 2019c. Quantum dots and their applications. In: Vakhrushev, A.V., Ameta, S.C., Susanto, H., Haghi, A.K. (Eds.), Advances in Nanotechnology and the Environmental Sciences: Applications, Innovations and Visions for the Future Series: AAP Research Notes on Nanoscience & Nanotechnology. CRC Press/Taylor & Francis Group; Apple Academic Press, Boca Raton.

Ameta, S.K., Rai, A.K., Hiran, D., Ameta, R., Ameta, S.C., 2020. Use of nanomaterials in food science. In: Ghorbanpour, M., Bhargava, P., Varma, A., Choudhary, D. (Eds.), Biogenic Nano - Particles and their Use in Agro-ecosystems. Springer Singapore, pp. 457−488.

Ardelean, I.I., Sarchizian, I., Manea, M., Damian, V., Apostol, I., Cîrnu, M., et al., 2011. CdSe/ZnS quantum dots cytotoxicity against phototrophic and heterotrophic bacteria. Proc. NANOCON 9, 21−23.

Armăşelu, A., 2017. Chapter 2: Recent developments in applications of quantum-dot based light-emitting diodes. In: Ghamsari, M.S. (Ed.), Quantum-Dot Based Light Emitting Diodes. IntechOpen, Rijeka, Croatia, pp. 7−24.

Armăşelu, A., 2019. Chapter 3: Recent advancement on the excitonic and biexcitonic properties of low-dimensional semiconductors. In: Thirumalai, J., Pokutnyi, S.I. (Eds.), Advances in Condensed-Matter and Materials Physics Rudimentary Research to Topical Technology. IntechOpen, Rijeka, Croatia, pp. 41−54.

Armăşelu, A., Popescu, A., Damian, V., Ardelean, I., Apostol, D., 2011a. Fluorescence properties of quantum dots used in the study of microorganism. J. Optoelectron. Adv. Mater. 13 (4), 439−443.

Armăşelu, A., Popescu, A., Apostol, I., Ardelean, I., Damian, V., Iordache, I., et al., 2011b. Passive nonspecific labeling of cyanobacteria in natural samples using quantum dots. Optoelectron. Adv. Mater. Rapid Commun. 5 (10), 1084−1090.

Bao, R., Chen, Z., Zhao, Z., Sun, X., Zhang, J., Hou, L., et al., 2018. Green and facile synthesis of nitrogen and phosphorus co-doped carbon quantum dots towards fluorescent ink and sensing applications. Nanomater 8 (6). Available from: https://doi.org/10.3390/nano8060386.

Bao, D., Kumar, V., Chandra, S., Singh, V.K., Mohan, S., Singh, D.K., et al., 2019. Synthesis of highly fluorescent nitrogen-rich carbon quantum dots and their application for the turn-off detection of cobalt (II). Opt. Mater. 92, 311−318.

Benitez-Martinez, S., Valcárcel, M., 2015. Graphene quantum dots in analytical science. Trends Analyt. Chem. 72, 93−113.

Benitez-Martinez, S., Lopez-Lorente, A.I., Valcárcel, M., 2014. Graphene quantum dots sensor for the determination of graphene oxide in environmental water samples. Anal. Chem. 86 (24), 12279–12284.

Benjamin, S., Sharma, S., Ameta, R., 2014. Nanomaterials. In: Ameta, S.C., Punjabi, P.B., Ameta, R., Ameta, C. (Eds.), Microwave—Assisted Organic Synthesis: A Green Chemical Approach, first ed. CRC Press/Taylor & Francis Group; Apple Academic Press, New York, p. 24.

Bhakat, A., Pal, A., Siddaramaiah, R., Chattopadhyay, A., 2021. Complexation-based super crystalline assembly of zinc oxide quantum dots for sensitive carbon dioxide gas sensing. J. Phys. Chem. C. 125, 12316–12323.

Bhatt, J., Benjamin, S., Ameta, R., Ameta, S.C., 2019a. Enhancement of photodegradation of picric acid (2, 4, 6-trintrophenol) by fabrication of visible-light-active SnO_2 quantum dots/TiO_2 nanospheres composite. J. Appl. Chem. 8 (4), 1805–1812.

Bhatt, J., Jat, K.K., Rai, A.V., Ameta, R., Ameta, S.C., 2019b. Photodegradation of 2-nitrophenol an endocrine disruptor, using TiO_2 nanosphere/SnO_2 quantum dots. In: Aquilar, C.N., Ameta, S.C., Haghi, A.K. (Eds.), Green Chemistry and Biodiversity: Principles, Technique and Correlations. CRC Press/Taylor & Francis Group; Apple Academic Press, New York, pp. 1–8.

Bhatt, J., Benjamin, S., Ameta, R., Ameta, S.C., 2019c. Enhanced visible light photocatalytic activity of TiO_2 nanospheres/SnO_2 quantum dots composite for degradation of 4—Nitrophenol. J. Nanosci. Technol. 5 (4), 748–750.

Bhatt, J., Jangid, M., Kapoor, N., Ameta, R., Ameta, S.C., 2020a. Detection and degradation of pesticides using nanomaterials. In: Ghorbanpour, M., Bhargava, P., Varma, A., Choudhary, D. (Eds.), Biogenic Nano-Particles and their Use in Agro-ecosystems. Springer, Singapore, pp. 431–455.

Bhatt, J., Jat, K.K., Rai, A.K., Ameta, R., Ameta, S.C., 2020b. Quantum dots and their sensing applications. In: Pogliani, L., Ameta, S.C., Haghi, A.K. (Eds.), Chemistry and Industrial Techniques for Chemical Engineers Innovations in Physical Chemistry: Monograph Series. CRC Press/Taylor & Francis Group; Apple Academic Press, New York, p. 18.

Chandra, S., Bano, D., Pradhan, P., Singh, V.K., Yadav, P.K., Sinha, D., et al., 2020. Nitrogen/sulfur-co-doped carbon quantum dots: a biocompatible material for the selective detection of picric acid in aqueous solution and living cells. Anal. Bioanal. Chem. 412 (15), 3753–3763.

Chen, T., Zhao, T., Wei, D., Wei, Y., Li, Y., Zhang, H., 2013. Core–shell nanocarriers with ZnO quantum dots-conjugated Au nanoparticle for tumor-targeted drug delivery. Carbohydr. Polym. 92 (2), 1124–1132.

Chen, X., Tang, Y., Cai, B., Fan, H., 2014. 'One-pot'synthesis of multifunctional GSH–CdTe quantum dots for targeted drug delivery. Nanotechnol 25 (23). Available from: https://doi.org/10.1088/0957-4484/25/23/235101.

Chen, Y., Hu, X., Sun, J., Zhou, Q., 2016. Specific nanotoxicity of graphene oxide during zebrafish embryogenesis. Nanotoxicology 10 (1), 42–52.

Chen, W., Xin, X., Zang, Z., Tang, X., Li, C., Hu, W., et al., 2017a. Tunable photoluminescence of $CsPbBr_3$ perovskite quantum dots for light emitting diodes application. J. Solid. State Chem. 255, 115–120.

Chen, F., Gao, W., Qiu, X., Zhang, H., Liu, L., Liao, P., et al., 2017b. Graphene quantum dots in biomedical applications: recent advances and future challenges. Front. Lab. Med. 1 (4), 192–199.

Chen, J., Qiu, H., Zhao, S., 2020. Fabrication of chemiluminescence resonance energy transfer platform based on nanomaterial and its application in optical sensing, biological imaging and photodynamic therapy. Trend. Anal. Chem. 122. Available from: https://doi.org/10.1016/j.trac.2019.115747.

Choi, H.-J., Montemagno, C.D., 2016. Convergence of nanotechnology and biotechnology. In: Bainbridge, W., Roco, M. (Eds.), Handbook of Science and Technology Convergence. Springer, Cham, pp. 253–277.

Dai, Y.-B., Jia, Y.-F., Chen, N., Bian, W.-P., Li, Q.-K., Ma, Y.-B., et al., 2014. Zebrafish as a model system to study toxicology. Environ. Toxicol. Chem. 33 (1), 11–17.

Dai, C., Zhang, S., Liu, Z., Wu, R., Chen, Y., 2017. Two-dimensional graphene augments nanosonosensitized sonocatalytic tumor eradication. ACS Nano 11, 9467–9480.

Damian, V., Ardelean, I., Armăşelu, A., Popescu, A., Apostol, I., Fourier transform spectra of quantumdots. In: Proc. SPIE 7469, ROMOPTO 2009: NinthConference on Optics: MicrotoNanophotonics II, 74690E, 17 May 2010. Available from: https://doi.org/10.1117/12.862053.

Damian, V., Udrea, C., Bojan, M., Luculescu, C., Armăşelu, A., Apostol, I., Aluminum nanoparticles production by laser ablation in liquids. In: Proc. SPIE 8001, International Conference on Applications of Optics and Photonics, 80012G, 26 July 2011. Available from: https://doi.org/10.1117/12.894525.

de França, C.C.L., Meneses, D., Silva, A.C.A., Dantas, N.O., de Abreu, F.C., Petroni, J.M., et al., 2021. Development of novel paper-based electrochemical device modified with CdSe/CdS magic-sized quantum dots and application for the sensing of dopamine. Electrochim. Acta 367. Available from: https://doi.org/10.1016/j.electacta.2020.137486.

Deng, S., Jia, P.P., Zhang, J.H., Junaid, M., Niu, A., Ma, Y.-B., et al., 2018. Transcriptomic response and perturbation of toxicity pathways in zebrafish larvae after exposure to graphene quantum dots (GQDs). J. Hazard. Mater. 357, 146–158.

Ding, Q., Zhang, X., Li, L., Lou, X., Xu, J., Zhou, P., et al., 2017. Temperature dependent photoluminescence of composition tunable $Zn_xAgInSe$ quantum dots and temperature sensor application. Opt. Express 25 (16), 19065–19076.

Ding, H., Tang, Z., Dong, Y., 2018. Synthesis of black phosphorus quantum dots doped ZnO nanoparticles and its electrogenerated chemiluminescent sensing application. ECS J. Solid. State Sci. Technol. 7 (9). Available from: https://doi.org/10.1149/2.0151809jss.

Dong, J., Wang, K., Sun, L., Sun, B., Yang, M., Chen, H., et al., 2018. Application of graphene quantum dots for simultaneous fluorescence imaging and tumor-targeted drug delivery. Sens. Actuators B. Chem. 256, 616–623.

Duran, G.M., Benavidez, T.E., Contento, A.M., Rios, A., Garcia, C.D., 2017. Analysis of penicillamine using Cu-modified graphene quantum dots, synthesized from uric acid as single precursor. J. Pharm. Anal. 7 (5), 324–331.

Erogbogbo, F., Yong, K.T., Roy, I., Xu, G., Prasad, P.N., Swihart, M.T., 2008. Biocompatible luminescent silicon quantum dots for imaging of cancer cells. ACS Nano 2 (5), 873–878.

Fasbender, S., Zimmermann, L., Cadeddu, R.P., Luysberg, M., Moll, B., Janiak, C., et al., 2019. The low toxicity of graphene quantum dots is reflected by marginal gene expression changes of primary human hematopoietic stem cells. Sci. Rep. 9. Available from: https://doi.org/10.1038/s41598-019-48567-6.

Felix, D.M., Alencar, L.M.R., de Menezes, F.D., Midlej, V.V.P., Aguilar, L., Piperni, S.G., et al., 2021. Graphene quantum dots decorated with imatinib for leukemia treatment. J. Drug. Deliv. Sci. Technol. 61. Available from: https://doi.org/10.1016/j.jddst.2020.102117.

Flak, D., Przysiecka, Ł., Nowaczyk, G., Scheibe, B., Kościński, M., Jesionowski, T., et al., 2018. GQDs-MSMs nanocomposite nanoparticles for simultaneous intracellular drug delivery and fluorescent imaging. J. Nanopart. Res. 20. Available from: https://doi.org/10.1007/s11051-018-4416-y.

Gao, L., Ju, L., Cui, H., 2017. Chemiluminescent and fluorescent dual-signal graphene quantum dots and their application in pesticide sensing arrays. J. Mater. Chem. C. 31, 7753–7758.

Ghosh, S., Ghosal, K., Mohammad, S.A., Sarkar, K., 2019. Dendrimer functionalized carbon quantum dot for selective detection of breast cancer and gene therapy. Chem. Eng. J. 373, 468–484.

Grunwald, D.J., Eisen, J.S., 2002. Headwaters of the zebrafish [mdash] emergence of a new model vertebrate. Nat. Rev. Genet. 3 (9), 717–724.

Gu, Z., Zhu, S., Yan, L., Zhao, F., 2019. Graphene-based smart platforms for combined cancer therapy. Adv. Mater. 31 (9). Available from: https://doi.org/10.1002/adma.201800662.

Gu, M., Dai, Z., Yan, X., Ma, J., Niu, Y., Lan, W., et al., 2021. Comparison of toxicity of Ti_3C_2 and Nb_2C Mxene quantum dots (QDs) to human umbilical vein endothelial cells. J. Appl. Toxicol. 41 (5), 745–754.

Guan, Q., Ma, J., Yang, W., Zhang, R., Zhang, X., Dong, X., et al., 2019. Highly fluorescent Ti_3C_2MXene quantum dots for macrophage labeling and Cu^{2+} ion sensing. Nanoscale 11 (30), 14123–14133.

Hallaj, T., Amjadi, M., Mirbirang, F., 2020. S, N-doped carbon quantum dots enhanced Luminol-Mn (IV) chemiluminescence reaction for detection of uric acid in biological fluids. Microchem. J. 156. Available from: https://doi.org/10.1016/j.microc.2020.104841.

Han, C., Zhang, X., Wang, F., Yu, Q., Chen, F., Shen, D., et al., 2021. Duplex metal co-doped carbon quantum dots-based drug delivery system with intelligent adjustable size as adjuvant for synergistic cancer therapy. Carbon 183, 789–808.

Hassanzadeh, J., Khataee, A., Lotfi, R., 2017. Sensitive fluorescence and chemiluminescence procedures for methamphetamine detection based on CdS quantum dots. Microchem. J. 132, 371–377.

Henna, T.K., Pramod, K., 2020. Graphene quantum dots redefine nanobiomedicine. Mater. Sci. Eng. C. 110. Available from: https://doi.org/10.1016/j.msec.2020.110651.

Hill, A.J., Teraoka, H., Heideman, W., Peterson, R.E., 2005. Zebrafish as a model vertebrate for investigating chemical toxicity. Toxicol. Sci. 86 (1), 6–19.

Ingale, A.G., Chaudhari, A.N., 2013. Biogenic synthesis of nanoparticles and potential applications: an eco-friendly approach. J. Nanomed. Nanotechol. 4 (1). Available from: https://doi.org/10.4172/2157-7439.1000165.

Irani-Nezhad, M.H., Khataee, A., Hassanzadeh, J., Orooji, Y., 2019. A chemiluminescent method for the detection of H_2O_2 and glucose based on intrinsic peroxidase-like activity of WS_2 quantum dots. Molecules 24 (4). Available from: https://doi.org/10.3390/molecules24040689.

Jahangir, M.A., Gilani, S.J., Muheem, A., Jafar, M., Aslam, M., Ansari, M.T., 2019. Quantum dots: next generation of smart nano-systems. Pharm. Nanotechnol. 7 (3), 234–245.

Jahdaly, B.A.A., Elsadek, M.F., Ahmed, B.M., Farahat, M.F., Taher, M.M., Khalil, A.M., 2021. Outstanding graphene quantum dots from carbon source for biomedical and corrosion inhibition applications: a review. Sustainability 13 (4). Available from: https://doi.org/10.3390/su13042127.

Jat, K.K., Bhatt, J., Ameta, S.C., 2019. Photodegradation of fast green by using SnO_2 quantum dots / TiO_2 nanoparticles composite. J. Appl. Chem. 8 (1), 139–145.

Jie, G., Zhou, Q., Jie, G., 2019. Graphene quantum dots-based electrochemiluminescence detection of DNA using multiple cycling amplification strategy. Talanta 194, 658–663.

Jlassi, K., Mallick, S., Eribi, A., Chehimi, M.M., Ahmad, Z., Touati, F., et al., 2021. Facile preparation of NS co-doped graphene quantum dots (GQDs) from graphite waste for efficient humidity sensing. Sens. Actuators B. Chem. 328. Available from: https://doi.org/10.1016/j.snb.2020.129058.

Justin, R., Tao, K., Román, S., Chen, D., Xu, Y., Geng, X., et al., 2016. Photoluminescent and superparamagnetic reduced graphene oxide–iron oxide quantum dots for dual-modality imaging, drug delivery and photothermal therapy. Carbon 97, 54–70.

Kateshiya, M.R., Malek, N.I., Kailasa, S.K., 2020. Facile synthesis of highly blue fluorescent tyrosine coated molybdenum oxide quantum dots for the detection of imidacloprid pesticide. J. Mol. Liq. 319. Available from: https://doi.org/10.1016/j.molliq.2020.114329.

Khataee, A., Hassanzadeh, J., Lotfi, R., Joo, S.W., 2018. Graphene quantum dots/bisulfite assisted chemiluminescence of rhodamine B-H_2O_2 system for sensitive recognition of HCHO. Sens. Actuators B: Chem. 254, 402–410.

Khosravanian, A., Moslehipour, A., Ashrafian, H., 2021. A review on bioimaging, biosensing and drug delivery systems based on graphene quantum dots. Prog. Chem. Biomed. Res. 4 (1), 44–56.

Kumari, A., Kumar, A., Sahu, S.K., Kumar, S., 2018. Synthesis of green fluorescent carbon quantum dots using waste polyolefins residue for Cu^{2+} ion sensing and live cell imaging. Sens. Actuators B. Chem. 254, 197–205.

Lei, C.W., Hsieh, M.L., Liu, W.R., 2019. A facile approach to synthesize carbon quantum dots with pH-dependent properties. Dye. Pigm 169, 73–80.

Li, H., Shih, W.Y., Shih, W.H., 2007. Synthesis and characterization of aqueous carboxyl-capped CdS quantum dots for bioapplications. Ind. Eng. Chem. Res. 46 (7), 2013–2019.

Li, Z., Fan, J., Tong, C., Zhou, H., Wang, W., Li, B., et al., 2019a. A smart drug-delivery nano-system based on carboxylated graphene quantum dots for tumor–targeted chemotherapy. Nanomedicine 14. Available from: https://doi.org/10.2217/nnm-2018-0378.

Li, Y., Hou, X., Dai, X., Yao, Z., Lv, L., Jin, Y., et al., 2019b. Stoichiometry-controlled InP-based quantum dots: synthesis, photoluminescence, and electroluminescence. J. Am. Chem. Soc. 141 (16), 6448–6452.

Liang, J., Huang, Q., Hua, C., Hu, J., Chen, B., Wan, J., et al., 2019. pH—responsive nanoparticles loaded with graphene quantum dots and doxorubicin for intracellular imaging, drug delivery and efficient cancer therapy. ChemistrySelect 4 (20), 6004–6012.

Liu, P., Wang, Q., Li, X., 2009. Studies on CdSe/L-cysteine quantum dots synthesized in aqueous solution for biological labeling. J. Phys. Chem. C. 113 (18), 7670–7676.

Liu, J., Hu, R., Liu, J., Zhang, B., Wang, Y., Liu, X., et al., 2015. Cytotoxicity assessment of functionalized CdSe, CdTe and InP quantum dots in two human cancer cell models. Mater. Sci. Eng. C. 57, 222–231.

Liu, T., Li, N., Dong, J.X., Luo, H.Q., Li, N.B., 2016. Fluorescence detection of mercury ions and cysteine based on magnesium and nitrogen co-doped carbon quantum dots and implication logic gate operation. Sens. Actuators B. Chem. 231, 147–153.

Liu, L., Jiang, H., Dong, J., Zhang, W., Dang, G., Yang, M., 2020a. PEGylated MoS_2 quantum dots for traceable and pH-responsive chemotherapeutic drug delivery. Colloids Surf. B: Biointerfaces 185. Available from: https://doi.org/10.1016/j.colsurfb.2019.110590.

Liu, W., Huang, G., Su, X., Li, S., Wang, Q., Zhao, Y., et al., 2020b. Zebrafish: a promising model for evaluating the toxicity of carbon dot—based nanomaterials. ACS Appl. Mater. Interfaces 12 (43), 49012–49020.

Liu, Y., Zhao, C.H., Sabirsh, A., Ye, L.L., Wu, X.Q., Lu, H.B., et al., 2021. A novel graphene quantum dot-based mRNA delivery platform. Chem. Open. Available from: https://doi.org/10.1002/open.202000200.

Lobo, F.A., Santos, T., Vieira, K.M., Osorio, V.M., Taylor, J.G., 2015. Determination of formaldehyde in hair creams by gas chromatography-mass spectrometry. Drug. Test. Anal. 7, 848–852.

Misra, R.D., 2008. Quantum dots for tumor-targeted drug delivery and cell imaging. Nanomedicine 3 (3). Available from: https://doi.org/10.2217/17435889.3.3.271.

Mondal, M.K., Mukherjee, S., Joardar, N., Roy, D., Chowdhury, P., Sinha Babu, S.P., 2019. Synthesis of smart graphene quantum dots: a benign biomaterial for prominent intracellular imaging and improvement of drug efficacy. Appl. Surf. Sci. 495. Available from: https://doi.org/10.1016/j.apsusc.2019.143562.

Murugan, N., Prakash, M., Jayakumar, M., Sundaramurthy, A., Sundramoorthy, A.K., 2019. Green synthesis of fluorescent carbon quantum dots from eleusine coracana and their application as a fluorescence 'turn-off' sensor probe for selective detection of Cu^{2+}. Appl. Surf. Sci. 476, 468–480.

Nasrollahi, F., Sana, B., Paramelle, D., Ahadian, S., Khademhosseini, A., Lim, S., 2020. Incorporation of graphene quantum dots, iron, and doxorubicin in/on ferritin nanocages for bimodal imaging and drug delivery. Adv. Ther. 3 (3). Available from: https://doi.org/10.1002/adtp.201900183.

Ng, O.T., Wong, Y., Chan, H.M., Cheng, J., Qi, X., Chan, W.H., et al., 2013. N-Acetyl-l-cysteine capped quantum dots offer neuronal cell protection by inhibiting beta (1–40) amyloid fibrillation. Biomater. Sci. 1 (6), 577–580.

Nikazar, S., Sivasankarapillai, V.S., Rahdar, A., Gasmi, S., Anumol, P.S., Shanavas, M.S., 2020. Revisiting the cytotoxicity of quantum dots: an in- depth overview. Biophys. Rev. 12 (3), 703–718.

Niu, H., Yang, X., Wang, Y., Li, M., Zhang, G., Pan, P., et al., 2020. Electroluminescence detection of sunset yellow by graphene quantum dots. Front. Chem. 8. Available from: https://doi.org/10.3389/fchem.2020.00505.

Palit, S., 2020. Frontiers of applications of nanotechnology in biological sciences and green chemistry. In: Dake, S.A., Shinde, R.S., Ameta, S.C., Haghi, A.K. (Eds.), Green Chemistry and Sustainable Technology: Biological, Pharmaceutical and Macromolecular Systems, first ed. CRC Press/Taylor & Francis Group; Apple Academic Press, New York, p. 25.

Pandey, A., Kalal, S., Ameta, C., Ameta, R., Kumar, S., Punjabi, P.K., 2015. Synthesis, characterization and application of naïve and nano-sized titanium dioxide as photocatalyst for degradation of methylene blue. J. Saudi Chem. Soc. 19 (5), 528–536.

Pang, C., Han, S., Li, Y., Zhang, J., 2018. Graphene quantum dot-enhanced chemiluminescence through energy and electron transfer for the sensitive detection of tyrosine. J. Chin. Chem. Soc. 65 (12), 1504–1509.

Perini, G., Palmieri, V., Ciasca, G., De Spirito, M., Papi, M., 2020. Unravelling the potential of graphene quantum dots in biomedicine and neuroscience. Int. J. Mol. Sci. 21 (10). Available from: https://doi.org/10.3390/ijms21103712.

Plaza, D.O., Gallardo, C., Straub, Y.D., Bravo, D., Perez-Donaso, J.M., 2016. Biological synthesis of fluorescent nanoparticles by cadmium and tellurite resistant Antarctic bacteria: exploring novel natural nanofactories. Microb. Cell Fact. 15 (76). Available from: https://doi.org/10.1186/s12934-016-0477-8.

Pramanik, S., Hill, S.K., Zhi, B., Hudson-Smith, N.V., Wu, J.J., White, J.N., et al., 2018. Comparative toxicity assessment of novel Si quantum dots and their traditional Cd-based counterparts using bacteria models *Shewanellaoneidensis* and *Bacillus subtilis*. Environ. Sci. Nano 5 (8), 1890–1901.

Qian, C., Yan, P., Wan, G., Liang, S., Dong, Y., Wang, J., 2018. Facile synthetic photoluminescent graphene quantum dots encapsulated β-cyclodextrin drug carrier system for the management of macular degeneration: detailed analytical and biological investigations. J. Photochem. Photobiol. B: Biol. 189, 244–249.

Qiu, J., Zhang, R., Li, J., Sang, Y., Tang, W., Gil, P.R., et al., 2015. Fluorescent graphene quantum dots as traceable, ph-sensitive drug delivery systems. Int. J. Nanomed. 10, 6709–6724.

Qu, Z., Liu, L., Sun, T., Hou, J., Sun, Y., Yu, M., et al., 2020. Synthesis of bifunctional carbon quantum dots for bioimaging and anti-inflammation. Nanotechnology 31 (17). Available from: https://doi.org/10.1088/1361-6528/ab6b9d.

Rai, S., Singh, B.K., Bhartiya, P., Singh, A., Kumar, H., Dutta, P.K., et al., 2017. Lignin derived reduced fluorescence carbon dots with theranostic approaches: nano-drug-carrier and bioimaging. J. Lumin. 190, 492–503.

Rasoulzadeh, F., Amjadi, M., 2021. The chemiluminescence of $AgInS_2$ quantum dots and its application as a sensing platform for glutathione assay. J. Photochem. Photobiol. A: Chem. 420. Available from: https://doi.org/10.1016/j.jphotochem.2021.113493.

Rathi, K., Pal, K., 2020. Ruthenium-decorated tungsten disulfide quantum dots for a CO_2 gas sensor. Nanotechnology 31 (13). Available from: https://doi.org/10.1088/1361-6528/ab5cd3.

Ray, P.C., Yu, H., Fu, P.P., 2009. Toxicity and environmental risks of nanomaterials: challenges and future needs. J. Environ. Sci. Health C. Envirom. Ecotoxicol. Rev. 27 (1). Available from: https://doi.org/10.1080/10590500802708267.

Ruzycka-Ayoush, M., Kowalik, P., Kowalczyk, A., Bujak, P., Nowicka, A.M., Wojewodzka, M., et al., 2021. Quantum dots as targeted doxorubicin drug delivery nanosystems. Cancer Nanotechnol. 12 (1). Available from: https://doi.org/10.1186/s12645-021-00077-9.

Sahub, C., Tuntulani, T., Nhujak, T., Tomapatanaget, B., 2018. Effective biosensor based on graphene quantum dots via enzymatic reaction for directly photoluminescence detection of organophosphate pesticide. Sens. Actuat. B: Chem. 258, 88–97.

Samantara, A.K., Maji, S., Ghosh, A., Bag, B., Dash, R., Jena, B.K., 2016. Good's buffer derived highly emissive carbon quantum dots: excellent biocompatible anticancer drug carrier. J. Mater. Chem. B. 4 (14), 2412–2420.

Sangam, S., Gupta, A., Shakeel, A., Bhattacharya, R., Sharma, A.K., Suhag, D., 2018. Sustainable synthesis of single crystalline sulphur-doped graphene quantum dots for bioimaging and beyond. Green. Chem. 20, 4245–4259.

Shahid, S., Mohiyuddin, S., Packirisamy, G., 2020. Synthesis of multi-color fluorescent carbon dots from mint leaves: a robust bioimaging agent with potential antioxidant activity. J. Nanosci. Nanotechnol. 20 (10), 6305–6316.

Shan, J., Li, R., Yan, K., Zhu, Y., Zhang, J., 2016. In situ anodic stripping of Cd (II) from CdS quantum dots for electrochemical sensing of ciprofloxacin. Sens. Actuators B: Chem. 237, 75–80.

Shao, D., Zeng, Q., Fan, Z., Li, J., Zhang, M., Zhang, Y., et al., 2012. Monitoring HSV-TK/ganciclovir cancer suicide gene therapy using CdTe/CdS core/shell quantum dots. Biomaterials 33 (17), 4336–4344.

Shao, D., Li, J., Xiao, X., Zhang, M., Pan, Y., Li, S., et al., 2014. Real-time visualizing and tracing of HSV-TK/GCV suicide gene therapy by near-infrared fluorescent quantum dots. ACS Appl. Mater. Interf. 6 (14), 11082–11090.

Smith, W.E., Brownell, J., White, C.C., Afsharinejad, Z., Tsai, J., Hu, X., et al., 2012. In vitro toxicity assessment of amphiphillic polymer-coated CdSe/ZnS quantum dots in two human liver cell models. ACS Nano 6 (11), 9475–9484.

Solanki, M.N., Benjamin, S., Ameta, S.C., 2018. Nanomaterials. In: Ameta, S.C., Ameta, R., Ameta, G. (Eds.), Sonochemistry: An Emerging Green Technology. CRC Press/Taylor & Francis Group; Apple Academic Press, Boca Raton, p. 37.

Sonthanasamy, R.S.A., Ahmad, W.Y.W., Fazry, S., Hassan, N.I., Lazim, A.M., 2016. Transformation of crystalline starch nanoparticles into highly luminescent carbon nanodots: toxicity studies and their applications. Carbohydr. Polym. 137, 488–496.

Su, W., Guo, R., Yuan, F., Li, Y., Li, X., Zhang, Y., et al., 2020. Red-emissive carbon quantum dots for nuclear drug delivery in cancer stem cells. J. Phys. Chem. Lett. 11 (4), 1357–1363.

Sun, H., Wu, L., Wei, W., Qu, X., 2013. Recent advances in graphene quantum dots for sensing. Mater. Today 16 (11), 433–442.

Tadyszak, K., Wychowaniec, J.K., Litowczenko, J., 2018. Biomedical applications of graphene-based structures. Nanomaterials 8 (11). Available from: https://doi.org/10.3390/nano8110944.

Tan, L., Wan, A., Li, H., 2013. Ag_2S quantum dots conjugated chitosan nanospheres toward light-triggered nitric oxide release and near-infrared fluorescence imaging. Langmuir 29 (48), 15032−15042.

Tang, Y.-M., Junaid, M., Niu, A., Deng, S., Pei, D.-S., 2017. Diverse toxicological risks of PAHs in surface water with an impounding level of 175m in the three Gorges Reservoir Area. Chin. Sci. Total. Environ. 580, 1085−1096.

Thovhogi, N., Sibuyi, N.R.S., Onani, M.O., Meyer, M., Madiehe, A.M., 2018. Peptide-functionalized quantum dots for potential applications in the imaging and treatment of obesity. Int. J. Nanomed. 13, 2551−2559.

Vahid, B., Hassanzadeh, J., Khodakarami, B., 2019. CdSe quantum dots-sensitized chemiluminescence system and quenching effect of gold nanoclusters for cyanide detection. Spectrochim. Acta Part. A: Mol. Biomol. Spectrosc. 212, 322−329.

Wang, Z., Xia, J., Zhou, C., Via, B., Xia, Y., Zhang, F., 2013a. Synthesis of strongly green-photoluminescent graphene quantum dots for drug carrier. Colloid. Surf. B 112, 192−196.

Wang, Y., Zhang, L., Liang, R.-P., Bai, J.-M., Qiu, J.-D., 2013b. Using graphene quantum dots as photoluminescent probes for protein kinase sensing. Anal. Chem. 85 (19), 9148−9155.

Wang, X.J., Sun, X., Lao, J., He, H., Cheng, T.T., Wang, M.Q., et al., 2014. Multifunctional graphene quantum dots for simultaneous targeted cellular imaging and drug delivery. Colloid Surf. B 122, 638−644.

Wang, S., Cole, I.S., Li, Q., 2016. The toxicity of graphene quantum dots. RSC Adv. 6 (92), 89867−89878.

Wang, Z., Ciacchi, L.C., Wei, G., 2017. Recent advances in the synthesis of graphene-based nanomaterials for controlled drug delivery. Appl. Sci. 7 (11). Available from: https://doi.org/10.3390/app7111175.

Wang, Y., He, L., Yu, B., Chen, Y., Shen, Y., Cong, H., 2018. ZnO quantum dots modified by pH-activated charge-reversal polymer for tumor targeted drug delivery. Polymers 10 (11). Available from: https://doi.org/10.3390/polym10111272.

Wang, D., Liang, Y., Su, Y., Shang, Q., Zhang, C., 2019a. Sensitivity enhancement of cloth-based closed bipolar electroluminescence glucose sensor via electrode decoration with chitosan/multi-walled carbon nanotubes/graphene quantum dots-gold nanoparticles. Biosens. Bioelectron. 130, 55−64.

Wang, Y., Xu, N., He, Y., Wang, J., Wang, D., Gao, Q., et al., 2019b. Loading graphene quantum dots into optical-magneto nanoparticles for real-time tracking in vivo. Mater. (Basel) 12 (13). Available from: https://doi.org/10.3390/ma12132191.

Wang, L.H., Bu, Y.M., Liu, Y., Yao, Y.P., Yang, Z.F., Chen, P., 2020. A strategy for microwave-controlled release of anticancer drugs: $(Fe_3O_4/nGO)@mSiO_2/GQDs$ nanocomposite carrier jointly enhanced by nGO and GQDs. Nano 15 (6). Available from: https://doi.org/10.1142/S179329202050071X.

Wei, M., Lin, P., Chen, Y., Lee, J.Y., Zhang, L., Li, F., et al., 2020. Applications of ion level nanosensors for neuroscience research. Nanomedicine 15 (29), 2871−2881.

Weng, C.I., Chang, H.T., Lin, C.H., Shen, Y.W., Unnikrishnan, B., Li, Y.J., et al., 2015. One-step synthesis of biofunctional carbon quantum dots for bacterial labeling. Biosens. Bioelectron. 68. Available from: https://doi.org/10.1016/j.bios.2014.12.028.

Wolcott, A., Gerion, D., Visconte, M., Sun, J., Schwartzberg, A., Chen, S., et al., 2006. Silica-coated CdTe quantum dots functionalized with thiols for bioconjugation to IgG proteins. J. Phys. Chem. B. 110 (11), 5779−5789.

Wu, P.J., Ou, K.L., Chen, J.K., Fang, H.P., Tzing, S.H., Lin, W.X., et al., 2014. Methotrexate-conjugated $AgInS_2$/ZnS quantum dots for optical imaging and drug delivery. Mater. Lett. 128, 412–416.

Wu, D., Liu, Y., Wang, Y., Hu, L., Ma, H., Wang, G., et al., 2016. Label-free electroluminescent immunosensor for detection of prostate specific antigen based on aminated graphene quantum dots and carboxyl graphene quantum dots. Sci. Rep. 6. Available from: https://doi.org/10.1038/srep20511.

Wychowaniec, J.K., Iliut, M., Zhou, M., Moffat, J., Elsawy, M.A., Pinheiro, W.A., et al., 2018. Designing peptide/graphene hybrid hydrogels through fine-tuning of molecular interactions. Biomacromolecules 19 (7), 2731–2741.

Xiang, Y., Liu, X., Mao, C., Liu, X., Cui, Z., Yang, X., et al., 2018. Infection-prevention on Ti implants by controlled drug release from folic acid/ZnO quantum dots sealed titania nanotubes. Mater. Sc. Eng. C. 85, 214–224.

Xiao, A., Wang, C., Chen, J., Guo, R., Yan, Z., Chen, J., 2016. Carbon and Metal Quantum Dots toxicity on the microalgae Chlorella pyrenoidosa. Ecotoxicol. Environ. Safe 133, 211–217.

Xie, R., Wang, Z., Zhou, W., Liu, Y., Fan, L., Li, Y., et al., 2016. Graphene quantum dots as smart probes for biosensing. Anal. Methods 8 (20), 4001–4016.

Xu, S., Li, D., Wu, P., 2015. One-pot, facile, and versatile synthesis of monolayer MoS_2/WS_2 quantum dots as bioimaging probes and efficient electrocatalysts for hydrogen evolution reaction. Adv. Funct. Mater. 25 (7), 1127–1136.

Xu, Q., Ding, L., Wen, Y., Yang, W., Zhou, H., Chen, X., et al., 2018. High photoluminescence quantum yield of 18.7% by using nitrogen-doped Ti_3C_2MXene quantum dots. J. Mater. Chem. C. 6 (24), 6360–6369.

Xue, B., Yang, Y., Sun, Y., Fan, J., Li, X., Zhang, Z., 2019. Photoluminescent lignin hybridized carbon quantum dots composites for bioimaging applications. Int. J. Biol. Macromol. 122, 954–961.

Xue, D., Zou, W., Liu, D., Li, L., Chen, T., Yang, Z., et al., 2022. Cytotoxicity and transcriptome changes triggered by $CuInS_2$/ZnS quantum dots in human glial cells. Neurotoxicology 88, 134–143.

Yahyai, I.A., Hassanzadeh, J., Al-Lawati, H.A.J., 2021. A novel and selective multi-emission chemiluminescence system for the quatification of delthamethrin in food samples. Sens. Actuat. B: Chem. 327. Available from: https://doi.org/10.1016/j.snb.2020.128927.

Yan, M., Zhang, Y., Xu, K., Fu, T., Qin, H., Zheng, X., 2011. An in vitro study of vascular endothelial toxicity of CdTe quantum dots. Toxicology 282 (3), 94–103.

Ye, S., Yu, M., Yan, W., Song, J., Qu, J., 2017. Enhanced photoluminescence of $CsPbBr_3$@ Ag hybrid perovskite quantum dots. J. Mater. Chem. C. 5 (32), 8187–8193.

Zhang, Q., Wu, Z., Li, N., Pu, Y., Wang, B., Zhang, T., et al., 2017. Advanced review of graphene-based nanomaterials in drug delivery systems: synthesis, modification, toxicity and application. Mater. Sci. Eng. C. 77, 1363–1375.

Zhao, C., Song, X., Liu, Y., Fu, Y., Ye, L., Wang, N., et al., 2020. Synthesis of graphene quantum dots and their applications in drug delivery. J. Nanobiotechnol. 18 (142). Available from: https://doi.org/10.1186/s12951-020-00698-z.

Zor, E., Morales-Narváez, E., Zamora-Gálvez, A., Bingol, H., Ersoz, M., Merkoçi, A., 2015. Graphene quantum dots—based photoluminescent sensor: a multifunctional composite for pesticide detection. ACS Apple. Mater. Interf. 7, 20272–20279.

Chapter 12

Application of quantum dots in solar cells

Shwetharani R[1], Chandan Hunsur Ravikumar[1,2], M.S. Jyothi[3] and R. Geetha Balakrishna[1]

[1]Centre for Nano and Material Sciences, Jain University, Bengaluru, Karnataka, India, [2]Pilot Plant Development and Training Institute, King Mongkut's University of Technology Thonburi, Thakam, Bangkok, Thailand, [3]Department of Chemistry, AMC Engineering College, Bengaluru, Karnataka, India

12.1 Introduction

The limited availability of fossil fuels and global warming are demanding the use of renewable energy. The potential of solar energy as an alternative for fossil fuels has been investigated over the past half century and its reliability along with marketability is understood thoroughly. The 4.3×10^{20} J h^{-1} of energy known to reach Earth from the Sun is sufficient to accomplish the annual energy consumption of Earth, 4.1×10^{20} J (Lewis and Crabtree, 2005). Highly efficient and low-cost solar cells were introduced to collect solar energy. Here, the photovoltaic cells (PVs) convert the solar energy into electrical and chemical energies (Kazacos et al., 1980). The first kind of solar cells were of p-n junction technology and Schottky barrier, which adopt the PV characteristics of appropriate semiconductor (Badawy et al., 1990). The best example is Si (Badawy and El-Dessouki, 1985; Decker et al., 1983).

Launching with Si-single crystals, and proceeding to bulk polycrystalline silica wafers, these cells are considered as first-generation cells. A 12%–16% conversion efficiency has been achieved for these cells and these are marketed widely, where the principle of energy storage is lead-acid batteries (Sharma et al., 2015). The second-generation solar cells evolved with the science of thin films. Si-wafers, CdTe, a-Si, $CuInSe_2$, and CdS are the key candidates for thin-film solar cells. In comparison with the first-generation solar cells, these thin-film solar cells presented a cost-efficient engineering process in association with integrated lower temperature progressions for the insulation of cells. Besides the use of flexible substrates helped to spread their

Quantum Dots. DOI: https://doi.org/10.1016/B978-0-12-824153-0.00012-4
© 2023 Elsevier Inc. All rights reserved.

accessibility for a wide spectra of applications. A conversion efficiency of nearly 20% was achieved for combination PVs such as CIGS (Cu/In/Ga/Se) (Schock and Noufi, 2000; Wada et al., 2001; Kaelin et al., 2004). However, due to the lesser stability, the thin-film solar cells shared a lower market and the efforts of researchers into improved versions of PVs were anticipated. A combination of polymers and semiconductors came into existence, where polymers were doped to form Schottky barriers (Amani-Ghadim et al., 2022; Gamboa et al., 1998). Nonetheless, the lower conversion efficiency restricted their practice.

An association of nanoscience, nanotechnology, and surface science resulted in sustainable energy conversions and consideration for third generation solar cells. Nanocrystals and nanoporous materials are employed to increase the efficiency as well as stability of solar cells. Attention to catalysts and light harvesting materials such as TiO_2, quantum dots, and many other nanocomposites has been increased to work on the nanostructured solar cells to bring out the breakthrough potentials. This chapter deals with the exercise on fabrication and advancements in one of such nanostructured materials, QDs involved solar cells.

QDs are the semiconductor clusters of nanoscale and are known for their extraordinary optoelectronic properties. The size-dependent quantum physical features of QDs present tunable optoelectronic properties attributed to the production of electron−hole pairs, which extend their use in solar cells. The cells also offer a tunable bandgap to match with the wavelength of illuminating light to generate more electricity (Badawy, 1993). QDs pose a simple method of synthesis and are economically feasible. The remarkable excitation coefficients and wide adsorption spectra depending on their size are attractive features for PV applications. The carrier multiplication phenomenon in QDs demonstrating the generation of more than one electron for an adsorption of one electron at broader wavelength spectra results in higher quantum efficiencies of QDs sensitized solar cells (QDSSCs) (Nozik, 2002; Sambur et al., 2010). This phenomenon is known as multiple exciton generation (MEG).

12.1.1 Basic structure of quantum dot sensitized solar cells

An elementary structure of QDSSCs is given in Fig. 12.1.

The key structure involves four major portions:

- photoanode;
- sensitizer, which is QD;
- electrolyte; and
- counter electrode (CE).

A photoanode is generally a semiconducting material deposited on transparent substrate and is usually a fluorine-doped tin oxide (FTO) and or

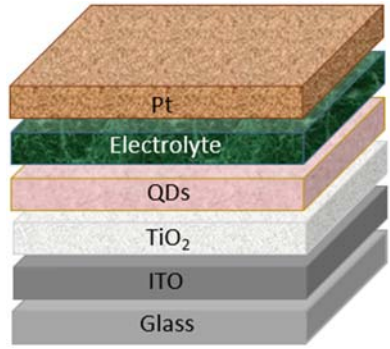

FIGURE 12.1 Primary structure of QDSSCs. *QDSSCs*, QD-sensitized solar cells.

indium tin oxide (ITO). FTO usually maintains the semiconducting layer and employs current collection. An ideal FTO should have higher transparency and lower electrical resistance, which allows the maximum transmittance of sunlight to facilitate an efficient charge transfer phenomena (Shin et al., 2019). The importance of a photoanode in QDSSCs is attributed to the contribution of a matrix for adsorption of QDs and it also acts as a charge transport medium, which could transport electrons from the sensitizer to the conducting oxide substrate. Photoanodes must have higher electron mobility and surface area and must not react with redox electrolytes. These ideal characteristics allow the maximum loading of QDs and reduce unwanted photon adsorption. TiO2 is considered as the best material as a photoanode due to its wider and tunable bandgap, low cost, stability, and nontoxicity, as well as its mesoporous features, higher surface area, conduction band edge, and greater electron affinity (Ahmad et al., 2017).

The second portion is a sensitizer. In QDSSCs it is QDs. QDs such as InP (Crisp et al., 2018), CdS (Vázquez et al., 2016), CdSe (Lee and Lo, 2009), Si (Hao et al., 2009), PbS (Park et al., 2019), PbSe (Zhang et al., 2014), CdTe (Badawi et al., 2013), graphene (Guo et al., 2010), $CuInS_2$ (Li et al., 2012), Bi_2S_3 (Zumeta-Dube et al., 2014), and many others have been used in QDSSCs. The QDs, which are stable upon visible light irradiation, with high adsorption efficiency and suitable bandgap energy, are the most preferred ones. These QDs are fabricated to act as sensitizers by two different methods. The first one is a successive ionic layer adsorption reaction (SILAR) method, and it is an example for in situ fabrication (Yang et al., 2015a,b). The other is a linker-assisted assembly method and it is an example for ex situ fabrication (Li and Zhong, 2015). However, in situ methods have shown improved performance (Bhambhani, 2018).

The third major part is a redox electrolyte, which transfers the charges between photoanodes and CEs and aids the restoration of oxidized QDs (Wu et al., 2015). These are also called hole conductors. As Cd chalcogenides

QDs are not stable in an iodide/triiodide electrolyte system, this system is most commonly practiced with an addition of suitable organic solvents (Yella et al., 2011). Several efforts have been tried out to stabilize the polysulfide electrolyte systems to avoid the leaching of QDs and the protective films have been coated (Shalom et al., 2009). Yet, the overall performance of the cell remained insignificant with just 3% of power conversion efficiency. However, polysulfide redox system (S_2/Sn^{2-}) is used instead with greater challenges like high redox potential (Hod and Zaban, 2014). To overcome this challenge, scientist have tried to control the concentration of polysulfide (Liao et al., 2015), varied solvent systems (Li et al., 2011), coupling with additives such as poly(vinyl pyrrolidone) (PVP) (Jiang et al., 2016), SiO_2 (Wei et al., 2016a), guanidine thiocyanate (Chou et al., 2011), etc. The research has been also concentrated on using a material that possesses lower redox potential like Mn poly(pyrazolyl) borate (Haring et al., 2014). Besides, the toxicity of liquid electrolytes vapor is another challenge, which arises due to leakage of solvents due to their lower boiling points. This aids to degradation of solvents and reduces the durability of the solar system. Hence solid-state electrolytes and/or quasisolid-state electrolytes are used as a substitute for liquid ones (Yu et al., 2010; Huo et al., 2015; Feng et al., 2016). Poly(ethylene oxide)/poly(vinylidene fluoride) (Yang and Wang, 2015), PVP (Jiang et al., 2016), and P3HT (poly-3-hexylthiophene) (Shaw et al., 2008) are the accomplished solid electrolytes. Some hydrogels (Zhang et al., 2017), ionic liquids (Jovanovski et al., 2011), and gels (Kim et al., 2014) are used as quasisolid-state electrolytes.

The last major portion is the CE, which allows the movement of electrons from therexternal circuit to electrolytes and also acts as a catalyst in reducing the oxidized electrolyte. The reduction reaction takes place at the interface of electrolyte and CE. For an ideal CE, the material must be highly electrical conductive with great electrocatalytic activity and also stability. Platinum is the widely used CE for QDSSCs with an electrolyte system of iodide/triiodide. But for a polysulfide system, the conversion efficiency decreased as the sulfur atoms are likely to adsorb on Pt. To overcome this, metal chalcogenides (Meng et al., 2015), many composite materials (Yang et al., 2012; Gopi et al., 2018), and also carbon-based materials (Zhang et al., 2010; Du et al., 2016) are emerging as new CEs for QDSSCs.

12.1.2 Working principle of quantum dot sensitized solar cells

QDSSCs work in a similar fashion to DSSCs. The schematic representation of the working principle of QDSSC is provided in Fig. 12.2. The photoexcitation of the sensitizer takes place with an irradiation of light. The excited electrons from QDs are transferred to the TiO_2 conduction band. These injected electrons breach through the TiO_2 nanocrystal film and reach the conducting substrate. These electrons then flow through the external circuit

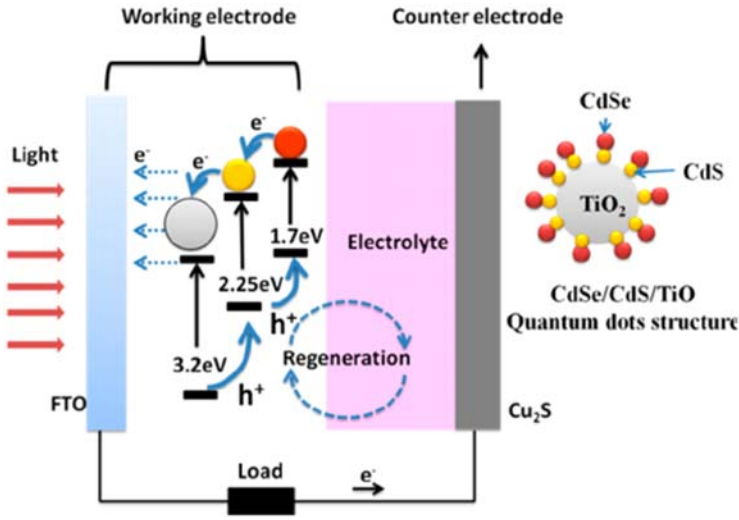

FIGURE 12.2 Working principle of QDSSCs. *QDSSCs*, QD-sensitized solar cells (Tian et al., 2012). *Adapted from Tian, J., Gao, R., Zhang, Q., Zhang, S., Li, Y., Lan, J., et al., 2012. Enhanced performance of CdS/CdSe quantum dot cosensitized solar cells via homogeneous distribution of quantum dots in TiO_2 film. J. Phys. Chem. C. 116 (35), 18655–18662. With permission.*

and reach the CE. Proceeding further, the reduction of oxidized compound of the electrolyte takes place at CE and hence the regeneration of sensitizer, that is, QDs are there for the continuing process.

12.2 Properties of quantum dots

12.2.1 Energy gap tuning

The bandgap of QDs plays a major role in QDSSCs, because an appropriate bandgap can enhance/control the photon absorption in the solar spectrum. QDs possess tunable bandgap energy, which can be tuned by varying the size of QDs because of the quantum confinement effect, which occurs in the particles having a smaller size than the exciton. QDs solution displays a different color that corresponds to the change in the particle size, which exhibits a different absorption band of light. This effect increases the bandgap along with a blueshift in photoluminescence (PL). Therefore, the selection of an appropriate absorber for designing an efficient solar cell is very important. Anttu (2015) have found that the balance limit for photon conversion efficiency in a single junction solar cell depends strongly on the bandgap of absorbing material. Literature reports that the driving force of 0.25 eV is sufficient for the electron injection into photoanode (Weller, 1991). Therefore for better electron transport, the conduction band (CB) of QDs absorber

should be 0.25 eV above the CB of the photoanode for efficient exciton dissociation and the valence band level of QDs should be lower than the redox level of the hole transporting material.

A decrease in size of CdSe QDs increases the bandgap (Fig. 12.3) and hence the emission of PL shifts from red to blue. A decrease in particle size of CdSe increases the photocurrent, attributed to the shift of the CB towards a more negative potential, which enhances the driving force for charge injection. However, the higher particle size materials shows better absorption in the visible region but the disadvantage of these materials is lower electron injection into TiO_2, unlike with small-sized QDs. Vogel et al. (1994) reported that the charge separation can be optimized through tuning the size of QDs and Kongkanand et al. (2008) demonstrated that the photoelectrochemical response and photoconversion efficiency (PCE) can be enhanced by varying the size of QDs.

The sufficiently small QD particles represent wider bandgap energy; consequently, the optical absorption and emission with regard to excitation across the bandgap shift to higher energy. Gorer and Hodes (1994) have investigated the quantum size effect in CdSe films and observed blueshift of the absorption spectra with the decrease in crystal size. This phenomenon is also reported in CdS QDs by Thambidurai et al. (2011). Jun et al. (2013) have suggested that the use of a combination of different sizes of QDs having a range of bandgaps in a solar cell may show better efficiency due to a

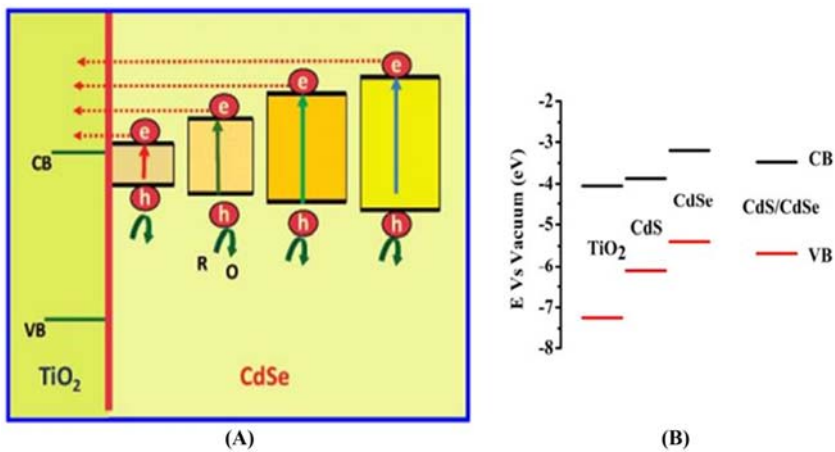

FIGURE 12.3 (A) Schematic illustration of energy band structure of different sized CdSe QDs and TiO_2. (B) Band energy of TiO_2, CdS, CdSe and co**sensitized** CdS/CdSe. *Adapted from Kongkanand, A., Tvrdy, K., Takechi, K., Kuno, M., Kamat, P. V., 2008. Quantum dot solar cells. Tuning photoresponse through size and shape control of CdSe − TiO_2 architecture. J. Am. Chem. Soc. 130 (12), 4007–4015; (B) Esparza, D., Zarazúa, I., López-Luke, T., Cerdán-Pasarán, A., Sánchez-Solís, A., Torres-Castro, A., et al., 2015. Effect of different sensitization technique on the photoconversion efficiency of CdS quantum dot and CdSe quantum rod sensitized TiO_2 solar cells. J. Phys. Chem. C. 119 (24), 13394–13403. With permission.*

wider absorption of light. Esparza et al. (2015) have sensitized two different QDs with a varied range of light absorption on TiO_2 and demonstrated that the PCE for CdS/CdSe (PCE = 4.7%) is higher than CdS alone (PCE = 2.5%), which are prepared by SILAR (CdS), electrophoretic deposition (CdSe), and pipetting (CdSe) methods, respectively. The use of different kinds of QDs sensitizers is a promising technique to enhance the light absorption wavelength region, increase electron injection, and also enhance the charge transport, which improves the photon conversion efficiency.

12.2.2 Multiple exciton generation

The effectual formation of more than one photoinduced electron−hole (e^-−h^+) pair upon absorption of a single photon is potentially important for the development of optoelectronic devices (photovoltaic and photoelectrochemical cells), which convert solar radiation (energy) into electricity. In some cases, stored chemical potential is there in solar-derived fuels like hydrogen, alcohols, and hydrocarbons. Several workers explain the dynamics of such a conversion process (Hanna and Nozik, 2006; Klimov, 2006). The conversion process increases because of the excess kinetic energy of the electrons and holes that are produced by the absorption of photons in a cell, with the energies above the bandgap energy for absorption, and can create additional e^- /h^+ pairs with at least the twice the bandgap energy (Nozik, 2008). The additional e^- /h^+ pair is created by the bandgap in a semiconductor and HOMO−LUMO energy difference in molecular systems. These extra e^- /h^+ pair can be separated, transported, and collected to yield higher photocurrent in the cells. In such a process, the excess kinetic energy is converted to heat and can become unavailable for conversion into electrical free energy, thus limiting the cell to achieve the maximum thermodynamic conversion efficiency. The hot carrier and relaxation of electrons in semiconductor is shown in Fig. 12.4. The creation of the (e^- - h^+) pair, which absorbs the proton, has been studied for over 50 years in bulk semiconductors. It has also been observed in photocurrent of bulk p-n junctions in Si, PbS, PbSe, PbTe, and InSb, and in these systems, they are termed as impact ionization (Tauc, 1959; Vavilov, 1959; Beattie, 1962; Christensen, 1976; Kolodinski et al., 1993). Nevertheless, the impact of ionization is not an effective process in bulk semiconductors and may require more multiples of photoenergy for threshold absorption of energy. For an Si-based semiconductor PV, which is dominant in the present-day photovoltaic market, impact ionization does not become significant until the incident photons energy exceeds 3.5 eV. This energy is an ultraviolet energy threshold, which is beyond the photon energies present in the solar spectrum. Even with absorption of 5 eV photons, impact ionization only generates a quantum yield (QY) of 1.3. Hence it is not a meaningful approach to increase the efficiency of conventional bulk Si PV with impact ionization.

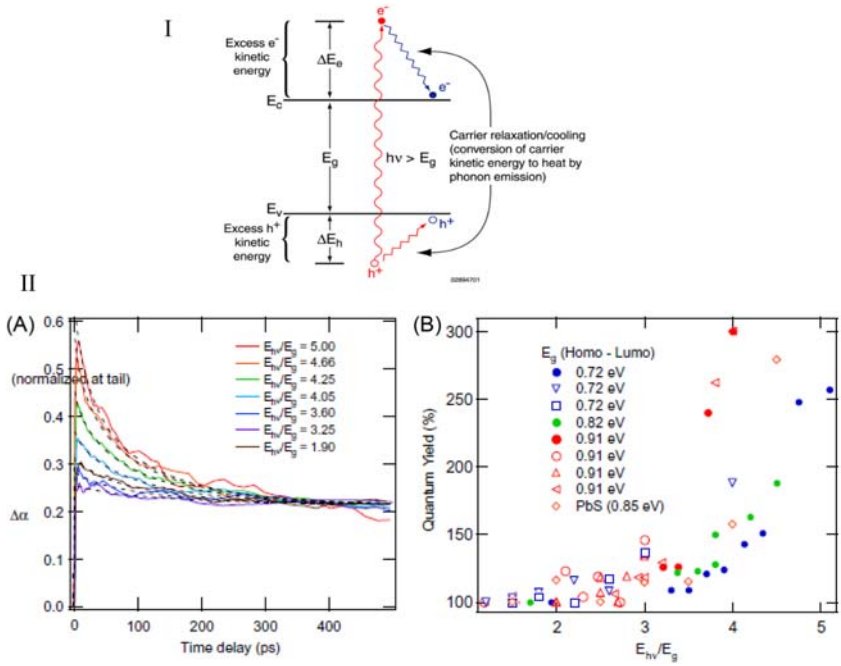

FIGURE 12.4 (I) Hot carrier relaxation/cooling in semiconductors. (II) (A) Exciton population decay dynamics obtained by probing intraband (intraexciton) transitions in the mid-IR at 5.0 μm for a sample of 5.7 nm diameter PbSe QDs, and (B) QY for exciton formation from a single photon versus photon energy expressed as the ratio of the photon energy to the QD bandgap (HOMO−LUMO energy) for three PbSe QD sizes and one PbS (dia. = 3.9, 4.7, 5.4, and 5.5 nm, respectively, and Eg = 0.91, 0.82, 0.73, and 0.85 eV, respectively). Solid symbols indicate data acquired using mid-infrared probe; open symbols indicate band edge probe energy. Quantum yield results were independent of the probe energy utilized (Beard et al., 2015). *Adapted (I) from Beard, M. C., Johnson, J. C., Luther, J. M., Nozik, A. J., 2015. Multiple exciton generation in quantum dots vs singlet fission in molecular chromophores for solar photon conversion. Phil. Trans. R. Soc. A: Maths, Phys. Eng. Sci. 373 (2044), doi: 10.1098/rsta.2014.0412.; (II) Ellingson, R. J., Beard, M. C., Johnson, J. C., Yu, P., Micic, O. I., Nozik, A. J., et al., 2005. Highly efficient multiple exciton generation in colloidal PbSe and PbS quantum dots. Nano Lett. 5 (5), 865−871. With permission.*

On the other side, the semiconductor nanocrystals (QDs) generating the multiple (e^- /h^+) pairs from a single photon are more efficient. The threshold photons required to generate become more efficient and such photon energy for the same process generates two (e^- /h^+) pairs per photon absorbed, which can approach values as low as twice the threshold energy for the absorption. In QDs, the rate of Auger recombination including the inverse Auger process of MEG can be increased. The enhancement is due to the carrier confinement and this correspondingly increases the (e^- /h^+) coulomb interaction with a time scale reported to be more than 100 fs (Ellingson

et al., 2005; Shabaev et al., 2006). The rate of velocity of generation of MEG is much faster than the hot exciton cooling rate produced during the process of recombination and thus MEG can be become more efficient. However, Nozik (2001) noted that crystal momentum is not a good quantum number and momentum need not to be conserved. This allows the threshold photon energy to generate two (e^- /h^+) pairs per photon absorbed. Lowering the threshold to absorb more photons would lower the kinetic energy lost due to heat and reflection. This allows the solar spectrum to contribute more photons with a particular ideal or particular bandgap of the material, which could possibly enhance the MEG.

MEG has been detected by several spectroscopic techniques and is consistent (Schaller and Klimov, 2004; Ellingson et al., 2005; Schaller et al., 2005). The first method is by using transient absorption spectroscopy, which measures with respect to time (can measure from femto to microsecond transition). It can measure the data from delays as low as 5 ps, by which in some material, the carrier multiplication and cooling are complete and probe pulse is catechizing the exciton population at their lowest possible state (band edges) (Schaller et al., 2006). It also monitors the interband bleach dynamics with excitation across the QD bandgap. In the other set of experiments, probe pulse is in mid-IR and monitors the interband transitions of the new excitons that are created. The peak magnitude of the initial time induced photon absorption change is created by the pump pulse and the Auger decay dynamics of the generated excitons and it is equal to the number of excitons generated. The dynamics of the mid IR interband absorptions are monitored after the pump pulse. Fig. 12.4B gives the excitation decay probing interband transition of PbSe QDs.

The exciton multiplication was first reported and presented by Schaller and Klimov (2004) for PbSe QDs. They showed that an excitation energy threshold for the efficient formation of two excitons per photon at 3 Eg, where Eg is the absorption energy gap of the QDs (HOMO-LUMO transition energy) commonly called bandgap in QDs. They also reported that the QY of 218% (118% Impact Ionization (I.I.) efficiency) at 3.8 Eg, and value of QYs above 200% indicates the formation of more than two excitons per photon absorbed. The research group from NREL (Ellingson et al., 2005) reported QY of 300% for 3.9 nm QDs at a photon energy of 4 Eg. This indicated that there is formation of three excitons per photon absorbed for every photoexcited QDs in the sample. They have also shown that the threshold Eg of MEG by optical excitation is 2 Eg. It was also revealed that efficient MEG occurs in PbS (Ellingson et al., 2005) and PbTe QDs (Murphy et al., 2006). MEG is also seen in other types QDs such as CdS, CdSe, CdTe, ZnS, ZnSe, CdSe/CdS, CdSe/CdTe, and CdTe/ZnS but it is not limited to these only. These core−shell type of QDs mentioned not only gives the stability to the core but also stabilizes the generation of MEG.

12.3 Synthesis of quantum dots

12.3.1 Chalcogenide quantum dots

The synthesis of QDs took a rapid phase of development from its discovery by Alexy Emikov (Ekimov and Onushchenko, 1981) in a glass matrix. It took almost a decade to synthesize these in a stable colloidal form by Murray et al. (1993). There are mainly two ways to synthesize the QDs and these are: (1) solution phase synthesis (colloidal route) and (2) vapor phase synthesis. The solution phase synthesis involves the hot injection method, where the precursor is injected into the hot solution of another precursor. This development in technique led to improved QD photophysical properties such as quantum confinement, reproducibility, and size-tunable PL. The main advantage of the colloidal method is that it uses injection and growth temperature to control the QD particle size. It is well known that nucleation and growth of the QDs depends on the time and temperature of the colloidal precursor solution, which can be controlled (Chandan and Geetha, 2013; Chandan et al., 2014). This led to the development of QDs such as CdSe, CdS, CdTe, ZnSe, and ZnS. This enhancement of photophysical properties with stability of QDs marked their presence and importance in photovoltaics, energy, biosensors, and bioimaging (D'Souza et al., 2015; Venkataramana et al., 2016; Kusuma et al., 2019; Ravikumar et al., 2019, 2020). Apart from these QDs, near infrared emitting QDs are InP, InAs, and other lead and copper chalcogenides (Micic et al., 1994, 1995; Allen and Bawendi, 2008; Tan et al., 2017).

The stable CdSe colloidal QDs were first synthesized and reported by Murray et al. (1993). They were the first to report the use of TOPO/TOP (Trioctyl phosphine oxide/Trioctyl phosphine) as a coordinating and stabilizing agent. They were successfully able to synthesize group II−VI QDs with PL. But this technique was plagued by Ostwald's ripening. To overcome this, Katari et al. (1994) replaced TOP with tributylphosphine, which allowed spontaneous nucleation with a relatively slow rate of growth; incidentally increasing the stability of the QDs with TOPO as capping agent. $CdMe_2$ was used previously as the precursor for the synthesis of QDs and needed to be replaced due to their pyrophoric and toxic nature. Peng and Peng (2001) solved this problem with use of less toxic CdO (cadmium oxide) along with a long-chain fatty acid, oleic acid. This reduced the use of the toxic phosphine derivative, paving the way for much greener solvents for the synthesis. Chandan et al. (2014) reported the use of more environment-friendly ligands such as oleic acid and octadecyl amine as growth and nucleating ligands for CdSe synthesis. They investigated the effect of these ligands on the nucleation and growth of CdSe QDs and found these were stable over months. Such QDs with increased stability are better suited for photovoltaic application, keeping in the mind that it has to be exposed to an outdoor

environment. QDs were also synthesized in an aqueous solution of respective salts. Even though, there are several research reports on such synthesis, they lack stability and better confinement is not possible due to an elongated reaction time. Some reactions can be as long as 6 days, which can lead to polydispersed QDs.

Electron−hole pair recombination and leaching is the main concern in QDs, which affects the performance and stability of the device. This can be mitigated by forming the shell structure or inserting the dopant on the surface of the core QDs structure. Such an introduction can reduce recombination and increase the stability. Thus plain core QDs (CdSe, CdS, ZnS and CdTe) have countered comparatively less attention than core−shell structures such as CdSe/CdS, CdSe/ZnS, CdTe/CdS, etc. but it is not limited to these only. The thickness of the shell can be monitored and controlled by varying the same ligand used by monitoring the injection time, concentration of the shell precursor, and capping material used (Zhu et al., 2010a,b). CdSe/CdZnS QDs were reported by Schrier et al. (2012) and the maximum QY was 100%, which is the highest reported QY for the chalcogenide series of QDs. If the shell coating on the core is smaller, then it can lead to complete transmittance of electromagnetic radiation (light) through the shell to reach the core. Such a process can increase the QY of the material and reduce the electron−hole pair recombination. Another strategy to increase the PL QY is to incorporate the dopant into the energy level of the QDs. Dopants such as Mn, Cu and Ag can significantly increase PL QY over 50% (Chen et al., 2009). Doped QDs can emit significantly in the visible region with large Stokes shifts and decay time ranging from micro- to milliseconds timescales (Wood et al., 2009). Fig. 12.5 shows the schematic representation of surface passivation and related surface chemistry.

Vapor phase synthesis of QDs is a rather less known technique than the hot injection method due to its complexity. It can be formed via deposition from vapor onto the appropriate substrates in molecular beam epitaxy (MBE) or metal organic chemical vapor deposition. There are two approaches to form the QDs. The first is Stranski−Krastinov (SK) growth, where nanosized islands are formed with several monolayers deposited upon one another. This leads to the large lattice mismatch between the two semiconductor materials. This was observed in Ge/Si, InP/AlGaAs, and InP/GaInP. For such highly strained system, growth initiates with the addition of layer by layer and thus minimizes the strain energy. Such islands then grow articulately on the substrate without any misfit until a critical strain density with corresponding to its critical size is exceeded. Incidentally, coherent SK islands can be overgrown with a suitable passivating and carrier confining epitaxial layer to produce QDs with better PL efficiency—typically colloidal QDs—which depend on the capping layer. The second method is to produce the near surface quantum well (QW) and then deposit coherent SK islands on to those wells. Such deposition has a large lattice mismatch with the barrier to

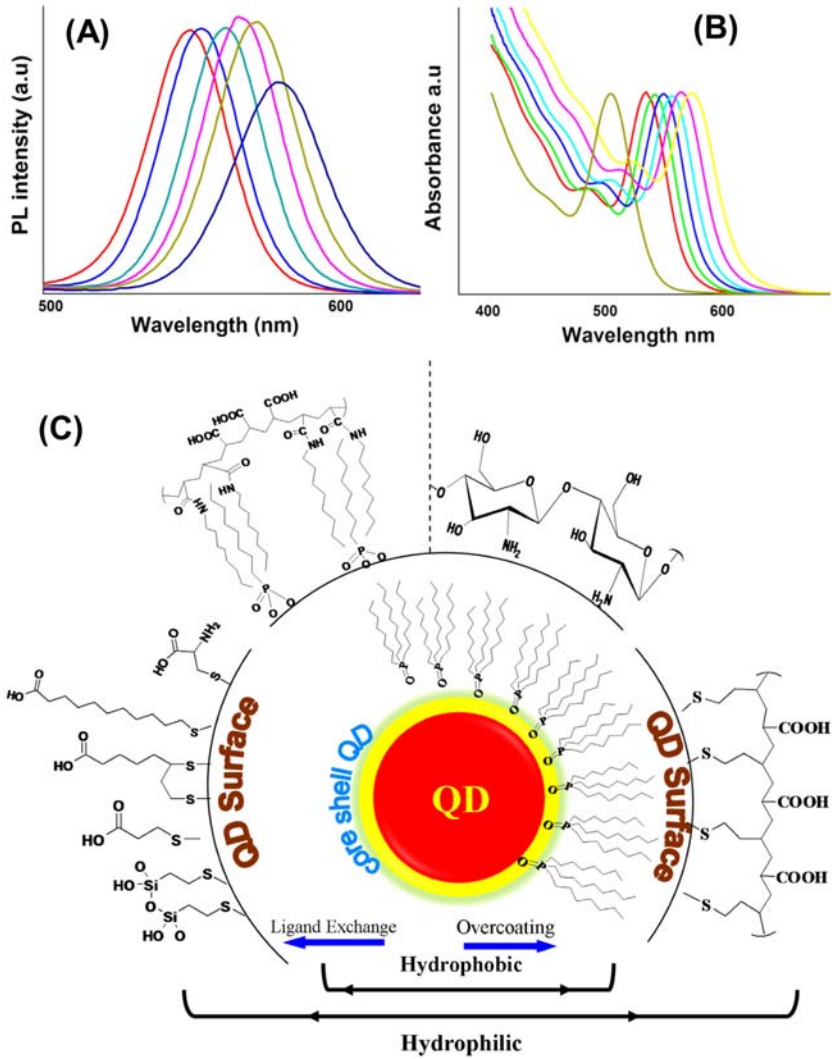

FIGURE 12.5 (A) PL; (B) UV−visible spectra of CdTe QDs; and (C) possible schemes for surface modification of QDs using ligand exchange and polymer coatings (Chandan et al., 2018). *Adapted from Chandan, H. R., Schiffman, J. D., Balakrishna, R. G., 2018. Quantum dots as fluorescent probes: synthesis, surface chemistry, energy transfer mechanisms, and applications. Sens. Actuator, B 258, 1191−1214. With permission.*

produce strain in the island formed. The strain created by the island can be extended to the QW and thus it can penetrate through its outer barrier and well region. Such a strain field can expand the lattice of the QW and lowers the bandgap below the SK island formed and thus produces the quantum

dots by confining its electrons three dimensionally. Such SK islands are referred to as stress islands. Stress-induced InGaAs and GaAs have been reported for InP stress islands on GaAs/InGaAs/GaAs QW and for InP stressor islands on an AlGaAs/GaAs/AlGaAs QW (Petroff and DenBaars, 1994; Willardson et al., 1999).

12.3.2 Perovskite quantum dots

Hybrid organic−inorganic perovskite quantum dots is the new entry to the QDs family with enhanced fluorescence intensity and QY. The metal halide perovskite has the simple ABX_3 structure. "A" is occupied by organic or inorganic materials such CH_3NH_3 (MA), $CH(NH_2)$ (FA), or Cs^+. "B" by a divalent metal cation such as lead, strontium, and germanium. "X" usually is halide ions. The octahedral BX_6 structure is the basis of the perovskite and "A" is occupied by the cation, which fills the voids between these structures. Synthesis of such a structure can be also achieved through the hot injection method. During the initial stage of the development, organic−inorganic halide perovskite, such as methyl ammonium lead halide ($MAPbI_3$) and formammonium lead halide ($FAPbI_3$), gained more attention (Choi et al., 2017; Lee et al., 2019). However, these PQDs are less stable due to the organic content and soon the focus was shifted toward inorganic halide perovskites (Xiang and Tress, 2019). But the toxicity of the lead limited their use in practical applications. Until recently, most of the studies shifted their focus from $CsPbX_3$ to lead-free structures (Han et al., 2019). Hot injection method is the most common method used for the synthesis of the PQDs, with OA and ODE being the predominant ligand system for the synthesis of the PQDs (Zhang et al., 2015; Sun et al., 2018). The temperature was adjusted ranging from 150 to 200°C depending on the type of the material. Typically, the Cs oleate precursor was injected into the degassed PX_3 (X = Cl, Br, I) solution. This hot injection leads to nucleation and growth of the particle. The reaction is arrested by reducing the reaction temperature using ice cold water (immersing the round bottom flask). The synthesis of lead-free perovskite gained more interest.

Zhou et al. (2018) demonstrated the synthesis of $Cs_2AgBiBr_6$ perovskite QDs. Typically, the Cs-oleate was injected into the mixture of $BiBr_3$, $AgNO_3$, ODE, OA, and HBr at 200°C under inert condition or N_2 atmosphere. This led to the formation of $Cs_2AgBiBr_6$ PQDs with a time span of 5 s. In fact, the morphology of the PQDs synthesized by hot injection method is monitored by three factors influencing it (Wang et al., 2016; Dolzhnikov et al., 2017; Zhou et al., 2018; Xu et al., 2019). This includes the reaction time of the two precursors, the temperature and the ratio of the ligands. Wang et al. (2015) reported the synthesis of Cs_2SnI_6 PQDs. They demonstrated that reaction time is very important in the hot injection method. Usually the reaction is short with less than a minute, and it results in cubic

structured PQDs. However, when the reaction time is progressed, a different morphology of the PQDs was formed. The formation of nanorods, nanowires, nanobelts, and nanoplatelets was reported with a time scan of 5, 10, 30, and 60 min, respectively (Zhou et al., 2018). Similarly, the effect on the morphology of PQDs by variation of temperature and ligand ration was also reported by Dolzhnikov et al. (2017) and Xu et al. (2019), respectively. Fig. 12.6 gives schematic presentation for hot injection method and effect of reaction time over morphology.

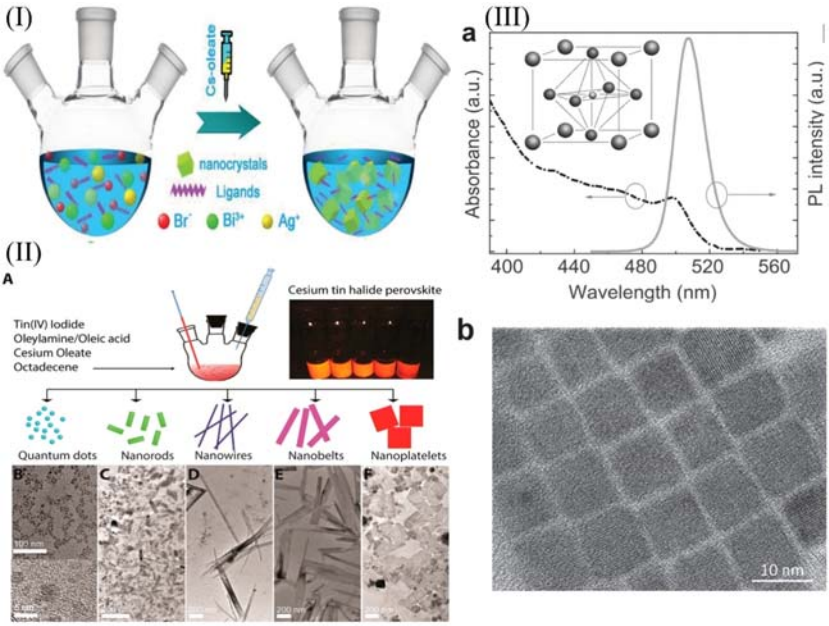

FIGURE 12.6 (I) Schematic illustration of the hot-injection method for the synthesis of $Cs_2AgBiBr_6$ QDs. (II) (a) Absorption and emission spectra of $CsPbBr_3$ IPQDs in solution. Inset: Cubic perovskite structure of $CsPbBr_3$ IPQDs: medium spheres in the centers of the cubic faces: Br; small sphere in the center of the cubic: Pb; large spheres in the cubic corners: Cs. (b) TEM image of $CsPbBr_3$ IPQDs. (III) Synthesis of Cs_2SnI_6 nanocrystals: (A) Schematic of procedures for the controlled synthesis of perovskite Cs_2SnI_6 nanocrystals (*left panel*) and photograph of the as-prepared Cs_2SnI_6 samples under UV light (*right panel*); (B−F) TEM images of Cs_2SnI_6 nanocrystals with different shapes (the inset of B gives an HRTEM image of Cs_2SnI_6 spherical quantum dots). *Adapted (I) from Zhou, L., Xu, Y. F., Chen, B. X., Kuang, D. B., Su, C. Y. 2018. Synthesis and photocatalytic application of stable lead-free Cs2AgBiBr6 perovskite nanocrystals. Small 14 (11) doi: 10.1002/smll.201703762. (II) from Wang, Y., Li, X., Song, J., Xiao, L., Zeng, H., Sun, H., 2015. All-inorganic colloidal perovskite quantum dots: a new class of lasing materials with favorable characteristics. Adv. Mater. 27 (44), 7101−7108. (III) from Wang, A., Yan, X., Zhang, M., Sun, S., Yang, M., Shen, W., et al., 2016. Controlled synthesis of lead-free and stable perovskite derivative Cs2SnI6 nanocrystals via a facile hot-injection process. Chem. Mater. 28 (22), 8132−8140. With permission.*

Another method of synthesizing PQDs is ligand-assisted synthesis. To solve some of the challenges associated with the hot injection method (high reaction temperature and low reproducibility for large-scale synthesis), this method came to existence. It is a simple synthetic process, which involves the principle of supersaturation in the presence of ligands. PQDs were synthesized by dropwise addition of precursor solution in polar solvent into a solvent containing ligands. The difference in the polarity of the solvent system influences the miscibility of solvents. Thus it resulted in two solvent systems, which cannot mix, and the precursor present encounters a nonequilibrium state. Due to this supersaturation, nucleation and growth occurs immediately even at room temperature and the product can be produced at gram scale with reproducibility.

Gram-scale synthesis of lead-based PQDs was reported using this method (Liang et al., 2016; Wei et al., 2016b). Yang et al. (2017) reported the synthesis of $Cs_3Bi_2Br_9$ PQDs by a one-step reaction without ligands. CsBr and $BiBr_3$ were dissolved in dimethylsulfoxide (DMSO) to form a precursor solution. As DMSO is a polar solvent, therefore when such a precursor solution was added to the less polar solvent such as isopropanol (which can act as antisolvent), a yellow-green colloidal solution was formed. This indicates the nucleation and growth of $Cs_3Bi_2Br_9$ PQDs formation even without the presence of ligands. Nevertheless, the low QY of 0.2% indicates the requirement of ligands.

Leng et al. (2018), synthesized $Cs_3Bi_2Br_9$ by this method using OA and oleylamine (OLA) as ligands. This protocol for the synthesis is similar to Yang et al. (2017) except for two reaction conditions. The first one is that actone was used as the antisolvent and second is that precursor solution was prepared using OLA and antisolvent OA. It resulted in PQDs $Cs_3Bi_2Br_9$ having an average diameter of 3.88 nm and QY of 19.4%. Even though the ligand-assisted method is advantageous in terms of reaction temperature, there are some issues that need to be addressed. Typical to chalcogenide QDs synthesis using hot injection method, the nucleation occurs at early stage of the reaction, which is followed by the growth. This allows one to arrest the reaction depending on time or temperature. But in ligand-assisted synthesis, the nucleation and growth stages cannot be separated, indicating the difficulties in controlling the size and morphology of the PQDs (Lignos et al., 2016). Another problem associated with halide PQDs is that the polar solvents are used in ligand-assisted reaction. The halide PQDs are vulnerable to the polar solvents with the possibility that PQDs may undergo degradation or aggregation losing their properties. Other than this method, one-step synthesis using an ultrasonication method has also been reported, where all the precursors have been dissolved in appropriate solvent and sonicated. The PQDs can be synthesized with the use of the same ligand system (Tong et al., 2016; Jang et al., 2016). Nevertheless, there is always scope to improve the synthetic route for better quality products.

12.4 Quantum dot sensitized solar cells

Several QDs are used in QDSSCs as sensitizers, which include $CsPbX_3$, CdS, CdSe, CdTe, ZnS, Ag_2Se, PbSeS, $AgInSe_2$, PbS, $CuInS_2$, and $MAPbX_3$ (Lin et al., 2020). Among all these QDs sensitizers, CdS and CdSe QDs are considered significant choice as stable materials in QDSSCs. The enhancement in PCE observed in QDSSCs are mainly contributed by the increase in size of QD, enhanced light harvesting, reduced defects, improved charge carrier migration and higher surface area covered by the QDs on the photoelectrode. Lee and Lo (2009) have used CdS/CdSe cosensitized photoelectrode for QDSSC application and reported that CdS and CdSe QDs exhibits complementary effect in light harvesting due to stepwise arrangement of band edge levels, which is beneficial for the injection of electron and recovery of hole between CdS and CdSe (Fig. 12.7) resulting in a PCE of 4.22% using a TiO_2/CdS/CdSe/ZnS electrode. Introduction of ZnS layer acted as a passivation layer to protect QD materials from photocorrosion and improves the photovoltaic effect of QDSSCs.

Archana et al. (2020) have studied the cosensitization effect of CdS and InSb QDs and reported an improved PCE for TiO_2/CdS/InSb QDSSC that is 0.8% (InSb) and 3.52% (CdS QDs) to 4.94% (InSb QDs and CdS QDs). The cosensitization of InSb improves the light absorption range along with reduced spectral overlap leading to better light harvesting and decreased defects causing suppressed recombination of charge carriers. Liu et al. (2019) have used zinc titanium mixed metal oxides as photoanodes with CdS/CdSe QDs for QDSSCs and reported PCE of 3.95%. Yu et al. (2012) have prepared CdSe/CdS core/shell nanocrystals and showed an improved Jsc, Voc, and η compared to single CdSe QDSSCs, due to higher light

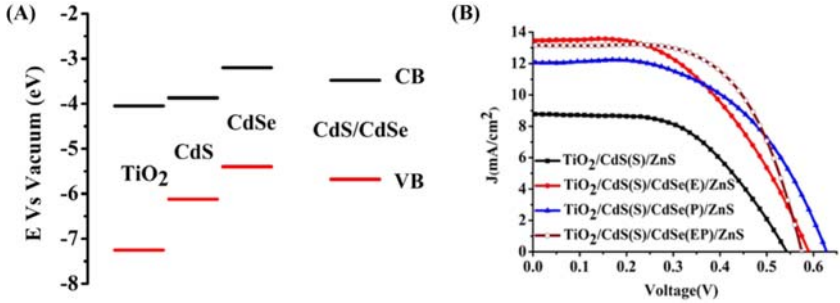

FIGURE 12.7 (A–B) Band edge structure for TiO_2, CdS and CdSe electrodes and (C) I–V curves for QDs sensitized solar cells. *Adapted from Esparza, D., Zarazúa, I., López-Luke, T., Cerdán-Pasarán, A., Sánchez-Solís, A., Torres-Castro, A., et al., 2015. Effect of different sensitization technique on the photoconversion efficiency of CdS quantum dot and CdSe quantum rod sensitized TiO_2 solar cells. J. Phys. Chem. C. 119 (24), 13394–13403. With permission.*

harvesting ability. In addition, CdSe/CdS prevents recombination of charges inside QDs by decreasing surface states and by accelerating charge separation, suggesting that cosensitized QDs are better than single QDs. Another approach to improve QDSSCs performance is by incorporating passivation layer like ZnS between TiO_2 (photoanode) and electrolyte in CdS QDs solar cell. The decreased recombination of charge carriers from TiO_2 to electrolyte was observed in the presence of passivation layer, leading to enhanced charge collection efficiency (Jung et al., 2012).

Li et al. (2020) have introduced TiO_2 as a passivation layer between ZnO hollow microspheres photoanode and CdS/CdSe/ZnS, which showed an improved PCE of 3.16% as compared to bare ZnO of 1.54%. This enhancement was attributed to improved light absorption and electron transport resulting from TiO_2 incorporation. Yu et al. (2012) studied effect of different annealing temperatures (100°C, 150°C, 200°C and 250°C). QDSSC performance in CdSe/CdS QDs, exhibited an increased IPCE from 0.46% to 2.83%. A significant enhancement in efficiency of 4.21% was observed with 300°C annealing temperature as compared to the photoanode, which was not treated with heat, which exhibited only 3.2%. In addition, CE and electrolyte can also be modified to enhance the properties of QDSSC. CoS (Yang et al., 2010) and Cu_2S are used as CE in ZnS/CdSe/CdS multilayer QDSSCs and they showed an increased efficiency of 2.7% and 1.9%, respectively in comparison to Pt CE with an efficiency of 1.6%. Furthermore, recently Cu_2S and rGO composites have open up new path for CE material choice for QDSSCs (Kusuma et al., 2018).

Huang et al. (2011) reported a flexible photoelectrode for CdS/CdSe quantum dot-QDSSCs with a PCE of 3.47% under AM 1.5G illumination using Cu_2S CE and polysulfide electrolyte between the electrodes. The conventional flexible transparent conductive oxides substrates like ITOs−polyethylene terephthalate (ITO-PET) cannot tolerate high temperature and hence they have also investigated a new technique of depositing the TiO_2 and FTO layer first, followed by PET substrate at lower temperature in order to avoid temperature issues for CdS/CdSe QDSSCs photoelectrodes. Yu et al. (2011) have used electrodeposition method to fabricate CdS/CdSe QDs with TiO_2 as a photoanode and reported an improved electron transport and electron collection efficiency with a PCE of 4.81%.

Li et al. (2011) have used modified polysulfide $[(CH_3)_4N]_2S/[(CH_3)_4N]_2S_n$, in organic solvent (3-methoxypropionitrile) to improve the QDSSCs performance. They observed an increased PCE of 3.2% under AM 1.5G irradiation by employing CdS QDSSCs. The modified polysulfide contributes in linking QDs with nanoporous TiO_2 through covalent bonds using thioglycolic acid resulting in high wettability and superior penetration capability of TiO_2 with an improved fill factor of 0.89. Pan et al. (2012) prepared CdS/CdSe inverted type-I core/shell structure deposited on TiO_2 photoanode with a bifunctional linker mercaptopropionic acid (MPA), which showed an

improved PCE of 5.32%. It was attributed to modified deposition technique using linker MPA.

Zhu et al. (2010a,b) have used Zn-doped TiO_2 screen printed on FTO as a photoanode for CdS QDSSCs and reported an improved PCE by 24% and it was attributed to reduced electron recombination and enhanced electron transport by Zn doping. Santra and Kamat (2012) have reported that QDSSCs exhibited a significant enhancement in PCE (5.4%) on doping Mn^{2+} to CdS. Mn-doped ZnS, ZnSe and CdS depicted emission at 585 nm resulting from d-d transition, but these transitions are both; spin and orbitally forbidden, leading to a very long lifetime in the range of several hundreds of micro seconds (Fig. 12.8). Hence it is advantageous to utilize long lived charge carriers to enhance the PCE in QDSSCs using Mn-doped QDs (Santra and Kamat, 2012). Some parameters of CdQDs-based solar cells are tabulated in Table 12.1.

12.4.1 Perovskite quantum dots-based quantum dot sensitized solar cells

Organometallic halide perovskites having the formula ABX_3 (where A is an organic cation, B is commonly Pb^{2+}, and X is a halide) have inspired photovoltaics field due to their unique photophysical properties like high emission efficiencies, long carrier diffusion lengths and low production cost. It makes them as potential candidate for photovoltaics and optoelectronics applications. The research in this field is highly focused on organic−inorganic hybrid perovskites, for example, $CH_3CH_3PbI_3$, $CH_3NH_3PbI_3$, etc. and later the volatile organic part is substituted by inorganic materials such as $CsPbX_3$, X = Cl, Br, and I with cubic perovskite structure. The organic−inorganic $CH_3CH_3PbI_3$ perovskites will dissociate into PbI_2 and CH_3NH_3I under environmental stress; the latter is volatile, and therefore,

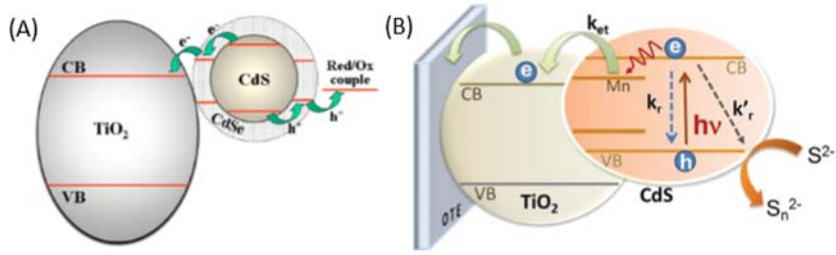

FIGURE 12.8 Band alignment for (A) Inverted type-I CdS/CdSe core/shell structure and (B) Mn-doped CdS QDSSC solar cells. *Adapted (A) from Pan, Z., Zhang, H., Cheng, K., Hou, Y., Hua, J., Zhong, X., 2012. Highly efficient inverted type-I CdS/CdSe core/shell structure QD-sensitized solar cells. ACS Nano 6(5), 3982−3991.; (B) Santra, P. K., Kamat, P. V., 2012. Mn-doped quantum dot sensitized solar cells: a strategy to boost efficiency over 5%. J. Am. Chem. Soc. 134 (5), 2508−2511. With permission.*

TABLE 12.1 Cd QDs-based solar cell parameter.

QDs material	Voc (V)	Jsc (mA cm^{-2})	Fill factor (%)	η (%)	References
$TiO_2/CdS_3/CdSe_4/ZnS$, Au	0.513	16.8	0.49	4.22	Lee et al. (2012)
TiO_2/CdS/InSb/CuS	0.533	18.58	49.88	4.94	Archana et al. (2020)
Zn−Ti/CdS/CdSe/ZnS	0.57	13.36	0.52	3.95	Liu et al. (2019)
$TiO_2/CdS_8/ZnS$	0.49	7.813	44.83	1.72	Jung et al. (2012)
ZnS/CdSe/CdS/TiO_2@ZnO	0.45	14.57	0.46	2.99	Li et al. (2020)
TiO_2/TGA/CdS-3	1.2	3	0.89	3.2	Li et al. (2011)
TiO_2/CdS/CdSe core shell structure-inverted Type-I	0.527	18.02	0.56	5.32	Pan et al. (2012)
Mn-doped-CdS/CdSe	0.558	20.7	0.47	5.42	Santra and Kamat (2012)
TiO_2/ZnSe/QDs/ZnSe (CdS/CdSe)	0.61	21.49	0.55	7.24	Huang et al. (2016)

replaced with inorganic material. The first perovskite-based solar cells was reported by Kojima et al. (2009) with PCE of 3.8% using $MAPbI_3$ and $MAPbBr_3$ as a liquid sensitizer in DSSC-based structure. Im et al. (2011) have used quantum dots of nanocrystalline material and enhanced the PCE to 6.54%. The incorporation of solid hole transporting layer (HTL) spiro-OMeTAD instead of liquid HTL has boosted the PCE in recent years. Presently, perovskites cells have reached an efficiency of 25.5% to convert sunlight into electricity and perovskite silicon tandem solar cells reached PCE of 29.5% as depicted in NREL chart (Fig. 12.9), which is at par with the best thin-film chalcogenide and silicon devices.

Swarnkar et al. (2016) have prepared phase stabilized $CsPbI_3$ QDs at lower temperature for photovoltaic applications. $CsPbI_3$ undergoes immediate transformation to orthorhombic phase, when exposed to ambient conditions. The phase stabilized $CsPbI_3$ QDs stable for months at ambient conditions are developed by modifying the purification process, which includes washing with methyl acetate, an antisolvent, which eliminates

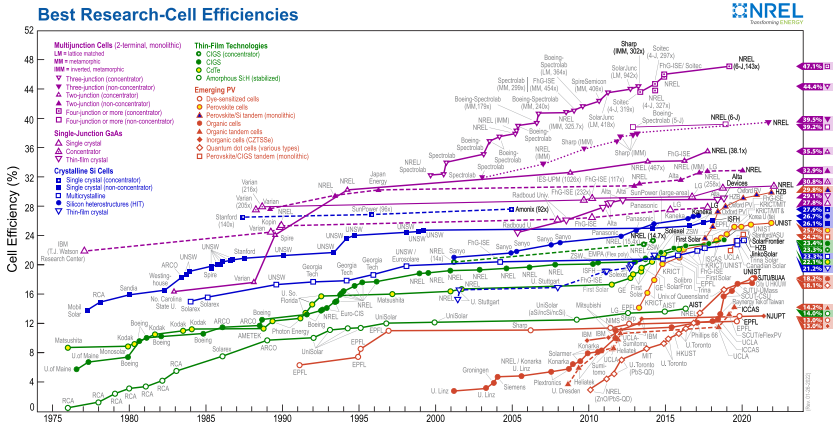

FIGURE 12.9 NREL cell efficiency chart.

unreacted precursor material without inducing agglomeration. Lee et al. (2012) have modified structure of device by replacing m- (mesoporous)-TiO_2 with insulating m-Al_2O_3, which is fabricated above the thin compact layer of TiO_2. It resulted in ten times faster charge collection with an enhanced photocurrent. Here, they concluded that mesoporous structure acts as a scaffold for perovskite structure.

Chen et al. (2017) reported that efficient vacuum deposited $CsPbI_3$ and $CsPbI_2Br$ enhances the PCE in solar cells to 11.8%. Sanehira et al. (2017) have reported that A-site cation halide salt treatment (formamidinium FA^+) enhances charge carriers mobility, resulting in increased photocurrent contributing to higher PCE of 13.43%. Here, the interaction of QDs and FA^+ might be a surface reaction or partial cation exchange resulting $Cs_xFA_{1-x}PbI_3$ QD core or a core shell structure formed by $FAPbI_3$ matrix around $CsPbI_3$ QDs, suggesting that individual QDs are no longer present. Frolova et al. (2017) have used coevaporation by thermal annealing of CsI and PbI_2 to fabricate $CsPbI_3$ perovskite solar cells, which delivered an enhanced power conversion efficiency of 10.5%. Thermal annealing contributes to phase changes in crystal structure and morphology in order to enhance the device performance by producing a well crystalline, uniform and highly pure perovskite film compared to solution-based process, where the film is affected by solvent, wetting, evaporation and deposition process (Fig. 12.10).

Lv et al. (2015) have used colloidal surface modified $CuInS_2$ QDs with improved carrier transport ability as hole transporting agent in TiO_2/$CH_3NH_3PbI_3$/HTM/Au solar cell, which showed an enhanced PCE of 8.38% along with ZnS as shell layer. The improved PCE is contributed by decreased charge recombination between TiO_2 and hole transporting material HTM. Stolterfoht et al. (2018) have visualized nonradiative recombination pathways in

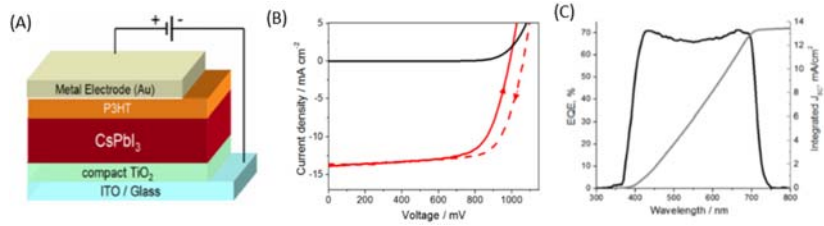

FIGURE 12.10 (A) Schematic of the PQDs solar cell, (B) current-voltage curve of device and (C) EQE spectrum. *Adapted from Frolova, L. A., Anokhin, D. V., Piryazev, A. A., Luchkin, S. Y., Dremova, N. N., Stevenson, K. J., et al., 2017. Highly efficient all-inorganic planar heterojunction perovskite solar cells produced by thermal coevaporation of CsI and PbI_2. J. Phys. Chem. Lett. 8 (1), 67−72. With permission.*

perovskite solar cells $(CsPbI_3)_{0.05}[(FAPbI_3)_{0.89}(MAPbBr_3)_{0.11}]_{0.95}$ using transient and absolute PL. They found quasi-Fermi-level splitting losses and interfacial recombination resulting in 135 and 80 meV, free energy loss. Incorporation of thin interlayers of PFN-P2—a conjugated polyelectrolyte and LiF between perovskite and transport layer contributes to a considerable decrease of these interfacial losses at both p and n contacts, by 65 and 35 meV respectively. The PCE has improved to 19.83% with a record fill factor of 81%. Zheng et al. (2020) have reported that introduction of long-chain surface anchoring alkylamine ligands into precursor solution suppressing the nonradiative recombination, which improves the optoelectronic properties of mixed-cation mixed-halide perovskite films. The resulting modified film shows (100) orientation, low trap state density in addition to improved charge carrier mobility and diffusion lengths leading to a highly enhanced efficiency of 22.3%. Some perovskite-based solar cell parameter are summarized in Table 12.2.

12.4.2 Other quantum dots-based quantum dot sensitized solar cells

QDSSCs are potential photovoltaic device systems, attributed to their low material requirements and simplicity. However, in order to achieve high efficiencies, complicated and expensive processes or toxic materials are used, which limit their large-scale application. By overcoming these limits, the QDSSCs can be used for commercial applications. Pan et al. (2014) have prepared green QDs that are free of Cd or Pb. They have applied surface passivation to the ternary $CuInS_2$ (CIS) QDs using ZnS and reported a high efficiency of 7.04% as compared to other green QDs-based QDSSCs, suggesting the possibility of better or comparable performance with green CIS QDs (Fig. 12.11). This enhanced efficiency was attributed to a high absorption range, more QDs loading, and reduced recombination with type-I core/shell structure.

TABLE 12.2 Perovskite-based solar cells characteristics.

QDs material	Voc (V)	Jsc (mA cm^{-2})	Fill factor (%)	η (%)	References
Phase stable $CsPbI_3$	1.23	13.47	0.65	10.77	Swarnkar et al. (2016)
$CH_3NH_3PbI_2Cl$	0.98	17.8	0.63	10.9	Singh and Nagarjuna (2014)
$CsPbI_2Br$	1.15	15.2	0.67	11.8	Chen et al. (2017)
$CsPbI_3$	1.06	13.8	71.6	10.5	Frolova et al. (2017)
$TiO_2/CH_3NH_3PbI_3/CuInS_2/ZnS/Au$	0.924	18.6	48.7	8.38	Lv et al. (2015)
$(CsPbI_3)_{0.05}[(FAPbI_3)_{0.89}(MAPbBr_3)_{0.11}]_{0.95}$	1.05	25.1	0.75	19.83	Stolterfoht et al. (2018)
$Cs_{0.05}(FA_{0.92}MA_{0.08})_{0.95}Pb(I_{0.92}Br_{0.08})_3$	1.14	23.9	0.82	22.34	Zheng et al. (2020)

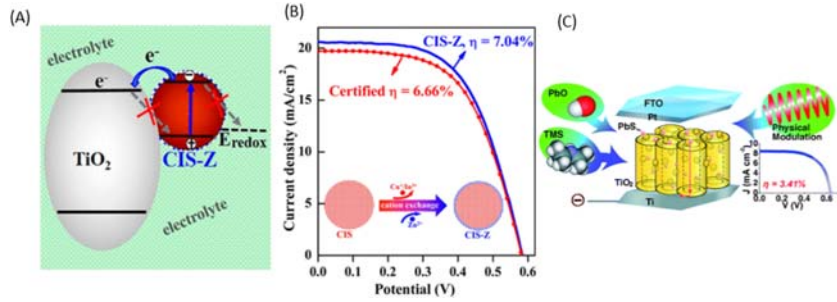

FIGURE 12.11 (A) Schematic of band structure of TiO_2 and $CuInS_2$ (CIS) QDs passivated by ZnS (B) I−V curves of CIS QDs solar cells and (C) Schematic of PbS QDs solar cell along with I−V curves. *Adapted from Tao, L., Xiong, Y., Liu, H., Shen, W. 2014. High performance PbS quantum dot sensitized solar cells via electric field assisted in situ chemical deposition on modulated TiO_2 nanotube arrays. Nanoscale. 6 (2), 931−938. With permission. Adapted from Pan, Z., Mora-Seró, I., Shen, Q., Zhang, H., Li, Y., Zhao, K., et al., 2014. High-efficiency "green" quantum dot solar cells. J. Am. Chem. Soc. 136 (25), 9203−9210. With permission.*

Tao et al. (2014) have prepared PbS QDs-based TiO_2 nanotube arrays (NTAs) through an in situ chemical bath deposition method controlled by low electric field. They could achieve an efficiency of 3.41%. These methods enhance QDs loading on the NTAs with high Voc and fill factor (FF) contributed by shorter electron path, less structural and electronic defects, optimal film thickness ($\sim 4\ \mu m$), and reduced recombination in the ordered TiO_2 NTAs produced by oscillating anodic voltage. Bi et al. (2018) could harvest the short-wave infrared range of the solar spectrum using PbS colloidal quantum dots for solar cells using hybrid inorganic−organic ligand treatment by combining ZnI_2 with 3-mercaptapropionic acid for surface passivation of PbS QDs. The modified PbS solar cell has delivered an efficiency of 7.9% and an additional 3.3% enhancement by placing this cell at the back of the $MAPbI_3$ perovskite film due to enhanced light absorption up to 750 nm. It suggests that the modification of a passivation layer can boost the PCE.

Inorganic nanostructured materials and hybrid carbon materials have attracted a potential interest and open an exciting field in the design and fabrication of efficient catalysts. Guo et al. (2014) have prepared a novel CE consisting of Co_9S_8 nanotube arrays grown on carbon fiber (CF) (Co_9S_8/CF) for fiber-shaped flexible QDSSCs and achieved high PCE of 3.79% as compared to CE and Pt. The redox mediator plays an important role in determining photovoltage and photocurrent in QDSSCs. As per kinetics, reduction of oxidized QDs by the redox mediator should happen faster than the back transfer of electron between TiO_2 and oxidized QDs to sustain the photocurrent. Thermodynamically, the redox mediator should possess effectively

positive reduction potential to provide high photovoltage. Haring et al. (2014) have investigated Mn(II/III) complexes as potential redox mediator for CdS/CdSe/ZnS QDSSCs. Mn poly(pyrazolyl)borates showed high photovoltages ~ 1 V with reduction potential of ~ 0.51 V versus Ag/AgCl. Reduction rates were slower compared to $Co(bpy)_3$, where bpy = 2,2′-bipyridine, which was confirmed by enhanced electron lifetimes up to four orders of magnitude longer as the low solubility prevents the sustaining of high current. The Mn(II/III) complexes redox mediator exhibited higher fill factor (~ 0.6) and photovoltage than $Co(bpy)_3$ and it can be ascribed to more positive reduction potential and reduced recombination.

Interface engineering is an important path to enhance the photovoltaic performance in QDSSCs. Zhang et al. (2019) have studied the interface modification between TiO_2 and QDs using ZnS and ZnSSe semiconductors. Here, the main limitations are the passivation effect and the matching of lattice with TiO_2 and QDs. Though, ZnS has a large energy bandgap due to higher CB edge, its lattice mismatch with TiO_2 and QDs largely leads to the formation of defect states. In contrast, ZnSe alloy exhibited a small lattice mismatch with TiO_2 and QDs with a lower CB edge. They have prepared ZnS_xSe_{1-x} alloy material as a passivation layer on the Zn−Cu−In−Se (ZCISe) QD-sensitized TiO_2 photoanode and reported that alloy material is more constructive for the inhibition of charge recombination between photoanode/electrolyte interfaces, and it also improves extraction of photogenerated electron leading to the photon efficiency improvement from 12.17% to 13.08%.

12.5 Recent developments

Solar cell parameters of some quantum dots-based solar cells are summarized in Table 12.3.

12.6 Conclusion

QDSSCs are a promising alternative for dye-sensitized solar cells due to unique properties of QDs. Numerous factors limit the PCE of QDSSCs, which include narrow absorption of solar spectrum, recombination at interfaces, lower QD deposition on semiconductor film, poor charge carrier transportation, photocorrosion of electrode, and low fill factor, because of the low performance of CE. The research work in QDSSCs has mainly focused on the improvement of PCE in recent years. Among all QDs sensitizers, Cd chalcogenide-based sensitizers, especially CdS and CdSe, are the preferred choice for solar cell devices. The researchers have investigated various modifications to improve the PCE of Cd-based QDSSCs and reported on the cosensitization of CdS/CdSe, introduction of passivation layer (ZnS), annealing temperature, CE modification (Cu_2S, CoS, and composites of Cu_2S/

TABLE 12.3 Some quantum dots-based solar cell parameters.

QDs material	V_{oc} (V)	J_{sc} (mA cm^{-2})	Fill factor (%)	η (%)	References
$CuInS_2$	0.586	20.65	58.1	7.04	Pan et al. (2014)
PbS	0.63	8.48	64	3.41	Tao et al. (2014)
CdS/CdSe	0.37	17.95	57	3.79	Guo et al. (2014)
CdS/CdSe	0.9	0.12	55	0.33	Haring et al. (2014)
Zn−Cu−In−Se (ZCISe) QD	0.733	26.49	68.52	13.08	Zhang et al. (2019)
Ag_2S (scattering layer)	0.33	7.3	40.8	0.98	Tubtimtae et al. (2010)
CdSe/ZnS	0.44	2.29	27	0.27	Ning et al. (2011)
$CuInSe_xS_{2-x}$	0.55	10.5	60.4	3.54	McDaniel et al. (2013a)
$CsPbBr_3$/CdS	0.77	9.88	40	3.59	Hunsur Ravikumar et al. (2022)
Mn/CdS	0.6	10.27	49	3.29	Shen et al. (2016)
$CuInSe_xS_{2-x}$	0.54	17.565	54.1	5.13	McDaniel et al. (2013b)
CdTe/CdSe core/shell QD	0.6	19.59	56.9	6.76	Wang et al. (2013)
ZnTe/CdSe	0.64	19.65	57	7.17	Jiao et al. (2015)
$AgInSe_2$/CdS/ZnS	0.654	18.27	52.5	6.27	Abate and Chang (2018)
$CuInS_2$−Mn-doped CdS	0.581	19.29	48	5.38	Luo et al. (2013)
$Cd_{1-X}Zn_XTe$/CdS core/shell	0.6	10.05	54	3.27	Lu et al. (2020)
PbSe	0.61	25.39	67	10.38	Liu et al. (2020)
N and S codoped carbon QDs	0.43	0.61	52	1.36	Riaz and Park (2022)
Gd-doped CdS@CdSe	0.71	16.34	65.2	7.57	Amani-Ghadim et al. (2022)
Mn-doped CdS@CdSe	0.558	20.7	47	5.42	Santra and Kamat (2012)

(*Continued*)

TABLE 12.3 (Continued)

QDs material	V_{oc} (V)	J_{sc} (mA cm^{-2})	Fill factor (%)	η (%)	References
Ni-doped CdS	0.643	8.91	54.3	3.11	Gopi et al. (2016)
Sn:InP	0.59	10.58	56.7	3.54	Yang et al. (2015a,b)

rGO), polysulfide electrolyte modification and doping of QDs (e.g., Mn), and wide bandgap semiconductor (TiO_2/ZnO). Apart from Cd chalcogenide QDs, other QDs also have promising properties as sensitizers, such as $CuInS_2$, PbS, and Zn-Cu-In-Se. Recently, PQDs and tandem silicon solar cells (PQDs and silicon) have gained significant importance due to the low production cost and high PCE (reported up to 29.5%). To further enhance PCE and to achieve breakthroughs in QDs solar cell device, the focus of investigation should be channeled to research on materials such as doping/composite/different tandem structure of wide bandgap material, QDs, surface treatment of electron transport layer, electrolytes, and CE modification.

References

Abate, M.A., Chang, J.-Y., 2018. Boosting the efficiency of $AgInSe_2$ quantum dot sensitized solar cells via core/shell/shell architecture. Sol. Energy Mater. Sol. Cell 182, 37–44.

Ahmad, M.S., Pandey, A.K., Abd Rahim, N., 2017. Advancements in the development of TiO_2 photoanodes and its fabrication methods for dye sensitized solar cell (DSSC) applications. A review. Renew. Sustain. Energy Rev. 77, 89–108.

Allen, P.M., Bawendi, M.G., 2008. Ternary I − III − VI quantum dots luminescent in the red to near-infrared. J. Am. Chem. Soc. 130 (29), 9240–9241.

Amani-Ghadim, A.R., Mohammad-Gholipour-Rezaei, E., Bayat, F., Agbolaghi, S., Khodam, F., 2022. Enhancement in photovoltaic properties of exciplex quantum dot sensitized solar cells via gadolinium doping and formation of type II Core/Shell (Gd-doped CdS@CdSe) structure. Sol. Energy 231, 402–413.

Anttu, N., 2015. Shockley–Queisser detailed balance efficiency limit for nanowire solar cells. ACS Photonics 2 (3), 446–453.

Archana, T., Vijayakumar, K., Subashini, G., Nirmala Grace, A., Arivanandhan, M., Jayavel, R., 2020. Effect of co-sensitization of InSb quantum dots on enhancing the photoconversion efficiency of CdS based quantum dot sensitized solar cells. RSC Adv. 10 (25), 14837–14845.

Badawi, A., Al-Hosiny, N., Abdallah, S., Negm, S., Talaat, H., 2013. Tuning photocurrent response through size control of CdTe quantum dots sensitized solar cells. Sol. Energy 88, 137–143.

Badawy, W.A., 1990. Improvement of n-Si/SnO_2/electrolyte photoelectrochemical cells by Ru deposits. J. Electroanal. Chem. Interfacial Electrochem. 281 (1), 85–95.

Badawy, W.A., 1993. Preparation and characterization of TiO_2/Sb thin films for solar energy applications. Sol. Energy Mater. Sol. Cell 28 (4), 293–303.

Badawy, W.A., El-Dessouki, M.S., 1985. A study of the stability of n-Si/SnO_2 solar cells under normal working conditions. Phys. Status Solidi 92 (2). Available from: https://doi.org/10.1002/pssa.2210920258.

Beattie, A.R., 1962. Quantum efficiency in InSb. J. Phys. Chem. Solids 23 (8), 1049–1056.

Beard, M.C., Johnson, J.C., Luther, J.M., Nozik, A.J., 2015. Multiple exciton generation in quantum dots vs singlet fission in molecular chromophores for solar photon conversion. Phil. Trans. R. Soc. A: Maths, Phys. Eng. Sci. 373 (2044). Available from: https://doi.org/10.1098/rsta.2014.0412.

Bhambhani, P., 2018. Quantum dot-sensitized solar cells: a review. Bull. Electr. Eng. Inform. 7 (1), 42–54.

Bi, Y., Pradhan, S., Gupta, S., Akgul, M.Z., Stavrinadis, A., Konstantatos, G., 2018. Infrared solution-processed quantum dot solar cells reaching external quantum efficiency of 80% at 1.35 μm and Jsc in Excess of 34 mA cm^{-2}. Adv. Mater. 30 (7). Available from: https://doi.org/10.1002/adma.201704928.

Chandan, H., Geetha, B.R., 2013. Study on precipitation efficiency of solvents in postpreparative treatment of nanocrystals. J. Mater. Res. 28 (21), 3003–3009.

Chandan, H., Saravanan, V., Pai, R.K., Balakrishna, R.G., 2014. Synergistic effect of binary ligands on nucleation and growth/size effect of nanocrystals: studies on reusability of the solvent. J. Mater. Res. 29 (14), 1556–1564.

Chandan, H.R., Schiffman, J.D., Balakrishna, R.G., 2018. Quantum dots as fluorescent probes: synthesis, surface chemistry, energy transfer mechanisms, and applications. Sens. Actuator, B 258, 1191–1214.

Chen, D., Viswanatha, R., Ong, G.L., Xie, R., Balasubramaninan, M., Peng, X., 2009. Temperature dependence of "elementary processes" in doping semiconductor nanocrystals. J. Am. Chem. Soc. 131 (26), 9333–9339.

Chen, C.Y., Lin, H.Y., Chiang, K.M., Tsai, W.L., Huang, Y.C., Tsao, C.S., et al., 2017. All-vacuum-deposited stoichiometrically balanced inorganic cesium lead halide perovskite solar cells with stabilized efficiency exceeding 11. Adv. Mater. 29 (12). Available from: https://doi.org/10.1002/adma.201605290.

Choi, J., Le, Q.V., Hong, K., Moon, C.W., Han, J.S., Kwon, K.C., et al., 2017. Enhanced endurance organolead halide perovskite resistive switching memories operable under an extremely low bending radius. ACS Appl. Mater. Interfaces 9 (36), 30764–30771.

Chou, C.-Y., Lee, C.-P., Vittal, R., Ho, K.-C., 2011. Efficient quantum dot-sensitized solar cell with polystyrene-modified TiO_2 photoanode and with guanidine thiocyanate in its polysulfide electrolyte. J. Power Sources 196 (15), 6595–6602.

Christensen, O., 1976. Quantum efficiency of the internal photoelectric effect in silicon and germanium. J. Appl. Phys. 47 (2), 689–695.

Crisp, R.W., Kirkwood, N., Grimaldi, G., Kinge, S., Siebbeles, L.D., Houtepen, A.J., 2018. Highly photoconductive InP quantum dots films and solar cells. ACS Appl. Energy Mater. 1 (11), 6569–6576.

D'Souza, L.P., Amoli, V., Chandan, H.R., Sinha, A.K., Krishna Pai, R., Balakrishna, G.R., 2015. Atomic force microscopic study of nanoscale interaction between N719 dye and CdSe quantum dot in hybrid solar cells and their enhanced open circuit potential. Sol. Energy 116, 25–36.

Decker, F., Fracastoro-Decker, M., Badawy, W., Doblhofer, K., Gerischer, H., 1983. The Photocurrent-voltage characteristics of the heterojunction combination n - Si/SnO_2 /redox - electrolyte. J. Electrochem. Soc. 130 (11), 2173–2179.

Dolzhnikov, D.S., Wang, C., Xu, Y., Kanatzidis, M.G., Weiss, E.A., 2017. Ligand-free, quantum-confined $CsSnI_6$ perovskite nanocrystals. Chem. Mater. 29 (18), 7901–7907.

Du, Z., Pan, Z., Fabregat-Santiago, F., Zhao, K., Long, D., Zhang, H., et al., 2016. Carbon counter-electrode-based quantum-dot-sensitized solar cells with certified efficiency exceeding 11%. J. Phys. Chem. Lett. 7 (16), 3103–3111.

Ekimov, A.I., Onushchenko, A.A., 1981. Quantum size effect in three-dimensional microscopic semiconductor crystals. Jetp Lett. 34 (6), 345–349.

Ellingson, R.J., Beard, M.C., Johnson, J.C., Yu, P., Micic, O.I., Nozik, A.J., et al., 2005. Highly efficient multiple exciton generation in colloidal PbSe and PbS quantum dots. Nano Lett. 5 (5), 865–871.

Esparza, D., Zarazúa, I., López-Luke, T., Cerdán-Pasarán, A., Sánchez-Solís, A., Torres-Castro, A., et al., 2015. Effect of different sensitization technique on the photoconversion efficiency of CdS quantum dot and CdSe quantum rod sensitized TiO_2 solar cells. J. Phys. Chem. C. 119 (24), 13394–13403.

Feng, W., Zhao, L., Du, J., Li, Y., Zhong, X., 2016. Quasi-solid-state quantum dot sensitized solar cells with power conversion efficiency over 9% and high stability. J. Mater. Chem. A. 4 (38), 14849–14856.

Frolova, L.A., Anokhin, D.V., Piryazev, A.A., Luchkin, S.Y., Dremova, N.N., Stevenson, K.J., et al., 2017. Highly efficient all-inorganic planar heterojunction perovskite solar cells produced by thermal coevaporation of CsI and PbI_2. J. Phys. Chem. Lett. 8 (1), 67–72.

Gamboa, S., Nguyen-Cong, H., Chartier, P., Sebastian, P., Calixto, M., Rivera, M., 1998. Photovoltaic structures based on polymer/semiconductor junctions. Sol. Energy Mater., Sol. Cell 55 (1–2), 95–104.

Gopi, C.V.V.M., Venkata-Haritha, M., Seo, H., Singh, S., Kim, S.-K., Shiratani, M., et al., 2016. Improving the performance of quantum dot sensitized solar cells through CdNiS quantum dots with reduced recombination and enhanced electron lifetime. Dalton Trans. 45 (20), 8447–8457.

Gopi, C.V.M., Singh, S., Eswar Reddy, A., Kim, H.-J., 2018. CNT@ rGO@ MoCuSe composite as an efficient counter electrode for quantum dot-sensitized solar cells. ACS Appl. Mater. Interface 10 (12), 10036–10042.

Gorer, S., Hodes, G., 1994. Quantum size effects in the study of chemical solution deposition mechanisms of semiconductor films. J. Phys. Chem. 98 (20), 5338–5346.

Guo, C.X., Yang, H.B., Sheng, Z.M., Lu, Z.S., Song, Q.L., Li, C.M., 2010. Layered graphene/quantum dots for photovoltaic devices. Angew. Chem. Int. (Ed.) 49 (17), 3014–3017.

Guo, W., Chen, C., Ye, M., Lv, M., Lin, C., 2014. Carbon fiber/Co_9S_8 nanotube arrays hybrid structures for flexible quantum dot-sensitized solar cells. Nanoscale 6 (7), 3656–3663.

Han, J.S., Le, Q.V., Choi, J., Kim, H., Kim, S.G., Hong, K., et al., 2019. Lead-free all-inorganic cesium tin iodide perovskite for filamentary and interface-type resistive switching toward environment-friendly and temperature-tolerant nonvolatile memories. ACS Appl. Mater. Interface. 11 (8), 8155–8163.

Hanna, M., Nozik, A., 2006. Solar conversion efficiency of photovoltaic and photoelectrolysis cells with carrier multiplication absorbers. J. Appl. Phys. 100 (7). Available from: https://doi.org/10.1063/1.2356795.

Hao, X., Cho, E.-C., Flynn, C., Shen, Y., Park, S.-C., Conibeer, G., et al., 2009. Synthesis and characterization of boron-doped Si quantum dots for all-Si quantum dot tandem solar cells. Sol. Energy Mater. Sol. Cell 93 (2), 273–279.

Haring, A.J., Pomatto, M.E., Thornton, M.R., Morris, A.J., 2014. MnII/III complexes as promising redox mediators in quantum-dot-sensitized solar cells. ACS Appl. Mater. Interface 6 (17), 15061–15067.

Hod, I., Zaban, A., 2014. Materials and interfaces in quantum dot sensitized solar cells: challenges, advances and prospects. Langmuir 30 (25), 7264–7273.

Huang, X., Huang, S., Zhang, Q., Guo, X., Li, D., Luo, Y., et al., 2011. A flexible photoelectrode for CdS/CdSe quantum dot-sensitized solar cells (QDSSCs). Chem. Commun. (Camb.) 47 (9). Available from: https://doi.org/10.1039/c0cc04419a.

Huang, F., Zhang, L., Zhang, Q., Hou, J., Wang, H., Wang, H., et al., 2016. High efficiency CdS/CdSe quantum dot sensitized solar cells with two ZnSe layers. ACS Appl. Mater. Interface. 8 (50), 34482–34489.

Hunsur Ravikumar, C., Maroli, N., Kulkarni, B., Kolandaivel, P., Balakrishna, R.G., 2022. Heterostructure of $CsPbBr_3$-CdS perovskite quantum dots for enhanced stability and charge transfer. Mater. Sci. Eng.: B 275. Available from: https://doi.org/10.1016/j.mseb.2021.115513.

Huo, Z., Tao, L., Wang, S., Wei, J., Zhu, J., Dong, W., et al., 2015. A novel polysulfide hydrogel electrolyte based on low molecular mass organogelator for quasi-solid-state quantum dot-sensitized solar cells. J. Power Sources 284, 582–587.

Im, J.-H., Lee, C.-R., Lee, J.-W., Park, S.-W., Park, N.-G., 2011. 6.5% efficient perovskite quantum-dot-sensitized solar cell. Nanoscale 3 (10), 4088–4093.

Jang, D.M., Kim, D.H., Park, K., Park, J., Lee, J.W., Song, J.K., 2016. Ultrasound synthesis of lead halide perovskite nanocrystals. J. Mater. Chem., C. 4 (45), 10625–10629.

Jiang, G., Pan, Z., Ren, Z., Du, J., Yang, C., Wang, W., et al., 2016. Poly (vinyl pyrrolidone): a superior and general additive in polysulfide electrolytes for high efficiency quantum dot sensitized solar cells. J. Mater. Chem. A 4 (29), 11416–11421.

Jiao, S., Shen, Q., Mora-Seró, I., Wang, J., Pan, Z., Zhao, K., et al., 2015. Band engineering in core/shell ZnTe/CdSe for photovoltage and efficiency enhancement in exciplex quantum dot sensitized solar cells. ACS Nano 9 (1), 908–915.

Jovanovski, V., González-Pedro, V., Giménez, S., Azaceta, E., Cabañero, G.N., Grande, H., et al., 2011. A sulfide/polysulfide-based ionic liquid electrolyte for quantum dot-sensitized solar cells. J. Am. Chem. Soc. 133 (50), 20156–20159.

Jun, H.K., Careem, M.A., Arof, A.K., 2013. Quantum dot-sensitized solar cells—perspective and recent developments: a review of Cd chalcogenide quantum dots as sensitizers. Renew. Sustain. Energy Rev. 22, 148–167.

Jung, S.W., Kim, J.-H., Kim, H., Choi, C.-J., Ahn, K.-S., 2012. ZnS overlayer on in situ chemical bath deposited CdS quantum dot-assembled TiO_2 films for quantum dot-sensitized solar cells. Curr. Appl. Phys. 12 (6), 1459–1464.

Kaelin, M., Rudmann, D., Tiwari, A., 2004. Low cost processing of CIGS thin film solar cells. Sol. Energy 77 (6), 749–756.

Katari, J.B., Colvin, V.L., Alivisatos, A.P., 1994. X-ray photoelectron spectroscopy of CdSe nanocrystals with applications to studies of the nanocrystal surface. J. Phys. Chem. 98 (15), 4109–4117.

Kazacos, M.S., McHenry, E., Heller, A., Miller, B., 1980. Fluorescent window for liquid junction solar cells. Sol. Energy Mater. 2 (3), 333–342.

Kim, H., Hwang, I., Yong, K., 2014. Highly durable and efficient quantum dot-sensitized solar cells based on oligomer gel electrolytes. ACS Appl. Mater. Interface 6 (14), 11245–11253.

Klimov, V.I., 2006. Detailed-balance power conversion limits of nanocrystal-quantum-dot solar cells in the presence of carrier multiplication. Appl. Phys. Lett. 89 (12). Available from: https://doi.org/10.1063/1.2356314.

Kojima, A., Teshima, K., Shirai, Y., Miyasaka, T., 2009. Organometal halide perovskites as visible-light sensitizers for photovoltaic cells. J. Am. Chem. Soc. 131 (17), 6050–6051.

Kolodinski, S., Werner, J.H., Wittchen, T., Queisser, H.J., 1993. Quantum efficiencies exceeding unity due to impact ionization in silicon solar cells. Appl. Phys. Lett. 63 (17), 2405–2407.

Kongkanand, A., Tvrdy, K., Takechi, K., Kuno, M., Kamat, P.V., 2008. Quantum dot solar cells. Tuning photoresponse through size and shape control of CdSe − TiO_2 architecture. J. Am. Chem. Soc. 130 (12), 4007–4015.

Kusuma, J., Balakrishna, R.G., Patil, S., Jyothi, M.S., Chandan, H.R., Shwetharani, R., 2018. Exploration of graphene oxide nanoribbons as excellent electron conducting network for third generation solar cells. Sol. Energy Mater. Sol. Cell 183, 211–219.

Kusuma, J., Chandan, H.R., Balakrishna, R.G., 2019. Conjugated molecular bridges: a new direction to escalate linker assisted QDSSC performance. Sol. Energy 194, 74–78.

Lee, Y.L., Lo, Y.S., 2009. Highly efficient quantum-dot-sensitized solar cell based on co-sensitization of CdS/CdSe. Adv. Funct. Mater. 19 (4), 604–609.

Lee, M.M., Teuscher, J., Miyasaka, T., Murakami, T.N., Snaith, H.J., 2012. Efficient hybrid solar cells based on meso-superstructured organometal halide perovskites. Science 338 (6107), 643–647.

Lee, S., Choi, J., Jeon, J.B., Kim, B.J., Han, J.S., Kim, T.L., et al., 2019. Conducting bridge resistive switching behaviors in cubic $MAPbI_3$, orthorhombic $RbPbI_3$, and their mixtures. Adv. Elect. Mater 5 (2). Available from: https://doi.org/10.1002/aelm.201800586.

Leng, M., Yang, Y., Zeng, K., Chen, Z., Tan, Z., Li, S., et al., 2018. All-inorganic bismuth-based perovskite quantum dots with bright blue photoluminescence and excellent stability. Adv. Funct. Mater. 28 (1). Available from: https://doi.org/10.1002/adfm.201704446.

Lewis, N. S., Crabtree, G., 2005. Basic research needs for solar energy utilization: report of the basic energy sciences workshop on solar energy utilization, April 18–21, 2005. US Department of Energy, Office of Basic Energy Science.

Li, W., Zhong, X., 2015. Capping ligand-induced self-assembly for quantum dot sensitized solar cells. J. Phys. Chem. Lett. 6 (5), 796–806.

Li, L., Yang, X., Gao, J., Tian, H., Zhao, J., Hagfeldt, A., et al., 2011. Highly efficient CdS quantum dot-sensitized solar cells based on a modified polysulfide electrolyte. J. Am. Chem. Soc. 133 (22), 8458–8460.

Li, T.-L., Lee, Y.-L., Teng, H., 2012. High-performance quantum dot-sensitized solar cells based on sensitization with $CuInS_2$ quantum dots/CdS heterostructure. Energy Environ. Sci. 5 (1), 5315–5324.

Li, Z., Yu, L., Wang, H., Yang, H., Ma, H., 2020. TiO_2 passivation layer on ZnO hollow microspheres for quantum dots sensitized solar cells with improved light harvesting and electron collection. Nanomater 10 (4), 631. Available from: https://doi.org/10.3390/nano10040631.

Liang, D., Peng, Y., Fu, Y., Shearer, M.J., Zhang, J., Zhai, J., et al., 2016. Color-pure violet-light-emitting diodes based on layered lead halide perovskite nanoplates. ACS Nano 10 (7), 6897–6904.

Liao, Y., Zhang, J., Liu, W., Que, W., Yin, X., Zhang, D., et al., 2015. Enhancing the efficiency of CdS quantum dot-sensitized solar cells via electrolyte engineering. Nano Energy 11, 88–95.

Lignos, I., Stavrakis, S., Nedelcu, G., Protesescu, L., deMello, A.J., Kovalenko, M.V., 2016. Synthesis of cesium lead halide perovskite nanocrystals in a droplet-based microfluidic platform: fast parametric space mapping. Nano Lett. 16 (3), 1869–1877.

Lin, X., Cui, D., Luo, X., Zhang, C., Han, Q., Wang, Y., et al., 2020. Efficiency progress of inverted perovskite solar cells. Energy Environ. Sci. 13 (11), 3823–3847.

Liu, D., Liu, J., Liu, J., Liu, S., Wang, C., Ge, Z., et al., 2019. The effect of CuS counter electrodes for the CdS/CdSe quantum dot co-sensitized solar cells based on zinc titanium mixed metal oxides. J. Mater. Sci. 54 (6), 4884–4892.

Liu, Y., Li, F., Shi, G., Liu, Z., Lin, X., Shi, Y., et al., 2020. PbSe quantum dot solar cells based on directly synthesized semiconductive inks. ACS Energy Lett. 5 (12), 3797–3803.

Lu, W., Song, B., Li, H., Zhou, J., Dong, W., Zhao, G., et al., 2020. Strategy for performance enhancement of $Cd_{1-X}Zn_XTe$/CdS core/shell quantum dot sensitized solar cells through band adjustment. J. Alloy. Comp. 826. Available from: https://doi.org/10.1016/j.jallcom.2020.154050.

Luo, J., Wei, H., Huang, Q., Hu, X., Zhao, H., Yu, R., et al., 2013. Highly efficient core–shell $CuInS_2$–Mn doped CdS quantum dot sensitized solar cells. Chem. Commun. 49 (37), 3881–3883.

Lv, M., Zhu, J., Huang, Y., Li, Y., Shao, Z., Xu, Y., et al., 2015. Colloidal $CuInS_2$ quantum dots as inorganic hole-transporting material in perovskite solar cells. ACS Appl. Mater. Interface 7 (31), 17482–17488.

McDaniel, H., Fuke, N., Pietryga, J.M., Klimov, V.I., 2013a. Engineered $CuInSe_xS_{2-x}$ quantum dots for sensitized solar cells. J. Phys. Chem. Lett. 4 (3), 355–361.

McDaniel, H., Fuke, N., Makarov, N.S., Pietryga, J.M., Klimov, V.I., 2013b. An integrated approach to realizing high-performance liquid-junction quantum dot sensitized solar cells. Nat. Commun. 4 (1). Available from: https://doi.org/10.1038/ncomms3887.

Meng, K., Chen, G., Thampi, K.R., 2015. Metal chalcogenides as counter electrode materials in quantum dot sensitized solar cells: a perspective. J. Mater. Chem. A 3 (46), 23074–23089.

Micic, O.I., Curtis, C.J., Jones, K.M., Sprague, J.R., Nozik, A.J., 1994. Synthesis and characterization of InP quantum dots. J. Phys. Chem. 98 (19), 4966–4969.

Micic, O., Sprague, J., Curtis, C., Jones, K., Machol, J., Nozik, A., et al., 1995. Synthesis and characterization of InP, GaP, and $GaInP_2$ quantum dots. J. Phys. Chem. 99 (19), 7754–7759.

Murphy, J.E., Beard, M.C., Norman, A.G., Ahrenkiel, S.P., Johnson, J.C., Yu, P., et al., 2006. PbTe colloidal nanocrystals: synthesis, characterization, and multiple exciton generation. J. Am. Chem. Soc. 128 (10), 3241–3247.

Murray, C., Norris, D.J., Bawendi, M.G., 1993. Synthesis and characterization of nearly monodisperse CdE (E = sulfur, selenium, tellurium) semiconductor nanocrystallites. J. Am. Chem. Soc. 115 (19), 8706–8715.

Ning, Z., Tian, H., Yuan, C., Fu, Y., Qin, H., Sun, L., et al., 2011. Solar cells sensitized with type-II ZnSe–CdS core/shell colloidal quantum dots. Chem. Commun. 47 (5), 1536–1538.

Nozik, A.J., 2001. Spectroscopy and hot electron relaxation dynamics in semiconductor quantum wells and quantum dots. Annu. Rev. Phys. Chem. 52 (1), 193–231.

Nozik, A.J., 2002. Quantum dot solar cells. Phys. E 14 (1–2), 115–120.

Nozik, A.J., 2008. Multiple exciton generation in semiconductor quantum dots. Chem. Phys. Lett. 457 (1–3), 3–11.

Pan, Z., Zhang, H., Cheng, K., Hou, Y., Hua, J., Zhong, X., 2012. Highly efficient inverted type-I CdS/CdSe core/shell structure QD-sensitized solar cells. ACS Nano 6 (5), 3982–3991.

Pan, Z., Mora-Seró, I., Shen, Q., Zhang, H., Li, Y., Zhao, K., et al., 2014. High-efficiency "green" quantum dot solar cells. J. Am. Chem. Soc. 136 (25), 9203–9210.

Park, D., Azmi, R., Cho, Y., Kim, H.M., Jang, S.-Y., Yim, S., 2019. Improved passivation of PbS quantum dots for solar cells using triethylamine hydroiodide. ACS Sustain. Chem. Eng. 7 (12), 10784–10791.

Peng, Z.A., Peng, X., 2001. Formation of high-quality CdTe, CdSe, and CdS nanocrystals using CdO as precursor. J. Am. Chem. Soc. 123 (1), 183–184.

Petroff, P., DenBaars, S., 1994. MBE and MOCVD growth and properties of self-assembling quantum dot arrays in III–V semiconductor structures. Superlattices Microstruct 15 (1). Available from: https://doi.org/10.1006/spmi.1994.1004.

Ravikumar, C.H., Gowda, M.I., Balakrishna, R.G., 2019. An "OFF–ON" quantum dot–graphene oxide bioprobe for sensitive detection of micrococcal nuclease of *Staphylococcus aureus*. Analyst 144 (13), 3999–4005.

Ravikumar, C.H., Shwetharani, R., Balakrishna, R.G., 2020. Surface modified glass substrate for sensing *E. coli* using highly stable and luminescent CdSe/CdS core shell quantum dots. J. Photochem. Photobiol. B: Biol. 204. Available from: https://doi.org/10.1016/j.jphotobiol.2020.111799.

Riaz, S., Park, S.-J., 2022. Thioacetamide-derived nitrogen and sulfur co-doped carbon quantum dots for "green" quantum dot solar cells. J. Ind. Eng. Chem. 105, 111–120.

Sambur, J.B., Novet, T., Parkinson, B., 2010. Multiple exciton collection in a sensitized photovoltaic system. Sci 330 (6000), 63–66.

Sanehira, E.M., Marshall, A.R., Christians, J.A., Harvey, S.P., Ciesielski, P.N., Wheeler, L., et al., 2017. Enhanced mobility $CsPbI_3$ quantum dot arrays for record-efficiency, high-voltage photovoltaic cells. Sci. Adv. 3 (10). Available from: https://doi.org/10.1126/sciadv.aao4204.

Santra, P.K., Kamat, P.V., 2012. Mn-doped quantum dot sensitized solar cells: a strategy to boost efficiency over 5%. J. Am. Chem. Soc. 134 (5), 2508–2511.

Schaller, R.D., Klimov, V.I., 2004. High efficiency carrier multiplication in PbSe nanocrystals: implications for solar energy conversion. Phys. Rev. Lett. 92 (18). Available from: https://doi.org/10.1103/PhysRevLett.92.186601.

Schaller, R.D., Petruska, M.A., Klimov, V.I., 2005. Effect of electronic structure on carrier multiplication efficiency: comparative study of PbSe and CdSe nanocrystals. Appl. Phys. Lett. 87 (25). Available from: https://doi.org/10.1063/1.2142092.

Schaller, R.D., Sykora, M., Pietryga, J.M., Klimov, V.I., 2006. Seven excitons at a cost of one: redefining the limits for conversion efficiency of photons into charge carriers. Nano Lett. 6 (3), 424–429.

Schock, H.W., Noufi, R., 2000. CIGS-based solar cells for the next millennium. Prog. Photovolt.: Res. 8 (1), 151–160.

Schrier, M., Zehnder, D., Treadway, J., Bartel, J., 2012. Preparation of stable, bright luminescent nanoparticles having compositionally engineered properties. Google Patents.

Shabaev, A., Efros, A.L., Nozik, A.J., 2006. Multiexciton generation by a single photon in nanocrystals. Nano Lett. 6 (12), 2856–2863.

Shalom, M., Dor, S., Ruhle, S., Grinis, L., Zaban, A., 2009. Core/CdS quantum dot/shell mesoporous solar cells with improved stability and efficiency using an amorphous TiO_2 coating. J. Phys. Chem. C. 113 (9), 3895–3898.

Sharma, S., Jain, K.K., Sharma, A., 2015. Solar cells: in research and applications—a review. Mater. Sci. Appl. 6 (12). Available from: https://doi.org/10.4236/msa.2015.612113.

Shaw, P.E., Ruseckas, A., Samuel, I.D., 2008. Exciton diffusion measurements in poly (3-hexylthiophene). Adv. Mater. 20 (18), 3516–3520.

Shen, T., Tian, J., Lv, L., Fei, C., Wang, Y., Pullerits, T., et al., 2016. Investigation of the role of Mn dopant in CdS quantum dot sensitized solar cell. Electrochim. Acta 191, 62–69.

Shin, S.S., Lee, S.J., Seok, S.I., 2019. Metal oxide charge transport layers for efficient and stable perovskite solar cells. Adv. Funct. Mater. 29 (47). Available from: https://doi.org/10.1002/adfm.201900455.

Singh, S.P., Nagarjuna, P., 2014. Organometal halide perovskites as useful materials in sensitized solar cells. Dalton Trans. 43 (14), 5247–5251.

Stolterfoht, M., Wolff, C.M., Márquez, J.A., Zhang, S., Hages, C.J., Rothhardt, D., et al., 2018. Visualization and suppression of interfacial recombination for high-efficiency large-area pin perovskite solar cells. Nat. Energy 3 (10), 847–854.

Sun, C., Xu, G., Jiang, X.-M., Wang, G.-E., Guo, P.-Y., Wang, M.-S., et al., 2018. Design strategy for improving optical and electrical properties and stability of lead-halide semiconductors. J. Am. Chem. Soc. 140 (8), 2805–2811.

Swarnkar, A., Marshall, A.R., Sanehira, E.M., Chernomordik, B.D., Moore, D.T., Christians, J. A., et al., 2016. Quantum dot–induced phase stabilization of α-$CsPbI_3$ perovskite for high-efficiency photovoltaics. Sci 354 (6308), 92–95.

Tan, L., Zhou, Y., Ren, F., Benetti, D., Yang, F., Zhao, H., et al., 2017. Ultrasmall PbS quantum dots: a facile and greener synthetic route and their high performance in luminescent solar concentrators. J. Mater. Chem. A 5 (21), 10250–10260.

Tao, L., Xiong, Y., Liu, H., Shen, W., 2014. High performance PbS quantum dot sensitized solar cells via electric field assisted in situ chemical deposition on modulated TiO_2 nanotube arrays. Nanoscale 6 (2), 931–938.

Tauc, J., 1959. Electron impact ionization in semiconductors. J. Phys. Chem. Solids 8, 219–223.

Thambidurai, M., Muthukumarasamy, N., Sabari Arul, N., Agilan, S., Balasundaraprabhu, R., 2011. CdS quantum dot-sensitized ZnO nanorod-based photoelectrochemical solar cells. J. Nanopart. Res. 13 (8), 3267–3273.

Tian, J., Gao, R., Zhang, Q., Zhang, S., Li, Y., Lan, J., et al., 2012. Enhanced performance of CdS/CdSe quantum dot cosensitized solar cells via homogeneous distribution of quantum dots in TiO_2 film. J. Phys. Chem. C. 116 (35), 18655–18662.

Tong, Y., Bladt, E., Aygüler, M.F., Manzi, A., Milowska, K.Z., Hintermayr, V.A., et al., 2016. Highly luminescent cesium lead halide perovskite nanocrystals with tunable composition and thickness by ultrasonication. Angew. Chem. Int. (Ed.) 55 (44), 13887–13892.

Tubtimtae, A., Wu, K.-L., Tung, H.-Y., Lee, M.-W., Wang, G.J., 2010. Ag_2S quantum dot-sensitized solar cells. Electrochem. Commun. 12 (9), 1158–1160.

Vavilov, V.S., 1959. On photo-ionization by fast electrons in germanium and silicon. J. Phys. Chem. Solids 8, 223–226.

Vázquez, C.I., Baruzzi, A.M., Iglesias, R.A., 2016. Charge extraction from TiO_2 nanotubes sensitized with CdS quantum dots by SILAR method. IEEE J. Photovolt. 6 (6), 1515–1521.

Venkataramana, M., Chandan, H.R., Kurkuri, M.D., Balakrishna, R., 2016. G. Simple quantum dot bioprobe/label for sensitive detection of *Staphylococcus aureus* TNase. Sens. Actuators, B Chem. 222, 1201–1208.

Vogel, R., Hoyer, P., Weller, H., 1994. Quantum-Sized PbS, CdS, Ag_2S, Sb_2S_3, and Bi_2S_3 particles as sensitizers for various nanoporous wide-bandgap semiconductors. J. Phys. Chem. 98 (12), 3183–3188.

Wada, T., Kohara, N., Nishiwaki, S., Negami, T., 2001. Characterization of the Cu (In, Ga) Se2/Mo interface in CIGS solar cells. Thin Solid. Films 387 (1–2), 118–122.

Wang, J., Mora-Seró, I., Pan, Z., Zhao, K., Zhang, H., Feng, Y., et al., 2013. Core/Shell Colloidal quantum dot exciplex states for the development of highly efficient quantum-dot-sensitized solar cells. J. Am. Chem. Soc. 135 (42), 15913–15922.

Wang, Y., Li, X., Song, J., Xiao, L., Zeng, H., Sun, H., 2015. All-inorganic colloidal perovskite quantum dots: a new class of lasing materials with favorable characteristics. Adv. Mater. 27 (44), 7101–7108.

Wang, A., Yan, X., Zhang, M., Sun, S., Yang, M., Shen, W., et al., 2016. Controlled synthesis of lead-free and stable perovskite derivative Cs_2SnI_6 nanocrystals via a facile hot-injection process. Chem. Mater. 28 (22), 8132–8140.

Wei, H., Wang, G., Shi, J., Wu, H., Luo, Y., Li, D., et al., 2016a. Fumed SiO_2 modified electrolytes for quantum dot sensitized solar cells with efficiency exceeding 11% and better stability. J. Mater. Chem. A 4 (37), 14194–14203.

Wei, S., Yang, Y., Kang, X., Wang, L., Huang, L., Pan, D., 2016b. Room-temperature and gram-scale synthesis of $CsPbX_3$ (X = Cl, Br, I) perovskite nanocrystals with 50–85% photoluminescence quantum yields. Chem. Commun. 52 (45), 7265–7268.

Weller, H., 1991. Quantum sized semiconductor particles in solution and in modified layers. Ber. Bunsen. Phys. Chem. 95 (11), 1361–1365.

Willardson, R.K., Weber, E.R., Sugawara, M., 1999. Self-Assembled InGaAs/GaAs Quantum Dots. Academic Press.

Wood, V., Halpert, J.E., Panzer, M.J., Bawendi, M.G., Bulovic, V., 2009. Alternating current driven electroluminescence from ZnSe/ZnS: Mn/ZnS nanocrystals. Nano Lett. 9 (6), 2367–2371.

Wu, M., Lin, X., Wang, Y., Ma, T., 2015. Counter electrode materials combined with redox couples in dye-and quantum dot-sensitized solar cells. J. Mater. Chem. A 3 (39), 19638–19656.

Xiang, W., Tress, W., 2019. Review on recent progress of all-inorganic metal halide perovskites and solar cells. Adv. Mater 31 (44). Available from: https://doi.org/10.1002/adma.201902851.

Xu, Y., Li, S., Zhang, Z., Hu, Y., Yuan, L., Chen, W., et al., 2019. Ligand-mediated synthesis of colloidal Cs_2SnI_6 three-dimensional nanocrystals and two-dimensional nanoplatelets. Nanotechnol 30 (29). Available from: https://doi.org/10.1088/1361-6528/ab13f6.

Yang, Y., Wang, W., 2015. A new polymer electrolyte for solid-state quantum dot sensitized solar cells. J. Power Sources 285, 70–75.

Yang, Z., Chen, C.Y., Liu, C.W., Chang, H.T., 2010. Electrocatalytic sulfur electrodes for CdS/CdSe quantum dot-sensitized solar cells. Chem. Commun. 46 (30). Available from: https://doi.org/10.1039/c0cc00642d.

Yang, Y., Zhu, L., Sun, H., Huang, X., Luo, Y., Li, D., et al., 2012. Composite counter electrode based on nanoparticulate PbS and carbon black: towards quantum dot-sensitized solar cells with both high efficiency and stability. ACS Appl. Mater. Interface. 4 (11), 6162–6168.

Yang, P., Tang, Q., Ji, C., Wang, H., 2015a. A strategy of combining SILAR with solvothermal process for In2S3 sensitized quantum dot-sensitized solar cells. Appl. Surf. Sci. 357, 666–671.

Yang, S., Zhao, P., Zhao, X., Qu, L., Lai, X., 2015b. InP and Sn:InP based quantum dot sensitized solar cells. J. Mater. Chem. A. 3 (43), 21922–21929.

Yang, B., Chen, J., Hong, F., Mao, X., Zheng, K., Yang, S., et al., 2017. Lead-free, air-stable all-inorganic cesium bismuth halide perovskite nanocrystals. Angew. Chem. 129 (41), 12645–12649.

Yella, A., Lee, H.-W., Tsao, H.N., Yi, C., Chandiran, A.K., Nazeeruddin, M.K., et al., 2011. Porphyrin-sensitized solar cells with cobalt (II/III)–based redox electrolyte exceed 12 percent efficiency. Sci 334 (6056), 629–634.

Yu, Z., Zhang, Q., Qin, D., Luo, Y., Li, D., Shen, Q., et al., 2010. Highly efficient quasi-solid-state quantum-dot-sensitized solar cell based on hydrogel electrolytes. Electrochem. Commun. 12 (12), 1776–1779.

Yu, X.Y., Liao, J.Y., Qiu, K.Q., Kuang, D.B., Su, C.Y., 2011. Dynamic study of highly efficient CdS/CdSe quantum dot-sensitized solar cells fabricated by electrodeposition. ACS Nano 5 (12), 9494–9500.

Yu, X.-Y., Lei, B.-X., Kuang, D.-B., Su, C.-Y., 2012. High performance and reduced charge recombination of CdSe/CdS quantum dot-sensitized solar cells. J. Mater. Chem. 22 (24), 12058–12063.

Zhang, Q., Zhang, Y., Huang, S., Huang, X., Luo, Y., Meng, Q., et al., 2010. Application of carbon counterelectrode on CdS quantum dot-sensitized solar cells (QDSSCs). Electrochem. Commun. 12 (2), 327–330.

Zhang, J., Gao, J., Miller, E.M., Luther, J.M., Beard, M.C., 2014. Diffusion-controlled synthesis of PbS and PbSe quantum dots with in situ halide passivation for quantum dot solar cells. ACS Nano 8 (1), 614–622.

Zhang, F., Zhong, H., Chen, C., Wu, X.-g, Hu, X., Huang, H., et al., 2015. Brightly luminescent and color-tunable colloidal $CH_3NH_3PbX_3$ (X = Br, I, Cl) quantum dots: potential alternatives for display technology. ACS Nano 9 (4), 4533–4542.

Zhang, H., Yang, C., Du, Z., Pan, D., Zhong, X., 2017. Graphene hydrogel-based counter electrode for high efficiency quantum dot-sensitized solar cells. J. Mater. Chem. A 5 (4), 1614–1622.

Zhang, L., Rao, H., Pan, Z., Zhong, X., 2019. ZnSxSe1−x alloy passivation layer for high-efficiency quantum-dot-sensitized solar cells. ACS Appl. Mater. Interface. 11 (44), 41415–41423.

Zheng, X., Hou, Y., Bao, C., Yin, J., Yuan, F., Huang, Z., et al., 2020. Managing grains and interfaces via ligand anchoring enables 22.3%-efficiency inverted perovskite solar cells. Nat. Energy 5 (2), 131–140.

Zhou, L., Xu, Y.F., Chen, B.X., Kuang, D.B., Su, C.Y., 2018. Synthesis and photocatalytic application of stable lead-free $Cs_2AgBiBr_6$ perovskite nanocrystals. Small 14 (11). Available from: https://doi.org/10.1002/smll.201703762.

Zhu, H., Song, N., Lian, T., 2010a. Controlling charge separation and recombination rates in CdSe/ZnS type I core − shell quantum dots by shell thicknesses. J. Am. Chem. Soc. 132 (42), 15038–15045.

Zhu, G., Cheng, Z., Lv, T., Pan, L., Zhao, Q., Sun, Z., 2010b. Zn-doped nanocrystalline TiO_2 films for CdS quantum dot sensitized solar cells. Nanoscale 2 (7), 1229–1232.

Zumeta-Dube, I., Ruiz-Ruiz, V.-F., Diaz, D., Rodil-Posadas, S., Zeinert, A., 2014. TiO_2 sensitization with Bi_2S_3 quantum dots: the inconvenience of sodium ions in the deposition procedure. J. Phys. Chem. C. 118 (22), 11495–11504.

This page intentionally left blank

Chapter 13

Application of quantum dots in sensors

Neelam Kunwar[1], Hetal Zala[2] and Kushnuma Parveen[3]
[1]*Department of Chemistry, PAHER University, Udaipur, Rajasthan, India,* [2]*1197-1, Uchigashimacho, A-101, Gunma, Ota-Shi, Japan,* [3]*Khamis Mushayt, Ahad Rafaidah, Kingdom of Saudi Arabia*

13.1 Introduction

Any change in biological or chemical environment is likely to affect the life of human beings, plants, animals, and aquatic plants and organisms. Similarly, humidity and temperature may also affect some physical or chemical phenomena. Therefore sometimes it becomes very much necessary to know the changes in these parameters. The slight variation in chemical environment can affect the health of living beings as some chemicals available in the atmosphere are toxic in nature if present even in very low concentrations. Sometimes, the presence of these chemicals can be fatal also and thus these should be detected in time otherwise any reaction may be totally undesirable. There are some limits on their concentrations, above which these are harmful and they may create disease or harm. Development of any disease or deformation in the body can be detected in advance if a proper sensing system is available. Then, such diseases can be diagnosed in a timely manner and treatment can be started at an early stage. Therefore, such chemical or biological changes should be monitored so as the protect the society from their adverse effects.

The variation of temperature and/or the presence of high humidity also affect some physical or chemical entities adversely, that is, corrosion of metals, stability of hygroscopic compounds, etc., depending on the circumstances. Hence, the correct measurement of humidity and temperature becomes necessary to safeguard certain materials or reactions from high humidity or temperature. Although various sensing systems are commercially available for sensing the presence of some chemical changes such as liquefied petroleum gas, ammonia, alcohol, carbon monoxide, etc., these have some other limits or demerits. Quantum dots (QDs) have some interesting properties like smaller size, large surface area-to-volume ratio, and

Quantum Dots. DOI: https://doi.org/10.1016/B978-0-12-824153-0.00013-6
© 2023 Elsevier Inc. All rights reserved.

fluorescence/photoluminescence, and as a result these QDs can find potential applications in fabricating effective, sensitive, and selective sensors. In this chapter, the development of chemical, biological, temperature, and humidity sensors has been discussed.

13.2 Sensors

QDs can find numerous applications in fabricating sensors such as temperature, humidity, alcohol, hydrogen sulfide, ammonia, carbon dioxide, nitrogen dioxide, pesticides, biosensors, etc.

13.2.1 Chemical sensors

Various chemicals are hazardous in nature and their presence in the atmosphere can affect the lives of human beings, animals, plants, aquatic organisms, etc. They can create a number of dreadful diseases including cancer. Therefore, it is very important to know their presence, even if they are present in very low concentrations. Here, QDs can help us in sensing their presence as their florescence or photoluminescence can be quenched by their presence. Very good and effective sensors are now available involving mainly QDs.

13.2.1.1 Alcohol sensors

A high-performance ethanol sensor based on iron (Fe)-doped titanium dioxide (TiO_2)/molybdenum disulfide (MoS_2) nanocomposite was demonstrated. Wu et al. (2018) synthesized flower-like MoS_2 and Fe-TiO_2 QDs by a facile hydrothermal route. Then they prepared Fe-TiO_2/MoS_2 composite via a layer-by-layer (LbL) self-assembly technique. As-fabricated Fe-TiO_2/MoS_2 film sensor was used to determine different concentrations of ethanol (gas) at room temperature. It was indicated that this sensor has a short response/recovery time, high response, excellent selectivity, stable repeatability, long-term stability, along with detection low limit (ppb level).

Abbasi and Alizadeh (2020) prepared a hybrid of ZnS:Mn^{2+} QDs and soluble N-methylpolypyrrole (NMPPy). It was reported that the determination of methanol can be carried out using as-prepared ZnS:Mn^{2+} QDs/NMPPy hybrid with high selectivity, sensitivity, and a limit of detection of 1 mM in the concentration range of 25−230 mM. As-fabricated hybrid was successfully used to determine the amount of methanol in real samples of alcoholic beverages.

Masemola et al. (2021) synthesized NGQDs via a microwave-assisted hydrothermal method. They used urea and citric acid as nitrogen and carbon sources, respectively. It was reported that uniformly distributed NGQDs (spherical) were obtained in 4 min. Then these dots were further loaded onto PANI/PAN to fabricate NGQDs/PANI/PAN composite. It was observed that

optimized electrospun composite fibers can be used for sensing of alcohol vapors.

13.2.1.2 Liquid petroleum gas sensor

Liquid petroleum gas-sensing behavior of graphene/SrO QDs composites was also investigated by Nemade and Waghuley (2013a). They evaluated gas-sensing properties of composites by the change in resistance as a function of gas concentration of LPG.

They also synthesized graphene/Bi_2O_3 QDs composites (Nemade and Waghuley 2013b). It was reported that as-prepared composites exhibited better performance toward the sensing of LPG. The graphene/CeO_2 QDs composite was synthesized by Nemade and Waghuley (2013c). They used this composite for sensing of liquid petroleum gas at room temperature. This composite of graphene/CeO_2 QDs was prepared on mixing 20 wt.% of graphene in CeO_2 (1 g). This composite shows excellent stability and sensing response.

Mishra et al. (2015) synthesized rGO/SnO_2 QDs and investigated its LPG gas sensing behavior. It was reported that this sensor exhibited a high response of ~92.4% to LPG (500 ppm) at 250°C. As-fabricated rGO/SnO_2 QDs-based sensor also has a good selectivity for LPG even in the presence of other chemicals such as chloroform, ammonia, benzene, toluene, acetone, formic acid, acetic acid, and *n*-butylacetate. It was observed that the gas response to LPG was about 17.8 times higher compared to formic acid. An excellent reproducibility was also observed in this sensor. Zhang et al. (2018b) prepared zinc oxide/polypyrrole/lead sulfide QDs (ZnO/PPy/PbS QDs) nanocomposite film and used it as a liquefied petroleum gas sensor. It was reported that it can detect LPG and the response at 1000 ppm LPG could reach 45.47%. It was also revealed that it showed excellent repeatability and good selectivity.

13.2.1.3 Ammonia (NH_3) sensors

Liu et al. (2016) prepared PbS QDs/TiO_2 nanotubes arrays (PbS QDs/TiO_2 NTARs) via ionic-layer adsorption. Then they fabricated a gas sensor for ammonia based on these. It was observed that PbS QDs/TiO_2 NTARs had a good response toward ammonia gas and could detect 17.49−100 ppm ammonia with a limit of detection of 2 ppm. It was also revealed that as-fabricated PbS QDs/TiO_2 NTARs show good selectivity toward ammonia as compared with methanol, ethanol, acetone, and toluene.

Hollow indium trioxide nanofibers were fabricated by Hong et al. (2021) via a combination of electrospinning and high-temperature calcinations. Then these were coated with nitrogen-doped graphene QDs (N-GQDs). As-prepared N-GQD-coated hollow In_2O_3 nanofibers served as a core for synthesizing polyaniline (PANI)/N-GQD/hollow In_2O_3 nanofiber ternary

composites using in situ chemical oxidative polymerization. It was observed that the response value of the PANI/20%N-GQD/hollow In_2O_3 nanofiber sensor was 15.2 on exposure to 1 ppm ammonia. This was almost 4.4 times more than the PANI sensor. It was revealed that this composite sensor proved to be very sensitive in the detection of NH_3 in the concentration range of 0.6−2.0 ppm at room temperature. This sensor also exhibited higher selectivity and repeatability in the range of 1.0−2.0 ppm NH_3. Hence, it was suggested that it will prove to be a good gas-sensing material in the case of human breath for detecting hepatic or kidney disease.

Kumar et al. (2018) fabricated poly(3, 3-dialkylquaterthiophene) (PQT-12) and CdSe QDs composite. It was based on back-gated organic thin-film transistors (OTFTs) SiO_2-coated heavily doped p-Si substrates. It was reported that an estimated gas response of ∼51% was obtained for sensing ammonia gas using a PQT-12/CdSe QDs composite, which was higher than an OTFT pristine PQT-12 OTFT-based sensor (41%). Liu et al. (2018) self-assembled 3-D cocoon-like architectures of PbS QDs−reduced graphene oxide composites. It was observed that 3-D PbS QDs/rGO nanococoons exhibited a good detection limit of 750 ppb toward sensing ammonia gas at room temperature, which was higher than rGO and pure PbS QDs. It was also revealed that these 3-D PbS QDs/rGO nanococoons show a good selectivity toward ammonia gas compared to ethanol, acetone, etc. with excellent sensing stability in the long term.

Ouyang et al. (2018) prepared monolayer WS_2 NSs modified with Pt QDs. It was reported that the response of nanocomposite to NH_3 (250 ppm) was almost ten times that of WS_2 NSs. Liu et al. (2019) self-assembled $CuSbS_2$ QDs/reduced graphene oxide composites via a hot-injection method. It was reported that a gas sensor based on $CuSbS_2$ QDs/rGO composites exhibited a good response toward ammonia with a limit of detection of 500 ppb with an average response time of 50 s at room temperature. It was revealed that the sensing performance of the composites was improved in the presence of visible light.

Wongrat et al. (2021) prepared ZnO nanostructures combined with GQDs. It was reported that GQDs have an average size distribution of 2.6 nm. It was revealed that as-prepared ZnO:GQD heterojunctions exhibited a selective response (high) to the vapor of ammonia. As-fabricated ZnO: GQDs sensors have the optimum sensor response at an ammonia concentration of 1000 ppm. This sensor was found to be highly responsive and gave a selective performance for sensing ammonia at room temperature. Bai et al. (2022) prepared flower-like MoS_2 decorated with SnO_2 QDs via a solvothermal method. It was reported that SnO_2 QDs have a uniform particle size of 2−4 nm and these were uniformly distributed on the ultrathin nanosheets of MoS_2 hierarchical architectures. It was found that as-prepared SnO_2 QDs@MoS_2 composites-based gas sensor exhibited a good response of 8.6 with short response and recovery times of 6 s/121 s, respectively to 100 ppm

ammonia with good selectivity, excellent repeatability, and outstanding long-term stability.

13.2.1.4 Hydrogen sulfide (H_2S) sensors

Keshtkar et al. (2018) synthesized SnO_2 QDs−fullerene (SnO_2 QDs-C_{60}) nanohybrid via a hydrothermal method. It was observed that the as-prepared hybrid could detect H_2S (70 ppm). This sensor exhibited a good selectivity toward H_2S gas in the range 5.4−70 ppm. Dun et al. (2019) prepared CdS QDs supported by ultrathin porous nanosheets and further assembled into hollowed-out Co_3O_4 microspheres (CdS QD/Co_3O_4 HMSs). It was observed that CdS QDs of ∼4.5 nm size were well dispersed on Co_3O_4 HMSs (ultrathin porous nanosheet). It was reported that this sensor exhibited a high response (12.7) for 100 ppm H_2S as well as fast response and recovery rates of 0.6−1.0 s, respectively.

Yang et al. (2019) prepared In_2O_3 colloidal QDs and then they deposited In_2O_3 QDs followed by surface ligand exchange treatment via Cu inorganic salts to fabricate H_2S sensor devices. It was reported that the as-prepared sensor exhibited a high response up to 90 for H_2S (5 ppm) with response and recovery time of 72 and 200 s, respectively. Xu et al. (2021) prepared carbon dots passivated with polyethylene glycol. These were then used for detection of H_2S. This proposed sensor can detect Na_2S with a concentration limit of detection approximately 7.0 nM. It was proposed that this probe can also be used successfully for the detection of H_2S in live cells.

13.2.1.5 Carbon dioxide (CO_2) sensors

Chu and Hsieh (2019) designed an optical fiber carbon dioxide sensor, which was based on the emission wavelength shift of $CuInS_2$/ZnS QDs. It was all due to changes in the absorption of α-naphtholphthalein (a pH indicator). With a change in concentration of CO_2. It allowed the detection of CO_2 concentration over the range of 0%−100%. Bhakat et al. (2021) assembled ZnO QDs. It was reported that as-prepared ZnO QD−phosphate was successfully used for designing a gas sensor that showed great sensitivity and selectivity toward CO_2 gas at room temperature. Hajikhanloo et al. (2021) created a valley in the core of the ring and then PbSe QDs were deposited in this valley. This sensor was used to detect CO_2 gas. It was reported that the refractive index of PbSe QDs was found to increase with the increase in the concentration of gas flow. It was revealed that the as-prepared sensor operated in a wide range of concentrations for CO_2 gas with a detection limit of 0.001%.

13.2.1.6 Nitrogen dioxide (NO_2) sensors

Wang et al. (2013) functionalized silica aerogels branched polyethyleniminecapped QDs. The fluorescence quantum yield of CQD-aerogel hybrid material yield was more than 40%. Its fluorescence was sensitively and

selectively quenched by NO_2 gas. Dong et al. (2018) synthesized germanium QDs (GeQDs)/graphene hybrids. They fabricated a NO_2 gas sensor by introducing GeQDs on graphene and the gas sensor sensitivity to NO_2 was improved substantially. With the optimization of the growth time of GeQDs (600 s), the response sensitivity to 10 ppm NO_2 can be as high as 3.88, which is 20 times higher than that of the graphene sensor without GeQDs decoration. The 600 s GeQDs/graphene hybrid sensor exhibited fast response and recovery rates as well as excellent stability.

Lv et al. (2021) prepared SnO_2 hierarchical hollow cubes (ultrathin mesoporous nanosheets) and then N-GQDs were decorated on the surface of SnO_2. It was reported that as-prepared N-GQDs modified SnO_2 (NG/Sn_x) exhibited an improved response toward 1 ppm NO_2, which was almost 2.2 times that of pure SnO_2. Thus sensing material exhibited long-term stability, fast response, recovery repeatability, and good selectivity. This NG/$Sn_{1.5}$ sensor can even detect lower concentrations of NO_2 at the level of 100 ppb.

Zhang et al. (2021) modified ZnO composite with N-GQDs. The sample G-Z-2 (N-GQD_S doping amount of 2 mL) exhibited excellent sensing performance for NO_2 compared with pure ZnO. It was found to be sensitive to 5 ppm NO_2, which was 11.6 times more than others. The detection limit of NO_2 was found to be 0.1 ppm. It was also revealed that there is selectivity, excellent reproducibility, and stability in this sensor for the detection of NO_2. Luo et al. (2022) modified MoS_2 with SnO_2. The MoS_2 nanoflowers were prepared via a hydrothermal method with a high surface/volume ratio and SnO_2 was fabricated using a solvothermal method. It was revealed that its response was increased by 1.5 times on modification, supported by fast response and recovery time for sensing of NO_2 gas.

13.2.1.7 Pesticide sensors

Liang et al. (2021) developed a fluorescence/colorimetric sensor, which was based on a nanocomposite of carbon QDs and gold nanoparticles (CQDs-GNPs). It was observed that fluorescence intensity increased, but absorption decreased with the addition of malathion, a pesticide. Finally, the approximate concentrations of malathion in cabbage samples were estimated by the standard arrays and the naked eye. It was revealed that malathion can be accurately detected in cabbage samples with two methods with recoveries of 89.9%−103.4% (fluorescence) and 88.7%−107.6% (colorimetric).

Nair et al. (2020) prepared a fluorescent sulfur-doped GQDs (S-GQDs)-based sensor. It was reported that the particle size distribution was uniform in the order of $\sim$5 nm with high crystallinity. It was revealed that green fluorescent S-GQDs exhibited a detection limit of 0.45 and 1.6 ppb for carbofuran and thiram, respectively. A sensor was developed by Liang et al. (2021) that was based on CQDs-GNPs. It was observed that fluorescence intensity was increased on the addition of malathion in the range of 1×10^{-9}

to 1×10^{-2} M. It was reported that concentrations of malathion in cabbage samples can also be determined. Alvandi et al. (2021) prepared multicolor fluorescent carbon dots via a hydrothermal method using greengage plums. These carbon dots were used to detect pesticides (duplosan, confidor, and dialen super). It was also revealed that the as-prepared nanosensor did not detect other pesticides such as diazinon, bromoxynil, malathion, glyphosate, and deltamethrin, confirming that it is sensitive and specific toward the three intended pesticides.

Ghiasi et al. (2021) fabricated a selective and sensitive electrochemical sensor based on the modification of activated glassy carbon electrode with nickel molybdate GQDs, and chitosan nanocomposites. It was reported that the as-fabricated sensor can be used in a concentration range between 0.1 and 330 μM with a limit of detection of 30 nM. The function of the sensor was also evaluated for the recovery analysis of diazinon in real samples of tomato and cucumber.

Yellowish-green emitting CQDs were prepared by Huo et al. (2021) via hydrothermal treatment. They used p-phenylenediamine and citric acid as precursors. It was observed that phoxim can quench the fluorescence emission of CQDs by an inner filter effect. As-prepared CQDs showed a good selectivity and sensitivity for detection of phoxim in the concentration ranges of 1−10 and 10−98 μM with a detection limit of 0.09 μM. It was revealed that phoxim can also be detected in real samples with satisfactory recoveries ranging between 93% and 105.9%. The low cytotoxicity and excellent biocompatibility of these CQDs was suitable for cell imaging also.

Yang et al. (2021b) synthesized cadmium telluride QDs. As-prepared CdTeQDs exhibited good water dispersion bright emission, and long emission wavelength as well as a unique response inhibition of organophosphorus pesticides (OPs) on acetylcholinesterase (AChE) activity. It was reported that the detection of OPs can be done with sensitivity, with the limit of detection of 0.027 ng mL^{-1}. It was observed that a CdTe-QD-based sensor can monitor methidathion in cultivated soil as well as Chinese cabbage.

Yi et al. (2021) first modified molybdenum disulfide QDs (MoS_2 QDs) with 3-aminophenyl boronic acid, and then it was functionalized with hydropropyl-β-cyclodextrin (β-CD), (β-CD functionalized MoS_2 QDs β-CD-MoS_2 QDs). It was used for fluorescent detection of parathion-methyl (MP), hydrolyzed to p-nitrophenol which can enter into the β-CD cavity; thus resulting in fluorescence quenching. It was reported that as-prepared β-CD-MoS_2 QDs nanoprobe exhibited a wide detection range of 0.01−18.0 ppm and a low detection limit of 3.3 ppb for the detection of parathion-methyl. An excellent selectivity was also reported for detection of MP, and it can be applied in real samples. Fluorescent CQDs (J-CQDs) were prepared by Chandra et al. (2022) using jatropha fruit via a hydrothermal route. The catalytic activity of AChE was inhibited in the presence of OPs, and a fluorescence signal was recovered. A sensitive and selective nanoprobe was designed as a sensor,

which can detect chlorpyrifos with a limit of detection (2.7 ng mL^{-1}). It was also revealed that this can be applied for pesticide detection in environmental and agricultural samples successfully with acceptable recovery.

13.2.1.8 Others

Lu et al. (2019) prepared a carbon dot-decorated hybrid nanocomposite (CD@RCC3) (chiral porous organic cage) and used it to fabricate a fluorescent sensor. It was reported that the as-fabricated sensor was used for the determination of isomers of nitrophenol. It could also differentiate phenylethanol and phenylalaninol enantiomers.

Yang et al. (2021c) prepared CdTeS QDs-coated silica shell (CdTeS QDs@SiO_2). Then ZnCdS QDs were encapsulated in a 3D network imprinted polymer (ZnCdS QDs@MIP) to give a response signal. It was observed that the fluorescence emission of ZnCdS QDs@MIP was quenched in the presence of ascorbic acid (1−500 μM) with a detection limit of 0.78 μM. It was reported that satisfactory results were obtained in the detection of ascorbic acid in vitamin C tablets.

Liu et al. (2021) designed an ECL sensor based on a dual-emission luminophore (NSGQDs-PEI-luminol-Pt). It was composed of nitrogen and sulfur codoped GQDs (NSGQDs) (main luminophore), luminol (auxiliary luminophore), platinum nanoparticles (coreaction accelerator), and polyetherimide linker of NSGQDs and luminal, respectively. This ECL senor can detect ascorbic acid in the concentration range of 10−360 nM with a limit of detection of 3.3 nM. It was also used for monitoring ascorbic acid in human serum.

Yanyan et al. (2021) fabricated a sensor based on N-GQDs. This sensor was used for the detection of H_2O_2 and glucose in the concentration range of 0.3−100.0 and 0.7−90.0 μM with a limit of detection of 63 nM. The sensitive detection of glucose is also realized in the concentration range (0.7−90.0 μM) with LOD of 96 nM, because the oxidation of glucose by glucose oxidase (GOx) produces H_2O_2.

A fluorescence sensor with dual-emission was developed by Gan et al. (2021) based on CQDs and Eu^{3+} complexes. It was observed that dual-emission fluorescence intensity was increased in the presence of Hg^{2+} ions. It was reported that the as-developed sensor exhibited an excellent sensitivity and selectivity in the concentration range of 1−20 nM with a detection limit of 0.2 nM. It was revealed that this sensor gave satisfactory recovery from 97.6% to 105.4% for the detection of Hg^{2+} ions in drinking water and milk samples.

A single-step synthesis of positively charged Pd NPs and green synthesis of GQDs from graphite was reported by Ahmed et al. (2021). An aptamer-induced fluorescence fluctuation of GQDs and palladium nanoparticles for the detection of tetracycline has been observed with a limit of detection of

45 ng mL^{-1}. CQDs were synthesized via a facile one-step hydrothermal treatment of purslane leaves by Amer et al. (2021). It was reported that a CQDs-based sensor could detect formaldehyde. It was revealed that the as-fabricated sensor exhibited a good reversibility and reproducibility.

Carneiro et al. (2021) synthesized CQDs via a hydrothermal route using the seed of *Caelsalpinia pulcherrima*. They could detect five food additives—lactic acid, citric acid, ascorbic acid, potassium sorbate, and sodium benzoate—with a detection limit of 252 ng mL^{-1}. They also successfully identified all these additives in a sample of a pickled olives with 100% of the combinations correctly identified.

Huangfu and Feng (2021) synthesized $CsPbBr_3$ QDs and used them to sense various solvents with different polarities. A good linear relationships was found between the fluorescence intensity of $CsPbBr_3$ QDs and the volume of different polar solvents, ethanol, methanol, and acetone. It is all due to the fast change of polarity, which makes perovskite QDs useful as polarity sensors. They used as-fabricated $CsPbBr_3$ QDs for total polar materials detection in edible oils. The quenching effect of fluorescence intensity was observed for soybean oil, olive oil, and sunflower oil, in the range of 17%−31.5%, 25%−31.5%, and 21.5%−33%, respectively.

Khose et al. (2021) synthesized novel red-fluorescent GQDs (G-GQD) using therapeutic guava (*Psidium guajava*) leaf. It was reported that the emission property of as-fabricated G-GQD can be used as a fluorescence turn-off probe for the determination of Hg^{2+} ions with a detection limit of 82 μM. It was also reported that other ions such as Co^{2+}, Cu^{2+}, Al^{3+}, and Fe^{2+}, are also known fluorescence quenchers, but they did not show any interference with the selectivity of Hg^{2+} ions. The G-GQD can be used as a sensor for Hg^{2+} ions even in polluted water sources.

Kongsanan et al. (2021) synthesized GQDs by pyrolyzing solid citric acid. The as-prepared sample can be used for the simultaneous detection of ferricyanide $[Fe(CN)_6]^{3-}$ and cyanide (CN^-) in wastewater samples (Fig. 13.1). It was reported that the fluorescence intensity of GQDs decorated with Hg^{2+} could be turned on in the presence of CN^- and back to turn-off mode by $[Fe(CN)_6]^{3-}$. These can be detected simultaneously in the range of 5.0−15.0 and 10.0−50.0 μM, with detection limits of 3.10 and 9.48 μM for CN^- ion and $[Fe(CN)_6]^{3-}$, respectively. This sensor was successfully used for CN^- and $[Fe(CN)_6]^{3-}$ detection (simultaneous and selective) in wastewater samples of municipal water reservoirs.

Lu et al. (2021) fabricated functionalized carbon nitride QDs (CNQDs) using a microwave-assisted solvothermal method. It was reported that these CNQDs were monodispersed with a narrow size distribution of particles with an average size of 3.5 nm. They exhibited excellent sensitivity and selectivity of fluorescence quenching for 2,4,6-trinitrophenol (TNP) in the range of 0.1−15 μM with a limit of detection of 87 nM. They also obtained satisfactory results with this probe for detecting TNP in spiked water samples.

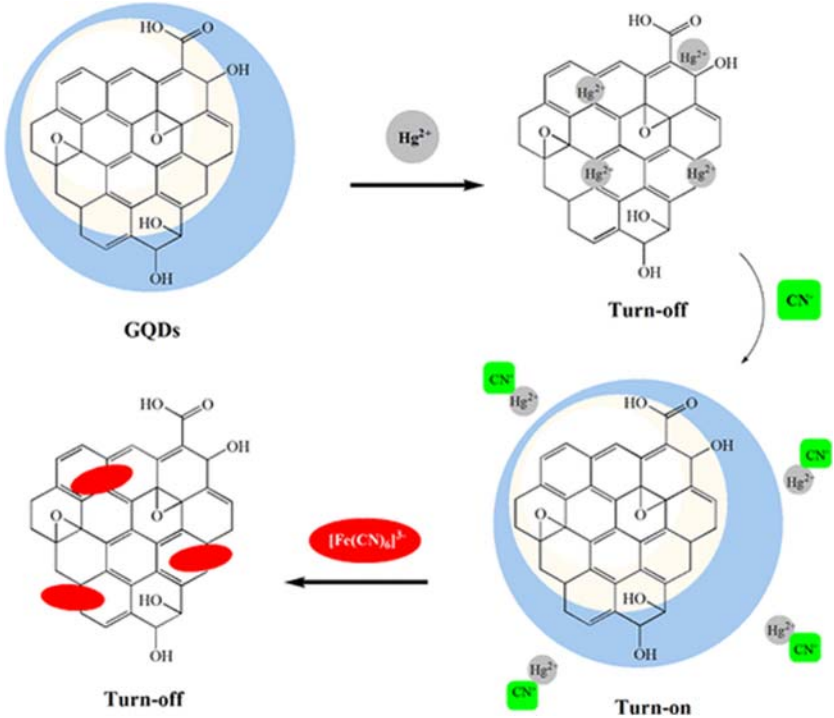

FIGURE 13.1 Use of GQDs for detection of ferricyanide and cyanide ions. *Adapted from Kongsanan, N., Pimsin, N., Keawprom, C., Sricharoen, P., Areerob, Y., Nuengmatcha, P., et al., 2021. A fluorescence switching sensor for sensitive and selective detections of cyanide and ferricyanide using mercuric cation-graphene quantum dots. ACS Omega 6(22), 14379–14393, with permission.*

Mehata and Biswas (2021) prepared GQDs–silver nanoparticles (GQDs@AgNPs) hybrid structure using GOD as a reducing and stabilizing agent. As-prepared composite exhibited strong surface plasmon resonance along with the absorption of GQDs. It was also reported in the sensing of hydrogen peroxide in an aqueous medium and therefore as-prepared GQDs@AgNPs nanohybrids can be used as a sensing probe.

The mannitol capped boron-doped CQDs (B-CQDs) were synthesized by Ali et al. (2021) and used for detection of sparfloxacin and orbifloxacin. As-prepared samples exhibited an increase of fluorescence intensity in the range of 1.5×10^{-9}–1.3×10^{-7} and 1.2×10^{-9}–1.1×10^{-7} M with limits of detection of 5.0×10^{-10} and 4.0×10^{-10} M for sparfloxacin and orbifloxacin, respectively. This probe gave satisfactory results determination for these antibiotics in milk and natural water samples. Zhang and Fan (2021) synthesized cerium–nitrogen codoped CQDs (Ce–N–CDs) via a hydrothermal method. They used cerium nitrate with citric acid, and ethylenediamine.

It was observed that as-prepared Ce−N−CDs exhibited excellent detection selectivity for tetracyclines (TCs). It was reported that this probe detected doxycycline (DC) in a concentration range of 0.4−35 μM with a limit of detection of 0.25 μM. This method was also used successfully for the determination of DC and total TCs in pork and milk. It was revealed that as-prepared Ce−N−CDs had low cytotoxicity and did not affect cell viability. It was proposed that as-prepared Ce−N−CDs can be used in cell imaging.

A dual-signal fluorescent sensor was developed for the detection of tetracycline in milk with excellent reproducibility and stability. Molybdenum disulfide QDs (blue fluorescence) and cadmium telluride QDs with yellow fluorescence were synthesized by (Liang et al., 2022). They prepared MoS_2/CdTe-based sensor with two fluorescence emission peaks at 433 and 573 nm. It was observed that the fluorescence of MoS_2/CdTe was quenched by photoinduced electron transfer. As-prepared CdTe QDs composite can be used for the determination of tetracyline in the concentration range of 0.1−1 μM. This sensor was also applied for the detection of tetracyline in milk samples with recovery of 95.53%−104.22%.

Şen et al. (2022) synthesized fluorescent polyethylenimine capped CQDs (PEI-C-dots) via microwave irradiation. They used polyethylenimine and citric acid as precursors for this purpose. It was observed that fluorescence quantum yield of as-synthesized PEI-C-dots was found to be 54% and the detection limit for 2,4,6-trinitrotoluene was 93 $\mu g\ L^{-1}$. It was interesting to note that that neither the HMX or RDX explosives interfered with this determination. Xu et al. (2022) prepared molecularly imprinted polymers based on Si QDs (Si QDs@SiO_2 @MIPs) via a sol−gel method. It was observed that as-prepared Si QDs@SiO_2 @MIPs exhibited a strong fluorescent emission at 447 nm, which was quenched in the presence of catechol. This sensor can be used to determine concentrations of catechol in the range of 0.018−100 μM with a limit of detection of 0.018 μM. This method was also applied by detecting catechol in real river water samples with satisfactory results.

Afshary et al. (2022) fabricated an electrochemiluminescence sensor based on nitrogen-doped CQDs (N-CQDs). It was reported that the as-prepared N-CQD-based sensor can be used for the determination of ceftazidime in the concentration range of 1×10^{-7} to 5×10^{-4} mol L^{-1} with a limit of detection of 2.3×10^{-8} mol L^{-1}. It was suggested that this ECL sensor is also applicable for the analysis of ceftazidime in some real samples (milk powder, bovine milk, and human serum).

Jiang et al. (2022) decorated 0D/2D heterostructure of ZnO QDs on nitrogen-doped Ti_3C_2 MXene (ZnO/N-Ti_3C_2). The size of ZnO QDs was found to be in the range of 2−5 nm. It was reported that the as-prepared sensor could be used for selective and sensitive detection of chloramphenicol in the concentration range of linear range (0.1−100 ng mL^{-1}) with a detection limit of 0.019 ng mL^{-1}. Praoboon et al. (2022) developed an

electrochemiluminescence sensor using tris(2,2′-bipyridyl)ruthenium(II) complex coupled with water-soluble thioglycolic acid-capped CdSe QDs. It was revealed that the trimethylamine can be determined using this sensor in the concentration range of 1×10^{-12} to 1×10^{-7} M with a limit of detection of 2.09×10^{-13} M. A rapid estimation of concentration of trimethylamine can be done in fish tissue using the as-prepared sensor.

13.2.2 Biosensors

Any disease has its origin in changes in biological environment and organs of the body, and therefore detecting such changes at an early stage can safeguard our health because one can plan the treatment of any disease in a timely manner. It is possible to sense these changes with the help of QDs, which are very sensitive to any variation in the biological environment.

Hwang et al. (2021) reported the synthesis of reduced graphene oxide QDs (rGOQDs) in perfluorotributylamine solution. It was observed that the as-prepared sample exhibited good photostability without any loss in intensity even after a month and it can be used for an optical device (Fig. 13.2). It was revealed that PL spectra from the rGOQDs-solution changed color from blue to green when mixed with GOx for glucose concentration of 0−2 mM. Thus rGOQDs can be used as colorimetric biosensors with the help of smartphone.

Mostafa et al. (2021) synthesized highly photoluminescent $Mn^{2+}{}_xZn_{2-x}S$ ($0 \leq x \leq 0.1$)-doped QDs. These QDs were capped with 3-mercaptopropionic acid. It was reported that ZnS and $Mn^{2+}{}_{0.04}Zn_{1.96}S$ QDs were of average particle size 13 and 16 nm, respectively. As-prepared Mn-doped ZnS QDs were used as an optical sensor for determination of bovine serum albumin with limit of detection of 1.56×10^{-7} M.

Pothipor et al. (2021) constructed an electrochemical biosensor based on gold nanoparticles/GQDs/graphene oxide (AuNPs/GQDs/GO) modified three-screen-printed carbon electrode to detect miRNA-21, miRNA-155, and

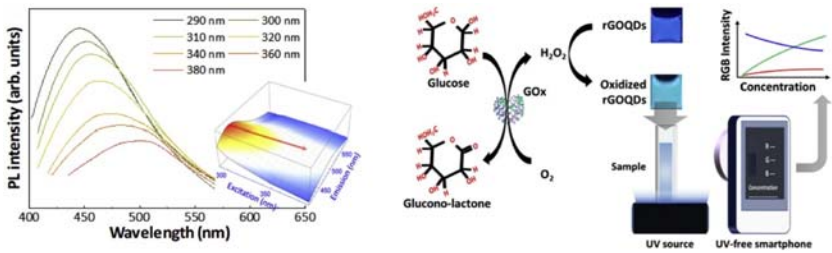

FIGURE 13.2 Use of reduced graphene oxide quantum dots in detection of glucose. *Adapted from Hwang, J., Le, A.D.D., Trinh, C.T., Le, Q.T., Lee, K.G., Kim, J., 2021. Green synthesis of reduced-graphene oxide quantum dots and application for colorimetric biosensor. Sens. Actuators A: Phys. 318. https://doi.org/10.1016/j.sna.2020.112495, with permission.*

miRNA-210 biomarkers. They used different redox species (polydopamine, anthraquinone, and methylene blue) as redox indicators for anchoring to capture miRNA probes, which are hybridized with the miRNA-21, miRNA-155, and miRNA-210. It was reported that the as-developed AuNPs/GQDs/GO-based biosensor exhibited an excellent performance for miRNA sensing simultaneously, in a wide concentration range (0.001−1000 pM) with a lower detection limit of 0.04, 0.33, and 0.28 fM for the detection of miRNA-21, miRNA-155, and miRNA-210, respectively. It was revealed that this method can be used with selectivity for the detection of miRNAs in human serum samples and such a multiplex label-free miRNA biosensor has a great potential for the diagnosis of breast cancer.

Van Tam et al. (2021) synthesized aniline functionalized GQDs (a-GQDs) via microwave-assisted pyrolysis of fructose. Then these GQDs were modulated with phenylboric acid (PBA). It was reported that the as-prepared fluorescent sensor using a-GQDs/PBA exhibited high selectivity and sensitivity toward glucose. Furthermore, a-GQD/PBA system exhibited excellent biocompatibility and can be satisfactorily applied to detect glucose in HeLa cells with a limit of detection of 2.1 μM. A highly compatible graphene nanofilm decorated with Prussian blue (PB) (electroactive) and photoelectric responsive QDs was prepared by Ma et al. (2022). An impressive biosensing performance could be obtained by as-prepared enzyme-modified PB-rGO-QDs film, which exhibited high sensitivity for H_2O_2. It was reported that wearable devices of PB-rGO-QDs films on textile showed flexible bending lifetime over several thousands of cycles, with photoelectronic properties and as a stable sensor.

A sensitive photoelectrochemical biosensor was fabricated by Tu et al. (2022) with ZnSe QDs (QDs)/Au nanoparticles. It was reported that ZnSe QDs were enhanced in the presence of light irradiation as a result of surface plasmon resonance of AuNPs. The photocurrent intensity of AuNPs/ZnSe QDs was also increased by six times that of ZnSe QDs only. This biosensor was able to detect target DNA in the range from 1 fM to 10 nM with a very low limit of detection of 0.33 fM. Acrylamide (AM) is a potential carcinogen produced during food thermal processing. Wei et al. (2021) developed a simple fluorescent biosensor that was based on single-stranded DNA (ssDNA). CQDs and ssDNA were preferentially bound to AM by hydrogen bonding. It was observed that the degree of reduction of fluorescence was smaller compared to in the absence of AM. This sensor could detect AM in the concentration range of 5×10^{-3} to 1×10^{-7} M with a detection limit of 2.41×10^{-8} M.

Deng et al. (2022) fabricated CQD functionalized solution-gated graphene transistors and used them for highly sensitive label-free detection of DNA. These CQDs were immobilized on the surface of the gate electrode using mercaptoacetic acid using its thiol group. The ssDNA probe can hybridize with the ssDNA target and form double-stranded DNA. It was

revealed that the detection limit was as low as 1 aM. The proposed sensor exhibited a good linear range (1 aM to 0.1 nM). It was interesting to note that it can effectively distinguish one-base mismatched target DNA and response time was only 326 s for 1 aM target DNA molecules. Mao et al. (2022) coated colloidal gold nanoparticles with polydopamines (PDA) to obtain Au@PDA nanoparticles. It was reported that Au@PDA nanoparticles mediated ZnCdSe/ZnS QDs fluorescence quenching and recovery, and it could assist in the detection, resulting in a reverse fluorescence enhancement detection format of carbendazim (CBD). It was observed that the sensitivity of lateral flow immunoassay (LFIA) of the fluorescence was 32 times higher compared to the colorimetry mode. A negligible cross reactivity was there for the determination of thiabendazole, benomyl, thiophanate-methyl, and thiophanate-ethyl on using LFIA. They could achieve satisfactory results in testing spiked strawberry and cucumber samples, which indicated that the as-prepared probe Au@PDAs-QDs-LFIA was more reliable.

The 3-mercaptopropionic acid capped CdSe QDs graphene nanocomposite (rGO-CdSe QDs/ITO) was fabricated by Khandelwal et al. (2022) and used as an electrochemical biosensor for the detection of low-density lipoprotein (LDL). It was reported that as-prepared immunoelectrodes could detect LDL in a wide concentration range ($2-125\ \text{mg dL}^{-1}$). Zhu et al. (2022) prepared CdTe QDs (CA-CdTe QDs) (cysteamine stabilized) and gold nanoparticles (sodium citrate stabilized). These CA-CdTe and Au NPs were self-assembled to from large clusters. The fluorescence of CA-CdTe was quenched as a result of fluorescence resonance energy transfer (FRET). It was reported that positive glutathione (GSH) could assemble with negative Au NPs through electrostatic interaction at pH 5.5 and it could destroy the FRET system of CA-CdTe and Au NPs. The recovered fluorescence efficiency of CA-CdTe shows a linear relationship with GSH concentrations in the range of 6.7 nM to 0.40 μM, with a limit of detection of 3.3 nM. It was revealed that this sensing system can be applied in the detection of GSH in real human blood plasma samples with good recovery (99.5%−102.3%).

13.2.3 Humidity sensors

Humidity of an area is a necessary parameter for knowing the moisture content, which can sometime adversely affect some materials. Therefore it is important to know about humidity. Various sensors are available for determining humidity in a particular area, but QDs can measure humidity more selectively as these are very sensitive toward any change in humidity.

Chaloeipote et al. (2021) synthesized GQDs and silver nanoparticles via a hydrothermal method and a green reducing agent route, respectively. They confirmed the successful formation of a core/shell-like AgNPs/GQDs structure. It was reported that a ratio of 1:1 of GQDs/AgNPs in nanocomposite exhibited the best humidity response of about 98.14%. Chaudhary et al. (2021)

synthesized CQDs of two types: (1) C-1 and (2) C-2, depending on carbonization temperatures. It was revealed that average particle size was 5.5 and 2 nm for samples C-1 and C-2, respectively. It was reported that C-2 gave an enhanced sensing performance with an average sensitivity of 254.861 pF/%RH with a fast response and recovery times of 7.3 and 4.7 s, respectively. Holemadlu et al. (2022) synthesized GQDs via carbonization of citric acid monohydrate. This process is low cost and has scalability. They fabricated a humidity sensor using GQD solution as the sensing material, which showed a rapid and high sensitivity to changes in humidity.

13.2.4 Temperature sensors

Temperature variation is a quite common feature but it is likely to affect some chemical and biochemical reactions, and therefore the correct measurement of temperature becomes necessary. Although various techniques are available for temperature measurement, QDs are very sensitive to such temperature changes and these are used in different devices for determining temperature at a particular site.

Zhang et al. (2018a) prepared lead sulfide QDs decorated zinc oxide nanorods. Then PbS QDs/ZnO film was fabricated by tuning deposition of PbS QDs on ZnO nanorods via a successive ionic-layer adsorption and reaction (SILAR) method. The sensor based on PbS QDs/ZnO nanorods can be used for sensing of room temperature.

Glass stabilized Mn-doped $CsPb(Cl/Br)_3$ QDs have been synthesized by Zhuang et al. (2019). They used a glass composition design and in situ glass crystallization for this purpose. It was reported that Mn-doped $CsPb(Cl/Br)_3$ QDs exhibited superior thermal stability and water resistance (about 100%). It is interesting to know that complete luminescence could be retained even after immersing this composite in water for a month or so. It was revealed that rapid thermal quenching for exciton recombination relative to Mn^{2+} d−d transition at lower temperatures (cryogenic) may provide it a promising position as a ratiometric temperature sensing medium.

Li et al. (2020) developed an optical thermometer with high sensitivity by using exciton recombination of $CsPbBr_3$ QDs for detecting a signal for temperature. It was reported that the fluorescence intensity ratio of exciton recombination and Eu^{3+} emission in nanocomposite exhibited a good temperature sensing property in as-prepared temperature ranging between 93K and 383K. It was observed that maximum absolute and relative temperature sensitivity could reach 0.0224% and $2.25\%K^{-1}$, respectively. It provides an effective pathway for developing a noncontact optical thermometric materials.

A simple one-pot strategy was reported by Lei et al. (2021) for preparing polyvinyl alcohol (PVA)-capped SQDs. They used low cost sulfur and PVA as a ligand. It was observed that as-prepared SQDs had sizes in the range of

1.5−5 nm. They also exhibited good water dispersibility and stability, good optical stability, bright fluorescence, and low cytotoxicity. As-prepared SQDs show selective and sensitive fluorescence quenching behavior toward Fe^{3+} ions with a detection limit of 9.2×10^{-9} M. SQDs also show temperature-dependent fluorescence. It was revealed that SQDs can be used for monitoring Fe^{3+} ions and also as a nanothermometer for temperature in the interior of cells.

Han et al. (2021) fabricated a highly sensitive ratiometric thermal sensor. This sensor was based on colloidal C-dots as these C-dots exhibited a temperature-dependent photoluminescence response. It was reported that C-dots@OH exhibited an absolute thermal sensitivity of $-0.082\ ^{\circ}C^{-1}$, which makes it a very promising candidate for high-sensitivity, and a self-calibrated nanoscale thermometer. These as-prepared C-dots@OH were used to monitor the intracellular temperature in the range of 32°C−42°C, with a clear trend for temperature variation in a single cell. It was reported that as-prepared thermal sensors can find potential application in nanoelectronic and optoelectronic devices.

Lee et al. (2021) developed nanothermometers based on luminescence of GQDs to probe temperature-sensitive processes at the nanoscale,. These QDs were synthesized via top-down (RGQDs) or bottom-up (N-GQDs) approaches using reduced graphene oxide and glucosamine as precursors, respectively. The average particle size of QDs was found to be 3−6 nm. It was reported that both GQDs exhibited temperature-sensitive fluorescence, which was photostable. A linear as well as reversible fluorescence quenching was observed up to 19.3% for the visible and near-infrared GQD emission in the temperature range 25°C−49°C. It was revealed that these GQD nanothermometers can give more than 40% quenching response in the range of 25°C−45°C, when internalized into the cytoplasm of HeLa cells. It was suggested that as-prepared sensors can be used for temperature sensing in microscopic subcellular biological environments.

Kumbhakar et al. (2021) synthesized Mn^{2+}-doped ZnS QDs (MZQDs) and used its reversible temperature-dependent PL emission quenching properties in the development of a smartphone-based optical thermometer. It was observed that temperature-dependent variations are present in PL intensity on using MZQDs in different forms, like powder form, aqueous dispersion, and polymer-encapsulated thin film. They have demonstrated a smartphone-based colorimetric imaging method for the measurement of temperature.

Yang et al. (2021a) synthesized N-GQDs with high blue fluorescence via a hydrothermal method using benzimidazoles as the precursor. It was reported that as-fabricated N-GQDs had a particle size of 3.8 nm with good water solubility, crystallinity, and photostability. It was observed that fluorescence of N-GQDs was quenched by tetracycline at elevated temperature and fluorescence intensity exhibited a linear reduction with temperature between 25°C and 100°C. They reported reversible and stable abilities of temperature sensing of as-prepared N-GQDs.

Sharma and Mehata (2022a) synthesized undoped as well as manganese-doped zinc selenide QDs in the temperature range of 77-300K. It was observed that intense blue and orange PL were exhibited by these as-prepared ZnSe and Mn@ZnSe QDs, respectively. It was found that PL intensity is dependent on temperature, decreasing with increasing temperature, and the maximum sensitivity values were 0.58% (225K) and 0.44%K^{-1} (250K) for ZnSe and Mn@ZnSe QDs, respectively.

13.3 Recent developments

Some recent developments in the use of QDs in fabricating different sensors have been summarized in Table 13.1.

TABLE 13.1 Recent advances in use of quantum dots in sensors.

Material	Application	Limit of detection	References
Carbon quantum dots	Detection of ammonia	10 nM	Ganesan et al. (2022)
Nitrogen-doped graphene quantum dots (N-GQDs) polyaniline (PANI)	Detection of ammonia	1500 ppm	Hakimi et al. (2018)
SnO_2 QDs	Detection of ammonia	–	Sahu et al. (2019)
Titanium dioxide quantum dots	Detection of hydrogen sulfide	500 ppb	Wu et al. (2022)
Graphene quantum dots	Detection of carbon dioxide	10–20 nm	Raeyani et al. (2020)
N-type nitrogen-doped carbon oxide quantum dots	Detection of humidity	20%–90%	Kondee et al. (2022)
Nitrogen-doped carbon quantum dots and red-emitting copper nanoclusters (CuNCs) complex	Detection of pesticide	7.49 and 3.03 nM	Chen et al. (2022)
Gold nanoparticles decorated quantum dots	Pesticide detection	Response range of 0.01–20 μM and limit of detection (LOD) of 7 nM	Jin et al. (2021)
MIP/$CsPbBr_3$ QDs	Detection of pesticide	0.10–500.0 μg L^{-1}	Zhang et al. (2022)
CdSe@CdS quantum dots	Detection of ochratoxin A	0.89 ng mL^{-1}	Jia et al. (2022)

(*Continued*)

TABLE 13.1 (Continued)

Material	Application	Limit of detection	References
ZnS/PbS core-shell quantum dots	Detection of hydrogen sulfide	300 ppm	Azimi and Rostami (2021)
Films of CdSe/ZnS core-shell type quantum dots	Detection of nitrogen dioxide	1–100 ppm	Ando et al. (2022)
PbS CQDs	Detection of nitrogen dioxide	–	Li et al. (2020)
Aptamer-modified quantum dots	Detection of *Staphylococcus aureus* in food and serum samples	2 CFU mL^{-1}	Tao et al. (2021)
CdSe/CdS/ZnS quantum dots	Detection of *Escherichia coli* and *P. Aeruginosa*	58 and 97 CFU mL^{-1}	Ye et al. (2022)
Tungsten trioxide quantum dots	Detection of *Listeria monocytogenes*	$1.3–1.3 \times 10^7$ CFU mL^{-1}	Zhu et al. (2021)
Carbon quantum dots	Detection of *E. coli* O157: H7 (*E. coli*)	487 CFU mL^{-1}	Hu et al. (2021) and Hong et al. (2021)
Fe_3O_4 nanoparticles and CdTe quantum dots	Detection of human serum albumin (HSA)	12 ng mL^{-1}	Liao et al. (2021)
S,N-CQDs	Detection of bendiocarb	0.02 μg mL^{-1}	Al Yahyai et al. (2021)
MoS_2 QDs and GQDs mixture (3:2)	Detection of cholesterol	35 nmol L^{-1}	Hassanzadeh and Khataee (2018)
3-Mercaptoproponic acid protected Mn@ZnSe QDs	Detection of Hg^{2+} and Pb^{2+} ions	Hg^{2+} and Pb^{2+} (0–100 μL)	Sharma and Mehata (2022b)
CdTe quantum dots	Thimerosal (TM), an organic mercury compound	26.6 μg L^{-1}	Tall et al. (2021)
CdZnTeS alloyed QDs	Detection of Pb^{2+} or Hg^{2+} ions	–	Hoang et al. (2022)

13.4 Conclusion

QDs are very sensitive toward any changes in chemical and biological environment, temperature, humidity, etc. Hence, these are successfully used for sensing the presence of certain chemicals. such as alcohol, liquefied petroleum gas, pesticides, drugs, hydrogen sulfide, ammonia. and many more, even if these are present in very low concentrations (ppm or even ppb level). The timely detection of any abnormality in body will help us in its immediate treatment. The leakage of toxic material can also be traced in time to have a safeguard. The list of sensors is not complete and it will continue increasing day by day.

References

Abbasi, F., Alizadeh, N., 2020. Highly selective detection of methanol in aqueous and ethanol medium based on hybrid ZnS: Mn^{2+} quantum dots/N-methylpolypyrrole as a fluorescence switchable sensor. Food Chem. 328. Available from: https://doi.org/10.1016/j.foodchem.2020.127091.

Afshary, H., Amiri, M., Bezaatpour, A., Wark, M., 2022. Electrochemiluminescence sensor based on N-doped carbon quantum dots for determination of ceftazidime in real samples. J. Electrochem. Soc. 169. Available from: https://doi.org/10.1149/1945-7111/ac53ce.

Ahmed, S.R., Kumar, S., Ortega, G.A., Srinivasan, S., Rajabzadeh, A.R., 2021. Target specific aptamer-induced self-assembly of fluorescent graphene quantum dots on palladium nanoparticles for sensitive detection of tetracycline in raw milk. Food Chem. 346. Available from: https://doi.org/10.1016/j.foodchem.2020.128893.

Al Yahyai, I., Al-Lawati, H.A., Hassanzadeh, J., 2021. A paper-based chemiluminescence detection device based on S, N-doped carbon quantum dots for the selective and highly sensitive recognition of bendiocarb. Anal. Methods. 13 (31), 3461–3470.

Ali, H.R.H., Hassan, A.I., Hassan, Y.F., El-Wekil, M.M., 2021. Mannitol capped magnetic dispersive micro-solid-phase extraction of polar drugs sparfloxacin and orbifloxacin from milk and water samples followed by selective fluorescence sensing using boron-doped carbon quantum dots. J. Environ. Chem. Eng. 9 (2). Available from: https://doi.org/10.1016/j.jece.2021.105078.

Alvandi, N., Assariha, S., Esfandiari, N., Jafari, R., 2021. Off–on sensor based on concentration-dependent multicolor fluorescent carbon dots for detecting pesticides. Nano-Struct. Nano-Objects 26. Available from: https://doi.org/10.1016/j.nanoso.2021.100706.

Amer, W.A., Rehab, A.F., Abdelghafar, M.E., Torad, N.L., Atlam, A.S., Ayad, M.M., 2021. Green synthesis of carbon quantum dots from purslane leaves for the detection of formaldehyde using quartz crystal microbalance. Carbon 179, 159–171.

Ando, M., Inagaki, K., Kawasaki, H., Shigeri, Y., 2022. Reversible sensing of nitrogen dioxide using photoluminescent CdSe/ZnS quantum dots and enhanced response by combination with noble metals. J. Ceram. Soc. Jpn. 130 (1), 180–186.

Azimi, M., Rostami, A.M. 2021. Room temperature chemiresistor H2S Gas sensor based on ZnS/PbS core-shell quantum dots. In: 2021 29th Iranian Conference on Electrical Engineering (ICEE). IEEE, pp. 65–68.

Bai, J., Shen, Y., Zhao, S., Chen, Y., Li, G., Han, C., 2022. Flower-like MoS2 hierarchical architectures assembled by 2D nanosheets sensitized with SnO_2 quantum dots for

high-performance NH3 sensing at room temperature. Sens. Actuators B: Chem. 353. Available from: https://doi.org/10.1016/j.snb.2021.131191.

Bhakat, A., Pal, A., Siddaramaiah, R., Chattopadhyay, A., 2021. Complexation-based super crystalline assembly of zinc oxide quantum dots for sensitive carbon dioxide gas sensing. J. Phys. Chem. C. 125 (22), 12316−12323.

Carneiro, S.V., Holanda, M.H.B., Cunha, H.O., Oliveira, J.J.P., Pontes, S.M.A., Cruz, A.A.C., 2021. Highly sensitive sensing of food additives based on fluorescent carbon quantum dots. J. Photochem. Photobiol. A: Chem. 411. Available from: https://doi.org/10.1016/j.jphotochem.2021.113198.

Chaloeipote, G., Samarnwong, J., Traiwatcharanon, P., Kerdcharoen, T., Wongchoosuk, C., 2021. High-performance resistive humidity sensor based on Ag nanoparticles decorated with graphene quantum dots. R. Soc. Open. Sci. 8 (7). Available from: https://doi.org/10.1098/rsos.210407.

Chandra, S., Bano, D., Sahoo, K., Kumar, D., Kumar, V., Yadav, P.K., 2022. Synthesis of fluorescent carbon quantum dots from Jatropha fruits and their application in fluorometric sensor for the detection of chlorpyrifos. Microchem. J. 172. Available from: https://doi.org/10.1016/j.microc.2021.106953.

Chaudhary, P., Maurya, D.K., Yadav, S., Pandey, A., Tripathi, R.K., Yadav, B.C., 2021. Ultrafast responsive humidity sensor based on roasted gram derived carbon quantum dots: experimental and theoretical study. Sens. Actuators B: Chem. 329. Available from: https://doi.org/10.1016/j.snb.2020.129116.

Chen, L., Lu, J., Luo, M., Yu, H., Chen, X., Deng, J., 2022. A ratiometric fluorescent sensing system for the selective and ultrasensitive detection of pesticide residues via the synergetic effects of copper nanoclusters and carbon quantum dots. Food Chem. 379. Available from: https://doi.org/10.1016/j.foodchem.2022.132139.

Chu, C.S., Hsieh, M.W., 2019. Optical fiber carbon dioxide sensor based on colorimetric change of α-naphtholphthalein and CIS/ZnS quantum dots incorporated with a polymer matrix. Opt. Mater. Express 9 (7), 2937−2945.

Deng, M., Li, J., Xiao, B., Ren, Z., Li, Z., Yu, H., 2022. Ultrasensitive label-free DNA detection based on solution-gated graphene transistors functionalized with carbon quantum dots. Anal. Chem. 94 (7), 3320−3327.

Dong, L., Zheng, P., Yang, Y., Zhang, M., Xue, Z., Wang, Z., 2018. NO_2 gas sensor based on graphene decorated with Ge quantum dots. Nanotechnology 30 (7). Available from: https://doi.org/10.1088/1361-6528/aaf3d7.

Dun, M., Tan, J., Tan, W., Tang, M., Huang, X., 2019. CdS quantum dots supported by ultrathin porous nanosheets assembled into hollowed-out Co_3O_4 microspheres: a room-temperature H2S gas sensor with ultra-fast response and recovery. Sens. Actuators B: Chem. 298. Available from: https://doi.org/10.1016/j.snb.2019.126839.

Ganesan, S., Kalimuthu, R., Kanagaraj, T., Kulandaivelu, R., Nagappan, R., Pragasan, L.A., 2022. Microwave-assisted green synthesis of multi-functional carbon quantum dots as efficient fluorescence sensor for ultra-trace level monitoring of ammonia in environmental water. Environ. Res. 206. Available from: https://doi.org/10.1016/j.envres.2021.112589.

Gan, Z., Hu, X., Huang, X., Li, Z., Zou, X., Shi, J., et al., 2021. A dual-emission fluorescence sensor for ultrasensitive sensing mercury in milk based on carbon quantum dots modified with europium (III) complexes. Sens. Actuators B: Chem. 328. Available from: https://doi.org/10.1016/j.snb.2020.128997.

Ghiasi, T., Ahmadi, S., Ahmadi, E., Olyai, M.R.T.B., Khodadadi, Z., 2021. Novel electrochemical sensor based on modified glassy carbon electrode with graphene quantum dots, chitosan

and nickel molybdate nanocomposites for diazinon and optimal design by the Taguchi method. Microchem. J. 160. Available from: https://doi.org/10.1016/j.microc.2020.105628.

Hajikhanloo, A.S., Sarraf, M.J., Rostami, A., Dolatyari, M., 2021. Micro ring resonator based CO_2 gas sensor using PbSe quantum dots. Opt. Quantum Electron. . Available from: https://doi.org/10.21203/rs.3.rs-638041/v1.

Hakimi, M., Salehi, A., Boroumand, F.A., Mosleh, N., 2018. Fabrication of a room temperature ammonia gas sensor based on polyaniline with N-doped graphene quantum dots. IEEE Sens. J. 18 (6), 2245–2252.

Han, Y., Liu, Y., Zhao, H., Vomiero, A., Li, R., 2021. Highly efficient ratiometric nanothermometers based on colloidal carbon quantum dots. J. Mater. Chem. B 9 (20), 4111–4119.

Hassanzadeh, J., Khataee, A., 2018. Ultrasensitive chemiluminescent biosensor for the detection of cholesterol based on synergetic peroxidase-like activity of MoS_2 and graphene quantum dots. Talanta 178, 992–1000.

Hoang, Q.B., Nguyen, T.N., Nguyen, T.P., Nguyen, A.D., Chu, N.H., Ta, V.T., 2022. Size-dependent reactivity of highly photoluminescent CdZnTeS alloyed quantum dots to mercury and lead ions. Chem. Phys. 552. Available from: https://doi.org/10.1016/j.chemphys.2021.111378.

Holemadlu, A., Keerthana, G., Purohit, K.B., Shaik, H., Nagaraja, V.S., 2022. Synthesis of graphene quantum dots and fabrication of humidity sensor. Emerging Research in Computing, Information, Communication and Applications. Springer, Singapore, pp. 407–415.

Hong, S.Z., Huang, Q.Y., Wu, T.M., 2021. The room temperature highly sensitive ammonia gas sensor based on polyaniline and nitrogen-doped graphene quantum dot-coated hollow indium oxide nanofiber composite. Polymers 13 (21). Available from: https://doi.org/10.3390/polym13213676.

Hu, X., Li, Y., Xu, Y., Gan, Z., Zou, X., Shi, J., et al., 2021. Green one-step synthesis of carbon quantum dots from orange peel for fluorescent detection of Escherichia coli in milk. Food Chem 339. Available from: https://doi.org/10.1016/j.foodchem.2020.127775.

Huangfu, C., Feng, L., 2021. High-performance fluorescent sensor based on CsPbBr3 quantum dots for rapid analysis of total polar materials in edible oils. Sens. Actuators B: Chem. 344. Available from: https://doi.org/10.1016/j.snb.2021.130193.

Huo, X., Liu, L., Bai, Y., Qin, J., Yuan, L., Feng, F., 2021. Facile synthesis of yellowish-green emitting carbon quantum dots and their applications for phoxim sensing and cellular imaging. Anal. Chim. Acta . Available from: https://doi.org/10.1016/j.aca.2021.338685.

Hwang, J., Le, A.D.D., Trinh, C.T., Le, Q.T., Lee, K.G., Kim, J., 2021. Green synthesis of reduced-graphene oxide quantum dots and application for colorimetric biosensor. Sens. Actuators A: Phys. 318. Available from: https://doi.org/10.1016/j.sna.2020.112495.

Jiang, D., Wei, M., Du, X., Qin, M., Shan, X., Chen, Z., 2022. One-pot synthesis of ZnO quantum dots/N-doped Ti_3C_2 MXene: tunable nitrogen-doping properties and efficient electrochemiluminescence sensing. Chem. Eng. J. 430. Available from: https://doi.org/10.1016/j.cej.2021.132771.

Jia, M., Jia, B., Liao, X., Shi, L., Zhang, Z., Liu, M., 2022. A CdSe@ CdS quantum dots based electrochemiluminescence aptasensor for sensitive detection of ochratoxin A. Chemosphere 287. Available from: https://doi.org/10.1016/j.chemosphere.2021.131994.

Jin, Y., Liu, K., Li, G., Li, C., Xiao, Z., Yuan, C., 2021. In situ reduction triggers the highly sensitive detection of pesticide by classic gold nanoparticle and quantum dots nanocomposite. Anal. Chim. Acta 1172. Available from: https://doi.org/10.1016/j.aca.2021.338679.

Keshtkar, S., Rashidi, A., Kooti, M., Askarieh, M., Pourhashem, S., Ghasemy, E., 2018. A novel highly sensitive and selective H_2S gas sensor at low temperatures based on SnO_2 quantum dots-C60 nanohybrid: experimental and theory study. Talanta 188, 531–539.

Khandelwal, D., Jain, D., Solanki, P.R., Ranjan, K.R., Mukherjee, M.D., 2022. A novel nanocomposite platform of mercaptopropionic acid stabilized CdSe quantum dots-graphene for impedimetric detection of low density lipoprotein. Mater. Lett. 308. Available from: https://doi.org/10.1016/j.matlet.2021.131236.

Khose, R.V., Chakraborty, G., Bondarde, M.P., Wadekar, P.H., Ray, A.K., Some, S., 2021. Red-fluorescent graphene quantum dots from guava leaf as a turn-off probe for sensing aqueous Hg (II). N. J. Chem. 45 (10), 4617–4625.

Kondee, S., Arayawut, O., Pon-On, W., Wongchoosuk, C., 2022. Nitrogen-doped carbon oxide quantum dots for flexible humidity sensor: experimental and SCC-DFTB study. Vacuum 195. Available from: https://doi.org/10.1016/j.vacuum.2021.110648.

Kongsanan, N., Pimsin, N., Keawprom, C., Sricharoen, P., Areerob, Y., Nuengmatcha, P., et al., 2021. A fluorescence switching sensor for sensitive and selective detections of cyanide and ferricyanide using mercuric cation-graphene quantum dots. ACS Omega 6 (22), 14379–14393.

Kumar, C., Rawat, G., Kumar, H., Kumar, Y., Kumar, A., Prakash, R., et al., 2018. Electrical and ammonia gas sensing properties of PQT-12/CdSe quantum dots composite-based organic thin film transistors. IEEE Sens. J. 18 (15), 6085–6091.

Kumbhakar, P., Karmakar, A.R., Das, G.P., Chakraborty, J., Tiwary, C.S., Kumbhakar, P., 2021. Reversible temperature-dependent photoluminescence in semiconductor quantum dots for the development of a smartphone-based optical thermometer. Nanoscale 13 (5), 2946–2954.

Lee, B.H., McKinney, R.L., Hasan, M., Naumov, A.V., 2021. Graphene quantum dots as intracellular imaging-based temperature sensors. Materials 14 (3). Available from: https://doi.org/10.3390/ma14030616.

Lei, J., Huang, Z., Gao, P., Sun, J., Zhou, L., 2021. Polyvinyl alcohol enhanced fluorescent sulfur quantum dots for highly sensitive detection of Fe^{3+} and temperature in cells. Part. Part. Syst. Charact. 38 (4). Available from: https://doi.org/10.1002/ppsc.202000332.

Liang, N., Hu, X., Li, W., Mwakosya, A.W., Guo, Z., Xu, Y., 2021. Fluorescence and colorimetric dual-mode sensor for visual detection of malathion in cabbage based on carbon quantum dots and gold nanoparticles. Food Chem. 343. Available from: https://doi.org/10.1016/j.foodchem.2020.128494.

Liang, N., Hu, X., Li, W., Wang, Y., Guo, Z., Huang, X., 2022. A dual-signal fluorescent sensor based on MoS_2 and CdTe quantum dots for tetracycline detection in milk. Food Chem. 378. Available from: https://doi.org/10.1016/j.foodchem.2022.132076.

Li, X., Yu, Y., Hong, J., Feng, Z., Guan, X., Chen, D., 2020. Optical temperature sensing of Eu3 + -doped oxyhalide glasses containing CsPbBr3 perovskite quantum dots. J. Lumin. 219. Available from: https://doi.org/10.1016/j.jlumin.2019.116897.

Liao, B.Y., Chang, C.J., Wang, C.F., Lu, C.H., Chen, J.K., 2021. Controlled antibody orientation on Fe_3O_4 nanoparticles and CdTe quantum dots enhanced sensitivity of a sandwich-structured electrogenerated chemiluminescence immunosensor for the determination of human serum albumin. Sens. Actuators B: Chem. 336. Available from: https://doi.org/10.1016/j.snb.2021.129710.

Liu, P., Meng, H., Han, Q., Zhang, G., Wang, C., Song, L., 2021. Determination of ascorbic acid using electrochemiluminescence sensor based on nitrogen and sulfur doping graphene quantum dots with luminol as internal standard. Microchim. Acta 188 (4). Available from: https://doi.org/10.1007/s00604-021-04761-w.

Liu, Y., Wang, H., Chen, K., Yang, T., Yang, S., Chen, W., 2019. Acidic site-assisted ammonia sensing of novel $CuSbS_2$ quantum dots/reduced graphene oxide composites with an ultralow detection limit at room temperature. ACS Appl. Mater. Interfaces 11 (9), 9573–9582.

Liu, Y., Wang, L., Wang, H., Xiong, M., Yang, T., Zakharova, G.S., 2016. Highly sensitive and selective ammonia gas sensors based on PbS quantum dots/TiO2 nanotube arrays at room temperature. Sens. Actuators B: Chem. 236, 529–536.

Liu, Y., Wang, H., Yang, S., Chen, K., Yang, T., Wei, J., et al., 2018. ppb Level ammonia detection of 3-D PbS quantum dots/reduced graphene oxide nanococoons at room temperature and Schottky barrier modulated behavior. Sens. Actuators B: Chem. 255, 2979–2987.

Luo, J., Li, C., Yang, Q., Yan, L., Zhang, B., Tao, R., et al., 2022. Facile fabrication of MoS2 nanoflowers/SnO2 colloidal quantum dots nanocomposite for enhanced NO_2 sensing at room temperature. IEEE Sens. J. . Available from: https://doi.org/10.1109/JSEN.2022.3151068.

Lu, Z., Lu, X., Zhong, Y., Hu, Y., Li, G., Zhang, R., 2019. Carbon dot-decorated porous organic cage as fluorescent sensor for rapid discrimination of nitrophenol isomers and chiral alcohols. Anal. Chim. Acta 1050, 146–153.

Lu, S., Xue, M., Tao, A., Weng, Y., Yao, B., Weng, W., 2021. Facile microwave-assisted synthesis of functionalized carbon nitride quantum dots as fluorescence probe for fast and highly selective detection of 2, 4, 6-trinitrophenol. J. Fluoresc. 31 (1), 1–9.

Lv, Y.K., Li, Y.Y., Yao, H.C., Li, Z.J., 2021. Nitrogen-doped graphene quantum dots-modified mesoporous SnO2 hierarchical hollow cubes for low temperature detection of nitrogen dioxide. Sens. Actuators B: Chem. 339. Available from: https://doi.org/10.1016/j.snb.2021.129882.

Mao, X., Wang, Y., Jiang, L., Zhang, H., Zhao, Y., Liu, P., et al., 2022. A Polydopamine-coated gold nanoparticles quenching quantum dots-based dual-readout lateral flow immunoassay for sensitive detection of carbendazim in agriproducts. Biosensors 12 (2). Available from: https://doi.org/10.1016/j.cej.2021.131824.

Masemola, C.M., Shumbula, N.P., Gqoba, S.S., Tetana, Z.N., Moloto, N., Linganiso, E.C. Electrospun NGQDs/PANI/PAN composite fibers for room temperature alcohol sensing. In: 2021 IEEE 3rd Eurasia Conference on IOT, Communication and Engineering (ECICE) IEEE, 2021, pp. 146–150.

Ma, J., Jiang, Y., Shen, L., Ma, H., Sun, T., Lv, F., et al., 2022. Oil-water self-assembly engineering of Prussian blue/quantum dots decorated graphene film for wearable textile biosensors and photoelectronic unit. Chem. Eng. J. 427. Available from: https://doi.org/10.1016/j.cej.2021.131824.

Mehata, M.S., Biswas, S., 2021. Synthesis of fluorescent graphene quantum dots from graphene oxide and their application in fabrication of GQDs@ AgNPs nanohybrids and sensing of H_2O_2. Ceram. Int. 47 (13), 19063–19072.

Mishra, R.K., Upadhyay, S.B., Kushwaha, A., Kim, T.H., Murali, G., Verma, R., et al., 2015. SnO_2 quantum dots decorated on RGO: a superior sensitive, selective and reproducible performance for a H_2 and LPG sensor. Nanoscale 7 (28), 11971–11979.

Mostafa, M., El Nady, J., Ebrahim, S.M., Elshaer, A.M., 2021. Synthesis, structural, and optical properties of Mn^{2+} doped ZnS quantum dots for biosensor application. Opt. Mater. 112. Available from: https://doi.org/10.1016/j.optmat.2020.110732.

Nair, R.V., Thomas, R.T., Mohamed, A.P., Pillai, S., 2020. Fluorescent turn-off sensor based on sulphur-doped graphene quantum dots in colloidal and film forms for the ultrasensitive detection of carbamate pesticides. Microchem. J. 157. Available from: https://doi.org/10.1016/j.microc.2020.104971.

Nemade, K.R., Waghuley, S.A., 2013a. LPG sensing application of graphene/CeO_2 quantum dots composite. AIP Conf. Proc. 1536 (1), 1258–1259.

Nemade, K.R., Waghuley, S.A., 2013b. LPG sensing application of graphene/Bi_2O_3 quantum dots composites. Solid. State Sci. 22, 27–32.

Nemade, K.R., Waghuley, S.A., 2013c. Strontium oxide quantum dot decorated graphene composites for liquid petroleum gas sensing. J. Chin. Adv. Mater. Soc. 1 (3), 219–228.

Ouyang, C., Chen, Y., Qin, Z., Zeng, D., Zhang, J., Wang, H., et al., 2018. Two-dimensional WS_2-based nanosheets modified by Pt quantum dots for enhanced room-temperature NH_3 sensing properties. App. Surf. Sci. 455, 45–52.

Pothipor, C., Jakmunee, J., Bamrungsap, S., Ounnunkad, K., 2021. An electrochemical biosensor for simultaneous detection of breast cancer clinically related microRNAs based on a gold nanoparticles/graphene quantum dots/graphene oxide film. Analyst 146 (12), 4000–4009.

Praoboon, N., Siriket, S., Taokaenchan, N., Kuimalee, S., Phaisansuthichol, S., Pookmanee, P., et al., 2022. Paper-based electrochemiluminescence device for the rapid estimation of trimethylamine in fish via the quenching effect of thioglycolic acid-capped cadmium selenide quantum dots. Food Chem. 366. Available from: https://doi.org/10.1016/j.foodchem.2021.130590.

Raeyani, D., Shojaei, S., Ahmadi-Kandjani, S., 2020. Optical graphene quantum dots gas sensors: experimental study. Mater. Res. Express 7 (1). Available from: https://doi.org/10.1088/2053-1591/ab637e.

Sahu, B.K., Juine, R., Das, A., 2019. Room temperature ammonia sensor using SnO2 quantum dots: an approach toward optical eye. AIP Conf. Proceed. 2115 (1). Available from: https://doi.org/10.1063/1.5112974.

Şen, F.B., Beğiç, N., Bener, M., Apak, R., 2022. Fluorescence turn-off sensing of TNT by polyethylenimine capped carbon quantum dots. Spectrochim. Acta—A: Mol. Biomol. 271. Available from: https://doi.org/10.1016/j.saa.2022.120884.

Sharma, V., Mehata, M.S., 2022a. A parallel investigation of un-doped and manganese ion-doped zinc selenide quantum dots at cryogenic temperature and application as an optical temperature sensor. Mater. Chem. Phys. 276. Available from: https://doi.org/10.1016/j.matchemphys.2021.125349.

Sharma, V., Mehata, M.S., 2022b. Photoluminescence turn-off based dual analytes (Hg^{2+} and Pb^{2+}) sensor in aqueous medium using 3-marcaptoproponic acid protected Mn2 + doped ZnSe quantum dots. Chem. Phys. Lett. 787. Available from: https://doi.org/10.1016/j.cplett.2021.139270.

Tall, A., da Costa, K.R., de Oliveira, M.J., Tapsoba, I., Rocha, U., Sales, T.O., 2021. Photoluminescent nanoprobes based on thiols capped CdTe quantum dots for direct determination of thimerosal in vaccines. Talanta 221. Available from: https://doi.org/10.1016/j.talanta.2020.121545.

Tao, X., Liao, Z., Zhang, Y., Fu, F., Hao, M., Song, Y., 2021. Aptamer-quantum dots and teicoplanin-gold nanoparticles constructed FRET sensor for sensitive detection of Staphylococcus aureus. Chin. Chem. Lett. 32 (2), 791–795.

Tu, Y.P., Wang, H.H., Long, D., Yuan, R., Chai, Y.Q., 2022. Highly sensitive photoelectrochemical biosensor based on Au nanoparticles sensitized zinc selenide quantum dots for DNA detection. Sens. Actuators B: Chem. 357. Available from: https://doi.org/10.1016/j.snb.2021.131255.

Van Tam, T., Hur, S.H., Chung, J.S., Choi, W.M., 2021. Novel paper-and fiber optic-based fluorescent sensor for glucose detection using aniline-functionalized graphene quantum dots. Sens. Actuators B: Chem. 329. Available from: https://doi.org/10.1016/j.snb.2020.129250.

Wang, R., Li, G., Dong, Y., Chi, Y., Chen, G., 2013. Carbon quantum dot-functionalized aerogels for NO_2 gas sensing. Anal. Chem. 85 (17), 8065–8069.

Wei, Q., Zhang, P., Liu, T., Pu, H., Sun, D.W., 2021. A fluorescence biosensor based on single-stranded DNA and carbon quantum dots for acrylamide detection. Food Chem. 356. Available from: https://doi.org/10.1016/j.foodchem.2021.129668.

Wongrat, E., Nuengnit, T., Panyathip, R., Chanlek, N., Hongsith, N., Choopun, S., 2021. Highly selective room temperature ammonia sensors based on ZnO nanostructures decorated with graphene quantum dots (GQDs). Sens. Actuators B: Chem. 326. Available from: https://doi.org/10.1016/j.snb.2020.128983.

Wu, J., Zhang, D., Cao, Y., 2018. Fabrication of iron-doped titanium dioxide quantum dots/molybdenum disulfide nanoflower for ethanol gas sensing. J. Colloid Interface Sci. 529, 556–567.

Wu, K., Zhang, W., Zheng, Z., Debliquy, M., Zhang, C., 2022. Room-temperature gas sensors based on titanium dioxide quantum dots for highly sensitive and selective H2S detection. Appl. Surf. Sci. 357. Available from: https://doi.org/10.1016/j.apsusc.2022.152744.

Xu, Y., Huang, T., Wang, S., Meng, M., Yan, Y., 2022. SiO_2-coated molecularly imprinted sensor based on Si quantum dots for selective detection of catechol in river water. J. Environ. Chem. Eng. 10 (1). Available from: https://doi.org/10.1016/j.jece.2021.106850.

Xu, Y., Yu, H., Chudal, L., Pandey, N.K., Amador, E.H., Bui, B., et al., 2021. Striking luminescence phenomena of carbon dots and their applications as a double ratiometric fluorescence probes for H2S detection. Mater. Today Phys. 17. Available from: https://doi.org/10.1016/j.mtphys.2020.100328.

Yang, Y., Liu, Z., Chen, D., Gu, B., Gao, B., Wang, Z., et al., 2021a. Multifunctional N-doped graphene quantum dots towards tetracycline detection, temperature sensing and high-performance WLEDs. J. Photochem. Photobiol. A: Chem. 405. Available from: https://doi.org/10.1016/j.jphotochem.2020.112977.

Yang, Q., Li, Q., Li, H., Li, F., 2021b. pH-response quantum dots with orange–red emission for monitoring the residue, distribution, and variation of an organophosphorus pesticide in an agricultural crop. J. Agri. Food Chem. 69 (9), 2689–2696.

Yang, S., Song, Z., Gao, N., Hu, Z., Zhou, L., Liu, J., et al., 2019. Near room temperature operable H2S sensors based on In2O3 colloidal quantum dots. Sens. Actuators B: Chem. 286, 22–31.

Yang, M., Wang, C., Liu, E., Hu, X., Hao, H., Fan, J., 2021c. A novel ascorbic acid ratiometric fluorescent sensor based on ZnCdS quantum dots embedded molecularly imprinted polymer and silica-coated CdTeS quantum dots. J. Mol. Liq. 337. Available from: https://doi.org/10.1016/j.molliq.2021.116438.

Yanyan, Z., Lin, J., Xie, L., Tang, H., Wang, K., Liu, J., 2021. One-step preparation of nitrogen-doped graphene quantum dots with anodic electrochemiluminescence for sensitive detection of hydrogen peroxide and glucose. Front. Chem. 9. Available from: https://doi.org/10.3389/fchem.2021.688358.

Ye, S., Han, T., Cheng, M., Dong, L., 2022. Wulff-type boronic acid-functionalized quantum dots for rapid and sensitive detection of Gram-negative bacteria. Sens. Actuators B: Chem. 356. Available from: https://doi.org/10.1016/j.snb.2021.131332.

Yi, Y., Zeng, W., Zhu, G., 2021. β-Cyclodextrin functionalized molybdenum disulfide quantum dots as nanoprobe for sensitive fluorescent detection of parathion-methyl. Talanta 222. Available from: https://doi.org/10.1016/j.talanta.2020.121703.

Zhang, D., Dong, G., Cao, Y., Zhang, Y., 2018a. Ethanol gas sensing properties of lead sulfide quantum dots-decorated zinc oxide nanorods prepared by hydrothermal process combining with successive ionic-layer adsorption and reaction method. J. Colloid Interface Sci. 528, 184–191.

Zhang, D., Dong, G., Wu, Z., Pan, W., Fan, X., et al., 2018b. Liquefied petroleum gas sensing properties of ZnO/PPy/PbS QDs nanocomposite prepared by self-assembly combining with SILAR method. IEEE Sens. J. 19 (8), 2855–2862.

Zhang, Z., Fan, Z., 2021. Application of cerium−nitrogen co-doped carbon quantum dots to the detection of tetracyclines residues and bioimaging. Microchem. J. 165. Available from: https://doi.org/10.1016/j.microc.2021.106139.

Zhang, R.R., Gan, X.T., Xu, J.J., Pan, Q.F., Liu, H., Sun, A.L., 2022. Ultrasensitive electrochemiluminescence sensor based on perovskite quantum dots coated with molecularly imprinted polymer for prometryn determination. Food Chem. 370. Available from: https://doi.org/10.1016/j.foodchem.2021.131353.

Zhang, Y.H., Wang, C.N., Yue, L.J., Chen, J.L., Gong, F.L., Fang, S.M., 2021. Nitrogen-doped graphene quantum dot decorated ultra-thin ZnO nanosheets for NO_2 sensing at low temperatures. Phys. E: Low-dimens. Syst. Nanostruct. 133. Available from: https://doi.org/10.1016/j.physe.2021.114807.

Zhuang, B., Liu, Y., Yuan, S., Huang, H., Chen, J., Chen, D., 2019. Glass stabilized ultra-stable dual-emitting Mn-doped cesium lead halide perovskite quantum dots for cryogenic temperature sensing. Nanoscale 11 (32), 15010−15016.

Zhu, Q., Du, J., Feng, S., Li, J., Yang, R., Qu, L., 2022. Highly selective and sensitive detection of glutathione over cysteine and homocysteine with a turn-on fluorescent biosensor based on cysteamine-stabilized CdTe quantum dots. Spectrochim. Acta A: Mol. Biomol. Spectrosc. 267. Available from: https://doi.org/10.1016/j.saa.2021.120492.

Zhu, L., Hao, H., Ding, C., Gan, H., Jiang, S., Zhang, G., et al., 2021. A novel photoelectrochemical aptamer sensor based on CdTe quantum dots enhancement and exonuclease I-assisted signal amplification for listeria monocytogenes detection. Foods 10 (12). Available from: https://doi.org/10.3390/foods10122896.

Chapter 14

Application of quantum dots in photosplitting of water

Luma M. Ahmed[1], Thaqeef M. Jawad[1], Hamad H. Kadium[1] and Jayesh P. Bhatt[2]
[1]*Department of Chemistry, College of Science, University of Kerbala, Karbala, Iraq,*
[2]*Department of Chemistry, PAHER University, Udaipur, Rajasthan, India*

14.1 Introduction

The whole world is facing scarcity of energy resources as presently available conventional fuels such as coal, kerosene, petrol, diesel, etc. will be reaching a point of complete exhaustion in the coming few decades. On the other hand, the demand for energy is increasing regularly, which cannot be fulfilled by the available resources, and therefore there is an urgent demand to find some alternate sources of energy, that are inexhaustible and/or renewable. Solar energy enters the scene here as it can fulfill the energy demands of society for many more centuries to come because it is abundantly available and free of cost. Hydrogen has a higher storage capacity than many other conventional fuels. There is a need for clean and eco-friendly energy sources as fossil fuel energy sources show adverse impacts on the environment also, whereas hydrogen is a clean energy source.

Hydrogen on combustion will produce water, which is a benign compound, and therefore it does not pollute our environment any more. Hydrogen has been very truly advocated as the fuel of the future and there is no doubt that it can fulfill the ever increasing requirement of energy and will replace the existing conventional fuels in the future. The use of hydrogen as a fuel for transportation and generation of electricity through fuel cells has been already established. Water covers almost three fourth of the Earth and if a method is developed to generate hydrogen gas from photosplitting of water, then it is welcome. Hydrogen produced from electrolysis of water is costly and does not help much because electricity is being used to decompose water. On the other hand, water is broken into hydrogen and oxygen by using solar energy as the source, which is freely and abundantly available.

Quantum Dots. DOI: https://doi.org/10.1016/B978-0-12-824153-0.00014-8
© 2023 Elsevier Inc. All rights reserved.

There are still some existing challenges in this direction, which should be overcome in order to improve efficiency, durability, and lower the cost. These are:

- Enhance absorption of sunlight and better catalysis on surface.
- Developing highly active and eco-friendly photocatalyst.
- Stability and durability for a longer time may be improved using protective surface coatings.
- Photocatalyst may be modified so that the higher recombination rate of photogeneration electron−hole pairs is lowered or completely checked.
- The costs of production of hydrogen should be lowered by using low-cost photocatalysts through lowering their processing costs.
- Quantum dots (QDs) have come to our rescue at this stage as these QDs have certain unique properties, such as larger surface area (high surface to volume ratio), quantum confinement effect, and shifting absorption wavelength in visible and near infrared regions.

14.2 Hydrogen production

Hydrogen has the potential to be a dependable renewable source of energy that can replace fossil fuels in the current energy crisis, because of its zero emissions and its enhanced energy content (Dahiya et al., 2020). In the few last years, the interest in producers of hydrogen gas production has increased with the growing human activity, because it is considered as a main fuel of the future, which is clean energy as it does not liberate any carbon dioxide during its combustion. It is also economic and very flexible in various applications compared to traditional energy sources such as fossil fuel or nuclear plant (Nemzer et al., 2003; Bičáková and Straka, 2010; Melo and Silva, 2011). Hydrogen gas is regarded as one of the common forms of renewable energy resources. It is produced in various ways with different sources like hydrocarbons, alcohol, or water, such as photodehydrogenation of methanol (Ahmed et al., 2016), electrochemical photolysis of water (Carey and Oliver, 1976), photolysis, sonolysis, and sonophotolysis of water (Penconi et al., 2015), and electrolysis of different materials that contain water, and it is used in photovoltaic solar energy (Slama, 2013).

The hydrogen gas was first liberated from the splitting of the water molecule by Fujishima and Honda (1972). They used an electrochemical cell and observed the hydrogen gas evaluation at the TiO_2 electrode, when the TiO_2 electrode surface was irradiated by light, generating an exciton, that is, a photoelectron (e^-)−photohole (h^+) pair. There is a key role played by this photoelectron (e^-)−photohole (h^+) pair in the redox reaction. This reaction occurs on the TiO_2 electrode surface and the photoelectron produces a proton

from water. This electron also reduced a proton at the Pt electrode surface to afford hydrogen gas (Eqs. 14.1–14.4):

$$TiO_2 + 2\,hv \rightarrow 2\,e^- + 2\,h^+ \tag{14.1}$$

$$2\,e^- + H_2O \rightarrow \frac{1}{2}O_2 + 2\,H^+ \tag{14.2}$$

$$2\,e^- + 2\,H^+ \rightarrow H_2 \tag{14.3}$$

Therefore, the overall reaction is:

$$2\,hv + H_2O \rightarrow \frac{1}{2}O_2 + H_2 \tag{14.4}$$

Wrighton et al. (1976) evolved hydrogen gas using an electrochemical cell that contains a Pt electrode and a Sb-SnO_2 single-crystal electrode, which was irradiated with ultraviolet light in an alkaline solution. Bockris et al. (1985) reported the possible routes of hydrogen production from the decomposition of water, such as electrolysis, plasmolysis, magnetolysis, biocatalysis, thermal method, use of light photolysis or photocatalyst, radiolysis, etc. However, the maximum purity for hydrogen produced was found to be 99.99% using the electrolysis method because it is one of the best methods and it is also regarded as a green method. The normal electrolysis of water uses direct current in two steps (Eqs. 14.5–14.6):

$$2\,H_2O \rightarrow \frac{1}{2}O_2 + 2\,H^+ + 2\,e^- \text{ at } E^o = 1.229\ (1.23)\ V \tag{14.5}$$

$$2\,e^- + 2\,H^+ \rightarrow H_2 \text{ at } E^o = 0.00\ V \tag{14.6}$$

14.2.1 Basic principle of overall water splitting

Over the years, there have been several proposals for water splitting. In the late 1970s, major attempts were made at photocatalytic water splitting (Fujishima and Honda, 1972; Bard, 1979; Van Damme and Hall, 1979; Domen et al., 1980; Kudo et al., 1988). The powdered semiconductor photocatalyst will be useful for the large-scale use of solar water splitting due to its simplicity (Jia et al., 2014). TiO_2 has been one of the most extensively researched photocatalysts for water splitting (Ma et al., 2014). Through water splitting, photon energy is transformed to chemical energy, with a largely positive change in Gibbs free energy $\left(\Delta G^o = 237\ kJ^{-1}\ mol\right)$ (Han et al., 2017). When a light is incident on a photocatalyst with energy larger than the bandgap, then electrons in the valance band (VB) are excited into the conductive band (CB) leaving holes in the valence band (Cao et al., 2017).

As the first step in the photocatalytic process, both excited electrons and holes are generated; which subsequently diffuse to the surface of the

semiconductor particles independently (Vaiano et al., 2018). Protons play a major role in hydrogen generation. Photogenerated electrons and holes promote redox processes that are comparable to electrolysis. Total water splitting into H_2 (reduced by the electrons) and O_2 (oxidized by the holes) on the photocatalyst surface can be achieved (Eqs. 14.7 and 14.8 and Fig. 14.1) (Liu et al., 2015; Qiao et al., 2020; Marschall, 2021).

$$H_2O + 2\,h^+ \rightarrow 2\,H^+ + \frac{1}{2}O_2 \tag{14.7}$$

$$2\,H^+ + 2\,e^- \rightarrow H_2 \tag{14.8}$$

Overall water splits into H_2 and O_2 (Eq. 14.9).

$$H_2O \rightarrow \frac{1}{2}O_2 + H_2 \tag{14.9}$$

The bandgap width and potentials of the conduction and valence bands of a semiconductor photocatalyst material are important. The bottom level of the CB must be located at a more negative potential than H^+/H_2 (0 V at pH 0), whereas the VB must be more positive than the O_2/H_2O energy level (1.23 V vs NHE). This indicates that the minimum photon energy thermodynamically necessary to cause photocatalytic water splitting is 1.23 eV (Strataki et al., 2007; Kudo and Miseki, 2009; Hisatomi et al., 2014; Peng et al., 2019; Niu et al., 2021).

A photocatalyst must fulfill these three requirements (Maeda et al., 2005; Hisatomi et al., 2014):

- it should have a bandgap smaller than 3 eV;
- it has stability during the photocatalytic process, and
- its band edge potentials are adequate for overall water splitting.

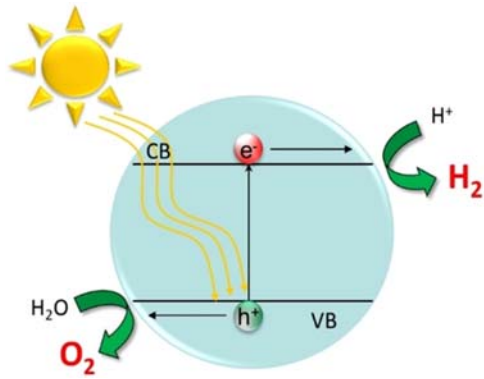

FIGURE 14.1 Schematic illustration of solar water splitting by using the photocatalyst. *Adapted from Marschall, R., 2021. 50 years of materials research for photocatalytic water splitting. Eur. J. Inorg. Chem. 2021(25), 2435–2441, with permission.*

The pure water splitting process exhibits a low efficiency because direct water splitting is still a difficult problem due to the inherent process drawbacks ($H_2 + O_2 = H_2O$) and it is a multistep process, in which four electrons are transferred. In addition, hydrogen is mostly created from fossil fuels such as natural gas, oil, and coal and only 2% is produced by water splitting (Miyoshi et al., 2018; Wang et al., 2018a; Fang et al., 2020; Dinda et al., 2020). Sacrificial reagents (as electron donors) are commonly used in water, such as alcohols (methanol, ethanol, and glycerol) to produce hydrogen efficiently by successfully scavenging photogenerated holes by suppressing back reaction, because O_2 is not evolved, and permitting a two-electron-transfer mechanism (Yang et al., 2013; Schneider and Bahnemann, 2013; Hisatomi et al., 2014).

Methanol is commonly employed as a sacrificial agent in photocatalysis for the evolution of H_2 from water under inert gas atmosphere, due to its strong reactivity, structural simplicity, and lack of C−C bonds (Cargnello et al., 2011). The water splitting reaction is a large uphill reaction with a ΔG° change. It is not an easy process compared to a reaction using a sacrificial agent (such as methanol), which is still an uphill reaction but less than that of water splitting. The energy change of sacrificial H_2 production is smaller than the energy change of water splitting. The use of sacrificial reagents leads to a significant decrease in ΔG° as it avoids the four-electron process of molecular oxygen formation. (Yasuda et al., 2018; Corredor et al., 2019) (Fig. 14.2).

Kawai and Sakata (1980) reported direct photocatalytic production of hydrogen from methanol and water over TiO_2-based catalysts, which produced H_2 and CO_2 from a mixture of H_2O/methanol (50:50 v/v %) after

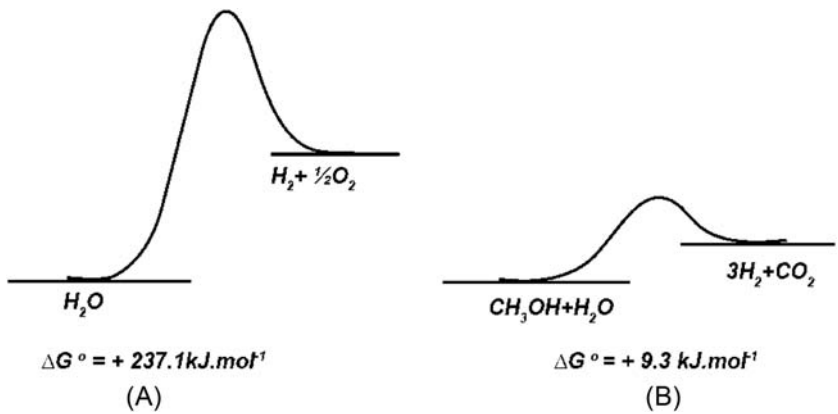

FIGURE 14.2 Comparison between H_2 production reaction: (A) from water splitting; and (B) from methanol. *Adapted from Yasuda, M., Matsumoto, T., Yamashita, T., 2018. Sacrificial hydrogen production over TiO_2-based photocatalysts: polyols, carboxylic acids, and saccharides. Renew. Sustain. Energy Rev. 81, 1627–1635, with permission.*

prolonged illumination. The absorption of photons from a light source with energy larger than the bandgap of the semiconductor photocatalyst promotes an electron from the VB of the semiconductor to the CB, generating an electron−hole pair. In this case, the photogenerated electrons are used to combine with protons in water to generate hydrogen (water reduction). The photogenerated holes are captured by sacrificial agents with a series of reactions (methanol oxidation) (Eqs. 14.10−14.14 and Fig. 14.3) (Wang et al., 2004; Puga, 2016; Huang et al., 2020; Zhao et al., 2020).

$$\text{Photocatalyst} \xrightarrow{hv} e^- + h^+ \tag{14.10}$$

$$CH_3OH + h^+ \rightarrow \cdot CH_2OH + H^+ \rightarrow HCHO + H \tag{14.11}$$

$$HCHO + H_2O + h^+ \rightarrow HCOOH + H_2 \tag{14.12}$$

$$HCOOH + h^+ \rightarrow CO_2 + H_2 \tag{14.13}$$

Overall process can be presented as Eq. (14.14).

$$CH_3OH + H_2O \xrightarrow{hv} CO_2 + 3H_2 \tag{14.14}$$

The reductive alkoxy radicals ($\bullet CH_2$-OH) are further oxidized to formaldehyde, formic acid, and carbon dioxide. The reductive alkoxy radicals $\bullet CH_2OH$ and $\bullet CO_2^-$ cannot react only with holes or hydroxyl radicals but also donate electrons to promote proton reduction to hydrogen, which is called the "doubling" effect. The same mechanisms are used for any other alcohol that carries a hydrogen atom on the carbon atom at the α-position of its OH group (Hainer et al., 2018). The by-products produced from methanol and other alcohols, such as formaldehyde, formic acid, and carbon dioxide, are also used as sacrificial agents for water splitting for hydrogen production

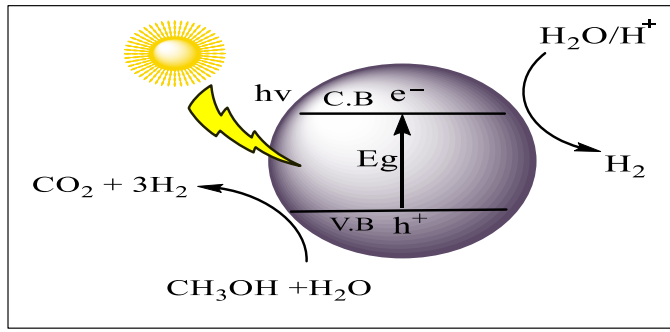

FIGURE 14.3 The photocatalytic hydrogen evolution process from aqueous methanol solution in the presence of inert gas (Kamat and Jin, 2018). *Adapted from Kamat, P.V., Jin, S., 2018. Semiconductor photocatalysis: tell us the complete story! ACS Energy Lett. 3, 622 − 623, with permission.*

(Bahruji et al., 2011; Coronado, 2013; Belhadj et al., 2017). The photocatalyst valence band potential has to be more positive than the sacrificial agent oxidation potential to oxidize such sacrificial agents (Luo et al., 2021).

Kumar et al. (2016) compared the activity for photocatalytic H_2 evolution under solar light irradiation in the presence of different scavengers. It was observed that hydrogen production was enhanced by using several organics such as ethylene glycol, because of the position of its oxidation potential with respect to the valence band potential of titania, and the generation of hydrogen was also found to be increased on increasing the polarity of alcohol. The photooxidation route of methanol depends on the molecular species adsorbed on the photocatalytic surface (Crampton et al., 2017). The carrier recombination rate was decreased after the traps of the hole by methanol on the catalytic surface; thus promoting the separation of electron−hole pairs (Chen et al., 2018).

Jitputti et al. (2008) have reported the photocatalytic evolution of H_2 from the water-splitting process using methanol as a sacrificial reagent in the presence of TiO_2 nanowires. The photogenerated holes or photogenerated oxygen are swiftly removed in an irreversible fashion, inhibiting mutual electron−hole recombination. Here, sacrificial reagents might compete with water in the reduction reaction. Fang et al. (2020) found that water was not the major source of hydrogen production in the photocatalytic process at Rh-loaded TiO_2 in the presence of sacrificial methanol at room temperature. It was found that the contribution of methanol decomposition ($\sim$60%) contributed even more than water splitting ($\sim$40%) because protons produced from both oxidation of methanol and ionization of water may be converted into hydrogen. In contrast, hydrogen generation was predominantly from water based on the combination of thermal and light energy over Rh-loading TiO_2.

Camacho et al. (2018) concluded that hydrogen production via water splitting is practically null compared to when methanol was added. It was revealed that the quantity of hydrogen produced increases with the increasing concentration of methanol. They could achieve the highest quantum efficiency under solar radiation of 7.7%. Gultom et al. (2017) reported that the highest activity could be achieved in 50% ethanol solution in the presence of ZnOS-10 with a hydrogen production rate of 14,800 $\mu mol\ g^{-1}\ h^{-1}$ and an apparent quantum yield (QY) of 31.5%. The QY and apparent quantum yield (AQY) are calculated by Eqs. (14.15 and 14.16), respectively, which define the stability and process efficiency of the photocatalytic system (Fukuzumi et al., 2018; Meng et al., 2020).

$$\text{QY}\ (\%) = \frac{\text{Number of reacted electrons}}{\text{Number of absorbed photons}} \times 100 \tag{14.15}$$

$$\text{AQY}\ (\%) = \frac{(\text{Number of photohydrogen molecules}) \times 2}{\text{Number of incident photons}} \times 100 \tag{14.16}$$

14.2.2 Photoelectrochemical cells

Photoelectrochemical (PEC) cells are one of the most efficient methods for converting solar energy into hydrogen (Landman et al., 2020). It was discovered that clean H_2 energy can be obtained by splitting water through a PEC cell using a TiO_2 photoanode. A typical PEC system consists of three electrodes:

- working electrode (photoanode);
- counter electrode (photocathode), for example, Pt or semiconductor, and
- reference electrode.

The typical PEC systems use photocatalysts [nanoparticles (NPs)] as photoelectrodes (such as TiO_2, ZnO, CdSe, CdS) (Gunasekaran et al., 2021). The electrodes are immersed in an aqueous electrolyte (Crespo-Quesada and Reisner, 2017). When a photoanode (semiconductor) comes in contact with an electrolyte, the Fermi energy level rises above the potential of electrocatalytic water splitting, which results in an upward band bending contact of a photocathode semiconductor with electrolyte. On the other hand, a downward band bending is present (Kibria et al., 2014; Guijarro et al., 2015). The difference in the electrochemical potential between the semiconductor electrode and the electrolyte causes a charge transfer process at the solid/liquid interface, resulting in an electric current flowing through the junction until an electronic equilibrium is reached (Jiang et al., 2017; Xiao and Liu, 2018).

The QDs having unique confined optical and electronic properties are applied to sensitize large bandgap photoanode materials (Zamiri and Bagheri, 2018). On irradiating the photoanode in the PEC cell, hydrogen is generated (Fig. 14.4) (Chen et al., 2016a).

They found that when photons are absorbed with an energy larger than their bandgap, the photoelectrons are excited and migrate into the unoccupied conduction band (CB) and holes are left in the valence band (VB) (exciton, i.e., electron−hole pairs generation). The exciton is separated by the built-in electric field, when photoexcited charge carriers have a longer lifetime and larger diffusion distance (Molaei, 2020), which leads to the higher process efficiencies due to easy separation and transport of the carriers (Xiao et al., 2019). Photoexcited electrons are swept toward the counter electrode through the back contact and an outside circuit, while the remaining holes participate in the oxidation reaction. In a PEC cell, electron−hole pairs produced by incident photons drive reduction−oxidation (redox) processes (Phang and Tan, 2019), in which holes oxidize the water/hole scavenger (HS) at the anode surface, while electrons travel to the counter electrode to reduce water and produce H_2 gas (Sahai et al., 2017).

The properties of the photoelectrode strongly influence the PEC efficiency of water splitting. An ideal photoelectrode should fulfill the following conditions:

- small bandgap for visible light absorption;

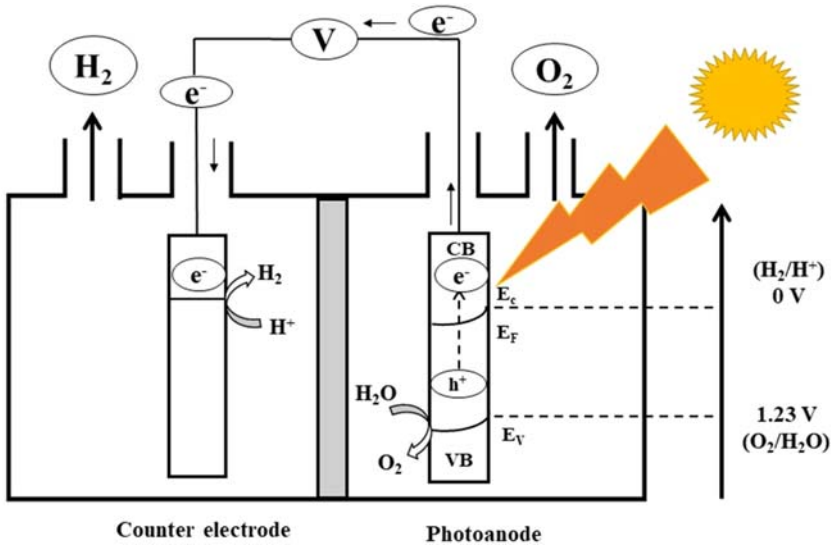

FIGURE 14.4 The basic principles of water splitting for a photoelectrochemical cell. E_F, Fermi level.

- photoelectrodes must be corrosion-resistant and chemically stable in aqueous solutions; under both conditions; dark and illumination;
- photogenerated charge separation ($e^- - h^+$) should be efficient; and
- the CB position of the semiconductor should be more negative than the (H^+/H_2) potential, and the VB should be more positive than the (O_2/H_2O) potential (1.23 V vs NHE) (Tamirat et al., 2016; Batubara and Zulys, 2019). It is shown in Fig. 14.5.

Semiconductor types, charge separation, transfer efficiency, crystal phases, and morphologies determine the efficiency for hydrogen production.

14.3 Metal-based quantum dots

14.3.1 Metals

Ye et al. (2012) prepared vertically oriented TiO_2 nanotube arrays (TNTAs) by a three-step electrochemical anodization technique. Then Pd QDs were prepared with uniform size and narrow size distribution on TiO_2 nanotubes by a modified hydrothermal method. It was reported that a high photocatalytic hydrogen production rate (592 $\mu mol\, h^{-1}\, cm^{-2}$) could be achieved with Pd@TNTAS. Chen et al. (2016b) prepared Ag QDs/g-C_3N_4 (Ag QDs/g-C_3N_4) photocatalysts via a novel one-step method using $AgNO_3$ and urea as precursors. As-composed Ag QDs with an average diameter of about 5 nm were found to be uniformly dispersed on the surface of g-C_3N_4 nanosheets.

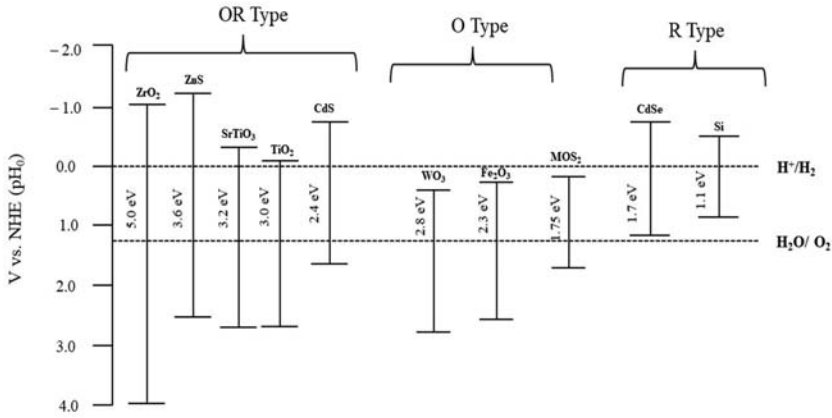

FIGURE 14.5 The band edge position and bandgaps for different semiconductors (OR, O, and R types). *OR*, oxidation and reduction; *O*, oxidation; *R*, reduction.

They used methanol as a sacrificial reagent. It was reported that as-prepared Ag QDs/g-C_3N_4 photocatalysts (0.5%) exhibited almost 4.6 times higher photoactivity for hydrogen production.

Kuang et al. (2016) embedded Au QDs in rimous cadmium sulfide nanospheres to synthesize hybrid photocatalyst via a simple hydrothermal process, which was followed by photoreduction. As rimous cadmium sulfide nanospheres had a rough surface and irregular fissures, these will strengthen their interaction and adhesion with Au QDs. It was revealed that the highest photocatalytic activity obtained for hydrogen generation was 601.2 $\mu mol\ h^{-1}\ g^{-1}$ by adjusting the Au loading. The synthesis of bimetallic (NiFe) quantum dot based electrocatalysts has been reported by Cirone et al. (2021). They optimized Ni:Fe ratio to tune QDs for increased electrochemical catalytic activity. The optimal compositions of these bimetallic QD based electrocatalysts was found to be 25.3% and 54.9% towards the hydrogen evolution reaction (HER) and oxygen evolution reaction (OER), respectively.

14.3.2 Oxides

Yang et al. (2009) have made use of N-doped ZnO concentrating on its PEC performance. The nitrogen has been commonly employed as a dopant to modify the electronic structures of metal oxide semiconductors as it resembles oxygen in size and low formation energy is required to replace oxygen (Zong et al., 2013). ZnO QDs dispersed in HS matrix were prepared by Xu et al. (2016). The HS contains S^{2-} and SO_3^{2-} groups. It was reported that as-synthesized ZnO QDs were hybridized with HS groups forming a stable ZnO QDs/HS hybrid hydrosol. This composite could produce H_2 with

a high rate of 260 μmol h^{-1} g^{-1}, which is almost 48-fold higher than for pure ZnO QDs.

Xie et al. (2017) decorated $BiVO_4$ QDs on the surface of screw-like SnO_2 nanostructures. They used the ionic layer absorption method for this purpose. It was revealed that the bandgap of $BiVO_4$ increases from 2.4 to 2.6 eV, when the particle size was decreased to about 5 nm. It was revealed that incident photon to current conversion efficiency was also increased up to 13.47%. It was reported that the rate of H_2 generation from splitting of water was 1.16 μmol h^{-1} cm^{-2} over $BiVO_4$ quantum dot/screw-like SnO_2 nanostructures in the presence of visible light. Liu et al. (2018) reported the synthesis of Co_3O_4 QDs TiO_2 nanobelts (NBs) hybrids via a facile hydrothermal method. They could obtain simultaneous production of H_2 and O_2 from pure water in the presence of light with high evolution rates of 22.0 and 41.8 μmol h^{-1} g^{-1}, respectively. It was observed that these production rates were higher compared to Co_3O_4 and TiO_2 NBs. The size of Co_3O_4 QDs was found to be ~3 nm, which not only improved the light sensitivity but also promoted the transfer of electrons from TiO_2 to Co_3O_4 QDs and as a result, H_2 generation was also enhanced.

Qian et al. (2018) reported the synthesis of p-type CuO/n-type CeO_2 heterojunction in situ grown on graphene. It was revealed that the H_2 evolution rate of the CeO_2−CuO QDs/graphene could reach 2481 μmol h^{-1} g^{-1} and remained unaffected for four consecutive hydrogen production cycles. The protonated graphitic carbon nitride (p-C_3N_4) loaded with IrO_2 QDs was fabricated by Wang and Li (2018) via a hydrothermal approach. It was found that IrO_2 QDs had an average diameter of approx 2 nm and these were highly dispersed and anchored on surfaces of p-C_3N_4. It was reported that as-prepared IrO_2/C_3N_4−0.6 wt.% photocatalyst could produce hydrogen and oxygen at a rate of 45 and 20 μmol h^{-1}, respectively.

Zhang et al. (2018a) constructed novel SnO_2 QDs modified TiO_2 nanorod arrays (NAs) by calcining $SnCl_2$-adsorbed on TiO_2 NAs. It was reported that photocurrent density of SnO_2 QDs/TiO_2 NAs was five times higher than that obtained with only TiO_2 NAs. It was also revealed that SnO_2 QDs/TiO_2 NAs exhibited a high photoelectrocatalytic activity for overall water splitting affording O_2 and H_2 at the rate of 11.87 and 27.85 μmol cm^{-2} h^{-1}, respectively. Such an excellent performance of water splitting may be due to its Z-scheme heterostructure. They also developed an effective strategy by distributing $BiVO_4$ QDs on nano tin oxide (Zhang et al., 2018a,b). They also used carbon QDs (CQDs) to enhance charge transfer and electrocatalytic properties at the $BiVO_4$-SnO_2 interface. It was observed that this composite afforded a hydrogen generation rate of 0.54 μmol h^{-1} without using any bias.

The dodecahedral nitrogen-doped carbon-coated CuO-In_2O_3 p−n heterojunction (DNCPH) was fabricated by Sun et al. (2019). As-prepared composite exhibited an excellent photocatalytic production efficiency of H_2. It was

revealed that improved separation efficiency of excitons (photogenerated electron/hole pairs) and coated N-doped C layer with CuO-In_2O_3 p−n heterojunction was responsible for enhanced photocatalytic hydrogen production efficiency of DNCPH. Reddy et al. (2020) prepared functionalized carbon nanotubes−titania QDs (FCNT-TQDs) and used them as photocatalysts in the presence of sunlight for hydrogen production. It was reported that the photocatalyst synthesized may be tuned by the addition of copper to achieve a highest hydrogen production rate up to 54.4 mmol $h^{-1}g^{-1}$, which was about 5.4 and 25 times higher than that obtained on using FCNT-TQDs composite and pristine TiO_2 QDs, respectively.

14.3.3 Metal sulfides

Although bulk CdSe produces H_2 from water under visible light irradiation, CdSe-nanoribbons were able to generate hydrogen from aqueous sodium sulfite/sulfide solution with a quantum efficiency (9.2%) at 440 nm (Frame and Osterloh, 2010). It was observed that ultrasonication and exfoliation of bulk MoS_2 can produce MoS_2 nanoplates. When the CdSe nanoribbons are chemically linked to these nanoplates, the activity was found to increase about four times. CdS quantum dot coupled graphitic carbon nitride photocatalysts were synthesized by Ge et al. (2012) through chemical impregnation. The effect of CdS content was observed on the rate of photocatalytic hydrogen evolution under visible light irradiation using platinum as a cocatalyst in aqueous solutions of methanol. It was revealed that the optimal CdS QD content was 30 wt.%, where H_2 evolution rate could reach 17.27 μmol h^{-1} in the presence of visible light, and it was about nine times more than that with pure g-C_3N_4.

The oil refineries are venting off almost 15%−20% H_2S and hardly 5% of it is utilized to produce sulfur and water. Apte et al. (2012) investigated a novel Q-CdS (highly monodispersed) germanate glass nanocomposite. The size of CdS QDs varied between 4−14 nm. A high rate of evolution of H_2 (3780 μmol h^{-1}) was obtained. It was also observed that as-prepared catalyst was stable and it can be also regenerated easily as compared to other catalysts. This glass nanocomposite also exhibited rapid methylene blue degradation in the presence of visible light. It was suggested that such orthorhombic QD−CdS−glass nanocomposites can find potential applications in LED, solar cells, and other optoelectronic devices.

Cao et al. (2013) grew well dispersed CdS QDs on g-C_3N_4 nanosheets via a solvothermal method. They used dimethyl sulfoxide. It was observed that as-prepared CdS−C_3N_4 nanocomposites exhibited an excellent efficiency for photocatalytic hydrogen evolution in the presence of visible light as compared to pure g-C_3N_4. It was revealed that composite with 2 wt.% CdS showed a higher hydrogen evolution rate (4.494 mmol h^{-1} g^{-1}), which is about 115 times more than that obtained with pure g-C_3N_4. Schweinberger et al. (2013)

synthesized Pt clusters of various sizes and embedded these on CdS quantum rods. They reported that the size of the Pt cluster had a significant impact on photocatalytic effectiveness. The highest efficiency could be achieved by a Pt cluster comprising Pt_{46}.

Li et al. (2014) decorated $ZnIn_2S_4$ microspheres (ZIS MSs) with CQDs as well as platinum NPs (dual cocatalysts). It was observed that ZIS MSs coloaded with Pt and CQDs exhibited a high photocatalytic production rate of H_2 of 1032.2 $\mu mol\ h^{-1}\ g^{-1}$ in triethanolamine aqueous solution in the presence of visible light, which was much higher compared to pure ZIS, CQDs-decorated ZIS, and Pt-loaded ZIS. The CdS QDs supported on two oxides (Ga_2O_3 and In_2O_3) were prepared by Pan et al. (2014) and used for the evolution of H_2 from aqueous solutions containing lactic acid under visible light. It was observed that H_2 evolution rates on CdS/Pt/In_2O_3 and CdS/Pt/Ga_2O_3 were 1032.2 and 995.8 $\mu mol\ h^{-1}$, respectively. These rates of H_2 evaluation were much higher compared to Pt/CdS (108.09 $\mu mol\ h^{-1}$), Pt/In_2O_3 (0.05 $\mu mol\ h^{-1}$), and Pt/Ga_2O_3 (0.12 $\mu mol\ h^{-1}$). It was suggested that the surface properties of the metal oxides played two important roles:

- anchoring of CdS QDs and Pt NPs; and
- efficient trapping of photogenerated electrons.

Wang et al. (2014) reported a photocatalyst, nickel-hybrid CdS QDs (Ni_h-CdS QDs), which was prepared in situ from nickel salts and CdS QDs. They used 3-mercaptopropionic acid as a stabilizer. It was found that 403.2 μmol of H_2 was obtained with a high evolution rate of 74.6 $\mu mol\ h^{-1}\ mg^{-1}$ under visible light irradiation for 20 h as compared to MPA-CdS QDs (mercaptopropionic-acid-stabilized CdS QDs). Cu_2S QDs coupled three-dimensional flower-like hierarchical BiOBr (Cu_2S QDs/BiOBr) were prepared by Wang et al. (2015) via a precipitation method. It was observed that Cu_2S QDs had an average diameter of 10 nm and these were uniformly attached on the surface of BiOBr. It was reported that as-prepared Cu_2SQDs/BiOBr composite exhibited higher water splitting and they could obtain 717 $\mu mol\ g^{-1}$ of H_2 with 3 wt.% Cu_2SQDs/BiOBr containing 1 wt.% Pt. This rate was about 3.1 times higher as compared to only Cu_2S NPs.

Yue et al. (2016) synthesized CdTe/CdS QDs using sulfur tolerant $[Mo_3S_{13}]^{2-}$ nanoclusters, which exhibited much better photocorrosion resistance than regular CdTe QDs for photocatalytic hydrogen generation. The sulfur compound covered CdTe/CdS QDs. It was observed that as-prepared composite exhibited higher visible light photocatalytic H_2 generation compared to CdTe QDs with cocatalyst Pt. A novel CdS/ZnO heterojunction was fabricated by Ma et al. (2017), which is composed of zero-dimensional CdS QDs and two-dimensional ZnO nanosheets (NSs). It was reported that as-obtained CdS/ZnO 0D/2D heterostructures exhibited excellent photocatalytic activity for the evolution of hydrogen from water splitting in comparison

with other CdS/ZnO heterostructures with different combinations (0D/3D, 2D/2D, and 3D/0D). It was observed that out of these, CdS/ZnO-12 (12 deposition cycles of CdS QDs) exhibited the highest evolution rate of hydrogen of 22.12 mmol g^{-1} h^{-1}, which was about 13 and 138 times higher than produced with single CdS (1.68 mmol g^{-1} h^{-1}) and ZnO (0.16 mmol g^{-1} h^{-1}), respectively. It was revealed that as-prepared CdS/ZnO-12 exhibited excellent stability without any significant loss for five cycles in 25 h.

A vertical self-assembly of ultrathin $CdIn_2S_4$ nanosheet arrays on the reduced graphene oxide (rGO) has been prepared by Xue et al. (2017) via a facile hydrothermal method. Here, ZnS QDs were in situ deposited on $CdIn_2S_4$ nanosheet arrays. It was reported that as-prepared 3D nanosheet arrays architecture with GO (13 wt.%) exhibited the optimum, highest hydrogen generation of 6.82 mmol g^{-1} h^{-1} corresponding to the photocurrent transient response (107.4 μA cm^{-2}). An inverse structure of $Cd_{0.5}Zn_{0.5}S$ QDs was reported by Zhou et al. (2017) loaded onto the onion-like carbon (OLC) matrix. It was observed that as-prepared $Cd_{0.5}Zn_{0.5}S$ QDs with average diameter of 6.9 nm were uniformly distributed on an OLC (30 nm) matrix. An optimum rate of H_2 generation, 58.6 and 2018 μmol h^{-1} g^{-1}, could be achieved on irradiation of visible light and 58.6 μmol h^{-1} g^{-1} under the irradiation of (550−900 nm), respectively using $Cd_{0.5}Zn_{0.5}S$/OLC composite samples. Such a reverse construction using hydrogen has a great potential for noble metal-free solar production of hydrogen.

Kitazono et al. (2017) photodeposited CdSe on a CdS-preloaded mesoporous TiO_2 nanocrystalline film. As a result, CdS(core)−CdSe(shell) QDs (CdS@CdSe/mp-TiO_2) were obtained with a heteroepitaxial nanojunction. They fabricated quantum-dot-sensitized PEC (QD-SPEC) cells with photoanode | 0.25 M Na_2S, 0.35 M Na_2SO_3 (in water)| cathode. It was observed that a CdS@CdSe QD-SPEC cell could achieve solar-to-current efficiency (STCE) of 0.03% under simulated sunlight (AM 1.5, one sol). An increase in STCE up to 0.048 was obtained on application of 0.1 V between the electrodes, far surpassing the CdSe/mp-TiO_2 and CdS/mp-TiO_2 photoanode cells. A WS_2/graphitic carbon nitride (CN) (2D/2D) nanosheet heterostructure was decorated with CdS QDs by Zou et al. (2018). It was observed that optimized CdS/WS_2/CN exhibited an excellent photocatalytic H_2 evolution rate of 1174.5 μmol h^{-1} g^{-1} without using any cocatalyst, which was about 67 times higher than for pure CN nanosheets. It was also revealed that CdS/WS_2/CN photocatalyst showed excellent stability as well as reusability without any significant loss role in photocatalytic H_2 evolution within four cycles in 20 h.

Hao et al. (2018) synthesized Bi_2WO_6 QDs decorated g-C_3N_4 nanoplates through a one-step hydrothermal method. The size of Bi_2WO_6 QDs was found to be about 3.5 nm. It was reported that a Bi_2WO_6 QDs/g-C_3N_4 Z-scheme not only increased the separation efficiency of charge, but it also enhanced the ability of PEC water splitting. Thick-shell CdSe/$CdSe_xS_{1-x}$/CdS QDs were synthesized by Zhao et al. (2018) with a pyramidal shape.

It was reported that these exhibited a QY of ~15%. As-prepared pyramidal QDs were then applied as light absorbers in a PEC system, leading to a saturated photocurrent density of ~12 mA cm^{-2}, which could provide an H_2 generation rate of 90 mL cm^{-2} day^{-1}.

Wang et al. (2018b) decorated TiO_2 nanotube arrays (TiO_2 NTAs) with MoS_2 QDs by an electrodeposition method. It was reported that as-prepared MoS_2 QDs/TiO_2 NTAs exhibited an increased photocatalytic activity compared to pristine TiO_2 NTAs for H_2 evolution in the presence of sunlight. They did not use any sacrificial agents or cocatalysts. The optimal H_2 evolution rates were observed to be 31.36, 5.29, and 1.67 μmol cm^{-2} h^{-1} in the presence of UV, visible, and near-infrared illumination, respectively. Such an enhanced photocatalytic activity may be due to decreased bandgap energy and surface plasmonic properties, which increased absorption capacity for visible and near-infrared light. Xue et al. (2018) fabricated high-density NiS_x QDs as a highly efficient cocatalyst on the surface of $Cd_{0.8}Zn_{0.2}S$/rGO nanosheet composites. It was reported that a two-dimensional (2D) $Cd_{0.8}Zn_{0.2}S$/rGO nanohybrid system with 2 wt.% NiSx loading could achieve H_2 evolution rate of 7.84 mmol g^{-1} h^{-1} under visible light irradiation, which is almost 1.4 times higher as compared to Pt/$Cd_{0.8}Zn_{0.2}S$/rGO.

The Se-doped CdS QDs with different Se doping levels were prepared via a solvothermal procedure (Shi et al., 2019). It was reported that photocatalytic performance of as-prepared $CdS_{0.9}Se_{0.1}$ QDs (without any cocatalysts) was enhanced to give a hydrogen evolution rate of 29.12 mmol h^{-1} g^{-1} under simulated solar irradiation, which was about 23.5 times higher as compared to CdS QDs. Yang et al. (2019) prepared a series of Zn−$AgIn_5S_8$/g-C_3N_4 (0D/2D) nanocomposites by growth (in situ) of the Zn−$AgIn_5S_8$ QDs (QDs) on g-C_3N_4 nanosheets. It was reported that the hydrogen production rate with Zn−$AgIn_5S_8$/g-C_3N_4 nanocomposites was found to be optimum, when the mass ratio of g-C_3N_4 was kept at 10%, which was 1.39, about 138.6 times higher than pure Zn−$AgIn_5S_8$ QDs and g-C_3N_4, respectively. It was also revealed that as-prepared Zn−$AgIn_5S_8$/g-C_3N_4 nanocomposites exhibited good cycle stability.

Yu et al. (2019) used Ag_2S QDs as both photocatalysts and electrocatalysts. It was observed that H_2 production rate could reach 858 μmol h^{-1} g_{catal}^{-1} under 100 mW cm^{-2}. Zheng et al. (2019) synthesized a p-n heterojunction photocatalyst for splitting of water. They incorporated p-type $CuInS_2$ QDs into n-type polymeric carbon nitride (CN) via a self-assembly and calcination method. It was reported that hydrogen evolution rate of $CuInS_2$/CN hybrid was two-fold more than that with pristine CN. A metal−organic framework (MOF)-derived synthesis was reported by Shi et al. (2020). They could obtain a controlled mixed-phase (rutile and anatase) of TiO_2 NPs, retaining MOF crystal morphology. It was observed that MOF-derived TiO_2 film, which was sensitized by core−shell CdSe@CdS QDs, exhibited an higher PEC device stability of +42.1% with PEC performance as +47.6%. It was suggested that

this protocol can improve the efficiency of the PEC system based on TiO_2-QDs heterojunction for hydrogen generation.

Chen et al. (2019) prepared ZnCdS QDs. It was reported that the photocatalytic H_2 production activity of as-prepared QDs can be optimized by adjusting their quantum sizes. It was revealed that maximum H_2 production rate of 3.70 mmol h^{-1} g^{-1} could be obtained with it, without using noble metal cocatalysts in the presence of visible light, which was much better than that of ZnCdS and ZnCdS-based catalysts. Miodyńska et al. (2020) increased the photoactivity of urchin-like rutile particles by decorating these with pristine as well as Er- or Yb-doped Bi_2S_3 QDs. They varied doping degrees (1−15 mol%), and QDs loadings (1−20 wt.%), and the best hydrogen evolution performance could be achieved with Er and Yb contents of 10 mol%. It was observed that hydrogen productivity of 1576.7 μmol g_{cat}^{-1} could be achieved for TiO_2 decorated by 10 mol% Yb-doped Bi_2S_3 QDs after 20 h irradiation. Su et al. (2020) reported that nickel in zinc blende cadmium−zinc sulfide QDs is an efficient and stable photocatalyst for splitting of water under sunlight. It was observed that finely tuned Ni atoms dispersed in these QDs exhibited H_2 production activity of 18.87 mmol h^{-1} g^{-1}.

14.3.4 Others

Chen et al. (2010) studied the utilization of CdTe quantum-dot-sensitized ZnO:nanowire arrays for water splitting. It was reported that photocurrent and stability was significantly improved. It was also revealed that the addition of nitrogen alters the electronic state, which improves the ability for water splitting. CoP QDs embedded in S,N-codoped graphite carbon (CoP@SNC) were reported by Meng et al. (2018). They used organophosphoric acid as a precursor of both phosphorus and carbon. Benefiting from the strong coupling and synergistic effect between CoP QDs and highly conductive S,N-codoped carbon, well-structured porosity and high specific surface area. It was observed that as-synthesized CoP@SNC exhibited excellent activities for HER, OER, and oxygen reduction reaction (ORR). It acts as a trifunctional electrocatalyst for overall splitting of water.

Zhu et al. (2018) loaded black phosphorus QDs (BP QDs) on MXene nanosheets. It was revealed that as-prepared BP QDs/MXene nanohybrids can serve as a bifunctional electrocatalyst in producing both hydrogen and oxygen. It was observed that a current density of 10 mA cm^{-2} was reached at a potential of only 1.78 V on using BP QDs/MXene nanohybrids cathode and anode in a full cell for overall water splitting. A composite consisting of CdSe QDs and indium-doped $BaTiO_3$ was synthesized by Zhong et al. (2019). The optimal load ratio of CdSe QDs with 2.5% indium (7.5 mol.%) was found to increase the production of hydrogen (0.437 mmol g^{-1} h^{-1}) as compared to undoped composite (0.258 mmol g^{-1} h^{-1}).

The $BiVO_4@ZnIn_2S_4/Ti_3C_2$ MXene QDs assembly (photocatalyst) was fabricated by Du et al. (2020). It was observed that $BiVO_4@ZnIn_2S_4/Ti_3C_2$ MXene QDs could achieve effective splitting of water into H_2 and O_2 in the presence of visible light with rates of 102.67 and 50.83 $\mu mol\ g^{-1}\ h^{-1}$, respectively. Yan and Jin (2021) derived NiP_2 QDs (n-type) in situ from the three-dimensional nanoflower NiAl-LDH. They also constructed n-type p-n heterojunction by coupling NiP_2 QDs and Cu_3P NPs (p-type) for hydrogen generation.

14.4 Carbon and graphene-based quantum dots

Yu et al. (2013) used an impregnation method to prepare graphene quantum dots (GQDs) anchored inside inversely structured TiO_2 nanotubes-array (TiO_2-NA) and CdS-modified TiO_2 nanotubes-array (CdS/TiO_2-NA). It was observed that the hydrogen evolution rate was greatly increased on loading GQDs into TiO_2-NA and CdS/TiO_2-NA. It was revealed that the light-filtering effect of graphene was inhibited as compared to graphene sheets, when graphene is broken into GQDs. However, the morphology of TiO_2 the nanotube array was still maintained even when anchoring GQDs inside, which favored mass transfer.

Nitrogen-doped graphene oxide QDs were prepared by Yeh et al. (2014). As-prepared catalyst samples exhibited both p- and n-type conductivities and overall water-splitting under visible light. It was reported that QDs contain p-n type photochemical diodes and active sites for O_2 and H_2 evolution were n- and p-domains, respectively. It was also revealed that this reaction mimics biological photosynthesis. Martindale et al. (2015) produced CQDs, as a homogeneous photocatalytic system with a Ni-bis(diphosphine) catalyst. It was observed that it could produce hydrogen at a rate of 398 $\mu mol\ (g_{CQD})^{-1}\ h^{-1}$. It was revealed that these CQDs exhibited activity in the visible region and maintained their photocatalytic activity for a day. Qu et al. (2015) prepared S,N-GQDs by doping GQDs with heteroatoms (S, N). It might be utilized as a sensitizer in photocatalytic processes. It was observed that loading of S,N-GQDs onto TiO_2 nanocrystals resulted in the generation of H_2 through splitting of water. They revealed that the H_2 generation rate was about 4.3 $mol\ h^{-1}$ under visible light.

CQDs were deposited by Li et al. (2016) onto graphite-like carbon nitride nanosheets (CNNS) to afford CNNS/CQDs composites. It was found that as-prepared CNNS/CQDs composites exhibited a much higher photocatalytic hydrogen production rate (116.1 $\mu mol\ h^{-1}$) under visible light irradiation, which was almost three times higher than with pure CNNS (37.8 $\mu mol\ h^{-1}$). The photoanodes were fabricated by Shi et al. (2016) consisting of WO_3 nanoflakes decorated with CQDs via seed-mediated solvothermal method and impregnation-assembling. It was revealed that the photocurrent density of 1.46 $mA\ cm^{-2}$ at 1.0 V versus Ag/AgCl could be achieved for CQDs/

WO_3 electrode, which was almost more than double as compared to only the WO_3 electrode. Such an enhancement was due to the increased light harvesting ability of CQDs and rapid charge transfer across the interface between the electrolyte and CQDs/WO_3 electrode.

Sulfur-doped graphene oxide QDs (S-GOQDs) were synthesized by Gliniak et al. (2017). They observed efficient photocatalytic hydrogen generation under direct sunlight irradiation. The doping of S atoms into the GOQDs was confirmed. They could achieve an initial rate of 18,166 and 30,519 $\mu mol\ h^{-1}\ g^{-1}$ in pure water and in 80% ethanol aqueous solution, respectively. Yan et al. (2017) prepared nitrogen-doped graphene QDs (NGQDs)-$ZnNb_2O_6$/g-C_3N_4 heterostructures and used them as hydrogen evolving catalysts. It was reported that as-prepared NGQDs-$ZnNb_2O_6$/g-C_3N_4 heterostructures could achieve a higher hydrogen evolution rate of 340.9 $\mu mol\ h^{-1}\ g^{-1}$, when the mole ratio Zn/gC_3N_4 and NGQDs were kept at 1:7 and 5%, respectively.

Pan et al. (2018) prepared CQDs modified porous g-C_3N_4/TiO_2 two-dimensional (2D) nanoheterojunctions. The TiO_2 NPs were introduced via a hydrothermal method while CQDs were successively introduced on the surface of the porous g-C_3N_4 and TiO_2 by coupling. It was observed that hydrogen production using these 2D nanoheterojunctions was almost double that obtained with unmodified samples. The cobalt carbide (Co_2C) was prepared by Guo et al. (2018). A combination of colloidal QDs/Co_2C can produce hydrogen at the rate of $\sim$18,000 $\mu mol\ g^{-1}\ h^{-1}$, which was about 10 times more than that of bare QDs under similar conditions.

Wang and Li (2018) and Wang et al. (2018a,b) reported that the coloading of graphene QDs and PdS on ZnCdS surface as cocatalysts can increase the efficiency of photocatalytic evolution of H_2 in the presence of visible light. This photocatalyst (GQDs/ZnCdS/PdS) was prepared by two steps: (1) hydrothermal coupling of GQDs on ZnCdS surface, and (2) an in situ chemical deposition of PdS. It was reported that as-prepared GQDs/ZnCdS/PdS exhibited an H_2 evolution rate of 517 $\mu mol\ h^{-1}$, which is about 15, 1.7, and 7 times higher as compared to ZnCdS, ZnCdS/PdS, and GQDs/ZnCdS respectively. This photocatalyst has a good stability. Enhancement of photocatalytic activity was attributed to coloading of the GQDs (reduction) and PdS (oxidation) as respective cocatalysts.

A facile method has been reported by Liu et al. (2019) to prepare efficient and robust Ru-M (M = Mn, Ni, Cu) bimetallic NPs and carbon quantum dot hybrid (RuM/CQDs). It was observed that RuNi/CQDs catalysts exhibited an excellent HER performance in all pH ranges. It was revealed that Ni doping resulted in a weakening of the hydrogen bonding energy of close surface Ru atoms, which played an important role in enhancing the HER activity. Zhang et al. (2019) reported that a dendrite-like plasmonic bimetal (CuNi) can be used as a photocatalyst, which is nonsemiconducting in nature. It produced electrons for photocatalytic splitting of water to

generate hydrogen, but when such a bimetal is supported by a catalyst like CQDs, then the photocatalytic water splitting rate was found to be highest at 55.19 μmol g^{-1} h^{-1}. The content of CQDs in the photocatalyst was kept at 3 wt.% for optimum conditions. It was reported that this photocatalyst was stable for four cycles over 20 h.

The B-doped g-C_3N_4 QDs (BCNQDs) were prepared by Wang et al. (2013) via a facile molten salt method. They used melamine and boron oxide as the precursors. The BCNQDs were introduced onto the surface of g-C_3N_4, via hydrothermal treatment and as a result a g-C_3N_4/BCNQDs heterojunction was constructed. As-prepared g-C_3N_4/BCNQDs heterojunction exhibited excellent hydrogen evolution performance for water splitting in the presence of visible light irradiation. *Bombyx mori* silk, a natural nitrogen-rich biopolymer protein, is earth-abundant and sustainable. Wang et al. (2020) derived nitrogen-doped CQDs (N-CQDs) from *Bombyx mori* silk fibroin and then immobilized them onto TiO_2 nanotube arrays (TiO_2 NTAs) using a hydrothermal approach. As-prepared N-CQDs decorated TiO_2 NTA heterostructures (N-CQDs@TiO_2 NTAs) could split water into H_2 and O_2 with production rates of 30.12 and 14.96 μmol cm^{-2} h^{-1}, respectively.

Liu et al. (2020) prepared N-doped CQDs (NCDs) modified defect-rich g-C_3N_4 (DCN) via an impregnation method. It was revealed that optimized NCDs/DCN exhibited excellent photocatalytic H_2 production with an evolution rate of 3.68 μmol h^{-1} g^{-1}. Nasir et al. (2020) prepared a 1D nanofiber of TiO_2 via electrospinning. Then they produced a needle-like structure on this fiber through an alkali hydrothermal method and chemical vapor deposition method. The g-C_3N_4 QDs and nanoflakes of $SnSe_2$ fiber (branched) were loaded on TiO_2 via a heterojunction. It was observed that the composite exhibited excellent photocatalytic performance for the production of hydrogen (2375 μmol g^{-1} h^{-1}) with quantum efficiency of HER (>16%).

Nitrogen-doped graphene QDs (N-GQDs) were synthesized by Tsai et al. (2020) via a hydrothermal cutting approach. The concentration of nitrogen was controlled with a change in concentration of nitrogen source urea. It was revealed that N-GQDs prepared by using 2 g of urea gave the highest photocurrent. They also observed that photocatalytic activity of 2N-GQDs (photocatalyst) for production of hydrogen was higher compared to pristine GQDs. Raza Naqvi et al. (2020) developed a nitrogen-doped carbon dots (NDCDs)-AgNi alloy. Then, it was used as an electrocatalyst for electrochemical water splitting. NDCDs-AgNi alloy NPs were synthesized by easy and scalable methods. NDCDs were prepared by the pyrolysis of ethanolamine. It acted as a good electrocatalyst for HER. It was also revealed that as-prepared NDCDs-AgNi alloy also exhibited superior OER activity.

Roy et al. (2020) demonstrated that chlorophyll(*a*)/CQDs (Chl/CQDs) bionanocomposite (b-NC)-decorated Si-nanowires (SiNWs) can surpass the efficiency for PEC generation of hydrogen. It was revealed that efficiency reaches ~7.86%, which is highest reported so far with hybrid Si-based

photocathodes. They measured the hydrogen evolution rate to be $\sim 113\ \mu mol\ h^{-1}$ at 0.8 V versus RHE under 1 sol illumination. Duan et al. (2021) developed a simple exfoliation−sonication approach to prepare nitrogen carbide QDs (CNQDs)-doped nitrogen carbide nanosheet (CNS) composite, which can be used as a photocatalyst to produce hydrogen in the presence of organic pollutants such as acridine orange, or aniline. In their presence, it was observed that hydrogen evolution efficiency was increased from 8.8 to 11.7 and 32.1 $mmol\ g^{-1}\ h^{-1}$ in the presence of aniline and acridine orange, respectively. It was revealed that heterojunction of CNQDs/CNS induced the separation of photogenerated electron−hole pairs, where electrons will migrate to CNQDs transforming protons into hydrogen molecules, and holes migrated to CNS, oxidizing organic pollutants, simultaneously.

Elsayed et al. (2021) have prepared N-doped carbon QDs (NCQDs) into polymer dots resulting in significant enhancement in their photocatalytic performance as well stability. The role of NCQDs was suggested to enhance the charge separation and the photocatalytic efficiency of the polymer dot. It was reported that NCQDs were easily introduced into the polymer dot, and as a result the hydrogen evolution rate was increased by about five times as compared to pure polymer dots.

Liang et al. (2021) prepared nitrogen doped graphene quantum dots as a photocatalyst dodecahedron nano-Au particles. It was revealed that as-obtained graphene@Au catalysts exhibited an efficient photocatalytic overall water splitting involving both; high valuable H_2O_2 and clean H_2 energy with generation rate as 49.7 and 65.6 $\mu mol\ g^{-1}\ h^{-1}$, respectively. The separation of hydrogen peroxide from hydrogen gas is easy as compared with most water splitting method that liberated hydrogen gas and oxygen gas, which further needs gas separation.

Nitrogen-doped graphene QDs (NGQDs) were prepared by Liu et al. (2021) and then used as a cocatalyst of $SrTiO_3(Al)/CoO_x$ for photocatalytic overall water splitting to generate hydrogen. It was found that as-prepared $NGQDs/SrTiO_3(Al)/CoO_x$ was highly active for splitting of water with an evolution rate of H_2 and O_2 as 18.8 and 9.0 $\mu mol\ h^{-1}$, respectively. Wu et al. (2021) synthesized an organic semiconductor (DAnTMS compound) using trimethylsilylacetylene (TMS) and 9,10-dibromoanthracene (DAn). Then, they designed a metal-free composite photocatalyst with carbon dots (DAnTMS/CD). It was reported that this DAnTMS/CD composite could achieve maximum production rates of H_2 and H_2O_2 of 265.0 and 396.7 $\mu mol\ g^{-1}\ h^{-1}$, respectively, with pure water.

14.5 Conclusion

QDs have many advantages compared to traditional materials as photocatalysts. These can create multiple excitons, which could lead to better control over the degree of charge. They can also be more efficient at producing hot

carriers with sufficient energy. Various surface atom ratios of QDs can modify the photoluminescence property. Dangling bonds or defects can reduce long-term photostability and reduce QY. As a result, passivating the surface is critical for enhancing stability and protecting its properties by the shelling of QDs and doping in the QDs.

The role of the quantum dot in photocatalysts developed for photocatalytic and PEC water splitting is a unique function. Water can be converted into hydrogen gas, when solar energy is applied to water in two technologies.

1. Indirectly through concentrated solar thermal and an electrolyzer, as well as solar-converted electricity, and electrolyzer, biological, and thermochemical processes. It has excessive costs, energy loss, and is unfeasible. Besides, the performance of electrolyzers, which have typical commercial efficiencies of around 73%, is always constrained when the energy conversion step is combined with electrolyzers.
2. Direct route including powdered photocatalysts and PEC cells, using photo-/photoelectrocatalysis of water.

The dispersion of powdered photocatalysts into water is ideal for major operations. The system needs to be motivated during the reaction and product separation after the reaction. PEC systems combined solar energy collection and water reduction in one device. Most hydrogen is generated from fossil fuels, including natural gas, oil, and coal. Electron donors like alcohols (methanol, ethanol, and glycerol) are commonly utilized as sacrificial reagents (SEDs) in water to efficiently generate hydrogen by successfully scavenging photogenerated holes to suppress the back reaction.

References

Ahmed, L.M., Alkaim, A.F., Halbus, A.F., Hussein, F.H., 2016. Photocatalytic hydrogen production from aqueous methanol solution over metallized TiO_2. Int. J. ChemTech Res. 9, 90−98.

Apte, S., Garaje, S., Valant, M., Kale, B., 2012. Eco-friendly solar light driven hydrogen production from copious waste H_2S and organic dye degradation by stable and efficient orthorhombic CdS quantum dots−GeO_2 glass photocatalyst. Green. Chem. 14 (5), 1455. Available from: https://doi.org/10.1039/c2gc16416g.

Bahruji, H., Bowker, M., Davies, P.R., Pedrono, F., 2011. New insights into the mechanism of photocatalytic reforming on Pd/TiO_2. Appl. Catal. B: Environ. 107 (1−2), 205−209.

Bard, A., 1979. Photoelectrochemistry and heterogeneous photocatalysis at semiconductors. J. Photochem. 10, 59−75.

Batubara, N.H., Zulys, A., 2019. Synthesis, Structural, spectroscopic, and morphology of metal-organic frameworks based on La (III) and ligand 2, 6-Napthalenedicarboxylic acid (La-MOFs) for hydrogen production. IOP Conf. Series: Mater. Sci. Eng. 546. Available from: https://doi.org/10.1088/1757-899X/546/4/042005.

Belhadj, H., Hamid, S., Robertson, P.K., Bahnemann, D.W., 2017. Mechanisms of simultaneous hydrogen production and formaldehyde oxidation in H_2O and D_2O over platinized TiO_2. Acs Catal. 7 (7), 4753−4758.

Bičáková, O., Straka, P., 2010. The resources and methods of hydrogen production. Acta Geodyn. Geomater. 7 (158), 175–188.

Bockris, J.O.M., Dandapani, B., Cocke, D., Ghoroghchian, J., 1985. On the splitting of water. Int. J. Hydrog. Energy 10 (3), 179–201.

Camacho, S.Y.T., Rey, A., Hernández-Alonso, M.D., Llorca, J., Medina, F., Contreras, S., 2018. Pd/TiO_2-WO_3 photocatalysts for hydrogen generation from water-methanol mixtures. Appl. Surf. Sci. 455, 570–580.

Cao, S., Yuan, Y., Fang, J., Shahjamali, M., Boey, F., Barber, J., et al., 2013. In-situ growth of CdS quantum dots on g-C_3N_4 nanosheets for highly efficient photocatalytic hydrogen generation under visible light irradiation. Int. J. Hydrog. Energy 38 (3), 1258–1266. Available from: https://doi.org/10.1016/j.ijhydene.2012.10.116.

Cao, S., Wang, C.J., Fu, W.F., Chen, Y., 2017. Metal phosphides as co-catalysts for photocatalytic and photoelectrocatalytic water splitting. ChemSusChem 10 (22), 4306–4323.

Carey, J.H., Oliver, B.G., 1976. Intensity effects in the electrochemical photolysis of water at the TiO_2 electrode. Nature 259 (5544), 554–556.

Cargnello, M., Gasparotto, A., Gombac, V., Montini, T., Barreca, D., Fornasiero, P., 2011. Photocatalytic H_2 and added-value by-products–the role of metal oxide systems in their synthesis from oxygenates. Eur. J. Inorg. Chem. 2011, 4309–4323.

Chen, H.M., Chen, C.K., Chang, Y.C., Tsai, C.W., Liu, R.S., Hu, S.F., et al., 2010. Quantum dot monolayer sensitized ZnO nanowire-array photoelectrodes: true efficiency for water splitting. Angew. Chem. 122 (34), 6102–6105.

Chen, X., Zhang, Z., Chi, L., Nair, A.K., Shangguan, W., Jiang, Z., 2016a. Recent advances in visible-light-driven photoelectrochemical water splitting: catalyst nanostructures and reaction systems. Nanomicro Lett. 8 (1). Available from: https://doi.org/10.1007/s40820-015-0063-3.

Chen, T., Quan, W., Yu, L., Hong, Y., Song, C., Fan, M., et al., 2016b. One-step synthesis and visible-light-driven H_2 production from water splitting of Ag quantum dots/g-C_3N_4 photocatalysts. J. Alloy. Comp. 686, 628–634. Available from: https://doi.org/10.1016/j.jallcom.2016.06.076.

Chen, Z., Zhang, Q., Luo, Y., 2018. Experimental identification of ultrafast reverse hole transfer at the interface of the photoexcited methanol/graphitic carbon nitride system. Angew. Chem. Int. (Ed.) 57 (19), 5320–5324.

Chen, J., Lv, S., Shen, Z., Tian, P., Chen, J., Li, Y., 2019. Novel ZnCdS Quantum dots engineering for enhanced visible-light-driven hydrogen evolution. ACS Sustain. Chem. Eng. 7 (16), 13805–13814.

Cirone, J., Dondapati, J., Chen, A., 2021. Design of bimetallic nickel-iron quantum dots with tunable compositions for enhanced electrochemical water splitting. Electrochim. Acta 392. Available from: https://doi.org/10.1016/j.electacta.2021.139016.

Coronado, J.M., 2013. Photons, electrons and holes: fundamentals of photocatalysis with semiconductors. Design of Advanced Photocatalytic Materials for Energy and Environmental Applications. Springer, London.

Corredor, J., Rivero, M.J., Rangel, C.M., Gloaguen, F., Ortiz, I., 2019. Comprehensive review and future perspectives on the photocatalytic hydrogen production. J. Chem. Technol. Biotechnol. 94 (10), 3049–3063.

Crampton, A.S., Cai, L., Janvelyan, N., Zheng, X., Friend, C.M., 2017. Methanol photooxidation on rutile TiO_2 nanowires: probing reaction pathways on complex materials. J. Phys. Chem. C. 121 (18), 9910–9919.

Crespo-Quesada, M., Reisner, E., 2017. Emerging approaches to stabilise photocorrodible electrodes and catalysts for solar fuel applications. Energy Environ. Sci. 10 (5), 1116–1127.

Dahiya, S., Chatterjee, S., Sarkar, O., Mohan, S.V., 2020. Renewable hydrogen production by dark-fermentation: current status, challenges and perspectives. Bioresour. Technol. Available from: https://doi.org/10.1016/j.biortech.2020.124354.

Dinda, D., Park, H., Lee, H.J., Oh, S., Park, S.Y., 2020. Graphene quantum dot with covalently linked Rhodamine dye: a high efficiency photocatalyst for hydrogen evolution. Carbon 167, 760–769.

Domen, K., Naito, S., Soma, M., Onishi, T., Tamaru, K., 1980. Photocatalytic decomposition of water vapour on an NiO–$SrTiO_3$ catalyst. J. Chem. Soc. Chem. Commun. 1980, 543–544.

Du, X., Zhao, T., Xiu, Z., Xing, Z., Li, Z., Pan, K., et al., 2020. $BiVO_4$@$ZnIn_2S_4$/Ti_3C_2 MXene quantum dots assembly all-solid-state direct Z-Scheme photocatalysts for efficient visible-light-driven overall water splitting. Appl. Mater. Today 20. Available from: https://doi.org/10.1016/j.apmt.2020.100719.

Duan, C., Xie, L., Wang, S., Dai, Y., Yin, L., 2021. Photocatalytic hydrogen evolution by degradation of organic pollutants over quantum dots doped nitrogen carbide. Chemosphere. Available from: https://doi.org/10.1016/j.chemosphere.2021.132873.

Elsayed, M.H., Jayakumar, J., Abdellah, M., Mansoure, T.H., Zheng, K., Elewa, A.M., et al., 2021. Visible-light-driven hydrogen evolution using nitrogen-doped carbon quantum dot-implanted polymer dots as metal-free photocatalysts. Appl. Catal. B: Environ. 283. Available from: https://doi.org/10.1016/j.apcatb.2020.119659.

Fang, S., Liu, Y., Sun, Z., Lang, J., Bao, C., Hu, Y.H., 2020. Photocatalytic hydrogen production over Rh-loaded TiO_2: what is the origin of hydrogen and how to achieve hydrogen production from water? Appl. Catal. B: Environ. 278. Available from: https://doi.org/10.1016/j.apcatb.2020.119316.

Frame, F.A., Osterloh, F.E., 2010. CdSe-MoS_2: a quantum size-confined photocatalyst for hydrogen evolution from water under visible light. J. Phys. Chem. C. 114 (23), 10628–10633.

Fujishima, A., Honda, K., 1972. Electrochemical photolysis of water at a semiconductor electrode. Nature. 238, 37–38.

Fukuzumi, S., Lee, Y.M., Nam, W., 2018. Thermal and photocatalytic production of hydrogen with earth-abundantmetal complexes. Coord. Chem. Rev. 355, 54–73.

Ge, L., Zuo, F., Liu, J., Ma, Q., Wang, C., Sun, D., 2012. Synthesis and efficient visible light photocatalytic hydrogen evolution of polymeric g-C_3N_4 coupled with CdS quantum dots. J. Phys. Chem. C. 116 (25), 13708–13714.

Gliniak, J., Lin, J., Chen, Y., Li, C., Jokar, E., Chang, C., et al., 2017. Sulfur-doped graphene oxide quantum dots as photocatalysts for hydrogen generation in the aqueous phase. Chemsuschem. 10 (16), 3260–3267.

Guijarro, N., Prévot, M.S., Sivula, K., 2015. Surface modification of semiconductor photoelectrodes. Phys. Chem. Chem. Phys. 17 (24), 15655–15674.

Gultom, N.S., Abdullah, H., Kuo, D.H., 2017. Enhanced photocatalytic hydrogen production of noble-metal free Ni-doped Zn (O, S) in ethanol solution. Int. J. Hydrog. Energy 42 (41), 25891–25902.

Gunasekaran, A., Anbarasan, N., Mukilan, N., 2021. CdS and CdSe nanoparticles activated 1D TiO_2 heterostructure nanoarray photoelectrodes for enhanced photoelectrocatalytic water splitting. Int. J. Hydrog. Energy. 46, 26381–26390.

Guo, Q., Liang, F., Gao, X.-Y., Gan, Q.-C., Li, X.-B., Li, J., et al., 2018. Metallic Co_2C: a promising co-catalyst to boost photocatalytic hydrogen evolution of colloidal quantum dots. ACS Catal. 8 (7), 5890–5895.

Hainer, A.S., Hodgins, J.S., Sandre, V., Vallieres, M., Lanterna, A.E., Scaiano, J.C., 2018. Photocatalytic hydrogen generation using metal-decorated TiO_2: sacrificial donors vs true water splitting. ACS Energy Lett. 3 (3), 542–545.

Han, B., Mo, J., Kang, Z., Yang, G., Barnhill, W., Zhang, F.Y., 2017. Modeling of two-phase transport in proton exchange membrane electrolyzer cells for hydrogen energy. Int. J. Hydrog. Energy 42 (7), 4478–4489.

Hao, H., Lu, D., Wang, Q., 2018. Photoelectrochemical study on charge separation mechanisms of Bi_2WO_6 quantum dots decorated g-C_3N_4. Int. J. Hydrog. Energy 43 (18), 8824–8834.

Hisatomi, T., Kubota, J., Domen, K., 2014. Recent advances in semiconductors for photocatalytic and photoelectrochemical water splitting. Chem. Soc. Rev. 43, 7520–7535.

Huang, C.W., Nguyen, B.S., Wu, J.C.S., Nguyen, V.H., 2020. A current perspective for photocatalysis towards the hydrogen production from biomass-derived organic substances and water. Int. J. Hydrog. Energy 45 (36), 18144–18159.

Jia, Q., Iwase, A., Kudo, A., 2014. $BiVO_4$–Ru/$SrTiO_3$: Rh composite Z-scheme photocatalyst for solar water splitting. Chem. Sci. 5 (4), 1513–1519.

Jiang, C., Moniz, S.J., Wang, A., Zhang, T., Tang, J., 2017. Photoelectrochemical devices for solar water splitting–materials and challenges. Chem. Soc. Rev. 46 (15), 4645–4660.

Jitputti, J., Suzuki, Y., Yoshikawa, S., 2008. Synthesis of TiO_2 nanowires and their photocatalytic activity for hydrogen evolution. Catal. Commun. 9 (6), 1265–1271.

Kamat, P.V., Jin, S., 2018. Semiconductor photocatalysis: tell us the complete story!. ACS Energy Lett. 3, 622–623.

Kawai, T., Sakata, T., 1980. Photocatalytic hydrogen production from liquid methanol and water. J. Chem. Soc. Chem. Commun. 1980 (15), 694–695.

Kibria, M.G., Zhao, S., Chowdhury, F.A., Wang, Q., Nguyen, H.P.T., Trudeau, M.L., et al., 2014. Tuning the surface fermi level on p-type gallium nitride nanowires for efficient overall water splitting. Nat. Commun. 5 (1), 1–6.

Kitazono, K., Akashi, R., Fujiwara, K., Akita, A., Naya, S., Fujishima, M., et al., 2017. Photocatalytic synthesis of CdS(core)-CdSe(shell) quantum dots with a heteroepitaxial junction on TiO_2: photoelectrochemical hydrogen generation from water. Chemphyschem 18 (20), 2840–2845.

Kuang, P., Zheng, P., Liu, Z., Lei, J., Wu, H., Li, N., et al., 2016. Embedding Au quantum dots in rimous cadmium sulfide nanospheres for enhanced photocatalytic hydrogen evolution. Small 12 (48), 6735–6744.

Kudo, A., Miseki, Y., 2009. Heterogeneous photocatalyst materials for water splitting. Chem. Soc. Rev. 38 (1), 253–278.

Kudo, A., Tanaka, A., Domen, K., Maruya, K.I., Aika, K.I., Onishi, T., 1988. Photocatalytic decomposition of water over NiO- $K_4Nb_6O_{17}$ catalyst. J. Catal. 111 (1), 67–76.

Kumar, D.P., Reddy, N.L., Srinivas, B., Durga kumari, V., Roddatis, V., Bondarchuk, O., 2016. Stable and active CuxO/TiO_2 nanostructured catalyst for proficient hydrogen production under solar light irradiation. Sol. Energy Mater. Sol. Cell 146, 63–71.

Landman, A., Halabi, R., Dias, P., Dotan, H., Mehlmann, A., Shter, G.E., 2020. Decoupled photoelectrochemical water splitting system for centralized hydrogen production. Joule 4 (2), 448–471.

Li, Q., Cui, C., Meng, H., Yu, J., 2014. Visible-Light photocatalytic hydrogen production activity of $ZnIn_2S_4$ microspheres using carbon quantum dots and platinum as dual co-catalysts. Chem. Asian J. 9 (7), 1766–1770.

Li, K., Su, F., Zhang, W., 2016. Modification of g-C_3N_4 nanosheets by carbon quantum dots for highly efficient photocatalytic generation of hydrogen. Appl. Surf. Sci. 375, 110–117. Available from: https://doi.org/10.1016/j.apsusc.2016.03.025.

Liang, J., Liu, Y., Si, Z., Wei, G., Weng, D., Kang, F., 2021. Graphene quantum dots piecing together into graphene on nano Au for overall water splitting. Carbon 178, 265–272.

Liu, J., Liu, Y., Liu, N., Han, Y., Zhang, X., Huang, H., et al., 2015. Metal-free efficient photocatalyst for stable visible water splitting via a two-electron pathway. Science 347, 970–974.

Liu, J., Ke, J., Li, Y., Liu, B., Wang, L., Xiao, H., et al., 2018. Co_3O_4 quantum dots/TiO_2 nanobelt hybrids for highly efficient photocatalytic overall water splitting. Appl. Catal. B: Env. 236, 396–403.

Liu, Y., Li, X., Zhang, Q., Li, W., Xie, Y., Liu, H., et al., 2019. A general route to prepare low-ruthenium-content bimetallic electrocatalysts for ph-universal hydrogen evolution reaction by using carbon quantum dots. Angew. Chem. Int. (Ed.) 59 (4), 1718–1726.

Liu, H., Liang, J., Fu, S., Li, L., Cui, J., Gao, P., et al., 2020. N doped carbon quantum dots modified defect-rich g-C3N4 for enhanced photocatalytic combined pollutions degradation and hydrogen evolution. Colloids Surf. A: Physicochem. Eng. Asp. 591. Available from: https://doi.org/10.1016/j.colsurfa.2020.124552.

Liu, Y., Xu, X., Lv, S., Li, H., Si, Z., Wu, X., et al., 2021. Nitrogen doped graphene quantum dots as a cocatalyst of $SrTiO_3$(Al)/CoOx for photocatalytic overall water splitting. Catal. Sci. Technol. 11 (9), 3039–3046.

Luo, H., Barrio, J., Sunny, N., Li, A., Steier, L., Shah, N., et al., 2021. Progress and perspectives in photo-and electrochemical-oxidation of biomass for sustainable chemicals and hydrogen production. Adv. Energy Mater. 11. Available from: https://doi.org/10.1002/aenm.202101180.

Ma, Y., Wang, X., Jia, Y., Chen, X., Han, H., Li, C., 2014. Titanium dioxide-based nanomaterials for photocatalytic fuel generations. Chem. Rev. 114 (19), 9987–10043.

Ma, D., Shi, J.W., Zou, Y., Fan, Z., Ji, X., Niu, C., 2017. Highly efficient photocatalyst based on a CdS quantum dots/ZnO nanosheets 0D/2D heterojunction for hydrogen evolution from water splitting. ACS Appl. Mater. Interf. 9 (30), 25377–25386.

Maeda, K., Teramura, K., Takata, T., Hara, M., Saito, N., Toda, K., et al., 2005. Overall water splitting on $(Ga_{1-x}\ Zn_x)(N_{1-x}\ O_x)$ solid solution photocatalyst: relationship between physical properties and photocatalytic activity. J. Phys. Chem. B 109 (43), 20504–20510.

Marschall, R., 2021. 50 years of materials research for photocatalytic water splitting. Eur. J. Inorg. Chem. 2021 (25), 2435–2441.

Martindale, B.C.M., Hutton, G.A.M., Caputo, C.A., Reisner, E., 2015. Solar Hydrogen production using carbon quantum dots and a molecular nickel catalyst. J. Am. Chem. Soc. 137 (18), 6018–6025. Available from: https://doi.org/10.1021/jacs.5b01650.

Melo, M., Silva, L., 2011. Review-photocatalytic production of hydrogen: an innovative use for biomass derivatives. J. Braz. Chem. Soc. 22. Available from: https://doi.org/10.1590/S0103-50532011000800002.

Meng, T., Hao, Y., Zheng, L., Cao, M., 2018. Organophosphoric acid-derived CoP quantum dots@S,N-codoped graphite carbon as a trifunctional electrocatalyst for overall water splitting and Zn–air batteries. Nanoscale 10 (30), 14613–14626.

Meng, X., Zhang, C., Dong, C., Sun, W., Ji, D., Ding, Y., 2020. Carbon quantum dots assisted strategy to synthesize Co@ NC for boosting photocatalytic hydrogen evolution performance of CdS. Chem. Eng. J. 389, 124432.

Miodyńska, M., Mikolajczyk, A., Bajorowicz, B., Zwara, J., Klimczuk, T., Lisowski, W., et al., 2020. Urchin-like TiO_2 structures decorated with lanthanide-doped Bi_2S_3 quantum dots to boost hydrogen photogeneration performance. Appl. Catal. B: Environ. 272. Available from: https://doi.org/10.1016/j.apcatb.2020.118962.

Miyoshi, A., Nishioka, S., Maeda, K., 2018. Water splitting on rutile TiO_2-based photocatalysts. Chem. A Eur. J. 24 (69), 18204–18219.

Molaei, M.J., 2020. The optical properties and solar energy conversion applications of carbon quantum dots: a review. Sol. Energy 196, 549–566.

Nasir, M., Yang, G., Ayub, I., Wang, S., Yan, W., 2020. Tin diselinide a stable co-catalyst coupled with branched TiO_2 fiber and g-C_3N_4 quantum dots for photocatalytic hydrogen evolution. Appl. Catal. B: Environ. 270. Available from: https://doi.org/10.1016/j.apcatb.2020.118900.

Nemzer, M., Page, D., Carter, A., 2003. CH 3 Energy for Keeps—Creating Clean Electricity from Renewable Resources, third ed. National Science Techers Association, Malaysia.

Niu, P., Dai, J., Zhi, X., Xia, Z., Wang, S., Li, L., 2021. Photocatalytic overall water splitting by graphitic carbon nitride. InfoMat 3 (9), 931−961.

Pan, Y., Zhuang, H., Hong, J., Fang, Z., Liu, H., Liu, B., et al., 2014. Cadmium sulfide quantum dots supported on gallium and indium oxide for visible-light-driven hydrogen evolution from water. Chemsuschem 7 (9), 2537−2544.

Pan, J., You, M., Chi, C., Dong, Z., Wang, B., Zhu, M., et al., 2018. The two dimension carbon quantum dots modified porous g-C_3 N_4/TiO_2 nano-heterojunctions for visible light hydrogen production enhancement. Int. J. Hydrog. Energy 43 (13), 6586−6593.

Penconi, M., Rossi, F., Ortica, F., Elisei, F., Gentili, P.L., 2015. Hydrogen production from water by photolysis, sonolysis and sonophotolysis with solid solutions of rare earth, gallium and indium oxides as heterogeneous catalysts. Sustainability 7 (7), 9310−9325.

Peng, R., Ma, Y., Huang, B., Dai, Y., 2019. Two-dimensional Janus PtSSe for photocatalytic water splitting under the visible or infrared light. J. Mater. Chem. A 7 (2), 603−610.

Phang, S.J., Tan, L.L., 2019. Recent advances in carbon quantum dots (CQDs)-based two dimensional materials for photocatalytic applications. Catal. Sci. Technol. 9, 5882−5905.

Puga, A.V., 2016. Photocatalytic production of hydrogen from biomass-derived feedstocks. Coord. Chem. Rev. 315. Available from: https://doi.org/10.1016/j.ccr.2015.12.009.

Qian, J., Chen, Z., Chen, F., Wang, Y., Wu, Z., Zhang, W., 2018. Exploration of CeO_2−CuO quantum dots in situ grown on graphene under hypha assistance for highly efficient solar-driven hydrogen production. Inorg. Chem. Available from: https://doi.org/10.1021/acs.inorgchem.8b0193.

Qiao, S., Feng, C., Guo, Y., Chen, T., Akram, N., Zhang, Y., et al., 2020. CdS nanoparticles modified Ni@ NiO spheres as photocatalyst for oxygen production in water oxidation system and hydrogen production in water reduction system. Chem. Eng. J. 395. Available from: https://doi.org/10.1016/j.cej.2020.125068.

Qu, D., Sun, Z., Zheng, M., Li, J., Zhang, Y., Zhang, G., et al., 2015. Three colors emission from S, N co-doped graphene quantum dots for visible light H_2 production and bioimaging. Adv. Opt. Mater. 3 (3), 360−367.

Raza Naqvi, S., Rasheed, T., Majeed, S., Hussain, D., Fatima, B., Najam ul Haq, M., et al., 2020. Nitrogen doped carbon quantum dots conjugated with AgNi alloy nanoparticles as potential electrocatalyst for efficient water splitting. J. Alloy. Comp. 847. Available from: https://doi.org/10.1016/j.jallcom.2020.156492.

Reddy, N., Bharagav, U., Kumari, M., Cheralathan, K., Shankar, M., Reddy, K., et al., 2020. Highly efficient solar light-driven photocatalytic hydrogen production over Cu/FCNTs-titania quantum dots-based heterostructures. J. Environ. Manag. 254, 109747. Available from: https://doi.org/10.1016/j.jenvman.2019.109747.

Roy, K., Ghosh, D., Sarkar, K., Devi, P., Kumar, P., 2020. Chlorophyll(a)/carbon quantum dot bio-nanocomposite activated nano-structured silicon as an efficient photocathode for photoelectrochemical water splitting. ACS Appl. Mater. Interf. Available from: https://doi.org/10.1021/acsami.0c10279.

Sahai, S., Ikram, A., Rai, S., Shrivastav, R., Dass, S., Satsangi, V.R., 2017. Quantum dots sensitization for photoelectrochemical generation of hydrogen: a review. Renew. Sust. Energy Rev. 68, 19−27.

Schneider, J., Bahnemann, D.W., 2013. Undesired role of sacrificial reagents in photocatalysis. J. Phys. Chem. Lett. 4, 3479–3483.

Schweinberger, F.F., Berr, M.J., Döblinger, M., Wolff, C., Sanwald, K.E., Crampton, A.S., et al., 2013. Cluster size effects in the photocatalytic hydrogen evolution reaction. J. Am. Chem. Soc. 135 (36), 13262–13265.

Shi, W., Zhang, X., Brillet, J., Huang, D., Li, M., Wang, M., et al., 2016. Significant enhancement of the photoelectrochemical activity of WO_3 nanoflakes by carbon quantum dots decoration. Carbon 105, 387–393. Available from: https://doi.org/10.1016/j.carbon.2016.04.051.

Shi, J., Sun, D., Zou, Y., Ma, D., He, C., Ji, X., et al., 2019. Trap-level-tunable Se doped CdS quantum dots with excellent hydrogen evolution performance without co-catalyst. Chem. Eng. J. 364, 11–19.

Shi, L., Benetti, D., Li, F., Wei, Q., Rosei, F., 2020. Phase-junction design of MOF-derived TiO_2 photoanodes sensitized with quantum dots for efficient hydrogen generation. Appl. Catal. B: Environ. 263. Available from: https://doi.org/10.1016/j.apcatb.2019.118317.

Slama, R.B., 2013. Production of hydrogen by electrolysis of water: effects of the electrolyte type on the electrolysis performances. Comput. Water, Energy, Environ. Eng. 2, 54–58.

Strataki, N., Bekiari, V., Kondarides, D.I., Lianos, P., 2007. Hydrogen production by photocatalytic alcohol reforming employing highly efficient nanocrystalline titania films. Appl. Catal. B: Env. 77 (1–2), 184–189.

Su, D.W., Ran, J., Zhuang, Z.W., Chen, C., Qiao, S.Z., Li, Y.D., et al., 2020. Atomically dispersed Ni in cadmium-zinc sulfide quantum dots for high-performance visible-light photocatalytic hydrogen production. Sci. Adv. 6 (33). Available from: https://doi.org/10.1126/sciadv.aaz8447.

Sun, L., Zhuang, Y., Yuan, Y., Zhan, W., Wang, X., Han, X., et al., 2019. Nitrogen-doped carbon-coated CuO-In_2O_3 p–n heterojunction for remarkable photocatalytic hydrogen evolution. Adv. Energy Mater. 9 (48). Available from: https://doi.org/10.1002/aenm.201902839.

Tamirat, A.G., Rick, J., Dubale, A.A., Su, W.N., Hwang, B.J., 2016. Using hematite for photoelectrochemical water splitting: a review of current progress and challenges. Nanoscale Horiz. 1 (4), 243–267.

Tsai, K.-A., Hsieh, P.-Y., Lai, T.-H., Tsao, C.-W., Pan, H., Lin, Y.-G., et al., 2020. Nitrogen-doped graphene quantum dots for remarkable solar hydrogen production. ACS Appl. Energy Mater. 3 (6), 5322–5332.

Vaiano, V., Lara, M.A., Iervolino, G., Matarangolo, M., Navío, J.A., Hidalgo, M.C., 2018. Photocatalytic H_2 production from glycerol aqueous solutions over fluorinated Pt-TiO_2 with high {001} facet exposure. J. Photochem. Photobiol. A: Chem. 365, 52–59.

Van Damme, H., Hall, W.K., 1979. Photoassisted decomposition of water at the gas-solid interface on titanium dioxide. J. Am. Chem. Soc. 101 (15), 4373–4374.

Wang, N., Li, X., 2018. Protonated carbon nitride nanosheet supported IrO_2 quantum dots for pure water splitting without sacrificial reagents. Inorg. Chem. Front. 5 (9), 2268–2275.

Wang, C.Y., Pagel, R., Bahnemann, D.W., Dohrmann, J.K., 2004. Quantum yield of formaldehyde formation in the presence of colloidal TiO_2-based photocatalysts: effect of intermittent illumination, platinization, and deoxygenation. J. Phys. Chem. B 108 (37), 14082–14092.

Wang, Y., Li, Y., Zhao, J., Wang, J., Li, Z., 2013. g-C_3N_4/B doped g-C_3N_4 quantum dots heterojunction photocatalysts for hydrogen evolution under visible light. Int. J. Hydrog. Energy 44 (2), 618–628.

Wang, J.J., Li, Z.J., Li, X.B., Fan, X.B., Meng, Q.Y., Yu, S., et al., 2014. Photocatalytic hydrogen evolution from glycerol and water over nickel-hybrid cadmium sulfide quantum dots under visible-light irradiation. ChemSusChem 7 (5), 1468–1475.

Wang, B., An, W., Liu, L., Chen, W., Liang, Y., Cui, W., 2015. Novel Cu_2S quantum dots coupled flower-like BiOBr for efficient photocatalytic hydrogen production under visible light. RSC Adv. 5 (5), 3224–3231.

Wang, F., Su, Y., Min, S., Li, Y., Lei, Y., Hou, J., 2018a. Synergistically enhanced photocatalytic hydrogen evolution performance of ZnCdS by co-loading graphene quantum dots and PdS dual cocatalysts under visible light. J. Solid. State Chem. 260, 23–30.

Wang, Q., Huang, J., Sun, H., Ng, Y., Zhang, K., Lai, Y., 2018b. MoS_2 quantum dots@TiO_2 nanotube arrays: an extended-spectrum-driven photocatalyst for solar hydrogen evolution. Chemsuschem 11 (10), 1708–1721.

Wang, Q., Cai, J., Biesold-McGee, G., Huang, J., Ng, Y., Sun, H., et al., 2020. Silk fibroin-derived nitrogen-doped carbon quantum dots anchored on TiO_2 nanotube arrays for heterogeneous photocatalytic degradation and water splitting. Nano Energy 78, 105313. Available from: https://doi.org/10.1016/j.nanoen.2020.105313.

Wrighton, M.S., Morse, D.L., Ellis, A.B., Ginley, D.S., Abrahamson, H.B., 1976. Photoassisted electrolysis of water by ultraviolet irradiation of an antimony doped stannic oxide electrode. J. Am. Chem. Soc. 98 (1), 44–48.

Wu, Z., Li, X., Zhao, Y., Li, Y., Wei, K., Shi, H., et al., 2021. Organic semiconductor/carbon dot composites for highly efficient hydrogen and hydrogen peroxide coproduction from water photosplitting. ACS Appl. Mater. Interf. 13 (50), 60561–60570.

Xiao, F.X., Liu, B., 2018. Plasmon-Dictated photo-electrochemical water splitting for solar-to-chemical energy conversion: current status and future perspectives. Adv. Mater. Inter. 5 (6). Available from: https://doi.org/10.1002/admi.201701098.

Xiao, M., Wang, Z., Lyu, M., Luo, B., Wang, S., Liu, G., et al., 2019. Hollow nanostructures for photocatalysis: advantages and challenges. Adv. Mater. 31 (38). Available from: https://doi.org/10.1002/adma.201801369.

Xie, M., Zhang, Z., Han, W., Cheng, X., Li, X., Xie, E., 2017. Efficient hydrogen evolution under visible light irradiation over $BiVO_4$ quantum dot decorated screw-like SnO_2 nanostructures. J. Mater. Chem. A. 5 (21), 10338–10346.

Xu, X., Zhou, G., Feng, B., Bao, Z., Hu, J., 2016. ZnO quantum dots arranged by hole scavenger groups for enhanced and stable photocatalyic hydrogen generation. Mater. Lett. 165, 196–199.

Xue, C., An, H., Yan, X., Li, J., Yang, B., Wei, J., et al., 2017. Spatial charge separation and transfer in ultrathin $CdIn_2S_4$/rGO nanosheet arrays decorated by ZnS quantum dots for efficient visible-light-driven hydrogen evolution. Nano Energy 39, 513–523.

Xue, C., Li, H., An, H., Yang, B., Wei, J., Yang, G., 2018. NiSx Quantum dots accelerate electron transfer in $Cd_{0.8}Zn_{0.2}S$ photocatalytic system viaan rgo nanosheet "bridge" toward visible-light-driven hydrogen evolution. ACS Catal. 8 (2), 1532–1545.

Yan, X., Jin, Z., 2021. Interface engineering: NiAl-LDH in-situ derived NiP_2 quantum dots and Cu_3P nanoparticles ingeniously constructed p-n heterojunction for photocatalytic hydrogen evolution. Chem. Eng. J. 420, 127682. Available from: https://doi.org/10.1016/j.cej.2020.127682.

Yan, M., Hua, Y., Zhu, F., Sun, L., Gu, W., Shi, W., 2017. Constructing nitrogen doped graphene quantum dots-$ZnNb_2O6$/g-C_3N_4 catalysts for hydrogen production under visible light. Appl. Catal. B: Environ. 206, 531–537.

Yang, X., Wolcott, A., Wang, G., Sobo, A., Fitzmorris, R.C., Qian, F., et al., 2009. Nitrogen-doped ZnO nanowire arrays for photoelectrochemical water splitting. Nano let. 9 (6), 2331–2336.

Yang, J., Wang, D., Han, H., Li, C., 2013. Roles of cocatalysts in photocatalysis and photoelectrocatalysis. Acc. Chem. Res. 46, 1900–1909 (2013).

Yang, Y., Mao, B., Gong, G., Li, D., Liu, Y., Cao, W., et al., 2019. In-situ growth of Zn–$AgIn_5S_8$ quantum dots on g-C_3N_4 towards 0D/2D heterostructured photocatalysts with enhanced hydrogen production. Int. J. Hydrog. Energy 44 (30), 15882–15891.

Yasuda, M., Matsumoto, T., Yamashita, T., 2018. Sacrificial hydrogen production over TiO_2-based photocatalysts: polyols, carboxylic acids, and saccharides. Renew. Sustain. Energy Rev. 81, 1627–1635.

Ye, M., Gong, J., Lai, Y., Lin, C., Lin, Z., 2012. High-efficiency photoelectrocatalytic hydrogen generation enabled by palladium quantum dots-sensitized TiO_2 nanotube arrays. J. Am. Chem. Soc. 134 (38), 15720–15723.

Yeh, T., Teng, C., Chen, S., Teng, H., 2014. Nitrogen-doped graphene oxide quantum dots as photocatalysts for overall water-splitting under visible light illumination. Adv. Mater. 26 (20), 3297–3303.

Yu, Y., Ren, J., Meng, M., 2013. Photocatalytic hydrogen evolution on graphene quantum dots anchored TiO_2 nanotubes-array. Int. J. Hydrog. Energy 38 (28), 12266–12272.

Yu, W., Yin, J., Li, Y., Lai, B., Jiang, T., Li, Y., et al., 2019. Ag_2S quantum dots as an infrared excited photocatalyst for hydrogen production. ACS Appl. Energy Mater. Available from: https://doi.org/10.1021/acsaem.9b00091.

Yue, D., Qian, X., Zhang, Z., Kan, M., Ren, M., Zhao, Y., 2016. CdTe/CdS core/shell quantum dots cocatalyzed by sulfur tolerant [Mo_3S13] 2–nanoclusters for efficient visible-light-driven hydrogen evolution. Acs Sustain. Chem. Eng. 4 (12), 6653–6658.

Zamiri, G., Bagheri, S., 2018. Fabrication of green dye-sensitized solar cell based on ZnO nanoparticles as a photoanode and graphene quantum dots as a photo-sensitizer. J. Colloid Inter. Sci. 511, 318–324.

Zhang, Z., Jiang, X., Mei, J., Li, Y., Han, W., Xie, M., et al., 2018a. Improved photoelectrocatalytic hydrogen generation through $BiVO_4$ quantum-dots loaded on nano-structured SnO_2 and modified with carbon quantum-dots. Chem. Eng. J. 331, 48–53.

Zhang, Y., Lin, Q., Tong, N., Zhang, Z., Zhuang, H., Zhang, X., et al., 2018b. Simple fabrication of SnO_2 quantum-dot-modified TiO_2 nanorod arrays with high photoelectrocatalytic activity for overall water splitting. Chemphyschem 19 (20), 2717–2723.

Zhang, P., Zeng, G., Song, T., Huang, S., Wang, T., Zeng, H., 2019. Synthesis of a plasmonic CuNi bimetal modified with carbon quantum dots as a non-semiconductor-driven photocatalyst for effective water splitting. J. Catal. 369, 267–275.

Zhao, H., Liu, G., Vidal, F., Wang, Y., Vomiero, A., 2018. Colloidal thick-shell pyramidal quantum dots for efficient hydrogen production. Nano Energy 53, 116–124.

Zhao, J., Shi, R., Li, Z., Zhou, C., Zhang, T., 2020. How to make use of methanol in green catalytic hydrogen production? Nano Sel. 1 (1), 12–29.

Zheng, Y., Chen, Y., Gao, B., Chen, J., Du, Z., Lin, B., 2019. Polymeric carbon nitride hybridized by $CuInS_2$ quantum dots for photocatalytic hydrogen evolution. Mater. Lett. 254, 81–84.

Zhong, D., Liu, W., Tan, P., Zhu, A., Qiao, L., Bian, Y., et al., 2019. Efficient hydrogen generation of indium doped $BaTiO_3$ decorated with CdSe quantum dots: novel understanding of the effect of doping strategy. Int. J. Hydrog. Energy 44 (3), 1627–1639.

Zhou, X., Wang, X., Feng, X., Zhang, K., Peng, X., Wang, H., et al., 2017. Loading $Cd_{0.5}Zn_{0.5}S$ quantum dots onto onion-like carbon nanoparticles to boost photocatalytic hydrogen generation. ACS Appl. Mater. Interf. 9 (27), 22560–22567.

Zhu, X., Xie, Y., Liu, Y., 2018. Exploring the synergy of 2D MXene-supported black phosphorus quantum dots in hydrogen and oxygen evolution reactions. J. Mater. Chem. A 6 (43), 21255–21260.

Zong, X., Sun, C., Yu, H., Chen, Z.G., Xing, Z., Ye, D., et al., 2013. Activation of photocatalytic water oxidation on N-doped ZnO bundle-like nanoparticles under visible light. J. Phys. Chem. C. 117 (10), 4937–4942.

Zou, Y., Shi, J., Ma, D., Fan, Z., Cheng, L., Sun, D., et al., 2018. WS_2/Graphitic carbon nitride heterojunction nanosheets decorated with CdS quantum dots for photocatalytic hydrogen production. Chemsuschem 11 (7), 1187–1197. Available from: https://doi.org/10.1002/cssc.201800053.

Index

Note: Page numbers followed by "*f*" and "*t*" refer to figures and tables, respectively.

A

Agriculture and horticulture, 226–228
Alcohol sensors, 314–315
Alloyed quantum dots, 5–6
Ammonia sensors, 315–317
Antimicrobial technology, 228–229
Application of quantum dots, 10*f*
  in biomedical and biotechnological fields, 12–13
    biolabeling and bioimaging, 246–248
    others, 261–264
    targeted drug delivery, 248–254
    toxicity of, 264–267
  developments, 329–330
  hydrogen generation, 12
  in light-emitting diodes, 11
    agriculture and horticulture, 226–228
    antimicrobial technology, 228–229
    data communication, 225–226
    developments, 229–230
    display and lighting, 206–224
    night vision, 224–225
  in photocatalysis, 11–12, 193*t*
    applications, 189–192
    hydrogen production, 189–192
    quantum dots, 170–171
    wastewater treatment, 171–188
  in photosplitting of water
    carbon and graphene-based QDs, 355–358
    hydrogen production, 340–347
    metal-based QDs, 347–355
  in sensors, 11, 314–329
  in solar cells, 10–11
    CdSe QDs and TiO_2, 282*f*
    developments, 300
    multiple exciton generation, 283–285
      hot carrier relaxation/cooling in semiconductors, 284*f*
    properties of, 281–285
    redox electrolyte, 279–280
    sensitized solar, 292–300
    structure of, 278–280, 279*f*
    synthesis of, 286–291
    working principle of, 280–281, 281*f*
Artificial nanocrystals possessing confinement, 205
Autoclave, 15–16

B

Bacteria
  on *Collembolans*, 99
  engineered *E. coli*, 98
  fluorescent *Bacillus subtilis*, 99
  isolated oxidative stress-resistant, 99
  low-cost hydroxypropyl starch (HPS), 100
  by nitric acid treatment, 101–102
  sulfate-reducing, 102
  volatile sulfur compounds, 101
Bandgap, 169–170
Bandgap in QDs, 285
Biogenic synthesis of quantum dots
  advantages, 94
  bacteria, 98–103
  disadvantages, 94
  fungi, 103–107
  plants, 94–98
Biolabeling and bioimaging, 246–248
Blue light-emitting diodes, 213–217

C

Carbon and graphene-based quantum dots
  coloading of graphene QDs, 356
  N-doped carbon, 358
  nitrogen-doped graphene oxide, 355
  sulfur-doped graphene oxide QDs, 356
Carbon and graphene quantum dots, 135
Carbon-based quantum dots, 21–26, 46–47, 159–162
Carbon dioxide sensors, 317

Chemical sensors, 314–324
Chemiluminescence sensors, 257–259
Classification of coprecipitation
  mechanical entrapment, 79
  mixed-crystal formation, 79
  occulation entrapment, 79
  surface adsorption, 79
Classification of quantum dots
  alloyed, 5–7
  core-shell, 5, 5*f*, 6*f*, 7*f*
  core-type, 4, 4*f*
Coprecipitation synthesis of quantum dots
  advantages, 77–78
  classification of, 78–79
  disadvantages, 78
  flow chart of, 78*f*
  synthesis of, 79–87
Cup horn, 150*f*

D

Data communication, 225–226
Dielectric heating, 116
Doubling effect, 344–345
Drugs, 181–185

E

Electroluminescence sensors, 259–261

F

Fluorescence quenchers, 321
Fungi
  cadmium selenide, 105
  cadmium selenium, 104
  cadmium sulfide, 103
  live yeast cell, 103
  polycrystalline ZnS, 104–105
  simple and efficient biosynthesis, 103

G

Galton whistle, 150*f*
Graphen-based quantum dots, 26–28
Green light-emitting diodes, 219–222

H

Hole conductors, 279–280
Humidity sensors, 326–327
Hydrogen production, 189–192
  band edge position and bandgaps, 348*f*
  H_2 reaction, 343*f*
  PEC efficiency of water splitting, 346–347
  photocatalytic hydrogen evolution process, 344*f*
  photoelectrochemical cell, 347*f*
  principle of overall water splitting, 341–345
  solar water splitting by using the photocatalyst, 342*f*
Hydrogen sulfide sensors, 317
Hydrothermal synthesis of quantum dots
  advantages, 17
  developments, 28
  disadvantages, 17
  metal-based quantum dots, 17–21
  nonmetal-based quantum dots, 21–28
  property of, 16
  teflon-lined autoclave reactor, 16*f*

I

Instrumentation, 149

L

Laser ablation
  advantages, 54
  disadvantages, 55
  for synthesis of quantum dots, 54*f*
Laser ablation synthesis of quantum dots
  developments, 68
  laser ablation, 53–55
  metal-based, 55–63
  nonmetal-based, 63–65
  others, 65–68
LED application of quantum dots, 229*t*
Light-emitting diode light, 11
Light-emitting diodes, 223–224
Lighting
  blue light-emitting diodes, 213–217
    luminescence efficiency of blue LEDs, 216*f*
  colored carbon quantum dots doped with heteroatoms, 214*f*
  display and, 206–224
  fabrication of silica-wrapped Mn-doped, 211*f*
  green light-emitting diodes, 219–222
  light-emitting diodes
    orange, 222–223
    other, 223–224
    red, 217–219
    white, 207–213
    yellow, 223
  night vision, 224–225
Liquid petroleum gas sensor, 315
Liquid whistle, 150*f*

M

MEG. *See* Multiple exciton generation
Metal-based quantum dots
  metal oxides, 56–59
  metals, 55–56, 347–348
  metal selenides, 62–63
  metal sulfides, 59–62, 350–354
  others, 21, 354–355
  oxides, 17–19, 348–350
  sulfide, 19–20
Metal oxide quantum dots, 17–19, 79–80
Metal selenide quantum dots, 83–84
Metal sulfide quantum dots, 19–20
Metal sulfides, 80–83, 350–354
Microwave-assisted synthesis of quantum dots
  advantages, 116–117, 117*f*
  carbon and graphene, 135
  developments, 135
  disadvantages, 117
  synthesis of
    alloyed, 133–135
    core-shell, 130–132
    core-type, 117–130
Multiple exciton generation, 278

N

Night vision, 224–225
Nitrogen dioxide sensors, 317–318
Nonmetal-based quantum dots
  biomass waste and detection of ferric ions, 25*f*
  B, N-doped, 24*f*
  carbon, 21–26, 63–64
  graphene, 26–28, 64–65
  by hydrothermal route, 28*t*

O

Orange light-emitting diodes, 222–223
Oxides, 37–44

P

Pesticides, 185–186
Pesticide sensors, 318–320
Photoluminescence sensors, 255–257
Piezoelectric transducer, 150*f*
Plants
  biosynthesis of luminescent ZnO, 95–96
  cadmium telluride quantum dots, 96
  extracts of medicinal plants, 97
  green chemical route for, 97
  Ocimumsanctum (Tulsi) leaf extract, 97
  water-soluble biocompatible, 94–95

Q

Quantum dots, 170–171
  advantages, 2–3
  applications of, 9–13
  classification of, 4–7
  color with size of, 2*f*
  disadvantages, 3
  energy or frequency of emitted light, 2*f*
  synthesis of, 8–9
  unique features of, 3–4
  wavelength of radiation, 2*f*
Quantum dots-based solar cell parameters, 301*t*
Quantum dot sensitized solar cells
  band edge structure for TiO_2, 292*f*
  Cd QDs-based solar cell parameter, 295*t*
  CdS and CdSe electrodes, 292*f*
  dots-based, 297–300
    band structure of TiO_2 and $CuInS_2$, 299*f*
  inverted type-I CdS/CdSecore/shell structure, 294*f*
  Mn-doped CdS QDSSC solar cells, 294*f*
  NREL cell efficiency chart, 296*f*
  perovskite-based solar cells characteristics, 298*t*
  perovskite quantum dots-based, 294–297
Quantum dots in sensors, 329*t*

R

Red light-emitting diodes, 217–219
Reduction of carbon dioxide, 188–189
Reverse type quantum dots, 5

S

Selenides, 157–158
Sensing
  chemiluminescence, 257–259
  electroluminescence, 259–261
  photoluminescence, 255–257
Sensors
  biosensors, 324–326
    graphene oxide quantum dots in detection of glucose, 324*f*
  chemical, 314–324
    alcohol, 314–315
    ammonia, 315–317
    ferricyanide and cyanide ions, 322*f*
    hydrogen sulfide, 317
    liquid petroleum gas, 315
    nitrogen dioxide, 317–318
    others, 320–324
    pesticide, 318–320

Sensors (*Continued*)
humidity, 326–327
temperature, 327–329
Sol formation, 36
Sol-gel synthesis of quantum dots
advantages, 37
disadvantages, 37
others, 47
in sol-gel and related processes, 36*f*
synthesis of, 37–47
Sonochemical synthesis of quantum dots
advantages, 148–149
disadvantage, 149
growth and implosion of a bubble, 148*f*
instrumentation, 149
reaction zone in cavitation process, 148*f*
synthesis of, 149–163
Sulfides, 44–46
Synthesis of alloyed quantum dots
MW treatment procedure, 134
Synthesis of core-shell quantum dots
core-shell-shell, 132
microwave-assisted preparation of CdTe, 133*f*
water-dispersed CdTe/CdS/ZnS core-shell-shell quantum dots, 133*f*
inverse type I, 131–132
inverse type II, 132
type I, 131
type II, 132
Synthesis of core-type quantum dots
other, 129–130
oxide quantum dots, 118–122
CeO_2, 121
CO_3O_4, 119–120
CuO, 122
MoO_2, 122
SiO_2, 121
SnO_2, 118–119
TiO_2, 122
WO_3, 121
ZnO, 120
selenide, 126–127
CdSe, 126–127
sulfide, 122–126
CdS, 122–123
PbS, 125
ZnS, 123–125
telluride, 127–129
CdTe, 128–129
ZnTe, 127–128
Synthesis of quantum dots
bottom-up approach, 9, 9*f*
carbon-based, 46–47, 84–85, 159–162
$BiVO_4$/CNQDs/NCDs, 86*f*
iron-based, 85*f*
rhodamine B and tetracycline, 86*f*
chalcogenide, 286–289
dye sensitized solar cells, 84*f*
graphene based, 47
graphene-based, 85–87
hot-injection method, 290*f*
metal oxides, 79–80, 151–153
metals, 149–151
metal selenide quantum dots, 83–84
metal sulfides, 80–83, 153–157
methods of synthesis, 9
under microwave irradiation, 136*t*
others, 87, 162–163
oxides, 37–44
perovskite, 289–291
selenides, 157–158
sulfides, 44–46
tellurides, 158–159
top-down approach, 8, 8*f*
UV-visible spectra of CdTe QDs, 288*f*

T

Targeted drug delivery
doses of anticancer drugs, 252–253
dual-functional NMs, 249–250
novel drug, 250
treatment of cancer, 248–249
triple negative breast cancer (TNBC), 252
to tumors, 249
Tellurides, 158–159
Temperature sensors, 327–329
Toxicity of quantum dots, 264–267

U

Ultrasonic cavitation, 147
Unique features of quantum dots
high surface-to-volume ratio, 3
quantum confinement effect, 4
surface plasmon resonance, 3–4

W

Wastewater treatment
control recovery, 172
degradation of rhodamine B, 178*f*
drugs, 181–185
dyes, 173–181
heteroatoms-doped, 179–180

indigo carmine and levofloxacin, 177*f*
pesticides, 185–186
photocatalytic degradation
of amoxicillin, 183*f*
of methyl orange, 179*f*
of rhodamine B, 182*f*
photocatalytic hydrogen generation, 176*f*
photocatalytic reduction of Cr, 173*f*
White light-emitting diodes, 207–213

Y

Yellow light-emitting diodes, 223

Quantum Dots

Fundamentals, Synthesis and Applications

With their adaptability and broad applicability, quantum dots have become an increasingly important tool for the development of new materials, approaches, and applications across a wide range of fields. Understanding the molecular fundamentals governing their structures, interactivity, and behaviors can provide a unique insight for researchers and help them design and apply quantum dots in novel ways. *Quantum Dots: Fundamentals, Synthesis and Applications* compiles such key information with practical guidance on quantum dot synthesis and applications.

Beginning with an introduction to quantum dots, Part 1 highlights foundational knowledge such as growth mechanisms, shape and composition, electrochemical properties, and production scale-up for quantum dots. Part 2 goes on to provide practical guides to key chemical, physical, and biological methods for the synthesis of quantum dots. Part 3 reviews a range of important applications of quantum dots, including photocatalysis, energy cells, and medical imaging.

Drawing on the knowledge of its expert authors, this book provides practical guidance for all those who already study, develop, or use quantum dots in their work and is a great introduction for anyone who would like to start doing so.

Key features

- Presents foundational information needed to effectively understand and manipulate quantum dot properties
- Consolidates key methods of quantum dot synthesis in a single volume
- Reviews both current and future practical applications of quantum dots across a range of important fields

About the editors

Dr. Rakshit Ameta has a thoroughly first-class career, securing first position in his MSc. and was awarded a Gold Medal. He was also given the Fateh Singh Award from Maharana Mewar Foundation, Udaipur for his meritorious performance. After completion of his Ph.D., he served in Hindustan Zinc Limited, Vedanta Group for 1 year. Under his supervision, 12 Ph.D. students have been completed their Ph.D. on various aspects of green chemistry. He has around 140 research publications to his credit in journals of national and international repute. Presently, he is the Director, Faculty of Science, J. R. N. Rajasthan Vidyapeeth (Deemed to be University), Udaipur.

Dr. Jayesh P. Bhatt received his MSc. from RSTM Nagpur University in 2011. He did his Ph.D. in the year 2019 from PAHER University, Udaipur and since 2019, he has been working as an Assistant Professor in the Department of Chemistry of the same university. Dr. Jayesh has published 11 research articles in various reputed national and international journals and contributed 12 chapters. Currently, four Ph.D. students are working under his supervision.

Prof. Suresh C. Ameta obtained his master's degree from the University of Udaipur and was awarded a gold medal in 1970. He obtained his Ph.D. degree from Vikram University in 1980. He has served as a Professor and Head of the Department of Chemistry, North Gujarat University, Patan (1994) and M. L. Sukhadia University, Udaipur (2002–05) and the Head of the Department of Polymer Science (2005–08). He has successfully guided 108 students through their course of Ph.D. Dr. Ameta has more than 400 research papers and 36 books to his credit.

ISBN 978-0-12-824153-0

9 780128 241530

ELSEVIER elsevier.com/books-and-journals

GRAPHENE-BASED CARBOCATALYSTS

SYNTHESIS, PROPERTIES AND APPLICATIONS

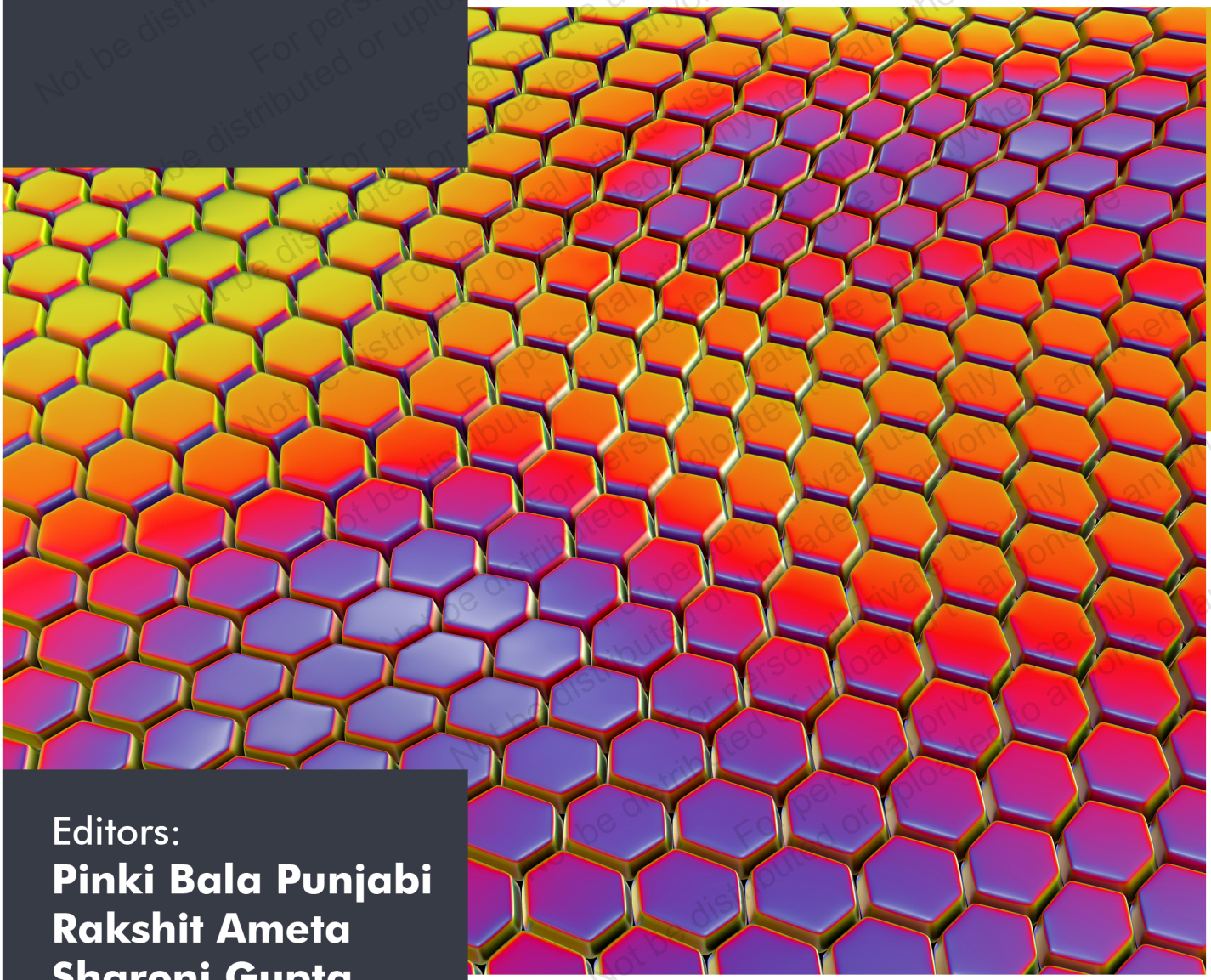

Editors:
Pinki Bala Punjabi
Rakshit Ameta
Sharoni Gupta

Bentham Books

Not be distributed or uploaded to anyone or anywhere
For personal private use only

Graphene-based Carbocatalysts: Synthesis, Properties and Applications

(Volume 1)

Edited by

Pinki Bala Punjabi
Department of Chemistry, University College of Science, Mohanlal Sukhadia University, Udaipur-313001, Rajasthan, India

Rakshit Ameta
Department of Chemistry, J.R.N. Rajasthan Vidyapeeth University, Udaipur-313001, Rajasthan, India

&

Sharoni Gupta
Department of Chemistry, University College of Science, Mohanlal Sukhadia University, Udaipur-313001, Rajasthan, India

For personal private use only
Not be distributed or uploaded to anyone or anywhere

Graphene-based Carbocatalysts: Synthesis, Properties and Applications (Volume 1)

Editors: Pinki Bala Punjabi, Rakshit Ameta & Sharoni Gupta

ISBN (Online): 978-981-5050-89-9

ISBN (Print): 978-981-5050-90-5

ISBN (Paperback): 978-981-5050-91-2

© 2023, Bentham Books imprint.

Published by Bentham Science Publishers Pte. Ltd. Singapore. All Rights Reserved.

First published in 2023.

For personal private use only
Not be distributed or uploaded to anyone or anywhere

BENTHAM SCIENCE PUBLISHERS LTD.

End User License Agreement (for non-institutional, personal use)

This is an agreement between you and Bentham Science Publishers Ltd. Please read this License Agreement carefully before using the ebook/echapter/ejournal (**"Work"**). Your use of the Work constitutes your agreement to the terms and conditions set forth in this License Agreement. If you do not agree to these terms and conditions then you should not use the Work.

Bentham Science Publishers agrees to grant you a non-exclusive, non-transferable limited license to use the Work subject to and in accordance with the following terms and conditions. This License Agreement is for non-library, personal use only. For a library / institutional / multi user license in respect of the Work, please contact: permission@benthamscience.net.

Usage Rules:

1. All rights reserved: The Work is the subject of copyright and Bentham Science Publishers either owns the Work (and the copyright in it) or is licensed to distribute the Work. You shall not copy, reproduce, modify, remove, delete, augment, add to, publish, transmit, sell, resell, create derivative works from, or in any way exploit the Work or make the Work available for others to do any of the same, in any form or by any means, in whole or in part, in each case without the prior written permission of Bentham Science Publishers, unless stated otherwise in this License Agreement.
2. You may download a copy of the Work on one occasion to one personal computer (including tablet, laptop, desktop, or other such devices). You may make one back-up copy of the Work to avoid losing it.
3. The unauthorised use or distribution of copyrighted or other proprietary content is illegal and could subject you to liability for substantial money damages. You will be liable for any damage resulting from your misuse of the Work or any violation of this License Agreement, including any infringement by you of copyrights or proprietary rights.

Disclaimer:

Bentham Science Publishers does not guarantee that the information in the Work is error-free, or warrant that it will meet your requirements or that access to the Work will be uninterrupted or error-free. The Work is provided "as is" without warranty of any kind, either express or implied or statutory, including, without limitation, implied warranties of merchantability and fitness for a particular purpose. The entire risk as to the results and performance of the Work is assumed by you. No responsibility is assumed by Bentham Science Publishers, its staff, editors and/or authors for any injury and/or damage to persons or property as a matter of products liability, negligence or otherwise, or from any use or operation of any methods, products instruction, advertisements or ideas contained in the Work.

Limitation of Liability:

In no event will Bentham Science Publishers, its staff, editors and/or authors, be liable for any damages, including, without limitation, special, incidental and/or consequential damages and/or damages for lost data and/or profits arising out of (whether directly or indirectly) the use or inability to use the Work. The entire liability of Bentham Science Publishers shall be limited to the amount actually paid by you for the Work.

General:

1. Any dispute or claim arising out of or in connection with this License Agreement or the Work (including non-contractual disputes or claims) will be governed by and construed in accordance with the laws of Singapore. Each party agrees that the courts of the state of Singapore shall have exclusive jurisdiction to settle any dispute or claim arising out of or in connection with this License Agreement or the Work (including non-contractual disputes or claims).
2. Your rights under this License Agreement will automatically terminate without notice and without the

need for a court order if at any point you breach any terms of this License Agreement. In no event will any delay or failure by Bentham Science Publishers in enforcing your compliance with this License Agreement constitute a waiver of any of its rights.

3. You acknowledge that you have read this License Agreement, and agree to be bound by its terms and conditions. To the extent that any other terms and conditions presented on any website of Bentham Science Publishers conflict with, or are inconsistent with, the terms and conditions set out in this License Agreement, you acknowledge that the terms and conditions set out in this License Agreement shall prevail.

Bentham Science Publishers Pte. Ltd.
80 Robinson Road #02-00
Singapore 068898
Singapore
Email: subscriptions@benthamscience.net



For personal private use only
Not be distributed or uploaded to anyone or anywhere

CONTENTS

FOREWORD i

PREFACE ii

DEDICATION iv

LIST OF CONTRIBUTORS v

CHAPTER 1 INTRODUCTION TO CARBOCATALYSIS 1

Pinki Bala Punjabi and *Sharoni Gupta*

INTRODUCTION 1

PROPERTIES OF CARBOCATALYSTS 4

Surface Properties 5

Pore Size Distribution 7

Thermal Conductivity 8

Electrical Properties 8

SYNTHETIC STRATEGIES FOR CARBOCATALYSTS 11

Active Carbon 11

Graphite 13

Fullerenes 14

Glassy Carbon 16

Carbon Black 16

Channel Black Process 17

Gas Black Process 17

Thermal Black Process 17

Acetylene Black Process 17

Lamp Black Process 17

Furnace Black Process 17

Carbon Nanomaterials 18

Carbon Nanofibres 18

Carbon Nanotubes 20

Nanodiamonds 21

Carbon Nano-onions 23

Graphene and Its Derivatives 24

SCOPE OF CARBOCATALYSTS 24

CONCLUDING REMARKS 28

LIST OF ABBREVIATIONS 29

CONSENT FOR PUBLICATION 30

CONFLICT OF INTEREST 30

ACKNOWLEDGEMENTS 30

REFERENCES 30

CHAPTER 2 STRUCTURE AND PROPERTIES OF GRAPHENE AND CHEMICALLY MODIFIED GRAPHENE MATERIALS 43

Manish Srivastava, Anjali Banger, Anamika Srivastava, Nirmala Kumari Jangid and *Priy Brat Dwivedi*

1. INTRODUCTION 44

2. FABRICATION OF GRAPHENE 46

2.1. Bottom-up Method 46

2.2. Top-down Method 46

3. STRUCTURE 46

4. PROPERTIES 47

Not be distributed or uploaded to anyone or anywhere For personal private use only

4.1. Electrical Properties 48
4.2. Mechanical Properties 48
4.3. Thermal Properties 49
4.4. Optical Properties 50
4.5. Chemical Properties 50
4.6. Biological Properties 50
Additional Properties 51
4.7. Functionality and Solubility 51
4.8. Surface Area 52
4.9. Fluorescence Quenching 52
4.10. Surface-Enhanced Raman Spectroscopy 52
5. APPLICATIONS 53
5.1. Storage Material 55
5.2. Actuators 56
5.3. Electrochemical Capacitors 56
6. GRAPHENE OXIDE 57
6.1. Fabrication of Graphene Oxide 57
7. QUANTUM DOTS OF GRAPHENE 60
7.1. Fabrication of Quantum Dots of Graphene 60
8. GRAPHENE AND DERIVED NANOFILLER 60
8.1. Fabrication of Graphene and Derived Nanofiller 60
8.2. Significance of Graphene and Derived Nanofiller 61
8.3. Application of Graphene and Derived Nanofiller in Energy and Electronics 61
9. GRAPHENE AEROGELS (GAS) 62
10. HYBRID GRAPHENE/MICROFIBER COMPOSITES 62
11. GRAPHENE BIOACTIVE COMPOSITES 63
12. CONCLUDING REMARKS 64
CONSENT FOR PUBLICATION 64
CONFLICT OF INTEREST 64
ACKNOWLEDGEMENTS 64
LIST OF ABBREVIATIONS 64
REFERENCES 66

CHAPTER 3 PREPARATION METHODS FOR GRAPHENE AND ITS DERIVATIVES 76
Sharoni Gupta, Pinki Bala Punjabi and *Rakshit Ameta*
INTRODUCTION 76
TOP-DOWN SYNTHESIS 79
Exfoliation Method 79
Mechanical Exfoliation 80
Chemical Exfoliation 83
Unzipping/Unrolling of Carbon Nanotubes 84
Electric Arc Discharge 86
Laser Ablation 87
Oxidative Exfoliation-Reduction of Graphene Oxide 88
Graphene Oxide Synthesis 89
Graphene Oxide Reduction 91
BOTTOM-UP SYNTHESIS 94
Chemical Vapour Deposition 94
Epitaxial Growth 95
Template Synthesis 97
Pyrolysis 98

For personal private use only
Not be distributed or uploaded to anyone or anywhere

Substrate Free Synthesis 99
Total Organic Synthesis 101
Biosynthesis of Graphene and its Derivatives 102
CONCLUDING REMARKS 103
LIST OF ABBREVIATIONS 104
CONSENT FOR PUBLICATION 105
CONFLICT OF INTEREST 105
ACKNOWLEDGEMENTS 105
REFERENCES 105

CHAPTER 4 CHARACTERIZATION TECHNIQUES FOR GRAPHENE-BASED MATERIALS 118
Vickramjeet Singh and *Ramesh L. Gardas*
1. INTRODUCTION 119
2. OPTICAL METHODS 119
2.1. Optical Microscopic Analysis 124
2.2. Transmission Electron Microscope (TEM) 125
2.3. Scanning Tunnelling Microscope (STM) 126
3. RAMAN SPECTROSCOPY 128
4. FT-IR SPECTROSCOPY 134
5. X-RAY PHOTOELECTRON SPECTROSCOPY (XPS) 135
6. THERMOGRAVIMETRIC ANALYSIS (TGA) 140
7. CONCLUDING REMARKS 144
LIST OF ABBREVIATIONS 144
CONSENT FOR PUBLICATION 145
CONFLICT OF INTEREST 145
ACKNOWLEDGEMENTS 145
REFERENCES 145

CHAPTER 5 FUNCTIONALIZATION OF GRAPHENE AND FACTORS AFFECTING CATALYTIC PERFORMANCE 154
Gopal Avashthi and *Man Singh*
INTRODUCTION TO CARBON CHEMISTRY 155
POLYMORPHISM OF CARBON 155
Natural Allotropes 156
Diamond 156
Graphite 158
Synthetic Allotropes 159
Fullerene 159
Carbon Nanotube 160
Graphene 161
REFINING OF GRAPHENE OXIDE 162
SURFACE FUNCTIONALIZATION OF GRAPHENE OXIDE FOR STRENGTHENING CATALYTIC PERFORMANCES 163
Covalent Functionalization 164
Nucleophilic Substitution Reaction 164
Electrophilic Substitution Reaction 166
Condensation Reaction 167
Cycloaddition Reaction (Pericyclic Reaction) 168
Noncovalent Functionalization 170
GRAPHENE OXIDE FUNCTIONALIZATION WITH AMINE SUBSTITUTED ORGANIC MOLECULES 171

Not be distributed or uploaded to anyone or anywhere
For personal private use only

ALTERNATIVES OF CONVENTIONAL METHODS FOR FUNCTIONALIZATION OF GRAPHENE OXIDE 172
Ultrasound-Assisted Functionalization: A Sustainable Technology 172
Microwave-Assisted Functionalization: A Green Chemical Transformations 173
CHEMICAL REDUCTION OF GRAPHENE OXIDE 174
GRAPHENE-BASED MATERIALS TOWARDS VARIOUS CATALYTIC PERFORMANCES 175
Biomedical Catalysis 176
Photoluminescent Catalysis 177
Magnetic Catalysis 178
Electrocatalysis and Photocatalysis For Energy Applications 178
PHYSICOCHEMICAL MECHANISM TOWARDS REINFORCING CATALYTIC PERFORMANCES 181
CONCLUSION AND PERSPECTIVES 183
CONSENT FOR PUBLICATION 183
CONFLICT OF INTEREST 184
ACKNOWLEDGEMENTS 184
REFERENCES 184

CHAPTER 6 GRAPHENE-BASED NANOCOMPOSITE CATALYSTS: SYNTHESIS, PROPERTIES AND APPLICATIONS 208
Pradeep Kumar Jaiswal, Munsaf Ali, Siddharth Sharma, Dinesh Kumar Yadav and *Nitinkumar Satyadev Upadhyay*
INTRODUCTION 208
APPROACHES TOWARDS GRAPHENE-BASED NANOCOMPOSITES SYNTHESES 210
Non-covalent Interactive Approach 210
Covalent Interactive Approach 210
In-situ Chemical Electroless Deposition-based Approach 211
Solvothermal and Hydrothermal-growth Based Approach 212
Microwave- assisted Approach 215
Electrochemical and Electrophoresis Deposition-based Approach 216
Chemical-vapor Deposition (CVD) Based Approach 217
Photochemical- based Approach 218
Physical Deposition/Mixing Based Approach 219
PROPERTIES AND APPLICATIONS OF GRAPHENE-BASED NANOCOMPOSITE CATALYSTS 220
For Energy Storage and Conversion 221
As a Basic Component in Lithium-ion Batteries (LIBs) 222
As a Basic Component in Supercapacitors 223
As an Electrocatalyst in Fuel Cells 224
As an Electrochemical Sensor 225
Catalytic Potential of Graphene-based Nanocomposites 227
CO Oxidation 227
Oxidation of Alcohols 228
Graphene-based Nanocomposite for Hydrogenation Reactions 230
Graphene Based Nanocomposite in Fischer–Tropsch Synthesis 233
Graphene-supported Nanocomposites for Hydrolysis of AB (Ammonia Borane) 234
Graphene-supported Nanocomposite for Coupling Reactions 236
CONCLUSION AND SUMMARY 238
LIST OF ABBREVIATIONS 239
CONSENT FOR PUBLICATION 240

For personal private use only
Not be distributed or uploaded to anyone or anywhere

CONFLICT OF INTEREST 240
ACKNOWLEDGEMENTS 240
REFERENCES 240

CHAPTER 7 GRAPHENE SUPPORTED PALLADIUM NANOCATALYST FOR CROSS-COUPLING REACTIONS 263
Mukesh Kumar, Meenakshi Singh Solanki and *Siddharth Sharma*
INTRODUCTION 263
GRAPHENE SUPPORTED PALLADIUM NANOPARTICLES (PDNPS/G) CATALYZED CROSS-COUPLING REACTIONS 265
GRAPHENE OXIDE (GO) SUPPORTED PALLADIUM NANOPARTICLES (PDNPS/GO) CATALYZED CROSS-COUPLING REACTIONS 273
REDUCED GRAPHENE OXIDE (RGO) SUPPORTED PALLADIUM NANOPARTICLES (PDNPS-RGO) CATALYZED COUPLING REACTIONS 279
CONCLUDING REMARKS 288
LIST OF ABBREVIATIONS 289
CONSENT FOR PUBLICATION 290
CONFLICT OF INTEREST 290
ACKNOWLEDGEMENTS 290
REFERENCES 290

CHAPTER 8 DOMINO AND MULTICOMPONENT REACTIONS BY GRAPHENE-BASED CARBOCATALYSTS – A BOON FOR ORGANIC TRANSFORMATIONS 297
S. Haripriya, K.M. Sreeranjan, Sagar Ulkesh Patil, G.S. Sahoo Navneet, H.S. Sushma, S. Ahallya, Rakesh R Panicker, Ivaturi Sai Vighnesh, Rajagopal Desikan, Vepa Jagannadha Rao and *Akella Sivaramakrishna*
1. INTRODUCTION 297
2. SYNTHESIS OF GRAPHENE-BASED CARBOCATALYSTS 298
3. ORGANIC TRANSFORMATIONS BY GRAPHENE-BASED CARBOCATALYSIS 300
3.1. Oxidation Reactions 300
3.2. Carbon-Carbon Bond Formation 303
3.3. Hydrogenation Reaction 306
3.4. Aza-Michael Addition 311
3.5. Dehydration-Hydrothiolation Reactions 313
3.6. Friedel-Crafts Alkylation 314
3.7. Other Useful Reactions 317
CONCLUSION AND FUTURE PROSPECTS 323
LIST OF ABBREVIATIONS 325
CONSENT FOR PUBLICATION 326
CONFLICT OF INTEREST 326
ACKNOWLEDGEMENTS 326
REFERENCES 326

CHAPTER 9 OXIDATION AND REDUCTION REACTIONS CATALYZED BY GRAPHENE BASED CATALYSTS 337
Chetna Ameta, Priyanka Chundawat, Yogeshwari Vyas, Reema Agarwal and *Dharmendra Dharmendra*
INTRODUCTION 337
SYNTHESIS OF GRAPHENE/GRAPHENE OXIDE 339
Graphene 339
Graphene Oxide and Reduced Graphene Oxide 339
Functionalized Graphene Oxide 342

Not be distributed or uploaded to anyone or anywhere
For personal private use only

N-Doped (Heteroatom-Doped) Graphene 342
CATALYTIC APPLICATIONS 343
Oxidation Reactions 344
Catalysis by Graphene Oxide and Graphite Oxide 344
Oxidation of Cis-Stilbene 346
Oxidation of Organosulfur Compounds 347
Oxidation of Thiols 348
Oxidation of Sulfides 350
Oxidation of Amines 352
Nitrogen-Doped Graphene Catalysts 353
Oxidation of Alkyl Arenes and Alcohols 354
Selective Oxidation of Olefins and Alcohols 356
REDUCTION REACTIONS 360
Reduction of Nitro Compounds 360
Graphene-Based (nano) Catalysts in the Reduction of Nitro Compounds 361
GO and RGO 361
Au/Graphene-Based Nanocomposites 361
Ag/Graphene-based Nanocomposites 362
Pd/Graphene-Based Nanocomposites 362
Ni/Graphene-based Nanocomposites 363
Pt/Graphene-based Nanocomposites 364
Cu/Graphene-based Nanocomposites 364
Bimetallic/Graphene-based Nanocomposites 365
CONCLUDING REMARKS 366
LIST OF ABBREVIATIONS 367
CONSENT FOR PUBLICATION 368
CONFLICT OF INTEREST 368
ACKNOWLEDGEMENTS 368
REFERENCES 368

CHAPTER 10 GRAPHENE BASED BIOCATALYSTS 378
Monika Jangid, Sunita Panchawat and *Abhilasha Jain*
INTRODUCTION 378
APPLICATIONS OF GRAPHENE BASED BIOCATALYSTS 379
Immobilization of Enzymes 379
Biofunctionalization of Protein 392
Biosensors 393
Enzymatic Biofuel Cells 397
CONCLUSION 399
CONSENT FOR PUBLICATION 400
CONFLICT OF INTEREST 400
ACKNOWLEDGEMENTS 400
REFERENCES 400

SUBJECT INDEX 406

For personal private use only
Not be distributed or uploaded to anyone or anywhere

FOREWORD

Graphene is an allotrope of carbon, which is in the form of a thin layer with a two-dimensional honeycomb-like structure. It exhibits unique properties such as lightweight, excellent thermal and electrical conductivities, large specific surface area, easy preparation and functionalization, high intrinsic mobility, chemical stability, simple recovery, recyclability, *etc*. Therefore, it has emerged as the most successful entity with a wide range of applications in various medical, chemical and industrial processes, such as flexible electric/photonics circuits, solar cells, drug delivery, tissue engineering, bioimaging, optoelectronics, photodetectors, generation and storage of energy, biosensors, removal of contaminants, catalyst, water and sound proofing, and many more. The editors have made a very judicious choice in selecting graphene and its applications as a topic covering major fields of interest. I appreciate their efforts in compiling the different areas related to graphene and putting them all in a single arena. I believe that this book will get an overwhelming response from the readers.

Suresh C. Ameta
Past President & Life Time Advisor
Indian Chemical Society, Kolkata
Professor of Eminence (Distinguished Professor)
Faculty of Science
PAHER University
Udaipur-313003 (Raj.) India

Not be distributed or uploaded to anyone or anywhere
For personal private use only

PREFACE

Catalysis is a fundamental and multidisciplinary phenomenon that has been ruling the energy sector and chemical industry for centuries impacting the world's economy. Not only production processes but even biological and natural reactions are catalytically controlled by enzymes and other substances to maintain life on Earth. Various manufacturing units including petrochemicals, pharmaceuticals, food, polymers, materials, and fine chemicals-based industries along with pollution-abating firms are highly dependent on catalysts. This is because catalysts offer green means for accelerating chemical transformations *via* energy-saving and atom economic pathways.Untill today, multitudes of homogeneous and heterogeneous catalysts have been explored for carrying out several conversions and enhancing the feasibility of reactions. However, the issues of catalyst recoverability and efficiency have been a cause of concern across the globe. More recently, the necessity of environmental conservation has further accentuated the search for sustainable catalysts. In such a scenario, graphene-based catalysts or carbocatalysts have emerged as a boon to meet the growing demand for efficacious, benign and inexpensive heterogeneous catalysts.

Graphene with its distinguished opto-electronic, thermo-mechanical, surface and chemical characteristics is renowned as the most invincible nanomaterial. Ever since the path-breaking discovery of graphene in 2004, the two-dimensional, honeycomb lattice-based material has enthralled the scientific community throughout the world. The exceptional conductivity, tensile strength, stability, large surface area, recoverability, recyclability and ease of functionalization of graphene materials have especially captivated the researchers working in the field of catalysis. Owing to the surge in demand for graphene-based catalysts, graphene research is being carried out at a very rapid pace. Every year new additions to the knowledge and scope of graphene carbocatalysts appear at a considerably large scale. Consequently, this book is an attempt to acquaint readers with the recent advances in the field of graphene carbocatalysis.

The book encapsulates the recent developments involving the syntheses, properties, characterizations, functionalization, and catalytic applications of graphene, its derivatives and composites. The book is in two volumes. The first volume is divided into 10 chapters. In Chapter 1, a brief introduction to carbocatalysis has been laid out. The properties, syntheses and scope of carbocatalysts have been discussed to highlight their significance. Chapter 2 discusses the fundamental structure and properties of graphene and chemically modified graphene contributing to their applications in diverse fields. Chapter 3 describes the diverse synthetic strategies for the preparation of graphene and its derivatives. The advantages of present methods and future challenges related to industrial-scale synthesis have also been outlined in this chapter. Chapter 4 focuses on the latest and most commonly employed characterization techniques used for investigating the morphological, structural, and thermal properties of graphene materials. In Chapter 5, recent trends in functionalization and its role in the catalytic activity of graphene have been put forward. Chapter 6 summarizes the recent progress in the synthesis of graphene-based composites along with their properties and applications in catalytic reactions. The future prospects and challenges towards the design and development of graphene-based nanocomposites for catalytic reactions have also been addressed in the chapter. Chapter 7 reviews the recent advances in graphene-supported palladium catalysts for coupling reactions. It also underscores the synthesis of these catalysts and their mechanistic aspects spanning across a variety of cross-coupling reactions. A comparison of graphene-supported catalysts with traditional catalysts has also been included in this chapter. Chapter 8 provides an in-depth review of recent applications of graphene-based catalysts in multicomponent and domino reactions. In Chapter 9, current progress made

in the field of oxidation and reduction reactions of organic molecules catalyzed by graphene materials has been explored. Chapter 10 accounts for the contemporary trends in the area of graphene-based biocatalysts.

The second volume includes six chapters. Chapter 1 of the second volume incorporates the most recent advances in photocatalytic applications of graphene-based materials such as graphene-based semiconductor photocatalysts for the degradation of various contaminants (treatment of waste water), production of hydrogen, and photocatalytic reduction of carbon dioxide to energy-rich synthetic fuels (combating against global warming and energy crisis), *etc*. Chapter 2 discusses the latest advances in electrocatalysis by graphene materials with a special focus on the electrocatalytic activities of non-metal doped graphene, graphene-2D materials heterostructures, and graphene-plasmonic nanostructures. Chapter 3 provides an overview of the recent advancement made by graphene-based materials including graphene oxide, reduced graphene oxide and graphene oxide quantum dots for hydrogen evolution from light-driven water splitting and future prospects. Chapter 4 highlights the modern trends in the fabrication of graphene-based smart energy materials for applications in various energy storage systems. The future trends and challenges have also been underlined. Chapter 5 underscores the potential utility of graphene materials in electrochemical sensing devices. Chapter 6 concludes the book and reports state-of-the-art graphene carbocatalysis with the future challenges accompanying graphene-based catalysts.

The book covers multidimensional applications of graphene-based materials cutting across various fields ranging from energy generation, chemical synthesis, and electrochemical sensing to photocatalysis. Hopefully, this book will serve as a reference work for all those researchers, students, industry workers and engineers who are interested in graphene research as well as its emerging applications in catalysis and beyond.

At last, we would like to thank all the authors of this book for their invaluable contribution to enriching the content of this book. We are also extremely indebted to the managers, editors, and reviewers of Bentham Science Publications for their magnanimous help throughout the creation and publication of this book. Finally, we are highly grateful to our families for their constant support and inspiration.

Pinki B Punjabi
Department of Chemistry,
University College of Science,
Mohanlal Sukhadia University,
Udaipur-313001, Rajasthan,
India

Rakshit Ameta
Department of Chemistry,
J.R.N. Rajasthan Vidyapeeth University,
Udaipur-313001, Rajasthan, India

&

Sharoni Gupta
Department of Chemistry,
University College of Science,
Mohanlal Sukhadia University,
Udaipur-313001, Rajasthan, India

DEDICATION

In fond memory of my beloved uncle Mr. Anil Kothari who taught me how to smile through difficult times.

Dr. Sharoni Gupta

For personal private use only
Not be distributed or uploaded to anyone or anywhere

List of Contributors

Abhilasha Jain	Department of Chemistry, St. Xavier's College (Autonomus), Mumbai, Maharashtra-400001, India
Akella Sivaramakrishna	Department of Chemistry, School of Advanced Sciences, Vellore Institute of Technology (VIT), Vellore 632014, Tamil Nadu, India
Anamika Srivastava	Department of Chemistry, Banasthali Vidyapith, Banasthali, Rajasthan, India
Anjali Banger	Department of Chemistry, Banasthali Vidyapith, Banasthali, Rajasthan, India
Chetna Ameta	Photochemistry Laboratory, Department of Chemistry, University College of Science, Mohanlal Sukhadia University, Udaipur (Raj.), India
Dharmendra Dharmendra	Photochemistry Laboratory, Department of Chemistry, University College of Science, Mohanlal Sukhadia University, Udaipur (Raj.), India
Dinesh Kumar Yadav	Department of Chemistry, Mohanlal Sukhadia University, Udaipur, 313001, India
G.S. Sahoo Navneet	Department of Chemistry, School of Advanced Sciences, Vellore Institute of Technology (VIT), Vellore 632014, Tamil Nadu, India
H.S. Sushma	Department of Chemistry, School of Advanced Sciences, Vellore Institute of Technology (VIT), Vellore 632014, Tamil Nadu, India
Ivaturi Sai Vighnesh	Department of Chemistry, School of Advanced Sciences, Vellore Institute of Technology (VIT), Vellore 632014, Tamil Nadu, India
K. M. Sreeranjan	Department of Chemistry, School of Advanced Sciences, Vellore Institute of Technology (VIT), Vellore 632014, Tamil Nadu, India
Manish Srivastava	Department of Chemistry, Banasthali Vidyapith, Banasthali, Rajasthan, India
Monika Jangid	Department of Chemistry, PAHER University, 313001-Udaipur, Rajasthan, India
Munsaf Ali	College of Nanoscale Science and Engineering, State University of New York, Polytechnic Institute - CNSE, 257 Fuller Rd., Albany, NY 12203, New York
Nirmala Kumari Jangid	Department of Chemistry, Banasthali Vidyapith, Banasthali, Rajasthan, India
Nitinkumar Satyadev Upadhyay	College of Nanoscale Science and Engineering, State University of New York, Polytechnic Institute - CNSE, 257 Fuller Rd., Albany, NY 12203, New York
Priyanka Chundawat	Photochemistry Laboratory, Department of Chemistry, University College of Science, Mohanlal Sukhadia University, Udaipur (Raj.), India
Pinki Bala Punjabi	School of Basic and Applied Sciences, Sangam University, Bhilwara-311001, Rajasthan, India
Pradeep Kumar Jaiswal	Department of Biochemistry and Biophysics, Texas A&M University, College Station, Texas 77843, USA

For personal private use only Not be distributed or uploaded to anyone or anywhere

Priy Brat Dwivedi	National University of Science and Technology, AlHail South, Seen 111, Muscat, Oman
Reema Agarwal	Photochemistry Laboratory, Department of Chemistry, University College of Science, Mohanlal Sukhadia University, Udaipur (Raj.), India
Rajagopal Desikan	Department of Chemistry, School of Advanced Sciences, Vellore Institute of Technology (VIT), Vellore 632014, Tamil Nadu, India
Rakesh R Panicker	Department of Chemistry, School of Advanced Sciences, Vellore Institute of Technology (VIT), Vellore 632014, Tamil Nadu, India
Rakshit Ameta	Department of Chemistry, J.R.N. Rajasthan Vidyapeeth University, Udaipur-313001, Rajasthan, India
Ramesh L. Gardas	Department of Chemistry, Indian Institute of Technology Madras, Chennai - 600 036, India
S. Ahallya	Department of Chemistry, School of Advanced Sciences, Vellore Institute of Technology (VIT), Vellore 632014, Tamil Nadu, India
S. Haripriya	Department of Chemistry, School of Advanced Sciences, Vellore Institute of Technology (VIT), Vellore 632014, Tamil Nadu, India
S. Sathish	Department of Physics, MVJ College of Engineering, Bangalore – 560067, India
Sagar Ulkesh Patil	Department of Chemistry, School of Advanced Sciences, Vellore Institute of Technology (VIT), Vellore 632014, Tamil Nadu, India
Siddharth Sharma	Department of Chemistry, Mohanlal Sukhadia University, Udaipur, 313001, India
Sharoni Gupta	Department of Chemistry, University College of Science, Mohanlal Sukhadia University, Udaipur-313001, Rajasthan, India
Sunita Panchawat	Department of Phatmaceutical Sciences, Mohanlal Sukhadia University, Udaipur, Rajasthan-313001, India
Vepa Jagannadha Rao	Department of Chemistry, Anil Neerukonda Institute of Technology and Sciences, Affiliated to Andhra University, Sanghivalasa, Visakhapatnam 531162, Andhra Pradesh, India
Vickramjeet Singh	Department of Chemistry, Dr B R Ambedkar National Institute of Technology, Jalandhar-144011, Punjab, India
Yogeshwari Vyas	Photochemistry Laboratory, Department of Chemistry, University College of Science, Mohanlal Sukhadia University, Udaipur (Raj.), India

Not be distributed or uploaded to anyone or anywhere
For personal private use only

CHAPTER 1

Introduction to Carbocatalysis

Pinki Bala Punjabi[1,*] and **Sharoni Gupta**[1]

[1] *Department of Chemistry, University College of Science, Mohanlal Sukhadia University, Udaipur-313001, Rajasthan, India*

Abstract: Carbocatalysis has emerged as a promising field of catalysis. The exceptional surface morphology, pore distribution, thermal conductivity, chemical inertness, electrical property and renewability of carbon materials have rendered them suitable for various catalytic processes namely, photocatalysis, electrocatalysis, biocatalysis and chemical catalysis. Therefore, the introductory chapter on carbocatalysis describes the useful properties of carbonaceous materials which govern their catalytic behaviour. Moreover, synthetic approaches for the fabrication of diverse carbon polymorphs such as active carbon, graphite, fullerene, glassy carbon, carbon black, carbon nanotubes, carbon nanofibres, nanodiamonds, carbon nano-onions, and graphene have also been briefly discussed in this chapter. The scope of carbocatalysts over broad areas has also been elucidated by quoting instances.

Keywords: Carbocatalysis, Electrical Properties, Surface Properties, Sustainability, Synthesis, Thermal Conductivity.

INTRODUCTION

Catalysis is the backbone of chemical transformations which facilitates a sustainable and efficacious means to convert starting raw materials to useful chemical compounds. One of the twelve principles of green chemistry states that the "use of catalysts should be encouraged as these enhance selectivity, reduce the formation of by-products, reaction time and energy requirements" [1]. Therefore, catalytic transformations have become an integral part of environmentally benign chemical processes. Homogenous and heterogeneous catalysts are the two main classes of catalysts that over the past several decades have served as a driving force in achieving high performance conversions by abating the activation energy. Both homogeneous and heterogeneous catalysts have their high points, for instance, homogeneous catalysts have excellent catalytic efficiency owing to

* **Corresponding author Pinki Bala Punjabi:** Department of Chemistry, University College of Science, Mohanlal Sukhadia University, Udaipur-313001, Rajasthan, India; E-mail: pb_punjabi@yahoo.com

Pinki Bala Punjabi, Rakshit Ameta & Sharoni Gupta (Eds.)
All rights reserved-© 2023 Bentham Science Publishers

readily accessible active sites [2] while heterogeneous catalysts are quite stable and easy to separate and recover [3]. However, with growing awareness of environmentally friendly protocols, the use of conventional catalysts has become a debatable topic. This is primarily because the traditional catalysis employs acids, bases, transition and non-transition metals which are toxic, expensive, get easily deactivated by impurities and non-reusable.

Sustainability being an essential element of modern chemistry has coerced researchers and chemists globally to look for renewable and cost-effective catalytic systems. The recent emergence of graphene based catalysts has paved way for a green alternative to conventional catalysts. Carbocatalysis *viz.* catalysis driven by carbonaceous materials is not a novel avenue of study. Several carbon based catalyst have been used in the past. Perhaps the beginning of carbocatalysis can be traced back to the year 1854 when Stenhouse observed that activated carbon was capable of oxidizing a mixture of organic gases coming from putrefied biomass [4]. Since then there have been several reports where carbon allotropes were used as catalytic materials. In 1925, Rideal and Wright employed charcoal as a catalyst for the oxidation of oxalic acid [5]. In the 1930s, Kutzelnigg and Kolthoff separately confirmed that activated charcoals were highly suitable for catalyzing the aerobic oxidation of ferrocyanide to ferricyanide [6, 7]. Thereafter in 1979, charcoal was used to catalyze the oxidative dehydrogenation (ODH) reaction of ethylbenzene to styrene [8]. Also, graphite catalyst was employed for the first time by Lucking and co-workers for the oxidative cleavage of 4-chlorophenol, which yielded CO_2, H_2O, and HCl [9]. In another instance, Fortuny *et al.* have also reported oxidation of phenol using active carbon as a catalyst [10]. Despite the good catalytic performance of carbonaceous materials attributable to their versatile porosity and surface properties, carbocatalysis did not achieve the desired level of attention until the discovery of fullerene, carbon nanotubes, and graphene. Further, mostly the carbon polymorphs such as charcoal [11], graphite [12], carbon black [13], and diamond [14] have been used as support in catalytic systems because of their advantages including ease of metal immobilization on carbon, resistance to attack by acids and bases, simple as well as cost-effective preparation, high thermal stability and straightforward recovery of the active phase. Regardless of the beneficial features, some shortcomings such as lack of active sites, microporous structure, hydrophobic character and poor resistance to oxidation stalled the growth of carbon based catalysts in earlier days [15]. However, the recent developments in the synthetic chemistry of carbon have allowed easy modification of the pore size distribution, surface chemistry, and hydrophilicity to afford carbocatalyst with desirable electronic and physicochemical properties, large surface to weight ratio, and better biocompatibility.

The discovery of fullerenes in 1985 was a landmark in the field of carbon science [16]. The unique three dimensional structure of fullerene comprises intricately arranged five and six membered rings of covalently bonded carbon atoms arranged to form spherical shape. The high conductivity (narrow band gap) of fullerene arises from the pi electron delocalization within carbon layers which favours its catalytic behaviour. Functionalization of fullerenes also aids in tuning their electrical properties and serves as a precursor for the preparation of fullerene based nanocatalyst. Ever since their discovery, fullerene based catalysts have been used to catalyze several reactions such as reduction [17], oxidation [18], photodegradation [19], dehydration [20], proton transfer [21], deallylation [22], *etc*.

The birth of nanotechnology proved to be a boon for carbocatalysis. The designing of nanodimensional carbon tubes with readily accessible sites on large surface area revolutionized the field of catalysis. The breakthrough invention of carbon nanotubes in 1991 by Iijima [23] followed by its use as catalyst support in 1994 [24] led to a new generation of catalysts dominated by carbon nanomaterials. Carbon nanotubes belong to the fullerene family and are basically graphite sheets rolled in the form of cylindrical shapes. The excellent electrical conductivity, striking mechanical and thermal stabilities, tolerance against poisoning effect, easily modifiable surface area, and ease of functionalization of carbon nanotubes make them promising catalytic systems [25]. Carbon nanotubes have been widely applied and employed in heterogeneous catalysis [26], photocatalysis [27], and electrocatalysis [28].

One of the lightest and strongest known materials, graphene is a single layered allotrope of carbon that has honeycomb structure and is the most famous carbocatalyst of recent times. The discovery of graphene dates back to 1859 when Brodie while examining the structure of graphite, observed graphene and named it "graphone" [29]. In 2004, the isolation of graphene sheets by Novoselov *et al.* brought about a storm in the field of carbonaceous materials [30]. The extraordinary physicochemical and thermoelectrical properties of graphene such as large specific surface area (theoretically 2630 m^2/g for single-layer graphene) [31], amazing electronic properties and electron transport potential [32, 33], unparalleled flexibility and impermeability [34, 35], sturdy mechanical property [36] and excellent thermal and electrical conductivities [37, 38] attracted enormous interest and resulted in an explosion of research studies in the domain of graphene based materials. In 2009, Lu *et al.* highlighted the use of gold embedded graphene based catalyst for oxidation of CO [39]. Jafri *et al.* also reported nitrogen doped graphene nanoplatelets as a potent catalyst for oxygen reduction reaction [40]. In 2010, Dreyer *et al.* demonstrated graphene oxide as a compatible carbocatalyst for oxidation and hydration reactions [41]. In the same

year, Li and his research group reported electro-oxidation of methanol promoted by Pt nanoparticles on reduced graphene oxide [42]. In another instance, Gao and co-workers used reduced graphene oxide as carbocatalyst for the reduction of nitrobenzene [43]. Since then, a plethora of literature has been available which showcases the abilities of graphene and its derivatives as potent carbocatalysts.

Thus, a bountiful of reusable and economically viable carbonaceous materials are available today which serve as heterogeneous and semi-homogeneous catalysts as well catalytic supports for a range of reactions that find significance in different areas namely, chemical manufacturing, environmental remediation, biomass production, water splitting, energy conversion and storage devices. In the present chapter, an effort has been made to acquaint the readers with the properties, syntheses and scope of carbocatalysts (Fig. **1**).

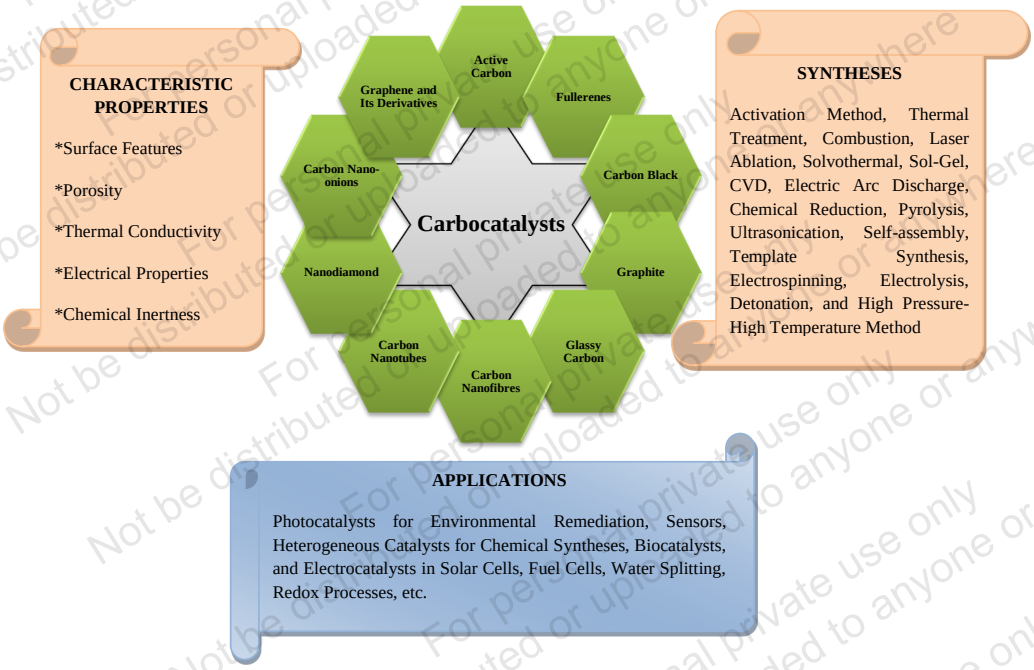

Fig. (1). Properties, syntheses and scope of carbocatalysts.

PROPERTIES OF CARBOCATALYSTS

Now let us delve into the properties of carbon materials that render them suitable as catalytic systems.

Not be distributed or uploaded to anyone or anywhere
For personal private use only

Surface Properties

It is well known that for any catalyst, surface features are crucial in governing its catalytic activity. The surface properties of carbon materials depend on the spatial arrangement of carbon atoms which in turn are based on the method of preparation or treatment used to synthesize these materials. The presence of a high density of pores and large surface area on carbonaceous materials play a key role in the adsorption of reactant molecules [44]. The introduction of defects in carbon atom layers present in carbon based materials and eases of their functionalization make their surface apt for catalysis. These structural defects particularly on the edges serve as active sites for binding of reaction molecules being easily accessible.

The defects in carbon materials can be introduced by thermal treatment or doping. For instance, Qiu *et al.* have reported that the amount of surface defects is directly related to the catalytic efficiency of activated carbons [45]. They used a simple thermal treatment method aided by a nitrate solid-phase oxidative method to increase the amount of surface defects on the activated carbons and observed their catalytic effect on the hydrochlorination of acetylene. It was reported that this treatment removed oxygen moieties and introduced defects on the edges of active carbons. Armchair and zigzag edges were observed in active carbon due to the stacking arrangement of nanosized graphitic layers, thereby populating the edges with active sites. In another study, it was reported that selective doping of carbon materials with heteroatoms induces catalytically beneficial defects. Chen *et al.* doped carbon nanosheets with B-N pairs and employed them as a catalyst to promote ammonia synthesis [46]. It was highlighted that the B-N doped carbon nanosheets showed superior activity compared to metallic catalysts for the nitrogen reduction reaction. The better electrocatalytic behavior of B-N doped carbon nanosheets was attributed to the fact that doping resulted in generating sufficient active sites at the edge carbon atoms.

The functionalization of carbon surfaces causes changes in the surface energy as well as chemical reactivity of the materials. Surface functional groups may increase free valences on the edges of the external surface, thereby increasing the catalytic activity [47]. The functional groups also assist in tuning the hydrophilicity of carbon materials and are capable of altering the acidic and basic character of these materials [48, 49]. Oxygen, nitrogen, hydrogen, sulphur, phosphorous and halogens functionalities are commonly used for this purpose. Chen *et al.* functionalized carbon nanotubes with oxygen functional groups [50]. Several oxidants like H_2O_2, $KMnO_4$, HNO_3/H_2SO_4 were used to functionalize the nanotubes. After functionalization, the pH_{pzc} (pH at which net surface charge on carbon is zero) was measured by the chemical titration method [51]. It was

reported that after functionalization the carbon surface became acidic due to the presence of functional groups like carboxyls which decreased the pH_{pzc} value making the surface more hydrophilic [52 - 54]. It was also reported that the presence of carboxylic functional groups also enhanced the dispersion of Pd and Pt metals on CNTs *via* the formation of chemical bonds, which hindered the agglomeration metal particles on CNTs and minimized the sintering propensity of the formed Pd–Pt particles across the CNT surface in the calcination and reduction process [55, 56]. This increased uniform dispersion of Pd-Pt on functionalized CNTs resulted in improved catalytic efficiency for hydrogenation of naphthalene to tetralin. In another study, it was reported that the functionalization of sulphonic acid group on graphene oxide improved its hydrophilicity as well as permeability [57].

It has been also reported that surface functionalization also improves the adsorption property of carbon materials. Sun *et al.* functionalized carbon beads *via* surface amination treatment and used it to study CO_2 capture [58]. It was demonstrated that the surface modifications enhanced the adsorption of CO_2 without compromising the desirable spherical morphology and mechanical strength of the activated carbon beads. This was attributed to surface modification of carbon, greater number of N-H functionalities resulted in stronger binding between CO_2 and C-N-H groups than that of C=N-C.

A study conducted by Arrigo *et al.* showed that the functionalization of nanocarbons aids in the regulation of their acidic/basic character [49]. They treated oxidized carbon nanofibres with ammonia and evaluated the surface acid-base properties. It was reported that the samples contained both O and N species on the surface which served as acidic and basic sites. It was further illustrated that the population of O and N functionalities depended on temperature and could be controlled to modify the acid-base properties of the carbon surface. At 473 K, nitrogen moieties were incorporated on the surface as a consequence of the reaction of carboxylic acid sites with ammonia, thereby generating a bifunctional hydrophilic material with both acidic and basic sites on the carbon surface. Further raising the temperature to 873 K resulted in strong basic sites leading to a hydrophobic carbon surface. Thus, it was proved that altering the surface functionalization once can modify the acid-base nature of the carbon surface.

The specific surface area of materials is one the most imperative factors that directly affect catalysis. Greater surface area means better ease of access to active sites. The size reduction of particles causes the enhancement in the surface area of a substance. The surfacing of nanotechnology has resulted in the development of methods through which one can get nanodimensional materials with extremely large surface area. The nanocarbon materials with higher surface to volume ratio

have therefore emerged as very effective carbocatalysts. For example, Pan *et al.* prepared porous N-doped carbon nanotubes (NCNTs) by pyrolysis of polypyrrole nanotubes and KOH activation at different temperatures 800 °C, 900 °C and 1000 °C [59]. The prepared nanotubes were used as electrocatalysts for the oxygen reduction reaction. A BET analysis was conducted to deduce the surface area of the nanotubes. It was reported that the specific surface area of polypyrrole nanotubes, NCNT-800, NCNT-900, and NCNT-1000 was 26, 1057, 1402, and 1137 m^2/g, respectively. The assessment of ORR in a standard three electrodes cell showed that the NCNT-900 and NCNT-1000 were the most efficient catalysts in promoting the reactions. Furthermore, the nanotubes exhibited superior catalytic activities as compared to the commercially available Pt/C catalyst. It was thus highlighted that the high surface areas in porous nanotubes afforded active sites for diffusing O_2 and KOH electrolyte thereby enhancing the rate of ORR.

Pore Size Distribution

The porosity of carbon materials is another important factor that influences their catalytic performance. Porous carbon materials can be classified as microporous (<2 nm), mesoporous (2-50 nm), and macroporous (>50 nm) on the basis of their pore diameters [60]. The pore volume and pore-size distribution play a crucial role in shape-selective catalysis [61]. Porosity in a material enhances catalytic activity not only by increasing accessibility to active sites albeit also by facilitating the mass transfer. Thus, by tuning the porosity one can induce desired catalytic properties in a material. Ferrero *et al.* investigated nitrogen-doped carbon microspheres with tunable porosity as electrocatalysts for the oxygen reduction reaction (ORR) [62]. It was reported that the catalyst was prepared by nanocasting using pyrrole as N-containing carbon precursor and porous silica microspheres as a template. Using two different silica samples as templates, the porosity of the microspheres was tuned from a micro- to a mesoporous network. The prepared catalytic system was applied to ORR and it was found that mesoporous electrocatalyst was more efficient than microporous one. This result was attributed to better accessibility of the active sites in the case of the mesoporous microspheres compared to the microporous ones. This is because in microporous materials the diffusion of reactant molecules becomes restricted due to small pore size and volume. It was further deciphered that the improved accessibility to the active sites on the surface of the mesoporous microspheres led to increase in mass-transfer reactions during the electrochemical process, thereby increasing the rate of catalytic reduction. Consequently, it can be said that pore size and volume are significant contributing factors in carbon based catalysis.

Thermal Conductivity

Thermal conductivity is another important criterion in carbocatalysis. Thermal conductivity is the ability of an object to conduct heat. Heat transfer is an important phenomenon in catalysis, particularly for strongly endo- and exothermic reactions in which fast heat management is advantageous for active sites [63]. Heat conduction in materials usually occurs due to the transmission of lattice vibrations known as phonons [64]. Carbonaceous materials like graphite, diamond, graphene, carbon fibres, and carbon nanotubes are well known for their thermal properties. The arrangement and coordination of carbon atoms along with defects in these materials are the main reasons for high thermal conductivities [65, 66]. A thermally conductive cobalt loaded graphite based catalyst for low temperature based highly exothermic Fischer-Tropsch synthesis (FTS) was reported [67]. It was reported that the use of this catalyst resulted in high productivity of hydrocarbons. This is because the incorporation of exfoliated graphite in the catalyst provides an amalgamation of extensive surface with high thermal conductivity and durability for the gasification process. Thermal analyses of graphite and aluminium based catalysts showed that the thermal conductivity of graphite is twice more than aluminum based catalyst and 30 times greater than a cobalt catalyst without heat conducting agents. It was further revealed that due to the high thermal stability of graphite, the catalyst survives overheating while the aluminum based counterpart is limited to 450 °C or even lower temperature because of irreversible effects such as metal pre-melting and oxidation. Hence, it is clear that thermally conductive as well as stable catalysts are perquisite for promoting reactions that require conduction of heat energy or heat removal.

Electrical Properties

To understand the electrical properties of carbonaceous materials, first, it is imperative to clarify the concepts of electrical resistivity and conductivity. Electric resistivity is a fundamental property of a material due to which it opposes the flow of electric current [68]. Mathematically, electric resistivity (ρ, Ωm) is defined as the ratio of electrical field (E, Vm^{-1}) inside the material to the electric current density (J, Am^{-1}), eq. (1). In other words, the resistivity is the resistance (R) offered by a material with unit cross sectional area (A) and unit length (l), eq. (2),

$$\rho = \frac{E}{J} \quad \textbf{(1)}$$

$$\rho = R.\frac{A}{l} \quad \textbf{(2)}$$

Not be distributed or uploaded to anyone or anywhere
For personal private use only

Electric conductivity (σ, $\Omega^{-1}m^{-1}$ or Sm^{-1}) is the property of a material by the virtue of which it conducts electricity. It is the reciprocal of electric resistivity. Consequently, both the terms resistivity and conductivity are interrelated and form the basis of the classification of materials [68]. On the basis of electric conductivity or resistivity, materials can be classified as conductors (materials that conduct electric current), insulators (materials that resist electric current) and semi-conductors (materials that intermediate between conductors and insulators).

The electrical properties of carbon materials are very much dependent on the structural attributes and type of treatment given to them. Different allotropes of carbon show different degrees of conductivities due to structural differences [69]. For instance, diamond exhibits low conductivity because each carbon atom is sp^3 hybridized and bonded to four carbon atoms by strong covalent bonds. Therefore, no electrons are available for conduction. It has a wide band gap of 5.5 eV [70]. While in graphite the sp^2 hybridized carbon atoms are arranged as two-dimensional hexagonal lattice structure with carbon sheets stacked one above another and each carbon has one free electron. The sheets are held by weak van der Waals forces, electrons freely move throughout the layered structure. Graphite, thus, has a small band gap (40 meV) between valence and conduction bands and behaves as a conductor similar to metal [71].

Fullerene, a carbon polymorph, is a large caged polyhedral molecule with either fcc or bcc packing of atoms. In fullerene sp^2 carbons are directly bonded to three neighbors in an arrangement of five- and six-membered rings. Fullerenes are basically semiconductors, however, by doping heteroatoms, superconductivity can be induced [72].

Carbon nanotubes (CNTs) are rolled-up graphene sheets with cylindrical structure. These are of two kinds, single-walled carbon nanotubes (SWCNT) with a diameter in the nanometer range and multi-walled carbon nanotubes (MWCNT) are nested single-walled carbon nanotubes held together by van der Waals forces with a diameter of less than 100 nm. The interlayer distance in multi-walled carbon nanotubes is 0.34-0.39 nm [73]. SWCNTs can have an armchair, chiral, and zigzag geometries depending on the wrapping of cylinders while MWCNTs are of two types Russian Doll model and the Parchment model [74]. When the diameter of the outer nanotube is greater than the inner nanotube then, it is called the Russian Doll model. Whereas, when a single graphene sheet wraps around itself multiple times just like a scroll of paper, it is called the Parchment model. On the basis of structural symmetry, carbon nanotubes can exhibit conducting or semiconducting nature [75].

Graphene is a two dimensional single sheet of carbon atoms arranged like a honeycomb lattice and displays unusual electrical properties. In graphene, each C atom is linked to three other carbon atoms, leaving an electron freely available for electronic conduction. These mobile electrons are called pi (π) electrons and are located above and below the graphene sheet. Graphene is a zero-gap semiconductor because its conduction and valence bands meet at the Dirac points, where the effective mass of electrons (or holes) is zero. The free electrons in graphene interact with the periodic potential of the honeycomb lattice, generating new quasiparticles that have lost their mass or rest mass and hence, called massless Dirac fermions. Thus, graphene conducts electrons with high velocity and the lattice symmetry inhibits direct backscattering of electrons, enhancing the electrical mobility and conductivity [76].

The remarkable electric conductivities of graphite, fullerenes, nanotubes, and graphene make them highly suitable as a catalyst for various redox reactions. The electrical properties of carbon materials arising from their unique structures can further be tuned by functionalization, heteroatom doping and controlling the temperature of graphitization or carbonization [77].

Functionalization of carbon surface alters the electrical behaviour of carbon material by modifying their structure. In one such instance, Suslova *et al.* have reported that the electrical conductivity of nitrogen doped carbon nanotubes increased considerably with an increase in oxygen functionalities on their surfaces owing to elevation in the density of defects in their structural arrangement [78]. In another example, it was shown that graphitized carbon nanofibre bearing oxygen functional groups demonstrated high electrocatalytic activity as bifunctional electrode for vanadium redox flow battery [79]. The high catalytic performance of carbon nanofibres was attributed to an increase in ion diffusion and electron transfer processes owing to improved electrical conductivity and surface area due to presence of surface functionalities.

Doping is a method by which introduction of heteroatom results in generation of holes or addition of an extra electron in a substance. This process leads to decrease in band gap of valence and conduction bands, thereby, improving the conductivity of semiconductors. Heteroatom doping is therefore a strong tool for tuning the electrical conductivities of carbon materials. Han *et al.* studied the effect of N-doping in carbon nano-onions [80]. The N-doped carbon nano-onions (N-CNOs) were prepared by a one-step, *in situ* flame synthesis technique using clarified butter and acetonitrile as precursors. The prepared N-CNO was than employed as catalyst for ORR process in a microbial fuel cell. It was reported that the catalytic activity of N-CNO was 5.4 times higher than CNO. This high performance was ascribed to the presence of nitrogen atoms in carbon framework.

Through electrochemical impedance spectroscopy, it was elucidated that the conductivity of N-CNO is higher than CNO due to N-doping. It has been explained that the sp^2–C atoms adjacent to N atoms and N atoms stimulate the electrostatic adsorption of oxygen molecules leading to sharp reduction in the kinetic barrier for the ORR process [81]. Simultaneously, N-doping causes electron excess in the delocalized π-system which results in enhancement of electrical conductivity. Finally, the high electrical conductivity induces electron transfer during catalysis, assisting the contribution of C-N active sites and improving the ORR activity on the whole [82]. As a result, the high ORR catalytic performance of N-CNO can be attributed to the high electrical conductivity arising from N-doping.

It has also been reported that thermal [83] and graphitization treatments [84] generally result in metallic conductivity in carbon materials while oxidation induces semi-conductivity due to π-electron delocalization [85]. Therefore, by applying different treatments one can tune the electrical properties of carbocatalysts.

SYNTHETIC STRATEGIES FOR CARBOCATALYSTS

As is well known that synthetic methods greatly influence the properties of a material, therefore, in this section some strategies employed for synthesis of carbocatalyst have been discussed. So many methods for synthesis of carbon materials are reported that a whole chapter can be devoted to the synthetic aspects of carbon allotropes. However, since the book deals with graphene here we have highlighted some important methods only.

Active Carbon

Activated carbon is highly porous form of carbon. Coal, wood, agricultural wastes or biomass, ionic liquids, salt solutions, *etc*. are used as precursors to prepared activated carbon or charcoal [86]. Physical and chemical activation methods are commonly used to prepare active carbon materials. Before activation, carbonization and de-ashing is performed as pre-treatment. In carbonization the raw materials are subjected to heat treatment or pyrolysis at high temperatures around 573.15 K to 1173.15 K in order to eliminate non-carbon materials and volatile impurities. This result in formation of char after rearrangement of carbon atoms into graphitic sheets stacked above one another to form rigid microcrystals with voids which constitute the pore structure [44]. Ahead of activation, ash and mineral content of the carbon materials is reduced by de-ashing or demineralization technique *via* chemical leaching. In this process, acid and alkali solutions are used to demineralize the carbon raw materials [87]. For instance,

Ahmad *et al*. performed acid treatment of cocoa shell pellets with 1M HCl which reduced the ash content to less than 10% [88]. In another study, it was reported that high ash content reduced the adsorption property of activated charcoal prepared from stone coal ore hence, to improve the adsorption. The stone coal ore was pre-treated with HF and H_2SO_4. The acid treatment reduced the contents of mineral atoms like Fe, Mg, Ca, Si, *etc*. resulting in stone coal ore with 74.76% carbon content [89]. Similarly, KOH promoted de-ashing of rice husk was reported by Shen and Fu which resulted in highly porous biochar [90].

Next step involved in formation of activated carbon is activation. Activation can be carried out in two methods: physical and chemical. Physical activation includes use of carbon dioxide, air, steam or other gaseous agents at 1073.15 to 1273.15 K to remove oxides of carbon from char and improving the porosity of carbonaceous materials. Zhou and co-workers have reported preparation of highly porous activated carbon from waste tea *via* physical activation with steam [91]. It was further highlighted that typically micropores were developed when the activation temperature was below 800 °C while activation above 800 °C enriched the carbon with both micropores and mesopores.

Chemical activation involves single-step carbonization and activation of carbon materials by impregnating them with chemical agents such as KOH, $ZnCl_2$, H_3PO_4, $FeCl_3$, $CaCl_2$, H_2SO_4, NaOH, $MgCl_2$, K_2CO_3, HNO_3, *etc*., followed by thermal treatment [86]. The chemical agents due to dehydrating property result in generation of a rigid framework which is less prone to reduction in volume during carbonization, thereby generating excellent yields of activated carbon [92, 93]. Moreover, since chemical activation is performed at lower temperature than physical activation, it offers better control of porous structure [94]. However, from environment point of view physical activation is better as it avoids use of chemical agents while chemically activated materials contain some amount of inorganic matter [95]. Recently, Chen *et al.* have demonstrated synthesis of activated carbon with large surface area from tobacco stem [96]. Chemical activation was performed using KOH, K_2CO_3 and $ZnCl_2$ as activating agents. It was reported that $ZnCl_2$ caused higher activation of tobacco stem compared to KOH and K_2CO_3. Further, increasing the concentration of $ZnCl_2$ enhanced the development of new pores and the widening of existing pores. Furthermore, activation of carbon with K_2CO_3 resulted in high oxygen functionalities on the surface. Thus, it is evident that nature of chemical agent and concentration affects the activation process as well as surface properties.

Graphite

Synthetically, graphite is prepared *via* thermal treatment of petroleum coke or coal-tar. Hydrothermal methods involving treatment of polymers and metal carbides can also be used to produce graphitic materials. Of late, graphite encapsulated nanoparticles have also emerged as potent carbocatalysts. These can be fabricated by several methods such as pyrolysis, template synthesis, chemical vapor deposition, arc discharge, laser ablation technique, *etc*. Li *et al.* have demonstrated hydrothermal synthesis of graphite encapsulated molybdenum carbides [97]. The graphite encased molybdenum carbide nanoparticles were prepared by the hydrothermal carbonization of a mixture of glucose solution and ammonium molybdate followed by temperature programmed reduction under mild conditions. The prepared graphite encapsulated nanoparticles showed high catalytic efficiency for conversion of guaiacol to phenolic compounds in methanolic medium. In another study, graphite encapsulated gold nanoparticles displaying excellent electrocatalytic activities towards oxidation reduction reaction were prepared by laser ablation method. The process of laser ablation involved installation of Au target in a vessel containing graphite precursor-acetone (16 mL). Thereafter, the revolving Au target was ablated by a focused beam of laser with wavelength of 1064 nm, 10 Hz pulse repetition rate and 100 mJ pulse energy for 30 min. Finally, the graphite encased Au nanoparticles were obtained by centrifugation followed by freeze drying. Thus, laser ablation technique afforded a facile and efficient route to synthesis of graphite encased nanoparticles.

Recently, expanded graphite has been employed as catalyst for oxidation reaction [98]. Expanded graphite is a type of graphite with interlayer spaces. The expanded graphite is prepared by oxidation of natural graphite flakes using acids like nitric acid and sulfuric acid and oxidants like potassium permanganate, chromic acid, hydrogen peroxide, *etc*. Then, the mixture is subjected to high temperature which causes expansion and swelling of graphite resulting in separation of layers leading to formation of its expanded form.

In recent past, hydroxylated high surface area graphite has also been used as carbocatalyst for ozonation. Usually, oxygen functionalized graphite are prepared *via* oxidation using strong acids and mechanical or thermal exfoliation methods. In a method reported by Bernat-Quesada *et al.*, the water soluble graphite was synthesized by oxidation of graphite by nitric acid [99]. Dispersion of graphite in nitric acid followed by heating at 83 °C for 20 h followed by filtration and drying resulted in formation of oxygen functionalized graphite on edges as well as basal planes [48]. In another method, the workers used ball milling technique to fabricate hydroxylated graphite. In this method, graphite, KOH and water were

loaded in a grinding jar of planetary ball mill. The jar was agitated at 300 rpm for 10 hours at ambient temperature. Later, the mixture was filtered and dried to obtain graphite functionalized with oxygen moieties on the edges.

Xu *et al.* have also reported the synthesis of functionalized graphite felts as catalyst for oxidation of hydrogen sulphide [100]. The commercial graphite felts bearing oxygen functionalities were prepared by treatment with nitric acid. According to the method, graphite felts were first heated at 500 °C for 1 hour in air. Then, the felts were loaded in a tubular reactor and heated at 250 °C using an external electric furnace [101]. The reactor loaded with the felts was connected to a round bottom flask (RBF) containing 65% HNO_3 solution (150 mL). The temperature of the RBF was maintained at 125 °C and the solution was continuously stirred magnetically. The gaseous acid passed through the felts for several hours causing their oxidation. The sample was then washed using deionized water and dried at 130 °C overnight. The acid treated functionalized graphite felts exhibited large surface area and it was concluded that the structural defects in graphite felts as well as oxygen groups on them served as active sites for oxidation of hydrogen sulphide.

Fullerenes

Fullerenes and their composites are widely used as catalysts. Fullerenes are giant caged carbon allotropes that are generally prepared by arc discharge and laser ablation of graphite, and combustion of hydrocarbons. In a typical arc discharge method, electric current is struck between graphite or carbon anode and cathode electrode in an inert atmosphere. The electric discharge produces soot which is collected and fullerene is then extracted from the soot by solvent extraction method, sublimation or supercritical fluid extraction technique. Generally for fullerene synthesis, an alternating current between the graphite electrodes in He atmosphere of about 200 Torr is used to produce soot containing C_{60} and C_{70} molecules [102].

The laser ablation technique makes use of a pulsed laser beam which is focused on the surface of carbon sample at high temperature (usually 1000 °C). Thus, the ablation of carbon results in fragments which form fullerenes [103]. Also, hydrocarbon combustion in presence of electric field acting on the flame is widely used to achieve soot-containing fullerene [104].

Additionally, several fullerene based complexes are also well known as catalysts and can be prepared by different methods. For instance, Sabounchei and co-workers have prepared mono- and bidentate palladium(0)- [60]fullerene based complexes as catalyst for Mizoroki-Heck coupling reaction [105]. The synthetic strategy involved a Schlenk tube containing C_{60} (0.05 mmol, 0.036 g) and

$Pd(dba)_2$ (0.05 mmol, 0.029 g) in 15 mL of toluene. The reaction mixture was stirred for 15 min at room temperature during which the color changed from purple to black. Thereafter, a phosphorus ylide solution (0.05 mmol) in toluene (5 mL) was injected into the reaction solution *via* a syringe pump. Further, a 2 hour stirring was continued at ambient temperature which resulted in deep green solution. Dark green crystals were obtained by treating the solution with n-hexane overnight and later washing with diethyl ether.

Further, several fullerene based composites fabricated by sol-gel method, chemical reduction, ultrasonication, hydro- or solvothermal technique, *etc*. serve as useful catalysts [106]. For example, Liu *et al.* have reported synthesis of silver (I) doped fullerene by liquid- liquid interfacial precipitation method [107]. The method involved mixing of saturated solution of fullerene (approx. 2.8 mg/mL) in toluene with isopropyl alcohol saturated with silver nitrate at ambient temperature. The bilayer so formed was kept still under room conditions for 3 hours. Thereafter, centrifugation of the mixture at 7000 rpm for 5 minutes resulted in precipitation of crystalline solid which was dried under nitrogen stream. Then, chemical reduction the $AgNO_3$ complex encapsulated fullerene crystals with hydrazine hydrate solution (1.3% wt.) resulted in formation of Ag(I)-fullerene composite. Finally, the composite was washed with deionized water and ethanol to remove excess silver ions. The prepared Ag(I)-fullerene composite was used as a catalytic system for reduction of 4-nitrophenol and photo-degradation of orange G dye.

A self assembled method based on hydrothermal mode for synthesis of amine functionalized fullerene decorated with palladium nanoflowers was reported by Li and Han [108]. Initially, amine functionalized fullerene was prepared by dissolving ethylenediamine in ethanol-water system (5:1). Then this solution was added drop by drop to toluene saturated with C_{60} fullerene and sodium hydroxide with continuous stirring. The stirring was continued for 5 days in argon atmosphere at room temperature, later the solution was filtered, centrifuged, and washed with ethanol and distilled water for a number of times. Eventually, dark brown solid products were obtained after drying in vacuum for 24 hours at 60 °C. For preparation of composite of fullerene, palladium chloride was dissolved in HCl and DMF and mixed with functionalized fullerene. The reaction mixture was then placed in autoclave for 6 hours at 140 °C in nitrogen atmosphere. The obtained product was washed with ethanol and vacuum dried overnight to yield amine functionalized fullerene decorated with palladium nanoflowers which displayed excellent electrocatalytic effect for reduction of *p*-nitrophenol.

Glassy Carbon

It is a type of carbon material which combines characteristics of both glass and ceramic materials with that of graphite. It is a commonly used electrocatalyst or electrode material. The strategy for fabrication of glassy carbon is based on pyrolysis of polymeric materials at elevated temperatures of about 3000 °C [44, 109]. The mechanism basically involves breakdown of carbon-heteroatom bonds in polymers and generation of C-C bonds [110 - 112]. Initially, hydrocarbon radicals are generated with their highest concentration at around 600 °C [113] and after 800 °C or higher temperature, a network of graphene fragments develop [114]. Further, annealing process results in formation of cross-linked carbon network and removal of volatile by-products like oxides of carbon, water, methane and small hydrocarbons [115]. For instance, Jurkiewicz *et al.* prepared glassy carbon by carrying out pyrolysis of polymeric furfuryl alcohol under Ar gas flow at varied temperatures ranging from 600 to 2500 °C at different heating rates [116]. The carbonized samples were then cooled in argon atmosphere resulting in glassy carbon with fullerene-like or nanotube-like elements in its structure. It was also reported that pyrolysis up to 1000 °C resulted in increase in fullerene-like non-planar sp^2 carbon bonds. But on further increase in pyrolysis temperature the amount of non-planar sp^2 bond content decreased.

Recently, a nitrogen enriched glassy carbon was prepared as an electrocatalyst for hydrogen evolution reaction by Thirukumaran and his research group [117]. Initially polybenzoxazine was synthesized by step-wise polymerization of benzoxazine. The carbonization of polybenzoxazine at 600 °C for 5 hours under nitrogen atmosphere was performed. The resultant carbonaceous material was then activated by adding KOH solution followed by water elimination through evaporation at 120 °C. Subsequently, the carbon material was heated in a tubular furnace for an hour at 600 °C to obtain nitrogen enriched glassy carbon. This method thus offered an efficient method for synthesis of glassy carbon electrocatalyst.

Carbon Black

Carbon black is composed of colloidal carbon particles and is usually synthesized *via* partial combustion or thermal decomposition of petroleum products. Carbon blacks are extensively used as electrocatalysts for redox processes. Diverse thermal methods for carbon black synthesis are summarized below [118].

Channel Black Process

In this process, combustion of natural gases using a continuous small wide luminous fan-shaped flame occurs. This process yields carbon black with a particle size of approximately 10-30 nm.

Gas Black Process

It involves thermal oxidative decomposition, where the formation of carbon black takes place in diffusion flame.

Thermal Black Process

In the thermal black process, thermal combustion of natural gas into elemental carbon and hydrogen takes place at high temperatures to produce carbon black and tail gas. The sizes of obtained carbon black particles are about 180 nm.

Acetylene Black Process

The method involves constant thermal decomposition of acetylene gas in the absence of oxygen gas to generate carbon black as aerosols.

Lamp Black Process

It includes partial combustion of carbon materials such as resins, fatty oils and acids, coal tar, *etc*., resulting in the deposition of carbon in the form of soot. Carbon black particles so obtained range in the size from 110 to 120 nm.

Furnace Black Process

In this process, aromatic oils are pyrolized by exposing them to a hot gas stream to produce carbon blacks with particle sizes of about 20-100 nm.

Besides these methods, carbon black is also obtained by plasma synthesis. An arc discharge plasma method coupled with thermal pyrolysis for the synthesis of carbon black was demonstrated by Sun *et al.* [119]. An apparatus composed of a plasma generator, thermal pyrolysis device, gas injector, power supply and collecting device was used for this purpose. Thermal plasma was generated by electrodes supplied with 10 kV power. Argon was injected into the device for 5 min. to firstly drain out oxygen and then mixed with propane at definite rate of volume. As the propane gas flowed into the plasma region, carbon black was produced instantly. Then the thermal pyrolysis furnace pyrolyzed the un-reacted propane. Finally, carbon black was collected from the bottom of sand core funnel connected with a vacuum pump.

Not be distributed or uploaded to anyone or anywhere
For personal private use only

Functionalized carbon black has also gained attention as catalyst. Recently, oxidized carbon black has been employed as a catalyst for the synthesis of benzodiazepines [119]. The oxygen functionalized carbon black was prepared by Hummer's method. In this method, sulphuric acid (120 mL) and sodium nitrate (2.5 g) were mixed with 5g of carbon black in a round bottom flask kept on an ice bath. The suspension was magnetically stirred and then 15 g potassium permanganate was added gradually. The mixture was subjected to heating at 35 °C and stirred for about 24 hours. Then, 700 mL deionized water was added in small portions resulting in black slurry for carbon black under stirring. Finally, 5 mL of hydrogen peroxide solution (30 wt%) was added to the slurry. The obtained sample was poured into deionized water and then centrifuged for 15 min at 10000 rpm. The sample was then washed with deionized water and HCl (5 wt %) and later dried to obtain oxidized carbon black. The optimal conditions for highly graphitized carbon black production were a discharge current of 0.8 A, 120 L/h of argon flow rate, 80 ml/min of propane flow rate and pyrolysis temperature at 700 °C.

Also, carbon black based composites to have found applications as electrocatalysts. In a work conducted by Lim *et al*., TiO_2/carbon black composite was prepared and used as a catalytic electrode in dye-sensitized solar cells [120]. The composite formation involved pulverization of carbon black followed by its calcination in a muffle furnace at 500°C for 2 hours by placing the carbon black in 80-unit mesh. The calcinated carbon black was again ground and thermally treated at 300 °C for 2 hours to obtain carbon black powder with a particle size of about 80 nm. Then, nano-TiO_2 was prepared by the modified Burnside method. Finally, TiO_2/carbon black composite was fabricated by mixing carbon black powder with TiO_2 NPs followed by ultrasonication for 10 min. at 750 W. Then, the addition of 100 µl of Triton X-100 to the mixture followed ultrasonic treatment for 10 min. yielded the TiO_2/carbon black composite. The prepared composite was subsequently used as the counter electrode material in solar cells.

Carbon Nanomaterials

Carbon Nanofibres

Carbon fibres are carbon containing fibres of diameter of the order of few micrometers that find applications in industries due to their enormous tensile strength and thermo-chemical conductivity and stability. In last few years nanodimensional carbon fibres have attracted huge attention in the field of catalysis due to their advanced chemical and electrical activities along with large surface area. Carbon nanofibres are usually prepared by chemical vapour deposition method (CVD), catalytically promoted CVD (CCVD), electrospinning

and template synthesis techniques. CVD is a well acknowledged method for synthesis of 2-dimensional nanomaterials. The method is based on decomposition of vapour or gaseous precursors on a substrate for preparation of materials at elevated temperature in presence of vacuum. The CVD method was explored by Hulicova-Jurcakova *et al.* for synthesis of carbon nanofibre [121]. Carbon precursors like methane and acetylene were used for this process and nickel supported on γ-alumina was used as substrate. The reaction was carried out in tubular furnace with a heating rate of 10 °C/min at 500°C and 700°C, respectively. The obtained carbon samples were purified in reflux system using 5 M nitric acid solution for 6 h, the obtained solution was filtered and dried to obtain carbon nanofibres. Highly graphitic carbon nanofibres were obtained by this CVD method.

Another important method that has emerged for nanofibre synthesis is CCVD, in which catalyst based chemical vapour decomposition, is carried out. Miniach and co-workers have reported a CCVD method for synthesis of carbon nanofibres [122]. They used hydroxyapatite-supported nickel catalyst (Ni/HAp) on which methane decomposition occurred resulting in the formation of herringbone bamboo-like carbon nanofibres. In this method, first Ni/Hap was loaded in a quartz tube placed inside a horizontal furnace. First the catalyst was reduced under H_2 flow (150 ml min^{-1}) at 450-650°C for 10-120 min. Afterwards, the methane and hydrogen gases were made to flow through the tubes at 650°C for 3-180 min. Later the nanofibres were cooled down to room temperature in N_2 atmosphere and then treated with 5% HCl in a sonication bath for 2 hours to remove the excess catalyst. Finally, the carbon nanofibres were washed with deionized water and dried.

Electrospinning is a commonly used method for the fabrication of nanofibres from polymeric materials using high power electric force. Recently, Alarifi *et al.* prepared carbon nanofibres from polyacrylonitrile (PAN) by electrospinning technique [123]. It was reported that a homogeneous solution of PAN was prepared by dissolving PAN in DMF and stirring it at 500 rpm for an hour. The solution was then transferred into a 10 mL syringe and using electrospinning technique with the electric field of 25kVat injection rate of 1 ml/h and a spinneret-to-collector distance of 25 cm, the nanofibres were formed. Thereafter, thermal treatment of nanofibres in oxygen atmosphere at 270°C for an hour followed by carbonization in argon atmosphere at different temperatures 750, 850, and 950°C was carried out resulting in high carbon content nanofibres.

Template synthesis is also one widely used method for synthesis of nanofibres. The strategy involves use of a nanoporous membrane as a template for synthesis of nanofibers from diverse materials such as carbon, polymers, semiconductors,

and metals [124 - 126] (Huczko, 2000; Hulteen and Martin, 1997; Toro and Buriak, 2014). A template based synthesis for carbon nanofibres were reported by Li *et al.* [127]. The method involved addition of anhydrous zinc acetate to ethylene glycol followed by stirring of the mixture at 150 ° C for 90 min. Then, the mixture was subjected to centrifugation and the obtained slurry was calcinated at 600 ° C for 2 hours in argon atmosphere. Later, the composite was immersed in a 2.0 M HCl solution with overnight stirring to obtain the nanofibres. The carbon nanofibres were then purified by washing with water and ethanol and then dried. Mesoporous carbon nanofibers were obtained after being washed with water and ethanol, and then dried at room temperature. The carbon nanofibres produced by this method were highly mesoporous and were used as electrodes.

Carbon Nanotubes

There are several methods for fabrication of carbon nanotubes (CNTs) namely, CVD, arc discharge, laser ablation, electrolysis, ultrasonication techniques, *etc*. Verma *et al.* have demonstrated CNT fabrication using CVD approach [128]. An automated CVD reactor was used and iron catalyst supported over magnesium oxide was loaded on quartz boats of the reactor. Argon and hydrogen gases were flown into the reactor at a rate of 100 ml/min. at 25 °C for 5 min. Then, temperature was raised to 750 °C and after 10 minutes acetylene along with hydrogen was flown in the reactor for 15 min. at the rate of 300 ml/min. and 100 ml/min., respectively, over the catalyst to develop CNTs.

Arc discharge method for CNTs is carried out at elevated temperatures usually above 1000 °C. Cu and Ni containing carbon nanotubes were prepared by Saravanan *et al.* using DC arc discharge method [129]. Firstly, the graphite anode was filled with mixture of graphite and metal powder in the ratio 1:1. A graphite rotating disc with a speed of 8-10 rpm was used as cathode on which soot deposition occurred. The electric arc was generated *via* a DC source of 20 V and 150 A. Owing to high temperature and energy, vaporization of graphite and metals in air took place. The graphene sheets rolled into CNTs due to elevated temperature and enormous energy while the metals upon condensation deposited in the inner walls of CNTs. The CNTs so formed were washed with distilled water and dried. Finally, treatment with toluene for 5 hours and annealation for an hour at 650°C led to metal encapsulated CNTs.

Laser ablation technique is primarily used to prepare single-walled CNTs (SWCNTs). But nowadays multi-walled CNTs (MWCNTs) are also prepared by this technique. Recently, Ismail *et al.* have demonstrated fabrication of MWCNTs using pulsed laser ablation method in aqueous medium [130]. In this method high grade graphite pellet was placed in the glass cell filled with double distilled water.

The laser beam from Q-switched Nd:YAG of two wavelengths: 532 and 1064 nm with pulse width of 9 ns were focused on the graphite target by using positive lens of focal length of 5 cm. The ablation time and laser repletion rate selected for the process were 30 min and 2 Hz, respectively. The ablation cell rotated during the ablation process by using DC motor with 25 rpm and was used to prevent the vapour from depositing on the lens. Finally, colloidal CNTs were collected in the glass cell. Thus, MWCNTs with diamond like structure were formed.

Electrolysis of carbon materials in molten salts are widely used to prepare CNTs. Thin walled CNTs from CO_2 using molten carbonate was prepared *via* electrolysis by Wang *et al*. [131]. Electrodes (Muntz brass sheet-cathode and Nichrome-anode) were immersed in a mixture of electrolytes (lithium carbonate, lithium oxide, calcium oxide, and boric acid) and a constant current of 0.1 A/cm^2 was applied for 4 hours. The electrolysis temperature was 770 °C and impure sample was collected at cathode which was later washed. The washed product was recovered by vacuum filtration and dried overnight at 60 °C to obtain pure CNTs. The method resulted in ultra-thin walled CNTs (22–42 nm diameter) consisting of about 25 concentric, cylindrical graphene walls.

Sonochemical treatment of carbonaceous materials also results in CNTs. For instance, Wang and his research group have developed CNTs from graphene oxide *via* ultrasonication method [132]. The method involved dispersion of graphene oxide into HNO_3 solution (70%) which was subjected to sonication in ultrasonic bath at ambient temperature for 4 hours. Thereafter, water was poured into the suspension and centrifugation was carried out at 15,000 rpm to obtain CNTs. The CNTs were further purified their dispersion in water followed by centrifugation at 12,000 rpm for an hour to obtain pure CNTs.

Nanodiamonds

Nanodiamonds are nanosized carbon particles with dimensions less than 100 nm and were first discovered in 1963 [133]. The nanodiamonds due to their remarkable features like high solidity, large surface area, chemical inertness, enormous strength, optical clarity, biocompatibility, and thermal conductivity are quite useful carbon materials and can be fabricated by diverse techniques [134]. Detonation, CVD, laser irradiation and high pressure-high temperature methods are commonly used strategies for nanodiamond synthesis.

A bulk production of nanodiamonds from tetryl, a low cost explosive, was demonstrated by Panich and co-workers [135]. The detonation method proceeded with pressing of tetryl or its mixture with TNT and RDX at 1000 to 2000 kg/cm^3 into a cylindrical disc of 60 mm diameter and 110 mm height to form an explosive charge. The explosive charge was kept in an explosive chamber in a plastic bag

and was detonated. Further, it was reported that after every fifth detonation the valve at the bottom opened and the diamond soot was washed off with water. The diamond soot was then filtered, magnetically separated and centrifuged to remove impurities. Then, the soot was dried and crushed to obtain nanodiamonds. Thus, it was elucidated that tetryl serves as an excellent explosive material for fabrication of nanodiamonds.

Recently, Tallaire and his research group have synthesized loose nanodiamonds by plasma-assisted CVD method [136]. The synthesis was carried out in a quartz bell jar microwave reactor. The plasma was generated by microwaves at 2.45 GHz in resonant cavity. The reactor operated using a mixture of gases ($H_2/CH_4/O_2$) along with high microwave energy to produce nanodiamonds which agglomerated on water cooled molybdenum holder exposed to plasma at 450-500 °C. The agglomerated nanodiamonds were then washed away by ethanol and collected in cavity of bell jar reactor. The nanodiamonds thus obtained by the CVD technique showed superior crystallinity and lower impurities, which make this method advantageous.

In another method, pulsed laser induced ablation was used for synthesis of nanodiamonds from graphite. Basso *et al.* reported that laser ablation of graphite with KrF excimer laser was carried out [137]. The graphite target was kept in vial made of glass filled with liquid nitrogen. The laser beam of 500 mJ energy was focused on the target. After completion of ablation, liquid nitrogen was evaporated and the nanodiamond powders were formed. Consequently, laser ablation process offered an inexpensive and controlled approach for nanodiamond synthesis.

High pressure and high temperature technique for fabrication of nanodiamonds from hydrocarbons has attained great significance nowadays. This is because this method affords nanodimensional diamonds with highest possible structural perfection and crystallinity. Ekimov and co-workers have recently synthesized nanodiamonds from adamantane under high temperature/pressure conditions [138]. The process was performed at 7.7 and 9.4 GPa pressure and temperatures at 300 to 1600°C. The adamantane sample pressed in the form of a disc of 5 mm diameter and 3 mm thickness was placed in a titanium capsule in Torrid chamber. The temperature was controlled using Chromel-Alumel thermocouple at <1350°C and tungsten-rhenium thermocouple at temperatures up to 1600°C. The thermocouple junction was held on the outer wall at the mid-height of the capsule. The high pressure/temperature treatment of adamantane caused carbonization of thus leading to formation of nanodiamonds. It was reported that at 7.7 GPa only diamond microcrystals were formed but on increasing the pressure to 9.4 GPa,

nanodiamonds were formed. Thus, high pressure conditions are very important for synthesis of nanodimensional diamonds.

Das and Saikia have highlighted a novel method of synthesis of nanodiamonds from low grade coal under ultrasound exposure [139]. In this method, coal (2 g) was added to 100 mL hydrogen peroxide solution in a Teflon beaker and exposed to ultrasound-waves for 3 hours. A senor probe was used to measure the reaction temperature. After 3 hours of exposure, the reaction mixture was filtered to remove sulphur and other mineral contaminants. The filtrate was then poured into a beaker full of crushed ice and neutralized. Then the neutral suspension was filtered *via* a polytetrafluoroethylene membrane (0.22 μm) and dialyzed for 5 days in a 1 kDa dialysis bag. Thereafter, the solution was concentrated in a rotator evaporator and collected. The nanodiamonds synthesized by this method were obtained as monocrystalline and polycrystalline carbon nanocrystals with 4-15 nm dimensions.

Carbon Nano-onions

Carbon nano-onions are concentric shell like nanostructures consisting of nested fullerenes. The carbon onions were discovered for the first time by Ugarte in 1992 [140] and ever since their emergence several methods have been developed for their synthesis. Some of these include arc discharge method, chemical vapour deposition, pyrolysis, laser technique and thermal treatment of nanodiamonds.

Alessandro and co-workers have demonstrated synthesis of carbon nano-onions by water based arc discharge method [141]. It was reported that in an electric discharge apparatus, two graphite electrodes (anode of 5 nm and cathode of 10 nm diameters) were immersed in water and a potential of 12 V and current 30 A were applied between them. This resulted in formation of a powder that was dispersed in water and floated or settled at the bottom in the beaker. The floating powder like sample was collected on a microscope slide, whereas the bottom sample was recovered by water evaporation at 80 °C. The samples were then subjected to ultrasonication in ethanol for half an hour at 100 W. Finally, annealation of the samples at 400°C in air resulted in carbon nano-onions free from amorphous carbon residues. Highly stable, polyhedral carbon nano-onions were obtained by this method.

CVD method was employed by Zhang and his research group to prepare carbon nano-onions [142]. The synthesis was carried out by decomposition of methane gas over Ni-Fe alloy based catalyst at 850 °C. The process yielded highly graphitic carbon nano-onions.

In another method, carbon nano-onions were prepared from waste frying oil by pyrolysis technique. Jung *et al.* pyrolyzed the oil using a cotton wick under stable air conditions [143]. Then, to collect the sooty material, a beaker was inverted above the flame and the powder was gathered by scrapping off the deposited material. Next, the soot was calcined at 900 °C for an hour in a muffle furnace which led to carbonization and graphitization of carbon nano-onions. The method thus offered an economical approach for preparation of carbon nano-onions for application in energy storage devices.

A laser ablation induced carbon nano-onions synthesis was demonstrated by Dorobantu and co-workers [144]. A pulsed laser from Compex Pro 205 (KrF) excimer laser with a wavelength of 248 nm, pulse length of 25 ns and repetition rate of 10 Hz was used. The laser beam was focused on a pure graphite target under an ambient pressure of 7 Torr. During the process argon gas flowed at about 300 L/h through the reactor and temperature was maintained at 900°C. The ablation products then condensed on the water cooled cold finger to finally obtain the carbon nano-onions. The carbon nano-onions formed by this technique were about 10-25 nm in diameter.

Recently, Bartolome and Fragoso have reported synthesis of carbon nano-onions *via* thermal annealing of nanodiamonds [145]. The method involved annealing of 300 mg of nanodiamond at 1200°C at a heating rate of 50°C min^{-1} under argon atmosphere for 6 hours. Thereafter, the annealed sample cooled down to room temperature and a portion of this sample was then treated with 30% H_2O_2 for 3 hours, washed and dried to obtain pure carbon nano-onions. The protocol afforded carbon nano-onions with a diameter of 3-4 nm and comprising 5-6 graphitic shells.

Graphene and Its Derivatives

A multitude of top-down and bottom-up strategies for fabrication of graphene and its derivatives are reported in literature. These methods have been described in detail in Chapter 3.

SCOPE OF CARBOCATALYSTS

As mentioned earlier the carbon materials due to their several interesting properties find applications as catalysts in various fields such as environmental remediation, solar cells, fuel cells, energy devices, water splitting, redox reactions, sensors, biocatalysis, synthesis of fine chemicals, *etc*. For instance, Christoforidis and co-workers have lately reported the use of carbon nanotubes supported on graphitic nitride as photocatalyst for hydrogen production [146]. It was elucidated that the carbon nitrides functionalized with SWCNTs were found

to be about 2-5 times more efficient in catalyzing hydrogen evolution as compared to DWCNTs (double-walled carbon nanotubes) and MWCNTs under both the illumination of solar as well as visible light. This was attributed to the fact that CNTs worked as acceptors of electrons and further it was reported that the charge transfer varied inversely with the number of walls in CNTs. Thus, the transfer of photogenerated electrons occurred more readily when SWCNTs were used, thereby promoting H_2 production by providing more electrons.

Removal of pollutants from environment is a big concern and nowadays carbon catalysts are being widely used to remediate environment. Pausova *et al.* have recently employed active carbon (AC)-TiO_2 based composites as catalyst for photodegradation of benzoic acid in water and toluene in air [147]. It was reported that the incorporation of active carbon in composite enhanced photocatalytic activity due to greater adsorption ability of AC which facilitates adhesion of the pollutants. Further, it was also illustrated that the enhanced catalytic efficiency of AC was due to the milling process which increased its surface area thereby causing better adsorption of the substrates. Thus, active carbon based composites have merged as efficient catalytic systems for elimination of water and air pollutants.

The high conductivity, surface property and high melting point of carbon materials favour their application as electrodes in solar cells and fuel cells. Recently, Don and his research group have demonstrated use of acetylene carbon black-graphite composite as electrode for dye sensitized solar cells (DSSCs) [148]. It was highlighted that the composite was prepared in different ratio of carbon black and graphite *viz.* 0:1, 1:0, 1:1, 1:3, and 3:1 and the highest conversion efficacy was found to 5.06% for DSSCs containing acetylene carbon black-graphite in the ratio 3:1 compared to conventional expensive Pt counter electrode. This was because the carbon black particles offered greater surface area for ekectrochemical reaction in DSSC. Further, it was elucidated that the incorporation of acetylene carbon black particles on graphite enhanced the electrocatalytic efficiency of triiodide ion reduction by enhancing the electric conductivity *via* linking of the graphite flakes. Thus, acetylene carbon black-graphite composite can be used as cost effective alternative to Pt counter electrode in DSSCs.

Similarly, Bhavani *et al.* have reported use of fullerene based electrocatalyst in direct alcohol fuel cells (DAFCs) [149]. They prepared bimetallic Pd-W nanoparticles anchored on fullerene-C_{60} catalyst (Pd-W@Fullerene-C_{60}) for electrooxidation of methanol and ethanol for DAFCs applications. It was reported that owing to large electrochemical surface area, excellent conductivity, high reproducibility and long standing durability, the electrocatalysts showed

enormous catalytic activity for oxidation reaction compared to monometallic catalyst and commonly used Pt/C catalyst. It was revealed that the remarkable activity of the catalyst for oxidation of alcohols in fuel cells was attributed to the synergistic relation between Pd-W nanoparticles and fullerene. The uniform distribution of nanoparticles on fullerene prevented their aggregation resulting in enhanced surface area and stability. Moreover, the outstanding electron conductivity of fullerenes contributed to the overall catalytic activity of the Pd-W@Fullerene-C_{60} electrocatalyst, making them highly suitable electrode material for fuel cells.

In recent past, Chen and co-workers have reported the use of PT-Ni nanoparticles decorated on carbon nanofibres (PtNi/CNFs) as potent electrocatalyst for water splitting [150]. The catalyst was fabricated by electrospinning technique and carbonization. The catalyst was used as electrode for water splitting. It was reported that for hydrogen evolution in acidic medium (0.5 M H_2SO_4), the electrocatalyst achieved a 10 mA cm^{-2} current density at low overpotentials of 34 mV and a Tafel slope of 31 mV dec^{-1} similar to that of commercially available Pt/C (20 wt%) electrocatalysts. In alkaline medium (1 M KOH), the PtNi/CNFs catalyst showed a low overpotential of 82 mV to attain a current density of 10 mA cm^{-2} a small Tafel slope corresponding to 34 mV dec^{-1}. In addition, the PtNi/CNFs also show good activity for oxygen evolution in alkaline medium displaying a small overpotential of 151 mV to reach a current density of 10 mA cm^{-2} and a Tafel slope at 159 mV dec^{-1}. In acidic medium, the PtNi/CNFs exhibited an overpotential of 451 mV and Tafel slope at 198 mV dec^{-1}. Thus, on the whole the PtNi/CNFs electrocatalysts showed tolerable electrocatlaytic activity for water splitting. The catalytic efficiency of the PtNi/CNFs was ascribed to the synergism which arises due to homogeneous dispersion of Pt and Ni nanoparticles on carbon nanofibres, elevated conductivity of the nanofibres and three-dimensional interlinked frameworks of the carbon nanofiber mats. Consequently, carbon nanofibres have surfaced as significant electrocatlytic material for water splitting.

Owing to the extraordinary electrochemical properties of carbon nanomaterials, they have become a commonly employed as sensors. Mohapatra and his research group have designed carbon nano-onions (CNOs) as electrochemical sensor for detection of glucose [151]. The carbon onions were obtained by combustion of natural oils and a hybrid nanocomposite bearing CNOs, Nafion and glucose oxidase enzyme was fabricated to be used as sensor. The enzymatic CNO composite displayed good sensitivity of 26.5 μA mM^{-1} cm^{-2} with 0.21 mM detection limit. Non-enzymatic CNO nanocomposite bearing Pt nanoparticles were also fabricated which showed superior sensitivity of about 21.6 μA mM^{-1} cm^{-2} and a lower detection limit of 0.09 mM than enzymatic CNOs for detection

of glucose. The good sensitivities of CNO based nanocomposites were attributed to due to the high surface area, excellent conductivity and catalytic behaviour of CNOs. Overall, the research findings highlighted that CNOs serve as facile, economical and effective carbon materials for development of glucose detecting sensors.

The immobilization of enzymes on carbon materials has resulted in a new class of biocatalysts which is used for various purposes such as biosensing [152], removal of pollutants [153], dye degradation [154], synthesis of organic compounds [155], *etc*. In a study carried out by Wang and co-workers a lipase-immobilized carbon nanotubes were reported as biocatalyst for production of biodiesel [156]. The multiwalled carbon nanotubes bearing *Candida antarctica* lipase B were designed by pickering emulsification method. The prepared biocatalyst was then used to manufacture biodiesel from *J. curcas* L. seed oil. The esterification and trans-esterification of *J. curcas* L. seed oil with methanol in presence of biocatalyst resulted in 95.2% yield of biodiesel in 11 hours and 6 seconds at low temperature of about 35 °C. Thus, the liapse immobilized MWCNTs showed excellent biocatalytic activity. Moreover, the study revealed that the use of MWCNTs provided stability to the enzyme as well as rendered the catalyst recyclable up to 10 runs without significant loss in catalytic performance. Hence, it can be concluded that use of carbon nanostructures in biocatalytic systems can add features such as enlarged surface area, thermo-chemical stability, conductivity and mechanical properties which are beneficial for catalytic materials.

Over the past few decades, the carbocatalysts have been extensively used for chemical transformations. Recently, Dam *et al*. have employed graphite oxide as a heterogeneous catalyst for synthesis of pyrimidines [157]. The pyrimidine derivatives were afforded from one pot reaction between 1 mmol each of substituted benzaldehyde/heteroaldehyde, dimedone and 2-amino-benzothiazole or 2-amino-imidazole under solvent-less condition in presence of graphite oxide (20 mg) at 60 °C. It was also revealed that the catalyst generated good yields in short time and was reusable for 9 cycles. The use of graphite oxide carbocatalyst offered several advantages such as efficient reaction, easy recovery, high recyclability of catalyst, facile work-up and inexpensive synthetic protocol with avoidance of toxic solvents and metal based catalyst.

Considering the above examples it is clear that carbon materials exhibit wide range of catalytic applications. The broad scope of carbocatalysts cover diverse spheres including photocatalysis, electrocatalysis, biocatalysis and heterogeneous chemical catalysis owing to their merits such as interesting surface features, porosity, thermal conductivity, stability and electrical properties. Moreover, the

sustainability factor due to their renewability also renders carbon materials as suitable catalytic materials.

CONCLUDING REMARKS

Carbon and its allotropes are incredible materials that have been an integral part of chemical and physical sciences for ages. The extraordinary surface properties, conductivity, chemical inertness and renewability of carbon materials have turned them into sustainable catalytic systems. Ever since the first use of activated carbon as a catalyst for oxidation reaction, there has been a continuous development in the field of carbocatalysis. The diversely synthesized carbon materials with exorbitantly useful properties exhibit broad applications as photocatalysts for the removal of pollutants in the environment, sensors, heterogeneous catalysts for chemical syntheses, biocatalysts, and electrocatalysts in solar cells, fuel cells, water splitting, redox processes, *etc*. Consequently, the properties, synthetic methods and the scope of carbocatalysts have been highlighted in this chapter. The carbon polymorphs due to their unique surface characteristics and porosity have received immense attention as catalyst or catalyst support. The presence of large surface area and pores on carbonaceous materials facilitate the binding of substrates. Additionally, by suitable functionalization, doping or thermal treatment, the surface features and porosity of carbon facets can further be tuned to introduce beneficial defects which serve as active sites for reactant molecules. The emergence of nanodimensional carbon materials has also revolutionized the field of carbocatalysis because a reduction in size enhances the surface area which in turn improves their catalytic activity. Furthermore, the exceptional thermal conductivities and electrical properties of active carbon, graphite, fullerene, glassy carbon, carbon black, carbon nanotubes, carbon nanofibres, nanodiaomonds, carbon nano-onions, graphene and its derivatives have contributed enormously to their catalytic applications. The thermal conductivity and electrical property of a carbon material depend on the coordination and arrangement of C atoms as well as defects in the structural framework. By controlling the degree of carbonization or structural defects one can achieve desired properties in a carbocatalyst.

To realize the desirable characteristics of a carbon material, one needs a proper synthetic strategy. Diverse synthetic approaches for the synthesis of carbocatalysts have been described in this chapter. Active carbons are mainly procured by physical or chemical activation of raw materials like wood, coal, biomass, *etc*. The activation process governs the surface features and pores of active carbon. Graphite is a natural allotrope of carbon but synthetically it is fabricated by thermal treatment of coke or coal tar and hydrothermal treatment of polymers or metal carbides. The thermal treatment controls the graphitization

process. Nowadays, graphite encapsulated nanoparticles are also prepared by pyrolysis, template synthesis, chemical vapor deposition, arc discharge, laser ablation technique, *etc*. Fullerenes are macro-caged structures that are prepared by arc discharge, laser ablation and combustion techniques. Further, functionalization of fullerenes can also be carried out by sol-gel, solvo-thermal, chemical reduction, self-assembly, and ultrsonication techniques, to develop composites with catalytic properties. Glassy carbon electrocatalysts are fabricated by pyrolysis of polymers.

Besides, there are several thermal methods such as furnace black method, lampblack method, *etc*. for the preparation of carbon black particles of nanosize. Plasma synthesis has also been employed for the synthesis of glassy carbon composites. Chemical vapor deposition (CVD), electrospinning and template synthesis are commonly used strategies for the synthesis of carbon nanofibre based catalysts. Carbon nanotubes with relevant features can be synthesized *via* CVD, arc discharge, laser ablation, ultrasonication, electrolysis, *etc*. Detonation, high pressure-high temperature, laser irradiation and CVD are typical methods for the synthesis of nanodiamonds with exceptional surface, mechanical, electrical and thermal properties. Several bottom-up strategies including pyrolysis, arc discharge, CVD, laser ablation and thermal treatment of nanodiamonds are available for designing catalytic carbon nano-onions.

Considering the ever growing interest in carbocatalysis and the emergence of numerous fabrication strategies, it is evident that the field of carbocatalysts will continue to bloom in the coming days. However, there are certain concerns that need to be settled. The industrial scale syntheses of carbon based catalysts and their application need to be more cost-effective and feasible. The incorporation of desired properties using more benign methods also needs to be looked into. Further, identification of specific active sites on the carbon surface and detailed study of structural intricacies of carbon materials, thermal and electrical properties that essentially drive the catalytic behaviour of carbon catalysts also need to be dealt with at atomic as well as molecular levels. Overcoming these challenges will surely help in the expansion of the application spectrum and scalability of carbocatalysts.

LIST OF ABBREVIATIONS

AC	Active carbon
bcc	Body centered cubic
BET	Brunauer-Emmett-Teller
CVD	Chemical vapour deposition
CCVD	Catalytically-promoted chemical vapour deposition

CNF	Carbon nanofibres
CNO	Carbon nano-onions
CNT	Carbon nanotube
DAFCs	Direct alcohol fuel cells
DC	Direct current
DMF	Dimethyl formamide
DWCNTS	Double-walled carbon nanotubes
fcc	Face centered cubic
FTS	Fischer-Tropsch synthesis
MWCNT	Multi-walled carbon nanotube
N-CNOs	Nitrogen doped carbon nano-onions
NCNTs	Nitrogen doped carbon nanotubes
ODH	Oxidative dehydrogenation
ORR	Oxygen reduction reaction
PAN	Polyacrylonitrile
RBF	Round bottom flask
RDX	Research Department Explosive
RPM	Rotations per minute
SWCNT	Single-walled carbon nanotubes
TNT- 2	4,6-Trinitrotoluene

CONSENT FOR PUBLICATION

Not applicable.

CONFLICT OF INTEREST

The author declares no conflict of interest, financial or otherwise.

ACKNOWLEDGEMENTS

Declared none.

REFERENCES

[1] Anastas, P.T.; Warner, J.C. *Green Chemistry: Theory and Practice*; Oxford University Press: New York, **1998**, p. 30.

[2] Cole-Hamilton, D.J. Homogeneous catalysis--new approaches to catalyst separation, recovery, and recycling. *Science,* **2003**, *299*(5613), 1702-1706. [http://dx.doi.org/10.1126/science.1081881] [PMID: 12637737]

[3] Sheldon, R.A.; Downing, R.S. Heterogeneous catalytic transformations for environmentally friendly

Not be distributed or uploaded to anyone or anywhere For personal private use only

production. *Appl. Catal. A Gen.,* **1999**, *189*(2), 163-183.
[http://dx.doi.org/10.1016/S0926-860X(99)00274-4]

[4] Stenhouse, J. Charcoal: On the deodorizing and disinfecting properties of charcoal, with the description of a charcoal respirator for purifying the air by filtration. *Chem. Gaz,* **1854**.

[5] Rideal, E.K.; Wright, W.M. CCCCXXX.—Low temperature oxidation at charcoal surfaces. Part III. The behaviour of blood charcoal and the influence of temperature on the reaction rate. *J. Chem. Soc.,* **1926**, *129*(0), 3182-3190.
[http://dx.doi.org/10.1039/JR9262903182]

[6] Kutzelnigg, A. Zur Kenntnis der sauerstoff-übertragenden Wirkung von Stoffen mit großer spezifischer Oberfläche. *Ber. Dtsch. Chem. Ges. B,* **1930**, *63*(7), 1753-1758.
[http://dx.doi.org/10.1002/cber.19300630721]

[7] Kolthoff, I.M.; Tomsicek, W.J. The oxidation potential of the system potassium ferrocyanide–potassium ferricyanide at various ionic strengths. *J. Phys. Chem.,* **1935**, *39*(7), 945-954.
[http://dx.doi.org/10.1021/j150367a004]

[8] Alkhazov, T.G.; Lisovskii, A.E.; Gulakhmedova, T.K. Oxidative dehydrogenation of ethylbenzene over a charcoal catalyst. *React. Kinet. Catal. Lett.,* **1979**, *12*(2), 189-193.
[http://dx.doi.org/10.1007/BF02071909]

[9] Lücking, F.; Köser, H.; Jank, M.; Ritter, A. Iron powder, graphite and activated carbon as catalysts for the oxidation of 4-chlorophenol with hydrogen peroxide in aqueous solution. *Water Res.,* **1998**, *32*(9), 2607-2614.
[http://dx.doi.org/10.1016/S0043-1354(98)00016-5]

[10] Fortuny, A.; Font, J.; Fabregat, A. Wet air oxidation of phenol using active carbon as catalyst. *Appl. Catal. B,* **1998**, *19*(3-4), 165-173.
[http://dx.doi.org/10.1016/S0926-3373(98)00072-1]

[11] Saha, J.; Kumar, A.; Pm, A.; Jakhad, V. Oxidised charcoal: an efficient support for NiFe layered double hydroxide to improve electrochemical oxygen evolution. *Chem. Commun. (Camb.),* **2020**, *56*(62), 8770-8773.
[http://dx.doi.org/10.1039/D0CC02880K] [PMID: 32618289]

[12] Xu, J.; Li, R.; Qian, X.; Ba, J.; Wu, Q.; Luo, W.; Meng, D. Nanoarray-structured nitrogen-doped graphite foil as the support of NiFe layered double hydroxides for enhancing oxygen evolution reaction. *J. Power Sources,* **2020**, *469*, 228419.
[http://dx.doi.org/10.1016/j.jpowsour.2020.228419]

[13] Celorrio, V.; Montes de Oca, M.G.; Plana, D.; Moliner, R.; Fermín, D.J.; Lázaro, M.J. Electrochemical performance of Pd and Au–Pd core–shell nanoparticles on surface tailored carbon black as catalyst support. *Int. J. Hydrogen Energy,* **2012**, *37*(8), 7152-7160.
[http://dx.doi.org/10.1016/j.ijhydene.2011.12.014]

[14] La-Torre-Riveros, L.; Guzman-Blas, R.; Méndez-Torres, A.E.; Prelas, M.; Tryk, D.A.; Cabrera, C.R. Diamond nanoparticles as a support for Pt and PtRu catalysts for direct methanol fuel cells. *ACS Appl. Mater. Interfaces,* **2012**, *4*(2), 1134-1147.
[http://dx.doi.org/10.1021/am2018628] [PMID: 22270177]

[15] Zhang, L.H.; Shi, Y.; Wang, Y.; Shiju, N.R. Nanocarbon catalysts: recent understanding regarding the active sites. *Adv. Sci. (Weinh.),* **2020**, *7*(5), 1902126.
[http://dx.doi.org/10.1002/advs.201902126] [PMID: 32154069]

[16] Kroto, H.W.; Heath, J.R.; O'Brien, S.C.; Curl, R.F.; Smalley, R.E. C60: Buckminsterfullerene. *Nature,* **1985**, *318*(6042), 162-163.
[http://dx.doi.org/10.1038/318162a0]

[17] María Girón, R.; Marco-Martínez, J.; Bellani, S.; Insuasty, A.; Comas Rojas, H.; Tullii, G.; Antognazza, M.R.; Filippone, S.; Martín, N. Synthesis of modified fullerenes for oxygen reduction

Not be distributed or uploaded to anyone or anywhere
For personal private use only

reactions. *J. Mater. Chem. A Mater. Energy Sustain.,* **2016**, *4*(37), 14284-14290.
[http://dx.doi.org/10.1039/C6TA06573B]

[18] Fukuzumi, S.; Imahori, H.; Okamoto, K.; Yamada, H.; Fujitsuka, M.; Ito, O.; Guldi, D.M. Uphill photooxidation of NADH analogues by hexyl viologen catalyzed by zinc porphyrin linked fullerenes. *J. Phys. Chem. A,* **2002**, *106*(10), 1903-1908.
[http://dx.doi.org/10.1021/jp011613g]

[19] Rogozea, E.A.; Meghea, A.; Olteanu, N.L.; Bors, A.; Mihaly, M. Fullerene-modified silica materials designed for highly efficient dyes photodegradation. *Mater. Lett.,* **2015**, *151*, 119-121.
[http://dx.doi.org/10.1016/j.matlet.2015.03.069]

[20] Ghosh, A.; Bhaduri, K.; Shah, S.; Auroux, A.; Pandey, J.K.; Chowdhury, B. Dehydration of isopropanol to propylene over fullerene[C_{60}] containing niobium phosphate catalyst: Study on catalyst recyclability. *Molecular Catalysis,* **2019**, *475*, 110470.
[http://dx.doi.org/10.1016/j.mcat.2019.110470]

[21] Varadwaj, P.R.; Varadwaj, A.; Marques, H.M. $_{70}$ Fullerene cage as a novel catalyst for efficient proton transfer reactions between small molecules: A theoretical study. *Sci. Rep.,* **2019**, *9*(1), 10650.
[http://dx.doi.org/10.1038/s41598-019-46725-4] [PMID: 31337790]

[22] Wang, S.; Dai, T.; Lu, Y.; Chen, Q.; Feng, L.; Sui, Z. Fullerene-bearing porous polymer *via* ball-milling approach and its palladium composite for catalytic deallylation. *Microporous Mesoporous Mater.,* **2020**, *302*, 110187.
[http://dx.doi.org/10.1016/j.micromeso.2020.110187]

[23] Iijima, S. Synthesis of Carbon Nanotubes. *Nature,* **1991**, *354*, 56-58.
[http://dx.doi.org/10.1038/354056a0]

[24] Planeix, J.M.; Coustel, N.; Coq, B.; Brotons, V.; Kumbhar, P.S.; Dutartre, R.; Geneste, P.; Bernier, P.; Ajayan, P.M. Application of carbon nanotubes as supports in heterogeneous catalysis. *J. Am. Chem. Soc.,* **1994**, *116*(17), 7935-7936.
[http://dx.doi.org/10.1021/ja00096a076]

[25] Yan, Y.; Miao, J.; Yang, Z.; Xiao, F.X.; Yang, H.B.; Liu, B.; Yang, Y. Carbon nanotube catalysts: recent advances in synthesis, characterization and applications. *Chem. Soc. Rev.,* **2015**, *44*(10), 3295-3346.
[http://dx.doi.org/10.1039/C4CS00492B] [PMID: 25855947]

[26] Abdolmohammadi, S.; Mirza, B.; Vessally, E. Immobilized TiO_2 nanoparticles on carbon nanotubes: an efficient heterogeneous catalyst for the synthesis of chromeno[*b*]pyridine derivatives under ultrasonic irradiation. *RSC Advances,* **2019**, *9*(71), 41868-41876.
[http://dx.doi.org/10.1039/C9RA09031B] [PMID: 35557875]

[27] Gopannagari, M.; Kumar, D.P.; Park, H.; Kim, E.H.; Bhavani, P.; Reddy, D.A.; Kim, T.K. Influence of surface-functionalized multi-walled carbon nanotubes on CdS nanohybrids for effective photocatalytic hydrogen production. *Appl. Catal. B,* **2018**, *236*, 294-303.
[http://dx.doi.org/10.1016/j.apcatb.2018.05.009]

[28] Xu, Y.; Deng, P.; Chen, G.; Chen, J.; Yan, Y.; Qi, K.; Liu, H.; Xia, B.Y. 2D Nitrogen-doped carbon nanotubes/graphene hybrid as bifunctional oxygen electrocatalyst for long-life rechargeable Zn-air batteries. *Adv. Funct. Mater.,* **2020**, *30*(6), 1906081.
[http://dx.doi.org/10.1002/adfm.201906081]

[29] Brodie, B.C. XIII. On the atomic weight of graphite. *Philos. Trans. R. Soc. Lond.,* **1859**, *149*, 249-259.
[http://dx.doi.org/10.1098/rstl.1859.0013]

[30] Novoselov, K.S.; Geim, A.K.; Morozov, S.V.; Jiang, D.; Zhang, Y.; Dubonos, S.V.; Grigorieva, I.V.; Firsov, A.A. Electric field effect in atomically thin carbon films. *Science,* **2004**, *306*(5696), 666-669.
[http://dx.doi.org/10.1126/science.1102896] [PMID: 15499015]

[31] Zhu, Y.; Murali, S.; Cai, W.; Li, X.; Suk, J.W.; Potts, J.R.; Ruoff, R.S. Graphene and graphene oxide:

Not be distributed or uploaded to anyone or anywhere
For personal private use only

synthesis, properties, and applications. *Adv. Mater.*, **2010**, *22*(35), 3906-3924.
[http://dx.doi.org/10.1002/adma.201001068] [PMID: 20706983]

[32] Castro Neto, A.H.; Guinea, F.; Peres, N.M.R.; Novoselov, K.S.; Geim, A.K. The electronic properties of graphene. *Rev. Mod. Phys.,* **2009**, *81*(1), 109-162.
[http://dx.doi.org/10.1103/RevModPhys.81.109]

[33] Akturk, A.; Goldsman, N. Electron transport and full-band electron-phonon interactions in graphene. *J. Appl. Phys.,* **2008**, *103*(5), 053702.
[http://dx.doi.org/10.1063/1.2890147]

[34] Berry, V. Impermeability of graphene and its applications. *Carbon,* **2013**, *62*, 1-10.
[http://dx.doi.org/10.1016/j.carbon.2013.05.052]

[35] Vekeman, J.; Sánchez-Marín, J.; Sánchez de Merás, A.; Garcia Cuesta, I.; Faginas-Lago, N. Flexibility in the graphene sheet: The influence on gas adsorption from molecular dynamics studies. *J. Phys. Chem. C,* **2019**, *123*(46), 28035-28047.
[http://dx.doi.org/10.1021/acs.jpcc.9b07503]

[36] Papageorgiou, D.G.; Kinloch, I.A.; Young, R.J. Mechanical properties of graphene and graphene-based nanocomposites. *Prog. Mater. Sci.,* **2017**, *90*, 75-127.
[http://dx.doi.org/10.1016/j.pmatsci.2017.07.004]

[37] Fugallo, G.; Cepellotti, A.; Paulatto, L.; Lazzeri, M.; Marzari, N.; Mauri, F. Thermal conductivity of graphene and graphite: collective excitations and mean free paths. *Nano Lett.,* **2014**, *14*(11), 6109-6114.
[http://dx.doi.org/10.1021/nl502059f] [PMID: 25343716]

[38] Murata, H.; Nakajima, Y.; Saitoh, N.; Yoshizawa, N.; Suemasu, T.; Toko, K. oko, K. High-electrica--conductivity multilayer graphene formed by layer exchange with controlled thickness and interlayer. *Sci. Rep.,* **2019**, *9*(1), 4068.
[http://dx.doi.org/10.1038/s41598-019-40547-0] [PMID: 30858422]

[39] Lu, Y.H.; Zhou, M.; Zhang, C.; Feng, Y.P. Metal-embedded graphene: a possible catalyst with high activity. *J. Phys. Chem. C,* **2009**, *113*(47), 20156-20160.
[http://dx.doi.org/10.1021/jp908829m]

[40] Imran Jafri, R.; Rajalakshmi, N.; Ramaprabhu, S. Nitrogen doped graphene nanoplatelets as catalyst support for oxygen reduction reaction in proton exchange membrane fuel cell. *J. Mater. Chem.,* **2010**, *20*(34), 7114-7117.
[http://dx.doi.org/10.1039/c0jm00467g]

[41] Dreyer, D.R.; Jia, H.P.; Bielawski, C.W. Graphene oxide: a convenient carbocatalyst for facilitating oxidation and hydration reactions. *Angew. Chem. Int. Ed.,* **2010**, *49*(38), 6686.
[http://dx.doi.org/10.1002/anie.201003238] [PMID: 20602388]

[42] Li, Y.; Gao, W.; Ci, L.; Wang, C.; Ajayan, P.M. Catalytic performance of Pt nanoparticles on reduced graphene oxide for methanol electro-oxidation. *Carbon,* **2010**, *48*(4), 1124-1130.
[http://dx.doi.org/10.1016/j.carbon.2009.11.034]

[43] Gao, Y.; Ma, D.; Wang, C.; Guan, J.; Bao, X. Reduced graphene oxide as a catalyst for hydrogenation of nitrobenzene at room temperature. *Chem. Commun. (Camb.),* **2011**, *47*(8), 2432-2434.
[http://dx.doi.org/10.1039/C0CC04420B] [PMID: 21170437]

[44] Serp, P.; Machado, B. Carbon (Nano)materials for Catalysis. In: *Nanostructured Carbon Materials for Catalysis*; Royal Society of Chemistry: London, **2015**; pp. 1-45.

[45] Qiu, Y.; Ali, S.; Lan, G.; Tong, H.; Fan, J.; Liu, H.; Li, B.; Han, W.; Tang, H.; Liu, H.; Li, Y. Defect-rich activated carbons as active and stable metal-free catalyst for acetylene hydrochlorination. *Carbon,* **2019**, *146*, 406-412.
[http://dx.doi.org/10.1016/j.carbon.2019.01.102]

[46] Chen, C.; Yan, D.; Wang, Y.; Zhou, Y.; Zou, Y.; Li, Y.; Wang, S. B-N Pairs enriched defective carbon

Not be distributed or uploaded to anyone or anywhere
For personal private use only

nanosheets for ammonia synthesis with high efficiency. *Small,* **2019**, *15*(7), 1805029. [http://dx.doi.org/10.1002/smll.201805029]

[47] Vidic, R.D.; Tessmer, C.H.; Uranowski, L.J. Impact of surface properties of activated carbons on oxidative coupling of phenolic compounds. *Carbon,* **1997**, *35*(9), 1349-1359. [http://dx.doi.org/10.1016/S0008-6223(97)00071-7]

[48] Speranza, G. The role of functionalization in the applications of carbon materials: an overview. *C- J Carbon Res,* **2019**, *5*(4), 84. [http://dx.doi.org/10.3390/c5040084]

[49] Arrigo, R.; Hävecker, M.; Wrabetz, S.; Blume, R.; Lerch, M.; McGregor, J.; Parrott, E.P.J.; Zeitler, J.A.; Gladden, L.F.; Knop-Gericke, A.; Schlögl, R.; Su, D.S. Tuning the acid/base properties of nanocarbons by functionalization *via* amination. *J. Am. Chem. Soc.,* **2010**, *132*(28), 9616-9630. [http://dx.doi.org/10.1021/ja910169v] [PMID: 20583786]

[50] Chen, J.; Chen, Q.; Ma, Q. Influence of surface functionalization *via* chemical oxidation on the properties of carbon nanotubes. *J. Colloid Interface Sci.,* **2012**, *370*(1), 32-38. [http://dx.doi.org/10.1016/j.jcis.2011.12.073] [PMID: 22280791]

[51] Boehm, H.P. Surface oxides on carbon and their analysis: a critical assessment. *Carbon,* **2002**, *40*(2), 145-149. [http://dx.doi.org/10.1016/S0008-6223(01)00165-8]

[52] Ros, T.G.; van Dillen, A.J.; Geus, J.W.; Koningsberger, D.C. Surface oxidation of carbon nanofibres. *Chemistry,* **2002**, *8*(5), 1151-1162. [http://dx.doi.org/10.1002/1521-3765(20020301)8:5<1151::AID-CHEM1151>3.0.CO;2-#] [PMID: 11891903]

[53] Moreno-Castilla, C.; Ferro-Garcia, M.A.; Joly, J.P.; Bautista-Toledo, I.; Carrasco-Marin, F.; Rivera-Utrilla, J. Ferro-Garcia, M.A. Joly, J.P. Bautista-Toledo, I. Carrasco- Marin, F. Rivera-Utrilla, J. Activated carbon surface modifications by nitric acid, hydrogen peroxide, and ammonium peroxydisulfate treatments. *Langmuir,* **1995**, *11*(11), 4386-4392. [http://dx.doi.org/10.1021/la00011a035]

[54] Boehm, H.P. Some aspects of the surface chemistry of carbon blacks and other carbons. *Carbon,* **1994**, *32*(5), 759-769. [http://dx.doi.org/10.1016/0008-6223(94)90031-0]

[55] Serp, P.; Corrias, M.; Kalck, P. Carbon nanotubes and nanofibers in catalysis. *Appl. Catal. A Gen.,* **2003**, *253*(2), 337-358. [http://dx.doi.org/10.1016/S0926-860X(03)00549-0]

[56] Rodríguez-reinoso, F. The role of carbon materials in heterogeneous catalysis. *Carbon,* **1998**, *36*(3), 159-175. [http://dx.doi.org/10.1016/S0008-6223(97)00173-5]

[57] Ayyaru, S.; Ahn, Y.H. Application of sulfonic acid group functionalized graphene oxide to improve hydrophilicity, permeability, and antifouling of PVDF nanocomposite ultrafiltration membranes. *J. Membr. Sci.,* **2017**, *525*, 210-219. [http://dx.doi.org/10.1016/j.memsci.2016.10.048]

[58] Sun, N.; Sun, C.; Liu, H.; Liu, J.; Stevens, L.; Drage, T.; Snape, C.E.; Li, K.; Wei, W.; Sun, Y. Synthesis, characterization and evaluation of activated spherical carbon materials for CO_2 capture. *Fuel,* **2013**, *113*, 854-862. [http://dx.doi.org/10.1016/j.fuel.2013.03.047]

[59] Pan, T.; Liu, H.; Ren, G.; Li, Y.; Lu, X.; Zhu, Y. Metal-free porous nitrogen-doped carbon nanotubes for enhanced oxygen reduction and evolution reactions. *Sci. Bull. (Beijing),* **2016**, *61*(11), 889-896. [http://dx.doi.org/10.1007/s11434-016-1073-3]

[60] Li, O.L.; Ishizaki, T. Development, challenges, and prospects of carbon-based electrode for lithium-air

Not be distributed or uploaded to anyone or anywhere
For personal private use only

batteries. In: *Emerging Materials for Energy Conversion and Storage*; Cheong, K.Y.; Impellizzeri, G.; Fraga, M.A., Eds.; Elsevier: Amsterdam, **2018**; pp. 115-152.
[http://dx.doi.org/10.1016/B978-0-12-813794-9.00004-1]

[61] Čejka, J.; Mintova, S. Perspectives of micro/mesoporous composites in catalysis. *Catal. Rev., Sci. Eng.,* **2007**, *49*(4), 457-509.
[http://dx.doi.org/10.1080/01614940701583240]

[62] Ferrero, G.A.; Preuss, K.; Fuertes, A.B.; Sevilla, M.; Titirici, M.M. The influence of pore size distribution on the oxygen reduction reaction performance in nitrogen doped carbon microspheres. *J. Mater. Chem. A Mater. Energy Sustain.,* **2016**, *4*(7), 2581-2589.
[http://dx.doi.org/10.1039/C5TA10063A]

[63] Vaccaro, S.; Malangone, L. Catalytic combustion for supplying energy for endothermic reaction. *J. Adv. Chem. Eng.,* **2014**, *4*, 1000107.

[64] Koh, Y.K. Thermal conductivity and phonon transport. In: *Encyclopedia of Nanotechnology*; Bhushan, B., Ed.; Springer: Berlin, **2012**.

[65] Liu, Y.; Hu, C.; Huang, J.; Sumpter, B.G.; Qiao, R. Tuning interfacial thermal conductance of graphene embedded in soft materials by vacancy defects. *J. Chem. Phys.,* **2015**, *142*(24), 244703.
[http://dx.doi.org/10.1063/1.4922775] [PMID: 26133445]

[66] Hung, N.T.; Nugraha, A.R.T.; Saito, R. N.; R. T. Nugraha, A.; Saito, R. Thermoelectric properties of carbon nanotubes. *Energies,* **2019**, *12*(23), 4561.
[http://dx.doi.org/10.3390/en12234561]

[67] Asalieva, E.; Sineva, L.; Sinichkina, S.; Solomonik, I.; Gryaznov, K.; Pushina, E.; Kulchakovskaya, E.; Gorshkov, A.; Kulnitskiy, B.; Ovsyannikov, D.; Zholudev, S.; Mordkovich, V. Exfoliated graphite as a heat-conductive frame for a new pelletized Fischer–Tropsch synthesis catalyst. *Appl. Catal. A Gen.,* **2020**, *601*, 117639.
[http://dx.doi.org/10.1016/j.apcata.2020.117639]

[68] Bogeat, A.B. Understanding and tuning the electrical conductivity of activated carbon: A state-of-the-art review. *Crit. Rev. Solid State,* **2019**, *46*(1), 1-37.
[http://dx.doi.org/10.1080/10408436.2019.1671800]

[69] Nasir, S.; Hussein, M.; Zainal, Z.; Yusof, N. Carbon-based nanomaterials/allotropes: a glimpse of their synthesis, properties and some applications. *Materials (Basel),* **2018**, *11*(2), 295.
[http://dx.doi.org/10.3390/ma11020295] [PMID: 29438327]

[70] Hausmann, B.J.M.; Bulu, I.; Venkataraman, V.; Deotare, P.; Lončar, M. Diamond nonlinear photonics. *Nat. Photonics,* **2014**, *8*(5), 369-374.
[http://dx.doi.org/10.1038/nphoton.2014.72]

[71] García, N.; Esquinazi, P.; Barzola-Quiquia, J.; Dusari, S. Evidence for semiconducting behavior with a narrow band gap of Bernal graphite. *New J. Phys.,* **2012**, *14*(5), 053015.
[http://dx.doi.org/10.1088/1367-2630/14/5/053015]

[72] Maruszewski, B.T. Fullerenes: Thermomechanics, Doping, Electrical Conductivity. In: *Encyclopedia of Thermal Stresses*; Hetnarski, R.B., Ed.; Springer: Dordrecht, **2014**.
[http://dx.doi.org/10.1007/978-94-007-2739-7_1030]

[73] Eatemadi, A.; Daraee, H.; Karimkhanloo, H.; Kouhi, M.; Zarghami, N.; Akbarzadeh, A.; Abasi, M.; Hanifehpour, Y.; Joo, S.W. Carbon nanotubes: properties, synthesis, purification, and medical applications. *Nanoscale Res. Lett.,* **2014**, *9*(1), 393.
[http://dx.doi.org/10.1186/1556-276X-9-393] [PMID: 25170330]

[74] Gupta, N.; Gupta, S.M.; Sharma, S.K. Carbon nanotubes: synthesis, properties and engineering applications. *Carbon Letters,* **2019**, *29*(5), 419-447.
[http://dx.doi.org/10.1007/s42823-019-00068-2]

[75] Bandaru, P.R. Electrical properties and applications of carbon nanotube structures. *J. Nanosci.*

Not be distributed or uploaded to anyone or anywhere
For personal private use only

Nanotechnol., **2007**, *7*(4), 1239-1267.
[http://dx.doi.org/10.1166/jnn.2007.307] [PMID: 17450889]

[76] Sreeprasad, T.S.; Berry, V. How do the electrical properties of graphene change with its functionalization? *Small,* **2013**, *9*(3), 341-350.
[http://dx.doi.org/10.1002/smll.201202196] [PMID: 23169614]

[77] Borchardt, L.; Zhu, Q.L.; Casco, M.E.; Berger, R.; Zhuang, X.; Kaskel, S.; Feng, X.; Xu, Q. Toward a molecular design of porous carbon materials. *Mater. Today,* **2017**, *20*(10), 592-610.
[http://dx.doi.org/10.1016/j.mattod.2017.06.002]

[78] Suslova, E.V.; Arkhipova, E.A.; Kalashnik, A.V.; Ivanov, A.S.; Savilov, S.V.; Xia, H.; Lunin, V.V. Effect of the functionalization of nitrogen-doped carbon nanotubes on electrical conductivity. *Russ. J. Phys. Chem. A. Focus Chem.,* **2019**, *93*(10), 1952-1956.
[http://dx.doi.org/10.1134/S0036024419100303]

[79] Jiang, Y.; Cheng, G.; Li, Y.; He, Z.; Zhu, J.; Meng, W.; Zhou, H.; Dai, L.; Wang, L. Superior electrocatalytic performance of porous, graphitic, and oxygen-functionalized carbon nanofiber as bifunctional electrode for vanadium redox flow battery. *Appl. Surf. Sci.,* **2020**, *525*, 146453.
[http://dx.doi.org/10.1016/j.apsusc.2020.146453]

[80] Han, F.D.; Yao, B.; Bai, Y.J. Preparation of carbon nano-onions and their application as anode materials for rechargeable lithium-ion batteries. *J. Phys. Chem. C,* **2011**, *115*(18), 8923-8927.
[http://dx.doi.org/10.1021/jp2007599]

[81] Li, X.; Cai, W.; An, J.; Kim, S.; Nah, J.; Yang, D.; Piner, R.; Velamakanni, A.; Jung, I.; Tutuc, E.; Banerjee, S.K.; Colombo, L.; Ruoff, R.S. Large-area synthesis of high-quality and uniform graphene films on copper foils. *Science,* **2009**, *324*(5932), 1312-1314.
[http://dx.doi.org/10.1126/science.1171245] [PMID: 19423775]

[82] Sawant, S.Y.; Somani, R.S.; Newalkar, B.L.; Choudary, N.V.; Bajaj, H.C. Synthesis of submicron size hollow carbon spheres by a chemical reduction — solvothermal method using carbon tetrachloride as carbon source. *Mater. Lett.,* **2009**, *63*(27), 2339-2342.
[http://dx.doi.org/10.1016/j.matlet.2009.07.066]

[83] Wang, Y.; Wang, Y.; Fei, H.; Cai, X. The effect of heat treatment on the electrical conductivity of highly conducting graphene films. *Carbon,* **2013**, *51*, 436.
[http://dx.doi.org/10.1016/j.carbon.2012.08.034]

[84] Mattia, D.; Rossi, M.P.; Kim, B.M.; Korneva, G.; Bau, H.H.; Gogotsi, Y. Effect of graphitization on the wettability and electrical conductivity of CVD-carbon nanotubes and films. *J. Phys. Chem. B,* **2006**, *110*(20), 9850-9855.
[http://dx.doi.org/10.1021/jp061138s] [PMID: 16706438]

[85] Špitalský, Z.; Krontiras, C.A.; Georga, S.N.; Galiotis, C. Effect of oxidation treatment of multiwalled carbon nanotubes on the mechanical and electrical properties of their epoxy composites. *Compos., Part A Appl. Sci. Manuf.,* **2009**, *40*(6-7), 778-783.
[http://dx.doi.org/10.1016/j.compositesa.2009.03.008]

[86] Iwanow, M.; Gärtner, T.; Sieber, V.; König, B. Activated carbon as catalyst support: precursors, preparation, modification and characterization. *Beilstein J. Org. Chem.,* **2020**, *16*, 1188-1202.
[http://dx.doi.org/10.3762/bjoc.16.104] [PMID: 32550932]

[87] Behera, S.K.; Chakraborty, S.; Meikap, B.C. Demineralization mechanism and influence of parameters on high ash Indian coal by chemical leaching of acid and alkali solution. *Int. J. Coal Sci. Technol.,* **2018**, *5*(2), 142-155.
[http://dx.doi.org/10.1007/s40789-018-0208-3]

[88] Ahmad, F.; Daud, W.M.A.W.; Ahmad, M.A.; Radzi, R. Cocoa (*Theobroma cacao*) shell-based activated carbon by CO_2 activation in removing of Cationic dye from aqueous solution: Kinetics and equilibrium studies. *Chem. Eng. Res. Des.,* **2012**, *90*(10), 1480-1490.
[http://dx.doi.org/10.1016/j.cherd.2012.01.017]

Not be distributed or uploaded to anyone or anywhere
For personal private use only

[89] Xie, T.; Liao, T.; Liu, C.; Xu, L.; Yang, J.; Zhu, Q.; Wang, J.; Zhang, X. Synthesis of multifunctional photocatalyst vanadium oxide/activated carbon *via in situ* utilization of stone coal ore. *Ceram. Int.,* **2019**, *45*(4), 4934-4944.
[http://dx.doi.org/10.1016/j.ceramint.2018.11.193]

[90] Shen, Y.; Fu, Y. KOH-activated rice husk char *via* CO_2 pyrolysis for phenol adsorption. *Mater. Today Energy,* **2018**, *9*, 397-405.
[http://dx.doi.org/10.1016/j.mtener.2018.07.005]

[91] Zhou, J.; Luo, A.; Zhao, Y. Preparation and characterisation of activated carbon from waste tea by physical activation using steam. *J. Air Waste Manag. Assoc.,* **2018**, *68*(12), 1269-1277.
[http://dx.doi.org/10.1080/10962247.2018.1460282] [PMID: 29667515]

[92] Hsu, L.Y.; Teng, H. Influence of different chemical reagents on the preparation of activated carbons from bituminous coal. *Fuel Process. Technol.,* **2000**, *64*(1-3), 155-166.
[http://dx.doi.org/10.1016/S0378-3820(00)00071-0]

[93] Ahmadpour, A.; Do, D.D. The preparation of active carbons from coal by chemical and physical activation. *Carbon,* **1996**, *34*(4), 471-479.
[http://dx.doi.org/10.1016/0008-6223(95)00204-9]

[94] Saleem, J.; Shahid, U.B.; Hijab, M.; Mackey, H.; McKay, G. Production and applications of activated carbons as adsorbents from olive stones. *Biomass Convers. Biorefin.,* **2019**, *9*(4), 775-802.
[http://dx.doi.org/10.1007/s13399-019-00473-7]

[95] Maciá-Agulló, J.A.; Moore, B.C.; Cazorla-Amorós, D.; Linares-Solano, A. Activation of coal tar pitch carbon fibres: Physical activation *vs.* chemical activation. *Carbon,* **2004**, *42*(7), 1367-1370.
[http://dx.doi.org/10.1016/j.carbon.2004.01.013]

[96] Chen, R.; Li, L.; Liu, Z.; Lu, M.; Wang, C.; Li, H.; Ma, W.; Wang, S. Preparation and characterization of activated carbons from tobacco stem by chemical activation. *J. Air Waste Manag. Assoc.,* **2017**, *67*(6), 713-724.
[http://dx.doi.org/10.1080/10962247.2017.1280560] [PMID: 28121516]

[97] Li, R.; Shahbazi, A.; Wang, L.; Zhang, B.; Hung, A.M.; Dayton, D.C. Graphite encapsulated molybdenum carbide core/shell nanocomposite for highly selective conversion of guaiacol to phenolic compounds in methanol. *Appl. Catal. A Gen.,* **2016**, *528*, 123-130.
[http://dx.doi.org/10.1016/j.apcata.2016.09.016]

[98] Lan, R.; Su, W.; Li, J. Preparation and catalytic performance of expanded graphite for oxidation of organic pollutant. *Catalysts,* **2019**, *9*(3), 280.
[http://dx.doi.org/10.3390/catal9030280]

[99] Bernat-Quesada, F.; Espinosa, J.C.; Barbera, V.; Álvaro, M.; Galimberti, M.; Navalón, S.; García, H. Catalytic ozonation using edge-hydroxylated graphite-based materials. *ACS Sustain. Chem.& Eng.,* **2019**, *7*(20), 17443-17452.
[http://dx.doi.org/10.1021/acssuschemeng.9b04646]

[100] Xu, Z.; Duong-Viet, C.; Ba, H.; Li, B.; Truong-Huu, T.; Nguyen-Dinh, L.; Pham-Huu, C. Gaseous nitric acid activated graphite felts as hierarchical metal-free catalyst for selective oxidation of H_2S. *Catalysts,* **2018**, *8*(4), 145.
[http://dx.doi.org/10.3390/catal8040145]

[101] Duong-Viet, C.; Liu, Y.; Ba, H.; Truong-Phuoc, L.; Baaziz, W.; Nguyen-Dinh, L.; Nhut, J.M.; Pham-Huu, C. Carbon nanotubes containing oxygenated decorating defects as metal-free catalyst for selective oxidation of H_2S. *Appl. Catal. B,* **2016**, *191*, 29-41.
[http://dx.doi.org/10.1016/j.apcatb.2016.03.018]

[102] Hariharan, Y.; Bharathi, A.; Sundar, C.S.; Sastry, V.S.; Yousuf, M.; Radhakrishnan, T.S.; Rao, G.V.N. GeethaKumary, T.; Subramanian, N.; Sahu, P.Ch.; Raghunathan V.S.; Valsakumar M.C. Synthesis and characterization of fullerenes C_{60} and C_{70} and superconductivity in K and Rb-doped C_{60}. *Curr. Sci.,*

1992, *63*, 25-33.

[103] Itagaki, H.; Fujiwara, Y.; Minowa, Y.; Ikehara, Y.; Kaneko, T.; Okazaki, T.; Iizumi, Y.; Kim, J.; Sakakita, H. Synthesis of endohedral-fullerenes using laser ablation plasma from solid material and vaporized fullerenes. *AIP Adv.,* **2019**, *9*(7), 075324.
[http://dx.doi.org/10.1063/1.5100980]

[104] Goel, A.; Hebgen, P.; Vander Sande, J.B.; Howard, J.B. Combustion synthesis of fullerenes and fullerenic nanostructures. *Carbon,* **2002**, *40*(2), 177-182.
[http://dx.doi.org/10.1016/S0008-6223(01)00170-1]

[105] Sabounchei, S.J.; Hosseinzadeh, M.; Zarepour-jevinani, M.; Ghanbari, B. Monodentate palladium(0)–[60]fullerene complexes of diphosphine ligands as efficient and sustainable nanocatalysts for the Mizoroki–Heck coupling reaction of aryl chlorides. *New J. Chem.,* **2017**, *41*(18), 9701-9709.
[http://dx.doi.org/10.1039/C7NJ00741H]

[106] Yao, S.; Yuan, X.; Jiang, L.; Xiong, T.; Zhang, J. Recent progress on fullerene-based materials: synthesis, properties, modifications, and photocatalytic applications. *Materials (Basel),* **2020**, *13*(13), 2924.
[http://dx.doi.org/10.3390/ma13132924] [PMID: 32629789]

[107] Liu, R.; Hou, Y.; Jiang, S.; Nie, B. Ag(I)-hived fullerene microcube as an enhanced catalytic substrate for the reduction of 4-nitrophenol and the photodegradation of Orange G dye. *Langmuir,* **2020**, *36*(19), 5236-5242.
[http://dx.doi.org/10.1021/acs.langmuir.0c00580] [PMID: 32306732]

[108] Li, Z.; Han, C. Palladium nanoflowers supported on amino-fullerene as novel catalyst for reduction of 4-nitrophenol. *Chin. Chem. Lett.,* **2020**, *31*(3), 818-820.
[http://dx.doi.org/10.1016/j.cclet.2019.06.047]

[109] Sharma, S. Glassy carbon: A promising material for micro- and nanomanufacturing. *Materials (Basel),* **2018**, *11*(10), 1857.
[http://dx.doi.org/10.3390/ma11101857] [PMID: 30274225]

[110] Jenkins, G.M.; Kawamura, K. *Polymeric carbons-carbon fibre, glass and char*; Cambridge University Press: Cambridge, UK: New York, **1976**.

[111] Dunn, J.G.; Chamberlain, A.C. The recovery of gold from refractory arsenopyrite concentrates by pyrolysis-oxidation. *Miner. Eng.,* **1997**, *10*(9), 919-928.
[http://dx.doi.org/10.1016/S0892-6875(97)00074-5]

[112] Hoffman, W.P.; Vastola, F.J.; Walker, P.L., Jr Pyrolysis of propylene over carbon active sites II. Pyrolysis products. *Carbon,* **1988**, *26*(4), 485-499.
[http://dx.doi.org/10.1016/0008-6223(88)90147-9]

[113] Sharma, S.; Rostas, A.M.; Bordonali, L.; MacKinnon, N.; Weber, S.; Korvink, J.G. Micro and nano patternable magnetic carbon. *J. Appl. Phys.,* **2016**, *120*(23), 235107.
[http://dx.doi.org/10.1063/1.4972476]

[114] Sharma, S.; Kumar, C.N.S.; Korvink, J.G.; Kübel, C. Evolution of glassy carbon microstructure: *In situ* transmission electron microscopy of the pyrolysis process. *Scientific Reports,* 2018, 8(1).

[115] Sharma, S.; Kamath, R.; Madou, M. Porous glassy carbon formed by rapid pyrolysis of phenol-formaldehyde resins and its performance as electrode material for electrochemical double layer capacitors. *J. Anal. Appl. Pyrolysis,* **2014**, *108*, 12-18.
[http://dx.doi.org/10.1016/j.jaap.2014.05.025]

[116] Jurkiewicz, K.; Pawlyta, M.; Zygadło, D.; Chrobak, D.; Duber, S.; Wrzalik, R.; Ratuszna, A.; Burian, A. Evolution of glassy carbon under heat treatment: correlation structure–mechanical properties. *J. Mater. Sci.,* **2018**, *53*(5), 3509-3523.
[http://dx.doi.org/10.1007/s10853-017-1753-7]

Not be distributed or uploaded to anyone or anywhere
For personal private use only

[117] Thirukumaran, P.; Balasubramanian, R.; Atchudan, R.; Shakila Parveen, A.; Lee, Y.R.; Kim, S.C. Metal-free nitrogen-rich glassy carbon as an electrocatalyst for hydrogen evolution reaction. *Mater. Res. Bull.,* **2020**, *124*, 110734.
[http://dx.doi.org/10.1016/j.materresbull.2019.110734]

[118] Bhagabati, P.; Rahaman, M.; Bhandari, S.; Roy, I.; Dey, A.; Gupta, P.; Ansari, M.A.; Dutta, A.; Chattopadhyay, D. Synthesis/Preparation of Carbon Materials. In: *Carbon-Containing Polymer Composites*; Rahaman, M.; Ali, D.K.; Aldalbahi, K., Eds.; Springer: Singapore, **2019**.
[http://dx.doi.org/10.1007/978-981-13-2688-2_1]

[119] Villano, R.; Acocella, M.R.; Guerra, G. Oxidized carbon black as catalyst for the enamine formation in solvent-free conditions: A green strategy to build the benzodiazepine scaffold. *ChemistrySelect,* **2017**, *2*(32), 10559-10564.
[http://dx.doi.org/10.1002/slct.201701711]

[120] Lim, J.; Ryu, S.Y.; Kim, J.; Jun, Y. A study of TiO_2/carbon black composition as counter electrode materials for dye-sensitized solar cells. *Nanoscale Res. Lett.,* **2013**, *8*(1), 227.
[http://dx.doi.org/10.1186/1556-276X-8-227] [PMID: 23672498]

[121] Hulicova-Jurcakova, D.; Li, X.; Zhu, Z.; de Marco, R.; Lu, G.Q. Graphitic carbon nanofibers synthesized by the chemical vapor deposition (CVD) method and their electrochemical performances in supercapacitors. *Energy Fuels,* **2008**, *22*(6), 4139-4145.
[http://dx.doi.org/10.1021/ef8004306]

[122] Miniach, E.; Śliwak, A.; Moyseowicz, A.; Gryglewicz, G. Growth of carbon nanofibers from methane on a hydroxyapatite-supported nickel catalyst. *J. Mater. Sci.,* **2016**, *51*(11), 5367-5376.
[http://dx.doi.org/10.1007/s10853-016-9839-1]

[123] Alarifi, I.M.; Khan, W.S.; Asmatulu, R. Synthesis of electrospun polyacrylonitrile- derived carbon fibers and comparison of properties with bulk form. *PLoS One,* **2018**, *13*(8), e0201345.
[http://dx.doi.org/10.1371/journal.pone.0201345] [PMID: 30091992]

[124] Huczko, A. Template-based synthesis of nanomaterials. *Appl. Phys., A Mater. Sci. Process.,* **2000**, *70*(4), 365-376.
[http://dx.doi.org/10.1007/s003390051050]

[125] Hulteen, J.C.; Chen, H.X.; Chambliss, C.K.; Martin, C.R. Template synthesis of carbon nanotubule and nanofiber arrays. *Nanostruct. Mater.,* **1997**, *9*(1-8), 133-136.
[http://dx.doi.org/10.1016/S0965-9773(97)00036-6]

[126] Toro, C.; Buriak, J.M. Template synthesis approach to nanomaterials. *Charles Martin. Chem. Mater.,* **2014**, *26*, 4889-4890.

[127] Li, W.; Zhang, F.; Dou, Y.; Wu, Z.; Liu, H.; Qian, X.; Gu, D.; Xia, Y.; Tu, B.; Zhao, D. A self-template strategy for the synthesis of mesoporous carbon nanofibers as advanced supercapacitor electrodes. *Adv. Energy Mater.,* **2011**, *1*(3), 382-386.
[http://dx.doi.org/10.1002/aenm.201000096]

[128] Verma, B.; Sewani, H.; Balomajumder, C. Synthesis of carbon nanotubes *via* chemical vapor deposition: an advanced application in the Management of Electroplating Effluent. *Environ. Sci. Pollut. Res. Int.,* **2020**, *27*(12), 14007-14018.
[http://dx.doi.org/10.1007/s11356-020-08002-0] [PMID: 32036530]

[129] Saravanan, M.S.S.; Nagaraj, T.; Mohan, S.; Singh, S.R.K.; Sivaprasad, K.; Babu, S.P.K.; Sajin, J.B. Synthesis of metal catalyst carbon nanotubes by arc-discharge method used for energy efficient applications. *AIP Conf. Proc.,* **2018**, *2039*, 020072.
[http://dx.doi.org/10.1063/1.5079031]

[130] Ismail, R.A.; Kadhim, R.G.; Abdulridha, W.M. Effect of multiwalled carbon nanotubes incorporation on the performance of porous silicon photodetector. *Optik (Stuttg.),* **2016**, *127*(19), 8144-8152.
[http://dx.doi.org/10.1016/j.ijleo.2016.06.018]

Not be distributed or uploaded to anyone or anywhere
For personal private use only

[131] Wang, X.; Liu, X.; Licht, G.; Licht, S. Calcium metaborate induced thin walled carbon nanotube syntheses from CO_2 by molten carbonate electrolysis. *Sci. Rep.,* **2020**, *10*(1), 15146.
[http://dx.doi.org/10.1038/s41598-020-71644-0] [PMID: 32934276]

[132] Wang, S.; Tang, L.A.; Bao, Q.; Lin, M.; Deng, S.; Goh, B.M.; Loh, K.P. Room-temperature synthesis of soluble carbon nanotubes by the sonication of graphene oxide nanosheets. *J. Am. Chem. Soc.,* **2009**, *131*(46), 16832-16837.
[http://dx.doi.org/10.1021/ja905968v] [PMID: 19873970]

[133] Chauhan, S.; Jain, N.; Nagaich, U. Nanodiamonds with powerful ability for drug delivery and biomedical applications: Recent updates on *in vivo* study and patents. *J. Pharm. Anal.,* **2020**, *10*(1), 1-12.
[http://dx.doi.org/10.1016/j.jpha.2019.09.003] [PMID: 32123595]

[134] Basso, L.; Cazzanelli, M.; Orlandi, M.; Miotello, A. Nanodiamonds: Synthesis and application in sensing, catalysis, and the possible connection with some processes occurring in space. *Appl. Sci. (Basel),* **2020**, *10*(12), 4094.
[http://dx.doi.org/10.3390/app10124094]

[135] Panich, A.M.; Shames, A.I.; Mogilyansky, D.; Goren, S.D.; Dolmatov, V.Y. Detonation nanodiamonds fabricated from tetryl: Synthesis, NMR, EPR and XRD study. *Diamond Related Materials,* **2020**, *108*, 107918.
[http://dx.doi.org/10.1016/j.diamond.2020.107918]

[136] Tallaire, A.; Brinza, O.; De Feudis, M.; Ferrier, A.; Touati, N.; Binet, L.; Nicolas, L.; Delord, T.; Hétet, G.; Herzig, T.; Pezzagna, S.; Goldner, P.; Achard, J. Synthesis of loose nanodiamonds containing nitrogen-vacancy centers for magnetic and thermal sensing. *ACS Appl. Nano Mater.,* **2019**, *2*(9), 5952-5962.
[http://dx.doi.org/10.1021/acsanm.9b01395]

[137] Basso, L.; Bazzanella, N.; Cazzanelli, M.; Miotello, A. On the route towards a facile fluorescent nanodiamonds laser-synthesis. *Carbon,* **2019**, *153*, 148-155.
[http://dx.doi.org/10.1016/j.carbon.2019.07.025]

[138] Ekimov, E.A.; Kondrina, K.M.; Mordvinova, N.E.; Lebedev, O.I.; Pasternak, D.G.; Vlasov, I.I. High-pressure, high-temperature synthesis of nanodiamond from adamantane. *Inorg. Mater.,* **2019**, *55*(5), 437-442.
[http://dx.doi.org/10.1134/S0020168519050042]

[139] Das, T.; Saikia, B.K. Nanodiamonds produced from low-grade indian coals. *ACS Sustain. Chem.& Eng.,* **2017**, *5*(11), 9619-9624.
[http://dx.doi.org/10.1021/acssuschemeng.7b02500]

[140] Ugarte, D. Curling and closure of graphitic networks under electron-beam irradiation. *Nature,* **1992**, *359*(6397), 707-709.
[http://dx.doi.org/10.1038/359707a0] [PMID: 11536508]

[141] Alessandro, F.; Scarcello, A.; Basantes Valverde, M.D.; Coello Fiallos, D.C.; Osman, S.M.; Cupolillo, A.; Arias, M.; Arias de Fuentes, O.; De Luca, G.; Aloise, A.; Curcio, E.; Nicotra, G.; Spinella, C.; Caputi, L.S. Selective synthesis of turbostratic polyhedral carbon nano-onions by arc discharge in water. *Nanotechnology,* **2018**, *29*(32), 325601.
[http://dx.doi.org/10.1088/1361-6528/aac4ca] [PMID: 29761791]

[142] Zhang, C.; Li, J.; Shi, C.; Liu, E.; Du, X.; Feng, W.; Zhao, N. The efficient synthesis of carbon nano-onions using chemical vapor deposition on an unsupported Ni–Fe alloy catalyst. *Carbon,* **2011**, *49*(4), 1151-1158.
[http://dx.doi.org/10.1016/j.carbon.2010.11.030]

[143] Jung, S.; Myung, Y.; Das, G.S.; Bhatnagar, A.; Park, J.W.; Tripathi, K.M.; Kim, T. Carbon nano-onions from waste oil for application in energy storage devices. *New J. Chem.,* **2020**, *44*(18), 7369-7375.

Not be distributed or uploaded to anyone or anywhere
For personal private use only

[http://dx.doi.org/10.1039/D0NJ00699H]

[144] Dorobantu, D.; Bota, P.M.; Boerasu, I.; Bojin, D.; Enachescu, M. Pulse laser ablation system for carbon nano-onions fabrication. *Surg. Eng. Appl. Electrochem.,* **2014**, *50*(5), 390-394. [http://dx.doi.org/10.3103/S1068375514050044]

[145] Bartolome, J.P.; Fragoso, A. Preparation and characterization of carbon nano-onions by nanodiamond annealing and functionalization by radio-frequency Ar/O_2 plasma. *Fuller. Nanotub. Carbon Nanostruct.,* **2017**, *25*(5), 327-334. [http://dx.doi.org/10.1080/1536383X.2017.1303604]

[146] Christoforidis, K.C.; Syrgiannis, Z.; La Parola, V.; Montini, T.; Petit, C.; Stathatos, E.; Godin, R.; Durrant, J.R.; Prato, M.; Fornasiero, P. Metal-free dual-phase full organic carbon nanotubes/g-C_3N_4 heteroarchitectures for photocatalytic hydrogen production. *Nano Energy,* **2018**, *50*, 468-478. [http://dx.doi.org/10.1016/j.nanoen.2018.05.070]

[147] Paušová, Š.; Pacileo, L.; Baudys, M.; Hrubantová, A.; Neumann-Spallart, M.; Dvoranová, D.; Brezová, V.; Krýsa, J. Active carbon/TiO_2 composites for photocatalytic decomposition of benzoic acid in water and toluene in air. *Catal. Today,* 2022 (9), 417-423. [http://dx.doi.org/10.1016/j.cattod.2020.06.048]

[148] Don, M.F.; Ekanayake, P.; Nakajima, H.; Mahadi, A.H.; Lim, C.M.; Atod, A. Acetylene carbon black-graphite composite as low-cost and efficient counter electrode for dye-sensitized solar cells (DSSCs). *Ionics,* **2019**, *25*(11), 5585-5593. [http://dx.doi.org/10.1007/s11581-019-03071-9]

[149] Bhavani, K.S.; Anusha, T.; Shanmukha Kumar, J.V.; Brahman, P.K. Enhanced electrocatalytic activity of methanol and ethanol oxidation in alkaline medium at bimetallic nanoparticles electrochemically decorated fullerene-C_{60} nanocomposite electrocatalyst: An efficient anode material for alcohol fuel cell applications. *Electroanalysis,* **2020**, *33*(1), 388-389. [http://dx.doi.org/10.1002/elan.202060154]

[150] Chen, J.; Wang, J.; Chen, J.; Wang, L. A bifunctional electrocatalyst of PtNi nanoparticles immobilized on three-dimensional carbon nanofiber mats for efficient and stable water splitting in both acid and basic media. *J. Mater. Sci.,* **2017**, *52*(22), 13064-13077. [http://dx.doi.org/10.1007/s10853-017-1410-1]

[151] Mohapatra, J.; Ananthoju, B.; Nair, V.; Mitra, A.; Bahadur, D.; Medhekar, N.V.; Aslam, M. Enzymatic and non-enzymatic electrochemical glucose sensor based on carbon nano-onions. *Appl. Surf. Sci.,* **2018**, *442*, 332-341. [http://dx.doi.org/10.1016/j.apsusc.2018.02.124]

[152] Lawrence, N.S.; Deo, R.P.; Wang, J. Biocatalytic carbon paste sensors based on a mediator pasting liquid. *Anal. Chem.,* **2004**, *76*(13), 3735-3739. [http://dx.doi.org/10.1021/ac049943v] [PMID: 15228348]

[153] Ji, C.; Hou, J.; Chen, V. Cross-linked carbon nanotubes-based biocatalytic membranes for micro-pollutants degradation: Performance, stability, and regeneration. *J. Membr. Sci.,* **2016**, *520*, 869-880. [http://dx.doi.org/10.1016/j.memsci.2016.08.056]

[154] Singh, R.S.; Chauhan, K.; Kennedy, J.F. Fructose production from inulin using fungal inulinase immobilized on 3-aminopropyl-triethoxysilane functionalized multiwalled carbon nanotubes. *Int. J. Biol. Macromol.,* **2019**, *125*, 41-52. [http://dx.doi.org/10.1016/j.ijbiomac.2018.11.281] [PMID: 30529206]

[155] Oliveira, S.F.; da Luz, J.M.R.; Kasuya, M.C.M.; Ladeira, L.O.; Correa Junior, A. Enzymatic extract containing lignin peroxidase immobilized on carbon nanotubes: Potential biocatalyst in dye decolourization. *Saudi J. Biol. Sci.,* **2018**, *25*(4), 651-659. [http://dx.doi.org/10.1016/j.sjbs.2016.02.018] [PMID: 29740229]

[156] Wang, L.; Liu, X.; Jiang, Y.; Zhou, L.; Ma, L.; He, Y.; Gao, J. Biocatalytic pickering emulsions stabilized by lipase-immobilized carbon nanotubes for biodiesel production. *Catalysts,* **2018**, *8*(12),

587.
[http://dx.doi.org/10.3390/catal8120587]

[157] Dam, B.; Jamatia, R.; Gupta, A.; Pal, A.K. Metal-free greener syntheses of pyrimidine derivatives using a highly efficient and reusable graphite oxide carbocatalyst under solvent-free reaction conditions. *ACS Sustain. Chem.& Eng.,* **2017**, *5*(12), 11459-11469.
[http://dx.doi.org/10.1021/acssuschemeng.7b02626]

For personal private use only
Not be distributed or uploaded to anyone or anywhere

CHAPTER 2

Structure and Properties of Graphene and Chemically Modified Graphene Materials

Manish Srivastava[1], Anjali Banger[2], Anamika Srivastava[2], Nirmala Kumari Jangid[2,*] and **Priy Brat Dwivedi[3]**

[1] *Department of Chemistry, Central University of Allahabad, Allahabad – 211002, Uttar Pradesh, India*

[2] *Department of Chemistry, Banasthali Vidyapith, Banasthali – 304022, Rajasthan, India*

[3] *National University of Science and Technology, AlHail South, Seen 111, Muscat, Oman*

Abstract: Graphene is an allotrope of carbon that is made up of very strongly bonded carbon atoms. The structure of graphene is a hexagonal lattice. Graphene shows sp^2 hybridization and an extremely thin atomic thickness of approximately 0.345Nm. This chapter deals with graphene structure, including hybridization, critical parameters of the unit cell, the formation of σ and π bonds, electronic band structure, edge orientations, and the number and stacking order of graphene layers. The remarkable characteristics of graphene occur because of the extended chain of π conjugation that results in high charge mobility, high conductivity & high Young's modulus value. Due to these attractive properties, graphene has gained much attention. Graphene, with the unique combination of bonded carbon atom structures with its myriad and complex physical properties is balanced to have a big impact on the future of material sciences, electronics, and nanotechnology. Graphene is converted to Graphene nanoparticles, Graphene oxide nanoparticles; Polymer-based graphene composite materials and Graphene nanoribbons, *etc* by chemical methods. Some of the application areas are batteries and ultracapacitors for energy storage and fuel cell and solar cell for energy generation and some of the possible future directions of research have been discussed.

Keywords: Actuators, Application of Graphene, Chemical Properties, Electrical Properties, Electrochemical Capacitors, Fabrication of Graphene Oxide, Functionality and Solubility, Graphene Aerogels, Graphene Composites, Graphene Derived Nanofiller, Graphene Oxide, Hybrid Graphene, Mechanical Properties, Optical Properties, Properties of Graphene, Quantum Dots of Graphene, Storage Material, Surface-Enhanced Raman Spectroscopy, Thermal Properties.

[*] **Corresponding author Nirmala Kumari Jangid:** Department of Chemistry, Banasthali Vidyapith, Banasthali – 304022, Rajasthan, India; E-mail:nirmalajangid.111@gmail.com

Pinki Bala Punjabi, Rakshit Ameta & Sharoni Gupta (Eds.)
All rights reserved-© 2023 Bentham Science Publishers

1. INTRODUCTION

The 6th element of the periodic table *i.e*., Carbon has always attracted researchers and technologists and the most studied allotrope of the Carbon family is Graphene. It is a single atomic planar layer of graphite [1]. By chemical vapor deposition, chemical or mechanical methods, can be obtained from graphite [2, 3].

Theoretically, for the last sixty years, graphene or two-dimensional graphite had been studied [4]. Earlier, it was assumed that graphene does not exist in the free state. Peierls and Landau contended that since two-dimensional crystals were chemically not stable so they do not exist [5, 6]. Hence, it was proclaimed that graphene has large three-dimensional structures [7]. Without a three-dimensional base, two-dimensional structures do not exist, later in 2004, Novoselov *et al*. accidentally discovered graphene. Using a micromechanical cleavage technique single-layer graphene was established [8].

After several broadcasts on nanotubes of carbon (1991) [9], fullerenes (1985) [10], and intercalated graphite [11], graphene gained immense interest [12, 13]. It is a flat sp^2 hybridized planar sheet of C atoms densely packed in a 2D hexagonal pattern. It can be coated into zero-dimensional fullerenes, twirled into a one-dimensional nanotube, or can be bundled into three-dimensional graphite.

The uncommon characteristics of graphene involve that its charge carriers behave as Dirac fermions, and under encompassing situations they scatter. This distinct attitude resulted in exceptional phenomenal changes [12]. Firstly, it is a two-dimensional semiconductor with minimal overlapping between the conduction band and valence band and has a bandgap of zero. Secondly, for measuring deviation in room temperature (up to 10000 cm^{-2} s^{-1}) and charge carrier concentration (up to 1013 cm^{-2}) it shows a strong bipolar electric field effect. Thirdly, by modifying chemical potential with the help of the electric field effect, exceptional half-integer QHE for hole and electrons carrier can be seen [13, 14]. At room temperature, a single layer of a sheet, shows great thermal conductivity (5000 WmK^{-1}). Additionally, it's transparent with 2.3% absorption towards visible light [15, 16]. Transistors can be produced with narrower (1-2 nm thick) ribbons of graphene having variable band gaps [17 - 19].

In past years, graphene is being used instead of carbon-based nanofiller in preparing nanocomposites of polymer and showed great thermal, electrical, and mechanical properties [20 - 27]. Chemically unstable indium tin oxide in displays and screens can be replaced by graphene [28, 29]. Hence, it is assumed that a single layer is responsible for the uniqueness of graphene although its preparation is severe in encompassing conditions. Due to inappropriate separation of graphene

sheets, it aggregates and restacks leading to the formation of graphite *via* Vander Waals interaction and p–p stacking [30, 31]. Graphene has vast applications in the fields of microwave absorption shields, nanocomposites of polymer, super-capacitor devices, drug delivery, biosensing, *etc*.

According to IUPAC, graphene can be explained as a single sheet of C with a graphitic structure and similar to a polycyclic aromatic hydrocarbon. During a discussion of various properties of monatomic sheets, graphene is prescribed [32, 33]. In 1987, for the first time, the word "graphene" was used by Mouras *et al*. [34], although in 1840 Schafhaeutl (German scientist) narrated the exfoliation and intercalation of graphite by making use of HNO_3 and H_2SO_4. From that time researchers predict the presence of graphene. But it was not until 2004 that two physicists at the University of Manchester, Andre Geim and Konstantin Novoselov, obtained graphene in the laboratory and could prove it. These researchers developed an easy procedure for obtaining graphene from graphite. Using tape, a thin sample of graphite was extracted from a greater one.

This procedure was repeated several times to finally obtain a monoatomic layer, which was then electrically isolated with a thin layer of silicon dioxide on a silicon wafer. The importance of this event lies in having isolated graphene at room temperature since in the past this material was considered thermodynamically unstable. For their innovative experiments, in 2010 they received the Nobel Prize in Physics [35].

The important discoveries of a few scientists have been summarized below (Table **1**).

Table 1. Scientists with their discoveries.

S.No.	SCIENTISTS	DISCOVERIES
1.	Schafhaeutl (1840)	Narrated exfoliation and intercalation of graphite by making use of HNO_3 and H_2SO_4.
2.	B.C. Brodie (1859)	First discovered graphite oxide properties [97].
3.	Brodie, Staudenmaier, Hummers and Offeman (1958)	First synthesized graphene oxide through graphitic oxidation [109 - 111].
4.	Mouras *et al*. (1987)	For the first time, used the word "graphene" [34].
5.	Andre Geim and Konstantin Novoselov (2004)	Fabricated graphene from graphite in the laboratory and received Nobel Prize in Physics (2010) for this.
6.	Novoselov *et al*. (2004)	Discovered graphene using a micromechanical cleavage technique [8].
7.	Wu *et al*. (2011)	Established remote control graphene-based robot in the presence and absence of IR radiations [89].

2. FABRICATION OF GRAPHENE

2.1. Bottom-up Method

Various synthetic criteria can be used to prepare graphene and its derivatives but usually bottom-up and top-down methods are used (Kim, 2010a). From the past ten years, productive work has been done for the advancement of bottom-up criteria to atomically brief graphene nanoribbons [36, 37]. Usually, chemical and epitaxial methods are used to generate large-sized, defect-free sheets of graphene in minimal quantities. With the help of the CVD method's low resistance, monolayered graphene films (30-inches) had been produced having higher potential and great optical transmission properties replacing commercially available transparent electrodes (Bae, 2010). They have useful applications in electronic and fundamental fields but are inapplicable in the case of nanocomposites of polymer since they require altered surface graphene sheets. By selecting the starting material of nanotubes size can be controlled by unzipped graphene ribbons but preparing composites of polymer is still an expensive procedure.

2.2. Top-down Method

In this method, graphene is prepared by the exfoliation of graphite and its derivatives. Since globally graphite is produced in bulk (1-2 million tons per annum) so starting from it (like from graphite oxide) is favorable and economically more advantageous than a bottom-up approach.

3. STRUCTURE

Carbon has six electrons in total, out of which four are in the outer orbit and two in the inner orbit. Outer four electrons are capable of forming chemical bonds but in graphene, one C atom is attached to three C atoms in a 2-D plane leaving one electron free for electronic conduction. Such movable electrons are known as pi (π) electrons present above and below the plane and their overlapping boost C-C bonding (Fig. **1**). It also governs the electronic properties of graphene and in general, these properties depend on the bonding and anti-bonding of this π orbital.

Graphene has a 2D structure (of monatomic thickness) and is formed by a regular honeycomb network of joined C atoms. The bond length of the C-C bond is about 0.142 nm. The interplanar distance of graphene sheets is 0.335 nm which further stacks and leads to the formation of graphite. It is light with 0.77 mg /m^2 surface density.

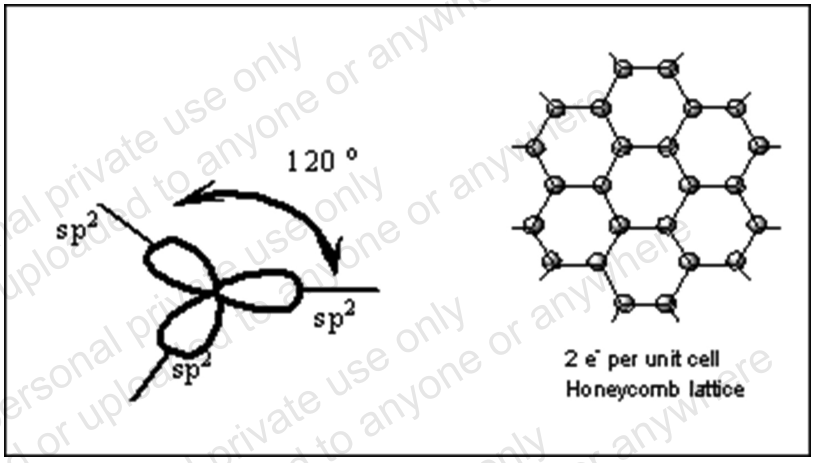

Fig. (1). Structure of graphene.

It is sp^2 hybridized and 0.345 nm thick. Since it shows normal electronic spectra, they are regarded as zero-band gap semiconductors. They can be rolled into a one-dimensional nanotube or in three-dimensional graphite. Its preparation is severe in encompassing conditions due to inappropriate separation of graphene sheets; it aggregates and restacks leading to the formation of graphite *via* Vander Waals interaction and p–p stacking [38, 39]. The aggregation *via* large-size or polar-polar interaction can be prevented if hydrophilic or hydrophobic groups are present [40].

Graphene can spontaneously repair voids present in its film when exposed to carbon-containing molecules [41]. Graphene sheets can be used to form other more complex carbon structures [42], like buckminsterfullerene, *etc*.

4. PROPERTIES

Due to its monatomic layer as well as the nature of the covalent bonds that can be extended making it no longer remain on the same plane, graphene is very flexible. Furthermore, it can be stretched up to 20% size [43].

The specific heat of graphene cannot be measured directly and is identical to that of graphite from 100 K, while for low temperatures graphene exceeds the contribution of phonons (vibrational modes of the crystal structure) of low frequency. At high temperatures, the specific heat is almost constant, approaching 25 $Jmol^{-1}K^{-1}$ (Dulong-Petit limit) [44].

Another feature to note is its impermeability to aqueous solutions, vapors, and gaseous medium, along with He (the smallest radius atom, 32 pm). However, it has been observed that water passes through the membranes of graphene [45].

Since graphene is flexible so it can be used in roller ball computers, heat-sensitive clothing, and flexible phones. It has a tendency of conducting electricity that's too better than Cu which is a boon to electronic applications for the next generation. It is transparent and thin (one-atom-thick *i.e.*, one million times thinner compared to a human hair). Graphene is associated with various properties shown in Fig. (**2**).

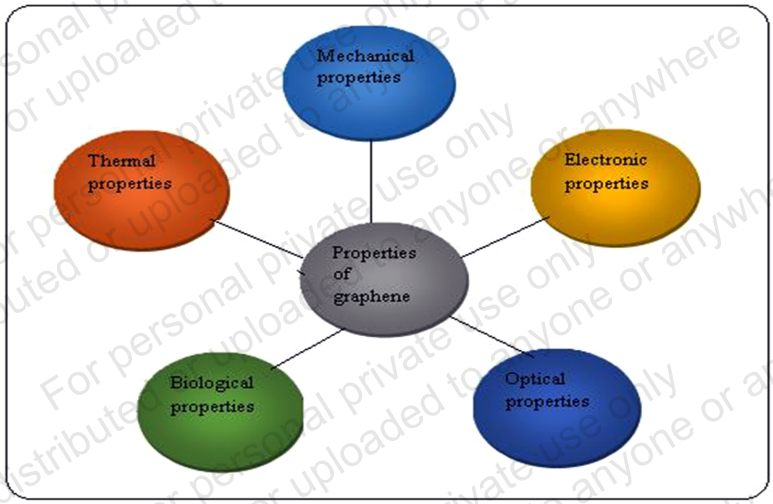

Fig. (2). Properties of graphene.

4.1. Electrical Properties

The symmetry & 2-D structure of graphene makes it interesting for research. It is illustrated as a zero-band gap semiconductor because, at the Brillouin zone's area, the meeting of its conduction & valance bond takes place. The charge carrier in graphene acts as relativistic or mass-less particles [46]. An ambipolar effect of the electric field is exhibited along with high concentrations [1013 cm^{-2}] in between electrons and the holes and have current mobility up to ~15000 $cm^2/(Vs)$ with interaction and electrical conduction between the substrate and the layers of graphene.

4.2. Mechanical Properties

Frank and his co-workers firstly reported the mechanical property of graphene. They used an atomic force microscope and calculated the spring constant. The

young modulus was found to be 0.5TPa and the spring constant between 1-5 N/m. Graphene is a highly used compound in the world. Graphene is a hundred times extra influential than steel and is harder than diamonds. Few mechanical properties include Poisson's ratio, tensile strength, and young's modulus. The mechanical conception should be placed in the continuous standard structure. Using a hypothesis, one can calculate its thickness. Graphene consists of a single layer of C atoms that makes its mechanical properties more significant. By using a traditional microscope or technique, it is hard to get efficient mechanical property while doing experiments because of its two-dimensional nature. So, for this, a new arrangement called atomic force nanoindentation has been achieved [47]. Generally, graphene is used to improve the mechanical properties of composites of polymer.

4.3. Thermal Properties

It generally causes vibrations that are created by the layered structure of graphene. Based on the dispersion curve of acoustic phonon & optical phonon, generally, six categories of polar phonons are recognized. These are the following [48]:

1. ZA mode phonons [Out of plane acoustic phonons] & ZO [optical phonons].

2. TA mode phonons [In plane transverse acoustic phonons] & TO [transverse optical phonons].

3. LA mode phonons [In plane longitudinal acoustic phonons] & LO [longitudinal optical phonons].

Currently, the most commonly used thermal conductive materials are copper, aluminum foil, carbon nano tubes, *etc*. Copper shows thermal conductivity of 380 W/mK, conductivity shown by Al foil is $160Wm^{-1}K$. Thermal conductivities of single-walled CNT & multiwalled carbon nano-tubes are $3500Wm^{-1}K$ and $3000Wm^{-1}K$ respectively. Diamond has the thermal conductivity ranging from $1000\text{-}2200Wm^{-1}K$ while that of single-layer graphene is $5000\ Wm^{-1}K$ [49].

Interplanar heat transfer processes within the two-dimensional plane of graphene are among the highest for known materials. It has been reported a value of $(4.84 \pm 0.44)103$ and $(5.30 \pm 0.48)103\ Wm^{-1}K^{-1}$ at ambient temperature, significantly higher than other carbon structures [50]. Processes for heat transfer perpendicular are to the plane; weak Vander Waals interactions limit the thermal conductivity. An approximate value of $6\ Wm^{-1}K^{-1}$ has been measured [51]. But in any case, both the presence of a substrate and defects in the structure of the graphene, condition their thermal properties significantly.

4.4. Optical Properties

The optical and outstanding charge carrier characteristics make it interesting. Over a vivid range of wavelengths, monolayer graphene can pass on 97% of the total incident light [52]. As the layers of graphene increase, the optical imaging & absorption of light is also increased [53]. Modulators, charge injectors, IR detectors, and emitters can also be formed from graphene [54]. When the light gets absorbed on the surface of graphene, some electron-hole pairs are generated that are based on the density of holes & electrons. These pairs can combine again and again very quickly, but the internal or external field that is generated close to the graphene-electron boundary can separate them [55]. To develop bioimaging techniques, this property of recombining & separating is very useful. Graphene can be cut into nano-ribbons which can make it luminous [56 - 58]. The recombining characteristic of the electron-hole pair can also make graphene a photo-luminescent material. Graphene has several applications in biomedical imaging & magnetic resonance imaging due to its high charge mobility, photo-luminescence, and high light transmittance [59, 60].

4.5. Chemical Properties

Graphene, the only allotrope of C whose every atom present on the two sides is responsible for chemical reactions because it is two-dimensional. As compared to other materials present in the environment graphene consists of maximum no. of C atoms present on the edge and they show specific reactivity towards chemical reactions and defects within them increase their reactive power.

4.6. Biological Properties

Sanchez and co-workers described the biological properties and the toxicity of nanocomposites of graphene [61]. Bianco also described this property recently [62]. A brief discussion of the interaction of cells and biomolecules with graphene is focused here. The nanomaterials based on graphene show a different kind of interaction with RNA & DNA. So, it is very interesting to use it in RNA or DNA delivery & sensing. Graphene oxide has better adsorption for single-strand DNA than double-strand DNA. It protects adsorbed nuclide against nuclease enzyme [63 - 66]. In high ion concentrated solution at low ph, the adsorption for small oligomers is increased because of negative charge interaction between graphene oxide and DNA [67]. Titov and his workers used coarse-grained molecules simulation of lipids and estimated that functional & stable hybrid structures can be formed of graphene [68]. Although these simulations have to be supported by

some data from experiments. For understanding the interaction between graphene & lipid bi-layer in the membrane of a cell, these studies are significant as shown in Fig. (**3**).

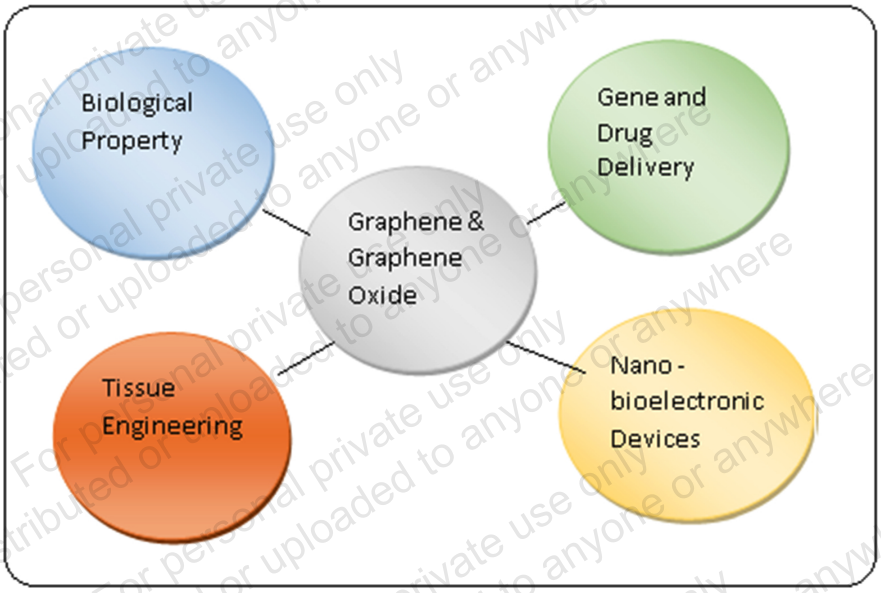

Fig. (3). Biological application of graphene.

Additional Properties

4.7. Functionality and Solubility

Graphene is insoluble in aqueous mediums like water, polymer resins. So, they require the attachment of some specific functional groups without affecting their physical and chemical properties. The functionalization of graphene has been carried out by different groups using various novel strategies [69]. Niyogy *et al*. *via* covalent bonding functionalized graphene [70]. To dissolve graphene in a non-polar solvent like CCl_4 and THF amidation was performed. When pristine graphene is treated with nitrating agents (sulfuric acid and nitric acid) it leads to the formation of aqueous graphene which remains stable for months. Si and Samulski performed a scalable and facile method to fabricate isolated, sparingly sulfonated liquid graphene [71].

Non-covalent bonding can also be performed for functionalizing graphene. This can be done by wrapping it with surfactants or *via* π-π bonding with aromatic molecules like PYBS [72]. This does not affect the electronic structure of graphene. When graphene is treated with surfactants like SDS and CTAB, it leads

to the formation of aqueous graphene or it can also be obtained by the interaction of acidified graphene with excessive PEG and concentrated hydrochloric acid under solvothermal conditions [73].

Liu and co-workers performed a single-step ionic liquid-aided electrochemical procedure to obtain ionic liquid functionalized graphene directly from graphite [74]. Here graphite works as cathode dipped in phase-separated water and ionic liquid (imidazolium-based) mixture with 10–20 V potential across electrodes. After half an hour graphitic anode produced ionic liquid functionalized graphene sheets with an average length of 700 nm and breadth of 500 nm. TEM images and AFM analysis confirmed the results.

4.8. Surface Area

Since graphene has a higher specific surface area and is highly porous, it makes it highly adsorptive for various gases like H_2, CH_4, and CO_2. Theoretically, the surface area of one graphene sheet is 2600 mg [75] but experimental results came around 270–1550 mg. Calculations performed using First-principle showed that carbon monoxide is present in a parallel configuration in hexagonal rings [75]. Calculations performed using First-principle showed that the hydrogen is present in parallel and perpendicular dimensions on cyclic rings of graphene and a single sheet of graphene use 7.7 weight% of H.

4.9. Fluorescence Quenching

Graphene is capable of light emission. It helps in the selective detection of biomolecules. This is directly linked with photo enhanced transfer of electrons. Quenching of porphyrin by graphene has been submitted [76].

Ramakrishna *et al*. worked on the light-emitting property of graphene [77]. During quenching of dye molecule when graphene was present, long-range energy transfer is considered.

4.10. Surface-Enhanced Raman Spectroscopy

SERS and simple Raman spectroscopy give almost similar information except that it provides enhanced signals. Fleischmann and co-workers (in 1974) enhanced a weak signal by introducing SERS [78]. After that, it came under focus and facilitates its identity in science. This enhancement effect follows two basic mechanisms *i.e*., electromagnetic enhancement mechanism (EM) and chemical enhancement mechanism (CM). The first one *i.e*., EM works based on exciting

surface plasmons while CM works based on the formation of a complex of the adsorbed molecule and its charge transfer. Experimentally separation of SERS and Raman spectroscopy is quite challenging. Preparation of SERS is done only in SERS research labs. By chemical reduction and electrochemical oxidation-reduction methods, active substrates of SERS can be obtained. Fabrication of nanostructures and nanowires too can be used as SERS substrates. After working on it, it was found that only "free-electron-like" metals *e.g*., silver, copper, and gold can be used as substrates for colloidal particles and rough surfaces. Limited substrates declined its applications. The SERS substrates are less biocompatible so, there is an urgent need to develop new ones. For an ideal SERS substrate, it should be cost-effective, easily accessible, biologically compatible, and chemically inert. Professor Ling and his co-workers reported the use of graphene as an efficient SERS substrate since it is chemically inert and biologically compatible. On depositing protoporphyrin IX, phthalocyanine (Pc), and crystal violate (CV) on the graphene surface, they found it useful as a substrate [79]. Further, the Raman Effect was examined on various layers and single-layered graphene was found to be most appropriate. With the increase in layers of graphene, the Raman signals decrease. The distance between the substrate and probe molecule should be lower than 0.2 nm in the case of the chemical enhancement mechanism. For transferring charge from molecules to metals and vice-versa the Fermi level of the substrate matches should be symmetrical to HOMO and LUMO of the probe. In the visible region, the optical transmission *via* the surface of graphene is greater than 95% and terahertz plasmon excitation. Because of these characteristics, it does not support the EM process. Now only CM is left for enhancing Raman signals. This is based on the fact that researchers worked on the possibility of charge transfer between molecule and graphene [80]. If graphene works as a SERS substrate, separation of CM and EM will be easily possible compared to other SERS substrates. Graphene can be easily synthesized, biocompatible, and cheap.

5. APPLICATIONS

Different types of applications in numerous fields associated with graphene as electronics, biomedicine, photonics, sensors and metrology, composites and coatings, generation & storage of energy, *etc*. shown in Fig. (**4**).

It possesses remarkable electronic properties and could replace silicon shortly by making use of itself in computer chips, ultrafast or quantum computers working at terahertz speed. Like photons, the electrons of graphene behave as massless particles. Unluckily, the complete study of electronic property is tricky.

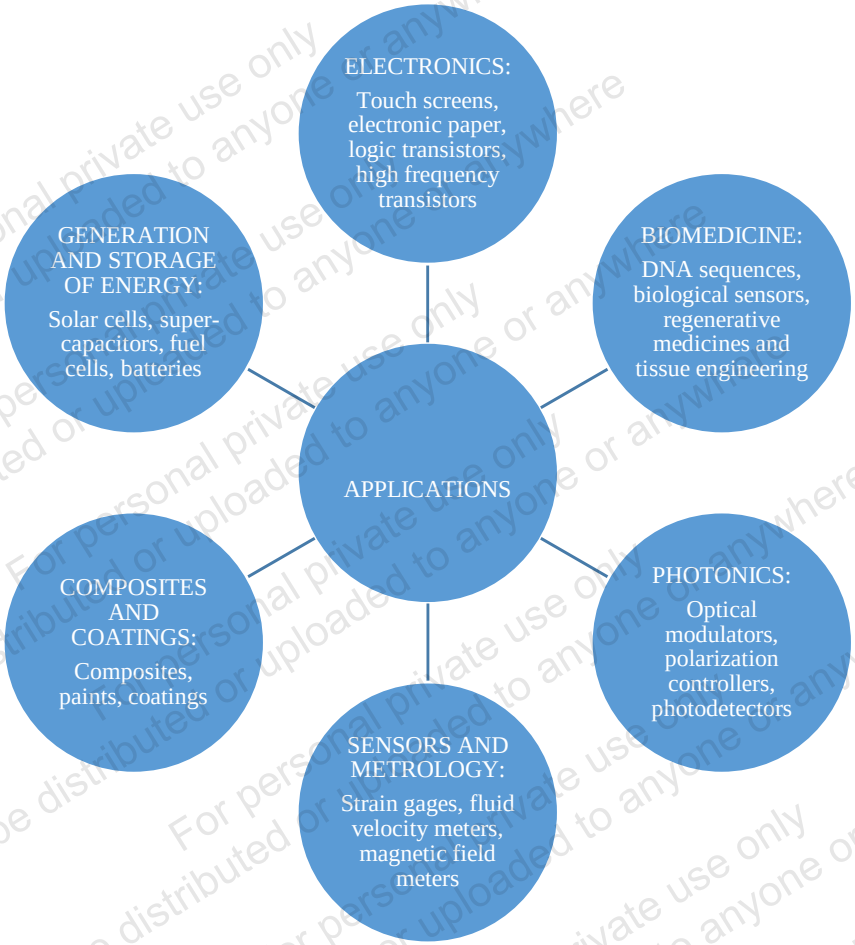

Fig. (4). Application of graphene.

Under the FET configuration, the transportation of electrons of graphene can be understood. FET is done by placing a sample of graphene on an oxidized silicon substrate and connecting it to the drain electrode and a source. The capacitance of the oxide layer is less than that of FET devices complicating the measurement of quantum capacitance.

The capability of a substance to store energy in the form of charge is known as capacitance. In physics, capacitance is resisted by electrically charged electrons. Although this capacitance is dominated by that of 2-D graphene. Pauli's Exclusion Principle explains quantum capacitance as a group of particles (which includes neutrons, electrons, and protons) that are unable to occupy the same energy stage at the same time. Only when an energy level is filled particles can excite to higher

energy levels. Xia *et al*. reported direct measurement of quantum capacitance of graphene in electrolytic ionic liquid media by making use of three electrodes of electrochemical configuration. It was published in Nature Nanotechnology in 2010 [81]. He attached two electrodes to graphene, and applied voltage across it with the help of the third electrode. The use of electrochemical gate and ionic liquid electrolyte reduced the Debye screening length to zero dominating quantum capacitance. The experimental data of Tao's experiment showed small graphene's capacitance. The plot of gate potential against quantum capacitance showed an asymmetric V-shape with a small Dirac point. This data grants theoretical prediction that signifies the quantum origin of interfacial capacitance in C-based electrodes.

The data provided by Tao declared the charged impurities are responsible for the declination of capacitance. This produces a low signal-to-noise ratio and found its application in chemical sensors and biosensors. The geometry of a single layer of graphene and low capacitance are boon to biosensors. By altering the electronic properties of the graphene, it can show when external biological substances interacted with the graphene layer. The study of antibody-antigen interaction by functionalizing the graphene's surface with antibodies can act as a useful application in biosensing. M. Shekhirev and co-workers reported that graphene nanoribbons having uniform electrical conductance can be produced on arbitrary high-temperature-resistant substrates, like metals, silicon dioxide, silicon, or its glasses, *via* the CVD method on basis of thermal decomposition of commercially accessible PTCDA molecules [82]. Polymer composites having a high thermal conductivity coefficient (λ) and excellent electrical and magnetic interference shielding efficiency have theoretical as well as potential practical applications [83, 84].

5.1. Storage Material

The energy density by mass of His high and that's why it is regarded as a basic carrier for energy. H storage is cost-effective and needs fast reaction kinetics, low adsorption temperature, high gravimetric and volumetric densities, and good reversibility. Since it is explosive so it requires stable storage conditions. It can be stored in solid materials (as adsorbed gas), pressurized cylinders (in gaseous form), and cryogenic liquid. The dissolution of hydrogen at high temperatures in metal hydrides is problematic so the chemical process is the safest method for storing H. Development in the field of nanomaterials can be useful because of the large surface-to-volume ratio and decreased diffusion path lengths of H.

Because of properties like high surface area, chemically stable and light graphene can be used. By chemical processes like chemisorption and physisorption, it can

be stored in graphene. Although practically it encompassed and normal temperature its storage is difficult. Therefore, to intensify the uptake of hydrogen C atom needs chemical modification. Palladium can strongly adsorb hydrogen and its role can be intensified three times under variable temperature and pressure. Graphene has a higher potential for storing H and can be used in fuel cell technology. Maidhily and co-workers made use of graphene for the proton exchange [85]. Subrahmanyam *et al*. reported the storage of H in graphene chemically [86].

5.2. Actuators

Researchers used the unique properties (optical, mechanical, and electrical) of graphene to study actuators. Park and co-workers prepared a bi-layer paper (graphene-based actuators) made of carbon nanotubes (multi-walled) and graphene oxide [87]. The curls of paper depend on temperature. Xie and co-workers by modifying two edges of a monolithic film of graphene with O_2 plasma and a six-membered ring prepared the surface asymmetrically graphene film actuator [88]. Based on graphene on organic hybrid film, a bimorph micro-actuator was established. It develops bending and capping motion that varies with frequency and potential. Wu and co-workers established remote control graphene-based robot. In the presence and absence of IR radiations, it can curl or uncurl [89]. It can pick and move any object in any direction. This is an exquisite manifestation of photochemical and thermal energy conversion by graphene-based actuators.

5.3. Electrochemical Capacitors

Nowadays, because of higher security, power output, fast charging and discharging efficiency, and ultra-long service life the electrochemical supercapacitors have been greatly advanced and contemplated as present generation devices [90 - 92].

They are also known as ultracapacitors/supercapacitors. They use fast surface redox reactions to store energy. In need of high-power delivery, they can replace batteries. A supercapacitor is high power and low-energy device and is useful in high-power pulse needs. They have a long-life cycle and higher power density and fill the space between dielectric capacitors and batteries. There are three types of supercapacitors divided based on conducting polymers, transition metal oxides, and C-C based. For higher capacitance blocking and electronically conducting electrodes are being used. Graphite-based carbon is electrochemically stable, highly conductive, and porous. The most used electrode material is activated

carbon since it is cheaper, capable, and has a high surface area. Graphene-based materials like fullerenes (0D), carbon nanotubes (1D), graphene (2D), and graphite (3D) are in focus because of their unique properties and structure. Since carbon nanotubes possess high electrical conductivity and surface area so they are being synthesized for supercapacitors. Although, CNT-based supercapacitors do not meet expectations but even after those experiments are being performed to improve their performance by growing them directly on bulk metals to remove resistance [93]. For supercapacitor applications, the graphene-based electrode material is being used [94] and on studying graphene supercapacitor, data revealed specific capacitance of 135 Fg^{-1} in aqueous electrolyte [95] and 117 Fg^{-1} in aqueous H_2SO_4 [94] on basis of multi-layered graphene. The effective surface area of graphene depends on the layer. So, graphene possesses high supercapacitor performance and surface area. Wang and co-workers [96] synthesized graphene-based supercapacitors and examined them. At room temperature, by the usage of gas-based hydrazine reduction of a single layer of graphene was performed. It showed low aggregation as compared to chemically modified liquid graphene. The capacitance of 205 F g^{-1} at 1.0 V in an aqueous electrolyte with an energy density of 28.5W h kg^{-1} has been observed and is the best data till now. Further, its power density was found to be 10 kW kg^{-1} greater than carbon nanotubes-based supercapacitors.

Poly pyrrole, polyaniline, polythiophene, and their derivatives are examined for supercapacitor electrodes. Wang and co-workers employed *in-situ* anodic electro-polymerization to synthesize flexible and free-standing graphene composite paper [96]. This paper electrode uses graphene sheets as building blocks having a tensile strength of 12.6 MPa and 233 F g^{-1} gravimetric capacitance and 135 F cm^{-1} volumetric capacitance respectively. This data is excellent as compared to other carbon-based flexible electrodes.

6. GRAPHENE OXIDE

6.1. Fabrication of Graphene Oxide

B.C. Brodie first discovered graphite oxide properties [97]. Although graphene oxide is synthesized by the treatment of graphite with strong oxidizing agents still it requires a reduction step which can be thermal or chemical to attain the properties of graphene.

The surface of GO was investigated under STM to obtain information regarding its structure [98, 99]. Due to bulky oxygen-containing functional groups, the width of the mono-layered graphene sheet is more than ~ 0.34 nm of ideal mono-layered graphene. Mono-layered graphene oxide has a width of ~ 1 nm; double-

layered has ~ 2 nm. Although their width varies with the degree of oxidation [100 - 102]. Xue and co-workers synthesized 3D framework structures with reduced GO on melamine foam (MF) frameworks [103].

Graphene oxide can be used in the synthesis of the ER dispersed phase since it has reduced electrical conductance and great polarizable property because of functional groups present on edges and planes. Although it has poor stability of dispersion because of the restacking of graphene sheets and in turn constrains utilization in engineering fields.

Hong and Jang reported a solvent exchange method for dispersing graphene oxide sheets in Si to intensify of stable dispersion of graphene sheets in non-polar solvents [104]. Through the drying process, the sheets agglomerated and restacked. Hummers' method was used to synthesize graphene sheets primarily. While for type II, the graphene oxide mixture was first dispersed in alcohol along with Si oil, and then it was centrifugated. They get stable in Si oil resulting in immensely stable graphene oxide suspension. Even after three months span, no specific sedimentation was seen [105].

Fabrication of graphene oxide involves two methods *i.e*., bottom-up approach where molecules of carbon form pristine graphene, and the other one is a top-down approach where layers of derivatives of graphene are synthesized from C-source, generally from graphite [106, 107]. The bottom-up approach (like epitaxial growth on silicon carbide wafers, chemical vapor deposition, *etc*.) is found to be time-consuming and unstably scalable [108]. Therefore, top-down approaches are much preferable which initially supports the generation of graphene oxide and reduced GO. Brodie [109], Staudenmaier [110], Hummers and Offeman [111] first synthesized graphene oxide through graphitic oxidation *via* different procedures. Hummers and Offeman further worked on it and improved it by using potassium permanganate as an oxidizing agent instead of potassium hypochlorite and adding $NaNO_3$. Usually, Hummers' method is being used because it is scalable and safe for the generation of graphene oxide. Any fabrication process which alters or shows improvement is termed as the "modified Hummers' method" [112]. Usually, a C-source is kept into a protonated solvent (like H_2SO_4, PO_4^{2-}, *etc*.) in the presence of a strong oxidizer (like potassium permanganate). For removing metal ions from it, dilution is performed resulting in a yellow-brown solution followed by separation and addition of HCl. Lastly washing and centrifugation are performed to neutralize its pH.

It is altered according to the researcher's needs. The morphology of GO depends on the dimensions of the carbon source obtained through modified Hummer's method [112]. In other words, the dimensions of synthesized graphene oxide

sheets depend on the diameter of the graphite powder. Huang and co-workers fabricated nanoribbons by unfastening carbon nanotubes (multi-walled) [113]. To lower the C/O ratio of the product often graphite is oxidized before the fabrication of graphene oxide. Few researchers follow Kovtyukhova and his co-workers [114], who treat graphite powder in potassium persulphate and phosphorous pentaoxide before using Hummers' method [115 - 117]. Others alter graphite into expanded graphite by thermal treatment or exposure to strong oxidizing agents [118, 119]. The famous alteration of this method is the "improved Hummers' method". It removes $NaNO_2$ *via* the addition of PO_4^{2-} and $KMnO_4$. It provides GO powders with a higher degree of oxidation at ambient temperature conditions and without the evolution of any toxic gas [120]. Novel work has been reported regarding the fabrication of graphene oxide. Zhang and his co-workers fabricated large graphene oxide sheets with an average size of 108 μm *via* stationary oxidation method [121]. The GO prepared by Hummer's method is relatively smaller than its graphite source. For synthesizing graphene oxide flakes of relatable size and morphology to graphite, sulfuric acid and potassium permanganate are added "without external mechanical agitations" hence forming a symmetrical three-dimensional structure later converting it into enlarged graphene oxide through "mild agitation". Enlarged graphene sheets are beneficial to composite materials. Dong and his co-workers reported an explanation for dispensable graphene oxide by forming GO slurries which could be scaled off and stored into flakes [122]. Single graphene oxide sheets bound *via* π-π stacking; although ion adsorption controls the aggregation of graphene oxide. By oxidizing their graphite pre-cursor and releasing it in a highly alkaline medium (pH 14), Vander Waals interaction is dominated by electrostatic repulsion hence, exfoliation leads to a slurry of low-viscosity instead of dispersion. It can be re-dispersed in N-methyl-2-pyrrolidone or alkaline medium, depicting a reliable method for storing and transporting graphene oxide flakes. Properties of graphene oxide and reduced form of graphene oxide given in Table **2**.

Table 2. Properties of graphene oxide and reduced form of graphene oxide.

Properties	GO	GO (in reduced form)
Fracture strength	120 MPa	-
Thermal conductivity	2000$Wm^{-1}K$ for pure 600W $m^{-1}K$ on Si/SiO_2	0.14-0.87W $m^{-1}K$
Electrical conductivity	10^{-1}S/cm	200-35000S/cm
Young's modulus	220 GPa	-
Optical transmittance	-	depends 60-90% on the synthesizing method and reducing agent

7. QUANTUM DOTS OF GRAPHENE

7.1. Fabrication of Quantum Dots of Graphene

Considering edge effects and quantum confinement of nano-graphene, its new derivatives have been evolved. Nanosheets of graphene having a lateral dimension below 100 nm and multi-layered stacks of graphene together are termed, graphene quantum dots [123]. Because of their flexible bandgap and fluorescence stability, they are of keen interest [123, 124]. Fabrication of these quantum dots requires alteration of graphene oxide and reduced graphene oxide *via* bottom-up and top-down approaches which include microwave-assisted thermal treatment, high-power ultrasonication, hydrothermal and liquid-phase exfoliation [125, 126]. Lu and co-workers reported the eco-friendly one-pot hydrothermal process for the fabrication of quantum dots (90 minutes) using black C [127]. By making use of H_2O_2 they can be made efficiently photo-stable and biologically compatible. Wang and co-workers demonstrated a single-step, one-pot hydrothermal procedure to fabricate quantum dots by making use of rice husk biomass. With the help of light-emitting quenchers, these quantum dots sensed iron's 3þ orbital [128]. A derivative of graphene is too diverse and involves varied fabrication processes and for fabricating graphene oxide, reduced graphene oxide, or quantum dots of graphene there is no “standard” procedure. It opens gates for many exclusive prospects.

8. GRAPHENE AND DERIVED NANOFILLER

8.1. Fabrication of Graphene and Derived Nanofiller

Because of the simple method of preparation, tunable property and wide application conductive polymer composites (CPCs) are of great interest (Fig. **5**). For synthesizing conductive polymer composites from non-conducting polymers, conducting fillers are inserted into them. They increase the conductivity of the material. This is known as an electrical percolation threshold (Pc). Both theoretically and experimentally it was found that with an increase in filler aspect ratio electrical percolation threshold decreases. So, by employing large aspect ratio conducting fillers conducting networks in a matrix can be synthesized [129]. Graphene composites possess great mechanical properties, extraordinary thermal conductivity, and higher electron portability at room temperature. For corresponding to electrical conductivity polymer composites use a 3D network. Wu and co-workers used a hot press method for the preparation of polystyrene composites having a three-dimensional network [130]. Chen and co-workers fabricated an excellent conducting composite film with the help of three-

dimensional graphene foam *via* template-assisted chemical vapor deposition method [131].

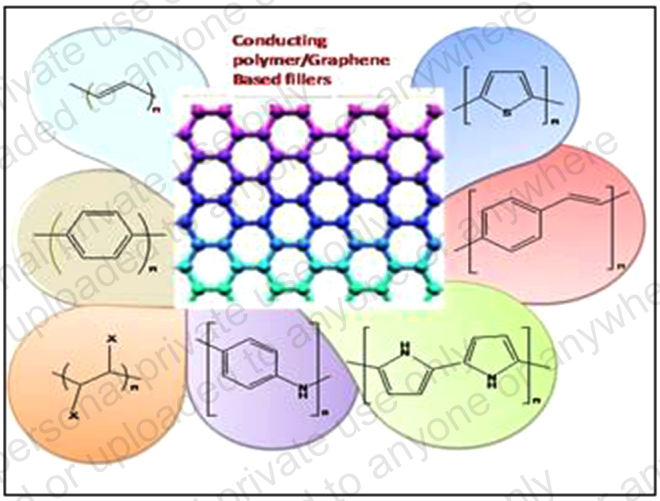

Fig. (5). Conducting graphene composite.

8.2. Significance of Graphene and Derived Nanofiller

As a nanofiller, graphene is preferred over other common nanofillers like exfoliated graphite, sodium montmorillonite, carbon nanotube, carbon nanofiber, and because of its higher aspect ratio, great surface area, low coefficient of thermal expansion tensile strength, electrical and thermal conductivity, transparency, flexibility, and shielding ability [132].

8.3. Application of Graphene and Derived Nanofiller in Energy and Electronics

Because of extraordinary microelectronic chips, high power densities they require conductivity issued as thermal pads, heat spreaders, and thermal interface materials. They are necessary compounds of thermal packaging and are responsible for maintaining a great relationship between metal sinks and chips [133]. The most important characteristic of graphene is modern electrical conductivity.

By inserting graphene into polymer matrix conductive polymer composites are being synthesized. Various polymers specifically polyvinyl chloride, polyvinyl alcohol, polymethyl methacrylate, polyethylene, polyamide, and polystyrene worked as matrices to fabricate graphene composites. They generally demonstrate

a non-linear improvement of the electrical conductance as a means of concentration of filler. They can be used to make sensors, solar cells, *etc*.

9. GRAPHENE AEROGELS (GAS)

It is a three-dimensional structure of graphene that produces porous and cheap structures of graphene. Various procedures including chemical-reduction methods [134, 135], hydrothermal methods [136, 137] Resorcinol (R), and Formaldehyde (F) sol-gel chemistry methods [138, 139] were suggested for the preparation of aerogels and monolithic aerogels on the basis of graphene oxide [140]. The chemical reduction method was found to be the most appropriate one since it is an eco-friendly and low-cost method. This method requires a low temperature without the need for a binder. Zhang and co-workers showed high electrical conductance of 102 S/m and a large surface area of 512 m^2g^{-1} was observed in synthesizing graphene aerogels through the chemical-reduction method [135].

10. HYBRID GRAPHENE/MICROFIBER COMPOSITES

An encouraging advance to ready graphene-based composites is by utilization of hybrid fillers that comprises an inorganic material and graphene-based materials. The hybrid combination gives an advantage such as synergistic effects between the fillers or final properties consequential from preservatives. The hybridization process will come across a few drawbacks of filler and progresses its interplay with the host matrix, it depends on its functioning criteria. Multifunctionality plays an important role in manufacturing composites (hybrid) since combined properties of diverse fillers correspond to a substance having a dissimilar set of characteristics as contrasted to characteristics of individually fabricated materials. In addition to this, the value of the ultimate product can be decreased by making use of fine microscale reinforcements like C and fibers of glass having lower levels of graphene where stress moves from micro to nano-scale reinforcement, hence improving the final properties.

Hybridizing graphene materials and the rest inorganic group showed outstanding properties at an atomic scale or nano or synergy can be exposed with complementarities. Hybrid graphene and other-two dimensional structures maintained the electronic properties and specifically, it can alter the bandgap of graphene. The zero-band gap of the unique graphene is unsuccessful in semiconductor materials; it is advantageous to its composites which can help in the manufacturing of graphene-based electronics. The addition of carbon to h-boron nitride increases electric conductance, which acts as an insulating agent in pristine form. The inductive band gap in graphene can effectively fabricate field-

effect transistors of graphene/ boron nitride films having 190-2000 $cm^2V^{-1}s^{-1}$ carrier mobilities. Cross-linking of graphene *via* chemicals and h-boron nitride composites could efficiently store energy. The (h-BN) Supercapacitors of graphene or boron nitride have B240 F/g specific capacitance. The bond formed between graphene and individual fillers affects the resulting physical and chemical characteristics of synthesized reinforced composites. To improve the efficiency amongst fillers various procedures were followed like solution blending, functionalization *via* chemicals, mechanical mixing, alternate growth, and many more. Aggregation of graphene takes place because of higher specific surface area and van der Waals interaction. The ornament of graphene is preferred since it avoids aggregation with other nanomaterials. Graphene's reactive sites got improved because of its functionalization which further improved its bond formation capability with the rest of the nanomaterials and finally led to the advancement of less significant covalent bonding between the matrix of host and hybrid-filler.

The functioning of multi-walled carbon nanotubes established effective bonds between multi-graphene platelets and fillers. The two-dimensional filler *i.e.*, multi-graphene platelets and one-dimensional filler *i.e.*, multiwalled carbon nanotubes combine to form a three-dimensional structure having a higher surface area. Thermal conductance of functionalized multiwalled carbon nanotube showed enlargement of >50% in comparison to pristine hybrid filler. Lin and co-workers accounted for the synthesis of Si/reduced GO hybrids through the electrostatic mechanism and then it is mechanical blending with BUNA-S (styrene-butadiene rubber) matrix. Great experimental distribution has been seen in hybrid materials in comparison to individual fillers having great matrix interaction.

11. GRAPHENE BIOACTIVE COMPOSITES

Various bio-sensors which depend on graphene for different sensing purposes consist of separate criteria for electrochemical and optical signals. Because of its quick response, elevated sensitivity, excellent electrochemical properties, straightforward operation, and low-cost graphene is used as a probable contender for biomolecule discovery. Zhou and co-workers examined the electrical and chemical activities of the graphene-modified electrode towards H_2O_2. In comparison to the exposed electrode, noteworthy enlargement in the rate of electron transmission of graphene-based electrodes has been obtained. Shao and co-workers accounted for superior electro-catalytic progress of (N-doped graphene) N-graphene towards reduction of H_2O_2 in comparison to graphene, responsible for the occurrence of N- containing groups, O- functional groups, and

structural defects. GO possess fluorescence over a broad array of wavelength *i.e*., 200 -1200 nm and it successfully quenched the light-emitting property of other fluorescing dyes.

12. CONCLUDING REMARKS

This 2D material which seemed to be of least research in past decades had now become a boon to society since it provides unique and reliable solutions to globally challenged environmental problems. In this chapter, we have briefly discussed its properties and application areas which makes it more content for scientists to depend on. The distinct and captivating properties of graphene make it unique in a way that could lead to substantial advancement in the near future. Its properties make it one of the most reliable materials in various applicable areas which include sensing, tissue engineering, electronics, *etc*. Although many interdisciplinary areas still seek its contribution in different ways which need to be discovered which will further accelerate a better understanding of graphene-based materials. Its properties have paced new ways for scientists working for the betterment of the global environmental progressions.

CONSENT FOR PUBLICATION

Not applicable.

CONFLICT OF INTEREST

The author declares no conflict of interest, financial or otherwise.

ACKNOWLEDGEMENTS

The authors would like to acknowledge Banasthali Vidyapith for providing an internet facility for the completion of this chapter. One of the authors Dr. Nirmala Kumari Jangid is thankful to Dr. Pinki Bala Punjabi and all editors for allowing her to write this chapter.

LIST OF ABBREVIATIONS

AFM	Atomic/Scanning force microscopy
BUNA-S	Styrene-butadiene rubber
CCl_4	Carbon tetrachloride
CM	Chemical enhancement mechanism
CNT	Carbon nanotubes
CPCs	Conductive polymer composites

Not be distributed or uploaded to anyone or anywhere For personal private use only

CTAB	Cetyltrimethylammonium bromide
CVD	Chemical vapor deposition
DNA	Deoxyribonucleic acid
EM	Electromagnetic enhancement mechanism
FET	Field-effect transistor
GO	Graphene oxide
HOMO	Highest occupied molecular orbital
IUPAC	International Union of Pure and Applied Chemistry
IR	Infra-red radiations
LA mode phonons	Longitudinal acoustic phonons
LO	Longitudinal optical phonons
LUMO	Lowest unoccupied molecular orbital
MGP	Multi graphene platelet
MF	Melamine foam
MWCNTs	Multi-walled carbon nanotubes
PC	Percolation threshold
PEG	Polyethylene glycol
PYBS	1- pyrenebutanoic acid succinimidyl ester
PTCDA	Perylenetetracarboxylic dianhydride
SDS	Sodium dodecyl sulfate
SERS	Surface Enhanced Raman Spectroscopy
STM	Scanning tunneling microscopy
TA mode phonons	Transverse acoustic phonons
TEM	Transmission electron microscopy
THF	Tetrahydrofuran
TO	Transverse optical phonons
TPa	Terapascal
QHE	Quantum Hall effect
RNA	Ribonucleic acid
ZA mode phonons	Out of plane acoustic phonons
ZO	Out of plane optical phonons
2D	Two-dimensional

For personal private use only Not be distributed or uploaded to anyone or anywhere

REFERENCES

[1] Geim, A.K. Graphene: Status and Prospects. *Science,* **2009**, *324*(5934), 1530-1534. [http://dx.doi.org/10.1126/science.1158877] [PMID: 19541989]

[2] Whitener, K.E., Jr; Sheehan, P.E. Graphene synthesis. *Diamond Related Materials,* **2014**, *46*, 25-34. [http://dx.doi.org/10.1016/j.diamond.2014.04.006]

[3] Choi, W.; Lahiri, I.; Seelaboyina, R.; Kan, Y.S. Synthesis of Graphene and Its Applications: A Review. *Crit. Rev.,* **2010**, 52-71.

[4] Wallace, P.R. The band theory of graphite. *Phys. Rev.,* **1947**, *71*(9), 622-634. [http://dx.doi.org/10.1103/PhysRev.71.622]

[5] Peierls, R.E. Quelques proprietes typiques des corpses solides. *Annales de l'Institut Henri Poincaré,* **1935**, *5*, 177-222.

[6] Landau, L.D. Zur theorie der phasenumwandlungen II, Physikalische Zeitschri under Sowjetunion. **1937**, 26-35.

[7] Evans, J.W.; Thiel, P.A.; Bartelt, M.C. Morphological evolution during epitaxial thin film growth: formation of 2D islands and 3D mounds, Surface Science Reports. **2006**, 1-28.

[8] Novoselov, K.S.; Geim, A.K.; Morozov, S.V.; Jiang, D.; Zhang, Y.; Dubonos, S.V.; Grigorieva, I.V.; Firsov, A.A. Electric field effect in atomically thin carbon films. *Science,* **2004**, *306*(5696), 666-669. [http://dx.doi.org/10.1126/science.1102896] [PMID: 15499015]

[9] Iijima, S. Helical microtubules of graphitic carbon. *Nature,* **1991**, *354*(6348), 56-58. [http://dx.doi.org/10.1038/354056a0]

[10] Kroto, H.W.; Heath, J.R.; O'Brien, S.C.; Curl, R.F.; Smalley, R.E. C60: Buckminsterfullerene. *Nature,* **1985**, *318*(6042), 162-163. [http://dx.doi.org/10.1038/318162a0]

[11] Lincoln Vogel, F. The electrical conductivity of graphite intercalated with superacid fluorides: experiments with antimony pentafluoride. *J. Mater. Sci.,* **1977**, *12*(5), 982-986. [http://dx.doi.org/10.1007/BF00540981]

[12] Novoselov, K.S.; Geim, A.K.; Morozov, S.V.; Jiang, D.; Zhang, Y.; Dubonos, S.V.; Grigorieva, I.V.; Firsov, A.A. Electric field effect in atomically thin carbon films. *Science,* **2004**, *306*(5696), 666-669. [http://dx.doi.org/10.1126/science.1102896] [PMID: 15499015]

[13] Novoselov, K.S.; Geim, A.K.; Morozov, S.V.; Jiang, D.; Katsnelson, M.I.; Grigorieva, I.V.; Dubonos, S.V.; Firsov, A.A. Two-dimensional gas of massless Dirac fermions in graphene. *Nature,* **2005**, *438*(7065), 197-200. [http://dx.doi.org/10.1038/nature04233] [PMID: 16281030]

[14] Zhang, Y.; Tan, Y.W.; Stormer, H.L.; Kim, P. Experimental observation of the quantum Hall effect and Berry's phase in graphene. *Nature,* **2005**, *438*(7065), 201-204. [http://dx.doi.org/10.1038/nature04235] [PMID: 16281031]

[15] Balandin, A.A.; Ghosh, S.; Bao, W.; Calizo, I.; Teweldebrhan, D.; Miao, F.; Lau, C.N. Superior thermal conductivity of single-layer graphene. *Nano Lett.,* **2008**, *8*(3), 902-907. [http://dx.doi.org/10.1021/nl0731872] [PMID: 18284217]

[16] Nair, R.R.; Blake, P.; Grigorenko, A.N.; Novoselov, K.S.; Booth, T.J.; Stauber, T.; Peres, N.M.R.; Geim, A.K. Fine structure constant defines visual transparency of graphene. *Science,* **2008**, *320*(5881), 1308. [http://dx.doi.org/10.1126/science.1156965] [PMID: 18388259]

[17] Li, X.; Wang, X.; Zhang, L.; Lee, S.; Dai, H. Chemically derived, ultrasmooth graphene nanoribbon semiconductors. *Science,* **2008**, *319*(5867), 1229-1232. [http://dx.doi.org/10.1126/science.1150878] [PMID: 18218865]

Not be distributed or uploaded to anyone or anywhere
For personal private use only

[18] Ritter, K.A.; Lyding, J.W. The influence of edge structure on the electronic properties of graphene quantum dots and nanoribbons. *Nat. Mater.,* **2009**, *8*(3), 235-242.
[http://dx.doi.org/10.1038/nmat2378] [PMID: 19219032]

[19] Cai, J.; Ruffieux, P.; Jaafar, R.; Bieri, M.; Braun, T.; Blankenburg, S.; Muoth, M.; Seitsonen, A.P.; Saleh, M.; Feng, X.; Müllen, K.; Fasel, R. Atomically precise bottom-up fabrication of graphene nanoribbons. *Nature,* **2010**, *466*(7305), 470-473.
[http://dx.doi.org/10.1038/nature09211] [PMID: 20651687]

[20] Ansari, S.; Giannelis, E.P. Functionalized graphene sheet-Poly(vinylidene fluoride) conductive nanocomposites. *J. Polym. Sci., B, Polym. Phys.,* **2009**, *47*(9), 888-897.
[http://dx.doi.org/10.1002/polb.21695]

[21] Ramanathan, T.; Abdala, A.A.; Stankovich, S.; Dikin, D.A.; Herrera-Alonso, M.; Piner, R.D.; Adamson, D.H.; Schniepp, H.C.; Chen, X.; Ruoff, R.S.; Nguyen, S.T.; Aksay, I.A.; Prud'Homme, R.K.; Brinson, L.C. Functionalized graphene sheets for polymer nanocomposites. *Nat. Nanotechnol.,* **2008**, *3*(6), 327-331.
[http://dx.doi.org/10.1038/nnano.2008.96]

[22] Stankovich, S.; Dikin, D.A.; Dommett, G.H.B.; Kohlhaas, K.M.; Zimney, E.J.; Stach, E.A.; Piner, R.D.; Nguyen, S.T.; Ruoff, R.S. Graphene-based composite materials. *Nature,* **2006**, *442*(7100), 282-286.
[http://dx.doi.org/10.1038/nature04969] [PMID: 16855586]

[23] Fan, H.; Wang, L.; Zhao, K.; Li, N.; Shi, Z.; Ge, Z.; Jin, Z. Fabrication, mechanical properties, and biocompatibility of graphene-reinforced chitosan composites. *Biomacromolecules,* **2010**, *11*(9), 2345-2351.
[http://dx.doi.org/10.1021/bm100470q] [PMID: 20687549]

[24] Zhang, K.; Zhang, L.L.; Zhao, X.S.; Wu, J. Graphene/Polyaniline Nanofiber Composites as Supercapacitor Electrodes. *Chem. Mater.,* **2010**, *22*(4), 1392-1401.
[http://dx.doi.org/10.1021/cm902876u]

[25] Zhao, X.; Zhang, Q.; Chen, D.; Lu, P. Enhanced Mechanical Properties of Graphene-Based Poly(vinyl alcohol) Composites. *Macromolecules,* **2010**, *43*(5), 2357-2363.
[http://dx.doi.org/10.1021/ma902862u]

[26] Kuila, T.; Bose, S.; Hong, C.E.; Uddin, M.E.; Khanra, P.; Kim, N.H.; Lee, J.H. Preparation of functionalized graphene/linear low density polyethylene composites by a solution mixing method. *Carbon,* **2011**, *49*(3), 1033-1037.
[http://dx.doi.org/10.1016/j.carbon.2010.10.031]

[27] Wu, J.; Becerril, H.A.; Bao, Z.; Liu, Z.; Chen, Y.; Peumans, P. Organic solar cells with solution-processed graphene transparent electrodes. *Appl. Phys. Lett.,* **2008**, *92*(26), 263302.
[http://dx.doi.org/10.1063/1.2924771]

[28] Huang, J.; Wang, X.; deMello, A.J.; deMello, J.C.; Bradley, D.D.C. Efficient flexible polymer light emitting diodes with conducting polymer anodes. *J. Mater. Chem.,* **2007**, *17*(33), 3551-3554.
[http://dx.doi.org/10.1039/b705918n]

[29] Park, H.; Rowehl, J.A.; Kim, K.K.; Bulovic, V.; Kong, J. Doped graphene electrodes for organic solar cells. *Nanotechnology,* **2010**, *21*(50), 505204.
[http://dx.doi.org/10.1088/0957-4484/21/50/505204] [PMID: 21098945]

[30] Li, D.; Müller, M.B.; Gilje, S.; Kaner, R.B.; Wallace, G.G. Processable aqueous dispersions of graphene nanosheets. *Nat. Nanotechnol.,* **2008**, *3*(2), 101-105.
[http://dx.doi.org/10.1038/nnano.2007.451] [PMID: 18654470]

[31] Shan, C.; Yang, H.; Han, D.; Zhang, Q.; Ivaska, A.; Niu, L. Water-soluble graphene covalently functionalized by biocompatible poly-L-lysine. *Langmuir,* **2009**, *25*(20), 12030-12033.
[http://dx.doi.org/10.1021/la903265p] [PMID: 19769343]

Not be distributed or uploaded to anyone or anywhere
For personal private use only

[32] McNaught, A.D.; Wilkinson, A. *Compendium of Chemical Terminology*; Blackwell Scientific Publications: Oxford, **1997**.

[33] Boehm, H.P.; Setton, R.; Stumpp, E. Nomenclature and terminology of graphite intercalation compounds (IUPAC Recommendations 1994). *Pure Appl. Chem.,* **1994**, *66*(9), 1893-1901. [http://dx.doi.org/10.1351/pac199466091893]

[34] Mouras, S.; Hamm, A.; Djurado, D.; Cousseins, J.C. Synthesis of first-stage graphite intercalation compounds with fluorides. *Revue de Chimie Minerale,* **1987**, *24*, 572-582.

[35] Bourzac, K. *Graphene wines nobel prize*; MIT Technology Review, **2010**.

[36] Narita, A.; Chen, Z.; Chen, Q.; Müllen, K. Solution and on-surface synthesis of structurally defined graphene nanoribbons as a new family of semiconductors. *Chem. Sci. (Camb.),* **2019**, *10*(4), 964-975. [http://dx.doi.org/10.1039/C8SC03780A] [PMID: 30774890]

[37] Clair, S.; de Oteyza, D.G. Controlling a Chemical Coupling Reaction on a Surface: Tools and Strategies for On-Surface Synthesis. *Chem. Rev.,* **2019**, *119*(7), 4717-4776. [http://dx.doi.org/10.1021/acs.chemrev.8b00601] [PMID: 30875199]

[38] *Graphene and doped graphene elaborated by pulsed laser deposition*; HAL Open Sciences, **2021**.

[39] Li, D.; Müller, M.B.; Gilje, S.; Kaner, R.B.; Wallace, G.G. Processable aqueous dispersions of graphene nanosheets. *Nat. Nanotechnol.,* **2008**, *3*(2), 101-105. [http://dx.doi.org/10.1038/nnano.2007.451] [PMID: 18654470]

[40] Si, Y.; Samulski, E.T. Synthesis of water soluble graphene. *Nano Lett.,* **2008**, *8*(6), 1679-1682. [http://dx.doi.org/10.1021/nl080604h] [PMID: 18498200]

[41] Smith, A.T.; LaChance, A.M.; Zeng, S.; Liu, B.; Sun, L. Synthesis, properties, and applications of graphene oxide/reduced graphene oxide and their nanocomposites. *Nano Materials Science,* **2019**, *1*(1), 31-47. [http://dx.doi.org/10.1016/j.nanoms.2019.02.004]

[42] Wang, Y.; Shi, Z.; Huang, Y.; Ma, Y.; Wang, C.; Chen, M.; Chen, Y. Supercapacitor devices based on graphene materials. *J. Phys. Chem. C,* **2009**, *113*(30), 13103-13107. [http://dx.doi.org/10.1021/jp902214f]

[43] Tomori, H.; Kanda, A.; Goto, H.; Ootuka, Y.; Tsukagoshi, K.; Moriyama, S.; Watanabe, E.; Tsuya, D. Introducing Nonuniform Strain to Graphene Using Dielectric Nanopillars. *Appl. Phys. Express,* **2011**, 4-7. [http://dx.doi.org/10.1143/APEX.4.075102]

[44] Pop, E.; Varshney, V.; Roy, A.K. Thermal properties of graphene: Fundamentals and applications. *MRS Bull.,* **2012**, *37*(12), 1273-1281. [http://dx.doi.org/10.1557/mrs.2012.203]

[45] Nair, R.R.; Wu, H.A.; Jayaram, P.N.; Grigorieva, I.V.; Geim, A.K. Unimpeded permeation of water through helium-leak-tight graphene-based membranes. *Science,* **2012**, *335*(6067), 442-444. [http://dx.doi.org/10.1126/science.1211694] [PMID: 22282806]

[46] Frank, I.W.; Tanenbaum, D.M.; van der Zande, A.M.; McEuen, P.L. Microelectronics and nanometer structures. J. *J. Vac. Sci. Technol. B,* **2007**, *25*, 2558-2561. [http://dx.doi.org/10.1116/1.2789446]

[47] Roos, W.H. How to perform a nanoindentation experiment on a virus. *Methods Mol. Biol.,* **2011**, *783*, 251-264. [http://dx.doi.org/10.1007/978-1-61779-282-3_14] [PMID: 21909893]

[48] Zou, J.H.; Ye, Z.Q. Phonon thermal properties of graphene from molecular dynamics using different potentials. *J. Chem. Phys,* **2016**, *145*, 134705.

[49] Singh, V.; Joung, D.; Zhai, L.; Das, S.; Khondaker, S.I.; Seal, S. Graphene based materials: Past,

present and future. *Prog. Mater. Sci.,* **2011**, *56*(8), 1178-1271.
[http://dx.doi.org/10.1016/j.pmatsci.2011.03.003]

[50] Chen, S.; Wu, Q.; Mishra, C. Thermal Properties of Isotopically Engineered Graphene. *Nat. Mater.,* **2012**, *11*, 203-207.
[http://dx.doi.org/10.1038/nmat3207] [PMID: 22231598]

[51] Sang, M.; Shin, J.; Kim, K.; Yu, K. Electronic and Thermal Properties of Graphene and Recent Advances in Graphene Based Electronics Applications. *Nanomaterials (Basel),* **2019**, *9*(3), 374.
[http://dx.doi.org/10.3390/nano9030374] [PMID: 30841599]

[52] Nair, R.R.; Blake, P.; Grigorenko, A.N.; Novoselov, K.S.; Booth, T.J.; Stauber, T.; Peres, N.M.R.; Geim, A.K. Fine structure constant defines visual transparency of graphene. *Science,* **2008**, *320*(5881), 1308.
[http://dx.doi.org/10.1126/science.1156965] [PMID: 18388259]

[53] Kravets, V.G.; Grigorenko, A.N.; Nair, R.R.; Blake, P.; Anissimova, S.; Novoselov, K.S.; Geim, A.K. Spectroscopic ellipsometry of graphene and an exciton-shifted van Hove peak in absorption. *Phys. Rev. B Condens. Matter Mater. Phys.,* **2010**, *81*(15), 155413.
[http://dx.doi.org/10.1103/PhysRevB.81.155413]

[54] Feng Wang, ; Hamdi, M. Strictly non-blocking conditions for the central-stage buffered Clos-network. *IEEE Commun. Lett.,* **2008**, *12*(3), 206-208.
[http://dx.doi.org/10.1109/LCOMM.2008.071752]

[55] Rana, F.; George, P.A.; Strait, J.H.; Dawlaty, J.; Shivaraman, S.; Chandrashekhar, M.; Spencer, M.G. Carrier recombination and generation rates for intravalley and intervalley phonon scattering in graphene. *Phys. Rev. B Condens. Matter Mater. Phys.,* **2009**, *79*(11), 115447.
[http://dx.doi.org/10.1103/PhysRevB.79.115447]

[56] Park, S.; Ruoff, R.S. Chemical methods for the production of graphenes. *Nat. Nanotechnol.,* **2009**, *4*(4), 217-224.
[http://dx.doi.org/10.1038/nnano.2009.58] [PMID: 19350030]

[57] Elias, D.C.; Nair, R.R.; Mohiuddin, T.M.G.; Morozov, S.V.; Blake, P.; Halsall, M.P.; Ferrari, A.C.; Boukhvalov, D.W.; Katsnelson, M.I.; Geim, A.K.; Novoselov, K.S. Control of graphene's properties by reversible hydrogenation: evidence for graphane. *Science*, **2009**, *323*(5914), 610-613.
[http://dx.doi.org/10.1126/science.1167130] [PMID: 19179524]

[58] Bonaccorso, F.; Sun, Z.; Hasan, T.; Ferrari, A.C. Graphene photonics and optoelectronics. *Nat. Photonics,* **2010**, *4*(9), 611-622.
[http://dx.doi.org/10.1038/nphoton.2010.186]

[59] Ma, X.; Tao, H.; Yang, K.; Feng, L.; Cheng, L.; Shi, X.; Li, Y.; Guo, L.; Liu, Z. A functionalized graphene oxide-iron oxide nanocomposite for magnetically targeted drug delivery, photothermal therapy, and magnetic resonance imaging. *Nano Res.,* **2012**, *5*(3), 199-212.
[http://dx.doi.org/10.1007/s12274-012-0200-y]

[60] Shen, A.J.; Li, D.L.; Cai, X.J.; Dong, C.Y.; Dong, H.Q.; Wen, H.Y.; Dai, G.H.; Wang, P.J.; Li, Y.Y. Multifunctional nanocomposite based on graphene oxide for *in vitro* hepatocarcinoma diagnosis and treatment. *J. Biomed. Mater. Res. A,* **2012**, *100*, 9.
[http://dx.doi.org/10.1002/jbm.a.34148] [PMID: 22623284]

[61] Sanchez, V.C.; Jachak, A.; Hurt, R.H.; Kane, A.B. Biological interactions of graphene-family nanomaterials: an interdisciplinary review. *Chem. Res. Toxicol.,* **2012**, *25*(1), 15-34.
[http://dx.doi.org/10.1021/tx200339h] [PMID: 21954945]

[62] Bianco, A. Graphene: safe or toxic? The two faces of the medal. *Angew. Chem. Int. Ed.,* **2013**, *52*(19), 4986-4997.
[http://dx.doi.org/10.1002/anie.201209099] [PMID: 23580235]

[63] Ren, H.; Wang, C.; Zhang, J.; Zhou, X.; Xu, D.; Zheng, J.; Guo, S.; Zhang, J. DNA cleavage system of

nanosized graphene oxide sheets and copper ions. *ACS Nano,* **2010**, *4*(12), 7169-7174. [http://dx.doi.org/10.1021/nn101696r] [PMID: 21082807]

[64] Lu, C.H.; Zhu, C.L.; Li, J.; Liu, J.J.; Chen, X.; Yang, H.H. Using graphene to protect DNA from cleavage during cellular delivery. *Chem. Commun. (Camb.),* **2010**, *46*(18), 3116-3118. [http://dx.doi.org/10.1039/b926893f] [PMID: 20424750]

[65] Wang, Y.; Li, Z.; Hu, D.; Lin, C.T.; Li, J.; Lin, Y. Aptamer/graphene oxide nanocomplex for *in situ* molecular probing in living cells. *J. Am. Chem. Soc.,* **2010**, *132*(27), 9274-9276. [http://dx.doi.org/10.1021/ja103169v] [PMID: 20565095]

[66] Xu, Y.; Wu, Q.; Sun, Y.; Bai, H.; Shi, G. Three-dimensional self-assembly of graphene oxide and DNA into multifunctional hydrogels. *ACS Nano,* **2010**, *4*(12), 7358-7362. [http://dx.doi.org/10.1021/nn1027104] [PMID: 21080682]

[67] Wu, M.; Kempaiah, R.; Huang, P.J.J.; Maheshwari, V.; Liu, J. Adsorption and desorption of DNA on graphene oxide studied by fluorescently labeled oligonucleotides. *Langmuir,* **2011**, *27*(6), 2731-2738. [http://dx.doi.org/10.1021/la1037926] [PMID: 21302946]

[68] Titov, A.V.; Král, P.; Pearson, R. Sandwiched graphene--membrane superstructures. *ACS Nano,* **2010**, *4*(1), 229-234. [http://dx.doi.org/10.1021/nn9015778] [PMID: 20025267]

[69] Rao, C.N.R.; Subrahmanyam, K.S.; Ramakrishna Matte, H.S.S.; Govindaraj, A. Graphene: synthesis, functionalization, and properties. *Mod. Phys. Lett. B,* **2011**, *25*(7), 427-451. [http://dx.doi.org/10.1142/S0217984911025961]

[70] Niyogi, S.; Bekyarova, E.; Itkis, M.E.; McWilliams, J.L.; Hamon, M.A.; Haddon, R.C. Solution properties of graphite and graphene. *J. Am. Chem. Soc.,* **2006**, *128*(24), 7720-7721. [http://dx.doi.org/10.1021/ja060680r] [PMID: 16771469]

[71] Si, Y.; Samulski, E.T. Exfoliated Graphene Separated by Platinum Nanoparticles. *Chem. Mater.,* **2008**, *20*(21), 6792-6797. [http://dx.doi.org/10.1021/cm801356a]

[72] Ghosh, A.; Rao, K.V.; George, S.J.; Rao, C.N.R. Noncovalent functionalization, exfoliation, and solubilization of graphene in water by employing a fluorescent coronene carboxylate. *Chemistry,* **2010**, *16*(9), 2700-2704. [http://dx.doi.org/10.1002/chem.200902828] [PMID: 20108284]

[73] Subrahmanyam, K.S.; Vivekchand, S.R.C.; Govindaraj, A.; Rao, C.N.R. A study of graphenes prepared by different methods: characterization, properties and solubilization. *J. Mater. Chem.,* **2008**, *18*(13), 1517-1523. [http://dx.doi.org/10.1039/b716536f]

[74] Liu, N.; Luo, F.; Wu, H.; Liu, Y.; Zhang, C.; Chen, J. One-step ionic-liquid-assisted electrochemical synthesis of ionic-liquid-functionalized graphene sheets directly from graphite. *Adv. Funct. Mater.,* **2008**, *18*(10), 1518-1525. [http://dx.doi.org/10.1002/adfm.200700797]

[75] Ghosh, A.; Subrahmanyam, K.S.; Krishna, K.S.; Datta, S.; Govindaraj, A.; Pati, S.K.; Rao, C.N.R. Uptake of H_2 and CO_2 by Graphene. *J. Phys. Chem. C,* **2008**, *112*(40), 15704-15707. [http://dx.doi.org/10.1021/jp805802w]

[76] Xu, Y.; Zhao, L.; Bai, H.; Hong, W.; Li, C.; Shi, G. Chemically converted graphene induced molecular flattening of 5,10,15,20-tetrakis(1-methyl-4-pyridinio)porphyrin and its application for optical detection of cadmium(II) ions. *J. Am. Chem. Soc.,* **2009**, *131*(37), 13490-13497. [http://dx.doi.org/10.1021/ja905032g] [PMID: 19711892]

[77] Ramakrishna Matte, H.S.S.; Subrahmanyam, K.S.; Venkata Rao, K.; George, S.J.; Rao, C.N.R. Quenching of fluorescence of aromatic molecules by graphene due to electron transfer. *Chem. Phys. Lett.,* **2011**, *506*(4-6), 260-264.

Not be distributed or uploaded to anyone or anywhere
For personal private use only

[http://dx.doi.org/10.1016/j.cplett.2011.03.031]

[78] Fleischmann, M.; Hendra, P.J.; McQuillan, A.J. Raman spectra of pyridine adsorbed at a silver electrode. *Chem. Phys. Lett.,* **1974**, *26*(2), 163-166.
[http://dx.doi.org/10.1016/0009-2614(74)85388-1]

[79] Ling, X.; Xie, L.; Fang, Y.; Xu, H.; Zhang, H.; Kong, J.; Dresselhaus, M.S.; Zhang, J.; Liu, Z. Can graphene be used as a substrate for Raman enhancement? *Nano Lett.,* **2010**, *10*(2), 553-561.
[http://dx.doi.org/10.1021/nl903414x] [PMID: 20039694]

[80] Manna, A.K.; Pati, S.K. Tuning the electronic structure of graphene by molecular charge transfer: a computational study. *Chem. Asian J.,* **2009**, *4*(6), 855-860.
[http://dx.doi.org/10.1002/asia.200800486] [PMID: 19322803]

[81] Xia, J.; Chen, F.; Li, J.; Tao, N. Measurement of the quantum capacitance of graphene. *Nat. Nanotechnol.,* **2009**, *4*(8), 505-509.
[http://dx.doi.org/10.1038/nnano.2009.177] [PMID: 19662012]

[82] Shekhirev, M.; Lipatov, A.; Torres, A.; Vorobeva, N.S.; Harkleroad, A.; Lashkov, A.; Sysoev, V.; Sinitskii, A. Highly Selective Gas Sensors Based on Graphene Nanoribbons Grown by Chemical Vapor Deposition. *ACS Appl. Mater. Interfaces,* **2020**, *12*(6), 7392-7402.
[http://dx.doi.org/10.1021/acsami.9b13946] [PMID: 32011111]

[83] aYousefi, N.; Sun, X.; Lin, X.; Shen, X.; Jia, J.; Zhang, B.; Tang, B.; Chan, M.; Kim, J.K. Highly aligned graphene/polymer nanocomposites with excellent dielectric properties for high-performance electromagnetic interference shielding. *Adv. Mater.,* **2014**, *26*(31), 5480-5487.
[http://dx.doi.org/10.1002/adma.201305293] [PMID: 24715671] bTang, L.; He, M.; Na, X.; Guan, X.; Zhang, R.; Zhang, J.; Gu, J. Functionalized glass fibers cloth/spherical BN fillers/epoxy laminated composites with excellent thermal conductivities and electrical insulation properties. *Composites Communications,* **2019**, *16*, 5-10.
[http://dx.doi.org/10.1016/j.coco.2019.08.007]

[84] Rohini, R.; Bose, S. Electromagnetic wave suppressors derived from crosslinked polymer composites containing functional particles: Potential and key challenges. *Nano-Structures & Nano-Objects,* **2017**, *12*, 130-146.
[http://dx.doi.org/10.1016/j.nanoso.2017.09.016]

[85] Maidhily, M.; Rajalakshmi, N.; Dhathathreyan, K.S. Electrochemical impedance diagnosis of micro porous layer in polymer electrolyte membrane fuel cell electrodes. *Int. J. Hydrogen Energy,* **2011**, *36*(19), 12352-12360.
[http://dx.doi.org/10.1016/j.ijhydene.2011.06.084]

[86] Subrahmanyam, K.S.; Kumar, P.; Maitra, U.; Govindaraj, A.; Hembram, K.P.S.S.; Waghmare, U.V.; Rao, C.N.R. Chemical storage of hydrogen in few-layer graphene. *Proc. Natl. Acad. Sci. USA,* **2011**, *108*(7), 2674-2677.
[http://dx.doi.org/10.1073/pnas.1019542108] [PMID: 21282617]

[87] Park, S.; An, J.; Suk, J.W.; Ruoff, R.S. Graphene-Based Actuators. *Small,* **2010**, *6*(2), 210-212.
[http://dx.doi.org/10.1002/smll.200901877] [PMID: 19924742]

[88] Xie, X.; Qu, L.; Zhou, C.; Li, Y.; Zhu, J.; Bai, H.; Shi, G.; Dai, L. An asymmetrically surface-modified graphene film electrochemical actuator. *ACS Nano,* **2010**, *4*(10), 6050-6054.
[http://dx.doi.org/10.1021/nn101563x] [PMID: 20828146]

[89] Wu, C.; Feng, J.; Peng, L.; Ni, Y.; Liang, H.; He, L.; Xie, Y. Large-area graphene realizing ultrasensitive photothermal actuator with high transparency: new prototype robotic motions under infrared-light stimuli. *J. Mater. Chem.,* **2011**, *21*(46), 18584-18591.
[http://dx.doi.org/10.1039/c1jm13311j]

[90] Nagamuthu, S.; Ryu, K.S. Synthesis of Ag/NiO honeycomb structured nanoarrays as the electrode material for high-performance asymmetric supercapacitor devices, Sci. *Sci. Rep.,* **2019**, *9*(1), 4864.
[http://dx.doi.org/10.1038/s41598-019-41446-0] [PMID: 30890740]

Not be distributed or uploaded to anyone or anywhere
For personal private use only

[91] Borenstein, A.; Hanna, O.; Attias, R.; Luski, S.; Brousse, T.; Aurbach, D. Carbon-based composite materials for supercapacitor electrodes: a review. *J. Mater. Chem. A Mater. Energy Sustain.,* **2017**, *5*(25), 12653-12672.
[http://dx.doi.org/10.1039/C7TA00863E]

[92] Li, H.; Wu, X.; Zhou, J.; Liu, Y.; Huang, M.; Xing, W.; Yan, Z.; Zhuo, S. Enhanced supercapacitive performance of $MnCO_3$@ rGO in an electrolyte with KI as Additive. *ChemElectroChem,* **2019**, *6*(2), 316-319.
[http://dx.doi.org/10.1002/celc.201801290]

[93] Talapatra, S.; Kar, S.; Pal, S.K.; Vajtai, R.; Ci, L.; Victor, P.; Shaijumon, M.M.; Kaur, S.; Nalamasu, O.; Ajayan, P.M. Direct growth of aligned carbon nanotubes on bulk metals. *Nat. Nanotechnol.,* **2006**, *1*(2), 112-116.
[http://dx.doi.org/10.1038/nnano.2006.56] [PMID: 18654161]

[94] Vivekchand, S.R.C.; Rout, C.S.; Subrahmanyam, K.S.; Govindaraj, A.; Rao, C.N.R. Graphene-based electrochemical supercapacitors. *J. Chem. Sci.,* **2008**, *120*(1), 9-13, 9-13.
[http://dx.doi.org/10.1007/s12039-008-0002-7]

[95] Stoller, M.D.; Park, S.; Zhu, Y.; An, J.; Ruoff, R.S. Graphene-Based Ultracapacitors. *Nano Lett.,* **2008**, *8*(10), 3498-3502.
[http://dx.doi.org/10.1021/nl802558y] [PMID: 18788793]

[96] Wang, D.W.; Li, F.; Zhao, J.; Ren, W.; Chen, Z.G.; Tan, J.; Wu, Z.S.; Gentle, I.; Lu, G.Q.; Cheng, H.M. Fabrication of graphene/polyaniline composite paper *via in situ* anodic electro polymerization for high-performance flexible electrode. *ACS Nano,* **2009**, *3*(7), 1745-1752.
[http://dx.doi.org/10.1021/nn900297m] [PMID: 19489559]

[97] Brodie, B.C. On the Atomic Weight of Graphite. *Philos. Trans. R. Soc. Lond.,* **1895**, *149*, 249-259.
[http://dx.doi.org/10.1098/rstl.1859]

[98] Wang, Y.; Shi, Z.; Fang, J.; Xu, H.; Ma, X.; Yin, J. Direct exfoliation of graphene in methanesulfonic acid and facile synthesis of graphene/polybenzimidazole nanocomposites. *J. Mater. Chem.,* **2011**, *21*(2), 505-512.
[http://dx.doi.org/10.1039/C0JM02376K]

[99] Wang, X.; Fulvio, P.F.; Baker, G.A.; Veith, G.M.; Unocic, R.R.; Mahurin, S.M.; Chi, M.; Dai, S. Direct exfoliation of natural graphite into micrometre size few layers graphene sheets using ionic liquids. *Chem. Commun. (Camb.),* **2010**, *46*(25), 4487-4489.
[http://dx.doi.org/10.1039/c0cc00799d] [PMID: 20485780]

[100] Stankovich, S.; Dikin, D.A.; Piner, R.D.; Kohlhaas, K.A.; Kleinhammes, A.; Jia, Y.; Wu, Y.; Nguyen, S.T.; Ruoff, R.S. Synthesis of graphene-based nanosheets *via* chemical reduction of exfoliated graphite oxide. *Carbon,* **2007**, *45*(7), 1558-1565.
[http://dx.doi.org/10.1016/j.carbon.2007.02.034]

[101] Zheng, Q.B.; Gudarzi, M.M.; Wang, S.J.; Geng, Y.; Li, Z.; Kim, J.K. Improved electrical and optical characteristics of transparent graphene thin films produced by acid and doping treatments. *Carbon,* **2011**, *49*(9), 2905-2916.
[http://dx.doi.org/10.1016/j.carbon.2011.02.064]

[102] Jung, I.; Vaupel, M.; Pelton, M.; Piner, R.; Dikin, D.A.; Stankovich, S.; An, J.; Ruoff, R.S. Characterization of thermally reduced graphene oxide by imaging ellipsometry. *J. Phys. Chem. C,* **2008**, *112*(23), 8499-8506.
[http://dx.doi.org/10.1021/jp802173m]

[103] Xue, F.; Lu, Y.; Qi, X.; Yang, J.; Wang, Y. Melamine foam-templated graphene nanoplatelet framework toward phase change materials with multiple energy conversion abilities. *Chem. Eng. J.,* **2019**, *365*, 20-29.
[http://dx.doi.org/10.1016/j.cej.2019.02.023]

Not be distributed or uploaded to anyone or anywhere
For personal private use only

[104] Hong, J-Y.; Jang, J. Highly stable, concentrated dispersions of graphene oxide sheets and their electro-responsive characteristics. *Soft Matter,* **2012**, *8*(28), 7348-7350.
[http://dx.doi.org/10.1039/c2sm25865j]

[105] Shin, K.Y.; Lee, S.; Hong, S.; Jang, J. Graphene size control *via* a mechanochemical method and electroresponsive properties. *ACS Appl. Mater. Interfaces,* **2014**, *6*(8), 5531-5537.
[http://dx.doi.org/10.1021/am405930k] [PMID: 24665987]

[106] Chua, C.K.; Pumera, M. Chemical reduction of graphene oxide: a synthetic chemistry viewpoint. *Chem. Soc. Rev.,* **2014**, *43*(1), 291-312.
[http://dx.doi.org/10.1039/C3CS60303B] [PMID: 24121318]

[107] Wang, Z.; Liu, J.; Wang, W.; Chen, H.; Liu, Z.; Yu, Q.; Zeng, H.; Sun, L. Aqueous phase preparation of graphene with low defect density and adjustable layers. *Chem. Commun. (Camb.),* **2013**, *49*(92), 10835-10837.
[http://dx.doi.org/10.1039/c3cc46809g] [PMID: 24121934]

[108] Wang, X.Y.; Narita, A.; Müllen, K. Precision synthesis *versus* bulk-scale fabrication of graphenes. *Nat. Rev. Chem.,* **2017**, 2.

[109] Brodie, B.C. *On the Atomic Weight of Graphite*; The Royal Society, **1859**, pp. 249-259.

[110] Staudenmaier, L. Verfahren zur Darstellung der Graphitsäure. *Ber. Dtsch. Chem. Ges.,* **1898**, *31*(2), 1481-1487.
[http://dx.doi.org/10.1002/cber.18980310237]

[111] Hummers, W.S., Jr; Offeman, R.E. Preparation of graphitic oxide. *J. Am. Chem. Soc.,* **1958**, *80*(6), 1339-1339.
[http://dx.doi.org/10.1021/ja01539a017]

[112] Pendolino, F.; Armata, N. *Graphene Oxide in Environmental Remediation Process*; Springer, **2017**.
[http://dx.doi.org/10.1007/978-3-319-60429-9]

[113] Huang, N.J.; Zang, J.; Zhang, G.D.; Guan, L.Z.; Li, S.N.; Zhao, L.; Tang, L.C. Efficient interfacial interaction for improving mechanical properties of polydimethylsiloxane nanocomposites filled with low content of graphene oxide nanoribbons. *RSC Advances,* **2017**, *7*(36), 22045-22053.
[http://dx.doi.org/10.1039/C7RA02439H]

[114] Kovtyukhova, N.I.; Ollivier, P.J.; Martin, B.R.; Mallouk, T.E.; Chizhik, S.A.; Buzaneva, E.V.; Gorchinskiy, A.D. Layer-by-layer assembly of ultrathin composite films from micron-sized graphite oxide sheets and polycations. *Chem. Mater.,* **1999**, *11*(3), 771-778.
[http://dx.doi.org/10.1021/cm981085u]

[115] Kuilla, T.; Bhadra, S.; Yao, D.; Kim, N.H.; Bose, S.; Lee, J.H. Recent advances in graphene based polymer composites. *Prog. Polym. Sci.,* **2010**, *35*(11), 1350-1375.
[http://dx.doi.org/10.1016/j.progpolymsci.2010.07.005]

[116] Pei, S.; Cheng, H.M. The reduction of graphene oxide. *Carbon,* **2012**, *50*(9), 3210-3228.
[http://dx.doi.org/10.1016/j.carbon.2011.11.010]

[117] Yoo, B.M.; Shin, H.J.; Yoon, H.W.; Park, H.B. Graphene and graphene oxide and their uses in barrier polymers. *J. Appl. Polym. Sci.,* **2014**, *131*, 1.
[http://dx.doi.org/10.1002/app.39628]

[118] Sun, L.; Fugetsu, B. Mass production of graphene oxide from expanded graphite. *Mater. Lett.,* **2013**, *109*, 207-210.
[http://dx.doi.org/10.1016/j.matlet.2013.07.072]

[119] Jalili, R.; Aboutalebi, S.H.; Esrafilzadeh, D.; Shepherd, R.L.; Chen, J.; Aminorroaya-Yamini, S.; Konstantinov, K.; Minett, A.I.; Razal, J.M.; Wallace, G.G. Chen, J.; AminorroayaYamini, S.; Konstantinov, K.; Minett, A.I.; Razal, J.M.; Wallace, G.G. Scalable one-step wet-spinning of graphene fibers and yarns from liquid crystalline dispersions of graphene oxide: towards multifunctional

Not be distributed or uploaded to anyone or anywhere
For personal private use only

textiles. *Adv. Funct. Mater.,* **2013**, *23*(43), 5345-5354.
[http://dx.doi.org/10.1002/adfm.201300765]

[120] Marcano, D.C.; Kosynkin, D.V.; Berlin, J.M.; Sinitskii, A.; Sun, Z.; Slesarev, A.; Alemany, L.B.; Lu, W.; Tour, J.M. Improved synthesis of graphene oxide. *ACS Nano,* **2010**, *4*(8), 4806-4814.
[http://dx.doi.org/10.1021/nn1006368] [PMID: 20731455]

[121] Zhang, J.; Liu, Q.; Ruan, Y.; Lin, S.; Wang, K.; Lu, H. Monolithic crystalline swelling of graphite oxide: a bridge to ultra-large graphene oxide with high scalability. *Chem. Mater.,* **2018**, *30*(6), 1888-1897.
[http://dx.doi.org/10.1021/acs.chemmater.7b04458]

[122] Dong, L.; Chen, Z.; Zhao, X.; Ma, J.; Lin, S.; Li, M.; Bao, Y.; Chu, L.; Leng, K.; Lu, H.; Loh, K.P. A non-dispersion strategy for large-scale production of ultra-high concentration graphene slurries in water. *Nat. Commun,* **2018**, 1-76.

[123] Li, L.; Wu, G.; Yang, G.; Peng, J.; Zhao, J.; Zhu, J.J. Focusing on luminescent graphene quantum dots: current status and future perspectives. *Nanoscale,* **2013**, *5*(10), 4015-4039.
[http://dx.doi.org/10.1039/c3nr33849e] [PMID: 23579482]

[124] Cheng, C.; Li, S.; Thomas, A.; Kotov, N.A.; Haag, R. Functional graphene nanomaterials-based architectures: bio interactions, fabrications, and emerging biological applications. *Chem. Rev.,* **2017**, *117*(3), 1826-1914.
[http://dx.doi.org/10.1021/acs.chemrev.6b00520] [PMID: 28075573]

[125] Melo, J.P.; Ríos, P.L.; Povea, P.; Morales-Verdejo, C.; Camarada, M.B. Graphene oxide quantum dots as the support for the synthesis of gold nanoparticles and their applications as new catalysts for the decomposition of composite solid propellants. *ACS Omega,* **2018**, *3*(7), 7278-7287.
[http://dx.doi.org/10.1021/acsomega.8b00837] [PMID: 31458888]

[126] Tian, P.; Tang, L.; Teng, K.S.; Lau, S.P. Graphene quantum dots from chemistry to applications. *Mater. Today Chem.,* **2018**, *10*, 221-258.
[http://dx.doi.org/10.1016/j.mtchem.2018.09.007]

[127] Lu, Q.; Wu, C.; Liu, D.; Wang, H.; Su, W.; Li, H.; Zhang, Y.; Yao, S. A facile and simple method for synthesis of graphene oxide quantum dots from black carbon. *Green Chem.,* **2017**, *19*(4), 900-904.
[http://dx.doi.org/10.1039/C6GC03092K]

[128] Wang, W.; Wang, Z.; Liu, J.; Peng, Y.; Yu, X.; Wang, W.; Zhang, Z.; Sun, L. One-pot facile synthesis of graphene quantum dots from rice husks for Fe3þ sensing. *Ind. Eng. Chem. Res.,* **2018**, *57*(28), 9144-9150.
[http://dx.doi.org/10.1021/acs.iecr.8b00913]

[129] Bauhofer, W.; Kovacs, J.Z. A review and analysis of electrical percolation in carbon nanotube polymer composites. *Compos. Sci. Technol.,* **2009**, *69*(10), 1486-1498.
[http://dx.doi.org/10.1016/j.compscitech.2008.06.018]

[130] Wu, C.; Huang, X.; Wang, G.; Lv, L.; Chen, G.; Li, G.; Jiang, P. Highly Conductive Nanocomposites with Three Dimensional, Compactly Interconnected Graphene Networks *via* a Self-Assembly Process. *Adv. Funct. Mater.,* **2013**, *23*, 506513.

[131] Chen, Z.; Xu, C.; Ma, C.; Ren, W.; Cheng, H.M. Lightweight and flexible graphene foam composites for high-performance electromagnetic interference shielding. *Adv. Mater.,* **2013**, *25*(9), 1296-1300.
[http://dx.doi.org/10.1002/adma.201204196] [PMID: 23300002]

[132] Wang, X.; Zhi, L.; Müllen, K. Transparent, conductive graphene electrodes for dye-sensitized solar cells. *Nano Lett.,* **2008**, *8*(1), 323-327.
[http://dx.doi.org/10.1021/nl072838r] [PMID: 18069877]

[133] Slack, G.A. Anisotropic thermal conductivity of pyrolytic graphite. *Phys. Rev.,* **1962**, *127*(3), 694-701.
[http://dx.doi.org/10.1103/PhysRev.127.694]

[134] Chen, W.; Yan, L. *In situ* self-assembly of mild chemical reduction graphene for three-dimensional

architectures. *Nanoscale,* **2011**, *3*(8), 3132-3137.
[http://dx.doi.org/10.1039/c1nr10355e] [PMID: 21698339]

[135] Zhang, X.; Sui, Z.; Xu, B.; Yue, S.; Luo, Y.; Zhan, W.; Liu, B. Mechanically strong and highly conductive graphene aerogel and its use as electrodes for electrochemical power sources. *J. Mater. Chem.,* **2011**, *21*(18), 6494-6497.
[http://dx.doi.org/10.1039/c1jm10239g]

[136] Xu, Y.; Sheng, K.; Li, C.; Shi, G. Self-assembled graphene hydrogel *via* a one-step hydrothermal process. *ACS Nano,* **2010**, *4*(7), 4324-4330.
[http://dx.doi.org/10.1021/nn101187z] [PMID: 20590149]

[137] Nguyen, S.T.; Nguyen, H.T.; Rinaldi, A.; Nguyen, N.P.V.; Fan, Z.; Duong, H.M. Morphology control and thermal stability of binderless-graphene aerogels from graphite for energy storage applications. *Colloids Surf. A Physicochem. Eng. Asp.,* **2012**, *414*, 352-358.
[http://dx.doi.org/10.1016/j.colsurfa.2012.08.048]

[138] Worsley, M.A.; Pauzauskie, P.J.; Kucheyev, S.O.; Zaug, J.M.; Hamza, A.V.; Satcher, J.H., Jr; Baumann, T.F. Properties of single-walled carbon nanotube-based aerogels as a function of nanotube loading. *Acta Mater.,* **2009**, *57*(17), 5131-5136.
[http://dx.doi.org/10.1016/j.actamat.2009.07.012]

[139] Worsley, M.A.; Olson, T.Y.; Lee, J.R.I.; Willey, T.M.; Nielsen, M.H.; Roberts, S.K.; Pauzauskie, P.J.; Biener, J.; Satcher, J.H., Jr; Baumann, T.F. High surface area, sp2- cross-linked three-dimensional graphene monoliths. *J. Phys. Chem. Lett.,* **2011**, *2*(8), 921-925.
[http://dx.doi.org/10.1021/jz200223x] [PMID: 26295629]

[140] Longo, S.; Mauro, M.; Daniel, C.; Musto, P.; Guerra, G. Rayleigh scattering by graphene-oxide in syndiotactic polystyrene aerogels. *Carbon,* **2014**, *77*, 896-905.
[http://dx.doi.org/10.1016/j.carbon.2014.06.003]

Not be distributed or uploaded to anyone or anywhere
For personal private use only

CHAPTER 3

Preparation Methods for Graphene and its Derivatives

Sharoni Gupta[1,*], **Pinki Bala Punjabi**[1] and **Rakshit Ameta**[2]

[1] *Department of Chemistry, University College of Science, Mohanlal Sukhadia University, Udaipur-313001, Rajasthan, India*

[2] *Department of Chemistry, J.R.N. Rajasthan Vidyapeeth University, Udaipur-313001, Rajasthan, India*

Abstract: Over the past few decades, graphene and its derivatives have carved a niche for themselves in material science. These carbon nanomaterials exhibit a broad range of applications owing to their enchanting features like high specific surface area, chemical inertness, astonishing electrical and thermal properties, elevated intrinsic mobility, inimitable optical properties, and huge mechanical strength. Considering the ubiquitous applications of graphene in different industries, diverse top-down and bottom-up methods have been developed. This chapter outlines the various methods used for the synthesis of graphene and graphene-based derivatives, such as exfoliation, unrolling or unzipping of carbon nanotubes, electric arc discharge method, laser ablation technique, oxidative exfoliation-reduction of graphene oxide, chemical vapour deposition, epitaxial growth, template synthesis, pyrolysis, substrate-free synthesis, total organic synthesis, and biological methods, highlighting the advantages of these methods. Upcoming challenges concerning the commercial synthesis of graphene have also been addressed in the concluding part.

Keywords: Bottom-up Strategies, Graphene, Graphene Oxide, Reduced Graphene Oxide, Top-down Methods.

INTRODUCTION

Graphene, a 2-D carbon allotrope, is one of the thinnest and strongest materials known. Graphene has a honeycomb lattice structure comprising a monolayer of sp^2 hybridized carbon atoms assembled as hexagonal rings [1]. In 1859, Brodie, while examining the structure of graphite for the first time, observed graphene and

* **Corresponding author Sharoni Gupta:** Department of Chemistry, University College of Science, Mohanlal Sukhadia University, Udaipur-313001, Rajasthan, India; E-mail:sharoni290490@gmail.com

Pinki Bala Punjabi, Rakshit Ameta & Sharoni Gupta (Eds.)
All rights reserved-© 2023 Bentham Science Publishers

coined the name "graphone" [2]. Later, Boehm *et al.* were the first to use the term 'graphene' [3]. For a long time since its first discovery, very little work has been reported on graphene. Then in 2004, Novoselov, Geim, and their research group isolated graphene from graphite with a simple exfoliation method [4]. The reinstating of graphene by Geim and Novoselov, who were awarded the Noble Prize in 2010 for their work on graphene [5], paved the way for "Graphene Science". Ever since then, a plethora of methods for the synthesis of graphene and its applications in various areas have been explored by researchers worldwide.

The incredible properties namely, enlarged specific surface area (up to 2630 m^2 g^{-1}), enormous intrinsic mobility (200,000 cm^2 v^{-1} s^{-1}), stupendous thermal conductivity (<5000W m^{-1} K^{-1}), extremely large Young's modulus (< 1.0 TPa), exceptional optical transmittance (< 97.7%), outstanding electrical conductivity, and tremendous chemical stability, displayed by graphene arise from its distinctive structure and arrangement of carbon framework [6 - 9].

The arrangement of mono graphitic lamellae of carbon particles in hexagonal planar sheet stacked in one or few layers forms bi-dimensional graphene. It has been reported that graphene lamella has a thickness of about 0.35 nm, comparable to 1/200,000th of the diameter of a strand of a human's hair [10]. The bi-layer and few-layer graphenes consist of two and three to ten layers of graphitic sheets, respectively. Graphene with twenty to thirty sheets is identified as multilayer or thick graphene or nanocrystalline thin graphite [11]. The monolayer graphene has a wavy sheet without any stacking. While, in the bi or few-layered graphene, the graphitic sheets are arranged in AA (hexagonal) or AB (Bernal) or ABC (rhombohedral) stacking [12]. Also, the few-layered graphene with no appreciable stacking order is commonly termed turbostratic [13].

The sp^2 bonding of carbon atoms in graphene exhibits three σ bonds (in-plane) formed by hybridization of s, p_x, and p_y orbitals and a π bond formed by p_z orbital perpendicular to the plane [10, 14]. The σ bonds form a firm backbone of hexagonal geometry, whereas the out-of-plane π bonds result in inter-lamellar interaction between graphene layers [10]. The existence of free electrons in the π bands is thus responsible for the exclusive electrical and optical properties of graphene [15]. Furthermore, the electrical conductivity of graphene is governed by the type of edges. Generally, armchair or zigzag edges exist in graphene. The variety and density of edges can generate metallic or semiconducting behaviour in graphene [16].

In spite of the desirable features of graphene, the lack of industrial-scale production is a major hindrance to its applicability in diverse fields. In such a scenario, the surfacing of graphene oxide and reduced graphene oxide has been a

relief for material chemists and industrial workers. This is because preparative protocols for GO and rGO are quite simple, require inexpensive starting materials, and result in mass production of these materials [17].

The oxidized form of graphene, *viz*. graphene oxide (GO), is structurally similar to graphene but with the presence of oxygen functionalities [17]. The precise structure of GO has been a highly controversial subject owing to its amorphous, berthollide character and hygroscopic nature [18]. Despite its debatable structure, several models have been proposed to elucidate the structural architecture of GO. Hofmann and Holst were the first to put forth a model suggesting that the epoxy groups exist at the basal planes of the graphite layer, with an overall molecular formula of C_2O [19]. Next, Ruess anticipated a model which elucidated that the carbon sheets were puckered instead of planar and the oxygen-containing groups like hydroxyl and ether-like oxygen formed bridges between the carbon atoms at positions 1 and 3 of the graphite framework [20]. Thereafter, Clause and co-workers [21], to explain the acidic nature of GO, further illustrated an enol- and keto-type model. In 1969, Scholz and Boehm [22] presented a novel arrangement of GO, which encompassed grooved carbon layers bearing hydroxyl and carbonyl functional groups. Nakajima and his research group [23, 24] also proposed a model elucidating the structural attributes of GO. According to them, GO comprises two carbon layers anchored to each other by sp^3 hybridized carbon-carbon bonds at right angles to the layers with the presence of relative numbers of carbonyl and hydroxyl groups based on the hydration scale. In 1997, Lerf and his colleagues [25] suggested the most widely accepted model for GO. As per their model, GO consists of haphazardly dispersed planar aromatic sections comprising un-oxidized benzene rings and crumpled zones of six-membered alicyclic rings with C=C, C−OH and ether groups at 1 and 2 positions [26]. Finally, Szabó *et al.* presented the most recent structural model for GO [27]. The model revealed that the carbon framework exhibits two kinds of zones, one with trans-linked cyclohexane chairs and the other one bearing ribbons of flat hexagonal rings with C=C bonds as well as functionalities, including tertiary OH, 1,3-ether, ketone, quinone, and phenol. Overall, it is clear that the structure of GO comprises graphitic regions, disordered oxidized areas, and regions with defects (which arise due to holes *via* the release of CO and CO_2 during the belligerent oxidation and exfoliation of the sheet in GO) [28].

Additionally, the partial reduction of graphene oxide restores the carbon framework of a graphene layer with the presence of a few oxygen functional groups. This form is known as reduced graphene oxide (rGO). The atomic structure of rGO was studied by Navarro *et al.* [29], and it was explicated that rGO sheets include large areas of undamaged graphene along with considerable regions rich in defects, namely, pentagonal-hexagonal pairs and planar, quasi

amorphous sp^2 bonded carbon clusters. It was reported that the defects occur due to imperfections in the crystallinity of graphene layers after GO reduction. Furthermore, through molecular dynamics simulations, it was revealed that carbonyl and ether groups are quite stable and hinder the complete reduction of GO [30]. Therefore, at low temperatures only, hydroxyl groups desorb without affecting the basal planes of graphene. While the more stable epoxy groups leave the GO surface at high temperatures, resulting in profound distortions in the graphene network. Thus, reinstating the extended π-conjugated network in rGO with some topological defects leads to superior electrical properties of rGO compared to GO. It is also noteworthy that owing to the existence of residual functional groups in rGO, the flow of charge carriers is disrupted *via* sp^2 networks, and thus, electric flow principally occurs by hopping, unlike graphene, where charge carriers flow ballistically [31 - 34]. Another feature of GO and rGO is hydrophilicity, which ascribes to the inclusion of functional groups that renders them soluble in water, organic solvents, and various other polar media [35].

Consequently, by fine-tuning the structural morphology, edges, number of sheets, defects, and functionalities in graphene or graphene oxide/reduced graphene oxide, one can realize desirable characteristic properties of graphene for diverse applications. To achieve this, one can adopt a cost-effective, reliable, simple, high-yielding, time-efficient, and scalable synthetic strategy for graphene synthesis. Considering the crucial inter-relationship between synthesis, property, and application of graphene, the chapter intends to highlight diverse top-down and bottom-up strategies available for designing graphene and its derivatives.

TOP-DOWN SYNTHESIS

Top-down methods are based on the breakdown of graphitic compounds into mono- or few-layer graphene [13]. The top-down approaches for graphene and its derivatives include exfoliation, unrolling or unzipping carbon nanotubes, electric arc discharge method, laser ablation technique, and oxidative exfoliation-reduction of graphene oxide.

Exfoliation Method

Exfoliation is the most cost-effective for the production of graphene from graphite. The process involves the un-stacking of graphite layers by increasing the inter-planar spacing *via* the breakdown of van der Waals forces and causing poor bonding in the direction orthogonal to the planes [36]. The exfoliation method is of two types: mechanical and chemical.

Mechanical Exfoliation

Mechanical exfoliation is also referred to as the "scotch tape" method. This is because in this technique, an adhesive tape is put on a graphite sample, and then the sample flakes are peeled off. The process involves preferential cleaving of flakes that stick to the tape along the crystal plane [37]. Furthermore, few- and single-layered graphene are obtained by pressing a fresh tape against the graphite flakes that adhere to the first piece of tape. Thereafter, the two tapes are peeled apart, slicing graphite into thinner sheets. By repeating the process several times, very thin graphite sheets are obtained [38]. In mechanical exfoliation, milling, stirring, ultrasonication or fluid dynamic techniques are employed to pull apart graphite layers [39].

For instance, Chen and co-workers have reported the synthesis of mono- and few-layer graphene using a three-roll mill machine and a polymer adhesive [40]. A three-roll mill with three adjacent cylindrical rolls (80 mm in diameter), which rotated at the same velocity, was employed, as shown in Fig. (**1**). The first (feed) and third (apron) cylindrical rolls moved in the same direction while the central roll rotated in the opposite direction. The mechanical force of the mill causes the S-shaped movement of the graphite sample in the rolls, causing continuous exfoliation of graphite. To prepare the polymer adhesive, poly vinyl chloride (PVC) was dispersed in dioctyl phthalate and magnetically stirred for half an hour. Then, the adhesive and graphite were placed in the mill. As the rolls rotated, the graphite sample gradually spread on the adhesive, followed by homogenous dispersion on the rolls and exfoliation of the graphite to form graphene. The process of exfoliation was performed for 12 h at ambient temperature. Finally, pure graphene was obtained by adding alcohol to impure graphene in order to remove dioctyl phthalate, followed by combustion in the muffle furnace at 500 ^{o}C for 3 h to burn PVC. The method offered a large-scale synthesis of homogeneous graphene sheets of a thickness of about 1.13-1.41 nm.

The use of acoustic cavitations for mechanical exfoliation of graphite flakes is also well known. The dispersion of graphite in suitable solvents like water, ethanol, DMF, *etc.* followed by ultrasonication leads to the breakdown of graphite sheets. The mechanism of ultrasonic exfoliation basically involves distribution of cavitation bubbles around the graphite flakes. The violent collapse of these bubbles generates shock waves which produce stress throughout the graphite material leading to splitting of graphite sheets. Additionally, the unbalanced lateral compressive stress may also separate two adjacent graphite layers by shear effect. The ultrasonic method offers low cost industrial scale production of graphene but sometimes it is deemed unfit because ultrasonic exfoliation in some cases results in fractures in graphene sheet and other undesirable defects.

However, by carefully controlling the reaction parameters like temperature, sonication power, solvent, and sonication time once can overcome this issue as well.

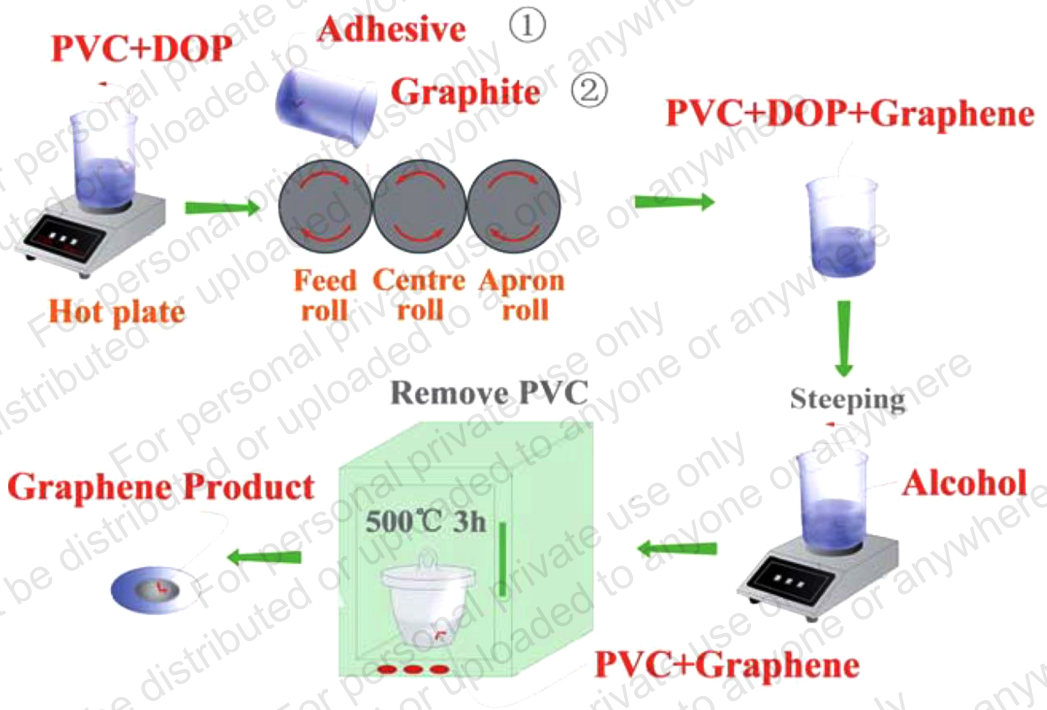

Fig. (1). The use of a three-roll mill machine for the synthesis of graphene by mechanical exfoliation. Reprinted with permission from [40]. Copyright 2012 The Royal Society of Chemistry.

Lately, Noroozi *et al.* demonstrated an ultrasonic exfoliation of graphite under environmentally benign conditions [41]. A mixture of polyvinyl pyrrolidone (PVP), hand soap-deionized water and graphite was stirred followed by sonication for 3 h. The reaction mixture was then kept still for 24 h leading to settling down of the large graphite aggregates at the bottom. A uniform dark suspension was obtained which was left undisturbed for five months. After that the suspension was washed with deionized water and centrifuged at 4,000 rpm for some hours which resulted in the formation of a gel like substance. The gel was dried overnight in a vacuum oven at 80°C followed by annealing at 1000°C for 5 min, to eliminate any residual PVP from the material. At last, pure few layered graphene sheets were obtained as black powder. Thus, graphene sheets were afforded by a low cost and simple sonication based exfoliation method.

Ball-milling of graphite for production of graphene has also gained much attention. Typically, two mechanisms are known for delamellation of graphite *via* ball milling [39]. In the first approach, shear force exerted for exfoliation is employed to produce large sized graphene flakes. The second approach makes use of the collisions or vertical forces applied by the balls in rolling actions to produce small flakes. Recently, Balasubramanyan and his research group have prepared graphene flakes using ball-milling technique for exfoliation [42]. A planetary ball-mill with 14 stainless steel balls was used for this purpose. In this method, sucrose and graphite were milled at 70 rpm for 30 h to obtain graphene-sucrose mixture. Thereafter, the mixture was calcinated for 3 h at 400 °C to obtain pure graphene. The method was high yielding and afforded graphene with fewer defects.

Nowadays, fluid dynamics methods are also employed for mechanical exfoliation. In this method, the graphite flakes flow with the liquid and are exfoliated frequently at different points [43]. An exfoliation method based on fluid dynamics was reported by Tran and his colleagues [44]. In this method, the Taylor-Couette flow reactor (Fig. **2**) consisting of two coaxial cylinders was used with a mixing vessel connected to a circulating chiller for prevention of heating up of the solvent.

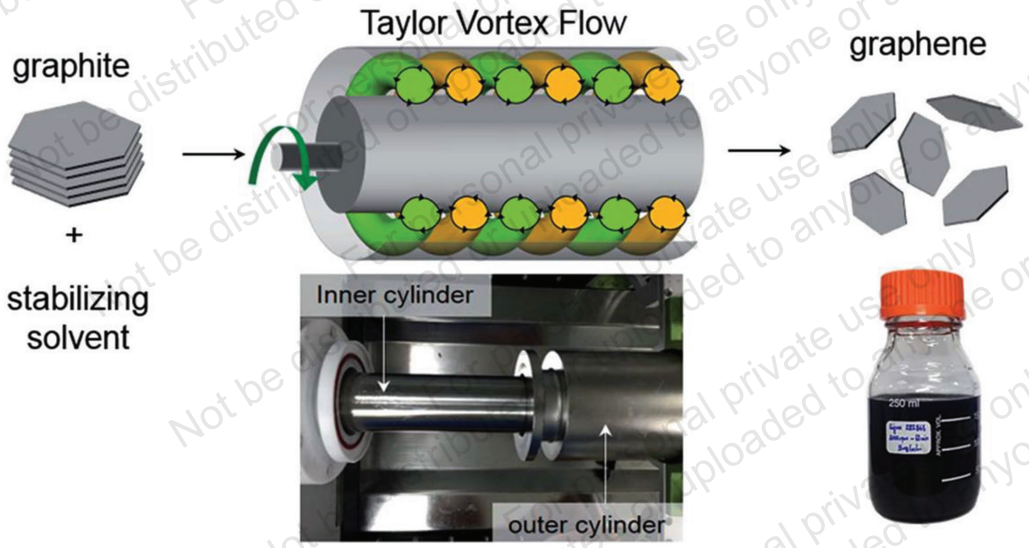

Fig. (2). Synthesis of graphene by using Taylor vortex flow. Reprinted with permission from [44]. Copyright 2016 The Royal Society of Chemistry.

The graphite powder and stabilizing solvents (N-Methyl-2-pyrrolidone and dimethylformamide) were injected into the space between the two cylinders of the

reactor. Then, as the inner cylinder of the reactor rotated at a speed of 500 to 3000 rpm for 10 to 120 min., shear mixing of graphite took place. The mixing resulted in the exfoliation of graphite and the resultant dispersion was centrifuged for half an hour at 1000 rpm to discard un-exfoliated graphite particles. Finally, exfoliated graphene was collected from the supernatant. The advantage of fluid dynamic method is that it affords high quality of graphene in short time.

Chemical Exfoliation

In chemical exfoliation, chemical agents are used to ablate graphite sheets. The chemicals first reduce van der Waals forces by increasing inter-layer spacing by intercalating themselves between the graphene layers. Then, thermal/high pressure treatment leads to breakdown of the intercalated graphite to form graphene [45].

Recently, a scalable fabrication of few-layer graphene by chemical exfoliation of graphite flakes has been demonstrated by Liu and his research group [46]. The process involved mixing of peroxyacetic acid with sulphuric acid followed by the addition of graphite to the binary system. The resultant mixture was stirred at room temperature to form a turbid liquid. During stirring, the decomposition of peroxyacetic acid took place accompanying oxygen evolution. Thereafter, the mixture was allowed to stand at ambient temperature and exfoliated graphene was obtained after 4 h. Pure graphene was obtained by filtration and washing with deionized water followed by air drying. In this method sulphuric acid intercalates between the graphite layers while the oxygen gas evolved by decomposition of peroxyacetic acid causes an increase in pressure that results in an increase in inter-layer distance to such an extent that van der Waals forces are conquered resulting in peeling off graphite layers to form graphene. This novel method produced graphene with an average of five layers.

In another chemical exfoliation method, microwave irradiation was used for rapid graphene synthesis [47]. The method involved two steps. In the first step, graphite intercalated with perchloric acid was prepared by mixing graphite with acid followed by 2 min. stirring under ambient conditions. Then, acetic anhydride was added to the mixture and the reaction mixture after stirring was subjected to microwaves for 30 s at 700 W resulting in $HClO_4$-intercalated graphite. In the second step, the intercalated graphite was suspended in deionized water and irradiated by microwaves for 80 s. This process led to large expansion of intercalated graphite's volume resulting in the formation of porous graphene aggregates. The aggregates were then subjected to ultrasonication for 5 min. at 100 W leading to the formation of exfoliated few-layer graphene.

It was reported that the use of perchloric acid with acetic anhydride increased its oxidation of graphite and thereby ensured intercalation of $HClO_4$ in graphite. Further, in the second step, the microwaves facilitated the decomposition of intercalated graphite due to a rapid increase in temperature. Thus, the use of microwaves in combination with sonication led to 100% exfoliated graphene. It was also reported that the few-layer garphene so produced had an average layer number of less than five and an average surface area of 256.8 μm^2.

In recent years, electrochemical exfoliation of graphite in aqueous solutions of inorganic substances and ionic liquids has gained a lot of significance over the years. Generally, the electrochemical exfoliation of graphite involves cleavage of intercalated graphite in solutions of salts or inorganic precursors undergoing insertion into graphite under electric current. The electrochemical exfoliation offers advantages such as better control of oxidation, intercalation and exfoliation of graphite sheets, hence generating good yields of less defective, high quality graphene [48].

An electrochemical exfoliation process for graphene preparation has been reported by Htwe *et al.* [49]. The method was based on the use of the traditional binary electrode system comprising graphite rod as a working electrode and platinum rod as a counter electrode for electrochemical processes. The two electrodes were immersed in an electrolyte solution containing sulphuric acid and phosphoric acid in one study and in another one, ammonium sulphate in distilled water was used as an electrolyte. A 10 V direct current bias voltage was applied until complete exhaustion of the graphitic anode. After electrochemical exfoliation, graphene is sonicated for about 15 to 60 minutes at ambient temperature and washed with distilled water *via* vacuum filtration. After vacuum drying at 80°C, pure graphene is obtained. In this exfoliation process, the inorganic compounds/ions from electrolyte solution are intercalated between graphite sheets *via* covalent or ionic bonds. Next, the graphite undergoes destruction due to electric potential and graphite sheets separated to form graphene. It was further reported that a comparative study of electrolytes and sonication time showed that the sulphuric acid electrolyte coupled with 45 min. of ultrasonication resulted in the most stable and least defective graphene with a few layers. Overall, from the above examples, it can be inferred that both mechanical and chemical exfoliation methods are cost-efficient and lead to high grade graphene in good yields.

Unzipping/Unrolling of Carbon Nanotubes

The unrolling of single-walled or multi-walled carbon nanotubes (SWCNT or MWCNT) is comparatively a new technique for graphene synthesis. Unzipping of

CNT results in the unfolding of a rolled cylindrical structure into planar graphitic sheets of single or few layers. By and large, a high strain rate of about $10^{8\text{-}10}$/s is the perquisite for breakdown of the C–C bond, leading to unrolling of CNT [50]. Laser irradiation, plasma etching, oxidizing agents, *etc.* are commonly used for the unzipping of SWCNT and MWCNT into mono- and few-layer graphene nanoribbons [51 - 53]. Graphene nanoribbons are basically quasi-monodimensional materials with armchair or zigzag edges [54].

In a recent study, nitrogen doped carbon nanotubes were unzipped to prepare graphene nanoribbons *via* a two-step process [55]. Firstly, an electrochemical process was carried out using 1 M H_2SO_4 solution as electrolyte for a three-electrode arrangement consisting of the nitrogen doped CNT array, platinum mesh, and mercury/mercury (I) sulfate (MMS) as the working, counter, and reference electrode, respectively. A potential of 0.8 V was applied at the working electrode for electrochemical unzipping of N-doped CNT. The unzipped CNTs were then washed thoroughly with deionized water to get rid of impurities. In the next step, the unzipped CNTs were suspended in N-methyl-2-pyrrolidone and subjected to sonication in an ice bath at different powers ranging from 40 W to 200 W (Fig. **3**). Finally, pure graphene nanoribbons were obtained by ultracentrifugation at 40000 rpm to discard the residual N-doped CNTs and other impurities. The method offered an efficient protocol for unzipping of CNTs, leading to graphene nanoribbons of 2 μm length.

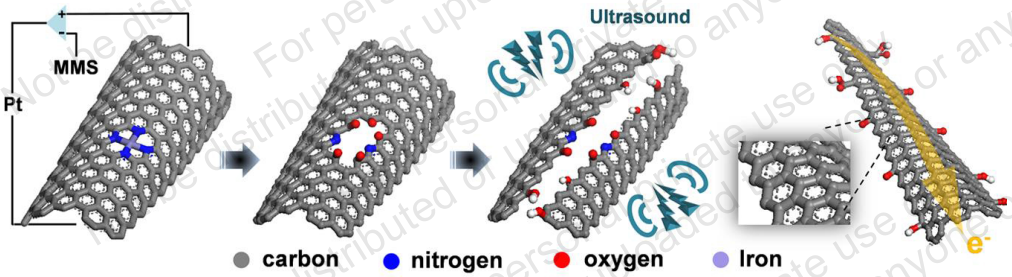

Fig. (3). Two-step synthesis of graphene nanoribbons *via* **(i)** Electrochemical unzipping **(ii)** Ultrasonication. Reprinted with permission from [55]. Copyright © 2019, American Chemical Society.

Plasma etching technique for graphene synthesis has been reported by Jiao *et al*. [56]. In this technique, the MWCNTs were dispersed in 1% aqueous Tween 20 solution and sonicated for 5 min. followed by centrifugation for 10 min. at 16,400*g* to eliminate the aggregates. The MWCNT dispersion was then mounted onto a pretreated Si substrate. Thereafter, the sample was calcined for 10 min. at 350 °C to get rid of the Tween 20. Next, a poly(methyl methacrylate) (PMMA) solution was spin-coated on MWCNTs at 3,000 rounds per minute for 60 s and then scorched at 170 °C on a hot plate for 2 h. This was followed by peeling off

the PMMA-MWCNT film in 1 M KOH solution at 80 °C [57]. Later, the film was cleaned with water and deposited onto a Si substrate by heating at 80 °C for 10 min in an oven. A10 W Ar plasma was employed by the workers to etch the PMMA-MWCNT film by applying a pressure of 40 mTorr. Subsequent to the etching process, the PMMA film was adhered to 3-aminopropyltriethoxysilane (APTES)-treated SiO_2/Si substrate with a preassembled Pt/W marker array. Finally, the PMMA was eliminated by acetone vapour followed by calcination for 10 min. at 300 °C to obtain graphene nanoribbons [57]. The graphene nanoribbons synthesized by this method were obtained with smooth edges and a slender width of 10-20 nm. This process has an advantage that it allows better control over the structure and quality of graphene.

Lately, Li and his research group have demonstrated longitudinal unrolling of carbon nanotubes (Fig. **4**) *via* intercalation of MWCNTs with KNO_3 and H_2SO_4 [58]. The advantage of this method is its scalable and mild protocol for the synthesis of graphene nanoribbons in excellent yields using less amount of H_2SO_4. The typical process involved magnetical stirring of MWCNTs with KNO_3 and H_2SO_4 for 2 h at 300 rpm. Thereafter, $KMnO_4$ was added gradually to the solution followed by stirring for another 2 h at ambient temperature. Then the unrolling reaction was carried out for 2 h in a water bath by slowly raising temperature from 30 °C to 70 °C. After completion of the reaction, the product was purified by sonication and centrifugation to yield pure graphene nanoribbons [59]. It was also revealed that the nanoribbons were single-layer to few-layer graphene with an average height of 2.1 nm and width of 101.8 nm.

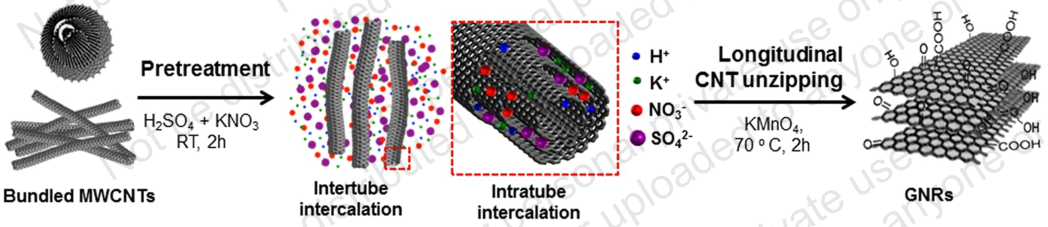

Fig. (4). Graphene nanoribbons are synthesized *via* stepwise longitudinal unzipping of CNTs. Reprinted with permission from [58]. Copyright © 2016, The Author(s).

Electric Arc Discharge

In a characteristic electric arc-discharge method, graphitic rods as a negative cathode and a positive anode are placed at a distance of few millimeters from each other and high current is applied to the electrodes to decompose the graphite rods to generate carbon nanostructures which pile up over the cathode or around the chamber walls [60]. The electric arc method for graphene synthesis has been investigated by several researchers. The advantage of electric arc method is that it results in the production of highly crystalline and pure graphene [61]. Recently a

gram scale synthesis of graphene has been established by Wu *et al*. [62]. The method was based on alternating current arc discharge method. An AC arc-discharge was performed in a water-cooled stainless steel chamber containing a mixture of nitrogen and hydrogen as buffer gas. Two graphite electrodes at a distance of 1 mm were used in the chamber. An AC of 150 A was applied at 400 Torr pressure. The electric discharge led to the consumption of two graphite electrodes in a short time of 4 min to 5 min and the carbon products were deposited on the inner and top wall of the chamber. The products were collected and annealed in air for an hour at 400 °C to obtain pure few-layer graphene. The method presented several advantages such as short reaction time, production of gram quantities of graphene and generation of high quality graphene sheets.

In another method, graphene and N-doped graphene were prepared *via* arc discharge by utilizing anodic carbon fillers *viz*. graphite, graphene oxide (GO) and polyaniline (PANi) [63]. In this method, an arc discharge apparatus was employed with graphite cathode and hollowed graphite anode positioned horizontally. Graphite powder, GO and PANi were homogeneously mixed and used as anodic carbon filler. For preparation of N-doped graphene, the arc chamber was first maintained at a pressure of 5×10^{-2} Torr, then filled with He, H_2, and NH_3 gases. The chamber pressure was then sustained at 550 Torr. For graphene, He and H_2 gases were used. A voltage of 30 V and current of 150 A were applied. The discharge resulted in the collection of graphene and N-doped graphene materials at the upper part of chamber. The graphene and N-doped graphene flakes produced by this method exhibited high crystallinity and large number of active edges that displayed super-capacitance.

Laser Ablation

Pulsed laser ablation or pulsed laser deposition is a reductive technique consisting of the production of micro or nanosized materials *via* removal of small portions of bulk substrates using a focused pulsed laser beam. In a typical laser ablation method, a pulsed beam is focused on graphite containing catalytic material in the presence of inert gas and high temperature resulting in ablation of carbon particles [64].

The main advantage of laser ablation techniques is that it yields highly porous graphene materials. A femtosecond laser ablation process for synthesis of extremely porous graphene has been demonstrated by Russo and co-workers [65]. In this approach, a highly oriented pyrolytic graphite (HOPG) was used as a target, placed at the bottom of a quartz cell filled with water and ablated by a femtosecond laser with a pulse duration of 35 fs. The HOPG was ablated continuously for 20 min. to produce highly porous graphene floating in the air-

water interface. It was further revealed that a six-layered spongy graphene with an irregular 3D porous structure with an average pore size of 15-20 nm was generated by this method.

A mechanism for graphene synthesis was also proposed by researchers. According to them, the laser beam simultaneously initiates decomposition of water, generates reactive molecules O_2, H_2, and H_2O_2 and exfoliates graphite, causing un-stacking of graphite sheets. Later, oxidation of graphene sheets takes place due to O_2 and H_2O_2 species producing several layered graphene oxide (GO) with sp^3 hybridized carbon atoms due to oxygen bonded atoms. Then, similar to the coal gasification mechanism, the sp^3 carbon atoms of the GO react with oxidized species. Subsequently, the formation of CO and CO_2 molecules occurs, leaving behind carbon vacancies and creating pores of nanodimension. This finally results in the production of porous graphene which floats at the water-air interface from where it is readily collected. Thus, this method affords large-scale synthesis of graphene in a short time and with high porosity.

Very recently, a novel single step liquid phase laser ablation technique has been used by Juvaid and his research group to produce a bilayer graphene [66]. In this method, a commercially graphite bar was suspended in deionized water (ablation medium) and ablated with a KrF excimer laser beam of 248 nm wavelength. The laser irradiation generated plasma which caused exfoliation of graphene films in water. Then, after half an hour of laser exfoliation, the Si/SiO_2 substrate was immersed in deionized water to collect the graphene films and later subjected to a natural drying process. Consequently, this cost-effective method produced bilayer graphene films with a high crystalline nature. Thus, it can be inferred that the laser beams produce high thermal energy which helps in overcoming the van der Waal bonds between the hexagonal sheets of graphite and leads to the formation of graphene.

Oxidative Exfoliation-Reduction of Graphene Oxide

Graphene oxide (GO) is generally prepared by oxidation of graphite using oxidants like $KClO_3$, $KMnO_4$, *etc.* in acidic media (HCl, H_2SO_4 and HNO_3, *etc.*). The first ever synthesis of graphene oxide *via* intercalation of graphite flakes was reported by Schafhacutl in 1840. Since then, various methods have been employed to synthesize graphene oxide including the Brodie's method [2], Staudenmaier method [67], Hofmann method [19, 68], Hummers method [69] and also other modified and improved methods [70, 71]. The reduction of graphene oxide leads to the production of graphene or reduced graphene oxide. In the following sections, oxidation and reduction methods have been briefly discussed.

Graphene Oxide Synthesis

Diverse methods used for oxidation of graphite to form graphene oxide (Fig. **5**) are as follows:

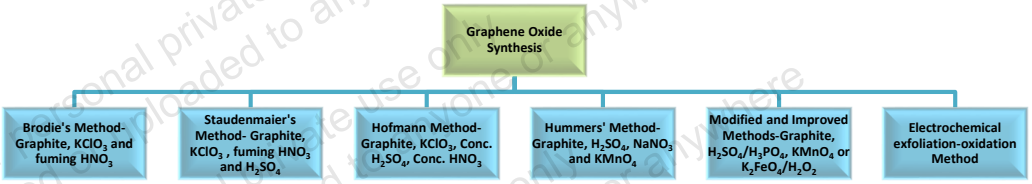

Fig. (5). Diverse methods for synthesis of graphene oxide.

a) Brodie's Method- Graphene oxide was fabricated by Brodie in 1859 using potassium chlorate and fuming nitric acid as oxidants. The synthesized product was a mixture of graphene and graphene oxide and soluble in water. The composition of the product as determined by elemental analysis was found to be 61.04% C, 1.85% H, 37.11% O. The shortcomings of this method were lengthy reaction time and evolution of hazardous gases.

b) Staudenmaier's Method- Staudenmaier's method (1898) was an upgrade to Brodie's method. This method used sulphuric acid in addition to fuming nitric acid and multiple aliquots of potassium chlorate solution, thereby escalating the acidity of the reaction mixture. This led to production of an extensively oxidized graphene oxide. However, this process was also time consuming and released toxic gases, hence it was not so suitable.

c) Hofmann's Method- In 1937, Hofmann and his research group demonstrated the use of concentrated nitric acid along with concentrated H_2SO_4 and $KClO_3$ to prepare graphene oxide.

d) Hummmers' Method- Hummers and Offeman in 1958 elucidated a novel method for the oxidation of graphite. The process was based on stirring of graphite powder with a combination of concentrated H_2SO_4, $NaNO_3$ and $KMnO_4$. When the stirring was complete, the reaction mixture was diluted with water and hydrogen peroxide and filtered. The product was then washed and dried to obtain pure graphene oxide. Although the method yielded highly oxidized graphene oxide in good yields, its major flaws were the explosive reaction process and the evolution of poisonous NO_2 and N_2O_4 gases.

e) Modified and Improved Methods- Over the past few years, improved and modified methods have been developed to conquer the drawbacks of the above mentioned routes and enhance the product yield. In 2010, Marcano and his co-

workers designed an improved method for GO synthesis [72]. In this method, they substituted sodium nitrate with a 9:1 mixture of H_2SO_4/H_3PO_4 and raised the concentration of $KMnO_4$. The highlight of this method was that a greater yield of hydrophilic graphene oxide was produced without the release of toxic nitrogenous gases. Recently, an improved Hummers method was demonstrated by Chen *et al.* [73] for GO synthesis using $KMnO_4$ and concentrated sulfuric acid. The advantage of this method was that $NaNO_3$ was not used, which prevented the evolution of hazardous gases Further, very recently an improved $NaNO_3$-free Hummers method was devised by Yu *et al.* employing $KMnO_4$, K_2FeO_4 and concentrated H_2SO_4 as oxidants and boric acid as a stabilizing agent [74]. This protocol was extremely efficacious and environmentally-friendly.

Another non-explosive improved method for GO synthesis was demonstrated by Ranjan *et al.* [75]. The method was a modification of Marcano's method. In this method, graphite flakes and $KMnO_4$ (taken in 1:6 ratio) were mixed using mortar and pestle for 5 min. and kept at 5 °C (the pre-cooling protocol). Next, a solution of sulphuric acid and phosphoric acid (taken in the ratio 9:1) was prepared separately and again pre-cooled at 5 °C. Both the solutions were mixed. At this step, no explosive reaction occurred and temperature also remained constant at room temperature. The suspension was then heated at 65 °C and was continuously stirred for 24 h. Later, the brown colored suspension was cooled down by adding 400 ml of deionized ice water. Then, H_2O_2 (7 mL) was added and stirred to obtain a golden yellow solution indicating the formation of graphene oxide. To the solution, distilled water was added and the precipitate was allowed to settle down. The precipitate was then washed with deionized water, HCl and ethanol, centrifuged and the suspension was decanted to obtain a gel-like substance. Finally, the gel was degassed for 24 h in a desiccator to obtain GO. Thus, the modified approach was cost-effective, free from toxic gas emission as well as non-explosive in nature, generating high purity GO.

Similarly, a modified Hummers approach using a mixture of sulfuric acid, phosphoric acid and nitric acid as intercalating sources and potassium permanganate and hydrogen peroxide as oxidants has been investigated by Al-Gaashani and co-workers [76]. This chemical oxidation method was free from poisonous gas expulsion, a low temperature process and reliable producing high quality of graphene.

f) Electrochemical Exfoliation-Oxidation Method- In a characteristic electrochemical exfoliation-oxidation method, two electrode system with graphite electrode as working or anodic electrode is used with an oxidizing electrolyte [77]. The basic approach is exfoliation of graphite by intercalation followed by oxidation to produce GO.

Of late, a high yielding electrochemical exfoliation procedure for GO preparation has been reported by Wang and his research group [78]. A two electrode system with graphite foil as a working electrode and Pt foil as a counter electrode placed at a distance of 3.0 cm was set-up. A low voltage of 4.0 V from a DC power source was applied and a mixture of H_2SO_4 (1 mol L^{-1}) and $KMnO_4$ (0.4 g) was used as electrolyte. The exfoliation was carried out for an hour. Thereafter, the electrolyte (retreated by sonication at 200 W of power for 30 min.) caused oxidation of the exfoliated graphene. The process continued for 10 hours. The GO was purified by washing with deionized water to remove the electrolyte ions and collected by vacuum filtration using a 0.22 mm microfiltration membrane. Finally, pure GO was obtained by drying at 60 °C for about 12 h. In this process, H_2SO_4 caused intercalation and exfoliation of graphite to afford graphene while $KMnO_4$ resulted in the oxidation of graphene to form hydrophilic graphene oxide. This method generated a 90% yield of GO.

A similar electrochemical oxidation process to produce graphene oxide was reported by Pei *et al*. using graphite intercalation compound paper as anode and Pt as cathode with a 5 V DC power supply, and diluted H_2SO_4 solution as an electrolyte [79]. Overall, the method presented a benign and efficient protocol for GO synthesis (Fig. **6**).

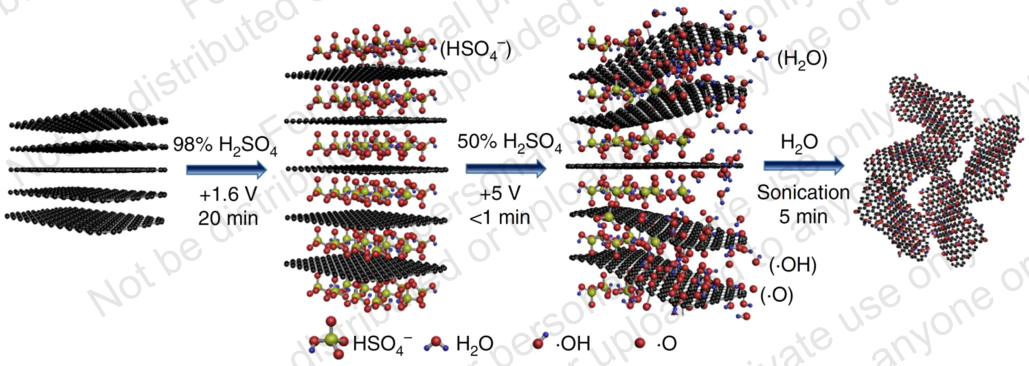

Fig. (6). Synthesis of graphene oxide *via* electrochemical oxidation process. Reprinted with permission from [79]. Copyright © The Author(s) 2018.

Graphene Oxide Reduction

The reduction of graphene oxide to reduced graphene oxide (rGO) or graphene can be accomplished by diverse methods such as chemical reduction, thermal annealing, photo or microwave reduction methods, electrochemical and solvothermal reduction (Fig. **7**). The reduction process removes oxygen functionalities from GO and re-establishes the aromatic framework of graphene.

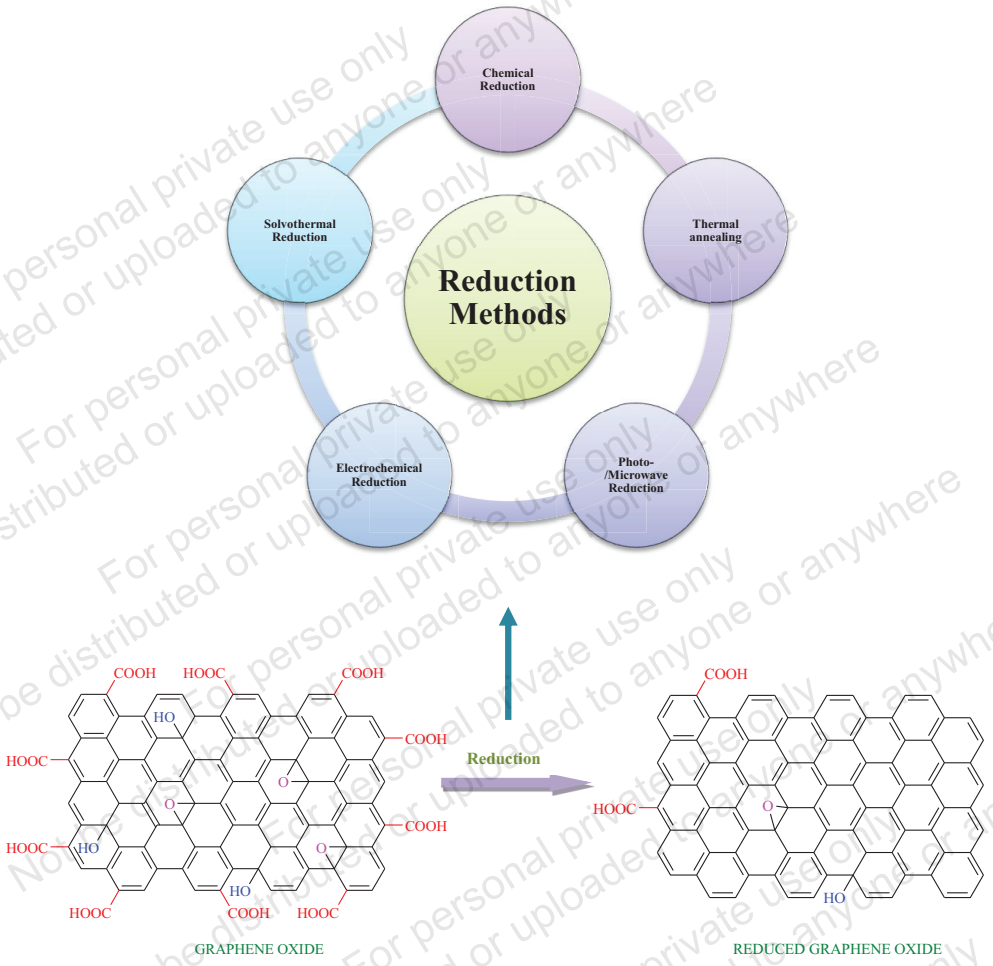

Fig. (7). Reduction of graphene oxide by diverse methods.

a) Chemical Reduction- The most commonly used method for reduction of graphene oxide is chemical reduction. The reduction of GO is basically carried out using chemical reductants in water. A variety of reducing agents such as hydrazine [80], lithium triethylborohydride [81] and elemental sulphur [82], L-ascorbic acid [83], glycine [84], starch [85], vanomycin [86], polydopamine [87], algal extracts [88], bacterium [89], artemisinin [90], green tea extract [91], *Aloe vera* [92], *etc.* have been used to prepare rGO from GO. Despite the scalability of this method, chemical reduction of GO suffers a setback because the rGO so obtained exhibits reasonably poor surface area and electronic conductivity [93].

b) Thermal Annealing- Annealing is a process which is usually carried out in vacuum [94], air [95], in inert [96] or reducing environment [97]. The rapid heating of GO at elevated temperature, not only exfoliates it but also removes oxygen functionality. Further, the thermal annealing introduces morphological defects and damages the graphene sheets due to the release of carbon dioxide [98] which enhances the electronic properties of the reduced form. Additionally, it has been proven that the more elevated the annealing temperature, the better is the reduction and the greater is the surface area of rGO [99].

c) Microwave and Photo-Reduction- The microwave reduction method is quite advantageous because using this method one can simultaneously carry out reduction as well as doping of GO along with fabrication of hybrid composites in short reaction time [100 - 102]. In an instance, it was reported that microwave reduction of graphene oxide powders produced rGO within just 3 minutes [103]. Recently, photo reduction of GO has also emerged as a neat and straightforward technique using solar light [104], ultraviolet light [105], and visible irradiation [106]. These methods lead to supreme quality rGO. Besides, by employing laser beam, the reduction is accomplished in femto-seconds [107].

d) Electrochemical Reduction- The prime highlight of this method is that GO reduction of GO can be achieved in aqueous buffer solution at ambient temperature without using hazardous chemical agents. In this method, the reduction process is performed in an electrochemical cell and reduction of GO occurs *via* the exchange of electrons between the electrodes and GO [108 - 110]. This method produces rGO with a high carbon to oxygen ratio and excellent electrical properties. However, the only concern is scalability that needs to be improved [111].

e) Solvothermal Reduction- In this approach, GO is dispersed in a solvent and reduction is carried out under supercritical conditions which arise due to heating in a sealed vessel [112, 113]. Moreover, solvothermal reduction aided by ultrasonication leads to rapid formation of rGO [114]. Supercritical water is a commonly used green solvent in this technique and results in elimination of functionalities in GO thereby restoring its aromatic framework [115]. The solvothermal route using water as solvent is also branded as hydrothermal reduction [116, 117].

In addition to the above methods, multi-step reductions are also well known for reduction of GO [118, 119]. The multi-step reduction is an extremely capable process which is known to generate high quality rGO. This method is nothing but an amalgamation of the above-mentioned methods.

BOTTOM-UP SYNTHESIS

The bottom-up approach deals with assembly of graphene from carbon precursors, *i.e*. step by step, building up graphene from carbon particles [120]. Chemical vapour deposition (CVD), epitaxial growth, template synthesis, pyrolysis, substrate free synthesis, and total organic synthesis are commonly used bottom-up strategies.

Chemical Vapour Deposition

Chemical vapour deposition (CVD) technique involves decomposition of volatile precursors on a substrate at elevated temperature in the presence of vacuum to prepare nanomaterials [121]. It is an extensively used method for industrial scale preparation of graphene. In this method, carbonaceous precursors undergo pyrolytic decomposition on crystalline substrate resulting in the creation of adsorption sites on the substrate's surface and thereby promoting the growth of high quality homogeneous thin films of graphene [122]. Generally, metals are used as substrates as well as catalysts, whereas carbonaceous precursors include hydrocarbons or biomass materials [123 - 125]. Recently, silicon carbide [126], boron nitride [127], quartz [128], silica [129], *etc.* have also been used as substrates for CVD. The greatest advantage of using CVD is that it produces high quality graphene with less defects, exceedingly cross-linked structure and higher surface area [130]. However, the method also suffers from some shortcomings like high production cost and, need for purification to remove catalysts which can be overcome by optimizing the process to low temperature and pressure [131].

Singh and his research group in their recent work have investigated nickel-catalyzed thermal chemical vapour decomposition of acetylene on steel (GCr15) for graphene synthesis [132]. The method typically involved the use of GCr15 alloy steel discs of 24 mm diameter. The discs were mechanically ground and immersed in acetone and isopropanol, respectively, followed by sonication. Thereafter, the surfaces of steel discs were electroplated with a nickel layer of 25 μm thickness to assist graphene deposition. Acetylene was used as a carbon source with hydrogen gas as a reducing medium. The discs were mounted in a ceramic boat and kept inside the quartz in the centre of the furnace. Then, a vacuum of 1.2×10-2 Torr was created inside the furnace and maintained. Next, the discs were heated at room temperature and at various growth temperatures ranging from 650 °C to 950 °C in 30 min. followed by annealation for 40 min under H_2 gas flow (20 sccm) at the growth temperature. Then, acetylene (6 sccm) was made to flow through the sample for 20 min. along with H_2 (20 sccm). At elevated temperature, the decomposed carbon atoms were absorbed by the nickel and acetylene flow was stopped after reaction completion. Then the cooling

process in a hydrogen-rich environment resulted in the formation of graphene due to carbon precipitation. Further, acetylene flow rates (6, 8, and, 10 sccm, growth temperature (850 °C and 950 °C) and reaction time (10 and 20 min.) were also optimized to afford the highest quality graphene. Overall, the study showed that the highest quality graphene over nickel was obtained at a growth temperature of 850 °C for a reaction time of 10 min. under 6 sccm acetylene gas flow rate. This is because at 850 °C, the graphene formed exhibits higher graphitization, and in a short reaction time, the number of graphene layers formed is less and at reduced flow of acetylene, graphene with low defects is formed [133].

In another study, graphene was prepared using a plasma enhanced CVD method. Munoz *et al.* for the first time have demonstrated growth of graphene on silicon dioxide *via* plasma CVD at a low temperature [134]. In this approach, the ASTEX AX 4500 ECR system was used as a microwave power source, a two zone chamber and a two-stage pumping system were also employed. Acetylene and hydrogen gas mixtures and silicon wafers (111) with native oxide as substrate were used in this process. The method involved two steps-(i) growth of high quality graphitic seeds with controlled treatment and density and (ii) promotion of edge growth leading to graphene film formation. In this method, hydrogen flow was adjusted at 50 sccm while acetylene flow was tuned in the range from 0.9 to 0.34 sccm for nucleation and from 0.8 to 0.24 sccm for growth of graphene films. Plasma was generated by applying a power of 200 W and a temperature ranging from 550°C to 650°C was set-up to carry out CVD. After completion of nucleation and growth steps, annealing of graphene films at 650°C was performed in vacuum for 2 h to produce supreme quality graphene films. This method resulted in the fabrication of a monolayer and a few layer graphene films with domain sizes ranging from 50 nm to >300 nm. Additionally, this strategy offered advantages including low temperature process, avoidance of film transfer and scalability.

Epitaxial Growth

The term epitaxial has been derived from two Greek words, “epi” (meaning above) and “taxis” (meaning arrangement), respectively [135]. In epitaxial growth technique, a crystalline film grows over a single crystalline substrate. There are usually two kinds of growth *viz*. homo-epitaxial (when film and substrate are of the same material) and hetero-epitaxial (when film and substrate are of different materials) [136]. For graphene synthesis, a mono crystal of silicon carbide is used as a substrate for epitaxial growth. This technique is usually performed at elevated temperatures under ultra-high vacuum (UHV) [137]. At high temperatures, silicon sublimes, leaving behind carbon atoms which undergo sp^2 hybridization and arrange to form aromatic hexagonal ring network, stimulating graphitization leading to the formation of graphene [138]. This method offers commercial

synthesis of graphene but it has certain drawbacks which include expensive protocols and production of graphene lacking uniformity [139]. However, in recent years, modified epitaxial growth methods have been developed to overcome these issues. Of late, Lalmi and his research group have demonstrated a large scale trilayer graphene synthesis *via* epitaxial growth on 6H-SiC (0001) [140]. The typical process included hydrogen etching of SiC at 1550°C to produce 6H-SiC (0001). Thereafter, 6H-SiC (0001) was heated at 1000°C in a semi-ultra high vacuum chamber and later heated at 1550°C in an atmosphere of argon, causing graphitization. An active graphene layer attached to the substrate was obtained and later cooled down for further processing. The method yielded flower-shaped and wrinkled three-layered graphene (Fig. **8**). The unique morphology of graphene is ascribed to partial dislocations between ABA and ABC stacking in trilayered graphene.

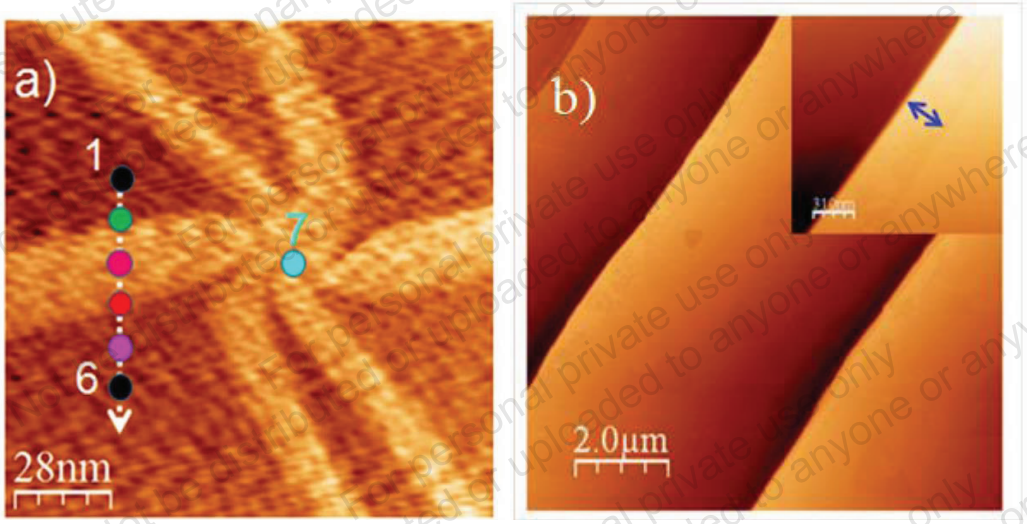

Fig. (8). STM images showing **(a)** flower-shaped domain of graphene **(b)** three-layered graphene. Reprinted with permission from [140] Copyright 2014, The Author(s).

In recent years, other than silicon carbide, boron nitride, metals like copper, nickel, *etc.* have also been used as substrates for epitaxial growth of graphene. For instance, Xu *et al.* reported epitaxial synthesis of graphene on commercially available Cu foil [141]. The method involved placing Cu foil on a quartz substrate and mounting it on a CVD furnace and annealing at 1030°C under the flow of Ar (500 sccm) to yield a Cu (111) crystal. The single Cu crystal (111) was then constantly moved past the furnace at a speed of 2.5 cm min^{-1}. For graphene growth, the CVD furnace was heated to 1030°C under the flow of Ar at 500 sccm and H_2 at 10 sccm. Then methane is made to flow at 1-5 sccm through the CVD

reactor. Graphitization leading to growth of graphene film was observed and upon completion of growth, the system was allowed to cool under the atmosphere of Ar (500 sccm) and H_2 (10 sccm). The method afforded ultra high quality graphene film in just 20 min. by epitaxial growth of graphene islands over a single crystal of Cu (111). These islands combine on the Cu surface to form a graphene film displaying exceptional crystallinity. On the whole, the technique presented a rapid and high yielding protocol for ultra-crystalline graphene film synthesis.

Template Synthesis

In template synthesis, an organic or inorganic material is employed as a template to express the growth of novel materials [142]. For graphene fabrication, carbon precursors are used along with pre-synthesized templates. This method is known as a hard-template synthesis. In hard template synthesis, a template works as a mold for replication of carbon materials, and no considerable chemical interactions occur between the template and the carbon precursor [143]. There is another approach in which molecular self-assembly of templates takes place *via* hydrogen bonding, hydrophobic/hydrophilic interactions, ion pairing, or dative bonding. This type of template synthesis involves chemical interactions between templates and carbon and is known as soft-template synthesis [144]. The synthesis of graphene *via* template synthesis using metal oxides [145], micelles [146], polymers [147], *etc.* has been reported to produce graphene with a well ordered structure and high quality.

Yang and co-workers have reported a simple soft-hard template method for the synthesis of graphene [148]. In this method, cetyltrimethyl ammonium bromide (CTAB) was employed as a soft template, silica (SiO_2) obtained from tetramethoxysilane (TMOS) was used as a hard template, and pyrene as a source of carbon (Fig. **9**). The process began with hydrolysis of TMOS in water under acidic conditions at pH=3 at ambient temperature of 2 h. Then, CTAB solution and pyrene were added to it and the reaction mixture was stirred for a few minutes. The homogenous sol so obtained was spin coated on quartz and silicon substrates. Subsequently, the films were thermally treated to vapourize the solvent and to further induce solidification of the composite. Later, the SiO_2/CTAB/pyrene composite was ground and annealed at 900°C for 2 h under N_2 atmosphere to obtain graphene loaded on silica substrate (SiO_2/graphene/SiO_2 composite). The silica was removed by treatment of the composite with HF (10% aqueous solution) for 48 h to obtain pure graphene. The graphene films obtained by template self assembly synthesis were of high quality and had thickness of the order of 1 nm and a size of about 5 μm.

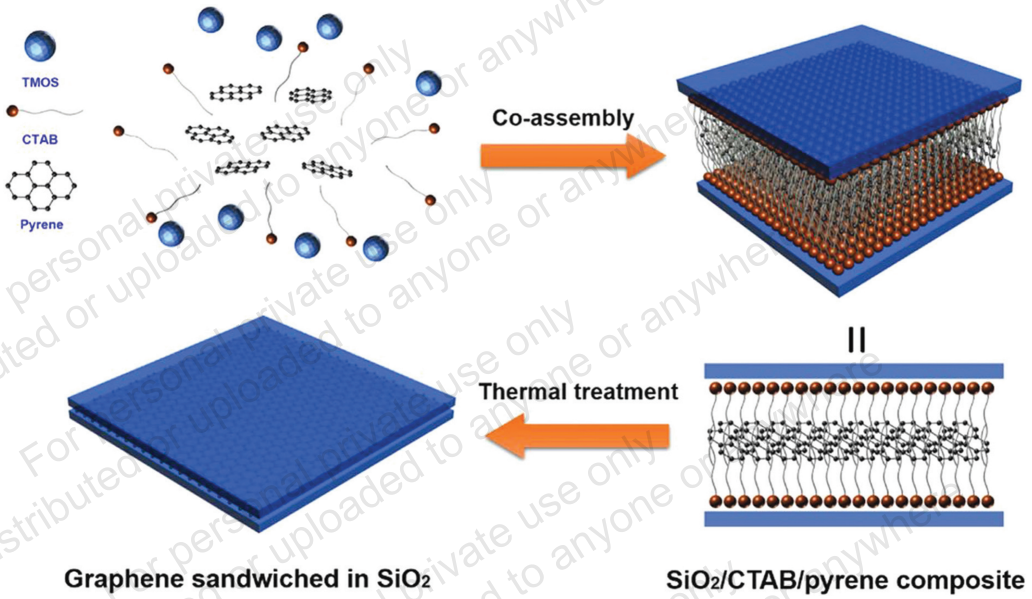

Fig. (9). Template synthesis of graphene film. Reprinted with permission from [148]. Copyright 2014, The Author(s).

In another method, micelle template based synthesis was used to fabricate N-doped mesoporous graphene [149]. Huang *et al.* first mixed 50 mL of GO suspension and 150 mL of hydrazine hydrate solution at ambient temperature *via* vigorous stirring for 12 h. Afterwards, 20 mL of F127 micellar solution was added to the above suspension and the reaction mixture was stirred for 2 h. Later, HCl (14 mL) was added and the mixture was briskly stirred for 24 h. The precipitate was collected by vacuum filtration and sintered at 350ºC for 5 h in argon atmosphere and for another 5 h at 900ºC to generate highly mesoporous graphene. In order to obtain N-doped graphene, 50 mg of graphene and 250 mg of cyanamide were mixed for 15 min. followed by sintering at 800ºC for 3 h in argon atmosphere. Thus, this method was quite efficient and afforded graphene with homogenously distributed mesopores, a large pore volume and a huge surface area.

Pyrolysis

Pyrolysis is a high temperature treatment involving thermal decomposition of a carbon source leading to the formation of C atoms that rearrange to form a graphitic carbon framework, leading to the formation of graphene. The method is inexpensive and produces graphene with superb purity but with few defects [150]. A gram scale synthesis of multi layer graphene was fabricated by Hong *et al.* [151]. This method involved pyrolysis of poly(methyl methacrylate) (PMMA) on

nickel microparticles in the restricted microzones created by organophilic montmorillonite (OMT). The typical process involved a pyrolysis apparatus with a quartz tube. The PMMA sample was placed in a quartz tube and placed inside a furnace fitted with a thermocouple under N_2 atmosphere. The carbonization was carried out at 1000°C for 8 min. and the product was obtained as black powder by cooling the reactor under N_2 flow. The product was further purified by etching the impure graphene powder with HF (10 wt.%) and HNO_3 (30 wt.%) under ultrasonication at ambient temperature followed by filtration, washing and drying at 80°C. Initially, PMMA sample was obtained by mixing methyl methacrylate, OMT and benzoyl peroxide under magnetic stirring followed by heating at 85°C under N_2 atmosphere. A thick paste was formed to which Ni particles were added and polymerization was carried out for 48 h at 60°C. Thus, wrinkled graphene sheets with a thickness of 1-4 nm and with few defects were achieved by this method. It was further reported that the addition of OMT restricts the pyrolytic carbon derivatives obtained by PMMA decomposition in microzones and improves yields of graphene produced catalytically by Ni particles in the microzones. Thus, the method offers inexpensive and scalable production of graphene.

Recently, the spray pyrolysis method has been used for the synthesis of graphene. In spray pyrolysis, a precursor solution is sprayed on a heated surface to produce aerosol droplets which undergo reaction and decompose to form particles and thin film [152]. Zou and his research group have demonstrated production of graphene nanosheets by spray pyrolysis of precursor's *viz*. iron carbonyl and pyridine [153]. In this process, the precursors (carbonyl and pyridine) were introduced into a quartz reactor at 5 mL min^{-1} flow rate. Also, N_2 was made to flow through the reactor at 600 L h^{-1}. The resultant sample was collected and mixed with excess ammonium chloride followed by heat treatment at 800°C for 30 min. in a quartz tube to remove the residual precursors. Finally, pure graphene nanosheets of good quality were obtained by washing, filtration and drying.

Substrate Free Synthesis

Substrate free synthesis is a comparatively newly developed strategy where graphene is synthesized *via* gas phase reactions in the absence of substrates, solvents and catalysts. In general, this method includes four strategies including carbonization, arc discharge, combustion, and atmospheric plasma [154]. The advantages of this method comprise scalability and production of high quality graphene with a tunable number of layers, low content of oxygen, and enhanced purity [154].

A substrate free, argon-plasma induced synthesis of graphene sheets was reported by Dato and his research group [155]. The researchers carried out the graphene synthesis in an atmospheric pressure microwave plasma reactor (Fig. **10a**) equipped with a quartz tube for conduction of argon gas stream (1.71 L/min.) *via* a microwave guide. This stream generates argon plasma. Further, with the aid of an alumina tube placed concentrically within the quartz tube, aerosols comprising argon gas (2 L/min.) and ethanol droplets (4×10^{-4} L/min.) were injected straightforwardly into the argon plasma. The ethanol droplets resided within the plasma for a very short time (10^{-1} s) during which these droplets evapourated and dissociated within the plasma forming a solid carbon material. Subsequently, the reaction product *i.e.* graphene after moving through the plasma was quickly cooled and collected on nylon filter membranes. It was reported that the rate of graphene sheets collected on filters was 2 mg/ min, for an input of carbon present in the ethanol of 164 mg/ min. Further, the graphene sheets collected on the filters were dispersed in methanol (Fig. **10b**) and sonicated for 5 min. to obtain a black homogenous suspension. The graphene sheets are composed of mono- and bi-layers as characterized by transmission electron microscopy (Fig. **10c**). The highlight of this method was continuous production of atomically thin graphene sheets.

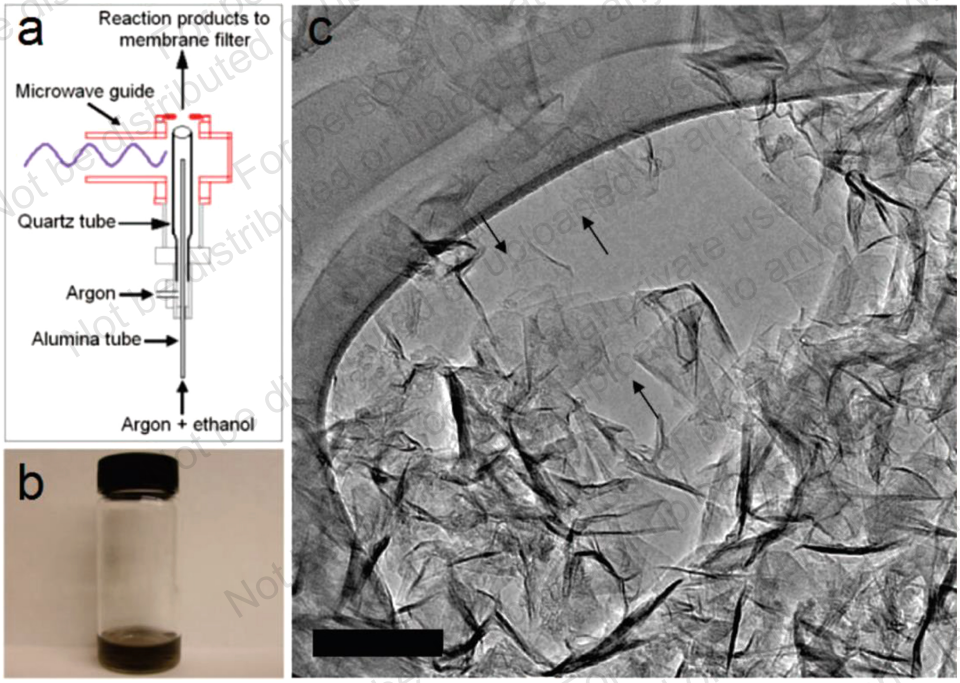

Fig. (10). (a) The microwave plasma reactor employed for graphene synthesis. **(b)** Image showing graphene dispersed in methanol. **(c)** TEM image of graphene sheets. Reprinted with permission from [155] Copyright © 2008, American Chemical Society.

Not be distributed or uploaded to anyone or anywhere
For personal private use only

In another instance, a multi-layer graphene sheet with a large specific surface area was produced by employing substrate free gas phase synthesis. Liu and Zhang have demonstrated a substrate free fabrication of graphene in a CVD reactor comprising quartz tube placed inside a horizontal furnace [156]. In the first step, camphor was put inside the tube and argon gas flowed through it at atmospheric pressure. The camphor sublimed on heating at 180°C and the volatilized camphor was pyrolyzed at 800-850°C in the furnace. The reaction was accomplished in 40 min., producing a graphene film which adhered to the wall of the chamber. The film was later scraped off and collected in the quartz tube. A graphene film of a large surface area of about 1 cm×1 cm was obtained by this method. Other advantages of this method include scalability and inexpensive production of graphene.

Total Organic Synthesis

The synthesis of graphene from polycyclic aromatic hydrocarbons (PAHs) constitutes total organic synthesis of graphene. PAHs are defined as 2D graphene fragments composed of all sp^2 hybridized carbons and can be readily modified by using appropriate aliphatic chains to tune the solubility of the product [157, 158]. In this method, suitable PAHs are chosen and used to prepare good quality graphene at high yields *via* a facile reaction pathway. Several reactions such as Suzuki coupling, Yamamoto coupling, Diels-Alder's cylcoaddition, *etc.* have been employed for synthesis of nano-graphene materials [159]. Recently, Vo and his research group have demonstrated a total organic synthesis of N-doped graphene nano ribbons [160]. The process involved several steps. In the first step, phenanthrene-9,10-dione was mixed with 98% sulfuric acid and N-bromosuccinimide was added to the mixture. The reaction mixture was then stirred vigorously at ambient temperature for 8 h. Then, ice-cold water was added to the reaction mixture and filtered to obtain orange colored 2,7-dibromophenanthrene-9,10-dione. In the next step, 5,10-dibromo-1,3-diphe-yl-2H-cyclopenta[l]phenanthren-2-one was synthesized by addition of 2,7-dibromophenanthrene-9,10-dione and 1,3-diphenylacetone methanol under stirring. Then, the reaction mixture was refluxed for 2h after addition of 0.3 M KOH solution drop-wise to the reaction mixture. After filtration, a green colored product was obtained. Next, 5-(phenylethynyl)pyrimidine was prepared by reaction between triethylamine, toluene, 5-bromopyrimidine, and triphenylphosphine in the presence of copper iodide. After degassing the suspension for 15 min., bis(triphenylphosphine)palladium (II) chloride was added. The reaction mixture was again constantly degassed for 15 min. followed by heating at 60 °C and stirring for 30 min. Later, phenylacetylene was added to the reaction mixture and heated at 65-70 °C for 18 h. After filtration and column chromatography, the product was isolated.

In the next step, a reaction between 5,10- dibromo-1,3-diphenyl-2H-cyclopenta[l]phenanthren-2-one, 5-(phenylethynyl)pyrimidine and diphenyl ether was carried out by refluxing for 24 h. this led to formation of 5-(6,11-dibromo-1,-,4-triphenyltriphenylen-2-yl)pyrimidine. Subsequently, bis(cyclooctadiene)nickel was added to a mixture of 2,2'-bipyridyl and 1,5-cyclooctandiene in dried N,N-Dimethylformamide as solvent and heated at 60 °C for 30 min. The degassed solution of 5-(6,11-dibromo-1,3,4-triphenyltriphenylen-2-yl)pyrimidine in toluene was added to the reaction mixture. The reaction mixture was then heated to 80 °C for 3 days and then cooled followed by the addition of methanol/water mixture (50mL/10mL). Thereafter, the slurry was filtered, washed with methanol, concentrated HCl, sodium hydroxide/methanol solution, water, and hexane, followed by drying. Finally, a polymer product was obtained. In the last step, the polymer and dichloromethane were sonicated. Then, iron (III) chloride dissolved in nitromethane was added to the above suspension. Next, nitrogen gas was passed through the reaction mixture for 15- 24 h under stirring condition. Then ethanol was added and the reaction mixture was filtered. The reaction product was then washed with concentrated HCl, water, and methanol/sodium hydroxide solution to obtain a black solid. This solid was dried at 50 °C for 24 h to yield a black powder of N-doped graphene nanoribbons. Thus, this method produces large quantities of high quality N-doped graphene *via* a strategy based on Yamamoto coupling of N-doped precursors and cyclodehydrogenation through Scholl reaction.

A similar scheme was reported by Dichtel *et al.* who used poly(phenylene ethynylene) to produce graphene nanoribbons [161]. The process was based on Asao-Yamamoto alkyne benzannulation [162] promoted by Cu(II) and Brønsted acid that proceeds *via* a benzopyrylium intermediate to generate precursors for nanographene which are further oxidized by Scholl reaction to produce nano graphene ribbons. In this process, diynes undergo benzannulation to form a polyaromatic hydrocarbon intermediate which undergoes oxidation to form nanographene derivatives. The process was quite efficient and resulted in the production of good quality graphene nanoribbons.

Biosynthesis of Graphene and its Derivatives

Besides the aforementioned methods, biosynthesis has also emerged as a sustainable strategy for of preparation of graphene and its derivatives. The biomolecules derived from living organisms or cells or plant extracts serve as reducing, capping as well as stabilizing agents for the synthesis of graphene materials thereby eliminating the use of hazardous chemical agents [163]. Recently, Khanam and Hasan have reported a benign biosynthesis of graphene using extracts of *Allium cepa* (onion) as non-toxic reducing agents [164]. In this

method GO was synthesized by modified Hummers method and then reduced by extracts of *Allium cepa* to produce graphene. The onion skins were first peeled off; the scales were chopped up and then blended to produce juice. Then, about 10 mL of the onion juice was added to GO and the suspension was sonicated for 30 min. Thereafter, the suspension of GO in juice was stirred for 6 h at ambient temperature and the color of dispersion changed from brown to black. This confirmed the transformation of GO to graphene. The mixture was then filtered and the impure graphene was washed with ethanol and water followed by drying to yield pure graphene. Thus, this method afforded a green route for efficacious and economically compatible production of graphene. It was further reported that the graphene so obtained was thin, crumpled and multilayer with a thickness of the order of 140 nm. In another report, green tea leaf extracts containing polyphenols which can serve as reducing and stabilizing agents were used for biofabrication of reduced graphene oxide.

The microbial reduction of graphene oxide is also an important biological method for production of rGO or graphene. For instance, Gurunathan and co-workers have reported reduction of GO using *Escherichia coli* biomass [165]. The *E. coli* bacteria were grown on LB medium (Luria-Bertani broth comprising 10 g tryptone, 5 g yeast extract, and 10 g/L NaCl) in an Erlenmeyer flask. The flask was incubated in a rotatory shaker agitating at a speed of 120 rpm/min for 21 h at 37°C. The bacterial culture after incubation was centrifuged at 10,000 rpm/min. then, the bacterial biomass was employed for reduction of GO. Next, to a GO dispersion, about 200 mg of *E. coli* biomass was added and the mixture was stirred for 72 h at 37°C. The reduction of GO produced a black suspension that was sonicated for 5 min. followed by centrifugation for 10 min. at 10,000 rpm/min to eliminate bacterial biomass as supernatant liquid. Thus, reduced graphene oxide was obtained as black pellets. This method resulted in highly efficient, large scale production water dispersible reduced graphene oxide by eliminating the use of toxic chemical reductants. Therefore, *E. coli* based reduction of GO presented an eco-friendly protocol. Similarly, an inexpensive and environmentally-benign synthesis of microbially reduced graphene oxide was also reported by Wang and his research group using *Shewanella oneidensis* MR-1 cell culture. Consequently, it is quite obvious that the bioproduction of graphene or reduced graphene oxide has gained great attention over the past few years owing to the simplicity, eco-compatibility, cost-effectiveness and sustainability of these methods.

CONCLUDING REMARKS

The superlative and desirable characteristics of graphene and its derivatives, including large specific surface area, high chemical stability, extraordinary

electrical and thermal properties, high intrinsic mobility, unique optical properties and enormous mechanical strength, have rendered them as the most useful carbonaceous nanomaterials. Considering the wide scope of these materials, several researchers from time to time have immersed themselves in developing simple, sustainable and efficacious synthetic strategies for graphene synthesis. In this chapter, we have summarized some of the most widely employed methods for fabrication of graphene and its derivatives. Several methods including exfoliation, unrolling or unzipping of carbon nanotubes, electric arc discharge method, laser ablation technique, oxidative exfoliation-reduction of graphene oxide, chemical vapour deposition, epitaxial growth, template synthesis, pyrolysis, substrate free synthesis, total organic synthesis, and biological methods have been used for efficient synthesis of high quality graphene and its derivatives. However, despite the rapidly expanding research in the field of graphene chemistry and availability of a large spectrum of methods, there are still a few challenges that need to be addressed for industrial scale synthesis of graphene. For instance, most of these methods largely yield few layer graphene. Scalable synthesis of monolayer graphene is still an area that needs to be worked upon. From economic perspective, designing of inexpensive modus operandi is the need of the hour for commercial graphene production. Also, eco-friendly graphene synthesis which minimizes the release of toxic gases, makes use of benign solvents and precursors, energy intensive protocols, and avoids further processing should be encouraged so at to reduce adverse impact on our environment. Overall, it can be said that in order to realize the dream of industrialization and commercialization of graphene and its derivatives, fabrication of scalable, reproducible, economically compatible and benign synthetic methods is of utmost significance. On a positive note, it is worth mentioning that the pace with which the graphene research is growing, it is quite certain that in near future a plethora of improved methodologies will be accessible for manufacturing of graphene with promising applications in our day to day life.

LIST OF ABBREVIATIONS

2-D	Two-dimensional
3-D	Three-dimensional
AC	Alternating current
APTES	3-Aminopropyl triethoxysilane
CNT	Carbon nanotubes
CTAB	Cetyltrimethyl ammonium bromide
CVD	Chemical vapour deposition
DC	Direct current

DMF	Dimethyl formamide
GO	Graphene oxide
HOPG	Highly oriented pyrolytic graphite
LB	Luria-Bertani
MMS	Mercury/Mercury (I) sulfate
MWCNT	Multi-walled carbon nanotubes
OMP	Organophilic montmorillonite
PAC	Polycyclic Aromatic Hydrocarbon
PANi	Polyaniline
PMMA	Polymethyl methacryalte
PVC	Polyvinyl chloride
PVP	Polyvinyl pyrrolidine
rGO	Reduced graphene oxide
SWCNT	Single-walled carbon nanotubes
TMOS	Tetramethoxysilane
UHV	Ultra high vacuum

CONSENT FOR PUBLICATION

Not applicable.

CONFLICT OF INTEREST

The author declares no conflict of interest, financial or otherwise.

ACKNOWLEDGEMENTS

The authors are grateful to the esteemed publishers for providing copyright permission to publish figures/diagrams/schemes used in this book chapter.

REFERENCES

[1] Allen, M.J.; Tung, V.C.; Kaner, R.B. Honeycomb carbon: a review of graphene. *Chem. Rev.,* **2010**, *110*(1), 132-145. [http://dx.doi.org/10.1021/cr900070d] [PMID: 19610631]

[2] Brodie, B.C. XIII. On the atomic weight of graphite. *Philos. Trans. R. Soc. Lond.,* **1859**, *149*, 249-259. [http://dx.doi.org/10.1098/rstl.1859.0013]

[3] Boehm, H.P.; Setton, R.; Stumpp, E. Nomenclature and terminology of graphite intercalation compounds. *Carbon,* **1986**, *24*(2), 241-245. [http://dx.doi.org/10.1016/0008-6223(86)90126-0]

[4] Novoselov, K.S.; Geim, A.K.; Morozov, S.V.; Jiang, D.; Zhang, Y.; Dubonos, S.V.; Grigorieva, I.V.; Firsov, A.A. Electric field effect in atomically thin carbon films. *Science,* **2004**, *306*(5696), 666-669.

Not be distributed or uploaded to anyone or anywhere For personal private use only

[http://dx.doi.org/10.1126/science.1102896] [PMID: 15499015]

[5] Gerstner, E. Nobel Prize 2010. *Andre Geim & Konstantin Novoselov. Nature Phys.,* **2020**, *6*, 836.

[6] Zhu, Y.; Murali, S.; Cai, W.; Li, X.; Suk, J.W.; Potts, J.R.; Ruoff, R.S. Graphene and graphene oxide: synthesis, properties, and applications. *Adv. Mater.,* **2010**, *22*(35), 3906-3924.
[http://dx.doi.org/10.1002/adma.201001068] [PMID: 20706983]

[7] Bharech, S.; Kumar, R.J. A review on the properties and applications of graphene. *Mat. Sci. Mech. Eng.,* **2015**, *2*, 70-73.

[8] Singh, R.K.; Kumar, R.; Singh, D.P. Graphene oxide: strategies for synthesis, reduction and frontier applications. *RSC Advances,* **2016**, *6*(69), 64993-65011.
[http://dx.doi.org/10.1039/C6RA07626B]

[9] Olenych, I.B.; Aksimentyeva, O.I.; Monastyrskii, L.S.; Horbenko, Y.Y.; Partyka, M.V. Electrical and photoelectrical properties of reduced graphene oxide-porous silicon nanostructures. *Nanoscale Res. Lett.,* **2017**, *12*(1), 272.
[http://dx.doi.org/10.1186/s11671-017-2043-7] [PMID: 28410550]

[10] Zhen, Z.; Zhu, H. Structure and properties of graphene. In: *Graphene: Fabrication, Characterizations, Properties and Applications*; Zhen, Z.; Zhu, H.; Xie, D.; Fang, Y., Eds.; Academic Press: Cambridge, **2018**.
[http://dx.doi.org/10.1016/B978-0-12-812651-6.00001-X]

[11] Zhang, Y.; Small, J.P.; Pontius, W.V.; Kim, P. Fabrication and electric-field-dependent transport measurements of mesoscopic graphite devices. *Appl. Phys. Lett.,* **2005**, *86*(7), 073104.
[http://dx.doi.org/10.1063/1.1862334]

[12] Yang, G.; Li, L.; Lee, W.B.; Ng, M.C. Structure of graphene and its disorders: a review. *Sci. Technol. Adv. Mater.,* **2018**, *19*(1), 613-648.
[http://dx.doi.org/10.1080/14686996.2018.1494493] [PMID: 30181789]

[13] Edwards, R.S.; Coleman, K.S. Graphene synthesis: relationship to applications. *Nanoscale,* **2013**, *5*(1), 38-51.
[http://dx.doi.org/10.1039/C2NR32629A] [PMID: 23160190]

[14] Tiwari, S.K.; Mishra, R.K.; Ha, S.K.; Huczko, A. Evolution of graphene oxide and graphene: from imagination to industrialization. *ChemNanoMat,* **2018**, *4*(7), 598-620.
[http://dx.doi.org/10.1002/cnma.201800089]

[15] Sang, M.; Shin, J.; Kim, K.; Yu, K. Electronic and thermal properties of graphene and recent advances in graphene based electronics applications. *Nanomaterials (Basel),* **2019**, *9*(3), 374.
[http://dx.doi.org/10.3390/nano9030374] [PMID: 30841599]

[16] Jia, X.; Campos-Delgado, J.; Terrones, M.; Meunier, V.; Dresselhaus, M.S. Graphene edges: a review of their fabrication and characterization. *Nanoscale,* **2011**, *3*(1), 86-95.
[http://dx.doi.org/10.1039/C0NR00600A] [PMID: 21103548]

[17] Chen, D.; Feng, H.; Li, J. Graphene oxide: preparation, functionalization, and electrochemical applications. *Chem. Rev.,* **2012**, *112*(11), 6027-6053.
[http://dx.doi.org/10.1021/cr300115g] [PMID: 22889102]

[18] Dreyer, D.R.; Park, S.; Bielawski, C.W.; Ruoff, R.S. The chemistry of graphene oxide. *Chem. Soc. Rev.,* **2010**, *39*(1), 228-240.
[http://dx.doi.org/10.1039/B917103G] [PMID: 20023850]

[19] Hofmann, U.; Holst, R. Über die Säurenatur und die Methylierung von Graphitoxyd. *Ber. Dtsch. Chem. Ges. B,* **1939**, *72*(4), 754-771.
[http://dx.doi.org/10.1002/cber.19390720417]

[20] Ruess, G. Uber das Graphitoxyhydroxyd (Graphitoxyd). *Monatsh. Chem.,* **1947**, *76*(3-5), 381-417.
[http://dx.doi.org/10.1007/BF00898987]

Not be distributed or uploaded to anyone or anywhere
For personal private use only

[21] Clause, A.; Plass, R.; Boehm, H-P.; Hofmann, U. Untersuchungen zur Struktur des Graphitoxyds. *Z. Anorg. Allg. Chem.,* **1957**, *291*(5-6), 205-220.
[http://dx.doi.org/10.1002/zaac.19572910502]

[22] Scholz, W.; Boehm, H.P. Untersuchungen am Graphitoxid. VI. Betrachtungen zur Struktur des Graphitoxids. *Z. Anorg. Allg. Chem.,* **1969**, *369*(3-6), 327-340.
[http://dx.doi.org/10.1002/zaac.19693690322]

[23] Nakajima, T.; Mabuchi, A.; Hagiwara, R. A new structure model of graphite oxide. *Carbon,* **1988**, *26*(3), 357-361.
[http://dx.doi.org/10.1016/0008-6223(88)90227-8]

[24] Nakajima, T.; Matsuo, Y. Formation process and structure of graphite oxide. *Carbon,* **1994**, *32*(3), 469-475.
[http://dx.doi.org/10.1016/0008-6223(94)90168-6]

[25] Lerf, A.; He, H.; Riedl, T.; Forster, M.; Klinowski, J. 13C and 1H MAS NMR studies of graphite oxide and its chemically modified derivatives. *Solid State Ion.,* **1997**, *101-103*, 857-862.
[http://dx.doi.org/10.1016/S0167-2738(97)00319-6]

[26] Lerf, A.; Buchsteiner, A.; Pieper, J.; Schöttl, S.; Dekany, I.; Szabo, T.; Boehm, H.P. Hydration behavior and dynamics of water molecules in graphite oxide. *J. Phys. Chem. Solids,* **2006**, *67*(5-6), 1106-1110.
[http://dx.doi.org/10.1016/j.jpcs.2006.01.031]

[27] Szabó, T.; Tombácz, E.; Illés, E.; Dékány, I. Enhanced acidity and pH-dependent surface charge characterization of successively oxidized graphite oxides. *Carbon,* **2006**, *44*(3), 537-545.
[http://dx.doi.org/10.1016/j.carbon.2005.08.005]

[28] Eigler, S.; Hirsch, A. Chemistry with graphene and graphene oxide-challenges for synthetic chemists. *Angew. Chem. Int. Ed.,* **2014**, *53*(30), 7720-7738.
[http://dx.doi.org/10.1002/anie.201402780] [PMID: 24962439]

[29] Gómez-Navarro, C.; Weitz, R.T.; Bittner, A.M.; Scolari, M.; Mews, A.; Burghard, M.; Kern, K. Electronic transport properties of individual chemically reduced graphene oxide sheets. *Nano Lett.,* **2007**, *7*(11), 3499-3503.
[http://dx.doi.org/10.1021/nl072090c] [PMID: 17944526]

[30] Bagri, A.; Mattevi, C.; Acik, M.; Chabal, Y.J.; Chhowalla, M.; Shenoy, V.B. Structural evolution during the reduction of chemically derived graphene oxide. *Nat. Chem.,* **2010**, *2*(7), 581-587.
[http://dx.doi.org/10.1038/nchem.686] [PMID: 20571578]

[31] Becerril, H.A.; Mao, J.; Liu, Z.; Stoltenberg, R.M.; Bao, Z.; Chen, Y. Evaluation of solution-processed reduced graphene oxide films as transparent conductors. *ACS Nano,* **2008**, 463-470.
[http://dx.doi.org/10.1021/nn700375n]

[32] Mattevi, C.; Eda, G.; Agnoli, S.; Miller, S.; Mkhoyan, K.A.; Celik, O.; Mastrogiovanni, D.; Granozzi, G.; Garfunkel, E.; Chhowalla, M. Evolution of Electrical, Chemical, and Structural Properties of Transparent and Conducting Chemically Derived Graphene Thin Films. *Adv. Funct. Mater.,* **2009**, *19*(16), 2577-2583.
[http://dx.doi.org/10.1002/adfm.200900166]

[33] Castro Neto, A.H.; Guinea, F.; Peres, N.M.R.; Novoselov, K.S.; Geim, A.K. The electronic properties of graphene. *Rev. Mod. Phys.,* **2009**, *81*(1), 109-162.
[http://dx.doi.org/10.1103/RevModPhys.81.109]

[34] Du, X.; Skachko, I.; Barker, A.; Andrei, E.Y. Approaching ballistic transport in suspended graphene. *Nat. Nanotechnol.,* **2008**, *3*(8), 491-495.
[http://dx.doi.org/10.1038/nnano.2008.199] [PMID: 18685637]

[35] Huang, X.; Yin, Z.; Wu, S.; Qi, X.; He, Q.; Zhang, Q.; Yan, Q.; Boey, F.; Zhang, H. Graphene-based materials: synthesis, characterization, properties, and applications. *Small,* **2011**, *7*(14), 1876-1902.

Not be distributed or uploaded to anyone or anywhere For personal private use only

[http://dx.doi.org/10.1002/smll.201002009] [PMID: 21630440]

[36] Kumar, R.; Sahoo, S.; Joanni, E.; Singh, R.K.; Tan, W.K.; Kar, K.K.; Matsuda, A. Recent progress in the synthesis of graphene and derived materials for next generation electrodes of high performance lithium ion batteries. *Pror. Energy Combust. Sci.,* **2019**, *75*, 100786.
[http://dx.doi.org/10.1016/j.pecs.2019.100786]

[37] Dresselhaus, M.S.; Dresselhaus, G. Intercalation compounds of graphite. *Adv. Phys.,* **2002**, *51*(1), 1-186.
[http://dx.doi.org/10.1080/00018730110113644]

[38] Whitener, K.E., Jr; Sheehan, P.E. Graphene synthesis. *Diamond Related Materials,* **2014**, *46*, 25-34.
[http://dx.doi.org/10.1016/j.diamond.2014.04.006]

[39] Yi, M.; Shen, Z. A review on mechanical exfoliation for the scalable production of graphene. *J. Mater. Chem. A Mater. Energy Sustain.,* **2015**, *3*(22), 11700-11715.
[http://dx.doi.org/10.1039/C5TA00252D]

[40] Chen, J.; Duan, M.; Chen, G. Continuous mechanical exfoliation of graphene sheets *via* three-roll mill. *J. Mater. Chem.,* **2012**, *22*(37), 19625-19628.
[http://dx.doi.org/10.1039/c2jm33740a]

[41] Noroozi, M.; Zakaria, A.; Radiman, S.; Abdul Wahab, Z. Environmental synthesis of few layers graphene sheets using ultrasonic exfoliation with enhanced electrical and thermal properties. *PLoS One,* **2016**, *11*(4), e0152699.
[http://dx.doi.org/10.1371/journal.pone.0152699] [PMID: 27064575]

[42] Balasubramanyan, S.; Sasidharan, S.; Poovathinthodiyil, R.; Ramakrishnan, R.M.; Narayanan, B.N. Sucrose-mediated mechanical exfoliation of graphite: a green method for the large scale production of graphene and its application in catalytic reduction of 4-nitrophenol. *New J. Chem.,* **2017**, *41*(20), 11969-11978.
[http://dx.doi.org/10.1039/C7NJ01900A]

[43] Yi, M.; Shen, Z.; Zhu, J. A fluid dynamics route for producing graphene and its analogues. *Chin. Sci. Bull.,* **2014**, *59*(16), 1794-1799.
[http://dx.doi.org/10.1007/s11434-014-0303-9]

[44] Tran, T.S.; Park, S.J.; Yoo, S.S.; Lee, T.R.; Kim, T. High shear-induced exfoliation of graphite into high quality graphene by Taylor–Couette flow. *RSC Advances,* **2016**, *6*(15), 12003-12008.
[http://dx.doi.org/10.1039/C5RA22273G]

[45] Bhuyan, M.S.A.; Uddin, M.N.; Islam, M.M.; Bipasha, F.A.; Hossain, S.S. Synthesis of graphene. *Int. Nano Lett.,* **2016**, *6*(2), 65-83.
[http://dx.doi.org/10.1007/s40089-015-0176-1]

[46] Liu, M.; Zhang, X.; Wu, W.; Liu, T.; Liu, Y.; Guo, B.; Zhang, R. One-step chemical exfoliation of graphite to ~100% few-layer graphene with high quality and large size at ambient temperature. *J. Mater. Chem. C Mater. Opt. Electron. Devices,* **2019**, *355*, 181-185.

[47] Wu, W.; Liu, M.; Gu, Y.; Guo, B.; Ma, H.; Wang, P.; Wang, X.; Zhang, R. Fast chemical exfoliation of graphite to few-layer graphene with high quality and large size *via* a two-step microwave-assisted process. *Chem. Eng. J.,* **2020**, *381*, 122592.
[http://dx.doi.org/10.1016/j.cej.2019.122592]

[48] Bakunin, E.S.; Obraztsova, E.Y.; Rukhov, A.V. Modern methods for synthesis of few-layer graphene structures by electrochemical exfoliation of graphite. *Inorg. Mater. Appl. Res.,* **2019**, *10*(2), 249-255.
[http://dx.doi.org/10.1134/S2075113319020047]

[49] Htwe, Y.Z.N.; Chow, W.S.; Suda, Y.; Thant, A.A.; Mariatti, M. Effect of electrolytes and sonication times on the formation of graphene using an electrochemical exfoliation process. *Appl. Surf. Sci.,* **2019**, *469*, 951-961.
[http://dx.doi.org/10.1016/j.apsusc.2018.11.029]

[50] Tiwary, C.S.; Javvaji, B.; Kumar, C.; Mahapatra, D.R.; Ozden, S.; Ajayan, P.M.; Chattopadhyay, K. Chemical-free graphene by unzipping carbon nanotubes using cryo-milling. *Carbon,* **2015**, *89*, 217-224.
[http://dx.doi.org/10.1016/j.carbon.2015.03.036]

[51] Kumar, P.; Yamijala, S.S.R.K.C.; Pati, S.K. Optical unzipping of carbon nanotubes in liquid media. *J. Phys. Chem. C,* **2016**, *120*(30), 16985-16993.
[http://dx.doi.org/10.1021/acs.jpcc.6b02524]

[52] Thomas, R.; Hembram, K.P.S.S.; Kumar, B.V.M.; Rao, G.M. High density oxidative plasma unzipping of multiwall carbon nanotubes. *RSC Advances,* **2017**, *7*(76), 48268-48274.
[http://dx.doi.org/10.1039/C7RA04318J]

[53] Dimiev, A.M.; Khannanov, A.; Vakhitov, I.; Kiiamov, A.; Shukhina, K.; Tour, J.M. Revisiting the mechanism of oxidative unzipping of multiwall carbon nanotubes to graphene nanoribbons. *ACS Nano,* **2018**, *12*(4), 3985-3993.
[http://dx.doi.org/10.1021/acsnano.8b01617] [PMID: 29578700]

[54] Xie, L.; Wang, H.; Jin, C.; Wang, X.; Jiao, L.; Suenaga, K.; Dai, H. Graphene nanoribbons from unzipped carbon nanotubes: atomic structures, Raman spectroscopy, and electrical properties. *J. Am. Chem. Soc.,* **2011**, *133*(27), 10394-10397.
[http://dx.doi.org/10.1021/ja203860a] [PMID: 21678963]

[55] Lee, H.J.; Lim, J.; Cho, S.Y.; Kim, H.; Lee, C.; Lee, G.Y.; Sasikala, S.P.; Yun, T.; Choi, D.S.; Jeong, M.S.; Jung, H.T.; Hong, S.; Kim, S.O. Intact crystalline semiconducting graphene nanoribbons from unzipping nitrogen-doped carbon nanotubes. *ACS Appl. Mater. Interfaces,* **2019**, *11*(41), 38006-38015.
[http://dx.doi.org/10.1021/acsami.9b08876] [PMID: 31544452]

[56] Jiao, L.; Zhang, L.; Wang, X.; Diankov, G.; Dai, H. Narrow graphene nanoribbons from carbon nanotubes. *Nature,* **2009**, *458*(7240), 877-880.
[http://dx.doi.org/10.1038/nature07919] [PMID: 19370031]

[57] Jiao, L.; Fan, B.; Xian, X.; Wu, Z.; Zhang, J.; Liu, Z. Creation of nanostructures with poly(methyl methacrylate)-mediated nanotransfer printing. *J. Am. Chem. Soc.,* **2008**, *130*(38), 12612-12613.
[http://dx.doi.org/10.1021/ja805070b] [PMID: 18763767]

[58] Li, Y.S.; Liao, J.L.; Wang, S.Y.; Chiang, W.H. Intercalation-assisted longitudinal unzipping of carbon nanotubes for green and scalable synthesis of graphene nanoribbons. *Sci. Rep.,* **2016**, *6*(1), 22755.
[http://dx.doi.org/10.1038/srep22755] [PMID: 26948486]

[59] Kosynkin, D.V.; Higginbotham, A.L.; Sinitskii, A.; Lomeda, J.R.; Dimiev, A.; Price, B.K.; Tour, J.M. Longitudinal unzipping of carbon nanotubes to form graphene nanoribbons. *Nature,* **2009**, *458*(7240), 872-876.
[http://dx.doi.org/10.1038/nature07872] [PMID: 19370030]

[60] Yang, L.; Zhang, L.; Webster, T.J. Carbon nanostructures for orthopedic medical applications. *Nanomedicine (Lond.),* **2011**, *6*(7), 1231-1244.
[http://dx.doi.org/10.2217/nnm.11.107] [PMID: 21929458]

[61] Agudosi, E.S.; Abdullah, E.C.; Numan, A.; Mubarak, N.M.; Khalid, M.; Omar, N. A review of the graphene synthesis routes and its applications in electrochemical energy storage. *Crit. Rev. Solid State Mater. Sci.,* **2020**, *45*(5), 339-377.
[http://dx.doi.org/10.1080/10408436.2019.1632793]

[62] Wu, X.; Liu, Y.; Yang, H.; Shi, Z. Large-scale synthesis of high-quality graphene sheets by an improved alternating current arc-discharge method. *RSC Advances,* **2016**, *6*(95), 93119-93124.
[http://dx.doi.org/10.1039/C6RA22273K]

[63] Pham, T.V.; Kim, J.G.; Jung, J.Y.; Kim, J.H.; Cho, H.; Seo, T.H.; Lee, H.; Kim, N.D.; Kim, M.J. High areal capacitance of n-doped graphene synthesized by arc discharge. *Adv. Funct. Mater.,* **2019**, *29*(48), 1905511.

Not be distributed or uploaded to anyone or anywhere
For personal private use only

[http://dx.doi.org/10.1002/adfm.201905511]

[64] Shojaei, T.R.; Azhari, S. *Emerging Applications of Nanoparticles and Architecture Nanostructures*; Barhoum, A.; Makhlouf, A.S.H., Eds.; Elsevier: Amsterdam, **2018**, pp. 501-531. [http://dx.doi.org/10.1016/B978-0-323-51254-1.00016-6]

[65] Russo, P.; Hu, A.; Compagnini, G.; Duley, W.W.; Zhou, N.Y. Femtosecond laser ablation of highly oriented pyrolytic graphite: a green route for large-scale production of porous graphene and graphene quantum dots. *Nanoscale,* **2014**, *6*(4), 2381-2389. [http://dx.doi.org/10.1039/C3NR05572H] [PMID: 24435549]

[66] Juvaid, M.M.; Kumar, D.; Ramachandra Rao, M.S. Realization of good quality bilayer graphene by single step laser ablation process. *Mater. Res. Bull.,* **2020**, *126*, 110840. [http://dx.doi.org/10.1016/j.materresbull.2020.110840]

[67] Staudenmaier, L. Verfahren zur Darstellung der Graphitsäure. *Ber. Dtsch. Chem. Ges.,* **1898**, *31*(2), 1481-1487. [http://dx.doi.org/10.1002/cber.18980310237]

[68] Hofmann, U.; König, E. Untersuchungen über Graphitoxyd. *Z. Anorg. Chem.,* **1937**, *234*(4), 311-336. [http://dx.doi.org/10.1002/zaac.19372340405]

[69] Hummers, W.S., Jr; Offeman, R.E. Preparation of graphitic oxide. *J. Am. Chem. Soc.,* **1958**, *80*(6), 1339. [http://dx.doi.org/10.1021/ja01539a017]

[70] Cao, N.; Zhang, Y. Study of reduced graphene oxide preparation by Hummers' method and related characterization. *J. Nanomater.,* **2015**, *2015*, 1-5. [http://dx.doi.org/10.1155/2015/168125]

[71] Alam, S.N.; Sharma, N.; Kumar, L. Synthesis of graphene oxide (GO) by modified Hummers method and its thermal reduction to obtain reduced graphene Oxide (rGO). *Graphene (Irvine, Calif.),* **2017**, *6*(1), 1-18. [http://dx.doi.org/10.4236/graphene.2017.61001]

[72] Marcano, D.C.; Kosynkin, D.V.; Berlin, J.M.; Sinitskii, A.; Sun, Z.; Slesarev, A.; Alemany, L.B.; Lu, W.; Tour, J.M. Improved synthesis of graphene oxide. *ACS Nano,* **2010**, *4*(8), 4806-4814. [http://dx.doi.org/10.1021/nn1006368] [PMID: 20731455]

[73] Chen, J.; Yao, B.; Li, C.; Shi, G. An improved Hummers method for eco-friendly synthesis of graphene oxide. *Carbon,* **2013**, *64*, 225-229. [http://dx.doi.org/10.1016/j.carbon.2013.07.055]

[74] Yu, H.; Zhang, B.; Bulin, C.; Li, R.; Xing, R. High-efficient synthesis of graphene oxide based on improved Hummers method. *Sci. Rep.,* **2016**, *6*(1), 36143. [http://dx.doi.org/10.1038/srep36143] [PMID: 27808164]

[75] Ranjan, P.; Agrawal, S.; Sinha, A.; Rao, T.R.; Balakrishnan, J.; Thakur, A.D. A low-cost non-explosive synthesis of graphene oxide for scalable applications. *Sci. Rep.,* **2018**, *8*(1), 12007. [http://dx.doi.org/10.1038/s41598-018-30613-4] [PMID: 30104689]

[76] Al-Gaashani, R.; Najjar, A.; Zakaria, Y.; Mansour, S.; Atieh, M.A. XPS and structural studies of high quality graphene oxide and reduced graphene oxide prepared by different chemical oxidation methods. *Ceram. Int.,* **2019**, *45*(11), 14439-14448. [http://dx.doi.org/10.1016/j.ceramint.2019.04.165]

[77] Liu, F.; Wang, C.; Sui, X.; Riaz, M.A.; Xu, M.; Wei, L.; Chen, Y. Synthesis of graphene materials by electrochemical exfoliation: Recent progress and future potential. *Carbon Energy,* **2019**, *1*(2), 173-199. [http://dx.doi.org/10.1002/cey2.14]

[78] Wang, H.; Fu, Q.; Pan, C. Green mass synthesis of graphene oxide and its MnO_2 composite for high performance supercapacitor. *Electrochim. Acta,* **2019**, *312*, 11-21.

Not be distributed or uploaded to anyone or anywhere
For personal private use only

[http://dx.doi.org/10.1016/j.electacta.2019.04.178]

[79] Pei, S.; Wei, Q.; Huang, K.; Cheng, H.M.; Ren, W. Green synthesis of graphene oxide by seconds timescale water electrolytic oxidation. *Nat. Commun.,* **2018**, *9*(1), 145. [http://dx.doi.org/10.1038/s41467-017-02479-z] [PMID: 29321501]

[80] Chua, C.K.; Pumera, M. The reduction of graphene oxide with hydrazine: elucidating its reductive capability based on a reaction-model approach. *Chem. Commun. (Camb.),* **2016**, *52*(1), 72-75. [http://dx.doi.org/10.1039/C5CC08170J] [PMID: 26525927]

[81] Xu, G.; Malmström, J.; Edmonds, N.; Broderick, N.; Travas-Sejdic, J.; Jin, J. Investigation of the reduction of graphene oxide by lithium triethylborohydride. *J. Nanomater.,* **2016**.

[82] Nam, K.H.; Kim, K.; Kim, S.G.; Lee, H.S.; Jung, H.; Yu, J.; Jang, S.G.; Ku, B-C.; Moon, B.; You, N-H. Sustainable production of reduced graphene oxide using elemental sulfur for multifunctional composites. *Compos., Part B Eng.,* **2019**, *176*, 107236. [http://dx.doi.org/10.1016/j.compositesb.2019.107236]

[83] Go, S.H.; Kim, H.; Yu, J.; You, N.H.; Ku, B.C.; Kim, Y.K. Synergistic effect of UV and l-ascorbic acid on the reduction of graphene oxide: Reduction kinetics and quantum chemical simulations. *Solid State Sci.,* **2018**, *84*, 120-125. [http://dx.doi.org/10.1016/j.solidstatesciences.2018.09.001]

[84] Khandelwal, M.; Kumar, A. Electrochemical behavior of glycine-mediated N-doped reduced graphene oxide. *New J. Chem.,* **2017**, *41*(16), 8333-8340. [http://dx.doi.org/10.1039/C7NJ01662J]

[85] Narayanan, K.B.; Kim, H.D.; Han, S.S. Biocompatibility and hemocompatibility of hydrothermally derived reduced graphene oxide using soluble starch as a reducing agent. *Colloids Surf. B Biointerfaces,* **2020**, *185*, 110579. [http://dx.doi.org/10.1016/j.colsurfb.2019.110579] [PMID: 31689675]

[86] Xu, L.Q.; Liao, Y.B.; Li, N.N.; Li, Y.J.; Zhang, J.Y.; Wang, Y.B.; Hu, X.F.; Li, C.M. Vancomycin-assisted green synthesis of reduced graphene oxide for antimicrobial applications. *J. Colloid Interface Sci.,* **2018**, *514*, 733-739. [http://dx.doi.org/10.1016/j.jcis.2018.01.014] [PMID: 29316529]

[87] Luo, F.; Wu, K.; Shi, J.; Du, X.; Li, X.; Yang, L.; Lu, M. Green reduction of graphene oxide by polydopamine to a construct flexible film: superior flame retardancy and high thermal conductivity. *J. Mater. Chem. A Mater. Energy Sustain.,* **2017**, *5*(35), 18542-18550. [http://dx.doi.org/10.1039/C7TA04740A]

[88] Ahmad, S.; Ahmad, A.; Khan, S.; Ahmad, S.; Khan, I.; Zada, S.; Fu, P. Algal extracts based biogenic synthesis of reduced graphene oxides (rGO) with enhanced heavy metals adsorption capability. *J. Ind. Eng. Chem.,* **2019**, *72*, 117-124. [http://dx.doi.org/10.1016/j.jiec.2018.12.009]

[89] Kalathil, S.; Katuri, K.P.; Alazmi, A.S.; Pedireddy, S.; Kornienko, N.; Costa, P.M.F.J.; Saikaly, P.E. Bioinspired synthesis of reduced graphene oxide-wrapped *Geobacter sulfurreducens* as a hybrid electrocatalyst for efficient oxygen evolution reaction. *Chem. Mater.,* **2019**, *31*(10), 3686-3693. [http://dx.doi.org/10.1021/acs.chemmater.9b00394]

[90] Hou, D.; Liu, Q.; Wang, X.; Quan, Y.; Qiao, Z.; Yu, L.; Ding, S. Facile synthesis of graphene *via* reduction of graphene oxide by artemisinin in ethanol. *Journal of Materiomics,* **2018**, *4*(3), 256-265. [http://dx.doi.org/10.1016/j.jmat.2018.01.002]

[91] Vatandost, E.; Ghorbani-HasanSaraei, A.; Chekin, F.; Naghizadeh Raeisi, S.; Shahidi, S.A. Green tea extract assisted green synthesis of reduced graphene oxide: Application for highly sensitive electrochemical detection of sunset yellow in food products. *Food Chem. X,* **2020**, *6*, 100085. [http://dx.doi.org/10.1016/j.fochx.2020.100085] [PMID: 32577617]

[92] Bhattacharya, G.; Sas, S.; Wadhwa, S.; Mathur, A.; McLaughlin, J.; Roy, S.S. *Aloe vera* assisted facile

green synthesis of reduced graphene oxide for electrochemical and dye removal applications. *RSC Advances,* **2017**, *7*(43), 26680-26688.
[http://dx.doi.org/10.1039/C7RA02828H]

[93] Reduced Graphene Oxide: Properties, Applications and Production Methods. *AZoNano,* https://www.azonano.com/article.aspx?ArticleID=4041

[94] Silipigni, L.; Salvato, G.; Di Marco, G.; Fazio, B.; Torrisi, A.; Cutroneo, M.; Torrisi, L. Band-like transport in high vacuum thermal reduced graphene oxide films. *Vacuum,* **2019**, *165*, 254-261.
[http://dx.doi.org/10.1016/j.vacuum.2019.04.025]

[95] Tian, S.; Sun, J.; Yang, S.; He, P.; Ding, S.; Ding, G.; Xie, X. Facile thermal annealing of graphite oxide in air for graphene with a higher C/O ratio. *RSC Advances,* **2015**, *5*(85), 69854-69860.
[http://dx.doi.org/10.1039/C5RA09388K]

[96] Sofer, Z.; Jankovský, O.; Šimek, P.; Sedmidubský, D.; Šturala, J.; Kosina, J.; Mikšová, R.; Macková, A.; Mikulics, M.; Pumera, M. Insight into the mechanism of the thermal reduction of graphite oxide: deuterium-labeled graphite oxide is the key. *ACS Nano,* **2015**, *9*(5), 5478-5485.
[http://dx.doi.org/10.1021/acsnano.5b01463] [PMID: 25894311]

[97] Kumar, R.; Kumar, R.M.; Lahiri, D.; Lahiri, I. Thermally reduced graphene oxide film on soda lime glass as transparent conducting electrode. *Surf. Coat. Tech.,* **2017**, *309*, 931-937.
[http://dx.doi.org/10.1016/j.surfcoat.2016.10.060]

[98] Schniepp, H.C.; Li, J.L.; McAllister, M.J.; Sai, H.; Herrera-Alonso, M.; Adamson, D.H.; Prud'homme, R.K.; Car, R.; Saville, D.A.; Aksay, I.A. Functionalized single graphene sheets derived from splitting graphite oxide. *J. Phys. Chem. B,* **2006**, *110*(17), 8535-8539.
[http://dx.doi.org/10.1021/jp060936f] [PMID: 16640401]

[99] Li, X.; Wang, H.; Robinson, J.T.; Sanchez, H.; Diankov, G.; Dai, H. Simultaneous nitrogen doping and reduction of graphene oxide. *J. Am. Chem. Soc.,* **2009**, *131*(43), 15939-15944.
[http://dx.doi.org/10.1021/ja907098f] [PMID: 19817436]

[100] Agusu, L.; Ahmad, L.O.; Anggara, D.; Alimin, ; Mitsudo, S.; Fujii, Y.; Kikuchi, H. Alimin, Mitsudo, S.; Fujii, Y.; Kikuchi, H. Microwave hydrothermal synthesis of reduced graphene oxide: effects of microwave power and irradiation time. *J. Phys. Conf. Ser.,* **2018**, *1011*, 012012.
[http://dx.doi.org/10.1088/1742-6596/1011/1/012012]

[101] Umrao, S.; Gupta, T.K.; Kumar, S.; Singh, V.K.; Sultania, M.K.; Jung, J.H.; Oh, I.K.; Srivastava, A. Microwave-assisted synthesis of boron and nitrogen co-doped reduced graphene oxide for the protection of electromagnetic radiation in Ku-band. *ACS Appl. Mater. Interfaces,* **2015**, *7*(35), 19831-19842.
[http://dx.doi.org/10.1021/acsami.5b05890] [PMID: 26287816]

[102] Wu, J.; Zhao, J.; Vaidhyanathan, B.; Zhang, H.; Anshuman, A.; Nare, A.; Saremi-Yarahmadi, S. Rapid microwave-assisted bulk production of high-quality reduced graphene oxide for lithium ion batteries. *Materialia (Oxf.),* **2020**, *13*, 100833.
[http://dx.doi.org/10.1016/j.mtla.2020.100833]

[103] Iskandar, F.; Hikmah, U.; Stavila, E.; Aimon, A.H. Microwave-assisted reduction method under nitrogen atmosphere for synthesis and electrical conductivity improvement of reduced graphene oxide (rGO). *RSC Advances,* **2017**, *7*(83), 52391-52397.
[http://dx.doi.org/10.1039/C7RA10013B]

[104] Mohandoss, M.; Gupta, S.S.; Nelleri, A.; Pradeep, T.; Maliyekkal, S.M. Solar mediated reduction of graphene oxide. *RSC Advances,* **2017**, *7*(2), 957-963.
[http://dx.doi.org/10.1039/C6RA24696F]

[105] He, X.; Zhang, S.; Pan, H.; Chen, J.; Xu, J. Horizontally aggregation of monolayer reduced graphene oxide under deep UV irradiation in solution. *Nanoscale Res. Lett.,* **2019**, *14*(1), 117.
[http://dx.doi.org/10.1186/s11671-019-2940-z] [PMID: 30941577]

Not be distributed or uploaded to anyone or anywhere
For personal private use only

[106] Hasani, A.; Dehsari, H.S.; Zarandi, A.A.; Salehi, A.; Taromi, F.A.; Kazeroni, H. Visible light-assisted photoreduction of graphene oxide using CdS nanoparticles and gas sensing properties. *J. Nanomater,* **2015**.

[107] Low, M.J.; Lee, H.; Lim, C.H.J.; Suchand Sandeep, C.S.; Murukeshan, V.M.; Kim, S.W.; Kim, Y.J. Laser-induced reduced-graphene-oxide micro-optics patterned by femtosecond laser direct writing. *Appl. Surf. Sci.,* **2020**, *526*, 146647.
[http://dx.doi.org/10.1016/j.apsusc.2020.146647]

[108] Feng, X.; Chen, W.; Yan, L. Electrochemical reduction of bulk graphene oxide materials. *RSC Advances,* **2016**, *6*(83), 80106-80113.
[http://dx.doi.org/10.1039/C6RA17469H]

[109] Tong, H.; Zhu, J.; Chen, J.; Han, Y.; Yang, S.; Ding, B.; Zhang, X. Electrochemical reduction of graphene oxide and its electrochemical capacitive performance. *J. Solid State Electrochem.,* **2013**, *17*(11), 2857-2863.
[http://dx.doi.org/10.1007/s10008-013-2195-z]

[110] Nia, P.M.; Abouzari-Lotf, E.; Arshad, A.; Nasef, M.M.; Ripin, A. Tunable electrochemical approach for reduction of graphene oxide: Taguchi-assisted chemical and structural optimization. *J. Electrochem. Soc.,* **2018**, *165*(9), E429-E438.
[http://dx.doi.org/10.1149/2.0031810jes]

[111] Ray, S.C. *Applications of Graphene and Graphene-Oxide Based Nanomaterials,* 1st ed; Elsevier Science: Amsterdam, **2015**.

[112] Dubin, S.; Gilje, S.; Wang, K.; Tung, V.C.; Cha, K.; Hall, A.S.; Farrar, J.; Varshneya, R.; Yang, Y.; Kaner, R.B. A one-step, solvothermal reduction method for producing reduced graphene oxide dispersions in organic solvents. *ACS Nano,* **2010**, *4*(7), 3845-3852.
[http://dx.doi.org/10.1021/nn100511a] [PMID: 20586422]

[113] Kim, S.; Choi, K.; Park, S. Solvothermal reduction of graphene oxide in dimethylformamide. *Solid State Sci.,* **2016**, *61*, 40-43.
[http://dx.doi.org/10.1016/j.solidstatesciences.2016.07.013]

[114] Mikhaylov, P.A.; Levin, I.S.; Lubenchenko, A.V.; Bondarenko, G.N.; Kulichihin, V.G. Ultrasonication-assisted ultrafast solvothermal reduction of graphene oxide. *IOP Conf. Ser.: Mater. Sci. Eng.,* 525 012039. **2019**.
[http://dx.doi.org/10.1088/1757-899X/525/1/012039]

[115] Torres, D.; Arcelus-Arrillaga, P.; Millan, M.; Pinilla, J.; Suelves, I. Enhanced reduction of few-layer graphene oxide *via* supercritical water gasification of glycerol. *Nanomaterials (Basel),* **2017**, *7*(12), 447.
[http://dx.doi.org/10.3390/nano7120447] [PMID: 29240720]

[116] Zheng, X.; Peng, Y.; Yang, Y.; Chen, J.; Tian, H.; Cui, X.; Zheng, W. Hydrothermal reduction of graphene oxide; effect on surface-enhanced Raman scattering. *J. Raman Spectrosc.,* **2017**, *48*(1), 97-103.
[http://dx.doi.org/10.1002/jrs.4998]

[117] Hayes, W.I.; Joseph, P.; Mughal, M.Z.; Papakonstantinou, P. Production of reduced graphene oxide *via* hydrothermal reduction in an aqueous sulphuric acid suspension and its electrochemical behaviour. *J. Solid State Electrochem.,* **2015**, *19*(2), 361-380.
[http://dx.doi.org/10.1007/s10008-014-2560-6]

[118] Wei, M.; Qiao, L.; Zhang, H.; Karakalos, S.; Ma, K.; Fu, Z.; Swihart, M.T.; Wu, G. Engineering reduced graphene oxides with enhanced electrochemical properties through multiple-step reductions. *Electrochim. Acta,* **2017**, *258*, 735-743.
[http://dx.doi.org/10.1016/j.electacta.2017.11.120]

[119] Lin, Y.; Hou, G.; Bi, S.; Su, X.; Li, H. Synthesis of reduced graphene oxide paper for EMI shielding

Not be distributed or uploaded to anyone or anywhere
For personal private use only

by a multi-step process. *Funct. Mater. Lett. (Singap.),* **2020**, *13*(5), 2051024.
[http://dx.doi.org/10.1142/S1793604720510248]

[120] Suraya Abdul Rashid, Tongling Tan. Recent Development on the Synthesis Techniques and Properties of Graphene Derivatives. In: *Synthesis, Technology and Applications of Carbon Nanomaterials*; Rashid, S.A.; Othman, R.N.I.R.; Hussein, M.Z., Eds. Elsevier: Amsterdam, **2019**; pp. 77-107.
[http://dx.doi.org/10.1016/B978-0-12-815757-2.00004-8]

[121] Martin, P.M. *Handbook of Deposition Technologies for Films and Coatings,* 3rd ed; William Andrew Publishing: New York, **2010**.

[122] Reinke, M.; Kuzminykh, Y.; Hoffmann, P. Low temperature chemical vapour deposition using atomic layer deposition chemistry. *Chem. Mater.,* **2015**, *27*(5), 1604-1611.
[http://dx.doi.org/10.1021/cm504216p]

[123] Fujita, J.; Hiyama, T.; Hirukawa, A.; Kondo, T.; Nakamura, J.; Ito, S.; Araki, R.; Ito, Y.; Takeguchi, M.; Pai, W.W. Near room temperature chemical vapor deposition of graphene with diluted methane and molten gallium catalyst. *Sci. Rep.,* **2017**, *7*(1), 12371.
[http://dx.doi.org/10.1038/s41598-017-12380-w] [PMID: 28959046]

[124] Jeong, H.; Hwang, W.T.; Song, Y.; Kim, J.K.; Kim, Y.; Hihath, J.; Chung, S.; Lee, T. Highly uniform monolayer graphene synthesis *via* a facile pretreatment of copper catalyst substrates using an ammonium persulfate solution. *RSC Advances,* **2019**, *9*(36), 20871-20878.
[http://dx.doi.org/10.1039/C9RA02689D] [PMID: 35515571]

[125] Seo, D.H.; Pineda, S.; Fang, J.; Gozukara, Y.; Yick, S.; Bendavid, A.; Lam, S.K.H.; Murdock, A.T.; Murphy, A.B.; Han, Z.J.; Ostrikov, K. Single-step ambient-air synthesis of graphene from renewable precursors as electrochemical genosensor. *Nat. Commun.,* **2017**, *8*(1), 14217.
[http://dx.doi.org/10.1038/ncomms14217] [PMID: 28134336]

[126] Strupinski, W.; Grodecki, K.; Wysmolek, A.; Stepniewski, R.; Szkopek, T.; Gaskell, P.E.; Grüneis, A.; Haberer, D.; Bozek, R.; Krupka, J.; Baranowski, J.M. Graphene epitaxy by chemical vapor deposition on SiC. *Nano Lett.,* **2011**, *11*(4), 1786-1791.
[http://dx.doi.org/10.1021/nl200390e] [PMID: 21438581]

[127] Tang, S.; Wang, H.; Wang, H.S.; Sun, Q.; Zhang, X.; Cong, C.; Xie, H.; Liu, X.; Zhou, X.; Huang, F.; Chen, X.; Yu, T.; Ding, F.; Xie, X.; Jiang, M. Silane-catalysed fast growth of large single-crystalline graphene on hexagonal boron nitride. *Nat. Commun.,* **2015**, *6*(1), 6499.
[http://dx.doi.org/10.1038/ncomms7499] [PMID: 25757864]

[128] Hwang, J.; Kim, M.; Cha, H.Y.; Spencer, M.G.; Lee, J.W. Metal free growth of graphene on quartz substrate using chemical vapor deposition (CVD). *J. Nanosci. Nanotechnol.,* **2014**, *14*(4), 2979-2983.
[http://dx.doi.org/10.1166/jnn.2014.8583] [PMID: 24734720]

[129] Zhou, L.; Wei, S.; Ge, C.; Zhao, C.; Guo, B.; Zhang, J.; Zhao, J. Ultrafast growth of uniform multi-layer graphene films directly on silicon dioxide substrates. *Nanomaterials (Basel),* **2019**, *9*(7), 964.
[http://dx.doi.org/10.3390/nano9070964] [PMID: 31266221]

[130] Min, B.H.; Kim, D.W.; Kim, K.H.; Choi, H.O.; Jang, S.W.; Jung, H.T. Bulk scale growth of CVD graphene on Ni nanowire foams for a highly dense and elastic 3D conducting electrode. *Carbon,* **2014**, *80*, 446-452.
[http://dx.doi.org/10.1016/j.carbon.2014.08.084]

[131] Lee, X.J.; Hiew, B.Y.Z.; Lai, K.C.; Lee, L.Y.; Gan, S.; Thangalazhy-Gopakumar, S.; Rigby, S. Review on graphene and its derivatives: Synthesis methods and potential industrial implementation. *J. Taiwan Inst. Chem. Eng.,* **2019**, *98*, 163-180.
[http://dx.doi.org/10.1016/j.jtice.2018.10.028]

[132] Singh, S.; Chen, X.; Zhang, C.; Gautam, R.K.; Tyagi, R.; Luo, J. Nickel-catalyzed direct growth of graphene on bearing steel (GCr15) by thermal chemical vapor deposition and its tribological behavior. *Appl. Surf. Sci.,* **2020**, *502*, 144135.
[http://dx.doi.org/10.1016/j.apsusc.2019.144135]

Not be distributed or uploaded to anyone or anywhere
For personal private use only

[133] Regmi, M.; Chisholm, M.F.; Eres, G. The effect of growth parameters on the intrinsic properties of large-area single layer graphene grown by chemical vapor deposition on Cu. *Carbon,* **2012**, *50*(1), 134-141.
[http://dx.doi.org/10.1016/j.carbon.2011.07.063]

[134] Muñoz, R.; Martínez, L.; López-Elvira, E.; Munuera, C.; Huttel, Y.; García-Hernández, M. Direct synthesis of graphene on silicon oxide by low temperature plasma enhanced chemical vapor deposition. *Nanoscale,* **2018**, *10*(26), 12779-12787.
[http://dx.doi.org/10.1039/C8NR03210F] [PMID: 29946620]

[135] Sze, S.M.; Ng, K.K. *Physics of Semiconductor Devices,* 3rd ed; John Wiley & Sons: New York, **1981**.

[136] Capper, P.; Irvine, S.; Joyce, T. Epitaxial Crystal Growth: Methods and Materials. In: *Springer Handbook of Electronic and Photonic Materials*; Kasap, S.; Capper, P., Eds.; Springer: Cham, New York, **2017**.
[http://dx.doi.org/10.1007/978-3-319-48933-9_14]

[137] Briggs, N.; Gebeyehu, Z.M.; Vera, A.; Zhao, T.; Wang, K.; De La Fuente Duran, A.; Bersch, B.; Bowen, T.; Knappenberger, K.L., Jr; Robinson, J.A. Epitaxial graphene/silicon carbide intercalation: a minireview on graphene modulation and unique 2D materials. *Nanoscale,* **2019**, *11*(33), 15440-15447.
[http://dx.doi.org/10.1039/C9NR03721G] [PMID: 31393495]

[138] Mishra, N.; Boeckl, J.; Motta, N.; Iacopi, F. Graphene growth on silicon carbide: A review (Phys. Status Solidi A 9/2016). *Phys. Status Solidi., A Appl. Mater. Sci.,* **2016**, *213*(9), 2269-2289.
[http://dx.doi.org/10.1002/pssa.201670657]

[139] Riedl, C.; Coletti, C.; Starke, U. Structural and electronic properties of epitaxial graphene on SiC(0 0 0 1): a review of growth, characterization, transfer doping and hydrogen intercalation. *J. Phys. D Appl. Phys.,* **2010**, *43*(37), 374009.
[http://dx.doi.org/10.1088/0022-3727/43/37/374009]

[140] Lalmi, B.; Girard, J.C.; Pallecchi, E.; Silly, M.; David, C.; Latil, S.; Sirotti, F.; Ouerghi, A. Flower-shaped domains and wrinkles in trilayer epitaxial graphene on silicon carbide. *Sci. Rep.,* **2015**, *4*(1), 4066.
[http://dx.doi.org/10.1038/srep04066] [PMID: 24513669]

[141] Xu, X.; Zhang, Z.; Dong, J.; Yi, D.; Niu, J.; Wu, M.; Lin, L.; Yin, R.; Li, M.; Zhou, J.; Wang, S.; Sun, J.; Duan, X.; Gao, P.; Jiang, Y.; Wu, X.; Peng, H.; Ruoff, R.S.; Liu, Z.; Yu, D.; Wang, E.; Ding, F.; Liu, K. Ultrafast epitaxial growth of metre-sized single-crystal graphene on industrial Cu foil. *Sci. Bull. (Beijing),* **2017**, *62*(15), 1074-1080.
[http://dx.doi.org/10.1016/j.scib.2017.07.005]

[142] Wade, T.L.; Wegrowe, J.E. Template synthesis of nanomaterials. *Eur. Phys. J. Appl. Phys.*, **2005**, *29*(1), 3-22.
[http://dx.doi.org/10.1051/epjap:2005001]

[143] Lu, A.H.; Schuth, F. Nanocasting: A versatile strategy for creating nanostructured porous materials. *Adv. Mater,* **2006**, 179-1805.

[144] Liang, C.; Li, Z.; Dai, S. Mesoporous carbon materials: synthesis and modification. *Angew. Chem. Int. Ed.,* **2008**, *47*(20), 3696-3717.
[http://dx.doi.org/10.1002/anie.200702046] [PMID: 18350530]

[145] Lei, L.; Wu, Z.; Liu, H.; Qin, Z.; Chen, C.; Luo, L.; Wang, G.; Fan, W.; Wang, J. A facile method for the synthesis of graphene-like 2D metal oxides and their excellent catalytic application in the hydrogenation of nitroarenes. *J. Mater. Chem. A Mater. Energy Sustain.,* **2018**, *6*(21), 9948-9961.
[http://dx.doi.org/10.1039/C8TA02338G]

[146] Huang, X.; Sun, B.; Su, D.; Zhao, D.; Wang, G. Soft-template synthesis of 3D porous graphene foams with tunable architectures for lithium–O_2 batteries and oil adsorption applications. *J. Mater. Chem. A Mater. Energy Sustain.,* **2014**, *2*(21), 7973-7979.

[http://dx.doi.org/10.1039/C4TA00829D]

[147] von Kugelgen, S.; Piskun, I.; Griffin, J.H.; Eckdahl, C.T.; Jarenwattananon, N.N.; Fischer, F.R. Templated synthesis of end-functionalized graphene nanoribbons through living ring-opening alkyne metathesis polymerization. *J. Am. Chem. Soc.,* **2019**, *141*(28), 11050-11058.
[http://dx.doi.org/10.1021/jacs.9b01805] [PMID: 31264864]

[148] Yang, Y.; Liu, R.; Wu, J.; Jiang, X.; Cao, P.; Hu, X.; Pan, T.; Qiu, C.; Yang, J.; Song, Y.; Wu, D.; Su, Y. Bottom-up fabrication of graphene on silicon/silica substrate *via* a facile soft-hard template approach. *Sci. Rep.,* **2015**, *5*(1), 13480.
[http://dx.doi.org/10.1038/srep13480] [PMID: 26311022]

[149] Huang, X.; Zhao, Y.; Ao, Z.; Wang, G. Micelle-template synthesis of nitrogen-doped mesoporous graphene as an efficient metal-free electrocatalyst for hydrogen production. *Sci. Rep.,* **2015**, *4*(1), 7557.
[http://dx.doi.org/10.1038/srep07557] [PMID: 25523276]

[150] Wang, F.; Wang, F.; Hong, R.; Lv, X.; Zheng, Y.; Chen, H. High-purity few-layer graphene from plasma pyrolysis of methane as conductive additive for $LiFePO_4$ lithium ion battery. *J. Mater. Res. Technol.,* **2020**, *9*(5), 10004-10015.
[http://dx.doi.org/10.1016/j.jmrt.2020.06.072]

[151] Hong, N.; Yang, W.; Bao, C.; Jiang, S.; Song, L.; Hu, Y. Facile synthesis of graphene by pyrolysis of poly(methyl methacrylate) on nickel particles in the confined microzones. *Mater. Res. Bull.,* **2012**, *47*(12), 4082-4088.
[http://dx.doi.org/10.1016/j.materresbull.2012.08.049]

[152] Perednis, D.; Gauckler, L.J. Thin film deposition using spray pyrolysis. *J. Electroceram.,* **2005**, *14*(2), 103-111.
[http://dx.doi.org/10.1007/s10832-005-0870-x]

[153] Zou, B.; Wang, X.X.; Huang, X.X.; Wang, J.N. Continuous synthesis of graphene sheets by spray pyrolysis and their use as catalysts for fuel cells. *Chem. Commun. (Camb.),* **2015**, *51*(4), 741-744.
[http://dx.doi.org/10.1039/C4CC08197H] [PMID: 25421428]

[154] Sun, Y.; Zhang, J. Strategies for scalable gas-phase preparation of free-standing graphene. *CCS Chem.,* **2020**, *2*, 1058-1077.

[155] Dato, A.; Radmilovic, V.; Lee, Z.; Phillips, J.; Frenklach, M. Substrate-free gas-phase synthesis of graphene sheets. *Nano Lett.,* **2008**, *8*(7), 2012-2016.
[http://dx.doi.org/10.1021/nl8011566] [PMID: 18529034]

[156] Liu, F.; Zhang, Y. Substrate-free synthesis of large area, continuous multi-layer graphene film. *Carbon,* **2010**, *48*(9), 2394-2400.
[http://dx.doi.org/10.1016/j.carbon.2010.02.033]

[157] Choi, W.; Lee, J. *Graphene: Synthesis and applications*; CRC Press: Ohio, **2016**.
[http://dx.doi.org/10.1201/b11259]

[158] Zheng, Q.; Kim, J-K. Synthesis, structure, and properties of graphene and graphene oxide. In: *Graphene for transparent conductors: synthesis, properties and applications*; Springer: New York, **2015**; pp. 29-94.
[http://dx.doi.org/10.1007/978-1-4939-2769-2_2]

[159] Narita, A.; Wang, X.Y.; Feng, X.; Müllen, K. New advances in nanographene chemistry. *Chem. Soc. Rev.,* **2015**, *44*(18), 6616-6643.
[http://dx.doi.org/10.1039/C5CS00183H] [PMID: 26186682]

[160] Vo, T.H.; Perera, U.G.E.; Shekhirev, M.; Mehdi Pour, M.; Kunkel, D.A.; Lu, H.; Gruverman, A.; Sutter, E.; Cotlet, M.; Nykypanchuk, D.; Zahl, P.; Enders, A.; Sinitskii, A.; Sutter, P. Axel Enders, Sinitskii, A.; Sutter, P. Nitrogen-doping induced self-assembly of graphene nanoribbon-based two-dimensional and three-dimensional metamaterials. *Nano Lett.,* **2015**, *15*(9), 5770-5777.

[http://dx.doi.org/10.1021/acs.nanolett.5b01723] [PMID: 26258628]

[161] Dichtel, W.R.; Arslan, H.; Uribe-Romo, F.J. Graphene nanoribbons derived from poly(phenylene ethynylene) polymer, methods of making same, and uses thereof. **2017**.

[162] Asao, N.; Nogami, T.; Lee, S.; Yamamoto, Y. Lewis acid-catalyzed benzannulation *via* unprecedented [4+2] cycloaddition of o-alkynyl(oxo)benzenes and enynals with alkynes. *J. Am. Chem. Soc.,* **2003**, *125*(36), 10921-10925.
[http://dx.doi.org/10.1021/ja036927r] [PMID: 12952473]

[163] Sharma, D.; Kanchi, S.; Bisetty, K. Biogenic synthesis of nanoparticles: A review. *Arab. J. Chem.,* **2019**, *12*(8), 3576-3600.
[http://dx.doi.org/10.1016/j.arabjc.2015.11.002]

[164] Noorunnisa Khanam, P.; Hasan, A. Biosynthesis and characterization of graphene by using non-toxic reducing agent from *Allium Cepa* extract: Anti-bacterial properties. *Int. J. Biol. Macromol.,* **2019**, *126*, 151-158.
[http://dx.doi.org/10.1016/j.ijbiomac.2018.12.213] [PMID: 30584937]

[165] Gurunathan, S.; Han, J.W.; Eppakayala, V.; Kim, J.H. Microbial reduction of graphene oxide by *Escherichia coli*: A green chemistry approach. *Colloids Surf. B Biointerfaces,* **2013**, *102*, 772-777.
[http://dx.doi.org/10.1016/j.colsurfb.2012.09.011] [PMID: 23107955]

Not be distributed or uploaded to anyone or anywhere
For personal private use only

CHAPTER 4

Characterization Techniques for Graphene-Based Materials

Vickramjeet Singh[1] and **Ramesh L. Gardas**[2,*]

[1] *Department of Chemistry, Dr B R Ambedkar National Institute of Technology, Jalandhar-144011, Punjab, India*

[2] *Department of Chemistry, Indian Institute of Technology Madras, Chennai - 600 036, India*

Abstract: Graphene bearing 2D (dimensional) layer of carbon atoms bonded in sp^2 hybridized state are only 1 atomic-scale thick. However, the graphene can be extended along the horizontal dimension. The alternate double bonds leading to perfect conjugation with sp^2 hybridization are exhibited in the hexagonal structure (*honeycomb*) of graphene. Theoretically and experimentally, the thicknesses of graphene have been determined and are in the nano-meter range. The extraordinary mechanical and electrical properties exhibited by such a 2D material have inspired scientists for device fabrication methodologies that can shift the synthesis from lab scale to large scale. It is considered the strongest material on earth, almost 100 times stronger (*i.e.*, strength) than the best steel. Since graphene is only 1 atomic-scale thick and transparent, the characterization of graphene is complex but essential. The thickness down to one atomic layer in graphene can be identified by the light interference causing color contrast. Thus, optical microscopy-based methods enable the identification of graphene or its derivatives; on the other hand, Raman spectroscopy, which is sensitive to molecular bonding and geometric structure, is commonly employed for the quality determination of graphene-based materials. In this chapter, various characterization techniques are discussed, enabling the characterization of graphene and graphene-based materials (GBMs).

Keywords: Characterization, Fourier-transform infra-red Spectroscopy (FT-IR), Graphene, Graphene Sayers, Graphene Oxide, Optical Microscopy, Raman Spectroscopy, Reduced Graphene Oxide, Scanning Tunneling Microscope (STM), Transmission Electron Microscope (TEM), X-ray Shotoelectron Spectroscopy (XPS).

[*] **Corresponding author Ramesh L. Gardas:** Department of Chemistry, Indian Institute of Technology Madras, Chennai - 600 036, India; E-mail:gardas@iitm.ac.in

Pinki Bala Punjabi, Rakshit Ameta & Sharoni Gupta (Eds.)
All rights reserved-© 2023 Bentham Science Publishers

1. INTRODUCTION

Graphene is a 2D nano crystallite material composed of a single carbon atom layer packed in a hexagonal arrangement (honeycomb) with alternating single and double bonds [1, 2]. The sp^2 hybridized state of carbon atoms has π-bonds (out-o--plane) responsible for conduction (delocalized π-electrons) and weak interaction between graphene layers [1, 2]. The strongest bond in this carbon allotrope is the in-plane C-C bond [2, 3]. The graphene is thus a 2D semiconductor with zero band gaps or nil band gap energy, *i.e.*, having a minor overlap among the conduction and valence bands [2, 4]. While maintaining the sp^2 hybridization, graphene sheets can be rolled up to make materials with dimensions as 3 D (graphite), 1 D (nanotubes), and 0D (fullerenes) [5]. Since graphene is 1 atomic layer thick, the first report of graphene discovery (structural analysis) was still based on optical microscopy [4, 6]. The ease of analysis by the visualization using an optical microscope is possible for graphene synthesized by mechanical peeling and transferred on a few layers of thick SiO_2 (onto a silicon surface) [6]; however, when deposited on cleaned Si surfaces, this visualization of graphene is lost [6]. The graphene-based materials (GBMs) can be single or multi-layered, graphene oxide, graphene reduced oxide, graphene ribbons, and graphene nano sheets [1, 6, 7]. Graphene with various layers or GBMs can be characterized by a number of techniques, and in this chapter following techniques are being discussed:

1. Optical Microscopic techniques

2. Raman Spectroscopy

3. FT-IR Spectroscopy

4. X-ray Photoelectron Spectroscopy

5. Thermogravimetric Analysis

2. OPTICAL METHODS

As mentioned above, optical methods can be used to characterise graphene synthesized by mechanical peeling unless the graphene is pasted onto a clean Si substrate [6]. The graphene layers onto a SiO_2 substrate can cause light interferences, so the color and the contrast depend upon graphene layers [3, 6, 8, 9]. Besides SiO_2-based surfaces, other substrates for supporting graphene layers that can be visibility distinct are polymethylmethacrylate and silicon nitrite (Si_3N_4) [3, 6, 8, 9]. Mechanical exfoliation may form flakes of various thicknesses; the image of graphite on SiO_2 substrate (oxide thickness of 500 nm)

Not be distributed or uploaded to anyone or anywhere For personal private use only

is shown in Fig. (**1**) [8]. Besides the optical image, the SEM (scanning electron microscope) and AFM (atomic force microscope) images are also shown in Fig. **1 b** and **c**, respectively. The picture shows the regions having varied thicknesses [8]. The rectangular box (broken lines) in these images indicates the region with a few monolayer thicknesses. The images can be resolved to get a better picture with an electron microscope, such as SEM with better electron detectors [8].

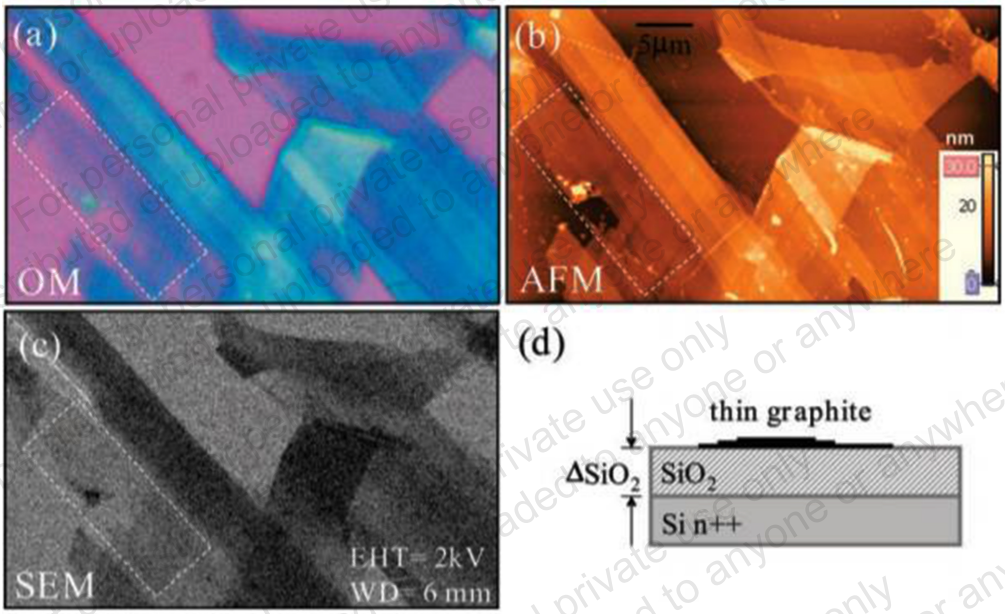

Fig. (1). The image of graphite flake having regions with different thicknesses, as obtained from **(a)** optical microscope (OM), **b)** AFM, **c)** SEM. The graphite was deposited on a Si substrate with a SiO_2 thickness of about 500 nm. Reprinted (adapted) with permission from ref [8]. Copyright (2007) American Chemical Society.

The AFM analysis can directly identify the layer number of graphene, but this technique can damage the crystal lattice while performing the measurement, and the true thickness cannot be estimated [10]. Ni *et al*. [10] developed a method based on contrasting graphene and the substrate onto which graphene layers were transferred. The light reflection makes graphene visible from ten layers down to one layer. Furthermore, experimental data were correlated with theoretical analysis and a good agreement was reported [10]. An analytical expression for determining the number of graphene layers was also provided [10]. Blake *et al*. [3] represented the optical microscopic images of graphene transferred onto the SiO_2 layer. It was demonstrated that the optically visualized contrast depends upon the opacity of graphene and the optical path, that is, the dependence on the SiO_2 layer as well as light wavelength [3]. The images of graphene obtained under

normal light illumination on SiO_2 layers (200 nm and 300 nm) are shown in Fig. (**2**) [3]. It was demonstrated from the images that contrast could be employed as a tool to quantitatively define the number of graphene layers deposited on a suitable substrate (in this case, a Si wafer) [3]. Moreover, the color contrast at different wavelengths of light and SiO_2 thickness is also shown in Fig. (**3**) [3]. The Fresnel theory was applied to show that by using appropriate filters, the contrast could be enhanced for various SiO_2 thicknesses [3].

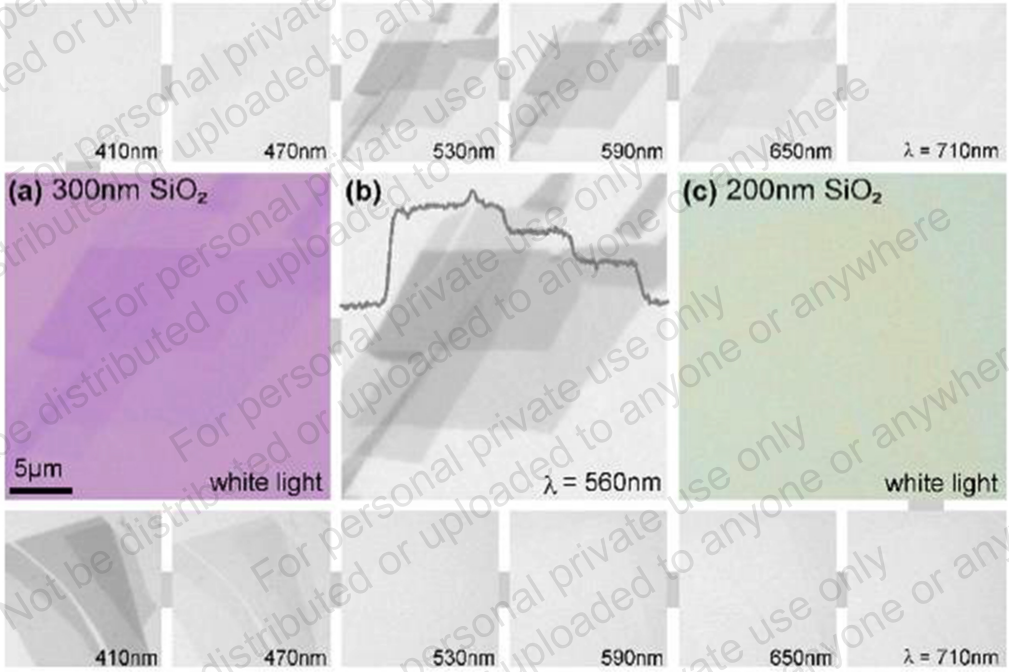

Fig. (2). The images of graphene crystallites **(a)** deposited onto Si wafer (SiO_2 thickness was 300 nm) obtained using normal white light, **(b)** deposited onto Si wafer (SiO_2 thickness was 300 nm) obtained using green light and **(c)** deposited onto SiO_2 (thickness 200 nm) obtained using normal white light, here in image **(c)** graphene is not visible. The images shown above and below those of a, b and c were taken by illumination through various narrow-band filters [3]. Reproduced from ref [3], with the permission of AIP Publishing.

Mechanically exfoliated graphene deposited on SiO_2 (300 nm thickness) was also observed using an optical microscope along with a scanning force microscopy (SFM) micrograph for the selected flakes, as reported previously [11]. The color and contrast were qualitatively correlated to the intensity of light (white to blue to violet light). The number of layers with an uncertainty of ± 1 layer estimated from SFM analysis; the uncertainty arises due to surface roughness and the difference in height between the first layer and the substrate [11]. A methodology was developed by Jia *et al*. [12] by which graphene domains/boundaries can be

optically identified on a surface other than SiO_2 layers. The copper oxide enhances the interference, leading to color contrast, thereby making the visible detection of graphene with an optical microscope possible [12] (see Fig. **4**).

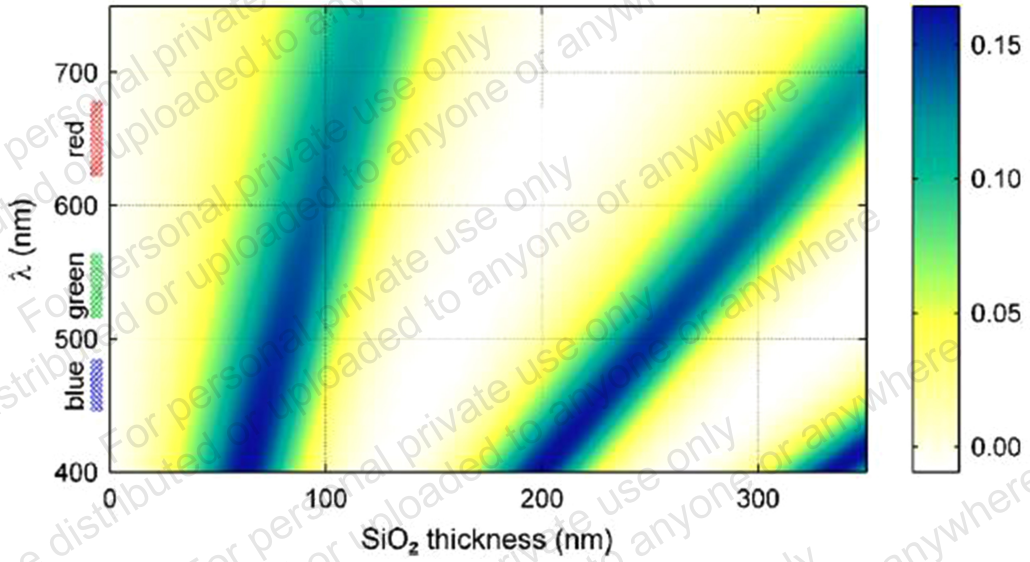

Fig. (3). The plot (colored) depicted by variation in wavelength as well as SiO_2 thickness. The scale in color on the right side depicts the expected contrast [3]. Reproduced from [3], with the permission of AIP Publishing.

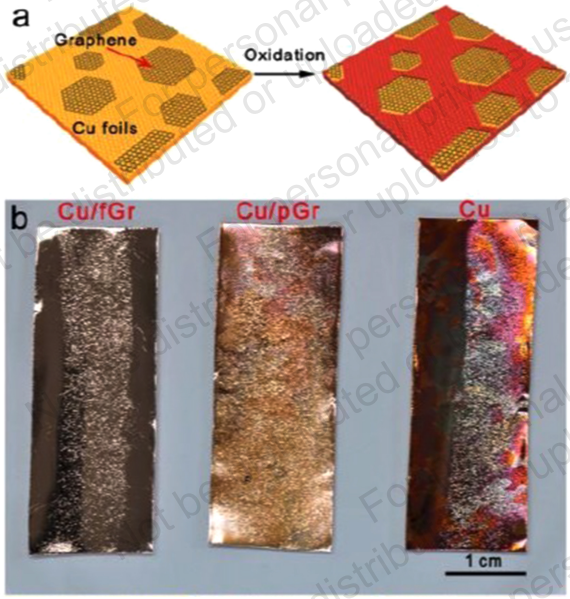

(Fig. 4) contd.....

Not be distributed or uploaded to anyone or anywhere
For personal private use only

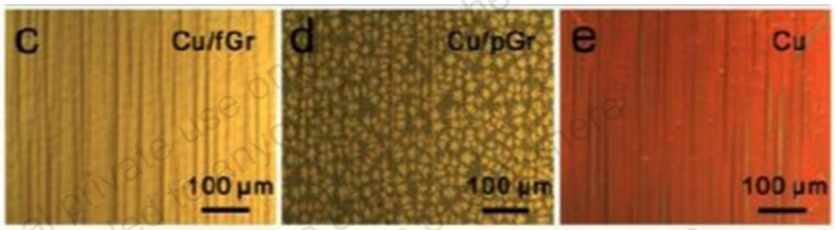

Fig. (4). The **(a)** schematic illustration of optical characterization and oxidation of graphene domains deposited on Cu substrate **(b)** pictures of Cu substate (foil) having fully grown graphene (represented as Cu/fGr), partially grown graphene (Cu/pGr), Cu without graphene after annealing at 160 ºC for 6 min. in air. The optical images of **(c)** Cu/fGr, **(d)** Cu/pGr, and **(e)** Cu foil after the annealing [12]. Reused with permission from ref [12]. under Creative Commons license.

Hong *et al*. [13] have visualized graphene deposited on Cu-foil by the area-specific atomic layer deposition (ALD) method. The optical images were shown for graphene on Cu substrate obtained by annealing at 200 ºC and with various cycles of ALD [13]. The underling Cu substrate was oxidized by water vapor, with selective deposition of single-layer graphene. The Al_2O_3 was used as a mask to cover single-layer graphene (SLG) and the area with multi-layer graphene (MLG). The MLG was removed by ion etching, and the copper substrate was thermally oxidized before visualization. The images of graphene on Cu substrate obtained by ALD as a function of time and ALD cycles were reported [13]. Overall, the process is a four-step involving chemical vapor deposition, area selective ALD, treatment with plasma, followed by thermal oxidation [13]. These combinations of surface modifications provide a way to demonstrate the spatial distribution of graphene multi-layers and control the growth and quality evaluation of graphene [13]. The multi-step process was monitored/characterized by TEM, Raman spectroscopy, and SEM [13].

Besides Cu and SiO_2, Ni surfaces have also been used for the growth of graphene multi-layers [14]. The chemical vapor deposition (CVD) method at 900 ºC was employed for graphene formation on polycrystalline as well as single Ni (111) crystals [14]. The thermal annealing rate was modulated for the growth of graphene on polycrystalline Ni. The X-ray diffraction (XRD) spectra collected from single as well as polycrystalline Ni with variable annealing rates and the optical images of graphene are shown in Fig. (**5**). Only mono- or bi-layer graphene was formed on a single Ni crystal [*i.e*., Ni (111)] due to a lack of grain boundaries (interplane) on a single crystal and thus reduction in the nucleation sites [14]. The multi-layer graphene (MLG) was depicted by the dark regions in the optical images, and the light regions depict the bilayer (or monolayer) graphene, and this was confirmed by Raman spectroscopic analysis [14]. The various samples were obtained with slow, medium, or fast annealing rates. It was reported [14] that with an increase in polycrystallinity of Ni, the growth of MLG

was enhanced. Bilayer or mono-layer graphene formed on central regions of larger crystalline grains, whereas the enhanced carbon segregation confined to polycrystalline grain boundaries was responsible for MLG formation [14].

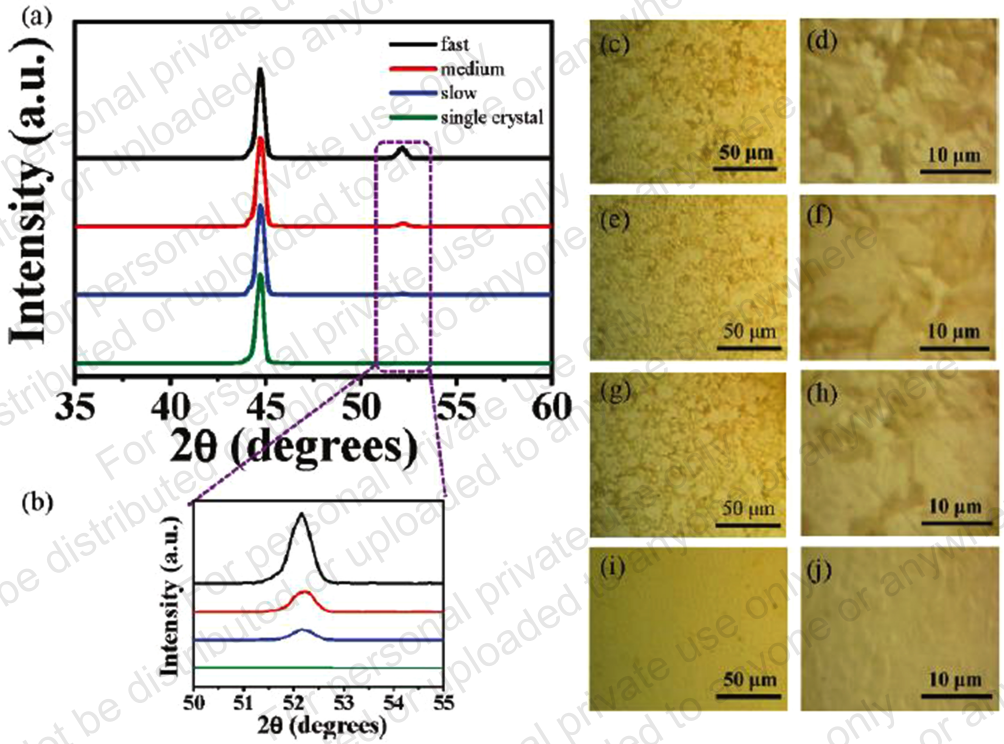

Fig. (5). a) XRD spectra from polycrystalline Ni with variable annealing rates {*i.e.* black (fast), red (medium), and blue (slow)} and XRD spectrum from single-crystal {Ni (111) (green)} after thermal annealing (XRD spectrum is identical for Ni (111) using different annealing rates). **(b)** XRD spectra (Zoomed-in) of peaks at 2θ = 52.16º (that is assigned as Ni (200)). **(c-j)** Optical images after CVD grown graphene on polycrystalline Ni with variable annealing rates {**c, d** (fast); **e, f** (medium); and **g, h** (slow)}; **i,j** optical images after CVD grown graphene on single crystal Ni (111) [14]. The figure has been reprinted (adapted) with permission from ref [14]. Copyright (2010) American Chemical Society.

2.1. Optical Microscopic Analysis

Due to the limited wavelength of visible light, the resolution of an optical microscope is low (~ 200 nm); therefore, to observe the structure at the atomic level after the basic optical microscopic analysis, the most popular tool for the characterization of graphene or graphene derivatives (Go, rGO *etc*.) is based on electron microscopic methods [15]. This way, structural morphology, quality, and crystal structure can be investigated [15]. The commonly used optical microscopic techniques are AFM, TEM or high-resolution electron microscope (HR-TEM), SEM, and scanning tunnelling microscope (STM) [15].

2.2. Transmission Electron Microscope (TEM)

The electrons which are transmitted through a thin sample kept on a TEM grid are analysed in the technique [15 - 17]. The local information at the atomic level about the bulk and surface of a sample is obtained by using TEM. The technique also provides information such as three-dimensional structure, electronic, and chemical properties [16]. In spite of a versatile technique for optical analysis, TEM demonstrates drawbacks such as a small relative area of view as compared to SEM [15, 16]. Very high magnification and a much better resolution down to a group of atoms or even a single atom are provided by HRTEM [15]. The advanced TEM provides various structural and material information as: a) in- real space; or b) reciprocal space or energy space (the spectroscopic mode) [16 - 19].

The C-C bond distance of about 0.142 nm [19] in graphene can be directly resolved by aberration-corrected TEM (AC-TEM), which employs accelerating voltage in the range of (60-80 kV) [16 - 19]. This voltage range is relatively low and avoids beam damage [19]. The better resolution images of graphene and carbon nanotubes were thus recorded by AC-TEM and reported by Suenaga and co-workers [20 - 25]. A lot of new information was provided for various nanomaterials, including graphene [19 - 25]. The image of graphene has been reported by Suenga and Koshino [25]. The TEM-based characterization of carbon-based material is explained in a review by Zhang and Su [16]. The sample preparation is required for TEM analysis; the support film used for materials like carbon nanotubes or graphene can produce a stronger contrast as compared to the sample under analysis [16 - 19]. Thus, various techniques have been employed for sample preparations, such as mechanical exfoliation and transfer of graphene onto TEM grids or CVD on grids [26]. The graphene or GBMs (graphene-based materials) can be synthesized by employing various methods, viz. mechanical exfoliation (top-down), reduction or oxidation of bulk graphite, CVD, and flash Joule heating [2, 26 - 29].

The recent report regarding the scalable synthesis of graphene from cheap sources (tyres, coal, carbon black, waste food) in a short period of time employs a flash joule heating process [30]. The process involves the heating of precursor carbon material above 3000 K for a period of < 100 ms. The heating is performed by means of high voltage electric discharge between two electrodes forming turbostratic graphene [30]. The graphene derived from the process was shown to have single-layer graphene, also graphene showing Moire pattern (interference pattern) [30]. The graphene thus produced does not require a purification step and, in addition to TEM, is also characterized by Raman spectroscopic technique [30]. Ding *et al*. [31] have reported the green synthesis process to obtain graphene *via* a

one-pot synthesis process. The precursor used is an alkaline mixture with lignin (called as black liquor) [31]. The graphene, called black liquid converted graphene (BL-G) with thickness between one to three atomic carbon layers, was obtained [31]. The BL-G obtained *via* this green process has a hexagonal lattice structure and thickness similar to reduced graphene sheets fabricated by the conventional chemical process [31]. The TEM and high-resolution TEM (HR-TEM) images of BL-graphene were recorded to analyse synthesized graphene. The BL-G was spin-coated on a flexible substrate with decreased transparencies and enhanced conductivity [31].

The remarkable properties of graphene oxide (GO) have led to extensive research on GO synthesis, characterization, and application [32 - 36]. The monolayer graphite oxide layer is considered as GO, typically fabricated by oxidation of graphite and then stored in dispersed form or as agglomerated (dried) form [36]. Wilson *et al*. [27] have performed the structural analysis of GO by electron microscopy. It was concluded that the hexagonal symmetry was maintained with order and the C-C bond length of the pristine (unmodified) graphene sheet. The GO was used as an underlying film for the study of the structure of macromolecules, and this has become possible as GO was stable under the electron beam and demonstrated transparency in the electron beam [36]. Thus, GO can be used as a TEM grid [36].

However, the structural characterization of GO is challenging owing to its non-stoichiometric structure and the structured dependency on the fabrication process [37, 38]. Moreover, surface contaminants (oxidative debris [39], amorphous airborne hydrocarbons [40]) influence not only the surface properties but also the chemical structure and defect density [38 - 41]. The image in the TEM detector may not be a direct image showing atomic position; rather can be a modification of the wave coming from behind the sample by the optical (electron) system of microscope or modification of incoming electron wave by the under studied sample [42]. In such a case, aberration-corrected TEM is employed [38, 42]. The direct image can be obtained for graphene but still cannot be successful for GO or GO with contaminants [38, 43]. Dave *et al*. [38] demonstrated a method to remove contaminants for a much better atomic resolution of GO. The *in-situ* heating (up to 700 °C) enables the elucidation of GO structure [38], which otherwise inhibits the sample imaging by adsorbed surface contamination [38].

2.3. Scanning Tunnelling Microscope (STM)

The graphene layers stack in a number of arrangements in graphite; the layer arrangement is described in detail by Mayer, Li and Andrei [43]. The atoms marked A in the top layer can reside above the B atoms of the lower layer in such

a manner that three stacking modes can occur: AA stacking, AB stacking (Bernal stacking) and twisted stacking (giving Moiré pattern). In the AA stacking, layers are stacked in such a way that all the carbon atoms of one layer are on top of the other carbon atoms; Bernal stacking or AB type stacking is done with a shifted second layer such that A atoms reside on top of atom B of the layer, which is twisted by some degree [43 - 45]. The twisted or rotated stacked layers form the Moiré pattern [43 - 45]. Lucian *et al*. [46] employed home build low-temperature STM to study the graphene layers. They employed CVD at ambient pressure for the growth of graphene layer on polycrystalline films. The graphene layers were mechanically supported by spin-coated polymethyl methacrylate (PMMA) layers; afterward, the graphene layers were transferred onto the TEM grid for analysis. It was demonstrated that the electronic properties (low energy) of twisted graphene layers were managed by Dirac femion [46].

The twisted graphene layers (TGL) (particularly bi layers) have also been analysed with an optical microscope, and it was demonstrated that various coloured regions variable in shape and size are present in a given sample [47]. The red-, blue-, and yellow-colored domains are shown in Fig. (**6**) [47]. The methodology for bilayer fabrication is depicted in Fig. (**6a**) and Fig. (**6b**) represents the coloured domains. Briefly, the fabrication involves the growth of graphene films onto Cu support by CVD at ambient pressure, then transferring the layers onto Si/SiO_2 substrate by a wet process using PMMA protection layer and etching process [47]. The process was repeated to grow a graphene bilayer onto an already transferred graphene layer supported on SiO_2/Si [47]. The distinct colored regions occur without the use of any filters; as shown in Fig. (**6b**), the graphene layers were annealed and chemically treated (solvent cleaning) to modify the extent of the color domains, but there is no change in colored regions suggesting that the colors do not produce by impurities or residues [47]. The colored regions are observed in the bilayer but not by the neighbouring single layer [47].

The scanning tunnelling spectroscopy provides tunnelling conductance as a function of the quantity considered proportional to the density (local) of states (DOS). This quantity is bias voltage [48, 49]. The tunnelling spectrum obtained in zero magnetic field and low temperature is obtained for graphene flakes and graphite. A V-shaped curved is obtained for graphene DOS in the proximity of the Fermi level and reaches a minimum (at zero bias voltage) at Dirac point [48, 49]. The graphene flakes obtained after mechanical exfoliation of highly oriented pyrolitic–graphite (HOPG) are obtained as loosely bound graphene after exfoliation on graphite surface [48]. The STM images of the graphene layers were recorded as well. It was concluded that graphite as a substrate for the growth of graphene could be used for studying the intrinsic properties of charge carriers in graphene [48].

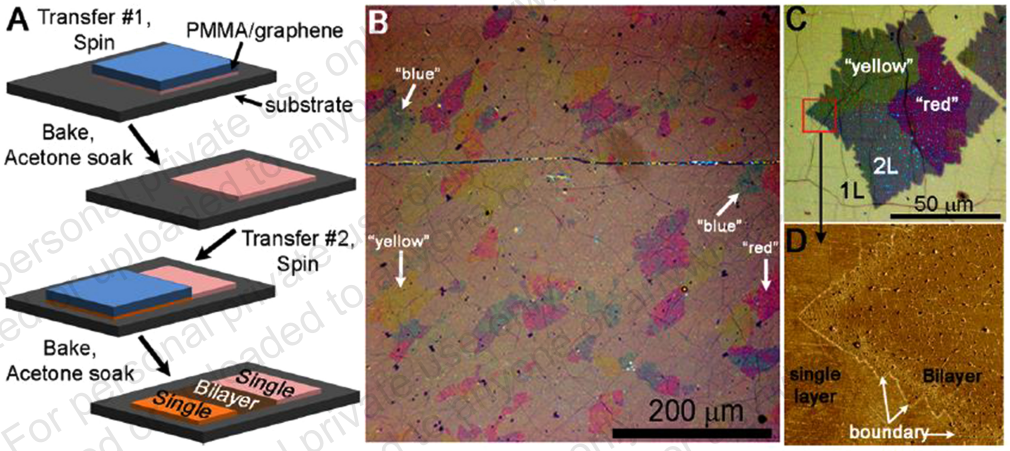

Fig. (6). The fabrication as well as characterization of stacked graphene films. **(a)** Schematic process for bilayer graphene preparation starting from single-layer CVD graphene films. **(b)** Images (Optical microscope) of a twisted bilayer graphene (TBG) film. The colored domains {"red", "blue" and "yellow") are depicted. **(c)** Sample showing top (second) graphene layer is only a partial layer, forming single-(1L) and bi-layer (2L) regions. **(d)** AFM images (15x15 μm^2) depicting the boundary between the single-layer and bilayer region highlighted by the red box in figure **(c)** [47]. Reprinted (adapted) with permission from ref [47]. Copyright (2013) American Chemical Society.

3. RAMAN SPECTROSCOPY

The identification of graphene or graphene-based materials has also been performed extensively by Raman spectroscopic technique [50, 51]. Simultaneous study of vibrational and electronic properties of graphene-based materials (GBM) is obtained from Raman spectroscopy [50, 51]. It is a reliable, rapid, non-destructive, sensitive analytical technique that provides high resolution and better precision [51 - 53]. The technique is based on the Raman Effect involving the Stokes process (absorption) and emission of phonons (anti-Stokes process) [50, 51]. The technique is sensitive to molecular structure and bonding in the molecule. The Raman bands obtained for graphite are influenced by the defect, flakes, layer of flakes, functionalization, doping, *etc* [53, 54]. Since the band gap is negligible in graphene, the incident wavelength resonates information regarding electronic and atomic levels [53, 55]. The position of the peaks, intensity and shape (of Raman band) varies with flake size, degree of doping, oxidation, number of layers, *etc* [51 - 55]. Thus, Raman spectroscopy quantitatively provides information that is mostly in agreement with microscopic analysis data [53 - 55].

The technique, which is based on Raman Effect, involves the phenomena in which light of wavelength (750-850 nm) excites the molecules in the sample. The incident light interacts with the sample, causing light to be reflected with different

frequencies (or wave numbers) [53 - 55]. The wave number change occurs due to molecular rotations and vibrations in the sample [55, 56]. The modulated frequency provides information regarding the molecular structure of the sample [55, 56]. In the case of graphene with a negligible band gap, the incident wavelength resonates, providing atomic and electronic information. Thus, peak shape, intensity, and position vary with oxidation, disorder, doping, layers and flakes of graphene [54, 55].

The absorption or emission of phonons that are observed in Raman spectroscopy occurs owing to the interaction between incident radiation (light) and vibrations causing energy shift. The shift causes a change in wave number of emission or absorption [50, 57]. The energy difference between absorption and emission is known as the Raman shift [58]. When an electron scattered by phonon leads to first-order Raman scattering or the scattering can be of higher-order (second or more), involving scattering by two or more than two phonons [58, 59] and these provide a lot of information regarding the phonon coupling in the studied material [58]. Thus, Raman spectroscopy is effectively used to evaluate carbon nanostructures ranging from amorphous carbon, and carbon nanotubes (CNTs) to graphene or GBMs [58]. Jorio *et al*. [60] have shown the Raman spectra of various carbon-based materials. The similarities among the spectra, as well as differences between the spectra, help to study various carbon allotropes [15].

For understanding the characterization process for graphene or graphene-based materials, the graphene with honeycomb structure (Fig. **7a**) having sp^2 hybridization [60 - 64] of carbon and the reciprocal space unit cell depicting the first Brillouin zone (phonon dispersions of graphene, Fig. (**7b**) are shown in Fig. (**7**). The monolayer graphene showing hexagonal symmetry belongs to D^1_{6h} (space group *P6/mmm*) [60, 61]. Graphene having six normal modes (2 are double degenerate) and 2 atoms per unit cell at the Brillouin zone (Γ) center with (Γ) = $A_{2u} + B_{2g} + E_{1u} + E_{2g}$ [50, 62]. The B_{2g} phonon is Raman and IR inactive, while E_{2g} phonons are active, showing Raman spectra [50]. In the case of graphene, the phonon dispersion (six phonon branches shown in Fig. (**7b**) from the non-equivalent 2 carbon atoms present in the unit cell [60, 63]. The characteristic peaks in Raman are of two types called the G (~ 1582 cm^{-1}) and the G' bands (~ 2670 cm^{-1}) [58]. The in-plane sp^2 C-C vibration of carbon atoms (C-C in-plane vibration) leads to the band called as G band (first-order Raman mode) [50, 51, 58, 60]. The G band is related to doubly degenerate phonon modes, namely iTO (in-plane transverse optic) and LO at the Brillouin zone center Γ point, with the E_{2g} symmetry [51, 58, 60]. The LO stands for longitudinal optic [51, 64]. The iTO and iLO phonons are causing the Raman active bands in the graphene [64]. The second-order Raman scattering *i.e*., G' band involves inelastic inter-valley scattering with iTO phonon close to the K point [51, 64].

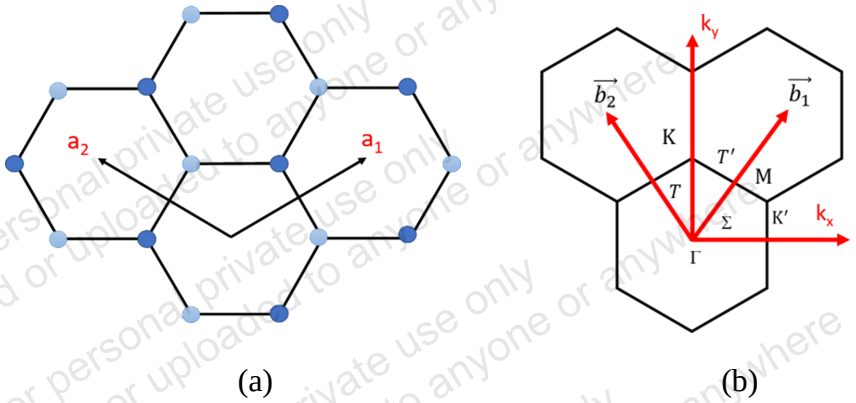

Fig. (7). (a) Monolayer graphene from a top view showing the unit vectors a_1 and a_2 and inequivalent atoms A and B; **(b)** reciprocal space unit cell depicting the first Brillouin zone (BZ) with high-symmetry points and lines. Reciprocal space coordinate axes are K_x and K_y (primitive vectors) [64].

The G' band is also known as 2 D mode [50]. The G, G', and D peak positions are used to study graphene layer or doping in graphene [50]. The GO obtained from oxidation of graphite having sp^3 hybridized carbon is characterized based on G and D bands [50]. The D and D' peaks are Raman bands (second-order); here D band is inter-valley scattering with iTO phonon and defect; in other words, it arises due to disordered C atoms [50, 51, 53]. Whereas D' band is intra-valley double resonance scattering phenomena with iLO phonon and the defect [50, 51]. So, the G band occurs due to bond stretching of carbon sp_2 atoms both in ring and chain compounds, whereas the D peak appeared owing to the breathing mode of the sp^2 hybridized atoms in the ring [55, 65, 66]. Since D mode is known to occur by disorder or defects in the graphene-based materials, the ratio of D band to G band intensities (I_D/I_G) denotes the disorder/defect level in graphene synthesis [53, 67]. The 2D band is a G' band but has a frequency twice that of the D band [51]. The 2D band is present in both graphite and graphene [53]. The D and G' band peaks change as the excitation wavelength of the laser changes [51, 53, 60].

The prominent G' (second-order) band ~ 2700 cm^{-1} is produced by two phonons which is the iTO (in-plane transversal optical) phonon close to the K point in the Brillouin zone [60, 63]. This phonon displays strong electron-phonon coupling and produces a prominent G' band [60, 63]. In graphene, other phonons can produce similar scattering processes, causing various smaller peaks to appear in Raman spectra [60, 68]. Tuinstra and Koenig [66] performed the Raman spectroscopic analysis of single-crystal graphite and other graphite materials. The peaks at ~1580 cm^{-1} are assigned to E_{2g} and at ~1350 cm^{-1}, to A_{1g} breathing mode

[66]. The former high-frequency peak and the mode at Brillouin Zone (BZ) boundary K are known as G and D peaks, respectively [66, 69, 70]. The Raman spectrum of graphene (crystalline) on SiO_2/Si substrate is shown in Fig. (**8a**); the excitation laser with 514.4 nm was employed [64, 68]. The spectrum has two Raman bands at 1580 cm^{-1} (G band) and another one at 2700 cm^{-1} {the G' band or termed at 2D band} [64, 68, 71]. The number of graphene layer influences the intensity of the 2D band, which is approximately four times as compared to the G band in the case of crystalline graphene single-layer atoms [10, 64, 68, 72 - 75]. The number of layers in graphene increases, causing variation in an electronic environment, and this change occurs due to interactions among adjacent layers [53]. This consequently results in the broadening of 2D peaks and decreasing of the peak intensity [53], as shown in Fig. (**8b**). After a few layers (five), graphene and graphite Raman spectra are indistinguishable [53, 68]. The D band is weak, and the presence of defects in graphene nanosheets makes the D band appear in the spectrum [64]. The intense D peak is observed for amorphous carbon isotopes, which are absent in graphitic material [64].

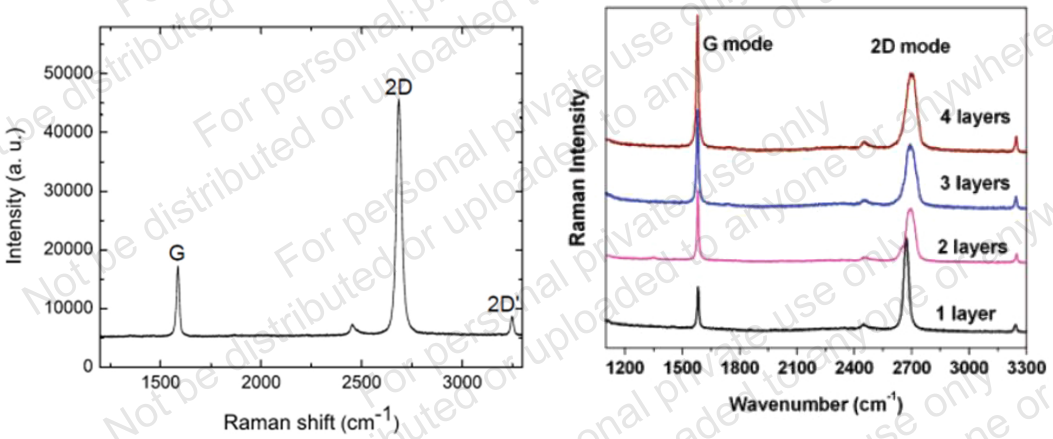

(a) (b)

Fig. (8). The Raman spectra of **a)** crystalline graphite, **(b)** few layer graphene. Reproduced/reprinted (adapted) from refs [10, 64].

Ni *et al*. [10] employed a 532 nm excitation source for recording Raman spectra of graphene having different staked layers [10]. The sharp 2D peak is observed for single-layer graphene, which is distinguishable from the 2D band of multi-layer graphene. But in the case of graphene with 2 to 4 layers, the difference in 2D peak is not noticeable, but a visible difference is observed in G band intensity [10]. The appearance or disappearance of D peaks corresponds to the defects or imperfections in the hexagonal sp^2 carbon network [60]. The Raman spectra are

shown for amorphous carbon materials with or without high-temperature treatments, with D band peaks appearing in the spectra having different peak widths and intensities [60]. With few defects in the structure will exhibit D, and in the case of crystalline ordered graphene or graphite, the D band was missing [60]. Luong *et al*. [30] fabricated the high-quality graphene by the flash Joule heating (FJH) process and observed that the I_{2D}/I_G is greater than 10. The D band with extremely low intensity is observed, indicating a low defect concentration [30]. The ratio I_{2D}/I_G was as high as 17 for graphene obtained from carbon black by the FJH process and was reported to be the highest value for any form of graphene [30]. This is due to the extremely high temperature achieved for graphene fabrication by the flash process [30].

Cancado *et al*. [70] studied the Raman spectra of single-layer graphene samples with various defect densities. The defect was created by the bombardment of the sample by Ar^+ ions. The Raman spectra of various SLG bombarded with different doses of Ar^+ ions are shown in Fig. (**9**). Thus, the measure of defects (point-like) in graphene was evaluated from the I_D/I_G ratio by Raman spectroscopy using different excitation laser energies [70].

The one-dimensional defects (or the amount of border) with respect to the crystalline area give the degree of disorder in a nano-crystallite and the measurement of L_a [70]. In the case of zero-dimension point-like defects, as in graphene, L_d is the distance between defects [70, 75]. Various methods can quantify the measure of the amount of disorder, *i.e*., L_d, by using Raman spectroscopic analysis [70, 75]. Thus, the influence of L_d on peak frequency, width, integrated area and intensity has been studied [70, 76, 77]. In Fig. (**9a**), the peaks at 1580 cm^{-1} and 1350 cm^{-1} correspond to G and D bands, respectively [70]. The strongly dispersive intervalley double resonance process having excitation energy due to Kohn Anomaly at K gives rise to the D peak [70]. The intervalley process can also occur by connecting the two points which belong to the same cone around the K or K' [78]. Thus, giving a peak at ~1620 cm^{-1} in a defective sample is obtained using a laser at 514.15 nm [70]. The second-order 2D peak appears as a single peak in graphene but breaks into four peaks in the case of BLG (bilayer graphene), indicating the electron band structure evolution [68, 70, 79]. Again, the second-order peak of D' known as 2D' and the 2D peak do not require any defects for their activation and are found in the Raman spectra [70]. However, the peak corresponding to ~ 2940 cm^{-1} (D + D') requires defect activation, and this peak is a combination of phonons having dissimilar momenta at K and Γ [70]. In Fig. (**9b**), the plot of I_D/I_G*vs.* L_D is represented [70]. The ratio increases with a decrease in L_D and reaches maxima at L_D ~ 3 nm and reaches a minimum (zero) at L_D < 3 nm [70]. Thus, Raman spectroscopy has been employed for the analysis of defects in graphene and related materials [80]. The detailed application of Raman

Spectroscopy is provided in the reference [51]. Kumar and Pattammattel [53] highlighted a few limitations and opportunities for errors in employing Raman spectroscopy; these are summarised previously in the literature [53]:

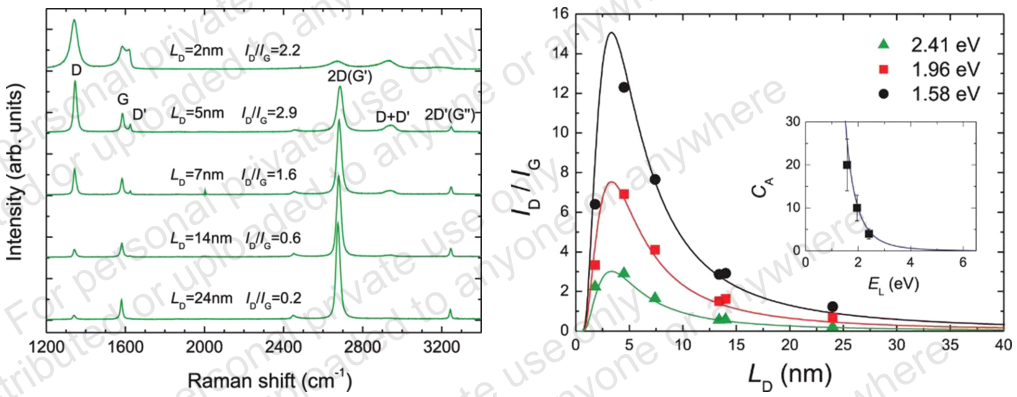

(a) (b)

Fig. (9). (a) Raman spectra of ion bombarded SLG with different L_D (measured at laser excitation energy, E_L = 2.41 eV and wavelength, λ_L = 514.5 nm). The L_D (distance between defects) is independently measured as per ref [70, 75]. The I_D/I_G values are shown for each spectrum. The notation, such as in the parentheses [2D(G´)], indicates two commonly used notations for the same peak (2D and G´); and **b)** I_D/I_G for all SLGs and E_L [70, 75]. The inset figure is the plot of C_A *vs.* E_L. Reprinted (adapted) with permission from ref [70]. Copyright (2011) American Chemical Society.

A) The sampling for Raman analysis is crucial; for instance, the spectroscopic analysis of exfoliated graphene samples can estimate the graphene layer. The transfer of exfoliated samples on glass slides can lead to the rest of the sheets, thus providing a rough evaluation of the number of layers [53]. The samples (films) fabricated from various stock solutions under dilute conditions can provide a better way of sample analysis. However, they may encounter problems related signal-to-noise ratio [53].

B) The particle size estimation (formed by exfoliation) from Raman analysis should be complemented with absorption spectroscopy and microscopic studies [53].

C) During spectroscopic analysis, samples can undergo photoreduction, as in the case of graphene oxide, influencing the conclusions drawn [53]. By reducing laser excitation energy (laser power) or by defocusing, the damage caused to samples can be minimized, and the same can be judged by optical analysis using an optical microscope [53].

4. FT-IR SPECTROSCOPY

FT-IR spectroscopic analysis is one of the efficient approaches for the detection of functional groups in the molecule [53]. The modification or functionalization of graphene or graphene oxide can be analysed by IR spectroscopy along with other spectroscopic techniques such as NMR, and XPS [6, 53, 81]. The 2D hexagonal arrangement of sp^2 hybridized carbons atoms is present in graphene [82, 83]. In the FTIR spectrum, no significant peak due to any functional group is observed [82, 83]. But in the case of graphene oxide, IR spectra provide information regarding -COOH, -OH, C-O and C=O functional groups, as shown in Fig. (**10**) [53, 84]. Fig. (**10**) shows spectra for crystalline graphite, GO and rGO [84]. The in-plane stretching vibration of C=C in graphite appears at ~1500–1600 cm^{-1} [81, 84]. In the case of GO, -OH peak appears at 3162 cm^{-1}, C=O peak at 1710 cm^{-1}, and for alkoxy and epoxy groups, the peaks are at 1050 cm^{-1} and 1220 cm^{-1}, respectively [53, 84]. The functionalization of graphene can be performed by a number of reagents, including amino acids, carboxylic acids, polymers, phosphates, *etc* [73, 84 - 87].

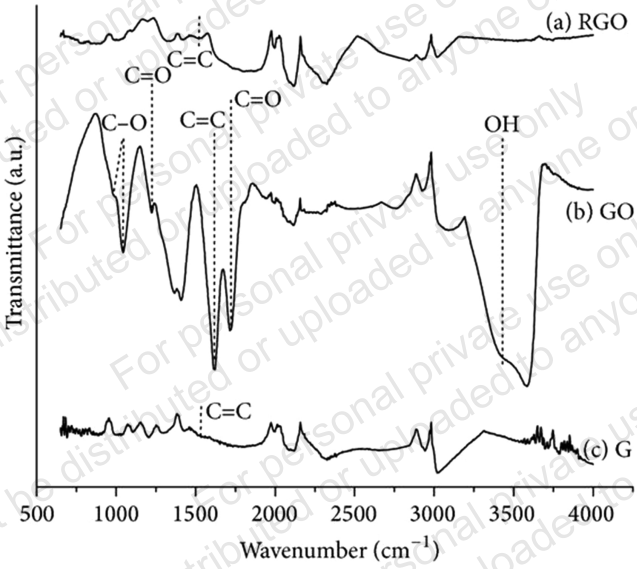

Fig. (10). The figure represents the IR spectra of **(a)** (RGO), **(b)** graphene oxide (GO), and **(c)** pure graphite (G). Reproduced with permission from ref [84]. under Creative Commons Attribution License.

Mittal *et al*. [88] performed thermal oxidation of graphene (a few layer) in the presence of oxygen, and the oxidized graphene was analysed by FT-IR spectroscopic technique. The attached oxygen groups onto the surface of oxidized graphene (called porous graphene) were confirmed by the peaks at 3418 cm^{-1} for -OH; similarly, the peaks at 1726 cm^{-1}, 1096 cm^{-1}, and 915 cm^{-1} ascribed to -COO-,

-C-O-, and -C-O-C- groups, respectively [88]. Kuila *et al*. [89] employed a green approach to reducing for the reduction of GO to rGO, by using carrot root (endophytic micro-organisms in the carrot root). The partial reduction of GO to graphene was confirmed by X-ray photoelectron and FT-IR [89]. The C=O stretching peak and -O-H deformation peaks at 1728 cm^{-1} and 1395 cm^{-1}, respectively, decrease significantly after carrot-assisted reduction of GO [89]. The intensities of epoxy and alkoxy C-O stretching peaks were unchanged after reduction, but the peaks' position was significantly altered [89], owing to a partial reduction of GO. New peaks due to carotene present in carrots appear at 2928 cm^{-1} and 2851 cm^{-1} [89].

Acik *et al*. [81] performed *in situ* transmission IR absorption analysis of GO during vacuum thermal annealing (temperature 60-850 ^{o}C). In this work, Acik *et al*. [81] have reported that the peak assignments (identification of chemical composition) in IR of GO are difficult and challenging due to conjugation and proximity effects. Modified Hummer's method was used for the fabrication of GO and analysed by the peaks at 3000-3600 cm^{-1} of hydroxyls C-OH (-COOH, H_2O contribution), ketones C=O at ~ 1750-1850 cm^{-1}, carboxyls (COOH) at ~ 1600-1750 cm^{-1}, in-plane C=C stretching at ~ 1500-1600 cm^{-1}, C-O-C epoxide peaks at ~1280-1330 cm^{-1} and 800-900 cm^{-1}, along with weak contributions by all these species in the region 900-1500 cm^{-1} [81]. The possible IR peak assignments of functional groups needed for the characterization of graphene-based materials are reviewed by Tucureanu *et al*. [82]. Since the IR analysis is complementary to other spectroscopic analyses, *e.g*., XPS, NMR, *etc*., the characterization of GBMs by XPS analysis is discussed in the next section.

5. X-RAY PHOTOELECTRON SPECTROSCOPY (XPS)

The characterization of surface functionalities is done using X-ray photoelectron spectroscopy (XPS). This is a quantitative technique for the evaluation of surface chemistry, the chemical and electronic state of elements, and also the elemental composition [43, 90 - 92]. The X-ray beam irradiates the material of interest; the surface generates a spectrum of electrons with characteristic kinetic energy [92]. The number and kinetic energy of released electrons are measured in XPS [93]. Thus, XPS peaks with characteristic binding energies are obtained by the various elements exposed to the X-ray beam [92]. The peaks provide information regarding electronic configuration within atoms [92]. The technique is based on the photoelectric effect [93], and for obtaining XPS spectra, the sample is irradiated with X-ray beams [91 - 93]. The law of energy can be used to understand the working principle of the XPS technique as [91 - 93]:

$$E_p = E_{ke} + \varphi + E_{bind} \quad \textbf{(1)}$$

In the above eq. (1), E_p, E_{ke}, φ, and E_{bind}, represent the energy of the incident X-ray radiation (*i.e.*, of incident photons), the kinetic energy of the photon emitted core electrons, the part of energy absorbed (work function), and ionization energy (binding energy) in eV, respectively [91 - 93]. So, the binding energy is calculated from the above equation [91, 93]. The photons of incident radiations eject core-level electrons from the atoms, and the kinetic energy of electrons depends upon the binding energy in the atoms and the elements from which electrons are ejected [91, 93]. The ejected electrons are collected from the uppermost 3 nm to 7 nm part of the material under study [91, 93].

XPS has been employed to characterize GBMs, GO, and rGO [53, 91, 93]. The representative binding energy of C1s, depending upon the chemical environment, is detected around 285 eV [53, 90]. The various C1s components of graphene with binding energy are shown in Table **1** [53].

Table 1. The binding energy (eV) of C1s components in graphene [92 - 97].

State	C1s Binding Energy (eV)
C-C	284.9-285.6
C=C	284.3-284.6
C=O	287.9-288.3
C-OH	285.4-286.7
C-O-C	285.6-286.9
COOR/COOH	288.3-289.4
O=C-O	288.5
O-C-O	285.6-286.9
π-π*	290.5-291.2
C-H	285.3
C=O	289
C-N (sp^3 N)	283.7
C=N	286.8

As shown in Table **1**, the common chemical state of carbon along with oxygen is used to identify or distinguish graphene from GO or rGO, heteroatom doped graphene [92 - 97]. The GO is rich in elemental oxygen, so in XPS analysis strong oxygen-bearing C1s peaks are observed [92]. Among the oxygen-bearing groups in GO, such as C-O, C=O, O-C=O, the most dominating XPS peak is C-O [92,

98]. Yu *et al*. [98] have reported improved Hummer's method for fabrication of GO in a high yield. The fabricated GO was characterized by various techniques of spectroscopic (FTIR, UV, XPS, Raman) [98]. XPS spectra for the fabricated GOs are shown in Fig. (**11**), in which the GO2 is the GO fabricated by their methodology, and GO1 is fabricated by improved Hummer's method reported by Kovtyukhova *et al*. [99]. Few XPS spectra indicate a strong peak of C=C [92 - 97, 99], and some report a strong main peak of the C-O bond [92, 98].

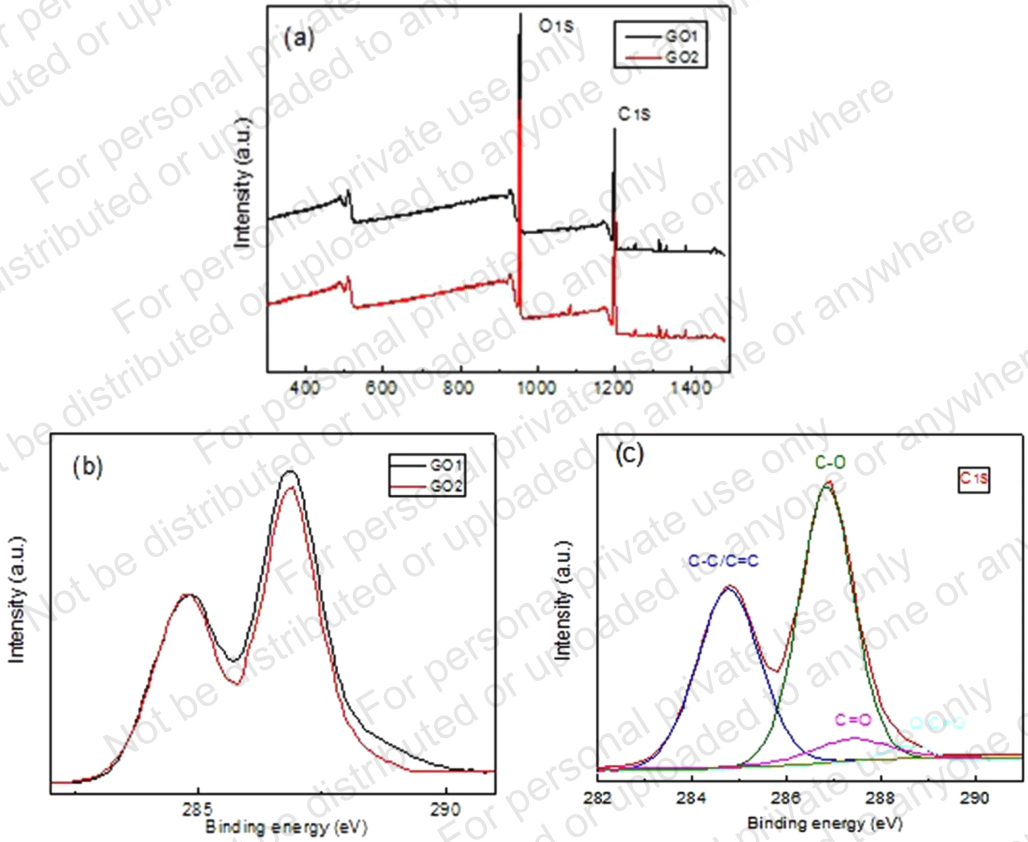

Fig. (11). The XPS of GO samples showing **(a)** GO1 and GO2, **(b)** C1s of GO1 and GO2 normalized to C=C peak, **(c)** deconvoluted C1s of GO2. Reused with permission from ref [98]. under Creative Commons CC BY license.

Ganguly *et al*. [100] reported *in situ* temperature-dependent XPS analysis of GO upon heat treatment process and observed that the unstable groups, such as the edge-plane COOH and C=O were stable and difficult to remove [100]. The C=O peak at 200 °C appears at ~ 288.3 eV, and the C-OH peak remains even at 1000 °C [100]. This peak indicates that thermally pyrolysis of the C-OH group is not

complete even at very high temperature and due to intercalating position of the C-OH group in the interlayer galleries, which is between intact conjugated regions [100, 101].

The C1s components in GO samples are a) carbon atoms of graphitic material with a peak at 284.5 eV, b) carbon atoms of alcohols (tertiary) and epoxides at 286. 5 eV, and c) the carboxylic acid groups at 289.2 eV [93]. The signal of ketones is placed between 287.7 to 288.1 eV [93, 102]. However, the interval has been placed either into 286.5 to 287.5 eV (along with alcohol and epoxides) or 288.5–289.2 eV interval (along with carboxyl groups) [93]. The deconvoluting integral C1s spectra are reported in various ways, for instance, the spectral deconvolutions of C-O-C and C-OH peaks [93, 100, 103]. Nonetheless, the overall oxidation level of GO or rGO can be interpreted with confidence using XPS analysis [93].

Siokuo *et al*. [104] have adopted two different methodologies to grow atomically clean graphene layers on Cu substrates. One of the methodologies is the stepwise annealing up to a temperature of 750 ºC and the second process is the treatment using mild Ar^+ sputtering under UHV conditions [104]. The XPS spectra of C1s of single-layer graphene grown on Cu foil treated at different temperatures. The XPS analysis in this report [104] has a much stronger C-OH peak. The sample of pristine graphene has peaks at 284.5 eV of C=C bonds, 285.6 eV for sp^3 hybridized carbon and peaks for C–OH and O–C–O bonds at 286.7 eV and 288.3 eV, respectively. The intensity of peaks corresponding to O-C-O and C-OH bonds indicates the presence of amorphous and oxidized carbon contamination [92, 104].

Rabchinksii *et al*. [105] have fabricated aminated graphene by simultaneous reduction and amination of GO under mild conditions. This facile and scalable fabrication involves treating GO with hydrobromic acid and ammonia solution [105]. The aminated graphene bears a low content of various other nitrogen species (graphitic N and pyridines), and this was confirmed from XAS (X-ray absorption studies) and XPS analysis [105]. The XPS spectra of brominated GO, rGO-Br, aminated graphene oxide, rGO-Am and precursor GO are shown in Fig. (**12**) [105].

The C1s peak in GO appears at ~284.7 eV, and O1s peaks in GO appear at ~ 532.6 eV, demonstrating no impurities were present [105]. The presence of bromine in the brominated GO demonstrates the Br3p doublet peaks at ~ 182eV and 189 eV, for the Br3d band at ~ 69 eV was confirmed from XPS analysis [105]. The absence of these Br-related peaks and the presence of N1s peak at ~ 400 eV indicated the amination of rGO-Br; furthermore, the incorporation of

nitrogen functionalities had a concentration of about 5.5 at. % [105]. The peaks appearing at 285.1 eV, 284.7 eV, and 283.9 eV correspond to sp^2 C=C domains, carbon atoms having bond distortion due to the presence of functional groups at the neighbouring C-C atoms vacancy defects in graphene lattice [105].

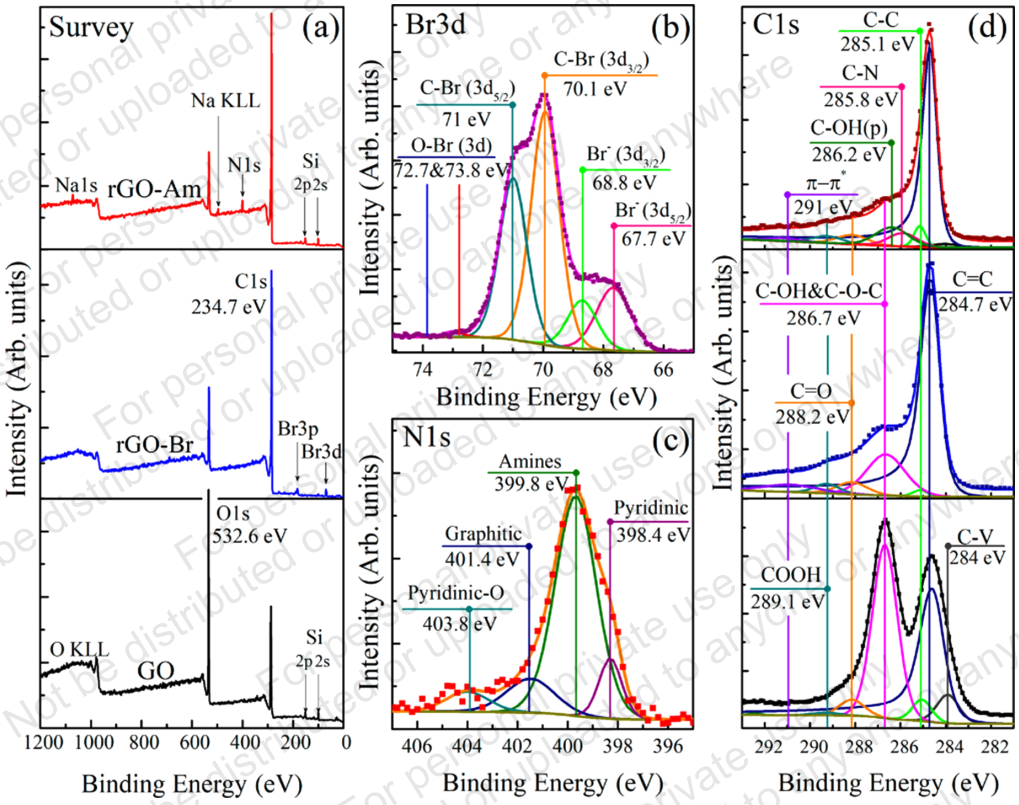

Fig. (12). (a) XPS survey spectra of the pristine GO, brominated rGO-Br and rGO-Am. **(b)** High-resolution XPS spectrum of rGO-Br (Br3d). **(c)** N1s XPS (high-resolution) of rGO-Am. **(d)** C1s spectra (high-resolution) of the initial GO and modified rGOs. For clarity, C1s spectrum and their fits are vertically offset from the fitting components [105]. Reused from ref [105]. under Creative Commons CC BY license.

Besides XPS, extended X-ray absorption fine structure (EXAFS) is also utilized as a powerful technique for structural characterization (bond length and coordination number) of GBMs [106 - 108]. The local structure around the element of interest can be evaluated using EXAFS; thus, metal coordination or metal absorption can be studied to evaluate the potential applications [106 - 108]. GBMs are employed for a number of applications related to environmental remediation, catalysis, energy, water desalination, *etc* [106 - 108]. For contamination absorption (*e.g.*, heavy metal) or the use of GBMs as a catalyst, the local structure around an element of interest can be studied using EXAFS [106 - 108].

The strength of X-ray absorbed by material as a function of energy provided by the X-ray radiations is measured [108]. The absorption of heavy metals [Pb(II), Cd(II), and U(VI)] using multi-layered graphene oxide (MLGO) was studied recently using XAFS [107]. Inner-sphere and the outer-sphere mechanisms were concluded to be the crucial mechanisms of heavy metal absorption onto MLGO [107]. EXAFS and Near-edge X-ray absorption fine-structure have also been used to study the structure of GBMs [107 - 110].

6. THERMOGRAVIMETRIC ANALYSIS (TGA)

Various techniques discussed above are used for the characterization of graphene or graphene-based materials, typically probing properties only of a small sample area. These localized analytical techniques can also characterize the industrially produced graphene materials; however, it has been shown that graphene material produced on a large scale may not be graphene [111, 112] but instead can be a few layers of graphene (FLG) having non-exfoliated graphitic materials or impurities [111, 112]. The FLG, as described by ISO (International Organization for Standardization) [113], is a 2-D material with 3-10 stacked graphene layers [111]. Recently, the TGA analysis of GBMs has been performed to demonstrate the analytical application of TGA for characterization by recording and analyzing TGA/DTA thermograms [111, 112]. TGA, a thermoanalytical technique, measures the mass change with respect to temperature rise. The mass change can occur due to oxidation, decomposition, moisture loss, or loss of volatiles [114]. In this regard, the TGA-DTG of materials, such as graphite, FLG, GO, and rGO was recorded, and the decomposition with temperature was analyzed in terms of various characteristic parameters, such as DTG (derivative thermogravimetry) peak-range and -shape, maximum mass decomposition rate (T_{max}) and thermal stability. These parameters closely related to intrinsic physical and chemical structures were studied to identify graphene-based materials [111, 112] undoubtedly. The authors [111, 112] designed a hypothesis of using TGA as an analytical method, and this hypothesis was verified by recording TGA/DTA of controlled, verified samples of FLG, GO and rGO. These samples were also characterized by XPS, SEM, TEM, particle size distribution (PSD) and XRD. The TGA/DTA characteristics of these samples were grouped into analytical parameters. These parameters (DTG peak range and shape, T_{max} and thermal stability) were further used for the identification of GBMs [111, 112].

The TGA-DTA signatures of GBMs involved the division of thermographs into three distinct temperature regions [111]. Region I (RGI): water evaporation region (temperature, $T < 100$ ° C); region II (RGII): decomposition of oxygen-bearing groups (T =100°-360°) and region III (RGIII): carbon combustion (T = 360°-

1000°). Three DTG peaks were reported [111] for GO samples in each region, with T_{max} values of 221.2 ± 1.2 °C in region II and 555.5 ± 5.0 °C in region III. For rGO, only one DTG peak with a different position and T_{max} was observed in region III. The T_{max} values in RIII for rGO, FLG, and graphite were observed at 536.5 ± 5.0 °C, 703.9 ± 0.5 °C, and 871.3 ± 0.1 °C, respectively [111, 112]. It was reported that the T_{max} values are highly distinct for the studied GBMs [111, 112]. The T_{max} values were different for these GBMs, and the values vary with their chemical structures and carbon structures. The highest T_{max} was reported for graphite, followed by FLG, rGO and GO with lower values, resulting in significant differences in carbon decomposition temperatures. The graphite decomposes at higher temperatures than FLG, rGO and GO. Graphite, which contains many stacked graphene layers, is more thermodynamically stable owing to additional van der Waals interactions within the layers [111]. Thus, graphite requires higher temperature treatment for its decomposition due to the strength provided due to coexisting covalent bonding and the van der Waals interactions. The three regions in thermographs of graphite, graphene, and GO are shown in Fig. (**13**) [112].

Not be distributed or uploaded to anyone or anywhere
For personal private use only

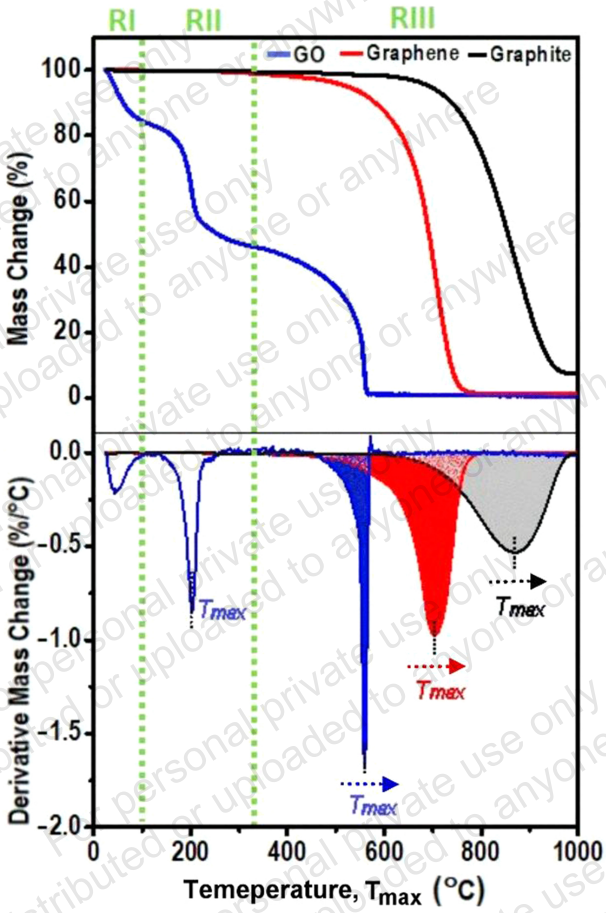

Fig. (13). The representative TGA-DTA thermographs along with T_{max} values of graphene, graphite, and GO [112].

The oxidation of graphite sp^2 hybridized carbon atoms forming GO leads to the conversion of the majority of sp^2 hybridized C-atoms to non-graphitic sp^3 hybridized carbon atoms. Additionally, the defects' density also increases due to extensive oxidation during the said conversion. The presence of defects and oxygenated groups leads to a reduction of GO strength, and GO decomposes at a lower temperature [111, 112]. The reduced-GO shows similar behavior in RGIII to that of GO, indicating that the sp^3 carbon framework has not recovered to the graphitic structure. The distinguished TGA/DTA behavior of GO and rGO was reported in RGII; here, no DTG peak was observed as most of the oxygen functional groups present in GO were removed during the reduction process when rGO was formed. It is worth mentioning that the authors have compared the results with available literature data and the data collected from more than

hundreds of samples from other laboratories [106]. Thus, DTG peaks and values of T_{max} can be used to distinguish and identify graphite, FLG, GO and rGO. For qualitative analysis, several samples (commercially available as well as synthesized in lab) were analyzed using TGA/DTA, and the results were compared with verified GBM samples. The TGA/DTA results used for quantitative and qualitative analysis of GBMs were also in good agreement with other commonly used characterization techniques such as Raman spectroscopy, TEM, AFM, XRD, SEM and XPS [111, 112].

Wang *et al*. [115] facilely fabricated and then characterized graphene nanosheets. The synthesis was performed by oxidation, ultrasonic exfoliation, and chemical reduction. The nanosheets were characterized using XRD, HRTEM, TEM, and selected area electron diffraction (SAED). The TGA analysis of graphene nanosheets, GO, and pristine graphite powders was also performed in dry air to characterize and study the thermal behavior [115]. GO shows two-step mass loss with the rise of temperatures, one at 200 ºC due to removing oxygenated groups and the other at a higher temperature of 500 ºC because of carbon oxidation [115]. The pristine graphite losses mass at a much higher temperature of 650 ºC, which was combustion to carbon dioxide. The mass loss in the case of less stable graphene nanosheet (as compared to graphite bulk powder) was reported at 250 ºC. Similarly, Shtein *et al*. [116] have also characterized graphene-nanoplatelets by thermogravimetry in addition to Raman spectroscopy, electron microscopy, AFM and XPS analysis.

Recently, GO and rGO were used as fillers for the synthesis of polymer composite with poly(vinyl alcohol) as the polymer matrix [117]. The composite was studied for IR shielding applications. The filler GO and rGO were characterized along with TGA analysis. The TGA/DTA was performed to check the thermal stability of GBMs [117]. Three peaks were observed for GO, the first peak corresponding to water loss, the second peak at 200 ºC due to the decomposition of GO as oxygen groups were removed and at 500 ºC, beyond which the GO was completely decomposed. The GO was reduced chemically (using citric acid or hydrazine) and thermally (at 200 ºC or 1000 ºC) GO, and the rGO was again analyzed by TGA/DTA. The analysis indicated that a strong reducing agent or higher temperature treatment was able to lower the oxygen content in rGO significantly [117], as supported by decomposition trends in thermographs. Thus TGA/DTA analysis has been used for the characterization of GBMs. The degree of oxidation during GO formation can also be evaluated facilely using TGA [106]. In oxidized graphene samples, the mass loss of the functional groups can be studied quantitatively by TGA, and when combined with mass spectra or FTIR, more accurate information can be obtained [106, 111, 112].

7. CONCLUDING REMARKS

The affinity of hydrocarbons toward graphene leads to hydrocarbon contamination [53]. The hydrocarbons can come from vacuum grease, solvents, oil pumps *etc* [53]. This contamination is a challenge for the characterization of graphene by XPS analysis. Furthermore, oxygen-rich functionalities are liable to get reduced in the presence of X-ray beams, so this issue needs to be considered while recording XPS spectra [53, 93]. Additionally, the sample analysis is performed under a vacuum compared to the ambient atmosphere required by other techniques, such as Raman analysis [53, 93].

The characterization techniques in this chapter provided crucial information regarding atomic level as well as surface, chemical, and electronic properties of graphene-based materials. Optical microscopic techniques can make the visible distinction between graphene layer-by-layer or stacking. The information regarding 3D structural integration along with simultaneous vibrational and electronic properties can be evaluated. For practical application of GBMs, which depends upon controlling surface contamination, tuning surface properties, gram-scale fabrication process, and modulating electronic properties can be possible by targeted fabrication/modification approach. In this regard, the characterization of the material, both raw and processed (synthesized), is highly desirable. Thus, a brief discussion is made in this chapter regarding some of the important GBMs characterization techniques.

LIST OF ABBREVIATIONS

AC-TEM	Aberration-corrected transmission electron microscope
AFM	Atomic force microscope
ALD	Atomic layer deposition
BLG	Bilayer graphene
BZ	Brillouin zone
CNTs	Carbon nanotubes
CVD	Chemical vapor deposition
DOS	Density of states
DTG	Derivative thermogravimetry
FJH	Flash Joule heating
FT-IR	Fourier-transform infra-red spectroscopy
GBMs	Graphene-based materials
GO	Graphene oxide

Not be distributed or uploaded to anyone or anywhere
For personal private use only

HOPG	Highly oriented pyrolitic graphite
HR-TEM	High-resolution electron microscope
ISO	International Organization for Standardization
LO	Longitudinal optic
MLG	Multi-layer graphene
NMR	Nuclear magnetic resonance
OM	Optical Microscope
PMMA	Polymethyl methacrylate
PSD	Particle size distribution
rGO	Reduced graphene oxide
SAED	Selected area electron diffraction
SFM	Scanning force microscopy
SLG	Single layer graphene
STM	Scanning tunneling microscope
TEM	Transmission electron microscope
TGA	Thermogravimetric analysis
TGL	Twisted graphene layers
XPS	X-ray photoelectron spectroscopy
XRD	X-ray diffraction

CONSENT FOR PUBLICATION

Not applicable.

CONFLICT OF INTEREST

The author declares no conflict of interest, financial or otherwise.

ACKNOWLEDGEMENTS

Declared none.

REFERENCES

[1] Lee, H.C.; Liu, W.W.; Chai, S.P.; Mohamed, A.R.; Aziz, A.; Khe, C.S.; Hidayah, N.M.S.; Hashim, U. Review of the synthesis, transfer, characterization and growth mechanisms of single and multilayer graphene. *RSC Advances,* **2017**, *7*(26), 15644-15693. [http://dx.doi.org/10.1039/C7RA00392G]

[2] Huang, X.; Yin, Z.; Wu, S.; Qi, X.; He, Q.; Zhang, Q.; Yan, Q.; Boey, F.; Zhang, H. Graphene-based materials: synthesis, characterization, properties, and applications. *Small,* **2011**, *7*(14), 1876-1902. [http://dx.doi.org/10.1002/smll.201002009] [PMID: 21630440]

For personal private use only Not be distributed or uploaded to anyone or anywhere

[3] Blake, P.; Hill, E.W.; Castro Neto, A.H.; Novoselov, K.S.; Jiang, D.; Yang, R.; Booth, T.J.; Geim, A.K. Making graphene visible. *Appl. Phys. Lett.,* **2007**, *91*(6), 063124. [http://dx.doi.org/10.1063/1.2768624]

[4] Novoselov, K.S.; Geim, A.K.; Morozov, S.V.; Jiang, D.; Zhang, Y.; Dubonos, S.V.; Grigorieva, I.V.; Firsov, A.A. Electric field effect in atomically thin carbon films. *Science,* **2004**, *306*(5696), 666-669. [http://dx.doi.org/10.1126/science.1102896] [PMID: 15499015]

[5] Arco, L.G.D.; Zhang, Y.; Zhou, C. Large scale graphene by chemical vapor deposition: synthesis, characterization and applications. In: *Graphene - synthesis, characterization, properties and applications*; Jian Ru Gong, Intech Open, **2011**; pp. 161-184. [http://dx.doi.org/10.5772/22358]

[6] Chen, Q.; Zhu, H. Structural characterizations of graphene. In: *Graphene Fabrication, Characterizations, Properties and Applications*; Zhu, H.; Xu, Z.; Xie, D.; Fang, Y., Eds.; Academic Press, **2018**; pp. 13-26.

[7] Kumar, V.; Lee, Y.S.; Shin, J.W.; Kim, K.H.; Kukkar, D.; Fai Tsang, Y. Potential applications of graphene-based nanomaterials as adsorbent for removal of volatile organic compounds. *Environ. Int.,* **2020**, *135*, 105356. [http://dx.doi.org/10.1016/j.envint.2019.105356] [PMID: 31881425]

[8] Roddaro, S.; Pingue, P.; Piazza, V.; Pellegrini, V.; Beltram, F. The optical visibility of graphene: interference colors of ultrathin graphite on $SiO_{(2)}$. *Nano Lett.,* **2007**, *7*(9), 2707-2710. [http://dx.doi.org/10.1021/nl071158l] [PMID: 17665963]

[9] Cheng, Y.; Song, Y.; Zhao, D.; Zhang, X.; Yin, S.; Wang, P.; Wang, M.; Xia, Y.; Maruyama, S.; Zhao, P.; Wang, H. Direct identification of multilayer graphene stacks on copper by optical microscopy. *Chem. Mater.,* **2016**, *28*(7), 2165-2171. [http://dx.doi.org/10.1021/acs.chemmater.6b00053]

[10] Ni, Z.H.; Wang, H.M.; Kasim, J.; Fan, H.M.; Yu, T.; Wu, Y.H.; Feng, Y.P.; Shen, Z.X. Graphene thickness determination using reflection and contrast spectroscopy. *Nano Lett.,* **2007**, *7*(9), 2758-2763. [http://dx.doi.org/10.1021/nl071254m] [PMID: 17655269]

[11] Graf, D.; Molitor, F.; Ensslin, K.; Stampfer, C.; Jungen, A.; Hierold, C.; Wirtz, L. Spatially resolved Raman spectroscopy of single- and few-layer graphene. *Nano Lett.,* **2007**, *7*(2), 238-242. [http://dx.doi.org/10.1021/nl061702a] [PMID: 17297984]

[12] Jia, C.; Jiang, J.; Gan, L.; Guo, X. Direct optical characterization of graphene growth and domains on growth substrates. *Sci. Rep.,* **2012**, *2*(1), 707. [http://dx.doi.org/10.1038/srep00707] [PMID: 23050091]

[13] Hong, K.P.; Lee, K.H.; Nam, J.; Kim, K.S.; Kim, S.H.; Kim, B.; Kim, K.; Park, J.S.; Lee, J.Y.; Jeong, T.; Song, Y.J.; Hwang, J.Y.; Choi, J.B.; Cho, S.; Kim, K.S.; Kim, H. Visualization of CVD-grown graphene on Cu film using area-selective ALD for quality management. *Appl. Surf. Sci.,* **2019**, *496*, 143614. [http://dx.doi.org/10.1016/j.apsusc.2019.143614]

[14] Zhang, Y.; Gomez, L.; Ishikawa, F.N.; Madaria, A.; Ryu, K.; Wang, C.; Badmaev, A.; Zhou, C. Comparison of graphene growth on single-crystalline and polycrystalline Ni by chemical vapor deposition. *J. Phys. Chem. Lett.,* **2010**, *1*(20), 3101-3107. [http://dx.doi.org/10.1021/jz1011466]

[15] Badruddoza, A.Z.M.; Chepyala, R.; Ashraf, K. State-of-the-Art characterization methods for graphene and its derivatives. In: *Micro and nano technologies, biomedical applications of graphene and 2D nanomaterials*; Nurunnabi, M.; McCarthy, J.R., Eds.; Elsevier, **2019**; pp. 43-86. [http://dx.doi.org/10.1016/B978-0-12-815889-0.00003-9]

[16] Zhang, B.; Su, D.S. Transmission electron microscopy and the science of carbon nanomaterials. *Small,* **2013**, 1-8.

Not be distributed or uploaded to anyone or anywhere
For personal private use only

[PMID: 23913822]

[17] Yang, J.C.; Small, M.W.; Grieshaber, R.V.; Nuzzo, R.G. Recent developments and applications of electron microscopy to heterogeneous catalysis. *Chem. Soc. Rev.,* **2012**, *41*(24), 8179-8194. [http://dx.doi.org/10.1039/c2cs35371g] [PMID: 23120754]

[18] Gai, P.L. Developments of electron microscopy methods in the study of catalysts. *Curr. Opin. Solid State Mater. Sci.,* **2001**, *5*(5), 371-380. [http://dx.doi.org/10.1016/S1359-0286(01)00036-5]

[19] Harris, P. J. F. Transmission electron microscopy of carbon: A brief history. **2018**, 1-17.

[20] Guan, L.; Suenaga, K.; Iijima, S. Smallest carbon nanotube assigned with atomic resolution accuracy. *Nano Lett.,* **2008**, *8*(2), 459-462. [http://dx.doi.org/10.1021/nl072396j] [PMID: 18186659]

[21] Suenaga, K.; Wakabayashi, H.; Koshino, M.; Sato, Y.; Urita, K.; Iijima, S. Imaging active topological defects in carbon nanotubes. *Nat. Nanotechnol.,* **2007**, *2*(6), 358-360. [http://dx.doi.org/10.1038/nnano.2007.141] [PMID: 18654307]

[22] Sato, Y.; Suenaga, K.; Okubo, S.; Okazaki, T.; Iijima, S. Structures of D5d-C80 and Ih-Er3N@C80 fullerenes and their rotation inside carbon nanotubes demonstrated by aberration-corrected electron microscopy. *Nano Lett.,* **2007**, *7*(12), 3704-3708. [http://dx.doi.org/10.1021/nl0720152]

[23] Liu, Z.; Suenaga, K.; Harris, P.J.F.; Iijima, S. Open and closed edges of graphene layers. *Phys. Rev. Lett.,* **2009**, *102*(1), 015501. [http://dx.doi.org/10.1103/PhysRevLett.102.015501] [PMID: 19257205]

[24] Sato, Y.; Yanagi, K.; Miyata, Y.; Suenaga, K.; Kataura, H.; Iijima, S. Chiral-angle distribution for separated single-walled carbon nanotubes. *Nano Lett.,* **2008**, *8*(10), 3151-3154. [http://dx.doi.org/10.1021/nl801364g] [PMID: 18729412]

[25] Suenaga, K.; Koshino, M. Atom-by-atom spectroscopy at graphene edge. *Nature,* **2010**, *468*(7327), 1088-1090. [http://dx.doi.org/10.1038/nature09664] [PMID: 21160475]

[26] Meyer, J.C. Transmission electron microscopy (TEM) of graphene. Graphene, Woodhead Publishing, **2014**; pp. 101-123.

[27] Wilson, N.R.; Pandey, P.A.; Beanland, R.; Young, R.J.; Kinloch, I.A.; Gong, L.; Liu, Z.; Suenaga, K.; Rourke, J.P.; York, S.J.; Sloan, J. Graphene oxide: structural analysis and application as a highly transparent support for electron microscopy. *ACS Nano,* **2009**, *3*(9), 2547-2556. [http://dx.doi.org/10.1021/nn900694t] [PMID: 19689122]

[28] Dong, L.X.; Chen, Q. Properties, synthesis, and characterization of graphene. *Front. Mater. Sci. China,* **2010**, *4*(1), 45-51. [http://dx.doi.org/10.1007/s11706-010-0014-3]

[29] Seekaew, Y.; Arayawut, O.; Timsorn, K.; Wongchoosuk, C. Synthesis, characterization, and applications of graphene and derivatives. In: *Carbon-Based Nanofillers and Their Rubber Nanocomposites*; Elsevier, **2019**.

[30] Luong, D.X.; Bets, K.V.; Algozeeb, W.A.; Stanford, M.G.; Kittrell, C.; Chen, W.; Salvatierra, R.V.; Ren, M.; McHugh, E.A.; Advincula, P.A.; Wang, Z.; Bhatt, M.; Guo, H.; Mancevski, V.; Shahsavari, R.; Yakobson, B.I.; Tour, J.M. Gram-scale bottom-up flash graphene synthesis. *Nature,* **2020**, *577*(7792), 647-651. [http://dx.doi.org/10.1038/s41586-020-1938-0] [PMID: 31988511]

[31] Ding, Z.; Yuan, T.; Wen, J.; Cao, X.; Sun, S.; Xiao, L.P.; Shi, Q.; Wang, X.; Sun, R. Green synthesis of chemical converted graphene sheets derived from pulping black liquor. *Carbon,* **2020**, *158*, 690-697. [http://dx.doi.org/10.1016/j.carbon.2019.11.041]

Not be distributed or uploaded to anyone or anywhere
For personal private use only

[32] Dreyer, D.R.; Park, S.; Bielawski, C.W.; Ruoff, R.S. The chemistry of graphene oxide. *Chem. Soc. Rev.,* **2010**, *39*(1), 228-240.
[http://dx.doi.org/10.1039/B917103G] [PMID: 20023850]

[33] Zhu, J.; Li, B.; Xu, M.; Liu, R.; Xia, T.; Zhang, Z.; Xu, Y.; Liu, S. Graphene oxide promotes cancer metastasis through associating with plasma membrane to promote TGF-β signaling-dependent epithelial–mesenchymal transition. *ACS Nano,* **2020**, *14*(1), 818-827.
[http://dx.doi.org/10.1021/acsnano.9b07891] [PMID: 31877027]

[34] Georgakilas, V.; Tiwari, J.N.; Kemp, K.C.; Perman, J.A.; Bourlinos, A.B.; Kim, K.S.; Zboril, R. Noncovalent functionalization of graphene and graphene oxide for energy materials, biosensing, catalytic, and biomedical applications. *Chem. Rev.,* **2016**, *116*(9), 5464-5519.
[http://dx.doi.org/10.1021/acs.chemrev.5b00620] [PMID: 27033639]

[35] Chen, D.; Feng, H.; Li, J. Graphene oxide: preparation, functionalization, and electrochemical applications. *Chem. Rev.,* **2012**, *112*(11), 6027-6053.
[http://dx.doi.org/10.1021/cr300115g] [PMID: 22889102]

[36] Tian, Y.; Yu, Z.; Cao, L.; Zhang, X.L.; Sun, C.; Wang, D.W. Graphene oxide: An emerging electromaterial for energy storage and conversion. *J. Energy.Chem.,* **2021**, *55*, 323-344.
[http://dx.doi.org/10.1016/j.jechem.2020.07.006]

[37] Dave, S.H.; Gong, C.; Robertson, A.W.; Warner, J.H.; Grossman, J.C. Correction to chemistry and structure of graphene oxide *via* direct imaging. *ACS Nano,* **2017**, *11*(1), 1121-1121.
[http://dx.doi.org/10.1021/acsnano.6b07705] [PMID: 28026164]

[38] Dave, S.H.; Gong, C.; Robertson, A.W.; Warner, J.H.; Grossman, J.C. Chemistry and structure of graphene oxide *via* direct imaging. *ACS Nano,* **2016**, *10*(8), 7515-7522.
[http://dx.doi.org/10.1021/acsnano.6b02391] [PMID: 27397115]

[39] Rourke, J.P.; Pandey, P.A.; Moore, J.J.; Bates, M.; Kinloch, I.A.; Young, R.J.; Wilson, N.R. The real graphene oxide revealed: stripping the oxidative debris from the graphene-like sheets. *Angew. Chem. Int. Ed.,* **2011**, *50*(14), 3173-3177.
[http://dx.doi.org/10.1002/anie.201007520] [PMID: 21432951]

[40] Gómez-Navarro, C.; Meyer, J.C.; Sundaram, R.S.; Chuvilin, A.; Kurasch, S.; Burghard, M.; Kern, K.; Kaiser, U. Atomic structure of reduced graphene oxide. *Nano Lett.,* **2010**, *10*(4), 1144-1148.
[http://dx.doi.org/10.1021/nl9031617] [PMID: 20199057]

[41] Li, Z.; Wang, Y.; Kozbial, A.; Shenoy, G.; Zhou, F.; McGinley, R.; Ireland, P.; Morganstein, B.; Kunkel, A.; Surwade, S.P.; Li, L.; Liu, H. Effect of airborne contaminants on the wettability of supported graphene and graphite. *Nat. Mater.,* **2013**, *12*(10), 925-931.
[http://dx.doi.org/10.1038/nmat3709] [PMID: 23872731]

[42] Skákalová, V.; Kaiser, A.B., Eds. Meyer. J. C. Transmission electron microscopy (TEM) of graphene. In: *Graphene*; Woodhead Publishing, **2014**; pp. 101-123.
[http://dx.doi.org/10.1533/9780857099334.2.101]

[43] Luican-Mayer, A.; Li, G.; Andrei, E.Y. Atomic scale characterization of mismatched graphene layers. *J. Electron Spectrosc. Relat. Phenom.,* **2017**, *219*, 92-98.
[http://dx.doi.org/10.1016/j.elspec.2017.01.005]

[44] Bottari, G.; Herranz, M.Á.; Wibmer, L.; Volland, M.; Rodríguez-Pérez, L.; Guldi, D.M.; Hirsch, A.; Martín, N.; D'Souza, F.; Torres, T. Chemical functionalization and characterization of graphene-based materials. *Chem. Soc. Rev.,* **2017**, *46*(15), 4464-4500.
[http://dx.doi.org/10.1039/C7CS00229G] [PMID: 28702571]

[45] Andrei, E.Y.; Li, G.; Du, X. Electronic properties of graphene: a perspective from scanning tunneling microscopy and magnetotransport. *Rep. Prog. Phys.,* **2012**, *75*(5), 056501.
[http://dx.doi.org/10.1088/0034-4885/75/5/056501] [PMID: 22790587]

[46] Luican, A.; Li, G.; Reina, A.; Kong, J.; Nair, R.R.; Novoselov, K.S.; Geim, A.K.; Andrei, E.Y. Single-

Not be distributed or uploaded to anyone or anywhere
For personal private use only

layer behavior and its breakdown in twisted graphene layers. *Phys. Rev. Lett.,* **2011**, *106*(12), 126802. [http://dx.doi.org/10.1103/PhysRevLett.106.126802] [PMID: 21517338]

[47] Robinson, J.T.; Schmucker, S.W.; Diaconescu, C.B.; Long, J.P.; Culbertson, J.C.; Ohta, T.; Friedman, A.L.; Beechem, T.E. Electronic hybridization of large-area stacked graphene films. *ACS Nano,* **2013**, *7*(1), 637-644. [http://dx.doi.org/10.1021/nn304834p] [PMID: 23240977]

[48] Luican, A.; Li, G.; Andrei, E.Y. Scanning tunneling microscopy and spectroscopy of graphene layers on graphite. *Solid State Commun.,* **2009**, *149*(27-28), 1151-1156. [http://dx.doi.org/10.1016/j.ssc.2009.02.059]

[49] Vázquez De Parga, A.L.; Miranda, R. Scanning tunneling microscopy (STM) of graphene. In: *Graphene: Properties, Preparation, Characterisation and Devices*; Skákalová, V.; Kaiser, A.B., Eds.; Woodhead Publishing, **2014**; pp. 124-155. [http://dx.doi.org/10.1533/9780857099334.2.124]

[50] Nanda, S.S.; Kim, M.J.; Yeom, K.S.; An, S.S.A.; Ju, H.; Yi, D.K. Raman spectrum of graphene with its versatile future perspectives. *Trends Analyt. Chem.,* **2016**, *80*, 125-131. [http://dx.doi.org/10.1016/j.trac.2016.02.024]

[51] Wu, J.B.; Lin, M.L.; Cong, X.; Liu, H.N.; Tan, P.H. Raman spectroscopy of graphene-based materials and its applications in related devices. *Chem. Soc. Rev.*, **2018**, *47*(5), 1822-1873. [http://dx.doi.org/10.1039/C6CS00915H] [PMID: 29368764]

[52] Hulman, M. Raman spectroscopy of graphene. In: *Graphene: Properties, Preparation, Characterization and Devices*; Skákalová, V.; Kaiser, A.B., Eds.; Woodhead Publishing, **2014**. [http://dx.doi.org/10.1533/9780857099334.2.156]

[53] Kumar, C.V.; Pattammattel, A. Characterization techniques for graphene. In: *Introduction to Graphene, Chemical and Biochemical Applications*; Kumar, C.V.; Pattammattel, A., Eds.; Elsevier, **2017**; pp. 45-74.

[54] Ferrari, A.C.; Basko, D.M. Raman spectroscopy as a versatile tool for studying the properties of graphene. *Nat. Nanotechnol.,* **2013**, *8*(4), 235-246. [http://dx.doi.org/10.1038/nnano.2013.46] [PMID: 23552117]

[55] Ferrari, A.C. Raman spectroscopy of graphene and graphite: Disorder, electron–phonon coupling, doping and nonadiabatic effects. *Solid State Commun.,* **2007**, *143*(1-2), 47-57. [http://dx.doi.org/10.1016/j.ssc.2007.03.052]

[56] Synetos, A.; Tousoulis, D. Invasive imaging techniques. In: *Coronary Artery Disease, from Biology to clinical practice*; Tousoulis, D., Ed.; Academic Press, **2018**; pp. 359-376. [http://dx.doi.org/10.1016/B978-0-12-811908-2.00018-0]

[57] Cardona, M. *Light Scattering in Solids II*; Springer: Berlin, **1982**, Vol. 50, pp. 19-176. [http://dx.doi.org/10.1007/3-540-11380-0_14]

[58] Wu, J.; Xie, L. Structural quantification for graphene and related two–dimensional materials by Raman spectroscopy. *Anal. Chem.,* **2019**, *91*(1), 468-481. [http://dx.doi.org/10.1021/acs.analchem.8b04991] [PMID: 30408419]

[59] Loudon, R. The Raman effect in crystals. *Adv. Phys.,* **2001**, *50*(7), 813-864. [http://dx.doi.org/10.1080/00018730110101395]

[60] Jorio, A.; Souza Filho, A.G. Raman studies of carbon nanostructures. *Annu. Rev. Mater. Res.,* **2016**, *46*(1), 357-382. [http://dx.doi.org/10.1146/annurev-matsci-070115-032140]

[61] Malard, L.M.; Guimarães, M.H.D.; Mafra, D.L.; Mazzoni, M.S.C.; Jorio, A. Group-theory analysis of electrons and phonons in N -layer graphene systems. *Phys. Rev. B Condens. Matter Mater. Phys.,* **2009**, *79*(12), 125426. [http://dx.doi.org/10.1103/PhysRevB.79.125426]

Not be distributed or uploaded to anyone or anywhere For personal private use only

[62] Nemanich, R.J.; Lucovsky, G.; Solin, S.A. Infrared active optical vibrations of graphite. *Solid State Commun.,* **1977**, *23*(2), 117-120.
[http://dx.doi.org/10.1016/0038-1098(77)90663-9]

[63] Jorio, A.; Dresselhaus, M.; Saito, R.; Dresselhaus, G. *Raman spectroscopy in graphene related systems*; Weinheim, Ger: Wiley-VCH, **2011**.
[http://dx.doi.org/10.1002/9783527632695]

[64] Lan, Y.; Zondode, M.; Deng, H.; Yan, J.A.; Ndaw, M.; Lisfi, A.; Wang, C.; Pan, Y.L. Basic Concepts and recent advances of crystallographic orientation determination of graphene by Raman spectroscopy. *Crystals (Basel),* **2018**, *8*(10), 375.
[http://dx.doi.org/10.3390/cryst8100375]

[65] Ferrari, A.C.; Robertson, J. Interpretation of Raman spectra of disordered and amorphous carbon. *Phys. Rev. B Condens. Matter,* **2000**, *61*(20), 14095-14107.
[http://dx.doi.org/10.1103/PhysRevB.61.14095]

[66] Tuinstra, F.; Koenig, J.L. Raman Spectrum of Graphite. *J. Chem. Phys.,* **1970**, *53*(3), 1126-1130.
[http://dx.doi.org/10.1063/1.1674108]

[67] Childres, I.; Jauregui, L.A.; Park, W.; Cao, H.; Chen, Y.P. Raman spectroscopy of graphene and related materials. In: *New Developments in Photon and Materials Research*; Jang, J.I., Ed.; Nova Science Publishers: Hauppauge, NY, **2013**.

[68] Ferrari, A.C.; Meyer, J.C.; Scardaci, V.; Casiraghi, C.; Lazzeri, M.; Mauri, F.; Piscanec, S.; Jiang, D.; Novoselov, K.S.; Roth, S.; Geim, A.K. Raman spectrum of graphene and graphene layers. *Phys. Rev. Lett.,* **2006**, *97*(18), 187401.
[http://dx.doi.org/10.1103/PhysRevLett.97.187401] [PMID: 17155573]

[69] Geim, A.K.; Novoselov, K.S. The rise of graphene. *Nat. Mater.,* **2007**, *6*(3), 183-191.
[http://dx.doi.org/10.1038/nmat1849] [PMID: 17330084]

[70] Cançado, L.G.; Jorio, A.; Ferreira, E.H.M.; Stavale, F.; Achete, C.A.; Capaz, R.B.; Moutinho, M.V.O.; Lombardo, A.; Kulmala, T.S.; Ferrari, A.C. Quantifying defects in graphene *via* Raman spectroscopy at different excitation energies. *Nano Lett.,* **2011**, *11*(8), 3190-3196.
[http://dx.doi.org/10.1021/nl201432g] [PMID: 21696186]

[71] Vidano, R.P.; Fischbach, D.B.; Willis, L.J.; Loehr, T.M. Observation of Raman band shifting with excitation wavelength for carbons and graphites. *Solid State Commun.,* **1981**, *39*(2), 341-344.
[http://dx.doi.org/10.1016/0038-1098(81)90686-4]

[72] Gupta, A.; Chen, G.; Joshi, P.; Tadigadapa, S.; Eklund, P.C. Raman scattering from high-frequency phonons in supported n-graphene layer films. *Nano Lett.,* **2006**, *6*(12), 2667-2673.
[http://dx.doi.org/10.1021/nl061420a] [PMID: 17163685]

[73] Park, J.S.; Cho, S.M.; Kim, W.J.; Park, J.; Yoo, P.J. Fabrication of graphene thin films based on layer-by-layer self-assembly of functionalized graphene nanosheets. *ACS Appl. Mater. Interfaces,* **2011**, *3*(2), 360-368.
[http://dx.doi.org/10.1021/am100977p] [PMID: 21207942]

[74] Liu, Y.; Liu, Z.; Lew, W.S.; Wang, Q.J. Temperature dependence of the electrical transport properties in few-layer graphene interconnects. *Nanoscale Res. Lett.,* **2013**, *8*(1), 335.
[http://dx.doi.org/10.1186/1556-276X-8-335] [PMID: 23885802]

[75] Lucchese, M.M.; Stavale, F.; Ferreira, E.H.M.; Vilani, C.; Moutinho, M.V.O.; Capaz, R.B.; Achete, C.A.; Jorio, A. Quantifying ion-induced defects and Raman relaxation length in graphene. *Carbon,* **2010**, *48*(5), 1592-1597.
[http://dx.doi.org/10.1016/j.carbon.2009.12.057]

[76] Jorio, A.; Lucchese, M.M.; Stavale, F.; Martins Ferreira, E.H.; Moutinho, M.V.O.; Capaz, R.B.; Achete, C.A. Raman study of ion-induced defects in *N* -layer graphene. *J. Phys. Condens. Matter,* **2010**, *22*(33), 334204-334208.

Not be distributed or uploaded to anyone or anywhere
For personal private use only

[http://dx.doi.org/10.1088/0953-8984/22/33/334204] [PMID: 21386494]

[77] Martins Ferreira, E.H.; Moutinho, M.V.O.; Stavale, F.; Lucchese, M.M.; Capaz, R.B.; Achete, C.A.; Jorio, A. Evolution of the Raman spectra from single-, few-, and many-layer graphene with increasing disorder. *Phys. Rev. B Condens. Matter Mater. Phys.,* **2010**, *82*(12), 125429-125437. [http://dx.doi.org/10.1103/PhysRevB.82.125429]

[78] Saito, R.; Jorio, A.; Souza Filho, A.G.; Dresselhaus, G.; Dresselhaus, M.S.; Pimenta, M.A. Probing phonon dispersion relations of graphite by double resonance Raman scattering. *Phys. Rev. Lett.,* **2001**, *88*(2), 027401-027404. [http://dx.doi.org/10.1103/PhysRevLett.88.027401] [PMID: 11801034]

[79] Cançado, L.G.; Reina, A.; Kong, J.; Dresselhaus, M.S. Geometrical approach for the study of G′ band in the Raman spectrum of monolayer graphene, bilayer graphene, and bulk graphite. *Phys. Rev. B Condens. Matter Mater. Phys.,* **2008**, *77*(24), 245408-245416. [http://dx.doi.org/10.1103/PhysRevB.77.245408]

[80] Jorio, A.; Cançado, L.G. Disorder and Defects in Two-Dimensional Materials Probed by Raman Spectroscopy. In: *Raman Spectroscopy of Two-Dimensional Materials. Springer Series in Materials Science*; Tan, P.H., Ed.; Springer: Singapore, **2019**; Vol. 276, pp. 99-110. [http://dx.doi.org/10.1007/978-981-13-1828-3_5]

[81] Acik, M.; Lee, G.; Mattevi, C.; Pirkle, A.; Wallace, R.M.; Chhowalla, M.; Cho, K.; Chabal, Y. The Role of oxygen during thermal reduction of graphene oxide studied by infrared absorption spectroscopy. *J. Phys. Chem. C,* **2011**, *115*(40), 19761-19781. [http://dx.doi.org/10.1021/jp2052618]

[82] Ţucureanu, V.; Matei, A.; Avram, A. M. FTIR spectroscopy for carbon family study, critical reviews in analytical chemistry. *Crit. Rev. Anal. Chem,* **2016**, *46*(6), 502-20.

[83] Sangermano, M.; Marchi, S.; Valentini, L.; Bon, S.B.; Fabbri, P. Transparent and conductive graphene oxide-polyethylenglycol diacrylate coatings obtained by photopolymerization. *Macromol. Mater. Eng.,* **2011**, *296*(5), 401-407. [http://dx.doi.org/10.1002/mame.201000372]

[84] Ramos-Galicia, L.; Mendez, L.N.; Martínez-Hernández, A.L.; Espindola-Gonzalez, A.; Galindo-Esquivel, I.R.; Fuentes-Ramirez, R.; Velasco-Santos, C. Improved performance of an epoxy matrix as a result of combining graphene oxide and reduced graphene. *Int. J. Polym. Sci.,* **2013**, *2013*, 1-7. [http://dx.doi.org/10.1155/2013/493147]

[85] Layek, R.K.; Nandi, A.K. A review on synthesis and properties of polymer functionalized graphene. *Polymer (Guildf.),* **2013**, *54*(19), 5087-5103. [http://dx.doi.org/10.1016/j.polymer.2013.06.027]

[86] Yu, S.; Liu, J.; Zhu, W.; Hu, Z.T.; Lim, T.T.; Yan, X. Facile room-temperature synthesis of carboxylated graphene oxide-copper sulfide nanocomposite with high photodegradation and disinfection activities under solar light irradiation. *Sci. Rep.,* **2015**, *5*(1), 16369. [http://dx.doi.org/10.1038/srep16369] [PMID: 26553709]

[87] Mallakpour, S.; Abdolmaleki, A.; Borandeh, S. Covalently functionalized graphene sheets with biocompatible natural amino acids. *Appl. Surf. Sci.,* **2014**, *307*, 533-542. [http://dx.doi.org/10.1016/j.apsusc.2014.04.070]

[88] Mittal, G.; Rhee, K.Y.; Park, S.J.; Hui, D. Generation of the pores on graphene surface and their reinforcement effects on the thermal and mechanical properties of chitosan-based composites. *Compos., Part B Eng.,* **2017**, *114*, 348-355. [http://dx.doi.org/10.1016/j.compositesb.2017.02.018]

[89] Kuila, T.; Bose, S.; Khanra, P.; Mishra, A.K.; Kim, N.H.; Lee, J.H. A green approach for the reduction of graphene oxide by wild carrot root. *Carbon,* **2012**, *50*(3), 914-921. [http://dx.doi.org/10.1016/j.carbon.2011.09.053]

Not be distributed or uploaded to anyone or anywhere
For personal private use only

[90] Penkov, O.V. Preparation and characterization of graphene. In: *Tribology of Graphene*; Elsevier, **2020**.

[91] Lefebvre, J.; Galli, F.; Bianchi, C.L.; Patience, G.S.; Boffito, D.C. Experimental methods in chemical engineering: X-ray photoelectron spectroscopy-XPS. *Can. J. Chem. Eng.,* **2019**, *97*(10), 2588-2593. [http://dx.doi.org/10.1002/cjce.23530]

[92] Chen, X.; Wang, X.; Fang, D. A review on C1s XPS-spectra for some kinds of carbon materials. *Fuller. Nanotub. Carbon Nanostruct.,* **2020**, *28*(12), 1048-1058. [http://dx.doi.org/10.1080/1536383X.2020.1794851]

[93] Eigler, S.; Dimiev, A.M. *Characterization techniques in graphene oxide fundamentals and applications*; Eigler, S.; Dimiev, A.M., Eds.; John Wiley & Sons, Inc., **2017**, pp. 85-118.

[94] Scardamaglia, M.; Aleman, B.; Amati, M.; Ewels, C.; Pochet, P.; Reckinger, N.; Colomer, J.F.; Skaltsas, T.; Tagmatarchis, N.; Snyders, R.; Gregoratti, L.; Bittencourt, C. Nitrogen implantation of suspended graphene flakes: Annealing effects and selectivity of sp^2 nitrogen species. *Carbon,* **2014**, *73*, 371-381. [http://dx.doi.org/10.1016/j.carbon.2014.02.078]

[95] Susi, T.; Pichler, T.; Ayala, P. X-ray photoelectron spectroscopy of graphitic carbon nanomaterials doped with heteroatoms. *Beilstein J. Nanotechnol.,* **2015**, *6*, 177-192. [http://dx.doi.org/10.3762/bjnano.6.17] [PMID: 25671162]

[96] Thermoscientific, X.P.S. http://xpssimplified.com/elements/carbon.php

[97] Cooper, A.J.; Wilson, N.R.; Kinloch, I.A.; Dryfe, R.A.W. Single stage electrochemical exfoliation method for the production of few-layer graphene *via* intercalation of tetraalkylammonium cations. *Carbon,* **2014**, *66*, 340-350. [http://dx.doi.org/10.1016/j.carbon.2013.09.009]

[98] Yu, H.; Zhang, B.; Bulin, C.; Li, R.; Xing, R. High-Efficient synthesis of graphene oxide based on improved hummers method. *Sci. Rep.,* **2016**, *6*(1), 36143. [http://dx.doi.org/10.1038/srep36143] [PMID: 27808164]

[99] Kovtyukhova, N.I.; Ollivier, P.J.; Martin, B.R.; Mallouk, T.E.; Chizhik, S.A.; Buzaneva, E.V.; Gorchinskiy, A.D. Layer-by-layer assembly of ultrathin composite films from micron-sized graphite oxide sheets and polycations. *Chem. Mater.,* **1999**, *11*(3), 771-778. [http://dx.doi.org/10.1021/cm981085u]

[100] Ganguly, A.; Sharma, S.; Papakonstantinou, P.; Hamilton, J. Probing the thermal deoxygenation of graphene oxide using high-resolution *in situ* x-ray-based spectroscopies. *J. Phys. Chem. C,* **2011**, *115*(34), 17009-17019. [http://dx.doi.org/10.1021/jp203741y]

[101] Szabó, T.; Berkesi, O.; Forgó, P.; Josepovits, K.; Sanakis, Y.; Petridis, D.; Dékány, I. Evolution of surface functional groups in a series of progressively oxidized graphite oxides. *Chem. Mater.,* **2006**, *18*(11), 2740-2749. [http://dx.doi.org/10.1021/cm060258+]

[102] Hofflund, G.B. Spectroscopic techniques: X-ray photoelectron spectroscopy (XPS), Auger electron spectroscopy (AES) and ion scattering spectroscopy (ISS). In: *Handbook of Surface and Interface Analysis*; Marcel Dekker: New York, **1998**.

[103] Chiu, P.L.; Mastrogiovanni, D.D.T.; Wei, D.; Louis, C.; Jeong, M.; Yu, G.; Saad, P.; Flach, C.R.; Mendelsohn, R.; Garfunkel, E.; He, H. Microwave- and nitronium ion-enabled rapid and direct production of highly conductive low-oxygen graphene. *J. Am. Chem. Soc.,* **2012**, *134*(13), 5850-5856. [http://dx.doi.org/10.1021/ja210725p] [PMID: 22385480]

[104] Siokou, A.; Ravani, F.; Karakalos, S.; Frank, O.; Kalbac, M.; Galiotis, C. Surface refinement and electronic properties of graphene layers grown on copper substrate: An XPS, UPS and EELS study. *Appl. Surf. Sci.,* **2011**, *257*(23), 9785-9790. [http://dx.doi.org/10.1016/j.apsusc.2011.06.017]

Not be distributed or uploaded to anyone or anywhere
For personal private use only

[105] Rabchinskii, M.K.; Ryzhkov, S.A.; Kirilenko, D.A.; Ulin, N.V.; Baidakova, M.V.; Shnitov, V.V.; Pavlov, S.I.; Chumakov, R.G.; Stolyarova, D.Y.; Besedina, N.A.; Shvidchenko, A.V.; Potorochin, D.V.; Roth, F.; Smirnov, D.A.; Gudkov, M.V.; Brzhezinskaya, M.; Lebedev, O.I.; Melnikov, V.P.; Brunkov, P.N. From graphene oxide towards aminated graphene: facile synthesis, its structure and electronic properties. *Sci. Rep.,* **2020**, *10*(1), 6902.
[http://dx.doi.org/10.1038/s41598-020-63935-3] [PMID: 32327708]

[106] Hu, M.; Yao, Z.; Wang, X. Characterization techniques for graphene-based materials in catalysis. *AIMS Mater. Sci.,* **2017**, *4*(3), 755-788.
[http://dx.doi.org/10.3934/matersci.2017.3.755]

[107] Showalter, A.R.; Duster, T.A.; Szymanowski, J.E.S.; Na, C.; Fein, J.B.; Bunker, B.A. An X-ray absorption fine structure spectroscopy study of metal sorption to graphene oxide. *J. Colloid Interface Sci.,* **2017**, *508*, 75-86.
[http://dx.doi.org/10.1016/j.jcis.2017.08.040] [PMID: 28822863]

[108] Bunker, G. *Introduction to XAFS: A Practical Guide to X-ray Absorption Fine Structure Spectroscopy*; Cambridge University Press: New York, **2010**.
[http://dx.doi.org/10.1017/CBO9780511809194]

[109] Papagno, M.; Fraile Rodríguez, A.; Girit, Ç.Ö.; Meyer, J.C.; Zettl, A.; Pacilé, D.; Polarization-dependent, C. Polarization-dependent C K near-edge X-ray absorption fine-structure of graphene. *Chem. Phys. Lett.,* **2009**, *475*(4-6), 269-271.
[http://dx.doi.org/10.1016/j.cplett.2009.05.054]

[110] Wahab, H.; Mertins, H.C.; Timmers, H.; Frankcombe, T.J. X-ray absorption fine structure of carboxyl and other adventitious moieties attached to copper-supported graphene. *Carbon,* **2019**, *141*, 457-466.
[http://dx.doi.org/10.1016/j.carbon.2018.09.086]

[111] Farivar, F.; Yap, P.L.; Hassan, K.; Tung, T.T.; Tran, D.N.H.; Pollard, A.J.; Losic, D. Unlocking thermogravimetric analysis (TGA) in the fight against "Fake graphene" materials. *Carbon,* **2021**, *179*, 505-513.
[http://dx.doi.org/10.1016/j.carbon.2021.04.064]

[112] Farivar, F.; Yap, P. L.; Karunagaran, R. U.; Losic, D. Thermogravimetric Analysis (TGA) of Graphene materials: effect of particle size of graphene, graphene oxide and graphite on thermal parameters. **2021**, *7*(2), 41.
[http://dx.doi.org/10.3390/c7020041]

[113] ISO. Nanotechnologies - Vocabulary - Part 13: Graphene and related two- dimensional (2D) materials. **2017**.

[114] Polini, A.; Yang, F. Physicochemical characterization of nanofiber composites. Ramakrishna, S.; Ramalingam, M. In: *Nanofiber composites for biomedical applications*; Woodhead Publishing, **2017**; pp. 97-115.

[115] Wang, G.; Yang, J.; Park, J.; Gou, X.; Wang, B.; Liu, H.; Yao, J. Facile synthesis and characterization of graphene nanosheets. *J. Phys. Chem. C,* **2008**, *112*(22), 8192-8195.
[http://dx.doi.org/10.1021/jp710931h]

[116] Shtein, M.; Pri-Bar, I.; Varenik, M.; Regev, O. Characterization of graphene-nanoplatelets structure *via* thermogravimetry. *Anal. Chem.,* **2015**, *87*(8), 4076-4080.
[http://dx.doi.org/10.1021/acs.analchem.5b00228] [PMID: 25796961]

[117] Mazurkiewicz-Pawlicka, M.; Nowak, M.; Malolepszy, A.; Witowski, A.; Wasik, D.; Hu, Y.; Stobinski, L. Graphene oxide with controlled content of oxygen groups as a filler for polymer composites used for infrared radiation shielding. *Nanomaterials (Basel),* **2019**, *10*(1), 32.
[http://dx.doi.org/10.3390/nano10010032] [PMID: 31877714]

Not be distributed or uploaded to anyone or anywhere
For personal private use only

CHAPTER 5

Functionalization of Graphene and Factors Affecting Catalytic Performance

Gopal Avashthi[1,2,3] and **Man Singh**[1,*]

[1] *School of Chemical Sciences, Central University of Gujarat, Gandhinagar-382030, Gujarat, India*

[2] *Department of Chemistry, Sankalchand Patel University, Visnagar-384315, Gujarat, India*

[3] *School of Sciences, P P Savani University, Kosamba-394125, Surat, Gujarat, India*

Abstract: Carbon and its driven materials have been a foundation of living and non-living systems for centuries due to their amazing experimental expressions in light, temperature, pressure, and pH. Being light-weighted and electronically active with equal energy partitioning in its four orbitals ($2s^1 2p_x^1 2p_y^1 2p_z^1$), the C atoms have been at the core of natural sciences, providing valuable resources like high-grade wood, cotton, and many others. Thus, carbon-driven materials like diamond, graphite, and graphene ink have been attracting the attention of scientists, researchers, and industries. The chapter reviews recent chemical methodologies for the synthesis and structural investigation of graphene and its derivatives by various analytical techniques that provide information about basic knowledge to understand the role of graphene and graphene-based composites in various qualitative and quantitative applications. Here, several methods have been enlisted for the surface alteration of graphene oxide by a synthetic approach, such as ultrasound, a microwave-assisted synthesis that avoids the use of hazardous chemicals. Also, conventional methods have been discussed, including various types of reactions, such as nucleophilic, electrophilic, condensation, and cycloaddition. This review article highlights the key points to understanding the 2D carbon material for researchers and users to learn about the chemical modification of graphene at the initial stage. This write-up also discusses a brief explanation of various carbon nanomaterials that concern graphene and its oxide forms. We have explained the synthetic value of 2D carbon materials so that it covers a lot of the needs of researchers for synthetic aspects in graphene and allied fields of interest. Currently, such unique experiments are noted as milestones in the field of material synthesis for various applications. So, a review of chemically altered graphene materials reinforced with structural multi-functionalities is highly informative as a ready reckoner for needed information and understanding.

* **Corresponding author Man Singh:** School of Chemical Sciences, Central University of Gujarat, Gandhinagar-382030, Gujarat, India. Tel: +91-079-23260210; Fax: +91-079-23260076. E-mail: mansingh50@hotmail.com

Pinki Bala Punjabi, Rakshit Ameta & Sharoni Gupta (Eds.)
All rights reserved-© 2023 Bentham Science Publishers

Keywords: Covalent Functionalization, Graphene, Non-covalent Functionalization, Surface Modified Carbon Materials, Utrasound and Microwave-assisted Functionalization.

INTRODUCTION TO CARBON CHEMISTRY

Carbon is the fourth most abundant chemical element in the universe and the second most abundant in the human body by mass [1]. The atomic number of carbon is six and it belongs to the second period of the fourteenth group [IVA group] of the periodic table. A carbon atom has six electrons with $1s^2$, $2s^2$, and $2p^2$ electronic configurations, which infer tetravalency. Two inner shell electrons are spherically symmetric; out of which, 1s orbital is tightly close to the nucleus. The energy difference between 1st and 2nd shells is far from the Fermi energy levels, and remaining four valence electrons ($2s^2$, $2p^2$) have very similar energy to silicon. The energy difference between the 2s and 2p orbitals of carbon is relatively low compared to the bond enthalpy. The tetravalent nature of carbon and its distinctive catenation property can be accessible for hybridization, forming new compounds. Thus, 2s and 2p orbitals hybridize (Fig. **1a,b**). The catenation property of carbon results in stable allotropes of 0D, 1D, 2D, and 3D dimensionality compared to other elements [2].

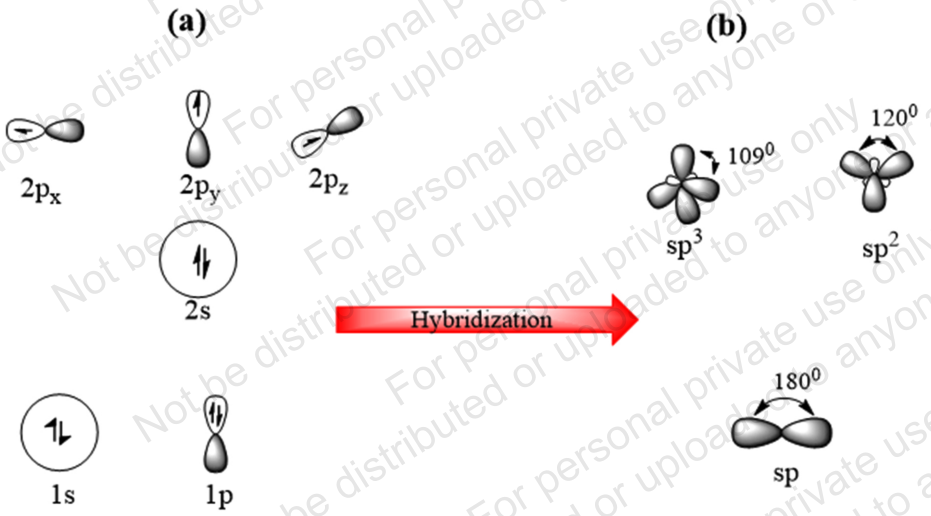

Fig. (1). (**a**) Diagram of atomic orbitals, and (**b**) hybrid orbitals of carbon.

POLYMORPHISM OF CARBON

Carbon has the ability to bind with various elements like H, Si according to optimal hybridization, supporting the synthesis of compounds with different

structural properties and applications. Therefore, newly synthesized compounds have different geometrical features, like sp hybridized carbon which is linear in nature, while sp^2 and sp^3 have trigonal planar and tetrahedral structures, respectively [2]. The one p and one s-orbital hybridize as sp while, two p and one s-orbital hybridize as sp^2 carbon, and remaining unhybridized orbitals participate in forming an additional π bond. Therefore, the tetrahedral lattice of the diamond (Greek 'adamant' meaning impossible to tame) belongs to sp^3-hybridized carbon atoms in terms of strong covalent bonding to itself [1, 2]. The wave function of four valence electrons ($2s^2$ and $2p^2$) of carbon, hybridize easily and it adds to the solid-state features of sp^2 hybridized graphite (Gt). The diamond and Gt are two natural allotropes of carbon. The diamond and Gt allotropes have been known since prehistoric times for their distinctive properties such as hardness, thermal conductivity, and lubrication behaviour [3, 4]. In the last few decades, the surprising discoveries of three artificial allotropes of carbon, *i.e.*, 0D fullerene, 1D carbon nanotube, and 2D graphene (Gr) have confirmed the efficiencies of carbon materials for their amazing applications [1 - 8] (Fig. **2a-e**).

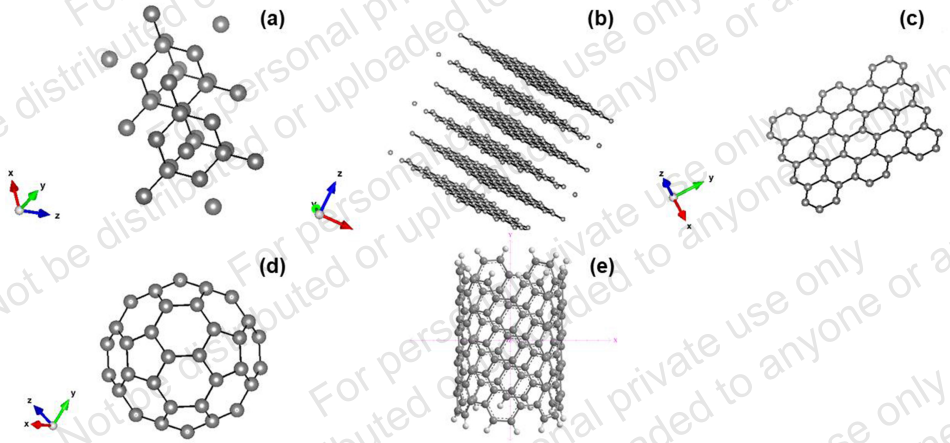

Fig. (2). Carbon allotropes (**a**) Diamond, (**b**) Graphite, (**c**) Graphene, (**d**) Fullerene, and (**e**) Carbon nanotube.

Natural Allotropes

Diamond

Diamond is a sp^3 hybridized natural allotrope of carbon with structurally strong C-C covalent bonds [1, 2]. The crystal structure (Figs. **3a, b**) of the diamond is known for its excellent properties; such as high Young's modulus, hardness (hardest material with a supreme Mohs value of 10), chemical inertness, low electrical conductivity, high thermal conductivity (900–2,320 W/m/K), high X-ray, and high optical scattering ability of visible spectrum 1-1.5 eV [1, 9, 10].

Natural diamond, high-pressure synthetic diamond, low-pressure synthetic diamond, and metastable carbon or diamond-like carbon are the four types of diamonds known to date [8]. Natural diamonds are produced at a high temperature and pressure in volcanic eruptions. Moreover, English chemist H. Davy proved that the burning of diamonds produced only CO_2. Initially, in 1955, the first unquestioned high-pressure synthetic diamond was synthesized in the Institute for High-Pressure Physics of the Soviet Union, the U.S. and Sweden. It was commercialized for various industrial applications such as wear, abrasive, and tools. The preparation of low-pressure synthetic diamond is based on chemical vapour deposition (CVD). A diamond-like carbon is produced by a thin coating at low pressure [8]. The C-C strong covalent bonds in diamond are responsible for the thermal conductivity as well as its valuable applications in microelectronics, optoelectronics, and carbon fibre electronics. Diamond acts as an insulator at RT with a resistivity 10^2 Ω and a wide bandgap (~5.5 eV) [11, 12].

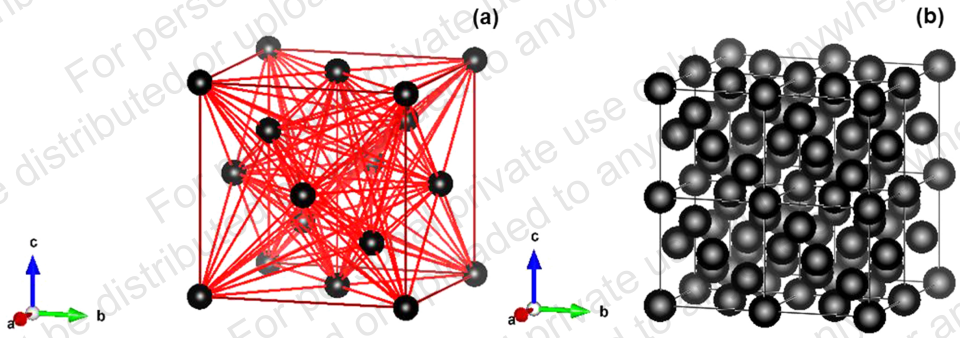

Where a, b, and c are primitive lattice vectors:

Fig. (3). (a) Crystal structure of diamond, and **(b)** fcc lattice with a set of primitive lattice vectors.

The direct lattice (linear combinations) for the diamond is stated to be face-centred cubic (fcc) (Fig. **3b**) with primitive lattice vectors a, b, and c. The dissimilarities of primitive lattice vectors shown in Figs. (**3a** and **b**) are given below:

$$a = (0, a/2, a/2),$$

$$b = (a/2, 0, a/2),$$

$$c = (a/2, a/2, 0),$$

where a, b, and c are the lengths of the edges of the smallest cube in the fcc lattice. The unit cube, or crystallographic unit cell, is the smallest cube of the direct lattice [10]. The CVD-synthesized diamonds have potential applications in

various fields such as electronics, optics, mechanics, thermals, chemicals, and others. The supreme hardness of a diamond is useful for cutting-edge applications. In chemical synthesis of nanodiamonds (NDs), the detonation process retains heterogeneous functional moieties such as carbonyl, alcohol, epoxy, ether, and unsaturated double bonds on ND surfaces. The surface functionalization of DNDs to produce highly unstable intermediates such as acyl and ester is accountable for amidation and esterification [12 - 14]. Thus, newly functionalized NDs have various applications in biomedical engineering, biophysics, electronics, optical devices, and mechanical studies. Recently, the NDs have been utilized as drug carriers due to their stable dispersibility subjected to drug and gene delivery and imaging systems [12 - 15].

Graphite

3D flakes of Gt are amorphous and crystalline in nature. The multi-layered planar hexagonal 2D sheets of Gr are stacked by weak Van der Waals forces. In each plane, the carbon atoms are arranged in such a way that each carbon atom is sp^2 hybridized along the hexagon lattice [16] (Fig. **4a,b**). The length of the hexagon lattice is 0.142 nm and the interplanar distance is 1 nm. Due to weak interactions between the sheets, the Gt is reported as the softest natural material (Mohs hardness of 1). Its electrons move over the sheets and, being a soft material, graphite is used as a lubricating agent in industries [1 - 5]. However, the reason for the interaction between the sheets is not entirely understood. Unlike diamond, the delocalized π-electron clouds over the sheets of Gt produce good electrical conductivity [17, 18]. Gt and graphite oxide (GtO) are used in the synthetic transformations as carbocatalysts to avoid hazardous organic reagents and solvents. The Gt acts as a carbocatalyst in microwave, conventional, and ultrasound-assisted synthesis, offering various synthetic transformations such as reduction of substituted nitro functionalities to their respective amines using hydrazine hydrate, cleavage of ethers followed by coupling with an acyl halide, Friedel-Crafts-type substitution, Diels-Alder reaction, cycloaddition reactions, and ene-cyclization. Also, GtO is used as a selective and highly efficient oxidant of thiols and sulphides [19 - 25]. Oxidation of Gt produces GtO which further facilitates ultrasound-assisted exfoliation into graphene oxide (GO) followed by surface functionalization [18, 26 - 31]. Birch reduction of Gt with lithium in liquid ammonia gives a highly reduced exfoliated product which is free from metal. The reduction is due to edge and interior hydrogenation [32]. Gt, GtO, reduced GtO and surface functionalized GO composites are found to be potentially applicable in electrical, optical, mechanical, energy storage devices, capacitors, and biological areas of research and industries [18, 27, 33, 34].

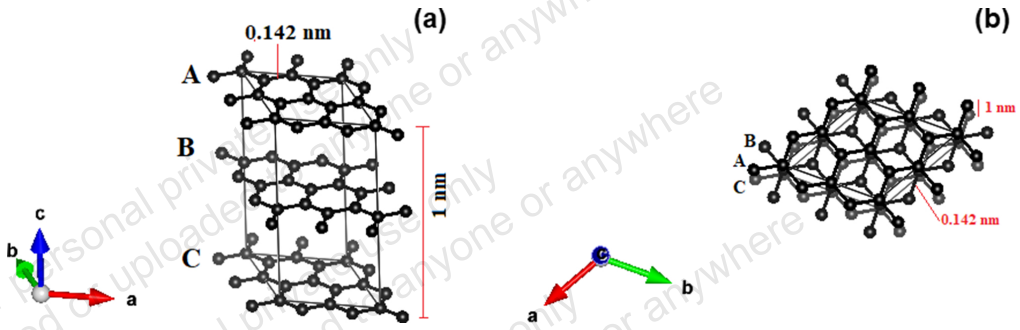

Fig. (4). (**a**) Layers sequencing in hexagonal, and (**b**) Rhombohedral graphite (front view).

Synthetic Allotropes

Fullerene

Fullerene is a 0D synthetic allotrope of carbon with a face-centred cubic crystal lattice. The credit of fullerene's discovery goes to a group of scientists including Richard Smalley, Robert Curl, Harry Kroto, and Heath and O'Brien, at Rice University, Huston, who compared the structure of fullerene with the geodesic dome model of American architect Buckminster fuller. In 1996, Richard Smalley, Robert Curl, and Harry Kroto were awarded the Nobel Prize in Physics [35]. They proposed the icosahedron shape of the molecule possessing 32 faces, 60 apexes (carbon atoms) and 90 ribs within 12 pentagons and 20 hexagon rings to make a spheroid shape of the molecule. The point group symmetry of this molecule is I_h [36]. The chemical stability of the closed-hollow-cell of C_{60} is proved by a large energy gap between HOMO and LUMO [36 - 38]. The Van der Waals diameter of fullerene is 10.1 Å and the nucleus-to-nucleus diameter of C_{60} is 7.09 Å. The C-C bond length between two hexagons is 1.40 Å. It is considered as a double bond and slightly shorter than the C-C bond length of hexagon-pentagon *i.e.* 1.46 Å [36 - 38]. The functionalization of fullerene comprises exohedral and endohedral orientations, depending on the added substituents outside and trapped inside the cages. The chemistry of fullerene covers a wider range of chemical reactions like nucleophilic addition, electrophilic addition, electrocyclic reactions, radical addition, metal doping, and supramolecular complexation [39 - 57]. The exohedral modification of fullerene cages has been done by reacting with sulphur-containing group thiols, thioethers to facilitate the adsorption on the metal surfaces [39] and explored for their applications in various research areas and industries. C_{60} acts like a 2π electron-deficient dienophile and dipolarophile, hence enduring cycloaddition reactions such as [2+2], [3+2], and [4+2] on the 6, 6-ring junctions of the fullerene skeleton, either thermally or photochemically [40, 41]. The reactive divalent species, a carbene, has synthesized new derivatives and

enhanced the reactivity of fullerene [42]. In a one-pot reaction, a charged zwitterion intermediate with added nucleophiles with multiple functional groups is fitted onto the fullerene [43]. Fullerene has been named "radical sponge" due to its extraordinary reactivity towards radical species. Therefore, the highly reactive species are very attractive for functionalization [44, 45]. Although fullerene is insoluble in water, treatment with hydrogen peroxide converts it into a water-soluble polyhydroxy functionalized fullerene. Apposite functionalization of fullerene also makes the molecule soluble in water. Hence, water-soluble derivatives interact with DNA, protein, and living cells and find biomedical applications [46, 47]. There is aggregation of fullerenes into colloidal crystals due to fullerene-fullerene and fullerene-water driving forces in an aqueous or biological medium. Most of the photoactivity of nC_{60} is lost during the process, whereas aggregates of hydrophilic functionalized nC_{60} may or may not have reduced photoactivity, depending on the functional characteristics [47, 48]. Fullerene-based Friedel-Crafts arylation, alkylation, and acylation are multistep procedures for functionalization in synthetic chemistry [49]. The hydrogenation reaction is accomplished *via* the Birch reduction. The reaction of fullerene with hydrogen atoms makes hydrofullerenes, similar to the addition of H_2 at the C=C double bond, which results in the adduct of two C-H bonds [50]. The radical derivative of the fullerene is analysed by the most efficient analytical technique, *i.e.*, electron spin resonance (ESR) spectroscopy [51]. Fullerene and its alkali-doped composites such as M_3C_{60} (M is an alkali metal) [37, 52 - 54] and organic ferromagnets have been found as superconductors [54, 55]. The vast array of chemical reactivity promises a growth of various fullerene-based materials with their uses in polymer chemistry [56], biological applications [57, 58], catalysts [59, 60], organic electronics [61], photovoltaic [62], and thin-film transistors [63, 64].

Carbon Nanotube

In the year 1991, Sumio Iijima discovered the multi-walled carbon nanotube (MWCNT) [65], with multiple coaxial tubular units of single-walled carbon nanotube (SWCNT) rolled up by Van der Waals forces [66, 67]. MWCNTs are multi-stacked structures with unique properties [65 - 68]. SWCNT can be synthesized by various methods, such as chemical approach (Fig. **5**) [67], arc discharge [68], laser ablation [68], and CVD [69]. The principle of SWCNT synthesis implies that the hexagonal honeycomb carbon lattice of single-layer Gr gets rolled up into cylindrical helical hexagonal microtubules with a diameter range of 1-2 nm [70, 71]. CNT acts as a nanomechanical resonator in water to enhance the viscosity at low temperatures. It also applies to the mass measurement of biological molecules and various sensing applications due to their lightweight

nature, characteristic ultrahigh mechanical strength, and high surface activity [72, 73].

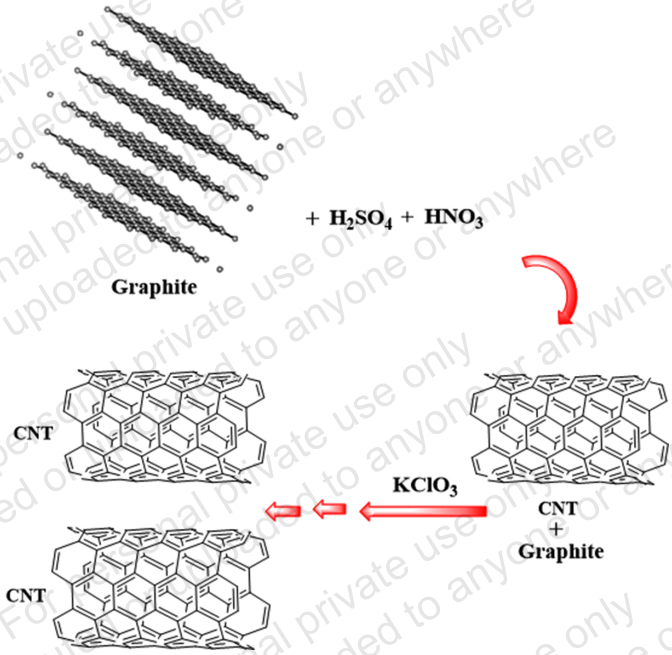

Fig. (5). Graphical representation of CNT synthesis by chemical approach.

The functionalization of CNT with organometallic compounds, metals, organic compounds, and biological molecules helps to manipulate the bandgap and heterojunction energetics [74 - 77]. Transformation of the assembled SWCNT into ultrathin long CNT fibrils has a great potential for applications as conductive wires and probe electrodes in industries [78]. The strength, small dimensions, and electronic, optical, and chemical properties of CNT-composite materials open a new direction for innovative applications, including [74 - 77, 79], energy storage electronic and semiconductor devices [80, 81], hydrogen storage media [82, 83], and high-performance hydrogen production devices [84].

Graphene

The Single-layered isolated sheet from Gt, is noted as Gr, which was first discovered through mechanical exfoliation using the “Scotch-tape” method from bulk Gt [85]. Epitaxial CVD [86] is also considered as a suitable method to grow Gr. The first experimental Gr was reported by Hanns-Peter Boehm in 1962, but it was not experimentally proven for so many years [87]. The comprehensive Gr study was started by Novoselov and Geim after getting the exfoliated single layer

Gr in 2004 and both were awarded the Nobel Prize in 2010 for ground-breakthrough research and its extraordinary properties. The atomic-level thin Gr possesses a 2D planar structure, having sp^2-hybridized carbon atoms with high charge mobility, mechanical properties (breaking strength ~40 N/m, Young's modulus~1.0 Tpa), thermal properties (at RT thermal conductivity~3000 $Wm^{-1}K^{-1}$), electronic, quantum hall effect, spin transport, and magnetism [85 - 94]. The electronic behaviour of materials is characterized in terms of the Fermi surface and controlled by external electric and magnetic fields [95 - 100]. However, due to the synergistic impact of nitrogen, N-doped Gr has become a promising material for various applications such as batteries, electronics, sensors, catalysis, and supercapacitors [96 - 100]. Furthermore, the ultrasound and microwave-assisted methods for surface modification of Gr have a wide range of applications [101 - 121]. In synthetic chemistry, unmodified Gt, GtO, and their derivatives catalyze redox reactions, alkylation, cycloaddition, and Friedel-Craft reactions [102 - 112]. The covalent functionalization of Gr could be demonstrated with the help of reactive intermediates such as radicals, nitrenes, carbenes, arynes, and nucleophilic substitutions like amidation or esterification [113 - 116]. The non-covalent approach for the surface modification of carbon-based materials comprises π-π stacking between the Gr surfaces and various biological molecules to synthesize bio-conjugates-proteins, enzyme-drug, DNA-protein complexes, and supra molecules-inorganic metallic complexes [119 - 121]. The impact of surface modification of Gr and graphene oxide (GO) demonstrates excellent electrical, mechanical, and optical properties, which could be further explored for the development of several biomedical devices, industrial metallic goods, conductors, energy storage devices, and transistors [120, 121]. The surface modification of Gr by using a robust chemical approach is the latest thrust area in the field of carbon nanotechnology to explore its several potential applications [102 - 116]. More-over, CNT and Gr are both carbon-based functional nanostructures, and they have different properties due to the diverse nature of their geometries which are planar in Gr and tubular in CNT.

REFINING OF GRAPHENE OXIDE

Initially, four methods were introduced in GtO synthesis. Each successive method has advancement in the simplicity, degree of oxidation, yields, and product quality. The impurities, *i.e.*, highly flammable salts and acids, are a major problem for GtO synthesis and purification, which makes it a dull procedure in GtO production. Multiple time washing, centrifugation, and filtration are important steps for the purification of GtO. Inorganic salts and acids are both quite water-soluble, but the purification of them is not easy since a gelatinous appearance of dispersed GtO is observed due to an increase in pH during washing

with water, which slows down the further purification, centrifugation, and especially filtration processes. Another best procedure for purification involves two-step washing with aqueous HCl and acetone to avoid gelation and accelerate the synthesis of purified GtO. Therefore, GtO is washed with an excess amount of HCl to remove salts and ions effectively, then acetone is used to eliminate the acid to make the pH neutral, which avoids gelation. The GtO is air-dried and allowed to disperse in acetone after 3 to 4 washes with HCl, followed by filtration and washing with more acetone, which removes residual HCl without gelation. In 1974, a similar purification process was described by Nikolaev *et al.* This purification method does not damage the various functionalities present over the surface. Thus, the solid GtO synthesis at a large scale can be achieved by filtration and vacuum drying. The salt content of GtO, washed with HCl and acetone 3 to 4 times, is measured. If the concentration is lower than 0.1 wt.%, then it goes unnoticed by Energy Dispersive X-Ray (EDX). Therefore, the purified GtO is quite stable against ignition. The GtO obtained by this method is utilized as a precursor in graphene synthesis [122].

SURFACE FUNCTIONALIZATION OF GRAPHENE OXIDE FOR STRENGTHENING CATALYTIC PERFORMANCES

Fabrication of Gr is cost-effective as compared to other carbon materials. Therefore, the researchers have focused their attention on exploring this material for various vital applications *via* surface modification of Gr, also known as the functionalization of Gr (f-Gr). Chemical functionalization of Gr avoids agglomeration and aids to sustain the intrinsic properties [122]. GtO is utilized as a starting material for the synthesis of Gr through chemical, thermal and photochemical reduction [123 - 127]. Oxidation of Gt helps to synthesize GtO, possessing various oxygenated functionalities over the surface, *i.e.*, hydroxyl, epoxide, diol, ketone, carboxyl, phenol, lactone and quinone [128 - 134]. The active functional groups expand the intercalative distance, to reduce interlayer Van der Waals forces. These help to improve the solubility and stability in water and organic solvents [135 - 139]. The presence of carbonyl and carboxyl groups at the edges of GtO sheets, makes it strongly hydrophilic and make stable dispersion in water using sound energy [135 - 137]. The different structures of GtO has been explained in the literature [128, 140]. But the stability of Gr is the necessity for chemical reduction of GtO due to rapid irreversible aggregation of the graphene sheet. Hence, the surface functionalization is linked with the composite materials which are synthesized by covalent and non-covalent functionalization [101].

Covalent Functionalization

Oxidation of the Gt produces various functionalities over the Gr surface. The numerous oxygenated functional groups on the Gr surface offer covalent modification. The aim of surface alteration of Gr in organic solvents is the stable dispersion to synthesize new composite materials for various applications. The principle of functionalization is to rehybridize one or more sp^2 carbon atoms into sp^3, which deals with the bandgap engineering by losing the conjugated electrons [2, 141]. The covalent modification of Gr can be achieved in four different ways [142 - 178].

1. Nucleophilic substitution reaction

2. Electrophilic substitution reaction

3. Condensation reaction

4. Addition reaction

Nucleophilic Substitution Reaction

The nucleophilic substitution reaction of GO is based on the accessibility of epoxy and carboxylic acid groups over the surface of dispersed GO in the aqueous and organic solvent phases. It has been reported that the epoxy and hydroxyl functional groups lie above and below, while the carboxyl group is at the edge of the carbon layer. Surface functionalization of GO with amine substituted organic compounds is simple at RT as a result of nucleophilic substitution and condensation reactions. Amide bond formation is one of the most vital reactions in organic chemistry because of its extensive applicability in the synthesis of modern biological and pharmaceutical compounds. The Lone pair electron of amine attacks the epoxy or electrophilic carbon center of the carboxyl group of GO. Since then, this method has been known for the large-scale production of functionalized (f) Gr. The acyclic and aromatic amines, amino acids, amine substituted biomolecules, ionic liquids, and small molecular weight polymeric compounds are functionalized with graphene oxide (f-GO) [101 - 104, 112 - 116, 120, 142 - 151]. Athanasios B. Bourlinos *et al.* explored the primary amines, possessing chemical formulas equivalent to $C_nH_{2n+1}NH_2$ (n = 2, 4, 8, 12, 18) of amino acids and nucleobases for surface modification of GtO and GO at RT [146 - 148]. Thus, the reaction condition depends upon the size of amine-substituted compounds. For a long-chain aliphatic amine, the reaction mixture is heated under reflux for several hours. The surface functionalization enhances the stability and dispersibility of f-GO in water and organic solvents. X-Ray Diffraction (XRD)

verified the functionalization of GtO at higher interlayer spacing (d-spacing) due to the amidation of GtO with amine substituted molecules [147]. The reaction between amino acids and GtO occurs in an alkaline solution due to the hydrophilicity of GtO. According to Bourlinos et al., the tilted orientation is more likely to occur due to its hydrophilicity [147]. Fan Zhang *et al.* for the first-time synthesized guanine-based covalently modified Gr. According to Fan Zhang, the amine group of guanines is covalently attached to the GOCl group, which is made *via* reacting COOH with $SOCl_2$. Thus, the synthesized compound is highly soluble in organic solvents with good potential in nanoelectronics [148]. The GO sheets were functionalized with the amine-end of the ionic liquid. The resulting composites were well dispersed in water, DMF, and DMSO without any addition of polymer or surfactant stabilizers [149].

Sang Hwa Shim *et al.* have shown a method to convert the hydrophilic groups of GO into alkyl or alkyl ether *via* a single-step bimolecular substitution reaction with alkyl bromide. Thus, the f-GO is dispersed as exfoliated sheets in various solvents, accomplished by covalent modification. The substitution of f-GO with solvophilic groups like polyethylene terephthalate (PET) on a small scale improves the electronic, mechanical tensile strength, and optical properties [152]. The dispersibility of GtO in organic solvents is potentially applicable to synthesizing polymeric-based composites [120, 153 - 157]. The GO surface was modified by an amidation reaction between carboxylic acid and amine substituted alkylamine [147], and esterification between carboxyl groups and alcohol polyvinyl alcohol [116]. Sungjin Park *et al.* produced a homogenous colloidal suspension of Gr sheets with the addition of polyallylamine to an aqueous suspension of GO sheet. Thus, this type of cross-linked sheet possesses outstanding mechanical stiffness and strength [153]. Wei-Hao Liao *et al.* have studied the fabrication of amine-substituted GO-polyimide composite film with high-performance capability using in-situ polymerization [154]. Zhiyuan Xu *et al.* made a polymeric composite of GO with 6-armed polyethylene glycol (PEG) by facile covalent amidation under mild conditions to make modified GO. GO-PEG was biocompatible in physiological solution and nontoxic to human lung cancer A-549 and human breast cancer MCF-7 cells. It was tested *via* cell feasibility examination [155]. Sunanda Roy *et al.* have established an effective chemical alteration with polyethylneimine (PEI) that converts into modified GO, which can extensively increase the overall strength of the nylon-12 composite. This method overcomes the drawbacks of developing advanced graphene-based polymer composites. Poor dispersibility is caused by factors such as restacking, weak interfacial bonding, and incompatibility with polymeric matrices, all of which suppress the potential action of Gr sheets [156]. GO esterification proceeds through converting the COOH of GO into an acyl chloride reacting with $SOCl_2$. Then, alcohol was substituted with organic molecules such as hydroxypropyl

cellulose or chitosan, which further covalently binds to the activated graphene oxide through esterification [116, 157].

Electrophilic Substitution Reaction

The synthesis of f-Gr or f-GO is based on an electrophilic substitution reaction in which a hydrogen atom is replaced by an electrophile [158 - 165]. The high electron density of the Gr induces more reactivity towards the strong electrophile. The substitution reaction was attained *via* grafting of aryldiazonium salt, Friedel–Crafts acylation and hydrogen–lithium exchange methods [158 - 165]. The diazonium salt of p-nitroaniline and 4-bromoaniline or para-nitro substituted aryl compounds have been embedded on the Gr surface [159 - 161]. M. Tour *et al.* have synthesized organic-soluble Gr by electrophilic substitution of aryldiazonium salt on the surfactant wrapped Gr surface [159, 160]. 4-bromoaniline was used for edge-selective functionalization [161]. Thus, chemically functionalized Gr is more dispersible than pristine Gr. The Friedel-Crafts acylation is still the only method for introducing the aryl ketone group onto the Gr surface [164]. A Friedel-Crafts acylation occurs through an intermediate of an acyl anion which is catalyzed in the presence of Lewis acid. Recently, T. Govindaraju *et al.* proposed the Friedel Crafts acylation of an exfoliated single-layer GO with ferrocene at RT. The reaction was achieved by making a solution of ferrocene in dichloromethane, which was adsorbed on acidic alumina by adding trifluoroacetic anhydride at RT [162].

Fang, Wang *et al.* have synthesized covalently f-GO using polystyrene through a three-step mechanism subsequently followed by oxidation of Gt, fixing of the atom through radical initiator and in-situ polymerization to the surface of a reduced Gr sheet [163]. In hydrogen-lithium exchange methods, the metal-substituted aromatic compounds (Ar-M) are more reactive than simple aromatic compounds (Ar-H). The metallated aromatic compounds are more reactive towards the electrophile for the formation of a covalent bond. It increases the length of the aromatic ring. Yan and co-workers proposed the functionalization of Gr using hydrogen-lithium exchange (deprotonation/carbometallation and subsequent electrophilic attack) method [165]. However, towards making a new solid catalyst with trimethylamine, it shows an electrophilic substitution reaction [164, 165]. The f-GO exhibited higher catalytic activity than sodium hydroxide for hydrolysis of ethyl acetate [164]. Jin Suk Chung *et al.* have proposed a new idea for the functionalization of Gr through a solvothermal process by using GO and NMP as precursors [166]. The solvothermal reduction and functionalization occur *via* generated free radicals from NMP and proceed similarly as in the functionalization of Gr by aryldiazonium salts [158 - 161, 166]. The restoration of electronic conjugation of C=C in Gr increases with reaction time. The f-Gr forms

a stable dispersion in organic solvents. Thus, the electrical conductivity of f-Gr is more efficient than pristine Gr [166].

Condensation Reaction

The condensation reaction is carried out by combining two compounds (functional groups) into a single molecule with a loss of energy. The condensation reaction of Gr takes place with isocyanate, diisocyanate, and amine through amide and carbamate ester linkages [164, 167 - 172]. Yanfei Xu *et al.* proposed a condensation reaction between 5-4-(aminophenyl)-10,15,20-triphenylporphyrin (TPP) and GO *via* an amide linkage. Modified GO was standardised and optimised for homogeneous dispersion in DMF. Consequently, the addition of the TPP-NH_2 has changed the electronic properties of GO, but no major effect is detected on the TPP-NH_2 part individually. The prevention of agglomeration is significant for processability and applications. Fluorescence quenching and energy loss occur as a result [167]. Zhuang Liu *et al.* have functionalized nanoscale graphene oxide (NGO) sheets (50 nm) by branching with biocompatible polyethylene glycol (PEG) to achieve higher aqueous solubility and stability in physiological solutions of serum. Thus, the unique features of Gr are revealed for drug delivery with water-insoluble aromatic drugs. The solubility of the drug decreases its efficacy. It revealed that PEGylated NGO (NGO-PEG) easily synthesizes complexes with water-insoluble drugs *via* noncovalent Van der Waals interaction. The hybrid NGO-PEG-SN38 composite displays excellent aqueous solubility and holds the high influence of free SN38 dissolved in organic solvents. The toxicity exceeds that of irinotecan (CPT-11, an FDA approved SN38 prodrug for colon cancer treatment) by 2-3 times [168]. Jianfeng Shen *et al.* functionalized GO nanosheets (GOS) with bovine serum albumin (BSA) *via* diimide-activated amidation. The GOS–BSA complex is highly water-soluble. BSA protein was used in this study; it contains 60 amino moieties in lysine and 26 arginine units in guanidino side chains. Infrared spectroscopy reveals the strong bands at 1690 and 1570 cm^{-1} for N-H stretching frequency of amide I and amide II, respectively. The thermogravimetric analysis (TGA) curves presented the lower thermal stability of f-GO compared to GO. AFM and Raman have demonstrated surface-functionalized GO. This method was used to synthesize the next generation of functionalized GO, with applicability for various applications [169].

Yuhua Xue *et al.* synthesized a polyhedral oligomeric silsesquioxane (POSS)-functionalized GO through an amide bond which is highly soluble in various organic solvents including tetrahydrofuran (THF), dichloromethane, chloroform, toluene, hexane, and acetone. Thus, POSS-Gr has developed super-hydrophobicity with a water/air contact angle of 157°. It could be utilized for the

construction of liquid marbles. The hybrid POSS-Gr was also used as nanofiller to raise the glass transition and decomposition temperature of polymers [170]. Sasha Stankovich *et al.* used several isocyanate compounds for surface functionalization of GO. Since the isocyanates functionalized graphene oxide (iGO) formed a stable dispersion in polar aprotic solvents, The functionalization of the hydroxyl and carboxyl groups in GO occurs through the formation of amides and carbamate esters, respectively. The efficiency of the functionalization is controlled by the isocyanates' reactivity or reaction time. iGO was not completely dispersed in the water. It was formed a colloidal dispersion in apolar aprotic solvents such as dimethyl sulfoxide (DMSO), hexamethylphosphoramide (HMPA), N-methyl pyrrolidone (NMP), and DMF using sonochemical technique. iGO material does not disperse in less polar solvents, such as THF, acetone, toluene, methylene chloride, or common polar solvents, such as ethanol and methanol. The stable brown dispersion of phenyl iGO in DMF contains no precipitate. Thus, the mechanism is very useful for the preparation of polymeric nanocomposites. Hence, isocyanate and diisocyanate are useful in GO modification through cross-linkage. The functionalization occurs through the formation of a covalent (amide linkage) bond between Ar-COCl (produced by the reaction of GO with $SOCl_2$) and the NH_2 functional group of octadecylamine (ODA) [171]. Mitra Yoonessi *et al.* proposed that the synthesized polyimide nanocomposite be shown to have superior mechanical properties and good compatibility with N-methyl-2-pyrrolidone. Since then, the thermal stability of polyimide nanocomposite has been enhanced by the addition of Gr [172].

Cycloaddition Reaction (Pericyclic Reaction)

The cycloaddition reaction differs from most of the organic reactions in which the formation of cation and anion is not essential. The electrons are moved cyclically, with the bond making and breaking spontaneously. The Cycloaddition reaction of Gr offers a new route for improving the bandgap, dispersibility, and solubility. There are four types of graphene cycloaddition reactions: 1,3 dipolar cycloaddition, [2+2] cycloaddition, Diels Alder reaction, and [2+1] cycloaddition reaction [101, 150, 164, 173 - 178]. The 1,3 dipolar cycloaddition reaction, also known as [3+2] cycloaddition, occurs *via* six electron cycloaddition between 1,3 dipolar and dipolarophile (graphene) to produce five-membered rings of azomethine ylides on Gr (functionalized Gr). Mildred Quintana *et al.* have prepared functionalized Gr by condensation of formaldehyde and protected a-amino acid, followed by a deprotection of the t-butyl carbamate group (Boc group). Meanwhile, functionalized Gr has developed a new method for making nanocomposite materials by using gold nanorods [164, 173]. The azomethine ylides are unstable in most of the cases of functionalization and are made by the decarboxylation of carbonyl species and an N-methylglycine (sarcosine). Other

than the edges, 1,3 dipolar reactions also occur at the C=C of the centre of the Gr sheet. Aijian Wang *et al.* proposed two possible routes for covalent functionalization of reduced GO (RGO) with porphyrin moieties by 1,3 dipolar reactions. The first method involves reacting RGO with sarcosine and 4-hydroxybenzaldehyde in dimethylformamide (DMF) at 145 °C, followed by nucleophilic substitution with w 5-[4-(2-bromoethoxy) phenyl]-10,15,2--triphenylporphyrin (TPP 1) in DMF and K_2CO_3 at 80 °C to derivatize RGO [174]. The second method involves making a formyl-inclosing porphyrin 5-[4--2-(4-formylphenoxy) ethyloxy) phenyl]-10,15,20-triphenylporphyrin (TPP 2) that is attached to the RGO through azomethine ylide. The attachment of RGO with porphyrin ensures efficient electron and energy transfer between them and improves the optical and electronic properties compared to the RGO and pristine Gr [174]. [2+2] cycloaddition comprises the four-electron cyclization process with Gr.

Zhong *et al.* have established a new efficient approach for the synthesis of chemically modified Gr by aryne cycloaddition under mild and neutral reaction conditions. Aryne modified Gr is highly thermally stable and well dispersed in water and organic solvents such as 1,2-dichlorobenzene, ethanol, and chloroform [175]. After the photochemical or thermal heat treatment, the Diels-Alder cycloaddition reaction or [4+2] cycloaddition has proceeded in a single step *via* six-membered ring formation. The reaction occurs between conjugated cis diene (electron-rich) and dienophile (electron-deficient). The reaction would take place favourably for dienophiles in the existence of an electron-withdrawing group. The interaction between the diene and dienophile is due to the good symmetrical overlapping between HOMO of the diene and LUMO of the dienophile. At high temperatures, Jeong-Min Seo and Jong-Beom Baek have developed the solvent-free mechanochemical approach for the Diels–Alder reaction of Gt (diene) with dienophile maleic anhydride (MA) or maleimide (MI) in a sealed glass bulb of argon at a high pressure of 160–220 °C. Dispersed in polar solvents, functionalized composites were used in a variety of applications [164, 176]. Hence, well-dispersed graphene function permits it to act as a more reactive dienophile or diene in Diels-Alder's reaction. Such a synthetic method has a high potential for reversible modification of Gr electronic properties *via* bandgap opening under mild conditions [177]. The unique method for the functionalization of Gr nanosheets is based on nitrene chemistry. This scheme is easy and efficient to introduce various functional groups (hydroxyl, amine, carboxyl, and bromine), long alkyl chains, and polymers, *e.g.*, poly (ethylene glycol, polystyrene) by covalent bond and stably stacked on the Gr surface to yield single-layer functionalized Gr from GO in a one-step reaction. Nitrenes are reactive intermediates that can be made from azide species through irradiation or thermolysis. Further, it can be tried for covalent functionalization with epitaxial

Gr and exfoliated Gt by [2+1] cycloaddition [178]. Thus, functionalized composites are confirmed with X-ray photoelectron spectroscopy (XPS), Atomic force microscopy (AFM), Scanning electron microscopy (SEM), EDX, XRD, Transmission electron microscopy (TEM), Brunauer–Emmett–Teller (BET), Fourier transform infrared spectroscopy (FTIR), Elemental analyzer (EA), and Solid-state nuclear magnetic resonance (SSNMR) spectroscopy techniques.

Noncovalent Functionalization

Noncovalent functionalization is an established technique for the surface modification of carbon-based nanomaterials. The noncovalent approach involves the hydrophobic Van der Waals interaction, which is prompted by an electrical interaction between two or more closely placed atoms, - interactions produced by the electronic cloud, and electrostatic force of interaction produced by electrically charged particles [101 - 121, 128, 140, 179 - 188]. Such functionalization requires the physical adsorption of suitable molecules on the Gr surface. Noncovalent functionalization is achieved by polymer wrapping, adsorption of surfactants [139] or small aromatic molecules, and interaction with sulfonated polyaniline [184], porphyrins [186], or biomolecules like proteins, enzyme-drug complexes, DNA-protein complexes, supramoleculars, and inorganic metallic complexes [117 - 119]. Surface modification of Gr and GO demonstrates excellent electrical, mechanical, and optical properties, which could be further explored for the development of several biomedical devices, industrial metallic goods, conductors, energy storage devices, and transistors [120, 121, 128, 140].

Surface modification of Gr using a robust chemical approach is the latest thrust area in the field of carbon nanotechnology to explore its several potential industrial applications [101 - 116]. The wet chemical dispersion of the Gr layer was prompted by multiple noncovalent functionalization in a suitable solvent, NMP. The first analysis was done on surfactants, *i.e.*, sodium cholate, sodium deoxycholate and dodecyl benzenesulfonate, for major alterations in material applications for enhancing efficiencies. In amphiphilic sodium dodecyl benzenesulfonate dispersion, the majority of the material uptake endorsements were observed. The utilisation of sodium deoxycholate leads by far to the uppermost level of individualization [139]. However, the selection of various matrices is an important factor for the incorporation and homogenous distribution of Gr to restore the electrical properties. Hence, adequate solubility of Gr-based materials in various solvents is a necessity for their future experimental applications [180, 181]. The stability of reduced Gr in various solvents is achieved *via* noncovalent functionalization of amine-terminated polymers [182]. The GO reduction is carried out in an aqueous medium by treating with hydrazine monohydrate and subsequently washing for the removal of agglomerated Gr

sheets and impurities. The amine-substituted polymer is solubilized in an organic solvent. The aqueous dispersion of RGO is added to the organic polymer solution [183, 184]. The electric biosensor was made by non-covalent functionalization of RGO with conducting polypyrrole, implant copolymer, *i.e.*, poly (styrenesulfonic acid-g-pyrrole) [183]. The sulfonated polyaniline functionalized Gr sheet enhanced the electrochemical activity and stability [184]. The dispersibility of Gr in water is increased by noncovalent functionalization of RGO with aromatic dyes like methylene blue [185] and porphyrin [186]. Its research is useful in the preparation of graphene-based electric conducting sheets [185, 186]. Gr has created a blue fluorescent material by combining coronene derivatives such as the tetrapotassium salt of coronene tetracarboxylic acid. Its liquid crystalline derivatives, ester and imide, exhibit high fluorescence emission in solution and solid phase [187]. Non-covalent functionalization of RGO with sulfanilic acid azocromotrop shows its applicability as a supercapacitor electrode material [188].

GRAPHENE OXIDE FUNCTIONALIZATION WITH AMINE SUBSTITUTED ORGANIC MOLECULES

Substituted organic compounds are highly attractive due to their importance in agrochemicals, pharmaceuticals, device manufacturing, supercapacitors, and nanomaterial synthesis. Amine substituted molecules may be either aromatic or nonaromatic, heterocyclic or non-heterocyclic, or aliphatic. The heterocyclic compounds are considered for their potency in various fields. Heterocyclic molecules are cyclic structures that bear one or two heteroatoms (other than carbon) in the ring. The ring size differs from three-membered onward and is most efficient up to eight members. The number of heterocyclic compounds is still increasing rapidly. Almost all natural drugs, such as papaverine, procaine, emetine, atropine, theophylline, morphine, reserpine, and codeine, are heterocyclic natural drugs. The most commonly known synthetic drugs such as chlorpromazine, antipyrine, metronidazole, methotrexate, captopril, diazepam, barbiturates, and azidothymidine are heterocyclic. Moreover, some pesticides, dyes, and herbicides are also heterocyclic [189 - 192]. The nucleobases of DNA and RNA are nitrogen-based heterocyclic compounds that are directly involved in the recording of genetic code for therapeutic applications [146]. The essential amino acids [115], natural pigments such as haemoglobin [193], chlorophyll [194] and some hormones have a heterocyclic core. These molecules have changed their potency after functionalization with Gr. The whole physiological process of life, such as the provision of energy, metabolism, respiration, hereditary transformation, and nerve impulse, is based on biochemical reactions in which many heterocyclic compounds are associated with vitamins, serotonin, enzymes, coenzymes, adenosine triphosphate [ATP], nucleic acids, and others. According to the literature survey, most of the natural products contain heterocyclic molecules,

revealing that nature itself likes heterocyclic compounds for equilibrating their life cycle because of their unique properties. The presence of heteroatoms in the heterocyclic compounds maintains the pH of many synthetic and biochemical reactions. The heterocyclic molecules undergo nucleophilic, electrophilic, condensation, and cycloaddition reactions. Such flexible reactivity is responsible for changing their electronic properties to enhance their efficiency for various applications.

ALTERNATIVES OF CONVENTIONAL METHODS FOR FUNCTIONALIZATION OF GRAPHENE OXIDE

The synthesis needs environmentally benign routes to maintain sustainability. Researchers are trying to develop a new chemical process for minimising the use of hazardous chemicals. The chemist is constantly looking for greener alternatives to traditional synthetic methods. Ultrasound-energy and microwave-irradiation are two of the thrust areas for achieving this goal. To explore new efficient and eco-friendly alternatives for chemical reactions to minimise the waste product by avoiding or reducing the use of conventional volatile organic solvents. Thus, several approaches have been reported, such as reaction under solvent-free (dry media) conditions, by the use of solid-supported reagents, mechanochemical mixing (grinding), and alternative activation and heating methods that utilize microwave and ultrasonic irradiation for synthesis. Therefore, to avoid overheating problems, the sonochemical approach is utilized for the synthesis of surface modified Gr-based nanomaterials [195 - 200].

Ultrasound-Assisted Functionalization: A Sustainable Technology

Ultrasound refers to sound waves (>20 kHz) higher than the upper limit of human hearing (16-18 kHz). The ultrasound frequency is generally kHz) higher than the upper limit of human hearing (16-18 kHz). The ultrasound frequency is generally considered to be between 20 and 100 MHz. The laboratory sonicator for performing chemical reactions generally has a frequency of 20 to 100 kHz, while the higher frequency of ultrasound waves is used in medical applications. The principle of ultrasound waves is based on the generation of acoustic cavitation, which favours a chemical reaction between 20 and 40 kHz. Higher ultrasound frequencies of 5 MHz and above do not produce cavitation, and this frequency range is used in medical imaging. The ultrasound waves are generated by the ultrasonic transducer, which converts the electrical and mechanical energy into sound energy.

The electromechanical transducer is made of quartz and is usually based on the piezoelectric effect. Applying equal and opposite electrical charges to the opposite faces of quartz tends to cause simultaneous expansion and contraction. The

speedily reversed charges put up a vibration that produces ultrasonic waves, *i.e.*, a piezoelectric effect. Recently, the piezoelectric transducer of ultrasonic equipment is made of ceramic impregnated barium titanate that transforms 95% of electrical energy into ultrasound energy [195, 196]. The proliferation of sound waves, with a continuous succession of compression and refraction, goes through the liquid medium, which permits the molecules to oscillate about their mean. Hence, the average distance between molecules decreases and increases simultaneously. In the refraction cycle, the average distance and attractive forces between the molecules in the liquid medium may be overwhelmed, causing the formation of bubbles. The bubbles continuously rise within a few cycles by taking some vapours or gases from the liquid medium to gain an equilibrium size which matches the frequency of bubbles to the resonance of applied ultrasound frequency. Therefore, the acoustic field experienced by the bubbles is not stable because of the interference of other bubbles forming and resonating around them. However, the internal forces are too high to confirm the violent collapsing of bubbles, producing a very high confined temperature of nearly 5000 K and a pressure of over 1000 bar. High temperatures and pressure can be involved in chemical reactions.

The term "sonochemistry" is used to explain the effect of sound energy through bond oscillation on chemical reactivity. Among several theories, the 'hot-spot' is the most acceptable for describing sonochemical reactions. It explains the release of energy through cavitation. A cavitation bubble acts as a localised microreactor in an aqueous system, generating thousands of kelvins of temperature and high pressure. The driving force for a chemical reaction under the influence of ultrasonic waves is driven by cavitation bubbles [197]. The broad applications of sonochemistry in synthesis have attracted the attention of many researchers. Interest has spread beyond academic laboratories into the industry and chemical engineering. Various ultrasound-assisted organic reactions, exfoliation of GtO [198] and nanomaterial synthesis, have been conducted in aqueous as well as in non-aqueous media and homogenous liquid mixtures. As a result, the wonderful properties of ultrasonic-irradiation have been highlighted for successful application in organic transformations.

Microwave-Assisted Functionalization: A Green Chemical Transformations

Microwave-assisted heating with a Bunsen burner is a 21st-century asset for its use in the synthesis of organic, nanomaterials, polymers, and inorganic materials. It is the homogeneous heating process that speeds up the reaction rate compared to conventional methods. The confined zone is electromagnetic radiation range of size 1 cm to 1 m, frequency 30 GHz to 300 MHz, and photonic energy 1.24 meV to 1.24 eV. The transition between infrared irradiation and radio frequency is

referred to as microwave irradiation [199, 200]. The mechanism of microwave irradiation is the interaction of electromagnetic radiation with dipolar molecules. Hence, the dipole moment directs it to become aligned and change its orientation due to electric field oscillations. Speedily reoriented molecules produce homogenous internal heating to proceed with the chemical reactions. Therefore, the choice of solvent is important for the microwave-assisted synthesis to consider a dipole moment [199, 200]. Surface modification of GO occurs in terms of an amide bond between the carboxyl group of GO and the amine group of chitosan, subsequently followed by reduction with hydrazine monohydrate. Thus, the dispersibility, aqueous solubility, and biocompatibility were enhanced by the grafting of chitosan on the GO sheet [201]. Therefore, a microwave is more valuable to get a quantifiable yield with more precision than conventional heating. The researchers are attempting to advance nanomaterial design and synthesis by monitoring all of these parameters such as temperature, pressure, temperature ramp, and polar solvent selection [199 - 201].

CHEMICAL REDUCTION OF GRAPHENE OXIDE

Most of the research work has been published for the functionalization of Gr using chemical, electrochemical, sonochemical, and microwave methods. GO functionalization has been done through the reduction of epoxy, carboxylic and ketone groups using reducing agents [124, 125]. The most commonly used reducing reagents are hydrazine monohydrate [126], sodium borohydride and their substituted derivatives [202, 203], lithium aluminium hydride [204], alkaline solution (KOH, NaOH) [205], metal iodides [123], hydrogen iodide [206], aluminium foil [207], alcohol [208], thiourea dioxide [209], p-phenylenediamine [210], L-ascorbic acid [211], nascent hydrogen [212], iron/hydrochloric acid [213], bacterial respiration [214] and pyrrole ring [215]. These chemicals are hazardous to the environment and living organisms. Hydrazine monohydrate, sodium borohydride, and lithium aluminium hydride are sensitive and explosive chemicals to moisture. The alkaline solution and organic solvents unbalance the whole aquatic system. Therefore, precautions are needed for Gr synthesis using bulk amounts of a strong reducing reagent. The alternative methods, *i.e.* metal/HCl-based reduction, such as Fe/HCl, are secure compared to explosive chemicals . But still, some problems exist due to the presence of an impurity in the reduced Gr. Recently, an acetic acid and HCl-based alternative method has been proposed, which is comparable to the reduction by hydrazine monohydrate. The elemental analysis of reduced Gr revealed a high C:O ratio vis-à-vis a loss of oxygen (reduction), high conductivity (4600 Sm^{-1}), and specific capacitance (35 Fg^{-1}) due to the attainment of unsaturation [208]. Green approaches such as microwave, ultrasound, and solvent-assisted, flash, thermal, and photochemical-based GO reduction have piqued the interest of researchers for large-scale Gr

production. Considering the literature review, the recent progress in Gr research is the enzymatic reduction of GO on a priority basis. For example, Martin Pumera *et al.* have proposed GO reduction by thiourea dioxide [209]. Aravind Dasari *et al.* have reported the dopamine-induced reduction and subsequently functionalization of the GO sheet [210]. Jingyan Zhang and Shouwu Guo *et al.* found the GO reduction using L-ascorbic acid [211], which is very close to that of hydrazine monohydrate [126]. James M. Tour *et al.* have shown bacterial respiration for GO reduction [214].

GRAPHENE-BASED MATERIALS TOWARDS VARIOUS CATALYTIC PERFORMANCES

The single-atom thick, 2D carbon hexagon network of Gr and its derivatives have remarkable applications in the fields of biomedicals [146, 148, 168, 216 - 225], nanoelectronics [226 - 230], energy storage devices [231 - 233] and organic synthesis [21, 110]. The magic material of the 21st century shows good mechanical [234, 235], optical [236 - 239], sensing [98, 121, 240 - 245] and adsorption [179, 246 - 255] properties. The amphiphilic nature of GO is seen from edge to centre in the dispersion of hydrophilic to hydrophobic domains. Therefore, GO acts as a surfactant and sticks to interfaces and lower interfacial energy sites [249]. The use of pure Gr is challenging due to its agglomeration and processing difficulties. So, the modification of Gr has attracted broad research interest. The grafting of polymers with GO increases the biocompatibility and stability in the cellular medium, and it is used as a nanocarrier for hydrophilic and hydrophobic drugs [220, 246]. Also, the GO functionalization with enzymes enhanced its thermostability, which has been extensively used in biotechnological applications to stabilise heat-sensitive enzymes [247]. Recently, the surface modification of GO has been utilized to make nanofiltration membranes for desalination purposes [248]. Still, there is not much research done to search for graphene in biological systems, despite much exertion in the area of CNT for *in vitro* and *in vivo* biological uses. f-GO has biocompatibility with organic molecules such as nucleobases [146, 148] to increase the high aqueous solubility and stability. A new hybrid nanomaterial was established as an exhibiting enzyme for *in vitro* analysis and therapeutic cure of cancer cells [168, 219]. Gr-based composites show a positive impact when imparting antimicrobial [222, 223] and antibacterial [224, 225] properties.

Arghya Paul *et al.* have discovered an injectable and biocompatible hydrogel of polyethylenimine (PEI) functionalized GO to easily deliver vascular endothelial growth factor-165 (VEGF) pro-angiogenic gene for myocardial therapy [221]. Self-assembled 3D Gr or functionalized Gr-based conducting nanostructures are suitable for designing flexible, thermally and electrically stable electronics [226 -

229], supercapacitors [227, 228, 230], energy storage devices [231, 232] and solar energy conversion schemes [233]. Gr-based nanomaterials are appropriate as highly efficient complexes with good mechanical properties such as high strength and modulus, which are prepared by adding a few numbers of fillers [234, 235]. Gr and Gr-based composites have sparked interest in optoelectronic applications such as photodetection [236], the synthesis of low-cost optical photovoltaic devices [237], and fluorescent nanocomposites [238, 239]. The most important application of f-Gr is to act as a sensor to diagnose the disease, which depends upon the large surface area of Gr. f-Gr can be sensitive to a particular disease. The dispersed f-Gr interacts with the biomolecules in the matrix. The more effective nanocomposites of GO are allowed to bond with single-stranded DNA, subsequently added by fluorescent molecules [98, 121, 240 - 245]. Tetiana Kurkina *et al*. established an f-GO-based device as an electrical biosensor for the immunodetection of amyloid-beta peptide [244]. Also, f-GO-based sensors have been developed for humidity and temperature sensing due to their suitable features such as flexibility, transparency, and bulk-scale production [245]. The porous nature of Gr and its derivatives is utilized as an adsorbent for hazardous chemicals, elements, and gases for environmental remediation. Gr-based composites decontaminate naphthalene and its derivatives [179], bisphenol A [250], toxic Cr (VI) [251], copper (II) [252], carbon dioxide [253] and mercury [254] from the ecosystem. The catalytic properties of unmodified Gt are found to be utilized for alkylation [21] and Friedel–Crafts acylation of aromatic compounds [20] to avoid the use of hazardous solvents and reagents. The fluorinated Gr acts as an electrophile, which substitutes amine and alcohol nucleophiles *via* covalent bond formation [255]. The excellent properties of Gr and its derivatives in several research inventions have given fruitful solutions. The synthesis of Gr-based composites by a robust chemical approach is a new and recent thrust area. The covalently modified Gr-based materials are further confirmed in the product with detailed analysis and electrical as well as photochemical applications [256, 257]. Hence The robust chemical approach for the surface functionalization of GO is suitable for synthesizing nanocomposites for biomedical applications [258 - 260].

Biomedical Catalysis

Gr-based modified materials have been extensively studied and reported for biomedical research like cell viability, cancer therapy, tissue implantation, antibacterial activities, antioxidant behaviour and as drug carriers due to their improved solvent processabilities. Furthermore, in the literature review, alginate-based functionalized GO has been selectively obstructed in the MDA-MB-231 cell line adhesion efficiency (human breast cancer cells) while promoting adhesion towards healthy murine fibroblasts (3T3) and human osteosarcoma

(HOS) [261]. There is variation in the adhesion efficiency towards the cancer cell MDA-MB-231. HOS is not similar to healthy cell 3T3 due to tumour cell specificity, but it is driven by topographical signals originated by alginate-GO based substrate. The use of various antibiotic medicines causes resistance against the pathogens, which needs to be modified with GO that endorses the stability with agglomeration reduction. So, the materials are used as drug carriers and antibacterial agents too [262 - 264]. The optimised nanosized GO function-alization with two derivatives, *i.e.*, polyethylene glycol and polyethyleneimine, is a new method for developing a si-RNA (si = small interfering) carrier-based delivery system. It improves the osseointegration implantation, which has been confirmed by cellular cytocompatibility investigation [265]. The modulation of the Gr surface as well as its functionalization have developed various functionalities like hydroxyl groups with surfaces' defects, which show excellent cytocompatibility with better mechanical strength. These facilitate cell differentiation and regeneration in the tissue engineering field [266 - 269]. The combination of highly electrically conductive Gr and titanium dioxide facilitates the separation of electrons and holes in the TiO_2 energy band and prevents recombination when ultrasound is applied. Thus, the TiO_2-graphene-based material is used as a nanosonosensitizer for therapeutic effects against tumours [270]. Therefore, biomedical science is essentially required for chemical modification of graphene to develop a new cost-effective artificial cytocompatible tissue that can be used as an alternative.

Photoluminescent Catalysis

The zero-bandgap has less applicability in optics. So, the oxidation of Gr opens the zero bandgap after generating various oxygen functionalities such as hydroxyl, carbonyl, carboxyl, and aldehyde to focus on the optical properties [271 - 277]. The photoluminescence (PL) of GO is seen in the visible or ultraviolet region, which is more intense than Gr. Two PL bands, one in blue and another in the red region (500-600 nm), are seen. The PL band of the GO is not yet simplified like organic molecules due to the presence of various electronic domains and uncertain functionality on the GO surface. The origin of PL bands is still being debated. The blue band has been observed due to the the π-π* transition of sp^2 electronic domains at the C-O sp^3 surface [277], while it is also claimed that π-π* transition has observed the broad long-wavelength (LW) band [278]. The broadband due to defects has caused a variation in the sp^2 domains' bandgap. The pH-dependent tunable PL bands of the GO resemble those of the polycyclic aromatic compound in a basic medium because the carboxylic functionalities are coupled with their neighbouring atoms of Gr. The blue band is intense at pH>8 and allocated for the optical-electronic transition from GO−COO* to GO−COO−. Hence, the LW band has developed an important factor at pH 8. It is ascribed to the LW band for an

optical-electronic transition from (GOCOOH)* to (GOCOOH) as an excited carboxyl group protonated into carboxylic acid. Further, the study concludes that the protonation and deprotonation of carboxyl and hydroxyl functionalities of GO were accountable for the dissimilar PL strength with pH of solutions [278, 279]. The COOH and OH are accountable for the blue and broadening the LW band [280, 281]. According to the theory of the red-edge effect, the performance of the blue PL band depends on the excitation wavelength. The red-edge-effect also explains that the solvation dynamics of GO in a polar medium decelerates miserably with the time scale of PL, resulting in a broadening of the red-shift of the PL band [282]. Hence, the surface-modified GO shows change in the PL bandgap as their corresponding PL peaks slightly differ compared to previously reported GO due to the difference in electronic domains at the GO surface. Therefore, the GO-based derived materials have attracted a lot of attention for PL and sensing applications due to their variable electronic structural insight and solubility in various solvents.

Magnetic Catalysis

The magnetic properties of the Gr and its composites are very challenging due to the absence of d and f shell electrons, which are accountable for the ferromagnetism. The theoretical and experimental studies infer that magnetism can be explored only in specified circumstances. Magnetism is attributed by density functional theory (DFT) calculations to the confinement of spin-polarized electronic states in Fermi energy levels. In honeycomb nanostructured, Gr "zig-zag" edges possess magnetic moments while zero magnetic moments are recognised at the "armchair" edge [283]. However, the temperature-dependent magnetic moment is also produced due to the point defects in the Gr lattice. It is found in the form of missing carbon from the continuous lattice or additional doping or functionalization on the surface to create vacancies [283 - 290]. Ion irradiation of atoms is bombarded on the carbon lattice to create defects, and it is susceptible to generating magnetism. The ferromagnetic behaviour at (room temperature) RT in Gr-based materials needs great attention to the inference of the doubts as well as the validity of results along with reproducibility. To get appropriate results, extra care is necessary to protect against impurities and contaminants [291]. Hence, we have initiated GO functionalization by a chemical approach to induce magnetic behaviour at RT. Understanding the thermal behaviour of defected Gr is closely related to magnetism.

Electrocatalysis and Photocatalysis For Energy Applications

Electrocatalysis was initiated by Kobosev and Monblanowa in 1936 [292, 293], to explain the electrochemical reactions which occur at the electrode surface. The

catalytic activity of the Gr can be modulated by various dopants like N, S, or O on the surface. The heteroatom dopants affect the electronic charge and spin density, which determine the catalytic activities. The electrocatalytic reactions of heterogeneous Gr have the efficiency to act as an intermediate or a reactant to interact with the electrodes. Also, the catalytic activity depends on the properties of the electrode like surface area, electron density, and thermal stability. To investigate electrocatalyst binding efficacy with electrode surfaces and to investigate new electrocatalytic applications. Pyridinic and quaternary N are the main dopants of chemically modified Gr. Several N-containing species are useful for doping on the Gr surface to explain the oxygen reduction reaction (ORR) [292]. The consumption of fuel cells (fcs) converts chemical energy into electricity. In ORR, the H_2 gas is produced at the anode. It splits into electrons and protons by a hydrogen oxidation reaction (HOR) in which the proton is diffused at the cathode with the motion of electrons throughout the cell to generate electricity. Consequently, the presence of cathodic O_2 reacts with protons and electrons to generate the water, which is generally known as ORR. Another electrocatalytic property of Gr-based materials is termed oxygen evolution reaction (OER), in which renewable natural energy is converted into chemical fuels like hydrocarbons and hydrogen energy (methanol, formic acid, methane, and butane, *etc*). OER is an excellent source of energy storage [293 - 300]. In OER, the water splits into H_2 and hydrocarbons by the reduction of CO_2. The mechanistic path of OER involves the generation of O_2 at the anode, which is important for energy storage devices like batteries, solar cells, and reversible fuel cells [293 - 300]. OER has an essential type of kinetics produced by numerous proton-coupled electron-transfer steps, which are successively made possible by the use of an active electrocatalyst to increase the reaction rate [301 - 304]. The noble metal oxide-based electrocatalysts act most efficiently [305 - 308], but due to the high cost of materials, a lot of transition metals have been applied as alternatives [303, 309, 310]. Thus, cost-effective heteroatoms doped with Gr have recently been reported for an efficient and novel class of electrocatalyst [302, 311]. Also, heterogeneous and homogenous electrocatalysts have attracted attention for OER applications due to their active electrocatalytic centres and simple OER mechanisms [304, 312 - 315].

Due to the availability of limited natural resources like petrol, diesel, coal, and others, scientists have intensified research for H_2 energy production. The accessibility of H_2O is much greater on earth than on water, which is only a workable and clean resource to produce H_2 energy in the future as an excellent source of energy within locally available resources. However, the extreme temperature (2000 °C) is required for water dissociation to produce H_2 and O_2 while avoiding instant recombining capability.The small overpotential is required for H_2O splitting to produce H_2 *via* the cathodic HER pathway of electrocatalytic

performance at ambient circumstances [293, 316]. The most effective platinum-based electrocatalyst exhibits potentially effective HER, but its high cost and lack of robustness prevent it from being commercialised [317, 318]. Therefore, scientists are highly motivated to identify alternatives to Pt-based electrocatalysts that are cost-effective, highly competent, and most durable for HER. A lot of investigations have been completed. But some are in continuation in the same direction. Transition metal-based homogenous or heterogeneous materials *e.g.* W, Co, Mo, Ni and their various derivatives like nitrides, phosphides, carbides and sulphides have been discovered, despite their corrosion vulnerability to acidic and basic electrolytes [319 - 323]. The preparation of the membrane electrode by an assembling method in which the powder form of catalyst is dissolvate in solvent with binders, subsequently forming ink on the surface with the support of copper foil and glassy carbon. As a result of the inevitable accumulation of catalyst mass and detachment from its chemical composition during the gas-based progression of HER, the dried membrane electrode has excellent catalytic activity as prepared [324, 325]. The electrocatalyst performance depends on the surface morphology, chemical constituents, pore size, electronic homogeneity or heterogeneity. Also, the architecture applied for the electrode preparation is important for HER applications.

The scientific community has focused on photocatalytic methods for photon-based energy generation in various chemical reactions. This energy solves the major global problems of pollutant remediation like water purification from toxic chemicals and dye degradation [326 - 332]. Simultaneously, it produces solar energy as a fuel substitute [298]. Photocatalysis occurs in the solar cell as a chemical bond that can be utilized in the future for various uses. Thus, photocatalysis is applicable, but there is a lack of efficiency for practical industrial application. Photocatalysis is an energy-storage device-based process. Therefore, a lot of procedures have been applied to enhance the photocatalytic activity of semiconductor-based photocatalysts, like architecture designing of materials [333, 334], doping of homo or heteroatoms [335, 336], metals and synthesis of semiconductor composites [337]. (Hydroxyl radical) attacks on organic pollutants like dyes to breakdown into nontoxic or less hazardous units that are released in gaseous form (CO_2, NO_2, N_2O, and HCO_3) and as H_2O also [327 - 332]. The toxicity of various metal-based photocatalysts forced researchers to develop metal-free carbon-based materials, especially heteroatom doped Gr, constituting carbon, nitrogen, oxygen, sulphur, and boron. So, a heterogeneous gr enhances the photoefficiency and degradation rate of organic pollutants. It makes the environment a benign water resource for the biotic community [329].

In conclusion (Fig. **6**), recent developments in the development of heteroatom-doped Gr-based materials have had a tremendous electrocatalysis application for

HER, OER, ORR, photocatalysis, and sonocatalysis to make energy storage devices: batteries, superconducting materials, and imprinting chips. Therefore, the excellent behaviour of Gr and its derivatives in many research areas has attracted us to initiate this research work. The chemically modified Gr-based materials explore out-of-the-box applications in the 21st century. Not only Gr but also GO and its derivatives have been investigated for structural studies and numerous industrial applications through several experimental conditions.

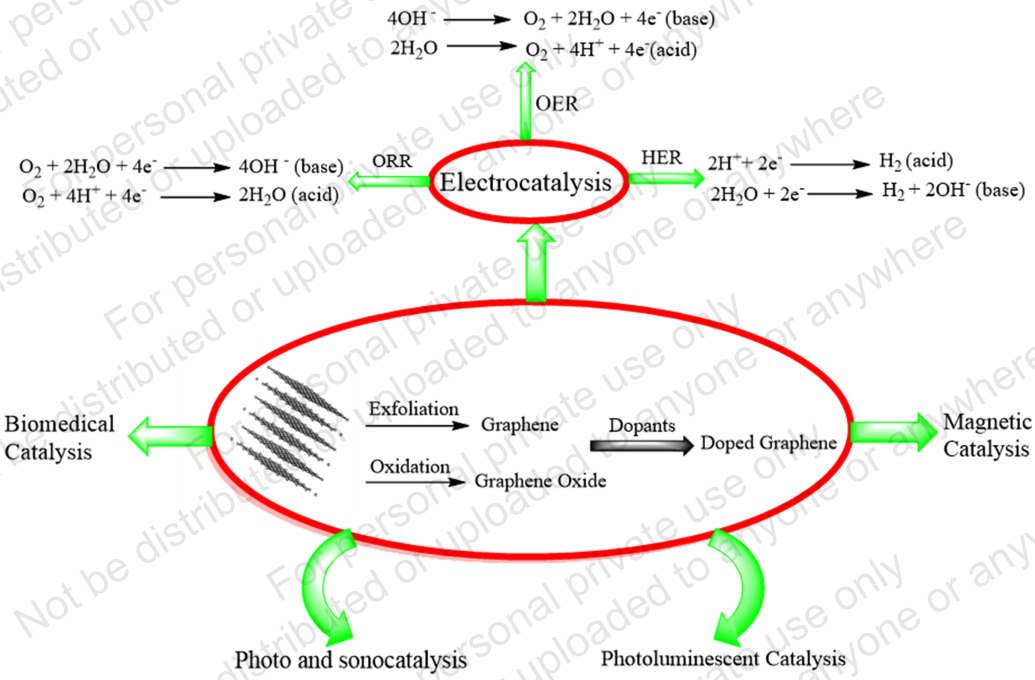

Fig. (6). Graphical representation of various catalytic performance of graphene-based materials.

We have thoroughly reviewed the initial research to explore the advanced understanding of a new dimension of the Gr and its wider derivatives and applications. Reportedly, a lot of studies have been done within the box model with certain *restrictions*. Therefore, our theme, hypothesis, and objectives have been at the cutting edge of research in the area of Gr research for enhancing industrial applications and processes.

PHYSICOCHEMICAL MECHANISM TOWARDS REINFORCING CATALYTIC PERFORMANCES

The Friccohesity is the most authentic physicochemical database to determine the structural stability, transitions, and electronic state with respect to temperature

(wrt), electrical field, magnetic field, UV light, and laser. It is found that Gt and GO are the most tunable nanofunctional materials which are structurally reorganised by these external forces. These forces could be studied with the GO sheet. The database with respect to temperature, electric field, and magnetic field, the G (Gibbs free energy) and friccohesity could be measured in certain solvents at variable stoichiometric ratios. The stoichiometric ratio determines the activity of the GO with its compositions where it is on the first order or has certain transitions in structure. This will also define the uniformity of sheet repetition. Currently, these are measured with the D and G characteristic peaks of Gt and GO with Raman spectroscopy.

However, this friccohesity tracks each and every chemical activity of the GO. The polarisation of the solvent could be studied. Normal energy could be studied. There are some intra-GO points where the solvent interacts more. This could generate the transitions in its fluid dynamics in the steady state because the force will be affected due to the different orientation of friccofluids owing to its natural flow. Hence, microfluids could also be studied. The structure of GO has an intersheet binding force which makes it difficult to weaken the intersheet Van der Waals force (ISVF) through the wet reaction procedures. As a result, before proceeding with the Gt oxidation, it could be treated with a suitable nondestructive solvent with mild interaction, allowing dipolar tuning in the ISVF, and the sheet could be slightly free with a higher surface area (HSA). The HSA develops low activation energy and higher activity. Thus, the soaked Gt could be the most economical model. There could be the possibility of reacting systems. Solvents should be explored for use before adding real reacting species. Different solvents take place one by one in the reaction medium. These could be studied to fix their impact on their interaction with ISVF. These forces are the key factors which are responsible for the sheet's togetherness. These forces originated where the Gt sheet was developed initially. At the normal energy scale, mixed solvent could also be used to identify specific solvated molecules dispersed within the sheets or out edges with moderate binding forces. Gt and GO sheets have specific spatial geometry to synchronise and synergize these structures. Thus, the points of functionalizing reagent create Lennard Jone potential distance The capillary sciences explore carbon-based functional nanomaterials (CFN). For checking the stability of the solvent-GO binding dynamics, van der Waals force theory (VFT) could be achieved. Further, the activation energy (Ea) with increased temperatures could be estimated to understand the economics of the GO functionalization. How much heat (q) is needed for functionalization could be studied by monodispersed GO in suitable solvents. Certain fluorescent dyes could also be added to understand the real science of their electronic linkages mutually. The activity coefficient could also depict the electrolyte behaviour of the GO solution in a specific solvent. The capillary action develops a remarkable alignment to have a

favourable geometrical orientation to receive maximum photons for photocatalysis of the materials. The friccofluids are different microfluids. Hence, more surface area is obtained by orienting the thinnest flat surface capillary so that it seems monodispersed . However, there could be a maximum frictional force. There is gradient flow where the GO is automatically sparsely dispersed and represents the photon O_2 cellular forces. The area of GO distribution for better electronic activity reflection investigates the various catalytic performances.

CONCLUSION AND PERSPECTIVES

Since inception, carbon nanomaterials have attracted enormous attention due to their extraordinary properties, moldability, and applications. Therefore, along with the natural allotropes of carbon, the artificial allotropes such as Fullerene, CNT, and Graphene have grown extensively in the last few decades to replace metallic devices to store energy. Because of their unique synergistic effects and physical properties such as optical, electrical, thermal, mechanical, piezoelectric, bionics, and supercatalytic, surface-modified carbon materials (SMCM) have become significant in the generation. The synergistic impacts of SMCM have emerged as the new avenues for biomedical application and catalytic activity with green environmental impact. The synthesis of graphene and surface-modified graphene oxide has both unlocked the latest thrust area in material sciences for space applications. The robust chemical approach for the surface modification of GO has been developed *via* direct amidation. Functionalized GO for semiconductor formulation has resolved the challenges to capturing solar energy. The sonochemical approach is employed for the greener surface modification of GO with unique edge intensities to design novel and state-of-the-art superconductor nanomaterials. The mechanism and outcome both lay a foundation for the formation of mechanistic intermediates with quasistatic irreversible and reversible states. For an insight into structural confirmation, the various high-end and sophisticated instrumentation techniques like ultraviolet-visible spectroscopy, FTIR, TGA, XRD AFM, SEM XPS, and HRTEM have been the assets to illustrate the sheet structures of the GO with an eye on ridging eutectic electronics for designing high-intensity CV (cyclic voltameter) sensors. Upgrading carbon footprints through surface plasmon resonance (SPR) and upconversion nanoparticles (UCNPs) out of the newly prepared functionalized graphene oxide (f-GO) could lay a foundation for the multifunctionalities for advanced and thermodynamically and kinetically stable nanoemulsion for stable electronic and heat-conducting nanoparticles for sensing thin-film technology.

CONSENT FOR PUBLICATION

Not applicable.

CONFLICT OF INTEREST

The authors declare no conflict of interest, financial or otherwise.

ACKNOWLEDGEMENTS

Authors are thankful to the Central University of Gujarat, India for providing infrastructural support. Authors acknowledge UGC-DAE CSR Indore for collaborative research scheme [Ref: CSR-IC-BL-79/CRS-196]. Authors are thankful to Principal Collaborators, Dr. Mukul Gupta, UGC-DAE CSR Indore, and Dr. S.N. Jha, Indus-2 RRCAT Indore, DAE India for extending their kind cooperation and support during the Collaborative Research Scheme. Mr. Gopal Avashthi is thankful to UGC-DAE CSR Indore for financial assistance in the form of Project Fellow.

REFERENCES

[1] Ren, Z.; Lan, Y.; Wang, Y. Aligned Carbon Nanotubes: Physics, Concepts, Fabrication and DevicesSpringer: Verlag Berlin Heidelberg, **2013**.

[2] Krueger, A. *Carbon Materials and Nanotechnology*; Wiley-VCH: Verlag GmbH and Co. KGaA, Weinheim, **2010**.

[3] Shenderova, O.A.; Zhirnov, V.V.; Brenner, D.W. Carbon Nanostructures. *Crit. Rev. Solid State Mater. Sci.,* **2002**, *27*(3-4), 227-356. [http://dx.doi.org/10.1080/10408430208500497]

[4] Delhaes, P. Carbon-based solids and materials. In: *ISTE Ltd and John Wiley & Sons*; ISTE Ltd and John Wiley & Sons, Inc.: UK and USA, **2011**.

[5] Serp, P.; Machado, B. *Nanostructured Carbon Materials for Catalysis*; Wiley-VCH: France, **2015**, pp. 1-45.

[6] Titirici, M.M.; White, R.J.; Brun, N.; Budarin, V.L.; Su, D.S.; del Monte, F.; Clark, J.H.; MacLachlan, M.J. Sustainable carbon materials. *Chem. Soc. Rev.,* **2015**, *44*(1), 250-290. [http://dx.doi.org/10.1039/C4CS00232F] [PMID: 25301517]

[7] Martín, N.; Guldi, D.M.; Echegoyen, L. Carbon nanostructures—Introducing the latest web themed issue. *Chem. Commun. (Camb.),* **2011**, *47*(2), 604-605. [http://dx.doi.org/10.1039/C0CC90122A] [PMID: 21125092]

[8] Miyoshi, K. *Structures and Mechanical Properties of Natural and Synthetic Diamonds,* **1998**.

[9] Liu, Y.; Gu, Z.; Margrave, J.L.; Khabashesku, V.N. Functionalization of nanoscale diamond powder: fluoro-, alkyl-, amino-, and amino acid-nanodiamond derivatives. *Chem. Mater.,* **2004**, *16*(20), 3924-3930. [http://dx.doi.org/10.1021/cm048875q]

[10] Yu, P.Y.; Cardona, M. *Electronic Band Structures: Fundamentals of Semiconductors: Physics and Materials Properties*; Springer: Verlag Berlin Heidelberg, **2010**, pp. 17-106.

[11] Motochi, I.; Makau, N.W.; Amolo, G.O. Metal–semiconductor ohmic contacts: An ab initio Density Functional Theory study of the structural and electronic properties of metal–diamond (111)-(1×1) interfaces. *Diamond Related Materials,* **2012**, *23*, 10-17. [http://dx.doi.org/10.1016/j.diamond.2011.12.021]

[12] Lafosse, A.; Bertin, M.; Azria, R. Electron driven processes in ices: Surface functionalization and

synthesis reactions. *Prog. Surf. Sci.,* **2009**, *84*(5-6), 177-198.
[http://dx.doi.org/10.1016/j.progsurf.2009.03.001]

[13] El Tall, O.; Hou, Y.; Abou-Hamad, E.; Raja, I.U.; Hedhili, M.N.; Peng, W.; Mahfouz, R.; Bakr, O.M.; Beaujuge, P.M. Direct functionalization of nanodiamonds with maleimide. *Chem. Mater.,* **2014**, *26*(9), 2766-2769.
[http://dx.doi.org/10.1021/cm500036x]

[14] Burleson, T.; Yusuf, N.; Stanishevsky, A. Surface modification of nanodiamonds for biomedical application and analysis by infrared spectroscopy. *J. Achiev. Mater. Manuf. Eng.,* **2009**, *37*, 258-263.

[15] Kaur, R.; Badea, I. Nanodiamonds as novel nanomaterials for biomedical applications: drug delivery and imaging systems. *Int. J. Nanomedicine,* **2013**, *8*, 203-220.
[PMID: 23326195]

[16] Lukovits, I. Resonance energy in graphite. *J. Chem. Inf. Comput. Sci.,* **2004**, *44*(5), 1565-1570.
[http://dx.doi.org/10.1021/ci049931a] [PMID: 15446813]

[17] Wallace, P.R. The band theory of graphite. *Phys. Rev.,* **1947**, *71*(9), 622-634.
[http://dx.doi.org/10.1103/PhysRev.71.622]

[18] Sengupta, R.; Bhattacharya, M.; Bandyopadhyay, S.; Bhowmick, A.K. A review on the mechanical and electrical properties of graphite and modified graphite reinforced polymer composites. *Prog. Polym. Sci.,* **2011**, *36*(5), 638-670.
[http://dx.doi.org/10.1016/j.progpolymsci.2010.11.003]

[19] Dreyer, D.R.; Bielawski, C.W. Carbocatalysis: Heterogeneous carbons finding utility in synthetic chemistry. *Chem. Sci. (Camb.),* **2011**, *2*(7), 1233-1240.
[http://dx.doi.org/10.1039/c1sc00035g]

[20] Kodomari, M.; Suzuki, Y.; Yoshida, K. Graphite as an effective catalyst for Friedel–Crafts acylation. *Chem. Commun. (Camb.),* **1997**, (16), 1567-1568.
[http://dx.doi.org/10.1039/a703947f]

[21] Sereda, G.A.; Rajpara, V.B.; Slaba, R.L. The synthetic potential of graphite-catalyzed alkylation. *Tetrahedron,* **2007**, *63*(34), 8351-8357.
[http://dx.doi.org/10.1016/j.tet.2007.05.005]

[22] Dreyer, D.R.; Jia, H.P.; Todd, A.D.; Geng, J.; Bielawski, C.W. Graphite oxide: a selective and highly efficient oxidant of thiols and sulfides. *Org. Biomol. Chem.,* **2011**, *9*(21), 7292-7295.
[http://dx.doi.org/10.1039/c1ob06102j] [PMID: 21909587]

[23] Bawaked, S.; He, Q.; Dummer, N.F.; Carley, A.F.; Knight, D.W.; Bethell, D.; Kiely, C.J.; Hutchings, G.J. Selective oxidation of alkenes using graphite-supported gold-palladium catalysts. *Catal. Sci. Technol.,* **2011**, *1*(5), 747-759.
[http://dx.doi.org/10.1039/c1cy00122a]

[24] Garrigues, B.; Laporte, C.; Laurent, R.; Laporterie, A.; Dubac, J. Microwave-assisted Diels-Alder reaction supported on graphite. *Liebigs Ann.,* **1996**, *1996*(5), 739-741.
[http://dx.doi.org/10.1002/jlac.199619960515]

[25] Vijay Kumar, A.; Rama Rao, K. Recyclable graphite oxide catalyzed Friedel–Crafts addition of indoles to α,β-unsaturated ketones. *Tetrahedron Lett.,* **2011**, *52*(40), 5188-5191.
[http://dx.doi.org/10.1016/j.tetlet.2011.08.002]

[26] Girard-Lauriault, P.L.; Illgen, R.; Ruiz, J.C.; Wertheimer, M.R.; Unger, W.E.S. Surface functionalization of graphite and carbon nanotubes by vacuum-ultraviolet photochemical reactions. *Appl. Surf. Sci.,* **2012**, *258*(22), 8448-8454.
[http://dx.doi.org/10.1016/j.apsusc.2012.03.012]

[27] Sadasivuni, K.K.; Ponnamma, D.; Thomas, S.; Grohens, Y. Evolution from graphite to graphene elastomer composites. *Prog. Polym. Sci.,* **2014**, *39*(4), 749-780.
[http://dx.doi.org/10.1016/j.progpolymsci.2013.08.003]

Not be distributed or uploaded to anyone or anywhere
For personal private use only

[28] Boukhvalov, D.W. Oxidation of a graphite surface: The role of water. *J. Phys. Chem.,* **2014**, *118*, 27594-27598.

[29] Dimiev, A.; Kosynkin, D.V.; Alemany, L.B.; Chaguine, P.; Tour, J.M. Pristine graphite oxide. *J. Am. Chem. Soc.,* **2012**, *134*(5), 2815-2822.
[http://dx.doi.org/10.1021/ja211531y] [PMID: 22239610]

[30] Dongil, A.B.; Bachiller-Baeza, B.; Guerrero-Ruiz, A.; Rodríguez-Ramos, I.; Martínez-Alonso, A.; Tascón, J.M.D. Surface chemical modifications induced on high surface area graphite and carbon nanofibers using different oxidation and functionalization treatments. *J. Colloid Interface Sci.,* **2011**, *355*(1), 179-189.
[http://dx.doi.org/10.1016/j.jcis.2010.11.066] [PMID: 21190698]

[31] Beckett, R.J.; Croft, R.C. The structure of graphite oxide. *J. Phys. Chem.,* **1952**, *56*(8), 929-935.
[http://dx.doi.org/10.1021/j150500a001]

[32] Yang, Z.; Sun, Y.; Alemany, L.B.; Narayanan, T.N.; Billups, W.E. Birch reduction of graphite. Edge and interior functionalization by hydrogen. *J. Am. Chem. Soc.,* **2012**, *134*(45), 18689-18694.
[http://dx.doi.org/10.1021/ja3073116] [PMID: 23072630]

[33] Liu, S.; Zeng, T.H.; Hofmann, M.; Burcombe, E.; Wei, J.; Jiang, R.; Kong, J.; Chen, Y. Antibacterial activity of graphite, graphite oxide, graphene oxide, and reduced graphene oxide: membrane and oxidative stress. *ACS Nano,* **2011**, *5*(9), 6971-6980.
[http://dx.doi.org/10.1021/nn202451x] [PMID: 21851105]

[34] Robledo, C.B.; Otero, M.; Luque, G.; Cámara, O.; Barraco, D.; Rojas, M.I.; Leiva, E.P.M. First-principles studies of lithium storage in reduced graphite oxide. *Electrochim. Acta,* **2014**, *140*, 232-237.
[http://dx.doi.org/10.1016/j.electacta.2014.07.013]

[35] Ulloa, E. Fullerenes and their Applications in Science and Technology. *Introduction to Nanotechnology,* **2013**, (Spring), 1-5.

[36] Sheka, E.F.; Razbirin, B.S.; Nelson, D.K. Continuous symmetry of C_{60} fullerene and its derivatives. *J. Phys. Chem. A,* **2011**, *115*(15), 3480-3490.
[http://dx.doi.org/10.1021/jp109128v] [PMID: 21449547]

[37] Haddon, R.C. Electronic structure, conductivity and superconductivity of alkali metal doped (C60). *Acc. Chem. Res.,* **1992**, *25*(3), 127-133.
[http://dx.doi.org/10.1021/ar00015a005]

[38] Lieber, C.M.; Zhang, Z. Physical properties of metal-doped fullerene superconductors. *Solid State Phys.,* **1994**, *48*, 349-384.
[http://dx.doi.org/10.1016/S0081-1947(08)60581-0]

[39] del Carmen Gimenez-Lopez, M.; Räisänen, M.T.; Chamberlain, T.W.; Weber, U.; Lebedeva, M.; Rance, G.A.; Briggs, G.A.D.; Pettifor, D.; Burlakov, V.; Buck, M.; Khlobystov, A.N. Functionalized fullerenes in self-assembled monolayers. *Langmuir,* **2011**, *27*(17), 10977-10985.
[http://dx.doi.org/10.1021/la200654n] [PMID: 21744819]

[40] Gogotsi, Y. Carbon Nanomaterials. *Taylor and Francis, CRC Press, USA,* **2006**.

[41] Hoke, S.H., II; Molstad, J.; Dilettato, D.; Jay, M.J.; Carlson, D.; Kahr, B.; Cooks, R.G. Reaction of fullerenes and benzyne. *J. Org. Chem.,* **1992**, *57*(19), 5069-5071.
[http://dx.doi.org/10.1021/jo00045a012]

[42] Yamada, M.; Akasaka, T.; Nagase, S. Carbene additions to fullerenes. *Chem. Rev.,* **2013**, *113*(9), 7209-7264.
[http://dx.doi.org/10.1021/cr3004955] [PMID: 23773169]

[43] Zhang, W.; Sprafke, J.K.; Ma, M.; Tsui, E.Y.; Sydlik, S.A.; Rutledge, G.C.; Swager, T.M. Modular functionalization of carbon nanotubes and fullerenes. *J. Am. Chem. Soc.,* **2009**, *131*(24), 8446-8454.
[http://dx.doi.org/10.1021/ja810049z] [PMID: 19480427]

Not be distributed or uploaded to anyone or anywhere
For personal private use only

[44] Tzirakis, M.D.; Orfanopoulos, M. Radical reactions of fullerenes: from synthetic organic chemistry to materials science and biology. *Chem. Rev.,* **2013**, *113*(7), 5262-5321. [http://dx.doi.org/10.1021/cr300475r] [PMID: 23570603]

[45] Kokubo, K.; Matsubayashi, K.; Tategaki, H.; Takada, H.; Oshima, T. Facile synthesis of highly water-soluble fullerenes more than half-covered by hydroxyl groups. *ACS Nano,* **2008**, *2*(2), 327-333. [http://dx.doi.org/10.1021/nn700151z] [PMID: 19206634]

[46] Nakamura, E.; Isobe, H. Functionalized fullerenes in water. The first 10 years of their chemistry, biology, and nanoscience. *Acc. Chem. Res.,* **2003**, *36*(11), 807-815. [http://dx.doi.org/10.1021/ar030027y] [PMID: 14622027]

[47] Snow, S.D.; Kim, K.C.; Moor, K.J.; Jang, S.S.; Kim, J.H. Functionalized fullerenes in water: a closer look. *Environ. Sci. Technol.,* **2015**, *49*(4), 2147-2155. [http://dx.doi.org/10.1021/es504735h] [PMID: 25632831]

[48] Zhang, G.; Liu, Y.; Liang, D.; Gan, L.; Li, Y. Facile synthesis of isomerically pure fullerenols and formation of spherical aggregates from $C_{60}(OH)_8$. *Angew. Chem. Int. Ed.,* **2010**, *49*(31), 5293-5295. [http://dx.doi.org/10.1002/anie.201001280] [PMID: 20575126]

[49] Iwashita, A.; Matsuo, Y.; Nakamura, E. $AlCl_{(3)}$-mediated mono-, di-, and trihydroarylation of [60]fullerene. *Angew. Chem. Int. Ed.,* **2007**, *46*(19), 3513-3516. [http://dx.doi.org/10.1002/anie.200700062] [PMID: 17385815]

[50] Talyzin, A.V.; Tsybin, Y.O.; Purcell, J.M.; Schaub, T.M.; Shulga, Y.M.; Noréus, D.; Sato, T.; Dzwilewski, A.; Sundqvist, B.; Marshall, A.G. Reaction of hydrogen gas with C_{60} at elevated pressure and temperature: hydrogenation and cage fragmentation. *J. Phys. Chem. A,* **2006**, *110*(27), 8528-8534. [http://dx.doi.org/10.1021/jp0557971] [PMID: 16821837]

[51] Morton, J.R.; Preston, K.F.; Krusic, P.J.; Hill, S.A.; Wasserman, E. ESR studies of the reaction of alkyl radicals with fullerene (C60). *J. Phys. Chem.,* **1992**, *96*(9), 3576-3578. [http://dx.doi.org/10.1021/j100188a006]

[52] Wang, H.H.; Kini, A.M.; Savall, B.M.; Carlson, K.D.; Williams, J.M.; Lathrop, M.W.; Lykke, K.R.; Parker, D.H.; Wurz, P.; Pellin, M.J.; Gruen, D.M.; Welp, U.; Kwok, W-K.; Fleshler, S.; Crabtree, G.W.; Schirber, J.E.; Overmyer, D.L. Superconductivity at 28.6 K in a rubidium-C_{60} fullerene compound, Rb_xC_{60}, synthesized by a solution-phase technique. *Inorg. Chem.,* **1991**, *30*(15), 2962-2963. [http://dx.doi.org/10.1021/ic00015a004]

[53] Glarum, S.H.; Duclos, S.J.; Haddon, R.C. Microwave study of superconductivity in alkali-metal-doped fullerene C60 films. *J. Am. Chem. Soc.,* **1992**, *114*(6), 1996-2001. [http://dx.doi.org/10.1021/ja00032a010]

[54] Komatsu, K.; Takimoto, N.; Murata, Y.; Wan, T.S.M.; Wong, T. Synthesis and properties of dialkyl derivatives of di[60]fullerenylbutadiyne and di[60]fullerenylacetylene: the buckydumbbells. *Tetrahedron Lett.,* **1996**, *37*(34), 6153-6156. [http://dx.doi.org/10.1016/0040-4039(96)01335-4]

[55] Innocenzi, P.; Brusatin, G. Fullerene-based organic-inorganic nanocomposites and their applications. *Chem. Mater.,* **2001**, *13*(10), 3126-3139. [http://dx.doi.org/10.1021/cm0110223]

[56] Giacalone, F.; Martín, N. Fullerene polymers: synthesis and properties. *Chem. Rev.,* **2006**, *106*(12), 5136-5190. [http://dx.doi.org/10.1021/cr068389h] [PMID: 17165684]

[57] Bakry, R.; Vallant, R.M.; Najam-ul-Haq, M.; Rainer, M.; Szabo, Z.; Huck, C.W.; Bonn, G.K. Medicinal applications of fullerenes. *Int. J. Nanomedicine,* **2007**, *2*(4), 639-649. [PMID: 18203430]

[58] Bosi, S.; Da Ros, T.; Spalluto, G.; Prato, M. Fullerene derivatives: an attractive tool for biological applications. *Eur. J. Med. Chem.,* **2003**, *38*(11-12), 913-923.

Not be distributed or uploaded to anyone or anywhere For personal private use only

[http://dx.doi.org/10.1016/j.ejmech.2003.09.005] [PMID: 14642323]

[59] Tohji, K.; Paul, A.; Moro, L.; Malhotra, R.; Lorents, D.C.; Ruoff, R.S. Selective and high-yield synthesis of higher fullerenes. *J. Phys. Chem.,* **1995**, *99*(50), 17785-17788.
[http://dx.doi.org/10.1021/j100050a018]

[60] Gan, L.; Huang, S.; Zhang, X.; Zhang, A.; Cheng, B.; Cheng, H.; Li, X.; Shang, G. Fullerenes as a tert-butylperoxy radical trap, metal catalyzed reaction of tert-butyl hydroperoxide with fullerenes, and formation of the first fullerene mixed peroxides C(60)(O)(OO(t)Bu)(4) and C(70)(OO(Bu)(10). *J. Am. Chem. Soc.,* **2002**, *124*(45), 13384-13385.
[http://dx.doi.org/10.1021/ja027714p] [PMID: 12418881]

[61] Bendikov, M.; Wudl, F.; Perepichka, D.F. Tetrathiafulvalenes, oligoacenenes, and their buckminsterfullerene derivatives: the brick and mortar of organic electronics. *Chem. Rev.,* **2004**, *104*(11), 4891-4946.
[http://dx.doi.org/10.1021/cr030666m] [PMID: 15535637]

[62] Imahori, H.; Fukuzumi, S. Porphyrin- and fullerene-baed molecular photovoltaic devices. *Adv. Funct. Mater.,* **2004**, *14*(6), 525-536.
[http://dx.doi.org/10.1002/adfm.200305172]

[63] Anthopoulos, T.D.; Singh, B.; Marjanovic, N.; Sariciftci, N.S.; Montaigne Ramil, A.; Sitter, H.; Cölle, M.; de Leeuw, D.M. High performance n-channel organic field-effect transistors and ring oscillators based on C_{60} fullerene films. *Appl. Phys. Lett.,* **2006**, *89*(21), 213504-3.
[http://dx.doi.org/10.1063/1.2387892]

[64] Haddon, R.C.; Perel, A.S.; Morris, R.C.; Palstra, T.T.M.; Hebard, A.F.; Fleming, R.M. C_{60} thin film transistors. *Appl. Phys. Lett.,* **1995**, *67*(1), 121-123.
[http://dx.doi.org/10.1063/1.115503]

[65] Iijima, S. Helical microtubules of graphitic carbon. *Nature,* **1991**, *354*(6348), 56-58.
[http://dx.doi.org/10.1038/354056a0]

[66] Ajayan, P.M.; Charlier, J.C.; Rinzler, A.G. Carbon nanotubes: From macromolecules to nanotechnology. *Proc. Natl. Acad. Sci. USA,* **1999**, *96*(25), 14199-14200.
[http://dx.doi.org/10.1073/pnas.96.25.14199] [PMID: 10588679]

[67] Lee, D.W.; Seo, J.W Preparation of carbon nanotubes from graphite powder at room temperature. **2010**.

[68] Journet, C.; Maser, W.K.; Bernier, P.; Loiseau, A.; de la Chapelle, M.L.; Lefrant, S.; Deniard, P.; Lee, R.; Fischer, J.E. Large-scale production of single-walled carbon nanotubes by the electric-arc technique. *Nature,* **1997**, *388*(6644), 756-758.
[http://dx.doi.org/10.1038/41972]

[69] Cassell, A.M.; Raymakers, J.A.; Kong, J.; Dai, H. Large scale CVD synthesis of single-walled carbon nanotubes. *J. Phys. Chem. B,* **1999**, *103*(31), 6484-6492.
[http://dx.doi.org/10.1021/jp990957s]

[70] Odom, T.W.; Huang, J.L.; Kim, P.; Lieber, C.M. Atomic structure and electronic properties of single-walled carbon nanotubes. *Nature,* **1998**, *391*(6662), 62-64.
[http://dx.doi.org/10.1038/34145]

[71] Tersoff, J.; Ruoff, R.S. Structural properties of a carbon-nanotube crystal. *Phys. Rev. Lett.,* **1994**, *73*(5), 676-679.
[http://dx.doi.org/10.1103/PhysRevLett.73.676] [PMID: 10057509]

[72] Aykol, M.; Hou, B.; Dhall, R.; Chang, S.W.; Branham, W.; Qiu, J.; Cronin, S.B. Clamping instability and van der Waals forces in carbon nanotube mechanical resonators. *Nano Lett.,* **2014**, *14*(5), 2426-2430.
[http://dx.doi.org/10.1021/nl500096p] [PMID: 24758201]

[73] Sawano, S.; Arie, T.; Akita, S. Carbon nanotube resonator in liquid. *Nano Lett.,* **2010**, *10*(9), 3395-

Not be distributed or uploaded to anyone or anywhere
For personal private use only

3398.
[http://dx.doi.org/10.1021/nl101292b] [PMID: 20681632]

[74] Wong, S.S.; Joselevich, E.; Woolley, A.T.; Cheung, C.L.; Lieber, C.M. Covalently functionalized nanotubes as nanometre- sized probes in chemistry and biology. *Nature,* **1998**, *394*(6688), 52-55.
[http://dx.doi.org/10.1038/27873] [PMID: 9665127]

[75] Blake, R.; Gun'ko, Y.K.; Coleman, J.; Cadek, M.; Fonseca, A.; Nagy, J.B.; Blau, W.J. A generic organometallic approach toward ultra-strong carbon nanotube polymer composites. *J. Am. Chem. Soc.,* **2004**, *126*(33), 10226-10227.
[http://dx.doi.org/10.1021/ja0474805] [PMID: 15315418]

[76] Biercuk, M.J.; Llaguno, M.C.; Radosavljevic, M.; Hyun, J.K.; Johnson, A.T.; Fischer, J.E. Carbon nanotube composites for thermal management. *Appl. Phys. Lett.,* **2002**, *80*(15), 2767-2769.
[http://dx.doi.org/10.1063/1.1469696]

[77] An, W.; Turner, C.H. Linking carbon and boron-nitride nanotubes: Heterojunction energetics and band gap tuning. *J. Phys. Chem. Lett.,* **2010**, *1*(15), 2269-2273.
[http://dx.doi.org/10.1021/jz100753x]

[78] Ma, J.; Tang, J.; Zhang, H.; Shinya, N.; Qin, L.C. Ultrathin carbon nanotube fibrils of high electrochemical capacitance. *ACS Nano,* **2009**, *3*(11), 3679-3683.
[http://dx.doi.org/10.1021/nn900787h] [PMID: 19877714]

[79] Bethune, D.S.; Kiang, C.H.; de Vries, M.S.; Gorman, G.; Savoy, R.; Vazquez, J.; Beyers, R. Cobalt-catalysed growth of carbon nanotubes with single-atomic-layer walls. *Nature,* **1993**, *363*(6430), 605-607.
[http://dx.doi.org/10.1038/363605a0]

[80] Xiong, H.; Slater, M.D.; Balasubramanian, M.; Johnson, C.S.; Rajh, T. Amorphous TiO_2 nanotube anode for rechargeable sodium ion batteries. *J. Phys. Chem. Lett.,* **2011**, *2*(20), 2560-2565.
[http://dx.doi.org/10.1021/jz2012066]

[81] Perebeinos, V.; Tersoff, J. Carbon nanotube deformation and collapse under metal contacts. *Nano Lett.,* **2014**, *14*(8), 4376-4380.
[http://dx.doi.org/10.1021/nl5012646] [PMID: 25014612]

[82] Dillon, A.C.; Heben, M.J. Hydrogen storage using carbon adsorbents: past, present and future. *Appl. Phys., A Mater. Sci. Process.,* **2001**, *72*(2), 133-142.
[http://dx.doi.org/10.1007/s003390100788]

[83] Chen, Y.; Shaw, D.T.; Bai, X.D.; Wang, E.G.; Lund, C.; Lu, W.M.; Chung, D.D.L. Hydrogen storage in aligned carbon nanotubes. *Appl. Phys. Lett.,* **2001**, *78*(15), 2128-2130.
[http://dx.doi.org/10.1063/1.1341224]

[84] Svedružić, D.; Blackburn, J.L.; Tenent, R.C.; Rocha, J.D.R.; Vinzant, T.B.; Heben, M.J.; King, P.W. High-performance hydrogen production and oxidation electrodes with hydrogenase supported on metallic single-wall carbon nanotube networks. *J. Am. Chem. Soc.,* **2011**, *133*(12), 4299-4306.
[http://dx.doi.org/10.1021/ja104785e] [PMID: 21384925]

[85] Novoselov, K.S.; Geim, A.K.; Morozov, S.V.; Jiang, D.; Zhang, Y.; Dubonos, S.V.; Grigorieva, I.V.; Firsov, A.A. Electric field effect in atomically thin carbon films. *Science,* **2004**, *306*(5696), 666-669.
[http://dx.doi.org/10.1126/science.1102896] [PMID: 15499015]

[86] Li, X.; Cai, W.; An, J.; Kim, S.; Nah, J.; Yang, D.; Piner, R.; Velamakanni, A.; Jung, I.; Tutuc, E.; Banerjee, S.K.; Colombo, L.; Ruoff, R.S. Large-area synthesis of high-quality and uniform graphene films on copper foils. *Science,* **2009**, *324*(5932), 1312-1314.
[http://dx.doi.org/10.1126/science.1171245] [PMID: 19423775]

[87] Dreyer, D.R.; Ruoff, R.S.; Bielawski, C.W. From conception to realization: an historial account of graphene and some perspectives for its future. *Angew. Chem. Int. Ed.,* **2010**, *49*(49), 9336-9344.
[http://dx.doi.org/10.1002/anie.201003024] [PMID: 21110353]

Not be distributed or uploaded to anyone or anywhere
For personal private use only

[88] Geim, A.K.; Novoselov, K.S. The rise of graphene. *Nat. Mater.,* **2007**, *6*(3), 183-191. [http://dx.doi.org/10.1038/nmat1849] [PMID: 17330084]

[89] Novoselov, K.S.; Geim, A.K.; Morozov, S.V.; Jiang, D.; Katsnelson, M.I.; Grigorieva, I.V.; Dubonos, S.V.; Firsov, A.A. Two-dimensional gas of massless Dirac fermions in graphene. *Nature,* **2005**, *438*(7065), 197-200. [http://dx.doi.org/10.1038/nature04233] [PMID: 16281030]

[90] Demming, A. Demming. *King of the elements.Nanotechnology,* **2010**. [http://dx.doi.org/10.1088/0957-4484/21/30/300201]

[91] Boyes, M.; Alieva, A.; Tong, J.; Nagyte, V.; Melle-Franco, M.; Vetter, T.; Casiraghi, C. Exploiting the surface properties of graphene for polymorph selectivity. *ACS Nano,* **2020**, *14*(8), 10394-10401. [http://dx.doi.org/10.1021/acsnano.0c04183] [PMID: 32692539]

[92] Xu, H.; Xie, L.; Zhang, H.; Zhang, J. Effect of graphene Fermi level on the Raman scattering intensity of molecules on graphene. *ACS Nano,* **2011**, *5*(7), 5338-5344. [http://dx.doi.org/10.1021/nn103237x] [PMID: 21678950]

[93] Neto, A.H.C.; Guinea, F.; Peres, N.M.R.; Novoselov, K.S.; Geim, A.K. *The electronic properties of graphene.,* **2009**, *109*(54), 81.

[94] Rao, C.N.R.; Matte, H.S.S.R.; Subrahmanyam, K.S. Synthesis and selected properties of graphene and graphene mimics. *Acc. Chem. Res.,* **2013**, *46*(1), 149-159. [http://dx.doi.org/10.1021/ar300033m] [PMID: 22738406]

[95] Kim, Y.A.; Fujisawa, K.; Muramatsu, H.; Hayashi, T.; Endo, M.; Fujimori, T.; Kaneko, K.; Terrones, M.; Behrends, J.; Eckmann, A.; Casiraghi, C.; Novoselov, K.S.; Saito, R.; Dresselhaus, M.S. Raman spectroscopy of boron-doped single-layer graphene. *ACS Nano,* **2012**, *6*(7), 6293-6300. [http://dx.doi.org/10.1021/nn301728j] [PMID: 22695033]

[96] Prathish, K.P.; Barsan, M.M.; Geng, D.; Sun, X.; Brett, C.M.A. Chemically modified graphene and nitrogen-doped graphene: Electrochemical characterisation and sensing applications. *Electrochim. Acta,* **2013**, *114*, 533-542. [http://dx.doi.org/10.1016/j.electacta.2013.10.080]

[97] Wang, H.; Maiyalagan, T.; Wang, X. Review on recent progress in nitrogen-doped graphene: Synthesis, characterization, and its potential applications. *ACS Catal.,* **2012**, *2*(5), 781-794. [http://dx.doi.org/10.1021/cs200652y]

[98] Wang, Y.; Shao, Y.; Matson, D.W.; Li, J.; Lin, Y. Nitrogen-doped graphene and its application in electrochemical biosensing. *ACS Nano,* **2010**, *4*(4), 1790-1798. [http://dx.doi.org/10.1021/nn100315s] [PMID: 20373745]

[99] Deng, D.; Pan, X.; Yu, L.; Cui, Y.; Jiang, Y.; Qi, J.; Li, W.X.; Fu, Q.; Ma, X.; Xue, Q.; Sun, G.; Bao, X. Toward N-doped graphene *via* solvothermal synthesis. *Chem. Mater.,* **2011**, *23*(5), 1188-1193. [http://dx.doi.org/10.1021/cm102666r]

[100] Usachov, D.; Vilkov, O.; Grüneis, A.; Haberer, D.; Fedorov, A.; Adamchuk, V.K.; Preobrajenski, A.B.; Dudin, P.; Barinov, A.; Oehzelt, M.; Laubschat, C.; Vyalikh, D.V. Nitrogen-doped graphene: efficient growth, structure, and electronic properties. *Nano Lett.,* **2011**, *11*(12), 5401-5407. [http://dx.doi.org/10.1021/nl2031037] [PMID: 22077830]

[101] Georgakilas, V.; Otyepka, M.; Bourlinos, A.B.; Chandra, V.; Kim, N.; Kemp, K.C.; Hobza, P.; Zboril, R.; Kim, K.S. Functionalization of graphene: covalent and non-covalent approaches, derivatives and applications. *Chem. Rev.,* **2012**, *112*(11), 6156-6214. [http://dx.doi.org/10.1021/cr3000412] [PMID: 23009634]

[102] Koehler, F.M.; Stark, W.J. Organic synthesis on graphene. *Acc. Chem. Res.,* **2013**, *46*(10), 2297-2306. [http://dx.doi.org/10.1021/ar300125w] [PMID: 23210633]

[103] Su, C.; Loh, K.P. Carbocatalysts: graphene oxide and its derivatives. *Acc. Chem. Res.,* **2013**, *46*(10),

2275-2285.
[http://dx.doi.org/10.1021/ar300118v] [PMID: 23270430]

[104] Quintana, M.; Vazquez, E.; Prato, M. Organic functionalization of graphene in dispersions. *Acc. Chem. Res.,* **2013**, *46*(1), 138-148.
[http://dx.doi.org/10.1021/ar300138e] [PMID: 22872046]

[105] Mirza-Aghayan, M.; Kashef-Azar, E.; Boukherroub, R. Graphite oxide: an efficient reagent for oxidation of alcohols under sonication. *Tetrahedron Lett.,* **2012**, *53*(37), 4962-4965.
[http://dx.doi.org/10.1016/j.tetlet.2012.07.016]

[106] Jia, H.P.; Dreyer, D.R.; Bielawski, C.W. C–H oxidation using graphite oxide. *Tetrahedron,* **2011**, *67*(24), 4431-4434.
[http://dx.doi.org/10.1016/j.tet.2011.02.065]

[107] Lücking, F.; Köser, H.; Jank, M.; Ritter, A. Iron powder, graphite and activated carbon as catalysts for the oxidation of 4-chlorophenol with hydrogen peroxide in aqueous solution. *Water Res.,* **1998**, *32*(9), 2607-2614.
[http://dx.doi.org/10.1016/S0043-1354(98)00016-5]

[108] Byung, H.H.; Dae, H.S.; Sung, Y.C. Graphite catalyzed reduction of aromatic and aliphatic nitro compounds with hydrazine hydrate. *Tetrahedron Lett.,* **1985**, *26*(50), 6233-6234.
[http://dx.doi.org/10.1016/S0040-4039(00)95060-3]

[109] Hu, F.; Patel, M.; Luo, F.; Flach, C.; Mendelsohn, R.; Garfunkel, E.; He, H.; Szostak, M. Graphene-catalyzed direct friedel–crafts alkylation reactions: mechanism, selectivity, and synthetic utility. *J. Am. Chem. Soc.,* **2015**, *137*(45), 14473-14480.
[http://dx.doi.org/10.1021/jacs.5b09636] [PMID: 26496423]

[110] Sachdeva, H. Recent advances in the catalytic applications of GO/rGO for green organic synthesis. *Green Processing and Synthesis,* **2020**, *9*(1), 515-537.
[http://dx.doi.org/10.1515/gps-2020-0055]

[111] Lombardi, L.; Bandini, M. Graphene oxide as a mediator in organic synthesis: a mechanistic focus. *Angew. Chem. Int. Ed.,* **2020**, *59*(47), 20767-20778.
[http://dx.doi.org/10.1002/anie.202006932] [PMID: 32516475]

[112] Zhao, J.; Wang, H.; Gao, B.; Wang, X.; Cai, Q.; Wang, X. Chemical functionalization of graphene *via* aryne cycloaddition: a theoretical study. *J. Mol. Model.,* **2012**, *18*(6), 2861-2868.
[http://dx.doi.org/10.1007/s00894-011-1309-8] [PMID: 22127614]

[113] Park, J.; Yan, M. Covalent functionalization of graphene with reactive intermediates. *Acc. Chem. Res.,* **2013**, *46*(1), 181-189.
[http://dx.doi.org/10.1021/ar300172h] [PMID: 23116448]

[114] Maktedar, S.S.; Mehetre, S.S.; Singh, M.; Kale, R.K. Ultrasound irradiation: A robust approach for direct functionalization of graphene oxide with thermal and antimicrobial aspects. *Ultrason. Sonochem.,* **2014**, *21*(4), 1407-1416.
[http://dx.doi.org/10.1016/j.ultsonch.2014.02.022] [PMID: 24613466]

[115] Mallakpour, S.; Abdolmaleki, A.; Borandeh, S. Covalently functionalized graphene sheets with biocompatible natural amino acids. *Appl. Surf. Sci.,* **2014**, *307*, 533-542.
[http://dx.doi.org/10.1016/j.apsusc.2014.04.070]

[116] Salavagione, H.J.; Gómez, M.A.; Martínez, G. Polymeric Modification of graphene through esterification of graphite oxide and poly(vinyl alcohol). *Macromolecules,* **2009**, *42*(17), 6331-6334.
[http://dx.doi.org/10.1021/ma900845w]

[117] Sanchez, V.C.; Jachak, A.; Hurt, R.H.; Kane, A.B. Biological interactions of graphene-family nanomaterials: an interdisciplinary review. *Chem. Res. Toxicol.,* **2012**, *25*(1), 15-34.
[http://dx.doi.org/10.1021/tx200339h] [PMID: 21954945]

[118] Chung, C.; Kim, Y.K.; Shin, D.; Ryoo, S.R.; Hong, B.H.; Min, D.H. Biomedical applications of

Not be distributed or uploaded to anyone or anywhere
For personal private use only

graphene and graphene oxide. *Acc. Chem. Res.,* **2013**, *46*(10), 2211-2224.
[http://dx.doi.org/10.1021/ar300159f] [PMID: 23480658]

[119] Mao, H.Y.; Laurent, S.; Chen, W.; Akhavan, O.; Imani, M.; Ashkarran, A.A.; Mahmoudi, M. Graphene: promises, facts, opportunities, and challenges in nanomedicine. *Chem. Rev.,* **2013**, *113*(5), 3407-3424.
[http://dx.doi.org/10.1021/cr300335p] [PMID: 23452512]

[120] Dai, L. Functionalization of graphene for efficient energy conversion and storage. *Acc. Chem. Res.,* **2013**, *46*(1), 31-42.
[http://dx.doi.org/10.1021/ar300122m] [PMID: 23030244]

[121] Liu, Y.; Dong, X.; Chen, P. Biological and chemical sensors based on graphene materials. *Chem. Soc. Rev.,* **2012**, *41*(6), 2283-2307.
[http://dx.doi.org/10.1039/C1CS15270J] [PMID: 22143223]

[122] Kim, F.; Luo, J.; Cruz-Silva, R.; Cote, L.J.; Sohn, K.; Huang, J. Self-propagating domino-like reactions in oxidized graphite. *Adv. Funct. Mater.,* **2010**, *20*(17), 2867-2873.
[http://dx.doi.org/10.1002/adfm.201000736]

[123] Liu, C.; Hao, F.; Zhao, X.; Zhao, Q.; Luo, S.; Lin, H. Low temperature reduction of free-standing graphene oxide papers with metal iodides for ultrahigh bulk conductivity. *Scientific Reports,* **2014**, *3996*(6), 4.

[124] Pei, S.; Cheng, H.M. The reduction of graphene oxide. *Carbon,* **2012**, *50*(9), 3210-3228.
[http://dx.doi.org/10.1016/j.carbon.2011.11.010]

[125] Chua, C.K.; Pumera, M. Chemical reduction of graphene oxide: a synthetic chemistry viewpoint. *Chem. Soc. Rev.,* **2014**, *43*(1), 291-312.
[http://dx.doi.org/10.1039/C3CS60303B] [PMID: 24121318]

[126] Gao, X.; Jang, J.; Nagase, S. Hydrazine and thermal reduction of graphene oxide: Reaction mechanisms, product structures, and reaction design. *J. Phys. Chem. C,* **2010**, *114*(2), 832-842.
[http://dx.doi.org/10.1021/jp909284g]

[127] Kim, M.; Hwang, Y.; Min, K.; Kim, J. Concentration dependence of graphene oxide–nanoneedle manganese oxide composites reduced by hydrazine hydrate for an electrochemical supercapacitor. *Phys. Chem. Chem. Phys.,* **2013**, *15*(37), 15602-15611.
[http://dx.doi.org/10.1039/c3cp52126e] [PMID: 23942656]

[128] Dreyer, D.R.; Park, S.; Bielawski, C.W.; Ruoff, R.S. The chemistry of graphene oxide. *Chem. Soc. Rev.,* **2010**, *39*(1), 228-240.
[http://dx.doi.org/10.1039/B917103G] [PMID: 20023850]

[129] Lee, D.W.; De Los Santos V, L.; Seo, J.W.; Felix, L.L.; Bustamante D, A.; Cole, J.M.; Barnes, C.H.W. The structure of graphite oxide: investigation of its surface chemical groups. *J. Phys. Chem. B,* **2010**, *114*(17), 5723-5728.
[http://dx.doi.org/10.1021/jp1002275] [PMID: 20380401]

[130] He, H.; Riedl, T.; Lerf, A.; Klinowski, J. Solid-state nmr studies of the structure of graphite oxide. *J. Phys. Chem.,* **1996**, *100*(51), 19954-19958.
[http://dx.doi.org/10.1021/jp961563t]

[131] Lerf, A.; He, H.; Forster, M.; Klinowski, J. Structure of graphite oxide revisited. *J. Phys. Chem. B,* **1998**, *102*(23), 4477-4482.
[http://dx.doi.org/10.1021/jp9731821]

[132] Casabianca, L.B.; Shaibat, M.A.; Cai, W.W.; Park, S.; Piner, R.; Ruoff, R.S.; Ishii, Y. NMR-based structural modeling of graphite oxide using multidimensional ^{13}C solid-state NMR and ab initio chemical shift calculations. *J. Am. Chem. Soc.,* **2010**, *132*(16), 5672-5676.
[http://dx.doi.org/10.1021/ja9030243] [PMID: 20359218]

[133] Cai, W.; Piner, R.D.; Stadermann, F.J.; Park, S.; Shaibat, M.A.; Ishii, Y.; Yang, D.; Velamakanni, A.;

An, S.J.; Stoller, M.; An, J.; Chen, D.; Ruoff, R.S. Synthesis and solid-state NMR structural characterization of ^{13}C-labeled graphite oxide. *Science,* **2008**, *321*(5897), 1815-1817. [http://dx.doi.org/10.1126/science.1162369] [PMID: 18818353]

[134] He, H.; Klinowski, J.; Forster, M.; Lerf, A. A new structural model for graphite oxide. *Chem. Phys. Lett.,* **1998**, *287*(1-2), 53-56. [http://dx.doi.org/10.1016/S0009-2614(98)00144-4]

[135] Ang, P.K.; Wang, S.; Bao, Q.; Thong, J.T.L.; Loh, K.P. High-throughput synthesis of graphene by intercalation-exfoliation of graphite oxide and study of ionic screening in graphene transistor. *ACS Nano,* **2009**, *3*(11), 3587-3594. [http://dx.doi.org/10.1021/nn901111s] [PMID: 19788171]

[136] Hernandez, Y.; Nicolosi, V.; Lotya, M.; Blighe, F.M.; Sun, Z.; De, S.; McGovern, I.T.; Holland, B.; Byrne, M.; Gun'Ko, Y.K.; Boland, J.J.; Niraj, P.; Duesberg, G.; Krishnamurthy, S.; Goodhue, R.; Hutchison, J.; Scardaci, V.; Ferrari, A.C.; Coleman, J.N. High-yield production of graphene by liquid-phase exfoliation of graphite. *Nat. Nanotechnol.,* **2008**, *3*(9), 563-568. [http://dx.doi.org/10.1038/nnano.2008.215] [PMID: 18772919]

[137] Parvez, K.; Wu, Z.S.; Li, R.; Liu, X.; Graf, R.; Feng, X.; Müllen, K. Exfoliation of graphite into graphene in aqueous solutions of inorganic salts. *J. Am. Chem. Soc.,* **2014**, *136*(16), 6083-6091. [http://dx.doi.org/10.1021/ja5017156] [PMID: 24684678]

[138] Paredes, J.I.; Villar-Rodil, S.; Martínez-Alonso, A.; Tascón, J.M.D. Graphene oxide dispersions in organic solvents. *Langmuir,* **2008**, *24*(19), 10560-10564. [http://dx.doi.org/10.1021/la801744a] [PMID: 18759411]

[139] Hirsch, A.; Englert, J.M.; Hauke, F. Wet chemical functionalization of graphene. *Acc. Chem. Res.,* **2013**, *46*(1), 87-96. [http://dx.doi.org/10.1021/ar300116q] [PMID: 22946482]

[140] Szabó, T.; Berkesi, O.; Forgó, P.; Josepovits, K.; Sanakis, Y.; Petridis, D.; Dékány, I. Evolution of surface functional groups in a series of progressively oxidized graphite oxides. *Chem. Mater.,* **2006**, *18*(11), 2740-2749. [http://dx.doi.org/10.1021/cm060258+]

[141] Niyogi, S.; Bekyarova, E.; Itkis, M.E.; Zhang, H.; Shepperd, K.; Hicks, J.; Sprinkle, M.; Berger, C.; Lau, C.N.; deHeer, W.A.; Conrad, E.H.; Haddon, R.C. Spectroscopy of covalently functionalized graphene. *Nano Lett.,* **2010**, *10*(10), 4061-4066. [http://dx.doi.org/10.1021/nl1021128] [PMID: 20738114]

[142] Pattabiraman, V.R.; Bode, J.W. Rethinking amide bond synthesis. *Nature,* **2011**, *480*(7378), 471-479. [http://dx.doi.org/10.1038/nature10702] [PMID: 22193101]

[143] Liu, L.H.; Lerner, M.M.; Yan, M. Derivitization of pristine graphene with well-defined chemical functionalities. *Nano Lett.,* **2010**, *10*(9), 3754-3756. [http://dx.doi.org/10.1021/nl1024744] [PMID: 20690657]

[144] Chen, D.; Feng, H.; Li, J. Graphene oxide: preparation, functionalization, and electrochemical applications. *Chem. Rev.,* **2012**, *112*(11), 6027-6053. [http://dx.doi.org/10.1021/cr300115g] [PMID: 22889102]

[145] Hsiao, M.C.; Liao, S.H.; Yen, M.Y.; Liu, P.I.; Pu, N.W.; Wang, C.A.; Ma, C.C.M. Preparation of covalently functionalized graphene using residual oxygen-containing functional groups. *ACS Appl. Mater. Interfaces,* **2010**, *2*(11), 3092-3099. [http://dx.doi.org/10.1021/am100597d] [PMID: 20949901]

[146] Vovusha, H.; Sanyal, S.; Sanyal, B. Interaction of nucleobases and aromatic amino acids with graphene oxide and graphene flakes. *J. Phys. Chem. Lett.,* **2013**, *4*(21), 3710-3718. [http://dx.doi.org/10.1021/jz401929h]

[147] Bourlinos, A.B.; Gournis, D.; Petridis, D.; Szabó, T.; Szeri, A.; Dékány, I. Graphite oxide: Chemical

Not be distributed or uploaded to anyone or anywhere
For personal private use only

reduction to graphite and surface modification with primary aliphatic amines and amino acids. *Langmuir,* **2003**, *19*(15), 6050-6055.
[http://dx.doi.org/10.1021/la026525h]

[148] Zhang, F.; Cao, H.; Yue, D.; Zhou, Z. Graphene covalently modified by DNA G-base. *J. Phys. Chem. C,* **2013**, *117*(7), 3513-3519.
[http://dx.doi.org/10.1021/jp307298p]

[149] Yang, H.; Shan, C.; Li, F.; Han, D.; Zhang, Q.; Niu, L. Covalent functionalization of polydisperse chemically-converted graphene sheets with amine-terminated ionic liquid. *Chem. Commun. (Camb.),* **2009**, *26*(26), 3880-3882.
[http://dx.doi.org/10.1039/b905085j] [PMID: 19662239]

[150] Georgakilas, V.; Bourlinos, A.B.; Zboril, R.; Steriotis, T.A.; Dallas, P.; Stubos, A.K.; Trapalis, C. Organic functionalisation of graphenes. *Chem. Commun. (Camb.),* **2010**, *46*(10), 1766-1768.
[http://dx.doi.org/10.1039/b922081j] [PMID: 20177643]

[151] McGrail, B.T.; Rodier, B.J.; Pentzer, E. Rapid functionalization of graphene oxide in water. *Chem. Mater.,* **2014**, *26*(19), 5806-5811.
[http://dx.doi.org/10.1021/cm5031409]

[152] Shim, S.H.; Kim, K.T.; Lee, J.U.; Jo, W.H. Facile method to functionalize graphene oxide and its application to poly(ethylene terephthalate)/graphene composite. *ACS Appl. Mater. Interfaces,* **2012**, *4*(8), 4184-4191.
[http://dx.doi.org/10.1021/am300906z] [PMID: 22764836]

[153] Park, S.; Dikin, D.A.; Nguyen, S.T.; Ruoff, R.S. Graphene oxide sheets chemically cross-linked by polyallylamine. *J. Phys. Chem. C,* **2009**, *113*(36), 15801-15804.
[http://dx.doi.org/10.1021/jp907613s]

[154] Liao, W.H.; Yang, S.Y.; Wang, J.Y.; Tien, H.W.; Hsiao, S.T.; Wang, Y.S.; Li, S.M.; Ma, C.C.M.; Wu, Y.F. Effect of molecular chain length on the mechanical and thermal properties of amine-functionalized graphene oxide/polyimide composite films prepared by *in situ* polymerization. *ACS Appl. Mater. Interfaces,* **2013**, *5*(3), 869-877.
[http://dx.doi.org/10.1021/am302494c] [PMID: 23286332]

[155] Xu, Z.; Wang, S.; Li, Y.; Wang, M.; Shi, P.; Huang, X. Covalent functionalization of graphene oxide with biocompatible poly(ethylene glycol) for delivery of paclitaxel. *ACS Appl. Mater. Interfaces,* **2014**, *6*(19), 17268-17276.
[http://dx.doi.org/10.1021/am505308f] [PMID: 25216036]

[156] Roy, S.; Tang, X.; Das, T.; Zhang, L.; Li, Y.; Ting, S.; Hu, X.; Yue, C.Y. Enhanced molecular level dispersion and interface bonding at low loading of modified graphene oxide to fabricate super nylon 12 composites. *ACS Appl. Mater. Interfaces,* **2015**, *7*(5), 3142-3151.
[http://dx.doi.org/10.1021/am5074408] [PMID: 25545112]

[157] Yang, Q.; Pan, X.; Clarke, K.; Li, K. Covalent functionalization of graphene with polysaccharides. *Ind. Eng. Chem. Res.,* **2012**, *51*(1), 310-317.
[http://dx.doi.org/10.1021/ie201391e]

[158] Bekyarova, E.; Itkis, M.E.; Ramesh, P.; Berger, C.; Sprinkle, M.; de Heer, W.A.; Haddon, R.C. Chemical modification of epitaxial graphene: spontaneous grafting of aryl groups. *J. Am. Chem. Soc.,* **2009**, *131*(4), 1336-1337.
[http://dx.doi.org/10.1021/ja8057327] [PMID: 19173656]

[159] Lomeda, J.R.; Doyle, C.D.; Kosynkin, D.V.; Hwang, W.F.; Tour, J.M. Diazonium functionalization of surfactant-wrapped chemically converted graphene sheets. *J. Am. Chem. Soc.,* **2008**, *130*(48), 16201-16206.
[http://dx.doi.org/10.1021/ja806499w] [PMID: 18998637]

[160] Zhu, Y.; Higginbotham, A.L.; Tour, J.M. Covalent functionalization of surfactant-wrapped graphene nanoribbons. *Chem. Mater.,* **2009**, *21*(21), 5284-5291.

[http://dx.doi.org/10.1021/cm902939n]

[161] Sun, Z.; Kohama, S.; Zhang, Z.; Lomeda, J.R.; Tour, J.M. Soluble graphene through edge-selective functionalization. *Nano Res.,* **2010**, *3*(2), 117-125. [http://dx.doi.org/10.1007/s12274-010-1016-2]

[162] Avinash, M.B.; Subrahmanyam, K.S.; Sundarayya, Y.; Govindaraju, T. Covalent modification and exfoliation of graphene oxide using ferrocene. *Nanoscale,* **2010**, *2*(9), 1762-1766. [http://dx.doi.org/10.1039/c0nr00024h] [PMID: 20820707]

[163] Fang, M.; Wang, K.; Lu, H.; Yang, Y.; Nutt, S. Covalent polymer functionalization of graphene nanosheets and mechanical properties of composites. *J. Mater. Chem.,* **2009**, *19*(38), 7098-7105. [http://dx.doi.org/10.1039/b908220d]

[164] Chua, C.K.; Pumera, M. Covalent chemistry on graphene. *Chem. Soc. Rev.,* **2013**, *42*(8), 3222-3233. [http://dx.doi.org/10.1039/c2cs35474h] [PMID: 23403465]

[165] Yuan, C.; Chen, W.; Yan, L. Amino-grafted graphene as a stable and metal-free solid basic catalyst. *J. Mater. Chem.,* **2012**, *22*(15), 7456-7460. [http://dx.doi.org/10.1039/c2jm30442b]

[166] Pham, V.H.; Cuong, T.V.; Hur, S.H.; Oh, E.; Kim, E.J.; Shin, E.W.; Chung, J.S. Chemical functionalization of graphene sheets by solvothermal reduction of a graphene oxide suspension in N-methyl-2-pyrrolidone. *J. Mater. Chem.,* **2011**, *21*(10), 3371-3377. [http://dx.doi.org/10.1039/C0JM02790A]

[167] Xu, Y.; Liu, Z.; Zhang, X.; Wang, Y.; Tian, J.; Huang, Y.; Ma, Y.; Zhang, X.; Chen, Y. A Graphene hybrid material covalently functionalized with porphyrin: Synthesis and optical limiting property. *Adv. Mater.,* **2009**, *21*(12), 1275-1279. [http://dx.doi.org/10.1002/adma.200801617]

[168] Liu, Z.; Robinson, J.T.; Sun, X.; Dai, H. PEGylated nanographene oxide for delivery of water-insoluble cancer drugs. *J. Am. Chem. Soc.,* **2008**, *130*(33), 10876-10877. [http://dx.doi.org/10.1021/ja803688x] [PMID: 18661992]

[169] Shen, J.; Shi, M.; Yan, B.; Ma, H.; Li, N.; Hu, Y.; Ye, M. Covalent attaching protein to graphene oxide *via* diimide-activated amidation. *Colloids Surf. B Biointerfaces,* **2010**, *81*(2), 434-438. [http://dx.doi.org/10.1016/j.colsurfb.2010.07.035] [PMID: 20728319]

[170] Xue, Y.; Liu, Y.; Lu, F.; Qu, J.; Chen, H.; Dai, L. Functionalization of graphene oxide with polyhedral oligomeric silsesquioxane (POSS) for multifunctional applications. *J. Phys. Chem. Lett.,* **2012**, *3*(12), 1607-1612. [http://dx.doi.org/10.1021/jz3005877] [PMID: 26285716]

[171] Stankovich, S.; Piner, R.D.; Nguyen, S.T.; Ruoff, R.S. Synthesis and exfoliation of isocyanate-treated graphene oxide nanoplatelets. *Carbon,* **2006**, *44*(15), 3342-3347. [http://dx.doi.org/10.1016/j.carbon.2006.06.004]

[172] Yoonessi, M.; Shi, Y.; Scheiman, D.A.; Lebron-Colon, M.; Tigelaar, D.M.; Weiss, R.A.; Meador, M.A. Graphene polyimide nanocomposites; thermal, mechanical, and high-temperature shape memory effects. *ACS Nano,* **2012**, *6*(9), 7644-7655. [http://dx.doi.org/10.1021/nn302871y] [PMID: 22931435]

[173] Quintana, M.; Spyrou, K.; Grzelczak, M.; Browne, W.R.; Rudolf, P.; Prato, M. Functionalization of graphene *via* 1,3-dipolar cycloaddition. *ACS Nano,* **2010**, *4*(6), 3527-3533. [http://dx.doi.org/10.1021/nn100883p] [PMID: 20503982]

[174] Wang, A.; Yu, W.; Xiao, Z.; Song, Y.; Long, L.; Cifuentes, M.P.; Humphrey, M.G.; Zhang, C. A 1,3-dipolar cycloaddition protocol to porphyrin-functionalized reduced graphene oxide with a push-pull motif. *Nano Res.,* **2015**, *8*(3), 870-886. [http://dx.doi.org/10.1007/s12274-014-0569-x]

[175] Zhong, X.; Jin, J.; Li, S.; Niu, Z.; Hu, W.; Li, R.; Ma, J. Aryne cycloaddition: highly efficient chemical

modification of graphene. *Chem. Commun. (Camb.),* **2010**, *46*(39), 7340-7342.
[http://dx.doi.org/10.1039/c0cc02389b] [PMID: 20820532]

[176] Seo, J.M.; Baek, J.B. A solvent-free Diels–Alder reaction of graphite into functionalized graphene nanosheets. *Chem. Commun. (Camb.),* **2014**, *50*(93), 14651-14653.
[http://dx.doi.org/10.1039/C4CC07173E] [PMID: 25314623]

[177] Sarkar, S.; Bekyarova, E.; Niyogi, S.; Haddon, R.C. Diels-Alder chemistry of graphite and graphene: graphene as diene and dienophile. *J. Am. Chem. Soc.,* **2011**, *133*(10), 3324-3327.
[http://dx.doi.org/10.1021/ja200118b] [PMID: 21341649]

[178] He, H.; Gao, C. General approach to individually dispersed, highly soluble, and conductive graphene nanosheets functionalized by nitrene chemistry. *Chem. Mater.,* **2010**, *22*(17), 5054-5064.
[http://dx.doi.org/10.1021/cm101634k]

[179] Yang, X.; Li, J.; Wen, T.; Ren, X.; Huang, Y.; Wang, X. Adsorption of naphthalene and its derivatives on magnetic graphene composites and the mechanism investigation. *Colloids Surf. A Physicochem. Eng. Asp.,* **2013**, *422*, 118-125.
[http://dx.doi.org/10.1016/j.colsurfa.2012.11.063]

[180] Kamada, S.; Nomoto, H.; Fukuda, K.; Fukawa, T.; Shirai, H.; Kimura, M. Noncovalent wrapping of chemically modified graphene with π-conjugated disk-like molecules. *Colloid Polym. Sci.,* **2011**, *289*(8), 925-932.
[http://dx.doi.org/10.1007/s00396-011-2414-z]

[181] Qi, X.; Pu, K.Y.; Li, H.; Zhou, X.; Wu, S.; Fan, Q.L.; Liu, B.; Boey, F.; Huang, W.; Zhang, H. Amphiphilic graphene composites. *Angew. Chem. Int. Ed.,* **2010**, *49*(49), 9426-9429.
[http://dx.doi.org/10.1002/anie.201004497] [PMID: 21031384]

[182] Choi, E.Y.; Han, T.H.; Hong, J.; Kim, J.E.; Lee, S.H.; Kim, H.W.; Kim, S.O. Noncovalent functionalization of graphene with end-functional polymers. *J. Mater. Chem.,* **2010**, *20*(10), 1907-1912.
[http://dx.doi.org/10.1039/b919074k]

[183] Zhang, J.; Lei, J.; Pan, R.; Xue, Y.; Ju, H. Highly sensitive electrocatalytic biosensing of hypoxanthine based on functionalization of graphene sheets with water-soluble conducting graft copolymer. *Biosens. Bioelectron.,* **2010**, *26*(2), 371-376.
[http://dx.doi.org/10.1016/j.bios.2010.07.127] [PMID: 20729055]

[184] Bai, H.; Xu, Y.; Zhao, L.; Li, C.; Shi, G. Non-covalent functionalization of graphene sheets by sulfonated polyaniline. *Chem. Commun. (Camb.),* **2009**, (13), 1667-1669.
[http://dx.doi.org/10.1039/b821805f] [PMID: 19294256]

[185] Liu, H.; Gao, J.; Xue, M.; Zhu, N.; Zhang, M.; Cao, T. Processing of graphene for electrochemical application: noncovalently functionalize graphene sheets with water-soluble electroactive methylene green. *Langmuir,* **2009**, *25*(20), 12006-12010.
[http://dx.doi.org/10.1021/la9029613] [PMID: 19764798]

[186] Geng, J.; Jung, H.T. Porphyrin functionalized graphene sheets in aqueous suspensions: From the preparation of graphene sheets to highly conductive graphene films. *J. Phys. Chem. C,* **2010**, *114*(18), 8227-8234.
[http://dx.doi.org/10.1021/jp1008779]

[187] Ghosh, A.; Rao, K.V.; George, S.J.; Rao, C.N.R. Noncovalent functionalization, exfoliation, and solubilization of graphene in water by employing a fluorescent coronene carboxylate. *Chemistry,* **2010**, *16*(9), 2700-2704.
[http://dx.doi.org/10.1002/chem.200902828] [PMID: 20108284]

[188] Jana, M.; Saha, S.; Khanra, P.; Samanta, P.; Koo, H.; Chandra Murmu, N.; Kuila, T. Non-covalent functionalization of reduced graphene oxide using sulfanilic acid azocromotrop and its application as a supercapacitor electrode material. *J. Mater. Chem. A Mater. Energy Sustain.,* **2015**, *3*(14), 7323-7331.
[http://dx.doi.org/10.1039/C4TA07009G]

Not be distributed or uploaded to anyone or anywhere
For personal private use only

[189] Komeilizadeh, H. Does Nature prefer heterocycles? *Iran. J. Pharm. Sci.,* **2006**, *4*, 229-230.

[190] Busto, E.; Gotor-Fernández, V.; Gotor, V. Hydrolases in the stereoselective synthesis of N-heterocyclic amines and amino acid derivatives. *Chem. Rev.,* **2011**, *111*(7), 3998-4035. [http://dx.doi.org/10.1021/cr100287w] [PMID: 21526748]

[191] Lawrence, S.A. Amines: Synthesis, properties and applications. *J. Am. Chem. Soc.,* **2005**, *127*, 9655-9658.

[192] Cheng, K.W.; Chen, F.; Wang, M. Heterocyclic amines: Chemistry and health. *Mol. Nutr. Food Res.,* **2006**, *50*(12), 1150-1170. [http://dx.doi.org/10.1002/mnfr.200600086] [PMID: 17131456]

[193] Liu, P.; Zhang, X.; Feng, L.; Xiong, H.; Wang, S. Direct electrochemistry of hemoglobin on graphene nanosheet-based modified electrode and its electrocatalysis to nitrite. *Am. J. Biomed. Sci.,* **2011**, *3*, 70-77. [http://dx.doi.org/10.5099/aj110100070]

[194] Chen, S.Y.; Lu, Y.Y.; Shih, F.Y.; Ho, P.H.; Chen, Y.F.; Chen, C.W.; Chen, Y.T.; Wang, W.H. Biologically inspired graphene-chlorophyll phototransistors with high gain. *Carbon,* **2013**, *63*, 23-29. [http://dx.doi.org/10.1016/j.carbon.2013.06.031]

[195] Wu, T.Y.; Guo, N.; Teh, C.Y.; Hay, J.X.W. *Advances in Ultrasound Technology for Environmental Remediation*; Springer: Dordrecht, Heidelberg, New York, London, **2013**, pp. 5-12. [http://dx.doi.org/10.1007/978-94-007-5533-8_2]

[196] Bang, J.H.; Suslick, K.S. Applications of ultrasound to the synthesis of nanostructured materials. *Adv. Mater.,* **2010**, *22*(10), 1039-1059. [http://dx.doi.org/10.1002/adma.200904093] [PMID: 20401929]

[197] Griffing, V. Ultrasonic chemical effects. *Ind. Eng. Chem.,* **1955**, *47*(6), 1180. [http://dx.doi.org/10.1021/ie50546a025]

[198] Yang, H.; Li, H.; Zhai, J.; Sun, L.; Yu, H. Simple synthesis of graphene oxide using ultrasonic cleaner from expanded graphite. *Ind. Eng. Chem. Res.,* **2014**, *53*(46), 17878-17883. [http://dx.doi.org/10.1021/ie503586v]

[199] de la Hoz, A. *Microwaves in Organic Synthesis, Wiley-VCH Verlag GmbH & Co. KGaA.,* **2012**.

[200] Gawande, M.B.; Shelke, S.N.; Zboril, R.; Varma, R.S. Microwave-assisted chemistry: synthetic applications for rapid assembly of nanomaterials and organics. *Acc. Chem. Res.,* **2014**, *47*(4), 1338-1348. [http://dx.doi.org/10.1021/ar400309b] [PMID: 24666323]

[201] Zuo, P.P.; Feng, H.F.; Xu, Z.Z.; Zhang, L.F.; Zhang, Y.L.; Xia, W.; Zhang, W.Q. Fabrication of biocompatible and mechanically reinforced graphene oxide-chitosan nanocomposite films. *Chem. Cent. J.,* **2013**, *7*(1), 39. [http://dx.doi.org/10.1186/1752-153X-7-39] [PMID: 23442350]

[202] Yang, Z.; Zheng, Q.; Qiu, H.; Li, J.; Yang, J. A simple method for the reduction of graphene oxide by sodium borohydride with CaCl2 as a catalyst. *N. Carbon Mater.,* **2015**, *30*(1), 41-47. [http://dx.doi.org/10.1016/S1872-5805(15)60174-3]

[203] Chua, C.K.; Pumera, M. Reduction of graphene oxide with substituted borohydrides. *J. Mater. Chem. A Mater. Energy Sustain.,* **2013**, *1*(5), 1892-1898. [http://dx.doi.org/10.1039/C2TA00665K]

[204] Ambrosi, A.; Chua, C.K.; Bonanni, A.; Pumera, M. Lithium aluminum hydride as reducing agent for chemically reduced graphene oxides. *Chem. Mater.,* **2012**, *24*(12), 2292-2298. [http://dx.doi.org/10.1021/cm300382b]

[205] Fan, X.; Peng, W.; Li, Y.; Li, X.; Wang, S.; Zhang, G.; Zhang, F. Deoxygenation of exfoliated graphite oxide under alkaline conditions: A green route to graphene preparation. *Adv. Mater.,* **2008**,

Not be distributed or uploaded to anyone or anywhere For personal private use only

20(23), 4490-4493.
[http://dx.doi.org/10.1002/adma.200801306]

[206] Cataldo, F.; Ursini, O.; Angelini, G. Graphite oxide and graphene nanoribbons reduction with hydrogen iodide. *Fuller. Nanotub. Carbon Nanostruct.,* **2011**, *19*(5), 461-468.
[http://dx.doi.org/10.1080/1536383X.2010.481064]

[207] Domingues, S.H.; Kholmanov, I.N.; Kim, T.; Kim, J.; Tan, C.; Chou, H.; Alieva, Z.A.; Piner, R.; Zarbin, A.J.G.; Ruoff, R.S. Reduction of graphene oxide films on Al foil for hybrid transparent conductive film applications. *Carbon,* **2013**, *63*, 454-459.
[http://dx.doi.org/10.1016/j.carbon.2013.07.007]

[208] Dreyer, D.R.; Murali, S.; Zhu, Y.; Ruoff, R.S.; Bielawski, C.W. Reduction of graphite oxide using alcohols. *J. Mater. Chem.,* **2011**, *21*(10), 3443-3447.
[http://dx.doi.org/10.1039/C0JM02704A]

[209] Chua, C.K.; Ambrosi, A.; Pumera, M. Graphene oxide reduction by standard industrial reducing agent: thiourea dioxide. *J. Mater. Chem.,* **2012**, *22*(22), 11054-11061.
[http://dx.doi.org/10.1039/c2jm16054d]

[210] Ma, H.L.; Zhang, H.B.; Hu, Q.H.; Li, W.J.; Jiang, Z.G.; Yu, Z.Z.; Dasari, A. Functionalization and reduction of graphene oxide with p-phenylene diamine for electrically conductive and thermally stable polystyrene composites. *ACS Appl. Mater. Interfaces,* **2012**, *4*(4), 1948-1953.
[http://dx.doi.org/10.1021/am201654b] [PMID: 22422027]

[211] Zhang, J.; Yang, H.; Shen, G.; Cheng, P.; Zhang, J.; Guo, S. Reduction of graphene oxide *via* l-ascorbic acid. *Chem. Commun. (Camb.),* **2010**, *46*(7), 1112-1114.
[http://dx.doi.org/10.1039/B917705A] [PMID: 20126730]

[212] Pham, V.H.; Pham, H.D.; Dang, T.T.; Hur, S.H.; Kim, E.J.; Kong, B.S.; Kim, S.; Chung, J.S. Chemical reduction of an aqueous suspension of graphene oxide by nascent hydrogen. *J. Mater. Chem.,* **2012**, *22*(21), 10530-10536.
[http://dx.doi.org/10.1039/c2jm30562c]

[213] Fan, Z.J.; Kai, W.; Yan, J.; Wei, T.; Zhi, L.J.; Feng, J.; Ren, Y.; Song, L.P.; Wei, F. Facile synthesis of graphene nanosheets *via* Fe reduction of exfoliated graphite oxide. *ACS Nano,* **2011**, *5*(1), 191-198.
[http://dx.doi.org/10.1021/nn102339t] [PMID: 21230006]

[214] Salas, E.C.; Sun, Z.; Lüttge, A.; Tour, J.M. Reduction of graphene oxide *via* bacterial respiration. *ACS Nano,* **2010**, *4*(8), 4852-4856.
[http://dx.doi.org/10.1021/nn101081t] [PMID: 20731460]

[215] Amarnath, C.A.; Hong, C.E.; Kim, N.H.; Ku, B.C.; Kuila, T.; Lee, J.H. Efficient synthesis of graphene sheets using pyrrole as a reducing agent. *Carbon,* **2011**, *49*(11), 3497-3502.
[http://dx.doi.org/10.1016/j.carbon.2011.04.048]

[216] Georgakilas, V.; Perman, J.A.; Tucek, J.; Zboril, R. Broad family of carbon nanoallotropes: classification, chemistry, and applications of fullerenes, carbon dots, nanotubes, graphene, nanodiamonds, and combined superstructures. *Chem. Rev.,* **2015**, *115*(11), 4744-4822.
[http://dx.doi.org/10.1021/cr500304f] [PMID: 26012488]

[217] Yin, P.T.; Shah, S.; Chhowalla, M.; Lee, K.B. Design, synthesis, and characterization of graphene-nanoparticle hybrid materials for bioapplications. *Chem. Rev.,* **2015**, *115*(7), 2483-2531.
[http://dx.doi.org/10.1021/cr500537t] [PMID: 25692385]

[218] Nguyen, P.; Berry, V. Graphene interfaced with biological cells: Opportunities and challenges. *J. Phys. Chem. Lett.,* **2012**, *3*(8), 1024-1029.
[http://dx.doi.org/10.1021/jz300033g] [PMID: 26286566]

[219] Maji, S.K.; Mandal, A.K.; Nguyen, K.T.; Borah, P.; Zhao, Y. Cancer cell detection and therapeutics using peroxidase-active nanohybrid of gold nanoparticle-loaded mesoporous silica-coated graphene. *ACS Appl. Mater. Interfaces,* **2015**, *7*(18), 9807-9816.

Not be distributed or uploaded to anyone or anywhere
For personal private use only

[http://dx.doi.org/10.1021/acsami.5b01758] [PMID: 25909624]

[220] Liu, X.; Ma, D.; Tang, H.; Tan, L.; Xie, Q.; Zhang, Y.; Ma, M.; Yao, S. Polyamidoamine dendrimer and oleic acid-functionalized graphene as biocompatible and efficient gene delivery vectors. *ACS Appl. Mater. Interfaces,* **2014**, *6*(11), 8173-8183.
[http://dx.doi.org/10.1021/am500812h] [PMID: 24836601]

[221] Paul, A.; Hasan, A.; Kindi, H.A.; Gaharwar, A.K.; Rao, V.T.S.; Nikkhah, M.; Shin, S.R.; Krafft, D.; Dokmeci, M.R.; Shum-Tim, D.; Khademhosseini, A. Injectable graphene oxide/hydrogel-based angiogenic gene delivery system for vasculogenesis and cardiac repair. *ACS Nano,* **2014**, *8*(8), 8050-8062.
[http://dx.doi.org/10.1021/nn5020787] [PMID: 24988275]

[222] de Faria, A.F.; Perreault, F.; Shaulsky, E.; Arias Chavez, L.H.; Elimelech, M. Antimicrobial electrospun biopolymer nanofiber mats functionalized with graphene oxide-silver nanocomposites. *ACS Appl. Mater. Interfaces,* **2015**, *7*(23), 12751-12759.
[http://dx.doi.org/10.1021/acsami.5b01639] [PMID: 25980639]

[223] Perreault, F.; de Faria, A.F.; Nejati, S.; Elimelech, M. Antimicrobial properties of graphene oxide nanosheets: Why size matters. *ACS Nano,* **2015**, *9*(7), 7226-7236.
[http://dx.doi.org/10.1021/acsnano.5b02067] [PMID: 26091689]

[224] Zhan, S.; Zhu, D.; Ma, S.; Yu, W.; Jia, Y.; Li, Y.; Yu, H.; Shen, Z. Highly efficient removal of pathogenic bacteria with magnetic graphene composite. *ACS Appl. Mater. Interfaces,* **2015**, *7*(7), 4290-4298.
[http://dx.doi.org/10.1021/am508682s] [PMID: 25634911]

[225] Musico, Y.L.F.; Santos, C.M.; Dalida, M.L.P.; Rodrigues, D.F. Surface modification of membrane filters using graphene and graphene oxide-based nanomaterials for bacterial inactivation and removal. *ACS Sustain. Chem.& Eng.,* **2014**, *2*(7), 1559-1565.
[http://dx.doi.org/10.1021/sc500044p]

[226] Chung, D.D.L. Electrical applications of carbon materials. *J. Mater. Sci.,* **2004**, *39*(8), 2645-2661.
[http://dx.doi.org/10.1023/B:JMSC.0000021439.18202.ea]

[227] Xu, Y.; Shi, G.; Duan, X. Self-assembled three-dimensional graphene macrostructures: Synthesis and applications in supercapacitors. *Acc. Chem. Res.,* **2015**, *48*(6), 1666-1675.
[http://dx.doi.org/10.1021/acs.accounts.5b00117] [PMID: 26042764]

[228] Lee, J.H.; Park, N.; Kim, B.G.; Jung, D.S.; Im, K.; Hur, J.; Choi, J.W. Restacking-inhibited 3D reduced graphene oxide for high performance supercapacitor electrodes. *ACS Nano,* **2013**, *7*(10), 9366-9374.
[http://dx.doi.org/10.1021/nn4040734] [PMID: 24001136]

[229] Guo, Y.; Guo, S.; Ren, J.; Zhai, Y.; Dong, S.; Wang, E. Cyclodextrin functionalized graphene nanosheets with high supramolecular recognition capability: synthesis and host-guest inclusion for enhanced electrochemical performance. *ACS Nano,* **2010**, *4*(7), 4001-4010.
[http://dx.doi.org/10.1021/nn100939n] [PMID: 20583782]

[230] Wu, W.; Li, Y.; Yang, L.; Ma, Y.; Pan, D.; Li, Y. A facile one-pot preparation of dialdehyde starch reduced graphene oxide/polyaniline composite for supercapacitors. *Electrochim. Acta,* **2014**, *139*, 117-126.
[http://dx.doi.org/10.1016/j.electacta.2014.06.166]

[231] Bhattacharjya, D.; Jeon, I.Y.; Park, H.Y.; Panja, T.; Baek, J.B.; Yu, J.S. Graphene nanoplatelets with selectively functionalized edges as electrode material for electrochemical energy storage. *Langmuir,* **2015**, *31*(20), 5676-5683.
[http://dx.doi.org/10.1021/acs.langmuir.5b00195] [PMID: 25942431]

[232] Goh, B.M.; Wang, Y.; Reddy, M.V.; Ding, Y.L.; Lu, L.; Bunker, C.; Loh, K.P. Filling the voids of graphene foam with graphene "eggshell" for improved lithium-ion storage. *ACS Appl. Mater. Interfaces,* **2014**, *6*(12), 9835-9841.

Not be distributed or uploaded to anyone or anywhere
For personal private use only

[http://dx.doi.org/10.1021/am5022655] [PMID: 24857682]

[233] Guldi, D.M.; Sgobba, V. Carbon nanostructures for solar energy conversion schemes. *Chem. Commun. (Camb.),* **2011**, *47*(2), 606-610.
[http://dx.doi.org/10.1039/C0CC02411B] [PMID: 20871887]

[234] Qiu, S.; Hu, W.; Yu, B.; Yuan, B.; Zhu, Y.; Jiang, S.; Wang, B.; Song, L.; Hu, Y. Effect of functionalized graphene oxide with organophosphorus oligomer on the thermal and mechanical properties and fire safety of polystyrene. *Ind. Eng. Chem. Res.,* **2015**, *54*(13), 3309-3319.
[http://dx.doi.org/10.1021/ie504511f]

[235] Lim, J.; Yeo, H.; Goh, M.; Ku, B.C.; Kim, S.G.; Lee, H.S.; Park, B.; You, N.H. Grafting of polyimide onto chemically-functionalized graphene nanosheets for mechanically-strong barrier membranes. *Chem. Mater.,* **2015**, *27*(6), 2040-2047.
[http://dx.doi.org/10.1021/cm5044254]

[236] Sun, Z.; Chang, H. Graphene and graphene-like two-dimensional materials in photodetection: mechanisms and methodology. *ACS Nano,* **2014**, *8*(5), 4133-4156.
[http://dx.doi.org/10.1021/nn500508c] [PMID: 24716438]

[237] Gupta, V.; Chaudhary, N.; Srivastava, R.; Sharma, G.D.; Bhardwaj, R.; Chand, S. Luminscent graphene quantum dots for organic photovoltaic devices. *J. Am. Chem. Soc.,* **2011**, *133*(26), 9960-9963.
[http://dx.doi.org/10.1021/ja2036749] [PMID: 21650464]

[238] Balcioglu, M.; Rana, M.; Robertson, N.; Yigit, M.V. DNA-length-dependent quenching of fluorescently labeled iron oxide nanoparticles with gold, graphene oxide and MoS_2 nanostructures. *ACS Appl. Mater. Interfaces,* **2014**, *6*(15), 12100-12110.
[http://dx.doi.org/10.1021/am503553h] [PMID: 25014711]

[239] Dinda, D.; Shaw, B.K.; Saha, S.K. Thymine functionalized graphene oxide for fluorescence "turn-of--on" sensing of Hg^{2+} and I^- in aqueous medium. *ACS Appl. Mater. Interfaces,* **2015**, *7*(27), 14743-14749.
[http://dx.doi.org/10.1021/acsami.5b02603] [PMID: 26094997]

[240] Cai, B.; Wang, S.; Huang, L.; Ning, Y.; Zhang, Z.; Zhang, G.J. Ultrasensitive label-free detection of PNA-DNA hybridization by reduced graphene oxide field-effect transistor biosensor. *ACS Nano,* **2014**, *8*(3), 2632-2638.
[http://dx.doi.org/10.1021/nn4063424] [PMID: 24528470]

[241] Alonso-Cristobal, P.; Vilela, P.; El-Sagheer, A.; Lopez-Cabarcos, E.; Brown, T.; Muskens, O.L.; Rubio-Retama, J.; Kanaras, A.G. Highly sensitive DNA sensor based on upconversion nanoparticles and graphene oxide. *ACS Appl. Mater. Interfaces,* **2015**, *7*(23), 12422-12429.
[http://dx.doi.org/10.1021/am507591u] [PMID: 25622622]

[242] Huang, K.J.; Niu, D.J.; Sun, J.Y.; Han, C.H.; Wu, Z.W.; Li, Y.L.; Xiong, X.Q. Novel electrochemical sensor based on functionalized graphene for simultaneous determination of adenine and guanine in DNA. *Colloids Surf. B Biointerfaces,* **2011**, *82*(2), 543-549.
[http://dx.doi.org/10.1016/j.colsurfb.2010.10.014] [PMID: 21050729]

[243] Zhan, L.; Zhang, Y.; Zeng, Q.L.; Liu, Z.D.; Huang, C.Z. Facile one-pot synthesis of folic acid-modified graphene to improve the performance of graphene-based sensing strategy. *J. Colloid Interface Sci.,* **2014**, *426*, 293-299.
[http://dx.doi.org/10.1016/j.jcis.2014.03.056] [PMID: 24863796]

[244] Kurkina, T.; Sundaram, S.; Sundaram, R.S.; Re, F.; Masserini, M.; Kern, K.; Balasubramanian, K. Self-assembled electrical biodetector based on reduced graphene oxide. *ACS Nano,* **2012**, *6*(6), 5514-5520.
[http://dx.doi.org/10.1021/nn301429k] [PMID: 22545858]

[245] Borini, S.; White, R.; Wei, D.; Astley, M.; Haque, S.; Spigone, E.; Harris, N.; Kivioja, J.; Ryhänen, T. Ultrafast graphene oxide humidity sensors. *ACS Nano,* **2013**, *7*(12), 11166-11173.

Not be distributed or uploaded to anyone or anywhere
For personal private use only

[http://dx.doi.org/10.1021/nn404889b] [PMID: 24206232]

[246] Kundu, A.; Nandi, S.; Das, P.; Nandi, A.K. Fluorescent graphene oxide *via* polymer grafting: an efficient nanocarrier for both hydrophilic and hydrophobic drugs. *ACS Appl. Mater. Interfaces,* **2015**, *7*(6), 3512-3523.
[http://dx.doi.org/10.1021/am507110r] [PMID: 25612470]

[247] Yao, K.; Tan, P.; Luo, Y.; Feng, L.; Xu, L.; Liu, Z.; Li, Y.; Peng, R. Graphene oxide selectively enhances thermostability of trypsin. *ACS Appl. Mater. Interfaces,* **2015**, *7*(22), 12270-12277.
[http://dx.doi.org/10.1021/acsami.5b03118] [PMID: 25985836]

[248] Wang, J.; Gao, X.; Wang, J.; Wei, Y.; Li, Z.; Gao, C. O-(carboxymethyl)-chitosan nanofiltration membrane surface functionalized with graphene oxide nanosheets for enhanced desalting properties. *ACS Appl. Mater. Interfaces,* **2015**, *7*(7), 4381-4389.
[http://dx.doi.org/10.1021/am508903g] [PMID: 25635511]

[249] Cote, L.J.; Kim, J.; Tung, V.C.; Luo, J.; Kim, F.; Huang, J. Graphene oxide as surfactant sheets. *Pure Appl. Chem.,* **2010**, *83*(1), 95-110.
[http://dx.doi.org/10.1351/PAC-CON-10-10-25]

[250] Xu, J.; Wang, L.; Zhu, Y. Decontamination of bisphenol A from aqueous solution by graphene adsorption. *Langmuir,* **2012**, *28*(22), 8418-8425.
[http://dx.doi.org/10.1021/la301476p] [PMID: 22571829]

[251] Dinda, D.; Gupta, A.; Saha, S.K. Removal of toxic Cr(vi) by UV-active functionalized graphene oxide for water purification. *J. Mater. Chem. A Mater. Energy Sustain.,* **2013**, *1*(37), 11221-11228.
[http://dx.doi.org/10.1039/c3ta12504a]

[252] Tan, M.; Liu, X.; Li, W.; Li, H. Enhancing sorption capacities for copper(II) and lead(II) under weakly acidic conditions by l-tryptophan-functionalized graphene oxide. *J. Chem. Eng. Data,* **2015**, *60*(5), 1469-1475.
[http://dx.doi.org/10.1021/acs.jced.5b00015]

[253] Li, P.; Xing, C.; Qu, S.; Li, B.; Shen, W. Carbon dioxide capturing by nitrogen-doping microporous carbon. *ACS Sustain. Chem.& Eng.,* **2015**, *3*(7), 1434-1442.
[http://dx.doi.org/10.1021/acssuschemeng.5b00291]

[254] Xu, H.; Qu, Z.; Zong, C.; Huang, W.; Quan, F.; Yan, N. MnO_x/graphene for the catalytic oxidation and adsorption of elemental mercury. *Environ. Sci. Technol.,* **2015**, *49*(11), 6823-6830.
[http://dx.doi.org/10.1021/es505978n] [PMID: 25922870]

[255] Whitener, K.E., Jr; Stine, R.; Robinson, J.T.; Sheehan, P.E. Jr.; Stine, R.; Robinson, J.T.; Sheehan, P.E. Graphene as electrophile: reactions of graphene fluoride. *J. Phys. Chem. C,* **2015**, *119*(19), 10507-10512.
[http://dx.doi.org/10.1021/acs.jpcc.5b02730]

[256] Mehetre, S.S.; Maktedar, S.S.; Singh, M. Understanding the mechanism of surface modification through enhanced thermal and electrochemical stabilities of N-doped graphene oxide. *Appl. Surf. Sci.,* **2016**, *366*, 514-522.
[http://dx.doi.org/10.1016/j.apsusc.2016.01.108]

[257] Maktedar, S.S.; Mehetre, S.S.; Avashthi, G.; Singh, M.; Jayaraman, T.; Jagannathan, M. Functionalized graphene oxide: an advanced material for the photocatalytic application. *Int. J. Phtochem.,* **2016**, *2*, 1-4.

[258] Maktedar, S.S.; Mehetre, S.S.; Avashthi, G.; Singh, M. In situ sonochemical reduction and direct functionalization of graphene oxide: A robust approach with thermal and biomedical applications. *Ultrason. Sonochem.,* **2017**, *34*, 67-77.
[http://dx.doi.org/10.1016/j.ultsonch.2016.05.015] [PMID: 27773294]

[259] Maktedar, S.S.; Avashthi, G.; Singh, M. Ultrasound assisted simultaneous reduction and direct functionalization of graphene oxide with thermal and cytotoxicity profile. *Ultrason. Sonochem.,* **2017**,

34, 856-864.
[http://dx.doi.org/10.1016/j.ultsonch.2016.07.016] [PMID: 27773313]

[260] Maktedar, S.S.; Avashthi, G.; Singh, M. Understanding the significance of O-doped graphene towards biomedical applications. *RSC Advances,* **2016**, *6*(115), 114264-114275.
[http://dx.doi.org/10.1039/C6RA23416J]

[261] Marrella, A.; Giannoni, P.; Pulsoni, I.; Quarto, R.; Raiteri, R.; Scaglione, S. Topographical features of graphene-oxide-functionalized substrates modulate cancer and healthy cell adhesion based on the cell tissue of origin. *ACS Appl. Mater. Interfaces,* **2018**, *10*(49), 41978-41985.
[http://dx.doi.org/10.1021/acsami.8b15036] [PMID: 30479135]

[262] Zhang, J.; Chen, L.; Chen, J.; Zhang, Q.; Feng, J. Stability, cellular uptake, and in vivo tracking of zwitterion modified graphene oxide as a drug carrier. *Langmuir,* **2019**, *35*(5), 1495-1502.
[http://dx.doi.org/10.1021/acs.langmuir.8b01995] [PMID: 30089359]

[263] Zhao, R.; Lv, M.; Li, Y.; Sun, M.; Kong, W.; Wang, L.; Song, S.; Fan, C.; Jia, L.; Qiu, S.; Sun, Y.; Song, H.; Hao, R. Stable nanocomposite based on pegylated and silver nanoparticles loaded graphene oxide for long-term antibacterial activity. *ACS Appl. Mater. Interfaces,* **2017**, *9*(18), 15328-15341.
[http://dx.doi.org/10.1021/acsami.7b03987] [PMID: 28422486]

[264] Szunerits, S.; Boukherroub, R. Antibacterial activity of graphene-based materials. *J. Mater. Chem. B Mater. Biol. Med.,* **2016**, *4*(43), 6892-6912.
[http://dx.doi.org/10.1039/C6TB01647B] [PMID: 32263558]

[265] Zhang, L.; Zhou, Q.; Song, W.; Wu, K.; Zhang, Y.; Zhao, Y. Dual-functionalized graphene oxide based sirna delivery system for implant surface biomodification with enhanced osteogenesis. *ACS Appl. Mater. Interfaces,* **2017**, *9*(40), 34722-34735.
[http://dx.doi.org/10.1021/acsami.7b12079] [PMID: 28925678]

[266] Sun, J.; Deng, Y.; Li, J.; Wang, G.; He, P.; Tian, S.; Bu, X.; Di, Z.; Yang, S.; Ding, G.; Xie, X. A new graphene derivative: hydroxylated graphene with excellent biocompatibility. *ACS Appl. Mater. Interfaces,* **2016**, *8*(16), 10226-10233.
[http://dx.doi.org/10.1021/acsami.6b02032] [PMID: 27052945]

[267] Wu, X.; Ding, S.J.; Lin, K.; Su, J. A review on the biocompatibility and potential applications of graphene in inducing cell differentiation and tissue regeneration. *J. Mater. Chem. B Mater. Biol. Med.,* **2017**, *5*(17), 3084-3102.
[http://dx.doi.org/10.1039/C6TB03067J] [PMID: 32263706]

[268] Upadhyay, R.; Naskar, S.; Bhaskar, N.; Bose, S.; Basu, B. Modulation of protein adsorption and cell proliferation on polyethylene immobilized graphene oxide reinforced HDPE bionanocomposites. *ACS Appl. Mater. Interfaces,* **2016**, *8*(19), 11954-11968.
[http://dx.doi.org/10.1021/acsami.6b00946] [PMID: 27108739]

[269] Akhavan, O. Graphene scaffolds in progressive nanotechnology/stem cell-based tissue engineering of the nervous system. *J. Mater. Chem. B Mater. Biol. Med.,* **2016**, *4*(19), 3169-3190.
[http://dx.doi.org/10.1039/C6TB00152A] [PMID: 32263253]

[270] Dai, C.; Zhang, S.; Liu, Z.; Wu, R.; Chen, Y. Two-dimensional graphene augments nanosonosensitized sonocatalytic tumor eradication. *ACS Nano,* **2017**, *11*(9), 9467-9480.
[http://dx.doi.org/10.1021/acsnano.7b05215] [PMID: 28829584]

[271] Liang, H.F.; Smith, C.T.G.; Mills, C.A.; Silva, S.R.P. The band structure of graphene oxide examined using photoluminescence spectroscopy. *J. Mater. Chem. C Mater. Opt. Electron. Devices,* **2015**, *3*(48), 12484-12491.
[http://dx.doi.org/10.1039/C5TC00307E]

[272] Du, D.; Song, H.; Nie, Y.; Sun, X.; Chen, L.; Ouyang, J. Photoluminescence of graphene oxide in visible range arising from excimer formation. *J. Phys. Chem. C,* **2015**, *119*(34), 20085-20090.
[http://dx.doi.org/10.1021/acs.jpcc.5b04529]

Not be distributed or uploaded to anyone or anywhere
For personal private use only

[273] Chiu, N.F.; Yang, C.D. Real-time and stepwise deoxidization processes to tune the photoluminescence properties of graphene oxide using EC-SPR spectroscopy. *RSC Advances,* **2018**, *8*(21), 11557-11565. [http://dx.doi.org/10.1039/C7RA13594G] [PMID: 35542802]

[274] Li, S.S.; Tu, K.H.; Lin, C.C.; Chen, C.W.; Chhowalla, M. Solution-processable graphene oxide as an efficient hole transport layer in polymer solar cells. *ACS Nano,* **2010**, *4*(6), 3169-3174. [http://dx.doi.org/10.1021/nn100551j] [PMID: 20481512]

[275] Bonaccorso, F.; Sun, Z.; Hasan, T.; Ferrari, A.C. Graphene photonics and optoelectronics. *Nat. Photonics,* **2010**, *4*(9), 611-622. [http://dx.doi.org/10.1038/nphoton.2010.186]

[276] Loh, K.P.; Bao, Q.; Eda, G.; Chhowalla, M. Graphene oxide as a chemically tunable platform for optical applications. *Nat. Chem.,* **2010**, *2*(12), 1015-1024. [http://dx.doi.org/10.1038/nchem.907] [PMID: 21107364]

[277] Eda, G.; Lin, Y.Y.; Mattevi, C.; Yamaguchi, H.; Chen, H.A.; Chen, I.S.; Chen, C.W.; Chhowalla, M. Blue photoluminescence from chemically derived graphene oxide. *Adv. Mater.,* **2010**, *22*(4), 505-509. [http://dx.doi.org/10.1002/adma.200901996] [PMID: 20217743]

[278] Chien, C.T.; Li, S.S.; Lai, W.J.; Yeh, Y.C.; Chen, H.A.; Chen, I.S.; Chen, L.C.; Chen, K.H.; Nemoto, T.; Isoda, S.; Chen, M.; Fujita, T.; Eda, G.; Yamaguchi, H.; Chhowalla, M.; Chen, C.W. Tunable photoluminescence from graphene oxide. *Angew. Chem. Int. Ed.,* **2012**, *51*(27), 6662-6666. [http://dx.doi.org/10.1002/anie.201200474] [PMID: 22623281]

[279] Kochmann, S.; Hirsch, T.; Wolfbeis, O.S. The pH dependence of the total fluorescence of graphite oxide. *J. Fluoresc.,* **2012**, *22*(3), 849-855. [http://dx.doi.org/10.1007/s10895-011-1019-8] [PMID: 22143963]

[280] Li, M.; Cushing, S.K.; Zhou, X.; Guo, S.; Wu, N. Fingerprinting photoluminescence of functional groups in graphene oxide. *J. Mater. Chem.*, **2012**, *22*(44), 23374-23379. [http://dx.doi.org/10.1039/c2jm35417a]

[281] Cushing, S.K.; Li, M.; Huang, F.; Wu, N. Origin of strong excitation wavelength dependent fluorescence of graphene oxide. *ACS Nano,* **2014**, *8*(1), 1002-1013. [http://dx.doi.org/10.1021/nn405843d] [PMID: 24359152]

[282] Demchenko, A.P. The red-edge effects: 30 years of exploration. *Luminescence,* **2002**, *17*(1), 19-42. [http://dx.doi.org/10.1002/bio.671] [PMID: 11816059]

[283] Enoki, T.; Takai, K. The edge state of nanographene and the magnetism of the edge-state spins. *Solid State Commun.,* **2009**, *149*(27-28), 1144-1150. [http://dx.doi.org/10.1016/j.ssc.2009.02.054]

[284] Diamantopoulou, A.; Glenis, S.; Zolnierkiwicz, G.; Guskos, N.; Likodimos, V. *Magnetism in pristine and chemically reduced graphene oxide.,* **2017**, 1-11.

[285] Tang, T.; Liu, F.; Liu, Y.; Li, X.; Xu, Q.; Feng, Q.; Tang, N.; Du, Y. Identifying the magnetic properties of graphene oxide. *Identifying the magnetic properties of graphene oxide.,* **2014**, *104*, 1-5. [http://dx.doi.org/10.1063/1.4869827]

[286] Miao, Q.; Wang, L.; Liu, Z.; Wei, B.; Xu, F.; Fei, W. Magnetic properties of N-doped graphene with high Curie temperature.*21832*, 1-10.**2016**,

[287] Sahoo, P.K.; Panigrahy, B.; Li, D.; Bahadur, D. *Magnetic properties of N-doped graphene with high Curie temperature.,* **2013**, *113*, 1-3.

[288] Zhang, H.; Zhao, M.; Yang, X.; Xia, H.; Liu, X.; Xia, Y. Diffusion and coalescence of vacancies and interstitials in graphite: A first-principles study. *Diamond Related Materials,* **2010**, *19*(10), 1240-1244. [http://dx.doi.org/10.1016/j.diamond.2010.06.010]

[289] Sahoo, R.K.; Jeyapandiarajan, P.; Devi Chandrasekhar, K.; Daniel, B.S.S.; Venimadhav, A.; Sant, S.B.; Jacob, C. Single-step synthesis of graphene-carbon nanofiber hybrid material and its synergistic

magnetic behaviour. *J. Alloys Compd.,* **2014**, *615*, 348-354.
[http://dx.doi.org/10.1016/j.jallcom.2014.06.171]

[290] Mansour, M.; Bechelany, M.; Habchi, R.; Eid, C. Influence of graphene oxide doping on the morphology and the magnetic properties of $Ni_{0.8}$ $Gd_{0.2}$ Fe_2 O_4 nanofibers prepared by electrospinning. *Phys. Lett. A,* **2017**, *381*(6), 658-662.
[http://dx.doi.org/10.1016/j.physleta.2016.12.014]

[291] Bahadur, J.; Pal, K. Structural and magnetic properties of reduced graphene oxide-TiO_2 nanoflower composite. *Physica E,* **2017**, *90*, 98-103.
[http://dx.doi.org/10.1016/j.physe.2017.02.022]

[292] Frumkin, A.; Polianovskaya, N.; Bagotskaya, I.; Grigoryev, N. Electrocatalysis and electrode surface properties. *J. Electroanal. Chem. Interfacial Electrochem.,* **1971**, *33*(2), 319-328.
[http://dx.doi.org/10.1016/S0022-0728(71)80120-1]

[293] Azzam, A.M.; Bockris, J.O.M. O'M. Cathodic evolution of hydrogen at very high current densities. *Nature,* **1950**, *165*(4193), 403-404.
[http://dx.doi.org/10.1038/165403b0]

[294] Xia, B.; Yan, Y.; Wang, X.; Lou, X.W.D. Recent progress on graphene-based hybrid electrocatalysts. *Mater. Horiz.,* **2014**, *1*(4), 379-399.
[http://dx.doi.org/10.1039/C4MH00040D]

[295] Duan, J.; Chen, S.; Jaroniec, M.; Qiao, S.Z. Heteroatom-doped graphene-based materials for energy-relevant electrocatalytic processes. *ACS Catal.,* **2015**, *5*(9), 5207-5234.
[http://dx.doi.org/10.1021/acscatal.5b00991]

[296] Debe, M.K. Electrocatalyst approaches and challenges for automotive fuel cells. *Nature,* **2012**, *486*(7401), 43-51.
[http://dx.doi.org/10.1038/nature11115] [PMID: 22678278]

[297] Armand, M.; Tarascon, J.M. Building better batteries. *Nature,* **2008**, *451*(7179), 652-657.
[http://dx.doi.org/10.1038/451652a] [PMID: 18256660]

[298] Gray, H.B. Powering the planet with solar fuel. *Nat. Chem.,* **2009**, *1*(1), 7.
[http://dx.doi.org/10.1038/nchem.141] [PMID: 21378780]

[299] Li, Y.; Dai, H. Recent advances in zinc–air batteries. *Chem. Soc. Rev.,* **2014**, *43*(15), 5257-5275.
[http://dx.doi.org/10.1039/C4CS00015C] [PMID: 24926965]

[300] Qiao, J.; Liu, Y.; Hong, F.; Zhang, J. A review of catalysts for the electroreduction of carbon dioxide to produce low-carbon fuels. *Chem. Soc. Rev.,* **2014**, *43*(2), 631-675.
[http://dx.doi.org/10.1039/C3CS60323G] [PMID: 24186433]

[301] Liang, Y.; Li, Y.; Wang, H.; Zhou, J.; Wang, J.; Regier, T.; Dai, H. Co_3O_4 nanocrystals on graphene as a synergistic catalyst for oxygen reduction reaction. *Nat. Mater.,* **2011**, *10*(10), 780-786.
[http://dx.doi.org/10.1038/nmat3087] [PMID: 21822263]

[302] Mirzakulova, E.; Khatmullin, R.; Walpita, J.; Corrigan, T.; Vargas-Barbosa, N.M.; Vyas, S.; Oottikkal, S.; Manzer, S.F.; Hadad, C.M.; Glusac, K.D. Electrode-assisted catalytic water oxidation by a flavin derivative. *Nat. Chem.,* **2012**, *4*(10), 794-801.
[http://dx.doi.org/10.1038/nchem.1439] [PMID: 23000992]

[303] Suntivich, J.; May, K.J.; Gasteiger, H.A.; Goodenough, J.B.; Shao-Horn, Y. A perovskite oxide optimized for oxygen evolution catalysis from molecular orbital principles. *Science,* **2011**, *334*(6061), 1383-1385.
[http://dx.doi.org/10.1126/science.1212858] [PMID: 22033519]

[304] Yin, Q.; Tan, J.M.; Besson, C.; Geletii, Y.V.; Musaev, D.G.; Kuznetsov, A.E.; Luo, Z.; Hardcastle, K.I.; Hill, C.L. A fast soluble carbon-free molecular water oxidation catalyst based on abundant metals. *Science,* **2010**, *328*(5976), 342-345.
[http://dx.doi.org/10.1126/science.1185372] [PMID: 20223949]

Not be distributed or uploaded to anyone or anywhere
For personal private use only

[305] Abdelhafiz, A.; Vitale, A.; Joiner, C.; Vogel, E.; Alamgir, F.M. Layer-by-layer evolution of structure, strain, and activity for the oxygen evolution reaction in graphene-templated Pt monolayers. *ACS Appl. Mater. Interfaces,* **2015**, *7*(11), 6180-6188.
[http://dx.doi.org/10.1021/acsami.5b00182] [PMID: 25730297]

[306] Ardizzone, S.; Fregonara, G.; Trasatti, S. "Inner" and "outer" active surface of RuO_2 electrodes. *Electrochim. Acta,* **1990**, *35*(1), 263-267.
[http://dx.doi.org/10.1016/0013-4686(90)85068-X]

[307] Cherevko, S.; Zeradjanin, A.R.; Topalov, A.A.; Kulyk, N.; Katsounaros, I.; Mayrhofer, K.J.J. Dissolution of noble metals during oxygen evolution in acidic media. *ChemCatChem,* **2014**, *6*(8), 2219-2223.
[http://dx.doi.org/10.1002/cctc.201402194]

[308] Jiao, Y.; Zheng, Y.; Jaroniec, M.; Qiao, S.Z. Design of electrocatalysts for oxygen- and hydrogen-involving energy conversion reactions. *Chem. Soc. Rev.,* **2015**, *44*(8), 2060-2086.
[http://dx.doi.org/10.1039/C4CS00470A] [PMID: 25672249]

[309] Bergmann, A.; Zaharieva, I.; Dau, H.; Strasser, P. Electrochemical water splitting by layered and 3D cross-linked manganese oxides: correlating structural motifs and catalytic activity. *Energy Environ. Sci.,* **2013**, *6*(9), 2745-2755.
[http://dx.doi.org/10.1039/c3ee41194j]

[310] Gong, M.; Li, Y.; Wang, H.; Liang, Y.; Wu, J.Z.; Zhou, J.; Wang, J.; Regier, T.; Wei, F.; Dai, H. An advanced Ni-Fe layered double hydroxide electrocatalyst for water oxidation. *J. Am. Chem. Soc.,* **2013**, *135*(23), 8452-8455.
[http://dx.doi.org/10.1021/ja4027715] [PMID: 23701670]

[311] Zhao, Y.; Nakamura, R.; Kamiya, K.; Nakanishi, S.; Hashimoto, K. Nitrogen-doped carbon nanomaterials as non-metal electrocatalysts for water oxidation. *Nat. Commun.,* **2013**, *4*, 1-7.
[http://dx.doi.org/10.1038/ncomms3390]

[312] Barnett, S.M.; Goldberg, K.I.; Mayer, J.M. A soluble copper–bipyridine water-oxidation electrocatalyst. *Nat. Chem.,* **2012**, *4*(6), 498-502.
[http://dx.doi.org/10.1038/nchem.1350] [PMID: 22614386]

[313] Fillol, J.L.; Codolà, Z.; Garcia-Bosch, I.; Gómez, L.; Pla, J.J.; Costas, M. Efficient water oxidation catalysts based on readily available iron coordination complexes. *Nat. Chem.,* **2011**, *3*(10), 807-813.
[http://dx.doi.org/10.1038/nchem.1140] [PMID: 21941254]

[314] Geletii, Y.V.; Botar, B.; Kögerler, P.; Hillesheim, D.A.; Musaev, D.G.; Hill, C.L. An all-inorganic, stable, and highly active tetraruthenium homogeneous catalyst for water oxidation. *Angew. Chem. Int. Ed. Engl.,* **2008**, *47*(21), 3896-3899.
[http://dx.doi.org/10.1002/anie.200705652] [PMID: 18351608]

[315] Thomas, J.G.N. Kinetics of electrolytic hydrogen evolution and the adsorption of hydrogen by metals. *Trans. Faraday Soc.,* **1961**, *57*, 1603-1611.
[http://dx.doi.org/10.1039/tf9615701603]

[316] Greeley, J.; Jaramillo, T.F.; Bonde, J.; Chorkendorff, I.; Nørskov, J.K. Computational high-throughput screening of electrocatalytic materials for hydrogen evolution. *Nat. Mater.,* **2006**, *5*(11), 909-913.
[http://dx.doi.org/10.1038/nmat1752] [PMID: 17041585]

[317] Sheng, W.; Zhuang, Z.; Gao, M.; Zheng, J.; Chen, J.G.; Yan, Y. *Correlating hydrogen oxidation and evolution activity on platinum at different pH with measured hydrogen binding energy.,* **2015**, *6*(5848), 1-6.
[http://dx.doi.org/10.1038/ncomms6848]

[318] McKone, J.R.; Sadtler, B.F.; Werlang, C.A.; Lewis, N.S.; Gray, H.B. Ni−Mo nanopowders for efficient electrochemical hydrogen evolution. *ACS Catal.,* **2013**, *3*(2), 166-169.
[http://dx.doi.org/10.1021/cs300691m]

Not be distributed or uploaded to anyone or anywhere
For personal private use only

[319] Jaramillo, T.F.; Jørgensen, K.P.; Bonde, J.; Nielsen, J.H.; Horch, S.; Chorkendorff, I. Identification of active edge sites for electrochemical H_2 evolution from MoS_2 nanocatalysts. *Science,* **2007**, *317*(5834), 100-102.
[http://dx.doi.org/10.1126/science.1141483] [PMID: 17615351]

[320] Huang, Z.; Chen, Z.; Chen, Z.; Lv, C.; Meng, H.; Zhang, C. $Ni_{12}P_5$ nanoparticles as an efficient catalyst for hydrogen generation *via* electrolysis and photoelectrolysis. *ACS Nano,* **2014**, *8*(8), 8121-8129.
[http://dx.doi.org/10.1021/nn5022204] [PMID: 25065948]

[321] Vrubel, H.; Hu, X. Molybdenum boride and carbide catalyze hydrogen evolution in both acidic and basic solutions. *Angew. Chem. Int. Ed.,* **2012**, *51*(51), 12703-12706.
[http://dx.doi.org/10.1002/anie.201207111] [PMID: 23143996]

[322] Xin, N.; Huang, H.; Zhang, J.; Dai, Z.; Gan, L. Fullerene doping: preparation of azafullerene C59NH and oxafulleroids $C_{59}O_3$ and $C_{60}O_4$. *Angew. Chem. Int. Ed.,* **2012**, *51*(25), 6163-6166.
[http://dx.doi.org/10.1002/anie.201202777] [PMID: 22573566]

[323] Tian, J.; Liu, Q.; Asiri, A.M.; Sun, X. Self-supported nanoporous cobalt phosphide nanowire arrays: an efficient 3D hydrogen-evolving cathode over the wide range of pH 0-14. *J. Am. Chem. Soc.,* **2014**, *136*(21), 7587-7590.
[http://dx.doi.org/10.1021/ja503372r] [PMID: 24830333]

[324] Duan, J.; Chen, S.; Jaroniec, M.; Qiao, S.Z. Porous C_3N_4 nanolayers@N-graphene films as catalyst electrodes for highly efficient hydrogen evolution. *ACS Nano,* **2015**, *9*(1), 931-940.
[http://dx.doi.org/10.1021/nn506701x] [PMID: 25559360]

[325] Putri, L.K.; Ong, W.J.; Chang, W.S.; Chai, S.P. Heteroatom doped graphene in photocatalysis: A review. *Appl. Surf. Sci.,* **2015**, *358*, 2-14.
[http://dx.doi.org/10.1016/j.apsusc.2015.08.177]

[326] Turchi, C.; Ollis, D.F. Photocatalytic degradation of organic water contaminants: Mechanisms involving hydroxyl radical attack. *J. Catal.,* **1990**, *122*(1), 178-192.
[http://dx.doi.org/10.1016/0021-9517(90)90269-P]

[327] Xiong, Z.; Zhang, L.L.; Ma, J.; Zhao, X.S. Photocatalytic degradation of dyes over graphene–gold nanocomposites under visible light irradiation. *Chem. Commun. (Camb.),* **2010**, *46*(33), 6099-6101.
[http://dx.doi.org/10.1039/c0cc01259a] [PMID: 20661492]

[328] Singh, P.; Shandilya, P.; Raizada, P.; Sudhaik, A.; Rahmani-Sani, A.; Hosseini-Bandegharaei, A. Review on various strategies for enhancing photocatalytic activity of graphene based nanocomposites for water purification. *Arab. J. Chem.,* **2020**, *13*(1), 3498-3520.
[http://dx.doi.org/10.1016/j.arabjc.2018.12.001]

[329] Posa, V.R.; Annavaram, V.; Koduru, J.R.; Bobbala, P.; V, M.; Somala, A.R. Preparation of graphene–TiO_2 nanocomposite and photocatalytic degradation of Rhodamine-B under solar light irradiation. *J. Exp. Nanosci.,* **2016**, *11*(9), 722-736.
[http://dx.doi.org/10.1080/17458080.2016.1144937]

[330] Posa, V.R.; Annavaram, V.; Somala, A.R. Fabrication of graphene–TiO_2 nanocomposite with improved photocatalytic degradation for acid orange 7 dye under solar light irradiation. *Bull. Mater. Sci.,* **2016**, *39*(3), 759-767.
[http://dx.doi.org/10.1007/s12034-016-1215-x]

[331] Khare, P.; Singh, A.; Verma, S.; Bhati, A.; Sonker, A.K.; Tripathi, K.M.; Sonkar, S.K. Sunlight-induced selective photocatalytic degradation of methylene blue in bacterial culture by pollutant soot derived nontoxic graphene nanosheets. *ACS Sustain. Chem.& Eng.,* **2018**, *6*(1), 579-589.
[http://dx.doi.org/10.1021/acssuschemeng.7b02929]

[332] Liu, G.; Sun, C.; Yang, H.G.; Smith, S.C.; Wang, L.; Lu, G.Q.M.; Cheng, H.M. Nanosized anatase TiO_2 single crystals for enhanced photocatalytic activity. *Chem. Commun. (Camb.),* **2010**, *46*(5), 755-

757.
[http://dx.doi.org/10.1039/B919895D] [PMID: 20087510]

[333] Wu, Z.; Dong, F.; Zhao, W.; Wang, H.; Liu, Y.; Guan, B. The fabrication and characterization of novel carbon doped TiO_2 nanotubes, nanowires and nanorods with high visible light photocatalytic activity. **2009**, *20*(235701), 1-9.

[334] Wang, J.; Tafen, D.N.; Lewis, J.P.; Hong, Z.; Manivannan, A.; Zhi, M.; Li, M.; Wu, N. Origin of photocatalytic activity of nitrogen-doped TiO_2 nanobelts. *J. Am. Chem. Soc.,* **2009**, *131*(34), 12290-12297.
[http://dx.doi.org/10.1021/ja903781h] [PMID: 19705915]

[335] Ullah, R.; Dutta, J. Photocatalytic degradation of organic dyes with manganese-doped ZnO nanoparticles. *J. Hazard. Mater.,* **2008**, *156*(1-3), 194-200.
[http://dx.doi.org/10.1016/j.jhazmat.2007.12.033] [PMID: 18221834]

[336] Sakthivel, S.; Shankar, M.V.; Palanichamy, M.; Arabindoo, B.; Bahnemann, D.W.; Murugesan, V. Enhancement of photocatalytic activity by metal deposition: characterisation and photonic efficiency of Pt, Au and Pd deposited on TiO_2 catalyst. *Water Res.,* **2004**, *38*(13), 3001-3008.
[http://dx.doi.org/10.1016/j.watres.2004.04.046] [PMID: 15261537]

[337] Arai, T.; Yanagida, M.; Konishi, Y.; Iwasaki, Y.; Sugihara, H.; Sayama, K. Efficient complete oxidation of acetaldehyde into CO_2 over $CuBi_2O_4/WO_3$ composite photocatalyst under visible and uv light irradiation. *J. Phys. Chem. C,* **2007**, *111*(21), 7574-7577.
[http://dx.doi.org/10.1021/jp0725533]

For personal private use only
Not be distributed or uploaded to anyone or anywhere

CHAPTER 6

Graphene-based Nanocomposite Catalysts: Synthesis, Properties and Applications

Pradeep Kumar Jaiswal[1,*], Munsaf Ali[2], Siddharth Sharma[3], Dinesh Kumar Yadav[3] and **Nitinkumar Satyadev Upadhyay[2]**

[1] *Department of Biochemistry and Biophysics, Texas A&M University, College Station, Texas 77843, USA*

[2] *Colleges of Nanoscale Science and Engineering, State University of New York, Polytechnic Institute, 257 Fuller Rd. Albany, NY 12203, New York, USA*

[3] *Department of Chemistry, Mohanlal Sukhadia University, Udaipur, 313001, India*

Abstract: In recent years, the progress of doped carbon catalysts (such as graphene-based nanocomposites), has attracted the tremendous attention of the scientific community because of their broad area of applications involving unique mechanical, electrical and industrial chemical production processes. The catalytic nature of metal-doped graphene-based nanocomposites has significantly improved, and provides alternatives to traditional transition metal-based catalysts. In addition, the progress of simple and easy synthetic approaches for graphene-based nanocomposites provides a wide range of opportunities for the synthesis of graphene-based nanocomposites *via* incorporating various metal or polymer-based nanomaterials for diverse applications. In this context, the recent development in the synthesis of graphene-based nanocomposites, their properties and applications are summarized in this chapter. The future insights and challenges towards the design and utilization of graphene-based nanocomposites with decent stability and enhanced catalytic performance are also outlined in this chapter.

Keywords: Electrochemical Biosensor, Graphene, Graphene Nanocomposite Catalysts, Graphene Oxide, Reduced Graphene Oxide.

INTRODUCTION

Since the discovery of carbon-related catalysts, the hydrocarbon-based compounds such as activated carbon, carbon fibers, graphite, and graphite-intercalation compounds, have gained significant attraction from chemists, in the last decades. Nowadays, carbon-based materials like graphene-based nanomaterial synthesis have become an attractive field in chemistry, physics, biology, and

* **Corresponding author Pradeep Kumar Jaiswal:** Department of Biochemistry and Biophysics, Texas A&M University, College Station, Texas 77843, USA; E-mail:pradeepjais@gmail.com

Pinki Bala Punjabi, Rakshit Ameta & Sharoni Gupta (Eds.)
All rights reserved-© 2023 Bentham Science Publishers

materials science [1]. Graphene is a two-dimensional carbon-based material having a single layer of sp^2 hybridized bonded carbon atoms that are closely packed in a honeycomb lattice [2]. Since the remarkable work of Prof. Novoselov's group in carbon-based chemistry research, the fast development in graphene-based research has envisioned the great potential of graphene in optoelectronics, nanoelectronics, electrochemical drug delivery, and biosensor applications due to its unique 2D structure, excellent electrical capacity, high adsorption susceptibility, high mechanical strength, and high thermal conductivity [3 - 5]. Although graphene sheets were well explored in fundamentals by a physicist at the discovery time, graphene metal-nanocomposites are drawing more attention to real applications for industry [6 - 9]. Until now, various synthetic procedures, such as covalent as well as non-covalent methods, electrochemical, micro-mechanical, solvo-thermal, chemical oxidation–reduction, chemical vapour deposition, photochemical reaction, physical deposition, and mixing [10 - 14] have been fabricated for the synthesis of well-defined functional graphene-based nanocomposites [15 - 20]. It was investigated that the graphene-based sheets can be doped with several components such as metal, metal oxides, or polymers [15, 21, 22] and developed as graphene-based-hybrids which can be employed in multiple applications [23 - 29]. In this view, extensive efforts have been devoted towards the study of graphene-based hybrids and many reviews on their design, development, synthesis, properties, characterization, and applications in recent decades are documented [29 - 32]. The significant potential growth of graphene-based nanocomposites toward their application in a variety of fields motivated us to present its synthesis, properties, and potential applications in a single chapter.

It is well established that the design of a heterogeneous catalyst plays an important role in its catalytic activity [33, 34]. As a new carbon family member, the extraordinary properties of graphene-based nanocomposites provide an ideal catalytic support [32, 35]. Therefore, we hope that this chapter will draw significant attention to the recent developments and advancements in the synthetic protocols and catalytic utilization of graphene-based nanocomposites. It is noteworthy that almost all graphene supports in the nanocomposites are developed *via* chemical reduction–oxidation methodology. The catalytic reactions, which are demonstrated, are an extension of the model reactions towards industrial-based reactions and the utilization of non-selective reactions towards more challenging and selective hydrogenation, coupling, oxidation, or reduction reactions. In the present chapter, a brief overview of the characteristic synthetic approaches and catalytic potential of graphene-based nanocomposites is presented, along with the enhanced catalytic behavior. A summary of some of the scientific opportunities and challenges is also presented at the end of the chapter.

APPROACHES TOWARDS GRAPHENE-BASED NANOCOMPOSITES SYNTHESES

Many versatile synthetic approaches have been documented to synthesize the graphene-based nanocomposites, such as covalent/non-covalent interaction, photochemical reactions, chemical/physical deposition or mixing, hydrothermal/solvothermal growth, electrophoresis, and electrochemical deposition. These developed approaches have several advantages as well as limitations, along with the improved recent development of specific graphene nanocomposites by adoption of appropriate preparation methods.

Non-covalent Interactive Approach

Non-covalent interaction is a leading applied methodology to design and synthesize graphene-based nanocomposites. Non-covalent association of organic and inorganic species with graphene leads to the attachment of organic and inorganic species on graphene incorporated surfaces. *in-situ* Small molecules, such as surfactants and polymers, are bonded to graphene surfaces *via* - stacking and/or hydrophobic interactions, providing an important way to modify graphene surfaces for graphene nanocomposites [36 - 40]. Because of the strong -stacking interaction with the graphene sheet of the pyrene moiety in the molecule, Xu and colleagues used PB- to synthesize enhanced hydrophilic graphene [40]. This was provided by *in-situ* chemical reduction of GO by hydrazine in the presence of 1-pyrenebutyrate (PB-).The resultant water-soluble graphene can be utilized to develop large scale conductive graphene films with higher conductivity in comparison to graphene oxide.

Metal ions can also be doped in graphene sheets through non-covalent congregation of graphene to form 3-D composites or hydrogel [41, 42]. For example, graphene oxide and metal precursors are hydrothermally decomposed to furnish three dimensional graphene-supported metal nanocomposites. Novel metal nanocomposites (Ag, Au, Pd, Rh, Ir, or Pt) on graphene material exhibit active sites, which enhance the porosity in graphene metal composites. The catalytic activity of 3-D composite with respect to Heck reaction has shown excellent and selective physical behavior [41]. GO sheets also undergo metal ions promoted self-assembly based reaction *via* the reduction of GO and produce magnetic Fe_3O_4 nanoparticles with macroscopic graphene based nanocomposites [42].

Covalent Interactive Approach

Another method that can be used to design and synthesis graphene nanocomposites is covalent reaction. Ionic liquids, polymers, porphyrin,

azidotrimethylsilane, *p*-phenyl-SO_3H, perfluorophenylazide (PFPA), and organic nitrite can all be covalently bonded to graphene *via* atom-transfer radical polymerization, amide-bonding, or click chemistry reaction. There are limited examples reported in the literature for the synthesis of graphene metal composites *via* covalent assembly [43-45].

Click chemistry is one of the best methods for the formation of covalent bond with metal composites and graphene surfaces. Various photo-induced moieties such as ruthenium-phenanthroline and zinc-porphyrin chromophores can be attached to graphene sheet using click chemistry. Firstly, the graphene surface was modified by unsaturated moieties *via* exposing alkyne groups followed by click chemistry reaction. In the result, these hybrids showed significantly improved photocurrent responses [46].

In-situ Chemical Electroless Deposition-based Approach

In the last few years, various efforts have been made to deposit nano-objects on graphene sheets to fabricate nanocomposites *via* chemical electroless deposition. Specific nanorod, nanoparticle and nanosheet can be fabricated *via* doping of metal on graphene surface, through *in situ* chemical deposition method, of the selective precursors. These process are straight forward and convenient for designing of a large number of graphene-based nanocomposites using metal oxides, metals and dichalcogenide precursors, such as, Au, Pt, Ag, Cu, TiO_2, Fe_2O_3, Mn_3O_4, SnO_2, and CdS [47 - 55]. Using the electroless chemical deposition method, Li *et al*. created graphene-based bimetallic nanocomposites with improved electrochemical surface area [48]. High-quality 3D-bimetallic nano-dendrites Pt-on-Pd were doped on graphene surfaces in two steps (Fig. **1**). Pt precursors (K_2PtCl_4) were reduced by earlier doped Pd-NPs on graphene-based material and fabricated into branched Pt-nano-dendrites with the number of branches being tunable with a synthetic framework [48]. Similarly, Ag-deposited graphene nanocomposites were created by heating a silver nitrate-graphene oxide aqueous solution at 75°C or by in situ reduction of silver precursor in the presence of GO by glucose or other reducing agents [50, 51, 56]. Copper-based graphene composites were also created by heating a copper precursor in the presence of graphene oxide and potassium borohydride [57].

The resultant Cu-nanoparticles are well dispersed on a graphene sheet having a diameter of about 20.8 nm. In another report, graphene-based macroscopic hydrogel-iron oxide nanocomposite with robust interconnected three-dimensional frame was constructed by the synergistic effect *via in-situ* reduction of graphene oxide from ferrous ions [42]. The amount of reducing agent and pH value play a very significant role in the synthesis of graphene-based nanocomposites. In

another investigation, TiO_2 deposited graphene nanocomposites have been designed and synthesized by *in-situ* hydrolysis of absorbed Ti (IV)-butoxide on rGO surfaces with oxygenated functional groups [74]. To achieve both better deposition and high conductivity of TiO_2 NPs, the oxidization time in the chemical exfoliation process was essential [53]. *In-situ* Metal chalcogenides like cadmium sulfide-NPs can be produced by *in-situ* chemical deposition on graphene sheets [58]. CdS nanoparticles were also synthesized from cadmium nitrate and CH_4N_2S at 150 °C heating in microwave irradiation [59]. This method was also used to synthesize graphene-zinc sulphide nanocomposites from zinc ions and H_2S gas reactions [54].

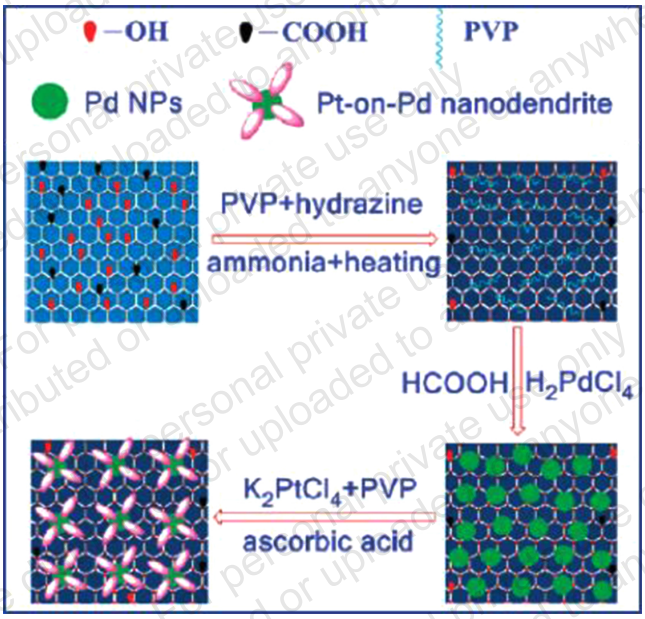

Fig. (1). Schematic representation for designing graphene nanosheet/Pt on Pd bimetallic nano-dendrite hybrids. (Reproduced with permission from Ref [48]. Copyright 2010, American Chemical Society).

Solvothermal and Hydrothermal-growth Based Approach

Solvothermal and hydrothermal methods are also extensively employed to construct graphene nanocomposites. Due to high pressure in solvothermal and hydrothermal methodologies, the acquired materials have close covalent network between deposited composites and graphene, which shows various useful applications.

To fabricate graphene metal composites by solvothermal or hydrothermal methodology, the metal/metal oxide precursor is mixed with graphene or GO in a solution followed by solvothermal/hydrothermal deposition of the precursor on

graphene sheet at high pressure in an autoclave. Solvothermal and hydrothermal processes are very flexible and can be used to design various kinds of nanomaterials (Fig. **2**) [60 - 65].

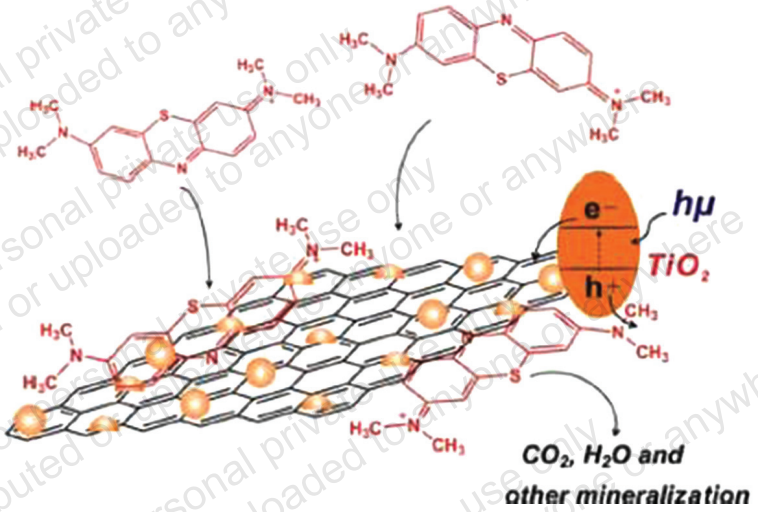

Fig. (2). Schematic representation of P25 nanoparticles and photodegradation of methylene blue (MB) over P25-GR. (Reproduced with permission from Ref [64]. Copyright 2010, American Chemical Society).

Metals like Ag and Pt-Ru, metal oxide (TiO_2, SnO_2, VO_2, Mn_3O_4), metal chalcogenides (*e.g*: ZnS, SnS) and complex compounds ($LiFePO_4$) based nanocomposites have been successfully decorated on the 2D carbon layer of graphene with well controlled solvothermal methods. Ye and his co-workers have reported a hydrothermal synthesis of reduced graphene oxide based Ag-nanocomposites by using ascorbic acid as a reducing agent and silver nitrate and graphene oxide as precursors [60]. Yoon and co-workers fabricated platinum–ruthenium (Pt-Ru) nanoparticles on graphene sheet *via* a hydrothermal process and the composites showed improved tolerance towards poisoning issues of oxidation of methanol with enhanced electrocatalytic activity [61].

Metal oxides are also used to synthesize graphene-based metal oxide composites on 2D carbon sheets by hydrothermal or solvothermal assembly. Zou *et al.* utilized seed-directed hydrothermal process to synthesize a large number of graphene-based metal oxide (such as TiO_2, ZnO, MnO_2, CuO, and ZrO_2) nanocomposites *via* designing a novel series of metal oxide-graphene-metal oxide hetero-structures. The hetero-structures exhibit four times increased photo-catalytic properties compared to pure metal oxide nanoparticles [62]. TiO_2 attached graphene nanocomposites were synthesized from GO and a reducing agent using a hydrothermal process (Fig. **3**) [63]. The crystal facets of TiO_2 nano-

objects in graphene based-nanocomposites, can also be controlled in a hydrothermal fashion [66]. Recently, graphene-based TiO_2 nanotubes and TiO_2 nanosheets with exposed facets were developed under a hydrothermal process in alkaline solution/ aqueous ethanol (Fig. **3**) [67, 68].

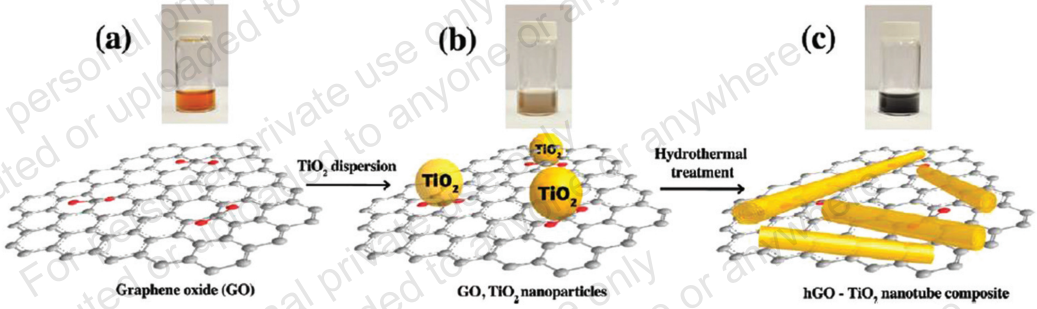

Fig. (3). Graphical presentation of the synthesis of TiO_2 nanotubes on rGO sheets. The GO sheets (a) coordinated with TiO_2 nanoparticles (b) converted to TNTs on hGO (c) The digital images show the color variations of the aqueous dispersions in each stage. (Reproduced with permission from Ref [68]. Copyright 2012, American Chemical Society).

After 2010, several research groups broadly investigated the synthesis of TiO_2 and VO_2 nanotubes, MoO_3 nano-objects, Mn_3O_4 and Fe_3O_4 nanoparticles having spherical geometry and hollow interiors with graphene *via* hydrothermal approach (Fig. **4**) [13, 65, 68 - 71]. Graphitic layers decorated with metal chalcogenides were also synthesized by solvothermal method. Cao and his co-workers have reported synthesis of CdS quantum dots attached to graphene sheets [72]. The nanocomposites formed have demonstrated tremendous performance in electron transfer from quantum dots (QDts) to graphene surfaces and have significant importance in optoelectronic materials. Later on, Gong *et al.* adopted the same methodology for the fabrication of graphene CdS nanocluster for hydrogen generation from water [72]. ZnSe mixed graphene nanocomposites were designed and synthesized by one-pot hydrothermal based methodology by using graphene-oxide (GO) and zinc-selenide (ZnSe) as precursors. The nanobelts were deposited from GO followed by heating at 180ºC temperature for 12 h under a solvothermal approach [73]. In addition, the complex compounds, such as $Li_4Ti_5O_{12}$, $LiFePO_4$ and $Bi_2WO_{6;}$ were also synthesized by hydrothermal and solvothermal processes [74 - 76].

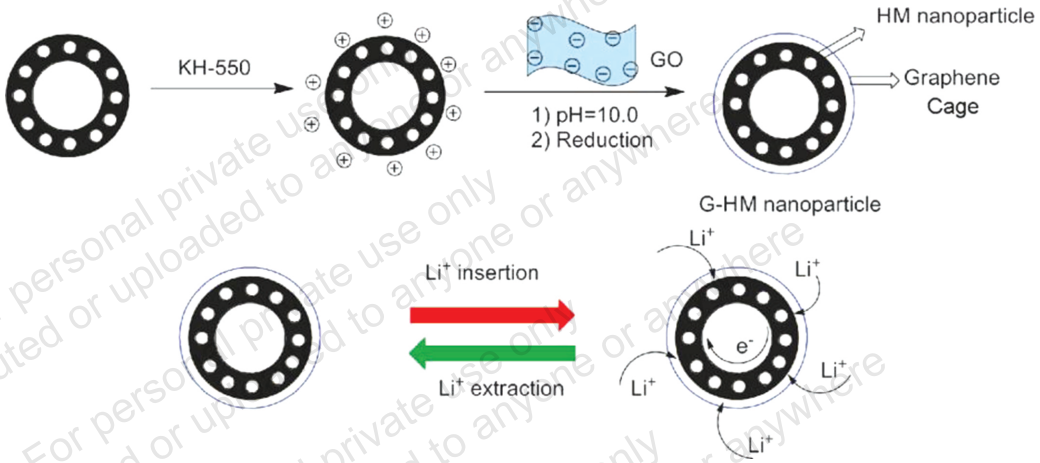

Fig. (4). Schematic illustration of the fabrication process along with the structure of the resulting graphene nanocomposite. (Reproduced with permission from Ref [69]. Copyright 2011, American Chemical Society).

Microwave- assisted Approach

Under this approach, microwave irradiation (MWI) is widely utilized towards the design and synthesis of graphene-based nanocomposites [8, 77, 78]. Particularly, the construction of graphene-based metal nanocomposites by *in-situ* reduction of various metal salts and graphitic materials, exhibited significant catalytic activity. In 2009, Hassan *et al.* reported the scalable synthesis of RG/NP composites by microwave-induced reduction [79]. This strategy represents a fast reduction of graphene oxide with several reducing agents in water and/or organic media, and the instantaneous reduction of GO with metal precursors furnishes the construction of metallic/bimetallic NPs doped graphene sheets. Under MWI conditions, metal- attached graphene nanocomposites of Pd, Cu, Ag, and Au have been made by *in-situ* reduction of appropriate metallic salts (Pd nitrate, $HAuCl_4$) and graphitic material with several reducing agents like ethylenediamine, ammonium hydroxide, and hydrazine hydrate [78]. *In-situ* reduction leads to homogeneous dispersions of nanostructures on graphene sheets *via* specific interaction and physical mixing between the graphene sheets and nanocomposites. In addition, the *in-situ* MWI approach has also been applied to fabricate graphene-based metal nanocomposites such as Graphene–SnO_2 nanocomposites. (Fig. **5**) [80]. Liu *et al.* investigated improved conditions for the synthesis of ZnS nanospheres on graphene, and the reaction was optimized in an aqueous medium induced by MWI [81]. Additionally, in 2014, a MWI-based approach for an ionic liquid supported Pd-Pt nanostructures on HRG sheets was investigated [82].

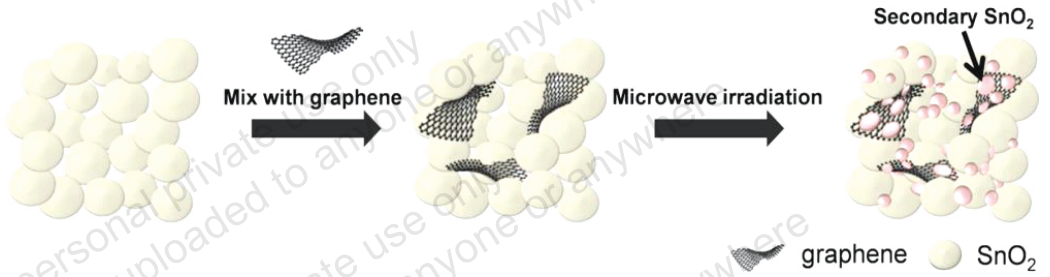

Fig. (5). Schematic illustration of the morphologies of the graphene−SnO_2 nanocomposites developed by the MWI. (Reproduced with permission from Ref [80]. Copyright 2011, American Chemical Society).

Electrochemical and Electrophoresis Deposition-based Approach

Electrochemical and electrophoresis depositions are another widely used methododologies for the synthesis of graphene-based metal nanostructures. Metal salts and oxides easily mix with 2D carbon layers by electrochemical assemblies [83 - 89].

Using electric current, electrochemical reduction of metal nanomaterial was also discovered. Some semiconductors such as Cd-Se was electrochemically doped on graphene surfaces and resulted the graphene nanocomposites. ZnO nanoparticles were also deposited on conductive reduced graphene oxide (rGO) under electrochemical deposition assembly [83]. In brief for the first time, a constant potential was used with ZnO on reduce graphene oxide for the synthesis of nanocomposite.

The conductivity of rGO has a strong influence on zinc oxide-based graphene nanocomposite. Particle-shaped nanocomposites were synthesized with rGO having low conductivity, whereas the hexagonal nanorods were constructed with rGO having greater conductivity. A graphene-based MnO_2 nanocomposite was also fabricated by electrochemical method (Fig. **6**) [85]. In 2011, Graphene composite having Cu_2O/ZrO_2 was also prepared by using electrochemical methodology [86, 90]. Metals like Ni, Cu, and Pt were doped on graphene sheet by an electrochemical approach [87, 91 - 93]. Yang *et al.* developed a mixed metal Au-Pd nanocomposite on graphene surface by constant-potential reduction using electrochemical approach with $HAuCl_4$, $PdCl_2$, and 0.1 M KCl [93]. In 2013, Ma and co-workers fabricated graphene-based NiOH nanocomposite under the electrophoresis method with Ni^{2+} ions and GO colloidal solutions. The positively charged graphene oxide, by nickel ions, was deposited on substrates *via* electrochemical reduction of GO to rGO under negative current [94].

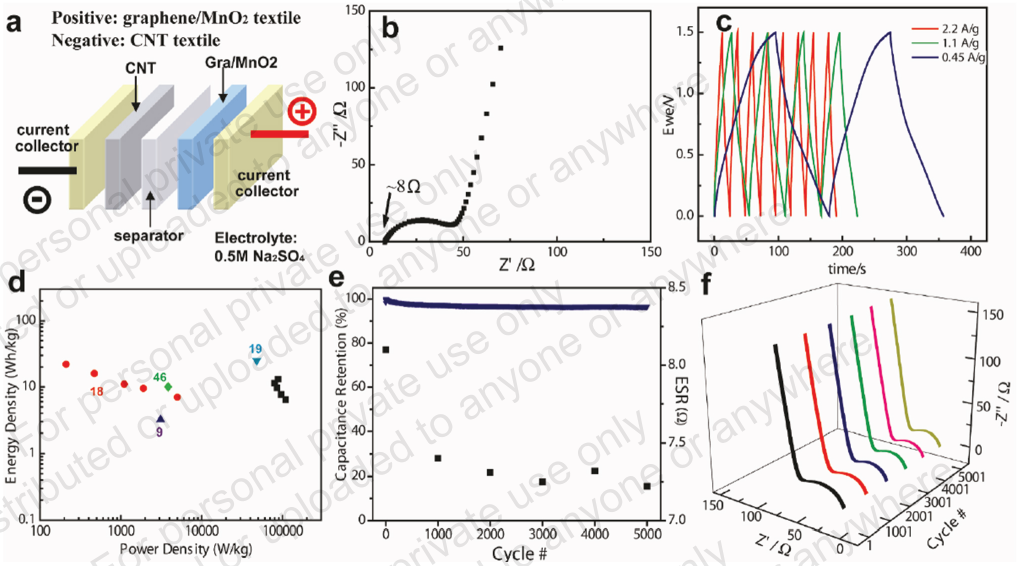

Fig. (6). An Asymmetric ECs based CNT-textile as negative electrode and graphene/MnO_2-textile as positive electrode. (a) Representation of the structure of hybrid EC-cells in an aqueous electrolyte (0.5 M Na_2SO_4). (b) Nyquist plot for hybrid EC (the frequency range was 100 kHz-0.1 Hz). (c) Galvanostatic discharge/charge curves with different current densities. (d) Ragone plot of energy-density vs power-density. (e) Cycling performance of hybrid ECs (capacitance retention having 95% after 5000 cycles). (f) Nyquist plots demonstrating the corresponding impedance curves for assembled ECs (observed after every 1000 cycles). (Reproduced with permission from Ref [85], Copyright 2011, American Chemical Society).

Chemical-vapor Deposition (CVD) Based Approach

Chemical-vapor deposition is another valuable approach for constructing graphene-based nanocomposites. Normally, graphene is utilized as a base material in the normal chemical-vapor deposition (CVD) based approach for the synthesis of graphene based hetero-nanostructures having other materials [95 - 102]. In 2009, Kim and his co-workers fabricated graphene-based ZnO nanoneedles employing vapor-phase epitaxy [95]. ZnO deposited graphene heterogeneous nano-objects were also synthesized by tuning the temperature in CVD assembly [96]. Recently, Fan and coworkers published a report on the CVD induced 3D CNTs/graphene sandwich compound prepared by using graphene oxide with uniform catalysts for CNT growth (which improved surface area) [97]. In the year 2010, pillared graphene mixed CNTs were also fabricated [98]. The same CVD processing was used to make metal-doped graphene-based CNTs composites and three-dimensional graphene mixed CNTs carpet micro supercapacitor electrodes [99, 100, 102]. Tavakkoli and colleagues recently developed a one-step catalytic CVD assembly to make a highly graphitized/CNT hybrid-material that was doped with single atoms (N-Co-GF/CNT). The enhanced surface area composites have

mesoporous structures, which facilitates oxygen mass transfer within the catalyst film and also act as an electrocatalyst for oxygen reduction in basic medium [101].

Photochemical- based Approach

Photochemical reaction is another approach for designing and synthesizing graphene-based metal-nanostructures [103 - 111]. Under UV light irradiation, graphene surfaces can be modified with reducing agents or metal precursors, which may provide the graphene-based nanoarchitectures. For example, the graphene-based TiO_2 nanocomposite was fabricated by mixing GO and TiO_2 NPs in ethanol under UV irradiation conditions. The photoactive TiO_2 transfers the electrons to graphene oxide and affords reduced graphene/TiO_2 nanocomposites. (Fig. **7**) [103].

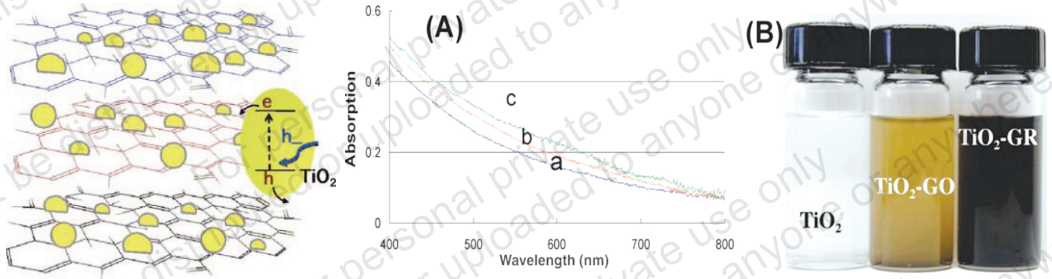

Fig. (7). (**A**) TiO_2-graphene nanocomposite having response in UV excitation/absorption spectra of GO and TiO_2 in ethanol suspension (a) before UV irradiation, (b) after 5 min (c) after 15 min under UV irradiation; (**B**) The color change of TiO_2 nanoparticles of 0.5 mg/mL GO of 10 mM solution before/ after UV irradiation. (Reproduced with permission from Ref [103], Copyright 2008, American Chemical Society).

In 2011, Amal and his co-workers adopted the same strategy to fabricate WO^{3-} and $BiVO^{4-}$ based graphene nanocomposites by irradiation with light amongst their precursors and graphene oxide [104]. Additionally, in metal nanoparticle based graphene nanocomposites, the precursors were doped on 2D carbon sheet under photochemical irradiation [104, 106 - 109, 111]. A photochemical strategy was also applied for the photolysis of phosphor-tungstic acid (PTA) to reduce GO for graphene based Au, Ag, and Pt NPs synthesis [105].

At the same time, two- step photochemical process was also developed for the dispersed noble metals (Pd, Ag, and Au) NPs on graphene sheet in dimethylformamide solvent. In the first step, the photolysis of phosphor-tungstate provides reduced graphene from graphene oxide. The noble metal ion precursors were doped with above metals to fabricate graphene-nano composites [106]. In

2012, Chen and his colleagues used an Hg lamp (450 W) to initiate the photochemical reaction for the synthesis of Ag/rG nano-structures using a mixture of $Ag(NH_3)_2OH$ complex and GO [107]. In the same year, the Ag NPs were also deposited on graphene oxide using similar methodology [108]. Ag NPs deposited on graphene oxide and Pt-graphene based-nanocomposites were synthesized *via* same method without using any reducing agent (Fig. **8**) [109 - 111].

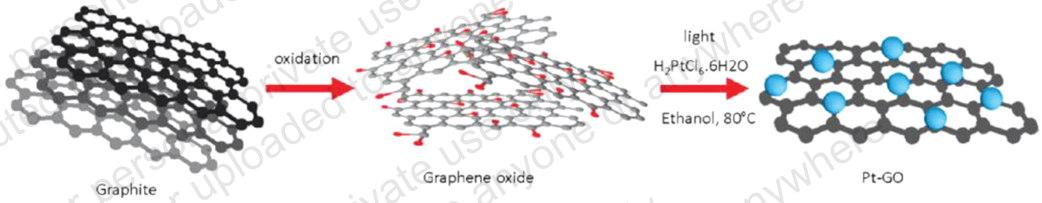

Fig. (8). Schematic depiction of light mediated Pt-Salt reduction on GO-sheet in ethanolic solution. (Reproduced with permission from Ref [110]. Copyright 2012, American Chemical Society).

Physical Deposition/Mixing Based Approach

The straight forward and simple process to construct graphene based-nanostructures, directly attached on 2D carbon sheet, *via* physical loading (physical vapor deposition/atomic layer deposition) is also discovered [112 - 116]. Metal oxides like Al_2O_3 was physically loaded on graphene sheet with atomic layer deposition (ALD) assembly (Fig. **9**) [112]. Metal based nanostructures were also doped physically on modified graphene surfaces under chemical environment by physical-vapor deposition based methodology [113]. The NPs growth on 2D (two dimensional) carbon layer was illustrated below, which exhibits significantly difference of activity for diverse metals (Ag, Fe, Au, Pt, Pd, Ti). Physical mixing is also one of the simplest approaches to synthesize the graphene-based nanocomposites. In the general procedure, the three-dimensional graphene material was obtained, when $LiFePO_4$ nanoparticles were loaded on graphene sheet by using annealing and spray-drying methodology [114].

Alternatively, the commercially available $LiFePO_4$ material was deposited on graphene sheet through a dropwise loading of $LiFePO_4$ particles at 180 ºC in DMF solution. This process was stimulated by a non-covalent interaction between the graphene surface and the amorphous carbon shell of $LiFePO_4$ particles. These modifications resulted improved stability and more efficient capacity of lithium battery of $LiFePO_4$ [115, 116].

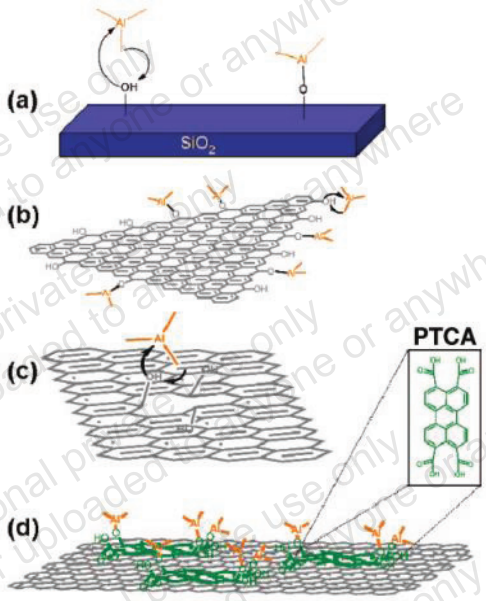

Fig. (9). Schematics representation using trimethylaluminum precursor for atomic layer deposition of aluminum oxide on (**a**) plain SiO_2 substrate, (**b**) a single-layered graphene sheet with their edges, (**c**) graphene having a defect site, (**d**) PTCA (perylene tetracarboxylic acid)-capped graphene. (Reproduced with permission from Ref [112], Copyright 2008, American Chemical Society).

PROPERTIES AND APPLICATIONS OF GRAPHENE-BASED NANOCOMPOSITE CATALYSTS

The diverse nature of graphene-based nanocomposites exhibits a huge range of properties towards various aspects. The novel properties and applications of graphene-based nanocomposites are the main criteria for catalyst design and synthesis. Therefore, only those potential graphene-based nanocomposites that exhibit significant catalytic potential are shortlisted and discussed in the present chapter.

Based on theoretical and experimental calculations for graphene and graphene-based nanocomposites (using carbon nanotubes (CNT)), the properties and applications were found to be outstanding with respect to several aspects. In graphene, the carbon atoms are arranged hexagonally, which results in a 2D honeycomb scaffold. While the strong bonds in graphene sheets lead to the stability and rigidity in hexagonal structures, the other out of plane π bonds provide interaction between different 2D carbon layers [117]. In addition, another significant property of graphene is the adsorption on the surfaces. It was found that the adsorption and interaction between 2D carbon surfaces and adsorbed objects are unique and specific parameters towards the design and synthesis of the

graphene-based nanocomposites. The theoretical calculations are of paramount importance in order to emphasize this property of graphene sheets. The stable configuration of embedded metal atoms in graphene displays the charge transfer between graphene and the adsorbed metal atoms. Generally, the binding of the adsorbed metal atom on graphene takes place *via* three sites of symmetry: a) at the center of a hollow hexagon (H); b) at the center of a C-C bond bridge (B); c) and directly on the carbon atom top (T) [118]. In 2010, Hu and his coworkers developed a good correlation between the adsorption of a huge number of doped metal atoms on graphene surface using DFT energy calculations [119]. They outlined that hollow hexagon sites are well suited for Ti, Sc, V, Co, Ni, and Fe deposition on graphene sheet, whereas B or T are the most striking sites for metals that have a completely filled or near- to- filled d-shell (Pd, Pt and Cu). Having half-filled d-shell transition metals (such as Au, Ag and Zn) has lesser adsorption energies. The preferred adsorption site is based on the intensity of the adsorption energy, which represents the remarkable effect on the chemical bond between the graphene surface and deposited materials. So, the adsorption of these metals (such as Ag, Au, and Cu) was reflected as physisorption, whereas the adsorption of Ni, Pt, Co, and Pd showed chemisorption on the graphene sheet surface. Similar results were reported for Ag, Au and Pt metals by Tang and his coworkers [120]. In 2011, the Nakada research group discovered the migration and adsorption energies for almost all atoms in the periodic table from H to Bi (except Ln, noble gases) on 2D carbon sheets using DFT calculations. The computational data demonstrated that the chemisorption of metals includes hybridization of d-orbitals of deposited atoms with the graphene surface. For the doped atom, there is a decrease in the magnetic moment for adsorbed metal atoms compared to the isolated metal atom, which depends on charge transfer between graphene and the adsorbed atom [119]. Several other research groups have also demonstrated the relationship between chemical/biologically privileged compounds with graphene sheet or metal deposited graphene sheet [121 - 123]. On the basis of theoretical as well as experimental observations, enormous works have been documented for the synthesis of graphene- based inorganic nanocomposites, typically using transition metal/metal oxide nanoparticles [8, 32, 78, 118, 124]. Moreover, massive interest has been reported in synthesizing graphene-based nanocomposites and utilizing them for diverse applications [8, 82, 91, 100, 125].

For Energy Storage and Conversion

The discovery of novel methodologies for the manufacturing of clean energy is an interesting and more challenging area for the scientific research community. Due to the increased air pollution and global warming conditions, the development of high energy density devices for energy storage and its conversion has increased tremendously [126, 127].

As a Basic Component in Lithium-ion Batteries (LIBs)

Graphene-based nanocomposites have attracted significant popularity in the electrochemical energy storage research area because of their unique physico-chemical properties, such as enhanced chemical and thermal stability, better electrical conducting behavior and mechanical properties. Graphene-based nanocomposites have been utilized as electrode materials and investigated for energy storage and conversion devices like lithium ion batteries (LIBs), supercapacitors, and fuel/solar cells [128 - 133]. TiO_2 has gained tremendous interest in high-performance LIBs. Several TiO_2 doped nanomaterials with increased lithium storage capabilities compared to non-doped pure TiO_2 have been developed [134, 135].

In 2011, Li *et al.* investigated a simple one-pot route *via* template free self-assembly methodology to fabricate mesoporous TiO_2 nanocomposite on a graphene surface. These TiO_2 nanocomposites are mono-crystalline in nature compared to the conventionally based poly-crystalline mesoporous anatase particles. The nanocomposite exhibits a significant improvement in the specific capacity, which is 6-fold higher than the pure TiO_2 [136]. Due to the layered structure and abundant availability in nature along with the high energy density, the vanadium pentoxide (V_2O_5) has been discovered as a cathode material in rechargeable LIBs. Therefore, a huge number of V_2O_5-based graphene nanocomposites have been investigated [137 - 139]. A V_2O_5 doped HRG nanocomposite having significant electrochemical properties was synthesized *via* hydrothermal reactions [140]. Yang *et al*. demonstrated in 2011 that graphene-based nanocomposites decorated with MoO_3 act like n-type semiconductors with energy storage in electrochromic and photochromic devices [141]. It was later investigated that MoO_3-based graphene nanocomposites showed enhanced discharge capacity and an outstanding high specific capacitance activity [142]. Mn_3O_4 has been investigated as an anode material for LIBs, having higher specific capacitance than graphite [143]. In order to achieve higher capacity, Wang *et al*. produced Mn_3O_4-based graphene materials in two steps.

The hybrid nanocomposites exhibited significant high capacity of ~ 900 mA h g^{-1} as well as good cycling stability and rate capability [144]. Fe_3O_4- based graphene nano-composite was developed by Su *et al.* with excellent reversible capacity, high cyclic performance, and enhanced rate capability compared to the Fe_3O_4 nanoparticles (Fig. **10**) [145]. Zou *et al.* reported Fe_2O_3 doped graphite nanocomposites as an anode material in LIBs. This metal nanocomposite revealed a good reversible capacity (1184 mA h g^{-1}) upon cycling along with an outstanding rate capability at increased currents [146]. In addition, graphene-

based nanocomposites of Fe_2O_3 and Fe_3O_4 and other iron-based precursors (like $LiFePO_4$) have also been utilized in LIBs [146 - 148]. Moreover, Qu *et al.* made sandwich-like Fe_3O_4 doped graphene nanocomposites *via* FeOOH nanostructures with graphene [149].

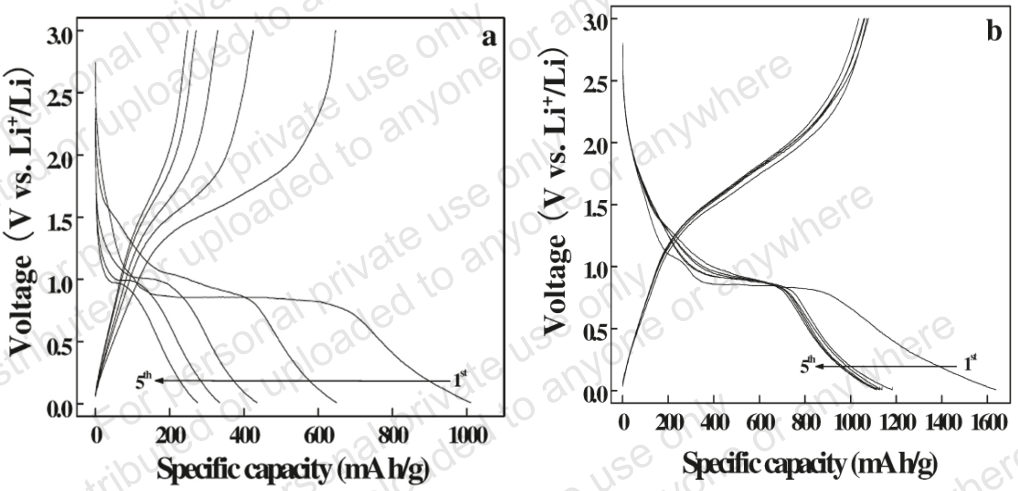

Fig. (10). Charge and discharge profiles of graphene oxide nanocomposite with Fe_3O_4 (**a**) GN-Fe_3O_4 nanocomposites (**b**) electrodes from one to fifth cycles. (Reproduced with permission from Ref [145], Copyright 2011, American Chemical Society).

As a Basic Component in Supercapacitors

Supercapacitors are utilized as brilliant energy storage materials and display enhanced power density and increased life cycle along with improved performance in comparison to common batteries. The energy storage capacity in supercapacitors contains a carbon-based EDL (electric double layer). In EDLCs, the charge storage depends on the material of electrode, because the stored energy depends on the adsorption of ionic charges. Therefore, the property of electrode material is highly responsible to increase the efficacy of capacitance of EDLCs. In this point of view, graphene as well as graphene-based nanocomposite was found to be a good alternative for making improved electrodes [150]. For example, the electrochemical capacity of RuO_2 hybrids with activated carbon, exfoliated graphite and CNTs, exhibited significant potential towards efficacy [151]. Wu *et al.* synthesized RuO_2 doped HRG nanocomposites by solvo-thermal process by varying the Ru loading amount [152]. Later on, using high theoretical capacitance, the expensive amorphous RuO_2 was replaced by cost effective and easily available $Ni(OH)_2$ and NiO [153, 154].

As an Electrocatalyst in Fuel Cells

Several graphene-based nanocomposites have been well explored as an electrocatalysts in ORR. Pd incorporated rGO nanocomposites were used as electrocatalysts in ORR along with the oxidation of alcohols in various fuel cells, such as DEFCs, DMFCs and DFAFCs [25, 155, 156]. Bimetallic Pt–Au graphene nanocomposites are an important electro-catalyst in DFAFCs fuel cells, which are also utilized for formic acid oxidation. Au loading on Pt nanoparticles has an specific effect on the direct oxidation to CO_2 from formic acid without CO intermediates [157]. Later on, Pt decorated graphene nanocomposites with perfluorosulfonic acid (PFSA) were utilized as electro-catalysts for ORR. PFSA accelerates the Pt–graphene interactions and opens more channels for H^+ on Pt surfaces, and thus generates more active catalytic property (Fig. **11**) [158]. In addition, PFSA activates the absorption of H_2O and CO on graphene composite surfaces and leads to an active Pt–OH compound's synthesis, which enables the oxidation to CO_2 from CO. Thus, PFSA-anchored HRG/Pt nanocomposites showed an enhanced catalytic oxidation of CO along with minimum electrochemical active area reduction. Rao and his coworkers discovered graphene-based Pt_3Cr and Pt_3Co nanocomposites, having 3 to 4 times enhanced catalytic activity than HRG/Pt, as electrocatalysts for ORR [159].

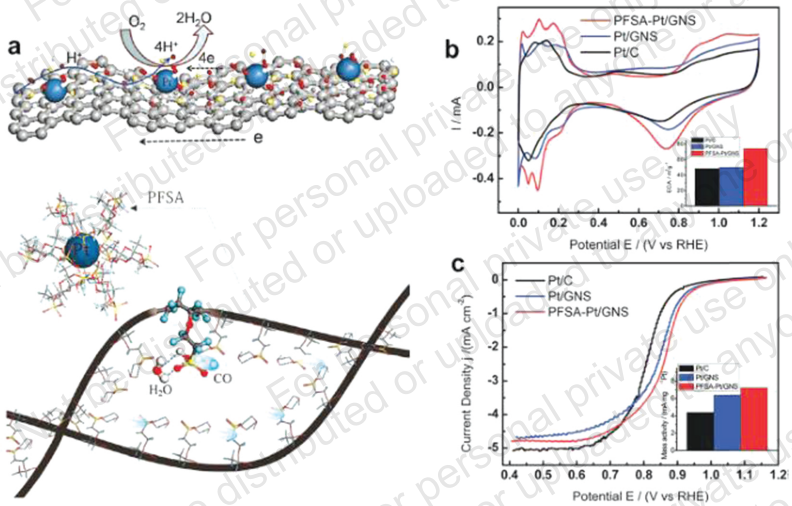

Fig. (11). (**a**) Schematic demonstration of the electrocatalytic mechanism with Graphene/Pt nanocomposites. (**b**) CV curves of nano-catalysts (PFSA–Pt/GNS, Pt/GNS and Pt/C). (**c**) Current potential curves for ORR and having comparisons between ORR mass-activities and specific-activity of catalysts. (Reproduced with permission from Ref [158], Copyright 2012, American Chemical Society).

Not be distributed or uploaded to anyone or anywhere
For personal private use only

As an Electrochemical Sensor

Various graphene-based nanocomposites have also been used as electrochemical sensors for detecting numerous chemicals. In 2011, Du and his co-workers synthesized ZrO_2 decorated graphene composites, where ZrO_2 nanoparticles were utilized as a selective sorbent for SPE (solid-phase extraction) and detection of pesticides (such as OP pesticides and nitroaromatic OP pesticides) [160]. Graphene based ZrO_2 electrochemical sensor was also utilized for rapid extraction for analyte, due to its strong affinity to phosphorus based species. Recently, Gong and his co-workers investigated HRG/ZrO_2 nanomaterial as SPE for enzyme less methyl parathion sensing [161]. Subramanian *et al.* discovered a non-enzymatic $Ni(OH)_2$ decorated graphene nanocomposite as a sensor for glucose detection. The nanocomposite is composed of leaf-shaped $Ni(OH)_2$ (diameter =~150 nm) dispersed between the graphene layers. The sensing limit (up to 0.6 mM) having a good linear range (2 mM-3.1 mM) was attained in this study [162]. Moreover, the excellent sensing capability of graphene and the detection capability of Pd nanoparticles have been also utilized simultaneously for numerous sensing applications [163]. The enhanced catalytic property of Pd-decorated graphene nanocomposites was achieved by charge transfer from molecules wrapped on graphene surface *via* change in the electrical conductive behavior of graphene. In 2010, Johnson and his co-workers investigated graphene-based Pd nanocomposites as hydrogen sensors in fuel cells [164]. This research group prepared multi-layered graphene as a nanoribbon *via* dispersing graphite material along with functionalized Pd-nanostructure in a water-surfactant solution. The nanoribbon, having porous structure, provides improved surface area, which permits better detection of the adsorbed gas. HRG based Au-nanocomposite was investigated as an electrochemical sensor, for sensing organic species, chemicals and metallic ions (such as lead, organophosphate pesticides, hydroquinone *etc*.) [165, 166]. The quenching potential of Au-nanocomposite was utilized for the detection of lead ions in organophosphate pesticides as a chemo-sensor. The composite electrode having acetylcholinesterase, was stabilized from aqueous soluble poly-diallyldimethylammonium chloride (PDDA electrolyte) [167]. The graphene and ZnO, together exhibit electronic and semiconducting nature so, a ZnO-graphene composite was used to fabricate a highly sensitive photo-sensor [168]. Graphene nanocomposites having ZnO NPs work as visible-blind UV-photosensors, where graphene behaves as a conductive matrix and the ZnO NPs were used as a charge carrier generating a UV absorbing material also [169]. The HRG nano-material having ZnO with photoluminescence (PL) nature was explored for gas detection [170]. HRG having ZnO nanocomposites showed optoelectronic and semiconducting features [171]. The ZnO nanomaterial with luminescent nature present between the graphene layers showed sensing property for various gases (such as NH_3, CO, and NO). In addition, SnO_2 based graphene

nanocomposites with excellent selectivity and sensitivity were also developed [172].

Lu and his co-workers discovered graphene-based Pd decorated electrode, for the detection of glucose, as an electrochemical biosensor [173]. This research group modified graphene with chitosan covalently which improved the solubility and biocompatibility [174]. Dey and his co-workers reported the synthesis of graphene-Pt based nanocomposite as an amperometry biosensor for detecting cholesterol and H_2O_2 *via* catalyzing H_2O_2 oxidation and electron transfer [175]. In 2012, Chen and his coworkers fabricated Cu decorated graphene nanocomposites for carbohydrate sensing *via* reduction of graphene oxide with KBH_4. (Fig. **12**) [176].

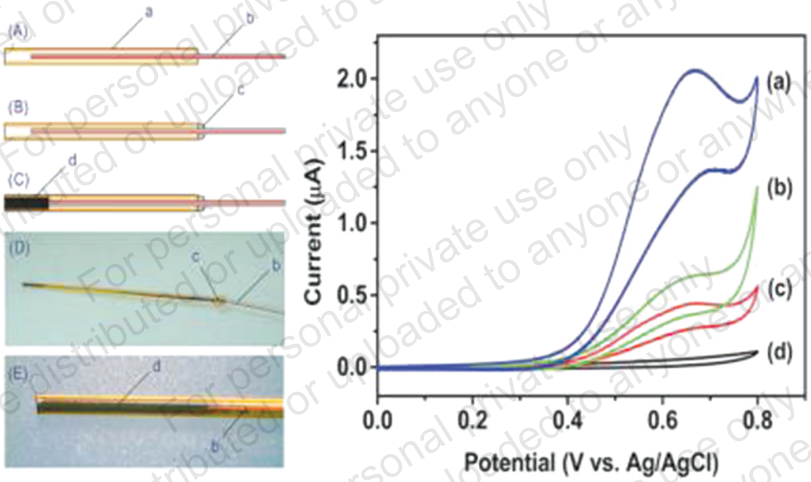

Fig. (12). (**A-E**): Schematic illustration of fabrication of graphene-copper nanoparticle composite electrode, and cyclic voltammetry diagram of graphene-copper nanocomposites. (Reproduced with permission from Ref [176], Copyright 2012, American Chemical Society).

Ag- based HRG nanocomposites were also prepared for sensing of H_2O_2, glucose and NO_2-based aromatic compounds [177, 178]. Graphene decorated with Ag nanocomposite was also explored for the detection of glucose, H_2O_2, and SERS substrate [179]. Zhang *et al.* investigated Au decorated graphene nanocomposites as an electrochemical bio-sensor, for sensing H_2O_2 (detection range 0.1mM to 2.3mM; and detection limit 0.01mM at 3s) in food *via* the reduction of H_2O_2 at pH 5.8 in buffer solution [180]. In 2012, another study was performed related to epinephrine (EP), an important neurotransmitter, using an Au- based GCE electrode with improved sensitivity [181].

Graphene-based nanomaterials also show significant biomedical applications [182]. Various studies have been reported towards the biomedical potential of

graphene such as drug and gene delivery systems, anti-tumor and antibacterial properties with scanning and imaging nature *etc* [183 - 186]. Paramagnetic Fe_2O_3 decorated graphene nanocomposites were applied for magnetic resonance imaging (MRI) and in hyperthermia therapy having improved physiological stability and biocompatibility [187 - 189]. In 2011, Zhang and his co-workers investigated aminodextran-coated Fe_3O_4 graphene nanocomposites for T2-weighted cellular MRI detection having improved T2 relativity *via* the aggregation of Fe_3O_4 nanoparticles on graphene surface (Fig. **13**) [190]. Oleylamine with Ag nanoparticles decorated on graphene oxide surface displayed improved antibacterial property compared to pristine based Ag NPs against Gram-negative bacteria [191]. In 2011, Ma and his co-workers reported the enhanced anti-bacterial activity of Ag-based graphene oxide due to H-bonding between GO and the cell membrane of *E. coli*., which prevents the nutrients uptake from the cell membrane and causes cell death [191].

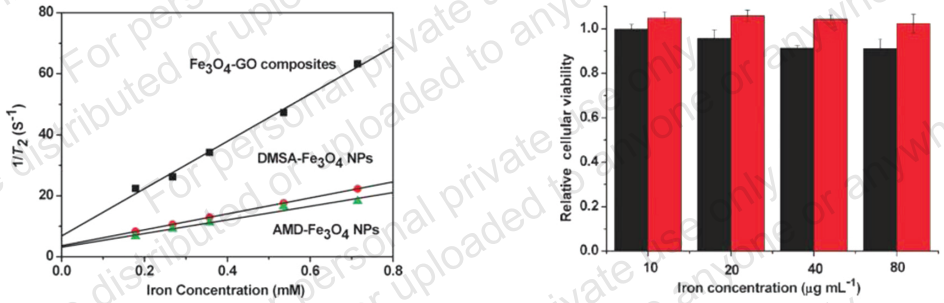

Fig. (13). (**a**) T-2 relaxation rates of the GO-Fe_3O_4, DMSA-Fe_3O_4NPs, AMD-Fe_3O_4NPs nanocomposites having iron concentration (mM) at 11.7 T. (**b**) Relative cellular viability of HeLa cells of AMD-Fe_3O_4 (red) and GO-Fe_3O_4 (black) incubated for 24 h, respectively. (Reproduced with permission from Ref [190], Copyright 2011, American Chemical Society).

Catalytic Potential of Graphene-based Nanocomposites

CO Oxidation

CO oxidation is one of the most useful reactions due to its significant potential towards the removal of CO and emission of pollutants [192].

In 2012, Liu and his co-workers synthesized a graphene-based Pd nanocomposite, loaded with 10 wt% Pd on graphitic material which showed the complete conversion of CO at 393 K, and improved stability without significant Pd size change [193]. El-Shall's research group developed bimetallic Pd–CoO based-graphene nanocomposites without using a chemical reductant [194]. They showed that the deoxygenation property of GO and light-induced metallic reduction property can be enhanced during the laser irradiation due to the formation of alloy

structure, which also improved the catalytic property of graphene surface in comparison to the separately deposited graphene surface with Pd or CoO. Similar catalytic performance was also reported for bimetallic Pt–Ni based graphene nanocomposite *via* high dispersion of Pt–Ni on graphene surface [195]. Liu and his co-workers showed that the positively charged Pd-Gr can display a good relation of temperature with CO oxidation (Fig. **14**) [196].

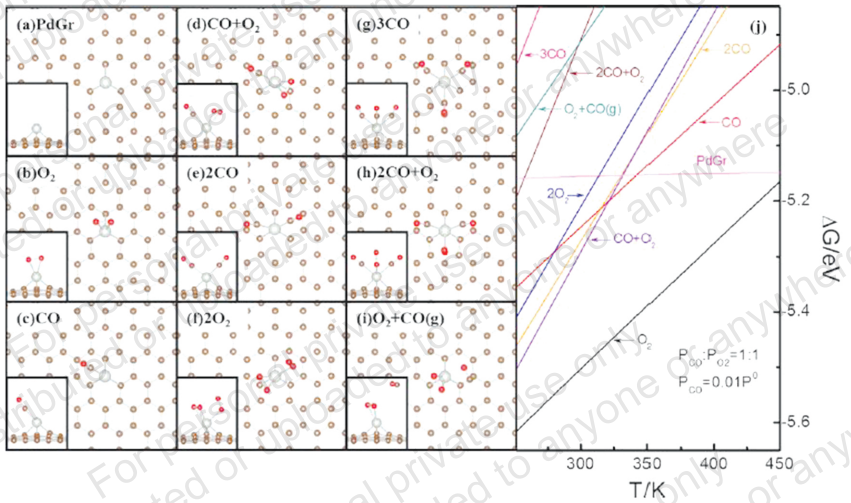

Fig. (14). Left and right-side panels show relation of atomic structures and temperature dependence with Gibbs free energies (ΔG) change over Pd-Gr in CO oxidation. (Reproduced with permission from Ref [196], Copyright 2020, American Chemical Society).

Oxidation of Alcohols

The carbonyl compounds (aldehydes and ketones) are an important group of compounds for the synthesis of several fine chemicals and biologically privileged molecules. The conventional oxidation of alcohol to carbonyl compounds is done by the use of homogeneous transition metal-based catalysts or several organometallic complexes (Fig. **15**). However, these homogeneous catalysts have several potential drawbacks such as moderate to high amount of catalyst loading, difficult removal of catalyst from the reaction medium (due to its toxic nature) and high cost [197]. To overcome these limitations, several research groups demonstrated that the Pd decorated on various carbon based material (like activated carbon [198], CNTs [199], and CMK-3) performed excellent catalytic property for oxidation of benzyl alcohol to benzaldehyde. In this context, graphene was utilized as a support for these transition metals for oxidation of alcohols to carbonyl compounds under a heterogeneous catalytic system.

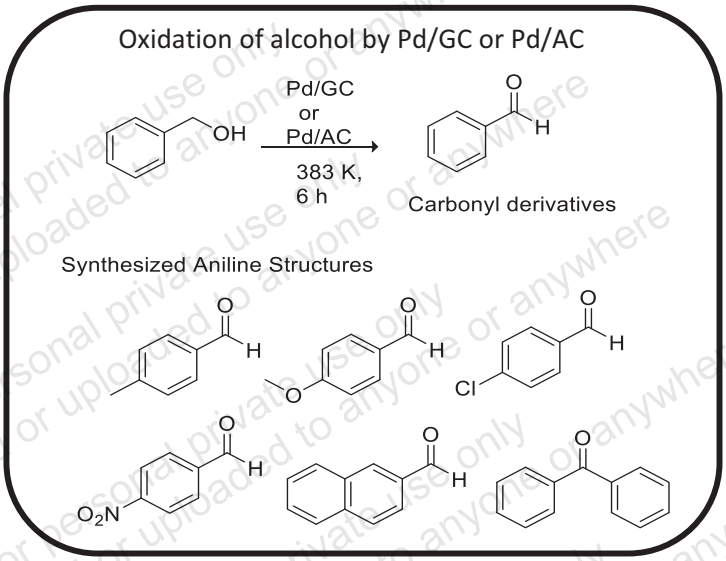

Fig. (15). Benzyl alcohol oxidation by palladium-based nanocomposite on different carbon-based material.

Li and his co-workers synthesized a Pd-based nanocomposite on carbon materials (such as carbon nanotubes, graphene (Pd/G), and activated carbon) *via* impregnation, which showed significant catalytic potential for benzyl alcohol oxidation [200]. The synthesized Pd-based nanocomposites having different carbon materials were approximately of the same size (≈ 4 nm) having the catalytic property in the following decreasing order: Pd/G > Pd/AC > Pd/CNT > commercial Pd/AC.

The observed catalytic activities of nanocomposites were significantly dependent on the use of carbon materials, and graphene was found superior in comparison to the other carbon materials. Huang *et al.* got similar results by decorating Au nanoparticles on several carbon materials, in which the rGO supported nanocomposite displayed the best catalytic performance (selectivity of 93% and conversion rate of 65%) for the oxidation of benzyl alcohol to benzaldehyde [201]. Furthermore, graphene-based metal oxides (eg: NiOx, CoOx, and FeOx,) [202], bimetallic Au–Pd based nanomaterial [203], and magnetically retrievable Fe_3O_4–Pt decorated rGO nanocomposites [204] were also synthesized and utilized for the selective oxidation to carbonyl compounds from alcohols. The bimetallic Au–Pd based graphene nanocomposites were found to be more active in comparison to the others towards selective oxidation to methyl formate from methanol [203].

Graphene-based Nanocomposite for Hydrogenation Reactions

The hydrogenation of various unsaturated organic compounds (such as alkenes, alkynes, nitriles, carbonyl compounds, and nitroarenes) to other privileged compounds is very challenging and has significant industrial applications [205]. In this context, the carbon- based catalytic hydrogenation is one of the most striking pathways due to its several advantages [206, 207] and in recent decades, graphene-based nanocomposites have displayed significant potential in this area.

Selective Reduction of Nitroarenes Using Graphene-based Nanocomposite

Aromatic amines are important precursors utilized for the synthesis of a variety of biologically important materials and industrial chemicals. Selective reduction of nitroarenes *via* catalytic hydrogenation is found to be one of the most effective routes for the synthesis of aromatic amines.

Pd-based nanocomposites display excellent catalytic potential for selective hydrogenation to amines from nitroarenes. In 2014, Wang and his co-workers synthesized graphene-based Pd nanocomposites *via* dispersion on graphene support by a hydrothermal process [206]. Pd-based rGO displayed improved catalytic potential in comparison to the commercial Pd/C towards the synthesis of 4-aminophenol (4-AP) from 4-nitrophenol (4-NP) with a reduction from $NaBH_4$.

Xu and his co-workers discovered similar findings *via* a simple redox reaction of H_2PdCl_4 and GO [208]. In addition, graphene-based Ni-Pd [209] or bimetallic Pd-Cu NPs [210] also displayed efficient catalytic properties towards the hydrogenation of nitroarenes (Fig. **16**).

Ni-Pd based graphene nanocomposites catalyze the tandem reduction of nitroarenes and dehydrogenation of ammonia borane (AB) [209]. Hou and his colleagues synthesized Pt-doped rGO *via* ethylene glycol reduction and used this composite to hydrogenate nitrobenzene *via* H_2 gas [211]. Additionally, it was also found that the hydrogenation efficacy was improved *via* the activation of H_2 gas by using a mixture of Pt and graphene [212]. Fan *et al.* synthesized Ru-decorated rGO nanocomposite *via* a hydrothermal process and utilized this nanocomposite for the selective hydrogenation of halo-nitroarenes [213].

Later on, the same research group also demonstrated higher selectivity of p-CAN over Ru anchored rGO nano-catalyst [214]. Other metal-based nanoparticles such as nickel [215, 216], gold [217, 218], silver [219] and Ni-Co alloy [220], metal oxide nanocomposites like Fe_3O_4 [221] were also anchored on the graphene surface and utilized for selective hydrogenation of aromatic nitro-compounds (Fig. **17**).

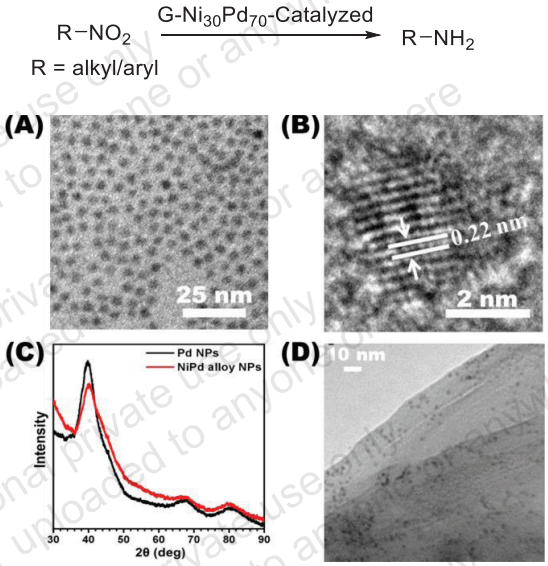

Fig. (16). (**A**) TEM (**B**) HRTEM diagram of $Ni_{30}Pd_{70}$ NPs, (**C**) XRD of Pd and Ni-Pd NPs, and (**D**) TEM image of Ni-Pd NPs decorated on graphene. (Reproduced with permission from Ref [209], Copyright 2014, American Chemical Society).

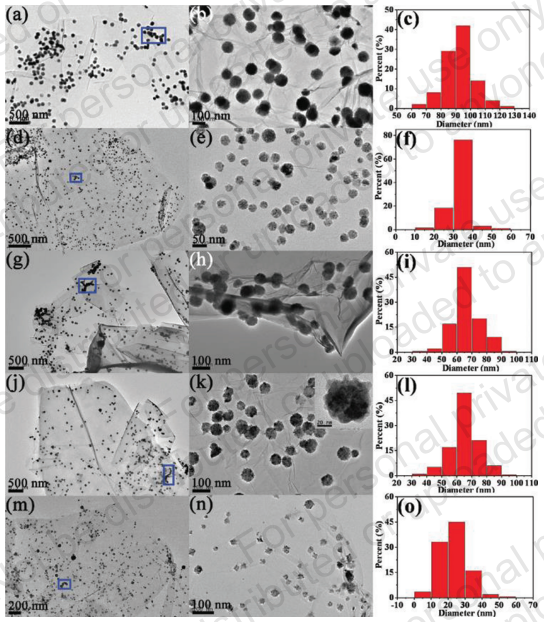

Fig. (17). Typical TEM images and Ni_xCo_{100-x} particle size distribution of RGO-Ni_xCo_{100-x} nanocomposites under different molar ratios of Ni/Co: (**a−c**) Co (**d−f**) $Ni_{25}Co_{75}$ (**g−i**) $Ni_{50}Co_{50}$ (**j−l**) $Ni_{75}Co_{25}$; and (**m−o**) Ni. (Reproduced with permission from Ref [220], Copyright 2012, American Chemical Society).

Not be distributed or uploaded to anyone or anywhere
For personal private use only

Magnetic retrievability and better recyclability are some of the advantageous features for catalysts. In this context, the magnetically separable catalysts were also synthesized by the use of metal NPs such as Pt, Pd, or Pt-Pd on Fe_3O_4/graphene surface, which was functionalized with L-lysine *via* selective doping. The NH_2 and COOH functional groups of L-lysine displayed unique roles as linkers between Fe_3O_4/graphene nanocomposites and the noble metals [222].

Hydrogenation of the C=C Bond using Graphene-based Nanocomposite

Conventionally, the hydrogenation of carbon-carbon unsaturated bonds is performed by metals such as Ru, Rh, Pt, Pd, and Au. In 2013, Maser and his co-workers developed Pd NPs based graphene nanocomposites having improved catalytic properties for the hydrogenation of unsaturated compounds [223].

In another study, graphene-based Pt nanocomposites were also prepared from H_2PtCl_6 having excellent catalytic reductive potential towards reduction of alkenes and alkynes to corresponding alkanes [224]. Han and his co-workers synthesized Ru NPs decorated with rGO for the hydrogenation of toluene [225]. Later on, several other Ru-decorated graphene nano-catalysts were also reported for the reduction of benzene/cyclohexene to cyclohexane [226, 227]. Begin and his co-workers fabricated graphene-based Pd nanocomposites for hydrogenation of cinnamaldehyde *via* H_2 reduction [228]. Furthermore, under microwave irradiated reduction conditions [229] and in solvothermal process [230], graphene anchored-Pd nanocomposites catalyst for the selective hydrogenation of the C=C bond of vinyl acetate and isophorone were reported.

Hydrogenation of the C=O Bond using Graphene-based Nanocomposite

The selective hydrogenation of the C=O bond of α,β-unsaturated carbonyl compounds over C=C bonds is more challenging due to comparably more favorable thermodynamic and kinetic stability of the C=O moiety over C=C bond [231, 232]. In 2014, Fu and his coworkers synthesized graphene-supported Pt nanocomposites for selective hydrogenation of cinnamic aldehyde (CAL) to cinnamyl alcohol (COL) [233]. The authors proposed that the electronic network of graphene based nanocomposite may form the inter-molecular π–π interactions with CAL and the aromatic moiety. Notably, the electron transfer behavior was also found for Pt decorated rGO nanocomposite [234]. The uniform dispersion of Pt on rGO in a specific solvent also displayed enhanced catalytic activity [235]. In addition, Fe [236] and Ni [237] based graphene nanocomposites for C=O over C=C hydrogenation were also reported. Furthermore, chiral-functionalized Ni [238] or Pd [239] nanocomposites based on rGO demonstrated exceptional

catalytic potential for asymmetric hydrogenation, yielding optically pure enantiomers from prochiral substrates. Furthermore, graphene-based Pd [240], Pt [241], and RuO_2 [242] nanocomposites were also reported for selective hydrogenation of cellulose to sorbitol [241], catalytic hydrodesulfurization [240], and selective hydrogenation of carbonyl compounds [242].

Graphene Based Nanocomposite in Fischer–Tropsch Synthesis

CO hydrogenation in Fischer-Tropsch synthesis (FTS) has received a lot of attention [243, 244], and carbon-based materials have been discovered to be good supports for FTS catalysts due to their low interaction with active metals. In this context, a variety of carbon supports (such as carbon spheres, activated carbon, CNTs, mesoporous carbon, and carbon nanofibers) have been utilized for the FTS catalyst synthesis (Fig. **18**) [245 - 247].

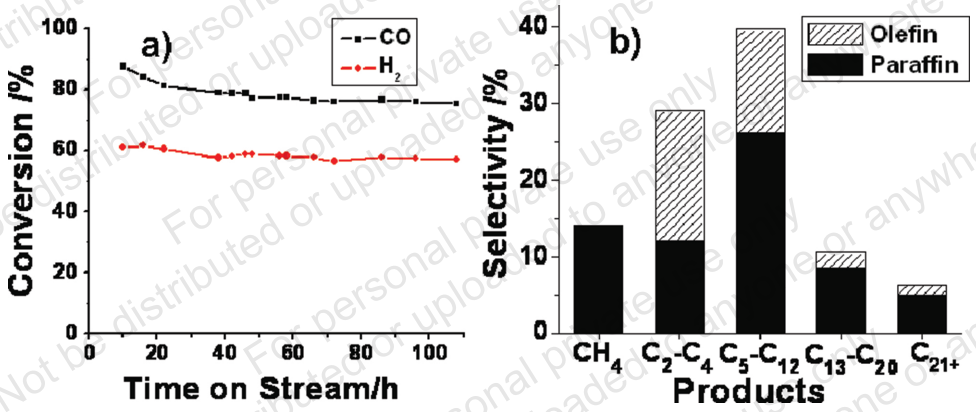

Fig. (18). Fischer–Tropsch synthesis (FTS) on reduced Fe*x*O*y*@C spheres. (**a**) conversion of CO and H_2 with time. (**b**) hydrocarbon selectivity. (Reproduced with permission from Ref [245], Copyright 2010, American Chemical Society).

Qiao and his co-workers synthesized Fe-based rGO nanocomposites *via* hydrothermal hydrolysis and reduction process by the use of GO and $Fe(acac)_3$ [248]. The nanocomposites synthesized demonstrated exceptional catalytic potential as well as thermodynamic stability. From p-rGO, a Fe-anchored pre-reduced GO (p-rGO) was synthesized, which demonstrated improved selectivity and stability to C_{5+} products. This was the first documented report which showed the application of graphene-based nanocomposite having mixed metals at high-temperatures. The role of the oxygen-containing functionalities on graphite support is authenticated over GO decorated with pyrolytic iron in the FTS process [249]. El-Shall and his colleagues created microwave-irradiated graphene-based K/Mn-functionalized iron nano-catalysts [250]. The graphene support improved the C_{8+} products as well as reduced the production of CO_2 and CH_4 as compared to

carbon nanotubes. The synthesis of CO_2 from CO was reduced from 14% to 2.6%. The catalytic selectivity (without CO_2) towards C_{8+} products increased (61.5% to 86.7%), and for CH_4, it was reduced (11.5% to 2.6%). In 2013, Yang and his co-workers fabricated cobalt-based graphene nanocomposites for the hydrogenation of CO_2 *via* a solvothermal process [251]. In the solvothermal process, as the temperature changed from 453 to 493 K, the cobalt nano-catalysts transformed from cubic shape to hexagonal shape, followed by an irregular arrangement to a sea-urchin like structure, and ultimately to a flower like final structure. In CO_2 reduction, the nanocomposites formed at 493 K displayed excellent catalytic properties due to the active hexagonal Co phase formation (Fig. **19**) [252].

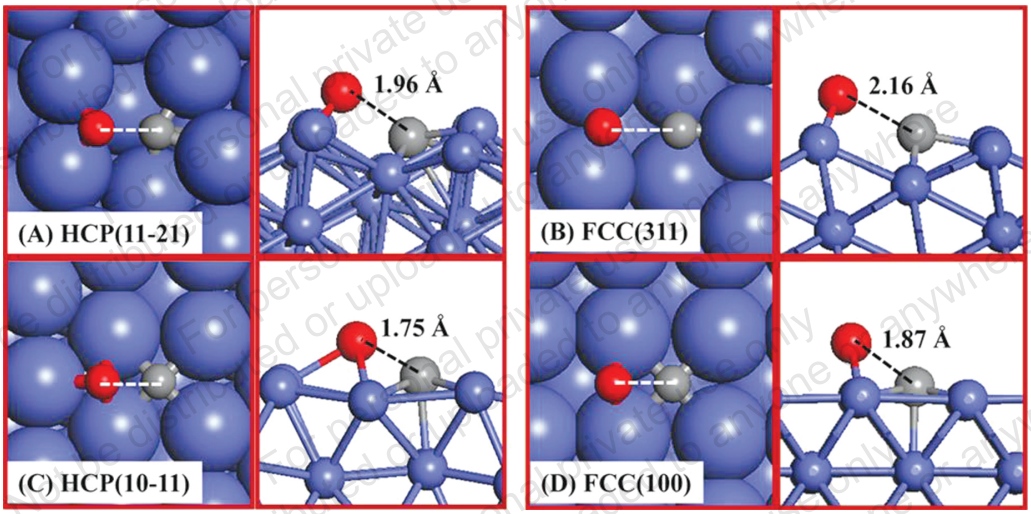

Fig. (19). Top and side views of CO dissociation from optimized TSs. (Blue balls represent Co, red balls represent O, and gray balls represent C atoms). (Reproduced with permission from Ref [252], Copyright 2013, American Chemical Society).

Graphene-supported Nanocomposites for Hydrolysis of AB (Ammonia Borane)

Hydrogen is a well-documented clean fuel due to its safe, efficient delivery and storage point of view [253]. The efficient chemical synthesis of H_2 was performed by using B–N based compounds, in which AB (ammonia borane) was found to be the best one due to its good stability, less hazardous nature, and high hydrogen content (up to 19.6 wt%) [254]. Thus, several research groups have worked towards the synthesis of modified graphene-based nanocomposites having good catalytic potential towards the hydrolysis of AB.

In 2012, Metin *et al.* fabricated Pd-anchored graphene nanocomposites for AB hydrolysis [255]. In the same year, Zeng and his co-workers synthesized Pd-anchored rGO nanocomposite *via* a solvothermal process [256]. Graphene-based

Co [257] and Cu [258] NPs were also developed using AB as a reductant, which displayed improved catalytic properties in comparison to the rGO-free Co or Cu NPs. Similarly, co-anchored rGO [259] and Ru- decorated rGO [260] nanocomposites were also synthesized from methylamine borane (Me-AB) using $NaBH_4$ [260]. Moreover, the bimetallic nanocomposites with graphene support were also fabricated and utilized for the hydrolysis of ammonia borane. Several research groups have fabricated bimetallic graphene-based nanocomposites (like Co-Fe [261], Ni-Co [262], Co-Cu [263], and Ru-Cu [264]. Ciftci and Metin reported Ni-Pd nanocomposites with rGO *via* reduction from $Pd(acac)_2$ and $Ni(OAc)_2$ [265]. Furthermore, other bimetallic graphene-supported nanocomposites such as Cu-Co [266], Ag-Co [267, 268], Pd-Co [269], Ru-Ni [270], and Ru-Co [271], were also synthesized *via* one-step co-reduction employing ammoniaborane as a reductant depending on the change of the two metal substrates in their reduction potentials (Fig. **20**).

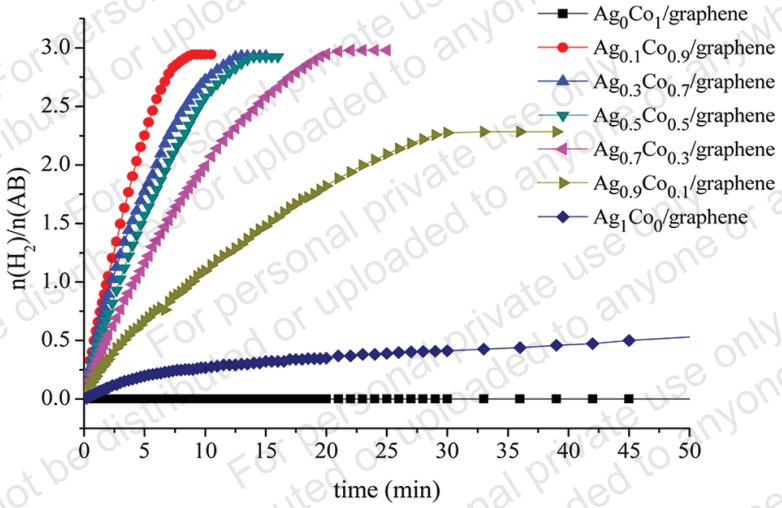

Fig. (20). Representation of H_2 gas generation after hydrolysis from graphene-based nano-catalysts. (Reproduced with permission from Ref [268], Copyright 2013, American Chemical Society).

It is also observed that the graphene-based nanocomposites show improved catalytic nature compared to their graphene-free counterparts. Recent studies have synthesized multi-metallic graphene-based nanocomposite such as Ni-Cu-Co [272], Ni-Ag-Co [273], and Fe-Ag-Co [274] *via* a co-reduction process using NaBH4, Me-AB, or AB as a reductant. In a similar study, it was reported that the catalytic property can be tuned according to the composite size by changing the graphite-based surface of the Ag-Co-Ni nanocomposite for AB hydrolysis [275]. Graphene-based nanocomposites were also utilized for H_2 production from $NaBH_4$ [276], Me-AB [268], and propane [277]. It is noteworthy that the design of

graphene-based nanocomposites was utilized as a key feature for the efficient hydrolysis of AB [278].

Graphene-supported Nanocomposite for Coupling Reactions

C–C bond construction in organic scaffolds *via* coupling reactions is a very demandable approach for both academic research and industrial production. In 2010, the Nobel Prize in Chemistry was awarded to Heck, Negishi, and Suzuki for their potential discovery of Pd-catalyzed cross-coupling reactions. In general, coupling reactions are carried out under homogeneous catalytic conditions; however, due to the severe toxicity profile, poor recovery and recyclability, as well as higher water and air-sensitive properties of homogeneous catalysts, their applications to large scale industrial processes are limited [279]. In this context, reusable heterogeneous catalysts provide potential benefits to overcome this problem.

Typically Pd NPs anchored on some materials like zeolites [280], activated carbon [281], and carbon nanotubes [282] have been utilized for coupling reactions. In recent years, a huge number of graphene-based nanocomposites have been synthesized and utilized for the coupling reactions. In 2009, Mülhaupt and his co-workers developed a Pd-functionalized graphene support by immobilizing the Pd^{2+} on GO *via* cation exchange followed by the reduction from $N_2H_4 \cdot H_2O$, H_2 or thermal reduction (Fig. **21**) [283].

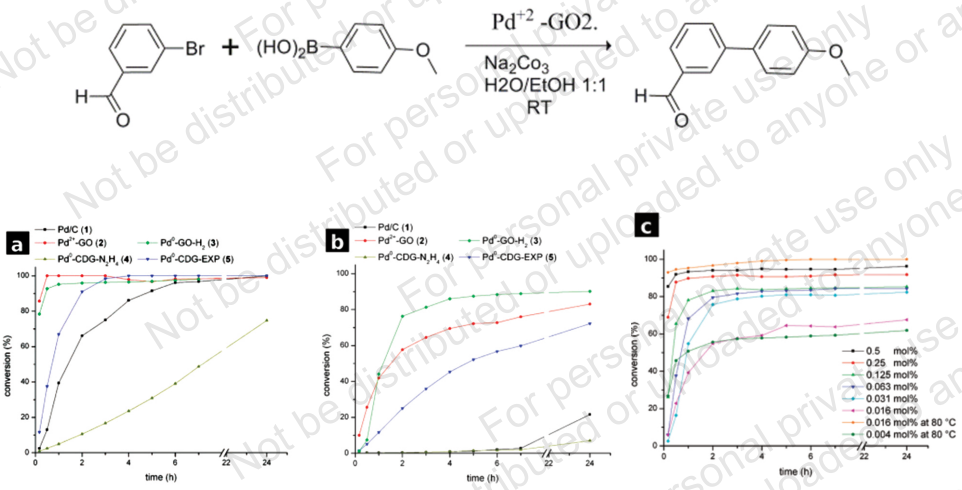

Fig. (21). Screening of Pd-GO/CDG catalysts for Suzuki-Miyaura reaction. Coupling reaction of 4-methoxyphenylboronic acid with (**a**) 4-bromo-1,2-difluorobenzene (**b**) 4-bromo-1,2-(methylenedioxy) benzene (**c**) 3-bromobenzaldehyde. (Reproduced with permission from Ref [283], Copyright 2009, American Chemical Society).

Not be distributed or uploaded to anyone or anywhere
For personal private use only

Furthermore, the graphene-based nanocomposites displayed enhanced catalytic activity in comparison to the typical Pd/C catalyst, and very little Pd leaching (<1 ppm) was found. Later on, graphene-based Pd nanocomposites having improved catalytic property were also synthesized with various reductants like H_2 [284], $NaBH_4$ [285], $N_2H_4 \cdot H_2O$ [286, 287], and ascorbic acid [288].

Other approaches were investigated, including CO-reduction with GO and H_2PtCl_6 from Ti^{3+} [289], electrochemical-based CO-deposition [290], thermal exfoliation process [291], and pulsed laser based irradiation [292]. The graphene support based mixed hybrid also demonstrated excellent catalytic properties for Sonogashira and Heck cross-coupling reactions. Notably, it was also documented that the Pd-based graphene nanocomposite displayed improved stability to polymeric materials like polyvinyl pyrrolidone, polystyrene-polyethylene oxide, and poly(amido-amine) dendrimers compared to the Pd nanoparticles (Fig. **22**) [292]. In 2013, Metin and his co-workers developed a synthetic route for graphene-based Ni/Pd nanocomposites *via* a two-step methodology and utilized this synthesized nanocomposite for Suzuki–Miyaura cross-coupling of phenyl iodide and phenylboronic acid [293]. Xu *et al.* developed graphene-supported Pd–Co nanocomposites, which were utilized in the Suzuki coupling reaction of phenylboronic acid with iodobenzene and conversion up to 96% and almost 100% selectivity with respect to biphenyl was achieved [294]. Fan *et al.* developed uniformly deposited Au NPs on graphene support having enhanced catalytic properties compared to unsupported Au NPs by reducing $HAuCl_4$ using sodium dodecyl sulfate [295, 296].

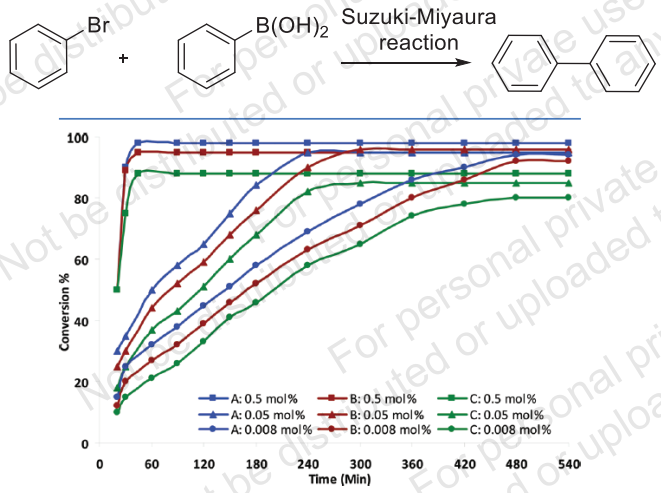

Fig. (22). Pd/PRGO catalytic effect on the conversion of Suzuki reaction. (Reproduced with permission from Ref [292], Copyright 2012, American Chemical Society).

In 2013, Wang and his co-workers investigated a facile synthetic route for Fe_3O_4 doped graphene nanocomposite synthesis *via* thermal decomposition of $Fe(CO)_5$ on GO surface [297]. In 2014, another report was published for graphene-based Ni nanocomposite synthesis and utilization of its catalytic potential in the Kumada-Corriu cross-coupling reaction of 4-iodoanisole and phenyl magnesium chloride. Therefore, the progress of graphene-based nanocomposites with improved catalytic activity and stability towards coupling reactions warrants further research and development.

CONCLUSION AND SUMMARY

Graphene is utilized as a two-dimensional solid support for the growth and nucleation of metal or metal oxide nano-particles, and the synergistic effects of these graphene-supported nanocomposites dramatically enhance the catalytic performance of the composite materials. The better knowledge of graphene surface-based chemistry leads to the development of potential synthetic routes for graphene-based inorganic nanocomposites synthesis by introducing several metal-based NPs. Thus, graphene-based metal nanocomposites with decorated, anchored, doped, encapsulated, layered, wrapped, and mixed structures have demonstrated huge potential for numerous industrial applications and are commercially achievable compared to less active nanocomposites using other carbon family members. The synergistic effects of graphene support and metal NPs in these nanocomposites result in improved catalytic potential in a variety of applications such as medicine, energy, biosensors, and industrial applications. The synthesis of these graphene-based nanocomposites, with well-defined shape and size along with the crystallinity of nanocomposites, not only prevents the restacking of graphene-based nanomaterial but also offers better support for the synthesis of 2D porous materials. This exceptional and remarkable catalytic potential of graphene-based nanocomposite has captured the scientific community's attention enormously, and as a result, a large number of publications and patents related to graphene as well as graphene-based nanocomposite synthesis and utilization have been reported in recent decades. In this context, the recent developments towards the synthesis of graphene-based metal nanocomposites and their catalytic utilization are broadly discussed in the present chapter.

Despite the significant advancement in the preparation of graphene-based nanocomposites, challenges still exist in their catalytic utilization on a large scale. For instance, advanced utilization of graphene-based metal nanocomposites needs further extensive exploration to understand the interactions between metal nanomaterials and the graphene/graphene oxide surface, which have a direct correlation with the catalytic nature of these nanocomposites. A thorough

investigation of these surface interactions will undoubtedly improve the catalytic potential of graphene-based nanocomposites in a variety of fields, including biosensing, drug delivery, imaging, and catalysis. Moreover, the advancement in graphene surface modification will ultimately allow the fabrication of mono/multi-layered nanocomposites and also improve the protocols for the production of graphene-based nanocomposites on a large scale to get an advanced form of nanotechnology to build devices for several potential applications.

LIST OF ABBREVIATIONS

2D structure	Two-dimensional structure
3D composites	Three-dimensional structure
CDG	Chemically derived graphene
CNTs	Carbon nanotubes
DEFCs	Direct ethanol fuel cells
DFAFCs	Direct formic acid fuel cells
DFT	Density functional theory
DMFCs	Direct methanol fuel cell
EDLC	Electric double layer carbon
ERGO	Electrochemically reduced graphene oxide
FLG	Few-layer graphene
GC	Graphene composites
GNP	Graphene nanoparticle
GNS	Graphene nano-sheet
GO	Graphene oxide
HRG	Highly reduced graphene oxide
MWI	Microwave irradiation
OP pesticides	Organophosphorus pesticides
ORR	Oxygen reduction reaction
Pd/AC	Palladium/activated carbon
Pd/PRGO	Pd-partially reduced graphene oxide catalysts
RG/NP	Reduced graphene nanoparticles
r-GO	Reduced graphene oxide

For personal private use only Not be distributed or uploaded to anyone or anywhere

CONSENT FOR PUBLICATION

Not applicable.

CONFLICT OF INTEREST

The authors declare no conflict of interest, financial or otherwise.

ACKNOWLEDGEMENTS

The corresponding author P. K. J. gratefully acknowledges Prof. (Dr.) James Sacchettini, Department of Biochemistry & Biophysics, Texas A&M University for support and encouragement and Dr. Aashish Srivastava, Senior Research Scientist, Department of Biochemistry and Biophysics for technical help and discussion.

REFERENCES

[1] Wallace, P.R. The Band Theory of Graphite. *Phys. Rev.,* **1947**, *71*(9), 622-634. [http://dx.doi.org/10.1103/PhysRev.71.622]

[2] Bodenmann, A.K.; MacDonald, A.H. Graphene: Exploring carbon flatland. *Phys. Today,* **2007**, *60*(8), 35-41. [http://dx.doi.org/10.1063/1.2774096]

[3] Rao, C.N.R.; Sood, A.K.; Subrahmanyam, K.S.; Govindaraj, A. Graphene: the new two-dimensional nanomaterial. *Angew. Chem. Int. Ed.,* **2009**, *48*(42), 7752-7777. [http://dx.doi.org/10.1002/anie.200901678] [PMID: 19784976]

[4] Allen, M.J.; Tung, V.C.; Kaner, R.B. Honeycomb carbon: a review of graphene. *Chem. Rev.,* **2010**, *110*(1), 132-145. [http://dx.doi.org/10.1021/cr900070d] [PMID: 19610631]

[5] Yuan, W.; Huang, L.; Zhou, Q.; Shi, G. Ultrasensitive and selective nitrogen dioxide sensor based on self-assembled graphene/polymer composite nanofibers. *ACS Appl. Mater. Interfaces,* **2014**, *6*(19), 17003-17008. [http://dx.doi.org/10.1021/am504616c] [PMID: 25208097]

[6] Stankovich, S.; Dikin, D.A.; Dommett, G.H.B.; Kohlhaas, K.M.; Zimney, E.J.; Stach, E.A.; Piner, R.D.; Nguyen, S.T.; Ruoff, R.S. Graphene-based composite materials. *Nature,* **2006**, *442*(7100), 282-286. [http://dx.doi.org/10.1038/nature04969] [PMID: 16855586]

[7] Ding, S.; Chen, J.S.; Luan, D.; Boey, F.Y.C.; Madhavi, S.; Lou, X.W.D. Graphene-supported anatase TiO_2 nanosheets for fast lithium storage. *Chem. Commun. (Camb.),* **2011**, *47*(20), 5780-5782. [http://dx.doi.org/10.1039/c1cc10687b] [PMID: 21494738]

[8] Mohan, V.B.; Lau, K.; Hui, D.; Bhattacharyya, D. Graphene-based materials and their composites: A review on production, applications and product limitations. *Compos., Part B Eng.,* **2018**, *142*, 200-220. [http://dx.doi.org/10.1016/j.compositesb.2018.01.013]

[9] Torres, T. Graphene chemistry. *Chem. Soc. Rev.,* **2017**, *46*(15), 4385-4386. [http://dx.doi.org/10.1039/C7CS90061A] [PMID: 28661520]

[10] Shang, N.G.; Papakonstantinou, P.; McMullan, M.; Chu, M.; Stamboulis, A.; Potenza, A.; Dhesi, S.S.; Marchetto, H. Catalyst-Free Efficient Growth, Orientation and Biosensing Properties of Multilayer Graphene Nanoflake Films with Sharp Edge Planes. *Adv. Funct. Mater.,* **2008**, *18*(21), 3506-3514.

Not be distributed or uploaded to anyone or anywhere For personal private use only

[http://dx.doi.org/10.1002/adfm.200800951]

[11] Su, C.Y.; Lu, A.Y.; Xu, Y.; Chen, F.R.; Khlobystov, A.N.; Li, L.J. High-quality thin graphene films from fast electrochemical exfoliation. *ACS Nano,* **2011**, *5*(3), 2332-2339. [http://dx.doi.org/10.1021/nn200025p] [PMID: 21309565]

[12] Novoselov, K.S.; Geim, A.K.; Morozov, S.V.; Jiang, D.; Zhang, Y.; Dubonos, S.V.; Grigorieva, I.V.; Firsov, A.A. Electric field effect in atomically thin carbon films. *Science,* **2004**, *306*(5696), 666-669. [http://dx.doi.org/10.1126/science.1102896] [PMID: 15499015]

[13] Wang, H.; Cui, L.F.; Yang, Y.; Sanchez Casalongue, H.; Robinson, J.T.; Liang, Y.; Cui, Y.; Dai, H. Mn3O4-graphene hybrid as a high-capacity anode material for lithium ion batteries. *J. Am. Chem. Soc.,* **2010**, *132*(40), 13978-13980. [http://dx.doi.org/10.1021/ja105296a] [PMID: 20853844]

[14] Li, H.; Chi, Z.; Li, J. Covalent bonding synthesis of magnetic graphene oxide nanocomposites for Cr(III) removal. *Desalination Water Treat.,* **2014**, *52*(10-12), 1937-1946. [http://dx.doi.org/10.1080/19443994.2013.806224]

[15] Singh, V.; Joung, D.; Zhai, L.; Das, S.; Khondaker, S.I.; Seal, S. Graphene based materials: Past, present and future. *Prog. Mater. Sci.,* **2011**, *56*(8), 1178-1271. [http://dx.doi.org/10.1016/j.pmatsci.2011.03.003]

[16] Tabarsa, M. ZareNezhad, B. An Eco-Friendly Air–Water Plasma Surface Treatment Technique for Improving the Stability of Graphene Oxide Nanosheets in Aqueous Solutions. *Mater. Today Commun.,* **2021**, *101940*, 26.

[17] Spilarewicz-Stanek, K.; Jakimińska, A.; Kisielewska, A.; Dudek, M.; Piwoński, I. Graphene Oxide Photochemical Transformations Induced by UV Irradiation during Photocatalytic Processes. *Mater. Sci. Semicond. Process.,* **2020**.

[18] Kuila, T.; Bose, S.; Mishra, A.K.; Khanra, P.; Kim, N.H.; Lee, J.H. Chemical functionalization of graphene and its applications. *Prog. Mater. Sci.*, **2012**, *57*(7), 1061-1105. [http://dx.doi.org/10.1016/j.pmatsci.2012.03.002]

[19] Velásquez-Rojas, M.M.; Contreras-Torres, F.F.; Meza-Laguna, V.; Álvarez-Zauco, E.; Farías, M.H.; Basiuk, V.A.; Basiuk, E.V. Solvent-free functionalization of graphene oxide powder and paper with aminobenzo-crown ethers and complexation with alkali metal cations. *Mater. Chem. Phys.,* **2021**, *260*, 124127. [http://dx.doi.org/10.1016/j.matchemphys.2020.124127]

[20] Garg, B.; Bisht, T.; Ling, Y.C. Graphene-based nanomaterials as heterogeneous acid catalysts: a comprehensive perspective. *Molecules,* **2014**, *19*(9), 14582-14614. [http://dx.doi.org/10.3390/molecules190914582] [PMID: 25225721]

[21] Huang, X.; Yin, Z.; Wu, S.; Qi, X.; He, Q.; Zhang, Q.; Yan, Q.; Boey, F.; Zhang, H. Graphene-based materials: synthesis, characterization, properties, and applications. *Small,* **2011**, *7*(14), 1876-1902. [http://dx.doi.org/10.1002/smll.201002009] [PMID: 21630440]

[22] Srivastava, S.; Jain, S.K.; Gupta, G.; Senguttuvan, T.D.; Gupta, B.K. Boron-doped few-layer graphene nanosheet gas sensor for enhanced ammonia sensing at room temperature. *RSC Advances,* **2020**, *10*(2), 1007-1014. [http://dx.doi.org/10.1039/C9RA08707A] [PMID: 35494469]

[23] Hong, W.; Xu, Y.; Lu, G.; Li, C.; Shi, G. Transparent graphene/PEDOT–PSS composite films as counter electrodes of dye-sensitized solar cells. *Electrochem. Commun.,* **2008**, *10*(10), 1555-1558. [http://dx.doi.org/10.1016/j.elecom.2008.08.007]

[24] La Notte, L.; Giordano, L.; Calabrò, E.; Bedini, R.; Colla, G.; Puglisi, G.; Reale, A. Hybrid and organic photovoltaics for greenhouse applications. *Appl. Energy,* **2020**, *278*, 115582. [http://dx.doi.org/10.1016/j.apenergy.2020.115582]

[25] Liu, M.; Zhang, R.; Chen, W. Graphene-supported nanoelectrocatalysts for fuel cells: synthesis,

properties, and applications. *Chem. Rev.,* **2014**, *114*(10), 5117-5160.
[http://dx.doi.org/10.1021/cr400523y] [PMID: 24666160]

[26] Yang, C.; Jiang, Q.; Huang, H.; He, H.; Yang, L.; Li, W.; Li, W. Polyelectrolyte-Induced Stereoassembly of Grain Boundary-Enriched Platinum Nanoworms on $Ti_3C_2T_x$ MXene Nanosheets for Efficient Methanol Oxidation. *ACS Appl. Mater. Interfaces,* **2020**, *12*(21), 23822-23830.
[http://dx.doi.org/10.1021/acsami.0c02806] [PMID: 32356656]

[27] Yang, H.; Li, S.; Feng, F.; Ou, S.; Li, F.; Yang, M.; Qian, K.; Jin, J.; Ma, J. Palladium Nanoparticles with Surface Enrichment of Palladium Oxide Species Immobilized on the Aniline-Functionalized Graphene As an Advanced Electrocatalyst of Ethanol Oxidation. *ACS Sustain. Chem.& Eng.,* **2019**, *7*(17), 14621-14628.
[http://dx.doi.org/10.1021/acssuschemeng.9b02397]

[28] Li, X.; Huang, X.; Liu, D.; Wang, X.; Song, S.; Zhou, L.; Zhang, H. Synthesis of 3D Hierarchical Fe_3O_4 /Graphene Composites with High Lithium Storage Capacity and for Controlled Drug Delivery. *J. Phys. Chem. C,* **2011**, *115*(44), 21567-21573.
[http://dx.doi.org/10.1021/jp204502n]

[29] Adepu, A.K.; Goskula, S.; Chirra, S.; Siliveri, S.; Gujjula, S.R.; Venkatathri, N. Magnetically separable porous titanosilicate/Fe3O4 hybrid nanocomposites with enhanced photocatalytic performance under UV light irradiation. *J. Porous Mater.,* **2019**, *26*(5), 1259-1267.
[http://dx.doi.org/10.1007/s10934-019-00719-9]

[30] Wu, Z.S.; Zhou, G.; Yin, L.C.; Ren, W.; Li, F.; Cheng, H.M. Graphene/metal oxide composite electrode materials for energy storage. *Nano Energy,* **2012**, *1*(1), 107-131.
[http://dx.doi.org/10.1016/j.nanoen.2011.11.001]

[31] Chen, D.; Zhang, H.; Liu, Y.; Li, J. Graphene and its derivatives for the development of solar cells, photoelectrochemical, and photocatalytic applications. *Energy Environ. Sci.,* **2013**, *6*(5), 1362-1387.
[http://dx.doi.org/10.1039/c3ee23586f]

[32] Hu, M.; Yao, Z.; Wang, X. Graphene-Based Nanomaterials for Catalysis. *Ind. Eng. Chem. Res.,* **2017**, *56*(13), 3477-3502.
[http://dx.doi.org/10.1021/acs.iecr.6b05048]

[33] Khodakov, A.; Olthof, B.; Bell, A.T.; Iglesia, E. Structure and Catalytic Properties of Supported Vanadium Oxides: Support Effects on Oxidative Dehydrogenation Reactions. *J. Catal.,* **1999**, *181*(2), 205-216.
[http://dx.doi.org/10.1006/jcat.1998.2295]

[34] Santander, P.; Bravo, L.; Pecchi, G.; Karelovic, A. The consequences of support identity on the oxidative conversion of furfural to maleic anhydride on vanadia catalysts. *Appl. Catal. A Gen.,* **2020**, *595*, 117513.
[http://dx.doi.org/10.1016/j.apcata.2020.117513]

[35] Luo, D.; Zhang, G.; Liu, J.; Sun, X. Evaluation Criteria for Reduced Graphene Oxide. *J. Phys. Chem. C,* **2011**, *115*(23), 11327-11335.
[http://dx.doi.org/10.1021/jp110001y]

[36] Xu, Y.; Bai, H.; Lu, G.; Li, C.; Shi, G. Flexible graphene films *via* the filtration of water-soluble noncovalent functionalized graphene sheets. *J. Am. Chem. Soc.,* **2008**, *130*(18), 5856-5857.
[http://dx.doi.org/10.1021/ja800745y] [PMID: 18399634]

[37] Su, Q.; Pang, S.; Alijani, V.; Li, C.; Feng, X.; Müllen, K. Composites of Graphene with Large Aromatic Molecules. *Adv. Mater.,* **2009**, *21*(31), 3191-3195.
[http://dx.doi.org/10.1002/adma.200803808]

[38] Kim, J.; Cha, J.; Chung, B.; Ryu, S.; Hong, S.H. Fabrication and mechanical properties of carbon fiber/epoxy nanocomposites containing high loadings of noncovalently functionalized graphene nanoplatelets. *Compos. Sci. Technol.,* **2020**, *192*, 108101.
[http://dx.doi.org/10.1016/j.compscitech.2020.108101]

Not be distributed or uploaded to anyone or anywhere
For personal private use only

[39] An, X.; Simmons, T.; Shah, R.; Wolfe, C.; Lewis, K.M.; Washington, M.; Nayak, S.K.; Talapatra, S.; Kar, S. Stable aqueous dispersions of noncovalently functionalized graphene from graphite and their multifunctional high-performance applications. *Nano Lett.,* **2010**, *10*(11), 4295-4301. [http://dx.doi.org/10.1021/nl903557p] [PMID: 20557029]

[40] Shang, X.; Park, C.H.; Jung, G.Y.; Kwak, S.K.; Oh, J.H. Highly Enantioselective Graphene-Based Chemical Sensors Prepared by Chiral Noncovalent Functionalization. *ACS Appl. Mater. Interfaces,* **2018**, *10*(42), 36194-36201. [http://dx.doi.org/10.1021/acsami.8b13517] [PMID: 30270614]

[41] Tang, Z.; Shen, S.; Zhuang, J.; Wang, X. Noble-metal-promoted three-dimensional macroassembly of single-layered graphene oxide. *Angew. Chem. Int. Ed.,* **2010**, *49*(27), 4603-4607. [http://dx.doi.org/10.1002/anie.201000270] [PMID: 20491102]

[42] Cong, H.P.; Ren, X.C.; Wang, P.; Yu, S.H. Macroscopic multifunctional graphene-based hydrogels and aerogels by a metal ion induced self-assembly process. *ACS Nano,* **2012**, *6*(3), 2693-2703. [http://dx.doi.org/10.1021/nn300082k] [PMID: 22303866]

[43] Stankovich, S.; Dikin, D.A.; Piner, R.D.; Kohlhaas, K.A.; Kleinhammes, A.; Jia, Y.; Wu, Y.; Nguyen, S.T.; Ruoff, R.S. Synthesis of graphene-based nanosheets *via* chemical reduction of exfoliated graphite oxide. *Carbon,* **2007**, *45*(7), 1558-1565. [http://dx.doi.org/10.1016/j.carbon.2007.02.034]

[44] Xu, Y.; Liu, Z.; Zhang, X.; Wang, Y.; Tian, J.; Huang, Y.; Ma, Y.; Zhang, X.; Chen, Y. A Graphene Hybrid Material Covalently Functionalized with Porphyrin: Synthesis and Optical Limiting Property. *Adv. Mater.,* **2009**, *21*(12), 1275-1279. [http://dx.doi.org/10.1002/adma.200801617]

[45] Liu, J.; Liang, Q.; Zhao, R.; Lei, S.; Hu, W. Application of organic–graphene hybrids in high performance photodetectors. *Mater. Chem. Front.,* **2020**, *4*(2), 354-368. [http://dx.doi.org/10.1039/C9QM00517J]

[46] Wang, H.X.; Zhou, K.G.; Xie, Y.L.; Zeng, J.; Chai, N.N.; Li, J.; Zhang, H.L. Photoactive graphene sheets prepared by "click" chemistry. *Chem. Commun. (Camb.),* **2011**, *47*(20), 5747-5749. [http://dx.doi.org/10.1039/c1cc11121c] [PMID: 21503310]

[47] Li, Y.; Tang, L.; Li, J. Preparation and electrochemical performance for methanol oxidation of pt/graphene nanocomposites. *Electrochem. Commun.,* **2009**, *11*(4), 846-849. [http://dx.doi.org/10.1016/j.elecom.2009.02.009]

[48] Guo, S.; Dong, S.; Wang, E. Three-dimensional Pt-on-Pd bimetallic nanodendrites supported on graphene nanosheet: facile synthesis and used as an advanced nanoelectrocatalyst for methanol oxidation. *ACS Nano,* **2010**, *4*(1), 547-555. [http://dx.doi.org/10.1021/nn9014483] [PMID: 20000845]

[49] Peng, X.; Lu, D.; Qin, Y.; Li, M.; Guo, Y.; Guo, S. Pt-on-Pd Dendritic Nanosheets with Enhanced Bifunctional Fuel Cell Catalytic Performance. *ACS Appl. Mater. Interfaces,* **2020**, *12*(27), 30336-30342. [http://dx.doi.org/10.1021/acsami.0c05868] [PMID: 32525299]

[50] Zhou, X.; Huang, X.; Qi, X.; Wu, S.; Xue, C.; Boey, F.Y.C.; Yan, Q.; Chen, P.; Zhang, H. *In Situ* Synthesis of Metal Nanoparticles on Single-Layer Graphene Oxide and Reduced Graphene Oxide Surfaces. *J. Phys. Chem. C,* **2009**, *113*(25), 10842-10846. [http://dx.doi.org/10.1021/jp903821n]

[51] Xu, C.; Wang, X. Fabrication of flexible metal-nanoparticle films using graphene oxide sheets as substrates. *Small,* **2009**, *5*(19), 2212-2217. [http://dx.doi.org/10.1002/smll.200900548] [PMID: 19662647]

[52] Gnanaprakasam, P.; Jeena, S.E.; Selvaraju, T. Hierarchical electroless Pt deposition at Au decorated reduced graphene oxide *via* a galvanic exchanged process: an electrocatalytic nanocomposite with

Not be distributed or uploaded to anyone or anywhere
For personal private use only

enhanced mass activity for methanol and ethanol oxidation. *J. Mater. Chem. A Mater. Energy Sustain.,* **2015**, *3*(35), 18010-18018.
[http://dx.doi.org/10.1039/C5TA04293C]

[53] Tang, Y.B.; Lee, C.S.; Xu, J.; Liu, Z.T.; Chen, Z.H.; He, Z.; Cao, Y.L.; Yuan, G.; Song, H.; Chen, L.; Luo, L.; Cheng, H.M.; Zhang, W.J.; Bello, I.; Lee, S.T. Incorporation of graphenes in nanostructured TiO_2) films *via* molecular grafting for dye-sensitized solar cell application. *ACS Nano,* **2010**, *4*(6), 3482-3488.
[http://dx.doi.org/10.1021/nn100449w] [PMID: 20455548]

[54] Nethravathi, C.; Nisha, T.; Ravishankar, N.; Shivakumara, C.; Rajamathi, M. Graphene - nanocrystalline metal sulphide composites produced by a one-pot reaction starting from graphite oxide. *Carbon,* **2009**, *47*(8), 2054-2059.
[http://dx.doi.org/10.1016/j.carbon.2009.03.055]

[55] Mao, S.; Wen, Z.; Kim, H.; Lu, G.; Hurley, P.; Chen, J. A general approach to one-pot fabrication of crumpled graphene-based nanohybrids for energy applications. *ACS Nano,* **2012**, *6*(8), 7505-7513.
[http://dx.doi.org/10.1021/nn302818j] [PMID: 22838735]

[56] Soysal, F.; Çıplak, Z.; Gökalp, C.; Getiren, B.; Yıldız, N. One-step hydrothermal synthesis of nitrogen doped reduced graphene oxide-silver nanocomposites: Catalytic performance. *Appl. Organomet. Chem.,* **2020**, *34*(5), 34.
[http://dx.doi.org/10.1002/aoc.5621]

[57] Gowthaman, N.S.K.; Raj, M.A.; John, S.A. Nitrogen-Doped Graphene as a Robust Scaffold for the Homogeneous Deposition of Copper Nanostructures: A Nonenzymatic Disposable Glucose Sensor. ACS Sustainable Chemistry &amp. *Engineering,* **2017**, *5*(2), 1648-1658.

[58] Chang, H.; Lv, X.; Zhang, H.; Li, J. Quantum dots sensitized graphene: *In Situ* growth and application in photoelectrochemical cells. *Electrochem. Commun.,* **2010**, *12*(3), 483-487.
[http://dx.doi.org/10.1016/j.elecom.2010.01.025]

[59] Liu, X.; Pan, L.; Lv, T.; Zhu, G.; Sun, Z.; Sun, C. Microwave-assisted synthesis of CdS–reduced graphene oxide composites for photocatalytic reduction of Cr(vi). *Chem. Commun. (Camb.),* **2011**, *47*(43), 11984-11986.
[http://dx.doi.org/10.1039/c1cc14875c] [PMID: 21960206]

[60] Shen, J.; Shi, M.; Yan, B.; Ma, H.; Li, N.; Ye, M. One-pot hydrothermal synthesis of Ag-reduced graphene oxide composite with ionic liquid. *J. Mater. Chem.,* **2011**, *21*(21), 7795-7801.
[http://dx.doi.org/10.1039/c1jm10671f]

[61] Lee, S.H.; Kakati, N.; Jee, S.H.; Maiti, J.; Yoon, Y.S. Hydrothermal synthesis of PtRu nanoparticles supported on graphene sheets for methanol oxidation in direct methanol fuel cell. *Mater. Lett.,* **2011**, *65*(21-22), 3281-3284.
[http://dx.doi.org/10.1016/j.matlet.2011.07.025]

[62] Zou, R.; Zhang, Z.; Yu, L.; Tian, Q.; Chen, Z.; Hu, J. A general approach for the growth of metal oxide nanorod arrays on graphene sheets and their applications. *Chemistry,* **2011**, *17*(49), 13912-13917.
[http://dx.doi.org/10.1002/chem.201101981] [PMID: 22038954]

[63] Shen, J.; Yan, B.; Shi, M.; Ma, H.; Li, N.; Ye, M. One step hydrothermal synthesis of TiO_2-reduced graphene oxide sheets. *J. Mater. Chem.,* **2011**, *21*(10), 3415-3421.
[http://dx.doi.org/10.1039/c0jm03542d]

[64] Zhang, H.; Lv, X.; Li, Y.; Wang, Y.; Li, J. P25-graphene composite as a high performance photocatalyst. *ACS Nano,* **2010**, *4*(1), 380-386.
[http://dx.doi.org/10.1021/nn901221k] [PMID: 20041631]

[65] Zou, Y.; Wang, Y. NiO nanosheets grown on graphene nanosheets as superior anode materials for Li-ion batteries. *Nanoscale,* **2011**, *3*(6), 2615-2620.
[http://dx.doi.org/10.1039/c1nr10070j] [PMID: 21523266]

Not be distributed or uploaded to anyone or anywhere
For personal private use only

[66] Wang, Z.; Huang, B.; Dai, Y.; Liu, Y.; Zhang, X.; Qin, X.; Wang, J.; Zheng, Z.; Cheng, H. Crystal facets controlled synthesis of graphene@TiO_2 nanocomposites by a one-pot hydrothermal process. *CrystEngComm,* **2012**, *14*(5), 1687-1692.
[http://dx.doi.org/10.1039/C1CE06193C]

[67] Xiang, Q.; Yu, J.; Jaroniec, M. Enhanced photocatalytic H_2-production activity of graphene-modified titania nanosheets. *Nanoscale,* **2011**, *3*(9), 3670-3678.
[http://dx.doi.org/10.1039/c1nr10610d] [PMID: 21826308]

[68] Perera, S.D.; Mariano, R.G.; Vu, K.; Nour, N.; Seitz, O.; Chabal, Y.; Balkus, K.J., Jr Hydrothermal Synthesis of Graphene-TiO_2 Nanotube Composites with Enhanced Photocatalytic Activity. *ACS Catal.*, **2012**, *2*(6), 949-956.
[http://dx.doi.org/10.1021/cs200621c]

[69] Chen, D.; Ji, G.; Ma, Y.; Lee, J.Y.; Lu, J. Graphene-encapsulated hollow Fe_3O_4 nanoparticle aggregates as a high-performance anode material for lithium ion batteries. *ACS Appl. Mater. Interfaces,* **2011**, *3*(8), 3078-3083.
[http://dx.doi.org/10.1021/am200592r] [PMID: 21749101]

[70] Nethravathi, C.; Viswanath, B.; Michael, J.; Rajamath, M. Hydrothermal synthesis of a monoclinic VO_2 nanotube–graphene hybrid for use as cathode material in lithium ion batteries. *Carbon,* **2012**, *50*(13), 4839-4846.
[http://dx.doi.org/10.1016/j.carbon.2012.06.010]

[71] Tang, Q.; Wang, L.; Zhu, K.; Shan, Z.; Qin, X. Synthesis and electrochemical properties of H-MoO3/graphene composite. *Mater. Lett.,* **2013**, *100*, 127-129.
[http://dx.doi.org/10.1016/j.matlet.2013.03.005]

[72] Cao, A.; Liu, Z.; Chu, S.; Wu, M.; Ye, Z.; Cai, Z.; Chang, Y.; Wang, S.; Gong, Q.; Liu, Y. A facile one-step method to produce graphene-CdS quantum dot nanocomposites as promising optoelectronic materials. *Adv. Mater.,* **2010**, *22*(1), 103-106.
[http://dx.doi.org/10.1002/adma.200901920] [PMID: 20217706]

[73] Chen, P.; Xiao, T.Y.; Li, H.H.; Yang, J.J.; Wang, Z.; Yao, H.B.; Yu, S.H. Nitrogen-doped graphene/ZnSe nanocomposites: hydrothermal synthesis and their enhanced electrochemical and photocatalytic activities. *ACS Nano,* **2012**, *6*(1), 712-719.
[http://dx.doi.org/10.1021/nn204191x] [PMID: 22136425]

[74] Shen, L.; Yuan, C.; Luo, H.; Zhang, X.; Yang, S.; Lu, X. *In Situ* synthesis of high-loading $Li_4Ti_5O_{12}$ –graphene hybrid nanostructures for high rate lithium ion batteries. *Nanoscale,* **2011**, *3*(2), 572-574.
[http://dx.doi.org/10.1039/C0NR00639D] [PMID: 21076732]

[75] Shi, Y.; Chou, S.L.; Wang, J.Z.; Wexler, D.; Li, H.J.; Liu, H.K.; Wu, Y. Graphene wrapped $LiFePO_4$/C composites as cathode materials for Li-ion batteries with enhanced rate capability. *J. Mater. Chem.,* **2012**, *22*(32), 16465-16470.
[http://dx.doi.org/10.1039/c2jm32649c]

[76] Gao, E.; Wang, W.; Shang, M.; Xu, J. Synthesis and enhanced photocatalytic performance of graphene-Bi_2WO_6 composite. *Phys. Chem. Chem. Phys.,* **2011**, *13*(7), 2887-2893.
[http://dx.doi.org/10.1039/C0CP01749C] [PMID: 21161101]

[77] Li, J.; Yang, Z.; Qiu, H.; Dai, Y.; Zheng, Q.; Zheng, G.P.; Yang, J. Microwave-assisted simultaneous reduction and titanate treatment of graphene oxide. *J. Mater. Chem. A Mater. Energy Sustain.,* **2013**, *1*(37), 11451-11456.
[http://dx.doi.org/10.1039/c3ta12228j]

[78] Huang, X.; Qi, X.; Boey, F.; Zhang, H. Graphene-based composites. *Chem. Soc. Rev.,* **2012**, *41*(2), 666-686.
[http://dx.doi.org/10.1039/C1CS15078B] [PMID: 21796314]

[79] Hassan, H.M.A.; Abdelsayed, V.; Khder, A.E.R.S.; AbouZeid, K.M.; Terner, J.; El-Shall, M.S.; Al-

Resayes, S.I.; El-Azhary, A.A. Microwave synthesis of graphene sheets supporting metal nanocrystals in aqueous and organic media. *J. Mater. Chem.,* **2009**, *19*(23), 3832-3837.
[http://dx.doi.org/10.1039/b906253j]

[80] Kim, H.W.; Na, H.G.; Kwon, Y.J.; Kang, S.Y.; Choi, M.S.; Bang, J.H.; Wu, P.; Kim, S.S. Microwave-Assisted Synthesis of Graphene–SnO_2 Nanocomposites and Their Applications in Gas Sensors. *ACS Appl. Mater. Interfaces,* **2017**, *9*(37), 31667-31682.
[http://dx.doi.org/10.1021/acsami.7b02533] [PMID: 28846844]

[81] Hu, H.; Wang, X.; Liu, F.; Wang, J.; Xu, C. Rapid microwave-assisted synthesis of graphene nanosheets–zinc sulfide nanocomposites: Optical and photocatalytic properties. *Synth. Met.,* **2011**, *161*(5-6), 404-410.
[http://dx.doi.org/10.1016/j.synthmet.2010.12.018]

[82] Li, M.; Bo, X.; Zhang, Y.; Han, C.; Guo, L. One-pot ionic liquid-assisted synthesis of highly dispersed PtPd nanoparticles/reduced graphene oxide composites for nonenzymatic glucose detection. *Biosens. Bioelectron.,* **2014**, *56*, 223-230.
[http://dx.doi.org/10.1016/j.bios.2014.01.030] [PMID: 24508545]

[83] Yin, Z.; Wu, S.; Zhou, X.; Huang, X.; Zhang, Q.; Boey, F.; Zhang, H. Electrochemical deposition of ZnO nanorods on transparent reduced graphene oxide electrodes for hybrid solar cells. *Small,* **2010**, *6*(2), 307-312.
[http://dx.doi.org/10.1002/smll.200901968] [PMID: 20039255]

[84] Nandi, D.; Mohan, V.B.; Bhowmick, A.K.; Bhattacharyya, D. Metal/metal oxide decorated graphene synthesis and application as supercapacitor: a review. *J. Mater. Sci.,* **2020**, *55*(15), 6375-6400.
[http://dx.doi.org/10.1007/s10853-020-04475-z]

[85] Yu, G.; Hu, L.; Vosgueritchian, M.; Wang, H.; Xie, X.; McDonough, J.R.; Cui, X.; Cui, Y.; Bao, Z. Solution-processed graphene/MnO_2 nanostructured textiles for high-performance electrochemical capacitors. *Nano Lett.,* **2011**, *11*(7), 2905-2911.
[http://dx.doi.org/10.1021/nl2013828] [PMID: 21667923]

[86] Wu, S.; Yin, Z.; He, Q.; Lu, G.; Zhou, X.; Zhang, H. Electrochemical deposition of Cl-doped n-type Cu_2O on reduced graphene oxide electrodes. *J. Mater. Chem.,* **2011**, *21*(10), 3467-3470.
[http://dx.doi.org/10.1039/C0JM02267E]

[87] Wu, S.; Yin, Z.; He, Q.; Lu, G.; Yan, Q.; Zhang, H. Nucleation Mechanism of Electrochemical Deposition of Cu on Reduced Graphene Oxide Electrodes. *J. Phys. Chem. C,* **2011**, *115*(32), 15973-15979.
[http://dx.doi.org/10.1021/jp201667p]

[88] Liu, A.; Li, C.; Bai, H.; Shi, G. Electrochemical Deposition of Polypyrrole/Sulfonated Graphene Composite Films. *J. Phys. Chem. C,* **2010**, *114*(51), 22783-22789.
[http://dx.doi.org/10.1021/jp108826e]

[89] Zhu, G.; Pan, L.; Lu, T.; Xu, T.; Sun, Z. Electrophoretic deposition of reduced graphene-carbon nanotubes composite films as counter electrodes of dye-sensitized solar cells. *J. Mater. Chem.,* **2011**, *21*(38), 14869-14875.
[http://dx.doi.org/10.1039/c1jm12433a]

[90] ReddyPrasad, P.; Naidoo, E.B.; Sreedhar, N.Y. Electrochemical preparation of a novel type of C-dots/ZrO2 nanocomposite onto glassy carbon electrode for detection of organophosphorus pesticide. *Arab. J. Chem.,* **2019**, *12*(8), 2300-2309.
[http://dx.doi.org/10.1016/j.arabjc.2015.02.012]

[91] Liu, S.; Wang, J.; Zeng, J.; Ou, J.; Li, Z.; Liu, X.; Yang, S. "Green" electrochemical synthesis of Pt/graphene sheet nanocomposite film and its electrocatalytic property. *J. Power Sources,* **2010**, *195*(15), 4628-4633.
[http://dx.doi.org/10.1016/j.jpowsour.2010.02.024]

[92] Zhang, Y.; Xiao, X.; Sun, Y.; Shi, Y.; Dai, H.; Ni, P.; Hu, J.; Li, Z.; Song, Y.; Wang, L.

Not be distributed or uploaded to anyone or anywhere
For personal private use only

Electrochemical Deposition of Nickel Nanoparticles on Reduced Graphene Oxide Film for Nonenzymatic Glucose Sensing. *Electroanalysis,* **2013**, *25*(4), 959-966.
[http://dx.doi.org/10.1002/elan.201200479]

[93] Yang, J.; Deng, S.; Lei, J.; Ju, H.; Gunasekaran, S. Electrochemical synthesis of reduced graphene sheet–AuPd alloy nanoparticle composites for enzymatic biosensing. *Biosens. Bioelectron.,* **2011**, *29*(1), 159-166.
[http://dx.doi.org/10.1016/j.bios.2011.08.011] [PMID: 21903376]

[94] Zhang, H.; Zhang, X.; Zhang, D.; Sun, X.; Lin, H.; Wang, C.; Ma, Y. One-step electrophoretic deposition of reduced graphene oxide and $Ni(OH)_2$ composite films for controlled syntheses supercapacitor electrodes. *J. Phys. Chem. B,* **2013**, *117*(6), 1616-1627.
[http://dx.doi.org/10.1021/jp305198j] [PMID: 22994913]

[95] Kim, Y.J.; Lee, J.H.; Yi, G.C. Vertically aligned ZnO nanostructures grown on graphene layers. *Appl. Phys. Lett.,* **2009**, *95*(21), 213101.
[http://dx.doi.org/10.1063/1.3266836]

[96] Lin, J.; Penchev, M.; Wang, G.; Paul, R.K.; Zhong, J.; Jing, X.; Ozkan, M.; Ozkan, C.S. Heterogeneous graphene nanostructures: ZnO nanostructures grown on large-area graphene layers. *Small,* **2010**, *6*(21), 2448-2452.
[http://dx.doi.org/10.1002/smll.201000250] [PMID: 20878792]

[97] Fan, Z.; Yan, J.; Zhi, L.; Zhang, Q.; Wei, T.; Feng, J.; Zhang, M.; Qian, W.; Wei, F. A three-dimensional carbon nanotube/graphene sandwich and its application as electrode in supercapacitors. *Adv. Mater.,* **2010**, *22*(33), 3723-3728.
[http://dx.doi.org/10.1002/adma.201001029] [PMID: 20652901]

[98] Paul, R.K.; Ghazinejad, M.; Penchev, M.; Lin, J.; Ozkan, M.; Ozkan, C.S. Synthesis of a pillared graphene nanostructure: a counterpart of three-dimensional carbon architectures. *Small,* **2010**, *6*(20), 2309-2313.
[http://dx.doi.org/10.1002/smll.201000525] [PMID: 20862676]

[99] Zhu, Y.; Li, L.; Zhang, C.; Casillas, G.; Sun, Z.; Yan, Z.; Ruan, G.; Peng, Z.; Raji, A.R.O.; Kittrell, C.; Hauge, R.H.; Tour, J.M. A seamless three-dimensional carbon nanotube graphene hybrid material. *Nat. Commun.,* **2012**, *3*(1), 1225.
[http://dx.doi.org/10.1038/ncomms2234] [PMID: 23187625]

[100] Yan, Z.; Ma, L.; Zhu, Y.; Lahiri, I.; Hahm, M.G.; Liu, Z.; Yang, S.; Xiang, C.; Lu, W.; Peng, Z.; Sun, Z.; Kittrell, C.; Lou, J.; Choi, W.; Ajayan, P.M.; Tour, J.M. Three-dimensional metal-graphen--nanotube multifunctional hybrid materials. *ACS Nano,* **2013**, *7*(1), 58-64.
[http://dx.doi.org/10.1021/nn3015882] [PMID: 23194106]

[101] Tavakkoli, M.; Flahaut, E.; Peljo, P.; Sainio, J.; Davodi, F.; Lobiak, E.V.; Mustonen, K.; Kauppinen, E.I. Mesoporous Single-Atom-Doped Graphene–Carbon Nanotube Hybrid: Synthesis and Tunable Electrocatalytic Activity for Oxygen Evolution and Reduction Reactions. *ACS Catal.,* **2020**, *10*(8), 4647-4658.
[http://dx.doi.org/10.1021/acscatal.0c00352]

[102] Lin, J.; Zhang, C.; Yan, Z.; Zhu, Y.; Peng, Z.; Hauge, R.H.; Natelson, D.; Tour, J.M. 3-Dimensional graphene carbon nanotube carpet-based microsupercapacitors with high electrochemical performance. *Nano Lett.,* **2013**, *13*(1), 72-78.
[http://dx.doi.org/10.1021/nl3034976] [PMID: 23237453]

[103] Williams, G.; Seger, B.; Kamat, P.V. TiO_2-graphene nanocomposites. UV-assisted photocatalytic reduction of graphene oxide. *ACS Nano,* **2008**, *2*(7), 1487-1491.
[http://dx.doi.org/10.1021/nn800251f] [PMID: 19206319]

[104] Ng, Y.H.; Iwase, A.; Bell, N.J.; Kudo, A.; Amal, R. Semiconductor/Reduced Graphene Oxide Nanocomposites Derived from Photocatalytic Reactions In: *Proceedings of the Catalysis Today*; Elsevier, **2011**; pp. 353-357.

Not be distributed or uploaded to anyone or anywhere
For personal private use only

[http://dx.doi.org/10.1016/j.cattod.2010.10.090]

[105] Pasricha, R.; Gupta, S.; Joshi, A.G.; Bahadur, N.; Haranath, D.; Sood, K.N.; Singh, S.; Singh, S. Directed nanoparticle reduction on graphene. *Mater. Today,* **2012**, *15*(3), 118-125. [http://dx.doi.org/10.1016/S1369-7021(12)70047-0]

[106] Moon, G.; Park, Y.; Kim, W.; Choi, W. Photochemical loading of metal nanoparticles on reduced graphene oxide sheets using phosphotungstate. *Carbon,* **2011**, *49*(11), 3454-3462. [http://dx.doi.org/10.1016/j.carbon.2011.04.042]

[107] Zhang, Y.; Yuan, X.; Wang, Y.; Chen, Y. One-pot photochemical synthesis of graphene composites uniformly deposited with silver nanoparticles and their high catalytic activity towards the reduction of 2-nitroaniline. *J. Mater. Chem.,* **2012**, *22*(15), 7245-7251. [http://dx.doi.org/10.1039/c2jm16455h]

[108] Moon, G.; Kim, H.; Shin, Y.; Choi, W. Chemical-free growth of metal nanoparticles on graphene oxide sheets under visible light irradiation. *RSC Advances,* **2012**, *2*(6), 2205-2207. [http://dx.doi.org/10.1039/c2ra00875k]

[109] Chen, J.; Zheng, X.; Wang, H.; Zheng, W. Graphene oxide-Ag nanocomposite: *In Situ* photochemical synthesis and application as a surface-enhanced Raman scattering substrate. *Thin Solid Films,* **2011**, *520*(1), 179-185. [http://dx.doi.org/10.1016/j.tsf.2011.07.012]

[110] Tjoa, V.; Chua, J.; Pramana, S.S.; Wei, J.; Mhaisalkar, S.G.; Mathews, N. Facile photochemical synthesis of graphene-pt nanoparticle composite for counter electrode in dye sensitized solar cell. *ACS Appl. Mater. Interfaces,* **2012**, *4*(7), 3447-3452. [http://dx.doi.org/10.1021/am300437g] [PMID: 22646232]

[111] Xu, F.; Sun, Y.; Zhang, Y.; Shi, Y.; Wen, Z.; Li, Z. Graphene–Pt nanocomposite for nonenzymatic detection of hydrogen peroxide with enhanced sensitivity. *Electrochem. Commun.,* **2011**, *13*(10), 1131-1134. [http://dx.doi.org/10.1016/j.elecom.2011.07.017]

[112] Wang, X.; Tabakman, S.M.; Dai, H. Atomic layer deposition of metal oxides on pristine and functionalized graphene. *J. Am. Chem. Soc.,* **2008**, *130*(26), 8152-8153. [http://dx.doi.org/10.1021/ja8023059] [PMID: 18529002]

[113] Pandey, P.A.; Bell, G.R.; Rourke, J.P.; Sanchez, A.M.; Elkin, M.D.; Hickey, B.J.; Wilson, N.R. Physical vapor deposition of metal nanoparticles on chemically modified graphene: observations on metal-graphene interactions. *Small,* **2011**, *7*(22), 3202-3210. [http://dx.doi.org/10.1002/smll.201101430] [PMID: 21953833]

[114] Zhou, X.; Wang, F.; Zhu, Y.; Liu, Z. Graphene modified LiFePO4 cathode materials for high power lithium ion batteries. *J. Mater. Chem.,* **2011**, *21*(10), 3353-3358. [http://dx.doi.org/10.1039/c0jm03287e]

[115] Lung-Hao Hu, B.; Wu, F.Y.; Lin, C.T.; Khlobystov, A.N.; Li, L.J. Graphene-modified LiFePO4 cathode for lithium ion battery beyond theoretical capacity. *Nat. Commun.,* **2013**, *4*(1), 1687. [http://dx.doi.org/10.1038/ncomms2705] [PMID: 23575691]

[116] Chang, H.; Wang, G.; Yang, A.; Tao, X.; Liu, X.; Shen, Y.; Zheng, Z. A Transparent, Flexible, Low-Temperature, and Solution-Processible Graphene Composite Electrode. *Adv. Funct. Mater.,* **2010**, *20*(17), 2893-2902. [http://dx.doi.org/10.1002/adfm.201000900]

[117] Geim, A.K.; Novoselov, K.S. The Rise of Graphene. In: *Nanoscience and Technology: A Collection of Reviews from Nature Journals*; World Scientific Publishing Co., **2009**; pp. 11-19. [http://dx.doi.org/10.1142/9789814287005_0002]

[118] Machado, B.F.; Serp, P. Graphene-based materials for catalysis. *Catal. Sci. Technol.,* **2012**, *2*(1), 54-75.

Not be distributed or uploaded to anyone or anywhere
For personal private use only

[http://dx.doi.org/10.1039/C1CY00361E]

[119] Hu, L.; Hu, X.; Wu, X.; Du, C.; Dai, Y.; Deng, J. Density functional calculation of transition metal adatom adsorption on graphene. *Physica B,* **2010**, *405*(16), 3337-3341. [http://dx.doi.org/10.1016/j.physb.2010.05.001]

[120] Tang, Y.; Yang, Z.; Dai, X. Noble metals induced magnetic properties of graphene. *J. Magn. Magn. Mater.,* **2011**, *323*(20), 2441-2447. [http://dx.doi.org/10.1016/j.jmmm.2011.05.004]

[121] Leenaerts, O.; Partoens, B.; Peeters, F.M. Adsorption of H_2O, NH_3, CO, NO_2, and NO on graphene: A first-principles study. *Phys. Rev. B Condens. Matter Mater. Phys.,* **2008**, *77*(12), 125416. [http://dx.doi.org/10.1103/PhysRevB.77.125416]

[122] Ma, F.; Zhang, Z.; Jia, H.; Liu, X.; Hao, Y.; Xu, B. Adsorption of cysteine molecule on intrinsic and Pt-doped graphene: A first-principle study. *J. Mol. Struct. THEOCHEM,* **2010**, *955*(1-3), 134-139. [http://dx.doi.org/10.1016/j.theochem.2010.06.007]

[123] Voloshina, E.N.; Mollenhauer, D.; Chiappisi, L.; Paulus, B. Theoretical study on the adsorption of pyridine derivatives on graphene. *Chem. Phys. Lett.,* **2011**, *510*(4-6), 220-223. [http://dx.doi.org/10.1016/j.cplett.2011.05.025]

[124] Bai, S.; Shen, X. Graphene–inorganic nanocomposites. *RSC Advances,* **2012**, *2*(1), 64-98. [http://dx.doi.org/10.1039/C1RA00260K]

[125] Chang, H.; Wu, H. Graphene-based nanocomposites: preparation, functionalization, and energy and environmental applications. *Energy Environ. Sci.,* **2013**, *6*(12), 3483-3507. [http://dx.doi.org/10.1039/c3ee42518e]

[126] Mahmood, N.; Zhang, C.; Yin, H.; Hou, Y. Graphene-based nanocomposites for energy storage and conversion in lithium batteries, supercapacitors and fuel cells. *J. Mater. Chem. A Mater. Energy Sustain.,* **2014**, *2*(1), 15-32. [http://dx.doi.org/10.1039/C3TA13033A]

[127] Chen, P.; Guo, L.; Wang, Y. Graphene wrapped SnCo nanoparticles for high-capacity lithium ion storage. *J. Power Sources,* **2013**, *222*, 526-532. [http://dx.doi.org/10.1016/j.jpowsour.2012.09.026]

[128] Li, Q.; Mahmood, N.; Zhu, J.; Hou, Y.; Sun, S. Graphene and its composites with nanoparticles for electrochemical energy applications. *Nano Today,* **2014**, *9*(5), 668-683. [http://dx.doi.org/10.1016/j.nantod.2014.09.002]

[129] Lee, J.; Kim, S.M.; Lee, I.S. Functionalization of hollow nanoparticles for nanoreactor applications. *Nano Today,* **2014**, *9*(5), 631-667. [http://dx.doi.org/10.1016/j.nantod.2014.09.003]

[130] Bonaccorso, F.; Colombo, L.; Yu, G.; Stoller, M.; Tozzini, V.; Ferrari, A.C.; Ruoff, R.S.; Pellegrini, V. *Graphene, Related Two-Dimensional Crystals, and Hybrid Systems for Energy Conversion and Storage. Science (80).,* **2015**, 347.

[131] Dubal, D.P.; Ayyad, O.; Ruiz, V.; Gómez-Romero, P. Hybrid energy storage: the merging of battery and supercapacitor chemistries. *Chem. Soc. Rev.,* **2015**, *44*(7), 1777-1790. [http://dx.doi.org/10.1039/C4CS00266K] [PMID: 25623995]

[132] Hu, C.; Song, L.; Zhang, Z.; Chen, N.; Feng, Z.; Qu, L. Tailored graphene systems for unconventional applications in energy conversion and storage devices. *Energy Environ. Sci.,* **2015**, *8*(1), 31-54. [http://dx.doi.org/10.1039/C4EE02594F]

[133] Peng, X.; Peng, L.; Wu, C.; Xie, Y. Two dimensional nanomaterials for flexible supercapacitors. *Chem. Soc. Rev.,* **2014**, *43*(10), 3303-3323. [http://dx.doi.org/10.1039/c3cs60407a] [PMID: 24614864]

[134] Qiu, B.; Xing, M.; Zhang, J. Mesoporous TiO_2 nanocrystals grown *in situ* on graphene aerogels for

high photocatalysis and lithium-ion batteries. *J. Am. Chem. Soc.,* **2014**, *136*(16), 5852-5855. [http://dx.doi.org/10.1021/ja500873u] [PMID: 24712676]

[135] Etacheri, V.; Yourey, J.E.; Bartlett, B.M. Chemically bonded TiO_2-bronze nanosheet/reduced graphene oxide hybrid for high-power lithium ion batteries. *ACS Nano,* **2014**, *8*(2), 1491-1499. [http://dx.doi.org/10.1021/nn405534r] [PMID: 24446910]

[136] Li, N.; Liu, G.; Zhen, C.; Li, F.; Zhang, L.; Cheng, H.M. Battery Performance and Photocatalytic Activity of Mesoporous Anatase TiO_2 Nanospheres/Graphene Composites by Template-Free Self-Assembly. *Adv. Funct. Mater.,* **2011**, *21*(9), 1717-1722. [http://dx.doi.org/10.1002/adfm.201002295]

[137] Lee, M.; Balasingam, S.K.; Jeong, H.Y.; Hong, W.G.; Lee, H.B.R.; Kim, B.H.; Jun, Y. One-step hydrothermal synthesis of graphene decorated V_2O_5 nanobelts for enhanced electrochemical energy storage. *Sci. Rep.,* **2015**, *5*(1), 8151. [http://dx.doi.org/10.1038/srep08151] [PMID: 25633147]

[138] Li, M.; Sun, G.; Yin, P.; Ruan, C.; Ai, K. Controlling the formation of rodlike V_2O_5 nanocrystals on reduced graphene oxide for high-performance supercapacitors. *ACS Appl. Mater. Interfaces,* **2013**, *5*(21), 11462-11470. [http://dx.doi.org/10.1021/am403739g] [PMID: 24138545]

[139] Cheng, J.; Wang, B.; Xin, H.L.; Yang, G.; Cai, H.; Nie, F.; Huang, H. Self-assembled V_2O_5 nanosheets/reduced graphene oxide hierarchical nanocomposite as a high-performance cathode material for lithium ion batteries. *J. Mater. Chem. A Mater. Energy Sustain.,* **2013**, *1*(36), 10814-10820. [http://dx.doi.org/10.1039/c3ta12066j]

[140] Liu, Q.; Li, Z.F.; Liu, Y.; Zhang, H.; Ren, Y.; Sun, C.J.; Lu, W.; Zhou, Y.; Stanciu, L.; Stach, E.A.; Xie, J. Graphene-modified nanostructured vanadium pentoxide hybrids with extraordinary electrochemical performance for Li-ion batteries. *Nat. Commun.,* **2015**, *6*(1), 6127. [http://dx.doi.org/10.1038/ncomms7127] [PMID: 25600907]

[141] Yang, X.; Ding, H.; Zhang, D.; Yan, X.; Lu, C.; Qin, J.; Zhang, R.; Tang, H.; Song, H. Hydrothermal synthesis of MoO_3 nanobelt-graphene composites. *Cryst. Res. Technol.,* **2011**, *46*(11), 1195-1201. [http://dx.doi.org/10.1002/crat.201100302]

[142] Lu, P.J.; Lei, M.; Liu, J. Graphene nanosheets encapsulated α-MoO_3 nanoribbons with ultrahigh lithium ion storage properties. *CrystEngComm,* **2014**, *16*(29), 6745-6755. [http://dx.doi.org/10.1039/C4CE00252K]

[143] Chen, C.; Jian, H.; Fu, X.; Ren, Z.; Yan, M.; Qian, G.; Wang, Z. Facile synthesis of graphene-supported mesoporous Mn_3O_4 nanosheets with a high-performance in Li-ion batteries. *RSC Advances,* **2014**, *4*(11), 5367-5370. [http://dx.doi.org/10.1039/c3ra45976d]

[144] Wang, B.; Park, J.; Wang, C.; Ahn, H.; Wang, G. Mn_3O_4 nanoparticles embedded into graphene nanosheets: Preparation, characterization, and electrochemical properties for supercapacitors. *Electrochim. Acta,* **2010**, *55*(22), 6812-6817. [http://dx.doi.org/10.1016/j.electacta.2010.05.086]

[145] Su, J.; Cao, M.; Ren, L.; Hu, C. Fe_3O_4–Graphene Nanocomposites with Improved Lithium Storage and Magnetism Properties. *J. Phys. Chem. C,* **2011**, *115*(30), 14469-14477. [http://dx.doi.org/10.1021/jp201666s]

[146] Zou, Y.; Kan, J.; Wang, Y. Fe_2O_3 -Graphene Rice-on-Sheet Nanocomposite for High and Fast Lithium Ion Storage. *J. Phys. Chem. C,* **2011**, *115*(42), 20747-20753. [http://dx.doi.org/10.1021/jp206876t]

[147] Kim, H.; Choi, W.; Yoon, J.; Um, J.H.; Lee, W.; Kim, J.; Cabana, J.; Yoon, W.S. Exploring Anomalous Charge Storage in Anode Materials for Next-Generation Li Rechargeable Batteries. *Chem. Rev.,* **2020**, *120*(14), 6934-6976.

[http://dx.doi.org/10.1021/acs.chemrev.9b00618] [PMID: 32101429]

[148] Yang, J.; Wang, J.; Tang, Y.; Wang, D.; Li, X.; Hu, Y.; Li, R.; Liang, G.; Sham, T.K.; Sun, X. $LiFePO_4$–graphene as a superior cathode material for rechargeable lithium batteries: impact of stacked graphene and unfolded graphene. *Energy Environ. Sci.,* **2013**, *6*(5), 1521-1528.
[http://dx.doi.org/10.1039/c3ee24163g]

[149] Qu, Q.; Yang, S.; Feng, X. 2D sandwich-like sheets of iron oxide grown on graphene as high energy anode material for supercapacitors. *Adv. Mater.,* **2011**, *23*(46), 5574-5580.
[http://dx.doi.org/10.1002/adma.201103042] [PMID: 22052661]

[150] Bharali, P.; Kuratani, K.; Takeuchi, T.; Kiyobayashi, T.; Kuriyama, N. Capacitive behavior of amorphous and crystalline RuO_2 composite electrode fabricated by spark plasma sintering technique. *J. Power Sources,* **2011**, *196*(18), 7878-7881.
[http://dx.doi.org/10.1016/j.jpowsour.2011.03.097]

[151] Vellacheri, R.; Pillai, V.K.; Kurungot, S. Hydrous RuO_2 –carbon nanofiber electrodes with high mass and electrode-specific capacitance for efficient energy storage. *Nanoscale,* **2012**, *4*(3), 890-896.
[http://dx.doi.org/10.1039/C2NR11479H] [PMID: 22159715]

[152] Wu, Z.S.; Wang, D.W.; Ren, W.; Zhao, J.; Zhou, G.; Li, F.; Cheng, H.M. Anchoring Hydrous RuO_2 on Graphene Sheets for High-Performance Electrochemical Capacitors. *Adv. Funct. Mater.,* **2010**, *20*(20), 3595-3602.
[http://dx.doi.org/10.1002/adfm.201001054]

[153] Wu, Z.S.; Sun, Y.; Tan, Y.Z.; Yang, S.; Feng, X.; Müllen, K. Three-dimensional graphene-based macro- and mesoporous frameworks for high-performance electrochemical capacitive energy storage. *J. Am. Chem. Soc.,* **2012**, *134*(48), 19532-19535.
[http://dx.doi.org/10.1021/ja308676h] [PMID: 23148416]

[154] Wang, Y.M.; Zhao, D.D.; Zhao, Y.Q.; Xu, C.L.; Li, H.L. Effect of electrodeposition temperature on the electrochemical performance of a $Ni(OH)_2$electrode. *RSC Advances,* **2012**, *2*(3), 1074-1082.
[http://dx.doi.org/10.1039/C1RA00613D]

[155] Liang, H.W.; Wei, W.; Wu, Z.S.; Feng, X.; Müllen, K. Mesoporous metal-nitrogen-doped carbon electrocatalysts for highly efficient oxygen reduction reaction. *J. Am. Chem. Soc.,* **2013**, *135*(43), 16002-16005.
[http://dx.doi.org/10.1021/ja407552k] [PMID: 24128393]

[156] Singh, R.N.; Awasthi, R. Graphene support for enhanced electrocatalytic activity of Pd for alcohol oxidation. *Catal. Sci. Technol.,* **2011**, *1*(5), 778-783.
[http://dx.doi.org/10.1039/c1cy00021g]

[157] Zhang, S.; Shao, Y.; Yin, G.; Lin, Y. Electrostatic self-assembly of a Pt-around-Au nanocomposite with high activity towards formic acid oxidation. *Angew. Chem. Int. Ed.,* **2010**, *49*(12), 2211-2214.
[http://dx.doi.org/10.1002/anie.200906987] [PMID: 20186901]

[158] He, D.; Cheng, K.; Li, H.; Peng, T.; Xu, F.; Mu, S.; Pan, M. Highly active platinum nanoparticles on graphene nanosheets with a significant improvement in stability and CO tolerance. *Langmuir,* **2012**, *28*(8), 3979-3986.
[http://dx.doi.org/10.1021/la2045493] [PMID: 22276697]

[159] Rao, C.V.; Reddy, A.L.M.; Ishikawa, Y.; Ajayan, P.M. Synthesis and electrocatalytic oxygen reduction activity of graphene-supported Pt_3Co and Pt_3Cr alloy nanoparticles. *Carbon,* **2011**, *49*(3), 931-936.
[http://dx.doi.org/10.1016/j.carbon.2010.10.056]

[160] Du, D.; Liu, J.; Zhang, X.; Cui, X.; Lin, Y. One-step electrochemical deposition of a graphene-ZrO_2 nanocomposite: Preparation, characterization and application for detection of organophosphorus agents. *J. Mater. Chem.,* **2011**, *21*(22), 8032-8037.
[http://dx.doi.org/10.1039/c1jm10696a]

[161] Zhu, M.; Chen, P.; Liu, M. Graphene oxide enwrapped Ag/AgX (X = Br, Cl) nanocomposite as a highly efficient visible-light plasmonic photocatalyst. *ACS Nano,* **2011**, *5*(6), 4529-4536.
[http://dx.doi.org/10.1021/nn200088x] [PMID: 21524132]

[162] Subramanian, P.; Niedziolka-Jonsson, J.; Lesniewski, A.; Wang, Q.; Li, M.; Boukherroub, R.; Szunerits, S. Preparation of reduced graphene oxide–Ni(OH) $_2$ composites by electrophoretic deposition: application for non-enzymatic glucose sensing. *J. Mater. Chem. A Mater. Energy Sustain.,* **2014**, *2*(15), 5525-5533.
[http://dx.doi.org/10.1039/C4TA00123K]

[163] Fu, L.; Yu, S.; Thompson, L.; Yu, A. Development of a novel nitrite electrochemical sensor by stepwise *in situ* formation of palladium and reduced graphene oxide nanocomposites. *RSC Advances,* **2015**, *5*(50), 40111-40116.
[http://dx.doi.org/10.1039/C5RA02661J]

[164] Johnson, J.L.; Behnam, A.; Pearton, S.J.; Ural, A. Hydrogen sensing using pd-functionalized multi-layer graphene nanoribbon networks. *Adv. Mater.,* **2010**, *22*(43), 4877-4880.
[http://dx.doi.org/10.1002/adma.201001798] [PMID: 20803539]

[165] Fu, X.; Lou, T.; Chen, Z.; Lin, M.; Feng, W.; Chen, L. "Turn-on" fluorescence detection of lead ions based on accelerated leaching of gold nanoparticles on the surface of graphene. *ACS Appl. Mater. Interfaces,* **2012**, *4*(2), 1080-1086.
[http://dx.doi.org/10.1021/am201711j] [PMID: 22264012]

[166] Wang, F.; Zhu, L.; Zhang, J. Electrochemical sensor for levofloxacin based on molecularly imprinted polypyrrole–graphene–gold nanoparticles modified electrode. *Sens. Actuators B Chem.,* **2014**, *192*, 642-647.
[http://dx.doi.org/10.1016/j.snb.2013.11.037]

[167] Wang, Y.; Zhang, S.; Du, D.; Shao, Y.; Li, Z.; Wang, J.; Engelhard, M.H.; Li, J.; Lin, Y. Self assembly of acetylcholinesterase on a gold nanoparticles–graphene nanosheet hybrid for organophosphate pesticide detection using polyelectrolyte as a linker. *J. Mater. Chem.,* **2011**, *21*(14), 5319-5325.
[http://dx.doi.org/10.1039/c0jm03441j]

[168] Liu, X.; Du, H.; Sun, X.W. High-performance photoresponse of carbon-doped ZnO/reduced graphene oxide hybrid nanocomposites under UV and visible illumination. *RSC Advances,* **2014**, *4*(10), 5136-5140.
[http://dx.doi.org/10.1039/c3ra46864j]

[169] Chang, H.; Sun, Z.; Ho, K.Y.F.; Tao, X.; Yan, F.; Kwok, W.M.; Zheng, Z. A highly sensitive ultraviolet sensor based on a facile *in situ* solution-grown ZnO nanorod/graphene heterostructure. *Nanoscale,* **2011**, *3*(1), 258-264.
[http://dx.doi.org/10.1039/C0NR00588F] [PMID: 20976323]

[170] Anand, K.; Singh, O.; Singh, M.P.; Kaur, J.; Singh, R.C. Hydrogen sensor based on graphene/ZnO nanocomposite. *Sens. Actuators B Chem.,* **2014**, *195*, 409-415.
[http://dx.doi.org/10.1016/j.snb.2014.01.029]

[171] Singh, G.; Choudhary, A.; Haranath, D.; Joshi, A.G.; Singh, N.; Singh, S.; Pasricha, R. ZnO decorated luminescent graphene as a potential gas sensor at room temperature. *Carbon,* **2012**, *50*(2), 385-394.
[http://dx.doi.org/10.1016/j.carbon.2011.08.050]

[172] Zhu, C.; Fang, Y.; Wen, D.; Dong, S. One-pot synthesis of functional two-dimensional graphene/SnO_2 composite nanosheets as a building block for self-assembly and an enhancing nanomaterial for biosensing. *J. Mater. Chem.,* **2011**, *21*(42), 16911-16917.
[http://dx.doi.org/10.1039/c1jm11612f]

[173] Lu, L.M.; Li, H.B.; Qu, F.; Zhang, X.B.; Shen, G.L.; Yu, R.Q. *In situ* synthesis of palladium nanoparticle–graphene nanohybrids and their application in nonenzymatic glucose biosensors. *Biosens. Bioelectron.,* **2011**, *26*(8), 3500-3504.

Not be distributed or uploaded to anyone or anywhere
For personal private use only

[http://dx.doi.org/10.1016/j.bios.2011.01.033] [PMID: 21342759]

[174] Zeng, Q.; Cheng, J.S.; Liu, X.F.; Bai, H.T.; Jiang, J.H. Palladium nanoparticle/chitosan-grafted graphene nanocomposites for construction of a glucose biosensor. *Biosens. Bioelectron.,* **2011**, *26*(8), 3456-3463.
[http://dx.doi.org/10.1016/j.bios.2011.01.024] [PMID: 21324668]

[175] Dey, R.S.; Raj, C.R. Development of an Amperometric Cholesterol Biosensor Based on Graphene−Pt Nanoparticle Hybrid Material. *J. Phys. Chem. C,* **2010**, *114*(49), 21427-21433.
[http://dx.doi.org/10.1021/jp105895a]

[176] Chen, Q.; Zhang, L.; Chen, G. Facile preparation of graphene-copper nanoparticle composite by *in situ* chemical reduction for electrochemical sensing of carbohydrates. *Anal. Chem.,* **2012**, *84*(1), 171-178.
[http://dx.doi.org/10.1021/ac2022772] [PMID: 22098222]

[177] Lu, X.; Qi, H.; Zhang, X.; Xue, Z.; Jin, J.; Zhou, X.; Liu, X. Highly dispersive Ag nanoparticles on functionalized graphene for an excellent electrochemical sensor of nitroaromatic compounds. *Chem. Commun. (Camb.),* **2011**, *47*(46), 12494-12496.
[http://dx.doi.org/10.1039/c1cc15697g] [PMID: 22024647]

[178] Huang, K.J.; Liu, Y.J.; Wang, H.B.; Wang, Y.Y. A sensitive electrochemical DNA biosensor based on silver nanoparticles-polydopamine@graphene composite. *Electrochim. Acta,* **2014**, *118*, 130-137.
[http://dx.doi.org/10.1016/j.electacta.2013.12.019]

[179] Zhang, Y.; Liu, S.; Wang, L.; Qin, X.; Tian, J.; Lu, W.; Chang, G.; Sun, X. One-pot green synthesis of Ag nanoparticles-graphene nanocomposites and their applications in SERS, H_2O_2, and glucose sensing. *RSC Advances,* **2012**, *2*(2), 538-545.
[http://dx.doi.org/10.1039/C1RA00641J]

[180] Zhang, B.; Cui, Y.; Chen, H.; Liu, B.; Chen, G.; Tang, D. A New Electrochemical Biosensor for Determination of Hydrogen Peroxide in Food Based on Well-Dispersive Gold Nanoparticles on Graphene Oxide. *Electroanalysis,* **2011**, *23*(8), 1821-1829.
[http://dx.doi.org/10.1002/elan.201100171]

[181] Cui, F.; Zhang, X. Electrochemical sensor for epinephrine based on a glassy carbon electrode modified with graphene/gold nanocomposites. *J. Electroanal. Chem. (Lausanne),* **2012**, *669*, 35-41.
[http://dx.doi.org/10.1016/j.jelechem.2012.01.021]

[182] Chen, Y.; Tan, C.; Zhang, H.; Wang, L. Two-dimensional graphene analogues for biomedical applications. *Chem. Soc. Rev.,* **2015**, *44*(9), 2681-2701.
[http://dx.doi.org/10.1039/C4CS00300D] [PMID: 25519856]

[183] Jakus, A.E.; Secor, E.B.; Rutz, A.L.; Jordan, S.W.; Hersam, M.C.; Shah, R.N. Three-dimensional printing of high-content graphene scaffolds for electronic and biomedical applications. *ACS Nano,* **2015**, *9*(4), 4636-4648.
[http://dx.doi.org/10.1021/acsnano.5b01179] [PMID: 25858670]

[184] Ahadian, S.; Estili, M.; Surya, V.J.; Ramón-Azcón, J.; Liang, X.; Shiku, H.; Ramalingam, M.; Matsue, T.; Sakka, Y.; Bae, H.; Nakajima, K.; Kawazoe, Y.; Khademhosseini, A. Facile and green production of aqueous graphene dispersions for biomedical applications. *Nanoscale,* **2015**, *7*(15), 6436-6443.
[http://dx.doi.org/10.1039/C4NR07569B] [PMID: 25779762]

[185] Dan, L.; Cheng, Q.; Narain, R.; Krause, B.; Pötschke, P.; Elias, A. Three-Dimensional Printed and Biocompatible Conductive Composites Comprised of Polyhydroxybutyrate and Multiwalled Carbon Nanotubes. *Indus & Eng. Chem. Res,* **2021**, *60*(2), 885-897.
[http://dx.doi.org/10.1021/acs.iecr.0c04753]

[186] Ajiteru, O.; Sultan, M.T.; Lee, Y.J.; Seo, Y.B.; Hong, H.; Lee, J.S.; Lee, H.; Suh, Y.J.; Ju, H.W.; Lee, O.J.; Park, H.S.; Jang, M.; Kim, S.H.; Park, C.H. A 3D Printable Electroconductive Biocomposite Bioink Based on Silk Fibroin-Conjugated Graphene Oxide. *Nano Lett.,* **2020**, *20*(9), 6873-6883.
[http://dx.doi.org/10.1021/acs.nanolett.0c02986] [PMID: 32794720]

Not be distributed or uploaded to anyone or anywhere
For personal private use only

[187] Shen, J.M.; Huang, G.; Zhou, X.; Zou, J.; Yang, Y.; Chen, Y.F.; Men, S.K. Safety evaluation of graphene oxide-based magnetic nanocomposites as MRI contrast agents and drug delivery vehicles. *RSC Advances,* **2014**, *4*(92), 50464-50477.
[http://dx.doi.org/10.1039/C4RA09657F]

[188] Ren, L.; Huang, S.; Fan, W.; Liu, T. One-step preparation of hierarchical superparamagnetic iron oxide/graphene composites *via* hydrothermal method. *Appl. Surf. Sci.,* **2011**, *258*(3), 1132-1138.
[http://dx.doi.org/10.1016/j.apsusc.2011.09.049]

[189] Fan, X.; Jiao, G.; Zhao, W.; Jin, P.; Li, X. Magnetic Fe_3O_4–graphene composites as targeted drug nanocarriers for pH-activated release. *Nanoscale,* **2013**, *5*(3), 1143-1152.
[http://dx.doi.org/10.1039/c2nr33158f] [PMID: 23288110]

[190] Chen, W.; Yi, P.; Zhang, Y.; Zhang, L.; Deng, Z.; Zhang, Z. Composites of aminodextran-coated Fe_3O_4 nanoparticles and graphene oxide for cellular magnetic resonance imaging. *ACS Appl. Mater. Interfaces,* **2011**, *3*(10), 4085-4091.
[http://dx.doi.org/10.1021/am2009647] [PMID: 21882840]

[191] Liu, L.; Liu, J.; Wang, Y.; Yan, X.; Sun, D.D. Facile synthesis of monodispersed silver nanoparticles on graphene oxide sheets with enhanced antibacterial activity. *New J. Chem.,* **2011**, *35*(7), 1418-1423.
[http://dx.doi.org/10.1039/c1nj20076c]

[192] Freund, H.J.; Meijer, G.; Scheffler, M.; Schlögl, R.; Wolf, M. CO oxidation as a prototypical reaction for heterogeneous processes. *Angew. Chem. Int. Ed.,* **2011**, *50*(43), 10064-10094.
[http://dx.doi.org/10.1002/anie.201101378] [PMID: 21960461]

[193] Li, Y.; Yu, Y.; Wang, J.G.; Song, J.; Li, Q.; Dong, M.; Liu, C.J. CO oxidation over graphene supported palladium catalyst. *Appl. Catal. B,* **2012**, *125*, 189-196.
[http://dx.doi.org/10.1016/j.apcatb.2012.05.023]

[194] Moussa, S.; Abdelsayed, V.; Samy El-Shall, M. Laser synthesis of Pt, Pd, CoO and Pd–CoO nanoparticle catalysts supported on graphene. *Chem. Phys. Lett.,* **2011**, *510*(4-6), 179-184.
[http://dx.doi.org/10.1016/j.cplett.2011.05.026]

[195] Zhang, C.; Lv, W.; Yang, Q.; Liu, Y. Graphene supported nano particles of Pt–Ni for CO oxidation. *Appl. Surf. Sci.,* **2012**, *258*(20), 7795-7800.
[http://dx.doi.org/10.1016/j.apsusc.2012.03.131]

[196] Liu, X.; Xu, M.; Wan, L.; Zhu, H.; Yao, K.; Linguerri, R.; Chambaud, G.; Han, Y.; Meng, C. Superior Catalytic Performance of Atomically Dispersed Palladium on Graphene in CO Oxidation. *ACS Catal.,* **2020**, *10*(5), 3084-3093.
[http://dx.doi.org/10.1021/acscatal.9b04840]

[197] Sheldon, R.A.; Arends, I.W.C.E.; Dijksman, A. New developments in catalytic alcohol oxidations for fine chemicals synthesis. *Catal. Today,* **2000**, *57*(1-2), 157-166.
[http://dx.doi.org/10.1016/S0920-5861(99)00317-X]

[198] Villa, A.; Wang, D.; Dimitratos, N.; Su, D.; Trevisan, V.; Prati, L. Pd on carbon nanotubes for liquid phase alcohol oxidation. *Catal. Today,* **2010**, *150*(1-2), 8-15.
[http://dx.doi.org/10.1016/j.cattod.2009.06.009]

[199] Harada, T.; Ikeda, S.; Miyazaki, M.; Sakata, T.; Mori, H.; Matsumura, M. A simple method for preparing highly active palladium catalysts loaded on various carbon supports for liquid-phase oxidation and hydrogenation reactions. *J. Mol. Catal. Chem.,* **2007**, *268*(1-2), 59-64.
[http://dx.doi.org/10.1016/j.molcata.2006.12.010]

[200] Wu, G.; Wang, X.; Guan, N.; Li, L. Palladium on graphene as efficient catalyst for solvent-free aerobic oxidation of aromatic alcohols: Role of graphene support. *Appl. Catal. B,* **2013**, *136-137*, 177-185.
[http://dx.doi.org/10.1016/j.apcatb.2013.01.067]

[201] Yu, X.; Huo, Y.; Yang, J.; Chang, S.; Ma, Y.; Huang, W. Reduced graphene oxide supported Au

Not be distributed or uploaded to anyone or anywhere
For personal private use only

nanoparticles as an efficient catalyst for aerobic oxidation of benzyl alcohol. *Appl. Surf. Sci.,* **2013**, *280*, 450-455.
[http://dx.doi.org/10.1016/j.apsusc.2013.05.008]

[202] Wu, Y.; Yu, H.; Wang, H.; Peng, F. Controllable synthesis and catalytic performance of graphene-supported metal oxide nanoparticles. *Chin. J. Catal.,* **2014**, *35*(6), 952-959.
[http://dx.doi.org/10.1016/S1872-2067(14)60114-5]

[203] Wang, R.; Wu, Z.; Chen, C.; Qin, Z.; Zhu, H.; Wang, G.; Wang, H.; Wu, C.; Dong, W.; Fan, W.; Wang, J. Graphene-supported Au–Pd bimetallic nanoparticles with excellent catalytic performance in selective oxidation of methanol to methyl formate. *Chem. Commun. (Camb.),* **2013**, *49*(74), 8250-8252.
[http://dx.doi.org/10.1039/c3cc43948h] [PMID: 23925488]

[204] Wu, S.; He, Q.; Zhou, C.; Qi, X.; Huang, X.; Yin, Z.; Yang, Y.; Zhang, H. Synthesis of Fe_3O_4 and Pt nanoparticles on reduced graphene oxide and their use as a recyclable catalyst. *Nanoscale,* **2012**, *4*(7), 2478-2483.
[http://dx.doi.org/10.1039/c2nr11992g] [PMID: 22388949]

[205] Pei, Y.; Zhou, G.; Luan, N.; Zong, B.; Qiao, M.; Tao, F.F. Synthesis and catalysis of chemically reduced metal–metalloid amorphous alloys. *Chem. Soc. Rev.,* **2012**, *41*(24), 8140-8162.
[http://dx.doi.org/10.1039/c2cs35182j] [PMID: 22907172]

[206] Sun, J.; Fu, Y.; He, G.; Sun, X.; Wang, X. Catalytic hydrogenation of nitrophenols and nitrotoluenes over a palladium/graphene nanocomposite. *Catal. Sci. Technol.,* **2014**, *4*(6), 1742-1748.
[http://dx.doi.org/10.1039/C4CY00048J]

[207] Zhang, H.; Zhao, Y.; Liu, W.; Gao, S.; Shang, N.; Wang, C.; Wang, Z. Preparation of magnetically separable Cu6/7Co1/7Fe_2O_4–graphene catalyst and its application in selective reduction of nitroarenes. *Catal. Commun.,* **2015**, *59*, 161-165.
[http://dx.doi.org/10.1016/j.catcom.2014.10.016]

[208] Yang, M.Q.; Pan, X.; Zhang, N.; Xu, Y.J. A facile one-step way to anchor noble metal (Au, Ag, Pd) nanoparticles on a reduced graphene oxide mat with catalytic activity for selective reduction of nitroaromatic compounds. *CrystEngComm,* **2013**, *15*(34), 6819-6828.
[http://dx.doi.org/10.1039/c3ce40694f]

[209] Göksu, H.; Ho, S.F.; Metin, Ö.; Korkmaz, K.; Mendoza Garcia, A.; Gültekin, M.S.; Sun, S. Tandem Dehydrogenation of Ammonia Borane and Hydrogenation of Nitro/Nitrile Compounds Catalyzed by Graphene-Supported NiPd Alloy Nanoparticles. *ACS Catal.,* **2014**, *4*(6), 1777-1782.
[http://dx.doi.org/10.1021/cs500167k]

[210] Feng, Y.S.; Ma, J.J.; Kang, Y.M.; Xu, H.J. PdCu nanoparticles supported on graphene: an efficient and recyclable catalyst for reduction of nitroarenes. *Tetrahedron,* **2014**, *70*(36), 6100-6105.
[http://dx.doi.org/10.1016/j.tet.2014.04.034]

[211] Nie, R.; Wang, J.; Wang, L.; Qin, Y.; Chen, P.; Hou, Z. Platinum supported on reduced graphene oxide as a catalyst for hydrogenation of nitroarenes. *Carbon,* **2012**, *50*(2), 586-596.
[http://dx.doi.org/10.1016/j.carbon.2011.09.017]

[212] Wu, J.; Ong, S.W.; Kang, H.C.; Tok, E.S. Hydrogen Adsorption on Mixed Platinum and Nickel Nanoclusters: The Influence of Cluster Composition and Graphene Support. *J. Phys. Chem. C,* **2010**, *114*(49), 21252-21261.
[http://dx.doi.org/10.1021/jp108517k]

[213] Fan, G.; Huang, W.; Wang, C. Insitu synthesis of Ru/RGO nanocomposites as a highly efficient catalyst for selective hydrogenation of halonitroaromatics. *Nanoscale,* **2013**, *5*(15), 6819-6825.
[http://dx.doi.org/10.1039/c3nr01532g] [PMID: 23771438]

[214] Fan, G.Y.; Huang, W.J. Synthesis of ruthenium/reduced graphene oxide composites and application for the selective hydrogenation of halonitroaromatics. *Chin. Chem. Lett.,* **2014**, *25*(2), 359-363.
[http://dx.doi.org/10.1016/j.cclet.2013.11.044]

Not be distributed or uploaded to anyone or anywhere
For personal private use only

[215] Ji, Z.; Shen, X.; Zhu, G.; Zhou, H.; Yuan, A. Reduced graphene oxide/nickel nanocomposites: facile synthesis, magnetic and catalytic properties. *J. Mater. Chem.,* **2012**, *22*(8), 3471-3477. [http://dx.doi.org/10.1039/c2jm14680k]

[216] Wu, Y.; Wen, M.; Wu, Q.; Fang, H. Ni/graphene Nanostructure and Its Electron-Enhanced Catalytic Action for Hydrogenation Reaction of Nitrophenol. *J. Phys. Chem. C,* **2014**, *118*(12), 6307-6313. [http://dx.doi.org/10.1021/jp412711b]

[217] Wang, W.; Gu, J.; Hua, W.; Jia, X.; Xi, K. A novel high efficiency composite catalyst: single crystal triangular Au nanoplates supported by functional reduced graphene oxide. *Chem. Commun. (Camb.),* **2014**, *50*(64), 8889-8891. [http://dx.doi.org/10.1039/C4CC03306J] [PMID: 24968811]

[218] Huang, J.; Zhang, L.; Chen, B.; Ji, N.; Chen, F.; Zhang, Y.; Zhang, Z. Nanocomposites of size-controlled gold nanoparticles and graphene oxide: Formation and applications in SERS and catalysis. *Nanoscale,* **2010**, *2*(12), 2733-2738. [http://dx.doi.org/10.1039/c0nr00473a] [PMID: 20936236]

[219] Ji, Z.; Shen, X.; Yang, J.; Zhu, G.; Chen, K. A novel reduced graphene oxide/Ag/CeO_2 ternary nanocomposite: Green synthesis and catalytic properties. *Appl. Catal. B,* **2014**, *144*, 454-461. [http://dx.doi.org/10.1016/j.apcatb.2013.07.052]

[220] Bai, S.; Shen, X.; Zhu, G.; Li, M.; Xi, H.; Chen, K. *In situ* growth of $Ni_{(x)}Co_{(100-x)}$ nanoparticles on reduced graphene oxide nanosheets and their magnetic and catalytic properties. *ACS Appl. Mater. Interfaces,* **2012**, *4*(5), 2378-2386. [http://dx.doi.org/10.1021/am300310d] [PMID: 22486337]

[221] Feng, C.; Zhang, H.Y.; Shang, N.Z.; Gao, S.T.; Wang, C. Magnetic graphene nanocomposite as an efficient catalyst for hydrogenation of nitroarenes. *Chin. Chem. Lett.,* **2013**, *24*(6), 539-541. [http://dx.doi.org/10.1016/j.cclet.2013.03.036]

[222] Li, X.; Wang, X.; Song, S.; Liu, D.; Zhang, H. Selectively deposited noble metal nanoparticles on Fe_3O_4/graphene composites: stable, recyclable, and magnetically separable catalysts. *Chemistry,* **2012**, *18*(24), 7601-7607. [http://dx.doi.org/10.1002/chem.201103726] [PMID: 22508188]

[223] Cano, M.; Benito, A.M.; Urriolabeitia, E.P.; Arenal, R.; Maser, W.K. Reduced graphene oxide: firm support for catalytically active palladium nanoparticles and game changer in selective hydrogenation reactions. *Nanoscale,* **2013**, *5*(21), 10189-10193. [http://dx.doi.org/10.1039/c3nr02822d] [PMID: 24056941]

[224] Sheng, B.; Hu, L.; Yu, T.; Cao, X.; Gu, H. Highly-dispersed ultrafine Pt nanoparticles on graphene as effective hydrogenation catalysts. *RSC Advances,* **2012**, *2*(13), 5520-5523. [http://dx.doi.org/10.1039/c2ra20400b]

[225] Yao, K.X.; Liu, X.; Li, Z.; Li, C.C.; Zeng, H.C.; Han, Y. Preparation of a Ru-Nanoparticles/Defectiv--Graphene Composite as a Highly Efficient Arene-Hydrogenation Catalyst. *ChemCatChem,* **2012**, *4*(12), 1938-1942. [http://dx.doi.org/10.1002/cctc.201200354]

[226] Zhao, J.; Hu, W.; Li, H.; Ji, M.; Zhao, C.; Wang, Z.; Hu, H. One-step green synthesis of a ruthenium/graphene composite as a highly efficient catalyst. *RSC Advances,* **2015**, *5*(10), 7679-7686. [http://dx.doi.org/10.1039/C4RA11397G]

[227] Marquardt, D.; Vollmer, C.; Thomann, R.; Steurer, P.; Mülhaupt, R.; Redel, E.; Janiak, C. The use of microwave irradiation for the easy synthesis of graphene-supported transition metal nanoparticles in ionic liquids. *Carbon,* **2011**, *49*(4), 1326-1332. [http://dx.doi.org/10.1016/j.carbon.2010.09.066]

[228] Truong-Huu, T.; Chizari, K.; Janowska, I.; Moldovan, M.S.; Ersen, O.; Nguyen, L.D.; Ledoux, M.J.; Pham-Huu, C.; Begin, D. Few-Layer Graphene Supporting Palladium Nanoparticles with a Fully

Not be distributed or uploaded to anyone or anywhere For personal private use only

Accessible Effective Surface for Liquid-Phase Hydrogenation Reaction In: *Proceedings of the Catalysis Today*; Elsevier, **2012**; Vol. 189, pp. 77-82.
[http://dx.doi.org/10.1016/j.cattod.2012.04.005]

[229] Yang, J.H.; Ma, D. Graphene-supported Pd nanoparticles: microwave-assisted synthesis and as microwave-active selective hydrogenation catalysts. *RSC Advances,* **2013**, *3*(26), 10131-10134.
[http://dx.doi.org/10.1039/c3ra41340c]

[230] Chandra, S.; Bag, S.; Das, P.; Bhattacharya, D.; Pramanik, P. Fabrication of magnetically separable palladium–graphene nanocomposite with unique catalytic property of hydrogenation. *Chem. Phys. Lett.,* **2012**, *519-520*, 59-63.
[http://dx.doi.org/10.1016/j.cplett.2011.11.017]

[231] Pei, Y.; Guo, P.; Qiao, M.; Li, H.; Wei, S.; He, H.; Fan, K. The modification effect of Fe on amorphous CoB alloy catalyst for chemoselective hydrogenation of crotonaldehyde. *J. Catal.,* **2007**, *248*(2), 303-310.
[http://dx.doi.org/10.1016/j.jcat.2007.03.024]

[232] Zhu, Y.; Tian, L.; Jiang, Z.; Pei, Y.; Xie, S.; Qiao, M.; Fan, K. Heteroepitaxial growth of gold on flowerlike magnetite: An efficacious and magnetically recyclable catalyst for chemoselective hydrogenation of crotonaldehyde to crotyl alcohol. *J. Catal.,* **2011**, *281*(1), 106-118.
[http://dx.doi.org/10.1016/j.jcat.2011.04.007]

[233] Ji, X.; Niu, X.; Li, B.; Han, Q.; Yuan, F.; Zaera, F.; Zhu, Y.; Fu, H. Selective Hydrogenation of Cinnamaldehyde to Cinnamal Alcohol over Platinum/Graphene Catalysts. *ChemCatChem,* **2014**, *6*(11), 3246-3253.
[http://dx.doi.org/10.1002/cctc.201402573]

[234] Sun, Z.; Rong, Z.; Wang, Y.; Xia, Y.; Du, W.; Wang, Y. Selective hydrogenation of cinnamaldehyde over Pt nanoparticles deposited on reduced graphene oxide. *RSC Advances,* **2014**, *4*(4), 1874-1878.
[http://dx.doi.org/10.1039/C3RA44962A]

[235] Shi, J.; Nie, R.; Chen, P.; Hou, Z. Selective hydrogenation of cinnamaldehyde over reduced graphene oxide supported Pt catalyst. *Catal. Commun.,* **2013**, *41*, 101-105.
[http://dx.doi.org/10.1016/j.catcom.2013.07.012]

[236] Stein, M.; Wieland, J.; Steurer, P.; Tölle, F.; Mülhaupt, R.; Breit, B. Iron Nanoparticles Supported on Chemically-Derived Graphene: Catalytic Hydrogenation with Magnetic Catalyst Separation. *Adv. Synth. Catal.,* **2011**, *353*(4), 523-527.
[http://dx.doi.org/10.1002/adsc.201000877]

[237] Xie, R.; Fan, G.; Ma, Q.; Yang, L.; Li, F. Facile synthesis and enhanced catalytic performance of graphene-supported Ni nanocatalyst from a layered double hydroxide-based composite precursor. *J. Mater. Chem. A Mater. Energy Sustain.,* **2014**, *2*(21), 7880-7889.
[http://dx.doi.org/10.1039/c4ta00395k]

[238] Ding, C.; Wei, W.; Sun, H.; Ding, J.; Ren, J.; Qu, X. Reduced graphene oxide supported chiral Ni particles as magnetically reusable and enantioselective catalyst for asymmetric hydrogenation. *Carbon,* **2014**, *79*, 615-622.
[http://dx.doi.org/10.1016/j.carbon.2014.08.022]

[239] Szőri, K.; Puskás, R.; Szőllősi, G.; Bertóti, I.; Szépvölgyi, J.; Bartók, M. Palladium Nanoparticle–Graphene Catalysts for Asymmetric Hydrogenation. *Catal. Lett.,* **2013**, *143*(6), 539-546.
[http://dx.doi.org/10.1007/s10562-013-1006-6]

[240] Xu, W.; Wang, X.; Zhou, Q.; Meng, B.; Zhao, J.; Qiu, J.; Gogotsi, Y. Low-temperature plasma-assisted preparation of graphene supported palladium nanoparticles with high hydrodesulfurization activity. *J. Mater. Chem.,* **2012**, *22*(29), 14363-14368.
[http://dx.doi.org/10.1039/c2jm16479e]

[241] Wang, D.; Niu, W.; Tan, M.; Wu, M.; Zheng, X.; Li, Y.; Tsubaki, N. Pt nanocatalysts supported on reduced graphene oxide for selective conversion of cellulose or cellobiose to sorbitol. *ChemSusChem,*

2014, *7*(5), 1398-1406.
[http://dx.doi.org/10.1002/cssc.201301123] [PMID: 24648252]

[242] Gopiraman, M.; Babu, S.G.; Khatri, Z.; Wei, K.; Endo, M.; Karvembu, R.; Kim, I.S. Facile and homogeneous decoration of RuO2 nanorods on graphene nanoplatelets for transfer hydrogenation of carbonyl compounds. *Catal. Sci. Technol.,* **2013**, *3*(6), 1485-1489.
[http://dx.doi.org/10.1039/c3cy20735h]

[243] Sun, B.; Qiao, M.; Fan, K.; Ulrich, J.; Tao, F.F. Fischer-Tropsch Synthesis over Molecular Sieve Supported Catalysts. *ChemCatChem,* **2011**, *3*(3), 542-550.
[http://dx.doi.org/10.1002/cctc.201000352]

[244] Xu, K.; Sun, B.; Lin, J.; Wen, W.; Pei, Y.; Yan, S.; Qiao, M.; Zhang, X.; Zong, B. ε-Iron carbide as a low-temperature Fischer–Tropsch synthesis catalyst. *Nat. Commun.,* **2014**, *5*(1), 5783.
[http://dx.doi.org/10.1038/ncomms6783] [PMID: 25503569]

[245] Yu, G.; Sun, B.; Pei, Y.; Xie, S.; Yan, S.; Qiao, M.; Fan, K.; Zhang, X.; Zong, B. Fe(x)O(y)@C spheres as an excellent catalyst for Fischer-Tropsch synthesis. *J. Am. Chem. Soc.,* **2010**, *132*(3), 935-937.
[http://dx.doi.org/10.1021/ja906370b] [PMID: 20028126]

[246] Sun, B.; Xu, K.; Nguyen, L.; Qiao, M.; Tao, F.F. Preparation and Catalysis of Carbon-Supported Iron Catalysts for Fischer-Tropsch Synthesis. *ChemCatChem,* **2012**, *4*(10), 1498-1511.
[http://dx.doi.org/10.1002/cctc.201200241]

[247] Sun, Z.; Sun, B.; Qiao, M.; Wei, J.; Yue, Q.; Wang, C.; Deng, Y.; Kaliaguine, S.; Zhao, D. A general chelate-assisted co-assembly to metallic nanoparticles-incorporated ordered mesoporous carbon catalysts for Fischer-Tropsch synthesis. *J. Am. Chem. Soc.,* **2012**, *134*(42), 17653-17660.
[http://dx.doi.org/10.1021/ja306913x] [PMID: 23020275]

[248] Sun, B.; Jiang, Z.; Fang, D.; Xu, K.; Pei, Y.; Yan, S.; Qiao, M.; Fan, K.; Zong, B. One-Pot Approach to a Highly Robust Iron Oxide/Reduced Graphene Oxide Nanocatalyst for Fischer-Tropsch Synthesis. *ChemCatChem,* **2013**, *5*(3), 714-719.
[http://dx.doi.org/10.1002/cctc.201200653]

[249] Zhao, H.; Zhu, Q.; Gao, Y.; Zhai, P.; Ma, D. Iron oxide nanoparticles supported on pyrolytic graphene oxide as model catalysts for Fischer Tropsch synthesis. *Appl. Catal. A Gen.,* **2013**, *456*, 233-239.
[http://dx.doi.org/10.1016/j.apcata.2013.03.006]

[250] Moussa, S.O.; Panchakarla, L.S.; Ho, M.Q.; El-Shall, M.S. Graphene-Supported, Iron-Based Nanoparticles for Catalytic Production of Liquid Hydrocarbons from Synthesis Gas: The Role of the Graphene Support in Comparison with Carbon Nanotubes. *ACS Catal.,* **2014**, *4*(2), 535-545.
[http://dx.doi.org/10.1021/cs4010198]

[251] He, F.; Niu, N.; Qu, F.; Wei, S.; Chen, Y.; Gai, S.; Gao, P.; Wang, Y.; Yang, P. Synthesis of three-dimensional reduced graphene oxide layer supported cobalt nanocrystals and their high catalytic activity in F–T CO2 hydrogenation. *Nanoscale,* **2013**, *5*(18), 8507-8516.
[http://dx.doi.org/10.1039/c3nr03038e] [PMID: 23892431]

[252] Liu, J.X.; Su, H.Y.; Sun, D.P.; Zhang, B.Y.; Li, W.X. Crystallographic dependence of CO activation on cobalt catalysts: HCP versus FCC. *J. Am. Chem. Soc.,* **2013**, *135*(44), 16284-16287.
[http://dx.doi.org/10.1021/ja408521w] [PMID: 24147726]

[253] Graetz, J. New approaches to hydrogen storage. *Chem. Soc. Rev.,* **2009**, *38*(1), 73-82.
[http://dx.doi.org/10.1039/B718842K] [PMID: 19088966]

[254] Hamilton, C.W.; Baker, R.T.; Staubitz, A.; Manners, I. B–N compounds for chemical hydrogenstorage. *Chem. Soc. Rev.,* **2009**, *38*(1), 279-293.
[http://dx.doi.org/10.1039/B800312M] [PMID: 19088978]

[255] Metin, Ö.; Kayhan, E.; Özkar, S.; Schneider, J.J. Palladium nanoparticles supported on chemically derived graphene: An efficient and reusable catalyst for the dehydrogenation of ammonia borane. *Int.*

Not be distributed or uploaded to anyone or anywhere
For personal private use only

J. Hydrogen Energy, **2012**, *37*(10), 8161-8169.
[http://dx.doi.org/10.1016/j.ijhydene.2012.02.128]

[256] Xi, P.; Chen, F.; Xie, G.; Ma, C.; Liu, H.; Shao, C.; Wang, J.; Xu, Z.; Xu, X.; Zeng, Z. Surfactant free RGO/Pd nanocomposites as highly active heterogeneous catalysts for the hydrolytic dehydrogenation of ammonia borane for chemical hydrogen storage. *Nanoscale,* **2012**, *4*(18), 5597-5601.
[http://dx.doi.org/10.1039/c2nr31010d] [PMID: 22732933]

[257] Yu-Wen, Y.A.N.G.; Gang, F.E.N.G.; Zhang-Hui, L.U.; Na, H.U.; Fei, Z.H.A.N.G.; Xiang-Shu, C.H.E.N. *In situ* Synthesis of Reduced Graphene Oxide Supported Co Nanoparticles as Efficient Catalysts for Hydrogen Generation from NH_3BH_3. *Wuli Huaxue Xuebao,* **2014**, *30*(6), 1180-1186.
[http://dx.doi.org/10.3866/PKU.WHXB201404141]

[258] Yang, Y.; Lu, Z.H.; Hu, Y.; Zhang, Z.; Shi, W.; Chen, X.; Wang, T. Facile *in situ* synthesis of copper nanoparticles supported on reduced graphene oxide for hydrolytic dehydrogenation of ammonia borane. *RSC Advances,* **2014**, *4*(27), 13749-13752.
[http://dx.doi.org/10.1039/C3RA47023G]

[259] Yang, L.; Cao, N.; Du, C.; Dai, H.; Hu, K.; Luo, W.; Cheng, G. Graphene supported cobalt(0) nanoparticles for hydrolysis of ammonia borane. *Mater. Lett.,* **2014**, *115*, 113-116.
[http://dx.doi.org/10.1016/j.matlet.2013.10.039]

[260] Cao, N.; Luo, W.; Cheng, G. One-step synthesis of graphene supported Ru nanoparticles as efficient catalysts for hydrolytic dehydrogenation of ammonia borane. *Int. J. Hydrogen Energy,* **2013**, *38*(27), 11964-11972.
[http://dx.doi.org/10.1016/j.ijhydene.2013.06.125]

[261] Qiu, F.; Li, L.; Liu, G.; Wang, Y.; An, C.; Xu, C.; Xu, Y.; Wang, Y.; Jiao, L.; Yuan, H. Synthesis of $Fe_{0.3}Co_{0.7}$/rGO nanoparticles as a high performance catalyst for the hydrolytic dehydrogenation of ammonia borane. *Int. J. Hydrogen Energy,* **2013**, *38*(18), 7291-7297.
[http://dx.doi.org/10.1016/j.ijhydene.2013.03.168]

[262] Feng, W.; Yang, L.; Cao, N.; Du, C.; Dai, H.; Luo, W.; Cheng, G. *In situ* facile synthesis of bimetallic CoNi catalyst supported on graphene for hydrolytic dehydrogenation of amine borane. *Int. J. Hydrogen Energy,* **2014**, *39*(7), 3371-3380.
[http://dx.doi.org/10.1016/j.ijhydene.2013.12.113]

[263] Yan, J.M.; Wang, Z.L.; Wang, H.L.; Jiang, Q. Rapid and energy-efficient synthesis of a graphene–CuCo hybrid as a high performance catalyst. *J. Mater. Chem.,* **2012**, *22*(22), 10990-10993.
[http://dx.doi.org/10.1039/c2jm31042b]

[264] Cao, N.; Hu, K.; Luo, W.; Cheng, G. RuCu nanoparticles supported on graphene: A highly efficient catalyst for hydrolysis of ammonia borane. *J. Alloys Compd.,* **2014**, *590*, 241-246.
[http://dx.doi.org/10.1016/j.jallcom.2013.12.134]

[265] Çiftci, N.S.; Metin, Ö. Monodisperse nickel–palladium alloy nanoparticles supported on reduced graphene oxide as highly efficient catalysts for the hydrolytic dehydrogenation of ammonia borane. *Int. J. Hydrogen Energy,* **2014**, *39*(33), 18863-18870.
[http://dx.doi.org/10.1016/j.ijhydene.2014.09.060]

[266] Du, Y.; Cao, N.; Yang, L.; Luo, W.; Cheng, G. One-step synthesis of magnetically recyclable rGO supported Cu@Co core–shell nanoparticles: highly efficient catalysts for hydrolytic dehydrogenation of ammonia borane and methylamine borane. *New J. Chem.,* **2013**, *37*(10), 3035-3042.
[http://dx.doi.org/10.1039/c3nj00552f]

[267] Du, C.; Su, J.; Luo, W.; Cheng, G. Graphene supported Ag@Co core–shell nanoparticles as efficient catalysts for hydrolytic dehydrogenation of amine boranes. *J. Mol. Catal. Chem.,* **2014**, *383-384*, 38-45.
[http://dx.doi.org/10.1016/j.molcata.2013.11.018]

[268] Yang, L.; Luo, W.; Cheng, G. Graphene-supported Ag-based core-shell nanoparticles for hydrogen generation in hydrolysis of ammonia borane and methylamine borane. *ACS Appl. Mater. Interfaces,*

2013, *5*(16), 8231-8240.
[http://dx.doi.org/10.1021/am402373p] [PMID: 23927435]

[269] Wang, J.; Qin, Y.L.; Liu, X.; Zhang, X.B. *In situ* synthesis of magnetically recyclable graphene-supported Pd@Co core–shell nanoparticles as efficient catalysts for hydrolytic dehydrogenation of ammonia borane. *J. Mater. Chem.,* **2012**, *22*(25), 12468-12470.
[http://dx.doi.org/10.1039/c2jm32229c]

[270] Cao, N.; Su, J.; Luo, W.; Cheng, G. Hydrolytic dehydrogenation of ammonia borane and methylamine borane catalyzed by graphene supported Ru@Ni core–shell nanoparticles. *Int. J. Hydrogen Energy,* **2014**, *39*(1), 426-435.
[http://dx.doi.org/10.1016/j.ijhydene.2013.10.059]

[271] Cao, N.; Su, J.; Luo, W.; Cheng, G. Graphene supported Ru@Co core–shell nanoparticles as efficient catalysts for hydrogen generation from hydrolysis of ammonia borane and methylamine borane. *Catal. Commun.,* **2014**, *43*, 47-51.
[http://dx.doi.org/10.1016/j.catcom.2013.09.003]

[272] Meng, X.; Yang, L.; Cao, N.; Du, C.; Hu, K.; Su, J.; Luo, W.; Cheng, G. Graphene-Supported Trimetallic Core-Shell Cu@CoNi Nanoparticles for Catalytic Hydrolysis of Amine Borane. *ChemPlusChem,* **2014**, *79*(2), 325-332.
[http://dx.doi.org/10.1002/cplu.201300336] [PMID: 31986590]

[273] Yang, L.; Su, J.; Meng, X.; Luo, W.; Cheng, G. *In situ* synthesis of graphene supported Ag@CoNi core–shell nanoparticles as highly efficient catalysts for hydrogen generation from hydrolysis of ammonia borane and methylamine borane. *J. Mater. Chem. A Mater. Energy Sustain.,* **2013**, *1*(34), 10016-10023.
[http://dx.doi.org/10.1039/c3ta11835e]

[274] Yang, L.; Su, J.; Luo, W.; Cheng, G. Strategic synthesis of graphene supported trimetallic Ag-based core–shell nanoparticles toward hydrolytic dehydrogenation of amine boranes. *Int. J. Hydrogen Energy,* **2014**, *39*(7), 3360-3370.
[http://dx.doi.org/10.1016/j.ijhydene.2013.12.089]

[275] Qiu, F.; Li, L.; Liu, G.; Xu, C.; An, C.; Xu, Y.; Wang, Y.; Huang, Y.; Chen, C.; Wang, Y.; Jiao, L.; Yuan, H. Synthesis of size-controlled Ag@Co@Ni/graphene core-shell nanoparticles for the catalytic hydrolysis of ammonia borane. *Chem. Asian J.,* **2014**, *9*(2), 487-493.
[http://dx.doi.org/10.1002/asia.201301034] [PMID: 24273129]

[276] Zhang, F.; Hou, C.; Zhang, Q.; Wang, H.; Li, Y. Graphene sheets/cobalt nanocomposites as low-cost/high-performance catalysts for hydrogen generation. *Mater. Chem. Phys.,* **2012**, *135*(2-3), 826-831.
[http://dx.doi.org/10.1016/j.matchemphys.2012.05.065]

[277] López Guerra, E.; Shanmugharaj, A.M.; Choi, W.S.; Ryu, S.H. Thermally reduced graphene oxide-supported nickel catalyst for hydrogen production by propane steam reforming. *Appl. Catal. A Gen.,* **2013**, *468*, 467-474.
[http://dx.doi.org/10.1016/j.apcata.2013.09.025]

[278] Sun, D.; Mazumder, V.; Metin, Ö.; Sun, S. Catalytic hydrolysis of ammonia borane *via* cobalt palladium nanoparticles. *ACS Nano,* **2011**, *5*(8), 6458-6464.
[http://dx.doi.org/10.1021/nn2016666] [PMID: 21766875]

[279] Bhowmik, K.; Sengupta, D.; Basu, B.; De, G. Reduced graphene oxide supported Ni nanoparticles: a high performance reusable heterogeneous catalyst for Kumada–Corriu cross-coupling reactions. *RSC Advances,* **2014**, *4*(67), 35442-35448.
[http://dx.doi.org/10.1039/C4RA04834B]

[280] Djakovitch, L.; Koehler, K. Heck reaction catalyzed by PD-modified zeolites. *J. Am. Chem. Soc.,* **2001**, *123*(25), 5990-5999.
[http://dx.doi.org/10.1021/ja001087r] [PMID: 11414833]

Not be distributed or uploaded to anyone or anywhere
For personal private use only

[281] Zhao, F.; Bhanage, B.M.; Shirai, M.; Arai, M. Heck reactions of iodobenzene and methyl acrylate with conventional supported palladium catalysts in the presence of organic and/or inorganic bases without ligands. *Chemistry,* **2000**, *6*(5), 843-848.
[http://dx.doi.org/10.1002/(SICI)1521-3765(20000303)6:5<843::AID-CHEM843>3.0.CO;2-G] [PMID: 10826606]

[282] Chen, X.; Hou, Y.; Wang, H.; Cao, Y.; He, J. Facile Deposition of Pd Nanoparticles on Carbon Nanotube Microparticles and Their Catalytic Activity for Suzuki Coupling Reactions. *J. Phys. Chem. C,* **2008**, *112*(22), 8172-8176.
[http://dx.doi.org/10.1021/jp800610q]

[283] Scheuermann, G.M.; Rumi, L.; Steurer, P.; Bannwarth, W.; Mülhaupt, R. Palladium nanoparticles on graphite oxide and its functionalized graphene derivatives as highly active catalysts for the Suzuki-Miyaura coupling reaction. *J. Am. Chem. Soc.,* **2009**, *131*(23), 8262-8270.
[http://dx.doi.org/10.1021/ja901105a] [PMID: 19469566]

[284] Li, N.; Wang, Z.; Zhao, K.; Shi, Z.; Xu, S.; Gu, Z. Graphene-Pd composite as highly active catalyst for the Suzuki-Miyaura coupling reaction. *J. Nanosci. Nanotechnol.,* **2010**, *10*(10), 6748-6751.
[http://dx.doi.org/10.1166/jnn.2010.2638] [PMID: 21137791]

[285] Jafar Hoseini, S.; Dehghani, M.; Nasrabadi, H. Thin film formation of Pd/reduced-graphene oxide and Pd nanoparticles at oil–water interface, suitable as effective catalyst for Suzuki–Miyaura reaction in water. *Catal. Sci. Technol.,* **2014**, *4*(4), 1078-1083.
[http://dx.doi.org/10.1039/c3cy01068f]

[286] Wang, P.; Zhang, G.; Jiao, H.; Liu, ; Deng, X.; Chen, Y.; Zheng, X. Pd/graphene nanocomposite as highly active catalyst for the Heck reactions. *Appl. Catal. A Gen.,* **2015**, *489*, 188-192.
[http://dx.doi.org/10.1016/j.apcata.2014.10.044]

[287] Siamaki, A.R.; Khder, A.E.R.S.; Abdelsayed, V.; El-Shall, M.S.; Gupton, B.F. Microwave-assisted synthesis of palladium nanoparticles supported on graphene: A highly active and recyclable catalyst for carbon–carbon cross-coupling reactions. *J. Catal.,* **2011**, *279*(1), 1-11.
[http://dx.doi.org/10.1016/j.jcat.2010.12.003]

[288] Kim, S.H.; Jeong, G.H.; Choi, D.; Yoon, S.; Jeon, H.B.; Lee, S.M.; Kim, S.W. Synthesis of noble metal/graphene nanocomposites without surfactants by one-step reduction of metal salt and graphene oxide. *J. Colloid Interface Sci.,* **2013**, *389*(1), 85-90.
[http://dx.doi.org/10.1016/j.jcis.2012.08.064] [PMID: 23026300]

[289] Xiang, G.; He, J.; Li, T.; Zhuang, J.; Wang, X. Rapid preparation of noble metal nanocrystals *via* facile coreduction with graphene oxide and their enhanced catalytic properties. *Nanoscale,* **2011**, *3*(9), 3737-3742.
[http://dx.doi.org/10.1039/c1nr10439j] [PMID: 21804982]

[290] Shendage, S.S.; Singh, A.S.; Nagarkar, J.M. Facile approach to the electrochemical synthesis of palladium-reduced graphene oxide and its application for Suzuki coupling reaction. *Tetrahedron Lett.,* **2014**, *55*(4), 857-860.
[http://dx.doi.org/10.1016/j.tetlet.2013.12.022]

[291] Nishina, Y.; Miyata, J.; Kawai, R.; Gotoh, K. Recyclable Pd–graphene catalyst: mechanistic insights into heterogeneous and homogeneous catalysis. *RSC Advances,* **2012**, *2*(25), 9380-9382.
[http://dx.doi.org/10.1039/c2ra21185h]

[292] Moussa, S.; Siamaki, A.R.; Gupton, B.F.; El-Shall, M.S. Pd-Partially Reduced Graphene Oxide Catalysts (Pd/PRGO): Laser Synthesis of Pd Nanoparticles Supported on PRGO Nanosheets for Carbon–Carbon Cross Coupling Reactions. *ACS Catal.,* **2012**, *2*(1), 145-154.
[http://dx.doi.org/10.1021/cs200497e]

[293] Metin, Ö.; Ho, S.F.; Alp, C.; Can, H.; Mankin, M.N.; Gültekin, M.S.; Chi, M.; Sun, S. Ni/Pd core/shell nanoparticles supported on graphene as a highly active and reusable catalyst for Suzuki-Miyaura cross-coupling reaction. *Nano Res.,* **2013**, *6*(1), 10-18.

Not be distributed or uploaded to anyone or anywhere
For personal private use only

[http://dx.doi.org/10.1007/s12274-012-0276-4]

[294] Feng, Y.S.; Lin, X.Y.; Hao, J.; Xu, H.J. Pd–Co bimetallic nanoparticles supported on graphene as a highly active catalyst for Suzuki–Miyaura and Sonogashira cross-coupling reactions. *Tetrahedron,* **2014**, *70*(34), 5249-5253.
[http://dx.doi.org/10.1016/j.tet.2014.05.083]

[295] Li, Y.; Fan, X.; Qi, J.; Ji, J.; Wang, S.; Zhang, G.; Zhang, F. Gold nanoparticles–graphene hybrids as active catalysts for Suzuki reaction. *Mater. Res. Bull.,* **2010**, *45*(10), 1413-1418.
[http://dx.doi.org/10.1016/j.materresbull.2010.06.041]

[296] Movahed, S.K.; Fakharian, M.; Dabiri, M.; Bazgir, A. Gold nanoparticle decorated reduced graphene oxide sheets with high catalytic activity for Ullmann homocoupling. *RSC Advances,* **2014**, *4*(10), 5243-5247.
[http://dx.doi.org/10.1039/c3ra45518a]

[297] Huo, X.; Liu, J.; Wang, B.; Zhang, H.; Yang, Z.; She, X.; Xi, P. A one-step method to produce graphene–Fe_3O_4 composites and their excellent catalytic activities for three-component coupling of aldehyde, alkyne and amine. *J. Mater. Chem. A Mater. Energy Sustain.,* **2013**, *1*(3), 651-656.
[http://dx.doi.org/10.1039/C2TA00485B]

For personal private use only
Not be distributed or uploaded to anyone or anywhere

CHAPTER 7

Graphene Supported Palladium Nanocatalyst for Cross-Coupling Reactions

Mukesh Kumar[1], Meenakshi Singh Solanki[2] and **Siddharth Sharma[3,*]**

[1] *Department of Chemistry. Sahu Jain College, Najibabad, Bijnor 246763, India*

[2] *Department of Chemistry, PAHER University, Udaipur, Rajasthan 313003, India*

[3] *Department of Chemistry. Mohanlal Sukhadia University Udaipur, Rajasthan 313001, India*

Abstract: The catalytic potential of graphene oxide (GO) and graphite oxide has been well explored in recent years. The reactivity of metal-supported graphite oxide as a solid-phase heterogeneous catalyst has started to be an exceptionally powerful tool for the construction of C-C bonds in synthetic organic chemistry. Among them, palladium has been widely used in different catalysts for a variety of cross-coupling reactions such as Mizoroki-Heck, Suzuki-Miyaura, Kumada, Stille, Negishi, Hiyama, and Buchwald-Hartwig, *etc.*, because of its high catalytic activity and the rapid installation of a complex molecular structure with selectivity in comparison to other transition metal catalysts. A description of recent advances in graphene-supported palladium nanocatalysts for cross-coupling reactions is presented in this chapter. Catalyst synthesis and mechanistic aspects are also given, followed by comparisons with traditional methods.

Keywords: C-C Bond Formation, Cross-coupling Reaction, Graphene Oxide, Graphite Oxide, Reduced Graphene Oxide (r-GO).

INTRODUCTION

Transition metal-catalyzed cross-coupling reactions have emerged as an exceptionally powerful tool for the construction of C-C and C-Hetero atoms bonds in synthetic organic chemistry and continue to have widespread application, especially in drug development programmes and agrochemicals [1, 2]. In the last decades, many transition metals have been employed to carry out cross-coupling reactions. Among them, palladium has been widely used in different catalysts for a variety of cross-coupling reactions such as Mizoroki-Heck, Suzuki-Miyaura, Kumada, Stille, Negishi, Hiyama, Buchwald-Hartwig, *etc.*, because of its high catalytic activity and the rapid installation of complex molecular structure with

* **Corresponding author Siddharth Sharma:** Department of Chemistry. Mohanlal Sukhadia University Udaipur, Rajasthan 313001, India; E-mail: siddharth@mlsu.ac.in

Pinki Bala Punjabi, Rakshit Ameta & Sharoni Gupta (Eds.)
All rights reserved-© 2023 Bentham Science Publishers

selectivity in comparison to other transition metal catalysts [3]. The impact of palladium-catalyzed reactions in the scientific community has been recognized after getting the Nobel Prize in chemistry by three renowned scientists in this area: Professor Richard F. Heck, Professor Eichi Negishi, and Professor Akira Suzuki [4].

Despite the high impact of homogenous palladium-catalyzed cross-coupling reactions in all fields of science, there are many issues associated with homogenous catalysis, such as the use of a high-cost catalytic system, lack of reusability of catalyst, and potential contamination of the drug by residual heavy metals, which strongly limit their use in the pharmaceutical industry [5, 6]. To address these issues, synthetic chemists started channeling their efforts to innovate environmentally benign processes by developing new catalysts with high efficiency and reusability, applying efficient energy sources, and avoiding the use of ligands and auxiliaries. For these reasons, synthetic chemists moved on to heterogeneous catalysis, in which palladium catalysts immobilized on solid support (organic, inorganic, and hybrid materials) have become an important alternative to address all the issues associated with homogenous catalysis. Several heterogeneous palladium catalysts have been generated using silica [7, 8], zeolites [9, 10], ionic liquids [11 - 13], alumina [14], clay [15], zinc ferrite [16], organic, and inorganic polymers as supports [17 - 22]. There are many carbon-based nanomaterials such as one-dimensional (1D) carbon nanotubes (CNTs), two-dimensional (2D) graphene, amorphous activated carbon (AC), and mesoporous carbon (MC), which have also been applied as supports for the synthesis of palladium nanoparticles catalysts [23 - 26].

Among them, graphene and modified graphene has recently become more attractive support in the field of catalysis and have attracted much attention from the scientific community because of their extraordinary properties. Graphene, a 2D material, is considered a "wonder material" formed by carbon atoms that are arranged in a hexagonal monolayer pattern (a honeycomb crystal lattice). Each carbon atom of graphene is sp^2 hybridized and 200 times harder than steel, very feathery, and flexible [27 - 29]. In addition, graphene possesses a large surface area, and excellent chemical, thermal and electrical stability. Moreover, it showed a strong hydrophobic interaction with metal and was easily modified to other forms [30]. Graphene-based architectures are highly desirable in the synthesis of metal nanoparticles, especially as a support for palladium nanoparticles (PdNPs), and displayed exceptional catalytic efficiency for C-C cross-coupling reactions because graphene has high binding energy with palladium and good charge storage performance [31]. Moreover, due to the presence of transparency and conductive properties of graphene it also plays a vital role in the areas of electrochemical applications such as sensors [32], electrodes [33], and fuel cells

[34]. Furthermore, graphene derivatives, such as graphene oxide (GO) and reduced graphene oxide (rGO) have also become useful support in nano metal-catalysis due to their structural defects, which allow an easy covalent and non-covalent (hydrogen-binding or π-stacking) functionalization of the material that can be used either as supports for immobilizing active species or as metal-free catalysts and enhancing the rate of interaction with anchored metal nanoparticles [35, 36]. Graphene oxide was first synthesized by oxidation of graphite in acidic conditions using the Hummers-Offeman method [37]. This method involves the treatment of graphite with sodium nitrite ($NaNO_3$), potassium permanganate ($KMnO_4$), and followed by hydrogen peroxide (H_2O_2).

Recently, Palladium nanoparticles (PdNPs) have established as an intensively investigated and rapidly growing area in ligand-free catalysis because of their high surface-to-volume ratio and highly active surface atoms in comparison to other bulk catalysts [38 - 42]. Palladium nanoparticles (PdNPs), used as a heterogeneous catalyst for the production of pharmaceutical agents, herbicides, fine chemicals, and polymers have a lot of advantages over the palladium-catalyzed homogenous reactions because of their remarkable features such as stability, selectivity, reusability, cost-effective, simple workup procedure and easy separation of the final product [43]. Palladium nanoparticles (PdNPs) supported on graphene/graphene oxide (GO) /reduced graphene oxide (rGO) increase the surface area of nanohybrids by expanding the distance between the sheets. This process enhances the catalytic performance of this type of heterogeneous catalyst. These heterogeneous catalysts have not only shown their catalytic efficiency for catalyzing the cross-coupling reactions in which carbon-carbon bond is formed but they have also been applied in other reactions, such as hydrogenation of alkenes, alkynes, and hydrogenation of carbonyl (-CO) and nitro ($-NO_2$) groups [44 - 52].

This chapter covers the graphene/graphene oxide (GO)/reduced graphene oxide (rGO) supported metal nanoparticles catalyzed cross-coupling reactions such as Suzuki, Heck, and Sonogashira, leading to the formation of biological importance molecules.

GRAPHENE SUPPORTED PALLADIUM NANOPARTICLES (PDNPS/G) CATALYZED CROSS-COUPLING REACTIONS

Palladium nanoparticles supported on graphene (PdNPs-G) and reduced graphene oxide (PdNPs-rGO) have been used as catalysts for Suzuki cross-coupling reactions between aryl bromides and potassium aryltrifluoroborates by Gómez-Martínez and his co-workers in 2015 [53]. Potassium aryl- and heteroaryl-trifluoroborates efficiently coupled with various aryl halides in the presence of 0.1

mol% catalyst, potassium carbonate as a base in MeOH:H_2O as solvent using conventional and microwave heating to generate a library of functionalized biphenyl derivatives in good to excellent yields (Scheme **1**). Sterically hindered substrate such as 2-bromo-1,3-dimethylbenzene was unable to provide the cross-coupling product in good yield with potassium phenyltrifluoroborate. Heterocyclic bromides such as 2-bromopyridine and 2-bromothiophene were smoothly coupled with potassium phenyltrifluoroborate to give the coupling products with slightly lower yields. However, less reactive chlorobenzene gave the lowest yield of coupling products. Microwave irradiation provides a lower accumulation of the PdNPs. Identical results of coupling products in terms of yields have been observed using microwave and conventional heating. It is interesting to note that this catalyst was used in Gram-scale synthesis and provides an excellent yield of Suzuki products without loss of catalytic activity. The reusability of the catalyst was also studied and found that the catalyst could be reused up to eight times without loss of significant activity under microwave irradiation, whereas four times when the conventional heating condition was applied.

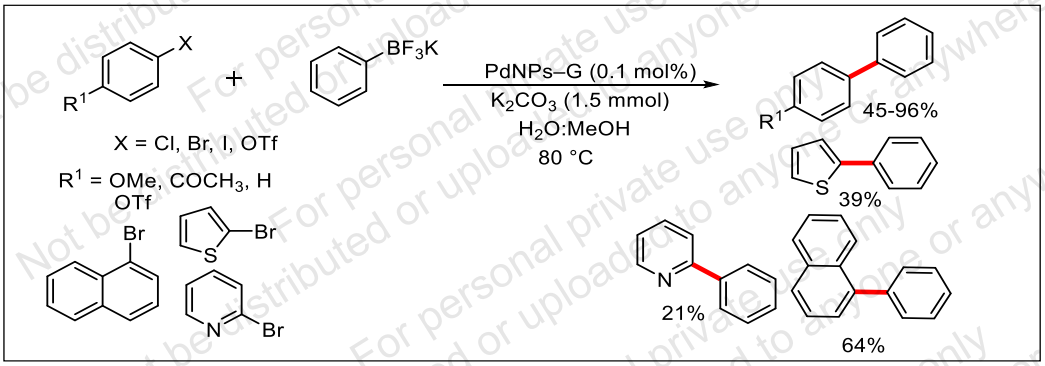

Scheme (1). Synthesis of biaryl derivatives using PdNPs-G catalyst.

Wang and co-workers disclosed the formation of graphene-supported Pd (Pd/graphene) catalyst derived from graphene oxide (GO) and $PdCl_2$ followed by reduction with hydrazine hydrate in an aqueous medium [54]. The performance of this catalyst was investigated in Heck cross-coupling reactions in which iodo- and bromobenzene efficiently coupled with *n*-butyl acrylate or styrene in the presence of 0.05 mol% Pd/G and K_2CO_3 as the base at 100 ^{0}C to provide the coupling products in good to excellent yields (Scheme **2**). However, chlorobenzene was unable to provide a satisfactory coupling product even after increasing the catalyst loading and reaction time. The reusability of the catalyst was also studied using the reaction between bromobenzene with *n*-butyl acrylate. The recycled catalyst could be used seven times without significant loss of activity. Pd NPs in

Pd/graphene were uniformly dispersed on the surface of graphene as displayed by the TEM image. The shape and size of Palladium nanoparticles were found to be spherical and ranged from 2-6, respectively.

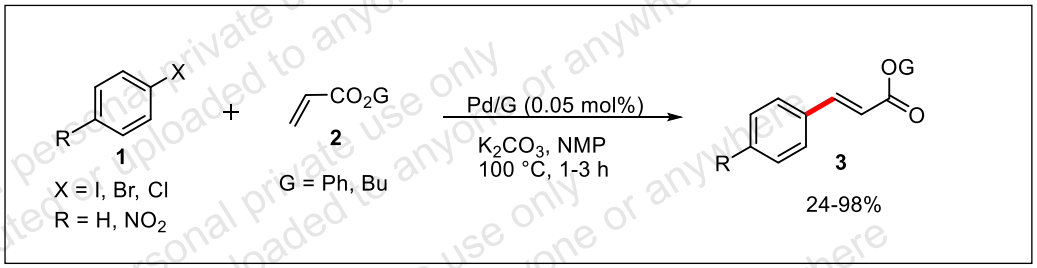

Scheme (2). Heck cross-coupling reaction catalyzed by Pd/G catalyst.

Siamaki *et al*. described a highly efficient protocol for the formation of graphene supported-palladium nanoparticles; in which an aqueous mixture of Pd $(NO_3)_2$ and GO sheets were reduced under microwave irradiation in the presence or absence of hydrazine hydrate respectively [55]. The catalytic exploration of these Pd/G and Pd/GO catalysts was tested using C-C cross-coupling reactions (Suzuki and Heck) without the use of any ligand in aqueous ethanol. The author observed that both catalysts (Pd/G and Pd/GO) exhibit excellent catalytic activity towards the cross-coupling reaction of phenylboronic acid with aryl halides (Scheme **3**), however, Pd/G displayed outstanding activity towards the Suzuki coupling even at low concentrations.

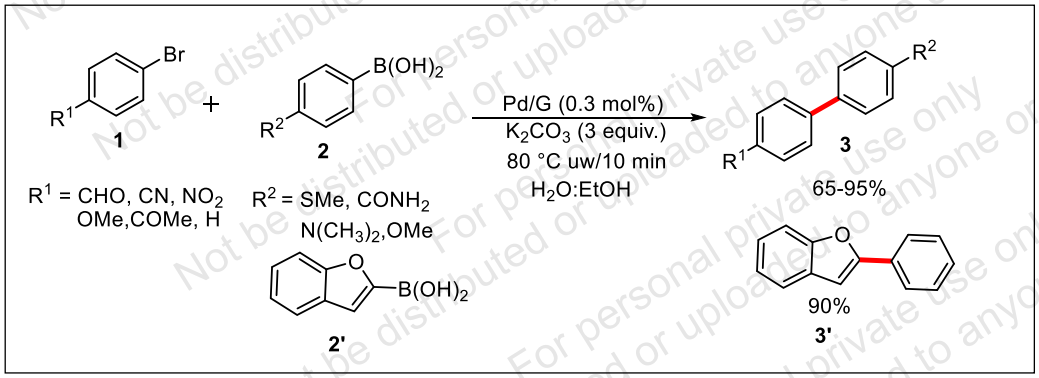

Scheme (3). Graphene-supported palladium catalyzed Suzuki reaction.

The Pd/G catalyst promotes the coupling reaction between bromobenzene and phenylboronic acid with a very low catalyst loading (0.007 mol% Pd/G) to form a biphenyl derivative with a TON of 9000, a TOF of 108 000 h^{-1}, and a 63%

conversion at 80 °C under microwave for 5 min radiation. It is interesting to note that this is the highest TOF for palladium-catalyzed Suzuki cross-coupling reaction under microwave irradiation. Pd/G catalyst also showed excellent catalytic activity towards the Heck cross-coupling. Many aryl bromides coupled with a variety of olefins in the presence of 0.3 mol% of Pd/G, K_2CO_3 as a base in H_2O:EtOH at 180 °C under microwave irradiation. Aryl bromides bearing electron-donating or electron-donating groups easily react with olefins even with inactivated olefins such as *tert*-butylstyrene to furnish excellent yield of the coupling products (Scheme **4**). The recyclability of the catalyst was also examined and found it could be reused eight times without loss of catalytic activity. The activity of the catalyst was dropped after eight times due to the agglomeration and accumulation of the Pd nanoparticles on the surface of graphene. The uniform dispersion of Pd nanoparticles on both graphene and graphene oxide was confirmed by TEM images. The size of NPs supported on graphene was found to be smaller than those supported on the GO sheets.

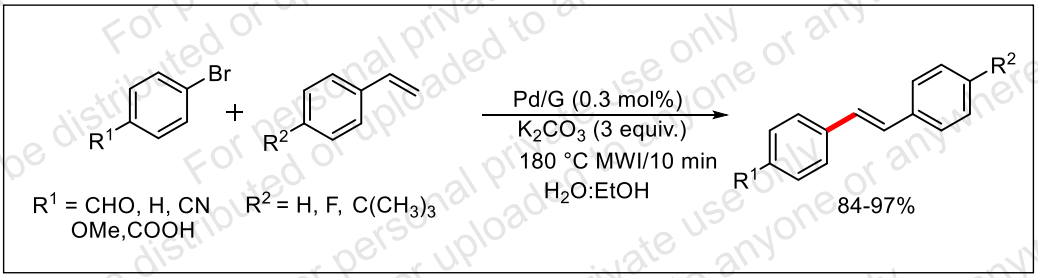

Scheme (4). Pd/G catalyzed Heck cross-coupling reactions.

Later, Gilliland III *et al*. research group developed the catalysts having several defect sites through strong electrostatic adsorption (SEA) with solvent-free microwave reduction method using four different types of commercially available graphene supports (graphene powder 1-5 layers, graphene oxide, reduced graphene oxide, and graphene Nanoplatelet aggregates) as starting materials [56]. The synthesized catalysts were characterized using different analytical techniques such as powder x-ray diffraction (XRD), transmission electron microscopy (TEM), and X-ray photoelectron spectroscopy (XPS). The prepared catalysts (graphene Nanoplatelet) were economical and showed excellent activity towards the Suzuki cross-coupling reactions than other graphene-based supports (Scheme **5**).

In 2013, Lee and co-workers demonstrated a multistep route for the synthesis of a high-performance graphene-based palladium nanoparticles catalyst and evaluated their catalytic power towards the copper and ligand-free Sonogashira reaction

[57]. The synthetic route involved the formation of multilayer Pd^{+2}/GO intermediate between the reaction of GO with $Pd(OAc)_2$ followed by reduction and exfoliation into Pd/G using H_2 gas as a reducing agent. TEM images displayed the uniform distribution of PdNPs on the surface of graphene sheets without aggregation. The mean particle size of PdNPs was found to be 1.4 ±0.6 nm with the help of ICP-MS. The synthesized catalyst exhibited excellent catalytic activity in the Sonogashira coupling reaction in which iodobenzene coupled with phenylacetate in the presence of the formed catalyst (Pd/G) without using any ligand to form biphenylacetylene derivative in a high (89%) yield. There are many advantages of this catalyst such as easy removal of catalyst from the reaction mixture and reusability; *i.e.* it can be reused five times without loss of significant activity.

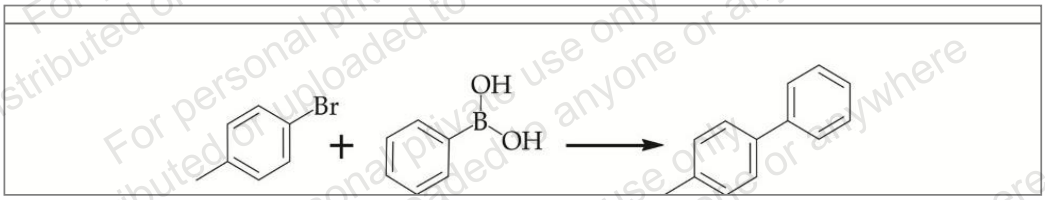

Scheme (5). Suzuki cross-coupling.

In 2015, Rana research groups fabricated a new type of nanocomposite catalyst by highly deposited PdNPs on organodiamine-functionalized graphene support. Organodiamine-functionalized graphene was synthesized by the reaction of [3-(--Aminoethylamino)propyl] trimethoxysilane (AAPTMS) with GO using toluene as solvent. Organodiamine-functionalized graphene-supported PdNPs were obtained by a reduction of $Pd(NO_3)_2$ using $NaBH_4$ as a reducing agent [58].

Organodiamine-functionalized graphene support worked as a stabilizer for Pd NPs and provides sufficient electron density to Pd(0) during oxidative addition of aryl halide. In addition, it also worked as excellent support that helped in eluding "Ostwald ripening". The newly fabricated catalyst exhibited outstanding activity toward the Suzuki cross-coupling reaction of aryl iodides with phenylboronic acids. The reaction was performed in the presence of 0.05 mol% of catalyst using $Ba(OH)_2$ or K_3PO_4 as a base in an aqueous medium providing 98% yield with 100% conversion of starting materials (aryl iodides with phenylboronic acids). 2-bromopyridine smoothly reacted with phenylboronic acid producing biaryl products in good yield, whereas chlorobenzene was unable to provide the desired products. The authors proposed the reaction mechanism in which oxidative addition of phenyl halide in the presence of a catalyst is the main step. The yield of coupling products was not increased when catalyst loading was increased from 0.05 mol% to 0.06 mol%. The catalyst was recycled up to six times without any

change in catalytic activity. However, noticeable changes can be seen in the catalytic activity of the catalyst after the seventh and eighth repetitive uses in cross-coupling reaction, the leached amount of Pd was ~10% and ~15% respectively, which indicated that the redeposition of the Pd species was not fully completed during the release-redeposition cycle. TEM images displayed that Pd nanoparticles (3-7 nm) were uniformly distributed on the surface of amine functionalized graphene.

Mahdavi *et al*. employed a similar strategy for the development of polyacrylamide (PAM) functionalized Graphene oxide supported palladium nanoparticles (PAM-g-rGO/Pd) catalyst using ammonium cerium (IV) sulphate $[(NH_4)_4Ce(SO_4)_4 \cdot 2H_2O]$ induced by redox polymerization [59]. PAM helps to make effective dispersion of graphene oxide because of its high polarity and hydrophilic nature. Then PdNPs were synthesized on the surface of PAM-g-rGO using $NaBH_4$ as a reducing agent. The synthesized catalyst was used for Suzuki cross-coupling reactions to observe its catalytic activity. The reactions were performed between different aryl halides and boronic acid in the presence of PAM-g-rGO/Pd using potassium carbonate as a base in an aqueous medium. Iodobenzene-bearing electron-withdrawing substituents efficiently coupled with boronic acid to furnish the corresponding biphenyl products in 100% yields. However, bromobenzene and chlorobenzene needed a long reaction time to couple with the boronic acid and provide the coupling products in excellent yields. Boronic acid that incorporated electron-donating substituents smoothly reacted with aryl halides to provide the corresponding products in excellent yield except methyl boronic acid gave 100% yield of coupling product with iodobenzene. The most important thing about this type of heterogeneous catalyst is its reusability. The catalyst can be recycled successfully up to eight times with a minimum loss of activity (Scheme **6**).

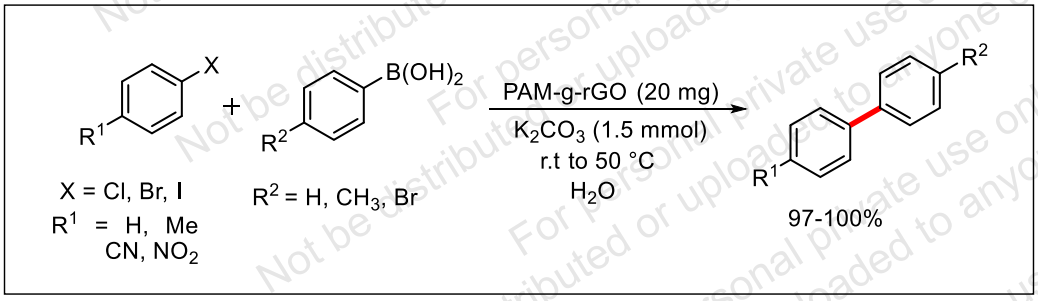

Scheme (6). Suzuki cross-coupling reaction catalyzed by PAM-g-rGO/Pd.

Another important approach has been described for the synthesis of reusable heterogeneous catalysts based on palladium nanoparticles supported on graphene-

benzimidazole(G-BI-Pd) by Sarvestani and co-workers [60]. The catalyst was prepared in the following steps. In the first step, graphene oxide-benzimidazole was prepared by the reaction of graphene oxide with an excess amount of *ortho*-phenylenediamine in the presence of polyphosphoric acid which subsequently underwent reduction of graphene oxide using hydrazine as a reducing agent to generate benzimidazole-grafted graphene (G-BI). Finally, PdNPs were immobilized on the surface of benzimidazole-grafted graphene to form (G-BI-Pd) *via* the formation of the N-Pd complex. Several analytical techniques have been used for the confirmation of synthesized catalysts. The developed catalyst demonstrated superb catalytic activity toward the Suzuki cross-coupling reaction of aryl halides with phenylboronic acids (Scheme **7**). The best results were obtained in terms of yield when the reaction was performed in the presence of 0.45 mol% of G-BI-Pd catalyst using potassium carbonate as a base in an aqueous medium at 80 ^{0}C. Bromobenzene/iodobenzene having electron-withdrawing or electron-donating substituents smoothly transformed into the corresponding biphenyl products in short reaction times with excellent yields. Aryl bromide required a longer reaction time to complete the reaction in comparison to iodobenzene. 2-bromofuran and α-bromo-naphthalene were smoothly converted into the corresponding products in excellent yields under the same catalytic system, except for chlorobenzene which was unable to provide good results in terms of yields. This heterogeneous catalyst showed high stability and could be reused up to five times without loss of their catalytic activity. The uniform distribution of palladium nanoparticles on the surface of G-BI and no aggregation was observed in TEM images.

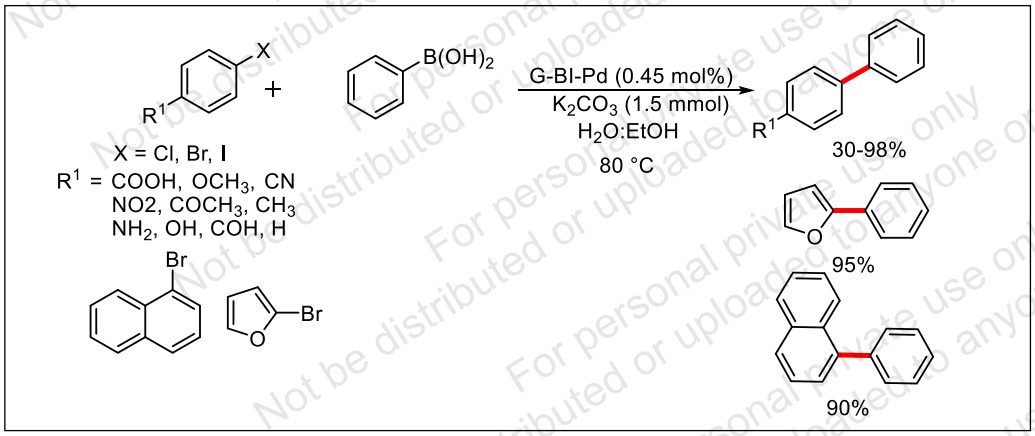

Scheme (7). Synthesis of biphenyl derivative using GBIPd catalyst.

In continuation, Fareghi-Alamdari and co-workers also applied a similar strategy for the construction of palladium nanoparticles catalyst decorated on the surface of phosphine functionalized graphene (PFG-Pd) and demonstrated its application as a highly efficient catalyst for the Suzuki cross-coupling reaction [61]. A phosphine functionalized graphene (PFG) was prepared by the treatment of graphene oxide (GO) with potassium hydroxide resulting in the formation of a free hydroxyl group on the surface of graphene (GOH). The generated hydroxy-functionalized graphene reacted with chlorodiphenylphosphine ($ClPPh_2$) to form phosphine grafted graphene oxide $GOPPh_2$ (PFG), which could be helpful in the preparation of reusable metal catalysts and for the stabilization of metal nanoparticles or the complexation of transition metals. The application of phosphine functionalized graphene (PFG-Pd) catalyst was tested for Suzuki cross-coupling reaction and found that different aryl halides bearing electron-donating or electron-withdrawing substituents smoothly reacted with arylboronic acids using 1.2 mol% of PFG-Pd catalyst and K_2CO_3 as a base in aqueous medium at 80 ^{0}C providing the corresponding biphenyl products in good to excellent yields. Heterocyclic substrates were also applied in place of aryl halides which smoothly coupled with arylboronic acid to furnish the coupling products in good to excellent yields but with more reaction time (Scheme **8**). It is interesting to note that this catalyst was also used for Heck cross-coupling and *N*-arylation. The catalyst can be consecutively recycled up to five times without significant leaching of the palladium catalyst.

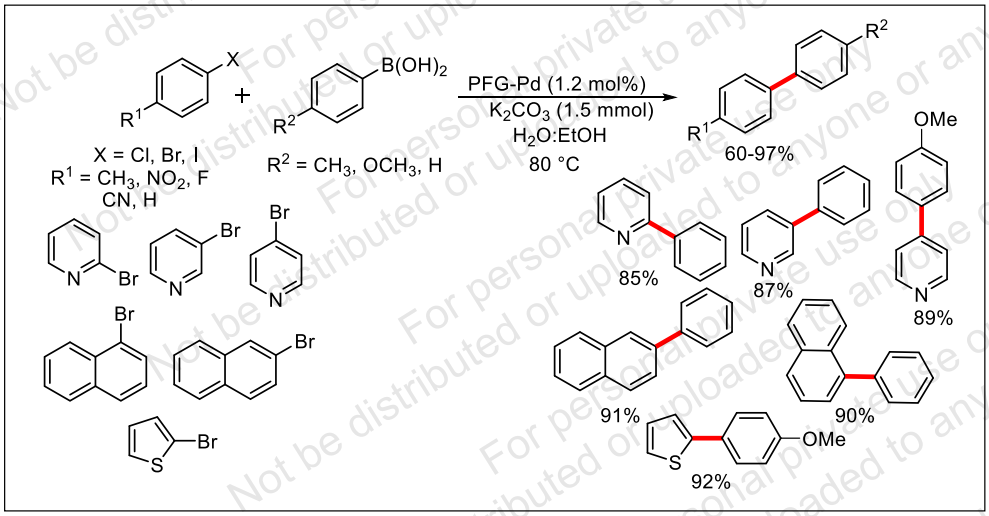

Scheme (8). Synthesis of biaryl derivatives using Suzuki cross-coupling reaction.

GRAPHENE OXIDE (GO) SUPPORTED PALLADIUM NANOPARTICLES (PDNPS/GO) CATALYZED CROSS-COUPLING REACTIONS

In 2014, Yamamoto and his research group described the synthesis of palladium nanoparticles supported on single layer oxide (Pd-slGO) using palladium (II) acetate ($Pd(OAc)_2$) and GO using ethanol as solvent [36]. Ethanol also acted as a reducing agent for palladium precursor at room temperature or 60 ^{0}C or 100 ^{0}C. TEM images displayed that Pd-slGO-60 (reaction at 60 ^{0}C) had a smaller particle size in comparison to PdslGO-100 (reaction at 100 ^{0}C), whereas Pd-slGO-r.t (reaction at room temperature) was not exit at room temperature. Pd-slGO-60 exhibited outstanding catalytic activity towards the Suzuki cross-coupling reaction between iodobenzenes/bromobenzenes with phenylboronic acids. Bromobenzene-bearing electron-withdrawing groups efficiently coupled with phenylboronic acids in the presence of 0.01 mol% of catalyst (Pd-slGO-60) using K_2CO_3 as a base in EtOH:H_2O at room temperature to furnish the corresponding biaryl products in moderate to excellent yields whereas bromobenzene with electron-donating substituents was less reactive towards the phenylboronic acids (Scheme **9**). However, heterocyclic bromides, such as thienyl bromide and indolyl bromide were easily transformed into the corresponding coupling products with phenylboronic acids using the same catalyst. It is interesting to note that iodobenzene showed much reactive towards the phenylboronic acid to provide the coupling product in good yield using 0.00016 mol% catalyst with a turnover number (TON) and TOF (h^{-1}) of 237 000. Moreover, the authors also proved that GO could be used as a scavenger to prevent Pd leaching and contamination of the product. The reusability of this catalyst was also investigated and found that the catalytic activity was dropped after three runs due to the aggregation of PdNPs on the surface of GO and reduction in particle size.

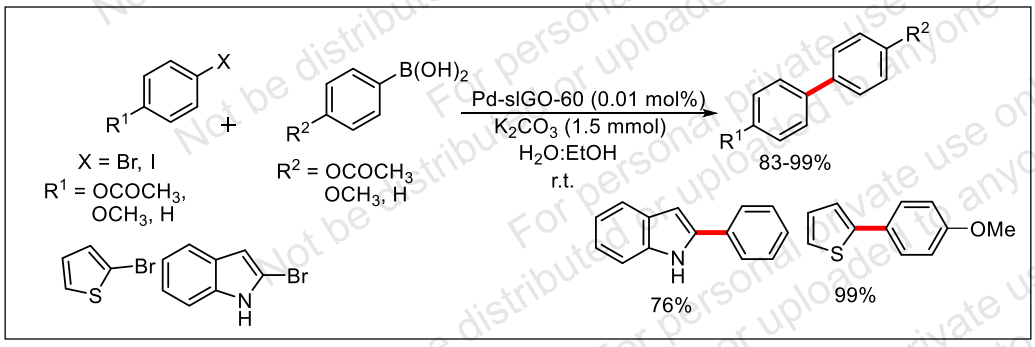

Scheme (9). Synthesis of the biaryl derivative using Pd-slGO-60 catalyst.

In recent years, three-dimensional graphene-based materials (3DGMs) have become an emerging support for the synthesis of heterogeneous nano-catalysts because of their high surface area, low mass density, mechanical strength, and flexible porosity [62]. The remarkable feature of this type of heterogeneous catalyst is its porous structure, which could be used in the stabilization of metal nanoparticles and control their growth [63, 64].

In 2017, Tran and co-workers have discovered a novel method for the preparation of palladium nanoparticles catalyst supported on graphene oxide framework (Pd@GOF) [65]. According to this approach, graphene oxide was first intercalated with benzene-1,4-diboronic through a covalent bond to achieve a three-dimensional (3D) structure. After that PdNPs were formed by the reduction of $PdCl_2$. The intercalation of graphene oxide (GO) with benzene-1,4-diboronic acid through a covalent link afforded a three-dimensional GOF structure having uniformly expanded interlayer spacing which provided thermal stability. The fabricated palladium nanoparticles were uniformly encapsulated and stabilized inside the rigid framework. The synthesized catalyst (Pd@GOF) was used for Suzuki's cross-coupling reaction of aryl halides with phenylboronic acids to evaluate its catalytic performance and found that it exhibits superb activity in both polar and non-polar solvents in terms of yields and could be recycled at least five times without significant loss of catalytic activity.

Functionalized graphene oxide-based materials have been considered as promising supports for nanoparticles and play a significant role in organic transformations such as C-C bond forming cross-coupling reactions [66]. The functional groups present in graphene oxide make the sorption and intercalation of ions and molecules possible and are very helpful in making promising materials for catalytic applications [67]. In 2014, a recyclable heterogeneous catalyst based on palladium nanoparticles supported on non-covalently functionalized graphene oxide (GO) using 1-pyrene carboxylic acid has been developed by Sharavath and Ghosh [68]. Graphene oxide was reacted with a 1-pyrene carboxylic acid in the presence of sodium hydroxide and hydrazine monohydrate to form functionalized graphene and was dispersed in ethanol for 30 min. After that, $PdCl_2$ was added to the above suspension which reduced to palladium nanoparticles (PdNPs). It is interesting to note that ethanol worked both as a solvent and as a reducing agent. The fabricated catalyst (PCA-GNS-Pd) was found to be effective in the promotion of the Suzuki cross-coupling reaction between aryl halides and phenylboronic acids in an aqueous medium. Aryl bromide-bearing electron-donating and electron-withdrawing substituents are easily coupled with phenylboronic acids to transform into the corresponding biphenyl products in good yields. The synthesized catalyst was also useful for unreactive substrates such as chlorobenzene, which reacted smoothly with arylboronic acids to provide

coupling products in good yields (see Table **1**). The application of the PCA-GN--Pd catalyst was further demonstrated for the Heck cross-coupling reaction of aryl halides and olefins. A series of Heck coupling products were obtained in good yields using 0.2 mol% of nanocatalyst in water.

Table 1. Synthesis of biaryl analogous *via* Suzuki cross-coupling of aryl halides with phenylboronic acid using PCA-GNS-Pd catalyst[a].

Entry	R^1	X	Yield (%)[b]	Time (h)
1	H	Br	97	2
2	*p*-CHO	Br	96, 98[d]	2.5, 2.5[d]
3	*p*-OMe	Br	85[f]	6
4	*p*-OH	Br	90	4
5	*p*-Me	Br	85	7
6	2,4-OMe	Br	80	9
7	1-Naphthyl[d]	Br	85	6
8	2-Pyridyl	Br	80	5
9	3-Pyridyl	Br	82	4.5
10	5-Pyrimidine	Br	80	4.5
11	*m*-NO_2	Br	90[e], 75[c]	2[e], 12[c]
12	H	Cl	80	15
13	*p*-CHO	Cl	85	18
14	2-Pyridyl	Cl	60	15
15	3-Pyridyl	Cl	67	15
16	*m*-NO_2	Cl	75	15
17	*p*-OH	Cl	70	10
18	2,4-OMe	Cl	65	15

[a]Reaction conditions:aryl halide (1.435 mmol), phenylboronic acid (1.722 mmol) Na_2CO_3 (2.153 mmol), water (5 mL), PCA-GNS-Pd (3 mg, 0.2 mol %) (mol% Pd *vs.* halide), heated to 90 °C. [b]Isolated yield. [c]PCA-GNS-Pd (3 mg, 0.6 mol% Pd *vs.* halide) was used. [d]Isolated yield and time using Et_3N as base. [e]4-Cyanophenylboronic acid was used instead of $PhB(OH)_2$. [f]2-Napthylboronic acid was used instead of $PhB(OH)_2$.

The nanocatalyst was recovered and successfully reused up to five times without loss of catalytic performance. The catalytic efficiency of the catalyst was dropped after the fifth run due to the leaching of PdNPs from the support during the reaction and their agglomeration on the catalyst support, which was analyzed by ICP-AES.

For personal private use only Not be distributed or uploaded to anyone or anywhere

Very recently, Mohazzab's research group has developed a novel and efficient method for the fabrication of separable palladium nanoparticles (PdNPs) supported on graphene oxide (GO)/stainless-steel mesh using a laser ablation in liquids (LAL) process and an electrophoretic deposition (EPD) technique [69]. In this method, no need of any chemical or capping agents was required during the preparation of a mesh-GO/Pd catalyst. The developed catalyst was characterized by using various analytical techniques. The catalytic performance of this catalyst was investigated for Suzuki cross-coupling reaction in ethanol-water without the use of any ligand. The results showed that aryl halides having either electron-attracting or electron-releasing groups smoothly coupled with phenylboronic acids and provided coupling products in excellent yields. In addition, less reactive chlorobenzene also reacted with phenylboronic acids affording the corresponding products in good yields. The reusability of this catalyst was also examined using the Suzuki cross-coupling reaction and found that it could be recycled up to five times with no remarkable loss of catalytic activity.

The research group of Premia has described another method for the functionalization of graphene oxide with heteroatoms such as sulfur and nitrogen on which Palladium nanoparticles (PdNPs) were uniformly dispersed [70]. The presence of functional groups in graphene oxide can increase the rate of dispersion of nanohybrids in organic solvents and can be used as a ligand to stabilize the active palladium species. The fabricated catalyst was applied for the Heck cross-coupling reaction to prove its catalytic performance. The coupling reactions between aryl iodides/bromides and substituted styrenes/acrylates were performed in the presence of 0.02 mol% of catalyst using potassium hydroxide as a base at 120 ^{0}C in DMF-H_2O (Scheme **10**).

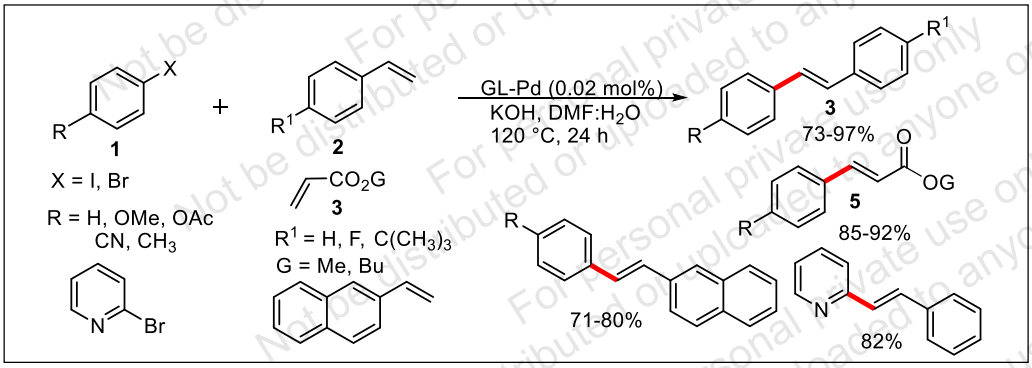

Scheme (10). GL-Pd catalyzed Heck coupling between aryl halides and olefins.

Under the catalytic system, aryl halides bearing electron-withdrawing groups reacted smoothly with olefins to give the corresponding stilbene derivatives,

whereas lower yields of coupling products were obtained with aryl halide bearing electron-donating substituents. Heteroaryl halides such as 2-bromo-pyridine are also easily coupled with styrene to afford the corresponding coupling products in moderate yields. In addition, polycyclic aryl halide was also used to increase the scope and versatility of the reaction. As shown in Scheme (**11**), the proposed reaction mechanism for the Heck cross-coupling reaction was initiated by the formation of GL-Pd complex I in which Pd is stabilized through coordination with sulfur and nitrogen. Then, aryl halide was activated through oxidative addition with Pd(0) to form complex II followed by the coordination of olefin to give π-complex III and then migratory insertion of olefin takes place to generate IV. Subsequently, *β*-hydride elimination takes place to afford coupling product with the regeneration of the catalyst. The nano-catalyst was recovered, and reused up to three times without any significant loss of its catalytic efficiency, but catalytic activity was dropped after the third cycle due to the aggregation of PdNPs.

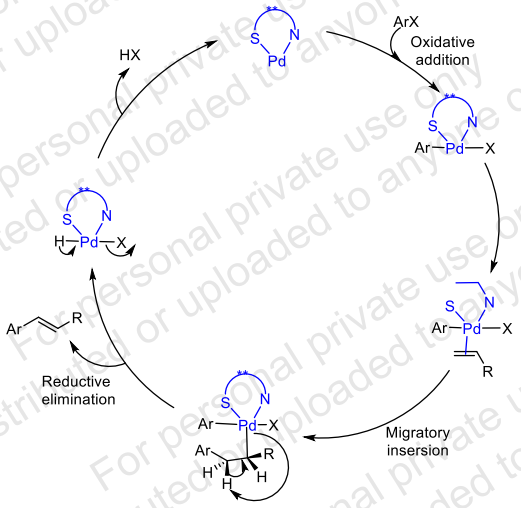

Scheme (11). Proposed mechanism for the Heck coupling reaction.

Recently, Veisi and co-workers reported the synthesis of palladium nanoparticles supported on the surface of graphene oxide, functionalized with metformin (MET) [71]. Metformin functionalized graphene oxide (Met-GO) was prepared between the condensation reaction of graphene oxide with metformin and then palladium nanoparticles (PdNPs) were decorated onto the surface of functionalized graphene oxide by the reduction of $PdCl_2$ using hydrazine hydrate as reducing agents. TEM and FESEM images showed that palladium nanoparticles were uniformly incorporated onto the surface of functionalized graphene oxide. The synthesized catalyst showed outstanding catalytic performance towards the Heck cross-coupling reaction of various aryl halides with olefins without the use of any

phosphine or ligand coordination. The coupling reaction proceeded in good to excellent yields of trans-stilbene derivatives between the reactions of aryl halides with olefins using 0.1 mol% of catalyst, triethylamine as a base in DMF at 120 ^{0}C. The catalyst was found to be the most effective in the Gram-scale synthesis of trans-stilbene product. The most impressive feature of this catalyst was its reusability, and it could be recycled up to seven cycles without a noticeable loss of its catalytic performance. A hot filtration test was carried out to determine the heterogeneity of this synthesized catalyst (Met-GO-Pd) using Heck cross-coupling reaction between aryl bromide and styrene under optimized reaction conditions. Then, coupling products were obtained in 54% yield and the catalyst was separated out. After separating the catalyst, the reaction was continued for another hour. However, no significant improvement was observed in the yield of the coupling product. This observation proved that the catalytic process was heterogeneous.

A novel approach for the construction of palladium nanoparticles (PdNPs) supported on a carbon-based graphene oxide (GO) monolith has been described by Nakhate and his co-workers [72]. It was fabricated by the carbonization of glucose with a small amount of graphene oxide as a structure directing agent, which offers a large surface area for the dispersion of palladium nanoparticles. The carbon-based graphene oxide monolith reduced the leaching of PdNPs into the reaction mixture and increased the rate of interaction between the support and the nanoparticles.

The developed catalyst was found to be effective for Sonogashira cross-coupling reaction and hydrogenation of alkene and nitrobenzene. The catalytic efficiency of the Pd@CGO monolith was compared with 5% Pd/C and 5% Pd@GO for the Sonogashira coupling of iodobenzene with phenyl-acetylene. The Pd@CGO monolith exhibited superb reactivity towards the Sonogashira cross-coupling reaction of iodobenzene with phenylacetylene leading to 93% conversion of the coupling products without the use of copper and ligand at 90 ^{0}C (Scheme **12**). Iodobenzene, substituted with electron-withdrawing groups easily transformed to the corresponding diphenylethyne as coupling products in good to excellent yields. Good to excellent yields of desired products were also obtained with iodobenzene, substituted with electron-donating groups. It is interesting to note that less reactive bromobenzenes smoothly reacted with phenylacetylene to furnish desired products in good yields. The author also proposed the reaction mechanism and kinetic equation. The hot filtration test showed that the catalyst has high stability and could be reused at least four times without loss of activity.

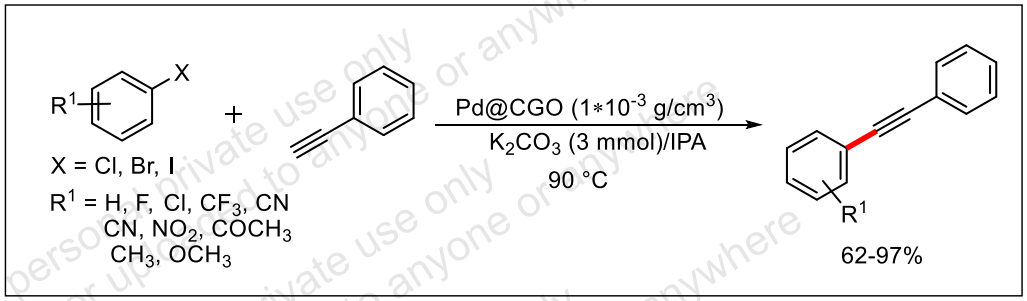

Scheme (12). Sonogashira cross-coupling catalyzed by Pd@CGO catalyst.

REDUCED GRAPHENE OXIDE (RGO) SUPPORTED PALLADIUM NANOPARTICLES (PDNPS-RGO) CATALYZED COUPLING REACTIONS

In 2014, Shendage and co-workers developed electrochemically co-deposited palladium nanoparticles (PdNPs) supported on a reduced graphene oxide (ERGO-Pd) catalyst and used for Suzuki cross-coupling reactions [73]. They observed that PdNPs with smaller sizes in ranges from 3 to 9 nm exhibited high catalytic activity. The prepared catalyst has major advantages such as a high degree of catalytic activity, chemical stability, selectivity, and reusability up to six times. This catalytic system generates a library of biphenyl derivatives using K_2CO_3 as a base in ethanol under reflux conditions, whereas lower yield was observed at room temperature (Scheme **13**). Several aryl halides having electron-withdrawing as well as electron-donating groups smoothly coupled with various phenylboronic acids to form coupling products in good to excellent. Aryl iodide provides better results in compassion to aryl bromides in terms of yield and time. There are many analytical techniques such as SEM (scanning electron microscopy), TEM (transmission electron microscopy), X-Ray analysis, and EDAX (energy dispersive X-ray analysis) have been used to characterize the catalyst.

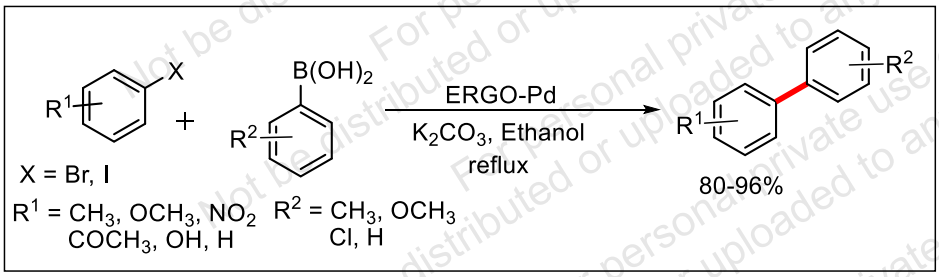

Scheme (13). Suzuki coupling reaction catalyzed by ERGO-Pd.

Later, the same research group reported co-deposited palladium nanoparticles (Pd NPs) supported on reduced graphene oxide (ERGO-Pd) catalyzed carbon-carbon cross-coupling Heck reactions [74]. Under this catalytic system, several aryl halide bearing either electron-withdrawing or electron-donating groups reacted with different styrene and acrylate to generate a series of substituted stilbenes and cinnamates in good to excellent yields (Scheme **14**). Aryl bromides take a longer time due to high bond dissociation energy in comparison to aryl iodide. The reusability of this catalyst is high and can be recycled up to four to five times without loss of activity.

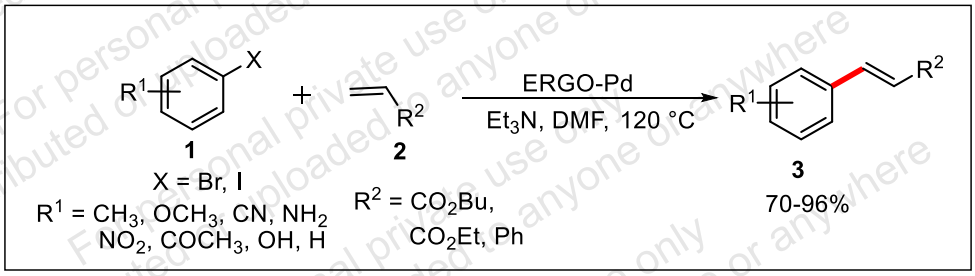

Scheme (14). Heck cross-coupling reaction catalyzed by ERGO-Pd.

In 2015, a new multi-step protocol for in-situ generation of palladium nanoparticles supported on reduced graphene oxide using 1-butyl-3-methylimidazolium hexafluorophosphate ([BMIM]PF_6) ionic liquid by phase-transfer method (Pd/rGO-IL) in aqueous medium was developed by Liu and co-workers [75]. In-situ generated catalyst having an average particle size of 2 nm and uniformly dispersed on the surface of reduced graphene oxide was confirmed by TEM images. The synthesized catalyst showed excellent activity for Heck cross-coupling reactions of iodobenzene with butyl acrylate. The reactions were performed using a catalytic amount of Pd/RGO-IL in the presence of Et_3N as a base at 130 ^{0}C; in which iodobenzene-bearing electron-withdrawing or electron-donating groups coupled with acrylate to provide a moderate yield of desired products with 76-87% conversion. However, neutral iodobenzene reacted with acrylate and styrene to give coupling products in excellent yields with 95% and 92% conversion respectively (Scheme **15**). The reusability of the catalyst was also studied and found that it can be recycled up to ten times without significant loss of catalytic activity, which showed that it has high catalytic stability. The high stability of the catalyst might be due to the double protection of the organic cation [BMIM]+ of IL and reduced graphene oxide (rGO) which could be helpful in the reduction of collision and agglomeration of Pd nanoparticles.

In 2015, the research group of Liu developed an effective and eco-friendly protocol for the synthesis of multimetallic nanoparticles catalyst, especially

magnetically separable Pd NPs supported on graphene oxide [76]. The polymetallic graphene oxide supported PdNPs ($NiFe_2O_4$@GO-Pd) hybrids were obtained from $PdCl_2$, $FeCl_3.6H_2O$, and $NiCl_2.4H_2O$ in ethanol-ethylene glycol using hydrothermal treatment. The $NiFe_2O_4$ were uniformly dispersed on the surface of graphene oxide without help of any linker molecules, which help in providing ion transport channels to bridge the NPs and the matrix. The authors have also demonstrated the catalytic power of this synthesized catalyst for Heck cross-coupling reactions of aryl halides with substituted olefins. Iodobenzene-bearing electron-donating or electron-withdrawing groups efficiently reacted with olefins in the presence of (0.08 mol% Pd) $NiFe_2O_4$@GO-Pd catalyst and 2.0 equiv. of K_2CO_3 as a base in EtOH-H_2O at 80°C to provide coupling products in excellent yield (Scheme **16**). A slightly decreased yield of the coupling product was obtained with iodobenzene having a methyl group at the ortho position. Bromobenzene reacted with styrene to furnish a moderate yield of coupling product under the same catalytic system. However, chlorobenzene provides a lower yield of the desired product even after increasing the catalyst loading and reaction time. The most attractive feature of this catalyst was its recyclability and stability, it can be recycled up to six times without the loss of catalytic activity supported by ICP-MS analysis. The $NiFe_2O_4$@GO-Pd catalyst showed high catalytic power and stability towards the Heck cross-coupling reactions in comparison to $NiFe_2O_4$-Pd catalyst because of the supportive role of graphene oxide for $NiFe_2O_4$@GO-Pd, which reduces the agglomeration of Pd nanoparticles.

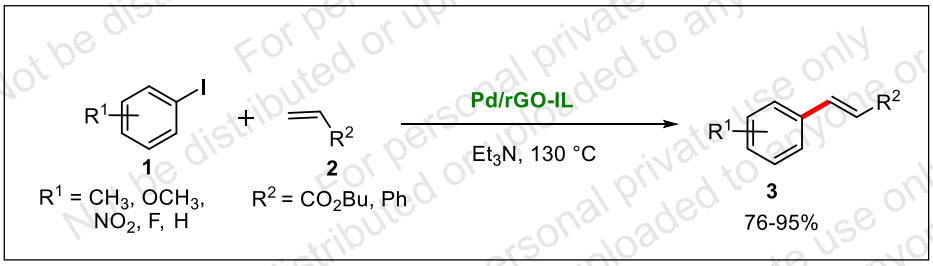

Scheme (15). Heck reaction catalyzed by Pd/RGO-IL.

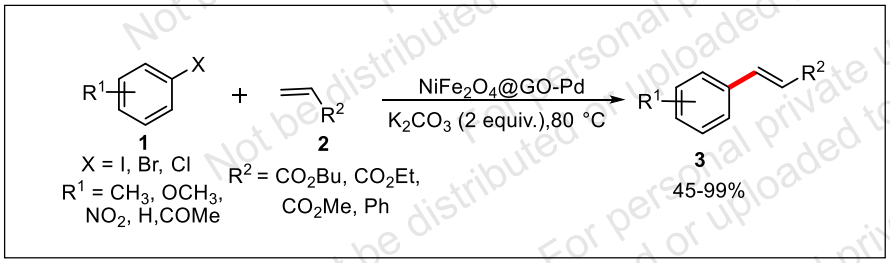

Scheme (16). $NiFe_2O_4$@GO-Pd catalyzed Heck cross-coupling reaction.

Another important approach for the construction of highly active Pd/Fe_3O_4 nanoparticles supported on graphene ($Pd/Fe_3O_4/G$) has been described by Elazab and co-workers in 2015 [77]. The catalyst ($Pd/Fe_3O_4/G$) was synthesized by microwave-assisted reduction of palladium nitrate, ferric nitrate, and graphene oxide using hydrazine hydrate as the reducing agent in an aqueous medium. The constructed magnetic catalyst ($Pd/Fe_3O_4/G$) showed exceptional catalytic activity for cross-coupling reactions (Heck and Suzuki cross-coupling reaction). The most striking feature of this magnetic catalyst is that it shows a high turnover number (TON) of 9250 and a turnover frequency (TOF) of 111,000 h^{-1} for Suzuki and Heck cross-coupling reactions. The catalytic performance was first studied for Suzuki cross-coupling reactions and found that a wide range of functionalized aryl halides efficiently coupled with aryl boronic acid in the presence of 0.3 mol% of catalyst using K_2CO_3 as a base in H_2O:EtOH as a solvent to provide the corresponding biphenyl products in moderate to excellent yield (Scheme **17**). Arylhalide-bearing electron-withdrawing groups such as aldehyde, ketone, nitro, and nitrile furnished the corresponding biphenyl derivatives in excellent yield, whereas chlorobenzene provided the Suzuki cross-coupling product in a relatively good yield. However, boronic acid containing electron-donating groups (dimethyl amino, thiomethyl, and *p*-methoxy) smoothly converted into biphenyl derivatives with aryl halides in excellent yield.

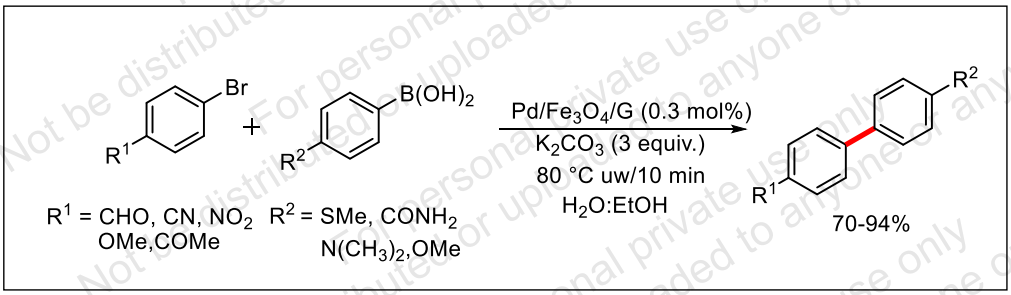

Scheme (17). Suzuki reaction catalyzed by $Pd/Fe_3O_4/G$.

The catalytic efficiency of this catalyst was further checked for Heck cross-coupling reactions. The catalyst was found to be highly active towards the Heck reactions of different aryl iodides/bromides with substituted styrenes/acrylates using 0.3 mol% of catalyst and K_2CO_3 (3 eq.) as a base in H_2O:EtOH at 150 ^0C under microwave irradiation. The reaction provided the corresponding products in excellent yields in cases of bromobenzene-bearing electron-donating and electron-withdrawing groups. These results prove the outstanding activity of this catalyst. The catalyst can be recovered and further used up to ten times without significant loss of catalytic activity (Scheme **18**).

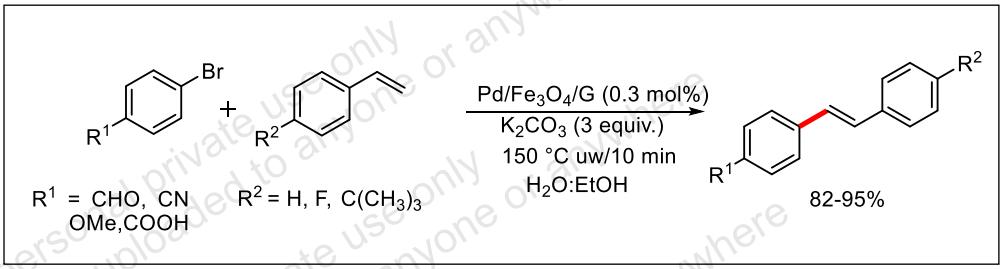

Scheme (18). Heck cross-coupling reaction catalyzed by $Pd/Fe_3O_4/G$.

Recently, a similar approach for the preparation of magnetically recoverable palladium nanoparticles supported on graphene oxide has been developed by Fu's research workers [78]. In the development of $Pd\text{-}Fe_3O_4/rGO$, $FeCl_2.4H_2O$ was used as a starting material reacting with ammonium hydroxide to form iron hydroxide followed by simultaneously oxidation and dehydration to form Fe_3O_4 nanoparticles at high temperature and pressure whereas Pd nanoparticles were dispersed onto the surface of graphene oxide using ethanol as the reducing agent under the ultrasonic and hydrothermal strategy. Concurrently, the Fe_3O_4 NPs were well dispersed on two-dimensional rGO nanosheets and formed $Pd\text{-}Fe_3O_4/rGO$ nanohybrids materials through a self-assembly approach. The synthesized catalyst was characterized using various analytical techniques. TEM images displayed that both palladium nanoparticles and iron oxide nanoparticles were homogeneously distributed onto the surface of reduced graphene oxide nanosheets, whereas HRTEM images indicate the size of nanoparticles up to 2 nm and no agglomeration on the surface of graphene oxide.

The formed catalyst was used to evaluate its catalytic efficiency for Heck cross-coupling of 4-iodoanisole and styrene. A wide range of iodobenzene reacted with styrenes in the presence of 0.06 mol% catalyst using triethylamine as a base in DMF as solvent at 120 ^{0}C to provide the corresponding coupling products in moderate to excellent yields. Iodobenzene-bearing electron-withdrawing groups efficiently coupled with styrene to give the cross-coupling products in excellent yields, whereas iodobenzene with an amino group at the para position provides the corresponding product in lower yield (Scheme **19**). The reusability of this catalyst was also examined and found that the recovered catalyst can be consecutively recycled up to six times without significant loss of catalytic power. These results indicate that this catalyst has high catalytic efficiency and is beneficial to both the environmental and economic perspectives.

Another important approach for the synthesis of palladium nanoparticles supported on graphene oxide using hydrogen gas as the reducing agent has been

developed by Hussain and his co-workers [79]. The catalyst was synthesized by the following methods, involving reduction of graphene oxide followed by dispersion of palladium nanoparticles on the surface of reduced graphene oxide nanosheets and simultaneously reduction of olefin. The synthesized catalyst was found to be more effective towards the cross-coupling reactions of aryl iodides with phenylboronic acids (Scheme **20**). Iodobenzene that incorporated electron-donating and electron-withdrawing substituents smoothly coupled with arylboronic acids under the catalytic system (Pd-rGO-H_2 (25 mg), Na_2CO_3 (2 mmol), H_2O:EtOH (10 mL, 1:1), r.t) providing the corresponding biphenyl analogous in moderate to excellent yields. It is interesting to note that phenylboronic acid neopentylglycol ester was used in place of boronic acid as a coupling partner for the Suzuki cross-coupling with bromobenzene to give the coupling product in an excellent yield under the same catalytic system. However, the use of chlorobenzene as a coupling partner with arylboronic acid gave a slightly lower yield of the coupling product even after increasing the reaction time and reaction temperature. The most important feature of this catalyst was its reusability. The recovered catalyst can be recycled up to four times without loss of catalytic activity for Suzuki cross-coupling reactions. However, the catalytic performance decreased up to 62% after the fourth run might be due to the decrease in the surface area.

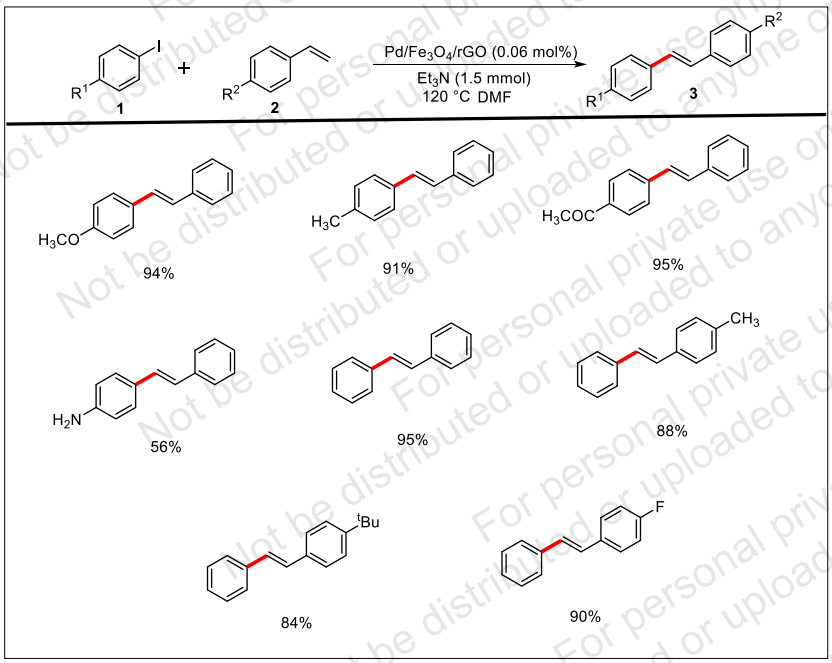

Scheme (19). Synthesis of biphenyl styrenes by Heck cross-coupling reaction using Pd-Fe_3O_4/rGO.

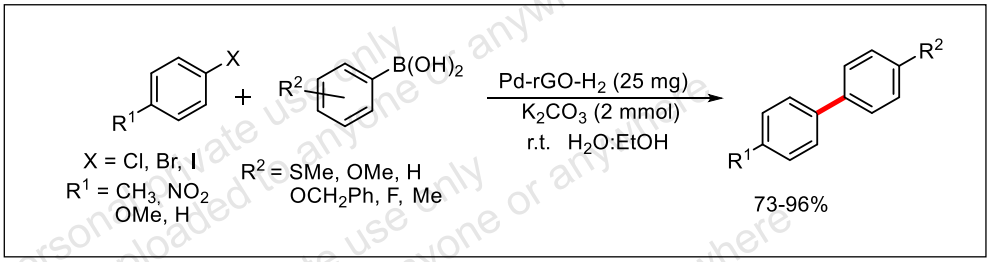

Scheme (20). Suzuki cross-coupling reaction catalyzed by Pd-rGO-H_2.

In 2018, the Raiza research group reported a biogenic one-pot strategy for the synthesis of graphene-supported palladium nanoparticle (Pd Nps/rGO) catalyst using reduced graphene oxide (rGO) and H_2PdCl_4 as starting material followed by reduction with *Ficus carica* fruit juice as the reducing agent and Poly(*N*-vinyl-2-pyrrolidone) (PVP) as stabilizing agent [80]. The Ultraviolet-Visible spectroscopy (UV-Vis) displaced the complete reduction of ions and the formation of PdNP and PdNP/rGO. TEM images showed the homogeneous distribution of PdNPs on the surface of rGO with a smaller particle size in a spherical shape. The HRTEM image confirmed the crystal lattice of PdNPs and the edges of rGO nanosheets to be ~16 nm. The crystalline nature of observed using the SAED image (Fig. **1**). The formed catalyst was examined in Suzuki cross-coupling reactions using aryl halides with phenylboronic acids. A variety of biphenyl derivatives have been synthesized in good to excellent yields using 0.96 mol%, K_2CO_3 as a base and water: ethanol as solvent at 180 ^{0}C. The reduced yield was observed after decreasing the catalyst loading from 0.96 mol% to 0.5 mol% whereas no yield of coupling products were observed after increasing catalyst loading. The reusability of the catalyst in Suzuki cross-coupling was examined and found that the catalyst can be used ten times without loss of activity.

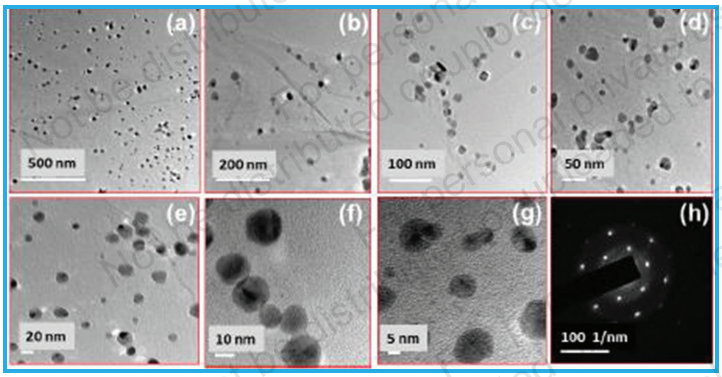

Fig. (1). Transmission electron microscopy images. (**a-e**) Images along with particle size distribution; (**g**) HETEM image along with fringe spacing; and (**f**) SAED image of the PdNP/rGO.

For personal private use only Not be distributed or uploaded to anyone or anywhere

In 2018, Kulkarni and co-workers developed an eco-friendly protocol for the synthesis of graphene oxide supported palladium nanoparticle catalyst using graphene oxide, $PdCl_2$ as the precursor, followed by reduction with aloe vera extract as the reducing agent in the presence of sunlight as an energy source [81]. The prepared catalyst was characterized using different analytical techniques.

SEM image confirmed the formation of PdNPs on reduced graphene oxide with a uniform dispersion of PdNPs whereas the TEM image indicated the presence of PdNPs on the surface of rGO with an average particle size of 2-19 nm. The catalytic performance of the synthesized catalyst was examined in Suzuki cross-coupling reactions. The authors obtained several coupling products in good to excellent yields, when the reaction was performed using aryl halides with phenylboronic acid in the presence of 0.2 mol% of catalyst K_2CO_3 as a base and water: ethanol as solvent at 80 ^{0}C (Scheme **21**). Aryl iodide having electron-donating or electron-withdrawing groups was more reactive towards the phenylboronic acid providing exceptional results in terms of yield and reaction time, whereas aryl bromide/aryl chloride was less reactive with phenyl boronic acid under same the reaction conditions. The recovery of the catalyst was also studied and found that it could be reused seven times without significant loss of activity. A considerable loss of activity of the catalyst was seen after the 7th cycle due to agglomeration and an increase in particle size of palladium nanoparticles on reduced graphene oxide.

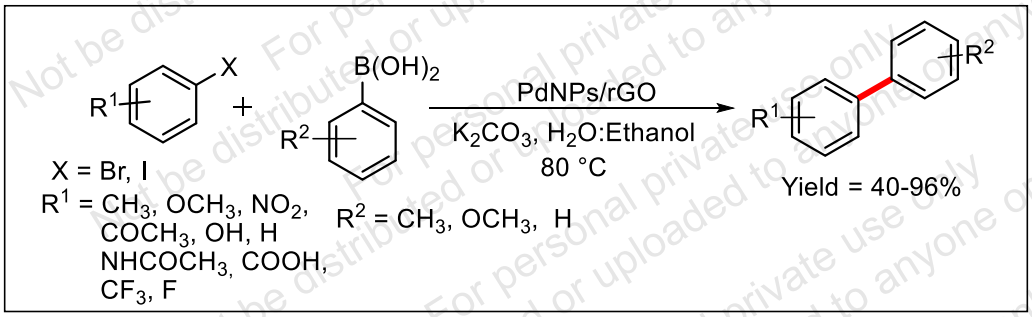

Scheme (21). Suzuki cross-coupling reaction catalyzed by PdNPs/rGO.

In 2016, Mahanta and co-workers described an eco-friendly copper-free Sonogashira cross-coupling reaction catalyzed by palladium nanoparticles supported on reduced graphene oxide at room temperature in ethanol [82]. PdNPs were synthesized using hydrogen gas as a reducing agent to generate PdNPs supported on reduced graphene oxide sheets. The catalytic performance of the catalyst was investigated for the Sonogashira cross-coupling reaction. The reactions proceeded smoothly using 5 wt% of the catalyst in the presence of

K_2CO_3 as a base at room temperature in ethanol to provide the coupling products with good to excellent yield (see Table 2). The alkyne bearing electron-donating or electron-withdrawing groups was coupled with aryl halides to furnish the biphenylacetylene derivatives in excellent to good yield. However, non-aromatic alkynes such as cyclohexylacetylene were coupled with different iodides to provide the coupling products in moderate yield under the same catalytic system. Moreover, bromobenzene did not provide a satisfactory yield of the coupling products even after increasing the reaction time (Table **2**, entries 11 and 12). The reusability of the catalyst was also studied and observed that it could be recycled up to six times without loss of minimal activity.

Recently, the research group of Tarahomi has employed the Pd catalyst supported on dendrimer-functionalized graphene oxide for Sonogashira cross-coupling reaction [83]. The dendrimer-based palladium catalyst was developed in multistep. The first step involves the reaction of GO with $FeCl_2.4H_2O$, and $FeCl_3.4H_2O$ followed by the addition of 1 mL of NH_3-H_2O to get magnetic graphene oxide (MGO), then MGO was covalently attached with modified PAMAM dendrimer (G. 2) in the presence of EDC/NHS [84].

Table 2. Scope of Sonogashira coupling reaction catalyzed by PdNPs@GO.

Entry	R^1	R^2	X	Time	Yield
1	4-NO_2	C_6H_5	I	7	94
2	3-Me	C_6H_5	I	7	96
3	4-Me	C_6H_5	I	8	95
4	3-NO_2	C_6H_5	I	8	95
5	4-OMe	C_6H_5	I	8	92
6	H	C_6H_5	I	7	96
7	4-Me	4-MeC_6H_5	I	7	98
8	4-Me	C_6H_{11}	I	10	85
9	H	C_6H_{11}	I	10	80
10	4-OMe	4-MeC_6H_5	I	7.5	98
11	4-NO_2	C_6H_5	Br	12	47
12	4-OMe	C_6H_5	Br	12	53

[a]Reaction conditions: acetylene (0.75 mmol), aryl halide (0.5 mmol) [b]Isolated yield: purified by column chromatography.

Subsequently, PdNPs were dispersed on the surface of dendrimer-functionalized graphene oxide through graft interactions between free chelating amino groups of dendrimer and Pd precursor. The most attractive feature of these nanocomposite

materials was not only solubility in an aqueous medium but also stabilized metal NPs on their surfaces. The structural characterization of this catalyst was confirmed by using different analytical techniques such as TEM, BET, FTIR, and elemental mapping analysis. The catalytic power of this catalyst was checked for the Sonogashira cross-coupling reaction. The Sonogashira cross-coupling reaction works very well for alkynes and aryl halides in the presence of dendrimer-supported palladium catalyst to furnish corresponding products in excellent yields, except for chlorobenzene which gave a lower yield of the desired product (Scheme **22**). Regarding the mechanism, it was proposed that the reaction is initiated by the coordination of the Pd@MGO-D-NH_2 catalyst to the C-C triple bond of phenylacetylene followed by the deprotonation of terminal C-H of alkyne with K_2CO_3 to form potassium acetylide. Pd@MGO-D-NH_2 catalyst also activates the aryl halide (ArX) and forms aryl palladium halide complex (ArPdX) and then halide displacement takes place to form an aryl palladium acetylide. Subsequently, reductive elimination takes place to give a cross-coupling product with a regeneration catalyst. The reusability of this catalyst was also studied and found that it could be reused up to four times without significant loss of catalytic power.

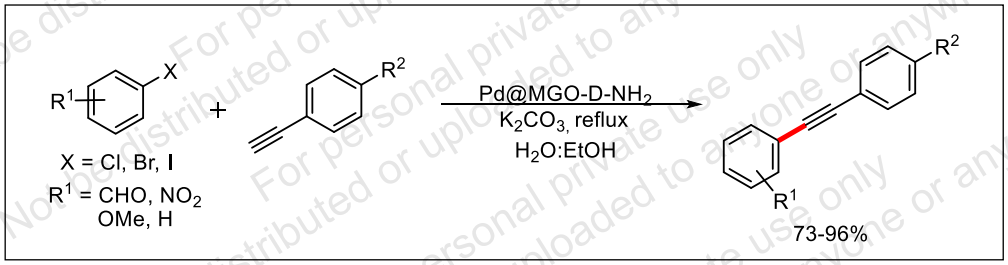

Scheme (22). Pd@MGO-D-NH_2 catalyzed Sonogashira coupling reaction.

CONCLUDING REMARKS

In this chapter, we focused on metal-supported graphene oxide for its catalytic potential. The prepared heterogeneous catalysts were beneficially used for C-C bond formation using different cross-coupling reactions such as Mizoroki-Heck, Suzuki-Miyaura, Kumada, Stille, Negishi, Hiyama, and Buchwald-Hartwig, *etc.* In a prevalent number of examples, the comparison of heterogeneous catalysts with corresponding homogeneous catalysts has been observed. The advantages of the discussed heterogeneous catalysts consisted of their simple preparation, inexpensive and easily available starting materials, their simple isolation, and the possibility of reuse. Easy performance of the reaction in aqueous media brings great benefits in the case of several cross-coupling reactions. Several of the described reactions possibly have a high potential for industrial usage, hence the

catalytic systems presented in this chapter significantly contribute to the further development of green chemical processes.

LIST OF ABBREVIATIONS

AAPTMS	[3-(2-Aminoethylamino)propyl] trimethoxysilane
BET	Brunauer–Emmett–Teller
$ClPPh_2$	Chlorodiphenylphosphine
2D	Two dimensional
EPD	Electrophoretic deposition
ERGO-Pd	Electrochemically codeposited palladium nanoparticles supported on reduced graphene oxide
EDAX	Energy dispersive X-ray analysis
EDC2	ethyl(dimethylaminopropyl) carbodiimide
FESEM	Field emission scanning electron microscopy
FTIR	Fourier Transform Infrared Spectroscopy
GO	Graphene oxide
G-BI-Pd	Graphene-benzimidazole
GOH	Hydroxyl group on the surface of graphene
GNS	Graphite nanosheet
HRTEM	High-resolution transmission electron microscopy
ICP-AES	Nductively coupled plasma atomic emission spectroscopy
LAL	Laser ablation in liquids
NHS	N-Hydroxysuccinimide
PdNPs	Palladium nanoparticles
PdNPs-G	Palladium nanoparticles supported on graphene
PdNPs-rGO	Palladium nanoparticles reduced graphene oxide
Pd/graphene	Graphene supported Pd
PFG	Phosphine functionalized graphene
PFG	Phosphine grafted graphene oxide
Pd-slGO	Palladium nanoparticles supported on single layer oxide
Pd@GOF	Palladium nanoparticles catalyst supported on graphene oxide framework
PCA-GNS-Pd	Pyrenecarboxylic acid graphite nanosheet supported Palladium
PVP	Poly(N-vinyl-2-pyrrolidone)
PAMAM	Polyamidoamine
r-GO	Reduced graphene oxide
SEA	Strong electrostatic adsorption

For personal private use only Not be distributed or uploaded to anyone or anywhere

SAED	Selected area diffraction
TEM	Transmission electron microscopy
XRD	Powder x-ray diffraction
XPS	X-ray photoelectron spectroscopy

CONSENT FOR PUBLICATION

Not applicable.

CONFLICT OF INTEREST

The authors declare no conflict of interest, financial or otherwise.

ACKNOWLEDGEMENTS

The authors thank the SERB SRG grant, grant no. SRG-0721 research grant for financial support.

REFERENCES

[1] (a) Ananikov, V.P.; Beletskaya, I.P. Toward the ideal catalyst: from atomic centers to a "cocktail" of catalysts. *Organometallics,* **2012**, *31*(5), 1595-1604. [http://dx.doi.org/10.1021/om201120n] (b) Negishi, E. Transition metal-catalyzed organometallic reactions that have revolutionized organic synthesis. *Bull. Chem. Soc. Jpn.,* **2007**, *80*(2), 233-257. [http://dx.doi.org/10.1246/bcsj.80.233] (c) Torborg, C.; Beller, M. Recent applications of palladium-catalyzed coupling reactions in the pharmaceutical, agrochemical, and fine chemical industries. *Adv. Synth. Catal.,* **2009**, *351*(18), 3027-3043. [http://dx.doi.org/10.1002/adsc.200900587]

[2] Magano, J.; Dunetz, J.R. Large-scale applications of transition metal-catalyzed couplings for the synthesis of pharmaceuticals. *Chem. Rev.*, **2011**, *111*(3), 2177-2250. [http://dx.doi.org/10.1021/cr100346g] [PMID: 21391570]

[3] Negishi, E.; Meijere, A. *Handbook of organo palladium chemistry for organic synthesis*; Wiley: New York, **2002**. Tsuji, J. *Perspective in Organo Palladium Chemistry for XXI Century*; Elsevier Science, **1999**. Malleron, J-L.; Fiaud, J-C.; Lagros, J.Y. *Handbook of Palladium Catalyzed Organic Reactions*; Academic Press: San Diego, **1997**.

[4] (a) Negishi, E. Magical power of transition metals: past, present, and future (Nobel Lecture). *Angew. Chem. Int. Ed.,* **2011**, *50*(30), 6738-6764. [http://dx.doi.org/10.1002/anie.201101380] [PMID: 21717531] (b) Suzuki, A. Cross-coupling reactions of organoboranes: an easy way to construct C-C bonds (Nobel Lecture). *Angew. Chem. Int. Ed.,* **2011**, *50*(30), 6722-6737. [http://dx.doi.org/10.1002/anie.201101379] [PMID: 21618370] (c) Nobelprize.org. **2013**. http://www.nobelprize. org/nobel_prizes/chemistry/laureates/2010/

[5] Astruc, D.; Lu, F.; Aranzaes, J.R. Nanoparticles as recyclable catalysts: the frontier between homogeneous and heterogeneous catalysis. *Angew. Chem. Int. Ed.,* **2005**, *44*(48), 7852-7872. [http://dx.doi.org/10.1002/anie.200500766] [PMID: 16304662]

[6] Yin, L.; Liebscher, J. Carbon-carbon coupling reactions catalyzed by heterogeneous palladium catalysts. *Chem. Rev.,* **2007**, *107*(1), 133-173. [http://dx.doi.org/10.1021/cr0505674] [PMID: 17212474]

Not be distributed or uploaded to anyone or anywhere For personal private use only

[7] Bedford, R.B.; Singh, U.G.; Walton, R.I.; Williams, R.T.; Davis, S.A. Nanoparticulate palladium supported by covalently modified silicas: Synthesis, characterization, and application as catalysts for the Suzuki coupling of aryl halides. *Chem. Mater.,* **2005**, *17*(4), 701-707.
[http://dx.doi.org/10.1021/cm048860s]

[8] Jana, S.; Dutta, B.; Bera, R.; Koner, S. Immobilization of palladium in mesoporous silica matrix: preparation, characterization, and its catalytic efficacy in carbon-carbon coupling reactions. *Inorg. Chem.,* **2008**, *47*(12), 5512-5520.
[http://dx.doi.org/10.1021/ic8004294] [PMID: 18459724]

[9] Djakovitch, L.; Koehler, K. Heterogeneously catalysed Heck reaction using palladium modified zeolites. *J. Mol. Catal. Chem.,* **1999**, *142*(2), 275-284.
[http://dx.doi.org/10.1016/S1381-1169(98)00292-1]

[10] Djakovitch, L.; Koehler, K. Heck reaction catalyzed by PD-modified zeolites. *J. Am. Chem. Soc.,* **2001**, *123*(25), 5990-5999.
[http://dx.doi.org/10.1021/ja001087r] [PMID: 11414833]

[11] Zhao, D.; Fei, Z.; Geldbach, T.J.; Scopelliti, R.; Dyson, P.J. Nitrile-functionalized pyridinium ionic liquids: synthesis, characterization, and their application in carbon-carbon coupling reactions. *J. Am. Chem. Soc.,* **2004**, *126*(48), 15876-15882.
[http://dx.doi.org/10.1021/ja0463482] [PMID: 15571412]

[12] Miao, T.; Wang, L.; Li, P.H.; Yan, J.C. A highly efficient and recyclable ionic liquid anchored pyrrolidine catalyst for enantioselective Michael additions. *Synthesis,* **2008**, 3828-3834.

[13] Lombardo, M.; Chiarucci, M.; Trombini, C. A recyclable triethylammonium ion-tagged diphenylphosphine palladium complex for the Suzuki–Miyaura reaction in ionic liquids. *Green Chem.,* **2009**, *11*(4), 574-579.
[http://dx.doi.org/10.1039/b815568b]

[14] Biffis, A.; Zecca, M.; Basato, M. Metallic Palladium in the Heck Reaction: Active Catalyst or Convenient Precursor? *Eur. J. Inorg. Chem.,* **2001**, *2001*(5), 1131-1133.
[http://dx.doi.org/10.1002/1099-0682(200105)2001:5<1131::AID-EJIC1131>3.0.CO;2-3]

[15] Ramchandani, R.K.; Vinod, M.P.; Wakharkar, R.D.; Choudhary, V.R.; Sudalai, A.; Sudalai, A. Pd–Cu–Exchanged montmorillonite K10 clay: an efficient and reusable heterogeneous catalyst for vinylation of aryl halides. *Chem. Commun. (Camb.),* **1997**, (21), 2071-2072.
[http://dx.doi.org/10.1039/a705870e]

[16] Singh, A.S.; Patil, U.B.; Nagarkar, J.M. Palladium supported on zinc ferrite: A highly active, magnetically separable catalyst for ligand free Suzuki and Heck coupling. *Catal. Commun.,* **2013**, *35*, 11-16.
[http://dx.doi.org/10.1016/j.catcom.2013.02.003]

[17] Ogasawara, S.; Kato, S. Palladium nanoparticles captured in microporous polymers: a tailor-made catalyst for heterogeneous carbon cross-coupling reactions. *J. Am. Chem. Soc.,* **2010**, *132*(13), 4608-4613.
[http://dx.doi.org/10.1021/ja9062053] [PMID: 20225817]

[18] Bai, L.; Wang, J.X. Reusable, polymer-supported, palladium-catalyzed, atom- efficient coupling reaction of aryl halides with sodium tetraphenylborate in water by focused microwave irradiation. *Adv. Synth. Catal.,* **2008**, *350*(2), 315-320.
[http://dx.doi.org/10.1002/adsc.200700361]

[19] Alacid, E.; Nájera, C. Kaiser oxime resin-derived palladacycle: A recoverable polymeric precatalyst in Suzuki–Miyaura reactions in aqueous media. *J. Organomet. Chem.,* **2009**, *694*(11), 1658-1665.
[http://dx.doi.org/10.1016/j.jorganchem.2009.01.016]

[20] Giacalone, F.; Gruttadauria, M. Covalently supported ionic liquid phases: An advanced class of recyclable catalytic systems. *ChemCatChem,* **2016**, *8*(4), 664-684.

Not be distributed or uploaded to anyone or anywhere
For personal private use only

[http://dx.doi.org/10.1002/cctc.201501086]

[21] Nasrollahzadeh, M.; Sajjadi, M.; Shokouhimehr, M.; Varma, R.S. Recent developments in palladium (nano)catalysts supported on polymers for selective and sustainable oxidation processes. *Coord. Chem. Rev.,* **2019**, *397*, 54-75.
[http://dx.doi.org/10.1016/j.ccr.2019.06.010]

[22] Nasrollahzadeh, M.; Motahharifar, N.; Ghorbannezhad, F.; Soheili Bidgoli, N.S.; Baran, T.; Varma, R.S. Recent advances in polymer supported palladium complexes as (nano)catalysts for Sonogashira coupling reaction. *Molecular Catalysis,* **2020**, *480*, 110645.
[http://dx.doi.org/10.1016/j.mcat.2019.110645]

[23] Ahmed, M.J. Application of agricultural based activated carbons by microwave and conventional activations for basic dye adsorption: Review. *J. Environ. Chem. Eng.,* **2016**, *4*(1), 89-99. [Review].
[http://dx.doi.org/10.1016/j.jece.2015.10.027]

[24] Harris, J.F. *Carbon Nanotubes Science: Synthesis, Properties and Applications Chap. 2*; Cambridge, **2009**.

[25] Wang, M.; Huang, Z-H.; Bai, Y.; Kang, F.; Inagaki, M. Porous Carbon Nanofibers: Preparation and Potential Applications. *Curr. Org. Chem.,* **2013**, *17*(13), 1434-1447.
[http://dx.doi.org/10.2174/1385272811317130010]

[26] Rao, C.N.R.; Sood, A.K. *Graphene: Synthesis, Properties and phenomena*; Wiley, **2012**.
[http://dx.doi.org/10.1002/9783527651122]

[27] Novoselov, K.S.; Geim, A.K.; Morozov, S.V.; Jiang, D.; Katsnelson, M.I.; Grigorieva, I.V.; Dubonos, S.V.; Firsov, A.A. Two-dimensional gas of massless Dirac fermions in graphene. *Nature,* **2005**, *438*(7065), 197-200.
[http://dx.doi.org/10.1038/nature04233] [PMID: 16281030]

[28] Geim, A.K. Graphene: Status and Prospects. *Science,* **2009**, *324*(5934), 1530-1534.
[http://dx.doi.org/10.1126/science.1158877] [PMID: 19541989]

[29] Geim, A.K.; Novoselov, K.S. The rise of graphene. *Nat. Mater.,* **2007**, *6*(3), 183-191.
[http://dx.doi.org/10.1038/nmat1849] [PMID: 17330084]

[30] Nasrollahzadeh, M.; Issaabadi, Z.; Tohidi, M.M.; Mohammad Sajadi, S. Recent progress in application of graphene supported metal nanoparticles in c-c and c-x coupling Reactions. *Chem. Rec.,* **2018**, *18*(2), 165-229.
[http://dx.doi.org/10.1002/tcr.201700022] [PMID: 28745452]

[31] Yang, Y.; Castano, C.E.; Gupton, B.F.; Reber, A.C.; Khanna, S.N. A fundamental analysis of enhanced cross-coupling catalytic activity for palladium clusters on graphene supports. *Nanoscale,* **2016**, *8*(47), 19564-19572.
[http://dx.doi.org/10.1039/C6NR06793J] [PMID: 27833943]

[32] Sakhaee-Pour, A.; Ahmadian, M.T.; Vafai, A. Potential application of single-layered graphene sheet as strain sensor. *Solid State Commun.,* **2008**, *147*(7-8), 336-340.
[http://dx.doi.org/10.1016/j.ssc.2008.04.016]

[33] Takamura, T.; Endo, K.; Fu, L.; Wu, Y.; Lee, K.J.; Matsumoto, T. Identification of nano-sized holes by TEM in the graphene layer of graphite and the high rate discharge capability of Li-ion battery anodes. *Electrochim. Acta,* **2007**, *53*(3), 1055-1061.
[http://dx.doi.org/10.1016/j.electacta.2007.03.052]

[34] Shendage, S.S.; Patil, U.B.; Nagarkar, J.M. Electrochemical deposition of highly dispersed palladium nanoparticles on nafion-graphene film in presence of ferrous ions for ethanol electrooxidation. *Fuel Cells (Weinh.),* **2013**, *13*(3), 364-370.
[http://dx.doi.org/10.1002/fuce.201300043]

[35] Groves, M.N.; Malardier-Jugroot, C.; Jugroot, M. Improving platinum catalyst durability with a doped graphene support. *J. Phys. Chem. C,* **2012**, *116*(19), 10548-10556.

Not be distributed or uploaded to anyone or anywhere
For personal private use only

[http://dx.doi.org/10.1021/jp203734d]

[36] Yamamoto, S.; Kinoshita, H.; Hashimoto, H.; Nishina, Y. Facile preparation of Pd nanoparticles supported on single-layer graphene oxide and application for the Suzuki–Miyaura cross-coupling reaction. *Nanoscale,* **2014**, *6*(12), 6501-6505.
[http://dx.doi.org/10.1039/C4NR00715H] [PMID: 24838740]

[37] Hummers, W.S., Jr; Offeman, R.E. Preparation of graphitic oxide. *J. Am. Chem. Soc.,* **1958**, *80*(6), 1339-1339.
[http://dx.doi.org/10.1021/ja01539a017]

[38] Djakovitch, L.; Koehler, K.; de Vries, J.G. *Nanoparticles and catalysis*; Wiley-VCH: Weinheim, **2009**.

[39] Narayanan, R. Recent advances in noble metal nanocatalysts for Suzuki and Heck cross-coupling reactions. *Molecules,* **2010**, *15*(4), 2124-2138.
[http://dx.doi.org/10.3390/molecules15042124] [PMID: 20428032]

[40] Balanta, A.; Godard, C.; Claver, C. Pd nanoparticles for C–C coupling reactions. *Chem. Soc. Rev.,* **2011**, *40*(10), 4973-4985.
[http://dx.doi.org/10.1039/c1cs15195a] [PMID: 21879073]

[41] Fihri, A.; Bouhrara, M.; Nekoueishahraki, B.; Basset, J.M.; Polshettiwar, V. Nanocatalysts for Suzuki cross-coupling reactions. *Chem. Soc. Rev.,* **2011**, *40*(10), 5181-5203.
[http://dx.doi.org/10.1039/c1cs15079k] [PMID: 21804997]

[42] Molnár, Á. Efficient, selective, and recyclable palladium catalysts in carbon-carbon coupling reactions. *Chem. Rev.,* **2011**, *111*(3), 2251-2320.
[http://dx.doi.org/10.1021/cr100355b] [PMID: 21391571]

[43] Taladriz-Blanco, P.; Hervés, P.; Pérez-Juste, J. Supported Pd nanoparticles for carbon–carbon coupling reactions. *Top. Catal.,* **2013**, *56*(13-14), 1154-1170.
[http://dx.doi.org/10.1007/s11244-013-0082-6]

[44] Scheuermann, G.M.; Rumi, L.; Steurer, P.; Bannwarth, W.; Mülhaupt, R. Palladium nanoparticles on graphite oxide and its functionalized graphene derivatives as highly active catalysts for the Suzuki-Miyaura coupling reaction. *J. Am. Chem. Soc.,* **2009**, *131*(23), 8262-8270.
[http://dx.doi.org/10.1021/ja901105a] [PMID: 19469566]

[45] Huang, Y.X.; Xie, J.F.; Zhang, X.; Xiong, L.; Yu, H.Q. Reduced graphene oxide supported palladium nanoparticles *via* photoassisted citrate reduction for enhanced electrocatalytic activities. *ACS Appl. Mater. Interfaces,* **2014**, *6*(18), 15795-15801.
[http://dx.doi.org/10.1021/am504664r] [PMID: 25153308]

[46] Sun, T.; Zhang, Z.; Xiao, J.; Chen, C.; Xiao, F.; Wang, S.; Liu, Y. Facile and green synthesis of palladium nanoparticles-graphene-carbon nanotube material with high catalytic activity. *Sci. Rep.,* **2013**, *3*(1), 2527.
[http://dx.doi.org/10.1038/srep02527] [PMID: 23982312]

[47] Scheuermann, G.M.; Rumi, L.; Steurer, P.; Bannwarth, W.; Mülhaupt, R. Palladium nanoparticles on graphite oxide and its functionalized graphene derivatives as highly active catalysts for the Suzuki-Miyaura coupling reaction. *J. Am. Chem. Soc.,* **2009**, *131*(23), 8262-8270.
[http://dx.doi.org/10.1021/ja901105a] [PMID: 19469566]

[48] Hu, J.; Wang, Y.; Han, M.; Zhou, Y.; Jiang, X.; Sun, P. A facile preparation of palladium nanoparticles supported on magnetite/s-graphene and their catalytic application in Suzuki–Miyaura reaction. *Catal. Sci. Technol.,* **2012**, *2*(11), 2332-2340.
[http://dx.doi.org/10.1039/c2cy20263h]

[49] Ioni, Y.V.; Lyubimov, S.E.; Korlyukov, A.A.; Antipin, M.Y.; Davankov, V.A.; Gubin, S.P. Activity of palladium nanoparticles on graphene oxide in the Suzuki—Miyaura reaction. *Russ. Chem. Bull.,* **2012**, *61*(9), 1825-1827.

Not be distributed or uploaded to anyone or anywhere
For personal private use only

[http://dx.doi.org/10.1007/s11172-012-0252-x]

[50] Morimoto, N.; Yamamoto, S.; Takeuchi, Y.; Nishina, Y. Palladium on graphene: the *in situ* generation of a catalyst for the chemoselective reduction of α,β-unsaturated carbonyl compounds. *RSC Advances,* **2013**, *3*(36), 15608-15612.
[http://dx.doi.org/10.1039/c3ra42150c]

[51] Wang, Z.; Xu, C.; Gao, G.; Li, X. Facile synthesis of well-dispersed Pd–graphene nanohybrids and their catalytic properties in 4-nitrophenol reduction. *RSC Advances,* **2014**, *4*(26), 13644-13651.
[http://dx.doi.org/10.1039/c3ra47721e]

[52] Yang, M.Q.; Pan, X.; Zhang, N.; Xu, Y.J. A facile one-step way to anchor noble metal (Au, Ag, Pd) nanoparticles on a reduced graphene oxide mat with catalytic activity for selective reduction of nitroaromatic compounds. *CrystEngComm,* **2013**, *15*(34), 6819-6828.
[http://dx.doi.org/10.1039/c3ce40694f]

[53] Gómez-Martínez, M.; Buxaderas, E.; Pastor, I.M.; Alonso, D.A. Palladium nanoparticles supported on graphene and reduced graphene oxide as efficient recyclable catalyst for the Suzuki–Miyaura reaction of potassium aryltrifluoroborates. J. Mole. Catal. *Anal. Chem.,* **2015**, *404*, 1-7.

[54] Wang, P.; Zhang, G.; Jiao, H.; Liu, ; Deng, X.; Chen, Y.; Zheng, X. Pd/graphene nanocomposite as highly active catalyst for the Heck reactions. *Appl. Catal. A Gen.,* **2015**, *489*, 188-192.
[http://dx.doi.org/10.1016/j.apcata.2014.10.044]

[55] Siamaki, A.R.; Khder, A.E.R.S.; Abdelsayed, V.; El-Shall, M.S.; Gupton, B.F. Microwave-assisted synthesis of palladium nanoparticles supported on graphene: A highly active and recyclable catalyst for carbon–carbon cross-coupling reactions. *J. Catal.,* **2011**, *279*(1), 1-11.
[http://dx.doi.org/10.1016/j.jcat.2010.12.003]

[56] Gilliland, S.E., III; Tengco, J.M.M.; Yang, Y.; Regalbuto, J.R.; Castano, C.E.; Gupton, B.F. Electrostatic adsorption-microwave synthesis of palladium nanoparticles on graphene for improved cross-coupling activity. *Appl. Catal. A Gen.,* **2018**, *550*, 168-175.
[http://dx.doi.org/10.1016/j.apcata.2017.11.007]

[57] Lee, K.H.; Han, S.W.; Kwon, K.Y.; Park, J.B. Systematic analysis of palladium–graphene nanocomposites and their catalytic applications in Sonogashira reaction. *J. Colloid Interface Sci.,* **2013**, *403*, 127-133.
[http://dx.doi.org/10.1016/j.jcis.2013.04.006] [PMID: 23673006]

[58] Rana, S.; Maddila, S.; Yalagala, K.; Jonnalagadda, S.B. Organo functionalized graphene with Pd nanoparticles and its excellent catalytic activity for Suzuki coupling reaction. *Appl. Catal. A Gen.,* **2015**, *505*, 539-547.
[http://dx.doi.org/10.1016/j.apcata.2015.07.018]

[59] Mahdavi, H.; Rahmani, O. Polyacrylamide-g-reduced graphene oxide supported pd nanoparticles as a highly efficient catalyst for Suzuki–Miyaura reactions in water. *Catal. Lett.,* **2016**, *146*(11), 2292-2305.
[http://dx.doi.org/10.1007/s10562-016-1851-1]

[60] Sarvestani, M.; Azadi, R. Palladium nanoparticles deposited on a graphene-benzimidazole support as an efficient and recyclable catalyst for aqueous-phase Suzuki-Miyaura coupling reaction. *Appl. Organomet. Chem.,* **2017**, *31*(8), e3667.
[http://dx.doi.org/10.1002/aoc.3667]

[61] Fareghi-Alamdari, R.; Haqiqi, M.G.; Zekri, N. Immobilized Pd(0) nanoparticles on phosphine-functionalized graphene as a highly active catalyst for Heck, Suzuki and N-arylation reactions. *New J. Chem.,* **2016**, *40*(2), 1287-1296.
[http://dx.doi.org/10.1039/C5NJ02227D]

[62] Novoselov, K.S.; Geim, A.K.; Morozov, S.V.; Jiang, D.; Zhang, Y.; Dubonos, S.V.; Grigorieva, I.V.; Firsov, A.A. Electric field effect in atomically thin carbon films. *Science,* **2004**, *306*(5696), 666-669.
[http://dx.doi.org/10.1126/science.1102896] [PMID: 15499015]

Not be distributed or uploaded to anyone or anywhere
For personal private use only

[63] Wu, Y.; Zhu, J.; Huang, L. A review of three-dimensional graphene-based materials: Synthesis and applications to energy conversion/storage and environment. *Carbon,* **2019**, *143*, 610-640. [http://dx.doi.org/10.1016/j.carbon.2018.11.053]

[64] Qiu, B.; Xing, M.; Zhang, J. Recent advances in three-dimensional graphene based materials for catalysis applications. *Chem. Soc. Rev.,* **2018**, *47*(6), 2165-2216. [http://dx.doi.org/10.1039/C7CS00904F] [PMID: 29412198]

[65] Tran, T.P.N.; Thakur, A.; Trinh, D.X.; Dao, A.T.N.; Taniike, T. Design of Pd@Graphene oxide framework nanocatalyst with improved activity and recyclability in Suzuki-Miyaura cross-coupling reaction. *Appl. Catal. A Gen.,* **2018**, *549*, 60-67. [http://dx.doi.org/10.1016/j.apcata.2017.09.026]

[66] Chua, C.K.; Pumera, M. Covalent chemistry on graphene. *Chem. Soc. Rev.,* **2013**, *42*(8), 3222-3233. [http://dx.doi.org/10.1039/c2cs35474h] [PMID: 23403465]

[67] Xiang, Q.; Cheng, B.; Yu, J. Graphene-based photocatalysts for solar-fuel generation. *Angew. Chem. Int. Ed.,* **2015**, *54*(39), 11350-11366. [http://dx.doi.org/10.1002/anie.201411096] [PMID: 26079429]

[68] Sharavath, V.; Ghosh, S. Palladium nanoparticles on noncovalently functionalized graphene-based heterogeneous catalyst for the Suzuki–Miyaura and Heck–Mizoroki reactions in water. *RSC Advances,* **2014**, *4*(89), 48322-48330. [http://dx.doi.org/10.1039/C4RA06868H]

[69] Feizi Mohazzab, B.; Jaleh, B.; Issaabadi, Z.; Nasrollahzadeh, M.; Varma, R.S. Stainless steel mesh-GO/Pd NPs: catalytic applications of Suzuki–Miyaura and Stille coupling reactions in eco-friendly media. *Green Chem.,* **2019**, *21*(12), 3319-3327. [http://dx.doi.org/10.1039/C9GC00889F]

[70] Premi, C.; Jain, N. A nitrogen and sulphur functionalized graphene oxide–palladium nanoparticle hybrid catalyst for an efficient Heck coupling. *RSC Advances,* **2016**, *6*(78), 74961-74967. [http://dx.doi.org/10.1039/C6RA09996C]

[71] Veisi, H.; Mirzaee, N. Ligand-free Mizoroki–heck reaction using reusable modified graphene oxide-supported Pd(0) nanoparticles. *Appl. Organomet. Chem.,* **2018**, *32*(2), 4067. [http://dx.doi.org/10.1002/aoc.4067]

[72] Nakhate, A.V.; Yadav, G.D. Palladium nanoparticles supported carbon based graphene oxide monolith as catalyst for Sonogashira coupling and hydrogenation of nitrobenzene and alkenes. *ChemistrySelect,* **2016**, *1*(13), 3954-3965. [http://dx.doi.org/10.1002/slct.201600819]

[73] Shendage, S.S.; Singh, A.S.; Nagarkar, J.M. Facile approach to the electrochemical synthesis of palladium-reduced graphene oxide and its application for Suzuki coupling reaction. *Tetrahedron Lett.,* **2014**, *55*(4), 857-860. [http://dx.doi.org/10.1016/j.tetlet.2013.12.022]

[74] Shendage, S.S.; Nagarkar, J.M. Electrochemically codeposited reduced graphene oxide and palladium nanoparticles: An efficient heterogeneous catalyst for Heck coupling reaction. *Colloid Interface Sci. Commun.,* **2014**, *1*, 47-49. [http://dx.doi.org/10.1016/j.colcom.2014.06.008]

[75] Liu, D.; Zhang, C.; Wang, F.; Huang, Z.; Zhang, N.; Zhou, H.; Kuang, Y. In situ preparation of graphene oxide supported Pd nanoparticles in an ionic liquid and the long-term catalytic stability for the Heck reaction. *J. Mater. Chem. A Mater. Energy Sustain.,* **2015**, *3*(32), 16583-16589. [http://dx.doi.org/10.1039/C5TA03767K]

[76] Liu, X.; Zhao, X.; Zhu, J.; Xu, J. One-pot synthesis of magnetic palladium-$NiFe_2O_4$-graphene oxide composite: an efficient and recyclable catalyst for Heck reaction. *Appl. Organomet. Chem.,* **2016**, *30*(5), 354-359.

[http://dx.doi.org/10.1002/aoc.3439]

[77] Elazab, H.A.; Siamaki, A.R.; Moussa, S.; Gupton, B.F.; El-Shall, M.S. Highly efficient and magnetically recyclable graphene-supported Pd/Fe3O4 nanoparticle catalysts for Suzuki and Heck cross-coupling reactions. *Appl. Catal. A Gen.,* **2015**, *491*, 58-69.
[http://dx.doi.org/10.1016/j.apcata.2014.11.033]

[78] Fu, W.; Zhang, Z.; Zhuang, P.; Shen, J.; Ye, M. One-pot hydrothermal synthesis of magnetically recoverable palladium/reduced graphene oxide nanocomposites and its catalytic applications in cross-coupling reactions. *J. Colloid Interface Sci.,* **2017**, *497*, 83-92.
[http://dx.doi.org/10.1016/j.jcis.2017.02.063] [PMID: 28273514]

[79] Hussain, N.; Borah, A.; Darabdhara, G.; Gogoi, P.; Azhagan, V.K.; Shelke, M.V.; Das, M.R. A green approach for the decoration of Pd nanoparticles on graphene nanosheets: An *in situ* process for the reduction of C–C double bonds and a reusable catalyst for the Suzuki cross-coupling reaction. *New J. Chem.,* **2015**, *39*(8), 6631-6641.
[http://dx.doi.org/10.1039/C5NJ01221J]

[80] Anasdass, J.R.; Kannaiyan, P.; Raghavachary, R.; Gopinath, S.C.B.; Chen, Y. Palladium nanoparticle-decorated reduced graphene oxide sheets synthesized using Ficus carica fruit extract: A catalyst for Suzuki cross-coupling reactions. *PLoS One,* **2018**, *13*(2), e0193281.
[http://dx.doi.org/10.1371/journal.pone.0193281] [PMID: 29466453]

[81] Kulkarni, P.A.; Shendage, S.S.; Awale, A.G. Carbon–carbon bond formation reaction with Pd/reduced graphene oxide composite. *Orient. J. Chem.,* **2018**, *34*, 881-886.
[http://dx.doi.org/10.13005/ojc/340236]

[82] Mahanta, A.; Hussain, N.; Das, M.R.; Thakur, A.J.; Bora, U. Palladium nanoparticles decorated on reduced graphene oxide: An efficient catalyst for ligand- and copper-free Sonogashira reaction at room temperature. *Appl. Organomet. Chem.,* **2017**, *31*(8), e3679.
[http://dx.doi.org/10.1002/aoc.3679]

[83] Tarahomi, M.; Alinezhad, H.; Maleki, B. Immobilizing Pd nanoparticles on the ternary hybrid system of graphene oxide, Fe_3O_4 nanoparticles, and PAMAM dendrimer as an efficient support for catalyzing sonogashira coupling reaction. *Appl. Organomet. Chem.,* **2019**, *33*(11), e5203.
[http://dx.doi.org/10.1002/aoc.5203]

[84] Alinezhad, H.; Tarahomi, M.; Maleki, B.; Amiri, A. SO_3 H-functionalized nano-MGO-D-NH_2 : Synthesis, characterization and application for one-pot synthesis of pyrano[2,3- *d*]pyrimidinone and tetrahydrobenzo[*b*]pyran derivatives in aqueous media. *Appl. Organomet. Chem.,* **2019**, *33*(3), e4661.
[http://dx.doi.org/10.1002/aoc.4661]

Not be distributed or uploaded to anyone or anywhere
For personal private use only

CHAPTER 8

Domino and Multicomponent Reactions by Graphene-Based Carbocatalysts – A Boon for Organic Transformations

S. Haripriya[1,ψ], K.M. Sreeranjan[1,ψ], Sagar Ulkesh Patil[1,ψ], G.S. Sahoo Navneet[1,ψ], H.S. Sushma[1], S. Ahallya[1], Rakesh R Panicker[1], Ivaturi Sai Vighnesh[1], Rajagopal Desikan[1], Vepa Jagannadha Rao[2] and **Akella Sivaramakrishna[1,*]**

[1] *Department of Chemistry, School of Advanced Sciences, Vellore Institute of Technology (VIT), Vellore 632014, Tamil Nadu, India*

[2] *Department of Chemistry, Anil Neerukonda Institute of Technology and Sciences, Affiliated to Andhra University, Sanghivalasa, Visakhapatnam 531162, Andhra Pradesh, India*

Abstract: The research on the development of high-performance metal-free carbocatalysis is one of the emerging areas in chemical sciences. The possible active sites of the surfaces of graphene, oxygenated, and reduced graphene oxide materials are responsible for diversified synthetic transformations, including redox reactions. At present, the advanced research is focused on scalable, sustainable, biocompatible, green, and cost-effective graphene-based carbocatalysts as wonderful alternatives over the noble metallic catalytic materials which are being employed despite their scarcity, high cost, and relative toxicity. The present chapter describes the utility of graphene-based carbocatalysts in multicomponent reactions.

Keywords: Catalytic Activity, Graphene Oxide Materials, Metal-Free Carbocatalysts, Multicomponent Reactions, Reduced Graphene Oxides.

1. INTRODUCTION

Numerous organic transformations have been reported by many homogeneous transition metal complexes including organometallics and heterogeneous catalysts [1 - 4]. Among these catalytic reactions, due to the significant medicinal properties of the reaction products, various multicomponent organic reactions yielding fused heterocyclic compounds have been designed employing a variety

* **Corresponding author Akella Sivaramakrishna:** Department of Chemistry, School of Advanced Sciences, Vellore Institute of Technology (VIT), Vellore 632014, Tamil Nadu, India; E-mail: asrkrishna@vit.ac.in
ψ All these authors have equal contributions to this Chapter.

Pinki Bala Punjabi, Rakshit Ameta & Sharoni Gupta (Eds.)
All rights reserved-© 2023 Bentham Science Publishers

of metal and non-metal-based catalysts [5]. It would be appropriate to design alternative non-metal catalysts derived from renewable resources in terms of sustainability. Because of this, carbon materials resulting from biomass have been considered sustainable pathways [6, 7]. The economic burden and toxicity are the other specific factors besides sustainability, which favor the carbocatalysts since some of the precious metals (in particular noble metals) are very expensive over the carbon feedstock materials. Furthermore, it is sometimes a very difficult task to remove the residual catalyst from the final product, which can lead to undesired toxicity. These aspects are the driving force in developing metal-free catalysts by researchers. Among them, "carbocatalysis" is one of the promising sustainable routes to reduce metal-based reactions [8 - 10]. It was found that these carbocatalysts, especially the heteroatom doped graphene-based carbocatalysts are considered the best promising alternates of noble metals as an efficient and green catalyst.

In general, carbocatalysts are non-molecular entities and contain mostly carbon framework as an active component with a large surface area. But these carbonaceous catalytic materials are completely different from organocatalysts, which are active organic molecules [7, 11]. Furthermore, the incorporation of the active sites into the carbon materials by appropriate modifications is the key aspect for carbocatalysts, which makes the utilization of metals non-essential. Carbocatalyst is better suited for heterogeneous reactions over homogeneous systems when the particle sizes are large. However, the particle size of the graphene material can be reduced to the carbon dots having 2D morphology; carbocatalysts facilitate the single phased homogeneous catalysis [12]. The graphene derivatives can offer wonderful catalytic properties due to the presence of functional groups with heteroatoms on the G-sheet as active catalytic centers [13, 14]. The importance of graphene as catalytic material is highlighted based on the adsorption capacity, electron density, and morphology of the sheets and its efficiency is strongly dependent on the position and nature of active sites on the graphene sheets.

2. SYNTHESIS OF GRAPHENE-BASED CARBOCATALYSTS

A large number of research articles have been reported on the method of preparation on various Gmat [12 - 33] and characterization techniques [17, 18, 23, 34], including their important structural properties for the applications in electronics [34 - 40] and conductivity [38 - 41]. Furthermore, the studies on electrocatalysis [42 - 47] and photocatalytic applications [48] of graphene derivatives have been widely carried out; however, there is a growing interest in the graphene oxide (GO) materials as semiconductors [49] and the synthesis of

organic heterocycles [50]. Notably, N and P double doped graphene carbon catalyst (NP-G) was employed for the reduction of nitrophenol over traditional graphene-based catalyst [14]. Nitrogen and sulfur co-doped graphene (NS-G) derived by one-pot thermal pyrolysis using heteroatom containing precursors like dopamine hydrochloride (DA) and 2-mercaptoethanol (ME) exhibits unusual catalytic activity due to its porous structure toward water splitting upon activation [51].

The synthesis of heteroatom donor graphene oxide (GO) is quite lengthy and cumbersome. Primarily, the modified Hummer's method [52] was employed to synthesize GO for the synthesis of N-doped rGO. By this process, GO was (1.0 g) dissolved in 50 mL ethanol, agitated for around 30 min, followed by sonication. After that, melamine (1.0 g) was incorporated into the mixture and the resulting suspension was heated to 50 °C on a hotplate while stirring (Scheme **1**). The desiccated mixture was heated at 450 °C and then calcination was done at varying temperatures of 600, 700, and 800 °C under an inert N_2 atmosphere for 1 h to obtain NG-600, NG-700, NG-800, respectively. Further washing with ultrapure water and ethanol and after overnight drying at 60 °C, the (N)G attains the catalytic activity [53].

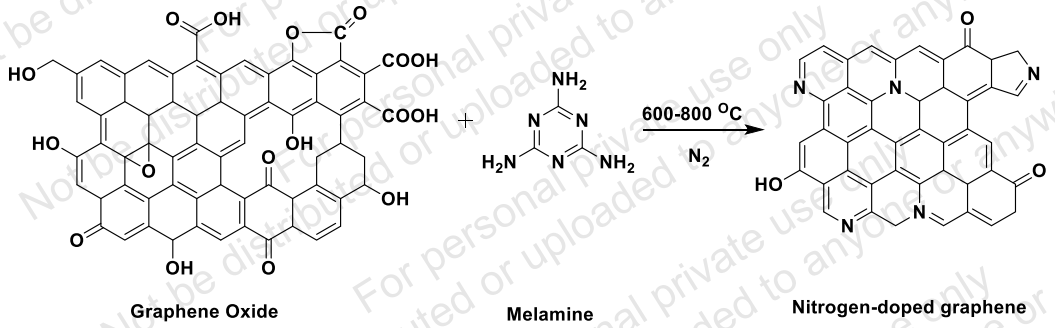

Scheme 1. Synthesis of N-doped graphene.

The graphene-based carbocatalytic reactions for various organic transformations are broadly classified into i) oxidation, ii) carbon-carbon bond formation, iii) hydrogenation, iv) aza-Michael addition, v) dehydration-hydrothiolation, and vi) Friedel-Crafts alkylation.

3. ORGANIC TRANSFORMATIONS BY GRAPHENE-BASED CARBOCATALYSIS

3.1. Oxidation Reactions

Similar to transition metal-based catalysts facilitating efficient incorporation of an oxygen atom into organic molecules by oxidation reactions, graphene oxide-based catalysts are also mild but effective carbocatalysts for oxidation reactions as given in Scheme **2** and Scheme **3** [54].

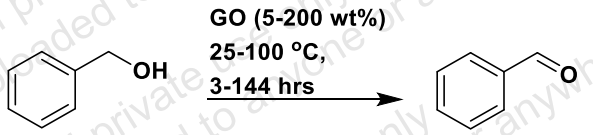

Scheme 2. Oxidation reaction of benzyl alcohol to benzaldehyde (92%) with GO catalyst.

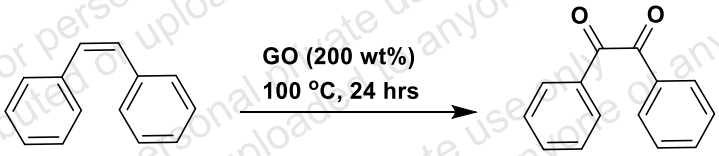

Scheme 3. Oxidation of *cis*-stilbene in to dione (49%) with GO catalyst.

The conversion of benzene to oxygen-containing aromatic compounds is one of the most active and still evolving fields of catalysis due to its industrial significance. But they are typically prepared by long processes that are both expensive and time-consuming (*e.g.* phenol produced by 3-step cumene processes as given in Scheme **4**). There are also other disadvantages, such as contamination and less selectivity towards compounds. A lot of changes and improvisations have been made to enhance this field of catalysis. Nano-sized carbon materials, such as graphene, have proven to be effective and selective catalysts for such reactions. The reason for the improved catalytic activity is due to the open π-electron system and the huge adsorption rate of graphene [55].

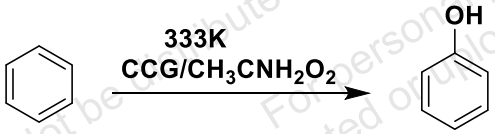

Scheme 4. Oxidation of benzene to phenol (> 99%) using CCG as a catalyst.

Traditionally the styrene was oxidized to benzaldehyde and benzoic acid by molecular oxygen, but it was investigated that the styrene oxide was also getting formed through epoxidation. So far it was extremely difficult to monitor the

reaction so that it should not form unpleasant side products and undergo detrimental reactions. The interest of this (S)G synthesis arrived in minds of researchers from the fact that the oxidation of the alkene in aerobic conditions using transition or noble metals as the catalysts, and, hence it would be exceptionally profitable to formulate such catalysts which must be metal-free for such processes. The monitored reaction was done in the absence of catalyst which has led to only 4% product formation. This is attributed due to auto-oxidation. Moreover, the reaction was assessed by oxidation of styrene under aerobic and non-solvent reaction conditions in presence of (S)G as a catalyst. Promisingly, 13% of conversion was achieved after 7 h with 70 and 20% of benzaldehyde and styrene oxide respectively (Scheme **5**). The hallmark of (S)G catalyst is that it could be reused or recycled two times with no considerable changes in selectivity and efficiency [56].

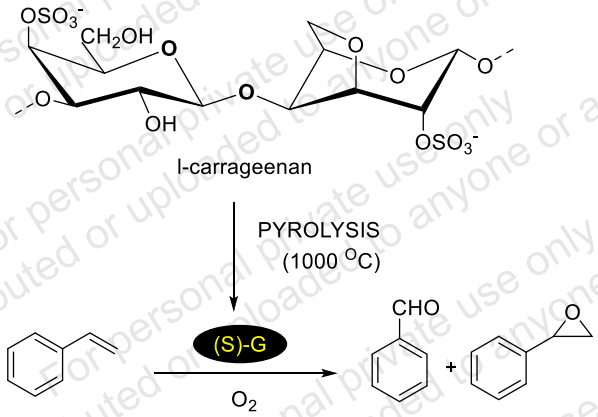

Scheme 5. Oxidation of styrene in the presence of graphene S-doped to benzaldehyde (100% selectivity at 100 ºC) and to styrene oxide (maxmum 20% selectivity).

Further, the use of a metal-free sulfonic acid-functionalized reduced graphene oxide (SA-rGO) material for catalytic synthesis of carboxylic acids and its corresponding bio-isosteres, 5-substituted-1H-tetrazoles, has been reported. As a catalytic material, SA-rGO combines the intriguing properties of graphene oxide with the added benefit of highly acidic sites due to sulfonic acid groups. H_2O_2 as a green oxidant with high TOF values (9.06–9.89 h^{-1}) was used to oxidize aldehydes to carboxylic acids very efficiently. Similarly, the 5-substituted-1H-tetrazoles could also be synthesized efficiently with high TOF values (12.08–16.96 h^{-1}). By employing the SA-rGO catalyst, both reactions could be carried out efficiently at the gram scale level (10 g). SA-rGO has high reusability of up to eight runs without a significant decrease in productivity. As a result of these features, SA-rGO is an attractive alternative from the industrial point of view [57].

Notably, the graphene oxide reduction method influences the activity of the resulting reduced graphene oxide (rGO) for the aerobic oxidation of benzylamine. Beginning with GO obtained *via* the Hummers method, a series of rGO samples was prepared *via* chemical (hydroquinone (HQ), hydrazine (HZ), or ascorbic acid (ASC)) or thermal reduction. The analysis reveals that the chemical reducing agents reduce GO with different functional groups affecting the catalytic activity of the resulting rGO for molecular oxygen activation in the oxidation of benzylamine. The rGO-HQ1 sample prepared with HQ as a reducing agent exhibited the optimum activity in the aerobic oxidation of benzylamine at 80 °C. It has been hypothesized that HQ introduces hydroquinone/*p*-benzoquinone-like moieties onto the graphene sheet and these active sites are responsible for the oxidation reaction. By selective masking of oxygen functional groups present in the most active rGO sample, indicates the activity of HQ and/or *p*-benzoquinone as organocatalysts. In five consecutive uses, the most active rGO sample displayed good reusability and stability. Hydroperoxyl radicals were presumed as the primary reactive oxygen species formed in the system, according to selective quenching tests [58].

Anumula *et. al*. reported glutathione-protected Ag_6 clusters using a simple green reaction, transferred them to graphene oxide (GO), and used them as a catalyst for cyclohexane oxidation under ambient conditions. With *t*-butyl hydroperoxide (TBHP) as the oxidant in an oxygen-flowing atmosphere, high selectivity and yield of cyclohexanone is obtained. It is demonstrated that using density functional theory calculations that both TBHP and oxygen interact with the Ag6 clusters supported by GO, resulting in the peroxide structure and thus facilitating catalysis cyclohexane oxidation. It is interesting to note that hydrogen-added hydroperoxyl (-OOH) has a significantly lower activation barrier for O-O bond dissociation. The O-O dissociated intermediate then reacts with cyclohexane to form cyclohexanol, which is then dehydrogenated by successive oxidative reactions to form cyclohexanone. This finding validates the enhanced catalysis of TBHP and O_2 for the conversion of cyclohexane to cyclohexanone and contributes to the development of heterogeneous metal cluster catalysts for efficient C-H activation [59].

Reports show that by reacting respective ultra-small colloidal metal oxide/hydroxide with partially reduced colloidal graphene oxide, surfactant-free MGN for distinct noble metals can be prepared for high-performance fuel cell catalysis. The resulting MGN is made up of widely distributed M-M^{+n} based nanoparticles with extremely small sizes that provide a strong and stable catalytic current for the oxidation of ethanol and formic acid [60].

3.2. Carbon-Carbon Bond Formation

Besides, *N*-doped defective graphene [(N)G] carbocatalyst was synthesized by pyrolysis of chitosan and employed as a basic catalyst for some C-C bond forming reactions which are nucleophilic Michael and Henry additions as shown in Scheme **6**. The most basic *N*-sites were detected by DFT calculations amongst pyridinic, pyrrolic, and graphitic residual nitrogen atoms of *N*-doped defective graphene [61].

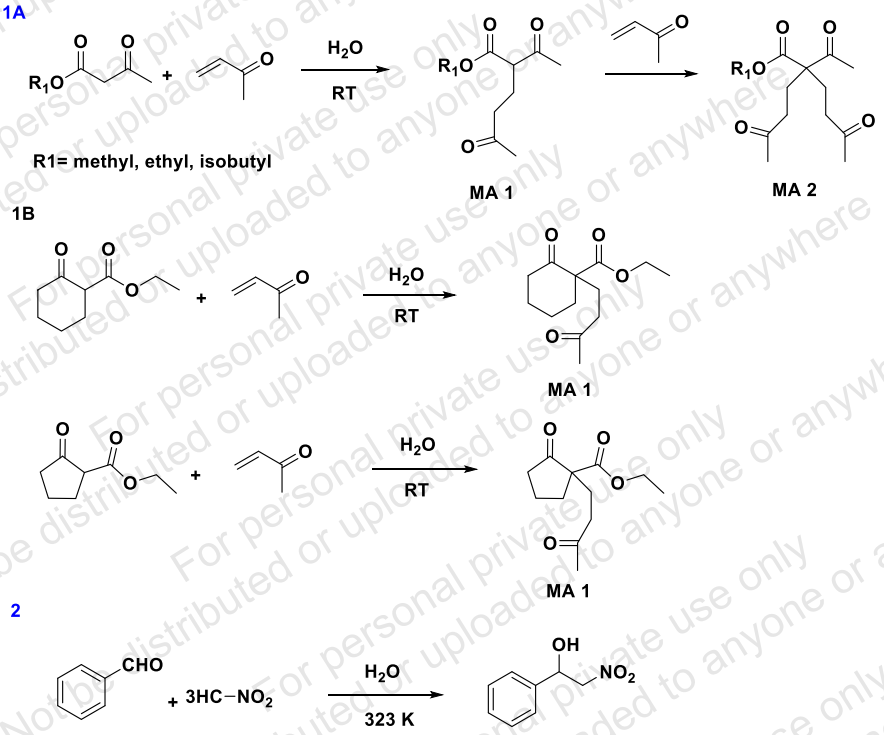

Scheme 6. Some C-C bond forming reactions through nucleophilic Michael and Henry additions by carbocatalysis.

Also, the fabrication of sulfur-doped graphene oxide (SA-GO) by the method of sulfuration and alkylation was reported [62].

Remarkably, GO-supported primary amine (AP-GO) facilitated one-pot Henry-Michael reactions provide synthetically profitable multi-functionalized nitroalkanes. Furthermore, the higher activity is recorded with GO-supported system more than those activated carbon-supported primary amine, and mesoporous silica-supported primary amine as catalysts. This predominant catalytic performance started from the interesting properties of AP-GO, which is based on the acid−base cooperative effect by the suitable primary amines on their

basal planes and the carboxyl acids along their edges. The decreased diffusion resistance of the reactants and intermediates are responsible for the multistep catalytic cycles. Also, it may be promptly reused by simple filtration and consequently recycled without significant loss of its catalytic activity. The organoamines were anchored on the basal planes of GO through a basic and simple silane-coupling reaction to manage GO-supported organic amines, as depicted in Scheme **7** [63].

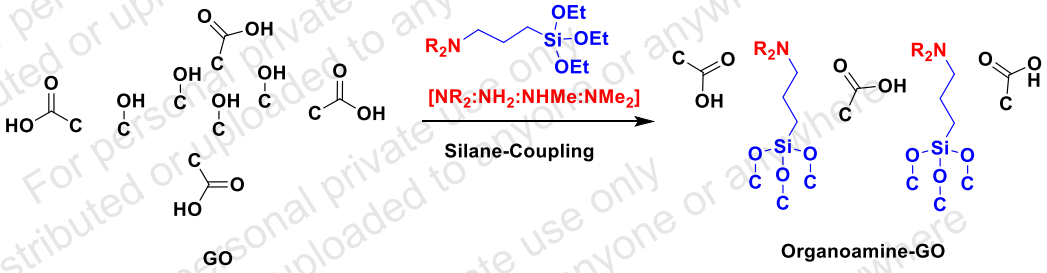

Scheme 7. Schematic illustration of organic amine-functionalized GO carbocatalysis.

The successful anchoring of organic amine groups onto GO surface was achieved by the Henry reaction between benzaldehyde and nitromethane to give the resulting products through nitroaldol addition and dehydration steps in the presence of different types of catalytic systems (Table **1**).

Table 1. Different catalysts in henry reaction.

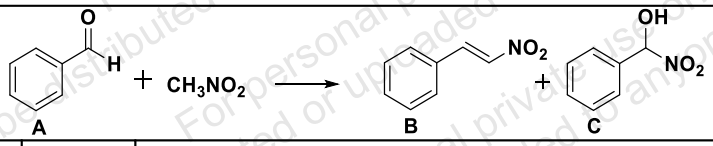

Carbocatalyst	Conversion of A (%)	Conversion to B (%)	Yield of C (%)
GO[2]	0	0	0
AP-GO	90	90	0
MAP-GO	91	76	15
DMAP-GO	84	53	31
PROPYLAMINE	39	39	0
GO+PROPYLAMINE	22	22	0
AP-GO-A[3]	13	13	0
AP-GO-B[4]	36	36	0

Interestingly, the catalytic reactions do not work with GO alone, but the GO-supported organic amines advanced to high conversion of products, showing that organic amines are important active species. The capability of the AP-GO catalyst among others to promote the one-pot Henry-Michael reaction is described in Table **2**. Initially, the carboxylic acids in the edges of GO activate the carbonyl group of benzaldehyde through hydrogen bonding, while the primary amines on the basal planes of GO attack the activated benzaldehyde to form the imine intermediates by the elimination of the water molecule. Eventually, nitromethane attacks this imine in the presence of carboxylic acids by following the elimination of amine species to generate *trans-β*-nitrostyrene. Finally, carboxylic acid activates *trans-β*-nitrostyrene again, to yield the targeted products as Michael adducts [63].

Table 2. Influence of different carbocatalysts in one-pot Henry-Michael reaction.

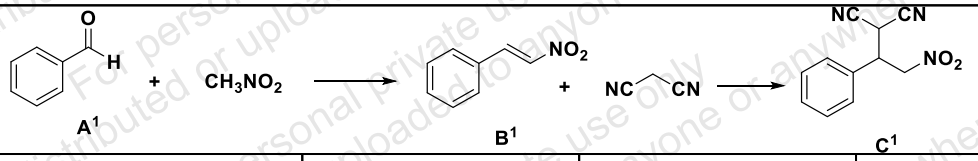

A^1 B^1 C^1

Carbocatalyst	Conversion of A^1 (%)	Conversion to B^1 (%)	Yield of C^1 (%)
AP-GO	90	97	87
Propylamine	39	49	19
AP-AC	53	58	31
AS-SBA-15	38	40	15
AP-GO-M[b]	34	39	13

Reaction conditions: 0.306 mL of benzaldehyde (3.0 mmol), 6.0 mL of nitromethane, 0.228 of malononitrile (3.6 mmol), a catalyst containing 0.075 mmol nitrogen species, 12 h. [b]Added 3.0 mL of methanol

Even though GO is inexpensive and has numerous remarkable mechanical and electronic properties, easy recovery, and metal-free reactivity from the reaction mixtures, the properties of GO have been relatively less explored as an oxidant or catalyst for facilitating various organic transformations. Eco-friendly synthesis of 2-amino-3-cyanopyridines *via* a GO catalyzed four-component condensation was studied [63] and the catalytic efficiency of GO over other catalysts is compared in Table **3**.

Table 3. A comparative analysis on the efficiency of carabocatalyst (GO) over other catalysts.

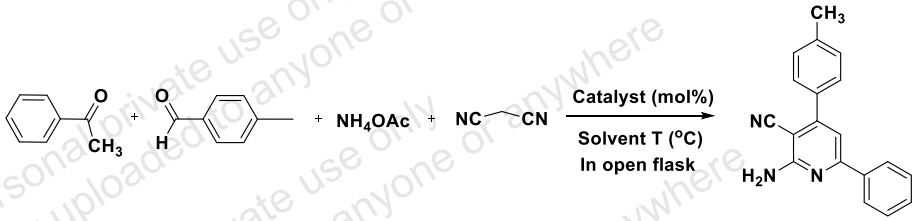

Entry	Catalyst (Mol %)	Reaction Conditions[1]	Time, h	Yield[2] (%)
1[3]	-	H_2O, 80°C	24	<10
2	GO (05)	H_2O, 80°C	05	81
3[4]	GO (10)	H_2O, 80°C	05	90
4	Graphite	H_2O, 80°C	24	20
5	r-GO	H_2O, 80°C	24	36
6	Activated carbon	H_2O, 80°C	24	57
7	Silica	H_2O, 80°C	05	49
8	H-beta Zeolite	H_2O, 80°C	05	66
9	TiO_2	H_2O, 80°C	05	40

[1]Reaction conditions: acetophenone (1 mmol), 4-methyl-benzaldehyde (1 mmol), ammonium acetate (1.5 mmol), malononitrile (1.3 mmol), catalyst (type indicated) in the presence of air
[2]Isolated yields
[3]r-GO-reduced graphene oxide

3.3. Hydrogenation Reaction

With regard to stability and safety issues associated with graphene oxide, when the compound is contaminated with potassium salts, its thermal stability is decreased. These potassium salts are obtained as GO synthesis products. These compounds are extremely flammable and unstable, therefore, a small spark is sufficient to burn down the entire GO film, resulting in a disastrous explosion. Since the compound's thermal instability in the presence of salts (by GO synthesis products) was observed, it was necessary to purify the GO material to prevent a fire hazard. In two phases, an acid wash proved to be a successful purification tool because it suppresses gelation, which is one of the major factors hindering purification. Furthermore, the energy produced from GO's self-propagating domino reactions can be used to generate other materials based on graphene that have high activity [64].

Among all the relevant graphene catalytic operations, its use as a composite photocatalyst for organic pollutant degradation is socially important. Graphene

has a honeycomb-like structure with sp^2 hybridized carbon arranged like a sheet. By chemically modifying the graphene, its surface properties like chemical adsorption, transparency, and conductivity will improve, which enhances its use as a composite material. Photocatalysts like TiO_2 can be chemically bonded to graphene by a one-step hydrothermal reaction. P25 is a TiO_2 photocatalyst that is bonded to graphene and can be used for the photodegradation of dyes. P25-Graphene photocatalyst possesses good absorptivity of dyes, a wide range of light absorption, and also charge separation properties, making it different and more efficient than normal TiO_2. Due to its giant 2-D planar structure, the improved activity of the P25-Graphene photocatalyst over normal P25 and other photocatalysts provided a better surface for dye adsorption and also separation charge [65].

Studies show that peroxymonosulfate (PMS) can be effectively activated by chemically reduced graphene oxide to produce active sulfate radicals, which is a powerful oxidizing species with a high oxidizing potential having enough potential to decompose various aqueous contaminants. In comparison with graphite powder (GP), graphene oxide (GO), activated carbon (AC), and multiwall carbon nanotube (MWCNT), graphene exhibits a higher activity. It was demonstrated that graphene catalysis is better than that of Co_3O_4 in the degradation of 2,4-dichlorophenol (DCP), phenol, and methylene blue (MB) in water, which is an efficient system for ecological remediation.

The activation of peroxy-monosulfate by graphene is more like those in oxidative dehydrogenation (ODH) and dehydrogenation (DH) reactions, in the presence of nanocarbon (Lewis base). The reduction of GO hydrothermally tunes the surface acidity/alkalinity by removing the oxygen moieties. By modifying the surface acidity of GO to alkaline by ammonia solution, the activity of graphene in the initiation of PMS improves significantly [66].

The sp^2 carbon atoms are placed in a hexagonal cell as a conjugated device in the case of a basal plane in perfect graphene. The curvature of stacked graphene layers and edge defects create non-six carbon rings. Two kinds of edges, zigzag and armchair, are created when C-C σ bonds are broken. The localized state at the zigzag edge means that their π electrons are not limited to edge carbons, hence the chemical activity is increased. The zigzag edges of reduced graphene oxides derived from chemical treatment hold a small number of oxygen-containing groups, and the remaining groups have a higher intrinsic activity than those at the end of the flat surface. Chemically reduced graphene oxide at zigzag edges hold a very small number of oxygen groups, and the remaining groups have a significantly higher intrinsic activity than those at the end of the flat surface.

Oxygen functional surface species, such as ketone (C=O) groups, are abundant and have a great deal to organize the redox phase.

PMS (HSO_5^-) is capable of activating graphene to yield two different types of sulfate radicals ($SO_4^{\bullet-}$ and $SO_5^{\bullet-}$). The former radical exhibits a higher oxidative potential value (2.5−3.1 V) and plays a vital role in phenol degradation. This reaction pathway is accompanied with the observations that the operation of different carbons follows the order: graphene > MWCNT > GP > GO, matching to the density of the graphite defects, (b) the action is closely related to the loading of the catalyst, (c) the influence of temperature is less which reflects the character of the graphene carrier, and (d) the similar catalysis analogs applicable to nanocarbons. The activity of graphene is higher than other carbon allotropes (GP, AC, MWCNT, and GO), and then it is on par with the activity of popular transition metal oxides.

Moreover, hydrogenation reactions of nitroarenes by reduced graphene oxide (RGO)-supported platinum (Pt) catalyst derived from the reduction of ethylene glycol (EG) and its characterization study demonstrated that EG as a reductant exhibits better advantages than the extensively used hydrated hydrazine to produce Pt nanoparticles that are small-sized and monodispersed on the entire surface of RGO. The results reveal that the yields of aniline over the Pt/RGO-EG catalyst are much higher than that of active carbon-supported and multi-walled carbon nanotube-based Pt catalysts. When the reaction temperature was changed to 20°C, the catalytic activity of Pt/RGO-EG was enhanced to 1138.3 mol (mol-Pt min), which proved to be extremely fruitful for the hydrogenation of nitroarene derivatives. The peculiar catalytic behavior of Pt/RGO-EG can be attributed to the well-scattered Pt clusters on the RGO sheets and the homogeneously dispersed Pt/RGO-EG in the reaction mixture. Thus, it is evident that RGO plays a vital role as a support to the catalyst and it is a better promoter than AC and MWCNT. Furthermore, Pt/RGO-EG appears to be a promisingly active and stable catalyst for the hydrogenation of NB (Scheme **8** and Scheme **9**).

The distinctive catalytic operation and simple fabrication process of GO and GO-based composites have the notable ability as heterogeneous catalysis [67].

The hydrothermal treatment of a mixed aqueous precursor solution of $PdCl_4^{2-}$, carbon nanotube (CNT), and GO, as well as the simultaneous spontaneous redox reaction between $PdCl_4^{2-}$ and CNTGO hybrid, resulted in the formation of a 3D macroscopic Pd-CNT-rGO hydrogel. The resulting Pd-CNT-rGO bifunctional nanocatalyst has a large surface area and excellent durability, and thus exhibits remarkably high and stable catalytic activity toward p-nitrophenol reduction, with 100 percent conversion in only 30s. The proposed simple synthetic route and

designed bifunctional catalysts will serve as a universal platform for the fabrication of nano-catalysts that can be used in a variety of catalysis, environmental protection, energy storage, drug delivery, chemical and biological sensing, and other applications [68].

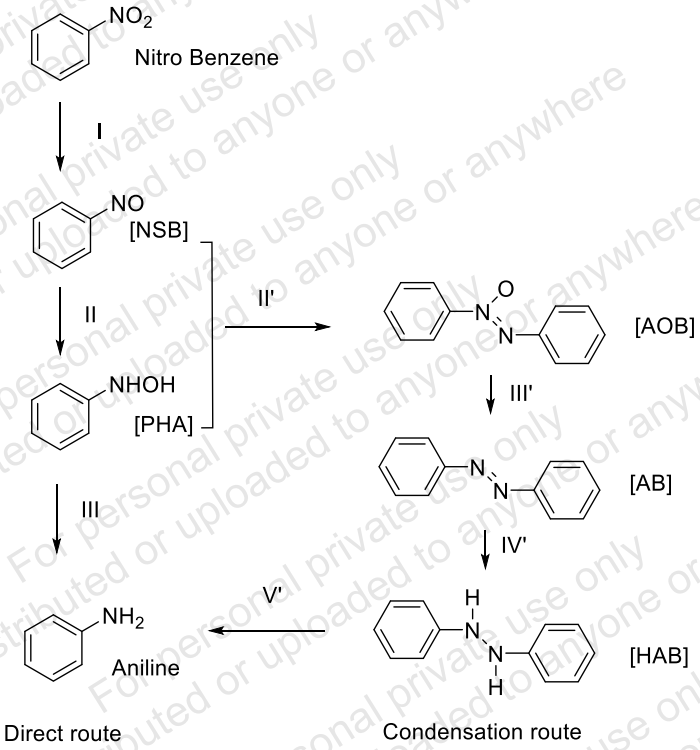

Scheme 8. Mechanistic steps for the hydrogenation of NB.

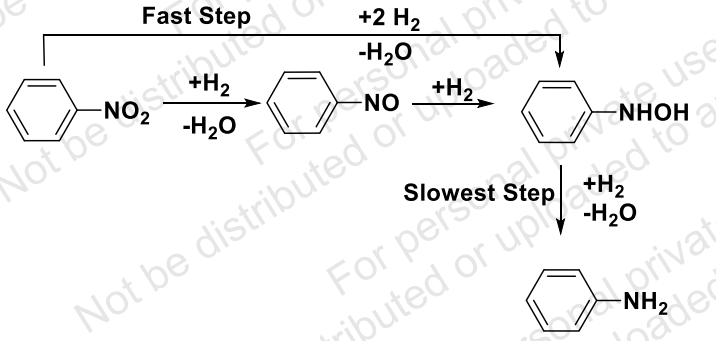

Scheme 9. Proposed mechanism for the hydrogenation of NB over Pt/RGO-EG catalyst.

Song *et.al.* reported the effect of capping agents on the catalytic function of rGO for redox reactions using nitrogen-containing surface modifiers with distinctly

different chemical structures, such as poly (diallyl dimethylammonium chloride), cetyltrimethylammonium chloride, and poly (allylamine hydrochloride), which can endow rGO with improved suspension stability. The reduction of graphene oxide with hydrazine in the presence of capping agents resulted in the facile preparation of functionalized rGOs. The results of model redox reactions, such as 4-nitrophenol and ferricyanide reduction reactions, catalyzed by functionalized rGOs, confirmed that the way capping agents functionalize rGO, which is highly correlated with their chemical structure, has a significant impact on overall reaction kinetics, such as induction time, reduction rate, total reaction time, and reaction order. This strongly shows that careful capping agent selection is essential for fully exploiting rGO's catalytic function and therefore designing innovative rGO-based non-metallic catalysts with controlled reaction kinetics [69].

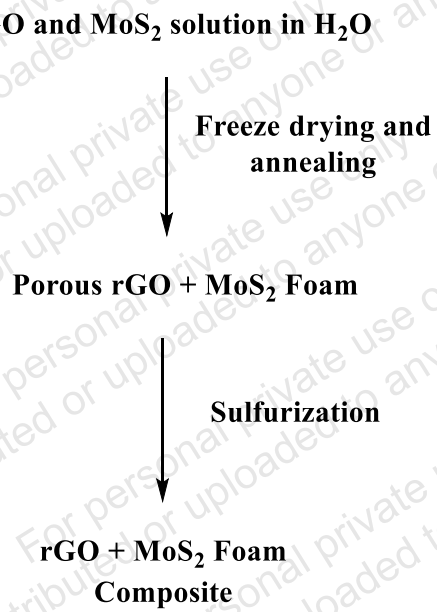

Scheme 10. Procedure of *in situ* growth of rGO supported MoS_2 with high defect density by sulfurization.

Joyner *et. al*. outlined a chemical vapor deposition (CVD) method for growing MoS_2 structures by sulfurizing rGO supported MoO_2 particles. On the basal plane of rGO supported MoS_2 structures, this approach created various morphologies of MoS_2 with large edges and high defect densities, which are considered active sites for hydrogen evolution reactions (HER) catalysis. Furthermore, MoS_2 nanostructures on the surface of the porous rGO network exhibit strong physical interactions, such as van der Waals and π−π interactions between MoS_2 and rGO. As a result of these features, the HER catalyst has been enhanced. With the duration of the sulfurization was 30 min, the 1rGO- 2MoS_2 composition provided

the lowest onset potential of -197 mV. Theoretical calculations show that defects on MoS_2's basal plane do indeed increase catalytic activity, resulting in more active sites. Due to alternative geometries other than triangle structures take longer to saturate the interactions with hydrogen atoms, having alternative MoS_2 geometries allows the system to be active for longer. According to the calculations, having MoS_2 crystals with diverse geometries and defects is favorable for hydrogen catalytic activity because the varied geometries allow the system to remain active for longer periods and the defects increase the number of active sites accessible for hydrogen interactions (Scheme **10**) [70].

Graphene doped with a heteroatom such as oxygen, nitrogen, boron, sulfur, and phosphorus yields a wide range of metal-free organocatalysts carrying improved catalytic performance. In this effort, Jiangbo Xi *et al*. synthesized an N and P-double-doped graphene (NPG) carbocatalyst by microwave-exfoliated graphite (MEG) in presence of hexachlorocyclotriphosphazene (HCCP) in a facile way, which in turn was used as N as well as a P source. This NPG showed a wonderful catalytic activity towards reduction reactions of nitroarenes, furthermore, excellent stability, selectivity, and recyclability [71].

3.4. Aza-Michael Addition

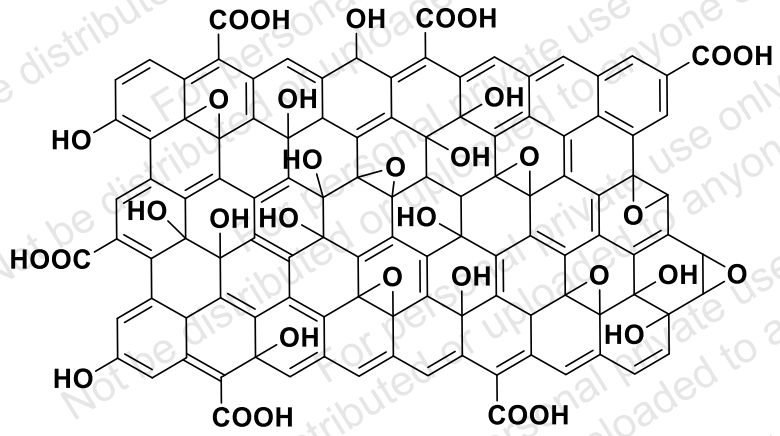

Fig. (1). A schematic design of graphene oxide (single sheet) showing active oxygen groups.

Oxygen-containing graphene oxide (GO) mainly functions as a precursor to the reduced graphene oxide. Various solvents including ionic liquids, water, and aprotic organic solvents, like dimethyl sulfoxide (DMSO), have been used as reaction media in the dehydration of carbohydrates to HMF. Further, ionic liquids are capable of solvents in terms of high selectivity in biomass conversion. For the

dehydration of fructose, graphene oxide can be an efficient carbocatalyst in the presence of isopropanol. Also, GO has been employed under various experimental conditions including strongly acidic and ultrasonic conditions [72]. The arrangement of new carbon-heteroatom bonds through *aza*-Michael expansion is a notable change in organic chemistry, which is of biological significance through active nitrogen-containing molecules, chiral auxiliaries, natural products, and antibiotics. The presence of oxygen-carrying functionalities in graphene oxide (Fig. **1**) facilitates hydrophilicity and allows dispersion in water and further polar solvents. The catalytic potential of graphene oxide nano-sheets was examined for the Aza-Michael addition reaction, as shown in Scheme **11**.

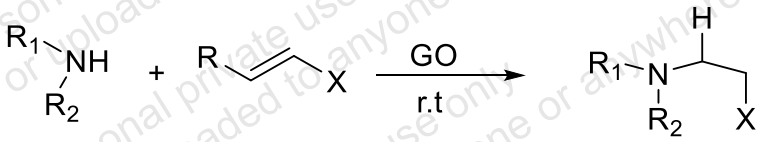

R= H, CH_3
R_1= Et, n-Bu, n-Pr, Bz
R_2= Et, n-Bu, n-Pr, Bz
X = CN, $CONH_2$, $COOCH_3$

Scheme 11. The catalytic Aza-Michael addition reaction by GO.

Further reaction scope was extended towards aromatic amines, such as aniline and *p*-anisidine, and was found to be less reactive and afforded moderate product yield in longer reaction times as given in Table **4** [73].

Table 4. Graphene oxide catalyzed aza-Michael addition of amines to α,β-unsaturated compounds.

Entry	Amine	Michael Acceptor	Reaction Time, Min	Yield (%)
1	Et, NH, Et	CN	35,[c] 150[d]	96, 94
		CN	30.0,[e] 5.0	95, 97
		$CONH_2$	5.0	97
		$COOCH_3$	7.0	96
		$COOCH_3$	7.0	95
2	NH_2	CN	5.0	95
		$CONH_2$	7.0	92
		$COOCH_3$	5.0	92
		$COOCH_3$	5.0	94

(Table 4) cont.....

3	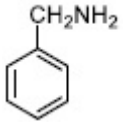		7.0	90
			10.0	89
			10.0	92
			10.0	92
4	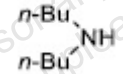		5.0	96
			10.0	85
			7.0	94
5	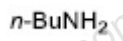		5.0	95
			5.0	94
6	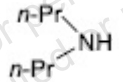		5.0	95
			5.0	96
7			5.0	94
			5.0	95
8			5.0	95
			5.0	94
9			45	65
10	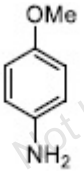		30	70

3.5. Dehydration-Hydrothiolation Reactions

To optimize the catalytic activity and observing the yields of the products, various combinations of the reactants were used under varied conditions like changing the amount of catalyst, time, temperature, and different aryl and alky groups. Thioethers can be utilized for synthesizing various biologically vital molecules. It was observed that the reactions with both long-chain and alicyclic thiols were reported (Scheme **12**). The electron-withdrawing group enhances dehydration-hydrothiolation reactions.

Not be distributed or uploaded to anyone or anywhere For personal private use only

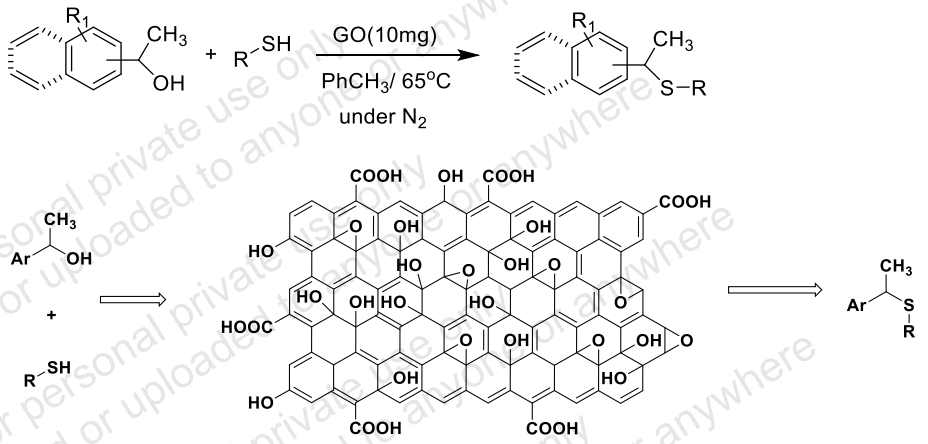

Scheme 12. Graphene oxide-catalyzed dehydration and hydrothiolation.

By this method, the catalyst can be retrieved from the product and can be reused at least 4-5 times without losing the catalytic activity. It was observed from the FT-IR spectrum of the GO catalyst and the GO's functional groups were not at all affected even after several cycles of catalytic reactions and they retained their functionality [74].

Peng *et. al*. developed a three-dimensional monolith of neat GO aerogel as a fixed-bed carbocatalyst for the synthesis of thiol compounds (Scheme **13**), demonstrating the advantages of ultrafast catalytic speed (5-8 h), high selectivity (100%), high yields (near 100%), easy product isolation, and long-life recyclability (> 18 times). For the first time, thiol compounds with halogen and hydroxyl functional groups that cannot be produced using conventional catalysts have been reported. The effective catalysis mechanism is primarily attributed to the protonic functional groups, ultra large size, and unpaired electrons of GO, as well as the "cage effect" in nanoscale constrained areas of aerogel cells, according to control experiments [75].

3.6. Friedel-Crafts Alkylation

The carbonyl functional sites in graphene can also be used as active sites for chemical reactions. The developed carbocatalysts are one without pH adjusted film (G1 film) and another pH adjusted film using ammonia (G2 film). Also, it was noticed that AA (L-ascorbic acid) plays a vital role in the preparation of carbocatalyst. The pH-mediated carbocatalyst enhances electrostatic repulsive interactions and it was observed that the pH and its effect can be seen only during

carbocatalyst formation with AA and after the reaction, the active edges are exposed (Scheme **14**) [76].

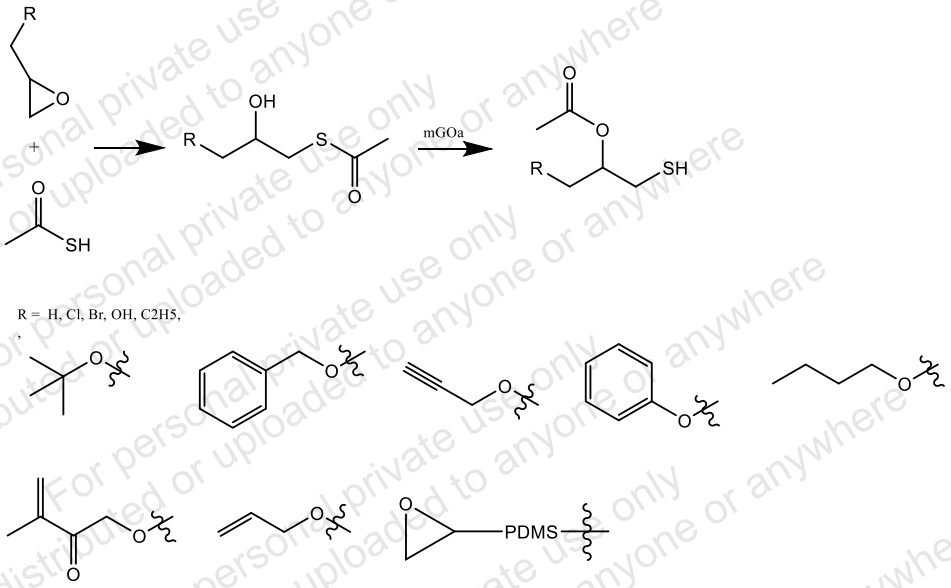

Scheme 13. Acetyl migration reaction of latent thiol compounds into thiol compounds catalyzed by mGO fixed-bed.

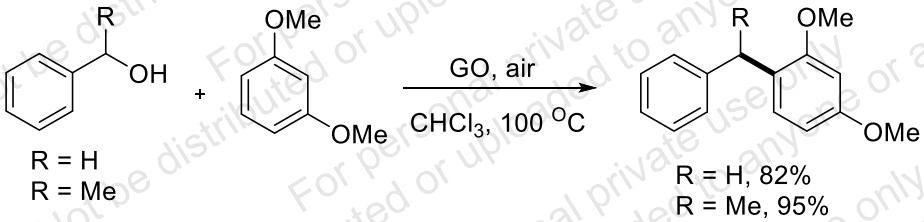

Scheme 14. GO-catalyzed direct Friedel-Crafts alkylation of arenes to alcohols.

Alkylation of arenes to diarylmethanes catalyzed by graphenes has been reported as shown in Fig. (**2**). The activation of the reactants on the catalyst surface is due to the active edges of aromatic polar functional groups on the surface of graphene.

It was observed that RGO can be used as a very effective catalyst in electrochemical and in-situ polymerization reactions of ABA whereas the GO can be used as an active catalyst for in-situ polymerization reaction of ABA only and in the case of electrochemical polymerization RGO, it enhances the formation of ABA rather than GO. Whereas in the case of *in-situ* both the carbocatalysts exhibits good efficacy and the reaction of polymerization depends on the concentration of monomer and oxidants on the surfaces (Scheme **15**) [77].

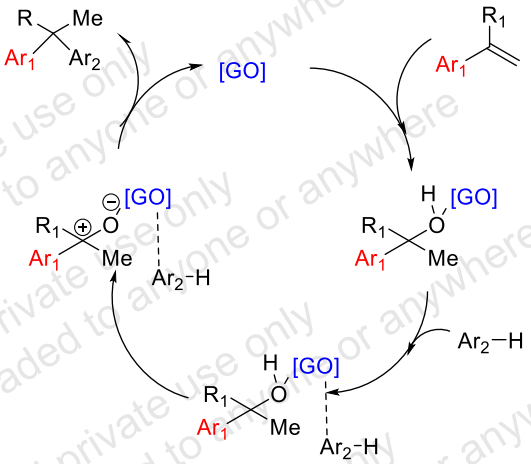

Fig. (2). Reaction pathway for the GO-catalysed alkylation of arenes.

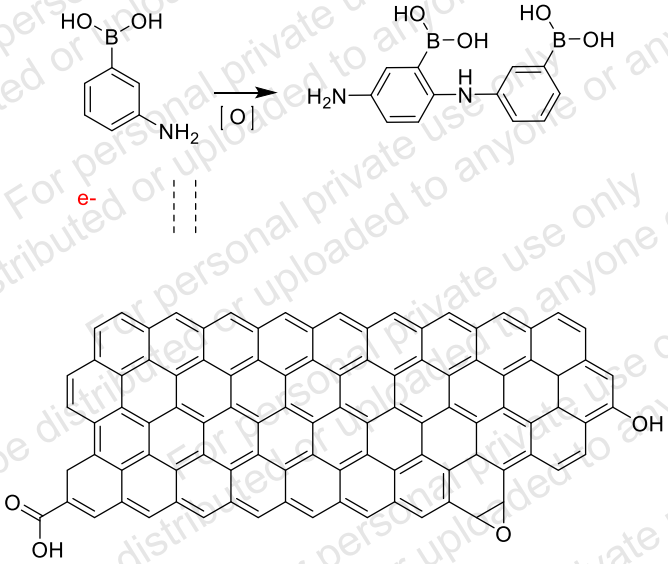

Scheme 15. Schematic illustration of the electron-withdrawing process from the RGO Substrate to ABA.

The preparation of graphene oxide (GO) carbocatalyst by the Hummers method is well-known. A graphite's oxidation in presence of strong acidic conditions and strong oxidizing agents gives GO. This method enhances the oxygen-functionalized groups on the GO surface. GO is can be retrieved back effectively after the reaction process and it is also be used as an acid catalyst for opening the ring of epoxides. The conversion of carbohydrates to 5-ethoxy methyl furfural (EMF) has been reported. The formation of 5-hydroxymethylfurfural (HMF) on etherification with ethanol and GO catalyst gives EMF. The yield of EMF is

affected by the loading capacity on the carbocatalyst surface and the temperature. This conversion of bio-mass compounds to useful chemicals using GO as a catalyst would open up a wide area of research (Scheme **16**) [78].

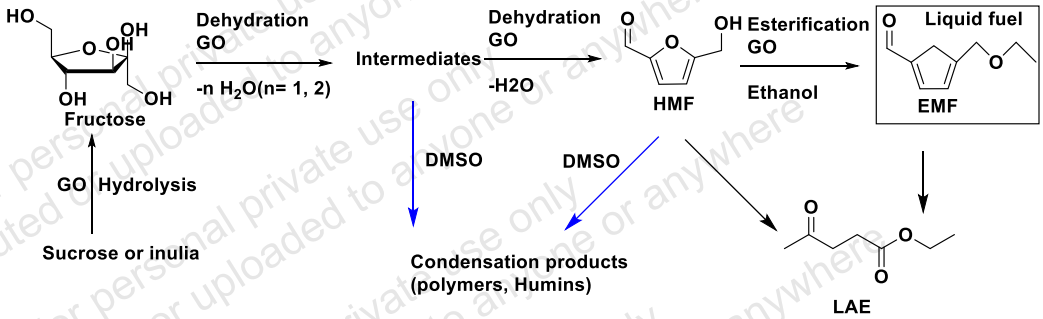

Scheme 16. The conversion of carbohydrates to EMF catalyzed by GO.

3.7. Other Useful Reactions

In a range of applications, graphene-based materials with hierarchical structures and multifunctionality have roused attention. Yang *et al*. reported a simple, yet universal, the method for making graphene-based composite cellular foams (GCCFs) using a mixture of redox reactions. Cationic polymers facilitate assembly and biomimetic mineralization. Cationic polymers (*e.g*., polyethyleneimine, lysozyme, *etc*.) could not only decrease and assemble graphene oxide (GO) into cellular foams, but they could also induce mineralization, allowing the formation of inorganic nanoparticles (silica, titania, silver, and so on). The GCCFs have a highly porous structure and adequate structural stability, with nanoparticles evenly distributed on the surface of the reduced GO. A series of GCCFs are synthesized by varying polymer/inorganic pairs, which exhibit significantly improved catalytic performance in enzyme catalysis, heterogeneous chemical catalysis, and photocatalysis when compared to nanoparticulate catalysts [79].

Furthermore, graphene oxide is good support for immobilizing lipase in an organic solvent for catalysis. Lipase was immobilized using carboxyl functionalized graphene oxide (GO-COOH). To characterize lipase immobilization, FTIR, UV-vis, and XPS spectra were measured. The immobilized lipase retains 80% of the hydrolytic activity of the native lipase at the optimum temperature of 40 °C. The catalysis efficiency of the immobilized lipase is 1.6 times that of native lipase. when catalyzing the enantioselective reaction in the organic solvent heptane at 50 °C (optimal), and the immobilized lipase retains the native lipase's selectivity [80].

Using a spray-drying approach, Z. Xu *et. al*. developed hollow reduced graphene oxide microspheres containing well-distributed Fe_2O_3 nanoparticles (Fe-rGOS). L-ascorbic acid was used to decrease graphite oxide (GO) and increase electron transfer velocity. The *in situ* Fe_2O_3 nanoparticles with a mean size of 5-10 nm were uniformly deposited on rGO support due to the L-ascorbic acid and spray-drying procedure, and the rGO migrated to the drop's surface to form microspheres. The well-dispersed nanoparticles not only generated more active sites and interface contact, which improved catalyst stability but also acted as pillars between the rGO layers, resulting in a mesoporous structure. The formed mesoporous frameworks significantly improved mass transfer, resulting in significantly higher catalytic efficiency. As a result, the prepared Fe-rGOS demonstrated remarkable photocatalytic activity across a wide pH range, as well as superior recyclability with low iron ion leaching [81].

The detailed syntheses of miscellaneous heterocyclic compounds catalyzed by graphene-based carbocatalysts were very well-reviewed [76]. The Cu–Cu_2O@RGO nanocomposite was studied as a promising reusable catalyst in a multicomponent reaction of halides and sodium azide with terminal alkynes for the synthesis of 1,4-disubstituted 1,2,3-triazoles [82] (Scheme **17**). Strikingly, the merging of RGO and Cu–Cu_2O nanocomposite prevents the aggregation of RGO but also enhances the improved stability and catalytic performance of the metal nanoparticles loaded at RGO.

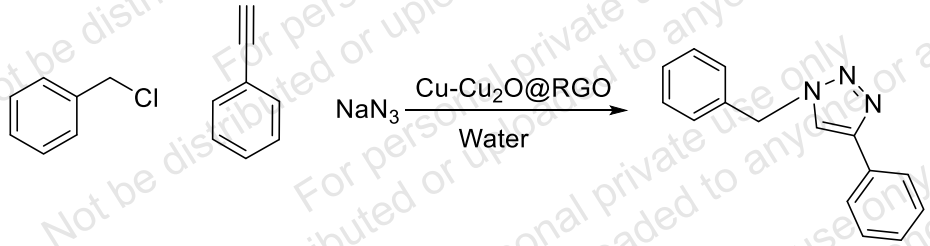

Scheme 17. Cu-Cu_2O@RGO catalyzed synthesis of triazoles by a facile cycloaddition.

Gupta *et al*. [83] described an effective and viable click reaction for the one-pot synthesis of hybrid molecules containing flavanone with triazole by amalgamating Michael addition using copper oxide/reduced graphene oxide (CuO/rGO) nanocomposite (Scheme **18**). A comparison of CuO/rGO with other catalysts was carried out.

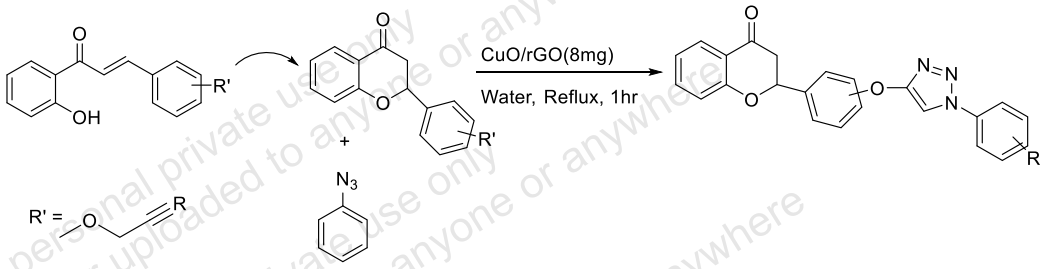

Scheme 18. CuO/rGO catalyzed synthesis of flavanone containing triazole derivatives.

A three-component reaction of sodium azide and alkyl halides in the presence of terminal alkynes was reported [84] by using functionalized graphene oxide copper(I) complex (GO–NH–IA–Cu(I)) under ultrasonic irradiation at room temperature (Scheme **19**).

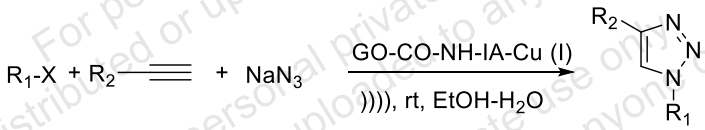

Where X = Cl, Br, I; R_1 = alkyl, benzyl, cinnamyl and R_2 = Ph, CH_3-Ph, $CH_3CH_2CH_3$

Scheme 19. Catalytic synthesis of triazole derivatives by functionalized graphene oxide-Cu(I) complex.

In addition to this, studies on the catalytic synthesis of β-hydroxy-1,2,3-triazole derivatives from aryl-substituted epoxide, phenylacetylene, and sodium azide by GO@polytriazole–Cu (GO@PTA–Cu) mediated by ultrasound irradiation were carried out [85] (Scheme **20**).



Where Ph = C_6H_5, 4-CH_3-C_6H_5 and $C_6H_5OCH_2$

Scheme 20. Catalytic synthesis of β-hydroxy-1,2,3-triazole derivatives using GO@polytriazole-Cu-catalyst.

Furthermore, Xiong *et al*. [86] used GO/Fe_3O_4–CuBr catalyst was employed as a special semi-heterogeneous catalyst for the multicomponent reaction of azide, alkyl halide, and alkyne through 1,3-dipolar cycloaddition by microwave irradiation to yield mono/bis-1,2,3-triazoles (Scheme **21**).

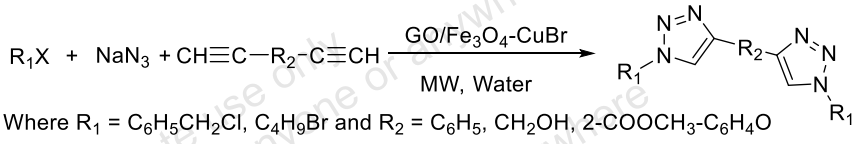

Scheme 21. Microwave-assisted catalytic synthesis of substituted-1,2,3-triazoles using GO/Fe_3O_4-CuBr.

Narayanan *et al*. [87] reported neat, effective, and simple Biginelli reactions of aryl aldehyde, ethyl acetoacetate, and urea in the presence of clay-graphene oxide as recyclable nanocatalyst (montmorillonite clay–GO) (Scheme **22**).

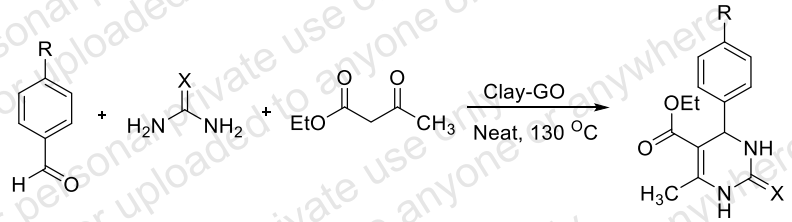

Scheme 22. Clay-GO nanocomposite catalyzed synthesis of 3,4-dihydropyrimidinone.

Similarly, Moitra *et al*. [88] reported a solvent-free preparation of 3,4-dihydropyrimidin-2(1H)-ones (Scheme **23**) in presence of $BiFeO_3$ nanowire-reduced graphene oxide (BFO-RGO) nanocatalyst. Furthermore, Akocak *et al*. [89] established an eco-friendly method for the synthesis of 2-amino--H-chromene derivatives *via* condensation of resorcinol, malononitrile, and diverse aromatic aldehydes in the presence of palladium nanoparticles loaded on graphene oxide (Pd@GO) (Scheme **24**).

Investigations were carried out on the usage of magnetically separable nanocatalyst, Fe_3O_4-supported-N-pyridin-4-amine-grafted graphene oxide for the synthesis of chromenes from a multicomponent reaction of malononitrile, dimedone, and aryl aldehydes [90] (Scheme **25**).

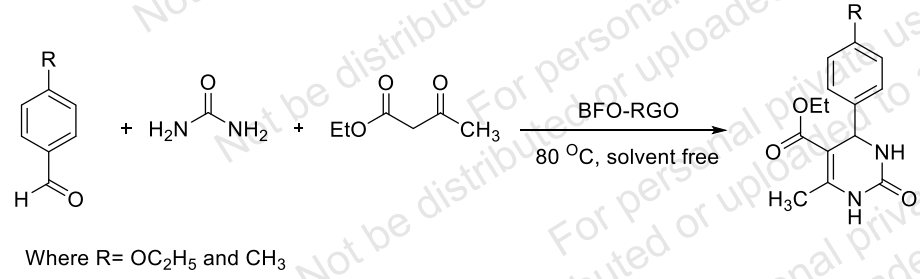

Scheme 23. Biginelli reaction catalyzed by $BiFeO_3$-reduced graphene oxide nanocatalyst.

Not be distributed or uploaded to anyone or anywhere
For personal private use only

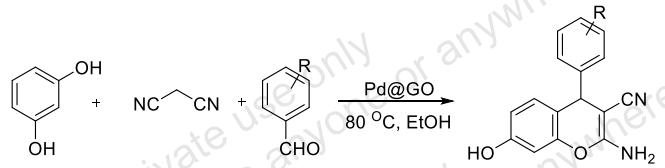

Where R= H, 4-CH_3, 4-$CH(CH_3)_2$, 4-CN, 4-OCH_3, 4-$N(CH_3)_2$, 3,4-OCH_3, 3,4,5-OCH_3, 3,5-CH_3 and 2,3,5,6-F

Scheme 24. Catalytic synthesis of 2-amino-4*H*-chromene by Pd@GO nanoparticles.

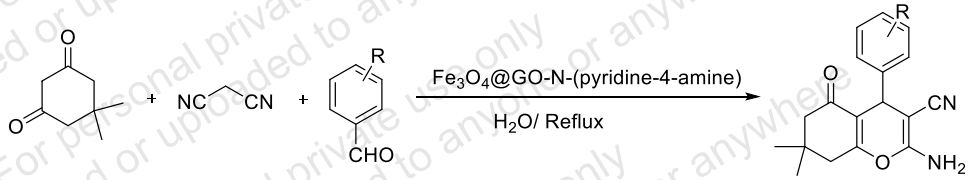

Where R= H, 4-F, 4-CH_3, 4-Cl, 2-Cl, 3-NO_2, 4-NO_2 and 4-OH

Scheme 25. Fe_3O_4@GO-*N*-(Pyridin-4-amine) catalytic synthesis of chromenes.

A multi-component reaction of aryl glyoxals with 4-hydroxycoumarin, and malononitrile was reported using metal-free graphene oxide (GO) nanosheets [91] (Scheme **26**).

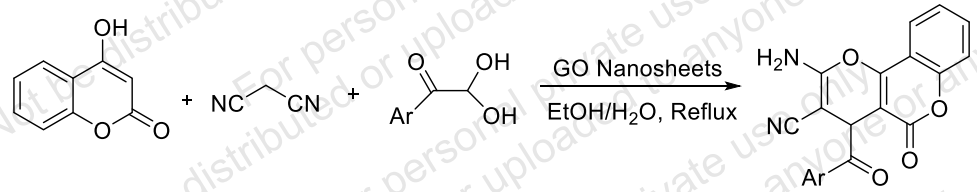

Where Ar= C_6H_5, 1-naphthyl, 2-Cl-C_6H_4, 4-NO_2-C_6H_4, 4-Br-C_6H_4 and 4-CH_3O-C_6H_4

Scheme 26. GO nanosheets catalyzed preparation of pyranocoumarins.

A four-component reaction of phenylhydrazine, aldehydes, ethyl acetoacetate, and 4-hydroxycoumarin was demonstrated for the preparation of highly functionalized benzylpyrazolyl coumarins employing mesoporous/biogenic graphene oxide nanoparticles by Siddiqui *et al*. [92] (Scheme **27**).

The catalytic preparation of a variety of 1-H spiro[isoindoline-1,2- quinazoline]-3,4-(3-H)-diones was reported by the reaction of aliphatic, or aromatic primary amines with isatoic anhydride in the presence of isatin using acidic magnetic graphene oxide nanosheets (Fe_3O_4–GO–SO_3H) by Abdi *et al*. [93] (Scheme **28**).

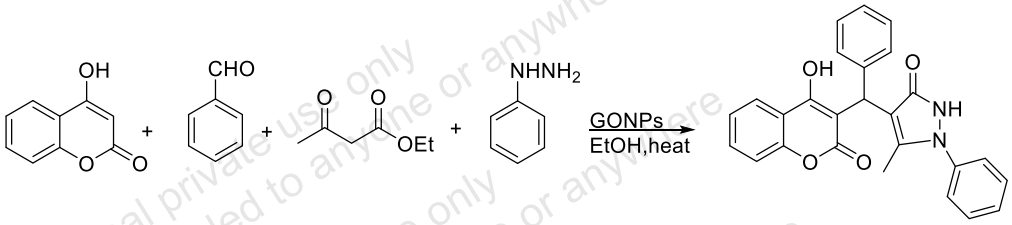

Scheme 27. GONPs catalyzed synthesis of benzyl pyrazolyl coumarins.

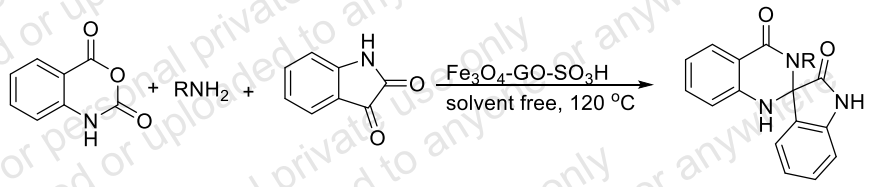

Where R= H, cyclohexyl, Ph, n-Bu, 4-CH_3-C_6H_4, 4-CH_{30}-C_6H_4, 3-CH_3O-C_6H_4, 4-Br-C_6H_4, 3-Cl-C_6H_4, 4-NO_2-C_6H_4

Scheme 28. Catalytic synthesis of 1-H spiro[isoindoline-1,2-quinazoline]-3,4-(3-*H*)-diones by Fe_3O_4-GO-SO_3H.

A tandem synthesis of benzo[b] [1, 4]diazepine derivatives was performed [94] by the reaction of ethyl-3-oxobutanoate,2-nitroaniline, isocyanide, and $TMSN_3$ as substrates using the bimetallic nanoparticles (AuCu and AgCu) supported on guanidine-grafted-rGO nanosheets (AuCu@G-rGO and AgCu@G-rGO) as catalysts and (Scheme **29**).

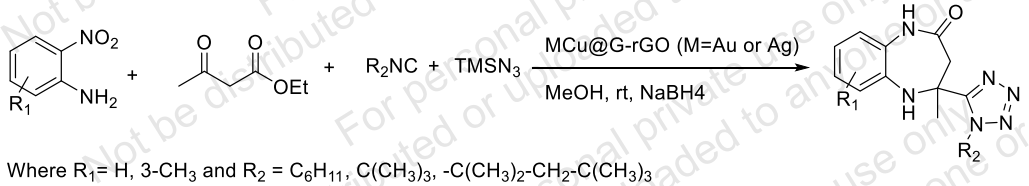

Where R_1= H, 3-CH_3 and R_2 = C_6H_{11}, $C(CH_3)_3$, -$C(CH_3)_2$-CH_2-$C(CH_3)_3$

Scheme 29. AuCu@G-rGO/AgCu@G-rGOcatalyzedsynthesis of benzo[b] [1, 4]diazepine derivatives.

Kausar *et al*. [95] reported a metal-free carbocatalyst to prepare a variety of dibenzo [1, 4] diazepine scaffolds from *o*-phenylene diamine, aldehydes, or ketones, and 1,3-diketo compounds (Scheme **30**) employing graphene oxide (GO) nanosheets as carbocatalyst to producedibenzo [1, 4]diazepines.

Several carbocatalysts have been examined for PMS activation for the oxidation of phenol in an aqueous medium. In absence of carbocatalyst, the PMS could unable to generate activated radicals for phenol degradation. In parallel, without PMS addition, hardly 4% of phenol was removed because of adsorption on the NG-700 surface.

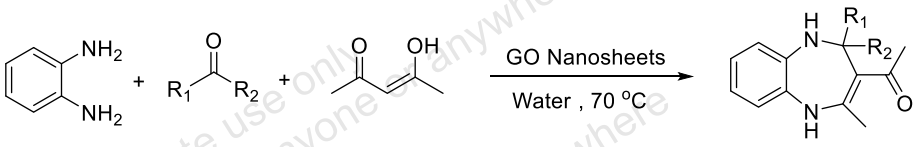

Where R_1 = H, CH_3 and R_2 = aryl, heteroaryl, alkyl and benzoyl

Scheme 30. GO nanosheet catalyzed preparation of dibenzo [1, 4]diazepines.

The GO and RGO catalysts usually are not that stable or soluble in an aqueous medium and there is a need for optimization of this catalytic activity of GO and RGO by incorporating a polymer PSSS (poly(sodium 4-styrene sulfonate)) which enhances the dispersion of this catalyst in an aqueous medium. PSSS is water-soluble which is incorporated into the graphene surface through a radical initiator (ATRP). ATRP use is that it facilitates the incorporation of PSSS on the graphene surface. Once this GO-g-PSSS catalyst is ready, it can be used as the catalyst for various chemical reactions. In the same way, RGO-*g*-PSSS is also improvised which also helps in the synthesis of isoamyl benzoate (Scheme **31**). Also, the PSSS is pH-sensitive, such that the introduction of any drugs to the surface can be released concerning the drug's response to the change of pH. This method is used to improvise the dispersion of graphene oxide and reduced graphene oxide in the aqueous solution [96].

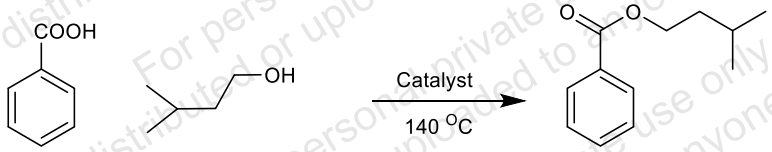

Scheme 31. Preparation of isoamyl benzoate.

CONCLUSION AND FUTURE PROSPECTS

With the development of several advanced catalytic systems for diverse chemical processes, carbocatalysts are one of the efficient classes of heterogeneous materials of high industrial significance. Several GO based catalysts employed for a wide range of organic transformations reported in the past are summarised in Table **5**. Owing to their remarkable properties, including high intrinsic mobility, large specific surface area, excellent electrical conductivity, high thermal conductivity, ease of preparation, chemical inertness, and facile functionalization, graphene-based materials have become promising recyclable and sustainable catalysts. In the light of this, the present chapter highlights the preparation of different types of carbocatalysts, the possible reaction mechanisms, and multi-

component organic transformations. Various graphene-based materials (graphene oxide/ reduced graphene oxide/ their nanosheets/metal-nanoparticles grafted on graphene/ functionalized graphene oxide/ quantum dots/ graphene oxide-spinel composites) have been employed for the preparation of a variety of heterocyclic molecules. Relatively faster synthesis of thiophenes, triazoles, aziridines, tetrazoles, pyrazoles, imidazoles, furans, oxindoles, pyrimidines, chromenes, coumarins, quinazolines, oxazoles, quinoxalines, xanthenes, pyridines, and diazepines was reported in good to excellent yields. The high catalytic activity of graphene-based catalysts is mainly attributed to the incorporation of Brønsted acid sites and/ or Lewis acid-base centers in these carbon materials, accompanied by π–π stacking and electrostatic interactions through the increased adsorption of reactants. Additionally, the advantage of these carbocatalysts is that they are very easy to recover by filtration/centrifugation and/or magnetic decantation. Moreover, the low catalyst loading, renewability, and solvent-free conditions make them very special catalytic systems concerning sustainability and environmentally benign processes. The major limitations of these graphene-based carbocatalysts are the identification of the actual reactive sites of graphene oxide, functionalities, defects, and edges. These problems can be overcome when suitable models are designed describing the structure of graphene-based materials at the molecular level. Still, better graphene-based carbocatalysts need to be developed with less complexity and cost-effectiveness by doping/ double doping with B/ B-N/ P-N and other appropriate dopants, as evident in the facile activation of molecular hydrogen at the periphery and holes with zigzag edges. This will be a promising field for future applications of catalysis by graphene-based materials.

Table 5. Previously reported graphene oxide catalyzed reactions.

S.no	Catalyst	Reaction	Reference
1	rGO	Oxidation of methylene blue, phenol, 2,4-dichlorophenol by H_2O_2	[97]
2	(B, N) doped rGO	Oxidation of phenol by peroxymonosulfate or H_2O_2	[98]
3	rGO	Hydrogenation	[99-100]
4	rGO or N-rGO	Reduction of 4-nitrophenol to 4-aminophenol by $NaBH_4$	[101-102]
5	rGO	Synthesis of dipyrromethene, calix [4] pyrrole and 5-substituted 1H-tetrazoles	[103-104]
6	rGO	Thermal dehydrogenation and re-hydrogenation of $LiBH_4$	[105]
7	rGO-NEt_3	Hydrolysis of ethyl acetate	[106]
8	rGO-PAMAM	Knoevenagel condensation	[107]
9	rGO-SO_3H	Dehydration of xylose to furfural, Esterification and transesterification, pechmann reaction, hydration of propylene oxide	[108-110]

(Table 5) cont.....

10	rGO-poly(styrene sulfonic acid)	Synthesis of isoamyl benzoate	[111]
11	rGO-Ar-SO_3H	Hydrolysis of ethyl acetate, synthesis of xanthenes and benzoxanthenes	[112-113]
12	GO	Aerobic oxidation of alcohols	[114-115]
13	GO	Dehydrogenation of propane to propene	[116]
14	GO	Aerobic oxidation of SO_2	[117]
15	GO or rGO	Polymerization of 3-aminophenylboronic acid	[118]
16	GO	Ring opening of epoxides	[119]
17	GO	Michael addition reaction	[120]
18	GO	Aza-michael addition of amines to alkenes	[121]
19	GO	Dehydrative esterification of benzyl alcohol	[122]

LIST OF ABBREVIATIONS

AC	Activated Carbon
AA	L-Ascorbic Acid
ABA	Azo Benzoic Acid
ATRP	Atom Transfer Radical Polymerization
ASC	Ascorbic acid
CDG	Chemically derived Graphene
CVD	Chemical Vapour Deposition
DH	Dopamine Hydrochloride
DCP	Dichlorophenol
DH	Dehydrogenation
DMSO	Dimethyl Sulfoxide
EG	Ethyleneglycol
EMF	5-Ethoxy Methyl Furfural
GO	Graphene Oxide
GP	Graphite Powder
GCCF	Graphene Composite Cellular Foam
HMF	5-Hydroxy Methyl Furfural
HCCP	Hexachlorocyclotriphosphazene
HQ	Hydroquinone
HZ	Hydrazine
HER	Hydrogen Evolution Reaction

For personal private use only Not be distributed or uploaded to anyone or anywhere

ME	2-Mercapto Ethanol
MWCNT	Multi Wall Carbon Nanotube
MB	Methylene Blue
MEG	Microwave Exfoliated Graphite
MGN	Metal Graphene Nanocomposite
NPG	N&P double doped Graphene
[(N)G]	N-doped defective Graphene
ODH	Oxidative Dehydrogenation
PMS	Peroxymonosulphate
PSSS	[Poly(Sodium-4-Styrene Sulfonate)]
rGO	Reduced Graphene Oxide
rGO-PAMAM	Poly(amidoamine)-modified Reduced Graphene Oxide
SA-GO	Sulfur Graphene Oxide
TBHP	Tert-Butyl Hydroperoxide
$TMSN_3$	Trimethylsilylazide
TOF	Turn Over Frequency

CONSENT FOR PUBLICATION

Not applicable.

CONFLICT OF INTEREST

The author declares no conflict of interest, financial or otherwise.

ACKNOWLEDGEMENTS

Declared none.

REFERENCES

[1] a) Stratakis, M.; Garcia, H. Catalysis by supported gold nanoparticles: beyond aerobic oxidative processes. *Chem. Rev.,* **2012**, *112*(8), 4469-4506. [http://dx.doi.org/10.1021/cr3000785] [PMID: 22690711] b) Sivaramakrishna, A.; Clayton, H.S.; Mogorosi, M.M.; Moss, J.R. Hydrocarbon (π- and σ-) complexes of nickel, palladium and platinum: Synthesis, reactivity and applications. *Coord. Chem. Rev.,* **2010**, *254*(23-24), 2904-2932. [http://dx.doi.org/10.1016/j.ccr.2010.05.021] c) Sivaramakrishna, A.; Suman, P.; Veerashekhar Goud, E.; Janardan, S.; Sravani, C.; Sandeep, T.; Vijayakrishna, K.; Clayton, H.S. Review: active homogeneous reagents and catalysts in *n* -alkane activation. *J. Coord. Chem.,* **2013**, *66*(12), 2091-2109. [http://dx.doi.org/10.1080/00958972.2013.797572]

[2] Sherry, B.D.; Fürstner, A. The promise and challenge of iron-catalyzed cross coupling. *Acc. Chem. Res.,* **2008**, *41*(11), 1500-1511. [http://dx.doi.org/10.1021/ar800039x] [PMID: 18588321]

Not be distributed or uploaded to anyone or anywhere For personal private use only

[3] Jana, R.; Pathak, T.P.; Sigman, M.S. Advances in transition metal (Pd, Ni, Fe)-catalyzed cross-coupling reactions using alkyl-organometallics as reaction partners. *Chem. Rev.,* **2011**, *111*(3), 1417-1492.
[http://dx.doi.org/10.1021/cr100327p] [PMID: 21319862]

[4] a) Punniyamurthy, T.; Velusamy, S.; Iqbal, J. Recent advances in transition metal catalyzed oxidation of organic substrates with molecular oxygen. *Chem. Rev.,* **2005**, *105*(6), 2329-2364.
[http://dx.doi.org/10.1021/cr050523v] [PMID: 15941216] b) Yan, Y.; Xia, B.Y.; Zhao, B.; Wang, X. A review on noble-metal-free bifunctional heterogeneous catalysts for overall electrochemical water splitting. *J. Mater. Chem. A Mater. Energy Sustain.,* **2016**, *4*(45), 17587-17603.
[http://dx.doi.org/10.1039/C6TA08075H]

[5] a) Dömling, A.; Wang, W.; Wang, K. Chemistry and biology of multicomponent reactions. *Chem. Rev.,* **2012**, *112*(6), 3083-3135.
[http://dx.doi.org/10.1021/cr100233r] [PMID: 22435608] b) Reddy, M.M.; Sivaramakrishna, A. Remarkably flexible quinazolinones—synthesis and biological applications. *J. Heterocycl. Chem.,* **2020**, *57*(3), 942-954.
[http://dx.doi.org/10.1002/jhet.3844] c) Rocha, R.O.; Rodrigues, M.O.; Neto, B.A.D. Review on the Ugi Multicomponent Reaction Mechanism and the Use of Fluorescent Derivatives as Functional Chromophores. *ACS Omega,* **2020**, *5*(2), 972-979.
[http://dx.doi.org/10.1021/acsomega.9b03684] [PMID: 31984252] d) José Climent, M.; Corma, A.; Iborra, S. Homogeneous and heterogeneous catalysts for multicomponent reactions. *RSC Advances,* **2012**, *2*(1), 16-58.
[http://dx.doi.org/10.1039/C1RA00807B] e) Saranya, S.; Rohit, K.R.; Radhika, S.; Anilkumar, G. Palladium-catalyzed multicomponent reactions: an overview. *Org. Biomol. Chem.,* **2019**, *17*(35), 8048-8061.
[http://dx.doi.org/10.1039/C9OB01538H] [PMID: 31410440]

[6] Titirici, M.M.; Antonietti, M. Chemistry and materials options of sustainable carbon materials made by hydrothermal carbonization. *Chem. Soc. Rev.,* **2010**, *39*(1), 103-116.
[http://dx.doi.org/10.1039/B819318P] [PMID: 20023841]

[7] Schaetz, A.; Zeltner, M.; Stark, W.J. Carbon Modifications and Surfaces for Catalytic Organic Transformations. *ACS Catal.,* **2012**, *2*(6), 1267-1284.
[http://dx.doi.org/10.1021/cs300014k]

[8] Dreyer, D.R.; Bielawski, C.W. Carbocatalysis: Heterogeneous carbons finding utility in synthetic chemistry. *Chem. Sci. (Camb.),* **2011**, *2*(7), 1233-1240.
[http://dx.doi.org/10.1039/c1sc00035g]

[9] Su, C.; Loh, K.P. Carbocatalysts: graphene oxide and its derivatives. *Acc. Chem. Res.,* **2013**, *46*(10), 2275-2285.
[http://dx.doi.org/10.1021/ar300118v] [PMID: 23270430]

[10] Pyun, J. Graphene oxide as catalyst: application of carbon materials beyond nanotechnology. *Angew. Chem. Int. Ed.,* **2011**, *50*(1), 46-48.
[http://dx.doi.org/10.1002/anie.201003897] [PMID: 20979072]

[11] Navalon, S.; Dhakshinamoorthy, A.; Alvaro, M.; Garcia, H. Heterogeneous fenton catalysts based on activated carbon and related materials. *ChemSusChem,* **2011**, *4*(12), 1712-1730.
[http://dx.doi.org/10.1002/cssc.201100216] [PMID: 22162405]

[12] Su, D.S.; Perathoner, S.; Centi, G. Nanocarbons for the development of advanced catalysts. *Chem. Rev.,* **2013**, *113*(8), 5782-5816.
[http://dx.doi.org/10.1021/cr300367d] [PMID: 23721498]

[13] Rao, C.N.R.; Sood, A.K.; Subrahmanyam, K.S.; Govindaraj, A. Graphene: the new two-dimensional nanomaterial. *Angew. Chem. Int. Ed.,* **2009**, *48*(42), 7752-7777.
[http://dx.doi.org/10.1002/anie.200901678] [PMID: 19784976]

Not be distributed or uploaded to anyone or anywhere
For personal private use only

[14] a) Blanita, G.; Lazar, M.D. Mater. Review of graphene-supported metal nanoparticles as new and efficient heterogeneous catalysts. *Micro Nanosyst.,* **2013**, *5*(2), 138-146. [http://dx.doi.org/10.2174/1876402911305020009] b) Zhu, Y.; Murali, S.; Stoller, M.D.; Velamakanni, A.; Piner, R.D.; Ruoff, R.S. Microwave assisted exfoliation and reduction of graphite oxide for ultracapacitors. *Carbon,* **2010**, *48*(7), 2118-2122. [http://dx.doi.org/10.1016/j.carbon.2010.02.001] c) Xi, J.; Wang, Q.; Liu, J.; Huan, L.; He, Z.; Qiu, Y.; Zhang, J.; Tang, C.; Xiao, J.; Wang, S. N,P-dual-doped multilayer graphene as an efficient carbocatalyst for nitroarene reduction: A mechanistic study of metal-free catalysis. *J. Catal.,* **2018**, *359*, 233-241. [http://dx.doi.org/10.1016/j.jcat.2018.01.003]

[15] Dreyer, D.R.; Park, S.; Bielawski, C.W.; Ruoff, R.S. The chemistry of graphene oxide. *Chem. Soc. Rev.,* **2010**, *39*(1), 228-240. [http://dx.doi.org/10.1039/B917103G] [PMID: 20023850]

[16] Jia, X.; Campos-Delgado, J.; Terrones, M.; Meunier, V.; Dresselhaus, M.S. Graphene edges: a review of their fabrication and characterization. *Nanoscale,* **2011**, *3*(1), 86-95. [http://dx.doi.org/10.1039/C0NR00600A] [PMID: 21103548]

[17] Kuila, T.; Bose, S.; Mishra, A.K.; Khanra, P.; Kim, N.H.; Lee, J.H. Chemical functionalization of graphene and its applications. *Prog. Mater. Sci.,* **2012**, *57*(7), 1061-1105. [http://dx.doi.org/10.1016/j.pmatsci.2012.03.002]

[18] Soldano, C.; Mahmood, A.; Dujardin, E. Production, properties and potential of graphene. *Carbon,* **2010**, *48*(8), 2127-2150. [http://dx.doi.org/10.1016/j.carbon.2010.01.058]

[19] Chua, C.K.; Pumera, M. Covalent chemistry on graphene. *Chem. Soc. Rev.,* **2013**, *42*(8), 3222-3233. [http://dx.doi.org/10.1039/c2cs35474h] [PMID: 23403465]

[20] Georgakilas, V.; Otyepka, M.; Bourlinos, A.B.; Chandra, V.; Kim, N.; Kemp, K.C.; Hobza, P.; Zboril, R.; Kim, K.S. Functionalization of graphene: covalent and non-covalent approaches, derivatives and applications. *Chem. Rev.,* **2012**, *112*(11), 6156-6214. [http://dx.doi.org/10.1021/cr3000412] [PMID: 23009634]

[21] Chen, L.; Hernandez, Y.; Feng, X.; Müllen, K. From nanographene and graphene nanoribbons to graphene sheets: chemical synthesis. *Angew. Chem. Int. Ed.,* **2012**, *51*(31), 7640-7654. [http://dx.doi.org/10.1002/anie.201201084] [PMID: 22777811]

[22] Chua, C.K.; Pumera, M. Chemical reduction of graphene oxide: a synthetic chemistry viewpoint. *Chem. Soc. Rev.,* **2014**, *43*(1), 291-312. [http://dx.doi.org/10.1039/C3CS60303B] [PMID: 24121318]

[23] Singh, V.; Joung, D.; Zhai, L.; Das, S.; Khondaker, S.I.; Seal, S. Graphene based materials: Past, present and future. *Prog. Mater. Sci.,* **2011**, *56*(8), 1178-1271. [http://dx.doi.org/10.1016/j.pmatsci.2011.03.003]

[24] Tunckol, M.; Durand, J.; Serp, P. Carbon nanomaterial–ionic liquid hybrids. *Carbon,* **2012**, *50*(12), 4303-4334. [http://dx.doi.org/10.1016/j.carbon.2012.05.017]

[25] Krishnan, D.; Kim, F.; Luo, J.; Cruz-Silva, R.; Cote, L.J.; Jang, H.D.; Huang, J. Energetic graphene oxide: Challenges and opportunities. *Nano Today,* **2012**, *7*(2), 137-152. [http://dx.doi.org/10.1016/j.nantod.2012.02.003]

[26] Hur, S.H.; Park, J.N. Graphene and its application in fuel cell catalysis: a review. *Asia-Pac. J. Chem. Eng.,* **2013**, *8*(2), 218-233. [http://dx.doi.org/10.1002/apj.1676]

[27] Malig, J.; Jux, N.; Guldi, D.M. Toward multifunctional wet chemically functionalized graphene-integration of oligomeric, molecular, and particulate building blocks that reveal photoactivity and

redox activity. *Acc. Chem. Res.,* **2013**, *46*(1), 53-64.
[http://dx.doi.org/10.1021/ar300124z] [PMID: 22916796]

[28] Rodríguez-Pérez, L.; Herranz, M.Á.; Martín, N. The chemistry of pristine graphene. *Chem. Commun. (Camb.),* **2013**, *49*(36), 3721-3735.
[http://dx.doi.org/10.1039/c3cc38950b] [PMID: 23539514]

[29] James, D.K.; Tour, J.M. Graphene: powder, flakes, ribbons, and sheets. *Acc. Chem. Res.,* **2013**, *46*(10), 2307-2318.
[http://dx.doi.org/10.1021/ar300127r] [PMID: 23276286]

[30] Zhang, Y.; Zhang, L.; Zhou, C. Review of chemical vapor deposition of graphene and related applications. *Acc. Chem. Res.,* **2013**, *46*(10), 2329-2339.
[http://dx.doi.org/10.1021/ar300203n] [PMID: 23480816]

[31] Wang, H.; Yuan, X.; Wu, Y.; Huang, H.; Peng, X.; Zeng, G.; Zhong, H.; Liang, J.; Ren, M. M. Graphene-based materials: fabrication, characterization and application for the decontamination of wastewater and wastegas and hydrogen storage/generation. *Adv. Colloid Interface Sci,* **2013**, 195−196-19-40.

[32] Ciesielski, A.; Samorì, P. Graphene *via* sonication assisted liquid-phase exfoliation. *Chem. Soc. Rev.,* **2014**, *43*(1), 381-398.
[http://dx.doi.org/10.1039/C3CS60217F] [PMID: 24002478]

[33] Loh, K.P.; Bao, Q.; Ang, P.K.; Yang, J. The chemistry of graphene. *J. Mater. Chem.,* **2010**, *20*(12), 2277-2289.
[http://dx.doi.org/10.1039/b920539j]

[34] Brownson, D.A.C.; Kampouris, D.K.; Banks, C.E. Graphene electrochemistry: fundamental concepts through to prominent applications. *Chem. Soc. Rev.,* **2012**, *41*(21), 6944-6976.
[http://dx.doi.org/10.1039/c2cs35105f] [PMID: 22850696]

[35] Zhu, Y.; Murali, S.; Cai, W.; Li, X.; Suk, J.W.; Potts, J.R.; Ruoff, R.S. Graphene and graphene oxide: synthesis, properties, and applications. *Adv. Mater.,* **2010**, *22*(35), 3906-3924.
[http://dx.doi.org/10.1002/adma.201001068] [PMID: 20706983]

[36] Shen, J.; Zhu, Y.; Yang, X.; Li, C. Graphene quantum dots: emergent nanolights for bioimaging, sensors, catalysis and photovoltaic devices. *Chem. Commun. (Camb.),* **2012**, *48*(31), 3686-3699.
[http://dx.doi.org/10.1039/c2cc00110a] [PMID: 22410424]

[37] Dirian, K.; Herranz, M.Á.; Katsukis, G.; Malig, J.; Rodríguez-Pérez, L.; Romero-Nieto, C.; Strauss, V.; Martín, N.; Guldi, D.M. Low dimensional nanocarbons – chemistry and energy/electron transfer reactions. *Chem. Sci. (Camb.),* **2013**, *4*(12), 4335-4353.
[http://dx.doi.org/10.1039/c3sc51100f]

[38] Agnoli, S.; Granozzi, G. Second generation graphene: Opportunities and challenges for surface science. *Surf. Sci.,* **2013**, *609*, 1-5.
[http://dx.doi.org/10.1016/j.susc.2012.11.016]

[39] Li, N.; Cao, M.; Hu, C. Review on the latest design of graphene-based inorganic materials. *Nanoscale,* **2012**, *4*(20), 6205-6218.
[http://dx.doi.org/10.1039/c2nr31750h] [PMID: 22961110]

[40] Wang, H.X.; Wang, Q.; Zhou, K.G.; Zhang, H.L. Graphene in light: design, synthesis and applications of photo-active graphene and graphene-like materials. *Small,* **2013**, *9*(8), 1266-1283.
[http://dx.doi.org/10.1002/smll.201203040] [PMID: 23554268]

[41] Zheng, Y.; Liu, J.; Liang, J.; Jaroniec, M.; Qiao, S.Z. Graphitic carbon nitride materials: controllable synthesis and applications in fuel cells and photocatalysis. *Energy Environ. Sci.,* **2012**, *5*(5), 6717-6731.
[http://dx.doi.org/10.1039/c2ee03479d]

[42] Sharma, S.; Pollet, B.G. Support materials for PEMFC and DMFC electrocatalysts—A review. *J.*

Not be distributed or uploaded to anyone or anywhere
For personal private use only

Power Sources, **2012**, *208*, 96-119.
[http://dx.doi.org/10.1016/j.jpowsour.2012.02.011]

[43] Candelaria, S.L.; Shao, Y.; Zhou, W.; Li, X.; Xiao, J.; Zhang, J.G.; Wang, Y.; Liu, J.; Li, J.; Cao, G. Nanostructured carbon for energy storage and conversion. *Nano Energy,* **2012**, *1*(2), 195-220.
[http://dx.doi.org/10.1016/j.nanoen.2011.11.006]

[44] Cheng, F.; Chen, J. Metal–air batteries: from oxygen reduction electrochemistry to cathode catalysts. *Chem. Soc. Rev.,* **2012**, *41*(6), 2172-2192.
[http://dx.doi.org/10.1039/c1cs15228a] [PMID: 22254234]

[45] Pumera, M. Graphene-based nanomaterials and their electrochemistry. *Chem. Soc. Rev.,* **2010**, *39*(11), 4146-4157.
[http://dx.doi.org/10.1039/c002690p] [PMID: 20623061]

[46] Chen, D.; Tang, L.; Li, J. Graphene-based materials in electrochemistry. *Chem. Soc. Rev.,* **2010**, *39*(8), 3157-3180.
[http://dx.doi.org/10.1039/b923596e] [PMID: 20589275]

[47] Chen, D.; Feng, H.; Li, J. Graphene oxide: preparation, functionalization, and electrochemical applications. *Chem. Rev.,* **2012**, *112*(11), 6027-6053.
[http://dx.doi.org/10.1021/cr300115g] [PMID: 22889102]

[48] a) Xiang, Q.; Yu, J.; Jaroniec, M. Graphene-based semiconductor photocatalysts. *Chem. Soc. Rev.,* **2012**, *41*(2), 782-796.
[http://dx.doi.org/10.1039/C1CS15172J] [PMID: 21853184] b) Sun, Z.; Ye, Q.; Chi, C.; Wu, J. Low band gap polycyclic hydrocarbons: from closed-shell near infrared dyes and semiconductors to open-shell radicals. *Chem. Soc. Rev.,* **2012**, *41*(23), 7857-7889.
[http://dx.doi.org/10.1039/c2cs35211g] [PMID: 22918297]

[49] Al Kausor, M.; Chakrabortty, D. Graphene oxide based semiconductor photocatalysts for degradation of organic dye in waste water: A review on fabrication, performance enhancement and challenges. *Inorg. Chem. Commun.,* **2021**, *129*, 108630.
[http://dx.doi.org/10.1016/j.inoche.2021.108630]

[50] Gupta, S.; Banu, R.; Ameta, C.; Ameta, R.; Punjabi, P.B. Emerging Trends in the Syntheses of Heterocycles Using Graphene-based Carbocatalysts: An Update. *Top. Curr. Chem. (Cham),* **2019**, *377*(3), 13.
[http://dx.doi.org/10.1007/s41061-019-0238-3] [PMID: 31054016]

[51] Li, X.; Duan, X.; Han, C.; Fan, X.; Li, Y.; Zhang, F.; Zhang, G.; Peng, W.; Wang, S. Chemical activation of nitrogen and sulfur co-doped graphene as defect-rich carbocatalyst for electrochemical water splitting. *Carbon,* **2019**, *148*, 540-549.
[http://dx.doi.org/10.1016/j.carbon.2019.04.021]

[52] Hummers, W.S., Jr; Offeman, R.E. Preparation of Graphitic Oxide. *J. Am. Chem. Soc.,* **1958**, *80*(6), 1339-1339.
[http://dx.doi.org/10.1021/ja01539a017]

[53] Duan, X.; Ao, Z.; Sun, H.; Indrawirawan, S.; Wang, Y.; Kang, J.; Liang, F.; Zhu, Z.H.; Wang, S. Nitrogen-doped graphene for generation and evolution of reactive radicals by metal-free catalysis. *ACS Appl. Mater. Interfaces,* **2015**, *7*(7), 4169-4178.
[http://dx.doi.org/10.1021/am508416n] [PMID: 25632991]

[54] Dreyer, D.R.; Jia, H.P.; Bielawski, C.W. Graphene Oxide: A Convenient Carbocatalyst for Facilitating Oxidation and Hydration Reactions. Angew. Chem. Intern. Ed. , **2010**; pp. 6813-6815.

[55] Yang, J.H.; Sun, G.; Gao, Y.; Zhao, H.; Tang, P.; Tan, J.; Lu, A.H.; Ma, D. Direct catalytic oxidation of benzene to phenol over metal-free graphene-based catalyst. *Energy Environ. Sci.,* **2013**, *6*(3), 793-798.
[http://dx.doi.org/10.1039/c3ee23623d]

Not be distributed or uploaded to anyone or anywhere
For personal private use only

[56] Dhakshinamoorthy, A.; Latorre-Sanchez, M.; Asiri, A.M.; Primo, A.; Garcia, H. Sulphur-doped graphene as metal-free carbocatalysts for the solventless aerobic oxidation of styrenes. *Catal. Commun.,* **2015**, *65*, 10-13.
[http://dx.doi.org/10.1016/j.catcom.2015.02.018]

[57] Mittal, R.; Kumar, A.; Awasthi, S.K. Practical scale up synthesis of carboxylic acids and their bioisosteres 5-substituted-1 *H* -tetrazoles catalyzed by a graphene oxide-based solid acid carbocatalyst. *RSC Advances,* **2021**, *11*(19), 11166-11176.
[http://dx.doi.org/10.1039/D1RA01053K] [PMID: 35423636]

[58] a) Espinosa, J.C.; Álvaro, M.; Dhakshinamoorthy, A.; Navalón, S.; García, H. Engineering active sites in reduced graphene oxide: Tuning the catalytic activity for aerobic oxidation. *ACS Sustain. Chem.& Eng.,* **2019**, *7*(19), 15948-15956.
[http://dx.doi.org/10.1021/acssuschemeng.9b02237] b) Kitano, M.; Yamaguchi, D.; Suganuma, S.; Nakajima, K.; Kato, H.; Hayashi, S.; Hara, M. Adsorption-enhanced hydrolysis of β-1,4-glucan on graphene-based amorphous carbon bearing SO3H, COOH, and OH groups. *Langmuir,* **2009**, *25*(9), 5068-5075.
[http://dx.doi.org/10.1021/la8040506] [PMID: 19397353]

[59] Anumula, R.; Cui, C.; Yang, M.; Li, J.; Luo, Z. Catalytic Oxidation of Cyclohexane on Small Silver Clusters Supported by Graphene Oxide. *J. Phys. Chem. C,* **2019**, *123*(35), 21504-21512.
[http://dx.doi.org/10.1021/acs.jpcc.9b04405]

[60] Mondal, A.; Jana, N.R. Surfactant-free, stable noble metal–graphene nanocomposite as high-performance electrocatalyst. *ACS Catal.,* **2014**, *4*(2), 593-599.
[http://dx.doi.org/10.1021/cs401032p]

[61] Candu, N.; Man, I.; Simion, A.; Cojocaru, B.; Coman, S.M.; Bucur, C.; Primo, A.; Garcia, H.; Parvulescu, V.I. Nitrogen-doped graphene as metal free basic catalyst for coupling reactions. *J. Catal.,* **2019**, *376*, 238-247.
[http://dx.doi.org/10.1016/j.jcat.2019.07.011]

[62] Ma, J.; Xiao, Y.; Sun, Y.; Hu, J.; Wang, Y. Sulfur-Doped Alkylated Graphene Oxide as High-Performance Lubricant Additive. *Nanoscale Res. Lett.,* **2020**, *15*(1), 26.
[http://dx.doi.org/10.1186/s11671-020-3257-7] [PMID: 32002704]

[63] a) Khalili, D. Graphene oxide: a reusable and metal-free carbocatalyst for the one-pot synthesis of 2-amino-3-cyanopyridines in water. *Tetrahedron Lett.,* **2016**, *57*(15), 1721-1723.
[http://dx.doi.org/10.1016/j.tetlet.2016.03.020] b) Zhang, F.; Jiang, H.; Wu, X.; Mao, Z.; Li, H. Organoamine-functionalized graphene oxide as a bifunctional carbocatalyst with remarkable acceleration in a one-pot multistep reaction. *ACS Appl. Mater. Interfaces,* **2015**, *7*(3), 1669-1677.
[http://dx.doi.org/10.1021/am507221a] [PMID: 25556875] c) Scheuermann, G.M.; Rumi, L.; Steurer, P.; Bannwarth, W.; Mülhaupt, R. Palladium nanoparticles on graphite oxide and its functionalized graphene derivatives as highly active catalysts for the Suzuki-Miyaura coupling reaction. *J. Am. Chem. Soc.,* **2009**, *131*(23), 8262-8270.
[http://dx.doi.org/10.1021/ja901105a] [PMID: 19469566]

[64] Kim, F.; Luo, J.; Cruz-Silva, R.; Cote, L.J.; Sohn, K.; Huang, J. Self-propagating domino-like reactions in oxidized graphite. *Adv. Funct. Mater.,* **2010**, *20*(17), 2867-2873.
[http://dx.doi.org/10.1002/adfm.201000736]

[65] Zhang, H.; Lv, X.; Li, Y.; Wang, Y.; Li, J. P25-graphene composite as a high performance photocatalyst. *ACS Nano,* **2010**, *4*(1), 380-386.
[http://dx.doi.org/10.1021/nn901221k] [PMID: 20041631]

[66] Sun, H.; Liu, S.; Zhou, G.; Ang, H.M.; Tadé, M.O.; Wang, S. Reduced graphene oxide for catalytic oxidation of aqueous organic pollutants. *ACS Appl. Mater. Interfaces,* **2012**, *4*(10), 5466-5471.
[http://dx.doi.org/10.1021/am301372d] [PMID: 22967012]

[67] Nie, R.; Wang, J.; Wang, L.; Qin, Y.; Chen, P.; Hou, Z. Platinum supported on reduced graphene

Not be distributed or uploaded to anyone or anywhere
For personal private use only

oxide as a catalyst for hydrogenation of nitroarenes. *Carbon,* **2012**, *50*(2), 586-596.
[http://dx.doi.org/10.1016/j.carbon.2011.09.017]

[68] Zhang, Z.; Sun, T.; Chen, C.; Xiao, F.; Gong, Z.; Wang, S. Bifunctional nanocatalyst based on three-dimensional carbon nanotube-graphene hydrogel supported Pd nanoparticles: one-pot synthesis and its catalytic properties. *ACS Appl. Mater. Interfaces,* **2014**, *6*(23), 21035-21040.
[http://dx.doi.org/10.1021/am505911h] [PMID: 25375195]

[69] Song, J.; Kang, S.W.; Lee, Y.W.; Park, Y.; Kim, J.H.; Han, S.W. Regulating the catalytic function of reduced graphene oxides using capping agents for metal-free catalysis. *ACS Appl. Mater. Interfaces,* **2017**, *9*(2), 1692-1701.
[http://dx.doi.org/10.1021/acsami.6b13970] [PMID: 27991751]

[70] Joyner, J.; Oliveira, E.F.; Yamaguchi, H.; Kato, K.; Vinod, S.; Galvao, D.S.; Salpekar, D.; Roy, S.; Martinez, U.; Tiwary, C.S.; Ozden, S.; Ajayan, P.M. Graphene supported MoS2 structures with high defect density for an efficient HER electrocatalyst. *ACS Appl. Mater. Interfaces,* **2020**, *12*(11), 12629-12638.
[http://dx.doi.org/10.1021/acsami.9b17713] [PMID: 32045208]

[71] Xi, J.; Wang, Q.; Liu, J.; Huan, L.; He, Z.; Qiu, Y.; Zhang, J.; Tang, C.; Xiao, J.; Wang, S. N,P-dua--doped multilayer graphene as an efficient carbocatalyst for nitroarene reduction: A mechanistic study of metal-free catalysis. *J. Catal.,* **2018**, *359*, 233-241.
[http://dx.doi.org/10.1016/j.jcat.2018.01.003]

[72] Wang, H.; Kong, Q.; Wang, Y.; Deng, T.; Chen, C.; Hou, X.; Zhu, Y. Graphene Oxide Catalyzed Dehydration of Fructose into 5-Hydroxymethylfurfural with Isopropanol as Cosolvent. *ChemCatChem,* **2014**, *6*(3), 728-732.
[http://dx.doi.org/10.1002/cctc.201301067]

[73] Basu, B.; Kundu, S.; Sengupta, D. Graphene oxide as a carbocatalyst: the first example of a one-pot sequential dehydration–hydrothiolation of secondary aryl alcohols. *RSC Advances,* **2013**, *3*(44), 22130-22134.
[http://dx.doi.org/10.1039/c3ra44712j]

[74] Hu, H.; Wang, X.; Miao, D.; Wang, Y.; Lai, C.; Guo, Y.; Wang, W.; Xin, J.H.; Hu, H. A pH-mediated enhancement of the graphene carbocatalyst activity for the reduction of 4-nitrophenol. *Chem. Commun. (Camb.),* **2015**, *51*(93), 16699-16702.
[http://dx.doi.org/10.1039/C5CC05826K] [PMID: 26434405]

[75] Peng, L.; Zheng, Y.; Li, J.; Jin, Y.; Gao, C. Monolithic neat graphene oxide aerogel for efficient catalysis of S→ O acetyl migration. *ACS Catal.,* **2015**, *5*(6), 3387-3392.
[http://dx.doi.org/10.1021/acscatal.5b00233]

[76] Hu, F.; Patel, M.; Luo, F.; Flach, C.; Mendelsohn, R.; Garfunkel, E.; He, H.; Szostak, M. Graphene-catalyzed direct Friedel–Crafts alkylation reactions: mechanism, selectivity, and synthetic utility. *J. Am. Chem. Soc.,* **2015**, *137*(45), 14473-14480.
[http://dx.doi.org/10.1021/jacs.5b09636] [PMID: 26496423]

[77] Tan, L.; Wang, B.; Feng, H. Comparative studies of graphene oxide and reduced graphene oxide as carbocatalysts for polymerization of 3-aminophenylboronic acid. *RSC Advances,* **2013**, *3*(8), 2561-2565.
[http://dx.doi.org/10.1039/c2ra22516f]

[78] Wang, H.; Deng, T.; Wang, Y.; Cui, X.; Qi, Y.; Mu, X.; Hou, X.; Zhu, Y. Graphene oxide as a facile acid catalyst for the one-pot conversion of carbohydrates into 5-ethoxymethylfurfural. *Green Chem.,* **2013**, *15*(9), 2379-2383.
[http://dx.doi.org/10.1039/c3gc41109e]

[79] Yang, D.; Zhao, J.; Shi, J.; Wang, X.; Zhang, S.; Jiang, Z. Combination of redox assembly and biomimetic mineralization to prepare graphene-based composite cellular foams for versatile catalysis. *ACS Appl. Mater. Interfaces,* **2017**, *9*(50), 43950-43958.

Not be distributed or uploaded to anyone or anywhere
For personal private use only

[http://dx.doi.org/10.1021/acsami.7b11601] [PMID: 29171256]

[80] Li, Q.; Fan, F.; Wang, Y.; Feng, W.; Ji, P. Enzyme immobilization on carboxyl-functionalized graphene oxide for catalysis in organic solvent. *Ind. Eng. Chem. Res.,* **2013**, *52*(19), 6343-6348. [http://dx.doi.org/10.1021/ie400558u]

[81] Xu, Z.; Li, W.; Zhang, Y.; Xue, Z.; Guo, X.; Zhang, G. Facile synthesis of mesoporous reduced graphene oxide microspheres with well-distributed Fe_2O_3 nanoparticles for photochemical catalysis. *Ind. Eng. Chem. Res.,* **2016**, *55*(40), 10591-10599. [http://dx.doi.org/10.1021/acs.iecr.6b01004]

[82] Li, Z.; Zhao, H.; Han, H.; Song, J.; Liu, Y.; Guo, W.; Sun, Z.; Chu, W. A one-pot method for synthesis of reduced graphene oxide-supported Cu-Cu $_2$ O and catalytic application in tandem reaction of halides and sodium azide with terminal alkynes. *Appl. Organomet. Chem.,* **2018**, *32*(4), e4301. [http://dx.doi.org/10.1002/aoc.4301]

[83] Gupta, A.; Jamatia, R.; Patil, R.A.; Ma, Y.R.; Pal, A.K. Copper Oxide/Reduced Graphene Oxide Nanocomposite-Catalyzed Synthesis of Flavanones and Flavanones with Triazole Hybrid Molecules in One Pot: A Green and Sustainable Approach. *ACS Omega,* **2018**, *3*(7), 7288-7299. [http://dx.doi.org/10.1021/acsomega.8b00334] [PMID: 31458889]

[84] Naeimi, H.; Shaabani, R. Ultrasound promoted facile one pot synthesis of triazole derivatives catalyzed by functionalized graphene oxide Cu(I) complex under mild conditions. *Ultrason. Sonochem.,* **2017**, *34*, 246-254. [http://dx.doi.org/10.1016/j.ultsonch.2016.05.043] [PMID: 27773242]

[85] Naeimi, H.; Ansarian, Z. Functionalized polytriazoles on graphene oxide-supported copper(I) complex as an effective reusable catalyst for sonochemical click synthesis of triazoles in aqueous media. *Inorg. Chim. Acta,* **2017**, *466*, 417-425. [http://dx.doi.org/10.1016/j.ica.2017.06.057]

[86] Xiong, X.; Chen, H.; Tang, Z.; Jiang, Y. Supported CuBr on graphene oxide/Fe_3O_4: a highly efficient, magnetically separable catalyst for the multi-gram scale synthesis of 1,2,3-triazoles. *RSC Advances,* **2014**, *4*(19), 9830-9837. [http://dx.doi.org/10.1039/c3ra45994b]

[87] Narayanan, D.P.; Gopalakrishnan, A.; Yaakob, Z.; Sugunan, S.; Narayanan, B.N. A facile synthesis of clay – graphene oxide nanocomposite catalysts for solvent free multicomponent Biginelli reaction. *Arab. J. Chem.,* **2020**, *13*(1), 318-334. [http://dx.doi.org/10.1016/j.arabjc.2017.04.011]

[88] Moitra, D.; Ghosh, B.K.; Chandel, M.; Ghosh, N.N. Synthesis of a BiFeO $_3$ nanowire-reduced graphene oxide based magnetically separable nanocatalyst and its versatile catalytic activity towards multiple organic reactions. *RSC Advances,* **2016**, *6*(100), 97941-97952. [http://dx.doi.org/10.1039/C6RA22077K]

[89] Akocak, S.; Şen, B.; Lolak, N.; Şavk, A.; Koca, M.; Kuzu, S.; Şen, F. One-pot three-component synthesis of 2-Amino-4H-Chromene derivatives by using monodisperse Pd nanomaterials anchored graphene oxide as highly efficient and recyclable catalyst. *Nano-Structures & Nano-Objects,* **2017**, *11*, 25-31. [http://dx.doi.org/10.1016/j.nanoso.2017.06.002]

[90] Azarifar, D.; Khaleghi-Abbasabadi, M. Fe_3O_4-supported N-pyridin-4-amine-grafted graphene oxide as efficient and magnetically separable novel nanocatalyst for green synthesis of 4H-chromenes and dihydropyrano[2,3-c]pyrazole derivatives in water. *Res. Chem. Intermed.,* **2019**, *45*(2), 199-222. [http://dx.doi.org/10.1007/s11164-018-3597-4]

[91] Khodabakhshi, S.; Karami, B. Graphene oxide nanosheets as metal-free catalysts in the three-component reactions based on aryl glyoxals to generate novel pyranocoumarins. *New J. Chem.,* **2014**, *38*(8), 3586-3590. [http://dx.doi.org/10.1039/C4NJ00228H]

[92] Siddiqui, T.A.J.; Ghule, B.G.; Shaikh, S.; Shinde, P.V.; Gunturu, K.C.; Zubaidha, P.K.; Yun, J.M.; O'Dwyer, C.; Mane, R.S.; Kim, K.H. Metal-free heterogeneous and mesoporous biogenic graphene-oxide nanoparticle-catalyzed synthesis of bioactive benzylpyrazolyl coumarin derivatives. *RSC Advances,* **2018**, *8*(31), 17373-17379.
[http://dx.doi.org/10.1039/C7RA12550J] [PMID: 35539260]

[93] Abdi, M.; Rostamizadeh, S.; Zekri, N. An efficient and green synthesis of 1′H spiro [isoindoline-1, 2′-quinazoline]-3, 4′ (3′H)-Dione derivatives in the presence of nano Fe_3O_4–GO–SO_3H. *Polycycl. Aromat. Compd.,* **2019**, *39*(5), 413-424.
[http://dx.doi.org/10.1080/10406638.2017.1340313]

[94] Shaabani, A.; Hezarkhani, Z.; Nejad, M.K. AuCu and AgCu bimetallic nanoparticles supported on guanidine-modified reduced graphene oxide nanosheets as catalysts in the reduction of nitroarenes: tandem synthesis of benzo[b][1,4]diazepine derivatives. *RSC Advances,* **2016**, *6*(36), 30247-30257.
[http://dx.doi.org/10.1039/C6RA03132C]

[95] Kausar, N.; Mukherjee, P.; Das, A.R. Practical carbocatalysis by graphene oxide nanosheets in aqueous medium towards the synthesis of diversified dibenzo[1,4]diazepine scaffolds. *RSC Advances,* **2016**, *6*(91), 88904-88910.
[http://dx.doi.org/10.1039/C6RA17520A]

[96] Sun, X.; Wang, W.; Wu, T.; Qiu, H.; Wang, X.; Gao, J. Grafting of graphene oxide with poly(sodium 4-styrenesulfonate) by atom transfer radical polymerization. *Mater. Chem. Phys.,* **2013**, *138*(2-3), 434-439.
[http://dx.doi.org/10.1016/j.matchemphys.2012.12.022]

[97] Gao, Y.; Hu, G.; Zhong, J.; Shi, Z.; Zhu, Y.; Su, Sheng Gao, Y.; Hu, G.; Zhong, J.; Shi, Z.; Zhu, Y.; Su, D.S.; Wang, J.; Bao, X.; Ma, D. Nitrogen-doped sp2-hybridized carbon as a superior catalyst for selective oxidation. *Angew. Chem. Int. Ed.,* **2013**, *52*(7), 2109-2113.
[http://dx.doi.org/10.1002/anie.201207918] [PMID: 23307693]

[98] Sun, H.; Wang, Y.; Liu, S.; Ge, L.; Wang, L.; Zhu, Z.; Wang, S. Facile synthesis of nitrogen doped reduced graphene oxide as a superior metal-free catalyst for oxidation. *Chem. Commun. (Camb.),* **2013**, *49*(85), 9914-9916.
[http://dx.doi.org/10.1039/c3cc43401j] [PMID: 23945634]

[99] Gao, Y.; Ma, D.; Wang, C.; Guan, J.; Bao, X. Reduced graphene oxide as a catalyst for hydrogenation of nitrobenzene at room temperature. *Chem. Commun. (Camb.),* **2011**, *47*(8), 2432-2434.
[http://dx.doi.org/10.1039/C0CC04420B] [PMID: 21170437]

[100] Perhun, T.I.; Bychko, I.B.; Trypolsky, A.I.; Strizhak, P.E. Catalytic properties of graphene material in the hydrogenation of ethylene. *Theor. Exp. Chem.,* **2013**, *48*(6), 367-370.
[http://dx.doi.org/10.1007/s11237-013-9282-1]

[101] Kong, X.; Chen, Q.; Lun, Z. Probing the influence of different oxygenated groups on graphene oxide's catalytic performance. *J. Mater. Chem. A Mater. Energy Sustain.,* **2014**, *2*(3), 610-613.
[http://dx.doi.org/10.1039/C3TA13946H]

[102] Kong, X.; Sun, Z.; Chen, M.; Chen, C.; Chen, Q. Metal-free catalytic reduction of 4-nitrophenol to 4-aminophenol by N-doped graphene. *Energy Environ. Sci.,* **2013**, *6*(11), 3260.
[http://dx.doi.org/10.1039/c3ee40918j]

[103] Singh Chauhan, S.M.; Mishra, S. Use of graphite oxide and graphene oxide as catalysts in the synthesis of dipyrromethane and calix[4]pyrrole. *Molecules,* **2011**, *16*(9), 7256-7266.
[http://dx.doi.org/10.3390/molecules16097256] [PMID: 21869753]

[104] Qi, G.; Zhang, W.; Dai, Y. An efficient synthesis of 5-substituted 1H-tetrazoles catalyzed by graphene. *Res. Chem. Intermed.,* **2015**, *41*(2), 1149-1155.
[http://dx.doi.org/10.1007/s11164-013-1260-7]

[105] Xu, J.; Meng, R.; Cao, J.; Gu, X.; Qi, Z.; Wang, W.; Chen, Z. Enhanced dehydrogenation and

rehydrogenation properties of LiBH4 catalyzed by graphene. *Int. J. Hydrogen Energy,* **2013**, *38*(6), 2796-2803.
[http://dx.doi.org/10.1016/j.ijhydene.2012.12.046]

[106] Yuan, C.; Chen, W.; Yan, L. Amino-grafted graphene as a stable and metal-free solid basic catalyst. *J. Mater. Chem.,* **2012**, *22*(15), 7456.
[http://dx.doi.org/10.1039/c2jm30442b]

[107] Wu, T.; Wang, X.; Qiu, H.; Gao, J.; Wang, W.; Liu, Y. Amino-grafted graphene as a stable and metal-free solid basic catalyst. *J. Mater. Chem.,* **2012**, *22*, 4772.
[http://dx.doi.org/10.1039/c2jm15311d]

[108] Lam, E.; Chong, J.H.; Majid, E.; Liu, Y.; Hrapovic, S.; Leung, A.C.W.; Luong, J.H.T. Carbocatalytic dehydration of xylose to furfural in water. *Carbon,* **2012**, *50*(3), 1033-1043.
[http://dx.doi.org/10.1016/j.carbon.2011.10.007]

[109] Liu, F.; Sun, J.; Zhu, L.; Meng, X.; Qi, C.; Xiao, F.S. Sulfated graphene as an efficient solid catalyst for acid-catalyzed liquid reactions. *J. Mater. Chem.,* **2012**, *22*(12), 5495.
[http://dx.doi.org/10.1039/c2jm16608a]

[110] Wang, L.; Wang, D.; Zhang, S.; Tian, H. Synthesis and characterization of sulfonated graphene as a highly active solid acid catalyst for the ester-exchange reaction. *Catal. Sci. Technol.,* **2013**, *3*(5), 1194.
[http://dx.doi.org/10.1039/c3cy20646g]

[111] Sun, X.; Wang, W.; Wu, T.; Qiu, H.; Wang, X.; Gao, J. Grafting of graphene oxide with poly(sodium 4-styrenesulfonate) by atom transfer radical polymerization. *Mater. Chem. Phys.,* **2013**, *138*(2-3), 434-439.
[http://dx.doi.org/10.1016/j.matchemphys.2012.12.022]

[112] Ji, J.; Zhang, G.; Chen, H.; Wang, S.; Zhang, G.; Zhang, F.; Fan, X. Sulfonated graphene as water-tolerant solid acid catalyst. *Chem. Sci. (Camb.),* **2011**, *2*(3), 484-487.
[http://dx.doi.org/10.1039/C0SC00484G]

[113] Shaabani, A.; Mahyari, M.; Hajishaabanha, F. The synthesis of xanthenes and benzoxanthenes on graphene oxide and sulfated graphene nanosheets in water. *Res. Chem. Intermed.,* **2014**, *40*(8), 2799-2810.
[http://dx.doi.org/10.1007/s11164-013-1129-9]

[114] Ramirez-Barria, C.S.; Isaacs, M.; Parlett, C.; Wilson, K.; Guerrero-Ruiz, A.; Rodríguez-Ramos, I. Ru nanoparticles supported on N-doped reduced graphene oxide as valuable catalyst for the selective aerobic oxidation of benzyl alcohol. *Catal. Today,* **2020**, *357*, 8-14.
[http://dx.doi.org/10.1016/j.cattod.2019.05.057]

[115] Boukhvalov, D.W.; Dreyer, D.R.; Bielawski, C.W.; Son, Y.W. A Computational Investigation of the Catalytic Properties of Graphene Oxide: Exploring Mechanisms by using DFT Methods. *ChemCatChem,* **2012**, *4*(11), 1844-1849.
[http://dx.doi.org/10.1002/cctc.201200210]

[116] Tang, S.; Cao, Z. Site-dependent catalytic activity of graphene oxides towards oxidative dehydrogenation of propane. *Phys. Chem. Chem. Phys.,* **2012**, *14*(48), 16558-16565.
[http://dx.doi.org/10.1039/c2cp41343d] [PMID: 22801590]

[117] Long, Y.; Zhang, C.; Wang, X.; Gao, J.; Wang, W.; Liu, Y. Oxidation of SO_2 to SO_3 catalyzed by graphene oxide foams. *J. Mater. Chem.,* **2011**, *21*(36), 13934.
[http://dx.doi.org/10.1039/c1jm12031j]

[118] Tan, L.; Wang, B.; Feng, H. Comparative studies of graphene oxide and reduced graphene oxide as carbocatalysts for polymerization of 3-aminophenylboronic acid. *RSC Advances,* **2013**, *3*(8), 2561.
[http://dx.doi.org/10.1039/c2ra22516f]

[119] Sreeprasad, T.S.; Berry, V. How do the electrical properties of graphene change with its functionalization? *Small,* **2013**, *9*(3), 341-350.

Not be distributed or uploaded to anyone or anywhere
For personal private use only

[http://dx.doi.org/10.1002/smll.201202196] [PMID: 23169614]

[120] Kim, Y.; Some, S.; Lee, H. Graphene oxide as a recyclable phase transfer catalyst. *Chem. Commun. (Camb.),* **2013**, *49*(50), 5702-5704.
[http://dx.doi.org/10.1039/c3cc42787k] [PMID: 23689290]

[121] Verma, S.; Mungse, H. P.; Kumar, N.; Choudhary, S.; Jain, S. L.; Sain, B., ; Khatri, O. P, Graphene oxide: an efficient and reusable carbocatalyst for aza-Michael addition of amines to activated alkenes. *Chem. Commun. (Camb.),* **2011**, *47*(47), 12673-12675.
[http://dx.doi.org/10.1039/c1cc15230k] [PMID: 22039588]

[122] Yu, H.; Wang, X.; Zhu, Y.; Zhuang, G.; Zhong, X.; Wang, J. Solvent-free catalytic dehydrative etherification of benzyl alcohol over graphene oxide. *Chem. Phys. Lett.,* **2013**, *583*, 146-150.
[http://dx.doi.org/10.1016/j.cplett.2013.08.011]

For personal private use only
Not be distributed or uploaded to anyone or anywhere

CHAPTER 9

Oxidation and Reduction Reactions Catalyzed by Graphene Based Catalysts

Chetna Ameta[1,*], **Priyanka Chundawat**[1], **Yogeshwari Vyas**[1], **Reema Agarwal**[1] and **Dharmendra Dharmendra**[1]

[1] *Photochemistry Laboratory, Department of Chemistry University College of Science, Mohanlal Sukhadia University, Udaipur (Raj.), India*

Abstract: Graphene has several features, such as charge mobility, high conductivity, and a large specific surface area with a two-dimensional structure. It also has exceptional electrical, mechanical, and thermal properties. Graphene has exceptional mechanical, physical, and chemical properties, which are responsible for the development of efficient graphene-based catalysts for selective organic synthesis. This chapter recapitulates the various applications of graphene-based catalysts in oxidation and reduction reactions. It gives a complete overview of graphene, reduced graphene oxide, functionalized graphene oxide, N-doped graphene oxide, and their catalytic applications in various oxidation and reduction reactions. The previous studies reveal that metal-free GO has many catalytic applications. Owing to its high surface area, graphene oxide has a high adsorption tendency for hydrocarbons, gases, and ions.When reacting with oxygenating functionalities, GO provides several paths for introducing and modifying various functional groups. The large potential is employed for the use of metal-free carbon catalysts to resolve the industrial problems arising from traditional catalysts. Since graphene/GO catalysts are synthesized from environmental-friendly material, their applications in green synthesis should be discovered vigorously. The graphene-based catalysts have several applications. They allow only selective, mild, and highly effective transformations and undergo the synthesis and synthesis in an easy, recyclable, regenerable, and environmentally friendly manner.

Keywords: Graphene, Reduced Graphene Oxide, Functionalized Graphene Oxide, Metal-free Structured Carbon Catalysts, Oxidation and Reduction Reactions, Green Method.

INTRODUCTION

In the last decade, the utilization of nanomaterials as catalysts and supporting catalysts has propagated immensely. More exciting is the fast development in the research on the application of structured carbon nanomaterial in catalysis.

[*] **Corresponding author Chetna Ameta:** Photochemistry Laboratory, Department of Chemistry University College of Science, Mohanlal Sukhadia University, Udaipur (Raj.), India; E-mail: chetna.ameta@yahoo.com

Pinki Bala Punjabi, Rakshit Ameta & Sharoni Gupta (Eds.)
All rights reserved-© 2023 Bentham Science Publishers

Graphene is composed of a two-dimensional carbon network and it is also used for the synthesis of other carbon materials such as single and multiwalled carbon tubes (1D), fullerenes (0D), and graphite (3D) [1]. All the above-mentioned carbon materials are used as a support system for catalytic active phase and metals, it can also be used as a metal-free catalyst.

Carbon nanomaterials own unique properties, such as electrochemical and chemical stability, the tendency for a high degree of functionalization, and high surface area. In the last few years, extensive studies have been done on single and multi-walled carbon nanotubes to explore their use in catalysis, energy and electronic devices, polymer fillers, biological applications, and drug delivery. In 2004 mechanically exfoliated single-layer graphene sheets were reported.

Graphene-based materials have a huge application in energy storage, photocatalysis, catalysis, solar cells, memory devices, drug delivery, nano circuitry, and sensing platforms [2]. Several unique thermal, electronic, mechanical, and optical properties are owned by pristine graphene, these above properties are different from other forms of carbon. But, pristine graphene has some limitations, such as complex synthesis procedures and poor processability. Graphene oxide, reduced graphene oxide, and chemically modified graphene can be used as alternatives to pristine graphene because they can be easily prepared and processed in large quantity and also they can be easily synthesized, processed and dispersed in water and other organic solvents. However, they have some mechanical and electrical properties which are somehow different from graphene and responsible for disturbance in few applications. Yet, they are the appropriate starting materials for several applications [3].

Pristine graphene has zero bandgap and is a stable and inert material, whereas graphene oxide and reduced graphene oxides are either insulators or semiconductors. Graphene consists of only carbon material, while graphene oxide and reduced graphene oxide contain several organic functional groups which can further undergo modifications. At present main function of GO, graphene, and CMGs (chemically modified Graphene) are to act as supporting materials for catalytically active transition metals. So, we need to find more striking alternatives concerning extended stability, low cost, flexibility, and ecological influence.

The biological grade synthesis processes are highly toxic processes which is a matter of great concern, particularly the leakage of metal from their supports. To solve these problems, heterogenous metal-free catalysts made up of carbon materials [4] and noncarbon materials [5] can be used as an alternative. Over the past two decades, innovation and growth in new forms of carbon like nanotubes,

fullerenes, graphene, and nanofibers have resulted in an emphasis on the development and use of metal-free carbon catalysts. Important applications of CMGs and metal-free graphene oxides are their use in various chemical reactions as green catalysts.

The application of graphene and graphene oxide in catalysis has been discovered recently. Because of their use in battery and fuel cells, these materials have gained much attention already, specially N-doped graphene shows excellent activity for electrocatalytic oxygen reduction reaction (ORR). In this chapter, we will emphasize recent development and synthesis and oxidation and reduction reactions catalyzed by GO, FGO (Functionalized graphene oxide), and heteroatom doped graphene, which does not gain much consideration.

SYNTHESIS OF GRAPHENE/GRAPHENE OXIDE

Graphene

The exfoliation method was used first time for the experimental research of a single atomic layer of graphene. But this synthesis method is not adaptable for producing high-quality graphene on a large scale. The development of graphene sheets from graphite is done by the use of various chemical methods. The solvent used in the chemical method can interrupt the p–p interaction between sheets and result in individual stabilization of graphene [6], another alternative method is the bottom-up method in which, at high-temperature organic precursors are used for the direct growth of graphene [7].

The above methods have a large number of limitations, such as poor solubility, which results in graphitization and an increase in defect sites, and the number of unwanted side reactions. Even with the lots of development in the above alternative techniques, the mechanical exfoliation route is still the best method to produce graphene sheets of good quality.

Graphene Oxide and Reduced Graphene Oxide

Brodie [8], Staudenmeier [9], and Hummers [10] proposed the most common method to prepare to GO. In this method, graphite is oxidized with a strong oxidizing agent and results in samples having the same degree of oxidation. In the last decade, a modified Hummers method has become much more popular because it does not produce hazardous ClO_2 gas, has a short reaction time, and peroxidation steps promote further oxidation.

In Modified Hummers method, oxidization of flake graphite powder takes place, in these method flake graphite powder is mixed with phosphorus peroxide (P_2O_5)

and potassium persulphate ($K_2S_2O_8$) and stirred after the above mixture is dissolved in concentrated sulfuric acid (H_2SO_4). Afterward, the further oxidation of graphite is done by adding a mixture of potassium permanganate ($KMnO_4$) and H_2SO_4 and it is cool down to remove the reaction heat. After that, exfoliation of oxidized graphene is done by sonication, or mechanically it is done by polymers or surface stabilizing solvents [11].

GO is made up of a carbon framework containing a variety of oxygenating functionalities. GO lacks well-defined stoichiometry or uniquely defined structure, and distribution, location, and density of different oxygenate functionalities are defined by the synthesis method and the starting graphite material. Lerf and Klinowski [12] proposed the most acceptable structural model of GO, as shown in Fig. (**1**). This model indicates that and epoxy and hydroxyl groups are present at the basal plane of a GO sheet, and carbonyl groups and carboxylic acid are present at the edges of GO sheets. The above groups disturb the delocalization of p electrons and make graphene oxide electrically insulating. The polarity of the above group and their capability to contribute to hydrogen bonding results in the hydrophilic nature of GO and make it easily soluble in polar solvents or water. The carboxylic acid groups present at the edges of graphene oxide sheet are ionizable in less acidic aqueous solution, and the suspension of GO sheets in polar and aqueous solvents are stabilized by electrostatic repulsion between above-charged groups, and this repulsion is also responsible for the separation of GO sheets.

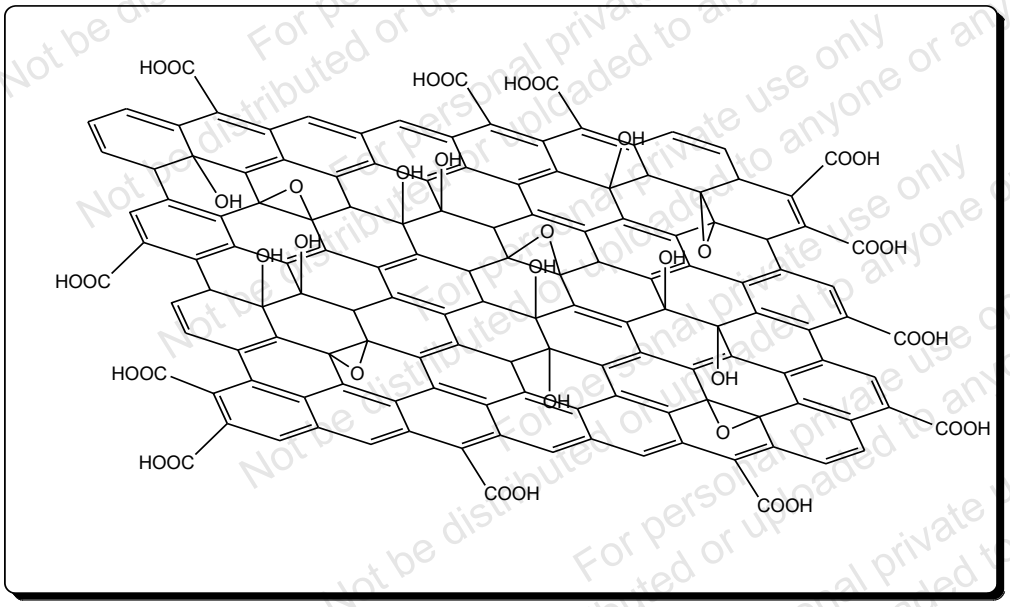

Fig. (1). Proposed structure of graphene oxide (honeycomb graphene lattice).

Few exceptional properties of graphene are retained by the reduction in oxygen functionalities. After reduction GO is signified as reduced graphene oxide, indicating the incomplete reduction. However, at a present complete reduction has not been achieved by researchers. Chemical, thermal and electrochemical methods are the commonly used method for the synthesis of rGO, and all the above methods retain the conjugated p-p bond up to some extent. For the chemical reduction of GO, lithium aluminum hydride is used as a strong reducing agent.

However, lithium aluminum hydride gives dangerous side reactions, so it cannot be used for the reduction of GO. So to avoid the above problems, less reactive chemicals such as hydrazine monohydrate are used for reduction of GO and reduction is also possible in aqueous solvents. Sodium borohydride, hydroquinone, and strong alkaline solutions are some other effective reducing agents employed for the reduction of GO. The main disadvantage associated with the chemical reduction is the incorporation of heteroatom impurities into the basal plane. The heteroatom nitrogen is incorporated into the basal plane by the reacting carbonyl group with hydrazine. This contamination affects the resulting electronic properties.

The ideal condition for effective reduction is achieved at high temperatures especially between 500-1,000°C using a dilute hydrogen atmosphere. Thermal reduction of graphene oxide and reduced graphene oxide is made in an inert atmosphere at a temperature above 500°C. More complete reduction is obtained at very high temperatures up to 1,000°C. This is because of the thermal cracking of C-C and C-O bonds in decarbonylation, dehydration, dehydrogenation, and decarboxylation reactions. Gas produced in reduction reaction is considered a byproduct, consisting of carbon dioxide, carbon monoxide, water, and perhaps hydrogen. Fast production of these gases creates pressure in the graphene oxide layers, which exfoliates the sample.

As the exfoliation process results in a higher surface area of the sample as compared to the area obtained by chemical reduction, it also has some drawbacks, such as it results in huge mass losses (30%) and it produces significant defects, these defects affect the electronic and chemical properties of rGO. These defects formation is controlled by employing successive reduction of chemical and thermal reduction. The third commonly used method for reduction is electrochemical reduction. In the above method, the electrode is prepared by placing a graphene oxide sample on the substrate, and this electrode is immersed in an electrolyte solution. The reduction process is completed by passing a current among a counter electrode and substrate [13]. The major drawback associated with this method is that the large-scale production of rGO is not possible.

Functionalized Graphene Oxide

To get a more adaptable material, various routes have been employed to change the GO surface through a change in a covalent bond. The various route which was employed to discover the functionalized carbon nanotubes can be used for graphene. For GO, numerous information is available that explains the functional group's nature, so the chemical reactions used to convert them into other functional groups have been employed.

Unfortunately, there are no particular techniques available for successful selective transformations, so effective transformation is not possible. However, these transformations are broadly used transformations, and the extensively used conversion reaction of an epoxy group and carboxylic acid are discussed below and also, several effective methods used for the synthesis of catalysts are discussed below. Unlike another organic synthesis, activation of surface carboxylic acid groups is necessary for their transformation. Once the carboxylic acid group gets stimulated, the carbon present in carboxylic acid becomes more susceptible to nucleophilic attack forming the covalent bond with nucleophiles.

Thionyl chloride ($SOCl_2$) [14, 15], 1-ethyl-3-(3-dimethyl aminopropyl) carbodiimide (EDC) or N-(3-dimethyl aminopropyl)-N-ethyl carbodiimide hydrochloride (EDCI) [16 - 19], and N,N-dicyclohexylcarbodiimide (DCC) are the commonly used activation or coupling reagents. Commonly used nucleophiles have a hydroxyl group or an amine that forms an ester and amide bond with graphene oxide and results in the formation of targeted entities on the graphene oxide surface. A ring-opening mechanism is used for the transformation of graphene oxide surface by its reaction with an epoxy group [20], but the above reaction is not much selective. For example, in the reaction of an amine with carboxylic acid, simultaneous aminolysis of epoxide may occur. Another method used for the activation of a carboxylic acid is the solvothermal method [21].

Other methods used to functionalize GO surface are the condensation of methoxy and ethoxy groups with surface hydroxyl group [22]; this is done by using the same method which is employed for fixing molecules on usual heterogeneous supports like Al_2O_3 and SiO_2. The rarely used method, which is the covalent functionalization of the graphitic area of reduced graphene oxide with diazonium salt is done by using a radical mechanism, and is also employed for catalyst synthesis.

N-Doped (Heteroatom-Doped) Graphene

Post-treatment of graphene or GO or in situ growth are generally used methods for the synthesis of heteroatom-doped graphene catalysts. In the last few years, N-

doping has become the most popular subject [23]. In the in-situ growth method, heteroatoms are integrated through the growth procedure by adding in an N-containing reagent, by CVD takes place. The key advantage of the in situ method is that it offers new catalytic properties and it also allows retains the intrinsic physical and chemical properties of pristine graphene. N-doped graphene can be synthesized by CVD by passing a gaseous mixture of CH_4, NH_3, and H_2 in an Ar carrier over a substrate.

The incorporation of nitrogen into graphene aromatic structures can be done by using various forms such as pyrrolic and pyridine nitrogen (Fig. **2**). Solvothermal synthesis processes are another type of in situ method. For example, during the pyrolysis process reaction of lithium nitride undergoes the reaction with tetrachloromethane by using stainless steel autoclave. In the post-treatment method heteroatoms are incorporated by indulging graphene oxide with various compounds by using a physical and chemical method like bypassing NH_3 over graphene oxide at high temperatures or combining graphene oxide with nitrogen sources such as dicyandiamide, melamine, and pyrrole, and then post-treatment method like thermal and chemical reduction is employed. Depending on the experimental details, nitrogen atoms can be merged into graphene oxide in various forms.

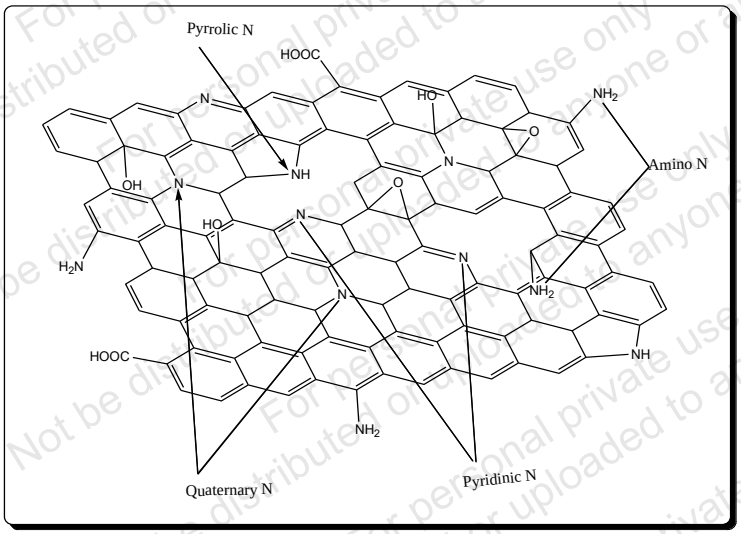

Fig. (2). Schematic illustration of the various forms of 'N' atom incorporation into the graphene structure.

CATALYTIC APPLICATIONS

As we already know that carbon and carbon-based materials like graphitic carbon and activated carbon play a very important role in catalysis and the functionalized carbons are generally more selective and active as compared to their

unfunctionalized counterparts. Since, because of heterogeneity of functionalized carbons, the determination of a detailed reaction mechanism is found to be very difficult, and their characterization at an atomic level is also, although functionalized carbons are found to be very active for several reactions such as oxidation of aromatic compounds, decarboxylation of fatty acids, and selective oxidation dehydrogenation of hydrocarbons [24]. Here we emphasize graphene and graphene oxide-based materials.

Oxidation Reactions

Catalysis by Graphene Oxide and Graphite Oxide

Dreyer and Bielawski [25] explained that synthesized graphene oxide and graphite oxide, which is exfoliated version of graphite oxide give a highly disrupted graphene network. GO has a huge application in catalysis like easy synthesis procedures, low cost, it can be easily recovered by filtration, and it also has a surface to volume ratio. As it is already mentioned that the edges and basal plane of GO contain numerous oxygen functional groups like carbonyl, epoxy, carboxylic acids, and hydroxyl, all these groups are responsible for the acidic character, chemical activity, oxidative nature, and catalytic activity of GO.

However, GO can be used as a catalyst in numerous reactions. Bielawski and his coworkers [26] reported the effect of GO on the oxidation of alkenes to diketones, alcohols to aldehyde and diketones, and oxidation of alkynes to hydrates at 75-150 °C in air. Above oxidation reactions are highly selective. For example, the yield in the oxidation of cis1,2-diphenylmethane-1,2-diol to 1,2-diphenylethan--1,2dione was 96%, and 98% for diphenylmethanol to benzophenone. Interestingly, whereas GO oxidized 1,2diphenylethene to 1,2-diphenylethane-1-2-dione with 56% conversion, it was either inactive or could only catalyze the isomerization of other alkene systems.

So, it is found that cis-1,2-diphenylethene is reactive because of a combination of cis geometry and aromatic substituents. To determine the catalytic activity of GO researchers performed several experiments inert nitrogen environment and found that absence of oxygen results in very little oxidation, and also GO can be extracted from the reaction mixture and reused up to several cycles. But, GO catalyst has very low activity and to obtain a reasonable yield in 24 h high carbon to substrate ratio up to 200% is required. Although GO catalyst requires high loading and has low activity, it has the main advantage that it has a high turnover frequency per dollar as compared to tetrapropyl ammonium per ruthenate oxidation catalyst.

GO was found to catalyze other reactions, such as oxidation of sulfides to sulfoxides and the coupling of thiols to disulfides [27], dehydrogenation of various hydrocarbons and oxidation of methylbenzenes to their respective aldehydes, diarylmethanes to their respective ketones, and other hydrocarbons with sp3-hybridized C–H bonds [28]. It has also shown high activities for the Claisen–Schmidt coupling reactions [29], Friedel-Crafts reactions [30], Aza-Michael additions [31], and ring-opening polymerization [32].

Oxidation of Various Alcohols

In the initial experiment, under ambient conditions and in the presence of 20 wt% of GO, benzyl alcohol ($PhCH_2OH$) is heated at 100 °C for 14 h (Scheme **1**). After that, it is filtered several times and gives the mixture of benzaldehyde ($PhCHO$)/$PhCH_2OH$ in the molar ratio of 1:3, as verified by 1H NMR spectroscopy. Under these conditions, the formation of any other by-products and benzoic acid ($PhCO_2H$) were not observed.

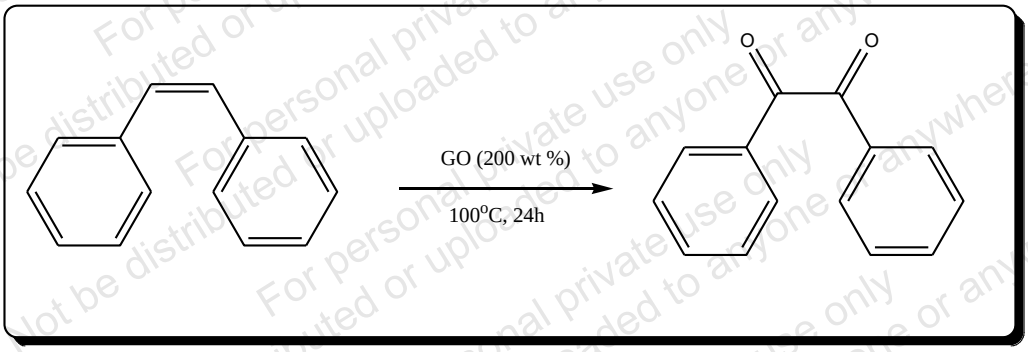

Scheme 1. Oxidation of benzyl alcohol using graphene oxide (GO).

The reactivity of the above carbocatalyst is studied by using various primary and secondary aliphatic and benzylic alcohols under ambient conditions such as 100°C, 24 h and 200 wt% GO, which results in the highest conversion of $PhCH_2OH$ into its oxidized products. Table **1**, entries 1–3 reveals that benzylic alcohols have moderate to high product conversion efficiency. Table **1**, entry 4 reveals the high catalytic power of GO to oxidize cyclohexanol. Table **1**, entry 5 explains the conversion of 2-thiophenemethanol into aldehyde, and the sulfur oxidation does not take place. The latter results explain that GO exhibit broad chemoselectivity and have a high tolerance towards functional groups, so GO can be used to overcome the challenges given by transition metal catalysts.

Table 1. Oxidation of Various Alcohols Using GO[a].

Entry	Alcohol	Product	Conversion (%)
1[b]	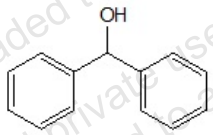	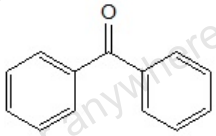	> 98
2[b]	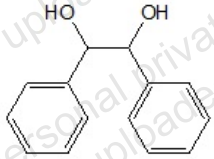	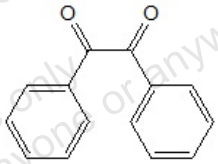	96
3[d]	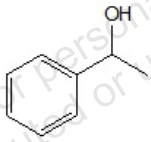	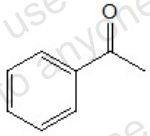	26
4		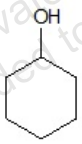	> 98
5[d]	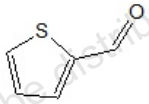	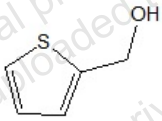	18

Oxidation of Cis-Stilbene

As mentioned above, GO can undergo the oxidation of various alcohols, so nowadays various efforts are used to explore the ability of GO to catalyze the oxidation of unsaturated hydrocarbons. As illustrated in Scheme **2**, under the optimized conditions on treatment of cis-stilbene at 100°C for 24 hours 49% benzil is isolated (56% conversion by NMR spectroscopy); in the crude reaction mixture, benzene or any oxidation product is not found.

For personal private use only Not be distributed or uploaded to anyone or anywhere

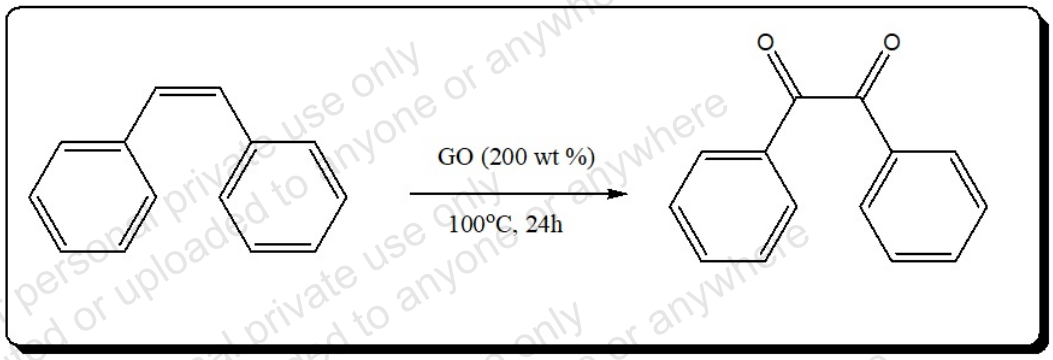

Scheme 2. Oxidation of cis-stilbene using GO.

To facilitate the oxidation process, it is necessary to combine cis geometry with aromatic substituents because when other alkenes (trans-stilbene, 3-hexene, cyclohexene, and b-methyl styrene) are used as substrates under the same environment, no reaction or isomerization is observed these may be due to orientation of the interaction tangled between catalyst surface and olefins or may be due to steric hindrance.

Oxidation of Organosulfur Compounds

The oxidation of sulfides and thiols resulted in various applications in drug metabolism, synthesis, and preparation of bioconjugates. Several methods have been investigated for the oxidation of organosulfur compounds but all the methods are associated with a major drawback of over-oxidation. For example, dimerization of thiols resulted in thiols and then it further undergoes the oxidation of disulfinates, thiosulfinates, disulfones, and sulfinylsulfones. Similarly, the oxidation of sulfides resulted in sulfoxides along with sulfones and sulfonic acid.

To solve this problem of overoxidation several advanced catalysts such as transition metal with active species are investigated. Among all the metals, catalyst based on palladium, iron, and molybdenum decreases the reaction time and increases the selectivity for the desired product. Despite this advantage, because of toxicity and separation issues, numerous metal catalysts cannot be used in biotechnological and pharmaceutical applications.

So for the organosulfur compounds, it is necessary to develop highly active metal-free oxidants. Furthermore, the heterogeneous catalysts allow not only the easy and facile separation of the target compounds by distillation and filtration but also reuse and recovery of the catalyst itself. We found that many of the above-mentioned challenges to ing organosulfur oxidants can be solved using a graphene oxide catalyst.

Oxidation of Thiols

In an initial experiment, 25 mg of thiophenol is reacted with 75 mg of GO by using 0.3 ml of $CHCl_3$ at 100 °C for 10 min in a closed vessel (Scheme **3**). After that, the above reaction mixture is dissolved in 50 ml of $CHCl_3$ and then it undergoes filtration to remove the volatile solvent, the thiol is determined by 1H NMR spectroscopy ($CDCl_3$) to convert them into diphenyl disulfide.

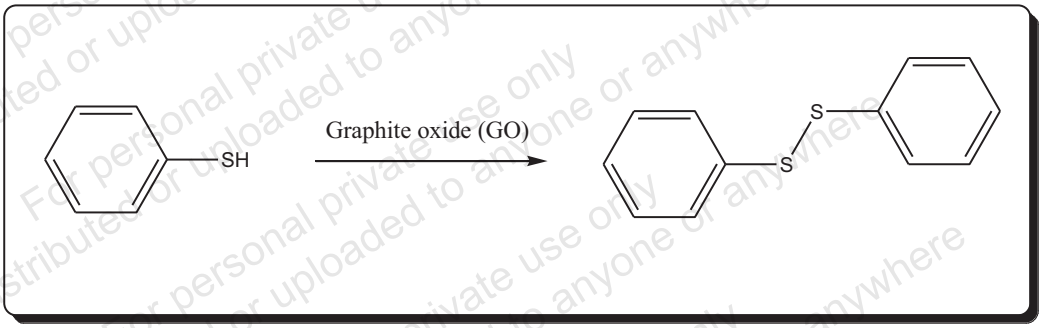

Scheme 3. Oxidation of thiol using graphene oxide (GO).

By using the above-mentioned experimental conditions (25 mg thiol, 15 mg GO, 0.3 mL $CHCl_3$, 100°C, 10 min), after that, we determined the substrate scope of this method. As presented in Table **2**, the reaction of various thiols with GO resulted in exceptional conversion to their disulfides, and by dissolving the reaction mixture in 50 ml $CHCl_3$, filtering the remaining carbon, removing the volatile solvent under close atmosphere, in some cases purification by using column chromatography resulted in the pure products.

Entries 1, 4–9 of Table **2** show that the aryl thiols have a longer reaction time of 30 min as compared to alkyl thiols which are 10 min (entries 2–3, 10), but the reactivity of aryl thiol is higher than alkyl thiol these is because of higher activity of GO towards arene functionalized substrate. To further indicate the superior reactivity of aryl thiol over alkyl thiols, 25 mg of thiophenol and 1-butanethiol in 1:l molar ratio is reacted with 60 wt% of GO at 100°C for 10 min. The 1HNMR spectroscopy revealed the 63% conversion of reactant into product and the product mixture contains a 1.0:5.0:2.9 molar ratio of dibutyl disulfide: butyl phenyl disulfide: diphenyl disulfide along with 34% unreacted 1-butylsulfide and a <5% unreacted thiophenol.

The incorporation of electron-donating or withdrawing substituents to the aromatic thiols does not influence the quantity of desired product. For example, electron-rich diols as given in entries 4–7 and electron deficient thiols as presented in entries 8–9 of Table **2** gives the exceptional 94-99% yield of their

respective disulfides, in all the above reaction, no over-oxidation and nitrogen oxidation in case of 2-amino thiophenol is detected, which has been occurred by use of chromic potassium sulfate ($CrK(SO_2)_2.12H_2O$) and other transition metal-based oxidation catalysts [33]. Although these challenges are overcome by the use of more advanced metal species such as cobalt porphyrins and imidazole [34], MOFs, and various bismuth species [35] but these catalysts do not show the extent of reactivity as shown by GO.

Table 2. Oxidation of various thiols using GO[a].

Entry	Starting material	Product	Reaction Time	Yield[b] (%)
1	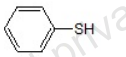	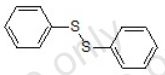	10 min	100
2	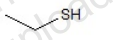	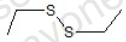	30 min[c]	77
3		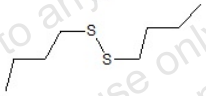	30 min[c]	90
4	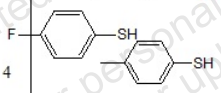	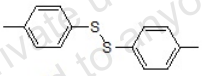	10 min	95
5	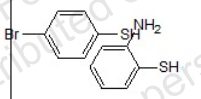	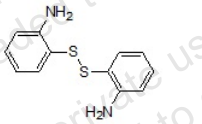	10 min	96
6	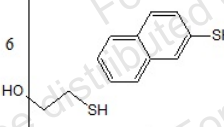	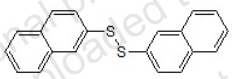	10 min	97
7	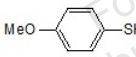	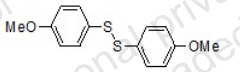	10 min	97
8	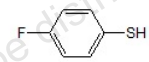	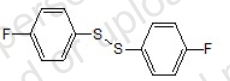	10 min	99
9	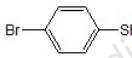	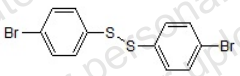	10 min	94
10		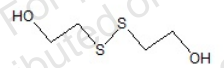	30 min[c]	75

[a]All reactions were performed at 100°C in sealed 7.5 mL vials using 25 mg thiol, 15 mg GO (60 wt%) and 0.3 mL $CHCl_3$ for the indicated reaction time. [b]Isolated yield after purification by column chromatography. [c]Relatively low yields (40–65%) were observed after 10 min; higher yields were obtained after 30 min.

Not be distributed or uploaded to anyone or anywhere
For personal private use only

Oxidation of Sulfides

In an initial experiment, diphenyl sulfide is oxidized to diphenyl sulfoxide at 100°C (300 wt% GO) after 24 h 86% isolated yield was obtained (Scheme **4**), and in the reaction mixture, no other oxidation product is observed. In the way illustrated above, the reaction is improved concerning reaction time, reaction temperature, and GO loading. It is found that GO concentration below 300 wt% does not give the desired product, yet with an increase in GO loading, no enhancement in isolated yield is observed.

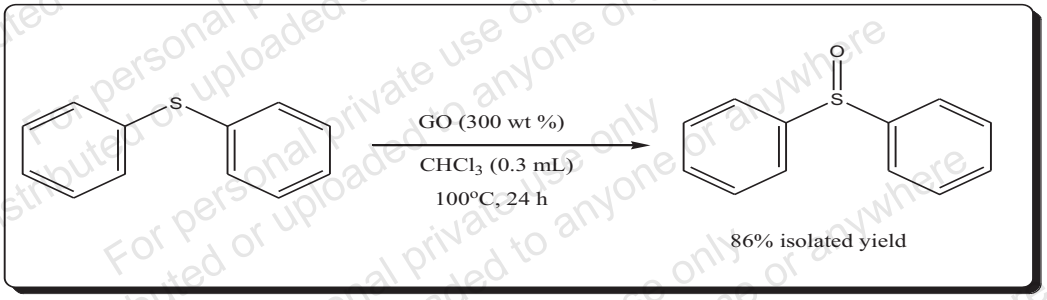

Scheme 4. Oxidation of diphenyl sulfide using GO.

Here the GO loadings required are much higher than that of metal catalysts but their heterogeneity and low cost make them more feasible to use. It is found that the used GO loadings which undergo the partial deoxygenation as given below, can be again reoxidized to GO by using the oxidation method, which was used by the graphite starting material. The above mention thiol coupling shows that when carbons other than GO are used, such as activated carbon, graphite, and hydrazine-reduced graphene oxide minimum reactivity is observed.

As shown in Table **3**, by using the optimum conditions like 75 mg GO, 25 mg sulfide, 0.3 mL $CHCl_3$, 24 h, and 100°C a large number of sulfides can be converted into their respective sulfoxides. In most cases, after purification by column chromatography exceptional yields of their subsequent products are gained. Differences in the electronic structure of the arene substituted sulfides slightly affect sulfoxide product yield. For example, an electron-rich sulfide (*p*-methoxythianisole, entry8) on oxidation gives a 96% product yield, while an electron deficient sulfides (*p*-chlorothianisole, entry 9) gives the 81% product yield. As Compared to Ru and Fe catalysts (using H_2O_2 or O_2 as the oxidant), GO resulted in an increase in selectivity and product yield for the sulfoxide over the sulfone.

Table 3. Oxidation of Various Sulfdies by Using GO[a].

Entry	Starting material	Product	Yield[b]
1	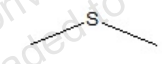	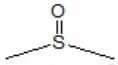	89%
2	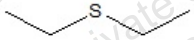	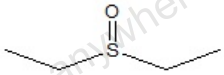	92%
3	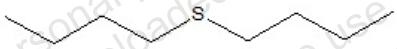	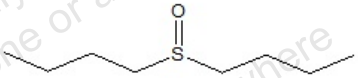	90%
4	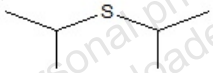	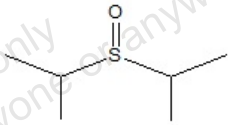	51%
5	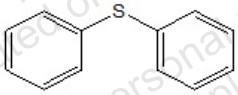	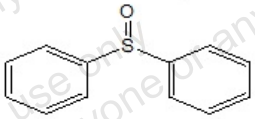	86%
6	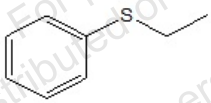	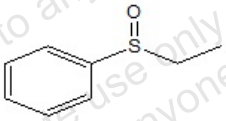	85%
7	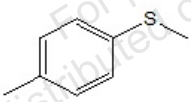	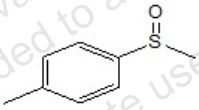	75%
8	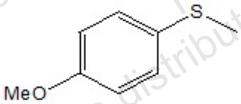	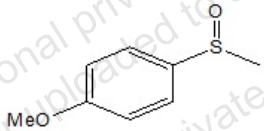	96%
9	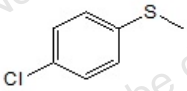	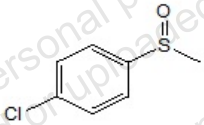	81%

[a]All reactions were performed at 100°C in sealed 7.5 mL vials using 25 mg sulfide, 75 mg GO (300 wt%), and 0.3 mL $CHCl_3$ for 24 h. [b]Isolated yield after purification by column chromatography.

For personal private use only Not be distributed or uploaded to anyone or anywhere

Oxidation of Amines

A large number of efficient methods have been for the oxidation of alcohols into their respective carbonyl groups but the methods for the catalytic oxidation of amines into imines are still not much studied, although imines are a good source of nitrogen in many chemical reactions [36 - 40]. In the conventional method, imine is prepared by condensation of primary amines and aldehyde and ketones [41], but this method requires some critical conditions like longer reaction time and catalyst Lewis as the catalyst [42]. In the last few years, to optimize these reaction conditions, many methods have been developed such as self-condensation of primary amines, oxidation of secondary amines, and direct coupling of amines and alcohols [43 - 47].

In recent years, a large number of catalysts have been explored for the oxidation of amines [48, 49]. But these catalysts still have some drawbacks, such as high toxicity, high cost, difficult preparation methods, and critical reaction conditions. Therefore, a catalyst with high selectivity, separability, and easy preparation procedure is required.

Recently, Go has drawn widespread attention [50 - 52]. Go along with its derivatives are widely used as a metal-free catalyst [53 - 58]. Because of the presence of a large number of oxygenated functional groups in GO, GO has high catalytic and oxidation capabilities [59]. Several advantages of GO like low toxicity, simple preparation method, and tendency to get separate makes it a good catalyst for oxidation of amine.

It is found that GO is an efficient catalyst for the oxidation of amines into imines but the effect of various functional groups on Go and their decreased activity in recycling experiments are not clarified [60]. Bermudez and co-workers [61] reported the use of hydrogen peroxide (H_2O_2) as the oxidant in GO-catalyzed oxidation of amines and disclose the effect of GO and H_2O_2 and GO on the selectivity of products.

But, in several reactions, the effect of free radical is uncertain so because of the above reason the mechanism of oxidation of amines catalyzed by carbocatalysts, which is necessary for efficiency and design of catalyst, is still in doubt. It is observed that GO and its derivative such as improved graphene oxide (IGO), can oxidize the amines into their respective imines in the absence of oxygen and catalyst and improved graphene oxide has higher reactivity for amine oxidation. GO can function as both catalyst and oxidant, the epoxy and hydroxyl groups present in GO act as an oxidant, and Carboxyl groups along with defects and edges play the role of catalyst.

This remarkable metal-free reactivity of graphene oxide has encouraged researchers to explore the probabilities offered for catalytic oxidation of amines into imines. Go is reported as an easily available, easily applicable, cheap, recyclable, and efficient catalyst for the direct conversion of amines into imines. It is the first suitable metal-free catalytic method that is used for the synthesis of imine from various amines by using molecular oxygen as the oxidant under neat conditions [62].

Benzylamine acts as an intermediate for several polymers, pharmaceuticals, and dyes, and it is also used to study the use of graphene oxide in the oxidative coupling reaction of amines. Entry 1 of Table **4** shows that the reaction of GO and benzylamine with p-xylene at 130°C in the air for 8 h resulted in 87.39% of N-benzylidene benzylamine product. Entry 2 of Table **4** shows that when a similar experiment is performed in the absence of GO, only 9.33% of product yield is obtained, which indicates that GO can catalyze the aerobic oxidation of benzylamine.

Table 4. Oxidation of Benzylamine to N-Benzylidene Benzylamine under various conditions[a].

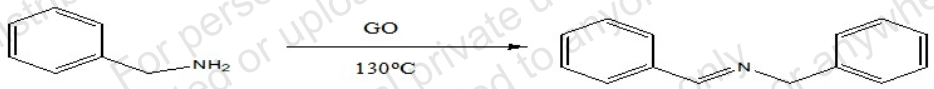

Entry	Condition	oxidant	yield (%)[b]
1	air	GO	87.39
2	air		9.33
3	air	IGO	99
4	argon	GO	46.32
5	argon		<5
6	argon	IGO	66.25

[a]Reaction conditions: benzylamine (2.5 mmol), GO (26 mg), and p xylene (5 mL) at 130°C for 8 h, entry 1−3 in air condition, entry 4− 6 in argon condition. [b]Isolated yield.

Entry 4 of Table **4** states that when the above reaction is carried out in the same condition in the presence of argon results in 46.32% of product yield. Entry 5 of Table **4** shows when the above reaction is carried out with argon in the absence of GO then less than 5% of the product is obtained which indicates that GO also plays the role of oxidant in this reaction.

Nitrogen-Doped Graphene Catalysts

Nowadays, N-doped graphene has become brilliant catalysts for oxygen reduction reaction (ORR) battery and fuel cell applications. The inclusion of nitrogen atom

changes the charge distribution of surrounding carbon, and spin density and broadens the bandgap of GO. Generally, the nitrogen can be incorporated into carbon lattice in three forms: pyridinic N, quaternary (graphitic) N and pyrrolic N. Since all the three forms of nitrogen affect the oxygen reduction reaction and the improvement in the reactivity is depends on the amount of quaternary and pyridinic nitrogen. Despite the above advantage use of N-doped graphene in various reactions is not much studied only a few studies like oxidation of benzene into phenol [63] and of a range of benzylic alcohols [64] are available. N-doped graphene is synthesized by flowing NH_3 over GO and it is found that the quaternary nitrogen increases the catalytic activity of oxidation of benzylic alcohol into their respective aldehyde. The incorporation of quaternary nitrogen into GO can be increased by increasing the temperature up to 900°C.

Oxidation of Alkyl Arenes and Alcohols

In organic synthesis, the selective oxidation of organic compounds at laboratory and industrial scales is a major challenge. In the aerobic oxidation reaction, there are generally three major considerable aspects are eradicating the requirement of the activators like inorganic bases and accomplishment of the reaction without activation in a green solvent at room temperature.

At an industrial scale, the grouping of these characteristics is highly challenging and this grouping provides benefits for chemical reactions. To solve the above challenge catalyst is the key, several studies are ongoing to get a suitable catalyst having all aforementioned aspects. Recently the researcher emphasis on the development of the catalyst by using the green and biometric principal. Because of this reason metal phthalocyanines and metal porphyrins are used as biomimetic catalysts in various oxidation reactions.

Zhang *et al*. [65] reported that the oxidation of alcohols and alkyl arenes in the solvent-free aerobic atmosphere with Pd@ N-doped carbon at 120°C resulted in very low product yield and the use of Pd in the catalyst as an active site also restrict its application. The aforementioned drawbacks lead to the development of new catalysts such as copper(II) tetrasulfo phthalocyanine reinforced on three-dimensional nitrogen-doped graphene-based frameworks (CuTSPc@3D-(N)GFs). The above catalyst is the first catalyst that was synthesized by using 3D-(N)GF--supported phthalocyanine and it has the unique property of selective aerobic oxidation of alcohols and alkyl arenes into their respective carbonyl groups. The selective aerobic oxidation reactions are conducted at room temperature in an ecofriendly environment for a short reaction time and resulted in excellent product yield.

To optimize the required amount of solvent and catalyst, the oxidation of 2,3-dihydro-1H-indene is carried out by using 0.4 mol% of H_2O and Cu as a solvent for both the reactions at room temperature and the results are given in Table **5**. The important advantage of 3D-(N)GFs support are: (i) They have high surface area, macroporous structures, good physical and chemical stability (ii) simple preparation method, (iii) the presence of a bifunctional heterogeneous catalyst (copper(II) as the active site and N as the base) eliminates the requirement of activators like inorganic bases, (iv) chemical modification of the surface with nitrogen doping increases the reactivity and in catalytic oxidation, they also improves the oxygen interaction with substrate and, and (v) because of its hydrophilic nature it is easily soluble in water which is used as a reaction solvent.

Entries 2-4 of Table **5** present the catalytic oxidation of benzaldehyde and 2,3-dihydro-1H-indene using GO, 3D-(N)GFs, and CuTSPc [66]. Entry 2 of Table **5** shows that when GO (0.005 g) is used as a catalyst under a mild condition in oxidation reaction results in a very low product yield.

Table 5. Comparison of the Results Obtained From Cutspc@3D-(N)Gfs with GO, Cutspc, and 3D-(N)Gfs for the Oxidation Reactions.

Entry	Catalyst	Product	Yield[b] (%)	Selectivity[b] (%)
1	CuTSPc@3D-(N)GFs	2,3-Dihydro-1*H*-indene	98	> 99
		Benzaldehyde	98	> 99
2	GO	2,3-Dihydro-1*H*-indene	24	> 99
		Benzaldehyde	30	> 99
3	3D-(N)GFs	2,3-Dihydro-1*H*-indene	33	> 99
		Benzaldehyde	35	> 99
4	CuTSPc	2,3-Dihydro-1*H*-indene	86	97
		Benzaldehyde	88	98
5	CuTSPc@MCM-41	2,3-Dihydro-1*H*-indene	75	98
		Benzaldehyde	81	99

[a]**Reaction conditions: 2,3-dihydro-1H-indene or benzyl alcohol (1.0 mmol), catalyst, H2O (4.0 mL), air (1 atm), r.t., 3 h.** [b]**Yield and selectivity determined by GC analysis.**

It is found that the use of 3D-(N)GFs support increases the adsorption of aromatic reactants these may be due to the p-p interaction between graphene and benzene skeleton of reactant. Furthermore, the interaction of 3D-(N)GFs with nitrogen-doped support resulted in the adsorption of oxygen on the bridge sites of graphene by using migration energy of more than 1.0 eV. Graphene contains mobile

oxygen, which endorses hydrogen elimination resulting in the enhancement of the aerobic oxidation of organic compounds. Entries 1 and 4 of Table **5** show the increase in the product yield as compared to the homogenous catalyst, several factors improve the yield, such as the presence of basic sites on solid and p-p interaction between support and aromatic groups favor the proximity of reagents with the catalytic site.

Selective Oxidation of Olefins and Alcohols

Although the selective oxidation of alcohols and olefins with molecular oxygen is very much important for the environment, life, and synthetic chemistry, it is still a very difficult task. Several reagents and methods have been discovered to accomplish these oxidation reactions. Most of the oxidation reaction uses the fixed amounts of heavy metal ions such as Mn, Cr, Co, and Fe and explosive oxidants such as hydrogen peroxide and peroxy acids. Because of environmental issues, there is a need to develop a safer and cheaper heterogeneous catalyst for oxidation. A large number of noble metal nanoparticles like Pd, Ru, Pt, and Au have been studied for use in the oxidation of alcohols and olefins.

Graphene has several advantages, such as it has a high surface area which helps in the transfer of reactant and product by scattering the metal nanoparticles micropore-free structure with one or a few sheet layers, it also has appropriate electrical conductivity, which helps in the transfer of electrons during catalysis process, and also have high chemical reactivity, and it is also found that the graphene has p character which is responsible for interaction between aromatic derivatives and graphene and this interaction makes the reactants available for active sites. Because of the large availability and low cost of graphite, it can be easily broken down into individual graphene by using chemical and physical methods. Traditionally it can be broken down into graphene using several methods such as liquid-phase exfoliation, use of graphite intercalation compound, oxidation exfoliation, and electrochemical exfoliation. In the last few years, it has become a great challenge to modify graphene's mechanical, chemical, and electronic properties by doping using N, B, and P elements.

It is found that N-dopants can decline the formation of “re-graphitized” carbon regions in the carbon skeleton and also, they are favorable sites to enhance the nucleation of particle and decreases particle size. be usually observed as favorable anchor sites or defects for enhancing particle nucleation and reducing the particle size. N dopants have several advantages, such as they can change the electronic structure of the carbon matrix, improve the interaction between the guest molecule and carbon, and also be responsible for the giving metal like d-band to carbon which hosts the reactive species. The effective heterogeneous oxidation

reaction of both alcohol and olefins is carried out by using molecular oxygen over a Co_3O_4/N-doped graphene hybrid (Co_3O_4/RGO-N) catalyst. It is observed that the dispersed Co_3O_4 NPs and well-exfoliated N-doped graphene can be grown simultaneously by employing a one-pot hydrothermal reaction using NH_3 solution. Here we discuss the structural characteristics of Co_3O_4/RGO-N and its performance in the green oxidation of olefins and alcohols [67].

Co_3O_4/RGO-N hybrid is used in the epoxidation of styrene. Entries 1 and 2 of Table **6** reveal that amides like DMF and DMA can be used to get the high conversion of styrene up to 97.7 and 86.2% and high epoxide selectivity of 72.7 and 63.8%. along with the desired product small amount of cleavage product like benzaldehyde is also observed.

Table 6. Epoxidation of Styrene by O_2 in Different Solvents Over Co_3O_4/RGO-N[a] in different solvents over.

Entry	Solvent	Conversion (%)	Epoxide selectivity (%)
1	DMF	97.7	72.7
2	DMA	86.2	63.8
3	Dioxane	77.7	55.7
4	DMSO	26.3	15.2
5	Toluene	0	0
6	n-Heptane	0	0
7	1-Butanol	0	0
8[b]	DMF	22.8	49.1
9[c]	DMF	79.9	66.0
10[d]	DMF	98.7	69.9

[a]Reaction conditions: temperature (100◦C), reaction time (3 h), Co_3O_4/ RGO-N (20 mg), styrene (8 mmol), DMF (25 mL), low rate of O_2 (20 mL min-1). [b]The reaction was carried out at 80◦C. [c]The reaction was carried out at 90◦C. dThe reaction was carried out at 110◦C.

Entries 3 and 4 of Table **6** show that by using DMSO and dioxane solvent certain amount of styrene conversion is obtained but their epoxide selectivity is very low. Entries 5-7 of Table **6** reveals that by using toluene, n-heptane, or 1-butanol

solvent, no products are obtained. Entries 8-10 of Table **6** present the temperature dependency of oxidation reaction and we found that at the temperature 80 -90°C both conversion and selectivity decrease and a small decrease in selectivity is observed at higher temperature (110°C).

Entry 2 of Table **7** shows that Co_3O_4/ RGO gives the relatively low activity (57.3%) and lower epoxide selectivity (70.3%) as compared to Co_3O_4/ RGO-N. Entry 3 of Table **7** shows that Co_3O_4 seems to be poorer in catalyzing the epoxidation of styrene. Entry 4 shows that significant catalytic activity can be observed over pure RGO-N alone. Entries 5-7 reveal that the use of commonly used oxidation catalysts such as MnO_2, Fe_3O_4, and CuO results in low activity and low epoxide selectivity. The above results show that separated Co_3O_4or RGO-N gives the lower catalytic activity while hybrids result in the superior catalytic activity suggests that Co_3O_4 and N-doped graphene play synergistic roles in the Co_3O_4/RGO-N hybrid for the selective epoxidation of styrene.

Table 7. Catalyst Screening in the Epoxidation of Styrene by O_2[a].

Entry	Catalyst	Conversion (%)	Epoxide selectivity (%)
1	Co_3O_4/RGO–N	97.7	72.7
2	Co_3O_4/RGO	57.3	70.9
3	Co_3O_4	38.6	67.6
4[b]	RGO–N	7.2	58.3
5	MnO_2	5.2	57.7
6	Fe_3O_4	32.2	63.4
7	CuO	3.5	42.9

[a]**Reaction conditions: temperature (100°C), reaction time (3 h), the amount of M (0.15 mmol), styrene (8 mmol), DMF (25 mL), low rate of O_2 (20 mL min-1).** [b]**Reaction conditions: 7.8 mg RGO-N was added.**

The flexibility of the Co_3O_4/RGO-N catalyst is further explained by using different types of olefins used as substrates under optimized conditions (Table **8**). Entry 2 reveals that using styrene with an electron-donating group such as 4-methylphenylene results in a similar conversion to styrene (entry 1), but it has

high epoxide selectivity of 80.6%. Entry 3 shows that the presence of electron-withdrawing group on styrene results in lower conversion and lower epoxide selectivity of 70.7% as compared to unsubstituted styrene. Entry 4 shows that the use of ethyl cinnamate results gives a lower conversion of 55.6% but gives a high epoxide selectivity of 83.9%.

Table 8. Selective Oxidation of Alkenes and Alcohols Over the Co3O4/RGO-N Catalyst[a].

Entry	Substrates	T (h)	Conversion (%)	Product	Selectivity (%)
1[b]	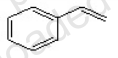	3	97.7	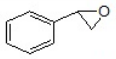	72.7
2	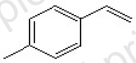	3	97.5	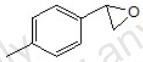	80.6
3		4	96.5	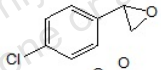	70.7
4	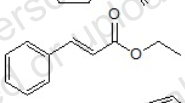	30	55.6	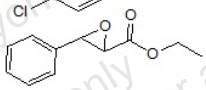	83.9
5	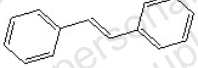	10	95.9	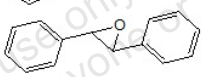	98.3
6[c]		2	>99.9	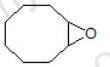	94.9
7[c]	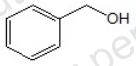	7	93.9	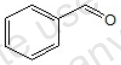	>99.9
8[c]	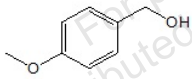	2	98.1	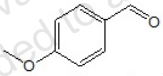	>99.9
9[c]	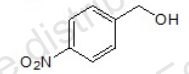	2	99.8	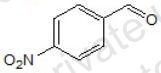	>99.9
10	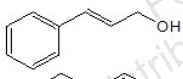	2.5	>99.9	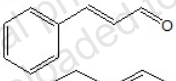	94.4
11[c]	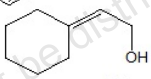	1	92.5	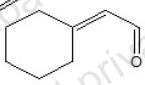	91.5
12[c]	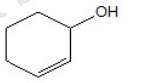	2	98.2	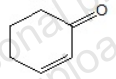	>99.9
13[c]	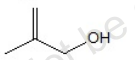	2	95.4	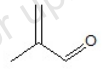	>99.9

[a]Reaction conditions: substrate (1.5 mmol), Co3O4/RGO-N (20 mg), DMF (25 mL), temperature (100◦C), low rate of O_2 (20 mL min-1). [b]8 mmol of the substrate was added. ‘sup> The reaction was carried out at 120◦C.

Entries 5 and 6 revels that by using trans-stilbene and cyclooctene higher selectivity (98.3% and 94.9%) and conversion (95.9% and >99.9%) is obtained.

Entries 7-9 show that the use of both electron-donating and electron-withdrawing substituents results in high conversion (>93%) and high selectivity (>99%). Entries 10-13 show that oxidation of allylic alcohols or other aliphatic unsaturated alcohols results in the respective unsaturated aldehydes/ketones without significant oxidation of the double bond.

REDUCTION REACTIONS

Reduction of Nitro Compounds

Nitro compounds such as 4-nitrophenol (4-NP) and 2-nitrophenol (2-NP) are highly soluble in water and are responsible for water pollution and they are referred to as priority pollutants. To date, several methods have been used to convert nitro pollutants into amines [68 - 72]. To remove the water pollutants generally used, three methods are photocatalytic degradation, catalytic reduction, and adsorption [73].

The catalytic reduction method is used to convert toxic nitrophenols into their corresponding amino phenols. The reduction process is an important method to remove toxic pollutants such as nitroarenes and convert them into amino arenes. The amino arenes play an important role in the synthesis of dyes, pesticides, pharmaceuticals, and have several advantages in the chemical industries [74 - 79]. Catalytic reduction is one of the most efficient methods used for the reduction of nitroarenes, by using the heterogenous catalysts the 4NP and 2-NP are converted into 4aminophenol (4-AP) and 2-aminophenol (2- respectively. Because simple processing, high efficiency, and economic nature of heterogenous catalyst make it a suitable reagent for the catalytic reduction of nitroarenes. Subsequently, the appropriate design and careful selection of the heterogeneous (nano) catalysts results in the enhancement of the reduction process.

At present several heterogeneous catalytic reduction processes have been discovered which does not use water-soluble toxic solvents [80 - 84]. Because of the presence of sp^2 hybridized carbon atomic layer in graphene, it becomes an appropriate candidate for catalytic reduction of nitroarenes. Geim and colleagues in 2004 reported that by using a peeling method having a scotch tape, single-layer graphene can be prepared [85]. Hexagonal flat layer carbon sheets of graphene have the special properties of material science, physics, mechanics, and chemistry [86 - 90] and it also has several advantages in hydrogen storage, catalysis, field emitters, and hydrogen storage. To prepare the heterogeneous catalyst graphene has a high tendency of immobilization of metal oxide between the layers or on the surface, because of above mention property graphene becomes an excellent (nano) catalyst support.

Graphene has very good conductivity, which is responsible for electron transfer during various transformations. In between the reaction steps, electric polarization is developed between the substrates and graphene, which is responsible for the generation of thermal and electrical conductivity that is useful in various processes [91 - 96]. In recent years several graphene derivatives such as functionalized graphene, reduced graphene oxide, and graphene oxide have gained significant attention [97 - 101]. Considering their excellent properties, graphene-based nanostructures with high catalytic activity are one of the outstanding selections for the synthesis of diverse organic compounds [102, 103]. With regards to the greener aspect of the catalytic (nano) systems, developing the most facile and environmentally benign strategies in the efficient remediation of toxic/hazardous nitroarenes is of specific significance worldwide [104].

Graphene-Based (nano) Catalysts in the Reduction of Nitro Compounds

GO and RGO

In 2012, Chen *et al*. reported that nitrogen-doped graphene (NG) can be used as a catalyst for electrochemical reduction of aromatic nitro compounds such as 2,4dinitrotoluene (2,4-DNT), 1,3-dinitrobenzene (1,3-DNB), 2,4,6-trinitrotoluene (TNT) and 1,3,5-trinitrobenzene (TNB) [105].

Colunga and his co-workers stated that using biogenic sulfide graphene oxide can undergo the catalytic reduction of various pollutants like 3-chloronitrobenzene (3CNB) and reactive red 2(RR2) [106]. It is found that the use of GO nanocatalyst in the reduction of 3-chloronitrobenzene results in a high product yield. Mahata and his co-workers, by using cashew leaf extract, discovered an economical, efficient, and described an efficient, economical, and green route for the synthesis of graphene oxide [108].

Au/Graphene-Based Nanocomposites

Adhikari and colleagues stated that GO-based supramolecular hydrogels can be prepared by using biologically active polyamines such as tris (aminoethyl) amine, spermine, and spermidine. Moreover, by using vitamin C reductant and greener route they synthesize the Ag, Au, Pt nanoparticles, and RGO-based hybrid hydrogels *via* the reduction of the metal ions and GO The obtained results reveal that metal nanoparticles are uniformly distributed on reduced graphene oxide nanosheet.

Fakhri and colleagues reported an easy and facile route for the synthesis of GO/Au NPs [109]. As shown in Scheme **5** that prepared GO/Au NPs undergo the

catalytic reduction of nitro compounds at ambient temperature and catalyst can be reused several times.

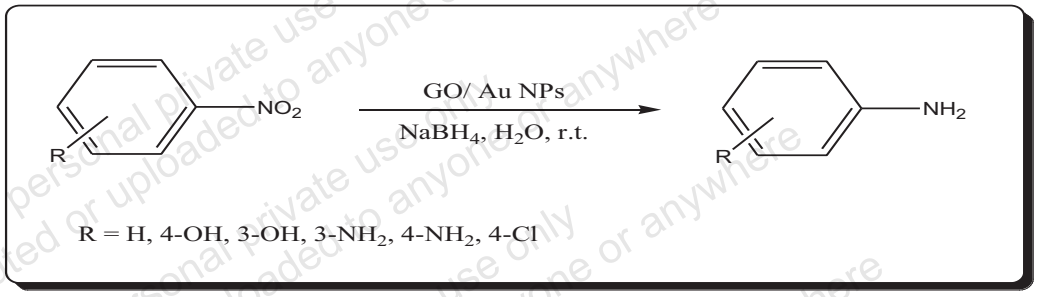

Scheme 5. Catalytic reduction of the nitroarenes using GO/AuNPs.

Ag/Graphene-based Nanocomposites

In 2013, Jeon and his co-workers suggested an easy and facile method for the synthesis of Ag nanoparticles decorated on GO surface-functionalized with them mussel inspired dopamine (GO-Dopa) [110]. It is found that the green synthesized Ag/GO- Dopa hybrid by using $NaBH_4$ undergoes the catalytic reduction of 4-NP to 4-AP. Paul and colleagues in 2016 reported a novel method for the hydrothermal synthesis of Ag/ Fe_2O_3 present on rGO surface by using urea as a hydroxylating agent and polyethylene glycol (PEG4000) as a surfactant [111]. As shown in Scheme **6** synthesized Ag/ Fe_2O_3 -rGO nanocomposite undergoes the effective catalytic reduction of nitro compounds into their respective amines and by using an external magnet catalyst can be reused five times.

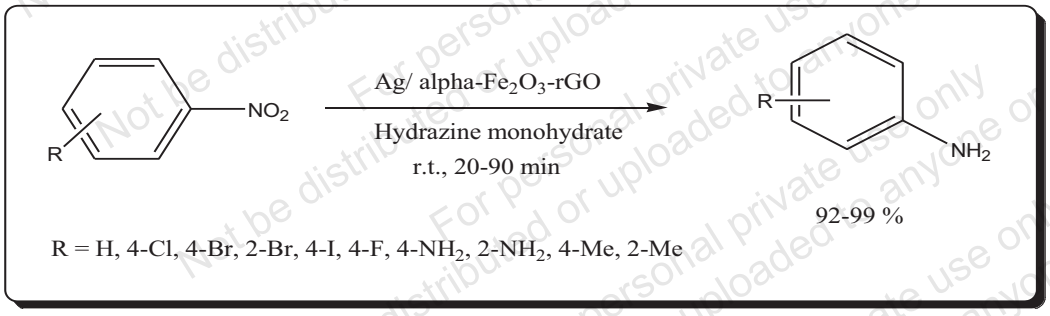

Scheme 6. Catalytic reduction of nitroarenes using Ag/Fe_2O_3-rGO nanocomposite.

Pd/Graphene-Based Nanocomposites

Li and his co-workers developed a synthesis method for the preparation of ultrafine Pd nanocrystals (PdNCs) immobilized on the SnO_2-decorated graphene nanosheets *via* immobilization of Pd NPs with 3.4 nm average size on the PDDA

functionalized SnO_2-GNS (SnO_2-GNS) [112]. As shown in Scheme **7** that by using $NaBH_4$.Pd NPs/ RGO the Pd NCs/ SnO_2 -GNS undergoes the extraordinary reduction of 4-nitrophenols by $NaBH_4$ in an EtOH and H_2O (1:2) mixture and the catalyst can be reused for 5 times.

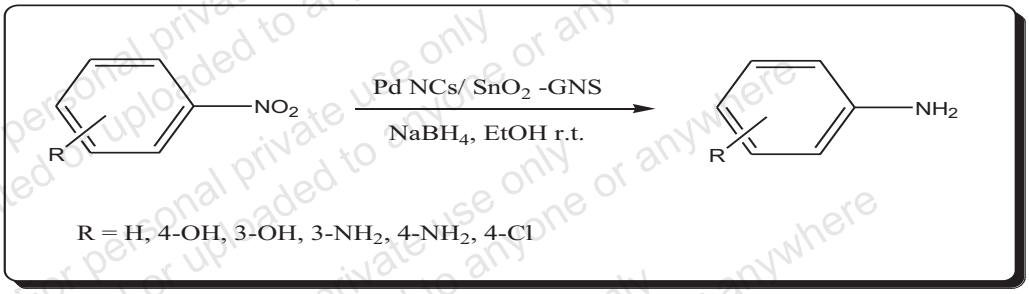

Scheme 7. The reduction of nitroarenes using Pd NPs/RGO.

Zhang *et al*. in 2014 reported an easy and facile route for the synthesis of Go nanocomposite decorated by Pd nanoparticles [113]. It is evident for Scheme **8** that Pd/GO nanocatalyst gives that exceptional catalytic activity during the reduction of aromatic nitro compounds by using $NaBH_4$. The catalyst can be reused 6 times.

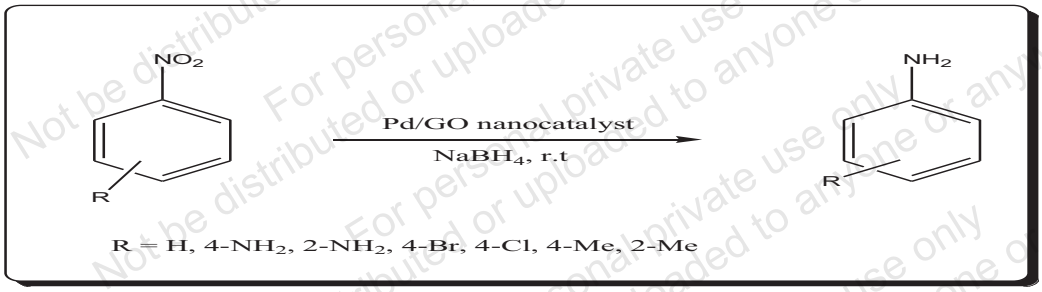

Scheme 8. The catalytic activity of Pd/GO nanocatalyst in nitroarenes reduction by $NaBH_4$.

Ni/Graphene-based Nanocomposites

Kubendhiran *et al*. in 2017 by employing reduction of GO with caffeic acid(CA) and the non-covalent π-π stacking interaction between Ni-TPP and RGO fabricated an RGO/nickel tetraphenyl porphyrin (GRGO/Ni-TPP) nanocomposite modified electrode [114]. The above-prepared nanocomposite GRGO/Ni-TPP is used for the reduction of nitrobenzene and it is found that GRGO/Ni-TPP modified electrode results in high product yield and high selectivity.

Karthik and his co-workers reported RGO-Ni nanocomposite is synthesized by using L-ascorbic acid as a reducing and capping agent by reduction of GO and $NiCl_2.6H_2O$ under hydrothermal conditions [115]. From Scheme **9** it is concluded that by using $NaBH_4$ the RGO-Ni heterogeneous catalyst results in high catalytic activity during the catalytic reduction of aromatic nitro compounds. By using the magnetic separation method, the above catalyst can be recovered and reused 5 times.

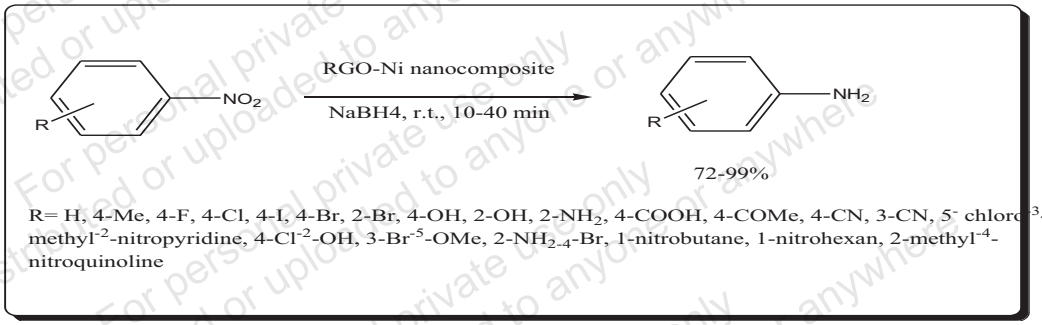

Scheme 9. Catalytic reduction of nitroarenes using RGO-N in a nanocomposite.

Pt/Graphene-based Nanocomposites

Li and his colleagues in 2015 reported a simple method for the fabrication of (Pt NCs/rGO) decorated on rGO by using a water-based, co-chemical reduction process using polyallylamine hydrochloride as a multi-functional agent in the functionalization of GO [116]. It is found that by using $NaBH_4$ the Pt-NCs/rGO composite results in high catalytic activity during the reduction of 4-Nitrophenols and the synthesized catalyst can be used 5 times.

In 2017, Sahoo and his co-workers by using graphene oxide and metal precursor, reported an efficient and green method for the synthesis of d metals (Au, Pd, and Pt)/ 3D-graphene nanocomposites [117]. The metals/3D-graphene nano-composites by using $NaBH_4$ at ambient temperature result in a high catalytic reduction of 4-NP and MB. The catalytic activity rate of metals is as Pt/>Pd/ >Au/3D-graphene for both the pollutants, showing a minimum number of metal nanoparticles results in excellent catalytic activity. The prepared catalyst can be reused 5 times.

Cu/Graphene-based Nanocomposites

In 2018, Liu and Guo developed a simple approach to fabricate the SH-β--D-RGO/Cu NSs nanocomposite by depositing the Cu nanospheres on thio---cyclodextrin (SH-βCD) functionalized RGO (SH-β-CD-RGO) [118]. The

aforementioned nanocomposite plays an important role in the catalytic reduction of 4-Nitrophenol.

Bimetallic/Graphene-based Nanocomposites

Feng and colleagues fabricated the graphene decorated Pd-Cu NPs by employing co-reduction of $CuCl_2.H_2O$ and $PdCl_2$ [119]. As shown in Scheme **10** that Pd Cu-graphene undergoes the effective nitroarene reduction by using $NaBH_4$ in EtOH: H_2O (1:2) at 50 °C. The obtained results reveal that the Pd Cu-graphene can be reused up to six times.

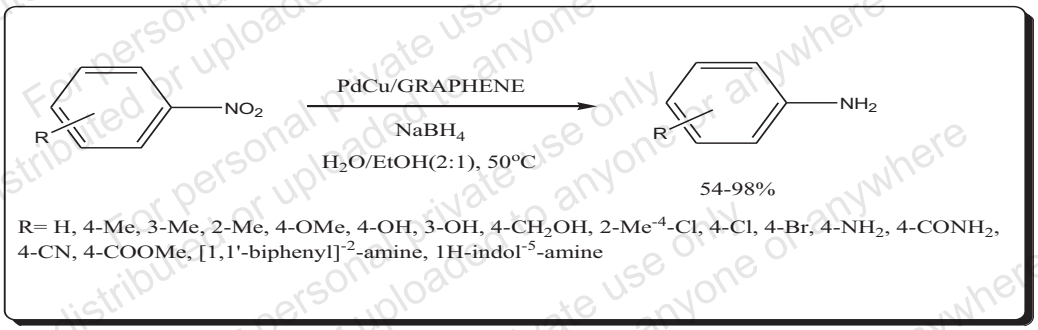

Scheme 10. Catalytic reduction of nitroarenes using Pd Cu-graphene.

In 2013, Goksu and co-workers reported an efficient method for the fabrication of rGO decorated $Co_{30}Pd_{70}$ alloy (rGO- $Co_{30}Pd_{70}$)NPs by co-reduction of cobalt(II) and Pd(II) acetyl acetates in borane-tertbutyl amine (BTB) and oleyl amine (OAm) mixture [120]. It is clear from Scheme **11** that rGO- $Co_{30}Pd_{70}$ catalyst by using ammonia borane in H_2O/methanol mixture undergoes the catalytic reduction of aromatic nitro compounds into their respective amines and results in good product yield.

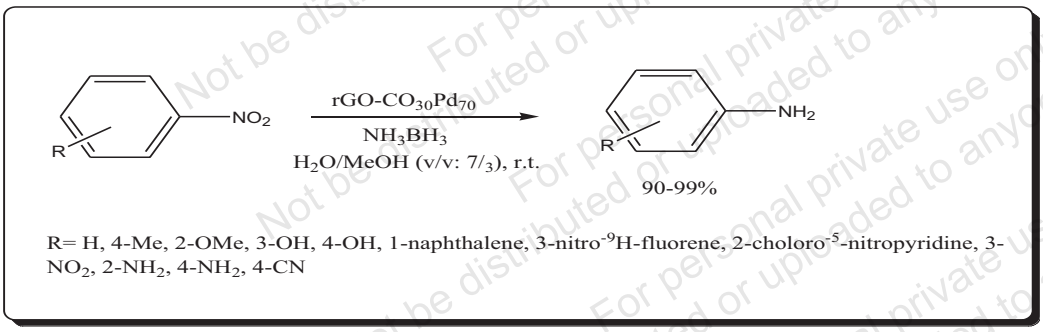

Scheme 11. Catalytic reduction of nitroarenes using rGO-Co30Pd70.

Fang and his coworkers developed an easy and eco-friendly method for the synthesis of graphene/CuNi nanocomposite. They synthesized the two-dimensional graphene decorated Cu Ni with 2D nanoparticles of particle size 2 nm. From Scheme **12** it is clear that the graphene/CuNi nanocomposite undergoes the selective catalytic reduction of aromatic nitro compounds by using $NaBH_4$ and the catalyst can be reused up to 25 times.

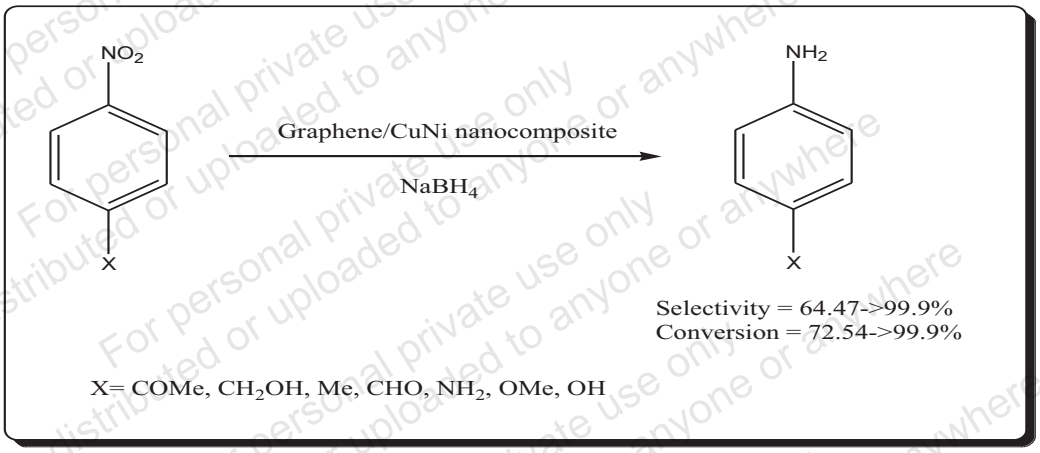

Scheme 12. Reduction of nitroarenes by graphene/CuNi nanocomposite.

CONCLUDING REMARKS

The previous studies reveal that the metal-free GO has many catalytic applications. The surface area of GO is high, the adsorption capacity of GO towards hydrocarbons, gases, and ions is very high, and also the reaction of GO with oxygenating functionalities resulted in various paths for the introduction and modification of various functional groups.

Although lots of studies are done on the numerous catalytic application of GO, still there are lots of challenges that should be examined and resolved. Among them, the three main important challenges are: (1) As we know that the performance of the GO catalytic system is mainly dependent on composition and structure, so there is a need to develop such methods which undergo the precise characterization for the identification of active sites. (2) Much care should be taken to eliminate the probability that the catalytic activity could be recognized to metal contaminants, even at a trace level. (3) Further understanding and more research are needed to describe the potential cooperative effect of Go on the catalytic activity. To design the balanced metal-free catalyst systems it is necessary to understand the advantages of graphene oxide over the activated carbon and traditional metal oxide. However, the metal-free carbon catalyst has

the above drawbacks. It can be used to solve the various industrial problems related to the traditional catalysts. Since graphene oxide catalysts are synthesized environmentally friendly material, their applications should be explored in green synthesis.

LIST OF ABBREVIATIONS

0D	Zero dimensional
1D	One dimensional
2D	Two dimensional
AP	Aminophenol
BTB	Borane-tertbutyl amine
CVD	Chemical vapor deposition
CuTSPc@3D-(N)GFs	Copper(II) tetrasulfo phthalocyanine reinforced on three-dimensional nitrogen-doped graphene-based frameworks
CNB	Chloronitrobenzene
Cu NSs	Copper nanospheres
CMGs	Chemically modified Graphenes
DCC	N,N-dicyclohexylcarbodiimide
DMF	Dimethylformamide
DMA	Dimethylacetamide
DMSO	Dimethyl sulfoxide
DNT	Dinitrotoluene
DNB	Dinitrobenzene
EDC	1-ethyl-3-(3-dimethyl aminopropyl) carbodiimide
EDCI	N-(3-dimethyl aminopropyl)-N-ethyl carbodiimide hydrochloride
FGO	Functionalized graphene oxide
GO	Graphene oxide
GNS	Graphene nanosheets
IGO	Improved graphene oxide
MOFs	Metal–organic frameworks
MB	Methylene Blue
NMR	Nuclear magnetic resonance
NP	Nitrophenol
NG	Nitrogen-doped graphene
NPs	Nanoparticles
NCs	Nanocrystals

For personal private use only Not be distributed or uploaded to anyone or anywhere

ORR	Oxygen reduction reaction
OAm	Oleyl amine
rGO	Reduced graphene oxide
RR	Reactive red
R.t.	Room temperature
SH-βCD	Thio-β-cyclodextrin
TNT	Trinitrotoluene
TNB	Trinitrobenzene
TPP	Tetraphenyl porphyrin

CONSENT FOR PUBLICATION

Not applicable.

CONFLICT OF INTEREST

The author declares no conflict of interest, financial or otherwise.

ACKNOWLEDGEMENTS

Declared none.

REFERENCES

[1] Geim, A.K.; Novoselov, K.S. The rise of graphene. *Nat. Mater.,* **2007**, *6*(3), 183-191. [http://dx.doi.org/10.1038/nmat1849] [PMID: 17330084]

[2] Georgakilas, V.; Otyepka, M.; Bourlinos, A.B.; Chandra, V.; Kim, N.; Kemp, K.C.; Hobza, P.; Zboril, R.; Kim, K.S. Functionalization of graphene: covalent and non-covalent approaches, derivatives and applications. *Chem. Rev.,* **2012**, *112*(11), 6156-6214. [http://dx.doi.org/10.1021/cr3000412] [PMID: 23009634]

[3] Huang, X.; Yin, Z.; Wu, S.; Qi, X.; He, Q.; Zhang, Q.; Yan, Q.; Boey, F.; Zhang, H. Graphene-based materials: synthesis, characterization, properties, and applications. *Small,* **2011**, *7*(14), 1876-1902. [http://dx.doi.org/10.1002/smll.201002009] [PMID: 21630440]

[4] Sun, X.; Wang, R.; Su, D. Research progress in metal-free carbon-based catalysts. *Chin. J. Catal.,* **2013**, *34*(3), 508-523. [http://dx.doi.org/10.1016/S1872-2067(11)60515-9]

[5] Yu, D.; Nagelli, E.; Du, F.; Dai, L. Metal-free carbon nanomaterials become more active than metal catalysts and last longer. *J. Phys. Chem. Lett.,* **2010**, *1*(14), 2165-2173. [http://dx.doi.org/10.1021/jz100533t]

[6] Lotya, M.; Hernandez, Y.; King, P.J.; Smith, R.J.; Nicolosi, V.; Karlsson, L.S.; Blighe, F.M.; De, S.; Wang, Z.; McGovern, I.T.; Duesberg, G.S.; Coleman, J.N. Liquid phase production of graphene by exfoliation of graphite in surfactant/water solutions. *J. Am. Chem. Soc.,* **2009**, *131*(10), 3611-3620. [http://dx.doi.org/10.1021/ja807449u] [PMID: 19227978]

[7] Kim, K.S.; Zhao, Y.; Jang, H.; Lee, S.Y.; Kim, J.M.; Kim, K.S.; Ahn, J.H.; Kim, P.; Choi, J.Y.; Hong, B.H. Large-scale pattern growth of graphene films for stretchable transparent electrodes. *Nature,* **2009**,

Not be distributed or uploaded to anyone or anywhere For personal private use only

457(7230), 706-710.
[http://dx.doi.org/10.1038/nature07719] [PMID: 19145232]

[8] Brodie, B.C. XIII. On the atomic weight of graphite. *Philos. Trans. R. Soc. Lond.,* **1859**, *149*, 249-259.
[http://dx.doi.org/10.1098/rstl.1859.0013]

[9] Staudenmaier, L. Verfahren zur Darstellung der Graphitsäure. *Ber. Dtsch. Chem. Ges.,* **1898**, *31*(2), 1481-1487.
[http://dx.doi.org/10.1002/cber.18980310237]

[10] Hummers, W.S., Jr; Offeman, R.E. Preparation of graphitic oxide. *J. Am. Chem. Soc.,* **1958**, *80*(6), 1339-1339.
[http://dx.doi.org/10.1021/ja01539a017]

[11] Stankovich, S.; Dikin, D.A.; Dommett, G.H.B.; Kohlhaas, K.M.; Zimney, E.J.; Stach, E.A.; Piner, R.D.; Nguyen, S.T.; Ruoff, R.S. Graphene-based composite materials. *Nature,* **2006**, *442*(7100), 282-286.
[http://dx.doi.org/10.1038/nature04969] [PMID: 16855586]

[12] Lerf, A.; He, H.; Forster, M.; Klinowski, J. Structure of graphite oxide revisited. *J. Phys. Chem. B,* **1998**, *102*(23), 4477-4482.
[http://dx.doi.org/10.1021/jp9731821]

[13] Zhou, M.; Wang, Y.; Zhai, Y.; Zhai, J.; Ren, W.; Wang, F.; Dong, S. Controlled synthesis of large-area and patterned electrochemically reduced graphene oxide films. *Chemistry,* **2009**, *15*(25), 6116-6120.
[http://dx.doi.org/10.1002/chem.200900596] [PMID: 19444826]

[14] Park, J.S.; Cho, S.M.; Kim, W.J.; Park, J.; Yoo, P.J. Fabrication of graphene thin films based on layer-by-layer self-assembly of functionalized graphene nanosheets. *ACS Appl. Mater. Interfaces,* **2011**, *3*(2), 360-368.
[http://dx.doi.org/10.1021/am100977p] [PMID: 21207942]

[15] Cao, H.; Wu, X.; Yin, G.; Warner, J.H. Synthesis of adenine-modified reduced graphene oxide nanosheets. *Inorg. Chem.,* **2012**, *51*(5), 2954-2960.
[http://dx.doi.org/10.1021/ic2022402] [PMID: 22356685]

[16] Liu, Q.; Shi, J.; Sun, J.; Wang, T.; Zeng, L.; Jiang, G. Graphene and graphene oxide sheets supported on silica as versatile and high-performance adsorbents for solid-phase extraction. *Angew. Chem. Int. Ed.,* **2011**, *50*(26), 5913-5917.
[http://dx.doi.org/10.1002/anie.201007138] [PMID: 21567667]

[17] Sun, X.; Liu, Z.; Welsher, K.; Robinson, J.T.; Goodwin, A.; Zaric, S.; Dai, H. Nano-graphene oxide for cellular imaging and drug delivery. *Nano Res.,* **2008**, *1*(3), 203-212.
[http://dx.doi.org/10.1007/s12274-008-8021-8] [PMID: 20216934]

[18] Jin, L.; Yang, K.; Yao, K.; Zhang, S.; Tao, H.; Lee, S.T.; Liu, Z.; Peng, R. Functionalized graphene oxide in enzyme engineering: a selective modulator for enzyme activity and thermostability. *ACS Nano,* **2012**, *6*(6), 4864-4875.
[http://dx.doi.org/10.1021/nn300217z] [PMID: 22574614]

[19] Kou, L.; He, H.; Gao, C. Click chemistry approach to functionalize two-dimensional macromolecules of graphene oxide nanosheets. *Nano-Micro Lett.,* **2010**, *2*(3), 177-183.
[http://dx.doi.org/10.1007/BF03353638]

[20] Lee, D.; Choi, M.C.; Ha, C.S. Polynorbornene dicarboximide/amine functionalized graphene hybrids for potential oxygen barrier films. *J. Polym. Sci. A Polym. Chem.,* **2012**, *50*(8), 1611-1621.
[http://dx.doi.org/10.1002/pola.25932]

[21] Wang, B.; Luo, B.; Liang, M.; Wang, A.; Wang, J.; Fang, Y.; Chang, Y.; Zhi, L. Chemical amination of graphene oxides and their extraordinary properties in the detection of lead ions. *Nanoscale,* **2011**, *3*(12), 5059-5066.

Not be distributed or uploaded to anyone or anywhere
For personal private use only

[http://dx.doi.org/10.1039/c1nr10901d] [PMID: 22041992]

[22] Zhang, W.; Wang, S.; Ji, J.; Li, Y.; Zhang, G.; Zhang, F.; Fan, X. Primary and tertiary amines bifunctional graphene oxide for cooperative catalysis. *Nanoscale,* **2013**, *5*(13), 6030-6033. [http://dx.doi.org/10.1039/c3nr01323e] [PMID: 23714770]

[23] Wang, H.; Maiyalagan, T.; Wang, X. Review on recent progress in nitrogen-doped graphene: synthesis, characterization, and Its potential applications. *ACS Catal.,* **2012**, *2*(5), 781-794. [http://dx.doi.org/10.1021/cs200652y]

[24] Fu, J.; Shi, F.; Thompson, L.T., Jr; Lu, X.; Savage, P.E. Activated carbons for hydrothermal decarboxylation of fatty acids. *ACS Catal.,* **2011**, *1*(3), 227-231. [http://dx.doi.org/10.1021/cs1001306]

[25] Dreyer, D.R.; Bielawski, C.W. Carbocatalysis: Heterogeneous carbons finding utility in synthetic chemistry. *Chem. Sci. (Camb.),* **2011**, *2*(7), 1233-1240. [http://dx.doi.org/10.1039/c1sc00035g]

[26] Dreyer, D.R.; Jia, H.P.; Bielawski, C.W. Graphene oxide: a convenient carbocatalyst for facilitating oxidation and hydration reactions. *Angew. Chem. Int. Ed.,* **2010**, *49*(38), 6686. [http://dx.doi.org/10.1002/anie.201003238] [PMID: 20602388]

[27] Dreyer, D.R.; Jia, H.P.; Todd, A.D.; Geng, J.; Bielawski, C.W. Graphite oxide: a selective and highly efficient oxidant of thiols and sulfides. *Org. Biomol. Chem.,* **2011**, *9*(21), 7292-7295. [http://dx.doi.org/10.1039/c1ob06102j] [PMID: 21909587]

[28] Jia, H.P.; Dreyer, D.R.; Bielawski, C.W. C–H oxidation using graphite oxide. *Tetrahedron,* **2011**, *67*(24), 4431-4434. [http://dx.doi.org/10.1016/j.tet.2011.02.065]

[29] Jia, H.P.; Dreyer, D.R.; Bielawski, C.W. Graphite oxide as an auto-tandem oxidation-hydration-aldol coupling catalyst. *Adv. Synth. Catal.,* **2011**, *353*(4), 528-532. [http://dx.doi.org/10.1002/adsc.201000748]

[30] Vijay Kumar, A.; Rama Rao, K. Recyclable graphite oxide catalyzed Friedel–Crafts addition of indoles to α,β-unsaturated ketones. *Tetrahedron Lett.,* **2011**, *52*(40), 5188-5191. [http://dx.doi.org/10.1016/j.tetlet.2011.08.002]

[31] Verma, S.; Mungse, H.P.; Kumar, N.; Choudhary, S.; Jain, S.L.; Sain, B.; Khatri, O.P. Graphene oxide: an efficient and reusable carbocatalyst for aza-Michael addition of amines to activated alkenes. *Chem. Commun. (Camb.),* **2011**, *47*(47), 12673-12675. [http://dx.doi.org/10.1039/c1cc15230k] [PMID: 22039588]

[32] Dreyer, D.R.; Jarvis, K.A.; Ferreira, P.J.; Bielawski, C.W. Graphite oxide as a carbocatalyst for the preparation of fullerene-reinforced polyester and polyamide nanocomposites. *Polym. Chem.,* **2012**, *3*(3), 757-766. [http://dx.doi.org/10.1039/c2py00545j]

[33] Supale, A.; Gokavi, G. Oxidation of thiols to disulfides using H_2O_2 catalyzed by recyclable chromic potassium sulphate at room temperature. *React. Kinet. Catal. Lett.,* **2008**, *93*(1), 141-148. [http://dx.doi.org/10.1007/s11144-008-5223-8]

[34] Goifman, A.; Gun, J.; Gelman, F.; Ekeltchik, I.; Worch, E.; Lev, O. Catalytic oxidation of thiol compounds by novel fuel cell□inspired Co□porphyrin and Co□imidazole catalysts. *Isr. J. Chem.,* **2006**, *46*(1), 17-26. [http://dx.doi.org/10.1560/8J05-UHG8-K6DN-VVB2]

[35] Postel, M.; Duñach, E. Bismuth derivatives for the oxidation of organic compounds. *Coord. Chem. Rev.,* **1996**, *155*, 127-144. [http://dx.doi.org/10.1016/0010-8545(96)90179-4]

[36] Qiu, X.; Len, C.; Luque, R.; Li, Y. Solventless oxidative coupling of amines to imines by using transition-metal-free metal-organic frameworks. *ChemSusChem,* **2014**, *7*(6), 1684-1688.

[http://dx.doi.org/10.1002/cssc.201301340] [PMID: 24801486]

[37] Jaiswal, G.; Landge, V.G.; Jagadeesan, D.; Balaraman, E. Sustainable iron-catalyzed direct imine formation by acceptorless dehydrogenative coupling of alcohols with amines. *Green Chem.,* **2016**, *18*(11), 3232-3238.
[http://dx.doi.org/10.1039/C6GC00565A]

[38] Zhang, B.; Guo, X.W.; Liang, H.; Ge, H.; Gu, X.; Chen, S.; Yang, H.; Qin, Y. Tailoring Pt–Fe_2O_3 Interfaces for Selective Reductive Coupling Reaction To Synthesize Imine. *ACS Catal.,* **2016**, *6*(10), 6560-6566.
[http://dx.doi.org/10.1021/acscatal.6b01756]

[39] Xu, Y.; Chen, Y.; Fu, W.F. Visible-light driven oxidative coupling of amines to imines with high selectivity in air over core-shell structured $CdS@C_3N_4$. *Appl. Catal. B,* **2018**, *236*, 176-183.
[http://dx.doi.org/10.1016/j.apcatb.2018.03.098]

[40] Chen, B.; Shang, S.; Wang, L.; Zhang, Y.; Gao, S. Mesoporous carbon derived from vitamin B_{12} : a high-performance bifunctional catalyst for imine formation. *Chem. Commun. (Camb.),* **2016**, *52*(3), 481-484.
[http://dx.doi.org/10.1039/C5CC06179B] [PMID: 26529323]

[41] Naya, S.; Kimura, K.; Tada, H. One-step selective aerobic oxidation of amines to imines by gold nanoparticle-loaded rutile titanium (iv) oxide plasmon photocatalyst. *ACS Catal.,* **2013**, *3*(1), 10-13.
[http://dx.doi.org/10.1021/cs300682d]

[42] Biswas, S.; Dutta, B.; Mullick, K.; Kuo, C.H.; Poyraz, A.S.; Suib, S.L. Aerobic oxidation of amines to imines by cesium-promoted mesoporous manganese oxide. *ACS Catal.,* **2015**, *5*(7), 4394-4403.
[http://dx.doi.org/10.1021/acscatal.5b00325]

[43] Tang, L.; Sun, H.; Li, Y.; Zha, Z.; Wang, Z. Highly active and selective synthesis of imines from alcohols and amines or nitroarenes catalyzed by Pd/DNA in water with dehydrogenation. *Green Chem.,* **2012**, *14*(12), 3423-3428.
[http://dx.doi.org/10.1039/c2gc36312g]

[44] Chen, B.; Wang, L.; Gao, S. Recent advances in aerobic oxidation of alcohols and amines to imines. *ACS Catal.,* **2015**, *5*(10), 5851-5876.
[http://dx.doi.org/10.1021/acscatal.5b01479]

[45] Largeron, M.; Fleury, M.B. A biologically inspired Cu(I)/topaquinone-like co-catalytic system for the highly atom-economical aerobic oxidation of primary amines to imines. *Angew. Chem. Int. Ed.,* **2012**, *51*(22), 5409-5412.
[http://dx.doi.org/10.1002/anie.201200587] [PMID: 22499249]

[46] Xu, J.; Zhuang, R.; Bao, L.; Tang, G.; Zhao, Y. KOH-mediated transition metal-free synthesis of imines from alcohols and amines. *Green Chem.,* **2012**, *14*(9), 2384-2387.
[http://dx.doi.org/10.1039/c2gc35714c]

[47] Zhang, H.; Wu, C.; Wang, W.; Bu, J.; Zhou, F.; Zhang, B.; Zhang, Q. Effect of Ceria on redox-catalytic property in mild condition: A solvent-free route for imine synthesis at low temperature. *Appl. Catal. B,* **2018**, *227*, 209-217.
[http://dx.doi.org/10.1016/j.apcatb.2018.01.012]

[48] Chen, B.; Wang, L.; Dai, W.; Shang, S.; Lv, Y.; Gao, S. Metal free and solvent-free oxidative coupling of amines to imines with mesoporous carbon from macrocyclic compounds. *ACS Catal.,* **2015**, *5*(5), 2788-2794.
[http://dx.doi.org/10.1021/acscatal.5b00244]

[49] Hirakawa, H.; Katayama, M.; Shiraishi, Y.; Sakamoto, H.; Wang, K.; Ohtani, B.; Ichikawa, S.; Tanaka, S.; Hirai, T. One-pot synthesis of imines from nitroaromatics and alcohols by tandem photocatalytic and catalytic reactions on Degussa (Evonik) P25 titanium dioxide. *ACS Appl. Mater. Interfaces,* **2015**, *7*(6), 3797-3806.
[http://dx.doi.org/10.1021/am508769x] [PMID: 25621386]

Not be distributed or uploaded to anyone or anywhere
For personal private use only

[50] Su, C.; Loh, K.P. Carbocatalysts: graphene oxide and its derivatives. *Acc. Chem. Res.,* **2013**, *46*(10), 2275-2285.
[http://dx.doi.org/10.1021/ar300118v] [PMID: 23270430]

[51] Xie, J.; Li, L.; Sun, L.; Pei, Z.; Wen, B.; Xing, B. Reduced graphene oxide-catalyzed oxidative coupling reaction of 4-methoxyphenol in aerobic aqueous solution. *Carbon,* **2017**, *121*, 418-425.
[http://dx.doi.org/10.1016/j.carbon.2017.06.016]

[52] Fan, X.; Peng, W.; Li, Y.; Li, X.; Wang, S.; Zhang, G.; Zhang, F. Deoxygenation of exfoliated graphite oxide under alkaline conditions: a green route to graphene preparation. *Adv. Mater.,* **2008**, *20*(23), 4490-4493.
[http://dx.doi.org/10.1002/adma.200801306]

[53] Pedrosa, M.; Pastrana-Martínez, L.M.; Pereira, M.F.R.; Faria, J.L.; Figueiredo, J.L.; Silva, A.M.T. N/S-doped graphene derivatives and TiO_2 for catalytic ozonation and photocatalysis of water pollutants. *Chem. Eng. J.,* **2018**, *348*, 888-897.
[http://dx.doi.org/10.1016/j.cej.2018.04.214]

[54] Marinescu, C.; Ben Ali, M.; Hamdi, A.; Cherifi, Y.; Barras, A.; Coffinier, Y.; Somacescu, S.; Raditoiu, V.; Szunerits, S.; Boukherroub, R. Cobalt phthalocyanine-supported reduced graphene oxide: A highly efficient catalyst for heterogeneous activation of peroxymonosulfate for rhodamine B and pentachlorophenol degradation. *Chem. Eng. J.,* **2018**, *336*, 465-475.
[http://dx.doi.org/10.1016/j.cej.2017.12.009]

[55] Su, C.; Acik, M.; Takai, K.; Lu, J.; Hao, S.; Zheng, Y.; Wu, P.; Bao, Q.; Enoki, T.; Chabal, Y.J.; Ping Loh, K. Probing the catalytic activity of porous graphene oxide and the origin of this behaviour. *Nat. Commun.,* **2012**, *3*(1), 1298-1306.
[http://dx.doi.org/10.1038/ncomms2315] [PMID: 23250428]

[56] Yang, F.; Fan, X.; Wang, C.; Yang, W.; Hou, L.; Xu, X.; Feng, A.; Dong, S.; Chen, K.; Wang, Y.; Li, Y. P-doped nanomesh graphene with high-surface-area as an efficient metal-free catalyst for aerobic oxidative coupling of amines. *Carbon,* **2017**, *121*, 443-451.
[http://dx.doi.org/10.1016/j.carbon.2017.05.101]

[57] Su, C.; Tandiana, R.; Balapanuru, J.; Tang, W.; Pareek, K.; Nai, C.T.; Hayashi, T.; Loh, K.P. Tandem catalysis of amines using porous graphene oxide. *J. Am. Chem. Soc.,* **2015**, *137*(2), 685-690.
[http://dx.doi.org/10.1021/ja512470t] [PMID: 25551171]

[58] Zhao, Q.; Chen, D.; Li, Y.; Zhang, G.; Zhang, F.; Fan, X. Rhodium complex immobilized on graphene oxide as an efficient and recyclable catalyst for hydrogenation of cyclohexene. *Nanoscale,* **2013**, *5*(3), 882-885.
[http://dx.doi.org/10.1039/C2NR33290F] [PMID: 23238302]

[59] Li, Y.; Chen, H.; Voo, L.Y.; Ji, J.; Zhang, G.; Zhang, G.; Zhang, F.; Fan, X. Synthesis of partially hydrogenated graphene and brominated graphene. *J. Mater. Chem.,* **2012**, *22*(30), 15021-15024.
[http://dx.doi.org/10.1039/c2jm32307a]

[60] Huang, H.; Huang, J.; Liu, Y.M.; He, H.Y.; Cao, Y.; Fan, K.N. Graphite oxide as an efficient and durable metal-free catalyst for aerobic oxidative coupling of amines to imines. *Green Chem.,* **2012**, *14*(4), 930-934.
[http://dx.doi.org/10.1039/c2gc16681j]

[61] Bermudez, J.M.; Menendez, J.A.; Arenillas, A.; Martinez-Palou, R.; Romero, A.A.; Luque, R. Selectivity matters: Graphene oxide-mediated oxidative coupling of benzylamine to N□benzylidine--phenylmethanamine under microwave irradiation. *J. Mol. Catal. Chem.,* **2015**, *406*, 19-22.
[http://dx.doi.org/10.1016/j.molcata.2015.05.010]

[62] He, H.; Li, Z.; Li, K.; Lei, G.; Guan, X.; Zhang, G.; Zhang, F.; Fan, X.; Peng, W.; Li, Y. Bifunctional Graphene-Based Metal-Free Catalysts for Oxidative Coupling of Amines. *ACS Appl. Mater. Interfaces,* **2019**, *11*(35), 31844-31850.
[http://dx.doi.org/10.1021/acsami.9b08741] [PMID: 31382740]

Not be distributed or uploaded to anyone or anywhere
For personal private use only

[63] Yang, J.H.; Sun, G.; Gao, Y.; Zhao, H.; Tang, P.; Tan, J.; Lu, A.H.; Ma, D. Direct catalytic oxidation of benzene to phenol over metal-free graphene-based catalyst. *Energy Environ. Sci.,* **2013**, *6*(3), 793-800.
[http://dx.doi.org/10.1039/c3ee23623d]

[64] Long, J.; Xie, X.; Xu, J.; Gu, Q.; Chen, L.; Wang, X. Nitrogendoped graphene nanosheets as metal-free catalysts for aerobic selective oxidation of benzylic alcohols. *ACS Catal.,* **2012**, *2*(4), 622-631.
[http://dx.doi.org/10.1021/cs3000396]

[65] Zhang, P.; Gong, Y.; Li, H.; Chen, Z.; Wang, Y. Solvent-free aerobic oxidation of hydrocarbons and alcohols with Pd@N-doped carbon from glucose. *Nat. Commun.,* **2013**, *4*(1), 1593-1604.
[http://dx.doi.org/10.1038/ncomms2586] [PMID: 23481401]

[66] Mahyari, M.; Laeini, M.S.; Shaabani, A. Aqueous aerobic oxidation of alkyl arenes and alcohols catalyzed by copper(II) phthalocyanine supported on three-dimensional nitrogen-doped graphene at room temperature. *Chem. Commun. (Camb.),* **2014**, *50*(58), 7855-7857.
[http://dx.doi.org/10.1039/C4CC01406E] [PMID: 24912023]

[67] Nie, R.; Shi, J.; Du, W.; Ning, W.; Hou, Z.; Xiao, F.S. A sandwich N-doped graphene/Co_3O_4 hybrid: an efficient catalyst for selective oxidation of olefins and alcohols. *J. Mater. Chem. A Mater. Energy Sustain.,* **2013**, *1*(32), 9037-9045.
[http://dx.doi.org/10.1039/c3ta11672g]

[68] Vellaichamy, B.; Prakash, P.; Thomas, J. Synthesis of AuNPs@RGO nanosheets for sustainable catalysis toward nitrophenols reduction. *Ultrason. Sonochem.,* **2018**, *48*, 362-369.
[http://dx.doi.org/10.1016/j.ultsonch.2018.05.012] [PMID: 30080561]

[69] Sarvestani, M.; Azadi, R. Efficient reduction of nitroarenes in water catalyzed by reusable Pd nanoparticles immobilized on chitosan-functionalized graphene oxide. *Can. J. Chem.,* **2019**, *97*(3), 191-196.
[http://dx.doi.org/10.1139/cjc-2018-0011]

[70] Ansar, S.M.; Kitchens, C.L. Impact of gold nanoparticle stabilizing ligands on the colloidal catalytic reduction of 4-nitrophenol. *ACS Catal.,* **2016**, *6*(8), 5553-5560.
[http://dx.doi.org/10.1021/acscatal.6b00635]

[71] Ayad, M.M.; Amer, W.A.; Kotp, M.G. Magnetic polyaniline-chitosan nanocomposite decorated with palladium nanoparticles for enhanced catalytic reduction of 4-nitrophenol. *Molecular Catalysis,* **2017**, *439*, 72-80.
[http://dx.doi.org/10.1016/j.mcat.2017.06.023]

[72] Naghdi, S.; Sajjadi, M.; Nasrollahzadeh, M.; Rhee, K.Y.; Sajadi, S.M.; Jaleh, B. Cuscuta reflexa leaf extract mediated green synthesis of the Cu nanoparticles on graphene oxide/manganese dioxide nanocomposite and its catalytic activity toward reduction of nitroarenes and organic dyes. *J. Taiwan Inst. Chem. Eng.,* **2018**, *86*, 158-173.
[http://dx.doi.org/10.1016/j.jtice.2017.12.017]

[73] Hu, H.; Xin, J.H.; Hu, H.; Wang, X.; Miao, D.; Liu, Y. Synthesis and stabilization of metal nanocatalysts for reduction reactions – a review. *J. Mater. Chem. A Mater. Energy Sustain.,* **2015**, *3*(21), 11157-11182.
[http://dx.doi.org/10.1039/C5TA00753D]

[74] Kariper, İ.A.; Çağlayan, M.O.; Üstündağ, Z. Heterogeneous Au/Ru hybrid nanoparticle decorated graphene oxide nanosheet catalyst for the catalytic reduction of nitroaromatics. *Res. Chem. Intermed.,* **2019**, *45*(2), 801-813.
[http://dx.doi.org/10.1007/s11164-018-3644-1]

[75] Lin, S-C.A.; Liu, Y.H.; Peng, S.M.; Liu, S.T. Diruthenium complex catalyzed reduction of nitroarenes-investigation of reaction pathway. *Molecular Catalysis,* **2019**, *466*, 46-51.
[http://dx.doi.org/10.1016/j.mcat.2019.01.005]

Not be distributed or uploaded to anyone or anywhere
For personal private use only

[76] Fiore, A.M.; Romanazzi, G.; Dell'Anna, M.M.; Latronico, M.; Leonelli, C.; Mali, M.; Rizzuti, A.; Mastrorilli, P. Mild and efficient synthesis of secondary aromatic amines by one-pot stepwise reductive amination of arylaldehydes with nitroarenes promoted by reusable nickel nanoparticles. *Molecular Catalysis,* **2019**, *476*, 110507-110516.
[http://dx.doi.org/10.1016/j.mcat.2019.110507]

[77] Romanazzi, G.; Fiore, A.M.; Mali, M.; Rizzuti, A.; Leonelli, C.; Nacci, A.; Mastrorilli, P.; Dell'Anna, M.M. Catalytic activities of heterogeneous catalysts obtained by copolymerization of metal-containing 2-(acetoacetoxy)ethyl methacrylate. *Mol. Catal.,* **2018**, *446*, 31-38.
[http://dx.doi.org/10.1016/j.mcat.2017.12.015]

[78] Metin, Ö.; Can, H.; Şendil, K.; Gültekin, M.S. Monodisperse Ag/Pd core/shell nanoparticles assembled on reduced graphene oxide as highly efficient catalysts for the transfer hydrogenation of nitroarenes. *J. Colloid Interface Sci.,* **2017**, *498*, 378-386.
[http://dx.doi.org/10.1016/j.jcis.2017.03.066] [PMID: 28343135]

[79] Goksu, H.; Sert, H.; Kilbas, B.; Sen, F. Recent advances in the reduction of nitro compounds by heterogenous catalysts. *Curr. Org. Chem.,* **2017**, *21*(9), 794-820.
[http://dx.doi.org/10.2174/1385272820666160525123907]

[80] Bustamante, T.M.; Dinamarca, R.; Torres, C.C.; Pecchi, G.; Campos, C.H. Pd-Co catalysts prepared from palladium-doped cobalt titanate precursors for chemoselective hydrogenation of halonitroarenes. *Molecular Catalysis,* **2020**, *482*, 110702-110715.
[http://dx.doi.org/10.1016/j.mcat.2019.110702]

[81] Jin, Q.; Shen, Y.; Li, X.; Zeng, Y. Resource utilization of waste deNOx catalyst for continuous-flow catalysis by supported metal reactors. *Molecular Catalysis,* **2020**, *480*, 110634-110640.
[http://dx.doi.org/10.1016/j.mcat.2019.110634]

[82] Hu, A.; Lu, X.; Cai, D.; Pan, H.; Jing, R.; Xia, Q.; Zhou, D.; Xia, Y. Selective hydrogenation of nitroarenes over MOF-derived Co@CN catalysts at mild conditions. *Molecular Catalysis,* **2019**, *472*, 27-36.
[http://dx.doi.org/10.1016/j.mcat.2019.04.008]

[83] Zhang, K.; Suh, J.M.; Choi, J.W.; Jang, H.W.; Shokouhimehr, M.; Varma, R.S. Recent advances in the nanocatalyst-assisted $NaBH_4$ reduction of nitroaromatics in water. *ACS Omega,* **2019**, *4*(1), 483-495.
[http://dx.doi.org/10.1021/acsomega.8b03051] [PMID: 31032469]

[84] Iijima, S.; Ichihashi, T. Single-shell carbon nanotubes of 1-nm diameter. *Nature,* **1993**, *363*(6430), 603-605.
[http://dx.doi.org/10.1038/363603a0]

[85] Castro Neto, A.H.; Guinea, F.; Peres, N.M.R.; Novoselov, K.S.; Geim, A.K. The electronic properties of graphene. *Rev. Mod. Phys.,* **2009**, *81*(1), 109-162.
[http://dx.doi.org/10.1103/RevModPhys.81.109]

[86] Shi, R.; Ren, M.; Li, H.; Zhao, J.; Liu, S.; Li, Z.; Ren, J. Graphene supported Cu nanoparticles as catalysts for the synthesis of dimethyl carbonate: Effect of carbon black intercalation. *Molecular Catalysis,* **2018**, *445*, 257-268.
[http://dx.doi.org/10.1016/j.mcat.2017.12.002]

[87] Gao, Z.; Liu, X.; Li, A.; Li, X.; Ding, X.; Yang, W. Bimetallic sites supported on N-doped graphene ((Fe,Co)/N-GN) as a new catalyst for NO oxidation: A theoretical investigation. *Molecular Catalysis,* **2019**, *470*, 56-66.
[http://dx.doi.org/10.1016/j.mcat.2019.03.024]

[88] Wang, R.; Liu, H.; Fan, C.; Gao, J.; Chen, C.; Zheng, Z. Selective oxidative esterification of alcohols over Au-Pd/graphene. *Molecular Catalysis,* **2020**, *484*, 110687-110699.
[http://dx.doi.org/10.1016/j.mcat.2019.110687]

[89] Li, D.; Li, W.; Zhang, J. Catalytic CO oxidation by Fe doped penta-graphene: A density functional

study. *Molecular Catalysis,* **2019**, *470*, 48-55.
[http://dx.doi.org/10.1016/j.mcat.2019.03.023]

[90] Behjatmanesh-Ardakani, R. Catalytic CO oxidation by Fe doped penta-graphene: A density functional study. *Mol. Catal.,* **2018**, *455*, 239-249.
[http://dx.doi.org/10.1016/j.mcat.2018.06.008]

[91] Kumar, K.V.A.; Chandana, L.; Ghosal, P.; Subrahmanyam, C. Simultaneous photocatalytic degradation of p -cresol and Cr (VI) by metal oxides supported reduced graphene oxide. *Molecular Catalysis,* **2018**, *451*, 87-95.
[http://dx.doi.org/10.1016/j.mcat.2017.11.014]

[92] Sharma, H.; Sharma, S.; Sharma, C.; Paul, S.; Clark, J.H. Magnetically recoverable graphene oxide supported Co@Fe_3O_4/L-dopa for C-C cross-coupling and oxidation reactions in aqueous medium. *Molecular Catalysis,* **2019**, *469*, 27-39.
[http://dx.doi.org/10.1016/j.mcat.2019.02.023]

[93] Yang, J.; Shen, X.; Ji, Z.; Zhou, H.; Zhu, G.; Chen, K. In situ growth of hollow CuNi alloy nanoparticles on reduced graphene oxide nanosheets and their magnetic and catalytic properties. *Appl. Surf. Sci.,* **2014**, *316*, 575-581.
[http://dx.doi.org/10.1016/j.apsusc.2014.08.097]

[94] Cheng, Y.; Fan, Y.; Pei, Y.; Qiao, M. Graphene-supported metal/metal oxide nanohybrids: synthesis and applications in heterogeneous catalysis. *Catal. Sci. Technol.,* **2015**, *5*(8), 3903-3916.
[http://dx.doi.org/10.1039/C5CY00630A]

[95] Samak, N.A.; Tan, Y.; Sui, K.; Xia, T.T.; Wang, K.; Guo, C.; Liu, C. CotA laccase immobilized on functionalized magnetic graphene oxide nano-sheets for efficient biocatalysis. *Molecular Catalysis,* **2018**, *445*, 269-278.
[http://dx.doi.org/10.1016/j.mcat.2017.12.004]

[96] Nayak, P.S.; Barik, B.; Achary, L.S.K.; Kumar, A.; Dash, P. Gold nanoparticles deposited on MnO2 nanorods modified graphene oxide composite: A potential ternary nanocatalyst for efficient synthesis of betti bases and bisamides. *Molecular Catalysis,* **2019**, *474*, 110415-110430.
[http://dx.doi.org/10.1016/j.mcat.2019.110415]

[97] Julkapli, N.M.; Bagheri, S. Graphene supported heterogeneous catalysts: An overview. *Int. J. Hydrogen Energy,* **2015**, *40*(2), 948-979.
[http://dx.doi.org/10.1016/j.ijhydene.2014.10.129]

[98] Fu, J.Y.; Chen, L.W.; Dai, Y.M.; Liu, F.Y.; Huang, S.T.; Chen, C.C. BiOmFn/BiOxIy/GO Nanocomposites: Synthesis, characterization, and photocatalytic activity. *Molecular Catalysis,* **2018**, *455*, 214-223.
[http://dx.doi.org/10.1016/j.mcat.2018.06.014]

[99] Zhu, Y.; Lin, B.; Hu, Y.; Cai, Z.; Xie, H.; Wang, K.; Zhou, Y. Enhanced stability of Pd/SPS catalyst over the one-pot liquid-phase synthesis of methyl isobutyl ketone by adding GO. *Molecular Catalysis,* **2019**, *478*, 110609-110617.
[http://dx.doi.org/10.1016/j.mcat.2019.110609]

[100] Tang, Y.; Zhou, J.; Chen, W.; Chai, H.; Li, Y.; Feng, Z.; Dai, X. Theoretical evaluation on single-atom Fe doped divacancy graphene for catalytic CO and NO oxidation by O_2 molecules. *Molecular Catalysis,* **2019**, *476*, 110524-110537.
[http://dx.doi.org/10.1016/j.mcat.2019.110524]

[101] Wu, C.; Gates, I.D. Methane activation by a single iron atom supported on graphene: Impact of substrates. *Molecular Catalysis,* **2019**, *469*, 40-47.
[http://dx.doi.org/10.1016/j.mcat.2019.03.002]

[102] Mohazzab, B.F.; Jaleh, B.; Nasrollahzadeh, M.; Issaabadi, Z.; Varma, R.S. Laser ablation-assisted synthesis of GO/TiO2/Au nanocomposite: Applications in $K_3[Fe(CN)_6]$ and Nigrosin reduction. *Molecular Catalysis,* **2019**, *473*, 110401-110411.

Not be distributed or uploaded to anyone or anywhere
For personal private use only

[http://dx.doi.org/10.1016/j.mcat.2019.110401]

[103] Lv, T.; Wang, H.; Hong, W.; Wang, P.; Jia, L. In situ self-assembly synthesis of sandwich-like TiO2/reduced graphene oxide/$LaFeO_3$ Z-scheme ternary heterostructure towards enhanced photocatalytic hydrogen production. *Molecular Catalysis,* **2019**, *475*, 110497-110509.
[http://dx.doi.org/10.1016/j.mcat.2019.110497]

[104] Li, X.; Qi, T.; Wang, J.; She, W.; Mao, G.; Yan, P.; Li, W.; Li, G. Enhanced catalytic performance of nitrogen-doped carbon supported FeOx-based catalyst derived from electrospun nanofiber crosslinked N, Fe-containing MOFs for efficient hydrogenation of nitroarenes. *Molecular Catalysis,* **2019**, *477*, 110544-110549.
[http://dx.doi.org/10.1016/j.mcat.2019.110544]

[105] Chen, T.W.; Xu, J.Y.; Sheng, Z.H.; Wang, K.; Wang, F.B.; Liang, T.M.; Xia, X.H. Enhanced electrocatalytic activity of nitrogen-doped graphene for the reduction of nitro explosives. *Electrochem. Commun.,* **2012**, *16*(1), 30-33.
[http://dx.doi.org/10.1016/j.elecom.2011.12.016]

[106] Colunga, A.; Rangel-Mendez, J.R.; Celis, L.B.; Cervantes, F.J. Graphene oxide as electron shuttle for increased redox conversion of contaminants under methanogenic and sulfate-reducing conditions. *Bioresour. Technol.,* **2015**, *175*, 309-314.
[http://dx.doi.org/10.1016/j.biortech.2014.10.101] [PMID: 25459837]

[107] Trandafir, M.M.; Florea, M.; Neaţu, F.; Primo, A.; Parvulescu, V.I.; García, H. Graphene from Alginate Pyrolysis as a Metal-Free Catalyst for Hydrogenation of Nitro Compounds. *ChemSusChem,* **2016**, *9*(13), 1565-1569.
[http://dx.doi.org/10.1002/cssc.201600197] [PMID: 27246529]

[108] Mahata, S.; Sahu, A.; Shukla, P.; Rai, A.; Singh, M.; Rai, V.K. Bio-inspired unprecedented synthesis of reduced graphene oxide: a catalytic probe for electro-/chemical reduction of nitro groups in an aqueous medium. *New J. Chem.,* **2018**, *42*(3), 2067-2073.
[http://dx.doi.org/10.1039/C7NJ04732K]

[109] Fakhri, P.; Nasrollahzadeh, M.; Jaleh, B. Graphene oxide supported Au nanoparticles as an efficient catalyst for reduction of nitro compounds and Suzuki–Miyaura coupling in water. *RSC Advances,* **2014**, *4*(89), 48691-48697.
[http://dx.doi.org/10.1039/C4RA06562J]

[110] Jeon, E.K.; Seo, E.; Lee, E.; Lee, W.; Um, M.K.; Kim, B.S. Mussel-inspired green synthesis of silver nanoparticles on graphene oxide nanosheets for enhanced catalytic applications. *Chem. Commun. (Camb.),* **2013**, *49*(33), 3392-3394.
[http://dx.doi.org/10.1039/c3cc00115f] [PMID: 23435315]

[111] Paul, B.; Purkayastha, D.D.; Dhar, S.S.; Das, S.; Haldar, S. Facile one-pot strategy to prepare Ag/Fe_2O_3 decorated reduced graphene oxide nanocomposite and its catalytic application in chemoselective reduction of nitroarenes. *J. Alloys Compd.,* **2016**, *681*, 316-323.
[http://dx.doi.org/10.1016/j.jallcom.2016.04.229]

[112] Li, H.; Gan, S.; Han, D.; Ma, W.; Cai, B.; Zhang, W.; Zhang, Q.; Niu, L. High performance Pd nanocrystals supported on SnO_2 -decorated graphene for aromatic nitro compound reduction. *J. Mater. Chem. A Mater. Energy Sustain.,* **2014**, *2*(10), 3461-3467.
[http://dx.doi.org/10.1039/C3TA14506A]

[113] Zhang, K.; Hong, K.; Suh, J.M.; Lee, T.H.; Kwon, O.; Shokouhimehr, M.; Jang, H.W. Facile synthesis of monodispersed Pd nanocatalysts decorated on graphene oxide for reduction of nitroaromatics in aqueous solution. *Res. Chem. Intermed.,* **2019**, *45*(2), 599-611.
[http://dx.doi.org/10.1007/s11164-018-3621-8]

[114] Kubendhiran, S.; Sakthinathan, S.; Chen, S.M.; Tamizhdurai, P.; Shanthi, K.; Karuppiah, C. Green reduction of reduced graphene oxide with nickel tetraphenyl porphyrin nanocomposite modified electrode for enhanced electrochemical determination of environmentally pollutant nitrobenzene. *J.*

Not be distributed or uploaded to anyone or anywhere
For personal private use only

Colloid Interface Sci., **2017**, *497*, 207-216.
[http://dx.doi.org/10.1016/j.jcis.2017.03.003] [PMID: 28285048]

[115] Karthik, M.; Suresh, P. Greener Synthesis of Reduced Graphene Oxide-Nickel Nanocomposite: Rapid and Sustainable Catalyst for the Reduction of Nitroaromatics. *ChemistrySelect,* **2017**, *2*(23), 6916-6928.
[http://dx.doi.org/10.1002/slct.201701314]

[116] Li, F.; Gao, X.; Xue, Q.; Li, S.; Chen, Y.; Lee, J.M. Reduced graphene oxide supported platinum nanocubes composites: one-pot hydrothermal synthesis and enhanced catalytic activity. *Nanotechnology,* **2015**, *26*(6), 065603.
[http://dx.doi.org/10.1088/0957-4484/26/6/065603] [PMID: 25612090]

[117] Kumar Sahoo, P.; Panigrahy, B.; Thakur, D.; Bahadur, D. Ice-templating synthesis of macroporous noble metal/3D-graphene nanocomposites: their fluorescence lifetimes and catalytic study. *New J. Chem.,* **2017**, *41*(16), 7861-7869.
[http://dx.doi.org/10.1039/C7NJ00128B]

[118] Liu, Z.; Guo, Y. Sensitive determination of trace 4-nitrophenol in water based on thio-β-cyclodextrin functionalized graphene/copper nanospheres. *J. Electroanal. Chem. (Lausanne),* **2018**, *825*, 57-64.
[http://dx.doi.org/10.1016/j.jelechem.2018.08.005]

[119] Feng, Y.S.; Ma, J-J.; Kang, Y-M.; Xu, H-J. PdCu nanoparticles supported on graphene: an efficient and recyclable catalyst for reduction of nitroarenes. *Tetrahedron,* **2014**, *70*(36), 6100-6105.
[http://dx.doi.org/10.1016/j.tet.2014.04.034]

[120] Fang, H.; Wen, M.; Chen, H.; Wu, Q.; Li, W. Graphene stabilized ultra-small CuNi nanocomposite with high activity and recyclability toward catalysing the reduction of aromatic nitro-compounds. *Nanoscale,* **2016**, *8*(1), 536-542.
[http://dx.doi.org/10.1039/C5NR05016B] [PMID: 26646949]

Not be distributed or uploaded to anyone or anywhere
For personal private use only

CHAPTER 10

Graphene Based Biocatalysts

Monika Jangid[1], Sunita Panchawat[2] and **Abhilasha Jain[3,*]**

[1] *Department of Chemistry, PAHER University, Udaipur, Rajasthan, 313001, India*

[2] *Department of Phatmaceutical Sciences, Mohanlal Sukhadia University, Udaipur, Rajasthan, 313001, India*

[3] *Department of Chemistry, St. Xavier's College (Autonomus), Mumbai, Maharashtra, 400001, India*

Abstract: Enzymes have catalytic properties and can be used for different purposes as biocatalysts in some industrial processes. However, their applications are limited due to some drawbacks, such as lack of long-term stability and recovery under conditions of any particular process. Enzymes can improve their catalytic activity, stability, reusability, and half life, if these are immobilized on some support. Graphene and graphene based nanomaterials are good supports for enzymes as they are also non-toxic materials in nature. Such materials can also find applications in the fields of medical diagnostics, biofuel cells, biosensors, *etc*. These particular aspects have been discussed in this chapter.

Keywords: Biocatalyst, Biofuel Cell, Biosensors, Graphene, Graphene Oxide, Immobilization, Reduced Graphene Oxide.

INTRODUCTION

Nowadays, graphene and its derivatives are attracting the attention of scientists all over the globe due to their unique properties such as chemical, optical, mechanical, electrical, *etc*. There could be multivalent functionalized and surface loaded efficiently with the number of biomolecules. Apart from it, abundance, easy synthesis, excellent solubility and processability, high surface area, conductivity, and biocompatibility are the added advantages of graphene-derivatives over other carbon-based materials like diamond, carbon nanotubes, fullerene, *etc*. Recent advancement in the synthesis and surface functionalization of this graphene or graphene-based nanostructured materials have opened up new horizons as a host material for polymers grafting and the designing of state-of-the-art nano-biocatalytic systems. Graphene-immobilized nanocatalyst varies from

* **Corresponding author Abhilasha Jain:** Department of Chemistry, St. Xavier's College (Autonomus), Mumbai, Maharashtra,400001, India; E-mail: jainabhilasha5@gmail.com

Pinki Bala Punjabi, Rakshit Ameta & Sharoni Gupta (Eds.)
All rights reserved-© 2023 Bentham Science Publishers

conventional nano-bioconjugates with respect to functional stability, catalytic efficacy, and applicability. Graphene-assisted biocatalysts find numerous applications in various fields such as enzyme engineering, biotransformation, biosensing, biofuel & energy production, and designing highly biocompatible, non-toxic (Arvidsson *et al*. [4]), and environmentally-friendly nanomaterials and assemblies.

The substances, which can catalyse different chemical reactions in living systems are called biocatalysts. Best examples are enzymes, which are biological compounds (derived from micro- organisms, plants or animal tissue) worked as nature's catalysts and promoted chemical reactions in biological as well as natural systems. Microbial lipases are a class of enzymes, well known as biocatalysts and these are used in a broad range of chemical and biological reactions. These enzymes find numerous applications such as pharmaceuticals, cosmetics, waste water treatments, foods, tanning, detergents, *etc*.

Various enzymes can be used as biocatalysts for different analytical purposes in medical diagnostics and manufacturing purposes in large-scale industrial processes. They have catalytic properties, but their industrial applications are limited due to a lack of long-term stability under process conditions. There is a demand to resolve the difficulties associated with recycling before the enzyme is implemented on an industrial scale. Here, immobilization of enzymes is a novel approach, which can improve half-life, stability, catalytic activity, and reusability of enzymes. Graphene-based nanomaterials are nanoscale and thermo stable inorganic carriers. There are also nontoxic materials and selective modulators for enzyme activity.

APPLICATIONS OF GRAPHENE BASED BIOCATALYSTS

Immobilization of Enzymes

Enzyme immobilization is an interesting field of research and many enzymes are useful in medical fields and food processing industries and this immobilization can improve their activity and stability. Immobilization has certain advantages such as increasing catalytic activity, improvement of stability, easy recovery of enzyme, reuse, *etc*.

A green and efficient Rassi has developed one-pot procedure and Baharfar [1] to achieve indole based amides using Passerini reaction, which involves indole--carboxylic acids, aromatic aldehydes and alkyl isocyanides in the presence of immobilized lipase on graphene oxide. This method has many advantages such as simple operation, mild reaction conditions, good to excellent yields, environmental compatibility and no side products.

The Passerini reaction was performed in the presence of GO@lipase as a green heterogeneous catalyst for the synthesis of indole based a-acyloxycarboxamide derivatives. Activity, efficiency and reusability of *Aspergillus Niger* Lipase (ANL) immobilized on graphene oxide (GO@lipase) were demonstrated. As-prepared nanobiocatalyst was found applicable in multi-component reactions (MCRs) as a heterogenous biocatalyst.

Adeel *et al*. [2] reported that graphene-based nanomaterials had attracted research interest in different fields related to proteins. They have exceptional physiochemical properties such as optical, thermal, electrical, and mechanical strength, so graphene-based nanostructured materials are considered suitable for many applications in varried fields such as electrochemical sensors, electroanalytical chemistry and immobilization of biomolecules and enzymes. Graphene oxide has different functionalities, such as epoxy, hydroxyl, and carboxylic group, which has opened new avenues to modify GO to achieve materials with desired properties.

Ariaeenejad *et al*. [3] reported bifunctional applications of a novel immobilized enzyme on the modified magnetic graphene oxide (GO) for the effective removal of dyes from water. The amine functionalized GO nano-carrier was covalently attached to a model enzyme (PersiManXyn1). It was observed that the specific activities of the free and immobilized enzymes were 856.05 and 1141.1 $\mu molmin^{-1}mg^{-1}$, respectively based an enzyme assays. The free enzyme showed only 5% of its maximum activity, while the immobilized PersiManXyn1 preserved more than 35% of its activity at 90°C. It was revealed that the free enzyme was deactivated after four weeks of storage, but the immobilized enzyme retained 54% of its initial activity. ImmobilizedPersiManXyn1 was applied for the removal of dye from water. The immobilized PersiManXyn1 could catalytically reduce the dye solutions (94% dye removal after 15th cycle), while pristine nano-carrier and free enzyme showed no considerable catalytic ability within 150s. It retained its superior reusability. This immobilized PersiManXyn1 finds its practical applications in the treatment of real textile effluent.

Graphene oxide is a potential candidate for enzyme immobilization, because it has large specific surface area. GO was first functionalized with L-aspartic acid (GO-Asp) by Monajati *et al*. [5]. Then L-asparaginase was immobilized on the GO-Asp either physically or through chemical conjugation. It was reported that a significant enzyme loading could be achieved through covalent immobilization (almost 100% immobilization efficiency). They also examined stability of free and immobilized L-asparaginase in a wide range of temperatures (20–60°C) and pH (5–9). It was revealed that covalently immobilized L-asparaginase exhibited higher enzyme activity than the free enzyme at pH 8, with the maximum

recovered activity of 100, 90.5 and 40.6% after 24h of incubation at 20, 40 and 60°C, respectively. The covalently immobilized L-asparaginase on GO-Asp was found to have 42% recovered activity even after eight continuous reaction cycles at 60°C. It was also indicated that no significant changes were there in the enzyme affinity through covalent conjugation. It was suggested that GO-Asp is suitable as a nanosheet support for L-asparaginase loading and later, it can find some industrial applications in future.

They synthesized a graphene-based matrix for immobilization of L-asparaginase. Asp was used for GO functionalization so that its dispersion and stability could be improved. Here, Asp acts as a spacer between graphene and immobilized enzyme to avoid any extensive structural damage of the enzyme. It was observed that thermal and pH stability of L-asparaginase was improved on immobilization. The covalent attachment of L-asparaginase on GO-Asp was found to retain the enzyme activity more at high temperature and pH 40.6% after 24 h heating at 60°C and pH 8 as compared to physical adsorption (25.1%) and free L-asparaginase (12.9%). It was reported that recovered activity of L-asparaginase retained about 29% and 42% of the initial activity for physically adsorbed and chemically conjugated L-asparaginase after 8 cycles at 60°C.

Dutta *et al*. [6] reported that immobilization conferred psychrostability to a cold active α-amylase (amy) enzyme using magnesium nanoparticle (Mg NP) and graphene oxide. It was revealed that GO-Mg NP-amy nanocomposite showed enhanced enzymatic activity and thermo stability at both; the temperature extremes; upper (90°C) and lower (8°C). The GO-Mg NP-amy exhibited increased affinity towards the substrate, which is reflected in the decline in its Km by 2.35 and 14.9-fold at 8° and 90°C, respectively, as-compared to untreated enzyme. They also found that GO-Mg NP-amy showed 2.34-fold and 4.29-fold increase in Vmax at 8° and 90°C, respectively, compared to the untreated enzyme. The half life of GO-Mg NP-amy was increased by 44-fold with simultaneous increase in E_d by 1.9-fold as compared to the native enzyme at 90°C. The same is true for8°C, half-life of GO-Mg NP-amy increased by 6.48-fold with the simultaneous increase in E_d by 2.21-fold as compared to the native enzyme. It was observed that enzymatic activity of GO-Mg NP-amy was retained even after 12 consecutive uses and had storage stability for more than 120 days at 4°C. The ability of GO-Mg NP to sustain and aggravate enzyme activity and stability at temperatures in a wide range can make it a better candidate in bioprocessing industries, which requires functioning at these extreme ranges of temperature.

Gür *et al*. [7] prepared graphene oxide and reduced graphene oxide (rGO) Langmuir-Blodgett (LB) films with specific surface properties and functional groups as negative ideal substrates. They immobilized polyphenol oxidase (PPO)

enzyme on these films by electrostatic interaction without any requirement of chemical bonding or surface modification. It was reported that catalytic performances of the enzyme immobilized on GO and rGO substrates were higher in GO-PPO LB films as compared to rGO-PPO LB films *in-vitro* media. It was revealed that the immobilized PPO enzyme on biodegradable GO was superior to the inorganic materials in terms of its use in biological systems. They prepared regular film structures with a single molecule thickness by LB film technique, which contributed to the stability and recycling of immobilization of PPO enzyme on GO and rGO. It was found that *in-vitro* storage stability of immobilization on both film structures was about one month at +4°C.

Li *et al*. [8] prepared three-dimensional magnetic graphene oxide-magnetite polyvinyl alcohol (3D-GO/PVA/Fe_3O_4) nanocomposites. It was reported that the specific surface and the average pore size of 3D-GO/PVA/Fe_3O_4 nanocomposites were 388.87 m^2g^{-1} and 9.6nm, respectively. The higher specific surface indicated that the three-dimensional structure avoided any aggregation for GO sheets. The saturation magnetization (Ms) of the nanocomposites was found to be large (30.5 $emug^{-1}$), which enabled the easy cycling of such nanocomposites. It was revealed that 3D-GO/PVA/Fe_3O_4 nanocomposites exhibited better performance for porcine pancreatic lipase (PPL) enzyme immobilization and it could reach the efficiency of 91%, and the enzyme immobilized nanocomposites reached up to 90% of their activities. It was observed that the activity of the immobilized enzyme retained 70.8% of its initial activity after 10 cycles. The activity of the immobilized enzyme remained up to 71.1% at 4°C for 56 days. Hydroxyl-rich PVA provided more binding sites for immobilizing enzyme and best-immobilized efficiency for (3D-GO/PVA/Fe_3O_4)-PPL (91%) was much more as compared to (GO/Fe_3O_4)-PPL (76%).

Immobilization of lipase was successfully achieved by Heidarizadeh *et al*. [9] on the surface of magnetically separable Fe_3O_4/graphene oxide through a post-modification. This modification was achieved in alternation to glutar aldehyde post-modification. It was revealed that the activity of immobilized lipase had no significant loss in the activity, and it can be simply separated (by keeping its major activity) from reaction crude using a magnet.

Dithiocarbamate can modify magnetic graphene oxide nanocomposite (Fe_3O_4-GO) for immobilization of covalent enzyme (lipase).Fabricated Fe_3O_4/GO-NHCS-Lip acts as a nanobiocatalyst for enzymatic hydrolysis of PNPD. It was reported that the recyclability of immobilized lipase is due to the fact that it is covalently attached to the surface and the leaching issue was not observed in this protocol.

The synthesis, characterization and biological application of reduced graphene oxide–chitosan (GC) based benign supramolecular scaffold (SMS) has been reported by Mondal *et al*. [10]. It was observed that immobilization of polyphenol oxidase (PPO) onto GC lowers the Michaelis-Menten constant (Km) value, which helps in achieving maximum velocity at lower substrate concentrations. In corporation of gold nanoparticles in GC (GCG) further strengthens the microbial resistance properties of GC and also improves its biocompatibility by reducing cytotoxicity.

A new rGO-chitosan (GC) based supramolecular scaffold (SMS) has desired thickness (55 nm), surface morphology and functionality for immobilization of enzyme and AuNP implantation. Its bio fabrication properties revealed that-

- Synthesized GC serves as an excellent enzyme (PPO) immobilizing matrix with low Km value and hence, a lesser amount of substrate is required to achieve maximum velocity,
- GC and GCG both possess antibacterial and antifungal activity and the presence of Au NP in GC (GCG) improved this antimicrobial activity as compared to GC alone,
- Biocompatibility study (MTT assay) on macrophage culture indicated that 91 and 98% cells are viable for GC and GCG, respectively and therefore, both the composite possesses no noticeable adverse effect on the cells and,
- It was also found that as-synthesized materials are suitable for *in vitro* cell growth.

Hence, these environmentally benign and biocompatible materials can be used in industries for the removal of phenolic, food packaging, biomedical coating and tissue engineering.

Magnetic graphene oxide (GO-MNP) was synthesized by Paz-Cedeno *et al*. [11] and used as the immobilization support for an industrial cellulase- and xylanase-containing preparation. The enzymatic preparation was immobilized utilizing carbodiimide cross-linking chemistry using 1-ethyl-3-(3-dimethylaminopropyl) carbodiimide and *N*-hydroxysuccinimide (NHS). It was revealed that the supported final biocatalyst (GO-MNP-Enz) exhibited higher activity for the hydrolysis of pretreated sugarcane bagasse (PSB). It presented relative β-glucosidase, endoglucanase, β-xylosidase and xylanase activities of 70, 66, 88, and 70%, respectively, after 10 cycles of hydrolysis of their respective substrates. It was also revealed that biocatalyst also maintained approximately 50 and 80% of its efficiency for cellulose and xylan hydrolysis, respectively. It was suggested that GO-MNP-Enz may be a prospective candidate for industrial applications such as second-generation ethanol production.

The yield, efficiency, and relative activity of the immobilization process ranked from 27–97, 37–113, and 24–110%, respectively, for the different enzymatic activities assessed. It was observed that cellulose conversion to glucose was diminished in comparison to the initial cycles, when GO-MNP-Enz was used multiple times in the hydrolysis of PSB, where xylan conversion to xylose remained high and stable at levels greater than 60% up to the tenth cycle. It was proposed that the use of GO-MNP-Enz is a cost-effective strategy for more competitive hydrolysis of PSB, and it has a potential for application in the production of second-generation ethanol, where the cost of enzymes is considered the bottleneck that prevents its economic viability.

Ameri *et al*. [12] immobilized thermo alkalophilic lipase from *Bacillus atrophaeus* (*Ba*L) onto amine-functionalized graphene oxide nanosheets, which were coated with the poly(maleic anhydride-alt-1-octadecene) copolymer (GO-NH_2-PMAO) and activated with glutaraldehyde as spacer arm through interfacial activation and subsequent multipoint covalent attachment. Immobilization conditions were optimized, such as GO-NH_2- concentration of PMAO, buffer & enzyme glutaraldehyde concentration, pH, time of sonication, concentration, time, and temperature. It was reported that specific activity of the immobilized *Ba*L (105.95 ± 2.37 Umg^{-1}) reached at 5 mg mL^{-1} for GO-NH_2-PMAO, 25 mM of buffer, pH 6.0, 60 min sonication time, 100 mM glutaraldehyde, 60 U mL^{-1} of the enzyme, and 4 h of immobilization time at 25°C, and it was very close to the predicted amount (106.08 ± 1.42 U mg^{-1}). Maximum immobilization yield and efficiency were found to be 81.35 and 277.63% in optimal immobilization conditions. It was indicated that the immobilized *Ba*L showed better stability at extreme temperature and pH than the free *Ba*L and it could retain more than 90% of the initial activity at a temperature of 90°C and pH 11 even after 10 days of storage and 6 cycles of application. It was revealed that maximum bioconversion of valeric acid to pentyl valerate was there in the xylene medium after 48 h of incubation at 60°C using the free *Ba*L (34.5%) and the immobilized *Ba*L (96.3%). This, *Ba*L immobilized on GO-NH_2-PMAO can be used as an effective biocatalyst to synthesize ester with the flavour of green apple.

Asmat *et al*. [13] treated *Candida rugosa* lipase (CRL) with surfactants and immobilized it onto the novel formulated magnetic graphene anchored silica nanocomposite (Fe_3O_4/SiO_2/Gr NC). The surface of lipase was initially coated with Triton-X 100 and cetyltrimethylammonium bromide (CTAB) surfactants to stabilize the enzyme in its open form and it was then adsorbed onto aminated Fe_3O_4/SiO_2/Gr NC. Here, glutaraldehyde (GA) was used to cross-link the adsorbed lipase onto the NC. It was reported that surfactant stabilized immobilized lipase exhibited significantly enhanced thermo stability, and also tolerance to various metal ions and inhibitors. The immobilization yield was remarkably enhanced by

6-folds and 3-folds using Triton X-100 and CTAB, respectively. As-fabricated nanobiocatalysts were used to synthesise green apple flavour ester, ethyl valerate *via* esterification reaction. It was found that Triton X-100 stabilized immobilized lipase performed better, giving about 90% ester yield as compared to 78% yield obtained with CTAB stabilized immobilized lipase.

A simple and effective method for lipase immobilization onto nanocellulose fused Ppy functionalized GO composite was developed by Asmat and Husain [14]. As-prepared nanobioconjugate exhibited significant catalytic performance, stability and solvent tolerance. This is an easy method of preparation and high stability nanobiocatalyst CRL@ Ppy/NCe/GO CRL immobilized on Ppy/NCe/GO, which exhibited enhanced catalytic performance and 160% of activity yield percentage was obtained. It was reported that immobilized lipase formulation (nanobiocatalyst) retained 85% of its original catalytic activity even after 10 cycles of application. It was employed for the synthesis of ethyl acetoacetate. The use of immobilized lipase gave flavour compounds with 27.5 and 75.5% ester yields in solvent-free media and n-hexane, respectively.

Jafarian *et al*. [15] synthesised graphene oxide nanosheets (GON) and its functionalization with 2, 4, 6-trichloro-1, 3, 5-triazine (TCT) through two different routes:

- Directly reaction of GON with TCT (GON-1), and
- Reaction of GON with pre-functionalized TCT with 3-aminopropyl-triethoxysilane (APTS) (GON-2).

Then GON, GON-1 and GON-2 were used as supports for immobilization of *Candida rugosa* lipase (CRL). The values of loading capacity, immobilization yield and leaching of CRL were found in the following order:

GON>GON-1>GON-2

But this order is reversed for a specific activity and recovered activity. It was found that storage stability was high with reasonable reusability for all the immobilized CRL, while the pH and thermal stability of CRL@GON-2 were higher than the remaining two. The advantages of these supports include biocompatibility, low toxicity, high enzyme stability, low cost production, convenient separation of the supports from the solution and relatively high reusability of the enzyme, which make them promising candidates for practical applications.

Kashefi *et al*. [16] synthesized graphene oxide by modified Hummer's method and used it as an ideal enzyme immobilization support because of its specific chemical and structural features. Then they covalently immobilized laccase from genetically modified Aspergillusonto GO (nanobiocatalyst). It exhibited interesting results such as laccase loading (156.5mgg^{-1}) and immobilization yield (64.6%) at laccase concentration (0.9mgmL^{-1}). Bioconversion of two anionic dyes; Direct red 23 (DR23) and acid blue 92 (AB92) was studied using nanobiocatalyst and optimized. It was found that average decolorization effectiveness of the nanobiocatalyst was more than 75% for both these dyes after six cycles, which indicated its excellent operational stability and good reusability.

Gao *et al*. [17] fabricated and characterized glucose oxidase (GOx) and chloroperoxidase (CPO) on the surface of MGO. The performance of as-synthesized immobilized CPO was enhanced by coupling with GOx providing required H_2O_2*in situ* through oxidation of glucose. The activity of MGO-GO--CPO for the decolorization of orange G was much higher (96.6%) than MGO-GOx+MGO-CPO (86.2%). It may be due to reduced mass transfer resistance between CPO and H_2O_2 generated from GOx molecules. It was found that MGO-GOx-CPO reached its highest activity (95.2%) in the temperature range 42-50°C as compared to 35°C for the free enzyme. It was attributed to dispersion of the otherwise stacked MGO below 42°C. This can be conveniently reused as it can be easily recovered in the presence of an external magnetic field, and retained ~38.5% activity even after 6 cycles of applications. Thus, as-synthesized MGO-GOx-CPO has potential applications in the environmental field.

Xylanaseenzyme was immobilized by Mehnati-Najafabadi*et al* [18]. on superparamagnetic garphene oxide nanosheets (GOMNP). It is a hydrolytic enzyme of xylan, which is widely used in industry. Asxylan is bulk, polyethylene glycol bisamine (PEGA) and, it was used as a spacer for functionalization of GOMNP to enhance the accessibility of active sites of the immobilized xylanase. It was reported that xylanase was attached to the functionalized nanocomposite with a yield of 273 mg enzyme g^{-1} PEGA-GOMNP. It was found that free and immobilized xylanase displayed an optimal enzymatic activity and pH 6.5 and 7.5, respectively, at 60°C. The immobilized enzyme retained about 40% of its initial activity even after 8 cycles. It was observed that immobilized and free enzymes retained 35 and 20% of initial catalytic activity after 90 days storage at 4 °C, respectively. The PEGA- modified GOMNP can be used as biodegradable and suitable support for bioengineering.

Desai *et al*. [19] immobilizedamylase on graphene oxide (GO)–magnetite (Fe_3O_4) nanoparticles through covalent bonding. Different operating parameters were optimized as concentrations of GO (1.3 mg), Fe_3O_4 (58 µg), and amylase (4.5 mg).

High loading capacity of 77.58 μg amylase over 1 μg GO-magnetite nanoparticles could be achieved under optimum conditions. The optimum pH remained the same (7), but alkalitolerance was increased by ~20% in relative activities upon immobilization. It was observed that half-life of soluble amylase was found to be 13 h, which was enhanced to 20 h upon immobilization in 20 mM phosphate buffer, pH 7 at 50°C. The immobilized amylase could be used for 11 consecutive runs.

Pectinase was immobilized by Dai *et al*. [20] onto sodium alginate/graphene oxide beads *via* amide bonds. They used *N*,*N*′-dicyclohexylcarbodiimide/*N*-hydroxysuccinimide as the activating agent. The activity of the as-prepared immobilized pectinase (1236.86±40.21 U g^{-1}) at optimal conditions had enzyme activity recovery 83.5%. The optimal pH of free pectinase was 4.5, which was shifted to 4.0 in the case of immobilized pectinase. The optimal temperature of immobilized pectinase was also increased by 10°C (60°C) as compared to the free form (50°C). It was observed that the immobilized pectinase had a superior thermal and storage stability than that of free pectinase. It was indicated that immobilized pectinase retained 73% of initial activity even after six cycles. Such immobilized pectinase may find various applications in the food industry.

Bifunctional acid urease is useful in reducing harmful substances in rice wine and it also effectively removes ethyl carbamate (EC). The acid urease was immobilized by Yang *et al*. [21] on graphene oxide/chitosan beads. It was observed that immobilized urease can be recovered to 77% from the graphene oxide/chitosan composite when it was coupled for 8 h with 5% glutaraldehyde. The optimum temperature for urease activity was found to be 37°C. The stability of the immobilized urease was improved at 37°C and the half-life of decay in urease activity was only 12 h, whereas it was 43 days for soluble and chitosan/graphene oxide immobilized urease at 4°C. The Km value for urea and EC in the free state was 9.14 mM and 386 mM, respectively, which were 5.28 mM and 180 mM, respectively, relatively lower in the immobilized state. The values of Vmax for immobilized EC and urea were observed to be 1.08 and 1.16 μmol min^{-1}, respectively, which were higher for soluble EC and urea 0.782 and 0.931 μmol min^{-1}, respectively. Furthermore, 90% of the initial activity of graphene oxide/chitosan–urease beads was retained after using the beads 10 times; thus, indicating its excellent reusability.

Dutta *et al*. purified an extracellular phytase from a strain of *Bacillus subtilis* obtained from cattle sheds in 24 Parganas (Kolkata, West Bengal) by Dutta *et al*. [22]. The native enzyme showed optimum activity at 42°C and pH 8.5. but it showed 2.40 fold increased activity at 42°C and more than 20-fold activity increment at 85°C in the presence of magnesium nanoparticle (Mg NP) graphene

oxide immobilized enzyme, respectively. The GO-Mg NP-phy complex (phytase coupled to Mg NP immobilized on graphene oxide) had a decrease in Km by 3.29 folds at 42°C and 6 folds at 85°C, and the enzyme system showed 3 fold and 5.5 fold increase in Vmax at 42°C and 85°C, respectively than the untreated enzyme. The energy of activation (Ea) was also lowered by 2.5 and 6 folds, respectively at 42°C and 85°C for GO-MgN-phy as compared to the untreated enzyme. The half life for GO-Mg NP-phy was found to be 29.5 times of that of the untreated enzyme. It was reported that enzymatic activity of GO-Mg NP-phy was retained by 86.6%, when it was tested for storage stability at 4°C after 140 days. This immobilization technique may be used in developing a thermostable phytase enzyme,which could withstand high temperatures during the pelleting of animal feeds and increased activity of the enzyme would also be beneficial to break down phytic acid during storage of feeds.

Different kinds of amino acids were used by Zhuang *et al*. [23] to reduce and modify GO. It was found that reduction and adsorption disparities of amino acids were responsible for the difference of structural heterogeneity such as density, thermal tolerance and disorder of the oxygen-containing groups of GO. This modification also resulted in changes in surface properties of the GO samples, such as hydrophobicity and surface charge. They functionalized GO as a carrier for the immobilization of lipase from *Thermomyces lanuginosus* (lipase TL). It was found that lipase immobilized on functionalized GO exhibited superior enzymatic loading and relative activity compared to GO, with a maximum increase of 70 and 47%, respectively. The relative activity of lipase immobilized on functionalized GO was reported to be 19.21 times more than commercial immobilized lipase TLIM.

Zhuang *et al*. [24] also used disodium guanosine 5′-monophosphate (GMP-2Na) as a reducing agent for the synthesis of functionalized GO (FGO) for lipase immobilization. This method could solve the toxic and hazardous issues of the agents in the chemical reduction process of graphene oxide.The degree of hydrophobicity of FGO was conducive to the formation of optimal conformation of lipase, when the concentration of GMP-2Na is 0.20mg mL^{-1}.The activity of the immobilized enzyme was enhanced by two folds of free enzyme after immobilization. Here, the protein loading reached 600mg g^{-1}. The immobilized enzyme has much durability as no significant decrease was observed after incubation for 8h at pH6.0 and 7.0. The activity of the GO-G@ enzyme was found to be 54.47% higher than that of free enzyme after storage for 35days.

Ariaeenejad *et al*. [25] presented a dual crosslinking (DC) strategy to synthesize novel 3D networks of carboxymethyl cellulose grafted copolymers of 2-acrylamido-2-methyl propane sulfonate and acrylamide (CMC-g-poly(AMPS-

co-AAm)) hydrogels. They utilized graphene oxide nano-sheets as nano-fillers and physical cross-linkers, making H-bondings between polymeric chains to prepare GO@CMC-g-poly(AMPS-co-AAm) networks. The effects of GO content on the performance of as-synthesized material was examined with a model enzyme (PersiCel1). It was revealed that persiCel1 immobilization on the GO reinforced hydrogels retained almost 60% of its maximum activity at 90°C. Its specific activity and storage stability were remarkably enhanced. The immobilized enzyme on the GO containing hydrogels showed a 154.8% increase in conversion of alkaline-treated sugar beet pulp compared with the free PersiCel1, while the PersiCel1/neat-hydrogel indicated only an increment of 66.7% under the same conditions.

Ranjbari *et al*. [26] reported the synthesis of graphene oxide nanosheets (GON) by a modified Hummer's method. Then they immobilized a protease purified from the *Penaeus*vannamei shrimp on the GON activated with glutaraldehyde. It was observed that immobilization of the protease on the GON activated with glutaraldehyde did not affect the optimum pH much, but it significantly improved thermal stability and stability at extreme pH values, as well as activity at 90°C. It was interesting to note that the free enzyme retained less than 10% of the activity, but immobilized enzyme could retain more than 90% of its original activity after 24h of incubation at 90°C. The immobilized enzyme exhibited higher activity for hydrolysis of casein at 70°C and in the presence of 2M urethane than that of the free enzyme.

The effect of the hydrophobicity of reduced graphene oxide (rGO) on the activity of candida rugose lipase (CRL) was studied by Chen *et al*. [27]. They observed that the higher hydrophobicity of rGO surface could increase CRL activity, but it decreased the activity. It was revealed that the rGOB showed a three-dimensional micro-nanoporous structure and surface hydrophobicity with improved adsorption properties and catalytic activity of CRL. It was reported that CRL was immobilized onto the beads by physical adsorption with the maximum adsorption capacity of 117.67 mg g^{-1}. The immobilized lipase (rGOB@CRL) exhibited good temperature, thermal, and reuse stability as compared to free CRL. The conversion rate of triglycerides (TG) in the free enzyme reaction system in the glycerolysis reaction of olive oil was found to be only 67.83%, while the conversion rate of TG in the $rGOB_4$@CRL reaction system could reach 74.87%. As-synthesised rGOB@CRL can be used to adsorb emulsified oil due to the excellent oil-absorbing ability of rGOB, producing monoglyceride (MG) and diglyceride (DG) *in situ* by catalyzing the glycerolysis reaction. The conversion rate of triglyceride (TG) could reach 89.70%, when the oil concentration was kept 4 mg mL^{-1}.

Agrawal *et al*. [28] immobilized *β*-amylase onto GQDs using 3-aminopropyltriethoxysilane and glutaraldehyde. It was reported that the predicted optimum immobilization efficiency (88.64%) was quite close to the actual value (87.98%), and it confirmed that the immobilization process was successful. The immobilized enzyme exhibited maximum activity at pH 5.0 and 57°C, The K_m and V_{max} were found to be 6.40 mg mL^{-1} and 714.28 μmol^{-1} min^{-1} mg, respectively. The enzyme could retain 75% activity even after 12 uses at 30°C. An increase in thermostability of immobilized fenugreek *β*-amylase and non-toxic nature of GQDs could be used for maltose production in beverage, food and pharmaceutical industries.

Laccase enzymes of *Aspergillus oryzae* were immobilized on graphene nanosheets by Skoronski *et al*. [29] *via* physical adsorption and covalent bonding. It was carried out through contact between graphene and a solution of laccase enzyme, which was dissolved in deionized water. It was reported that this adsorption process followed a Freundlich model, while the process of immobilization by covalent bonding was carried out by nitration of graphene. It was followed by a reduction of sodium borohydride and crosslinking with glutaraldehyde. It was observed that process of immobilization by both these techniques increased the pH range of its activity as compared to the free enzyme and also its operating temperature. It was found that the enzyme quickly lost its activity after the second reaction cycle, when it was immobilized *via* physical adsorption. It retained about 80% of it activity after six cycles.

Wang *et al*. [30] fabricated hydrophilic polyethylenimine (PEI) modified magnetic graphene oxide composite (Fe_3O_4@PDA@GO-PEI) and used it as efficient solid support for the immobilization of dextranase, so as to improve stability and recyclable performance. It was reported that GO nanosheet component not only provided abundant binding sites for decorating PEI molecules, but it increased the loading capacity of immobilized dextranase further and acted as a soft matrix to enhance its stability. A combination of the magnetic separation property and the recyclable ability of immobilized dextranase was found to be further improved. The loading amount of immobilized dextranase on as-developed Fe_3O_4@PDA@GO-PEI was determined to be 305.1 mg g^{-1}, and it was about 1.61 times that without GO component. It was revealed that as-developed Fe_3O_4@PDA@GO-PEI-dextranase exhibited high immobilization efficiency (76.27%) enzymatic activity (83.67%), improved stabilities in a wide range of temperature and pH conditions.It retained 85.78% of its initial activity even after 20 cycles. It was suggested that the immobilized dextranase has a potential for various applications in biocatalytic engineering fields.

Alpha-amylase was immobilized by Mulko *et al*. [31] inside three different polymeric matrices (polyacrylamide hydrogel) PAAm; polyacrylamide-graphene oxide nanocomposite, PAAm-GO; and alginate so that effect of the matrix on the catalytic performance can be compared. They also studied morphology, swelling, mechanical properties, retention efficiency, and the catalytic behaviour of supported biocatalysts. It was found that nanocomposite made of PAAm-GO matrix incorporated 98% of the enzyme, which may be due to cooperative effect, while alginate gels incorporated only 30%. The enzyme retention using PAAm-GO could achieve a value of 97.5%. It was reported that PAAm matrices protect the biocatalyst so that it can be reused. An improvement in catalytic properties of enzyme *via* immobilization makes it an excellent candidate in bioindustrial applications. It will therefore be possible to produce sequential or simultaneous saccharification and fermentation using it.

Atiroğlu [32] made some efforts to develop stability in *lipase B Candida antarctica* as Cross-Linked Enzyme Aggregates (CLEAs). Grapheneoxide nanoparticles (GO-MNPs) were prepared for this purpose. Different operating conditions were compared, such as temperature, pH, storage stability, reusability, and organic solvents. It was reported that saturated ammonium sulfate (55%) and cross-linked with 125mM glutaraldehyde for 10h at 4°C were found to optimize the synthesis of lipase-GO-MNPs-CLEAs with the maximum activity recovery of 96.5%. Hyaluronicacid (HA) was used to modify MNPs, which improved the stability and nano-biocatalytic performance so that it can be used in industrial applications.

D-Psicose (D-ribo-2-hexulose or D-allulose), (an epimer of D-fructose) is considered as a rare low-calorie sugar and its enzymatic production using ketose 3-epimerases is a feasible process for the production of D-Psicose. But there are some drawbacks in the application of ketose 3-epimerases, such as bioconversion efficiency and reusability of the enzyme. Dedania *et al*. [33] immobilized ketose 3-epimerases from *Agrobacterium tumefaciens (agtu)* D-psicose 3-epimerase (DPEase) on graphene oxide. It was reported that graphene oxide immobilized *agtu*-DPEase (GO-*agtu*-DPEase) had optimal pH 7.5 and temperature 60°C. A significant improvement in thermal stability was observed, which showed a half-life of 720 min at 60°C, while *Agrobacterium tumefaciens (agtu)* DPEase displayed only 3.99 min. The bioconversion efficiency accounted for graphene oxide immobilized DPEase at equilibrium, 40:60 (D-psicose: D-fructose), which is higher than the *agtu*-DPEase. It was observed that graphene oxide immobilized DPEase exhibited bioconversion efficiency up to 10 cycles of consecutive uses.

A simple, and efficient approach has been reported by Lin *et al*. [34] to fabricate a biocatalytic system by immobilizing the enzyme onto graphene oxide nanosheets

by two methods for the practical application of Bacillus licheniformis γ-glutamyltranspeptidase (BlGGT) *via* both; non-covalent (GO-BlGGT) and covalent (GO/GA-BlGGT) bonds. It was found that the enzyme-loading capacity for the prepared GO/GA nanomaterial was 3.47mg mg^{-1} support, corresponding to a 68.7% recovery of the initial activity. The immobilized enzymes exhibited significantly higher activity as compared to the free form of BlGGT, may be due to the beneficial effect of the layered GO carrier. It was revealed that covalently immobilized enzyme had comparable stability with respect to free enzyme during a storage period of 30days and it could be recycled nine times, retaining about 45.3% of its initial activity. Apart from it, the biocatalytic synthesis of γ--glutamyl-phenylalanine and γ-l-glutamyl-leucine by immobilized enzymes resulted in a yield > 31%.

Orfanakis *et al*. [35] synthesized hybrid nanostructures of magnetic iron nanoparticles and graphene oxide. They used these as nano supports for the covalent immobilization of β-glucosidase. It was revealed that the immobilization efficiency depends on the structure as well as the surface chemistry of nanostructures used. As-obtained hybrid nanostructure-based biocatalysts exhibited a two to four-fold higher thermostability as compared to the free enzyme, and also an enhanced performance at higher temperatures (up to 70°C); that too in a wide pH range. It was claimed that these biocatalysts retained up to 40% of their bioactivity after twelve cycles.

Biofunctionalization of Protein

As biological macromolecules have an essential role in our daily life; thus, it is important to control the activity and stability of such macromolecules. The most promising mothed for enhancing in activity and stability is to immobilize proteins on different support materials. Furthermore, large surface area and surface functional groups are the important features that are required for a better support system. Chaudhary *et al*. [36] opined that these features of graphene oxide and reduced graphene oxide make them ideal support materials for protein immobilization. The successful formation of GO/RGO-protein complexes with enhancement in structural/thermal stability may be due to various interactions at the nano-bio interface, making their utilization in various functional applications. It was emphasized that mechanism and interactions (hydrophilic, hydrophobic, electrostatic, local protein-protein, hydrogen bonding and van der Walls) between protein and GO/RGO influence structural stability and activity of enzymes/proteins. Furthermore, GO/RGO-protein complexes are utilized in various applications such as biosensors, bioimaging and theranostic agent, targeted drug delivery agents, and nanovectors for drug and protein delivery.

Wang *et al*. [37] constructed a hybrid composite of gold nanoparticles, phospholipids bilayer membrane, and graphene and there used this composite as matrices for microperoxidase-11 (MP11) immobilization. They also investigated direct electrochemistry and corresponding bioelectrocatalysis of the enzyme electrode. Phospholipid bilayer membrane was found to protect gold nanoparticles (Au NPs) assembled on polyelectrolyte functionalized graphene sheets may be due to electrostatic attraction to form a hybrid bionanocomposite. Due to the biocompatible microenvironment, which was (provided by the mimetic biomembrane) microperoxidase-11 entrapped in this matrix retained its original structure well and thus, exhibited higher bioactivity. The Au NPs–graphene assemblies, could also promote the direct electron transfer efficiently between the immobilized MP11 and the substrate electrode. As-prepared enzyme electrodes exhibited good direct electrochemistry and electrocatalytic responses to the reduction of hydrogen peroxide. The resulting H_2O_2 biosensor showed a low detection limit (2.6×10^{-6} M), broad linear range (2.0×10^{-5}–2.8×10^{-4} M), stability and good reproducibility. This sensor was used for real-time detection of H_2O_2 dynamically released from the tumor cells MCF-7 in response to a pro-inflammatory stimulant.

Biosensors

Narwal and Pundir [38] fabricated an improved amperometric biosensor by immobilizing glycerol kinase (GK) and glycerol-3-phosphate oxidase (GPO) nanoparticles (NPs) onto graphene oxide nanoparticles (GrO NPs) modified pencil graphite (PG) electrode. It was reported that this biosensor exhibited optimal current response at an applied potential of 0.45V and pH8.0 at 35°C. It displayed a wide linear response for glycerol concentration 0.001-60mM with a detection limit of 0.002μM. A very high sensitivity ($121.45\mu A \cdot mM^{-1} \cdot cm^{-2}$) and rapid response time (2s) were there. It was revealed that 98.5% analytical recovery was there on adding glycerol to the sera samples. The biosensor was used to measure blood serum glycerol levels in patients suffering from hyperglyceridemia. It was indicated that 25% of its initial activity was lost after its regular use for a period of 210 days or more at 4°C under storage conditions.

Two-dimensional GO nanosheets and one-dimensional lysozyme nanofibrils were hybridized by Wu *et al*. [39] through electrostatic interaction to obtain a novel amyloid-GO composite. It provides a biocompatible immobilization platform for Au nanocatalysts as well as enzymes, which could load a large and tunable amount of Au NPs and its high catalytic activity was also maintained. These immobilized catalysts showed high electrochemical behaviors, which is ideal as glucose sensing systems. It was reported that enzymes could also be immobilized

on the residual bare surfaces of amyloid-GO, which could serve as a sensitive and selective analytical glucose-detecting platform.

A competitive-displacement reaction strategy based on target-induced dissociation of gold nanoparticle coated graphene nanosheet (Au NPs/GN) from CdS quantum dot functionalized mesoporous titanium dioxide (CdS QDs/TiO_2) was designed by Cai *et al*. [40] for the sensitive photoelectrochemical (PEC) aptasensing of prostate-specific antigen (PSA) through the exciton–plasmon interaction (EPI) between CdS QDs and AuNPs. To construct such an aptasensing system, capture DNA was initially conjugated covalently onto CdS QDs/TiO_2-modified electrode, and then Au NPs/GN-labeled PSA aptamer was bound onto biofunctionalized CdS QDs/TiO_2 *via* hybridization chain reaction of partial bases with capture DNA. The introduction of AuNPs/GN efficiently quenched the photocurrent of CdS QDs/TiO_2 due to energy transfer. Upon addition of target PSA, the sandwiched aptamer between CdS QDs/TiO_2 and AuNPs/GN reacted with the analyte; thus, resulting in the dissociation of Au NPs/GN from the CdS QDs/TiO_2 to increase the photocurrent. Under optimum conditions, the aptasensing platform exhibited a high sensitivity for PSA detection within a dynamic linear range of 1.0 pg mL^{-1} to 8.0 ng mL^{-1} at a low limit of detection of 0.52 pg mL^{-1}. The interparticle distance of exciton–plasmon interaction and contents of AuNPs corresponding to the EPI effect in this system were also studied. Good selectivity and high reproducibility were obtained for the analysis of the target PSA. Importantly, the accuracy and matrix effect of the PEC aptasensor was evaluated for the determination of human serum specimens and newborn calf serum-diluted PSA standards, giving a well-matched result with the referenced PSA ELISA kit.

A simple and versatile method has been described by Liu *et al*. [41] to construct high-performance three-dimensional (3D) graphene-based enzyme biosensor. They used carbon nanotubes (CNTs) as carriers of methylene blue molecules to immobilize them on 3D graphene surface through strong π-π stacking force. The polydopamine (PDA) layer could also effectively prevent the leakage of inner electron mediators. The as-fabricated biosensor exhibited an outstanding performance for reagentless detection of hydrogen peroxide in terms of wide linear range (0.2 M-1.1 mM), high sensitivity (227.8 μA mM^{-1} cm^{-2}), low detection limit (58.0 nM), and fast response (reaching 95% of the steady current within 3 s). It was also revealed that biosensors exhibited high reproducibility and stability also.

Au nanoparticles and TiO_2 nanosheets co-modified reduced graphene oxide nanocomposite (Au-TiO_2NSs-rGO) were synthesized by Liu *et al*. [42] *via* a simple synthetic route and then used to immobilize hemoglobin (Hb) in order to fabricate a mediator-free biosensor. It was revealed that the Au-TiO_2NSs-rGO

would act as immobilization support for Hb, which afforded good protein stability and bioactivity. It was reported that direct electron transfer of Hb was facilitated with the special structure of Au-TiO_2NSs-rGO. This biosensor displayed good performance for the detection of H_2O_2 in a wide linear range of 7.5~250 μM with a low detection limit of 3 μM, supported by fast response and good stability.

Various multi-tapered (four, five, and eight tapered) optical fiber sensors (OFSs) have been developed by Zhu *et al*. [43]. They immobilized different nanomaterials, such as gold nanoparticles (Au NPs) and graphene oxide (GO) over the bare probe. These nanomaterials immobilized probes were then functionalized with ascorbate oxidase. The Au NPs were found to be well-suited for biosensing applications. GO-based materials were also equally promising in nanostructure-based optical sensing due to their good chemical stability,broad surface area, high electrical conductivity, and excellent mechanical behavior. The performance parameters of this sensor were found to be greatly improved such as sensitivity (8.3 $nmmM^{-1}$), correlation correlator (0.9724), and limit of detection (51.94 μM).

A novel and sensitive electrochemical biosensor were constructed by He and Liu [44] for detecting phosphate using AuNRs@Cu_2O-NDs loaded poly (diallyldimethylammonium chloride) (PDDA) functionalized graphene immobilized pyruvate oxidase (PyO). PDDA-Gr (which has good conductive ability) was used to increase the active site and supporting substrate of biosensor. Then AuNRs@Cu_2O-NDs composite material was prepared to enhance the capability for PyO immobilization and achieved fast electron transfer between hydrogen peroxide and Cu_2O-NDs to amplify the electrical signal. The proposed biosensor showed a wide linearity range from 0.01-80μM and a low detection limit of 0.4nM under optimal conditions. This biosensor exhibited satisfactory anti-interference, good stability, and excellent reproducibility when it was applied to the monitoring of phosphate content in food.

Centeno *et al* [45]. isolated a new plant peroxidase from the leaves of guinea grass (Panicum maximum). This peroxidase had a specific activity of 408 U mg^{-1} and a molecular weight of 30 kDa. It showed optimum activity at pH 8.0 and high thermostability at 66°C. The best substrates for this peroxidase from guinea grass are o-dianisidine and 2,2′-azino-bis-(3-ethylbenzthiazoline-6-sulfonic acid). The graphene-modified electrode exhibited excellent electrocatalytic activity for reduction of H_2O_2, with a linear response in the range (100 μM-3.5 mM)with detection limit of 150 μM.

Liu *et al*. [46] reported a hydrothermal method to prepare reduced graphene oxide (rGO)-based hydrogel (GelrGONR), using neutral red (NR) to mediate the

assembly of rGO sheets and tune the pore size of GelrGONR. A large pore size of up to 20 μm and interconnected porous structure of GelrGONR were observed. The GelrGONR-M was used as a biocatalyst for establishing a BOD biosensor and it exhibited a linear range of 2–64 mg O L^{-1} and a detection limit 0.4 mg O^{-1} for glucose–glutamic acid (GGA). This BOD detection strategy had long-term viability over one year and stability up to 2 months with a relative standard deviation of 2.1%.

A novel nanocomposite material prepared by Povedano *et al*. [47], which consists of reduced graphene oxide/Rh nanoparticles through a one-pot reaction process. It involved simultaneous reduction of both; $RhCl_3$ and graphene oxide with $NaBH_4$ as well as in situ deposition of the metal nanoparticles on the 2D carbon nanomaterial planar sheets. Glassy carbon electrode was coated with this nanocomposite and it was used as nanostructured support for the cross-linking of the enzyme laccase with glutaraldehyde to provide a voltammperometric biosensor for 17β-estradiol in the 0.9^{-11}pM range. This biosensor showed excellent analytical performance with high sensitivity of 25.7 A μM^{-1} $cm^{-1}$with a very low detection limit of 0.54 pM and high selectivity. It was applied to fast determination of the hormone in spiked synthetic and real human urine samples.

Amperometric biosensors based on glassy carbon electrodes (GCE) were modified with graphene oxide (GO) and multi-walled carbon nanotubes (MWCNTs) by Vlamidis *et al*. [48]. Two types of biosensors were realized using tyrosinase (Tyr) or laccase (Lac). The enzyme immobilisation on the modified GC was optimised employing different agents (bovine serum albumin and glutaraldehyde as crosslinking agent, Nafion, and chitosan). The conditions for the fabrication and the storage of the biosensors were established in order to obtain high sensitivities, good enzyme retention, and long-life devices. This biosensor was used for the determination of catechol, pyrogallol, epicatechin, gallic acid, 1,2-dihydroxybenzoic acid, caffeic acid, chlorogenic acid, rutin, catechin and dopamine. These were also used for the determination of total polyphenols concentration in juice samples.

Hashim *et al*. [49] used the spin coating technique for the preparation of tyrosinase immobilized graphene oxide thin film on a gold surface. It was revealed that the thin film is homogeneous, where the surface of graphene oxide is covered by tyrosinase as evident for AFM studies. The thin film has high absorbance value with a band gap of 4.082 eV. This modified thin film could sense the sensing presenceof phenol with a sensitivity of 0.00234° μM-1 and the ability to detect phenol down to 1 μM.

Zrinski *et al*. [50] developed a simple and highly sensitive electrochemical biosensor based on laccase immobilized onto a gold nanoparticles/graphene nanoplatelets-modified screen-printed carbon electrode (LACC/AuNP/GN-Pl/SPCE), and then it was used for the determination of hydroquinone (HQ) and other phenolic compounds. This biosensor shows excellent electrocatalytic activity towards the oxidation of hydroquinone at a potential of -0.05V (vs Ag/AgCl, 3M KCl) in phosphate buffer as supporting electrolyte (0.1M, pH 7.0) using hydrodynamic amperometry.

The biosensor was then applied to the determination of phenolic antioxidant capacity (AOC) in wine and blueberry syrup based on Trolox (6-hydroxy-2,5,7-8-tetramethylchromane-2-carboxylic acid) and hydroquinone equivalents. The results were found to be satisfactory and agreed well with the results of the reference method.

Enzymatic Biofuel Cells

Biofuel cell is a bioenergy device, which is useful in areas of biomedicine, bioelectronics, *etc*. Enzymatic biofuel cells are a class of biofuel cells which utilizes enzymes to generate energy from renewable sources.

Graphene has excellent electrical conductivity and ease of functionalization. As a result, it is considered a promising material for use in enzymatic bioelectrodes and biofuel cells. Such biofuel cells have attracted the attention of scientists due to their potential to harvest energy from organic materials.

Xie and Huang [51] encapsulated magnetic Fe_3O_4 nanoparticles in graphene oxides, and then these were employed as a magnetic carrier for the immobilization of lipase from *Candida rugosavia* interfacial activation of enzyme on hydrophobic surfaces. It was reported that activity recovery of 64.9% and enzyme immobilization efficiency of 85.5% could be achieved using the immobilization strategy. It was observed that Fe_3O_4 nanoparticles were successfully encapsulated into GO, and the lipase was tethered on this magnetic support. The immobilized lipase could efficiently catalyze the transesterification of soybean oil with methanol and produce biodiesel and the yield was 92.8% at 40°C. It was claimed that immobilized lipase could be easily recovered and recycling of the biocatalyst was possible five times without any significant loss of its activity.

Babadi *et al*. [52] fabricated 3-dimensional graphene (3DG)/glucose oxidase (GOx) bio-nanocomposite just to improve enzyme immobilisation and enzyme lifetime with an enhanced electron transfer rate. These enhancements were attributed to the unique physical properties of 3DG, (high porosity, large surface area, and excellent electrical conductivity). They could achieve a power density of

164 μW cm^{-2} at 0.4 V from this enzymatic biofuel cell (EBFC), which is comparable to that of the other glucose biofuel cells (GBFCs). This 3DG enhanced the enzyme lifetime, but decreased enzyme leaking and as a result, its good conductivity facilitates the electron harvest and transfer from the enzyme active site to the electrode.

Microfluidic microbial fuel cells (μMFC) combine the microfluidic technology and biocatalysts anchored at the electrode, representing an emerging bio-power generator. However, a major challenge towards further development is their low bio-catalysts loading on the electrodes. It has already been revealed that bioelectrode structure and nutrient-feeding type played a significant role in the power generation of μMFC. Yang *et al*. [53] fabricated a membrane-free μMFC with a piece of graphene-decorated nickel mesh as bio-anode. It was indicated that mixed bacteria grow densely on the surface of the electrode. Due to enriched bacterial colonization and sufficient nutrient supply, μMFC produces a remarkably high areal power density of 1.11 W m^{-2} at a current density of 2.15 A m^{-2}, which was higher than those obtained with conventional two-dimensional electrodes and flow-over architectures.

A nanocomposite comprised of graphene (G) supported manganese dioxide (MnO_2) incorporated into the network of polythioaniline (MnO_2-G/PTA) was synthesized by Perveen *et al*. [54]. This hybrid composite was applied as an electrode material for the development of a bioanode, which was fabricated by the electrochemical entrapment of ferritin (Frt) as mediator and glucose oxidase (GOx) enzyme in the matrix of the as-synthesized MnO_2-G/PTA deposited on glassy carbon electrode (GCE) surface. It was revealed that this hybrid electroactive support (MnO_2-G/PTA) used for the immobilization of the enzyme (GOx) provides appropriate electrical cabling between the redox enzyme (GOx) and the electrode surface. The as-developed GCE/MnO_2-G/PTA/Frt/GOx bioanode attained a maximum current density of 3.68 $mAcm^{-2}$ at 35 mM glucose concentration at a scan rate of 100 mVs^{-1}. This modified electrode possesses a high potential and good biocompatibility for production of bio-electricity from glucose.

Yaqoob *et al*. [55] used oil palm biomass waste-derived graphene derivatives (L-GO) as an anode in a double chamber of MFCs. This composite based anode (L-GO/ZnO) was fabricated to generate energy and remove Pb^{2+} from wastewater. It was reported that L-GO/ZnO anode showed 91.07% removal efficiency of lead ions, while only 85% removal efficiency was exhibited by L-GO anode. It was found that the composite anode (L-GO/ZnO) showed maximum power density (1350×10^{-3} mW m^{-2}) and current density (142.98 mA m^{-2}), which was relatively

many times higher than the L-GO anode (power density = 20×10^{-3}mW m^{-2} and current density = 17.54 mA m^{-2}).

There are a number of reactions, which involve biotransformations/organic transformations by the biocatalysts. Normally, the activity of an enzyme is limited because of its mobility; therefore, immobilization of such entity is necessary to enhance its activity. Graphene and graphene based materials such as graphene oxide and reduced graphene oxide have a good potential in this respect. These biocatalysts can effectively promote some bioreactions. Other applications of such biocatalyst are biosensors, biofuels, *etc*. It will prove to be a promising area of research in coming decades.

Some recent development in the fields of immobilization of enzymes, biofunctionalization of protein, biosensors, enzymatic biofuel cells, *etc*. have been summarized in Table **1**.

Table 1. Recent applications of graphene- based biocatalayst.

SUPPORT	APPLICATION	REFERENCE
Graphene oxide	Immobilization of Adenylate cyclase	[56]
Reduced graphene oxide	Immobilization of Geotrichumcandidum acetophenone reductase	[57]
Graphene oxide	Functionalized by loading laccase	[58]
Reduced graphene oxide	Biosensor for detection of sarcosine	[59]
N-Doped graphene	High-energy enzyme biofuel cells	[60]
Graphene	Xylose-fueled microbial fuel cells	[61]
Graphene oxide	Adsorption of dyes through immobilized lipase	[62]
Graphene oxide	Biosensor for detection of doxorubicin hydrochloride	[63]

CONCLUSION

There are a number of reactions that involve biotransformations/organic transformations by the biocatalyst. Normally, the activity of an enzyme is limited because of its mobility; therefore, immobilization of such entity is necessary to enhance its activity. Graphene and -based material such as graphene oxide and reduced graphene oxide have a good potential in this respect. These biocatalysts can effectively promote some bioreactions. Other applications such as biosensors, biofuels *etc*. will surface as a promising area of research in the coming decades.

CONSENT FOR PUBLICATION

Not applicable.

CONFLICT OF INTEREST

The author declares no conflict of interest, financial or otherwise.

ACKNOWLEDGEMENTS

Declared none.

REFERENCES

[1] Rassi, S.; Baharfar, R. Synthesis of indole based amides using immobilized lipase on graphene oxide (GO@lipase) as a retrievable heterogeneous nano biocatalyst. *Polyhedron,* **2019**, *174*, 114153. [http://dx.doi.org/10.1016/j.poly.2019.114153]

[2] Adeel, M.; Bilal, M.; Rasheed, T.; Sharma, A.; Iqbal, H.M.N. Graphene and graphene oxide: Functionalization and nano-bio-catalytic system for enzyme immobilization and biotechnological perspective. *Int. J. Biol. Macromol.,* **2018**, *120*(Pt B), 1430-1440. [http://dx.doi.org/10.1016/j.ijbiomac.2018.09.144] [PMID: 30261251]

[3] Ariaeenejad, S.; Motamedi, E.; Hosseini Salekdeh, G. Application of the immobilized enzyme on magnetic graphene oxide nano-carrier as a versatile bi-functional tool for efficient removal of dye from water. *Bioresour. Technol.,* **2021**, *319*, 124228. [http://dx.doi.org/10.1016/j.biortech.2020.124228] [PMID: 33254455]

[4] Arvidsson, R.; Boholm, M.; Johansson, M.; de Montoya, M.L. "Just carbon": ideas about graphene risks by graphene researchers and innovation advisors. *NanoEthics,* **2018**, *12*(3), 199-210. [http://dx.doi.org/10.1007/s11569-018-0324-y] [PMID: 30546498]

[5] Monajati, M.; Borandeh, S.; Hesami, A.; Mansouri, D.; Tamaddon, A.M. Immobilization of -asparaginase on aspartic acid functionalized graphene oxide nanosheet: Enzyme kinetics and stability studies. *Chem. Eng. J.,* **2018**, *354*, 1153-1163. [http://dx.doi.org/10.1016/j.cej.2018.08.058]

[6] Dutta, N.; Biswas, S.; Saha, M.K. Nano-magnesium aided activity enhancement and biophysical characterization of a psychrophilic α-amylase immobilized on graphene oxide nanosupport. *J. Biosci. Bioeng.,* **2017**, *124*(1), 15-22. [http://dx.doi.org/10.1016/j.jbiosc.2017.02.002] [PMID: 28268061]

[7] Gür, B.; Ayhan, M.E.; Türkhan, A.; Gür, F.; Kaya, E.D. A facile immobilization of polyphenol oxidase enzyme on graphene oxide and reduced graphene oxide thin films: An insight into in-vitro activity measurements and characterization. *Colloids Surf. A Physicochem. Eng. Asp.,* **2019**, *562*, 179-185. [http://dx.doi.org/10.1016/j.colsurfa.2018.11.041]

[8] Li, Y.; Jing, T.; Xu, G.; Tian, J.; Dong, M.; Shao, Q.; Wang, B.; Wang, Z.; Zheng, Y.; Yang, C.; Guo, Z. 3-D magnetic graphene oxide-magnetite poly(vinyl alcohol) nanocomposite substrates for immobilizing enzyme. *Polymer (Guildf.),* **2018**, *149*, 13-22. [http://dx.doi.org/10.1016/j.polymer.2018.06.046]

[9] Heidarizadeh, M.; Doustkhah, E.; Rostamnia, S.; Rezaei, P.F.; Harzevili, F.D.; Zeynizadeh, B. Dithiocarbamate to modify magnetic graphene oxide nanocomposite (Fe_3O_4-GO): A new strategy for covalent enzyme (lipase) immobilization to fabrication a new nanobiocatalyst for enzymatic hydrolysis of PNPD. *Int. J. Biol. Macromol.,* **2017**, *101*, 696-702. [http://dx.doi.org/10.1016/j.ijbiomac.2017.03.152] [PMID: 28363653]

Not be distributed or uploaded to anyone or anywhere For personal private use only

[10] Mondal, M.K.; Mukherjee, S.; Saha, S.K.; Chowdhury, P.; Sinha Babu, S.P. Design and synthesis of reduced graphene oxide based supramolecular scaffold: A benign microbial resistant network for enzyme immobilization and cell growth. *Mater. Sci. Eng. C,* **2017**, *75*, 1168-1177. [http://dx.doi.org/10.1016/j.msec.2017.02.136] [PMID: 28415403]

[11] Paz-Cedeno, F.R.; Carceller, J.M.; Iborra, S.; Donato, R.K.; Godoy, A.P.; Veloso de Paula, A.; Monti, R.; Corma, A.; Masarin, F. Magnetic graphene oxide as a platform for the immobilization of cellulases and xylanases: Ultrastructural characterization and assessment of lignocellulosic biomass hydrolysis. *Renew. Energy,* **2021**, *164*, 491-501. [http://dx.doi.org/10.1016/j.renene.2020.09.059]

[12] Ameri, A.; Shakibaie, M.; Khoobi, M.; Faramarzi, M.A.; Gholibegloo, E.; Ameri, A.; Forootanfar, H. Optimization of immobilization conditions of Bacillus atrophaeus FSHM2 lipase on maleic copolymer coated amine-modified graphene oxide nanosheets and its application for valeric acid esterification. *Int. J. Biol. Macromol.,* **2020**, *162*, 1790-1806. [http://dx.doi.org/10.1016/j.ijbiomac.2020.08.101] [PMID: 32814102]

[13] Asmat, S.; Husain, Q.; Shoeb, M.; Mobin, M. Tailoring a robust nanozyme formulation based on surfactant stabilized lipase immobilized onto newly fabricated magnetic silica anchored graphene nanocomposite: Aggrandized stability and application. *Mater. Sci. Eng. C,* **2020**, *112*, 110883. [http://dx.doi.org/10.1016/j.msec.2020.110883] [PMID: 32409040]

[14] Asmat, S.; Husain, Q. Exquisite stability and catalytic performance of immobilized lipase on novel fabricated nanocellulose fused polypyrrole/graphene oxide nanocomposite: Characterization and application. *Int. J. Biol. Macromol.,* **2018**, *117*, 331-341. [http://dx.doi.org/10.1016/j.ijbiomac.2018.05.216] [PMID: 29857098]

[15] Jafarian, F.; Bordbar, A.K.; Zare, A.; Khosropour, A. The performance of immobilized *Candida rugosa* lipase on various surface modified graphene oxide nanosheets. *Int. J. Biol. Macromol.,* **2018**, *111*, 1166-1174. [http://dx.doi.org/10.1016/j.ijbiomac.2018.01.133] [PMID: 29371152]

[16] Kashefi, S.; Borghei, S.M.; Mahmoodi, N.M. Covalently immobilized laccase onto graphene oxide nanosheets: Preparation, characterization, and biodegradation of azo dyes in colored wastewater. *J. Mol. Liq.,* **2019**, *276*, 153-162. [http://dx.doi.org/10.1016/j.molliq.2018.11.156]

[17] Gao, F.; Guo, Y.; Fan, X.; Hu, M.; Li, S.; Zhai, Q.; Jiang, Y.; Wang, X. Enhancing the catalytic performance of chloroperoxidase by co-immobilization with glucose oxidase on magnetic graphene oxide. *Biochem. Eng. J.,* **2019**, *143*, 101-109. [http://dx.doi.org/10.1016/j.bej.2018.12.013]

[18] Mehnati-Najafabadi, V.; Taheri-Kafrani, A.; Bordbar, A.K. Xylanase immobilization on modified superparamagnetic graphene oxide nanocomposite: Effect of PEGylation on activity and stability. *Int. J. Biol. Macromol.,* **2018**, *107*(Pt A), 418-425. [http://dx.doi.org/10.1016/j.ijbiomac.2017.09.013] [PMID: 28888544]

[19] Desai, R.P.; Dave, D.; Suthar, S.A.; Shah, S.; Ruparelia, N.; Kikani, B.A. Immobilization of α-amylase on GO-magnetite nanoparticles for the production of high maltose containing syrup. *Int. J. Biol. Macromol.,* **2021**, *169*, 228-238. [http://dx.doi.org/10.1016/j.ijbiomac.2020.12.101] [PMID: 33338531]

[20] Dai, X.Y.; Kong, L.M.; Wang, X.L.; Zhu, Q.; Chen, K.; Zhou, T. Preparation, characterization and catalytic behavior of pectinase covalently immobilized onto sodium alginate/graphene oxide composite beads. *Food Chem.,* **2018**, *253*, 185-193. [http://dx.doi.org/10.1016/j.foodchem.2018.01.157] [PMID: 29502820]

[21] Yang, L.; Liu, X.; Zhou, N.; Tian, Y. Characteristics of refold acid urease immobilized covalently by graphene oxide-chitosan composite beads. *J. Biosci. Bioeng.,* **2019**, *127*(1), 16-22. [http://dx.doi.org/10.1016/j.jbiosc.2018.06.012] [PMID: 30139654]

Not be distributed or uploaded to anyone or anywhere
For personal private use only

[22] Dutta, N.; Raj, D.; Biswas, N.; Mallick, M.; Omesh, S. Nanoparticle assisted activity optimization and characterization of a bacterial phytase immobilized on single layer graphene oxide. *Biocatal. Agric. Biotechnol.,* **2017**, *9*, 240-247.
[http://dx.doi.org/10.1016/j.bcab.2017.01.008]

[23] Zhuang, W.; Quan, X.; Wang, Z.; Zhou, W.; Yang, P.; Ge, L.; Villacorta Hernandez, B.; Wu, J.; Li, M.; Zhou, J.; Zhu, C.; Ying, H. Interfacial microenvironment for lipase immobilization: Regulating the heterogeneity of graphene oxide. *Chem. Eng. J.,* **2020**, *394*, 125038.
[http://dx.doi.org/10.1016/j.cej.2020.125038]

[24] Zhuang, W.; Gu, W.; Zhu, Q.; Zhu, J.; Wang, Z.; Niu, H.; Liu, D.; Wu, J.; Chen, Y.; Li, M.; Zhu, C.; Ying, H. Surface functionalization of graphene oxide by disodium guanosine 5′-monophosphate and its excellent performance for lipase immobilization. *Appl. Surf. Sci.,* **2019**, *492*, 27-36.
[http://dx.doi.org/10.1016/j.apsusc.2019.05.166]

[25] Ariaeenejad, S.; Motamedi, E.; Hosseini Salekdeh, G. Stable cellulase immobilized on graphene oxide@CMC-g-poly(AMPS-co-AAm) hydrogel for enhanced enzymatic hydrolysis of lignocellulosic biomass. *Carbohydr. Polym.,* **2020**, *230*, 115661.
[http://dx.doi.org/10.1016/j.carbpol.2019.115661] [PMID: 31887893]

[26] Ranjbari, N.; Razzaghi, M.; Fernandez-Lafuente, R.; Shojaei, F.; Satari, M.; Homaei, A. Improved features of a highly stable protease from Penaeus vannamei by immobilization on glutaraldehyde activated graphene oxide nanosheets. *Int. J. Biol. Macromol.,* **2019**, *130*, 564-572.
[http://dx.doi.org/10.1016/j.ijbiomac.2019.02.163] [PMID: 30831167]

[27] Chen, M.; Wu, H.; Li, Z.; Wu, K.; Jiao, Y.; Zhou, C. Preparation of reduced graphene oxide porous beads for lipase immobilization and its application for oil adsorption and glycerolysis reaction *in situ*. *Micropor. Mesopo. Mater,* **2020**, 294.

[28] Agrawal, D.C.; Yadav, A.; Kesarwani, R.; Srivastava, O.N.; Kayastha, A.M. Immobilization of fenugreek β-amylase onto functionalized graphene quantum dots (GQDs) using Box-Behnken design: Its biochemical, thermodynamic and kinetic studies. *Int. J. Biol. Macromol.,* **2020**, *144*, 170-182.
[http://dx.doi.org/10.1016/j.ijbiomac.2019.12.033] [PMID: 31843605]

[29] Skoronski, E.; Souza, D.H.; Ely, C.; Broilo, F.; Fernandes, M.; Fúrigo, A.; Ghislandi, M.G. Immobilization of laccase from Aspergillus oryzae on graphene nanosheets. *Int. J. Biol. Macromol.,* **2017**, *99*, 121-127.
[http://dx.doi.org/10.1016/j.ijbiomac.2017.02.076] [PMID: 28237573]

[30] Wang, Y.; Wang, Q.; Song, X.; Cai, J. Hydrophilic polyethylenimine modified magnetic graphene oxide composite as an efficient support for dextranase immobilization with improved stability and recyclable performance. *Biochem. Eng. J.,* **2019**, *141*, 163-172.
[http://dx.doi.org/10.1016/j.bej.2018.10.015]

[31] Mulko, L.; Pereyra, J.Y.; Rivarola, C.R.; Barbero, C.A.; Acevedo, D.F. Improving the retention and reusability of Alpha-amylase by immobilization in nanoporous polyacrylamide-graphene oxide nanocomposites. *Int. J. Biol. Macromol.,* **2019**, *122*, 1253-1261.
[http://dx.doi.org/10.1016/j.ijbiomac.2018.09.078] [PMID: 30219512]

[32] Atïroğlu, V. Lipase immobilization on synthesized hyaluronic acid-coated magnetic nanoparticle-functionalized graphene oxide composites as new biocatalysts: Improved reusability, stability, and activity. *Int. J. Biol. Macromol.,* **2020**, *145*, 456-465.
[http://dx.doi.org/10.1016/j.ijbiomac.2019.12.233] [PMID: 31883900]

[33] Dedania, S.R.; Patel, M.J.; Patel, D.M.; Akhani, R.C.; Patel, D.H. Immobilization on graphene oxide improves the thermal stability and bioconversion efficiency of D-psicose 3-epimerase for rare sugar production. *Enzyme Microb. Technol.,* **2017**, *107*, 49-56.
[http://dx.doi.org/10.1016/j.enzmictec.2017.08.003] [PMID: 28899486]

[34] Lin, L.L.; Chi, M.C.; Lan, Y.J.; Lin, M.G.; Juang, T.Y.; Wang, T.F. Facile immobilization of Bacillus licheniformis γ-glutamyltranspeptidase onto graphene oxide nanosheets and its application to the

biocatalytic synthesis of γ-l-glutamyl peptides. *Int. J. Biol. Macromol.,* **2018**, *117*, 1326-1333. [http://dx.doi.org/10.1016/j.ijbiomac.2017.11.153] [PMID: 29183740]

[35] Orfanakis, G.; Patila, M.; Catzikonstantinou, A.V.; Lyra, K.M.; Kouloumpis, A.; Spyrou, K.; Katapodis, P.; Paipetis, A.; Rudolf, P.; Gournis, D.; Stamatis, H. Hybrid nanomaterials of magnetic iron nanoparticles and graphene oxide as matrices for the immobilization of β-glucosidase: synthesis, characterization, and biocatalytic properties. *Front. Mater.,* **2018**, *5*, 25. [http://dx.doi.org/10.3389/fmats.2018.00025]

[36] Chaudhary, K.; Kumar, K.; Venkatesu, P.; Masram, D.T. Protein immobilization on graphene oxide or reduced graphene oxide surface and their applications: Influence over activity, structural and thermal stability of protein. *Adv. Colloid Interface Sci.,* **2021**, *289*, 102367. [http://dx.doi.org/10.1016/j.cis.2021.102367] [PMID: 33545443]

[37] Wang, T.; Liu, J.; Ren, J.; Wang, J.; Wang, E. Mimetic biomembrane–AuNPs–graphene hybrid as matrix for enzyme immobilization and bioelectrocatalysis study. *Talanta,* **2015**, *143*, 438-441. [http://dx.doi.org/10.1016/j.talanta.2015.05.022] [PMID: 26078181]

[38] Narwal, V.; Pundir, C.S. Development of glycerol biosensor based on co-immobilization of enzyme nanoparticles onto graphene oxide nanoparticles decorated pencil graphite electrode. *Int. J. Biol. Macromol.,* **2019**, *127*, 57-65. [http://dx.doi.org/10.1016/j.ijbiomac.2018.12.253] [PMID: 30594620]

[39] Wu, X.; Li, M.; Li, Z.; Lv, L.; Zhang, Y.; Li, C. Amyloid-graphene oxide as immobilization platform of Au nanocatalysts and enzymes for improved glucose-sensing activity. *J. Colloid Interface Sci.,* **2017**, *490*, 336-342. [http://dx.doi.org/10.1016/j.jcis.2016.11.058] [PMID: 27914332]

[40] Cai, G.; Yu, Z.; Ren, R.; Tang, D. Exciton–plasmon interaction between AuNPs/graphene nanohybrids and CdS quantum dots/TiO_2 for photoelectrochemical aptasensing of prostate-specific antigen. *ACS Sens.,* **2018**, *3*(3), 632-639. [http://dx.doi.org/10.1021/acssensors.7b00899] [PMID: 29465232]

[41] Liu, J.; Wang, T.; Wang, J.; Wang, E. Mussel-inspired biopolymer modified 3D graphene foam for enzyme immobilization and high performance biosensor. *Electrochim. Acta,* **2015**, *161*, 17-22. [http://dx.doi.org/10.1016/j.electacta.2015.02.034]

[42] Liu, H.; Gao, J.; Duan, C.; Wu, K.; Guo, K. A novel mediator-free biosensor based on hemoglobin immobilized in the Au nanoparticals and TiO_2 nanosheets co-modified graphene nanocomposite. *Mater. Lett.,* **2020**, *275*, 128142. [http://dx.doi.org/10.1016/j.matlet.2020.128142]

[43] Zhu, G.; Agrawal, N.; Singh, R.; Kumar, S.; Zhang, B.; Saha, C.; Kumar, C. A novel periodically tapered structure-based gold nanoparticles and graphene oxide – Immobilized optical fiber sensor to detect ascorbic acid. *Opt. Laser Technol.,* **2020**, *127*, 106156. [http://dx.doi.org/10.1016/j.optlastec.2020.106156]

[44] He, B.; Liu, H. Electrochemical biosensor based on pyruvate oxidase immobilized AuNRs@Cu_2O-NDs as electroactive probes loaded poly (diallyldimethylammonium chloride) functionalized graphene for the detection of phosphate. *Sens. Actuators B Chem.,* **2020**, *304*, 127303. [http://dx.doi.org/10.1016/j.snb.2019.127303]

[45] Centeno, D.A.; Solano, X.H.; Castillo, J.J. A new peroxidase from leaves of guinea grass (Panicum maximum): A potential biocatalyst to build amperometric biosensors. *Bioelectrochemistry,* **2017**, *116*, 33-38. [http://dx.doi.org/10.1016/j.bioelechem.2017.03.005] [PMID: 28384528]

[46] Liu, L.; Zhai, J.; Zhu, C.; Gao, Y.; Wang, Y.; Han, Y.; Dong, S. One-pot synthesis of 3-dimensional reduced graphene oxide-based hydrogel as support for microbe immobilization and BOD biosensor preparation. *Biosens. Bioelectron.,* **2015**, *63*, 483-489. [http://dx.doi.org/10.1016/j.bios.2014.07.074] [PMID: 25129511]

Not be distributed or uploaded to anyone or anywhere
For personal private use only

[47] Povedano, E.; Cincotto, F.H.; Parrado, C.; Díez, P.; Sánchez, A.; Canevari, T.C.; Machado, S.A.S.; Pingarrón, J.M.; Villalonga, R. Decoration of reduced graphene oxide with rhodium nanoparticles for the design of a sensitive electrochemical enzyme biosensor for 17β-estradiol. *Biosens. Bioelectron.,* **2017**, *89*(Pt 1), 343-351.
[http://dx.doi.org/10.1016/j.bios.2016.07.018] [PMID: 27450540]

[48] Vlamidis, Y.; Gualandi, I.; Tonelli, D. Amperometric biosensors based on reduced GO and MWCNTs composite for polyphenols detection in fruit juices. *J. Electroanal. Chem. (Lausanne),* **2017**, *799*, 285-292.
[http://dx.doi.org/10.1016/j.jelechem.2017.06.012]

[49] Hashim, H.S.; Fen, Y.W.; Omar, N.A.S.; Daniyal, W.M.E.M.M.; Saleviter, S.; Abdullah, J. Structural, optical and potential sensing properties of tyrosinase immobilized graphene oxide thin film on gold surface. *Optik (Stuttg.),* **2020**, *212*, 164786.
[http://dx.doi.org/10.1016/j.ijleo.2020.164786]

[50] Zrinski, I.; Pungjunun, K.; Martinez, S.; Zavašnik, J.; Stanković, D.; Kalcher, K.; Mehmeti, E. Evaluation of phenolic antioxidant capacity in beverages based on laccase immobilized on screen-printed carbon electrode modified with graphene nanoplatelets and gold nanoparticles. *Microchem. J.,* **2020**, *152*, 104282.
[http://dx.doi.org/10.1016/j.microc.2019.104282]

[51] Xie, W.; Huang, M. Immobilization of Candida rugosa lipase onto graphene oxide Fe_3O_4 nanocomposite: Characterization and application for biodiesel production. *Energy Convers. Manage.,* **2018**, *159*, 42-53.
[http://dx.doi.org/10.1016/j.enconman.2018.01.021]

[52] Babadi, A.A.; Wan-Mohtar, W.A.A.Q.I.; Chang, J.S.; Ilham, Z.; Jamaludin, A.A.; Zamiri, G.; Akbarzadeh, O.; Basirun, W.J. High-performance enzymatic biofuel cell based on three-dimensional graphene. *Int. J. Hydrogen Energy,* **2019**, *44*(57), 30367-30374.
[http://dx.doi.org/10.1016/j.ijhydene.2019.09.185]

[53] Yang, Y.; Ye, D.; Zhu, X.; Liao, Q.; Li, J.; Chen, R. Boosting power density of microfluidic biofuel cell with porous three-dimensional graphene@nickel foam as flow-through anode. *Int. J. Hydrogen Energy,* **2018**, *43*(39), 18516-18520.
[http://dx.doi.org/10.1016/j.ijhydene.2018.08.052]

[54] Perveen, R.; Nasar, A.; Inamuddin, ; Asiri, A.M.; Mishra, A.K. Optimization of MnO_2-Graphene/polythioaniline (MnO_2-G/PTA) hybrid nanocomposite for the application of biofuel cell bioanode. *Int. J. Hydrogen Energy,* **2018**, *43*(32), 15144-15154.
[http://dx.doi.org/10.1016/j.ijhydene.2018.06.070]

[55] Yaqoob, A.A.; Ibrahim, M.N.M.; Yaakop, A.S.; Umar, K.; Ahmad, A. Modified graphene oxide anode: A bioinspired waste material for bioremediation of Pb^{2+} with energy generation through microbial fuel cells. *Chem. Eng. J.,* **2021**, *417*, 128052.
[http://dx.doi.org/10.1016/j.cej.2020.128052]

[56] Zhou, W.; Rao, Y.; Zhuang, W.; Ge, L.; Lin, R.; Tang, T.; Wu, J.; Li, M.; Yang, P.; Zhu, C.; Wang, H.; Ying, H. Improved enzymatic activity by oriented immobilization on graphene oxide with tunable surface heterogeneity. *Compos., Part B Eng.,* **2021**, *216*, 108788.
[http://dx.doi.org/10.1016/j.compositesb.2021.108788]

[57] Kamogawa, R.; Issasi, C.S.C.; Sasaki, M.; Matsuda, T. Geotrichumcandidum acetophenone reductase immobilization on reduced graphene oxide: A promising biocatalyst for green asymmetric reduction of ketones. *Biochem. Eng. J.,* **2022**, *177*.
[http://dx.doi.org/10.1016/j.bej.2021.108263]

[58] Noreen, S.; Perveen, S.; Shafiq, N.; Aslam, S.; Iqbal, H.M.N.; Ashraf, S.S.; Bilal, M. Laccase-loaded functionalized graphene oxide assemblies with improved biocatalytic properties and decolorization performance. *Environmental Technology & Innovation,* **2021**, *24*, 101884.

Not be distributed or uploaded to anyone or anywhere For personal private use only

[http://dx.doi.org/10.1016/j.eti.2021.101884]

[59] Rajarathinam, T.; Kwon, M.; Thirumalai, D.; Kim, S.; Lee, S.; Yoon, J.H.; Paik, H.; Kim, S.; Lee, J.; Ha, H.K.; Chang, S.C. Polymer-dispersed reduced graphene oxide nanosheets and Prussian blue modified biosensor for amperometric detection of sarcosine. *Anal. Chim. Acta,* **2021**, *1175*, 338749. [http://dx.doi.org/10.1016/j.aca.2021.338749] [PMID: 34330447]

[60] Xu, J.; Wang, Y.H.; Wei, Z.; Wang, F.T.; Huang, K.J. Significantly improving the performance of self-powered biosensor by effectively combining with high-energy enzyme biofuel cells, N-doped graphene, and ultrathin hollow carbon shell. *Sens. Actuators B Chem.,* **2021**, *327*, 128933. [http://dx.doi.org/10.1016/j.snb.2020.128933]

[61] Moradian, J.M.; Mi, J.L.; Dai, X.; Sun, G.F.; Du, J.; Ye, X.M.; Yong, Y.C. Yeast-induced formation of graphene hydrogels anode for efficient xylose-fueled microbial fuel cells. *Chemosphere,* **2022**, *291*(Pt 2), 132963. [http://dx.doi.org/10.1016/j.chemosphere.2021.132963] [PMID: 34800508]

[62] Yao, L.W.; Ahmed Khan, F.S.; Mubarak, N.M.; Karri, R.R.; Khalid, M.; Walvekar, R.; Abdullah, E.C.; Mazari, S.A.; Ahmad, A.; Dehghani, M.H. Insight into immobilization efficiency of Lipase enzyme as a biocatalyst on the graphene oxide for adsorption of Azo dyes from industrial wastewater effluent. *J. Mol. Liq.,* **2022**, *354*, 118849. [http://dx.doi.org/10.1016/j.molliq.2022.118849]

[63] Hashemi, S.A.; Mousavi, S.M.; Bahrani, S.; Gholami, A.; Chiang, W.H.; Yousefi, K.; Omidifar, N.; Rao, N.V.; Ramakrishna, S.; Babapoor, A.; Lai, C.W. Bio-enhanced polyrhodanine/graphene Oxide/Fe_3O_4 nanocomposite with kombucha solvent supernatant as ultra-sensitive biosensor for detection of doxorubicin hydrochloride in biological fluids. *Mater. Chem. Phys.,* **2022**, *279*, 125743. [http://dx.doi.org/10.1016/j.matchemphys.2022.125743]

Not be distributed or uploaded to anyone or anywhere
For personal private use only

SUBJECT INDEX

A

Absorption spectroscopy 133
Acid(s) 13, 14, 21, 25, 51, 83, 84, 90, 102, 134, 138, 143, 165, 166, 178 300, 301, 305, 340, 342, 344, 345, 347, 363, 379, 384 396, 397
  benzoic 25, 300, 345
  boric 21, 90
  brønsted 102
  caffeic 363, 396
  carboxylic 134, 165, 178, 301, 305, 340, 342, 344, 379, 397
  chlorogenic 396
  chromic 13
  citric 143
  gallic 396
  hydrobromic 138
  lewis 166
  nitric 13, 14, 51, 90
  perchloric 83, 84
  sulfonic 347
  valeric 384
AFM images 128
Arc discharge method 14, 20, 23, 76, 79, 104
  electric 76, 79, 104
Arc discharge plasma method 17
Argon gas 101
Atomic force 49, 120, 124, 143, 167, 170, 396
  microscopy (AFM) 120, 124, 143, 167, 170, 396
  nanoindentation 49
Atomic layer deposition (ALD) 123, 219, 220
Atoms, adsorbed metal 221
Azidothymidine 171

B

Bacillus subtilis 387
Benzyl alcohol oxidation 229, 345
Benzylamine acts 353
BET analysis 7
Bifunctional acid urease 387
Biomass 11, 28, 103, 298, 398
  bacterial 103
  oil palm 398
Biomedical 50, 162, 170, 383
  coating 383
  devices 162, 170
  imaging 50
Biosensor(s) 171, 176, 394, 399
  electric 171
  electrical 176
  for detection of sarcosine 399
  graphene-based enzyme 394
Bovine serum albumin (BSA) 167, 396
Brodie's method 88, 89
BSA protein 167

C

Cancer therapy 176
Candida rugosa lipase (CRL) 384, 385, 389
Carbocatalysts 2, 3, 4, 11, 27, 28, 29, 158, 298, 303, 304, 305, 314, 322, 323
  pH-mediated 314
Carbon, 1, 2, 9, 10, 11, 23, 24, 26, 27, 28, 180, 233, 264
  based materials, metal-free 180
  mesoporous 233, 264
  nano-onions (CNOs) 1, 10, 11, 23, 24, 26, 27, 28
  polymorphs 2, 9, 28
Carbon nanofibres 1, 10, 18, 19, 20, 26, 28
  graphitic 19
Catalyst 5, 19, 20, 26, 208, 228, 269, 274, 276, 280, 298, 300, 302, 317, 339, 342, 393
  fabricated 269, 274, 276
  green 298, 339
  heteroatom-doped graphene 342
  heterogeneous metal cluster 302
  hydroxyapatite-supported nickel 19
  immobilized 393

All rights reserved-© 2023 Bentham Science Publishers

iron 20
metal-based 208, 228, 300
metallic 5
monometallic 26
multimetallic nanoparticles 280
nanocomposite 269
nanoparticulate 317
Catalytic 7, 209, 233, 268, 281, 283, 288, 297, 301, 305, 314, 319, 321, 322, 355, 360, 361, 362, 365,
hydrodesulfurization 233
oxidation 355
power 268, 281, 283, 288
reactions 209, 297, 305, 314
reduction 7, 360, 361, 362, 365
synthesis 301, 319, 321, 322
Catalyzed coupling reactions 279
Chemical 5, 62, 83, 84, 211
deposition method 211
exfoliation methods 83, 84
reduction method 62
titration method 5
Chemical vapor deposition (CVD) 18, 19, 20, 21, 29, 94, 95, 96, 123, 124, 125, 127, 217, 310, 343
method 18
Combustion 14, 17, 26, 29, 80, 99, 143
hydrocarbon 14
techniques 29
Composites 63, 165
polymeric-based 165
synthesized reinforced 63
Condensation reaction 164, 167, 277
Conductive polymer composites (CPCs) 60, 61
Conductivity 8, 9, 10, 11, 18, 25, 27, 28, 60, 61, 216, 298, 307
electric 9, 10, 25
metallic 11
thermo-chemical 18
Copper-based graphene composites 211
Coupling reactions 236, 238, 267, 276, 278, 353
oxidative 353
Cross-coupling reactions, 264 palladium-catalyzed 264
Cross-linked enzyme aggregates (CLEAs) 391

D

Density functional theory (DFT) 178, 302
Deposition 13, 29, 44, 58, 123, 210, 211, 212, 276, 310
chemical 212
chemical electroless 211
chemical vapor 13, 29, 44, 58, 123, 310
electrochemical 210
electrophoretic 276
Diels-Alder cycloaddition reaction 169
Direct alcohol fuel cells (DAFCs) 25
DNA-protein complexes 162, 170
Drying process 58
Dual crosslinking (DC) 388
Dye 25, 27, 180
degradation 27, 180
sensitized solar cells (DSSCs) 25

E

Electric 86, 174
arc method 86
field oscillations 174
Electrocatalysis 1, 3, 27, 178, 298
Electrocatalyst(s) 7, 16, 18, 25, 26, 28, 179, 218, 224
in fuel cells 224
mesoporous 7
oxide-based 179
Electrochemical biosensor 208, 226
Electrode material 16, 26, 56, 222, 223, 398
Electron(s) 10, 25, 26, 63, 160, 168, 280, 318
conductivity 26
cycloaddition 168
graphene conducts 10
mobile 10
photogenerated 25
spin resonance (ESR) 160
transfer velocity 318

Not be distributed or uploaded to anyone or anywhere For personal private use only

transmission 63
withdrawing, iodobenzene-bearing 280
Electron microscopy 100, 126, 143, 170, 268, 279
transmission 100, 170, 268, 279
Electrophilic 154, 159, 164, 166, 172
addition 159
substitution reaction 164, 166
Electrophoresis 210, 216
depositions 216
Electrostatic 11, 59, 340, 393
adsorption 11
attraction 393
repulsion 59, 340
Emission, toxic gas 90
Energy 169, 172, 173, 179, 355, 394
electrical 173
mechanical 172
migration 355
photonic 173
renewable natural 179
transfer 169, 394
Environment, electronic 131
Enzymatic bioelectrodes 397

F

Flash Joule heating (FJH) 125, 132
Friedel-Crafts reactions 162, 345
FT-IR 119, 134
spectroscopic technique 134
spectroscopy 119, 134
Fuel cell technology 56

G

Gas 17, 180
based progression 180
black process 17
Glucose 225, 226, 398
biofuel cells 398
detection of 225, 226
Glycerol kinase (GK) 393
Graphene-based 218, 299, 300, 324, 337
carbocatalysis 300
carbocatalytic reactions 299
catalysts 324, 337
metal-nanostructures 218

H

Heck cross-coupling reactions 237, 266, 267, 276, 277, 278, 280, 281, 282, 283, 284
Heck reactions 210, 280, 281, 282
catalyzed carbon-carbon cross-coupling 280
Hummers method 88, 302, 316
Hydration reactions 3
Hydrazine 92, 143, 158, 170, 174, 175, 210, 215, 266, 267, 271, 274, 277, 282, 302, 310, 341
hydrate 158, 215, 266, 267, 277, 282
monohydrate 170, 174, 175, 274, 341
Hydrogen 166, 179, 225
lithium exchange methods 166
oxidation reaction (HOR) 179
sensors 225
Hydrolysis 97, 166, 234, 235, 236, 382, 383, 384, 389
enzymatic 382
Hydrophilic nature 270, 340, 355
Hydrothermal 60, 213, 214, 222, 233, 362
one-pot 214
hydrolysis 233
reactions 222
synthesis 213, 362
Hydrothermal process 60, 213, 214, 230
one-pot 60

I

Immobilization 380, 384, 390, 392
efficiency 380, 392
process 384, 390
Immobilized lipase 317, 379, 382, 385, 389, 397, 399
Industrial processes 378
Industries 18, 76, 154, 158, 159, 161, 173, 209, 379, 381, 383, 386

For personal private use only Not be distributed or uploaded to anyone or anywhere

bioprocessing 381
food processing 379
Ionic liquid electrolyte 55
Iron 60, 102, 233, 347
pyrolytic 233
sensed 60
Irradiated reduction conditions 232

L

Lamp black process 17
Laser ablation technique 13, 14, 20, 29, 76, 79, 87, 104

M

Magnetic 50, 227, 364
resonance imaging (MRI) 50, 227
separation method 364
Mass-transfer reactions 7
Mechanism 16, 63, 80, 82, 88, 140, 168, 174, 183, 224, 277, 288, 309
coal gasification 88
electrocatalytic 224
electrostatic 63
Mesoporous 7, 20, 233, 264
carbon (MC) 20, 233, 264
microspheres 7
Metal 139, 353
absorption 139
free catalytic method 353
Microwave 91, 311
exfoliated graphite (MEG) 311
reduction methods 91
Microwave-assisted 173, 320
catalytic synthesis 320
heating 173
Microwave plasma reactor 100
atmospheric pressure 100
MRI detection 227
MTT assay 383
Multi-component reactions (MCRs) 380
Multi-layered graphene oxide (MLGO) 140
Myocardial therapy 175

N

Nanodiamonds, thermal treatment of 23, 29
Nanomaterial synthesis, graphene-based 208
Nanoparticles, magnetic iron 392
Nanoribbons, fabricated 59
Nanoscale graphene oxide (NGO) 167
Nitrogen reduction reaction 5
NMR spectroscopy 345, 346, 348

O

One-pot 305, 357
Henry-Michael reaction 305
hydrothermal reaction 357
Optical 118, 395
fiber sensors (OFSs) 395
microscopy-based methods 118
Oxidation process 91, 347
electrochemical 91
Oxidation reactions 13, 26, 28, 300, 302, 344, 354, 355, 356, 358
aerobic 354
Oxygen evolution reaction (OER) 179, 181

P

Pauli's exclusion principle 54
Photocatalytic activity 180, 318
Photolysis 218
Photo-reduction-the microwave reduction method 93
Phthalocyanine 53
Plasma etching 85
PMMA protection layer and etching process 127
Poisoning effect 3
Polycyclic aromatic hydrocarbons (PAHs) 101
Poly vinyl chloride (PVC) 80
Porcine pancreatic lipase (PPL) 382
Precursors 211, 223, 339
dichalcogenide 211
high-temperature organic 339
iron-based 223

For personal private use only Not be distributed or uploaded to anyone or anywhere

Pressure, atmospheric 101
Pretreated sugarcane bagasse (PSB) 383, 384
Procedures 52, 60 182, 318
  liquid-aided electrochemical 52
  one-pot hydrothermal 60
  spray-drying 318
  wet reaction 182
Process, electrochemical 7, 84, 85

R

Radiations, electromagnetic 174
Radicals 16, 162
  hydrocarbon 16
Raman 52, 53, 118, 119, 123, 128, 129, 131, 132, 133, 143, 182
  spectroscopy 52, 53, 118, 119, 123, 128, 129, 132, 133, 143, 182
  spectrum of graphene 131
Raman spectroscopic 123, 125, 128, 132
  analysis 123, 132
  technique 125, 128
Reactions 159, 178, 179, 212, 264, 302, 317, 341, 385, 389
  decarboxylation 341
  electrocatalytic 179
  electrochemical 178
  electrocyclic 159
  enantioselective 317
  esterification 385
  gas 212
  glycerolysis 389
  green 302
  palladium-catalyzed 264
Resonance 160, 173, 183
  electron spin 160
  surface plasmon 183
RT thermal conductivity 162

S

Scanning 57, 118, 121, 124, 126
  force microscopy (SFM) 121
  tunneling microscope (STM) 57, 118, 124, 126
SERS and Raman spectroscopy 53
Single-layer graphene (SLGs) 3, 44, 49, 123, 125, 131, 132, 133, 138, 338, 360
Solid-state nuclear magnetic resonance (SSNMR) 170
Sonocatalysis 181
Sonochemical treatment of carbonaceous materials 21
Sonogashira cross-coupling reaction 286, 287, 288
Spectroscopy 11, 127, 167, 170, 183, 285
  electrochemical impedance 11
  infrared 167, 170
  scanning tunnelling 127
  techniques 170
  ultraviolet-visible 183, 285
Surface plasmon resonance (SPR) 183
Suzuki 236, 265, 268, 270, 272, 273, 274, 276, 279, 282, 284, 285, 286
  and heck cross-coupling reactions 282
  coupling reaction 279
  cross-coupling reactions 265, 268, 270, 272, 273, 274, 276, 279, 282, 284, 285, 286
  Miyaura reaction 236
Synthesis, nanofibre 19

T

Techniques 19, 26, 29, 44, 45, 140, 168
  electrospinning 19, 26
  micromechanical cleavage 44, 45
  sonochemical 168
  thermoanalytical 140
  ultrsonication 29
Thermogravimetric analysis (TGA) 119, 140, 143, 167, 183
Toxic gases 59, 104
Transmission electron microscope 118, 125
Twisted 127, 128
  bilayer graphene (TBG) 128
  graphene layers (TGL) 127

For personal private use only Not be distributed or uploaded to anyone or anywhere

U

Ultrasonication techniques 20
UV light irradiation 218

V

Vacuum 21, 84, 91, 98, 163
  drying 84, 163
  filtration 21, 84, 91, 98

W

Waals 63, 141, 167, 170, 182
  force theory 182
  interactions 63, 141, 167, 170

X

X-ray 118, 119, 123, 135, 140, 143, 164, 170, 268
  diffraction (XRD) 123, 140, 143, 164, 170, 268
  photoelectron spectroscopy 119, 135, 170, 268
  shotoelectron spectroscopy 118

Not be distributed or uploaded to anyone or anywhere For personal private use only

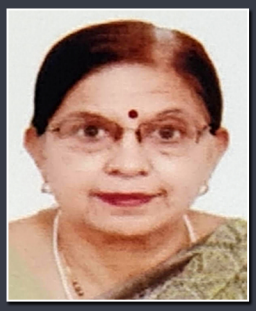

Pinki Bala Punjabi

Prof. Pinki Bala Punjabi obtained her M.Sc., M. Phil. and Ph.D. degrees from Vikram University, Ujjain (M.P.), India. She secured the first position in M.Sc. (1980) as well as in M.Phil. (1981). She has 34 years of research and teaching experience and superannuated from the Department of Chemistry, Mohanlal Sukhadia University, Udaipur (Raj.) in 2019. She is also a lifetime member of various societies namely, the Indian Chemical Society, Kolkata; Indian Council of Chemists, Agra; Indian Science Congress, Kolkata; and Indian Association of Chemistry Teachers, Mumbai. She has published around 139 research papers in journals of international and national repute. She has authored several chapters and books for renowned publishers such as Taylor and Francis, Elsevier, Apple Academic Press, CRC Press, Materials Research Forum, Nova Science Publishers, etc. She is also a reviewer of several international journals. She has completed two major research projects sponsored by University Grants Commission, New Delhi. Prof. Pinki Bala Punjabi has delivered invited lectures and chaired technical sessions at various national and international conferences. She has also organized two national-level conferences. Her expertise includes nanochemistry, particularly graphene chemistry, photocatalysis, organic synthesis, and polymer synthesis.



Rakshit Ameta

Dr. Rakshit Ameta has a first-class career throughout securing the first position in the M. Sc. and was awarded a Gold Medal. He was also conferred Fateh Singh Award by Maharana Mewar Foundation, Udaipur for his meritorious performance. After completing his Ph.D., he served at Hindustan Zinc Limited, Vedanta Group for one year. He has served at M. L. Sukhadia University, Udaipur; University of Kota, Kota, PAHER University, Udaipur, and presently J. R. N. Rajasthan Vidyapeeth (Deemed to be University) Udaipur. 16 Ph.D. students have been awarded their Ph.D. degrees under his supervision in various aspects of green chemistry. He has around 150 research publications to his credit in the journals of national and international repute. He also has a patent to his credit. He is a reviewer of around 50 international journals.

Dr. Rakshit has successfully organized many national conferences at the University of Kota, Kota; PAHER University, Udaipur, and JRN Rajasthan Vidyapeeth, Udaipur. He has delivered invited lectures and chaired sessions at 20 national conferences in different parts of the country. Dr. Rakshit served as a Council Member (2011-2013 & 2020-2022) and an Associate Editor of Physical Chemistry Section (2014-16), a Scientist-in-Charge in the Industrial and Applied Chemistry Section (2014-2016) of the Indian Chemical Society, Kolkata, and an Executive Council Member (2012-2014). He was also a Zonal Secretary (2016-18) of the Indian Council of Chemists, Agra.

He has written books and chapters published by CRC Press (Taylor & Francis), UK; Academic Press, Elsevier; Nova Publishers, USA; and Trans-Tech Publications, Switzerland. In 2017, he received Prof. U.C. Pant Memorial Award instituted by the Indian Chemical Society for his significant contribution. His research specialization includes photochemistry, green chemistry, microwave-assisted reactions, environmental chemistry, waste-water treatment, nanochemistry, solar cells, bioactive and conducting polymers. Recently, he has been elected as the Vice-President of the Indian Chemical Society, India.

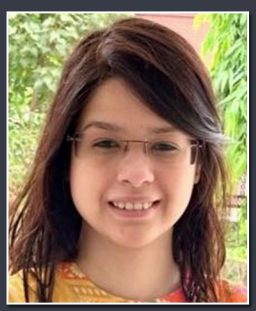

Sharoni Gupta

Sharoni Gupta obtained her Ph.D. degree from Mohanlal Sukhadia University, Udaipur (Raj.), India in the year 2020. She was awarded the University Gold Medal for securing the first position in M.Sc. (Chemistry) in the year 2015. She was also a recipient of the Maulana Azad National Fellowship from the University Grants Commission, New Delhi. She has contributed 10 articles and chapters to the journals and books of leading international publishers such as Apple Academic Press, CRC Press, Bentham Science, Elsevier, Springer Nature and Wiley & Sons. Her specialization fields include graphene-based chemistry, nanocatalysis, and sustainable organic synthesis.

ISSN No 2347-7075
Impact Factor- 7.328
Volume-3 Issue-2

INTERNATIONAL JOURNAL of ADVANCE and APPLIED RESEARCH



Publisher: P. R. Talekar
Secretary,
Young Researcher Association
Kolhapur(M.S), India

Young Researcher Association

International Journal of Advance and Applied Research (IJAAR)
Peer Reviewed Bi-Monthly

ISSN – 2347-7075
Impact Factor –7.328
Vol.3 Issue-2 Sept-Oct- 202

International journal of advance and applied research (IJAAR)

A Multidisciplinary International Level Referred and Peer Reviewed Journal

Volume-3 *Issue-2*

Chief Editor

P. R. Talekar
Secretary,
Young Researcher Association, Kolhapur(M.S), India

Executive Editor

Dr. M. S. Shinde
I/C Principal,
IQAC Coordinator and HOD,
Department of Physics
Mahant Jamanadas Maharaj
Art's, Commerce and Science College Karanjali

Editor

Dr. P.T. Wankhedkar Department of Zoology Mahant Jamanadas Maharaj Art's, Commerce and Science College Karanjali	**Dr. N. R. Giri** HOD,Department of Zoology Mahant Jamanadas Maharaj Art's, Commerce and Science College Karanjali

Editorial & Advisory Board

Dr. S. D. Shinde	Dr. M. B. Potdar	Dr. P. K. Pandey
Dr. L. R. Rathod	Mr. V. P. Dhulap	Dr. A. G. Koppad
Dr. S. B. Abhang	Dr. S. P. Mali	Dr. G. B. Kalyanshetti
Dr. M. H. Lohgaonkar	Dr. R. D. Bodare	Dr. D. T. Bornare

Published by: Young Researcher Association, Kolhapur, Maharashtra, India

The Editors shall not be responsible for originality and thought expressed in the papers. The author shall be solely held responsible for the originality and thoughts expressed in their papers.

© All rights reserved with the Editors

International Journal of Advance and Applied Research (IJAAR)
Peer Reviewed Bi-Monthly

ISSN – 2347-7075
Impact Factor –7.328
Vol.3 Issue-2 Sept-Oct-2022

CONTENTS

Sr No	Paper Title	Page No.
1	A Geographal Study of Sex Ratio in Latur **S. B. Ashture**	1-4
2	A Study on Factors Influencing Individual Investment Decisions Towards Indian Share Market **Mrs. Abilasha N, Dr. Madhu Tyagi**	5-11
3	A Relative Study on The Decalogue of Ronald Knox and The Earlier Novels in The Dublin Murder Squad Series of Tana French **Janani P R, Dr. Preetha C**	12-13
4	The Ecocentric Environmental Paradigm In Coehlo's The Alchemist **Mantha Padmabandhavi Prakashrao**	14-17
5	A Study On Environmental Perspectives Of Amitav Ghosh's The Hungry Tide **G. Prema**	18-21
6	Mobile Apps Of Libraries: Boon For Library Users **Dr. Sangaraj Hosamani**	22-25
7	Voices Of The Subaltern Female Protagonist In Vikas Swarup's The Accidental Apprentice **Prashant Jambhulkar, Dr. Vivek V. Joshi**	26-30
8	"A Study Of Modern Teaching Techniques In Acquiring English Language With Global Perspective" **Dr.P.R.V.N.Kesava Kumar**	31-36
9	Study Of Interactions Of 2-{[2-(Cyclohexylcarbamoyl) Benzoyl] Amino}-3-Methylbutanoic Acid (2ca3mba) With Bsa At Different Ph Using Ultrasonic Interferometer And Ft-Ir Techniques **Shrikant B. Thakare**	37-42
10	Effect Of Child Exploitation On The Socio-Economic Status In India **Dr. Sanjay Kumar Das**	43-48
11	Very Rare Sp. Of Odonates (Dragonflies And Damselflies) At Salim Ali Lake (Aurangabad City) **JB Aghade, SA Saraf**	49-52
12	New Media Use By Academic College Librarians To Provide Information To Library Users During Covid-19 Pandemic Period **Amol Bhaudas Meshram, Dr. Kishorsingh R. Chungade**	53-58
13	Skill Impact Bonds In Enhancing Youth Population In India **Kaleeshwari.S, Dr.M. Jegadeeshwaran**	59-61
14	Padmini As An Existential Woman In Girish Karnad's Play Hayavadana **Priti Nilkanth Bhandekar, Dr. Vivek V. Joshi**	62-64

15	The Study On Significance Of Dramatic Techniques In Roy Williams's Depiction Of Realistic Content In Joe Guy **Mr. Samadhan M. Jadhav, Dr. Prabhanjan B. Mane**	65-70
16	Study Of Zooplankton Diversity, Abundance And Seasonal Variations From Nakana Lake,Dhule (Ms) India **Patil, M. U., Patole, S. S.**	71-76
17	The Desperate Femeinsts **Swetta Rajendra Singh Gautam, Dr.Vivek V.Joshi**	77-79
18	Environmental Accounting And Reporting: A Disclosure Of Business Impact On Environment **Lt. Dr. Vijay Kumar Madugu**	80-84
19	Understanding Lifelong Learning And Its Prevalence Among College Students **Swati Tulshan, Susmita Neogi**	85-88
20	Feature And Use Of Open Source Software For Library **Mr. Satish K. Chandel, Dr. Kishorsingh R. Chungade**	89-91
21	The Role Of Photojournalism In Empowering Women To Achieve Sustainable Development **Nithish P**	92-95
22	A Survey On Impact Of Cement Industry In Gadchandur In Chandapur District **Dr. Farukh Ahemad Sheikh, Prof Rima Potdukhe**	96-100
23	Issues And Challenges Of Child Labour **Dr. Nandini N**	101-104
24	Wastewater Management And Its Challenges **Dr. Kavita Hingane**	105-109
25	Isolation Of Antimicrobial Resistance Bacteria From The External Body Surface Of Houseflies Collected From Civil Hospital Malegaon **Mohammad Ismail Ansari, Fariha Shafaq, Azra Ghayasuddin**	110-114
26	Impact Of Migration On The Sugarcane Cutter Labourers In Maharashtra **Supriya Chandrakant Gaikwad**	115-118
27	Automation In Estimation Of Land Surface Temperature Based On Landsat Satellites In The Upper Mutha Basin, Pune District **Kishor R. Sonawane, Jyotiram C. More**	119-126
28	Effect of Cypermethrin and Oxyfluorfen on alimentary canal of earthworm, Eisenia foetida **D. S. Patil, P. K. Bagul, P. A. Suryawanshi , B. C. More**	127-132
29	Status Of Academic College Libraries Regarding Sustainable Library Service Provision To Its Users **Shyamkumar S. Gorde, Prof. Dr. Harshal R. Nimbhorkar**	133-136
30	Impact Of Natyashastra On Indian Folk Theatres **Dr.Sarika Sinha, Akash Dahariya**	137-139
31	Retirement Planning: Awareness Among Individuals **Ms. Sanampreet Kaur Kapoor, Dr. Sangeeta**	140-152

32	Sustainable Development: A Call For A Change **Dr. Maneesh. B**	153-155
33	The Consequence Of Chemical Use On Cerastus Moussonianus Hatchability **Prakash Tanaji Wankhedkar, Niranjan Ramesh Giri, Shaikh Hasim Mohammed Isak**	159-163
34	Impact Of Climate Change On Agriculture Production And It's Sustainable Solutions **Dr. Nandini Pandurang Wagh**	164-166
35	Synthesis And Structural Properties Of Zinc Ferrite **Rahul Upalaikar**	167-169
36	A Study On Awareness Of Early Adolescent Boys Regarding Genral Information And Changes In Morality During Early Adolscent Stage **Nita B. Gaikwad, Gaytri Tiwari**	170-175
37	Survival Of Ankita Sharma In Preeti Shenoy's Life Is What You Make It **Harini P.**	176-179
38	"A Study On Industrial Pollution And Environment In Ghugus" **Dr Sarika Baban Nande, Prof Rima Potdukhe**	180-186
39	Analyzing Energy Efficiency In Office Building: A Case Study In Raipur, Chhattisgarh **Shanta Dash, Mahendra Joshi**	187-196
40	Recent Trends And Development In The Livestock Sector: A Descriptive Analysis **Susanthika S**	197-204
41	Natural Resources And Laws! **Dr. Prakash Laxmanrao Dompale**	205-208
42	Research Methodology: An Introduction **Dr. Vaishali E. Aher**	209-212
43	"A Comparative Analysis Of Health Status And Level Of Awareness In Pregnant Women In Jind District " **Poonam Lohan, Rinku Kharb**	213-223
44	Zinc Oxide Nanoparticles: Investigation On The Parameters Affecting The Structure Of Zno Nps In Sol -Gel Synthesis **JOSÉ, Basílio José Augusto, SHINDE, Mahendra Devidas**	224-233
45	Recent Changes In Msmes Sector And It's Impact On Economic Development In India **Miss Subhalaxmi Joshi, Dr. Bandana Pathak**	234-238
46	Investigation On The Tube Well Water Quality Of A Village From Daryapur Taluka, Dist. Amravati, Maharashtra, India **S.R.Bansod**	239-244
47	Social And Cultural Crises Between The Arvind Adiga's The White Tiger And Last Man In Tower **Ashwini M.Ingale, Prof. Dr. Kishor K. Wagh**	245-247
48	A Study Of Drinking Water Quality Impact On Human Health : Special Reference To Balapur Tahisal District Akola In The State Of Maharashtra **Dr. Alpana Deokar**	248-252
49	Status Of Agro-Tourism Centers: A Geographical Study Of Selected Area Of Maharashtra **Prof. Santosh Maruti Shinde**	253-257
50	Vaishnavism in West Bengal and its Environmental Ethics **Mrs. Ipsita Chakraborty, Dr. P. Ganesan, Dr. Debaprashad Chatterjee**	258-262
51	Carrier Mobility in The Field Effect Transistor Channel in The Single Walled Carbon Nanotubes **Jay Shankar Kumar, Versha Joshi, Vimal Sagar**	263-267
52	Information Literacy: - An Overview **Mr. Ashok B Nagare**	268-270
53	' Shiva ' The Hero Of ' The Shiva Trilogy '– By Amish Tripathi **Kavita Vasantrao Kakde, Dr.Kishor K Wagh**	271-273

54	A Geographical Analysis Of LULC In Pachora Tehsil Of Jalgaon District (MH) **Prof. Rahul V. Patil, Dr. S. N. Bharambe**	274-276
55	Record Of The Predatory Stink Bug Andrallus Spinidens (Fabricus) (Heteroptera: Pentatomidae: Aesopinae) From Goa State, India **Ayesha E. Shetkar, Vijaykumar S. Gadekar, Aishwarya S. Naik, S. V. More**	277-279
56	Quantum Machine Learning - A Study **Mr. K. VigneshKumar, Dr. N. Sumathi, Mrs. B. Vidhya, Ms. A. Subhasheni**	280-287
57	Land Resources of Wasteland Development in Mizoram State, India- A Geographical Perspective **Dr. Amol S. Shinde**	288-291
58	श्रीकृष्ण जन्मलीला विमर्शः **डॉ.रुरुकुमार महापात्र**	292-294
59	नगरीय आकारिकी की अवधारणा और नगरों/नगरीयकरण की उत्पत्ति एवं विकास का अध्ययन **डॉ. भूपेन्द्र कुमार जाँगिड.**	295-311
60	"पाचवीच्या गाण्यातील आदिवासी कोकणांच्या धारणा व संस्कार' ' **डॉ. मधुचंद्र लक्ष्मण भुसारे**	312-316
61	पर्यटन रोजगार, विकास की संभावनाऐं नीतियाँ एवं सुझाव (बिलासपुर संभाग के सन्दर्भ में) **श्रीमति सपना नामदेव**	317-322
62	"कृषी आणि जल संसाधन व्यवस्थापन " **सहा. प्रा .) कुमारे लक्ष्मण नागोराव, (सहा.प्रा.) अशोक प्रबती कांबळे**	323-327
63	भारत में समावेशी शिक्षा – एक मूल्यॉकन **डॉ. राजेश मौर्य**	328-334
64	A Facile Synthesis Of (1r,2r)-1,2-Cyclohexan Dimethanol, A Key Intermediate Of Lurasidone Hydrochloride-An Atypical Antipsychotic Drug **Pramod A. Dhokrat, Pavankumar V. Solanki, Tejas C. Gaikwad, Radhakrishnan M. Tigote**	335-341
65	जलवायु परिवर्तन एवं संपोषणीय विकास की ओर बढ़ते कदम Dr. Nisha Sharma	342-346
66	म्यूचुअल फंड **डॉ. मोनिका बाबेल**	347-352
67	Exact Study of Transient Thermoelastic Deformation of a Thick Circular Plate **Gaikwad Priyanka B.**	353-359

Based on NEP2020
As per Latest Syllabus of Chemistry (Semester-I)
for Mohanlal Sukhadia University, Udaipur

CHEMISTRY-I

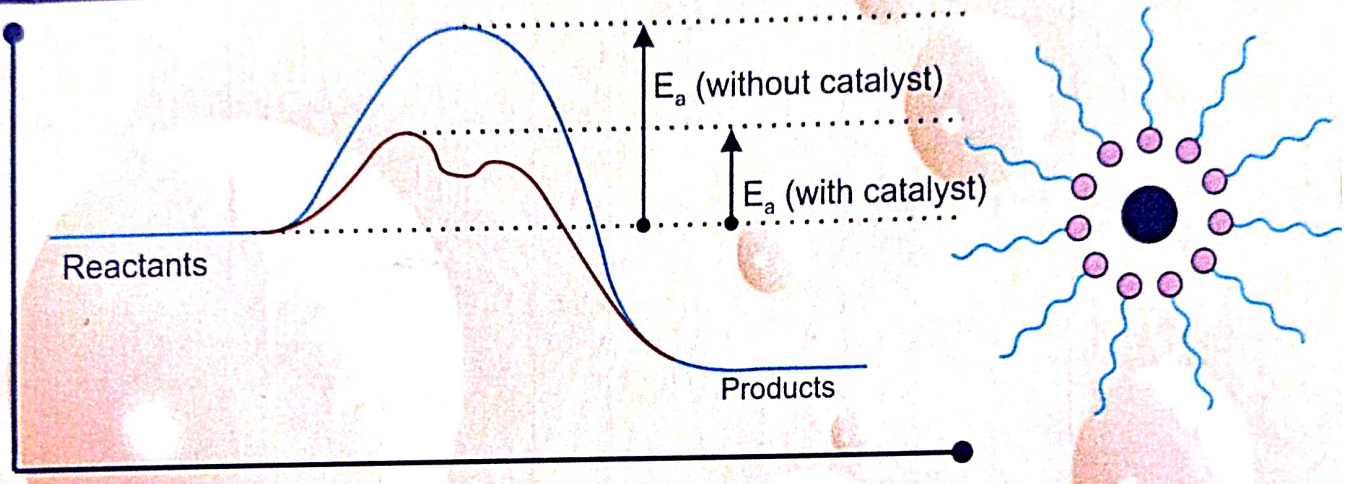

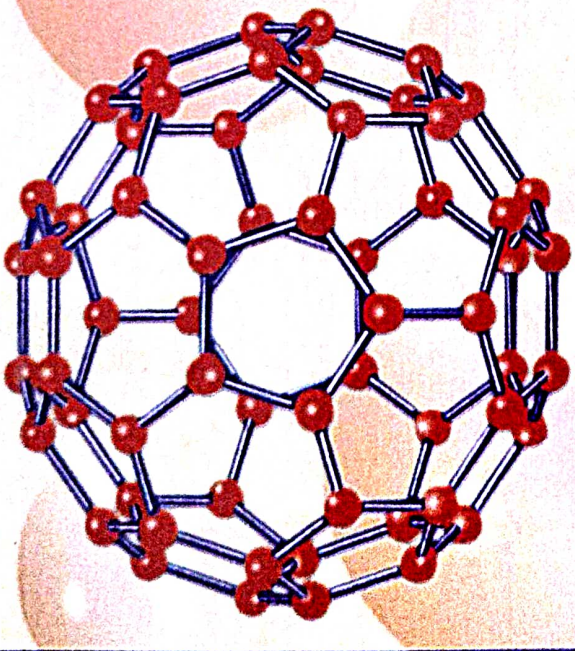

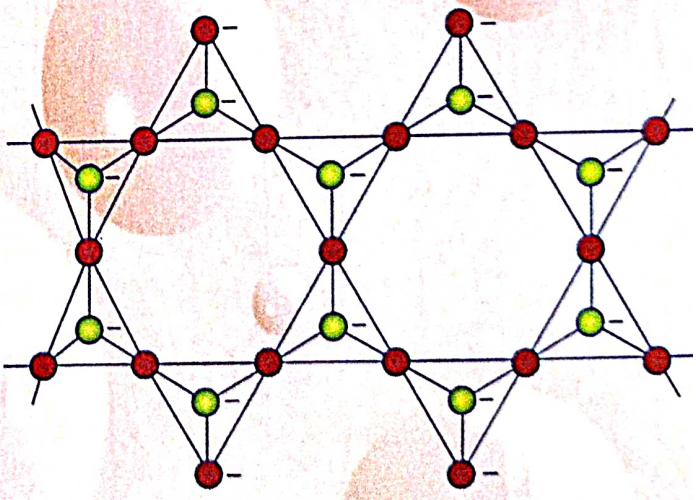

Suresh Ameta

Ajay Sharma Rakshit Ameta Anil Chohadia

Chetna Ameta Siddharth Sharma

Chemistry-I

As per Latest Syllabus of Chemistry (Semester-I) for
Mohanlal Sukhadia University, Udaipur

Prof. SURESH AMETA
Former Professor and Head
Department of Chemistry
M.L. Sukhadia University, Udaipur

Prof. AJAY SHARMA
Principal
Government College
Sirohi

Prof. RAKSHIT AMETA
Department of Chemistry
Pacific University
Udaipur

Dr. ANIL CHOHADIA
Associate Professor
M.P. Govt. College
Chittaurgarh

Dr. CHETNA AMETA
Assistant Professor
Department of Chemistry
M.L. Sukhadia University, Udaipur

Dr. SIDDHARTH SHARMA
Assistant Professor
Department of Chemistry
M.L. Sukhadia University, Udaipur

HIMANSHU Publications

HIMANSHU PUBLICATIONS

Udaipur ❑ New Delhi

Copyright © Publisher

All rights reserved. No part of this book may be reproduced or utilised in any form or by any means, electronic or mechanical, including photocopying, recording or by any information storage or retrieval system, without permission in writing from the publisher.



HIMANSHU PUBLICATIONS

First Floor, 2-D, Hajareshwar Colony, Near Krishna Complex, Udaipur (Raj.); Phone : 0294-2421087
4379/4-B, Prakash House, Ansari Road, Daryaganj, New Delhi - 2; Phone : +91-96109-73739
e-mail : *himanshupublications@gmail.com;* web: *www.himanshupublications.com*

ISBN : 978-93-87201-93-4

Edition : 2024

Price : 465.00

Distributor

ARYAS PUBLISHERS DISTRIBUTORS (P) LTD.

2-D, Hazareshwar Colony, Near Court Choraha, Udaipur (Raj.) - 313 001;
Phone : 0294-2421087; E-mail : apdpl.2012@gmail.com

Printed at : R.K. Offest Process, Delhi

ISSN No 2347-7075
Impact Factor- 7.328
Volume-3 Issue-2

INTERNATIONAL JOURNAL of ADVANCE and APPLIED RESEARCH



Publisher: P. R. Talekar
Secretary,
Young Researcher Association
Kolhapur(M.S), India

Young Researcher Association

	Dr. Arpana Deokar	
49	Status Of Agro-Tourism Centers: A Geographical Study Of Selected Area Of Maharashtra **Prof. Santosh Maruti Shinde**	253-257
50	Vaishnavism in West Bengal and its Environmental Ethics **Mrs. Ipsita Chakraborty, Dr. P. Ganesan, Dr. Debaprashad Chatterjee**	258-262
51	Carrier Mobility in The Field Effect Transistor Channel in The Single Walled Carbon Nanotubes **Jay Shankar Kumar, Versha Joshi, Vimal Sagar**	263-267
52	Information Literacy: - An Overview **Mr. Ashok B Nagare**	268-270
53	' Shiva ' The Hero Of ' The Shiva Trilogy '– By Amish Tripathi **Kavita Vasantrao Kakde, Dr.Kishor K Wagh**	271-273

54	A Geographical Analysis Of LULC In Pachora Tehsil Of Jalgaon District (MH) **Prof. Rahul V. Patil, Dr. S. N. Bharambe**	274-276
55	Record Of The Predatory Stink Bug Andrallus Spinidens (Fabricus) (Heteroptera: Pentatomidae: Aesopinae) From Goa State, India **Ayesha E. Shetkar, Vijaykumar S. Gadekar, Aishwarya S. Naik, S. V. More**	277-279
56	Quantum Machine Learning - A Study **Mr. K. VigneshKumar, Dr. N. Sumathi, Mrs. B. Vidhya, Ms. A. Subhasheni**	280-287
57	Land Resources of Wasteland Development in Mizoram State, India- A Geographical Perspective **Dr. Amol S. Shinde**	288-291
58	श्रीकृष्ण जन्मलीला विमर्श: **डॉ.रुरुकुमार महापात्र**	292-294
59	नगरीय आकारिकी की अवधारणा और नगरों/नगरीयकरण की उत्पत्ति एवं विकास का अध्ययन **डॉ. भूपेन्द्र कुमार जॉमिड.**	295-311
60	"पाचवीच्या गाण्यातील आदिवासी कोकणांच्या धारणा व संस्कार' ' **डॉ. मधुचंद्र लक्ष्मण भुसारे**	312-316
61	पर्यटन रोजगार, विकास की संभावनाऐं नीतियाँ एवं सुझाव (बिलासपुर संभाग के सन्दर्भ में) **श्रीमति सपना नागदेव**	317-322
62	"कृषी आणि जल संसाधन व्यवस्थापन " **सहा. प्रा .) कुमारे लक्ष्मण नागोराव, (सहा.प्रा.) अशोक प्रवती कांबळे**	323-327
63	भारत में समावेशी शिक्षा – एक मूल्यांकन **डॉ. राजेश गौर्य**	328-334
64	A Facile Synthesis Of (1r,2r)-1,2-Cyclohexan Dimethanol, A Key Intermediate Of Lurasidone Hydrochloride-An Atypical Antipsychotic Drug **Pramod A. Dhokrat, Pavankumar V. Solanki, Tejas C. Gaikwad, Radhakrishnan M. Tigote**	335-341
65	जलवायु परिवर्तन एवं संपोषणीय विकास की ओर बढ़ते कदम Dr. Nisha Sharma	342-346
66	म्यूचुअल फंड **डॉ. मोनिका बाबेल**	347-352
67	Exact Study of Transient Thermoelastic Deformation of a Thick Circular Plate **Gaikwad Priyanka B.**	353-359

International Journal of Advance and Applied Research (IJAAR)
Peer Reviewed Bi-Monthly

ISSN – 2347-7075
Impact Factor –7.328
Vol.3 Issue-2 Sept-Oct-2022

CONTENTS

Sr No	Paper Title	Page No.
1	A Geographal Study of Sex Ratio in Latur **S. B. Ashture**	1-4
2	A Study on Factors Influencing Individual Investment Decisions Towards Indian Share Market **Mrs. Abilasha N, Dr. Madhu Tyagi**	5-11
3	A Relative Study on The Decalogue of Ronald Knox and The Earlier Novels in The Dublin Murder Squad Series of Tana French **Janani P R, Dr. Preetha C**	12-13
4	The Ecocentric Environmental Paradigm In Coehlo's The Alchemist **Mantha Padmabandhavi Prakashrao**	14-17
5	A Study On Environmental Perspectives Of Amitav Ghosh's The Hungry Tide **G. Prema**	18-21
6	Mobile Apps Of Libraries: Boon For Library Users **Dr. Sangaraj Hosamani**	22-25
7	Voices Of The Subaltern Female Protagonist In Vikas Swarup's The Accidental Apprentice **Prashant Jambhulkar, Dr. Vivek V. Joshi**	26-30
8	"A Study Of Modern Teaching Techniques In Acquiring English Language With Global Perspective" **Dr.P.R.V.N.Kesava Kumar**	31-36
9	Study Of Interactions Of 2-[[2-(Cyclohexylcarbamoyl) Benzoyl] Amino]-3-Methylbutanoic Acid (2ca3mba) With Bsa At Different Ph Using Ultrasonic Interferometer And Ft-Ir Techniques **Shrikant B. Thakare**	37-42
10	Effect Of Child Exploitation On The Socio-Economic Status In India **Dr. Sanjay Kumar Das**	43-48
11	Very Rare Sp. Of Odonates (Dragonflies And Damselflies) At Salim Ali Lake (Aurangabad City) **JB Aghade, SA Saraf**	49-52
12	New Media Use By Academic College Librarians To Provide Information To Library Users During Covid-19 Pandemic Period **Amol Bhaudas Meshram, Dr. Kishorsingh R. Chungade**	53-58
13	Skill Impact Bonds In Enhancing Youth Population In India **Kaleeshwari.S, Dr.M. Jegadeeshwaran**	59-61
14	Padmini As An Existential Woman In Girish Karnad's Play Hayavadana **Priti Nilkanth Bhandekar, Dr. Vivek V. Joshi**	62-64

15	The Study On Significance Of Dramatic Techniques In Roy Williams's Depiction Of Realistic Content In Joe Guy **Mr. Samadhan M. Jadhav, Dr. Prabhanjan B. Mane**	65-70
	Study Of Zooplankton Diversity, Abundance And Seasonal Variations From Nakana	

International Journal of Advance and Applied Research
www.ijaar.co.in
ISSN – 2347-7075 Impact Factor – 7.328
Peer Reviewed Bi-Monthly
Vol.3 No.2 Sept – Oct 2022

जलवायु परिवर्तन एवं संपोषणीय विकास की ओर बढ़ते कदम

Dr. Nisha Sharma
Teaching Consultant, Faculty of Education
Mohan Lal Sukhadia University, Udaipur (Raj.)
E-mail : nishasharma06021983@gmail.com
***Corresponding Author* - Dr. Nisha Sharma**
Email:- nishasharma06021983@gmail.com

प्रस्तावना

वायु जल भूमि वनस्पति पेड़ पौधे पशु मानव सब मिलकर पर्यावरण बनाते हैं प्रकृति में इन सब की माया और इनकी रचना कुछ इस प्रकार से व्यवस्थित है कि पृथ्वी पर एक संतुलन 20वीं सदी की शुरुआत से पृथ्वी की जलवायु में देखे गए परिवर्तन मुख्य रूप से मानवीय गतिविधियों, विशेष रूप से जीवाश्म ईंधन के जलने से प्रेरित हैं, जो पृथ्वी के वायुमंडल में गर्मी-ट्रैपिंग ग्रीनहाउस गैस के स्तर को बढ़ाता है, जिससे पृथ्वी की सतह का औसत तापमान बढ़ जाता है। इन मानव-उत्पादित तापमान वृद्धि को आमतौर पर ग्लोबल वार्मिंग के रूप में जाना जाता है। आंतरिक परिवर्तनशीलता (उदाहरण के लिए, अल नीनो, ला नीना और प्रशांत डेकाडल ऑसीलेशन जैसे चक्रीय महासागर पैटर्न) और बाहरी बल (जैसे, ज्वालामुखी गतिविधि, सूर्य के ऊर्जा उत्पादन में परिवर्तन, पृथ्वी की कक्षा में बदलाव सहित) जलवायु परिवर्तन में प्राकृतिक प्रक्रियाएं भी योगदान दे सकती हैं।) अतीत, वर्तमान और भविष्य के जलवायु परिवर्तन की निगरानी और अध्ययन के लिए वैज्ञानिक सैद्धांतिक मॉडल के साथ-साथ जमीन, वायु और अंतरिक्ष से टिप्पणियों का उपयोग करते हैं। जलवायु डेटा रिकॉर्ड जलवायु परिवर्तन के प्रमुख संकेतकों का प्रमाण प्रदान करते हैं, जैसे कि वैश्विक भूमि और समुद्र के तापमान में वृद्धि; समुद्र का स्तर बढ़ना; पृथ्वी के ध्रुवों और पर्वतीय हिमनदों में बर्फ की हानि; चरम मौसम में आवृत्ति और गंभीरता में परिवर्तन जैसे तूफान, गर्मी की लहरें, जंगल की आग, सूखा, बाढ़ और वर्षा; और बादल और वनस्पति आवरण परिवर्तन

भूमंडलीय तापक्रम में वृद्धि

ग्लोबल वार्मिंग, मानव गतिविधियों के कारण पूर्व-औद्योगिक काल (1850 और 1900 के बीच) के बाद से पृथ्वी की जलवायु प्रणाली का दीर्घकालिक ताप है, मुख्य रूप से जीवाश्म ईंधन के जलने से, जो पृथ्वी के वायुमंडल में गर्मी-फंसाने वाले ग्रीनहाउस गैस के स्तर को बढ़ाता है। इस शब्द का प्रयोग अक्सर जलवायु परिवर्तन शब्द के साथ एक दूसरे के स्थान पर किया जाता है, हालांकि बाद वाला मानव और प्राकृतिक रूप से उत्पादित वार्मिंग और हमारे ग्रह पर इसके प्रभाव दोनों को संदर्भित करता है। इसे आमतौर पर पृथ्वी के वैश्विक सतह के तापमान में औसत वृद्धि के रूप में मापा जाता है।

पूर्व-औद्योगिक काल के बाद से, मानव गतिविधियों का अनुमान है कि पृथ्वी के वैश्विक औसत तापमान में लगभग 1 डिग्री सेल्सियस (1.8 डिग्री फ़ारेनहाइट) की वृद्धि हुई है, एक संख्या जो वर्तमान में प्रति दशक 0.2 डिग्री सेल्सियस (0.36 डिग्री फ़ारेनहाइट) बढ़ रही

है। यह स्पष्ट है कि मानव प्रभाव ने वातावरण, महासागर और भूमि को गर्म कर दिया है।

ग्लोबल वार्मिंग औद्योगिक क्रांति के बाद से औसत वैश्विक तापमान में वृद्धि को दर्शाता है। 1880 के बाद से औसत वैश्विक तापमान में लगभग एक डिग्री सेल्सियस की वृद्धि हुई है। ग्लोबल वार्मिंग एक सतत प्रक्रिया है, वैज्ञानिकों को आशंका है कि 2035 तक औसत वैश्विक तापमान अतिरिक्त 0.3 से 0.7 डिग्री

बढ़ी हुई वर्षा से कृषि को लाभ हो सकता है, लेकिन एक ही दिन में अधिक तीव्र तूफानों के रूप में वर्षा होने से, फसल, संपत्ति, बुनियादी ढांचे को नुकसान होता है और प्रभावित क्षेत्रों में जन-जीवन का भी नुकसान हो सकता है।

ग्लोबल वार्मिंग के कारण समुद्री सतह का तापमान भी बढ़ जाता है क्योंकि पृथ्वी के वातावरण की अधिकांश गर्मी समुद्र द्वारा अवशोषित हो जाती है। गर्म समुद्री सतह के

International Journal of Advance and Applied Research (IJAAR)
Peer Reviewed Bi-Monthly

ISSN – 2347-7075
Impact Factor –7.328
Vol.3 Issue-2 Sept-Oct- 202

International journal of advance and applied research (IJAAR)

A Multidisciplinary International Level Referred and Peer Reviewed Journal

Volume-3 *Issue-2*

Chief Editor

P. R. Talekar
Secretary,
Young Researcher Association, Kolhapur(M.S), India

Executive Editor

Dr. M. S. Shinde
I/C Principal,
IQAC Coordinator and HOD,
Department of Physics
Mahant Jamanadas Maharaj
Art's, Commerce and Science College Karanjali

Editor

Dr. P.T. Wankhedkar Department of Zoology Mahant Jamanadas Maharaj Art's, Commerce and Science College Karanjali	**Dr. N. R. Giri** HOD,Department of Zoology Mahant Jamanadas Maharaj Art's, Commerce and Science College Karanjali

Editorial & Advisory Board

Dr. S. D. Shinde	Dr. M. B. Potdar	Dr. P. K. Pandey
Dr. L. R. Rathod	Mr. V. P. Dhulap	Dr. A. G. Koppad
Dr. S. B. Abhang	Dr. S. P. Mali	Dr. G. B. Kalyanshetti
Dr. M. H. Lohgaonkar	Dr. R. D. Bodare	Dr. D. T. Bornare

Published by: Young Researcher Association, Kolhapur, Maharashtra, India

The Editors shall not be responsible for originality and thought expressed in the papers. The author shall be solely held responsible for the originality and thoughts expressed in their papers.

© All rights reserved with the Editors

NEP2020 पर आधारित
मोहनलाल सुखाड़िया विश्वविद्यालय, उदयपुर
के नवीनतम पाठ्यक्रमानुसार Chemistry (Semester-I) के लिए

रसायन-I

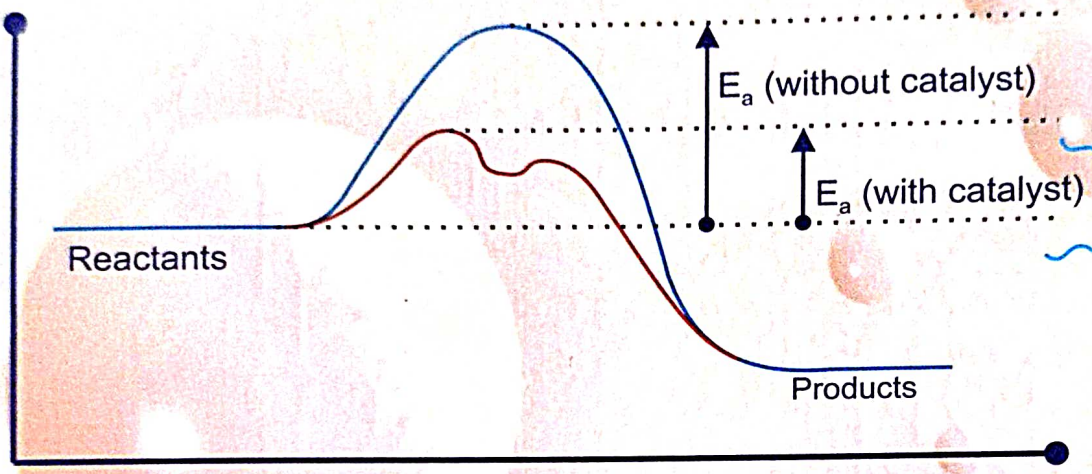

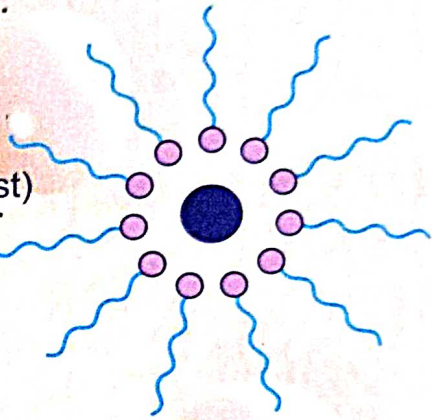

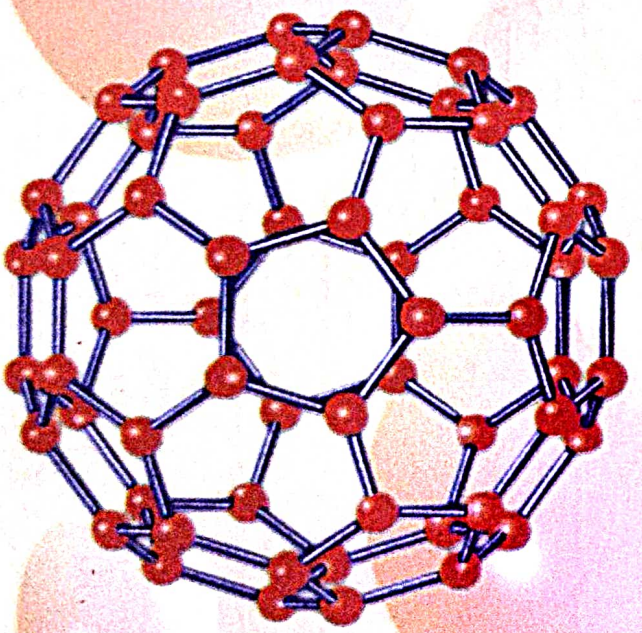

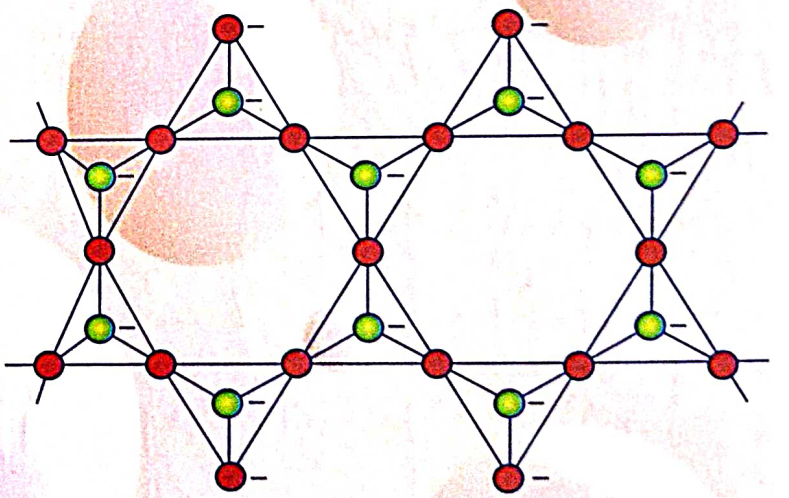

सुरेश आमेटा

अजय शर्मा रक्षित आमेटा अनिल चोहाड़िया

चेतना आमेटा सिद्धार्थ शर्मा

रसायन-I

As per Latest Syllabus of Chemistry (Semester-I) for
Mohanlal Sukhadia University, Udaipur

SPECIMEN COPY

प्रो. सुरेश आमेटा
पूर्व आचार्य एवं विभागाध्यक्ष, रसायन विभाग
मोहनलाल सुखाड़िया विश्वविद्यालय, उदयपुर

प्रो. अजय शर्मा
प्राचार्य
राजकीय महाविद्यालय
सिरोही

प्रो. रक्षित आमेटा
रसायन विभाग
पेसिफिक विश्वविद्यालय
उदयपुर

डॉ. अनिल चोहाड़िया
सहआचार्य, रसायन विभाग
एम.पी. राजकीय महाविद्यालय
चित्तौड़गढ़

डॉ. चेतना आमेटा
सहायक आचार्य, रसायन विभाग
मोहनलाल सुखाड़िया विश्वविद्यालय
उदयपुर

डॉ. सिद्धार्थ शर्मा
सहायक आचार्य, रसायन विभाग
मोहनलाल सुखाड़िया विश्वविद्यालय, उदयपुर

HIMANSHU Publications

हिमांशु पब्लिकेशन्स

उदयपुर ❑ नई दिल्ली

© सर्वाधिकार सुरक्षित

इस पुस्तक के किसी भी अंश की किसी भी रूप में प्रतिकृति करना या किसी भी साधन-इलेक्ट्रॉनिक, मेकैनिकल या अन्य प्रकार, फोटोकॉपी, रिकॉर्डिंग या सूचना संचयन और पुनः प्राप्ति पद्धति - द्वारा प्रसारित करना प्रकाशक की लिखित अनुमति के बिना मना है।



हिमांशु पब्लिकेशन्स

प्रथम तल, 2-D, हजारेश्वर कॉलोनी, कृष्णा कॉम्पलेक्स के पास, उदयपुर (राज.), फोन: 0294-2421087
4379/4-B, प्रकाश हाऊस, अंसारी रोड़, दरियागंज, नई दिल्ली-2, मोबाईल: 96109-73739
Web : *himanshupublications.com;* email : *himanshupublications@gmail.com*

ISBN : 978-93-87201-57-6
संस्करण : 2024
मूल्य : 395.00

Distributor
ARYA'S PUBLISHERS DISTRIBUTORS (P) LTD.
2-D, Hazareshwar Colony, Near Court Choraha, Udaipur (Raj.) - 313 001;
Phone : 0294-2421087; E-mail : apdpl.2012@gmail.com
Printed at : R.K. Offset Process, Delhi

Language and Digital Media

Editors
Dr. Rishikesh Kumar Gautam • Dr. Renuka
Dr. Prabha Gour • Ms. Chetna Kumari Joshi

Publisher

Radhika Books

B-637/7, Rajvir Colony,
Gharoli, New Delhi-110096
Phone: 09990790224
Email: radhikabooks2009@gmail.com
radhikabooks198@gmail.com

Branch Office:
Flate No. 303, Petels Residence
Plot No. 5152, Welcome City
Shahberi, Gautam Budh Nagar-201308 (Noida)
Phone: 9643592549

Language and Digital Media

Disclaimer

The publisher has fully tried to follow the copyright law. However, if any work is found to be similar, it is unintentional and the same should not be used as defamatory or to file legal suit against the editor/publisher.

If the readers find any mistake/s, they may kindly point out those to us, and we shall gratefully correct them in the next edition.

© *Editors, 2023*

ISBN: 978-93-91819-21-7

Price : ₹850/-

Laser Typesetting: Aadil Printographics, Delhi

7. The Rising Trend of Multilingualism in Digital Media 95
— *Ankur Prakash*
8. The Role of Social Media in Shaping Literary Narratives 109
— *Dr. Jaydip Kumar Deva Bhai Pandya*
9. Impact of Digital Media on Languages 116
— *Dr Ritu Singh Mahiyaria*
10. Language and Digital Media 121
— *J. Samuel Santhosh*
11. The Political Communication of BJP in Digital Era 129
— *Prof. Dr. Dilip Kumar & Sorabh Kumar Aggarwal*
12. अन्तर्राष्ट्रीय फलक पर उड़ान भरती हिन्दी भाषा और डिजीटल माध्यम 142
— *प्रो. (डॉ) गीता सक्सेना*
13. मोबाइल पत्रकारिता और भाषा 152
— *डॉ. आरती भट्ट एवं दीपिका रावत*
14. सोशल मीडिया और हिंदी भाषा 163
— *डॉ. रेणुका*
15. सोशल मीड़िया और हिन्दी 175
— *ममता तिवाड़ी*

ISBN: 978-93-91260-89-7



AMAZON #1 BESTSELLER

Reimagining Education

Editors:
Dr. Riya Tiwari
Dr. Sujankumar Kanubhai Patel
Dr. Shefaliben Kanubhai Patel

Eureka Publications

ffort has been made to trace copyright holders and obtain permission, this has not been all cases. Any omissions brought to our attention will be remedied in future editions.

All rights reserved.

of this publication may be reproduced, transmitted, or stored in a retrieval system, in any form or by any means, electronic, mechanical, photocopying, recording or otherwise, without the prior permission of the publisher.

ISBN: 978-93-91260-89-7

First Edition - 2023

The moral right of the authors has been asserted.

k is sold subject to the condition that it shall not, by way of trade or otherwise, esold, hired out, or otherwise circulated, without the publisher's prior consent, n any form of binding or cover other than that in which it is published.

Published By:

Eureka Publications

(A Division of EnTo Tech Pvt. Ltd.)

ia Office: 604, The Poorva, Pimple Saudagar, Pune, Maharashtra - 411027
Office: 9495, Bankal Street, Lopez Village, Batong Malake, Laguna, 4031, Philippines.
alaysia Office: No 26, Jalan Pulau Indah, u10/53 Taman Sandaran Permai, Seksyen u10, Shah Alam 40170, Malaysia.
Phone No: +91-9826601628
E-mail Id: info@eurekajournals.com, editor@eurekajournals.com

Publisher Disclaimers

bility for the content/opinions provided in the articles published in the present book is the author(s) of the book is not

23. Role of Innovative Pedagogical Strategies in Education
Dr. Ritu Singh Mahiyaria 241-248

24. Status of Future Challenges of Higher Education in India
Dr. Arun Kumar Mishra, Dr. Santosh Narain Pandey 249-255

25. Student Centered Approaches: The Role and Significance in Today's Academic System
Prof. Iranna Ronad 256-262

26. The Role of Innovative Teaching Methods in Modern Education
Jige Sandipan Babasaheb 263-277

27. Unlocking Work-Life Balance: The POWER-C LIFESTYLE Framework for Teaching Professionals
Akhila Rao, Shailashri V. T. 278-304

28. Ushering Service Learning from the Syllabus to Classroom
Vidya Krishnamoorthy 305-313

29. Vedic to Modernistic-A Study on India and Strategic Way of Inclusive Education
Partha Sarathi Sarkar 314-322

30. समकक्ष आकलन (Peer Assessment)
Dr. Jyotika Kharbanda 323-330

About the Authors



Prof. Shurveer S. Bhanawat has been working as a Professor and Head, Department of Accountancy and Business Statistics, Mohanlal Sukhadia University, Udaipur. Sixty eight research articles have been published. He was awarded by ICAI international research award in 2021 and 2022.



Dr. Avinash Panwar is currently working as Associate Professor, Department of Comp. Sc., Course Director, Informatics and Computational Sciences Programme, Nodal Officer College of Engineering and Architecture & Director, Computer Center at Mohanlal Sukhadia University, Udaipur.



Dr. Shilpa Vardia has been working as an Assistant Professor in the Department of Accountancy and Business Statistics, Mohanlal Sukhadia University, Udaipur. She is the convener of the Master of Finance and Control and Post-Graduation Diploma in Taxation Programme. She has contributed thirty-four research papers and also received ICAI International Research award in 2020.



Dr. Shilpa Lodha is Assistant Professor at Department of Accountancy and Statistics, Mohanlal Sukhadia University, Udaipur (Raj). Her more than 25 research papers have been published in journals of national and international repute. She is Convener of B. Com. Honours.



Dr. Asha Sharma is Assistant Professor in the Department of Accountancy and Business Statistics at Mohanlal Sukhadia University, Udaipur. She is the convener of Bachelor of Vocation and Master of Vocation (Accounting, taxation, and auditing). She has contributed more than 85 research papers.



Dr. Parul Dashora is an Assistant Professor in Department of Accountancy and Business Statistics, Mohanlal Sukhadia University, Udaipur, [RAJ]. She is also Convener of Certification Programmes of the department. She also has two patents to her credit.



Pushpraj Meena is an Assistant Professor in Department of Accountancy and Business Statistics, University College of Commerce and Management Studies at Mohanlal Sukhadia University, Udaipur (Rajasthan). He has 6 years of experience in practical field of Accounting, Auditing and Taxation.

Published by
Weser Books, No. 79737
Äussere Weberstr. 57
02763 Zittau, Germany
Email: weserbooks@gmail.com

ISBN 9783964925503
9 783964 925503
Price - € 18

BLOCOUNTING

A Futuristic Approach

Prof. Shurveer S. Bhanawat

Dr. Avinash Panwar
Dr. Shilpa Vardia
Dr. Shilpa Lodha
Dr. Asha Sharma
Dr. Parul Dashora
Pushpraj Meena



Weser Books

About the Authors



Prof. Shurveer S. Bhanawat has been working as a Professor and Head, Department of Accountancy and Business Statistics, Mohanlal Sukhadia University, Udaipur. Sixty eight research articles have been published. He was awarded by ICAI international research award in 2021 and 2022.



Dr. Avinash Panwar is currently working as Associate Professor, Department of Comp. Sc., Course Director, Informatics and Computational Sciences Programme, Nodal Officer College of Engineering and Architecture & Director, Computer Center at Mohanlal Sukhadia University, Udaipur.



Dr. Shilpa Vardia has been working as an Assistant Professor in the Department of Accountancy and Business Statistics, Mohanlal Sukhadia University, Udaipur. She is the convener of the Master of Finance and Control and Post-Graduation Diploma in Taxation Programme. She has contributed thirty-four research papers and also received ICAI International Research award in 2020.



Dr. Shilpa Lodha is Assistant Professor at Department of Accountancy and Statistics, Mohanlal Sukhadia University, Udaipur (Raj). Her more than 25 research papers have been published in journals of national and international repute. She is Convener of B. Com. Honours.



Dr. Asha Sharma is Assistant Professor in the Department of Accountancy and Business Statistics at Mohanlal Sukhadia University, Udaipur. She is the convener of Bachelor of Vocation and Master of Vocation (Accounting, taxation, and auditing). She has contributed more than 85 research papers.



Dr. Parul Dashora is an Assistant Professor in Department of Accountancy and Business Statistics, Mohanlal Sukhadia University, Udaipur, [RAJ]. She is also Convener of Certification Programmes of the department. She also has two patents to her credit.



Pushpraj Meena is an Assistant Professor in Department of Accountancy and Business Statistics, University College of Commerce and Management Studies at Mohanlal Sukhadia University, Udaipur (Rajasthan). He has 6 years of experience in practical field of Accounting, Auditing and Taxation.

Published by
Weser Books, No. 79737
Äussere Weberstr. 57
02763 Zittau, Germany
Email: weserbooks@gmail.com

ISBN 9783964925503
9 783964 925503
Price - € 18

BLOCOUNTING

A Futuristic Approach

Prof. Shurveer S. Bhanawat

Dr. Avinash Panwar
Dr. Shilpa Vardia
Dr. Shilpa Lodha
Dr. Asha Sharma
Dr. Parul Dashora
Pushpraj Meena



Weser Books

About the Authors



Prof. Shurveer S. Bhanawat has been working as a Professor and Head, Department of Accountancy and Business Statistics, Mohanlal Sukhadia University, Udaipur. Sixty eight research articles have been published. He was awarded by ICAI international research award in 2021 and 2022.



Dr. Avinash Panwar is currently working as Associate Professor, Department of Comp. Sc., Course Director, Informatics and Computational Sciences Programme, Nodal Officer College of Engineering and Architecture & Director, Computer Center at Mohanlal Sukhadia University, Udaipur.



Dr. Shilpa Vardia has been working as an Assistant Professor in the Department of Accountancy and Business Statistics, Mohanlal Sukhadia University, Udaipur. She is the convener of the Master of Finance and Control and Post-Graduation Diploma in Taxation Programme. She has contributed thirty-four research papers and also received ICAI International Research award in 2020.



Dr. Shilpa Lodha is Assistant Professor at Department of Accountancy and Statistics, Mohanlal Sukhadia University, Udaipur (Raj). Her more than 25 research papers have been published in journals of national and international repute. She is Convener of B. Com. Honours.



Dr. Asha Sharma is Assistant Professor in the Department of Accountancy and Business Statistics at Mohanlal Sukhadia University, Udaipur. She is the convener of Bachelor of Vocation and Master of Vocation (Accounting, taxation, and auditing). She has contributed more than 85 research papers.



Dr. Parul Dashora is an Assistant Professor in Department of Accountancy and Business Statistics, Mohanlal Sukhadia University, Udaipur, [RAJ]. She is also Convener of Certification Programmes of the department. She also has two patents to her credit.



Pushpraj Meena is an Assistant Professor in Department of Accountancy and Business Statistics, University College of Commerce and Management Studies at Mohanlal Sukhadia University, Udaipur (Rajasthan). He has 6 years of experience in practical field of Accounting, Auditing and Taxation.

Published by
Weser Books, No. 79737
Äussere Weberstr. 57
02763 Zittau, Germany
Email: weserbooks@gmail.com

ISBN 9783964925503
9 783964 925503
Price - € 18

BLOCOUNTING

A Futuristic Approach

Prof. Shurveer S. Bhanawat

Dr. Avinash Panwar
Dr. Shilpa Vardia
Dr. Shilpa Lodha
Dr. Asha Sharma
Dr. Parul Dashora
Pushpraj Meena



Weser Books

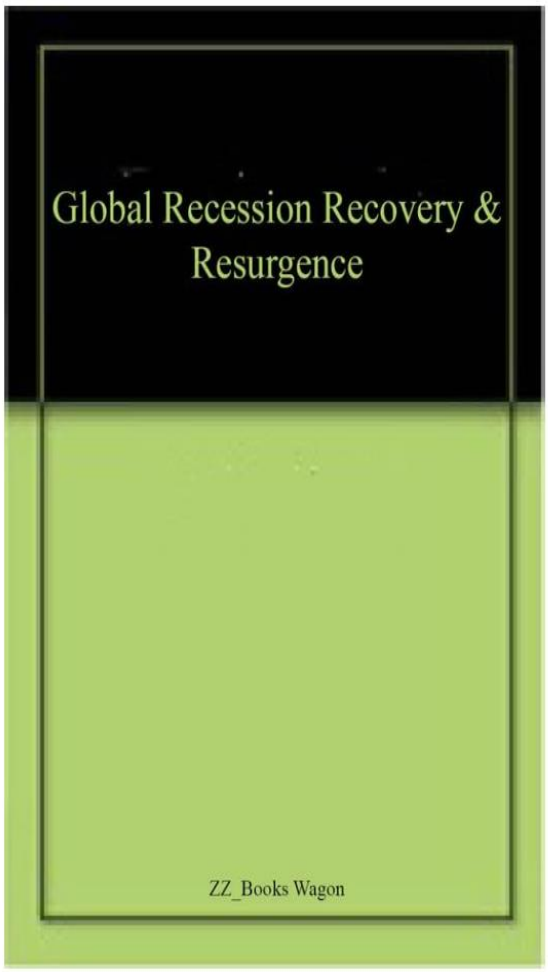

Global Recession Recovery and Resurgence: An Opportunities, Challengs a Strategic for Sustainable Growth in India

ISBN : 978-81-937067-2-5

GOVERNANCE REFORMS AND DEVELOPMENT IN INDIA



PROF. (DR.) S.S. MODI

INSPIRA (IRA)
JAIPUR - INDIA

GOVERNANCE REFORMS AND DEVELOPMENT IN INDIA
Prof. (Dr.) S.S. Modi



INSPIRA™

Reg. No. SH-481 R- 9-V P-76/2014

Printed in India by **Prof. (Dr.) S. S. Modi** at Aakrati Advertisers, Jaipur, Rajasthan and published by him on behalf of the Inspira Research Association, Jaipur, Rajasthan

Website : inspirajournals.com

₹ 600.00

ISBN : 978-81-937067-2-5



GOVERNANCE REFORMS
AND
DEVELOPMENT IN INDIA

Edited by:
Professor (Dr.) S.S. Modi
Former Head
Department of Accountancy and Business Statistics
Faculty of Commerce,
PG School of Commerce
University of Rajasthan, Jaipur-302004 Rajasthan (India)
25, Modi Sadan, Sudama Nagar, Opp. Glass Factory,
Tonk Road, Jaipur-302018 Rajasthan
Email ID: chiefeditorija@gmail.com, profdrssmodi@gmail.com
Mobile No. +91-98293 21067

INSPIRA®
Reg. No. SH-481 R- 9-V P-76/2014
JAIPUR - 302018 (INDIA)

Published by
INSPIRA
25, Modi Sadan
Sudama Nagar
Tonk Road
Jaipur-302018
Rajasthan, India

© Editor

ISBN: 978-81-937067-2-5

First Edition: June, 2018

All rights reserved. No part of this book may be reproduced in any form without the prior permission in writing from the Publisher.

Price: Rs. 600/-

Laser Type Setting by
INSPIRA
Tonk Road, Jaipur
Ph.: 0141-2710264

Printed at
Akrati Advertisers, Jaipur

CONTENTS

Chapter	Name of Chapter	Page No.
1	The Study of Micro Finance Related to Government Initiative Mission Mangalam ***Pratik Paun & Prof. (Dr.) Pratapsingh Chauhan***	01-07
2	Factors Affecting the Quality of Work Life of Women Employees: A Study of Small and Medium Enterprises (SMEs) in IT Sector in Rajasthan ***Aparna Soni & Dr. Meera Mathur***	08-20
3	Business Value Development: A Strategic Approach for Business Management ***Rajendra Deshpande***	21-28
4	Corporate Social Responsibility and Consumer Behaviour ***Dr. (Mrs.) Asha Sharma***	29-34
5	Women Empowerment in India: Challenges and Issues ***Dr. Mahesh Singh Rajput***	35-40
6	Hedge Ratio and Hedging Effectiveness Estimates for Stock Futures on NSE India ***Kerkar Puja Paresh & Dr. P. Sriram***	41-48
7	Oil Sector: Current Perspective of India ***CS Pradyumna Sharma & Dr. D.C. Jain***	49-57
8	Devising Suitable Models for Inclusive Finance ***Dr. Nitin Raj***	58-68
9	Issues and Challenges on Infrastructure Sector with Overview on Indian Economy ***Dr. Rohitash Lal Bairwa***	69-74
10	GST: Issues and Impact on Indian Banking Sector ***Dr. Naresh Kumar & Mamta Bhushan***	75-82
11	Bridging the Gender Gap: Empowering Women through Financial Inclusion ***Dr. Shaifali Mathur***	83-96
12	Role of Women Entrepreneurs in Make in India Campaign ***Miss Monika Talreja & Dr. Anurodh Godha***	97-102
13	Karz Mafi (Loan Waivers): Is it the Right Solution to the Woes of Indian Farmers? ***Ms. Pooja Pareek & Dr. R.K. Sharma***	103-106

14	Role of Tourism & Hotel Industry in Development of Jodhpur City (Rajasthan): An Overview ***Dr. Ashok Kumar & Nisha Sankhla***	107-115
15	A Study on Rural Development ***Dr. J. Venugopal***	116-120
16	Aim of Economic Growth and Its Analogous Share in National Economy: With Special Reference to Rajasthan ***Rita Soni***	121-124
17	Fair Value Measurement Concept of IFRS: Problems and Prospects in Corporate Reporting in India ***Manisha***	125-136
18	Role of Literature in Advancing Women's Economic Empowerment ***Dr. Ruchi Goyal***	137-142
19	Merger and Acquisition of Selected Indian Company ***Prof. (Dr). Mahendra H. Maisuria***	143-148
20	Impact of GST on Economy and Marketers in India ***Ms. Chandni Seth***	149-154
21	An Evaluative Study of Microfinance and Women Empowerment in Rajasthan ***Ekta & Salim Khan***	155-160
22	Empowerment of Women: Strategies and Governmental Efforts ***Dr. Piali Biswas***	161-166
23	Government Reforms for Developing Women Entrepreneurs ***Dr. Neha Khatri***	167-182
24	Analysis of Oilseed Crops Scenario in Rajasthan ***Sunil Kumar & Anuj Kumar***	183-191
25	The Amendment in GST: An Attempt to Give Relief to Ordinary Consumer ***Kavita Bharti***	192-198
26	Impact of Demonetization on Society and Economy ***Sunita Sharma*** & ***Prof. D.S. Rathore***	199-201
27	CSR and Sustainable Business Strategies: Global Growth Phenomenon in View of Environmental Concerns ***Dr. Kamlesh Pritwani***	202-206

♦❐♦

Advances in Commerce and Management

Advances in Commerce and Management

Editors:
Dr. Shalendra Singh Rao
Dr. Manish Dadhich
Dr. Renu Sharma

DISHA INTERNATIONAL PUBLISHING HOUSE
Greater Noida

Published by
DISHA INTERNATIONAL PUBLISHING HOUSE
Plot No.: 31 S, Bhunna Taga, P.S. Rabupura,
Greater Noida-203209
Mob. : 7080806934, 9760316934
E-mail : diph.india@gmail.com
Website : www.dishainternationalpublishing.com

Also Available at:

amazon.in
For Amazon Scan QR Code

snapdeal.com
For Snapdeal Scan QR Code

© Editors
Advances in Commerce and Management
Publishing Year: 2021
ISBN:978-93-91251-01-7

All rights are reserved with the editors and publisher, including the right to translate or reproduce this book or parts thereof except for brief quotations in critical or reviews. Editors are responsible for all the materials.

Printed by Disha International Publishing House

Contents

1.	Investment perspective of investors in share market-Case study of working women in Udaipur city	
	Prof. P.K.Singh	1
2	Election Tourism in India: A Niche Market to Encash India's Biggest Festival of Worlds Largest Democracy	
	Priyanka Payal	
	Dr. Rajeev K. Saxeena	15
3.	Measuring Effectiveness of Supply Chain Management and Its Impact on Financial Performance	
	Dr. Asha Sharma	25
4.	Impact of Expert System's on Audit Efficiency	
	Pushpraj Meena	
	Dr. Vinod Kumar Meena	38
5.	Implementation of CSR Practices and Challenges in its Development	
	Dr. Raja Bhoj Sharma	
	Nikhar Goyal	51
6.	Artificial Intelligence and Blockchain Technology: A Disruptive integration for Accounting and Auditing Profession	
	Gourav Surana	
	Shurveer S. Bhanawat	60
7.	Carbon Accounting Practices in Select European Companies	
	Neelam Yadav	
	Durga Singh Gour	
	Shurveer S. Bhanawat	68

8. Implementation of IFRS in India as IND AS and Significant Carve-outs
Nikhar Goyal
Dr. Raja Bhoj Sharma 87
9. Revealed Accounting Treatment under Cloud Computing Arrangement
Neelam Yadav
Mukesh Kumar
Shurveer S. Bhanawat 96
10. A Critical Study on Indian Banking System towards Digital Finance and Development of Business in India
Dr. Lokesh Mali 106
11. Challenges and Issues on Implementation and Value Relevance of IFRC (with special reference to Indian Accounting System)
Vikram Singh 112
12. Role of Artificial Intelligence for Agriculture Development: An Emerging Era of Research
Dr. Rakesh Birda 119
13. Study of Factors Influencing Consumer's Online Shopping Behavior with Special Reference to Organized Retail Market
Dr. Abhineet Saxena
Dr. Ashish Sharma 128
14. Readiness Indices for Adoption for Industry 4.0
Dr. Narendra Goyal 147
15. Digital Transformation and User's Awareness & Attitudes towards Artificial Intelligence Technology in the Banking Industry
Dr. Renu Sharma
Neha Khandelwal 155
16. Comprehensive Analysis of E-Commerce in India
Dr. Rajesh Meena
Dr. Manish Dadhich 170
17. Prospect of Micro Finance in Entrepreneurship Development in Zambia
Robert Mwiinga
Dr. Manish Dadhich 181

18. Marketing of Information Products and Services in the Electronic Era
Dr. Surendra Sethy 194
19. Challenges and Issues on Implementation and Value Relevance of IFRC With Special Reference to Indian Accounting System
Dr. Y. R. Goswami 204

ScienceDirect



Plant-Microbe Interaction - Recent Advances in Molecular and Biochemical Approaches

Volume 2 : Agricultural Aspects of Microbiome Leading to Plant Defence

Book • 2023

Edited by:
Prashant Swapnil, Mukesh Meena, ... Andleeb Zehra

Browse book content

About the book

Search in this book

Search in this book

Table of contents

Full text access

Front Matter, Copyright, Contributors, About the editors, Preface, Acknowledgments

Book chapter ○ Abstract only

Chapter 1 - Pathogen effectors: Biochemical and structural targets during plant-microbe interactions

Steffi Pulikondan Francis, L. Rene Christena and P.F. Mishel
Pages 1-19

Purchase View abstract

Book chapter ○ Abstract only

Chapter 2 - PGPMs-mediated improvement of crops under abiotic stress

Pankaj Kumar, Rima Kumari, ... Arun Kumar
Pages 21-31

Purchase View abstract

Book chapter ○ Abstract only

FEEDBACK

Chapter 3 - Endurance of microbes against nitrogen starvation by altering the biochemical and physiological activities of plants

Reshma Devi Ramesh, Kalaiselvi Selvaraj, ... Vijayalakshmi Selvakumar

Pages 33-63

Purchase View abstract

Book chapter ○ Abstract only

Chapter 4 - Destructive role of chemicals secreted by plants to diminish harmful microbes

Subhesh Saurabh Jha and L.S. Songachan

Pages 65-77

Purchase View abstract

Book chapter ○ Abstract only

Chapter 5 - Biodegradation and bioaugmentation of pesticides using potential fungal species

S. Gomathi, V. Ambikapathy and A. Panneerselvam

Pages 79-94

Purchase View abstract

Book chapter ○ Abstract only

Chapter 6 - Agricultural management by improving beneficial microflora

Shalini Tailor, Khushboo Jain, ... Anita Mishra

Pages 95-116

Purchase View abstract

Book chapter ○ Abstract only

Chapter 7 - Ameliorative characteristics of plant growth-enhancing microbes to revamp plant growth in an intricate environment

T. Savitha and A. Sankaranarayanan

Pages 117-135

Purchase View abstract

Book chapter ○ Abstract only

Chapter 8 - Immune signaling networks in plant-pathogen interactions

Andleeb Zehra, Mukesh Meena and Prashant Swapnil

Pages 137-147

Purchase View abstract

Book chapter ○ Abstract only

Chapter 9 - Quorum quenching strategies of endophytic bacteria: Role in plant protection

Etisha Paul, Parikshana Mathur, ... Payal Chaturvedi

Pages 149-166

Purchase View abstract

Book chapter ○ Abstract only

Chapter 10 - Peeking into plant-microbe interactions during plant defense

Shriniketan Puranik, Vindhya Bundela, ... Sandeep Kumar Singh
Pages 167-200

Purchase View abstract

Book chapter ○ Abstract only

Chapter 11 - Understanding plant-plant growth-promoting rhizobacteria (PGPR) interactions for inducing plant defense

Kunal Seth, Pallavi Vyas, ... Harish
Pages 201-226

Purchase View abstract

Book chapter ○ Abstract only

Chapter 12 - Revitalization of PGPR through integrating nanotechnology for sustainable development in agriculture

Gunja Vasant, Shweta Bhatt, ... Preetam Joshi
Pages 227-248

Purchase View abstract

Book chapter ○ Abstract only

Chapter 13 - Potential scope and prospects of plant growth-promoting microbes (PGPMs) in micropropagation technology

Sagar Teraiya, Dhaval Nirmal and Preetam Joshi
Pages 249-277

Purchase View abstract

Book chapter ○ Abstract only

Chapter 14 - Advantageous features of plant growth-promoting microorganisms to improve plant growth in difficult conditions

Mukesh Meena, Garima Yadav, ... Andleeb Zehra
Pages 279-296

Purchase View abstract

Book chapter ○ Abstract only

Chapter 15 - Plant-microbe interactions to reduce salinity stress in plants for the improvement of the agricultural system

Yashika Maheshwari, Shalini Tailor, ... Anita Mishra
Pages 297-309

Purchase View abstract

Book chapter ○ Abstract only

Chapter 16 - Metabolomic studies of medicinal plant-fungi interaction

Mahinder Partap, Abhishek Kumar, ... Ashish R. Warghat
Pages 311-330

Purchase View abstract

Book chapter ○ Abstract only

Chapter 17 - Sustainable agricultural approach to study interaction of plants and microbes

Parul Tyagi, Ayushi Singh, ... Rajiv Ranjan

Pages 331-361

Purchase View abstract

Book chapter ○ Abstract only

Chapter 18 - Plant-microbe interactions: Role in sustainable agriculture and food security in a changing climate

Diksha Tokas, Siril Singh, ... Anand Narain Singh

Pages 363-391

Purchase View abstract

Book chapter ○ Abstract only

Chapter 19 - Microbial interventions for improving agricultural performance under salt stress

Anisha Shashidharan and Lhea Blue

Pages 393-406

Purchase View abstract

Book chapter ○ Full text access

Index

Pages 407-421

Download PDF

About the book

Description

Plant-Microbe Interaction - Recent Advances in Molecular and Biochemical Approaches: Agricultural Aspects of Microbiome Leading to Plant Defence, Volume Two continues the work of Volume One, covering the role of these plant microbes and their interaction between plants and microbes. These beneficial microbes, such as bacteria and fungi are also known as plant growth-promoting

Show more

Key Features

- Covers agricultural aspects in which the biochemistry in between plants and microbes helps us understand interactions in the rhizosphere
- Helps readers understand the molecular and biochemical approaches of plant-microbe interactions

Show more

Details

ISBN

978-0-323-91876-3

Language

English

Published

2023

Copyright

Copyright © 2023 Elsevier Inc. All rights reserved.

Imprint

Academic Press

DOI

https://doi.org/10.1016/C2021-0-00317-5

Purchase book

Editors

Prashant Swapnil

Department of Botany, School of Basic Sciences, Central University of Punjab, Bhatinda, Punjab, India

Department of Botany, Acharya Narendra Dev College, Delhi University, New Delhi, India

Mukesh Meena

Department of Botany, Mohanlal Sukhadia University, Udaipur, Rajasthan, India

Harish

Department of Botany, Mohanlal Sukhadia University, Udaipur, Rajasthan, India

Avinash Marwal

Department of Biotechnology, Vigyan Bhawan - Block B, New Campus, University College of Science, Mohanlal Sukhadia University, Udaipur, Rajasthan, India

Selvakumar Vijayalakshmi

School of Food Science and Biotechnology, Kyungpook National University, Daegu, Republic of Korea

Andleeb Zehra

Department of Botany, Institute of Science, Banaras Hindu University, Varanasi, Uttar Pradesh, India

Related publications

Why related?

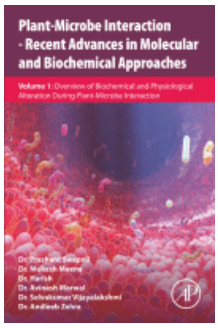

Book

Plant-Microbe Interaction - Recent Advances in Molecular and Biochemical Approaches

Editors-in-Chief: Prashant Swapnil, Mukesh Meena, ... Andleeb Zehra

2023



Book

Sustainable Agriculture and the Environment

Editors-in-Chief: Muhammad Farooq, Nirmali Gogoi and Michele Pisante

2023

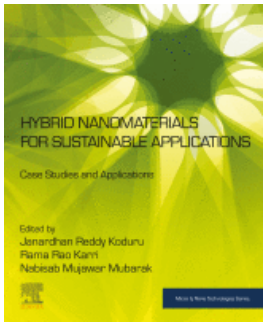

Book

Hybrid Nanomaterials for Sustainable Applications

Editors-in-Chief: Janardhan Reddy Koduru, Rama Rao Karri and Nabisab Mujawar Mubarak

A volume in Micro and Nano Technologies • 2023

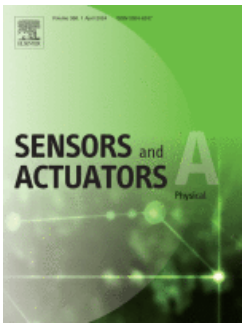

Journal

Sensors and Actuators A: Physical

ELSEVIER

All content on this site: Copyright © 2024 Elsevier B.V., its licensors, and contributors. All rights are reserved, including those for text and data mining, AI training, and similar technologies. For all open access content, the Creative Commons licensing terms apply.

RELX™

ScienceDirect



Plant-Microbe Interaction - Recent Advances in Molecular and Biochemical Approaches

Volume 1 : Overview of Biochemical and Physiological Alteration During Plant-Microbe Interaction

Book • 2023

Edited by:
Prashant Swapnil, Mukesh Meena, ... Andleeb Zehra

Browse book content

About the book

Search in this book

Search in this book

Table of contents

Full text access

Front Matter, Copyright, Contributors, About the editors, Preface, Acknowledgments

Book chapter ○ Abstract only

Chapter 1 - Plant growth-promoting microbiomes: History and their role in agricultural crop improvement

Vijay Vardhan Pandey, Arpita Bhattacharya and Amit Pandey
Pages 1-44

Purchase View abstract

Book chapter ○ Abstract only

Chapter 2 - Role of plant growth-promoting microorganisms in phytoremediation efficiency

M. Veerapagu, K.R. Jeya and A. Sankaranarayanan
Pages 45-61

Purchase View abstract

Book chapter ○ Abstract only

FEEDBACK

Chapter 3 - Physiological and biochemical studies of plant-pathogen interactions

Sana Sheikh, M. Vaishali Rai and Sareen Sheikh

Pages 63-72

Purchase View abstract

Book chapter ○ Abstract only

Chapter 4 - Biochemical process associated with plants and beneficial microbes

K.E. Poorni, Mehwish Roy, ... T.S. Gnanendra

Pages 73-85

Purchase View abstract

Book chapter ○ Abstract only

Chapter 5 - An introduction to current and future aspect on growth promoting microbiome

Sugandha Mishra, Asha Sharma, ... Dhirendra Kumar

Pages 87-110

Purchase View abstract

Book chapter ○ Abstract only

Chapter 6 - Advances in plant-pathogen interactions in terms of biochemical and molecular aspects

Rima Kumari, Arun Kumar, ... Dan Singh Jakhar

Pages 111-122

Purchase View abstract

Book chapter ○ Abstract only

Chapter 7 - Relevance of the antioxidative mechanism during plant-microbe interaction

Priyanka Choudhary and Priti Upadhyay

Pages 123-140

Purchase View abstract

Book chapter ○ Abstract only

Chapter 8 - Chemical communication between plant roots and microbes within the rhizosphere

Thenmozhi Manivel, T. Sandhiya, ... Rex Jeya Rajkumar Sandavid Thanapaul

Pages 141-164

Purchase View abstract

Book chapter ○ Abstract only

Chapter 9 - Chemical talk within plant holobiont: A fascinating conversation

Sandeep Kumar Singh, G.S. Srikanth, ... Livleen Shukla

Pages 165-203

Purchase View abstract

Book chapter ○ Abstract only

Chapter 10 - Advanced study of plant-microbe interactions in photosynthesis

T. Karpagam, A. Shanmugapriya, ... Jannathul Firdous

Pages 205-228

Purchase View abstract

Book chapter ○ Abstract only

Chapter 11 - PGPR-mediated synthesis and alteration of different secondary metabolites during plant-microbe interactions

Mukesh Meena, Tushar Mehta, ... Priyankaraj Sonigra

Pages 229-255

Purchase View abstract

Book chapter ○ Abstract only

Chapter 12 - Mycotoxins produced in plant-pathogen interactions

Yesmin Kaur and Rajnish Kumar Verma

Pages 257-279

Purchase View abstract

Book chapter ○ Abstract only

Chapter 13 - Improvement of soil fertility through plant microbial interaction

G. Gayathri, S. Gomathi, ... A. Panneerselvam

Pages 281-301

Purchase View abstract

Book chapter ○ Abstract only

Chapter 14 - Manipulation of cell wall components and enzymes on plant-microbe interactions

B. Varalakshmi, V. Suganya, ... M. Abinaya

Pages 303-326

Purchase View abstract

Book chapter ○ Abstract only

Chapter 15 - Acinetobacter: A versatile plant growth-promoting rhizobacteria (PGPR)

Shilpa Mujumdar, Jayshree Bhoyar, ... Smita Bhuyan

Pages 327-362

Purchase View abstract

Book chapter ○ Abstract only

Chapter 16 - *Exserohilum turcicum* [Pass.] resistance in maize: A sustainable agricultural approach for studying plant-microbe interactions

Dan Singh Jakhar, Rima Kumari, ... Arun Kumar

Pages 363-373

Purchase View abstract

Book chapter ○ Abstract only

Chapter 17 - Mechanistic basis of the symbiotic signaling pathway between the host and the pathogen

Mukesh Meena, Adhishree Nagda, ... Priyankaraj Sonigra

Pages 375-387

Purchase View abstract

Book chapter ○ Abstract only

Chapter 18 - Diversity of methylobacterium species in the plant phytosphere and their different strategies to mitigate biotic and abiotic stress responses

Ramswaroop Saini and Sourabh Karwa

Pages 389-410

Purchase View abstract

Book chapter ○ Abstract only

Chapter 19 - Calcium/calmodulin-mediated signaling mechanism of symbiotic relationship between plants and microbes

Pankaj Kumar, Rima Kumari, ... Arun Kumar

Pages 411-419

Purchase View abstract

Book chapter ○ Abstract only

Chapter 20 - Plant-microbe interactions in photosynthesis, nutrient acquisition, and plant growth

Anita Mishra and Shalini Tailor

Pages 421-434

Purchase View abstract

Book chapter ○ Abstract only

Chapter 21 - Beneficial metabolite production, a comparative account of medicinal plants and fungal interaction

N.M. Sudheep and N.K. Shahina

Pages 435-442

Purchase View abstract

Book chapter ○ Full text access

Index

Pages 443-455

Download PDF

About the book

Description

Plant-Microbe Interaction - Recent Advances in Molecular and Biochemical Approaches: Overview of Biochemical and Physiological Alteration During Plant-Microbe Interaction, Volume One covers the role of these plant microbes and their interaction between plants and microbes. These beneficial microbes, such as bacteria and fungi are also known as plant growth-promoting

Show more

Key Features

- Covers agricultural aspects in which the biochemistry in between plants and microbes helps us understand interactions in the rhizosphere
- Helps readers understand the molecular and biochemical approaches of plant-microbe interactions

Show more

Details

ISBN

978-0-323-91875-6

Language

English

Published

2023

Copyright

Copyright © 2023 Elsevier Inc. All rights reserved.

Imprint

Academic Press

DOI

https://doi.org/10.1016/C2021-0-00316-3

Purchase book

Editors

Prashant Swapnil

Department of Botany, School of Basic Sciences, Central University of Punjab, Bhatinda, Punjab, India

Department of Botany, Acharya Narendra Dev College, Delhi University, New Delhi, India

Mukesh Meena

Department of Botany, Mohanlal Sukhadia University, Udaipur, Rajasthan, India

Harish

Department of Botany, Mohanlal Sukhadia University, Udaipur, Rajasthan, India

Avinash Marwal

Department of Biotechnology, Vigyan Bhawan - Block B, New Campus, University College of Science, Mohanlal Sukhadia University, Udaipur, Rajasthan, India

Selvakumar Vijayalakshmi

School of Food Science and Biotechnology, Kyungpook National University, Daegu, Republic of Korea

Andleeb Zehra

Department of Botany, Institute of Science, Banaras Hindu University, Varanasi, Uttar Pradesh, India

Related publications

Why related?



Journal

Pesticide Biochemistry and Physiology

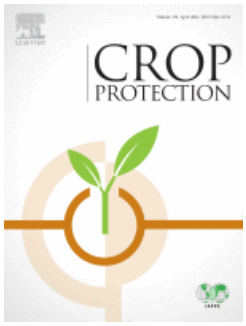

Journal

Crop Protection



Journal

Heliyon

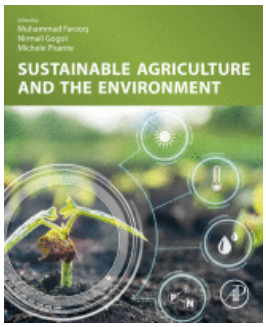

Book

Sustainable Agriculture and the Environment

Editors-in-Chief: Muhammad Farooq, Nirmali Gogoi and Michele Pisante

2023

ELSEVIER

All content on this site: Copyright © 2024 Elsevier B.V., its licensors, and contributors. All rights are reserved, including those for text and data mining, AI training, and similar technologies. For all open access content, the Creative Commons licensing terms apply.

RELX™

ScienceDirect



Plant-Microbe Interaction - Recent Advances in Molecular and Biochemical Approaches

Volume 2 : Agricultural Aspects of Microbiome Leading to Plant Defence

Book • 2023

Edited by:
Prashant Swapnil, Mukesh Meena, ... Andleeb Zehra

Browse book content

About the book

Search in this book

Search in this book

Table of contents

Full text access

Front Matter, Copyright, Contributors, About the editors, Preface, Acknowledgments

Book chapter ○ Abstract only

Chapter 1 - Pathogen effectors: Biochemical and structural targets during plant-microbe interactions

Steffi Pulikondan Francis, L. Rene Christena and P.F. Mishel
Pages 1-19

Purchase View abstract

Book chapter ○ Abstract only

Chapter 2 - PGPMs-mediated improvement of crops under abiotic stress

Pankaj Kumar, Rima Kumari, ... Arun Kumar
Pages 21-31

Purchase View abstract

Book chapter ○ Abstract only

FEEDBACK

Chapter 3 - Endurance of microbes against nitrogen starvation by altering the biochemical and physiological activities of plants

Reshma Devi Ramesh, Kalaiselvi Selvaraj, ... Vijayalakshmi Selvakumar

Pages 33-63

Purchase View abstract

Book chapter ○ Abstract only

Chapter 4 - Destructive role of chemicals secreted by plants to diminish harmful microbes

Subhesh Saurabh Jha and L.S. Songachan

Pages 65-77

Purchase View abstract

Book chapter ○ Abstract only

Chapter 5 - Biodegradation and bioaugmentation of pesticides using potential fungal species

S. Gomathi, V. Ambikapathy and A. Panneerselvam

Pages 79-94

Purchase View abstract

Book chapter ○ Abstract only

Chapter 6 - Agricultural management by improving beneficial microflora

Shalini Tailor, Khushboo Jain, ... Anita Mishra

Pages 95-116

Purchase View abstract

Book chapter ○ Abstract only

Chapter 7 - Ameliorative characteristics of plant growth-enhancing microbes to revamp plant growth in an intricate environment

T. Savitha and A. Sankaranarayanan

Pages 117-135

Purchase View abstract

Book chapter ○ Abstract only

Chapter 8 - Immune signaling networks in plant-pathogen interactions

Andleeb Zehra, Mukesh Meena and Prashant Swapnil

Pages 137-147

Purchase View abstract

Book chapter ○ Abstract only

Chapter 9 - Quorum quenching strategies of endophytic bacteria: Role in plant protection

Etisha Paul, Parikshana Mathur, ... Payal Chaturvedi

Pages 149-166

Purchase View abstract

Book chapter ○ Abstract only

Chapter 10 - Peeking into plant-microbe interactions during plant defense

Shriniketan Puranik, Vindhya Bundela, ... Sandeep Kumar Singh
Pages 167-200

Purchase View abstract

Book chapter ○ Abstract only

Chapter 11 - Understanding plant-plant growth-promoting rhizobacteria (PGPR) interactions for inducing plant defense

Kunal Seth, Pallavi Vyas, ... Harish
Pages 201-226

Purchase View abstract

Book chapter ○ Abstract only

Chapter 12 - Revitalization of PGPR through integrating nanotechnology for sustainable development in agriculture

Gunja Vasant, Shweta Bhatt, ... Preetam Joshi
Pages 227-248

Purchase View abstract

Book chapter ○ Abstract only

Chapter 13 - Potential scope and prospects of plant growth-promoting microbes (PGPMs) in micropropagation technology

Sagar Teraiya, Dhaval Nirmal and Preetam Joshi
Pages 249-277

Purchase View abstract

Book chapter ○ Abstract only

Chapter 14 - Advantageous features of plant growth-promoting microorganisms to improve plant growth in difficult conditions

Mukesh Meena, Garima Yadav, ... Andleeb Zehra
Pages 279-296

Purchase View abstract

Book chapter ○ Abstract only

Chapter 15 - Plant-microbe interactions to reduce salinity stress in plants for the improvement of the agricultural system

Yashika Maheshwari, Shalini Tailor, ... Anita Mishra
Pages 297-309

Purchase View abstract

Book chapter ○ Abstract only

Chapter 16 - Metabolomic studies of medicinal plant-fungi interaction

Mahinder Partap, Abhishek Kumar, ... Ashish R. Warghat
Pages 311-330

Purchase View abstract

Book chapter ○ Abstract only

Chapter 17 - Sustainable agricultural approach to study interaction of plants and microbes

Parul Tyagi, Ayushi Singh, ... Rajiv Ranjan

Pages 331-361

Purchase View abstract

Book chapter ○ Abstract only

Chapter 18 - Plant-microbe interactions: Role in sustainable agriculture and food security in a changing climate

Diksha Tokas, Siril Singh, ... Anand Narain Singh

Pages 363-391

Purchase View abstract

Book chapter ○ Abstract only

Chapter 19 - Microbial interventions for improving agricultural performance under salt stress

Anisha Shashidharan and Lhea Blue

Pages 393-406

Purchase View abstract

Book chapter ○ Full text access

Index

Pages 407-421

Download PDF

About the book

Description

Plant-Microbe Interaction - Recent Advances in Molecular and Biochemical Approaches: Agricultural Aspects of Microbiome Leading to Plant Defence, Volume Two continues the work of Volume One, covering the role of these plant microbes and their interaction between plants and microbes. These beneficial microbes, such as bacteria and fungi are also known as plant growth-promoting

Show more

Key Features

- Covers agricultural aspects in which the biochemistry in between plants and microbes helps us understand interactions in the rhizosphere
- Helps readers understand the molecular and biochemical approaches of plant-microbe interactions

Show more

Details

ISBN

978-0-323-91876-3

Language

English

Published

2023

Copyright

Copyright © 2023 Elsevier Inc. All rights reserved.

Imprint

Academic Press

DOI

https://doi.org/10.1016/C2021-0-00317-5

Purchase book

Editors

Prashant Swapnil

Department of Botany, School of Basic Sciences, Central University of Punjab, Bhatinda, Punjab, India

Department of Botany, Acharya Narendra Dev College, Delhi University, New Delhi, India

Mukesh Meena

Department of Botany, Mohanlal Sukhadia University, Udaipur, Rajasthan, India

Harish

Department of Botany, Mohanlal Sukhadia University, Udaipur, Rajasthan, India

Avinash Marwal

Department of Biotechnology, Vigyan Bhawan - Block B, New Campus, University College of Science, Mohanlal Sukhadia University, Udaipur, Rajasthan, India

Selvakumar Vijayalakshmi

School of Food Science and Biotechnology, Kyungpook National University, Daegu, Republic of Korea

Andleeb Zehra

Department of Botany, Institute of Science, Banaras Hindu University, Varanasi, Uttar Pradesh, India

Related publications

Why related?

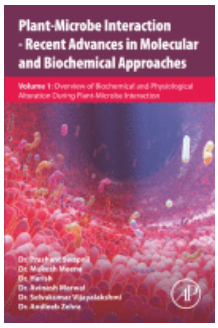

Book

Plant-Microbe Interaction - Recent Advances in Molecular and Biochemical Approaches

Editors-in-Chief: Prashant Swapnil, Mukesh Meena, ... Andleeb Zehra

2023



Book

Sustainable Agriculture and the Environment

Editors-in-Chief: Muhammad Farooq, Nirmali Gogoi and Michele Pisante

2023

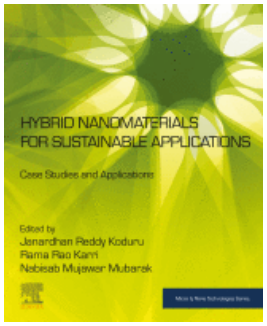

Book

Hybrid Nanomaterials for Sustainable Applications

Editors-in-Chief: Janardhan Reddy Koduru, Rama Rao Karri and Nabisab Mujawar Mubarak

A volume in Micro and Nano Technologies • 2023

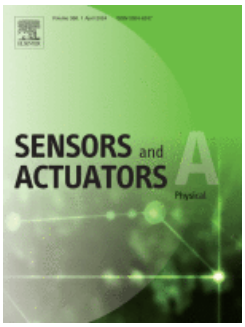

Journal

Sensors and Actuators A: Physical

ELSEVIER

All content on this site: Copyright © 2024 Elsevier B.V., its licensors, and contributors. All rights are reserved, including those for text and data mining, AI training, and similar technologies. For all open access content, the Creative Commons licensing terms apply.

RELX™

CONTEMPORARY ISSUES IN ACCOUNTING

(Including Blockchain Technology)

Editors

Shurveer S. Bhanawat, Ph.D.

Professor and Head, Department of Accountancy & Business Statistics,
Mohanlal Sukhadia University, Udaipur, Rajasthan

Shilpa Vardia

Assistant Professor,
Department of Accountancy and Business Statistics,
Mohanlal Sukhadia University,
Udaipur, Rajasthan

Shilpa Lodha

Assistant Professor,
Department of Accountancy and Business Statistics,
Mohanlal Sukhadia University,
Udaipur, Rajasthan

Bharti Publications

New Delhi- 110002 (INDIA)

Copyright © 2023, Editors

Title: Contemporary Issues in Accounting (Including Blockchain Technology)

Editors: Prof. Shurveer S Bhanawat, Dr. Shilpa Vardia and Dr. Shilpa Lodha

All rights reserved. No part of this publication may be reproduced or transmitted, in any from or by any means, without permission. Any person who does any unauthorised act in relation to this publication may be liable to criminal prosecution and civil claims for damages.

First Published, February 2023

ISBN: 978-81-19079-03-2

Published by :

Bharti Publications

4819/24, 2nd Floor, Mathur Lane

Ansari Road, Darya Ganj, New Delhi-110002

Phone: 011-46172797, 011-23247537, 9899897381

E-mail : bhartipublications@gmail.com

Website : www.bhartipublications.com

Printed in India, by Sagar Color Scan, Delhi

Disclaimer: The views expressed in the book are of the contributing authors and not necessarily of the Publisher and Editors. Authors are themselves responsible for any kind of plagiarism found in their paper or chapter and any related issues in book.

CONTENTS

Preface *iii-vi*

List of Contributors *ix-x*

1. Carbon Disclosure Ratings and Market Performance: Evidence from Carbon Disclosure Project (CDP)India **1-7**
Leo Themjung Makan and K. C. Kabra

2. Working Capital Prediction Model for Indian Corporate Sector **8-14**
Ritika Chittora and Shurveer S Bhanawat

3. Integrated Reporting Practices in South Africa **15-34**
Shiv Lal Parmar and Shilpa Vardia

4. Herd Behaviour: A Psychological bias of Behavioural Finance Theory **35-48**
Shilpa Lodha and Charu Sharma

5. Impact of Covid-19 on Goods and Services Tax Revenue Collection in India **49-57**
Ram Prasad Suthar and Parul Dashora

6. Crowdfunding: A Conceptual Understanding **58-68**
Shilpa Lodha and Babu Lal Gedar

7. Impact of XBRL Reporting System on the Reliability of Financial Reporting in India **69-80**
Apporva Mamodiya and Shilpa Lodha

8. Financial Analysis of Online Fantasy Sports Platform: A Case Study on Dream 11 **81-86**
Ashok Kumar Sharma and Shurveer S. Bhanawat

9. A Comparative Analysis of Composition Levy Scheme and Normal Tax Regime for Traders in GST **87-92**
Hemant Kaduniya and Palash Birla

10. A Financial analysis of two big FMCG companies of India: Proctor and Gamble & Nestle India **93-99**
Hemant Kaduniya and Ashok Singh Rana

11. A Study of Application of Blockchain Technology in India **100-110**
Geetanjali Sharma and Asha Sharma

12. Applications of Blockchain Technology in Various Fields **111-121**
Samta Ordia and Shurveer S. Bhanawat

13. Blockchain: A Revolutionary Technology Changing Life **122-133**
Ashok Kumar Gupta, Meenu Maheshwari and Ashish Chittora

14. Triple Entry Accounting (TEA) System & Blockchain Technology: A Theoretical Working Model **134-144**
Pushpraj Meena

4

Herd Behaviour: A Psychological Bias of Behavioural Finance Theory

Dr. Shilpa Lodha[1] | Charu Sharma[2]

ABSTRACT:

This paper provides a detailed description of the herd behaviour, one of the emotional biases of behavioural finance theory. Due to the challenges and contradictions faced by efficient market hypothesis, behavioural finance has become a very important research field. Various authors have contributed in the field of behaviour finance theory so the present study is focused on the concept of herd behaviour, its evolution, causes, types and relevance of further research in the field of herd behaviour. The paper has concluded that herd behaviour could be of great relevance in the stock market as the same has been observed as most common psychological bias among all other anomalies.

Keywords: *Behavioural Finance, Herd Behaviour, Emotional Bias*

I.INTRODUCTION

Investment decisions are vital for the success and survival of an investor. When an individual decides and invests his sum of money, he becomes investor. Individual investors accumulate their savings and convert them into investments. Institutional investors try to earn maximum returns by investing their idle funds. Investment helps in protecting the value of money which an individual possesses as the value of money decreases with the passage of time due to inflation effect. An investor is required to invest their money in such a way so that he should be able to earn such rate of return which is greater than the inflation rate. Therefore, investors need to analyze the investment

1 Assistant Professor, Department of Accountancy and Business Statistics, Mohanlal Sukhadia University, Udaipur, Rajasthan

2 Senior Research Fellow, Department of Accountancy and Business Statistics, Mohanlal Sukhadia University, Udaipur, Rajasthan

CONTEMPORARY ISSUES IN ACCOUNTING

(Including Blockchain Technology)

Editors

Shurveer S. Bhanawat, Ph.D.

Professor and Head, Department of Accountancy & Business Statistics,
Mohanlal Sukhadia University, Udaipur, Rajasthan

Shilpa Vardia

Assistant Professor,
Department of Accountancy and Business Statistics,
Mohanlal Sukhadia University,
Udaipur, Rajasthan

Shilpa Lodha

Assistant Professor,
Department of Accountancy and Business Statistics,
Mohanlal Sukhadia University,
Udaipur, Rajasthan

Bharti Publications

New Delhi- 110002 (INDIA)

Copyright © 2023, Editors

Title: Contemporary Issues in Accounting (Including Blockchain Technology)

Editors: Prof. Shurveer S Bhanawat, Dr. Shilpa Vardia and Dr. Shilpa Lodha

All rights reserved. No part of this publication may be reproduced or transmitted, in any from or by any means, without permission. Any person who does any unauthorised act in relation to this publication may be liable to criminal prosecution and civil claims for damages.

First Published, February 2023

ISBN: 978-81-19079-03-2

Published by :

Bharti Publications

4819/24, 2nd Floor, Mathur Lane

Ansari Road, Darya Ganj, New Delhi-110002

Phone: 011-46172797, 011-23247537, 9899897381

E-mail : bhartipublications@gmail.com

Website : www.bhartipublications.com

Printed in India, by Sagar Color Scan, Delhi

Disclaimer: The views expressed in the book are of the contributing authors and not necessarily of the Publisher and Editors. Authors are themselves responsible for any kind of plagiarism found in their paper or chapter and any related issues in book.

CONTENTS

Preface *iii-vi*

List of Contributors *ix-x*

1. Carbon Disclosure Ratings and Market Performance: Evidence from Carbon Disclosure Project (CDP)India **1-7**
Leo Themjung Makan and K. C. Kabra

2. Working Capital Prediction Model for Indian Corporate Sector **8-14**
Ritika Chittora and Shurveer S Bhanawat

3. Integrated Reporting Practices in South Africa **15-34**
Shiv Lal Parmar and Shilpa Vardia

4. Herd Behaviour: A Psychological bias of Behavioural Finance Theory **35-48**
Shilpa Lodha and Charu Sharma

5. Impact of Covid-19 on Goods and Services Tax Revenue Collection in India **49-57**
Ram Prasad Suthar and Parul Dashora

6. Crowdfunding: A Conceptual Understanding **58-68**
Shilpa Lodha and Babu Lal Gedar

7. Impact of XBRL Reporting System on the Reliability of Financial Reporting in India **69-80**
Apporva Mamodiya and Shilpa Lodha

8. Financial Analysis of Online Fantasy Sports Platform: A Case Study on Dream 11 **81-86**
Ashok Kumar Sharma and Shurveer S. Bhanawat

9. A Comparative Analysis of Composition Levy Scheme and Normal Tax Regime for Traders in GST **87-92**
Hemant Kaduniya and Palash Birla

10. A Financial analysis of two big FMCG companies of India: Proctor and Gamble & Nestle India **93-99**
Hemant Kaduniya and Ashok Singh Rana

11. A Study of Application of Blockchain Technology in India **100-110**
Geetanjali Sharma and Asha Sharma

12. Applications of Blockchain Technology in Various Fields **111-121**
Samta Ordia and Shurveer S. Bhanawat

13. Blockchain: A Revolutionary Technology Changing Life **122-133**
Ashok Kumar Gupta, Meenu Maheshwari and Ashish Chittora

14. Triple Entry Accounting (TEA) System & Blockchain Technology: A Theoretical Working Model **134-144**
Pushpraj Meena

6

Crowdfunding: A Conceptual Understanding

Dr. Shilpa Lodha[1] | Babu Lal Gedar[2]

ABSTRACT

Crowdfunding (CF) is an emerging platform for financial help and a new way to collect money. It's a good medium of financial assistance for any person, an organization, NGO, new startups and others. In this paper, one would get to know about a conceptual understanding of crowdfunding. Aim of the study is to explore conceptual framework of crowdfunding and it covered introduction, history and types of crowdfunding, legal framework of crowdfunding in India and other countries, process of generating fund from crowdfunding, benefits and challenges of crowdfunding. It is concluded that crowdfunding is growing very fast in many countries whereas in India there is a need to spread more awareness about it.

Keywords: *Crowdfunding, Equity Crowdfunding, Debt Crowdfunding*

INTRODUCTION

In finance, procuring funds is the basic step for investment and distribution decisions. Of late,crowdfunding is emerging as an alternative way of procuring funds for start-ups and entrepreneurial projects. Several authors have tried to define crowdfunding.

"Crowdfunding is solicitation of funds (small amount) from multiple investors through a web-based platform or social networking site for a specific project, business venture or social cause." (SEBI Consultation Paper, 2014)[1].

Crowdsourcing occurs when a profit-driven company outsources specific tasks critical to the production or sale of its product to the general public (the crowd)

1 Assistant Professor, Department of Accountancy and Business Statistics, Mohanlal Sukhadia University, Udaipur, Rajasthan

2 Senior Research Fellow, Department of Accountancy and Business Statistics, Mohanlal Sukhadia University,Udaipur, Rajasthan

CONTEMPORARY ISSUES IN ACCOUNTING

(Including Blockchain Technology)

Editors

Shurveer S. Bhanawat, Ph.D.

Professor and Head, Department of Accountancy & Business Statistics,
Mohanlal Sukhadia University, Udaipur, Rajasthan

Shilpa Vardia

Assistant Professor,
Department of Accountancy and Business Statistics,
Mohanlal Sukhadia University,
Udaipur, Rajasthan

Shilpa Lodha

Assistant Professor,
Department of Accountancy and Business Statistics,
Mohanlal Sukhadia University,
Udaipur, Rajasthan

Bharti Publications

New Delhi- 110002 (INDIA)

Copyright © 2023, Editors

Title: Contemporary Issues in Accounting (Including Blockchain Technology)

Editors: Prof. Shurveer S Bhanawat, Dr. Shilpa Vardia and Dr. Shilpa Lodha

All rights reserved. No part of this publication may be reproduced or transmitted, in any from or by any means, without permission. Any person who does any unauthorised act in relation to this publication may be liable to criminal prosecution and civil claims for damages.

First Published, February 2023

ISBN: 978-81-19079-03-2

Published by :

Bharti Publications

4819/24, 2nd Floor, Mathur Lane

Ansari Road, Darya Ganj, New Delhi-110002

Phone: 011-46172797, 011-23247537, 9899897381

E-mail : bhartipublications@gmail.com

Website : www.bhartipublications.com

Printed in India, by Sagar Color Scan, Delhi

Disclaimer: The views expressed in the book are of the contributing authors and not necessarily of the Publisher and Editors. Authors are themselves responsible for any kind of plagiarism found in their paper or chapter and any related issues in book.

CONTENTS

Preface *iii-vi*

List of Contributors *ix-x*

1. Carbon Disclosure Ratings and Market Performance: Evidence from Carbon Disclosure Project (CDP)India **1-7**
Leo Themjung Makan and K. C. Kabra

2. Working Capital Prediction Model for Indian Corporate Sector **8-14**
Ritika Chittora and Shurveer S Bhanawat

3. Integrated Reporting Practices in South Africa **15-34**
Shiv Lal Parmar and Shilpa Vardia

4. Herd Behaviour: A Psychological bias of Behavioural Finance Theory **35-48**
Shilpa Lodha and Charu Sharma

5. Impact of Covid-19 on Goods and Services Tax Revenue Collection in India **49-57**
Ram Prasad Suthar and Parul Dashora

6. Crowdfunding: A Conceptual Understanding **58-68**
Shilpa Lodha and Babu Lal Gedar

7. Impact of XBRL Reporting System on the Reliability of Financial Reporting in India **69-80**
Apporva Mamodiya and Shilpa Lodha

8. Financial Analysis of Online Fantasy Sports Platform: A Case Study on Dream 11 **81-86**
Ashok Kumar Sharma and Shurveer S. Bhanawat

9. A Comparative Analysis of Composition Levy Scheme and Normal Tax Regime for Traders in GST **87-92**
Hemant Kaduniya and Palash Birla

10. A Financial analysis of two big FMCG companies of India: Proctor and Gamble & Nestle India **93-99**
Hemant Kaduniya and Ashok Singh Rana

11. A Study of Application of Blockchain Technology in India **100-110**
Geetanjali Sharma and Asha Sharma

12. Applications of Blockchain Technology in Various Fields **111-121**
Samta Ordia and Shurveer S. Bhanawat

13. Blockchain: A Revolutionary Technology Changing Life **122-133**
Ashok Kumar Gupta, Meenu Maheshwari and Ashish Chittora

14. Triple Entry Accounting (TEA) System & Blockchain Technology: A Theoretical Working Model **134-144**
Pushpraj Meena

7

Impact of XBRL Reporting System on the Reliability of Financial Reporting in India

Apporva Mamodiya[1] | Dr. Shilpa Lodha[2]

ABSTRACT

XBRL is a very dynamic and modern financial reporting language which is being used around the world to communicate the results of operational and financial performance of the business organisations. It ensures accuracy, reliability, timeliness and decision usefulness to various stakeholders. This paper focuses on the impact on the XBRL reporting on the reliability and transparency of the financial reporting system in India. The data was obtained through a questionnaire survey of 34 accounting professionals. Collected data was analysed with the help of descriptive statistics and concludes that XBRL reporting positively impacts on the reliability of financial reporting system in India. It is also assumed that the use of XBRL will provide stakeholders and recipients of the financial statements with financial information about the companies that are credible.

Keywords: *XBRL, Financial reporting, Reliability, Transparency.*

INTRODUCTION

XBRL is a state-of-the-art tool for digitized disclosure of business and financial information ofbusiness houses. And this is the emerging reporting trend around the world. This new tool removes almost all the disadvantages of traditional formats of financial reports like paper- based, PDF, HTML, Word etc., these are static in nature which does not enable the preparers and users to easily compare, analyse and reuse past reports to prepare reports for the current years. But Extensible Business Reporting Language benefits both the creators and the

1 Research Scholar, Department of Accountancy and Business Statistics, Mohanlal Sukhadia University, Udaipur, Rajasthan

2 Assistant Professor, Department of Accountancy and Business Statistics, Mohanlal Sukhadia University, Udaipur, Rajasthan



MYCOTOXINS IN FOOD AND FEED

Detection and Management Strategies

Edited by
Pradeep Kumar, Madhu Kamle, and Dipendra Kumar Mahato

CRC Press
Taylor & Francis Group

First edition published 2023
by CRC Press
6000 Broken Sound Parkway NW, Suite 300, Boca Raton, FL 33487-2742

and by CRC Press
4 Park Square, Milton Park, Abingdon, Oxon, OX14 4RN

CRC Press is an imprint of Taylor & Francis Group, LLC

© 2023 Pradeep Kumar, Madhu Kamle, and Dipendra Kumar Mahato

Reasonable efforts have been made to publish reliable data and information, but the author and publisher cannot assume responsibility for the validity of all materials or the consequences of their use. The authors and publishers have attempted to trace the copyright holders of all material reproduced in this publication and apologize to copyright holders if permission to publish in this form has not been obtained. If any copyright material has not been acknowledged please write and let us know so we may rectify in any future reprint.

Except as permitted under U.S. Copyright Law, no part of this book may be reprinted, reproduced, transmitted, or utilized in any form by any electronic, mechanical, or other means, now known or hereafter invented, including photocopying, microfilming, and recording, or in any information storage or retrieval system, without written permission from the publishers.

For permission to photocopy or use material electronically from this work, access www.copyright.com or contact the Copyright Clearance Center, Inc. (CCC), 222 Rosewood Drive, Danvers, MA 01923, 978-750-8400. For works that are not available on CCC please contact mpkbookspermissions@tandf.co.uk

Trademark notice: Product or corporate names may be trademarks or registered trademarks and are used only for identification and explanation without intent to infringe.

Library of Congress Cataloging-in-Publication Data
Names: Kumar, Pradeep (Professor of biotechnology), editor. | Kamle, Madhu, editor. | Mahato, Dipendra Kumar, editor.
Title: Mycotoxins in food and feed : detection and management strategies / edited by Pradeep Kumar, Madhu Kamle, and Dipendra Kumar Mahato.
Description: First edition. | Boca Raton : CRC Press, 2023. | Includes bibliographical references and index.
Identifiers: LCCN 2022032433 (print) | LCCN 2022032434 (ebook) | ISBN 9781032113920 (hardback) | ISBN 9781032150352 (paperback) | ISBN 9781003242208 (ebook)
Subjects: LCSH: Mycotoxins. | Food contamination. | Food—Toxicology.
Classification: LCC RA1242.M94 M9644 2023 (print) | LCC RA1242.M94 (ebook) | DDC 615.9/5295—dc23/eng/20221114
LC record available at https://lccn.loc.gov/2022032433
LC ebook record available at https://lccn.loc.gov/2022032434

ISBN: 978-1-032-11392-0 (hbk)
ISBN: 978-1-032-15035-2 (pbk)
ISBN: 978-1-003-24220-8 (ebk)

DOI: 10.1201/9781003242208

Typeset in Kepler
by Apex CoVantage, LLC

Contents

Preface ix
Author Biographies xi
List of Contributors xiii

1 Aflatoxins in Food and Feed: Occurrence, Detection, and Mitigating Strategies 1
Namita Ashish Singh, Jyoti, Vidhi Jain

2 Fumonisins in Food and Feed: Their Detection and Management Strategies 29
Shubhangi Srivastava, Ashok Kumar Yadav, Mousumi Ghosh, Dipendra Kumar Mahato, Madhu Kamle, Pooja Pandey, Sreemoyee Chakraborty, Pradeep Kumar

3 Ochratoxins in Food and Feed: Detection and Management Strategies 51
Arun Kumar Pandey, Rahul Vashishth, Dipendra Kumar Mahato, Madhu Kamle, Raman Selvakumar, Monika Mathur, Pradeep Kumar

4 Trichothecene Concerns in Food and Feed: Detection and Management Strategies 87
Madhvi Singh, Chayanika Sarma, Pinky Deka, Ramzan Ahmed, Jayabrata Saha, Sourav Chakraborty

5 Detection and Management Strategies for Deoxynivalenol in Food and Feed: An Overview 119
Raman Selvakumar, Dalasanuru Chandregowda Manjunathagowda, Arun Kumar Pandey, Dipendra Kumar Mahato, Akansha Gupta, Shikha Pandhi, Raveena Kargwal, Madhu Kamle, Pradeep Kumar

6 Occurrence, Detection, and Management of T-2 Toxin and HT-2 Toxin in Food and Feed 157
Pooja Yadav, Nabendu Debnath, Shalini Arora, Ashok Kumar Yadav

7 Detection and Management of Ergot Alkaloids and Their Therapeutic Applications 189
Nabendu Debnath, Pooja Yadav, Shalini Arora, Ashok Kumar Yadav

8 Roquefortines in Food and Feed: Detection and Management Strategies 213
Saloni, Dinesh Chandra Rai, Himanshu Kumar Rai, Arvind Kumar, Urvashi Vikranta, Shikha Pandhi, Akansha Gupta, Dipendra Kumar Mahato

9 PR Toxins: Concerns in Food and Feed with Their Detection and Management Strategies 239
Mousumi Ghosh, Sreemoyee Chakraborty, Sourav Misra, Shubhangi Srivastava, Sourabh Bondre, Madhu Kamle, Pradeep Kumar, Dipendra Kumar Mahato

10 Occurrence, Production, Determination, Toxicity, and Control Strategies of Cyclopiazonic Acid in Food Products 265
Sourav Misra, Sitesh Kumar, Pooja Pandey, Shubham Mandliya, Mousumi Ghosh, Shubhangi Srivastava, Dipendra Kumar Mahato

11 Tremorgenic Mycotoxin Concerns in Food and Feed: Detection and Management Strategies 287
Himani, Mitali Madhumita, Mohit Singla, Pramod K Prabhakar

12 Zearalenone in Food and Feed: Occurrence, Biosynthesis, Detection and Management Strategies 311
Shikha Pandhi, Ashok Kumar Yadav, Vidhi Tyagi, Saloni, Akansha Gupta, Surabhi Pandey, Dipendra Kumar Mahato, Pradeep Kumar, Arun Kumar Pandey, Arvind Kumar

13 Mycotoxins in Stored Foods 333
Preeti Sharma, Kanishka Chawla, Kamakshi Kalia, Vanshika Saini, Aastha Bhardwaj, Vasudha Bansal, Nitya Sharma

14 Climate Change's Impact on Mycotoxin Production in Food and Feed 361
Monika Mathur, Raveena Kargwal, Raman Selvakumar, Dipendra Kumar Mahato, Madhu Kamle, Pradeep Kumar

15 Nano-Biosensors for the Monitoring of Toxic Contaminants in Food and it's Products 429
Namita Ashish Singh, Nimisha Tehri, Amit Vashishth, Pradeep Kumar

Index 449

Chapter 1

Aflatoxins in Food and Feed

Occurrence, Detection, and Mitigating Strategies

Namita Ashish Singh, Jyoti, Vidhi Jain

CONTENTS

1.1 Introduction 2
1.2 Aflatoxin Contamination in Food and Feed 4
1.3 Methods Available for Detection of Aflatoxins 4
1.3.1 Chromatographic Methods 4
1.3.2 Immunoassays 8
1.3.2.1 Radioimmunoassay 8
1.3.2.2 Enzyme Linked Immunosorbent Assay 8
1.3.2.3 Lateral Flow Immunoassay 9
1.3.3 Biosensors Based on Immunoassay 9
1.3.3.1 Immunoassay with Amperometric Technique 9
1.3.3.2 Electrochemical Immunosensor 9
1.3.3.3 Impedimetric Immunosensor 10
1.3.4 Nanobiosensor-Based Method 10
1.4 Management Strategies for Mitigation of Aflatoxin 11
1.4.1 Pre-harvest Agricultural Management of Aflatoxins 11
1.4.1.1 Biological Control 11
1.4.1.2 Improved Plant Resistance against Aflatoxins 11
1.4.1.2.1 Resistance Breeding against *Aspergillus flavus* and Aflatoxin 11
1.4.1.2.2 Transgenic Approaches for *Aspergillus flavus* 12
1.4.2 Post-harvest Agricultural Management of Aflatoxins 12
1.4.2.1 Degradation of Aflatoxins by Physical Means 12
1.4.2.1.1 Irradiation 12
1.4.2.1.2 Cold Plasma 14
1.4.2.1.3 Treatment with Heat 15

DOI: 10.1201/9781003242208-1

Chapter 15

Nano-Biosensors for the Monitoring of Toxic Contaminants in Food and it's Products

Namita Ashish Singh, Nimisha Tehri,
Amit Vashishth, Pradeep Kumar

CONTENTS

15.1 Introduction
15.1.1 Toxic Contaminants 430
15.1.1.1 Mycotoxins 430
15.1.1.2 Pesticides 430
15.1.1.3 Heavy Metals 432
15.2 Need for Nanosensors 432
15.3 Nanobiosensors for Detection of Toxic Contaminants 433
15.4 Nanobiosensors for Monitoring Mycotoxins 433
15.4.1 Optical 435
15.4.2 Electrochemical 435
15.5 Nanobiosensors for Monitoring Pesticides 438
15.5.1 Optical 439
15.5.2 Electrochemical 439
15.5.3 Piezoelectric 440
15.6 Nanobiosensors for Heavy Metal Detection 440
15.6.1 Optical 441
15.6.2 Electrochemical 441
15.7 Conclusion 442
442

DOI: 10.1201/9781003242208-15

MYCOTOXINS IN FOOD AND FEED

Detection and Management Strategies

Mycotoxins represent an assorted range of secondary fungal metabolites that extensively occur in numerous food and feed ingredients at any stage during pre- and post-harvest conditions. Mycotoxin contamination in food and feed cause acute and chronic mycotoxicosis, including teratogenic, carcinogenic, oestrogenic, neurotoxic, and immunosuppressive effects and several others health issues. ***Mycotoxins in Food and Feed*** presents an overview of all the major mycotoxins, sources of production, chemistry and biosynthesis, occurrence in food and feed, effect on agriculture, effect on human health, detection technique, masked mycotoxins, and management and control strategies.

Key Features

- Provides broad coverage of mycotoxins and their effects on food and feed
- Includes comprehensive information of occurrence, chemistry, detections methods and management strategies for each toxin
- Discusses recent development in detection technologies for major mycotoxins
- Explores agricultural practices and post-harvest management strategies for managing mycotoxin infestations

Food Science & Technology

CRC Press
Taylor & Francis Group
an Informa business
www.routledge.com

CRC Press titles are available as eBook editions in a range of digital formats

ISBN 978-1-032-11392-0



MYCOTOXINS IN FOOD AND FEED

Detection and Management Strategies

Edited by
Pradeep Kumar, Madhu Kamle, and Dipendra Kumar Mahato

CRC Press
Taylor & Francis Group

First edition published 2023
by CRC Press
6000 Broken Sound Parkway NW, Suite 300, Boca Raton, FL 33487-2742

and by CRC Press
4 Park Square, Milton Park, Abingdon, Oxon, OX14 4RN

CRC Press is an imprint of Taylor & Francis Group, LLC

© 2023 Pradeep Kumar, Madhu Kamle, and Dipendra Kumar Mahato

Reasonable efforts have been made to publish reliable data and information, but the author and publisher cannot assume responsibility for the validity of all materials or the consequences of their use. The authors and publishers have attempted to trace the copyright holders of all material reproduced in this publication and apologize to copyright holders if permission to publish in this form has not been obtained. If any copyright material has not been acknowledged please write and let us know so we may rectify in any future reprint.

Except as permitted under U.S. Copyright Law, no part of this book may be reprinted, reproduced, transmitted, or utilized in any form by any electronic, mechanical, or other means, now known or hereafter invented, including photocopying, microfilming, and recording, or in any information storage or retrieval system, without written permission from the publishers.

For permission to photocopy or use material electronically from this work, access www.copyright.com or contact the Copyright Clearance Center, Inc. (CCC), 222 Rosewood Drive, Danvers, MA 01923, 978-750-8400. For works that are not available on CCC please contact mpkbookspermissions@tandf.co.uk

Trademark notice: Product or corporate names may be trademarks or registered trademarks and are used only for identification and explanation without intent to infringe.

Library of Congress Cataloging-in-Publication Data
Names: Kumar, Pradeep (Professor of biotechnology), editor. | Kamle, Madhu, editor. | Mahato, Dipendra Kumar, editor.
Title: Mycotoxins in food and feed : detection and management strategies / edited by Pradeep Kumar, Madhu Kamle, and Dipendra Kumar Mahato.
Description: First edition. | Boca Raton : CRC Press, 2023. | Includes bibliographical references and index.
Identifiers: LCCN 2022032433 (print) | LCCN 2022032434 (ebook) | ISBN 9781032113920 (hardback) | ISBN 9781032150352 (paperback) | ISBN 9781003242208 (ebook)
Subjects: LCSH: Mycotoxins. | Food contamination. | Food—Toxicology.
Classification: LCC RA1242.M94 M9644 2023 (print) | LCC RA1242.M94 (ebook) | DDC 615.9/5295—dc23/eng/20221114
LC record available at https://lccn.loc.gov/2022032433
LC ebook record available at https://lccn.loc.gov/2022032434

ISBN: 978-1-032-11392-0 (hbk)
ISBN: 978-1-032-15035-2 (pbk)
ISBN: 978-1-003-24220-8 (ebk)

DOI: 10.1201/9781003242208

Typeset in Kepler
by Apex CoVantage, LLC

Contents

Preface ix
Author Biographies xi
List of Contributors xiii

1 Aflatoxins in Food and Feed: Occurrence, Detection, and Mitigating Strategies 1
Namita Ashish Singh, Jyoti, Vidhi Jain

2 Fumonisins in Food and Feed: Their Detection and Management Strategies 29
Shubhangi Srivastava, Ashok Kumar Yadav, Mousumi Ghosh, Dipendra Kumar Mahato, Madhu Kamle, Pooja Pandey, Sreemoyee Chakraborty, Pradeep Kumar

3 Ochratoxins in Food and Feed: Detection and Management Strategies 51
Arun Kumar Pandey, Rahul Vashishth, Dipendra Kumar Mahato, Madhu Kamle, Raman Selvakumar, Monika Mathur, Pradeep Kumar

4 Trichothecene Concerns in Food and Feed: Detection and Management Strategies 87
Madhvi Singh, Chayanika Sarma, Pinky Deka, Ramzan Ahmed, Jayabrata Saha, Sourav Chakraborty

5 Detection and Management Strategies for Deoxynivalenol in Food and Feed: An Overview 119
Raman Selvakumar, Dalasanuru Chandregowda Manjunathagowda, Arun Kumar Pandey, Dipendra Kumar Mahato, Akansha Gupta, Shikha Pandhi, Raveena Kargwal, Madhu Kamle, Pradeep Kumar

6 Occurrence, Detection, and Management of T-2 Toxin and HT-2 Toxin in Food and Feed 157
Pooja Yadav, Nabendu Debnath, Shalini Arora, Ashok Kumar Yadav

7 Detection and Management of Ergot Alkaloids and Their Therapeutic Applications 189
Nabendu Debnath, Pooja Yadav, Shalini Arora, Ashok Kumar Yadav

8 Roquefortines in Food and Feed: Detection and Management Strategies 213
Saloni, Dinesh Chandra Rai, Himanshu Kumar Rai, Arvind Kumar, Urvashi Vikranta, Shikha Pandhi, Akansha Gupta, Dipendra Kumar Mahato

9 PR Toxins: Concerns in Food and Feed with Their Detection and Management Strategies 239
Mousumi Ghosh, Sreemoyee Chakraborty, Sourav Misra, Shubhangi Srivastava, Sourabh Bondre, Madhu Kamle, Pradeep Kumar, Dipendra Kumar Mahato

10 Occurrence, Production, Determination, Toxicity, and Control Strategies of Cyclopiazonic Acid in Food Products 265
Sourav Misra, Sitesh Kumar, Pooja Pandey, Shubham Mandliya, Mousumi Ghosh, Shubhangi Srivastava, Dipendra Kumar Mahato

11 Tremorgenic Mycotoxin Concerns in Food and Feed: Detection and Management Strategies 287
Himani, Mitali Madhumita, Mohit Singla, Pramod K Prabhakar

12 Zearalenone in Food and Feed: Occurrence, Biosynthesis, Detection and Management Strategies 311
Shikha Pandhi, Ashok Kumar Yadav, Vidhi Tyagi, Saloni, Akansha Gupta, Surabhi Pandey, Dipendra Kumar Mahato, Pradeep Kumar, Arun Kumar Pandey, Arvind Kumar

13 Mycotoxins in Stored Foods 333
Preeti Sharma, Kanishka Chawla, Kamakshi Kalia, Vanshika Saini, Aastha Bhardwaj, Vasudha Bansal, Nitya Sharma

14 Climate Change's Impact on Mycotoxin Production in Food and Feed 361
Monika Mathur, Raveena Kargwal, Raman Selvakumar, Dipendra Kumar Mahato, Madhu Kamle, Pradeep Kumar

15 Nano-Biosensors for the Monitoring of Toxic Contaminants in Food and it's Products 429
Namita Ashish Singh, Nimisha Tehri, Amit Vashishth, Pradeep Kumar

Index 449

Chapter 1

Aflatoxins in Food and Feed

Occurrence, Detection, and Mitigating Strategies

Namita Ashish Singh, Jyoti, Vidhi Jain

CONTENTS

1.1 Introduction 2
1.2 Aflatoxin Contamination in Food and Feed 4
1.3 Methods Available for Detection of Aflatoxins 4
1.3.1 Chromatographic Methods 4
1.3.2 Immunoassays 8
1.3.2.1 Radioimmunoassay 8
1.3.2.2 Enzyme Linked Immunosorbent Assay 8
1.3.2.3 Lateral Flow Immunoassay 9
1.3.3 Biosensors Based on Immunoassay 9
1.3.3.1 Immunoassay with Amperometric Technique 9
1.3.3.2 Electrochemical Immunosensor 9
1.3.3.3 Impedimetric Immunosensor 10
1.3.4 Nanobiosensor-Based Method 10
1.4 Management Strategies for Mitigation of Aflatoxin 11
1.4.1 Pre-harvest Agricultural Management of Aflatoxins 11
1.4.1.1 Biological Control 11
1.4.1.2 Improved Plant Resistance against Aflatoxins 11
1.4.1.2.1 Resistance Breeding against *Aspergillus flavus* and Aflatoxin 11
1.4.1.2.2 Transgenic Approaches for *Aspergillus flavus* 12
1.4.2 Post-harvest Agricultural Management of Aflatoxins 12
1.4.2.1 Degradation of Aflatoxins by Physical Means 12
1.4.2.1.1 Irradiation 12
1.4.2.1.2 Cold Plasma 14
1.4.2.1.3 Treatment with Heat 15

DOI: 10.1201/9781003242208-1

Chapter 15

Nano-Biosensors for the Monitoring of Toxic Contaminants in Food and it's Products

Namita Ashish Singh, Nimisha Tehri,
Amit Vashishth, Pradeep Kumar

CONTENTS

15.1 Introduction
15.1.1 Toxic Contaminants 430
15.1.1.1 Mycotoxins 430
15.1.1.2 Pesticides 430
15.1.1.3 Heavy Metals 432
15.2 Need for Nanosensors 432
15.3 Nanobiosensors for Detection of Toxic Contaminants 433
15.4 Nanobiosensors for Monitoring Mycotoxins 433
15.4.1 Optical 435
15.4.2 Electrochemical 435
15.5 Nanobiosensors for Monitoring Pesticides 438
15.5.1 Optical 439
15.5.2 Electrochemical 439
15.5.3 Piezoelectric 440
15.6 Nanobiosensors for Heavy Metal Detection 440
15.6.1 Optical 441
15.6.2 Electrochemical 441
15.7 Conclusion 442
442

DOI: 10.1201/9781003242208-15

MYCOTOXINS IN FOOD AND FEED

Detection and Management Strategies

Mycotoxins represent an assorted range of secondary fungal metabolites that extensively occur in numerous food and feed ingredients at any stage during pre- and post-harvest conditions. Mycotoxin contamination in food and feed cause acute and chronic mycotoxicosis, including teratogenic, carcinogenic, oestrogenic, neurotoxic, and immunosuppressive effects and several others health issues. ***Mycotoxins in Food and Feed*** presents an overview of all the major mycotoxins, sources of production, chemistry and biosynthesis, occurrence in food and feed, effect on agriculture, effect on human health, detection technique, masked mycotoxins, and management and control strategies.

Key Features

- Provides broad coverage of mycotoxins and their effects on food and feed
- Includes comprehensive information of occurrence, chemistry, detections methods and management strategies for each toxin
- Discusses recent development in detection technologies for major mycotoxins
- Explores agricultural practices and post-harvest management strategies for managing mycotoxin infestations

Food Science & Technology

CRC Press
Taylor & Francis Group
an Informa business
www.routledge.com

CRC Press titles are available as eBook editions in a range of digital formats

ISBN 978-1-032-11392-0

Graphene-based Carbocatalysis: Synthesis, Properties and Applications

(Volume 1)

Edited by

Pinki Bala Punjabi
Department of Chemistry, University College of Science, Mohanlal Sukhadia University, Udaipur-313001, Rajasthan, India

I have not published any books, chapters and conference proceedings in session 2022-23

Dr. Vivek Jain

Department of Pharmaceutical Sciences

MLSU

Taylor & Francis Group
an informa business

T&F eBooks | Search for keywords, authors, titles, ISBN

Login

Advanced Search

About Us | Subjects | Browse | Products | Request a trial | Librarian Resources | What's New!!



Chapter

Antarctic Climate History and Its Relationship with Global Climate Changes

Evidence from Ice Core Records

By Ashutosh K. Singh, Devesh K. Sinha, Ankush Shrivastava, Vikram Pratap Singh, Kirtiranjan Mallick, Tushar Kaushik

Book Climate Change and Geodynamics in Polar Regions

Edition	1st Edition
First Published	2022
Imprint	CRC Press
Pages	44
eBook ISBN	9781003284413

Share

You do not have access to this content currently. Please click 'Get Access' button to see if you or your institution have access to this content.

GET ACCESS

To purchase a print version of this book for personal use or request an inspection copy »

GO TO ROUTLEDGE.COM

ABSTRACT

The long and continuous ice cores obtained from drilling thick ice sheets of Antarctica provide us with one of the best high-resolution records of climate change during the last 800 kilo years. Away from anthropogenic activities, the ice core records are relatively uncorrupted and well preserved. The interior of Antarctica becomes still far away from the moist warm climate of the coastal region further reducing the moisture transport due to continentality. Despite being so dry, the desert continent holds 70% of the freshwater of the Earth. Much of the early history of the Antarctic ice sheet is revealed not from Antarctica but from the marine sedimentary record in the Southern Ocean surrounding Antarctica. However, for the last few thousand years, several ice cores reveal a direct record of Antarctic climate. The history of origin and subsequent permanent establishment of the Antarctic ice sheet has been well constrained by the oxygen isotope record of the benthic foraminifera from the marine sediments.

किन्नर विमर्श

शिक्षा, समाज और साहित्य



प्रधान संपादक
डॉ. विन्द कुमार चौहान

संपादक
संगीता कुमारी पासी
जैवेन्द्र चौहान

किन्नर विमर्श

शिक्षा, समाज और साहित्य

प्रधान संपादक

डॉ. बिन्द कुमार चौहान

संपादक

संगीता कुमारी पासी

जैनेन्द्र चौहान

हंस प्रकाशन

हंस प्रकाशन

नई दिल्ली (भारत)

प्रथम संस्करण : 2022

ISBN : 978-93-91118-02-0

© संपादकगण

मूल्य : 995.00/-

प्रकाशक

हंस प्रकाशन

(पब्लिशर्स एण्ड डिस्ट्रीब्यूटर्स)

बी-336/1, गली नं. 3, दूसरा पुस्ता,

सोनिया विहार, नई दिल्ली-110094

दूरभाष : 9868561340, 7217610640

E-mail : hansprakashan88@gmail.com

Website : www.hansprakashan.com

विक्रय कार्यालय :

4648/21, अंसारी रोड, दरियागंज,

नई दिल्ली-110002

दूरभाष : 7217610640

टाईप सेटिंग : मुस्कान कम्प्यूटर्स, दिल्ली-94

मुद्रक : एस. के. ऑफसेट, दिल्ली

अनुक्रमणिका

समर्पण (v)

संपादकीय (vii)

1. संस्कृत साहित्य एवं किन्नर : एक अध्ययन 1
–डॉ. डॉली जैन

2. अंधेरों से संघर्ष करता एक उपेक्षित दिया : 'यमदीप' 13
–डॉ. नीता त्रिवेदी

3. किन्नर समाज - उत्थान में साहित्य का योगदानः
"किन्नर : मुनिया मौसी" के विशेष संदर्भ में 22
–डॉ. प्रभा शर्मा

4. किन्नर समुदाय और उनकी संस्कृति 33
–संगीता कुमारी पासी

5. किन्नर समाज का दर्द और अपेक्षित आकांक्षाएँ
(हिन्दी कथा साहित्य में व्याप्त किन्नर वर्ग की
समस्याओं के विशेष संदर्भ में) 40
–डॉ. सुरेश कुमार बैरागी

6. समाज और साहित्य में किन्नर 48
–डॉ. लूनेश कुमार वर्मा

7. हिन्दी कहानियों में किन्नर विमर्श 55
–डॉ. उदय भान भगत

2

अंधेरों से संघर्ष करता एक उपेक्षित दिया : 'यमदीप'

डॉ. नीता त्रिवेदी

हमारी दुनिया के समानांतर चलती एक उपेक्षित दुनिया जो हमारे आसपास होते हुए भी, नजरों से दृष्टिगत होते हुए भी, हमारे दृष्टिकोण का हिस्सा नहीं बन पाती। यह दुनिया हमारे आसपास चलते-रहते-जीते नजर तो आती है पर हमारे विचारों तक उस दुनिया की पहुंच नहीं है। हां, एक पूरी की पूरी दुनिया हमारे आसपास ताली बजाती हुई, हमारे मांगलिक उत्सवों पर खुशियां मनाते हुए दुआएं देती और नेग लेकर गाती बजाती हमारे आसपास चलती है, किंतु यह हमारे लिए केवल भय, कौतूहल और घृणा का ही भाव उत्पन्न करती है विमर्श का नहीं। जी हां मैं बात कर रही हूँ– किन्नर समाज की जो सदियों से उपेक्षित, संघर्षशील रहा है। इस समाज में रहता हुआ समाज से दूर। यह समाज सृष्टि की उत्पत्ति से ही हमारे मध्य रहा है। सभ्यता के विकास के साथ मानव ने कई स्तरों पर उत्तरोत्तर प्रगति की है किंतु यह समाज आज भी अपनी अस्मिता के लिए संघर्षरत है। विमर्श के इस दौर में किन्नर विमर्श पर भी साहित्य ने सुधि ली है जिस कारण से इनके जीवन संघर्ष, यातनाओं-भावनाओं आदि ने बौद्धिक मानस पर अपनी उपस्थिति दर्ज करवाई है।

साहित्य में किन्नर विमर्श पर नीरजा माधव कृत 'यमदीप' उपन्यास भारतीय हिंदी साहित्य में अब तक ज्ञात प्रकाशित उपन्यासों में पहला उपन्यास माना जाता है। समकालीन स्त्री साहित्यकारों में नीरजा माधव एक सशक्त नाम है। आपने कथा साहित्य एवं कथेतर गद्य साहित्य में अपनी लेखनी द्वारा एक अलग विशिष्ट पहचान बनाई है। आपने समसामयिक विषयों पर गंभीर चिंतन प्रस्तुत किया है। आपके कहानी संग्रह हैं- 'चिटके आकाश का सूरज', 'अभी ठहरो अंधी सदी', 'आदिम गंध तथा अन्य कहानियां', 'चुप चंतारा रोना नहीं', 'पथदंश', 'वाया पांडेपुर चौराहा'। आप के प्रसिद्ध उपन्यास हैं - 'यमदीप', 'तेभ्यः स्वध', 'ईहानृग', 'अवर्ण महिला कॉन्स्टेबल की डायरी', 'अनुपमेय शंकर', 'गेशे जम्पा', 'मृगदाय के अहेरी', 'धन्यवाद सिवनी', 'रात्रिकालीन संसद'। आपके निबंध संग्रह हैं- 'चौत चित मन महुआ', 'रुकोगी नहीं भागीरथी', 'सांझी फूलन चिति', 'यह राम कौन है'? 'प्रस्थानत्रयी' नाम से आपका एक काव्य संग्रह भी प्रकाशित हुआ है। आपका रचना कर्म आपकी बहुमुखी प्रतिभा को अभिव्यक्त करता है। आपकी औपन्यासिक कृति 'यमदीप' सन 2002 में प्रकाशित उपन्यास है। यह उपन्यास किन्नर समाज एवं स्त्री अस्मिता पर आधारित एक महत्वपूर्ण हस्ताक्षर है।

'यमदीप' उपन्यास का शीर्षक ही पाठक को कथा की मूल संवेदना से सराबोर कर देता है। 'यमदीप' अर्थात यम के लिए जलाया गया दीप। प्रकाश-पर्व की पूर्व संध्या पर घर से बाहर घूरे (कूड़ा करकट की जगह) पर यमदीप रखा जाता है। इस दीप की कोई पूजा-अर्चना, आरती कुछ नहीं होती। यहां तक की उस दीप को रखने के बाद पलट कर उस ओर भी नहीं देखा जाता। ऐसा उपेक्षित दीप यमदीप है जो उस सांध्य कालीन घनघोर अंधेरे से अकेला ही संघर्ष करता है। प्रकाश का नन्हा स्त्रोत उस गहन अंधकार में भी कई पथिकों को मार्ग दिखाता किंतु स्वयं में अकेला जलता रहता है।

नीरजा माधव अपने उपन्यास 'यमदीप' की भूमिका में स्पष्ट लिखती है- "प्रकाश-पर्व की पूर्व संध्या में दरवाजे के बाहर रात-भर टिमटिमाते उसी यम दीपक की भांति जो उपेक्षित होते हुए भी याद दिलाता है

आलोकित कल का। नहीं छूटती उसकी प्रदीप्त होने पर फुलझड़ियां और पटाखे, नहीं होती पूजा अर्चना या चढ़ते थाल पर भोग, पर काली रात के विरोध में टिमटिमाता रहता है चुपचाप, निःशब्द। सूखता रहता है अंतसरस बँद- बँद -बँद।"[1] यदि इस 'यमदीप' के आलोक में हम महताब गुरु, नाजबीबी, छैलू, चमेली, शबनम, अकरम, मंजू आदि को प्रतीकार्थ में देखें तो इस शीर्षक की सार्थकता, उसकी संवेदना को उसकी व्यापकता में देख पाएंगे। क्या यह सभी वह यमदीप नहीं जो अपने घर के बाहर घूरे पर छोड़ दिए गए हैं और परिवार का कोई सदस्य मुड़कर उस दिए को नहीं देख सकता क्योंकि वह दिया अभिशप्त है। परिवार का कोई सदस्य पीछे मुड़कर फिर कभी नहीं जान पाता या जानना चाहता है कि वह दिया उस कूड़े करकट भरी दुर्गंध युक्त उपेक्षित एवं गहन अंधकार में जल भी रहा है या बुझ गया है। दिये का संघर्ष उसका नितांत वैयक्तिक बन जाता है। 'यमदीप' किन्नरों के जीवन को उसकी व्यापकता, गहराई एवं संपूर्णता में व्यक्त करता एक जीवंत दस्तावेज है।

'यमदीप' में नाजबीबी तथा मानवी की कथा दो समानांतर ध्रुवों पर चलती है। नीरजा जी 'यमदीप' की भूमिका में ही मानवी के संबंध में स्त्री विमर्श का एक नया आयाम प्रस्तुत करती है– "मानवी का पूरा का पूरा स्त्री विमर्श है। अपनी अस्मिता और स्वीकार के लिए एक अंतहीन जिजीविषा लिए। आदर्श भारतीय स्त्रीत्व-गरिमा की राह से एक पग भी लड़खड़ाए बिना। पितृसत्ता के सह-अस्तित्व को बिना नकारे, अपने अस्तित्व के लिए पूर्णतया चौतन्य। स्त्री के संघर्षों और जुझारूपन को तथाकथित नारी-मुक्ति आंदोलन की आयातित दृष्टि से नहीं, बल्कि अपने बौद्धिक और तार्किक दृष्टिकोण से जांचती-परखती, पर सहानुभूति के स्थान पर स्वानुभूति से तथ्यों तक पहुंचने के बाद ही कोई निर्णय लेती हुई।"[2] मानवी उपन्यास में एक संवेदनशील पत्रकार है जो वंचितों एवं शोषितों के प्रति सहानुभूति रखते हुए उनके उद्धार के लिए प्रयत्नशील दिखाई पड़ती है। वह पारिवारिक एवं सामाजिक स्तर पर संघर्षशील रहते हुए स्त्री-अस्मिता के प्रति जागरूक नारी है।

नाजबीबी उर्फ नंदरानी भी अपने अस्तित्व के प्रति संघर्षशील, भावुक, मानवीय गुणों से ओतप्रोत, संवेदनशील किंतु सर्जक एवं सुदृढ़ व्यक्तित्व की किन्नर है। उपन्यास के प्रथम अध्याय से ही उसके भावुक मन की झलक मिल जाती है। प्रसव पीड़ा से तड़पती एक पगली स्त्री को जब गली- मोहल्ले के लोग तमाशबीन बनकर देख रहे थे। स्त्रियां अपने घरों से छुप-छुप कर देख रही थी। जब कोई भी उस स्त्री की मदद को नहीं आता तब नाजबीबी अपने साथियों के साथ वहीं उसका प्रसव कराती है। प्रसव पीड़ा से जब उस पगली की मृत्यु हो जाती है और कोई भी उसकी सद्य:जात पुत्री को नहीं अपनाता तब नाजबीबी उसे अपने साथ ले आती है। उसके साथी जब उसे लड़की को साथ ले चलने के लिए मना करते हैं तब वह कहती है– "किसके भरोसे छोड़ें वह बच्ची को? कोई पालने को तैयार नहीं। ऐसे छोड़ देने पर कहीं कुत्ते-कौवे नोंचकर... नहीं... नहीं।"[3] थोड़ी आनाकानी के बाद मेहताब गुरु उस बच्ची को नाजबीवी के साथ रहने की इजाजत दे देते हैं तथा सभी को यह हिदायत भी देते हैं कि बस्ती के बाहर किसी को भी पता ना चले कि यहाँ टेपकी (लड़की) पल रही है।

बच्ची का नाम 'सोना' रखा गया तथा नंदरानी अर्थात नाजबीवी सोना की मां बन जाती है। किन्नरों के मन की ममता, उनकी भावना, उनका मानवतावादी स्वरूप पाठकों को उनके प्रति एक नई दृष्टि देता है। वे अपने परिवार एवं समाज से कटकर अपना एक नया समाज बनाते हैं जहां मानवीय समाज की घृणा, उपेक्षा, तिरस्कार के बदले भी वे उनके प्रति अमानवीय तथा क्रूर नहीं हो सकते। नाजबीबी सोना को बड़े यत्न से पालती है तथा उसे उसी सभ्य समाज के मध्य रहने के लिए, उस के उत्थान के लिए उसे स्कूल में भी भेजती है। वह जब सोना के एडमिशन के लिए स्कूल जाती है तब चपरासी, शिक्षिकाएं तथा प्रिंसिपल तक उस पर व्यंग्य करती है, उसका मजाक बनाती है। सब कुछ होते हुए भी वह सोना को स्कूल भेजती है किंतु सोना को स्कूल में उसके किन्नर होने पर शर्मिंदा ना होना पड़े इसलिए वह छैलू किन्नर जो पुरुष ही लगता है उसे सोना को स्कूल लाने एवं छोड़ने के लिए भेजती है।

इस प्रसंग के माध्यम से लेखिका यह भी बताना चाहती है कि इसी कारण किन्नर जो कि मुख्यधारा में आने का प्रयास भी करना चाहते हैं, समाज के अन्य वर्गों की तो बात ही क्या शिक्षित एवं बौद्धिक वर्ग ही उन्हें हीनता का बोध कराते हैं। नाजबीबी को कभी-कभी अपना अतीत भी याद आ जाता है। वह सोचती है कि समाज के इन्हीं तानों एवं तिरस्कार के कारण उसे आठवीं कक्षा के बाद स्कूल छोड़ना पड़ा था। वह पढ़ना चाहती थी, आगे बढ़ना चाहती थी किंतु सामाजिक उपेक्षा एवं परिवार की बदनामी के डर से उसे स्वयं ही अपना घर छोड़कर किन्नरों की बस्ती में आना पड़ा क्योंकि उसे लग रहा था कि उसके कारण उसकी बड़ी बहन के विवाह में अड़चन आ रही हैं, उसके पिता को समाज में अपमानित होना पड़ रहा है। इन्हीं सब कारणों से नंदरानी स्वयं ही घर छोड़कर चली जाती है। लेखिका ने परत-दर-परत टूटते नंदरानी के मन को बड़ी ही संवेदना से उकेरा है साथ ही उतनी ही क्रूरता से समाज का घृणित चेहरा भी रखा है। कैसी विडंबना है जहां किसी किन्नर को उसका परिवार अपना रहा है, शिक्षा के द्वारा उसकी उन्नति के मार्ग खोलना चाहता है वहां सामाजिक विभेद उसे अवनति के गर्त में ढकेल देता है। नंदरानी के माता-पिता बच्ची को तब भी नहीं छोड़ते। वे नंदरानी का पता प्राप्त कर एक बार उस बस्ती में भी जाते हैं जहां उनकी नंदरानी जो अब नाजबीबी बन चुकी है, रहती है। मां तो नंदरानी की स्थिति देखते ही बेहोश हो जाती है पिता भी आंसू बहाते हैं। वे नंदरानी को वहां से निकाल कर कहीं पक्का घर बना कर देना भी चाहते हैं पर मजबूरी यह भी है कि वे नंदरानी को साथ नहीं ले जा पाते। नंदरानी के भाई-भाभी उसकी उपस्थिति उनके घर में नहीं चाहते। तब सभी किन्नर भावुक हो जाते हैं उन्हें लगता है कि किसी के माता-पिता तो उन्हें मिलने आए वरना कईयों के तो माता-पिता ने हीं उन्हें यहां छोड़ दिया था। इस स्थिति में हिजड़ों के गुरु मेहताब गुरु नंदरानी के पिता को समझाते हुए तथा वास्तविक स्थिति का बोध कराते हुए किन्नर जीवन की त्रासदी को, उनके दर्द को बयां करते हुए कहते हैं– "आप इस बस्ती में रह नहीं सकते बाबूजी, और अपनी बेटी को अपने साथ रख भी नहीं सकते... दुनिया में बदनामी और हँसी-हँसारत के डर से। हिजड़ी के बाप कहलाना न आप बर्दाश्त कर पाएंगे और ना आपके परिवार के

लोग। लूली- लंगड़ी होती यह, कानी-कोतर होती, तो भी आप इसे अपने साथ रख सकते थे... इसीलिए इसे अब इसके हाल पर छोड़ दीजिए। यही उसका भाग्य था, यही बदा... था। सोच लीजिए, मर गई, सब्र कर लिया।"[4]

नाजबीबी उनके साथ नहीं जाती किंतु जब उसे पता चलता है कि उसकी मां की तबीयत बहुत खराब है। उसका अंतिम क्षण निकट आ गया है। तब वह अपने आप को नहीं रोक पाती। बस्ती में बिना किसी को बताए वह अपनी मां से मिलने जाती है। रास्ते में पता लिखा कागज भी उड़ जाता है तब उसकी संवेदनाएं और मुखर हो जाती है। किसी तरह घर पहुंचने पर उसे पता चलता है कि मां की मृत्यु हो गई है तब वह शोक विह्वल हो श्मशान पहुंचती है। यह प्रसंग भी नीरजा जी ने इतना मार्मिक बनाया है जिसे पढ़कर पाठकों का दिल भी पसीजने लगता है। नाजबीबी का अपने पिता के गले लग कर रोना, भैया का समाज के समक्ष उसे अपमानित एवं तिरस्कृत करना और पिता की व्यथा तथा उसका पुनः डेरे की ओर लौटना।

उसके पश्चात नाजबीबी अपनी ममता और प्रेम का पूरा कोष सोना पर लुटाती उसी को अपना जीवन मान पूर्ण तन्मयता से उसके लालन-पालन में जुट जाती है। बस्ती में सभी का सहयोग और महताब गुरु के संरक्षण में सोना बड़ी होने लगती है। एक दिन बस्ती के बाहर कोने का एक डॉक्टर पुलिस को खबर कर देता है कि हिजड़ों की बस्ती में एक लड़की पल रही है। उसके बाद पुलिस वाले हिजड़ों की बस्ती में जाकर सब को धमकाते हैं उन्हीं के दबाव में आकर नाजबीबी को सोना को नारी उद्धार गृह में छोड़ना पड़ता है। नारी उद्धार गृह की संरक्षिका रीता देवी पुलिस एवं नेताओं के साथ मिलकर आश्रम की बालिकाओं का दैहिक शोषण करती है। नाजबीबी को जब आश्रम की स्थिति का वास्तविक परिचय अखबारों के माध्यम से पता चलता है तब वह मानवी की सहायता से सोना को वहां से निकाल पाती है। साथ ही वह इस पूरे घटनाक्रम में मानवी पर नेताओं के तथा पुलिस के दबाव से हमला भी होता है। नाजबीबी उस परिस्थिति में मानवी के जीवन को बचाते हुए उसे हॉस्पिटल भी लेकर जाती है। मानवी के माध्यम से ही आश्रम की बालिकाओं की स्थिति का पता चलता है

कि किस प्रकार कोई लड़की अपने घर की दहलीज को चाहे वह किसी भी कारण से हो, लांघे तो वह पुनः अपने घर नहीं जा पाती। समाज के डर से माता-पिता भी उसे वापस नहीं ले जाते और इस प्रकार शोषण के चक्र में पिसते रहना उनकी नियति बन जाती है।

'यमदीप' उपन्यास में लेखिका ने हिजड़ों के जीवन पर, उनके रीति-रिवाजों आदि पर संपूर्ण प्रकाश डाला है। लेखिका हिजड़ों के समाज से अलग-थलग रहने, उनके मुख्य धारा से ना जुड़ पाने के साथ उनके सामाजिक स्तर पर भी चर्चा करती है। उनकी आय का मुख्य साधन मांगलिक अवसरों पर नाचना गाना, बधाई मांगना है। यजमान द्वारा जो मिल जाए उसी पर उन्हें आश्रित रहना पड़ता है। समाज के आधुनिकीकरण से इन पर आर्थिक संकट आ रहा है। इसके अतिरिक्त रोजगार इन्हें कोई देता नहीं अतः मजबूरन इन्हें देह व्यापार, भीख, डराकर लूटना आदि कृत्य करने पड़ते हैं। इसी संदर्भ में लेखिका कहती हैं– "धंधों में आ रही इस गिरावट को देखते हुए गिरिया रखने तक की छूट तो अब ना चाहते हुए भी स्वीकृति पा चुकी थी उनकी बस्ती में। समलैंगिक भूख से बेचैन कोई-कोई समर्थ पुरुष जो इसका कोती (स्त्री वेशधारी हिजड़ा) के रूप में भरण पोषण कर सके, इसके लिए अपनी इच्छित या अनिच्छत स्वीकृति कोई भी हिजड़ा दे सकता था। पेट पालने की इसी विवशता में कितने तो छिपे मुंदे तौर पर इसे वेश्यावृत्ति की तरह अपना चुके थे, क्योंकि एक तो गिरिया कम लोग बनते थे और दूसरे केवल गिरिया द्वारा दी गई सीमित धनराशि में इनका खर्च चलना मुश्किल हो जाता था। कभी-कभी ट्रेनों और बसों में चढ़कर भी यह धन उगाही करने लगते, लेकिन ऐसे हिजड़ों का पता चलते ही उन्हें बिरादरी से बहिष्कृत करने जैसा दंड भी गुरुजी द्वारा दे दिया जाता क्योंकि उनके समुदाय में भीख मांगना, चोरी हिंसा करना भयंकर पाप माना जाता है।"[5]

आर्थिक स्तर पर विपन्न होने के बावजूद भी देशभक्ति, धर्मनिरपेक्षता आदि पर उनके विचार उन्हें और भी महान बना देते हैं। नाजबीबी मानवी के प्रश्न के जवाब में कहती है– "अपने देश के लिए तो देखिए, हम लोग मर मिटेंगे। जिस तरह फौज में एक सिपाही भर्ती होता है, पुलिस होता है

...सरकार हमें भी हथियार दे दे। मैं तो लड़ूँगी। लड़ते-लड़ते हिंदुस्तान के पीछे अपना जान दे दूँगी। बस, मेरी यही तमन्ना है। मैं मेजर की लड़की हूँ, मेजर की।"[6] उनकी इसी भावना एवं विचारों को देखते हुए मानवी अंत में नाजबीबी का संकल्प उनके चुनाव में खड़े होने को मानती है। और नाजबीबी देश हित के लिए तत्पर मानवी को कहती है – "जैसा कहोगी, मेम साहब, वैसा ही होगा। जैसा भी काम होगा, मैं जनता की भलाई के लिए करूंगी, क्योंकि अपने तो आगे पीछे कोई नहीं है जिसके लिए दूसरों की रोटियां छीनूँगी और अपना घर भरूंगी। जरूरत पड़ी तो भ्रष्ट लोगों के खिलाफ हथियार भी उठाऊंगी। हर गंदगी को जड़ से साफ कर दूँगी। दुनिया में शांति रहे, और क्या चाहिए किसी को?"[7]

नीरजा जी ने 'यमदीप' में किन्नरों के रीति-रिवाज उनकी भाषा-शैली पर विस्तार से वर्णन किया है। नाजबीबी मानवी को बताती है कि – "हम लोगों की एक बेसरा माता है यानी हिजड़ों की देवी। उनका मंदिर अहमदाबाद में है। वहीं गुजरात में। तो वर्ष में एक बार वहां हम सब लोग जुटते हैं। भंडारा करते हैं, नाचते गाते हैं। यानी एक साथ दो चार दिन रहते हैं। हर जिले में हम लोगों के एक गुरु होते हैं। हम लोग जो रोज,कमाई करते हैं, उसका एक बड़ा हिस्सा बेसरा माता के नाम पर गुरुजी के पास जमा करते जाते हैं। उसी में से सब मिलाकर हो जाता है।"[8] हिजड़ों की अपनी एक सांकेतिक भाषा होती है। प्रतीकात्मक एवं संकेत भाषा के प्रयोग द्वारा लेखिका शिल्प को विशिष्टता प्रदान करती हैं। डॉ. विजेंद्र प्रताप सिंह ने अपने लेख में इसे स्पष्ट किया है – "नीरजा माधव ने 'यमदीप' में से चाय के लिए भांपकी, रिक्शा के लिए लुढ़कनी, ढोल के लिए डामरी, लड़की के लिए टेपकी, घुंघरू के लिए छमकने, पुरुषवेश के लिए कड़े ताल में, पिता के लिए सुड्डा, माता के लिए सुड्डी, सौ रुपये के नोट के लिए बड़मा, रखैल हिजड़ा के लिए कोती, किसी को टालने के लिए चिस्सेर पतवाईदास आदि शब्द इनके दैनंदिन भाषा का हिस्सा है जिसे लेखिका नीरजा माधव ने पूरी खोजबीन के साथ प्रस्तुत किया है। हिजड़ों की अनेक सांकेतिक भाषा जैसे– सेवा-समाखन, निहारन, वीला, पानकी, कातका, धौंकनी आदि अनेक नए शब्दों से लेखिका रूबरू करवाती हैं।"[9]

इस प्रकार यह उपन्यास किन्नरों के उदात्त चरित्र, संवेदनशील मन, कर्तव्यबोध, उनकी मानवता, नैतिकता अपने समाज के प्रति उनकी कौटुंबिक भावना, राष्ट्रप्रेम तथा अपनी आराध्या बेसरा माता और अपने हिजड़ा गुरु की आज्ञा पालन सभी से पाठकों का विस्तार से परिचय कराता है। 'यमदीप' इस उपन्यास के अंत में पथ प्रदर्शित करने वाले आलोक का प्रतिनिधि बनकर उभरता है। यही इस उपन्यास का मूल संदेश है।

संदर्भ

1. नीरजा माधव : 'यमदीप', सुनील साहित्य सदन, दरियागंज, नई दिल्ली, संस्करण 2009, भूमिका, पृ. 6
2. वही, पृ.6
3. नीरजा माधव : 'यमदीप', सुनील साहित्य सदन, दरियागंज, नई दिल्ली, संस्करण 2009, पृ. 13
4. वही, पृ. 93
5. वही, पृ. 42
6. वही, पृ. 163
7. वही, पृ. 288
8. वही, पृ.164
9. डॉ. विजेंद्र प्रताप सिंह : हिंदी उपन्यासों के आईने में थर्ड जेंडर, (नीरजा माधव कृत 'यमदीप') अमन प्रकाशन, कानपुर, सं. 2017, पृ. 27

योगदान कर्ता सूची

1. **डॉ. डॉली जैन,** एसोसिएट प्रोफेसर, संस्कृत विभाग, राजस्थान विश्वविद्यालय, जयपुर (राज.)
2. **डॉ. नीता त्रिवेदी,** सहायक आचार्य, हिन्दी विभाग, मोहनलाल सुखाड़िया विश्वविद्यालय, उदयपुर (राज.)
3. **डॉ. प्रभा शर्मा,** सह आचार्य, हिन्दी विभाग, राजकीय कला कन्या महाविद्यालय, कोटा
4. ***संगीता कुमारी पासी,*** पीएच.डी, शोध-प्रज्ञा, हिन्दी विभाग, कॉटन विश्वविद्यालय, पानबाजार, गुवाहाटी (असम)
5. **डॉ. सुरेश कुमार बैरागी**, (सी.ए.सी.) ज.शि.के. खिलचीपुर जिला-राजगढ़ (ब्यावरा) म.प्र.
6. **डॉ. लूनेश कुमार वर्मा,** छत्तीसगढ़
7. **डॉ. उदय भान भगत,** सहकारी अध्यापक, हिन्दी विभाग, नगाँव गर्ल्स कॉलेज, नगाँव, असम 782002, भारत।
8. **पूनम गुप्ता,** पद : पी. जी. टी (माउंट लिटरा जी स्कूल हावड़ा)
9. **डॉ. मोहिनी दहिया,** प्राचार्य, व्याख्याता, हिन्दी साहित्य, माता जीतो जी कन्या महाविद्यालय, सूरतगढ़
10. **अनुज कुमार,** शोधार्थी, हिन्दी विभाग, दिल्ली विश्वविद्यालय
11. **नवल पाल,** पीएच.डी शोधार्थी, गुरू काज़ी विश्वविद्यालय, तलवंडी साबो, बठिंडा, पंजाब।



डॉ. बिन्द कुमार चौहान
01 जनवरी, 1980

ग्राम : 4 नं. नवाईबिल, जिला-पश्चिम कार्बी आंगलंग (असम)

शिक्षा : बी. ए. - होजाई कॉलेज, होजाई
एम. ए. (हिंदी) - गौहाटी विश्वविद्यालय, गुवाहाटी (असम)
बी. एड. - कृष्ण बोरा बी. एड. कॉलेज, लंका (असम)
एम. एड. - केंद्रीय हिंदी संस्थान, आगरा
पी-एच. डी. (हिंदी) - असम विश्वविद्यालय, सिलचर (असम)

जे. एन. भी., आर. सी. घाट, खोवाई, त्रिपुरा, कृष्ण बोरा बी. एड. कॉलेज, लंका, (असम), कुमारी लक्ष्मी बधाला महिला बी. एड. कॉलेज, गोविंदगढ़, जयपुर (राजस्थान), होजाई कॉलेज, होजाई (असम), कपिली कॉलेज, खेरनी, प. कार्बी आंगलंग (असम) व केंद्रीय हिंदी संस्थान, क्षेत्रीय केंद्र गुवाहाटी में अध्यापन-अनुभव।

संपादन- 1. 'नाट्य सहचरी' 2. 'उपन्यास वीथिका'

संप्रति : सन् 2016 से बंगाईगाँव कॉलेज, बंगाईगाँव के स्नातकोत्तर हिंदी विभाग में असिस्टेंट प्रोफेसर के रूप में अध्यापन।

संपर्क : सावित्री निवास, वार्ड नं. 16, आर. के. मीशन रोड, नतुनपारा, बंगाईगाँव (असम) पिन - 783380

चलभाष : 8638283868

हंस प्रकाशन
E-mail : hansprakashan56@gmail.com
Website : www.hansprakashan.com

₹ 995
ISBN 978-93-91118-02-0
9 789391 118020

हिन्दी के समकालीन कवि

सर्जना के आयाम

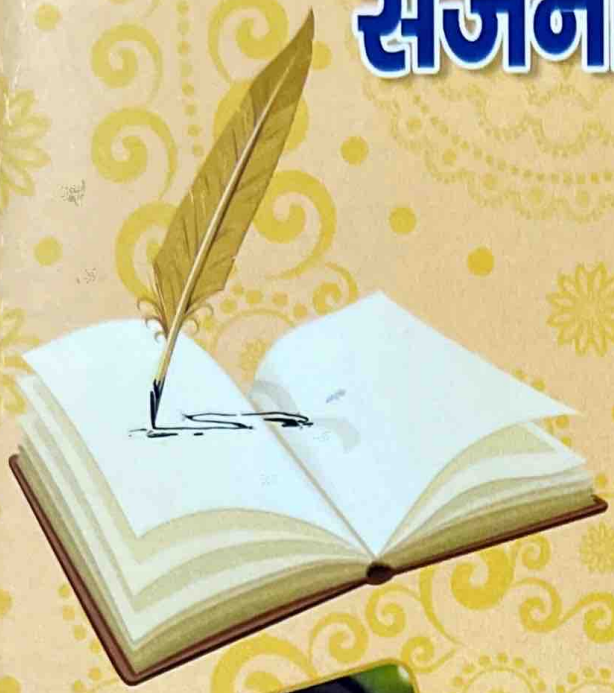

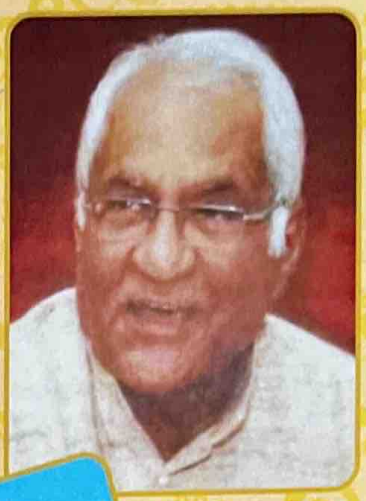







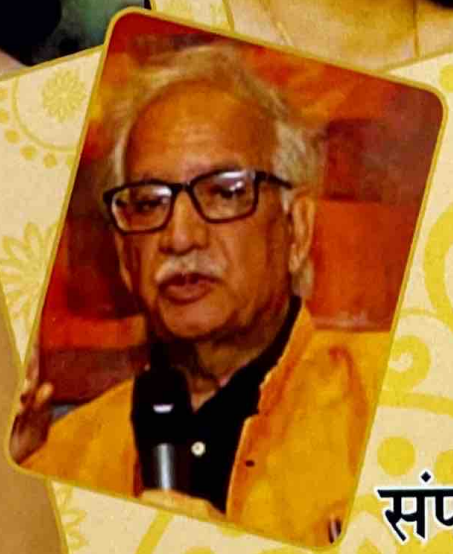

संपादक
डॉ. नीतू परिहार

हिंदी के समकालीन कवि : सर्जना के आयाम

संपादक

डॉ० नीतू परिहार

9413528299

अंकुर प्रकाशन

ANKUR PRAKASHAN

हिंदी के समकालीन कवि : सर्जना के आयाम
ISBN : *978-81-86064-88-7*
© : लेखक
मूल्य : पाँच सौ रुपये
संस्करण : 2022
प्रकाशक : अंकुर प्रकाशन
1/1 कांजी का हाटा, गायत्री मार्ग
उदयपुर (राज.) 313001
फोन नं. : (0294) 2417094, 2417039
(मो.) 9413528299
ईमेल : ankurprakashan15@gmail.com
आवरण : एन.वी.आर्ट, उदयपुर
टाईपसेटिंग : देवेन्द्र कम्प्यूटर, दिल्ली
मुद्रक : आर्यन डिजिटल प्रेस,दिल्ली

Hindi Ke Samkaleen Kavi : Sarjana Ke Ayam (Hindi Literature)
Edited By : Dr. Neetu Parihar
₹ 500

अनुक्रम

1	विश्वास के दीये-सी टिमटिमाती : वर्तिका नन्दा—*डॉ. नीतू परिहार*	13
2	अनुज लुगुन की कविताओं में आदिवासी जीवन—*डॉ० नवीन नन्दवाना*	22
3	आखर अनन्त और जीवन में आस्था के कवि : विश्वनाथ प्रसाद तिवारी—*डॉ० प्रीति भट्ट*	33
4	धूमिल : स्वातन्त्र्योत्तर कविता के उज्ज्वल 'मोची राम'—*डॉ० महेश चन्द्र तिवारी*	42
5	पवन करण की कविताओं में प्रतिबिम्बित नारी—*डॉ० नीता त्रिवेदी*	50
6	ममता कालिया की कविताओं में स्त्री-संघर्ष की गूँज—*डॉ० उषा शर्मा*	64
7	मंगलेश डबराल की कविताओं का सामाजिक स्वर—*डॉ० ममता पानेरी*	71
8	विजयदेव नारायण साही : सरल धरती का अभिलाषी कवि—*डॉ० कैलाश गहलोत*	77
9	अनामिका के काव्य में स्त्रियों की सामाजिक स्थिति—*एकता देवी*	86
10	समकालीन बोध और धूमिल की कविता—*विद्याप्रभाकर डॉ० कनुप्रिया प्रचंडिया*	94
11	अनामिका : काव्यगत पृष्ठभूमि—*डॉ० वसुन्धरा उपाध्याय*	102

5

पवन करण की कविताओं में प्रतिबिम्बित नारी

—डॉ० नीता त्रिवेदी

पवन करण आधुनिक हिंदी कविता के महत्त्वपूर्ण हस्ताक्षर हैं। आपकी कविताएँ दर्शन, समाज, राजनीति, पुराख्यान, जीवन के प्रत्येक क्षण, मानव मन की सूक्ष्म भावनाओं को जिस सहजता से अभिव्यक्त करती हैं उसमें प्रत्येक व्यक्ति अपने मन का दर्शन बड़े ही निश्चल भाव से कर पाता है। यह आपकी लेखनी की महत्त्वपूर्ण उपलब्धि है जो व्यक्ति से उसके ही मन का साक्षात्कार निर्विकार भाव से करा पाता है। आप की कविताएँ व्यक्ति के मन का वह दर्पण है जहाँ वह अपनी सभी सूक्ष्मातिसूक्ष्म मनोभावों के साथ नितान्त एकाकी खड़ा है। मन का दर्पण केवल उसके बाह्य आवरण को ही नहीं, मन की परतों के नीचे दबे छिपे सभी भावों का अपने नग्न रूप में दर्शन कराता है। व्यक्ति ना तो अपनी आँखें बन्द कर उस दर्पण से दूर जा सकता है और न ही सहज भाव से अपने ही मनोभावों से नजरें हटा सकता है। पाठक केवल तिलमिलाकर, बड़ी बेचैनी के साथ मूक दृष्टा बन उन सभी भावों के सामने खड़ा बेबस सा दिखाई पड़ता है।

पवन करण की कविताओं में स्त्री जीवन, उसके मन के विविध भावों, अनुभावों, संघर्षों तथा अभावों की सहज अभिव्यक्ति है। पवन करण की कविताओं में स्त्री मन अपने सभी द्वन्द्वों, संघर्षों, आत्मविश्वास, आस्था, जीवन मूल्यों के साथ मुखरित हुआ है।

18 जून, 1964 ई. को ग्वालियर (म.प्र.) में जन्मे पवन करण समकालीन कविताओं के एक सशक्त हस्ताक्षर हैं। आपने जनसंचार एवं मानव संसाधन विकास में स्नातकोत्तर की उपाधि प्राप्त की। आपके 8 काव्य-संग्रह प्रकाशित

हैं—'इस तरह मैं', ''स्त्री मेरे भीतर'', 'अस्पताल के बाहर टेलीफोन', 'कहना नहीं आता', ''कोट के बाजू पर बटन'', 'कल की थकान' और 'स्त्री शतक' (दो खंडों में)। आपका कविता संग्रह ''स्त्री मेरे भीतर'' मलयालम, मराठी, उड़िया, पंजाबी, उर्दू तथा बाँग्ला में प्रकाशित हो चुका है। इस संग्रह की कविताओं का नाट्यानुवाद एवं मंचन भी हो चुका है। आपकी कविताओं का भारतीय भाषाओं के अतिरिक्त रूसी और अंग्रेजी में भी अनुवाद हुआ है।

आपने नवभारत ग्वालियर में साहित्यिक पृ. 'सृजन' का 5 वर्षों तक संपादन किया। नई दुनिया में साहित्य पर केन्द्रित साप्ताहिक स्तंभ 'शब्द प्रसंग' का लेखन भी आपने किया। आपको अपनी साहित्यिक कृतियों के लिए कई सम्मान भी मिले हैं—'इस तरह मैं' पर रामविलास शर्मा पुरस्कार (म. प्र. साहित्य अकादमी 2000) एवं रजा पुरस्कार (म.प्र. कला अकादमी 2002) प्राप्त हुआ।''स्त्री मेरे भीतर'' पर वागीश्वरी सम्मान (म.प्र. हिंदी साहित्य सम्मेलन 2004), मास्को (रूस) का पुश्किन सम्मान (भारत मित्र समाज, मास्को 2006), शीला सिद्धांतकर स्मृति सम्मान (राग विराग कला केन्द्र, दिल्ली 2007), परम्परा ऋतुराज सम्मान (परम्परा, दिल्ली 2009), केदार सम्मान (केदार शोध संस्थान, बाँदा 2012) तथा स्पन्दन सम्मान आदि अनेक सम्मान आपको मिले हैं।

पवन करण की कविताएँ जीवन की कविता है, जहाँ जीवन का प्रत्येक क्षण, मानव मन की सूक्ष्म भावनाएँ अपनी सहजता में परिव्याप्त है। ये कविताएँ जीवनानुभवों के उस प्राकृतिक सोते के समान हैं जो अपनी राह स्वयं बनाता, उन सभी अनगढ़ रास्तों के बीच से सहज ही निर्बाध गति से आगे बढ़ता चलता है। उनकी कविताएँ अभिधा में हमसे बात करती है, बिना किसी लाग लपेट के। पवन करण का कविता संग्रह 'अस्पताल के बाहर टेलीफोन' के फ्लैप पर उद्धृत पंक्तियाँ भी इसी को स्पष्ट करती है—''ये कविताएँ उन्हीं लोगों के शब्दों और मुहावरों में बात करती हैं जिनकी ये कविताएँ हैं यानी हम और आप। यहीं हमारे सामने से शुरू होकर और हमारे देखते ही देखते हमारी दृष्टि सीमा से ऊंचे, कहीं अबूझ और अपार होती व्यवस्था के प्रति हमारी प्रतिक्रिया भी इन कविताओं में है, और विषाद भी। हमारे जीने का उछाह भी इनमें है और अवसाद भी। इनमें हमारा बड़ा होना भी है और छोटा होना भी, हमारी हिंसा भी और हमारी करुणा भी।''[1]

पवन करण अपनी कविताओं की भाषा में जितने सहज, सरल एवं संवेदी हैं उनकी कविताओं के विषय चयन में वे उतने ही अलग हैं और बाकी कवियों से विशिष्ट भी। वे अपनी कविता के विषय चयन को लेकर सारी वर्जना के

विपरीत किसी पुरानी परम्परा का अन्धानुकरण न करते हुए अपने नए मानक, नए विषय, जीवन के प्रत्येक क्षण का यथार्थ बहुत ही सहजता से व्यक्त कर देते हैं। यही कारण है कि हिंदी कविता में शायद पहली बार 'प्यार में डूबी हुई माँ' ने प्रवेश पाया है। 'स्त्री मेरे भीतर' कविता संग्रह की भूमिका में विष्णु नागर कहते हैं—"एक औरत जो अपनी युवावस्था में अचानक विधवा हो गयी हो, जिसने वर्षों उस अकेलेपन और निराशा में गुजारे हों, जिसमें दुनिया की हर खुशी में सिर्फ अपने व्यक्तिगत दु:ख की छाया ही नजर आती है, उसके जीवन में अचानक चुपके से कोई पुरुष आए (वह पुरुष विवाहित है या अविवाहित, यह मायने नहीं रखता और बहुत उचित ही पवन ने इस बारे में कविता में मौन बरता है।) और उसके इस तरह आने का सिर्फ मौन स्वागत ही उसकी बेटी न करे, इस कारण अपने को केवल दुनिया की सबसे खुशनसीब लड़की ही न समझे, बल्कि इस वजह से बौराई-पगलाई-सी रहे और उसे अपनी प्रेम करती हुई माँ उसके स्कूल की ही कोई शरारती, चंचल और हंसमुख लड़की लगने लगे, इस तरह की बात इससे पहले कहने और समझने का साहस किसी कवि ने नहीं किया।"[2]

जिस सहज भाषा में एक पुत्री अपने मृत पिता की फ्रेम से बात करते हुए अपनी माँ के प्रेम को व्यक्त करती है वह पवन करण की कविता के कथ्य की एक महत्त्वपूर्ण उपलब्धि है। जिस गहन संवेदना को सहज शब्दों में एक पुत्री के माध्यम से प्रस्तुत करना बिना किसी अश्लीलता के विषय को एक महत्त्वपूर्ण स्थान देती है—

अब तुम्हें वाकई नहीं मालूम पिता कि माँ
इस उम्र में कितनी खूबसूरत देती है दिखाई
और प्रेम करती हुई माँ को देखती
मैं क्यों न फिरूँ बौराई
प्रेम करती हुई माँ इन दिनों
बिल्कुल मुझ जैसी लगने लगी है
जैसे मेरी स्कूल की कोई सहेली
शरारती चंचल और हंसमुख[3]

पवन करण की कविताओं ने स्त्री मन को एक मुखर अभिव्यक्ति दी है। उनकी कविताओं में झांकता स्त्री मन अपनी हर घुटन, हर चीत्कार, अपना हर दर्द, हर संवेदना को बड़े ही संयत और सहज रूप में प्रस्तुत करता है। यह सहजता ही उन पात्रों से आत्मीयता जुड़ाती है, पाठक को उन अहसासों का साझी बनाती है।

पवन करण की कविताओं में आई नारी पात्र केवल अपनी व्यथा कथा ही नहीं बताती, केवल संवेदना का विषय ही नहीं बन कर आती, वह अपने सम्पूर्ण अस्तित्व के साथ कविताओं का केन्द्र बिन्दु बनकर उभरती हैं। उनकी कविताओं में नारी-मन की अनेक परते हैं जहाँ वह पारिवारिक -सामाजिक अंकुशों के भीतर भी अपनी परवाज तोल रही है। अपने आत्मविश्वास को परख रही है। अपना विरोध, अपना विद्रोह व्यक्त कर रही है किन्तु बहुत ही संयम और धैर्य के साथ। बड़ी सहजता से परम्पराओं को करवट देते हुए परिवर्तित कर रही है। वह स्त्री विमर्श का बिगुल बजाते हुए क्रान्ति की अलख नहीं जगाती किन्तु अपने आप को बदलते हुए, यथार्थ को स्वीकार करते हुए अपने जीवन मूल्यों के साथ आगे बढ़ रही है। हाँ, स्त्री शतक के दो खंडों में उन्होंने पौराणिक स्त्री पात्रों के माध्यम से प्रश्न तो उपस्थित किए हैं इस पुरुष वर्चस्ववादी समाज के समक्ष। मैं अपने आलेख के माध्यम से पवन करण की कविताओं में व्याप्त इसी नारी मन की अभिव्यक्ति को स्पष्ट करने का प्रयास करूँगी।

पवन करण की कविताओं में स्त्री-पुरुष संबंधों के अनेक भाव चित्र बिखरे हुए हैं। ये सभी विषय हमारे आसपास के जीवन में बिखरे हुए मिल जाएँगे इसी कारण हम इन्हें पढ़कर असहज नहीं होते बल्कि इन विषयों को कविता के विषय के रूप में देख कर आगे बढ़ने से पहले कुछ रुक कर गम्भीर होकर चिन्तन अवश्य करते हैं। पवन करण के काव्य-संग्रह 'कोट के बाजू पर बटन' के फ्लैप पर उल्लिखित उद्धरण से शायद बहुत अधिक स्पष्ट हो पाए—"भले ही टेकनोलॉजी और मैनेजमेंट के प्रशिक्षण ने बहुत जगहों पर आदमी को ही हाशिए पर सरका दिया हो किन्तु मध्यवर्गीय भद्रलोक की वर्जनाओं से भिड़न्त की धमक वाली ये कविताएँ पाठक के संवेदनतन्त्र में कुछ अलग ही प्रकार से हलचल पैदा करती हैं, क्योंकि भारतीय समाज अभी अपना नग्न फोटोसेशन कराने को उत्सुक प्रेमिका तथा बेटी और प्रेमिका के बीच पिता के प्यार के अन्तर तथा विवाह की तैयारी करती प्रेमिका से पति की आन्तरिकता को जानने को उत्सुक आहत प्रेमी को अपने संस्कारों के बीच जगह नहीं दे पाया है।"[4]

अपनी कई कविताओं में पवन करण ने पुरुष मन के माध्यम से स्त्री को समझाया है। पुरुष की सोच में स्त्री के मनोभावों की अभिव्यक्ति बड़े ही निश्चल रूप से की है। 'अपने विवाह की तैयारी करती प्रेमिका' कविता में प्रेमिका अन्तर्द्वंद तो स्पष्ट ही दीखता है जो अपने ऑफिस में कार्यरत अपने प्रेमी से अपने ही विवाह की तैयारी करते रहने के बीच भी अपने प्रेम को अभिव्यक्त करती है

साथ ही होने वाले पति के प्रति उसमें तनिक भी अनुरक्तता नहीं दीखती। प्रेमी न तो उसे अपना सकता है और उसे किसी और का होते देखने का दुःख भी कविता में पुरजोर दिखाई देता है। प्रेमिका की अभिव्यक्ति का खुलापन भी परिवर्तन की सौंधी-सी खुशबू का झोंका सा लगता है—

मगर मैं उसके साथ एक दिन भी नहीं रहने वाली
तुम्हारे और अपने घर के कहने पर मैं यह शादी कर रही हूँ
तुम जानते हो न तुम्हारे बिना नहीं रह सकती मैं
छोड़ कर चली आऊँगी सब, सुन रहे हो न
मैं हताश उसकी बेचैनी पर हाँ मैं हिला देता हूँ अपना सिर[6]

'फोटोसेशन' कविता में अवश्य स्त्री की बहुत ही नितान्त वैयक्तिक अभिव्यक्ति, खुलापन, स्त्री स्वातन्त्र्य का एक अलग पक्ष उभरता है, किन्तु इस कविता में स्त्री विमर्श के कई नए आयाम भी दृष्टिगत होते हैं—

जिसे तुम बार-बार मुझ पर लुटा देने की कहते हो
मुझे तुम्हारी वह जान नहीं चाहिए
नहीं चाहिए मुझे तुम्हारी वह ओट
जिसके पीछे मैं खुद को सुरक्षित मानतीआई हूँ
मैं उस ओट से बाहर आकर/तुम्हारे आगे खड़ी होना चाहती हूँ[6]

स्त्री के जीवन का यह एक क्रान्तिकारी पक्ष है जहाँ वह अपनी देह को बन्धन नहीं मानती और ना ही सात जन्मों के रिश्तों पर विश्वास करती है वह इस एक जीवन को ही खुलकर, भरपूर जीना चाहती है अपनी सभी इच्छाओं और कामनाओं की पूर्ति के साथ—

मुझ पर बहुत भार है अपनी इस देह का
मैं खुद को हल्का महसूस करना चाहती हूँ,
तुम्हारे साथ सपनों और चाहतों से लबालब सात नहीं
बस एक जीवन जीना चाहती हूँ
और उसी चाहत भरे जीवन से निकलकर बाहर आई
यह मेरी एक इच्छा है जिसे मैं पूरा करना चाहती हूँ
मैं तुम्हें ये भी बता देना चाहती हूँ ये कोई
ऐसी पहली और अन्तिम इच्छा नहीं मेरी
इसके बाद भी मैं इच्छाओं और कामनाओं से
लबालब एक लड़की ही रहूँगी
मैं इस इच्छा के पूरी होते ही कोई कैवल्य नहीं पा लूँगी[7]

साथ ही होने वाले पति के प्रति उसमें तनिक भी अनुरक्तता नहीं दीखती। प्रेमी न तो उसे अपना सकता है और उसे किसी और का होते देखने का दुःख भी कविता में पुरजोर दिखाई देता है। प्रेमिका की अभिव्यक्ति का खुलापन भी परिवर्तन की सौंधी-सी खुशबू का झोंका सा लगता है—

मगर मैं उसके साथ एक दिन भी नहीं रहने वाली
तुम्हारे और अपने घर के कहने पर मैं यह शादी कर रही हूँ
तुम जानते हो न तुम्हारे बिना नहीं रह सकती मैं
छोड़ कर चली आऊँगी सब, सुन रहे हो न
मैं हताश उसकी बेचैनी पर हाँ मैं हिला देता हूँ अपना सिर[6]

'फोटोसेशन' कविता में अवश्य स्त्री की बहुत ही नितान्त वैयक्तिक अभिव्यक्ति, खुलापन, स्त्री स्वातन्त्र्य का एक अलग पक्ष उभरता है, किन्तु इस कविता में स्त्री विमर्श के कई नए आयाम भी दृष्टिगत होते हैं—

जिसे तुम बार-बार मुझ पर लुटा देने की कहते हो
मुझे तुम्हारी वह जान नहीं चाहिए
नहीं चाहिए मुझे तुम्हारी वह ओट
जिसके पीछे मैं खुद को सुरक्षित मानतीआई हूँ
मैं उस ओट से बाहर आकर/तुम्हारे आगे खड़ी होना चाहती हूँ[6]

स्त्री के जीवन का यह एक क्रान्तिकारी पक्ष है जहाँ वह अपनी देह को बन्धन नहीं मानती और ना ही सात जन्मों के रिश्तों पर विश्वास करती है वह इस एक जीवन को ही खुलकर, भरपूर जीना चाहती है अपनी सभी इच्छाओं और कामनाओं की पूर्ति के साथ—

मुझ पर बहुत भार है अपनी इस देह का
मैं खुद को हल्का महसूस करना चाहती हूँ,
तुम्हारे साथ सपनों और चाहतों से लबालब सात नहीं
बस एक जीवन जीना चाहती हूँ
और उसी चाहत भरे जीवन से निकलकर बाहर आई
यह मेरी एक इच्छा है जिसे मैं पूरा करना चाहती हूँ
मैं तुम्हें ये भी बता देना चाहती हूँ ये कोई
ऐसी पहली और अन्तिम इच्छा नहीं मेरी
इसके बाद भी मैं इच्छाओं और कामनाओं से
लबालब एक लड़की ही रहूँगी
मैं इस इच्छा के पूरी होते ही कोई कैवल्य नहीं पा लूँगी[7]

बिना किसी लाग लपेट, बिना किसी आवरण के नारी मुक्ति का सहज जयघोष पवन करण की कविताओं को महत्त्वपूर्ण बना देता है। 'दरअसल उसको समझना खुद को समझना है' कविता में कवि ने पुरुषों के माध्यम से स्त्री चरित्र को समझा है। एक पुरुष अपनी पत्नी के उसके प्रेमी के साथ रंगे हाथों पकड़े जाने के बाद की स्थिति पर अपने मित्र के साथ विचार कर रहा है। कवि मित्र के माध्यम से पुरुष मन को आईना दिखाता है कि जब तुम किसी और की पत्नी के साथ प्रेम में रत रहते हो तब उस स्त्री के पति और हम प्रेमी क्या अलग-अलग पुरुष हैं?—

दरअसल उसे समझना खुद को समझना है
इस बात का कोई अर्थ नहीं कि तुम्हीं-
इसके शिकार क्यों हुए मैं तुम्हीं से पूछता हूँ
तुम्हें ही इस सब का शिकार क्यों नहीं होना चाहिए था[8]

पवन करण ने अपनी कविताओं में नारी मन को कभी नारी की नजर से देखा है तो कहीं पुरुष चरित्रों की नजर से भी स्त्री संबंधों के कई कई रूप उकेरे हैं। ऐसी ही एक कविता है—'एक खूबसूरत बेटी का पिता' जहाँ पिता अपनी बेटी की सुन्दरता पर चिंतित है। यह कविता बड़े ही सुन्दर एवं भावुक शब्दों में एक पिता की अभिव्यक्ति है। अपनी युवा बेटी के भविष्य, उसके सपनों, उसके प्रेम को सहारा देता एक पिता अन्त में आश्वासन देता अपनी पुत्री को—

सिर्फ भय ही नहीं एक खूबसूरत बेटी का पिता होने का
जो उल्लास होना चाहिए मेरे भीतर
वह मेरे भीतर है और दो गुना है
फिर भी मेरी चिन्ता में मेरी बेटी की खूबसूरती
शामिल है और शामिल है यह दृढ़ता
यदि इस सब के बावजूद भी
उससे कोई गलती होती है तो हो जाए
उसके पीछे उसे उबारने के लिए मैं खड़ा हूँ तत्पर[9]

पिता-पुत्री के संबंधों की कई कविताएँ पवन करण ने लिखी है। 'वह अब मुझसे भी डरने लगी है' कविता में पिता का अपनी बेटी की उम्र की लड़की से प्रेम करना तथा अपनी बेटी की नजरों में अपने पिता के प्रति भय को पवन करण ने एक अलग ही भूमि पर रचा है। जहाँ पिता अपनी बेटी की आँखों में अपने लिए भय को पाता है—

मैं अब उसके लिए पिता नहीं रहा
मुझमें अब उसे एक पुरुष नजर आने लगा है
उसे मेरे चेहरे में अब उस औरत का चेहरा
दिखाई देने लगा है जिसे लेकर इन दिनों
उसकी माँ की साँस गले में अटकी है
जिसके प्रेम मे में इन दिनों बेतहाशा डूबा हूँ[10]

पिता को यह खीझ है कि उसकी बेटी अब उससे नजरें चुराती है। उसके मन में यह संकोच है कि शायद इन दिनों में उसे उन आवारा, मनचले लड़कों जैसा लगता हूँ जो उसे रास्ते चलते छेड़ते हैं। पिता को लगता है कि मैंने अपने प्रेम को पाकर, बेटी की नजरों में अपना पिता होना खो दिया है। पिता के लिए अपनी बेटी की उम्र की प्रेमिका द्वारा बेटी से खुद की तुलना करना भी संकुचित करता है—

और उस वक्त तो खुद को लेकर
बेटी के भीतर पैदा हुआ भय
मुझे सच लगने लगता है
जब वह जिसके प्रेम में इन दिनों
खोया हूँ मैं अगाध, अपनी तुलना
मेरी युवा बेटी से करते हुए
मुझसे पूछती है, बताओ दोनों में से
तुम किसे ज्यादा प्यार करते हो
अपनी बेटी को या मुझे[11]

इस कविता में पिता अपनी पुत्री के मनोभावों को समझ रहा है। उसकी संवेदना से जुड़ा है पुत्री के प्रति उसका मन। यहाँ पिता बेटी के मन को पढ़ने का प्रयास कर रहा है। इसी प्रकार की एक और कविता है—'पिता की आँख में पराई औरत'। इस कविता में बेटी अपने पिता के मन को पढ़ रही है स्थिति कमोबेश वही है बस नजरिया थोड़ा सा बदला है। इसमें पुत्री अपने पिता के प्रेम के प्रति कहीं न कहीं संवेदनशील भी है। वह अपनी माँ और पिता के संबंधों की कई प्रकार से व्याख्या करती है। वह पिता से झगड़ा भी करना चाहती हैं पर पिता के प्रेम को समझने का प्रयास भी करती है—

एक बार तो उसके मन में आया वह अपने सामने बिठाकर
पिता को डांट दे बुरी तरह, ज्यादा हो तो झापड़ जड़ दे दो-चार
उनसे कहे क्या हो रहा है ये सब

पापा यह सब आपको अच्छा नहीं लगता अब
देखो मैं भी अब बड़ी हो गयी हूँ।
यह सब करने की तो अब मेरी उम्र है
मगर जब अपने भीतर किसी नवयुवक-सी बेचैनी लिए
सज-धजकर घर से बाहर
भागते पिता को देख तो खुद को समझाती है
नहीं यार मेरे बड़े हो जाने का मतलब
यह नहीं कि चुक गये हैं पिता शायद
उनका जीवन शुरू हुआ यहीं से[12]

पिता-पुत्री संबंधों के कई-कई आयाम पवन करण की कविताओं में स्वतन्त्र एवं निर्बाध रूप से अभिव्यक्त हुए हैं। अभिव्यक्ति की स्वतन्त्रता का एक और पक्ष है जहाँ पुत्री अपने मृत पिता को अपनी माँ के प्रेम के बारे में बताती है। इस कविता में कवि ने पुत्री के माध्यम से स्त्री के प्रति जो उदार संवेदनशीलता दिखाई है वह समकालीन हिंदी कविता की एक महत्त्वपूर्ण उपलब्धि है। इस कविता में उस पुत्री की खुशी में संवेदना की वह उजास है जो उसकी माँ के जीवन में कई वर्षों के बाद आई है। वह पुत्री साक्षी है अपनी माँ के उन दु:खों भरे वर्षों की जो उसने वैधव्य के कारण बिताए हैं वह माँ के अपने मृत पति के प्रेम को भी जानती है तभी वह खुश है। विष्णु नागर के शब्दों में—''पूरी कविता में कवि कहीं हस्तक्षेप करता नहीं दीखता, अन्धेरे में दिया लेकर चलने का अभिनय करता नहीं दीखता, वह अपनी कविता को पूरी तरह प्यार में डूबी हुई माँ की बेटी के हवाले कर देता है और उसे ही बोलने देता है। यह कविता उस लड़की की कविता है या कहें गीत है, उसकी गुनगुनाहट है, उसके बौराएपन का संगीत है।''[13]

स्त्री-पुरुष संबंधों के अतिरिक्त स्त्री से जब सामाजिक संबंध टकराए, जहाँ परिवार और स्त्री के विचार आमने- सामने आए उन कविताओं में स्त्री मन अपनी तमाम वर्जनाओं के बावजूद उभर कर आया। पवन करण की कविताओं में स्त्री अपने हक के लिए आवाज उठाना शुरू कर देती है। 'हक' कविता में स्त्री का अपने परिवार से संघर्ष मुखर है—

मैंने अपनी पसन्द के पुरुष को प्रेम- पत्र लिखा
तुमने मेरी पढ़ाई बन्द करवा दी
मैं अपनी चाहत के पुरुष से छुपकर मिली
तुमने घर के दरवाजों में कैद कर दिया मुझे

मैंने अपनी इच्छा के पुरुष से
प्रेम-विवाह करने को कहा, तुमने कोशिश की
मेरी जुबान पर ताला डालने की
मैंने तुम्हारी इच्छा के खिलाफ जाकर अपना ब्याह रचाया
तुमने मेरे साथ-साथ उसे भी मार डाला
या फिर मुझे मरा मान लिया हमेशा के लिए[14]

स्त्री का विरोध यहीं समाप्त नहीं होता। वह प्रश्न करती है, अपने परिवार से अपना हक माँगती है—

तुम भले ही मुझे मरा मान लो
और कभी मेरा चेहरा ना देखो
मगर उससे पहले मेरे हिस्से का पैसा तो मुझे दो
मेरे पूछने पर तुम ही तो कहते थे
हम अपने हक के लिए लड़ते आए हैं
प्रेम पर मेरा हक था तो पैसे पर भी तो मेरा हक है
क्या मुझे अब इसके लिए भी लड़ना पड़ेगा[15]

यह अपने अधिकार के प्रति सचेत स्त्री का स्वर है जो अपेक्षाकृत अधिक मुखर है। सभी स्त्रियाँ इतनी मुखर नहीं हो पाती। कुछ स्त्रियाँ विद्रोह नहीं करती, बस अचानक अपनी उड़ान से अपनी सोच समाज को सौंपती है। 'उड़ान' कविता में स्त्री की उसी सोच को कवि ने वाणी दी है। घर-परिवार स्त्री पर पाबन्दी लगाता है, वह नहीं जान पाता कि स्त्री अपने सपनों की उड़ान को, अपने परों को सबसे छुपा कर खुले आकाश में उड़ना सीख रही है। एक दिन वह अपने पूरे आत्मविश्वास के साथ सपनों के आकाश में उड़ जाती है। कवि सन्देश देता है—

जो घर स्त्री की उड़ान को
नहीं पहचानते
उनसे उड़कर जाने वाली स्त्रियाँ
कभी वापस नहीं लौटती
आकाश छूकर
बस उनकी उड़ान लौटती है[16]

ये सभी स्त्रियाँ समकालीन काव्य जगत की आधुनिक स्त्रियाँ हैं जो समाज के बीच अपनी स्थिति को स्वयं स्थापित करती हैं। पवन करण ने इसके अतिरिक्त इतिहास के पन्नों से उपेक्षित, विस्मृत करा दी गयी उन पौराणिक स्त्री पात्रों को

अपनी कविता में स्थान दिया है। पवन करण का प्रसिद्ध काव्य-संग्रह है—स्त्री' शतक'। यह दो खंडों में प्रकाशित है इसके प्रत्येक खंड में सौ कविताएँ हैं। ये सभी कविताएँ उन मिथकीय स्त्री पात्रों के प्रश्न हैं इस पुरुष वर्चस्ववादी समाज से कि क्यों उन्हें इस तरह बिसरा दिया गया? पवन करण का 'स्त्री-शतक' उनके काव्य जीवन की सबसे महत्त्वपूर्ण उपलब्धि है। यह काव्य-संग्रह स्त्री की वेदना, उसकी करुणा, उसकी निराशा या द्वन्द्व की ही अभिव्यक्ति नहीं है यह उसकी चैतन्य शक्ति, उसके साहस, उसके जीवन का जीवन्त आख्यान है। 'स्त्री-शतक' पुरुषवादी सत्ता के अहंकार पर एक प्रहार है।

'स्त्री-शतक' में कई-कई नारी पात्रों की कथा है जो अपने आँचल में कई-कई विमर्श छुपाए हुए हैं। पौराणिक आख्यान के अनुसार 'तारा' कविता में तारा बृहस्पति की पत्नी थी, जिसे बृहस्पति का शिष्य चन्द्रमा भगाकर ले जाता है और उन दोनों के अनैतिक संबंध से बुध का जन्म होता है—

यदि तुम्हें कभी तारा मिले तो उससे पूछना
तो वह बताएगी चमक का घर
गहरे अन्धेरे में डूबा रहता है
किसी पुरुष का किसी स्त्री के चेहरे में चन्द्र देख लेना चन्द्र को
खुद उसके चेहरे का पता बता देना है[17]

इसी सन्दर्भ में 'ममता' कविता में एक और स्त्री चरित्र उभरता है जो देव गुरु बृहस्पति के एक अन्य रूप से हमारी पहचान कराता है। ममता बृहस्पति के भाई उतथ्य की पत्नी जिसके साथ गर्भावस्था के दौरान बृहस्पति ने सम्भोग किया। वह बृहस्पति से प्रश्न करती है—

तुम कौन सा मुँह लेकर चन्द्र से
तारा को वापस माँगने जा रहे हो
भाई की पत्नी होते हुए भी तुमने
जिस तरह, अपमानित किया मुझे
चन्द्र ने तो वैसा नहीं किया तुम्हारे साथ[18]

इन सभी प्रश्नों के सामने हमारा इतिहास मौन है किन्तु पवन करण की कविताओं में ये सभी स्त्रियाँ दिल खोलकर अपनी व्यथा कथा कहती है। इन दुखिनी नारियों में केवल ऋषिकुल की नारियाँ ही नहीं, राजा-महाराजाओं की रानियाँ-दासियाँ, देव पत्नी तथा देव पुत्रियाँ, साथ ही पुरुषोत्तम कहलाने वाले देवताओं की बहनें भी हैं। मर्यादा पुरुषोत्तम दशरथ नन्दन राम की बहन शान्ता भी

दुःखी है। सरमा (रावण की दासी), सीता से शान्ता के बारे में प्रश्न करती है—

जब दशरथ उसे ऋषयश्रंग
को सौंप रहे थे तब क्या उसने
तुमसे कहा कि मैं किसी
ऋषि से नहीं राम भैया जैसे किसी
राजकुमार से ब्याह करना चाहती हूँ
भाभी तुम इन आर्यों को समझाओ न
कि वे मुझे यज्ञदान में नहीं सौंपे
मेरी पसन्द भी पूछे मुझसे, चलने दें
मेरी भी ब्याह की बात किसी योद्धा से[19]

एक और भी बहन है—एकानंगा (एकाँगा) जो गोकुल में कृष्ण की बहन है—

जैसे नाम सुनकर सब शान्ता का
जताते आश्चर्य/कि राम की बहन भी थी एक
अरे हमने तो सुना ही नहीं कभी
बारे में उस लुप्त भगिनी के
खुद की अनदेखी वे बहनें थीं हम
जो अपने-अपने कालखंड की
स्मृतियों में छूटती गयी सबसे पीछे
जबकि हम में से एक
कृष्ण की बहन थी और एक राम की[20]

देवराज इन्द्र, राजा बलि से धरती हथियाने के लिए अपनी पुत्री जयन्ति को वृद्ध शुक्र को दे देते हैं। तब कवि जयन्ति से प्रश्न करता है—

जयन्ति बूढ़े शुक्र की अंकशायिनी होने से पहले
तुमने खुद के बारे में नहीं सोचा
तुम्हें पिता की बात मानने से पहले
माँ शचि एक बार भी याद नहीं आई
नहुष से खुद को बचाने में सफल शचि
तुम्हें पितृ-आज्ञा न मानने का सुझाव देती
तुम्हें बताती कि तुम्हारे पिता को स्त्री-शीलता
दाँव पर लगाने में हिचक नहीं होती

नंदिनी और उर्वशी में अन्तर नहीं उसके लिए[21]

स्त्री शतक की स्त्रियाँ अपने अस्तित्व के प्रति अधिक जागरूक व सचेत मालूम पड़ती है। ऋषि दधीचि जिन्होंने अपनी हड्डियों का दान इन्द्र को दिया था वज्र निर्माण हेतु, उनकी पत्नी सुवर्चा का प्रश्न कितना सटीक है। 'सुवर्चा' कविता में वह अपने पति से प्रश्न करती है—

वज्र निर्माण के लिए अपनी हड्डियाँ
इन्द्र को सौंपते समय तुमने
मुझसे एक बार भी नहीं पूछा ऋषिवर
क्या बस मैं ही तुम्हारी अर्धांगिनी थी
तुम अर्धांग नहीं थे मेरे
क्या मेरी ही देह पर तुम्हारा
अधिकार था, तुम्हारी देह पर
कोई अधिकार नहीं था मेरा
फिर तुमने मेरी सहमति लिए बिना
अपना देह-आधार
कैसे दे दिया किसी को
तुम्हारी आज्ञा के बिना क्या मैं
कभी किसी को स्वयं का
कुछ सौंप सकती थी[22]

इसी प्रकार इस काव्य-संग्रह में कई मुखर नारी पात्र हैं—धृतराष्ट्र की दासी नयना, बाल विधवा उलूपी, घटोत्कच की पत्नी मोर्वी, विदुर की माँ इन्दु, राजा पृथु की पत्नी अर्ची, राजा शर्याति की पुत्री सुकन्या, शर्मिष्ठा, दुर्योधन की पत्नी भानुमति, भीम की पत्नी हिडिम्बा, कृष्ण की आठों पत्नियाँ, रायाणी आदि की अन्य-अन्य कथाएँ हैं। 'स्त्री-शतक' की भूमिका में राधावल्लभ त्रिपाठी जी लिखते हैं—"पवन करण ने इस शतक में आख्यानों को खंगालते हुए, मिथकों में गोता लगाते हुए ऐसे स्त्री पात्र हमारे सामने खड़े कर दिए हैं जिनकी अथाह व्यथा कथा प्राय: उपेक्षित अनजानी रह गयी है।"[23]

अत: निष्कर्ष रूप से कहा जा सकता है कि पवन करण की कविताएँ स्त्री मन का वह आइना है जहाँ से व्यक्ति स्त्री-जीवन को उसकी पूर्ण संवेदना के साथ

देख-सुन महसूस कर सकता है। आपकी कविताएँ स्त्री जीवन के विविध सन्दर्भों को नए-नए विषयों से रूबरू कराती हैं।

सन्दर्भ—

1. पवन करण : 'अस्पताल के बाहर टेलीफोन', राजकमल प्रकाशन, नई दिल्ली, सं. 2009, फ्लैप
2. पवन करण : 'स्त्री मेरे भीतर', राजकमल प्रकाशन, नई दिल्ली, सं. 2006, भूमिका 6-7
3. पवन करण : 'स्त्री मेरे भीतर', 'प्यार में डूबी हुई मां' राजकमल प्रकाशन, नई दिल्ली, सं. 2006, पृ. 92
4. पवन करण : 'कोट के बाजू पर बटन', राधाकृष्ण प्रकाशन, नई दिल्ली, सं. 2013, फ्लैप
5. पवन करण : 'कोट के बाजू पर बटन', 'अपने विवाह की तैयारी करती प्रेमिका' राधाकृष्ण प्रकाशन, नई दिल्ली, सं. 2013, पृ. 89-90
6. पवन करण : 'कोट के बाजू पर बटन', 'फोटो सेशन' राधाकृष्ण प्रकाशन, नई दिल्ली, सं. 2013, पृ. 45
7. वही पृ. 45
8. पवन करण : 'स्त्री मेरे भीतर', 'दरअसल उसे समझना खुद को समझना है' राजकमल प्रकाशन, नई दिल्ली, सं. 2006, पृ. 90
9. पवन करण : 'स्त्री मेरे भीतर', 'एक खूबसूरत बेटी का पिता' राजकमल प्रकाशन, नई दिल्ली, सं. 2006, पृ. 21
10. पवन करण : 'कोट के बाजू पर बटन', 'वह अब मुझसे भी डरने लगी है' राधाकृष्ण प्रकाशन, नई दिल्ली, सं. 2013, पृ. 20
11. वही पृ. 22
12. पवन करण : 'अस्पताल के बाहर टेलीफोन', 'पिता की आँख में पराई औरत' राजकमल प्रकाशन, नई दिल्ली, सं. 2009,पृ. 21-22
13. पवन करण : 'स्त्री मेरे भीतर', 'प्यार में डूबी हुई मां' राजकमल प्रकाशन, नई दिल्ली, सं. 2006, भूमिका 8-9
14. पवन करण : 'कल की थकान', 'हक' वाणी प्रकाशन, नई दिल्ली, सं. 2017, पृ. 62
15. वही पृ. 62-63
16. पवन करण : 'स्त्री मेरे भीतर', 'उड़ान' राजकमल प्रकाशन, नई दिल्ली, सं. 2006, पृ. 70
17. पवन करण : 'स्त्री-शतक' (प्रथम खंड), 'तारा', भारतीय ज्ञानपीठ प्रकाशन, नई दिल्ली, तृतीय सं. 2019 पृ. 17-18
18. पवन करण : 'स्त्री-शतक' (प्रथम खंड), 'ममता', भारतीय ज्ञानपीठ प्रकाशन, नई दिल्ली, तृतीय सं. 2019 पृ. 148
19. पवन करण : 'स्त्री-शतक' (प्रथम खंड), 'सरमा', भारतीय ज्ञानपीठ प्रकाशन, नई दिल्ली,

तृतीय सं. 2019 पृ. 47
20. पवन करण : 'स्त्री-शतक' (प्रथम खंड), 'एकानंगा', भारतीय ज्ञानपीठ प्रकाशन, नई दिल्ली, तृतीय सं. 2019 पृ. 130-131
21. पवन करण : 'स्त्री-शतक' (प्रथम खंड), 'जयन्ति', भारतीय ज्ञानपीठ प्रकाशन, नई दिल्ली, तृतीय सं. 2019 पृ. 24
22. पवन करण : 'स्त्री-शतक' (प्रथम खंड), 'सुवर्चा', भारतीय ज्ञानपीठ प्रकाशन, नई दिल्ली, तृतीय सं. 2019 पृ. 188
23. पवन करण : 'स्त्री-शतक' (प्रथम खंड), भारतीय ज्ञानपीठ प्रकाशन, नई दिल्ली, तृतीय सं. 2019 भूमिका 9-10

—सम्पर्क :
सहायक आचार्य, हिंदी विभाग
मोहनलाल सुखाड़िया विश्वविद्यालय,
उदयपुर (राज.)—पिन : 313001
फोन न. : 9950960999
ईमेल : nkntrivedi@gmail-com

❑❑❑



डॉ. नीतू परिहार
सह आचार्य एवं विभागाध्यक्ष,
हिन्दी-विभाग,
मोहनलाल सुखाड़िया विश्वविद्यालय, उदयपुर
मो. नं. : 9413864055
Email : neetuparihar11@gmail.com

लेखक परिचय

नाम : **डॉ. नीतू परिहार**

जन्म : 26 नवम्बर, 1974

शिक्षा : पीएच. डी., एम. ए (हिंदी, संस्कृत)

संप्रति : सह आचार्य एवं विभागाध्यक्ष हिंदी विभाग, मोहनलाल सुखाड़िया विश्वविद्यालय, उदयपुर (राजस्थान)

प्रकाशन : समकालीन हिंदी कविता का काव्यशास्त्र-2002, हिंदी नाट्य साहित्य और रंगमंच-2015, वागड़ का लोक साहित्य, (ई-पुस्तक)-2021, विभिन्न पत्र-पत्रिकाओं में साहित्य, संस्कृति और समाज विषयक शोध आलेख, समीक्षाएँ, समकालीन कविता पर शोध। वर्तमान में आप शिक्षा मंत्रालय के राष्ट्रीय उच्चतर शिक्षा अभियान प्रोजेक्ट 'वागड़ का लोक साहित्य' के सह अन्वेषक हैं।

अनुभव : गत 18 वर्षों से अध्यापन, शोध एवं शोध निर्देशन।

अक्षर प्रकाशन

ISBN : 978-81-86064-88-7

₹ : 500.00



कृष्ण साहित्य

(विविध संदर्भ)

सम्पादक
डॉ. नीतू परिहार

कृष्ण साहित्य : विविध संदर्भ

संपादक

डॉ० नीतू परिहार

अंकुर प्रकाशन
ANKUR PRAKASHAN

प्रतिलिप्याधिकार प्रकाशक व लेखक के अधीन सुरक्षित है। इनकी पूर्व लिखित अनुमति के बिना इस पुस्तक के किसी भी भाग का पुनः प्रकाशन वर्जित है। इस पुस्तक में व्यक्त विचार लेखकों के व्यक्तिगत हैं। इनसे किसी भी प्रकार की होने वाली हानि के लिए संपादक और प्रकाशक उत्तरदायी नहीं हैं। किसी भी विवादास्पद स्थिति में न्यायालय क्षेत्र उदयपुर मान्य होगा।

कृष्ण साहित्य : विविध संदर्भ

ISBN : *978-81-86064-98-6*

© : संपादक

मूल्य : चार सौ रुपये

संस्करण : 2023

प्रकाशक : अंकुर प्रकाशन
1/1 कांजी का हाटा, गायत्री मार्ग
उदयपुर (राज.) 313001
फोन नं. : (0294) 2417094, 2417039
(मो.) 9413528299
ईमेल : ankurprakashan15@gmail.com

आवरण : डॉ. शंकर शर्मा, उदयपुर

टाईपसेटिंग : देवेन्द्र कम्प्यूटर, दिल्ली

मुद्रक : रिसर्च प्रेस इण्डिया, दिल्ली

Krishna Sahitya : Vividh Sandarbh *(Hindi Literature)*

Edited By : Neetu Parihar

₹ 400

अनुक्रम

1	आत्म प्रबंधन : कृष्ण और गीता—प्रो. बी.एल. चौधरी	13
2	कृष्णभक्ति-परंपरा में सखी-भाव : प्रेमलक्षणा भक्ति का उत्कर्ष—डॉ. कृष्णचंद्र गोस्वामी 'विभास'	16
3	संप्रदाय मुक्त कृष्ण काव्य: चिंतन और चेतना के संदर्भ—प्रो. श्रद्धा सिंह	30
4	भक्ति साहित्य में कृष्ण—प्रो. कृष्ण कुमार शर्मा	37
5	राजस्थान में पुष्टिमार्गीय परम्परा एवं वल्लभाचार्य के सिद्धान्तों की व्यावहारिकता—डॉ. चन्द्रशेखर शर्मा	50
6	कृष्णभक्ति सरोवर में तैरता हंस : रसखान—डॉ. नीतू परिहार	64
7	मध्यकालीनकृष्ण भक्ति काव्यधारा: प्रमुख कवि और काव्य वैशिष्ट्य—डॉ. नवीन नंदवाना	71
8	भक्ति का लोक मार्ग : पुष्टि भक्ति संदर्भ—सूरसागर एवं पुष्टिवर्धन—डॉ. नवनीतप्रिया शर्मा	83
9	श्रीमद्भगवद्गीता में प्रतिपादित कर्मयोग एवं पुष्टिमार्ग —डॉ. प्रीति भट्ट	97
10	जैन आगमों में श्रीकृष्ण —डॉ. आशीष सिसोदिया	103
11	राधा की अंतरंग अनुभूतियों का गायन : कनुप्रिया —डॉ. नीता त्रिवेदी	111
12	रीतिकाल में कृष्ण भक्ति काव्य स्वरूप (बिहारी एवं घनानंद के विशेष संदर्भ में)—डॉ. कैलाश गहलोत	127

11

राधा की अंतरंग अनुभूतियों का गायन : कनुप्रिया

—डॉ. नीता त्रिवेदी

आधुनिककाल में कृष्ण साहित्य की दो महत्त्वपूर्ण कृतियाँ हैं—'अंधा युग' और 'कनुप्रिया'। इन दोनों कृतियों के रचनाकार एक ही है सर्वतो मुखी प्रतिभा संपन्न प्रख्यात कवि एवं कथाकार डॉ. धर्मवीर भारती। आपने साहित्य की कई विधाओं यथा कविता, कहानी, उपन्यास, नाटक, निबंध, आलोचना, अनुवाद, रिपोर्ताज आदि में अपनी लेखनी से विशिष्ट छाप छोड़ी है।

'अंधा युग' तथा 'कनुप्रिया' दोनों ही युद्ध और शांति के चरम क्षणों का काव्य है। दोनों में ही महाभारत के युद्ध और उसके बाद की अशांति, थकन, विवशता आदि पर लेखक के विचार हैं किंतु दोनों ही काव्य दो अलग-अलग ध्रुवों पर खड़े होकर युद्ध की विभीषिका को देख रहे हैं। कनुप्रिया में प्रेम की तन्मयता अपने चरम पर है। धर्मवीर भारती 'कनुप्रिया' की भूमिका में लिखते हैं दृश्लेखक के पिछले दृश्य काव्य में एक बिंदु से इस समस्या पर दृष्टिपात किया जा चुका है। गांधारी, युयुत्सु और अश्वत्थामा के माध्यम से। कनुप्रिया उनसे सर्वथा पृथक् बिल्कुल दूसरे बिंदु से चलकर उसी समस्या तक पहुँचती है, उसी प्रक्रिया को दूसरे भाव स्तर से देखती है और अपने अनजान में ही प्रश्न के ऐसे संदर्भ उद्घाटित करती है जो पूरक सिद्ध होते हैं। पर यह सब उसके अनजान में होता है क्योंकि उसकी मूल वृत्ति संशय या जिज्ञासा नहीं, भावाकुल तन्मयता है। कनुप्रिया की सारी प्रतिक्रियाएँ उसी तन्मयता की विभिन्न स्थितियाँ हैं।[1]

कनुप्रिया अर्थात कृष्ण की प्रिया, उनकी आराधिका-राधा। यह संपूर्ण काव्य राधा कृष्ण के प्रणयप्रसंग, कृष्ण के विरह में राधा की स्थिति, राधा की दृष्टि से कृष्ण, उनके प्रेम का अवलोकन करता है। उपमा ऋचा ने अपने एक लेख में

लिखा है—''कृष्ण को शरण देने वाला ये हृदय उसी आराधिका का है, जो पहले राधिका बनी और फिर राधिका से कृष्ण की आराध्या हो गई। कृष्ण आराधना करते हैं, इसलिए ये राधा है या ये कृष्ण की आराधना करती है, इसलिए राधिका कहलाती है। सच, बहुत कठिन है इसको परिभाषित करना क्योंकि इसकी परिभाषा स्वयं कृष्ण है खुद को असाधारण होने की सीमा तक साधारण बनाए रखने वाली ये किशोरी कृष्ण को अनायास ही मिली थी भागवत में। भागवत, रस का गीत है। उस गीत का रस भी और कोई नहीं, यही आराधिका है।''[12] पुरुष और प्रकृति के विविध प्रतीकों के माध्यम से सृष्टि के रहस्योद्घाटन के साथ ही प्रेम की तन्मयता और राधा की सहजता, विराटता और मन के कई सहज सुलभ प्रश्न हैं कनुप्रिया में जिनके प्रति उत्तर न तो इतिहास के पास है न ही वर्तमान के पास।

डॉ. धर्मवीर भारती 'कनुप्रिया' की भूमिका में इसे स्पष्ट करते हैं—''ऐसे तो क्षण होते ही हैं जब लगता है कि इतिहास की दुर्दांत शक्तियाँ अपनी निर्मम गति से बढ़ रही हैं, जिनमें कभी हम अपने को विवश पाते हैं, कभी विक्षुब्ध, कभी विद्रोही और प्रतिशोध युक्त, कभी वल्गाएँ हाथ में लेकर गतिनायक या व्याख्याकार, तो कभी चुपचाप शाप या सलीब स्वीकार करते हुए आत्मबलिदानी उद्धारक यात्राता[3], लेकिन ऐसे भी क्षण होते हैं जब हमें लगता है कि यह सब जो बाहर का उद्वेग है। महत्त्व उसका नहीं है। महत्त्व उसका है जो हमारे अंदर साक्षात्कृत होता है—चरम तन्मयता का क्षण जो एक स्तर पर सारे बाह्य इतिहास की प्रक्रिया से ज्यादा मूल्यवान सिद्ध होता है, जो क्षण हमें सीपी की तरह खोल गया है। इस तरह कि समस्त बाह्य,अतीत, वर्तमान और भविष्य, सिमटकर उस क्षण में पुंजीभूत हो गया है, और हम हम नहीं रहे।''[13]

'अंधायुग' में बाहर का उद्वेग अधिक है। 'कनुप्रिया' तो केवल चरम तन्मयता के उसी क्षण का काव्य है जिसके आलोक में बाह्य जगत भी उसी क्षण में समाहित हो जाता है। वैसे तो संपूर्ण काव्य ही राधा का आत्मकथन है किंतु जिस सहजता, जिस प्रेम की कसौटी पर राधा इस बाह्य जगत को, अपनी सृष्टि के केंद्र कान्हा को समझती है, परखती है वहीं राधा की तन्मयता संपूर्ण काव्य, समस्त चराचर से बड़ी हो जाती है इसी संदर्भ में भारती जी 'कनुप्रिया' की भूमिका में आगे लिखते हैं—''लेकिन वह क्या करें जिसने अपने मन से जीवन जिया है, तन्मयता के क्षणों में डूब कर सार्थकता पाई है, और जो अब उद्घोषित महानताओं से अभिभूत और आतंकित नहीं होता बल्कि आग्रह करता है कि वह उस सहज की कसौटी पर समस्त को कसेगा। ऐसा ही आग्रह है कनुप्रिया का।''[14]

'कनुप्रिया' राधा के मन की अंतरंग अनुभूतियों का गायन है, राधा का, उसके प्रेम का, सहज प्रस्फुटन है। प्रेम की सहजता से परिपक्वता की स्थिति तक की यात्रा है कनुप्रिया। भारती जी ने संपूर्ण काव्य को पाँच खंडों में विभक्त किया है—पूर्वराग-मंजरी, परिणय, सृष्टि-संकल्प, इतिहास तथा समापन, पूर्वराग-मंजरी, परिणय और सृष्टि-संकल्प के अंतर्गत राधा कृष्ण के बहुमुखी प्रणय के विविध आयामों से प्रेम की निर्मल अजस्र धारा प्रवाहित हो रही है जो इतिहास तथा समापन में कई मोड़ो से गुजरती हुई राधा और कृष्ण को एक नए रूप में व्याख्यायित करती है। एक नई दृष्टि प्रदान करती है। डॉ. परविंदर कौर के अनुसार—"कनुप्रिया राधा-कृष्ण के प्रेम का मनोवैज्ञानिक विकास है। पूर्वराग मंजरी, परिणय, सृष्टि-संकल्प, इतिहास और समापन के अंतर्गत राधा की प्रेमाभिव्यक्ति में कहीं भी अस्वाभाविकता का आभास नहीं होता, अपितु मनोवैज्ञानिक भाव-बोध है।"[5]

कृष्ण, महाभारत युद्ध के बाद नितांत एकाकी, थके हुए, व्याकुल, संशयग्रस्त होकर अपनी राधा को पुकारते हैं और राधा इसी क्षण की प्रतीक्षा में उसी अशोक वृक्ष के नीचे कृष्ण की प्रतीक्षा करती है कि कब उसके कृष्ण उन्हें पुकारे और राधा उन्हें अपने आंचल की छाया में विश्राम देकर सुला दे।

भारती जी ने 'कनुप्रिया' का प्रारंभ राधा के कैशोर्य-सुलभ मानवीय भावों से किया है धीरे.धीरे भावों का विकास एवं उनकी परिपक्वता उत्तरोत्तर विकसित होती है। लेखक ने भूमिका में लिखा है। "पूर्वरागा और मंजरी-परिणय उस विकास का प्रथम चरण, सृष्टि-संकल्प द्वितीय चरण तथा महाभारत काल से जीवन के अंत तक शासक, कूटनीतिज्ञ, व्याख्याकार कृष्ण के इतिहास निर्माण को 'कनुप्रिया' की दृष्टि से देखने वाले खंड-इतिहास तथा समापन इस विकास का तृतीय चरण चित्रित करते हैं।"[6]

पूर्वराग के पाँच गीत तथा मंजरी परिणय के तीन गीत राधा के प्रेम के सहज उच्छ्वास हैं जहाँ राधा के प्रेम की तन्मयता तथा किशोरावस्था का सहज एवं सरल मन अपनी समस्त कमनीयता के साथ मुखर है। सृष्टि-संकल्प में राधा कृष्ण का प्रेम एक अलौकिक आह्लाद, प्रकृति एवं पुरुष के विविध प्रतीकों के माध्यम से पल्लवित एवं प्रस्फुटित होता है। इतिहास खंड में इतिहास निर्माता, द्वारकाधीश, कूटनीतिज्ञ, गीतोपदेशक कृष्ण को कनुप्रिया अपने सहज प्रेम की कसौटी पर देखती है, समझती है, व्याख्यायित करती है। समापन राधा और कृष्ण के उसी प्रेम पर होता है जहाँ राधा कृष्ण की प्रतीक्षा में है और कृष्ण महाभारत युद्ध के पश्चात्

नितांत एकाकी, क्लांत और दुखी हैं। कृष्ण अधूरे हैं राधा के बिना और उन्हीं क्षणों में कृष्ण की पुकार पर प्रतीक्षारत राधा आती है कृष्ण से मिलने, उनकी थकान को दूर करने और उनके एकाकीपन को दूर करने।

भारती जी ने 'कनुप्रिया' में श्रीमद्भागवत के योगीश्वर कृष्ण को दृष्टि में रखते हुए वर्तमान संदर्भों को, समस्याओं को भावनात्मक रूप से समझाने का सार्थक प्रयास किया है। इसमें राधा-कृष्ण दोनों ही नवीन संदर्भों एवं नूतन रूप से उपस्थित हुए हैं। 'कनुप्रिया' के प्रारंभिक गीतों में कृष्ण के प्रेम की दिव्यता, अलौकिकता कई कई रूपों में प्रस्फुटित होती है। राधा-कृष्ण की प्रिया है। कनुप्रिया है, वह कृष्ण की आद्या शक्ति है, प्रकृति स्वरूपा है तथा कृष्ण पुरुष रूप में हैं। राधा प्रकृति के कण-कण में जीवन बनकर परिव्याप्त है। पूर्व राग के प्रथम गीत में ही अशोक वृक्ष राधा के चरणों के स्पर्श की प्रतीक्षा में जन्मों से पुष्पहीन खड़ा है—

ओपथ के किनारे खड़े
छायादार पावन अशोक-वृक्ष
तुम यह क्यों कहते हो कि
तुम मेरे चरणों के स्पर्श की प्रतीक्षा में
जन्मों से पुष्पहीन खड़े थे

प्रकृतिस्वरूपा राधा अशोक वृक्ष को समझाती है कि मैं तो कई कई रूपों में तुम्हीं में समाई हूँ—

तुम को क्या मालूम कि
मैं कितनी बार केवल तुम्हारे लिए।
धूल में मिली हूँ
धरती में गहरे उतर
जड़ों के सहारे
तुम्हारे कठोर तने के रेशों में
कलियाँ बन, कोंपलबन, सौरभ बन, लाली बन।
चुपके से सो गई हूँ
कि कब मधुमास आए और तुम कब मेरे
प्रस्फुटन से छा जाओ।[8]

कृष्ण राधा की सांसो में संगीत बनकर समाए हुए हैं। यह राधा के प्रेम की दिव्यता है जहाँ कृष्ण उनसे दूर होकर भी उन्हीं में समाहित है—

यह जो अकस्मात
आज मेरे जिस्म के सितार के
एक-एक तार में तुम झंकार उठे हो—
सच बतलाना मेरे स्वर्णिम संगीत
तुम कब से मुझ में छिपे सो रहे थे।[9]

इन गीतों में राधा कृष्ण के प्रेम की कई कई लीलाएं अभिव्यक्त हुई है। कृष्ण के प्रेम का सम्मोहनए राधा का समर्पण कई कई रूपों में मुखर होता है। एक रूपक दृष्टव्य है—

घाट से लौटते हुए
तीसरे पहर की अलसायी बेला में
मैंने अक्सर तुह्में कदंब के नीचे
चुपचाप ध्यानमग्न खड़े पाया
मैंने कोई अज्ञात वनदेवता समझ
कितनी बार तुह्में प्रणाम कर सिर झुकाया
पर तुम खड़े रहे अडिग, निर्लिप्त, वीतराग, निश्चल!
तुमने कभी उसे स्वीकारा ही नहीं।[10]

पर क्या ऐसा हो सकता है कि राधा का अभिवादन कृष्ण अस्वीकार कर दें। राधा भी मान करते हुए कृष्ण को प्रणाम करना छोड़ देती है पर क्या कृष्ण के सम्मोहन से छूटना इतना भी आसान हो सकता है। राधा के ही शब्दों में—

और क्या मुझे मालूम था कि
तुम केवल निश्चल खड़े नहीं रहे
तुह्में वह प्रणाम की मुद्रा और हाथों की गति
इस तरह भा गयी कि
तुम मेरे एक-एक अंग की एक-एक गति को
पूरी तरह बांध लोगे
इस संपूर्ण के लोभी तुम
भला उस प्रणाम मात्र को क्यों स्वीकारते?
और मुझ पगली को देखो कि मैं
तुह्में समझती थी कि तुम कितने वीतराग हो
कितने निर्लिप्त।[11]

राधा कृष्ण के प्रेम में इतनी बेसुध है कि उसे यमुना के सांवले जल में भी

कृष्ण का आभास होता है। उसे लगता है—

मानो यह यमुना की सांवली गहराई नहीं है
यह तुम हो जो सारे आवरण दूर कर
मुझे चारों ओर से कण-कण, रोम-रोम
अपने श्यामल प्रगाढ़ अथाह आलिंगन में पोर-पोर
कसे हुए हो।[12]

राधा के कृष्ण हर समय, हर पल उसके आसपास ही हैं। उनकी उपस्थिति का आभास राधा को प्रकृति के हर कण-कण में हो रहा है। राधा को रास की पूर्वस्मृति आती है तो उन्हें पश्चाताप भी होता है कि वह रास की रात में कृष्ण के पास से लौट क्यों आयी—

मैं उस दिन लौटी क्यों—
कण-कण अपने को तुम्हें देकर रीत क्यों नहीं गई?
तुमने तो उस रास की रात
जिसे अंशतरू भी आत्मसात किया
उसे संपूर्ण बनाकर
वापस अपने.अपने घर भेज दिया।[13]

पूर्वराग के इन पाँचों गीतों में राधा द्वारा कृष्ण की स्मृति के माध्यम से प्रेम के विविध दृश्य उपस्थित होते हैं। सुलभा बाजीराव ने इन गीतों के संबंध में कहा है—"पूर्वराग के पाँचों गीत स्त्री पुरुष के बीच उत्पन्न होने वाले अनुराग के उत्तरोत्तर अबाध गति से विकसित होने की कथा कहते हैं।"[14]

मंजरी परिणय के अंतर्गत तीन लंबे गीत हैं जिसमें राधा कृष्ण प्रेम के कई-कई बिम्ब, कई रूपक, कई प्रतीक, लौकिक-अलौकिक, कई-कई संकेत अभिव्यक्त होते हैं। राधा कैशोर्य की बाल सुलभ भावना में कई संकेत तो समझ जाती है और कई संकेत जिनके अर्थ उसे कृष्ण के जाने के बाद समझ आते हैं जिस कारण वह दुखी भी है, व्यथित भी। राधा कई-कई रूपों में अपने मनोभाव कृष्ण को समझाती है—

तुम्हारी जन्म-जन्मांतर की रहस्यमयी लीला की
एकांत-संगिनी मैं
इन क्षणों में अकस्मात
तुमसे पृथक नहीं हो जाती मेरे प्राण,
तुम यह क्यों नहीं समझ पाते कि लाज

सिर्फ जिस्म की नहीं होती
मन की भी होती है
एक मधुर भय
एक अनजान संशय
एक आग्रह भरा गोपन,
एक निर्व्याख्या वेदना या उदासी,
जो मुझे बार-बार चरमसुख के क्षणों में भी
अभिभूत कर लेती है।[15]

राधा को दुख है कि कृष्ण के बार-बार बांसुरी बजा कर बुलाने पर भी वह उस शाम आम्र मंजरियों के नीचे नहीं पहुँच पाई। कृष्ण द्वारा उदास मन से पगडंडी पर आम्र मंजरी को चूर-चूर कर बिखेर देने पर राधा कहती है—

यह तुमने क्या किया प्रिय!
क्या अपने अनजाने में ही
उस आम के बौर से मेरी क्वांरी उजली
पवित्र माँग भर रहे थे साँवरे![16]

राधा व्यथित है कि वह कृष्ण के आम के बोर का संकेत नहीं समझ पाई। वह कृष्ण से कहती है—

कतनी बार जब तुमने अर्द्धोन्मीलित कमल भेजा
तो मैं तुरंत समझ गई कि तुमने संझाबिरिया बुलाया है
कितनी बार जब तुमने अंजुरी भर-भर बेले के फूल भेजें
तो मैं समझ गई कि तुह्मारी अंजुरियों ने
किसे याद किया है
कितनी बार जब तुमने अगस्त्य के दो
उजले कटावदार फूल भेजें
तो मैं समझ गई कि
तुम फिर मेरे उजले कटावदार पाँवों में
तीसरे पहर—टीले के पास वाले
सहकार की घनी छांव में
बैठकर महावर लगाना चाहते हो।
आज अगर आम के बोर का संकेत नहीं भी
समझ पायी तो क्या इतना बड़ा मान ठान लोगे ?[17]

राधा कई-कई अर्थों, कई-कई रूपकों से कृष्ण को मनाती है। साथ ही 'तुम मेरे कौन हो?' गीत में कृष्ण के साथ अपने कई-कई संबंध जोड़ती है। हर संबंध में एक नया बिम्ब उभरता है और अंत में इन सभी संबंधों के मध्य से राधा का स्वयं से साक्षात्कार होता है और फिर समस्त सृष्टि, कृष्ण की हर लीला राधा में ही समाहित हो जाती है—

तो मुझे अकस्मात लगा है
कि मेरे अंग-अंग से ज्योति फूटी पड़ रही है
तुह्मारी शक्ति तो मैं ही हूँ
तुह्मारा संबल,
तुह्मारी योगमाया,
इस निखिल पारावार में ही परिव्याप्त हूँ
विराट,
सीमाहीन,
अदम्य,
दुर्दांत[18]

राधा और कृष्ण का प्रेम जब उस विराट स्वरूप को धारण कर लेता है जहाँ उन दोनों के अतिरिक्त समस्त सृष्टि में और किसी का अस्तित्व नहीं है। जहाँ राधा अपने आप से परिचित होती है। वह कहती है।

पर जब मुझे चेत हुआ
तो मैंने पाया कि हाय सीमा कैसी,
मैं तो वह हूँ जिसे दिग्वधू कहते हैं, कालवधू—
समय और दिशाओं की सीमाहीन पगडंडियों पर
अनंत काल से, अनंत दिशाओं में
तुह्मारे साथ-साथ चलती चली आ रही हूँ, चलती
चली जाऊँगी...
इस यात्रा का आदि न तो तुह्में स्मरण है न मुझे
और अंत तो इस यात्रा का है ही नहीं मेरे
सहयात्री![19]

भारती जी ने 'कनुप्रिया के सृष्टि-संकल्प के तीनों गीतों के माध्यम से राधा कृष्ण के प्रेम की विराटता को वाणी दी है। 'सृजन-संगिनी' गीत में सृष्टि के प्रत्येक कण में, उसकी गति-लय में, सृजन-विनाश, प्रवाह सभी में कृष्ण की इच्छा उनकी संकल्प शक्ति का विस्तार है और कृष्ण की संपूर्ण इच्छा का अर्थ

केवल और केवल राधा है—

और यह प्रवाह में बहती हुई
तुह्मारी असंख्य सृष्टियों का क्रम
महज हमारे गहरे प्यार
प्रगाढ़ विलास
और अतृप्त क्रीड़ा की अनंत पुनरावृत्तियाँ हैं—
ओ मेरे स्त्रष्टा
तुह्मारे संपूर्ण अस्तित्व का अर्थ है
मात्र तुह्मारी सृष्टि
तुह्मारी संपूर्ण सृष्टि का अर्थ है
मात्र तुह्मारी इच्छा
और तुह्मारी संपूर्ण इच्छा का अर्थ हूँ
केवल मैं!
केवल मैं!!
केवल मैं!!![20]

समस्त चराचर के प्रत्येक कण में राधा कृष्ण ही है। प्रकृति के संपूर्ण विस्तार में राधा कृष्ण का असीम प्रेम ही परिव्याप्त है। राधा कहती है—

अगर यह निखिल सृष्टि
मेरा ही लीलातन है
तुह्मारे आस्वादन के लिए।[21]

फिर भी राधा के मन में एक आदिम भय व्याप्त है। यह भय प्रकृति स्वरूपा राधा में सहज रूप से उदित होता है। वह अपनी शक्तियों को भी पहचानती है फिर भी एक आदिम भय उसमें है। वह कृष्ण से पूछती है—

और अगर यह चंद्रमा मेरी उंगलियों के
पोरों की छाप है
और मेरे इशारे पर घटता और बढ़ता है
और अगर यह आकाशगंगा मेरे ही
केश-विन्यास की शोभा है
और मेरे एक इंगित पर इसके अनंत
ब्रह्मांड अपनी दिशा बदल सकते हैं—
तो मुझे डर किससे लगता है

मेरे बंधु![22]

'केलिसखी' गीत प्रेम की, अभिसार की अभिव्यक्ति का गीत है। इस गीत में प्रेम की उद्दाम, उत्कंठा, व्याकुलता व्यक्त हुई है—

और भय,
आदिम भय,
तर्कहीन, कारणहीन भय जो
मुझे तुमसे दूर ले गया था, बहुत दूर—
क्या इसीलिए कि मुझे
दुगने आवेग से तुह्मारे पास लौटा लावे
और क्या यह भयकी ही काँपती उंगलियाँ हैं
जो मेरे एक-एक बंधन को शिथिल
करती जा रही हैं
और मैं कुछ कह नहीं पाती![23]

राधा स्वयं को, अपनी शक्तियों को भूल केवल उस क्षण में जीवंत होना चाहती है। प्रकृति अपनी बाह्य शक्तियों को समेट स्वयं में ही समा जाना चाहती है।

यह बाहर फैला-फैला समुद्र मेरा है
पर आज मैं उधर नहीं देखना चाहती
यह प्रगाढ़ अंधेरे के कंठ में झूमती
ग्रहों-उपग्रहों और नक्षत्रों की
ज्योतिर्माला मैं ही हूँ
और असंख्य ब्रह्माण्डों का
दिशाओं का,
समय का
अनंत प्रवाह! मैं ही हूँ
पर आज मैं अपने को भूल जाना चाहती हूँ[24]

इन अंतरंग क्षणों में, समय को बांधकर, दिशाओं को रोककर समस्त ब्रह्मांड में केवल कृष्ण और राधा ये दोनों ही हैं—

आओ मेरे अधैर्य !
दिशाएं घुल गई है
जगत लीन हो चुका है

समय मेरे अलक-पाश में बंध चुका है।
और इस निखिल सृष्टि के
अपार विस्तार में
तुह्मारे साथ मैं हूँ। केवल मैं—
तुह्मारी अंतरंग केलिसखी![25]

राधा कृष्ण की अंतरंग केलिसखी जिनके मिलने से सृष्टि का निर्माण होता है और राधा के थक कर सो जाने पर यह निखिल सृष्टि लय हो जाती है। कृष्ण पुनः अपने संकल्प और इच्छा के द्वारा राधा को जगाते हैं और पुनः सृष्टि का सृजन होता है। इस प्रकार असंख्य सृष्टियों का लय एवं पुनः सृजन राधा कृष्ण के अलौकिक प्रेम के संकल्प एवं इच्छा पर निर्भर है। अतः इस 'सृष्टि-.संकल्प' शीर्षक में राधा कृष्ण का प्रेम केवल लौकिक एवं दैहिक स्तर पर न होकर प्रकृति-पुरुष के दिव्य रूप से ओतप्रोत हो जाता है।

'इतिहास' शीर्षक से कृष्ण अब द्वारकाधीश, कूटनीतिज्ञ, महाभारत के नायक के रूप में उभरते हैं। यह शीर्षक कथा के चरमोत्कर्ष का केन्द्रीय बिंदु है जहाँ से कथा समापन की ओर आकर विराम लेती है। इतिहास खंड में सात गीत हैं 'विप्रलब्धा', 'सेतु : मैं', 'उसी आम के नीचे', 'अमंगल छाया', 'एक प्रश्न', 'शब्द : अर्थहीन' तथा 'समुद्र-स्वप्न'। 'समुद्र-स्वप्न' की ही अंतिम कड़ी समापन है।

'इतिहास' खंड में राधा का विरह मुखर है। कृष्ण के विरह में राधा अपना दर्प खोती जा रही है। 'विप्रलब्धा' कविता में राधा कहती है—

अब सिर्फ मैं हूँ, यह तन है, और याद है
खाली दर्पण में धुंधला-सा एक प्रतिबिंब
मुड़-मुड़ लहराता हुआ
निज को दोहराता हुआ![26]

'सेतु : मैं' कविता में राधा को इतिहास से शिकायत है, कान्हा से शिकायत है। इतिहास राधा को सेतु बनाकर कृष्ण को उससे छीनकर ले गया—

नीचे की घाटी से
ऊपर के शिखरों पर
जिसको जाना था वह चला गया—
हाय मुझी पर पग रख
मेरी बाहों से
इतिहास तुह्में ले गया![27]

राधा कृष्ण से प्रश्न करती है कि हे कनु, क्या मैं तुह्मारे लिए सिर्फ एक सेतु थी—

सुनो कनु, सुनो
क्या मैं सिर्फ एक सेतु थी तुह्मारे लिए
लीलाभूमि और युद्ध क्षेत्र के
अलंघ्य अंतराल में![28]

कृष्ण के द्वारकाधीश बनने में, सदी के महानायक बनने में बहुत कुछ ऐसा था जो पीछे छूट गया था। राधा उसी छूटे हुए बिंदु पर खड़े होकर कृष्ण से प्रश्न करती है—

तुह्मारे महान बनने में
क्या मेरा कुछ टूट कर बिखर गया है कनु![29]

कृष्ण के जीवन में आए परिवर्तन से राधा के मन में ऐसा बहुत कुछ है जो टूटकर बिखर गया है। राधा अब भी पथ के किनारे खड़े छायादार पावन अशोक-वृक्ष के नीचे कृष्ण की प्रतीक्षा में रोज आती है। आम के नए बौरों के पास हर रोज जाती है किंतु अब उसे वे सब अर्थहीन प्रतीत होते हैं—

नया है
केवल मेरा
सूनी माँग आना
सूनी माँग, शिथिल चरण, असमर्पिता
ज्यों का त्यों लौट जाना...[30]

'अमंगल छाया' गीत में राधा को युद्ध एक अमंगल छाया के रूप में दिखाई पड़ता है जो उसके गाँव पर छा रही है। कवि राधा से कहते हैं कि कृष्ण को पाने के लिए उस कदंब की राह से होकर ना जाना जहाँ कभी ध्यानमग्न कान्हा राधा को बाँसुरी बजा कर बुलाते थे क्योंकि आज उधर से कृष्ण की अठारह अक्षौहिणी सेनाएं युद्ध में भाग लेने जा रही है। यह भारती जी की मौलिक कल्पना है। कवि राधा को समझाता है कि कृष्ण तुह्मारा प्रिय है लेकिन तुह्मारे गाँव को रौंदती ये सेना तुह्में नहीं पहचानती क्योंकि सेना युद्ध का प्रतीक है और राधा प्रेम का पर्याय। स्वाभाविक है कि युद्ध प्रेम के प्रति अपरिचित बना रहे—

उदास क्यों होती है नासमझ
कि इस भीड़-भाड़ में
तू और तेरा प्यार नितांत अपरिचित
छूट गए हैं[31]

राधा कृष्ण के इस स्वरूप से नितांत अपरिचित है। वह तो केवल प्रेम जानती है या उतना ही जितना कृष्ण ने उसे समझाया है। राधा चाहती है कि अर्जुन की तरह कृष्ण उसे भी गीता ज्ञान समझा दे जिससे वह युद्ध, धर्माधर्म, पाप-पुण्य, न्याय-दंड, क्षमाशीलता आदि की सार्थकता समझ पाए—

जितनी समझ तुमसे अब तक पाई है कनु
उतनी बटोर कर भी
कितना कुछ है जिसका
कोई भी अर्थ मुझे समझ नहीं आता है
अर्जुन की तरह कभी
मुझे भी समझा दो
सार्थकता है क्या बंधु ?[32]

'शब्द : अर्थहीन' गीत में राधा कहती है कि इस सार्थकता को तुम मुझे कैसे समझोगे कनु ? क्योंकि ये सभी शब्द मेरे लिए अर्थहीन है—

कर्म, स्वधर्म, निर्णय, दायित्व...
मुझ तक आते-आते सब बदल गए हैं
मुझे सुन पड़ता है केवल
राधन्, राधन्, राधन्
शब्द, शब्द, शब्द,
तुह्मारे शब्द अगणित हैं कनु-संख्यातीत
पर उनका अर्थ मात्र एक है—
मैं, / मैं, / केवल मैं! फिर उन शब्दों से
मुझी को
इतिहास कैसे समझाओगे कनु ?[33]

'समुद्र-स्वप्न' गीत में कवि ने राधा को लक्ष्मी-स्वरूपा दर्शाया है। जो युग-युगों से विष्णु के साथ विराजित हैं। राधा उसी क्षीर-समुद्र को स्वप्न में देखती है। कृष्ण महाभारत युद्ध में जीतने के बाद भी उदास, कभी क्लांत, कभी विस्मित, कभी आहत होकर उसी समुद्र किनारे बैठे हैं। सब कुछ पाकर इतने खिन्न। कृष्ण के मन में अंतर्द्वंद्व है और यहाँ पुरुष पुनः प्रकृति की शरण में जाता है जहाँ प्रकृति स्वरूपा राधा कृष्ण को अपने प्रेम का अभयदान देती है। वह कहती है—

और चारों ओर
एक खिन्न दृष्टि से देख कर

एक गहरी सांस लेकर
तुमने असफल इतिहास को
जीर्णवसन की भाँति त्याग दिया है[34]

उस असफल इतिहास को त्यागने के बाद ही कृष्ण को पुनः राधा की याद आती है—

और अब इस क्षण तुम
केवल एक भरी हुई
पकी हुई
गहरी पुकार हो...
सब त्याग कर
मेरे लिए भटकती हुई...[35]

इसी का विस्तार 'समापन' गीत में होता है। कृष्ण की पुकार पर राधा आती है अपने कनु से मिलने—

और जनमांतरों की अनंत पगडंडी के
कठिनतम मोड़ पर खड़ी होकर
तुह्मारी प्रतीक्षा कर रही हूँ।
कि, इस बार इतिहास बनाते समय
तुम अकेले न छूट जाओ।[36]

राधा कृष्ण से प्रश्न करती है—

सुनो मेरे प्यार!
प्रगाढ़ केलिक्षणों में अपनी अंतरंग
सखी को तुमने बाहों में गूंथा
पर उसे इतिहास में गूंथने से हिचक क्यों गए प्रभु ?[37]

शायद इसी कारण कृष्ण उद्विग्न हो रहे थे क्योंकि राधा के बिना इतिहास कभी पूर्ण नहीं हो सकता क्योंकि प्रेम के बिना शब्द अर्थहीन ही रहते हैं। राधा कहती है—

बिना मेरे कोई भी अर्थ कैसे निकल पाता
तुह्मारे इतिहास का
शब्द, शब्द, शब्द ...
राधा के बिना
सब

रक्त के प्यासे
अर्थहीन शब्द![38]

अतः 'कनुप्रिया' के बिना कान्हा का इतिहास असफल ही रह जाएगा। सारी सृष्टि को शरण देने की सामर्थ्य भले ही कृष्ण में हो लेकिन कृष्ण को शरण देने की सामर्थ्य केवल 'कनुप्रिया' के हृदय में है। इस प्रकार भारती जी ने राधा कृष्ण की पौराणिक कथा को मौलिक परंपरा एवं नवीन बौद्धिकता प्रदान की है। 'कनुप्रिया' युद्ध पर प्रेम की जीत के साथ ही प्रेम का महाराग बनकर दिगंत पर छा जाता है। 'कनुप्रिया' की राधा वर्तमान संदर्भों में नारी चेतना, उसकी शक्ति, प्रेम के विस्तार, राधा की आल्हादिनी शक्ति का विस्तार है। राधा कृष्ण के प्रेम, उनकी लौकिक लीलाओं का अलौकिक विस्तार, पुरुष और प्रकृति के प्रेम का विस्तार 'कनुप्रिया' में सहज रूप से अभिव्यक्त होता है। भारती जी युद्ध की समस्या को प्रेम के दृष्टिकोण से देखते हैं।

संदर्भ—

1. धर्मवीर भारती : कनुप्रिया : भूमिका, भारतीय ज्ञानपीठ, लोदी रोड, नई दिल्ली, इक्कीसवाँ संस्करण, 2015
2. उपमा ऋचा : बूझत श्याम कौन तू गौरी, अहा! जिन्दगी, अगस्त 2012, सं. आलोक श्रीवास्तव, पृ. 26-27
3. धर्मवीर भारती : कनुप्रिया : भूमिका, भारतीय ज्ञानपीठ, लोदी रोड, नई दिल्ली, इक्कीसवां संस्करण, 2015
4. वही
5. डॉ. परविंदर कौर : कृष्ण काव्य परंपरा में धर्मवीर भारती का स्थान, भारतीय ग्रन्थ निकेतन, दरियागंज, नई दिल्ली, 2005 पृ. 48
6. धर्मवीर भारती : कनुप्रिया : भूमिका, भारतीय ज्ञानपीठ, लोदी रोड, नई दिल्ली, इक्कीसवाँ संस्करण, 2015
7. धर्मवीर भारती : कनुप्रिया, भारतीय ज्ञानपीठ, लोदी रोड, नई दिल्ली, इक्कीसवाँ संस्करण, 2015, पृ. 11
8. वही पृ. 11
9. वही पृ. 13
10. वही पृ. 14
11. वही पृ. 14-15
12. वही पृ. 16
13. वही पृ. 17
14. सुलभा बाजीराव पाटील, कनुप्रिया : एक मूल्यांकन, पंचशील प्रकाशन, जयपुर, सं. 1981,

पृ. 34
15. धर्मवीर भारती : कनुप्रिया, भारतीय ज्ञानपीठ, लोदी रोड, नई दिल्ली, इक्कीसवां संस्करण, 2015, पृ. 21
16. वही पृ. 23
17. वही पृ. 26
18. वही पृ. 36
19. वही पृ. 37
20. वही पृ. 44
21. वही पृ. 45
22. वही पृ. 47-48
23. वही पृ. 50-51
24. वही पृ. 52
25. वही पृ. 54
26. वही पृ. 57-58
27. वही पृ. 60
28. वही पृ. 60
29. वही पृ. 63
30. वही पृ. 63
31. वही पृ. 66
32. वही पृ. 68-69
33. वही पृ. 72
34. वही पृ. 76
35. पृ. 77
36. वही पृ. 81
37. वही पृ. 82
38. वही पृ. 82

सहायक आचार्य (हिंदी विभाग)
मोहनलाल सुखाड़िया विश्वविद्यालय,
उदयपुर (राज.)

❑



ISBN : 978-81-86064-98-6

9 788186 064986

₹ : 400.00

अंकुर
प्रकाशन

Pharmacognosy And Phytochemistry-I

Dr. Mukesh Kumar Meena, Ms. Pooja S Murkute, Dr. Mangilal Chouhan and Mr. M Mohammed Sahinsha

© 2023 @ Authors

All rights reserved. No part of this publication may be reproduced or transmitted in any form or by any means, without permission of the author. Any person who does any unauthorised act in relation to this Publication may be liable for criminal prosecution and civil claims for damage. [The responsibility for the facts stated, the conclusion reached, etc., is entirely that of the author. The publisher is not responsible for them, whatsoever.]

ISBN – 978-81-19152-11-7

Published by:

AGPH Books (Academic Guru Publishing House)

Bhopal, M.P. India

Contact: +91-7089366889

FIRST EDITION

PHARMACOGNOSY AND PHYTOCHEMISTRY -I



Dr. Mukesh Kumar Meena
Ms. Pooja S Murkute
Dr. Mangilal Chouhan
M Mohammed Sahinsha.

AGPH BOOKS
ACADEMIC GURU PUBLISHING HOUSE

Content

CHAPTER-1: Introduction to Pharmacognosy 1

1.1. Definition 1

1.2. History 6

1.3. Scope and Development of Pharmacognosy 9

1.4. Sources of Drugs – Plants, Animals, Marine & Tissue culture 12

1.5. Organized drugs 24

1.6. Unorganized drugs 25

1.7. Classification of drugs 26

1.8. Adulteration of drugs of natural origin 42

1.9. Evaluation by organoleptic, microscopic, physical, chemical, and biological methods and properties, camera lucida. 51

CHAPTER-2: Cultivation, Collection, Processing, and storage of drugs of natural origin **66**

2.1. Factors influencing cultivation of medicinal plants 66

2.2. Plant Hormones and their applications 78

2.3. Polyploidy, mutation, and hybridization

MEDICINAL CHEMISTRY

Published By: AGPH Books
(AG Publishing House)
Bhopal, M.P. India
Email : editor@agphbooks.com,
books@academicguru24x7.com
Website : www.agphbooks.com
Contact : **+91-7089366889**

Copyright © **2023 @ Authors**
Author Proof: Dr. Jaidev Kumar, Dr. Nisha Singh, Dr. Mangilal Chouhan and Dr. Santosh Kumar Nathsharma.
Layout & Cover: AGPH Books

ISBN: 978-81-19338-28-3

All rights reserved. No part of this publication may be reproduced or transmitted in any form or by any means, without permission of the author. Any person who does any unauthorized act in relation to this Publication may be liable to criminal prosecution and civil claims for damage.
[The responsibility for the facts stated, conclusion reaches, etc., is entirely that of the author. The publisher is not responsible for them, whatsoever]

Dr. Jaidev
Hariom Sa
(Uttarakhar
on topic "P
Potability a
Ground W
University,
Ambedkar U
"Analysis o
Research Pa
have been pu
in various N
500 National
written 10 bo
of being the
Research A
Horticulture
(H.R), M.Phil
Degree holde

Dr. Nisha Si
PhD in che
government s
2011 from G
teaching expe
in the

First Edition

MEDICINAL CHEMISTRY



Dr. Jaidev Kumar
Dr. Nisha Singh
Dr. Mangilal Chouhan
Dr. Santosh Kumar Nathsharma

AG PUBLISHING HOUSE
An ISO 9001:2015 Certified Company

TABLE OF CONTENT

CHAPTER-1: Introduction to Medicinal Chemistry 1

1.1. Introduction 1

1.2. History and development of medicinal chemistry. 3

1.3. Physicochemical properties in relation to biological action.....6

1.4. Drugs.....20

1.5. Properties of drugs relevant to controlled release formulations.....39

CHAPTER-2: Drug discovery process 42

2.1. A brief introduction to bioinformatics and chemoinformatics, Molecular modeling: 42

2.2. Drug discovery process.....47

2.4. Drug Receptors.....

2.5. Molecular docking: Rigid docking, flexible docking, manual docking 74

2.6. Biotransformation of drugs - Definition, types of biotransformation reactions, factors influencing drug metabolisms 81

CHAPTER-3: Pharmacokinetics and Pharmacodynamic 87

3.1. Pharmacokinetics 87

3.2. Pharmacodynamics.....100

CHAPTER-4: Drug Actions 132

4.1. General Introduction to Drug Action.....132

4.2. Antibacterial drugs 146

4.3. Antifungal drugs.....153

4.4. Antiviral drugs 158

4.5. Anticancer drugs.....

FIRST EDITION

PHARMACOGNOSY AND PHYTOCHEMISTRY -I



Dr. Mukesh Kumar Meena
Ms. Pooja S Murkute
Dr. Mangilal Chouhan
M Mohammed Sahinsha.

AGPH BOOKS

Content

CHAPTER-1: Introduction to Pharmacognosy 1

1.1. Definition.....1

1.2. History 6

1.3. Scope and Development of Pharmacognosy.....9

1.4. Sources of Drugs – Plants, Animals, Marine & Tissue culture.....12

1.5. Organized drugs 24

1.6. Unorganized drugs.....25

1.7. Classification of drugs.....26

1.8. Adulteration of drugs of natural origin 42

1.9. Evaluation by organoleptic, microscopic, physical, chemical, and biological methods and properties, camera lucida. 51

CHAPTER-2: Cultivation, Collection, Processing, and storage of drugs of natural origin 66

2.1. Factors influencing cultivation of medicinal plants 66

2.2. Plant Hormones and their applications 78

2.3. Polyploidy, mutation, and hybridization

Pharmacognosy And Phytochemistry-I

Dr. Mukesh Kumar Meena, Ms. Pooja S Murkute, D
Mangilal Chouhan and Mr. M Mohammed Sahinsha

© 2023 @ Authors

All rights reserved. No part of this publication may be
reproduced or transmitted in any form or by any mean
without permission of the author. Any person who doe
any unauthorised act in relation to this Publication may be
liable for criminal prosecution and civil claims for damage
[The responsibility for the facts stated, the conclusion
reached, etc., is entirely that of the author. The publisher is
not responsible for them, whatsoever.]

ISBN – 978-81-19152-11-7

Published by:

AGPH Books (Academic Guru Publishing House)

Bhopal, M.P. India

Contact: +91-7089366889

SPRINGER LINK

Log in

Menu Search Cart

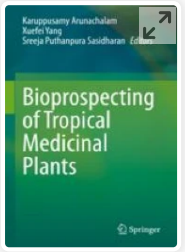

Bioprospecting of Tropical Medicinal Plants pp 767–788

Plant Metabolites as New Leads to Herbal Drug Discovery: Approaches and Challenges

Kapish Kapoor, Priyal Jain & Joohee Pradhan

Chapter | First Online: 31 August 2023

247 Accesses

Abstract

Natural products and structural counterparts have long played an important role in pharmacotherapy. Nonetheless, designing novel leads for drug discovery utilising natural chemicals is a difficult challenge. It covers the phytochemical analysis, characterisation, and pharmacological research of bioactive substances originating from natural resources. Because plant-derived metabolites and bioactive chemicals are readily available in a wide range of forms at low cost and do not cause major immune system responses, indigenous wisdom has

a wealth of information about many plants with various medicinal properties. That is why they are a viable and preferable alternative to synthetic substances as therapeutic medications. Drug discovery research requires the development of robust and viable lead molecules that go from a screening hit to a drug candidate by structural elucidation and structure identification using GC–MS, NMR, IR, HPLC, and HPTLC. The discovery of new medications has been transformed by the introduction of new technology for screening natural compounds. Utilising these tools, we will be able to conduct research into new molecule screening using software and databases, establishing natural products as a primary source for drug development. It eventually leads to the identification of lead structures. As research progresses, difficulties are thoroughly investigated in order to overcome the obstacles to obtaining therapeutic plant metabolites and then large-scale production of the same must be designed for industrial purposes. Here, we review recent technological advances that have made natural product-based drug discovery possible, highlight certain applications, and identify major potential.

Keywords

Herbal **Drug discovery** **Characterisation**

Phyto-chemistry **phytochemical analysis**

natural compounds

Kapish Kapoor, Priyal Jain, and Joohee Pradhan died before publication of this work was completed.

This is a preview of subscription content, log in via an institution.

Chapter EUR 29.95
Price includes VAT (India)

- Available as PDF
- Read on any device
- Instant download
- Own it forever

Buy Chapter

eBook EUR 213.99

Hardcover Book EUR 249.99

Tax calculation will be finalised at checkout

Purchases are for personal use only

Learn about institutional subscriptions

References

1. Lee ON, Ak G, Zengin G, Cziáky Z, Jekő J, Rengasamy KRR et al (2020) Phytochemical composition, antioxidant capacity, and enzyme inhibitory activity in callus, Somaclonal variant, and Normal green shoot tissues of Catharanthus roseus (L) G. Don. Molecules 25(21):4945

2. Rutterschmidt D, Kovács Z, Lorantfy L, Misek Z, Rajsch G (2015) Taxol purification with centrifugal partition chromatography. Planta Med 81(16):PW_152

3. Wang X, Tanaka M, Krstin S, Peixoto HS, Moura CCM, Wink M (2016) Cytoskeletal interference – a new mode of action for the anticancer drugs camptothecin and topotecan. Eur J Pharmacol 789:265–274

4. Balandrin MF, Kinghorn AD, Farnsworth NR (1993) Plant-derived natural products in drug discovery and development. Human medicinal agents from plants, ACS symposium series, 534. American Chemical Society, pp 2–12

5. Zhan ZJ, Bian HL, Wang JW, Shan WG (2010) Synthesis of physostigmine analogues and evaluation of their anticholinesterase activities. Bioorg Med Chem Lett 20(5):1532–1534

6. Landazuri P, Loango N, Restrepo B (2017) Medicinal plants used in the management hypertension. J Anal Pharm Res 5

7. Kumar A, Singh B, Sharma PR, Bharate SB, Saxena AK, Mondhe DM (2016) A novel microtubule depolymerizing colchicine analogue triggers apoptosis and autophagy in HCT-116 colon cancer cells. Cell Biochem Funct 34(2):69–81

8. Mcleod IK (2017) Local anesthetics. Medscape. Mechanism of action: hormones with intracellular receptors

9. Waldman HJ (1994) Centrally acting skeletal muscle relaxants and associated drugs. J Pain Symptom Manag 9(7):434–441

10. Fields A, Wiegand TJ (2014) Opium and the constituent opiates. In: Wexler P (ed) Encyclopedia of toxicology, 3rd edn. Academic Press, Oxford, pp 698–701

11. Raymon LP (2013) Pharmacology and mechanism of action of drugs. In: Siegel JA, Saukko PJ, Houck MM (eds) Encyclopedia of forensic sciences, 2nd edn. Academic Press, Waltham, pp 210–217

12. Woods KL (1986) The mode of action of cardiac glycosides. J Clin Hosp Pharm 11(1):11–13

13. Katiyar C, Gupta A, Kanjilal S, Katiyar S (2012) Drug discovery from plant sources: an integrated approach. Ayu 33(1):10–19

14. Ganesan A (2008) The impact of natural products upon modern drug discovery. Curr Opin Chem Biol 12(3):306–317

15. Sasidharan S, Chen Y, Dharmaraj S, Karupiah S, Lachimanan Y (2011) Extraction, isolation and characterization of bioactive compounds from plants? Extracts. Afr J Tradit Complement Altern Med 8:1–10

16. Chiu S, Wang T, Belski M, Abourashed EA (2016) HPLC-guided isolation, purification and characterization of Phenylpropanoid and phenolic constituents of nutmeg kernel

(Myristica fragrans). Nat Prod Commun 11(4):1934578X1601100416

17. Shah B, Seth A (2012) Textbook of pharmacognosy and phytochemistry – E-book. Elsevier Health Sciences

18. Konappa N, Udayashankar AC, Krishnamurthy S, Pradeep CK, Chowdappa S, Jogaiah S (2020) GC–MS analysis of phytoconstituents from Amomum nilgiricum and molecular docking interactions of bioactive serverogenin acetate with target proteins. Sci Rep 10(1):16438

19. Sharma M, Kaushik P (2021) Vegetable phytochemicals: an update on extraction and analysis techniques. Biocatal Agric Biotechnol 36:102149

20. Pavia D, Lampman G, Kriz G, Vyvyan J (2015) Introduction to spectroscopy. In: Pavia DL, Lampman GM, Kriz GS, Vyvyan JR (eds) A small scale approach to organic laboratory techniques. Cengage Learning

21. Rakhee MJ, Sharma RK, Misra K (2018) Chapter 9 – Characterization techniques for herbal products. In: Misra K, Sharma P, Bhardwaj A

(eds) Management of High Altitude Pathophysiology. Academic Press, pp 171–202

22. Bashir RA (2020) Phytochemical screening and Fourier transformed infrared spectroscopy(FT-IR) analysis of Vernonia amygdalina del. Methanol Leaf Extract

23. Hazra K (2019) Phytochemical investigation of terminalia bellirica fruit inside. J Pharm Clin Res 12(8):191–194

24. Velázquez Ríos IO, González-García G, Mellado-Mojica E, Veloz García RA, Dzul Cauich JG, López MG et al (2019) Phytochemical profiles and classification of agave syrups using (1)H-NMR and chemometrics. Food Sci Nutr 7(1):3–13

25. Barupal T, Meena M, Sharma K (2019) Inhibitory effects of leaf extract of Lawsonia inermis on Curvularia lunata and characterization of novel inhibitory compounds by GC–MS analysis. Biotechnol Rep 23:e00335

26. Padma MGS, Jayaseelan T, Azhagumadhavan S, Sasikala P, Senthilkumar S, Mani P (2019) Phytochemical screening and GC–MS analysis

of bioactive compounds present in ethanolic leaves extract of Silybum marianum (L). JDDT [Internet] 9(1):85–89

27. Shakya A, Correspondence A (2016) Medicinal plants: future source of new drugs. Int J Herb Med 4:59–64

28. Bernhoft A (2010) A brief review. In: Bernhoft A (ed) Bioactive compounds in plants—benefits and risks for man and animals. The Norwegian Academy of Science and Letters, Oslo, pp 11–17

29. Nema R, Khare S, Jain P, Pradhan A, Gupta A, Singh D (2013) Natural products potential and scope for modern cancer research. Am J Plant Sci 4:1270–1277

30. Kaur R, Kapoor K, Kaur HP (2011) Plants as a source of anticancer agents. J Nat Prod Plant Resour 1:119–124

31. Kumar S, Mishra A, Pandey AK (2013) Antioxidant mediated protective effect of Parthenium hysterophorus against oxidative damage using in vitro models. BMC Complement Altern Med 13(1):120

32. Khazir J, Mir BA, Pilcher L, Riley DL (2014) Role of plants in anticancer drug discovery. Phytochem Lett 7:173–181

33. Prakash O, Kumar A, Kumar P, Ajeet A (2013) Anticancer potential of plants and natural products: a review. Am J Pharmacol Sci 1(6):104–115

34. Cragg GM, Boyd MR, Cardellina JH 2nd, Newman DJ, Snader KM, McCloud TG (1994) Ethnobotany and drug discovery: the experience of the US National Cancer Institute. Ciba Found Symp 185:178–190; discussion 90-6

35. Rao PV, Nallappan D, Madhavi K, Rahman S, Jun Wei L, Gan SH (2016) Phytochemicals and biogenic metallic nanoparticles as anticancer agents. Oxidative Med Cell Longev 2016:3685671

36. Greenwell M, Rahman PKSM (2015) Medicinal plants: their use in anticancer treatment. Int J Pharm Sci Res 6(10):4103–4112

37. Lohani A, Verma A, Joshi H, Yadav N, Karki N (2014) Nanotechnology-based cosmeceuticals. ISRN. Dermatology 2014:843687

38. Alonso-Castro AJ, Villarreal ML, Salazar-Olivo LA, Gomez-Sanchez M, Dominguez F, Garcia-Carranca A (2011) Mexican medicinal plants used for cancer treatment: pharmacological, phytochemical and ethnobotanical studies. J Ethnopharmacol 133(3):945–972

39. Jena J, Gupta AK (eds) (2012) Ricinus communis linn: a phytopharmacological review

40. Pashaei-Asl F, Pashaei-Asl R, Khodadadi K, Akbarzadeh A, Ebrahimie E, Pashaiasl M (2018) Enhancement of anticancer activity by silibinin and paclitaxel combination on the ovarian cancer. Artif Cells Nanomed Biotechnol 46(7):1483–1487

41. Umadevi M, Rajeswari R, Rahale CS, Selvavenkadesh S, Pushpa R, Kumar KPS, Bhowmik D (2012) Traditional and medicinal uses of Withania Somnifera. Pharm Innov 1(9):102–110

42. Gajalakshmi S, Rajeswari D (2013) Pharmacological activities of Catharanthus

roseus: A perspective review. Int J Pharm Biosci 4:431–439

43. Sharma V, Sarkar IN (2013) Bioinformatics opportunities for identification and study of medicinal plants. Brief Bioinform 14(2):238–250

44. Akhtar MS, Swamy MK (2018) Anticancer plants: natural products and biotechnological implements, vol 2. Springer, Singapore

45. Rathinamoorthy R, Thilagavathi G (2014) Terminalia chebula – review on pharmacological and biochemical studies. Int J PharmTech Res 6:97–116

46. Raina H, Soni G, Jauhari N, Sharma N, Bharadvaja N (2014) Phytochemical importance of medicinal plants as potential sources of anticancer agents. Turk J Bot 38:1027–1035

47. Song Y-H, Sun H, Zhang A, Yan G-L, Han Y, Wang X-J (eds) (2014) Plant-derived natural products as leads to anti-cancer drugs

48. Atanasov AG, Waltenberger B, Pferschy-Wenzig EM, Linder T, Wawrosch C, Uhrin P et al (2015) Discovery and resupply of

pharmacologically active plant-derived natural products: a review. Biotechnol Adv 33(8):1582–1614

49. Zhou J, Du G, Chen J (2014) Novel fermentation processes for manufacturing plant natural products. Curr Opin Biotechnol 25:17–23

50. Fernando DR, Marshall AT, Forster PI, Hoebee SE, Siegele R (2013) Multiple metal accumulation within a manganese-specific genus. Am J Bot 100(4):690–700

51. Joshi K, Chavan P, Warude D, Patwardhan B (2004) Molecular markers in herbal drug technology. Curr Sci 87(2):159–165

52. Kala CPFN, Dhar U (2005) Traditional uses and conservation of Timur (Zanthoxylum armatum DC.) through social institutions in Uttaranchal Himalaya. India Conservat Soc 3:224–230

53. Rao MR, Palada MC, Becker BN (2004) Medicinal and aromatic plants in agroforestry systems. Agrofor Syst 61(1):107–122

54. Kala CP, Dhyani PP, Sajwan BS (2006) Developing the medicinal plants sector in

northern India: challenges and opportunities. J Ethnobiol Ethnomed 2(1):32

55. Cordell GA (2011) Sustainable medicines and global health care. Planta Med 77(11):1129–1138

56. Kingston DGI (2011) Modern natural products drug discovery and its relevance to biodiversity conservation. J Nat Prod 74(3):496–511

57. Narula A, Kumar S, Bansal K., Srivastava P (2004) Biotechnological approaches towards improvement of medicinal plants. In Plant biotechnology and molecular markers

58. Alam G, Peppelenbos L (2009) Cultivation of medicinal plants in Uttarakhand. Econ Polit Wkly 99–104

59. Ghayur MN, Gilani AH (2005) Gastrointestinal stimulatory and uterotonic activities of dietary radish leaves extract are mediated through multiple pathways. Phytotherapy research: An international journal devoted to pharmacological and toxicological evaluation of natural product derivatives 19(9):750–755

60. Cragg GM, Katz F, Newman DJ, Rosenthal J (2012) The impact of the United Nations convention on biological diversity on natural products research. Nat Prod Rep 29(12):1407–1423

61. Morrison C, Humphries F, Lawson C (2021) A regional review of genetic resource access and benefit sharing – key issues and research gaps. Environ Policy Law 51:1–24

62. David B, Wolfender J-L, Dias DA (2015) The pharmaceutical industry and natural products: historical status and new trends. Phytochem Rev 14(2):299–315

63. Koehn FE, Carter GT (2005) The evolving role of natural products in drug discovery. Nat Rev Drug Discov 4(3):206–220

64. Newman DJ (2008) Natural products as leads to potential drugs: an old process or the new Hope for drug discovery? J Med Chem 51(9):2589–2599

65. Evans BE, Rittle KE, Bock MG, DiPardo RM, Freidinger RM, Whitter WL et al (1988) Methods for drug discovery: development of potent, selective, orally effective

cholecystokinin antagonists. J Med Chem 31(12):2235–2246

66. Duarte CD, Barreiro EJ, Fraga CA (2007) Privileged structures: a useful concept for the rational design of new lead drug candidates. Mini Rev Med Chem 7(11):1108–1119

67. Mason JS, Morize I, Menard PR, Cheney DL, Hulme C, Labaudiniere RF (1999) New 4-point pharmacophore method for molecular similarity and diversity applications: overview of the method and applications, including a novel approach to the design of combinatorial libraries containing privileged substructures. J Med Chem 42(17):3251–3264

68. Kinghorn AD, Chin Y-W, Swanson SM (2009) Discovery of natural product anticancer agents from biodiverse organisms. Curr Opin Drug Discov Devel 12(2):189–196

69. Tsang CK, Qi H, Liu LF, Zheng XF (2007) Targeting mammalian target of rapamycin (mTOR) for health and diseases. Drug Discov Today 12(3-4):112–124

Author information

Authors and Affiliations

Department of Pharmaceutical Sciences, MLSU, Udaipur, Rajasthan, India

Kapish Kapoor & Joohee Pradhan

School of Pharmacy, Devi Ahilya Vishwavidyalaya, Indore, Madhya Pradesh, India

Priyal Jain

Corresponding author

Correspondence to Joohee Pradhan .

Editor information

Editors and Affiliations

Center for Studies in Stem Cells Cell Therapy and Toxicological Genetics (CeTroGen), Graduate Program in Health and Development in the Midwest RegionFaculty of Medicine (FAMED)Federal University of Mato Grosso do Sul (UFMS) Campo Grande, Cidade Universitária, Pioneiros, Mato Grosso do Sul, Brazil

Karuppusamy Arunachalam

Key Laboratory for Wild Plant Resources, Kunming Institute of Botany, Kunming, Yunnan, China

Xuefei Yang

Department of Botany, NSS College Nemmara, Palakkad, Kerala, India

Sreeja Puthanpura Sasidharan

Rights and permissions

Reprints and permissions

Copyright information

© 2023 The Author(s), under exclusive license to Springer Nature Switzerland AG

About this chapter

Cite this chapter

Kapoor, K., Jain, P., Pradhan, J. (2023). Plant Metabolites as New Leads to Herbal Drug Discovery: Approaches and Challenges. In: Arunachalam, K., Yang, X., Puthanpura Sasidharan, S. (eds) Bioprospecting of Tropical Medicinal Plants. Springer, Cham. https://doi.org/10.1007/978-3-031-28780-0_31

.RIS .ENW .BIB

DOI	Published	Publisher Name
https://doi.org/10.1007/978-3-031-28780-0_31	31 August 2023	Springer, Cham

Print ISBN	Online ISBN	eBook Packages
978-3-031-28779-4	978-3-031-28780-0	Biomedical and Life Sciences Biomedical and Life Sciences (R0)

Publish with us

Policies and ethics

SPRINGER LINK

Log in

Menu Search Cart

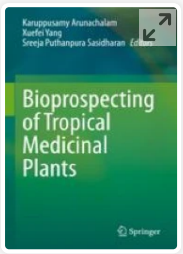

Bioprospecting of Tropical Medicinal Plants pp 821–861

Phyto-Constituents as Potential Leads for the Development of Novel Antiepileptic Drugs

Joohee Pradhan, Purnima Paliwal, Sunita Panchawat, Rohini Trivedi & Devshree Gayakwad

Chapter | First Online: 31 August 2023

250 Accesses

Abstract

Epilepsy is the major cause of morbidity and mortality despite the availability of varied drugs. The current antiepileptic drugs (AEDs), however, solve numerous problems, but still many adverse reactions are observed in patients for instance; enzyme induction; impact of these drugs on growth and bone metabolism; effect on visual performance, etc. Along with this, the drug resistance epilepsy still remains a problem. Most of the antiepileptic therapies focus on combined administration of two

or more AEDs, but this is still not the solution to existing complications. These facts dictate a clear-cut need of a novel, third-generation, safe, and effective AED. The safety and efficacy of herbal drugs in treatment of various ailments including epilepsy have been supported by a vast literature published time to time. The phyto-constituents present in these herbal sources, e.g., *Bacopa monnierie*, *Acanthus montanus*, *Alchornea laxiflora*, *Berberine*, and many others, were found to act potentially on AED targets, which are voltage-gated Ca^{2+} channel, voltage-gated K^{+} channels (A- or M-type), voltage-gated sodium channel, $GABA_A$ receptors, Nicotinic cholinergic receptors, Glycine receptor, NMDA receptor, AMPA receptor, and ionotropic glutamate receptors, etc. Thus, we have a large database of phyto-constituents, which are effective against various types of epilepsies; and through a systematic approach involving structure–activity relationship study, computational approach such as molecular docking and pharmacophore modeling, new and safer AED can be developed. Along with the pharmacological therapy of Epilepsy and problems associated with the use of AEDs, this chapter includes the antiepileptic activity of various herbal drugs available through literarure. Those phyto-constituents which are responsible for anti epileptic activity, can serve as possible leads for the development of new, safer third-generation antiepileptic drugs.

Keywords

Epilepsy **Antiepileptic drugs**

Herbal sources **Phyto-constituents**

Computer-aided drug design

This is a preview of subscription content, log in via an institution.

Chapter EUR 29.95
Price includes VAT (India)

- Available as PDF
- Read on any device
- Instant download
- Own it forever

Buy Chapter

eBook EUR 213.99

Hardcover Book EUR 249.99

Tax calculation will be finalised at checkout

Purchases are for personal use only

Learn about institutional subscriptions

References

1. Tripathi K (2018) Essential of medical pharmacology. Jaypee Brothers, Medical Publishers Pvt. Limited, New Delhi

2. WHO (2005) Epilepsy: the disorder. Epilepsy Atlas, pp 15–28. http://www.who.int/mental_health/neurology/Epilepsy_disorder_rev1.pdf

3. Devinsky O, Vezzani A, O'Brien TJ, Jette N, Scheffer IE, De Curtis M, Perucca P (2018) Epilepsy. Nat Rev Dis Prim 4:18024

4. Berkovic FS, Mulley CJ, Scheffer EI, Petrou S (2006) Human epilepsies: interaction of genetic and acquired factor. Trends Nuerosci 29(7):391–397. https://doi.org/10.1016/j.tins.2006.05.009

5. Engle J Jr (1989) Commission on classification and terminology of the international league against epilepsy, "Proposal for revised classification of epilepsies and epileptic syndromes". Epilepsia 30:389–399

6. Ciecka J (1982) Book reviews: book reviews. Rev Soc Econ 40(1):76–78. https://doi.org/10.1080/00346768200000024

7. Sirven Joseph I (2015) Epilepsy: a spectrum disorder. Cold Spring Harb Perspect Med 5. https://doi.org/10.1101/cshperspect.a022848

8. Perucca P, Scheffer IE, Kiley M (2018) The management of epilepsy in children and adult. Med J Aust:226–233. https://doi.org/10.5694/mja17.00951

9. Giridhar BN, Srinivasu CC, Raju PT, Lakshmana DN (2015) Estimation of trace elements concentration in anti-epileptic medicinal plants by using EDXRF. Int J Sci Res (IJSR) 4(2):211–216. https://doi.org/10.21275/SUB15931

10. Beghi E (2019) The epidemiology of epilepsy. Neuroepidemiology:1–7. https://doi.org/10.1159/000503831

11. Patrick K, Steven SC, Martin BJ (2011) Drug resistance epilepsy. Eng J Med:919–926. https://doi.org/10.1056/NEJMra1004418

12. Rajakulendran S, Hanna MG (2016) The role of calcium channels in epilepsy. Cold Spring Harb Perspect Med. https://doi.org/10.1101/cshperspect.a022723

13. Kohl M, Paulsen O (2010) The roles of $GABA_B$ receptor in cortical network activity. Adv Pharmacol:205–229. https://doi.org/10.1016/S1054-3589(10)58009-8

14. Go T (2004) Carbamazepine-induced IgG1 and IgG2 deficiency associated with B cell maturation defect. Seizure:187–190. https://doi.org/10.1016/S1059-1311(03)00086-4

15. Lasoń W, Chlebicka M, Rejdak K (2013) Research advances in basic mechanisms of seizures and antiepileptic drug action. Pharmacol Rep:787–801. https://doi.org/10.1016/S1734-1140(13)71060-0

16. Hass M, Forbush B III (2009) The Na-K-Cl cotrnasporte of secretory epithelia. Annu Rev Physiol 62:15–34

17. Sen A, Martinian L, Nikolic M, Walker MC, Thom M, Sisodiya SM (2007) Increased NKCC1 expression in refractory human epilepsy. Epilepsy Res:220–227. https://doi.org/10.1016/j.eplepsyres.2007.01.004

18. Arun SK, Ekta R, Abdul W, Satyendra RK (2015) Pharmacoresistant epilepsy: a current update on non-conventional pharmacological and non-pharmacological interventions. J Epilepsy Res 5(1). https://doi.org/10.14581/jer.15001

19. Meador KJ, Gilliam FG, Kanner AM, Pellock JM (2001) Cognitive and behavioral effects of antiepileptic drugs. Epilepsy Behav 2:SS1–SS17. https://doi.org/10.1006/ebeh.2001.0235

20. Karaya A, Burak O, Selçuk İ, Co M (2019) Epilepsy & behavior serum NGF levels may be associated with intrauterine antiepileptic exposure-related developmental problems. Epilepsy Behav:60–66. https://doi.org/10.1016/j.yebeh.2019.05.013

21. Dana-Haeri J, Oxley J, Richens A (1984) Pitutary responsiveness to gonadotrophin-releasing and thyrotrophin-releasing hormone in epileptic patients reciving carbamazepine or phenytoin. Clin Endocrinol:163–168. https://doi.org/10.1111/j.1365-2265.1984.tb00071.x

22. Spina E, Perucca E (2002) Clinical significance of pharmacokinetic interactions between antiepileptic and psychotropic drugs. Epilepsia:37–44.

https://doi.org/10.1046/j.1528-1157.2002.043s2037.x

23. Vecht JC, Wagner LG, Wilms BE (2003) Interaction between antiepilectic and chemotherapeutic drugs. Lancet Neurol:404–409. https://doi.org/10.1016/S1474-4422(03)00435-6

24. Isojärvi JIT (1993) Serum lipid levels during carbamazepine medication. Arch Neurol:17–20. https://doi.org/10.1001/archneur.1993.00540060030012

25. Mintzer S, Mattson RT (2009) Should enzyme-inducing antiepileptic drugs be considered first-line agents. Epilepsia:42–50. https://doi.org/10.1111/j.1528-1167.2009.02235.x

26. Ahmed SN, Siddiqi AZ (2006) Antiepileptic drugs and liver disease. Seizure:156–164. https://doi.org/10.1016/j.seizure.2005.12.009

27. Arroyo S, Morena A (2001) Life-threatening adverse events of antiepileptic drugs. Epilepsy Res:155–174. https://doi.org/10.1016/S09201211(01)00306-0

28. Sheth RD (2004) Bone health in epilepsy. Lancet Neurol:516. https://doi.org/10.1016/S1474-4422(04)00848-8

29. Musa A, Haluk S, Ercan M (2003) Evaluation of bone mineral density with dual x-ray absorptiometry for osteoporosis in children with bladder augmentation. J Pediatr Surg:230–232. https://doi.org/10.1053/jpsu.2003.50050

30. Ludwig B, Marsan CA (1975) Clinical ictal pattern in epileptic patients with occipital electroencephalographic foci. Neurology:463–471. https://doi.org/10.1212/wnl.25.5.463

31. Hermann B, Meador JK, Gaillard DW, Cramer AJ (2010) Cognition across the lifespan: antiepileptic drugs, epilepsy, or both? Epilepsy Behav:1–5. https://doi.org/10.1016/j.yebeh.2009.10.019

32. Blumer D, Montouris G, Hermann B (1995) Psychiatric morbidity in seizure patients on a neurodiagnostic monitoring unit. Neuropsychiatry Clin Neurosci:445–456. https://doi.org/10.1176/jnp.7.4.445

33. Cramer JA, Mintzer S, Wheless J, Mattson RH (2010) Adverse effects of antiepileptic drugs: a brief overview of important issues. Expert Rev Neurother:885–891. https://doi.org/10.1586/ern.10.71

34. Besag Frank MC (2004) Behavioural effects of the newer antiepileptic drugs: an update. Expert Opin Drug Saf:1–8. https://doi.org/10.1517/14740338.3.1.1

35. Parker WA, Shearee CA (1979) Phenytoin hepatotoxicity: a case report and review. Neurology:175–178. https://doi.org/10.1212/wnl.29.2.175

36. Anderson GD (2002) Children versus adults: pharmacokinetic and adverse-effect differences. Epilepsia:53–59. https://doi.org/10.1046/j.15281157.43.s.3.5.x

37. Arif H, Buchsbaum R, Weintraub D, Koyfman S, Salas-Humara C, Bazil CW, Resor SR, Hirsch LJ (2007) Comparision and predictors of rash associated with 15 antiepileptic drugs. Neurology:1701–1709. https://doi.org/10.1212/01.wnl.0000261917.83337.db

38. Perucca P, Gilliam GF (2012) Adverse effects of antiepileptic drugs. Lancet Neurol:792–802. https://doi.org/10.1016/S1474-4422(12)70153-9

39. Fricke-Galindo I, Jung-cook H, Lerena A, Lopez-Lopez M (2018) Pharmacogenetics of adverse reactions to antiepileptic drugs. Neurologia:165–176. https://doi.org/10.1016/j.nrl.2015.03.005

40. Moore TJ, Weiss SR, Kaplan S Blaisdell CJ (2002) Reported adverse drug events in infants and children under 2 years of age. Pediatrics:1–5. https://doi.org/10.1542/peds.110.5.e53

41. Mathis LL, Lyasu S (2007) Safety monitoring of drugs granted exclusivity under the best pharmaceuticals for children act: what the FDA has learned. Clin Pharm Therap:133–134. https://doi.org/10.1038/sj.clpt.6100285

42. McSherry E (1978) Acidosis and growth in nonuremic renal disease. Kidney Int:349–354. https://doi.org/10.1038/ki.1978.135

43. Camfield P, Camfield C (2006) Monitoring for adverse effects of antiepileptic drugs. Epilepsia:31–34.

https://doi.org/10.1111/j.15281167.2006.00657.x

44. Liu W, Ge T, Pan Z, Leng Y, Lv J, Li B (2017) The effects of herbal medicine on epilepsy. Oncotarget:48385–48397. https://doi.org/10.18632/oncotarget.16801

45. Pradhan J, Sunita P (2018) Herbal therapies for epilepsy: chemistry, biology and potential applications of selected plants and compounds. Chem Biol Interface 8(4):205–224

46. Tripathi M, Reddy P, Rawat D (2014) Chemistry and biology interface. Chem Biol 4:1–22

47. Ragsdale D, McPhee J, Scheuer T, Catterall W (1994) Molecular determinants of state-dependent block of Na^+ channels by local anesthetics. Science:1724–1728. https://doi.org/10.1126/science.8085162

48. Ragsdale D, McPhee J, Scheuer T, Catterall W (1996) Common molecular determinants of local anesthetic, antiarrhythmic, and anticonvulsant block of voltagegated Na+ channels. Proc Natl Acad Sci:9270–9275. https://doi.org/10.1073/pnas.93.17.9270

49. Yarov-Yarovoy V, Brown J, Sharp EM, Clare JJ, Scheuer T, Catterall WA (2001) Molecular determinants of voltage-dependent gating and binding of pore-blocking drugs in transmembrane segment IIIS6 of the Na+ channel alpha subunit. J Biol Chem:20–27. https://doi.org/10.1074/jbc.M006992200

50. Drew CDM (2000) Instant pharmacology. Postgrad Med J 76(896):381–381a. https://doi.org/10.1136/pmj.76.896.381a

51. Ffrench-Mullen JM, Barker JL, Rogawski MA (1993) Calcium current block by (−)-pentobarbital, phenobarbital, and CHEB but not (+)-pentobarbital in acutely isolated hippocampal CA1 neurons: comparison with effects on GABA-activated Cl- current. J Neurosci 13(8):3211–3221. https://doi.org/10.1523/jneurosci.1308-03211.1993

52. Stefani A, Spadoni F, Siniscalchi A, Bernardi G (1996) Lamotrigine inhibits Ca2+ currents in cortical neurons: functional implications. Eur J Pharmacol 307:113–116. https://doi.org/10.1016/0014-2999(96)00265-8

53. Pisani A, Bonsi P, Martella G, De Persis C, Costa C, Pisani F, Bernardi G, Calabresi P (2004)

Intracellular calcium increase in epileptiform activity. Epilepsia 45(7):719–728. https://doi.org/10.1111/j.0013-9580.2004.02204.x

54. Hainsworth HA, Nicolle MCL, Alexey P, Toni S, Andrew RD (2003) Actions of sipatrigine, 202W92 and lamotrigine on R-type and T-type Ca2+ channel currents. Eur J Pharmacol 467(1–3):77–80. https://doi.org/10.1016/S0014-2999(03)01625-X

55. Arias RL, Bowlby RM (2005) Pharmacological characterization of antiepileptic drugs and experimental analgesics on low magnesium-induced hyperexcitability in rat hippocampal slices. Brain Res 1047(2):233–244. https://doi.org/10.1016/j.brainres.2005.04.052

56. Monaghan EP, McAuley JW, Data JL (1999) Ganaxolone: a novel positive allosteric modulator of the GABA(A) receptor complex for the treatment of epilepsy. Expert Opin Investig Drugs 8(10):1663–1671. https://doi.org/10.1517/13543784.8.10.1663

57. Scheffer IE, Bhatia KP, Lopes-Cendes I, Fish DR, Marsden CD, Andermann E, Andermann F, Desbiens R, Keene D, Cendes F, Manson JI, Constantinou JEC, McIntosh A, Berkovic SF

(1995) Autosomal dominant nocturnal frontal lobe epilepsy. Brain 118(1):61–73. https://doi.org/10.1093/brain/118.1.61

58. Steinlein OK, Mulley JC, Propping P, Wallace RH, Phillips HA, Sutherland GR, Scheffer IE, Berkovic SF (1995) A missense mutation in the neuronal nicotinic acetylcholine receptor α4 subunit is associated with autosomal dominant nocturnal frontal lobe epilepsy. Nat Genet 11(2):201–203. https://doi.org/10.1038/ng1095-201

59. Mayer ML, Armstrong N (2004) Structure and function of glutamate receptor ion channels. Annu Rev Physiol 66(1):161–181. https://doi.org/10.1146/annurev.physiol.66.050802.084104

60. Bowery NG, Smart TG (2006) GABA and glycine as neurotransmitters: a brief history. Br J Pharmacol 147:109–119. https://doi.org/10.1038/sj.bjp.0706443

61. Bowery NG, Hill DR, Hudson AL, Middlemiss DN, Shaw J, Turnbull M (1980) (−)Baclofen decreases neurotransmitter release in the mammalian CNS by an action at a novel GABA receptor. Nature 283(5742):92–94. https://doi.org/10.1038/283092a0

62. Brogi S (2019) Computational approaches for drug discovery. Molecules 24(17):3061. https://doi.org/10.3390/molecules24173061

Author information

Purnima Paliwal, Sunita Panchawat, Rohini Trivedi and Devshree Gayakwad contributed equally with all other contributors.

Authors and Affiliations

Department of Pharmaceutical Sciences, Mohanlal Sukhadia University, Udaipur, Rajasthan, India
Joohee Pradhan & Sunita Panchawat

School of Pharmacy, Devi Ahilya Vishwavidyalaya, Indore, Madhya Pradesh, India
Purnima Paliwal

Department of Botany, Mohanlal Sukhadia University, Udaipur, Rajasthan, India
Rohini Trivedi

Acropolis Institute of Pharmaceutical Education and Research, Indore, Madhya Pradesh, India
Devshree Gayakwad

Corresponding author

Correspondence to Joohee Pradhan .

Editor information

Editors and Affiliations

Center for Studies in Stem Cells Cell Therapy and Toxicological Genetics (CeTroGen), Graduate Program in Health and Development in the Midwest RegionFaculty of Medicine (FAMED)Federal University of Mato Grosso do Sul (UFMS) Campo Grande, Cidade Universitária, Pioneiros, Mato Grosso do Sul, Brazil

Karuppusamy Arunachalam

Key Laboratory for Wild Plant Resources, Kunming Institute of Botany, Kunming, Yunnan, China

Xuefei Yang

Department of Botany, NSS College Nemmara, Palakkad, Kerala, India

Sreeja Puthanpura Sasidharan

Rights and permissions

Reprints and permissions

Copyright information

© 2023 The Author(s), under exclusive license to Springer Nature Switzerland AG

About this chapter

Cite this chapter

Pradhan, J., Paliwal, P., Panchawat, S., Trivedi, R., Gayakwad, D. (2023). Phyto-Constituents as Potential Leads for the Development of Novel Antiepileptic Drugs. In: Arunachalam, K., Yang, X., Puthanpura Sasidharan, S. (eds) Bioprospecting of Tropical Medicinal Plants. Springer, Cham. https://doi.org/10.1007/978-3-031-28780-0_34

.RIS .ENW .BIB

DOI	Published	Publisher Name
https://doi.org/10.1007/978-3-031-28780-0_34	31 August 2023	Springer, Cham

Print ISBN	Online ISBN	eBook Packages
978-3-031-28779-4	978-3-031-28780-0	Biomedical and Life Sciences Biomedical and Life Sciences (R0)

Publish with us

Policies and ethics

alzheimersanddementia.com Volume 19, Issue S13

Alzheimer's & Dementia

THE JOURNAL OF THE ALZHEIMER'S ASSOCIATION

AAIC 2023 ABSTRACTS

Basic Science and Pathogenesis – Part 2



ALZHEIMER'S ASSOCIATION | AAIC 23

WILEY

Alzheimer's & Dementia

THE JOURNAL OF THE ALZHEIMER'S ASSOCIATION

Volume 19, Issue S13 December 2023

EDITORIAL BOARD

Editor-in-Chief

Donna M. Wilcock
Indianapolis, IN
E-mail: dwilcock@iu.edu

Deputy Editor

Lisa L. Barnes
Chicago, IL

Founding Editor

Zaven S. Khachaturian
Rockville, MD

Emeritus Editor-in-Chief

Zaven S. Khachaturian
Rockville, MD

Emeritus Executive Editor

Ara S. Khachaturian
Rockville, MD

Senior Associate Editors

Susan Abushakra, Boston, MA
Liana Apostolova, Indianapolis, IN
Maria Corrada, Irvine, CA
Barry Greenberg, Baltimore, MD
Samuel Gandy, New York, NY
Harald Hampel, Woodcliff Lake, NJ
Pei Jung Lin, Boston, MA
Rima Kaddurah-Daouk, Durham, NC
Walter Kukull, Seattle, WA
Michael Lutz, Durham, NC
Soeren Mattke, Los Angeles, CA
M Marsel Mesulam, Chicago, IL
Michelle Mielke, Winston-Salem, NC
Richard Mohs, Chicago, IL
Yi Tang, Beijing, China
Stefan Teipel, Rostock, Germany
Henrik Zetterberg, Stockholm, Sweden

Associate Editors

Lars Bertram, Lübeck, Germany
Paul Coleman, Tempe, AZ
Brittany Duggar, Davis, CA
Michael Ewers, Frankfurt, Germany
Margaret Ellen Flanagan, Chicago, IL
Michael Gold, Chicago, IL
Hector González, San Diego, CA
Deborah Gustafson, New York, NY
John Kauwe, Provo, UT
Lewis Kuller, Pittsburgh, PA
Virginia Lee, Philadelphia, PA
Samuel Lockhart, Winston-Salem, NC
José Luís Molinuevo Guix, Barcelona, Spain
John Morris, St. Louis, MO
Rachel Nosheny, San Fransisco, CA
Brea Louise Perry, Bloomington, IN
Julie Robillard, Vancouver, BC
Dominic Trepel, Dublin, Ireland
Michael Weiner, San Francisco, CA
Sharon Xie, Philadelphia, PA
Julie Zissimopoulos, Los Angeles, CA

Science Editors

Daniel Burns, Durham, NC
Alexander Ehrenberg, San Francisco, CA
Emma Nichols, Baltimore, MD
Yakeel Quiroz, Boston, MA
Nilufer Taner, Jacksonville, FL
Auriel Willette, Ames, IA

15525279, 2023, S13, Downloaded from https://alz-journals.onlinelibrary.wiley.com/doi/10.1002/alz.13648, Wiley Online Library on [19/02/2024]. See the Terms and Conditions (https://onlinelibrary.wiley.com/terms-and-conditions) on Wiley Online Library for rules of use; OA articles are governed by the applicable Creative Commons License

Alzheimer's & Dementia

THE JOURNAL OF THE ALZHEIMER'S ASSOCIATION

Volume 19, Issue S13 **December 2023**

Statistical Editors

Hiroko Dodge, Portland, OR
Richard Jones, Providence, RI
Max Petzold, Gothenburg, Sweden

Editorial Advisory Board

Michael Agadjanyan, Los Angeles, CA
Philippe Amouyel, Lille, France
Carol Barnes, Tucson, AZ
Anders Björklund, Lund, Sweden
Francois Boller, Paris, France
Heiko Braak, Frankfurt, Germany
John Breitner, Montreal, Canada
Monique Breteler, Bonn, Germany
Henry Brodaty, Sydney, Australia
Louis Burgio, Chapel Hill, NC
Shengdi Chen, Shanghai, China
Carl Cotman, Irvine, CA
Peggye Dilworth-Anderson, Chapel Hill, NC
Serge Gauthier, Montreal, Canada
Alison Goate, New York, NY
Michel Goedert, Cambridge, United Kingdom
Patrick Griffith, Nashville, TN
Jianping Jia, Beijing, China
Sterling Johnson, Madison, WI
Jeffrey Kaye, Portland, OR
Miia Kivipelto, Stockholm, Sweden
Jae-Young Koh, Seoul, South Korea
Walter A. Kukull, Seattle, WA
Lewis Kuller, Pittsburgh, PA
Weidong Le, Shanghai, China
Constantine Lyketsos, Baltimore, MD
Eckhard Mandelkow, Hamburg, Germany
Eva Mandelkow, Hamburg, Germany
Richard Mayeux, New York, NY
M Marsel Mesulam, Chicago, IL
Thomas Montine, Stanford, CA
George Perry, San Antonio, TX
Ronald Petersen, Rochester, MN
Steve Post, Stony Brook, NY
Teresa Radebaugh, El Dorado, KS
Joseph Rogers, Phoenix, AZ
Barbara Sahakian, Cambridge, United Kingdom
Mary Sano, New York, NY
Dennis Selkoe, Boston, MA
Sudha Seshadri, San Antonio, TX
Philip Sloane, Chapel Hill, NC
Christine van Broeckhoven, Antwerp, Belgium
Sandra Weintraub, Chicago, IL
Kathleen Welsh-Bohmer, Durham, NC
Bengt Winblad, Huddinge, Sweden

15525279, 2023, S13, Downloaded from https://alz-journals.onlinelibrary.wiley.com/doi/10.1002/alz.13648, Wiley Online Library on [19/02/2024]. See the Terms and Conditions (https://onlinelibrary.wiley.com/terms-and-conditions) on Wiley Online Library for rules of use; OA articles are governed by the applicable Creative Commons License

Alzheimer's Association International Conference® (AAIC®) 2023 SCIENTIFIC PROGRAM COMMITTEE

The Alzheimer's Association recognizes the following individuals for their valuable contributions of time and expertise in the development of the scientific program for AAIC 2023.

Chairs

Sergio Ferreira, Brazil
Wiesje van der Flier, Netherlands

Committee Members

Rufus Akinyemi, Nigeria
Kaarin Anstey, Australia
Delphine Boche, United Kingdom
José Brás, USA
Luc Buée, France
Adelina Comas-Herrera, United Kingdom
María M. Corrada, USA
Jeffrey Cummings, USA
Jeffrey Dage, USA
Nilufer Ertekin-Taner, USA
Cameron Gettel, USA
Crystal Glover, USA
Michael Gold, USA
Rebecca Gottesman, USA
Lea Grinberg, USA
Agustín Ibáñez, Ireland
Zahinoor Ismail, Canada
Takeshi Iwatsubo, Japan
Michelle Mielke, USA
Moyra Mortby, Australia
Catherine Mummery, United Kingdom
Melissa Murray, USA
Sebastian Palmqvist, Sweden
Tharick Pascoal, USA
Alexa Pichet Binette, Sweden
Rema Raman, USA
Christopher Rowe, Australia
Sietske Sikkes, Netherlands
John Sims, USA
Sudhir Sivakumaran, USA

Ex-officio members

Bruce Lamb, USA, Chair, Alzheimer's Association Medical and Scientific Advisory Group
Renaud La Joie, USA, Immediate Past Chair, Neuroimaging PIA
Paulo Caramelli, Brazil, Chair, ISTAART Advisory Council

15525279, 2023, S13, Downloaded from https://alz-journals.onlinelibrary.wiley.com/doi/10.1002/alz.13648, Wiley Online Library on [19/02/2024]. See the Terms and Conditions (https://onlinelibrary.wiley.com/terms-and-conditions) on Wiley Online Library for rules of use; OA articles are governed by the applicable Creative Commons License

Alzheimer's & Dementia

THE JOURNAL OF THE ALZHEIMER'S ASSOCIATION

ALZHEIMER'S AND DEMENTIA, (ISSN: 1552-5260), is published monthly on behalf of the Alzheimer's Association by Wiley Perodicals LLC, 111 River St., Hoboken, NJ 07030-5774.

Postmaster: Send all address changes to Alzheimer's and Dementia, Wiley Periodicals LLC, C/O The Sheridan Press, PO Box 465, Hanover, PA 17331 USA. All journals are normally despatched direct from the country in which they are printed by surface air-lifted delivery. All journals are normally despatched direct from the country in which they are printed by surface air-lifted delivery.

Editorial correspondence should be addressed to Donna M. Wilcock: dwilcock@iu.edu

Information for subscribers: Alzheimer's and Dementia is published in 12 issues per year. Institutional subscription prices for 2023 are: Print & Online: US$792 (US and Rest of World), €688 (Europe), £613 (UK). Prices are exclusive of tax. Asia-Pacific GST, Canadian GST/HST and European VAT will be applied at the appropriate rates. For more information on current tax rates, please go to https://onlinelibrary.wiley.com/library-info/products/price-lists/payment. The price includes online access to the current and all online backfiles to for previous 5 years, where available. For other pricing options, including access information and terms and conditions, please visit https://onlinelibrary.wiley.com/library-info/products/price-lists. Terms of use can be found here: https://onlinelibrary.wiley.com/terms-and-conditions

Delivery Terms and Legal Title: Where the subscription price includes print issues and delivery is to the recipient's address, delivery terms are Delivered at Place (DAP); the recipient is responsible for paying any import duty or taxes. Title to all issues transfers Free of Board (FOB) our shipping point, freight prepaid.

Claims for Missing or Damaged Print Issues: Our policy is to replace missing or damaged copies within our reasonable discretion, subject to print issue availability, and subject to the following terms: Title to all issues transfers Freight on Board ("FOB") to the address specified in the order; (1) Freight costs are prepaid by Wiley; and (2) Claims for missing or damaged copies must be submitted by the Customer or Subscription Agent within the claims window, as noted below.

Claims window - General: Claims for missing print issues must be sent to cs-agency@wiley.com (and the Subscription Agent or Customer may be referred to a society) within three months of whichever of these dates is the most recent: date of subscription payment; or date of issue publication.

Claims window - India: Both Subscription Agents and Customers in India have 48 hours after receipt of goods to confirm that all content listed on the packing label has been received. In the event of any discrepancy, SPUR Infosolutions, Wiley's delivery partner in India, needs to be notified within forty-eight (48) hours using this email address: support@spurinfo.com. All claims will be checked against SPUR Infosolutions delivery records before the claim is accepted. The above terms for Wiley's claims policy otherwise apply.

Journal Customer Services: For ordering information, claims and any inquiry concerning your journal subscription please go to https://wolsupport.wiley.com/s/contactsupport?tabset-a7d10=2 or contact your nearest office.

Americas: E-mail: cs-journals@wiley.com; Tel: +1 877 762 2974.

Europe, Middle East and Africa: E-mail: cs-journals@wiley.com; Tel: +44 (0) 1865 778315; 0800 1800 536 (Germany).

Germany, Austria, Switzerland, Luxembourg, Liechtenstein: cs-germany@wiley.com; Tel: 0800 1800 536 (Germany).

Asia Pacific: E-mail: cs-journals@wiley.com; Tel: +65 3165 0890.

Japan: For Japanese speaking support, E-mail: cs-japan@wiley.com

Visit our Online Customer Help at https://wolsupport.wiley.com/s/contactsupport?tabset-a7d10=2

Production Editor: Aakriti Saini (email: alz@wiley.com)

Advertising representative: Beverly Lawrence, PO Box 90758, San Diego, CA 92169-2758, E-mail blawrence@wiley.com for details.

Back issues: Single issues from current and recent volumes are available at the current single issue price from cs-journals@wiley.com. Earlier issues may be obtained from Periodicals Service Company, 351 Fairview Avenue – Ste 300, Hudson, NY 12534, USA. Tel: +1 518 822-9300, Fax: +1 518 822-9305, E-mail: psc@periodicals.com

Abstracting and Indexing Services: The journal is indexed by Index Medicus/MEDLINE, Scopus, Science Citation Index Expanded (SciSearch®), Current Contents®/Clinical Medicine, Neuroscience Citation Index®, and Journal Citation Reports/Science Edition.

Reprints: Should you wish to purchase additional copies of your article, please follow the instructions provided at: www.sheridan.com/wiley/eoc. Corresponding authors are invited to inform their coauthors of the reprint options available. Please note that regardless of the form in which they are acquired, reprints should not be resold, nor further disseminated in electronic form, nor deployed in part or in whole in any marketing, promotional or educational contexts without authorization from Wiley. Permissions requests should be directed to mail to: permissionsus@wiley.com

For information about 'Pay-Per-View and Article Select', go to the following link: https://onlinelibrary.wiley.com/researchers/how-to-access/ppv and https://onlinelibrary.wiley.com/library-info/products/articleselect.

Open Access: *Alzheimer's and Dementia* accepts articles for Open Access publication. Please visit https://authorservices.wiley.com/author-resources/Journal-Authors/open-access/hybrid-open-access.html for further information about OnlineOpen.

Disclaimer: The Publisher, Alzheimer's Association, and Editors cannot be held responsible for errors or any consequences arising from the use of information contained in this journal; the views and opinions expressed do not necessarily reflect those of the Publisher, Alzheimer's Association, or Editors, neither does the publication of advertisements constitute any endorsement by the Publisher, Alzheimer's Association, or Editors of the products advertised.

Publisher: ALZHEIMER'S AND DEMENTIA is published by Wiley Perodicals LLC, 111 River St.,Hoboken, NJ 07030-5774.

Copyright and Copying (in any format): Copyright © 2023 Alzheimer's Association. All rights reserved. No part of this publication may be reproduced, stored or transmitted in any form or by any means without the prior permission in writing from the copyright holder. Authorization to copy items for internal and personal use is granted by the copyright holder for libraries and other users registered with their local Reproduction Rights Organisation (RRO), e.g. Copyright Clearance Center (CCC), 222 Rosewood Drive, Danvers, MA 01923, USA (www.copyright.com), provided the appropriate fee is paid directly to the RRO. This consent does not extend to other kinds of copying such as copying for general distribution, for advertising or promotional purposes, for republication, for creating new collective works or for resale. Permissions for such reuse can be obtained using the RightsLink "Request Permissions" link on Wiley Online Library. Special requests should be addressed to: permissions@wiley.com

Aims and Scope: The mission of *Alzheimer's & Dementia*: Journal of the Alzheimer's Association is to bridge the knowledge gaps across a wide range of bench-to-bedside investigation. The journal publishes the results of studies in: behavior, biochemistry, genetics, molecular biology, pharmacology, physiology, protein chemistry, neurology, neuropathology, psychiatry, geriatrics, neuropsychology, epidemiology, sociology, health services research, health economics, political science and public policy. Content emphasizes interdisciplinary investigations, integrative/translational articles, related to: etiology, risk factors, early detection, disease modifying interventions, prevention of dementia and applications of new technologies in health services.

Wiley's Corporate Citizenship: Wiley's Corporate Citizenship initiative seeks to address the environmental, social, economic, and ethical challenges faced in our business and which are important to our diverse stakeholder groups. Since launching the initiative, we have focused on sharing our content with those in need, enhancing community philanthropy, reducing our carbon impact, creating global guidelines and best practices for paper use, establishing a vendor code of ethics, and engaging our colleagues and other stakeholders in our efforts. Follow our progress at www.wiley.com/go/citizenship

Wiley is a founding member of the UN-backed HINARI, AGORA, and OARE initiatives. They are now collectively known as Research4Life, making online scientific content available free or at nominal cost to researchers in developing countries. Please visit Wiley's Content Access – Corporate Citizenship site: http://www.wiley.com/WileyCDA/ Section/id-390082.html

View this journal online at wileyonlinelibrary.com/ALZHEIMER'S AND DEMENTIA/alz.

Hobbs: Printed in the UK by Hobbs the Printers Ltd.

For submission instructions, subscription and all other information visit: https://alz-journals.onlinelibrary.wiley.com/.

15525279, 2023, S13, Downloaded from https://alz-journals.onlinelibrary.wiley.com/doi/10.1002/alz.13648, Wiley Online Library on [19/02/2024]. See the Terms and Conditions (https://onlinelibrary.wiley.com/terms-and-conditions) on Wiley Online Library for rules of use; OA articles are governed by the applicable Creative Commons License

Check for updates

DOI: 10.1002/alz.078118

BASIC SCIENCE AND PATHOGENESIS

POSTER PRESENTATION

Alzheimer's & Dementia®
THE JOURNAL OF THE ALZHEIMER'S ASSOCIATION

MOLECULAR AND CELL BIOLOGY

Syzigium aromaticum may protect against paraquat mediated toxicity via p53 and Sestrin2 modulation

Nitish Rai[1] | Sharmistha Dey[2]

[1]Mohanlal Sukhadia University, Udaipur, Rajasthan, India

[2]All India Institute of Medical Sciences, AIIMS, New Delhi, CA, India

Correspondence
Nitish Rai, Mohanlal Sukhadia University, Udaipur, Rajasthan, India.
Email: nits6691@gmail.com

Abstract

Background: Numerous environmental risk factors, particularly neurotoxins, have been linked to the development of sporadic Parkinson's disease (PD), even though its exact cause is still unknown. The common spice Syzigium aromaticum has the greatest ORAC (Oxygen Radical Absorbance Capacity) value according to the National Institute on Aging. One of the three components of healthy ageing, vata, is calmed by Syzigium aromaticum while also stimulates nerves. The study investigated the rescue effect of Syzigium aromaticum ethanolic extract against paraquat (PQ) mediated PD type toxicity and elucidated the underlying molecular mechanism using the cell line.

Method: The cold extraction method was used to prepare the Syzigium aromaticum ethanolic extract by powdering, soaking in ethanol and stirring for 72 h. Then the supernatant was gradually aliquoted and filtered with Whatman filter paper no 1. Paraquat, at different doses, was used to generate PD type toxicity in SH-SY5Y cells for 24, 48, and 72 hours, and MTT test was used to measure the cytotoxicity. The rescue effect was demonstrated by simultaneously treating cells with 100 mM PQ and various doses of Syzigium aromaticum and then performing MTT assay. The protein expression studies was done using western blot technique to elucidate the underlying mechanism.

Result: The toxicity experiment showed that PQ-treated cells exhibited significant cell death, with the maximal toxicity occurring after 72 hours. However, the cells treated with Syzigium aromaticum were protected from the PQ-induced cell death. Syzigium aromaticum exhibited rescue effect in proportion to its dose. The western blot analysis of PQ treated SH-SY5Y cells demonstrated a dose-dependent increase in the levels of p53, Setrin2, and phosphorylated AMPK (P-AMPK). The levels of AMPK, mTOR and p70S6K remain unchanged, however, the phosphorylated p70S6K (P-p70S6K) levels were declined. When cells were simultaneously treated with PQ and increasing dose of Syzigium aromaticum, the levels of p53, Sesn2, and P-AMPK lowered similar to control. Further, there was an increase in the level of phosphorylated p70S6K (P-p70S6K) in proportion to the dose of Syzigium aromaticum.

Conclusion: The current study showed that the Syzigium aromaticum ethanolic extract prevented PQ-induced cell death in SH-SY5Y by targeting p53 and sestrin2.

© 2023 the Alzheimer's Association.

Plant-Microbe Interaction - Recent Advances in Molecular and Biochemical Approaches

Volume 2: Agricultural Aspects of Microbiome Leading to Plant Defence



Dr. Prashant Swapnil
Dr. Mukesh Meena
Dr. Harish
Dr. Avinash Marwal
Dr. Selvakumar Vijayalakshmi
Dr. Andleeb Zehra

Academic Press is an imprint of Elsevier
125 London Wall, London EC2Y 5AS, United Kingdom
525 B Street, Suite 1650, San Diego, CA 92101, United States
50 Hampshire Street, 5th Floor, Cambridge, MA 02139, United States
The Boulevard, Langford Lane, Kidlington, Oxford OX5 1GB, United Kingdom

Copyright © 2023 Elsevier Inc. All rights reserved.

No part of this publication may be reproduced or transmitted in any form or by any means, electronic or mechanical, including photocopying, recording, or any information storage and retrieval system, without permission in writing from the publisher. Details on how to seek permission, further information about the Publisher's permissions policies and our arrangements with organizations such as the Copyright Clearance Center and the Copyright Licensing Agency, can be found at our website: www.elsevier.com/permissions.

This book and the individual contributions contained in it are protected under copyright by the Publisher (other than as may be noted herein).

Notices

Knowledge and best practice in this field are constantly changing. As new research and experience broaden our understanding, changes in research methods, professional practices, or medical treatment may become necessary.

Practitioners and researchers must always rely on their own experience and knowledge in evaluating and using any information, methods, compounds, or experiments described herein. In using such information or methods they should be mindful of their own safety and the safety of others, including parties for whom they have a professional responsibility.

To the fullest extent of the law, neither the Publisher nor the authors, contributors, or editors, assume any liability for any injury and/or damage to persons or property as a matter of products liability, negligence or otherwise, or from any use or operation of any methods, products, instructions, or ideas contained in the material herein.

ISBN 978-0-323-91876-3

For information on all Academic Press publications
visit our website at https://www.elsevier.com/books-and-journals

Publisher: Nikki P. Levy
Acquisitions Editor: Nancy J. Maragioglio
Editorial Project Manager: Kyle Gravel
Production Project Manager: Nadhiya Sekar
Cover Designer: Christian Bilbow

Typeset by STRAIVE, India



4. Destructive role of chemicals secreted by plants to diminish harmful microbes

Subhesh Saurabh Jha and L.S. Songachan

1. Introduction 65
2. Detrimental interactions between plants 67
   - 2.1 Allelopathy 67
   - 2.2 Biological invasions at the community level and the novel weapons' theory 68
   - 2.3 Associations of parasitic plants with their hosts 69
3. Detrimental interactions between plants and microbes 70
   - 3.1 Antimicrobial effects 70
   - 3.2 Environmental associations of plants and microbes 70
   - 3.3 Root exudates' influence on surrounding nematodes 71
4. Techniques used for studying various associations arbitrated by root exudates 72
5. Conclusions 73

References 74

5. Biodegradation and bioaugmentation of pesticides using potential fungal species

S. Gomathi, V. Ambikapathy, and A. Panneerselvam

1. Introduction 79
2. Fungi 81
3. As natural scavengers 81
4. Humus formation 82
5. Nitrogen fixation and biological control 82
6. Role of Mycorrhizae 82
7. Inorganic pesticides 83
8. Toxicological classification of pesticides 84
9. Fungi in removal and degradation of pesticides 85
10. Isolation of fungi from soil 85
11. Observations 86
12. Identification 86
13. TLC and HPLC analyses 86
14. GC-MS analysis 87
15. Biodegradation 87
16. Strategies for biodegradation 87
17. Enzymes involved in the biodegradation process 90
18. Conclusions 91

References 92

6. Agricultural management by improving beneficial microflora

Shalini Tailor, Khushboo Jain, Avinash Marwal, Mukesh Meena, and Anita Mishra

1. Introduction 95

Chapter 6

Agricultural management by improving beneficial microflora

Shalini Tailor[a], **Khushboo Jain**[a], **Avinash Marwal**[a], **Mukesh Meena**[b], **and Anita Mishra**[c]

[a]*Department of Biotechnology, Mohanlal Sukhadia University, Udaipur, Rajasthan, India,* [b]*Laboratory of Phytopathology and Microbial Biotechnology, Department of Botany, Mohanlal Sukhadia University, Udaipur, Rajasthan, India,* [c]*Department of Science (Biotechnology), Biyani Girls College, University of Rajasthan, Jaipur, Rajasthan, India*

1 Introduction

The living beings from the primitive ones to the most developed all require food for their survival and growth. Food being the major component for living is cultivated and harvested throughout the world using various agricultural techniques. For agriculture practice, one requires land which is composed of soil. Hence, it could be said that without the soil, there is no existence of food. Soil has the greatest affinity and dwelling place for a wide range of microflora which in turn is found to be beneficial or harmful, in some cases, for the growth of the plants. The presence or the absence of these microorganisms in the soil totally depends on the soil quality, texture, region where it is present, and the various abiotic factors of that ecosystem. The soil of a specific region may grow certain sort of plant types better as compared to the other soil type since the soil varies from region to region [1]. Soil possesses several vital characteristics and functions such as nutrient recycling, growth of plants and crops, the dwelling place for living creatures, especially microbes, water-holding capacity, filtration, degradation of organic as well as inorganic matter, and many others [1]. Soil serves as the raw material for any kind of agricultural activity in order to produce food or fiber. A soil particle gets surrounded by a large population of microbes in an ecosystem. One gram of soil approximately contains 10 billion bacteria and builds the highest number as well as the biomass of the soil microflora [2].

In India, 60% of the land is under cultivation means that a large population depends majorly on the agricultural produce for their daily requirement of food and feed. Not only India but also most of the countries around the world are

Plant-Microbe Interaction—Recent Advances in Molecular and Biochemical Approaches
https://doi.org/10.1016/B978-0-323-91876-3.00004-X
Copyright © 2023 Elsevier Inc. All rights reserved.

Plant-Microbe Interaction - Recent Advances in Molecular and Biochemical Approaches

Volume 2: Agricultural Aspects of Microbiome Leading to Plant Defence



Dr. Prashant Swapnil
Dr. Mukesh Meena
Dr. Harish
Dr. Avinash Marwal
Dr. Selvakumar Vijayalakshmi
Dr. Andleeb Zehra

Academic Press is an imprint of Elsevier
125 London Wall, London EC2Y 5AS, United Kingdom
525 B Street, Suite 1650, San Diego, CA 92101, United States
50 Hampshire Street, 5th Floor, Cambridge, MA 02139, United States
The Boulevard, Langford Lane, Kidlington, Oxford OX5 1GB, United Kingdom

Copyright © 2023 Elsevier Inc. All rights reserved.

No part of this publication may be reproduced or transmitted in any form or by any means, electronic or mechanical, including photocopying, recording, or any information storage and retrieval system, without permission in writing from the publisher. Details on how to seek permission, further information about the Publisher's permissions policies and our arrangements with organizations such as the Copyright Clearance Center and the Copyright Licensing Agency, can be found at our website: www.elsevier.com/permissions.

This book and the individual contributions contained in it are protected under copyright by the Publisher (other than as may be noted herein).

Notices

Knowledge and best practice in this field are constantly changing. As new research and experience broaden our understanding, changes in research methods, professional practices, or medical treatment may become necessary.

Practitioners and researchers must always rely on their own experience and knowledge in evaluating and using any information, methods, compounds, or experiments described herein. In using such information or methods they should be mindful of their own safety and the safety of others, including parties for whom they have a professional responsibility.

To the fullest extent of the law, neither the Publisher nor the authors, contributors, or editors, assume any liability for any injury and/or damage to persons or property as a matter of products liability, negligence or otherwise, or from any use or operation of any methods, products, instructions, or ideas contained in the material herein.

ISBN 978-0-323-91876-3

For information on all Academic Press publications
visit our website at https://www.elsevier.com/books-and-journals

Publisher: Nikki P. Levy
Acquisitions Editor: Nancy J. Maragioglio
Editorial Project Manager: Kyle Gravel
Production Project Manager: Nadhiya Sekar
Cover Designer: Christian Bilbow

Typeset by STRAIVE, India



7. Abiotic stress tolerance in plants 231
8. Macronutrients and micronutrients 231
8.1 Potassium 232
8.2 Phosphorus 232
8.3 Calcium 232
8.4 Magnesium 233
8.5 Iron 233
8.6 Zinc 234
8.7 Manganese 234
8.8 Copper 234
9. Nanotechnology and PGPR 235
9.1 Silver nanoparticles 235
9.2 Zinc oxide nanoparticles 240
9.3 Silicon oxide nanoparticles 240
9.4 Iron oxide nanoparticles 241
9.5 Other nanomaterials 241
10. Conclusions 242
References 242

13. Potential scope and prospects of plant growth-promoting microbes (PGPMs) in micropropagation technology
Sagar Teraiya, Dhaval Nirmal, and Preetam Joshi

1. Introduction 249
2. Plant tissue culture 250
3. Challenges in plant tissue culture 253
4. Plant growth-promoting microbes 254
5. Application of PGPM in micropropagation technology 256
5.1 Biotization with plant growth-promoting fungi 256
5.2 Biotization with plant growth-promoting (rhizo)bacteria (PGPB or PGPR) 258
5.3 Biotization to elevate in vitro secondary metabolite production 266
6. Future prospects of biotization 269
7. Conclusions 269
References 270

14. Advantageous features of plant growth-promoting microorganisms to improve plant growth in difficult conditions
Mukesh Meena, Garima Yadav, Priyankaraj Sonigra, Adhishree Nagda, Tushar Mehta, Prashant Swapnil, Avinash Marwal, and Andleeb Zehra

1. Introduction 279
2. Plant growth-promoting microorganisms (PGPMs) and plant growth 280

Chapter 14

Advantageous features of plant growth-promoting microorganisms to improve plant growth in difficult conditions

Mukesh Meena[a], Garima Yadav[a], Priyankaraj Sonigra[a], Adhishree Nagda[a], Tushar Mehta[a], Prashant Swapnil[b], Avinash Marwal[c], and Andleeb Zehra[d]

[a]*Laboratory of Phytopathology and Microbial Biotechnology, Department of Botany, Mohanlal Sukhadia University, Udaipur, Rajasthan, India,* [b]*School of Basic Sciences, Department of Botany, Central University of Punjab, Bathinda, Punjab, India,* [c]*Department of Biotechnology, Mohanlal Sukhadia University, Udaipur, Rajasthan, India,* [d]*Laboratory of Mycopathology and Microbial Technology, Department of Botany, Centre of Advanced Study in Botany, Institute of Science, Banaras Hindu University, Varanasi, Uttar Pradesh, India*

1 Introduction

The microbial community is a major uncovered pool of the Earth's biodiversity, of which only a tiny fraction is known [1]. Microbes comprise the major part of life on the planet and also play a vital role in the life of other living organisms [2]. Nowadays, climate change is appearing as a major issue because it affects life forms on the Earth. These changes are usually seen in the morphology, metabolic rate, photosynthetic rate, activity, and interactions of plant roots with their surrounding plants and microorganisms [3,4]. Growth and development of plants diminishes due to disturbed conditions of soils such as water deficiency, acidity, salinity, shortage of organic and inorganic nutrients mainly essential micronutrients (P, Ca, Mg, and molybdenum). Microorganisms that live in this type of soil enable plants to cope with these conditions [5–9]. The plant roots affect the rhizosphere through the exudation of substances in soil and influence microbial activity. Plant roots offer niches for a multitude of microorganisms, including viruses, fungi, bacteria, protists, and nematodes. Among different phyla, some of the phyla that are included in the plant growth-promoting microbe family are Cyanobacteria, Actinobacteria, Firmicutes, Bacteroidetes, *Bacillus* spp.,

Plant-Microbe Interaction—Recent Advances in Molecular and Biochemical Approaches
https://doi.org/10.1016/B978-0-323-91876-3.00019-1
Copyright © 2023 Elsevier Inc. All rights reserved.

Plant-Microbe Interaction - Recent Advances in Molecular and Biochemical Approaches

Volume 2: Agricultural Aspects of Microbiome Leading to Plant Defence



Dr. Prashant Swapnil
Dr. Mukesh Meena
Dr. Harish
Dr. Avinash Marwal
Dr. Selvakumar Vijayalakshmi
Dr. Andleeb Zehra

Academic Press is an imprint of Elsevier
125 London Wall, London EC2Y 5AS, United Kingdom
525 B Street, Suite 1650, San Diego, CA 92101, United States
50 Hampshire Street, 5th Floor, Cambridge, MA 02139, United States
The Boulevard, Langford Lane, Kidlington, Oxford OX5 1GB, United Kingdom

Copyright © 2023 Elsevier Inc. All rights reserved.

No part of this publication may be reproduced or transmitted in any form or by any means, electronic or mechanical, including photocopying, recording, or any information storage and retrieval system, without permission in writing from the publisher. Details on how to seek permission, further information about the Publisher's permissions policies and our arrangements with organizations such as the Copyright Clearance Center and the Copyright Licensing Agency, can be found at our website: www.elsevier.com/permissions.

This book and the individual contributions contained in it are protected under copyright by the Publisher (other than as may be noted herein).

Notices

Knowledge and best practice in this field are constantly changing. As new research and experience broaden our understanding, changes in research methods, professional practices, or medical treatment may become necessary.

Practitioners and researchers must always rely on their own experience and knowledge in evaluating and using any information, methods, compounds, or experiments described herein. In using such information or methods they should be mindful of their own safety and the safety of others, including parties for whom they have a professional responsibility.

To the fullest extent of the law, neither the Publisher nor the authors, contributors, or editors, assume any liability for any injury and/or damage to persons or property as a matter of products liability, negligence or otherwise, or from any use or operation of any methods, products, instructions, or ideas contained in the material herein.

ISBN 978-0-323-91876-3

For information on all Academic Press publications
visit our website at https://www.elsevier.com/books-and-journals

Publisher: Nikki P. Levy
Acquisitions Editor: Nancy J. Maragioglio
Editorial Project Manager: Kyle Gravel
Production Project Manager: Nadhiya Sekar
Cover Designer: Christian Bilbow

Typeset by STRAIVE, India



3. Some advantageous features of plant growth-promoting microorganisms 283
4. Biological nitrogen fixation 283
5. Production of phytohormone 285
6. Solubilization of minerals 285
7. As biocontrol agents 286
8. In phytoremediation 287
9. ACC deaminase activity 287
10. PGPMs as biofertilizers and biopesticides 287
11. Conclusions 289
Acknowledgments 289
References 289

15. Plant-microbe interactions to reduce salinity stress in plants for the improvement of the agricultural system
Yashika Maheshwari, Shalini Tailor, Avinash Marwal, and Anita Mishra

1. Introduction 297
2. Types and causes of salinity 298
3. Salinity impact on the agricultural system 299
4. Detection of salinity 301
4.1 Visual diagnosis of saline and sodic soils 304
5. Strategies to tolerate salinity in flora 304
6. Plant-bacteria interaction to reduce salinity 305
7. Plant-fungi interaction to reduce salinity 305
8. Conclusions 306
References 306

16. Metabolomic studies of medicinal plant-fungi interaction
Mahinder Partap, Abhishek Kumar, Pankaj Kumar, Shiv Shanker Pandey, and Ashish R. Warghat

1. Literature search process 311
2. Introduction 311
3. Plant-fungi interactions 312
4. Metabolomics approach 313
5. Fungi elicitors and their action in medicinal plants 315
6. Case studies on medicinal plant-fungi interaction 322
6.1 *Catharanthus roseus* (L.) G. Don (Madagascar periwinkle) 322
6.2 *Withania somnifera* L. (Indian ginseng or Ashwagandha) 322
6.3 *Artemisia annua* L. (sweet wormwood) 322

Chapter 15

Plant-microbe interactions to reduce salinity stress in plants for the improvement of the agricultural system

Yashika Maheshwari[a], Shalini Tailor[b], Avinash Marwal[b], and Anita Mishra[c]

[a]*Department of Biotechnology, School of Science, GSFC University, Vadodara, Gujarat, India,*
[b]*Department of Biotechnology, Mohanlal Sukhadia University, Udaipur, Rajasthan, India,*
[c]*Department of Science (Biotechnology), Biyani Girls College, University of Rajasthan, Jaipur, Rajasthan, India*

1 Introduction

The world is rich in plant biodiversity and to protect this enormous number of species, many researchers have studied the effects of plant hormones and factors responsible for encouraging and limiting agricultural crop productivity. Eventually, as the research carried further, they discovered many points that have an outcome on plant development in both positive and negative manner such as proper sunlight, water, fertile soil, nutrients, drought, salinity, high temperature, cold, high winds, flood, and pH. Researchers recognized that salinization is the major abiotic stress to the environment [1]. Stress is a limitation that restricts the metabolic processes as well as decreases the ability of plants by converting energy into a nonrenewable energy source [2]. Stress affects one billion hectares of land globally [3]. Salt stress is an undesirable outcome of redundant minerals like Na^+ along with Cl^- or either one of them on the plant [2], and accrual of sodium and chloride ions on the Earth's surface results in natural salinity [3]. An inappropriate practice of irrigation exerts influence on 50% of the total fertile area, which is the major reason for increase in salt concentrations which further cause plant impairment [3]. On the basis of the living world, the quality, and the relation of the plant growth in the salinity area, Szabolcs [4] coined two main types of soils [2], which are as follows: (1) brackish soils—sodium chloride and sodium sulfate are the salts with good solubility, and often this soil

Plant-Microbe Interaction—Recent Advances in Molecular and Biochemical Approaches
https://doi.org/10.1016/B978-0-323-91876-3.00002-6
Copyright © 2023 Elsevier Inc. All rights reserved.

Plant-Microbe Interaction - Recent Advances in Molecular and Biochemical Approaches

Volume 1: Overview of Biochemical and Physiological Alteration During Plant-Microbe Interaction



Dr. Prashant Swapnil
Dr. Mukesh Meena
Dr. Harish
Dr. Avinash Marwal
Dr. Selvakumar Vijayalakshmi
Dr. Andleeb Zehra

Academic Press is an imprint of Elsevier
125 London Wall, London EC2Y 5AS, United Kingdom
525 B Street, Suite 1650, San Diego, CA 92101, United States
50 Hampshire Street, 5th Floor, Cambridge, MA 02139, United States
The Boulevard, Langford Lane, Kidlington, Oxford OX5 1GB, United Kingdom

Copyright © 2023 Elsevier Inc. All rights reserved.

No part of this publication may be reproduced or transmitted in any form or by any means, electronic or mechanical, including photocopying, recording, or any information storage and retrieval system, without permission in writing from the publisher. Details on how to seek permission, further information about the Publisher's permissions policies and our arrangements with organizations such as the Copyright Clearance Center and the Copyright Licensing Agency, can be found at our website: www.elsevier.com/permissions.

This book and the individual contributions contained in it are protected under copyright by the Publisher (other than as may be noted herein).

Notices

Knowledge and best practice in this field are constantly changing. As new research and experience broaden our understanding, changes in research methods, professional practices, or medical treatment may become necessary.

Practitioners and researchers must always rely on their own experience and knowledge in evaluating and using any information, methods, compounds, or experiments described herein. In using such information or methods they should be mindful of their own safety and the safety of others, including parties for whom they have a professional responsibility.

To the fullest extent of the law, neither the Publisher nor the authors, contributors, or editors, assume any liability for any injury and/or damage to persons or property as a matter of products liability, negligence or otherwise, or from any use or operation of any methods, products, instructions, or ideas contained in the material herein.

ISBN 978-0-323-91875-6

For information on all Academic Press publications
visit our website at https://www.elsevier.com/books-and-journals

Publisher: Nikki P. Levy
Acquisitions Editor: Nancy J. Maragioglio
Editorial Project Manager: Kyle Gravel
Production Project Manager: Nadhiya Sekar
Cover Designer: Vicky Esser Pearson

Typeset by STRAIVE, India



Plant-Microbe Interaction - Recent Advances in Molecular and Biochemical Approaches

Volume 2: Agricultural Aspects of Microbiome Leading to Plant Defence



Dr. Prashant Swapnil
Dr. Mukesh Meena
Dr. Harish
Dr. Avinash Marwal
Dr. Selvakumar Vijayalakshmi
Dr. Andleeb Zehra

Academic Press is an imprint of Elsevier
125 London Wall, London EC2Y 5AS, United Kingdom
525 B Street, Suite 1650, San Diego, CA 92101, United States
50 Hampshire Street, 5th Floor, Cambridge, MA 02139, United States
The Boulevard, Langford Lane, Kidlington, Oxford OX5 1GB, United Kingdom

Copyright © 2023 Elsevier Inc. All rights reserved.

No part of this publication may be reproduced or transmitted in any form or by any means, electronic or mechanical, including photocopying, recording, or any information storage and retrieval system, without permission in writing from the publisher. Details on how to seek permission, further information about the Publisher's permissions policies and our arrangements with organizations such as the Copyright Clearance Center and the Copyright Licensing Agency, can be found at our website: www.elsevier.com/permissions.

This book and the individual contributions contained in it are protected under copyright by the Publisher (other than as may be noted herein).

Notices

Knowledge and best practice in this field are constantly changing. As new research and experience broaden our understanding, changes in research methods, professional practices, or medical treatment may become necessary.

Practitioners and researchers must always rely on their own experience and knowledge in evaluating and using any information, methods, compounds, or experiments described herein. In using such information or methods they should be mindful of their own safety and the safety of others, including parties for whom they have a professional responsibility.

To the fullest extent of the law, neither the Publisher nor the authors, contributors, or editors, assume any liability for any injury and/or damage to persons or property as a matter of products liability, negligence or otherwise, or from any use or operation of any methods, products, instructions, or ideas contained in the material herein.

ISBN 978-0-323-91876-3

For information on all Academic Press publications
visit our website at https://www.elsevier.com/books-and-journals

Publisher: Nikki P. Levy
Acquisitions Editor: Nancy J. Maragioglio
Editorial Project Manager: Kyle Gravel
Production Project Manager: Nadhiya Sekar
Cover Designer: Christian Bilbow

Typeset by STRAIVE, India



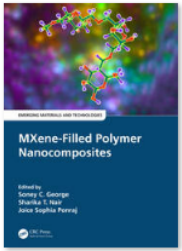

Chapter

Self-Healing Activity of MXene/Polymer Nanocomposites

By Shikha Agarwal, Ayushi Sethiya, Divyani Gandhi, Jay Soni

Book MXene-Filled Polymer Nanocomposites

Edition	1st Edition
First Published	2022
Imprint	CRC Press
Pages	20
eBook ISBN	9781003164975

Share

You do not have access to this content currently. Please click 'Get Access' button to see if you or your institution have access to this content.

GET ACCESS

To purchase a print version of this book for personal use or request an inspection copy >>

GO TO ROUTLEDGE.COM

ABSTRACT

MXenes, a new class of two-dimensional (2D) materials and composites, have engrossed tremendous interest of researchers because of their promising characteristics, namely, high conductivity, tunable band gaps,

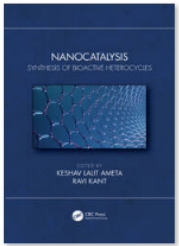

Chapter

Nanocatalysed Synthesis of Pyrazoles, Indazoles, and Pyrazolines

By Divyani Gandhi, Ayushi Sethiya, Nusrat Sahiba, Dinesh Kumar Jangid, Shikha Agarwal

Book Nanocatalysis

Edition	1st Edition
First Published	2022
Imprint	CRC Press
Pages	25
eBook ISBN	9781003141488

Share

You do not have access to this content currently. Please click 'Get Access' button to see if you or your institution have access to this content.

GET ACCESS

To purchase a print version of this book for personal use or request an inspection copy >>

GO TO ROUTLEDGE.COM

ABSTRACT

This chapter provides an extensive overview of the emerging field of nanomaterials in synthetic applications

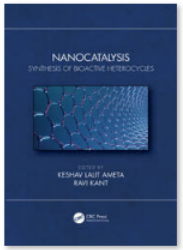

Chapter

Nanocatalysed Synthesis and Biological Significance of Imidazoles, Hydantoins, Oxazoles, and Thiazoles

By Surbhi Dhadda, Nidhi Jangir, Shikha Agarwal, Arvnabh Mishra, Dinesh Kumar Jangid

Book Nanocatalysis

Edition	1st Edition
First Published	2022
Imprint	CRC Press
Pages	18
eBook ISBN	9781003141488

Share

You do not have access to this content currently. Please click 'Get Access' button to see if you or your institution have access to this content.

GET ACCESS

To purchase a print version of this book for personal use or request an inspection copy >>

GO TO ROUTLEDGE.COM

ABSTRACT

The Multidisciplinary Perspectives in Geography

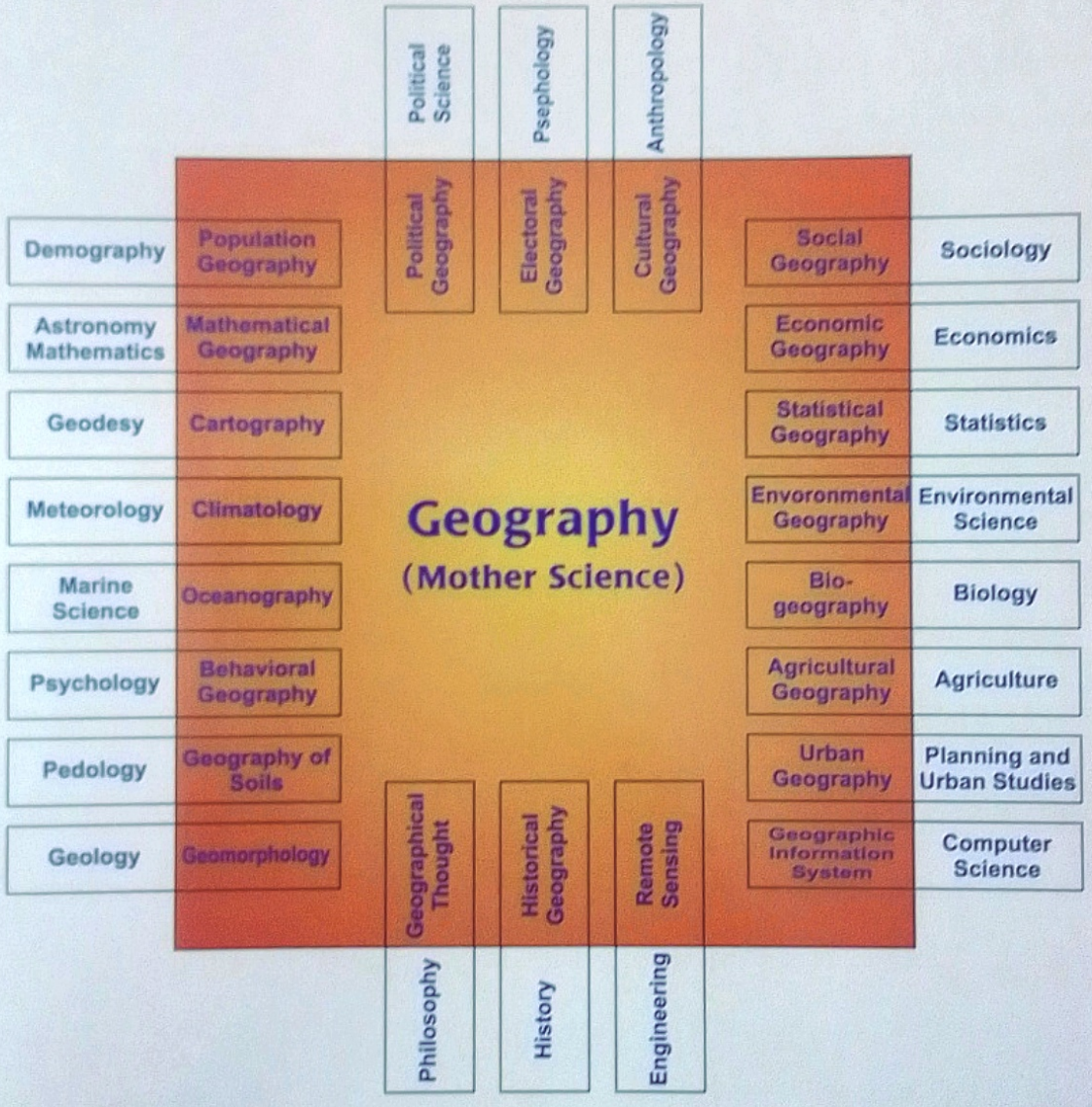

Editor
Dr. Purnima Singh

Contents

S.No.	Title of the Chapter and Author/ Authors	Page No.
1.	Trend of Urbanization and Emerging Environmental Problems in Towns of Rajasthan. –Dr. Preeti Mishra	1-15
2.	Application of Statistical Methods in Applied Economic Geography. –Dr. Nidhi Khinduka Jain	16-24
3.	Geotourism: Future of Travel. – Dr. Ravinder Kumar	25-32
4.	Some Promising Plants in Rajasthan for Phytoremediation. –Bhavika Kunwar and Vartika Jain	33-50
5.	Modern Agriculture Practices and Land Degradation. –Dr Savitri Patidar	51-57
6.	Ecotourism: Conserving Environment with Responsibility. –Dr. Shweta Khandelwal	58-80
7.	History of Lakes of Udaipur. –Rahul Kumar	81-86
8.	Geography as Human Ecology. –Dr. Sandhya Pathania	87-103
9.	Elderly in India: Concerning issues. –Dr. Shruti Tandon	104-111
10.	Feasibility of Wind Energy in Rajasthan. --Dr. Palak Bhardwaj	112-115
11.	भू-सतही जल क्षेत्र में परिवर्तन का भू-स्थानिक अध्ययन: झालरापाटन तहसील, झालावाड़, राजस्थान –भरत कुमार सोनी, निमीष नारायण गौतम, डॉ. शिवानी स्वर्णकार	116-125
12.	मानव पर्यावरण संबंध –डॉ. सबीहा खान	126-136

12. मानव-पर्यावरण संबंध

डॉ. सबीहा खान

सहायक आचार्य, भूगोल विभाग, मोहनलाल सुखाड़िया विश्वविद्यालय, उदयपुर

शोध सारांश

मानव-पर्यावरण संबंध का अध्ययन एक समकालीन विषय है। दोनों घटकों का पूरक संबंध इनके अस्तित्व का प्रमाण है। सौर मंडल के एकमात्र ग्रह - पृथ्वी पर ही मानव जीवन संभव है परंतु इसके साथ ही इसी मानव जीवन के द्वारा ही पृथ्वी के अस्तित्व का महत्व है। मानव, पर्यावरण के प्रत्येक घटक को एवं पर्यावरण, मानव के प्रत्येक पक्ष को सदा प्रभावित करते रहें है और अनवरत करते रहेंगे। प्रागैतिहासिक युग में जहां प्रकृति सर्वोपरि थी एवं मानव अपने जीवन के अस्तित्व के लिए संघर्षरत था। वर्तमान में मानव ने अत्यधिक तकनीकी एवं प्रौद्योगिक विकास के साथ प्राकृतिक घटकों को अपने अनुरूप रूपांतरित करके, अपने जीवन के प्रत्येक पक्ष को मजबूत बनाया है। परंतु प्रकृति के अत्याधिक विदोहन के फलस्वरूप जलवायु परिवर्तन जैसी विकट समस्या ने संपूर्ण विश्व को सोचने पर मजबूर कर दिया है। इस समस्या के निराकरण हेतु मनुष्य को अपनी महत्वाकांक्षाओं पर काबू करना होगा।

कुंजी शब्द: मानव, पर्यावरण, प्राकृतिक घटक, प्रभाव।

मानव पर्यावरण संबंध (Man & Environment Relationship)

मानव पर्यावरण संबंधों का अध्ययन एक प्राचीन विषय के साथ ही समकालीन भी है। मानव सभ्यता के विकास के साथ ही इस प्राकृतिक एवं स्वाभाविक संकल्पना का प्रादुर्भाव हुआ क्योंकि उपलब्ध अनुकूल पर्यावरणीय दशाओं के फलस्वरूप ही मानव सभ्यता का उद्भव एवं विकास संभव हुआ है। बदलते हुए कालचक्र क्रम के साथ ही इस मानव पर्यावरण संबंध के प्रारूपों में परिवर्तन सदैव होते रहे हैं एवं भविष्य में भी होते रहेंगे।

यह संकल्पना विभिन्न वैज्ञानिकों, इतिहासकारों, भूगोलवेत्ताओं, दार्शनिकों के लिए सदैव महत्वपूर्ण विषय रहा है। अतः संकल्पना अंतर विषयक स्वरूप लिए हुए हैं। प्राचीन काल से आधुनिक काल तक यूनानी, रोमन, अरब, भारतीय, चीनी, फ्रांसीसी, जर्मन, ब्रिटिश, रशियन एवं अमेरिकी भूगोलवेत्ता ने इस संबंध में अपने ज्ञान को उजागर किया है। 19वीं सदी के उत्तरार्ध में चार्ल्स डार्विन की पर्यावरण के 'प्राकृतिक चयन' पर आधारित वैज्ञानिक संकल्पना- "विकासवाद सिद्धांत" के साथ ही मानव-पर्यावरण संबंध के अध्ययन का काल प्रारंभ हो गया था।

पृथ्वी पर मानव के जन्म से ही, मनुष्य पर्यावरण को एवं पर्यावरण मनुष्य को प्रभावित करता रहा है। इस संबंध के ऐतिहासिक क्रम पर यदि दृष्टि डाली जाए, तो पाएंगे कि प्रारंभिक काल में पर्यावरण के साथ आदि-मानव का कार्यात्मक संबंध था, जिसमें मानव की भूमिका दो तरफा थी। जहां मानव एक ओर ग्राही के रूप में भौतिक पर्यावरण से अन्य जीवो की भांति विभिन्न प्राकृतिक

MATRICES

A BOOK FOR HIGHER COMPETITIVE EXAMINATION



KHEMRAJ MEENA
DR. RAKESHWAR PUROHIT
HRISHIKESH PALIWAL

MATRICES

For

NET / IIT – JAM / GATE / TIFR

KHEMRAJ MEENA

(RESEARCH SCHOLAR)

DR. RAKESHWAR PUROHIT

(ASSISTANT PROFESSOR)

HRISHIKESH PALIWAL

(RESEARCH SCHOLAR)

Department of Mathematics & Statistics

Mohanlal Sukhadia University, Udaipur

published by

HSRA Publications 2022
#02, Sri Annapoorneshwari Nilaya, 1st Main,
Byraveshwara Nagar, Laggere,
Bangalore – 560058
Ph- 7892793054

Sales Headquarters – Bangalore

Copyright © AUTHORS 2022

This book has been published with all reasonable efforts taken to make the material error-free after the consent of the respective authors. No part of this book shall be used, reproduced in any manner whatsoever without written permission from the editors, except in the case of brief quotations embodied in critical articles and reviews. The Authors of the respective chapters of this bookies solely responsible and liable for its content.

All rights reserved.

No part of this publication may be reproduced, transmitted, or storedin any digital or Electronic form. Also photocopying, recording or otherwise without the prior permission of the editor and publisher is strictly prohibited.

ISBN: 978-93-5506-043-3

First Edition 2022

No. of Pages -158

₹499. 00

CALCULUS

(A Book for Higher Competitive Examinations)

Dr. Rakeshwar Purohit, Khemraj Meena
Hrishikesh Paliwal

CALCULUS

For

NET / IIT – JAM / GATE / TIFR

DR. RAKESHWAR PUROHIT

(ASSISTANT PROFESSOR)

KHEMRAJ MEENA

(RESEARCH SCHOLAR)

HRISHIKESH PALIWAL

(RESEARCH SCHOLAR)

Department of Mathematics & Statistics

Mohanlal Sukhadia University, Udaipur

published by

HSRA Publications 2022
#02, Sri Annapoorneshwari Nilaya, 1st Main,
Byraveshwara Nagar, Laggere,
Bangalore – 560058
Ph- 7892793054

Sales Headquarters – Bangalore

Copyright © AUTHORS 2022

This book has been published with all reasonable efforts taken to make the material error-free after the consent of the respective authors. No part of this book shall be used, reproduced in any manner whatsoever without written permission from the editors, except in the case of brief quotations embodied in critical articles and reviews. The Authors of the respective chapters of this bookies solely responsible and liable for its content.

All rights reserved.

No part of this publication may be reproduced, transmitted, or storedin any digital or Electronic form. Also photocopying, recording or otherwise without the prior permission of the editor and publisher is strictly prohibited.

ISBN: 978-93-5506-044-0

First Edition 2022

No. of Pages -162

₹499. 00

Dilip Kumar,
Yuri Luchko
G. Suresh Singh *Editors*

Recent Advances in Mathematical Analysis and their Applications

Department of Mathematics
University of Kerala
Thiruvananthapuram, Kerala-695 581, India
2022

TABLE OF CONTENTS

List of Symbols 7

1. *Bilateral Generating Relations Involving Gegenbauer Polynomials*
   – *M.A. Pathan* 9

2. *A Survey on ${}_pR_q(\alpha, \beta; z)$ Function and its Applications*
   –*Ankit Pal, Rachana Desai, R.K. Jana & A. K. Shukla* . 19

3. *A quick survey of the bicomplex integral transforms and their applications*
   – *Ritu Agarwal, U.P. Sharma & M.P. Goswami* 55

4. *A Time Series Approach to Model Multiple Entropy of a Physical System Using Wright Distribution*
   – *Shanoja R. Naik* 89

5. *$\mathcal{P}$-transform on McBride Space*
   – *Deepa H. Nair* 115

Index 129

Recent Advances in Mathematical Analysis and their Applications
Dr Dilip Kumar, Dr Yuri Luchko, Dr Suresh Singh G., Editors

Copyright©2022. Department of Mathematics, University of Kerala, Thiruvuananthapuram, Kerala, India

All rights reserved.

No part of this book may be reproduced or transformed in any form or any other means, electronic or mechanical, by photostat, microfilm, xerography, recording, or incorporated into any information storage or retrieval system, without prior permission in writing from the copyright owner.

ISBN: 978-81-86660-48-5 81-86660-48-8
Published for Department of Mathematics, University of Kerala by:
Southern Book Star, T.C.7/2047-1, S.B. Tower, Medical College P.O.,
Ulloor, Thiruvananthapuram, Kerala, India

A quick survey of the bicomplex integral transforms and their applications

Ritu Agarwal[1], Urvashi Purohit Sharma[2], & Mahesh Puri Goswami[3]

[1,2]Department of Mathematics, Malaviya National Institute of Technology, Jaipur-302017, INDIA

[2]Department of Science and Humanities, Kalaniketan Polytechnic College, Jabalpur-482001, INDIA

[3] Department of Mathematics & Statistics, Mohanlal Sukhadia University, Udaipur, INDIA

E-mail: [1]*ragarwal.maths@mnit.ac.in*, [2]*urvashius100@gmail.com*, [3]*maheshgoswami1989@gmail.com*

Abstract: Various authors have defined a number of the integral transforms in the bicomplex space. This paper presents a review of the research on the bicomplex integral transformations. These transformations' varied applications are also highlighted here. The formula for the bicomplex version of the generalized Stieltjes transform been derived in light of recent advancements in the integral transforms in bicomplex space. Its basic operational properties are also addressed.

Keywords: Bicomplex numbers, integral transform, bicomplex Stieltjes transform.

AMS Subject Classification(2020): 44A05, 30G35.

1 *Introduction*

For a long time, bicomplex numbers have been investigated, and a lot of work has been done in this area. Between 1848 and 1850, Cockle [1, 2] introduced *Tessarines*, after which Segre [3] introduced bicomplex numbers.

Many bicomplex number properties have been identified. Researchers have been studying the various algebraic and geometric features of bicomplex numbers, as well as their applications, for the past few years (see, e.g. [4, 5, 6, 7, 8, 9]). In the recent developments, efforts have been






Publishers:
Thanuj International Publishers,
8/173-B, Vengayapalayam, Rasipuram,
Namakkal, Tamil Nadu, India – 637406.
E-mail: thanujinternationalpublishers@gmail.com

Printers:
Dhazh Computers
No: 442- A, 10th East Cross Street,
Munthirithoppu, Annanagar,
Madurai – 20, Tamil Nadu, India.
E-mail: narennarayanasamy@gmail.com

ISBN: 978-93-94638-19-8

Copyright@Thanuj International Publishers, 2022.

Current and Future Perspectives of Environmental Pollution and It's Remediation

CURRENT AND FUTURE PERSPECTIVES OF ENVIRONMENTAL POLLUTION AND IT'S REMEDIATION

First Edition

Editors
Dr. Azad Kumar
Mr. Vinod Kumar Singh
Dr. Akhilesh Sharma



THANUJ INTERNATIONAL PUBLISHERS,
TAMIL NADU, INDIA.

CONTENT TABLE

Chapter No.	Authors	Title of chapter	Page no.
1	[1]Amar Nath, [2]Anamica and [2]P.P. Pande,[3] Vinod Kumar Singh	COAGULANTS AND FLOCCULNTS FOR WASTEWATER TREATMENT	1-25
2	Tanushree Kain and Devendra Singh Rathore*	AIR POLLUTANTS EMISSION FROM THE BRICK KILN INDUSTRY, ITS IMPACT, AND REMEDIAL MEASURES	26-35
3	Manisha Khandelwal, Deeksha Sharma, Gangotri Pemawat, and Rama Kanwar Khangarot*	MECHANISTIC INSIGHTS INTO PHOTODEGRADATION OF ORGANIC DYES USING COPPER OXIDE NANOCATALYST	36-49
4	Prity Mehta and Sanjay Yadav*	DAIRY EFFLUENTS: SOURCES, CHARACTERISTICS AND ITS ENVIRONMENTAL IMPACT	50-57
5	Safana Asma'u Ibrahim[1]& Tijjani Sabi'u Imam[2]	POTENTIALS OF MICROALGAE IN BIOFUEL PRODUCTION	58-66
6	Kapil Kumar, Bhavya Singh, Rama Kanwar khangarot and Devendra Singh Rathore*	NANOTECHNOLOGY AND ITS APPLICATIONS AND IMPACT ON THE ENVIRONMENT	67-78
7	Shiv Mahendra Singh and Rashida Khatoon	OVERPOPULATION AND ITS IMPACT ON ENVIRONMENT	79-91
8	Pranoy Dey	OZONE LAYER DEPLETION: ITS CAUSES AND CONSEQUENCES	92-101
9	Ayushi Bhatnagar[1], Dr. Rama	PHOTODEGRADATION OF PHENOL USING PHYSIOCHEMICAL AND BIOLOGICAL METHODS	102-117

	Kanwar Khangarot[1], Kiran Meena[1], and Dr. Gangotri Pemawat[1*]		
10	Lokesh Baloat	RECENT PROGRESS IN APPLICATION AND IMPLICATIONS OF ENVIRONMENTAL NANOTECHNOLOGY	118-124
11	Subhamoy Das[1], Surekha Chowdhury[2], Avishek Dolai[3]	SUSTAINABLE AND ADAPTIVE APPROACHES TO SALINITY CHANGE IN WATER: A CASE STUDY FROM SOUTH BENGAL, INDIA	125-140
12	Vinod Kumar Singh	THE STUDY OF THE RADON, THORON LEVEL CONCENTRATION IN AND AROUND THE THERMAL POWER PLANT	141-144
13	Almas Khanam and Mohammad Akmal*	TOXIC HEAVY METAL REMOVAL FROM WATER USING SOME ADSORBENTS	145-173
14	Dr. Moon Mandal,*‡ Dr. Mahmuda Khannam*‡	SANITARY PRACTICES AND WASTE MANAGEMENT AMONG ADOLESCENT GIRLS & WOMEN IN RURAL AREA OF DALGAON CONSTITUENCY UNDER DARRANG DISTRICT, ASSAM: A CASE STUDY	174-185
15	Zaheen Hasan* and D.D.Tewari	EFFECT OF INDUSTRIALIZATION AND FERTILIZERS ON WATER QUALITY	186-195
16	Bhavya Singh[1], Kapil Kumar[1], Dr. Rama Kanwar Khangarot[2], and Dr. Devendra Singh Rathore[1*]	COPPER-BASED NPS: SOURCES, FATE AND BIOAVAILABILITY IN AGROECOSYSTEM	196-210
17	Capt. Mukesh Kumar	ADSORPTION OF TOXIC METALS FROM WATER BY ADSORBENT	211-215
18	SK. Kamruzzaman	RECENT TRENDS IN SOLID WASTE MANAGEMENT AND ITS RECYCLING IN INDIA	216-222

CHAPTER:16
COPPER-BASED NPS: SOURCES, FATE AND BIOAVAILABILITY IN AGROECOSYSTEM

Bhavya Singh[1], Kapil Kumar[1], Dr. Rama Kanwar Khangarot[2], and Dr. Devendra Singh Rathore[1*]

[1]Department of Environmental Sciences, Mohanlal Sukhadia University, Udaipur- 313001, Rajasthan, India

[2]Department of Chemistry, University College of Science, Mohanlal Sukhadia University, Udaipur-313001, Rajasthan, India

*Corresponding author: dsrathore@mlsu.ac.in

Abstract

Nanotechnology has broadened its horizon by incorporating nanoproducts in agriculture, as it is the primary source of income in developing nations. These nanoparticles (NPs) are incorporated with conventional fertilizers, fungicides, biocides, pesticides, etc., increasing their bioavailability in soil, sediments, and trophic levels. Various kinds of NPs are used in agriculture, for example, inorganic (Cu, Zn, CuO, ZnO, Fe_3O_4, etc.) and organic. This chapter summarizes, the application of copper-based NPs in agroecosystems. After exposure to the biological system, NPs fate depends on exposure, dissolution, transportation, chemical composition, and interaction with other plants. Their fate can alter depending on the properties of the respective ecosystem they are entering. NPs might aggravate toxic effects on non-targeted plants. Thousands and tons of NPs released into the environment yearly, yet, their interaction with biological systems is needed more systematic and methodical research.

Keywords: Nanotechnology, Copper-based NPs, Agroecosystems, Fate, Bioavailability

Introduction

Advancement in nanotechnology has made advantageous progress in science and technology at the industrial level, especially in biological sciences, agriculture, medicine, computing and microelectronics, environment and bioremediation, chemical manufacturing, transportation, energy, military, and consumer products (textiles, food packaging, cosmetics, paints, etc.). Nanoparticles (NPs) are the particles with at least one dimension in the array of 1-100 nm. These nanoparticles have well-known chemical and physical properties comprising antimicrobial and biocidal, photovoltaic and superconductivity, and relative stability by boosting the effectiveness of the products despite their small size. Extensive usage of nano-based agriproducts to control pests and improve fertility and growth has waked researchers to dwell






Publishers:
Thanuj International Publishers,
8/173-B, Vengayapalayam, Rasipuram,
Namakkal, Tamil Nadu, India – 637406.
E-mail: thanujinternationalpublishers@gmail.com

Printers:
Dhazh Computers
No: 442- A, 10th East Cross Street,
Munthirithoppu, Annanagar,
Madurai – 20, Tamil Nadu, India.
E-mail: narennarayanasamy@gmail.com

ISBN: 978-93-94638-19-8

Copyright@Thanuj International Publishers, 2022.

Current and Future Perspectives of Environmental Pollution and It's Remediation

CURRENT AND FUTURE PERSPECTIVES OF ENVIRONMENTAL POLLUTION AND IT'S REMEDIATION

First Edition

Editors
Dr. Azad Kumar
Mr. Vinod Kumar Singh
Dr. Akhilesh Sharma



THANUJ INTERNATIONAL PUBLISHERS,
TAMIL NADU, INDIA.

CONTENT TABLE

Chapter No.	Authors	Title of chapter	Page no.
1	[1]Amar Nath, [2]Anamica and [2]P.P. Pande,[3] Vinod Kumar Singh	COAGULANTS AND FLOCCULNTS FOR WASTEWATER TREATMENT	1-25
2	Tanushree Kain and Devendra Singh Rathore*	AIR POLLUTANTS EMISSION FROM THE BRICK KILN INDUSTRY, ITS IMPACT, AND REMEDIAL MEASURES	26-35
3	Manisha Khandelwal, Deeksha Sharma, Gangotri Pemawat, and Rama Kanwar Khangarot*	MECHANISTIC INSIGHTS INTO PHOTODEGRADATION OF ORGANIC DYES USING COPPER OXIDE NANOCATALYST	36-49
4	Prity Mehta and Sanjay Yadav*	DAIRY EFFLUENTS: SOURCES, CHARACTERISTICS AND ITS ENVIRONMENTAL IMPACT	50-57
5	Safana Asma'u Ibrahim[1]& Tijjani Sabi'u Imam[2]	POTENTIALS OF MICROALGAE IN BIOFUEL PRODUCTION	58-66
6	Kapil Kumar, Bhavya Singh, Rama Kanwar khangarot and Devendra Singh Rathore*	NANOTECHNOLOGY AND ITS APPLICATIONS AND IMPACT ON THE ENVIRONMENT	67-78
7	Shiv Mahendra Singh and Rashida Khatoon	OVERPOPULATION AND ITS IMPACT ON ENVIRONMENT	79-91
8	Pranoy Dey	OZONE LAYER DEPLETION: ITS CAUSES AND CONSEQUENCES	92-101
9	Ayushi Bhatnagar[1], Dr. Rama	PHOTODEGRADATION OF PHENOL USING PHYSIOCHEMICAL AND BIOLOGICAL METHODS	102-117

	Kanwar Khangarot[1], Kiran Meena[1], and Dr. Gangotri Pemawat[1*]		
10	Lokesh Baloat	RECENT PROGRESS IN APPLICATION AND IMPLICATIONS OF ENVIRONMENTAL NANOTECHNOLOGY	118-124
11	Subhamoy Das[1], Surekha Chowdhury[2], Avishek Dolai[3]	SUSTAINABLE AND ADAPTIVE APPROACHES TO SALINITY CHANGE IN WATER: A CASE STUDY FROM SOUTH BENGAL, INDIA	125-140
12	Vinod Kumar Singh	THE STUDY OF THE RADON, THORON LEVEL CONCENTRATION IN AND AROUND THE THERMAL POWER PLANT	141-144
13	Almas Khanam and Mohammad Akmal*	TOXIC HEAVY METAL REMOVAL FROM WATER USING SOME ADSORBENTS	145-173
14	Dr. Moon Mandal,*‡ Dr. Mahmuda Khannam*‡	SANITARY PRACTICES AND WASTE MANAGEMENT AMONG ADOLESCENT GIRLS & WOMEN IN RURAL AREA OF DALGAON CONSTITUENCY UNDER DARRANG DISTRICT, ASSAM: A CASE STUDY	174-185
15	Zaheen Hasan* and D.D.Tewari	EFFECT OF INDUSTRIALIZATION AND FERTILIZERS ON WATER QUALITY	186-195
16	Bhavya Singh[1], Kapil Kumar[1], Dr. Rama Kanwar Khangarot[2], and Dr. Devendra Singh Rathore[1*]	COPPER-BASED NPS: SOURCES, FATE AND BIOAVAILABILITY IN AGROECOSYSTEM	196-210
17	Capt. Mukesh Kumar	ADSORPTION OF TOXIC METALS FROM WATER BY ADSORBENT	211-215
18	SK. Kamruzzaman	RECENT TRENDS IN SOLID WASTE MANAGEMENT AND ITS RECYCLING IN INDIA	216-222

CHAPTER:6
NANOTECHNOLOGY AND ITS APPLICATIONS AND IMPACT ON THE ENVIRONMENT

Kapil Kumar, Bhavya Singh, Rama Kanwar khangarot and Devendra Singh Rathore*

Department of Environmental Sciences, Mohanlal Sukhadia University, Udaipur-313001, Rajasthan, India

*Corresponding Author: dsrathore@mlsu.ac.in

Abstract: - Nanotechnology is science, engineering, and technology conducted at the nanoscale which is about 1-100nm. Different techniques are there to synthesize the nanoparticles and modify them as per requirement. The types of nanoparticles and their enormous number of applications have crucial importance in the emerging field of nanotechnology. Although it's an emerging field but has less knowledge about the behaviour of nanoparticles which can lead to the generation of nano waste which may cause an adverse impact on the environment.

Keywords: - Nanotechnology, engineering, technology, nanoparticles, nano waste.

Introduction: -

Nanotechnology and nanoscience are emerging areas with enormous potential to enhance many areas of study and applications. What is truly novel about nanoscience is that developments in material science and characterisation technologies now allow for monitoring materials at the nanometre (nm = 10^{-9}m) scale, allowing for unique insights into atomic interactions [1]. Nanomaterials (NMs) are defined as materials that have particles with at least one dimension of 1-100 nm in length. Their unique physical and chemical properties have made them advantageous in a variety of applications [2]. Depending on the overall shape these materials can be 0D, 1D, 2D or 3D [3]. Nanoparticles have an interesting history. Their production is not solely the outcome of current science, nor is it limited to man-made materials. Organic nanoparticles (proteins, polysaccharides, viruses, among others) and inorganic nanoparticles (iron oxyhydroxides, aluminosilicates, metals, among others) are created naturally by weathering, volcano eruptions, wildfires, or microbiological processes [4]. The production of nanoscale materials with unique physicochemical properties has resulted in powerful nanotechnology in the twenty-first century, allowing existing technologies to realize their full potential. The unique features of these






Publishers:
Thanuj International Publishers,
8/173-B, Vengayapalayam, Rasipuram,
Namakkal, Tamil Nadu, India – 637406.
E-mail: thanujinternationalpublishers@gmail.com

Printers:
Dhazh Computers
No: 442- A, 10th East Cross Street,
Munthirithoppu, Annanagar,
Madurai – 20, Tamil Nadu, India.
E-mail: narennarayanasamy@gmail.com

ISBN: 978-93-94638-19-8

Copyright@Thanuj International Publishers, 2022.

Current and Future Perspectives of Environmental Pollution and It's Remediation

CURRENT AND FUTURE PERSPECTIVES OF ENVIRONMENTAL POLLUTION AND IT'S REMEDIATION

First Edition

Editors
Dr. Azad Kumar
Mr. Vinod Kumar Singh
Dr. Akhilesh Sharma



THANUJ INTERNATIONAL PUBLISHERS,
TAMIL NADU, INDIA.

CONTENT TABLE

Chapter No.	Authors	Title of chapter	Page no.
1	[1]Amar Nath, [2]Anamica and [2]P.P. Pande,[3] Vinod Kumar Singh	COAGULANTS AND FLOCCULNTS FOR WASTEWATER TREATMENT	1-25
2	Tanushree Kain and Devendra Singh Rathore*	AIR POLLUTANTS EMISSION FROM THE BRICK KILN INDUSTRY, ITS IMPACT, AND REMEDIAL MEASURES	26-35
3	Manisha Khandelwal, Deeksha Sharma, Gangotri Pemawat, and Rama Kanwar Khangarot*	MECHANISTIC INSIGHTS INTO PHOTODEGRADATION OF ORGANIC DYES USING COPPER OXIDE NANOCATALYST	36-49
4	Prity Mehta and Sanjay Yadav*	DAIRY EFFLUENTS: SOURCES, CHARACTERISTICS AND ITS ENVIRONMENTAL IMPACT	50-57
5	Safana Asma'u Ibrahim[1]& Tijjani Sabi'u Imam[2]	POTENTIALS OF MICROALGAE IN BIOFUEL PRODUCTION	58-66
6	Kapil Kumar, Bhavya Singh, Rama Kanwar khangarot and Devendra Singh Rathore*	NANOTECHNOLOGY AND ITS APPLICATIONS AND IMPACT ON THE ENVIRONMENT	67-78
7	Shiv Mahendra Singh and Rashida Khatoon	OVERPOPULATION AND ITS IMPACT ON ENVIRONMENT	79-91
8	Pranoy Dey	OZONE LAYER DEPLETION: ITS CAUSES AND CONSEQUENCES	92-101
9	Ayushi Bhatnagar[1], Dr. Rama	PHOTODEGRADATION OF PHENOL USING PHYSIOCHEMICAL AND BIOLOGICAL METHODS	102-117

	Kanwar Khangarot[1], Kiran Meena[1], and Dr. Gangotri Pemawat[1*]		
10	Lokesh Baloat	RECENT PROGRESS IN APPLICATION AND IMPLICATIONS OF ENVIRONMENTAL NANOTECHNOLOGY	118-124
11	Subhamoy Das[1], Surekha Chowdhury[2], Avishek Dolai[3]	SUSTAINABLE AND ADAPTIVE APPROACHES TO SALINITY CHANGE IN WATER: A CASE STUDY FROM SOUTH BENGAL, INDIA	125-140
12	Vinod Kumar Singh	THE STUDY OF THE RADON, THORON LEVEL CONCENTRATION IN AND AROUND THE THERMAL POWER PLANT	141-144
13	Almas Khanam and Mohammad Akmal*	TOXIC HEAVY METAL REMOVAL FROM WATER USING SOME ADSORBENTS	145-173
14	Dr. Moon Mandal,*‡ Dr. Mahmuda Khannam*‡	SANITARY PRACTICES AND WASTE MANAGEMENT AMONG ADOLESCENT GIRLS & WOMEN IN RURAL AREA OF DALGAON CONSTITUENCY UNDER DARRANG DISTRICT, ASSAM: A CASE STUDY	174-185
15	Zaheen Hasan* and D.D.Tewari	EFFECT OF INDUSTRIALIZATION AND FERTILIZERS ON WATER QUALITY	186-195
16	Bhavya Singh[1], Kapil Kumar[1], Dr. Rama Kanwar Khangarot[2], and Dr. Devendra Singh Rathore[1*]	COPPER-BASED NPS: SOURCES, FATE AND BIOAVAILABILITY IN AGROECOSYSTEM	196-210
17	Capt. Mukesh Kumar	ADSORPTION OF TOXIC METALS FROM WATER BY ADSORBENT	211-215
18	SK. Kamruzzaman	RECENT TRENDS IN SOLID WASTE MANAGEMENT AND ITS RECYCLING IN INDIA	216-222

CHAPTER: 9
PHOTODEGRADATION OF PHENOL USING PHYSIOCHEMICAL AND BIOLOGICAL METHODS

Ayushi Bhatnagar[1], Dr. Rama Kanwar Khangarot[1], Kiran Meena[1], and Dr. Gangotri Pemawat[1*]

[1]Department of Chemistry, University College of Science, Mohanlal Sukhadia University, Udaipur, Rajasthan, India 313001.

*Correspondence: drgpemawat@mlsu.ac.in; Tel.: 9929614067

Abstract:

Industrial effluents are one of the major provenances of continuous input of pollutants in aquatic ecosystems. The treatment of such contaminated systems requires several techniques, which include both conventional methods and some special techniques. Phenolic compounds are one of the persistent and lethal components found in wastewater. The contamination due to phenol and its compounds has moderately appeared. The degradation of such compounds can be achieved by using solar energy. Photodegradation or photolysis is a significant process in which pollutants are disclosed to sunlight. The process of photodegradation is enhanced by utilizing photocatalysts, which are regularly modified by incorporating nanoscience. Several physiochemical and biological methods have been developed which are environment friendly and bring complete mineralization of toxic compounds. Researchers have proved that several microorganisms can transmute organic pollutants into simpler compounds. Such methods proved sustainable and cost-effective.

Keywords: Phenol, Phenolic compounds, wastewater, physiochemical methods, biological methods.

Introduction:

Phenol is a crucial material in industries and is generally used in petrochemical industries, medicine, pesticide, dye, paper, and coal industries. Phenol acts as a forebearer in the production of several pharmaceutical drugs, plastics, epoxies, polycarbonates, and detergents. Its extensive use and noxious nature have generated serious health issues, as well as contamination of soil and water[1]. The carcinogenic and mutagenic effects affect humans, plants, and animals even at a very low concentration level[2]. In aqueous environments, the presence of phenol creates serious problems because of its perseverance and toxicity. Due to its carcinogenic nature, phenol causes mouth sores, darkening of urine, blood diarrhea, nausea, and vomiting with varying levels[3]. On top of that, while






Publishers:
Thanuj International Publishers,
8/173-B, Vengayapalayam, Rasipuram,
Namakkal, Tamil Nadu, India – 637406.
E-mail: thanujinternationalpublishers@gmail.com

Printers:
Dhazh Computers
No: 442- A, 10th East Cross Street,
Munthirithoppu, Annanagar,
Madurai – 20, Tamil Nadu, India.
E-mail: narennarayanasamy@gmail.com

ISBN: 978-93-94638-19-8

Copyright@Thanuj International Publishers, 2022.

Current and Future Perspectives of Environmental Pollution and It's Remediation

CURRENT AND FUTURE PERSPECTIVES OF ENVIRONMENTAL POLLUTION AND IT'S REMEDIATION

First Edition

Editors
Dr. Azad Kumar
Mr. Vinod Kumar Singh
Dr. Akhilesh Sharma



THANUJ INTERNATIONAL PUBLISHERS,
TAMIL NADU, INDIA.

CONTENT TABLE

Chapter No.	Authors	Title of chapter	Page no.
1	[1]Amar Nath, [2]Anamica and [2]P.P. Pande,[3] Vinod Kumar Singh	COAGULANTS AND FLOCCULNTS FOR WASTEWATER TREATMENT	1-25
2	Tanushree Kain and Devendra Singh Rathore*	AIR POLLUTANTS EMISSION FROM THE BRICK KILN INDUSTRY, ITS IMPACT, AND REMEDIAL MEASURES	26-35
3	Manisha Khandelwal, Deeksha Sharma, Gangotri Pemawat, and Rama Kanwar Khangarot*	MECHANISTIC INSIGHTS INTO PHOTODEGRADATION OF ORGANIC DYES USING COPPER OXIDE NANOCATALYST	36-49
4	Prity Mehta and Sanjay Yadav*	DAIRY EFFLUENTS: SOURCES, CHARACTERISTICS AND ITS ENVIRONMENTAL IMPACT	50-57
5	Safana Asma'u Ibrahim[1]& Tijjani Sabi'u Imam[2]	POTENTIALS OF MICROALGAE IN BIOFUEL PRODUCTION	58-66
6	Kapil Kumar, Bhavya Singh, Rama Kanwar khangarot and Devendra Singh Rathore*	NANOTECHNOLOGY AND ITS APPLICATIONS AND IMPACT ON THE ENVIRONMENT	67-78
7	Shiv Mahendra Singh and Rashida Khatoon	OVERPOPULATION AND ITS IMPACT ON ENVIRONMENT	79-91
8	Pranoy Dey	OZONE LAYER DEPLETION: ITS CAUSES AND CONSEQUENCES	92-101
9	Ayushi Bhatnagar[1], Dr. Rama	PHOTODEGRADATION OF PHENOL USING PHYSIOCHEMICAL AND BIOLOGICAL METHODS	102-117

	Kanwar Khangarot[1], Kiran Meena[1], and Dr. Gangotri Pemawat[1*]		
10	Lokesh Baloat	RECENT PROGRESS IN APPLICATION AND IMPLICATIONS OF ENVIRONMENTAL NANOTECHNOLOGY	118-124
11	Subhamoy Das[1], Surekha Chowdhury[2], Avishek Dolai[3]	SUSTAINABLE AND ADAPTIVE APPROACHES TO SALINITY CHANGE IN WATER: A CASE STUDY FROM SOUTH BENGAL, INDIA	125-140
12	Vinod Kumar Singh	THE STUDY OF THE RADON, THORON LEVEL CONCENTRATION IN AND AROUND THE THERMAL POWER PLANT	141-144
13	Almas Khanam and Mohammad Akmal*	TOXIC HEAVY METAL REMOVAL FROM WATER USING SOME ADSORBENTS	145-173
14	Dr. Moon Mandal,*‡ Dr. Mahmuda Khannam*‡	SANITARY PRACTICES AND WASTE MANAGEMENT AMONG ADOLESCENT GIRLS & WOMEN IN RURAL AREA OF DALGAON CONSTITUENCY UNDER DARRANG DISTRICT, ASSAM: A CASE STUDY	174-185
15	Zaheen Hasan* and D.D.Tewari	EFFECT OF INDUSTRIALIZATION AND FERTILIZERS ON WATER QUALITY	186-195
16	Bhavya Singh[1], Kapil Kumar[1], Dr. Rama Kanwar Khangarot[2], and Dr. Devendra Singh Rathore[1*]	COPPER-BASED NPS: SOURCES, FATE AND BIOAVAILABILITY IN AGROECOSYSTEM	196-210
17	Capt. Mukesh Kumar	ADSORPTION OF TOXIC METALS FROM WATER BY ADSORBENT	211-215
18	SK. Kamruzzaman	RECENT TRENDS IN SOLID WASTE MANAGEMENT AND ITS RECYCLING IN INDIA	216-222

CHAPTER:3
MECHANISTIC INSIGHTS INTO PHOTODEGRADATION OF ORGANIC DYES USING COPPER OXIDE NANOCATALYST

Manisha Khandelwal, Deeksha Sharma, Gangotri Pemawat,and Rama Kanwar Khangarot*

Department of Chemistry, University College of Science, Mohanlal Sukhadia University, Udaipur 313001, Rajasthan, India.
*Correspondence: ramakanwar@mlsu.ac.in

Abstarct

Photocatalysis is a promising method for eradicating organic dyes from wastewater. Among the admired photocatalyst, copper oxide nanoparticles (CuO-NPs) are widely used for the photodegradation of organic dyes in wastewater treatment due to their low cost, abundance, less-toxic, ability to proceed at ambient temperature, and high photonic efficiency. This chapter includes a brief overview of dyes as a pollutant, applications of dyes, and dyes classification. Further, the photodegradation mechanism of dyes and kinetics using CuO nano photocatalyst is also discussed. It emphasizes the operational parameters affecting the photodegradation of cationic or anionic dyes and the charge carrier properties of the CuO nanocatalyst under visible or UV irradiation. In addition, we have discussed the photodegradation of organic dyes such as anionic dyes- methyl orange (MO) and congo red (CR) and cationic dyes- methylene blue (MB) and rhodamine B (RhB) using CuO nano photocatalyst.

Keywords: Copper oxide nanoparticles (CuO-NPs), photocatalyst, organic dyes, photodegradation, scavengers

1 Introduction

Ironically 'there is a reason we don't see the world black and white.' (Celeries Kemble)

Colours have always fascinated human beings since the Neolithic period (6000-3500 BC) from cave painting to acrylic advancements [1], [2]. Back then, a few plant-based colourants such as madder, indigo, woad, and saffron were cultivated and used as trade-in economies over Europe and the Asian continent especially. The use of these natural colouring agents came to a check, after the discovery of synthetic dyes by William Henry Perkin in 1856 [3]. This was one of the revolutionary works done in organic chemistry with its economical applications. Synthetic dyes are the most important colouring agent used in

Climate Change and Sustainable Development

Om Prakash
Gaurav Kumar Jain
Govind Singh
Lalit Singh Jhala



SCIENTIFIC PUBLISHERS®

Climate Change and Sustainable Development

Our Related Books

Title	Author
Agriculture and Climate Change	FAO
Agroforestry for Climate Resilience and Rural Livelihood	Inder Dev
Antarctica: Environment and Conservation	Neloy Khare
Atmospheric Pollution By Aerosols	V.K. Sharma
Bioclimatology and Plant Geography of Peninsular India	V.M. Meher-Homji
Climate Change & Himalayan Ecosystem: Indicator, Bio & Water Resources	J. Sundaresan
Climate Change & Himalayan Informatics	J. Sundaresan
Climate Change Adaptation Strategies in Agriculture and Allied Sectors	GSLHV Prasad Rao
Climate Change and Environment	J. Sundaresan
Climate Change and Himalaya: Natural Hazards and Mountain Resources	J. Sundaresan
Climate Change and Its Ecological Implications for The Western Himalaya	V.L. Chopra
Climate Change Impact on Ecosystem	J. Sundaresan
Climate, Agriculture and Man (Shrinking Biodiversity and Sustainability)	V.K. Sehgal
Climate-Smart Agriculture Source Book	FAO
Climate-Smart Agriculture Training Manual for Agricultural Extension	FAO
Combating Desertification Land Degradation and Climate Change: Management of Dry Lands	T.S. Chouhan
Communication for Rural Development Source Book	Mario Acunzo
Crop Growth Simulation Modelling and Climate Change	Nishant K. Sinha
Crop Protection Strategies Under Climate Change Scenarios	P.P. Reddy
Disaster Management: A Disaster Manager's Handbook	W.Nick Carter
Drought Mitigation and Management	Suresh Kumar
Earth and Ocean: Useful Resources (Hindi)	D.D. Ojha
Emergency Response Manual	USDA
Introductory Agrometeorology	Sevak Das
Objective Environmental Pollution and Climate Change	M. Prasanthrajan
Objective Environmental Studies and Disaster Management	M. Prasanthrajan
Organic Agriculture and Climate Change Mitigation	URS Niggli
Pollution Risks, Impacts & Management Social, Economic and Environmental Perspectives	Golam Kibria
Principles of Agricultural Meteorology	B.M. Mote
Questions and Answers in Environmental Science Practical	R.K. Kamble
Rainwater Management: Theory and Practice	M.L. Jat
Space Technology and GIS for Disaster Monitoring and Mitigation	T.S. Chouhan
Text Book of Disaster Management	Ajay Kumar Srivastava
Thar Desert in Retrospect and Prospect	R.P. Dhir

For more details visit our website

Climate Change and Sustainable Development

Edited By

Om Prakash, Gaurav Kumar Jain,
Govind Singh, Lalit Singh Jhala

Department of Geography,
Jai Narain Vyas University Jodhpur,
Rajasthan (*India*)

SCIENTIFIC PUBLISHERS

Published by
SCIENTIFIC PUBLISHERS (INDIA)
5 A, New Pali Road, P.O. Box 91
Jodhpur 342 001 (INDIA)
E-mail: info@scientificpub.com
Website: http://www.scientificpub.com

© 2023 Author

All rights reserved. No part of this publication or the information contained herein may be reproduced, adapted, abridged, translated, stored in a retrieval system, computer system, photographic or other systems or transmitted in any form or by any means, electronic, mechanical, by photocopying, recording or otherwise, without written prior permission from the publisher.

Disclaimer: Whereas every effort has been made to avoid errors and omissions, this publication is being sold on the understanding that neither the editors (or authors) nor the publishers nor the printers would be liable in any manner to any person either for an error or for an omission in this publication, or for any action to be taken on the basis of this work. Any inadvertent discrepancy noted may be brought to the attention of the publisher, for rectifying it in future editions, if published.

This book contains information obtained from authentic and highly regarded sources. Reasonable efforts have been made to publish reliable data and information, but the editors and publisher cannot assume responsibility for the validity of all materials or the consequences of their use. The editors and publisher have attempted to trace and acknowledge the copyright holders of all material reproduced in this publication and apologize to copyright holders if permission and acknowledgment to publish in this form have not been obtained. If any copyright material has not been acknowledged please write and let us know so that we may rectify it.

Trademark Notice: Product or corporate names may be trademarks or registered trademarks, and are used only for identification and explanation without intent to infringe.

ISBN: 978-93-90749-29-4 (HB)
eISBN: 978-93-90749-31-7 (EBook)

Printed in India

Editors' Introduction



Dr. Om Prakash

M.A., Ph.D. in Geography from Jai Narain Vyas University Jodhpur, UGC NET-JRF in Geography, UGC NET in Population Studies, RPSC SET in Geography, NNRMS certificate course IIRS-ISRO. He has been working as an Assistant Professor in the Department of Geography at Jai Narain Vyas University, Jodhpur since 2013. He is also the coordinator of the Nodal Centre for the IIRS outreach program. At present, four research scholars are pursuing PhDs under his supervision. He has participated and presented papers in various international and national seminars and conferences and has published many research papers in reputed journals.



Dr. Gaurav Kumar Jain

M.A., M.Phil., NET-JRF, RPSC-SET in Geography, Ph.D. from Jai Narain Vyas University, Jodhpur. He has been working as an Assistant Professor in the Department of Geography at Jai Narain Vyas University, Jodhpur since 2013. At present, five scholars are pursuing research degrees under his supervision. He has participated and presented papers in various international and national seminars and conferences and has published many research papers in reputed journals.



Mr. Govind Singh

M.A. UGC-NET in Geography, RPSC-SET in Geography and Population Studies both. Born in 1983 in the village of Bhawanda in the Nagaur district of Rajasthan. Vagdevi's spiritual practice and literary interest turned him towards writing. He has a spontaneous inclination towards poetry, drama and various co-curricular activities. Due to his deep interest in geographical analysis and culture writing, various research articles and contemporary papers have been presented as well as published in various journals by him. He has been working as an Assistant Professor at the Department of Geography at Jai Narain Vyas University, Jodhpur since 2013.



Dr. Lalit Singh Jhala

M.A., NET, SET, Ph.D. in Geography from Mohan Lal Sukhadia University, Udaipur. Currently, he is working as an Assistant Professor in the Department of Geography at Jai Narain Vyas University, Jodhpur. His books, titled "Regional Disparities in Tribal Area" (single author) and "Tourism Development in Desert and Humid Zones" (co-authored), were published in 2012 & 2016 respectively. Dr. Jhala, is the recipient of the "Young Geographer Award" (2008) at the Rajasthan Geographical Association (RGA) national conference. He has also served as the Vice-President of RGA from 2020 to 2022. He has participated and presented papers in various international and national conferences, seminars and workshops; and has published 15 research papers in reputed journals. He has also supervised four Ph.D. scholars from Mohanlal Sukhadia University, Udaipur and JNV University, Jodhpur, respectively.

Preface

Climate change has become an agenda of key concern and requires our utmost attention. There are several factors which collectively attribute to climate change but anthropogenic activities since the early 1700s, could be considered the major cause of it. These anthropogenic activities not only degrade the quality of the water, air and soil around it, but are also responsible for several adverse health effects on animals and humans. Recent accelerated climate change has exacerbated existing environmental problems around the globe that are caused by the combination of changes in land use, increasing pollution and declining biodiversity. Climate change can be said to be a threat multiplier. It intensifies existing threats, aggravating complications for the environment, economy and thus, the entire society. The recent global warming is already producing negative influences on natural and human systems, seriously impeding progress toward some sustainable development goals (SDGs). Sustainable development is development that meets the needs of the existing generation without compromising with the capabilities of the future generations to meet their own needs. Climate change causes hindrance in the sustainable development of the society which not only affects mankind but all the species existing in an ecosystem.

This bilingual book emphasises on the several issues regarding climate change and how these issues are interlinked with sustainable development. The 20 chapters of this book revolve around how plants and animals are affected by climate change and how they can be used as indicators of climate change, how the agriculture sector is affected by it and what policies could be brought into account to stop the climate change and lead to betterment of all via working on sustainable development goals.

We would like to thank all the authors for coming forward and presenting their ideas which helped us in moulding this book. Their efforts would help the present and future generations in understanding the importance of this topic and would open gateways of new and better research.

Foreword



Earth, life and climate have always changed and climate change itself may have been crucial for the evolution of human being. The climate system is a complex interactive system consisting of the atmosphere, hydrosphere, lithosphere, cryosphere and outer space. Climate change is a global challenge with diverse implication at the national and regional levels, through impacts on various sectors such as agriculture, water resources, forestry and biodiversity, human health, energy and infrastructure. The scientific studies indicate that climate change is inevitable. The climate has transformed in the past, is varying in the present and is bound to change in the future. Today we are erroneously worried about the global warming and the impacts it is likely to bring. Contrary to it, some scientists forecast that 'global cooling' would be more disastrous in future.

The scientists are debating on the causes of climate change. The natural scientists believe that climate changes are due to several natural forces like changes in the obliquity of earth's axis, its rotational speed, solar variability or sunspot and volcanic activities. On the contrary, some scientists who believe in global warming say that increase in the emission of green house gases after industrial revolution has been mainly responsible for global warming and climate changes. It is beyond doubt that since 1850 A.D. the temperature is rising at such a rate that it was never experienced during last 800,000 years during geological past. The 'pro-warming lobby' advocates that the earth's warming occur not only in response to external forcing but also due to release of GHG's in the atmosphere by human beings especially the burning fossil fuels.

This book **"Climate Change and Sustainable Development"** presents a systematic work on the issues of climate change. The backdrop ranges from biology, agriculture, renewable energy to human health. All of these are very important aspects of human life as impacted by the rapid change in the climate of the earth. The book offers a wide variety of topics ranging from the global scenario of climate change, the bio monitoring properties of a plant that can be symptomatic of climate change and its impacts, the issue of solid waste management, the problems of agricultural pollution, the scenario of potential and challenges of biomass energy. The wider academic and geographical area of the problems discussed in the various chapters ensures that the book is wide in its scope, methods, approaches, spatial coverage and variety of problems faced.

I take immense pleasure in congratulating all the editors, as well as, the contributing authors of this book. The editors **Dr. Om Prakash, Dr. Gaurav Kumar Jain, Mr. Govind Singh and Dr. Lalit Singh Jhala** have, through persistent hard work and academic assiduity produced a well-balanced piece of literature that is varied in its approach and perspectives.

Hence, my compliments for their ardor and zeal.

Prof. H. S. Sharma
Formerly Professor and Head Department of Geography
University of Rajasthan, Jaipur
hssharma358@gmail.com

Contents

Editors' Introduction (*v*)

Preface (*vii*)

Foreword (*ix*)

1. Bryophytes: Pollution Indicators and Biomonitoring Agents 1–6
   G. S. Deora, Monika K. Shekhawat And Saraswati
2. Monograph of Commiphora Wightii: 7–20
   A Critically Endangered Medicinal Plant
   Kunal Seth, Vishambhar Sangela, Sandhya Deora, Priyanka Faroda, Sunita Choudhary, Nikita Gautam, Amit Kumar Gupta, Harish
3. Changes in Irrigated Land Utilization: A Spatio-Temporal Analysis of Kopai River Basin, Eastern India 21–30
   Tanmoy Das
4. Teredolites: The Wood-Boring Tracefossils From Fatehgarh Formation of The Barmer Basin, Western Rajasthan, India 31–42
   V. S. Parihar, Pawan Kumar, Anshul Harsh, C. P. Khichi And S. L. Nama
5. Climate Change Policy of India 43–54
   Chandraveer Singh Bhati
6. Impact of Solid Waste on Global Climate Change 55–70
   Kundan Kunwar Chouhan
7. Sustainable Development and Enviromental Issues: 71–82
   Save The Enviroment Save The Life
   Dalpat Singh
8. Understanding Impact of Shifting Wild Fire Regime on Environment and Climate 83–94
   Anuya Verma, Rohini Trivedi And Sanjay Meghwal
9. Climate Change: An Overview of The Global Scenario 95–104
   Bhavya Singh, Chirmaie Nagda, Kapil Kumar, Monika Rathore, Girima Nagda, Lalit Singh Jhala And Devendra Singh Rathore
10. Agricultural Pollution 105–114
    Sanjay Parihar
11. Geopolitics of Indian Ocean 115–120
    Jyotiraditya Singh Bhati

12. Scenario of Mining Industry in Western Rajasthan: An Environmental Issue 121–128
Indu Deval, O.P. Dewasi
13. Sustainable Growth of Agriculture in Rajasthan 129–138
Pramila Jangid, Jai Singh
14. Urbanisation Changing Morphology of Alwar City of Rajasthan 139–146
Yudhister Sharma, Aakanksha Bali
15. The Evolving Pattern of Agriculture in Changing Climatic Conditions (In Two Decades): A Review in The Context of Pali District 147–156
Sukhdev Meghwal, Lalit Singh Jhala
16. The Jawai Dam: Lifeline of Marwar 157–160
Ummed Kumar Choudhary
17. Impact of Climate Change on Medicinal Plants: A Case Study of Karnataka State 161–172
Pragnya. S. Hangaragi
18. Impact of Biodiversity on Food Security: A Geographical Study of India 173–176
Yudhister Sharma, Aakanksha Bali
19. Climate Change, Human Health and Sustainable Development: The Interlinked Trinity 177–192
Girima Nagda, Chirmaie Nagda, Devendra Singh Rathore and Bhavya Singh
20. Energy Generation from Biomass in Rajasthan: An Overview of Potential, Policies and Challenges 193–205
Shrikant, Om Prakash

Chapter 9

Climate Change: An Overview of The Global Scenario

Bhavya Singh[1], Chirmaie Nagda[1], Kapil Kumar[1], Monika Rathore[1], Girima Nagda[2], Lalit Singh Jhala[3] and Devendra Singh Rathore[1]*

Abstract

Climate change is the variability among climatic statistics such as temperature, precipitation, wind circulation patterns, oceanic currents, and hot and cold snaps. Climate phenomena are accelerating at an alarming pace due to anthropogenic forces. It's a global pandemic of the 21st century that demands to act collectively in unison to curtail the changes that adversely affect the environment and the climate. These global alterations pose a threat to Earth and earthlings due to over-flourishing industrialization, unplanned development, and degradation of forests, population explosion, over-exploitation of natural resources, and increased pollution concentration in an ambient environment. Outcomes of these anthropogenic driven forces are devastating and detrimental, which speeds up the ecosystem disruption to its collapsing level. These events are impacting the ecosystems, ecological niches and habitats, shifting of geographical realms, altering weather patterns, sea level upsurging, melting of permafrost, biodiversity, changing hydrological and nutrient cycling, reducing ecosystem services, the outbreak of diseases, nations economy, and lives and livelihoods of people, etc. around the planet.

Keywords: Climate change, GHGs (Greenhouse gases), climatic systems, earthlings, pandemic, global, threats, over-exploitation.

Introduction

Climate change has become a crucial concern around every corner of the globe, which must be discussed and mentioned at the scientific and academic level and the societal level from a broader perspective as these climatic events worsen in the 21st century. Climatic changes across the globe have escalated the frequency and magnitude of altered unprecedented events such as wind circulation patterns across the northern and southern hemispheres, oceanic flow from equator to poles, and greenhouse gas

[1] Department of Environmental Sciences, Mohanlal Sukhadia University, Udaipur
[2] Department of Zoology, Mohanlal Sukhadia University, Udaipur
[3] Department of Geography, Jai Narain Vyas University, Jodhpur
[1*] Corresponding author

concentration in the ambient atmosphere. The events mentioned above cascading detrimental effects on Earth and earthlings in varied ways, for instance, affect and impact the life and livelihoods, biodiversity, seasonal variations, local weather patterns, freshwater availability, energy, and food security, etc. by altering the ambient environment. We are now getting used to this climate emergency as we have seen and heard about it everywhere. But, do we care about this climatic emergency?

Climate is an ancient Greek word that means ***Klima***, meaning inclination. Climate is simply the standard average of 30 years of weather over a long period of any considered/studying area. According to IPCC (Intergovernmental Panel on Climate Change), 2001 glossary:

Climate in a narrow sense is usually defined as the "average weather," or more rigorously, as the statistical description in terms of the mean and variability of relevant quantities over a period ranging from months to thousands or millions of years. The classical period is 30 years, as defined by the World Meteorological Organization (WMO). These quantities are most often surface variables such as temperature, precipitation, and wind. Climate in a wider sense is the state, including a statistical description, of the climate system. (IPCC, 2001). The World Meteorological Organization (WMO) describes ***climate "normals" as"reference points used by climatologists to compare current climatological trends to that of the past or what is considered 'normal'. A Normal is defined as the arithmetic average of a climate element (e.g. temperature) over a 30-year period"*** (WMO).

Earth's climate comprises of five main climate systems, which are atmosphere (air), hydrosphere (water), cryosphere (ice and permafrost), lithosphere (upper earth layer, i.e., soil/land), and biosphere (living entity). The industrial revolution started back in the 1950s has gradually escalated the ambient atmospheric temperature, which has reached a level that is massively contributing to global climate change. The industrialization has popped up the concentration of atmospheric greenhouse gases to many folds than pre-industrialization. Climate change is a remarkable long-term change across the globe. Climatic changes are paving their way beyond thermal stress, disrupting ecosystems, and influencing the resources we depend on for our daily lives, such as water, energy, transportation, wildlife, agriculture, forest, and human health. Climate is one of the most important factors that affect species behavioral, productivity and distribution, and has an enormous impact on habitat and ecosystem ecology.

India is the 2nd most populated country with 1.3 billion population and lies at 6° 44' and 35° 33' latitude and 68° 71' and 97° 25' longitude. It's a mega-diverse nation. India is exceptionally prone to climate change impacts mainly due to its unique geography (IPCC, 2017). According to Global Climate Risk Index 2020, the top 10 most affected countries in 2018 are Japan, Philippines, Germany, Madagascar, India (14 in 2017), Sri Lanka, Kenya, Rwanda, Canada, and Fiji in chronology (Eckstein et al., 2019).

Climate change is the outcome of global warming due to the excess release of GHGs (Greenhouse gases). Global warming is the warming or heating up of Earth's environment naturally. But what we did is accelerate this gradual heating process and make the Earth's temperature rise by 2-3° Celsius. Since the pre-industrial period, anthropogenic greenhouse gases emissions have risen significantly propelled by economic and population growth, and nowhere are they: at their peak. This has

contributed to unparalleled atmospheric amounts of CO_2 (Carbon dioxide), CH_4 (Methane), N_2O (Nitrous oxide), as well as some anthropogenic induced gases such as HFCs (Hydro-fluoro carbon), PFCs (Perfluorocarbon), and SF_6 (Sulfur hexafluoride) over the last 100 years. The impacts were found in the climate system and other human-driven forces and were likely to be the primary cause of the observed warming since the mid- 20th century. Global warming has the potential to induce extreme, pervasive, and irreversible impacts with greater magnitude in the future.

The CO_2 concentration in Earth's atmosphere has increased from pre-industrial time and has reached 405ppm (Parts Per Million) in 2017 to 414.11ppm in February 2020, the concentration of methane was 1849.95 ppb (Parts Per Billion), and nitrous oxide was 330.30 ppb in the year 2017 (NOAA). According to WMO (World Meteorological Organisation), since 1990, the warming consequences of stable greenhouse gases on our planet have risen by 41% (WMO). 2019 was the second warmest year measuring Earth's average global surface temperature at 1.71° F (0.95°C) of the 20th century. After 2005 nine of the ten warmest years on record have taken place (NOAA).

First-time climate change was addressed at the first earth summit, i.e., the Rio convention in 1992 held in Rio de Janerio adopted by UNFCCC (United Nations Framework Convention on Climate Change). UNFCCC came into force on 21 March 1994. The primary objective of this conference was to stipulate greenhouse gas emissions at a level that would prohibit the release of harmful anthropogenic driven gases entering into climate systems

The Inter governmental Panel on Climate Change (IPCC) has already forecasted in its 'Fifth Assessment Report' released in 2014 that threats associated with extreme events will continue to increase as the global mean temperature rises. IPCC is a United Nations governing body established in 1988 by WMO (World Meteorological Organisation) and UNEP (United Nations Environment Program). It produces reports which contribute to the work of UNFCCC**.**

"IPCC prepares comprehensive assessment reports on the state of scientific, technical and socio-economic knowledge on climate change, its impact and future risk and options for reducing the rate at which climate change is taking place." IPCC has been assigned to prepare a document on climate change, a detailed description of scientific assessment covering a broad spectrum of aspects of climate change, its impacts, and its variability.

Effects of climate change

Climate change affects every arena globally, mainly social, economic, and cultural aspects, at an alarming pace. Climatic events surpassed in the last 2-3 decades, affecting billions of people's lives, biodiversity, retreating glaciers, coral reefs, agricultural and food industry, forest, economy, etc. Increase in average global temperature since the pre-industrial era has substantially increased the frequency of storms, wildfires, cyclones, heatwaves, desertification, floods, droughts, famines, lowering of groundwater level, sea-level rise, disrupting wind and ocean currents, seasonal variations, crop patterns and production, depleting forest cover, the breakout of deadly diseases, increasing pests, affecting livelihoods of coastal region people, etc.

Greenhouse gas emissions were the largest in 3 million years when the Earth's

temperature was 3 degrees higher and the sea level 15 meters higher, which leads to the loss of earthlings and their livelihoods from droughts, wildfires, floods, severe storms, freshwater, and air crisis as well as a breakout of deadly diseases. State of the climate report 2019 emphasized the substantial effects of climate change such as thermal stress rising between land and ocean, upsurged sea levels, retreating glaciers as well as their influence towards socio-economic growth, human health, migration and relocation, food and water security, and land and marine ecosystem (WMO).

Effect of climate change on the coastal region

Corals are key indicator species for the health of the marine ecosystem worldwide. Approximately 50-70% of coral reefs are directly impacted by human-driven global climate change (Hoegh-Guldberg, 1999). Over the years, however, an inflated demand for coastal and marine goods and services ended in the unacceptable depletion of such vital assets, thereby diminishing the potential of those habitats themselves. Coastal erosion, beach erosion, damaging the flood management protection of coastal areas, loss of biodiversity has affected the livelihood and economy of agricultural, forestry, and fisheries dependent sectors. Coral reefs went through dramatic destruction because of varied anthropogenic and natural events in the last 3-4 decades. Coral reefs are a highly bio-diversified ecosystem on Earth, home to several species globally, and provide a livelihood to approximately 500 million people in economically poor countries or developing nations (IUCN).

Coral reefs host more than one-quarter of overall marine fish species (according to other marine species) despite covering less than 0.1% of the ocean floor (Spalding et al., 2001). Coral bleaching could recover if rising sea temperature between 1-2°C normalizes within some days. If this temperature rise persists for a longer duration, it will lead to coral death. 24% of coral bleaching was observed with 16% of mortality, which has reduced 23% of coral cover in India between March to June 2016 in Gulf of Munnar (Down-to-Earth, 2018). Coral mortality deviates as per species variability and varied responses towards climatic events; for instance, fast-growing coral species *Acropora, Montipora,* and *Pacillopora* faced severe mortality due to resistance towards temp rising. In 2010 and 2016, coral bleaching caused severe mortality in the wake of global climate change (global coral bleaching events). SAC (Space Application Centre) produced an alert report on coral bleaching. They evaluated the mass bleaching in 1998, 2010, and 2016 in 5 coral reefs of India, i.e., Andaman, Nicobar, Gulf of Kutch, and Gulf of Munnar (Down-to-Earth, 2018)

Corals are deteriorating by cascading climatic events occurring in the last 2-3 decades, for instance; increase in temperature (1-2°C), light level/high solar irradiance, salinity, and low water quality due to agricultural and storm run-off other pollutants, acidification due to elevated CO_2 levels in oceans. The ocean absorbs around 30% of the world's carbon dioxide, which is being released into the atmosphere from the burning of fossil fuels by various sectors. This, in turn, is accelerating the acidification of oceans damaging marine life to a great extent. The increase in sea level will result in the influx of salt water and salinity of groundwater and surface water in coastal regions. Saltwater in agricultural plains may lead to food shortages, further spread of water-borne diseases, and lack of freshwater supply (Climate Change Report, 2009).

Effects of climate change on glaciers

Global climatic patterns have significantly impacted the Himalayan glaciers leads to the melting of ice caps since post-glacial time. Most of the river system is originating from the Himalayas Karakoram Range in India is home to almost 13,700 glaciers. Sea level is rising due to the melting of glaciers, the reason being global warming (warming air and increasing ocean temperature) which is cascading other disruptions, for instance, coastal erosion and storm surges (hurricanes and typhoons), as well as showing detrimental effects on the livelihoods of downstream people. Thawing of glaciers due to thermal distress and retreating land ice sheets has led to a rise in sea level, which has posed a severe threat of erosion and storm surge.

As surveyed by the Geological Survey of India, the glaciers of Satluj river basins such as Gara, Gor Garang, Shaune Garang, NagpoTokpo retreated at an average rate of 4.22-6.8m/year. At the same time, the Chenab river basin glaciers such as Bara Shigri, Chhota Shigri, Miyar, Hamtah, NagpoTokpa, Triloknath, and Sonapani retreated at an average rate between 6.81-29.78m/year. It can be concluded from above that the Bara Shigri glacier and Chhota Shigri glacier were recorded as the highest and lowest retreated glaciers (Vohra, 1981). Vohra (1981) monitored the Siachen and Pindari glaciers retreated with the rate of 31.5m and 23.5m/year. Thakur et al. (1991) found that the Gangotri glacier has retreated at the rate of 18m/year. Shukla and Siddiqui (1999) evaluated the 9.1m/year retreating rate for Milam Glaciers in the Kumaon Himalaya. Matny (2000) evaluated that Dokriani Bamak glaciers retreated at a rate of 20m compared to the average rate of 16.5m over the span of 35 years. Dobhal et al. (1999) observed the shifting of the Dokriani Bamak glacier by 586m in Garhwal Himalayas from 1962 to 1997.

Philip and Sah (2004) studied the Shaune Garang Glacier, which has shifted its place vertically by 100 m and similarly shifted horizontally by 1500m in 37 years. From 1780 to 2001, the Gangotri Glacier snout was moved around 2 km vertically and changing its place continuously. Kulkarni and others observed the retreating of many glaciers such as Janapa glacier by 646m, Jorya Garang by 425m, Naradu Garang by 550m, Bilare Bange by 90m, Karu Garang by 800m, Baspa Bamak by 380m, and Parbati Glacier in Kullu district by 608km from 1962 to 2000. They also concluded that in 39 years, the glaciated area was retreated by 19% and glacier volume by 23% (Kulkarni et al., 2004). In the Himalayan region, GLOF (Glacial Lake Outburst Flood) observed every 3-10 years resulted in the loss of lives and damaged the roads, houses, forests, bridges, and fields (Bajracharya et al., 2008)

Effects of climate change on agriculture

In India, 15% of GDP coming from the agricultural sector (other than forestry and fisheries), which engages 55% of the labour force. Furthermore, according to the 2011 census, 69% of the rural population is still closely associated with this sector. The rest of the economy also has significant forward and backward linkages with agriculture (Gupta et al., 2012). Around the world's one-third of the land area comes under cultivation. Agriculture in India is dependent on optimum weather conditions as crops are produced seasonally, such as Rabi and Kharif crops. Climate change brings altered rainfall patterns, thermal stress, proliferates pests and diseases and, irregular

crop cycle leads to a reduction in plant growth and yield.

A rise in the winter temperature of 0.5° Celsius is expected to decrease the wheat yield by 0.45 tons per hectare. A recent World Bank study analyzed the impacts of climate change on two drought susceptible regions in Andhra Pradesh and Maharashtra and one flood susceptible area in Orissa and concluded that Dryland farmers in Andhra Pradesh could see their income plummeting by 20%, sugarcane produce in Maharashtra can drop drastically by 25-30% and in some districts of Orissa substantial increase in floods leading to declining in rice production by 12% (Guiteras, 2009). Guiteras (2009) studied the effects of changing climatic variables such as temperature and precipitation in overall out-turn for rice, wheat, jawar, bajra, maize, and sugarcane. He depicted that without proper adapting and mitigating strategies, these alarming changes over the globe can decrease the out-turn by 4-9% in the short-run (2010-39) and by 25% in the future (2070-2099).

Effects of climate change on biodiversity

Climate change is a significant threat to biodiversity, rising pressure on genetic diversity, communities, and ecosystems. As per the report of the Ministry of Environment, Forest and Climate Change, India, a mega-diverse nation that contributes 7 to 8% of documented species, including 45,000 species of plants and 91,000 species of animals worldwide through India only accounts for 2.4% of the global area. India is among the 17 mega-diverse countries home to many plants, birds, fishes, mammals, reptiles, amphibians, insects species, and microorganisms (MOEFCC, 2014). Changing in climatic systems such as pollution, overpopulation, anthropogenic emissions, overexploitation of natural resources, heat storms, land-ocean thermal stress, droughts, floods, cyclones, seasonal variations, sea-level rise, coastal upwelling, rising of ambient temperature, annual and seasonal precipitation variations, changing intensity and frequency of solar irradiance and soil erosion, etc. are directly affecting the growth, habitats, reproduction, breeding seasons, migration of biodiversity.

Bates et al. (2008) stated that habitat loss in the wake of changing climate might severely affect approximately 5,000 plant species Thuiller (2007) mentioned that every 10□ increase in temperature would cause the occurrence zone of several specialist species to move by 160 meters vertically and 160km horizontally. Around 27,000 specioes are expected to become extinct every year. If thuis continues, 30 percent of the world's animals by the year 2050 will become extinct. The global rate of extinction is 100 to 1000 times that of natural death. Invading species (*Lantana camara, Partheniumhys terophorous, Ageratumconyzoides*) are dangerous to more climate-tolerant native species. Seasonal changes due to ever-increasing climatic conditions affect the normal plant life cycle by changing leaf fall, bud formation, flowering, fertilization, synchrony during pollination, fruiting and production, etc. Early flowering, fruiting, and ripening in crops showed less grain production. Due to the increase in land thermal stress, forest fires have escalated in recent years (Sharma, 2011)

In its most recent evaluation, the IPCC underlines that 20-30% of the species assessed so far are likely to be at increased risk of extinction if global average warming increases by 1.5-2.5°C (relative to 1980-1999). If global average temperature

increases around 3.5°C, 40-70% of the species assessed become extinct majorly across the globe (IPCC, 2001). As a result of high ocean thermal stress, more female turtles are produced than male turtles. As well as some threatened species, e.g., elephants, frogs, toads, amphibians, and tigers, are more prone to vulnerability due to climate change. Some findings observed the decreased weight of the polar bears from 325kg to 253kg between 1980 to 2004 (Bellard et al., 2012).

Parmesan (2006) and Bellard et al. (2012) confirmed that climate change is responsible for significant consequences throughout various biodiversity levels such as genetic, species, organismal, and ecosystem. Some species, such as *Berberisasiatica, Taraxacumofficinale*, *Jasminumofficinale,* etc., have moved to the elevation from 1000 to 2000m in Nanital (Anonymous, 2009).

Effects of climate change on humans

Climate variability impacts the human race and generates interfering warming pressure by increasing morbidity and mortality. Climate change can directly affect human health, such as thermal stress, cold snaps, death/injury during floods and storms, and indirectly through disease-spreading vectors, e.g., mosquitoes, viruses, bacteria, and various pathogens. The local environment, social, behavioral, and economic aspects are strongly influenced due to climate variability. The numerous health effects such as traumatic, infectious, nutritional, and psychological and other that emerge in shells hocked and distress communities amid climate induced economic dislocation, environmental degradation and conflict.

Changing climate is affecting all the species on our planet. Even the human race cannot withstand this ever-increasing climate crisis persistently for the last 50 years. Climate crisis brings our notice to breaking out diseases such as dengue, malaria, plague, Ebola virus, Nipah virus, Zica virus, etc. Recently COVID-19 (Coronavirus disease 2019) outbreak in central china has spread its roots across the globe as a pandemic leading to active cases toll 191,733,410 and death toll is 4,113,054 last week of July, 2021 (WHO, 2021). This disease is very contagious and transmits through contact from patients to their caregivers.

As a whole, 12000 severe weather incidents worldwide leads to 4 95,000 causalities between the years 1999 and 2018, which costs up to US$3.54 trillion. The annual monsoon in 2018 hit worst over hundreds of years, and it devastated Kerala state severely, which damaged 80 dams, 20000 houses with 324 causalities, and 2,20,000 people were forced to vacate their abode primarily due to flooding, which costs up to EUR 2.4 billion (US$ 2.8 billion). Moreover, Cyclone Titli and Gaja hit the east coast of India in October- November 2018 with 150km/h wind speed leads to 8 deaths and set off 4,50,000 without electricity. As per the Global Climate Risk Index 2020, in 2018, a sum of 2,928 people officially died from heat-related impacts, compared to 3,622 causalities due to flood and 2,463 death tolls from extreme storms (Eckstein et al., 2019). According to the MOEFCC report, around 2400 casualties occurred in the year 2018-2019 due to consecutive floods and cyclones in the face of altered meteorological systems. India recorded a temperature near 50°C; this intense water stress was omnipresent. Because of droughts in Chennai, around a million occupants could only be provided with water by trains and trucks.

Effects of climate change on the economy

According to a Stanford report showing that how Earth's increased thermal stress has raised disparity, global warming has slowed down the Indian economy by 31% (Economic Times). Over the last 15 years (2005-2019), the U.S. has endured 156 different weather or climate disasters causing a combined $1.16 trillion over damages (NOAA). As per Global Climate Risk Index 2020, India's death tolls are 2081, and total losses in US$ 37807.82 million (in PPP- Purchasing Power Parities). The IPCC evaluates in its current report on "Global Warming of 1.5°C that the "average net cost of the warming risk at 1.5°C and 2°C in 2100 (Mention global warming-induced business and non – business effects, seal level effects, and significant spectrum discontinuity effects) is US$ 54 trillion and US$ 69 trillion, significantly, concerning 1961-1990. Existing figures for potential losses and mitigation needs for climate finance spectrum between US$ 290 billion to US$ 580 billion in 2030. As forecasts in UNEP (United Nations Environment Programme) Adaptation Gap Report 2016, that expenditure for global climate change adaptation strategies will be accelerating by twice to thrice fold for the year 2030 and four to fivefold for the year 2050 than the current scenario. In 2018, heat resulted in a total cumulative loss of US$ 60.42 billion (in PPP) worldwide (Eckstein et al., 2019).

Conclusion

This ever-increasing global warming has paved its way towards extreme climatic changes around the globe, and it's knocking–off the unprecedented events over India and the world. These variations have increased the frequency and magnitude of wind patterns, cold waves, ocean currents, cyclones, EL-Nino, La-Nina, droughts, hot spell winds, famines, precipitation, thermal stress, shifting of geographical realms, and a severe scarcity of water and food which is in turn affecting the earthlings at genetic, species, population and, community level by curtailing their livelihoods, growth, reproduction, mating, reducing their geographical territory, depleting water regimes, degrading ecosystems and ecosystem services as well as increasing morbidity and death toll. It's an urgency to think about the possible solution not just virtually but practicing all the possible solutions at the grass-roots level individually and collectively to reduce the magnitude of these extreme harsh events before it's too late to survive. We need to takes action at full-tilt because climate change would not wait for our preparedness. 2030 and 2050 agenda to reduce global emission by 2-3° C is necessary to achieve before time to delay the next mass extinction.

References

1. Anonymous. (2009). Impact of climate change on the vegetation of Nainital and its surroundings, NBRI Newsletter, Vol. 36, pp. 25-31.
2. Bajracharya, S. R., Mool, K. P. and Shrestha, R. B. (2008). Global Climate Change and Melting of Himalayan Glaciers, Research Gate, pp. 28-46.
3. Bates, B. C., Kundzewicz, Z. W., Wu, S. and Palutikof, J. P. (2008). Climate Change and Water, Technical Paper of the Intergovernmental Panel on Climate Change, IPCC Secretariat, Geneva.

4. Bellard, C., Bertelsmeier, C., Leadley, P., Thuiller, W. and Courchamp, F. (2012). Impacts of climate change on the future of biodiversity, Ecology Letters, vol. 15, pp. 365-377.
5. Dobhal, D. P., Gergan, J. T. and Thayyen, R. J. (1999). Recession of Dokriani Glacier, Garhwal Himalaya' - An overview. Symp. On snow, ice and glaciers. In A Himalayan Perspective. Geological Survey of India, pp. 30-33.
6. Down to Earth. (May, 2018). http:// www.downtoearth.org.in/news/climatechange
7. Eckstein, D., Kunzel, V., Schafer, L. and Winges, M. (2019). Global Climate Risk Index, German Watch.
8. Economic Times. Global warming shrank Indian economy by 31 per cent: Study,https://economictimes.indiatimes.com.
9. Guiteras. (2009). The Impact of Climate Change on India Agriculture, University of Maryland.
10. Gupta, S. Partha, S. and Srinivasan, S. (2012). Impact of Climate Change on The Indian Economy: Evidence from food Grain Yields, Research Gate, doi : 10.2139/ssrn. 2191010.
11. Hoegh-Guldberg, O., (1999). Climate Change, Coral Bleaching and The Future of The Worlds Coral Reefs, Marine Fresh Water Research Vol. 50(8), pp. 839-866.
12. IPCC (International Panel on Climate Change). (2001). http://www.ipcc.ch.
13. IPCC (International Panel on Climate Change). (2017). Appendix I: Glossary. Archived 2017-01-26 at the Wayback Machine, https://www.ipcc.ch/.
14. IUCN (International Union for Conservation of Nature), https://www.iucn.org/sites
15. Kulkarni, A.V., Rathore, B. P. and Suja. A. (2004). Monitoring of glacial mass balance in the Baspa basin using Accumulation Area Ratio method. Current Science, Vol. 86(1), pp. 101-106.
16. Matny, L. (2000). Melting of Earth's Ice Cover Reaches New High, In Worldwatch News Brief, 06 March 2000.
17. MOEFCC (Ministry of Environment Forest and Climate Change). (2014). report.
18. NOAA (National Oceanic and Atmospheric Administration). https://www.noaa.gov/
19. Parmesan, C. (2006). Ecological and evolutionary responses to recent climate change, Ecology Evolution, Vol. 37, pp. 637-669.
20. Philip, G. and Sah, M. P. (2004). Mapping Repeated Surges and Retread of Glaciers Using IRS1C/1D Data: A Case Study of Shaune Garang Glacier, Northwestern Himalaya. In International Journal of Applied Earth Observation and Geoinformation Vol. 6(2), pp. 127-141.
21. Sharma, U. (2011). Effect of Global Warming on Biodiversity in India, APCCF, IT, U.P., National Conference on Forest Biodiversity : Earth's Living Treasures,.

22. Shukla, S. P. and Siddiqui, M. A. (1999). Recession of The Snout Front of Milam Glacier, Goriganga valley, District Pithoragah, Uttar Pradesh. In Symp. on snow, ice and glaciers'. A Himalayan Perspective. Geological Survey India, pp. 27-29.
23. Spalding, M. D., Ravilious, C. and Green, E. P. (2001). World Atlas Coral Reefs, UNEP, World Conservation Monitoring Centre, University of California Press: Berkeley, pp. 416.
24. Thakur, V. C., Virdi, N. S., Gergan, J. T., Mazari, R. K., Chaujar, R. K., Bartarya, S. K. and Philip, G. (1991). Report on Gaumukh. The snout of the Gangotri glacier (Unpublished Report submitted to DST, New Delhi).
25. Thuiller, W. (2007). Climate change and the ecologist. Nature, Vol. (2), pp. 550-552.
26. Vohra, C. P. (1981). Note on recent glaciological expedition in Himachal Pradesh, Geological Survey of India. Sp. Vol., 6, pp. 26-29.
27. WHO (World Health Organisation). (2021). https://www.who.int.
28. WMO (World Meteorological Organisation). http://ncdc.noaa.gov/sotc/global/201913.
29. WMO (World Meteorological Organisation). https://public.wmo.int/en.

❑❑❑

Climate Change and Sustainable Development

Om Prakash
Gaurav Kumar Jain
Govind Singh
Lalit Singh Jhala

Climate change has become an agenda of key concern and requires our utmost attention. There are several factors which collectively attribute to climate change but anthropogenic activities since the early 1700s, could be considered the major cause. Climate change causes hindrance in the sustainable development of the society which not only affects mankind but all the species existing in an ecosystem.

This book highlights the connection between climate change and sustainable development, exploring the impacts of climate change on the environment, economy, and society. It is a result of contributions from multiple authors, aimed at raising awareness and encouraging further research on the topic.

Other Related Book

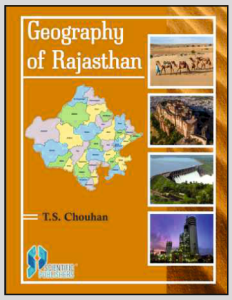

ISBN: 978-93-89184-28-0

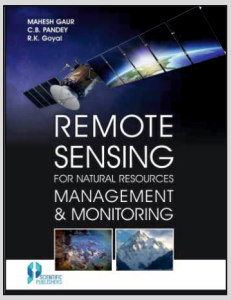

ISBN: 978-93-86102-72-0

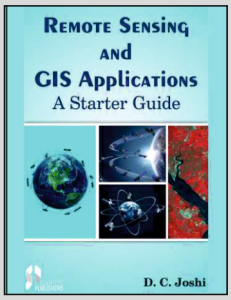

ISBN: 978-93-88172-54-7

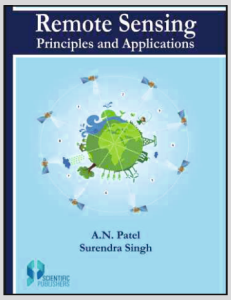

ISBN: 978-81-72335-90-8

SCIENTIFIC® PUBLISHERS

For more details visit
www.scientificpubonline.com

ISBN: 978-93-90749-29-4

Climate Change and Sustainable Development

Om Prakash
Gaurav Kumar Jain
Govind Singh
Lalit Singh Jhala



SCIENTIFIC PUBLISHERS®

Climate Change and Sustainable Development

Our Related Books

Title	Author
Agriculture and Climate Change	FAO
Agroforestry for Climate Resilience and Rural Livelihood	Inder Dev
Antarctica: Environment and Conservation	Neloy Khare
Atmospheric Pollution By Aerosols	V.K. Sharma
Bioclimatology and Plant Geography of Peninsular India	V.M. Meher-Homji
Climate Change & Himalayan Ecosystem: Indicator, Bio & Water Resources	J. Sundaresan
Climate Change & Himalayan Informatics	J. Sundaresan
Climate Change Adaptation Strategies in Agriculture and Allied Sectors	GSLHV Prasad Rao
Climate Change and Environment	J. Sundaresan
Climate Change and Himalaya: Natural Hazards and Mountain Resources	J. Sundaresan
Climate Change and Its Ecological Implications for The Western Himalaya	V.L. Chopra
Climate Change Impact on Ecosystem	J. Sundaresan
Climate, Agriculture and Man (Shrinking Biodiversity and Sustainability)	V.K. Sehgal
Climate-Smart Agriculture Source Book	FAO
Climate-Smart Agriculture Training Manual for Agricultural Extension	FAO
Combating Desertification Land Degradation and Climate Change: Management of Dry Lands	T.S. Chouhan
Communication for Rural Development Source Book	Mario Acunzo
Crop Growth Simulation Modelling and Climate Change	Nishant K. Sinha
Crop Protection Strategies Under Climate Change Scenarios	P.P. Reddy
Disaster Management: A Disaster Manager's Handbook	W.Nick Carter
Drought Mitigation and Management	Suresh Kumar
Earth and Ocean: Useful Resources (Hindi)	D.D. Ojha
Emergency Response Manual	USDA
Introductory Agrometeorology	Sevak Das
Objective Environmental Pollution and Climate Change	M. Prasanthrajan
Objective Environmental Studies and Disaster Management	M. Prasanthrajan
Organic Agriculture and Climate Change Mitigation	URS Niggli
Pollution Risks, Impacts & Management Social, Economic and Environmental Perspectives	Golam Kibria
Principles of Agricultural Meteorology	B.M. Mote
Questions and Answers in Environmental Science Practical	R.K. Kamble
Rainwater Management: Theory and Practice	M.L. Jat
Space Technology and GIS for Disaster Monitoring and Mitigation	T.S. Chouhan
Text Book of Disaster Management	Ajay Kumar Srivastava
Thar Desert in Retrospect and Prospect	R.P. Dhir

For more details visit our website

Climate Change and Sustainable Development

Edited By

Om Prakash, Gaurav Kumar Jain,
Govind Singh, Lalit Singh Jhala

Department of Geography,
Jai Narain Vyas University Jodhpur,
Rajasthan (*India*)

SCIENTIFIC PUBLISHERS

Published by
SCIENTIFIC PUBLISHERS (INDIA)
5 A, New Pali Road, P.O. Box 91
Jodhpur 342 001 (INDIA)
E-mail: info@scientificpub.com
Website: http://www.scientificpub.com

© 2023 Author

All rights reserved. No part of this publication or the information contained herein may be reproduced, adapted, abridged, translated, stored in a retrieval system, computer system, photographic or other systems or transmitted in any form or by any means, electronic, mechanical, by photocopying, recording or otherwise, without written prior permission from the publisher.

Disclaimer: Whereas every effort has been made to avoid errors and omissions, this publication is being sold on the understanding that neither the editors (or authors) nor the publishers nor the printers would be liable in any manner to any person either for an error or for an omission in this publication, or for any action to be taken on the basis of this work. Any inadvertent discrepancy noted may be brought to the attention of the publisher, for rectifying it in future editions, if published.

This book contains information obtained from authentic and highly regarded sources. Reasonable efforts have been made to publish reliable data and information, but the editors and publisher cannot assume responsibility for the validity of all materials or the consequences of their use. The editors and publisher have attempted to trace and acknowledge the copyright holders of all material reproduced in this publication and apologize to copyright holders if permission and acknowledgment to publish in this form have not been obtained. If any copyright material has not been acknowledged please write and let us know so that we may rectify it.

Trademark Notice: Product or corporate names may be trademarks or registered trademarks, and are used only for identification and explanation without intent to infringe.

ISBN: 978-93-90749-29-4 (HB)
eISBN: 978-93-90749-31-7 (EBook)

Printed in India

Editors' Introduction



Dr. Om Prakash

M.A., Ph.D. in Geography from Jai Narain Vyas University Jodhpur, UGC NET-JRF in Geography, UGC NET in Population Studies, RPSC SET in Geography, NNRMS certificate course IIRS-ISRO. He has been working as an Assistant Professor in the Department of Geography at Jai Narain Vyas University, Jodhpur since 2013. He is also the coordinator of the Nodal Centre for the IIRS outreach program. At present, four research scholars are pursuing PhDs under his supervision. He has participated and presented papers in various international and national seminars and conferences and has published many research papers in reputed journals.



Dr. Gaurav Kumar Jain

M.A., M.Phil., NET-JRF, RPSC-SET in Geography, Ph.D. from Jai Narain Vyas University, Jodhpur. He has been working as an Assistant Professor in the Department of Geography at Jai Narain Vyas University, Jodhpur since 2013. At present, five scholars are pursuing research degrees under his supervision. He has participated and presented papers in various international and national seminars and conferences and has published many research papers in reputed journals.



Mr. Govind Singh

M.A. UGC-NET in Geography, RPSC-SET in Geography and Population Studies both. Born in 1983 in the village of Bhawanda in the Nagaur district of Rajasthan. Vagdevi's spiritual practice and literary interest turned him towards writing. He has a spontaneous inclination towards poetry, drama and various co-curricular activities. Due to his deep interest in geographical analysis and culture writing, various research articles and contemporary papers have been presented as well as published in various journals by him. He has been working as an Assistant Professor at the Department of Geography at Jai Narain Vyas University, Jodhpur since 2013.



Dr. Lalit Singh Jhala

M.A., NET, SET, Ph.D. in Geography from Mohan Lal Sukhadia University, Udaipur. Currently, he is working as an Assistant Professor in the Department of Geography at Jai Narain Vyas University, Jodhpur. His books, titled "Regional Disparities in Tribal Area" (single author) and "Tourism Development in Desert and Humid Zones" (co-authored), were published in 2012 & 2016 respectively. Dr. Jhala, is the recipient of the "Young Geographer Award" (2008) at the Rajasthan Geographical Association (RGA) national conference. He has also served as the Vice-President of RGA from 2020 to 2022. He has participated and presented papers in various international and national conferences, seminars and workshops; and has published 15 research papers in reputed journals. He has also supervised four Ph.D. scholars from Mohanlal Sukhadia University, Udaipur and JNV University, Jodhpur, respectively.

Preface

Climate change has become an agenda of key concern and requires our utmost attention. There are several factors which collectively attribute to climate change but anthropogenic activities since the early 1700s, could be considered the major cause of it. These anthropogenic activities not only degrade the quality of the water, air and soil around it, but are also responsible for several adverse health effects on animals and humans. Recent accelerated climate change has exacerbated existing environmental problems around the globe that are caused by the combination of changes in land use, increasing pollution and declining biodiversity. Climate change can be said to be a threat multiplier. It intensifies existing threats, aggravating complications for the environment, economy and thus, the entire society. The recent global warming is already producing negative influences on natural and human systems, seriously impeding progress toward some sustainable development goals (SDGs). Sustainable development is development that meets the needs of the existing generation without compromising with the capabilities of the future generations to meet their own needs. Climate change causes hindrance in the sustainable development of the society which not only affects mankind but all the species existing in an ecosystem.

This bilingual book emphasises on the several issues regarding climate change and how these issues are interlinked with sustainable development. The 20 chapters of this book revolve around how plants and animals are affected by climate change and how they can be used as indicators of climate change, how the agriculture sector is affected by it and what policies could be brought into account to stop the climate change and lead to betterment of all via working on sustainable development goals.

We would like to thank all the authors for coming forward and presenting their ideas which helped us in moulding this book. Their efforts would help the present and future generations in understanding the importance of this topic and would open gateways of new and better research.

Foreword



Earth, life and climate have always changed and climate change itself may have been crucial for the evolution of human being. The climate system is a complex interactive system consisting of the atmosphere, hydrosphere, lithosphere, cryosphere and outer space. Climate change is a global challenge with diverse implication at the national and regional levels, through impacts on various sectors such as agriculture, water resources, forestry and biodiversity, human health, energy and infrastructure. The scientific studies indicate that climate change is inevitable. The climate has transformed in the past, is varying in the present and is bound to change in the future. Today we are erroneously worried about the global warming and the impacts it is likely to bring. Contrary to it, some scientists forecast that 'global cooling' would be more disastrous in future.

The scientists are debating on the causes of climate change. The natural scientists believe that climate changes are due to several natural forces like changes in the obliquity of earth's axis, its rotational speed, solar variability or sunspot and volcanic activities. On the contrary, some scientists who believe in global warming say that increase in the emission of green house gases after industrial revolution has been mainly responsible for global warming and climate changes. It is beyond doubt that since 1850 A.D. the temperature is rising at such a rate that it was never experienced during last 800,000 years during geological past. The 'pro-warming lobby' advocates that the earth's warming occur not only in response to external forcing but also due to release of GHG's in the atmosphere by human beings especially the burning fossil fuels.

This book **"Climate Change and Sustainable Development"** presents a systematic work on the issues of climate change. The backdrop ranges from biology, agriculture, renewable energy to human health. All of these are very important aspects of human life as impacted by the rapid change in the climate of the earth. The book offers a wide variety of topics ranging from the global scenario of climate change, the bio monitoring properties of a plant that can be symptomatic of climate change and its impacts, the issue of solid waste management, the problems of agricultural pollution, the scenario of potential and challenges of biomass energy. The wider academic and geographical area of the problems discussed in the various chapters ensures that the book is wide in its scope, methods, approaches, spatial coverage and variety of problems faced.

I take immense pleasure in congratulating all the editors, as well as, the contributing authors of this book. The editors **Dr. Om Prakash, Dr. Gaurav Kumar Jain, Mr. Govind Singh and Dr. Lalit Singh Jhala** have, through persistent hard work and academic assiduity produced a well-balanced piece of literature that is varied in its approach and perspectives.

Hence, my compliments for their ardor and zeal.

Prof. H. S. Sharma
Formerly Professor and Head Department of Geography
University of Rajasthan, Jaipur
hssharma358@gmail.com

Contents

Editors' Introduction (*v*)

Preface (*vii*)

Foreword (*ix*)

1. Bryophytes: Pollution Indicators and Biomonitoring Agents 1–6
   G. S. Deora, Monika K. Shekhawat And Saraswati
2. Monograph of Commiphora Wightii: 7–20
   A Critically Endangered Medicinal Plant
   Kunal Seth, Vishambhar Sangela, Sandhya Deora, Priyanka Faroda, Sunita Choudhary, Nikita Gautam, Amit Kumar Gupta, Harish
3. Changes in Irrigated Land Utilization: A Spatio-Temporal Analysis of Kopai River Basin, Eastern India 21–30
   Tanmoy Das
4. Teredolites: The Wood-Boring Tracefossils From Fatehgarh Formation of The Barmer Basin, Western Rajasthan, India 31–42
   V. S. Parihar, Pawan Kumar, Anshul Harsh, C. P. Khichi And S. L. Nama
5. Climate Change Policy of India 43–54
   Chandraveer Singh Bhati
6. Impact of Solid Waste on Global Climate Change 55–70
   Kundan Kunwar Chouhan
7. Sustainable Development and Enviromental Issues: 71–82
   Save The Enviroment Save The Life
   Dalpat Singh
8. Understanding Impact of Shifting Wild Fire Regime on Environment and Climate 83–94
   Anuya Verma, Rohini Trivedi And Sanjay Meghwal
9. Climate Change: An Overview of The Global Scenario 95–104
   Bhavya Singh, Chirmaie Nagda, Kapil Kumar, Monika Rathore, Girima Nagda, Lalit Singh Jhala And Devendra Singh Rathore
10. Agricultural Pollution 105–114
    Sanjay Parihar
11. Geopolitics of Indian Ocean 115–120
    Jyotiraditya Singh Bhati

12. Scenario of Mining Industry in Western Rajasthan: An Environmental Issue 121–128
Indu Deval, O.P. Dewasi
13. Sustainable Growth of Agriculture in Rajasthan 129–138
Pramila Jangid, Jai Singh
14. Urbanisation Changing Morphology of Alwar City of Rajasthan 139–146
Yudhister Sharma, Aakanksha Bali
15. The Evolving Pattern of Agriculture in Changing Climatic Conditions (In Two Decades): A Review in The Context of Pali District 147–156
Sukhdev Meghwal, Lalit Singh Jhala
16. The Jawai Dam: Lifeline of Marwar 157–160
Ummed Kumar Choudhary
17. Impact of Climate Change on Medicinal Plants: A Case Study of Karnataka State 161–172
Pragnya. S. Hangaragi
18. Impact of Biodiversity on Food Security: A Geographical Study of India 173–176
Yudhister Sharma, Aakanksha Bali
19. Climate Change, Human Health and Sustainable Development: The Interlinked Trinity 177–192
Girima Nagda, Chirmaie Nagda, Devendra Singh Rathore and Bhavya Singh
20. Energy Generation from Biomass in Rajasthan: An Overview of Potential, Policies and Challenges 193–205
Shrikant, Om Prakash

Chapter 19

Climate Change, Human Health and Sustainable Development: The Interlinked Trinity

Girima Nagda[1*], Chirmaie Nagda[2], Devendra Singh Rathore[2], and Bhavya Singh[2]

Abstract

In modern times, climate change is one of the greatest challenges we are facing. Besides natural phenomenon, a major chunk of climatic changes can be attributed to anthropogenic activities which have subsequently resulted in myriad devastating effects. Every aspect of climate change has negative impacts which thus break the well knitted chain of ecology of the well-balanced ecosystem of the earth. Human beings as an integral part of the ecosystem are also susceptible to the dreaded physical, biological and socio-economic effects of climate change. The very existence of human life and livelihood is affected by climate change. There are innumerable evidences which have shown that human activities are responsible for changing the climate and this change will produce some major impacts on health, both on national and global level. These climate changes and health regarding issues move beyond national borders and the impact of health hazards related to these changes affects several people as well as communities to a large extent. There are unprecedented and immense risks of climate change and environmental degradation on human population. Thus, the viscous circle of human influences on climate resulting in climate change and affecting human health and development needs to be checked for better environment to live in and sought for more eco-friendly development "sustainable development". It is necessary to understand the intricate linkage of climate change, public health and development.

Keywords: Climate change, human health, sustainable development, infectious diseases

Introduction

Climate change along with environmental degradation is amongst the biggest challenges being faced by the world today. Rise in temperature, growing intensity and incidences of extreme weather events, the destruction of forests, wildfires, the risk of extinction of a million species, spread of infectious diseases, the warming up of oceans and the disruption of ecosystem services which sustain life on this planet are amongst the major threats and challenges faced today. Events like frequent droughts, floods,

[1] Department of Zoology, [2]Department of Environmental Sciences, University College of Science, Mohanlal Sukhadia University, Udaipur, Rajasthan

* Corresponding author

hurricanes and cyclones, forest fires like the recent one in Australian region leading to massive destruction of wild animals, resurgence of diseases etc. have presented a glimpse of devastation that can be caused by climate change and environmental degradation.

Changing climate is not a new phenomenon. Over the course of evolution, the Earth's climate has undergone a continuous change. The present scenario of climate change is quite different from the traditional one as the latter makes the earth as a whole either hotter or colder. Systematic global warming is believed to be one of the major causes of climate change today. This has made the climate much more erratic making the Earth hotter and drier at some places and cooler and wetter at others, thus breaking its constancy. In a nutshell, climate change means that drastic changes will be seen in the weather conditions in the near future.

To a much greater extent anthropogenic activities have brought about the major climatic changes and subsequently it results in myriad effects on human health and development. Current trends of climate change are alarming both in terms of environment loss and human damage as impairment of livelihood, income and damage to the properties by extreme events is faced by millions of people around the world. Furthermore, as climate change negatively affects agriculture, it leads to undernourishment and deteriorates the economic conditions of the people especially in areas where it is the mainstay.

As climate change has a global effect it should be given due emphasis. Thus, it is important to promote a better understanding about climate change and create awareness of its impacts and influence on the well-being of humans, ecosystems and the development, so that the significant challenges it poses can be dealt with easily.

How climate change affects human health which in turn hampers the sustainable development approach is being discussed here.

Climate Change : Current Scenario

As per the World Meteorological Organization (WMO) the global mean temperature for 2019 was around 1.1 ± 0.1 °C above the 1850–1900 baseline, used as an approximation of preindustrial levels. The year 2019 is likely to be the second warmest on record (WMO, 2019). The Intergovernmental Panel on Climate Change (IPCC) has issued an extensive warning, stating that the Earth will face catastrophic consequences if the current trends of rising global temperatures are not reversed immediately. The report also states that an increase of 1.5°C in Earth's temperatures will affect the population disproportionately, especially the vulnerable and disadvantaged ones, by causing rise in food prices, food insecurity, unemployment, adverse impacts on health, and displacement of population (Awasthi, 2018).

Earlier report of IPCC states that by 2100, the global mean sea level rise will be around 10cm higher for a rise of 2°C as compared to 1.5°C thus, up to 10 million more people will be affected by the risk of rising seas. Similarly, in context of heat waves, a rise of 1.5°C, would expose 14% of the population to heat wave every five years and it will increase to 37% of the population at 2°C. Figure 1 shows that how the increase in temperature would affect different sectors like species, coral reefs, crops and floods.

It is suggestive from the figure that if the rise in temperature is kept below 1.5°C the Earth would have far better survival options than above it as every bit of rise will make a huge difference (McGrath**,** 2018).

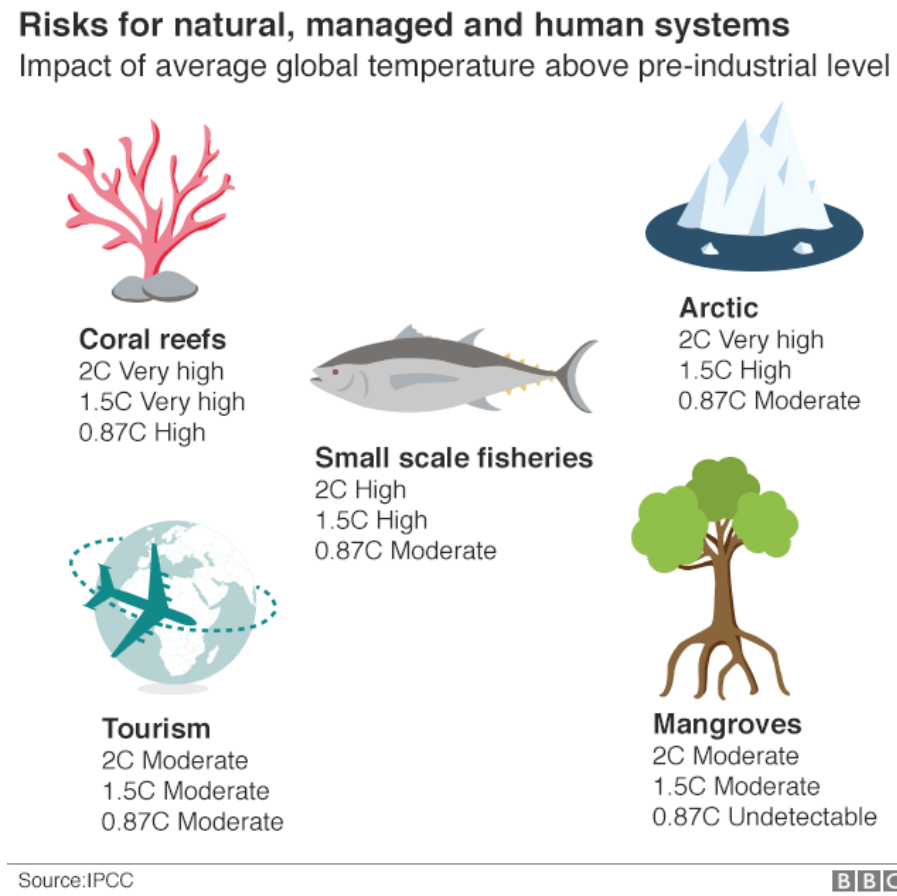

Figure 1: Impact of average global temperature rise above the pre-industrial level (Source: McGrath, 2018)

India is most significantly affected by climate change due to its large population, inequality and poverty. The impact of destabilization on India could be devastating. A report by Germanwatch, an environmental think tank, has ranked India as the fifth-most vulnerable country in terms of extreme weather events. It is believed that the current level of efforts to slow down global warming in India will result in a rise of 1-2° C in average temperatures by 2050. Thus, India is facing a dual pressure to mitigate climate change by controlling its emission growth and simultaneously needs to adapt to increased water scarcity, floods, droughts, cyclones and other natural disasters. In spite of a fairly good disaster management system, it requires more resources to develop further and is in need to set ambitious targets on renewable energy (Goswami, 2020).

A warmer Earth certainly must be avoided because of its adverse implications on ecosystems, water resources, agriculture, biodiversity, human health, economic

growth and development. Unplanned development has led to emission of greenhouse gases over decades leading to climate change. As a result, development itself suffers, because lots of resources get wasted to cope up with adversities of climate change which otherwise would have added to better health, education, and better socio-economic status of people.

Climate Change and Human Health

Human health is influenced by the climate. The environment and socioeconomic systems vital to human health and development, are sensitive to the rate and magnitude of climate change (IPCC 1996). Climate variability and climate change threatens human health and well-being in numerous ways especially by affecting the environment that provides with clean air, food, water, shelter, and security.

Climate change has both direct and indirect impact on human health. The direct impacts are due to extreme weather conditions, air pollution, heat waves etc., which can cause injuries, thermal stress, death etc. The indirect impact on human health can be either ecologically or socially mediated which can cause infectious diseases, under-nutrition, mental stress etc.

Following 11 human health issues occurring as a result of climate change have been reported (IWGCCH 2010):

1. Weather-related diseases and mortality
2. Vector-borne and zoonotic diseases
3. Water-borne diseases
4. Food-borne diseases and nutrition
5. Heat-related morbidity and mortality
6. Human developmental effects
7. Mental health and stress-related disorders
8. Asthma, respiratory allergies, and airway diseases
9. Neurological diseases and disorders
10. Cardiovascular disease and stroke
11. Cancer

Climate vulnerability includes three different properties of the human community: exposure, susceptibility to harm and the capacity of adapting to such harm (IPCC 2014). All these three properties are time dependent and are site and system specific (IPCC 2014; NRC 2012; USGCRP 2016). Thus, climate change alters the natural environment and affects the health of people by causing malnutrition, various infectious and zoonotic diseases like vector borne diseases, food & water borne diseases, diseases associated with air pollutants & aero-allergens, mental health and stress related disorders, increased respiratory and cardiovascular disease, injuries and premature deaths related to extreme weather events. (Figure 2). It is suspected that the risk to health of people by these diseases will increase significantly in coming decades (Ruhil 2016; Confalonieri et al., 2007). Figure 2. Gives an account of the impact of climate change on human health.

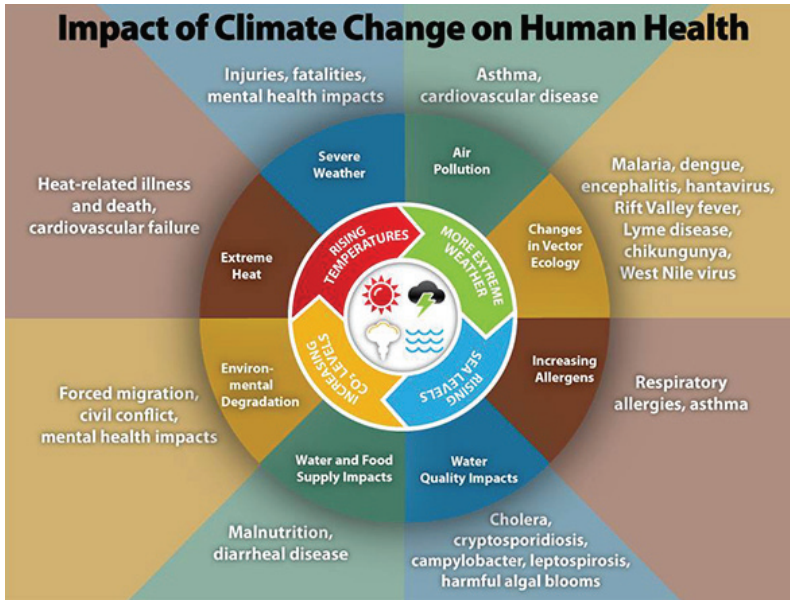

Figure 2: The impact of climate change on human health (Source: CDC, 2019 a)

Zoonotic and infectious diseases are highly sensitive to climate change. Temperature, precipitation and humidity play an important role in reproduction & survival of vectors & infectious agents. Dynamics of vector-borne diseases are influenced by multiple factors like environmental (vegetation, climate, hydrology); biological (the life cycles of insects that are vectors for infectious agents); sociodemographic (migrations and population density); and medico-social (the immunological conditions of the population; the effectiveness of local health systems, etc.), which potentialize their effects on human health (OPAS 2008). Climate change results in abnormal patterns of precipitation, humidity & temperatures, which results in mosquito breeding sites, increased survival & development of mosquitoes. Thus, prevalence of malaria and dengue has increased over recent years (WHO, 2011; Kleef and Hales, 2010). Conditions favorable to outbreaks of infectious diseases are created by the changing weather events. The incidence of mosquito-borne diseases, such as malaria, dengue, and viral encephalitis, are most sensitive to climate (Houghton, 1997). Climate change directly affects disease transmission by shifting the vector's geographic range, increasing the reproductive and biting rates and shortening the pathogen incubation period. Climate change also causes extensive spread of pests and diseases. Figure 3 shows how the burden of zoonotic diseases increases with the climate change

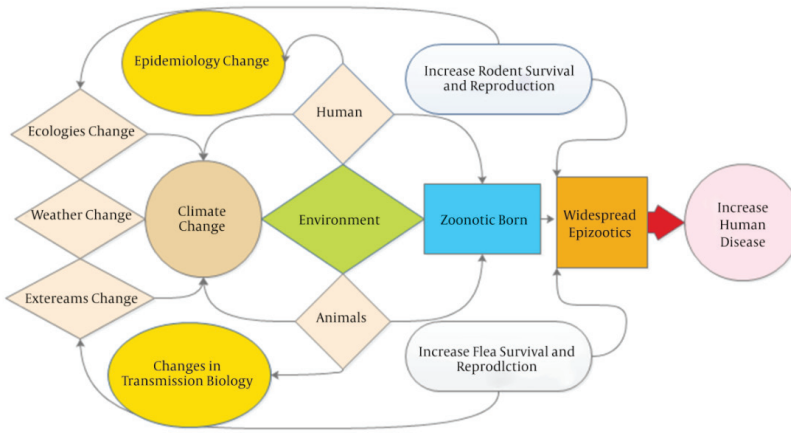

Figure 3: Concept of climate change and increased burden of zoonotic diseases (Source: Esmaeilnejad et al., 2018)

Climate change mediated increase in surface temperature of sea and sea level rise leads to higher incidence of waterborne infectious diseases like cholera and toxin-related illnesses such as shellfish poisoning. Figure 4 shows how diverse environmental changes affect the occurrence of various infectious diseases in humans.

Environmental changes	Example diseases	Pathway of effect
Dams, canals, irrigation	Schistosomiasis	▲ Snail host habitat, human contact
	Malaria	▲ Breeding sites for mosquitoes
	Helminthiasies	▲ Larval contact due to moist soil
	River blindness	▼ Blackfly breeding, ▼ disease
Agricultural intensification	Malaria	Crop insecticides and ▲ vector resistance
	Venezuelan haemorraghic fever	▲ rodent abundance, contact
Urbanization, urban crowding	Cholera	▼ sanitation, hygiene; ▲ water contamination
	Dengue	Water-collecting trash, ▲ *Aedes aegypti* mosquito breeding sites
	Cutaneous leishmaniasis	▲ proximity, sandfly vectors
Deforestation and new habitation	Malaria	▲ Breeding sites and vectors, immigration of susceptible people
	Oropouche	▲ contact, breeding of vectors
	Visceral leishmaniasis	▲ contact with sandfly vectors
Reforestation	Lyme disease	▲ tick hosts, outdoor exposure
Ocean warming	Red tide	▲ Toxic algal blooms
Elevated precipitation	Rift valley fever	▲ Pools for mosquito breeding
	Hantavirus pulmonary syndrome	▲ Rodent food, habitat, abundance

▲ increase ▼ reduction

Figure 4: Diverse environmental change and occurrence of various infectious diseases in humans (Source: Patz et al., 2000)

Food and water borne diseases are a major public health issue. Disease transmission is known to be affected by air and water temperatures, precipitation patterns, extreme rainfall events, and seasonal variations. Diseases like salmonellosis and campylobacteriosis, diarrhea occur more frequently with high temperature and unusual precipitation. As a result of climate change, disasters have become more frequent; such as hurricanes, typhoons, earthquakes, tsunamis and floods. During disasters epidemic outbreaks occur, particularly of cholera and other diarrhoeal diseases (UNICEF & WHO, 2012).

Meningococcal meningitis is another seasonal infectious disease favoured by dry, hot and dusty climate. Hunger, draught, extreme climate events, and regional conflicts also are a few factors increasing the incidence and severity of diseases, as well as contributing to other adverse impacts on health.

High temperature itself is a threat to human health particularly for elderly, chronically ill and children. It is projected that by 2050s, heat events will be very frequent (IPCC, 2012). Excessive exposure to UV radiations of sun results in premature ageing of skin and more severe outcomes like skin cancer.(Ferlay et al., 2008).

Air pollution is also directly related to morbidity and mortality, particularly exposure to unsafe levels of fine particulate matter has severe consequences to health (Ruhil, 2016). According to WHO, due to climate change, seasons of pollens start earlier and last longer, leading to more cases of asthma associated with pollen allergens. The sources of indoor air pollution include inefficient use of solid fuels for cooking (WHO, 2009) and tobacco smoke (Lin et al., 2007). Wild fires and forest fires have become very frequent. Emissions from fires contain gas and particle pollutant which has adverse health outcomes for humans and animals. Health impacts of climate change are felt globally but these health impacts are more severely felt by poor and vulnerable. Thus, poverty is both a catalyst and consequence of climate change & poor health.

Mental illness is a major cause of suffering in the advancing world today, and extreme weather events affect mental health in numerous ways. As a result of disasters, mental health problems like high levels of anxiety and post-traumatic stress disorder increase, both among people with no history of mental illness, and those at risk, a phenomenon known as "common reactions to abnormal events." Climate change like extreme weather, rising temperatures are suggestive of potential impacts on depression and other mental illnesses. Some mental illness patients like those suffering from schizophrenia are at risk during hot weather because their medications may interfere with temperature regulation or even directly cause hyperthermia (CDC, 2019b).

Global environmental changes, such as bioaccumulation of chemicals in air, water and soil, global warming, species extinction caused by destruction of natural habitats leading to reduction of genetic resources, etc. cumulatively affect the human health directly or indirectly. Reproductive problems; weakening of the immune system; behavioral anomalies; thyroid malfunction, hormonal imbalances; tumors and cancer; and congenital malformations are some of the direct effects of global changes on human health. The indirect effects are often hard to quantify because of the complex involvement of ecological mechanisms and social processes (Confalonieri et al. 2002).

Climate change is known to affect human health in two possible ways: firstly, by increasing the severity and the occurrence rate of health issues which are already affected by climatic factors and secondly by generating unforeseen health problems (USGCRP 2016).

Sustainable Development and Climate Change

Sustainable development is a development pattern which involves judicious use of resources. It aims to protect and preserve the environment while fulfilling human needs effectively in the present as well as in the indefinite future (McKeever and James, 2009). According to Robert Repetto, "Sustainable development is a developmental strategy that increases long-term wealth and human and environmental well-being by managing all the natural resources, human resources, as well as financial and physical assets. It rejects policies and practices that support current living standards at the cost of depleting the existing resources that leaves future generations with poorer prospects and greater risks than our own" (Repetto, 1986). Sustainable development implies economic growth as well as the protection of environmental quality, each reinforcing the other. It includes adoption of green technologies in all fields, which are market-driven solutions for reducing harmful impact of industries on environment (Reddy, 2010). It denies economic and social development at the cost of environmental degradation and it implies that development should not lead to the scarcity of natural resources.

The guiding rule of sustainable development is to care for the Earth. Humanity must take only that much from nature which can be replenished. This means adopting lifestyles and development paths that respect and work within nature's limits. It can be done without rejecting the many benefits that modern technology has brought, provided that technology also works within those limits"(IUCN, 1991).

Sincere concerns for environment came into existence for the first time in a global conference on the "environment and development" in Stockholm in 1972 where the challenges of economic growth towards environmental sustainability were addressed. Later, it became a regular practice and sustainable development plans were formulated in Agenda 21, Earth Summit 1992, Kyoto protocol 1997, Johannesburg summit2002, millennium development goals and now sustainable development goals (Blewitt, 2015; Elliot, 2006). At the Rio +20 Summit in June 2012 Sustainable Development Goals (SDGs) were adopted (Sachs, 2012) amongst which SDG13 particularly focuses on climate issues and climate action which need to be addressed in an interdisciplinary and holistic way.

Development is a time-consuming process but a few moments of disastrous effects of climate change could undo all the development efforts and poor countries are particularly vulnerable to the destructive effects of climate change (Thomas and Twyman, 2005; IPCC, 2007). Climate change increases shortages of potable water, sanitation and health services (Bierbaum and Fay, 2010) and also threatens food security due to direct impact on agriculture & crop yield (DFID, 2005) thus in turn hampering development.

In most of the developing countries, agriculture is dependent on rain water for irrigation. Decreasing precipitation over the years has increased the burden on

fresh water supplies. In addition, increasing environmental exploitation through processes like overgrazing, deforestation, desertification and mineral extraction has led to degradation of a large portion (about 40%) of land globally (Klugman, 2011). Moreover, poor and underdeveloped countries have limited resources to cope with climate change and its destructive effects (Thomas and Twyman, 2005; IPCC, 2007). Such episodes of extreme climate change events lead to epidemic outbreaks and thus loss of productivity (WHO, 2005). Resources which could be better utilized for development of a country are wasted in coping with disasters and the effects of climate change. The world is already facing the devastating effects of climate change; thus, cumulative efforts to mitigate harmful consequences of climate change should come from all spheres of human development.

Link Between Climate Change, Human Health and Sustainable Development

Environment and human beings are interdependent. At one hand human beings are increasingly altering the environment and on the other hand climate change is adversely affecting health of people (Lang and Raynor, 2012). Furthermore, environment and development are inseparable because the "environment" is where we live; and "development" is what we all do in attempting to improve our lot within that abode (WCED, 1987). Thus, climate change is a ubiquitous challenge for the world.

The environmental impacts on human health are enormous. The links between people, nature and economies are inescapable when looking at environmental security and environmental risks as they relate to human health and security. Aspirations for security and development therefore must be directed towards efforts to protect individuals from environmental threats. They must also be based on practical steps to seize upon the opportunities presented by the environment, in recognition of its inherent value, and its deep connections to human beings, societies and economies (Khagram et al., 2003). Sustainability science focuses on linking the human imprint on the biosphere to the co-evolving human-environment condition, as it pertains to a transition towards sustainability.

Adverse climatic condition affects human life and livelihood badly and in turn threat to human security. Now-a-days human security is defined through the vocabulary of development. Better livelihood, employment, health facilities, education, etc. are considered to be new milestones of development as well as human security. Procuring these determinants however triggers serious environmental degradation and in turn climate change.

Paradoxically, development causes climate change which in turn slows down the former. Thus, it appears to be a vicious circle. Development ensures human health and security, but it also causes climate change which ultimately threatens human health. Therefore, a proper balance is needed to bring harmony among these determiners (Parvizian et al., 2011).

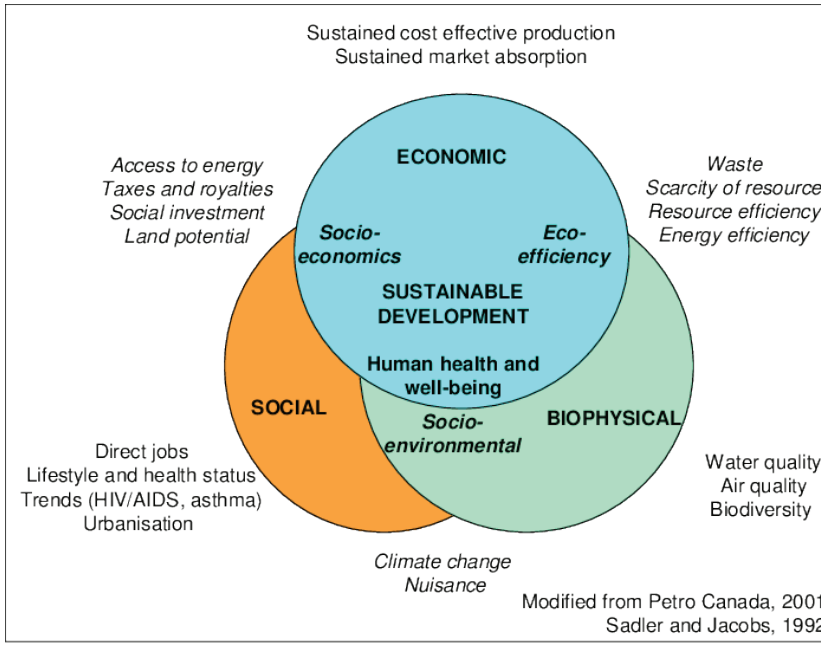

Figure 5: Three pillars of Sustainable development and their interaction (Source: Boer and O'Beirne, 2005)

Figure 5 represents:

- The 3 pillars of sustainable development i.e., economic, social and biophysical,
- Human health and well-being as central concern of sustainable development,
- Interrelationship and interaction between the pillars of sustainable development (socioenvironmental, eco-efficiency, socio-economic),

Human health is central to the three dimensions of sustainable development. Health is a beneficiary of and a contributor to development. Sustainable development focuses on a balanced relationship between anthropogenic activities and the environment, so that the benefits of the future generations are not hampered (ECO, 1999). Thus, human health and welfare are the principal consideration of environmental management and sustainable development.

Human health, as a "sustainable state" (King, 1990), requires continuous support of a rich and well-balanced ecology and protective environment. Although the socioeconomic changes over the past few decades, have improved human health but as a counter effect of this, global environmental conditions have deteriorated and affected the human health (WHO, 1995). Anthropogenically induced climatic changes have compromised the sustainability of human development, by threatening the ecological support systems on which human life depends (McMichael, 1993) and affecting the human health and well-being.

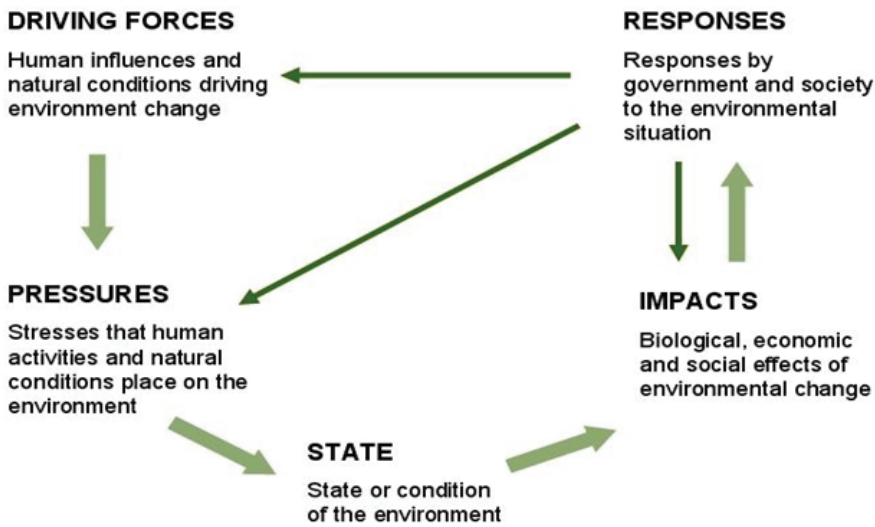

Figure 6: DPSIR framework related to interaction of human and climate

Figure 6 shows the DPSIR (Driver, Pressure, State, Impact Response) framework indicating that human influences are the main driving forces and pressures which bring about the state of climate change which in turn has biological, social and economic impact affecting the overall human health and growth to reduce these impacts favorable responses like sustainable development should be taken into account. Thus, climate change, human health and sustainable development are intricately linked.

'Health' and 'sustainable development' are complex interlinked entities. Good health usually assists development, and development often results in improved health. Equally important is the fact that our attitude towards the environment, lifestyle and consumption patterns need to be in consonance with the sustainability of the development process. Thus, human health and quality of life depends on the quality of the environment we live in (Leff, 2004).

Specific Actions to be taken to Combat Climate Change

Climate change has deep socio-economic impacts. It has been reported that unchecked climate change can result in 2.5-4.5 % decrease in GDP. To meet the challenges of climate change and environmental degradation and to achieve the 2030 Sustainable Development Goals a transformation of the economy is required. A switch from use of fossil fuels to renewable sources of energy, from traditional agriculture practices to organic farming, judicious use of our natural resources, adopting the concept of green buildings etc., are a few well known measures which can help us reduce the increasing pressure of population on our limited resources.

One of the major worldwide impacts of climate change is its effect on public health. Public health officials need to look into the matter and act accordingly to improve the overall health status of the population.

A new concept called as Building Resilience Against Climate Effects (BRACE) framework if taken into account will allow health officials to develop effective

strategies and programs to combat the health effects of climate change (Marinucci et al., 2014). BRACE is a five-step process which helps in the public health planning and response activities by incorporating complex atmospheric data, climate projections and combining it with the epidemiologic analysis. Health officials can effectively predict and respond to various climate-induced and climate sensitive health impacts by using the BRACE concept.

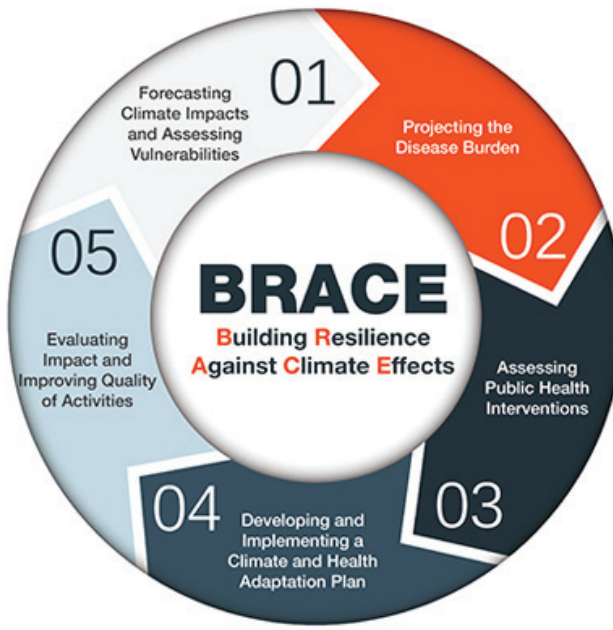

Figure 7: The BRACE framework (Source: CDC, 2019c)

The five sequential steps of the BRACE framework include:

1. Anticipating the Impacts of Climate and Assessing the Vulnerabilities: It involves identification of the scope of climate impacts, associated possible health outcomes and vulnerable populations and locations.
2. Projecting the Disease Burden: It involves estimation or quantification of the additional burden of health impacts associated with climate change.
3. Assessing Public Health Interventions: Identification of the most suitable health interventions for the identified health impacts of greatest concern.
4. Developing and Implementing Climate and Health Adaptation Plan: this step aims to develop an adaptation plan and its effective dissemination and implementation.
5. Evaluating the impact and improving the Quality of Activities : this step involves evaluation of the entire process and also determines the value of information attained and activities undertaken.

As environment and health are interdependent and inseparable, they should be priorities to development and be given precedence in the everyday management of government policies (WHO 1991).

Conclusion

As already known that climate change has multiple effects on human community which includes human health, security and overall well-being which in turn is intricately linked to the socio economic development we should work in unison towards protecting our environment. Effective environmental management and sustainable development is principally about placing humans and their needs at the forefront. For the effectiveness of public policies participation from industrial sector, public health sector, NGOs, local communities is crucial. Development should be environmentally, socially and economically sustainable. A recent example of effective replenishment of the environment comes from the COVID-19 pandemic which has resulted in a world over lockdown. It has been found that as a consequence of massive lockdown the pollution levels are lowered and the air quality has improved, the water resources are replenished and clean. Thus, public involvement and sensitivity towards environment plays a major role.

It's time to bring in more effective climate-related governance and climate change management. A shift from a fossil fuel-based energy system to a more efficient and renewable energy system, judicious use of resources and the adoption of 3Rs i.e., reduce, reuse and recycle should be brought into practice. There is a dire need to support the global efforts toward handling the causes and the many impacts of a changing climate on both human health and sustainable development.

References

1. Awasthi, A. (2018) Why India needs to worry about climate change, https://www.bbc.com/news/world-asia-india-45949323, Date accessed 17/04/2020.
2. Bierbaum R & Fay M. World Development Report 2010: Development and Climate Change. Washington: World Bank, 2010.
3. Blewitt J. (2005) Understanding sustainable development. Routledge 2015; 2nd edition.
4. Boer Annarie and O'Beirne Sean (2005), Human health impacts – temperamental pathogens for sustainable development? IAIAsa 2005, Thaba 'Nchu, https://pdfs.semanticscholar.org/2546/ae65c64992c786256df4106a4112d61961f9.pdf
5. CDC, (2019a) Centre for Disease Control and Prevention, Climate effects on Health; https://www.cdc.gov/climateandhealth/effects/default.htm, Date accessed 18/04/2020.
6. CDC, (2019b) Centre for Disease Control and Prevention, Mental Health and Stress-Related Disorders, https://www.cdc.gov/climateandhealth/effects/mental_health_disorders.htm, Date accessed 18/04/2020.
7. CDC, (2019c) Centre for Disease Control and Prevention, CDC's Building Resilience Against Climate Effects (BRACE) Framework, https://www.cdc.gov/climateandhealth/BRACE.htm, Date accessed: 20/04/2020.
8. Confalonieri U et al. (2007), Human Health. In: Parry ML et al (eds). Climate Change 2007: Impacts, adaptation and vulnerability. Contribution of working

group II to the fourth assessment report of the intergovernmental panel on climate change. Cambridge University Press 2007; 391- 431.

9. Confalonieri UEC, Chame M, Najar A, Chaves SAM, Krug T, Nobre C, Miguez JDG, Cortesão J, Hacon S (2002), "Mudanças Globais e Desenvolvimento: Importancia para a Saúde. Informe Epidemiol do" SUS 11(3):139–154. http://scielo.iec.gov.br/pdf/iesus/v11n3/v11n3a04.pdf
10. DFID (Department for International Development), (2005), DFID's Draft strategy for Research on Sustainable Agriculture (SRSA) 2006-2016. [Internet] http://www.dfi d.gov.uk/ research/srsa-consultation.pdf
11. Economic Cooperation Organization, Directorate of Human Resources & Sustainable Development (1999), "Sustainable Development", Tehran, Iran, Accessed 15th October 2008, URL:http://www.ecosecretariat.org/Directorates/dhr.htm
12. Elliott JA (2006), An introduction to sustainable development. Routledge 2006; 3rd edition.
13. Esmaeilnejad M, Bazrafshan E, Ansari-Moghaddam A. (2018), 'Effect of Climatic Changes on Spatial Distribution of Zoonoses: A Case Study from South Khorasan Province, Iran', Health Scope. 2018 ; 7(1):e56045. doi: 10.5812/jhealthscope.56045.
14. Ferlay J et al. GLOBOCAN 2008 U1.2, Cancer incidence and mortality worldwide: IARC Cancer Base No. 10 (Internet). Lyon, France: International agency for research on cancer; 2010. Available from: h□ p://globocon.iarc.fr accessed 16 April, 2015.
15. Goswami Urmi (2020), View: Climate change distress should reflect in budget 2020 https://economictimes.indiatimes.com/news/economy/policy/view-climate-change-distress-should-reflect-in-budget-2020/articleshow/73779537.cms?utm_source= contentofinterest&utm_medium=text&utm_campaign=cppst, Date accessed:17/04/
16. Houghton MJ (1997) Global warming: the complete briefing. 2nd ed. Cambridge: Cambridge University Press; 1997.
17. IPCC (1996) Intergovernmental Panel on Climate Change. In: Watson RT et al., eds. Climate change 1995: Impacts, adaptations, and mitigation of climate change: scientific-technical analyses. New York, Cambridge University Press, 1996.
18. IPCC (2007) Intergovernmental Panel on Climate Change. Climate Change 2007: Impacts, adaptation and vulnerability. Summary for policy makers. http://www.ipcc.ch/pdf/assessment-report/ar4_syr_spm.pdf
19. IPCC (2012) Intergovernmental Panel on Climate Change. Managing the risks of extreme events and disasters to advance climate change adaptation. Special report of working groups I and II of the intergovernmental panel on climate change. Cambridge, UK & New York, USA: Cambridge University Press 2012.
20. IPCC (2014) Intergovernmental Panel on Climate Change. Climate Change 2014: impacts, adaptation, and vulnerability. Part A: global and sectoral aspects. Contribution of working group II to the fifth assessment report of

the intergovernmental panel on climate change. Cambridge University Press, Cambridge/New York, p 1132. http://www.ipcc.ch/report/ar5/wg2/

21. IUCN (1991), International Union for Conservation of Nature, "Principles of a Sustainable Society, Caring for the Earth: A Strategy for Sustainable Living", Accessed 15thn December 2008, URL: http://www.globalleamingnj.org/global_ ata/ principles_of_a_sustainable_society.htm
22. IWGCCH (2010) – Interagency Working Group on Climate Change and Health , A human health perspective on climate change. A report outlining the research needs on the human health effects of climate change. Environmental Health Perspectives and the National Institute of Environmental Health Sciences, Triangle Park. ISSN 0091-6765. https://data.globalchange.gov/ assets/be/e7/ e8af30e920e7a4c27c173af785a6/ climatere port2010.pdf
23. Khagram, Sanjeev, William C. Clark, and Dana Firas Raad. (2003) "From the Environment and Human Security to Sustainable Security and Development." Journal of Human Development ,4(2): 289-313.
24. King M (1990). Health is a sustainable state. Lancet, 336: 664-667.
25. Klugman J (2011). Human Development Report 2011. Sustainability and Equity: A better future for All, Basingstoke: Palgrave Macmillan.
26. Lang T and Raynor G (2012). Ecological public health: The 21st century's big idea? An essay by Tim Lang and Geof Raynor. BMJ 2012; 345: e5466. doi: 10.1136bmj.e5466.
27. Leff E (2004) Saber ambiental: sustentabilidade, racionalidade, complexidade, poder, 3a edn. Vozes, Petrópolis
28. Lin HH, Ezzati M, Murray M.(2007) Tobacco smoke, indoor air pollution and tuberculosis: A systematic review and meta-analysis. PLoS Medicine 2007.
29. McGrath, M. (2018) Five things we have learned from the IPCC report, https://www.bbc.com/news/science-environment-45784892, Date accessed 23/04/2020
30. McKeever, Patrick James (2009), The UNESCO Global Network of National Geoparks:Geological Heritage and Sustainability, LESTARI Public Lecture No. 7. Bangi: LESTARI, UKM, URL: http://www. wcf2009.org/program/ down/106_S7-110-l_Puay_Liu_Ong.doc.
31. McMichael AJ. (1993) Planetary overload: global environmental change and the health of the human species. Cambridge, Cambridge University Press, 1993.
32. NRC (2012) Disaster resilience: a national imperative. National Academies Press, Washington, DC. https:// doi.org/10.17226/13457
33. OPAS/OMS (2008) Mudanças climáticas e ambientais e seus efeitos na saúde: cenários e incertezas para o Brasil. Disponível em, Brasilia. http://bvsms.saude. gov. br/bvs/publicacoes/mudancas_climaticas_ambientais_ efeitos.pdf
34. Parvizian Ganje Firouz and el al, (2011) "Evaluation of the Effects of Climate Change in Destruction Procedure on Iran's Historic Buildings", World Academy of Science, Engineering and Technology, 59.

35. Patz, J.A., et al., (2000) Effects of environmental change on emerging parasitic diseases. Int J Parasitol, 30(12-13): p. 1395-405.
36. Reddy PLS (2010). Promoting Green Technologies: A way Forward. In: Climate change, society & sustainable development. New Delhi: Times Group Books 2010; 124-141.
37. Repetto, R. (1986), World enough and Time, New Haven: Yale University Press, p-15.
38. Ruhil R (2016) Climate Change, Public Health and Sustainable Development: The Interlinkages., Indian Journal of Public Health Research & Development, Vol. 7, No. 3 141-146
39. Sachs JD (2012). From millennium development goals to sustainable development goals. Lancet 2012; 379: 2206-11.
40. Thomas DSG & Twyman C (2005). Equity and justice in climate change adaptation amongst natural resources dependent societies. Global Environmental Change, 15: 115-24.
41. UNICEF & WHO (2012). JMP Biennial Report. Progress on drinking water and sanitation, 2012 update. New York & Geneva: UNICEF & WHO. www.wssinfo.org
42. USGCRP (2016) The impacts of climate change on human health in the United States: a scientific assessment. In: Crimmins A, Balbus J, Gamble JL, Beard CB, Bell JE, Dodgen D, Eisen RJ, Fann N, Hawkins MD, Herring SC, Jantarasami L, Mills DM, Saha S, Sarofim MC, Trtanj J, Ziska L (eds). U.S. Global Change Research Program, Washington, DC, p 312. https://doi.org/10.7930/J0R49NQX
43. Van Kleef E, Bambrick H, Hales S. (2010) The geographic distribution of dengue fever and the potential infl uence of global climate change. Tropl K Anet
44. WCED (1987) World Commission on Environment and Development (1987), Our Common Future, Oxford University Press: New York, p-8. \
45. WHO (1991) Sundsvall statement on supportive environments for health. In: Third international conference on health promotion, Sundsva
46. WHO (1995), World health report 1995. Geneva, World Health Organization, 1995.
47. WHO (2005). Using climate to predict infectious disease epidemics. Geneva: World Health Organisation 2005.
48. WHO (2009) (World Health Organisation). Global risks: mortality and burden of disease attributable to selected major risks. Geneva: World Health Organisation 2009.
49. WHO (2011) (World Health Organisation). World Malaria Report. Geneva: World Health Organisation 2011.
50. WMO 2019, WMO Statement on the State of the Global Climate in 2019 (WMO No. 1248) https://library.wmo.int/doc_num.php?explnum_id=10211

❑❑❑

Climate Change and Sustainable Development

Om Prakash
Gaurav Kumar Jain
Govind Singh
Lalit Singh Jhala

Climate change has become an agenda of key concern and requires our utmost attention. There are several factors which collectively attribute to climate change but anthropogenic activities since the early 1700s, could be considered the major cause. Climate change causes hindrance in the sustainable development of the society which not only affects mankind but all the species existing in an ecosystem.

This book highlights the connection between climate change and sustainable development, exploring the impacts of climate change on the environment, economy, and society. It is a result of contributions from multiple authors, aimed at raising awareness and encouraging further research on the topic.

Other Related Book

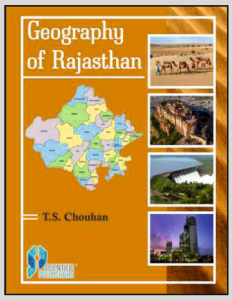

ISBN: 978-93-89184-28-0

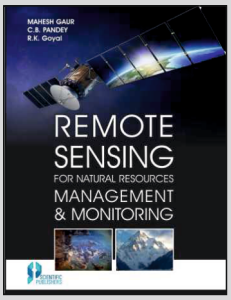

ISBN: 978-93-86102-72-0

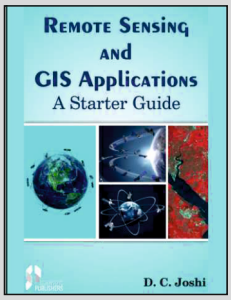

ISBN: 978-93-88172-54-7

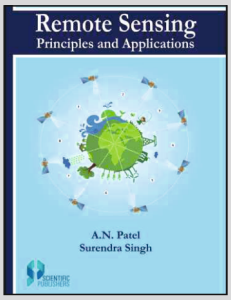

ISBN: 978-81-72335-90-8

SCIENTIFIC® PUBLISHERS

For more details visit
www.scientificpubonline.com

ISBN: 978-93-90749-29-4

GLOBAL ENVIRONMENTAL SCIENCE: ISSUES AND SOLUTIONS

(PART-D : Eco-Friendly Perspectives)



Books Available on :

amazon flipkart.com

Dr. Anil Kumar Chohadia
Dr. Narendra Nirwan
Dr. Chandresh Pareek
Dr. Gayatri



Dr. Chohadia obtained his Post-Graduation in Chemistryfrom Seth Mathuradas Binani Government PG College, Nathdwara in 2003. He has been awarded Ph.D. degree in the field of photochemistry from Mohanlal Sukhadia University, Udaipur in 2009. Apart from this, he has presented research papers in many National and International level seminars, conferences and workshops and has also been awarded the best research paper. Many of his articles have been published in Scopus, Web-science indexing and UGC-CARE Listed International and National Journals and his chapters have also been published in many edited books of National and International repute. Apart from this, he has also worked as an adjudicator in many National and International conferences.



Dr. Nirwan obtained his Post-Graduation degree in Chemistry from the Department of Chemistry, University of Rajasthan, Jaipur with a position of branch topper. He has been awarded the Ph.D. degree in "Heterocyclic Synthesis and their Biological Activity" from Maharshi Dayanand Saraswati University, Ajmer in 2020. He has published more than 30 research papers in various Scopus, Web-science indexing and UGC-CARE-Listed National and International journals. His more than 10 chapters have also been published in many edited books of National and International repute. He has participated and presented research papers in more than 80 National and International conferences. He organized a National workshop titled **"Use of Technology in the Field of Education"** in 2021 during the National Science Day celebration programme. Apart from this, he has also been an invited speaker in National conferences. His area of research is Organic Synthesis and Green Chemistry.



Dr. Pareek obtained his Post-Graduation degree in Chemistry from MaharshiDayanandSaraswati University, Ajmer with a position of University topper. He has been awarded the Ph.D. degree in "Physico-Analytical studies of some new derivatives of oxazines and thiazine series" from the MDS University, Ajmer in 2009. He has published more than 25 research papers in various Scopus, Web-science indexing and UGC-CARE-Listed National and International journals. More than 7 chapters have also been published in many edited books of National and International repute. He has participated and presented research papers in more than 20 National and International conferences including Poland and is conference chair in Belgium. Apart from this, he has also been an invited speaker in many National conferences. He was awarded as a "Master of Reiki" by USUI Shiki Ryoho and an Award of Appreciation by ECB in Poland.



Dr. Gayatri obtained her Post-Graduation degree in Political Science from the SPC Government College Ajmer. She has been awarded Ph.D. degree in Political Science from Maharshi Dayanand Saraswati University, Ajmer. She has published more than 12 research papers in various Scopus, Web-science indexing and UGC-CARE-listed National and International journals. Hermore than 8 chapters have also been published in many edited books of National and International repute. She has participated and presented research papers in more than 30 National and International conferences. She organized a National Webinar in 2020 on the topic **"Challenges before Democracy"**. Apart from this, she has also been an invited speaker in National conferences. Her area of research is Local self-Government and Environmental Issues and Solutions.

₹ 995.00 $ 9.95

ISBN 978-93-91777-61-6

9 789391 777616

Raj Publishing House
44, Parnami Mandir, Govind Marg,
Jaipur-302 004, Mob. 9414051782
email : shreerajpublishing@gmail.com

Global Environmental Science: Issues and Solutions

(Part-D: Eco-Friendly Perspectives)

Editors

Dr. Anil Kumar Chohadia
Assistant Professor
Department of Chemistry
M.P. Govt. PG College, Chittorgarh

Dr. Narendra Nirwan
Assistant Professor
Department of Chemistry
S.P.C. Government College, Ajmer

Dr. Chandresh Pareek
Associate Professor
Department of Chemistry
J.D.B. Government Girls College, Kota

Dr. Gayatri
Assistant Professor
Department of Political Science
S.P.C. Government College, Ajmer

RAJ PUBLISHING HOUSE
Jaipur

Publisher:
Mrs. Kiran Parnami
Raj Publishing House
44, Parnami Mandir, Govind Marg, Jaipur-302004
Cell : 09414051782
Email : shreerajpublishing@gmail.com

Global Environmental Science: Issues and Solutions

(Part-D: Eco-Friendly Perspectives)

Editors
Dr. Anil Kumar Chohadia
Dr. Narendra Nirwan
Dr. Chandresh Pareek
Dr. Gayatri

© Subject to the content of the chapter

Peer Reviewed International Standard Book No. (ISBN) Book
978-93-91777-61-6
Edition : 2022

Jurisdiction of book distribution : All India

All rights reserved by the editor.
No part of this publication can be reproduced or transmitted in any from or by means, without written permission of the editor.

The responsibility of the facts stated, conclusions and plagiarism, if any, in this book is entirely that of the contributors (authors and co-authors). And editor and publisher bear no responsibility for them, whatsoever.

Printed at
Trident Enterprises, Delhi

Contents

S.No.	Chapter Name	Page No.
	Preface	(i)
1.	Development of Traditional System of Medicine in India, Prospects of Traditional Medicine **Dinesh Kumar Yadav, Hina Mathur, Neetu Kumari Vineet K. Maurya, Mohammad Faheem Khan Devendra P. Mishra**	1
2.	Coronaviruses a Pandemic: Symptom, Treatment, Its Influence, Future Challenges Towards the World and India **Charul Somani, Dinesh K. Yadav, Mahesh Meena, Neetu Kumari, Gunmala Gugalia**	16
3.	Alternative System of Medicine: A Holistic Approach to Cure Human Being **Dinesh Kumar Yadav, Hina Mathur, Neetu Kumari, Vineet K. Maury, Mohammad Faheem Khan Devendra P. Mishra**	41
4.	Characterization of Biodiesel **Jyoti Pathak**	54
5.	Green Recovery: A Solution for Green Economy in Post Covid Era **Dr. Vineeta Arora**	61
6.	Biodiversity, Sustainability and Conservation **Dr. Anita Lubana, Dr. Gayatri, Dr. Narendra Nirwan**	69

GLOBAL ENVIRONMENTAL SCIENCE: ISSUES AND SOLUTIONS

(PART-D : Eco-Friendly Perspectives)



Books Available on :

amazon flipkart.com

Dr. Anil Kumar Chohadia
Dr. Narendra Nirwan
Dr. Chandresh Pareek
Dr. Gayatri



Dr. Chohadia obtained his Post-Graduation in Chemistryfrom Seth Mathuradas Binani Government PG College, Nathdwara in 2003. He has been awarded Ph.D. degree in the field of photochemistry from Mohanlal Sukhadia University, Udaipur in 2009. Apart from this, he has presented research papers in many National and International level seminars, conferences and workshops and has also been awarded the best research paper. Many of his articles have been published in Scopus, Web-science indexing and UGC-CARE Listed International and National Journals and his chapters have also been published in many edited books of National and International repute. Apart from this, he has also worked as an adjudicator in many National and International conferences.



Dr. Nirwan obtained his Post-Graduation degree in Chemistry from the Department of Chemistry, University of Rajasthan, Jaipur with a position of branch topper. He has been awarded the Ph.D. degree in "Heterocyclic Synthesis and their Biological Activity" from Maharshi Dayanand Saraswati University, Ajmer in 2020. He has published more than 30 research papers in various Scopus, Web-science indexing and UGC-CARE-Listed National and International journals. His more than 10 chapters have also been published in many edited books of National and International repute. He has participated and presented research papers in more than 80 National and International conferences. He organized a National workshop titled **"Use of Technology in the Field of Education"** in 2021 during the National Science Day celebration programme. Apart from this, he has also been an invited speaker in National conferences. His area of research is Organic Synthesis and Green Chemistry.



Dr. Pareek obtained his Post-Graduation degree in Chemistry from MaharshiDayanandSaraswati University, Ajmer with a position of University topper. He has been awarded the Ph.D. degree in "Physico-Analytical studies of some new derivatives of oxazines and thiazine series" from the MDS University, Ajmer in 2009. He has published more than 25 research papers in various Scopus, Web-science indexing and UGC-CARE-Listed National and International journals. More than 7 chapters have also been published in many edited books of National and International repute. He has participated and presented research papers in more than 20 National and International conferences including Poland and is conference chair in Belgium. Apart from this, he has also been an invited speaker in many National conferences. He was awarded as a "Master of Reiki" by USUI Shiki Ryoho and an Award of Appreciation by ECB in Poland.



Dr. Gayatri obtained her Post-Graduation degree in Political Science from the SPC Government College Ajmer. She has been awarded Ph.D. degree in Political Science from Maharshi Dayanand Saraswati University, Ajmer. She has published more than 12 research papers in various Scopus, Web-science indexing and UGC-CARE-listed National and International journals. Hermore than 8 chapters have also been published in many edited books of National and International repute. She has participated and presented research papers in more than 30 National and International conferences. She organized a National Webinar in 2020 on the topic **"Challenges before Democracy"**. Apart from this, she has also been an invited speaker in National conferences. Her area of research is Local self-Government and Environmental Issues and Solutions.

₹ 995.00 $ 9.95

ISBN 978-93-91777-61-6

9 789391 777616

Raj Publishing House
44, Parnami Mandir, Govind Marg,
Jaipur-302 004, Mob. 9414051782
email : shreerajpublishing@gmail.com

Global Environmental Science: Issues and Solutions

(Part-D: Eco-Friendly Perspectives)

Editors

Dr. Anil Kumar Chohadia
Assistant Professor
Department of Chemistry
M.P. Govt. PG College, Chittorgarh

Dr. Narendra Nirwan
Assistant Professor
Department of Chemistry
S.P.C. Government College, Ajmer

Dr. Chandresh Pareek
Associate Professor
Department of Chemistry
J.D.B. Government Girls College, Kota

Dr. Gayatri
Assistant Professor
Department of Political Science
S.P.C. Government College, Ajmer

RAJ PUBLISHING HOUSE
Jaipur

Publisher:
Mrs. Kiran Parnami
Raj Publishing House
44, Parnami Mandir, Govind Marg, Jaipur-302004
Cell : 09414051782
Email : shreerajpublishing@gmail.com

Global Environmental Science: Issues and Solutions

(Part-D: Eco-Friendly Perspectives)

Editors
Dr. Anil Kumar Chohadia
Dr. Narendra Nirwan
Dr. Chandresh Pareek
Dr. Gayatri

© Subject to the content of the chapter

Peer Reviewed International Standard Book No. (ISBN) Book
978-93-91777-61-6
Edition : 2022

Jurisdiction of book distribution : All India

All rights reserved by the editor.
No part of this publication can be reproduced or transmitted in any from or by means, without written permission of the editor.

The responsibility of the facts stated, conclusions and plagiarism, if any, in this book is entirely that of the contributors (authors and co-authors). And editor and publisher bear no responsibility for them, whatsoever.

Printed at
Trident Enterprises, Delhi

Contents

S.No.	Chapter Name	Page No.
	Preface	(i)
1.	Development of Traditional System of Medicine in India, Prospects of Traditional Medicine **Dinesh Kumar Yadav, Hina Mathur, Neetu Kumari Vineet K. Maurya, Mohammad Faheem Khan Devendra P. Mishra**	1
2.	Coronaviruses a Pandemic: Symptom, Treatment, Its Influence, Future Challenges Towards the World and India **Charul Somani, Dinesh K. Yadav, Mahesh Meena, Neetu Kumari, Gunmala Gugalia**	16
3.	Alternative System of Medicine: A Holistic Approach to Cure Human Being **Dinesh Kumar Yadav, Hina Mathur, Neetu Kumari, Vineet K. Maury, Mohammad Faheem Khan Devendra P. Mishra**	41
4.	Characterization of Biodiesel **Jyoti Pathak**	54
5.	Green Recovery: A Solution for Green Economy in Post Covid Era **Dr. Vineeta Arora**	61
6.	Biodiversity, Sustainability and Conservation **Dr. Anita Lubana, Dr. Gayatri, Dr. Narendra Nirwan**	69

योग एवं खेल

[Yoga and Sports]



डॉ. रवि कुमार शर्मा • डॉ. वर्षा शर्मा

Scanned with CamScanner

योग एवं खेल

[Yoga and Sports]

डॉ. रवि कुमार शर्मा
एम.एससी. (योग एवं प्रेक्षा मेडिटेशन)
पीएच.डी. (मनोविज्ञान एवं जनसंचार)
पोस्ट डॉक्टरेट (मनोविज्ञान)

डॉ. वर्षा शर्मा
एम.ए. (मनोविज्ञान, स्वर्ण पदक सहित)
पीएच.डी. (मनोविज्ञान)
पोस्ट डॉक्टरेट

हिमांशु पब्लिकेशन्स
उदयपुर □ दिल्ली

Scanned with CamScanner

© प्रकाशकाधीन

इस पुस्तक के किसी भी अंश की किसी भी रूप में प्रतिकृति करना या किसी भी साधन-इलेक्ट्रॉनिक, मेकैनिकल या अन्य प्रकार, फोटोकॉपी, रिकॉर्डिंग या सूचना संचयन और पुनः प्राप्ति पद्धति - द्वारा प्रसारित करना प्रकाशक की लिखित अनुमति के बिना मना है।



हिमांशु पब्लिकेशन्स

464, हिरण मगरी, सेक्टर 11, उदयपुर 313 002 (राज.), फोन: 0294-2421087
4379/4-B, प्रकाश हाऊस, अंसारी रोड़, दरियागंज, नई दिल्ली-2, मोबाईल: 96109-73739
Web : himanshupublications.com; email : himanshupublications@gmail.com

ISBN : 978-93-94954-10-6

मुद्रण : 2022

मूल्य : ₹ 225.00

Distributor
ARYAS PUBLISHERS DISTRIBUTORS (P) LTD.
2-D, Hazareshwar Colony, Near Court Choraha, Udaipur (Raj.) - 313 001
Phone : 0294-2526160; E-mail : apdpl.2012@gmail.com

Scanned with CamScanner

अनुक्रमणिका

1. **योग एवं यौगिक क्रियाएं: एक परिचय** 1
(Introduction to Yoga & Yogic Practices)
योग का अर्थ, परिभाषा, स्वरूप, ऐतिहासिक पृष्ठभूमि, योग की विधाएं, अष्टांग योग, राजयोग, ध्यान एवं व्यक्तित्व विकास।

2. **यौगिक पाठ्य** (Yogic Texts) 12
एक विधा के रूप में योग, यौगिक पाठ्य के वर्गीकरण, हठ योग पद्धति।

3. **योग एवं स्वास्थ्य** (Yoga & Health) 24
स्वास्थ्य का अर्थ, परिभाषा, योग एवं स्वास्थ्य में संबध, स्वास्थ्य को प्रभावित करने वाले कारक, स्वास्थ्य एवं अस्वस्थ्य का समप्रत्यय, अस्वस्थता की कसौटी एवं सकारात्मक स्वास्थ्य।

4. **स्वास्थ्य एवं खुशहाली में मनोविज्ञान की भूमिका** 37
(Role of Psychology in Health and Well-Being)
स्वास्थ्यवर्धक एवं हानिकारक जीवन शैली, प्राचीन योग साहित्य के अनुसार सकारात्मक स्वास्थ्य में योग की भूमिका।

5. **सकारात्मक मनोविज्ञान एवं स्वास्थ्य** 50
(Positive Psychology & Health)
सकारात्मक मनोविज्ञान का अर्थ, परिभाषा, स्वास्थ्य उन्नयन में सकारात्मक मनोविज्ञान की भूमिका, स्वस्थ्य जीवन के लिए यौगिक क्रियाएं।

6. **ध्यान-स्वास्थ्य उन्नत करने का उपाय** 58
(Meditation-Solution for Health Promotion)
ध्यान का अर्थ, परिभाषा, ध्यान के विभिन्न प्रकार एवं पद्धतियाँ, ध्यान के लाभ।

Scanned with CamScanner

7. **व्यक्तित्वः एक परिचय** (Personality: An Introduction) 64
व्यक्तित्व का अर्थ, परिभाषा, प्रकार, श्रेणीकरण, व्यक्तित्व को प्रभावित करने वाले कारक, व्यक्तित्व विकास की प्रक्रिया।

8. **तनाव का परिचय** (Stress: An Introduction) 86
तनाव का अर्थ, परिभाषा, तनाव के कारण, तनाव के प्रभाव, जीएएस।

9. **योग द्वारा व्यक्तित्व विकास एवं तनाव प्रबंधन** (Personality Development & Stress Management Through Yoga) 99
तनाव प्रबंधन की विधीयाँ, तनाव प्रबंधन हेतु योगासन, पद्हस्तासन, त्रिकोणासन, शशांकासन, उष्ट्रासन, अर्द्ध मत्स्येन्द्रासन, भुजांगासन, मकरासन, सर्वांगासन, मत्स्यासन, शवासन, प्राणायाम, भामरी प्राणायाम, शीतली प्राणायाम, शीर्षासन, बकासन, मयूरासन, हंसासन, व्यक्तित्व विकास हेतु आसन-सूर्य नमस्कार, ताडासन, सिंहासन, कुकुटासन, धनुरासन।

10. **गुणवत्तापूर्ण जीवन के लिए नैतिक मूल्य अवधारणा** (Moral Values Concept for Living Quality Life) 132
आहार-विहार, आचार-विचार, संकल्पना, व्यवहार, अर्थ, स्वरूप, व्यवहार का वैज्ञानिक अध्ययन- नैतिक मूल्य; प्रामाणिकता, करूणा, आत्मानुशासन, आत्मसंयम, सहिष्णुता।

11. **खेल का मनोविज्ञान** (Psychology of Sports) 146
खेल, खेल की आवश्यकता, खेल एवं खुशहाली, व्यक्तित्व एवं खेल प्रदर्शन में संबध, खिलाड़ियों के मानसिक स्वास्थ्य को उन्नत करने में मनोविज्ञान की भूमिका।

12. **खेल एवं जीवन दर्शन** (Sports and Life Philosophy) 154
खेल मूल्य, खेल प्रदर्शन के कौशल।

13. **सन्दर्भ सूची** (References) 158

Scanned with CamScanner

पुस्तक के बारे में

योग एंव खेल, स्वस्थ जीवन शैली की आधारशिला हैं। आपाधापी के इस दौर में जब व्यक्ति तनाव से परिपूर्ण हो जाता हैं तो मानसिक सुख एंव शांति प्राप्त करने के लिए योग एंव खेल अचूक उपाय की तरह सामनें आते हैं। दिन ब दिन बढती प्रतिस्पर्धा, व्यस्त होती दिनचर्या औऱ लगातार बदलते सामाजिक परिवेश के चलते प्राणी मात्र में मानसिक स्वास्थ्य हेतु कई चुनौतियाँ उत्पन्न हुई हैं। प्रस्तृत पुस्तक योग एंव खेल के अभ्यास द्वारा मानसिक स्वास्थ्य को उन्नत करने के उपाय सुझाती हैं। यह पुस्तक सकारात्मक मनोविज्ञान की उपयोगिता को स्पष्ट करने के साथ ही जीवनदर्शन एंव जीवन कौशल को विकसित करने के उपाय के रुप में योग और खेल की विस्तृत व्याख्या प्रस्तृत करती है। इस पुस्तक को विभिन्न विश्वविद्यालय के पाठ्यक्रमों के अनुरुप विधार्थी हितार्थ लेखनबद्द किया गया हैं। विभिन्न प्रतियोगी परिक्षाओं को ध्यान में रखते हुए पुस्तक में लघु उत्तरीय एंव निबंधात्मक प्रश्नों का भी समावेश है। ऐसे में यह पुस्तक विधार्थीयों, शिक्षाविदों एंव प्रबुद्ध पाठकों के आशानुरुप होगी।

लेखक के बारे में



डॉ. रवि कुमार शर्मा प्रदेश के पत्रकारिता जगत का जाना पहचाना नाम हैं, जो पिछले 16 वर्षों से भी अधिक समय से समाज के उत्थान के लिए इलेक्ट्रॉनिक मीडीया के क्षेत्र में अपनी सेवाएं और महत्वपूर्ण योगदान दे रहे हैं। ई.टी.वी राजस्थान, जी-न्यूज और फिलहाल फर्स्ट इंडिया न्यूज जैसे प्रतिष्ठित मीडीया घरानों में विभिन्न पदो पर रहते हुए, आपने राजस्थान के आदिवासी बाहुल्य दक्षिणांचल में प्रचलित मौताणा, मानव तस्करी, बाल श्रम और ऐसी [illegible] सामाजिक कुरीतियों से जुडे संवेदनशील मसलों को प्रमुखता से कवर करते हुए कमजो[illegible] मजबूत करने का महत्वपूर्ण कार्य किया हैं। आपने आई.सी.एस.एस.आर., नई [illegible] डॉक्टरेट की उपाधि हासिल करने के साथ ही मनोविज्ञान और पत्रकारिता एंव जनसंचार विषय में दो पीएच.डी की डिग्रीयाँ हासिल की हैं। डॉ. शर्मा नें राजस्थान विश्वविद्यालय, जयपुर से पत्रकारिता में स्नात्तकोत्तर की डिग्री प्राप्त करने के साथ ही सांइस ऑफ लिविंग, योगा एंड मेडिटेशन में भी स्नात्तकोत्तर की डिप्लोमा हैं। आपने जयनारायण विश्वविद्यालय,जोधपुर से मास कम्यूनिकेशन एंड विडियो प्रोडक्शन में स्नातक की डिग्री प्राप्त [illegible] डॉ. शर्मा के 10 से अधिक शोध पत्र राष्ट्रीय और अंतर्राष्ट्रीय स्तर के जर्नल्स में प्रकाशित हो चुके हैं। आपने अब तक दो पुस्तकों का लेखन करने के साथ ही कई राष्ट्रीय और अंतर्राष्ट्रीय स्तर की सेमिनार और कॉफ्रेंसेज में पत्र-वाचन किये हैं। आपको पत्रकारिता के क्षेत्र में उल्लेखनीय कार्य के लिए प्रदेश और राष्ट्रीय स्तर के अवार्ड के साथ ही अन्तर्राष्ट्रीय स्तर पर दुबई एक्सीलेंस अवार्ड से भी सम्मानित किया जा चुका है। आप राजस्थान सरकार के सूचना एंव जनसंपर्क विभाग द्वारा अधिस्वीकृत पत्रकार भी हैं। डॉ. शर्मा शैक्षणिक उन्नयन के कार्य हेतु सिंगापुर, श्रीलंका और दुबई की यात्रा भी कर चुके हैं।



डॉ. वर्षा शर्मा वर्तमान में मोहनलाल सुखाडिया विश्वविद्यालय, उदयपुर के मनोविज्ञान विभाग में असिस्टेंट प्रोफेसर के पद पर कार्यरत है और जानी मानी क्लिनीकल साइकोलोजिस्ट हैं। डॉ. शर्मा ने सुखाडिया विश्वविद्यालय से 2009 में एम. ए. की डिग्री प्राप्त की और विश्वविधालय गोल्ड मेडल प्राप्त किया हैं। डॉ. शर्मा ने NET, SLET, परीक्षा उत्तीर्ण करने के साथ ही यू.जी.सी से JRF औऱ SRF प्राप्त किया हैं।आपने एमबीए इन ह्यूमन रिसोर्स मैनेजमेंट की डिग्री भी हासिल की और सुखाड़िया विश्वविद्यालय से पीएचडी की उपाधि प्राप्त की हैं।डॉ.वर्षा आई.सी.एस.एस.आर, नई दिल्ली से पोस्ट डॉक्टरेट की उपाधि हासिल करने के साथ ही अब तक 2 पुस्तकों का लेखन कर चुकी है। डॉ शर्मा ने बतौर अनुसंधान अधिकारी पापुलेशन रिसर्च सेंटर जो कि मिनिस्ट्री ऑफ हेल्थ एंड फैमिली वेलफेयर नई दिल्ली की इकाई है, में अपनी सेवाएं दी है। डॉ शर्मा द्वारा वैलबिइंग इंडेक्स नामक स्टैंडर्डराइज साइक्लोजिकल टूल का निर्माण किया है, जिसे वैश्विक स्तर पर समाज विज्ञानियों द्वारा अपने शोध अनुसन्धान में प्रयोग किया जा रहा है। आपके 11 से अधिक शोध पत्रों का प्रकाशन राष्ट्रीय एवं अन्तराष्ट्रीय स्तर के जर्नल में हो चुका है। साथ ही आपने 21 से ज्यादा राष्ट्रीय एवं अंतराष्ट्रीय स्तर के सेमिनार- कॉन्फ्रेंस में शोध पत्र प्रस्तुत किये है।कई अवॉर्ड अपने नाम करने वाली डॉ. शर्मा को गार्गी सम्मान, महाराणा मेवाड़ फतेहसिंह अवार्ड , एम .के. सिंघवी अवार्ड, विश्विद्यालय गोल्ड मैडल, गुजरात एकेडमी ऑफ साइकोलॉजी से रजत पदक और विप्र फांउडेशन का राष्ट्रीय स्तर का तेजस्वनी सम्मान भी प्राप्त है।

हिमांशु पब्लिकेशन्स

464, हिरण मगरी, सेक्टर 11, उदयपुर 313 002 (राज.), फोन: 0294-2421087
4379/4-B, प्रकाश हाऊस, अंसारी रोड़, दरियागंज, नई दिल्ली-2, मोबाईल: +91-96109-73739
Web : himanshupublications.com; email : himanshupublications@gmail.com

ISBN 978-93-94954-10-6

Scanned with CamScanner

BOARD OF OPEN SCHOOLING
& SKILL EDUCATION
(Established under Act No.14 of 2020 by Govt of Sikkim)

F.No. BOSSE /SLM Sr. Sec. Psycho./2022/848
Date: 10/10/ 2022

CERTIFICATE OF APPRECIATION

This is to certify that ***Dr. Varsha Sharma,*** *Assistant Professor, Department of Psychology, University College of Social Sciences & Humanities, Mohanlal Sukhadia University, Udaipur, Rajasthan has* contributed towards the content development of Self Learning Material for the **Board of Open Schooling and Skill Education (BOSSE), Sikkim.**

In accordance with the specific requirements of the curriculum, she has authored the following chapter in the subject *Psychology at Senior Secondary Level:*

1. Psychotherapy
2. Ramifications of Mental Health

We wish her all the best for future endeavours.

Kuldeep A

Dr. Kuldeep Agarwal,
Vice-Chairperson,
BOSSE, SIKKIM

Scanned with CamScanner

28

PSYCHOTHERAPY

INTRODUCTION

In the previous chapter you have learned about the concept of Abnormality, difference between normal and abnormal and also about neurotic and psychotic behaviour and their assessment. In this chapter you will learn about meaning and definition of psychotherapies, different types of psychotherapeutic procedures as well as approaches, common mental health conditions which can be effectively treated by psychotherapies. Psychotherapies are those scientific procedures which are used by the trained psychotherapists in order to provide the professional help to the client or patient. Though Psychotherapies differ on the basis of their procedures and approaches but all are focused to enhance the level of self awareness, self competence and coping skills of the clients so that they can have better and effective adjustment in day today life. In this chapter we will discuss some of the major forms of psychotherapies.

28.1 LEARNING OBJECTIVES:

After reading this chapter you will be able to:

- ✓ Understand the basic nature and process of psychotherapy
- ✓ Understand the difference between different psychotherapies
- ✓ Learn that how psychotherapies are helpful to solve the psychological issues of everyday life
- ✓ Learn that how psychotherapies are helpful to assist different mental disorders

© Not To Be Republished

28.2 PSYCHOTHERAPY- MEANING/ DEFINITION, NATURE, PROCESS & GOALS

28.2.1 Meaning/ Definition

Psychotherapy is a psychological intervention based on the scientific procedures and principles of psychology, which is provided by trained psychologists, psychiatrist or mental health practitioners. It is also known as 'talk therapy'. The literal meaning of psychotherapy indicates that it is made up of two Greek words 'psyche' means soul and sprit and 'therapeia' meaning healing. The major technique used in psychotherapies is talking about the

Scanned with CamScanner

BOARD OF OPEN SCHOOLING & SKILL EDUCATION

(Established under Act No.14 of 2020 by Govt of Sikkim)

F.No. BOSSE /SLM Sr. Sec. Psycho./2022/848
Date: 10/10/ 2022

CERTIFICATE OF APPRECIATION

This is to certify that ***Dr. Varsha Sharma,*** *Assistant Professor, Department of Psychology, University College of Social Sciences & Humanities, Mohanlal Sukhadia University, Udaipur, Rajasthan has* contributed towards the content development of Self Learning Material for the **Board of Open Schooling and Skill Education (BOSSE), Sikkim.**

In accordance with the specific requirements of the curriculum, she has authored the following chapter in the subject *Psychology at Senior Secondary Level:*

1. Psychotherapy
2. Ramifications of Mental Health

We wish her all the best for future endeavours.

Kuldeep A

Dr. Kuldeep Agarwal,
Vice-Chairperson,
BOSSE, SIKKIM

Near Indira Bypass, NH-10, Gangtok, East Sikkim- 737102 | Ph: 03592-295335

Scanned with CamSca

23

RAMIFICATIONS OF MENTAL HEALTH

INTRODUCTION

In the previous chapter you have learned about the concept of Meditation for Health and Well Being. In this chapter you will learn about Ramifications of Mental Health in which we will discuss about concept of mental health its meaning, definition and importance as well. Mental health is always overlooked in our concerns we bother about physical health, but plight of the hour is we are not yet aware about the importance of mental health. This chapter will explain the ramifications of mental health on intellectual health, emotional health, social health, moral health and spiritual health.

23.1 LEARNING OBJECTIVES

After reading this chapter you will be able to:

- ✓ Understand the meaning and definition of mental health
- ✓ Learn about the importance of mental health
- ✓ Understand how mental health acts as an instrument for achieving the goal of overall health and happiness
- ✓ Understand the ramifications of mental health
- ✓ Learn the concept of intellectual health, emotional health, social health, moral health and spiritual health.

© Not To Be Republished

23.2 Mental Health – Concept, Definitions and Importance

Before we discuss about mental health it is important for us to understand about the concept of health first. What is Health? It is not only the absence of any physical ailment or disease. **According to WHO**, "Health is a state of complete physical, mental, and social well-being and not merely the absence of disease or infirmity."

As per the definition of health it is clear that mental health is an important aspect of all over health. Mental health is nothing but a state of emotional, social and psychological wellbeing. In other words,mental health is an indicator of having good understanding about our own thoughts, emotions and actions.Let's learn some definitions of mental health-

Scanned with CamScanner

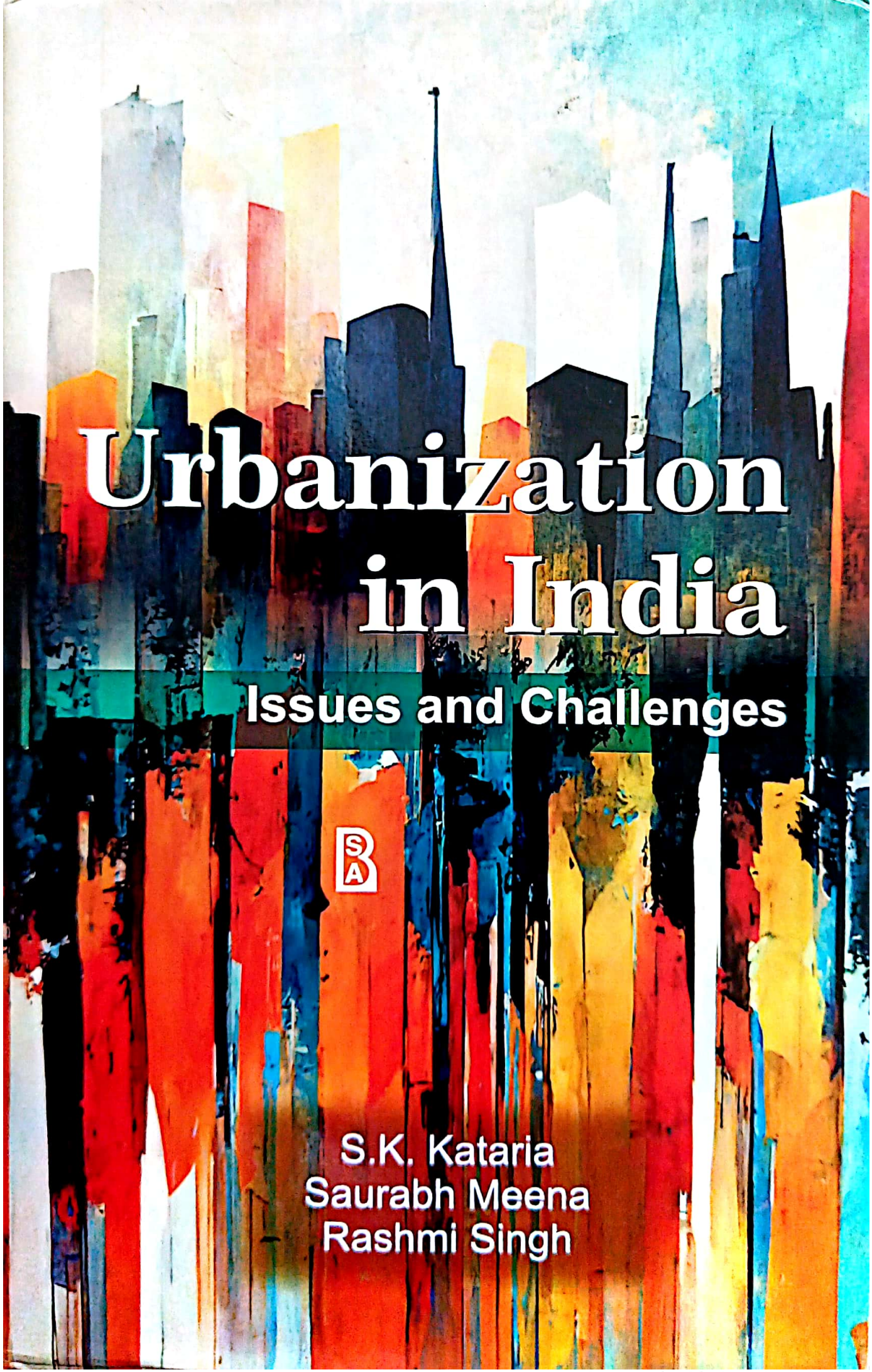

Scanned with CamScanner

URBANIZATION IN INDIA
ISSUES AND CHALLENGES

S.K. Kataria
Saurabh Meena
Rashmi Singh

❑

Published by :

RBSA Publishers
340, Fatehpuriyon ka Darwaza,
Chaura Rasta, Jaipur – 302 003
Phone : 0141-2575826, 2571702

❑

© Authors
First Edition : 2023

ISBN : 978-93-92064-36-4

❑

Laser Typesetting by :
Madan Computers, Jaipur

❑

Printed at :
Sheetal Printers, Jaipur

All Rights Reserved. No part of this publication may be reproduced, stored in a retrieval system, or transmitted in any form or by any means, electronic, mechanical, photocopying, recording, scanning or otherwise, without the prior written permission of the copyright owner. Responsibility for the facts stated, opinions expressed, conclusions reached and plagiarism, if any, in this volume is entirely that of the author/editor. The publishers bear no responsibility for them, whatsoever.

Scanned with CamScanner

Contents

Preface *v*

1. **Urbanization in India : Evolution and Impacts** 1
   - Multiplicity of Urban Development Agencies / 19
2. **Parsi Community: The Modern Makers of India** 31
3. **Urban Infrastructure and Civic Amenities** 46
   - Urban Planning in India / 46
   - Poor Urban Infrastructure and Civic Mess / 65
   - Urban Transportation / 72
   - Solid Waste Management / 80
   - Urban Housing / 90
   - Urban Policing / 97
4. **Social Development in Urban India** 113
   - Urban Health in Globalized India / 113
   - Towards Total Sanitized Cities / 123
   - Slums in India: Issues and Policies / 132
   - Empowering Street Vendors / 139
   - Socio-Administrative Aspects of Tourism Sector / 144
   - Scientific Temper in Urbanites: A KAP Study on COVID-19 / 153
   - Begging and Vagrancy / 167
   - Genext Communication: Trends and Threats / 174
   - Towards Safe Workplace for Women Employees / 183
   - Transgender Persons in Urban India / 191
5. **Municipal Government and Urban Development** 204
   - Subsidiarity and Urban Local Government / 204

Scanned with CamScanner

- Municipal Capacity Building / 212
- Future of Municipal Governments in India / 221

Annexures

- *The Constitution (Seventy-fourth Amendment) Act, 1992* 233
- *The Real Estate (Regulation and Development) Act, 2016* 247

Bibliography 309

Scanned with CamScanner

21st Century Business Management

Reshaping the Business World Post-COVID-19

Management Strategies for Sustainable Behavior Change

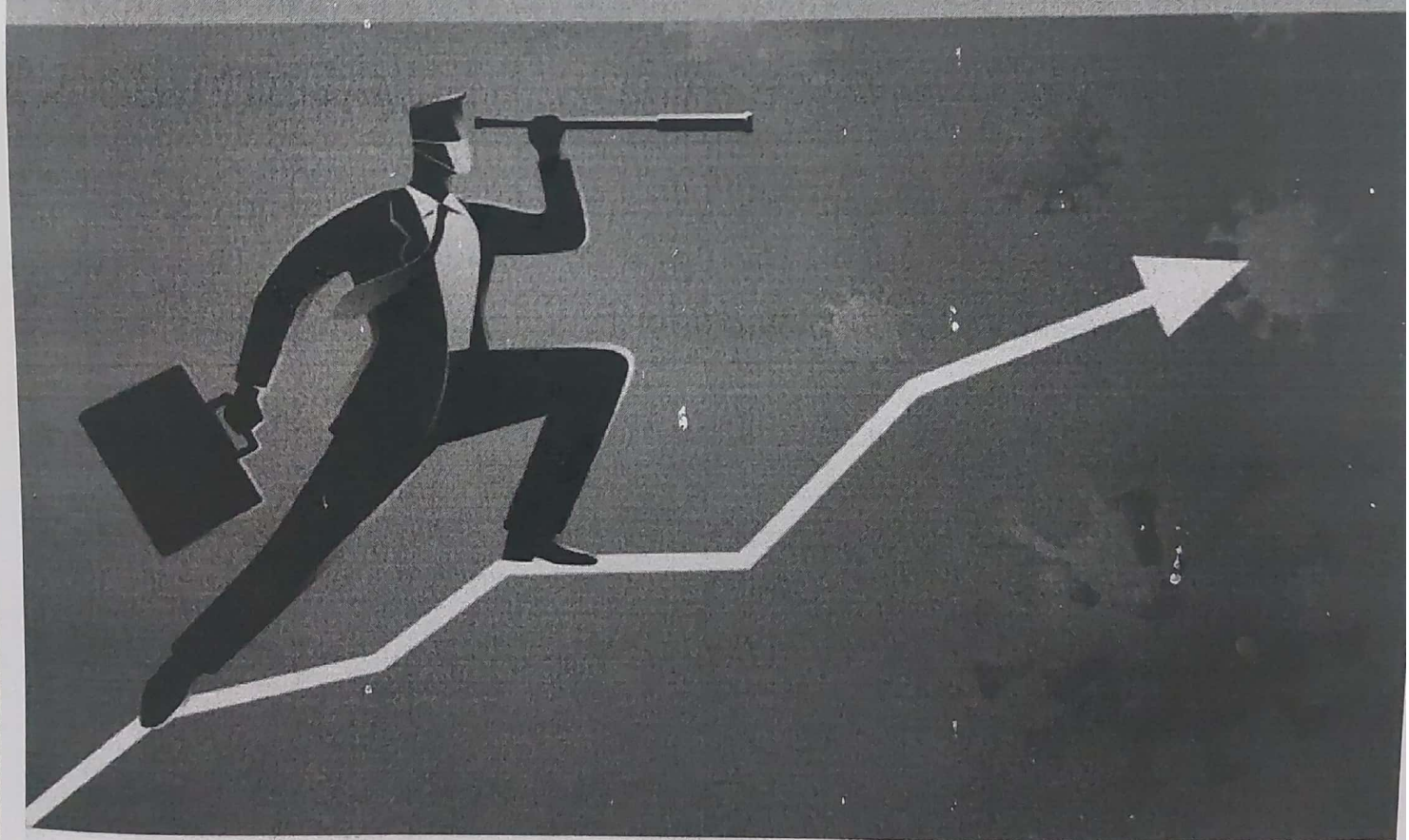

Arvind K. Birdie | Ruchi Joshi

Editors

CRC Press
Taylor & Francis Group
APPLE ACADEMIC PRESS

Scanned with CamSca

Contents

Contributors
Abbreviations
Preface

1. **COVID-19 and Employee Satisfaction with Leadership Influencing the Future Competitiveness of Organizations**
   Maja Rožman, Anita Peša, Mladen Rajko, and Tjaša Štrukelj
2. **Hybrid Working: The Future of Organizations**
   Tarun Kumar Sharma
3. **Mapping the Nature of Workplace Incivility in Post-COVID Work Culture**
   Suyesha Singh and Rimjhim
4. **Changes of Collaboration Platforms' Use Perceived by Users Because of COVID: A Research Study of Changes in User Experience of Microsoft Teams Platform**
   Zdenko Deželak, Simona Sternad Zabukovšek, and Samo Bobek
5. **The Culture Shock of COVID-19: A Study to Understand the Effects of Pandemic on the Art and Culture Industry**
   Chirmi Acharya
6. **Is Resilience a Predictor of Psychological Well-Being Among Employees Amid Lockdown? A Literature Review-Based Study**
   Monika Gwalani
7. **Impact of the Pandemic on Street Food Vendors Globally: Challenges and Coping Strategies**
   Vismita Paliwal, Ruchi Joshi, and Nida Nafees
8. **Work and Life Allies or Enemies: A COVID Pandemic Perspective**
   Varsha Sharma
9. **Effect of Autogenic Relaxation and Self-Management Training on Internet Addiction Among Red Collar Employees in Post-COVID-19**
   Neharshi Srivastava and Neeta Gupta
10. **Paradigm Shift in Consumer Shopping Behavior During the COVID-19 Pandemic**
    Priya Vij, Kashish Kakra, and Attin Kumar

Index

Scanned with CamSca

Contributors

Chirmi Acharya
Assistant Professor, Department of Psychology, Manipal University, Jaipur, Rajasthan, India

Samo Bobek
University of Maribor, Faculty of Economics and Business, Slovenia

Zdenko Deželak
University of Maribor, Faculty of Economics and Business, Slovenia

Neeta Gupta
Associate Professor, DAVPG College, Dehradun, Uttarakhand, India

Monika Gwalani
Assistant Professor, Amity University, Jaipur, Rajasthan, India

Ruchi Joshi
Assistant Professor, Department of Psychology, Manipal University Jaipur, India

Kashish Kakra
IND Analyst II-HCS, Aon Consulting Pvt. Ltd., Gurgaon, India

Attin Kumar
Cluster Manager, Reliance Trends, Gurgaon, India

Nida Nafees
Assistant Professor, Amity Institute of Behavioral and Allied Sciences, Amity University, Rajasthan, India

Vismita Paliwal
Associate Professor and Coordinator, Amity Institute of Behavioral and Allied Sciences, Amity University, Rajasthan, India

Anita Peša
University of Zadar, Department of Economics, Croatia

Mladen Rajko
University of Zadar, Department of Economics, Croatia

Rimjhim
Mphil Clinical Psychology, Department of Psychiatry, Government Medical College and Hospital, Chandigarh

Maja Rožman
University of Maribor, Faculty of Economics and Business, Slovenia

Tarun Kumar Sharma

Scanned with CamSca

Assistant Professor, Department of Psychology, Mohanlal Sukhadia University, Udaipur, Rajasthan, India

Varsha Sharma

Assistant Professor, Department of Psychology, Mohanlal Sukhadia University, Udaipur, Rajasthan

Suyesha Singh

Assistant Professor, Department of Psychology, Manipal University Jaipur, Rajasthan, India

Neharshi Srivastava

Assistant Professor, Amity Institute of Behavioral and Allied Sciences, Amity University, Jaipur, Rajasthan, India

Tjaša Štrukelj

University of Maribor, Faculty of Economics and Business, Slovenia

Priya Vij

Professor, Economics, Chandigarh University, Punjab, India

Simona Sternad Zabukovšek

University of Maribor, Faculty of Economics and Business, Slovenia

Scanned with CamScanner

DE GRUYTER

Ajay Kumar Goswami, Prabhat Kumar Baroliya

HEAVY METALS ADSORPTION

LOW-COST ADSORBENTS



Ajay Kumar Goswami, Prabhat Kumar Baroliya
Heavy Metals Adsorption

Also of interest

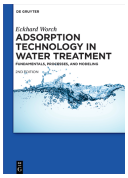

Adsorption Technology in Water Treatment.
Fundamentals, Processes, and Modeling
Eckhard Worch, 2021
ISBN 978-3-11-071542-2, e-ISBN (PDF) 978-3-11-071550-7

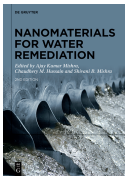

Nanomaterials for Water Remediation
Ajay Kumar Mishra, Chaudhery M. Hussain and Shivani B. Mishra (Eds.), 2020
ISBN 978-3-11-064336-7, e-ISBN (PDF) 978-3-11-065060-0

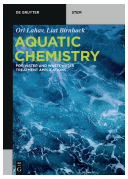

Aquatic Chemistry.
for Water and Wastewater Treatment Applications
Ori Lahav and Liat Birnhack, 2019
ISBN 978-3-11-060392-7, e-ISBN (PDF) 978-3-11-060395-8

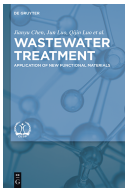

Wastewater Treatment.
Application of New Functional Materials
Jianyu Chen, Jun Luo, Qijin Luo und Zhihua Pang, 2018
In cooperation with: China Environment Publishing Group
ISBN 978-3-11-054278-3, e-ISBN (PDF) 978-3-11-054438-1

Ajay Kumar Goswami,
Prabhat Kumar Baroliya

Heavy Metals Adsorption

Low-Cost Adsorbents

DE GRUYTER

Authors
Prof. Ajay Kumar Goswami
5 Anugraha 132 Road Nr
UDAIPUR-313001
Rajasthan
India
akumargoswami56@gmail.com

Dr. Prabhat Kumar Baroliya
Mohanlal Sukhadia University
Department of Chemistry
Ganesh Nagar
University Road
Udaipur-313001
India
prabhatkbaroliya@mlsu.ac.in

ISBN 978-3-11-077455-9
e-ISBN (PDF) 978-3-11-077465-8
e-ISBN (EPUB) 978-3-11-077476-4

Library of Congress Control Number: 2022945036

Bibliographic information published by the Deutsche Nationalbibliothek
The Deutsche Nationalbibliothek lists this publication in the Deutsche Nationalbibliografie; detailed bibliographic data are available on the internet at http://dnb.dnb.de.

© 2023 Walter de Gruyter GmbH, Berlin/Boston
Cover image: Sadasiba behera/iStock/Getty Images Plus
Typesetting: Integra Software Services Pvt. Ltd.
Printing and binding: CPI books GmbH, Leck

www.degruyter.com

About the authors



Dr. A. K. Goswami, retired professor and BSR faculty fellow is a known name in the field of analytical and coordination chemistry. Over a span of 33 years of his teaching and research career he had enormously contributed to his field. Starting from electrochemistry as his field of doctoral research, he moved on to spectrophotometric studies and metal complexes. Thoroughly and exhaustively working on development of analytical reagents, particularly hydroxytriazenes, for transition metal determination via spectrophotometric or complexometry, he focused on medicinally important complexes or ligands, adsorption corrosion or even theoretical drug designing of late. Prof. Goswami has more than 135 research publication in journals with high impact, 33 doctoral students and more than 7 books to his credit. The present book is his third book with De Gruyter, and he is working on more such books to his list.



Dr. P. K. Baroliya, Assistant Professor at the Mohanlal Sukhadia University, Udaipur, since 2012. His research interests include medicinal chemistry, water treatment by adsorption and catalysis. He has been part of numerous research groups, and is a well-known lecture and author of scientific papers of national and international repute.

https://doi.org/10.1515/9783110774658-204

Contents

Foreword —— V

About the authors —— IX

Chapter 1
Paradigm of removing toxic heavy metals using low-cost adsorbents —— 1
Introduction —— **1**
1.1 Heavy metals: a menace to environment and human health —— **1**
1.2 Heavy metal removal: a brief overview —— **3**
1.3 Adsorption: state-of-the-art —— **5**
1.4 Review of various low-cost adsorbents in recent years —— **7**
References —— **12**

Chapter 2
Removal of heavy metals using mineral-based adsorbents —— 17
Introduction —— **17**
2.1 Preparation of adsorbent —— **18**
2.2 Various process parameters —— **19**
2.3 Right choice of adsorbent —— **20**
2.4 Methods of removing heavy metals using low-cost adsorbents —— **21**
References —— **57**

Chapter 3
Removal of heavy metals using low-cost bioadsorbents —— 63
Introduction —— **63**
3.1 Biosorption of metals —— **63**
3.2 Fruit cortex/peel as adsorbent —— **65**
3.3 Leaves as bioadsorbent —— **67**
3.4 Sawdust and bark as adsorbent —— **70**
3.5 Rice husk as adsorbent —— **70**
3.6 Peat moss adsorbent —— **72**
3.7 Nut shell as adsorbent —— **74**
3.8 Egg shell as adsorbent —— **76**
3.9 Agricultural/forestry waste as adsorbent —— **76**
3.10 Animal shell as adsorbent —— **80**
3.11 Microbes as adsorbent —— **81**
3.12 Bone waste as adsorbent —— **84**
References —— **90**

Chapter 4
Removal of heavy metals using low-cost biochars — 95
Introduction — **95**
4.1 Biochar from forestry and agricultural waste — **95**
4.2 Biochar from dairy manure — **100**
4.3 Algal biochar — **101**
4.4 Biochar from oil cake carbon — **103**
References — **108**

Index — 111



कृष्ण साहित्य

(विविध संदर्भ)

सम्पादक
डॉ. नीतू परिहार

कृष्ण साहित्य : विविध संदर्भ

संपादक
डॉ० नीतू परिहार

अंकुर प्रकाशन
ANKUR PRAKASHAN

प्रतिलिप्याधिकार प्रकाशक व लेखक के आधीन सुरक्षित है। इनकी पूर्व लिखित अनुमति के बिना इस पुस्तक के किसी भी भाग का पुनः प्रकाशन वर्जित है। इस पुस्तक में व्यक्त विचार लेखकों के व्यक्तिगत हैं। इनसे किसी भी प्रकार की होने वाली हानि के लिए संपादक और प्रकाशक उत्तरदायी नहीं हैं। किसी भी विवादास्पद स्थिति में न्यायालय क्षेत्र उदयपुर मान्य होगा।

कृष्ण साहित्य : विविध संदर्भ
ISBN : *978-81-86064-98-6*
© : संपादक
मूल्य : चार सौ रुपये
संस्करण : 2023
प्रकाशक : अंकुर प्रकाशन
1/1 कांजी का हाटा, गायत्री मार्ग
उदयपुर (राज.) 313001
फोन नं. : (0294) 2417094, 2417039
(मो.) 9413528299
ईमेल : ankurprakashan15@gmail.com
आवरण : डॉ. शंकर शर्मा, उदयपुर
टाईपसेटिंग : देवेन्द्र कम्प्यूटर, दिल्ली
मुद्रक : रिसर्च प्रेस इण्डिया, दिल्ली

Krishna Sahitya : Vividh Sandarbh *(Hindi Literature)*
Edited By : Neetu Parihar ₹ 400

13	सूरदास के काव्य में लोकसंस्कृति के आगाम— डॉ. प्रिया ए.	135
14	वल्लभ सम्प्रदाय एवं नाथद्वारा का ऐतिहासिक संबंध— डॉ. शिल्पा मेहता	144
15	राजस्थानी साहित्य परम्परा में श्रीकृष्ण— डॉ. सुरेश सालवी	151
16	सूरसागर का समापन : मानवीय प्रेम की करुण त्रासदी— डॉ. देवेन्द्र शर्मा	161
17	कृष्ण-कथा का उत्तरार्ध और आधुनिक युग बोध: (नाटक सूर्यमुख के संदर्भ में)—डॉ. मंजू त्रिपाठी	168
18	मीरां के पदों में कृष्ण के विभिन्न नाम—रीना मेनारिया	173
19	जैन प्राकृत साहित्य में अंकित श्रीकृष्ण और उनका वासुदेवत्व —डॉ. सुमत कुमार जैन	185
20	द्रौपदी : एक निर्वचनात्मक विश्लेषण—डॉ. सुमित्रा शर्मा	196
21	कृष्ण की अनन्य साधिका : भक्तिमती मीरा— डॉ. ममता पानेरी	206
22	रांगेय राघव के कथा साहित्य में कृष्ण —डॉ. अनुपम	211

15

राजस्थानी साहित्य परम्परा में श्रीकृष्ण

—डॉ. राकेश सालवी

भारतीय भाषाओं, साहित्य एवं संस्कृति में ही नहीं वरन् विदेशी भाषाओं एवं साहित्य में भी श्रीकृष्ण का विशिष्ट स्थान है। भारतीय भाषाओं में श्रीकृष्ण का चरित्र प्रबन्ध काव्यों, खण्ड काव्यों में रचा बसा है। राजस्थानी भाषा में भी कई के रचनाकारों ने श्रीकृष्ण के जीवन पर आधारित काव्य रचे। चाहे शिष्ट साहित्य हो या लोकसाहित्य सभी में श्रीकृष्ण का चरित्र एक नायक के रूप में अंकित हुआ है। श्रीमद्भागवतगीता भारतीयों के हृदय में रची बसी है। श्रीकृष्ण हैं ब्धा तो आमजन की जिव्हा पर रची बसी है। प्राचीन एवं मध्यकालीन राजस्थानी साहित्य में तो श्रीकृष्ण पर साहित्य सृजना हुई है पर आधुनिक साहित्यकार आधुनिक चिन्तन के साथ श्रीकृष्ण पर काव्य एवं गद्य में रचनाएं कर रहें हैं।

राजस्थानी साहित्य में कृष्ण भक्ति हो, राम भक्ति, शिव भक्ति या शक्ति की रचना हो। इस दृष्टि से राजस्थानी भक्ति साहित्य बहुत ही समृद्ध है। राजस्थानी साहित्य में कृष्ण से संबंधित सगुण एवं निर्गुण भक्ति का स्वरूप हमें दिखाई देता कृष्ण साहित्य में हमें रस की दृष्टि से शांत, शृंगार, वीर, वीभत्स एवं करुण रस का आस्वादन होता है। राजस्थानी साहित्य जैन शैली, चारण शैली एवं लौकिक में में श्रीकृष्ण के जीवन पर आधारित ग्रन्थ में रचे गए। ''जैन साहित्यकारों में न कृत हरिवंश-पुराण (र.का. 11वीं शताब्दी वि.), रविसागर कृत प्रद्युम्न-रास (र.का. 1207 वि.), यशकीर्ति कृत पाण्डव-पुराण (र.का. 1497 वि.), यशकीर्ति कृत द्रौपदी रास (र.का. 1693 वि.)'' जिसमें श्रीकृष्ण का चरित्रांकन किया गया है।

मीराबाई श्रीकृष्ण की भक्त परम्परा की उपासक रही हैं। मीराबाई की भाषा

बोलचाल की राजस्थानी है। मीरा के पदों में प्रेम भक्ति, मीरा की उपासना दंपति भाव की थी। इनकी कविता में भक्ति और शृंगार दोनों रूप नजर आता है।

जाओ हरि निरमाहना रे, जाणी थारी प्रीत।
तेरा कोई नहँ रोकरणहार, मगन होय मीरा चली।
ह्मारो जनम-मरण रो साथी, थाँने नहँ बिसरुँ दिन राती।
राणाजी ह्माँणै या बदनामी लागे मीठी।
ह्माँरे सिर पर साळगराम, राणाजी ह्माँरो काँई करसी।

ईसरदास का जन्म सं. 1595 में जोधपुर के भाद्रेस गाँव में हुआ था। इन्होंने राजस्थानी की डिंगल शैली में हरिरस एक उत्कृष्ट कोटि का आध्यात्मिक ग्रंथ रचा। दोहा, गाथा, मातीदाम, बिअखरी और छप्पय छंदों में रचित है।

विखो ब्रज मांझ पड़यौ बोह बार
धरै नख वार किता गिर धार
बजाड़ि तु वार किताइक वंस
किता तैं फेरां जीत्योहि कंसंप

ईसरदास कृत वि.स. 1595-1676 गुण भागवत, माधोदास कृत वि.स. 1960 भाषा दसमस्कंध, खेतसी सांदू कृत भाषा-भारथ र.का. वि.स. 1760 श्रीकृष्ण संबंधी डिंगल शैली के काव्य है। श्रीकृष्ण संबंधी पौराणिक साहित्य में सोढ़ीनाथी (अमरकोट) कृत बालचरित्र सं.1731, और कंसलीला सं.1731, भीम कवि कृत हरिलीला र.का. सं.1541 तथा श्रीमद्भागवत्, हरिवंशपुराण उल्लेखनीय रचनाएँ है। मीरां और चन्द्रसखी के भजन भी कृष्ण से संबंधित है। निम्बार्क संप्रदाय के परशुरामजी का श्रीकृष्ण चरित सं. 1677 प्रमुख रचना है।

सांखला करमसी रुणेचा रचित 'क्रिसनजी री वेलि' की हस्तलिखित प्रति सं.1635 प्राप्त हुई थी। 22 पद्यों की रचना है। जिसमें रुखमणी का नख-शिख वर्णन है।

''सीस तरुणि श्री फल सारिषउ
भाल मुगत सिंदूर भरि
नषत्र माल सोहंति कि निसि भरि
चँदन तिलिक कि चंद परि।।''

पृथ्वीराज राठौड़ बीकानेर नरेश राव कल्याणमल के पुत्र और राव जैतसी के पोते थे। राजस्थानी भाषा की डिंगल शैली के कवियों में पृथ्वीराज का स्थान बहुत ऊंचा है। इनके रचे ग्रन्थों में क्रिसन रुकमणी री वेली, दसम भागवत रा दूहा,

वसदेरावउत रादूहा भगवान श्रीकृष्ण भक्ति पर है। क्रिसन रुकमणी री वेलि में रुकमणी की बाल्यावस्था से लेकर कृष्ण के परिवार तक की कथा समाहित है। यह शान्त, शृंगार एवं वीर रस की रचना है। यह एक खंड काव्य है।

''परमेसर प्रणवि, प्रणवि सरसति, पुणि
सद-गुरु प्रणवि, त्रिण्हे तत-सार
मंगळ-रूप गाइजइ माहव्
चार सु अे - ही मंगळचार।

शान्त रस में कवि ने मंगलाचरण प्रस्तुत किया है—

आरोपित हार घणउ थ्यउ अंतर
ऊर-स्थळि कुंभ-स्थळि आज
सु-जु मोती नहि न लहइ सोभा,
रज तिणि सिरि नाखइ गज-राज।

कवि पृथ्वीराज राठौड़ ने इसमें रुकमणी के शृंगार का वर्णन किया है।

चोटियाळी कूदइ चउसठी चाचरि,
धू ढळियइ ऊकसइ धड़
अनंत अनइ सिसुपाळ अउझड़इ
झड़ मातउ माँडियउ झड़।।''

वेलि में कवि ने वीर रस के अन्तर्गत युद्ध का वर्णन किया है।

ठकुर जी रा दूहा पृथ्वीराज राठौड़ की कृष्ण भक्ति की रचना है। कृष्ण के दोहों के अंत में वसदेव राव उत आता है।

''प्रभु दे फण फण पाग, थेइ थेइ तनु करता थया।
नचायौ तै नाग, विहबल वसदेरावउत।।''

सायांजी झूला शाखा के चारण थे। इनका जन्म सं.1632 में हुआ। साँयाजी श्रीकृष्ण के भक्त थे। इनके काव्य कृष्ण भक्ति पर थे। काव्यों की भाषा राजस्थानी है डिंगल शैली की इन रचनाओं पर गुजराती भाषा का प्रभाव है क्योंकि साँयाजी काठियावाड़ी थे। रुक्मिणी-हरण और नागदमण इनकी उत्कृष्ट रचनायें हैं।

सायांजी का रुक्मिणी-हरण वीर रस का वर्णनात्मक खंड काव्य है। अकबर संबंधी प्रवाद के अनुसार पृथ्वीराज कृत क्रिसन रुखमणी री वेलि से भी रुक्मिणी हरण को श्रेष्ठ काव्य कहा गया है। रुक्मिणी हरण का आधार श्रीमद्भगवत महापुराण है। रचना में वीर रस के साथ कही-कही पर शान्त, शृंगार और वीभत्स रसों का भी वर्णन हुआ है। वैणसगाई अलंकार का निर्वाह हुआ है।

भेटतां अंबिका हुओ मन-भावीयो।
अंतरीप येडि रथ महमहण आवीयो।।
दुलहणी झालि वैसारतो देपीयो।
एवडो सेन पण चित्र आलेपीयो।।

सायांजी का नागदमण श्रीकृष्ण की बाललीला पर आधारित एक चरित्र काव्य है। श्रीकृष्ण और कालिया नाग इस आख्यान के विशिष्ट पात्र है। वीर रस प्रधान यह एक खंड काव्य है।

जदुनाथ काली समी वाथ जोड़ै,
घंणी भोम चाली चढी वात घोडै।
ऊभा गाय गोवाळ झूरंत आरै,
ळहाकार हक्कार संसार सारै।।

श्रीकृष्ण पर 'हरि लीला सोलह कला' की रचना भीम कवि ने सं. 1541 में दोहों, चौपाइयों और पदों में की।

''वृंदावन गोपी नाचेरि तेणि रंगे राचे राम।
श्राग मधूर स्वर आलवे री गाए हरी वीलाश।।''

अलूनाथ कविया का जन्म 1560 वि. के आसपास हुआ। अलूनाथ के कवित्त (षट्पदियां) राजस्थानी कवि समाज में अजोड़ गिनाये गए है। इनकी प्राप्त कविताएं मुक्तक ही है। इनकी रचनाओं में नए-नए प्रतीकों पौराणिक कथाओं का बखान है। राजस्थानी भाषा में ओज, प्रसाद गुण के साथ शान्त रस की रचना है। हर षट्पदी का स्वतंत्र आस्तित्व है।

''काराग्रहि जामेवि कणय मणि भूषण धारण
अर्द्ध निसा अस्टमी क्रस्ण भूअ और उतारण
क्रस्ण करिहिं संमिले मात जसुदा तिणि रखखय
वे कंस निरवंस हिये पित मात हरखखय
कप्पूर हलिद्रा कुम-कुमा मिलय संग गोकुल मही
निसि दिवस द्वार नंदराइ रै दधि कादव ममना वही।।''

परशुराम का रचना काल सं. 1677 के लगभग है। इन्होंने 22 ग्रन्थ और 750 फुटकर पद रचे। श्रीकृष्ण चरित, सिंगार सुदामा चरित, द्रौपदी का जोड़ा ग्रंथ राजस्थानी भाषा की पिंगल शैली की रचना है। 'बलभद्र वेलि' के रचविता सालिग 16 वीं शती के कवि थे। यह 28 छंदों की छोटी रचना है। इसमें बलभद्र और कृष्ण की अन्तिम जीवन झांकी दिखाई गई है।

''द्वारिका नयरी नीकल्या, वे बंधव इक ठाय।
त्रिखा ऊपनी कृष्णनई, बंधव पाणी पाय।।''

नरहरिदास रोहड़िया शाखा के चारण लक्खाजी के पुत्र थे। इनकी रचना अवतार चरित्र में राम के साथ कृष्णावतार, कपिलावतार, बुद्धावतार का बखान है। भाषा शैली पिंगल है। कल्याणदास रचित गुण गोविन्द में श्रीकृष्ण के साथ श्रीराम की विविध लीलाओं का सरस और भक्ति भाव के साथ बखान है। डिंगल शैली में रचित यह ग्रन्थ 197 छंदो की रचना है। कुशलधीर सोजत निवासी जैन कवि थे। इन्होंने क्रिसन रुखमणी री वेली की टीका सं.1696 में की। जो गद्य में है।

''हिव रुक्मिणी माता नउ कथा प्रसंग कहई। दक्षिण दिसिइ विदर्भ नामा देस दीपइ। तीयइ देस विषद कुंदणपुर नामइ पुर नगर अत्यन्त सर्वोत्कृष्ट पणइ शोभइ। तणि नगर विषद भीषमक एक राजा राज करइ।''

किशनगढ़ महाराज राजसिंह के पुत्र नागरीदास का जन्म सं. 1756 को हुआ। इनका मूल नाम सावंतसिंह था। कविता में नागरी, नागर, नागरिया और नागरीदास लिखा करते थे। ये संस्कृत, फारसी और ब्रजभाषा के ज्ञानी थे। इनकी कृष्ण जन्मोत्सव कवित्त, गोवर्धनधारक के कवित्त, फाग गोकुलाष्टक रचनाएँ हैं। इन्होंने वैष्णव संप्रदाय के कृष्णोपासक की भांति राधाकृष्ण शृंगार रसात्मक कविता रची।

पुष्कर क्षेत्र निवासी हित वृंदावनदास गौड़ ब्राह्मण थे। इनका जन्म सं. 1765 में हुआ। वृंदावनदास श्रीकृष्ण के भक्त थे। इन्होंने श्रीकृष्ण लीला पर छोटे बड़े कई ग्रन्थ बनाए। कृष्ण गिरि पूजन वेलि, कृष्ण गिरिपूजन मंगल, कृष्ण सुमिरन पचीसी, कृष्ण विवाह उत्कंठा, राधा जन्म उत्सव वेलि, राधा बाल विनोद आदि मुख्य ग्रन्थ हैं।

''न्याइ काम करवट व्है निकसत, पिय अरु रूप गुमानी।
वृंदावन हितरूप, कियो वस, सो कानन की रानी।।''

गवरीबाई का जन्म सं. 1815 में डूँगरपुर में हुआ। बचपन में ही ये विधवा हो गई। इन्होंने भागवत, गीता के साथ धार्मिक ग्रन्थों का अध्ययन किया। गवरीबाई को मीरा का दूसरा अवतार माना जाता है। इन्होने 610 फुटकर पद लिखे। इनकी भाषा राजस्थानी पर गुजराती और ब्रजभाषा का प्रभाव है। माखन चोरी, डाणलीला, रास लीला का मनोहारी वर्णन आपके पदों में मिलता है।

''गवरी गउ गोपाल की, चरण चारा रस च्हाय
वंकी टेंढी जो चले तो करे गोपाल सहाय
गवरी कर गोपाल सहाय ज्युं बालक के मात
कालो, घेलो बावरो, तो हुँ न छाडे तात।।''

हरिजी रो ब्यांवलो अथवा रुकमणी मंगल पदम तेली की रचना है। 17वीं शताब्दी में रचित यह विविध राग-रागिनियों में लिखा गया है। गायक मंडलियाँ रात्रि में इसे गाया करती है। जसनाथी संप्रदाय की किसनजी रो विवाहलो रचना है। जवान सिंह मेवाड़ के महाराणा भीमसिंह के पुत्र थे। जवान सिंह ने ब्रजभाषा में अनेक कवित्त, सवैया, पद बनाए जो ब्रजराज पद्यावली के नाम से विख्यात है। इनके काव्य में आत्म समर्पण, श्रृंगार और भक्ति स्पष्ट दिखाई देती है।

''उद्धव आय गए ब्रज में सुनि गोपिन के तन में सुख छायौ।
आनंद सौ उमगी सगरी चलि प्रेम भरी दधि आन बँधायौ।।
पूछति है मन मोहन की सुधि बोलता ही दृग नीर चलायौ।
देखि सनेह सखा हरि के घनश्याम वियोग कछू न सुनायौ।।''

बूंदी निवासी जीवनलाल का जन्म सं. 1870 में हुआ था। सोलह वर्ष की आयु में इन्होंने बारह हजार श्लोकों का 'कृष्ण-खंड' नामक ग्रन्थ बनाया। रचना में भक्ति और श्रृंगार की प्रधानता है। गुलाबजी बूंदी के दरबारी कवि थे। इनकी रचनाओं में ध्यान रूप सवतिका बद्ध कृष्णचरित्र, कृष्ण लीला, कृष्ण चरित्र उल्लेखनीय हैं।

जयपुर के राजा आनंदराम कछवाहा की पुत्री ब्रजदासी रानी बांकावती का जन्म वि.सं. 1760 को हुआ। इनकी रचना श्रीमद्भागवत रचना राजस्थानी में अनुवाद है, जिसमें भागवत महात्म्य के साथ राधा-कृष्ण का चरित्र वर्णन है। इनकी 'विवाह विलास रचना' में राधा-कृष्ण का वर्णन है। सूरज कँवर की रचनाएँ कृष्ण कीर्तन और कृष्ण निंद्रालीला में राधा-कृष्ण के मिलन प्रसंग, युगल लीलाओं का बखान है। जामसुता जाडेची जी प्रताप बाला की रचना प्रताप कुंअरी पद रत्नावली नामक पुस्तक मिलती है। बाघेली रणछोड़ कुंअरी कृष्ण भक्त हरजस बनाकर गाया करती थी।

बावजी चतुरसिंह जी ने श्रीमद् भगवद् गीता पर गंगाजळी टीका की रचना की। अर्जुन जब महाभारत के युद्ध से विमुख होना चाह रहा था। तब श्रीकृष्ण आत्मा की अमरता की बात कहते हुए समझाते हैं।

''नीं जन्म लेवै न मरे कदी यो
वणै नहीं तो वगड़ै कदी यो
सदा अनाशी अज अेक भांत
मारयाँ मरै यो नहिं देह साथ।''

भक्त कवयित्री मीरांबाई रचित मीरा बृहत्पदावली कृष्ण भक्ति का एक ग्रन्थ है। जिसमें मीरांबाई की कृष्ण के प्रति सगुण और निर्गुण भक्ति काव्य में दृष्टिगत होती है।

''मोर मुकुट पीताम्बर सोहे, गले बैजन्ती माला।
मीरां के प्रभु गिरधर नागर, ठाकुर बंसीवाला।।
यांकी सूरत पर बलिहारी माय।।'' काव्य में मीरां का विरह, भक्ति भाव का रूप नजर आता है।

श्री रामनाथ कविया का जन्म चोरवा का बास सीकर में सं. 1865 वि. में हुआ। इनकी द्रौपदी विनय (करुण बहत्तरी) 72 छंदों की एक व्यंग्य काव्य है। जिसमें द्रौपदी के चीरहरण के प्रसंग पर द्रौपदी द्वारा सभा में मौजूद सभी सभासदों पर व्यंग्य करते हुए श्रीकृष्ण को सहायता करने की प्रार्थना करती है। सोरठा छंद में रचित एक खंड काव्य है।

''चित में दुस्ट कुचाव, औ निलज्ज लायौ अठै।
अब गिरधर झट आव, साय करण नै साँवरा।।''

राजस्थानी भाषा का ''मानखो'' गिरधारी सिंह पड़िहार का खंड काव्य है। काव्य में गन्धर्व चित्रसेन की पान की पीक गालव ऋषि पर गिरती है। श्रीकृष्ण उसे दण्डित करने का निश्चय करते हैं। कृष्ण की बहिन और अर्जुन की पत्नी चित्रसेन की पत्नी का विलाप सुनती है। सुभद्रा श्रीकृष्ण के सामने युद्ध करने के लिए अर्जुन को तैयार कर देती है। श्रीकृष्ण और अर्जुन में भयंकर युद्ध होता है अर्जुन जब पाशुपत शस्त्र उठाता है। नारद और गालव ऋषि आकर मानवता की रक्षा के लिए युद्ध बन्द करने का अनुरोध करते है।

''ह्यारै तो हिंवड़ै में खड़कै,
एक चढै उतरै है।
धरती रो थंभो हालै है,
गिरधर जुलम करै है।।''

नारी के वीर चरित्र के साथ मानवता का संदेश देने वाला यह काव्य ऊँच कोटि का है।

आधुनिक काल के स्त्री कवियों में समान बाई का नाम उल्लेखनीय है। कृष्ण बाळ लीला रचना में भक्ति संबंधी अनूठे पद हैं। वि.सं. 1882 में सीकर जिले के नरसिंहपुरा गाँव में समान बाई का जन्म हुआ।

''यह उपमा है सब कृष्ण योग, औरन कूं लिखनूं है अजोग।
पति परमेश्वर समझैं जु तीय, उनकूं है लिखनू वाजबीय।।''

नारायण सिंह भाटी रचित 'मीरां' काव्य में मीरां के दुःख, दर्द के साथ भक्ति का रूप उजागर किया गया है।

''अरे गायाँ रा ग्वाळ
इण सिंघासण बैठ
थूं ही करण लागौ
कांई गूजरी सूं भेद
कांई मांखण मंगायाँ ही मूंडै बोलसी ?''

सत्यप्रकाश जोशी का सन् 1960 में रचित काव्य ''राधा'' काव्य में राधा के माध्यम से महाभारत के विनाशकारी युद्ध टालने की विनति दिखाई देती है।

''मन रा मीत कान्हा रै—
जग मे जे मडग्यौ घमसाण, तौ
भाई पर भाई करसी वार
आपस में लड़सी, मरसी मानखौ।
चुडला फेडैला काळ्ा ओढ,
अमर सुहागण थारी गोपिया।
कामणिया विकसी बीच बजार,
कुण तौ उघडी बैं ना नैं ढाकसी।
पिरथी पुरखा मू होसी हीण,
टाबर कहासी विना बाप रा।''

अम्बु शर्मा कृष्णायण हिंदी महाकाव्य में राजस्थानी काव्य छंदो और लोक शब्दों का समावेश कर कुल 684 पृष्टों में 95 लीलाओं को सम्मिलित किया है। कृष्ण लीला—गोपिका गीत की रचना की।

''जुगाँ जुगाँ वढ़ जाय घटै घर पाछा आयां
व गोधूळ्यै वेल जिवै मुख कृष्ण दिखायां।।''

लोक साहित्य के अन्तर्गत भक्ति भावना लोक गीतों में हर-जस के रूप में अभिव्यक्त होती है। हर-जस में कृष्ण-लीला पर आधारित गीत प्रचुर मात्रा में

उपलब्ध होते है। जो माखन चोरी, गो-चारण, नाग-दमण, चीर-हरण, रास और मथुरा गमन आदि लीला लोक में लोकानुरंजक और लोक रक्षक के रूप में लोक में व्याप्त है। लौकिक काव्यों में रतन खाती की नरसीजी रो माहेरो में नरसीजी की पुत्री नानीबाई के ससुराल में भात भरने की कथा है। मेवाड़ अंचल के गवरी लोक नृत्य-नाट्य में भी कान्ह-गुजरी नाट्य आज भी प्रस्तुत किया जाता है। लोक-भारत स्यावकरण घोड़ों (श्यामकर्ण घोड़ा) लोक गाथा में महाभारत विजय के बाद अर्जुन जब अभिमानी बन जाता है तो स्यावकरण घोडा सिर्फ श्रीकृष्ण का ही अपनी पीठ पर बैठने देता है। द्रौपदी के कहने पर घोड़ा अर्जुन को बिठाकर वायुमण्डल में से समुन्द्र में जा गिरा। फिर दानव नगरी में अर्जुन को सूली पर चढ़ाने का आदेश दिया गया। अर्जुन श्रीकृष्ण का स्मरण करने लगा। श्रीकृष्ण नीलकण्ठ पक्षी का रूप धर कर अर्जुन को बचाते हैं।

राजस्थानी साहित्य में श्रीकृष्ण से संबंधित साहित्य रचा गया है। जैन शैली, चारण शैली, संत शैली एवं लौकिक शैली के अन्तर्गत श्रीकृष्ण का चरित्र उद्घाटित हुआ है। राजस्थानी साहित्य में प्राचीन काल से लेकर आधुनिक काल में श्रीकृष्ण से संबंधित साहित्य की एक समृद्ध परम्परा रही है।

सन्दर्भ—

1. रुक्मिणी - हरण सायांजी झूला कृत - सं. मुनि जिनविजय, प्र. राजस्थान प्राच्य विद्या प्रतिष्ठान, जोधपुर, पृष्ट -13
2. राजस्थानी भाषा और साहित्य - डॉ. मोतीलाल मेनारिया, प्र. राजस्थानी ग्रन्थागार, जोधपुर, सं. 2014, पृष्ट-92
3. भगत कवि ईसरदास बारहठ प्रणीत हरिरस- सु. बदरीप्रसाद साकरिया, प्र. राजस्थानी ग्रन्थागार, जोधपुर, तृतीय सं. 2010, पृष्ट - 48
4. राजस्थानी भाषा और साहित्य- हीरालाल माहेश्वरी,प्र. आधुनिक पुस्तक भवन, कलकत्ता, सं. 1980, पृष्ट - 165
5. किसन रुकमणी री वेली-सं. नरोत्तमदास स्वामी, प्र. राजस्थानी ग्रन्थागार, जोधपुर, सं. 1998, पृष्ट - 1,48,63
6. राजस्थानी भाषा और साहित्य- हीरालाल माहेश्वरी, प्र. आधुनिक पुस्तक भवन, कलकत्ता, सं.1980, पृष्ट - 168
7. रुक्मिणी -हरण सायांजी झूला कृत - सं. मुनि जिनविजय, प्र. राजस्थान प्राच्य विद्या प्रतिष्ठान, जोधपुर, पृष्ट -37
8. वचनिका-सं. मूलचन्द 'प्राणेश' प्रं. भारतीय विद्या मन्दिर शोध प्रतिष्ठान, बीकानेर, राजस्थान, प्र. संस्करण 1966, पृष्ट - 51

9. राजस्थानी भाषा और साहित्य - हीरालाल माहेश्वरी, प्र. आधुनिक पुस्तक भवन, कलकत्ता, सं.1980, पृष्ट - 193
10. राजस्थानी साहित्य का आदिकाल सं. नारायण सिंह भाटी, राजस्थानी ग्रन्थागार, जोधपुर, द्वि.सं. 2016, पृष्ट 47
11. राजस्थानी वेलि साहित्य - डॉ. नरेन्द्र भानावत, प्र. राजस्थान साहित्य अकादमी संगम,उदयपुर, सं.1965, पृष्ट - 287
12. राजस्थानी भाषा और साहित्य - डॉ. मोतीलाल मेनारिया,,प्र. राजस्थानी ग्रन्थागार,जोधपुर, सं.2014, पृष्ट - 132
13. राजस्थानी भाषा और साहित्य - डॉ. मोतीलाल मेनारिया, प्र. राजस्थानी ग्रन्थागार, जोधपुर, सं. 2014, पृष्ट - 149
14. गवरी बाई - मथुराप्रसाद अग्रवाल, ज्योतिपुंज, प्र. साहित्य अकादेमी, नवी दिल्ली, सं. 1996, पृष्ट - 63
15. राजस्थानी भाषा और साहित्य - डॉ. मोतीलाल मेनारिया, प्र. राजस्थानी ग्रन्थागार, जोधपुर, सं. 2014, पृष्ट - 170
16. बावजी चतुरसिंहजी - कन्हैयालाल राजपुरोहित, प्र. साहित्य अकादेमी, दिल्ली, सं. 1996, पृष्ट - 77
17. भक्त कवयित्री मीरांबाई रचित - मीरां बृहत्पदावली- सं. हरिनारायण पुरोहित, प्र. राजस्थान प्राच्य विद्या प्रतिष्ठान, जोधपुर, सं. 1989, पृष्ट- 19
18. द्रौपदी विनय अथवा करुण बहत्तरी श्री रामनाथ कविया -सं. डॉ. कन्हैयालाल सहल, प्र. राजस्थानी ग्रन्थागार, जोधपुर, सं. 1999, पृष्ट -36
19. मानखो- गिरधारीसिंह पड़िहार प्र.जगजीवन सर्वोदय आश्रम ट्रस्ट श्री कोलायतजी, बीकानेर, सं. 1964, पृष्ट -49
20. भक्तिमति समान बाई जीवन और काव्य - सं. डॉ. मंजुला बारैठ प्र. कमला प्रकाशन, बीकानेर सं. 2015, पृष्ट-95
21. मीरां - नारायणसिंह भाटी, प्र. गिरधर प्रकासण, जोधपुर, सं. 1980, पृष्ट- 65
22. राधा- सत्यप्रकाश जोशी, प्र. राजस्थानी ग्रन्थागार,जोधपुर, सं. 1988, पृष्ट- 49
23. राजस्थानी साहित्य रा आगीवाण- महाकवि अम्बु शर्मा, विनिबंध स. ओंकार श्री, प्र. राजस्थानी भाषा, साहित्य एवं संस्कृति अकादमी, बीकानेर, सं. 2014, पृष्ट-36

सहायक आचार्य एवं प्रभारी अध्यक्ष
राजस्थानी विभाग,
मोहनलाल सुखाड़िया विश्वविद्यालय, उदयपुर
मो.न. : 9214569756
ई मेल : dr.sureshsalvi@gmail.com



हिन्दी के समकालीन कवि
सर्जना के आयाम

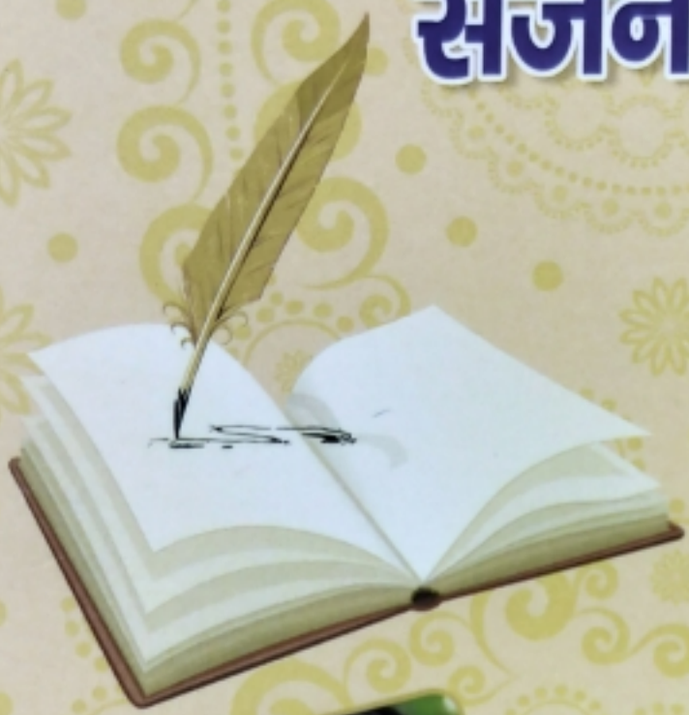











संपादक

डॉ. नीतू परिहार

Shot on OnePlus
2024.02.20 13:00

हिंदी के समकालीन कवि : सर्जना के आयाम
ISBN : *978-81-86064-88-7*
© : लेखक
मूल्य : पाँच सौ रुपये
संस्करण : 2022
प्रकाशक : अंकुर प्रकाशन
1/1 कांजी का हाटा, गायत्री मार्ग
उदयपुर (राज.) 313001
फोन नं. : (0294) 2417094, 2417039
(मो.) 9413528299
ईमेल : ankurprakashan15@gmail.com
आवरण : एन.वी.आर्ट, उदयपुर
टाईपसेटिंग : देवेन्द्र कम्प्यूटर, दिल्ली
मुद्रक : आर्यन डिजिटल प्रेस,दिल्ली

Hindi Ke Samkaleen Kavi : Sarjana Ke Ayam *(Hindi Literature)*
Edited By : Dr. Neetu Parihar
₹ 500

Shot on OnePlus
2024.02.20 13:00

अनुक्रम

1	विश्वास के दीये-सी टिमटिमाती : वर्तिका नन्दा—*डॉ. नीतू परिहार*	13
2	अनुज लुगुन की कविताओं में आदिवासी जीवन—*डॉ० नवीन नन्दवाना*	22
3	आखर अनन्त और जीवन में आस्था के कवि : विश्वनाथ प्रसाद तिवारी—*डॉ० प्रीति भट्ट*	33
4	धूमिल : स्वातन्त्र्योत्तर कविता के उज्ज्वल 'मोची राम'—*डॉ० महेश चन्द्र तिवारी*	42
5	पवन करण की कविताओं में प्रतिबिम्बित नारी—*डॉ० नीता त्रिवेदी*	50
6	ममता कालिया की कविताओं में स्त्री-संघर्ष की गूँज—*डॉ० उषा शर्मा*	64
7	मंगलेश डबराल की कविताओं का सामाजिक स्वर—*डॉ० ममता पानेरी*	71
8	विजयदेव नारायण साही : सरल धरती का अभिलाषी कवि—*डॉ० कैलाश गहलोत*	77
9	अनामिका के काव्य में स्त्रियों की सामाजिक स्थिति—*एकता देवी*	86
10	समकालीन बोध और धूमिल की कविता—*विद्याप्रभाकर डॉ० कनुप्रिया प्रचंडिया*	94
11	अनामिका : काव्यगत पृष्ठभूमि—*डॉ० वसुन्धरा उपाध्याय*	102

Shot on OnePlus
2024.02.20 13:00

1

विश्वास के दीये-सी टिमटिमाती : वर्तिका नन्दा

—डॉ० नीतू परिहार

आधुनिक हिंदी कविता में वर्तिका नन्दा का नाम अपरिचित नहीं है। पंजाब में जन्मी वर्तिका ने अपराध पत्रकारिता जैसे चुनौतीपूर्ण क्षेत्र को चुना। इस क्षेत्र में कई नये प्रयोग भी किए। पत्रकारिता के क्षेत्र में नये-नये प्रयोगों के माध्यम से अपराधों के प्रति जागरुकता लाने का प्रयास किया। जेल में बन्द सजायफ्ता और अपराधियों को लेकर मीडिया का उपयोग सकारात्मकता से किया। मीडिया और साहित्य के जरिये महिला अपराधों के प्रति जागरुकता लाने के लिए वर्तिका को कई पुरुस्कार/सम्मान प्राप्त हुए।

वर्तिका कई विषयों पर लिखती हैं। उनके काव्य जो चर्चित रहे वे हैं 'मधुर दस्तक', 'थी, हूँ ... रहूँगी', 'रानियाँ सब जानती हैं', यह आलेख 'थी, हूँ...रहूँगी' संग्रह में संकलित कविताओं पर केन्द्रित है। इस संग्रह में वर्तिका ने अपराध पर काम करते-करते जो देखा, सुना, महसूस किया उन्हें शब्दों में उतारा है। उनकी कविताएँ, उनके अनुभव से उपजी हैं। वे अपने अनुभव को शब्द देती हैं। उनकी कविता 'बस यों ही' में वे अपने इसी अनुभव को बताती हैं। ईश्वर को हम सब मानते हैं। जब भी उसे याद करते हैं। फरमाइश कर देते हैं। कोई कभी कष्ट हो झट से ईश्वर से उसे हर लेने को कहते हैं कोई भी कमी हो हमें प्रभु याद आ जाते हैं। वर्तिका ने इन्हीं बातों पर गौर किया और उसे कविता में बस यों ही कह दिया। वे कहती हैं हम भगवान को अपनी फरमाइशों की लिस्ट बना कर ऐसे दे देते हैं जैसे परचून के समान की लिस्ट हो। मोल-भाव भी सब्जी मंडी की तरह ही करते हैं—

मोल भाव भी किया वैसे ही
कि पहली नहीं है

Shot on OnePlus
2024.02.20 13:01

देहरी से पार

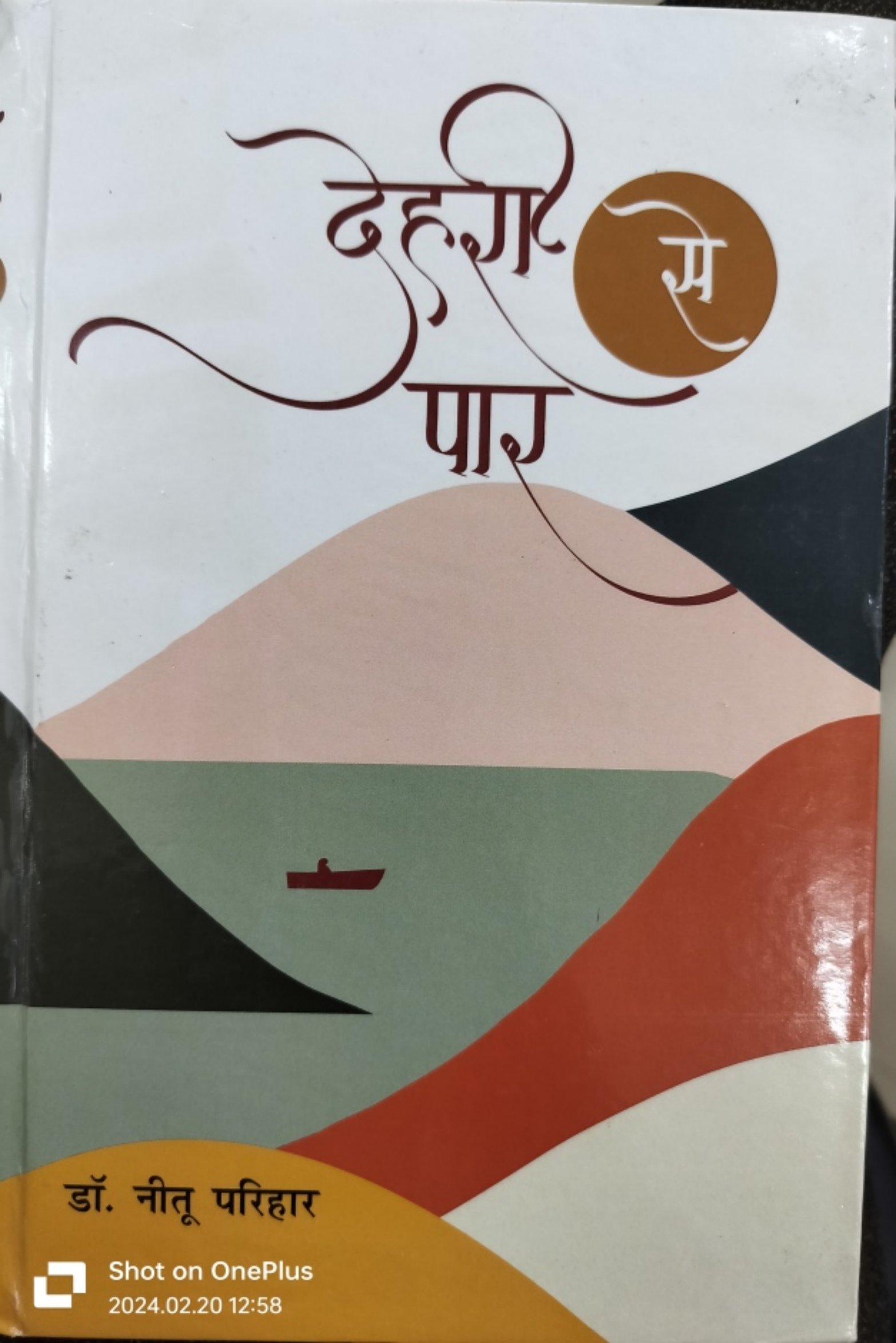

डॉ. नीतू परिहार

Shot on OnePlus
2024.02.20 12:58

ISBN : 978-93-94649-23-1

✦

प्रथम संस्करण 2022

✦

© सुरक्षित

✦

मूल्य: ₹ 200.00 (दो सौ रुपये मात्र)

✦

प्रकाशक :

राजस्थानी ग्रन्थागार

प्रकाशक एवं वितरक

प्रथम मंजिल, गणेश मंदिर के सामने

सोजती गेट, जोधपुर-342001

Ph: 0291-2623933, 2657531 (O)

E-mail : info@rgbooks.net

Website : www.rgbooks.net

✦

राजस्थानी ग्रन्थागार के लिए कम्पोजिंग एम.एस. कम्प्यूटर, मुद्रक- भारत प्रिण्टर्स, जोधपुर

✦

Dehri Se Paar (Hindi Kavita Ke Vividh Swar)

By **Neetu Parihar**

Rajasthani Granthagar, Sojati Gate, Jodhpur (Raj.) INDIA

First Edition : 2022 Price ₹ 200.00

Shot on OnePlus 2024.02.20 12:58

अनुक्रमणिका

1. स्त्री-विमर्श का दृढ आधार : अनामिका की कविताएँ 7
2. देहरी से देह तक पहुँचती : शैलजा पाठक की कविताएँ 16
3. स्त्री के स्वप्न, संसार और यातना : रंजना जायसवाल की कविताएँ 23
4. विश्वास के दीये से टिमटिमाती : वर्तिका नन्दा 32
5. समझदारों की दुनिया और 'माँएँ । 40
6. समकालीन कविता को नया स्वर देती अरुण कमल की कविताएँ 47
7. आधुनिक चुनौतियाँ और कैलाश वाजपेयी की कविता 54
8. अथाह प्रेम की थाह ढूँढते : कवि नागार्जुन 60
9. धरती से जुड़े कवि : भगवती लाल व्यास 66
10. पारम्परिक साँचे को तोड़ती पवन करण की कविता 72
11. स्त्री जीवन के विविध रंग समकालीन कविता के कैनवास में 77
12. नई सदी की कविता में सार्वभौमिकता 85
13. आधुनिक कविता और राष्ट्रीयता 92
14. इक्कीसवी सदी : आदिवासी चिंतन और हिन्दी कविता 97
15. आधुनिक कविता और रामायण के विविध संदर्भ 104

Shot on OnePlus
2024.02.20 12:58



कृष्ण साहित्य का व्यापक परिदृश्य

संपादक : डॉ. नीतू परिहार

प्रतिलिप्याधिकार प्रकाशक व लेखक के अधीन सुरक्षित है। इनकी पूर्व लिखित अनुमति के बिना इस पुस्तक के किसी भी भाग का पुनः प्रकाशन वर्जित है। इस पुस्तक में व्यक्त विचार लेखकों के व्यक्तिगत हैं। इनसे किसी भी प्रकार की होने वाली हानि के लिए संपादक और प्रकाशक उत्तरदायी नहीं हैं। किसी भी विवादास्पद स्थिति में न्यायालय क्षेत्र उदयपुर मान्य होगा।

कृष्ण साहित्य का व्यापक परिदृश्य

ISBN **:** ***978-81-963416-3-3***

© **:** **संपादक**

मूल्य **:** **सात सौ रुपये**

संस्करण **:** **2023**

प्रकाशक **:** **अंकुर प्रकाशन**

1/1 कांजी का हाटा, गायत्री मार्ग

उदयपुर (राज.) 313001

फोन नं. : (0294) 2417094, 2417039

(मो.) 9413528299

ईमेल : ankurprakashan15@gmail.com

आवरण **:** डॉ. शंकर शर्मा, उदयपुर

टाईपसेटिंग **:** देवेन्द्र कम्प्यूटर, दिल्ली

मुद्रक **:** आर्यन डिजिटल प्रेस, दिल्ली

Krishna Sahitya ka Vyapak Paridrishya *(Hindi Literaturre)*

Edited By : Neetu Parihar **₹ 700**

लघुकथाओं का वृहद संसार

(समीक्षात्मक आलेख)

संपादक
डॉ. नीता त्रिवेदी

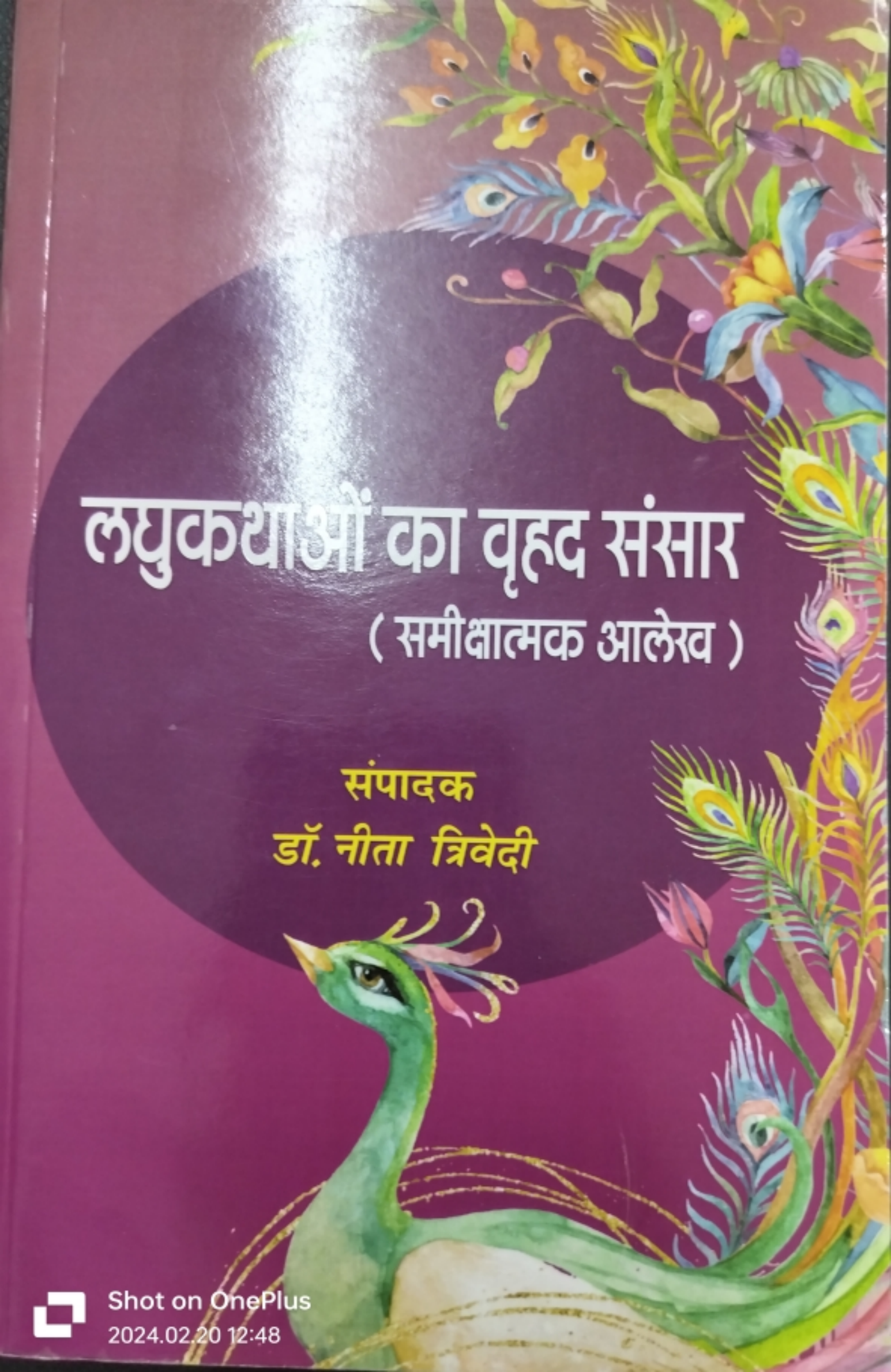

Shot on OnePlus
2024.02.20 12:48

ISBN : 978-81-930537-3-7
© डॉ. नीता त्रिवेदी
प्रथम संस्करण : 2022
लघुकथाओं का वृहद् संसार

प्रकाशक :
रैना बुक सेन्टर
उदयपुर (राज.)

आवरण :
एन. वी. आर्ट, उदयपुर

टाइप सेटिंग :
देवेन्द्र कम्प्यूटर, दिल्ली

मूल्य : ₹500

Shot on OnePlus
2024.02.20 12:48

अनुक्रम

1. खड़ी बोली का कथा—गद्य और लघुकथा का पुनर्प्रस्फुटन
—डॉ. बलराम अग्रवाल 11
2. मुट्ठी भर आसमान के लिए : लघुकथा में स्त्री विमर्श—
भगीरथ परिहार 22
3. लघुकथा : संश्लिष्ट सृजन-प्रक्रिया—*डॉ. कमल चोपड़ा* 28
4. आधुनिक हिंदी लघुकथा की अवधारणा, विकास एवं परिभाषा
—डॉ. रामकुमार घोटड़ 44
5. लघुकथाओं में प्रतिबिम्बित मानवीय संवेदनाएँ—*डॉ. नीतू परिहार* 60
6. संवेदनाओं की सुगन्ध से महकती लघुकथाएँ—*डॉ. नवीन नन्दवाना* 69
7. लघुकथा की भूमिका और माधव नागदा की संवेदना
—डॉ.आशीष सिसोदिया 79
8. लघुकथा साहित्य : कुछ विचार-बिन्दु—*डॉ. कुलवन्त सिंह* 88
9. व्यवस्था की विसंगतियों की धारदार अभिव्यंजना :
असगर वजाहत की लघुकथाएँ—*डॉ. प्रीति भट्ट* 96
10. सामाजिक सरोकारों का आईना : बोनसाई—*डॉ. नीता त्रिवेदी* 104
11. घाव करे गम्भीर : सामाजिक विसंगतियों को अभिव्यक्त
करती लघुकथाएँ—*डॉ. ममता पानेरी* 114
12. पद्मजा शर्मा की लघुकथाओं में मानवीय संवेदना—*डॉ. उषा शर्मा* 121
13. संवेदना और सामाजिक समरसता से जुड़ी लघुकथाएँ :
फूलों वाली दूब—*डॉ. शगुफ्ता सैफी* 128
14. लघुकथाकार गोपी भैया कहिन (उवाच)—*शेख शहजाद उस्मानी* 136
15. लघुकथा : हास्य एवं व्यंग्य—*रोहित बंसल* 145
16. हिंदी के लघुकथाकार एवं उनकी विशाल कथादृष्टि—*बबीता गुप्ता* 151
17. हिंदी लघुकथा : लघु कलेवर में व्याप्त गुरुत्तर वैश्विक मूल्य —
डॉ. ज्योत्सना स्वर्णकार 155
18. हिंदी लघुकथा : परिचय, स्वरूप और परिदृश्य—
तरुण पालीवाल, शोधार्थी 162

Shot on OnePlus
2024.02.20 12:48

5

लघुकथाओं में प्रतिबिम्बित मानवीय संवेदनाएँ

—डॉ. नीतू परिहार
सह आचार्य एवं विभागाध्यक्ष
हिन्दी विभाग
मोहनलाल सुखाड़िया विश्वविद्यालय
उदयपुर (राज०)

लघुकथा साहित्य की वह गद्य-विधा है जिसमें बहुआयामी मानव-जीवन के किसी एक पक्ष का सहज, स्वभाविक एवं प्रभावी रूप व्यक्त होता है। आकार की लघुता, लघुकथा की अनिवार्य शर्त है। लघुकथा का फलक छोटा होता है, किन्तु छोटा आकार कथा की संवेदना को सीमित नहीं करता। लघुकथा के लिए भूमिका का स्थान नहीं होता लेखक सीधे विषय पर आता है। लघुकथा में यह विशेषता रहती है कि वह कम शब्दों में अधिक बात कहती है। बिहारी के दोहों के समान 'देखन में छोटे लागे, घाव करे गम्भीर'। वरिष्ठ साहित्यकार कमल किशोर गोयनका ने लघुकथा को परिभाषित करते हुए कहा है—"लघु का अर्थ यह है कि वह कहानी की तुलना में निश्चित ही ऐसी विधा है जिसका आकार लघु है और लघु आकार के लिए उसकी कथा का लघु होना अनिवार्य है क्योंकि कथा की लघुता ही प्रमुख रूप से 'लघुकथा' की एक विशिष्ट कथागत विधा का स्वरूप प्रदान करती है।"[1]

लघुकथा अपनी बात को बहुत छोटे से में कहने का सशक्त माध्यम है। आज के व्यस्तमय जीवन में लघुकथा के पाठकों की संख्या निरन्तर बढ़ती जा रही है, कारण कम समय में लघुकथा का पढ़ा जा पाना। आज के समय में लघुकथा

Shot on OnePlus
Udaipur | 2024.02.20 12:48

मध्यकालीन संत कवि



सम्पादक

डॉ. नवीन नन्दवाना

Shot on OnePlus
2024.02.20 13:01

लोकभारती प्रकाशन
पहली मंजिल, दरबारी बिल्डिंग, महात्मा गांधी मार्ग
प्रयागराज-211 001

वेबसाइट : www.lokbhartiprakashan.com
ईमेल : info@lokbhartiprakashan.com

शाखाएँ : 1-बी, नेताजी सुभाष मार्ग, दरियागंज
नई दिल्ली-110 002
अशोक राजपथ, साइंस कॉलेज के सामने
पटना-800 006

पहला संस्करण : 2023 | **मूल्य :** ₹795

© लेखक/सम्पादक

बी.के. ऑफसेट
नवीन शाहदरा, दिल्ली-110 032
द्वारा मुद्रित

MADHYAKALEEN SANT KAVI
Edited by Dr. Naveen Nandwana

ISBN : 978-81-19133-17-8

Shot on OnePlus
2024.02.20 13:01

संत-साहित्य परम्परा में गुरु नानक वाणी : विविध पक्ष 122
प्रो. गुरमीत सिंह एवं डॉ. नरेन्द्र कुमार

संत पीपा का जीवन दर्शन 134
डॉ. नीता त्रिवेदी

महामति प्राणनाथ और उनकी साहित्य-साधना 144
प्रो. आनन्द प्रकाश त्रिपाठी

संत चरणदास की भक्ति चेतना 168
डॉ. नीतू परिहार

संत कवि लालदास : भक्ति और सरोकार 180
प्रो. देवेन्द्र कुमार गुप्ता

रामसनेही सम्प्रदाय एवं संतकवि दयालदास 187
डॉ. बंशीलाल

विराट व्यक्तित्व के धनी श्रीमन्त शंकरदेव 198
प्रो. दिनेश कुमार चौबे

संतकाव्य और महिला संतकाव्य-परम्परा 210
प्रदीप कुमार ठाकुर

संत कवयित्री दया बाई और सहजो बाई की भक्ति चेतना 220
डॉ. आशीष सिसोदिया

राजस्थान के मध्यकालीन संत और उनका काव्य 234
डॉ. कामिनी ओझा

लेखक परिचय *243*

Shot on OnePlus
2024.02.20 13:02

संत चरणदास की भक्ति चेतना

डॉ. नीतू परिहार

ईश्वर से प्रेम करना या ईश्वर में अपने को रत करना या डुबाना ही भक्ति है। दूसरे शब्दों में यह भी कह सकते हैं नित्यानुसार सांसारिक व्यवहार करते हुए, परमात्मा में लीन रहना भक्ति है। भक्ति की भावना निश्छल और शुद्ध हृदय में ही जाग्रत होती है, जहाँ स्वार्थ और अभिमान जैसे विकारों का स्थान नहीं। यह भी सच है कि भगवान की कृपा के बिना हम उसकी ओर आकृष्ट नहीं हो सकते। जब तक हमारे भीतर अच्छे संस्कारों का उदय नहीं होता, तब तक ईश्वर की अनुकम्पा भी नहीं होती।

हिन्दी साहित्य में भक्तिकाल को स्वर्ण युग कहा गया है। इस युग में भक्ति के अनेक रूप देखने को मिले हैं। भक्ति की अनेक धाराएँ बहती हुई दिखाई दीं। मार्ग चाहे कोई भी रहा हो, सबकी मंजिल एक ही थी—वो थी, उस परमात्मा की प्राप्ति। भक्तिकाल में ही निर्गुण भक्ति में ज्ञानाश्रयी शाखा को संत काव्य के नाम से जाना जाता है। संत साहित्य ने हिन्दी साहित्य को बहुत समृद्ध किया है। अनेक संतों की वाणियों ने भक्ति की जो धारा बहाई उसमें जनसमूह आकंठ डूबता-तिरता रहा। कबीर, नानक, रैदास, दादू, सुन्दरदास, मलूकदास आदि अनेक ऐसे संत हैं, जिन्होंने अपनी बाणियों से भक्ति का प्रचार-प्रसार किया तथा समाज को मिथ्या आडम्बरों, रूढ़ियों से मुक्त कराने का प्रयास किया। संत बहुसंख्यक जनता के वास्तविक प्रतिनिधि थे। उन्होंने जनता को जात-पाँत, अन्धविश्वासों से ऊपर उठाकर ईश्वर-भक्ति की ओर उन्मुख किया। समाज के विविध वर्गों के बीच की खाई को भी संतों ने पाटने का काम किया। संतों के विषय में डॉ. रांगेय राघव कहते हैं—"जब संसार में कार्ल मार्क्स नहीं था, जब संसार में द्वंद्वात्मक भौतिकवाद का चिन्तन नहीं था, तब भी मनुष्य अन्याय के प्रति लड़ता था और यह संघर्ष मध्यकाल के संतों में हमें दिखाई देता है। वे सब निम्न जातियों की मुक्ति के लिए हुए स्वर थे।"

मध्यकाल में भ्रमित जनता को संतों ने अपनी बाणियों से सहज भक्ति से ईश्वर की ओर ले जाने का प्रयास किया। घोर निराशा के समय में संतों ने समाज में फैली कुरीतियों पर गहरी चोट की, जाति-पाँति के भेदों से परे जाकर हर वर्ग को

Shot on OnePlus
2024.02.20 13:02

डॉ. 'निशंक' का साहित्य सृजन मनन एवं मूल्यांकन

(डॉ. निशंक का रचना संसार ऑनलाइन शृंखला एम्पावेज 2)

संपादक

डॉ. योगेन्द्र नाथ शर्मा 'अरुण'

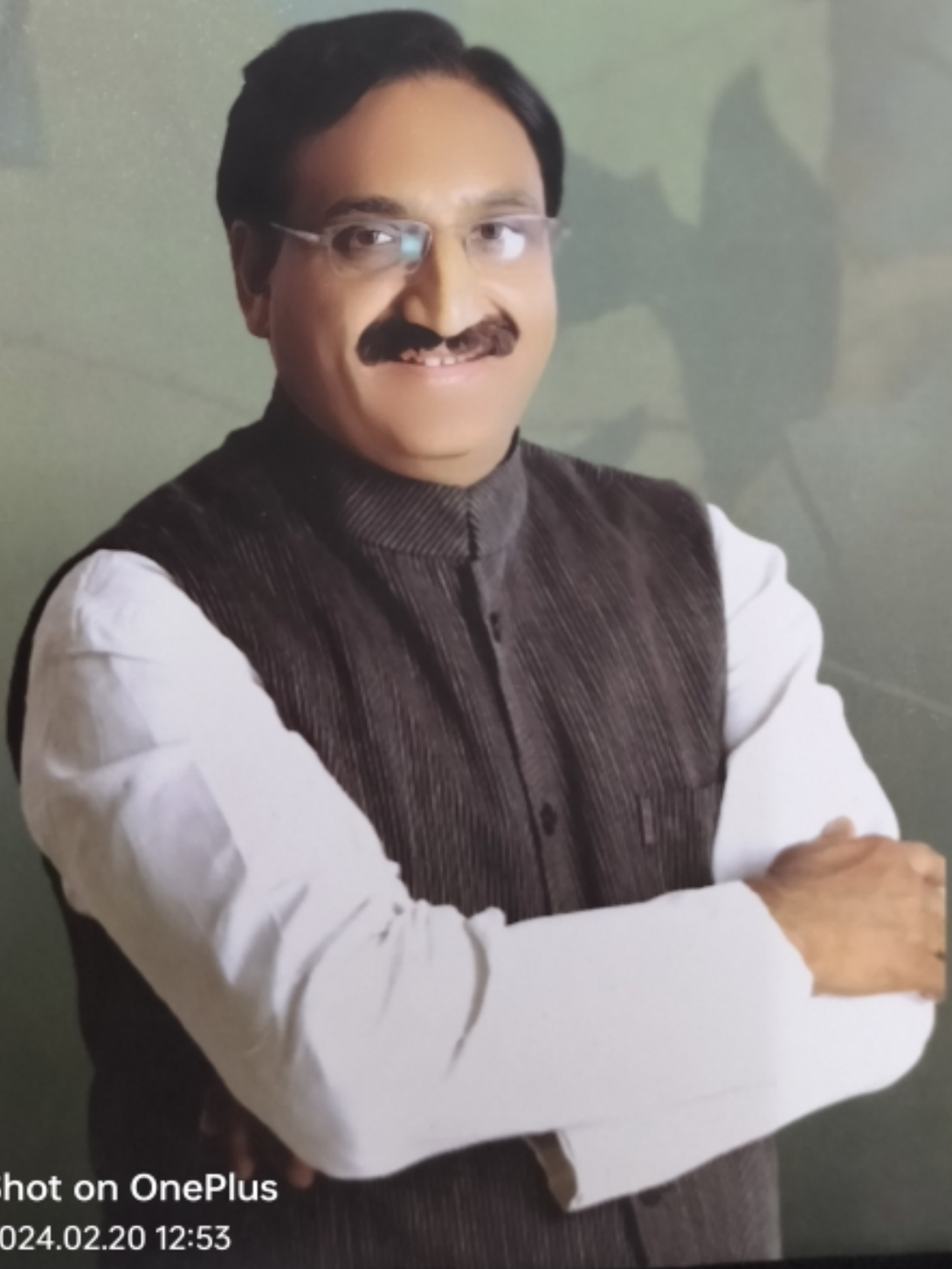

Shot on OnePlus
2024.02.20 12:53

ISBN : 978-93-80845-24-1

मुख्य वितरक
स्याही ब्लू बुक्स, दिल्ली
syahiblue.books@gmail.com

शाखा
अनंग प्रकाशन / ठा. गजराज सिंह, भगतपुर,
पोस्ट - भगतपुर, जिला- अलीगढ़ 203132 (उ.प्र.) भारत

अनंग प्रकाशन

फोन नं. 09350563707, 9540176542

सर्वाधिकार : संपादक

प्रथम संस्करण : 2022
मूल्य : 995 रुपये

ई-मेल : anangprakashan@gmail.com
anangbooks@gmail.com

अनंग प्रकाशन, बी-107/1, गली मन्दिर वाली, समीप रबड़ फैक्ट्री, उत्तरी घोण्डा, दिल्ली-110053, शब्द-संयोजन : सिद्ध-भभूति ग्राफिक्स, दिल्ली- 110053, मुद्रक : राजोरिया प्रिन्टर्स, दिल्ली-32 से मुद्रित।

Shot on OnePlus
2024.02.20 12:54

Shot on OnePlus
2024.02.20 12:54

अनुभूति की समता और निशंक का कवितालोक 96
– डॉ. सुनीता देवी

डॉ. निशंक काव्योद्यान का प्रथम पुष्प : समर्पण 104
– प्रो. सुशील कुमार शर्मा

डॉ. निशंक का रचना संसार परीक्षा लेती जिंदगी (काव्य संग्रह) 110
– डॉ. नीतू शर्मा

डॉ. निशंक का काव्य संग्रह मृगतृष्णा : दर्पण अंतर्मन का 119
– डॉ. आशा कुमारी

डॉ. निशंक की कविता में राष्ट्र-प्रेम की अभिव्यक्ति 128
– सिमरन

डॉ. निशंक की कविताओं में राष्ट्रीय भावना 138
– डॉ. अमर कान्त कुमार

रमेश पोखरियाल 'निशंक' की कविताओं का विश्लेष्णात्मक अध्ययन 156
– रमन कुमार

कथा-साहित्य खण्ड

'जीने का नाम जिंदगी' एक साहित्यिक अवलोकन
– डॉ. कुसुम कुंज मालाकार 167

जनसामान्य का संघर्ष और निशंक की कहानियां
– डॉ. स्नेह लता नेगी 178

'अंतहीन' नारी चिंतन के बहुआयामी पक्ष
– डॉ. नीरज भारद्वाज 183

डॉ. रमेश पोखरियाल निशंक के उपन्यासों में 'पहाड़ी जीवन'
– सुषमा चौहान 194

देश प्रेम और आँचलिकता का दस्तावेज : डॉ. निशंक का मेजर निराला
– डॉ. नीतू परिहार 198

देश प्रेम और आँचलिकता का दस्तावेज : डॉ. निशंक का मेजर निराला

डॉ. नीतू परिहार

डॉ. रमेश पोखरियाल 'निशंक' जाने-माने साहित्यकार हैं। उनका लेखन के प्रति लगाव, निष्ठा उन्हें सतत क्रियाशील बनाये रखता है। 'मेजर निराला' निशंक जी का चर्चित और प्रसिद्ध उपन्यास है। यह आलेख इसी उपन्यास पर केन्द्रित है।

उपन्यास के कथानक का प्रारम्भ फ्लैश बैक स्टोरी अर्थात् पूर्व दीप्ति से होता है। मेजर निराला पन्द्रह वर्ष जेल में सजा काट चुकने के बाद, जेल से रिहा होने वाला है। रिहा होने से पूर्व ही वह अपने बीते हुए समय पर विचार कर रहा है।

मेजर निराला जांबाज, बहादुर और देशभक्त मेजर था फौज का। वह अपने सीनियर अफसरों की आँखों का तारा था। भारत-पाक युद्ध में उसने अपनी वीरता से सबको बहुत प्रभावित किया। यही कारण था कि निराला के अफसरों ने युद्ध के लम्बा चलने की आशंका के चलते उसे जबरन छुट्टी पर भेज दिया ताकि युद्ध के अंतिम समय में उसका उपयोग कर सके।

मेजर निराला जितना अपने देश से प्रेम करता है उतना ही प्रेम वह अपने गाँव और परिवार से भी करता है। छुट्टियों में जब गाँव आता तो पूरे मन से वहीं रहता। मेजर को उसके साथी जब छुट्टियों में घूमने-फिरने को कहते हैं और अपने यहाँ बुलाते हैं तो वह कहता है, मेरी छुट्टियाँ तो गाँव के

Shot on OnePlus
2024.02.20 12:54

Green Sustainable Process for Chemical and Environmental Engineering and Science

Biomedical Applications of Green Composites

2023, Pages 21-34



Chapter 2 - Applications of bioresins and biopolymers derived from natural resources as composites in drug delivery

Garima Joshi [a], Khushwant S. Yadav [b]

Show more

+ Add to Mendeley Share Cite

https://doi.org/10.1016/B978-0-323-95169-2.00007-9

Get rights and content

Abstract

Recent years have witnessed awareness of environmental issues which has led to the development of green materials for drug delivery which are environment friendly. The pharmaceutical industry has paid close attention to bioresins and biopolymers as a means of developing new drugs and drug delivery systems. The biomedical scientists are looking forward to use bioresin and biopolymer composites in drug delivery as they are non-toxic, biodegradable, and affordable. They have broad range of release characteristics and do not have serious side effects on human body which are associated with synthetic polymers. Plant derived bioresins and plant and animal derived biopolymers have applications in drug delivery as beads, microparticles, implants, nanoparticles. They are employed as biomatrix in composites to control the drug release, to modify the release, gelling agents and viscosity enhancers etc. Food grade bioresins and biopolymers are employed in formulation of nutraceuticals. Further nanocomposites of bioresins and biopolymers are employed for treatment of various diseases like cancer, cardiovascular diseases, diabetes and other chronic metabolic diseases.

CHAPTER 16

Bioresorbable polymers for wound healing

Sheikh Shahnawaz Quadir[1], Dinesh Puri[2], Garima Joshi[1], Deepak Choudhary[1], Sanket Kumar[1], Monika Singh[3], Shalini K. Sawhney[3]

[1]Department of Pharmaceutical Sciences, Mohanlal Sukhadia University, Udaipur, Rajasthan, India
[2]School of Pharmacy, Graphic Era Hill University, Dehradun, Uttarakhand, India
[3]I.T.S. College of Pharmacy, Ghaziabad, Uttarpradesh, India

UNCORRECTED PROOF

16.1 Introduction

Over the last decade, polymers have played a vital role in medicine. Among these, bioresorbable polymers have gained increased attention due to their unique potential in medicinal formulations and represent a diverse family in the field of biomaterials. The term biomaterial was coined in 1982 at NIH Consensus Development Conference, describing clinical uses of biomaterials. It is defined as "any substances or a combination of the substances other than drug which is either natural or synthetic in nature can be used in any period of time for the treatment, replacement or augmentation of any tissue, organ or a function of the body." Other definitions include that in the William Dictionary of Biomaterials (1999), which states that "nonviable materials which is utilized in the medical devices, intended to interact with the biological system", and also "A material which is synthetic, natural or modified natural material (other than drug) intended to interact with the biological system or a part of system that are able to treat, replace or augment a tissue, organ or a function of the body" as described in Dorland's Medical Dictionary (Pertici, 2017).

Bioresorbable compounds are those compounds which alter their chemical and physical structure when they came into contact with a biological system. If a compound is bioresorbable in nature, by applying correct conditions in the presence of fungi, bacteria, or microorganisms, it will automatically break down to its basic structure. The key benefits of such compounds include that they degrade without leaving any toxins behind. The word bioresorbable means biodegradable or naturally ab-

Bioresorbable Polymers and their Composites
© 2024.
ISBN 978-0-443-18915-9, DOI: 10.1016/B978-0-443-18915-9.00008-2

sorbing, which is used to define the process of breaking down by nature. However, bioresorption highlights the process which leads to the slowly disintegration of a compound into fractions inside the human body. When this compound comes into contact with body fluids, it alters its physicochemical properties resulting in physical, chemical, biological, and mechanical characteristics among the compounds and neighboring environment. These compounds are easily metabolized without showing any toxic effects and then cleared from the body (Agubata et al., 2021).

The major utilized bioresorbable compounds in medicine are ceramics, and polymeric and metallic materials. Bioresorbable polymers have been described as "today's material." In the current era, bioresorbable polymers have attracted the attention of researchers and scientists due to their potential in the tissue engineering and biomaterials fields. Meanwhile, in medicine, bioresorbable polymers possess significant applications in wound healing (i.e., sutures, adhesives, staples, etc.) and controlled drug delivery. They are also used in ligaments for orthopedic devices, along with nonwoven materials and scaffolds in tissue engineering. These bioresorbable polymers also offer great applications in a number of domains such as dental, drug delivery, biological devices, biosensors, nanoparticles, and nanocarriers, as well as for in vitro diagnostic tools, etc. (Daniel, 2021).

Wounds can be defined as any lesion which occurs to the skin or other body tissues either by cuts, scratches, scrapes, or other accidental damage. Hence, for the treatment of such wounds, wound healing is needed. To regenerate and repair dermal and epidermal tissues, dressings are widely used in the wound-healing process. Wound dressing materials are materials which act as a barrier to foreign particles, oxygen, and moisture to combat and protect against microorganisms (Mogoşanu and Grumezescu, 2014). A passive dressing is important for maintaining optimum moisture, which helps in stimulating the wound-healing process. An ideal passive dressing material is one which influences the local cellular response for the treatment of wounds and burns such as cellulose, collagen, alginates, hydrogels, foams, cotton, hydrocolloids, etc. (Cornelius et al., 2006). These materials offer various key benefits in wound healing, e.g., maintenance of suitable moisture levels in wounds, minimizing the pain and itching, cleansing of damaged tissues, and eliminating dead spaces and nonviable tissues (Sawant et al., 2012). Some of these materials which are naturally available can progressively improve

UNCORRECTED PROOF

wound healing due to their emollient, antimicrobial, antiinflammatory, antioxidant and epithelializing properties.

Skin tissues have their own key potential, including structural organization and self-repairing ability. However, once they become injured by sufficiently large lesions, healing and recovery become suboptimal. In such cases, bioresorbable polymers play a vital role by restoring the native tissues or replacing them with engineered alternatives. This chapter emphasizes the factors which influence the healing process and the important applications of bioresorbable polymers in wound healing. It provides a framework for understanding the strategies of such polymers that could be key in the development of future therapeutic applications.

16.2 Wound-healing process

A wound is a skin lesion which occurs due to physical, chemical, thermal, or other tissue or systemic pathology. A wound is categorized on the basis of its severity, such as partial, superficial, or full thickness. The partial-thickness wound may have damage to the superficial layer, i.e. the epidermis (up to the dermal layer), and healing can take a few weeks. Superficial wounds only affect the epidermis, but healing can be successful through unaffected keratinocytes. The most difficult to treat and severe wounds are full-thickness wounds which can take several weeks to heal and still be suboptimal. These wounds include major damage to both the tissues of the epidermis and dermis (Mogoşanu and Grumezescu, 2014). The above-listed wounds occurs in three stages, i.e., inflammation, proliferation, and remodeling (Danti et al., 2017).

Inflammation: In the inflammatory process, platelets play a vital role by forming a fibrin clot soon after the injury which permits the infiltrating cells to gather in the lesion area to prevent bleeding. Additionally, these platelets attract growth factors by initiating a cascade of events such as monocytes, neutrophils, and fibroblasts. They also induce fibroblasts to secrete fresh extracellular matrix.

Proliferation: The second process of wound healing is categorized as reepithelialization and connective tissue regeneration. Reepithelialization is a process started by proliferating keratinocytes which travel toward the lesion site. These new blood vessels develop side by side and fibroblasts gather from nearby areas to deposit extracellular matrix molecules (collagen fibers, elastin, glycosaminoglycan) and granulocytic tissues.

UNCORRECTED PROOF

Remodeling: The final step in wound healing may take many year until the restoration of the entire dermis through constant tissue remodeling. This step proceeds by replacing collagen type III with collagen type I through the secretion of matrix metalloproteinase. There are also some wounds which occur due to pathological and disease conditions, such as diabetes, which are unable to heal completely. Hence, such wounds become chronic by sustaining inflammatory events which become difficult for the growth factors to perform a healing function, resulting in the development of pathological constraints such as tumors and persistent infections.

16.3 Factors affecting wound healing

There are various factors that may impede the wound-healing process. In simple terms, those factors which affect the repair mechanism are divided into local and systemic. The local factors are those which directly damage or influence the process of wound healing by altering its characteristics, and systemic factors are those which affect the healing abilities of an individual in healthy or diseased condition (Fig. 16.1). In the majority of cases systemic factors occur due to local factors which influence wound healing (Guo and DiPietro, 2010).

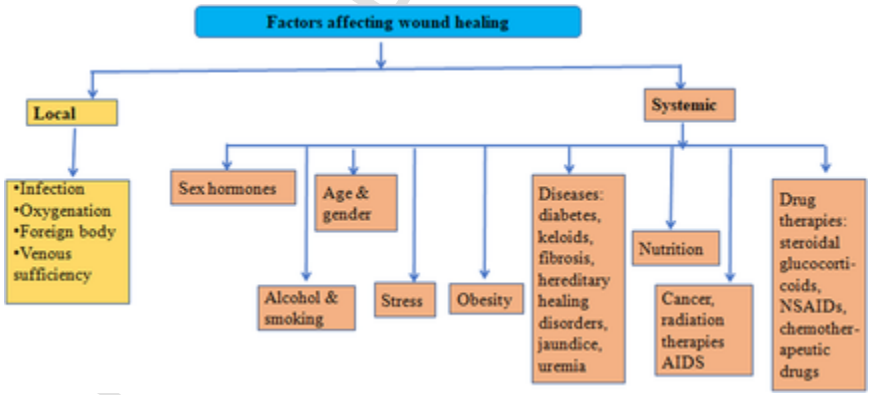

Figure 16.1 Factors affecting wound healing.

UNCORRECTED PROOF

16.3.1 Local factors that influence the healing process

16.3.1.1 Oxygenation

Oxygenation is crucial for the production of energy by means of ATP, cell metabolism, and for recovery from almost all types of wounds. It possesses several benefits in healing, such as the protection of wounds from infection by promoting angiogenesis, enhancing keratinocyte uptake, migration, and reepithelialization. It also promotes fibroblast proliferation around wounds along with the formation of collagen. Moreover, it increases the level of superoxide production with the help of polymorphonuclear leukocytes as a primary dependent oxygen factor (Bishop, 2008). There are several systemic conditions such as age and diabetes which can decrease the vascular flow, resulting in the development of hypoxic wounds due to poor tissue oxygenation.

Healing is diminished for those wounds which are unable to restore oxygen. A temporary lack of oxygen (hypoxia) can activate wound healing only if it happens for a long time, otherwise wound healing can be delayed. A lack of oxygen can impact cytokine and growth factor production. Cytokines formed due to a lack of oxygen include transforming growth factor-beta, platelet-derived growth factor, vascular endothelial growth factor, tumor necrosis factor, etc. ROS such as hydrogen peroxide and superoxide are majorly involved in normal wound healing and behave as cellular messengers to promote the wound-healing process, cell motility, cytokine action, and angiogenesis. Hypoxia and hyperoxia are responsible for enhancing ROS demand. However, on other hand, a higher level of ROS production can damage tissues (Rodriguez et al., 2008). To conclude, proper oxygen supply is essential for the success of the wound-healing process.

16.3.1.2 Infection and foreign bodies

Once a lesion is present on the skin, microorganisms gather at the skin surface and enter the underlying tissues. The level of the infection and replication state of the microorganisms affect whether the wounds are colonized, contaminated, or spread the invasive infection. The availability of nonreplicating microorganisms on wounds is identified as contamination. Meanwhile, the presence of replicating microorganisms on a wound without any tissue damage is described as colonization. Local infection and critical colonization are found at an intermediate stage where

UNCORRECTED PROOF

microorganisms can replicate and local tissue actions are started. An invasive infection is defined as the availability of replicating microorganisms inside a wound (Harding and Edwards, 2004).

On the other hand, inflammation is a basic response in the wound-healing process and an essential factor for the removal of contaminated microorganisms. If microbial removal is not completed, inflammation is sustained for a longer duration. Due to such conditions, bacteria and endotoxins both enhance cytokine production (IL-1 and TNF-alpha) which increase the inflammatory phase. If this happens for a longer time, the wound is considered as chronic and is difficult to heal. Moreover, such a prolonged inflammatory state may elevate the production of metalloproteases which are responsible inhibiting the extracellular matrix in wounds (Menke et al., 2007).

16.3.2 Systemic factors that influence the healing process

16.3.2.1 Age

As per WHO, the over 60 years age group is growing faster than any other age group. Higher age of individuals is one of the critical risk factors in the impaired wound-healing process. Many clinical and animal studies conducted at the molecular level have revealed that higher age can adversely impact wound healing (Keylock et al., 2008). In the aged individual, altered inflammatory reactions, i.e., T-cell infiltration, chemokine formation, and lower phagocytic volume around the wound environment, can delay the wound healing. An animal study in aged mice compared with young mice revealed delayed angiogenesis, collagen production, and reepithelialization. In general, there are small differences between young and aged individuals in terms of wound healing. A review study of age-related changes revealed that the each step of wound healing for aged persons showed higher platelet aggregation, higher uptake of inflammatory mediators, delayed permeation of macrophages and lymphocytes, lowered growth factor secretions, and delayed reepithelialization, angiogenesis, and collagen production (Gosain and DiPietro, 2004).

16.3.2.2 Sex hormones in aged individuals

Compared to aged females, aged males are more affected by delays in the wound-healing process due to sex hormones. A female estrogen (estrone), male androgen (testosterone), and there steroidal precursor (dehy-

UNCORRECTED PROOF

droepiandrosterone) have significant effects on the wound-healing process (Gilliver et al., 2007). A study revealed that the expression of genes among elderly men and young women was totally estrogen regulated. Numerous genes associated with wound healing are affected by estrogen, which enables matrix production, and inhibits protease and regeneration of tissues, and the genes those are involved in inflammation (Hardman and Ashcroft, 2008).

16.3.2.3 Stress

Stress has a significant effect on human health and social behavior. Several diseases are associated with stress, such as diabetes, wounds, CVS, and cancer (Vileikyte, 2007). Clinical research has revealed that both humans and animals with physiological stress can have a hampered wound-healing process. A student with the stress of academic examinations and a caretaker for a person with Alzheimer's have delayed wound-healing processes. Stress is responsible for the up-regulation of glucocorticoid hormones as well as lowering the amount of proinflammatory cytokines (IL-1β, TNF-α, and IL-6) at the wound area. It also inhibits the progression of chemoattractants (IL-8 and IL1-α) which are essential for the initial inflammatory step during the wound-healing process (Boyapati and Wang, 2007).

Moreover, Th1 responses are essential during the starting phase of wound healing, and are regulated by the glucocorticoid cortisol as an antiinflammatory agent. Hence, physiological stress can impair and delay healing at the wound site via reduced cell-mediated immunity (Godbout and Glaser, 2006). Other negative stress factors such as anxiety and depression affect health and behavior as well as being responsible for delaying wound healing. The effects of stress on wound healing are summarized in Fig. 16.2.

16.3.2.4 Diabetes

An individual who is affected by diabetes shows an impaired healing process in acute wounds. Much of this population is affected by chronic nonhealing diabetic foot ulcers (DFUs). DFUs are a severe condition of diabetes that occur in about 15% of the total diabetic population. A patient with diabetes can experience poor wound healing from both DFUs as well as acute cutaneous wounds due to a variety of intricate pathophysiological processes. DFUs arise to hypoxia, as with venous stasis ill-

UNCORRECTED PROOF

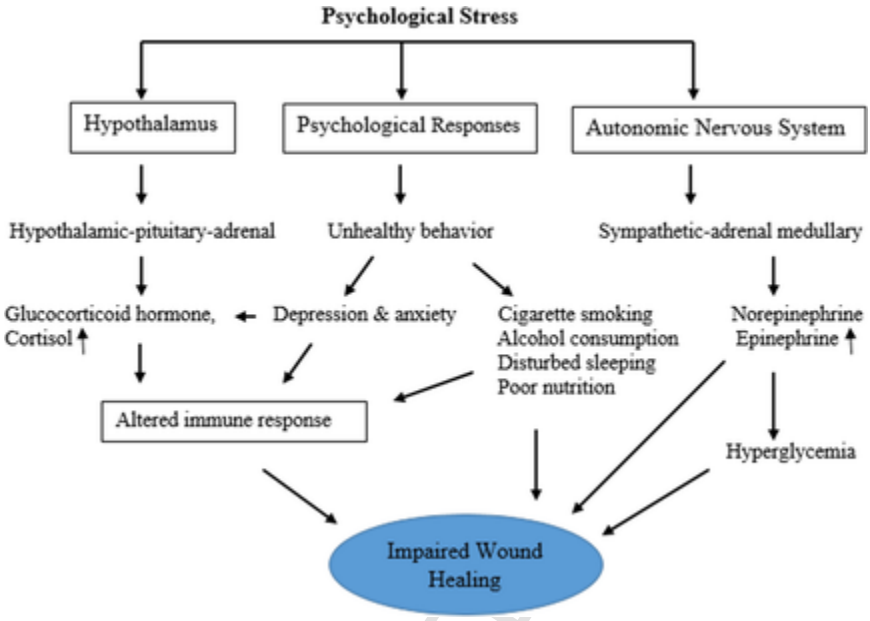

Figure 16.2 The effects of stress on wound healing.

ness and chronic nonhealing wounds. By elevating the concentration of oxygen radicals, hypoxia can exacerbate the primary inflammatory actions and lengthen the healing process. Diabetes-associated wounds are considered to have a number of dysregulated cellular causes, including inadequate T-cell immunity, faulty leukocyte chemotaxis, phagocytosis, bactericidal activity, and dysfunctioning of epidermal cells and fibroblasts (Woo et al., 2007). Some of the other causes are described in Fig. 16.3.

16.3.2.5 Medications

Numerous drugs have the potential to alter the wound-healing process, including those that hamper platelet function, clot development, inflammatory action, and cell proliferation. Only those drugs categories that are frequently taken and possess major effects on healing are discussed here, such as NSAIDs, glucocorticoid steroids, and chemotherapy therapies.

16.3.2.5.1 Glucocorticoid steroids

The glucocorticoids are systemic antiinflammatory drugs that are well recognized as hindering wound healing by suppressing cellular wound

UNCORRECTED

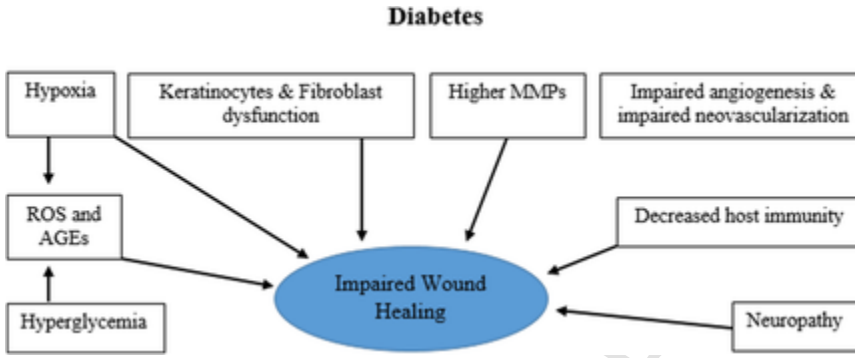

Figure 16.3 Effects of wound healing in diabetes. *AGEs*, advanced glycation end products; *MPPs*, matrix metalloproteases; *ROS*, reactive oxygen species.

responses. i.e., the proliferation of fibroblast and collagen production. These steroids form inadequate granulating tissues and lower wound contraction in the healing process. A critical transcriptional factor associated with wound healing, i.e., HIF-1 (Hypoxia-inducible factor-1), is also inhibited by glucocorticoids (Wagner et al., 2008). Compared to systemic application, topical application of glucocorticoids has quite different effects as it promotes the wound-healing process. Chronic wounds treated with topical low-dose corticosteroids have been shown to heal more rapidly, cause less pain and exudate, and encourage hypergranulation tissue formation in almost 79% of instances (Hofman et al., 2007).

16.3.2.5.2 NSAIDs

Ibuprofen is one of the nonsteroidal antiinflammatory drugs (NSAIDs) frequently used to treat inflammation, control pain, and treat rheumatoid arthritis. A low dose of aspirin is frequently used as a primary preventive treatment option for cardiovascular disease but not as an antiinflammatory drug due to its antiplatelet properties (Pertici, 2017). There is little evidence to support the claim that short-term use of NSAIDs impairs wound recovery. However, it remains unclear whether long-term NSAIDs affect how well wounds heal. Moreover, in animal studies, ibuprofen has been shown to have antiproliferative properties on wounds, resulting in lowering of fibroblast content and wound contraction, along with delayed epithelialization and impaired angiogenesis (Pieringer et al., 2007).

UNCORRECTED PR

16.3.2.5.3 Chemotherapeutic drugs

The majority of chemotherapies work by slowing down the cellular metabolism, accelerating cell division, and promoting angiogenesis, all of which are essential for an effective wound-healing process. These drugs prevent the production of DNA, RNA, and proteins, which lower the fibroplasia and neovascularization of tissues. Chemotherapeutic drugs delay cell migration into the wound, decrease early wound matrix formation, lower collagen production, impair the proliferation of fibroblasts, and inhibit the contraction of wounds (Kirchner et al., 2003).

16.3.2.6 Obesity

Numerous infections or diseases, as well as health issues such as diabetes, ischemic heart disease, cancer, hypertension, and delayed wound healing, are known to be made more likely by obesity. People affected by obesity experience several wound complications, such as venous and pressure ulcers, skin wound infections, seroma, and hematoma development. Obese patients receiving bariatric and nonbariatric procedures have been shown to have a higher frequency of wound problems. Obese people experience a higher rate of surgical site infections and many of these issues occur in subcutaneous adipose tissues due to hypoperfusion and ischemia. This situation also occurs due to lowered intake of antibiotics. Increased tension on the edges of surgical wounds typically occurs in obese patients, resulting in wound dehiscence. Due to wound tension, tissue pressure rises significantly, which hampers the microperfusion process and lowers the capabilities of wounds to consume oxygen (Franz et al., 2007).

16.3.2.7 Alcohol consumption

The use of alcohol hinders the wound-healing process and enhances the risk of infection as per a clinical and animal study report (Anaya and Dellinger, 2006). Due to alcohol exposure, either acute or chronic, in more than half of traumatic events, the impact of alcohol on the repair mechanism is extremely clinically significant. The consumption of alcohol lowers the defense mechanism and being intoxicated at the time of injury increases the likelihood of wound infection (Szabo and Mandrekar, 2009).

UNCORRECTED PROOF

16.3.2.8 Smoking

Smoking increases the risk of various malignancies, such as stroke, heart, vascular disease, lung disease ,etc. Similarly, smoking has long been recognized as having detrimental impacts on wound healing (Choudhry and Chaudry, 2006). One study revealed that patients who smoke after surgery experience delayed wound healing and also a number of issues such as wound rupture, infection, leaking, necrosis, epidermolysis, and lowered tensile strength of wounds. In the field of oral surgery, smokers have been found to have lower recovery after both conventional oral surgery and the installation of dental implants (Ahn and Mulligan, 2008).

16.3.2.9 Nutrition

Nutrition has been acknowledged for more than a century as a critical component that influences the wound-healing process. It is clear that inadequate nutrition or specific nutrient deficiency can significantly affect wound healing following trauma and surgery. Patients who are malnourished and have chronic or delayed healing frequently require specialized nourishment. The healing process can be impacted by the metabolism of carbohydrates, proteins, fats, vitamins, and minerals (Balaji, 2008).

16.4 Properties of bioresorbable polymers

For the manufacturing of engineered tissue products, the choice of biopolymer is crucial. Although the traditional selection principle for secure, stable, and inert substances still applies, it has been found that any artificial substances ingested by the patient will have biological reactions. As each biopolymer application necessitates a different environment for cell–cell communication, it is crucial for the engineered tissue product manufacturer to have a variety of biopolymer options available (Zhang et al., 2014). Such applications include:

A. It should support the development of new tissues through the interaction among cells and their potential to obtain nutrients, growth factor, and optimized active pharmaceutically ingredients.

B. It should inhibit the cellular properties of tissue growth where surgically induced adhesions are detrimental.

UNCORRECTED PROOF

C. It must lead to tissue responses by increasing the cellular reaction of one and inhibiting the other.
D. It should improve cell–cell connections and cellular activity, such as the formation of ECM, proliferation, and fibroblast attachment.
E. It should inhibit cellular connectivity, such as the connectivity of platelets to vascular grafts.
F. Inhibition of biological activity such as in organ transplantations by blocking antibodies against grafted cells.

When tissue recovery or modifications are the prime object of engineered tissue products, bioresorbable polymers are appropriate; however, they are not appropriate when long-lasting material stability is needed. Hence, bioresorbable polymers also require features such as:

A. Manufacturing feasibility, as well as an excess amount of polymers available commercially.
B. The proficiency to convert the polymer into the final product.
C. The mechanical characteristic that interact in short-term functioning but do not interfere with long-term functioning.
D. Minimum or nontoxicity of breakdown products, in both systemic and local tissue reactions.
E. Possibilities for the development of drug-delivery systems for use in the sustained release of active pharmaceutical ingredients.

Natural and engineered natural substances, along with metals, synthetic polymers, ceramics, and composites, are among the various substances that are mostly used in clinical applications. Metals, including their alloys, are employed for implants in dental and orthopedic use because of their mechanical potential, such as ductility, toughness, and increased strength. Nevertheless, a metallic implant may have issues that are serious enough to necessitate a second surgery to remove the device, such as irritation brought on by corrosive and erosive conditions in biological systems, secondary fracture of conducted bone, and development of sterile implants. Ceramics and glasses, which can be chemically bioactive or nonbioactive in nature, are utilized in a number of biomedical applications, mostly for rebuilding missing bones, but because of their brittle nature, they are avoided in load-bearing applications (Arnold and Barbul, 2006).

Polymers are less strong and ductile than ceramics, glasses, and metals, however they are commonly utilized for exchanging, increasing, supporting, or fixing live tissues due to their diversity, simplicity, and bio-

UNCORRECTED PROOF

compatible nature. It is feasible to develop composites by mixing polymers, ceramics, and metals to acquire unique qualities which are not present in a single material to develop customized devices for use in numerous biological sectors. Due to the structural similarity in living tissues which are formed of macromolecular composites, synthetic polymer composites are widely appealing biomaterials. The formation of engineered scaffolds, simple sutures, fixing screws, gauze strip, and bone replacements using bioresorbable polymers is a common practice. They do not require any secondary method to remove the implant or to initiate the tissue recovery in the matrix. The major outcome in the development of biomaterial research in the last 30 years has been the gradual transition from bio-stable prostheses to bioresorbable implants (Zhang et al., 2014).

16.5 Bioresorbable polymers for wound healing

Natural polymers offer a variety of benefits in regenerative medicinal therapy for the enhancement of wound healing, such as biodegradability, biocompatibility, and similarity to the extracellular matrix. Natural polymers are engaged in the repair of injured tissues and subsequently in skin regeneration by initiating and promoting the wound-healing process (Huang and Fu, 2010). Biomaterial hydrogels are used commercially, such as in pharmaceuticals and biomedicals, due to their unique 3D cross-linked structures that are soaked in aqueous or biological fluids for wound treatment, drug administration, organ replacement, and engineered tissue products (Das et al., 2012). Additionally, radioactivity studies are used to create innovative biomaterials based on biodegradability, nontoxicity, and bio-renewable polymers. As a result, hydrogels made of naturally cross-linked polymers are utilized for the healing of wounds and skin burns (Haji-Saeid et al., 2010). The natural bioresorbable polymers for wound healing are described in the following subsections.

16.5.1 Polysaccharides

Polysaccharides are mainly introduced in the form of hydrogels. Some are primarily used for the treatment of wounds and skin burns. The polysaccharides are divided on the basis of their nature, such as those are neutral in nature, i.e., dextrans, glucans, cellulose; acidic in nature, i.e.,

UNCORRECTED PROOF

alginic, hyaluronic acids; basic in nature, i.e., chitin, chitosan; or sulfated in nature, i.e., heparin, keratin, chondroitin, etc. (Kennedy et al., 2001).

16.5.1.1 Homoglycans

Homoglycans are biocompatible biopolymers that are utilized locally to alter the cellular activities involved in wound healing. Starch, dextran, cellulose, or their modified compositions can be used in the manufacture of nanofiber matrices in the regenerative medicinal therapies sector, such as for wound healing and tissue engineering (Lee et al., 2009).

16.5.1.1.1 α-Glucans

The common yeast-like fungus *Aureobasidium pullulans* forms pullulan (1-4),(1-6)-d-glucan from starch (Dothioraceae). A pullulan by-product was synthesized using a chemical cross-linking method for antibacterial release during wound healing via a superabsorbent polysaccharide-based hydrogel. Hydrogels possess extraordinary water-absorbing capabilities, with a swelling ratio up to 4000% and are also noncytotoxic, offering rapid hemostasis, while inhibiting fluid aggregation and enabling wound bed dryness. Additionally, drugs such as antibacterials or antimycotic therapies may be encapsulated into hydrogels to protect wounds and skin burns against microbial biofilm invasion (Li et al., 2011).

16.5.1.1.2 β-Glucans

β-Glucans possess the capabilities to form single and triple helical durable gel structures, while numerous forms of (1-3)-d-glucans can be isolated from fungi, yeast, and grains to identify the pharmacological and immunological properties. A study conducted by Lehtovaara et al. revealed that highly pure yeast-derived insoluble (1-3)-d-glucan considerably minimized skin irritation, blocked adipogenic division, and aided the wound-healing process (Lehtovaara and Gu, 2011; Vetvicka and Vetvickova, 2011).

16.5.1.1.3 Dextrans

Dextran that has been modified to possess heparin-like qualities is known as carboxymethyl benzalamide sulfonate dextran (CMDBS), which is utilized for the treatment of wounds and skin burns. In general, CMDBS is a soluble polymer which possesses structural similarity with glycosaminoglycan heparin by enhancing the wound-healing process. In the majority of in vivo studies, it has been shown to be capable of inhibiting

UNCORRECTED PROOF

Staphylococcus aureus biofilms and promoting the cell proliferation and metabolism of various cells such as tumor, smooth muscle, and endothelial cells. Recently, cyclodextrins (hydrated) have been utilized as odor-control dressings due to their bucket-shaped structure which is capable of trapping and neutralizing water-insoluble particles. Cyclodextrin can be active for a long time than charcoal or serum proteins, which makes them excellent candidates to absorb odors more effectively (Logeart-Avramoglou and Jozefonvicz, 1999).

16.5.1.1.4 Cellulose

For chronic wound dressings, bioengineered cellulose is utilized superficially as a healing scaffold or matrix material, which minimizes discomfort and pain, and accelerates the healing process. Cellulose also possesses key benefits in wound healings such as enhancing granulation and epithelialization of partial- and full-thickness wounds. Various bioactive molecules, such as enzymes, hormones, vitamins, antioxidants, and antimicrobials, can be incorporated through a co-immobilization process using engineered cellulose for wound healing (Medusheva et al., 2007).

16.5.1.1.5 Chitin and chitosan

The most common natural amino polysaccharide is chitin (polu-N-acetyl-glucosamine), which is readily accessible throughout the year like cellulose. It makes up the majority of the exoskeletons of insects, crustaceans, and vertebrates, and also the cell walls of fungi. Chitin is transformed into chitosan (poly-N-acetyl-glycosaminoglycan) via the alkaline deacetylation process and by reacting the shells of shrimps with sodium hydroxide (Morganti et al., 2011). Several chitin and chitosan compositions with local hemostatic, antimicrobial, antiinflammatory, and wound-healing characteristic have been developed, such as water-soluble chitin ointment for wound-healing treatment (Han, 2005) and chitin-loaded silver nanoparticles as a bactericidal film for wound healing (Madhumathi et al., 2010).

16.5.1.2 Heteroglycans

Heteroglycans offer various potentials in the biomedical sector. Heteroglycans, namely pectins, agarose, alginates, gums, carrageenans, and glycosaminoglycans, are biodegradable, biocompatible, and possess unusual physicochemical properties, i.e., film/gel forming and thickening proper-

UNCORRECTED PROOF

ties of electrostatic composites. The development of heteroglycan fibers in the nanometric range using electrospinning technology may be advantageous for drug delivery and also regenerative medicinal therapies (Lee et al., 2009).

16.5.1.2.1 Alginates

Alginates are long repeating-unit polysaccharides with varying concentrations of residues from D-mannuronic and L-guluronic acid that are (1-4)-linked. Due to their hemostatic qualities, alginate-based wound dressings are frequently applied on skin burns and exuding or bleeding wounds. Alginates such as calcium, calcium-sodium, collagen, and gelatin are extremely absorbent natural fiber dressing materials developed from processed algae.

16.5.1.2.2 Agar and agarose

Agar and agarose fibers are developed by wet-spinning technology and are mainly utilized in biomedical and biomaterial applications for wound healing. A solvent containing DMSO:water in a ratio of 9:1 was used to construct continuous fibers in an ethanol coagulation bath. Agarose fibers that were homogeneous and of smooth texture exhibited significant water-swelling capabilities of 400%–500% as well as tensile strength of 30–50 MPa. Agarose fibers have been shown to be superior for swelling in water than agar fibers. Meanwhile, agaropectin has been shown to have flexibility issues (Bao et al., 2010).

16.5.1.2.3 Carrageenan

Carrageenan or carrageenins are a family of natural linear polysaccharides that are extracted from red edible seaweeds. They offer several potentials in the pharmaceutical, biomaterial, and food industries for thickening, gelling, and stabilizing properties. PVP-KC hydrogels were created by subjecting a combination of water systems such as poly(N-vinyl-2-pyrrolidone), kappa-carrageenan (KC), potassium chloride, and PEG to various gamma radiation dosages. These hydrogels were evaluated on various factors such as temperature, mechanical behavior, fluid uptake, swelling factor, pH, electrical conductivity, and bioadhesive property on the human skin to predict their potential in wound healing (Şen and Avcı, 2005).

UNCORRECTED PROOF

16.5.2 Glycolipids

Glycolipids are the complex lipids comprising carbohydrates linked via a glycosidic bond. Their main qualities include providing stability to the cell membrane and enhancing cellular recognition, which is important in terms of cell immunity as it permits cells to form bonds to develop tissues. Patients suffering from skin burns and wounds can benefit from topical glycolipids therapy consisting of galactose liposomes because of the rapid uptake of neutrophils and macrophages. The ability of macrophages to release cytokines and growth factors promotes tissue remodeling and the repair mechanism which is a key approach to wound healing. When compared to a control group, an experiment on mutant mice using 1-3-galactosyl transferase revealed the beneficial response of –Gal liposome at a daily dose of 10 mg (Galili et al., 2010).

16.5.3 Proteoglycans

Proteoglycans are essential proteins, covalently linked with the glycosaminoglycan chain that have a significant amount of macromolecules in the composition of extracellular matrix. Neoproteoglycans are the most biocompatible and biodegradable synthetic glycoconjugates developed from essential nanomaterials, proteins, or polymers that are covalently linked to the glycosaminoglycan chain and connected with the cells and proteins. Conjugates such as protein glycosaminoglycan, nano-glycosaminoglycan, and polymer glycosaminoglycan complexes are the three basic forms of neoproteoglycan which possess in vivo and in vitro tissue-engineered applications (Weyers and Linhardt, 2013).

16.5.4 Proteins and peptides

16.5.4.1 Vegetal proteins

Vegetal proteins are proteins available naturally from plants. These include soya, pulses, seeds, certain grains etc. These foods contain all the amino acids in an acceptable quantity. The treatment of wounds and skin burns can also be aided by some vegetal proteins. An ex vivo study performed on excised skin of rat using a combinational biomaterial composite of soya protein and sago starch which was cross-linked with glutaraldehyde was found to be effective in wound healing (Ramnath et al., 2012). Additionally, vegetal proteins such as soya and sodium caseinate-derived biomaterials offer significant advantages in wound healing and

UNCORRECTED PROOF

drug delivery due to their biocompatible and biodegradable natures (Silva et al., 2003).

16.5.4.2 Collagen

One of the most prevalent proteins found in the human body and skin is formed by fibroblasts and is known as collagen. Collagen offers several potential qualities such as enhanced wound-healing process at the cellular and molecular levels as well as aiding the development of new tissues and epithelialization of wounds. For the prevention and cure of partial/full-thickness wounds with low to high exudates, collagen dressings formulated from bovine, pig, or avian sources are mainly utilized. However, these dressings are avoided in severe skin burns and for the patients who are sensitive or allergic to these products (Murali et al., 2011). There have been many research works on the use of various collagen-based dressings and compositions for the treatment of wounds and burns, such as for deep wounds (collagen sponges), gingival wounds (collagen–glycosaminoglycan complex), oral wounds (resorbable collagen membrane), wound healing (DNA salmon–collagen film complex) (Shen et al., 2008), cutaneous wounds (collagen–minocycline hydrogels) (Ghica et al., 2011), skin grafting (collagen microfiber scaffolds) (Kempf et al., 2011for vascular grafts and wound repairing (collagen electrospun nanofiber scaffolds) (Fullana and Wnek, 2012), and modified collagen–alginic thermostable biopolymers for the treatment of wounds (Mitra et al., 2011).

16.5.4.2.1 Gelatin

Gelatin is a naturally available biopolymer mainly obtained from collagen, and also from various animal by-products. Nowadays, gelatin is mainly used in the pharmaceutical and biomedical industries for the development of drug-delivery applications and for wound healing due to its biocompatible and biodegradable dressings. To identify its healing properties, various gelatin-containing composition studies have been performed on the dorsal skin of rats, such as cross-linked gelatin-alginates, gelatin-hyaluronic acid sponges, and EGF-gelatin-based wound healing in conditions including excess tissue loss and nonhealed wounds, i.e., burns, diabetic foot ulcers, trauma, and static ulcers; bioresorbable gelatin films have also been used for the treatment of trauma and orthopedic injuries.

UNCORRECTED PROOF

16.5.4.2.2 Keratin

The intermediary fibrin proteins present in vertebrate epithelia and corneous tissues such as hooves, horns, and claws are collectively referred to as keratin. Due to its potential to treat proteolytic injuries, keratin and its derivatives have been utilized in chronic wounds to speed up healing. Keratin-based novel wound dressings with optimum potential have demonstrated controlled release behavior of growth factors and antibiotics.

16.5.4.2.3 Silk fibroin

Silk fibrin offers exceptional characteristics in the wound-healing process such as adhesion, absorption of exudates as well as being biodegradable and biocompatible with less inflammatory responses. Additionally, silk fibroin is utilized for the management of skin grafts, artificial ligaments, tendons, etc. It also serves as an excellent candidate in regenerative medicinal therapies such as silk fibroin and chitosan complex scaffolds for tissue regeneration (Gobin et al., 2005), carbon nanotubes for wound healing, SF–alginate combinational sponges for full-thickness wounds, and SF film biomaterials for wound treatment (de Moraes and Beppu, 2013).

16.5.4.2.4 Bovine serum albumin (BSA)

BSA is a protein derived from cattle. Due to anionic charge, BSA act as an intermediate bridge between tissues and cells and also acts as a carrier to transport fatty acids, vitamins, hormones, etc. Because of its binding capabilities, it also acts as a scavenger for the removal of toxic material such as pyrogens from the medium. BSA nanofibers are developed from the globular proteins in BSA medium without utilizing any chemical cross-linkers. Because of the fibrous characteristic of BSA it possesses various benefits in wound healing, suturing, and wound closure. It is used in various biomedical and pharmaceutical applications due to its biocompatible, biodegradable, and effective mechanical qualities (Zhu et al., 2011).

16.5.4.2.5 Enzymes

Enzymes are proteins that offer several applications in wound healing. Proteolytic and fibrinolytic enzymes, along with collagenase and papain, are effectively utilized in the epithelialization of wounds. In pectin film

UNCORRECTED PROOF

applied for wound healing, the development of prostaglandin H was drastically enhanced (Dror et al., 2008). Lysostaphin, a cell lytic enzyme, was formulated as antiinfective bandages immobilized on electrospun fibers through a solution of cellulose, such as cellulose–chitosan and cellulose–poly-methacrylate. However, enzymes are avoided in wound healing for patients affected by coagulation disorders (Miao et al., 2011).

16.5.5 Synthetic polymers

Synthetic polymers were developed chemically in laboratories, and are described as manmade polymers (Gobi et al., 2021). By increasing the mechanical and biocompatible potentials of individual components, synthetic and natural polymers can be used to create new kinds of materials.

A hydrophilic synthetic polymer, polyvinyl alcohol (PVA), is widely employed in a variety of biomedical applications (Gyles et al., 2017). PVA is possible due to the availability of hydroxyl molecules, which can help to form hydrogen bonds (Norouzi et al., 2021). Due to its poor hydrophilic properties, thick membrane, and inadequate flexibility, PVA is only occasionally used as a polymeric wound-dressing material (Venkataprasanna et al., 2020). A synthetic hydrophilic polymer is known as poly(ethylene glycol) (PEG) (Sahana and Rekha, 2018). Growth factors such as macromeres and epidermal growth factor are interlinked to each other through significant attraction. These can be used directly at the wound site. Mechanical, thermal, and PEG crystalline features are preserved by mixing polymer with chitosan and PLGA. Such PEG-based treatments are effective in diabetic wounds. These treatments speed up the healing process by promoting skin cell development, collagen deposition, and proliferation (Shahverdi et al., 2014). Methacrylic acid is a monomer used to develop the synthetic polymer known as poly(methacrylic acid) (PMAA). In order to merge bioactive compounds with carboxylic groups, such as drugs and inorganic nanoparticles, PMAA is highly recommended in biomedical applications due to its water-soluble and biocompatible nature (Lumbreras-Aguayo et al., 2019). This substances can alter noticeably in response to changes in the pH and iconic strength of the solution as well as having high swelling capabilities in water. N-vinylpyrrolidone (monomer) was used to develop a hydrophilic linear chain polymer known as polyvinylpyrrolidone (PVP) (Kausar, 2019). A lipophilic and semicrystalline synthetic polymer

UNCORRECTED PROOF

known as polycaprolactone (PCL) has significant crystalline and morphological properties (Mohamed and Yusoh, 2016). To enhance its mechanical capabilities, PCL has been formed by mixing with other polymers or combined with them. Another of the most widely utilized synthetic polymers in the biomedical sector is poly(lactic acid (PLA). Several other derivatives of PLA are available with its chiral structure, such as poly-L-lactide (PLLA) formed by L-polymerization and called L-lactide.

Electrospinning technology is the primary method to obtain synthetic polymers which have micropores and a highly specified surface area for the treatment of wounds and skin burns. Synthetic polymers for wound dressing offer occlusive or semiocclusive characteristics enabling them to act as a barrier to protect against the infiltration of microorganisms. They may be in the form of hydrogels, foams, or hydrocolloids. Exudates are entrapped by the polymer film which provides a moist environment to the wound. Various authors have developed synthetic polymer-based wound dressing materials, such as ciprofloxacin HCL-loaded polyurethane and dextran electrospun nanofiber. Carrageenan-hydrophilic polymer hydrogels, cellulose acetate, PLA, and PLGA infused with shikonin have been used for wound recovery due to their antimicrobial, antiinflammatory, and antitumor activities, in addition to PVP-based nanosilver alginate hydrogels. One study revealed that carboxy methyl-chitosan provides various in vitro and in vivo characteristics in wound healing, such as stimulation of fibroblasts and macrophages and the secretion of various cytokines.

16.6 Nanocomposites for wound healing

In the area of wound healing, an increasing number of novel nano-therapies have surfaced and are presently undergoing clinical research studies. Numerous nano tactics have been investigated focusing on various stages of wound repair, such as nanoparticles, nanocarriers, and nanomaterials. Nanoparticles (NPs) are one of the options that researchers are studying for wound healing due to their wide spectrum of antibacterial properties and quick efficiency with a minimum dose. Due to the inability to permit a cell barrier, conventional therapies for wound healing have limited success as compared to nanoparticles, which can permit entry effectively (Khan et al., 2019). Disruption of the cell membrane, changes to the

UNCORRECTED PROOF

genes, and inhibition of enzyme production are aspects of NPs' antimicrobial activity, which leads to cell apoptosis. In addition, nanomaterials (NMs) are smooth, flexible, and biocompatible wound-healing materials that act as a gas barrier, absorbent for exudates, and a shielding material against further damages or heat. There are two primary types of NMs used in wound healing: (1) NMs with inherent qualities useful for treating wounds and (2) NMs used as drug-delivery systems (Bhattacharya et al., 2019).

16.6.1 Nonpolymeric

There are several nonpolymeric NPs that are utilized in wound healing, including metal and metallic NPs, lipid NPs, and ceramic NPs, as discussed next.

16.6.1.1 Metal and metallic nanoparticles

Various metal-based NPs such as gold (AuNPs), copper (CuNPs), silver (AgNPs), zinc oxide (ZnO NPs), titanium dioxide (TiO_2), cerium oxide (CeO_2), yttrium oxide (Y_2O_3), and other metal-based NPs have been reported for their antibacterial and wound-healing properties. Silver has been used as a medicine for a very long time. For the management of open wounds, burns, and chronically infected wounds, many types of silver components, i.e., metallic silver, silver nitrate, and silver sulfadiazine are used currently (Rai et al., 2009). The use of AgNPs has recently drawn attention, particularly for the treatment of open wounds, as a result of the rise in pathogenic bacteria that are multidrug resistant and to reduce the use of antibiotics. Silver nanoparticles are the most researched nanomaterial of all nanoparticles because of their exceptional antibacterial properties. Silver NPs are more effective at demonstrating higher antibacterial property than traditional therapies because they have a large surface area to volume ratio, which improves their interaction with microbes. The phosphorus-containing compounds in microbial cells, such as DNA ,can also bind with silver NPs, as can sulfur-containing proteins anchored in bacterial membranes.

A study performed by Orlowski and co-workers formulated tannic acid modified silver NPs possessing higher antibacterial action against *P. aeruginosa* and *E. coli*. The data revealed that the prepared NPs showed better wound closure, formation of granulating tissues, and angiogenesis in a mouse wound model (Orlowski et al., 2018). Another study per-

UNCORRECTED PROOF

formed by Peng and co-workers developed CS-coated silver NPs. Their data showed that the prepared formulation possessed excellent biocompatibility and was effective against meticillin-resistant *S. aureus* in contrast to polyvinyl-coated silver NPs (Peng et al., 2017). Silver NPs with CS polyethylene glycol hydrogel have been produced as a treatment for diabetic chronic wounds (Masood et al., 2019).

16.6.1.2 Lipid nanoparticles

Researchers and scientists have become interested in lipid-based NPs recently due to their potential use as drug-delivery systems. In addition, lipid NPs can be modified to suit certain health issues and routes of administration. These systems are risk-free, economical, and provide protection to drugs from biological deterioration. Due to their minimal toxicity and excellent efficacy, lipid NPs are employed as drug-delivery carriers in sensitive tissues (Attama et al., 2012). Such lipid NPs include solid lipid nanoparticles (SLNs), nanostructured lipid carriers (NLCs) and drug–lipid conjugates.

In addition to reducing pain and infection, essential oil offers several properties in wound healing such as an antibacterial, relaxing, and quick recovery from wounds (Saporito et al., 2018). Although rosemary and eucalyptus leaf extract have the ability to heal wounds, these essential oil are naturally volatile and are rapidly broken down by oxidation, heat, light, and volatilization (Apostolides et al., 2013). Hence, SLN- and NLC-based carriers are employed that enclose these essential oils and maintain their biological activity (Gokce et al., 2012). A study by Saporito and co-workers (Saporito et al., 2018) developed eucalyptus and rosemary oil-loaded NLCs. They used coco butter and olive oil as solid and liquid lipids which possess higher natural stability, biocompatibility, and rapid wound-healing properties through dermal fibroblasts. This study revealed that the prepared formulation effectively provided higher healing and antimicrobial properties showing a synergistic effect between olive oil and eucalyptus oil.

16.6.1.3 Ceramic nanoparticles

Ceramic NPs represent one of the most commonly employed inorganic NPs for wound healing. These NPs are mostly known for their wound healing, tissue regeneration, and antibacterial properties (Urie et al., 2018). Nanohydroxyapatite and calcium triphosphate as ceramic NPs of-

UNCORRECTED PROOF

fer broad applications in drug delivery and wound healing processes. the sol–gel formulation method is generally used for the development of ceramic NPs. Furthermore, these NPs are extensively utilized in the development of tissue-engineered formulations. Various authors has revealed the potential of ceramic NPs, such as Deepthi and co-workers who described the use of ceramic-CS-based NPs for bone rejuvenation (Deepthi et al., 2016). When combined with CS, components such as hydroxyapatite, silicon dioxide, bioglass ceramic, titanium dioxide, and zirconium oxide formed nano-scaffolds that are very effective in regenerating bone. To cure bone abnormalities in traditional therapies, artificial materials were implanted surgically, although this had several negative side effects. Hence, ceramic nanoparticles are employed to clear the way for tissue regeneration to overcome these problems. A bioactive ceramics and bioresorbable polymer mixture creates an extracellular matrix for the healing of bone tissue.

16.6.2 Polymeric nanoparticles

In the current era, strategies for the treatment of chronic wounds have been developed to deliver drugs and biomolecules in bioresorbable polymeric NPs with controlled release, such as PLGA, alginate, gelatin, chitosan, PEG, and polycaprolactones. Polymeric NPs avoid frequent dosing, extend the therapeutic effectiveness, and provide controlled drug delivery in wound healing (Masood, 2016).

16.6.2.1 Synthetic

PLGA offers one of the most widely used synthetic polymers due to its biodegradability, biocompatibility, hydrophobic property, and for entrapping the growth factor in chronic wound therapy among all polymeric NPs. It offers sustained drug release through NPs because it absorbs less water and enhances the degradation time (Masood, 2016). Additionally, the breakdown of PLGA yields lactate, which promotes pro-COL factors, angiogenesis, and the recruitment of endothelial cells to the wound site. A combinational therapy of PLGA–curcumin NPs revealed a twofold higher potential in wound healing than PLGA and curcumin alone.

Polyurethane is utilized to develop the bioresorbable polyester known as polycaprolactone (PCL). It is well known for its controlled intracellular reabsorption mechanism and its cell-specific responsiveness. In contrast to various available synthetic polymers, it is simple to use and can

UNCORRECTED PROOF

form a variety of nanostructures, including scaffolds and micro- and nano-carriers (Guarino et al., 2002). The antibacterial, antimicrobial, and wound-healing properties of PCL have been illustrated in numerous investigations to be enhanced by their combination with any metal or metal-based NPs. One study conducted on a skin model using zinc NPs which were developed by electrospun polycaprolactone provided scar-free wound healing by enhancing fibroblast proliferation (Augustine et al., 2014).

16.6.2.2 Natural

Chitosan (CS) is available from the shells of crustaceans and is made up of N-acetyl-D-glucosamine and randomly dispersed D-glucosamine. CS offers numerous potential in wound-healing applications, such as biodegradability, biocompatibility, cellular binding capacity, wound healing, etc. (Li et al., 2012). The study performed by Piran and co-workers developed electrospun PCL nanoscaffolds loaded with chitosan. The effect of the CS NPs scaffold topography and drug release behavior on skin fibroblasts has been investigated (Piran et al., 2018). Another prominent natural polymer used in wound healing is alginate, which is found in the cell wall of brown algae and which possesses maximum scaffold capacity. A study by Liao and co-workers developed porous alginate hydrogels. These hydrogels contains PCL, PEG, and calcium gluconate crystals which are effectively deposited in the pores of microspheres. The data revealed that the prepared hydrogel effectively enhanced the growth of fibroblasts, which led to providing new areas for skin tissue engineering (Liao et al., 2018).

16.6.3 Hydrogels

Hydrogels are among the most prevalent wound-healing systems because they trap moisture at the wound surface, develop an optimum environment for healing, and keep the skin hydrated. They are easily formulated and also allow prolonged drug release. Chitosan, fibrin, hyaluronic acid, or synthetic polymer, either as cellulose compounds or poloxamers, can be used to make hydrogels. These hydrogels are able to create a cool and moist environment that promotes the wound-healing process as well as water vapor permeability and inhibiting microorganisms from entering the wound.

UNCORRECTED PROOF

A study performed by Khorasani and co-workers developed a CS-ZnO-PVA-based hydrogel which progressively enhanced the antibacterial properties without any cellular toxicity (Khorasani et al., 2018). Another study performed by Hsu and co-workers developed gel-based adipose-derived stem cell hydrogels for the treatment of wounds. This in vivo study revealed enhanced wound healing on both mouse and porcine skin models (Hsu et al., 2019).

16.6.4 Nanofibers

Nanofibers (NFs) are the key nanomaterial utilized for the wound-healing process. NFs have a diameter of 10–100 nm and a large specific surface area (Abrigo et al., 2014). They are formulated using the process of electrospinning technology, where various polymer solutions are processed into nanometric fibers using electric force. These fibers have the capability to create a porous network forming a mesh. Due to the tough network and higher surface area to volume ratio, NFs are suitable candidates to use as scaffolds. They can be synthesized from natural or synthetic polymers as well as carbon-based and semiconductor materials. These fibers are renowned for their use in biological sensing, wound dressing, drug delivery, and tissue engineering formulations along with regenerative drug therapies (Chen et al., 2017).

A study by Kandhasamy and co-workers developed a nanofiber scaffold using COL-coated ostholamide for wound treatment. The prepared formulation possessed excellent mechanical characteristic and antimicrobial property against *P. aeruginosa* and *S. aureus*. The prepared system offers controlled delivery of ostholamide and provides stability against enzymatic degradation. In another study, a PLGA-aloe vera gel-growth factor scaffold was formed by electrospinning technology. In vivo studies on a mice model showed excellent wound-healing properties by reducing the inflammation (Garcia-Orue et al., 2017).

16.7 Conclusion and future perspectives

In pharmaceutical and biomedical applications, bioresorbable polymers offer excellent potential. Bioresorbable polymers for wound healing must be mechanically strong, have good antibacterial activity, and have hemostatic, water vapor permeability, appropriate gas exchange as well as higher free radical scavenging properties. Such characteristics can en-

UNCORRECTED PROOF

hance the wound-healing process. Additionally, the dressing should be easy to remove after healing and should be nontoxic, biocompatible, nonallergic, bio-stable, and biodegradable. Natural and synthetic bioresorbable polymers offer their own advantages while treating wound. Many researchers and scientists have proved the capabilities of such polymers by encapsulating them in nanocomposites such as nanoparticles, nanocarriers, hydrogels, metal and metal oxide components, etc. for tissue regeneration, and healing of skin burns and wounds, particularly using in vitro models. Wound healing has attracted the attention of many researchers as it is difficult to treat chronic wounds. The market is constantly expanding, driven by the rise in the number of patients globally, requiring new tactics and materials. Polymer- and hydrogel-based dressings make up the majority of competitive technologies available today for advanced wound care. Advanced dressings typically serve a purpose beyond merely concealing and covering wounds. By using the bioactive qualities of polymers, it is feasible to speed up tissue remodeling and regeneration, improving skin conditions while minimizing the appearance or size of any associated scars.

Despite the broad variety of solutions already in the market, bioresorbable dressings have a low impact on the healing of complex and chronic wounds, although they remain essential components of acute wound care. Recently, enormous progress has been made in our understanding of the molecular mechanisms underlying wound healing, and we may now use this expertise to create novel therapeutic strategies for nonhealing wounds. Also, employing natural resources can effectively overcome these issues. Tissue engineering techniques use 3D hybrid scaffolds which are both synthetic and natural that interact with human cells effectively. The possible advantages of this strategy include the capacity to increase the in vivo properties which enhance bone formation, reducing donor site morbidity, shortening the surgical time, and decreasing the technical difficulty of the repair. A 3D reconstruction will significantly reduce the amount of time needed for healing. Additionally, it ensures optimal contact between the graft and the recipient site for better integration. Another benefit is increased permeability with particular hybrid materials, which is essential for tissue remodelling and replacement. As a result, theblood can easily flow through the graft's internal chambers without any resistance Hence, because of such tactics, the healing process is significantly enhanced because of cell attachments.

UNCORRECTED PROOF

References

Abrigo, M., McArthur, S.L., Kingshott, P., June 2014. Electrospun nanofibers as dressings for chronic wound care: advances, challenges, and future prospects. Macromol. Biosci. 14 (6), 772–792.

Agubata, C.O., Mbah, M.A., Akpa, P.A., Ugwu, G., September 2, 2021. Application of self-healing, swellable and biodegradable polymers for wound treatment. J. Wound Care 30 (Suppl. 9a), IVi-x.

Ahn, C., Mulligan, P., May 1, 2008. Smoking-the bane of wound healing: biomedical interventions and social influences. Adv. Skin Wound Care 21 (5), 227–236.

Anaya, D.A., Dellinger, E.P., October 1, 2006. The obese surgical patient: a susceptible host for infection. Surg. Infect. 7 (5), 473–480.

Apostolides, N.A., El Beyrouthy, M., Dhifi, W., Najm, S., Cazier, F., Najem, W., Labaki, M., AbouKaïs, A., April 1, 2013. Chemical composition of aerial parts of *Rosmarinus officinalis* L. essential oil growing wild in Lebanon. J. Essent. Oil Bear. Plants 16 (2), 274–282.

Arnold, M., Barbul, A., June 1, 2006. Nutrition and wound healing. Plast. Reconstr. Surg. 117 (7S), 42S–58S.

Attama, A.A., Momoh, M.A., Builders, P.F., October 31, 2012. Lipid nanoparticulate drug delivery systems: a revolution in dosage form design and development. In: Recent Advances in Novel Drug Carrier Systems, 5. pp. 107–140.

Augustine, R., Dominic, E.A., Reju, I., Kaimal, B., Kalarikkal, N., Thomas, S., 2014. Electrospun polycaprolactone membranes incorporated with ZnO nanoparticles as skin substitutes with enhanced fibroblast proliferation and wound healing. RSC Adv. 4 (47), 24777–24785.

Balaji, S.M., October 1, 2008. Tobacco smoking and surgical healing of oral tissues: a review. Indian J. Dent. Res. 19 (4), 344.

Bao, X., Hayashi, K., Li, Y., Teramoto, A., Abe, K., November 30, 2010. Novel agarose and agar fibers: fabrication and characterization. Mater. Lett. 64 (22), 2435–2437.

Bhattacharya, D., Ghosh, B., Mukhopadhyay, M., October 2019. Development of nanotechnology for advancement and application in wound healing: a review. IET Nanobiotechnol. 13 (8), 778–785.

Bishop, A., September 2008. Role of oxygen in wound healing. J. Wound Care 17 (9), 399–402.

Boyapati, L., Wang, H.L., June 2007. The role of stress in periodontal disease and wound healing. Periodontol. 2000 44 (1), 195–210.

Chen, S., Liu, B., Carlson, M.A., Gombart, A.F., Reilly, D.A., Xie, J., June 2017. Recent advances in electrospun nanofibers for wound healing. Nanomedicine 12 (11), 1335–1352.

Choudhry, M.A., Chaudry, I.H., January 1, 2006. Alcohol intoxication and post-burn complications. Front. Biosci. - Landmark 11 (1), 998–1005.

Cornelius, V.J., Majcen, N., Snowden, M.J., Mitchell, J.C., Voncina, B., December 22, 2006. Preparation of SMART wound dressings based on colloidal microgels and textile fibres. In: Smart Materials IV, vol 6413. SPIE, pp. 211–218.

Daniel, S., 2021. Biodegradable polymeric materials for medicinal applications. In: Green Composites. pp. 351–372.

Danti, S., D'Alessandro, D., Mota, C., Bruschini, L., Berrettini, S., January 1, 2017. Applications of bioresorbable polymers in skin and eardrum. In: Bioresorbable Polymers for Biomedical Applications. pp. 423–444.

Das, N.I., Bera, T., Mukherjee, A., 2012. Biomaterial hydrogels for different biomedical applications. Int. J. Pharma Bio Sci. 3 (3), 586–597.

de Moraes, M.A., Beppu, M.M., December 5, 2013. Biocomposite membranes of sodium

UNCORRECTED PROOF

alginate and silk fibroin fibers for biomedical applications. J. Appl. Polym. Sci. 130 (5), 3451–3457.
Deepthi, S., Venkatesan, J., Kim, S.K., Bumgardner, J.D., Jayakumar, R., December 1, 2016. An overview of chitin or chitosan/nano ceramic composite scaffolds for bone tissue engineering. Int. J. Biol. Macromol. 93, 1338–1353.
Dror, Y., Ziv, T., Makarov, V., Wolf, H., Admon, A., Zussman, E., October 13, 2008. Nanofibers made of globular proteins. Biomacromolecules 9 (10), 2749–2754.
Franz, M.G., Steed, D.L., Robson, M.C., November 2007. Optimizing healing of the acute wound by minimizing complications. Curr. Probl. Surg. 44 (11), 691–763.
Fullana, M.J., Wnek, G.E., October 2012. Electrospun collagen and its applications in regenerative medicine. In: Drug Delivery and Translational Research, 2. pp. 313–322.
Galili, U., Wigglesworth, K., Abdel-Motal, U.M., March 1, 2010. Accelerated healing of skin burns by anti-Gal/α-gal liposomes interaction. Burns 36 (2), 239–251.
Garcia-Orue, I., Gainza, G., Gutierrez, F.B., Aguirre, J.J., Evora, C., Pedraz, J.L., Hernandez, R.M., Delgado, A., Igartua, M., May 25, 2017. Novel nanofibrous dressings containing rhEGF and Aloe vera for wound healing applications. Int. J. Pharm. 523 (2), 556–566.
Ghica, M.V., Albu, M.G., Leca, M., Popa, L., Moisescu, S.T., November 1, 2011. Design and optimization of some collagen-minocycline based hydrogels potentially applicable for the treatment of cutaneous wound infections. Pharmazie 66 (11), 853–861.
Gilliver, S.C., Ashworth, J.J., Ashcroft, G.S., January 1, 2007. The hormonal regulation of cutaneous wound healing. Clin. Dermatol. 25 (1), 56–62.
Gobi, R., Ravichandiran, P., Babu, R.S., Yoo, D.J., June 13, 2021. Biopolymer and synthetic polymer-based nanocomposites in wound dressing applications: a review. Polymers 13 (12), 1962.
Gobin, A.S., Froude, V.E., Mathur, A.B., September 1, 2005. Structural and mechanical characteristics of silk fibroin and chitosan blend scaffolds for tissue regeneration. J. Biomed. Mater. Res. A 74 (3), 465–473.
Godbout, J.P., Glaser, R., December 2006. Stress-induced immune dysregulation: implications for wound healing, infectious disease and cancer. J. Neuroimmune Pharmacol. 1, 421–427.
Gokce, E.H., Korkmaz, E., Dellera, E., Sandri, G., Bonferoni, M.C., Ozer, O., April 11, 2012. Resveratrol-loaded solid lipid nanoparticles versus nanostructured lipid carriers: evaluation of antioxidant potential for dermal applications. Int. J. Nanomed. 7, 1841–1850.
Gosain, A., DiPietro, L.A., March 2004. Aging and wound healing. World J. Surg. 28, 321–326.
Guarino, V., Gentile, G., Sorrentino, L., Ambrosio, L., July 15, 2002. Polycaprolactone: synthesis, properties, and applications. In: Encyclopedia of Polymer Science and Technology. pp. 1–36.
Guo, S.A., DiPietro, L.A., March 2010. Factors affecting wound healing. J. Dent. Res. 89 (3), 219–229.
Gyles, D.A., Castro, L.D., Silva, J.O., Jr., Ribeiro-Costa, R.M., March 1, 2017. A review of the designs and prominent biomedical advances of natural and synthetic hydrogel formulations. Eur. Polym. J. 88, 373–392.
Haji-Saeid, M., Safrany, A., Sampa, M.H., Ramamoorthy, N., March 1, 2010. Radiation processing of natural polymers: the IAEA contribution. Radiat. Phys. Chem. 79 (3), 255–260.
Han, S.S., 2005. Topical formulations of water-soluble chitin as a wound healing assistant-evaluation on open wounds using a rabbit ear model. Fibers Polym. 6 (3), 219–223.

UNCORRECTED PROOF

Harding, K.G., Edwards, R., April 2004. Bacteria and wound healing. Curr. Opin. Infect. Dis. 17, 91–96.

Hardman, M.J., Ashcroft, G.S., May 2008. Estrogen, not intrinsic aging, is the major regulator of delayed human wound healing in the elderly. Genome Biol. 9 (5), 1–7.

Hofman, D., Moore, K., Cooper, R., Eagle, M., Cooper, S., May 2007. Use of topical corticosteroids on chronic leg ulcers. J. Wound Care 16 (5), 227–230.

Hsu, L.C., Peng, B.Y., Chen, M.S., Thalib, B., Ruslin, M., Tung, T.D., Chou, H.H., Ou, K.L., February 2019. The potential of the stem cells composite hydrogel wound dressings for promoting wound healing and skin regeneration: in vitro and in vivo evaluation. J. Biomed. Mater. Res. B Appl. Biomater. 107 (2), 278–285.

Huang, S., Fu, X., March 3, 2010. Naturally derived materials-based cell and drug delivery systems in skin regeneration. J. Contr. Release 142 (2), 149–159.

Kausar, A., May 24, 2019. Poly (methyl methacrylate) nanocomposite reinforced with graphene, graphene oxide, and graphite: a review. Polym.-Plast. Technol. Mater. 58 (8), 821–842.

Kempf, M., Miyamura, Y., Liu, P.Y., Chen, A.C., Nakamura, H., Shimizu, H., Tabata, Y., Kimble, R.M., McMillan, J.R., July 1, 2011. A denatured collagen microfiber scaffold seeded with human fibroblasts and keratinocytes for skin grafting. Biomaterials 32 (21), 4782–4792.

Kennedy, J.F., Knill, C.J., Thorley, M., January 1, 2001. Natural polymers for healing wounds. In: Recent Advances in Environmentally Compatible Polymers. Woodhead Publishing, pp. 97–104.

Keylock, K.T., Vieira, V.J., Wallig, M.A., DiPietro, L.A., Schrementi, M., Woods, J.A., January 2008. Exercise accelerates cutaneous wound healing and decreases wound inflammation in aged mice. Am. J. Physiol. Regul. Integr. Comp. Physiol. 294 (1), R179–R184.

Khan, I., Saeed, K., Khan, I., November 1, 2019. Nanoparticles: properties, applications and toxicities. Arab. J. Chem. 12 (7), 908–931.

Khorasani, M.T., Joorabloo, A., Moghaddam, A., Shamsi, H., MansooriMoghadam, Z., July 15, 2018. Incorporation of ZnO nanoparticles into heparinised polyvinyl alcohol/chitosan hydrogels for wound dressing application. Int. J. Biol. Macromol. 114, 1203–1215.

Kirchner, L.M., Meerbaum, S.O., Gruber, B.S., Knoll, A.K., Bulgrin, J., Taylor, R.A., Schmidt, S.P., March 2003. Effects of vascular endothelial growth factor on wound closure rates in the genetically diabetic mouse model. Wound Repair Regen. 11 (2), 127–131.

Lee, K.Y., Jeong, L., Kang, Y.O., Lee, S.J., Park, W.H., October 5, 2009. Electrospinning of polysaccharides for regenerative medicine. Adv. Drug Deliv. Rev. 61 (12), 1020–1032.

Lehtovaara, B.C., Gu, F.X., July 13, 2011. Pharmacological, structural, and drug delivery properties and applications of 1,3-β-glucans. J. Agric. Food Chem. 59 (13), 6813–6828.

Li, H., Yang, J., Hu, X., Liang, J., Fan, Y., Zhang, X., July 2011. Superabsorbent polysaccharide hydrogels based on pullulan derivate as antibacterial release wound dressing. J. Biomed. Mater. Res. 98 (1), 31–39.

Li, X., Kong, X., Zhang, Z., Nan, K., Li, L., Wang, X., Chen, H., June 1, 2012. Cytotoxicity and biocompatibility evaluation of N, O-carboxymethyl chitosan/oxidized alginate hydrogel for drug delivery application. Int. J. Biol. Macromol. 50 (5), 1299–1305.

Liao, J., Jia, Y., Wang, B., Shi, K., Qian, Z., February 6, 2018. Injectable hybrid poly (ε-caprolactone)-b-poly (ethylene glycol)-b-poly (ε-caprolactone) porous microspheres/alginate hydrogel cross-linked by calcium gluconate crystals deposited in the pores of

UNCORRECTED PROOF

microspheres improved skin wound healing. ACS Biomater. Sci. Eng. 4 (3), 1029–1036.
Logeart-Avramoglou, D., Jozefonvicz, J., 1999. Carboxymethyl benzylamide sulfonate dextrans (CMDBS), a family of biospecific polymers endowed with numerous biological properties: a review. J. Biomed. Mater. Res. 48 (4), 578–590.
Lumbreras-Aguayo, A., Meléndez-Ortiz, H.I., Puente-Urbina, B., Alvarado-Canché, C., Ledezma, A., Romero-García, J., Betancourt-Galindo, R., February 1, 2019. Poly (methacrylic acid)-modified medical cotton gauzes with antimicrobial and drug delivery properties for their use as wound dressings. Carbohydr. Polym. 205, 203–210.
Madhumathi, K., Sudheesh Kumar, P.T., Abhilash, S., Sreeja, V., Tamura, H., Manzoor, K., Nair, S.V., Jayakumar, R., February 2010. Development of novel chitin/nanosilver composite scaffolds for wound dressing applications. J. Mater. Sci. Mater. Med. 21, 807–813.
Masood, F., March 1, 2016. Polymeric nanoparticles for targeted drug delivery system for cancer therapy. Mater. Sci. Eng. C 60, 569–578.
Masood, N., Ahmed, R., Tariq, M., Ahmed, Z., Masoud, M.S., Ali, I., Asghar, R., Andleeb, A., Hasan, A., March 25, 2019. Silver nanoparticle impregnated chitosan-PEG hydrogel enhances wound healing in diabetes induced rabbits. Int. J. Pharm. 559, 23–36.
Medusheva, E.O., Filatov, V.N., Ryl'tsev, V.V., Kazakova, N.A., Filatov, N.V., Kulagina, A.S., Avagyan, A.A., July 2007. New medical materials with an integral lasting effect based on fibre-forming polymers. Fibre Chem. 39 (4), 268–271.
Menke, N.B., Ward, K.R., Witten, T.M., Bonchev, D.G., Diegelmann, R.F., January 1, 2007. Impaired wound healing. Clin. Dermatol. 25 (1), 19–25.
Miao, J., Pangule, R.C., Paskaleva, E.E., Hwang, E.E., Kane, R.S., Linhardt, R.J., Dordick, J.S., December 1, 2011. Lysostaphin-functionalized cellulose fibers with antistaphylococcal activity for wound healing applications. Biomaterials 32 (36), 9557–9567.
Mitra, T., Sailakshmi, G., Gnanamani, A., Raja, S.T., Thiruselvi, T., Gowri, V.M., Selvaraj, N.V., Ramesh, G., Mandal, A.B., March 1, 2011. Preparation and characterization of a thermostable and biodegradable biopolymers using natural cross-linker. Int. J. Biol. Macromol. 48 (2), 276–285.
Mogoşanu, G.D., Grumezescu, A.M., March 25, 2014. Natural and synthetic polymers for wounds and burns dressing. Int. J. Pharm. 463 (2), 127–136.
Mohamed, R.M., Yusoh, K., 2016. A review on the recent research of polycaprolactone (PCL). Adv. Mater. Res. 1134, 249–255.
Morganti, P., Morganti, G., Morganti, A., December 6, 2011. Transforming nanostructured chitin from crustacean waste into beneficial health products: a must for our society. Nanotechnol. Sci. Appl. 4, 123–129.
Murali, R., Anumary, A., Ashokkumar, M., Thanikaivelan, P., Chandrasekaran, B., August 2011. Hybrid biodegradable films from collagenous wastes and natural polymers for biomedical applications. Waste Biomass Valorization 2, 323–335.
Norouzi, M.A., Montazer, M., Harifi, T., Karimi, P., January 1, 2021. Flower buds like PVA/ZnO composite nanofibers assembly: antibacterial, in vivo wound healing, cytotoxicity and histological studies. Polym. Test. 93, 106914.
Orlowski, P., Zmigrodzka, M., Tomaszewska, E., Ranoszek-Soliwoda, K., Czupryn, M., Antos-Bielska, M., Szemraj, J., Celichowski, G., Grobelny, J., Krzyzowska, M., 2018. Tannic acid-modified silver nanoparticles for wound healing: the importance of size. Int. J. Nanomed. 13, 991.
Peng, Y., Song, C., Yang, C., Guo, Q., Yao, M., 2017. Low molecular weight chitosan-coated silver nanoparticles are effective for the treatment of MRSA-infected wounds.

UNCORRECTED PROOF

Int. J. Nanomed. 12, 295.
Pertici, G., January 1, 2017. Introduction to bioresorbable polymers for biomedical applications. In: Bioresorbable Polymers for Biomedical Applications. Woodhead Publishing, pp. 3–29.
Pieringer, H., Stuby, U., Biesenbach, G., April 1, 2007. Patients with rheumatoid arthritis undergoing surgery: how should we deal with antirheumatic treatment? In: Seminars in Arthritis and Rheumatism, 36(5). WB Saunders, pp. 278–286.
Piran, M., Vakilian, S., Piran, M., Mohammadi-Sangcheshmeh, A., Hosseinzadeh, S., Ardeshirylajimi, A., October 31, 2018. In vitro fibroblast migration by sustained release of PDGF-BB loaded in chitosan nanoparticles incorporated in electrospun nanofibers for wound dressing applications. Artif. Cell Nanomed. Biotechnol. 46 (Suppl. 1), 511–520.
Rai, M., Yadav, A., Gade, A., January 1, 2009. Silver nanoparticles as a new generation of antimicrobials. Biotechnol. Adv. 27 (1), 76–83.
Ramnath, V., Sekar, S., Sankar, S., Sastry, T.P., Mandal, A.B., 2012. In vivo evaluation of composite wound dressing material containing soya protein and sago starch. Int. J. Pharm. Sci. 4 (2), 414–419.
Rodriguez, P.G., Felix, F.N., Woodley, D.T., Shim, E.K., September 2008. The role of oxygen in wound healing: a review of the literature. Dermatol. Surg. 34 (9), 1159–1169.
Sahana, T.G., Rekha, P.D., December 2018. Biopolymers: applications in wound healing and skin tissue engineering. Mol. Biol. Rep. 45, 2857–2867.
Saporito, F., Sandri, G., Bonferoni, M.C., Rossi, S., Boselli, C., Cornaglia, A.I., Mannucci, B., Grisoli, P., Vigani, B., Ferrari, F., 2018. Essential oil-loaded lipid nanoparticles for wound healing. Int. J. Nanomed. 13, 175.
Sawant, S.V., Sankpal, S.V., Jadhav, K.R., Kadam, V.J., 2012. Hydrogel as drug delivery system. Res. J. Pharm. Technol. 5 (5), 561–569.
Şen, M., Avcı, E.N., 2005. Radiation synthesis of poly (N-vinyl-2-pyrrolidone)–κ-carrageenan hydrogels and their use in wound dressing applications. I. Preliminary laboratory tests. J. Biomed. Mater. Res. A 74 (2), 187–196.
Shahverdi, S., Hajimiri, M., Esfandiari, M.A., Larijani, B., Atyabi, F., Rajabiani, A., Dehpour, A.R., Gharehaghaji, A.A., Dinarvand, R., October 1, 2014. Fabrication and structure analysis of poly (lactide-co-glycolic acid)/silk fibroin hybrid scaffold for wound dressing applications. Int. J. Pharm. 473 (1–2), 345–355.
Shen, X., Nagai, N., Murata, M., Nishimura, D., Sugi, M., Munekata, M., December 2008. Development of salmon milt DNA/salmon collagen composite for wound dressing. J. Mater. Sci. Mater. Med. 19, 3473–3479.
Silva, G.A., Vaz, C.M., Coutinho, O.P., Cunha, A.M., Reis, R.L., December 2003. In vitro degradation and cytocompatibility evaluation of novel soy and sodium caseinate-based membrane biomaterials. J. Mater. Sci. Mater. Med. 14, 1055–1066.
Szabo, G., Mandrekar, P., February 2009. A recent perspective on alcohol, immunity, and host defense. Alcohol Clin. Exp. Res. 33 (2), 220–232.
Urie, R., Ghosh, D., Ridha, I., Rege, K., June 4, 2018. Inorganic nanomaterials for soft tissue repair and regeneration. Annu. Rev. Biomed. Eng. 20, 353–374.
Venkataprasanna, K.S., Prakash, J., Vignesh, S., Bharath, G., Venkatesan, M., Banat, F., Sahabudeen, S., Ramachandran, S., Venkatasubbu, G.D., January 15, 2020. Fabrication of Chitosan/PVA/GO/CuO patch for potential wound healing application. Int. J. Biol. Macromol. 143, 744–762.
Vetvicka, V., Vetvickova, J., September 2011. β (1-3)-D-glucan affects adipogenesis, wound healing and inflammation. Orient. Pharm. Exp. Med. 11, 169–175.
Vileikyte, L., January 1, 2007. Stress and wound healing. Clin. Dermatol. 25 (1), 49–55.
Wagner, A.E., Huck, G., Stiehl, D.P., Jelkmann, W., Hellwig-Bürgel, T., July 25, 2008.

UNCORRECTED PROOF

Dexamethasone impairs hypoxia-inducible factor-1 function. Biochem. Biophys. Res. Commun. 372 (2), 336–340.
Weyers, A., Linhardt, R.J., May 2013. Neoproteoglycans in tissue engineering. FEBS J. 280 (10), 2511–2522.
Woo, K., Ayello, E.A., Sibbald, R.G., February 1, 2007. The edge effect: current therapeutic options to advance the wound edge. Adv. Skin Wound Care 20 (2), 99–117.
Zhang, Z., Ortiz, O., Goyal, R., Kohn, J., January 1, 2014. Biodegradable polymers. In: Handbook of Polymer Applications in Medicine and Medical Devices. pp. 303–335.
Zhu, X.Y., Li, Y.L., Xie, F., Zhang, Y.J., Huang, S.N., Li, M.Z., Qiu, Y.H., September 17, 2011. Activation of T lymphocytes on local trauma after implantation of regenerated porous silk fibroin film. Chin. J. Tissue Eng. Res. 15 (38), 7061.

UNCORRECTED PROOF

WOODHEAD PUBLISHING SERIES IN BIOMATERIALS



BIORESORBABLE POLYMERS AND THEIR COMPOSITES

CHARACTERIZATION AND FUNDAMENTAL PROCESSING FOR PHARMACEUTICAL AND MEDICAL DEVICE DEVELOPMENT

Edited by
DEEPAK VERMA
MANUNYA OKHAWILAI
KHENG-LIM GOH
SEERAM RAMAKRISHNA
POORIA PASBAKHSH
MOHIT SHARMA

ELSEVIER

BIORESORBABLE POLYMERS AND THEIR COMPOSITES

This page intentionally left blank

Woodhead Publishing Series in Biomaterials

BIORESORBABLE POLYMERS AND THEIR COMPOSITES

Characterization and Fundamental Processing for Pharmaceutical and Medical Device Development

Edited by

DEEPAK VERMA

Nanoscience and Technology, Chulalongkorn University, Bangkok, Thailand; GEHU, Dehradun, India

MANUNYA OKHAWILAI

Metallurgy and Materials Science Research Institute, Chulalongkorn University, Bangkok, Thailand

KHENG LIM GOH

Newcastle University in Singapore, Singapore

SEERAM RAMAKRISHNA

National University of Singapore (NUS), Singapore

POORIA PASBAKHSH

Monash University Malaysia, Selangor Darul Ehsan, Malaysia

MOHIT SHARMA

A*STAR (Agency for Science, Technology and Research), Singapore





Woodhead Publishing is an imprint of Elsevier
50 Hampshire Street, 5th Floor, Cambridge, MA 02139, United States
The Boulevard, Langford Lane, Kidlington, OX5 1GB, United Kingdom

Copyright © 2024 Elsevier Ltd. All rights reserved.

No part of this publication may be reproduced or transmitted in any form or by any means, electronic or mechanical, including photocopying, recording, or any information storage and retrieval system, without permission in writing from the publisher. Details on how to seek permission, further information about the Publisher's permissions policies and our arrangements with organizations such as the Copyright Clearance Center and the Copyright Licensing Agency, can be found at our website: www.elsevier.com/permissions.

This book and the individual contributions contained in it are protected under copyright by the Publisher (other than as may be noted herein).

Notices

Knowledge and best practice in this field are constantly changing. As new research and experience broaden our understanding, changes in research methods, professional practices, or medical treatment may become necessary.

Practitioners and researchers must always rely on their own experience and knowledge in evaluating and using any information, methods, compounds, or experiments described herein. In using such information or methods they should be mindful of their own safety and the safety of others, including parties for whom they have a professional responsibility.

To the fullest extent of the law, neither the Publisher nor the authors, contributors, or editors, assume any liability for any injury and/or damage to persons or property as a matter of products liability, negligence or otherwise, or from any use or operation of any methods, products, instructions, or ideas contained in the material herein.

ISBN: 978-0-443-18915-9

For information on all Woodhead Publishing publications visit our website at https://www.elsevier.com/books-and-journals

Publisher: Matthew Deans
Acquisitions Editor: Sabrina Webber
Editorial Project Manager: Rafael Guilherme Trombaco
Production Project Manager: Prem Kumar Kaliamoorthi
Cover Designer: Matthew Limbert

Typeset by TNQ Technologies



Dedication

Dedicated to my beloved parents, my wife, Shalini, and my sweet daughters, Aadya and Anaya, who motivate and support me throughout the entire journey of this book publication.

— **Deepak Verma**

This page intentionally left blank

Contents

Contributors *xv*
About the editors *xxi*
Preface *xxv*

SECTION 1 Fundamentals, processing, and modelling

1. Introduction to bioresorbable polymers: Types and biomedical applications **3**

Deepak Verma, Manunya Okhawilai, Kheng Lim Goh, Mohit Sharma, Pooria Pasbakhsh and Seeram Ramakrishna

1.1 Introduction 3
1.2 Bioresorbable polymers and their classifications: An overview 5
1.3 Polymer degradation: An overview 10
1.4 Bioresorbable polymer resorption process 11
1.5 Bioresorbable polymers and their biomedical applications 14
1.6 Conclusion 17
References 18

2. Bioresorbable polymers and their composites for biomedical applications **23**

Oludaisi Adekomaya and Thokozani Majozi

2.1 Introduction 23
2.2 Salient properties of bioresorbable materials for biomedical application 28
2.3 Performance of bioresorbable materials in medical interventions 33
2.4 Conclusion 37
Acknowledgments 39
References 39

3. Processing techniques for bioresorbable-based composites for medical device applications **41**

Nadda Chiaoprakobkij and Manunya Okhawilai

3.1 2D structure 41
3.2 3D structure 48
3.3 Micro-molding 55
3.4 Particulate structures 57

3.5 Conclusion and outlook 59
References 59

4. PCL-based composites and their utilizations in the medical sector 63

Deepak Gupta, Vaishally Dogra, Deepak Verma, Arun Kumar Chaudhary and Maneesh Tewari

4.1 Introduction to biopolymer composites 63
4.2 Development and synthesis of PCL 64
4.3 Advantages of PCL-based composites in the medical sector 67
4.4 Applications of PCL in different medical sectors 68
4.5 Challenges and future of PCL in the medical sector 77
4.6 Conclusion 78
References 78

5. Processing of PLA/PLLA-based composites for medical device applications 85

Deepak Gupta, Vaishally Dogra, Deepak Verma, Arun Kumar Chaudhary and Maneesh Tewari

5.1 Introduction 85
5.2 The chemical structure and synthesis of PLA/PLLA polymers 87
5.3 The physical and thermal characteristics of PLA/PLLA polymers 88
5.4 PLA/PLLA-based composites fabrication methods 90
5.5 Biocompatibility and biodegradability of PLA/PLLA composites 92
5.6 Applications of PLA/PLLA composites in the medical sector 92
5.7 Future perspectives 101
5.8 Conclusion 101
References 101

6. PHA/PHB/PHBV-based composites: development and biomedical applications 107

Ivana Cesarino, Ivan Moroz, Afonso Freitas Carbonera, Guilherme de Oliveira Martins, Luís Guilherme Leite Fernandes and Alcides Lopes Leao

6.1 Introduction 107
6.2 Polyhydroxyalkanoates (PHA) 108
6.3 Polyhydroxybutyrate (PHB) 112
6.4 Poly(hydroxybutyrate-co-hydroxyvalerate) (PHBV) 115
6.5 Conclusion 120
References 120

7. Synthesis and applications of bioresorbable polymers for tissue engineering scaffolds 125

Emenike George Okonkwo, Jesus Romo-Rico, Chinemerem Jerry Ozoude and Kingsley Job Obasi

7.1 Introduction 125
7.2 Synthesis of bioresorbable polymers 126
7.3 Applications of bioresorbable tissue scaffold 135
7.4 Future trends 138
7.5 Conclusion 139
References 140

8. Gelation and fabrication of bioresorbable-based hydrogels for drug-release applications 147

Chuanchom Aumnate, Chaimongkol Saengow and Manunya Okhawilai

8.1 Introduction 147
8.2 Cross-linking of hydrogels 148
8.3 Hydrogel fabrication 157
8.4 Conclusion 165
References 166

9. Molecular modeling of polymers for efficient drug-carrier applications 169

Rosaline Mishra, Dinesh Puri, Radha Goel, Praveen Kumar Gaur, Prasoon Kumar Saxena, Niharika Lal and Kanak Lata

9.1 Introduction 169
9.2 Methods for molecular simulation for designing polymers 171
9.3 Applications of the polymer-based smart nanocarriers 175
9.4 Conclusion 188
References 189
Further reading 194

10. Electrospinning technique: A potential method to develop bioresorbable-based medical devices 197

Senthilkumar Nangan, Natesan Thirumalaivasan and Ramasubburayan Ramasamy

10.1 Introduction 197
10.2 Fundamentals of electrospinning 198

10.3 Application of electrospun nanofiber membranes in medical protective equipment 205
10.4 Conclusion 209
References 210

11. Modeling of drug release from a bioresorbable polymer matrix system 213

Mohd Yasir, Dinesh Puri, Manikandan Arumugam, Wondesen G. Gobena, Mohammed Hussien Wondabo, S. Roshan and K.M. Noorulla

11.1 Introduction 213
11.2 Biodegradable/bioresorbable polymers 214
11.3 Factors affecting drug release from polymers 216
11.4 Diffusion law 217
11.5 Fundamentals of drug-release kinetics 219
11.6 Need for and objectives of mathematical models 221
11.7 Release kinetic modeling 222
11.8 How to select the best-fitting model 242
11.9 Conclusion and future perspectives 248
List of abbreviations 249
References 250

SECTION 2 Biomedical applications

12. Bioresorbable polymers: A prospective utilization as an implant 259

Shuai Chen, K. M. Faridul Hasan and Xiaoyi Liu

12.1 Introduction 259
12.2 Characteristics of bioabsorbable polymers as implants 262
12.3 Application of bioabsorbable polymers 264
12.4 Conclusion 272
References 272

13. Polymeric (PLGA-based) nanocomposites for application in drug delivery: Current state of the art and forthcoming perspectives 277

Sanket Kumar, Supriya Singh, Sheikh Shahnawaz Quadir, Garima Joshi, Mangilal Chouhan, Dinesh Puri and Deepak Choudhary

13.1 Introduction 277
13.2 PLGA properties 280

13.3 PLGA nanocomposite carriers: fabrication techniques 284
13.4 Applications of PLGA nanocomposites 293
13.5 Conclusions and future prospects 312
Abbreviations 313
References 314

14. Bioresorbable polymers: Challenges and opportunities for development and applications of medical devices 325

Pornnapa Kasemsiri, Kaewta Jetsrisuparb, Jesper T.N. Knijnenburg and Manunya Okhawilai

14.1 Introduction 325
14.2 Bioresorbable polymers for drug-delivery systems 326
14.3 Bioresorbable polymers for medical devices 330
14.4 Bioresorbable polymers for tissue engineering 330
14.5 Conclusions 346
References 347

15. Bioresorbable polymers for wound healing 353

Sheikh Shahnawaz Quadir, Dinesh Puri, Garima Joshi, Deepak Choudhary, Sanket Kumar, Monika Singh and Shalini K. Sawhney

15.1 Introduction 353
15.2 Wound-healing process 355
15.3 Factors affecting wound healing 356
15.4 Properties of bioresorbable polymers 363
15.5 Bioresorbable polymers for wound healing 364
15.6 Nanocomposites for wound healing 372
15.7 Conclusion and future perspectives 377
References 378

16. Bioresorbable polymers/HNT blend composite wound dressings 385

Deepak Gupta, Arun Kumar Chaudhary, Deepak Verma and Mohit Sharma

16.1 Introduction to bioresorbable polymers 385
16.2 Classifications of bioresorbable polymers 389
16.3 Halloysite nanotubes 391

16.4 Bioresorbable polymer-based HNT composites 393
16.5 Mechanical properties of HNT-reinforced polymer blends 394
16.6 Antibacterial activity of HNT—polymer blends 395
16.7 Drug-delivery capacity of HNT—polymer blends 397
16.8 Wound dressings based on HNT—polymer blends 405
16.9 Challenges and limitations of HNT—polymer blends 412
16.10 Future prospects of HNT—polymer blends in biomedical applications 413
16.11 Conclusion 414
References 414

17. Biobehavioral structure, elastic, optical, and thermoluminescence properties of $Al_xCa_{y-x}Nd_{01}P_{70}$ bioglasses 421

Ravi Kumar Guntu

17.1 Introduction 421
17.2 Methods and measurements 422
17.3 Results and discussion 423
17.4 Summary and conclusion 439
References 439

18. A prospective utilization of biodegradable polymers for controlled drug-delivery applications 443

Dinesh Puri, Deepak Choudhary, Mohd Yasir, Rosaline Mishra, Sanjay Sharma, Radha Goel and Praveen Kumar Gaur

18.1 Introduction 443
18.2 Classification of biodegradable polymers for CDDS 445
18.3 Application of biodegradable polymers in drug delivery 451
18.4 Mechanism involved in controlled release through polymers 452
18.5 Release kinetic 457
18.6 Examples of commercially available biodegradable polymer base products 457
18.7 Conclusion 460
References 460

19. Bioresorbable polymer-based sensors for medical applications 469

Thirumalaivasan Natesan, Senthilkumar Nangan and Ramasubburayan Ramasamy

19.1 Introduction 469
19.2 The essential principles of biodegradable polymers and their pertinent physiochemical attributes for medical utilization 470
19.3 A comprehensive review of current biodegradable sensing devices, classified according to their healthcare functionalities such as cardiac surveillance, glycemic level monitoring, and ophthalmic pressure assessment 473
19.4 An overview of the fabrication techniques for bioresorbable polymer-based sensors 476
19.5 Physical sensors 481
19.6 Chemical sensors 486
19.7 Conclusion 487
References 488

Index *495*

This page intentionally left blank

Contributors

Oludaisi Adekomaya
Sustainable Process Engineering, School of Chemical and Metallurgical Engineering, Faculty of Engineering and Built Environment, University of the Witwatersrand, Johannesburg, South Africa

Manikandan Arumugam
Department of Pharmaceutical Engineering and Technology, Indian Institute of Technology, BHU, Varanasi, Uttar Pradesh, India

Chuanchom Aumnate
Metallurgy and Materials Science Research Institute, Chulalongkorn University, Bangkok, Thailand; Center of Excellence in Responsive Wearable Materials, Chulalongkorn University, Bangkok, Thailand

Afonso Freitas Carbonera
São Paulo State University (UNESP), School of Agriculture, Botucatu, Brazil

Ivana Cesarino
São Paulo State University (UNESP), School of Agriculture, Botucatu, Brazil

Arun Kumar Chaudhary
Department of Industrial and Production Engineering, College of Technology, Govind Ballabh Pant University of Agriculture and Technology, Pantnagar, Uttarakhand, India

Shuai Chen
Department of Biochemistry and Molecular Biology, College of Basic Medical Sciences, Guizhou Medical University, Guiyang, China

Nadda Chiaoprakobkij
Metallurgy and Materials Science Research Institute, Chulalongkorn University, Bangkok, Thailand

Deepak Choudhary
Department of Pharmaceutical Sciences, Mohanlal Sukhadia University, Udaipur, Rajasthan, India

Mangilal Chouhan
Department of Pharmaceutical Sciences, Mohanlal Sukhadia University, Udaipur, Rajasthan, India

Vaishally Dogra
Department of Mechanical Engineering, Graphic Era Deemed to be University, Dehradun, Uttarakhand, India; Department of Mechanical Engineering, Graphic Era Hill University, Dehradun, Uttarakhand, India

Luís Guilherme Leite Fernandes
São Paulo State University (UNESP), Institute of Biosciences, Botucatu, Brazil

Praveen Kumar Gaur
Metro College of Health Sciences and Research, Greater Noida, Uttar Pradesh, India

Wondesen G. Gobena
Department of Pharmacy, College of Health Sciences, Arsi University, Asella, Ethiopia

Radha Goel
Lloyd Institute of Management and Technology, Greater Noida, Uttar Pradesh, India

Kheng Lim Goh
Faculty of Science, Agriculture and Engineering, Newcastle University, Newcastle Upon Tyne, United Kingdom; Newcastle University in Singapore, Singapore

Ravi Kumar Guntu
Department of Physics, Sreenidhi Institute of Science and Technology, JNT University, Hyderabad, Telangana, India

Deepak Gupta
Department of Industrial and Production Engineering, College of Technology, Govind Ballabh Pant University of Agriculture and Technology, Pantnagar, Uttarakhand, India

K. M. Faridul Hasan
Simonyi Károly Faculty of Engineering, University of Sopron, Sopron, Hungary

Kaewta Jetsrisuparb
Sustainable Infrastructure Research and Development Center and Department of Chemical Engineering, Faculty of Engineering, Khon Kaen University, Khon Kaen, Thailand

Garima Joshi
Department of Pharmaceutical Sciences, Mohanlal Sukhadia University, Udaipur, Rajasthan, India

Pornnapa Kasemsiri
Sustainable Infrastructure Research and Development Center and Department of Chemical Engineering, Faculty of Engineering, Khon Kaen University, Khon Kaen, Thailand

Jesper T.N. Knijnenburg
Biodiversity and Environmental Management Division, International College, Khon Kaen University, Khon Kaen, Thailand

Sanket Kumar
Department of Pharmaceutical Sciences, Mohanlal Sukhadia University, Udaipur, Rajasthan, India

Niharika Lal
Metro College of Health Sciences and Research, Greater Noida, Uttar Pradesh, India

Kanak Lata
Metro College of Health Sciences and Research, Greater Noida, Uttar Pradesh, India

Alcides Lopes Leao
São Paulo State University (UNESP), School of Agriculture, Botucatu, Brazil

Xiaoyi Liu
The Key Laboratory of Environmental Pollution Monitoring and Disease Control, Ministry of Education, Department of Nutrition and Food Hygiene, School of Public Health, Guizhou Medical University, Guizhou, China

Thokozani Majozi
Sustainable Process Engineering, School of Chemical and Metallurgical Engineering, Faculty of Engineering and Built Environment, University of the Witwatersrand, Johannesburg, South Africa

Guilherme de Oliveira Martins
São Paulo State University (UNESP), School of Agriculture, Botucatu, Brazil

Rosaline Mishra
Metro College of Health Sciences and Research, Greater Noida, Uttar Pradesh, India

Ivan Moroz
São Paulo State University (UNESP), School of Agriculture, Botucatu, Brazil

Senthilkumar Nangan
Department of Chemistry, Graphic Era (Deemed to be University), Dehradun, Uttarakhand, India

Thirumalaivasan Natesan
Department of Periodontics, Saveetha Dental College and Hospitals, Saveetha Institute of Medical and Technical Sciences (SIMATS), Saveetha University, Chennai, Tamil Nadu, India

K.M. Noorulla
Department of Pharmacy, College of Health Sciences, Arsi University, Asella, Ethiopia

Kingsley Job Obasi
Department of Mechanical Engineering, University of Nigeria, Nsukka, Enugu, Nigeria

Manunya Okhawilai
Metallurgy and Materials Science Research Institute, Chulalongkorn University, Bangkok, Thailand; Research Unit in Polymeric Materials for Medical Practice Devices, Department of Chemical Engineering, Faculty of Engineering, Chulalongkorn University, Bangkok, Thailand; Center of Excellence in Polymeric Materials for Medical Practice Devices, Department of Chemical Engineering, Faculty of Engineering, Chulalongkorn University, Bangkok, Thailand; Center of Excellence in Responsive Wearable Materials, Chulalongkorn University, Bangkok, Thailand

Emenike George Okonkwo
College of Science and Engineering, James Cook University, Townsville, QLD, Australia; Department of Metallurgical and Materials Engineering, University of Nigeria, Nsukka, Enugu, Nigeria

Chinemerem Jerry Ozoude
Department of Metallurgical and Materials Engineering, University of Nigeria, Nsukka, Enugu, Nigeria; Department of Materials Science and Engineering, University of North Texas, Denton, TX, United States

Pooria Pasbakhsh
Mechanical Engineering Discipline, School of Engineering, Monash University Malaysia, Subang Jaya, Selangor, Malaysia

Dinesh Puri
School of Pharmacy, Graphic Era Hill University, Dehradun, Uttarakhand, India

Sheikh Shahnawaz Quadir
Department of Pharmaceutical Sciences, Mohanlal Sukhadia University, Udaipur, Rajasthan, India

Seeram Ramakrishna
Department of Mechanical Engineering, National University of Singapore, Singapore

Ramasubburayan Ramasamy
Marine Biomedical Research Laboratory & Environmental Toxicology Unit, Department of Prosthodontics, Saveetha Dental College and Hospitals (SIMATS), Saveetha University, Chennai, Tamil Nadu, India

Jesus Romo-Rico
Electronics Materials Lab, College of Science and Engineering, James Cook University, Townsville, QLD, Australia

S. Roshan
Deccan School of Pharmacy, Darussalam Aghapura, Hyderabad, Telangana, India

Chaimongkol Saengow
Beckman Institute for Advanced Science and Technology, University of Illinois at Urbana-Champaign, Urbana, IL, United States

Shalini K. Sawhney
I.T.S. College of Pharmacy, Ghaziabad, Uttarpradesh, India

Prasoon Kumar Saxena
Sunder Deep Pharmacy College, Ghaziabad, Uttar Pradesh, India

Mohit Sharma
Institute of Materials Research and Engineering (IMRE), Agency for Science, Technology and Research (A*STAR), Singapore, Singapore

Sanjay Sharma
Shobhaben Pratapbhai Patel School of Pharmacy and Technology Management, SVKM's Narsee Monjee Institute of Management Studies, Mumbai, Maharashtra, India

Supriya Singh
Department of Pharmaceutical Sciences, Mohanlal Sukhadia University, Udaipur, Rajasthan, India

Monika Singh
I.T.S. College of Pharmacy, Ghaziabad, Uttarpradesh, India

Maneesh Tewari
Department of Industrial and Production Engineering, College of Technology, Govind Ballabh Pant University of Agriculture and Technology, Pantnagar, Uttarakhand, India

Natesan Thirumalaivasan
Department of Periodontics, Saveetha Dental College and Hospitals, Saveetha Institute of Medical and Technical Sciences (SIMATS), Saveetha University, Chennai, Tamil Nadu, India

Deepak Verma
International Graduate Program of Nanoscience and Technology, Chulalongkorn University, Bangkok, Thailand; Department of Mechanical Engineering, Graphic Era Hill University, Dehradun, Uttarakhand, India

Mohammed Hussien Wondabo
Department of Pharmacy, College of Health Sciences, Arsi University, Asella, Ethiopia

Mohd Yasir
Department of Pharmacy, College of Health Sciences, Arsi University, Asella, Ethiopia

This page intentionally left blank

About the editors

Deepak Verma

Deepak Verma is currently working as a Research Assistant in the Department of Nanoscience and Technology, Graduate School, Chulalongkorn University, Bangkok, Thailand. He also served as an Assistant Professor, in the Department of Mechanical Engineering, at Graphic Era Hill University, Dehradun, India. He received his MTech from the College of Technology, GBPUA&T Pantnagar, India. He has over 13 year of teaching and research experience in developing advanced materials such as electrospun membranes for biomedical applications and natural fiber-based polymer composites or green composites for advanced and sustainable applications. Deepak Verma was the editor of *Biomass, Biopolymer-Based Materials, and Bioenergy*, Woodhead Publishing House, Elsevier; and *Sustainable Biopolymer Composites*, Woodhead Publishing House, Elsevier. He is currently working in the area of medical devices and their applications. Overall, he has published more than 35 book chapters with Elsevier and other publishers, and more than 25 international journal papers in reputed journals with high impact factors.

Manunya Okhawilai

Dr. Manunya Okhawilai, Head of Materials and Advanced Polymer Technology Laboratory, is a Research Professor at Metallurgy and Materials Science Research Institute, Chulalongkorn University, Bangkok, Thailand. She effectively attained her doctoral degree with a dedicated emphasis on the field of Chemical Engineering specialization. She is particularly interested in polymer blends and polymer composites. Her main research areas are focusing on quasi and solid-state polymer electrolyte and separator for metal ion batteries and flow batteries as well as electrode for hydrogen production and electricity. Furthermore, she has dedicated her research efforts to the development of bioactive packaging using biopolymers and smart strain sensors. She has published book chapters and more than 50 research articles in reputed peer reviewed journals with high impact factors.

Kheng Lim Goh

Dr. Kheng Lim Goh is an Associate Professor and Reader in Mechanics of Composite Materials and Director of Research at Newcastle University in Singapore. He is a Fellow of the Institute of Mechanical Engineers

(FIMechE) and Fellow of the Institute of Physics (FInstP), Chartered Engineer (CEng) and Chartered Physicist (CPhys). He has a long-standing interest in composite materials. His research aims to understand the physical properties of natural and synthetic composite materials and to use this understanding to engineer nanocomposite materials and repair damaged composite materials. Dr. Goh has authored and coauthored over 120 papers in peer-reviewed journals, edited 3 books, and delivered plenary/keynote lectures at several international conferences. Dr. Goh is the author of the book entitled *Discontinuous-Fibre Reinforced Composites: Fundamentals of Stress Transfer and Fracture Mechanics*, published in 2017. Before joining Newcastle University, Dr. Goh held the post of Assistant Professor in Bioengineering at Nanyang Technological University and Senior Lecturer in Mechanical Engineering at Monash University. Dr. Goh received his BSc (Physics, Honors) degree from the National University of Singapore, MSc degree (National University of Singapore) in bioengineering, MSc degree (Aberdeen University) in Medical Physics, followed by Ph.D. (at the University of Aberdeen scholarship) in Biomedical Physics and Bioengineering.

Seeram Ramakrishna

Professor Seeram Ramakrishna is a world-renowned scholar of materials and cross-fields at the National University of Singapore (NUS). He is named among the World's Most Influential Minds (Thomson Reuters); and Top 1% Highly Cited Researchers in the world (Clarivate Analytics). Ioannidis/Stanford University C-score ranks him among top six impactful researchers of the world in materials, biomedical engineering, and enabling and strategic technologies. His publications to date have an H-index of 182 and over 165,152 citations. He is advocating sustainable | living | intelligent biomedical materials. He is the Biomaterials Section Editor of the Elsevier journal *Current Research* in Biomedical Engineering (https://www.sciencedirect.com/journal/current-opinion-in-biomedical-engineering/about/editorial-board), and editorial board member of the Elsevier journal *Biomaterials Advances*. He is an elected Fellow of the American Association for Advancement of Science (AAAS); ASM International; ASME; AIMBE, USA; and UK Royal Academy of Engineering (FREng). He is an elected Fellow of the International Union of Societies of Biomaterials Science and Engineering (*FBSE*).

Pooria Pasbakhsh

Dr. Pooria Pasbakhsh has been an Associate Professor in the School of Engineering at Monash University Malaysia. His research interests include polyurea, clay nanoparticles, self-healing materials, polymer nanocomposites, material characterization, and industrial applications of polymer composites. Dr. Pasbakhsh has published over 100 journal or conference papers, edited/coedited four books, and participated as an invited speaker or chair at several conferences. He has also participated in numerous collaborations aiming to integrate industry needs into academic research, and to support composite and nanomaterial industry applications. Dr. Pasbakhsh is one of the editorial boards of the journal of *Applied Clay Science* and he has been among the Top 2% scientists (Stanford List) from 2020 to 2022.

Mohit Sharma

Dr. Mohit Sharma is working as a Principal Scientist at Advanced Composite Engineering Group at the Institute of Materials Research and Engineering (IMRE), a leading research institute from Singapore's Agency for Science, Technology and Research (A*STAR). His current assignments are focused on lead technology acquisition for advanced composites innovations. He is building team competencies by leading key research activities in liaison with industries, which aim to create social impact and value capture. He is associated with Singapore graduate academy to nurture foreign talent and Ph.D. student training. His focused research includes sustainable and scalable composite material technologies, structural health monitoring, specialty polymers, bioresorbable and bio-compatible composites, composites recycling, and materials for harsh utilities and green initiatives.

This page intentionally left blank

Preface

Bioresorbable materials have been noticed in the last 10 years because of their suitable properties for biomedical applications. Dozens of materials are available, termed bioresorbable, but very few of them are recognized for medical device applications. The bioresorbable materials suitable for medical devices are glycolide-lactide polymers and copolymers, polycaprolactone, polydioxanone, and poly trimethylene carbonate. The applications of bioresorbable materials include but not limited to surgical sutures, orthopedic pins, screws, rods and plates, cardiovascular stents, etc. This book is divided into two parts. Part I is Fundamentals, Processing, and Modeling and Part II is Biomedical Applications. Part I describes an introduction to bioresorbable polymers and their utilizations as tissue scaffolds, drug delivery, implants, and molecular modeling. In Part II, bioresorbable-based polymer composites and their biomedical applications are described.

This book also focuses on the characterization techniques such as SEM, AFM, FTIR, etc. This book also focuses on the variety of biomaterials, their processing, and their usefulness in biomedical sectors. Also, we tried to include some chapters related to bioresorbable polymer processing and its properties. Moreover, this book should represent an indispensable resource for the growing number of scientists, engineers, physicists, and chemists interested in the preparation and applications of bio-based composites and nanocomposites for different final applications; it would be useful for those interested in finding new ideas for potential applications such as medical devices and for industrial scientists active in formulation, fabrication, and repairing of polymer products based on renewable resources.

This book will not be limited to developing polymer composites or nanocomposites. As we can notice from the other available books (listed above), these books only focus on bioresorbable materials and their utilization in the biomedical field. They were not discussing the other useful applications of the bioresorbable polymer-based composites, such as drug release, implants, wound healing, and wound dressing materials. The proposed book will focus on the vast domain of bioresorbable polymers, such as synthetic and biopolymers. The current theme will discuss the drug release mechanism/analysis of the nanomedicine blended with bioresorbable polymers. We will also discuss applications like biosensor

implants and their medical applications as medical devices, drug release, medical textiles, implants, and dressing materials. So, we can say that this book is the blending of the development/processing of the different types (bioresorbable polymers) of composite materials, their analysis (characterization and fracture), modeling of the composites, and biosensors, frequently utilized in the medical sectors.

This book also addresses the sustainable composites development process, including biocompatibility, tissue repair, scaffold development, recyclability, and systematic procedures and methods. It helps as a pertinent reference for readers, undergraduate and postgraduate students, doctors, academicians, researchers, engineers, and scientists interested in this imperative research area. This book's content will be divided into various chapters addressing the key concerns and interpretations. The researchers/readers will benefit by following the content of the different modules and chapters written by expert scientists of the related research areas. They are skillful individuals who own these technologies and/or suggest viable solutions for key associated problems. So, this book will be useful for graduate and postgraduate research scholars to identify the current/existing problems related to implants, wound dressing materials, bone graft materials, dental materials, and suggested tissue repairing and healing methods. A futuristic conclusion will be strategies for adopting novel nanocomposite processing, biocompatibility, ease of production, etc.

We appreciate all the global contributors' commitment and acceptance of chapter invitations, knowledge sharing, and integration of their research skills for writing the chapters and following editorial inputs to make this book project successful. We also thank Woodhead Publishing house and the Elsevier team for their generous cooperation at every book production stage.

CHAPTER 1

Introduction to bioresorbable polymers: Types and biomedical applications

Deepak Verma[1,2], Manunya Okhawilai[3,4], Kheng Lim Goh[5,6], Mohit Sharma[7], Pooria Pasbakhsh[8] and Seeram Ramakrishna[9]

[1]International Graduate Program of Nanoscience and Technology, Chulalongkorn University, Bangkok, Thailand; [2]Department of Mechanical Engineering, Graphic Era Hill University, Dehradun, Uttarakhand, India; [3]Metallurgy and Materials Science Research Institute, Chulalongkorn University, Bangkok, Thailand; [4]Center of Excellence in Polymeric Materials for Medical Practice Devices, Department of Chemical Engineering, Faculty of Engineering, Chulalongkorn University, Bangkok, Thailand; [5]Faculty of Science, Agriculture and Engineering, Newcastle University, Newcastle Upon Tyne, United Kingdom; [6]Newcastle University in Singapore, Singapore; [7]Institute of Materials Research and Engineering (IMRE), Agency for Science, Technology and Research (A*STAR), Singapore, Singapore; [8]Mechanical Engineering Discipline, School of Engineering, Monash University Malaysia, Subang Jaya, Selangor, Malaysia; [9]Department of Mechanical Engineering, National University of Singapore, Singapore

1.1 Introduction

This book is about biomaterials for biomedical applications. The first and foremost requirement of a biomaterial or bioresorbable material is that it should be nontoxic, biocompatible, and can be used for specific applications. The degradation of the polymer in the body is through cellular activity under the biological environment. Enzymes and microbes dominate the biodegradation process, remodeling the human body's degraded part (Ottenbright and Scott, 1992). Not all degradable materials need to be absorbed into the body; it may depend on the transformative step that alters the material's physiological properties/conditions, leading to the transformation/disappearance of the material/implant (Tormala et al., 1986). The most significant condition for an implant material is that it should be biocompatible and nontoxic, and exhibit good physical structure and biomechanical properties (Pulapura and Kohn, 1992). Based on this, different generations of materials have been developed, e.g., first-generation and second-generation materials. The first-generation materials were developed explicitly for good mechanical strength and relatively acceptable "bio-inertness." However, it is difficult for any material to have total

Bioresorbable Polymers and their Composites
ISBN 978-0-443-18915-9
https://doi.org/10.1016/B978-0-443-18915-9.00020-3
© 2024 Elsevier Ltd.
All rights reserved.

inertness, therefore, based on this, second-generation materials have been developed (Pertici, 2017). These materials consider and elicit the specific reactions and responses from the biomaterials and particular cells within the body. Metals and their alloys, ceramics, synthetic polymers, and composites are some other materials primarily utilized for implants because of their excellent mechanical properties, such as toughness, ductility, and high strength. However, the metallic-based implant must be removed after its intended use, requiring second surgery (Agrawal and Ray, 2001).

Conversely, ceramics and glass can serve as substitutes for bones, yet their fragility renders them unsuitable for weight-bearing functions. Polymers, while displaying inferior attributes in comparison to metals, ceramics, and glass, find effective use in bone replacement and fixation due to their ease of manipulation and compatibility with the body (Hench et al., 1971). Polymers should be reinforced with metals, nanoparticles, ceramics, or glasses to attain the specific properties of specific applications. Bioresorbable polymers do not create a corrosion effect as metallic implants may do (Pertici, 2017). Polylactide, polyglycolide, and their copolymers are bioresorbable polymers frequently utilized as surgical implants because of their suitability and chemical stability (Chatterjee et al., 2019). Bioresorbable polymers are also proposed for stent manufacturing and applications. Also, synthetic or natural bioresorbable polymers have found their applications in tissue engineering, regeneration, and tissue scaffolding (Tormala et al., 1986).

Bioresorbable materials have diverse applications in biomedical areas, i.e., implants and suture applications and wearable electronic devices for monitoring health conditions. Microelectromechanical systems-based implants are some examples developed using bioresorbable polymers for real-time monitoring of body parameters, such as temperature, pressure, and cardiovascular activities (Chen et al., 2010). Another significant application of bioresorbable-based implants is drug delivery, associated with the required dosages to fully treat the patient (Millard and Shepherd, 2007). These implant devices themselves select the drug in required/prescribed dosages and deliver it by simulating the nervous system in the body (Park et al., 2015). There may be a problem of infection caused by permanent implants because of the formation of biofilm on the device (Hall-Stoodley et al., 2004). This may result in resurgery of the affected site to remove the infected device, causing further major complications (Kuhn et al., 2012). This problem creates a financial and physical burden for the patient. However, material advancement develops a new class of material with a meager chance of biofilm generation causing infections as they dissolve in

the body after a specific or stipulated timeframe. Also, the patient does not require a second surgery to remove the infected implant device (Boutry et al., 2019; Shin et al., 2019). The potential application of bioresorbable polymers is considered for orthopedic implants because of their significant mechanical properties. Also, due to their bioresorbability, they showing superior application as cardiac stents (Oosterbeek et al., 2022). Additive manufacturing or 3D printing provides more accuracy in developing bioresorbable implants for biomedical applications (Culbreath et al., 2020). This chapter discusses bioresorbable polymers and their classifications and degradation mechanics. Various factors that affect the bioresorption process and the influence of porosity on the bioresorbability are discussed. Clinical applications of bioresorbable polymers and their composites are also explored.

1.2 Bioresorbable polymers and their classifications: An overview

Bioresorbable polymers undergo degradation within the physiological milieu upon fulfillment of their intended functional role (Petersen et al., 2020). Compared to the other conventional materials (for implants), they do not require a second surgery to remove the implant. Bioresorbable polymers have shown excellent applications in the biomedical sectors, specifically drug delivery and implants. The following is a general classification of the bioresorbable materials.

1.2.1 Natural bioresorbable materials

Various natural bioresorbable polymers encompass chitin and chitosan, alginates, and cellulose, as discussed here.

1.2.1.1 Chitin and chitosan

Chitin and chitosan are polysaccharides that are abundantly available worldwide. Chitin is commonly found in crustacean shells/skeletons. There are three general classifications of chitin: α-chitin, β-chitin, and γ-chitin" (Muzzarelli, 1977). It is the most produced polysaccharide worldwide after cellulose. Chitin is mostly used in biomedical applications, particularly wound-healing applications. It shows excellent wound-healing properties. Numerous researches have been carried out in utilizing chitin for wound-healing applications in hydrogel films, sponges, nanofibers, etc. Chitin consists of acetylglucosamine groups, where the acetyl group is connected

with each glucosamine molecule. Chitosan is derived from chitin. The deacetylation of chitin provides chitosan. Chitosan consists of amino groups and provides polycationic behavior to the polymer (Rinaudo, 2006). Chitosan, a mucopolysaccharide, exhibits structural properties resembling those of glycosaminoglycans. Chitosan is found in numerous varieties with different deacetylation degrees and molecular weights (Lehr et al., 1992). Chitosan can be prepared by decalcifying crustacean shells in dilute HCl, leading to deproteination using dilute NaOH at boiling point. After that, the deacetylation of chitin takes place in concentrated NaOH solution at boiling point. This deacetylation is repeated until biomedical-grade chitosan is obtained. Pure chitosan for pharma purposes can be obtained at 90%–95% deacetylation (Jayakumar et al., 2007).

Chitosan and its derivatives are mostly used in biomedical applications, specifically in drug delivery, hemostatic agents, wound dressings/healing, surgical sutures, etc. Chitosan is easily available and possesses biodegradable characteristics (Chandy and Sharma, 1990). It also exhibits low toxicity and is considered to be biocompatible. Chitosan also shows antibacterial properties, which makes it a significant material to be utilized for biomedical applications. Fig. 1.1 shows the structures of chitin and chitosan.

1.2.1.2 Alginates

Alginates represent a binary copolymer comprising L-guluronic acid (G) and D-mannuronic acid (M). Alginate is primarily found in brown seaweed, with calcium, sodium, magnesium, and potassium salts present in the kelp wall of the cells. These two monomers (G and M) are connected with each other and provide the physical and chemical properties of the alginates. Two bacterial species, *Azotobacter* and *Pseudomonas*, are also used for synthesizing alginates; however, at an industrial level, alginates are the

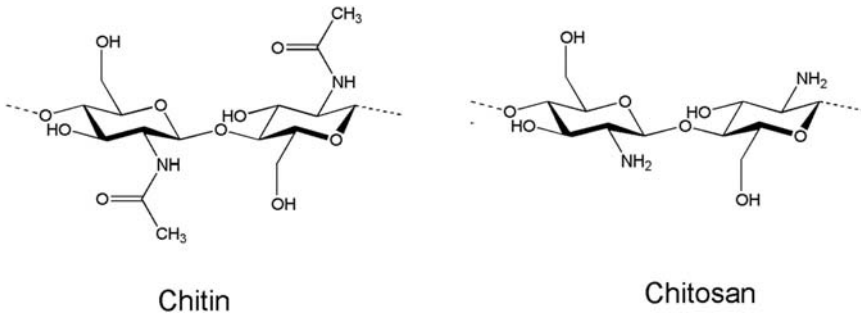

Figure 1.1 Chitin and chitosan. *(Reproduced with permission from Hahn et al. (2020).)*

extracted from brown algae. The quality of alginates primarily depends upon the molecular weight, and M and G proportion/ratios. The biomedical applications of alginates are particularly focused on wound dressings. Calcium alginates are natural hemostats and can be used for treating bleeding wounds (Paul and Sharma, 2008). The alginate's main phenomenon is that it transforms into a gel, and when it is applied to wounds and during removal/changing of dressings, the patient does not experience any pain. The moisture environment of alginates helps reepithelization and fast granulation, which are required for rapid wound healing. Alginates have good absorptivity, gelling ability, hemostat quality, and biocompatibility, making them an effective option for wound dressing (Ikarashi et al., 1992) (Fig. 1.2).

1.2.1.3 Cellulose

Cellulose, a complex polysaccharide obtained from β-glucose and comprised of 1,4-glycosidic bonds, is abundantly available in plants. Within plant cell walls, cellulose is a structural material primarily found in trees. Cellulose is commercially produced using a chemical pulping process. Wood and cotton are the main sources of commercial cellulose production, comprising around 90%–99% and 40%–50% cellulose, respectively (Hon, 1996). Cellulose is a straight-chain polymer whose microfibrils consist of multiple –OH groups connected via hydrogen bonds with glucose, resulting in an increase in tensile strength (Kim et al., 2006). There are numerous biomedical applications of cellulose, e.g., drug delivery, wound dressings, dialysis membranes, etc. Cellulose's good mechanical properties and permeability make it suitable for dialysis applications. It has been observed that cellulose has poor hemocompatibility, which can be improved by applying some modification techniques. Because of strong inter- and intramolecular interactions, cellulose has been found to be insoluble in water (Kai et al., 2000). Chemical etherification and

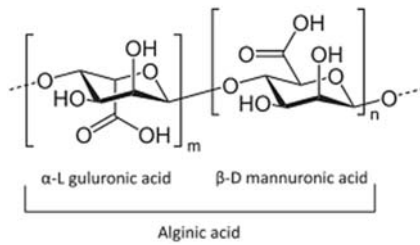

Figure 1.2 Alginate structure. *(Reproduced with permission from Liang et al. (2015).)*

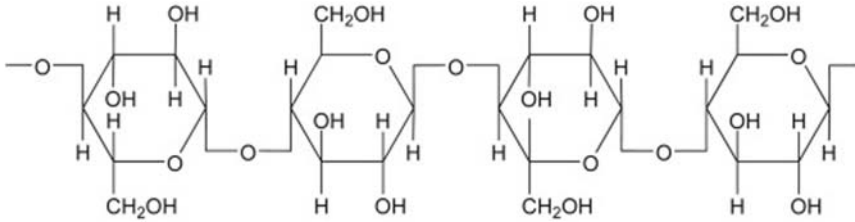

Figure 1.3 Cellulose structure. *(Reproduced with permission from Gilbert (2017).)*

esterification resolve its insolubility problem with water. Carboxymethyl cellulose has very good biomedical applications (Paul and Sharma, 2008) (Fig. 1.3).

1.2.2 Synthetic bioresorbable polymers

Synthetic biopolymers play a significant role in biomedical applications. The advantage of utilizing synthetic biopolymers is that they allow for better control of the properties of these polymers, such as molecular weight, mechanical, and degradation properties. One can develop and select the desired polymer for biomedical applications based on the specific requirements.

The following are some examples of synthetic biopolymers.

1.2.2.1 Polyvinyl alcohol (PVA)

The hydrolysis of polyvinyl acetate yields polyvinyl alcohol. The degree of polymerization and hydrolysis decides the physical properties of the polyvinyl alcohol (Roberts and Martens, 2016). Hydrolysis results in stronger inter- and intramolecular hydrogen bonds because of repeated hydroxyl groups (Chaouat et al., 2008). PVA exhibits higher water content, solubility, biocompatibility, and elasticity, and is mostly recommended for biomedical and pharmaceutical applications. Because of the numerous hydroxyl groups present, PVA macromers can be easily modified. Different groups, such as methacrylates, aldehydes, hydrazides, etc., can modify PVA, etc., which helps with in situ gelation (Lim et al., 2013). This means that different functional and cross-linking groups can be attached to the PVA, which helps further cross-linking and degradation. PVA is most suitable and has found its application for cell encapsulation because of its lower adhering properties with proteins (Dini et al., 2005). Because of biocompatibility and low toxicity, PVA has different applications, such as in contact lenses and cartilage replacement (Singh et al., 2020).

1.2.2.2 Polyethylene glycol (PEG)

Polyethylene glycol, also known as polyethylene oxide, is one of the most versatile polymers utilized for pharmaceutical and biomedical applications (Roberts and Martens, 2016). The major application of PEG is in hydrogel development because of its quick solubility in water and solvents (organic). The US FDA also has approved PEG because of its nontoxicity and less adhesion to protein, which is necessary for biomedical applications (Peppas et al., 2006). Thiols and methacrylate functional groups can easily modify PEG (Fairbanks et al., 2009; Gould and Anseth, 2016). If the molecular weight of the ethylene oxide macromolecules is less than 20,000 g/mol, then it is called polyethylene glycol. However, if the molecular weight is higher than 20,000 g/mol, then it is known as polyethylene oxide (Lee et al., 2008). Because of the hydrophilic nature of PEG, it is effectively utilized in medicine and therapeutic applications (Kucharska, 2022). The major applications of PEG, because of its biocompatibility, are cosmetics, pharma, tissue engineering, drug delivery, etc. (Aied et al., 2018).

1.2.2.3 Polylactic acid (PLA)

Polylactic acid is a biodegradable polymer/plastic derived from lactic acid (Singh et al., 2020). Lactic acid is a source found in starch, sugar cane, and cassava starch, respectively. Lactic acid is mainly derived from fermentation. Also, PLA is derived from isomers like L-lactide, D-lactide, and DL-lactide, showing different forms like PLLA, PDLA, and PDLLA. Of these classes, PLLA and PDLA are semicrystalline, and PDLLA is amorphous. Two processes, polycondensation and ring opening of lactic acid, are used to obtain PLA. The difference between these processes is the molecular weights. Polycondensation of lactic acid gives lower-molecular-weight PLA; however, ring opening of lactic acid gives higher-molecular-weight PLA (Auras et al., 2022). PLA exhibits excellent biocompatibility, mechanical properties, and low toxicity (Laoutid et al., 2018). PLA has low biodegradability, which may be an issue for some biomedical applications such as tissue regeneration (after implantation) (Lett et al., 2020). The PLA surface is hydrophobic, which can also sometimes limit its applications for biomedical purposes. This can be avoided or limited by blending it with another biopolymer, such as PEG, which helps to make its surface hydrophilic (Hendrick and Frey, 2014).

1.2.2.4 Polycaprolactone (PCL)

Polycaprolactone is a synthetic bioresorbable polymer that is derived by a ring-opening polymerization process of ε-caprolactone. PCL has a melting point of 59–64°C (Middleton and Tipton, 2000) and it has superior mechanical properties, such as tensile modulus and strength of 400 and 16 MPa, respectively (Daniels et al., 1990). Its lower melting temperature makes it suitable for diverse applications, and the mechanical properties of PCL can be easily improved by incorporating some nanofillers or nanoparticles. Because of the hydrophobic nature of PCL, it has durability also, i.e., it has the longest degradation time, and this polymer can be used for applications where a long degradation time of the biopolymer is of primary importance (Mano et al., 2004). Bone tissue engineering is the major application for efficiently utilizing this polymer (Cameron and Kamvari-Moghaddam, 2012).

1.3 Polymer degradation: An overview

There are two key processes governing polymer degradation (Pan, 2015), namely chemical hydrolysis and organism degradation (Casalini et al., 2019). In the first classification, water comes into contact with the polymer matrix. It interacts with the hydrolysable bonds and breaks the long chain of the polymer into small oligomers, which are water-soluble, that can easily diffuse through the polymer matrix leading to degradation of the polymer. In the second classification, organs remove the degraded products by themselves, which entirely depends upon the type of material used. Examples of polyanhydride and polylactic acids utilization as implants can help us understand this. Hydrolysis of polyanhydride results in aromatic monomers which are discharged without any metabolic transformations (Katti et al., 2002); however, the particles of PLA are transformed into monomers by the enzymes and then metabolized by following the citric acid cycle (Pan, 2015).

However, if the characteristic time of penetration (water) is less than the hydrolysis time, it may result in bulk degradation. In contrast, if the hydrolysis time is longer than the characteristic time, it may result in surface degradation. This means the surface is degraded without affecting the bulk of the matrix (Burkersroda et al., 2002). Also, there is a difference between degradation and erosion. Considering the erosion of the polymer matrix, there are two different types of erosion possible, i.e., bulk erosion and surface erosion. Diffusion of the mass (monomers and oligomers) toward

the neighboring environment, which causes mass loss, is known as erosion. Drug delivery/release can be directly linked with polymer erosion (Göpferich and Langer, 1995; Göpferich, 1996).

Factors affecting the degradation rates are matrix composition, pH, thickness, molecular weight, crystal structure, and compound addition (Alexis, 2005).

Matrix composition generally affects the level of the hydrophilic behavior of polymers. If the level is high, then it is more prone to degradation.

pH level is also a deciding factor for polymer degradation. It is also true that the rate of degradation may differ in acidic and basic environments. Degradation causes a decrease in pH level (Alexis, 2005).

Thickness is another factor that determines the degradation rate. If the characteristic length exceeds the critical value it may result in surface degradation (Burkersroda et al., 2002).

Increasing *molecular weight* causes a decrease in degradation rate. A high molecular weight may result in low swellability of the polymer, ultimately resulting in low or less degradation of the polymer (Li, 1999; Alexis, 2005).

The *crystalline structure* level affects the polymer degradation. Amorphous polymers exhibit higher degradation rates than crystalline ones (Alexis, 2005).

Compound addition also affects degradation rates. In the case of acidic compounds, degradation follows hydrolysis, however, the basic compounds cause degradation through base catalysts (Elkharraz et al., 2006).

1.4 Bioresorbable polymer resorption process

The resorption process is complicated. In this process, the cells use the endocytosis process to devour the particulate and macromolecules. The cell plasma membrane completely covers the particulate matter, and compresses and develops a vesicle enclosed by the cell cytoplasm. The endocytosis process is better understood by phagocytosis that devours larger particulate materials. Two phagocytosis cells, macrophages and neutrophiles, are present in the body that not only help restrict the interactions of microorganisms but also consume damaged cells. Antibodies recognize the degradable implant's extraneous material and initiate phagocytic activity. The fusion of lysosomes with the phagocytic vesicle activates the degradation (particulate) by following through various oxidative and hydrolytic enzymes, speeding up the material breakdown. The bioresorption process is observed intracellularly; however, distribution of the enzymatic protein is

provided extracellularly, helping to degrade the degradable implants, if any. The phagocytosis process is effective on degradable substances. Hydrolytic activity also helps in the degradation process as it forms a large number of pores and voids through which enzymes enter and initiate catalytic degradation (Burg and Orr, 2008; Buchanan, 2008).

1.4.1 In vitro methods of bioresorbability evaluation

Bioresorbable polymers exhibit numerous applications in biomedical fields such as tissue repair/regeneration, drug delivery, surgery, etc. Aliphatic polyesters are mainly degraded by hydrolytic degradation, consisting of a complex physicochemical phenomenon evaluated using different in-vitro and in-vivo methods. The following section describes the bioresorbability evaluation of the bioresorbable polymers.

1.4.1.1 Physico-chemical methods

Various physicochemical test methods are used to evaluate the bioresorbability of polymers. These methods are as follows.

- Environmental scanning electron microscope (ESEM):

  The changes in the surface morphology of degraded polymers are identified/evaluated using the ESEM technique. The ESEM technique provides natural images. In this method, it is not necessary to apply a coating and high vacuum to obtain the specimen's morphology.
- SEC (size-exclusion chromatography):

  During degradation, this method observes changes in the average molecular weight, average number molecular weight, and molecular weight distribution of the polymer. Polymer chain cleavage results in a reduction in molecular weight. On the other hand, a change in molecular weight distribution is observed under rapid internal degradation, degradation-induced crystallization, and preferential amorphous degradation.
- XRD (X-ray diffraction):

  This is another method for evaluating the bioresorbability of polymers. The morphology of the polymers, such as amorphous or semicrystalline, plays a primary role during the degradation process. The XRD technique is used to observe changes in the crystalline structure of the polymer during the degradation process.
- DSC (differential scanning calorimetry)

  This is another method for evaluating the morphology of polymers, as with XRD. In this method, two scans of 10°C/min are performed.

After the first scan, the polymer rush is quenched, instantly followed by a second scan. This helps in evaluating the thermal properties of polymers.

- ^{1}H NMR (proton nuclear magnetic resonance):

  This method is used to the changes in the chemical composition of a polymer during degradation.
- ESI—MS (electron spray injection mass spectroscopy):

  This method is used to evaluate the molecular weight of polymers. It follows the appearance of a low-molecular-weight polymer during degradation.
- Weight loss:

  Weight loss exhibits the oligomer release from the bulk polymer during the degradation process.

1.4.1.2 Biological methods

The biological resorbability of polymers is determined by using cell culture techniques. Generally, this depends on the cell culture at the material surface and the types of cells used. The selection of a specific cell type is required, which comes in contact with the biomaterial after the implantation process. The appropriate shape and size of the material is the next step after cell selection. The material selection is a significant step as it determines the adhesion and nonadhesion ability of the cells. After implantation, biological fluids consisting of proteins are adsorbed on the material surface.

The adsorption of proteins depends on the material properties, such as the thickness and quantity of the protein layer. Material roughness also plays a major role. The greater the roughness, the higher the concentration of protein deposited on the surface. The adhesion ability also depends on the material's positively and negatively charged surfaces. A positively charged surface induces cell adhesion and proliferation; however, a negatively charged surface shows a very low amount of cell adhesion. The pH of the cell culture medium can modify the surface charge.

Scanning electron microscopy (SEM), transmission electron microscopy (TEM), contact microscopy such as profilometry, and scanning probe microscopy (AFM) can be used to evaluate the bioresorbability of polymers.

1.5 Bioresorbable polymers and their biomedical applications

There are numerous applications of bioresorbable polymers and their composites. Generally, bioresorbable polymers find their applications in the biomedical sectors. Drug delivery, tissue scaffolds, tissue repair/regeneration, implants, etc., are some examples of bioresorbable composite applications. The following section discusses the research and applications based on bioresorbable polymers and their composites.

Hao Yang Zhang and co-workers (Zhang et al., 2020) developed magnesium-based PLA bioresorbable membranes for guided bone/tissue regeneration. The hot pressing method was used for developing the membrane. Two PLA membrane with AZ91 was hot pressed to make a PLA-fluoride AZ91 bioresorbable membrane. The developed membrane exhibits a higher maximum load and stiffness than the PLA-only membrane. FAZ91 exhibits a major degradation, so PLA-FAZ91 is completely degraded within 16−20 weeks. Based on this, the developed membrane is a better option than the PLA membrane for guided bone/regeneration applications.

Anjumol Joy and co-workers (Joy et al., 2023) have developed graphene-based gold nanostructures with polycaprolactone nanocomposites exhibiting potential biological and physicochemical properties. Different characterization techniques (SEM, TEM, XRD, XPS) confirmed the adhesion of gold nanoparticles over the graphene sheets. The biocompatibility of the developed nanocomposite was confirmed using hemolysis tests. Also, the developed nanocomposite exhibited biodegradability, biomineralization, and cell viability for bone tissue engineering.

Bioresorbable polymers exhibit magnificent applications in biomedical fields. Neural tissue engineering is another significant field in which biopolymers are frequently utilized. Yurena Polo and co-workers (Polo et al., 2021) fabricated bioresorbable polymer PLCL with graphene oxide using compression molding. Murine neural stem cells are attached to the surface of the scaffolds without any extracellular matrix coating. The neural stem cells bring immature neurons and glial cells over the scaffolds, advancing their migration into cell groups. The developed scaffold exhibits potential in cellular therapy and nerve tissue regeneration.

Bioresorbable-based polymer composites have been found to be one of the most promising replacements for metal-based implants. An in situ polymerization and laminate stacking process followed by compression

molding process are used to develop phosphate-based glass fiber-based polycaprolactone composites (Chen et al., 2016). Different phosphate fiber volume fractions were used for developing the bioresorbable composites. Figs. 1.4a and b exhibit the pH variation (PBS solution) for PCL and PCL-PGF composites developed by using laminate stacking and in situ polymerization. pH neutrality for both PCL composites (laminate stacking and in situ polymerization) was observed at 7.4 ± 0.2 until degradation. This pH neutral value is observed until the 11th day, followed by a gradual decrease until 28 days (Fig. 1.4).

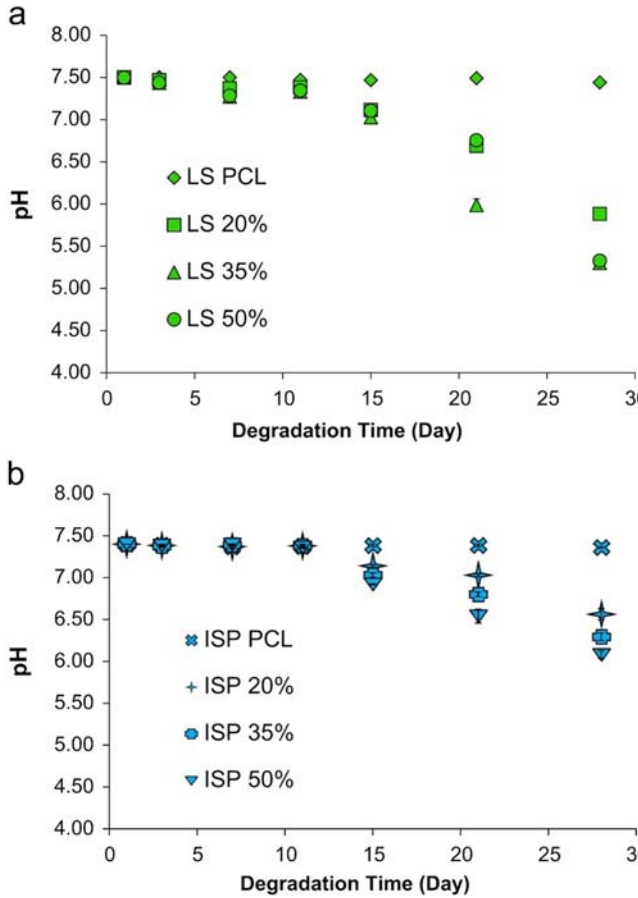

Figure 1.4 pH-based degradation of composites (PBS media): (a) Laminate stacked PCL and PCL-PGF composite; (b) in situ polymerized PCL and PCL-PGF composites. *(Reproduced with permission from Chen et al. (2016).)*

Katarzyna and co-workers (Polak-Kraśna et al., 2021) analyzed bioresorbable semicrystalline PLLA for stent application. Mass reduction, molecular weight, thermal properties, crystallinity, and tensile properties were evaluated by immersing in PBS at 50°C for 112 days. It has been observed that the tensile strain decreases rapidly at day 49; however, other tensile properties remain constant. This polymer has been observed to be one of the optimum options for vascular stent applications.

Constantino Fiuza and co-workers (Fiuza et al., 2022) evaluated the mechanical, micromechanical, and physical properties of Reva Fantom Encore bioresorbable scaffolds. These bioresorbable scaffolds were immersed in a PBS solution at 50°C for around 112 days. Radial compression testing, nanoindentation, DSC, and mass loss were evaluated at different intervals. Three phases of degradation are observed. One phase was observed from 0 to 21 days, the second phase was observed from 35 to 54 days, and the third phase was observed between 63 and 112 days. During the first phase, bioresorbable scaffolds' radial strength, stiffness, and melt temperature increase, and the molecular weight decreases. However, during the second phase, the radial strength becomes constant as in the first phase, but molecular weight again decreases. During the third or final phase, continuous reductions in radial strength, stiffness, and load-bearing capacity were observed.

Oosterbeek and co-workers (Oosterbeek et al., 2022) studied the mechanical properties of bioresorbable polymer–glass composites at degradation. Polylactide polymer is reinforced with 15–30 wt.% of the phosphate glass fiber, which results in an 80% increase in modulus. However, 15 wt.% glass incorporation holds comparable ductility to pure polymer. Ductility and stiffness are the two most significant properties required for stent applications. Including glass fiber suppresses polymer embrittlement, resulting in a controlled reduction in mechanical properties that gradually permits the load transfer to the healed tissue.

Chaigneau and co-workers (Chaigneau et al., 2023) developed PLA-bioactive glass-based composite scaffolds using fused filament. Because of the deficient mechanical properties of the bioactive glass–PLA composites, the bioactive glass is coated with a thin layer of gold which not only improves the mechanical properties of the PLA–BG composite but also shows good cytotoxicity.

Boccaccini and Maquet (Boccaccini and Maquet, 2003) developed a bioresorbable polymer–bioglass-based composite for tissue engineering applications. A bioactive glass particle-incorporated PLGA-based foam

composite was developed by using a thermally induced phase separation technique. The developed foam composite exhibits interconnected, well-defined porosity. Phosphate buffer solution (PBS) was used to check the degradation rate of the developed foam structure after a maturation period of 7 weeks. It has been observed that bioactive glass slows down the degradation rate of the foam structure for the suggested time period of investigation. Hence, the incorporation of bioactive glass could be the controlling factor for the evaluation of the degradation rate of a polymer.

1.6 Conclusion

The role of bioresorbable polymers in biomedical uses has become noteworthy due to their application in areas such as tissue healing, cardiovascular stents, neural stem cells, tissue scaffolding, drug release, dental work, and surgical implants. The major advantage of bioresorbable or degradable implants is that a second surgery is not required for their removal. Bioresorbable polymers find numerous applications in organ transplant, tissue engineering, orthopedic autografts, alternate tissue, and cell grafts/constructs. Numerous cases of organ transplants are observed each year. Bioresorbable polymer-based implants could be a boon for those waiting for organ transplants, including in emergency situations.

The technology is still developing in neural tissue engineering/regeneration. Bioresorbable-based drug-eluting stents are showing magnificent advantages/benefits for those who suffering from cardiovascular blockages, as they provide easy flow through the blood arteries to the heart. Apart from these, there remain some challenges into which numerous researches are ongoing. These challenges are related to the properties of the bioresorbable polymers/materials used for implant applications.

Detailed knowledge of material characteristics related to material degradation is required for tissue regeneration applications. Various factors influence the properties of bioresorbable polymers, such as drug incorporation, growth factors, enzymes, and proteins. Based on such factors, the application of the bioresorbable polymer-based implant for specific organ replacement is decided. Implant degradation and tissue regeneration are the primary objectives of a bioresorbable implant. However, one should still have proper knowledge of the degradable polymers and their characteristics for designing tissue engineering for future physiological functions.

References

Agrawal, C.M., Ray, R.B., 2001. Biodegradable polymeric scaffolds for musculoskeletal tissue engineering. J. Biomed. Mater. Res. 55 (2), 141–150. https://doi.org/10.1002/1097-4636(200105)55:2<141::AID-JBM1000>3.0.CO;2-J.

Aied, A., Song, W., Wang, W., Baki, A., Sigen, A., 2018. 3D Bioprinting of stimuli-responsive polymers synthesised from DE-ATRP into soft tissue replicas. Bioprinting 9, 37–43. https://doi.org/10.1016/j.bprint.2018.02.002.

Alexis, F., 2005. Factors affecting the degradation and drug-release mechanism of poly(lactic acid) and poly[(lactic acid)-co-(glycolic acid)]. Polym. Int. 54 (1), 36–46. https://doi.org/10.1002/pi.1697.

Auras, R.A., Lim, L.T., Selke, S.E.M., Tsuji, H., 2022. In: Auras, R.A., Lim, L.T., Selke, S.E.M., Tsuji, H. (Eds.), Poly(lactic Acid): Synthesis, Structures, Properties, Processing, Applications, and End of Life, second ed., vol. 1. Wiley.

Boccaccini, A.R., Maquet, V., 2003. Bioresorbable and bioactive polymer/bioglass® composites with tailored pore structure for tissue engineering applications. Compos. Sci. Technol. 63 (16), 2417–2429. https://doi.org/10.1016/S0266-3538(03)00275-6.

Boutry, C.M., Beker, L., Kaizawa, Y., Vassos, C., Tran, H., Hinckley, A.C., Pfattner, R., Niu, S., Li, J., Claverie, J., Wang, Z., Chang, J., Fox, P.M., Bao, Z., 2019. Biodegradable and flexible arterial-pulse sensor for the wireless monitoring of blood flow. Nat. Biomed. Eng. 3 (1), 47–57. https://doi.org/10.1038/s41551-018-0336-5.

Buchanan, F., 2008. In: Buchanan, F. (Ed.), Degradation Rate of Bioresorbable Materials: Prediction and Evaluation, first ed. CRC Woodhead.

Burg, K.J.L., Orr, D.E., 2008. An overview of bioresorbable materials. In: Degradation Rate of Bioresorbable Materials: Prediction and Evaluation, pp. 3–18. https://doi.org/10.1533/9781845695033.1.3.

Burkersroda, F. Von, Schedl, L., Göpferich, A., 2002. Why degradable polymers undergo surface erosion or bulk erosion. Biomaterials 23 (21), 4221–4231. https://doi.org/10.1016/S0142-9612(02)00170-9.

Cameron, R.E., Kamvari-Moghaddam, A., 2012. Synthetic bioresorbable polymers. Durab Reliab Med Polym 96–118. https://doi.org/10.1533/9780857096517.1.96.

Casalini, T., Rossi, F., Castrovinci, A., Perale, G., 2019. A perspective on polylactic acid-based polymers use for nanoparticles synthesis and applications. Front. Bioeng. Biotechnol. 7 (October), 1–16. https://doi.org/10.3389/fbioe.2019.00259.

Chaigneau, L., Perrot, A., Brezulier, D., Coulon, J.F., Chevire, F., Lebullenger, R., 2023. Bioresorbable polylactic acid (PLA) and bioactive glasses (BG) composite: influence of gold coated of BG powder on mechanical properties and chemical reactivity. J. Mech. Behav. Biomed. Mater. 138, 105571. https://doi.org/10.1016/J.JMBBM.2022.105571.

Chandy, T., Sharma, C.P., 1990. Chitosan — as a biomaterial. Biomater. Artif. Cell Artif. Organs 18 (1), 1–24. https://doi.org/10.3109/10731199009117286.

Chaouat, M., Le Visage, C., Baille, W.E., Escoubet, B., Chaubet, F., Mateescu, M.A., Letourneur, D., 2008. A novel cross-linked poly(vinyl alcohol) (PVA) for vascular grafts. Adv. Funct. Mater. 18 (19), 2855–2861. https://doi.org/10.1002/adfm.200701261.

Chatterjee, S., Saxena, M., Padmanabhan, D., Jayachandra, M., Pandya, H.J., 2019. Futuristic medical implants using bioresorbable materials and devices. Biosens. Bioelectron. 142, 111489. https://doi.org/10.1016/J.BIOS.2019.111489.

Chen, M., Parsons, A.J., Felfel, R.M., Rudd, C.D., Irvine, D.J., Ahmed, I., 2016. In-situ polymerisation of fully bioresorbable polycaprolactone/phosphate glass fibre composites: in vitro degradation and mechanical properties. J. Mech. Behav. Biomed. Mater. 59, 78–89. https://doi.org/10.1016/J.JMBBM.2015.12.019.

Chen, P.J., Saati, S., Varma, R., Humayun, M.S., Tai, Y.C., 2010. Wireless intraocular pressure sensing using microfabricated minimally invasive flexible-coiled LC sensor

implant. J. Microelectromech. Syst. 19 (4), 721–734. https://doi.org/10.1109/JMEMS.2010.2049825.

Culbreath, C.J., Gaerke, B., Taylor, M.S., McCullen, S.D., Mefford, O.T., 2020. Effect of infill on resulting mechanical properties of additive manufactured bioresorbable polymers for medical devices. Materialia 12, 100732. https://doi.org/10.1016/J.MTLA.2020.100732.

Daniels, A.U., Chang, M.K., Andriano, K.P., 1990. Mechanical properties of biodegradable polymers and composites proposed for internal fixation of bone. J. Appl. Biomater. 1 (1), 57–78. https://doi.org/10.1002/jab.770010109.

Dini, L., Panzarini, E., Miccoli, M.A., Miceli, V., Protopapa, C., Ramires, P.A., 2005. In vitro study of the interaction of polyalkilimide and polyvinyl alcohol hydrogels with cells. Tissue Cell 37 (6), 479–487. https://doi.org/10.1016/j.tice.2005.09.002.

Elkharraz, K., Faisant, N., Guse, C., Siepmann, F., Arica-Yegin, B., Oger, J.M., Gust, R., Goepferich, A., Benoit, J.P., Siepmann, J., 2006. Paclitaxel-loaded microparticles and implants for the treatment of brain cancer: preparation and physicochemical characterization. Int. J. Pharm. 314 (2), 127–136. https://doi.org/10.1016/J.IJPHARM.2005.07.028.

Fairbanks, B.D., Schwartz, M.P., Bowman, C.N., Anseth, K.S., 2009. Photoinitiated polymerization of PEG-diacrylate with lithium phenyl-2,4,6-trimethylbenzoylphosphinate: polymerization rate and cytocompatibility. Biomaterials 30 (35), 6702–6707. https://doi.org/10.1016/j.biomaterials.2009.08.055.

Fiuza, C., Polak-Kraśna, K., Antonini, L., Petrini, L., Carroll, O., Ronan, W., Vaughan, T.J., 2022. An experimental investigation into the physical, thermal and mechanical degradation of a polymeric bioresorbable scaffold. J. Mech. Behav. Biomed. Mater. 125, 104955. https://doi.org/10.1016/J.JMBBM.2021.104955.

Gilbert, M., 2017. Cellulose plastics. In: Brydson's Plastics Materials, eighth ed., pp. 617–630. https://doi.org/10.1016/B978-0-323-35824-8.00022-0.

Göpferich, A., 1996. Mechanisms of polymer degradation and erosion. Biomaterials 17 (2), 103–114. https://doi.org/10.1016/0142-9612(96)85755-3.

Göpferich, A., Langer, R., 1995. Modeling of polymer erosion in three dimensions: rotationally symmetric devices. AIChE J. 41 (10), 2292–2299. https://doi.org/10.1002/aic.690411012.

Gould, S.T., Anseth, K.S., 2016. Role of cell–matrix interactions on VIC phenotype and tissue deposition in 3D PEG hydrogels. J Tissue Eng. Regenerat. Med. 10 (10), E443–E453. https://doi.org/10.1002/term.1836.

Hahn, T., Tafi, E., Paul, A., Salvia, R., Falabella, P., Zibek, S., 2020. Current state of chitin purification and chitosan production from insects. J. Chem. Technol. Biotechnol. 95 (11), 2775–2795. https://doi.org/10.1002/jctb.6533. John Wiley and Sons Ltd.

Hall-Stoodley, L., Costerton, J.W., Stoodley, P., 2004. Bacterial biofilms: from the natural environment to infectious diseases. Nat. Rev. Microbiol. 2 (2), 95–108. https://doi.org/10.1038/nrmicro821.

Hench, L.L., Splinter, R.J., Allen, W.C., Greenlee, T.K., 1971. Bonding mechanisms at the interface of ceramic prosthetic materials. J. Biomed. Mater. Res. 5 (6), 117–141. https://doi.org/10.1002/jbm.820050611.

Hendrick, E., Frey, M., 2014. Increasing surface hydrophilicity in poly(lactic acid) electrospun fibers by addition of pla-b-peg Co-polymers. J. Eng. Fibers Fabrics 9 (2), 153–164. http://www.jeffjournal.org.

Ikarashi, Y., Toyoda, K., Ohsawa, N., Uchima, T., Tsuchiya, T., Kaniwa, M.A., Sato, M., Takahashi, M., Nakamura, A., 1992. Comparative studies by cell culture and in vivo implantation test on the toxicity of natural rubber latex materials. J. Biomed. Mater. Res. 26 (3), 339–356. https://doi.org/10.1002/jbm.820260306.

Jayakumar, R., Nwe, N., Tokura, S., Tamura, H., 2007. Sulfated chitin and chitosan as novel biomaterials. Int. J. Biol. Macromol. 40 (3), 175–181. https://doi.org/10.1016/J.IJBIOMAC.2006.06.021.

Joy, A., Unnikrishnan, G., Megha, M., Haris, M., Thomas, J., Kolanthai, E., Senthilkumar, M., 2023. Hybrid gold/graphene oxide reinforced polycaprolactone nanocomposite for biomedical applications. Surface. Interfac. 40, 103000. https://doi.org/10.1016/J.SURFIN.2023.103000.

Kai, Y., Hamada, J.-I., Morioka, M., Todaka, T., Hasegawa, S., Ushio, Y., 2000. The utility of the microcrystalline cellulose sphere as a particulate embolic agent: an experimental study. AJNR Am J Neuroradiol 21, 1160–1163.

Katti, D.S., Lakshmi, S., Langer, R., Laurencin, C.T., 2002. Toxicity, biodegradation and elimination of polyanhydrides. Adv. Drug Deliv. Rev. 54 (7), 933–961. https://doi.org/10.1016/S0169-409X(02)00052-2.

Kim, J., Yun, S., Ounaies, Z., 2006. Discovery of cellulose as a smart material. Macromolecules 39 (12), 4202–4206. https://doi.org/10.1021/ma060261e.

Kucharska, B., 2022. Polymers for 3D bioprinting. In: Polymers for 3D Printing: Methods, Properties, and Characteristics. Elsevier, pp. 337–349. https://doi.org/10.1016/B978-0-12-818311-3.00003-3.

Kuhn, J.R., Bush, R., Emilio, M., Scholl, I.F., 2012. The precise solar shape and its variability. Science 337 (6102), 1638–1640. https://doi.org/10.1126/science.1223231.

Laoutid, F., Vahabi, H., Shabanian, M., Aryanasab, F., Zarrintaj, P., Saeb, M.R., 2018. A new direction in design of bio-based flame retardants for poly(lactic acid). Fire Mater. 42 (8), 914–924. https://doi.org/10.1002/fam.2646.

Lee, H., Venable, R.M., MacKerell, A.D., Pastor, R.W., 2008. Molecular dynamics studies of polyethylene oxide and polyethylene glycol: hydrodynamic radius and shape anisotropy. Biophys. J. 95 (4), 1590–1599. https://doi.org/10.1529/BIOPHYSJ.108.133025.

Lehr, C.M., Bouwstra, J.A., Schacht, E.H., Junginger, H.E., 1992. In vitro evaluation of mucoadhesive properties of chitosan and some other natural polymers. Int. J. Pharm. 78 (1–3), 43–48. https://doi.org/10.1016/0378-5173(92)90353-4.

Lett, J.A., Sagadevan, S., Paiman, S., Mohammad, F., Schirhagl, R., Léonard, E., Alshahateet, S.F., Oh, W.C., 2020. Exploring the thumbprints of Ag-hydroxyapatite composite as a surface coating bone material for the implants. J. Mater. Res. Technol. 9 (6), 12824–12833. https://doi.org/10.1016/J.JMRT.2020.09.037.

Li, S., 1999. Hydrolytic degradation characteristics of aliphatic polyesters derived from lactic and glycolic acids. J. Biomed. Mater. Res. 48 (3), 342–353. https://doi.org/10.1002/(SICI)1097-4636(1999)48:3<342::AID-JBM20>3.0.CO;2-7. John Wiley & Sons Inc.

Liang, Y., Kashdan, T., Sterner, C., Dombrowski, L., Petrick, I., Kröger, M., Höfer, R., 2015. Algal biorefineries. Industr. Bioref. White Biotechnol 35–90. https://doi.org/10.1016/B978-0-444-63453-5.00002-1.

Lim, K.S., Alves, M.H., Poole-Warren, L.A., Martens, P.J., 2013. Covalent incorporation of non-chemically modified gelatin into degradable PVA-tyramine hydrogels. Biomaterials 34 (29), 7097–7105. https://doi.org/10.1016/j.biomaterials.2013.06.005.

Mano, J.F., Sousa, R.A., Boesel, L.F., Neves, N.M., Reis, R.L., 2004. Bioinert, biodegradable and injectable polymeric matrix composites for hard tissue replacement: state of the art and recent developments. Compos. Sci. Technol. 64 (6), 789–817. https://doi.org/10.1016/J.COMPSCITECH.2003.09.001.

Middleton, J.C., Tipton, A.J., 2000. Synthetic biodegradable polymers as orthopedic devices. Biomaterials 21 (23), 2335–2346.

Millard, R.E., Shepherd, R.K., 2007. A fully implantable stimulator for use in small laboratory animals. J. Neurosci. Methods 166 (2), 168–177. https://doi.org/10.1016/J.JNEUMETH.2007.07.009.

Muzzarelli, R.A.A., 1977. Stereochemistry and physical characterization. Chitin 45–86. https://doi.org/10.1016/B978-0-08-020367-6.50008-8.

N-S Hon, D., 1996. In: Dumitriu, S. (Ed.), Cellulose and its Derivatives: Structures, Reactions, and Medical Uses, first ed., vol. 1. Routledge, Taylor and Francis.

Oosterbeek, R.N., Zhang, X.C., Best, S.M., Cameron, R.E., 2022. The evolution of the structure and mechanical properties of fully bioresorbable polymer-glass composites during degradation. Compos. Sci. Technol. 218, 109194. https://doi.org/10.1016/J.COMPSCITECH.2021.109194.

Ottenbright, R.M., Scott, G., 1992. In: Vert, M., Feijen, J., Albertsson, A., Scott, G., Chiellini, E. (Eds.), Biodegradable Polymers and Plastics, first ed., vol. 1. Royal Society of Chemistry.

Pan, J., 2015. In: Pan, J. (Ed.), Modelling Degradation of Bioresorbable Polymeric Medical Devices, first ed., vol. 1. Woodhead Publishing.

Park, S.I., Brenner, D.S., Shin, G., Morgan, C.D., Copits, B.A., Chung, H.U., Pullen, M.Y., Noh, K.N., Davidson, S., Oh, S.J., Yoon, J., Jang, K.I., Samineni, V.K., Norman, M., Grajales-Reyes, J.G., Vogt, S.K., Sundaram, S.S., Wilson, K.M., Ha, J.S., Rogers, J.A., 2015. Soft, stretchable, fully implantable miniaturized optoelectronic systems for wireless optogenetics. Nat. Biotechnol. 33 (12), 1280–1286. https://doi.org/10.1038/nbt.3415.

Paul, W., Sharma, C.P., 2008. Natural bioresorbable polymers. In: Degradation Rate of Bioresorbable Materials: Prediction and Evaluation, pp. 67–94. https://doi.org/10.1533/9781845695033.2.67.

Peppas, N.A., Hilt, J.Z., Khademhosseini, A., Langer, R., 2006. Hydrogels in biology and medicine: from molecular principles to bionanotechnology. Adv. Mater. 18 (11), 1345–1360. https://doi.org/10.1002/adma.200501612.

Pertici, G., 2017. Introduction to bioresorbable polymers for biomedical applications. Biores. Polyme. Biomed. Appl. From Funda. Transla. Med. 3–29. https://doi.org/10.1016/B978-0-08-100262-9.00001-X.

Petersen, R.S., Nielsen, L.H., Rindzevicius, T., Boisen, A., Keller, S.S., 2020. Controlled drug release from biodegradable polymer matrix loaded in microcontainers using hot punching. Pharmaceutics 12 (11), 1–13. https://doi.org/10.3390/pharmaceutics12111050.

Polak-Kraśna, K., Abaei, A.R., Shirazi, R.N., Parle, E., Carroll, O., Ronan, W., Vaughan, T.J., 2021. Physical and mechanical degradation behaviour of semi-crystalline PLLA for bioresorbable stent applications. J. Mech. Behav. Biomed. Mater. 118, 104409. https://doi.org/10.1016/J.JMBBM.2021.104409.

Polo, Y., Luzuriaga, J., Iturri, J., Irastorza, I., Toca-Herrera, J.L., Ibarretxe, G., Unda, F., Sarasua, J.R., Pineda, J.R., Larrañaga, A., 2021. Nanostructured scaffolds based on bioresorbable polymers and graphene oxide induce the aligned migration and accelerate the neuronal differentiation of neural stem cells. Nanomed. Nanotechnol. Biol. Med. 31. https://doi.org/10.1016/j.nano.2020.102314.

Pulapura, S., Kohn, J., 1992. Trends in the development of bioresorbable polymers for medical applications. J. Biomat. Appl. 6 (3), 216–250.

Rinaudo, M., 2006. Chitin and chitosan: properties and applications. Prog. Polym. Sci. 31 (7), 603–632. https://doi.org/10.1016/J.PROGPOLYMSCI.2006.06.001.

Roberts, J.J., Martens, P.J., 2016. Engineering biosynthetic cell encapsulation systems. In: Biosynthetic Polymers for Medical Applications. Elsevier Inc, pp. 205–239. https://doi.org/10.1016/B978-1-78242-105-4.00009-2.

Shin, J., Yan, Y., Bai, W., Xue, Y., Gamble, P., Tian, L., Kandela, I., Haney, C.R., Spees, W., Lee, Y., Choi, M., Ko, J., Ryu, H., Chang, J.K., Pezhouh, M., Kang, S.K., Won, S.M., Yu, K.J., Zhao, J., Rogers, J.A., 2019. Bioresorbable pressure sensors protected with thermally grown silicon dioxide for the monitoring of chronic diseases

and healing processes. Nat. Biomed. Eng. 3 (1), 37–46. https://doi.org/10.1038/s41551-018-0300-4.

Singh, R., Kumar, N., Mehrotra, T., Bisaria, K., Sinha, S., 2020. Environmental hazards and biodegradation of plastic waste: challenges and future prospects. In: Bioremediation for Environmental Sustainability: Toxicity, Mechanisms of Contaminants Degradation, Detoxification and Challenges. Elsevier, pp. 193–214. https://doi.org/10.1016/B978-0-12-820524-2.00009-2.

Tormala, P., Laiho, J., Helevirta, P., Rokkanen, P., Vainionpaa, S., Bostman, O., Kilpikari, J., 1986. Resorbable surgical devices. In: Proceedings of the Vth International Conference on Polymers in Medicine and Surgery, PIMS. Leeuewenhorst Congress Center, Holland, pp. 16/1–16/6.

Zhang, H.Y., Jiang, H.B., Kim, J.E., Zhang, S.X., Kim, K.M., Kwon, J.S., 2020. Bioresorbable magnesium-reinforced PLA membrane for guided bone/tissue regeneration. J. Mech. Behav. Biomed. Mater. 112, 104061. https://doi.org/10.1016/J.JMBBM.2020.104061.

CHAPTER 2

Bioresorbable polymers and their composites for biomedical applications

Oludaisi Adekomaya and Thokozani Majozi
Sustainable Process Engineering, School of Chemical and Metallurgical Engineering, Faculty of Engineering and Built Environment, University of the Witwatersrand, Johannesburg, South Africa

2.1 Introduction

Adaptation and full integration of bioresorbable materials in medical applications has been described in a number of published works (Adekomaya et al., 2017b; Lambert and Wagner, 2017). This is against the backdrop of their applications in many energy-saving devices, most importantly, their vast use in building and vehicle component parts. The use of bioresorbable materials has been widely promoted basically for their lightness and fast degradation properties (Sun et al., 2016). These materials serve largely to protect the environment amid global climate change and the attendant repercussions. This has also resulted in several measures being evolved in which bioenergy and biobased materials were promoted as part of stopgap measures, thereby creating the opportunity to explore key qualities ascribed to their renewable properties and sustainable characteristics (Szendiuch, 2011). The biobased industries have explored the intrinsic biocompatibility and biodegradability of bioresorbable materials to alleviate human problems in a number of areas, where efforts have been made to use some of their salient properties to combat climate threats, thereby leading to a reduction in greenhouse gases emissions (Cheung et al., 2009). The use of synthetic fibers as a complementary materials in the medical field has been a subject of debate in the literature (Adekomaya et al., 2017a) in which their key advantages of low cost and high strength have been criticized on the basis of prevailing recycling and reuse complexities when trialing their use over many years. Part of the issue raised involves the structural problems associated with the use of these materials, culminating in a serious environmental problem as has been reported in several developing and emerging countries (McCullen et al., 2010). The awareness of climate change is reverberating throughout the planet, necessitating a new modern method

Bioresorbable Polymers and their Composites
ISBN 978-0-443-18915-9
https://doi.org/10.1016/B978-0-443-18915-9.00017-3
© 2024 Elsevier Ltd.
All rights reserved.

of recycling and reclamation of composite materials (Lau et al., 2010). Environmental legislation is now part of the fulcrum on which sustainable development has been built, thereby creating a discourse around materials with less risk to the environment. The human impact on the environment is huge and unprecedented, as the world struggles to cope with the increasing global population (Adekomaya and Majozi, 2020). This had led to competition among species, in which human activities take a large toll on the environment. There has also been a paradigm shift and material diversification in the production and manufacturing industries. This has been fully implemented in many developing countries around the world in which companies and production factories take ownership of the environmental impacts of their products. The law also mandates each company to file returns for every action taken to mitigate the environmental crisis arising from their operation. The policy is in line with a sustainable approach to material evolution and to protect the environment from unnecessary attack and degradation. Some of these policy actions were created in the United States where manufacturers are mandated to evolve best practices in terms of materials and products by adopting the 4Rs, in line with internal best practices: (1) reduce the quantity and proportion of toxic wastes to be disposed of (sourced reduction); (2) reclamation approach in which materials and used products are reused in an environmentally friendly manner; (3) repairing the environment in a sustainable manner; and (4) recycling approach in which measures are put in place to buy products made from recycled materials (RameshKumar et al., 2020; Adekomaya and Majozi, 2019). It is also important to continuously use all these aforementioned methods before waste materials are sent for open disposal or landfilling.

Natural fibers and bioresorbable composites continue to enjoy patronage in regenerative medicine and other related applications, in view of their biocompatibility, biodegradation rate, and ability to degrade into nontoxic components, which are often traceable to natural polymers, such as polysaccharides and synthetic reinforced polymers. Considering the safety of materials and the efficacy of the results desired for the application of bioresorbable materials, it is necessary to study the inherent properties of these materials before application. This must be considered in the deployment of biomedical applications in view of their direct contact with the human body. There are also clear-cut specifications which must be adhered to before they can be used. The use of polymers and natural fiber reinforced composites has given considerable leverage to their biomedical

application as they are flexible in terms of materials sourcing and life cycle assessment. In several papers published on this subject, the findings have shown that natural materials have been identified as among the most attractive options, which may be connected with their extracellular matrix and compatible characteristics with the human body. These materials are chemically stable in nature, are modifiable where necessary using chemical methods, and are capable of showing result-oriented biological performance. Generally, bioresorbable materials occur in nature and are mostly processed from plants, animals (invertebrates and vertebrates), or microorganisms. In other papers (Adekomaya, 2020), they are often referred to as polysaccharides, proteins, or glycosaminoglycans (GAGs). Natural polymers in other areas are modified structurally and can also be extracted from synthetic materials and used for medical aids, with ingredients embedded in them to complement medical and industrial uses. Findings have shown that most bioresorbable materials have been accepted for biomedical research as studies show their effectiveness and non-immunogenic properties when subjected to several tests. In other works, they are also noted for their preference over synthetic polymers, where the latter often pose an environmental challenge (Adekomaya et al., 2020). Going by the characteristic tendencies of synthetic biodegradable materials, one may be tempted to believe that these are commercially competitive polymers with similar emerging results, as they are often produced in a cost-effective manner. It can also be seen that, in commercial products, one of the most notable materials is polyesters, which acts as a biologically inert material in the sense that it reinforces materials or it can be modified to support other contending issues such as low cell compatibility, hydrophobicity, and inflammatory impacts. In many other papers (Upgupta et al., 2015), it has been reported that the preferred materials being used for biomedical applications are largely obtained from biodegradable sources due to their effectiveness in the healing process. These materials have been used as a stopgap measure, considering the reclamation and environmental disruption associated with natural resources. The world is faced with an existential threat and the indiscriminate use of natural resources could complicate the already dire situation that we face currently (Yang et al., 2015). Biodiversity losses are of great concern across the globe and these follow disruption in climatic weather conditions occasioned by the loss of fauna and flora (van Gameren and Zaccai, 2015). In order to explore natural polymers for the purpose of biomedical applications, it may be necessary to dissect some of the available materials being used and discuss how best to improve their functionalities.

In some cases, materials like polysaccharides exhibit products in the form of cellulose and starch, whereas, in other cases, these polymers are regenerated by fungi and nature. However, findings have shown that other natural polymers, such as proteins, could be deployed to produce natural fiber materials which would be suitable for biomedical applications. In this chapter, a detailed review of the bioresorbable biopolymers and their contributing impact in the biomedical field is discussed in this section detailing the properties of the materials in tackling human deficiencies as reported in many earlier works (Lau et al., 2018). It is also very important to discuss the contributing impact of the adjoining matrices in the entire value chain, so that if the reinforced natural fiber is to used, one is able to know whether the supporting materials could pose a danger to the application in which they are meant to be used. This has been the major concern in much of the literature, because materials production has been complicated by the evolution of composite materials containing various amounts of similar and different elements as constituent materials (Ayrilmis et al., 2011). The involvement of bioresorbable materials in biomedical applications has many advantages. The bioresorbable materials are also not reputed to posses serious threat to the environment since its component parts naturally decomposes with no side-effects to the nature. Bioengineering, as conceptualized in many biomedical applications, refers to any concepts and methods in which science and mathematics play a critical role in solving problems related to the repair and reconstruction of parts of the human body which may have been either lost, damaged, or contain dead tissue. The process of applying materials suitable for addressing these gaps can be regarded as biomaterials. As discussed in several published works, a biomaterial is a material deployed for medical devices, that aims at addressing the shortcomings occasioned by inadequacies in human parts, and is directed to interact with biological human systems. Several of the medical devices available for these applications are seeing breakthroughs in the evolution of artificial hearts and hips, in which these products are bioresorbable. A substantial part of the advantages of biomaterials is that they can be tailored based on the existing complications prevailing in the human system with the aim of meeting the deficiencies as reported (Xie et al., 2010). In the past, the most common conventional materials used were produced from synthetic compounds ranging from phenolic reinforced compounds to those reinforced with natural fibers (Faruk et al., 2012). These have led to several complications in regenerative medicine where the composite structures of these materials do not serve their

intended functionalities after their shelf-life, as the components are closely interconnected, and are thereby difficult to reuse after operational use. In the bone reconstruction method, several papers have recommended stainless steel and titanium as a sustainable bone plate materials due to their quick recovery tendency. However, there have been concerns about the side effects of these materials for bone replacement as unconfirmed reports have claimed that many surgical operations aimed at removing the bone and replacing it with commensurate biomaterial fasteners have resulted in delayed recovery and healing. This had reportedly caused uneven growth of bone cells underneath and round the bone plates, causing porosis. Refracture of bones around the insert may also occur after plate removal occasioned by differential stiffness between the bone and the plates. As shown in Table 2.1, the mechanical properties of some of these materials have been analyzed based on their implant application. This analysis also shows the detailed analysis of bone structure and properties, with detailed prediction of other materials for the same use. As shown in this table, it can be seen that less stiff materials should be deployed for bone fixation. Another material of high interest is poly(lactic acid) (PLA), which has considerable properties similar to biodegradable and bioresorbable materials (Amulya et al., 2021). Their strong advantages over other materials include that they can serve as a dual purpose without inflicting pain on the human body. However, studies have shown that a degradable implant may be removed naturally after the operation is completed, thereby making

Table 2.1 Mechanical tendencies of implant materials for regenerative medicine.

	Elastic modulus (GPa)	**Yield strength (MPa)**	**Tensile strength (MPa)**	**Elongation to failure (%)**
Al_2O_3	350	—	1000 −10,000	0
CoCr alloy	225	525	735	10
Stainless steel 316	210	240	600	55
	120	830	900	18
Ti-6Al-4V	15−30	30−70	70−150	0−8
Bone (cortical)	3.0	—	35−50	0.5
PMMA	0.6−1.8	—	23−40	200−400
HDPE	Strong	—	26.8	20
cartilage	viscoelastic			

bioresorbable polymers the most sought-after materials for biomedical applications (Suddell, 2008). The only concern about bioresorbable materials is the possibility of them becoming susceptible to external and internal moisture if chemical treatment fails. There have been several rebuttals in the literature in which this shortcoming has been shown to be minimal and to not occur in the operation theater. Another concern is the poor strength of the bioresorbable polymers which could inhibit their wider application.

2.2 Salient properties of bioresorbable materials for biomedical application

Over the last few decades, the use of bioresorbable materials has experienced wide patronage in all areas of human endeavor (Abiola et al., 2014). This has taken a toll on the use of natural fibers, with these becoming the immediate casualties among the types of materials used for biomedical applications. The key part of this work is to preserve natural resourses from severe threat and other anthropogenic activities. Findings have also shown that they are environmentally friendly composites in which the waste products constitute a lower or negligible effect on the environment (Jayaramudu et al., 2011). Further advances in natural fiber development have been reported in the literature, most importantly, in the areas of genetic engineering and composites science. Some of these approaches have created significant opportunities in the medical field, in which plant materials are interchangeably used to ensure environmental conservation. It is important to take cognizance of their nature, so as to mitigate biodiversity loss as we explore natural resources for medical improvements. In order to achieve precision in some of these giant strides, it is imperative to study the properties of bioresorbable fibers to know precisely some of the salient properties that can be explored for medical use (Liu et al., 2013).

Table 2.2 illustrates the physical properties of some of the bioresorbable fibers used in medical applications. These features also make their application attractive in other areas of human endeavors. A material of biomedical engineering must possess many specific characteristics, which are different in terms of what was originally designed. In the case of domestic-used plastic products, a lot of work needs to have been done to ascertain the chemical properties of the materials prior to their being adapted for any other purpose, most importantly medical needs. One of the most fundamental requirements revolves round biocompatibility, taking into consideration its adverse effects on host tissues (Asokan et al., 2009).

Table 2.2 Properties of bioresorbable materials for medical applications.

	Tensile strength (MPa)	Elongation at break (%)	Young's modulus (GPa)
Natural fibers			
Flax	300–1500	1.3–10	24–80
Jute	200–800	1.16–8	10–55
Sisal	80–840	2–25	9–38
Kenaf	295–1191	3.35	2.85
Pineapple	170–1627	2.4	60–82
Banana	529–914	3	27.32
Coir	106–175	14.21–49	4–6
Oil palm (empty fruit)	130–248	9.7–14	3.58
Oil palm (fruit)	80	17	
Ramie	348–938	1.2–8	44–128
Hemp	310–900	1.6–6	30–70
Wool	120–174	25–35	2.3–3.4
Spider silk	875–972	17–18	11–13
Cotton	264–800	3–8	
Skin	7.6	77–81	

Hence, the properties of the parent materials provide a detailed and overview analysis of their component elements before they can be subjected to further analysis or use. In the case that there are variations in the composite materials with poor reinforcement, they could be replaced with bio-engineered composites. In another analysis, as presented in Tables 2.3 and 2.4, the properties of polymers, and bioresorbable and biocompatible materials with their illustrative applications are presented. This could provide the basis for the in-depth analysis of bioresorbable materials in their quest to solve a growing gap in the deployment of these materials for other needs (Leal-Egaña and Scheibel, 2010). The properties of materials provide a clear understanding of the nature, origin, and behavior of materials after years of applications. Fig. 2.1 is a typical illustration of the chemical properties of some bioresorbable polymers. Polyethylene (PE) in high-density (HDPE) form, as it appears in some of the most common applications, is a lightweight material that may not cope with the sterilization temperature range. Polypropylene (PP) is one of the isotactic crystalline polymer materials with a high possibility of being rigid, with moderate chemical resistance and considerable strength, and the possibility of

Table 2.3 Properties of polymers.

Type	Thermal properties	Construction/useful form
Synthetic polymers		
Polyethylene (PE)	$T_m = 203-208°C$	Heath care products, lightweight
Polypropylene (PP)	$T_m = 223-233°C$	orthopedic casts, ligament prostheses
Poly(tetrafluoro-ethylene) (PTFE)	$T_m = 313-315°C$	Surgical drapes, and gowns
Nylon 6	$T_g = 45°C$, $T_m = 220°C$	Vascular fabrics, heart valve sewing
Poly(ethylene terephthalate (PET))		rings, orthopedic ligaments
		Sutures
	$T_g = 65-105°C$, $T_m = 265°C$	Sutures
Bio-absorbable synthetic polymers		
Poly(glycolide) (PGA)	$T_g = 40-45°C$, $T_m = 225°C$	Absorbable sutures and meshes
Poly(p-dioxanone) (PDS)	$T_g = 10°C$, $T_m = 205°C$	Sutures, intramedullary pins
Poly(lactic-acid) (PLA)	$T_g = 60°C$, $T_m = 166°C$	Bone fixtures

Table 2.4 Physical properties of medically inclined polymers.

Polymer	Water absorption (%)	Bulk modulus (GPa)	Tensile strength (MPa)	Elongation at break (%)	T_g (°C)	T_m (°C)
Polyethylene (PE)	0.001–0.02	0.8–2.2	30–40	130–500	71–76	203–208
Polypropylene (PP)	0.01–0.035	1.6–2.5	21–40	50–800	117–132	222–233
Polyurethane (PU)	0.1–0.9	1.5–2	28–40	600–720	93–121	233–272
Polytetrafluoro ethylene (PTFE)	0.01–0.05	1–2	15–40	250–550	145–146	312–315
Polyvinyl-chloride	0.04–0.75	3.4	10–75	10–400	121–183	217
Polyamides	0.25–3.5	2.4–3.3	44–90	40–250	145–185	256–282
Polycarbonate (PC)	0.15–0.7	2.8–4.6	56–75	8–130	214	258–273
Bombyx mori silk	0.2–1	0.015–0.017	610–690	4–16	–	–

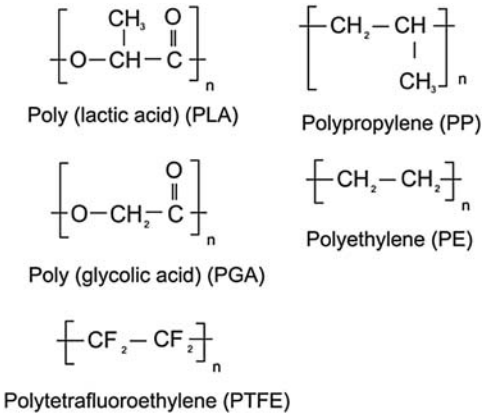

Figure 2.1 Chemical structures and behavioral properties of some bioresorbable and bio-degradable polymers.

possessing a higher fracture toughness as compared with HDPE. Polytetrafluoroethylene (PTFE) is also reputed to have a high melting point ($T_m = 312°C$) and moderate crystallinity as its features. PLA and PGA are often used in resorbable surgical sutures together with their copolymers. In many earlier works, the findings have shown that the degradation process and the emerging products are endogenous compounds and may not be toxic. As shown in these tables, it is noted that those synthetic materials being used in biomedical applications possess good thermal properties as compared with bioresorbable polymers. However, other findings and analyses indicate that the mechanical properties of some polymers are comparatively high when compared with existing materials for use in regenerative medicine (Sanjayan et al., 2015). However, a great deal of improvement has been reported in the enhancement of the physical properties of polymer materials but some lapses and drawbacks remain largely unaddressed. Generally, biocomposites are made up of synthetic polymer as matrix and natural fibers to support the fibers' moderate toughness, good specific strength, high thermal properties, separation flexibility, and biodegradable tendency. Bio-fibers, if they possess the highlighted properties, are often chosen as reinforcements since these features enable them to improve the tool wear properties when used for respiratory interventions. In another report (ul Haq et al., 2014), these fibers were constrained as a result of their small cross-sectional dimensions and they were unable to perform optimally in engineering applications which made them become embedded in matrix layers to form biocomposites. The

matrix may be used as a binder to bind the fibers intact and convey the loads to the fibers. An understanding of the chemistry of natural and synthetic materials is necessary to fully understand how their physicomechanical properties behave in biomedical applications (Li et al., 2007).

2.3 Performance of bioresorbable materials in medical interventions

The human body system is comprised of several tissue structures which may be classified according to the musculoskeletal system involving the integration of other human structural members ranging from skin, ligaments, nerves, and muscles, etc. In order for adjoining bones to co-exist in the human system, including fibrous and adjoining layers, this involves the integration of synovial and diarthrodial joints in which some degree of kinetic activity is activated (Davis and Song, 2006). The plan to use bioresorbable materials as a leverage for diarthrodial joints is an intervention approach for the protection of articular cartilage, which presents itself in translucent tissue parts, with the possibility of forming articulating surfaces in the diarthrodial joints (Amulya et al., 2021). The articular cartilage is composed of a tissue-related cellular matrix comprising of a sparse composition of embedded chondrocytes. The extracellular matrix (ECM) is naturally designed in such a manner that it forms insoluble tightly woven fibers, in the form of water and proteoglycan distributed to create the shape of a biphasic matrix. The involvement of fibrils is partly because of their ability to withstand tension but they can be susceptible to compression in application, and it is advisable that the matrix possesses high tensile strength, and in the case of proteoglycan macromolecules, they are reinforced with articular cartilage, making them able to withstand compression in the event of moisture interaction. The reinforcement of the cartilage structure, being a support system, is meant to support the joints' interactions with other organs, thereby reducing their wear resistance. This makes articular cartilage involved in steady compression which is often viscoelastic at every relaxation. Reports claim that its disadvantages are characterized by chronic diseases, child growth retardation, complicated trauma disorder, and other complications. These deficiencies could bring about the distortion of tissue to conform with the self-recovery effort, resulting in a full-thickness disorder. It is also important to examine the nature of some of these tissues in most regenerative procedures (Mayer et al., 2019). This also makes it difficult for them to have contact with blood, making them display a low

cell-to-matrix ratio. The findings have shown that more than 900,000 Americans display some form of articular cartilage injuries every year that require several transplants. This makes the situation worse in organs transplanted from similar donors due to the shortage of compatible donors. Given the circumstances arising from organ transplants, tissue regeneration through biomaterials offers a sustainable method for bridging the gap with the prospect for exploring more viable alternatives in biomedical materials as against surgical procedures (La Mantia and Morreale, 2011). Several years ago, a number of surgical operations were deployed to improve fractured cartilage which are now aimed at the treatment of injuries arising from tissue relief and dysfunctional cell structures. As it stands, three approaches are currently being activated in regenerative engineering: (1) the application of cell parts to serve as a replacement for damaged cells; (2) the application of cell materials in a specific location with a clear focus on modifying diverse factors; and (3) cultivating new cells in three diverse scaffolds. In a related development, three general principles are generally adopted for joint repair, these include: (1) reinforcement of different healing potentials of cartilage, (2) development of new cartilage with objective transplants, and (3) restoration of the cartilage interface with the adjoining cartilage. However, the findings have shown that the use of suspended cells for interfacing with chondrocytes in some transplants has certain limitations in theory and laboratory simulations. In addition, in vivo cells may display three-dimensional layers, in the form of cells in three-dimensional substrates that showcase scenarios that may reflect the results. To reduce these challenges, three-dimensional structural cells with matrices could be investigated for tissue engineering to study their features depending in vivo implantation or to promote cell repair.

The application of regenerative medicine has been shown to be effective in therapeutic control for the thorough replacement of damaged tissues and organs. Part of this method involves the production and replacement of scaffold materials in the place of a surrogate framework which aids tissue populations in order to translate them into equivalent and complementary cell parts. The adaptation of scaffold-based strategies in regenerative medicine has been shown to be most useful in three-dimensional platforms incorporating some of the features such as biocompatibility and biodegradability in some of the operational structures in order to provide an effective in vivo cell expansion for maturation. This may also aid in natural tissue development and the healing of many tissues in relation to their biochemical composition, morphological adaptation, and physiologic

function. The involvement of biomaterials in medicine has incorporated several methods, including naturally induced, synthetic, and hybrid bioresorbable materials to promote regenerative and safe healing (Adekomaya et al., 2017a). For these materials to be fully adapted into scaffolding, taking into consideration the process of tissue replacement, some techniques have been explored in the literature to develop materials with three-dimensional structures for cell growth, which provides an underlying tissue property with mechanical stability of the cell. The structural and background discourses for tissue replacement have been directed at damaged cells, with the aim of using scaffold biomaterials that are similar in chemical and physical composition to the isotropic nature of the materials including their considerable mechanical properties. It is important to adopt sustainable approaches and methods to develop scaffolds that have similar properties to the original tissue with some features such as nanoscale representation and biocompatibility, that continue to generate reactions and new methodologies for material fabrication. Scaffolding in cell repairs has focused on different approaches while accommodating bulk hydrogel materials or plant materials. Bulk hydrogels have been developed to provide a three-dimensional homogeneous platform that is suitable to bridge a fracture in the tissue adjacent to in vivo growth (Cheung et al., 2009). Hydrogel materials have been tailored through their chemical composition in such a manner that the pore size and mechanics of their structures are properly aligned. Some of these materials can be processed in microenvironmental structures depending on their properties and physical composition which may capture natural and synthetic components of the materials. In the case of synthetic hydrogels, these were fabricated from poly(ethylene glycol) and have been reported in a number of works depending on their decomposition mechanism and bioactive properties. Several of these processes have been undertaken in such a way that the growth factors or biomolecules are based on their interaction between the density and chemical composition of individual materials (McCullen et al., 2010). Some of the hydrogel materials which are often naturally occurring may be examined to provide sources such as hyaluronic acid-modified hydrogels and agarose. Part of the advantage of these materials is that they have been tested in practice to sustain equal cell conformity and a high tissue viability in cell repair. Also, there have been restrictions in the efficacies of these materials due to their heterogenic nature as indicated in batch-to-batch processing of some of their products. Substantial shrinkage has also been reported in some of these adaptive materials due to compatibility errors and poor mechanical

properties. There are several other ways in which these biomaterial properties can be structured by cross-linking, resulting in gel networks characterized by weak properties with moderate moduli depending on the transition from Pa to kPa. Moreover, in an attempt to increase the aggregate modulus, findings have shown that some of the resulting products could be limited in terms of permeability, diffusion, and the inability of repaired tissues to absorb nutrients and discharge unwanted products. There are also reported cases of structural heterogeneity in some of these products, making it a major disadvantage in the usage of hydrogel systems. Several other new approaches have been advanced to produce tissue materials with different geometries, including mechanical properties and uniformity in porosity, and anisotropy. The relationship of cells among other extracellular matrices is part of the effect in multi-cell matrix deposition, along with other resultant properties of the cellular materials. Several techniques have been recommended for the progression of scaffold fabrication in tissue-related medicine. Fiber-reinforced materials have long been used as replacement options in tissue repairs with complicated applications ranging from vascular grafts, hernia replacement tissue, etc. Fiber reinforcement could be adapted to suit particular operations depending on the properties of biomaterials needed to complement tissue repair applications. Findings have also shown that fiber reinforcement can be tailored to a variety of configurations in order to enhance the physical structure and mechanical properties of biomaterials based on the specific application and interest. In other areas, fibers are often arranged from monofilament yarns and could also be substituted to fit many substrates that can accommodate woven, knitted, braided, and randomly aligned materials. In the case of aligned fibers, the method could also be used in a spatial oriented arrangement that can be structured into any patterns ranging from angle-ply and cross-ply arrangements. The use of fibers as component parts of biomaterials depends largely on the orientation of the fibers, fiber volume fraction, physical attributes of the matrix, fiber—fiber contacts, and fiber—matrix ratio (Lau et al., 2018). The importance of using fibrous or natural materials including fiber and silk materials is that they can be tailored depending on the specific area of application in which the properties, such as extremely high porosity and good mechanical properties, are desired.

Several advances have been made to improve the fabrication techniques of biomaterials leading to diverse new ideas for both emerging products and therapies as they are used in the biomedical field. This has led to the development of many biomedical materials that have been deployed in

medical trials. Many studies were carried out a number of years ago to explore the possibilities of using natural materials, together with different types of fiber materials, to evolve a new class of biocomposite. This was done to create a clear departure from synthetic fibers that have been adapted for medical use (Rana and Jayachandran, 2000). The use of natural fibers has created a new area of knowledge in which several discoveries have been made on the use of bioresorbable materials and the progress needed for these to be advanced in the foreseeable future. Reports have also shown that some biological requirements may enhance the growth of cells and the porosity of the natural materials to fast-track cell growth and healing, nontoxicity of fibers, and fabrication techniques. Cellulose, which is one of the most highly sourced materials from processed cotton, is the most common fiber-forming biopolymer. Considering its absorbent nature, it is used in the production of hygiene products, diapers, and other absorbable applications. Some reports have also noted that they could not be used in vivo because of the highly inflammatory reactions associated with these materials. Findings have also created a growing interest in some of the natural fibers sourced from polysaccharide compounds comprising alginates, chitosan, dextran, and cellulose. Apart from cellulose, it is also important to source complementary resources which are dependent on natural fibers and more abundant, in the form of animal filaments. Their properties are of considerable interest to material engineers due to their rare structural properties, and by extension as reinforcement materials (Zaman et al., 2012).

2.4 Conclusion

This chapter has discussed the potential properties of biodegradable materials in regenerative and biomedical applications. Bioresorbable materials are derivable from natural fibers and are a suitable medium for several human needs. Natural fibers being biodegradable materials are faced with reclamation and replenishment challenges, including environmental vulnerability and biodiversity loss. Bioresorbable materials have been extensively used in the automotive industry in view of their lightness and payload reduction. This role has made natural fibers of high demand in several areas of human activities. Several features of biodegradable materials have made them complementary to regenerative medicine but there is always a shortfall in the procurement of these materials for further medical uses. this review chapter has also illuminated how important polysaccharides

and protein-based materials could be in the medical field and also to examine the potential of nanocellulose-based materials for biomedical applications. In the future, the demand for natural polymers in regenerative medicine will surpass the current demand thereby making natural material susceptable to environmental degradation and natural disasters. While natural fibers continue to find a market in biomedical applications, including wound dressings, tissue engineering, and scaffolds remolding, this may not be applicable to synthetic materials. There are also conflicting findings on their in vivo use as a complimentary support for biomaterials, where reports from the field run contrary to this claim. Bioresorbable materials, as reported in this chapter, provide a source for alternative materials for biomedical engineering in which alternative materials can easily be deployed where necessary. In consideration of bioresorbable materials for medical interventions, there is always concern about the characterization of materials to meet the required objectives. Natural materials are biodegradable in nature and as a results they tend to support the healing process better than other materials. Part of the shortcoming of natural fiber-reinforced composites is their water absorption tendency, which can result in poor compatibility. This effect may inhibit their performance in the medical field as pointed out in much of the literature. However, chemical treatments of these materials have shown good modification and better results in many cases. In order to enhance the properties of bioresorbable materials for the medical field, one may have to devise techniques to produce high-strength and improved inherent properties of these materials to conform with some of the regenerative drugs and other therapies required for the entire ecosystem. It is also important to consider other properties of natural fibers, such as pore size, degradation rate, and surface morphology, in order to ascertain the direction of application and sustainability of these materials in term of their high strength and compatibility to support healing and regenerative medicine. This may support the replacement of synthetic polymer and metallic-based materials in the medical field. The use of bioresorbable materials as a reinforcement to produce basic natural materials as well as control their biodegradability/bioresorbability is one of the most promising ongoing research areas. This research is multi-faceted, comprising diverse backgrounds to resolve how best to produce materials that can meet multiple requirements in all applications.

Acknowledgments

The lead author acknowledges the financial and institutional support provided by University of the Witwatersrand, South Africa, through the Research Office and the University Research Committee, upon which the postdoctoral fellowship was funded. The authors also appreciate the anonymous reviewers whose comments contributed positively to the final manuscript.

References

Abiola, O.S., Kupolati, W.K., Sadiku, E.R., Ndambuki, J.M., 2014. Utilisation of natural fibre as modifier in bituminous mixes: a review. Construct. Build. Mater. 54, 305–312.

Adekomaya, O., 2020. Adaption of green composite in automotive part replacements: discussions on material modification and future patronage. Environ. Sci. Pollut. Control Ser. 1–7.

Adekomaya, O., Jamiru, T., Sadiku, R., Huan, Z., 2017a. Minimizing energy consumption in refrigerated vehicles through alternative external wall. Renew. Sustain. Energy Rev. 67, 89–93.

Adekomaya, O., Jamiru, T., Sadiku, R., Huan, Z., 2017b. Negative impact from the application of natural fibers. J. Clean. Prod. 143, 843–846.

Adekomaya, O., Majozi, T., 2019. Sustainability of surface treatment of natural fibre in composite formation: challenges of environment-friendly option. Int. J. Adv. Des. Manuf. Technol. 105, 3183–3195.

Adekomaya, O., Majozi, T., 2020. Compatibility of natural fiber and hydrophobic matrix in composite modification. In: Kharissova, O.V., Martínez, L.M.T., Kharisov, B.I. (Eds.), Handbook of Nanomaterials and Nanocomposites for Energy and Environmental Applications. Springer International Publishing, Cham.

Adekomaya, O., Majozi, T., Adedoyin, S., 2020. Bio-based and biodegradable plastic materials: life cycle assessment. In: Kharissova, O.V., Martínez, L.M.T., Kharisov, B.I. (Eds.), Handbook of Nanomaterials and Nanocomposites for Energy and Environmental Applications. Springer International Publishing, Cham.

Amulya, K., Katakojwala, R., Ramakrishna, S., Venkata Mohan, S., 2021. Low carbon biodegradable polymer matrices for sustainable future. Compos. C Open Access 4, 100111.

Asokan, P., Osmani, M., Price, A.D.F., 2009. Assessing the recycling potential of glass fibre reinforced plastic waste in concrete and cement composites. J. Clean. Prod. 17, 821–829.

Ayrilmis, N., Jarusombuti, S., Fueangvivat, V., Bauchongkol, P., White, R.H., 2011. Coir fiber reinforced polypropylene composite panel for automotive interior applications. Fibers Polym. 12, 919–926.

Cheung, H.-Y., Ho, M.-P., Lau, K.-T., Cardona, F., Hui, D., 2009. Natural fibre-reinforced composites for bioengineering and environmental engineering applications. Compos. B Eng. 40, 655–663.

Davis, G., Song, J.H., 2006. Biodegradable packaging based on raw materials from crops and their impact on waste management. Ind. Crop. Prod. 23, 147–161.

Faruk, O., Bledzki, A.K., Fink, H.-P., Sain, M., 2012. Biocomposites reinforced with natural fibers: 2000–2010. Prog. Polym. Sci. 37, 1552–1596.

Jayaramudu, J., Maity, A., Sadiku, E.R., Guduri, B.R., Varada Rajulu, A., Ramana, C.V.V., Li, R., 2011. Structure and properties of new natural cellulose fabrics from *Cordia dichotoma*. Carbohydr. Polym. 86, 1623–1629.

La Mantia, F., Morreale, M., 2011. Green composites: a brief review. Compos. Appl. Sci. Manuf. 42, 579–588.
Lambert, S., Wagner, M., 2017. Environmental performance of bio-based and biodegradable plastics: the road ahead. Chem. Soc. Rev. 46, 6855–6871.
Lau, K.-T., Ho, M.-P., AU-Yeung, C.-T., Cheung, H.-Y., 2010. Biocomposites: their multifunctionality. Int. J. Soc. Netw. Min. 1, 13–27.
Lau, K.-T., Hung, P.-Y., Zhu, M.-H., Hui, D., 2018. Properties of natural fibre composites for structural engineering applications. Compos. B Eng. 136, 222–233.
Leal-Egaña, A., Scheibel, T., 2010. Silk-based materials for biomedical applications. Biotechnol. Appl. Biochem. 55, 155–167.
Li, X., Tabil, L.G., Panigrahi, S., 2007. Chemical treatments of natural fiber for use in natural fiber-reinforced composites: a review. J. Polym. Environ. 15, 25–33.
Liu, X.-D., Sheng, D.-K., Gao, X.-M., Li, T.-B., Yang, Y.-M., 2013. UV-assisted surface modification of PET fiber for adhesion improvement. Appl. Surf. Sci. 264, 61–69.
Mayer, F., Bhandari, R., Gäth, S., 2019. Critical review on life cycle assessment of conventional and innovative waste-to-energy technologies. Sci. Total Environ. 672, 708–721.
Mccullen, S.D., Haslauer, C.M., Loboa, E.G., 2010. Fiber-reinforced scaffolds for tissue engineering and regenerative medicine: use of traditional textile substrates to nanofibrous arrays. J. Mater. Chem. 20, 8776–8788.
Rameshkumar, S., Shaiju, P., O'connor, K.E., 2020. Bio-based and biodegradable polymers - State-of-the-art, challenges and emerging trends. Curr. Opin. Green Sustain. Chem. 21, 75–81.
Rana, A., Jayachandran, K., 2000. Jute fiber for reinforced composites and its prospects. Mol. Cryst. Liq. Cryst. 353, 35–45.
Sanjayan, J.G., Nazari, A., Chen, L., Nguyen, G.H., 2015. Physical and mechanical properties of lightweight aerated geopolymer. Construct. Build. Mater. 79, 236–244.
Suddell, B., 2008. Industrial fibres: recent and current developments. In: Proceedings of the Symposium on Natural Fibres. FAO and CFC Rome, pp. 71–82.
Sun, H.-S., Chiu, Y.-C., Chen, W.-C., 2016. Renewable polymeric materials for electronic applications. Polym. J. 49, 61–73.
Szendiuch, I., 2011. Development in electronic packaging–moving to 3D system configuration. Radioengineering 20, 214–220.
Ul Haq, E., Kunjalukkal Padmanabhan, S., Licciulli, A., 2014. Synthesis and characteristics of fly ash and bottom ash based geopolymers–A comparative study. Ceram. Int. 40, 2965–2971.
Upgupta, S., Sharma, J., Jayaraman, M., Kumar, V., Ravindranath, N.H., 2015. Climate change impact and vulnerability assessment of forests in the Indian Western Himalayan region: a case study of Himachal Pradesh, India. Clim. Risk Manag. 10, 63–76.
Van Gameren, V., Zaccai, E., 2015. Private forest owners facing climate change in Wallonia: adaptive capacity and practices. Environ. Sci. Pol. 52, 51–60.
Xie, Y., Hill, C.A., Xiao, Z., Militz, H., Mai, C., 2010. Silane coupling agents used for natural fiber/polymer composites: a review. Compos. Appl. Sci. Manuf. 41, 806–819.
Yang, L., Sáez, E.R., Nagel, U., Thomason, J.L., 2015. Can thermally degraded glass fibre be regenerated for closed-loop recycling of thermosetting composites? Compos. Appl. Sci. Manuf. 72, 167–174.
Zaman, H.U., Khan, M.A., Khan, R.A., 2012. Comparative experimental studies on the mechanical and degradation properties of natural fibers reinforced polypropylene composites. Compos. Interfac. 19, 59–70.

CHAPTER 3

Processing techniques for bioresorbable-based composites for medical device applications

Nadda Chiaoprakobkij[1] **and Manunya Okhawilai**[1,2]
[1]Metallurgy and Materials Science Research Institute, Chulalongkorn University, Bangkok, Thailand;
[2]Research Unit in Polymeric Materials for Medical Practice Devices, Department of Chemical Engineering, Faculty of Engineering, Chulalongkorn University, Bangkok, Thailand

3.1 2D structure

Thin film is one of the most common 2D structures. The materials are dissolved in solvents and cast in a flat template. The solvent is removed from the film's structure by evaporation. Recently, different types of thin films have become of great demand as they have the potential for low-priced processing with minimal materials usage. Thin films are small in size, and so they can be used to create small and portable medical devices. Thin films can be flexible and lightweight. They are also good candidates where mechanical flexibility and low weight are required. Thin films also allow direct integration of other components on the substrate. Multi-layer systems are possible without the need for bonding.

An implantable and ultra-flexible bone fracture electrostimulation device (FED) from bioresorbable soft and metallic materials has been researched (Yao et al., 2021). The device component was constructed with island-bridge electrodes and pyramid base microstructures. The device was able to adhere to uneven tissue surfaces and generate steady electric pulses reacting to the movements of knee joints. Figs. 3.1 and 3.2 illustrate the design, structural characterization, and fabrication procedure for the FED. The FED consisted of two modules: (1) triboelectric nanogenerator (TENG) and (2) interdigitated dressing electrodes. Both components were set up on the same PLGA substrate. Si wafer mold with inverse square pyramid arrays was produced by lithography technique.

Lithography is the process of transferring a pattern from one object onto another. Electrobeam and optical photolithography are used to transfer a

Bioresorbable Polymers and their Composites
ISBN 978-0-443-18915-9
https://doi.org/10.1016/B978-0-443-18915-9.00016-1
© 2024 Elsevier Ltd.
All rights reserved.

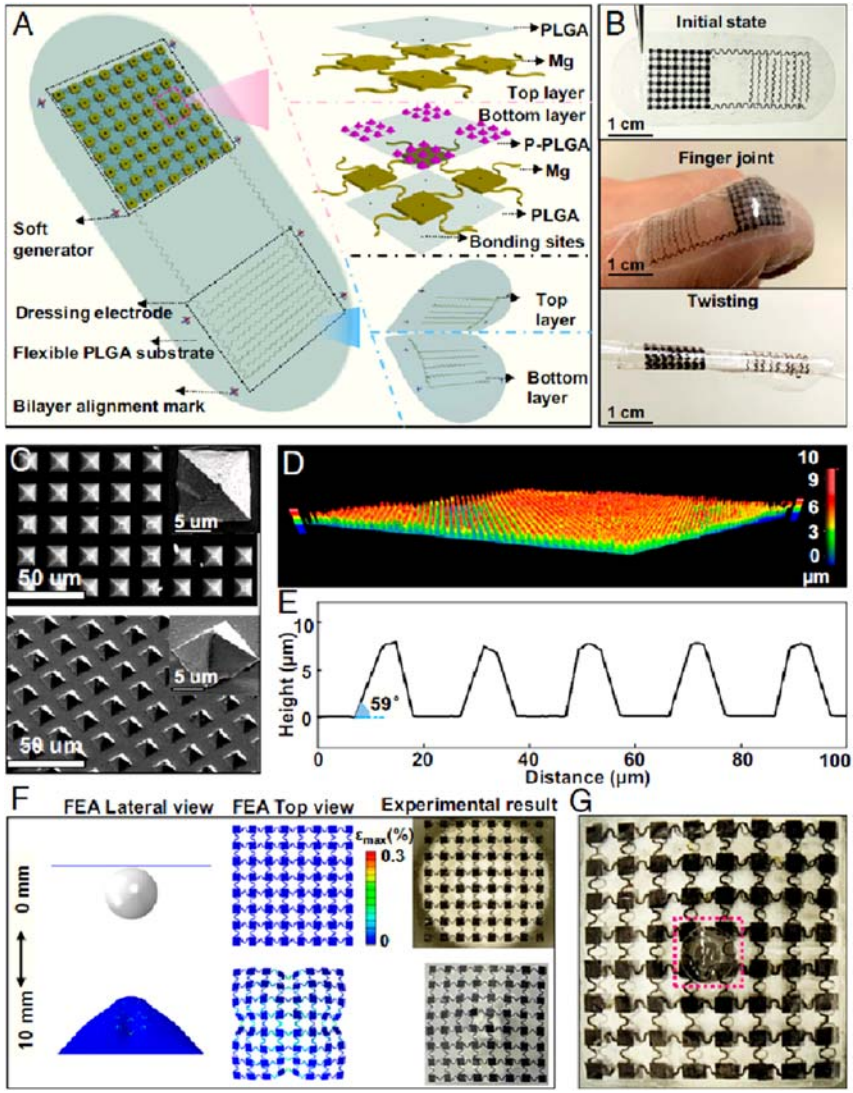

Figure 3.1 Configuration and characterization of the device. (a) Layout of the device structure (*left*) and illustration of the components, main materials, and microstructures (*right*). (b) Physical appearance of the device (*top*) being fully bent (middle) and being twisted (*bottom*). (c) Top and side-view SEM images of the microstructures onto the PLGA surface. Insets show enlarged views of a single pyramid. (d) 3D microscope. (e) The height profile of the PLGA microstructures. (f) Studies of the Mg electrode under different pressing heights. (g) Water droplet on the hydrophobic TENG (pressing height of 10 mm). *(Reproduced from Yao et al. (2021).)*

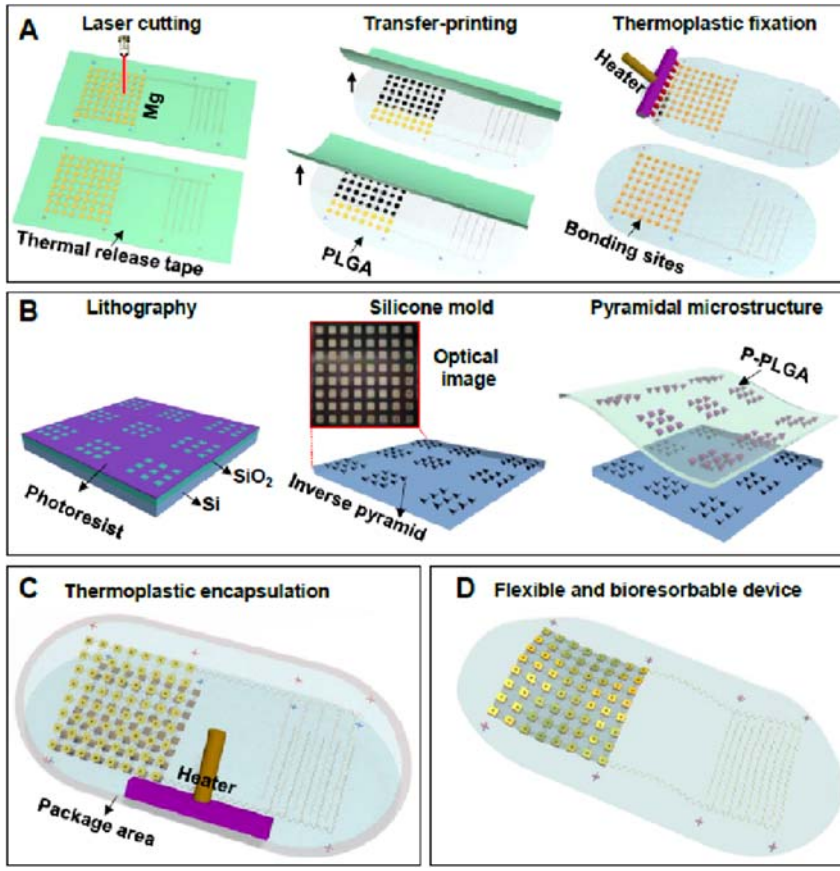

Figure 3.2 The schematic of the FED. (a) Mg foils attached to the thermal release tape. The Mg electrodes were printed onto PLGA substrates at 120°C and then fixed by a dot-matrix electric soldering iron. (b) The Si wafer mold was produced by lithography and wet-etching and the P-PLGA substrate was carefully peeled off the mold. (c) The device was thermoplastically encapsulated with the P-PLGA inserted in Mg electrodes. (d) Illustration of the bioresorbable and stretchable FED. *(Reproduced from Yao et al. (2021).)*

two-dimensional pattern onto a substrate. Imprint photolithography is used to transfer three-dimensional patterns and structures onto the substrate.

The PLGA polymer solution was spin-coated onto an Si wafer mold and then dried in an oven at 50−100°C overnight to evaporate the solvent. PLGA films were carefully peeled off as P-PLGA layer. Laser cutting technology prepared 2 Mg electrodes with an island-bridge structure.

Cointe and coworkers developed ultrathin and super-stretchable neural probes from the bioresorbable silk layer. A neural probe is one of the key tools in neuroscience for recording electrical brain activity. A flexible probe is in conformity with the surrounding neural tissue. The probes are made of a silk-parylene bilayer. The fabrication procedure and the probe are shown in Fig. 3.3. The fabrication processes consisted of the following three stages: (1) cellulose acetate (CA) is coated with a silk layer, (2) a super-thin parylene-based structure tops the silk layer using the lithography technique, and (3) the whole silk-parylene probe enables microscale shaping by a reaction ion etching (RIE) process.

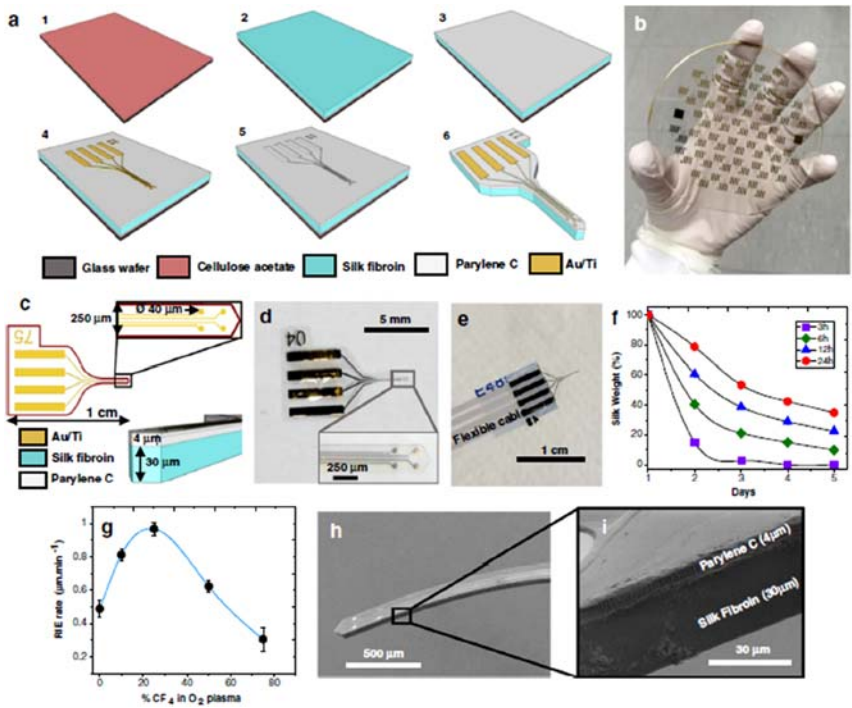

Figure 3.3 Production of the parylene-silk probes. (a) Illustration of the fabrication on a glass wafer: (1) cellulose acetate deposition, (2) silk deposition, (3) parylene deposition, (4) gold microelectrode patterning, (5) parylene top layer deposition, and (6) probe final shaping. (b) Photograph of a glass substrate after microfabrication. (c) Illustration of the bilayered silk-parylene probe with characteristic dimensions. (d) Photograph of the implant. The inset shows the magnified view of the microelectrodes. (e) Photograph of the silk-parylene probe. (f) Biodegradation of silk fibroin after immersion in methanol. (g) Etching rate of silk fibroin versus percent of CF_4 in O_2 plasma at 500 W and 20 mTorr. (h) SEM micrograph of the final bilayered silk-parylene shank, and (i) the magnified SEM micrograph. *(Reproduced from Cointe et al. (2022).)*

RIE, a standard method of dry etching, is used as a micro-structuring process that combines chemical and physical processes. In a sputtering process, ions activate the substrate surface and supply the energy to allow a chemical reaction with the etching gas. The RIE method is attractive due to its well-controlled etching behavior. This etching process provides good control of uniformity, etching profiles, and selectivity. Isotropic (direction independent) and anisotropic directed etching can be achieved.

The bioresorbable magnesium membrane has been fabricated and studied as a barrier membrane for dental surgical guided bone regeneration (GBR) (Rider et al., 2022). The magnesium barrier membrane and its insertion protocol are illustrated in Fig. 3.4.

The barrier membranes were produced from a hot-rolled magnesium sheet. The sheet was trimmed to the desired shapes using a stamping press and die, and each membrane was etched. The membrane was decontaminated by gamma irradiation after etching. The size of each membrane was 30 × 40 mm, with a thickness of 140 μm.

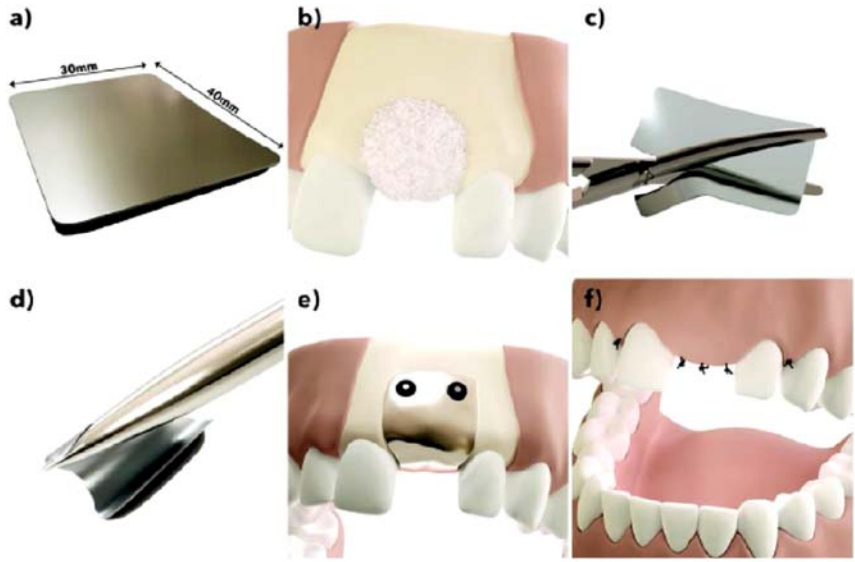

Figure 3.4 The insertion protocol of the Mg barrier membrane (NOVA-Mag membrane, botiss biomaterials GmbH, Germany). (a) The Mg membrane. (b) The defect sites are filled with a bone augmentation material. (c) The Mg membrane is trimmed by a pair of scissors (NOVAMag scissors). (d) The Mg membrane is twisted to fit the defect site contours. (e) The membrane is attached on the buccal and palatial sides. (f) The mucoperiosteal flap is sutured closed over the membrane for closed wound healing. *(Reproduced from Rider et al. (2022).)*

Choi and coworkers developed bioresorbable and stretchable electronic stimulators to promote neuromuscular regeneration. The device is made of bioresorbable polycaprolactone-based polyurethane (b-DCPU) and PLGA. A strip of bioresorbable molybdenum (Mo) in a serpentine geometry with an end opening acts as an electrical extension and connection to convey electrical stimuli from the receiver antenna to nerve tissues. An illustration of a device is depicted in Fig. 3.5. In vivo and in vitro studies revealed that the device could stimulate nerve regeneration.

Lee and coworkers reported a thin, flexible, and bioresorbable nerve simulator for electrical nerve block and pain mitigation (Lee et al., 2022). The developed devices combined bioresorbable metals and polymers. Electrodes and electrical interconnect traces were made of magnesium and molybdenum. A 40 μm-thick layer of PLGA acted as a support for the electrodes. All elements were between a pair of 400 μm-thick polyanhydride (PA). The favorable properties of PA over PLGA mean that it serves as a barrier to prevent the system from interacting with body fluids.

A thin film can also function like a selective nanomembrane. Li and coworker studied a bioresorbable and extremely stretchable electrochemical sensor for nitric oxide monitoring (Li et al., 2020). The device successfully senses the nitric oxide level in living mammals. The sensor consisted of polylactic acid and poly(trimethylene carbonate) (PLLA-PTMC), super-

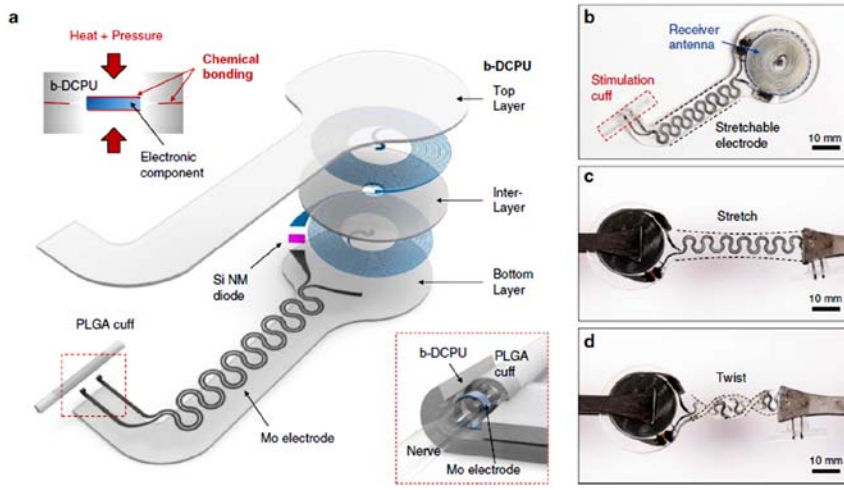

Figure 3.5 (a) The overall design of the device. (b) The photograph of a completed device. (c, d) Photographs of stretched (30%) and twisted (360 degrees) devices. *(Reproduced from Choi et al. (2020).)*

thin gold electrodes, and polyeugenol films. Thin films of PLLA-PTMC were fabricated by being drop-cast on glass substrates followed by gold sputtering.

Another example of integrated biomedical devices using the 2D structure casting method is a strain and pressure sensor. Boutry and coworkers reported the bioresorbable pressure and strain sensor for orthopedic rehabilitation monitoring (Boutry et al., 2018). The thin films of poly glycerol secabate (PGS) were used as a stretchable and nonsticking dielectric for the capacitor. Thin films of poly(octamethylene maleate (anhydride) citrate) (POMac) were employed for strain sensor and packaging. Thin films of PLLA were used as the layer for the magnesium electrodes.

Boutry and coworkers developed a sophisticated bioresorbable and flexible wireless pressure sensor to monitor blood flow (Boutry et al., 2019). The thin film of magnesium interconnected together with the thin film of poly(glycerol scabate) (PGS) for a pressure-sensitive layer. The thin layer of POMac and polyhydroxybutyrate-polyhydroxyvalerate (PHB-PHV) and PLLA were used for the binary coils. The PGS layer enhanced the sensitivity and response time of the sensor. The soft layer of POMac was in contact with the artery. The stiff layer of PHB-PHV was in contact with surrounding muscles. The integrated device was sensitive to artery expansion. The PLLA layer prevented short circuiting between the coil. In vivo studies revealed that the device has minimal hysteresis, fast response time, as well as being wirelessly operated.

A bioresorbable silicon electronic device for the brain has been reported (Kang et al., 2016). A thin membrane of PLGA was adhered onto the thin layer of nanoporous silicon. The silicon nanomembranes were patterned via photolithography and etching. The 100 nm-thick layer of silicon oxide was overcoated by an electron-beam evaporator. In vivo studies in rat showed that the devices could sense pressure, temperature, motion, flow, pH, and thermal properties that were compatible with the body's acute traumatic injuries.

A silicon nanomembrane was also developed into an NO_x sensing system for medical implants (Ko et al., 2020). The devices were equipped with patterned silicon nanomembrane, magnesium contact pad, and polycaprolactone (PCL) substrate. In vitro tests showed that the device was stable in harsh conditions and very hydrated environments for temporary implants.

A bioresorbable spectrometer consisting of a silicon nanomembrane, zinc electrodes, and PLGA optical fibers was studied (Bai et al., 2019).

In vivo studies in mice proved that the device is an intriguing option for measuring the temperature, neural activity, and oxygenation in brain monitoring.

A molybdenum disulfide (MoS_2) bioresorbable sensor was developed by Chen and coworkers (Chen et al., 2018). A monolayer of MoS_2 was patterned by photolithography. The mesh structure was formed by RIE and transferred onto a PLGA thin film. In vivo studies of severe traumatic brain injury in mice confirmed that the developed device was a potential sensor for pressure, temperature, strain, and motion through intracranial monitoring.

Silk fibroin was reported as ultrathin and conformable electrode arrays for neural mapping experiments (Kim et al., 2010). The device was developed and studied in a feline model. The results showed high conformal contact on the brain model with good response to signal amplitude and signal-to-noise ratio.

The bioresorbable composite of PLA-PLGA was integrated with magnesium electrodes as wireless anticancer drug-loaded patches for the treatment of brain tumors (Lee et al., 2019). Tumor volume suppression was observed in canine model studies.

PLGA pads integrated with magnesium electrodes were developed as battery-free implantable cardiac pacemakers (Choi et al., 2021). In vitro studies in rat, rabbit, and canine models showed favorable effective pacing of hearts.

Magnesium-iodine encapsulated with polyanhydride composites were reported as bioresorbable batteries (Huang et al., 2022). The constructed batteries were found to be potential power supplies for cardiac pacemakers.

3.2 3D structure

Solvent casting, in combination with patterning fabrication, works only for thin membranes or 3D samples with a very thin wall. 3D printing is a high-precision technique to produce complex 3D objects that accurately define and control the structure of the manufactured parts. This process is also known as additive manufacturing. It creates three-dimensional solid objects from 3D model files using materials such as powdered metal and polymers, by printing them layer by layer. 3D-printed objects can be printed into any desired shapes and geometric characteristics. The 3D printing technique can be categorized into fused deposition modeling, selective laser sintering, and stereo-lithography, as described below.

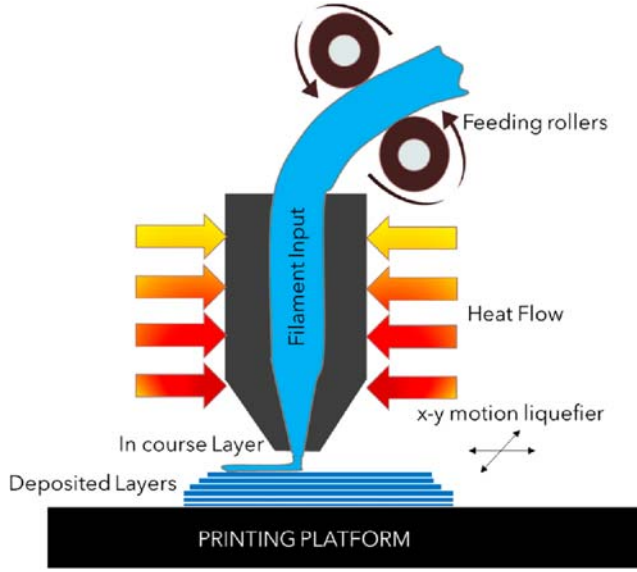

Figure 3.6 Illustration of fused deposition modeling (FDM). *(Reproduced from Ali et al. (2022).)*

3.2.1 Fused deposition modeling (FDM)

Fig. 3.6 shows a schematic diagram of fused deposition modeling.

The filamentous hot-melt material is heated and melted. Then the three-dimensional nozzle can accurately cover the material according to the cross-sectional profile information and set up a layer after a swift cooling procedure. The entire process is under the control of a computer.

3.2.2 Selective laser sintering (SLS)

A schematic diagram of SLS is shown in Fig. 3.7.

The SLS technique uses an infrared laser. This method is carried out by powder spreading. A layer of powder material is spread on the upper surface of the molded part. The temperature required by this technique is just below the sintering point of the material. The temperature of the material increases to the melting point, sintering and bonding with the molded part below after scanning. The control system directs the laser beam according to the cross-sectional profile of the layer.

3.2.3 Stereolithography apparatus (SLA)

The laser used in this method is an ultraviolet laser. A schematic of an SLA is shown in Fig. 3.8.

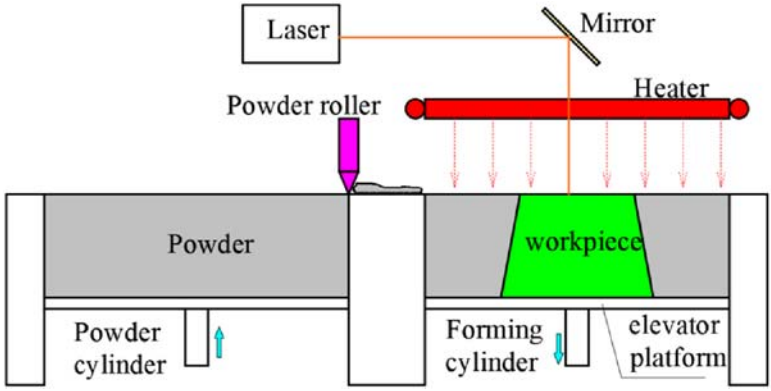

Figure 3.7 Schematic diagram of selective laser sintering (SLS). *(Reproduced from Zheng et al. (2022).)*

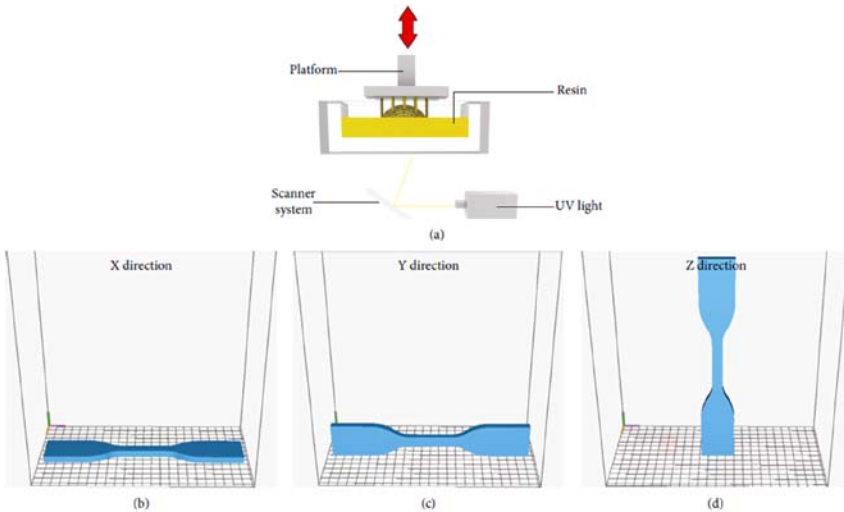

Figure 3.8 (a) Illustration of the SLA process: (b) face up (*X* direction), (c) edge up (*Y* direction), and (d) upright (*Z* direction) of tensile test specimens. *(Reproduced from Feng et al. (2019).)*

The liquid photosensitive resin is stuffed in the tank. It quickly cures under the ultraviolet laser beam. The laser beam scans the cross-sectional profile along the liquid surface. The liquid resin in the scanning is quickly solidified to complete the process of a layer of cross-section and obtains a layer of the sheet. The 3D printing technique is a fast prototyping and customized design with wide material options.

3.2.4 Advantages

3.2.4.1 Flexible design

3D printing can deliver a product with novel designs that can be uniquely shaped and much more intricate than those manufactured using traditional methods. Flexible, semirigid, and bioresorbable materials that are difficult to process through traditional means can be produced by the 3D printing technique.

3.2.4.2 Fast design and production

3D printing is low-cost and fast at producing manufactured parts, allowing for individual design modifications to be efficiently completed.

3.2.4.3 Minimizing waste

This fabrication technique can reduce wastage production, and less scrap is produced compares to conventional methods. It also reduces the cost of material usage. Despite many promising benefits, there are some disadvantages to the 3D printing technique.

3.2.5 Disadvantages

3.2.5.1 Limited materials

Despite 3D printing being able to produce parts in a selection of metals, synthetic polymers, and biopolymers, the available selection of raw materials remains limited. This is due to the fact that not all materials can endure 3D printing as the 3D printing process may alter the properties of raw materials and end-products.

3.2.5.2 Post-processing

3D-printed parts need some form of finishing. The purpose of finishing is to remove support material and to smooth the surface to complete the finished product. Generally, finishing methods include chemical rinsing and air or heating drying. Post-processing may affect the properties of end-products. Despite allowing rapid production, the entire manufacturing process's speed can be slowed down by post-processing.

3.2.5.3 Large volumes

Conventional techniques like injection molding can produce large volumes for mass production, which may be more cost-effective. 3D printing is more suitable for customized products.

Chiesa and coworkers developed a bioresorbable, super-stretchable, and self-adhesive piezoelectric device from a 3D printing technique that sensed

the motility whenever it was applied onto the phantom intestine and hand gesture by signal translation. The device is made of regenerative silk (RS), tannin from chestnut (T), and graphite nanoplatelets (GNP). The 3D-printed grids are illustrated in Fig. 3.9. It is promising for use in gastrointestinal tract motility monitoring and for motility disorder diagnosis.

Bioresorbable segmented poly(ester-urethanes) (SPEU)-glass ceramic scaffolds were fabricated using the FDM printing technique (Lores et al., 2022). The printed scaffold showed high dimensional accuracy.

Dave and coworkers reported the 3D-printed composite of PLA and carbon quantum dots scaffold fabricated via the FDM technique (Dave and Gomes, 2022). The developed scaffolds were photoluminescent. They could be used as alternatives in renewal, restoration, rejuvenation, and monitoring of tissues.

The bioresorbable stent is a medical device that has undergone continuous development processes. 3D printing technology has attracted a good deal of interest for the development of stents. Fig. 3.10 shows the available commercial bioresorbable stents.

Currently, PLLA is most regularly used in bioresorbable stents (Jinnouchi et al., 2019). Bioresorbable poly(p-dioxanone) (PPDO) was combined with PLLA to fabricate artery bioresorbable stents via the 3D-printing technique (Lu et al., 2022). The stents were improved in hydrolytic stability and endothelial cell growth.

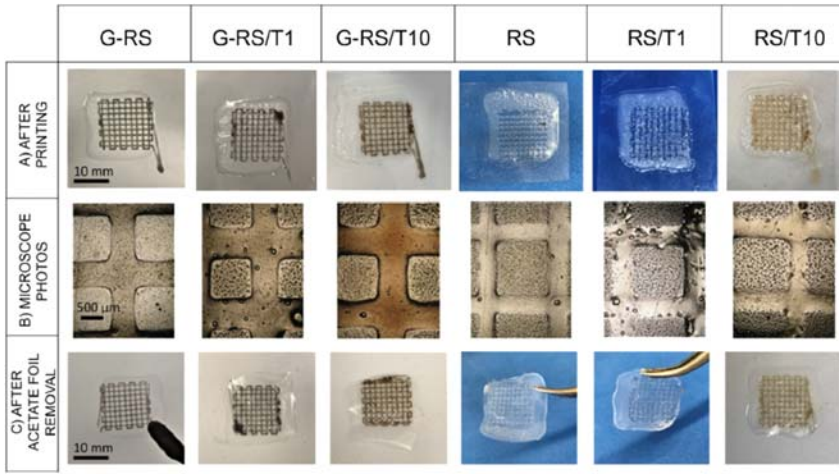

Figure 3.9 Physical appearances of 3D-printed grids. (a) Photographs taken as soon as printing ended. (b) Photographs taken with a brightfield microscope. (c) Photographs of the specimens after acetate foil removal. *(Reproduced from Chiesa et al. (2022).)*

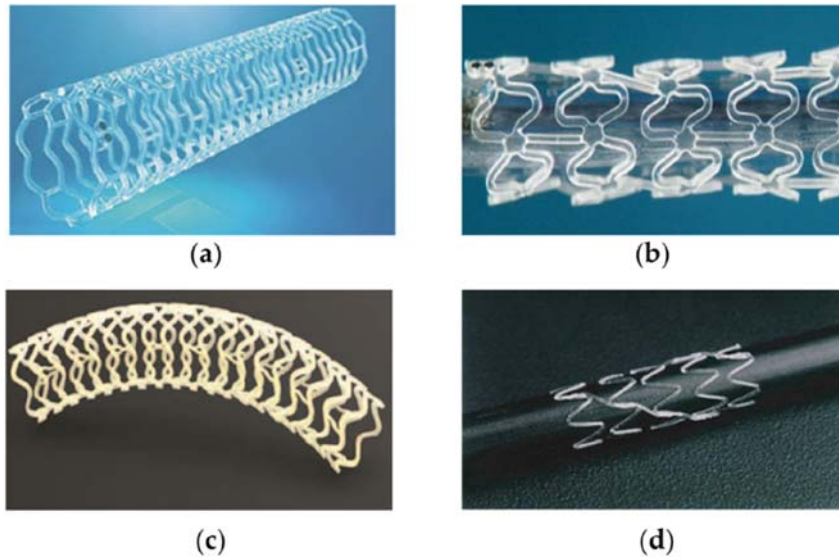

Figure 3.10 Examples of bioresorbable stents: (a) Abbott ABSORB stent; (b) DESolve stent; (c) Fantom stent; and (d) Igaki-Tamai stent. *(Reproduced from Wang et al. (2021).)*

Qiu and coworkers developed a bioresorbable stent from polycaprolactone (PCL)-sulfated chitosan via a 3D printing technique. Their results suggested that the fabricated stents could potentially be used for coronary artery disease. The 3D printing method is shown in Fig. 3.11.

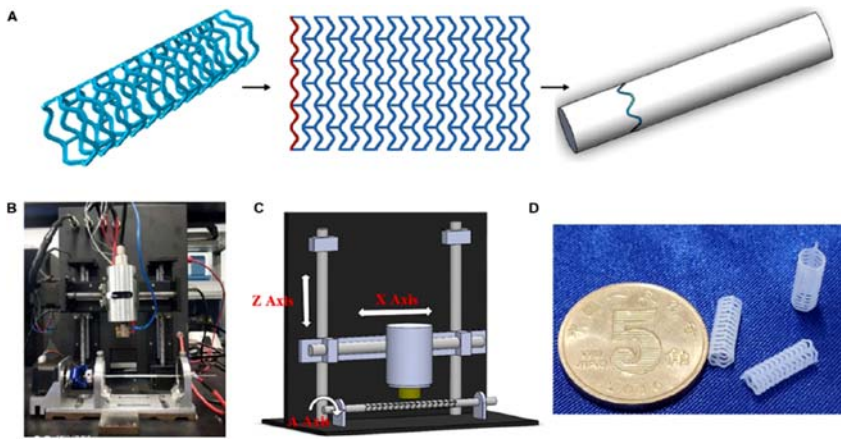

Figure 3.11 (a) Illustration of a 3D-printing process. (b) 3D-printing machine. (c) 3D-printing machine components. (d) Examples of 3D-printed PCL stents. *(Reproduced from Qiu et al. (2020).)*

Yu and coworkers developed personalized bioresorbable airway external splints from polycaprolactone (PCL) via a 3D-printing method. The device could provide functional support for at least 6 months in patients. No complications such as infection or device erosion occurred. The device remained intact throughout the follow-up period. Hence, the device is considered to be nontoxic, reliable, and practical. A personalized 3D-printed bioresorbable airway external splint is shown in Fig. 3.12. Patient-specific external airway splints with a "C"-shaped lumen were designed in SOLIDWORKS. The designed splints were processed by a selective laser sintering system (SLS). This technique can create layer-by-layer custom-made splints following the complex shape and 3D contours of the trachea.

In order to obtain better clinical outcomes for a bare stent, a nitric oxide-eluting hydrogel coating has been developed (Chen et al., 2021). The hydrogel consisted of gelatin and alginate. The hydrogel was applied onto the stents by a dip-coating process. The dip-coated stents could specifically promote the adhesion of endothelial cells along with inhibited smooth muscle cells. In vivo studies in leporine and swine models showed that the developed stents suppressed inflammation as well as promoting endothelium restoration.

Another case of the surface modification of a bare stent was a copper-incorporated polydopamine (PDA) top coating (Li et al., 2022). In vivo studies in rabbit abdominal aorta showed favorable clinical outcomes as well as prolonged structural durability of the stents.

Radiopaque bioresorbable stents with strong X-ray visibility were fabricated by a 3D-printing technique (Ding et al., 2022). Iodixanol was

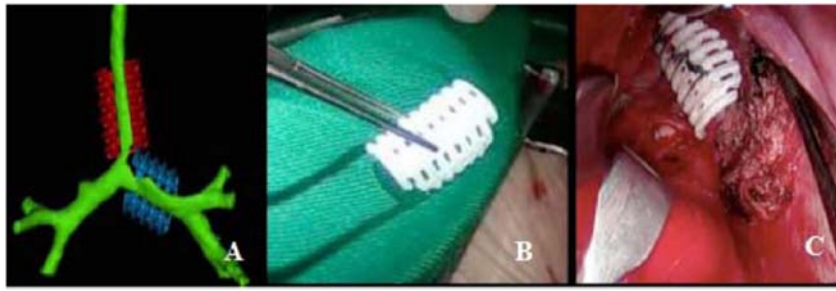

Figure 3.12 (a) Design of a customized 3D-printed airway external splint. (b) The physical appearance of the 3D-printed bioresorbable airway external splint. (c) Intra-operative placement of the splint overlying the malacia tracheal segment. *(Reproduced from Yu et al. (2022).)*

incorporated into citrate-based polymer to make radiopaque ink for 3D printing. The prepared stents appeared to be highly biocompatible in vitro. The stent visualization enabled less invasive follow-up monitoring.

The 3D printing of bioresorbable stents of PLLA and poly(lactic-co-ε-caprolactone) (PLCL) composite was studied by Chausse and coworkers (Chausse et al., 2023). The stents were found to be unaltered by ethylene oxide sterilization.

Sophisticated smart stents integrated with wireless pressure sensor have been developed (Park et al., 2019). These complicated forms of stents were fabricated via a 3D-printing technique, and the stents were made of PCL. The devices efficiently measured intravascular blood pressure in a rat model.

Heart disease in children is different from that in adults to some extent. Zhao and coworkers developed bioresorbable stents for pediatric patients with coronary artery disease (Zhao et al., 2021). The stents were the composites of polycaprolactone-poly(*p*-dioxanone). They showed a suitable degradation rate for vascular remodeling and the healing process.

PLGA and PLA were fabricated as tubular urethral stents via a 3D-printing method (Jaworska et al., 2022). PLGA stents were found to be more stable in an artificial urine.

Aside from stents, the diced cartilage grafts of bioresorbable PCL were successfully shaped with the help of a 3D-printing technique (Canli et al., 2022). The printed grafts were produced into the desired complex shapes which were helpful for utilization in operations such as nasal reconstruction and orbital floor fracture repair.

A bioresorbable composite of PLA and PCL and hydroxyapatite (HA) was developed to provide customized material for bone defect treatment via fused deposition modeling (FDM) (Åkerlund et al., 2022).

3.3 Micro-molding

Micro-molding is a highly specialized fabrication process that produces markedly small high-precision components with micron tolerances. The process starts where a mold is created that has a cavity in the shape of the part desired. Micro-molding is capable of molding more than one material on the same part at the same time. The different materials can be molded together, requiring only one mold cycle. Additives or functional materials can be added during the process.

Microneedles (MNs) are medical devices that have attracted favorable interest in the medical field. They possess microstructures that are spiky and

sufficiently robust for skin penetration. Their application produces a microsized pathway for transferring molecules, including biomedical antigens and cells (Rad et al., 2021). Blood and interstitial fluid can be drawn by this device. Either low- or high-molecular-weight biotherapeutic drugs and vaccines can be delivered through the skin.

Bioresorbable MNs are usually fabricated by micro-molding. Generally, a polymeric solution is poured into the mold. Air voids are removed by vacuum or centrifuge. Molds are then dried, and then MNs are detached after cooling. The micro-molding technique is shown in Fig. 3.13.

Yuan and coworkers developed MNs for diabetic wound healing. The MNs consisted of gelatin-methacryloyl (GelMA) and poly(ethylene glycol) diacrylate (PEGDA). Tazarotene (a wound repair drug) and exosomes were added to the MNs. In vivo studies in diabetic mice showed that the fabricated MNs could promote cell migration and angiogenesis in full-thickness cutaneous wounds. The preparation process and the morphology of MNs are shown in Fig. 3.14.

Yan and coworkers studied two-layered sodium hyaluronate MNs loaded with huperzine powder for Alzheimer disease (AD) treatment. In vivo tests in rats showed that the designed MNs are a promising alternative for AD treatment. A schematic of the preparation process and the morphology of MNs is provided in Fig. 3.15.

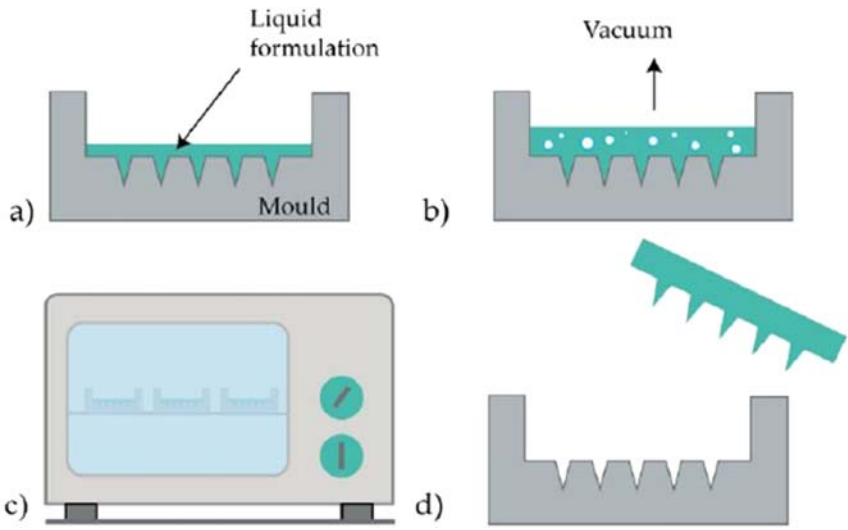

Figure 3.13 MN production using micro-molding: (a) pouring the polymer solution, (b) vacuum degasification, (c) drying, and (d) MNs removal from the mold. *(Reproduced from Tucak et al. (2020).)*

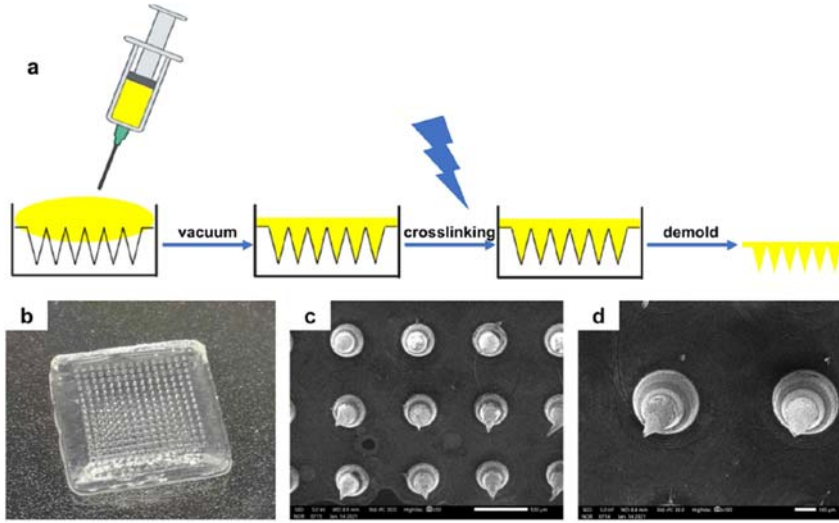

Figure 3.14 (a) Preparation of GelMA MNs. (b) Photographs of an MN patch. (c, d) SEM micrographs of MNs. (c) Scale bar is 500 μm; (d) scale bar is 100 μm. *(Reproduced from Yuan et al. (2022).)*

Integrated stretchable gold-doped graphene microneedles were successfully developed by Lee and coworkers (Lee et al., 2016). The developed microneedles were capable of monitoring sweat-based glucose and pH, along with being thermally activated to deliver Metformin and reduce blood glucose levels in diabetic mice.

A carboxymethylcellulose (CMC) and hyaluronan bioresorbable composite was reported for use in fast-dissolving microneedles for transcutaneous vaccination devices (Ono et al., 2017). These authors found that the developed microneedles were not completely dissolved in human skin. They suggested incorporating a hydration enhancer such as sugar alcohol to speed up microneedle dissolution. Sodium alginate—polyvinyl alcohol (PVA)—polyvinylpyrrolidone (PVP) bioresorbable composite was fabricated into two-layer microneedles for diabetes treatment (Liu et al., 2022).

A sodium hyaluronic acid—sodium alginate—gelatin composite incorporated with curcumin was studied as dual functional microneedles for melanoma treatment and wound healing (Shan et al., 2022).

3.4 Particulate structures

Particulate structures such as nano/microparticles have high surface area homogeneity in size, shape, distribution, and controllable degradation.

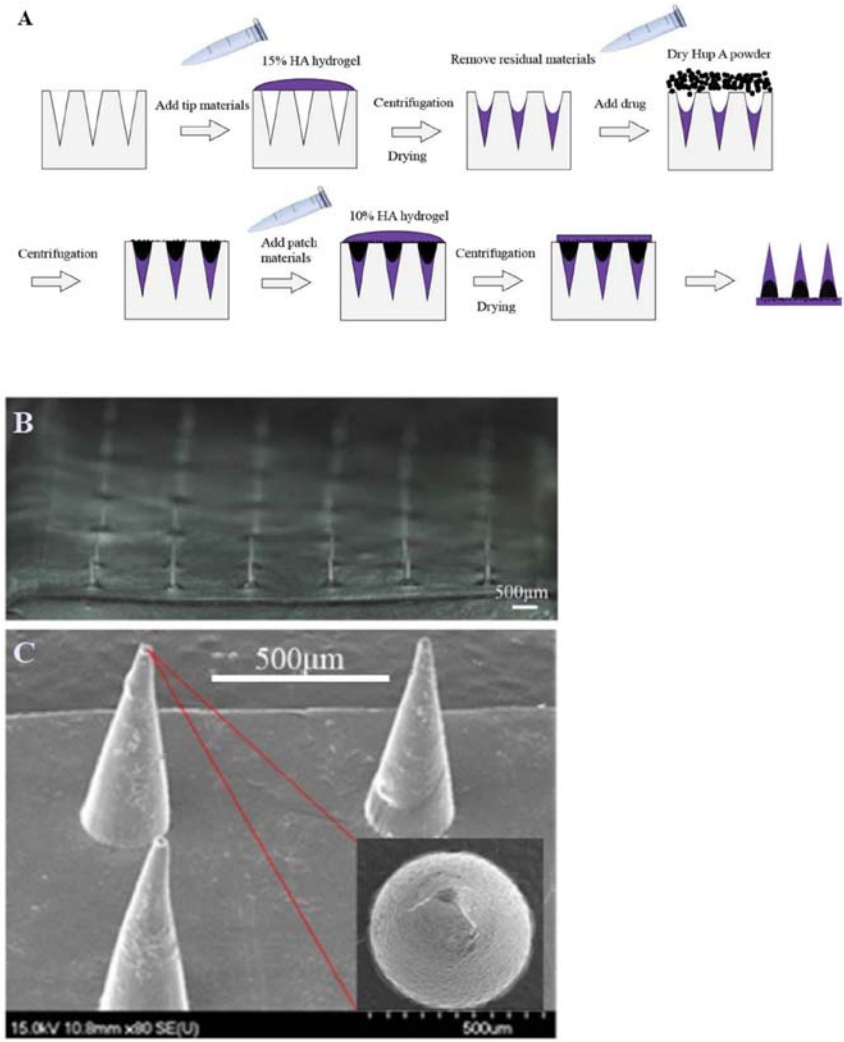

Figure 3.15 (a) Preparation of MNs; (b) the overall appearance of the 6 × 6 DMNP; (c) SEM micrographs of the MNs. *(Reproduced from Yan et al. (2020).)*

Zareei and coworkers developed bioresorbable and super-stretchable paper-based flexible bioelectronics devices with a mix of micro/nano conductive zinc paste. These devices were found to be promising as a wearable wireless heater for drug delivery (Zareei et al., 2022).

3.5 Conclusion and outlook

Current medical devices have undergone significant development in terms of manufacturing techniques. Materials consideration and processing methods are important for long-term success. A product's functionality depends on selecting and processing methods with mechanical properties for the product to perform as designed. The demand for customized medical devices continues to grow. The choice of fabrication technique depends on the device's properties, design, and function. The accuracy and versatility of 3D printing, combined with other fabrication techniques and patterning methods, are attracting favorable interest from both the research and industrial sectors. The benefit of 3D printing technology is apparent and growing rapidly. It is likely to be one of the crucial technologies driving invention, especially with the growth of tissue engineering, bioprinting, and regenerative medicine. The key benefits for manufacturing are that individual modifications can be made to the desired designs, and the speed at which methods can be amended and printed. Modifications can be made rapidly, and tools can be created to optimize specific functions for specific operative techniques.

References

Åkerlund, E., Diez-Escudero, A., Grzeszczak, A., Persson, C., 2022. The effect of PCL addition on 3D-printable PLA/HA composite filaments for the treatment of bone defects. Polymers 14 (16), 3305. https://doi.org/10.3390/polym14163305.

Ali, U., Saeed, H.A., Ahmed, B.A., Butt, S.U., Khan, R., 2022. Investigation of the impact resistance behavior of customized hair clipper comb fabricated by fused deposition modeling. Sustainability 14 (13), 8071. https://doi.org/10.3390/su14138071.

Bai, W., Shin, J., Fu, R., Kandela, I., Lu, D., Ni, X., Park, Y., Liu, Z., Hang, T., Wu, D., Liu, Y., 2019. Bioresorbable photonic devices for the spectroscopic characterization of physiological status and neural activity. Nat. Biomed. Eng. 3 (8), 644–654. https://doi.org/10.1038/s41551-019-0435-y.

Boutry, C.M., Beker, L., Kaizawa, Y., Vassos, C., Tran, H., Hinckley, A.C., Pfattner, R., Niu, S., Li, J., Claverie, J., Wang, Z., 2019. Biodegradable and flexible arterial-pulse sensor for the wireless monitoring of blood flow. Nat. Biomed. Eng. 3 (1), 47–57. https://doi.org/10.1038/s41551-018-0336-5.

Boutry, C.M., Kaizawa, Y., Schroeder, B.C., Chortos, A., Legrand, A., Wang, Z., Chang, J., Fox, P., Bao, Z., 2018. A stretchable and biodegradable strain and pressure sensor for orthopaedic application. Nat. Electron. 1 (5), 314–321. https://doi.org/10.1038/s41928-018-0071-7.

Canli, M., Karasoy Yesilada, A., Ulağ, S., Dobral, A., Yalçin, Ö., Gündüz, O., 2022. Evaluation of diced cartilage grafts shaped with three-dimensionally-printed bioresorbable polycaprolactone molds. Plast. Reconstr. Surg. 150 (4), 800e–809e. https://doi.org/10.1097/PRS.0000000000009572.

Chausse, V., Iglesias, C., Bou-Petit, E., Ginebra, M.P., Pegueroles, M., 2023. Chemical vs thermal accelerated hydrolytic degradation of 3D-printed PLLA/PLCL bioresorbable stents: characterization and influence of sterilization. Polym. Test. 117, 107817. https://doi.org/10.1016/j.polymertesting.2022.107817.

Chen, X., Park, Y.J., Kang, M., Kang, S.K., Koo, J., Shinde, S.M., Shin, J., Jeon, S., Park, G., Yan, Y., MacEwan, M.R., 2018. CVD-grown monolayer MoS2 in bioabsorbable electronics and biosensors. Nat. Commun. 9 (1), 1–12. https://doi.org/10.1038/s41467-018-03956-9.

Chen, Y., Gao, P., Huang, L., Tan, X., Zhou, N., Yang, T., Qiu, H., Dai, X., Michael, S., Tu, Q., Huang, N., 2021. A tough nitric oxide-eluting hydrogel coating suppresses neointimal hyperplasia on vascular stent. Nat. Commun. 12 (1), 1–16. https://doi.org/10.1038/s41467-021-27368-4.

Chiesa, I., De Maria, C., Ceccarini, M.R., Mussolin, L., Coletta, R., Morabito, A., Valentini, L., 2022. 3D printing silk-based bioresorbable piezoelectric self-adhesive holey structures for in vivo monitoring on soft tissues. ACS Appl. Mater. Interfaces 14 (17), 19253–19264. https://doi.org/10.1021/acsami.2c04078.

Choi, Y.S., Hsueh, Y.Y., Koo, J., Yang, Q., Avila, R., Hu, B., Rogers, J.A., 2020. Stretchable, dynamic covalent polymers for soft, long-lived bioresorbable electronic stimulators designed to facilitate neuromuscular regeneration. Nat. Commun. 11 (1), 1–14. https://doi.org/10.1038/s41467-020-19660-6.

Choi, Y.S., Yin, R.T., Pfenniger, A., Koo, J., Avila, R., Benjamin Lee, K., Chen, S.W., Lee, G., Li, G., Qiao, Y., Murillo-Berlioz, A., 2021. Fully implantable and bioresorbable cardiac pacemakers without leads or batteries. Nat. Biotechnol. 39 (10), 1228–1238. https://doi.org/10.1038/s41587-021-00948-x.

Cointe, C., Laborde, A., Nowak, L.G., Arvanitis, D.N., Bourrier, D., Bergaud, C., Maziz, A., 2022. Scalable batch fabrication of ultrathin flexible neural probes using a bioresorbable silk layer. Microsyst. Nanoeng. 8 (1), 1–11. https://doi.org/10.1038/s41378-022-00353-7.

Dave, K., Gomes, V.G., 2022. Bioresorbable poly (lactic acid) and organic quantum dot-based nanocomposites: luminescent scaffolds for enhanced osteogenesis and real-time monitoring. J. Nanostruct. Chem. 12 (5), 951–962. https://doi.org/10.1007/s40097-021-00456-z.

Ding, Y., Fu, R., Collins, C.P., Yoda, S.F., Sun, C., Ameer, G.A., 2022. 3D-Printed radiopaque bioresorbable stents to improve device visualization. Adv. Healthcare Mater. 11 (23), 2201955. https://doi.org/10.1002/adhm.202201955.

Feng, Z., Li, Y., Hao, L., Yang, Y., Tang, T., Tang, D., Xiong, W., 2019. Graphene-reinforced biodegradable resin composites for stereolithographic 3D printing of bone structure scaffolds. J. Nanomater. 2019. https://doi.org/10.1155/2019/9710264.

Huang, I., Zhang, Y., Arafa, H.M., Li, S., Vazquez-Guardado, A., Ouyang, W., Liu, F., Madhvapathy, S., Song, J.W., Tzavelis, A., Trueb, J., 2022. High performance dual-electrolyte magnesium–iodine batteries that can harmlessly resorb in the environment or in the body. Energy Environ. Sci. 15 (10), 4095–4108. https://doi.org/10.1039/D2EE01966C.

Jaworska, J., Stojko, M., Włodarczyk, J., Janeczek, H., Godzierz, M., Musiał-Kulik, M., Bryniarski, P., Kasperczyk, J., 2022. Docetaxel-loaded scaffolds manufactured by 3D printing as model, biodegradable prostatic stents. J. Appl. Polym. Sci. 139 (23), 52283. https://doi.org/10.1002/app.52283.

Jinnouchi, H., Torii, S., Sakamoto, A., Kolodgie, F.D., Virmani, R., Finn, A.V., 2019. Fully bioresorbable vascular scaffolds: lessons learned and future directions. Nat. Rev. Cardiol. 16 (5), 286–304. https://doi.org/10.1038/s41569-018-0124-7.

Kang, S.K., Murphy, R.K., Hwang, S.W., Lee, S.M., Harburg, D.V., Krueger, N.A., Shin, J., Gamble, P., Cheng, H., Yu, S., Liu, Z., 2016. Bioresorbable silicon electronic sensors for the brain. Nature 530 (7588), 71–76. https://doi.org/10.1038/nature16492.

Kim, D.H., Viventi, J., Amsden, J.J., Xiao, J., Vigeland, L., Kim, Y.S., Blanco, J.A., Panilaitis, B., Frechette, E.S., Contreras, D., Kaplan, D.L., 2010. Dissolvable films of silk fibroin for ultrathin conformal bio-integrated electronics. Nat. Mater. 9 (6), 511–517. https://doi.org/10.1038/nmat2745.

Ko, G.J., Han, S.D., Kim, J.K., Zhu, J., Han, W.B., Chung, J., Yang, S.M., Cheng, H., Kim, D.H., Kang, C.Y., Hwang, S.W., 2020. Biodegradable, flexible silicon nanomembrane-based NOx gas sensor system with record-high performance for transient environmental monitors and medical implants. NPG Asia Mater. 12 (1), 1–9. https://doi.org/10.1038/s41427-020-00253-0.

Lee, G., Ray, E., Yoon, H.J., Genovese, S., Choi, Y.S., Lee, M.K., Sahin, S., Yan, Y., Ahn, H.Y., Bandodkar, A.J., Kim, J., 2022. A bioresorbable peripheral nerve stimulator for electronic pain block. Sci. Adv. 8 (40), eabp9169. https://doi.org/10.1126/sciadv.abp9169.

Lee, H., Choi, T.K., Lee, Y.B., Cho, H.R., Ghaffari, R., Wang, L., Choi, H.J., Chung, T.D., Lu, N., Hyeon, T., Choi, S.H., 2016. A graphene-based electrochemical device with thermoresponsive microneedles for diabetes monitoring and therapy. Nat. Nanotechnol. 11 (6), 566–572. https://doi.org/10.1038/nnano.2016.38.

Lee, J., Cho, H.R., Cha, G.D., Seo, H., Lee, S., Park, C.K., Kim, J.W., Qiao, S., Wang, L., Kang, D., Kang, T., 2019. Flexible, sticky, and biodegradable wireless device for drug delivery to brain tumors. Nat. Commun. 10 (1), 1–9. https://doi.org/10.1038/s41467-019-13198-y.

Li, L.Y., Yang, Z., Pan, X.X., Feng, B.X., Yue, R., Yu, B., Zheng, Y.F., Tan, J.Y., Yuan, G.Y., Pei, J., 2022. Incorporating copper to biodegradable magnesium alloy vascular stents via a Cu (II)-Eluting coating for synergistic enhancement in prolonged durability and rapid re-endothelialization. Adv. Funct. Mater. 32 (47), 2205634. https://doi.org/10.1002/adfm.202205634.

Li, R., Qi, H., Ma, Y., Deng, Y., Liu, S., Jie, Y., Jing, J., He, J., Zhang, X., Wheatley, L., Huang, C., 2020. A flexible and physically transient electrochemical sensor for real-time wireless nitric oxide monitoring. Nat. Commun. 11 (1), 1–11. https://doi.org/10.1038/s41467-020-17008-8.

Liu, H., Zhang, S., Zhou, Z., Xing, M., Gao, Y., 2022. Two-layer sustained-release microneedles encapsulating exenatide for type 2 diabetes treatment. Pharmaceutics 14 (6), 1255. https://doi.org/10.3390/pharmaceutics14061255.

Lores, N.J., Hung, X., Talou, M.H., Ballarre, J., Abraham, G.A., Caracciolo, P.C., 2022. Additive manufacturing of bioresorbable poly (ester-urethane)/glass-ceramic composite scaffolds. Polym. Compos. 43 (8), 5611–5622. https://doi.org/10.1002/pc.26875.

Lu, J., Hu, X., Yuan, T., Cao, J., Zhao, Y., Xiong, C., Li, K., Ye, X., Xu, T., Zhao, J., 2022. 3D-Printed poly (P-dioxanone) stent for endovascular application: in vitro evaluations. Polymers 14 (9), 1755. https://doi.org/10.3390/polym14091755.

Ono, A., Ito, S., Sakagami, S., Asada, H., Saito, M., Quan, Y.S., Kamiyama, F., Hirobe, S., Okada, N., 2017. Development of novel faster-dissolving microneedle patches for transcutaneous vaccine delivery. Pharmaceutics 9 (3), 27. https://doi.org/10.3390/pharmaceutics9030027.

Park, J., Kim, J.K., Kim, D.S., Shanmugasundaram, A., Park, S.A., Kang, S., Kim, S.H., Jeong, M.H., Lee, D.W., 2019. Wireless pressure sensor integrated with a 3D printed polymer stent for smart health monitoring. Sensor. Actuator. B Chem. 280, 201–209. https://doi.org/10.1016/j.snb.2018.10.006.

Qiu, T., Jiang, W., Yan, P., Jiao, L., Wang, X., 2020. Development of 3D-printed sulfated chitosan modified bioresorbable stents for coronary artery disease. Front. Bioeng. Biotechnol. 8, 462. https://doi.org/10.3389/fbioe.2020.00462.

Rad, Z.F., Prewett, P.D., Davies, G.J., 2021. An overview of microneedle applications, materials, and fabrication methods. Beilstein J. Nanotechnol. 12 (1), 1034–1046. https://doi.org/10.3762/bjnano.12.77.

Rider, P., Kačarević, Ž.P., Elad, A., Tadic, D., Rothamel, D., Sauer, G., Witte, F., 2022. Biodegradable magnesium barrier membrane used for guided bone regeneration in dental surgery. Bioact. Mater. 14, 152–168. https://doi.org/10.1016/j.bioactmat.2021.11.018.

Shan, Y., Tan, B., Zhang, M., Xie, X., Liao, J., 2022. Restorative biodegradable two-layered hybrid microneedles for melanoma photothermal/chemo co-therapy and wound healing. J. Nanobiotechnol. 20 (1), 1–16. https://doi.org/10.1186/s12951-022-01426-5.

Tucak, A., Sirbubalo, M., Hindija, L., Rahić, O., Hadžiabdić, J., Muhamedagić, K., Vranić, E., 2020. Microneedles: characteristics, materials, production methods and commercial development. Micromachines 11 (11), 961. https://doi.org/10.3390/mi11110961.

Wang, L., Jiao, L., Pang, S., Yan, P., Wang, X., Qiu, T., 2021. The development of design and manufacture techniques for bioresorbable coronary artery stents. Micromachines 12 (8), 990. https://doi.org/10.3390/mi12080990.

Yan, Q., Wang, W., Weng, J., Zhang, Z., Yin, L., Yang, Q., Yang, G., 2020. Dissolving microneedles for transdermal delivery of huperzine A for the treatment of Alzheimer's disease. Drug Deliv. 27 (1), 1147–1155. https://doi.org/10.1080/10717544.2020.1797240.

Yao, G., Kang, L., Li, C., Chen, S., Wang, Q., Yang, J., Wang, X., 2021. A self-powered implantable and bioresorbable electrostimulation device for biofeedback bone fracture healing. Proc. Natl. Acad. Sci. USA 118 (28). https://doi.org/10.1073/pnas.2100772118 e2100772118.

Yu, D., Peng, W., Mo, X., Zhang, Y., Zhang, X., He, J., 2022. Personalized 3D-printed bioresorbable airway external splint for tracheomalacia combined with congenital heart disease. Front. Bioeng. Biotechnol. 758. https://doi.org/10.3389/fbioe.2022.859777.

Yuan, M., Liu, K., Jiang, T., Li, S., Chen, J., Wu, Z., Chen, Z., 2022. GelMA/PEGDA microneedles patch loaded with HUVECs-derived exosomes and tazarotene promote diabetic wound healing. J. Nanobiotechnol. 20 (1), 1–18. https://doi.org/10.1186/s12951-022-01354-4.

Zareei, A., Selvamani, V., Gopalakrishnan, S., Kadian, S., Maruthamuthu, M.K., He, Z., Rahimi, R., 2022. A biodegradable hybrid micro/nano conductive zinc paste for paper-based flexible bioelectronics. Adv. Mater. Technol. 2101722. https://doi.org/10.1002/admt.202101722.

Zhao, F., Sun, J., Xue, W., Wang, F., King, M.W., Yu, C., Jiao, Y., Sun, K., Wang, L., 2021. Development of a polycaprolactone/poly (p-dioxanone) bioresorbable stent with mechanically self-reinforced structure for congenital heart disease treatment. Bioact. Mater. 6 (9), 2969–2982. https://doi.org/10.1016/j.bioactmat.2021.02.017.

Zheng, X., Meng, J., Liu, Y., 2022. Strain rate dependence of compressive mechanical properties of polyamide and its composite fabricated using selective laser sintering under saturated-water conditions. Micromachines 13 (7), 1041. https://doi.org/10.3390/mi13071041.

CHAPTER 4

PCL-based composites and their utilizations in the medical sector

Deepak Gupta[1], Vaishally Dogra[2,3], Deepak Verma[3,4], Arun Kumar Chaudhary[1] and Maneesh Tewari[1]

[1]Department of Industrial and Production Engineering, College of Technology, Govind Ballabh Pant University of Agriculture and Technology, Pantnagar, Uttarakhand, India; [2]Department of Mechanical Engineering, Graphic Era Deemed to be University, Dehradun, Uttarakhand, India; [3]Department of Mechanical Engineering, Graphic Era Hill University, Dehradun, Uttarakhand, India; [4]International Graduate Program of Nanoscience and Technology, Chulalongkorn University, Bangkok, Thailand

4.1 Introduction to biopolymer composites

Bio-based polymers are those polymers which have biodegradable behavior and can be categorized by their different physicochemical properties and biodegradability activity (Pan et al., 2016; Imre and Pukánszky, 2013). Biopolymers can be of synthetic or natural origin, while their biodegradability and biocompatibility enhance their utility in food packaging, biomedical, tissue engineering, structural applications, and more (Kim et al., 2022; Alhanish and Ali, 2023). Different forms of biopolymers include nanocomposites, films, hydrogels, and scaffolds that find use in many biomedical applications (Varma and Gopi, 2021).

Polycaprolactone (PCL) is a type of poly (α-ester) which is hydrolytically degradable as well as highly sensitive to even typical humidity (Geoghegan et al., 2023). PCL is a polyester which is flexible at body and room temperatures because of its melting temperature of around 60°C. PCL has amorphous and crystalline domains and provides many interesting benefits due to its sticky quality (Burg, 2014). PCL has a ring-like structure (Fig. 4.1), is prepared by the ring opening polymerization (ROP) method, and is used for the encapsulation of different drugs for targeted drug delivery and controlled release (McKeen, 2017).

PCL belongs to the aliphatic polymers and is commonly used for tissue engineering, dental implants, orthopedics, vascular grafts, nerve repair, ear implants, etc. in the medical sector (Ulery et al., 2011). It exhibits natural breakdown processes within the human body over time (Dias et al., 2022).

Bioresorbable Polymers and their Composites
ISBN 978-0-443-18915-9
https://doi.org/10.1016/B978-0-443-18915-9.00012-4
© 2024 Elsevier Ltd.
All rights reserved.

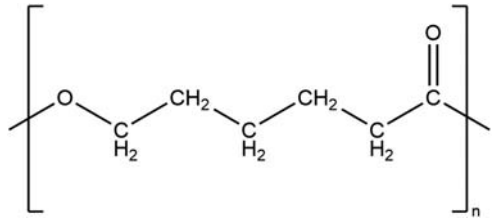

Figure 4.1 Polycaprolactone (PCL) structure. *(Reproduced with permission from Elsevier from McKeen (2017).)*

This property is particularly helpful for its utilization in temporary support or scaffolding in tissue engineering (Scaffaro et al., 2016). PCL is also acknowledged for its biocompatibility nature which means that it does not induce any adverse effects when interacting with biological systems (Álvarez-Ortega et al., 2021). PCL possesses a semicrystalline structure, which contributes to its favorable mechanical properties for utilization in medical applications (Jeong et al., 2018). It has a relatively low glass transition temperature (T_g), rendering it flexible and easily deformable at room temperature (Dell'Erba et al., 2001). PCL also exhibits good elongation, tensile strength, and impact resistance (Peponi et al., 2013). It offers excellent processability and can be utilized in various fabrication techniques, including melt blending, solution blending, electrospinning, and 3D printing (Dwivedi et al., 2020). This versatility allows for the production of PCL-based composites with customized properties and complex geometries, making it suitable for specific medical applications (Patrício et al., 2014). PCL displays hydrophobic properties, which are beneficial for medical purposes, particularly as a drug carrier that necessitates controlled release of hydrophobic drugs. The hydrophobic behavior of PCL enables encapsulation and also the sustained release of drugs (Ahmad Shariff et al., 2023).

4.2 Development and synthesis of PCL

The synthesis of polycaprolactone can be done by either of condensation of 6-hydroxycaproic acid or ROP of ε-caprolactone (Cama et al., 2017), both of which are discussed below.

4.2.1 Polycondensation

Polycondensation is a successive reaction, where two molecule groups can rejoin, resulting in the synthesis of a polymer and often producing a

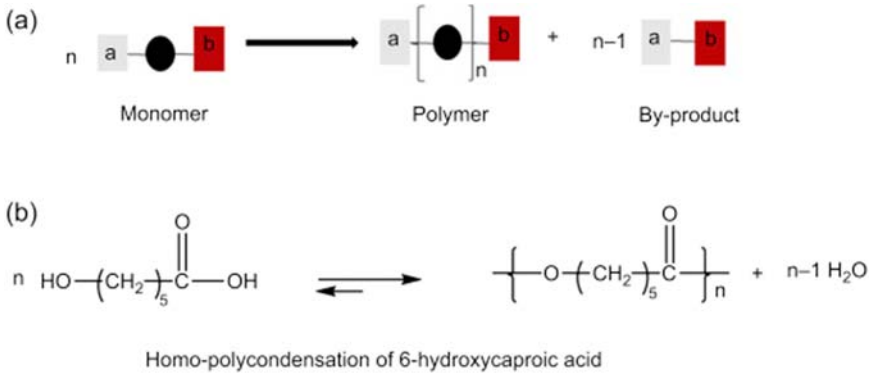

Figure 4.2 Polycondensation reaction for PCL synthesis. *(Reproduced with permission from Elsevier from Cama et al. (2017).)*

low-molecular-weight by-product as a result (Mousavifard et al., 2023). The increasing polymer chain of 6-hydroxycaproic rejoins with other molecules, while the alcohol group in a polycondensation reaction (Fig. 4.2) of PCL, releases water as a by-product and an ester bond is formed (Kaluzynski et al., 2022). This method is rarely used for synthesis of PCL as compared to ROP which results in inflated molecular weight with low polydispersity.

4.2.2 Ring-opening polymerization

ROP is as a chain-growth polymerization where one end of the polymer chain acts as the reactive center for addition of cyclic monomers and forms a longer chain (Cama et al., 2017). The polymer resulting from the reaction encloses end groups that depend on end reactions occurring and an applied initiator. Initiator and catalyst applications can be understood as:

- *Catalyst:* any metallic compound which is used to enhance a polymerization reaction process.
- *Initiator:* amine-alcohol groups that initiate the ROP reaction process.
- *Catalyst initiator:* the first part initiates the reaction of the molecule, while the secondary part catalyzes the reaction. These are used for reactions where only one compound is used.

Depending on the catalyst, the ROP process can be divided into four different processes (Fig. 4.3), each of which has different end groups, polydispersity, and molecular weights (Labet and Thielemans, 2009).

- *Anionic ROPs:* Anionic ROPs are generated during the ROP process, which subsequently attack the carbonyl carbon atom of monomers,

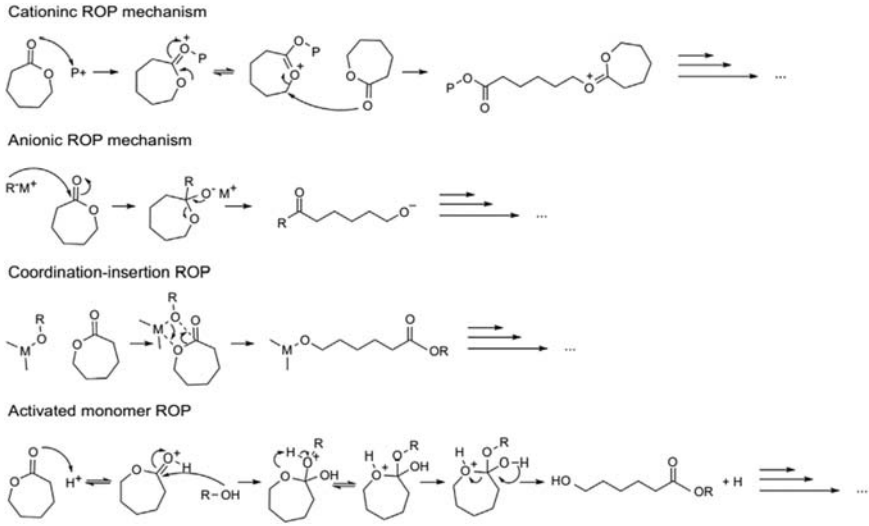

Figure 4.3 Different ring-opening polymerization mechanisms. *(Reproduced with permission from Elsevier from Cama et al. (2017).)*

leading to cleavage of the acyl-oxygen bond along with ring opening (Sudo, 2013; Ageyeva et al., 2018). The occurrence of significant intramolecular reactions is a major drawback, resulting in low-molecular-weight or cyclic polymers, although the effect of this drawback can be controlled at an early stage of polymerization (Penczek and Pretula, 2016).

- *Cationic ROPs:* Cationic ROPs are formed during the ROP process, which are attacked by the monomer's carbonyl oxygen by a bimolecular nucleophilic replacement reaction. Controlling the reactions is a major drawback, while the challenge is to increase the molecular weight (Penczek and Pretula, 2021).
- *Coordination-insertion ROPs:* This involves coordination of the monomer with the catalyst along with the insertion of a monomer through the associated monomer's oxygen—metal bond during propagation in a pseudo-anionic manner (Nifant'ev and Ivchenko, 2019). The alkoxide bond helps in attaching the growth chain to metal during the propagation process.
- *Activated monomer ROPs:* In this type of ROP, a catalyst is associated in galvanizing the monomer molecules, which is further followed by a polymer chain and then it is attacked by an activated monomer.

4.3 Advantages of PCL-based composites in the medical sector

The utilization of PCL composites in the medical sector offers numerous advantages, as outlined below.

4.3.1 Mechanical properties

The incorporation of fillers, such as ceramics and nanoparticles, into PCL can considerably enhance its mechanical properties, which can make it suitable for tissue engineering and load-bearing applications (Yang et al., 2021). In a study of PCL scaffolds, both neat and with chitosan nanofibrils, they were developed using solvent casting, to improve the mechanical properties and cellular compatibility of PCL nanocomposite scaffolds. The findings revealed that the incorporation of chitosan exhibited an important reinforcing effect on the structure, along with noticeable morphological changes. The addition of chitosan positively affects the surface wettability, swelling ratio, and weight loss of PCL, along with improved cell viability, adhesion, and spreading. The proposed PCL/chitosan nanocomposite showed potential for utilization as biocompatible scaffolds for various tissue engineering applications (Fadaie and Mirzaei, 2018).

4.3.2 Biological functionality

PCL-based composites can be modified to have bioactive properties. The cell adhesion, proliferation, and tissue integration can be improved by incorporation of growth factors, peptides, or surface modifications of PCL composites, which can promote tissue regeneration and facilitate the necessary biological interactions for successful medical applications (Dwivedi et al., 2020).

4.3.3 Drug-delivery carrier

The degradation rate can be controlled with the incorporation of specific fillers or additives into PCL. This ability ensures optimal performance and controlled degradation in the body (Liu et al., 2020). PCL-based composites offer flexibility in designing drug-delivery systems. Due to PCL's hydrophobic nature, it is suitable for encapsulating and releasing hydrophobic drugs. The composite material's degradation can be controlled for sustained discharge of therapeutic agents, enabling targeted drug delivery and improved therapeutic outcomes (Homaeigohar and Boccaccini, 2022).

4.4 Applications of PCL in different medical sectors

PCL and its copolymers, namely poly(lactide-co-ε-caprolactone) (PLCL) and poly(glycolide-co-ε-caprolactone) (PGCL) are the most commonly used in the medical sector, particularly for bone growth, vascular implants, fracture fixation, dental treatment, etc. (Zhang et al., 2021). PCL is mainly used as an additive for resins, hence improving their properties including impact resistance (Niaounakis, 2015). The common applications of PCL and its polymers (Fig. 4.4) are summarized in the following subsections.

4.4.1 Tissue engineering

Tissue engineering is a process for regenerating damaged tissues by designing 3D scaffolds that copy the natural extracellular matrix along with cell attachment facilitation (Chan and Leong, 2008). PCL polymer composites recently have gained attention for utilization as scaffold materials because of their biocompatibility (Dong et al., 2021a). In one study, the electro-spinning technique was used to fabricate the PCL scaffold. The prepared scaffolds were then examined for stem cell growth that can be further used for maintenance and generation of many tissues. The investigation revealed that 15% w/v PCL has higher stem cell growth, which also confirms its suitability for repairing soft tissues along with its regenerative medicine applicability (Jabur et al., 2017). Some PCL-based composite application models on animals for wound repair and tissue regenerating are tabulated in Table 4.1.

A study by Ajmal et al. investigated a composite fabricated by the incorporation of quercetin and ciprofloxacin hydrochloride in to PCL-gelatin by an electrospinning method, whereas nanofibers exhibited an average diameter of 725.943 ± 201.965 nm. The scaffolds exhibited antibacterial behavior when exposed to *Staphylococcus aureus* along with antioxidant properties. Gelatin/ciprofloxacin-hydrochloride/quercetin

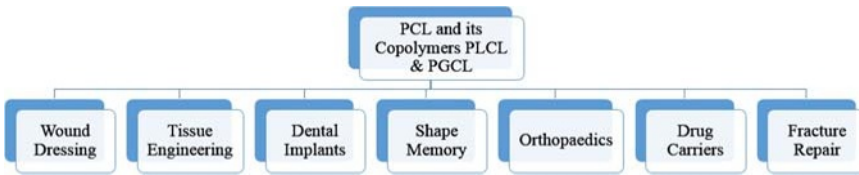

Figure 4.4 Common application fields of PCL and its copolymers.

Table 4.1 PCL composite applications.

Polymers blended with PCL	Animal model	Results
Gelatin (gel)	Balb/c mice	Hybrid nanofibers were created using a two-nozzle electrospinning method, with incorporation of cellulose nanocrystals. The addition of cellulose nanocrystals improved the tensile strength and modulus of the nanofibers by 60% and 80%, respectively. The incorporation of cellulose nanocrystals exhibited a 25% rapid degradation of scaffolds. Meanwhile, the scaffolds exhibited better wound-healing capabilities
Chitosan (cs)	Balb/c mice	Chitosan, lidocaine hydrochloride, and mupirocin were combined with PCL to create scaffolds. Mupirocin discharge was sustained, as well as indicating effective antibacterial properties. The investigation results confirmed collagen deposition, which leads to enhanced wound repairing
Gum tragacanth	Rats	The fabricated scaffolds demonstrated remarkable mechanical strength. Mesenchymal stem cells exhibited adhesion and propagation, promoting tissue regeneration. After 15 days, the scaffolds facilitated re-epithelization and collagen formation. Consequently, these engineered nanofiber scaffolds hold promise as a potential approach for the treatment of diabetic ulcers, particularly in wound healing
Polyethylene glycol	Male Wistar rats	3D nanofibrous fabricated scaffolds, having larger pore size and greater porosity compared with 2D mats made of PCL-PEG-PCL, were used. The porous structure of 3D nanofibrous scaffolds improved water storage and absorption properties. The results confirmed the ability of 3D nanofibrous scaffolds to promote cellular adhesion and migration as well as their importance in wound-repairing applications

Continued

Table 4.1 PCL composite applications.—cont'd

Polymers blended with PCL	Animal model	Results
Polyvinyl alcohol	Female minipig	In this study, PCL was incorporated with PVA polymers to develop the scaffolds. The investigation results confirmed its suitability for wound repair application with minimized scarring

Reproduced with permission from Raina et al. (2022).

incorporation improved the hydrophilicity and biodegradation speed. The scaffold exhibited good biocompatibility as confirmed by hemocompatibility and fibroblast viability tests. The scaffold promoted complete wound healing within 16 days while regulating hydroxyproline and superoxide dismutase, and suggesting its potential application for wound healing (Ajmal et al., 2019). In tissue engineering, the incorporation of bioactive agents into PCL during composite development is very important for improving cellular reactions, tissue regeneration, and scaffold performance. Growth factors regulate the cellular activities and propagation (Yun et al., 2010). Controlled discharge of growth factors from the PCL-composite scaffold offers bioactive indications which influence cell behavior and tissue reconstruction (Goonoo and Bhaw-Luximon, 2019).

In another study, synthesized L-lysine-coated magnetite (Lys@Fe_3O_4) was incorporated into PCL polymer to produce a tissue scaffold for liver cells. The nanoparticles of Lys@Fe_3O_4 were 7 nm in diameter. The incorporation of Lys@Fe_3O_4 reduced the hydrophobicity along with increasing the tensile strength of the developed scaffold. The cell sustainability on the developed scaffolds was increased by 150% compared with individual PCL scaffolds over the 3-day examination. This presence of magnetite nanoparticles helped in faster cell attachment and growth. The investigation results confirmed the usability of the incorporation of Lys@Fe_3O_4 nanoparticles in improving the physical, chemical, and biological characteristics of the PCL scaffolds regarding liver tissue engineering (Rezaei et al., 2021).

4.4.2 Drug-delivery application

PCL polymers provide a favorable platform for the development of drug-delivery carriers because of their biocompatibility and biodegradability nature, which also support a safe interaction with living tissues (Kurakula et al., 2021). Several drugs, including hydrophobic and hydrophilic compounds, proteins, and nucleic acids, can effectively be encapsulated with PCL polymer composites. Biopolymer composites have supported and contributed to the pharmaceutical and medical sectors in multiple applications, with drug delivery being one of them (Wróblewska-Krepsztul et al., 2019). Excipient material fabricated from PCL for drug delivery exhibits characteristics such as low toxicity, biodegradability, durability, and renewable nature (Prabu et al., 2021). In one study, a gelatin-PCL-based composite was evaluated for pore size distribution and thermodynamic property, and the behavior was studied for customized drug delivery. SEM analysis showed that an increase in PCL concentration reduces the porosity of the developed composite (Kanungo et al., 2015). The drug discharge profile (Fig. 4.5) showed that the steady-state phase was delayed with PCL concentration. Also, the composite drug release was at a slower rate as compared to pure gelatin.

In another study, coaxial techniques were used for constructing an NP (nanoparticle) Ag-chitosan/PCL composite as a dual-drug-delivery carrier. The chemical composition, morphological test, and mechanical and thermal analyses were investigated. Study outcomes confirmed the practicality

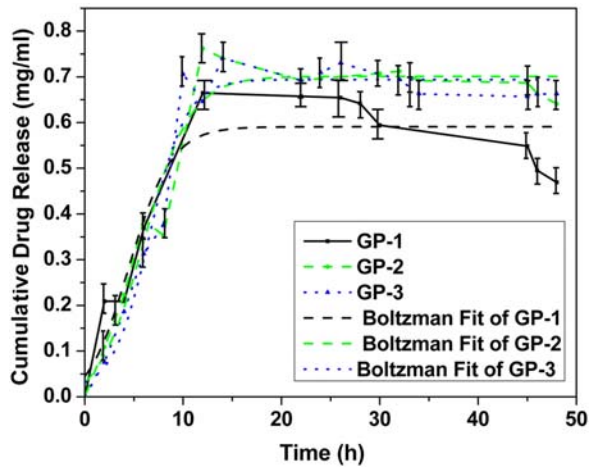

Figure 4.5 Drug-release profile of a gelatin–PCL composite at 310 K. *(Reproduced with permission from Elsevier from Kanungo et al. (2015).)*

of a dual-drug carrier for wound-dressing/healing along with tissue regeneration (Mohamady Hussein et al., 2021). Investigation of the diblock copolymers fabricated from poly-ethylene-glycol (PEG) incorporated with PCL included examination for various usage applicabilities, which revealed that PEG was responsible for enhancing the biocompatibility and PCL promoted the decay of cargo complex. The prepared NPs can be effectively used for targeting tumor cells with less toxicity to normal tissues (Behl et al., 2020). Another study by Faraji et al. investigated the impact of quercetin (Q) on the properties, antimicrobacterial behavior, and cell sustainability of electrospun scaffolds made from a combination of PCL and graphene oxide (GO). NIH/3 T3 fibroblast cells confirmed greater viability of 95% and durable attachment to the scaffolds. Among the scaffolds, the one with the highest quercetin release (0.5% GO/PCL and 43% Q/GO) exhibited approximately 70% released over 15 days as well as a confirmed 50% reduction in bacterial growth after 12 h, indicating the effectiveness against bacteria along with wound repair performance of GO/Q within the PCL nanofibers (Faraji et al., 2020). Furthermore, due to their low degradation polymers, they can also be applied for anticancer drugs for long-term delivery.

4.4.3 Wound healing/dressing

In one study, PCL/oregano oil/gelatin scaffolds were developed via an electro-spinning method to investigate their applicability in wound dressing. XRD, FESEM, and FTIR characterization were examined for the scaffolds, as well as cytotoxicity, antimicrobial, mechanical, and antioxidant properties, which were also studied. Cross-linking of the scaffolds were done using glutaraldehyde vapor to avoid suspension of gelatin at body temperature. The results revealed that increasing incorporation of oregano essential oil (OEO), increases the fiber diameter from 229.6 to 377.03 μm, and also the antibacterial activity, along with higher antioxidant activity. With these enhanced properties, PCL/oregano oil/gel scaffold has been confirmed and supported in its utility for the best wound dressing material without cytotoxicity (El Fawal et al., 2021). A human skin cross-section representation and the phases involved in wound healing are illustrated in Fig. 4.6.

Biopolymers and their composites can be used on skin due to their biodegradable and biocompatible nature. Biopolymer composites are used as hydrogels and healing compounds such as antioxidants, antiseptics, antimicrobials, and growth factors including in inhibitory agents, for accelerating and promoting the process of wound repair

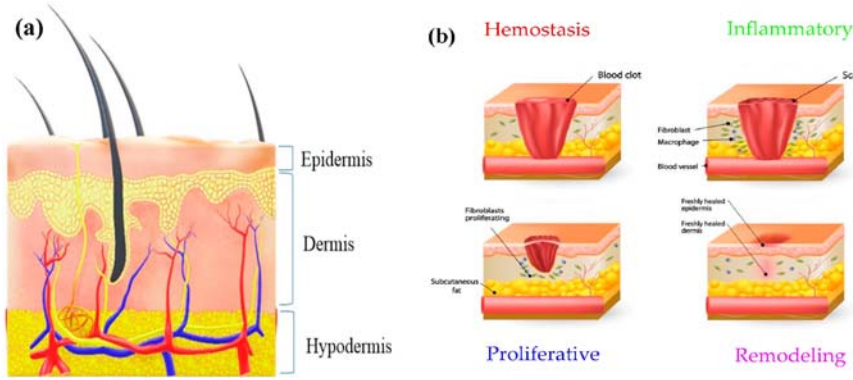

Figure 4.6 (a) Cross-section view of human skin and (b) the wound-healing phases. *(Reproduced with permission from Gobi et al. (2021).)*

(Suarato et al., 2018). A novel composite drug-eluting suture, commonly used as a medical device for wound closure, based on keratin, chitosan, polyethylene glycol (PEG), and PCL, was fabricated by the technique of hot-melt extrusion (Deng et al., 2021). Different tests for physiochemical characterization, drug release, and cytotoxicity were performed on the prepared suture and the results illustrated that the prepared PCL-based composite was a useful application for wound healing.

In one study, wound bandages were designed based on cerium nanoparticle (CeNP)-loaded chitosan/PCL on a cotton fabric surface, wherein the cotton acted as the supporting layer for hydrogel. The prepared hydrogel bandages illustrated antibacterial properties even at low temperatures, with a slower rate of releases. The results from one study suggested that Ce-CS/PCL could be a promising material for scar prevention and wound closure (Dong et al., 2021b).

In another study, copper oxide nanoparticles (NPs) infused PCL/gelatin nanofibers (NF) were fabricated for antibacterial dressing of wounds (Karuppannan et al., 2021). The prepared NFs had dimensions in the range of 130−160 nm and were investigated for biocompatibility and antibacterial activity with the help of MTT assay and disk diffusion assay, respectively. The NFs did not exhibit any bacterial activity in opposition to wound pathogens, including both Gram-negative and Gram-positive bacteria; also the nanofibers exhibited mechanical competence, hydrophilicity, and support for fibroblast growth and attachment. Biocompatibility tests revealed that prepared the NFs were non-cytotoxic and also enhanced its spreading and proliferation.

Table 4.2 Degradation and weight loss performance of PCL polymer and PCL composites.

Matrix	Weight loss (%)	Degradation time (days)
Poly-capro-lactone	4	28
(Poly-capro-lactone)/ 20% (bioactive glass) and 6 wt.% SIM	40	
Poly-capro-lactone	18	30
(Poly-capro-lactone)/ 6 wt.% ZnO	42	
Poly-capro-lactone	0	14
(Poly-capro-lactone)/ gelatin	15.5	

Reproduced with permission from Joseph et al. (2019).

The degradation behavior of composites is an important factor in wound healing, therefore is taken into considerable account. The PCL and its incorporated composites' degradation behavior are tabulated in Table 4.2.

4.4.4 Implantable medical devices

Suitable functioning of the skeleton and proper gliding between bones is regulated by articular cartilage. Less surface friction, shock absorbance, and load bearing are the functions of articular cartilage, which depends on collagen type II and proteoglycans. When a degenerative condition occurs, this cartilage has less self-repair capability, for which tissue engineering is used. Starch-polycaprolactone (SPCL) scaffolds offer a substitute to the restoration of cartilage (GOMES et al., 2008).

PCL/hydroxyapatite composites were synthesized by dispersion of hydroxyapatite particles into PCL with different weight percentage for which hydroxyapatite was derived from eggshell waste (Trakoolwannachai et al., 2019). FTIR/XRD tests were examined to investigate the composite's structural characteristics. Furthermore, thermos = gravimetric analysis revealed that the composite formed had a higher thermal stability of up to 300°C and increased melting temperature as compared to PCL alone. Morphology tests were carried out to show the presence of hydroxyapatite on PCL surface and the composited revealed a lower percentage of degradation and higher swelling behaviors. An innovative approach for the fabrication of PCL 3D scaffolds was introduced (Xu et al., 2021). The fabricated scaffolds consist of hierarchically and interconnected structured

macropores of sizes about 300 μm, and increased and high porosity of around 96.4%. SEM results illustrated that the PCL nanofibrous mats have random nanofibers that are overlaid and have diameters ranging between 200 nm and 1 μm. The prepared samples showed good ductility with no shattering or fracturing during compressive tests.

Oral diseases caused by inflammation due to pathologies can result in destruction of the periodontium (tooth-supporting apparatus) that leads to tooth loss. Dental tissue engineering is widely used for treating these pathologies, for which PCL is widely being studied and used in dental implants. An electrospinning method was used for fabricating PCL/PLA and zeolite-based nanofibers, and their efficiency on human dental pulp stem cells (hDPSCs) was studied (Mohandesnezhad et al., 2020). The prepared powders were studied for their morphology by FE-SEM (field emission scanning electron microscopy) examination, and phase formation was studied by XRD analysis. The fabricated scaffolds were investigated by FTIR analysis for the presence of functional groups. The results revealed that the feasibility of hDPSCs on prepared scaffolds was enhanced over 1, 7, and 14 days, and a cell viability increment was observed after 3 days. The prepared nanofibers loaded with zeolite were the most preferred and suitable for both tissue and bone engineering applications.

In an investigation, a nanocomposite coating of PCL/fluoride-substituted-hydroxyapatite (FHA) on Ti_6Al_4V substrate via sol—gel was studied as a biocompatible, bio-active, and non-cytotoxic coating for dental implant application. The consequence of FHA content on the hydrophilicity, morphology, surface roughness, corrosion behavior, and adhesion strength of the coated specimen was also studied and evaluated for cell vitality and bioactive potential. The outcomes revealed that the fabricated nanocomposite coating over the substrate improved its electrochemical, physical, and biological properties such as bioactivity, surface roughness, better cell adhesion, and higher corrosion resistance (Ansari et al., 2020). With all these enhanced properties, this nanocomposite coating could be used for applications in dental implants.

A ring-like inculcated device encapsulated by an antibacterial agent for implants was studied and evaluated. Calcium-alginate hydrogels and PCL, biodegradable and biocompatible polymers, enclosed with metronidazole for agent delivery at the implant site were used for making scaffolds. The high content of PCL in the formulation of the composite ring helped in minimizing the effects of burst release and providing a carrier for release of metronidazole over a time period of 30 days (Lan et al., 2013).

Wall fractures are related to the repair of fractured bones for which orbital implants are needed. The current most commonly used materials for this are associated with some complications such as exposure and migration over time, infections, hemorrhage, and inflammation. PCL emerges as a biodegradable and hydrophobic polymer with some characteristics that are beneficial in fracture repair, such as reduced degradation rate, less reaction to foreign bodies, greater flexibility. and sufficient mechanical strength. A three-dimensionally printed PCL mesh was developed (Kim, 2019) and a study was carried out on patients with wall fracture surgery. The PCL mesh was manufactured by the multi-head method of deposition with the use of 100% PCL and sterilized with gamma irradiation. For evaluation of surface characteristics, porosity, and microscopic morphology of the PCL mesh, FESEM (Fig. 4.7) was used, and molding and bending simulations were carried out to evaluate the biochemical properties. This study found that a PCL mesh leads to outstanding aesthetic and functional outcomes and is an effective and suitable alternative to the bioresorbable implants used for orbital wall fracture reconstruction.

Grafting of bone is a surgical course of action that restores bone with a material. Bone grafting is categorized as allogenous, autogenous, xenogenous, synthetic, or artificial, of which artificial and synthetic grafts are the most popular. PCL is the most studied and preferred polymer because it is economically viable, and has beneficial mechanical properties and a slower degradation rate. A study was carried out on encapsulated melatonin in PCL which emerges as a promising and effective graft material for bone regeneration. an electro-spraying process was used for synthesizing

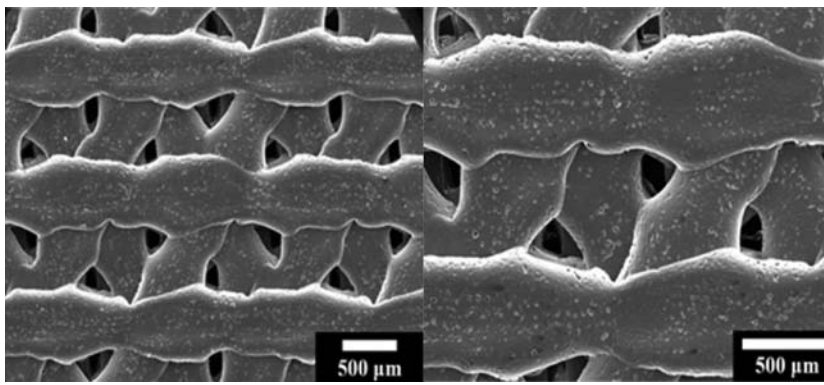

Figure 4.7 SEM images of PCL mesh. *(Reproduced with permission from Elsevier from Kim (2019).)*

microparticles of melatonin and PCL. The findings of this study indicated that bone remodeling is supported by encapsulated melatonin in polycaprolactone and is a very promising and favorable material for synthetic grafts (Gurler et al., 2019).

Different concentrations of trans-anethole (TA) were loaded on polyvinylpyrrolidone (PVP)/PCL fibers with the help of an electrospinning technique (PranavKumar Shadamarshan et al., 2018). Material and physiochemical characterization were done for the developed fibers. Incorporation of TA to the fibers exhibited 0% effectiveness for protein adsorption, swelling, biomineralization, degradation, and thickness of the fiber. The results showed that TA helps in supporting in vitro osteoblast differentiation, which aids in the regeneration and repair of bone tissue.

Another study aimed at improving the characteristics of PCL for tissue engineering by investigating the use of dimethyl sulfone ($DMSO_2$) as a composite with varying concentrations by weight (10%, 20%, and 30%) and was examined for thermal, hydrophilicity, mechanical, and degradation behaviors. The results revealed that the inclusion of $DMSO_2$ enhanced the hydrophilicity and mechanical strength of the composites compared to pure PCL. Increasing the $DMSO_2$ concentration resulted in a reduction in the water contact angle, indicating improved hydrophilicity. Additionally, the composite having 30% $DMSO_2$ exhibited a degradation time 18 times more rapid than that of pure PCL (Jang et al., 2023).

4.5 Challenges and future of PCL in the medical sector

Control over the degradation behavior of PCL-composites has become an important challenge (Malikmammadov et al., 2018). To overcome this challenge, future investigation is required of the variation in properties through fillers, additives integration, and surface modifications (El Yousfi et al., 2023; Ilyas et al., 2022). The incorporation of bioactive compounds improves the bioactivity for tissue regeneration (Lee et al., 2014; Ashammakhi et al., 2022). Scalability, along with cost optimization, is needed for practical application (Molina et al., 2021). Collaboration among researchers, doctors, and medical industries and patients is essential for correct feedback analysis regarding medical product developments. Advanced unconventional synthesis techniques are highly desirable to achieve customized and optimized results (Dalton et al., 2013).

4.6 Conclusion

This study comprises a comprehensive overview of PCL-based composites and their applicability in the medical sector. The characteristics of PCL such as biocompatible behavior, biodegradable nature, and mechanical strength make it suitable for medical applications. PCL polymers have confirmed acceptability in the healthcare sector, with benefits of customizable designs, controlled bio-degradation, and release of drugs. PCL polymers and associated composites also support in tissue/cell integration, adhesion, and proliferation. PCL composites successfully provide therapeutic healing and enable ease of fabrication using electrospinning and 3D printing techniques. However, challenges are related to optimizing recently investigated results for better medical treatment.

References

Ageyeva, T., Sibikin, I., Karger-Kocsis, J., 2018. Polymers and related composites via anionic ring-opening polymerization of lactams: recent developments and future trends. Polymers 10 (4), 357. https://doi.org/10.3390/polym10040357.

Ahmad Shariff, S.H., Daik, R., Haris, M.S., Ismail, M.W., 2023. Hydrophobic drug carrier from polycaprolactone-b-poly(ethylene glycol) star-shaped polymers hydrogel blend as potential for wound healing application. Polymers 15 (9), 2072. https://doi.org/10.3390/polym15092072.

Ajmal, G., Bonde, G.V., Mittal, P., Khan, G., Pandey, V.K., Bakade, B.V., et al., 2019. Biomimetic PCL-gelatin based nanofibers loaded with ciprofloxacin hydrochloride and quercetin: a potential antibacterial and anti-oxidant dressing material for accelerated healing of a full thickness wound. Int. J. Pharm. 567, 118480. https://doi.org/10.1016/J.IJPHARM.2019.118480.

Alhanish, A., Ali, G.A.M., 2023. Biodegradable polymers. Handbook of Biodegradable Materials, pp. 263–291. https://doi.org/10.1007/978-3-031-09710-2_13.

Álvarez-Ortega, O., Ruiz-Ramírez, L.R., Garibay-Alvarado, J.A., Donohue-Cornejo, A., Espinosa-Cristóbal, L.F., Cuevas-González, J.C., et al., 2021. Preliminary biocompatibility tests of poly-ε-caprolactone/silver nanofibers in Wistar rats. Polymers 13 (7). https://doi.org/10.3390/POLYM13071135.

Ansari, Z., Kalantar, M., Kharaziha, M., Ambrosio, L., Raucci, M.G., 2020. Polycaprolactone/fluoride substituted-hydroxyapatite (PCL/FHA) nanocomposite coatings prepared by in-situ sol-gel process for dental implant applications. Prog. Org. Coating 147 (June), 105873. https://doi.org/10.1016/j.porgcoat.2020.105873.

Ashammakhi, N., Ghavaminejad, A., Tutar, R., Fricker, A., Roy, I., Chatzistavrou, X., et al., 2022. Highlights on advancing frontiers in tissue engineering. Tissue Eng. B Rev. 28 (3), 633–664. https://doi.org/10.1089/TEN.TEB.2021.0012/ASSET/IMAGES/LARGE/TEN.TEB.2021.0012_FIGURE6.JPEG.

Behl, A., Parmar, V.S., Malhotra, S., Chhillar, A.K., 2020. Biodegradable diblock copolymeric PEG-PCL nanoparticles: synthesis, characterization and applications as anticancer drug delivery agents. Polymer 207, 122901. https://doi.org/10.1016/j.polymer.2020.122901.

Burg, K., 2014. Poly(α-ester)s. In: Natural and Synthetic Biomedical Polymers. Elsevier, pp. 115–121. https://doi.org/10.1016/B978-0-12-396983-5.00006-5.

Cama, G., Mogosanu, D.E., Houben, A., Dubruel, P., 2017. Synthetic biodegradable medical polyesters. In: Science and Principles of Biodegradable and Bioresorbable Medical Polymers. Elsevier, pp. 79–105. https://doi.org/10.1016/B978-0-08-100372-5.00003-9.

Chan, B.P., Leong, K.W., 2008. Scaffolding in tissue engineering: general approaches and tissue-specific considerations. Eur. Spine J. 17 (S4), 467–479. https://doi.org/10.1007/s00586-008-0745-3.

Dalton, P.D., Vaquette, C., Farrugia, B.L., Dargaville, T.R., Brown, T.D., Hutmacher, D.W., 2013. Electrospinning and additive manufacturing: converging technologies. Biomater. Sci. 1 (2), 171–185. https://doi.org/10.1039/C2BM00039C.

Dell'Erba, R., Groeninckx, G., Maglio, G., Malinconico, M., Migliozzi, A., 2001. Immiscible polymer blends of semicrystalline biocompatible components: thermal properties and phase morphology analysis of PLLA/PCL blends. Polymer 42 (18), 7831–7840. https://doi.org/10.1016/S0032-3861(01)00269-5.

Deng, X., Gould, M., Ali, M.A., 2021. Fabrication and characterisation of melt-extruded chitosan/keratin/PCL/PEG drug-eluting sutures designed for wound healing. Mater. Sci. Eng. C 120 (November), 111696. https://doi.org/10.1016/j.msec.2020.111696.

Dias, J.R., Sousa, A., Augusto, A., Bártolo, P.J., Granja, P.L., 2022. Electrospun polycaprolactone (PCL) degradation: an in vitro and in vivo study. Polymers 14 (16), 3397. https://doi.org/10.3390/polym14163397.

Dong, Q., Zhang, M., Zhou, X., Shao, Y., Li, J., Wang, L., et al., 2021a. 3D-printed Mg-incorporated PCL-based scaffolds: a promising approach for bone healing. Mater. Sci. Eng. C 129, 112372. https://doi.org/10.1016/j.msec.2021.112372.

Dong, H., Liang, W., Song, S., Xue, H., Fan, T., Liu, S., 2021b. Engineering of cerium oxide loaded chitosan/polycaprolactone hydrogels for wound healing management in model of cardiovascular surgery. Process Biochem. 106 (37), 1–9. https://doi.org/10.1016/j.procbio.2021.03.025.

Dwivedi, R., Kumar, S., Pandey, R., Mahajan, A., Nandana, D., Katti, D.S., et al., 2020. Polycaprolactone as biomaterial for bone scaffolds: review of literature. J. Oral Biol. Craniofac. Res. 10 (1), 381–388. https://doi.org/10.1016/j.jobcr.2019.10.003.

El Fawal, G., Hong, H., Mo, X., Wang, H., 2021. Fabrication of scaffold based on gelatin and polycaprolactone (PCL) for wound dressing application. J. Drug Deliv. Sci. Technol. 63 (March), 102501. https://doi.org/10.1016/j.jddst.2021.102501.

El Yousfi, R., Brahmi, M., Dalli, M., Achalhi, N., Azougagh, O., Tahani, A., et al., 2023. Recent advances in nanoparticle development for drug delivery: a comprehensive review of polycaprolactone-based multi-arm architectures. Polymers 15 (8). https://doi.org/10.3390/POLYM15081835.

Fadaie, M., Mirzaei, E., 2018. Nanofibrillated chitosan/polycaprolactone bionanocomposite scaffold with improved tensile strength and cellular behavior. Nanomed. J. 5 (2), 77–89. https://doi.org/10.22038/NMJ.2018.005.004.

Faraji, S., Nowroozi, N., Nouralishahi, A., Shabani Shayeh, J., 2020. Electrospun polycaprolactone/graphene oxide/quercetin nanofibrous scaffold for wound dressing: evaluation of biological and structural properties. Life Sci. 257, 118062. https://doi.org/10.1016/j.lfs.2020.118062.

Geoghegan, N., O'Loughlin, M., Delaney, C., Rochfort, K.D., Kennedy, M., Kolagatla, S., et al., 2023. Controlled degradation of polycaprolactone-based micropillar arrays. Biomater. Sci. 11 (9), 3077. https://doi.org/10.1039/D3BM00165B.

Gobi, R., Ravichandiran, P., Babu, R.S., Yoo, D.J., 2021. Biopolymer and synthetic polymer-based nanocomposites in wound dressing applications: a review. Polymers 13 (12), 1962. https://doi.org/10.3390/polym13121962.

Gomes, M.E., Oliveira, J.T., Rodrigues, M.T., Santos, M.I., Tuzlakoglu, K., Viegas, C.A., et al., 2008. Starch-polycaprolactone based scaffolds in bone and cartilage tissue engineering approaches. In: Natural-Based Polymers for Biomedical Applications. Elsevier, pp. 337–356. https://doi.org/10.1533/9781845694814.3.337.

Goonoo, N., Bhaw-Luximon, A., 2019. Mimicking growth factors: role of small molecule scaffold additives in promoting tissue regeneration and repair. RSC Adv. 9 (32), 18124–18146. https://doi.org/10.1039/C9RA02765C.

Gurler, E.B., Ergul, N.M., Ozbek, B., Ekren, N., Oktar, F.N., Haskoylu, M.E., et al., 2019. Encapsulated melatonin in polycaprolactone (PCL) microparticles as a promising graft material. Mater. Sci. Eng. C 100, 798–808. https://doi.org/10.1016/j.msec.2019.03.051.

Homaeigohar, S., Boccaccini, A.R., 2022. Nature-derived and synthetic additives to poly(ϵ-caprolactone) nanofibrous systems for biomedicine; an updated overview. Front. Chem. 9, 809676. https://doi.org/10.3389/fchem.2021.809676.

Ilyas, R., Zuhri, M., Norrrahim, M., Misenan, M., Jenol, M., Samsudin, S., et al., 2022. Natural fiber-reinforced polycaprolactone green and hybrid biocomposites for various advanced applications. Polymers 14 (1), 182. https://doi.org/10.3390/polym14010182.

Imre, B., Pukánszky, B., 2013. Compatibilization in bio-based and biodegradable polymer blends. Eur. Polym. J. 49 (6), 1215–1233. https://doi.org/10.1016/j.eurpolymj.2013.01.019.

Jabur, A.R., Al-Hassani, E.S., Al-Shammari, A.M., Najim, M.A., Hassan, A.A., Ahmed, A.A., 2017. Evaluation of stem cells' growth on electrospun polycaprolactone (PCL) scaffolds used for soft tissue applications. Energy Proc. 119, 61–71. https://doi.org/10.1016/j.egypro.2017.07.048.

Jang, J.-W., Min, K.-E., Kim, C., Wern, C., Yi, S., 2023. PCL and DMSO2 composites for bio-scaffold materials. Materials 16 (6), 2481. https://doi.org/10.3390/ma16062481.

Jeong, H., Rho, J., Shin, J.-Y., Lee, D.Y., Hwang, T., Kim, K.J., 2018. Mechanical properties and cytotoxicity of PLA/PCL films. Biomed. Eng. Lett. 8 (3), 267–272. https://doi.org/10.1007/s13534-018-0065-4.

Joseph, B., Augustine, R., Kalarikkal, N., Thomas, S., Seantier, B., Grohens, Y., 2019. Recent advances in electrospun polycaprolactone based scaffolds for wound healing and skin bioengineering applications. Mater. Today Commun. 19, 319–335. https://doi.org/10.1016/j.mtcomm.2019.02.009.

Kaluzynski, K., Pretula, J., Lewinski, P., Kaźmierski, S., Penczek, S., 2022. Synthesis and properties of functionalized poly(ε-caprolactone); chain polymerization followed by polycondensation in one pot with initiator and catalyst in one molecule. Synthesis and molecular structures. Macromolecules 55 (6), 2210–2221. https://doi.org/10.1021/ACS.MACROMOL.1C02325/ASSET/IMAGES/MEDIUM/MA1C02325_0024.GIF.

Kanungo, I., Chellappa, N., Fathima, N.N., 2015. Microfabrication of gelatin–polycaprolactone composites for customized drug delivery. Mater. Sci. Eng. C 49, 597–603. https://doi.org/10.1016/j.msec.2015.01.058.

Karuppannan, S.K., Ramalingam, R., Mohamed Khalith, S.B., Musthafa, S.A., Dowlath, M.J.H., Munuswamy-Ramanujam, G., et al., 2021. Copper oxide nanoparticles infused electrospun polycaprolactone/gelatin scaffold as an antibacterial wound dressing. Mater. Lett. 294, 129787. https://doi.org/10.1016/j.matlet.2021.129787.

Kim, S.Y., 2019. Application of the three-dimensionally printed biodegradable polycaprolactone (PCL) mesh in repair of orbital wall fractures. J. Cranio-Maxillofacial Surg. 47 (7), 1065–1071. https://doi.org/10.1016/j.jcms.2019.03.009.

Kim, H.-K., Jang, S.-J., Cho, Y.-S., Park, H.-H., 2022. Fabrication of nanostructured polycaprolactone (PCL) film using a thermal imprinting technique and assessment of antibacterial function for its application. Polymers 14 (24), 5527. https://doi.org/10.3390/polym14245527.

Kurakula, M., Rao, G.S.N.K., Yadav, K.S., 2021. Fabrication and characterization of polycaprolactone-based green materials for drug delivery. In: Applications of Advanced Green Materials. Elsevier, pp. 395–423. https://doi.org/10.1016/B978-0-12-820484-9.00016-7.

Labet, M., Thielemans, W., 2009. Synthesis of polycaprolactone: a review. Chem. Soc. Rev. 38 (12), 3484. https://doi.org/10.1039/b820162p.

Lan, S., Kehinde, T., Zhang, X., Khajotia, S., Schmidtke, D.W., Starly, B., 2013. Controlled release of metronidazole from composite poly-ε-caprolactone/alginate (PCL/alginate) rings for dental implants. Dent. Mater. 29 (6), 656–665. https://doi.org/10.1016/j.dental.2013.03.014.

Lee, E.J., Kasper, F.K., Mikos, A.G., 2014. Biomaterials for tissue engineering. Ann. Biomed. Eng. 42 (2), 323–337. https://doi.org/10.1007/s10439-013-0859-6.

Liu, S., Qin, S., He, M., Zhou, D., Qin, Q., Wang, H., 2020. Current applications of poly(lactic acid) composites in tissue engineering and drug delivery. Compos. B Eng. 199, 108238. https://doi.org/10.1016/j.compositesb.2020.108238.

Malikmammadov, E., Tanir, T.E., Kiziltay, A., Hasirci, V., Hasirci, N., 2018. PCL and PCL-based materials in biomedical applications. J. Biomater. Sci. Polym. Ed. 29 (7–9), 863–893. https://doi.org/10.1080/09205063.2017.1394711.

McKeen, L.W., 2017. Environmentally friendly polymers. In: Permeability Properties of Plastics and Elastomers. Elsevier, pp. 305–323. https://doi.org/10.1016/B978-0-323-50859-9.00013-0.

Mohamady Hussein, M.A., Guler, E., Rayaman, E., Cam, M.E., Sahin, A., Grinholc, M., et al., 2021. Dual-drug delivery of Ag-chitosan nanoparticles and phenytoin via core-shell PVA/PCL electrospun nanofibers. Carbohydr. Polym. 270 (February), 118373. https://doi.org/10.1016/j.carbpol.2021.118373.

Mohandesnezhad, S., Pilehvar-Soltanahmadi, Y., Alizadeh, E., Goodarzi, A., Davaran, S., Khatamian, M., et al., 2020. In vitro evaluation of Zeolite-nHA blended PCL/PLA nanofibers for dental tissue engineering. Mater. Chem. Phys. 252, 123152. https://doi.org/10.1016/j.matchemphys.2020.123152.

Molina, M.I.E., Malollari, K.G., Komvopoulos, K., 2021. Design challenges in polymeric scaffolds for tissue engineering. Front. Bioeng. Biotechnol. 9, 617141. https://doi.org/10.3389/fbioe.2021.617141.

Mousavifard, S.M., Ghermezcheshme, H., Mirzaalipour, A., Mohseni, M., de With, G., Makki, H., 2023. PolySMart: a general coarse-grained molecular dynamics polymerization scheme. Mater. Horiz. 10 (6), 2281–2296. https://doi.org/10.1039/D3MH00088E.

Niaounakis, M., 2015. Medical, dental, and pharmaceutical applications. In: Biopolymers: Applications and Trends. Elsevier, pp. 291–405. https://doi.org/10.1016/B978-0-323-35399-1.00007-7.

Nifant'ev, I., Ivchenko, P., 2019. Coordination ring-opening polymerization of cyclic esters: a critical overview of DFT modeling and visualization of the reaction mechanisms. Molecules 24 (22), 4117. https://doi.org/10.3390/molecules24224117.

Pan, Y., Farmahini-Farahani, M., O'hearn, P., Xiao, H., Ocampo, H., 2016. An overview of bio-based polymers for packaging materials. J. Bioresour. Bioprod. 1 (3), 106–113.

Patrício, T., Domingos, M., Gloria, A., D'Amora, U., Coelho, J.F., Bártolo, P.J., 2014. Fabrication and characterisation of PCL and PCL/PLA scaffolds for tissue engineering. Rapid Prototyp. J. 20 (2), 145–156. https://doi.org/10.1108/RPJ-04-2012-0037.

Penczek, S., Pretula, J.B., 2016. Ring-opening polymerization. In: Reference Module in Chemistry, Molecular Sciences and Chemical Engineering. Elsevier. https://doi.org/10.1016/B978-0-12-409547-2.11351-4.

Penczek, S., Pretula, J., 2021. Activated monomer mechanism (AMM) in cationic ring-opening polymerization. The origin of the AMM and further development in polymerization of cyclic esters. ACS Macro Lett. 10 (11), 1377–1397. https://doi.org/10.1021/ACSMACROLETT.1C00509/ASSET/IMAGES/LARGE/MZ1C00509_0006.JPEG.

Peponi, L., Navarro-Baena, I., Sonseca, A., Gimenez, E., Marcos-Fernandez, A., Kenny, J.M., 2013. Synthesis and characterization of PCL–PLLA polyurethane with shape memory behavior. Eur. Polym. J. 49 (4), 893–903. https://doi.org/10.1016/j.eurpolymj.2012.11.001.

Prabu, G., Muthusamy, S., Selvaganesh, B., Sivakumar, N., Hosseini-bandegharaei, A., Loke, P., 2021. Biopolymers and composites : properties , characterization and their applications in food, medical and pharmaceutical industries. J. Environ. Chem. Eng. 9 (4), 105322. https://doi.org/10.1016/j.jece.2021.105322.

PranavKumar Shadamarshan, R., Balaji, H., Rao, H.S., Balagangadharan, K., Viji Chandran, S., Selvamurugan, N., 2018. Fabrication of PCL/PVP electrospun fibers loaded with trans-anethole for bone regeneration in vitro. Colloids Surf. B Biointerfaces 171, 698–706. https://doi.org/10.1016/j.colsurfb.2018.08.005.

Raina, N., Pahwa, R., Khosla, J.K., Gupta, P.N., Gupta, M., 2022. Polycaprolactone-based materials in wound healing applications. Polym. Bull. 79 (9), 7041–7063. https://doi.org/10.1007/s00289-021-03865-w.

Rezaei, V., Mirzaei, E., Taghizadeh, S.-M., Berenjian, A., Ebrahiminezhad, A., 2021. Nano iron oxide-PCL composite as an improved soft tissue scaffold. Processes 9 (9), 1559. https://doi.org/10.3390/pr9091559.

Scaffaro, R., Lopresti, F., Botta, L., Rigogliuso, S., Ghersi, G., 2016. Integration of PCL and PLA in a monolithic porous scaffold for interface tissue engineering. J. Mech. Behav. Biomed. Mater. 63, 303–313. https://doi.org/10.1016/j.jmbbm.2016.06.021.

Suarato, G., Bertorelli, R., Athanassiou, A., 2018. Borrowing from nature: biopolymers and biocomposites as smart wound care materials. Front. Bioeng. Biotechnol. 6 (OCT), 137. https://doi.org/10.3389/FBIOE.2018.00137.

Sudo, A., 2013. Anionic ring-opening polymerization. Encyclopedia of Polymeric Nanomaterials, pp. 1–11. https://doi.org/10.1007/978-3-642-36199-9_172-1.

Trakoolwannachai, V., Kheolamai, P., Ummartyotin, S., 2019. Characterization of hydroxyapatite from eggshell waste and polycaprolactone (PCL) composite for scaffold material. Composites, Part B 173, 106974. https://doi.org/10.1016/j.compositesb.2019.106974.

Ulery, B.D., Nair, L.S., Laurencin, C.T., 2011. Biomedical applications of biodegradable polymers. J. Polym. Sci. B Polym. Phys. 49 (12), 832. https://doi.org/10.1002/POLB.22259.

Varma, K., Gopi, S., 2021. Biopolymers and their role in medicinal and pharmaceutical applications. In: Biopolymers and Their Industrial Applications. Elsevier, pp. 175–191. https://doi.org/10.1016/B978-0-12-819240-5.00007-9.

Wróblewska-Krepsztul, J., Rydzkowski, T., Michalska-Pożoga, I., Thakur, V.K., 2019. Biopolymers for biomedical and pharmaceutical applications: recent advances and overview of alginate electrospinning. Nanomaterials 9 (3). https://doi.org/10.3390/NANO9030404.

Xu, T., Miszuk, J.M., Yao, Q., Liang, Z., Sun, H., Fong, H., 2021. Electrospun three-dimensional nanofibrous scaffolds based on polycaprolactone for stem cells differentiation and bone regeneration. In: Electrospun Polymers and Composites. Elsevier, pp. 179–215. https://doi.org/10.1016/B978-0-12-819611-3.00006-6.

Yang, X., Wang, Y., Zhou, Y., Chen, J., Wan, Q., 2021. The application of polycaprolactone in three-dimensional printing scaffolds for bone tissue engineering. Polymers 13 (16), 2754. https://doi.org/10.3390/polym13162754.

Yun, Y.-R., Won, J.E., Jeon, E., Lee, S., Kang, W., Jo, H., et al., 2010. Fibroblast growth factors: biology, function, and application for tissue regeneration. J. Tissue Eng. 1 (1), 218142. https://doi.org/10.4061/2010/218142.

Zhang, M., Chang, Z., Wang, X., Li, Q., 2021. Synthesis of poly(L-lactide-co-ε-caprolactone) copolymer: structure, toughness, and elasticity. Polymers 13 (8), 1270. https://doi.org/10.3390/POLYM13081270/S1.

This page intentionally left blank

CHAPTER 5

Processing of PLA/PLLA-based composites for medical device applications

Deepak Gupta[1], Vaishally Dogra[2,3], Deepak Verma[3,4], Arun Kumar Chaudhary[1] and Maneesh Tewari[1]

[1]Department of Industrial and Production Engineering, College of Technology, Govind Ballabh Pant University of Agriculture and Technology, Pantnagar, Uttarakhand, India; [2]Department of Mechanical Engineering, Graphic Era Deemed to be University, Dehradun, Uttarakhand, India; [3]Department of Mechanical Engineering, Graphic Era Hill University, Dehradun, Uttarakhand, India; [4]International Graduate Program of Nanoscience and Technology, Chulalongkorn University, Bangkok, Thailand

5.1 Introduction

In clinics, biodegradable polymer materials are already often employed. Their molecular weight, polydispersity, crystallinity, degradation, and thermal transition all play a significant role in determining their characteristics. The principal synthetic polymers that degrade into natural substances include PCL (polycaprolactone), PLA, PGA [poly(glutamic acid)], polyanhydrides, poly(glycerol sebacate), polyurethanes, and a few synthetic hydrogels (Liu et al., 2020). Electro-spun fibers that are biodegradable and biocompatible have garnered a lot of interest recently due to their numerous medicinal uses. The most promising and extensively researched polymeric biomaterials are PCL and PLA (Liao et al., 2012). Poly-L-lactide (PLLA) is an aliphatic polyester that is known for its biodegradability. It is considered to be the most favorable material for fracture repair because of its relatively high strength and moderate rate of deterioration (McKeen, 2017). However PLLA has some drawbacks, including acidic breakdown products, a low degree of hydrophilicity, and a low compressive strength. The in vivo degraded acidic monomers were discovered to have a negative clinical effect in that they may trigger allergy or inflammatory responses (Balla et al., 2021). PLA has several industrial applications such as in packaging and textiles, and it has also become an important component in bioengineering (Fig. 5.1).

Bioresorbable Polymers and their Composites
ISBN 978-0-443-18915-9
https://doi.org/10.1016/B978-0-443-18915-9.00013-6
© 2024 Elsevier Ltd.
All rights reserved.

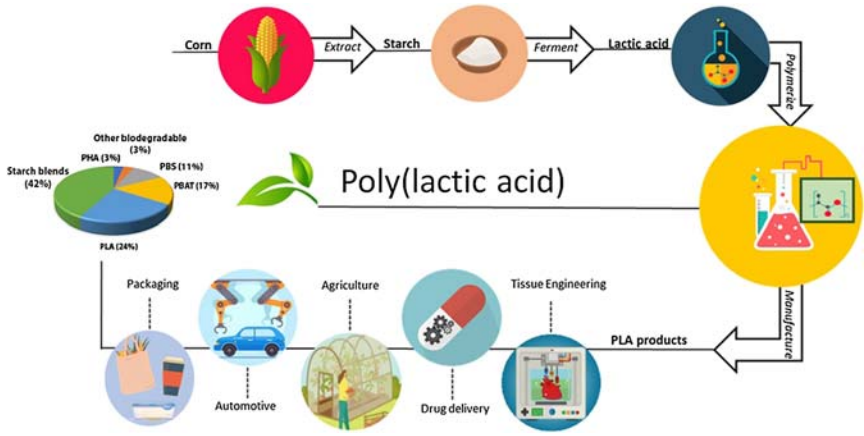

Figure 5.1 PLA and PLA-based composites processing and usability potential overview. *(Reproduced with permission from Balla et al. (2021).)*

The chemical moderation of PLLA, together with blending and copolymerization modification, has been thoroughly investigated as a means of overcoming the aforementioned shortcomings (Wan et al., 2014). In physiologic settings, PLA, a natural intermediary in the metabolism of carbohydrates, can degrade to lactic acid due to its superior biocompatibility and mechanical qualities. Orthopedics and oral and maxillofacial surgery have both employed medical equipment constructed of PLA in clinical settings, including as bone screws (Zhao et al., 2017). PLA can be produced through two main methods, the first is direct polycondensation of lactic acid, while the second is chain-growth or ring-opening polymerization (ROP) of lactide. Lactide is a cyclic ester formed by the di-cyclization of lactic acid (Fig. 5.2) (Augé et al., 2023).

Both PLA and its thermoplastic properties are biodegradable. Applications in orthopedics, cardiology, and dentistry are just a few examples of relevant medical fields. Because of the inherent properties of PLA, 3D-printed constructions may be manufactured quickly and effectively. Advantages of PLA include its ease of production, environment-friendliness, biocompatibility, recyclability, and more, with no toxic or carcinogenic effects. Wheat, carbon dioxide, rice, and corn are a few examples of renewable resources which could be processed to make PLA. Therefore, its by-products are not toxic to the environment or humans. Compared to polymers made from gasoline, PLA requires 25%–55% less energy to make. The low cost and extensive availability of the basic ingredients contribute to the ease of making PLA. The direct contact of PLA with biological fluids has also been permitted by the FDA

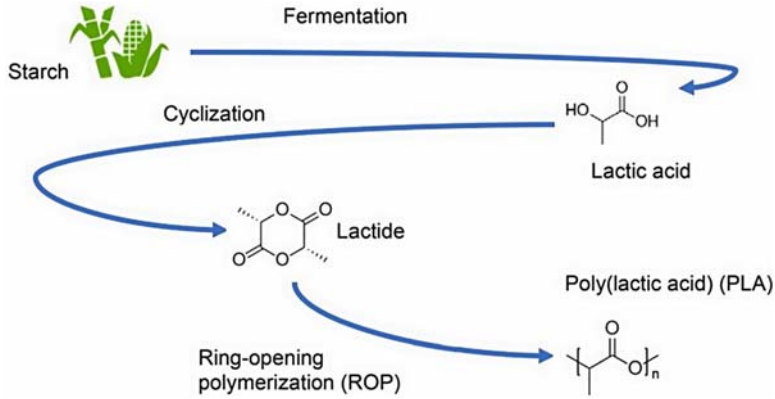

Figure 5.2 Chain-growth polymerization of PLA. *(Reproduced with permission from Augé et al. (2023).)*

(Destefano et al., 2020). PLA and PLLA exhibit a biodegradable nature, which has been gaining major attention for medical device applications (Neumann et al., 2017). PLA/PLLA is a derivative product of sustainable sources such as corn starch and sugarcane, which offers it several advantages, including biocompatibility and sustainable environmental impact, resulting in growing importance in the medical devices field (Farah et al., 2016).

5.2 The chemical structure and synthesis of PLA/PLLA polymers

The chemical structure of PLA/PLLA is important in determining the properties and behavior of by-products. PLA is a rectilinear aliphatic polyester composed by lactic acid units, while PLLA is a stereoisomer of PLA, consisting exclusively of L-lactic acid units (Fig. 5.3) (McKeen, 2012).

The organization of lactic acid monomers within the polymer chain impacts the crystallinity, mechanical strength, and degradation behavior. Additionally, PLLA properties are influenced by the L-lactic acid to D-lactic acid ratio, thus it is important to be considered for controlling the material characteristics for specific medical applications. Several synthesis methods are available to develop PLA/PLLA polymers. Direct condensation polymerization involves the lactic acid monomers reaction, and ROP utilizes lactide. Meanwhile, melt polymerization involves the linear polymerization of lactide in the molten phase. Each synthesis method has its advantages and limitations. Exploring these different synthesis techniques provides acknowledgment of their impacts on the PLA/PLLA polymer properties (Lopes et al., 2014).

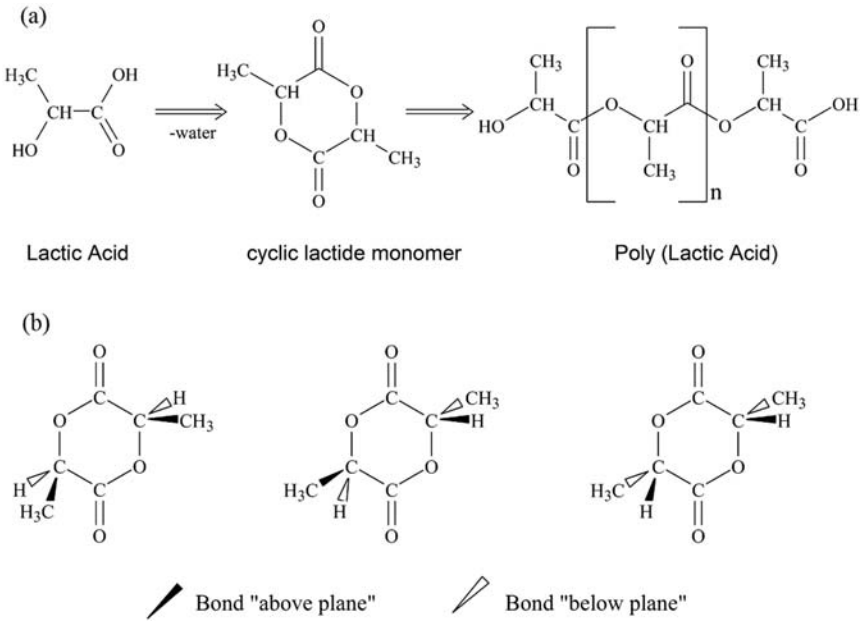

Figure 5.3 (a) Transformation of lactic acid to polylactic acid, and (b) stereoisomeric structures of the lactide dimer. *(Reproduced with permission from McKeen (2012).)*

5.3 The physical and thermal characteristics of PLA/PLLA polymers

The physical properties of PLA polymers are important factors to be considered for their use in medical applications. The related physical properties found in the literature are discussed in Table 5.1.

The various nanoparticle incorporations affect the PLA properties, which are discussed in Table 5.2.

The thermal properties of PLA/PLLA polymers such as the glass transition temperature (T_g), melting temperature (T_m), crystallization, and thermally stable behavior have an important role in their processing, shaping, and medical applications (Teixeira et al., 2021; Cheerarot and Baimark, 2015). T_g is responsible for the polymer undergoing the transition from a glassy state to an elastic state. This transition significantly impacts the flexibility as well as processability of the polymer (Xie et al., 2020). T_m reveals the temperature at which the polymer melts and can be molded, while the crystallization behavior affects the strength and crystallinity (Kulkarni, 2022). Additionally, thermal

Table 5.1 Physical characteristics of PLA.

Characteristics	Values
Specific gravity	1–1.5
Surface energy (dynes)	36–40
Melting temperature (°C)	140–210
Molecular weight (Daltons)	Approx. 1.6×10^5
Melt flow index (g/10 min)	4–22
Crystallinity (%)	5–35
Glass transition temperature (°C)	50–75
Solubility parameters ($J^{0.5}/cm^{1.5}$)	21

Reproduced with permission from Ranakoti et al. (2022).

Table 5.2 Nanoparticle effects on PLA properties.

	PLA mechanical properties alteration			
Nanoparticle added in PLA	Tensile strength (%)	Young's modulus (%)	Melting point (%)	Crystallization temperature (%)
1% TiO_2	2.8	4.3	0.2	5.9
1% HNT	1.58	5.28	−0.68	–
1% ZnO-Cu-Ag	−30.15	−22.5	0.6	−16.8
1% ZnO	−2.3	7.4	1.1	2.7
1% MgO	16.8	27.5	−0.5	4.6
1% GO-ZnO	20.5	–	–	–
1% ZiF 8 MOF	9.6	44.7	–	–

Reproduced with permission from Ranakoti et al. (2022).

stability indicates the polymer's resistance to degradation at higher temperatures. At high shear, PLA remains a non-Newtonian pseudoplastic fluid. Rheological models such as the Carreau–Yasuda model and Cross-WLF model were followed to study the rheological properties of PLA. Thermodynamics refers to the investigation of energy transport and conversion. Understanding the workability of PLA requires an understanding of its rheological and thermal characteristics (Liu et al., 2020). At room temperature, PLA is a rigid polymer. T_g commonly lies between 55°C and 65°C, while T_m having

only an L/D-isomeric arrangement lies from 160°C to 170°C. Its low melting temperature in comparison to poly(ethyleneterephthalate) (PET) highlights one of PLA's primary limitations in creating acceptable applications. PLA properties may be improved by changing the distribution and ratio of L/D isomers along with alteration of the melting points for the lowest at 130°C and the highest at 220°C (Farrington et al., 2008).

5.4 PLA/PLLA-based composites fabrication methods

It is necessary to properly acknowledge the co-relationship between PLA characteristics along with their reinforcement (fibers, additives, nano- and micro-fillers, etc.) for adaptability and degradation effects (Fig. 5.4) (Murariu and Dubois, 2016).

5.4.1 Additive manufacturing

Various additive manufacturing techniques are available for general PLA/PLLA-based composites development, , and of these some are widely used, such as fused deposition modeling (FDM), stereo-lithography (SLA), and selective laser sintering (SLS) (Kafle et al., 2021). Pharmaceutical items are frequently made via 3D printing which is a computerized process that has vital applications for individualized dosage medication because of its low cost and precise free form. FDM, SLS, SLA, direct ink writing, polyjet, and digital light processing are the most common 3D printing methods currently in use for the medical sector. PLA has a wide temperature range for hot extrusion (Azad et al., 2020). Prior to FDM printing, drug components are frequently incorporated with polymer filaments as there is relatively less capability of drug loading by FDM (Quodbach et al., 2022).

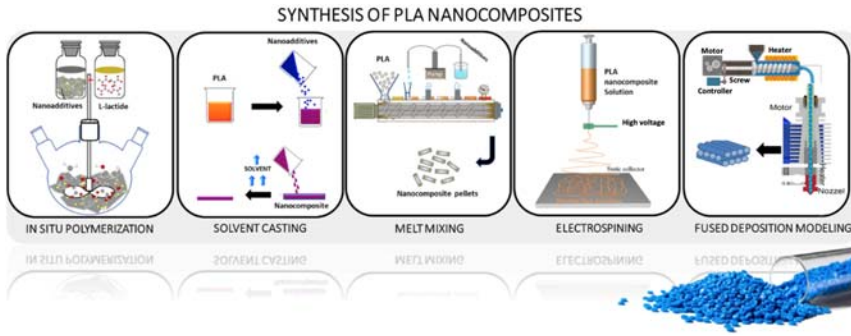

Figure 5.4 PLA composites fabrication methods. *(Reproduced with permission from Bikiaris et al. (2023).)*

Medication discharge properties of FDM-produced tablets may completely be modified based on the form, polymer used, and drug payload (Tan et al., 2018).

5.4.2 Solvent-based methods

Solvent processing delivers an alternative method for shaping PLA/PLLA-based composites. This method involves dissolving PLA/PLLA polymers in an appropriate solvent and afterward shaping and solidifying the composite resulting in the formation of thin films (Sousa et al., 2019). Electrospinning, another solvent-based technique, offers the advantage of controlled porosity, surface morphology, and mechanical properties (Casasola et al., 2014; Bambole and Yakhmi, 2016). The processes of pore creation during electrospinning mostly comprises temperature, and humidity with phase separation.

5.4.3 Melt compounding

Melt processing methods are usually followed for PLA/PLLA-based composites because of their simplicity, versatility, and cost-effectiveness. They involve melting the PLA/PLLA polymer and integrating reinforcing additives. This mixture can be extruded into desired shapes (De Santis and Pantani, 2015). Another widely used melting technique is the injection molding method, where the molten polymer is injected through a mold. On the other hand, blow molding is also used sometimes to produce hollow-type assemblies. In a study investigating the effectiveness of plasticizers collected from renewable sources, specifically epoxidized palm oil (EPO) and epoxidized soybean oil (ESO), on PLA, the results illustrated that EPO was more efficient at lower concentrations, while ESO exhibited higher effectiveness for greater concentrations of 10 wt.% and 15 wt.% with significant enhancements in impact strength and processing efficiency for PLA. Additionally, EPO and ESO indicated their suitability as alternatives to traditional plasticizers in the PLA processing industry (Tee et al., 2014).

5.4.4 Miscellaneous methods

Hybrid/miscellaneous processing methods combine different techniques to overcome limitations. Hybrid processing offers new possibilities for advanced PLA/PLLA-based composites in medical device applications. Low-pressure microcellular injection, rotary jet spinning, melt extrusion, tube drawing, melt blending, solvent casting, etc. are some of the methods that can be used for the production of PLA-based composites.

5.5 Biocompatibility and biodegradability of PLA/PLLA composites

The biocompatibility and biodegradability of PLA/PLLA composites are important considerations in medical applications. Studies of the biocompatibility and degradation behaviors of PLA/PLLA composites are described next.

5.5.1 Biocompatibility

The biocompatibility of materials indicates the capability of a composite to cooperate with human tissues without causing infection or toxicity. PLA/PLLA exhibited excellent biocompatibility, which makes them suitable for various medical applications. The biocompatible nature of composites ensures their safe and effective use inside the human body (Yoon et al., 2017). Multiple factors influence the biocompatibility of PLA/PLLA composites, including their chemical structure, surface characteristics, degradation products, and interactions with biological systems. For evaluating cytotoxicity, hemocompatibility, and tissue response along with cell feasibility inspection, blood compatibility tests are crucial to ensuring the biocompatibility of PLA composites (Pawar et al., 2014).

5.5.2 Biodegradability

Biodegradability refers to the degradation behavior over time through natural processes. PLA/PLLA are biodegradable in nature and undergo hydrolysis when exposed to water. The biodegradation behavior of PLA/PLLA composites exhibits a significance role for temporary medical devices and implants that must be absorbed or replaced (Narayanan et al., 2016). PLA/PLLA composite degradability is influenced by various factors including the molecular weight of the polymer along with its composition, processing techniques, as well as environmental conditions, etc. Meanwhile, the addition of reinforcement fillers and additives can also influence the biodegradability of PLA/PLLA composites (da Silva et al., 2018; Naser et al., 2021).

5.6 Applications of PLA/PLLA composites in the medical sector

PLA/PLLA have undergone increased consideration as important probable materials for medical applications. This study investigated recent case studies that reveal the effective medical applications of PLA/PLLA-based composites.

5.6.1 Scaffolds for tissue reengineering

PLA/PLLA-based composites are extensively used as scaffolds for tissue reengineering. PLA-based composites offer a 3D assembly that enables the growth of cells along with tissue regeneration. The mechanical characteristics of PLA composites are customizable as per the targeted tissue requirements. Additionally, the biodegradability of PLA enables its steady replacement by natural tissue over time.

The crystallinity of PLLA, which ranges from 37% to 42%, depends on the processing variables and molecular weight. This polymer has a melting temperature of around 175°C and T_g ranging between 60°C and 65°C. Also, PLA/PLLA have high tensile properties and elongation, along with superior bioresorbability and biocompatibility, which makes them perfect for applications that bear loads such as the closure of wounds, sutures, controlled-release systems, tissue culture, and orthopedic fixation (Sheikh et al., 2015). The addition of functional nanoparticles to the PLA matrix increase its physical properties with alterations in its surface properties. They are useful in artificial bone regeneration and tissue engineering (Mohammad et al., 2016). In the in vitro testing of a novel biocomposite polymer, PLLA augmented with short phosphate glass fibers (PGFs), showed PGFs' presence to have a rapid osteoinductive influence for a 3-week duration, without compromising the mechanical capabilities over an 8-week timeframe (Melo et al., 2019). The typical semicrystalline PLLA produced by compression molding exhibited peaks on an XRD diffraction test (Fig. 5.5).

New 3D-printed shape-memory PLLA-TMC/GA-TMC scaffolds having superior mechanical characteristics and degradability for bone tissue engineering have been created and examined for physiochemical properties

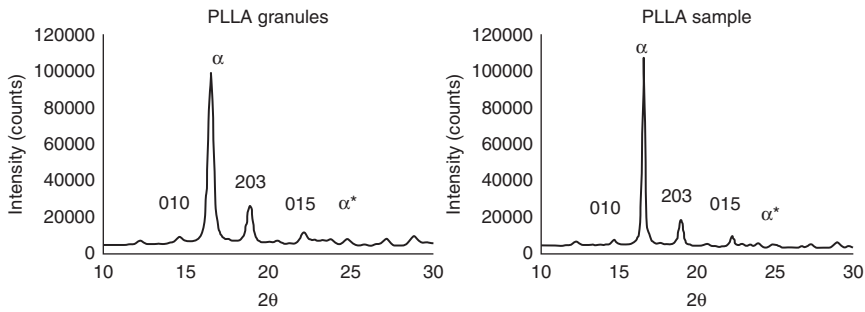

Figure 5.5 Exhibited XRD diffraction arrangements by PLLA granules and a PLLA specimen. *(Reproduced with permission from Melo et al. (2019).)*

and confirmed their potential for future use in the clinic for the repair of bone defects (Hu et al., 2023).

PLA/Kef-based hybrid scaffolds coated on electrospun fibers via air-plasma treatment have vast applications in skin tissue engineering (Lopresti et al., 2021). The reinforcement action of a Kefiran coating was mechanically analyzed by a tensile test. Morphological and gravimetric analyses were used to evaluate the water resistance of the prepared coating at 37°C, which clearly indicated that the solubilization of PLA fibers coated with Kefiran was faster than for P-PLA (pretreated PLA) fibers. The in vitro experiments conducted demonstrated the important promise of the PLA-Kef hybrid scaffold for applications in skin tissue re-engineering (Lopresti et al., 2021). In another study, composite scaffolds were prepared via FDM technology by PLA and n-HA (nano-hydroxyapatite) for bone muscle manufacturing (Wang et al., 2021). The optimization of prepared scaffolds was done by mechanical test, material characterization, a and stem cell biocompatibility test. The proposed composite for study was found to be highly printable, with good mechanical strength, and the biocompatibility was much higher compared with neat PLA scaffold. Thus, the prepared n-HA-PLA scaffold proved to be a good and promising material for the repair of large bone defects.

Pisanti et al. examined the scaffold microstructure effect on human mesenchymal stem cells (hMSCs). PLLA scaffolds were created using SC-CO_2 gel drying, resulting in nanostructured scaffolds. Porogen leaching led to the formation of microporous scaffolds, characterized by mean pore sizes measuring 100, 250, and 500 μm. The results revealed the successful attachment of hMSCs on all scaffolds, with greater proliferation in the 250 and 500 μm pore size scaffolds in the bioreactor, and the 100 μm pore size scaffolds in the static culture (Pisanti et al., 2012). Another research work investigated PLLA scaffolds and the effects of pore size on cultured human articular as well as nasoseptal chondrocytes. The feasibility, attachment, morphology, and extracellular matrix production were evaluated. Both types of chondrocytes confirmed feasibility, while the smaller pore sizes facilitated chondrocyte distinction. The thermally induced phase separation (TIPS) method was utilized to produce homogeneous scaffolds with specific pore sizes, preserving the chondrocyte phenotype. A minor difference in pore size affected the expression of

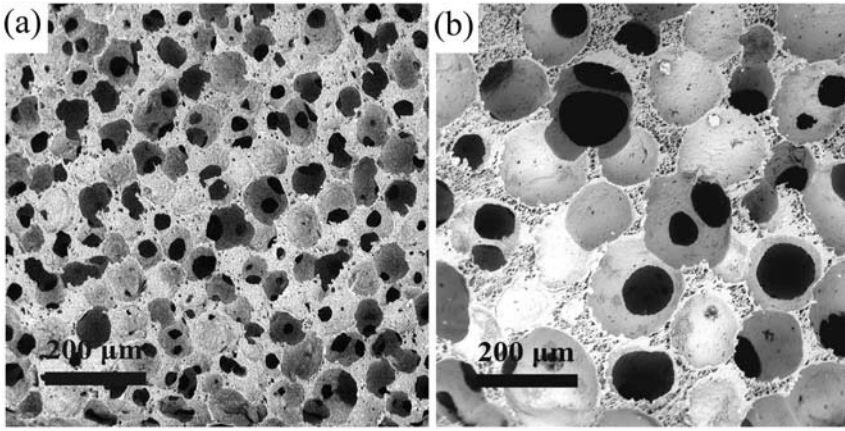

Figure 5.6 SEM images of a PLLA scaffold: mean pore dimension (a) 100 μm and (b) 200 μm. *(Reproduced with permission from Conoscenti et al. (2017). Scale bars 200 μm.)*

cartilage markers, with 100 μm pores stimulating chondrogenesis in PLLA scaffolds (Fig. 5.6) (Conoscenti et al., 2017).

5.6.2 Stent development

PLA/PLLA-based composites are useful in cardiovascular medical devices including stents and vascular grafts. Controlled degradation behavior by PLA composites reduces the associated risk of future difficulties related with permanent implants (Naseem et al., 2017). A study has investigated the surface-modified magnesium hydroxide nanoparticles (nMH), synthesized by nucleophilic addition reaction (nGTMH) and ROP of DL-lactide. The results revealed that the modified nMH incorporated into PLLA composite exhibited higher Young's modulus. The modified nMH confirmed low cytotoxicity, antiinflammatory properties, greater albumin/fibrinogen ratio, reduced platelet activation, as well as excellent hemocompatibility. The investigation concluded that the use of surface-modified nMH as an additive showed potential in enhancing the composite's mechanical/biological characteristics for medical purposes, particularly for vascular stents and orthopedic implants (Kang et al., 2020).

While metallic stents are helpful for avoiding acute occlusion with lowered late restenosis following coronary angioplasty, thrombosis and restenosis remain major issues. Bioresorbable stents had been developed

with benefits such as 100% bioresorption and mechanical flexibility. Many materials are now being studied for the construction of biodegradable stents, with PLLA and magnesium being the most favorable and promising. The process parameter effects over physical characteristics have been explored in order to create a PCL/PLA polymer tube for stent requirements (Guerra et al., 2017). The results demonstrated that polymer concentration and withdrawal speed have a considerable impact on the tube characteristics. PLA and PCL exhibited limited opportunities as stent materials during DMA testing and degradation analysis, while the PCL/PLA composite tube demonstrated favorable behavior for stent requirements.

Another study of biodegradable stents made from a self-reinforced poly-L,D-lactide copolymer (SR-PLA 96) in double-helical spiral structure was evaluated for its appropriateness in ureteral stenting. Temporary kidney function changes were observed in a few cases with SR-PLA 96 and C-Flex stents. Kidney washout times were prolonged in pigtail-stented ureters but remained normal with SR-PLA 96 stents. Renal function was confirmed as normal after ureteral repair with SR-PLA 96 stents. The results exhibited the potential use of SR-PLA 96 stents for ureteral repair (Lumiaho et al., 1999).

5.6.3 Drug-delivery systems and orthopedic implants

PLA/PLLA-based composites have established effective applications in orthopedic implants, including plates, screws, and anchors. These implants offer impermanent structural support during the healing practice and steadily degrade as new bone tissue develops (Amini et al., 2011). The integration of Mg particles into PLLA may have a favorable biological impact on bone repair. The alkaline environment created by magnesium breakdown could counteract the damage caused by acidic by-products of PLLA, resulting in inflammation relief (Chandra and Pandey, 2020). In one study, two composites, Mg/PLLA and MgF_2/PLLA, were developed by extrusion and injection molding. The impact of Mg inclusion was investigated as well as degradation and cytotoxicity being assessed for prospective use as orthopedic implants. The results illustrated that cell survival was improved by 37% when the amounts of MgF_2 and Mg were raised along with a suitable degradation rate, which confirms that magnesium incorporation has a significant capability for orthopedic transplant use (Wan et al., 2014). In another study on Mg-PLA composites, the in vitro breakdown as well as bio-mineralization were studied. The findings showed that the degradation of Mg particulates effectively

countered the acidic nature of PLA, along with controlled degradation behavior based on the quantity of Mg particulates (Zhao et al., 2017).

PLA is a thermoplastic polymer having an elevated elastic modulus, and low elongation at the tensile and break strength. Compared with other thermoplastics in commercial industries, PLA exhibits higher brittleness and lower overall strength as well as its processing properties also being less favorable, including susceptibility to hydrolysis along with a relatively slow crystallization rate (Ramlee and Tominaga, 2019; Li et al., 2023). PLA's stereochemical structure and physical characteristics can be easily adjusted by modifying the ratios of monomer feed, adjusting the stereochemistry of monomers, and optimizing polymerization conditions (de França et al., 2022; Worch et al., 2019). Because of their proclivity to rupture when the programming stains approach 10%, the shape-memory effect is often limited to small deformations. To increase the degradability of nondegradable shape-memory polymers (SMPs) for use as resorbable SMP transplants, lactic acid can be incorporated into the polymeric chains (Xu and Song, 2015). the shape-memory effects of PLA-based polymer hybrid have been studied for its glass-transition behavior, mechanical and thermal properties, miscibility, shape-memory property, and phase structure (Zhang et al., 2013). A study of (styrene-butadiene-styrene) SBS/DL-PLA composite was investigated for nontoxicity and biocompatibility of the materials which also has the shape-memory system of dual domain. The composite exhibited that as SBS exceeds 50% by weight for the elastic domain and 30% by weight for the thermo-switch domain, it offered good shape memory for DL-PLA ranging between 30% and 70% by weight (Zhang et al., 2013).

PLA/PLLA-based composites are widely used in drug-delivery applications. The PLA composites have been considered for encapsulating therapeutic agents along with controlled release. A study of four formulations of polylactide-co-glycolide (PLGA) nanoparticles loaded with Tamoxifen citrate (TNPs) were conducted. TNPs loaded for $27.16\% \pm 2.08\%$ w/w confirmed significant drug loading with sustained-release ability, and efficient uptake by breast cancer cells in the laboratory. The results indicated that the formulation exhibited breast cancer treatment qualities, with potential drug-loading ability (Maji et al., 2014). In another study, novel nanocomposites were fabricated by incorporating PLA-nanofibers with tetraheptylammonium-capped Fe_3O_4 magnetic nanoparticles for improving the growth of daunorubicin medicine over the cancer cells. The results showed improved interaction and accumulation of daunorubicin and subsequent cancer cell death (Lv et al., 2008).

5.6.4 Surgical tools/meshes developments and dental materials

PLA/PLLA-based composites can be used as surgical meshes for hernia repair and soft-tissue reinforcement. Compared to nondegradable meshes, PLA composite exhibits higher biocompatibility and reduces the associated long-term complication risks (Davachi et al., 2016). The bone screws developed through injection molding by PLA were improved and simulated by limiting shrinkage and warpage (Davachi et al., 2016). Based on the findings of injection molding simulations, the design of the experiment, along with a structural examination, the investigation confirmed that the composite consisting of 5% PLLA/TC (30% triclosan and 70% PLLA composite) and nano-hydroxyapatite by 5 wt.%, is the best alternative for biomedical applications among others (Davachi et al., 2016).

In another investigation, nanocomposites were fabricated with TiO_2-reinforced PLA matrix by a sonication process (Salahuddin et al., 2019). Encapsulation in PLA of TiO_2 nanospheres after being loaded with norfoxacin (NOR) drug was carried out. Different ratios of TiO_2 in the prepared nanocomposite were studied and evaluated for several morphologies and compared with PLA loading. No changes in the IR peak of NOR were observed, which indicated the absence of chemicals. All the results supported and confirmed the suitability of the prepared nanocomposite as a good alternative regarding tumor cell line carriers and it also exhibited antibacterial behavior which could be used in treating related infections.

PLA/PLLA-based composites have exhibited several applications in dentistry, such as dental implants, bone graft replacements, and guided tissue restoration films. The PLA composites contribute to enhanced dental treatment and reduce any required additional interventions (Cai et al., 2023).

Titanium is a widely used material for dental implant applications because of its constructive biological reaction (Özcan and Hämmerle, 2012). Implant failures resulting in infections remain an important concern (Silva et al., 2022). A study on the release behavior of chlorhexidine (CHX), which possesses broad-spectrum antimicrobial properties, from polylactide (PLA)-coated titanium was investigated. The method involved anodizing commercially pure titanium and subsequently coating over the PLA-CHX. The results showed that using a CHX-containing PLA-coated titanium implant has the probable effect of diminishing bacterial colonization during implant surgery (Kim et al., 2008).

Various PLLA-based composite applications along with reinforcement materials with composite properties are discussed in Table 5.3.

Table 5.3 Various applications of PLLA-based composites.

Application	Composite	Synthesis method	Characteristics
Bone tissue	(Poly-L-lactic acid)/(carbon nanotubes)/hydroxyapatite	TIPS	Young's modulus = 12.5 MPa Mean porosity = 87%
	Poly-L-lactic acid	TIPS + porogen leaching	MP = 97%
	(Poly lactic-co-glycolic acid)/(poly-L-lactic acid)/(poly-D-lactic acid)	Electrospinning	Young's modulus = 1.55 MPa Tensile strength = 2.04 MPa
	(Poly-L-lactic acid)/(poly-caprolactone)	TIPS	Degradation = 3 weeks
	(Poly-L-lactic acid)/hydroxyapatite	Electrospinning	Mean porosity = <90%
	(Poly-L-lactic acid)/hydroxyapatite	Additive manufacturing	Young's modulus = 17.2 −40.8 MPa Mean porosity = >90% Degradation = 24 weeks
	(Poly-L-lactic acid)/hydroxyapatite	Thermally induced phase separation	Young's modulus = 3−5 MPa Mean porosity = >90%
	(Poly-L-lactic acid)/hydroxyapatite	Porogen leaching	Young's modulus = 0.4 MPa
	(Poly-L-lactic acid)/hydroxyapatite	TIPS + porogen leaching	Young's modulus = 37−56.2 KPa Mean porosity = 88−98
	(Poly-L-lactic acid)/(bioactive glass)	TIPS	Young's modulus = 6−8 MPa Mean porosity = 88.5% Degradation = 28 days
	(Poly-L-lactic acid)/(bioactive glass)	Porogen leaching	Young's modulus = 55−81 MPa Tensile strength = 2.7−4.2 MPa Mean porosity = 69%−71% Degradation = 90 days
	PLLA/(poly-caprolactone)/hydroxyapatite	Porogen leaching + freeze drying	Young's modulus = 1−2 MPa Tensile strength = 0.2 MPa Mean porosity = 90% Degradation = 78 weeks

Continued

Table 5.3 Various applications of PLLA-based composites.—cont'd

Application	Composite	Synthesis method	Characteristics
Cartilage tissue	(Poly-L-lactic acid)/(poly-caprolactone)	TIPS	Young's modulus = 90–110 kPa Mean porosity = 93%–95%
	(Poly-L-lactic acid)	Thermally induced phase separation	Mean porosity = 93%
	(Poly-L-lactic acid)/chitosan	Freeze-drying	Tensile strength = 0.3–0.5 MPa Mean porosity = 73–93% Degradation = 28 days
	(Poly-L-lactic acid)/(silk fibroin)	Electrospinning	Tensile strength = 1.5 MPa Degradation = 12 weeks
Blood vessels	(Poly-L-lactic acid)/gelatin	Electrospinning	Young's modulus = 6–20 MPa Tensile strength = 5–7 MPa Mean porosity = 73–75% Degradation = 7 days
	(Poly-L-lactic acid)/(poly-caprolactone)/collagen	Electrospinning	Mean porosity = 20–80%
	(Poly-L-lactic acid)/chitosan/collagen	Electrospinning	Tensile strength = 2.13 MPa
Skin tissue	(Poly-L-lactic acid)/collagen	Freeze-drying	Young's modulus = 43–55 MPa Tensile strength = 5 MPa
	(Poly-L-lactic acid)/gelatin	Electrospinning	Tensile strength = 20 MPa Mean porosity = 72%
	(Poly-L-lactic acid)/gelatin	Freeze-drying	Young's modulus = 41–43 MPa Tensile strength = 5.7 MPa Degradation = 12 weeks

Reproduced with permission from Capuana et al. (2022).

5.7 Future perspectives

The application and usability of PLA and PLA/PLLA-based composites for medical devices has seen growth, and research into future perspectives is required. Unconventional methods such as 4D printing, biofabrication, and nanotechnology aid better material control, and thus need to be explored more. Multifunctional PLA polymers include antimicrobial characteristics that result in allowing complex tissue to be manufactured, and implants need further research to be more precise and optimized.

5.8 Conclusion

PLA/PLLA-based polymer applications for medical devices have revealed favorable developments. Synthesis methods such as melt processing, solvent processing, and additive manufacturing are widely used. PLA polymer composites are biocompatible and biodegradable, which makes them suitable for temporary implants. PLA/PLLA polymers have extensive scope in medicinal/therapeutic applications, such as muscle re-engineering, orthopedics, drug loading/delivery, stent development, dentistry, etc. Challenges include optimizing the constraints and achieving controlled drug release. Advanced research is desirable to improve the mechanical properties and discover new techniques for better patient care.

References

Amini, A.R., Wallace, J.S., Nukavarapu, S.P., 2011. Short-term and long-term effects of orthopedic biodegradable implants. J. Long Term Eff. Med. Implants 21 (2), 93. https://doi.org/10.1615/JLONGTERMEFFMEDIMPLANTS.V21.I2.10.

Augé, M.-O., Roncucci, D., Bourbigot, S., Bonnet, F., Gaan, S., Fontaine, G., 2023. Recent advances on reactive extrusion of Poly(lactic acid). Eur. Polym. J. 184 (December 2022), 111727. https://doi.org/10.1016/j.eurpolymj.2022.111727.

Azad, M.A., Olawuni, D., Kimbell, G., Badruddoza, A.Z.M., Hossain, M.S., Sultana, T., 2020. Polymers for extrusion-based 3D printing of pharmaceuticals: a holistic materials–process perspective. Pharmaceutics 12 (2), 124. https://doi.org/10.3390/pharmaceutics12020124.

Balla, E., Daniilidis, V., Karlioti, G., Kalamas, T., Stefanidou, M., Bikiaris, N.D., et al., 2021. Poly(lactic acid): a versatile biobased polymer for the future with multifunctional properties—from monomer synthesis, polymerization techniques and molecular weight increase to PLA applications. Polymers 13 (11), 1822. https://doi.org/10.3390/polym13111822.

Bambole, V., Yakhmi, J.V., 2016. Tissue engineering. In: Nanobiomaterials in Soft Tissue Engineering. Elsevier, pp. 387–455. https://doi.org/10.1016/B978-0-323-42865-1.00014-3.

Bikiaris, N.D., Koumentakou, I., Samiotaki, C., Meimaroglou, D., Varytimidou, D., Karatza, A., et al., 2023. Recent advances in the investigation of poly(lactic acid) (PLA) nanocomposites: incorporation of various nanofillers and their properties and applications. Polymers 15 (5). https://doi.org/10.3390/POLYM15051196.

Cai, H., Xu, X., Lu, X., Zhao, M., Jia, Q., Jiang, H.-B., et al., 2023. Dental materials applied to 3D and 4D printing technologies: a review. Polymers 15 (10), 2405. https://doi.org/10.3390/polym15102405.

Capuana, E., Lopresti, F., Ceraulo, M., La Carrubba, V., 2022. Poly-l-lactic acid (PLLA)-based biomaterials for regenerative medicine: a review on processing and applications. Polymers 14 (6), 1153. https://doi.org/10.3390/polym14061153.

Casasola, R., Thomas, N.L., Trybala, A., Georgiadou, S., 2014. Electrospun poly lactic acid (PLA) fibres: effect of different solvent systems on fibre morphology and diameter. Polymer 55 (18), 4728–4737. https://doi.org/10.1016/j.polymer.2014.06.032.

Chandra, G., Pandey, A., 2020. Biodegradable bone implants in orthopedic applications: a review. Biocybern. Biomed. Eng. 40 (2), 596–610. https://doi.org/10.1016/J.BBE.2020.02.003.

Cheerarot, O., Baimark, Y., 2015. Thermal and mechanical properties of biodegradable star-shaped/linear polylactide stereocomplexes. J. Chem. 2015. https://doi.org/10.1155/2015/206123.

Conoscenti, G., Schneider, T., Stoelzel, K., Carfi Pavia, F., Brucato, V., Goegele, C., et al., 2017. PLLA scaffolds produced by thermally induced phase separation (TIPS) allow human chondrocyte growth and extracellular matrix formation dependent on pore size. Mater. Sci. Eng. C 80, 449–459. https://doi.org/10.1016/J.MSEC.2017.06.011.

Davachi, S.M., Seyfi, J., Bahrami, M., 2016. Simulation of Mechanical Behavior and Optimization of Simulated Injection Molding Process for PLA Based Antibacterial Composite and Nanocomposite Bone Screws Using Central Composite Design. Elsevier. https://doi.org/10.1016/j.jmbbm.2016.08.008.

Destefano, V., Khan, S., Tabada, A., 2020. Applications of PLA in modern medicine. Eng. Regen. 1 (September), 76–87. https://doi.org/10.1016/j.engreg.2020.08.002.

Farah, S., Anderson, D.G., Langer, R., 2016. Physical and mechanical properties of PLA, and their functions in widespread applications — a comprehensive review. Adv. Drug Deliv. Rev. 107, 367–392. https://doi.org/10.1016/j.addr.2016.06.012.

Farrington, D.W., Lunt, J., Davies, S., Blackburn, R.S., 2008. Poly(lactic acid) fibers (PLA). In: Polyesters and Polyamides. Elsevier, pp. 140–170. https://doi.org/10.1533/9781845694609.1.140.

de França, J.O.C., da Silva Valadares, D., Paiva, M.F., Dias, S.C.L., Dias, J.A., 2022. Polymers based on PLA from synthesis using D,L-lactic acid (or racemic lactide) and some biomedical applications: a short review. Polymers 14 (12), 2317. https://doi.org/10.3390/polym14122317.

Guerra, A.J., San, J., Ciurana, J., 2017. Fabrication of PCL/PLA composite tube for stent manufacturing. Proc. CIRP 65, 231–235. https://doi.org/10.1016/j.procir.2017.03.339.

Hu, X., Zhao, W., Zhang, Z., Xie, J., He, J., Cao, J., et al., 2023. Novel 3D printed shape-memory PLLA-TMC/GA-TMC scaffolds for bone tissue engineering with the improved mechanical properties and degradability. Chin. Chem. Lett. 34 (1), 107451. https://doi.org/10.1016/j.cclet.2022.04.049.

Kafle, A., Luis, E., Silwal, R., Pan, H.M., Shrestha, P.L., Bastola, A.K., 2021. 3D/4D printing of polymers: fused deposition modelling (FDM), selective laser sintering (SLS), and stereolithography (SLA). Polymers 13 (18), 3101. https://doi.org/10.3390/polym13183101.

Kang, E.Y., Park, S.B., Choi, B., Baek, S.W., Ko, K.W., Rhim, W.K., et al., 2020. Enhanced mechanical and biological characteristics of PLLA composites through surface

grafting of oligolactide on magnesium hydroxide nanoparticles. Biomater. Sci. 8 (7), 2018–2030. https://doi.org/10.1039/C9BM01863H.

Kim, W.H., Lee, S.B., Oh, K.T., Moon, S.K., Kim, K.M., Kim, K.N., 2008. The release behavior of CHX from polymer-coated titanium surfaces. Surf. Interface Anal. 40 (3–4), 202–204. https://doi.org/10.1002/SIA.2809.

Kulkarni, A., 2022. Effect of ionic interactions on crystallization of star telechelic poly(l-lactide) ionomers. Polymer 252, 124939. https://doi.org/10.1016/j.polymer.2022.124939.

Li, X., Lin, Y., Liu, M., Meng, L., Li, C., 2023. A review of research and application of polylactic acid composites. J. Appl. Polym. Sci. 140 (7), e53477. https://doi.org/10.1002/APP.53477.

Liao, G., Zhou, X., Chen, L., Zeng, X., Xie, X., Mai, Y., 2012. Electrospun aligned PLLA/PCL/functionalised multiwalled carbon nanotube composite fibrous membranes and their bio/mechanical properties. Compos. Sci. Technol. 72 (2), 248–255. https://doi.org/10.1016/j.compscitech.2011.11.009.

Liu, S., Qin, S., He, M., Zhou, D., Qin, Q., Wang, H., 2020. Current applications of poly(lactic acid) composites in tissue engineering and drug delivery. Compos. B Eng. 199, 108238. https://doi.org/10.1016/j.compositesb.2020.108238.

Lopes, M.S., Jardini, A.L., Filho, R.M., 2014. Synthesis and characterizations of poly (lactic acid) by ring-opening polymerization for biomedical applications. Chem. Eng. Trans. 38, 331–336. https://doi.org/10.3303/CET1438056.

Lopresti, F., Campora, S., Tirri, G., Capuana, E., Carfi, F., Brucato, V., et al., 2021. Core-shell PLA/Kef hybrid scaffolds for skin tissue engineering applications prepared by direct kefiran coating on PLA electrospun fibers optimized via air-plasma treatment. Mater. Sci. Eng. C 127 (May), 112248. https://doi.org/10.1016/j.msec.2021.112248.

Lumiaho, J., Heino, A., Tunninen, V., Ala-Opas, M., Talja, M., Välimaa, T., et al., 1999. New bioabsorbable polylactide ureteral stent in the treatment of ureteral lesions: an experimental study. J. Endourol. 13 (2), 107–112. https://doi.org/10.1089/END.1999.13.107.

Lv, G., He, F., Wang, X., Gao, F., Zhang, G., Wang, T., et al., 2008. Novel nanocomposite of nano Fe 3 O 4 and polylactide nanofibers for application in drug uptake and induction of cell death of leukemia cancer cells. Langmuir 24 (5), 2151–2156. https://doi.org/10.1021/la702845s.

Maji, R., Dey, N.S., Satapathy, B.S., Mukherjee, B., Mondal, S., 2014. Preparation and characterization of Tamoxifen citrate loaded nanoparticles for breast cancer therapy. Int. J. Nanomed. 9 (1), 3107–3118. https://doi.org/10.2147/IJN.S63535.

McKeen, L., 2012. Renewable resource and biodegradable polymers. In: The Effect of Sterilization on Plastics and Elastomers, pp. 305–317. https://doi.org/10.1016/B978-1-4557-2598-4.00012-5.

McKeen, L.W., 2017. Environmentally friendly polymers. In: Permeability Properties of Plastics and Elastomers. Elsevier, pp. 305–323. https://doi.org/10.1016/B978-0-323-50859-9.00013-0.

Melo, P., Tarrant, E., Swift, T., German, M., Ferreira, A., Dalgarno, K., 2019. Short phosphate glass fiber-PLLA composite to promote bone mineralization. Mater. Sci. Eng. C 104, 109929. https://doi.org/10.1016/j.msec.2019.109929.

Mohammad, S., Kaffashi, B., Zamanian, A., Torabinejad, B., Ziaeirad, Z., 2016. Investigating composite systems based on poly L-lactide and poly L-lactide/triclosan nanoparticles for tissue engineering and medical applications. Mater. Sci. Eng. C 58, 294–309. https://doi.org/10.1016/j.msec.2015.08.026.

Murariu, M., Dubois, P., 2016. PLA composites: from production to properties. Adv. Drug Deliv. Rev. 107, 17–46. https://doi.org/10.1016/j.addr.2016.04.003.

Narayanan, G., Vernekar, V.N., Kuyinu, E.L., Laurencin, C.T., 2016. Poly (lactic acid)-based biomaterials for orthopaedic regenerative engineering. Adv. Drug Deliv. Rev. 107, 247. https://doi.org/10.1016/J.ADDR.2016.04.015.

Naseem, R., Zhao, L., Liu, Y., Silberschmidt, V.V., 2017. Experimental and computational studies of poly-L-lactic acid for cardiovascular applications: recent progress. Mech. Adv. Mater. Mod. Process. 3 (1), 1–18. https://doi.org/10.1186/S40759-017-0028-Y.

Naser, A.Z., Deiab, I., Darras, B.M., 2021. Poly(lactic acid) (PLA) and polyhydroxyalkanoates (PHAs), green alternatives to petroleum-based plastics: a review. RSC Adv. 11 (28), 17151–17196. https://doi.org/10.1039/D1RA02390J.

Neumann, I.A., Flores-Sahagun, T.H.S., Ribeiro, A.M., 2017. Biodegradable poly (l-lactic acid) (PLLA) and PLLA-3-arm blend membranes: the use of PLLA-3-arm as a plasticizer. Polym. Test. 60, 84–93. https://doi.org/10.1016/J.POLYMERTESTING.2017.03.013.

Özcan, M., Hämmerle, C., 2012. Titanium as a reconstruction and implant material in dentistry: advantages and pitfalls. Materials 5 (9), 1528. https://doi.org/10.3390/MA5091528.

Pawar, R.P., Tekale, S.U., Shisodia, S.U., Totre, J.T., Domb, A.J., 2014. Biomedical Applications of poly(lactic acid). Recent Pat. Regen. Med. 4 (1), 40–51. https://doi.org/10.2174/22102965046661404022350 24.

Pisanti, P., Yeatts, A.B., Cardea, S., Fisher, J.P., Reverchon, E., 2012. Tubular perfusion system culture of human mesenchymal stem cells on poly-L-lactic acid scaffolds produced using a supercritical carbon dioxide-assisted process. J. Biomed. Mater. Res. 100A (10), 2563–2572. https://doi.org/10.1002/JBM.A.34191.

Quodbach, J., Bogdahn, M., Breitkreutz, J., Chamberlain, R., Eggenreich, K., Elia, A.G., et al., 2022. Quality of FDM 3D printed medicines for pediatrics: considerations for formulation development, filament extrusion, printing process and printer design. Ther. Innov. Regul. Sci. 56 (6), 910–928. https://doi.org/10.1007/s43441-021-00354-0.

Ramlee, N.A., Tominaga, Y., 2019. Mechanical and degradation properties in alkaline solution of poly(ethylene carbonate)/poly(lactic acid) blends. Polymer 166, 44–49. https://doi.org/10.1016/J.POLYMER.2019.01.043.

Ranakoti, L., Gangil, B., Mishra, S.K., Singh, T., Sharma, S., Ilyas, R.A., et al., 2022. Critical review on polylactic acid: properties, structure, processing, biocomposites, and nanocomposites. Materials 15 (12), 4312. https://doi.org/10.3390/ma15124312.

Salahuddin, N., Abdelwahab, M., Gaber, M., Elneanaey, S., 2019. Synthesis and design of Norfloxacin drug delivery system based on PLA/TiO2 nanocomposites: antibacterial and antitumor activities. Mater. Sci. Eng. C 108, 110337. https://doi.org/10.1016/j.msec.2019.110337.

De Santis, F., Pantani, R., 2015. Melt compounding of poly (lactic acid) and talc: assessment of material behavior during processing and resulting crystallization. J. Polym. Res. 22 (12), 242. https://doi.org/10.1007/s10965-015-0885-1.

Sheikh, Z., Najeeb, S., Khurshid, Z., Verma, V., Rashid, H., Glogauer, M., 2015. Biodegradable materials for bone repair and tissue engineering applications. Materials 8 (9), 5744–5794. https://doi.org/10.3390/ma8095273.

da Silva, D., Kaduri, M., Poley, M., Adir, O., Krinsky, N., Shainsky-Roitman, J., et al., 2018. Biocompatibility, biodegradation and excretion of polylactic acid (PLA) in medical implants and theranostic systems. Chem. Eng. J. 340, 9–14. https://doi.org/10.1016/j.cej.2018.01.010.

Silva, R.C.S., Agrelli, A., Andrade, A.N., Mendes-Marques, C.L., Arruda, I.R.S., Santos, L.R.L., et al., 2022. Titanium dental implants: an overview of applied nanobiotechnology to improve biocompatibility and prevent infections. Materials 15 (9). https://doi.org/10.3390/MA15093150.

Sousa, S., Costa, A., Silva, A., Simões, R., 2019. Poly(lactic acid)/cellulose films produced from composite spheres prepared by emulsion-solvent evaporation method. Polymers 11 (1), 66. https://doi.org/10.3390/polym11010066.

Tan, D., Maniruzzaman, M., Nokhodchi, A., 2018. Advanced pharmaceutical applications of hot-melt extrusion coupled with fused deposition modelling (FDM) 3D printing for personalised drug delivery. Pharmaceutics 10 (4), 203. https://doi.org/10.3390/pharmaceutics10040203.

Tee, Y.B., Talib, R.A., Abdan, K., Chin, N.L., Basha, R.K., Yunos, K.F.M., 2014. Toughening poly(lactic acid) and aiding the melt-compounding with bio-sourced plasticizers. Agric. Agric. Sci. Procedia 2, 289–295. https://doi.org/10.1016/j.aaspro.2014.11.041.

Teixeira, S., Eblagon, K.M., Miranda, F., Pereira, M.F.R., Figueiredo, J.L., 2021. Towards controlled degradation of poly(lactic) acid in technical applications. C 7 (2), 42. https://doi.org/10.3390/c7020042.

Wan, P., Yuan, C., Tan, L., Li, Q., Yang, K., 2014. Fabrication and evaluation of bio-resorbable PLLA/magnesium and PLLA/magnesium fluoride hybrid composites for orthopedic implants. Compos. Sci. Technol. 98, 36–43. https://doi.org/10.1016/j.compscitech.2014.04.011.

Wang, W., Zhang, B., Li, M., Li, J., Zhang, C., Han, Y., et al., 2021. 3D printing of PLA/n-HA composite scaffolds with customized mechanical properties and biological functions for bone tissue engineering. Composites, Part B 224 (July), 109192. https://doi.org/10.1016/j.compositesb.2021.109192.

Worch, J.C., Prydderch, H., Jimaja, S., Bexis, P., Becker, M.L., Dove, A.P., 2019. Stereochemical enhancement of polymer properties. Nat. Rev. Chem 3 (9), 514–535. https://doi.org/10.1038/s41570-019-0117-z.

Xie, R., Weisen, A.R., Lee, Y., Aplan, M.A., Fenton, A.M., Masucci, A.E., et al., 2020. Glass transition temperature from the chemical structure of conjugated polymers. Nat. Commun. 11 (1), 893. https://doi.org/10.1038/s41467-020-14656-8.

Xu, J., Song, J., 2015. Polylactic acid (PLA)-based shape-memory materials for biomedical applications. In: Shape Memory Polymers for Biomedical Applications. Elsevier, pp. 197–217. https://doi.org/10.1016/B978-0-85709-698-2.00010-6.

Yoon, S.-D., Kwon, Y.-S., Lee, K.-S., 2017. Biodegradation and biocompatibility of poly L-lactic acid implantable mesh. Int. Neurourol. J. 21 (Suppl. 1), S48–S54. https://doi.org/10.5213/inj.1734882.441.

Zhang, H., Chen, Z., Zheng, Z., Zhu, X., Wang, H., 2013. Shape memory polymer hybrids of SBS/dl -PLA and their shape memory effects. Mater. Chem. Phys. 137 (3), 750–755. https://doi.org/10.1016/j.matchemphys.2012.10.006.

Zhao, C., Wu, H., Ni, J., Zhang, S., Zhang, X., 2017. Development of PLA/Mg composite for orthopedic implant: tunable degradation and enhanced mineralization. Compos. Sci. Technol. https://doi.org/10.1016/j.compscitech.2017.04.037.

This page intentionally left blank

CHAPTER 6

PHA/PHB/PHBV-based composites: development and biomedical applications

Ivana Cesarino[1], Ivan Moroz[1], Afonso Freitas Carbonera[1], Guilherme de Oliveira Martins[1], Luís Guilherme Leite Fernandes[2] and Alcides Lopes Leao[1]

[1]São Paulo State University (UNESP), School of Agriculture, Botucatu, Brazil; [2]São Paulo State University (UNESP), Institute of Biosciences, Botucatu, Brazil

6.1 Introduction

The development of materials with specific properties allied to the search for sustainability has increased the demand for materials with biodegradable characteristics and low environmental impact in their processing. For medical and pharmaceutical applications, these materials must still be biocompatible and present mechanical properties that meet the needs of each application (Mukherjee et al., 2023). Polyhydroxyalkanoates (PHAs) are good examples of components present in materials with these characteristics, due to their form of synthesis and behavior, and they have increasingly been the subject of research for the optimization of biomaterials (Kalia et al., 2023).

Among the analyzed market forecasts, there is no consensus on the exact market value of PHAs or its growth, but the literature reports values in the range between 80 and 90 million dollars for 2020 and 2021 (DMBR, 2022; GMI, 2022; Marketsandmarkets, 2022). Furthermore, among the analyses, a compound annual growth rate (CAGR) value ranging from 5.4% to 11.5% was reported, with the total market value potentially exceeding hundreds of millions of dollars by the end of this decade or the beginning of the next (DMBR, 2022; GMI, 2022; Stratview Research, 2021; TMR, 2021). This increase is due to the growing demand for bioplastics today, and their renewable properties, such as biodegradability. Although most plastic production still has a fossil origin, the environmental problems associated

Bioresorbable Polymers and their Composites
ISBN 978-0-443-18915-9
https://doi.org/10.1016/B978-0-443-18915-9.00001-X
© 2024 Elsevier Ltd.
All rights reserved.

with these sources are also contributing to the endeavor for the development of renewable technologies and products (DMBR, 2022; GMI, 2022).

The market research of Global Market Insights (2022) shows that most PHAs produced are known to have short or medium carbon chains. The main types are PHB, PHBH, and PHBV. The PHB market exceeded, in 2021, the value of USD 20 million, while PHBV has a CAGR exceeding 9% in the forecast for 2030. Europe is the largest market region for PHA, followed by North America, presenting a CAGR of 9.5% in the forecast until 2030, due to European policies related to plastic which in turn drive companies to invest in these bioplastics. However, the Asia–Pacific region has the greatest growth potential in the 2030 forecast, with a CAGR value that exceeds 10%. As for the areas of application, PHA production is widely focused on the food packaging industry, but other sectors have been gaining prominence and showing potential for growth in the coming years. Agriculture, biofuels, and biomedical industries are among the potential applications for PHA. In fact, the biomedical industry is the second largest market for PHA, with a CAGR forecast higher than 9% for the period between 2022 and 2030. The potential increase in this specific field is due to properties such as biodegradability, biocompatibility, and low toxicity, allowing wide application of PHA in technologies such as implants, tissue engineering, drug delivery, etc. (GMI, 2022).

Another market research study brought similar results in terms of market size, with the market cap forecast to reach US$167 million in 2027, thus having a CAGR of 15%. This study also shows that, despite the many factors that influence the growth of the PHA market, there are still barriers that slow down this growth, with the main one being the high relative cost of production compared to conventional plastics, in addition to the production technology still being in the early stages of development (Marketsandmarkets, 2022).

6.2 Polyhydroxyalkanoates (PHA)

Polyhydroxyalkanoates are biodegradable and biocompatible aliphatic polyesters synthesized by microorganisms because of the fermentation of at least 75 different species of bacteria, including *Bacillus cereus*, *Pseudomonas putida*, *Bacillus pumilus*, *Pseudomonas huttiensis*, *Yersinia frederiksenii*, *Aeromonas ichthiosmia*, and *Sphingopyxis terrae*, among others. They are produced intracellularly when there is excess carbon and limitation of nutrients (phosphorus, nitrogen, and oxygen) in the medium. They are produced in

solid form in the cytoplasm of the microorganism, do not dissolve, and can be accumulated in high concentrations. The composition of the synthesized polymer is governed mainly by three factors: the specificity of the enzyme that will synthesize the PHA, the carbon source supplied, and the pathway by which this carbon is metabolized (Kaniuk and Stachewicz, 2021; Wampfler et al., 2010).

PHAs are composed of monomers consisting of 4—5 carbons or 6—14 carbons. The chemical structure and chain size of these polymers allow a division into two main groups: short-chain PHAs are relatively brittle, have high crystallinity and high melting point; while medium-chain PHAs have elastomeric properties, low melting point and low crystallinity (Norhafini et al., 2017; Wampfler et al., 2010).

PHA polymers are isotactic, hydrophobic, water-insoluble, resistant to hydrolytic degradation, and have piezoelectric properties and some resistance to UV degradation. There is a diversity of monomers that make up the structure of PHA, including polyhydroxybutyrate (PHB) and poly-3-hydroxybutyrate-*co*-poly-3-hydroxyvalerate (PHBV). Fig. 6.1 shows some of these short-chain (SCL-PHA) and medium-chain (MCL-PHA) structures.

Polymeric biomaterials offer some advantages in various applications due to their biocompatible and biodegradable characteristics. PHA-based composites have potential medical applications, due to their ability to be broken down after their complete functionality, they can be used in implants, sutures, tissue regeneration, and as drug-delivery systems. When employed in the formulation of drug carriers, PHAs allow for good distribution to target sites and diffusion into cells. For medical applications, when PHAs are isolated, special attention must be paid to contamination by pyrogenic compounds, which are endotoxins (lipopolysaccharides) from the outer cell membrane of some groups of bacteria. Filtration and activated carbon processes can be used to remove these endotoxins (Lam et al., 2017; Wampfler et al., 2010).

Besides biocompatibility, appropriate mechanical properties for each specific application are a key feature for biopolymers in the medical area. For example, in bone treatments of various kinds, the material must possess some properties similar to bone, such as: (1) the ability to permeate the site of the defect; (2) the capacity to induce osteoblasts and other cells to produce bone material; and (3) biodegradability, or the ability to degrade naturally within the organism without inducting inflammatory or other

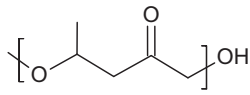

Polyhydroxybutyrate (PHB)

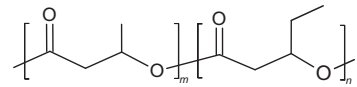

Poly(3-hydroxybutyrate-co-3-hydroxyvalerate) (PHBV)

(SCL-PHA)

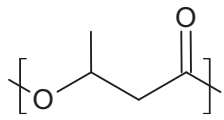

Poly(3-hydroxybutyrate) (P(3HB))

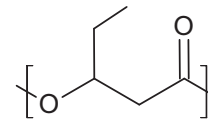

Poly(3-hydroxyvalerate) (P(3HV))

(MCL-PHA)

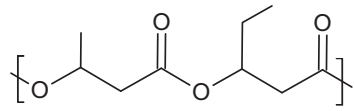

Poly(3-hydroxybutyrate-co-3-hydroxyvalerate) PHBV

Figure 6.1 Chemical structures of some short- and medium-chain length PHAs. *(Figure created by the authors.)*

adverse reactions in the patient (Shishatskaya et al., 2006). Table 6.1 describes the thermal and mechanical properties of some PHA films.

The degradability of PHA compared to polymers of synthetic origin (produced from petroleum) is also an important and attractive property for medical and pharmaceutical applications. Some enzymes are responsible for breaking the molecular bonds of these polymers, using them as a carbon source for their growth. An example is depolymerase, the main degradation enzyme of PHA, which is reduced to monomers and oligomers after being hydrolyzed. The crystallinity of the polymer structures and external factors such as pH, humidity, temperature, and degree of microbial activity influence the speed of degradation of these compounds. The occurrence of PHBV, for example, can affect this process. Under aerobic conditions, PHAs can be fully degraded into water and carbon dioxide, and under anaerobic conditions, they can be transformed into methane by an infinity of decomposing microorganisms (Lam et al., 2017).

Table 6.1 Thermal and mechanical parameters of PHA films.

Samples	Melting temperature (°C)	Glass transition temperature (°C)	Tensile strength (MPa)	Elongation (%)	Elastic modulus (GPa)
P(3HB)	175–180	4–9	40–45	4–5	3.5–3.8
P(3HB-*co*-3% 3HV)	170		38		2.9
P(3HB-co-20% 3HV)	114–145	−5 to (−1)	20–32	27–50	0.8–1.9
P(3HB-*co*-3% 4HB)	166		28	45	
P(3HB-*co*-64% 4HB)	50		17	591	30

Adapted from Kaniuk and Stachewicz (2021).

The polymer production and processing industry has been paying attention to two main points: the reduction in the use of synthetic chemicals in a growing trend toward sustainability, and the end of the life cycle of these products combined with their degradability. In this case, PHA shows more promise in relation to conventional matrices such as polypropylene and polystyrene, for example.

Finally, depending on the requirements for the material to be produced, PHA group polymers can be modified, blended, surface-modified, and combined with inorganic materials to improve their properties and potential use. These combinations can change the polymer structure, affecting its crystallinity, thermal and mechanical properties, and most importantly, its rate of degradation.

6.3 Polyhydroxybutyrate (PHB)

Considering their significant mechanical strength, PHAs also represent an important research subject in orthopedics. In fact, a selection of different types of PHAs, including polymer of hydroxybutyric acid (PHB), copolymers of hydroxybutyric and hydroxyvaleric acids (PHB/PHV or PHBV), and copolymers of hydroxybutyric and hydroxyhexanoic acids (PHB/PHHx) have been demonstrated to serve as matrices in which osteogenic cells can be cultured in vitro (Köse et al., 2003; Deng et al., 2003; Yang et al., 2004; Wang et al., 2004).

The research by Shishatskaya et al. (2006) was among the pioneering works to report the production and characterization of a PHB matrix composite with the addition of hydroxyapatite (HA). HA is a biocompatible material which has some disadvantages, such as high rigidity and low elasticity, and these disadvantages can be tackled by associating the material with less rigid, more elastic polymers. In this sense, traditional fossil-based polymers significantly hinder the biocompatibility of the composite, and thus polymers which occur naturally are preferable for associating with HA. In this study, bacteria were used for synthesizing PHB, and the HA was obtained from bovine cortical bones, configuring a truly biological originated composite. The hybrid composite was fabricated by the mechanical-physical method, involving cold-molding at high pressure and with weight percentage ratios ranging from 10% to 50% HA. The characterization included physical and mechanical properties as well as in vitro and in vivo tests to evaluate the osteogenic characteristics of the composites. When compared to native PHB, the composites displayed the same temperature

properties and crystallinity while possessing a more hydrophilic surface. From an osteogenic point of view, the optimal compositions were those with 10% and 20% HA, which yielded the best growth and differentiation characteristics of murine marrow osteoblasts; these results suggest that hybrid PHB/HA composites are feasible possibilities for bone tissue reconstruction applications.

Other materials can be associated with PHB for producing composite materials, such as, for example, the research concerning PHB/kaolin nanocomposites (Ankush et al., 2022). The solvent casting method was applied in this study to add different contents of polyethylene glycol and kaolin to the PHB matrix. By adding kaolin in contents of up to 10% in weight, the following results were obtained: decrease of the contact angle (representing an improvement in wettability); melting temperature was raised; increased blood clotting time; and surface characteristics, such as protein adsorption, platelet adhesion, and complement activation, were shown to be improved in the nanocomposite. Optimal mechanical properties were obtained for the 10% kaolin sample, similar to those of bone. Finally, in vitro and cytotoxic tests demonstrated the formation of hydroxyapatite on the optimal composition and the safety of biological use of this nanocomposite.

One of the first manuscripts to investigate the feasibility of PHB in biomedical applications was published in 2003 (Volova et al., 2003). The authors compared the in vivo biological reactions of PHB and PHBV sutures in comparison to reactions caused by silk and catgut sutures. In addition to displaying satisfactory strength during the healing period, PHB and PHBV sutures caused a tissue reaction considered usual for foreign-body invasion—and less pronounced than the reaction observed for catgut sutures.

PHB composites are interesting options also as drug-delivery scaffolds, due to their biocompatibility, biodegradability, and piezoelectric characteristics. Recently, Pryadko et al. (2022) reported the production of PHB composites using gelatin and magnetite as components, aiming to obtain magnetoactive scaffolds for biomedical use. The authors described the formation of core—shell-structured composite scaffolds, where PHB acts as the core and the shell is gelatin, where PHB crystallinity is decreased during this process. Additionally, cytotoxicity studies revealed that both human cervix adenocarcinoma cells and primary fibroblasts displayed a cellular response to the scaffolds similar to that of the control sample (pure PHB), indicating the nontoxic characteristic of the composites. Finally, the

saturation magnetization of the scaffolds occurred in a satisfactory range for use as magnetoactive materials, thus rendering these composites as interesting possibilities for wound treatment, tissue engineering, and drug-delivery scaffolds activated with an external magnetic field.

Another interesting characteristic of PHB composites is the ability to conduct electricity, as reported by (El-Hadi and Elbary, 2018). This article describes the fabrication of a blend material containing PHB, poly(-propylene carbonate) (PPC), multiwalled carbon nanotubes (MWCNTs), and plasticizers. PHB, among other biopolymers, has been researched as a promising material for the electronic industry as a matrix with the addition of conductive fillers as an alternative for conductive metals, because these biopolymers can be cheaper, lighter, and display corrosion resistance. Also, this addition enhances the mechanical and physical properties of pure PHB, which is known to be brittle and thermally unstable. In biomedical applications, these biopolymer blends are suitable for use as biosensors, drug-delivery systems, and in tissue engineering. Maintaining fixed contents of plasticizer and PPC, the authors produced blends with varying contents of PHB and MWCNTs via solution casting and posterior melting in a hot hydraulic press. Differential scanning calorimetry results showed that MWCNTs can act as nucleating agents in the PHB matrix, causing an increase in the crystallization rate of the material when compared to pure PHB; however, the blends displayed lower thermal stability than the pure material. Also, MWCNT addition increased the electrical conductivity of the blends which is an interesting result considering practical applications.

PHB can act in composites for biomedical applications as the matrix, but also as the added material to obtain specific properties. Rodríguez-Contreras et al. (2016) aimed to use PHB nano- and microspheres containing antibiotics in association with titanium and poly(ethylene glycol) (PEG) to produce antibacterial implant surfaces. The idea was to minimize postoperative infections that can happen in this type of application. Titanium surfaces were subjected to chemical activation via oxygen plasma or sodium hydroxide, and alkoxysilanes posteriorly to allow for PHB and PEG reactions and forming of covalent bonds. The results of in vitro bacterial tests indicated the attainment of antimicrobial properties in the titanium surfaces for both chemical strategies.

The employment of PHB in surface modification for biomedical applications was reported earlier, in 2011, in research targeted at reducing the corrosion rate of magnesium inside the human body (Ma et al., 2011). This metal ranks as one of the lightest available, and its elastic modulus is close to

the average modulus of human bone. This fact represents an important advantage in implant materials since the similarity in stiffness avoids the occurrence of stress shielding, an undesirable phenomenon in which bone does not heal optimally. In this scenario, the main disadvantage of magnesium is its high corrosion rate in body fluids, limiting the time window of its application. This study sought the development of a poly(3-hydroxybutyrate) coating on the surface of magnesium aiming to reduce the corrosion rate of the material. The authors verified the lower corrosion rate of the PHB-coated magnesium when compared to the pure metal. Additionally, the corrosion process occurred almost uniformly, allowing for possible adjustments of these coatings for specific time periods desired for the material application.

A more recent example of research involving PHB as a composite component for surface coatings was published by Mathina et al. (2022). In this article, the authors describe the importance of PHB addition to promote the biocompatibility of this composite material, which also contains HA from crab shell, aloe vera, and strontium oxide. The material was deposited via electrophoresis on a 316L stainless steel surface, a traditional material used in orthopedic applications. Structural, morphological, antibacterial, and biocompatibility properties assays indicated the potential of this composite coating to enhance the biomedical applications of 316L stainless steel. PHB has also been reported in the literature (Lin et al., 2021) as a promising composite component in addition to poly-epsilon-caprolactone (PCL) in fibrous membranes which can be tailored to be hydrophobic or hydrophilic, depending on additional HCl and NH_4OH treatments.

6.4 Poly(hydroxybutyrate-co-hydroxyvalerate) (PHBV)

Poly(3-hydroxybutyric acid-co-3-hydroxyvaleric acid) is a biodegradable, biocompatible, and nontoxic material produced by bacteria under certain conditions. It is a thermoplastic material, well established as an alternative to nonbiodegradable polymers (Kaniuk and Stachewick, 2021). The PHBV activity is highly dependent on its characteristics, such as the mean size, shape, surface electrical charge, and capacity to interact with proteins (Tebaldi et al., 2019). Due to its properties, several studies evaluating biopolymer suitability for medical and biological applications have been conducted.

One of the main advantages of PHBV is the fact that, just like other PHAs, PHBV is easily modified or combined with other compounds, enabling several different applications (Kaniuk and Stachewicz, 2021). Many studies have reported the combined use of PHBV with other natural polymers, such as gelatin (Meng et al., 2008), keratin (Yuan et al., 2009), polylactic acid (He et al., 2014), and collagen (Liu et al., 2019), among others. Other studies have reported the incorporation of inorganic compounds and mixtures, such as magnetite (Vilos et al., 2013), hydroxyapatite (Karbowniczek et al., 2022), and titanium dioxide (Karbowniczek et al., 2022), generating materials with superparamagnetic behavior.

One of the challenges of PHBV use in medical applications, however, is the fact that this polymer is hydrophobic. This property might affect cell activity, such as cell adhesion, where hydrophilic materials are preferred (Yuan et al., 2009). Most studies described in the literature aim to develop a material with enhanced hydrophilicity, promoting a better environment for cell fixation and growth (He et al., 2014).

Electrospinning has been widely reported as an effective method for obtaining PHBV nanofibers. This method consists of submitting a solution containing the biopolymer to high voltages. The solution is then ejected through a needle, accelerating toward a grounded collector. The solvent is evaporated, and the charged polymer fiber is deposited on the collector, forming a nanofibrous structure (Meng et al., 2008). Several parameters, such as PHBV concentration, the possibility of incorporating other compounds, and the solvents used in the process might affect the results.

Liu et al. (2019) also reported a method for obtaining nanofibrous PHBV-based materials. Forcespinning is a procedure where a polymer solution is ejected from spinnerets at high rotational speeds onto collecting frames, allowing the production of fibers from various materials at higher rates than electrospinning. This method is also cheaper than electrospinning since high voltages are not required.

PHBV can be used to obtain films for medical purposes, such as tissue engineering and wound dressing (Meng et al., 2008). Methodologies described in the scientific literature indicate the obtention of PHBV-based films via solvent evaporation of a polymer solution. However, the usage of nanofibrous materials instead of films may enhance the cell activity, due to the larger surface areas present in the fibers as compared to films. Yuan et al. (2009) could demonstrate how NIH 3T3 cells interacted with different substrates. In the SEM pictures, it is possible to observe how cells were able to adhere and grow at higher rates in fibers than on film surfaces. The

presence of keratin, which enhances biomaterial hydrophilicity, also contributed to cellular activity.

The application of PHBV-based nanofibrous materials is mainly related to structural functions, such as tissue engineering scaffolds and wound dressing. This is due to PHBV biocompatibility, biodegradability, and nontoxicity, which allow it to perform in recovery therapies for different tissues. Inorganic materials can also be incorporated, improving physical properties and developing enhanced materials. Karbowniczek et al. (2022) were able to successfully add ceramic nanoparticles of hydroxyapatite (HA) and titanium dioxide (TiO_2) into PHBV scaffolds. The results showed that the incorporation of HA significantly increased the mechanical properties of the material, while TiO_2 addition reduced these properties. However, the best results were achieved when both nanoparticles were incorporated into PHBV scaffolds. The authors related this behavior to the better distribution presented by hydroxyapatite than that presented by titanium dioxide. In addition, HA formed smaller agglomerations. Larger agglomerations formed by TiO_2 were related to a defect-like behavior in the structure, thus reducing its mechanical resistance. Fig. 6.2 presents the structure of scaffolds of different compositions.

The coating of compounds with magnetic and superparamagnetic activity is also a part of PHBV possible employment. Magnetic nanoparticles have several applications for scientific and clinical purposes. They may be used as biosensors, protein and cell separation systems, and magnetic carriers for hyperthermia and tissue-specific drug delivery (Vilos et al., 2013). An efficient coating of the magnetic material, such as iron oxide (magnetite), is important because, even though it is biocompatible, it is easily cleaned by the body, preventing it from being used in medical applications. The PHBV coating and its lower degrading rate allow the iron oxide to achieve its potential. However, to enhance PHBV coating properties, it is necessary to overcome its hydrophobicity. A possibility is the modification of its surface with a fatty acid, such as oleic acid or lauric acid (Idris et al., 2018). In fact, the surface modification of superparamagnetic iron oxide nanoparticles allowed for better encapsulation with PHBV. The resulting material showed great potential for drug delivery of tetracycling hydrochloride, being able to successfully be loaded with the drug and release it in a diffusion-controlled manner (Li et al., 2016).

Magnetic resonance imaging (MRI) is a nonradiating biomedical imaging technique where gadolinium is currently used as a contrast agent. However, magnetite nanoparticles have been extensively tested as

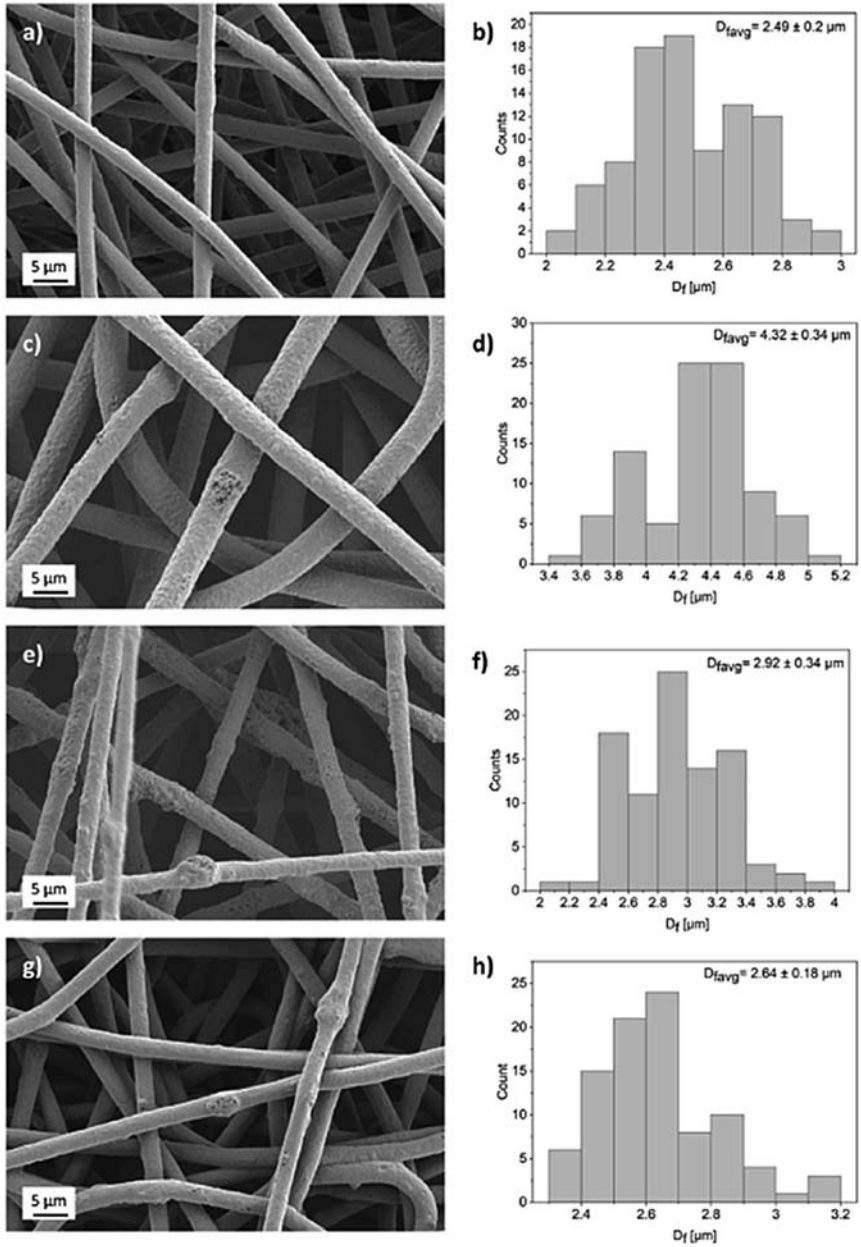

Figure 6.2 SEM micrographs of electrospun nanofiber morphology and corresponding histograms of their fiber diameters: (a, b) PHBV; (c, d) PHBV + HA; (e, f) PHBV + TiO_2; and (g, h) PHBV + HA + TiO_2. *(Source: Karbowniczek et al. (2022).)*

replacements because they present higher magnetic susceptibility among other advantages. In addition, when working with sufficiently small particles, it is possible to orient each particle by using an external magnetic field, causing them to lose their magnetic stability in the process. Changing the magnetization direction several times during a measurement interval will make the measurement zero at zero external fields. This phenomenon is called superparamagnetism. Superparamagnetic particles respond rapidly to an external field, which can be used to heat up the surrounding tissue, thus generating hyperthermia. This behavior shows that nuclear MRI is a promising tool for cancer therapy.

PHBV/PLA multifilament fibers have been also a potential material for medical sutures. He et al. (2014) described the use of the filament for muscular and subcutaneous tissue sutures in rats. No toxic symptoms were noticed at the implantation sites. The presence of inflammation was much less severe as compared to the control sample, a commercial alternative. Signs of polymer degradation started to appear 6 weeks after the procedure. From 12 to 48 weeks, the filament was loosened and lost its bundle structure but kept a uniform diameter. The results showed that PHBV compounds presented superior biocompatibility and its degradation products, such as 3-hydroxybutyrate (3-HB), 3-hydroxyvalerate (3-HV), and 3-hydroxyhexanoate (3-HHx), were completely nontoxic and even beneficial for the growth of vascular smooth muscle cells.

PHBV compounds can also be used as controlled drug-delivery systems. Prodigiosin (PG) is a bacterial pigment with strong anticancer activity. When incorporated into the biopolymer, it affected its thickness, making it more compact, but with a rougher surface and more distinctive topographical features. The primary role of a drug-delivery system is to provide controlled drug release in terms of time and location; at the same time, it should prevent the drug from suffering premature metabolic degradation, increase its bioavailability, and prevent drug availability fluctuation. The PG incorporation in PHBV resulted in film samples with improved physical properties and functionality in comparison with PHBV alone. The treatment with PHBV did not have any effect on cancer cells. However, all samples containing PG exhibited statistically significantly higher anticancer effects. Better anticancer potential was observed with higher concentrations of PG. PG exhibits strong anticancer activity against HCT116, colon cancer cells, according to its concentration. Compounds used in anticancer therapies are usually highly toxic and hydrophobic, so PHAs are suitable carriers for this type of drug-delivery system.

Bacterial pigment PG was successfully incorporated into PHBV. Apart from conferring a lively color to the compound, the incorporation improved not only the biopolymer's physical properties but also its functionality. It has affected PHBV's degree of crystallinity, thermal stability, and morphology. Films were also cytotoxic against cancer cells, indicating that the resulting material might be used in anticancer therapy (Ponjavic et al., 2023).

6.5 Conclusion

PHAs are being consolidated as interesting alternatives to fossil-derived polymers in medical and biomedical applications. Their set of characteristics are very interesting in this scenario, because they combine good mechanical properties with biodegradability and biocompatibility; thus, PHAs are reported in the literature in applications such as sutures, electrically conductive material for composites, bone tissue engineering and drug-delivery goals, fibrous membranes, composite coatings for metallic implants, and finally as components for composite blends aimed at additive manufacturing. The global market displays positive signs, reaching monetary values of up to USD 90 million in 2021 and CAGRs in the order of 9%–10% until 2030. Therefore, this class of biodegradable polymers is expected to experience continuous growth in the next decade and to replace a number of traditional polymers already in use in pharmaceutical, medical, and biomedical applications.

References

Ankush, K., Pugazhenthi, G., Vasanth, D., 2022. Fabrication and properties of polyhydroxybutyrate/kaolin nanocomposites and evaluation of their biocompatibility for biomedical applications. J. Appl. Polym. Sci. 139 (11), e51803. https://doi.org/10.1002/app.51803.

Data Bridge Market Research (Gurgaon), 2022. Global Polyhydroxyalkanoates (PHA) Market: Industry Trends and Forecast to 2029. Industry Trends and Forecast to 2029. Available at: https://www.databridgemarketresearch.com/reports/global-polyhydroxyalkanoate-pha-market#74848. (Accessed 12 May 2023).

Deng, Y., Lin, X.-S., Zheng, Z., Deng, J.-G., Chen, J.-C., Ma, H., Chen, G.-Q., 2003. Poly(hydroxybutyrate-co-hydroxyhexanoate) promoted production of extracellular matrix of articular cartilage chondrocytes in vitro. Biomaterials 24, 4273–4281. https://doi.org/10.1016/S0142-9612(03)00367-3.

El-Hadi, A.M., Elbary, A.M.A., 2018. Design of the electrically conductive PHB blends for biomedical applications. J. Mater. Sci. Mater. Electron. 29, 16496–16506. https://doi.org/10.1007/s10854-018-9743-3.

Global Market Insights (Selbyville, Delaware), 2022. Polyhydroxyalkanoate (PHA) Market Size – By Product (Short Chain Length, Medium Chain Length, Long Chain Length), PHA Type, Production Methods (Sugar Fermentation, Vegetable Oil Fermentation, Heterogeneous Waste Streams), Application & Forecast, 2022–2030. Available at: https://www.gminsights.com/industry-analysis/polyhydroxyalkanoate-market. (Accessed 10 May 2023).

He, Y., Hu, Z., Ren, M., Ding, C., Chen, P., Gu, Q., Wu, Q., 2014. Evaluation of PHBHHx and PHBV/PLA fibers used as medical sutures. J. Mater. Sci. Mater. Med. 25 (2), 561–571. https://doi.org/10.1007/s10856-013-5073-4.

Idris, M.I., Zaloga, J., Detsch, R., Roether, J.A., Unterweger, H., Alexiou, C., Boccaccini, A.R., 2018. Surface modification of SPIONs in PHBV microspheres for biomedical applications. Sci. Rep. 8 (1), 7286. https://doi.org/10.1038/s41598-018-25243-9.

Kalia, V.C., Patel, S.K.S., Lee, J.-K., 2023. Exploiting polyhydroxyalkanoates for biomedical applications. Polymers 15, 1937. Available at: https://www.mdpi.com/2073-4360/15/8/1937.

Kaniuk, Ł., Stachewicz, U., 2021. Development and advantages of biodegradable PHA polymers based on electrospun PHBV fibers for tissue engineering and other biomedical applications. ACS Biomater. Sci. Eng. 7, 5339–5362. https://doi.org/10.1021/acsbiomaterials.1c00757.

Karbowniczek, J.E., Ura, D.P., Stachewicz, U., 2022. Nanoparticles distribution and agglomeration analysis in electrospun fiber based composites for desired mechanical performance of poly(3-hydroxybuty-rate-co-3-hydroxyvalerate (PHBV) scaffolds with hydroxyapatite (HA) and titanium dioxide (TiO2) towards medical applications. Compos. B Eng. 241, 110011. https://doi.org/10.1016/j.compositesb.2022.110011.

Köse, G.T., Kenar, H., Hasirci, N., Hasirci, V., 2003. Macroporous poly(3-hydroxybutyrate-co-3-hydroxyvalerate) matrices for bone tissue engineering. Biomaterials 24 (11), 1949–1958. https://doi.org/10.1016/s0142-9612(02)00613-0.

Lam, W., Wang, Y., Chan, P.L., Chan, S.W., Tsang, Y.F., Chua, H., Yu, P.H.F., 2017. Production of polyhydroxyalkanoates (PHA) using sludge from different wastewater treatment processes and the potential for medical and pharmaceutical applications. Environ. Technol. 38, 1779–1791.

Li, W., Zaloga, J., Ding, Y., Liu, Y., Janko, C., Pischetsrieder, M., Alexiou, C., Boccaccini, A.R., 2016. Facile preparation of multifunctional superparamagnetic PHBV microspheres containing SPIONs for biomedical applications. Sci. Rep. 6, 23140. https://doi.org/10.1038/srep23140.

Lin, X., Li, S., Wang, Y., Yang, X., Jung, J., Li, Z., Ren, X., Sun, Y., 2021. Fabrication of pH-responsive hydrophobic/hydrophilic antibacterial polyhydroxybutyrate/poly-ε-caprolactone fibrous membranes for biomedical application. Mater. Chem. Phys. 260, 124087. https://doi.org/10.1016/j.matchemphys.2020.124087.

Liu, D., Long, W., Wu, M., Qi, K., Pu, J., 2019. Microstructure evolution and lifetime extension mechanism of Sn-added Fe-based pre-alloy brazing coating in diamond tools. Coatings 9 (6), 350. https://doi.org/10.3390/coatings9060350.

Ma, X., Lv, Y., Gao, Z., Cheng, G., 2011. Surface modification of biomedical magnesium alloys by PHB. Adv. Mater. Res. 146–147, 1170–1173. https://doi.org/10.4028/www.scientific.net/AMR.146-147.1170.

Marketsandmarkets (Pune, Maharashtra), 2022. Polyhydroxyalkanoate (PHA) Market: By Type, Production Methods, Application and Region – Global Forecast to 2027. Available at: https://www.marketsandmarkets.com/Market-Reports/pha-market-395.html. (Accessed 29 May 2023).

Mathina, M., Shinyjoy, E., Ramya, S., Kavitha, L., Gopi, D., 2022. Multifunctional crab shell derived hydroxyapatite/metal oxide/polyhydroxybutyrate composite coating on

316L SS for biomedical applications. Mater. Lett. 313, 131701. https://doi.org/10.1016/j.matlet.2022.131701.

Meng, W., Xing, Z.C., Jung, K.H., Kim, S.Y., Yuan, J., Kang, I.K., Yoon, S.C., Shin, H.I., 2008. Synthesis of gelatin-containing PHBV nanofiber mats for biomedical application. J. Mater. Sci. Mater. Med. 19 (8), 2799–2807. https://doi.org/10.1007/s10856-007-3356-3.

Mukherjee, C., Varghese, D., Krishna, J.S., Boominathan, T., Rakeshkumar, R., Dineshkumar, S., Brahmananda Rao, C.V.S., Sivaramakrishna, A., 2023. Recent Advances in Biodegradable Polymers – Properties, Applications and Future Prospects. Elsevier Ltd.

Norhafini, H., Thinagaran, L., Shantini, K., Huong, K.H., Syafiq, I.M., Bhubalan, K., Amirul, A.A., 2017. Synthesis of poly(3-hydroxybutyrate-co-4-hydroxybutyrate) with high 4HB composition and PHA content using 1,4-butanediol and 1,6-hexanediol for medical application. J. Polym. Res. 24, 189. https://doi.org/10.1007/s10965-017-1345-x.

Ponjavic, M., Malagurski, I., Lazic, J., Jeremic, S., Pavlovic, V., Prlainovic, N., Maksimovic, V., Cosovic, V., Atanase, L.I., Freitas, F., Matos, M., Nikodinovic-Runic, J., 2023. Advancing PHBV biomedical potential with the incorporation of bacterial biopigment prodigiosin. Int. J. Mol. Sci. 24, 1906. https://doi.org/10.3390/ijms24031906.

Pryadko, A.S., Botvin, V.V., Mukhortova, Y.R., Pariy, I., Wagner, D.V., Laktionov, P.P., Chernonosova, V.S., Chelobanov, B.P., Chernozem, R.V., Surmeneva, M.A., Kholkin, A.L., Surmenev, R.A., 2022. Core-shell magnetoactive PHB/gelatin/magnetite composite electrospun scaffolds for biomedical applications. Polymers 14, 529. https://doi.org/10.3390/polym14030529.

Rodríguez-Contreras, A., Marqués-Calvo, M.S., Gil, F.J., Manero, J.M., 2016. Modification of titanium surfaces by adding antibiotic-loaded PHB spheres and PEG for biomedical applications. J. Mater. Sci. Mater. Med. 27, 124. https://doi.org/10.1007/s10856-016-5723-4.

Shishatskaya, E.I., Khlusov, I.A., Volova, T.G., 2006. A hybrid PHB–hydroxyapatite composite for biomedical application: production, in vitro and in vivo investigation. J. Biomater. Sci. Polym. Ed. 17 (5), 481–498. https://doi.org/10.1163/156856206776986242.

Stratview Research (Detroit, Michigan), 2021. Polyhydroxyalkanoate (PHA) Market Size, Share, Trend, Forecast, & Industry Analysis – 2021–2026. Available at: https://www.stratviewresearch.com/1343/polyhydroxyalkanoate-(PHA)-market.html. (Accessed 12 May 2023).

Tebaldi, M.L., Maia, A.L.C., Poletto, F., DE Andrade, F.V., Soares, D.C.F., 2019. Poly(-3-hydroxybutyrate-co-3-hydroxyvalerate) (PHBV): current advances in synthesis methodologies, antitumor applications and biocompatibility. J. Drug Deliv. Sci. Technol. 51, 115–126. https://doi.org/10.1016/j.jddst.2019.02.007.

Transparency Market Research (Albany, New York), 2021. Polyhydroxyalkanoate Market. Available at: https://www.transparencymarketresearch.com/polyhydroxyalkanoate-market.html. (Accessed 12 May 2023).

Vilos, C., Gutiérrez, M., Escobar, R.A., Morales, F., Denardin, J.C., Velasquez, L., Altbir, D., 2013. Superparamagnetic Poly (3-hydroxybutyrate-co-3 hydroxyvalerate) (PHBV) nanoparticles for biomedical applications. Electron. J. Biotechnol. 16 (5). https://doi.org/10.2225/vol16-issue5-fulltext-8.

Volova, T., Shishatskaya, E., Sevastianov, V., Efremov, S., Mogilnaya, O., 2003. Results of biomedical investigations of PHB and PHB/PHV fiber. Biochem. Eng. J. 16, 125–133. https://doi.org/10.1016/S1369-703X(03)00038-X.

Wampfler, B., Ramsauer, T., Rezzonico, S., Hischier, R., Köhling, R., Thöny-Meyer, L., Zinn, M., 2010. Isolation and purification of medium chain length poly(3-hydroxyalkanoates) (mcl-PHA) for medical applications using nonchlorinated solvents. Biomacromolecules 11, 2716–2723. https://doi.org/10.1021/bm1007663.

Wang, Y.-W., Wu, Q., Chen, G.-Q., 2004. Attachment, proliferation and differentiation of osteoblasts on random biopolyester poly(3-hydroxybutyrate-co-3-hydroxyhexanoate) scaffolds. Biomaterials 25, 669–675. https://doi.org/10.1016/S0142-9612(03)00561-1.

Yang, M., Zhu, S., Chen, Y., Chang, Z., Chen, G., Gong, Y., Zhao, N., Zhang, X., 2004. Studies on bone marrow stromal cells affinity of poly (3-hydroxybutyrate-co-3-hydroxyhexanoate). Biomaterials 25, 1365–1373. https://doi.org/10.1016/j.biomaterials.2003.08.018.

Yuan, J., Xing, Z.-C., Park, S.-W., Geng, J., Kang, I.-K., Shen, J., Meng, W., Shim, K.-J., Han, I.-S., Kim, J.-C., 2009. Fabrication of PHBV/keratin composite nanofibrous mats for biomedical applications. Macromol. Res. 17, 850–855. https://doi.org/10.1007/BF03218625.

This page intentionally left blank

CHAPTER 7

Synthesis and applications of bioresorbable polymers for tissue engineering scaffolds

Emenike George Okonkwo[1,2], Jesus Romo-Rico[3], Chinemerem Jerry Ozoude[2,5] and Kingsley Job Obasi[4]

[1]College of Science and Engineering, James Cook University, Townsville, QLD, Australia; [2]Department of Metallurgical and Materials Engineering, University of Nigeria, Nsukka, Enugu, Nigeria; [3]Electronics Materials Lab, College of Science and Engineering, James Cook University, Townsville, QLD, Australia; [4]Department of Mechanical Engineering, University of Nigeria, Nsukka, Enugu, Nigeria; [5]Department of Materials Science and Engineering, University of North Texas, Denton, TX, United States

7.1 Introduction

Loss of tissues and organs to injuries and degeneration caused by chronic diseases are the most prevalent challenges in modern medicine. Although common, conventional treatment approaches such as removal of damaged tissues/organs, replacement and regeneration via grafting, transplants, and biomedical implants have several obvious drawbacks, including donor accessibility, probable immuno-induced rejection of implants/transplants, poor compatibility, implant vulnerability, poor integration, and ethical/religious issues, among others (Francis et al., 2023; Hajebi et al., 2020; Saska et al., 2021). This often leads to loss of life or a significant reduction in health-related quality of life. A better therapy option with fewer risks is to replace or rejuvenate damaged tissues by utilizing biocompatible platforms that can sustain cell development or contain living cells (Hajebi et al., 2020; Naseem et al., 2022; Saska et al., 2021).

Tissue engineering (TE), a multidisciplinary field that integrates engineering, chemistry, and biology, has emerged as an alternative to traditional methods of treating damaged tissues (Capuana et al., 2022; Emily Hartley et al., 2022; Hetal Patel et al., 2011). Herein, 3-D structures that support cell growth are used. These structures, called scaffolds, are designed to imitate the extracellular environment while providing mechanical support, promoting cellular growth and proliferation by fostering cell adhesion and

Bioresorbable Polymers and their Composites
ISBN 978-0-443-18915-9
https://doi.org/10.1016/B978-0-443-18915-9.00010-0
© 2024 Elsevier Ltd.
All rights reserved.

movement, and aiding the diffusion of nutrients and products and overall tissue development (Capuana et al., 2022; Duan et al., 2022). Scaffolds are generally made from biocompatible biomaterials (Hetal Patel et al., 2011). However, advances in the mechanistic understanding of the interactions occurring in the extracellular matrix and the need to avoid secondary surgical operations to remove temporary implants have led to increased demand for materials that can be tailored to suit specific needs. These needs include biodegradability, in vivo resorption, compatible elastomeric properties, etc. (Duan et al., 2022; Kennedy et al., 2023)

Bioresorbable polymers have emerged as a special class of biodegradable and biocompatible materials that can be tailored to meet the current needs of TE scaffolds (Hajebi et al., 2020; Mahdavi et al., 2017). Bioresorbable polymer scaffolds (BPSs) can be tuned to undergo mediated hydrolytic or enzymatic degradation to form nontoxic products that the body can eliminate via excretion or metabolic pathways (Afshar et al., 2022; Mendibil et al., 2019). The emergence of BPSs has led to a reduction in the number of surgeries required during tissue regeneration and reduced use of suppressant drugs (Chew et al., 2017; Tawade et al., 2022).

As polymers, the synthesis of BPSs typically involves the use of chemical or physical methods. Herein, traditional techniques such as extrusion, injection molding, among others are dominant. However, the increasing need for tailoring to suit specific applications and cellular environments, high sensitivity of some bioresorbable polymers to traditional techniques, etc. have prompted the emergence of newer techniques such as electrospinning, 3D and 4D printing, and lithography (Kirillova et al., 2021; Saska et al., 2021). The selection of an appropriate bioresorbable polymer and fabrication technique is crucial to successful tissue regeneration, as properties of scaffolds are dependent on the choice of material and fabrication technique. This chapter offers an overview of the traditional and current methods of synthesizing BPSs and areas of application. The influence of fabrication technique on the area of application and degradation of the polymers are emphasized. Future perspectives on the synthesis and applications of BPSs are also discussed.

7.2 Synthesis of bioresorbable polymers

The synthesis of bioresorbable polymers for scaffolds involves a combination of contemporary materials science and biomedical engineering techniques to produce polymers with specific characteristics that can be tailored

to a broad range of tissue engineering applications. It is widely acknowledged that achieving a balance between the required structural and dimension properties, biodegradability, and biocompatibility is essential for the performance of tissue scaffolds (Kirillova et al., 2021; Li et al., 2019a). Several techniques have been developed and conventional fabrication techniques modified to suit the increasing needs of modern tissue scaffolds. This section presents the different methods of synthesizing BPSs. A comparison of various approaches is made to present the distinct benefits and drawbacks of various methods.

7.2.1 Molding

Compression and injection molding are traditional polymer fabrication techniques (Okonkwo et al., 2020). Compression molding utilizes both heat and pressure to melt a thermoplastic polymer or cure a partly polymerized thermosetting resin in a mold (Okonkwo et al., 2020; Viera Rey and St-Pierre, 2019). It has a short cycle time and low material loss. In injection molding, pressurized polymer melts are fed into a mold to solidify and form the desired shape. An advanced form of injection molding is reaction injection molding, which utilizes low viscous resins and allows for in situ polymerization to occur in the mold. Due to their simplicity, these two melt processing techniques have been used in fabricating scaffolds from an array of bioresorbable polymer-based scaffolds and composites (Kirillova et al., 2021; Quiles-Carrillo et al., 2018; Viera Rey and St-Pierre, 2019).

Zhang et al. (2016) reported the fabrication of a high-modulus composite scaffold made of PLLA, PLGA, and HA for healing cranial bone defects via a high-pressure compression molding and salt leaching technique (Zhang et al., 2016). Fabricated scaffolds were observed to possess compressive strength and modulus comparable to cranial bones and excellent osteogenic properties. Salmoria et al. (2017) reported the fabrication of PCL and PCL/ibuprofen (IBP) with excellent cytocompatibility and drug-release properties via injection molding (Salmoria et al., 2017). The fabrication of PLLA-based noncytotoxic interference screws via injection molding has also been reported (Brown and Farrar, 2013).

Compression and injection molding allow for the production of complex shapes with high mechanical properties from all kinds of bioresorbable polymers. Both processes are easy to automate and scale up. Nonetheless, inhomogeneity and unsteady clamping pressure during the fabrication of scaffolds from highly viscous polymer melts, high tooling costs, entrapment of air bubbles, polymer degradation at high temperature and pressure, and

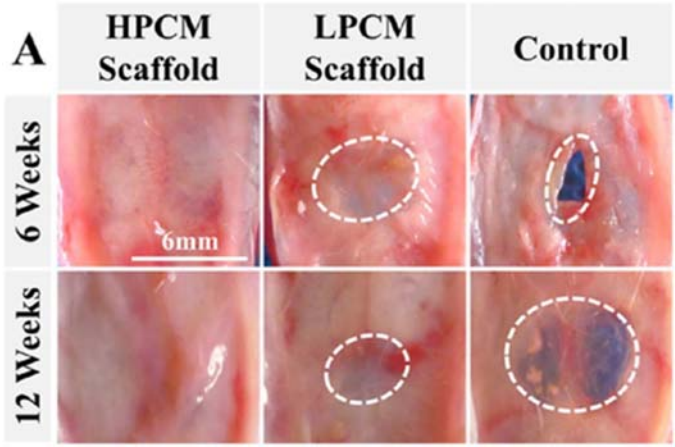

Figure 7.1 Pictures of revived skull defects at 6 and 12 weeks after implantation of high-pressure compression-molded (HPCM) polymeric biodegradable scaffolds. *(© 2016, American Chemical Society (Zhang et al., 2016).)*

residence time are some major drawbacks (Pertici, 2017; Viera Rey and St-Pierre, 2019). Processing parameters (pressure, temperature, and time) have been shown to significantly influence the properties and performance of BPSs fabricated via these molding techniques. PLLA/PLGA/HA scaffolds fabricated at high pressure were found to exhibit more impressive mechanical, cytocompatibility, and tissue regenerative properties as compared to those fabricated under lower pressure (Zhang et al., 2016) (Fig. 7.1). Injection molding has also been shown to impact the crystallinity of PLLA screws (Sadeghi-Avalshahr et al., 2016). As such, variants of the original techniques including the use of cyclic pressure, which Betanzos et al. observed can lead to a 30% improvement in strength as compared to conventional compression molded scaffolds and microwave-assisted compression molding (Barrera Betanzos et al., 2016; Singh et al., 2019), have been suggested. Furthermore, the molding process might be unable to produce scaffolds with a similar degree of porosity and interconnectivity as other methods, such as electrospinning. This is an important consideration for tissue engineering applications, as porosity and interconnectivity are critical for cell infiltration and proliferation. Therefore, molding techniques are normally combined with other techniques including particle leaching and supercritical gas foaming (Ozkoc et al., 2009; Zhang et al., 2016).

7.2.2 Melt extrusion

In melt extrusion, profiles (sheet, porous fiber, film, etc.) are made by forcing polymer melt through a die under regulated conditions. Extrusion machines adopt either the ram or screw extrusion approach, of which twin-screw extrusion is the most common and widely used mixing and compounding method. Extrusion is a widely used technique for fabricating bioresorbable polymer composites. It is used in making precursor (feed material) for other techniques (Casarin et al., 2011). The heating and agitation lead to the production of a homogeneous mix and eliminate the need for drying. In addition, no solvent is required, hence there is lower toxicity and no need for later washing/cleaning (Kenny et al., 2015).

Although solvent-free nanofibers can be produced via extrusion, it is specific to thermoplastic polymers. In addition, bioresorbable polymers are heat- and moisture-sensitive and hence need not be kept molten for a long time. This and the inability to produce scaffolds with consistent pores are some of the drawbacks of the melt extrusion technique. As such, it is often merged with other techniques such as particle leaching. Mendibil et al. (2019) reported the fabrication of PLCL bioresorbable polymer scaffold using sodium chloride as porogen particles. Long (300 mm) and thick (400 μm) microporous PLCL tubes with similar mechanical properties to nerves and veins were achieved. The authors noted that the particle size and proportion of NaCl porogen affected the scaffold's porosity and mechanical properties.

7.2.3 Solvent casting and particle leaching

Another straightforward method for creating porous scaffolds is solvent casting. Solvent casting involves dissolving a polymer in an appropriate organic solvent to create a slurry, casting the slurry on a membrane, and then evaporating the solvent (Kirillova et al., 2021; Viera Rey and St-Pierre, 2019). Solvent casting can be used to produce drug-loaded scaffolds or blend polymers. Particle leaching can also be used to introduce porosity in nonporous prefabricated scaffolds. Herein, particulates (porogens) are added to a polymer melt or slurry prior to casting and, afterward, washed out to yield well-defined pores. Together with particle leaching, porous scaffolds with interconnected pores can be made using this technique (Kirillova et al., 2021). Particle leaching is often called salt leaching because NaCl, owing to its high thermal stability, resistance to organic solvents, and solubility in water, is the most widely used porogen (Modolo et al., 2022; Ozkoc et al., 2009). Nonetheless, the use of organic particles including sucrose, gelatin,

and stearic acid has been reported (Kirillova et al., 2021; Viera Rey and St-Pierre, 2019). This technique presents a simple approach to engineer interconnected pores; however, the achieved pore size is influenced by the porogen size. The settling of the porogen during solvent evaporation can cause nonuniformity in the porosity of the scaffold. More importantly, this approach is not suitable for producing thick scaffolds because of the limitation on the thickness of the produced scaffolds (<3 mm). Due to the potential cytotoxicity of residual solvents and porogen, post-processing is frequently required (Viera Rey and St-Pierre, 2019).

7.2.4 Gas foaming

Porous structures with distinct and interconnected pores of precise sizes are essential for tissue vascularization. Gas foaming is another method often used to produce scaffolds. Herein, gas bubbles are blown into solid polymeric samples to form pores (de Matos et al., 2015). Various gases including supercritical CO_2 and N_2 have been used (Kosowska et al., 2022). Compared to solvent casting and particle leaching, no toxic chemical reagents that can cause cytotoxicity are used (Francis et al., 2023). It can also be performed at room temperature, although heating may be required if combined with molding techniques or for better pore formation (Kosowska et al., 2022).

Several research groups have combined gas foaming with other techniques to fabricate tailored scaffolds. Salerno et al. (2017) combined supercritical CO_2 gas foaming and freeze drying to synthesize scaffolds loaded with drugs (Salerno et al., 2017). In another study, a combination of supercritical CO_2 gas foaming and particulate leaching was used to fabricate a bimodal PCL scaffold with both macro- and microporosity (Salerno et al., 2012). It should be noted that foaming parameters and choice of porogen can influence the architecture, crystallinity, and mechanical properties of the fabricated scaffold. Kosowska et al. (2022) investigated the influence of foaming parameters and porogen type on the properties of PCL. These authors observed that pore morphology, including diameter and density, was dependent on the porogen, whereas mechanical strength and polymer crystallinity depend on foaming parameters such as the saturation time, temperature, and pressure. Porogens increased the nucleation sites, and improved both mechanical strength and degree of crystallization.

One major drawback of gas foaming is the poor control of the pores' characteristics. Similarly, reproducibility of pore architecture is poor. While

the use of microfluidic devices might mitigate this challenge, it will also increase the processing cost.

7.2.5 Electrospinning

Electrospinning is another common method of fabricating biodegradable scaffolds for tissue engineering applications. An electric field is utilized in electrospinning to deposit a polymer solution or melt through a small nozzle, creating a stream of polymer fibers. These fibers are then deposited on a grounded collector to form a nonwoven or woven scaffold (Lannutti et al., 2007). One of the main benefits of the electrospinning technique is the capacity to create highly porous scaffolds with precise control over the pore size and interconnectivity. Scaffolds of various shapes can be formed by altering the collector, which is a critical feature for TE applications, as shapes of scaffolds allow for better cell infiltration and proliferation (Ameer et al., 2019). When combined with solvent casting and particulate leaching, scaffolds with specific mechanical properties can be created.

Electrospinning has been used to fabricate scaffolds from an array of biodegradable polymers, including polyglycolic acid (PGA), polylactic acid (PLA), poly(ethylene oxide) (PEO), polycaprolactone (PCL), as well as composites and blends (Kirillova et al., 2021; Zhao et al., 2019). An electrospun composite scaffold made from a blend of acrylated L-lactide-co-trimethylene carbonate (aPLA-co-TMC) and polycaprolactone (PCL) was found to possess mechanical properties akin to human blood vessels. The scaffold promoted the development and adherence of human mesenchymal stem cells and so has potential in blood vessel repair (Stefani and Cooper-White, 2016). Electrospun poly-4-hydroxybutyrate (P4HB) nanofiber membranes have been reported to exhibit good mechanical properties, degradation behavior, and cytocompatibility with neural cells, and thus is a potential biodegradable substitute for dural tissue in neurosurgery (Ma et al., 2021). Another study reported the fabrication of a novel hydroxy-functionalized polyester with poly[(hydroxymethyl glycolide)-co-(e-caprolactone)] (pHMGCL) scaffold via electrospinning. In vitro tests showed that they degrade faster than a similar scaffold made from PCL. In addition, chondrocytes adhered to the fibers and the presence of important cartilage-related molecules like GAGs and collagen II was noticed. The excellent degradation, cell adhesion, and differentiation properties of electrospun pHMGCL scaffolds attests to their prospective role in tissue engineering cartilage (Seyednejad et al., 2011). A study by Beck et al. (2021) found that electrospun PU-PCL scaffold loaded with sacrificial PEO

particles showed potential as a scaffold for the correction of congenital heart defects (CHDs) (Beck et al., 2021). PEO particles improved pore size, and decreased stiffness and the inflammatory response of the scaffold, which led to better cell infiltration when compared to the PU—PCL blend without PEO particles.

Electrospun scaffolds have also been reported to possess wound-healing properties. Electrospun PCL/Gel scaffold, when used as a sublayer in a bilayer dressing in an animal wound model, was observed to accelerate wound closure and collagen deposition. This can be ascribed to the excellent biodegradability, biocompatibility, and significant antibacterial activity of the scaffolds (Eskandarinia et al., 2020). A similar observation was noted in electrospun PCL—collagen scaffold. The scaffold mimicked the natural architecture of skin and exhibited similar mechanical and physical attributes. When cocultured with keratinocytes and fibroblasts to promote growth and ECM deposition, the scaffolds promoted regeneration of all three skin layers without scar formation (Ghosh et al., 2022).

Several process parameters, including the nature of the polymer, voltage, solvent, needle dimension, needle-to-collector distance, flowrate, humidity, presence or absence of a rotating collector drum, etc., determine the diameter and alignment of electrospun fibers. Both fiber diameter and alignment affect the degree of cell attachment and proliferation.

7.2.6 3D printing

3D printing is a versatile method of fabricating bioresorbable polymeric TE scaffolds (Sousa et al., 2022). It enables the development of intricate and very permeable scaffolds with precise control over both size and shape (Choudhary et al., 2022). Herein, the scaffold is built layer by layer using a resorbable polymer material (Zopf et al., 2015). The most common polymers for 3D-printed BPSs for bone and cartilage applications are PLA, PGA, and PCL, and a variety of blends (Yeo et al., 2021; Zhang et al., 2021; Shuai et al., 2021; Chen et al., 2020). For instance, interference screws with excellent degradation and bone tissue production properties for bone repairs were successfully fabricated from PDLLA and PDLLA-β-TCP blend via 3D-printing (Shuai et al., 2021). Similarly, 3D printing was able to fabricate a PGA/hydroxyapatite scaffold that promoted bone regeneration and improved bone mineral density (Yeo et al., 2021). An in vivo study of the degradability of 3D-printed interference screws made PDLLA and PDLLA and beta-tricalcium phosphate (beta-TCP) was also observed

to exhibit good degradability, and enhanced the production of bone tissues in sheep (ewes) while showing no adverse histological reactions (Scorsato et al., 2022).

3D-printed scaffolds are easily tailored to meet specific needs. To improve their biocompatibility, Chen et al. (2020) successfully modified the biocompatibility of the tarsal plate scaffolds created using 3D printing by coating them with a matrix of adipose-derived mesenchymal stromal cells. The scaffolds exhibited high biocompatibility with sebocytes, decreased inflammatory and apoptotic gene expression, as well as promoted neutral lipid secretion, thus showcasing the potential of this scaffold as a suitable replacement for the tarsal plate (Chen et al., 2020). Yang et al. (2016) showed that the antibacterial and osteogenic activity of a 3D-printed poly(lactic-co-glycolic acid) (PLGA)—hydroxyapatite (HA) composite can be enhanced by grafting stem cells on the fabricated porous scaffold. The scaffold exhibited improved biocompatibility suitable for orthopedic applications with the presence of stem cells significantly increasing the scaffold's antibacterial property and osteogenic activity (Yang et al., 2016) (Fig. 7.2).

3D printing of resorbable scaffolds offers several advantages over traditional fabrication methods, including the ability to create complex, highly porous structures with explicit control of the shape and size of the scaffold. It also allows for a high degree of customization, making it possible to create

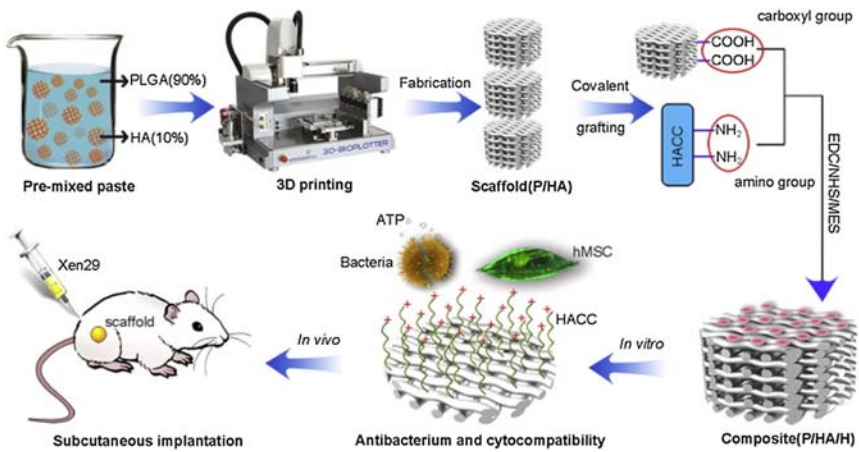

Figure 7.2 Synthesis and antibacterial mechanism of 3D-printed PHA/H composite scaffolds. *(© 2016 Acta Materialia Inc. Published by Elsevier (Yang et al., 2016).)*

scaffolds that can be adapted to the unique requirements of the patient and the tissue engineering application.

7.2.7 Hybrid techniques

The drawbacks and strengths of several techniques in synthesizing tailored scaffolds led to interest in the hybridization of conventional techniques and the development of newer ones. A soft lithographic technique such as microcontact printing, which permits the application of a molecular ink transferred from an elastomeric stamp to a surface, has been shown to be a simple and effective approach to tailor scaffolds. Altomare et al. (2010) reported the microprinting of fibronectin stripes of varied width on L-lactide/trimethylene carbonate copolymer (PLLA-TMC) films. Microscopic examination revealed a stable pattern of fibronectin on the PLLA-TMC surface. The C2C12 cells were well aligned along the pattern 24 h after seeding, and cell alignment was observed after 7 days, which shows that fibronectin patterning can induce cell alignment and improve myotube formation (Altomare et al., 2010).

Some nonconventional techniques and a blend of fabrication methods have been utilized to create bioresorbable polymer scaffolds with specific properties and geometries capable of being used in a variety of tissue engineering applications. For example, vacuum heating-press sintering was used to fabricate a b-TCP-based composite as scaffold for bone defect repair. The presence of magnesium in the scaffold improved the degradation and mechanical properties as well as the osteogenic activity of the composites. In addition, in vivo studies have revealed that these composites are promising materials for clinical bone repair (Yao et al., 2023). Shishatskaya et al. (2022) employed a combination of solvent casting and electrostatic spinning techniques in fabricating films and nanomembranes of poly-3-hydroxybutyrate [P(3HB)] and its copolymers for skin regeneration. The films and nanomembranes exhibited biocompatibility and aided the adhesion, proliferation, and preservation of cells for nearly 1 week. Furthermore, the type 1 collagen-coated polymeric nanomembranes were effective in the regeneration of skin defects, notably the electrospun non-oriented nanomembranes of low-crystalline P(3HB-co-4HB) copolymers (Shishatskaya et al., 2022) (Fig. 7.3).

The thermally induced phase separation (TIPS) technique is another method for preparing scaffolds with linked porous structures. It has been successfully used to produce a BPS from PLGA and a combination of PLGA and polyethylene glycol (PEG) (Yousefi et al., 2019).

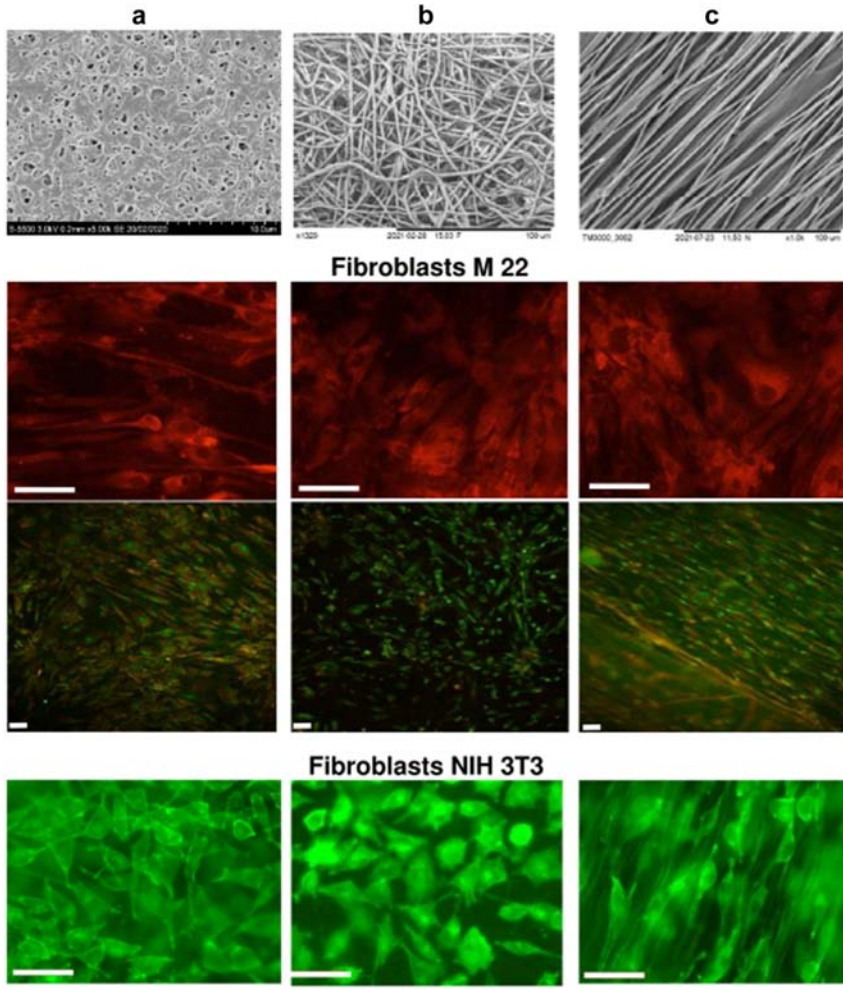

Figure 7.3 A combination of polymer casting and electrospinning were used to fabricate nanomembranes. This figure shows fibroblasts cultivated on P(3HB-co-4HB) polymer carriers: (a) Solvent-cast film; (b) random nanomembranes; (c) aligned nanomembranes. *(© 2022 by the authors (Shishatskaya et al., 2022).)*

7.3 Applications of bioresorbable tissue scaffold

Bioresorbable polymers have been utilized in different areas of tissue engineering ranging from wound dressing, skin regeneration, bone repair, to cartilage and other blood vessel regeneration (Hajebi et al., 2020). This section highlights some of the main areas of the applications of BPSs in

regenerative medicine with a focus on areas where the resorbability and mechanical properties of the polymer scaffolds play a critical role.

7.3.1 Vascular grafts and stents

Following their high tunability and resorbability, BPSs gained a lot of attention as next-generation materials for stents and grafts in the treatment of cardiovascular diseases. Against the drawbacks of traditional stents such as the risk of vascular inflammation, neoatherosclerosis, incomplete endothelialization, and poor suitability to noninvasive imagining, BPSs can provide transient support, allow for vasomotor function, maintenance of vessel geometry, and mitigate the occurrences of stent thrombosis in the hemodynamic environment (Jinnouchi et al., 2019; Sharma et al., 2018; Wiebe et al., 2014). Challenges of traditional grafts such as thromboembolic complications and calcification, and high failure rate can also be mitigated using these polymeric scaffolds. In addition, the growth of new tissue is also promoted, which mitigates the need for maintaining permanent grafts in the body.

The performance of BPSs as vascular grafts and stents has been extensively reported in in vivo and in vitro studies (Fukunishi et al., 2017; Nelson et al., 2008; Wiebe et al., 2014; Zamiri et al., 2010). Fukunishi et al. (2017) evaluated the performance of 3D-printed electrospun PGA/PLCL scaffolds as a bypass graft for the inferior vena cava (IVC) using a sheep model. The authors observed that all the animals survived the implantation, and no extracellular matrix deposition or endothelialization occurred. The fabricated scaffolds were almost resorbed at the end of the trial (6 months). In addition, the newly developed tissues exhibited similar mechanical properties as the native one. Zamiri et al. (2010) evaluated the biocompatibility of several BPSs for vascular stents in vitro and in vivo in pigs. In vitro studies showed that the fast-degrading PLGA materials showed significant mass loss in the first weeks, while PLA braids exhibited only minimal degradation. An in vivo study showed that tested polymers such as 10:90 L-PLGA and PDO with an absorption time of less than a year illustrated excellent vascular biocompatibility and hence are suitable for intravascular stents. Polak-Krasna et al. (2021) evaluated the behavior of medical-grade PLLA for medical stents under accelerated degradation conditions for absorbable stent application over a 112-day test period. The samples were found to consistently have lower molecular weights and only slightly altered mechanical characteristics in the first 30 days. A further decrease in molecular

weight and substantial reduction in tensile strain occurred after 70 days, while mechanical properties such as elastic modulus, yield, and tensile strength were unaffected. After 112 days, the samples became too brittle, thus indicating substantial loss of their load-bearing capacity. Across the test duration, the degree of crystallinity and melt temperature decreased and there were minor changes in glass transition temperature.

While these studies buttress the already established potentials of BPSs, some clinical trials such as Absorb BVS, Igaki-Tamai, ART-BRS, and DeSolve show that some complications attributable to scaffold design exist. To meet the radical strength requirement, BPSs are often designed to have a large strut thickness. However, delayed healing and risk of malapposition have been found to increase with strut thickness. It is pertinent to state that scaffold design and material selection will be key, as shown in on-going clinical trials (Fioretta et al., 2021; Jinnouchi et al., 2019). Herein, the incorporation of nanofillers to tailor the properties of already known polymers such as PLA, polymer blending, and virtual testing of cell shapes will be beneficial (Mahmud et al., 2021; Okereke et al., 2021).

7.3.2 Bone and cartilage tissue fixation

BPSs in the form of plates, screws, bars, and pins can be used as implants for bone and cartilage tissue repair, where they can provide mechanical support and accelerate the healing process. Time-dictated deterioration of mechanical properties due to degradation of BPSs averts stresses which are common during bone healing using conventional implants (Brown and Farrar, 2013). Different research groups have investigated the performance of BPSs in orthopedics. It is widely acknowledged that scaffolds made from bioresorbable polymers such as PLA and its derivatives possess properties that enhance bone tissue repair, and challenges such as low mechanical properties, poor osteogenic differentiation capacity, incompatible degradation rate, and acidic degradation product-induced inflammatory responses can occur. Using rabbits with distal ulna defect, Weng et al. showed that while PLLA/PCL and PLLA scaffolds can be used for bone regeneration, the degradation rate was low and the polymers lacked osteoinducibility (Weng et al., 2014). Surface modification with nanoparticles such as nano-bioactive glass, as reported by Mahdavi et al. (2017), can be used to improve the osteogenic differentiation capacity. Other $Ca_3(PO4)_2$-based compounds such as hydroxyapatite, β-TCP, and calcium sulfate either blended, coated, or grafted have also been reported to improve the

osteogenic properties of polymer scaffolds (Hussain et al., 2022). Recently, the addition of metals such as magnesium and metal oxides to the polymers has been used to improve both biocompatibility and mechanical properties. Chan et al. (2019) observed that the presence of oxides of hafnium, titanium, zirconium, and silicon in electrospun PLLA scaffolds improved both the mechanical and osteogenic properties of PLLA. Blending with other polymers has been utilized to tailor the degradation rate, mechanical properties, and nature of the formed degradation products. With more alkaline polymers such as PPC and PTMC, less acidic degradation products with a reduced risk of inflammatory reactions are achieved. Hua et al. (2009) observed that PLLA blended with PTMC reduced the acidity of the formed degradation product. Further, the addition of PGA-TMC into PLLA-TMC enabled the fabrication of scaffolds with improved degradability and mechanical properties suitable for bone tissue engineering applications. These scaffolds can be fabricated through a low-temperature 3D-printing method (Hu et al., 2023).

Scaffolds such as polycaprolactone have been reported to find application in cartilage regeneration. Gruber et al. (2022) showcased the potential of PCL scaffolds embedded with PLA microspheres bearing decellularized cartilage matrix for osteochondral regeneration. The scaffolds were observed to provide mechanical support and to aid seeded mesenchymal stem cells in forming mesenchymal condensates, which is a biochemical marker of cartilage development (Gruber et al., 2022). A chitosan/poly ε-caprolactone polymer blend was reported to facilitate neo-cartilage formation (Neves et al., 2011). PCL increased the mechanical properties and reduced the swelling ratio of the scaffold. Zhao et al. found a PLGA scaffold bearing icariin to be effective in inhibiting the progression of osteoarthritis. A histological evaluation revealed that the scaffold repressed the resorption of subchondral bone trabeculae and preserved the shape of the articular cartilage (Zhao et al., 2019).

7.4 Future trends

The field of scaffold fabrication is constantly evolving, with new advancements in materials science, biotechnology, and manufacturing technology shaping the future of this subject. One of the key trends in scaffold fabrication is biomimicry, where researchers aim to develop scaffolds that mimic the structure, composition, and mechanical properties of the native extracellular matrix (ECM) of the tissue being regenerated. By replicating

the natural environment of the tissue, these scaffolds can promote cell migration, proliferation, and differentiation, leading to more efficient and effective tissue regeneration.

Another trend in scaffold fabrication is the development of tissue-specific scaffolds, designed to meet the specific needs of different types of tissue such as bone, cartilage, or nerve tissue. Tailoring the environment to the specific needs of cells improves the efficiency and effectiveness of tissue regeneration. This, in combination with bioprinting, where functional tissue constructs bear living cells together with a hydrogel support material are printed using 3D printing technology, will further enhance the field of TE. Bioprinting enables precise control over the mechanical and surface properties, as well as the degradation rates of the scaffold, thus making it ideal for specific TE applications.

Smart scaffolds are also becoming increasingly popular. These are designed to react to changes in temperature, pH, or specific molecules in their environment. The poor adaptability of traditional scaffolds is one of their main limitations, hence engineering scaffolds with the ability to change will ultimately improve their efficiency and effectiveness in regenerating tissues. Similar to smart scaffolds, the use of nanotechnology to create scaffolds with precise control over the size, shape, and composition is a current trend that will continue to dominate. With nanotechnology, customized scaffolds can be easily made.

Composite scaffolds made through the combination of different materials such as polymers, ceramics, and natural materials is another important area of scaffold fabrication with huge prospects. Composite materials have been known for their exceptional properties (Aigbodion et al., 2019), thus, scaffolds with improved properties such as degradation rate, mechanical strength, and biocompatibility, that can further enhance tissue regeneration, can be made using composites. The future of scaffold fabrication will be marked by the increasing use of advanced materials and technologies to create scaffolds that are highly specific and customized to the needs of different types of tissue, leading to more efficient and effective tissue regeneration (Samadian et al., 2020).

7.5 Conclusion

Numerous methods, including molding, electrospinning, and 3D printing, are available for creating bioresorbable scaffolds; however, the properties of the scaffolds fabricated using these techniques are often limited. Therefore,

creating scaffolds with specific properties and geometries by combining different fabrication techniques will likely dominate the future of bioresorbable scaffolds for tissue engineering. By combining different methods, scaffolds with enhanced properties can be produced while inherent limitations of individual fabrication techniques are minimized. For example, electrospinning can be used to create scaffolds with high porosity, while solvent casting can be used to create scaffolds with more complex geometries and controlled pore sizes. By combining the two methods, it may be possible to produce scaffolds that have both high porosity and complex geometries (Li et al., 2019b). Similarly, the combination of microcontact printing with electrospinning or 3D printing could be used to create scaffolds that have specific patterns of growth factors or other molecules on the surface to promote cell adhesion and tissue growth (Si et al., 2022).

Besides the combination of fabrication techniques, the use of advanced materials such as biodegradable polymers with tunable mechanical and degradation properties is also likely to become more widespread in the future. The development of biodegradable polymers that can mimic the properties of natural tissue is an important goal in the field of tissue engineering, and the combination of different fabrication techniques with these advanced materials is likely to lead to the production of more effective scaffolds for an array of tissue engineering applications (Ciardulli et al., 2021).

The future of bioresorbable scaffolds will require a multidisciplinary approach, involving collaboration between materials scientists, engineers, and biologists, to fabricate scaffolds for effective regeneration of tissues.

References

Afshar, A., Gultekinoglu, M., Edirisinghe, M., 2022. Binary polymer systems for biomedical applications. Int. Mater. Rev. 1–41.

Aigbodion, V.S., Okonkwo, E.G., Akinlabi, E.T., 2019. Eco-friendly polymer composite: state-of-arts, opportunities and challenge. In: Sustainable Polymer Composites and Nanocomposites, pp. 1233–1265.

Altomare, L., Riehle, M., Gadegaard, N., Tanzi, M., Farè, S., 2010. Microcontact printing of fibronectin on a biodegradable polymeric surface for skeletal muscle cell orientation. Int. J. Artif. Organs 33 (8), 535–543.

Ameer, J.M., Pr, A.K., Kasoju, N., 2019. Strategies to tune electrospun scaffold porosity for effective cell response in tissue engineering. J. Funct. Biomater. 10 (3).

Barrera Betanzos, F., Gimeno-Fabra, M., Segal, J., Grant, D., Ahmed, I., 2016. Cyclic pressure on compression-moulded bioresorbable phosphate glass fibre reinforced composites. Mater. Des. 100, 141–150.

Beck, E.C., Jarrell, D.K., Lyons, A.C., Vanderslice, E.J., VeDepo, M.C., Jacot, J.G., 2021. Assessment of electrospun cardiac patches made with sacrificial particles and polyurethane-polycaprolactone blends. J. Biomed. Mater. Res., A 109 (11), 2154–2163.

Brown, M., Farrar, D., 2013. Development of bioresorbable polymers in orthopaedics. Plast., Rubber Compos. 37 (2–4), 46–49.
Capuana, E., Lopresti, F., Ceraulo, M., La Carrubba, V., 2022. Poly-l-Lactic acid (PLLA)-based biomaterials for regenerative medicine: a review on processing and applications. Polymers 14 (6), 1153.
Casarin, S.A., Malmonge, S.M., Kobayashi, M., Agnelli, J.A.M., 2011. Study on in-vitro degradation of bioabsorbable polymers poly (hydroxybutyrate-co-valerate) – (PHBV) and poly (caprolactone) – (PCL). J. Biomaterials Nanobiotechnol. 02 (03), 207–215.
Chan, K., Tsoi, J.K., Wu, O.K., Yon, M.J., Wong, R.W., 2019. Mechanical and biological evaluations of novel electrospun PLLA composite scaffolds doped with oxide ceramics. J. Mech. Behav. Biomed. Mater. 97, 229–237.
Chen, L., Yan, D., Wu, N., Zhang, W., Yan, C., Yao, Q., Sun, H., Fu, Y., 2020. 3D-Printed poly-caprolactone scaffolds modified with biomimetic extracellular matrices for tarsal plate tissue engineering. Front. Bioeng. Biotechnol. 8, 219-219.
Chew, S.A., Hinojosa, V.A., Arriaga, M.A., 2017. Bioresorbable polymer microparticles in the medical and pharmaceutical fields. In: Bioresorbable Polymers for Biomedical Applications, pp. 229–264.
Choudhary, R., Bulygina, I., Lvov, V., Zimina, A., Zhirnov, S., Kolesnikov, E., Leybo, D., Anisimova, N., Kiselevskiy, M., Kirsanova, M., Senatov, F., 2022. Mechanical, structural, and biological characteristics of polylactide/wollastonite 3D printed scaffolds. Polymers 14 (19), 3932.
Ciardulli, M.C., Lovecchio, J., Scala, P., Lamparelli, E.P., Dale, T.P., Giudice, V., Giordano, E., Selleri, C., Forsyth, N.R., Maffulli, N., Della Porta, G., 2021. 3D biomimetic scaffold for growth factor controlled delivery: an in-vitro study of tenogenic events on Wharton's jelly mesenchymal stem cells. Pharmaceutics 13 (9), 1448.
de Matos, M.B., Puga, A.M., Alvarez-Lorenzo, C., Concheiro, A., Braga, M.E., de Sousa, H.C., 2015. Osteogenic poly(epsilon-caprolactone)/poloxamine homogeneous blends prepared by supercritical foaming. Int. J. Pharm. 479 (1), 11–22.
Duan, R., Wang, Y., Su, D., Wang, Z., Zhang, Y., Du, B., Liu, L., Li, X., Zhang, Q., 2022. The effect of blending poly (l-lactic acid) on in vivo performance of 3D-printed poly(l-lactide-co-caprolactone)/PLLA scaffolds. Biomater. Adv. 138, 212948.
Eskandarinia, A., Kefayat, A., Agheb, M., Rafienia, M., Amini Baghbadorani, M., Navid, S., Ebrahimpour, K., Khodabakhshi, D., Ghahremani, F., 2020. A novel bilayer wound dressing composed of a dense polyurethane/propolis membrane and a biodegradable polycaprolactone/gelatin nanofibrous scaffold. Sci. Rep. 10 (1), 3063.
Fioretta, E.S., Motta, S.E., Lintas, V., Loerakker, S., Parker, K.K., Baaijens, F.P.T., Falk, V., Hoerstrup, S.P., Emmert, M.Y., 2021. Next-generation tissue-engineered heart valves with repair, remodelling and regeneration capacity. Nat. Rev. Cardiol. 18 (2), 92–116.
Francis, A.P., Augustus, A.R., Chandramohan, S., Bhat, S.A., Priya, V.V., Rajagopalan, R., 2023. A review on biomaterials-based scaffold: an emerging tool for bone tissue engineering. Mater. Today Commun. 34.
Fukunishi, T., Best, C.A., Sugiura, T., Opfermann, J., Ong, C.S., Shinoka, T., Breuer, C.K., Krieger, A., Johnson, J., Hibino, N., 2017. Preclinical study of patient-specific cell-free nanofiber tissue-engineered vascular grafts using 3-dimensional printing in a sheep model. J. Thorac. Cardiovasc. Surg. 153 (4), 924–932.
Ghosh, S., Haldar, S., Gupta, S., Chauhan, S., Mago, V., Roy, P., Lahiri, D., 2022. Single unit functionally graded bioresorbable electrospun scaffold for scar-free full-thickness skin wound healing. Biomater. Adv. 139, 212980.
Gruber, S.M.S., Murab, S., Ghosh, P., Whitlock, P.W., Lin, C.J., 2022. Direct 3D printing of decellularized matrix embedded composite polycaprolactone scaffolds for cartilage regeneration. Biomater. Adv. 140, 213052.

Hajebi, S., Mohammadi Nasr, S., Rabiee, N., Bagherzadeh, M., Ahmadi, S., Rabiee, M., Tahriri, M., Tayebi, L., Hamblin, M.R., 2020. Bioresorbable composite polymeric materials for tissue engineering applications. Int. J. Polym. Mater. Polym. Biomater. 70 (13), 926–940.

Hartley, E., Harrison, M., Ana, I., Neves, S., 2022. Biodegradable synthetic polymers for tissue engineering: a mini-review. Reinvention 15 (1).

Hu, X., Zhao, W., Zhang, Z., Xie, J., He, J., Cao, J., Li, Q., Yan, Y., Xiong, C., Li, K., 2023. Novel 3D printed shape-memory PLLA-TMC/GA-TMC scaffolds for bone tissue engineering with the improved mechanical properties and degradability. Chin. Chem. Lett. 34 (1).

Hua, J., Gebarowska, K., Dobrzynski, P., Kasperczyk, J., Wei, J., Li, S., 2009. Influence of chain microstructure on the hydrolytic degradation of copolymers from 1,3-trimethylene carbonate and L-lactide. J. Polym. Sci. Polym. Chem. 47 (15), 3869–3879.

Hussain, M., Khan, S.M., Al-Khaled, K., Ayadi, M., Abbas, N., Chammam, W., 2022. Performance analysis of biodegradable materials for orthopedic applications. Mater. Today Commun. 31.

Jinnouchi, H., Torii, S., Sakamoto, A., Kolodgie, F.D., Virmani, R., Finn, A.V., 2019. Fully bioresorbable vascular scaffolds: lessons learned and future directions. Nat. Rev. Cardiol. 16 (5), 286–304.

Kennedy, S.W., Roy Choudhury, N., Parthasarathy, R., 2023. 3D Printing Soft Tissue Scaffolds Using Poly(caprolactone). Bioprinting.

Kenny, E.K., Gately, N.M., Killion, J.A., Devine, D.M., Higginbotham, C.L., Geever, L.M., 2015. Melt extruded bioresorbable polymer composites for potential regenerative medicine applications. Polym.-Plast. Technol. Eng. 55 (4), 432–446.

Kirillova, A., Yeazel, T.R., Asheghali, D., Petersen, S.R., Dort, S., Gall, K., Becker, M.L., 2021. Fabrication of biomedical scaffolds using biodegradable polymers. Chem. Rev. 121 (18), 11238–11304.

Kosowska, K., Krzysztoforski, J., Henczka, M., 2022. Foaming of PCL-based composites using scCO(2): structure and physical properties. Materials 15 (3).

Lannutti, J., Reneker, D., Ma, T., Tomasko, D., Farson, D., 2007. Electrospinning for tissue engineering scaffolds. Mater. Sci. Eng. C 27 (3), 504–509.

Li, T., Tian, L., Liao, S., Ding, X., Irvine, S.A., Ramakrishna, S., 2019a. Fabrication, mechanical property and in vitro evaluation of poly (L-lactic acid-co-epsilon-caprolactone) core-shell nanofiber scaffold for tissue engineering. J. Mech. Behav. Biomed. Mater. 98, 48–57.

Li, W., Shi, L., Zhou, K., Zhang, X., Ullah, I., Ou, H., Zhang, W., Wu, T., 2019b. Facile fabrication of porous polymer fibers via cryogenic electrospinning system. J. Mater. Process. Technol. 266, 551–557.

Ma, H., Sun, Y., Tang, Y., Shen, Y., Kan, Z., Li, Q., Fang, S., Lu, Y., Zhou, X., Li, Z., 2021. Robust electrospun nanofibers from chemosynthetic poly(4-hydroxybutyrate) as artificial dural substitute. Macromol. Biosci. 21 (7), e2100134.

Mahdavi, F.S., Salehi, A., Seyedjafari, E., Mohammadi-Sangcheshmeh, A., Ardeshirylajimi, A., 2017. Bioactive glass ceramic nanoparticles-coated poly(l-lactic acid) scaffold improved osteogenic differentiation of adipose stem cells in equine. Tissue Cell 49 (5), 565–572.

Mahmud, Z., Nasrin, A., Hassan, M., Gomes, V.G., 2021. 3D-printed polymer nanocomposites with carbon quantum dots for enhanced properties and in situ monitoring of cardiovascular stents. Polym. Adv. Technol. 33 (3), 980–990.

Mendibil, X., Ortiz, R., Viteri, V.S., Ugartemendia, J.M., Sarasua, J.R., Quintana, I., 2019. High throughput manufacturing of bio-resorbable micro-porous scaffolds made of

poly(L-lactide-co-epsilon-caprolactone) by micro-extrusion for soft tissue engineering applications. Polymers 12 (1).
Modolo, L.P., França, W.R., Simbara, M.M.O., Malmonge, S.M., Santos, A.R., 2022. Dense, porous, and fibrous scaffolds composed of PHBV, PCL, and their 75:25 blend: an in vitro morphological and cytochemical characterization. Int. J. Polym. Anal. Char. 28 (1), 73–87.
Naseem, R., Montalbano, G., German, M.J., Ferreira, A.M., Gentile, P., Dalgarno, K., 2022. Influence of PCL and PHBV on PLLA thermal and mechanical properties in binary and ternary polymer blends. Molecules 27 (21).
Nelson, G.N., Tamar Mirensky, Brennan, M.P., Roh, J.D., Yi, T., Wang, Y., Christopher, K., Breuer, 2008. Functional small-diameter human tissue–engineered arterial grafts in an immunodeficient mouse model – preliminary findings. Arch. Surg. 143 (5), 488–494.
Neves, S.C., Moreira Teixeira, L.S., Moroni, L., Reis, R.L., Van Blitterswijk, C.A., Alves, N.M., Karperien, M., Mano, J.F., 2011. Chitosan/poly(epsilon-caprolactone) blend scaffolds for cartilage repair. Biomaterials 32 (4), 1068–1079.
Okereke, M.I., Khalaj, R., Tabriz, A.G., Douroumis, D., 2021. Development of 3D printable bioresorbable coronary artery stents: a virtual testing approach. Mech. Mater. 163.
Okonkwo, E.G., Aigbodion, V.S., Akinlabi, E.T., Daniel-Mkpume, C.C., 2020. Starch-based composites and their applications. In: Advanced Applications of Polysaccharides and their Composites, 73, p. 198.
Ozkoc, G., Kemaloglu, S., Quaedflieg, M., 2009. Production of poly(lactic acid)/organo-clay nanocomposite scaffolds by microcompounding and polymer/particle leaching. Polym. Compos. 31, 674–683.
Patel, H., Bonde, M., Srinivasan, G., 2011. Biodegradable polymer scaffold for tissue engineering. Trends Biomater. Artif. Organs 25 (1), 20–29.
Pertici, G., 2017. Introduction to bioresorbable polymers for biomedical applications. In: Bioresorbable Polymers for Biomedical Applications, pp. 3–29.
Polak-Krasna, K., Abaei, A.R., Shirazi, R.N., Parle, E., Carroll, O., Ronan, W., Vaughan, T.J., 2021. Physical and mechanical degradation behaviour of semi-crystalline PLLA for bioresorbable stent applications. J. Mech. Behav. Biomed. Mater. 118, 104409.
Quiles-Carrillo, L., Blanes-Martínez, M.M., Montanes, N., Fenollar, O., Torres-Giner, S., Balart, R., 2018. Reactive toughening of injection-molded polylactide pieces using maleinized hemp seed oil. Eur. Polym. J. 98, 402–410.
Sadeghi-Avalshahr, A.R., Khorsand-Ghayeni, M., Nokhasteh, S., Molavi, A.M., Sadeghi-Avalshahr, M., 2016. Physical and mechanical characterization of PLLA interference screws produced by two stage injection molding method. Prog. Biomater. 5 (3–4), 183–191.
Salerno, A., Zeppetelli, S., Di Maio, E., Iannace, S., Netti, P.A., 2012. Architecture and properties of bi-modal porous scaffolds for bone regeneration prepared via supercritical CO2 foaming and porogen leaching combined process. J. Supercrit. Fluids 67, 114–122.
Salerno, A., Domingo, C., Saurina, J., 2017. PCL foamed scaffolds loaded with 5-fluorouracil anti-cancer drug prepared by an eco-friendly route. Mater. Sci. Eng. C., Mater. Biol. Appl. 75, 1191–1197.
Salmoria, G.V., Sibilia, F., Gindri, I.M., Roesler, C.R.M., Farè, S., Tanzi, M.C., 2017. Ibuprofen-loaded PCL meshes manufactured using rapid tooling for ocular orbital repair. Polym. Test. 62, 33–40.
Samadian, H., Farzamfar, S., Vaez, A., Ehterami, A., Bit, A., Alam, M., Goodarzi, A., Darya, G., Salehi, M., 2020. A tailored polylactic acid/polycaprolactone biodegradable

and bioactive 3D porous scaffold containing gelatin nanofibers and Taurine for bone regeneration. Sci. Rep. 10 (1), 13366.
Saska, S., Pilatti, L., Blay, A., Shibli, J.A., 2021. Bioresorbable polymers: advanced materials and 4D printing for tissue engineering. Polymers 13 (4).
Scorsato, P.S., Rahal, S.C., Cestari, T.M., Mamprim, M.J., Doiche, D.P., Teixeira, D.d.B., Siqueira, R.C., Felix, M., 2022. Evaluation of the degradation of two bioabsorbable interference screws: an in-vivo study in sheep. Acta Cir. Bras. 37 (4).
Seyednejad, H., Ji, W., Schuurman, W., Dhert, W.J.A., Malda, J., Yang, F., Jansen, J.A., van Nostrum, C., Vermonden, T., Hennink, W.E., 2011. An electrospun degradable scaffold based on a novel hydrophilic polyester for tissue-engineering applications. Macromol. Biosci. 11 (12), 1684–1692.
Sharma, U., Concagh, D., Core, L., Kuang, Y., You, C., Pham, Q., Zugates, G., Busold, R., Webber, S., Merlo, J., Langer, R., Whitesides, G.M., Palasis, M., 2018. The development of bioresorbable composite polymeric implants with high mechanical strength. Nat. Mater. 17 (1), 96–103.
Shishatskaya, E.I., Dudaev, A.E., Volova, T.G., 2022. Resorbable nanomatrices from microbial polyhydroxyalkanoates: design strategy and characterization. Nanomaterials 12 (21), 3843.
Shuai, C., Yang, W., Feng, P., Peng, S., Pan, H., 2021. Accelerated degradation of HAP/PLLA bone scaffold by PGA blending facilitates bioactivity and osteoconductivity. Bioact. Mater. 6 (2), 490–502.
Si, B.M., Yang, J.C., Hazarika, D., Byeon, J.W., Lee, G.B., Park, J., 2022. Fabrication and sensing properties of fibrous-like chlorophenoxy herbicide-imprinted polymeric matrix via microcontact printing. Macromol. Res. 30 (10), 731–736.
Singh, M.K., Zafar, S., Talha, M., 2019. Development and characterisation of poly-L-lactide-based foams fabricated through microwave-assisted compression moulding. J. Cell. Plast. 55 (5), 523–541.
Sousa, A.M., Amaro, A.M., Piedade, A.P., 2022. 3D printing of polymeric bioresorbable stents: a strategy to improve both cellular compatibility and mechanical properties. Polymers 14 (6), 1099.
Stefani, I., Cooper-White, J.J., 2016. Development of an in-process UV-crosslinked, electrospun PCL/aPLA-co-TMC composite polymer for tubular tissue engineering applications. Acta Biomater. 36, 231–240.
Tawade, P., Tondapurkar, N., Jangale, A., 2022. Biodegradable and biocompatible synthetic polymers for applications in bone and muscle tissue engineering. J. Med. Sci. 91 (3).
Viera Rey, D.F., St-Pierre, J.-P., 2019. Fabrication techniques of tissue engineering scaffolds. In: Handbook of Tissue Engineering Scaffolds: Volume One, pp. 109–125.
Weng, W., Song, S., Cao, L., Cai, Y., Li, H., Zhou, Q., Zhang, J., Su, J., 2014. A comparative study of bioartificial bone tissue poly-L-lactic acid/polycaprolactone and PLLA scaffolds applied in bone regeneration. J. Nanomater. 1–7. https://doi.org/10.1155/2014/935149. In this issue.
Wiebe, J., Nef, H.M., Hamm, C.W., 2014. Current status of bioresorbable scaffolds in the treatment of coronary artery disease. J. Am. Coll. Cardiol. 64 (23), 2541–2551.
Yang, Y., Yang, S., Wang, Y., Yu, Z., Ao, H., Zhang, H., Qin, L., Guillaume, O., Eglin, D., Richards, R.G., Tang, T., 2016. Anti-infective efficacy, cytocompatibility and biocompatibility of a 3D-printed osteoconductive composite scaffold functionalized with quaternized chitosan. Acta Biomater. 46, 112–128.
Yao, R., Zhao, Y., Han, S., Shan, R., Liu, L., Sun, Y., Yao, X., Wang, X., Hang, R., 2023. Microstructure, mechanical properties, in vitro degradation behavior and in vivo osteogenic activities of Zn-1Mg-β-TCP composites for bone defect repair. Mater. Des. 225, 111494.

Yeo, T., Ko, Y.-G., Kim, E.J., Kwon, O.K., Chung, H.Y., Kwon, O.H., 2021. Promoting bone regeneration by 3D-printed poly(glycolic acid)/hydroxyapatite composite scaffolds. J. Ind. Eng. Chem. (Seoul, Repub. Korea) 94, 343–351.

Yousefi, A.-M., Liu, J., Sheppard, R., Koo, S., Silverstein, J., Zhang, J., James, P.F., 2019. I-optimal design of hierarchical 3D scaffolds produced by combining additive manufacturing and thermally induced phase separation. ACS Appl. Bio Mater. 2 (2), 685–696.

Zamiri, P., Kuang, Y., Sharma, U., Ng, T.F., Busold, R.H., Rago, A.P., Core, L.A., Palasis, M., 2010. The biocompatibility of rapidly degrading polymeric stents in porcine carotid arteries. Biomaterials 31 (31), 7847–7855.

Zhang, J., Liu, H., Ding, J.-X., Wu, J., Zhuang, X.-L., Chen, X.-S., Wang, J.-C., Yin, J.-B., Li, Z.-M., 2016. High-pressure compression-molded porous resorbable polymer/hydroxyapatite composite scaffold for cranial bone regeneration. ACS Biomater. Sci. Eng. 2 (9), 1471–1482.

Zhang, Z., He, F., Wang, B., Zhao, Y., Wei, Z., Zhang, H., Sang, L., 2021. Biodegradable PGA/PBAT blends for 3D printing: material performance and periodic minimal surface structures. Polymers 13 (21), 3757.

Zhao, C.F., Li, Z.H., Li, S.J., Li, J.A., Hou, T.T., Wang, Y., 2019. PLGA scaffold carrying icariin to inhibit the progression of osteoarthritis in rabbits. R. Soc. Open Sci. 6 (4), 181877.

Zopf, D.A., Mitsak, A.G., Flanagan, C.L., Wheeler, M., Green, G.E., Hollister, S.J., 2015. Computer aided–designed, 3-dimensionally printed porous tissue bioscaffolds for craniofacial soft tissue reconstruction. Otolaryngol. Head Neck. Surg. 152 (1), 57–62.

This page intentionally left blank

CHAPTER 8

Gelation and fabrication of bioresorbable-based hydrogels for drug-release applications

Chuanchom Aumnate[1,2], Chaimongkol Saengow[3] and Manunya Okhawilai[1,2]

[1]Metallurgy and Materials Science Research Institute, Chulalongkorn University, Bangkok, Thailand; [2]Center of Excellence in Responsive Wearable Materials, Chulalongkorn University, Bangkok, Thailand; [3]Beckman Institute for Advanced Science and Technology, University of Illinois at Urbana-Champaign, Urbana, IL, United States

8.1 Introduction

Hydrogels are three-dimensional network structures with cross-linking, which usually are constructed from synthetic or natural hydrophilic polymers. The hydrogels can be cross-linked chemically and physically through covalent bonds, hydrogen bonds, crystallized domains, or hydrophobic interactions (Li, 2003; Li et al., 2005). Normally, hydrogel networks are formed via chemical reactions of monomers, creating bonds between polymer chains. As a result, the absorption of water could be up to hundreds or thousands of times without dissolution in water (Hu et al., 2012). The recent development of hydrogels aims to achieve unique characteristics such as controllable swelling behavior, capability to retain water, improved degradation and mechanical properties, mild processing conditions, and outstanding biocompatibility, thereby overcoming deficiencies found in traditional hydrogels. Thereby, enhancing their broad applicability and expanding the potential tasks of hydrogels in health and biomedical applications such as bone and cartilage regeneration, tissue engineering, biosensor, wound injury, and target delivery of drugs (Hu et al., 2012; Wang et al., 2019; Kesharwani et al., 2021; Ahmed, 2015). Typically, hydrogels can be sorted by the source of materials, including natural polymers, synthetic polymers, and semisynthetic or a combination of natural and synthetic polymers. Various naturally derived polymers have been used to form hydrogel networks, such as polysaccharides, collagens, gelatin,

Bioresorbable Polymers and their Composites
ISBN 978-0-443-18915-9
https://doi.org/10.1016/B978-0-443-18915-9.00005-7
© 2024 Elsevier Ltd.
All rights reserved.

fibrin, chitosan, alginate, and cellulose, which offers drug delivery, biocompatibility, and biodegradability (Kesharwani et al., 2021; Nele et al., 2020; Peng et al., 2011; Chatterjee et al., 2018; Mondal et al., 2020). However, these naturally derived polymers have some drawbacks, such as immunogenicity, limited mechanical performance, and uncertainties due to batch-to-batch variations. As a result, synthetic polymers based on poly(ethylene glycol) (PEG), polyacrylic, poly(vinyl alcohol) (PVA), and poly(acrylamide) (PAM) have been seen as potential materials for hydrogel forming due to their high physical strengths and desirable flexibility, which are vital features for expanding hydrogel utilization (Singhal and Gupta, 2015). Synthetic polymers offer ease of functionalization and design, as well as increased mechanical properties. However, they lack biocompatibility and biodegradability. As a result, to merge the strengths of synthetic and natural-derived polymers, a raft of semisynthetic materials, such as gelatin methacrylate (GelMA) and hyaluronic acid methacrylate (HAMA), have been established.

Bioresorbable hydrogels have gained extensive consideration in targetable drug release and therapeutic applications as excellent carriers. The unique characteristics of hydrogels, such as the controllable swelling properties, biodegradability, and biocompatibility, have boosted their utilization, particularly in controlled drug-delivery applications. Also, their porous structures facilitate their ability for drug loading and ultimate release through the hydrogel networks. Typically, the loaded drug is delivered through hydrogels by being slowly eluted, maintaining a high drug concentration in the target for a considerable duration. Hydrogel-based delivery systems can be applied for many areas, such as oral, topical, ocular, vaginal, and rectal. The considerable functions of the hydrogels are prolonging drug release and reproducing drug-releasing profiles.

8.2 Cross-linking of hydrogels

Various techniques have been applied for hydrogel formation with the main principle of cross-linking polymer chains. Traditionally, hydrogels are broadly classified into physically and chemically cross-linked hydrogels (Zafar et al., 2021). Conventional and controlled radical polymerization techniques are used to prepare hydrogels with different compositions, sizes, and morphologies. Applying functional initiators and macroinitiators enables the contribution of functional groups, both inside and on the surface of the hydrogels, thus facilitating multivalent bio-conjugation. In addition,

hydrogels may consist of a double network in which both physical and chemical cross-linking occur, as shown in Fig. 8.1.

8.2.1 Physical cross-linking

Physically cross-linked hydrogels have gained much attention due to their ease of production, prevention of toxic cross-linking agents, and involvement of biopolymers. The physical networks can be concurrently connected by molecular entanglements, hydrogen bonds, ionic forces, and van der Waals interactions. Physical cross-linkers, for example, chitosan, carrageenan, and hyaluronan, can be used to entrap integral materials such as proteins and drugs, making physical hydrogels receive significant attention currently, mainly in the functional food and drug-delivery sectors (Kesharwani et al., 2021). Several methods, such as charge interactions, crystallization, and stereocomplex formation, are typically used to fabricate physically cross-linked hydrogels (Zafar et al., 2021).

8.2.1.1 Stereocomplexation

Stereocomplex formation is a well-established phenomenon found in the co-precipitation of poly(L-lactide), so-called PLLA, and poly(D-lactide), so-called PLDA, in solution, through cooling from their melts, or during their hydrolytic degradation. Hydrogel based on water-soluble PLA-based copolymers has been explored in drug-delivery systems and temporary therapeutic applications, including internal fixation devices and drug-

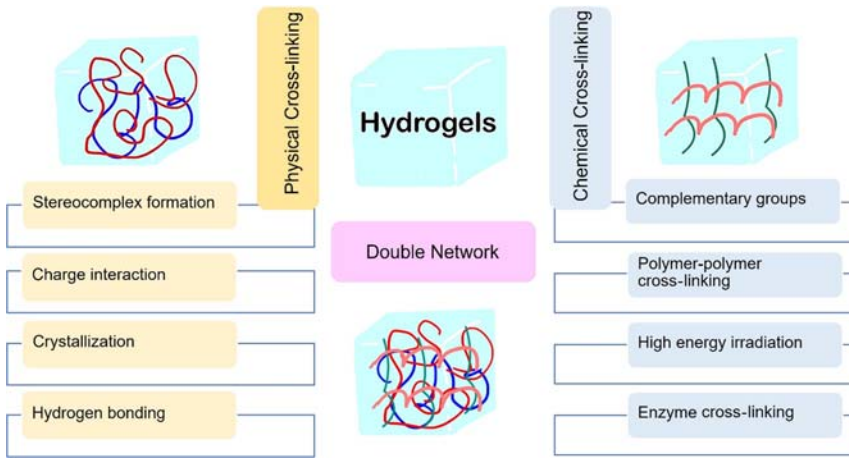

Figure 8.1 Cross-linking strategies in hydrogel forming: physical, chemical, and double networking.

delivery devices (Hu et al., 2012). For example, Zhang et al. suggested the fabrication of bioresorbable hydrogels for drug-delivery systems from water-soluble PLA—PEG—PLA triblock copolymers through stereocomplexation of PLLA and PDLA chains. However, the conventional stereocomplex process, such as solution blending, is relatively slow. Im et al. developed a novel process based on oil-in-water (O/W) emulsion blending, considerably improving the efficiency and speed of the reactions. The PLA hydrogel obtained from O/W emulsion blending exhibited superior mechanical and chemical properties (Im et al., 2020). Fig. 8.2 displays a schematic of O/W emulsion blending for stereocomplexation between PLLA and PDLA induced by O/W emulsion blending. Several considerations, such as copolymer concentration, copolymer composition, type of drug, and the difference between sol and gel characteristics, affect the efficiency of drug delivery. Higher copolymer concentration and molar mass lead to a slower rate of releasing and less bursting effect due to a more compact structure, which disfavors drug diffusion. In addition, the presence of both PLLA/PEG and PDLA/PEG in hydrogels slows the release rates compared to those of single-copolymer solutions.

Interestingly, chitosan-graft-polylactide copolymer (CS-g-PLA) hydrogels can be produced based on the stereocomplexation strategy to obtain a highly efficient drug carrier. By mixing aqueous solutions of CS-g-PLLA and CS-g-PDLA, a hydrogel network can be formed via stereocomplexation of PLLA and PDLA blocks (Hu et al., 2012). The CS-g-PLA hydrogel was reported as a great potential material for drug release, with 82% of TP5

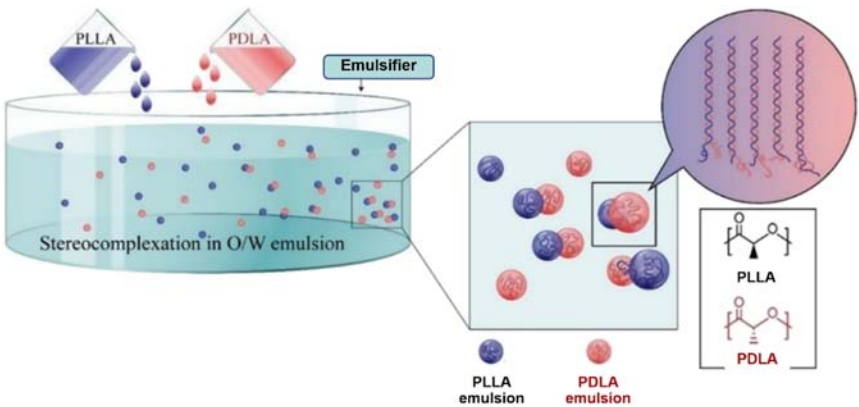

Figure 8.2 Schematic of oil-in-water (O/W) emulsion blending for hydrogel formation from stereocomplexation between PLLA and PDLA blocks. *(Reprinted with permission from Im et al. (2020).)*

(Thymopentin, a model drug) released from the hydrogel within 6 h. Consequently, the inner porous structure of the hydrogel controlled the more rapid release capability. The pores were well interconnected and thus benefited drug diffusion. In general, drug-release mechanisms can be identified as diffusion- or degradation-controlled drug-delivery behaviors. Also, drug diffusion is prevalent, which may be attributed to the reliable water solubility of TP5 and the favorably porous structure of hydrogels. The time scale for TP5 release is shorter than the degradation rate of PLA-based hydrogels, indicating that the developed CS-g-PLA hydrogels are promising candidates for bioactive molecules delivery, particularly hydrophilic drugs such as TP5 and insulin (Hu et al., 2012).

In addition, a simple physical cross-linked hydrogel can be formed by simply warming block-copolymer solutions such as the block-copolymer of poly(ethylene glycol), polylactic acid, and poly(ethylene oxide)−poly(propylene oxide)−poly(ethylene oxide) hydrogels (Wang et al., 2019; Im et al., 2020).

8.2.1.2 Cross-linking by charge interactions

Charge interaction can occur between two or multiple opposite-charged polymers and small molecules, resulting in a temporary hydrogel formulation such as the alginate hydrogel cross-linked by divalent cations, for example, calcium (Ca^{2+}), barium (Ba^{2+}), and magnesium (Mg^{2+}) (Zafar et al., 2021; Hu et al., 2019). Ionic hydrogels, cationic hydrogels, and anionic hydrogels have cross-linking of ionic polymers involved by adding divalent or trivalent counterions. Electrostatic interactions take place between the opposite-charged polymers, which then network with each other, generating polyelectrolyte complexes. The swelling of ionic hydrogel is typically dominated by the pH of the aqueous medium, which further defines the degree of dissociation of the ionic chains (Kesharwani et al., 2021; Singhal and Gupta, 2015; Hu et al., 2019). Examples of hydrogels fabricated based on ionic interaction cross-linking are chitosan−dextran hydrogels and chitosan−glycerol phosphate salt. The particular benefit of ionic interaction is its self-healing ability. Thus, when the physical network of hydrogel is broken at high stress, it can be reformed once the stress is removed. However, the mechanical performance of hydrogel remains limited due to the cross-linking strategy of the ionic interaction (Hu et al., 2019).

8.2.1.3 Cross-linking by crystallization

The crystallization of polymeric chains acts as a physical cross-linking site for hydrogel formation. For example, the hydrogel can be formed from the freeze–thawing process of the aqueous PVA solution. The obtained hydrogel properties can be altered with polymer molecular weight and concentration, freezing time, and temperature, as well as the number of freeze–thaw cycles. For example, a PVA/sodium alginate (SA) hydrogel was formed via freeze–thawing, using an NaCl solution. The obtained hydrogel was found to be improved in strength and conductivity. In addition, a physical double network (PDN) hydrogel can be prepared based on the crystallization-induced physically cross-linked PVA and polyacrylamide (HAPAM) by one-pot in situ polymerization and subsequent freeze–thawing cycling, as shown in Fig. 8.3. The obtained PDN hydrogel exhibited improved mechanical strength, owing to the substantial crystallization of PVA combined with the presence of an H-bond between the PVA and PAM chains (Hu et al., 2019).

8.2.1.4 Cross-linking by hydrogen bonding (H-bonding)

H-bonding is one of the most significant noncovalent interactions that can stabilize a hydrogel formation. Some examples include the hydrogel beads from carboxymethylcellulose (CMC) filled with graphene oxide (GO) nanoparticles prepared by lowering the pH of aqueous polymeric solutions surrounding carboxyl groups. The CMC/GO hydrogel was physically cross-linked by $FeCl_3.6H_2O$. Due to the H-bonding between GO and

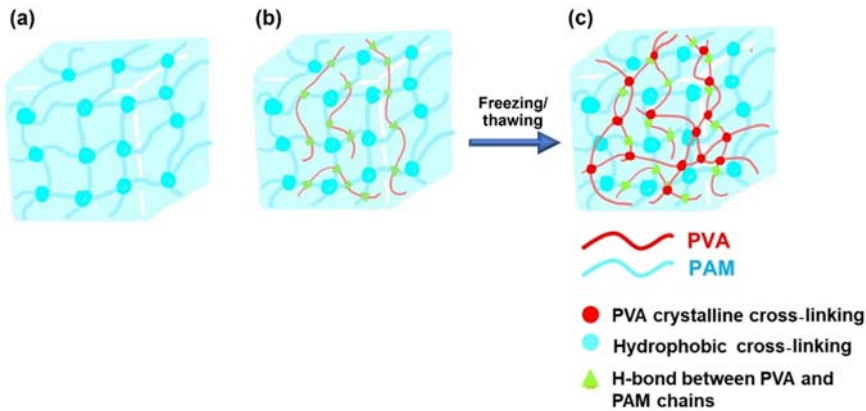

Figure 8.3 The hydrogel network structures developed from the freezing–thawing process: (a) HAPAM hydrogel, (b) semi-IPN HAPAM/PVA hydrogel, (c) PDN hydrogel after freezing–thawing. *(Adapted with permission from Hu et al. (2019).)*

water molecules and carboxyl groups of CMC hydrogels, the swelling ratio of the CMC/GO nanocomposite hydrogel increased compared to the neat CMC hydrogel, indicating the better drug-loading capacity compared to the neat CMC hydrogel (Rasoulzadeh and Namazi, 2017). In addition, cellulose-based hydrogels are typically formed via H-bonding. For example, two biopolymers, pectin and mucin, were incorporated into the hydrogel network in NaOH/urea aqueous solvent system. The obtained cellulose-based hydrogels provided more controlled release at different pH levels, ranging from 1.2 to 10, which allow further advancement of controlled drug-delivery systems (Islam et al., 2022). Moreover, H-bonding could be formed by active groups such as amide, carboxylic acid, and hydroxyl groups, or interact with electron donor groups, such as pyridine and imidazole. So far, a single H-bond is generally not strong enough to maintain the hydrogel structure. A novel self-healing hydrogel with a strong network can be prepared based on the interactions of ureidopyrimidinone (UPy). As shown in Fig. 8.4, a multiblock PEG-UPy copolymer was synthesized through physical cross-linking between UPy-UPy dimers which are surrounded in the PEG matrix. The UPy units could further assemble into dimers via four-fold H-bonding, resulting in network reinforcement with high strength, resiliency, and shape memory behavior (Hu et al., 2019).

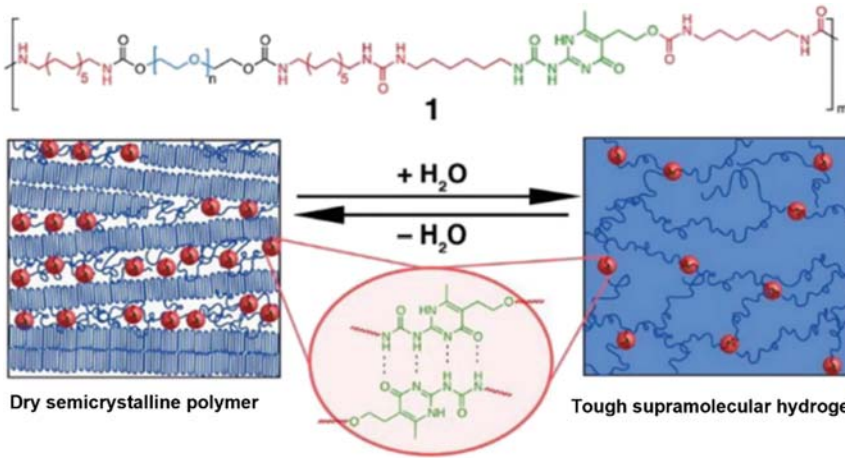

Figure 8.4 Schematic illustration of hydrogel cross-linked via H-bonding between two UPy segments in PEG-UPy hydrogel. *(Adapted with permission from Guo et al. (2014).)*

8.2.2 Chemical cross-linking

Chemical cross-linking is a straightforward and practical approach to obtaining hydrogels. Chemical cross-linking requires grafting polymers or connecting two polymeric chains with cross-linking agents. Covalent bonds are the primary mechanism involved in chemically cross-linked hydrogels which are more substantial and more permanent compared to those of physically cross-linked hydrogels. Numerous approaches have been reported, including the chemical reaction of complementary groups, polymer—polymer cross-linking, high-energy irradiation, and enzyme cross-linking. Compared to physically cross-linked hydrogels, chemically cross-linked hydrogels usually exhibit enhanced stability under physiological conditions, excellent mechanical properties, and tunable degradation behavior.

Some examples of chemically cross-linked hydrogels include the complex hydrogels composed of whey protein isolate (WPI), and chitosan (CS) prepared by cross-linking with a naturally derived cross-linking agent, genipin (GP), via cold gelation. The obtained complex hydrogels show excellent properties for the application of controlled release, in particular, bioactive materials in functional foods and pharmaceutical products (Liu et al., 2018). Another proposed area for hydrogel utilization is artificial skin that affords site-specific medicament delivery. Chemically cross-linked carboxymethylcellulose (CMC) hydrogels were successfully used for targeted drug delivery through the skin (Kesharwani et al., 2021).

8.2.2.1 Chemical reaction of complementary groups

For aqueous-soluble polymers, respective functional groups, including carboxylic (COOH), hydroxyl (OH), and amide (NH_2) groups, are accountable for hydrogel formation. Covalent links between polymeric chains can be created by Schiff-based formation, or reaction of complementary groups, such as a hyaluronic acid hydrogel cross-linked using poly(ethylene glycol) propionaldehyde. The formulated hydrogel is a potential candidate for carrying antibacterial and antiinflammatory properties in wound-dressing applications. In addition, hydrogels can be cross-linked by bis or higher functional cross-linking agents, such as 1,6-hexamethylene diisocyanate, divinyl sulfone, and 1,6-hexane dibromide. The cross-linking reaction is typically undertaken in organic solvents to avoid the reaction of water and the cross-linking agents. The formed hydrogels need to be extracted to remove the trace of unreacted reagents due to the toxicity of such cross-linking reagents, for example, a degradable hydrogel from cross-

linking of polyethylene glycol-dithiol and polyethylene glycol-acrylate. In addition, condensation reactions have also been widely used to prepare polyester/polyamide-based hydrogels. The condensation reaction was conducted through several groups, in particular, $-OH$ or $-NH_2$ with carboxylic acids and their derivatives, for example, hydrogel formulated from alginate and PEG-diamine. The hydrogel formulated via this cross-linking strategy typically exhibits superior mechanical properties compared with the ionically cross-linked counterparts (Zafar et al., 2021; Hu et al., 2019).

8.2.2.2 Polymer–polymer cross-linking

For polymer–polymer cross-linking, the reactive groups of prefunctionalized polymeric chains are utilized for creating the hydrogel network. A well-known example is the chitosan and hyaluronic acid polymer-based in situ hydrogels formed by Schiff-bases reaction at physiological pH, which resulted in a hydrogel that maintained stability for up to 4 weeks. Moreover, Michael addition is a reaction between a nucleophile, the donor with sufficient nucleophilicity, such as amines. The activated electrophilic olefins or alkenes as an acceptor with electron-withdrawing and resonance ability can stabilize the anionic intermediate. This approach offers mild reaction conditions, rapid gel formation, and flexibility in forming multiple bonding. In addition, this cross-linking method eliminates the necessity of low-molecular-weight cross-linkers; however, the limitation is the requirement for multi-step synthesis and purification processes. Fig. 8.5 illustrates the Michael addition of chitosan-based hydrogels cross-linked with poly(ethylene glycol-*b*-caprolactone-*b*-ethylene glycol) (PECL) micelles. Herein, drugs can be trapped inside the PECL micelles, promoting excellent delivery performance (Hu et al., 2019).

8.2.2.3 Cross-linking by photopolymerization

Photopolymerization has been extensively utilized for hydrogel construction in therapeutic applications. The speedy creation of hydrogel networks under mild conditions and the tunable mechanical properties make this method more interesting. Under light exposure, only light-exposed regions are polymerized and promote cross-linking. Typically, the presence of unsaturated groups, for example, the conjugated carbons in methacrylates, are greatly reactive, promoting a free radical chain-growth polymerization under light exposure. Various photoinitiators such as Irgacure 2959, Irgacure 819, Irgacure 1173, LAP, and so on, which can be absorbed by precise

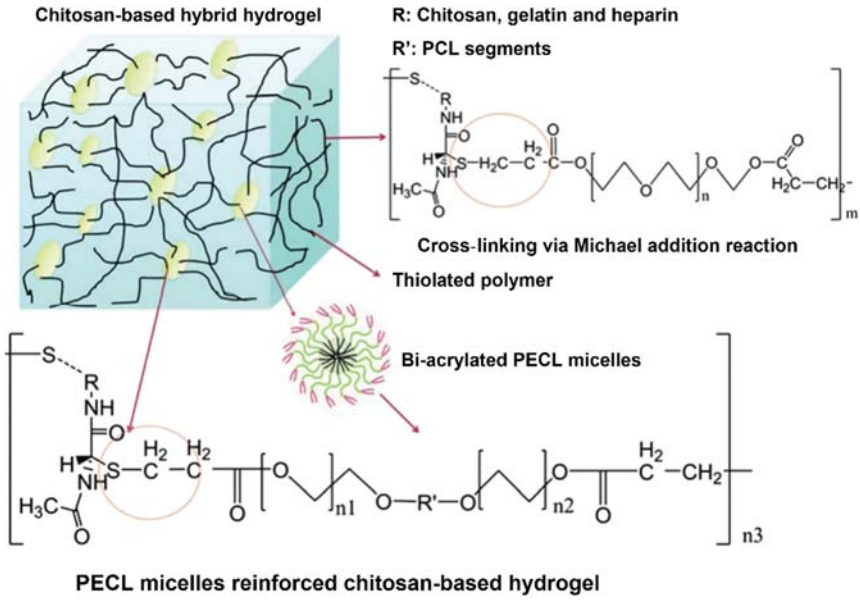

Figure 8.5 Schematic illustration of chitosan-based hydrogel cross-linked with PECL micelles via polymer–polymer cross-linking. *(Adapted with permission from Hu et al. (2019).)*

light at different wavelengths, including UV light at 250–370 nm, visible blue and purple light at 405–550 nm, and red light at 750–810 nm, are typically incorporated to initiate the photopolymerization. In addition, the chemical modification of photoinitiators has recently been more stimulating as it could enhance the photoinitiation performance. For example, using a carboxylated-modified camphorquinone photoinitiator significantly increases the photoactivity and cross-link density with better mechanical properties of the fabricated hydrogels (Hu et al., 2019).

8.2.2.4 High-energy irradiation cross-linking

High-intensity and energy irradiations, including gamma, UV, electron beams, and microwave, can be employed to create permanent hydrogels. Irradiation-mediated chemical cross-linking allows the formation of hydrogels under mild conditions, including pH and temperature, without using toxic cross-linking agents. Thus, the removal of unreacted species from the final product is not required. In the high-energy irradiation cross-linking technique, the produced free radicals attack the hydrophilic part of the polymer chains, generating macroradicals with the consequent creation

of cross-linked networks. Polyacrylic acid (PAA), polyethylene glycol (PEG), and polyvinyl alcohol (PVA) hydrogels are examples of hydrogels formed using this method. In addition, polymethyl vinyl ether aqueous solutions can be irradiated above the phase transition temperature to obtain a thermosensitive hydrogel. The factors influenced the swelling ratio and permeability of the resultant hydrogels are typically the irradiation dose and polymer concentration (Zafar et al., 2021).

8.2.2.5 Enzyme cross-linking

Recently, enzymes have been utilized for formulating hydrogels, for example, PEG-based hydrogels. Numerous enzymes, such as transglutaminases, tyrosinase, peroxidases, plasma amine oxidase, and phosphatases, have been widely used. For example, transglutaminase, along with calcium ions as a cofactor, can promote the formation of amide linkages between carboxamide and amine groups (Zafar et al., 2021). In addition, collagen can be conjugated with tyramine to form an injectable hydrogel in the presence of horseradish peroxidase and hydrogen peroxide (Hu et al., 2019).

8.3 Hydrogel fabrication

Hydrogel fabrication methods are typically based on physical and chemical cross-linking. Different cross-linked networks can be constructed and the properties, particularly the drug-delivery performance, can be designed as required (Kesharwani et al., 2021). The hydrogels for drug-delivery applications fabricated via different routes are described in Table 8.1.

8.3.1 Mold casting

Mold casting is a relatively simple fabrication strategy in which a hydrogel precursor solution is placed into a mold, cross-linked, and demolded. It can be used to produce shape-defined hydrogel structures from various hydrogel systems, for example, enzymatically cross-linked collagen/fibrinogen, photo-cross-linked acrylate PEG, and acrylamide (Nele et al., 2020). In addition, the mold casting method can be assisted by freeze drying, which is called freeze casting. For example, gelatin/chitosan hydrogel can be formed by freeze casting by first dissolving chitosan in acetic acid, then adding a gelatin solution to obtain gelatin/chitosan, which is then stirred until homogeneous blending is obtained. After that, the proper cross-linker, for example, glutaraldehyde (GA), is slowly added. The mixture solution is

Table 8.1 Physically and chemically cross-linked hydrogels for drug-delivery applications.

Cross-linking hydrogels	Cross-linking methods	Materials	References
Physically cross-linked hydrogels	H-bonding	Cyclodextrin, hyaluronic acid, polypseudorotaxane, gelatin	Kesharwani et al. (2021), Feng et al. (2016), and Ye et al. (2017)
	Ionic interaction	Cellulose microfibrils, chitosan	Masruchin et al. (2015) and Ishii-Mizuno et al. (2017)
		Sodium alginate-polyacrylamide	Zhou et al. (2018)
	Stereocomplexation	Polyethylene glycol, polylactic acid, dextran	Wang et al. (2015)
Chemically cross-linked hydrogels	Condensation	Cellulose nanofibers, B-cyclodextrin	Kobe et al. (2016)
	Radiation grafting	Carboxymethyl cellulose, chitosan, styrene sulfonate, N-vinyl caprolactam	Tran et al. (2017)

then poured into plastic molds, allowed to dry for 72−120 h at room temperature, and then dried at −40°C for 24 h to obtain a porous structure. The obtained hydrogels showed a significant reduction in the swelling behavior with increased chitosan cross-linking reagent contents, contributing to the formation of a more rigid network (Peng et al., 2011).

Another interesting example is a novel hydrogel applying drug molecules as cross-linking agents. A small drug solution is introduced into a graphene oxide (GO) dispersion to fabricate the hydrogel under mild conditions (Tao et al., 2012). The GO and drug molecules are dispersed in water and mixed in this process, and the mixture is then shaken for a period of time to form a hydrogel. Then, the drug molecules can be encapsulated in the hydrogel matrix. The freeze-dried and air-dried GO-based hydrogels were seen as prospective candidates for the controlled release of drugs in the strongly acidic environment of the stomach. The GO-based hydrogel with the drug as the cross-linker can be expanded to other hydrophilic drugs containing amino acids and nucleoside peptides.

8.3.2 Prilling or laminar jet break-up

The prilling process is used to prepare monodispersed hydrogel beads based on the dispersion of the solution through pressure-controlled injection in a specific gelation or coagulation medium. It is generally applied for producing polysaccharide-based hydrogels. The polysaccharide solution will transition from the sol phase to the gel phase as a gel particle. The sol phase breaks apart into mono-sized drops through a vibrating nozzle device, as shown in Fig. 8.6 (Auriemma et al., 2020).

This process is generally used for producing polysaccharide-based hydrogel microparticles with designed characteristics, for example, inner structures and diverse configurations, such as mono-layered or multi-layered. The obtained polysaccharide-based hydrogels can be used to control drug release. It should be noted that the hydrogel drying method is a key factor governing the morphology and inner structure characteristics, hence controlling the swelling and releasing properties, in particular for antibiotic and antiinflammatory drugs (Auriemma et al., 2020; Tran et al., 2011).

8.3.3 Nanoparticle-templated nanogel fabrication

Nanometer-sized hydrogels or nanogels have become known as versatile drug-delivery substances which permit large biomolecules to be

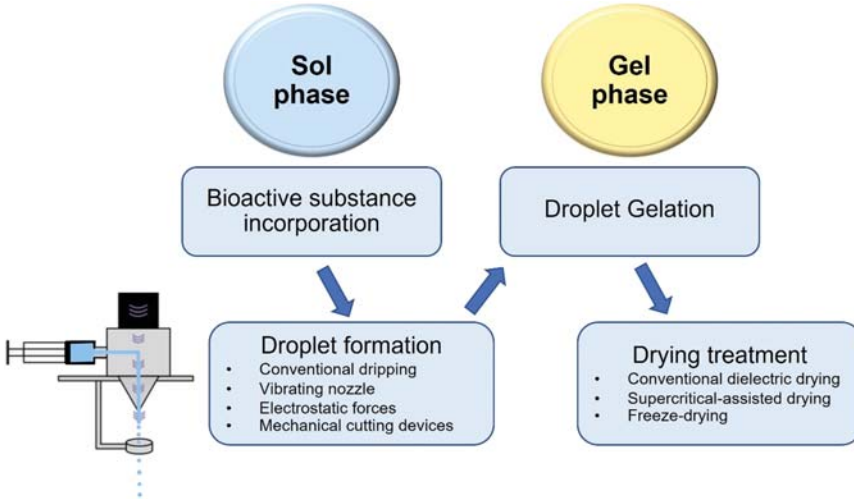

Figure 8.6 Illustration of the typical procedure for producing hydrogels via the prilling process.

encapsulated and released (Nele et al., 2020; Molina et al., 2015; Yan et al., 2017; Torres-Martinez et al., 2019). Conventional methods normally involve inverse emulsion polymerization of cross-linked amphiphilic polymer nanostructures. Instead, nanogel production can be templated by nanoparticles. For instance, liposome-templated nanogels were fabricated by rehydration of liposomes in a polylactide-PEG-polylactide diacrylate copolymer in the presence of a photoinitiator. The suspension was then irradiated with UV light. Similarly, PAM-based nanogels can be formed by encapsulating acrylamide monomers, *N, N′*-methylene-bisacrylamide cross-linker, and photo-initiator in the presence of phosphatidylcholine liposome. The photo-cross-linking then took place during liposome extrusion (Chacko et al., 2012). Furthermore, magnetically responsive liposomes containing maghemite nanocrystals or iron oxide nanoparticles have been prepared to release drugs under applied magnetic fields. The molecular nanogel based on liposomes can also be pH-triggered, in which a change in pH leads to the cross-linking formation. After removing the lipid, liposome-based hydrogel particles with potential uses in environmentally sensitive drug release were achieved (Torres-Martinez et al., 2019). Furthermore, liposomes which are composed of one or more lipid bilayer structures can be used to encapsulate drugs. A micelle with a hydrophilic shell and a hydrophobic core was responsible for carrying drugs. Also, the

nanocapsules can be used to encapsulate a drug in their matrix, as shown in Fig. 8.7.

8.3.4 Three-dimensional printing (3DP)

Recently, the 3D printing of bio-based hydrogels and other polymers has been considered a viable path toward ultimate regenerative treatment. The 3D structure allows liquid recognition for developing a swelled hydrogel form. The fluid core may stop the polymer material from failing, presenting features comparable to those of weak tissues. Conventional hydrogel manufacture processes like the mold casting method can only produce simple structures through molds. Thus, it is difficult to prepare drugs with complex structures. 3D printing of hydrogel drugs is gradually increasing, however, the current 3D-printed hydrogel drugs still face some challenges, including poor shape fidelity, limitations in drug type and load, and the requirement for soaking the hydrogels in drug solution (Zu et al., 2022). Hydrogels have been applied in numerous printing systems, such as droplet bioprinting, stereolithography, and two-photon polymerization.

Extrusion-based printing is a common 3DP technique used to manufacture hydrogel constructs using materials that undertake sol–gel transitions including before extrusion, during extrusion, or after deposition (Nele et al., 2020). For example, Pluronic F127 has been used to offer rapid thermal gelation of alginate-based hydrogel systems in extrusion printing. The reversible characteristic of the sol–gel allows its release during electrostatic cross-linking of the alginate component. A similar approach used the reversible thermosetting of gelatin to fabricate interconnected channel

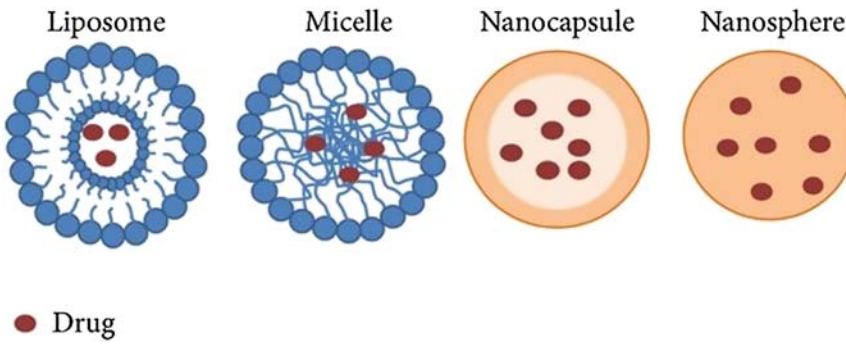

Figure 8.7 Structure of liposomes, micelles, nanocapsules, and nanospheres incorporating a drug in the matrix. *(Reprinted with permission from Neophytou and Constantinou (2015).)*

networks throughout GelMA hydrogels (Ouyang et al., 2022). Another approach is partially cross-linking bioinks into soft and extrudable hydrogels that can be further cross-linked post-printing, typically via photo-cross-linking, such as the hydrogel fabricated from methacrylate-, acrylate-, or norbornene-modified biopolymers (Fig. 8.8) (Ouyang et al., 2017).

Numerous additives have recently been incorporated into hydrogel bioinks to enhance printability or impart additional structural or functional properties. Furthermore, 3D/4D-printed hydrogel capsules have become more attractive for expanding the utility of hydrogel drugs, particularly the design of hydrogel capsules for smart controlled drug release. For example, poly(N-isopropylacrylamide) (PNIPAAM), a thermosensitive hydrogel,

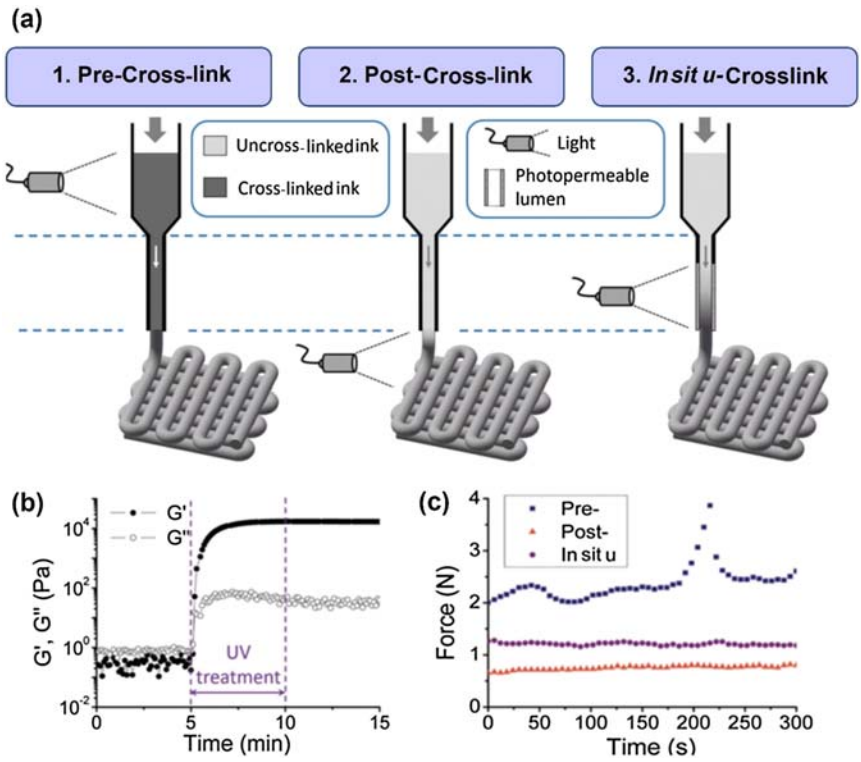

Figure 8.8 (a) Schematic of three different cross-linking strategies for extrusion-based bioprinting photo-cross-linkable inks (5 wt.% MeHA), where cross-linking occurs before (pre-cross-link), after (post-cross-link), or during (in situ cross-link) extrusion; (b) representative curves of storage (G') and loss (G'') moduli during irradiation of 5 wt.% MeHA with UV light (10 mW cm^{-2}); (c) driving force consistency. *(Adapted with permission from Ouyang et al. (2017).)*

was produced via extrusion 3D printing as the capsule shell (Zu et al., 2022). Fig. 8.9 illustrates the 4D/3D printing process for hydrogel.

3DP techniques are a new technology in developing medical devices for drug delivery. The main advantage of 3DP is the custom design, providing ideal devices with less fabrication and postprocessing time, reduced waste material, and lower cost. 3DP is the layer-by-layer deposition of slurry inks

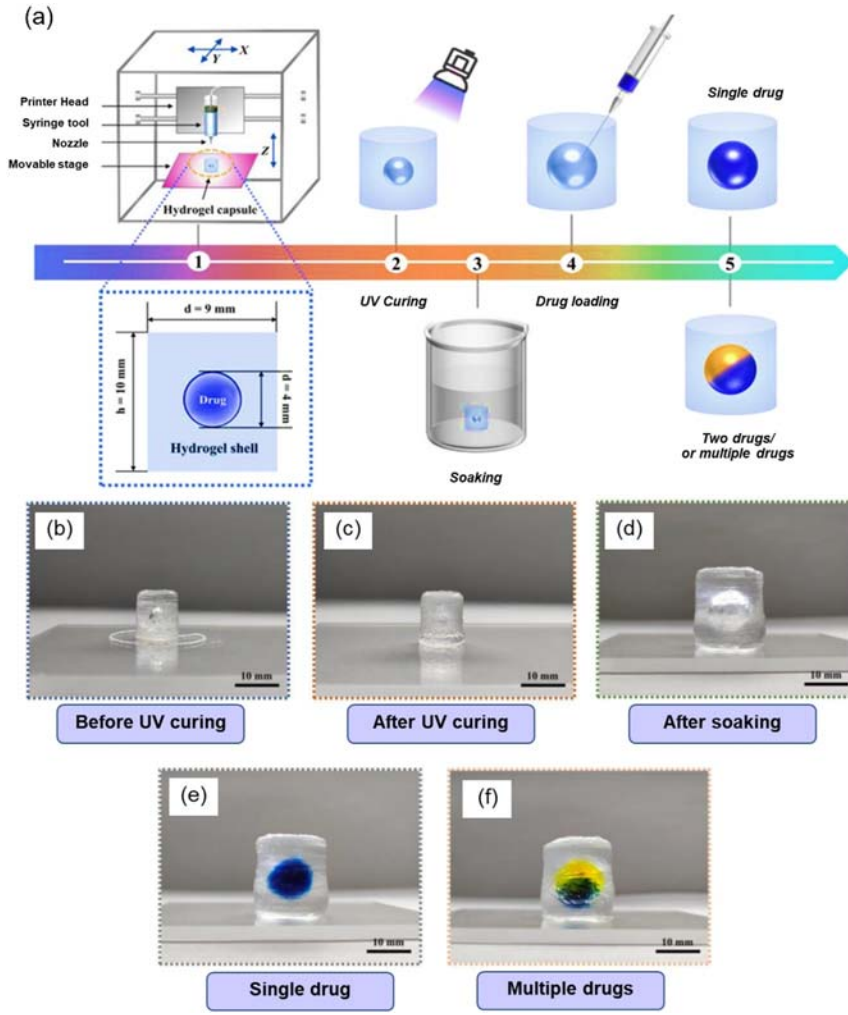

Figure 8.9 (a) Schematic diagram of the 3D-printed hydrogels and photographs of 3D-printed hydrogels, (b) before UV curing, (c) after UV curing, (d) after soaking in water for 96 h, (e) 3D-printed hydrogel loaded with a single drug, and (f) 3D-printed hydrogel loaded with multiple drugs. *(Adapted with permission from Zu et al. (2022).)*

and the burning out of liquid inks to obtain the final shape. Hence, the rheological parameters of the printing ink, viscosity, yield stress, and dynamic elastic modulus are essential for determining the final properties (Gritsch et al., 2021). In addition, 3DP has other vital factors in determining the shape, including nozzle speed and extrusion pressure. The pressure must be sufficient for a continuous strand at the given speed. In addition, the effect of hydrogel fabrication techniques, casting hydrogel (conventional fabrication), and 3D printing hydrogel impact the achieved mechanical properties. For example, 3D-printed chitosan exhibited ductility behavior with a significant drop in strength compared to those of the cast hydrogels due to the less homogeneous structure of the 3D-printed lattice. This can cause weakness in 3D printing due to stress distributions leading to failure, which can be overcome by incorporating higher-strength materials or reinforcements (Zolfagharian et al., 2018). Fig. 8.10 displays an example of 3D-printed gelatin-based hydrogels with designed structures.

8.3.5 Rheological toolbox

Hydrogels are networks of polymers that imbibe a significant portion of water. Depending on the chain stiffness and loadings, they are generally soft, and cross-linking is required to stabilize the network as well as improve the mechanical and rheological properties. When the cross-link density exceeds a threshold, yield stress arises—a representative critical stress at which hydrogels flow if applied stress exceeds this value. There are several approaches to use to measure yield stress but the most common is to use large-amplitude oscillatory shear flow (LAOS).

In LAOS, the frequency is fixed and flow strength—either stress or strain amplitudes—is increased. Taken that the cross-linked hydrogels are

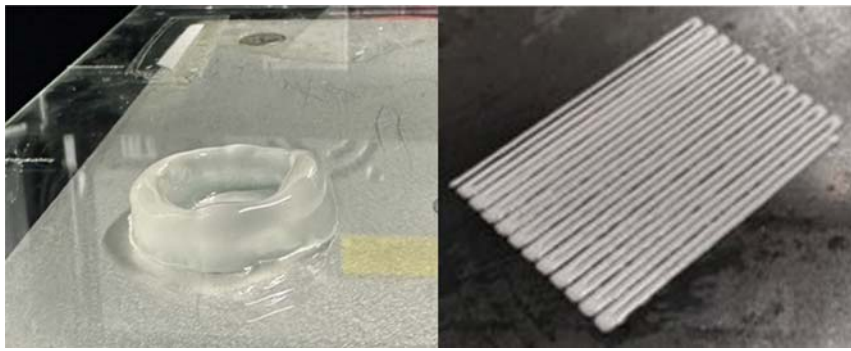

Figure 8.10 3D-printed gelatin-based hydrogels.

solid-like, the on-set amplitude, that is, elastic modulus (G') or the magnitude of complex modulus (G^*) drop, defines yield stress. This on-set splits the amplitude regime into two: (1) low-amplitude regime where the hydrogels exhibit their linear viscoelastic behaviors and (2) high-amplitude regime where nonlinear viscoelasticity arises. As mentioned above, both stress- or strain-controlled tests can be used to estimate the yield stress, but technically, stress-controlled is encouraged as it is a direct measurement and the amplitude spacing can be specified for better resolution (Ewoldt and McKinley, 2017).

Alternating between low- and high-amplitude oscillatory strengths can give an insight into the recoverability. For this, the low- and high-amplitude regimes must be identified first using LAOS, as described above. The test time Δt of each substep and number of repeats can be adjusted to reveal the material properties of interest. For example, this recovery is linked to shape retention of the filament on the substrate in direct-ink writing (Diloksumpan et al., 2020; Corker et al., 2019).

For injectable hydrogels, the steady-state viscosity as a function of shear rate, $\eta\left(\dot{\gamma}\right)$—also referred to as flow curves—can also be reported. However, for cross-linked hydrogels, flow instabilities, e.g., shear banding and edge fracture, can occur in the high shear rate regime. A detailed explanation of such phenomena can be found elsewhere (Divoux et al., 2016).

8.4 Conclusion

Bioresorbable polymers represent a diverse family of biomaterials, which can be absorbed by the body and then disappear when, after healing, the device is no longer needed. Innovative hydrogel products have been developed as carriers for specific applications or biomedical devices, including regenerative medicine, wound-healing dressings, and controlled-release drug-delivery systems. Recently, resorbable hydrogel has been variously applied in controlled-release drug delivery and wound-healing dressings as it can be degraded in the human body and also undergoes time degradation, depending on the materials. Bioresorbable hydrogel can be synthesized by several fabrication techniques. Many hydrogel systems have been developed, and fundamental studies have significantly contributed to understanding this unique class of materials. Many cross-linking methods are currently available to prepare hydrogels. Among these cross-linking methods, the physically cross-linked hydrogels are of greatest

interest, particularly when the hydrogels are fabricated under mild conditions without organic solvents. Although several interesting physical methods are known, 3D printing of hydrogel drugs is gradually increasing. However, some challenges remain, including poor shape fidelity, drug type and load limitations, and the requirement for soaking the hydrogels in the drug solution. It is expected that the current design and fabrication of bioresorbable-based hydrogels used for drug-release applications, along with some representative examples emphasized in this chapter, could further benefit in their development and application for biomedical purposes, in particular drug-release applications.

References

Ahmed, E.M., 2015. Hydrogel: preparation, characterization, and applications: a review. J. Adv. Res. 6 (2), 105–121.

Auriemma, G., et al., 2020. Technologies and formulation design of polysaccharide-based hydrogels for drug delivery. Molecules 25 (14), 3156.

Chacko, R.T., et al., 2012. Polymer nanogels: a versatile nanoscopic drug delivery platform. Adv. Drug Deliv. Rev. 64 (9), 836–851.

Chatterjee, S., Hui, P.C., Kan, C.W., 2018. Thermoresponsive hydrogels and their biomedical applications: special insight into their applications in textile based transdermal therapy. Polymers 10 (5).

Corker, A., et al., 2019. 3D printing with 2D colloids: designing rheology protocols to predict 'printability' of soft-materials. Soft Matter 15 (6), 1444–1456.

Diloksumpan, P., et al., 2020. Combining multi-scale 3D printing technologies to engineer reinforced hydrogel-ceramic interfaces. Biofabrication 12 (2), 025014.

Divoux, T., et al., 2016. Shear banding of complex fluids. Annu. Rev. Fluid Mech. 48 (1), 81–103.

Ewoldt, R.H., McKinley, G.H., 2017. Mapping thixo-elasto-visco-plastic behavior. Rheol. Acta 56 (3), 195–210.

Feng, W., et al., 2016. Tough polypseudorotaxane supramolecular hydrogels with dual-responsive shape memory properties. J. Mater. Chem. B 4 (11), 1924–1931.

Gritsch, L., et al., 2021. Combining bioresorbable polyesters and bioactive glasses: orthopedic applications of composite implants and bone tissue engineering scaffolds. Appl. Mater. Today 22.

Guo, M., et al., 2014. Tough stimuli-responsive supramolecular hydrogels with hydrogen-bonding network junctions. J. Am. Chem. Soc. 136 (19), 6969–6977.

Hu, Y., et al., 2012. Novel bioresorbable hydrogels prepared from chitosan-graft-polylactide copolymers. Polym. Int. 61 (1), 74–81.

Hu, W., et al., 2019. Advances in crosslinking strategies of biomedical hydrogels. Biomater. Sci. 7 (3), 843–855.

Im, S.H., et al., 2020. Strategy for stereocomplexation of polylactide using O/W emulsion blending and applications as composite fillers, drug carriers, and self-nucleating agents. ACS Sustain. Chem. Eng. 8 (23), 8752–8761.

Ishii-Mizuno, Y., et al., 2017. Improved sustained release of antigen from immunostimulatory DNA hydrogel by electrostatic interaction with chitosan. Int. J. Pharm. 516 (1–2), 392–400.

Islam, F., et al., 2022. Pectin and mucin modified cellulose-based superabsorbent hydrogel for controlled curcumin release. Cellulose 29 (9), 5207–5222.
Kesharwani, P., et al., 2021. Biomedical applications of hydrogels in drug delivery system: an update. J. Drug Deliv. Sci. Technol. 66, 102914.
Kobe, R., Yoshitani, K., Teramoto, Y., 2016. Fabrication of elastic composite hydrogels using surface-modified cellulose nanofiber as a multifunctional crosslinker. J. Appl. Polym. Sci. 133 (4).
Li, S., 2003. Bioresorbable hydrogels prepared through stereocomplexation between poly(L-lactide) and poly(D-lactide) blocks attached to poly(ethylene glycol). Macromol. Biosci. 3 (11), 657–661.
Li, S., El Ghzaoui, A., Dewinck, E., 2005. Rheology and drug release properties of bioresorbable hydrogels prepared from polylactide/poly(ethylene glycol) block copolymers. Macromol. Symp. 222 (1), 23–36.
Liu, H., et al., 2018. A functional chitosan-based hydrogel as a wound dressing and drug delivery system in the treatment of wound healing. RSC Adv. 8 (14), 7533–7549.
Masruchin, N., Park, B.-D., Causin, V., 2015. Influence of sonication treatment on supramolecular cellulose microfibril-based hydrogels induced by ionic interaction. J. Ind. Eng. Chem. 29, 265–272.
Molina, M., et al., 2015. Stimuli-responsive nanogel composites and their application in nanomedicine. Chem. Soc. Rev. 44 (17), 6161–6186.
Mondal, S., Das, S., Nandi, A.K., 2020. A review on recent advances in polymer and peptide hydrogels. Soft Matter 16 (6), 1404–1454.
Nele, V., et al., 2020. Tailoring gelation mechanisms for advanced hydrogel applications. Adv. Funct. Mater. 30 (42), 2002759.
Neophytou, C.M., Constantinou, A.I., 2015. Drug delivery innovations for enhancing the anticancer potential of vitamin E isoforms and their derivatives. BioMed Res. Int. 2015, 584862.
Ouyang, L., et al., 2017. A generalizable strategy for the 3D bioprinting of hydrogels from nonviscous photo-crosslinkable inks. Adv. Mater. 29 (8).
Ouyang, L., et al., 2022. Tunable microgel-templated porogel (MTP) bioink for 3D bioprinting applications. Adv. Healthcare Mater. 11 (8), e2200027.
Peng, Z., Peng, Z., Shen, Y., 2011. Fabrication and properties of gelatin/chitosan composite hydrogel. Polym.-Plast. Technol. Eng. 50 (11), 1160–1164.
Rasoulzadeh, M., Namazi, H., 2017. Carboxymethyl cellulose/graphene oxide bionanocomposite hydrogel beads as anticancer drug carrier agent. Carbohydr. Polym. 168, 320–326.
Singhal, R., Gupta, K., 2015. A review: Tailor-made hydrogel structures (classifications and synthesis parameters). Polym.-Plast. Technol. Eng. 55 (1), 54–70.
Tao, C.-a., et al., 2012. Fabrication of pH-sensitive graphene oxide–drug supramolecular hydrogels as controlled release systems. J. Mater. Chem. 22 (47).
Torres-Martinez, A., et al., 2019. Liposome-enveloped molecular nanogels. Langmuir 35 (41), 13375–13381.
Tran, V.T., Benoit, J.P., Venier-Julienne, M.C., 2011. Why and how to prepare biodegradable, monodispersed, polymeric microparticles in the field of pharmacy? Int. J. Pharm. 407 (1–2), 1–11.
Tran, T.H., et al., 2017. Removal of metal ions from aqueous solutions using carboxymethyl cellulose/sodium styrene sulfonate gels prepared by radiation grafting. Carbohydr. Polym. 157, 335–343.
Wang, R., et al., 2015. Kinetically stable metal ligand charge transfer complexes as crosslinks in nanogels/hydrogels: physical properties and cytotoxicity. Acta Biomater. 26, 136–144.

Wang, K., et al., 2019. Functional hydrogels and their application in drug delivery, biosensors, and tissue engineering. Int. J. Polym. Sci. 2019, 1–14.
Yan, S., et al., 2017. Templated fabrication of pH-responsive poly(l-glutamic acid) based nanogels via surface-grafting and macromolecular crosslinking. RSC Adv. 7 (24), 14888–14901.
Ye, X., et al., 2017. Self-healing pH-sensitive cytosine- and guanosine-modified hyaluronic acid hydrogels via hydrogen bonding. Polymer 108, 348–360.
Zafar, S., et al., 2021. Role of crosslinkers for synthesizing biocompatible, biodegradable and mechanically strong hydrogels with desired release profile. Polym. Bull. 79 (11), 9199–9219.
Zhou, Q., et al., 2018. Influence of different divalent ions cross-linking sodium alginate-polyacrylamide hydrogels on antibacterial properties and wound healing. Carbohydr. Polym. 197, 292–304.
Zolfagharian, A., et al., 2018. Polyelectrolyte soft actuators: 3D printed chitosan and cast gelatin. 3D Print. Addit. Manuf. 5 (2), 138–150.
Zu, S., et al., 2022. A bioinspired 4D printed hydrogel capsule for smart controlled drug release. Mater. Today Chem. 24, 100789.

CHAPTER 9

Molecular modeling of polymers for efficient drug-carrier applications

Rosaline Mishra[1], Dinesh Puri[2], Radha Goel[3], Praveen Kumar Gaur[1], Prasoon Kumar Saxena[4], Niharika Lal[1] and Kanak Lata[1]

[1]Metro College of Health Sciences and Research, Greater Noida, Uttar Pradesh, India; [2]School of Pharmacy, Graphic Era Hill University, Dehradun, Uttarakhand, India; [3]Lloyd Institute of Management and Technology, Greater Noida, Uttar Pradesh, India; [4]Sunder Deep Pharmacy College, Ghaziabad, Uttar Pradesh, India

9.1 Introduction

Molecular modeling is the discipline of numerically depicting molecular structures and replicating their behavior using quantum and traditional physics formulae. Polymer experts are able to directly create and collect molecular data such as energies, geometries, electronic characteristics, spectral characteristics, and bulk characteristics using computer tools. The characteristics of materials are well known to be closely linked to their makeup and bulk condition at the level of the molecular structure. Molecular modeling may be the only technique capable of directly revealing the structure of materials at the molecular level (Zuilhof et al., 2018).

In this chapter, we have made an effort to highlight important recent developments in the discipline of molecular modeling and demonstrate the ideas, techniques, and potential uses for smart polymer-based medication delivery. We propose a road map highlighting the possibilities and constraints of employing reliable multiscale molecular modeling approaches to accelerate the process of improved polymer-driven drug-delivery systems. These computational methods allow forecasts and interpretations of empirically known macromolecular frameworks, interactions, and micro- and macro-material characteristics. Polymer simulations, with recent advances in computational capacity, can educate, guide, and enhance empirical macromolecular component design and discovery activities. We also provide an overview of key design approaches for creating improved

Bioresorbable Polymers and their Composites
ISBN 978-0-443-18915-9
https://doi.org/10.1016/B978-0-443-18915-9.00007-0
© 2024 Elsevier Ltd.
All rights reserved.

multidimensional polymer structures, highlighting how the unique structure and chemistry of a few polymer-based drug-delivery systems can provide excellent drug-delivery platforms.

The effectiveness of a drug is usually hampered by poor water solubility and short residence time in the body's tissues (Zuilhof et al., 2018). Conventional drug distribution forms have made significant contributions to disease therapy. Several factors have increased the demand for smart transportation methods such as low effectiveness, trouble maintaining drug levels within desired ranges, reducing adverse reactions and toxicities, and the rise of particular biological therapies.

The requirement for better bioavailability, customized transport, long-term action, and other factors motivate the development of innovative pharmacological forms based on established therapeutic compounds. Biodegradable polymers, which are excellent candidates, have been extensively researched in recent years, especially as carriers for renal, long-circulating, and pH-sensitive drugs, in order to enable bone tissue engineering applications (Andreopoulos and Tarantili, 2002; Berendsen et al., 1984; Bourassa et al., 2011). Medication carriers with specific characteristics that are adapted for a given biological target are the foundation of effective medication delivery. Drug carriers with unique qualities that are matched to a specific cellular target are the foundation of effective drug transportation. Three primary qualities can be highlighted, namely:

(1) The ability of a polymer and a medication substance to mix together.
(2) The interactive force among the polymer chain and the drug molecule is identified by the nonbond intermolecular polymer—drug interaction energy.
(3) Polymer chain flexibility to describe the drug molecule's capacity to be coated and protected for prolonged circulation.

The smart polymers are classified broadly into organic and inorganic systems, and by varying their compositions, shapes, dimensions, and surface properties, it is possible to modify the physiochemical features of these systems. Polymer micelles, glycopeptides, etc. constitute the organic category, whereas carbon-, silica-, and silver-based ones fall into the inorganic category.

Computer modeling techniques that are properly evaluated and parameterized can provide the required molecular specifics to develop better knowledge of the process by which the Active Pharmaceutical Ingredient (API) is formulated and supplied.

There are numerous macro-molecular modeling methodologies accessible for application, including quantum mechanics (QM), molecular mechanics (MM), Monte Carlo (MC), molecular dynamics (MD), and other famous methods such as meso scale (MS).

9.2 Methods for molecular simulation for designing polymers

A computational scientist has specific problems when working with the class of complex fluids known as polymers as they display fascinating and important features over an extensive spectrum of scaling range, from the monomer to the polymer's radius of gyration. Numerous software and algorithm breakthroughs, as well as major advancements in computer hardware, have been made to overcome these computational challenges (McCrackin, 1967).

Nowadays, molecular simulation approaches are crucial tools for the computational devising of new material designs as well as for the synthesis and prediction of the structure—property relationships of molecular systems.

The polymer community has faced enormous challenges in the present era due to the search for innovative materials with improved performance, less environmental impact, and/or characteristics that imitate bio-systems (Frenkel, 2013). We have briefly discussed the relevant simulation techniques that are suited for each type of model, but in general, the polymers are MC and MD. The MC methods often incorporate uncorrelated random numbers to comprise a significant number of stochastic computer operations (Piscitelli et al., 2010). It must be noted that MC approaches are not restricted to the atomic size and can be utilized at any level if the appropriate logical model is provided. Three distinct phases are a common component of MC techniques:

(1) Converting the observed physical phenomenon into a comparable statistical model.

(2) Dealing with the derived logical model by numerous numerical stochastic sampling trials.

(3) Statistically examining the informative data. A basic sample method or a weighted sample method can be used as the sampling method. Simple sampling employs random numbers distributed equally, whereas weight sampling creates random numbers depending on the distribution tailored to the subject under investigation.

9.2.1 Simulation with Monte Carlo

This simulation is a potent method for predicting the essential physico-chemical features of complex systems and balancing their dense phases. It is especially well suited for modeling chain-like systems' bulk phases. Early MC simulations were carried out on lattice models because of challenges with eliminated quantity interactions, chain interactions, and conformational firmness (Mavrantzas, 2004), but emerged soon in continuous space. Nowadays, we can broadly divide the MC moves created for polymers as follows:

(1) Simple MC moves
(2) Complex MC moves
(3) Advanced MC moves.

(1) Simple MC moves

Repetition (McCrackin, 1967), libration or flip (Theodorou et al., 2004), dimer flip (Mavrantzas, 2004), concerted rotation (Vacatello et al., 1980), intrachain and interchain concerted rotation (Mavrantzas et al., 1999), general repetition (Peristeras et al., 2005), parallel rotation (Mavrantzas et al., 1999), pivot (Rosenbluth and Rosenbluth, 1955), end-mer rotation atom identity exchange (Dodd et al., 1993), and quantity fluctuation (Lal, 1969) are examples of basic MC moves. These operations are restricted to a lone polymer cycle, and general repetition, configurational bias, and end-mer rotation only work at the ends of the chain.

(2) Complex MC moves

Large interior regions of one or two polymer chains undergo simultaneous dramatic reconfigurations as a result of complex MC motions. They first show as chain-breaking steps (Olaj and Lantschbauer, 1982) in MC simulations of polymers on a cluster, ultimately leading to the discovery of chain connectivity altering moves. The following movements are incorporated in a group of complex MC moves: targeted internal bridging, targeted end-bridging, self-end-bridging, and fusion-scission (Zervopoulou et al., 2001).

(3) Advanced MC moves

Intramolecular double rebridging (IDR) and double bridging (DB) are examples of advanced MC maneuvers (Karayiannis et al., 2002). These are end-bridging move generalizations in that they entail the concurrent or sequential development of two trimer structures (instead of one).

9.2.2 Recent Monte Carlo computer software

These MC moves are available in a few software programs for general polymer design. Readily available MC software include:

(a) Using the enhanced MC code (Halverson et al., 2013) to simulate semicrystalline polymers (Kumar et al., 2017)
(b) Towhee (Martin, 2013)
(c) Cassandra (Shah et al., 2017)
(d) RASPA (Dubbeldam et al., 2016).

In recent years, Chameleon, one of the latest simulation programs in C++ with many chains, was presented by Alexiadis et al. (2019). This new tool can characterize polymer structures including polyethylene (PE), polyvinyl chloride (PVC), and polystyrene (PS) using either an all-atom, united-atom, or coarse-grained framework. It can also handle a wide range of polymer schemes, such as straight and branching polymers. DICE, an MC technique for molecular modeling of large stretchy molecules, has been updated by Cezar et al. (2020) for solute–solvent systems in the liquid or gas phase. This version is based on a more effective use of the configurationally biased move.

MC was used by Dodd and Jayaraman (2012) to examine the effects of polydispersity on the arrangement of polymers on rounded surfaces. They looked at the distribution of free-end monomers inside the grafted layer as well as the shape of the grafted polymer chains and the thickness of the layer created.

Based on single-chain Metropolis MC simulations, Tzounis et al. (2017) proposed a method for computing the unperturbed chain measurement of any polymer chain, independent of its chemical or architectural complexity.

Mendonça et al. (2016) developed the configurationally biased MC method as a replacement for the dissipative particle dynamics (DPD) technique to investigate hassle between grafted polymers with suitable solvents. The primary finding was that the shear force at which slip occurs decreased significantly with the flexibility of the polymer layer.

The tensile blob was previously supported by MC simulations of long, single linear polymer chains stretched uniformly by Pierleoni et al. (1997).

Metropolis MC has now developed into a potent computational tool that is capable of addressing many physicochemical aspects of genuine polymers (structural, conformational, thermodynamic, and morphological) with surprising precision.

9.2.3 Molecular dynamics

Despite the limitless potential of MC, the technique still needs to address some flaws and problems to mature to the same degree as molecular dynamics.

For the most part, "molecular dynamics" is effective at simulating systems with many atoms, such as polymers. The benefit of MD is that it can quickly determine a system's dynamics by analyzing the motion of its atoms according to classical mechanics.

MD simulation, which initially appeared in the late 1970s, has progressed from demonstrating a few hundred atoms to biologically relevant systems; totally dissolved proteins with distinct solvent representations, membrane-embedded proteins, or massive macromolecular structures like nucleosomes or ribosomes are examples of these types of structures.

In particular, the advantage of MD simulations is that they can directly and quantitatively predict both the structure and dynamic features of a molecular system.

Newton's second rule governs each atom's motion in atomistic MD simulations (aMDs), making it possible to determine each atom's position as a function of time. Simulations can be used to improve structures, identify the attributes at equilibrium states, and/or comprehend the dynamic behavior of the system.

A typical straightforward MD algorithm's flowchart shows the steps listed below (Binder, 1995):

1. The method begins with the selection or building of a configuration that reflects a molecular-level snapshot of the relevant physical system (starting locations and velocities of each particle inside the system).
2. After that, the total force exerted by the system's particles is calculated.
3. Using the proper methodology, integrating the motion equations follows.
4. Measurements are made with accuracy (velocities, positions, energies)
5. When the central loop is complete, the mean of all of the quantities and the necessary characteristics are calculated and printed (N steps).

$$m_i\ddot{\mathbf{r}}_i \equiv m_i\dot{\mathbf{q}}_i = \mathbf{F}_i$$

where $\mathbf{F}i$ represents the force pulling on atom i. Differential equations of second order in 3N are then used to solve motion equations.

The following elements (Binder, 1995) need to be taken into account while choosing an algorithm:

- The algorithm should not necessitate an excessively high volume of force evaluations for each integration time step.
- The algorithm needs to adhere to the energy conservation law.
- The algorithm ought to allow for the usage of a big-time step dt.
- The algorithm should run quickly and use little memory.

An MD simulation's primary goal is to predict thermodynamic parameters as time averages and determine temporal correlation functions that are descriptive of the dynamics, not to trace the precise configuration of a system over a lengthy period of time.

In the field of research and development, quantum ATK polymer simulator software is used to create polymers with enhanced thermal conductivity, thermomechanical and optical properties for products like photo-resist, transparent polymers, rubber-like polymers for tire manufacturing, along with thermoset polymers for the insulation industry. Quantum ATK's polymer construction and equilibration tools create trustworthy polymer models, which can subsequently be simulated utilizing fully automated processes and an MPI parallelized MD engine.

9.3 Applications of the polymer-based smart nanocarriers

Polymer particles have shown their usefulness in maintaining and keeping drug molecules safe, including proteins and DNA molecules against degradation caused by various environmental hazards (Kawashima, 2001). Thus, these polymers offer different possibilities for the delivery of proteins and genes. There are many ways to make nanoparticles, dependent on the polymer's physical and chemical characteristics, as well as the active component (Panyam and Labhasetwar, 2003). The aspects that need to be taken into synergistic account for a smart, regulated delivery system are listed in Fig. 9.1.

Trying to classify nanocarriers precisely is a daunting task. Since there is no clear boundary between the biomedical and pharmaceutical nanotechnology fields, different viewpoints may be relevant. They can also be categorized based on where they came from, such as natural or synthesized polymeric nanoparticles. Since they simultaneously perform polymer design and colloidal measurements (1000 nm), these are usually identified as polymer nanoparticles (biodegradable and biocompatible), nanoemulsions,



Figure 9.1 . Multiple variables must be taken when building a polymeric nanoparticle for a smart drug-delivery system.

dendrimers, polymersomes, polymer micelles or complexes, or cubosomes (Li et al., 2016). Polymer drugs, polymer–drug conjugates, polymer–protein conjugates, polymer micelles (drugs covalently bound to polymer carriers), and complexes (designed as nonviral vectors) are all examples of polymer therapies (Lal et al., 2022). Materials are selected for the creation of polymer-based nanocarriers not only for their biological behavior but also for their functional qualities, such as their capacity to construct designed nanostructures. Biocompatible and recyclable polymers are generally preferred.

Large numbers of available and/or easily synthesized polymers with good potential are used in medicine, while only a few have achieved regulatory approval (Lal and Verma, 2021). In order to increase medication specificity and decrease systemic toxicity, a number of nano-drug delivery systems have been created and assessed. They are now thought to be the most common and promising methods. For the treatment of cancer and other inflammatory illnesses, nanocarriers employ increased permeability and retention (EPR) to selectively concentrate at areas of disease. To progress toward more advanced nano drug-delivery systems (DDSs), research has focused on improving the performance of polymer carriers by developing smart, stimuli-responsive nanocarriers (SRNs). Such carriers change their composition as a result of internal or external stimuli, leading to dissociation of the carrier and release of the drug, based on

pharmacokinetics and pharmacodynamics when reaching the site of action after administration (Kawashima, 2001). The pH and presence of certain enzymes within cells or inside the pathological microenvironment are the two most significant and commonly used internal stimuli. Reduced glutathione stimulating hormone in the cytosol is also extensively utilized in the development and manufacture of reduction-sensitive polymer nano DDS (Cui and Mumper, 2002).

These multifunctional polymeric nanocarriers can solve current nanoparticle-based drug formulation problems, such as drug formulation and encapsulation, long-term stability, cell internalization, site targeting, increase in cellular uptake, intracellular targeting, and drug release. These double- and multi-activation response properties provide exciting new control over drug-release kinetics with improved efficacy (Cao et al., 2001). Due to their nonbiodegradable carriers, poor encapsulation, and unsuitability for clinical therapy, all mentioned studies of stimuli-responsive dual and diverse drug-delivery systems are primarily trial-and-error models. Fig. 9.2 provides descriptions of dual-response and multiple-response nanoparticle systems. It should be emphasized that the stimulus and the response occur simultaneously in the same place or in different ways (Kreuter, 1994). This multi-stimuli-responsive polymeric nanocarriers have the ability to regulate drug-release profiles and enhance anticancer effectiveness in both in vitro and in vivo models, while also allowing control of nanocarrier formulation and drug loading under controlled conditions. We briefly discuss a few cases in this section (Kasagana et al., 2011).

In particular, dual-response triblock copolymers functionalized by raising the temperature and remaining below the decreasing critical solution temperature followed by cross-linking have been developed as multifunctional nanoparticle systems for drug delivery that is sensitive to reduction and temperature (Lal et al., 2021). These multifunctional nanoparticle systems are triggered by a reduction—oxidation mechanism that causes the decross-linking, disruption, and disintegration of the nanoparticle system, which releases the active components. These nanoparticle systems have been developed to target cancer cells.

For greater drug release and accumulation in cancer targets, multifunctional disulfide cross-linked micelles with dual pH/redox stimulation have been generated. Intracellular pH and the redox environment of cells/lysosomes facilitate drug release (Lal et al., 2017).

Improved biodegradable as well as biocompatible, nonimmunogenic, and nontoxic smart polymer nanoparticles, capable of effectively capturing

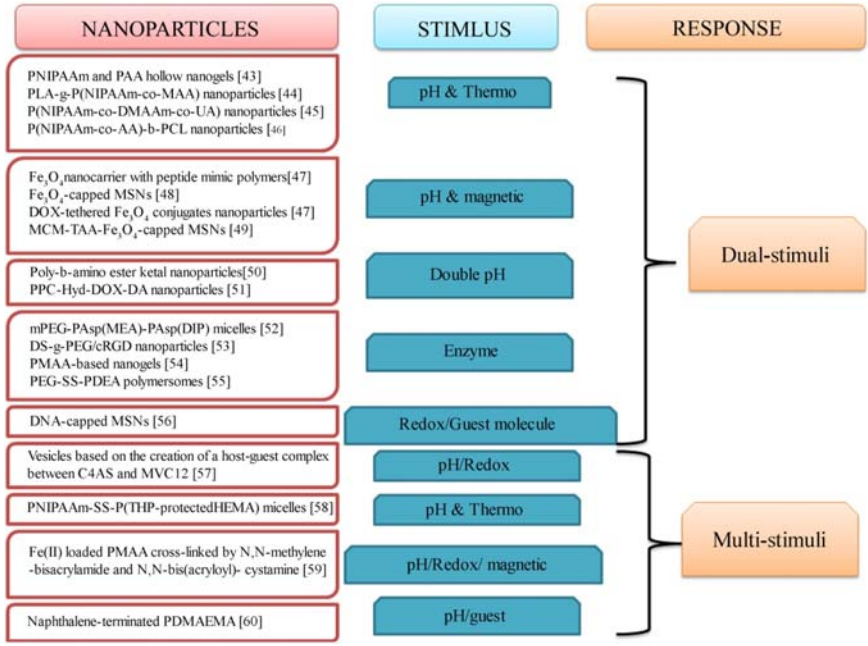

Figure 9.2 An overview of materials that respond to dual or multiple stimuli for nanocarriers used in several smart drug-delivery systems.

and maintaining the release of drugs into the systemic circulation, improving the accumulation of cancer targets, and with effective release kinetics in response to external or internal stimuli are the immediate targets to overcome any adverse conditions (Lo et al., 2005). In addition, smart polymer nanoparticle technology does not cause any collateral damage or damage to healthy cells. To determine the actual mode of action of anti-cancer targets, clinical studies of dual and multiple stimulus—response systems are needed. Additionally, smart nanoparticle systems with dual and multiple stimuli responses are bound to show promise in cancer treatment. This will consist of targeting ligands and nanoparticles responsive to dual/multiple stimuli to treat multidrug-resistant cancers through site targeting, site-specific delivery, and rapid or sustained release (Zhang et al., 2011; Loh et al., 2012). Fig. 9.3 presents images describing responsive nanocarriers.

The development of smart stimuli-responsive nano DDSs is an important new area of drug delivery. The most extensively studied concern endogenous triggers (enzymes, pH, and redox potential) that exploit certain intracellular or microenvironmental conditions present at the diseased area to accomplish controlled drug release (Heller, 1984). In addition to

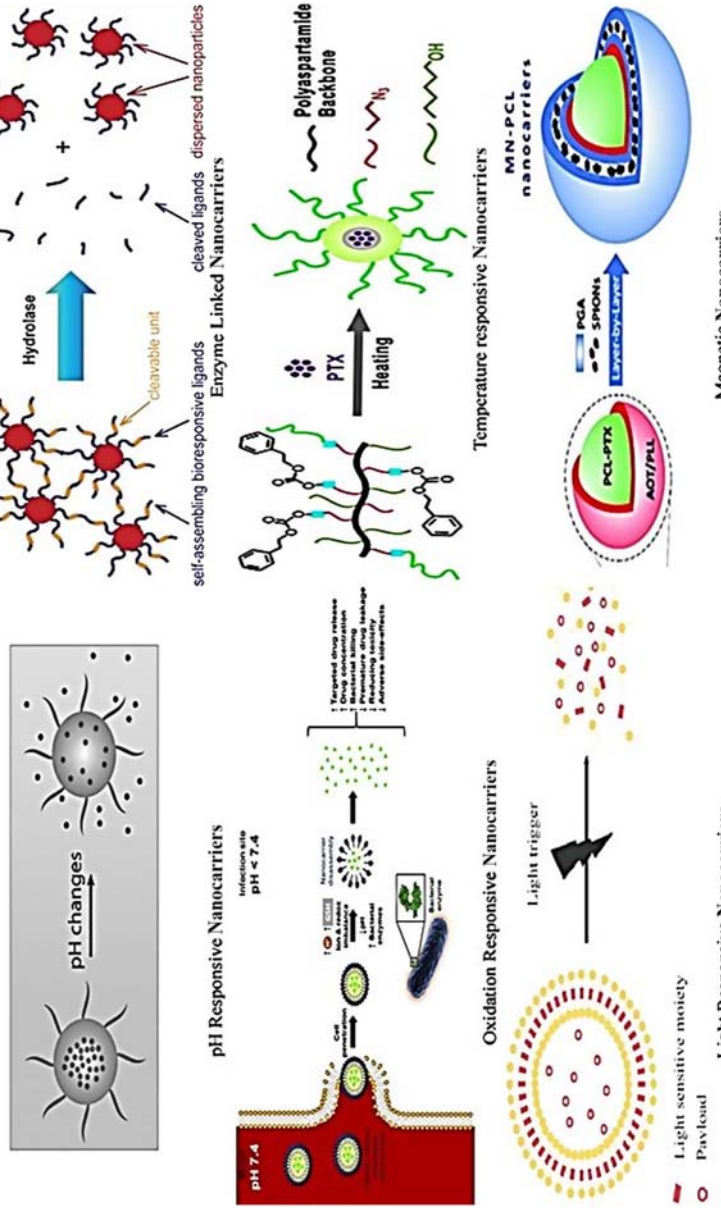

Figure 9.3 Different types of responsive nanocarriers.

endogenous stimuli, there is a growing interest in externally applied stimuli, often using methods currently used clinically for other purposes, such as ultrasound and magnetic fields. Despite the fact that this strategy appears to be promising, the main problem is coordinating drug accumulation with the application of exogenous stimuli with sufficient force to initiate drug release (You et al., 2003).

This approach is frequently used in conjunction with imaging methods to detect the distribution of nano DDS bodies, resulting in effective companion diagnostics similar to those already existing in the clinical setting. The development of personalized or patient-centered therapies could benefit from this strategy. New methods are needed to enable classification of patients and to identify those who may benefit from specific treatments due to patient heterogeneity (Tyle and Agrawala, 1989). To achieve site-specific drug release, probes for molecular imaging are activated under specific triggers with intraindividual, interindividual, and cell-to-cell variability, the application of stimuli-responsive DDS is essential. Therefore, they can be used to identify functional biomarkers needed to predict treatment effects (Schmaljohann, 2006).

Table 9.1 presents recent development program in the creation of smart nano DDS. Most of the research published till date remains proof-of-concept work, and the safety and efficacy of these nanocarriers in vivo have yet to be determined.

9.3.1 The era of smart polymer revolution

Resins known as smart polymers (SPs) change or respond in a particular manner to their surroundings. Since they are composed of polymers, even the slightest environmental changes cause them to react drastically. The terms "stimuli-responsive polymers," "intelligent polymers," and "environmentally sensitive polymers" are also used to describe them. What basically makes these polymers stand out as "smart" materials is their exceptional ability to react to extremely minute changes in their surroundings. These SPs are "smart" because they can modify their physical shape in response to stimuli with slight environmental changes, such as changes in pH or temperature, increases in ionic strength, the presence of particular metabolic chemicals, the inclusion of an opposite-charged polymer and the formation of polycation–polyanion complexes, and changes in an external force and alterations in a magnetic and electric field, radiation forces, or light (Vargas et al., 2018).

Table 9.1 List of responsive nanocarriers with respect to their functional attributes.

- **pH-responsive nanocarriers**

Dependent: pH

Example: Anticancer drugs are released selectively, taking into account the temporary or persistent acidity of tumors and areas of inflammation as compared to normal (Kato et al., 2013)

Mechanism: Based on two approaches:

1. In the initial strategy, either a pH-sensitive polymer is applied, or it degrades, resulting in the release of the drug, or the change in pH causes a change in the physicochemical properties (i.e., polarity) of the polymer, which destabilizes the nanocarrier and leads to the simultaneous release of the drug
2. Using an acid-cleavable linker, the drug is affixed to the polymeric base (Erdmann and Uhrich, 2000; Pang et al., 2016)

- **Enzyme-responsive nanocarriers**

Dependent: Catalytic activity of enzymes

Examples: Biocatalysis, sensing, imaging, controlled drug release and diagnostics (Gendelman et al., 2015)

Mechanism: Based on two approaches:

- Enzymatic transition is dependent on the nanocarrier itself

In enzyme-activated solutions, surface modification of nanocarriers with molecules results in modifications to the carrier's physical characteristics (Lammers et al., 2012; Zhao et al., 2018)

- **Oxidation-responsive nanocarriers**

Dependent: Redox potential variations between the outside of the cell and inside the cell habitat

Examples: Proteins, siRNA, intracellular DNA, low-molecular-weight drugs, and cancer treatments (Phillips and Gibson, 2014)

Mechanism: Based on two approaches:

The main components of these systems are cationic polymers, which can link DNA and siRNA to form complexes, and disulfide cross-linkers, which are specifically reduced inside the cell and lead to the cargo release and transfection efficiency (Cai et al., 2015; Wang et al., 2011b)

(Continued)

Table 9.1 List of responsive nanocarriers with respect to their functional attributes.—cont'd

- **Temperature-responsive nanocarriers**

Dependent: Temperature fluctuations instead help with self-assembly rather than drug release
Example: Cancer treatments (Jochum and Theato, 2013)
Mechanism: When a drug is encapsulated, local hypo/hyperthermia allows for its release. This results in a modification of the temperature-sensitive polymer's state and the dissociation of the micellar structure (Hu et al., 2015)

- **Light-responsive nanocarriers**

Dependent: Photoresponsive response to irradiation
Example: Precise spatial and temporal application (Linsley and Wu, 2017)
Mechanism: Azibenzene and o-nitrobenzyl are the two most often employed photosensitive compounds. Polymeric micelles and vesicles that enable release upon illumination have also been produced using photosensitive moieties including copolymers, owing to polarity shifts (Marturano et al., 2017)

- **Ultrasound-responsive nanocarriers**

Dependent: One option is to use ultrasound to facilitate drug release from nanocarriers
Examples: Tumor regression and reduced cardiotoxicity (Xia et al., 2016)
Mechanism: Ultrasound waves cause oscillating bubbles to form, which eventually burst, disrupting the polymer assemblies nearby. According to reports, using ultrasonic to biodegradable polymers may speed up the process of disintegration (Concellón et al., 2016; Ulbrich et al., 2016)

- **Magnetic-field-responsive nanocarriers**

Dependent: Paramagnetic or superparamagnetic nanoparticles are used to create magnetically responsive nanocarriers within a polymeric vehicle (Revia and Zhang, 2016)
Example: MRI (image-guided drug delivery), incredibly effective at destroying cancer through hyperthermia (Baeza et al., 2012)
Mechanism: It can function as a dual therapeutic agent, releasing drugs through the dissociation of nanocarriers and destroying cancer cells through hyperthermia (Yigit et al., 2012)

Electrical currents caused smart polymers to very quickly change their viscosity. The phrase "smart polymers" was first used in this context, and applications of environmentally sensitive polymers were assessed (Pan et al., 2012; Linsley and Wu, 2017; Galaev and Mattiasson, 1999). The key advantages of smart polymers are their simplicity in production, ability to maintain medication stability and level within the therapeutic window, and ability to promote patient compliance. Targeted drug-delivery systems, tissue engineering, microfluidic processes, gene carriers and bioseparation, reversible biocatalysts as actuators, protein folding, and several more important applications are just a few examples of the pharmaceutical industry's utilization of these technologies.

Scientists are currently chemically forming novel polymeric materials that can sense specific changes in the environment in biological systems and modify them reliably. These materials could be used as instruments for delivering medications or controlling other metabolic mechanisms (Gil and Hudson, 2004).

Smart polymers are simple to make, can be administered in situ as a liquid that gels at body temperature, are excellent carriers for providing nutrients to cellular and products from cells, can be readily changed with cell adhesion ligands, and are used for blood-contacting applications. They also improve patient cooperation, maintain drug stability, keep the drug level in the therapeutic range, and are nonthrombogenic, biocompatible, robust, pliable, and tough (Kumar et al., 2007). However, these polymers do have significant drawbacks, including the fact that they are frequently mechanically fragile and challenging to load with cells and medications.

Drug delivery is just one application for smart polymers. They are particularly well suited for bioseparations because of their characteristics. By utilizing smart polymers that change quickly and reversibly as a result of an alteration in the characteristics of the medium, the time and money required to purify proteins may be greatly decreased. Another approach for controlling biological reactions with smart polymers is to create recombinant proteins containing integrated polymer-binding sites adjacent to the ligand-binding sites. The technology of self-adaptive wound dressings depends greatly on smart polymers (Linsley and Wu, 2017; Zardad et al., 2016).

According to a published study, the dressing design uses patented, highly absorbent synthetic smart polymers that are immobilized in a matrix of three-dimensional fibers. Hydrogel is also incorporated into the material's core to provide additional hydration functionality.

One of the best examples of a thermally reversible, multifunctional polymer that is soluble-insoluble is poly(N-isopropylacrylamide), along with PNIPAAm, which, in an aqueous solution, has a lower critical solution temperature (LCST) of 32°C (Concellón et al., 2016; Galaev and Mattiasson, 1999).

9.3.1.1 Classification

The classification of smart polymers is as follows:

(I) "Smart" polymer categorization based on structural conformation

The triggers that cause the reaction or the type of conformation chosen for their application can both be used to categorize SPs. Many SPs can be described as:

(1) Chain-free state in the solution
(2) Trans-linked hydrogels
(3) Chains mounted on a surface, depending on their physiochemical makeup and distinctive structural traits.

(1) Chain-free state in the solution

SPs offered as a chain-free state in the solution are typically integrated into water-based systems. Two phases can be seen forming inside the system when these polymers are subjected to their stimuli. When external cues, such as temperature, are applied, the polymer-free chains of relevance in this class show reversible morphological changes. Thus, the motivation behind PNIPAAM's behavior appears (Hoffmann et al., 2002) in poly(ethylene oxide), poly(ethylene glycol), poly(propylene oxide), and poly(N-vinylcaprolactam). The bioprocessing application that employs SPs with this physical form most frequently is the production of ATPS.

(2) Trans-linked hydrogels

A hydrogel is a network of chains in three dimensions comprised of hydrophilic polymers, some of which are solvated by water atoms and others which bond together chemically or physically. Poly(2-hydroxyethyl methacrylate) (PHEMA) hydrophilic networks were proposed by Wichterle and Lim for use in contact lenses and the hydrogels used in the biomedical sector (Liu and Urban, 2010). In reaction to alterations in environmental stimuli, hydrogels with SPs in their structure can "swell" and then "deswell" or contract. The use of hydrogels has previously been

limited to the biomedical sector (i.e., drug delivery). New SP generations, however, may allow for the expansion of its application into new fields such as bioprocessing. Polymeric materials, both synthetic and natural, have been used to engineer a variety of hydrogels. For instance, some of the most well-known natural biopolymers include gelatin, chitosan, hyaluronic acid, alginic acid, and dextran. The most widely utilized natural polymer is chitosan (Zhou et al., 2013).

(3) Grafted chains on a surface

Chain-absorbed conformation, also referred to as "smart brushes" or "smart surfaces," is a category where polymers are covalently connected to the support (Da Silva et al., 2007). There are two possible reactions when these SPs come into contact with their stimuli: either the chains spread out while exposed, or they fall over the support.

(II) Sorting of "smart" polymers based on their activating stimuli

Stimuli-responsive polymers are capable of changing their structural characteristics in regarding to modifications in environmental factors such as pH, temperature, solvent, salt ionic strength, light field, and electrical field. Recent research has focused greatly on stimuli-responsive polymers because of their inventive response characteristics. They have been frequently used as drug-delivery carriers, coatings, membranes, synthetic organs, sensor technology, etc. All-atom molecular dynamics (AAMD) was one of the techniques that was introduced followed by coarse grained molecular dynamics (CGMD), and other methods that gained immense popularity were DPD and MC (Hu et al., 2014).

When studying the single-chain behaviors of stimuli-responsive polymers, AAMD was typically used; however, for larger block copolymers and blended systems, recent modeling developments, including simulations of temperature-, pH-, solvent-, and photo-responsive polymers, have been presented in order to understand the conformation transitions of stimuli-responsive polymers (You et al., 2016). The mechanism at the molecular level and theoretical framework for building intelligent materials may be provided by multiple scale modeling and simulations of stimuli-responsive polymers. Below, various simulation techniques are discussed, such as MC, DPD, AAMD, and theoretical techniques. The outcomes of simulations with stimulus-responsive polymers are then assessed in response to various stimuli (Appold et al., 2017).

9.3.2 Multiple scale simulations of sensitive polymers

9.3.2.1 Polymers with a pH response in simulations

The stimuli-responsive polymers known as pH-responsive polymers can alter in conformation and property in response to variations in the solution pH. The majority of pH-responsive polymers have ionizable groups, which can collect or release protons in response to modifications in the pH of the surrounding environment. Weak bases and acids like carboxylic acids, phosphoric acids, and amines are examples of commonly ionizable groups that change their ionization state when the pH changes (Ulbrich et al., 2016). DDSs, antifouling coatings, intelligent membranes, biosensors, super-hydrophilic surfaces, and other applications have all made extensive use of pH-responsive polymers. A polymer with pH sensitivity is assumed to have a fixed charge at each pH condition in the majority of molecular simulation studies (Hao et al., 2019; Lin et al., 2017). According to the observations of Longo et al., the charge variations are disregarded in applications. One way to solve this issue is to codify the charge regulation process brought on by proton fluctuations using statistical mechanical perturbation theory (Longo et al., 2019). Silva and Jonsson, in contrast, used semiquantitative analyses and MC simulations which are based on perturbation theory to investigate the charge-regulating protein interactions with polyelectrolytes (Gan et al., 2000). Their findings emphasized the significance of the charge regulation system and quantified when the ion−dipole term or charge control dominated the complexation. These techniques could be used to research pH-responsive polymer systems in the future.

A hydrophobic core with many functional groups that can be ionized can give or take protons as a result of pH variations is a pH-responsive SP. The ionization of pH-responsive polymers can cause a variety of structural alterations. Polyacrylic acid (PAA) is the widely recognized pH-responsive SP that has been the subject of most research.

Mesoscale modeling method DPD has been extensively used to comprehend how they change behavior under various pH environments. For example, the self-assembly of amphiphilic copolymers (PAE-g-PEG) found in vesicles, as well as the chemical load and release of doxorubicin drug molecules at various pH environments, have been widely investigated using DPD and MD models (Shao et al., 2012). It should be noted that the polymers in these DPD and MD models have set charges based on the pH level condition, which overlooks charge fluctuation in actuality. Nonetheless, these molecular modeling findings provide a quantitative grasp of

the pH-responsive polymers' controlled drug-release patterns at the molecular level.

Polymers with temperature response in simulations

Since temperature changes are very simple to achieve and to manage in both internal and exterior settings, temperature is a stimulus that is employed most frequently in stimulus-responsive polymer systems. Upper critical solution temperature (UCST)/lower critical solution temperature (LCST) are typically present in temperature-responsive polymers (Ramos et al., 2011). Since UCST polymers are rather uncommon, we concentrate mostly on the explanation of LCST polymers in this section. Water and the polymer would be mixable at temperatures below the LCST, forming a highly inflated, coil-like chain configuration, demonstrating hydrophilicity; at temperatures above the LCST, the polymer chain contracts and curls and additional phase separation takes place, demonstrating hydrophobicity (Ashraf et al., 2016).

The thermos-responsive polymer poly(N-isopropylacrylamide) is among the most common (PNIPAM). Amide groups (-CONH) and isopropyl groups (-$CH(CH_3)_2$), which are hydrophilic and hydrophobic, respectively, make up PNIPAM. At roughly 32°C, the LCST of PNIPAM is close to the temperature of the human body (305K). The structure of PNIPAM changes when the temperature crossed the LCST in an aqueous solution. As a result, drug-delivery systems frequently use it (Deshmukh et al., 2014). Using a variety of force-fields over the past 10 years, on an atomic scale, molecular dynamics simulations were utilized to investigate the coil-to-globule transition of PNIPAM (Li et al., 2014).

Polymers with a photo-response in simulations

Among the most thermos-responsive materials is a type of intelligent material known as photo-responsive polymers which use light to induce changes in color, chemical polarity, and conformation (Darvishmanesh et al., 2015). They have the advantages of environmental protection, remote controllability, and transitory qualities over other stimuli-responsive polymers. Hence, the usage of photo-responsive polymers in materials science has increased recently. Azolbenzene, stilbene, spiropyran, and other light-sensitive compounds are frequently found in the most researched light-responsive polymers. The photo-mechanical capabilities of the photo-responsive polymer azobenzene were studied by Choi and colleagues (Choi et al., 2018). There is a possibility of azobenzene moiety isomerization

having a significant impact on the orientation and conformity of the PRPN material, according to the results of AAMD simulations of the nanocomposites reinforced with gold nanoparticles, which showed that as the isomerization ratio increased, the rigidity and melting temperature decreased (Quan et al., 2016).

Simulations of other responsive polymers

Other responsive polymers, such as salt-responsive, electro-responsive, and dual-responsive polymers, have also been examined through computer simulations in addition to those described above. Ionizable groups are found in a class of polymers called salt-responsive polymers (Chen et al., 2019).

With the addition of saline ions, these polymers' solubility and conformation can adapt to the ionic strength in solutions. Dual-responsive polymers have drawn increasing interest in recent years because some applications may call for a combined response to several stimuli (Hao et al., 2019; Longo et al., 2019).

Dual-responsive polymers have been commonly used, and these include those that respond to heat, salt, and pH, and others (Chen et al., 2019). Using CGMD models, Liu et al. looked into the diblock copolymers PAAPDMAEMA's thermos-responsive and pH-responsive characteristics in aqueous liquids. They found that the molecular weight of PAA-PDMAEMA appeared to have a greater influence on the behavior of aggregation than did the makeup of the polymer (Han et al., 2014). Chen et al. examined the switching behavior of nanopores changed with double-responding block polymers using DPD models (PNIPAM and PAA). The influence of block proportion, chain length, grafting density, and block succession on a nanopore switching effect was thoroughly investigated. The findings showed that under different circumstances with high grafting density, medium block ratio and proper chain length, the wall-PNIPAM-PAA block pattern alone could accomplish the switching effect of nanopores (Chen et al., 2019). These publications have been valuable tools for further computer modeling studies on dual-responsive polymers.

9.4 Conclusion

Through the lens of advances in predictive modeling-led design, we have examined and investigated the most recent thrilling developments in smart multifaceted polymer-based nanoparticles (NPs). We discovered some major challenges and opportunities for future study, and we hope that our

findings will motivate more modeling-guided research into the synthesizing, self-assembly, and uses of smart polymer-based NPs. Because of the rapid advancement of computer technology, computer models such as CGMD, DPD, AAMD, and MC have been widely used to investigate the conformation transformations of stimuli-responsive polymers produced by external cues at the molecular level. External cues can be readily replicated by changing the ambient temperature, solvent setting, force field of view, or bonded properties. As a consequence, multiscale modeling and simulation have evolved toward effective methods for investigating stimuli-responsive materials at the micro- and mesoscopic levels, which could aid in the creation of innovative smart materials while reducing the expense and duration of experiments. A mixture of simulations and trials would help future studies into more complicated stimuli-responsive systems.

References

Alexiadis, O., Cheimarios, N., Peristeras, L.D., Bick, A., Mavrantzas, V.G., Theodorou, D.N., et al., 2019. Chameleon: a generalized, connectivity altering software for tackling properties of realistic polymer systems. WIREs Comput. Mol. Sci. 9, e1414. https://doi.org/10.1002/wcms.1414.

Andreopoulos, A.G., Tarantili, P.A., 2002. Study of biopolymers as carriers for controlled repase. J. Macromol. Sci. B41, 559–578.

Appold, M., Mari, C., Lederle, C., Elbert, J., Schmidt, C., Ott, I., Stu¨hn, B., Gasser, G., Gallei, M., 2017. Multi-stimuli responsive block copolymers as a smart release platform for a polypyridyl ruthenium complex. Polym. Chem. 8, 890–900.

Ashraf, S., Park, H.-K., Park, H., Lee, S.-H., 2016. Snapshot of phase transition in thermoresponsive hydrogel PNIPAM: role in drug delivery and tissue engineering. Macromol. Res. 24, 297–304.

Baeza, A., et al., 2012. Magnetically triggered multidrug release by hybrid mesoporous silica nanoparticles. Chem. Mater. 24 (3), 517–524. 10.1021/cm203000u. ISSN 0897-4756 1520-5002.

Berendsen, H.J.C., Postma, J.P.M., van Gunsteren, W.F., DiNola, A., Haak, J.R., 1984. Molecular dynamics with coupling to an external bath. J. Chem. Phys. 81, 3684–3690.

Binder, K. (Ed.), 1995. MC and Molecular Dynamics Simulations in Polymer Science. Oxford University Press, New York.

Bourassa, P., Dubeau, S., Maharvi, G.M., Fauq, A.H., Thomas, T.J., Tajmir-Riahi, H.A., 2011. Locating the binding sites of anticancer tamoxifen and its metabolites 4-hydroxytamoxifen and endoxifen on bovine serum albumin. Eur. J. Med. Chem. 6, 4344–4353.

Cai, K., et al., 2015. Redox-responsive self-assembled chain-shattering polymeric therapeutics. Biomater. Sci. 3 (7), 1061–1065. ISSN 2047-4849 (Electronic).

Cao, X., Lai, S., Lee, L.J., 2001. Design of a self-regulated drug delivery device. Biomed. Microdevices 3 (2), 109–118.

Cezar, H.M., Canuto, S., Coutinho, K., 2020. DICE: a MC code for molecular simulation including the configurational bias MC method. J. Chem. Inf. Model. 60, 3472–3488. https://doi.org/10.1021/acs.jcim.0c00077.

Chen, Z., Wang, L., Zhou, J., 2019. Computer simulations on the switching effect of nanopores modified by dual-responsive block polymers. CIESC J. 70, 271–279.
Choi, J., Shin, H., Cho, M., 2018. Multiscale multiphysical analysis of photomechanical properties of interphase in light-responsive polymer nanocomposites. Compos. Sci. Technol. 160, 32–41.
Concellón, A., et al., 2016. Light-responsive self-assembled materials by supramolecular post-functionalization via hydrogen bonding of amphiphilic block copolymers. Macromolecules 49 (20), 7825–7836. 10.1021/acs.macromol.6b01112. ISSN 0024-9297.
Cui, Z., Mumper, R.J., 2002. Plasmid DNA-entrapped nanoparticles engineered from microemulsion precursors: in vitro and in vivo evaluation. Bioconjugate Chem. 13 (6), 1319–1327.
Da Silva, R.M., Mano, J.F., Reis, R.L., 2007. Smart thermoresponsive coatings and surfaces for tissue engineering: switching cell material boundaries. Trends Biotechnol. 25 (12), 577–583. https://doi.org/10.1016/j.tibtech.2007.08.014.
Darvishmanesh, S., Qian, X., Wickramasinghe, S.R., 2015. Responsive membranes for advanced separations. Curr. Opin. Chem. Eng. 8, 98–104.
Deshmukh, S.A., Kamath, G., Mancini, D.C., Sankaranarayanan, S.K.R.S., 2014. Effect of methanol/water mixtures on the lower critical solution temperature of poly(n-isopropylacrylamide). MRS Proc. 1622, 25–30.
Dodd, P.M., Jayaraman, A., 2012. MC simulations of polydisperse polymers grafted on spherical surfaces. J. Polym. Sci. B Polym. Phys. 50, 694–705. https://doi.org/10.1002/polb.23057.
Dodd, L.R., Boone, T.D., Theodorou, D.N., 1993. A concerted rotation algorithm for atomistic MC simulation of polymer melts and glasses. Mol. Phys. 78, 961–996.
Dubbeldam, D., Calero, S., Ellis, D.E., Snurr, R.Q., 2016. RASPA: molecular simulation software for adsorption and diffusion in flexible nanoporous materials. Mol. Simul. 42, 81–101. https://doi.org/10.1080/08927022.2015.1010082.
Erdmann, L., Uhrich, K.E., 2000. Synthesis and degradation characteristics of salicylic acid-derived poly(anhydride-esters). Biomaterials 21 (19), 1941–1946. 10.1016/s0142-9612(00)00073-9. ISSN 0142-9612.
Frenkel, D., 2013. Simulations: the dark side. Eur. Phys. J. Plus 13010–13018.
Galaev, I.Y., Mattiasson, B., 1999. 'Smart' polymers and what they could do in biotechnology and medicine. Trends Biotechnol. 17 (8), 335–340. https://doi.org/10.1016/s0167-7799(99)01345-1.
Gan, L.H., Gan, Y.Y., Roshan Dean, G., 2000. Poly (N-acrylol-N propylpiperazine): a new stimuli responsive polymer. Macromolecules J 33, 7893–7897. 10.1021/ma000928b.
Gendelman, H.E., et al., 2015. Nanoneuromedicines for degenerative, inflammatory, and infectious nervous system diseases. Nanomedicine 11 (3), 751–767. ISSN 1549- 9642 (Electronic) 1549-9634 (Linking). Available at: http://www.ncbi.nlm.nih.gov/pubmed/25645958.
Gil, E.S., Hudson, S.M., 2004. Stimuli-responsive polymers and their bioconjugates. Prog. Polym. Sci. 29 (12), 1173–1222. https://doi.org/10.1016/j.progpolymsci.2004.08.003.
Halverson, J.D., Brandes, T., et al., 2013. ESPResSo++: a modern multiscale simulation package for soft matter systems. Comput. Phys. Commun. 184 (4), 1129–1149. 10.1016/j.cpc.2012.12.004.
Han, X., Feng, J., Dong, F., Zhang, X., Liu, H., Hu, Y., 2014. Thermo-/pH-responsive behaviours of base-rich diblock polyampholytes in aqueous solution: experiment and simulation. Mol. Phys. 112, 2046–2057.
Hao, L., Lin, L., Zhou, J., 2019. pH-responsive zwitterionic copolymer DHA-PBLG-PCB for targeted drug delivery: a computer simulation study. Langmuir 35, 1944–1953.
Heller, J., 1984. Biodegradable polymers in controlled drug delivery. Crit. Rev. Ther. Drug Carrier Syst. 1 (1), 39–90.

Hoffmann, A.S., Stayton, P.S., Murthy, N., 2002. Design of smart polymers that can direct intracellular drug delivery. Polym. Adv. Technol. 13, 992–999. 10.1002/pat.232.

Hu, J., Zhang, G., Ge, Z., Liu, S., 2014. Stimuli-responsive tertiary amine methacrylate-based block copolymers: synthesis, supramolecular self-assembly and functional applications. Prog. Polym. Sci. 39, 1096–1143.

Hu, Q., et al., 2015. Complete regression of breast tumour with a single dose of docetaxel entrapped core-cross-linked polymeric micelles. Biomaterials 53, 370–378. ISSN 1878-5905 (Electronic) 0142-9612 (Linking). Available at: http://www.ncbi.nlm.nih.gov/pubmed/25890735.

Jochum, F.D., Theato, P., 2013. Temperature- and light-responsive smart polymer materials. Chem. Soc. Rev. 42 (17), 7468–7483. ISSN 1460-4744 (Electronic) 0306-0012 (Linking). Available at: http://www.ncbi.nlm.nih.gov/pubmed/22868906.

Karayiannis, N.C., Mavrantzas, V.G., Theodorou, D.N., 2002. A novel MC scheme for the rapid equilibration of atomistic model polymer systems of precisely defined molecular architecture. Phys. Rev. Lett. 88, 105503. https://doi.org/10.1103/PhysRevLett.88.105503.

Kasagana, V.N., Karumuri, S.S., Thirumal, M., 2011. Recent advances in smart drug delivery systems. Int. J. Pharm. Biotechnol. 1 (3), 201–207.

Kato, Y., et al., 2013. Acidic extracellular microenvironment and cancer. Cancer Cell Int. 13 (1), 89. ISSN 1475-2867 (Print) 1475-2867 (Linking). Available at: http://www.ncbi.nlm.nih.gov/pubmed/24004445.

Kawashima, Y., 2001. Nanoparticulate systems for improved drug delivery. Adv. Drug Deliv. Rev. 47 (1), 1–2.

Kreuter, J., 1994. Nanoparticles. In: Swarbrick, J., Boylan, J.C. (Eds.), Encyclopedia of Pharmaceutical Technology. Marcel Dekker Inc, New York, NY, pp. 165–190.

Kumar, A., Srivastava, A., Galaev, I.Y., Mattiasson, B., 2007. Smart polymers: physical forms and bioengineering applications. Prog. Polym. Sci. 32 (10), 1205–1237. https://doi.org/10.1016/j.progpolymsci.2007.05.003.

Kumar, V., Locker, C.R., in t' Veld, P.J., Rutledge, G.C., 2017. Effect of short chain branching on the interlamellar structure of semicrystalline polyethylene. Macromolecules 50, 1206–1214. https://doi.org/10.1021/acs.macromol.6b02458.

Lal, M., 1969. 'MC' computer simulation of chain molecules. I. Mol. Phys. 17, 57–64. https://doi.org/10.1080/00268976900100781.

Lal, N., Verma, N., 2021. The effect of combination of functional and nonfunctional acrylic polymers on transdermal patches of: in vitro permeation, in vivo evaluation using biochemical parameters, and stability studies. Future J. Pharm. Sci. 7, 127. 10.1186/s43094-021-00272.

Lal, N., Dubey, J., Gaur, P., Verma, N., Verma, A., 2017. Chitosan based in situ forming polyelectrolyte complexes: a potential sustained drug delivery polymeric carrier for high dose drugs. Mater. Sci. Eng. C 79, 491–498.

Lal, N., Nair, A., Verma, N., 2021. The use of natural polymers in formation of polyelectrolyte Complexation. Bull. Fac. Pharm. Cairo Univ. 59 (1), 1. Article.

Lal, N., Gaur, P.K., Rastogi, S., Lata, K., 2022. Current novel nanocarriers in drug delivery: a review. Hacet. Univ. J. Fac. Pharm. 42 (4), 238–256. https://doi.org/10.52794/hujpharm.1075668.

Lammers, T., et al., 2012. Drug targeting to tumours: principles, pitfalls and (pre-) clinical progress. J. Contr. Release 161 (2), 175–187. 10.1016/j.jconrel.2011.09.063. ISSN 0168-3659.

Li, Z., Wang, P., Liu, B., Wang, Y., Zhang, J., Yan, Y., Ma, Y., 2014. Unusual, photo-induced self-assembly of azobenzene-containing amphiphiles. Soft Matter 10, 8758–8764.

Li, Z., et al., 2016. pH- and NIR light-responsive polymeric prodrug micelles for hyperthermia-assisted site-specific chemotherapy to reverse drug resistance in cancer treatment. Small 12 (20), 2731–2740. ISSN 1613-6829 (Electronic) 1613-6810 (Linking). Available at: http://www.ncbi.nlm.nih.gov/pubmed/27043935.

Lin, W., Yao, N., Qian, L., Zhang, X., Chen, Q., Wang, J., Zhang, L., 2017. PH-responsive unimolecular micelle-gold nanoparticles-drug nanohybrid system for cancer theranostics. Acta Biomater. 58, 455–465.

Linsley, C.S., Wu, B.M., 2017. Recent advances in light-responsive on-demand drug-delivery systems. Ther. Deliv. 8 (2), 89–107. ISSN 2041-6008 (Electronic) 2041-5990 (Linking). Available at: http://www.ncbi.nlm.nih.gov/pubmed/28088880.

Liu, F., Urban, M.W., 2010. Recent advances and challenges in designing stimuli-responsive polymers. Prog. Polym. Sci. 35 (1), 3–23. 10.1016/j.progpolymsci.2009.10.002.

Lo, C.L., Lin, K.M., Hsiue, G.H., 2005. Preparation and characterization of intelligent core-Shell nanoparticles based on poly(D, L-lactide)-g-poly(N-isopropyl-acryl-amide-co-methacrylic acid). J. Contr. Release 104 (3), 477–488.

Loh, X.J., Jesus del, B., Toh, P.P.C., Lee, T.C., Jiao, D.Z., Rauwald, U., Appel, E.A., Scherman, O.A., 2012. Triply triggered doxorubicin release from supramolecular nanocontainers. Biomacromolecules 13 (1), 84–91.

Longo, G.S., Pe´rez-Cha´vez, N.A., Szleifer, I., 2019. How protonation modulates the interaction between proteins and pH-responsive hydrogel films. Curr. Opin. Colloid Interface Sci. 41, 27–39.

Martin, M.G., 2013. MCCCS towhee: a tool for MC molecular simulation. Mol. Simul. 39, 1212–1222. https://doi.org/10.1080/08927022.2013.828208.

Marturano, V., et al., 2017. Light-responsive polymer micro- and Nano-capsules. Polymer 9 (1), 8. ISSN 2073-4360. Available at: http://www.mdpi.com/2073-4360/9/1/8.

Mavrantzas, V.G., 2004. MC simulation of chain molecules. In: Yip, S. (Ed.), The Encyclopedia of Modeling for Advanced Materials. Marcel Dekker, New York, NY.

Mavrantzas, V.G., Boone, T.D., Zervopoulou, E., Theodorou, D.N., 1999. End-Bridging MC: a fast algorithm for atomistic simulation of condensed phases of long polymer chains. Macromolecules 32, 5072–5096. https://doi.org/10.1021/ma981745g.

McCrackin, F.L., 1967. Configuration of isolated polymer molecules adsorbed on solid surfaces studied by Monte-Carlo computer simulation. J. Chem. Phys. 47 (6), 1980–1986. https://doi.org/10.1063/1.1712225.

Mendonça, A.C.F., Goujon, F., Malfreyt, P., Tildesley, D.J., 2016. MC simulations of the static friction between two grafted polymer brushes. Phys. Chem. Chem. Phys. 18, 6164. https://doi.org/10.1039/C5CP07374J.

Olaj, O.F., Lantschbauer, W., 1982. Simulation of chain arrangement in bulk polymer, 1. Chain dimensions and distribution of the end-to-end distance. Macromol. Chem. Rapid Commun. 3, 847–858. https://doi.org/10.1002/marc.1982, 030031202.

Pan, Y.J., Chen, Y.Y., Wang, D.R., Wei, C., Guo, J., Lu, D.R., Chu, C.C., Wang, C.C., 2012. Redox/pH dual stimuli-responsive biodegradable nnanohydrogels with varying responses to dithiothreitol and glutathione for controlled drug release. Biomaterials 33 (27), 6570–6579.

Pang, X., et al., 2016. pH-responsive polymer-drug conjugates: design and progress. J. Contr. Release 222 (Suppl. C), 116–129. ISSN 0168-3659. Available at: http://www.sciencedirect.com/science/article/pii/S0168365915302765.

Panyam, J., Labhasetwar, V., 2003. Biodegradable nanoparticle from drug and gene delivery to cells and tissue. Adv. Drug Deliv. Rev. 55 (3), 329–347.

Peristeras, L.D., Economou, I.G., Theodorou, D.N., 2005. Structure and volumetric properties of linear and triarm star polyethylenes from atomistic MC simulation using

new internal rearrangement moves. Macromolecules 38, 386–397. https://doi.org/10.1021/ma048364p.

Phillips, D.J., Gibson, M.I., 2014. Redox-sensitive materials for drug delivery: targeting the correct intracellular environment, tuning release rates, and appropriate predictive systems. Antioxid. Redox Signal 21 (5), 786–803. ISSN 1557-7716 (Electronic) 1523-0864 (Linking). Available at: http://www.ncbi.nlm.nih.gov/pubmed/24219144.

Pierleoni, C., Arialdi, G., Ryckaert, J.P., 1997. On the signature of tensile blobs in the scattering function of a stretched polymer. Phys. Rev. Lett. 79, 2990–2993. https://doi.org/10.1103/PhysRevLett.79.2990.

Piscitelli, F., Posocco, P., Toth, R., et al., 2010. Sodium montmorillonite silylation: unexpected effect of the aminosilane chain length. J. Colloid Interface Sci. 351, 108–115. https://doi.org/10.1016/j.jcis.2010.07.059.

Quan, X., Peng, C., Dong, J., Zhou, J., 2016. Structural properties of polymerbrush-graftedgoldnanoparticlesattheoil–waterinterface:insights from coarse-grained simulations. Soft Matter 12, 3352–3359.

Ramos, J., Imaz, A., Callejas-Ferna´ ndez, J., Barbosa-Barros, L., Estelrich, J., Quesada-Pe´ rez, M., Forcada, J., 2011. Soft nanoparticles (thermo-responsive nanogels and bicelles) with biotechnological applications: from synthesis to simulation through colloidal characterization. Soft Matter 7, 5067–5082.

Revia, R.A., Zhang, M., 2016. Magnetite nanoparticles for cancer diagnosis, treatment, and treatment monitoring: recent advances. Mater. Today 19 (3), 157–168. ISSN 1369-7021 (Print) 1369-7021 (Linking). Available at: http://www.ncbi.nlm.nih.gov/pubmed/27524934.

Rosenbluth, M.N., Rosenbluth, A.W., 1955. MC calculation of the average extension of molecular chains. J. Chem. Phys. 23, 356–359. https://doi.org/10.1063/1.1741967.

Schmaljohann, D., 2006. Thermo-and pH-responsive polymers in drug delivery. Adv. Drug Deliv. Rev. 58 (15), 1655–1670.

Shah, J.K., Marin-Rimoldi, E., Mullen, R.G., et al., 2017. Cassandra: an open source MC package for molecular simulation. J. Comput. Chem. 38, 1727–1739. https://doi.org/10.1002/jcc.24807.

Shao, Y., Huang, W., Shi, C., Atkinson, S.T., Luo, J., 2012. Reversibly crosslinked nanocarriers for on-demand drug delivery in cancer treatment. Ther. Deliv. 3 (12), 1409–1427.

Theodorou, D.N., 2004. Variable-connectivity MC algorithms for the atomistic simulation of long-chain polymer systems. In: Nielaba, P., Mareschal, M., Ciccotti, G. (Eds.), Bridging Time Scales: Molecular Simulations for the Next Decade. Springer Verlag, pp. 64–127. https://doi.org/10.1007/978-1-4020-3286-8_137.

Tyle, P., Agrawala, P., 1989. Drug delivery by phonophoresis. Pharmaceut. Res. 6 (5), 355–361.

Tzounis, P.N., Anogiannakis, S.D., Theodorou, D.N., 2017. General methodology for estimating the stiffness of polymer chains from their chemical constitution: a single unperturbed chain MC algorithm. Macromolecules 50, 4575–4587. https://doi.org/10.1021/acs.macromol.7b00645.

Ulbrich, K., et al., 2016. Targeted drug delivery with polymers and magnetic nanoparticles: covalent and noncovalent approaches, release control, and clinical studies. Chem. Rev. 116 (9), 5338–5431. ISSN 1520-6890 (Electronic) 0009-2665 (Linking). Available at: http://www.ncbi.nlm.nih.gov/pubmed/27109701.

Vacatello, M., Avitabile, G., Corradini, P., Tuzi, A., 1980. A computer model of molecular arrangement in a n-paraffinic liquid. J. Chem. Phys. 73, 548–552. https://doi.org/10.1063/1.439853.

Vargas, G.H., León, C.A., Valdez, J.G., 2018. Smart" polymers: physicochemical characteristics and applications in bio-separation strategies. Separ. Purif. Rev. 47 (3), 199–213. https://doi.org/10.1080/15422119.2017.1356332.

Wang, Y.-C., et al., 2011b. Redox-responsive nanoparticles from the single disulfide bond bridged block copolymer as drug carriers for overcoming multidrug resistance in cancer cells. Bioconjugate Chem. 22 (10), 1939–1945. 10.1021/bc200139n. ISSN 1043-18021520-4812.

Xia, H., Zhao, Y., Tong, R., 2016. Ultrasound-mediated polymeric micelle drug delivery. Adv. Exp. Med. Biol. 880, 365–384. ISSN 0065-2598 (Print) 0065-2598 (Linking). Available at: http://www.ncbi.nlm.nih.gov/pubmed/26486348.

Yigit, M.V., Moore, A., Medarova, Z., 2012. Magnetic nanoparticles for cancer diagnosis and therapy. Pharm. Res. (N. Y.) 29 (5), 1180–1188. 10.1007/s11095-012-0679-7. ISSN 0724-87411573-904.

You, L.-C., Lu, F.-Z., Li, Z.-C., Zhang, W., Li, F.-M., 2003. Glucose-sensitive aggregates formed by poly(ethylene oxide)-block-poly(2-glucosyloxyethyl acrylate) with concanavalin A in dilute aqueous medium. Macromolecules 36 (1), 1–4.

You, M., Wang, P., Xu, M., Yuan, T., Meng, J., 2016. Fouling resistance and cleaning efficiency of stimuli-responsive reverse osmosis (RO) membranes. Polymer 103, 457–467.

Zardad, A.-Z., et al., 2016. A review of thermo- and ultrasound-responsive polymeric systems for delivery of chemotherapeutic agents. Polymer 8 (10), 359. ISSN 2073-4360. Available at: http://www.mdpi.com/2073-4360/8/10/359.

Zervopoulou, E., Mavrantzas, V.G., Theodorou, D.N., 2001. A new MC simulation approach for the prediction of sorption equilibria of oligomers in polymer melts: solubility of long alkanes in linear polyethylene. J. Chem. Phys. 115, 2860–2875. https://doi.org/10.1063/1.1383050.

Zhang, J.C., Wu, L.L., Meng, F.H., Wang, Z.J., Deng, C., Liu, H., Zhong, Z., 2011. pH and reduction dual-bioresponsive polymersomes for efficient intracellular protein delivery. Langmuir 28 (4), 2056–2065.

Zhao, J., Koay, E.J., Li, T., Wen, X., Chun, L., 2018. A hindsight reflection on the clinical studies of poly (l-glutamic acid)-paclitaxel. Wiley Interdiscip. Rev. Nanomed. Nanobiotechnol. 10 (3), e1497.

Zhou, T., Xiao, C., Fan, J., et al., 2013. A nanogel of on-site tunable pH-response for efficient anticancer drug delivery. Acta Biomater. 9 (1), 4546–4557. https://doi.org/10.1016/j.actbio.2012.08.017.

Zuilhof, H., Yu, S.H., Sholl, D.S., 2018. Writing theory and modeling papers for Langmuir: the good, the bad, and the ugly. Langmuir 34 (5), 1817–1818. https://doi.org/10.1021/acs.langmuir.7b04236.

Further reading

Bahadur, K.C.R., Thapa, B., Xu, P., 2012. pH and redox dual responsive nanoparticle for nuclear targeted drug delivery. Mol. Pharm. 9 (9), 2719–2729.

Barick, K.C., Singh, S., Jadhav, N.V., Bahadur, D., Pandey, B.N., Hassan, P.A., 2012. pH-responsive peptide mimic shell cross-linked magnetic nanocarriers for combination therapy. Adv. Funct. Mater. 22 (23), 4975–4984.

Bilalis, P., Chatzipavlidis, A., Tziveleka, L.A., Boukos, N., Kordas, G., 2012. Nanodesigned magnetic polymer containers for dual stimuli actuated drug controlled release and magnetic hyperthermia mediation. J. Mater. Chem. 22 (27), 13451–13454.

Chen, C., Geng, J., Pu, F., Yang, X.J., Ren, J.S., Qu, X.G., 2011. Polyvalent nucleic acid/meso-porous silica nanoparticle conjugates: dual stimuli-responsive vehicles for intracellular drug delivery. Angew. Chem. 123 (4), 912–916.

Du, J.Z., Du, X.J., Mao, C.Q., Wang, J., 2011. Tailor-made dual pH-sensitive polymer-doxorubicin nanoparticles for efficient anticancer drug delivery. J. Am. Chem. Soc. 133 (44), 17560–17563.

Gan, Q., Lu, X.Y., Yuan, Y., Qian, J.C., Zhou, H.J., Lu, X., Shi, J., Liu, C., 2011. A magnetic, reversible pH-responsive nnanogated ensemble based on Fe3O4 nanoparticles-capped mesoporous silica. Biomaterials 32 (7), 1932–1942.

Gan, Q., Lu, X.Y., Dong, W.J., Yuan, Y., Qian, J.C., Li, Y.S., Shi, J., Liu, C., 2012. Endosomal pH-activatable magnetic nanoparticle-capped mesoporous silica for intracellular controlled release. J. Mater. Chem. 22 (31), 15960–15968.

Klaikherd, A., Nagamani, C., Thayumanavan, S., 2009. Multi-stimuli sensitive amphiphilic block copolymer assemblies. J. Am. Chem. Soc. 131 (13), 4830–4838.

Roccatano, D., Barthel, A., Zacharias, M., 2007. Structural flexibility of the nucleosome core particle at atomic resolution studied by molecular dynamics simulation. Biopolymers 85 (5–6), 407–421. https://doi.org/10.1002/bip.20690.

Sankaranarayanan, J., Mahmoud, E.A., Kim, G., Morachis, J.M., Almutairi, A., 2010. Multi-response strategies to modulate burst degradation and release from nanoparticles. ACS Nano 4 (10), 5930–5936.

Smith, A.E., Xu, X., McCormick, C.L., 2010. Stimuli-responsive amphiphilic (co)polymers via raft polymerization. Prog. Polym. Sci. 35, 45–93.

Soppimath, K.S., Tan, D.C.W., Yang, Y.Y., 2005. pH-triggered thermally responsive polymer core-shell nanoparticles for drug delivery. Adv. Mater. 17 (3), 318–323.

Wang, K., Guo, D.S., Wang, X., Liu, Y., 2011a. Multistimuli responsive supramolecular vesicles based on the recognition of P-sulfonatocalixarene and its controllable release of doxorubicin. ACS Nano 5 (4), 2880–2894.

Xing, Z.M., Wang, C.L., Yan, J., Zhang, L., Li, L., Zha, L.S., 2011. Dual stimuli responsive hollow nanogels with IPN structure for temperature controlling drug loading and pH triggering drug release. Soft Matter 7 (18), 7992–7997.

Zhang, L.Y., Guo, R., Yang, M., Jiang, X.Q., Liu, B.R., 2007. Thermo and pH dual-responsive nanoparticles for anti-cancer drug delivery. Adv. Mater. 19 (19), 2988–2992.

This page intentionally left blank

CHAPTER 10

Electrospinning technique: A potential method to develop bioresorbable-based medical devices

Senthilkumar Nangan[1], Natesan Thirumalaivasan[2] and Ramasubburayan Ramasamy[3]

[1]Department of Chemistry, Graphic Era (Deemed to be University), Dehradun, Uttarakhand, India; [2]Department of Periodontics, Saveetha Dental College and Hospitals, Saveetha Institute of Medical and Technical Sciences (SIMATS), Saveetha University, Chennai, Tamil Nadu, India; [3]Marine Biomedical Research Laboratory & Environmental Toxicology Unit, Department of Prosthodontics, Saveetha Dental College and Hospitals (SIMATS), Saveetha University, Chennai, Tamil Nadu, India

10.1 Introduction

Over the past few decades, there has been profound research and development in nanotechnology, leading to remarkable breakthroughs. The creation of nanomaterials using electrospinning technology has gained immense recognition because of their superior qualities, bringing about transformative effects in various sectors, especially healthcare (Abadi et al., 2022). According to data from "Research and Markets," the global nanofiber industry is expected to reach a value of one billion U.S. dollars in the future. The electrospinning technique, an adaptable and uncomplicated method for producing fibers at the micro and nano levels, showcases the vast potential of this field and adds to its flourishing progress (Zulkifli et al., 2023). The fusion of electrospray and spinning methodologies has given birth to the adaptable technique called electrospinning (Schneider et al., 2021). By subjecting a fluid droplet—whether in the form of a solution or melt—extruded from the tip of a die (serving as an electrode) to a robust electric field, the droplet undergoes deformation. This intricate sequence results in the emission of a charged jet from the apex of the cone, propelled toward the opposing electrode. This intricate yet efficient process leads to the creation of uninterrupted fibers. Distinguishing characteristics of electrospinning encompass the production of exceedingly thin fibers, frequently

Bioresorbable Polymers and their Composites
ISBN 978-0-443-18915-9
https://doi.org/10.1016/B978-0-443-18915-9.00022-7
© 2024 Elsevier Ltd.
All rights reserved.

on a nanoscale, possessing extensive surface areas, adaptable utility for diverse applications, exceptional mechanical properties, and a straightforward procedural essence, all of which have been affirmed by domain experts (Abadi et al., 2022).

Electrospun nanofibers have received significant interest for a variety of uses. These include functional fabrics, specific clothing, skincare products, cosmetics, electronics, sound management, composite materials, filtration systems, and medical tools (Fadil et al., 2021). While electrospinning was primarily used for air purification and protective clothing, its applications have widened over the years. It has found utility in areas like healthcare, water purification, sturdy composite materials, lightweight structures, noise reduction, energy production and storage, photonics, electronics, and wearable gadgets. Particularly in the bioengineering and biomedical fields, there is a notable similarity between electrospun nanofibers and the fibrous matrices present in human tissues (Si et al., 2023). In biomedicine, these nanofibers provide numerous benefits such as a vast array of polymer choices, precise substance release controls, small fiber diameter, large surface area, and customizable pore designs. Electrospinning allows for the design of three-dimensional nanofiber structures that resemble the natural extracellular matrix, making it especially beneficial for chronic wound treatment and tissue engineering (Jin et al., 2018).

Recently, the equipment used for electrospinning has transformed from simple lab setups to viable market solutions. Manufacturers, by adapting and innovating conventional methods, have greatly enhanced the production effectiveness of products derived from electrospinning. Such advancements now make it simpler to produce nanofiber items through electrospinning. Notably, the medical domain has witnessed substantial advancements in creating nanofiber membranes using electrospinning. These materials, having secured patents, have also made their way into large-scale commercial production. They play various roles in medicine, including being used in surgical implants, wound care, and different medical instruments. This section delves into the core techniques of electrospinning, the production of nanofibers, and their diverse applications in the realm of medical equipment (Wang et al., 2021).

10.2 Fundamentals of electrospinning

Over the past decade, electrospinning has emerged as a pivotal technique for producing polymer nanofibers smaller than a micron. Achieving this is

notably difficult using conventional mechanical fiber-producing methods. Electrospinning facilitates the formation of continuous polymer fibers, derived from polymer melts or solutions, with diameters spanning from the nano to micro scales. The versatility of this method applies to both natural and synthetic polymers, as well as blends, composites containing metals or ceramics, and nanocomposites. The process also results in enhanced surface areas, broadening the scope for innovative material design and uses in diverse areas, such as the creation of filtration systems, catalytic nanofibers, and fiber-based sensors (Yang et al., 2018).

10.2.1 Principles of electrospinning

The primary elements involved in electrospinning consist of a high-voltage electrical source, a flow control mechanism, a spinneret (made up of a syringe pump and needle), and a grounded gathering device, as depicted in Fig. 10.1. During the electrospinning process, the regulated flow of either a polymer solution or melt is released from the spinneret via the syringe

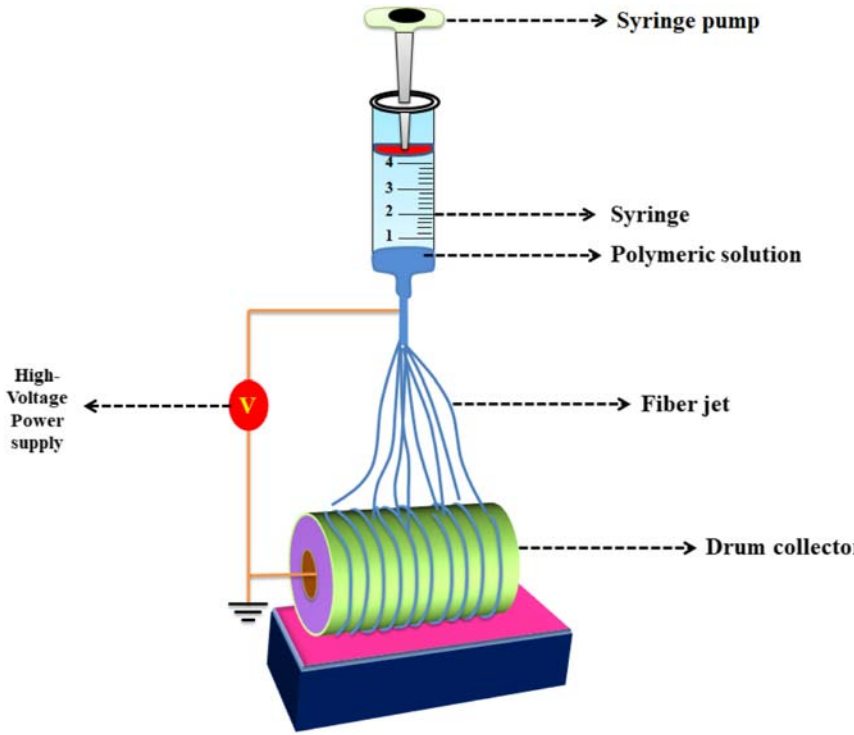

Figure 10.1 Schematic representation of electrospinning equipment.

pump. Initially, due to the effects of surface tension, the released substance appears as hanging spherical droplets. When the high-voltage source is turned on, a significant electric charge forms between the spinneret's tip and the grounded gathering device. This increased voltage results in repulsive electrostatic forces that cause the droplet at the end of the needle to stretch, assuming a cone shape, often referred to as the Taylor cone. When the voltage exceeds a certain limit, the electric field surpasses the droplet's surface tension, causing a thread to extend from the top of the cone. Consequently, one or multiple streams of charged polymer solution emerge. During this jet formation, various aspects affect the process, such as evaporation of the solvent in solution-based electrospinning or solidification of the polymer during melt electrospinning. The electric field's impact on the charged stream also induces it to stretch and waver unevenly. As the process continues, the charged stream quickly becomes more refined and solidified. Eventually, these solidified strands move toward and are captured by a gathering device with the opposite electric charge. This systematic procedure allows for the creation of polymer strands that vary in size from nano to submicron levels (Khan et al., 2013).

10.2.2 Effects of different electrospinning parameters

The investigation into the electrospinning process parameters holds significant importance. By comprehending these variables, it becomes feasible to produce nanofibers with diverse morphologies and diameters, as well as to fine-tune experimental configurations to achieve a variety of fibrous structures and patterns.

10.2.2.1 Solution parameters

Polymer solution properties are largely determined by the molecular weight of the polymer chains. These properties include viscosity, surface tension, conductivity, dielectric strength, and the structure of electrospun fibers (Munir et al., 2009). In general, a greater molecular weight results in improved viscosity, aiding in effective fiber formation. Previous reports explained how molecular weight affects the structural properties of membranes. While maintaining a consistent concentration, clear structural shifts with increasing molecular weight can be achieved. These shifts started with bead-like structures, evolved to beaded fibers, and eventually matured into fully formed fibers and flat ribbons. Nonetheless, a higher molecular weight is not always beneficial for achieving a specific fiber diameter due to the complex interactions among the polymer molecules. In electrospinning,

viscosity and polymer concentration jointly influence the size and shape of the produced fibers. Low viscosity can prevent the formation of continuous fibers, resulting in droplets, whereas high viscosity can cause the polymer solution to dry too quickly at the needle tip. The ideal viscosity varies among polymer types and polymer–solvent combinations (Huan et al., 2015). Polymer solution concentration is a crucial factor affecting fiber morphology. Numerous studies on different synthetic and natural polymer–solvent combinations have found that reduced polymer concentrations lead to an interrupted jet, causing bead formation on the fibers. On the other hand, too much solvent can produce tacky, wet fibers. Higher concentrations might enlarge the fiber diameter or block the jet due to increased polymer surface tension. The relationship among viscosity, surface tension, and the solution's rheology is closely connected to concentration, highlighting the need for the right concentration to obtain consistent fibers. For naturally occurring polymers with an ionic nature, concentration directly affects fiber spinnability and structure. Regarding inorganic solvent concentration, early studies have primarily focused on the chitosan biopolymer because of its solubility in slightly acidic water solutions, which also influences the conductivity of the polymer solution (Gradinaru et al., 2022). Numerous investigations focusing on polymer–solvent interactions have demonstrated that enhancing solution conductivity contributes to the creation of uniform fibers. The introduction of inorganic salts (such as NaCl, $CaCl_2$, $FeCl_3$) has been proven to elevate solution conductivity, even when these salts are incorporated at very low concentrations, leading to the removal of beads within the fibers (Su et al., 2011). The type of salt significantly impacts this conductivity improvement. Salts with smaller ionic diameters exhibit higher charge density and greater ion mobility under an electric field. Consequently, this results in increased elongation force and the production of finer fibers.

The role of the solvent or combination of solvents is vital in determining the conductivity of a solution, as discussed earlier. Using methylene chloride as a solvent for electrospinning PCL solutions, the resultant fibers had a consistent diameter close to 5500 nm, even though this was not the best method. However, when methylene chloride was mixed with DMF, the electrospinning process became more efficient, leading to a notable reduction in fiber diameter as the DMF ratio increased. This was believed to be due to the enhanced dielectric constant and conductivity of the mixed solution (Patlolla et al., 2010). In addition to adding inorganic salts, integrating biomolecules or surfactants can be beneficial. For example, as the

concentration of DNA in DNA/PEO solutions increased, there was a marked increase in their ionic conductivity. Remarkably, solutions with both DNA and PEO showed promising characteristics for electrospinning, producing very fine fibrous mats with diameters between 50 and 250 nm (Liu et al., 2007). Surface tension is majorly determined by the properties of the solvent rather than the polymer itself. The way a polymer solution demonstrates surface tension can vary based on how the polymer interacts with the solvent and the solvent's quantity present. By adjusting the concentration of the solution, either by adding more solvent or mixing solvents, one can prevent the formation of droplets and challenges in forming Taylor's cone. Reducing surface tension also enables the use of a milder electric field. However, adding more solvent changes the solution's thickness, which could lead to uneven fibers with droplets on them (Avossa et al., 2022).

10.2.2.2 Processing parameters

The relationship between the flow rate of a polymer solution and the electric field it experiences is tightly interconnected, with this correlation being particularly distinct based on the specific polymer—solvent pairing. Amplifying the rate at which the polymer solution is delivered leads to the alteration of Taylor's cone, concluding in the development of bead formations. However, this bead formation can be prevented by elevating the applied voltage. Nevertheless, this solution comes with an adjustment: avoiding bead formation through heightened voltage gives rise to uneven diameters and dispersion of the primary fiber. Furthermore, increased voltage accentuates the electrostatic forces within the charged solution, hindering the complete evaporation of the solvent. Conversely, a slower feed rate presents issues, including the inability to eject a polymer solution jet from the needle's end due to rapid droplet evaporation. It is crucial to keep an exact gap between the needle end and the collector to allow adequate drying time for the fibers before they touch the collector. Too short or too long gaps lead to uneven fiber structures. The ideal gap is determined by elements like the polymer solution's density and the voltage used. Essentially, while the electric field determines the fiber's thickness, its importance varies depending on factors like the polymer solution density and the gap between the needle and the collector (Tan et al., 2005).

The magnitude of the electric field not only dictates the size and structure of the fibers but also shapes their biological behavior, including the effect of the field's polarity (Ura and Stachewicz, 2022). The voltage

polarity can alter the performance of fibrous nanocomposite scaffolds in biological settings. It is confirmed that scaffolds with both positive and negative polarities promoted cell expansion and triggered the emergence of filopodia. Notably, scaffolds with negative polarity showed a boost in cell growth, ALP activity, and mineralization in contrast to those with a positive polarity. The design and organization of the collector play a pivotal role in dictating the morphology of electrospun fibers. Diverse collector types have been employed to achieve this, including materials like aluminum foil, conductive paper, and wire mesh, as well as configurations like pins, parallel bars, rotating rods, and rotating cylinders. Additionally, nonsolvents like methanol and ammonium hydroxide have also found utility in this context. In the field of tissue engineering, the most sought-after fiber arrangement mimics the consistent and oriented structure found in collagen fibers within the extracellular matrix. To realize this parallel alignment of fibers, collectors such as parallel bars or a rotating cylinder, have been effectively utilized. It is worth noting that in the case of a rotating cylinder, precise control over the rotation speed is imperative to achieve the intended alignment outcome (Vellayappan et al., 2016).

10.2.2.3 Environmental parameters

Apart from the innate qualities of materials and specific operational parameters, external elements like temperature and ambient moisture play a pivotal role in determining the outcome of the electrospinning method and the characteristics of the nanofibers produced (Phutane et al., 2023). The electrospinning process is significantly impacted by ambient moisture levels. Extremely low moisture conditions can lead to swift solvent evaporation, posing a risk of needle blockage. On the other hand, very high moisture conditions can interrupt the polymer stream, leading to electrospraying. Furthermore, the level of ambient moisture can alter the fiber's structure, a feature that is linked to whether the polymer attracts or repels water. For water-soluble and water-attracting polymers, tweaking moisture levels can help modify the fiber's thickness. When the air is more humid and the temperature drops, the drying speed of the solvent decreases. This extends the journey of the jet, resulting in finer fiber widths. On the other hand, when the humidity decreases, the drying process accelerates, producing coarser fibers. Moreover, elevated humidity can obstruct the drying of the water-based solvent, leading to the creation of bead-like structures. Solvent evaporation speeds up in hotter environments. Additionally, the ambient temperature can affect various properties of the polymer solution or melt,

such as its viscosity, surface tension, and conductivity (Wongsasulak et al., 2007). Furthermore, temperature is also crucial in determining the structure of nanofibers, influencing the solvent evaporation speed and viscosity, which lead to the formation of thinner fibers at both extremely low and high temperatures relative to moderate ones. At cooler temperatures, slower solvent evaporation caused the fiber jet to stretch more. On the other hand, hotter environments lowered the viscosity, enabling the creation of thinner nanofibers. It is worth noting that these effects are specific to the material in question, meaning different polymers might behave differently. Multiple research efforts have highlighted the indirect role of temperature on the diameter and structure of fibers. This suggests a possible use of the interplay between temperature and viscosity in tailoring nanofibers. Meanwhile, for hydrophobic polymers, increased humidity can lead to the formation of porous nanofibers. This is attributed to the complex interactions between water, the polymer's moisture-attracting solvent, and the polymer itself (Mailley et al., 2021).

10.2.3 Improvement and development of electrospinning technology in recent years

Producing laboratory-scale tools for needle electrospinning efficiently is a challenge, making it unsuitable for expansive industrial applications. In recent times, there has been a surge in efforts by scientists to improve the output of the electrospinning process. Various design approaches, adapting both individual and multiple needle setups, have been explored. An example includes using a single nozzle with a ridged end to produce multiple jets, as opposed to the traditional single needle, with the goal of boosting production speed. However, these innovations have not achieved the desired outcomes. The modification using a singular needle did not substantially enhance the output, and the design with several needles encountered issues such as electrostatic clashes among the needles and obstructions (Tan et al., 2022).

Innovatively, needle-free technology has emerged as a promising solution. This approach uses alternative spinnerets instead of traditional needles, tackling issues related to electrostatic disruptions and obstructions. The primary categories of spinnerets in needle-free electrospinning are rotating and stationary spinnerets (Schulte-Werning et al., 2021). Rotating spinnerets bring about mechanical disruption to the polymer mixture, whereas fixed spinnerets use methods like magnetism or bubbles to start the process. Various iterations of autonomous, multi-nozzle needle-free

electrospinning have shown great potential in enhancing the productivity of nanofiber membrane materials. Since 2004, the emergence of alternating current (AC) electrospinning technology has showcased its superiority over the traditional direct current (DC) electrospinning technique. AC electrospinning claims improved efficiency, making it possible to produce multiple jets on droplet surfaces at the same time (Balogh et al., 2015). When compared under the same experimental parameters, AC electrospinning yields results that are more than 20-fold higher than for its DC counterpart. The jets formed through AC methods are more stable during elongation, and due to the utilization of high AC voltage, they carry a reduced charge. This means there is no need for grounding conductive collectors. The natural propensity of the fiber stream to group together makes the creation of consistent nanofiber threads simpler. Furthermore, AC electrospinning offers enhanced precision; the electric or corona breeze surrounding the metal electrode plays a role in the fiber streams stretching. By tweaking the AC voltage and frequency, one can effectively dictate the nanofiber's shape and properties. However, AC electrospinning does have its limitations, which lead to relatively thicker fiber diameters (ranging from 300 to 500 nm) when compared to the ultra-fine 1 nm that can be achieved through DC electrospinning. It is worth noting that recent focus has been on nanofibrous yarn materials created through the AC electrospinning process, especially in the biomedicine sector. These materials consist of interconnected bundles of extremely fine nanofibers, creating structurally strong substances that find utility in diverse biomedical applications. The continuous progress of AC electrospinning technology unquestionably possesses the potential to attract substantial attention in times ahead (Sivan et al., 2022).

10.3 Application of electrospun nanofiber membranes in medical protective equipment

The worldwide outbreak of COVID-19 has led to a deficit in vital medical protection equipment, placing the health of medical professionals at risk. This challenge emphasizes the importance of innovative and accessible solutions that offer both antimicrobial and antiviral defenses. An emerging approach involves using electrospun nanofiber layers to produce medical items like masks and protective wear (Wu et al., 2022). These layers are preferred due to their high surface porosity, chemically modified surfaces that boost filtration capabilities, and their lightweight, breathable

characteristics. Lately, there has been a significant increase in research focused on leveraging electrospun nanofiber layers for healthcare protective purposes. In this field, a notable advancement is the development of a multifunctional composite made from electrospun nanofibers which includes polymethyl methacrylate (PMMA), ZnO nanorods, and silver (Ag) particles, termed PMMA/ZnO−Ag particles. This mixture serves as a decorative element for crafting protective padding. It has properties that can resist bacteria and viruses, helps in breaking down organic pollutants via photocatalysis, and can be reused (Ivanoska-Dacikj et al., 2023). Inspired by the above a biodegradable multi-layered mask with a filtration section formed from nanofibers of polylactic acid was proposed (Patil et al., 2021). These fibers were produced without the use of needles in the electrospinning process and proved potent against pandemics. Also, a unique Janus fiber membrane based mask, which provides holistic protection, tackling both airborne particulates and allowing for one-way water transfer, has been prepared. Another study demonstrated the feasibility of designing a superhydrophobic microporous layer through electrospinning, which is both water-resistant and breathable, and ideal for protective uses. Together, these examples highlight the critical significance of electrospun nanofiber membranes in various sectors for promoting health and safety.

10.3.1 Medical device and implant coating

The potential integration of electrospun nanofibers into medical implants offers considerable potential, aiming to improve biocompatibility and introduce innovative features. This strategy involves producing a nanofiber-based layer on the implant's surface, imparting unique surface qualities that enable interaction with neighboring cells and tissues. Through the incorporation of bioactive compounds or even cells within these nanofibers, the creation of adaptable coatings for medical devices, including advanced controlled drug-delivery systems, becomes feasible. For instance, application of this technique in depositing a porous PCL layer onto biodegradable magnesium prostheses using electrospinning was demonstrated. This porous coating not only facilitated better cell adhesion but also provided a platform for the controlled release of medications, particularly aimed at addressing infections (Matsuzaki et al., 2020). Another illustration pertains to Biotronik's PK Papyrus coronary stent system, which integrates a polyurethane coating to enhance its flexibility. Furthermore, in the field of aneurysm treatment, a stent was enveloped in

nanofibers comprising of poly(L-lactide-co-ε-caprolactone) (PLCL) to promote anticoagulation and swift growth of endothelial cells. This distinctive coating exhibited a central-core and outer-sheath arrangement, allowing a gradual discharge of enclosed compounds such as heparin and vascular endothelial growth factors over an extended period, avoiding any immediate rapid emission. Integrating nanofibrous coatings functions as an intermediate layer situated between implants and host tissues, effectively tackling the important issue of stiffness mismatch at the junction. This problem is particularly noteworthy when considering the potential risks associated with the malfunction of rigid tissue prostheses (Naseem et al., 2019).

10.3.2 In-vitro 3D cancer models

In the field of cancer research, in vitro models have proven to be a valuable asset for a range of purposes, including drug screening, understanding anticancer mechanisms, and exploring tumor cell biology. Traditional two-dimensional (2D) cancer models involve growing tumor cells as a single layer in flat containers, which provides some insights into cancer cell behavior. However, it is important to acknowledge that the behavior of tumor cells varies significantly between 2D and 3D models. The limitations of 2D models become apparent in their inability to replicate the intricate interactions between cells and their surrounding matrix, both on a cellular level and within the matrix itself. This is precisely where three-dimensional (3D) models come into play, offering a more comprehensive perspective on how cells collectively behave within the complex cell—matrix environment. This enhanced understanding enables a more effective control of tumor activities. Electrospun nanofibers possess a remarkable capacity to mimic the natural structure and composition of the extracellular matrix (ECM). This is a crucial factor for tissue regeneration and replicating stem cell environments. Similarly, in the realm of creating three-dimensional in vitro tumor models, the employment of electrospun nanofibers plays a pivotal role in accurately recreating the genuine extracellular environment for tumor cells. By incorporating biochemical signals through surface modifications involving biomolecules or enclosed medications, electrospun nanofibers effectively mirror the cues found in the native tumor ECM (Yang et al., 2015). This combination has led to the development of a pharmacokinetic model for prostate cancer.

Nonetheless, it is imperative to acknowledge the intricate and varied physiological composition of the tumor's ECM. The current predicament

introduces challenges regarding the fabrication of electrospun 3D tumor models, as they face limitations in faithfully reproducing essential components like tumor angiogenesis, intercellular communication, mechanical impacts, and efficient cell penetration (Monteiro et al., 2019). The integration of bioreactors into the model development process is being investigated as a promising approach to mechanically stimulate cancer cells. Furthermore, a more advanced tactic encompasses the fusion of electrospinning with bioprinting technology, holding the potential to craft more intricate 3D cancer models.

10.3.3 Filtration membranes for biomedical applications and wearables

The exceptional qualities of electrospun nanofiber networks include their remarkable surface-to-volume ratio, lightweight composition, significant porosity, interconnected structure, and microscale gaps. These attributes make them an ideal option for filtration applications, particularly in personal protective equipment. Unlike traditional protective clothing that prioritizes creating a complete barrier, but struggles with being heavy and retaining moisture, electrospun nanofibers offer the potential to develop textiles that are both incredibly lightweight and breathable. These textiles allow the passage of air and water vapor while effectively blocking undesirable agents. Biomedical scenarios widely utilize filtration membranes like protective masks. Electrospun nanofibrous membranes provide an opportunity not just to hinder, but also potentially to neutralize chemical and biological hazards such as nerve agents, bacteria, and viruses by integrating active substances into the nanofiber structure. For instance, the infusion of silver nanoparticles into electrospun nonwoven PAN nanofibrous matrices resulted in a 99% bacterial filtration efficiency, alongside notable antibacterial characteristics (Selvam and Nallathambi, 2015).

During the COVID-19 pandemic, the need for face masks grew significantly, leading to shortages in supply. In response, researchers at the Korea Advanced Institute of Science and Technology (KAIST) developed reusable masks using nanofiber filters that could be washed and utilized again. These masks incorporate nanofibers arranged in a crisscross pattern, ranging in dimensions from 100 to 500 nm. After conducting 20 rounds of tests to assess their antibacterial properties using ethanol, these masks exhibited an impressive filtration efficiency of over 94%. They maintained their hydrophobic features and retained their shape despite repeated usage. Additionally, Inovenso Ltd. contributed to the cause by manufacturing

masks with nanofibers, employing multiple layers of nonwoven electrospun material. These particular masks showcased an outstanding filtration efficiency of 99.9%. Nanofiber masks possess unique characteristics such as small pore size, large surface area, and lightweight nature, positioning them as a promising advancement in the realm of protective face masks. This innovation holds promise in meeting the demand for effective and reusable protection against viral particles and other contaminants (Persano et al., 2013).

10.4 Conclusion

The technique of electrospinning presents considerable benefits, foremost among which is the production of ultra-thin fibers with extensive surface areas. This approach also enables tailoring for various purposes, showcases impressive mechanical properties, and is characterized by its straightforward procedural elements. These advantages collectively open up a wide array of possibilities for implementation in the biomedicine sector. The applications of this technique span diverse fields, including tissue engineering, controlled drug release, implantology, biotransformation, and wound healing. By adjusting the electrospinning process, material properties can be seamlessly integrated with distinct morphological structures, effectively meeting the requirements of these diverse applications. Despite the growing body of literature in this domain, it is important to acknowledge that the use of electrospinning for biomedical purposes is still in its nascent stages of advancement. The capability for nanoscale surface modifications and the versatility in material selection for electrospinning empower researchers to create innovative scaffold designs. These innovations have led to breakthroughs in areas such as bone and cartilage regeneration, vascular grafts, artificial heart valves, and artificial myocardial tissue. Noteworthy is the clear advantage of the fine diameters and adjustable pore sizes found in electrospun nanofiber films, particularly in crafting wound dressings and medical protective equipment. Biological evaluation studies highlight that the electrospinning process conditions do not compromise the effectiveness of integrated growth factors and other functional biomolecules, including anticancer agents, proteins, DNA, and living cells. Unquestionably, electrospun materials are poised to play a pivotal role in the future of biomedical applications. However, it is crucial to develop methods and materials that can be scaled up to meet the technical demands of these applications.

References

Abadi, B., Goshtasbi, N., Bolourian, S., Tahsili, J., Adeli-Sardou, M., Forootanfar, H., 2022. Electrospun hybrid nanofibers: fabrication, characterization, and biomedical applications. Front. Bioeng. Biotechnol. 10 (December). https://doi.org/10.3389/fbioe.2022.986975.

Avossa, J., Herwig, G., Toncelli, C., Itel, F., Rossi, R.M., 2022. Electrospinning based on benign solvents: current definitions, implications and strategies. Green Chem. 24 (6), 2347–2375. https://doi.org/10.1039/d1gc04252a.

Balogh, A., Cselkó, R., Démuth, B., Verreck, G., Mensch, J., Marosi, G., Nagy, Z.K., 2015. Alternating current electrospinning for preparation of fibrous drug delivery systems. Int. J. Pharm. 495 (1), 75–80. https://doi.org/10.1016/j.ijpharm.2015.08.069.

Fadil, F., Affandi, N.D.N., Misnon, M.I., Bonnia, N.N., Harun, A.M., Alam, M.K., 2021. Review on electrospun nanofiber-applied products. Polymers 13 (13), 1–29. https://doi.org/10.3390/polym13132087.

Gradinaru, L.M., Bercea, M., Vlad, S., Barbalata Mandru, M., Drobota, M., Aflori, M., Ciobanu, R.C., 2022. Preparation and characterization of electrospun magnetic poly(ether urethane) nanocomposite mats: relationships between the viscosity of the polymer solutions and the electrospinning ability. Polymer (Guildf). 256 (March), 125186. https://doi.org/10.1016/j.polymer.2022.125186.

Huan, S., Liu, G., Han, G., Cheng, W., Fu, Z., Wu, Q., Wang, Q., 2015. Effect of experimental parameters on morphological, mechanical and hydrophobic properties of electrospun polystyrene fibers. Materials 8 (5), 2718–2734. https://doi.org/10.3390/ma8052718.

Ivanoska-Dacikj, A., Oguz-Gouillart, Y., Hossain, G., Kaplan, M., Sivri, C., Ros-Lis, J.V., Mikucioniene, D., Munir, M.U., Kizildag, N., Unal, S., Safarik, I., Akgül, E., Yıldırım, N., Bedeloğlu, A.Ç., Ünsal, Ö.F., Herwig, G., Rossi, R.M., Wick, P., Clement, P., Sarac, A.S., 2023. Advanced and smart textiles during and after the COVID-19 pandemic: issues, challenges, and innovations. Healthcare 11 (8). https://doi.org/10.3390/healthcare11081115.

Jin, G., He, R., Sha, B., Li, W., Qing, H., Teng, R., Xu, F., 2018. Electrospun three-dimensional aligned nanofibrous scaffolds for tissue engineering. Mater. Sci. Eng. C 92 (November 2017), 995–1005. https://doi.org/10.1016/j.msec.2018.06.065.

Khan, W.S., Asmatulu, R., Ceylan, M., Jabbarnia, A., 2013. Recent progress on conventional and non-conventional electrospinning processes. Fibers Polym. 14 (8), 1235–1247. https://doi.org/10.1007/s12221-013-1235-8.

Liu, Y., Chen, J., Misoska, V., Wallace, G.G., 2007. Preparation of novel ultrafine fibers based on DNA and poly(ethylene oxide) by electrospinning from aqueous solutions. React. Funct. Polym. 67 (5), 461–467. https://doi.org/10.1016/j.reactfunctpolym.2007.02.008.

Mailley, D., Hébraud, A., Schlatter, G., 2021. A review on the impact of humidity during electrospinning: from the nanofiber structure engineering to the applications. Macromol. Mater. Eng. 306 (7), 2100115. https://doi.org/10.1002/mame.202100115.

Matsuzaki, Y., Iwaki, R., Reinhardt, J.W., Chang, Y.C., Miyamoto, S., Kelly, J., Zbinden, J., Blum, K., Mirhaidari, G., Ulziibayar, A., Shoji, T., Breuer, C.K., Shinoka, T., 2020. The effect of pore diameter on neo-tissue formation in electrospun biodegradable tissue-engineered arterial grafts in a large animal model. Acta Biomater. 115, 176–184. https://doi.org/10.1016/j.actbio.2020.08.011.

Monteiro, C.F., Custódio, C.A., Mano, J.F., 2019. Three-dimensional osteosarcoma models for advancing drug discovery and development. Adv. Ther. 2 (3), 1800108. https://doi.org/10.1002/adtp.201800108.

Munir, M.M., Suryamas, A.B., Iskandar, F., Okuyama, K., 2009. Scaling law on particle-to-fiber formation during electrospinning. Polymer (Guildf). 50 (20), 4935–4943. https://doi.org/10.1016/j.polymer.2009.08.011.

Naseem, R., Zhao, L., Silberschmidt, V.V., Liu, Y., Zhang, X., 2019. Experimental study of synthesized co-polymer for stent application. Procedia Struct. Integr. 15, 55–59. https://doi.org/10.1016/j.prostr.2019.07.011.

Patil, N.A., Gore, P.M., Jaya Prakash, N., Govindaraj, P., Yadav, R., Verma, V., Shanmugarajan, D., Patil, S., Kore, A., Kandasubramanian, B., 2021. Needleless electrospun phytochemicals encapsulated nanofibre based 3-ply biodegradable mask for combating COVID-19 pandemic. Chem. Eng. J. 416 (December 2020), 129152. https://doi.org/10.1016/j.cej.2021.129152.

Patlolla, A., Collins, G., Livingston Arinzeh, T., 2010. Solvent-dependent properties of electrospun fibrous composites for bone tissue regeneration. Acta Biomater. 6 (1), 90–101. https://doi.org/10.1016/j.actbio.2009.07.028.

Persano, L., Camposeo, A., Tekmen, C., Pisignano, D., 2013. Industrial upscaling of electrospinning and applications of polymer nanofibers: a review. Macromol. Mater. Eng. 298 (5), 504–520. https://doi.org/10.1002/mame.201200290.

Phutane, P., Telange, D., Agrawal, S., Gunde, M., Kotkar, K., Pethe, A., 2023. Biofunctionalization and applications of polymeric nanofibers in tissue engineering and regenerative medicine. Polymers 15 (5), 1–38. https://doi.org/10.3390/polym15051202.

Schneider, R., Facure, M.H.M., Chagas, P.A.M., Andre, R.S., dos Santos, D.M., Correa, D.S., 2021. Tailoring the surface properties of micro/nanofibers using 0D, 1D, 2D, and 3D nanostructures: a review on post-modification methods. Adv. Mater. Interfaces 8 (13), 2100430. https://doi.org/10.1002/admi.202100430.

Schulte-Werning, L.V., Murugaiah, A., Singh, B., Johannessen, M., Engstad, R.E., Škalko-Basnet, N., Holsæter, A.M., 2021. Multifunctional nanofibrous dressing with antimicrobial and anti-inflammatory properties prepared by needle-free electrospinning. Pharmaceutics 13 (9). https://doi.org/10.3390/pharmaceutics13091527.

Selvam, A.K., Nallathambi, G., 2015. Polyacrylonitrile/silver nanoparticle electrospun nanocomposite matrix for bacterial filtration. Fibers Polym. 16 (6), 1327–1335. https://doi.org/10.1007/s12221-015-1327-8.

Si, Y., Shi, S., Hu, J., 2023. Applications of electrospinning in human health: from detection, protection, regulation to reconstruction. Nano Today 48, 101723. https://doi.org/10.1016/j.nantod.2022.101723.

Sivan, M., Madheswaran, D., Valtera, J., Kostakova, E.K., Lukas, D., 2022. Alternating current electrospinning: the impacts of various high-voltage signal shapes and frequencies on the spinnability and productivity of polycaprolactone nanofibers. Mater. Des. 213, 110308. https://doi.org/10.1016/j.matdes.2021.110308.

Su, P., Wang, C., Yang, X., Chen, X., Gao, C., Feng, X.X., Chen, J.Y., Ye, J., Gou, Z., 2011. Electrospinning of chitosan nanofibers: the favorable effect of metal ions. Carbohydr. Polym. 84 (1), 239–246. https://doi.org/10.1016/j.carbpol.2010.11.031.

Tan, S.H., Inai, R., Kotaki, M., Ramakrishna, S., 2005. Systematic parameter study for ultra-fine fiber fabrication via electrospinning process. Polymer (Guildf). 46 (16), 6128–6134. https://doi.org/10.1016/j.polymer.2005.05.068.

Tan, S.M., Teoh, X.Y., Le Hwang, J., Khong, Z.P., Sejare, R., Almashhadani, A.Q., Assi, R.A., Chan, S.Y., 2022. Electrospinning and its potential in fabricating pharmaceutical dosage form. J. Drug Deliv. Sci. Technol. 76 (August), 103761. https://doi.org/10.1016/j.jddst.2022.103761.

Ura, D.P., Stachewicz, U., 2022. The significance of electrical polarity in electrospinning: a nanoscale approach for the enhancement of the polymer fibers' properties. Macromol. Mater. Eng. 307 (5), 2100843. https://doi.org/10.1002/mame.202100843.

Vellayappan, M.V., Venugopal, J.R., Ramakrishna, S., Ray, S., Ismail, A.F., Mandal, M., Manikandan, A., Seal, S., Jaganathan, S.K., 2016. Electrospinning applications from diagnosis to treatment of diabetes. RSC Adv. 6 (87), 83638–83655. https://doi.org/10.1039/c6ra15252j.

Wang, Y., Chen, G., Zhang, H., Zhao, C., Sun, L., Zhao, Y., 2021. Emerging functional biomaterials as medical patches. ACS Nano 15 (4), 5977–6007. https://doi.org/10.1021/acsnano.0c10724.

Wongsasulak, S., Kit, K.M., McClements, D.J., Yoovidhya, T., Weiss, J., 2007. The effect of solution properties on the morphology of ultrafine electrospun egg albumen-PEO composite fibers. Polymer (Guildf). 48 (2), 448–457. https://doi.org/10.1016/j.polymer.2006.11.025.

Wu, S., Dong, T., Li, Y., Sun, M., Qi, Y., Liu, J., Kuss, M.A., Chen, S., Duan, B., 2022. State-of-the-art review of advanced electrospun nanofiber yarn-based textiles for biomedical applications. Appl. Mater. Today 27. https://doi.org/10.1016/j.apmt.2022.101473.

Yang, G., Wang, J., Wang, Y., Li, L., Guo, X., Zhou, S., 2015. An implantable active-targeting micelle-in-nanofiber device for efficient and safe cancer therapy. ACS Nano 9 (2), 1161–1174. https://doi.org/10.1021/nn504573u.

Yang, G., Li, X., He, Y., Ma, J., Ni, G., Zhou, S., 2018. From nano to micro to macro: electrospun hierarchically structured polymeric fibers for biomedical applications. Prog. Polym. Sci. 81, 80–113. https://doi.org/10.1016/j.progpolymsci.2017.12.003.

Zulkifli, M.Z.A., Nordin, D., Shaari, N., Kamarudin, S.K., 2023. Overview of electrospinning for tissue engineering applications. Polymers 15 (11), 1–27. https://doi.org/10.3390/polym15112418.

CHAPTER 11

Modeling of drug release from a bioresorbable polymer matrix system

Mohd Yasir[1], Dinesh Puri[2], Manikandan Arumugam[3], Wondesen G. Gobena[1], Mohammed Hussien Wondabo[1], S. Roshan[4] and K.M. Noorulla[1]

[1]Department of Pharmacy, College of Health Sciences, Arsi University, Asella, Ethiopia; [2]School of Pharmacy, Graphic Era Hill University, Dehradun, Uttarakhand, India; [3]Department of Pharmaceutical Engineering and Technology, Indian Institute of Technology, BHU, Varanasi, Uttar Pradesh, India; [4]Deccan School of Pharmacy, Darussalam Aghapura, Hyderabad, Telangana, India

11.1 Introduction

The emergence of innovative controlled drug-delivery methods, such as nano-drug-delivery systems (NDDSs), has significantly improved drug delivery. Polymers perform a vital role in manipulative controlled-release drug-delivery system (CRDDS) and sustained-release drug-delivery system (SRDDS). Since the invention of biodegradable (bioresorbable) polymers, a fantastic improvement in drug-delivery applications has taken place (Prajapati et al., 2019). Biodegradable polymers originating from synthetic and natural sources have been developed and applied for the design of controlled, sustained, and delayed-release drug-delivery carriers. The use of biodegradable polymers in drug delivery and drug targeting is extremely challenging due to problems with compatibility between biological tissue and biodegradable polymers as well as the release kinetics of biodegradable nanoparticles (Jacob et al., 2022). Following water absorption and swelling, the drug release primarily depends on whether polymer depletion controls it or occurs during migration. It has been claimed that the polymer's capacity for medication delivery has changed (Trucillo, 2022).

Bioresorbable Polymers and their Composites
ISBN 978-0-443-18915-9
https://doi.org/10.1016/B978-0-443-18915-9.00011-2
© 2024 Elsevier Ltd.
All rights reserved.

11.2 Biodegradable/bioresorbable polymers

Biodegradable/bioresorbable polymers showed a significant role in the improvement of pharmacokinetics as well as in reducing the side effects of active pharmaceutical ingredients (APIs) as they developed harmless or biocompatible products after degradation either enzymatically or non-enzymatically inside the body (Gavasane and Pawar, 2014). Recent advancements in tissue engineering, regenerative medicine, vaccination, CRDDS, SRDDS, nucleic acid, protein, and anticancer drug delivery have focused on the application of biodegradable biomaterials/polymers (George et al., 2019). As their name indicates, after the biodegradation of these polymers, the resulting product is not harmful either to the body or the environment after excretion. To date, researchers have reported and employed a number of biodegradable polymers with either natural or synthetic origins (Rancan et al., 2014). Natural biodegradable polymers involve polysaccharides of non-human origin such as chitosan and its derivatives including glycol chitosan, hyaluronic acid, sodium alginate, etc., and protein and polypeptide-based ones like collagen, albumin, gelatin, elastin, etc. (Prajapati et al., 2019; George et al., 2019; Idrees et al., 2020) (Fig. 11.1).

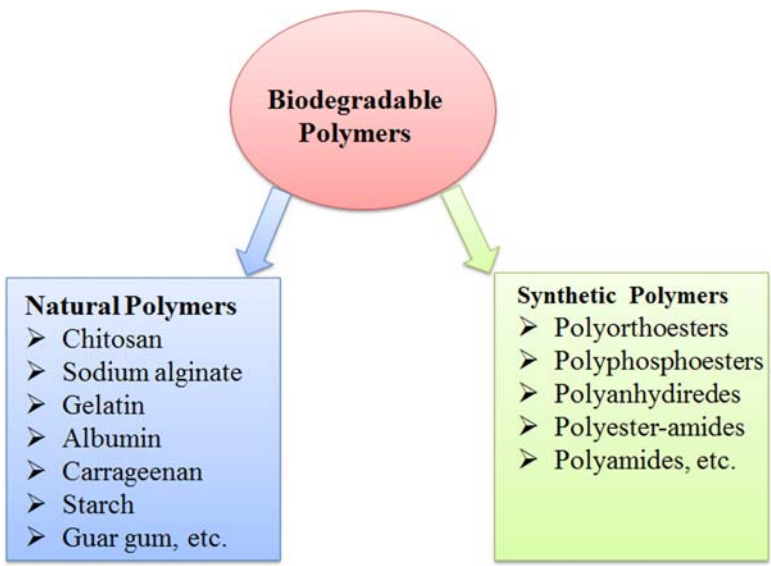

Figure 11.1 General classifications of biodegradable polymers used for the preparation of CRDDS.

Synthetic polymers involve poly(α-esters) such as poly(glycolic acid) (PGA), poly(lactic acid-co-glycolic acid) (PLGA), polydioxanone (PDS), polyanhydrides, polyurethanes, and poly trimethyl carbonates) (George et al., 2019; Anwar et al., 2021) (Fig. 11.1).

Researchers utilized both natural and synthetic polymers to develop pharmaceutical formulations like *Illicium verum* polymeric nanoparticles were developed using PLGA as biodegradable polymers and the in vitro release pattern was studied. It was concluded that polymeric nanoparticles showed an initial burst release for 1 h and then there was a controlled release for up to 30 h (Kumari et al., 2022). Poly(ester anhydride)s polymeric nanoparticles containing propranolol were developed and the findings suggested that the drug release mechanism for the developed formulation was primarily controlled by surface erosion (Mönkäre et al., 2012). Recently, researchers have used biodegradable polymers for the development of nanoparticles such as PLGA (Shamarekh et al., 2020; Musumeci et al., 2018), thiolated chitosan (Bari et al., 2015), chitosan (Shah et al., 2016; Elnaggar et al., 2015), PEG-PLGA (Pachauri et al., 2015), and carboxy methyl chitosan (Liu et al., 2018).

There are two *vital* factors, namely biodegradation and drug release from a polymeric matrix, that play an imperative role in the fruitful development of nanoformulations. Mechanisms like drug solubility, matrix diffusion, desorption of drug adsorbed, matrix erosion, matrix swelling, and a combination of two or more mechanisms affect the rate at which drugs are released from the polymeric matrix. The drug will be released through erosion or diffusion of the matrix if it is uniformly distributed throughout the matrix system (Begines et al., 2020). When a drug diffuses more quickly than the matrix, the term "burst release" is employed, which is often used to describe a drug that is poorly attached to the surface of polymeric nanoparticles (PNs). In contrast, if the drug is loaded via the incorporation method, the system exhibits a sustained/controlled release pattern (Bruschi, 2015a). The diffusivity and solubility of the drug become the key considerations for drug release if the nanoparticles are coated with a polymer, which acts as a barrier to the release of the drug. If a supplement is added, the way in which the supplement interacts with the drug will impact the rate at which it is released. Various techniques are used to examine a drug's in vitro release, but the dialysis bag diffusion approach, which is carried out with the use of a dissolving apparatus, is the most popular (George et al., 2019).

11.3 Factors affecting drug release from polymers

The prediction of drug release and the drug-release mechanism is an essential step to ensure the goal of the designed CRDDS or SRDDS formulation. Drug release from the drug carrier essentially depends upon the polymer's physicochemical features and physiological medium (Fig. 11.2). The possible detrimental factors for drug release from polymers are; (1) the medium and its pH; (2) the dissolution and diffusion of the drug from the drug carrier; (3) polymer and drug nature, i.e., hydrophilic or hydrophobic; (4) pattern of drug distribution in the polymer; (5) particle size of the drug and the developed system; and (6) the molecular weight of the polymers. Using both hydrophilic and hydrophobic polymer mixtures can avoid burst release and modulate the pattern of the drug's release (Fu and Kao, 2010).

The drug-release features of a polymer can be adjusted by using different viscosity-grade polymers like hydroxyl propyl methyl cellulose (HPMC) or by selecting a desired viscosity polymer (Siepmann and Peppas, 2012). Drug diffusivity from the polymeric system decreases with the molecular weight the polymer and hence retards drug release (Dhaliwal and Dosanjh, 2018). Drug to polymer ratios also play a role in releasing the drug. Hydrophilic polymers promote the burst release phenomena. Additionally, some excipients may be present in the formulation for a variety of reasons. For instance, PVA and mannitol are added to a formulation as a stabilizer and diluent/sweetening agent, respectively. PVA can reduce the

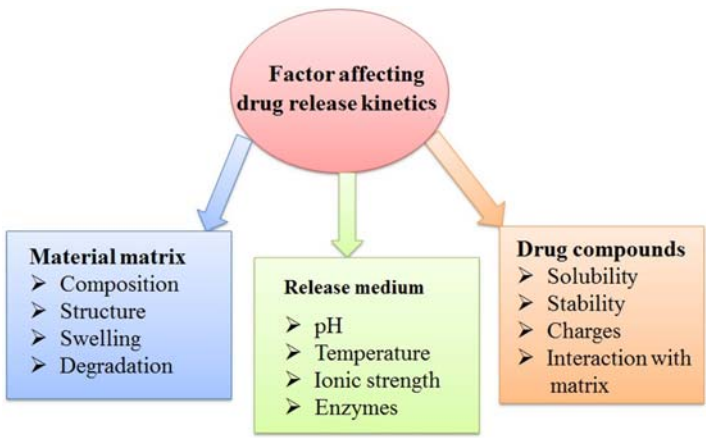

Figure 11.2 Factor affecting drug-release kinetics from a polymeric matrix.

burst release effect, while mannitol can improve the porosity of the matrix and, consequently, the drug-release rate (Joshi and Patel, 2012).

For the development of an effective nanoparticulate system, the biodegradation of the polymer and drug release from the polymer are necessary. The drug's solubility, matrix diffusion, adsorbed drug desorption, matrix erosion, and a combination of two or more mechanisms all have an impact on how a drug is released from a polymer system (Idrees et al., 2020). It is known that the drug will be released via erosion or diffusion mechanism if it is evenly distributed throughout the nanospheres/matrix. The phrase "burst release" is applied if API diffuses quicker than the matrix and is typically applied to weakly bound API on the surface of PNPs (Su and Kang, 2020).

11.4 Diffusion law

Diffusion is the result of intermixing of molecules due to Brownian motion caused by molecular kinetic energy. The unique distribution of dye in water is the simplest example of diffusion. The movement of dye molecules takes place in water until the establishment of equilibrium leads to the development of uniform color in the whole solution. At equilibrium, there is no net movement of dye molecules in the water. A similar phenomenon happens in the body as a drug is distributed, but in this case, equilibrium does not exist due to the establishment of the in vivo sink condition which ensures complete drug absorption from the dissolution site to the systemic circulation. In the case of CRDDS/SRDDS, diffusion is responsible for the passage of drug from the polymer matrix to the in vitro or in vivo medium. This process was explained by Fick (1855) by providing two separate laws. "These laws are useful to determine the flux and drug concentration across the biological membrane."

11.4.1 Fick's first law of diffusion

According to this law, "When the system is at steady state, the flux travels (with a magnitude that is proportional to the concentration gradient) from the area of highest concentration to the area of lowest concentration". Mathematically this law can be stated as follows:

$$J = -D\frac{dC}{dX} \tag{11.1}$$

where D is the diffusivity/diffusion coefficient of the drug, which can be expressed by the units m^2/s or cm^2/s, $\frac{dc}{dx}$ is the concentration gradient, and J is known as flux which indicates the drug amount moving perpendicularly over the unit surface area/time. The unit of J is $kg/m^2/s$ or $g/cm^2/s$. J is not a negative value. A negative sign in Eq. (11.1) indicates a concentration drop with distance, otherwise, flux is not a negative value. If there is no change in concentration (mean uniform concentration) with distance (x)/position, there will be no flux.

The diffusion rate (flux) through the unit area is a time-independent process in steady state. In this term, Fick's first law can be presented as follows:

$$J = \frac{dM}{S.dt} \tag{11.2}$$

After combining both equations, a new Eq. (11.3) will be generated that represents the rate of mass transfer as per Fick's law:

$$\frac{dM}{dt} = -DS\frac{dC}{dX} \tag{11.3}$$

D generally does not remain constant. Factors like concentration, temperature, pressure, solvent characteristics, and the chemical makeup of the drug all have an impact on D.

11.4.2 Fick's second law of diffusion

This is applicable under an unsteady state condition and represents how the concentration of diffusant alters with time. It states that "the concentration of diffusant alters with time ($\Delta C/\Delta t$) as the flux or diffusant amount alters with distance ($\Delta J/\Delta x$) in the x direction."

$$\frac{\Delta C}{\Delta t} = -\frac{\Delta J}{\Delta X} \tag{11.4}$$

Eq. (11.4) indicates the first form of Fick's second law. Another form can be differentiated as per Eq. (11.5).

$$\frac{dC}{dt} = -\frac{dJ}{dX} \tag{11.5}$$

By incorporating $J\left\{J=-D\frac{dC}{dX}\right\}$ value from Fick's first law, another form of Fick's second law can be obtained as follows:

$$\frac{dC}{dt}=-\frac{d}{dX}\left[=-D\frac{dC}{dX}\right] \tag{11.6}$$

It is assumed that D is constant and independent of X. It can be taken out from the differential:

$$-\frac{dJ}{dX}=D\frac{d^2C}{dX^2} \tag{11.7}$$

$$-\frac{dC}{dt}=D\frac{d^2C}{dX^2} \tag{11.8}$$

This is the third form of Fick's second law (Eq. 11.8). It states that any variable if its differential coefficient concerning time is related to second differential coefficient concerning space through a constant like D is known as a diffusion equation.

11.4.2.1 Outcomes of Fick's second law

- According to Fick's second law, the gradient of the concentration change at a given region in the system is proportional to the change in concentration over time in that region.
- This law is useable when the initial amount of drug per unit volume is lesser than the dimensional solubility of a drug.
- It narrates the temporal and spatial distributions of a drug concentration.

11.5 Fundamentals of drug-release kinetics

Drug-release patterns from the delivery system play an important role in the maintenance of the desired drug concentration at the receptor site/blood (Dash et al., 2010).

Noyes and Whitney conducted a dissolution experiment on two sparingly soluble compounds, namely benzoic acid and lead chloride (Noyes and Whitney, 1897). During the performance of experiment, both temperature and stirring speed were kept constant (Dokoumetzidis and Macheras, 2006). The experiment concluded that the dissolution rate was proportional to the concentration gradient, i.e., the difference between the

instantaneous concentration (C) at time t, and the saturation solubility (Cs) and modulated in the mathematical term as

$$\frac{dC}{dt} = k\,(Cs - C) \tag{11.9}$$

where k was considered a constant. The authors concluded that during drug dissolution, a thin layer was developed around the solid drug surface. The movement/diffusion of the drug was taken place from the solid surface to this layer to saturate it, followed by from this layer to the bulk of the solvent/solution (Dokoumetzidis and Macheras, 2006).

In 1900, Erich Brunner and Stanislaus von Tolloczko incorporated the surface area in the equation given by Noyes and Whitney and proposed the following equation (Bruner and Tolloczko, 1900):

$$\frac{dC}{dt} = k_1 S\,(Cs - C) \tag{11.10}$$

where $k = k_1 S$. They postulated that the exposed surface area of the drug to the dissolution medium, surface structure, and apparatus configuration all had an impact on the dissolution rate.

Brunner (1904) and Nernst (1904) modified Eq. (11.10) by utilizing the diffusion layer concept and Fick's second law and provided the following equation:

$$\frac{dC}{dt} = \frac{DS}{Vh}(Cs - C) \tag{11.11}$$

Here, D denotes the diffusion coefficient, h denotes the thickness of the diffusion layer, and V denotes the volume of dissolution medium (Gouda et al., 2017). According to Eq. (11.11), dissolution followed the first-order kinetic rate. Here, the concentration gradient i.e., $(Cs - C)$, acts as a driving force for drug dissolution. There is a chance to establish equilibrium, especially under nonsink/poor-sink condition in the case of in vitro dissolution. Due to the continuous circulation of blood in vivo, there is a better chance of the establishment of sink condition as compared to in vitro, and C is always approaching zero. If all other parameters keep constant, Eq. (11.11) reduces as $dC/dt = K$. Here, K is considered an overall constant that contains all the constants of Eq. (11.11). In this case, dissolution followed the zero-order kinetics.

In 1931, Hixson and Crowell modified Eq. (11.11) by utilizing the surface area (S) in terms of weight (w) (Hixson and Crowell, 1931).

They considered the surface area to be proportional to $w^{2/3}$. The generated equation after integration was applicable for the dissolution of compact material.

$$w_0^{1/3} - w^{1/3} = k_2 t \tag{11.12}$$

Here, w^0 is the initial weight, and k_2 is considered a constant. As a physical explanation for the process of dissolution, the aforementioned methods can be categorized as various expressions of the diffusion layer concept. The diffusion of molecules through a stationary film of liquid around the solid surface has been proposed as the limiting step. An interfacial barrier model for dissolution was proposed by Wilderman (1909), who was followed by Zdanovskii (1946), by taking interfacial transport into account rather than diffusion through the film. A third model of dissolution, the Danckwerts model, was presented by Danckwerts in 1951. This model states that constantly renewed macroscopic solvent packets reach the solid surface and absorb molecules of a solute, delivering them to the solution (Dokoumetzidis and Macheras, 2006).

11.6 Need for and objectives of mathematical models

New DDS can be designed by choosing the best size, formulation approaches, and geometry, and using the mathematical model equation. By choosing the best size, formulation approaches, and geometry, one can optimize new systems using the mathematical model equation. By fitting an appropriate model, the mathematical modeling approach assists in forecasting the drug-release rates and diffusion behavior from developed drug carriers, hence reducing the number of trials needed to optimize the DDS. The mathematical simulation of CDD can help scientists better understand the mass transport systems involved in the regulation of drug release (Ramteke et al., 2014; Siepmann and Siepmann, 2013). Therefore, mathematical modeling can greatly aid in the development of novel pharmaceutical goods as well as the optimization of already existing ones. Models can be used systematically to save time and money. Researchers may be able to create more precise dosing regimens and more effective therapeutic compositions with the use of mathematical methodologies (Costa and Sousa Lobo, 2001). Several mathematical model equations are described in the literature as described below (Trucillo, 2022; Dash et al., 2010; Costa and Sousa Lobo, 2001; Bhansali, 2021; Bruschi, 2015b; Elmas et al., 2020).

11.7 Release kinetic modeling

To describes the general drug release from dosage forms, different kinetic models have been devised. Because qualitative and quantitative changes in a formulation may alter drug release and in vivo performance, it is typically preferred to develop approaches that facilitate product development by reducing the requirement for biostudies. In this way, the rational development of CRDDS could be viewed as the use of in vitro drug dissolution data to predict in vivo bio-performance (Dash et al., 2010; Shaikh et al., 2015). As illustrated in Fig. 11.3, three different approaches can be utilized to assess the kinetics of drug release from CRDDS:

- Statistical approach
- Model-dependent approach
- Model-independent approach

11.7.1 Statistical approach

11.7.1.1 Explanatory data analysis approach

Although exploratory data analysis methods are not currently endorsed by the FDA, the method is useful in obtaining an improved understanding of the dissolution data of controlled release formulation, and therefore, its use is recommended (Dash et al., 2010; OíHara et al., 1998). This method can be used in the first step to compare dissolution profile data in both graphical and numerical manner.

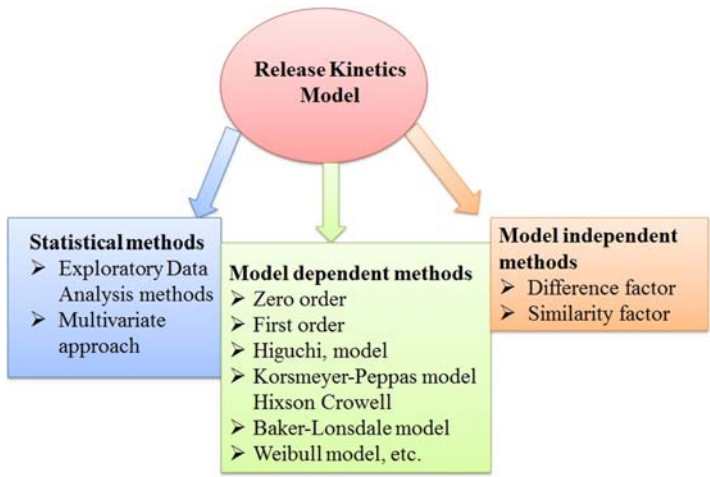

Figure 11.3 Classification of drug-release kinetic models.

11.7.1.2 Multivariate approach

Its foundation is based on the concept of repeated measure design. Here drug dissolution (%) is a dependent factor, while time is a repeating component. It is the standard method for determining whether a set of response measurements differs among the various population groups. Specifically, MANOVA examines both the statistical significance of the overall effect as well as the statistical significance of a specific main effect or an interaction on each of the response measurements. The level of connection between the group of dependent variables taken into account in a given study can also be determined using MANOVA (Liu, 2016).

11.7.2 Model-dependent approach

Designing controlled-release dosage forms requires the use of mathematical models for release kinetics (Gao, 2011). Mathematical models can be used to theoretically estimate the proportions of the drug, polymer, and other excipients as well as the optimal system size and shape to achieve the desired release profile in addition to assisting assessment of the physical aspects like the diffusion coefficient (Bhansali, 2021). The dissolution profile is described by many mathematical functions that form the foundation of model-dependent approaches. Once a suitable function has been chosen, the generated model parameters are used to evaluate the dissolution profiles. The model-dependent approach includes the various kinetic model, as listed in Fig. 11.3 and Table 11.1 (summary of various model-dependent approaches). Each model offers a unique equation that can convert the data from the release profile into a function that allows quantitative interpretation of the dissolution data.

11.7.2.1 Zero-order model

Eq. (11.13), which uses zero-order kinetics to describe the release rate of the nondisintegrating system, shows that the release rate is independent of the initial concentration or amount.

$$Q_t = Q_0 - KT \tag{11.13}$$

Here, Q_0 denotes the initial drug concentration, Q_t is the concentration of drug released from the system at time t, and K denotes the zero-order release constant (concentration * time^{-1}). In this instance, a graph of time (X-axis) and cumulative drug release (CDR, %) (Y-axis) results in a straight line whose slope will provide the value of the release constant,

Table 11.1 Summary of different kinetic release models.

Model	Mathematical relation	Plotting parameters	Assumptions	Application	References
Zero-order	$Q_t = Q_0 - Kt$	Time versus CDR (%)	Drug release form delivery system is independent of initial concentration (constant release).	Followed diffusion mechanism, Used for transdermal matrix system, Coated tablet with low water-soluble API, etc.	AlMajed et al. (2022)
First-order	$\text{Log } Q_t = \text{Log } Q_0 - Kt/2.303$	Time versus log % drug remained to release	Concentration-dependent, factors like exposed surface area and its structure, Physical factors like temperature, stirring speed, geometry of apparatus, etc. influence dissolution.	Followed diffusion mechanism, Describe drug-release form modified-release DDS containing water-soluble drug in porous medium, etc.	Dash et al. (2010)

Higuchi model	$Q_t = K_H\sqrt{t}$	Square root of time versus CDR (%)	Pseudo-steady-state condition for planar system, Volume change should be negligible, Establishment of sink condition, Smaller drug molecules with respect to DS thickness.	Followed diffusion mechanism, Solid or semi-solid DDS containing soluble API, Planar, variable geometrics, and porous DDS, Matrix DS with soluble polymer, etc.	Bhansali (2021)
Hixson –Crowell cube root law	$w_0^{\frac{1}{3}} - w^{\frac{1}{3}} = k_2 t$	Time versus $w_0^{\frac{1}{3}} - w^{\frac{1}{3}}$	Drug release is limited by dissolution of drug particle rather diffusion.	Erodible matrix DDS, Valid for DDS with diminished SA and thickness, Maintenance of constant initial geometry, etc.	Shaikh et al. (2015)
Korsmeyer –Peppas	$\frac{M_t}{M_\infty} = Kt^n$	Log time versus log M_t/M_∞	DDS with different geometries, DDS where	Semiempirical approach, Based on exponent value,	Ramteke et al. (2014)

Continued

Table 11.1 Summary of different kinetic release models.—cont'd

Model	Mathematical relation	Plotting parameters	Assumptions	Application	References
			one-dimensional diffusion cannot be assumed.	It differentiates release in Fickian and non-Fickian diffusion, Applied for wide dosage forms like hydrogels, etc.	
Weibull distribution	$m = 1 - e\left[-(t - T_i)^{\frac{b}{a}}\right]$	Log time versus log CDR (%)	Empirical approach	Empirical approach, May be applied for majority of DDS with more emphasis on matrix DDS.	Bruschi (2015b)
Hopfenburg model	$\frac{M_t}{M_\infty} = 1 - \left[1 - \frac{K_0 t}{C_0 a_0}\right]^n$	Time versus log M_t/M_∞	Drug release from erodible DDS that maintains constant SA during degradation.	Semiempirical approach, Erosion mechanism, Applied for oily spheres dispersed in biphasic DDS, etc.	Siepmann and Siepmann (2008)

Baker −Lonsdale model	$f_1 = \frac{3}{2}\left[1-\left(1-\frac{M_t}{M_\infty}\right)^{2/3}\right]-\frac{M_t}{M_\infty} = KT$	Root of time inverse versus $d\left(\frac{M_t}{M_\infty}\right)\Big/dt$	Drug release from spherical matrix, Negligible drug release initially.	Drug release from homogeneous nonfractured spherical matrices like microspheres, microcapsules, etc.	Trucillo (2022)
Peppas −Sahlin model	$\frac{M_t}{M_\infty} = K_1 t^m + K_2 t^{2m}$	Time versus log M_t/M_∞	Fickian diffusional and relaxational contribution.	Swellable polymeric devices	Shaikh et al. (2015)
Gompertz model	$M_t = M_{\max}\exp\left(-\alpha\, e^{\beta \log t}\right)$	Time versus $M_t/M_{\max}$	–	Compares the release profile of API with good solubility and intermediate release rate, etc.	Dash et al. (2010)

which is a function of time and is utterly independent of initial drug concentration (Bhansali, 2021).

The zero-order release approach can be applied to oral delivery when the drug core is covered by a water-permeable barrier. The system is hydrated as soon as it comes into contact with gastrointestinal fluid. The drug then builds a saturated reservoir as water moves toward the core of the object. Following partitioning into the membrane, the drug is then diffused into the GI fluids. The drug-saturated reservoir is responsible for maintaining the drug release regularly and constantly. The release rate decreases until it reaches zero after the drug concentration falls below the saturation concentration (Costa and Sousa Lobo, 2001; Gao, 2011).

Shivanand Puthli and coworkers developed levonorgestrel (LNG)-loaded microspheres using PLGA. The release kinetics of LNG from microspheres was found to be zero-order kinetics with the highest R^2 (Puthli and Vavia, 2009). Mariz et al. developed an ocular insert with PCL-PEG-PCL block copolymers using two different concentrations of PEG (24% and 33%). Both formulations exhibited zero-order release kinetics followed by the super-case-II transport release mechanism as the release exponent value (n) was more than 0.85 (Mariz et al., 2022). As mentioned in the literature, such a type of transport is usually observed in erodible and/or swelling matrixes or osmotically CRDDS (Mariz et al., 2022). Ulya Badilli and coworkers developed etofenamate-loaded topically administered semisolid lipid nanoparticles (SLNs) with an antiinflammatory activity using precirol ATO 5 and other lipids. The formulation developed by precirol ATO 5 displayed zero-order release kinetics. The release mechanism was found to be super-case-II transport release mechanism as the release exponent value (n) was more than 0.85 for all the formulations along with optimized formulation prepared with precirol ATO 5, indicating erosion as a release mechanism (Badilli et al., 2015).

11.7.2.2 First-order model

The release rate of a nondisintegrating system is dependent on the concentration/amount of the drug at a specific point. This model was created by Gibaldi and Feldman (1967) and afterward Wagner (Ramteke et al., 2014). Release kinetics and even drug absorption, distribution, elimination, and many more processes in pharmacy can be described by first-order kinetics as represented by the following equation:

$$\text{Log } Q_t = \text{Log } Q_0 - Kt/2.303 \tag{11.14}$$

In this instance, the plot between time (X-axis) and log of drug remaining to be released generates a straight line with a slope of $-K/2.303$. From the slope, K value can be calculated.

A variety of drug-delivery systems such as a porous matrix with a uniform distribution of drugs utilize the first-order drug-release model. Moreover, the drug release decreases as the drug concentration present in the delivery carriers is depleted (Bhansali, 2021).

A research work was reported by Malihe Pooresmaeil and associates for the preparation of carboxymethyl cellulose/mesoporous magnetic graphene oxide containing poorly water-soluble drug (Ibuprofen/IBU). Their result demonstrated that the first-order release kinetics model was the best-fitted among the all applied models with the non-Fickian release mechanism (Pooresmaeil et al., 2020). Chitosan microspheres containing methotrexate (MTX) were developed by Rajesh R. Dubey. The release kinetic of MTX from the microspheres was found to be collectively following the first-order and Higuchi's release model (Dubey and Parikh, 2004). Another study was conducted by Marilisa G. Lara for the development of cubic phase gels containing salicylic acid using a glyceryl monooleate/water system. The system followed the first-order and Higuchi's release model (Lara et al., 2005). Other researchers have reported different kinetic models to be fitted in various developed formulations such as drug release followed by the square root of time dependence, utilizing GMO/water systems, which is suggestive of a diffusion-regulated release mechanism (Chang and Bodmeier, 1997). Tinnabhop Santadkha developed curcumin nanomicelles using Pluronic F127/oleic acid(OA)-Fe_3O_4. The drug was released by first-order and the mechanism was a Fickian type of diffusion (Santadkha et al., 2022). *Illicium verum* polymeric nanoparticles were developed using PLGA. The drug-release experiment was conducted in PBS pH6.8. The results showed that the drug's swelling and diffusion affect its release (first-order). In this case, the release mechanism was non-Fickian (Case II transport) with a 1.03 value for the release exponent (Kumari et al., 2022).

11.7.2.3 Higuchi's model

The initial mathematical model for drug release from a matrix was presented by Higuchi. His work was associated with planar systems like ointment bases, and was started in 1961 and finalized in 1962. Higuchi eventually put forth the "mechanism of sustained-action medication" in 1963. Higuchi gave the following Eq. (11.15) to represent mathematically the release from the lipophilic planar matrix system:

$$Q = \sqrt{D\,(2C - C_s)C_s t} \tag{11.15}$$

This equation provides the relation between Q = amount of drug release/unit area at the time, C is the initial drug concentration, C_s = solubility of the drug in the matrix, and D = diffusion coefficient. For drug carriers holding a modest dose of the drug, an analogous connection was hypothesized, where release is controlled by the system's porosity as follows:

$$Q = \sqrt{\frac{D\varepsilon}{\tau}(2C - C_s)C_s t} \tag{11.16}$$

Here, ε and τ are the porosity and tortuosity, respectively, of the matrix. A simpler version of both Eqs. (11.15) and (11.16) is given by the following:

$$Q_t = K_H\sqrt{t} \tag{11.17}$$

where K_H is known as Higuchi's release constant. Eq. (11.17) shows a directly proportional relationship between the rate of drug release (water-soluble and poorly water-soluble) from different matrixes and the square root of time (Jain and Jain, 2016; Siepmann and Peppas, 2011). To obtain Higuchi's curve, a graph should be plotted between $\sqrt{t}$ (square root of time, X-axis) and Q_t (%CDR, Y-axis). The slope of the straight line gives the value of Higuchi's release constant, which is the function of the square root of time. Moreover, Higuchi's model followed the drug release by diffusion process as mentioned by Fick's law (Siepmann and Peppas, 2012; Jain and Jain, 2016). There are some assumptions to be followed by a system to exhibit Higuchi's model, as presented below:

- The initial drug concentration in the matrix needs to be sufficiently higher than the drug's solubility therein.
- The diffusion is unidirectional because the edge effects are negligible.
- The thickness of the dosage form is clearly greater than the size of the drug molecules.
- The matrix didn't swell or dissolve at all or very little.
- The diffusivity of the drug is constant.
- Establishing a perfect sink condition.

Any formulation that follows the above-said assumptions can follow the drug release by Higuchi's model. Researchers utilized Higuchi's model to describe the drug-release pattern. 5-FU liposomes were prepared using PL

90H and cholesterol and incorporated into a 1% chitosan solution after lyophilization to develop the liposomal gel. 5-FU was released from the developed liposomal gel following Higuchi's model (Glavas-dodov et al., 2005). The pH-sensitive hydrogel was developed for levothyroxine-Na pentahydrate using chitosan/arabinogalactan. Higuchi's model, which uses a Fickian diffusion release mechanism and has the greatest R^2 value (0.968), was deemed to be the best release model (Tapdiqov et al., 2022). Ciprofloxacin-loaded nano-biodegradable capsules were developed using chitosan + dextran sulfate. An in vitro release investigation was carried out in distilled water and PBS with pH values of 1.2, 4.5, and 7.4. The Higuchi model was found to be the most closely matched model across all media (Geetha Devi et al., 2021). Nimodipine-containing PLGA nanoparticles were created to treat posthemorrhagic cerebral vasospasm. A mixture of ethanol and PBS (1:1) was used to conduct the in vitro release examination, and the Higuchi model was determined to be the best-fitted model (Bege et al., 2013). Similarly, Higuchi kinetics was reported by various researchers such as docetaxel NPs prepared with chitosan (Jain et al., 2014), aceclofenac NPs using Eudragit RL-100 (Katara and Majumdar, 2013), ellagic acid NPs using PLGA-polycaprolactone (Sonaje et al., 2007), alpha lipoic acid cubosomes using glyceryl mono-oleate (Sherif et al., 2014), capsaicin cube phase gels using GMO and propylene glycol (Peng et al., 2010), carbamazepine nanoemulsion using castor oil (Kelmann et al., 2007), curcuminoid SLNs using GMS and stearic acid (Tiyaboonchai et al., 2007), bixin SLNs using GMS (Prathyusha et al., 2014), gatifloxacin SLNs using compritol/gelucire/stearic acid (Kalam et al., 2013), and metronidazole liposomes (Go, 2006), etc.

11.7.2.4 Hixson and Crowell's cube root law

Hixson and Crowell developed an equation that represents the rate of dissolution based on the cube root of particle weight and does not require that particle radius be constant for drug powder with uniformly sized particles (Hixson and Crowell, 1931). The generated equation after integration was applicable for the dissolution of compact material:

$$w_0^{1/3} - w^{1/3} = K_{\mathrm{HC}} t \tag{11.18}$$

where, w_0 denotes the initial weight of drug in the formulation, w denotes the weight of drug remaining to be released in the system at a specific time, and K_{HC} denotes the Hixson and Crowell release constant. For this model, a graph can be obtained by plotting the cube root of the amount of the

drug still to be released or present in the drug carrier versus time. The slope of the graph will reveal the release constant value (Ramteke et al., 2014).

The aforementioned formula is applicable to delivery systems like tablets in which dissolution takes place in planes parallel to the dosage form surface, and this surface reduces correspondingly with time while the geometric form is constant.

Regarding the concentration, density, and number of spherical particles (N) the above equation can be modified as

$$w_0^{\frac{1}{3}} - w^{\frac{1}{3}} = K' \frac{\sqrt[3]{NDC_s t}}{\delta} \tag{11.19}$$

where C_s is the saturation solubility at a given temperature, N is the number of particles, K' is a constant relating surface, form, and particle density, D is the diffusion coefficient, and δ is the thickness of the diffusion layer (Bruschi, 2015b).

It is well-known that surface factors of cubic or spherical particles are considered constant if the dissolution is constant throughout the entire system.

For irregular particles, the above equation can be modified. Moreover, dividing by $w_0^{1/3}$ the equation can be further simplified as follows:

$$\sqrt[3]{1} - f_i = 1 - K_\beta t \tag{11.20}$$

where K_β is known as the release constant, $f_i = 1 - (w/w_0)$ = fraction of drug release at time t. When the nonreleased fraction's cubic root is related to time, the above-mentioned equation reflects a linear function. This is accurate if the equilibrium circumstances remain unchanged and the particle's surface continues to gradually degrade with time (Bruschi, 2015b). The drug release is thought to be constrained by dissolution velocity in this model rather than diffusion, which can take place via the polymeric matrix (Bruschi, 2015b).

Danielly L.A. Sittaa and co-workers developed cross-linked albumin microparticles containing vitamin B12. A dissolution study was conducted in a dissolution medium of different pHs (2, 6, and 10) using a dialysis technique to evaluate the effect of the erosion matrix. Application of the Hixson–Crowell model confirmed the erosion mechanism (Sitta et al., 2014).

11.7.2.5 Korsmeyer–Peppas model

A more comprehensive semiempirical method created by Korsmeyer and coworkers (1983) and Ritger and Peppas (1987) to characterize the release of drugs from the polymeric system is also referred to as a power law (Bhansali, 2021; Bruschi, 2015b). An exponential correlation between the percentage of drugs released and time was established by the Korsmeyer–Peppas model (Korsmeyer et al., 1983; Ritger and Peppas, 1987):

$$f_i = \frac{M_t}{M_\infty} = Kt^n \tag{11.21}$$

Taking the log of the above equation:

$$\log\left(\frac{M_t}{M_\infty}\right) = \log K + n \log t \tag{11.22}$$

where M_t and M_∞ denote the amount of drug released at time t and after the establishment of equilibrium or infinite time, respectively. The ratio of M_t/M_∞ is known as the fraction of drug release (f_i). K denotes the release velocity constant. It is associated with the structural modification and geometrical characteristics of the system, n is known as the release exponent as a function of time. It is helpful to decide the release mechanism. The power law is applicable to depict the release of drugs from a polymeric system like hydrogels. A number of researchers have utilized a modified version of this equation that included the latency time (l) which indicates the time taken by the formulation to start drug release from the system.

$$\frac{M_{(i-l)}}{M_\infty} = K(t-l)^n \tag{11.23}$$

Taking the log of the above equation

$$\log\left(\frac{M_{(i-l)}}{M_\infty}\right) = \log K + n \log(t-l) \tag{11.24}$$

This equation was further modified by incorporation of the concept of the burst effect (b), i.e., an abrupt increase in the initial drug release as follows:

$$f_i = \frac{M_t}{M_\infty} = Kt^n + b \tag{11.25}$$

When a polymeric system comprises an unknown drug-release mechanism or more than one sort of release mechanism, researchers do well by applying the power law.

Researchers do justice with the application of power law when there is an unknown release mechanism or more than one sort of release mechanism involved in a polymeric system.

Simply, It is presumed that two independent drug transport mechanisms are involved *viz* relaxation and diffusion. The value of the release exponent (n), as given in Table 11.2, determines the drug's release profile in a matrix. Two mechanisms could be involved:

(a) Fickian type (case I)

(b) Non-Fickian type (case II, anomalous and super case II)

- Fickian diffusion (case I) describes DDS where the rate of diffusion is higher compared to the rate of polymer relaxation and swelling. Therefore, the release is managed by the diffusion process.
- DDS with non-Fickian diffusion (case II) has the release regulated by polymer relaxation and swelling.
- Last but not the least, super case II transport is an extreme example of a transport mechanism in which the polymer chains snap (known as solvent crazing) during sorption of the solvent.

In the literature, the applicability of the Korsmeyer—Peppas model is well justified. C.S. Dhanya and coworkers developed rhodamine B lauric

Table 11.2 Mechanism of drug release from the polymeric matrix based on the value of release exponent and geometry (Bruschi, 2015b; Kosmidis et al., 2013).

S. no.	Drug transport mechanism	Shape	Value of n
1	Fickian model	Planar (thin film)	0.50
		Cylinders	0.45
		Spheres	0.43
	Non-Fickian model		
2	Anomalous type	Planar (thin film)	$0.5 < n < 1.0$
		Cylinders	$0.45 < n < 0.89$
		Spheres	$0.43 < n < 0.85$
3	Case I transport	Planar (thin film)	1.0
		Cylinders	0.89
		Spheres	0.85
4	Super case II transport	Planar (thin film)	>1
		Cylinders	>0.89
		Spheres	>0.85

acid SLNs for lymphatic absorption via oral delivery. The drug-release study was conducted in pH 7.4 PBS and various models were applied to investigate the drug-release kinetics. Korsmeyer–Peppas's model was found to fit best with an R^2 value of 0.984. The release exponent (n) was 0.222, indicating the Fickian type of drug diffusion (Dhanya et al., 2023). Chitosan nanoparticles for doxorubicin were reported by Muhammad Usman Akram. The initial drug release followed the Korsmeyer–Peppas model with the highest R^2 value of 0.995 followed by the Fickian-type diffusion with a release exponent value of 0.420 (Akram et al., 2023). Utilizing HPMC, chitosan, Carbopol 934P, and NaCMC, rivastigmine in situ gels have been produced. An in vitro drug-release study was conducted in a simulated nasal electrolyte solution (SNES, pH 5.5) at 35°C ± 0.5. Release kinetics followed the Korsmeyer–Peppas model with a non-Fickian (anomalous) mechanism indicating that drug release was controlled by the erosion-diffusion mechanism (Abouhussein et al., 2018).

11.7.2.6 Baker and Lonsdale model

In 1974, a model was put up by Baker and Lansdale to explain how drug is released from a spherical-type DDS. This is also known as the modified Higuchi's model.

$$f_1 = \frac{3}{2}\left[1 - \left(1 - \frac{M_t}{M_\infty}\right)^{2/3}\right] - \frac{M_t}{M_\infty} = KT \tag{11.26}$$

where, M_t and M_∞ are the amount of drug released at time t and infinity, respectively. K is known as the release constant that corresponds to the angular coefficient of the curve (inclination). The slope of a graph obtained from the curve plotted between $d(\frac{M_t}{M_\infty})/dt$ and root of time inverse can be used to determine the value of K. The linearization of drug-release data from spherical systems, such as microspheres and microcapsules, is possible using this approach (Costa and Sousa Lobo, 2001; Shaikh et al., 2015). Shailesh and associates developed anionic drug containing pellets for CDD. Various models have been applied to find the release kinetics, but that of Baker and Lonsdale was found to be the best-fitting model (Singh et al., 1996).

11.7.2.7 Brazel and Peppas model

Many attempts have been made to describe solvent penetration and drug release from the polymeric matrix system. According to this model, the

diffusional Deborah number (De) and swelling interface number (Sw) are two dimensionless parameters that are used to describe the water absorption/penetration, swelling, and drug release for many polymer and solvent systems. De establishes a relation between the motion of water and polymer relaxation rate (Elmas et al., 2020; Brazel and Peppas, 2000). Sw measures water penetration in the polymer chain relative to the diffusion of a dispersed drug out of the polymer. Both constraints are influenced by the properties of the polymer and drug. Mathematically,

$$\mathrm{De} = \frac{\Lambda}{\Theta} = \frac{\Lambda D_{1.2}}{(\partial(t))^2} = \frac{\text{Relaxation time}}{\text{Time of solvent diffusion}} \tag{11.27}$$

where Λ is known as the relaxation time when subjected to swelling stress, Θ is the diffusion time of the swelling matrix. In this case, the Fickian process, which is a function of time, will determine whether water diffusion ($D >> 1$) or relaxation time ($D1$) dominates the swelling. If D is nearly 1, then two processes will occur simultaneously leading to the anomalous transport mechanism (Brazel and Peppas, 2000).

On the other hand, the swelling interface number (Sw) is the balance/equilibrium/ratio of water (solvent) penetration to drug (solute) release.

$$\mathrm{Sw} = \frac{\nabla \partial_r}{D3,21} = \frac{\Lambda D_{1.2}}{(\partial(t))^2} = \frac{\text{Solvent mobility}}{\text{Drug diffusion}} \tag{11.28}$$

where Λ denotes the velocity of the moving glassy/rubbery front, ∂ denotes swollen gel layer thickness, and $D3,21$ denotes the diffusion coefficient. Sw depends upon polymer and drug properties. In both situations of Sw values, either $<<1$ or $>>1$, the water penetration or diffusion controls the release, and time dependence will be as per the Fickian law. If Sw is close to 1, the release is directed by anomalous transport (Brazel and Peppas, 2000).

11.7.2.8 Hopfenburg model

In order to forecast drug release from polymers with eroding surfaces, Hopfenburg developed a mathematical model. During the erosion, the surface area remains constant. The release of poorly water-soluble drugs takes place through an erosion mechanism (Costa and Sousa Lobo, 2001; Jain and Jain, 2016). He examined how drugs are released from surfaces that have a variety of geometries, and he created a generic mathematical equation (Eq. 11.29) that describes how drugs are released from slabs,

spheres, and infinite cylinders that have heterogeneous erosion (Ramteke et al., 2014; Shaikh et al., 2015; Katzhendler, 1997).

$$\frac{M_t}{M_\infty} = 1 - \left[1 - \frac{K_0 t}{C_0 a_0}\right]^n \tag{11.29}$$

where, $\frac{M_t}{M_\infty}$ denotes the drug released fraction, K_0 denotes erosion grade constant, C_0 denotes initial drug concentration at time zero, a_0 denotes initial radius depending upon the geometry of the matrix, namely sphere ($a_0 = 3$) or cylinder ($a_0 = 2$), or half of the thickness of the film ($a_0 = 1$).

The preceding equation was updated by El-Arini and Leuenberger (1998) to compute the latency time (l) as follows:

$$\frac{M_t}{M_\infty} = 1 - [1 - K_1 t\,(t - l)]^n \tag{11.30}$$

where $K_1 = \frac{K_0}{C_0 a_0}$. According to this model, matrix erosion is considered as the rate-controlling step in the drug release. Time-dependent diffusing resistance internal and external to the eroded matrix does not have any influence on the drug release kinetics (Katzhendler, 1997). The drug release mechanism from optimized oily spheres which exhibited the site-specific biphasic release pattern that can be evaluated by the application of this model (Dash et al., 2010; Sibanda et al., 2004).

11.7.2.9 Weibull model

This is a distribution function-based model and was first put forward by Weilbull (1951), and which Langenbucher (1972) modified to its present form. This model explains the events and processes occurring within a limited time frame (Dash et al., 2010; Ramteke et al., 2014; Costa and Sousa Lobo, 2001). Drug accumulated in a solution system at time t can be explained by the following equation:

$$m = 1 - \exp\left(\frac{(t - T_i)^n}{a}\right) \tag{11.31}$$

In another format:

$$m = 1 - \exp^{-(t - T_i)^{\frac{b}{a}}} \tag{11.32}$$

where a and T_i represent the time scale parameter of the process and localization parameters and is known as the latency of the release process (maybe

zero also), respectively, and b denotes the shape of the dissolution curve (form parameter). The value of the form parameter b is a variable such as:

(a) $b = 1$ (exponential) = In this case the shape of the curve corresponds to the exponential profile k (constant) value $1/a$

(b) $b > 1$ = In this case the shape of the curve will be sigmoid, with ascendant curvature delimited by an inflection point

(c) $b < 1$ = In this case the shape of the curve will be parabolic, displaying high initial slope and a consistent exponential character.

The drug release from the matrix systems is compared using this model. Sittaa and co-workers developed cross-linked albumin microparticles containing vitamin B12. The release study was conducted at different pHs (2, 6, and 10). They concluded that the Weibull equations govern the release profile of vitamin B12 from the matrix during the preliminary stage of the investigation (pH 2), whereas the super case II transport mechanism results from diffusion, relaxation, and erosion during the second stage of the study (pH 6 and 10) (Sitta et al., 2014).

11.7.2.10 Peppas–Sahlin model

According to this model, during drug release in an anomalous process, the two contributing mechanisms, namely diffusional and relaxational, are involved. This can be seen by the following equation:

$$\frac{M_t}{M_\infty} = K_1 t^m + 2_2 t^{2m} \tag{11.33}$$

where, $K_1, K_2,$ and m are constants.

The first component in the equation stands for the Fickian diffusional contribution (F) and the second term stands for the Case II relaxational contribution (R). For any system with any geometrical shape and a controlled release pattern, the coefficient m is the exponent of pure Fickian diffusion (Shaikh et al., 2015; Peppas and Sahlin, 1989). Another coefficient m is related to the power law coefficient (n) and can be given for any shape, such as films, cylinders, and spheres (Bruschi, 2015b).

11.7.2.11 Gompertz model

This is the simple exponential model used to describe the drug-release mechanism, which can be mathematically presented as follows:

$$M_t = M_{\max} \exp\left(- \alpha \, e^{\beta \log t} \right) \tag{11.34}$$

where M_t is the percentage drug dissolved/100, M_{max} is the maximum amount of drug dissolved, α is the location or scale parameter, indicating the undissolved drug at time $t = 1$, and β denotes the shape parameter indicating the dissolution rate/time. This model begins with a sharp increase and converges gradually to the asymptotic maximal dissolution. This approach is more explicitly applicable in the case of an intermediate-release formulation of a drug with good solubility (Dash et al., 2010; Costa and Sousa Lobo, 2001; Shaikh et al., 2015; AlMajed et al., 2022).

11.7.3 Regression model analysis

Regression model analysis is used for the optimization of pharmaceutical formulation using various software such as Minitab, expert design, etc. Data (response) associated with dissolution/release is fitted to certain models like linear, 2F, and quadratic models, to detect the value of the regression coefficient (R^2) (Ladani Ravi, 2010). The model that exhibited the highest R^2 value is considered an optimized model. In the case of regression modeling, responses (like drug dissolved, disintegration, entrapment efficiency, particle size, etc.) are chosen as dependent parameters, and independent parameters may include polymer concentration, surfactant concentration, etc. (Li et al., 2008). The effect of independent constraints is observed on dependent constraints and can be displayed by diagrams (3D, contour), polynomial equations, etc. The following models are mainly used.

11.7.3.1 Polynomial equation for the linear, first-order, and quadratic models

The polynomial equation for the linear model exhibited the individual and interaction effect of independent parameters (X, $X2$, $X3$) on the dependent parameters (Y, response) effect (Noorulla et al., 2022; Yasir et al., 2022). The equation carries the charge, negative or positive. A positive charge displayed a positive effect of the independent parameter on the dependent parameter (response) while a negative sign showed an adverse influence on the response. The polynomial equation for the linear model can be depicted as:

$$Y = \beta_0 + \beta_1 X_1 + \beta_2 X_2 - \beta_3 X_3 - \beta_{12} X_1 X_2 + \beta_{13} X_1 X_3 + \beta_{23} X_2 X_3 \tag{11.35}$$

where, Y is the response (like CDR), β_0 is a constant obtained from the intercept, $\beta_1, \beta_2, \beta_3$ are regression coefficients, whereas $\beta_{12}, \beta_{13}, \beta_{23}$ are known as the interaction coefficient. X_1, X_2, X_3 are the formulation factors (independent parameters) that influence the response (like CDR). In the

above model equation positive signs like $+\beta_1 X_1$ mean the factor X_1 exhibited a positive effect on response Y i.e., if X_1 value will increase simultaneously Y will also increase, or vice versa. In the above model equation, negative signs like $-\beta_2 X_2$ mean the factor X_2 exhibited a negative effect on response Y, i.e., if X_2 value will increase simultaneously Y will decrease, or vice versa.

Similarly, the polynomial equation for the quadratic model (Yasir et al., 2018) can be represented by adding the quadratic term (X^2) in the above equation as:

$$Y = \beta_0 + \beta_1 X_1 + \beta_2 X_2 - \beta_3 X_3 - \beta_{12} X_1 X_2 + \beta_{13} X_1 X_3 + \beta_{23} X_2 X_3 - \beta_{11} X_1^2 + \beta_{22} X_2^2 + \beta_{33} X_3^2 \tag{11.36}$$

11.7.4 Nonlinear regression models

For the comparison of certain characteristics like amount of drug diffused or dissolved or the rate of dissolution, the percentage of drug released or dissolved at a specific point, analysis of variance (ANOVA) can be used. In this case, two types of effects are considered, namely fixed and random effects. The variables like the nature of the dissolution medium (pH, presence of enzyme/presence of surfactants), temperature, spindle speed, etc (Qazi et al., 2003). that researchers can control are called fixed effects. Typically, selection of levels from a large population is used to create random effects (Dash et al., 2010). In the case of dissolution, DDS like tablets or capsules act as a random effect. Each tablet is chosen from a larger population of tablets, and assumptions about the population variance from which the sample has been taken can be made based on the tablet-to-tablet variation in each scenario (Qazi et al., 2003). However, once the ANOVA analysis has determined the key components, a nonlinear regression model can be used to demonstrate the link between the important parameters. Nonlinear regression models have the advantage of allowing for the differentiation of dissolution parameters even when the overall dissolution profiles are comparable. This is due to the fact that the dissolution process in the nonlinear regression model depends on the kinetic constant and diffusion exponent, and that different combinations of the two parameters might lead to profiles of dissolution that are identical. Nonlinear regression

can be applied with the aid of the JMP software (Dash et al., 2010; Qazi et al., 2003). The relationship between important factors will be clarified through the data analysis utilizing nonlinear regression models, which will also guarantee that future preparations will not exceed permissible dissolution requirements (Qazi et al., 2003).

11.7.5 Model-independent approach

Moore and Flanner established two model-independent indices in 1996 for identifying similarities and differences between the release profile for two formulations (one may be standard and the other may be a test formulation). These are known as similarity (f_2) and dissimilarity (f_1) factors. Differences in the release profile of two formulations at each time point can be determine by the dissimilarity (f_1). This estimates the relative error of the two curves. Mathematically, the dissimilarity (f_1) factor can be denoted by Eq. (11.37) (Dash et al., 2010; Costa and Sousa Lobo, 2001; Jain and Jain, 2016):

$$f_1 = \frac{\left[\sum_{t=1}^{n}(R_t - T_t)\right]}{\sum_{t=1}^{n} R_t} \times 100 \tag{11.37}$$

where n denotes the number of time points for the dissolution study, and R_t and T_t denote the amount (or %) of drug dissolved at each of the selected n time points for the reference and test product, respectively (Costa and Sousa Lobo, 2001; Bhansali, 2021). Mathematically, the similarity factor (f_2) can be calculated by the following equation:

$$f_2 = 50 \log \left\{ \left[1 + \frac{1}{n} \sum_{t=1}^{n} (R_t - T_t)^2 \right]^{-0.5} \times 100 \right\} \tag{11.38}$$

Similarity and dissimilarity factors determine how similar two release profiles are at particular time points. There should be a minimum of 12 units of each product compared to at least three separate time periods. The standard deviation should not be greater than 10% at any given time point for the test or reference. According to guidelines of Food and Drug Administration (FDA) range of f_1 and f_2 should be 0–15 and 50–100 respectively, to indicate the similarity between the two profiles

(e.g. dissolution profile, drug release profile, etc.) (Sheth, 2021; FDA Guidance for Industry, December 2017). Tulsi Sagar Sheth and co-workers optimized the similarity factor by utilizing linear regression (Costa and Sousa Lobo, 2001; Sheth, 2021). The value of the similarity factor was found to be 40.

Paramita Saha and co-workers developed rotigotine redispersible nanoemulsion for brain targeting via the nasal route. In a PBS 6.4 pH buffer, a comparative in vitro dissolution test for pure drug and rotigotine-loaded lyophilized nanosuspension was performed, and the similarity factor was calculated. The fact that the f_2 was below 50 indicates that the two dissolution profiles are not comparable (Saha et al., 2023). The dissolution profiles of various brands of amoxicillin were compared with the amoxicillin innovator capsules by Kassaye and colleagues. The USP-II dissolution apparatus was used to conduct the investigation in 900 mL of water. The f_2 was much lower than 50, illustrating the divergence from the innovator's dissolution profile (Kassaye and Genete, 2013).

11.8 How to select the best-fitting model

Coefficient of determination (R^2) is the most suitable parameter to select the best-fitting release model. For different models, the R^2 value is calculated and compared to others. The model that has the highest value closest to 1 is considered the best-fitting model. However, this is applicable when model equation parameters are similar. In the case of increasing the comparing parameters, the adjusted coefficient (R^2_{adj}), which can be determined by the following equation, is used to select the best-fitted model.

$$R^2_{adj} = 1 - \frac{n-1}{n-p}(1 - R^2) \tag{11.39}$$

Correspondingly, other statistical methods are employed to compare and select the most suitable models, including the correlation coefficient (R), analysis of variance (ANOVA), and multivariate analysis of variance (MANOVA) (Shaikh et al., 2015). A summary of the literature associated with various model and drug release mechanisms is presented in Table 11.3.

Table 11.3 The literature associated with various models and release mechanisms of certain formulations with the major polymers involved in their preparation.

API	Formulation type	Main excipient	Release study	Release model	References
Levonorgestrel	Microspheres	PLGA	DM: 0.9% w/v in distilled water + 0.5% sodium dodecyl sulfate DA: Stoppered Flask	Zero-order	Puthli and Vavia (2009)
Poly (ε-caprolactone)	Ocular insert	PCL-PEG-PCL	DM: PBS 7.4 DA: Closed glass bottle	Zero-order	Mariz et al. (2022)
Etofenamate	SLN	Precirol ATO 5	DM: PBS pH 7.4: ethanol (70:30) DA: Franz diffusion cell	Zero-order	Badilli et al. (2015)
Ibuprofen	Carboxymethyl cellulose/ mesoporous magnetic graphene oxide carriers	Carboxymethyl cellulose, graphene oxide	DM: Intestinal Fluid (pH 7.4) DA: Franz diffusion cell	First-order	Pooresmaeil et al. (2020)
Methotrexate (MTX)	Microspheres	Chitosan	DM: PBS pH 7.4	First-order and Higuchi's model	Dubey and Parikh (2004)

Continued

Table 11.3 The literature associated with various models and release mechanisms of certain formulations with the major polymers involved in their preparation.—cont'd

API	Formulation type	Main excipient	Release study	Release model	References
Salicylic acid	Cubic phase gel	GMO Myverol 18—99 distilled monoglycerides	DM: Isotonic PB DA: USP-I app	First-order and Higuchi's model	Lara et al. (2005)
Curcumin	Nanomicelles	Pluronic F127/ oleic acid(OA)-Fe_3O_4	DM: PBS pH 7.4 DA: Beaker	First-order and diffusion	Santadkha et al. (2022)
Illicium verum	Polymeric nanoparticles	PLGA	DM: PBS pH 6.8 DA: Dialysis bag	First-order	Kumari et al. (2022)
5FU	Liposomal gel	PL 90H + cholesterol liposomes in 1% chitosan	DM: PBS pH 7.4 DA: Dialysis tube	Higuchi's model	Glavas-dodov et al. (2005)
Levothyroxine-Na pentahydrate	p- sensitive gel	Chitosan/ arabinogalactane	DM: deionized water or pH 7 PBS DA: Vial	Higuchi's model	Tapdiqov et al. (2022)
Ciprofloxacin HCL	Biodegradable capsules	Chitosan + dextran sulfate	DM: Water and PBS 7.4 DA: Dialysis tube	Higuchi's model	Geetha Devi et al. (2021)
Nimodipine Coumarin	Microparticles	PLGA	DM: ethanol + PBS (7.4) (1:1 ratio)	Higuchi's model	Bege et al. (2013)

Clonazepam	Chitosan-coated niosomes	Chitosan	DM: simulated nasal fluid DA: Dialysis tube	Higuchi's model with Fickian diffusion ($n = 0.380$)	Nerli et al. (2023)
Rhodamine B	SLNs	Lauric acid	DM: PBS 7.4 DA: Dialysis bag	Korsmeyer −Peppas model with Fickian diffusion ($n = 0.222$)	Dhanya et al. (2023)
Doxorubicin	Polymeric NP	Chitosan	DM: PB 5.3 DA: Dialysis bag	Korsmeyer −Peppas model with Fickian diffusion ($n = 0.42$)	Akram et al. (2023)
Docetaxel	PEGylated	Stearic acid + mPEG200	DM: 5.5 DA: Beaker	Higuchi model followed by Fickian diffusion ($n = 0.0.321$)	Korake et al. (2023)
5 FU	Polymeric NP	Chitosan	DM: PBS 7.4 DA: Dialysis bag	Higuchi model followed by Fickian diffusion ($n < 0.5$)	Badran et al. (2017)
Rivastigmine	In situ gel	HPMC, CS, CP 934, and NaCMC	DM: simulated nasal electrolyte Solution (pH = 5.5) DA: Dialysis tube	Korsmeyer −Peppas model followed by non-Fickian (anomalous release). Drug release is controlled by erosion-diffusion mechanism	Abouhussein et al. (2018)

Continued

Table 11.3 The literature associated with various models and release mechanisms of certain formulations with the major polymers involved in their preparation.—cont'd

API	Formulation type	Main excipient	Release study	Release model	References
Triamcinolone acetonide	Buccal patches	Modified pectin/ alginate	DM: simulated salivary pH 6.8 DA: Franz diffusion cell	Korsmeyer −Peppas model followed by non-Fickian release mechanism	Özbas et al. (2022)
Rivastigmine	Nasal insert	Gelatin/HPMC	DM: SNF (pH7.4) DA: Dialysis tube	Korsmeyer −Peppas model followed by non-Fickian release mechanism (anomalous transport)	Shaghlil et al. (2022)
Itraconazole	Hybrid NP	Chitosan + GMS	DM: 0.1 N HCl, PB pH 7.4 DA: Dialysis bag	Korsmeyer −Peppas model followed by non-Fickian diffusion model	Yousaf et al. (2023)
Vitamin B12	Microparticles	BSA	DM: Dialysis bag DM: pH 2, pH 6, and pH 10 buffers	First stage: Power law and Weibull equations Second stage: Super Case II transport mechanism, as a	Sitta et al. (2014)

				result of diffusion, relaxation, and erosion, Application of Hixson–Crowell model confirmed the erosion mechanism	
Rotigotine	Nanosuspension	Ethanol and Poloxamer 407	DM: PB pH 6.4 DA: Modified USP type I	Dissimilar dissolution profile ($f_2 < 50$) of formulation form pure drug	Saha et al. (2023)
Amoxicillin	Capsule (marketed brand compared with innovator)	–	DM: Water DA: USP-II	Dissimilar dissolution profile ($f_2 < 50$) form innovator	Kassaye and Genete (2013)
Ibuprofen and ketokonazole	Tablets	–	DM: FaSSGF, FeSSGF, FaSSIF-V2, and FeSSIF-V2 Volume: 500, 300, 40 mL	Dissolution profiles of Ibuprofen and ketoconazole differ in different dissolution mediums and in different volumes also	Jamil et al. (2021)

11.9 Conclusion and future perspectives

The chapter summarizes drug-release modeling from the bioresorbable polymeric matrix system. A huge number of natural and synthetic bioresorbable/biodegrdable polymers have been used for the design of DDSs based on sustained and controlled drug-release patterns. These polymers should be nontoxic, biocompatible, nonallergic, bio-stable, etc. Many researchers and scientists have designed and proven their capabilities to encapsulate the drug and transform them into nanocomposites such as nanoparticles, nanocarriers, hydrogels, metal, and metal oxide components, etc. In vitro release studies have been recognized as one of the main criteria to evaluate and optimize the formulation. In vitro release studies have shown the structure—function relationship of the material matrix, helped customize the materials for the best-regulated release, and also provided an idea about the in vivo performance of the developed formulations. Several mathematical models are reported in the literature, which have been used to describe the relevant kinetics and mechanisms of drug release from the biodegradable polymer matrix or biodegradable DDS. Mathematical modeling provides the relation between the drug dissolution/release and the geometry of the matrix. Statistical models, model-dependent approaches, and model-independent approaches are used currently. Application of the statistical approach is somewhat complicated, while model-dependent approaches offer an acceptable and are commonly used for drug-release kinetic studies. This approach provides a true correlation between dependent and independent dissolution parameters. The model-independent approach, on the other hand, is based on the value of similarity (f_2) and dissimilarity (f_1) factors, which are sensitive to the dissolution point taken during the study. However, the established similarity or dissimilarity between the dissolution profiles is not clear. Additionally, the goal of mathematical modeling is to explain drug-release kinetics and mechanisms, especially in association with the structure—function relationship of the material system. They can also be helpful in establishing the relationship between in vitro dissolution with in vivo absorption. Therefore, having a solid understanding of the principles will help with future device and material development.

Regarding future perspectives, a perfect model that can establish a better correlation between in vitro and in vivo dissolution is unavailable. This might be due to differences in the dissolution medium of in vivo atmosphere and in vitro condition. Body physiological conditions are highly

complex as compared to the PB used for the in vitro dissolution. After reaching the DDS in the body, the release profile of a drug may be influenced by different proteins, cells, and enzymes present at the site of drug dissolution. Therefore, mathematical models that can provide a real correlation of physiological conditions with an in vitro medium are still required to be developed (Fu and Kao, 2010).

The release pattern of SRDDS or CRDDS is usually characterized by the initial burst release, and typically followed by sustained release. The burst release helps to keep the appropriate drug-loading concentration fairly quickly. Burst release is frequently associated with the device's shape, the coating material's surface characteristics, the distribution pattern of API within the polymer matrix, the intrinsic dissolving rate of the API, the heterogeneity of the matrices (pore density), and other parameters. There have not been many investigations into the development of mathematical models for burst release that are based on mechanisms. Therefore, it would be beneficial to create models that explain the burst release mechanisms in order to improve the prediction of the burst release.

List of abbreviations

API	Active pharmaceutical ingredient (drug)
CDR	Cumulative drug release
CR	Controlled release
CRDDS	Controlled-released drug-delivery system
DDS	Drug-delivery system
DS	Delivery system
NDDSs	Nano-drug-delivery systems
NLC	Nanostructured lipid carrier
NP	Nanoparticle
PCL	Polycaprolactone
PDS	Polydioxanone
PGA	Poly(glycolic acid)
PLGA	Poly(lactic acid-co-glycolic acid)
PN	Polymeric nanoparticle
PVA	Polyvinyl alcohol
SA	Surface area
SLN	Semi-solid lipid nanoparticle
SR	Sustained release
SRDDS	Sustained-release drug-delivery system

References

Abouhussein, D.M.N., Khattab, A., Bayoumi, N.A., Mahmoud, A.F., Sakr, T.M., 2018. Brain targeted rivastigmine mucoadhesive thermosensitive in situ gel: optimization, in vitro evaluation, radiolabeling, in vivo pharmacokinetics and biodistribution. J. Drug Deliv. Sci. Technol. 43, 129–140. https://doi.org/10.1016/j.jddst.2017.09.021.

Akram, M.U., Abbas, N., Farman, M., Manzoor, S., Khan, M.I., Osman, S.M., Luque, R., Shanableh, A., 2023. Tumor micro-environment sensitive release of doxorubicin through chitosan based polymeric nanoparticles: an in-vitro study. Chemosphere 313, 137332. https://doi.org/10.1016/j.chemosphere.2022.137332.

AlMajed, Z., Salkho, N.M., Sulieman, H., Husseini, G.A., 2022. Modeling of the in vitro release kinetics of sonosensitive targeted liposomes. Biomedicines 10, 3139. https://doi.org/10.3390/biomedicines10123139.

Anwar, M., Muhammad, F., Akhtar, B., 2021. Biodegradable nanoparticles as drug delivery devices. J. Drug Deliv. Sci. Technol. 64, 102638. https://doi.org/10.1016/j.jddst.2021.102638.

Badilli, U., Tuba, C., Turk, S., Onay-besikci, A., Tarimci, N., 2015. Development of etofenamate-loaded semisolid SLN dispersions and evaluation of anti-inflammatory activity for topical application. Curr. Drug Deliv. 12, 200–209. https://doi.org/10.2174/1567201811666140613112721.

Badran, M.M., Mady, M.M., Ghannam, M.M., Shakeel, F., 2017. Preparation and characterization of polymeric nanoparticles surface modified with chitosan for target treatment of colorectal cancer. Int. J. Biol. Macromol. 95, 643–649. https://doi.org/10.1016/j.ijbiomac.2016.11.098.

Bari, N.K., Fazil, M., Hassan, Q., Haider, R., Gaba, B., Narang, J.K., Baboota, S., Ali, J., November 2015. Brain delivery of buspirone hydrochloride chitosan nanoparticles for the treatment of general anxiety disorder. Int. J. Biol. Macromol. 81, 49–59. https://doi.org/10.1016/j.ijbiomac.2015.07.041.

Bege, N., Renette, T., Endres, T., Beck-broichsitter, M., Hänggi, D., Kissel, T., 2013. In situ forming nimodipine depot system based on microparticles for the treatment of posthemorrhagic cerebral vasospasm. Eur. J. Pharm. Biopharm. 84, 99–105. https://doi.org/10.1016/j.ejpb.2012.12.016.

Begines, B., Ortiz, T., Mart, G., Merinero, M., Argüelles-arias, F., Alcudia, A., 2020. Polymeric nanoparticles for drug delivery: recent developments and future prospects. Nanomaterials 10 (7), 1403. https://doi.org/10.3390/nano10071403.

Bhansali, M., 2021. Solid oral controlled-release formulations. In: Modeling and Control of Drug Delivery Systems. Elsevier Inc., pp. 313–331. https://doi.org/10.1016/B978-0-12-821185-4.00007-5

Brazel, C.S., Peppas, N.A., 2000. Modeling of drug release from swellable polymers. Eur. J. Pharm. Biopharm. 49, 47–58.

Bruner, L., Tolloczko, S., 1900. Uber die Auflo sungsgeschwindigkeit FesterKorper. Z. Phys. Chem. 35, 283–290. https://doi.org/10.1515/zpch-1900-3517.

Brunner, E., 1904. Reaktionsgeschwindigkeit in heterogenen Systemen. Z. Phys.Chem. 43, 56–102. https://doi.org/10.1515/zpch-1904-4705.

Bruschi, M.L., 2015a. Main mechanisms to control the drug release. In: Strategies to Modify the Drug Release from Pharmaceutical Systems, pp. 37–62. https://doi.org/10.1016/b978-0-08-100092-2.00004-7.

Bruschi, M.L., 2015b. Mathematical models of drug release. In: Strategies to Modify the Drug Release from Pharmaceutical Systems, pp. 63–86. https://doi.org/10.1016/B978-0-08-100092-2.00005-9.

Chang, C.-M., Bodmeier, R., 1997. Swelling of and drug release from monoglyceride-based drug delivery systems. J. Pharm. Sci. 86, 747–752. https://doi.org/10.1021/js960256w.

Costa, P., Sousa Lobo, J.M., 2001. Modeling and comparison of dissolution profiles. Eur. J. Pharm. Sci. 13, 123–133. https://doi.org/10.1016/s0928-0987(01)00095-1.

Dash, S., Murthy, P.N., Nath, L., Chowdhury, P., 2010. Kinetic modeling on drug release from controlled drug delivery systems. Acta Pol. Pharm. Drug Res. 67, 217–223.

Dhaliwal, K., Dosanjh, P., 2018. Biodegradable polymers and their role in drug delivery systems. Biomed. J. Sci. Tech. Res. 5, 8315–8320. https://doi.org/10.26717/BJSTR.2018.11.002056.

Dhanya, C.S., Paul, W., Rekha, M.R., Joseph, R., 2023. Solid lipid nanoparticles of lauric acid: a prospective drug carrier for oral drug delivery. J. Mol. Liq. 380, 121738. https://doi.org/10.1016/j.molliq.2023.121738.

Dokoumetzidis, A., Macheras, P., 2006. A century of dissolution research: from Noyes and Whitney to the biopharmaceutics classification system. Int. J. Pharm. 321, 1–11. https://doi.org/10.1016/j.ijpharm.2006.07.011.

Dubey, R.R., Parikh, R.H., 2004. Two-stage optimization process for formulation of chitosan microspheres. AAPS PharmSciTech 5, 1–9. https://doi.org/10.1208/pt050105.

El-Arini, S.K., Leuenberger, H., 1998. Dissolution properties of praziquantel-PVP systems. Pharm. Acta Helv. 73, 89–94. https://doi.org/10.1016/s0031-6865(97)00051-4.

Elmas, A., Akyüz, G., Bergal, A., Andaç, M., Andaç, Ö., 2020. Mathematical modelling of drug release. Res. Eng. Struct. Mater. 6, 327–350. https://doi.org/10.17515/resm2020.178na0122.

Elnaggar, Y.S.R., Etman, S.M., Abdelmonsif, D.A., Abdallah, O.Y., 2015. Intranasal piperine-loaded chitosan nanoparticles as brain-targeted therapy in Alzheimer's disease: optimization, biological efficacy, and potential toxicity. J. Pharm. Sci. 104, 3544–3556. https://doi.org/10.1002/jps.24557.

FDA Guidance for Industry December 2017. Waiver of in vivo bioavailability and bioequivalence studies for immediate-release solid oral dosage forms based on a biopharmaceutics classification System, U.S. Department of Health and Human Services, Food and Drug Administration, Center for Drug Evaluation and Research (CDER). https://www.gmp-compliance.org/files/guidemgr/UCM070246.pdf.

Fick, A., 1855. On liquid diffusion. Lond. Edinb. Dublin Philos. Mag. J. Sci. 10 (63), 30–39. https://doi.org/10.1080/14786445508641925.

Fu, Y., Kao, W.J., 2010. Drug release kinetics and transport mechanisms of non-degradable and degradable polymeric delivery systems. Expert Opin. Drug Deliv. 7, 429–444. https://doi.org/10.1517/17425241003602259.

Gao, Z., 2011. Mathematical modeling of variables involved. J. Pharm. Sci. 100, 4934–4942. https://doi.org/10.1002/jps.

Gavasane, A.J., Pawar, H.A., 2014. Synthetic biodegradable polymers used in controlled drug delivery system: an overview. Clin. Pharmacol. Ther. 3, 121. https://doi.org/10.4172/2167-065X.1000121.

Geetha Devi, M., Dutta, S., Al Hinai, A.T., Feroz, S., 2021. Nano engineered biodegradable capsules for the encapsulation and kinetic release studies of ciprofloxacin hydrochloride. J. Indian Chem. Soc. 98, 100109. https://doi.org/10.1016/j.jics.2021.100109.

George, A., Shah, P.A., Shrivastav, P.S., 2019. Natural biodegradable polymers based nanoformulations for drug delivery: a review. Int. J. Pharm. 561, 244–264. https://doi.org/10.1016/j.ijpharm.2019.03.011.

Gibaldi, M., Feldman, S., 1967. Establishment of sink conditions in dissolutionrate determinations. Theoretical considerations and application to nondisintegratingdosage forms. J. Pharm. Sci. 56, 1238–1242. https://doi.org/10.1002/jps.2600561005.

Glavas-dodov, M., Fredro-kumbaradzi, E., Goracinova, K., Simonoska, M., 2005. The effects of lyophilization on the stability of liposomes containing 5-FU. Int. J. Pharm. 291, 79–86. https://doi.org/10.1016/j.ijpharm.2004.07.045.

Go, E.H., 2006. Release and diffusional modeling of metronidazole lipid matrices. Eur. J. Pharm. Biopharm. 63, 331–339. https://doi.org/10.1016/j.ejpb.2006.02.005.

Gouda, R., Baishya, H., Qing, Z., 2017. Application of mathematical models in drug release kinetics of carbidopa and levodopa ER tablets. J. Dev. Drugs 6, 1–8. https://doi.org/10.4172/2329-6631.1000171.

Hixson, A.W., Crowell, J.H., 1931. Dependence of reaction velocity upon surface andagitation: I–Theoretical consideration. Ind. Eng. Chem. 23, 923–931. https://doi.org/10.1021/ie50262a025.

Idrees, H., Zohaib, S., Zaidi, J., Sabir, A., Khan, R.U., Zhang, X., Hassan, S., 2020. A review of biodegradable natural polymer-based nanoparticles for drug delivery applications. Nanomaterials (Basel) 10 (10), 1970. https://doi.org/10.3390/nano10101970.

Jacob, S., Nair, A.B., Shah, J., Gupta, S., Boddu, S.H.S., Sreeharsha, N., Joseph, A., Shinu, P., Morsy, M.A., 2022. Lipid nanoparticles as a promising drug delivery carrier for topical ocular therapy; an overview on recent advances. Pharmaceutics 14, 533. https://doi.org/10.3390/pharmaceutics14030533.

Jain, A., Jain, S.K., 2016. In vitro release kinetics model fitting of liposomes: an insight. Chem. Phys. Lipids 201, 28–40. https://doi.org/10.1016/j.chemphyslip.2016.10.005.

Jain, A., Thakur, K., Kush, P., Jain, U.K., 2014. Docetaxel loaded chitosan nanoparticles: formulation, characterization and cytotoxicity studies. Int. J. Biol. Macromol. 69, 546–553. https://doi.org/10.1016/j.ijbiomac.2014.06.029.

Jamil, R., Xu, T., Shah, H.S., Adhikari, A., Sardhara, R., Nahar, K., Morris, K.R., Polli, J.E., 2021. Similarity of dissolution profiles from biorelevant media: assessment of interday repeatability, interanalyst repeatability, and interlaboratory reproducibility using ibuprofen and ketoconazole tablets. Eur. J. Pharm. Sci. 156, 105573. https://doi.org/10.1016/j.ejps.2020.105573.

Joshi, J.R., Patel, R.P., 2012. Role of biodegradable polymers in drug delivery. Int. J. Curr. Pharm. Res. 4, 74–81.

Kalam, M.A., Sultana, Y., Ali, A., Aqil, M., Mishra, A.K., Aljuffali, I.A., Alshamsan, A., 2013. Part I: development and optimization of solid-lipid nanoparticles using Box-Behnken statistical design for ocular delivery of gatifloxacin. J. Biomed. Mater. Res., Part A 101 A, 1813–1827. https://doi.org/10.1002/jbm.a.34453.

Kassaye, L., Genete, G., 2013. Evaluation and comparison of in-vitro dissolution profiles for different brands of amoxicillin capsules. Afr. Health Sci. 13, 369–375. https://doi.org/10.4314/ahs.v13i2.25. http://www.embase.com/search/results?subaction=viewrecord&from=export&id=L369785006%5Cn. http://www.ajol.info/index.php/ahs/article/download/93524/82949%5Cn.

Katara, R., Majumdar, D.K., 2013. Eudragit RL 100-based nanoparticulate system of aceclofenac for ocular delivery. Colloids Surf. B Biointerfaces 103, 455–462. https://doi.org/10.1016/j.colsurfb.2012.10.056.

Katzhendler, I., 1997. Modeling of drug release from erodible tablets. J. Pharm. Sci. 86, 6–11. https://doi.org/10.1021/js9600538.

Kelmann, R.G., Kuminek, G., Teixeira, H.F., Koester, S., 2007. Carbamazepine parenteral nanoemulsions prepared by spontaneous emulsification process. Int. J. Pharm. 342, 231–239. https://doi.org/10.1016/j.ijpharm.2007.05.004.

Korake, S., Bothiraja, C., Pawar, A., 2023. Design, development, and in-vitro/in-vivo evaluation of docetaxel-loaded PEGylated solid lipid nanoparticles in prostate cancer

therapy. Eur. J. Pharm. Biopharm. 189, 15–27. https://doi.org/10.1016/j.ejpb.2023.05.020.
Korsmeyer, R.W., Gurny, R., Doelker, E.M., Buri, P, Peppas, N.A., 1983. Mechanism of solute release from porous hydrophilic polymers. Int. J. Pharm. 15, 25–35. https://doi.org/10.1016/0378-5173(83)90064-9.
Kosmidis, K., Argyrakis, P., Macheras, P., 2013. Fractal kinetics in drug release from finite fractal matrices. J. Chem. Phys. 119, 6373–6377. https://doi.org/10.1063/1.1603731.
Kumari, V., Tyagi, P., Sangal, A., 2022. Proceedings in-vitro kinetic release study of Illicium verum (Chakraphool) polymeric nanoparticles. Mater. Today Proc. 60, 14–20. https://doi.org/10.1016/j.matpr.2021.11.014.
Ladani Ravi, K., 2010. Modern optimization techniques in field of pharmacy. Res. J. Pharm. Biol. Chem. Sci. 1, 148–157.
Langenbucher, F., 1972. Linearization of dissolution rate curves by the Weibull distribution. J. Pharm. Pharmacol. 24, 979–981. https://doi.org/10.1111/j.2042-7158.1972.tb08930.x.
Lara, M.G., Vit, M., Bentley, L.B., Collett, J.H., 2005. In vitro drug release mechanism and drug loading studies of cubic phase gels. Int. J. Pharm. 293, 241–250. https://doi.org/10.1016/j.ijpharm.2005.01.008.
Li, H., Hardy, R.J., Gu, X., 2008. Effect of drug solubility on polymer hydration and drug dissolution from polyethylene oxide (PEO) matrix tablets. AAPS PharmSciTech 9, 437–443. https://doi.org/10.1208/s12249-008-9060-x.
Liu, X., 2016. Traditional methods of longitudinal data analysis. In: Methods and Applications of Longitudinal Data Analysis, pp. 19–59. https://doi.org/10.1016/B978-0-12-801342-7/00002-2.
Liu, S., Yang, S., Ho, P.C., 2018. Intranasal administration of carbamazepine-loaded carboxymethyl chitosan nanoparticles for drug delivery to the brain. Asian J. Pharm. Sci. 13, 72–81. https://doi.org/10.1016/j.ajps.2017.09.001.
Mariz, M., Murta, J., Gil, M.H., Ferreira, P., 2022. An ocular insert with zero-order extended delivery: release kinetics and mathematical models. Eur. J. Pharm. Biopharm. 181, 79–87. https://doi.org/10.1016/j.ejpb.2022.10.023.
Mönkäre, J., Pajander, J., Hakala, R.A., Savolainen, P., Järveläinen, M., Korhonen, H., V Seppälä, J., Järvinen, K., 2012. Characterization of internal structure, polymer erosion and drug release mechanisms of biodegradable poly (ester anhydride)s by X-ray microtomography. Eur. J. Pharmaceut. Sci. 47, 170–178. https://doi.org/10.1016/j.ejps.2012.05.013.
Musumeci, T., Serapide, M.F., Pellitteri, R., Ferraro, L., Magro, R.D., Bonaccorso, A., Veiga, F., Sancini, G., Puglisi, G., 2018. Oxcarbazepine free or loaded PLGA nanoparticles as effective intranasal approach to control epileptic seizures in rodents. Eur. J. Pharm. Biopharm. 133, 309–320. https://doi.org/10.1016/j.ejpb.2018.11.002.
Nerli, G., Robla, S., Bartalesi, M., Luceri, C., Ambrosio, M.D., Csaba, N., Maestrelli, F., 2023. Chitosan coated niosomes for nose-to-brain delivery of clonazepam: formulation, stability and permeability. Carbohydr. Polym. Technol. Appl., 100332 https://doi.org/10.1016/j.carpta.2023.100332.
Nernst, W., 1904. Theorie der Reaktionsgeschwindigkeit in heterogenen Systemen. Z. Phys. Chem. 47, 52–55. https://doi.org/10.1515/zpch-1904-4704.
Noorulla, K.M., Yasir, M., Muzaffar, F., Roshan, S., Ghoneim, M.M., Almurshedi, A.S., Tura, A.J., Alshehri, S., Gebissa, T., Mekit, S., Ahmed, M.M., Zafar, A., 2022. Intranasal delivery of chitosan decorated nanostructured lipid carriers of Buspirone for brain targeting: formulation development, optimization and in-vivo preclinical evaluation. J. Drug Deliv. Sci. Technol. 67, 102939. https://doi.org/10.1016/j.jddst.2021.102939.
Noyes, A.A., Whitney, W.R., 1897. The rate of solution of solid substances in their own solutions. J. Am. Chem. Soc. 19, 930–934. https://doi.org/10.1021/ja02086a003.

OíHara, T., Dunne, A., Butler, J., Devane, J., 1998. A review of methods used to compare dissolution profile data. Pharm. Sci. Technol. Today 1 (5), 214–223. https://doi.org/10.1016/S1461-5347(98)00053-4.

Özbas, Z., Özkahraman, B., Akgüner, Z.P., Bal-Öztürk, A., 2022. Evaluation of modified pectin/alginate buccal patches with enhanced mucoadhesive properties for drug release systems: in-vitro and ex-vivo study. J. Drug Deliv. Sci. Technol. 67, 1–8. https://doi.org/10.1016/j.jddst.2021.102991.

Pachauri, M., Gupta, E.D., Ghosh, P.C., 2015. Piperine Loaded PEG-PLGA Nanoparticles: Preparation, Characterization and Targeted Delivery for Adjuvant Breast Cancer Chemotherapy. Elsevier Ltd. https://doi.org/10.1016/j.jddst.2015.08.009.

Peng, X., Wen, X., Pan, X., Wang, R., Chen, B., Wu, C., 2010. Design and in vitro evaluation of capsaicin transdermal controlled release cubic phase gels. AAPS PharmSciTech 11, 1405–1410. https://doi.org/10.1208/s12249-010-9481-1.

Peppas, N.A., Sahlin, J.J., 1989. A simple equation for the description of solute release. III. Coupling of diffusion and relaxation. Int. J. Pharm. 57, 169–172. https://doi.org/10.1016/0378-5173(89)90306-2.

Pooresmaeil, M., Javanbakht, S., Behzadi, S., Namazi, H., 2020. Carboxymethyl cellulose/mesoporous magnetic graphene oxide as a safe and sustained ibuprofen delivery biosystem: synthesis, characterization, and study of drug release kinetic. Colloids Surf., A 594, 124662. https://doi.org/10.1016/j.colsurfa.2020.124662.

Prajapati, S.K., Jain, A., Jain, A., Jain, S., Tirth, B., College, P., 2019. Biodegradable polymers and constructs: a novel approach in drug delivery. Eur. Polym. J. 120, 109191. https://doi.org/10.1016/j.eurpolymj.2019.08.018.

Prathyusha, M., Manjunath, K., Tippanna, S., Shivanandappa, B., 2014. Bixin loaded solid lipid nanoparticles for enhanced hepatoprotection – preparation, characterisation and in vivo evaluation. Int. J. Pharm. 473, 485–492. https://doi.org/10.1016/j.ijpharm.2014.07.027. Elsevier B.V.

Puthli, S., Vavia, P., 2009. Formulation and performance characterization of radio-sterilized "progestin-only" microparticles intended for contraception. AAPS PharmSciTech 10, 443–452. https://doi.org/10.1208/s12249-009-9226-1.

Qazi, S., Samuel, N.K.P., Venkatachalam, T.K., Uckun, F.M., 2003. Evaluating dissolution profiles of an anti-HIV agent using ANOVA and non-linear regression models in JMP software. Int J Pharm 252, 27–39. https://doi.org/10.1016/s0378-5173(02)00603-8.

Ramteke, K.H., Dighe, P.A., Kharat, A.R., V Patil, S., 2014. Mathematical models of drug dissolution: a review. Scholars Acad. J. Pharm. 3, 388–396.

Rancan, F., Blume-peytavi, U., Vogt, A., 2014. Utilization of biodegradable polymeric materials as delivery agents in dermatology. Clin. Cosmet. Investig. Dermatol. 7, 23–34. https://doi.org/10.2147/CCID.S39559.

Ritger, P.L., Peppas, N.A., 1987. A simple equation for describing of solute release. I. Fickian and non-Fickian release from non-swellable devices in the form of slabs, spheres, cylinders or discs. J. Control. Release 5, 23–36. https://doi.org/10.1016/0168-3659(87)90035-6.

Saha, P., Kathuria, H., Monohar, M., 2023. Nose-to-brain delivery of rotigotine redispersible nanosuspension: in vitro and in vivo characterization. J. Drug Deliv. Sci. Technol. 79, 104049. https://doi.org/10.1016/j.jddst.2022.104049.

Santadkha, T., Skolpap, W., Thitapakorn, V., 2022. Diffusion modeling and in vitro release kinetics studies of curcumin À loaded superparamagnetic nanomicelles in cancer drug delivery system. J. Pharm. Sci. 111, 1690–1699. https://doi.org/10.1016/j.xphs.2021.11.015.

Shaghlil, L., Alshishani, A., Sa'aleek, A.A., Abdalkader, H., Al-ebini, Y., 2022. Formulation and evaluation of nasal insert for nose-to-brain drug delivery of rivastigmine tartrate. J. Drug Deliv. Sci. Technol. 76, 103736. https://doi.org/10.1016/j.jddst.2022.103736.

Shah, B., Khunt, D., Misra, M., Padh, H., 2016. Application of Box-Behnken design for optimization and development of quetiapine fumarate loaded chitosan nanoparticles for brain delivery via intranasal route. Int. J. Biol. Macromol. 89, 206–218. https://doi.org/10.1016/j.ijbiomac.2016.04.076.

Shaikh, H.K., V Kshirsagar, R., Patil, S.G., 2015. Mathematical models for drug release characterization: a review. World J. Pharm. Pharmaceut. Sci. 4, 324–338. Corpus ID: 110048879.

Shamarekh, K.S., Gad, H.A., Soliman, M.E., Sammour, O.A., 2020. Development and evaluation of protamine-coated PLGA nanoparticles for nose-to-brain delivery of tacrine: in-vitro and in-vivo assessment. J. Drug Deliv. Sci. Technol., 101724 https://doi.org/10.1016/j.jddst.2020.101724.

Sherif, S., Bendas, E.R., Badawy, S., 2014. The clinical efficacy of cosmeceutical application of liquid crystalline nanostructured dispersions of alpha lipoic acid as anti-wrinkle. Eur. J. Pharm. Biopharm. 86, 251–259. https://doi.org/10.1016/j.ejpb.2013.09.008.

Sheth, T.S., 2021. Optimizing similarity factor of in vitro drug release profile for development of early stage formulation of drug using linear regression model. J. Math. Industry. 9. https://doi.org/10.1186/s13362-021-00104-9.

Sibanda, W., Pillay, V., Danckwerts, M.P., Viljoen, A.M., Van Vuuren, S., Riaz, A., 2004. Experimental design for the formulation and optimization of novel cross- linked oilispheres developed for in vitro site-specific release of Mentha piperita oil. AAPS PharmSciTech 5, 1–14. https://doi.org/10.1208/pt050118.

Siepmann, J., Peppas, N.A., 2011. Higuchi equation: derivation, applications, use and misuse. Int. J. Pharm. 418, 6–12. https://doi.org/10.1016/j.ijpharm.2011.03.051.

Siepmann, J., Peppas, N.A., 2012. Modeling of drug release from delivery systems based on hydroxypropyl methylcellulose (HPMC). Adv. Drug Deliv. Rev. 64, 163–174. https://doi.org/10.1016/j.addr.2012.09.028.

Siepmann, J., Siepmann, F., 2008. Mathematical modeling of drug delivery. Int. J. Pharm. 364, 328–343. https://doi.org/10.1016/j.ijpharm.2008.09.004.

Siepmann, J., Siepmann, F., 2013. Mathematical modeling of drug dissolution. Int. J. Pharm. 453, 12–24. https://doi.org/10.1016/j.ijpharm.2013.04.044.

Singh, S.K., Reddy, I.K., Khan, M.A., 1996. Optimization and characterization of controlled release pellets coated with an experimental latex. II. Cationic drug. Int. J. Pharm. 141, 179–195. https://doi.org/10.1016/0378-5173(96)04635-2.

Sitta, D.L.A., Guilherme, M.R., da Silva, E.P., Valente, A.J.M., Muniz, E.C., Rubira, A.F., 2014. Drug release mechanisms of chemically cross-linked albumin microparticles: effect of the matrix erosion. Colloids Surf. B Biointerfaces 122, 404–413. https://doi.org/10.1016/j.colsurfb.2014.07.014.

Sonaje, K., Italia, J.L., Sharma, G., Bhardwaj, V., Tikoo, K., Kumar, M.N.V.R., 2007. Development of biodegradable nanoparticles for oral delivery of ellagic acid and evaluation of their antioxidant efficacy against cyclosporine A-induced nephrotoxicity in rats. Pharm. Res. (N. Y.) 24, 899–908. https://doi.org/10.1007/s11095-006-9207-y.

Su, S., Kang, P.M., 2020. Systemic review of biodegradable nanomaterials in nanomedicine. Nanomaterials (Basel) 10 (4), 656. https://doi.org/10.3390/nano10040656.

Tapdiqov, S., Taghiyev, D., Zeynalov, N., Safaraliyeva, S., 2022. Cumulative release kinetics of levothyroxine-Na pentahydrate from chitosan/arabinogalactane based pH sensitive hydrogel and it's toxicology. React. Funct. Polym. 178, 105334. https://doi.org/10.1016/j.reactfunctpolym.2022.105334.

Tiyaboonchai, W., Tungpradit, W., Plianbangchang, P., 2007. Formulation and characterization of curcuminoids loaded solid lipid nanoparticles. Int. J. Pharm. 337, 299–306. https://doi.org/10.1016/j.ijpharm.2006.12.043.

Trucillo, P., 2022. Drug carriers: a review on the most used mathematical models for drug release. Processes 10. https://doi.org/10.3390/pr10061094.

Weilbull, W., 1951. A statistical distribution function of wide applicability. J. Appl. Mech. 18, 293–297. https://doi.org/10.1115/1.4010337.

Wilderman, M., 1909. Uber die Geschwindigkeit molekularer und chemischer Reaktionen in heterogenen Systemen. Erster Teil. Z. Phys. Chem. 66, 445–495. https://doi.org/10.1515/zpch-1909-6625.

Yasir, M., Sara, U.V.S., Chauhan, I., Gaur, P.K., Singh, A.P., Puri, D., Ameeduzzafar, A., 2018. Solid lipid nanoparticles for nose to brain delivery of donepezil: formulation, optimization by Box–Behnken design, in vitro and in vivo evaluation. Artif. Cells Nanomed. Biotechnol. 46, 1838–1851. https://doi.org/10.1080/21691401.2017.1394872.

Yasir, M., Zafar, A., Noorulla, K.M., Tura, A.J., Sara, U.V.S., Panjwani, D., Khalid, M., Haji, M.J., Gobena, W.G., Gebissa, T., Dalecha, D.D., 2022. Nose to brain delivery of donepezil through surface modified NLCs: formulation development, optimization, and brain targeting study. J. Drug Deliv. Sci. Technol. 75, 103631. https://doi.org/10.1016/j.jddst.2022.103631.

Yousaf, R., Khan, M.I., Akhtar, M.F., Madni, A., Sohail, M.F., Saleem, A., Irshad, K., Sharif, A., Rana, M., 2023. Development and in-vitro evaluation of chitosan and glyceryl monostearate based matrix lipid polymer hybrid nanoparticles (LPHNPs) for oral delivery of itraconazole. Heliyon 9, e14281. https://doi.org/10.1016/j.heliyon.2023.e14281.

Zdanovskii, A.B., 1946. The role of the interphase solution in the kinetics of the solution of salts. Zhur. Fiz. Khim. (USSR) 20, 869–880.

CHAPTER 12

Bioresorbable polymers: A prospective utilization as an implant

Shuai Chen[1], K. M. Faridul Hasan[2] and Xiaoyi Liu[3]
[1]Department of Biochemistry and Molecular Biology, College of Basic Medical Sciences, Guizhou Medical University, Guiyang, China; [2]Simonyi Károly Faculty of Engineering, University of Sopron, Sopron, Hungary; [3]The Key Laboratory of Environmental Pollution Monitoring and Disease Control, Ministry of Education, Department of Nutrition and Food Hygiene, School of Public Health, Guizhou Medical University, Guizhou, China

12.1 Introduction

A bioabsorbable polymer is a kind of polymer material that can be degraded by enzyme or chemical action in vivo (Li et al., 1998). According to the source, bioabsorbable polymers can be divided into natural polymers and artificial polymers, among which natural bioabsorbable polymers mainly include chitosan, collagen, etc. (Li et al., 2021). They are mainly isolated from biological tissues; artificial absorbable polymers include polyglycolide, poly-lactide and poly-hydroxybutyrate. The main general formula is the derivative of α-hydroxy acid of HO-CHR-COOH, and the R groups of H and CH_3 correspond to glycolic acid and lactic acid, respectively (Mukherjee and Pietrzak, 2011).

The development of modern medical science is often inseparable from materials science, especially the development of medical biomaterials. With their own characteristics, bioabsorbable polymers are widely used as implants in cosmetic shell, tissue repair, cardiovascular intervention, tissue engineering, and other major medical fields. Bioabsorbable polymers can be decomposed by enzyme or chemical decomposition after implantation, so there is no need for concerns about permanent implantation or surgical removal, so they can be implanted temporarily to promote the repair and fixation of damaged tissue. These include bioabsorbable sutures and small bones, for example, Li and Sun (2022) indicated that silk fibroin-based biomaterials could be used in tissue engineering, playing a very important

Bioresorbable Polymers and their Composites
ISBN 978-0-443-18915-9
https://doi.org/10.1016/B978-0-443-18915-9.00014-8
© 2024 Elsevier Ltd.
All rights reserved.

role in tooth and mandible tissue, cartilage, skeletal muscle, and vascular tissue. Meanwhile, De la Harpe et al. (2022) synthesized a new type of bioabsorbable suture with sodium alginate, pectin, and gelatin. This product did not only meet the basic requirements of suture materials, but also filled the gap of bioabsorbable polymer sutures in the medical market. In addition, Kim et al., (2022) synthesized a new type of fatty amide polyurethane urea elastomer and coated it on a biodegradable metal coil to prepare a bioabsorbable embolization device for cerebral saccular aneurysms. The biodegradable metal coil was used to protect against cerebral aneurysms. In general, bioabsorbable polymers are a kind of biomaterial that can be used as implants to replace injured or diseased tissues and organs, promote wound healing, such as absorbable sutures, bone nails, and bone plates, and even improve and correct tissue function.

In addition, the development of bioabsorbable polymers as implants also benefits from the rise of technologies such as 3D printing. 3D biological printing has become a new method to obtain complex biological structures, through accurate and controlled layer-by-layer assembly, using cells, bioabsorbable polymers, or bioactive molecules as biological ink, and finally obtain their own biological structure. For example, cold atmosphere plasma surface modification can quickly and cheaply enhance 3D printing potential applications of polylactic acid bone tissue engineering materials (Wang et al., 2016). Yi et al. (2016) claimed that 3D printing patches composed of bioabsorbable polymers could be used for long-term delivery of anticancer drugs, suggesting that 3D printing might be an effective method for local delivery of chemotherapy to treat cancer. Sun et al. (2020) found that a new biocompatible absorbable material (lactide-ethanol ester-1myr3-trimethylene carbonate; LA-GA-TMC) could be used to manufacture a cardiac septal defect occluder using 3D printing technology.

Natural bioabsorbable polymers have better bioabsorption and low toxicity, while artificial bioabsorbable polymers have good mechanical strength and controllability of chemical and physical properties such as the polymer degradation rate (Mohammadi Nasr et al., 2020; Hong et al., 2021). Also, with the progress in manufacturing technology, such as 3D biological printing, the emergence of technology has brought ideas for the production of more complex structures, which is extremely helpful for the application of bioabsorbable polymers (Abasalizadeh et al., 2020; Jammalamadaka and Tappa, 2018). As implants, bioabsorbable polymers can be

hydrolyzed or enzymatically hydrolyzed into small molecules and then excreted from the body, removing concerns about the risk of permanent implantations and so they are widely used as temporary implants to promote the repair of damaged tissue. The most common example is bioabsorbable sutures. With an understanding of biomaterials, various methods can be used to change the mechanical strength of bioabsorbable polymers, giving them more application prospects. For example, the mechanical strength can be enhanced so that they can be used in orthopedic fixation devices such as screws and plates, and then used to treat fractures, or in orthodontics and orthopedic surgery. Bioabsorbable polymers can also be made into artificial skin, such as chitosan, which can be used to cover a wound to stop bleeding, fight infection, and promote wound healing (Jiménez-Gómez and Cecilia, 2020). Bioabsorbable polymers as implants are widely used in surgery, and the scope of applications for biomaterials with different properties is also different. Bioabsorbable polymers are used as temporary implants to heal the injured tissue, their main function being to reduce the wound size and promote healing. When used in orthodontics or plastic surgery, they mainly are used in a supporting or fixed role. Bioabsorbable polymers degrade slowly with the growth of the tissue, with new tissue filling the space of the original bioabsorbable polymer.

Natural or artificial bioabsorbable polymers can also be used as implants as carriers or media for drug release in the body, so that drugs can reach a specific concentration in a specific time and space to achieve therapeutic purposes (Langer, 1990). For example, Wei-Hong Jian et al. used nanohybrid hydrogel of sulfated glycosylamine polyelectrolyte composite nanoparticles (PCNs) to control the transmission of matrix-derived factor-1 α (SDF-1 α) and basic fibroblast factor (bFGF) to regulate the transmission of endogenous neural stem cells to treat brain injury, and confirmed their conjecture through systematic in vivo and in vitro experiments (Jian et al., 2018). The bioabsorbable polymer drug-delivery device realizes local control of the drug concentration and greatly reduces the nonspecific distribution of drugs in normal tissues, so as to improve the therapeutic effect and reduce drug side effects. However, at the same time, there are some shortcomings such as unexpected degradation products (Khandare and Haag, 2010). As widely used biomaterials, bioabsorbable polymers are also used regularly in tissue engineering. The purpose of tissue engineering is to develop tissue or organ substitutes with biological functions (Guo and Ma, 2018).

Three conditions are needed to reorganize the damaged tissue: (1) seed cells of damaged tissue; (2) suitable scaffold material; and (3) chemical signals that induce cell proliferation and differentiation (Janoušková, 2018). By combining seed cells with scaffold materials, scaffolds act as extracellular matrix, and chemical signals induce cells to proliferate and differentiate into functionally mature adult cells to achieve the purpose of artificial organs. Scaffolds play a key role in tissue engineering (Lekshmi et al., 2020). Excellent bioabsorbable polymers can also be used as scaffolds for a variety of tissue engineering purposes. For example, polycaprolactone (PCL) is used not only in bone (Park et al., 2020), skeletal (Choi et al., 2008), muscle, and nerve tissue regeneration (Alvarez-Perez et al., 2010), but also in cardiovascular regeneration (Tillman et al., 2009). The emergence of tissue engineering provides a new method to speed up tissue healing and improve the quality of life of patients with organ defects, and provides a new way to solve the shortage of organ transplant donors.

Next, the characteristics of bioabsorbable polymers as implants, focusing on their applications in various aspects, in order to provide some reference for follow-up research, are discussed.

12.2 Characteristics of bioabsorbable polymers as implants

The most significant role of bioabsorbable polymers is mainly based on their characteristics (Fig. 12.1).

12.2.1 Good biocompatibility

Biocompatibility is a biological characteristic in which a material that is in the process of dynamic change in an organism, can withstand the action of the host system and remain relatively stable and not be rejected or destroyed, which is also known as biological adaptability and biological acceptability. The interaction and influence between the implant and the body continue until balance is reached or the implant disappears completely. Generally speaking, an implant reacts with the host's body, as determined by the physical or chemical properties of the implant, including inflammation, cytotoxicity, or corrosion of the implant (Zhiqiang et al., 2022).

12.2.2 Sufficient mechanical strength

Bioabsorbable polymers can provide support and fixation through compression and bending strength, and should be easy to implant (Liu et al., 2022),

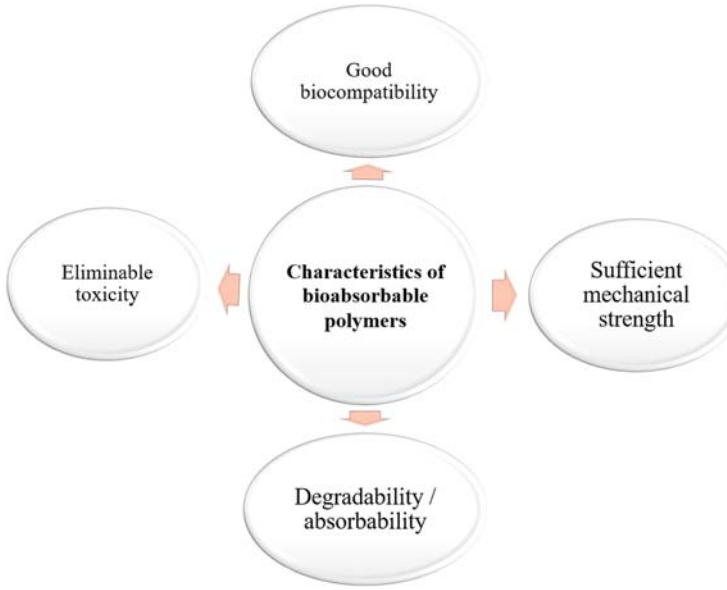

Figure 12.1 Characteristics of bioabsorbable polymers.

such as for fixation in orthopedics (Figueiredo et al., 2020), vascular scaffolding (Albaghdadi et al., 2017), and other areas of the use.

12.2.3 Degradability/absorbability

When the body tissue recovers, it is gradually degraded and replaced by normal tissue, therefore it does not need to be removed by a second operation. Also, it can be used as a drug-delivery system to release the drug locally and achieve the desired therapeutic effect (Mouriño and Boccaccini, 2010), such as bone repair that is carried out using bioabsorbable polymers containing antibiotics (Coraca-Huber et al., 2012).

12.2.4 Eliminable toxicity

Effective antiinfection protection in the process of implantation and recovery means that it can be used as an implant in various nonpermanent fixations, such as maxillofacial surgery (On et al., 2020) or bone remodeling (Majeed and Chowdhury, 2022), and it also can be used as a drug-delivery system to better control drug release and achieve a better therapeutic effect (Adekoya et al., 2022). Moreover, bioabsorbable polymers are also important materials in tissue engineering, which have an important impact on the construction of artificial tissues and organs (Li and Sun, 2022).

12.3 Application of bioabsorbable polymers

12.3.1 Application in implants for temporary fixation

By virtue of their characteristics, bioabsorbable polymers are widely used as temporary implants to help the body repair wounds, lift equipment for the body to support, and eventually degrade into nontoxic small molecules that can be excreted from the body. The main applications include absorbable sutures, drug-delivery devices, and orthopedic fixation devices, such as nails, plates, and needles. In addition, bioabsorbable polymers can also add drugs such as growth factors or antibiotics to further promote wound repair or antiinfection (Rousselle et al., 2019). Bioabsorbable polymers are mainly used in three areas, as shown in Fig. 12.2.

12.3.1.1 Application in orthopedics

Bioabsorbable polymer fixators have been used as a substitute for inert implants in orthopedics to prevent stress shielding and subsequent surgical removal of implants (Kainan, 2010). These bioabsorbable polymers are mainly made using polylactic acid and/or polyglycolic acid polymers, and self-reinforcing techniques are used to produce implants with sufficient

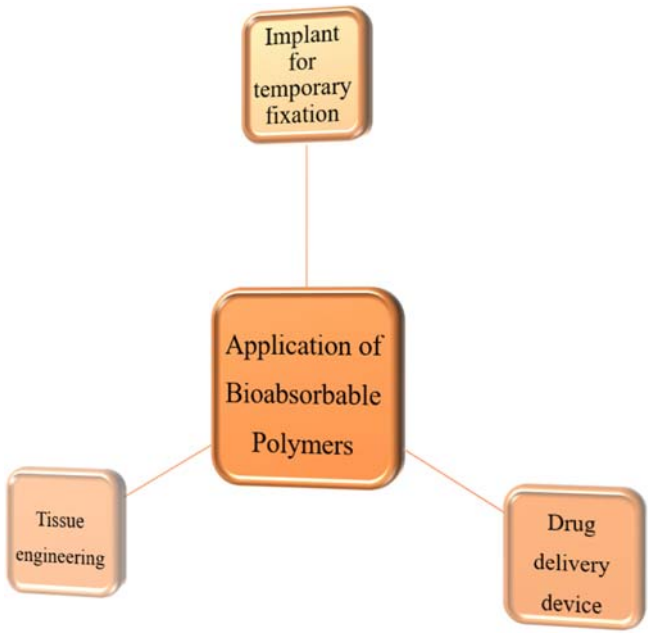

Figure 12.2 Applications of bioabsorbable polymers.

mechanical strength. The biological absorption time and treatments of different bioabsorbable polymers vary. There are bioabsorbable implants used for adults, some for children, and even different bioabsorbable polymers that are used at different sites, such as in the mandible, or in the extremities and skull (Peltoniemi et al., 2002).

Bioabsorbable polymers are increasingly accepted by orthopedic patients. They can be used to stabilize bone-to-bone fixation such as fracture, osteotomy, bone transplantation, and even to reconnect tendons, ligaments, meniscus fragmentation, and other soft tissues. They can be completely absorbed in the body, and so do not need to be removed by a second operation, thereby avoiding long-term interference in the surrounding tissue. Knee joint injury, cruciate ligament surgery, and meniscus injury have become the most common indications (Waris et al., 2004).

Hydroxyapatite poly-L-lactide (HPLLA) is a classical bioabsorbable polymer, which is composed of hydroxyapatite and poly-L-lactide (PLLA). Hydroxyapatite is widely used in craniofacial, hand, and joint repair operations (Sukegawa et al., 2016). HPLLA has good bone conductivity and can be uniformly degraded so that the body has little reaction to this foreign body. Satoshi Yanagibayashi's research showed that HPLLA screw pins could be used as fixation devices for phalangeal fractures, and also for comminuted fractures. The hydroxyapatite contained in HPLLA can be gradually and uniformly degraded and absorbed. In contrast, PLLA was not a complex, so its degradation rate was faster than HPLLA, and its degradation products were irregular and tended to gather in the same place, thus causing adverse foreign body reactions (Yanagibayashi et al., 2020).

In addition, RegJoint is also a bioabsorbable polylactic acid material introduced in 2011 and used in scapular and metacarpal interposition after trapezius resection of osteoarthritis. Dietrich et al. verified that the insertion of RegJoint implants did not cause adverse effects in 46 thumbs of 43 patients with symptomatic thumb arthritis who were treated with separate suspension arthroplasty (SA) and RegJoint insertiz (RJ) and followed up for at least 2 years (Dietrich et al, 2022).

In recent years, increasing attention has been paid to the adverse effects of inert in vivo implants, prompting clinicians and researchers to find more suitable fixators to improve the treatment, and a variety of bioabsorbable polymers have been developed for orthopedic treatment. Morandi et al. (2013) performed herringbone osteotomy to correct hallux valgus deformity from 2005 to 2010, and in their study group, 251 patients were fixed with distal metatarsal osteotomy with bioabsorbable needles (made of poly-

L-lactide and poly-DL- lactide), while those in the control group were fixed with conventional inert metal nails. After several years of follow-up, it was found that both bioabsorbable implant nails and metal nails could play a reliable role in fixation, not only for correction of hallux valgus deformity from a larger angle, but also for fewer foreign body reactions and a lower incidence of complications.

Bioabsorbable polymers can also be used for anterior cruciate ligament reconstruction to play a fixed role in surgery. The anterior cruciate ligament (ACL) is the inner ligament of the knee joint, which connects the femur and tibia and has important physiological functions such as maintaining the stability of the joint and helping to complete various movements. However, long-term strenuous lower limb movement or other factors can lead to its fracture, resulting in the interruption of the connection between the two bones, joint instability, and other sequelae (Zhichang, 2018). In the study by Thompson et al. (2016) by implanting Endobutton (Smith & Nephew) into the proximal end of the patient and fixing the distal end with a bioabsorbable screw made of amorphous low crystallinity PLLA, and after 16 years of continuous evaluation, they found that all patients had new bone formation after 16 years, although three patients developed cysts. However, it was not found that bioabsorbable screw implantation was related to adverse reactions such as survival or instability of anterior cruciate ligament implants.

12.3.1.2 Application in neurosurgery

Surgical treatment of complete transection of the sciatic nerve is usually by amputation, but this generally results in the patient spending the rest of their life in a wheelchair. Although limb salvage treatment is the first choice in some cases, especially in children or adolescents, patients often lose the opportunity for limb salvage due to various factors. Inada et al. (2017) not only provided objective evidence to prove that the sciatic nerve has strong potential for regeneration, but also selectively elongated the nerve to repair the nerve gap through the connection between the collagen-filled bioabsorbable nerve tube PGA-C and the broken end of the sciatic nerve, and gradually recovered the motor and sensory functions after operation, which greatly improved the quality of life of the patients.

Since Wigand first reported the repair of endoscopic cerebrospinal fluid (CSF) leakage in 1981, reconstruction of the skull base through nasal endoscopy in neurosurgery has gradually matured, successfully avoiding many complications such as meningitis, pneumocerebrosis, and cerebrospinal fluid

leakage. The conventional repair materials used in this operation include autogenous tissue and artificial materials, with the latter including bioabsorbable polymers such as fibrin glue and dura mater patches (Al-Asousi et al., 2017). Seaman et al. (2021) used a bioabsorbable polymer (DMAE L) lactic acid plate (Resorb-X Sellar Wall Plate; KLS Martin; Jacksonville, FL) to repair the skull base of the patient through a nasal endoscope. It has been demonstrated that a bioabsorbable polymer lactic acid plate could be used as a rigid implant for skull base repair through nasal endoscopic interventional implantation, and it has been objectively proved that this method has a good therapeutic effect for long-term integrity repair of exposed bone with a low complication rate.

12.3.1.3 Application in plastic surgery

The continuous updating of science and technology can also promote people to fulfill cosmetic surgery wishes, with breast reconstruction with implants are becoming increasingly acceptable. The acellular dermal matrix is an important part of breast reconstruction, but complete implantation of the acellular dermal matrix greatly increases the cost of operation. Sigalove et al. (2022) reduced the cost of surgery by using GalaFLEX-AlloDerm reconstruction; GalaFLEX is a biosynthetic grid derived from poly-4-hydroxybutyrate, which can be naturally degraded into water and carbon dioxide in vivo and completely absorbed within 18—24 months. Because it is harder and stronger than the acellular dermal matrix, it is particularly suitable for breast reconstruction, and this stability also reduces the implantation risks. By comparing GalaFLEX-AlloDerm reconstruction with AlloDerm reconstruction alone, they found that GalaFLEX-AlloDerm reconstruction not only did not increase the incidence of complications, but also had a lower rate of skin necrosis in the GalaFLEX-AlloDerm reconstruction group.

Augmentation rhinoplasty is usually used as a solution to indications such as wide lobule, deviation of the nasal septum structure, or frequent columella retraction, but the choice of rhinoplasty materials often determines the success of the operation. It also poses a challenge for surgeons to choose suitable implants and techniques. Autologous transplantation material is an ideal material for this graft, but the existing problems cannot be ignored, with the most direct problem being that the source is limited, and the site of implantation also carries a risk of infection. In recent years, bioabsorbable polymers have gradually replaced or supplemented other implant materials in rhinoplasty. Polycaprolactone (PCL) not only has good

flexibility, but also has the advantages of a slow degradation rate and good biocompatibility compared with other bioabsorbable polymers. Kim et al. reported that the implantation of fibrin/chondrocytes into PCL scaffolds designed by 3D printing can be used as implant materials for rhinoplasty, and the fusion of 3D printing and rhinoplasty will be the key to the realization of personalized rhinoplasty (Kim et al., 2015). Park et al. (2019) performed rhinoplasty with implants in patients with primary or secondary rhinoplasty using 3D-designed PCL stents, and verified the safety and effectiveness of PCL as a bioabsorbable implant in rhinoplasty through long-term follow-up. This can not only maintain its suitable shape, but also there is no foreign body reaction after operation. In addition, the function of patients with airway obstruction was also improved after the operation. As a kind of scaffold, PCL implants could improve the shape of the nose by migrating adjacent chondrocytes to form new cartilage tissue.

12.3.1.4 Application in the artificial skin

Artificial skin made of chitosan and its derivatives has good histocompatibility, softness, and antiinfection ability, which promotes wound healing (Liu et al., 2006). Yuan et al. (2021) used bioabsorbable poly(4-hydroxybutyrate) (P4HB) as a skin substitute, and SD rats as the research object to explore the relationship between P4HB and body-related inflammatory reaction. They found that P4HB could be used as a good skin substitute, which was very helpful in improving skin defects and wound healing.

12.3.2 Application in drug-delivery devices

The function of bioabsorbable polymer is not only that it can also be used as a carrier of bioactive substances such as growth factors, antibiotics, or various drugs. When a bioabsorbable polymer is slowly degraded in the body, the active substances or drugs are released locally, which makes the local drug concentration reach the therapeutic level, and avoids the adverse effects of drugs acting on the whole body. There are many kinds of polymers that can be used as drug carriers, including synthetic polymers such as polylactic acid co-glycolic acid (PLGA), poly(glycolic acid) (PGA), polylactic acid (PLA), polycaprolactone (PCL), and natural polymers such as chitosan, sodium alginate, gelatin, etc. The polymer represented by chitosan has become a research hotspot because it can be used as the carrier of macromolecular drugs such as vaccines, peptides, or proteins. As a drug-delivery device, bioabsorbable polymer has the advantages of high efficiency, low toxicity, and targeting.

12.3.2.1 Absorbable implant coating application in orthopedics

Despite the continuous optimization of surgical methods and implants, various complications of orthopedic surgery still affect the postoperative healing and return to health of patients. The most common complications in orthopedics include delayed healing, osteoporosis, and bone infection. It is well known that antibiotics are the key to the prevention and treatment of infection. However, systemic administration of antibiotics can cause a variety of sequelae, such as superinfection, systemic allergy, and drug-resistant bacteria. For this reason, local drug delivery with a higher drug concentration where the drugs are needed is the key to avoiding systemic drug side effects and achieving therapeutic effects. Fuchs et al. (2008) mixed bioactive substances into bioabsorbable poly(D-lactide) (PDLLA), which could be applied to the surface of metal fixtures by a "cold" coating process. This could be used not only as a bone material, but also as a drug carrier. Ideal results had been achieved in animal and clinical experiments using this method. Bioabsorbable polymers can be used as drug carriers to apply coating technology to various implants, which not only does not affect the mechanical stability of each implant, but also can increase the local drug concentration of the body to promote wound repair, reduce the incidence of sequelae, and avoid systemic drug effects. In addition, because all kinds of implants with different materials can be coated, this treatment idea will also be widely used clinically.

12.3.2.2 A novel bioabsorbable drug-eluting scaffold

In recent years, due to the changes in the social environment, dietary structure, and living habits, the incidence of coronary heart disease has also increased annually. Percutaneous coronary drug-eluting stent (DES) implantation has become a major breakthrough in the interventional treatment of heart disease (Zhang et al., 2020). Postoperative sequelae such as in-stent restenosis and in-stent thrombosis are important factors influencing postoperative death. In order to overcome these difficulties, the emergence of first- and second-generation drug-eluting stents has greatly reduced the incidence of stent restenosis and subsequent vascular remodeling. Despite the updating of implants and surgical techniques, in-stent thrombosis cannot be completely avoided (Kuramitsu et al., 2021). The polymer is made from two trimer molecules of salicylic acid using oxalic acid as a connecting molecule. In the process of being absorbed, the polymer releases salicylic acid, which acts on the surrounding vascular parietal cells. As a nonsteroidal antiinflammatory drug, salicylic acid can not only reduce the

inflammatory response of the stent to vascular wall stimulation, but also, as a bioabsorbable material, there is no need for concerns about the permanent retention of the implant after implantation. It may also help to prevent late complications of drug-eluting stents.

12.3.3 Application in tissue engineering

Tissue engineering is an interdisciplinary field, which mainly involves materials science, biology, reactor engineering, and clinical research. Its purpose is to cultivate or create new tissues or organs (Lavik and Langer, 2004), then transplant this tissue or organ into the body, replacing the tissue or organ in the original pathological state. These are a kind of artificially obtained tissues and organs, which can reduce mismatching between the recipient and the donor to a certain extent. After years of development, the technology of in vitro cell culture has gradually matured, but it remains a difficult problem to make cells arrange correctly into typed tissues and organs, although the emergence of 3D printing brings a solution to this problem (Zhu et al., 2016). In order for cells to grow according to certain rules, bioabsorbable polymers play a very important role. During cell culture, the cells are attached to a bioabsorbable polymer, and then the polymer cell scaffold is implanted into the body (Langer and Vacanti, 2016). This enables the implant not only to have the shape that is required, but also to perform some biological functions of the cells attached to it.

12.3.3.1 Application in bone tissue engineering

The emergence of bioresorbable polymers has triggered the exploration of bone tissue engineering (Wubneh et al., 2018), which provides scaffolds for cell growth and plays a very important role in cell localization and tissue regeneration. The biocompatibility and controllable absorptivity of polymers are also critical. Its surface should not only allow cells to complete biological activities such as adhesion, proliferation, and differentiation, but also must be able to transmit mechanical signals and have suitable mechanical strength (Vieira et al., 2017).

Natural bioabsorbable polymer chitosan meets these requirements. Chitosan is a kind of linear polysaccharide, which is commonly found in crustacean shells, insect bones, and fungal cell walls. It is widely used in biomedicine because of its unique biological characteristics. The positive charge on the chitosan skeleton makes it have hemostatic activity, it can produce an analgesic effect inflamed sites, and also has an antiinfection property. Therefore, it is

usually used as a wound coating or for artificial skin. In recent years, a large number of studies have shown that chitosan can promote cell adhesion, proliferation, osteoblast differentiation, and mineralization (Ho et al., 2014; Brun et al., 2021). Hu et al. (2021) also cross-linked chitosan, vanillin, and bioglass particles to form a new scaffold, namely chitosan—vanillin—bioglass (CVB) scaffold. After a series of in vivo and in vitro experiments, they found that this new scaffold could not only promote cell proliferation and differentiation, and mineralization into bone, it also had significant mechanical strength and antibacterial properties.

12.3.3.2 Application in ligament/tendon tissue engineering

Ligaments and tendons are a kind of fibrous tissue with only a small number of blood vessels, and their regeneration ability is poor (Nau and Teuschl, 2015). At present, the treatment of ligament or tendon injury is usually autologous or allogeneic transplantation, which may be accompanied by adverse outcomes such as infection, disease transmission, and immune rejection by the host (Cooper et al., 2005; Leong et al., 2014). These have a significant impact on the health and economy of patients, which has promoted the search for substitutes.

Natural bioabsorbable polymers such as collagen, fibrin, and cellulose have good biocompatibility and are good substitutes for extracellular matrix, which can be hydrolyzed into normal metabolic small molecules in vivo, and so it is a scaffold material often considered in tissue engineering. Collagen, as the main component of ligament, has become the first selected material for ligament tissue engineering (Leong et al., 2014; Yilgor et al., 2012). Dunn et al. (1995) seeded rabbit fibroblasts on bioabsorbable fiber scaffolds to produce ligament analogs similar to normal ligaments in vitro and verified their feasibility in vivo.

Artificial bioabsorbable polymers are easy to process and widely available biomaterials, and are used often in tissue engineering scaffolds of tendons and ligaments (Goh and Sahoo, 2010). Compared with natural bioabsorbable polymers, artificial bioabsorbable polymers are widely used, and the physical or chemical properties of polymers can be controlled by means of chemical modification (Rodrigues et al., 2013). Araque-Monrós et al. (2020) developed a ligament/tendon tissue engineering scaffold using artificial bioabsorbable materials. This kind of scaffold is a hollow reticular structure woven with polylactic acid, with microspheres containing cells in the middle, so as to regenerate tissue from the inside to the outside and replace the original aging or diseased tissue.

12.4 Conclusion

This chapter mainly describes the application prospects of bioabsorbable polymers as implants in nonpermanent implantation, as a drug-delivery device, and as a scaffold material for tissue engineering. The biomaterials used are divided into natural and artificial bioabsorbable polymers. Bioabsorbable polymer materials from different sources have different properties. Natural bioabsorbable polymers are more popular as implants because of their better biocompatibility and lower toxicity, especially plant-derived bioabsorbable polymers because of their wide availability, easy extraction, low cost, and the absence of ethical issues. Through the in-depth understanding of the physical and chemical properties of different bioabsorbable polymers, the properties of bioabsorbable polymers can be changed by chemical modification or compounding of different materials, so that bioabsorbable polymers can not only have wider application areas, they also can be more in line with the expected results of their use. Although bioabsorbable polymers have been widely studied as implants, there remain few clinical applications, and therefore more in-depth investigations are needed.

References

Abasalizadeh, F., Moghaddam, S.V., Alizadeh, E., Akbari, E., Kashani, E., Fazljou, S.M.B., Torbati, M., Akbarzadeh, A., 2020. Alginate-based hydrogels as drug delivery vehicles in cancer treatment and their applications in wound dressing and 3D bioprinting. J. Biol. Eng. 14, 8.

Adekoya, O.C., Adekoya, G., Sadiku, E.R., Hamam, Y., Ray, S.S., 2022. Application of DFT calculations in designing polymer-based drug delivery systems: an overview. Pharmaceutics 14, 1972.

AL-Asousi, F., Okpaleke, C., Dadgostar, A., Javer, A., 2017. The use of polydioxanone plates for endoscopic skull base repair. Am. J. Rhinol. Allergy 31, 122–126.

Albaghdadi, M.S., Yang, J., Brown, J.H., Mansukhani, N.A., Ameer, G.A., Kibbe, M.R., 2017. A tailorable in-situ light-activated biodegradable vascular scaffold. Adv. Mater. Technol. 2, 1600243.

Alvarez-Perez, M.A., Guarino, V., Cirillo, V., Ambrosio, L., 2010. Influence of gelatin cues in PCL electrospun membranes on nerve outgrowth. Biomacromolecules 11, 2238–2246.

Araque-Monrós, M.C., García-Cruz, D.M., Escobar-Ivirico, J.L., Gil-Santos, L., MonleóN-Pradas, M., MáS-Estellés, J., 2020. Regenerative and resorbable PLA/HA hybrid construct for tendon/ligament tissue engineering. Ann. Biomed. Eng. 48, 757–767.

Brun, P., Zamuner, A., Battocchio, C., Cassari, L., Todesco, M., Graziani, V., Iucci, G., Marsotto, M., Tortora, L., Secchi, V., Dettin, M., 2021. Bio-functionalized chitosan for bone tissue engineering. Int. J. Mol. Sci. 22, 5916.

Choi, J.S., Lee, S., Christ, G.J., Atala, A., Yoo, J.J., 2008. The influence of electrospun aligned poly(epsilon-caprolactone)/collagen nanofiber meshes on the formation of self-aligned skeletal muscle myotubes. Biomaterials 29, 2899–2906.

Cooper, J.A., Lu, H., Ko, F.K., Freeman, J.W., Laurencin, C.T., 2005. Fiber-based tissue-engineered scaffold for ligament replacement: design considerations and in vitro evaluation. Biomaterials 26, 1523–1532.

Coraca-Huber, D.C., Duek, E., Etchebehere, M., Magna, L.A., Amstalden, E.M., 2012. The use of vancomycin-loaded poly-l-lactic acid and poly-ethylene oxide microspheres for bone repair: an in vivo study. Clinics 67, 793–798.

De La Harpe, K.M., Marimuthu, T., Kondiah, P.P.D., Kumar, P., Ubanako, P., Choonara, Y.E., 2022. Synthesis of a novel monofilament bioabsorbable suture for biomedical applications. J. Biomed. Mater. Res. B Appl. Biomater. 110, 2189–2210.

Dietrich, A., Winkelmann, M., O'loughlin, P.F., Krettek, C., Gaulke, R., 2022. Arthroplasty of the trapeziometacarpal joint with or without bioabsorbable polylactide scaffold (RegJoint™) interposition. Hand Surg. Rehabil. 41, 65–72.

Dunn, M.G., Liesch, J., Tiku, M.L., Zawadsky, J.P., 1995. Development of fibroblast-seeded ligament analogs for ACL reconstruction. J. Biomed. Mater. Res. 29, 1363–1371.

Figueiredo, L., Fonseca, R., Pinto, L.F.V., Ferreira, F.C., Almeida, A., Rodrigues, A., 2020. Strategy to improve the mechanical properties of bioabsorbable materials based on chitosan for orthopedic fixation applications. J. Mech. Behav. Biomed. Mater. 103, 103572.

Fuchs, T., Schmidmaier, G., Raschke, M.J., Stange, R., 2008. Bioactive-coated implants in trauma surgery. Eur. J. Trauma Emerg. Surg. 34, 60–68.

Goh, J.C.H., Sahoo, S., 2010. Scaffolds for Tendon and Ligament Tissue Engineering. Regenerative Medicine and Biomaterials for the Repair of Connective Tissues. National University of Singapore, Singapore (Woodhead Publishing Series in Biomaterials).

Guo, B., Ma, P., 2018. Conducting polymers for tissue engineering. Biomacromolecules 19, 1764–1782.

Ho, M.H., Liao, M., Lin, Y.L., Lai, C.H., Lin, P.I., Chen, R.M., 2014. Improving effects of chitosan nanofiber scaffolds on osteoblast proliferation and maturation. Int. J. Nanomed. 9, 4293–4304.

Hong, S.H., Park, J., Kim, O.Y., Hwang, S.H., 2021. Preparation of chemically modified lignin-reinforced PLA biocomposites and their 3D printing performance. Polymers 13, 667.

Hu, J., Wang, Z., Miszuk, J.M., Zhu, M., Lansakara, T.I., Tivanski, A.V., Banas, J.A., Sun, H., 2021. Vanillin-bioglass cross-linked 3D porous chitosan scaffolds with strong osteopromotive and antibacterial abilities for bone tissue engineering. Carbohydr. Polym. 271, 118440.

Inada, Y., Moroi, K., Morimoto, S., Fujikawa, T., Tateuchi, H., Nakamura, T., 2017. Regeneration of a completely transected sciatic nerve with use of a bioabsorbable nerve conduit filled with collagen with a 14-year follow-up: a case report. JBJS Case Connect 7, e77.

Jammalamadaka, U., Tappa, K., 2018. Recent advances in biomaterials for 3D printing and tissue engineering. J. Funct. Biomater. 9, 22.

Janoušková, O., 2018. Synthetic polymer scaffolds for soft tissue engineering. Physiol. Res. 67, S335–S348.

Jian, W.H., Wang, H., Kuan, C.H., Chen, M.H., Wu, H.C., Sun, J.S., Wang, T.W., 2018. Glycosaminoglycan-based hybrid hydrogel encapsulated with polyelectrolyte complex nanoparticles for endogenous stem cell regulation in central nervous system refegeneration. Biomaterials 174, 17–30.

Jiménez-Gómez, C.P., Cecilia, J., 2020. Chitosan: a natural biopolymer with a wide and varied range of applications. Molecules 25, 3981.

Kainan, L., 2010. Research progress in biodegradable and absorbable materials PLA in orthopedics. Mod. Clin. Med. 36, 3.
Khandare, J., Haag, R., 2010. Pharmaceutically used polymers: principles, structures, and applications of pharmaceutical delivery systems. Handb. Exp. Pharmacol. 197, 221–250.
Kim, Y.S., Shin, Y., Park, D.Y., Choi, J.W., Park, J.K., Kim, D.H., Kim, C.H., Park, S.A., 2015. The application of three-dimensional printing in animal model of augmentation rhinoplasty. Ann. Biomed. Eng. 43, 2153–2162.
Kim, S., Nowicki, K., Ye, S., Jang, K., Elsisy, M., Ibrahim, M., Chun, Y., Gross, B.A., Friedlander, R.M., Wagner, W.R., 2022. Bioabsorbable, elastomer-coated magnesium alloy coils for treating saccular cerebrovascular aneurysms. Biomaterials 290, 121857.
Kuramitsu, S., Sonoda, S., Ando, K., Otake, H., Natsuaki, M., Anai, R., Honda, Y., Kadota, K., Kobayashi, Y., Kimura, T., 2021. Drug-eluting stent thrombosis: current and future perspectives. Cardiovasc. Interv. Ther. 36, 158–168.
Langer, R., 1990. New methods of drug delivery. Science 249, 1527–1533.
Langer, R., Vacanti, J., 2016. Advances in tissue engineering. J. Pediatr. Surg. 51, 8–12.
Lavik, E., Langer, R., 2004. Tissue engineering: current state and perspectives. Appl. Microbiol. Biotechnol. 65, 1–8.
Lekshmi, G., Sana, S., Nguyen, V.H., Nguyen, T.H.C., Nguyen, C., Le, Q.V., Peng, W., 2020. Recent progress in carbon nanotube polymer composites in tissue engineering and regeneration. Int. J. Mol. Sci. 21, 6440.
Leong, N.L., Petrigliano, F., Mcallister, D.R., 2014. Current tissue engineering strategies in anterior cruciate ligament reconstruction. J. Biomed. Mater. Res. 102, 1614–1624.
Li, G., Sun, S., 2022. Silk fibroin-based biomaterials for tissue engineering applications. Molecules 27, 2757.
Li, X., P, Y., Zhou, Z., 1998. Bioabsorbable polymers and their applications in dentistry. J. Oral Maxillofac. Surg. 8, 3.
Li, Y., Y, X., Nie, Z., Zhang, J., Li, C., Nie, W., Jiang, H., 2021. The characteristics of bioabsorbable materials and their applications in orthopedics. China Tissue Eng. Res. 25, 6.
Liu, L., L, M., Shi, S., Shiyao, M.A., 2006. The application of biodegradable polymers in the pharmaceutical field. Chin. J. Hosp. Pharm. 26, 3.
Liu, C., Huang, L., Zhang, H., Chang, F., Li, S., Ma, S., Zhang, Y., Ren, L., 2022. Biomechanical comparison between bioabsorbable and medical titanium screws in distal chevron osteotomy of first metatarsal in hallux valgus treatment. J. Mech. Behav. Biomed. Mater. 13, 105260.
Majeed, H., Chowdhury, Y., 2022. Percutaneous Transluminal Angioplasty and Balloon Catheters. StatPearls Publishing, Treasure Island, FL.
Mohammadi Nasr, S., Rabiee, N., Hajebi, S., Ahmadi, S., Fatahi, Y., Hosseini, M., Bagherzadeh, M., Ghadiri, A.M., Rabiee, M., Jajarmi, V., Webster, T.J., 2020. Biodegradable nanopolymers in cardiac tissue engineering: from concept towards nanomedicine. Int. J. Nanomed. 15, 4205–4224.
Morandi, A., Ungaro, E., Fraccia, A., Sansone, V., 2013. Chevron osteotomy of the first metatarsal stabilized with an absorbable pin: our 5-year experience. Foot Ankle Int. 34, 380–385.
Mouriño, V., Boccaccini, A., 2010. Bone tissue engineering therapeutics: controlled drug delivery in three-dimensional scaffolds. J. R. Soc. Interface 7, 209–227.
Mukherjee, D.P., Pietrzak, W., 2011. Bioabsorbable fixation: scientific, technical, and clinical concepts. J. Craniofac. Surg. 22, 679–689.
Nau, T., Teuschl, A., 2015. Regeneration of the anterior cruciate ligament: current strategies in tissue engineering. World J. Orthoped. 6, 127–136.

On, S.W., Cho, S., Byun, S.H., Yang, B.E., 2020. Bioabsorbable osteofixation materials for maxillofacial bone surgery: a review on polymers and magnesium-based materia. Biomedicines 8, 300.

Park, Y.J., Cha, J., Bang, S.I., Kim, S.Y., 2019. Clinical application of three-dimensionally printed biomaterial polycaprolactone (PCL) in augmentation rhinoplasty. Aesthetic Plast. Surg. 43, 437–446.

Park, J.H., Jung, S., Lee, C.K., Ban, M.J., Lee, S.J., Kim, H.Y., Oh, H.J., Kim, B.K., Park, H.S., Jang, S.H., Kim, H.S., 2020. A 3D-printed polycaprolactone/β-tricalcium phosphate mandibular prosthesis: a pilot animal study. Laryngoscope 130, 358–366.

Peltoniemi, H., Ashammakhi, N., Kontio, R., Waris, T., Salo, A., Lindqvist, C., Grätz, K., Suuronen, R., 2002. The use of bioabsorbable osteofixation devices in craniomaxillofacial surgery. Oral Surg. Oral Med. Oral Pathol. Oral Radiol. Endod. 94, 5–14.

Rodrigues, M.T., Reis, R., Gomes, M.E., 2013. Engineering tendon and ligament tissues: present developments towards successful clinical products. J. Tissue Eng. Regen. Med. 7, 673–686.

Rousselle, S.D., Ramot, Y., Nyska, A., Jackson, N.D., 2019. Pathology of bioabsorbable implants in preclinical studies. Toxicol. Pathol. 47, 358–378.

Seaman, S.C., Moline, M., Graham, S.M., Greenlee, J.D.W., 2021. Endoscopic extrasellar skull base reconstruction using bioabsorbable plates. Am. J. Otolaryngol. 42, 102750.

Sigalove, S., O'Rorke, E., Maxwell, G.P., Gabriel, A., 2022. Evaluation of the safety of a GalaFLEX-AlloDerm construct in prepectoral breast reconstruction. Plast. Reconstr. Surg. 150, 75S–81S.

Sukegawa, S., Kanno, T., Katase, N., Shibata, A., Takahashi, Y., Furuki, Y., 2016. Clinical evaluation of an unsintered hydroxyapatite/poly-L-lactide osteoconductive composite device for the internal fixation of maxillofacial fractures. J. Craniofac. Surg. 27, 1391–1397.

Sun, Y., Xia, Y., Zhang, X., Li, W., Xing, Q., 2020. An innovative occluder for cardiac defect: 3D printing and a biocompatibility research based on self-developed bioabsorbable material-LA-GA-TMC. J. Biomed. Mater. Res. B Appl. Biomater. 108, 2108–2118.

Thompson, S.M., Fung, S., Wood, D.G., 2016. The natural history of biointerference screw cyst and new bone formation in anterior cruciate ligament reconstruction: 16-year follow-up. Am. J. Sports Med. 44, 113–117.

Tillman, B.W., Yazdani, S., Lee, S.J., Geary, R.L., Atala, A., Yoo, J.J., 2009. The in vivo stability of electrospun polycaprolactone-collagen scaffolds in vascular reconstruction. Biomaterials 30, 583–588.

Vieira, S., Vial, S., Reis, R.L., Oliveira, J.M., 2017. Nanoparticles for bone tissue engineering. Biotechnol. Prog. 33, 590–611.

Wang, M., Favi, P., Cheng, X., Golshan, N.H., Ziemer, K.S., Keidar, M., Webster, T.J., 2016. Cold atmospheric plasma (CAP) surface nanomodified 3D printed polylactic acid (PLA) scaffolds for bone regeneration. Acta Biomater. 46, 256–265.

Waris, E., Konttinen, Y., Ashammakhi, N., Suuronen, R., Santavirta, S., 2004. Bioabsorbable fixation devices in trauma and bone surgery: current clinical standing. Expet Rev. Med. Dev. 1, 229–240.

Wubneh, A., Tsekoura, E., Ayranci, C., Uludağ, H., 2018. Current state of fabrication technologies and materials for bone tissue engineering. Acta Biomater. 80, 1–30.

Yanagibayashi, S., Nishijima, A., Yoshida, R., Sasaki, K., Yamamoto, N., Takikawa, M., 2020. Intramedullary fixation with bioabsorbable and osteoconductive hydroxyapatite/poly-L-lactide threaded pin in digital replantation. J. Plast. Surg. Hand Surg. 54, 177–181.

Yi, H.G., Choi, Y., Kang, K.S., Hong, J.M., Pati, R.G., Park, M.N., Shim, I.K., Lee, C.M., Kim, S.E., Cho, D.W., 2016. A 3D-printed local drug delivery patch for pancreatic cancer growth suppression. J. Contr. Release 28, 231–241.

Yilgor, C., Huri, P.Y., Huri, G., 2012. Tissue engineering strategies in ligament regeneration. Stem Cell. Int. 2012, 374676.

Yuan, S., Sun, X., Shen, Y., Li, Z., 2021. Bioabsorbable poly(4-hydroxybutyrate) (P4HB) fibrous membranes as a potential dermal substitute. J. Mater. Chem. B 9, 8074–8080.

Zhang, F., L, L., Song, X., Xie, Y., Qingqing, H., Dang, Y., Qi, X., 2020. Clinical analysis of drug-coated balloons and drug-eluting stents in the treatment of in-stent restenosis in elderly patients with coronary heart disease. Chinese J. Geriatr. Cardiovasc. Dis. 22, 3.

Zhichang, P., 2018. Progress in transplantation materials for anterior cruciate ligament reconstruction. World's Latest Med. Inform. Dig. 18, 4.

Zhiqiang, Z., Xiaosong, D., Yin, L., Zheng, H., 2022. Biodegradable polymeric materials for flexible and degradable electronics. Front. Electron. 3, 985681.

Zhu, W., Ma, X., Gou, M., Mei, D., Zhang, K., Chen, S., 2016. 3D printing of functional biomaterials for tissue engineering. Curr. Opin. Biotechnol. 40, 103–112.

CHAPTER 13

Polymeric (PLGA-based) nanocomposites for application in drug delivery: Current state of the art and forthcoming perspectives

Sanket Kumar[1], Supriya Singh[1], Sheikh Shahnawaz Quadir[1], Garima Joshi[1], Mangilal Chouhan[1], Dinesh Puri[2] and Deepak Choudhary[1]

[1]Department of Pharmaceutical Sciences, Mohanlal Sukhadia University, Udaipur, Rajasthan, India; [2]School of Pharmacy, Graphic Era Hill University, Dehradun, Uttarakhand, India

13.1 Introduction

The development of nanocomposite biomaterials with tailored compatibility, bioabsorbability, and degradation behavior has been mostly investigated and researched over the past few decades for human health applications. FDA/EMA (European Medicines Agency)-approved PLGA (polylactic-co-glycolic acid) has drawn the most focus for clinical uses (Nair and Laurencin, 2007; Makadia and Siegel, 2011). PLGA is a PLA (polylactic acid)-based copolymer obtained most efficiently by ring-opening copolymerization of poly-lactide monomer (PLA) and polyglycolic acid (PGA) nowadays resulting in high-molecular-weight PLA-based copolymers. PLGA is an abbreviation for poly D,L-lactic-co-glycolic acid in which the D/L-lactic acid forms are in the same ratio (Dechy et al., 2004; Sharma et al., 2016) (Fig. 13.1).

PLA is a linear aliphatic polyester obtained from corn, sugar, potatoes, and other agricultural renewable resources (Nampoothiri et al., 2010) and is of three kinds based on their microstructure, PDLA is poly(D-lactic acid), PLLA is poly(L-lactic acid), and PDLLA is a racemic blend of both D-PLA and L-PLA [poly-(D,L-lactic acid)] in monophasic structure (Swider et al., 2018). Each kind PLA has a unique structure and applications. PLA does

Bioresorbable Polymers and their Composites
ISBN 978-0-443-18915-9
https://doi.org/10.1016/B978-0-443-18915-9.00004-5
© 2024 Elsevier Ltd.
All rights reserved.

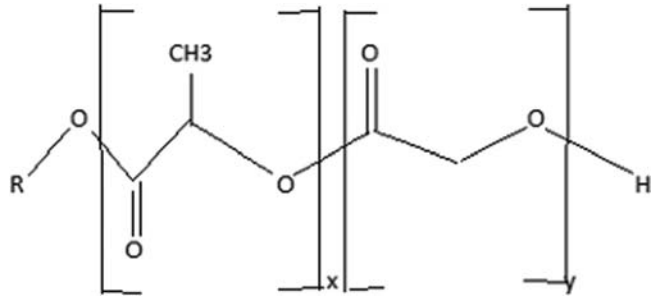

Figure 13.1 Poly-lactic-co-glycolic acid's structure (PLGA) (where *x* and *y* are number of lactic acid and number of glycolic acid units, respectively).

not cause any harm in humans as it degrades into water and carbon dioxide and can be totally cleared from the human body (Wu and Wang, 2001a). However, the most important reason for not using pure PLA instead of PLGA is due to PLA having deficient qualities, such as it is easily broken (Qi et al., 2019), has poor osteo-induction, and an unrestrained degradation rate (Go et al., 2019; Lee et al., 2016). Hence, PLA copolymer-based nanocomposites are mostly investigated as these nanocomposites meet all the requirements to improve cell adhesion and the ratio of cell propagation superficially on materials as per the current state of the art (Tang et al., 2013). These PLA copolymer-based nanocomposites are in nanometer sizes and act as a matrix in nanofillers with great potential uses in repairing and substituting synthesized bone (Sokolova et al., 2020), engineering of tissues (Davies et al., 2008), and importantly in the development of drug-delivery systems. Pinto et al. (2013) showed the effect of graphene nanosheets and graphene oxide (0.2−1 mass %) on the functional properties of poly-lactic acid films and the outcomes in yield strength, Young's modulus, and resulting nanocomposite impermeability were better than those with pristine PLA. Polymer nanocomposites such as PLA-based PLGA nanocomposites have revealed improved properties compared with pure PLA polymer (Holderegger et al., 2015).

With the help of nanotechnology, PLGA nanocomposites are greatly increasing the applications of PLA materials by providing suitable biocompatibility, as delivery vehicles for drugs, proteins, DNA, RNA, vaccines, peptides, and metallic as well as magnetic nanoparticles, and also have uses in tissue engineering and other functional properties (Mundargi et al., 2008a; Hans and Lowman, 2002; Allison, 2008). PLGA nanocomposites are physically strong and popular biodegradable polymers owing

to their long durability in clinical research and experience, showing promising degradation features and maintaining sustained drug release by implantation without the requirement for a surgical operation (Martou and Antonyshyn, 2011). The overall physical characteristics of PLGA nanocomposites are tunable by controlling the molecular weight of polymer, the lactide-to-glycolide ratio (Maquet et al., 2003), and when making the polymer–drug matrix by altering the drug concentration, which also helps in creating the desired dosage-release interval profile which depends on the type of drug (Mohamed and van der Walle, 2008). The present study shows the major applicability and forthcoming practices of PLGA nanocomposites in facilitating drug-delivery applications.

PLGA are commercially accessible in diverse molecular weights and copolymer ratios, and can be scaled into any shape and size with enhanced water solubility and tunable drug release dose-dependent profiles (Danhier et al., 2012; Lü et al., 2009). They have nonlinear biodistribution and pharmacokinetics profile (Panagi et al., 2001) and are obtained in an atactic configuration in which no regular stereochemical configuration is found in repeating units showing mutable stereochemical configurations (Cheng et al., 2007a). The PLGA degradation rate depends on the unit sequence of PLGA as random units degrade faster than sequenced units (Grizzi et al., 1995).

PLGA copolymer degrades via hydrolysis or biodegradation through the cleavage of its ester-linked backbone into oligomers, then monomers. This has been shown in vivo and in vitro for a variety of drugs and proteins with varying polymer ratios (Schliecker et al., 2003; Witt, 2001). These polymers degrade mainly by the matrix's consistent bulk degradation where water penetrating into the matrix is greater than the rate of polymer degradation. Furthermore, the process is autocatalyzed by an increase in carboxylic end-groups caused by biodegradation. Degradation of PLGA copolymer is a multistep process that includes both bulk/surface diffusion and erosion (Holy, 1999; Anderson and Shive, 1997).

PLGA has potential to encapsulate therapeutic agents such as antiseptics, antiinflammatories, and antioxidants, and can target drugs in form of the gels or micro/nano-particles (Mundargi et al., 2008b; Ding and Zhu, 2018; Arvizo et al., 2012).

The use of PLGA nanocomposites of with inorganic nanoparticles has the potential to reduce toxicity and extend PLGA's clinical applications. In recent years, researchers have thoroughly investigated the applications of PLGA-based nanocomposite materials in cancer therapy, diagnosis,

imaging, protein delivery, and gene therapy (Rezwan et al., 2006; Sun et al., 2008; Zare et al., 2019). As is discussed in this chapter, PLGA nanocomposites have also been investigated for vaccine delivery to the brain and CNS, treatment of inflammatory diseases, and scaffolds for tissue engineering (Wu and Wang, 2001b). Nonetheless, investigational efforts into PLGA nanocomposite development and marketability are still required for biomedical applications because of several issues related to scale-up, such as poor drug loading, high burst release, and production costs (Mir et al., 2017). This chapter aims to investigate recent advancements in this field, beginning with a brief analysis of PLGA properties, PLGA-based approved medicines, and an overview of the primary production methods of PLGA magnetic/nanoparticles.

13.2 PLGA properties (Martin and Averous, 2001; Nijenhuis et al., 1996; Tsuji et al., 2000; Passerini and Craig, 2001)

There are multiple factors on which PLGA's physical characteristics are dependent, such as the initial molecular weight, the lactide-to-glycolide ratio, device size, water exposure, and temperature of storage. In Table 13.1, PLGA physiochemical and biological properties and their description and parameters on which they influenced are discussed.

13.2.1 Copolymers of PLGA

The necessity for developing various types of block copolymers of polyesters with polyethylene glycol is based on their better delivery formulations that encapsulate a variety of drugs and methods of administration. Both triblock ABA (PLGA/PEG/PLGA) and BAB (PEG/PLGA/PEG) types of copolymers have been processed with diblock (PLGA/PEG) types in which PEG chains facing toward the outer hydrophilic phase in micelles are surrounded by encapsulated drug(s) (Allahyari and Mohit, 2016). The composition of PLA:PGA in a ratio of 1:1, as in PLGA 50:50, is mostly used in nanotechnology and a variety of PLGA forms can be obtained by changing the PLA:PGA ratio during polymerization (Kissel et al., 2002; Choi and Park, 2002).

Table 13.1 Physiochemical and biological properties of PLGA polymers.

S. No.	Properties	Description	Influences on
1.	PLGA formation	Ester-linked LA and GA unit's ring-opening catalyzed copolymerization	Biodegradability
2.	Metabolism	Nontoxic byproducts, such as water and carbon dioxide yielding via Krebs cycle	Biodegradability
3.	PLGA hydrolysis	With time, there are considerable changes in the formulation and various descriptions have been provided	Copolymerization of crystalline poly-glycolic acid with poly-lactic acid results in reduced PLGA degree of crystallinity, glass transition temperature (T_g), moisture content, and molecular weight
4.	Glass transition temperature (T_g)	Glassy appearance at 37°C	In copolymer composition, T_g decreases with a decrease in lactide content and molecular weight
5.	PLGA's melting point and degree of crystallinity	—	Molecular weight, mechanical strength, behavior of swelling, hydrolysis capacity, and polymer biodegradation rate
6.	Mechanical strength	—	Molecular weight and poly-dispersity index

Continued

Table 13.1 Physiochemical and biological properties of PLGA polymers.—cont'd

S. No.	Properties	Description	Influences on
7.	Shape and size	Encapsulating almost any size of molecule	—
8.	Copolymers	Copolymers with higher PLA are less hydrophilic in nature	By absorbing less water, the degradation period is longer
9.	Solubility	Soluble	Soluble in chloroform, acetone, ethyl acetate, and tetrahydrofuran (THF)
10.	PLGA copolymers	Diblock or triblock copolymer conformations	PLGA-PEG, PLGA-PEG-PLGA or PEG-PLGA-PEG
11.	PLGA bio-distribution and pharmacokinetics	Nonlinearity and dose-dependent profile	Carrier degradation is carried out in the initial stage with around 30% and clear-out by respiration in the lungs eventually
12.	Clearance	From blood uptake by the mononuclear phagocyte system (MPS)	Depends on drug dose and PLGA carriers' composition with systems

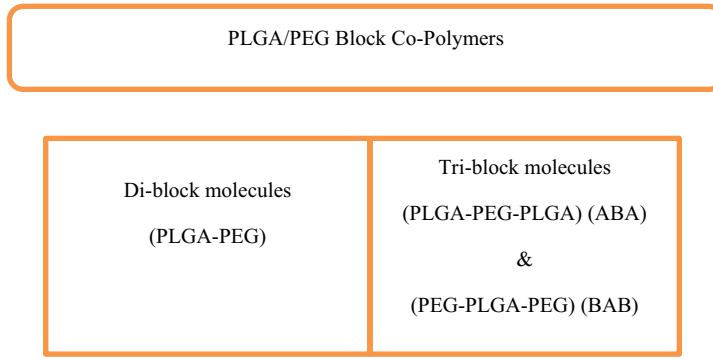

Release of encapsulated drug(s) and proteins from copolymers is done through two mechanisms (Uhrich et al., 1999):

(i) Initial release phase: Hydrogel diffuses the drug

(ii) Later phase: Hydrogel matrix erosion facilitates drug release

By reducing collaboration with external molecules through steric and hydration repulsion, this layer of PEG serves as a barrier and improves shelf stability. With effective fabrication, the further addition of PEG leads to a reduction in drug effectiveness and encapsulating proteins (Frank et al., 2005). A lower drug incorporation may be caused by the PEG chains' steric interference with the drug/protein−polymer interaction. Diblock copolymer formulations have been shown to have better release kinetics than PLGA alone. There have also been reports of numerous methods for diblock nanoparticle-based targeted medication delivery (Choi et al., 2011). For developing a thermogel system of triblock of ABA and BAB; A-block and B-blocks were covalently linked by ester bond. At body temperature, these block copolymers are a highly viscous gel but they act as a free-flowing solution at low temperature.

The ABA and BAB block copolymers, which are temperature-responsive, are made up of hydrophobic PLGA segments and hydrophilic PEG segments. The hydrophobic PLGA segments create associative cross-links, while the hydrophilic PEG units remain in solution. When the temperature decreases, the hydrophilic solution results in more hydrogen bonding between water and PEG hydrophobic units and dissolution occurs (Alexis, 2005; Zolnik and Burgess, 2007). Greater loss of PEG component mass has been observed during degradation of BAB gel. Hence the hydrophobic nature of gel with a lower water content has been seen in aqueous solution. The solution-to-gel transition is caused by a decrease in hydrogen bonding and an increase in hydrophobic forces among the PLGA

segments as the temperature rises. Such thermo-responsive polymers are desirable options due to their responsive polymers and the simplicity of handling during scale-up, formulation, filtering, and filling, etc. (Meikle et al., 2016).

13.3 PLGA nanocomposite carriers: fabrication techniques

Since 1989, many PLGA materials have already been commercialized. PLGA nanocomposite preparation methods are still being improved by scientists to design a close-control copolymer with the desired inherent characteristics. In pharmaceuticals, drug/protein delivery is the most rapidly developing class aimed at constant or aimed delivery with lower toxicity and decreased treatment-associated risks with increased specificity. During the synthesis of PLGA particles, their physicochemical characteristics and uses can be controlled by manipulating different methods to obtain optimized products (D'Mello et al., 2006). In preparation inconsistent particle behavior may be reported through grinding devices that do not allow batch-to-batch reproducibility and phase separation in case of emulsion system, extraction of solvents, and uniformity of particles when organic solvent used are not chosen carefully (Anton et al., 2008). The PLGA MP/NP (microparticles/nanoparticles) and implants are prepared by emulsification-solvent evaporation, electrospinning, salting out, nanoprecipitation, solvent diffusion—emulsification, drying spraying and extrusion, etc. techniques are commonly employed summarized in Table 13.2 (Jain, 2000; Schoubben et al., 2019).

The challenges associated with the stability and delivery of these copolymers have limited the number of marketed products available, as listed in Table 13.3.

Table 13.2 PLGA nanocomposite and implant preparation techniques, with descriptions and limitations/applications.

S. No.	Techniques	Description	Limitations/applications
1.	Emulsification–solvent evaporation (ESE) method: (Rosca et al., 2004; Bilati et al., 2005a; Yang et al., 2001; Freitas et al., 2005) ❖ Single emulsion oil-in-water (O/W) emulsification ❖ Double (multiple) emulsion method (microparticle preparation technique)	Dissolved PLGA polymer in organic vehicles such as dichloromethane, $CHCl_3$, or ethyl acetate. Drugs (particle size around 20–30 μm), imaging probes and NPs if loaded, also codissolved in the organic vehicles. Then emulsified with surfactants (for example PVA) with continuous stirring. Then evaporate the organic phase with stirring at a suitable temperature or by reducing pressure. Multi-wash the outcome particles (such as injectable microparticle formulation) to remove polymer/surfactant residue and freeze-dry in storage for long-term use **Double emulsion method**: Generally drugs or materials to be encapsulated are emulsified with PLGA organic phase under vigorous stirring to produce primary water-in-oil emulsion. This is added to surfactant aqueous solution with continuous stirring. At a suitable temperature, evaporate the organic phase by stirring or by reducing the pressure	For intended hydrophobic loading of particles, single emulsion (O/W) emulsification method is used, e.g., steroids. Oil-in-oil emulsion is used for loading of drugs which are water insoluble. This method has a very limited % of encapsulation of hydrophilic compounds W/O/W emulsion by double emulsion method Hao et al. synthesized PLGA NPs loaded with docetaxel (DTX) adapted with poly-ethyleneimine (PEI) and gold shell NPs with targeting glioma peptide angiopep-2 (ANG/GS/PLGA/DTX NPS) (Hao et al., 2015)

Continued

Table 13.2 PLGA nanocomposite and implant preparation techniques, with descriptions and limitations/applications.—cont'd

S. No.	Techniques	Description	Limitations/applications
2.	Salting-out method (nanoparticle preparation technique)	The compounds to be loaded and water-miscible organic solvent of PLGA solution are mixed to an aqueous phase with a salting-out agent such as chloride salt of calcium and as a stabilizer polyvinyl alcohol under continuous stirring. Formation of oil-in-water emulsion takes place, and then excess water is added to the emulsion for complete diffusion of organic solvent into the aqueous phase. This results in the formation of PLGA matrix particles with loaded compounds. By filtration, the salting-out agent and stabilizer are removed with washing of the particles (Reis et al., 2006)	Best suited method to encapsulate thermosensitive materials and when a high concentration of PLGA is required (Leroux et al., 1996)
3.	Emulsification—solvent diffusion (ESD) method	To achieve thermodynamic equilibrium at room temperature, mutually saturate the organic solvent and water. In organic solvent dissolve polymer and then emulsify the aqueous solution containing a stabilizer such as PVA in a high-speed homogenizer (Esmaeili et al., 2007) After complete homogenization, water is incorporated into the oil-in-water emulsion with regular stirring; this facilitates the solvent to diffuse out	Principally prepared by Quintanar-Guerrero et al. (Quintanar-Guerrero et al., 1998) Advanced form of salting-out method High reproducibility and high % encapsulation efficiency of hydrophobic drugs Takahashi et al. settled Ag-decorated PLGA NPs of 300 nm size (Takahashi et al., 2017)

		from the internal phase. Nano-precipitation of PLGA polymer leads to the production of colloid particles. By evaporation or steam distillation (vacuum applied), remove excess solvent (Murakami et al., 1999)	
4.	Nano-precipitation method	The polymer and encapsulating compounds are liquefied in acetone/ethanol or acetonitrile. The resultant solution is added drop-wise to surfactant or emulsifier aqueous solution. Diffusion of the organic phase takes place and formation of PLGA NPs is immediate. Excess solvent is removed by reducing the pressure (Bilati et al., 2005b)	Also called the solvent displacement method Simply entrap hydrophobic drugs in a single-step process with high reproducibility in PLGA NPs (Morales-Cruz et al., 2012) A two-step method reported to have high encapsulation efficiency of PLGA NPs, proteins, and enzymes (Miladi et al., 2016)
5.	Spray-drying method (Arpagaus, 2019; Gavini et al., 2004; Nie et al., 2008)	PLGA particle formation is done when PLGA emulsion of water-in-oil is sprayed into a jet of heated air in a spray dryer Compounds to be loaded as in a W/O dispersion with PLGA polymer may affect the choice of solvent due to their hydrophobicity	Rapid and suitable method for mass production of PLGA particles and to encapsulate all varieties of drugs/proteins/peptides into microparticles A major drawback is loss in resultant total weight of particles due to spray dryer inner wall adherence

Continued

Table 13.2 PLGA nanocomposite and implant preparation techniques, with descriptions and limitations/applications.—cont'd

S. No.	Techniques	Description	Limitations/applications
6.	Electro-spinning method	With application of a high electric voltage by syringe injecting PLGA aqueous solution through a needle. The unstabilized needle then produces nanofibers with jet spinning. These nanofibers are collected in a conducting substrate. By controlling the voltage, the type of collector used, and injection rate, the diameter of these nanofibers can be fixed (Yang et al., 2005)	Method is more versatile, simpler, and low cost Mostly utilized in tissue engineering scaffold fabrication (Yang et al., 2005) Usually produces nanofibers ranging from nanometers to several micrometers A flexible nanocomposite with cotton-wool-like appearance has been successfully prepared by Schneider et al. (Schneider et al., 2011)
7.	Phase separation (coacervation) technique (Wang et al., 2011; Otsuka et al., 2003; Kumari et al., 2010; Thomasin et al., 1998)	Both the coacervate phase of polymer and the supernatant phase are washed-out in polymer. Then drug is dispersed/dissolved in solution of polymer which is coacervate-coated In polymer—drug solvent phase, gradual addition of organic medium with stirring. After this, extracts of the polymer solvent result in soft drug coacervate droplets by phase separation of polymer. Then the prepared soft coacervate is quickly dipped into	With the technique of liquid—liquid phase separation, this method is best for the fabrication of biodegradable encapsulated polymer preparations in micrometer scale Steroids (Thomasin et al., 1998) (hydrophobic drug) are solubilized or distributed in the polymer—drug solvent phase (oil-in-water emulsion) whereas peptides and proteins (hydrophilic

		insoluble solvent for quenching of these microdroplets. In the quenching bath, the soaking time controls the hardness/coarsening of the droplets. Finally, microspheres are collected via water wash, straining, filtering, and centrifugation or lyophilization	drugs) are dissolved in water and distributed in the polymer solution (emulsion of water-in-oil)
8.	Solvent-casting and compression molding method (batch-to-batch operation) (implant preparation methods)	With the desired ratio, dissolve the polymer and drug in acetone then the solvent is cast at 60°C until the process of evaporation is complete resulting in a composite material of drug–polymer which is subjected to compression molding into its tunable geometry at approximately 80°C and 25,000 psi pressure until the final density of 1 g/cc is obtained (Durán et al., 2016)	It is best to fabricate a macroscopic formulation in millimeter sizing as an implant that is subcutaneous delivers the drug in the body (Hua et al., 2002) This process requires a large amount of organic solvents and takes an extended time for the resulting material to have complete removal of solvents
9.	Extrusion method (continuous operation) (implant preparation methods) (Widmer, 1998)	The heating of polymer–drug mixture results in a semiliquid phase using heating sources and with an extrusion screw for applying stress which pushes the mixture through the die. This is then cooled and solidified, and then cut into the required length for implants	This method is done without using solvent, the mixture of polymer–drug is drawn through a die to fabricate implants (Wang et al., 2010)

Table 13.3 FDA-approved marketed brands of PLGA MP/NPs with active principles and applications (Wang et al., 1888; Zhong et al., 2018; Garner et al., 2015; WCG, 1067).

Form/active principle	Brand	Delivery	Application	Approved year
Implant/goserelin acetate	Zoladex®	Subcutaneous	Prostate carcinoma	1989
Microparticle/leuprolide acetate	Lupron®	Intramuscular	Central precocious puberty/endometriosis	1995
Microparticle/octreotide	Sandostatin® LAR	Subcutaneous	Secreting tumors (VIP) and metastatic tumors with associated severe diarrhea	1997
Nanogel/leuprolide acetate	Eligard®	Subcutaneous	Prostate cancer—advanced	2002
Microparticle/buserelin acetate	Suprecur®	Intramuscular	Endometriosis	2002
Microparticle/risperidone	Consta®	Intramuscular	Schizophrenia and bipolar disorder	2003
Implant/dexamethasone	Ozurdex®	Subcutaneous	Macular edema	2009
Microparticle/pasireotide pamoate	Signifor® LAR	Intramuscular	Acromegaly and Cushing syndrome	2014
Microparticle/triamcinolone acetonide	Zilretta®	Intraarticular	Osteoarthritis	2017
Nanoparticle/buprenorphine	Sublocade®	Subcutaneous	Moderate to severe opioid addiction	2017

13.3.1 Factors influencing the degradation of PLGA

To design a drug-delivery device with PLGA's tunable properties, it is necessary to understand the factors influencing the degradation of PLGA which makes it more efficient and effective.

Composition's effect	For tunable hydrophilicity and degradation rate, composition of the polymer is the prime factor to determine	Studies related to accelerating weight loss of polymer, enhanced glycolic acid percentage in oligomer unit. Higher hydrophilicity leads to superior degradation of glycolic acid such as PLGA in ratio of 65:35 shows less degradation than PLGA in ratio of 50:50 (PLA/PGA) and faster degradation than PLGA in ratio of 75:25 and so on with PLGA 85:15 (Park, 1995)
Crystallinity (Bouissou et al., 2006)	Crystallinity and glass transition temperature both have indirect effects on the rate of degradation. Copolymer composition effects on these properties	Degradation rate increases with enhanced crystalline characteristic of polymer such as semicrystalline PLGA polymer due to increased hydrophilicity
Molecular weight (Mw)	Molecular weight is directly related to the chain size of the polymer. With higher molecular weight, polymer degrades more slowly and requires more time for degradation than polymer with short chains	Exception is PLLA where the molecular weight is inversely proportional to the degree of crystallinity (Castelli et al., 1996; Park, 1994).
Drug type (Siegel et al., 2006)	From surface degradation to bulk erosion, the presence of	In a biodegradable polymer system, the effect of the drug's chemical properties

(*Continued*)

—cont'd

	drugs will affect both the degradation mechanism and also the matrix rate of degradation	explains the overall drug-release behaviors (Ghitman et al., 2020)
Effect of size and shape of the matrix	A higher degradation rate has been seen in polymer devices with higher surface areas	A polymer device with a higher surface-area-to-volume ratio makes the release of the drug faster. PLGA bulk degradation is faster than surface one (Grayson et al., 2005; Gallo et al., 2014).
Effect of pH	Strongly acidic and alkaline media both accelerate PLGA in vitro hydrolysis (Li and Chang, 2005)	PLGA autocatalysis in slightly acidic and neutral media is less noticeable due to carboxylic end groups
Effect of enzymes (Esmaeili et al., 2008)	There is conflicting published data on in vitro and in vivo degradation mechanism observations which cannot be closely correlated due to the effect of enzymes as both hydrolytic and enzymatic cleavage	Proposed studies showed that the hydrolytic degradation primarily degrades PLGA rather than as suggested by enzymes
Loading of drug	Polymer matrices have a high drug load owing to a greater initial burst release than those with a low amount of drug-loading matrices	Drug type decides the level of drug content which is attenuated at a certain level (Crotts and Park, 1998)
Toxicological studies	For mild toxicological reactions, PLGA is one of the safe polymers at micro/macro-scaling and also better for application at the nanoscale	Toxicological investigation with PLGA devices shows that at the application site local tissue reactions may occur (Mura et al., 2011)

13.4 Applications of PLGA nanocomposites

13.4.1 Synthetic bone substitute and repair

With the improvement in living standards over the past few decades, there has been an increase in the prevalence of various bone disorders and the frequency of traffic accidents, which has led to a growing demand for artificial bone replacements or bone repair materials. Human bones are highly susceptible to damage or loss through pathological changes, trauma, or both. Currently, the creation of materials that aid in bone regeneration and in healing bone defects chiefly focus on preclinical investigation and utility in clinical areas. Orthopedic surgeons frequently fix bone defects using artificial bone substitutes which are placed in the body, so it is vital for selection of appropriate replacements.

Outstanding biocompatibility, osteoinductive, and osteoconductive qualities are essential for a good bone substitute (Bakhshalian et al., 2014). In earlier research, nontoxic bioabsorbable polymer implants were employed extensively in orthopedic surgery, including bone replacement and fracture repair. In dental, orthopedic, and craniofacial procedures, polymer devices such as pins, plates, and screws are often employed. For the preparation of porosity scaffolds and the repair of broken bones, PLA and PLGA are two promising copolymers that have been investigated most (Jo et al., 2015).

With the purpose of reducing patient suffering, the greater degradation of PLA materials eradicates the necessity for a second operative procedure and avoids the removal of implants. Additionally, using PLA materials lowers the likelihood of operation failure, thereby reduces the stress burden of patient. Pure PLA materials do not have the same bone-bonding strength as PLA-based nanocomposites, and their regeneration efficiency and degradation behavior are not as good (Lee et al., 2019). The PLGA (PLGA/TCP60:40) was mixed with tricalcium phosphate nanoparticles in amorphous form (TCP). Through its exceptional moldability, the material's characteristically cotton-like shape can be fitted to any bone deficiency. The matrix behavior of PLGA/TCP-calvarial defects significantly enhanced the compressive mechanical strength in all nine white rabbits (New Zealand) when compared to PLGA-treated calvarial defects after 4 weeks followed by implantation grafting, the graft material resorption was also seen (Gentile et al., 2014). Calcium phosphate ceramic (hydroxyapatite: HAp) has been primarily employed as artificial bone materials in various surgical procedures due to its great biocompatibility and similarity to human

bone (Hasegawa et al., 2006). Additionally, HAp has been frequently mixed with a PLA polymer matrix, and the resulting HAp-PLLA matrix showed enhanced biotic performance. In situ polymerization of L-lactide and glycolide was successfully completed by Takeoka et al. Numerous PLGA/HAp composites with various PLA:PGA ratios in porous discs of HAp have been produced (Takeoka et al., 2015).

Bioglass 45S5 application (Lu et al., 2014) has drawn a lot of interest because it is crucial to control the rate at which the polylactic acid matrix used as the fixation for bone devices and the degradation rate can be controlled by the crystalline behavior, molecular weight, size, and shape. Numerous studies have illustrated the breakdown of polymer in the presence of bioglass resulting in primary rapid loss of weight as the bioglass dissolves (Kranz et al., 2000). The local environment eventually becomes alkaline as the bioglass salts-out when it comes into touch with bodily fluids, neutralizing lactic acid, and the rate of polymer degradation decline. In general, almost all investigations demonstrate a direct connection between bioglass and the breakdown of the polymer matrix, in other words, weight loss. The results showed that the presence of bioglass in composites significantly speeds up polymer breakdown, and a 30% bioglass content encourages osseointegration in bones within a month after implantation. After 1 month, X-ray tomography and 3D images show a white line clearly indicating the process of new bone development around the implant (Vergnol et al., 2016). All of these findings suggest that this composite, which contains 30 wt.% bioglass particles, has significant potential for use in the medical field. Although bone allograft has good osteo-conduction and osteo-induction, and also has many of the same chemical components as bone autograft, its clinical usage has been constrained by its challenging shape, poor porosity, and unfavorable degrading behavior (Dimitriou et al., 2011). In this circumstance, demineralized bone matrix (DBM) forms collagen, and the bone growth elements are beneficial for bone regeneration (Zhang et al., 2015). Demineralized bone matrix formulations are available in a variety of forms in the market, including granules, powdered, gel, putty, and paste. Porous PLA/DBM composite biomaterials were created by Zhang and Ma (1999) using the supercritical CO_2 approach, a novel preparation technology that is well suited to the processing of bioactive materials nourished with growth modulators. The X-ray result and histological analysis showed that the healing process of PLA/DBM composite to bone formation is significantly better than PLA. Finally, the authors proposed the viability of using PLA/DBM to mend bone

deformities. The rate of degradation, products of degradation, and bioactive mechanical characteristics are best suited for bone replacement and repair. Nano-sized tricalcium phosphate, HAp, bioactive glass, or formulations containing DBM are enhanced with PLA/PLGA qualities (Araujo et al., 2014).

13.4.2 Tissue engineering

A new field in human healthcare focuses mainly on tissue regeneration and organ development. The sustained focus on the structural, functional, and growth mechanisms of tissues in biological environments against the backdrop of science related to cell development and biological engineering advancement has created innumerable benefits. Scaffolds are used for tissue engineering, and involve bone, blood vessel, and neural system regeneration (Kim and Martin, 2006), where they work as the cell transporter for attachment and development. Cell functioning is influenced by the base environment, involving biochemical and mechanical signals, while scaffolds have tunable structural advantages for cells, enabling a number of biological functions. Hence, as PLA materials are very biocompatible, they are frequently employed as scaffolds. It has been examined on the basis of alignment that PLLA micro/nano-fibrous scaffolds for their effectiveness in brain tissue engineering (Sundback et al., 2005). The findings demonstrated that neural stem cells (NSCs) with their outgrowth neurite expand in a parallel way to PLLA fibers so that aligned scaffolds appeared to have no relationship with the rate of differentiation of cells and arrangement of fibers (Table 13.4).

Additionally, nanofibers outperformed microfibers in terms of differentiation performance, highlighting the tremendous potential of PLLA scaffolds (with nanofibers aligned) for stem cell engineering. Numerous different biomaterials, including collagen and oxide of graphene, are slowly introduced for polymerization of PLAor PLGA for the design and construction of ideal scaffolds.

The electrospinning technique prepares such scaffolds effectively with the capability for mass production enabling a greater scaffold core area.

Investigation efforts have been made for a scaffold surface with increased cell adhesion and proliferation that will change the field concept of tissue engineering. For additives such as collagen, etc. it allows an increase in the core activity in poly-lactic acid and PLGA scaffolds. In the future, technological maturation of tissue regeneration needs further experiments into

Table 13.4 Researched PLGA nanocomposites/microparticles/implants.

S. no.	Investigators	Researched PLGA nanocomposites/ microparticles/implants	Preparation technique	Field of application
1.	Shin et al. (2012)	GO was used to create hybrid fiber matrices from PLGA and collagen (GO-PLGA-Col matrices)	Electrospinning process	In tissue engineering, these hybrid candidates are best used to induce spontaneous myogenesis
2.	Ziabari et al. (2010)	Demineralized bone particles (DBPs) were used to create scaffolds of PLGA copolymer	Solvent cast method or salt leach-out method	DBP was used on a PLGA scaffold to increase the smooth muscle cell growth and gene expression
3.	Ardjomandi et al. (2015)	The topography and angularity of the produced scaffolds were examined after a succession of coatings of tricalcium phosphate scaffolds had been prepared	Dip-and-dry coating	—
4.	Shim et al. (2015)	Resorbable membrane of polycaprolactone was created shaped in a semi-domed form (PCL/PLGA-TCP)	CADD 3D printing	Using this, the problem associated with the organic solvents used in preparation of scaffolds that cause impairments to cells and tissues has been solved
5.	Davachi et al. (2016)	Nearly 30% encapsulation of triclosan was observed in a melt mix of PLLA of high molecular weight and low molecular weight		Results indicated that the use of PLA3 with 5% LAT30 was the most viable choice for bone tissue engineering, primarily because triclosan's adverse effects were lessened by its encapsulation close to the tissue environment

6.	Shafiq et al. (2015)	Star-shaped conjugates of P-(LA-co-CL) and P (SP-) copolymer were mixed in the correct ratios to create nonwoven meshes. Then, Sprague–Dawley rats were implanted subcutaneously with P-(LA-co-CL) and SP-meshes	Electro-spinning	When doing a hematoxylin and eosin staining test, it was discovered that meshes of SP and P-(LA-co-CL) had become cellularized. These cutting-edge scaffolds must be used in soft tissue regeneration
7.	Mikael et al. (2014)	Using MWCNT (inorganic) for the fabrication of functionalized PLGA-MP-based scaffolds		Engineering of bone and tissue regeneration process: both show good cellular compatibility
8.	Sheikh et al. (2015)	Hybrid PLGA with silk fibroin fabrication of scaffolds embedded with HAp NPs		Upon implantation, these scaffolds of PLGA–silk–HAp showed good swelling and water uptake capacity by which they can retain biological fluids also.
9.	Selvaraju et al. (2018)	Instead of using silk, scaffolds were prepared using collagen composite-PLGA embedded in HAp nanoparticles		Result showed that the composite acts as a scaffold, being nontoxic to cells and utilized for engineering of bone and tissue development and their translation at a clinical level

Continued

Table 13.4 Researched PLGA nanocomposites/microparticles/implants.—cont'd

S. no.	Investigators	Researched PLGA nanocomposites/ microparticles/implants	Preparation technique	Field of application
10.	Pelaseyed et al. (2020)	Scaled scaffolds as a foam base with PLGA-nanopowder of TiO_2 embedded		These scaffolds were presented for attachment of the cell, their proliferation enabled transferring nutrients with best mechanical properties and wide applicability in the regeneration of bone
11.	Haider et al. (2015)	PLGA-CuO antibacterial nanoparticles with nanofiber composite scaffolds were developed		Results reported antibacterial properties in scaffolds utilized as internal/external dressing components for wounds

the feasibility of PLGA-based composites which might be the novel future candidate for nanocomposites being used also in the neuronal and vesicular systems (Dhandayuthapani et al., 2011).

13.4.3 Drug-delivery system

An uncontrollable level of drug after administration several times a day was a major drawback which still cannot guarantee a cure with a conventional drug formulation. This burden with undesirable side effects has created opportunities for scientists to develop such a drug-delivery system that pivotally links drug therapy with the aim of retaining a sustained drug concentration in the blood while acting on the targeted area. These novel systems deliver the drug in a defined time at gradual level & evading the drug's decomposition (Yu et al., 2009) (Table 13.5).

Currently, nanocomposites made by PLGA nano/microparticles with primary characteristics of being biodegradable, biocompatible, and nontoxic, with prolonged circulation and a wide payload capacity to hold drugs, both water-soluble and water-insoluble, have been used in the healthcare market and are undergoing continued research.

The most exploited biodegradable PLGA polymers are fabricated nanocomposite formulations created through techniques such as evaporating the solvent, salting-out, displacement of solvent, and diffusion methods. The resultant carriers are excellent for encapsulation of savoxepine (psychotic drug), tyrphostins (restenosis drug), the progesterone hormone, oridonin, and BSA protein. Also, these PLG nanocomposites have been utilized in sustained-release systems for drug delivery due to their gradual degradation with an extended retention time (Tansik et al., 2014). The remaining challenge is the preparation and storage of these PLGA polymers with drugs that do not create a surrounding acidic, environmentally negative result with a negative effect on protein stability when degradation begins. Further research should be conducted to overcome the drawbacks associated with drug—PLGA polymer matrices.

13.4.4 Therapy and theranostic agents

Nanoscaled PLGA nano-inorganic, biodegradable, biocompatible, and nontoxic combinations (described in Table 13.3) have been previously employed for clinical advancements in the treatment of many conditions due to their expanded functionalities in several areas of application (described in Table 13.6).

Table 13.5 Drug-delivery systems of PLGA nanocomposites.

S. no.	Researchers	Study	Method used	Observation
1.	Tobio et al. (1998)	Discovered that polymerized PLA/TCP carriers may retain gentamicin for up to 4 weeks while releasing 60% of it in the first week	–	Numerous copolymers of PLA, as well as single polylactic acid carriers have been the subject of research
2.	Ueng et al. (2002)	Prepared PLGA polymerized nanospheres	–	Determined the optimal drug-loading of materials
3.	Govender et al. (1999)	Investigated PLGA nanoparticles with procaine HCl	Nano-precipitation	By adjusting the pH of the watery phase, switching procaine HCl for procaine dehydrate, or involving excipients in sizing, one can also modifying the efficacy of the drug delivery
4.	Khodaverdi et al. (2012)	Prepared in situ gelling matrices of thermosensitive triblock copolymers of ABA	–	Release rate of drug, copolymer concentration, and formulation microstructure by molecular weight, according to in vitro drug-release experiments. Emphasized that the system for controlled release of naltrexone-HCl and vitamin B12 is best suited to ABA copolymer in a PLA-to-PGA ratio of 5:1
5.	Lal and Datta (2015)	Recently prepared montmorillonite-PLGA (Mt-PLGA) nanocomposites scaled by using Mt-ATN units (ATN-03 and ATN-05) and PLGA	Double emulsion solvent evaporation method for water-in-oil-in-water system	Developed for the administration of atenolol (ATN) by sustained-release oral dosage

Table 13.6 PLGA-based nanocomposites used in therapy and as theranostic agents.

Author	Field of application	PLGA nano composites	Utilization
Fazio et al. (2015)	Cancer therapy	Inventor used a diblock copolymer of PEG–PLGA nanoplatform embedded with gold nanoparticles and SLB	Gold nanoparticles are able to absorb heat and this phenomenon of absorption is utilized in hyper- and photo-thermal therapy and drug delivery
Fang et al. (2015)	Cancer therapy	Synthesized microspheres of drug DOX-containing PLGA in Fe_3O_4 coating. (DOXMMS)	Results showed increased release of DOX from the microsphere after exposure to an AMF, resulting in the destruction of cancer cells. DOX-MMS treated 81.6% of viable 4T1 cells versus AMF exposure of 10% of treated viable cells
Saengruengrit et al. (2018)	Immunotherapy	Fe_3O_4/PLGA nanoparticles	PLGA nanoparticles coated with Fe_3O_4-encapsulated BSA were adopted by macrophages and dendritic cells of bone marrow after exposure to AMF
Stankovic et al. (2016)	Observed to be bacteriostatic against Gram-negative and Gram-positive bacteria and the yeast *Candida albicans*	Zn-oxide–PLGA nanoparticles and silver organic hybrid materials have been developed	Reported use of such nanoparticles in suppression of growth of microorganisms

Continued

Table 13.6 PLGA-based nanocomposites used in therapy and as theranostic agents.—cont'd

Author	Field of application	PLGA nano composites	Utilization
Takahashi et al. (2017)	Antibacterial activity	PLGA—silver nanoparticles' efficacy tested against *Staphylococcus epidermidis* biofilms which have an extracellular shield with a dense film of polymeric substances (EPS)	Drug-delivery system with high antibacterial activity, treating biofilm infections
Mehta et al. (2020)	Neurodegenerative disorders and cardiovascular diseases	Nanoceria—CNPs were encapsulated in PLGA MPs involving SOD and catalase	Proficient targeting of macrophages and shielding action was clearly observed
Bennewitz et al. (2011)	Cellular MR imaging	PLGA-encapsulated MnO nanocrystals	PLGA-MnO based nano composites have been used as an MRI-based cell tracking T_1 agent. When injected by I.V. route, the nanocomposite release Mn^{2+} so bright contrast was observed by T_1 weighted MRI images
Nkansah et al. (2011)	Tracking of cells on the basis of MRI	Encapsulating magnetite in PLGA nano/micro- particles	Best suited for clinical translation of cells (Pelaseyed et al., 2020)
Granot et al. (2014)	MRI-based cell tracking	Fe_3O_4-encapsulating PLGA NPs	Proved labeling efficiency
Lu et al. (2018)	PA/MRI dual modal tracking of tendon stem cells (TSCs)	Utilized PLGA MPs containing iron oxide	—

Lee et al. (2017)	Theranostic PLGA/INP composite	Conjugated PLGA with core magnetite, complexed with Ce6 and mPEG	Significant inhibition of the growth of tumors
Ye et al. (2014)	Cancer theranostic agents	Tailored chemotherapeutics in vesicles of PLGA containing SPIONs, Mn:ZnS QDs	PLGA-SPION-Mn:ZnS vesicles
Hao et al. (2015)	Cancer theranostics and X-ray imaging applications	PLGA nanoparticles designed with PEI involving Au-nanoshells and angiopep-2 with DTX	DTX-loaded PLGA@Au nanocomposites
Song et al. (2012)	PA image-guided photothermal therapy as favorable agents for translation at clinical level for forthcoming image-based cancer therapy	Proposed AuNRs—PLGA conjugation with gold	AuNRs@PEG/PLGA nanocomposites

13.4.5 Applications of PLGA composites with core–plasmonic NPs

Several representative studies offering dissimilar groupings of PLGA and plasmonic NPs, available in customized micro-, nano-, and macroscopic assemblies are discussed here (Table 13.7).

13.4.6 Applications of PLGA-nano/magnetic nanocomposites

Recent decades have seen the development of customized magnetic NPs (MNPs), which exhibit a specific reaction for use in the applied magnetics field. Magnetized nanoparticles have been employed as agents for various MRI applications since the 1990s (De Moura et al., 2020) (Table 13.8). Magnetic nanoparticles have been utilized to produce energy in the AMFs field, which is advantageous for controlled delivery in medicines as well as being applicable for reducing malignancies by magnetized hyperthermia (Vieira Rocha et al., 2020). Some MNPs also exhibit sensitivity patterns to influence acidic and basic environments and oxidation–reduction conditions.

Due to their applicable magnetic-physiochemical properties and simplicity of development, as seen in FeO nanoparticles, also called SPIONs, are mostly utilized in scaling of medicines at nano-level (Ribeiro et al., 2021; Zhang et al., 2011). They are comprised under 20 nm diameters crucially with supermagnetized involving all magnetic characteristics inside of it. In order to develop functional nanocomposites as therapeutic utility in diagnosis through MRI/PA (Zhang et al., 2020), a number of techniques have been devised to embed magnetized nanoparticles in PLGA NPs/MPs form.

13.4.7 Applications of other PLGA/inorganic-NP-based composites

Combinational PLGA polymeric composites have been used with inorganic nanoparticles such as Zn, Ce, C, Cu, and Ti but most medical applications are with HAps. PLGA–inorganic nanoparticulate composites when scaled-up using ZnO additionally provide optical, semiconductive, and catalytic features of inorganic Zn, and as a biocomposite it is biochemically stable, nontoxic, and medically used against microbes and both Gram-positive and Gream-negative bacteria (Lanao et al., 2013; Houchin and Topp, 2009; Cheng et al., 2007b; Tang and Dong, 2009) (Table 13.9).

Another targeted inorganic–PLGA composite is nanoceria (CeO_2-NPs), which scavenges ROS to regenerate the oxidative state under severe

Table 13.7 Applications of dDifferent PLGA—-Pplasmonic NPs in researched.

Investigator	PLGA—plasmonics	Size of nanocomposites	Method of preparation	Applications
Hao et al. (2015)	Reported synthesis of PLGA-loaded modified docetaxel with polyethyleneimine with a covering of gold nanoparticles in the presence of angiopep-2 which is a targeting peptide in glioma	Approx. 200 nm	Improved emulsification solvent evaporation method	As chemophotothermal agents for DTX + PTT drug detection; as an agent for X-ray imaging in the treatment of tumors
Song et al. (2012)	Developed plasmonic composite PLGA vesicles where gold nanorods (AuNRs) were embedded in the vesicle shell formed by PLGA, with PEG molecules extending to the interior and exterior of the vesicle, providing stability (PLGA/AuNRs)	Approx. 60 nm in size	Emulsification solvent evaporation method	Nanocomposites were used as theranostic agents
Topete et al. (2014)	Scaled PLGA nanocomposite embedded with DTX (doxorubicin) as an anticancer agent consistently covered with a porous-shell (BGNSH) which was activated by HAS-ISG and complex folic acid	125 nm approx. size	Nano-precipitation method	Reported composite used for extended-release pattern mapping and also in optical image contrasting by fluorescence characteristics

Continued

Table 13.7 Applications of dDifferent PLGA−-Pplasmonic NPs in researched.—cont'd

Investigator	PLGA−plasmonics	Size of nanocomposites	Method of preparation	Applications
Takahashi et al. (2017)	Synthesized composite decorated with silver in PLGA NPs form (Ag PLGA)	Mean 300 nm	ESD method	Utilized biologically in film infection as a working delivery system for drugs and having antimicrobial action due to the presence of silver
Lee et al. (2017)	Reported development of chemically coated PLGA with gold nanoscaffolds with nanofiber composition	30 nm size	Electrospinning technique	Composite design is used as controlled-release scaffolds in regeneration of bone/tissue
Almajhdi et al. (2014)	Reported activity of fibers used in different percentages to develop a nanofiber sheet of PLGA with silver nanoparticles at a size of 5−10 nm	Diameter of sheet around 100−200 nm	Electrospinning technique	Nanosheet of fibers used for delivery of anticancer agents as well as antibiotics in tissue/bone scaffolding

Table 13.8 Listed PLGA—magnetic nanocomposites used in various applications.

Investigator	Research	Size of composite	Method of preparation	Applications
Wang et al. (2016)	Developed composite nanoparticles were coated in PLGA embedded with SPIONs while the core was filled with a liquid phase	Nonuniform size of approximately 900 nm microcapsules	ESE double technique	Developed composite as theranostic agents for MRI and ultrasound analysis and also in detection of efficiency in high-intensity focused ultrasound
Schleich et al. (2013)	Reported scale-up of PLGA-PEGylated-NPs embedded with SPIONs with PTX/DOX drug	Two sizes available reported as 250 and 290 nm	Coprecipitation method of iron salts in an alkaline medium	MRI contrasting and drug delivery studies
Ruggiero et al. (2016)	Reported development of PLGA NPs embedded with Fe_3O_4 NPs and PTX	Magnetized core sizing around 15—20 nm and resultant size was 120—160 nm	Coprecipitation	Drug = release monitoring in triggered magnetic hyperthermia and as a contrast agent in MRI
Nkansah et al. (2011)	Composite fabrication was done at the water phase with varying % of PVA weight by volume as PLGA-MPS/NPS	—	Coprecipitation/ homogenization	—

Continued

Table 13.8 Listed PLGA—magnetic nanocomposites used in various applications.—cont'd

Investigator	Research	Size of composite	Method of preparation	Applications
Lee et al. (2017)	Complexed multifunction PLGA —core magnetite	Approximate size of 2.4 nm	Steglich esterification method	Applied for prompt drug release in magnetic hyperthermia and thermal chemo treatment
Chen et al. (2016b)	Water-in-oil-in-water emulsion, with added PLGA-MNPs in organic side	—	Double emulsion method	An emulsion form act as the drug-delivery vehicle of theranostic agents for MRI dual-mode imaging
Saengruengrit et al. (2018)	Magnetized core—shell PLGA-SPIONs embedded nano-scaffolds having BSA drug in the core's hydrophilic composition	500 and 300 nm sizing scaled-up	Classic thermal decomposition method	The composite's applicability as contrast enhancers in T1-MRI noted antigen delivery to excite adaptive immune reaction when in contact with a magnetic field
Nkansah et al. (2011)	PLGA-NPs/MPs-MnO nanosized crystals form (pH-sensitive)	15—20 nm size	Single ESE with minor modifications	System is used in MRI imaging at cellular and molecular levels

Table 13.9 Inorganic nanoparticle-based PLGA nanocomposites with the method of preparation and applications.

Investigator	Preparation of PLGA composites	Method	Resultant size	Applications
Markovic et al. (2016)	Synthesized ZnO-loaded PLGA inorganic nanoparticles	Modified synthesis using assisted microwave (solvent/nonsolvent method)	Approximately 200 nm uniform spherical particles	Transporting drug and bacterial infection treatment
Mehta (1995)	Developed microparticles of PLGA-nanoceria-catalase (as an enzyme scavenging)	One-stage double emulsion method	800 nm average diameter	PLGA microcomposites reduce oxidative stress and protect cells
Singh et al. (2012)	Developed microparticles of nanoceria with PLGA (CNP-PLGA)	Standard double emulsion	Mean size of 60 μm	Useful in attenuating damage by bacterial infection and radiation
Mikael et al. (2014)	Reported fabrication of microspheres of PLGA-MWCNT composite	Single emulsion method (O/W)	Size range of 425−600 μm	PLGA-MWCNTs are mechanically strong and biodegradable microspheres for bone-tissue engineering, rounded using the thermal-sintering technique
Ye et al. (2014)	Developed PLGA nanovesicles by encapsulating manganese-zinc sulfide (Mn:ZnS) and quantum dots with busulfan (PLGA-SPION-Mn:ZnS-QDs-busulfan)	Thermal decomposition nucleation-doping strategy	–	Cancer treatment; QDs used in optical imaging, SPIONs in MRI, and Mn and ZnS both used as agents for inorganic imaging

Continued

Table 13.9 Inorganic nanoparticle-based PLGA nanocomposites with the method of preparation and applications.—cont'd

Investigator	Preparation of PLGA composites	Method	Resultant size	Applications
Li et al. (2001)	Finalized nanocomposite core–shell with PLGA-embedded silver/gold nanoparticles (PLGA@Ag/AuNPs)	Stabilizer-free technique	Spherical shaped, nearly 200 nm	SERS, enhanced signaling in surface-enhanced Raman spectroscopy analysis by nanoshell particles
Pelaseyed et al. (2020)	Developed scaffolds in different ratios of commercialized nano-PLGA-TiO_2 nanoparticles	Resultant microporous design developed by a process of air–liquid foaming in which bubbles of gas were created using nucleation	–	These scaffolds were best for regenerated bone engineering
Sheikh et al. (2015)	Scaffolds prepared using composites with hybridization of PLGA-fibroin silk-HAp scaffolds	–	180–250 mm	Regenerative engineering
Selvaraju et al. (2018)	Processed PLGA-collagen with inorganic HAp nanoparticles	–	Modified chemical precipitation method	HAp facilitates PLGA composite's physicochemical properties and stability for molding into porous scaffolds applied for bone and tissue regeneration

Haider et al. (2015)	Developed scaffolds of PLGA hybrid fiber in nano-sizing, comprises CuO-NPs	Electrospinning method	Mean span was 550 nm	Investigated CuO-NPs for antibacterial activity
Wang et al. (2017)	Prepared double-coated PLGA nanoparticles (primary coat of CTAB with secondary coat of manganese dioxide nanofilm at ultrascale) embedded with DTX-AuNRs (PLGA-AuNRs/DTX@MnO_2 NPs)	Simple ESE method	Mean size of 280 nm	Proposed application of nanocomposites in MRI-dual modeling, diagnosis for Mn and Au detection by CT X-ray and utilities as theranostic and diagnostically in RF-induced hyperthermia chemotherapy

biological conditions with reusable antioxidative activity which reduces the activity of the superoxide dismutase and initiates both superoxide radicals and hydrogen peroxide's conversion with the resultant availability of water and oxygen (Luo et al., 2019).

PLGA-CNT scaffolds have been scaled due to their enhanced surface area, low density, and higher mechanical integration. Nanomaterials developed as CNTs make ideal scaffolds such as CuO nanoparticles providing greater research benefits optically, electrically, and medicinally due to Cu^{2+} ions in metal form (Kuang et al., 2016). The scaffolds design are used as nanoscale medicine as antimicrobial by releasing of copper ions (Ahamed et al., 2014).

Engineering for bone implant fabrication with resultant tunable biocompatibility and superior mechanical properties has resulted in the use of titanium dioxide (TiO_2) in scaffold fabrication for bone implants enabling excellent physical and biological properties, for example resistance due to corrosion, reduced weight, nontoxicity, and increased cell proliferation and adhesion (Chen et al., 2016a).

The most important naturally bioactive and powerful are inorganic HAp NPs, the nanostructure of which is extensively utilized in combination with PLGA as a component for the fabrication of bone scaffolds with greater biocompatibility, decreased immunogenicity, etc. (Furukawa et al., 2000).

13.5 Conclusions and future prospects

At both the industrial and research scales, PLGA composites have been created for biomedical applications. The varieties of inorganic hybrid nanoparticles/composites based on PLGA in the present study show the adaptability of this family of materials, which spans the nano, micro, and macro ranges. The physicochemical characteristics, biocompatibility, shape, and multi-functionality of these PLGA hybrids have demonstrated their importance. The majority of the discussed hybrid materials have easy-to-follow synthesis methods, which gives them significant benefits over other types because the follow-up scaling can be quickly modified for a range of applications. In general, increased hydrophilicity, chemical collaboration between the hydrolytic functional groups, and decreased crystalline behaviors of the materials can speed up PLGA degradation and release of drug(s). To adjust drug release and degradation mechanisms for the desired application, all of these parameters should be strictly monitored and

considered. Hence it is advised to customize the amorphous polymer(s) with increased hydrophilicity for short-term release requirements of up to a month.

Numerous studies have shown that PLGA can be simply formulated as a drug-transporting device at all scales as micro/nano-spheres, and even as implants of millimeter size. PLGA can be used in a variety of drugs, peptides, and proteins, and can be transported over different ranges within a specified timeframe using a variety of delivery routes.

The final uses of PLGA are frequently determined by the inorganic components that will be mixed with it, as well as by the organic therapeutic agents such as drugs, proteins, peptides, vaccines, and DNA loaded on the PLGA platform. To avoid the uncomfortable surgical insertion of implants, PLGA particles such as micro/nanospheres and micro/nanocapsules can be used for controlled delivery as injectable, biodegradable, and biocompatible forms. PLGA composites are simple to produce, made in a variety of shape and sizes, with biocompatibility, drug compatibility, acceptable biodegradation kinetics, and superior mechanical qualities.

Multiple applications can be combined using multifunctional PLGA-based composite materials to improve diagnostic and therapeutic outcomes. A significant advancement in the field of biomedicine, PLGA materials and nanocomposites hold considerable potential for future advancements in the tissues engineering, therapeutics, theranostic, and diagnostic fields.

Abbreviations

%EE	% Encapsulation efficiency
AgNPs	Silver nanoparticles
AMF	Altering magnetic field
AuNPs	Gold nanoparticles
AuNRs	Gold nanorods
BPLP	Biodegradable photoluminescent polyester
CAs	Contrast agents
CNPs	Cerium oxide nanoparticles
CNTs	Carbon nanotubes
CTAB	Cetyl-trimethyl-ammonium bromide
DCM	Dichloromethane
DOX	Doxorubicin
DTX	Docetaxel
EMA	European Medicines Agency
ESD	Emulsification solvent diffusion

ESE	Emulsification solvent evaporation
FDA	U.S. Food & Drug Administration
GSH	Glutathione
HAp	Hydroxyapatite
HIFU	High-intensity focused ultrasound
INPs	Inorganic nanoparticles
MRI	Magnetic resonance imaging
MWCNTs	Multiwalled carbon nanotubes
PDT	Photodynamic therapy
PLGA	Poly-lactic-co-glycolic acid
PTT	Photothermal therapy
SOD	Superoxide dismutase
SPIONs	Superparamagnetic iron oxide nanoparticles
SPR	Surface plasmon resonance
W/O/W	Water-in-oil-in-water

Conflicts of interest

The authors declare that there is no conflict of interest regarding the publication of this chapter.

References

Ahamed, M., Alhadlaq, H.A., Khan, M.A.M., Karuppiah, P., Al-Dhabi, N.A., 2014. Synthesis, characterization, and antimicrobial activity of copper oxide nanoparticles. J. Nanomater. 2014, 637858.

Alexis, F., 2005. Factors affecting the degradation and drug-release mechanism of poly (lactic acid) and poly [(lactic acid)-co-(glycolic acid)]. Polym. Int. 54, 36–46.

Allahyari, M., Mohit, E., 2016. Peptide/protein vaccine delivery system based on PLGA particles. Hum. Vaccines Immunother. 12, 806–828.

Allison, S.D., 2008. Effect of structural relaxation on the preparation and drug release behavior of poly (lactic-co-glycolic) acid microparticle drug delivery systems. J. Pharmaceut. Sci. 97, 2022–2035.

Almajhdi, F.N., Fouad, H., Khalil, K.A., Awad, H.M., Mohamed, S.H.S., Elsarnagawy, T., Albarrag, A.M., Al-Jassir, F.F., Abdo, H.S., 2014. In-vitro anticancer and antimicrobial activities of PLGA/silver nanofiber composites prepared by electrospinning. J. Mater. Sci. Mater. Med. 25, 1045–1053.

Anderson, J.M., Shive, M.S., 1997. Biodegradation and biocompatibility of PLA and PLGA microspheres. Adv. Drug Deliv. Rev. 28, 5–24.

Anton, N., Benoit, J.P., Saulnier, P., 2008. Design and production of nanoparticles formulated from nano-emulsion templates – a review. J. Contr. Release 128, 185–199.

Araujo, A., Botelho, G., Oliveira, M., Machado, A.V., 2014. Influence of clay organic modifier on the thermal-stability of PLA based Nanocomposites. Appl. Clay Sci. 88–89, 144–150.

Ardjomandi, N., Henrich, A., Huth, J., et al., 2015. Coating of β-tricalcium phosphate scaffolds-a comparison between graphene oxide and poly-lactic-co-glycolic acid. Biomed. Mater. 10 (04), 45018.

Arpagaus, C., 2019. PLA/PLGA nanoparticles prepared by nano spray drying. J. Pharm. Investig. 49, 405–426.

Arvizo, R.R., Bhattacharyya, S., Kudgus, R.A., Giri, K., Bhattacharya, R., Mukherjee, P., 2012. Intrinsic therapeutic applications of noble metal nanoparticles: past, present and future. Chem. Soc. Rev. 41, 2943–2970.

Bakhshalian, N., Nowzari, H., Ahn, K.M., Arjmandi, B.H., 2014. Demineralized dentin matrix and bone graft: a review of literature. J. West Soc. Periodontol. Periodontal. Abstr. 62 (02), 35–38.

Bennewitz, M.F., Lobo, T.L., Nkansah, M.K., Ulas, G., Brudvig, G.W., Shapiro, E.M., 2011. Biocompatible and PH-sensitive PLGA encapsulated MnO nanocrystals for molecular and cellular MRI. ACS Nano 5, 3438–3446.

Bilati, U., Allémann, E., Doelker, E., 2005a. Poly-(D, L-lactide-co-glycolide) protein-loaded nanoparticles prepared by the double emulsion method-processing and formulation issues for enhanced entrapment efficiency. J. Microencapsul. 22 (2), 205–214.

Bilati, U., Allémann, E., Doelker, E., 2005b. Development of a nanoprecipitation method intended for the entrapment of hydrophilic drugs into nanoparticles. Eur. J. Pharmaceut. Sci. 24, 67–75.

Bouissou, C., Rouse, J.J., Price, R., Van der walle, C.F., 2006. The influence of surfactant on PLGA microsphere glass transition and water sorption: remodeling the surface morphology to attenuate the burst release. Pharm. Res. 23, 1295–1305.

Castelli, F., Conti, B., Conte, U., Puglisi, G., 1996. Effect of molecular weight and storage times on tolmetin release from poly-lactide microspheres to lipid model membrane. A calorimetric study. J. Contr. Release 40, 277–284.

Chen, Z.M., Cong, J., Hu, Z., Yang, Chen, Z., 2016a. Preparation of functionalized TiO2 nanotube arrays and their applications. Sci. Adv. Mater. 8 (6), 1231–1241.

Chen, Z., Zhang, A., Hu, J., Wang, X., Yang, Z., 2016b. Electrospun nanofibers for cancer diagnosis and therapy. Biomater. Sci. 04 (06), 922–932.

Cheng, J., Teply, B.A., Sherifi, I., Sung, J., Luther, G., Gu, F.X., Levy-Nissenbaum, E., Radovic-Moreno, A.F., Langer, R., Farokhzad, O.C., 2007a. Formulation of functionalized PLGA-PEG Nanoparticles for in vivo targeted drug delivery. Biomaterials 28, 869–876.

Cheng, J., Teply, B.A., Sherifi, I., Sung, J., Luther, G., Gu, F.X., Levy Nissenbaum, E., Radovic-Moreno, A.F., Langer, R., Farokhzad, O.C., 2007b. Formulation of functionalized PLGA-PEG nanoparticles for in vivo targeted drug delivery. Biomaterials 28, 869–876.

Choi, S.H., Park, T.G., 2002. Synthesis and characterization of elastic PLGA/PCL/PLGA tri-block copolymers. J. Biomater. Sci. Polym. Ed. 13, 1163–1173.

Choi, Y., Joo, J.R., Hong, A., Park, J.S., 2011. Development of drug-loaded PLGA microparticles with different release patterns for prolonged drug delivery. Bull. Kor. Chem. Soc. 32, 867–872.

Crotts, G., Park, T.G., 1998. Protein delivery from poly (lactic-co-glycolic acid) biodegradable microspheres: release kinetics and stability issues. J. Microencapsul. 15, 699–713.

Danhier, F., Ansorena, E., Silva, J.M., Coco, R., Le, B.A., Préat, V., 2012. PLGA-based nanoparticles: an overview of biomedical applications. J. Contr. Release 161, 505–522.

Davachi, S.M., Kaffashi, B., Zamanian, A., Torabinejad, B., Ziaeirad, Z., 2016. Investigating composite systems based on poly l-lactide and poly l-lactide/triclosan nanoparticles for tissue engineering and medical applications. Mater. Sci. Eng. C 58, 294–309.

Davies, O.R., Lewis, A.L., Whitaker, M.J., Tai, H., Shakesheff, K.M., Howdle, S.M., 2008. Applications of supercritical CO_2 in the fabrication of polymer systems for drug delivery and tissue engineering. Adv. Drug Deliv. Rev. 60, 373–387.

De Moura, C.L., Gallo, J., García-Hevia, L., Pessoa, O.D.L., Ricardo, N.M.P.S., Bañobre-López, M., 2020. Magnetic hybrid wax nanocomposites as externally controlled theranostic vehicles: high MRI enhancement and synergistic magnetically assisted thermo/chemo therapy. Chem. Eur J. 26, 4531–4538.

Dechy, C.O., Martin, V.B., Bourissou, D., 2004. Controlled ring-opening polymerization of lactide and glycolide. Chem. Rev. 104, 6147–6176.

Dhandayuthapani, B., Yoshida, Y., Maekawa, T., Kumar, D.S., 2011. Polymeric scaffolds in tissue engineering application: a review. Int. J. Polym. Sci., 290602

Dimitriou, R., Jones, E., McGonagle, D., Giannoudis, P.V., 2011. Bone regeneration: current concepts and future directions. BMC Med. 09, 66.

Ding, D., Zhu, Q., 2018. Recent advances of PLGA micro/nanoparticles for the delivery of biomacromolecular therapeutics. Mater. Sci. Eng. C 92, 1041–1060.

Durán, N., Durán, M., de Jesus, M.B., Seabra, A.B., Fávaro, W.J., Nakazato, G., 2016. Silver nanoparticles: a new view on mechanistic aspects on antimicrobial activity. Nanomed. Nanotechnol. Biol. Med. 12, 789–799.

D'Mello, S.R., Das, S.K., Das, N.G., 2006. Polymeric nanoparticles for small-molecule drugs: biodegradation of polymers and fabrication of nanoparticles. In: Drug Delivery Nanoparticles Formulation and Characterization. Informa Healthcare, Indianapolis, IN, pp. 16–30.

Esmaeili, F., Atyabi, F., Dinarvand, R., 2007. Preparation of PLGA nanoparticles using TPGS in the spontaneous emulsification solvent diffusion method. J. Exp. Nanosci. 2, 183–192.

Esmaeili, F., Ghahremani, M.H., Esmaeili, B., Khoshayand, M.R., Atyabi, F., Dinarvand, R., 2008. PLGA nanoparticles of different surface properties: preparation and evaluation of their body distribution. Int. J. Pharm. 349, 249–255.

Fang, K., Song, L., Gu, Z., Yang, F., Zhang, Y., Gu, N., 2015. Magnetic field activated drug release system based on magnetic PLGA microspheres for chemo-thermal therapy. Colloids Surf. B Biointerfaces 136, 712–720.

Fazio, E., Scala, A., Grimato, S., Ridolfo, A., Grassi, G., Neri, F., 2015. Laser light triggered smart release of silibinin from a PEGylated-PLGA gold nanocomposite. J. Mater. Chem. B 3, 9023–9032.

Frank, A., Rath, S.K., Venkatraman, S.S., 2005. Controlled release from bioerodible polymers: effect of drug type and polymer composition. J. Contr. Release 102, 333–344.

Freitas, S., Merkle, H.P., Gander, B., 2005. Microencapsulation by solvent extraction/evaporation: reviewing the state of the art of microsphere preparation process technology. J. Contr. Release 102, 313–332.

Furukawa, T., Matsusue, Y., Yasunaga, T., et al., 2000. Histomorphometric study on high-strength hydroxyapatite/poly(L-lactide) composite rods for internal fixation of bone fractures. J. Biomed. Mater. Res. 50 (3), 410–419.

Gallo, J., Alam, I.S., Lavdas, I., Wylezinska-Arridge, M., Aboagye, E.O., Long, N.J., 2014. RGD-targeted MnO nanoparticles as T1 contrast agents for cancer imaging-the effect of PEG length in vivo. J. Mater. Chem. B 2, 868–876.

Garner, J., Skidmore, S., Park, H., Park, K., Choi, S., Wang, Y.A., 2015. Protocol for assay of poly (lactide-co-glycolide) in clinical products. Int. J. Pharm. 495, 87–92.

Gavini, E., Chetoni, P., Cossu, M., Alvarez, M.G., Saettone, M.F., Giunchedi, P., 2004. PLGA microspheres for the ocular delivery of a peptide drug, vancomycin using emulsification/spray-drying as the preparation method: in vitro/in vivo studies. Eur. J. Pharm. Biopharm. 57, 207–212.

Gentile, P., Chiono, V., Carmagnola, I., Hatton, P.V., 2014. An overview of poly (lactic-co-glycolic) acid (PLGA)-based biomaterials for bone tissue engineering. Int. J. Mol. Sci. 15, 3640–3659.

Ghitman, J., Biru, E.I., Stan, R., Iovu, H., 2020. Review of hybrid PLGA nanoparticles: future of smart drug delivery and theranostics medicine. Mater. Des. 193, 108805.
Go, E.J., Kang, E.Y., Lee, S.K., Park, S., Kim, J.H., Park, W., Kim, I.H., Choi, B., Han, D.K., 2019. An osteoconductive PLGA scaffold with bioactive -TCP and anti-inflammatory Mg(OH)2 to improve: in vivo bone regeneration. Biomater. Sci. 8, 937−948.
Govender, T., Stolnik, S., Garnett, M.C., Illum, L., Davis, S.S., 1999. PLGA nanoparticles prepared by nanoprecipitation: drug loading and release studies of a water soluble drug. J. Contr. Release 57 (02), 171−185.
Granot, D., Nkansah, M.K., Bennewitz, M.F., Tang, K.S., Markakis, E.A., Shapiro, E.M., 2014. Clinically viable magnetic poly (lactide-co-glycolide) particles for MRI-based cell tracking. Magn. Reson. Med. 71, 1238−1250.
Grayson, A.C.R., Cima, M.J., Langer, R., 2005. Size and temperature effects on poly (lactic-co-glycolic acid) degradation and microreservoir device performance. Biomaterials 26, 2137−2145.
Grizzi, I., Garreau, H., Li, S., Vert, M., 1995. Hydrolytic degradation of devices based on poly (DL-lactic acid) size-dependence. Biomaterials 16, 305−311.
Haider, A., Kwak, S., Gupta, K.C., Kang, I.K., 2015. Antibacterial activity and cytocompatibility of PLGA/CuO hybrid nanofiber scaffolds prepared by electrospinning. J. Nanomater. 2015, 832762.
Hans, M.L., Lowman, A.M., 2002. Biodegradable nanoparticles for drug delivery and targeting. Curr. Opin. Solid State Mater. Sci. 6, 319−327.
Hao, Y., Zhang, B., Zheng, C., Ji, R., Ren, X., Guo, F., Sun, S., Shi, J., Zhang, H., Zhang, Z., 2015. The tumor-targeting core-shell structured DTX-loaded PLGA@Au nanoparticles for C photothermal therapy and X-ray imaging. J. Contr. Release 220, 545−555.
Hasegawa, S., Ishii, S., Tamura, J., et al., 2006. A 5-7 year in vivo study of high-strength hydroxyapatite/poly (L-lactide) composite rods for the internal fixation of bone fractures. Biomaterials 27 (08), 1327−1332.
Holderegger, C., Schmidlin, P.R., Weber, F.E., Mohn, D., 2015. Preclinical in vivo performance of novel biodegradable, electrospun poly(lactic acid) and poly(lactic-co-glycolic acid) nanocomposites: a review. Materials 8 (8), 4912−4931.
Holy, C., 1999. In vitro degradation of a novel poly(lactide-co-glycolide) 75/25 foam. Biomaterials 20, 1177−1185.
Houchin, M.L., Topp, E.M., 2009. Physical properties of PLGA films during polymer degradation. J. Appl. Polym. Sci. 114, 2848−2854.
Hua, F.J., Kim, G.E., Lee, J.D., Son, Y.K., Lee, D.S., 2002. Macroporous poly (L-lactide) scaffold 1. Preparation of a macroporous scaffold by liquid−liquid phase separation of a PLLA-dioxane-water system. J. Biomed. Mater. Res. 63, 161−167.
Jain, R.A., 2000. The manufacturing techniques of various drug loaded biodegradable poly(lactide-coglycolide) (PLGA) devices. Biomaterials 21, 2475−2490.
Jo, H., Hong, M., Shim, J.B., et al., 2015. The role of demineralized bone particle in a PLGA scaffold designed to create a media equivalent for a tissue engineered blood vessel. Macromol. Res. 23 (11), 986−993.
Khodaverdi, E.F., Tekie, S.M., Mohajeri, S.A., Ganji, F., Zohuri, G., Hadizadeh, F., 2012. Preparation and investigation of sustained drug delivery systems using an injectable, thermosensitive, in-situ forming hydrogel composed of PLGA-PEG-PLGA. AAPS PharmSciTech 13 (02), 590−600.
Kim, D.H., Martin, D.C., 2006. Sustained release of dexamethasone from hydrophilic matrices using PLGA nanoparticles for neural drug delivery. Biomaterials 27 (15), 3031−3037.

Kissel, T., Li, Y., Unger, F., 2002. ABA-triblock copolymer from biodegradable polyester A-blocks and hydrophilic poly(ethylene oxide) B-blocks as a candidate for in situ forming hydrogel delivery systems for proteins. Adv. Drug Deliv. Rev. 54 (1), 99–134.

Kranz, H., Ubrich, N., Maincent, P., Bodmeier, R., 2000. Physicomechanical properties of biodegradable poly(D,L-lactide) and poly(D,L-lactide-co-glycolide) films in the dry and wet states. J. Pharmaceut. Sci. 89, 1558–1566.

Kuang, T., Chang, L., Chen, F., Sheng, Y., Fu, D., Peng, X., 2016. Facile preparation of lightweight high-strength biodegradable polymer/multi-walled carbon nanotubes nanocomposite foams for electromagnetic interference shielding. Carbon 105, 305–313.

Kumari, A., Yadav, S.K., Yadav, S.C., 2010. Biodegradable polymeric nanoparticles based drug delivery systems. Colloids Surf. B Biointerfaces 75 (01), 1–18.

Lal, S., Datta, M., 2015. In vitro prolonged gastric residence and sustained release of atenolol using novel clay polymer nanocomposite. Appl. Clay Sci. 114, 412–421.

Lanao, R.P.F., Jonker, A.M., Wolke, J.G.C., Jansen, J.A., van Hest, J.C.M., Leeuwenburgh, S.C.G., 2013. Physicochemical properties and applications of poly (lactic-co-glycolic acid) for use in bone regeneration. Tissue Eng. B Rev. 19 (4), 380–390.

Lee, D., Heo, D.N., Kim, H.J., Ko, W.K., Lee, S.J., Heo, M., Bang, J.B., Lee, J.B., Hwang, D.S., Do, S.H., 2016. Inhibition of osteoclast differentiation and bone resorption by bisphosphonate-conjugated gold nanoparticles. Sci. Rep. 6, 27336.

Lee, D., Heo, D.N., Lee, S.J., Heo, M., Kim, J., Choi, S., Park, H.K., Park, Y.G., Lim, H.N., Kwon, I.K., 2017. Poly(lactide-co-glycolide) nanofibrous scaffolds chemically coated with gold-nanoparticles as osteoinductive agents for osteogenesis. Appl. Surf. Sci. 432, 300–307.

Lee, S.K., Han, C.M., Park, W., Kim, I.H., Joung, Y.K., Han, D.K., 2019. Synergistically enhanced osteoconductivity and anti-inflammation of PLGA/TCP/Mg(OH)2 composite for orthopedic applications. Mater. Sci. Eng. C 94, 65–75.

Leroux, J.C., Allemann, E., De Jaeghere, F., Doelker, E., Gurny, R., 1996. Biodegradable nanoparticles from sustained release formulations to improved site specific drug delivery. J. Contr. Release 39 (2–3), 339–350.

Li, H., Chang, J., 2005. pH-compensation effect of bioactive inorganic fillers on the degradation of PLGA. Compos. Sci. Technol. 65 (14), 2226–2232.

Li, Y., Pei, Y., Zhang, X., Gu, Z., Zhou, Z., Yuan, W., Zhou, J., Zhu, J., Gao, X., 2001. PEGylated PLGA nanoparticles as protein carriers: synthesis, preparation and biodistribution in rats. J. Contr. Release 71, 203–211.

Lü, J.M., Wang, X., Marin-Muller, C., Wang, H., Lin, P.H., Yao, Q., Chen, C., 2009. Current advances in research and clinical applications of PLGA-based nanotechnology. Expert Rev. Mol. Diagn. 9, 325–341.

Lu, W., Ji, K., Kirkham, J., et al., 2014. Bone tissue engineering by using a combination of polymer/bioglass composites with human adipose-derived stem cells. Cell Tissue Res. 356 (01), 97–107.

Lu, M., Cheng, X., Jiang, J., Li, T., Zhang, Z., Tsauo, C., Liu, Y., Wang, Z., 2018. Dual-modal photoacoustic and magnetic resonance tracking of tendon stem cells with PLGA/iron oxide microparticles in vitro. PLoS One 13, e0193362.

Luo, H., Zhang, Y., Gan, D., Yang, Z., Ao, H., Zhang, Q., Yao, F., Wan, Y., 2019. Incorporation of hydroxyapatite into nanofibrous PLGA scaffold towards improved breast cancer cell behavior. Mater. Chem. Phys. 226, 177–183.

Makadia, H.K., Siegel, S.J., 2011. Poly lactic-co-glycolic acid (PLGA) as biodegradable controlled drug delivery carrier. Polymers 3, 1377–1397.

Maquet, V., Boccaccini, A.R., Pravata, L., Notingher, I., Jerome, R., 2003. Preparation, characterization, and in vitro degradation of bioresorbable and bioactive composites based on Bioglass-filled polylactide foams. J. Biomed. Mater. Res. A 66 (2), 335–346.

Markovic, S., Rajic, V., Stankovic, A., Veselinovic, L., Beloševic-C, A.J., Batalovic, K., Abazovic, N., Škapin, S.D., Uskokovic, D., 2016. Effect of PEO molecular weight on sunlight induced photocatalytic activity of ZnO/PEO composites. Sol. Energy 127, 124–135.

Martin, O., Averous, L., 2001. Poly (lactic acid): plasticization and properties of biodegradable multiphase systems. Polymer 42 (14), 6209–6219.

Martou, G., Antonyshyn, O.M., 2011. Advances in surgical approaches to the upper facial skeleton. Curr. Opin. Otolaryngol. Head Neck Surg. 19, 242–247.

Mehta, R., 1995. The potential for the use of cell proliferation and oncogene expression as intermediate markers during liver carcinogenesis. Cancer Lett. 93, 85–102.

Mehta, A., Scammon, B., Shrake, K., Bredikhin, M., Gil, D., Shekunova, T., Baranchikov, A., Ivanov, V., Reukov, V., 2020. Nanoceria: metabolic interactions and delivery through PLGA-encapsulation. Mater. Sci. Eng. C 114, 111003.

Meikle, S.T., Piñeiro, Y., Bañobre López, M., Rivas, J., Santin, M., 2016. Surface functionalization superparamagnetic nanoparticles conjugated with thermoresponsive poly(epsilon-lysine) dendrons tethered with carboxybetaine for the mild hyperthermia-controlled delivery of VEGF. Acta Biomater. 40, 235–242.

Mikael, P.E., Amini, A.R., Basu, J., Arellano-Jimenez, M.J., Laurencin, C.T., Sanders, M.M., Carter, C.B., Nukavarapu, S.P., 2014. Functionalized carbon nanotube reinforced scaffolds for bone regenerative engineering: fabrication, in vitro and in vivo evaluation. Biomed. Mater. 9, 1–13.

Miladi, K., Sfar, S., Fessi, H., Elaissari, A., 2016. Nanoprecipitation process: from particle preparation to in vivo applications. In: Polymer Nanoparticles for Nanomedicines. Springer International Publishing, Berlin/Heidelberg, pp. 17–53.

Mir, M., Ahmed, N., Rehman, A.U., 2017. Recent applications of PLGA based nanostructures in drug delivery. Colloids Surf. B Biointerfaces 159, 217–231.

Mohamed, F., van der Walle, C.F., 2008. Engineering biodegradable polyester particles with specific drug targeting and drug release properties. J. Pharmaceut. Sci. 97, 71–87.

Morales-Cruz, M., Flores-Fernández, G.M., Morales-Cruz, M., Orellano, E.A., Rodriguez-Martinez, J.A., Ruiz, M., Griebenow, K., 2012. Two-step nanoprecipitation for the production of protein-loaded PLGA nanospheres. Results Pharma. Sci 2, 79–85.

Mundargi, R.C., Babu, V.R., Rangaswamy, V., Patel, P., Aminabhavi, T.M., 2008a. Nano/micro technologies for delivering macromolecular therapeutics using poly (D, L-lactide-coglycolide) and its derivatives. J. Contr. Release 125 (3), 193–209.

Mundargi, R., Babu, V., Rangaswamy, V., Patel, P., Aminabhavi, T., 2008b. Nano/micro technologies for delivering macromolecular therapeutics using poly(D,L-lactide-co-glycolide) and its derivatives. J. Contr. Release 125, 193–209.

Mura, S., Hillaireau, H., Nicolas, J., Le, D.B., Gueutin, C., Zanna, S., Tsapis, N., Fattal, E., 2011. Influence of surface charge on the potential toxicity of PLGA nanoparticles towards Calu-3 cells. Int. J. Nanomed. 6, 2591–2605.

Murakami, H., Kobayashi, M., Takeuchi, H., Kawashima, Y., 1999. Preparation of poly (D, L-lactide-co-glycolide) nanoparticles by modified spontaneous emulsification solvent diffusion method. Int. J. Pharm. 187, 143–152.

Nair, L.S., Laurencin, C.T., 2007. Biodegradable polymers as biomaterials. Prog. Polym. Sci. 32, m762–m798.

Nampoothiri, K.M., Nair, N.R., John, R.P., 2010. An overview of the recent developments in polylactide (PLA) research. Bioresour. Technol. 101 (22), 8493–8501.

Nie, H., Lee, L.Y., Tong, H., Wang, C.H., 2008. PLGA/Chitosan composites from a combination of spray drying and supercritical fluid Foaming techniques: new carriers for DNA delivery. J. Contr. Release 129, 207–214.

Nijenhuis, A.J., Colstee, E., Grijpma, D.W., Pennings, A.J., 1996. High molecular weight poly(L-lactide) and poly(ethylene oxide) blends: thermal characterization and physical properties. Polymer 37 (26), 5849–5857.

Nkansah, M.K., Thakral, D., Shapiro, E.M., 2011. Magnetic poly (lactide-co-glycolide) (PLGA) and cellulose particles for MRI-based cell tracking. Magn. Reson. Med. 65, 1776–1785.

Otsuka, Y., Nagasaki, Kataoka, K., 2003. PEGylated nanoparticles for biological and pharmaceutical applications. Adv. Drug Deliv. Rev. 55 (03), 403–419.

Panagi, Z., Beletsi, A., Evangelatos, G., Livaniou, E., Ithakissios, D.S., Avgoustakis, K., 2001. Effect of dose on the biodistribution and pharmacokinetics of PLGA and PLGA-mPEG nanoparticles. Int. J. Pharm. 221, 143–152.

Park, T.G., 1994. Degradation of poly (D, L-lactic acid) microspheres: effect of molecular weight. J. Contr. Release 30, 161–173.

Park, T.G., 1995. Degradation of poly (lactic- co-glycolic acid) microspheres: effect of copolymer composition. Biomaterials 16, 1123–1130.

Passerini, N., Craig, D.Q.M., 2001. An investigation into the effects of residual water on the glass transition temperature of polylactide microspheres using modulated temperature DSC. J. Contr. Release 73, 111–115.

Pelaseyed, S.S., Madaah Hosseini, H.R., Samadikuchaksaraei, A., 2020. A novel pathway to produce biodegradable and bioactive PLGA/TiO_2 nanocomposite scaffolds for tissue engineering: air-liquid foaming. J. Biomed. Mater. Res. 108, 1390–1407.

Pinto, A.M., Cabral, J., Tanaka, D.A.P., Mendes, A.M., Magalhaes, F.D., 2013. Effect of incorporation of graphene oxide and graphene nanoplatelets on mechanical and gas permeability properties of poly (lactic acid) films. Polym. Int. 62 (1), 33–40.

Qi, F., Wu, J., Li, H., Ma, G., 2019. Recent research and development of PLGA/PLA microspheres/nanoparticles: a review in scientific and industrial aspects. Front. Chem. Sci. Eng. 13, 14–27.

Quintanar-Guerrero, D., Allémann, E., Fessi, H., Doelker, E., 1998. Preparation techniques and mechanisms of formation of biodegradable nanoparticles from preformed polymers. Drug Dev. Ind. Pharm. 24, 1113–1128.

Reis, C.P., Neufeld, R.J., Ribeiro, A.J., Veiga, F., Nanoencapsulation, I., 2006. Methods for preparation of drug-loaded polymeric nanoparticles. Nanomed. Nanotechnol. Biol. Med. 2 (1), 8–21.

Rezwan, K., Chen, Q.Z., Blaker, J.J., Boccaccini, A.R., 2006. Biodegradable and bioactive porous polymer/inorganic composite scaffolds for bone tissue engineering. Biomaterials 27 (18), 3413–3431.

Ribeiro, M., Boudoukhani, M., Belmonte-Reche, E., Genicio, N., Sillankorva, S., Gallo, J., Rodríguez-Abreu, C., Moulai-Mostefa, N., Bañobre-López, M., 2021. Xanthan-Fe_3O_4 nanoparticle composite hydrogels for non-iinvasive magnetic resonance imaging and magnetically assisted drug delivery. ACS Appl. Nano Mater. 4, 7712–7729.

Rosca, I.D., Watari, F., Uo, M., 2004. Microparticle formation and its mechanism in single and double emulsion solvent evaporation. J. Contr. Release 99, 271–280.

Ruggiero, M.R., Crich, S.G., Sieni, E., Sgarbossa, P., Forzan, M., Cavallari, E., Stefania, R., Dughiero, F., Aime, S., 2016. Magnetic hyperthermia efficiency and 1H-NMR relaxation properties of iron oxide/paclitaxel-loaded PLGA nanoparticles. Nanotechnology 27, 285104.

Saengruengrit, C., Ritprajak, P., Wanichwecharungruang, S., Sharma, A., Salvan, G., Zahn, D.R.T., Insin, N., 2018. The combined magnetic field and iron oxide-PLGA

composite particles: effective protein antigen delivery and immune stimulation in dendritic cells. J. Colloid Interface Sci. 520, 101–111.
Schleich, N., Sibret, P., Danhier, P., Ucakar, B., Laurent, S., Muller, R.N., Jérôme, C., Gallez, B., Préat, V., Danhier, F., 2013. Dual anticancer drug/superparamagnetic iron oxide-loaded PLGA-based nanoparticles for cancer therapy and magnetic resonance imaging. Int. J. Pharm. 447, 94–101.
Schliecker, G., Schmidt, C., Fuchs, S., Wombacher, R., Kissel, T., 2003. Hydrolytic degradation of poly (lactide-co-glycolide) films: effect of oligomers on degradation rate and crystallinity. Int. J. Pharm. 266, 39–49.
Schneider, O.D., Mohn, D., Fuhrer, R., et al., 2011. Biocompatibility and bone formation of flexible, cotton wool-like PLGA/calcium phosphate nanocomposites in sheep. Open Orthop. J. 5, 63–71.
Schoubben, A., Ricci, M., Giovagnoli, S., 2019. Meeting the unmet: from traditional to cutting-edge techniques for poly lactide and poly lactide-co-glycolide microparticle manufacturing. J. Pharm. Investig. 49, 381–404.
Selvaraju, S., Ramalingam, S., Rao, J.R., 2018. Inorganic apatite nanomaterial: modified surface phenomena and its role in developing collagen based polymeric bio-composite (Coll-PLGA/HAp) for biological applications. Colloids Surf. B Biointerfaces 172, 734–742.
Shafiq, M., Jung, Y., Kim, S.H., 2015. Stem cell recruitment, angiogenesis, and tissue regeneration in substance P-conjugated poly (l-lactide-co-ε-caprolactone) nonwoven meshes. J. Biomed. Mater. Res. 103 (08), 2673–2688.
Sharma, S., Parmar, A., Kori, S., Sandhir, R., 2016. PLGA-based nanoparticles: a new paradigm in biomedical applications. TrAC, Trends Anal. Chem. 80, 30–40.
Sheikh, F.A., Ju, H.W., Moon, B.M., Lee, O.J., Kim, J.H., Park, H.J., Kim, D.W., Kim, D.K., Jang, J.E., Khang, G., 2015. Hybrid scaffolds based on PLGA and silk for bone tissue engineering. J. Tissue Eng. Regen. Med. 10, 209–221.
Shim, J.H., Won, J.Y., Sung, S.J., et al., 2015. Comparative efficacies of a 3D-printed PCL/PLGA/β-TCP membrane and a titanium membrane for guided bone regeneration in beagle dogs. Polymers 7 (10), 2061–2077.
Shin, S.H., Purevdorj, O., Castano, O., Planell, J.A., Kim, H.W., 2012. A short review: recent advances in electrospinning for bone tissue regeneration. J. Tissue Eng. 3, 1–11.
Siegel, S.J., Kahn, J.B., Metzger, K., Winey, K.I., Werner, K., Dan, N., 2006. Effect of drug type on the degradation rate of PLGA matrices. Eur. J. Pharm. Biopharm. 64, 287–293.
Singh, V., Singh, S., Das, S., Kumar, A., Self, W.T., Seal, S., 2012. A facile synthesis of PLGA encapsulated cerium oxide nanoparticles: release kinetics and biological activity. Nanoscale 4, 2597–2605.
Sokolova, V., Kostka, K., Shalumon, K.T., Prymak, O., Chen, J.P., Epple, M., 2020. Synthesis and characterization of PLGA/HAP scaffolds with DNA-functionalised calcium phosphate nanoparticles for bone tissue engineering. J. Mater. Sci. Mater. Med. 31, 1–12.
Song, J., Zhou, J., Duan, H., 2012. Self-assembled plasmonic vesicles of SERS-encoded amphiphilic gold nanoparticles for cancer cell targeting and traceable iintracellular drug delivery. J. Am. Chem. Soc. 134, 13458–13469.
Stankovic, A., Sezen, M., Milenkovic, M., Kaišarevic, S., Andric, N., Stevanovic, M., 2016. PLGA/nano-ZnO composite particles for use in biomedical applications: preparation, characterization, and antimicrobial activity. J. Nanomater. 2016, 9425289.
Sun, B., Ranganathan, B., Feng, S., 2008. Multifunctional poly (D, L-lactide- co-glycolide)/montmorillonite (PLGA/MMT) nanoparticles decorated by Trastuzumab for targeted chemotherapy of breast cancer. Biomaterials 29, 475–486.

Sundback, C.A., Shyu, J.Y., Wang, Y., Faquin, W.C., Langer, R.S., Vacanti, J.P., Hadlock, T.A., 2005. Biocompatibility analysis of poly (glycerol sebacate) as a nerve guide material. Biomaterials 26, 5454–5464.

Swider, E., Koshkina, O., Tel, J., Cruz, L.J., de Vries, I.J.M., Srinivas, M., 2018. Customizing poly(lactic-co-glycolic acid) particles for biomedical applications. Acta Biomater. 73, 38–51.

Takahashi, C., Matsubara, N., Akachi, Y., Ogawa, N., Kalita, G., Asaka, T., Tanemura, M., Kawashima, Y., Yamamoto, H., 2017. Visualization of silver-decorated poly (D,L-lactide-co-glycolide) nanoparticles and their efficacy against staphylococcus epidermidis. Mater. Sci. Eng. C 72, 143–149.

Takeoka, Y., Hayashi, M., Sugiyama, N., Yoshizawa-Fujita, M., Aizawa, M., Rikukawa, M., 2015. In situ preparation of poly (l-lactic acid-co-glycolic acid)/hydroxyapatite composites as artificial bone materials. Polym. J. 47 (02), 164–170.

Tang, E., Dong, S., 2009. Preparation of styrene polymer/ZnO nanocomposite latex via miniemulsion polymerization and its antibacterial property. Colloid Polym. Sci. 287, 1025–1032.

Tang, K.S., Hashmi, S.M., Shapiro, E.M., 2013. The effect of cryoprotection on the use of PLGA encapsulated iron oxide nanoparticles for magnetic cell labeling. Nanotechnology 24, 125101.

Tansik, G., Yakar, A., Gündüz, U., 2014. Tailoring magnetic PLGA nanoparticles suitable for doxorubicin delivery. J. Nanoparticle Res. 16, 2171.

Thomasin, C., Nam-Trân, H., Merkle, H.P., Gander, B., 1998. Drug microencapsulation by PLA/PLGA coacervation in the light of thermodynamics. 1. Overview and theoretical considerations. J. Pharmaceut. Sci. 87, 259–268.

Tobio, M., Gref, R., Sanchez, A., Langer, R., Alonso, M.J., 1998. Stealth PLA-PEG nanoparticles as protein carriers for nasal administration. Pharm. Res. 15, 270–275.

Topete, A., Alatorre-Meda, M., Iglesias, P., Villar-Alvarez, E.M., Barbosa, S., Costoya, J.A., Taboada, P., Mosquera, V., 2014. Fluorescent drug-loaded, polymeric-based, branched gold nanoshells for localized multimodal therapy and imaging of tumoral cells. ACS Nano 8, 2725–2738.

Tsuji, H., Mizuno, A., Ikada, Y., 2000. Properties and morphology of poly (L-lactide). III. Effects of initial crystallinity on long-term in vitro hydrolysis of high molecular weight poly (L-lactide) film in phosphate-buffered solution. J. Appl. Polym. Sci. 77, 1452–1464.

Ueng, S.W.N., Yuan, L.J., Lee, N., et al., 2002. In vivo study of hot compressing molded 50:50 poly (DL-lactide-co-glycolide) antibiotic beads in rabbits. J. Orthop. Res. 4, 654–661.

Uhrich, K.E., Cannizzaro, S.M., Langer, R.S., Shakesheff, K.M., 1999. Polymeric systems for controlled drug release. Chem. Rev. 99, 3181–3198.

Vergnol, G., Ginsac, N., Rivory, P., et al., 2016. In vitro and in vivo evaluation of a polylactic acid-bioactive glass composite for bone fixation devices. J. Biomed. Mater. Res. B Appl. Biomater. 104 (01), 180–191.

Vieira Rocha, C., Costa da Silva, M., Bañobre-López, M., Gallo, J., 2020. (Para) magnetic hybrid nanocomposites for dual MRI detection and treatment of solid tumours. Chem. Commun. 56, 8695–8698.

Wang Y, Qu W, Choi SH. FDA's Regulatory Science Program for Generic PLA/PLGA-Based Drug Products. Available online: https://www.americanpharmaceuticalreview.com/Featured-Articles/188841-FDA-s-Regulatory-Science-Program-for-Generic-PLA-PLGA-Based-Drug-Products/. (Accessed on 1 September 2022).

Wang, C., Wang, W., Meyer, R.F., Liang, Y., Winey, K.I., Siegel, S.J., 2010. A rapid method for creating drug implants: Translating laboratory-based methods into a scalable manufacturing process. J. Biomed. Mater. Res. B Appl. Biomater. 93, 562–572.

Wang, J.J., Zhao, W.Z., Ren, Z.X., et al., 2011. Recent advances of chitosan nanoparticles as drug carriers. Int. J. Nanomed. 06, 765–774.
Wang, Y., Strohm, E.M., Sun, Y., Wang, Z., Zheng, Y., Wang, Z., Kolios, M.C., 2016. Biodegradable polymeric nanoparticles containing gold nanoparticles and paclitaxel for cancer imaging and drug delivery using photoacoustic methods. Biomed. Opt Express 7, 4125.
Wang, L., Li, D., Hao, Y., Niu, M., Hu, Y., Zhao, H., Chang, J., Zhang, Z., Zhang, Y., 2017. Gold nanorod-based poly(lactic-co-glycolic acid) with manganese dioxide core-shell structured multifunctional nanoplatform for cancer theranostic applications. Int. J. Nanomed. 12, 3059–3075.
WCG. CenterWatch FDA Approved Drugs. Available online: https://www.centerwatch.com/directories/1067. (Accessed on 1 September 2022).
Widmer, M., 1998. Manufacture of porous biodegradable polymer conduits by an extrusion process for guided tissue regeneration. Biomaterials 19, 1945–1955.
Witt, C., 2001. Morphological characterization of microspheres, films and implants prepared from poly(lactide-co-glycolide) and ABA triblock copolymers: is the erosion controlled by degradation, swelling or diffusion? Eur. J. Pharm. Biopharm. 51, 171–181.
Wu, X.S., Wang, N., 2001a. Synthesis, characterization, biodegradation, and drug delivery application of biodegradable lactic/glycolic acid polymers. Part II: biodegradation. J. Biomater. Sci. Polym. Ed. 12, 21–34.
Wu, X.S., Wang, N., 2001b. Synthesis, characterization, biodegradation, and drug delivery application of biodegradable lactic/glycolic acid polymers. Part II: biodegradation. J. Biomater. Sci. Polym. Ed. 12, 21–34.
Yang, Y.Y., Chung, T.S., Ng, N.P., 2001. Morphology, drug distribution, and in vitro release profiles of biodegradable polymeric microspheres containing protein fabricated by double-emulsion solvent extraction/evaporation method. Biomaterials 22, 231–241.
Yang, F., Murugan, R., Wang, S., Ramakrishna, S., 2005. Electrospinning of nano/micro scale poly(l-lactic acid) aligned fibers and their potential in neural tissue engineering. Biomaterials 26 (15), 2603–2610.
Ye, F., Barrefelt, Å., Asem, H., Abedi-Valugerdi, M., El-Serafi, I., Saghafian, M., Abu-Salah, K., Alrokayan, S., Muhammed, M., Hassan, M., 2014. Biodegradable polymeric vesicles containing magnetic nanoparticles, quantum dots and anticancer drugs for drug delivery and imaging. Biomaterials 35, 3885–3894.
Yu, D.G., Zhu, L.M., White, K., Branford-White, C., 2009. Electrospun nanofiber-based drug delivery systems. Health 1, 67–75.
Zare, E.N., Jamaledin, R., Naserzadeh, P., Afjeh-Dana, E., Ashtari, B., Hosseinzadeh, M., Vecchione, R., Wu, A., Tay, F.R., Borzacchiello, A., 2019. Metal-based nanostructures/PLGA nanocomposites: antimicrobial activity, cytotoxicity, and their biomedical applications. ACS Appl. Mater. Interfaces 12, 3279–3300.
Zhang, R., Ma, P.X., 1999. Poly (hydroxyl acids)/hydroxyapatite porous composites for bone-tissue engineering. I. Preparation and morphology. J. Biomed. Mater. Res. 44, 446–455.
Zhang, W., Li, Y., Zhang, H., Zhou, X., Zhong, X., 2011. Facile synthesis of highly luminescent Mn-doped ZnS nanocrystals. Inorg. Chem. 50, 10432–10438.
Zhang, Y., Wang, J., Wang, J., et al., 2015. Preparation of porous PLA/DBM composite biomaterials and experimental research of repair rabbit radius segmental bone defect. Cell Tissue Bank. 16 (4), 615–622.
Zhang, Y., García-Gabilondo, M., Rosell, A., Roig, A., 2020. MRI/Photoluminescence dual-modal imaging magnetic PLGA nanocapsules for theranostics. Pharmaceutics 12, 16.
Zhong, H., Chan, G., Hu, Y., Hu, H., Ouyang, D.A., 2018. Comprehensive map of FDA-approved pharmaceutical products. Pharmaceutics 10, 263.

Ziabari, M., Mottaghitalab, V., Haghi, A.K., 2010. A new approach for optimization of electrospun nanofiber formation process. Kor. J. Chem. Eng. 27 (01), 340–354.
Zolnik, B.S., Burgess, D.J., 2007. Effect of acidic pH on PLGA microsphere degradation and release. J. Contr. Release 122, 338–344.

CHAPTER 14

Bioresorbable polymers: Challenges and opportunities for development and applications of medical devices

Pornnapa Kasemsiri[1], Kaewta Jetsrisuparb[1], Jesper T.N. Knijnenburg[2] and Manunya Okhawilai[3]

[1]Sustainable Infrastructure Research and Development Center and Department of Chemical Engineering, Faculty of Engineering, Khon Kaen University, Khon Kaen, Thailand; [2]Biodiversity and Environmental Management Division, International College, Khon Kaen University, Khon Kaen, Thailand; [3]Metallurgy and Materials Science Research Institute, Chulalongkorn University, Bangkok, Thailand

14.1 Introduction

Bioresorbable polymers are designed to have retentive properties during their shelf life and can be degraded over time by dissolving directly and slowly in body fluids. In the degradation process, bioresorbable polymers are metabolized or degraded via urinary excretion or the citric acid cycle without any risk associated with foreign body reactions (Low et al., 2020; Ramakrishna et al., 2001). Examples are the degradation of poly(glycolic acid) (PGA) and poly(lactic acid) (PLA) (Fig. 14.1). The hydrolytic cleavage of PGA and PLA produces glycolic acid (GA) and lactic acid (LA), respectively. Some of the produced GA is then transformed into oxalic acid and excreted via urine. Another part of the GA is further converted into glyoxylate and subsequently into glycine via glycine transaminase. The glycerin is transformed into pyruvic acid and finally converted to CO_2 and water in the citric acid cycle (On et al., 2020; Pappalardo et al., 2019).

Recently, bioresorbable materials based on polymers have attracted much attention due to their wide ranges of physical, mechanical, and chemical properties. Such bioresorbable polymers are frequently also designed to have smart functions such as shape memory, controllable release, and self-healing (Maitz, 2015). To produce bioresorbable polymers for medical devices, both natural and petroleum-based polymers have been used (Park et al., 2017; Ramakrishna et al., 2001). In this chapter,

Bioresorbable Polymers and their Composites
ISBN 978-0-443-18915-9
https://doi.org/10.1016/B978-0-443-18915-9.00011-2
© 2024 Elsevier Ltd.
All rights reserved.

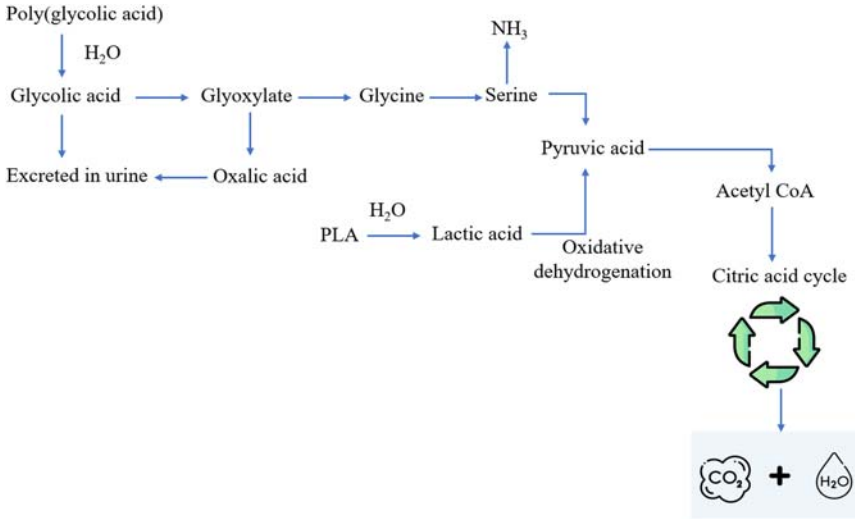

Figure 14.1 The degradation pathway of poly(glycolic acid) (PGA) and poly(lactic acid) (PLA) (On et al., 2020; Pappalardo et al., 2019).

bioresorbable polymers used in medical devices are classified into three groups according to their applications: drug delivery, medical devices, and tissue engineering, as illustrated in Fig. 14.2.

14.2 Bioresorbable polymers for drug-delivery systems

The drug release from bioresorbable polymers can occur through two mechanisms: (1) erosion, in which the polymer matrix slowly disintegrates resulting in pore formation, and (2) diffusion of drug molecules through water in the polymer matrix, driven by the osmotic pressure and differences in chemical potential (Fredenberg et al., 2011; Varde and Pack, 2004). These drug-release mechanisms are schematically depicted in Fig. 14.3.

A number of bioresorbable polymers for drug delivery have been investigated, including aliphatic polyesters (Washington et al., 2017), alginate (Srikhao et al., 2022), chitosan (Bernkop-Schnürch and Dünnhaupt, 2012), polyvinyl alcohol (PVA) (Rivera-Hernandez et al., 2021), polyamide, poly(N-isopropylacrylamide) (Gheysoori et al., 2023), and dextran (Prasher et al., 2022). The properties of the polymers are key parameters that affect drug release. For example, the molecular weight, crystallinity, and hydrophobicity/hydrophilicity influence the water absorption, hydrolysis, and erosion rate, which ultimately control the drug release (Kamaly et al., 2016; Stiepel et al., 2022). This is discussed in more detail in the following sections.

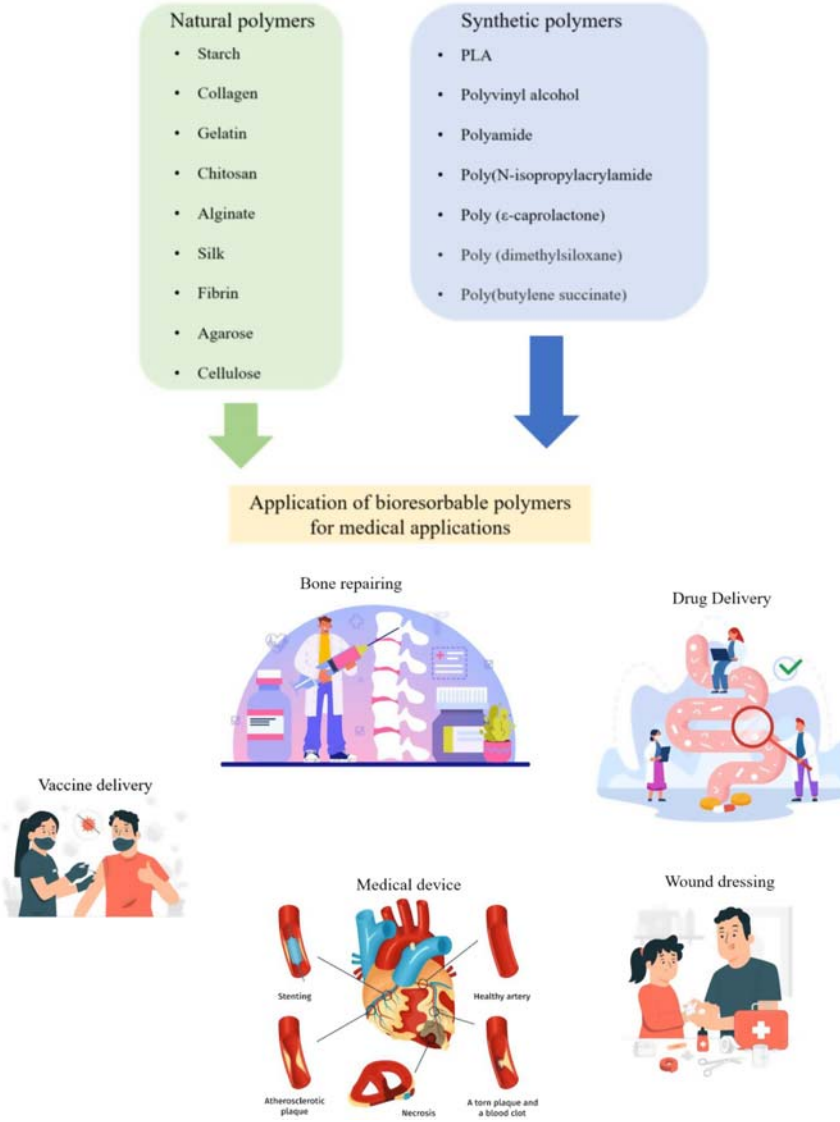

Figure 14.2 Bioresorbable polymers for medical applications.

14.2.1 Degree of crystallinity

Drug molecules are most frequently entrapped in amorphous sections of the polymer, which are more accessible to water and more permeable than the crystalline sections. Therefore, the degree of crystallinity of the polymer greatly influences the swelling and biodegradability in drug-delivery

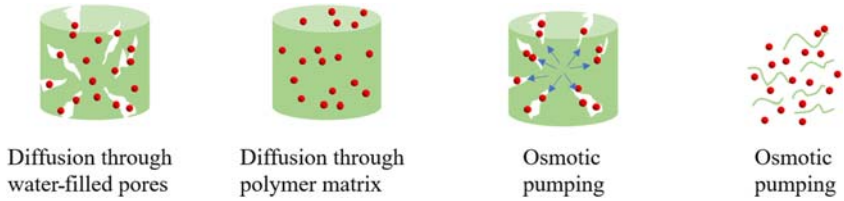

Figure 14.3 Model of drug release from bioresorbable polymers.

systems. Generally, a polymer with lower crystallinity provides a higher drug release rate (Karavelidis et al., 2011; Miles et al., 2021). Table 14.1 presents the relationship between the degree of crystallinity and the release of ropinirole. The degrees of crystallinity of poly(propylene glutarate) and poly(propylene adipate) are higher than for poly(propylene azelate) and poly(propylene pimalate), resulting in higher drug-release rates. The high crystallinity of the polymer matrix may negatively affect the drug release since the lamellar phase in the crystallized regions may hinder water penetration during drug diffusion. Furthermore, the crystallinity may also affect the mechanical properties and resorption rate, with a higher crystallinity resulting in better mechanical properties but a lower resorption rate (Tesfamariam, 2016).

In addition to the degree of crystallinity, the crystallite size is another factor that may influence drug release. Miles et al. (2021) observed more rapid drug release for larger crystallites. Smaller crystallites could increase tortuosity (and thus the path length for drug diffusion), resulting in slower drug release.

14.2.2 Hydrophobicity/hydrophilicity

The hydrophobicity and hydrophilicity of a polymer are used to design its degradability during drug release. The blending of hydrophobic and hydrophilic polymers is one approach that can control polymer degradation,

Table 14.1 Relationship between the degree of crystallinity of polyesters and ropinirole release (Karavelidis et al., 2011).

Types of polyesters	Degree of crystallinity (%)	Release of ropinirole (%) at 40 h
Poly(propylene azelate)	29.8	100
Poly(propylene pimalate)	43.9	98
Poly(propylene glutarate)	55.4	40
Poly(propylene adipate)	67.5	20

drug release rate (Kamaly et al., 2016), as well as degradation of drug molecules (Makadia and Siegel, 2011). An earlier study found that for poly(lactic-co-glycolic) acid (PLGA), an increase in the ratio of hydrophobic PLA segments to PGA segments reduced the hydrophilicity of PLGA, and hence a polymer with lower water absorbency and lower rate of polymer degradation (Makadia and Siegel, 2011). Fig. 14.4 shows that an increase in the LA/GA ratio greatly enhanced the degradation rate owing to its higher hydrophilicity. In addition, a higher LA/GA ratio prolonged the release of risperidone entrapped in the copolymer (Amann et al., 2010).

14.2.3 Molecular weight

The molecular weight of a polymer is related to properties such as the solubility, crystallinity, viscosity, glass transition temperature, mechanical strength, and degradability (Stiepel et al., 2022). Takeuchi et al. (2017) studied the effect of the molecular weight of poly(lactide-co-glycolide) (PLCG) on drug release. When compared under identical release conditions, the release of rifampicin decreased when the molecular weight of PLCG increased (Table 14.2). Based on the free volume model, the drug release depends on the molecular chain movement ability. The increase in

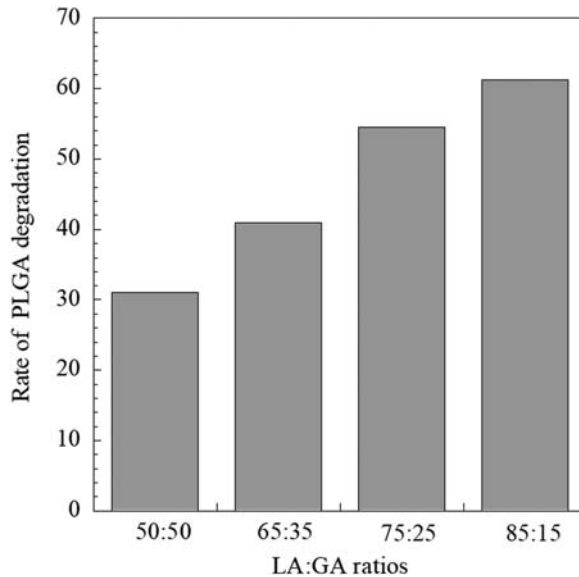

Figure 14.4 Rate of PLGA degradation at different LA:GA ratios. *(Data taken from Amann et al. (2010).)*

Table 14.2 Effect of PLCG molecular weight on rifampicin release (Takeuchi et al., 2017).

PLCG molecular weight	Cumulative release of rifampicin (%)	
	8 h	48 h
10,000	95	95
15,000	87	90
20,000	70	83

molecular weight led to a higher crystallinity and degree of polymerization which hindered the molecular chain mobility.

14.3 Bioresorbable polymers for medical devices

Bioresorbable polymers have been developed and applied as devices in the medical field, especially surgery. Because bioresorbable polymers slowly dissolve in the human body, they do not need to be removed in a second surgical procedure (Oliveira and Mano, 2011). Bioresorbable polymers have mostly been used to prepare valves, stents, screws, and pins, as summarized in Table 14.3.

14.4 Bioresorbable polymers for tissue engineering

Tissue engineering is a rapidly emerging biomedical field that focuses on the development of suitable biocompatible materials to repair or create tissues, or improve damaged tissues or organs via cell transplantation (Biswal, 2021), as depicted in Fig. 14.5.

To apply a polymer in tissue engineering, the suitable properties of the polymer are important and should meet the following requirements:

- A suitable topography and biocompatible surfaces for adhesion and propagation of cells.
- Appropriate mechanical properties that facilitate cell growth and biomechanical functionality.
- Matching of the polymer degradation rate and the tissue formation rate (Biswal, 2021; Ravichandran et al., 2012).

Recently, most polymers in tissue engineering have been constructed in several forms for various applications such as porous scaffolds, hydrogels, and micro/nanoparticles (Biswal, 2021). The characteristic properties and preparation methods of different constructed polymers are discussed in this section.

Table 14.3 Examples of bioresorbable polymers used in medical devices.

Applications	Polymers	Properties	References
Heart valve	Bis-urea-modified polycarbonate	Successful application in sheep with sustained functionality of up to 1 year	Kluin et al. (2017)
Coronary artery stents	3D-printed polycaprolactone functionalized with heparin	Good mechanical strength and biocompatibility for up to 12 weeks in rabbits.	Shen et al. (2022b)
Bone screw	Poly(glycerol-succinate)	Good mechanical strength (122.01 ± 8.82 MPa). Supported cell adhesion and proliferation Good osseointegration in the implanted rabbits	Cai et al. (2019)
Pin	Poly-L-co-D-lactide reinforced with bioresorbable glass fibers	Load bearing and substrate for a bone-like apatite formation.	Cao et al. (2019)

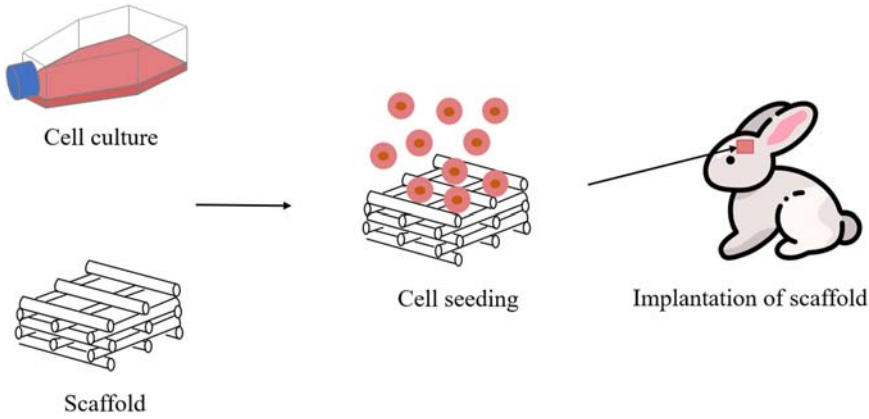

Figure 14.5 Schematic of scaffold-based tissue engineering.

14.4.1 Scaffolds

Scaffolds are porous materials that can deliver biofactors (such as cells, genes, and/or proteins) and repair tissues. The basic required properties for scaffolds include: (1) suitable topology for nutrient transport, cell attachment, proliferation, and differentiation; (2) controllable degradation without risk of cell inflammation; (3) suitable mechanical properties for formation of new tissue; and (4) minimal/no inflammation or in vivo toxicity (Thorrez et al., 2008). The porosity (including both pore size and structure/interconnectivity) of the scaffold is critical for successful integration of cells. Large pores lead to good mass transfer properties of nutrients, oxygen, and waste products, but cell adhesion is low. Small pores, on the other hand, have good integration of cells but poor mass transfer properties. It is therefore crucial to optimize the porous structure of scaffolds. Optimal pore size greatly depends on the site of application; for example, the optimal pore size is 20–80 μm for hepatocyte in-growth, 150–200 μm for fibroblast in-growth, and 100–500 μm for bone regeneration (Salerno et al., 2012).

Scaffolds can be prepared from various materials. Compared to rigid materials such as metals and ceramics, polymeric scaffolds have the advantages of superior processability, adjustable degradation rate, wettability, and good mechanical properties including flexibility, making them especially attractive for applications in organs such as the skin, liver, heart, and bladder (Ambekar and Kandasubramanian, 2019).

Polymer-based scaffolds have been fabricated by techniques such as solvent casting/particulate leaching (SCPL), freeze-drying, gas foaming,

thermally induced phase separation (TIPS), and electrospinning (Mabrouk et al., 2020). The advantages and limitations of these scaffold fabrication methods are summarized in Table 14.4.

SCPL is the oldest technique for scaffold preparation (Mabrouk et al., 2020). In a typical SCPL process, the target polymer is dissolved in a suitable solvent and cast into a mold containing a porogen (most commonly NaCl), after which the solvent and the porogen are removed. This way, highly porous scaffolds have been made from, e.g., PLA (Huang et al., 2014; Zeng et al., 2017), PCL (Yang et al., 2006), polyurethane (PU) (Sin et al., 2010; Sola et al., 2019), and silk fibroin (Raggio et al., 2018). For example, Zeng et al. (2017) prepared a three-dimensional porous PLA scaffold via vacuum-assisted SCPL. The PLA was dissolved in a dioxane/water mixture and cast into a NaCl preform under vacuum. The composite blend was then frozen at −20 to −80°C, after which the dioxane was removed by solvent extraction in ethanol followed by removal of the NaCl by leaching in DI water. The resulting porous PLA scaffold was dried and subsequently coated with chitosan and biofunctionalized with osteogenic growth peptide (OGP). The porous PLA/chitosan/OGP scaffold had a good interconnected network structure with porosity >90% and could accelerate osteoblast proliferation.

Freeze-drying or lyophilization is a simpler technique for the preparation of scaffolds, for example, based on PCL (Fereshteh et al., 2016), poly(hydroxybutyrate-co-valerate) (Sultana and Wang, 2008), poly(lactide-co-glycolide) (Qi et al., 2020), gelatin (Wu et al., 2010), and mixed polymers (Haghbin et al., 2020). In this process, a liquid sample is first frozen and then transferred to a freeze drier, which removes the frozen solvent by sublimation. The sublimation process results in the creation of pores in the spaces that were previously occupied by the ice crystals. Most freeze-drying processes have been carried out in aqueous solution, although organic solvents have also been used (Hou et al., 2003). Important parameters that can affect the resulting material properties are the solution properties (such as concentration, viscosity, solvent) and the freezing conditions (e.g., temperature, pressure, and direction of freezing). For example, smaller pores are formed at lower freezing temperatures. In the work of Mandal and Kundu (2009), silk fibroin protein scaffolds prepared by freeze drying had a porosity of 86% and pore sizes of 200−250 μm when frozen at −20°C. Decreasing the freezing temperature to −196°C resulted in a higher porosity of 96% and smaller pore size of 80−100 μm. Both the porosity and pore size decreased with increasing solution concentrations.

Table 14.4 Advantages and limitations of scaffold fabrication methods (Mabrouk et al., 2020).

Methods	Polymers	Advantages	Limitations	References
Solvent casting/ particulate leaching	Polycaprolactone Silk fibroin PLA	Simplicity Controlled pore size and pore distribution Low cost	Potential impurities from solvent and porogen Nonuniform distribution of porogen in polymer solution	Dhandayuthapani et al. (2011), Yang et al. (2006), and Zeng et al. (2017)
Freeze-drying	Poly(hydroxybutyrate-co-valerate) Polycaprolactone/chitosan/ gelatin Poly(lactide-co-glycolide)/ poly(trimethylene carbonate)	Water can often be used as solvent Highly interconnected pores	Uncontrolled pore size Slow process High energy consumption	Haghbin et al. (2020), Qi et al. (2020), and Sultana and Wang (2008)
Gas foaming	Poly (propylene carbonate) Polyurethane Polycaprolactone/ magnesium hydroxide	One-step process Porosity control without toxic solvents	Closed and unconnected pores Relatively poor mechanical properties	Han et al. (2021) and Manavitehrani et al. (2019)

Thermally induced phase separation (TIPS)	Poly(lactic-co-glycolic acid)	Simple equipment and procedure Intrinsically interconnected polymer network Scalable Good mechanical properties	Potential impurities from organic solvent	McKenna et al. (2020)
Electrospinning	Poly (ε-caprolactone) Polyethylene oxide Gelatin/polycaprolactone	Simple and inexpensive setup Highly interconnected pores High surface area to volume ratio	Limited scaffold thickness Relatively poor mechanical properties	Feng et al. (2019), Hodge and Quint (2019), and Surmenev et al. (2022)

Similar results were found for other polymers (Perez-Puyana et al., 2019; Reys et al., 2017). Furthermore, a lower freezing temperature increased the compressive modulus of chitosan scaffolds (Reys et al., 2017).

In the gas foaming process, gas bubbles are utilized to generate pores. These bubbles can be produced in situ by chemical reactions, or an inert gas like N_2 or CO_2 can be externally introduced (Dehghani and Annabi, 2011). Commonly, a surfactant is added to improve the stability of the foam. Important parameters to control the material properties include the foaming temperature, pressure, and depressurization rate. Scaffolds have been prepared by gas foaming using various polymers (Dehghani and Annabi, 2011) such as PCL (Salerno et al., 2012), PLA (Sheng et al., 2015), alginate (Catanzano et al., 2018; Costantini et al., 2016), and poly(propylene carbonate) (PPC) (Manavitehrani et al., 2019).

Salerno et al. (2012) prepared PCL scaffolds via a gas foaming technique. Thermoplastic gelatin (TG) was blended with PCL and pressed into 3 mm-thick plates, which were solubilized with the blowing agent [N_2/CO_2 (4/1 vol.% ratio) mixture] in an autoclave. The autoclave was then heated to 70–110°C and the pressure was reduced to ambient pressure. After rapid cooling to room temperature, the samples were placed in water for leaching of TG followed by drying. Higher foaming temperatures produced PCL foams with a higher porosity (ranging from 60.2% to 90.3%) and larger mean pore size (from 264 to 1830 μm). At the same time, the elastic modulus was reduced from 9.4 to 1.4 MPa. Biocompatibility tests confirmed the good interaction between the porous scaffold and human mesenchymal stem cells.

Manavitehrani et al. (2019) prepared porous scaffolds from PPC blended with starch and bioglass particles. The porous scaffolds were prepared by gas foaming through the introduction of CO_2 and the effect of parameters such as temperature (25–40°C), pressure (50–125 bar), and depressurization rate (0.02–10 bar/s) on the porosity and compressive modulus was studied. Higher porosity and smaller pores were obtained for higher pressures and lower depressurization rates, and increasing the pressure decreased the compressive modulus. The in vitro evaluations confirmed the safety and biocompatibility of the scaffold and in vivo evaluation in mice demonstrated good tissue infiltration.

Han et al. (2021) prepared a PU foam scaffold via a one-pot process with PCL diol/triol as polyol, hexamethylene diisocyanate (HMDI) as diisocyanate, water or aqueous gelatin as blowing agent, and silicone surfactant as foam stabilizer. Polymerization took place between PCL diol/

triol and HMDI, and CO_2 gas was generated by the reaction between HMDI and water. The resulting highly porous scaffolds were further treated with sulfuric acid to enhance the outer porosity. The influence of the polyol structure, blowing agent, and surfactant concentration on the porosity, mechanical properties, and biodegradability were investigated.

In the TIPS process, the polymer is first dissolved at elevated temperature and then cast into a specific shape. Next, the solution is cooled, during which the polymer solidifies. The solvent is then removed and a microporous polymer structure is formed as a result (Liu et al., 2016). This simple, scalable technique has been widely employed to produce porous scaffolds of various polymers. For example, Rowlands et al. (2007) prepared PU, PLGA, and PU/PLGA composite scaffolds by TIPS. The authors report that the composite scaffold had superior porosity, mechanical, and fibroblast adhesion properties over scaffolds prepared from individual polymers. Zhang et al. (2015) prepared silk fibroin (SF)/sodium alginate (SA) composite scaffold by TIPS. Scaffolds with an SF/SA ratio of 5:1 and 3:1 had high porosity and nanofibrous structure with physical interactions between SF and SA. Cell studies with MG-63 osteoblast cells showed good cellular adhesion and growth. McKenna et al. (2020) prepared thin, porous, high-strength biphasic scaffolds by encapsulation of PLGA mesh into a porous PLGA network by TIPS. The authors carefully optimized several synthesis parameters such as the nucleation temperature, template material, and scaffold assembly temperature. According to the optimized procedure, PLGA mesh strips (1×4 cm) were mounted on microscope slides and kept at 40°C. The degassed PLGA + EC solution was then poured into the pores of the PLGA mesh strips, which was then closed with a second microscope slide. The scaffolds and molds were cooled to 4°C, after which nucleation was manually stimulated. The scaffolds were then transferred to water to remove the EC phase at 4°C for 4 days, followed by drying at room temperature. The thin biphasic scaffold had a high porosity with small pore size, high tensile strength, rapid in vitro degradation, and supported the proliferation of HaCaT cells. The authors suggested that the scaffold may have applications for repairing dermal wounds or tubular organs.

Electrospinning has gained wide attention over the last 30 years due to its ease of operation, and more than 200 different polymers have been prepared into fibers by electrospinning (Mabrouk et al., 2020). In the electrospinning process, a polymeric solution is injected into a thin capillary over which a high voltage is applied. Repulsion of electric charges within

the solution counteracts the surface tension of the liquid, after which a jet erupts. The solvent in the jet evaporates and the formed fibers are deposited on a grounded collector (Pham et al., 2006). The properties of the fibers can be controlled by varying solution parameters (e.g., concentration, surface tension, and conductivity), polymer properties (such as the molecular weight), experimental conditions (such as the voltage, flow rate, and distance between the needle tip and collector), and ambient parameters (for example the temperature and humidity) (Pham et al., 2006). Feng et al. (2019) prepared a gelatin/PCL nanofiber composite membrane via electrospinning. The fibers had an average diameter of 441 nm and the average pore size of the membrane was 5.6 μm. The breaking strength and Young's modulus were measured in wet (3.2 and 1.5 MPa, respectively) and dry states (4.6 and 28.9 MPa, respectively). A study in a rabbit cardiac adhesion model demonstrated that the membrane was well incorporated. The composite membrane effectively prevented postcardiac operative adhesions and may have applications as pericardial substitutes.

Hodge and Quint (2019) prepared scaffolds by electrospinning of PGA, PLGA, and PCL. To enhance the porosity of the fibers, polyethylene oxide (PEO) microparticles were electrosprayed simultaneously with the electrospun fibers. The PEO microparticles acted as sacrificial material (porogen) and were removed from the scaffolds using ethanolic solutions. The porous fibers had high porosity (83%–90%), good mechanical strength (ultimate tensile strength 2.5–6.0 MPa) with low elasticity (Young's modulus 9–86 kPa), and improved cell infiltration and proliferation of human fibroblasts.

14.4.2 Hydrogels

Hydrogels are water-swollen cross-linked polymer networks that can be used to accelerate tissue formation, absorb body fluids, and control the release of active agents (Ounkaew et al., 2020, 2023). Two types of cross-links can exist in hydrogels, namely chemical and physical cross-links (Fig. 14.6). Chemical cross-links are formed via covalent bonding, whereas physical cross-links involve noncovalent interactions and entanglement of the polymeric chains. Recently, hydrogels integrated with smart properties have been developed that are triggered by stimuli such as a change in pH or temperature. Cross-linked hydrogels with reversible or noncovalent cross-links can create smart functions such as self-healing and shear-thinning behavior (Spicer, 2020). For example, the cross-linked hydrogel based on carboxymethyl starch and polyvinyl alcohol via boric

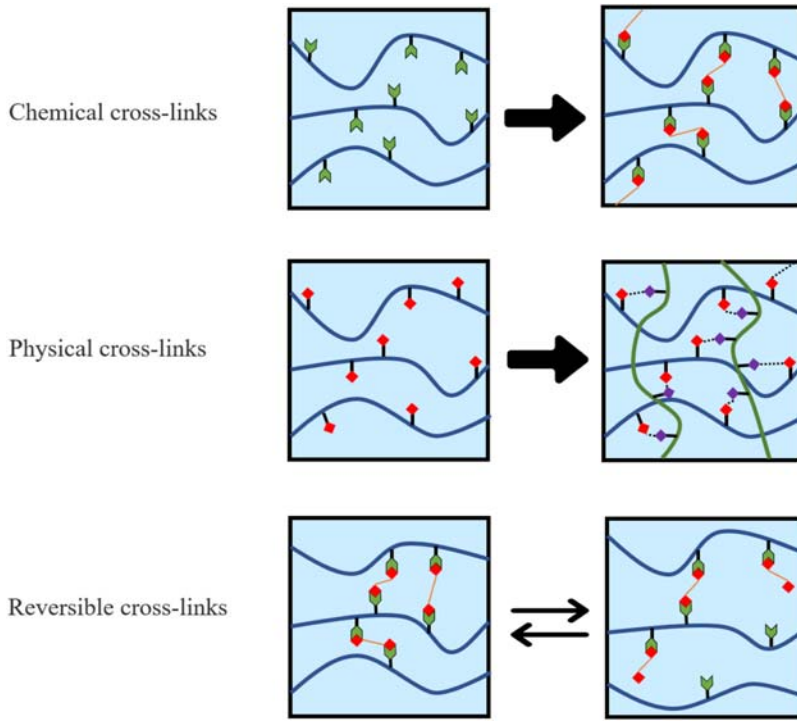

Figure 14.6 Types of cross-linking networks of hydrogels.

ester had self-healing ability (Ounkaew et al., 2022; Taesuwan et al., 2022). To prepare hydrogels, both synthetic polymers and polymers derived from natural resources have been used. Examples of hydrogels and their applications are provided in Table 14.5.

Hydrogel preparation methods can be roughly classified into physical cross-linking and chemical cross-linking techniques. In the case of physical cross-linking, the hydrogel is formed by an interaction between molecules such as ionic interaction, hydrogen bond, crystallization, and hydrophobic interactions. The preparation of hydrogels via physical cross-linking could provide outstanding properties such as ionic conductivity, response to external stimuli, and self-healing ability. However, the prepared hydrogels generally have poor mechanical properties for some applications and complex preparation. Chemical cross-linking processes have been developed to fabricate hydrogels with good mechanical properties and stability (Ahmed, 2015). The preparation methods of hydrogels are summarized in Tables 14.6 and 14.7.

Table 14.5 Hydrogels and their applications.

Polymers	Properties	References
Synthetic polymers		
Glass fiber-reinforced polyvinyl alcohol hydrogel	Cartilage repair for tissue engineering Enhancement of cell recruitment and proliferation	Zhu et al. (2023)
Poly (ε-caprolactone)/polyethylene glycol copolymer	Drug delivery for tissue regeneration	Dethe et al. (2022)
Methacrylated star poly(dimethylsiloxane) cross-linked with diacrylated poly(ethylene glycol)	Formation of hydroxyapatite for bone bonding	Frassica et al. (2019)
Polymers derived from natural resources		
Aloe vera/carboxymethyl cellulose/tannic acid nanocomposite	pH-responsive tannic acid release Antibacterial activity against *Staphylococcus aureus* and *Escherichia coli* Enhancement of human fibroblast cell proliferation Possibly applied as wound dressing	Ounkaew et al. (2023)
Carboxymethyl chitosan/sodium alginate/oxidized dextran hydrogel	Good hemostasis in rat liver injury and tail amputation models Antibacterial activity against *Staphylococcus aureus*	Xie et al. (2022)
Injectable hydrogel based on chitosan/hyaluronic acid	Encapsulated and transplanted cell for tissue regeneration	Tan et al. (2009)

Table 14.6 Preparation of hydrogels by chemical cross-linking

Preparation methods	Process	References
Conjugation reaction	Conjugation by Michael addition reaction, Schiff's base reaction, and Diels—Alder addition reaction. These reactions could take place under mild conditions	Lu et al. (2021)
Free radical polymerization	Free radicals are generated by various techniques i.e., heating, electrolysis, ultraviolet or high-energy radiation, and plasma initiation. After initiation of the free radicals, these functional groups further polymerize or cross-link under suitable conditions by heating or light irradiation to form covalent bonds	Darge et al. (2019), Eke et al. (2017), and Kang et al. (2018)

14.4.3 Micro/nanoparticles

Micro- and nanoparticles are particles with sizes of 1—100 μm and 1—100 nm, respectively. Their smaller size results in a larger surface area, mobility, and high reactivity compared to the bulk materials (Kohane, 2007). The large surface-to-volume ratio of micro- or nanoparticles increases the number of reaction sites compared to macro-size particles. The particle size is of prime importance and largely depends on preparation techniques and applications. For example, injected particles should have a size between 20 and 300 nm in order to prevent rapid elimination by the liver, spleen, and kidneys (Arruebo et al., 2007; Moscatelli and Sponchioni, 2017).

Among the different polymers, polyesters and their copolymers have been widely investigated. Particularly, PLA, PGA, and PLGA have been

Table 14.7 Preparation of hydrogel by physical cross-linking

Preparation methods	Process	References
Ionic interaction	Ionic interactions can be formed by dynamic interaction between positive and negative charged groups of polymer or metal–ligand interactions Examples: **(1)** the use of negatively charged acrylic acid monomers and positively charged 2-hydroxypropyl trimethylammonium chloride chitosan and **(2)** the introduction of divalent metal ions into the hydrogel, which could create interactions with functional groups of the polymers such as amino, carboxyl and hydroxyl.	Shen et al. (2022a)
Hydrogen bonds	The fabrication of hydrogen-bonding interactions in hydrogel could provide smart properties such as self-healing. The hydrogen-bonding interactions in hydrogel have a dissociation/association behavior. To design hydrogen bonding for hydrogel, several types of polymers such as amides, ureas, urethanes, proteins, saccharides, and DNA would be options for the preparation of supramolecular gelators	Lim et al. (2019)
Crystallization	The freeze–thaw method is commonly used. During the freeze process, ice crystals are formed and the polymer chains become arranged. During thawing, the ice melts and creates a microporous polymer structure. The pore size, mechanical properties, and morphology of the hydrogel depend on the number of freeze–thaw cycles	Su et al. (2021)

studied extensively in medical applications such as drug delivery, bone plates, and abdominal meshes (Lee et al., 2016). PLA and PLGA nanoparticles have also been shown to be useful in drug delivery for tumors. These polymer nanoparticles are particularly attractive as drug delivery vehicles for targeting cancer cells because they can overcome challenges related to the low solubility, stability, and rapid clearance, hence imparting high efficiency. To obtain the desirable properties of PLGA nanoparticles such as particle size, shape, biodegradability, as well as suitable chemical properties, the LA:GA ratio can be easily adjusted. Loading of active pharmaceutical ingredients is usually achieved through homogeneous dispersion in the PLA matrix (Danhier et al., 2012). However, a high initial burst release for drug delivery can be problematic (Kamaly et al., 2012). Some synthesis methods for polyester nanoparticles are summarized in this section.

Various techniques have been carried out to prepare micro- and nanoparticles of the polyesters (such as PLA, PCL, and PGA). The conventional technique is the emulsification-evaporation method. In the single emulsion method, polymers and hydrophobic drugs are dissolved in organic solvents and subsequently added to a mixture of water and surfactants to form an oil-in-water (o/w) emulsion. To form a nanosized dispersion of particles, homogenization, milling, and sonication at ultrasonic frequency are applied. The agitation rate among other parameters is used to control the particle size. Extraction of solvents is subsequently carried out by evaporation under low pressure. The limitation of this method lies in its poor encapsulation of hydrophilic compounds.

The double emulsion process is suitable when hydrophilic compounds such as proteins or peptides drugs are used. This method allows a higher drug loading for water-soluble compounds such as insulins. This process involves an additional step where water-soluble drugs are dissolved in the water mixture containing a proper stabilizer to form an aqueous phase. The water-soluble drug solution is then added to organic solvents containing polymers to form a w/o (water-in-oil) emulsion or an o/w emulsion. This emulsion is subsequently added to a mixture of water and a stabilizer, resulting in w/o/w or o/w/o emulsions. Finally, the removal of organic solvents is carried out under vacuum (Lee et al., 2016).

Emulsions such as o/w, o/o (oil-in-oil), or w/o can produce particles with various sizes from the nano- to micrometer scale. Although these techniques are simple, they suffer from several negative aspects including the production process, the use of potentially toxic solvents and surfactants,

wide size distribution, low solid content, and the need for high-molecular-weight polyesters (Moscatelli and Sponchioni, 2017). In addition, a polymeric shell needs to be rapidly formed in the first emulsification step in the double emulsion method to avoid diffusion of the hydrophilic compound into the outer (bulk) aqueous phase (Moscatelli and Sponchioni, 2017).

Salting out is a different approach to emulsification in which no heating step is required. In this process, the polymers are mixed with water-miscible solvents and added to a salting-out agent (often $MgCl_2$ or $CaCl_2$) in the presence of a stabilizer under high-speed stirring to form a colloid. Subsequently, this o/w emulsion is diluted in water to allow the miscible solvent to diffuse into the aqueous phase. Lastly, the particles are separated from the liquid phase by centrifugation or cross-flow filtration. This technique is particularly interesting for heat-sensitive drugs.

Nanoprecipitation is another means of polymer nanoparticle preparation. This facile technique does not require any high-energy source stirring device and offers nanoparticles with narrow size distribution where less toxic solvents can be used. The nanoparticles can be obtained with the aid of antisolvents followed by solvent removal under reduced pressure. The particle size and drug encapsulation yield can be controlled by the injection rate of the organic phase into the antisolvent and the solvent types. The limitation of this technique is the narrow condition of the Ouzo region used to form nanoparticles with high drug encapsulation efficiency (Anton et al., 2008; Ganachaud and Katz, 2005; Sah and Sah, 2015). In a similar category as the nanoprecipitation technique, other techniques based on precipitation such as dialysis have also been used to achieve particles with a narrow size distribution.

Spray drying has been used to improve the stability of protein encapsulates (Wischke and Schwendeman, 2008). Solutions containing the drug and polymer are sprayed into ultra-fine droplets followed by rapid evaporation of the solvent, after which nanoparticles are obtained.

Microparticles can also be produced through thermal treatment. Hot melt encapsulation is a suitable method to produce particles ranging from 1 to 1000 μm with a narrow size distribution (Sinchaipanid et al., 2004). In addition, no solvent is needed since the drug is dispersed in the molten polymer. The drug/polymer melt is then cooled to solidify and ground or milled to obtain the desired particle size. Although hot melt encapsulation is an attractive technique for large-scale production (Sinchaipanid et al., 2004), denaturation and degradation of the molecules are the main concerns because of the high temperatures involved.

Table 14.8 Applications of micro- and nanoparticles in tissue engineering.

Key factors	Polymers	Properties	Applications	References
Particle size	Alginate/calcium phosphate cement (CPC) paste containing human umbilical cord mesenchymal stem cells	Microbeads (73 −465 μm) provided a four- to seven-fold higher mechanical strength when compared to larger beads (2−3 mm)	Bone repair	Zhao et al. (2010)
Surface topography	Poly(ethylene glycol) diacrylate	Wrinkled surface on the particles promoted cell attachment with a larger surface area when compared to smooth ones	Cell carriers	Li et al. (2016)
Pore size	Polycaprolactone porous beads	After 7 days of testing, beads with pore sizes of 50−100 μm showed higher cell growth than those of 25−50 μm. The suitable pore size provided more efficient transport of nutrients or metabolites for cell growth	Cell carriers	Lim et al. (2009)

The supercritical fluid technique is an attractive and environmentally friendly method in which CO_2 is used as a nonsolvent. This technique overcomes the drawbacks of the conventional methods as it uses mild temperature, avoids the necessity of toxic solvents, and is capable of fabricating nanoparticles with narrow size distribution and uniform drug distribution. The products are free of any residual solvents and the structure and functionality of the active ingredients are unaltered. To produce micro/nanoparticles, the solution containing polymer and bioactive agent is sprayed into a supercritical fluid (typically supercritical CO_2). The solvent dissolves in the supercritical fluid and the polymer (nano)particles form by precipitation. Fine-tuning of the product properties can be done by optimizing process conditions such as temperature and pressure. The major drawback of this method is the high cost and poor solvent power of CO_2 (Paliwal et al., 2014).

Different synthesis approaches have been developed to produce micro/nanoparticles with remarkable properties and versatile structures. Apart from the discussed manufacturing techniques, there are other techniques such as electrospraying, coacervation, gelation, grinding, and microfabrication, which have been considered for micro/nanoparticle production, suitable for certain applications. Moreover, innovative methods to produce micro/nanoparticles with desired particle size using the emulsion-polymerization method are discussed by Moscatelli and Sponchioni (2017).

The medical applications of micro/nanoparticles started with drug delivery and were further developed as cell support in tissue engineering. Some examples of the use of micro/nanoparticles in tissue engineering can be seen in Table 14.8.

14.5 Conclusions

Bioresorbable polymers have shown great promise in medical devices and provide significant advantages over traditional devices, especially in short-term applications. Due to the wide range of both synthetic and especially natural polymers available, the polymers and their composites can be carefully designed through careful tuning of material properties such as crystallinity, molecular weight, and hydrophobicity in order to meet the requirements for specific applications. However, bioresorbable polymers are still under development and have primarily been tested in controlled laboratory environments. Their functioning needs to be demonstrated on a larger scale in more realistic settings before they can be used in practical applications.

References

Ahmed, E.M., 2015. Hydrogel: preparation, characterization, and applications: a review. J. Adv. Res. 6 (2), 105–121.

Amann, L.C., Gandal, M.J., Lin, R., Liang, Y., Siegel, S.J., 2010. In vitro–in vivo correlations of scalable PLGA-risperidone implants for the treatment of schizophrenia. Pharmaceut. Res. 27, 1730–1737.

Ambekar, R.S., Kandasubramanian, B., 2019. Progress in the advancement of porous biopolymer scaffold: tissue engineering application. Ind. Eng. Chem. Res. 58 (16), 6163–6194.

Anton, N., Benoit, J.P., Saulnier, P., 2008. Design and production of nanoparticles formulated from nano-emulsion templates-A review. J. Contr. Release 128 (3), 185–199.

Arruebo, M., Fernández-Pacheco, R., Ibarra, M.R., Santamaría, J., 2007. Magnetic nanoparticles for drug delivery. Nano Today 2 (3), 22–32.

Bernkop-Schnürch, A., Dünnhaupt, S., 2012. Chitosan-based drug delivery systems. Eur. J. Pharm. Biopharm. 81 (3), 463–469.

Biswal, T., 2021. Biopolymers for tissue engineering applications: a review. Mater. Today: Proc. 41, 397–402.

Cai, M., Liu, H., Jiang, Y., Wang, J., Zhang, S., 2019. A high-strength biodegradable thermoset polymer for internal fixation bone screws: preparation, in vitro and in vivo evaluation. Colloids Surf. B Biointerfaces 183, 110445.

Cao, X.-Y., Tian, N., Dong, X., Cheng, C.-K., 2019. Polylactide composite pins reinforced with bioresorbable continuous glass fibers demonstrating bone-like apatite formation and spiral delamination degradation. Polymers 11 (5), 812.

Catanzano, O., Soriente, A., La Gatta, A., Cammarota, M., Ricci, G., Fasolino, I., Schiraldi, C., Ambrosio, L., Malinconico, M., Laurienzo, P., Raucci, M.G., Gomez d'Ayala, G., 2018. Macroporous alginate foams crosslinked with strontium for bone tissue engineering. Carbohydr. Polym. 202, 72–83.

Costantini, M., Colosi, C., Mozetic, P., Jaroszewicz, J., Tosato, A., Rainer, A., Trombetta, M., Wieszkowski, W., Dentini, M., Barbetta, A., 2016. Correlation between porous texture and cell seeding efficiency of gas foaming and microfluidic foaming scaffolds. Mater. Sci. Eng. C 62, 668–677.

Danhier, F., Ansorena, E., Silva, J.M., Coco, R., Le Breton, A., Préat, V., 2012. PLGA-based nanoparticles: an overview of biomedical applications. J. Contr. Release 161 (2), 505–522.

Darge, H.F., Andrgie, A.T., Tsai, H.C., Lai, J.Y., 2019. Polysaccharide and polypeptide based injectable thermo-sensitive hydrogels for local biomedical applications. Int. J. Biol. Macromol. 133, 545–563.

Dehghani, F., Annabi, N., 2011. Engineering porous scaffolds using gas-based techniques. Curr. Opin. Biotechnol. 22 (5), 661–666.

Dethe, M.R., Prabakaran, A., Ahmed, H., Agrawal, M., Roy, U., Alexander, A., 2022. PCL-PEG copolymer based injectable thermosensitive hydrogels. J. Contr. Release 343, 217–236.

Dhandayuthapani, B., Yoshida, Y., Maekawa, T., Kumar, D.S., 2011. Polymeric scaffolds in tissue engineering application: a review. Int. J. Polym. Sci. 2011, 290602.

Eke, G., Mangir, N., Hasirci, N., MacNeil, S., Hasirci, V., 2017. Development of a UV crosslinked biodegradable hydrogel containing adipose derived stem cells to promote vascularization for skin wounds and tissue engineering. Biomaterials 129, 188–198.

Feng, B., Wang, S., Hu, D., Fu, W., Wu, J., Hong, H., Domian, I.J., Li, F., Liu, J., 2019. Bioresorbable electrospun gelatin/polycaprolactone nanofibrous membrane as a barrier to prevent cardiac postoperative adhesion. Acta Biomater. 83, 211–220.

Fereshteh, Z., Fathi, M., Bagri, A., Boccaccini, A.R., 2016. Preparation and characterization of aligned porous PCL/zein scaffolds as drug delivery systems via improved unidirectional freeze-drying method. Mater. Sci. Eng. C 68, 613–622.

Frassica, M.T., Jones, S.K., Diaz-Rodriguez, P., Hahn, M.S., Grunlan, M.A., 2019. Incorporation of a silicon-based polymer to PEG-DA templated hydrogel scaffolds for bioactivity and osteoinductivity. Acta Biomater. 99, 100–109.

Fredenberg, S., Wahlgren, M., Reslow, M., Axelsson, A., 2011. The mechanisms of drug release in poly (lactic-co-glycolic acid)-based drug delivery systems—a review. Int. J. Pharm. 415 (1–2), 34–52.

Ganachaud, F., Katz, J.L., 2005. Nanoparticles and nanocapsules created using the ouzo effect: spontaneous emulsification as an alternative to ultrasonic and high-shear devices. ChemPhysChem 6 (2), 209–216.

Gheysoori, P., Paydayesh, A., Jafari, M., Peidayesh, H., 2023. Thermoresponsive nanocomposite hydrogels based on Gelatin/poly (N–isopropylacrylamide) (PNIPAM) for controlled drug delivery. Eur. Polym. J. 186, 111846.

Haghbin, M., Esmaeilzadeh, J., Kahrobaee, S., 2020. Freeze dried biodegradable polycaprolactone/chitosan/gelatin porous scaffolds for bone substitute applications. Macromol. Res. 28, 1232–1240.

Han, S.K., Song, M., Choi, K., Choi, S.W., 2021. Fabrication of biodegradable polyurethane foam scaffolds with customized shapes and controlled mechanical properties by gas foaming technique. Macromol. Mater. Eng. 306 (7), 2100114.

Hodge, J., Quint, C., 2019. The improvement of cell infiltration in an electrospun scaffold with multiple synthetic biodegradable polymers using sacrificial PEO microparticles. J. Biomed. Mater. Res., Part A 107 (9), 1954–1964.

Hou, Q., Grijpma, D.W., Feijen, J., 2003. Preparation of interconnected highly porous polymeric structures by a replication and freeze-drying process. J. Biomed. Mater. Res. B Appl. Biomater. 67 (2), 732–740.

Huang, R., Zhu, X., Tu, H., Wan, A., 2014. The crystallization behavior of porous poly(lactic acid) prepared by modified solvent casting/particulate leaching technique for potential use of tissue engineering scaffold. Mater. Lett. 136, 126–129.

Kamaly, N., Xiao, Z., Valencia, P.M., Radovic-Moreno, A.F., Farokhzad, O.C., 2012. Targeted polymeric therapeutic nanoparticles: design, development and clinical translation. Chem. Soc. Rev. 41 (7), 2971–3010.

Kamaly, N., Yameen, B., Wu, J., Farokhzad, O.C., 2016. Degradable controlled-release polymers and polymeric nanoparticles: mechanisms of controlling drug release. Chem. Rev. 116 (4), 2602–2663.

Kang, S., Kim, T., Kim, B., Jeong, Y., Park, Y.I., Noh, S.M., Park, J., 2018. Novel thermal radical initiators based on a triazene moiety for radical polymerization. J. Ind. Eng. Chem. 68, 1–5.

Karavelidis, V., Karavas, E., Giliopoulos, D., Papadimitriou, S., Bikiaris, D., 2011. Evaluating the effects of crystallinity in new biocompatible polyester nanocarriers on drug release behavior. Int. J. Nanomed. 6, 3021–3032.

Kluin, J., Talacua, H., Smits, A.I., Emmert, M.Y., Brugmans, M.C., Fioretta, E.S., Dijkman, P.E., Söntjens, S.H., Duijvelshoff, R., Dekker, S., 2017. In situ heart valve tissue engineering using a bioresorbable elastomeric implant–from material design to 12 months follow-up in sheep. Biomaterials 125, 101–117.

Kohane, D.S., 2007. Microparticles and nanoparticles for drug delivery. Biotechnol. Bioeng. 96 (2), 203–209.

Lee, B.K., Yun, Y., Park, K., 2016. PLA micro- and nano-particles. Adv. Drug Deliv. Rev. 107, 176–191.

Li, M., Joung, D., Hughes, B., Waldman, S.D., Kozinski, J.A., Hwang, D.K., 2016. Wrinkling non-spherical particles and its application in cell attachment promotion. Sci. Rep. 6, 30463.

Lim, J.Y.C., Lin, Q., Xue, K., Loh, X.J., 2019. Recent advances in supramolecular hydrogels for biomedical applications. Mater. Today Adv. 3, 100021.
Lim, S.M., Lee, H.J., Oh, S.H., Kim, J.M., Lee, J.H., 2009. Novel fabrication of PCL porous beads for use as an injectable cell carrier system. J. Biomed. Mater. Res. B Appl. Biomater. 90 B (2), 521–530.
Liu, M., Liu, S., Xu, Z., Wei, Y., Yang, H., 2016. Formation of microporous polymeric membranes via thermally induced phase separation: a review. Front. Chem. Sci. Eng. 10 (1), 57–75.
Low, Y.J., Andriyana, A., Ang, B.C., Zainal Abidin, N.I., 2020. Bioresorbable and degradable behaviors of PGA: current state and future prospects. Polym. Eng. Sci. 60 (11), 2657–2675.
Lu, C.H., Yu, C.H., Yeh, Y.C., 2021. Engineering nanocomposite hydrogels using dynamic bonds. Acta Biomater. 130, 66–79.
Mabrouk, M., Beherei, H.H., Das, D.B., 2020. Recent progress in the fabrication techniques of 3D scaffolds for tissue engineering. Mater. Sci. Eng. C 110, 110716.
Maitz, M.F., 2015. Applications of synthetic polymers in clinical medicine. Biosurf Biotribol 1 (3), 161–176.
Makadia, H.K., Siegel, S.J., 2011. Poly Lactic-co-Glycolic Acid (PLGA) as biodegradable controlled drug delivery carrier. Polymers 3 (3), 1377–1397.
Manavitehrani, I., Le, T.Y., Daly, S., Wang, Y., Maitz, P.K., Schindeler, A., Dehghani, F., 2019. Formation of porous biodegradable scaffolds based on poly (propylene carbonate) using gas foaming technology. Mater. Sci. Eng. C 96, 824–830.
Mandal, B.B., Kundu, S.C., 2009. Cell proliferation and migration in silk fibroin 3D scaffolds. Biomaterials 30 (15), 2956–2965.
McKenna, E., Klein, T.J., Doran, M.R., Futrega, K., 2020. Integration of an ultra-strong poly(lactic-co-glycolic acid) (PLGA) knitted mesh into a thermally induced phase separation (TIPS) PLGA porous structure to yield a thin biphasic scaffold suitable for dermal tissue engineering. Biofabrication 12 (1), 015015.
Miles, C.E., Bernstein, A.D., Osborn Popp, T.M., Murthy, N.S., Nieuwkoop, A.J., Gormley, A.J., 2021. Control of drug release from microparticles by tuning their crystalline textures: a structure–activity study. ACS Appl. Polym. Mater. 3 (12), 6548–6561.
Moscatelli, D., Sponchioni, M., 2017. Bioresorbable polymer nanoparticles in the medical and pharmaceutical fields: a promising field. In: Bioresorbable Polymers for Biomedical Applications: From Fundamentals to Translational Medicine, pp. 265–283.
Oliveira, M.B., Mano, J.F., 2011. Polymer-based microparticles in tissue engineering and regenerative medicine. Biotechnol. Prog. 27 (4), 897–912.
On, S.-W., Cho, S.-W., Byun, S.-H., Yang, B.-E., 2020. Bioabsorbable osteofixation materials for maxillofacial bone surgery: a review on polymers and magnesium-based materials. Biomedicines 8 (9), 300.
Ounkaew, A., Jarensungnen, C., Jaroenthai, N., Boonmars, T., Artchayasawat, A., Narain, R., Chindaprasirt, P., Kasemsiri, P., 2023. Fabrication of hydrogel-nano silver based on aloe vera/carboxymethyl cellulose/tannic acid for antibacterial and pH-responsive applications. J. Polym. Environ. 31 (1), 50–63.
Ounkaew, A., Kasemsiri, P., Jetsrisuparb, K., Uyama, H., Hsu, Y.I., Boonmars, T., Artchayasawat, A., Knijnenburg, J.T.N., Chindaprasirt, P., 2020. Synthesis of nanocomposite hydrogel based carboxymethyl starch/polyvinyl alcohol/nanosilver for biomedical materials. Carbohydr. Polym. 248, 116767.
Ounkaew, A., Kasemsiri, P., Srichiangsa, N., Jetsrisuparb, K., Knijnenburg, J.T.N., Okhawilai, M., Hiziroglu, S., Theerakulpisut, S., 2022. Multifunctional gluten/guar gum copolymer with self-adhesion, self-healing, and remolding properties as smart strain sensor and self-powered device. Express Polym. Lett. 16 (6), 607–623.

Paliwal, R., Babu, R.J., Palakurthi, S., 2014. Nanomedicine scale-up technologies: feasibilities and challenges. Ageing Int. 15 (6), 1527–1534.
Pappalardo, D., Mathisen, T.r., Finne-Wistrand, A., 2019. Biocompatibility of resorbable polymers: a historical perspective and framework for the future. Biomacromolecules 20 (4), 1465–1477.
Park, S.-B., Lih, E., Park, K.-S., Joung, Y.K., Han, D.K., 2017. Biopolymer-based functional composites for medical applications. Prog. Polym. Sci. 68, 77–105.
Perez-Puyana, V., Felix, M., Romero, A., Guerrero, A., 2019. Influence of the processing variables on the microstructure and properties of gelatin-based scaffolds by freeze-drying. J. Appl. Polym. Sci. 136 (25), 47671.
Pham, Q.P., Sharma, U., Mikos, A.G., 2006. Electrospinning of polymeric nanofibers for tissue engineering applications: a review. Tissue Eng. 12 (5), 1197–1211.
Prasher, P., Sharma, M., Singh, S.K., Haghi, M., McLoughlin, R., Chellappan, D.K., Gupta, G., Paudel, K.R., Hansbro, P.M., Oliver, B.G.G., 2022. Advances and applications of dextran-based nanomaterials targeting inflammatory respiratory diseases. J. Drug Deliv. Sci. Technol. 74, 103598.
Qi, J., Zhang, Y., Liu, X., Zhang, Q., Xiong, C., 2020. Preparation and properties of a biodegradable poly (lactide-co-glycolide)/poly (trimethylene carbonate) porous composite scaffold for bone tissue engineering. New J. Chem. 44 (34), 14632–14641.
Raggio, R., Bonani, W., Callone, E., Dirè, S., Gambari, L., Grassi, F., Motta, A., 2018. Silk fibroin porous scaffolds loaded with a slow-releasing hydrogen sulfide agent (GYY4137) for applications of tissue engineering. ACS Biomater. Sci. Eng. 4 (8), 2956–2966.
Ramakrishna, S., Mayer, J., Wintermantel, E., Leong, K.W., 2001. Biomedical applications of polymer-composite materials: a review. Compos. Sci. Technol. 61 (9), 1189–1224.
Ravichandran, R., Sundarrajan, S., Venugopal, J.R., Mukherjee, S., Ramakrishna, S., 2012. Advances in polymeric systems for tissue engineering and biomedical applications. Macromol. Biosci. 12 (3), 286–311.
Reys, L.L., Silva, S.S., Pirraco, R.P., Marques, A.P., Mano, J.F., Silva, T.H., Reis, R.L., 2017. Influence of freezing temperature and deacetylation degree on the performance of freeze-dried chitosan scaffolds towards cartilage tissue engineering. Eur. Polym. J. 95, 232–240.
Rivera-Hernandez, G., Antunes-Ricardo, M., Martínez-Morales, P., Sanchez, M.L., 2021. Polyvinyl alcohol based-drug delivery systems for cancer treatment. Int. J. Pharm. 600, 120478.
Rowlands, A.S., Lim, S.A., Martin, D., Cooper-White, J.J., 2007. Polyurethane/poly(lactic-co-glycolic) acid composite scaffolds fabricated by thermally induced phase separation. Biomaterials 28 (12), 2109–2121.
Sah, E., Sah, H., 2015. Recent trends in preparation of poly(lactide-co-glycolide) nanoparticles by mixing polymeric organic solution with antisolvent. J. Nanomater. 2015, 794601.
Salerno, A., Di Maio, E., Iannace, S., Netti, P.A., 2012. Tailoring the pore structure of PCL scaffolds for tissue engineering prepared via gas foaming of multi-phase blends. J. Porous Mater. 19 (2), 181–188.
Shen, J., Dai, Y., Xia, F., Zhang, X., 2022a. Role of divalent metal ions in the function and application of hydrogels. Prog. Polym. Sci. 135, 101622.
Shen, Y., Tang, C., Sun, B., Zhang, Y., Sun, X., Mohamed, E.-N., Hany, E.-H., Morsi, Y., Gu, H., Wang, W., 2022b. 3D printed personalized, heparinized and biodegradable coronary artery stents for rabbit abdominal aorta implantation. Chem. Eng. J. 450, 138202.
Sheng, S.J., Wang, F., Ma, Q.Y., Hu, X., 2015. Impact of foaming air on melting and crystallization behaviors of microporous PLA scaffolds. J. Therm. Anal. Calorim. 122 (3), 1077–1088.

Sin, D., Miao, X., Liu, G., Wei, F., Chadwick, G., Yan, C., Friis, T., 2010. Polyurethane (PU) scaffolds prepared by solvent casting/particulate leaching (SCPL) combined with centrifugation. Mater. Sci. Eng. C 30 (1), 78–85.

Sinchaipanid, N., Junyaprasert, V., Mitrevej, A., 2004. Application of hot-melt coating for controlled release of propranolol hydrochloride pellets. Powder Technol. 141 (3), 203–209.

Sola, A., Bertacchini, J., D'Avella, D., Anselmi, L., Maraldi, T., Marmiroli, S., Messori, M., 2019. Development of solvent-casting particulate leaching (SCPL) polymer scaffolds as improved three-dimensional supports to mimic the bone marrow niche. Mater. Sci. Eng. C 96, 153–165.

Spicer, C.D., 2020. Hydrogel scaffolds for tissue engineering: the importance of polymer choice. Polym. Chem. 11 (2), 184–219.

Srikhao, N., Chirochrapas, K., Kwansanei, N., Kasemsiri, P., Ounkaew, A., Okhawilai, M., Likitaporn, C., Theerakulpisut, S., Uyama, H., 2022. Multi-responsive optimization of novel pH-sensitive hydrogel beads based on basil seed mucilage, alginate, and magnetic particles. Gels 8 (5), 274.

Stiepel, R.T., Pena, E.S., Ehrenzeller, S.A., Gallovic, M.D., Lifshits, L.M., Genito, C.J., Bachelder, E.M., Ainslie, K.M., 2022. A predictive mechanistic model of drug release from surface eroding polymeric nanoparticles. J. Contr. Release 351, 883–895.

Su, J., Li, J., Liang, J., Zhang, K., Li, J., 2021. Hydrogel preparation methods and biomaterials for wound dressing. Life 11 (10), 1016.

Sultana, N., Wang, M., 2008. Fabrication of HA/PHBV composite scaffolds through the emulsion freezing/freeze-drying process and characterisation of the scaffolds. J. Mater. Sci. Mater. Med. 19 (7), 2555–2561.

Surmenev, R.A., Ivanov, A.N., Saveleva, M.S., Kiriiazi, T.S., Fedonnikov, A.S., Surmeneva, M.A., 2022. The effect of different sizes of cross-linked fibers of biodegradable electrospun poly(ε-caprolactone) scaffolds on osteogenic behavior in a rat model in vivo. J. Appl. Polym. Sci. 139 (22).

Taesuwan, I., Ounkaew, A., Okhawilai, M., Hiziroglu, S., Jarernboon, W., Chindaprasirt, P., Kasemsiri, P., 2022. Smart conductive nanocomposite hydrogel containing green synthesized nanosilver for use in an eco-friendly strain sensor. Cellulose 29 (1), 273–286.

Takeuchi, I., Yamaguchi, S., Goto, S., Makino, K., 2017. Drug release behavior of hydrophobic drug-loaded poly (lactide-co-glycolide) nanoparticles: effects of glass transition temperature. Colloids Surf. A Physicochem. Eng. Asp. 529, 328–333.

Tan, H., Chu, C.R., Payne, K.A., Marra, K.G., 2009. Injectable in situ forming biodegradable chitosan-hyaluronic acid based hydrogels for cartilage tissue engineering. Biomaterials 30 (13), 2499–2506.

Tesfamariam, B., 2016. Bioresorbable vascular scaffolds: biodegradation, drug delivery and vascular remodeling. Pharmacol. Res. 107, 163–171.

Thorrez, L., Shansky, J., Wang, L., Fast, L., VandenDriessche, T., Chuah, M., Mooney, D., Vandenburgh, H., 2008. Growth, differentiation, transplantation and survival of human skeletal myofibers on biodegradable scaffolds. Biomaterials 29 (1), 75–84.

Varde, N.K., Pack, D.W., 2004. Microspheres for controlled release drug delivery. Expert Opin. Biol. Ther. 4 (1), 35–51.

Washington, K.E., Kularatne, R.N., Karmegam, V., Biewer, M.C., Stefan, M.C., 2017. Recent advances in aliphatic polyesters for drug delivery applications. Wiley Interdiscip. Rev. Nanomed. Nanobiotechnol. 9 (4), e1446.

Wischke, C., Schwendeman, S.P., 2008. Principles of encapsulating hydrophobic drugs in PLA/PLGA microparticles. Int. J. Pharm. 364 (2), 298–327.

Wu, X., Liu, Y., Li, X., Wen, P., Zhang, Y., Long, Y., Wang, X., Guo, Y., Xing, F., Gao, J., 2010. Preparation of aligned porous gelatin scaffolds by unidirectional freeze-drying method. Acta Biomater. 6 (3), 1167–1177.

Xie, M., Zeng, Y., Wu, H., Wang, S., Zhao, J., 2022. Multifunctional carboxymethyl chitosan/oxidized dextran/sodium alginate hydrogels as dressing for hemostasis and closure of infected wounds. Int. J. Biol. Macromol. 219, 1337–1350.

Yang, Q., Chen, L., Shen, X., Tan, Z., 2006. Preparation of polycaprolactone tissue engineering scaffolds by improved solvent casting/particulate leaching method. J. Macromol. Sci., Part B: Phys. 45 (6), 1171–1181.

Zeng, S., Ye, J., Cui, Z., Si, J., Wang, Q., Wang, X., Peng, K., Chen, W., 2017. Surface biofunctionalization of three-dimensional porous poly (lactic acid) scaffold using chitosan/OGP coating for bone tissue engineering. Mater. Sci. Eng. C 77, 92–101.

Zhang, H., Liu, X., Yang, M., Zhu, L., 2015. Silk fibroin/sodium alginate composite nanofibrous scaffold prepared through thermally induced phase-separation (TIPS) method for biomedical applications. Mater. Sci. Eng. C 55, 8–13.

Zhao, L., Weir, M.D., Xu, H.H.K., 2010. An injectable calcium phosphate-alginate hydrogel-umbilical cord mesenchymal stem cell paste for bone tissue engineering. Biomaterials 31 (25), 6502–6510.

Zhu, C., Zhang, W., Shao, Z., Wang, Z., Chang, B., Ding, X., Yang, Y., 2023. Biodegradable glass fiber reinforced PVA hydrogel for cartilage repair: mechanical properties, ions release behavior and cell recruitment. J. Mater. Res. Technol. 23, 154–164.

CHAPTER 15

Bioresorbable polymers for wound healing

Sheikh Shahnawaz Quadir[1], Dinesh Puri[2], Garima Joshi[1], Deepak Choudhary[1], Sanket Kumar[1], Monika Singh[3] and Shalini K. Sawhney[3]

[1]Department of Pharmaceutical Sciences, Mohanlal Sukhadia University, Udaipur, Rajasthan, India; [2]School of Pharmacy, Graphic Era Hill University, Dehradun, Uttarakhand, India; [3]I.T.S. College of Pharmacy, Ghaziabad, Uttarpradesh, India

15.1 Introduction

Over the last decade, polymers have played a vital role in medicine. Among these, bioresorbable polymers have gained increased attention due to their unique potential in medicinal formulations and represent a diverse family in the field of biomaterials. The term biomaterial was coined in 1982 at NIH Consensus Development Conference, describing clinical uses of biomaterials. It is defined as "any substances or a combination of the substances other than drug which is either natural or synthetic in nature can be used in any period of time for the treatment, replacement or augmentation of any tissue, organ or a function of the body." Other definitions include that in the William Dictionary of Biomaterials (1999), which states that "nonviable materials which is utilized in the medical devices, intended to interact with the biological system", and also "A material which is synthetic, natural or modified natural material (other than drug) intended to interact with the biological system or a part of system that are able to treat, replace or augment a tissue, organ or a function of the body" as described in Dorland's Medical Dictionary (Pertici, 2017).

Bioresorbable compounds are those compounds which alter their chemical and physical structure when they came into contact with a biological system. If a compound is bioresorbable in nature, by applying correct conditions in the presence of fungi, bacteria, or microorganisms, it will automatically break down to its basic structure. The key benefits of such compounds include that they degrade without leaving any toxins behind. The word bioresorbable

Bioresorbable Polymers and their Composites
ISBN 978-0-443-18915-9
https://doi.org/10.1016/B978-0-443-18915-9.00003-3
© 2024 Elsevier Ltd.
All rights reserved.

means biodegradable or naturally absorbing, which is used to define the process of breaking down by nature. However, bioresorption highlights the process which leads to the slowly disintegration of a compound into fractions inside the human body. When this compound comes into contact with body fluids, it alters its physicochemical properties resulting in physical, chemical, biological, and mechanical characteristics among the compounds and neighboring environment. These compounds are easily metabolized without showing any toxic effects and then cleared from the body (Agubata et al., 2021).

The major utilized bioresorbable compounds in medicine are ceramics, and polymeric and metallic materials. Bioresorbable polymers have been described as "today's material." In the current era, bioresorbable polymers have attracted the attention of researchers and scientists due to their potential in the tissue engineering and biomaterials fields. Meanwhile, in medicine, bioresorbable polymers possess significant applications in wound healing (i.e., sutures, adhesives, staples, etc.) and controlled drug delivery. They are also used in ligaments for orthopedic devices, along with nonwoven materials and scaffolds in tissue engineering. These bioresorbable polymers also offer great applications in a number of domains such as dental, drug delivery, biological devices, biosensors, nanoparticles, and nanocarriers, as well as for in vitro diagnostic tools, etc. (Daniel, 2021).

Wounds can be defined as any lesion which occurs to the skin or other body tissues either by cuts, scratches, scrapes, or other accidental damage. Hence, for the treatment of such wounds, wound healing is needed. To regenerate and repair dermal and epidermal tissues, dressings are widely used in the wound-healing process. Wound dressing materials are materials which act as a barrier to foreign particles, oxygen, and moisture to combat and protect against microorganisms (Mogosanu and Grumezescu, 2014). A passive dressing is important for maintaining optimum moisture, which helps in stimulating the wound-healing process. An ideal passive dressing material is one which influences the local cellular response for the treatment of wounds and burns such as cellulose, collagen, alginates, hydrogels, foams, cotton, hydrocolloids, etc. (Cornelius et al., 2006). These materials offer various key benefits in wound healing, e.g., maintenance of suitable moisture levels in wounds, minimizing the pain and itching, cleansing of damaged tissues, and eliminating dead spaces and nonviable tissues (Sawant et al., 2012). Some of these materials which are naturally available can progressively improve wound healing due to their emollient, antimicrobial, antiinflammatory, antioxidant and epithelializing properties.

Skin tissues have their own key potential, including structural organization and self-repairing ability. However, once they become injured by sufficiently large lesions, healing and recovery become suboptimal. In such cases, bioresorbable polymers play a vital role by restoring the native tissues or replacing them with engineered alternatives. This chapter emphasizes the factors which influence the healing process and the important applications of bioresorbable polymers in wound healing. It provides a framework for understanding the strategies of such polymers that could be key in the development of future therapeutic applications.

15.2 Wound-healing process

A wound is a skin lesion which occurs due to physical, chemical, thermal, or other tissue or systemic pathology. A wound is categorized on the basis of its severity, such as partial, superficial, or full thickness. The partial-thickness wound may have damage to the superficial layer, i.e. the epidermis (up to the dermal layer), and healing can take a few weeks. Superficial wounds only affect the epidermis, but healing can be successful through unaffected keratinocytes. The most difficult to treat and severe wounds are full-thickness wounds which can take several weeks to heal and still be suboptimal. These wounds include major damage to both the tissues of the epidermis and dermis (Mogosanu and Grumezescu, 2014). The above-listed wounds occurs in three stages, i.e., inflammation, proliferation, and remodeling (Danti et al., 2017).

Inflammation: In the inflammatory process, platelets play a vital role by forming a fibrin clot soon after the injury which permits the infiltrating cells to gather in the lesion area to prevent bleeding. Additionally, these platelets attract growth factors by initiating a cascade of events such as monocytes, neutrophils, and fibroblasts. They also induce fibroblasts to secrete fresh extracellular matrix.

Proliferation: The second process of wound healing is categorized as reepithelialization and connective tissue regeneration. Reepithelialization is a process started by proliferating keratinocytes which travel toward the lesion site. These new blood vessels develop side by side and fibroblasts gather from nearby areas to deposit extracellular matrix molecules (collagen fibers, elastin, glycosaminoglycan) and granulocytic tissues.

Remodeling: The final step in wound healing may take many year until the restoration of the entire dermis through constant tissue remodeling.

This step proceeds by replacing collagen type III with collagen type I through the secretion of matrix metalloproteinase. There are also some wounds which occur due to pathological and disease conditions, such as diabetes, which are unable to heal completely. Hence, such wounds become chronic by sustaining inflammatory events which become difficult for the growth factors to perform a healing function, resulting in the development of pathological constraints such as tumors and persistent infections.

15.3 Factors affecting wound healing

There are various factors that may impede the wound-healing process. In simple terms, those factors which affect the repair mechanism are divided into local and systemic. The local factors are those which directly damage or influence the process of wound healing by altering its characteristics, and systemic factors are those which affect the healing abilities of an individual in healthy or diseased condition (Fig. 15.1). In the majority of cases systemic factors occur due to local factors which influence wound healing (Guo and DiPietro, 2010).

15.3.1 Local factors that influence the healing process

15.3.1.1 Oxygenation

Oxygenation is crucial for the production of energy by means of ATP, cell metabolism, and for recovery from almost all types of wounds. It possesses several benefits in healing, such as the protection of wounds from infection by promoting angiogenesis, enhancing keratinocyte uptake, migration, and

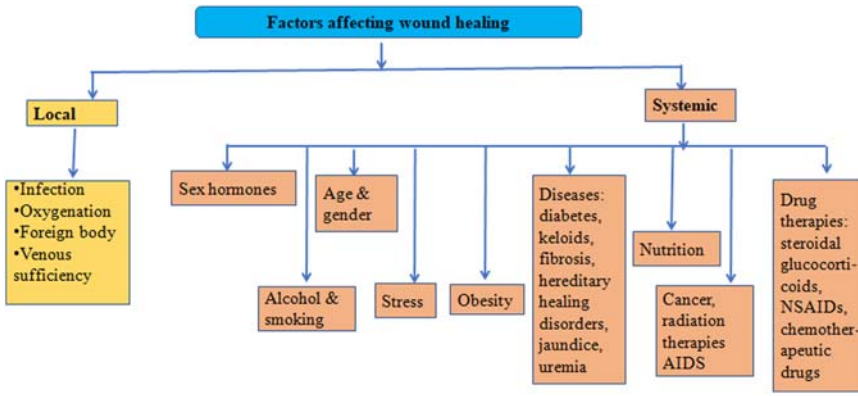

Figure 15.1 Factors affecting wound healing.

reepithelialization. It also promotes fibroblast proliferation around wounds along with the formation of collagen. Moreover, it increases the level of superoxide production with the help of polymorphonuclear leukocytes as a primary dependent oxygen factor (Bishop, 2008). There are several systemic conditions such as age and diabetes which can decrease the vascular flow, resulting in the development of hypoxic wounds due to poor tissue oxygenation.

Healing is diminished for those wounds which are unable to restore oxygen. A temporary lack of oxygen (hypoxia) can activate wound healing only if it happens for a long time, otherwise wound healing can be delayed. A lack of oxygen can impact cytokine and growth factor production. Cytokines formed due to a lack of oxygen include transforming growth factor-beta, platelet-derived growth factor, vascular endothelial growth factor, tumor necrosis factor, etc. ROS such as hydrogen peroxide and superoxide are majorly involved in normal wound healing and behave as cellular messengers to promote the wound-healing process, cell motility, cytokine action, and angiogenesis. Hypoxia and hyperoxia are responsible for enhancing ROS demand. However, on other hand, a higher level of ROS production can damage tissues (Rodriguez et al., 2008). To conclude, proper oxygen supply is essential for the success of the wound-healing process.

15.3.1.2 Infection and foreign bodies

Once a lesion is present on the skin, microorganisms gather at the skin surface and enter the underlying tissues. The level of the infection and replication state of the microorganisms affect whether the wounds are colonized, contaminated, or spread the invasive infection. The availability of nonreplicating microorganisms on wounds is identified as contamination. Meanwhile, the presence of replicating microorganisms on a wound without any tissue damage is described as colonization. Local infection and critical colonization are found at an intermediate stage where microorganisms can replicate and local tissue actions are started. An invasive infection is defined as the availability of replicating microorganisms inside a wound (Harding and Edwards, 2004).

On the other hand, inflammation is a basic response in the wound-healing process and an essential factor for the removal of contaminated microorganisms. If microbial removal is not completed, inflammation is sustained for a longer duration. Due to such conditions, bacteria and endotoxins both enhance cytokine production (IL-1 and TNF-alpha) which increase the inflammatory phase. If this happens for a longer time, the

wound is considered as chronic and is difficult to heal. Moreover, such a prolonged inflammatory state may elevate the production of metalloproteases which are responsible inhibiting the extracellular matrix in wounds (Menke et al., 2007).

15.3.2 Systemic factors that influence the healing process

15.3.2.1 Age

As per WHO, the over 60 years age group is growing faster than any other age group. Higher age of individuals is one of the critical risk factors in the impaired wound-healing process. Many clinical and animal studies conducted at the molecular level have revealed that higher age can adversely impact wound healing (Keylock et al., 2008). In the aged individual, altered inflammatory reactions, i.e., T-cell infiltration, chemokine formation, and lower phagocytic volume around the wound environment, can delay the wound healing. An animal study in aged mice compared with young mice revealed delayed angiogenesis, collagen production, and reepithelialization. In general, there are small differences between young and aged individuals in terms of wound healing. A review study of age-related changes revealed that the each step of wound healing for aged persons showed higher platelet aggregation, higher uptake of inflammatory mediators, delayed permeation of macrophages and lymphocytes, lowered growth factor secretions, and delayed reepithelialization, angiogenesis, and collagen production (Gosain and DiPietro, 2004).

15.3.2.2 Sex hormones in aged individuals

Compared to aged females, aged males are more affected by delays in the wound-healing process due to sex hormones. A female estrogen (estrone), male androgen (testosterone), and there steroidal precursor (dehydroepiandrosterone) have significant effects on the wound-healing process (Gilliver et al., 2007). A study revealed that the expression of genes among elderly men and young women was totally estrogen regulated. Numerous genes associated with wound healing are affected by estrogen, which enables matrix production, and inhibits protease and regeneration of tissues, and the genes those are involved in inflammation (Hardman and Ashcroft, 2008).

15.3.2.3 Stress

Stress has a significant effect on human health and social behavior. Several diseases are associated with stress, such as diabetes, wounds, CVS, and

cancer (Vileikyte, 2007). Clinical research has revealed that both humans and animals with physiological stress can have a hampered wound-healing process. A student with the stress of academic examinations and a caretaker for a person with Alzheimer's have delayed wound-healing processes. Stress is responsible for the up-regulation of glucocorticoid hormones as well as lowering the amount of proinflammatory cytokines (IL-1β, TNF-α, and IL-6) at the wound area. It also inhibits the progression of chemoattractants (IL-8 and IL1-α) which are essential for the initial inflammatory step during the wound-healing process (Boyapati and Wang, 2007).

Moreover, Th1 responses are essential during the starting phase of wound healing, and are regulated by the glucocorticoid cortisol as an antiinflammatory agent. Hence, physiological stress can impair and delay healing at the wound site via reduced cell-mediated immunity (Godbout and Glaser, 2006). Other negative stress factors such as anxiety and depression affect health and behavior as well as being responsible for delaying wound healing. The effects of stress on wound healing are summarized in Fig. 15.2.

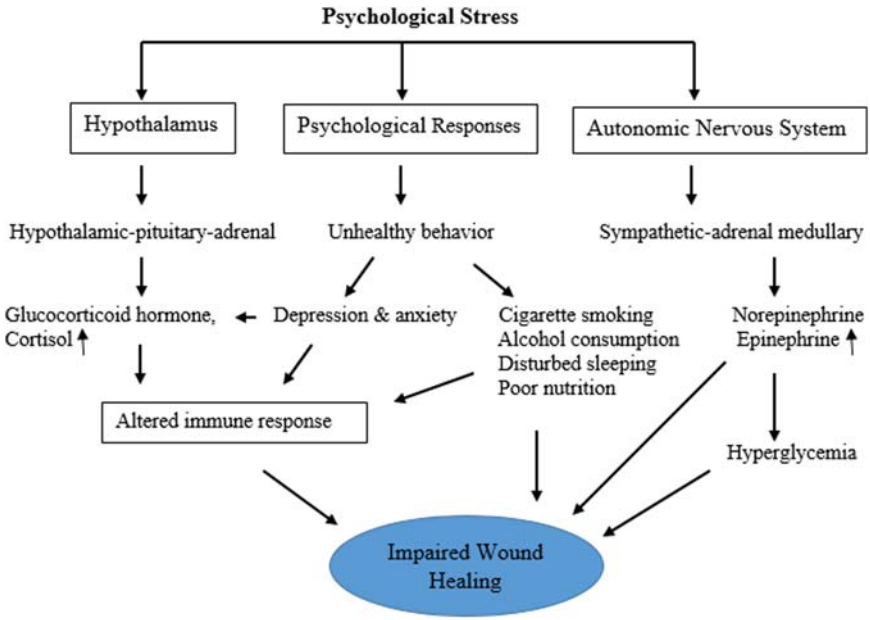

Figure 15.2 The effects of stress on wound healing.

15.3.2.4 Diabetes

An individual who is affected by diabetes shows an impaired healing process in acute wounds. Much of this population is affected by chronic nonhealing diabetic foot ulcers (DFUs). DFUs are a severe condition of diabetes that occur in about 15% of the total diabetic population. A patient with diabetes can experience poor wound healing from both DFUs as well as acute cutaneous wounds due to a variety of intricate pathophysiological processes. DFUs arise to hypoxia, as with venous stasis illness and chronic nonhealing wounds. By elevating the concentration of oxygen radicals, hypoxia can exacerbate the primary inflammatory actions and lengthen the healing process. Diabetes-associated wounds are considered to have a number of dysregulated cellular causes, including inadequate T-cell immunity, faulty leukocyte chemotaxis, phagocytosis, bactericidal activity, and dysfunctioning of epidermal cells and fibroblasts (Woo et al., 2007). Some of the other causes are described in Fig. 15.3.

15.3.2.5 Medications

Numerous drugs have the potential to alter the wound-healing process, including those that hamper platelet function, clot development, inflammatory action, and cell proliferation. Only those drugs categories that are frequently taken and possess major effects on healing are discussed here, such as NSAIDs, glucocorticoid steroids, and chemotherapy therapies.

Glucocorticoid steroids

The glucocorticoids are systemic antiinflammatory drugs that are well recognized as hindering wound healing by suppressing cellular wound

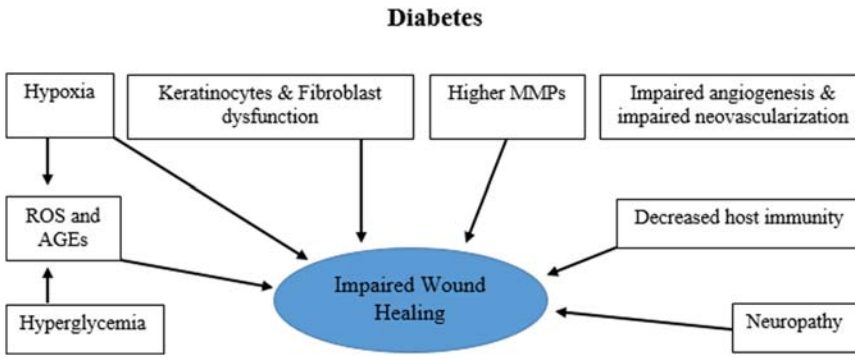

Figure 15.3 Effects of wound healing in diabetes. *AGEs*, advanced glycation end products; *MPPs*, matrix metalloproteases; *ROS*, reactive oxygen species.

responses. i.e., the proliferation of fibroblast and collagen production. These steroids form inadequate granulating tissues and lower wound contraction in the healing process. A critical transcriptional factor associated with wound healing, i.e., HIF-1 (Hypoxia-inducible factor-1), is also inhibited by glucocorticoids (Wagner et al., 2008). Compared to systemic application, topical application of glucocorticoids has quite different effects as it promotes the wound-healing process. Chronic wounds treated with topical low-dose corticosteroids have been shown to heal more rapidly, cause less pain and exudate, and encourage hypergranulation tissue formation in almost 79% of instances (Hofman et al., 2007).

NSAIDs

Ibuprofen is one of the nonsteroidal antiinflammatory drugs (NSAIDs) frequently used to treat inflammation, control pain, and treat rheumatoid arthritis. A low dose of aspirin is frequently used as a primary preventive treatment option for cardiovascular disease but not as an antiinflammatory drug due to its antiplatelet properties (Pertici, 2017). There is little evidence to support the claim that short-term use of NSAIDs impairs wound recovery. However, it remains unclear whether long-term NSAIDs affect how well wounds heal. Moreover, in animal studies, ibuprofen has been shown to have antiproliferative properties on wounds, resulting in lowering of fibroblast content and wound contraction, along with delayed epithelialization and impaired angiogenesis (Pieringer et al., 2007).

Chemotherapeutic drugs

The majority of chemotherapies work by slowing down the cellular metabolism, accelerating cell division, and promoting angiogenesis, all of which are essential for an effective wound-healing process. These drugs prevent the production of DNA, RNA, and proteins, which lower the fibroplasia and neovascularization of tissues. Chemotherapeutic drugs delay cell migration into the wound, decrease early wound matrix formation, lower collagen production, impair the proliferation of fibroblasts, and inhibit the contraction of wounds (Kirchner et al., 2003).

15.3.2.6 Obesity

Numerous infections or diseases, as well as health issues such as diabetes, ischemic heart disease, cancer, hypertension, and delayed wound healing, are known to be made more likely by obesity. People affected by obesity experience several wound complications, such as venous and pressure

ulcers, skin wound infections, seroma, and hematoma development. Obese patients receiving bariatric and nonbariatric procedures have been shown to have a higher frequency of wound problems. Obese people experience a higher rate of surgical site infections and many of these issues occur in subcutaneous adipose tissues due to hypoperfusion and ischemia. This situation also occurs due to lowered intake of antibiotics. Increased tension on the edges of surgical wounds typically occurs in obese patients, resulting in wound dehiscence. Due to wound tension, tissue pressure rises significantly, which hampers the microperfusion process and lowers the capabilities of wounds to consume oxygen (Franz et al., 2007).

15.3.2.7 Alcohol consumption

The use of alcohol hinders the wound-healing process and enhances the risk of infection as per a clinical and animal study report (Anaya and Dellinger, 2006). Due to alcohol exposure, either acute or chronic, in more than half of traumatic events, the impact of alcohol on the repair mechanism is extremely clinically significant. The consumption of alcohol lowers the defense mechanism and being intoxicated at the time of injury increases the likelihood of wound infection (Szabo and Mandrekar, 2009).

15.3.2.8 Smoking

Smoking increases the risk of various malignancies, such as stroke, heart, vascular disease, lung disease ,etc. Similarly, smoking has long been recognized as having detrimental impacts on wound healing (Choudhry and Chaudry, 2006). One study revealed that patients who smoke after surgery experience delayed wound healing and also a number of issues such as wound rupture, infection, leaking, necrosis, epidermolysis, and lowered tensile strength of wounds. In the field of oral surgery, smokers have been found to have lower recovery after both conventional oral surgery and the installation of dental implants (Ahn and Mulligan, 2008).

15.3.2.9 Nutrition

Nutrition has been acknowledged for more than a century as a critical component that influences the wound-healing process. It is clear that inadequate nutrition or specific nutrient deficiency can significantly affect wound healing following trauma and surgery. Patients who are malnourished and have chronic or delayed healing frequently require specialized nourishment. The healing process can be impacted by the metabolism of carbohydrates, proteins, fats, vitamins, and minerals (Balaji, 2008).

15.4 Properties of bioresorbable polymers

For the manufacturing of engineered tissue products, the choice of biopolymer is crucial. Although the traditional selection principle for secure, stable, and inert substances still applies, it has been found that any artificial substances ingested by the patient will have biological reactions. As each biopolymer application necessitates a different environment for cell–cell communication, it is crucial for the engineered tissue product manufacturer to have a variety of biopolymer options available (Zhang et al., 2014). Such applications include:

A. It should support the development of new tissues through the interaction among cells and their potential to obtain nutrients, growth factor, and optimized active pharmaceutically ingredients.
B. It should inhibit the cellular properties of tissue growth where surgically induced adhesions are detrimental.
C. It must lead to tissue responses by increasing the cellular reaction of one and inhibiting the other.
D. It should improve cell–cell connections and cellular activity, such as the formation of ECM, proliferation, and fibroblast attachment.
E. It should inhibit cellular connectivity, such as the connectivity of platelets to vascular grafts.
F. Inhibition of biological activity such as in organ transplantations by blocking antibodies against grafted cells.

When tissue recovery or modifications are the prime object of engineered tissue products, bioresorbable polymers are appropriate; however, they are not appropriate when long-lasting material stability is needed. Hence, bioresorbable polymers also require features such as:

A. Manufacturing feasibility, as well as an excess amount of polymers available commercially.
B. The proficiency to convert the polymer into the final product.
C. The mechanical characteristic that interact in short-term functioning but do not interfere with long-term functioning.
D. Minimum or nontoxicity of breakdown products, in both systemic and local tissue reactions.
E. Possibilities for the development of drug-delivery systems for use in the sustained release of active pharmaceutical ingredients.

Natural and engineered natural substances, along with metals, synthetic polymers, ceramics, and composites, are among the various substances that are mostly used in clinical applications. Metals, including their alloys, are

employed for implants in dental and orthopedic use because of their mechanical potential, such as ductility, toughness, and increased strength. Nevertheless, a metallic implant may have issues that are serious enough to necessitate a second surgery to remove the device, such as irritation brought on by corrosive and erosive conditions in biological systems, secondary fracture of conducted bone, and development of sterile implants. Ceramics and glasses, which can be chemically bioactive or nonbioactive in nature, are utilized in a number of biomedical applications, mostly for rebuilding missing bones, but because of their brittle nature, they are avoided in load-bearing applications (Arnold and Barbul, 2006).

Polymers are less strong and ductile than ceramics, glasses, and metals, however they are commonly utilized for exchanging, increasing, supporting, or fixing live tissues due to their diversity, simplicity, and biocompatible nature. It is feasible to develop composites by mixing polymers, ceramics, and metals to acquire unique qualities which are not present in a single material to develop customized devices for use in numerous biological sectors. Due to the structural similarity in living tissues which are formed of macromolecular composites, synthetic polymer composites are widely appealing biomaterials. The formation of engineered scaffolds, simple sutures, fixing screws, gauze strip, and bone replacements using bioresorbable polymers is a common practice. They do not require any secondary method to remove the implant or to initiate the tissue recovery in the matrix. The major outcome in the development of biomaterial research in the last 30 years has been the gradual transition from bio-stable prostheses to bioresorbable implants (Zhang et al., 2014).

15.5 Bioresorbable polymers for wound healing

Natural polymers offer a variety of benefits in regenerative medicinal therapy for the enhancement of wound healing, such as biodegradability, biocompatibility, and similarity to the extracellular matrix. Natural polymers are engaged in the repair of injured tissues and subsequently in skin regeneration by initiating and promoting the wound-healing process (Huang and Fu, 2010). Biomaterial hydrogels are used commercially, such as in pharmaceuticals and biomedicals, due to their unique 3D cross-linked structures that are soaked in aqueous or biological fluids for wound treatment, drug administration, organ replacement, and engineered tissue products (Das et al., 2012). Additionally, radioactivity studies are used to create innovative biomaterials based on biodegradability, nontoxicity, and

bio-renewable polymers. As a result, hydrogels made of naturally cross-linked polymers are utilized for the healing of wounds and skin burns (Haji-Saeid et al., 2010). The natural bioresorbable polymers for wound healing are described in the following subsections.

15.5.1 Polysaccharides

Polysaccharides are mainly introduced in the form of hydrogels. Some are primarily used for the treatment of wounds and skin burns. The polysaccharides are divided on the basis of their nature, such as those are neutral in nature, i.e., dextrans, glucans, cellulose; acidic in nature, i.e., alginic, hyaluronic acids; basic in nature, i.e., chitin, chitosan; or sulfated in nature, i.e., heparin, keratin, chondroitin, etc. (Kennedy et al., 2001).

15.5.1.1 Homoglycans

Homoglycans are biocompatible biopolymers that are utilized locally to alter the cellular activities involved in wound healing. Starch, dextran, cellulose, or their modified compositions can be used in the manufacture of nanofiber matrices in the regenerative medicinal therapies sector, such as for wound healing and tissue engineering (Lee et al., 2009).

α-Glucans

The common yeast-like fungus *Aureobasidium pullulans* forms pullulan (1-4),(1-6)-d-glucan from starch (Dothioraceae). A pullulan by-product was synthesized using a chemical cross-linking method for antibacterial release during wound healing via a superabsorbent polysaccharide-based hydrogel. Hydrogels possess extraordinary water-absorbing capabilities, with a swelling ratio up to 4000% and are also noncytotoxic, offering rapid hemostasis, while inhibiting fluid aggregation and enabling wound bed dryness. Additionally, drugs such as antibacterials or antimycotic therapies may be encapsulated into hydrogels to protect wounds and skin burns against microbial biofilm invasion (Li et al., 2011).

β-Glucans

β-Glucans possess the capabilities to form single and triple helical durable gel structures, while numerous forms of (1-3)-d-glucans can be isolated from fungi, yeast, and grains to identify the pharmacological and immunological properties. A study conducted by Lehtovaara et al. revealed that highly pure yeast-derived insoluble (1-3)-d-glucan considerably minimized skin irritation, blocked adipogenic division, and aided

the wound-healing process (Lehtovaara and Gu, 2011; Vetvicka and Vetvickova, 2011).

Dextrans

Dextran that has been modified to possess heparin-like qualities is known as carboxymethyl benzalamide sulfonate dextran (CMDBS), which is utilized for the treatment of wounds and skin burns. In general, CMDBS is a soluble polymer which possesses structural similarity with glycosaminoglycan heparin by enhancing the wound-healing process. In the majority of in vivo studies, it has been shown to be capable of inhibiting *Staphylococcus aureus* biofilms and promoting the cell proliferation and metabolism of various cells such as tumor, smooth muscle, and endothelial cells. Recently, cyclodextrins (hydrated) have been utilized as odor-control dressings due to their bucket-shaped structure which is capable of trapping and neutralizing water-insoluble particles. Cyclodextrin can be active for a long time than charcoal or serum proteins, which makes them excellent candidates to absorb odors more effectively (Logeart-Avramoglou and Jozefonvicz, 1999).

Cellulose

For chronic wound dressings, bioengineered cellulose is utilized superficially as a healing scaffold or matrix material, which minimizes discomfort and pain, and accelerates the healing process. Cellulose also possesses key benefits in wound healings such as enhancing granulation and epithelialization of partial- and full-thickness wounds. Various bioactive molecules, such as enzymes, hormones, vitamins, antioxidants, and antimicrobials, can be incorporated through a co-immobilization process using engineered cellulose for wound healing (Medusheva et al., 2007).

Chitin and chitosan

The most common natural amino polysaccharide is chitin (polu-N-acetyl-glucosamine), which is readily accessible throughout the year like cellulose. It makes up the majority of the exoskeletons of insects, crustaceans, and vertebrates, and also the cell walls of fungi. Chitin is transformed into chitosan (poly-N-acetyl-glycosaminoglycan) via the alkaline deacetylation process and by reacting the shells of shrimps with sodium hydroxide (Morganti et al., 2011). Several chitin and chitosan compositions with local hemostatic, antimicrobial, antiinflammatory, and wound-healing characteristic have been developed, such as water-soluble chitin ointment for

wound-healing treatment (Han, 2005) and chitin-loaded silver nanoparticles as a bactericidal film for wound healing (Madhumathi et al., 2010).

15.5.1.2 Heteroglycans

Heteroglycans offer various potentials in the biomedical sector. Heteroglycans, namely pectins, agarose, alginates, gums, carrageenans, and glycosaminoglycans, are biodegradable, biocompatible, and possess unusual physicochemical properties, i.e., film/gel forming and thickening properties of electrostatic composites. The development of heteroglycan fibers in the nanometric range using electrospinning technology may be advantageous for drug delivery and also regenerative medicinal therapies (Lee et al., 2009).

Alginates

Alginates are long repeating-unit polysaccharides with varying concentrations of residues from D-mannuronic and L-guluronic acid that are (1-4)-linked. Due to their hemostatic qualities, alginate-based wound dressings are frequently applied on skin burns and exuding or bleeding wounds. Alginates such as calcium, calcium-sodium, collagen, and gelatin are extremely absorbent natural fiber dressing materials developed from processed algae.

Agar and agarose

Agar and agarose fibers are developed by wet-spinning technology and are mainly utilized in biomedical and biomaterial applications for wound healing. A solvent containing DMSO:water in a ratio of 9:1 was used to construct continuous fibers in an ethanol coagulation bath. Agarose fibers that were homogeneous and of smooth texture exhibited significant water-swelling capabilities of 400%–500% as well as tensile strength of 30–50 MPa. Agarose fibers have been shown to be superior for swelling in water than agar fibers. Meanwhile, agaropectin has been shown to have flexibility issues (Bao et al., 2010).

Carrageenan

Carrageenan or carrageenins are a family of natural linear polysaccharides that are extracted from red edible seaweeds. They offer several potentials in the pharmaceutical, biomaterial, and food industries for thickening, gelling, and stabilizing properties. PVP-KC hydrogels were created by subjecting a combination of water systems such as poly(N-vinyl-2-pyrrolidone), kappa-carrageenan (KC), potassium chloride, and PEG to various gamma radiation dosages. These hydrogels were evaluated on various factors such as

temperature, mechanical behavior, fluid uptake, swelling factor, pH, electrical conductivity, and bioadhesive property on the human skin to predict their potential in wound healing (Sen and Avcı, 2005).

15.5.2 Glycolipids

Glycolipids are the complex lipids comprising carbohydrates linked via a glycosidic bond. Their main qualities include providing stability to the cell membrane and enhancing cellular recognition, which is important in terms of cell immunity as it permits cells to form bonds to develop tissues. Patients suffering from skin burns and wounds can benefit from topical glycolipids therapy consisting of galactose liposomes because of the rapid uptake of neutrophils and macrophages. The ability of macrophages to release cytokines and growth factors promotes tissue remodeling and the repair mechanism which is a key approach to wound healing. When compared to a control group, an experiment on mutant mice using 1-3-galactosyl transferase revealed the beneficial response of −Gal liposome at a daily dose of 10 mg (Galili et al., 2010).

15.5.3 Proteoglycans

Proteoglycans are essential proteins, covalently linked with the glycosaminoglycan chain that have a significant amount of macromolecules in the composition of extracellular matrix. Neoproteoglycans are the most biocompatible and biodegradable synthetic glycoconjugates developed from essential nanomaterials, proteins, or polymers that are covalently linked to the glycosaminoglycan chain and connected with the cells and proteins. Conjugates such as protein glycosaminoglycan, nano-glycosaminoglycan, and polymer glycosaminoglycan complexes are the three basic forms of neoproteoglycan which possess in vivo and in vitro tissue-engineered applications (Weyers and Linhardt, 2013).

15.5.4 Proteins and peptides

15.5.4.1 Vegetal proteins

Vegetal proteins are proteins available naturally from plants. These include soya, pulses, seeds, certain grains etc. These foods contain all the amino acids in an acceptable quantity. The treatment of wounds and skin burns can also be aided by some vegetal proteins. An ex vivo study performed on excised skin of rat using a combinational biomaterial composite of soya protein and sago starch which was cross-linked with glutaraldehyde was

found to be effective in wound healing (Ramnath et al., 2012). Additionally, vegetal proteins such as soya and sodium caseinate-derived biomaterials offer significant advantages in wound healing and drug delivery due to their biocompatible and biodegradable natures (Silva et al., 2003).

15.5.4.2 Collagen

One of the most prevalent proteins found in the human body and skin is formed by fibroblasts and is known as collagen. Collagen offers several potential qualities such as enhanced wound-healing process at the cellular and molecular levels as well as aiding the development of new tissues and epithelialization of wounds. For the prevention and cure of partial/full-thickness wounds with low to high exudates, collagen dressings formulated from bovine, pig, or avian sources are mainly utilized. However, these dressings are avoided in severe skin burns and for the patients who are sensitive or allergic to these products (Murali et al., 2011). There have been many research works on the use of various collagen-based dressings and compositions for the treatment of wounds and burns, such as for deep wounds (collagen sponges), gingival wounds (collagen−glycosaminoglycan complex), oral wounds (resorbable collagen membrane), wound healing (DNA salmon−collagen film complex) (Shen et al., 2008), cutaneous wounds (collagen−minocycline hydrogels) (Ghica et al., 2011), skin grafting (collagen microfiber scaffolds) (Kempf et al., 2011for vascular grafts and wound repairing (collagen electrospun nanofiber scaffolds) (Fullana and Wnek, 2012), and modified collagen−alginic thermostable biopolymers for the treatment of wounds (Mitra et al., 2011).

Gelatin

Gelatin is a naturally available biopolymer mainly obtained from collagen, and also from various animal by-products. Nowadays, gelatin is mainly used in the pharmaceutical and biomedical industries for the development of drug-delivery applications and for wound healing due to its biocompatible and biodegradable dressings. To identify its healing properties, various gelatin-containing composition studies have been performed on the dorsal skin of rats, such as cross-linked gelatin-alginates, gelatin-hyaluronic acid sponges, and EGF-gelatin-based wound healing in conditions including excess tissue loss and nonhealed wounds, i.e., burns, diabetic foot ulcers, trauma, and static ulcers; bioresorbable gelatin films have also been used for the treatment of trauma and orthopedic injuries.

Keratin

The intermediary fibrin proteins present in vertebrate epithelia and corneous tissues such as hooves, horns, and claws are collectively referred to as keratin. Due to its potential to treat proteolytic injuries, keratin and its derivatives have been utilized in chronic wounds to speed up healing. Keratin-based novel wound dressings with optimum potential have demonstrated controlled release behavior of growth factors and antibiotics.

Silk fibroin

Silk fibrin offers exceptional characteristics in the wound-healing process such as adhesion, absorption of exudates as well as being biodegradable and biocompatible with less inflammatory responses. Additionally, silk fibroin is utilized for the management of skin grafts, artificial ligaments, tendons, etc. It also serves as an excellent candidate in regenerative medicinal therapies such as silk fibroin and chitosan complex scaffolds for tissue regeneration (Gobin et al., 2005), carbon nanotubes for wound healing, SF—alginate combinational sponges for full-thickness wounds, and SF film biomaterials for wound treatment (de Moraes and Beppu, 2013).

Bovine serum albumin (BSA)

BSA is a protein derived from cattle. Due to anionic charge, BSA act as an intermediate bridge between tissues and cells and also acts as a carrier to transport fatty acids, vitamins, hormones, etc. Because of its binding capabilities, it also acts as a scavenger for the removal of toxic material such as pyrogens from the medium. BSA nanofibers are developed from the globular proteins in BSA medium without utilizing any chemical cross-linkers. Because of the fibrous characteristic of BSA it possesses various benefits in wound healing, suturing, and wound closure. It is used in various biomedical and pharmaceutical applications due to its biocompatible, biodegradable, and effective mechanical qualities (Zhu et al., 2011).

Enzymes

Enzymes are proteins that offer several applications in wound healing. Proteolytic and fibrinolytic enzymes, along with collagenase and papain, are effectively utilized in the epithelialization of wounds. In pectin film applied for wound healing, the development of prostaglandin H was drastically enhanced (Dror et al., 2008). Lysostaphin, a cell lytic enzyme, was formulated as antiinfective bandages immobilized on electrospun fibers through a solution of cellulose, such as cellulose—chitosan and cellulose—

poly-methacrylate. However, enzymes are avoided in wound healing for patients affected by coagulation disorders (Miao et al., 2011).

15.5.5 Synthetic polymers

Synthetic polymers were developed chemically in laboratories, and are described as manmade polymers (Gobi et al., 2021). By increasing the mechanical and biocompatible potentials of individual components, synthetic and natural polymers can be used to create new kinds of materials.

A hydrophilic synthetic polymer, polyvinyl alcohol (PVA), is widely employed in a variety of biomedical applications (Gyles et al., 2017). PVA is possible due to the availability of hydroxyl molecules, which can help to form hydrogen bonds (Norouzi et al., 2021). Due to its poor hydrophilic properties, thick membrane, and inadequate flexibility, PVA is only occasionally used as a polymeric wound-dressing material (Venkataprasanna et al., 2020). A synthetic hydrophilic polymer is known as poly(ethylene glycol) (PEG) (Sahana and Rekha, 2018). Growth factors such as macromeres and epidermal growth factor are interlinked to each other through significant attraction. These can be used directly at the wound site. Mechanical, thermal, and PEG crystalline features are preserved by mixing polymer with chitosan and PLGA. Such PEG-based treatments are effective in diabetic wounds. These treatments speed up the healing process by promoting skin cell development, collagen deposition, and proliferation (Shahverdi et al., 2014). Methacrylic acid is a monomer used to develop the synthetic polymer known as poly(methacrylic acid) (PMAA). In order to merge bioactive compounds with carboxylic groups, such as drugs and inorganic nanoparticles, PMAA is highly recommended in biomedical applications due to its water-soluble and biocompatible nature (Lumbreras-Aguayo et al., 2019). This substances can alter noticeably in response to changes in the pH and iconic strength of the solution as well as having high swelling capabilities in water. N-vinylpyrrolidone (monomer) was used to develop a hydrophilic linear chain polymer known as polyvinylpyrrolidone (PVP) (Kausar, 2019). A lipophilic and semicrystalline synthetic polymer known as polycaprolactone (PCL) has significant crystalline and morphological properties (Mohamed and Yusoh, 2016). To enhance its mechanical capabilities, PCL has been formed by mixing with other polymers or combined with them. Another of the most widely utilized synthetic polymers in the biomedical sector is poly(lactic acid (PLA). Several other derivatives of PLA are available with its chiral structure, such as poly-L-lactide (PLLA) formed by L-polymerization and called L-lactide.

Electrospinning technology is the primary method to obtain synthetic polymers which have micropores and a highly specified surface area for the treatment of wounds and skin burns. Synthetic polymers for wound dressing offer occlusive or semiocclusive characteristics enabling them to act as a barrier to protect against the infiltration of microorganisms. They may be in the form of hydrogels, foams, or hydrocolloids. Exudates are entrapped by the polymer film which provides a moist environment to the wound. Various authors have developed synthetic polymer-based wound dressing materials, such as ciprofloxacin HCL-loaded polyurethane and dextran electrospun nanofiber. Carrageenan-hydrophilic polymer hydrogels, cellulose acetate, PLA, and PLGA infused with shikonin have been used for wound recovery due to their antimicrobial, antiinflammatory, and antitumor activities, in addition to PVP-based nanosilver alginate hydrogels. One study revealed that carboxy methyl-chitosan provides various in vitro and in vivo characteristics in wound healing, such as stimulation of fibroblasts and macrophages and the secretion of various cytokines.

15.6 Nanocomposites for wound healing

In the area of wound healing, an increasing number of novel nano-therapies have surfaced and are presently undergoing clinical research studies. Numerous nano tactics have been investigated focusing on various stages of wound repair, such as nanoparticles, nanocarriers, and nanomaterials. Nanoparticles (NPs) are one of the options that researchers are studying for wound healing due to their wide spectrum of antibacterial properties and quick efficiency with a minimum dose. Due to the inability to permit a cell barrier, conventional therapies for wound healing have limited success as compared to nanoparticles, which can permit entry effectively (Khan et al., 2019). Disruption of the cell membrane, changes to the genes, and inhibition of enzyme production are aspects of NPs' antimicrobial activity, which leads to cell apoptosis. In addition, nanomaterials (NMs) are smooth, flexible, and biocompatible wound-healing materials that act as a gas barrier, absorbent for exudates, and a shielding material against further damages or heat. There are two primary types of NMs used in wound healing: (1) NMs with inherent qualities useful for treating wounds and (2) NMs used as drug-delivery systems (Bhattacharya et al., 2019).

15.6.1 Nonpolymeric

There are several nonpolymeric NPs that are utilized in wound healing, including metal and metallic NPs, lipid NPs, and ceramic NPs, as discussed next.

15.6.1.1 Metal and metallic nanoparticles

Various metal-based NPs such as gold (AuNPs), copper (CuNPs), silver (AgNPs), zinc oxide (ZnO NPs), titanium dioxide (TiO_2), cerium oxide (CeO_2), yttrium oxide (Y_2O_3), and other metal-based NPs have been reported for their antibacterial and wound-healing properties. Silver has been used as a medicine for a very long time. For the management of open wounds, burns, and chronically infected wounds, many types of silver components, i.e., metallic silver, silver nitrate, and silver sulfadiazine are used currently (Rai et al., 2009). The use of AgNPs has recently drawn attention, particularly for the treatment of open wounds, as a result of the rise in pathogenic bacteria that are multidrug resistant and to reduce the use of antibiotics. Silver nanoparticles are the most researched nanomaterial of all nanoparticles because of their exceptional antibacterial properties. Silver NPs are more effective at demonstrating higher antibacterial property than traditional therapies because they have a large surface area to volume ratio, which improves their interaction with microbes. The phosphorus-containing compounds in microbial cells, such as DNA ,can also bind with silver NPs, as can sulfur-containing proteins anchored in bacterial membranes.

A study performed by Orlowski and co-workers formulated tannic acid modified silver NPs possessing higher antibacterial action against *P. aeruginosa* and *E. coli*. The data revealed that the prepared NPs showed better wound closure, formation of granulating tissues, and angiogenesis in a mouse wound model (Orlowski et al., 2018). Another study performed by Peng and co-workers developed CS-coated silver NPs. Their data showed that the prepared formulation possessed excellent biocompatibility and was effective against meticillin-resistant *S. aureus* in contrast to polyvinyl-coated silver NPs (Peng et al., 2017). Silver NPs with CS polyethylene glycol hydrogel have been produced as a treatment for diabetic chronic wounds (Masood et al., 2019).

15.6.1.2 Lipid nanoparticles

Researchers and scientists have become interested in lipid-based NPs recently due to their potential use as drug-delivery systems. In addition, lipid NPs can be modified to suit certain health issues and routes of administration. These systems are risk-free, economical, and provide protection to drugs from biological deterioration. Due to their minimal toxicity and excellent efficacy, lipid NPs are employed as drug-delivery carriers in sensitive tissues (Attama et al., 2012). Such lipid NPs include solid lipid nanoparticles (SLNs), nanostructured lipid carriers (NLCs) and drug−lipid conjugates.

In addition to reducing pain and infection, essential oil offers several properties in wound healing such as an antibacterial, relaxing, and quick recovery from wounds (Saporito et al., 2018). Although rosemary and eucalyptus leaf extract have the ability to heal wounds, these essential oil are naturally volatile and are rapidly broken down by oxidation, heat, light, and volatilization (Apostolides et al., 2013). Hence, SLN- and NLC-based carriers are employed that enclose these essential oils and maintain their biological activity (Gokce et al., 2012). A study by Saporito and co-workers (Saporito et al., 2018) developed eucalyptus and rosemary oil-loaded NLCs. They used coco butter and olive oil as solid and liquid lipids which possess higher natural stability, biocompatibility, and rapid wound-healing properties through dermal fibroblasts. This study revealed that the prepared formulation effectively provided higher healing and antimicrobial properties showing a synergistic effect between olive oil and eucalyptus oil.

15.6.1.3 Ceramic nanoparticles

Ceramic NPs represent one of the most commonly employed inorganic NPs for wound healing. These NPs are mostly known for their wound healing, tissue regeneration, and antibacterial properties (Urie et al., 2018). Nanohydroxyapatite and calcium triphosphate as ceramic NPs offer broad applications in drug delivery and wound healing processes. the sol—gel formulation method is generally used for the development of ceramic NPs. Furthermore, these NPs are extensively utilized in the development of tissue-engineered formulations. Various authors has revealed the potential of ceramic NPs, such as Deepthi and co-workers who described the use of ceramic-CS-based NPs for bone rejuvenation (Deepthi et al., 2016). When combined with CS, components such as hydroxyapatite, silicon dioxide, bioglass ceramic, titanium dioxide, and zirconium oxide formed nanoscaffolds that are very effective in regenerating bone. To cure bone abnormalities in traditional therapies, artificial materials were implanted surgically, although this had several negative side effects. Hence, ceramic nanoparticles are employed to clear the way for tissue regeneration to overcome these problems. A bioactive ceramics and bioresorbable polymer mixture creates an extracellular matrix for the healing of bone tissue.

15.6.2 Polymeric nanoparticles

In the current era, strategies for the treatment of chronic wounds have been developed to deliver drugs and biomolecules in bioresorbable polymeric NPs with controlled release, such as PLGA, alginate, gelatin, chitosan,

PEG, and polycaprolactones. Polymeric NPs avoid frequent dosing, extend the therapeutic effectiveness, and provide controlled drug delivery in wound healing (Masood, 2016).

15.6.2.1 Synthetic

PLGA offers one of the most widely used synthetic polymers due to its biodegradability, biocompatibility, hydrophobic property, and for entrapping the growth factor in chronic wound therapy among all polymeric NPs. It offers sustained drug release through NPs because it absorbs less water and enhances the degradation time (Masood, 2016). Additionally, the breakdown of PLGA yields lactate, which promotes pro-COL factors, angiogenesis, and the recruitment of endothelial cells to the wound site. A combinational therapy of PLGA—curcumin NPs revealed a twofold higher potential in wound healing than PLGA and curcumin alone.

Polyurethane is utilized to develop the bioresorbable polyester known as polycaprolactone (PCL). It is well known for its controlled intracellular reabsorption mechanism and its cell-specific responsiveness. In contrast to various available synthetic polymers, it is simple to use and can form a variety of nanostructures, including scaffolds and micro- and nano-carriers (Guarino et al., 2002). The antibacterial, antimicrobial, and wound-healing properties of PCL have been illustrated in numerous investigations to be enhanced by their combination with any metal or metal-based NPs. One study conducted on a skin model using zinc NPs which were developed by electrospun polycaprolactone provided scar-free wound healing by enhancing fibroblast proliferation (Augustine et al., 2014).

15.6.2.2 Natural

Chitosan (CS) is available from the shells of crustaceans and is made up of N-acetyl-D-glucosamine and randomly dispersed D-glucosamine. CS offers numerous potential in wound-healing applications, such as biodegradability, biocompatibility, cellular binding capacity, wound healing, etc. (Li et al., 2012). The study performed by Piran and co-workers developed electrospun PCL nanoscaffolds loaded with chitosan. The effect of the CS NPs scaffold topography and drug release behavior on skin fibroblasts has been investigated (Piran et al., 2018). Another prominent natural polymer used in wound healing is alginate, which is found in the cell wall of brown algae and which possesses maximum scaffold capacity. A study by Liao and co-workers developed porous alginate hydrogels. These hydrogels contains PCL, PEG, and calcium gluconate crystals which are effectively deposited

in the pores of microspheres. The data revealed that the prepared hydrogel effectively enhanced the growth of fibroblasts, which led to providing new areas for skin tissue engineering (Liao et al., 2018).

15.6.3 Hydrogels

Hydrogels are among the most prevalent wound-healing systems because they trap moisture at the wound surface, develop an optimum environment for healing, and keep the skin hydrated. They are easily formulated and also allow prolonged drug release. Chitosan, fibrin, hyaluronic acid, or synthetic polymer, either as cellulose compounds or poloxamers, can be used to make hydrogels. These hydrogels are able to create a cool and moist environment that promotes the wound-healing process as well as water vapor permeability and inhibiting microorganisms from entering the wound.

A study performed by Khorasani and co-workers developed a CS-ZnO-PVA-based hydrogel which progressively enhanced the antibacterial properties without any cellular toxicity (Khorasani et al., 2018). Another study performed by Hsu and co-workers developed gel-based adipose-derived stem cell hydrogels for the treatment of wounds. This in vivo study revealed enhanced wound healing on both mouse and porcine skin models (Hsu et al., 2019).

15.6.4 Nanofibers

Nanofibers (NFs) are the key nanomaterial utilized for the wound-healing process. NFs have a diameter of 10−100 nm and a large specific surface area (Abrigo et al., 2014). They are formulated using the process of electro-spinning technology, where various polymer solutions are processed into nanometric fibers using electric force. These fibers have the capability to create a porous network forming a mesh. Due to the tough network and higher surface area to volume ratio, NFs are suitable candidates to use as scaffolds. They can be synthesized from natural or synthetic polymers as well as carbon-based and semiconductor materials. These fibers are renowned for their use in biological sensing, wound dressing, drug delivery, and tissue engineering formulations along with regenerative drug therapies (Chen et al., 2017).

A study by Kandhasamy and co-workers developed a nanofiber scaffold using COL-coated ostholamide for wound treatment. The prepared formulation possessed excellent mechanical characteristic and antimicrobial property against *P. aeruginosa* and *S. aureus*. The prepared system offers

controlled delivery of ostholamide and provides stability against enzymatic degradation. In another study, a PLGA-aloe vera gel-growth factor scaffold was formed by electrospinning technology. In vivo studies on a mice model showed excellent wound-healing properties by reducing the inflammation (Garcia-Orue et al., 2017).

15.7 Conclusion and future perspectives

In pharmaceutical and biomedical applications, bioresorbable polymers offer excellent potential. Bioresorbable polymers for wound healing must be mechanically strong, have good antibacterial activity, and have hemostatic, water vapor permeability, appropriate gas exchange as well as higher free radical scavenging properties. Such characteristics can enhance the wound-healing process. Additionally, the dressing should be easy to remove after healing and should be nontoxic, biocompatible, nonallergic, biostable, and biodegradable. Natural and synthetic bioresorbable polymers offer their own advantages while treating wound. Many researchers and scientists have proved the capabilities of such polymers by encapsulating them in nanocomposites such as nanoparticles, nanocarriers, hydrogels, metal and metal oxide components, etc. for tissue regeneration, and healing of skin burns and wounds, particularly using in vitro models. Wound healing has attracted the attention of many researchers as it is difficult to treat chronic wounds. The market is constantly expanding, driven by the rise in the number of patients globally, requiring new tactics and materials. Polymer- and hydrogel-based dressings make up the majority of competitive technologies available today for advanced wound care. Advanced dressings typically serve a purpose beyond merely concealing and covering wounds. By using the bioactive qualities of polymers, it is feasible to speed up tissue remodeling and regeneration, improving skin conditions while minimizing the appearance or size of any associated scars.

Despite the broad variety of solutions already in the market, bioresorbable dressings have a low impact on the healing of complex and chronic wounds, although they remain essential components of acute wound care. Recently, enormous progress has been made in our understanding of the molecular mechanisms underlying wound healing, and we may now use this expertise to create novel therapeutic strategies for nonhealing wounds. Also, employing natural resources can effectively overcome these issues. Tissue engineering techniques use 3D hybrid scaffolds which are both synthetic and natural that interact with human cells

effectively. The possible advantages of this strategy include the capacity to increase the in vivo properties which enhance bone formation, reducing donor site morbidity, shortening the surgical time, and decreasing the technical difficulty of the repair. A 3D reconstruction will significantly reduce the amount of time needed for healing. Additionally, it ensures optimal contact between the graft and the recipient site for better integration. Another benefit is increased permeability with particular hybrid materials, which is essential for tissue remodelling and replacement. As a result, the blood can easily flow through the graft's internal chambers without any resistance. Hence, because of such tactics, the healing process is significantly enhanced because of cell attachments.

References

Abrigo, M., McArthur, S.L., Kingshott, P., June 2014. Electrospun nanofibers as dressings for chronic wound care: advances, challenges, and future prospects. Macromol. Biosci. 14 (6), 772–792.

Agubata, C.O., Mbah, M.A., Akpa, P.A., Ugwu, G., September 2, 2021. Application of self-healing, swellable and biodegradable polymers for wound treatment. J. Wound Care 30 (Suppl. 9a), IVi-x.

Ahn, C., Mulligan, P., May 1, 2008. Smoking-the bane of wound healing: biomedical interventions and social influences. Adv. Skin Wound Care 21 (5), 227–236.

Anaya, D.A., Dellinger, E.P., October 1, 2006. The obese surgical patient: a susceptible host for infection. Surg. Infect. 7 (5), 473–480.

Apostolides, N.A., El Beyrouthy, M., Dhifi, W., Najm, S., Cazier, F., Najem, W., Labaki, M., AbouKaïs, A., April 1, 2013. Chemical composition of aerial parts of *Rosmarinus officinalis* L. essential oil growing wild in Lebanon. J. Essent. Oil Bear. Plants 16 (2), 274–282.

Arnold, M., Barbul, A., June 1, 2006. Nutrition and wound healing. Plast. Reconstr. Surg. 117 (7S), 42S–58S.

Attama, A.A., Momoh, M.A., Builders, P.F., October 31, 2012. Lipid nanoparticulate drug delivery systems: a revolution in dosage form design and development. In: Recent Advances in Novel Drug Carrier Systems, vol. 5, pp. 107–140.

Augustine, R., Dominic, E.A., Reju, I., Kaimal, B., Kalarikkal, N., Thomas, S., 2014. Electrospun polycaprolactone membranes incorporated with ZnO nanoparticles as skin substitutes with enhanced fibroblast proliferation and wound healing. RSC Adv. 4 (47), 24777–24785.

Balaji, S.M., October 1, 2008. Tobacco smoking and surgical healing of oral tissues: a review. Indian J. Dent. Res. 19 (4), 344.

Bao, X., Hayashi, K., Li, Y., Teramoto, A., Abe, K., November 30, 2010. Novel agarose and agar fibers: fabrication and characterization. Mater. Lett. 64 (22), 2435–2437.

Bhattacharya, D., Ghosh, B., Mukhopadhyay, M., October 2019. Development of nanotechnology for advancement and application in wound healing: a review. IET Nanobiotechnol. 13 (8), 778–785.

Bishop, A., September 2008. Role of oxygen in wound healing. J. Wound Care 17 (9), 399–402.

Boyapati, L., Wang, H.L., June 2007. The role of stress in periodontal disease and wound healing. Periodontol. 2000 44 (1), 195–210.
Chen, S., Liu, B., Carlson, M.A., Gombart, A.F., Reilly, D.A., Xie, J., June 2017. Recent advances in electrospun nanofibers for wound healing. Nanomedicine 12 (11), 1335–1352.
Choudhry, M.A., Chaudry, I.H., January 1, 2006. Alcohol intoxication and post-burn complications. Front. Biosci. - Landmark 11 (1), 998–1005.
Cornelius, V.J., Majcen, N., Snowden, M.J., Mitchell, J.C., Voncina, B., December 22, 2006. Preparation of SMART wound dressings based on colloidal microgels and textile fibres. In: Smart Materials IV, vol 6413. SPIE, pp. 211–218.
Daniel, S., 2021. Biodegradable polymeric materials for medicinal applications. In: Green Composites, pp. 351–372.
Danti, S., D'Alessandro, D., Mota, C., Bruschini, L., Berrettini, S., January 1, 2017. Applications of bioresorbable polymers in skin and eardrum. In: Bioresorbable Polymers for Biomedical Applications, pp. 423–444.
Das, N.I., Bera, T., Mukherjee, A., 2012. Biomaterial hydrogels for different biomedical applications. Int. J. Pharma Bio Sci. 3 (3), 586–597.
de Moraes, M.A., Beppu, M.M., December 5, 2013. Biocomposite membranes of sodium alginate and silk fibroin fibers for biomedical applications. J. Appl. Polym. Sci. 130 (5), 3451–3457.
Deepthi, S., Venkatesan, J., Kim, S.K., Bumgardner, J.D., Jayakumar, R., December 1, 2016. An overview of chitin or chitosan/nano ceramic composite scaffolds for bone tissue engineering. Int. J. Biol. Macromol. 93, 1338–1353.
Dror, Y., Ziv, T., Makarov, V., Wolf, H., Admon, A., Zussman, E., October 13, 2008. Nanofibers made of globular proteins. Biomacromolecules 9 (10), 2749–2754.
Franz, M.G., Steed, D.L., Robson, M.C., November 2007. Optimizing healing of the acute wound by minimizing complications. Curr. Probl. Surg. 44 (11), 691–763.
Fullana, M.J., Wnek, G.E., October 2012. Electrospun collagen and its applications in regenerative medicine. In: Drug Delivery and Translational Research, 2, pp. 313–322.
Galili, U., Wigglesworth, K., Abdel-Motal, U.M., March 1, 2010. Accelerated healing of skin burns by anti-Gal/α-gal liposomes interaction. Burns 36 (2), 239–251.
Garcia-Orue, I., Gainza, G., Gutierrez, F.B., Aguirre, J.J., Evora, C., Pedraz, J.L., Hernandez, R.M., Delgado, A., Igartua, M., May 25, 2017. Novel nanofibrous dressings containing rhEGF and Aloe vera for wound healing applications. Int. J. Pharm. 523 (2), 556–566.
Ghica, M.V., Albu, M.G., Leca, M., Popa, L., Moisescu, S.T., November 1, 2011. Design and optimization of some collagen-minocycline based hydrogels potentially applicable for the treatment of cutaneous wound infections. Pharmazie 66 (11), 853–861.
Gilliver, S.C., Ashworth, J.J., Ashcroft, G.S., January 1, 2007. The hormonal regulation of cutaneous wound healing. Clin. Dermatol. 25 (1), 56–62.
Gobi, R., Ravichandiran, P., Babu, R.S., Yoo, D.J., June 13, 2021. Biopolymer and synthetic polymer-based nanocomposites in wound dressing applications: a review. Polymers 13 (12), 1962.
Gobin, A.S., Froude, V.E., Mathur, A.B., September 1, 2005. Structural and mechanical characteristics of silk fibroin and chitosan blend scaffolds for tissue regeneration. J. Biomed. Mater. Res. A 74 (3), 465–473.
Godbout, J.P., Glaser, R., December 2006. Stress-induced immune dysregulation: implications for wound healing, infectious disease and cancer. J. Neuroimmune Pharmacol. 1, 421–427.
Gokce, E.H., Korkmaz, E., Dellera, E., Sandri, G., Bonferoni, M.C., Ozer, O., April 11, 2012. Resveratrol-loaded solid lipid nanoparticles versus nanostructured lipid carriers:

evaluation of antioxidant potential for dermal applications. Int. J. Nanomed. 7, 1841–1850.
Gosain, A., DiPietro, L.A., March 2004. Aging and wound healing. World J. Surg. 28, 321–326.
Guarino, V., Gentile, G., Sorrentino, L., Ambrosio, L., July 15, 2002. Polycaprolactone: synthesis, properties, and applications. In: Encyclopedia of Polymer Science and Technology, pp. 1–36.
Guo, S.A., DiPietro, L.A., March 2010. Factors affecting wound healing. J. Dent. Res. 89 (3), 219–229.
Gyles, D.A., Castro, L.D., Silva Jr., J.O., Ribeiro-Costa, R.M., March 1, 2017. A review of the designs and prominent biomedical advances of natural and synthetic hydrogel formulations. Eur. Polym. J. 88, 373–392.
Haji-Saeid, M., Safrany, A., Sampa, M.H., Ramamoorthy, N., March 1, 2010. Radiation processing of natural polymers: the IAEA contribution. Radiat. Phys. Chem. 79 (3), 255–260.
Han, S.S., 2005. Topical formulations of water-soluble chitin as a wound healing assistant-evaluation on open wounds using a rabbit ear model. Fibers Polym. 6 (3), 219–223.
Harding, K.G., Edwards, R., April 2004. Bacteria and wound healing. Curr. Opin. Infect. Dis. 17, 91–96.
Hardman, M.J., Ashcroft, G.S., May 2008. Estrogen, not intrinsic aging, is the major regulator of delayed human wound healing in the elderly. Genome Biol. 9 (5), 1–7.
Hofman, D., Moore, K., Cooper, R., Eagle, M., Cooper, S., May 2007. Use of topical corticosteroids on chronic leg ulcers. J. Wound Care 16 (5), 227–230.
Hsu, L.C., Peng, B.Y., Chen, M.S., Thalib, B., Ruslin, M., Tung, T.D., Chou, H.H., Ou, K.L., February 2019. The potential of the stem cells composite hydrogel wound dressings for promoting wound healing and skin regeneration: in vitro and in vivo evaluation. J. Biomed. Mater. Res. B Appl. Biomater. 107 (2), 278–285.
Huang, S., Fu, X., March 3, 2010. Naturally derived materials-based cell and drug delivery systems in skin regeneration. J. Contr. Release 142 (2), 149–159.
Kausar, A., May 24, 2019. Poly (methyl methacrylate) nanocomposite reinforced with graphene, graphene oxide, and graphite: a review. Polym.-Plast. Technol. Mater. 58 (8), 821–842.
Kempf, M., Miyamura, Y., Liu, P.Y., Chen, A.C., Nakamura, H., Shimizu, H., Tabata, Y., Kimble, R.M., McMillan, J.R., July 1, 2011. A denatured collagen microfiber scaffold seeded with human fibroblasts and keratinocytes for skin grafting. Biomaterials 32 (21), 4782–4792.
Kennedy, J.F., Knill, C.J., Thorley, M., January 1, 2001. Natural polymers for healing wounds. In: Recent Advances in Environmentally Compatible Polymers. Woodhead Publishing, pp. 97–104.
Keylock, K.T., Vieira, V.J., Wallig, M.A., DiPietro, L.A., Schrementi, M., Woods, J.A., January 2008. Exercise accelerates cutaneous wound healing and decreases wound inflammation in aged mice. Am. J. Physiol. Regul. Integr. Comp. Physiol. 294 (1), R179–R184.
Khan, I., Saeed, K., Khan, I., November 1, 2019. Nanoparticles: properties, applications and toxicities. Arab. J. Chem. 12 (7), 908–931.
Khorasani, M.T., Joorabloo, A., Moghaddam, A., Shamsi, H., MansooriMoghadam, Z., July 15, 2018. Incorporation of ZnO nanoparticles into heparinised polyvinyl alcohol/chitosan hydrogels for wound dressing application. Int. J. Biol. Macromol. 114, 1203–1215.
Kirchner, L.M., Meerbaum, S.O., Gruber, B.S., Knoll, A.K., Bulgrin, J., Taylor, R.A., Schmidt, S.P., March 2003. Effects of vascular endothelial growth factor on wound

closure rates in the genetically diabetic mouse model. Wound Repair Regen. 11 (2), 127–131.

Lee, K.Y., Jeong, L., Kang, Y.O., Lee, S.J., Park, W.H., October 5, 2009. Electrospinning of polysaccharides for regenerative medicine. Adv. Drug Deliv. Rev. 61 (12), 1020–1032.

Lehtovaara, B.C., Gu, F.X., July 13, 2011. Pharmacological, structural, and drug delivery properties and applications of 1,3-β-glucans. J. Agric. Food Chem. 59 (13), 6813–6828.

Li, H., Yang, J., Hu, X., Liang, J., Fan, Y., Zhang, X., July 2011. Superabsorbent polysaccharide hydrogels based on pullulan derivate as antibacterial release wound dressing. J. Biomed. Mater. Res. 98 (1), 31–39.

Li, X., Kong, X., Zhang, Z., Nan, K., Li, L., Wang, X., Chen, H., June 1, 2012. Cytotoxicity and biocompatibility evaluation of N, O-carboxymethyl chitosan/oxidized alginate hydrogel for drug delivery application. Int. J. Biol. Macromol. 50 (5), 1299–1305.

Liao, J., Jia, Y., Wang, B., Shi, K., Qian, Z., February 6, 2018. Injectable hybrid poly (ε-caprolactone)-b-poly (ethylene glycol)-b-poly (ε-caprolactone) porous microspheres/alginate hydrogel cross-linked by calcium gluconate crystals deposited in the pores of microspheres improved skin wound healing. ACS Biomater. Sci. Eng. 4 (3), 1029–1036.

Logeart-Avramoglou, D., Jozefonvicz, J., 1999. Carboxymethyl benzylamide sulfonate dextrans (CMDBS), a family of biospecific polymers endowed with numerous biological properties: a review. J. Biomed. Mater. Res. 48 (4), 578–590.

Lumbreras-Aguayo, A., Meléndez-Ortiz, H.I., Puente-Urbina, B., Alvarado-Canché, C., Ledezma, A., Romero-García, J., Betancourt-Galindo, R., February 1, 2019. Poly (methacrylic acid)-modified medical cotton gauzes with antimicrobial and drug delivery properties for their use as wound dressings. Carbohydr. Polym. 205, 203–210.

Madhumathi, K., Sudheesh Kumar, P.T., Abhilash, S., Sreeja, V., Tamura, H., Manzoor, K., Nair, S.V., Jayakumar, R., February 2010. Development of novel chitin/nanosilver composite scaffolds for wound dressing applications. J. Mater. Sci. Mater. Med. 21, 807–813.

Masood, F., March 1, 2016. Polymeric nanoparticles for targeted drug delivery system for cancer therapy. Mater. Sci. Eng. C 60, 569–578.

Masood, N., Ahmed, R., Tariq, M., Ahmed, Z., Masoud, M.S., Ali, I., Asghar, R., Andleeb, A., Hasan, A., March 25, 2019. Silver nanoparticle impregnated chitosan-PEG hydrogel enhances wound healing in diabetes induced rabbits. Int. J. Pharm. 559, 23–36.

Medusheva, E.O., Filatov, V.N., Ryl'tsev, V.V., Kazakova, N.A., Filatov, N.V., Kulagina, A.S., Avagyan, A.A., July 2007. New medical materials with an integral lasting effect based on fibre-forming polymers. Fibre Chem. 39 (4), 268–271.

Menke, N.B., Ward, K.R., Witten, T.M., Bonchev, D.G., Diegelmann, R.F., January 1, 2007. Impaired wound healing. Clin. Dermatol. 25 (1), 19–25.

Miao, J., Pangule, R.C., Paskaleva, E.E., Hwang, E.E., Kane, R.S., Linhardt, R.J., Dordick, J.S., December 1, 2011. Lysostaphin-functionalized cellulose fibers with antistaphylococcal activity for wound healing applications. Biomaterials 32 (36), 9557–9567.

Mitra, T., Sailakshmi, G., Gnanamani, A., Raja, S.T., Thiruselvi, T., Gowri, V.M., Selvaraj, N.V., Ramesh, G., Mandal, A.B., March 1, 2011. Preparation and characterization of a thermostable and biodegradable biopolymers using natural cross-linker. Int. J. Biol. Macromol. 48 (2), 276–285.

Mogosanu, G.D., Grumezescu, A.M., March 25, 2014. Natural and synthetic polymers for wounds and burns dressing. Int. J. Pharm. 463 (2), 127–136.

Mohamed, R.M., Yusoh, K., 2016. A review on the recent research of polycaprolactone (PCL). Adv. Mater. Res. 1134, 249–255.

Morganti, P., Morganti, G., Morganti, A., December 6, 2011. Transforming nanostructured chitin from crustacean waste into beneficial health products: a must for our society. Nanotechnol. Sci. Appl. 4, 123–129.

Murali, R., Anumary, A., Ashokkumar, M., Thanikaivelan, P., Chandrasekaran, B., August 2011. Hybrid biodegradable films from collagenous wastes and natural polymers for biomedical applications. Waste Biomass Valorization 2, 323–335.

Norouzi, M.A., Montazer, M., Harifi, T., Karimi, P., January 1, 2021. Flower buds like PVA/ZnO composite nanofibers assembly: antibacterial, in vivo wound healing, cytotoxicity and histological studies. Polym. Test. 93, 106914.

Orlowski, P., Zmigrodzka, M., Tomaszewska, E., Ranoszek-Soliwoda, K., Czupryn, M., Antos-Bielska, M., Szemraj, J., Celichowski, G., Grobelny, J., Krzyzowska, M., 2018. Tannic acid-modified silver nanoparticles for wound healing: the importance of size. Int. J. Nanomed. 13, 991.

Peng, Y., Song, C., Yang, C., Guo, Q., Yao, M., 2017. Low molecular weight chitosan-coated silver nanoparticles are effective for the treatment of MRSA-infected wounds. Int. J. Nanomed. 12, 295.

Pertici, G., January 1, 2017. Introduction to bioresorbable polymers for biomedical applications. In: Bioresorbable Polymers for Biomedical Applications. Woodhead Publishing, pp. 3–29.

Pieringer, H., Stuby, U., Biesenbach, G., April 1, 2007. Patients with rheumatoid arthritis undergoing surgery: how should we deal with antirheumatic treatment?. In: Seminars in Arthritis and Rheumatism, vol. 36(5). WB Saunders, pp. 278–286.

Piran, M., Vakilian, S., Piran, M., Mohammadi-Sangcheshmeh, A., Hosseinzadeh, S., Ardeshirylajimi, A., October 31, 2018. In vitro fibroblast migration by sustained release of PDGF-BB loaded in chitosan nanoparticles incorporated in electrospun nanofibers for wound dressing applications. Artif. Cell Nanomed. Biotechnol. 46 (Suppl. 1), 511–520.

Rai, M., Yadav, A., Gade, A., January 1, 2009. Silver nanoparticles as a new generation of antimicrobials. Biotechnol. Adv. 27 (1), 76–83.

Ramnath, V., Sekar, S., Sankar, S., Sastry, T.P., Mandal, A.B., 2012. In vivo evaluation of composite wound dressing material containing soya protein and sago starch. Int. J. Pharm. Sci. 4 (2), 414–419.

Rodriguez, P.G., Felix, F.N., Woodley, D.T., Shim, E.K., September 2008. The role of oxygen in wound healing: a review of the literature. Dermatol. Surg. 34 (9), 1159–1169.

Sahana, T.G., Rekha, P.D., December 2018. Biopolymers: applications in wound healing and skin tissue engineering. Mol. Biol. Rep. 45, 2857–2867.

Saporito, F., Sandri, G., Bonferoni, M.C., Rossi, S., Boselli, C., Cornaglia, A.I., Mannucci, B., Grisoli, P., Vigani, B., Ferrari, F., 2018. Essential oil-loaded lipid nanoparticles for wound healing. Int. J. Nanomed. 13, 175.

Sawant, S.V., Sankpal, S.V., Jadhav, K.R., Kadam, V.J., 2012. Hydrogel as drug delivery system. Res. J. Pharm. Technol. 5 (5), 561–569.

Sen, M., Avcı, E.N., 2005. Radiation synthesis of poly (N-vinyl-2-pyrrolidone)–κ-carrageenan hydrogels and their use in wound dressing applications. I. Preliminary laboratory tests. J. Biomed. Mater. Res. A 74 (2), 187–196.

Shahverdi, S., Hajimiri, M., Esfandiari, M.A., Larijani, B., Atyabi, F., Rajabiani, A., Dehpour, A.R., Gharehaghaji, A.A., Dinarvand, R., October 1, 2014. Fabrication and structure analysis of poly (lactide-co-glycolic acid)/silk fibroin hybrid scaffold for wound dressing applications. Int. J. Pharm. 473 (1–2), 345–355.

Shen, X., Nagai, N., Murata, M., Nishimura, D., Sugi, M., Munekata, M., December 2008. Development of salmon milt DNA/salmon collagen composite for wound dressing. J. Mater. Sci. Mater. Med. 19, 3473–3479.

Silva, G.A., Vaz, C.M., Coutinho, O.P., Cunha, A.M., Reis, R.L., December 2003. In vitro degradation and cytocompatibility evaluation of novel soy and sodium caseinate-based membrane biomaterials. J. Mater. Sci. Mater. Med. 14, 1055–1066.

Szabo, G., Mandrekar, P., February 2009. A recent perspective on alcohol, immunity, and host defense. Alcohol Clin. Exp. Res. 33 (2), 220–232.

Urie, R., Ghosh, D., Ridha, I., Rege, K., June 4, 2018. Inorganic nanomaterials for soft tissue repair and regeneration. Annu. Rev. Biomed. Eng. 20, 353–374.

Venkataprasanna, K.S., Prakash, J., Vignesh, S., Bharath, G., Venkatesan, M., Banat, F., Sahabudeen, S., Ramachandran, S., Venkatasubbu, G.D., January 15, 2020. Fabrication of Chitosan/PVA/GO/CuO patch for potential wound healing application. Int. J. Biol. Macromol. 143, 744–762.

Vetvicka, V., Vetvickova, J., September 2011. β (1-3)-D-glucan affects adipogenesis, wound healing and inflammation. Orient. Pharm. Exp. Med. 11, 169–175.

Vileikyte, L., January 1, 2007. Stress and wound healing. Clin. Dermatol. 25 (1), 49–55.

Wagner, A.E., Huck, G., Stiehl, D.P., Jelkmann, W., Hellwig-Bürgel, T., July 25, 2008. Dexamethasone impairs hypoxia-inducible factor-1 function. Biochem. Biophys. Res. Commun. 372 (2), 336–340.

Weyers, A., Linhardt, R.J., May 2013. Neoproteoglycans in tissue engineering. FEBS J. 280 (10), 2511–2522.

Woo, K., Ayello, E.A., Sibbald, R.G., February 1, 2007. The edge effect: current therapeutic options to advance the wound edge. Adv. Skin Wound Care 20 (2), 99–117.

Zhang, Z., Ortiz, O., Goyal, R., Kohn, J., January 1, 2014. Biodegradable polymers. In: Handbook of Polymer Applications in Medicine and Medical Devices, pp. 303–335.

Zhu, X.Y., Li, Y.L., Xie, F., Zhang, Y.J., Huang, S.N., Li, M.Z., Qiu, Y.H., September 17, 2011. Activation of T lymphocytes on local trauma after implantation of regenerated porous silk fibroin film. Chin. J. Tissue Eng. Res. 15 (38), 7061.

This page intentionally left blank

CHAPTER 16

Bioresorbable polymers/HNT blend composite wound dressings

Deepak Gupta[1], Arun Kumar Chaudhary[1], Deepak Verma[2,3] and Mohit Sharma[4]

[1]Department of Industrial and Production Engineering, College of Technology, Govind Ballabh Pant University of Agriculture and Technology, Pantnagar, Uttarakhand, India; [2]International Graduate Program of Nanoscience and Technology, Chulalongkorn University, Bangkok, Thailand; [3]Department of Mechanical Engineering, Graphic Era Hill University, Dehradun, Uttarakhand, India; [4]Institute of Materials Research and Engineering (IMRE), Agency for Science, Technology and Research (A*STAR), Singapore, Singapore

16.1 Introduction to bioresorbable polymers

Bioresorbable polymers are a category of polymers that experience metabolic degradation within the human body upon implantation. They include polylactide (PLA), polyglycolide (PGA), and copolymers of PLA/PGA. These polymers can be modified to attain specific mechanical properties and degradation, making them suitable for medical applications such as drug delivery, resorbable screws, anchors, etc. (Implantable Formulations, 1499).

Bioresorbable polymers are synthetic polymers which can be broken down (Fig. 16.1) into nontoxic elements and eliminated through natural metabolic pathways from the body. They have gained remarkable attention aimed at wound-healing applications due to their biocompatibility and

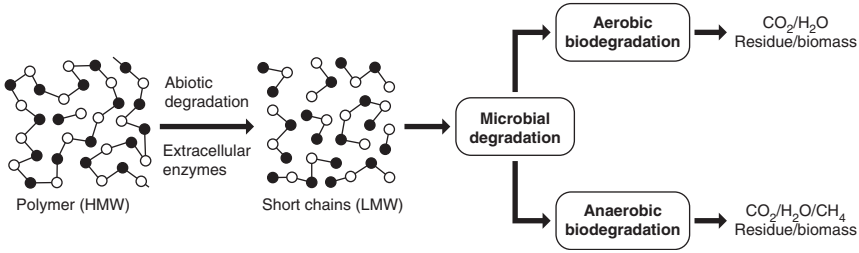

Figure 16.1 Graphical representation of the biodegradation process of polymers. *(Reproduced with permission from Samir et al. (2022).)*

Bioresorbable Polymers and their Composites
ISBN 978-0-443-18915-9
https://doi.org/10.1016/B978-0-443-18915-9.00008-2
© 2024 Elsevier Ltd.
All rights reserved.

biodegradability. Nevertheless, bioresorbable polymers often exhibit lower mechanical properties and drug delivery capability for optimal wound healing compared to the requirements (Khot et al., 2021). To overcome these obstacles, researchers have recently discovered bioresorbable polymer/halloysite nanotube (HNT) blend composite wound dressings, which have good mechanical strength and improved drug delivery, and also enhanced antibacterial activity (Khot et al., 2021).

The bioresorbable polymers in the context of medicine could be a diversifying event regarding biomaterials. Biomaterials have the capability to restore function, related to joint replacement, fixation of fracture-related devices and dental or canal root implants, etc.; the success rates of biomaterials vary significantly and range from excellent in full replacement of the hip area to less successful rates of other types of body joints and parts; therefore biomaterials used in devices are being improved through a greater understanding of the related consequences [The National Institutes of Health (NIH) Consensus Development Program, 1982]. Recent research shows that the demand for bioresorbable polymer implants is growing continuously because of their biodegradability and unconventional implants ability in several applications according to duration of utilization for weeks to months as per the necessity (McKeen, 2014). However, the benefits of bioabsorbable implants have been improved in recent decades; mostly implants are produced using synthetic materials which results in problems related to toxicity and chronic inflammatory reactions, which can effectively be reduced through the use of natural materials (Pertici, 2017).

16.1.1 Properties of bioresorbable polymers

Bioresorbable polymers can also be understood as biodegradable or absorbable polymers as they are polymers that break down and can be absorbed by the body over time. They have shown significant interest in medical-related applications, including drug delivery, tissue reengineering, and implantable medical devices (Gleadall, 2015). Some of the highly desirable and noted properties of bioresorbable polymers are listed here.

(i) Biocompatibility: Bioresorbable polymers have been designed to be biocompatible, which ensures that they are nontoxic and do not cause an immune response when introduced into the body (Ulery et al., 2011).

(ii) Biodegradability: These polymers having the advantage of being broken down into smaller components size at the micro level over time through a process called hydrolysis. The degradation products

are typically water and carbon dioxide, which are naturally acting and occurring substances inside the body (Nanda et al., 2022).

(iii) Mechanical properties: The properties relevant to the mechanical strength of bioresorbable polymers usually vary and are dependent on the particular type of polymer used. They can be developed to produce varieties related to stiffness, elasticity, and strength which are suitable to be used in various applications (Alhanish and Ali, 2023).

(iv) Processing: Injection molding, solvent casting, and electrospinning are most common techniques associated with bioresorbable polymers processing (Casalini and Perale, 2012).

(v) Rate of degradation: Absorption of bioresorbable polymers depends on several factors such as body type, body condition, body parts, etc., and thus the degradation behavior also varies according to the polymer used, and the size and shape of the device (Pappalardo et al., 2019).

(vi) Biostability: This refers to the period of time during which any bioresorbable polymer product functions efficiently and maintains its mechanical properties until it finally begins to degrade (Wang and Wang, 2012).

Bioresorbable polymers are typically biocompatible and do not cause any harm to the body, although a few studies have suggested that the degradation products may cause inflammation in some cases. Meanwhile, the properties related to bioresorbable polymers make them very impressive and attractive materials for use in medical applications. However, care and serious consideration must be observed in the specific type of polymer used and the implantation site to ensure the maximum possible performance and safety (Deng et al., 2023).

16.1.2 Applications of bioresorbable polymers

Bioresorbable polymers have huge possibilities to be used in medical applications due to their ability to degrade or be absorbed within the body over time. Some widely used applications of bioresorbable polymers are listed here:

(i) Drug delivery: Bioresorbable polymers are employed for their targeted drug-delivery capability within the human body over a prolonged duration. They have been designed to degrade at an optimum time to control the release of drugs (Fig. 16.2).

(ii) Tissue reengineering: Bioresorbable polymers can be used to reengineer new tissue developments. These recreated products/scaffolds have to be

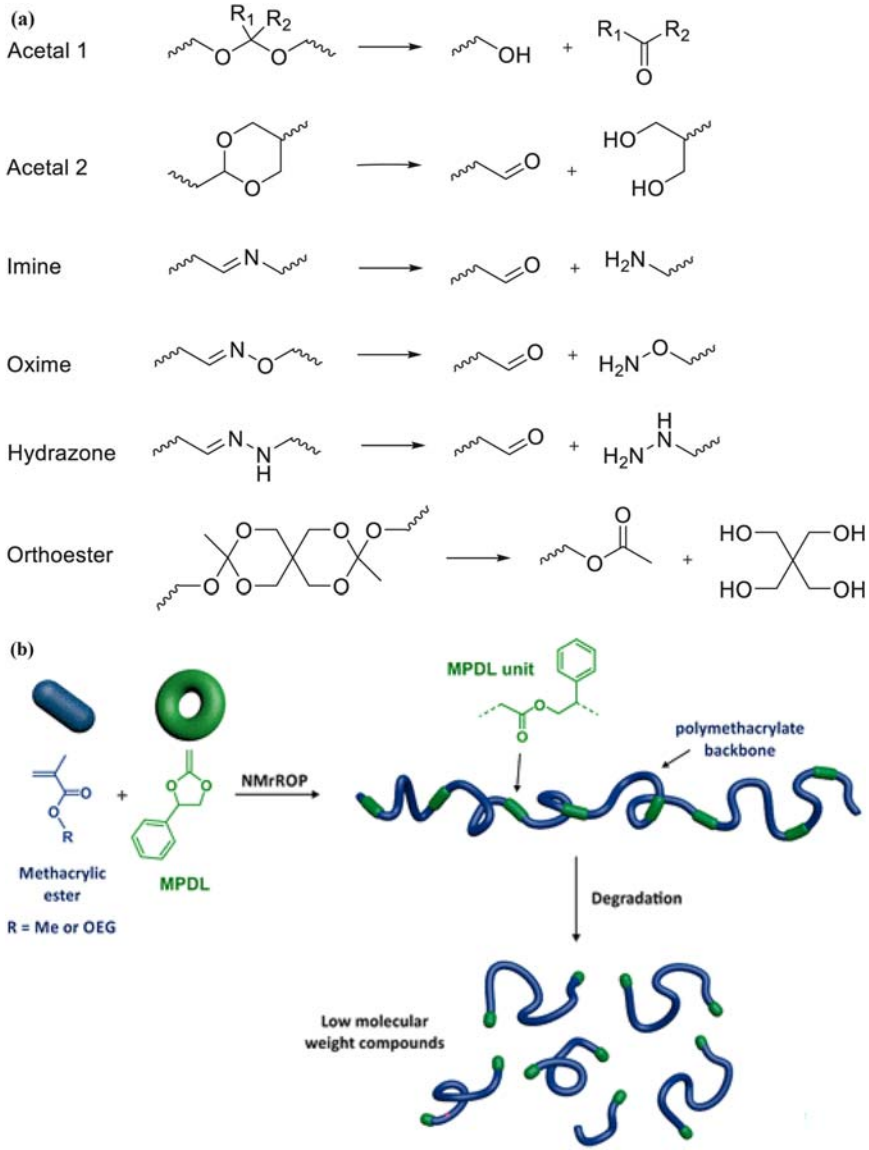

Figure 16.2 (a) Degradable functions and hydrolysis of common acids in an acidic aqueous atmosphere, (b) blending the degradable copolymers using nitroxide-mediated radical ring-opening copolymerization (NMrROP) with methacrylic esters and 2-methylene-4-phenyl-1,3-dioxolane (MPDL) as an ester-bound precursor incorporated into the copolymer backbone. *(Reproduced with permission from Rust et al. (2023).)*

implanted in the body and allow it to degrade according to a predefined time frame through behaving like functional tissue (Socci et al., 2023).

(iii) Surgical sutures: Bioresorbable polymers are used to develop surgical sutures which will break down over time, which eliminates any suture removal requirements and associated risk of infection (Afewerki et al., 2023).

(iv) Implants: Bioresorbable polymers are being used to create body part implants that degrade over a certain time period and are absorbed by the body. The main examples include screws, plates, and pins which have been used to repair fractured bones (Abbas et al., 2021; Bioresorbable Polymers Market to Expand, 2023).

(v) Stents: Advanced bioresorbable polymers are being used to develop stents that are inserted into blood vessels to allow smooth blood flow in the treatment of narrowed or blocked arteries and which degrades over time (Kim et al., 2021).

(vi) Wound dressings: Bioresorbable polymers can be used to develop wound dressings which will promote the healing capacity and be absorbed by the body over a predefined time frame (Nguyen et al., 2023).

The acceptable or desirable applications of bioresorbable polymers are having a wide range of opportunities therefore, it is yet to be explored for new materials development along with new fabrication processes inventions. The capability to self-degrade or be absorbed within the body heralds a demanding unconventional opportunity toward the traditional approach to permanent implants and devices, as it will reduce the risk of associated long-term medical complications and the need for additional surgeries.

16.2 Classifications of bioresorbable polymers

Bioresorbable polymers, also known as biodegradable polymers, belong to a category of polymers that undergo natural degradation processes in the body, resulting in harmless compounds (Hajebi et al., 2021). These polymers can be classified based on their chemical structure and origin.

Natural polymers: The polymers which are obtained from natural origins are called natural polymers (Fig. 16.3).

Examples include: animal, plant, or microbial origin, such as collagen, gelatin, chitosan, starch, and cellulose.

Synthetic polymers: Those polymers are developed or synthesized chemically in research laboratories are called synthetic polymers (Dirauf et al., 2022).

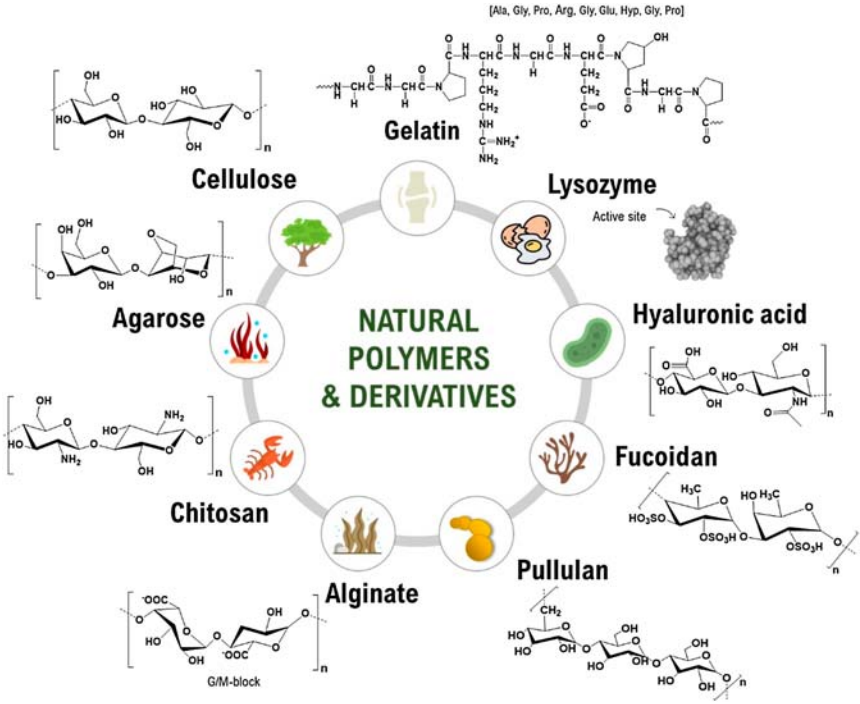

Figure 16.3 Examples of naturally available polymers with their potential derivatives. *(Reproduced with permission from Silva et al. (2021).)*

Examples include: PLA, PGA, polycaprolactone (PCL), and their co-polymers, etc.

Hybrid polymers: The polymers which are made by conjoining natural and synthetic polymers are called hybrid polymers (Zhiraslanovna Ozkan et al., 2018).

Examples include: silk fibroin and chitosan blends, collagen—PLA blends, and gelatin—PCL blends, etc.

Inorganic polymers: The polymers which are fabricated by inorganic elements such as silicon, phosphorus, and calcium are called inorganic polymers.

Examples include: bioactive glass and hydroxyapatite, etc.

Protein-based polymers: The polymers which are derived through proteins such as elastin, collagen, and silk are called protein-based polymers. These polymers are biocompatible and can also be broken down by enzymes in the body (Fig. 16.4).

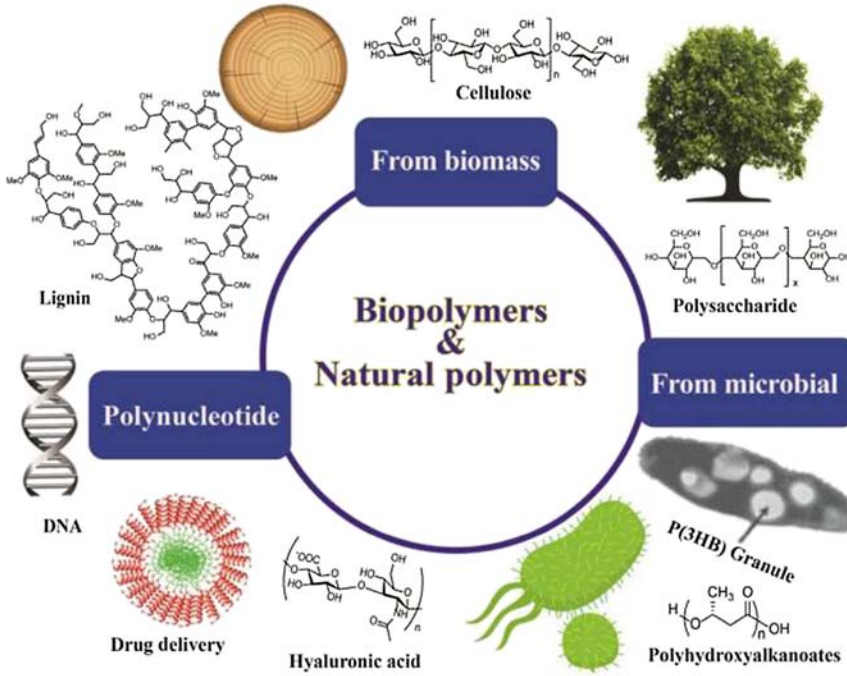

Figure 16.4 Some selective biopolymers with their classifications. *(Reproduced with permission from Alaswad et al. (2022).)*

16.3 Halloysite nanotubes

Halloysite nanotubes (HNTs) have gained major consideration in recent years due to their excellent properties (Table 16.1) and favorable applications. HNTs are tubular nanomaterials composed of hydrated aluminosilicate clay, characterized by an inner diameter of approximately 10−30 nm (Fig. 16.5), an outer diameter of 40−70 nm, and a length ranging between 200 and 2000 nm (Abdullayev and Lvov, 2013; Pereira et al., 2021).

16.3.1 Properties of HNTs

- **Biocompatibility**: HNTs exhibit the capability to be biocompatible which makes them favorable for biomedical applications (Lvov and Abdullayev, 2013).
- **High aspect ratio**: HNTs typically possess a high aspect ratio, meaning a higher ratio of surface area to volume. This characteristic makes HNTs an ideal choice for medical applications due to properties such as adsorption and catalysis (Wu et al., 2019).

Table 16.1 Common analytical data regarding HNTs for the fabrication of polymer nanocomposites.

HNT composition	$Al_2Si_2O_5(OH)_4 \cdot nH_2O$
HNT outer diameter	40–70 nm
HNT mean particle size in aqueous solution	143 nm
HNT pore space	14%–46.8%
HNT inner diameter	10–40 nm
HNT aspect ratio (L/D)	10–50
HNT length	0.2–2 μm
HNT density	2.14–2.59 g/cm^3
HNT particle size range in aqueous solution	50–400 nm
HNT lumen space	11%–39%
HNT average pore size	79.7–100.2 Å
HNT elastic modulus (theoretical value)	140 GPa (230–340 GPa)
HNT BET surface area	22.1–81.6 m^2/g
HNT structural water release temperature	400–600°C

Adapted with permission from Liu et al. (2014).

- **Thermal stability**: HNTs are thermally very stable and have a high melting point, thus making them highly suitable for high-temperature applications (Du et al., 2010).
- **Chemical stability**: HNTs are very chemically stable thus they have high demand in the field of drug deliveries and as reinforcement materials in polymer composites (Ganapathy et al., 2022).

16.3.2 Applications of HNTs

- **Drug delivery**: The utilization of HNTs in pharmaceuticals is in high demand because of their wide surface area and potential porosity (Guo et al., 2019; Santos et al., 2018).
- **Catalysis**: High aspect ratio and chemically stable properties increase HNT capability to be used as catalysis (Lvov et al., 2016a; Barman et al., 2020).
- **Reinforcement material**: HNTs have the capability to function as a reinforcing material in polymer composites, aiming to enhance their mechanical properties (Namathoti and Vakkalagadda, 2023).
- **Environmental remediation**: HNTs are helpful in controlling pollution due to their ability to adsorb pollutants and heavy metals from the atmosphere (Li et al., 2022).
- **Cosmetics development**: HNTs have been found to be suitable for use as cosmetics ingredients as natural fillers or adsorbents (Suh, 2015).

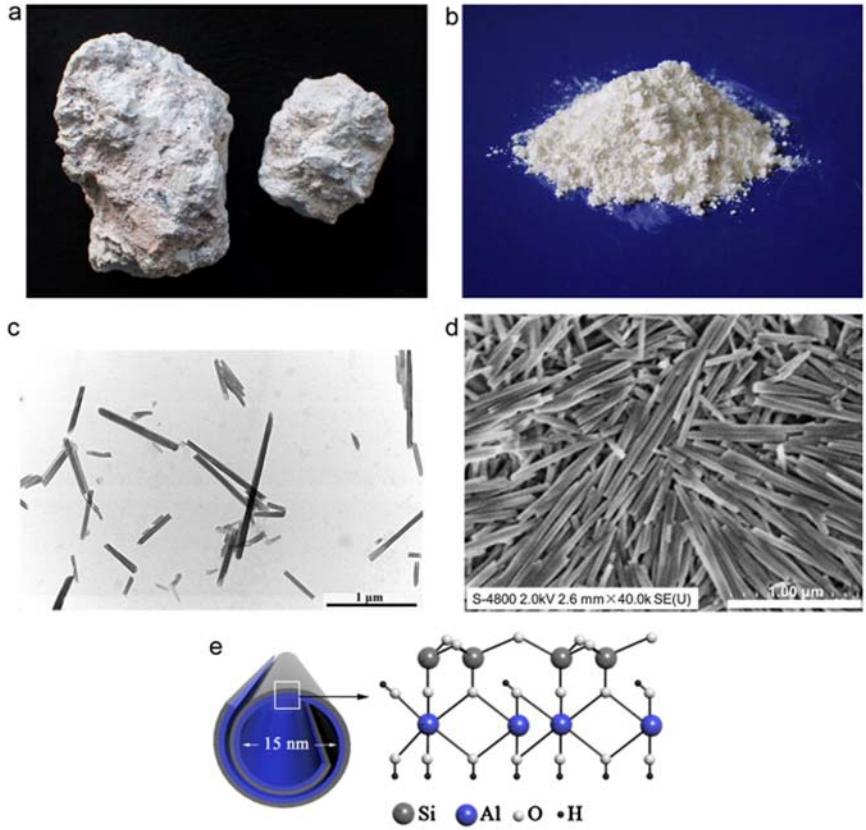

Figure 16.5 (a) Halloysite in its raw form, (b) halloysite after grinding, (c) transmission electron microscopy (TEM) image, (d) scanning electron microscopy (SEM) image, (e) photographs of halloysite nanotubes (HNTs) extracted from Hunan Province, China, and a schematic representation of the crystalline structure of HNTs. *(Reproduced with permission from Liu et al. (2014).)*

16.4 Bioresorbable polymer-based HNT composites

Bioresorbable polymer-based HNT composites are an emerging area of research in nanomaterials development because of their ability to deliver the collective advantages of both HNTs and bioresorbable polymers. This ability appeals to their usability in several fields, such as biomedical products, drug deliveries, and tissue reengineering (Asghari et al., 2017). The integration of HNTs into bioresorbable polymer matrix would expand their mechanical, thermal, and biological characteristics. HNTs as a reinforcement material would enrich the stiffness, strength, and toughness of the polymer matrix (Cheng et al., 2020a). Numerous bioresorbable

polymers have recently been used to develop HNT- based composites, for example, poly-lactic acid, poly-glycolic acid, and poly-caprolactone. These composite-based investigations have revealed favorable outcomes in terms of mechanical properties, bio-medicine, and biodegradability. Research has shown that HNT and N,N′-ethylenebis (stearamide) in a weight ratio of 2.33:1, respectively, in a polymethylmethacrylate matrix improved the properties related to scratch resistance, mechanical properties, and the dispersion of nanoparticles in the matrix without losing other properties (Vuluga et al., 2018). Encapsulated aspirin drug into the HNT lumen in a weight ratio of 1:1 and 2:1 (HNTs/aspirin) was reinforced to the PLA matrix, and the results revealed that aspirin in a 1:1 ratio could be successfully loaded in the HNT lumen with successive release of aspirin from the nanocomposite as well as the addition of HNT increasing the mechanical properties which also aids in use HNT as a drug-eluting agent (Venkatesh et al., 2019).

16.5 Mechanical properties of HNT-reinforced polymer blends

The mechanical properties of polymer blends reinforced with HNTs are influenced by various factors, such as the type and quantity of polymer used, aspect ratio of HNTs, concentration of HNTs, and the processing techniques employed (Gaaz et al., 2017). The literature has evidenced that fabricated nanocomposite by the ultrasonification dispersion technique for HNT reinforced in five proportions (0, 1, 2, 3, and 4 by weight%) to lapox L-12 epoxy matrix delivered increased mechanical properties with the best mechanical properties found at 3 wt.% of HNT reinforcement which also revealed that properties can be modified by the filler present and the dispersion condition alteration (Ravichandran et al., 2019). A Takayanagi model-based research study on determining the modulus of HNT polymer nanocomposites evidenced that HNT reinforcement is not suitable for polymers for an HNT volume fraction and interphase depth less than 0.01 and 5 nm, respectively, although 2.88 relative modulus was found at the 0.04 proportion of HNT volume and at 20 nm interphase depth, which indicates that the lower values of the associated matrix modulus and degradation initiation are appropriate to reinforce, while a higher polymer's modulus results in poor strengthening and affects the system modulus significantly (Zare and Rhee, 2022). In this context, the mechanical properties of some nanocomposites are discussed in Table 16.2.

Table 16.2 The influence of variations in hexadecyl-tri-methyl-ammonium-bromide (HEDA), silane, and urea on the mechanical properties of HNT/polypropylene nanocomposites.

Blend composition	σ_b (MPa)	E (MPa)
Neat polypropylene	36.3 ± 0.4	1340 ± 45
Polypropylene + 5 wt.% untreated halloysite nanotubes	36.5 ± 0.4	1440 ± 84
Polypropylene + 5 wt.% halloysite nanotubes modified HEDA	36.5 ± 0.3	1547 ± 35
Polypropylene + 5 wt.% halloysite nanotubes modified silane	36.2 ± 0.6	1495 ± 65
Polypropylene + 5 wt.% halloysite nanotubes modified urea	36.5 ± 0.8	1449 ± 30

Adapted with permission from Khunova et al. (2013).

The higher aspect ratio of HNTs supports its high suitability for reinforcement in the polymer matrix. HNT integration into the polymer matrix may improve the properties related to mechanical strength. The consequences of HNT concentration over the mechanical strength of HNT-reinforced polymer nanocomposites have been examined and concluded that increasing the HNT concentration results in increased stiffness along with improved strength of the nanocomposite. Conversely, a higher concentration of HNTs can result in clustering, negatively affecting the mechanical properties of the nanocomposite. The impact of HNT concentration on mechanical properties is discussed in detail in Table 16.3.

The type of polymer used in the blend also has a significant impact on the mechanical properties calculation related to the composite and as evidenced by literature that PLA–HNT composites exhibit higher stiffness and strength than polyethylene glycol (PEG)–HNT composites (Naser et al., 2021; Nedaipour et al., 2020; Cavallaro et al., 2013). Processing methods also influence the properties of HNT–polymer blends as it has been observed that the solvent casting method can deliver more uniform dispersion of the NTs, leading to improved mechanical properties (Guo et al., 2009; Modesti et al., 2005; Esawi et al., 2010).

16.6 Antibacterial activity of HNT–polymer blends

Incorporating HNTs into polymer blends can enhance the antibacterial activity of the composite due to the integral antibacterial properties of

Table 16.3 Mean values of Young's modulus (E), yield stress (σ_Y), ultimate stress (σ_{break}), and elongation at break (ϵ_{break}) are reported for various concentrations of high-density polyethylene (HDPE)/halloysite nanotubes nanocomposites, and also for pure HDPE (Cecílio et al., 2023).

Specimen	HNT content (wt.%)	E (MPa)	σ_Y (MPa)	σ_{break} (MPa)	ϵ_{break} (%)
High-density polyethylene	0	415 ± 12	18.5 ± 0.4	40 ± 2	840 ± 50
[Halloysite nanotubes]−[methylaluminoxane (MAO)]-N5	5	440 ± 15	14.0 ± 0.5	28 ± 2	600 ± 60
[Halloysite nanotubes]−[methylaluminoxane] -N8	8	450 ± 18	15.0 ± 0.5	38 ± 4	740 ± 50
[Halloysite nanotubes]−[methylaluminoxane] -N15	15	475 ± 20	15.5 ± 0.6	43 ± 4	930 ± 60
[Halloysite nanotubes]−[methylaluminoxane] -N23	23	515 ± 20	17.0 ± 0.7	33 ± 4	770 ± 70
[Halloysite nanotubes]−[supported activator (SA)]-N5	5	555 ± 20	18.5 ± 0.5	41 ± 1	670 ± 40
[Halloysite nanotubes]−[supported activator]-N9	9	605 ± 20	19.0 ± 0.5	44 ± 1	730 ± 40
Halloysite nanotubes −[supported activator]-N16	16	680 ± 20	20.5 ± 0.8	44 ± 2	910 ± 60
Halloysite nanotubes−[supported activator]-N20	20	710 ± 25	20.5 ± 0.8	36 ± 3	840 ± 40

HNTs. A high aspect ratio of HNTs allows for interaction with bacterial cells, leading to disruption of their cell membrane and subsequent bacterial death. The concentration and aspect ratio of HNTs can affect their antibacterial activity. A research study on erythromycin (ERY)−HNT-reinforced polycaprolactone (PCL) matrix composite developed by the electrospinning method evaluated the antibacterial action on a sterile zone in place of poly-caprolactone nanofibers holding 7.0 wt.% halloysite nanotubes/erythromycin (Fig. 16.6) when used against *Escherichia coli* and *Staphylococcus aureus* bacteria (Table 16.4); an additional improvement of the mechanical properties was also accomplished (Khunová et al., 2022).

An investigation reported on developed nanocomposites of polydimethylsiloxane (PDMS)−halloysite nanotubes by solvent swelling (Table 16.5) and revealed that these nanocomposites have great potential for use as a coating over antibacterial invasive devices to prevent possible infections as the polydimethylsiloxane−HNT nanocomposite showed improved performance over commercial catheters at preventing bacterial growth (Fig. 16.7) and also revealed that a higher concentration of HNTs in the composite leads to higher antibacterial activity (Boyer et al., 2018).

16.7 Drug-delivery capacity of HNT−polymer blends

HNTs possess a higher aspect ratio and porosity, which supports their suitability for drug-delivery applications (Ahuja and Pathak, 2009). The incorporation of HNTs into polymer blends can enhance the drug-delivery capacity of the composite, and numerous researchers have investigated the applicability of HNT−polymer blends in regard to drug-delivery applications (Hasani et al., 2021). A drug-delivery system responsive to H_2O_2 was developed by integrating a hydrogel (based on halloysite) using the coprecipitation method, which exhibits a "turn-on" fluorescence characteristic upon exposure to H_2O_2. The investigation results revealed that the hydrogel initiated fragmentation when in contact with H_2O_2, with subsequent degradation ongoing, and in that way a responsive drug was released (Fig. 16.8). The drug discharge were increased at ($[H_2O_2] = 0.02\ \mu M$) physiological concentration, whereas more than 90% drug was released at ($[H_2O_2] = 200\ \mu M$) pathological concentration. Therefore, HNTs can be loaded for countless drug types and the drug discharge can be well-ordered by changing the HNT concentration. HNTs work as a reservoir for the drug and provide sustained discharge over time, leading to improved therapeutic efficacy (Cheng et al., 2020b).

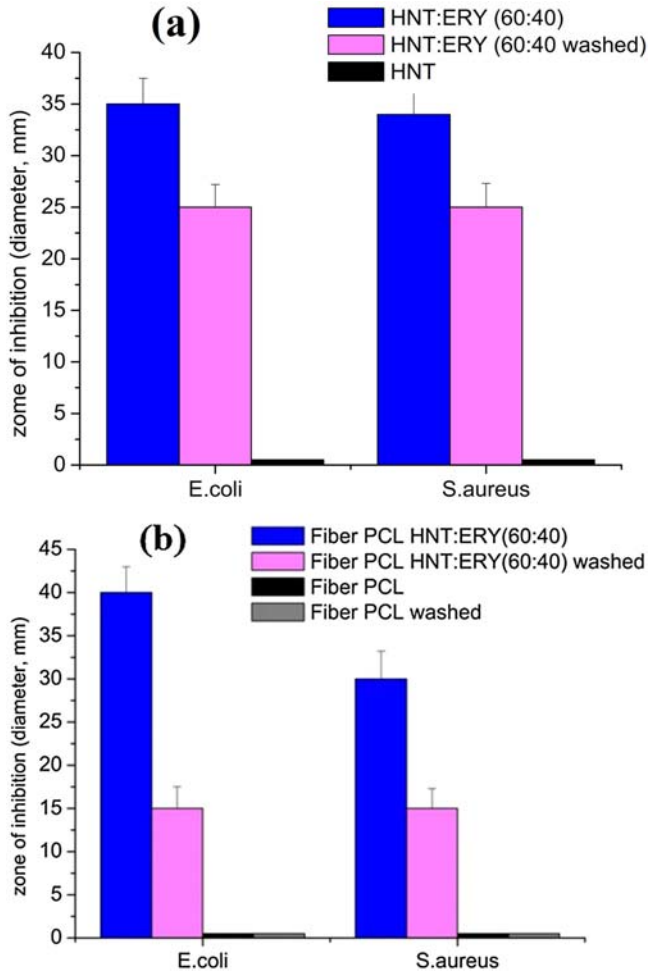

Figure 16.6 Disk diffusion-based examination of *Escherichia coli* and *Staphylococcus aureus* for the antibacterial effect of (a) halloysite nanotubes (HNTs) loaded with erythromycin, both before and after removing erythromycin from the external surface of HNTs, which was evaluated by measuring the inhibition zone diameter ± SE (standard error). (b) The antibacterial activity of poly-capro-lactone (PCL)/halloysite nanotube (HNT) fibers, with and without washing, and containing erythromycin was assessed by measuring the inhibition zone diameter ± SE (standard error) (Khunová et al., 2022).

HNTs have been investigated for their safe utilization and have been found to be relatively harmless for the human body and to prevent bacterial cell cultures in vivo (Lvov et al., 2016b). In this context, a related study of nanocomposites fabricated with chitosan−HNTs to deliver the drug

Table 16.4 Antibacterial activity of poly-caprolactone/halloysite nanotubes and erythromycin fiber after 3× replacement.

		Zone of inhibition (mm)	
Model bacteria	**Mode of application**	**Fiber PCL/ HNT**	**Fiber PCL/ HNT and ERY**
Escherichia coli	Positioned on the growth medium	0	40
	Substituted for the first time	0	35
	Substituted for the second time	0	21
	Substituted for the third time	0	0
Staphylococcus aureus	Positioned on the growth medium	0	30
	Substituted for the first time	0	30
	Substituted for the second time	0	0
	Substituted for the third time	0	0

Adapted with permission from Khunová et al. (2022).

Table 16.5 Assessment of protein adsorption on polydimethylsiloxane (PDMS) and PDMS—10% halloysite nanotube (HNT) composites was conducted using the Micro BCA protein assay. The presence of surface-adsorbed fibrinogen was reduced upon treatment of PDMS−HNT surfaces with polyethylene oxide (PEO).

Material	**Absorbance (562 nm)**
Polydimethylsiloxane	0.839 ± 0.024
Polydimethylsiloxane−[halloysite nanotubes]	0.992 ± 0.047
Polydimethylsiloxane−[halloysite nanotubes]−1% polyethylene oxide	0.526 ± 0.089
Polydimethylsiloxane−[halloysite nanotubes]−2.5% polyethylene oxide	0.492 ± 0.052
Polydimethylsiloxane−[halloysite nanotubes]−5% polyethylene oxide	0.245 ± 0.028

Adapted with permission from Boyer et al. (2018).

diclofenac investigated in vitro diffusion studies and confirmed the safe and sustained delivery of the drug. Cytotoxicity with MTT assay investigation confirmed the biocompatibility of this nanocomposite and drug loading over the tubular morphology of HNTs observed via SEM examination.

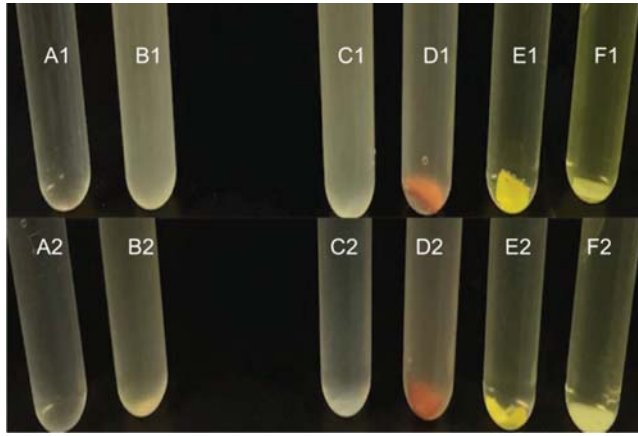

Figure 16.7 Photographs depicting the analysis of Mueller–Hinton broth against *Escherichia coli* and *Staphylococcus aureus* after 24 h: (1) *Escherichia coli*, (2) *Staphylococcus aureus*: (A1) broth, (B1) control group for *Escherichia coli*, (C1) 100% polydimethylsiloxane catheter, (D1) silver-coated catheter, (E1) antibacterial catheter, (F1) polydimethylsiloxane–HNT–polyethylene oxide–nitrofurantoin, (A2) broth, (B2) control group for *Staphylococcus aureus*, (C2) 100% polydimethylsiloxane catheter, (D2) silver-coated catheter, (E2) antibacterial catheter, (F2) polydimethylsiloxane–HNT–polyethylene oxide–nitrofurantoin. *(Reproduced with permission from Boyer et al. (2018).)*

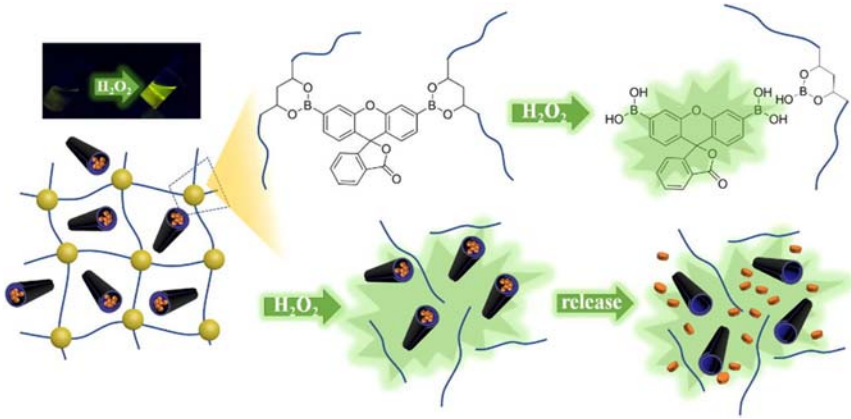

Figure 16.8 Release phenomena of hydrogel under pathological concentration. *(Reproduced with permission from Cheng et al. (2020b).)*

Drug loading of diclofenac has been confirmed on HNT nanotubes after XRD examination, while an FTIR report also illustrated the encapsulation of the drug (Paul et al., 2022). A discussion of loaded drugs with HNTs and the loading method is provided in Table 16.6.

Table 16.6 Utilization of halloysite nanotubes in drug delivery.

Drug	HNT and modifier	Advantages	Drug loading (wt.%)	Site of drug loading	Release rate (wt.%/mg g^{-1} h^{-1})	Release kinetics model	Application
Diclofenac sodium	Sodium alginate/ hydroxyapatite/ halloysite nanotube nanocomposite hydrogel beads	Cumulative discharge behavior	74.63 ± 1.65	Lumen	9.19 mg g^{-1} h^{-1}	–	Controlled drug delivery
Ibuprofen	APTES-modified HNT	Gradual release attributed to the robust electrostatic interaction and affinity	14.8	Lumen and partially on outer surface	–	Korsmeyer –Peppas model	Controlled discharge of drug
Aspirin	APTES modified or natural halloysite nanotubes	Enhanced loading capacity for aspirin	11.98	Lumen pores	–	Higuchi kinetic model	Controlled release of drug
Amoxicillin, brilliant green, chlorhexidine doxycycline, gentamicin sulfate, iodine, and potassium clavulanate	Halloysite nanotubes–PCL scaffolds	Promoters of structural integrity Suppression of bacterial growth	–	Lumen	–	–	Sutures and surgical dressings

Continued

Table 16.6 Utilization of halloysite nanotubes in drug delivery.—cont'd

Drug	HNT and modifier	Advantages	Drug loading (wt.%)	Site of drug loading	Release rate (wt.%/mg g^{-1} h^{-1})	Release kinetics model	Application
Thermo-responsive curcumin	Poly (*N*-isopropyla crylamide)-halloysite nanotubes	Temperature-dependent Brownian diffusion and electro phoretic mobility	3.6	Lumen	Approximately 10 pH 6.8	—	Biocompatible thermosensitive materials for controlled release
Curcumin	Dual-responsive nanocarrier	Formation of covalent bonds via GSH- or pH-responsive mechanisms Effective preservation of curcumin's antioxidant activity and stability	2.9 wt.%	Covalently linked to outer surface	Approximately 25% in acidic pH	Power fit equation	Controlled release of prodrug for anticancer therapy
Rabeprazol	—	Protects against acid-induced degradation of RAB in the stomach	8.355 ± 1.542	Lumen	94% up to 24 h	—	Increased bioavailability and sustained drug release

Paclitaxel	Poly(methacrylic acid-co-methyl methacrylate) polymer-coated halloysite nanotubes with pH-responsive characteristics	Delayed release under acidic pH conditions and enhanced release under basic pH conditions	7.5 ± 0.5	Lumen	40% at 120 h	Korsmeyer −Peppas model	Sustained discharge for anticancer therapy
Doxorubicin	3-Mercaptopropyl) trimethoxysilane (MPTS)- halloysite nanotubes	Targeted drug delivery facilitated by folate-mediated interaction and redox-responsive mechanisms Induces apoptosis in cancer cells in vitro	14.8	Outer surface	40% at 79 h	–	Anticancer therapy
Ciprofloxacin	Aminopropyl triethoxysilane (APTES) functionalized HNTs	Improved drug loading Reduces iron absorption upon complexation with CIP	70% ± 1.7%	Outer surface	92% ± 3%	–	Increased bioavailability of the drug upon administration

Continued

Table 16.6 Utilization of halloysite nanotubes in drug delivery.—cont'd

Drug	HNT and modifier	Advantages	Drug loading (wt.%)	Site of drug loading	Release rate (wt.%/mg g^{-1} h^{-1})	Release kinetics model	Application
Camptothecin	Chitosan oligosaccharide-magnetic halloysite nanotubes conjugated with folic acid	Exhibits enhanced inhibition of cell growth in colon cancer cells	227.10 mg g^{-1}	Lumen	Sustained release up to 60 h	—	Tumor-targeted drug delivery
Chlorogenic acid, ibuprofen, and salicylic acid	Dendrimer functionalized halloysite nanotubes	Serves as a carrier for small-sized drugs Exhibits no harmful effects on living organisms	123.16 mg g^{-1} (chlorogenic acid); 182.72 mg g^{-1} (IBU); 39.52 mg g^{-1} (salicylic acid)	Outer surface	—	—	Controlled discharge of drugs
Sodium salicylate	Utilizing acid treatment and composite polymer halloysite modification	Increased the inner cavity size of HNT Caused delayed release of the drug	—	Lumen	—	Zero order First order Higuchi model Korsmeyer —Peppas model	Controlled discharge of drugs.
Quercetin	(Polyethylene glycol) PEG amine-grafted halloysite nanotubes	Enhanced drug loading	278.36 mg g^{-1}	Outer surface	—	—	Controlled release with antitumor targeted drug delivered

With permission (Satish et al., 2019).

16.8 Wound dressings based on HNT–polymer blends

Wound dressings include the constituents that contain ingredients that protect a wound, and can include a barrier to pathogens. Usually, the wound dressing should have suitable biodegradability to speed up the healing process in addition to preventing any threats related to infections and bacterial invasion (O'Donnell and Lau, 2006). Wound dressings are part of the wound care process to ensure healing. HNT composites can be used in wound dressing development due to their antibacterial capability, biocompatibility, and drug-carrying properties. Wound dressings can broadly be classified into two system, namely primary and secondary dressings. The first layer directly surrounds the wound area and is the primary wound dressing, while successive covering up of the primary dressing layer is known as secondary dressing (Stoica et al., 2020). Wound dressings can be categorized into four main types based on their applications: traditional passive dressings, skin substitutes, interactive artificial dressings, and bioactive dressings (Fig. 16.9) (Ndlovu et al., 2021).

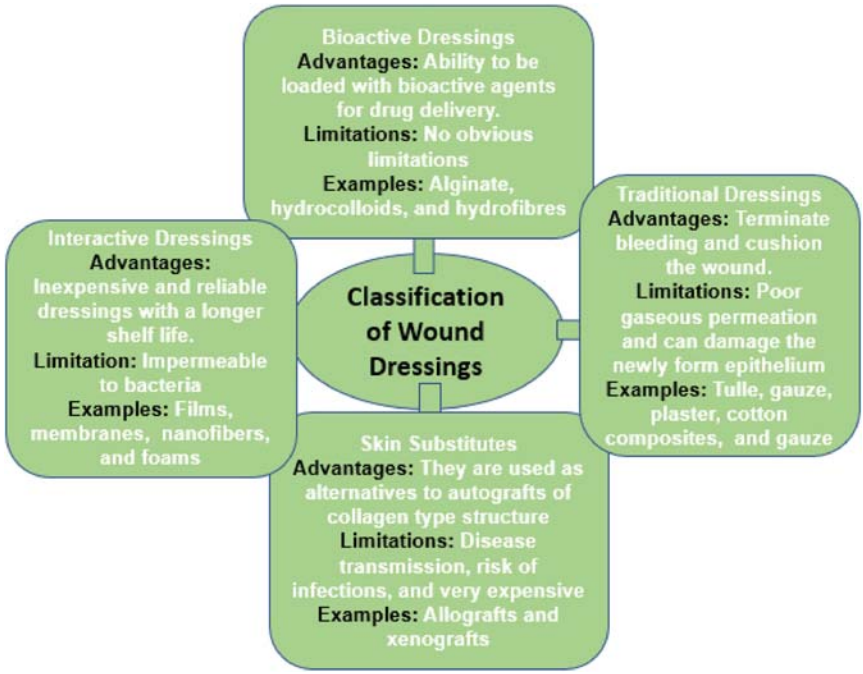

Figure 16.9 Wound dressing classifications. *(Reproduced with permission from Ndlovu et al. (2021).)*

The incorporation of HNTs into polymer blends can be a good option for wound dressing and healing processes (Fig. 16.10). A study on burn wound healing explored the use of a nanocomposite consisting of minocycline and APTES surface-modified HNTs to reinforce a PVA coating for wound dressing. The nanocomposites were thoroughly characterized using techniques such as FTIR, scanning electron microscopy (SEM), X-ray diffraction (XRD), zeta potential analysis, TGA, and field emission scanning electron microscopy (FESEM). Additionally, antibacterial tests and water absorption assessments were conducted to further examine the properties of the nanocomposites. The results revealed a tubular structure with uniformly distributed halloysite nanotubes and minocycline, along with sustained drug releasing, biodegradability and good water absorption capacity (Fig. 16.11) were observed, which is also apt for dealing with wound secretions to prevent infection. Minocycline incorporation with HNT-PVA showed enhanced antibacterial effects to Gram-positive and Gram-negative bacteria. This investigation supports HNT-PVA nanocomposite use regarding wound dressings for open or highly possibly infected wounds. The degradation rate of nanocomposite against the

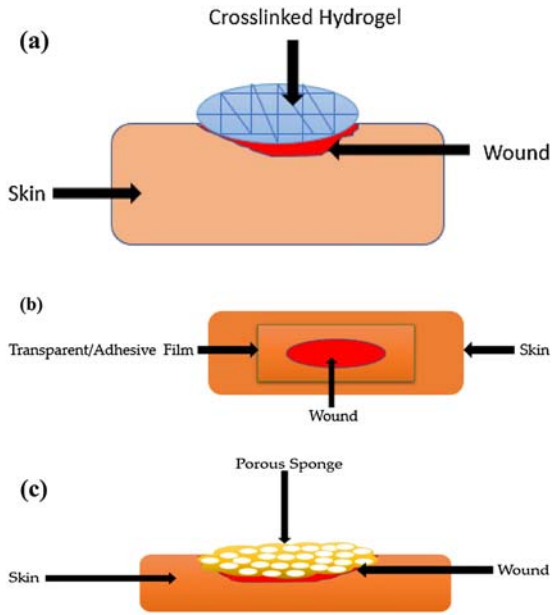

Figure 16.10 (a) Cross-linked hydrogel on skin wound, (b) utilization of transparent film dressing for skin wounds, (c) use of microporous sponge for skin wound treatment. *(Reproduced with permission from Ndlovu et al. (2021).)*

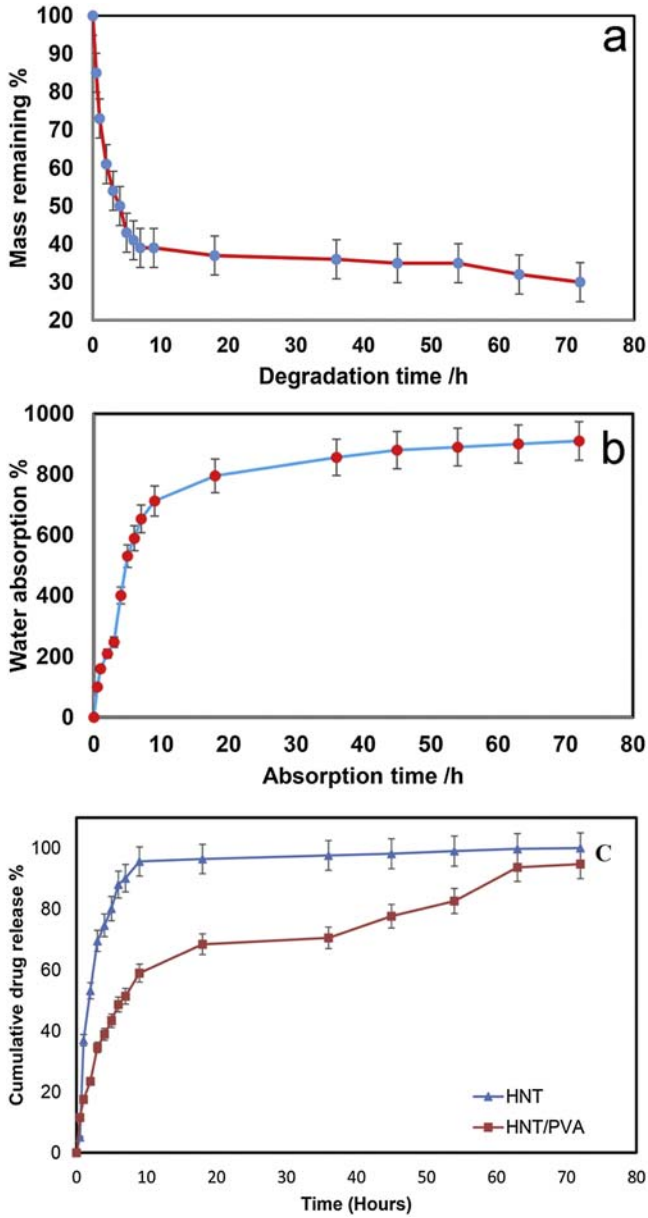

Figure 16.11 (a) Mass loss degradation (b) water absorption of halloysite nanotubes/PVA/minocycline nanocomposite in phosphate buffer saline, (c) in vitro drug discharge profile of halloysite nanotubes and halloysite nanotubes/PVA. *(Reproduced with permission from Mohebali et al. (2020).)*

absorption time can be seen in Fig. 16.9. Rapid degradation, for 8 h, shows the release of minocycline, whereas between 8 and 10 h breaking of polymer chains and sustained drug release occur for the next 3 days without much weight loss, which means that the proposed wound dressing could sustain its erection for up to a maximum of 3 days (Mohebali et al., 2020).

Therefore, HNT–polymer nanocomposites could be useful in wound dressing development, including films, fibers, hydrogels, etc. HNT–polymer-based wound dressings may deliver several benefits related to moisture retention, antibacterial activity, and as a drug carrier. Wound dressing is a part of tissue repair which means that wound healing can be considered as tissue reengineering (Cialdai et al., 2017; Wilkinson and Hardman, 2020). A study on wound dressing for skin healing for astronauts or skin injuries associated with space mission programs has been reported. The HNTs and thymol (Thy) integrated with poly 2-hydroxyethyl methacrylate (pHEMA) for developing nanocomposites further examined the chemical–physical properties to ensure Thy-HNT lumen integration and healing capacity because thymol accumulated with natural healing ingredients in addition to the drug release rate. The results revealed that the maximum swelling ability for 90 mg of dried sponge was 5.5 mg of Thy along with 62% of charged Thymol released in over a 1-week duration which indicated controlled drug release, and the calculation of efficiency in respect of drug released was calculated as follows (Zagni et al., 2023):

$$\text{Drug release efficiency } (\%) = \frac{\text{Mass released drug}}{\text{Mass loaded drug}} \times 100$$

Growth in cryogel swelling (Fig. 16.12) would support the burst effect which is very desirable in wound healing as a sustained release of drug prevents bacteria formation and infections (Fig. 16.13).

A nanocomposite sponge based on natural substances was developed to address injuries associated with the liver and tail of rats. This was achieved by combining carboxymethyl chitosan (CMC), sericin–silver nanoparticles (Ser-Ag), and halloysite nanotubes (Fig. 16.14). Different amounts of HNT powder (0.5, 1, and 2 g) were separately mixed with silver nitrate powder (8.5 mg) and a sericin solution (50 mL or approximately 0.1%). The resulting solutions (50 mL each) were then mixed with a carboxymethyl chitosan (CMC) solution (approximately 6%) to create the nanocomposite samples called CMC/Ser-Ag/HNT1, CMC/Ser-Ag/HNT2, and CMC/Ser-Ag/HNT4, as shown in Fig. 16.15. The investigation revealed that the

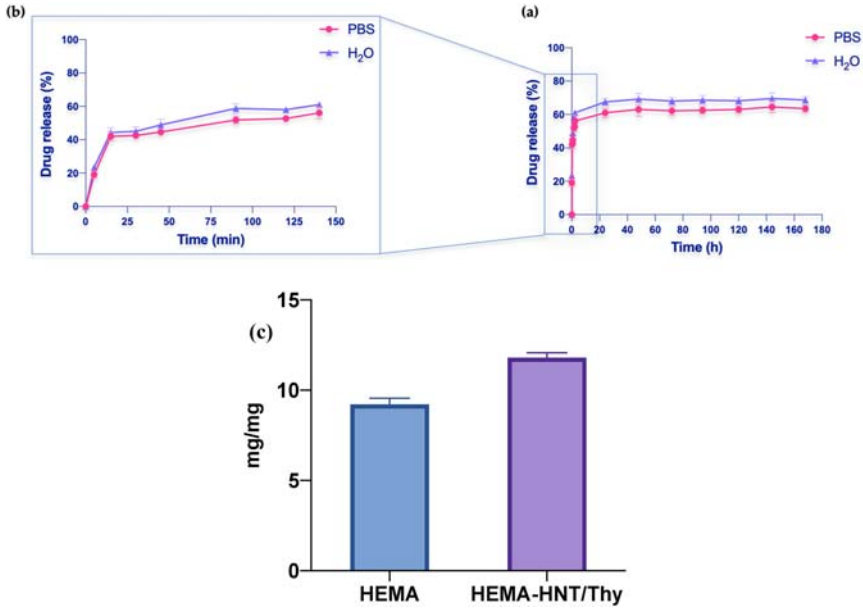

Figure 16.12 (a) Thymol release (%) from nanocomposite (hydroxyethyl methacrylate-HNT/thymol) within 1 week. (b) growth of thymol release (%) in the first 140 min. (c) Swelling capacity of hydroxyethyl-methacrylate and HEMA-HNT/thymol cryogels. *(Reproduced with permission from Zagni et al. (2023).)*

integration of HNTs into the CMC sponge resulted in a mechanical compressive strength of 100 kPa. Meanwhile, the hemostatic capacity (hemostasis time) was observed to be 15 ± 3 s and 12 ± 3 s in liver and caudal injuries, respectively. The sericin–silver nanoparticles (Ser-Ag) were found to be effective against bacteria such as *Escherichia coli* and *Staphylococcus aureus*. Additionally, experiments conducted on a full-thickness skin defect and injury model in rats confirmed the ability of the CMC/Ser-Ag/HNT4-based sponge to promote epithelialization and collagen formation. Immuno-fluorescence (IF) staining analyses revealed acceptable effectiveness for inflammation reduction after downregulating the expression of interleukin-6 (IL-6) along with improved angiogenesis after upregulating vascular endothelial growth factor (Li et al., 2023).

Ideally, achieving low cytotoxicity is important for promoting effective wound healing (Hao et al., 2022). In the case of the CMC/Ser-Ag/HNT4 group, minimal differences in cell survival were observed compared with the control group, and a low hemolysis rate (less than 5%) was observed, indicating low cytotoxicity and good hemo-compatibility

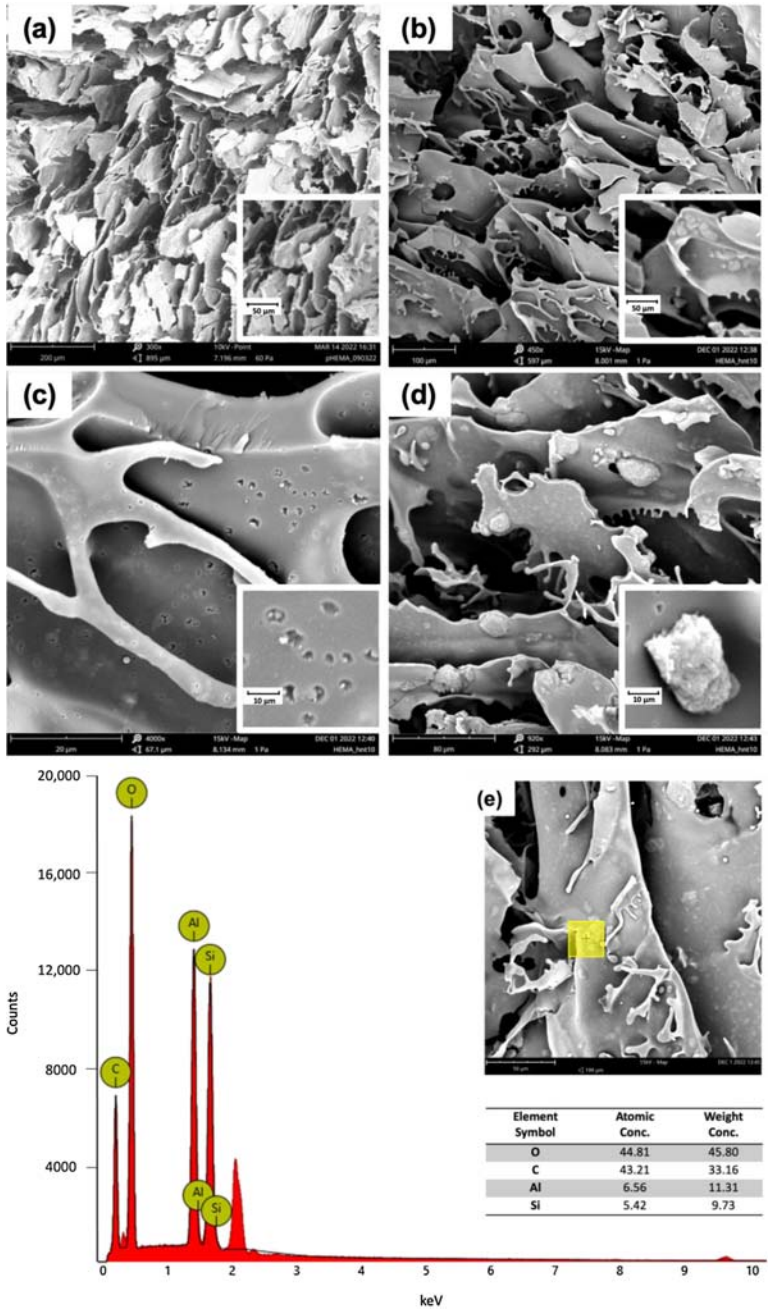

Figure 16.13 Scanning electron microscopy (SEM) images were captured to examine various samples, including: (a) cryogel of hydroxyethyl-methacrylate, (b) cryogel of hydroxyethyl-methacrylate with HNT/thymol, (c) inclusion of HNTs, (d) aggregates of halloysite, (e) energy-dispersive X-ray spectroscopy (EDX) analysis was performed on a selected area (indicated by a yellow square) of the hydroxyethyl-methacrylate with HNT/thymol cryogel. It is noteworthy that the presence of unlabeled peaks at 2.1 and 9.6 keV corresponds to gold, which was used to enhance conductivity during the examination. *(Reproduced with permission from Zagni et al. (2023).)*

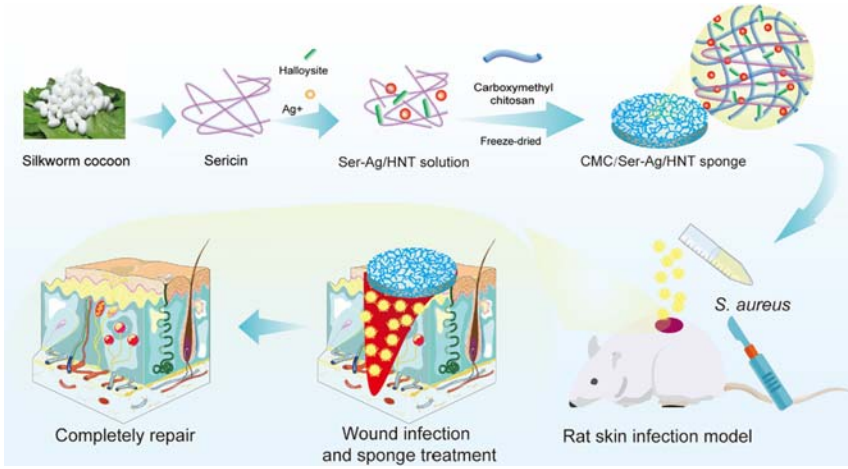

Figure 16.14 (a) Integration of carboxy-methylation with chitosan. (b) The formation of a composite sponge, CMC/Ser-Ag/HNT, for wound healing. *(Reproduced with permission from Li et al. (2023).)*

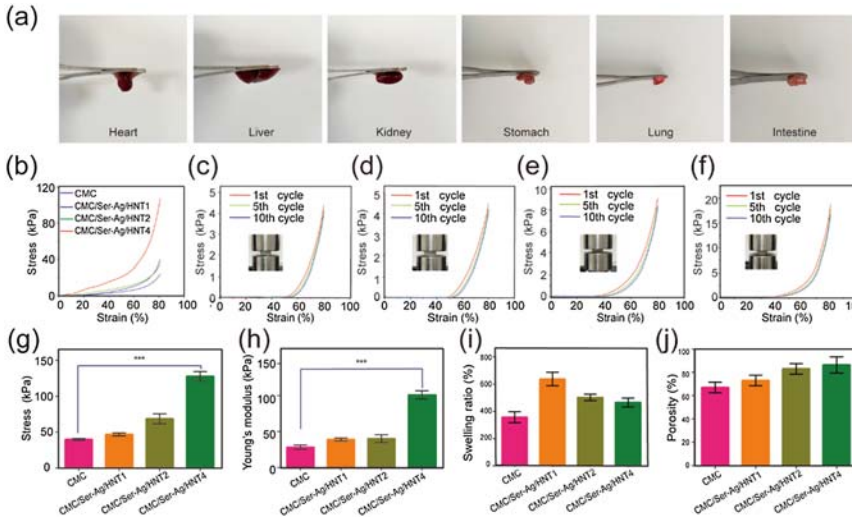

Figure 16.15 (a) Images showing the adherence of CMC/Ser-Ag/HNT4 sponge to the surfaces of six major organs in mice, (b) Stress—strain curves depicting the compression behavior of CMC and CMC/Ser-Ag/HNT sponges. Cyclic compression stress—strain curves of (c) CMC, (d) CMC/Ser-Ag/HNT1, (e) CMC/Ser-Ag/HNT2, and (f) CMC/Ser-Ag/HNT4 sponges. (g) Maximum stress; (h) Young's modulus; (i) swelling ratio; (j) porosity measurements of CMC and CMC/Ser-Ag/HNT sponges. *(Reproduced with permission from Liang et al. (2021).)*

(Chin et al., 2019; Wen et al., 2016). Effective control of bleeding is a crucial and desirable property of wound dressings, which is evidenced by the CMC/Ser-Ag/HNT4 sponge's high hemostatic effect (Udangawa et al., 2019; Yu et al., 2019a). Additionally, the CMC/Ser-Ag/HNT4 sponge has shown promising results in terms of timely bleeding control, antibacterial capability, and wound infection healing capability, as evidenced by a rat model of full-thickness skin defect wound healing (Matoori et al., 2021; Yu et al., 2019b). The CMC/Ser-Ag/HNT4 sponge has also shown the ability to promote the formation of newly created collagen fibers in wounds, which is favorable for wound healing (Chen et al., 2021).

An alginate-based wound dressing with vancomycin over the HNTs revealed that the release of vancomycin from gel is sustained with the integration of gelatin as compared to the incorporation of silica. The three samples were included in the research with the incorporation of vancomycin to HNTs, hydrochloric acid-activated HNTs (HNT-HCL), and 3-aminopropyl-trimethoxysilane-modified HNTs (HNT-APTS), respectively. However, the integration of gelatin in alginate gels is good for slowing the vancomycin-HNT-APTS drug release but resulted in poor antibacterial activity. On the other hand, encapsulated vancomycin-HNTs-APTS in alginate gel without gelatin showed good results in drug release capability and against microbacteria, which makes it a potential wound dressing material for treatment (Kurczewska et al., 2017).

Another study suggested that microfibrous mats have excellent biocompatibility along with sustained antimicrobial protection. The mat was prepared via the electrospinning method with tetracycline hydrochloride (TCH) loaded to the HNTs with regenerated silk fibroin (RSF) (Wu et al., 2021). Many more applications are available regarding HNT−polymer composite wound dressings, and some are included in Table 16.7.

16.9 Challenges and limitations of HNT−polymer blends

Despite the encouraging properties of HNTs and HNT−polymer blends, there are also some challenges and restrictions that require careful attention. The primary challenge is to succeed in uniform HNT distribution in the polymer. The agglomeration or random distribution of ingredients in the nanocomposite can have a significant impact on its mechanical, thermal, and optical properties. Modified HNTs' surface/structure could be an alternative to overcoming this challenge, but better optimization is

Table 16.7 HNT/polymer nanocomposite applications for wound healing.

Polymer composites	Drugs loading	Type of wound dressing/ healing
Poly(lactic-co-glycolic acid) (PLGA)	Tetracycline hydrochloride	Electrospun nanofiber mats
Poly(lactic-co-glycolic acid), chitosan	Amoxicillin	Electrospun nanofiber mats
Polyvinyl alcohol	Minocycline	Film
Cellulose ether, polyvinyl alcohol	Gentamicin sulfate	Electrospun nanofiber mats
PCL	Brilliant green, amoxicillin, and potassium clavulanate	Electrospun nanofiber mats
PCL, gelatin	NA	Electrospun nanofiber mats
Gelatin	Ciprofloxacin and polymyxin B sulfate	Film
Carrageenan	NA	Film
Chitosan	Doxorubicin	Hydrogel mold
Chitosan	NA	Sponges
Gelatin, sericin	Zinc and copper ions	Electrospun nanofiber mats
Poly(lactic-co-glycolic acid), chitosan	Minocycline	Film

Adapted with permission from Fakhruddin et al. (2021).

necessary before this. Another challenge is the probable toxicity of HNTs. Although HNTs are generally considered biocompatible and nontoxic, using them in medical areas for a long time raises some concerns in a few cases. HNTs and the related drug's size, aspect ratio, and surface modification variation can affect the toxicity as per the available research reports. The cost and compatibility of polymers to HNTs are other considerable challenges that have been seen because HNTs are new in nanocomposites and thus the availability of HNTs and the best suitable polymer to incorporate with HNTs need to be explore.

16.10 Future prospects of HNT–polymer blends in biomedical applications

The excellent properties of HNT–polymer blends place HNT composites as a favorable material for biomedical engineering and medical applications.

There is an increasing necessity for modernization in tissue reengineering by HNT incorporation. HNT–polymer composites have exhibited great potential in creating scaffolds that reproduce the natural extracellular matrix, providing a suitable environment for cell growth and tissue regeneration. The higher aspect ratio and porosity characteristics of HNTs support and enhance the cell adhesion and production, resulting in enhanced tissue regeneration naturally. Improving the drug-loading capability for a variety of drugs would support safer cancer treatment in the future through HNT–polymers.

16.11 Conclusion

HNT-based composites have exhibited potential positive results for wound dressings and wound care applications. The integration of HNTs with bioresorbable polymer matrices exhibited significant enhancements in drug delivery and antibacterial activities. HNTs have a tubular structure with a higher aspect ratio, which supports their drug-loading capability and controlled release of drugs. Alteration of the synthesis methods enables control over the properties of HNTs, polymers, and composites for medical purposes. The biodegradability of HNT composites exhibits suitable degradation rates, gradual absorption, and elimination from the body. These characteristics reduce the repeated requirement for dressing removal, resulting in better patient comfort and wound care management. Further optimization of the blending process, achieving reliable dispersion of HNTs, and improving stability are desirable.

References

Abbas, M., Alqahtani, M.S., Almohiy, H.M., Alqahtani, F.F., Alhifzi, R., Jambi, L.K., 2021. The potential contribution of biopolymeric particles in lung tissue regeneration of COVID-19 patients. Polymers 13 (22), 4011. https://doi.org/10.3390/polym13224011.

Abdullayev, E., Lvov, Y., 2013. Halloysite clay nanotubes as a ceramic "skeleton" for functional biopolymer composites with sustained drug release. J. Mater. Chem. B 1 (23), 2894–2903. https://doi.org/10.1039/C3TB20059K.

Afewerki, S., Harb, S.V., Stocco, T.D., Ruiz-Esparza, G.U., Lobo, A.O., 2023. Polymers for surgical sutures. In: Advanced Technologies and Polymer Materials for Surgical Sutures. Elsevier, pp. 95–128. https://doi.org/10.1016/B978-0-12-819750-9.00004-8.

Ahuja, G., Pathak, K., 2009. Porous carriers for controlled/modulated drug delivery. Indian J. Pharmaceut. Sci. 71 (6), 599. https://doi.org/10.4103/0250-474X.59540.

Alaswad, S.O., Mahmoud, A.S., Arunachalam, P., 2022. Recent advances in biodegradable polymers and their biological applications: a brief review. Polymers 14 (22). https://doi.org/10.3390/POLYM14224924.

Alhanish, A., Ali, G.A.M., 2023. Biodegradable polymers. In: Handbook of Biodegradable Materials, pp. 263–291. https://doi.org/10.1007/978-3-031-09710-2_13.

Asghari, F., Samiei, M., Adibkia, K., Akbarzadeh, A., Davaran, S., 2017. Biodegradable and biocompatible polymers for tissue engineering application: a review. Artif. Cell Nanomed. Biotechnol. 45 (2), 185–192. https://doi.org/10.3109/21691401.2016.1146731.

Barman, M., Mahmood, S., Augustine, R., Hasan, A., Thomas, S., Ghosal, K., 2020. Natural halloysite nanotubes/chitosan based bio-nanocomposite for delivering norfloxacin, an anti-microbial agent in sustained release manner. Int. J. Biol. Macromol. 162, 1849–1861. https://doi.org/10.1016/J.IJBIOMAC.2020.08.060.

Bioresorbable Polymers Market to Expand at a CAGR of ~13% Assessment for the Driving Factors, Size, Revenue, Segments, Expansion, Demand, and Opportunities During 2023–2035 – Digital Journal. https://www.digitaljournal.com/pr/bioresorbable-polymers-market-to-expand-at-a-cagr-of-13-assessment-for-the-driving-factors-size-revenue-segments-expansion-demand-and-opportunities-during-2023-2035. (Accessed 23 March 2022).

Boyer, C., Ambrose Jr, J., Das, S., Humayun, A., Chappidi, D., Giorno, R., et al., 2018. Antibacterial and antibiofouling clay nanotube–silicone composite. Med. Dev. Evid. Res. 11, 123–137. https://doi.org/10.2147/MDER.S146248.

Casalini, T., Perale, G., 2012. Processing of bioresorbable and other polymers for medical applications. In: Durability and Reliability of Medical Polymers, pp. 49–76. https://doi.org/10.1533/9780857096517.1.49.

Cavallaro, G., De Lisi, R., Lazzara, G., Milioto, S., 2013. Polyethylene glycol/clay nanotubes composites: thermal properties and structure. J. Therm. Anal. Calorim. 112 (1), 383–389. https://doi.org/10.1007/S10973-012-2766-8.

Cecílio, D.M., Cerrada, M.L., Pérez, E., Fernandes, A., Lourenço, J.P., McKenna, T.F.L., et al., 2023. A novel approach for preparation of nanocomposites with an excellent rigidity/deformability balance based on reinforced HDPE with halloysite. Eur. Polym. J. 184, 111765. https://doi.org/10.1016/J.EURPOLYMJ.2022.111765.

Chen, T.Y., Wen, T.K., Dai, N.T., Hsu, S.H., 2021. Cryogel/hydrogel biomaterials and acupuncture combined to promote diabetic skin wound healing through immunomodulation. Biomaterials 269. https://doi.org/10.1016/J.BIOMATERIALS.2020.120608.

Cheng, C., Song, W., Zhao, Q., Zhang, H., 2020a. Halloysite nanotubes in polymer science: purification, characterization, modification and applications. Nanotechnol. Rev. 9 (1), 323–344. https://doi.org/10.1515/NTREV-2020-0024.

Cheng, C., Gao, Y., Song, W., Zhao, Q., Zhang, H., Zhang, H., 2020b. Halloysite nanotube-based H_2O_2-responsive drug delivery system with a turn on effect on fluorescence for real-time monitoring. Chem. Eng. J. 380, 122474. https://doi.org/10.1016/J.CEJ.2019.122474.

Chin, J.S., Madden, L., Chew, S.Y., Becker, D.L., 2019. Drug therapies and delivery mechanisms to treat perturbed skin wound healing. Adv. Drug Deliv. Rev. 149–150, 2–18. https://doi.org/10.1016/J.ADDR.2019.03.006.

Cialdai, F., Vignali, L., Morbidelli, L., Colciago, A., Celotti, F., Santi, A., et al., 2017. Modeled microgravity affects fibroblast functions related to wound healing. Microgravity Sci. Technol. 29 (1–2), 121–132. https://doi.org/10.1007/S12217-016-9532-7.

Deng, S., Chen, A., Chen, W., Lai, J., Pei, Y., Wen, J., et al., 2023. Fabrication of biodegradable and biocompatible functional polymers for anti-infection and augmenting wound repair. Polymers 15 (1). https://doi.org/10.3390/POLYM15010120.

Dirauf, M., Muljajew, I., Weber, C., Schubert, U.S., 2022. Recent advances in degradable synthetic polymers for biomedical applications – beyond polyesters. Prog. Polym. Sci. 129, 101547. https://doi.org/10.1016/J.PROGPOLYMSCI.2022.101547.

Du, M., Guo, B., Jia, D., 2010. Newly emerging applications of halloysite nanotubes: a review. Polym. Int. 59 (5), 574–582. https://doi.org/10.1002/PI.2754.

Esawi, A.M.K., Salem, H.G., Hussein, H.M., Ramadan, A.R., 2010. Effect of processing technique on the dispersion of carbon nanotubes within polypropylene carbon nanotube-composites and its effect on their mechanical properties. Polym. Compos. 31 (5), 772–780. https://doi.org/10.1002/PC.20859.

Fakhruddin, K., Hassan, R., Khan, M.U.A., Allisha, S.N., Razak, S.I.A., Zreaqat, M.H., et al., 2021. Halloysite nanotubes and halloysite-based composites for biomedical applications. Arab. J. Chem. 14 (9), 103294. https://doi.org/10.1016/J.ARABJC.2021.103294.

Gaaz, T., Sulong, A., Kadhum, A., Al-Amiery, A., Nassir, M., Jaaz, A., 2017. The impact of halloysite on the thermo-mechanical properties of polymer composites. Molecules 22 (5), 838. https://doi.org/10.3390/molecules22050838.

Ganapathy, D., Shanmugam, R., Pitchiah, S., Murugan, P., Chinnathambi, A., Alharbi, S.A., et al., 2022. Potential applications of halloysite nanotubes as drug carriers: a review. J. Nanomater. 2022. https://doi.org/10.1155/2022/1068536.

Gleadall, A., 2015. Mechanical properties of biodegradable polymers for medical applications. In: Modelling Degradation of Bioresorbable Polymeric Medical Devices, pp. 163–199. https://doi.org/10.1533/9781782420255.2.163.

Guo, B., Zou, Q., Lei, Y., Jia, D., 2009. Structure and performance of polyamide 6/halloysite nanotubes nanocomposites. Polym. J. 41 (10), 835–842. https://doi.org/10.1295/polymj.PJ2009110.

Guo, S., Fu, D., Utupova, A., Sun, D., Zhou, M., Jin, Z., et al., 2019. Applications of polymer-based nanoparticles in vaccine field. Nanotechnol. Rev. 8 (1), 143–155. https://doi.org/10.1515/NTREV-2019-0014.

Hajebi, S., Nasr, S.M., Rabiee, N., Bagherzadeh, M., Ahmadi, S., Rabiee, M., et al., 2021. Bioresorbable composite polymeric materials for tissue engineering applications. Int. J. Polym. Mater. Polym. Biomater. 70 (13), 926–940. https://doi.org/10.1080/00914037.2020.1765365.

Hao, Y., Zhao, W., Zhang, H., Zheng, W., Zhou, Q., 2022. Carboxymethyl chitosan-based hydrogels containing fibroblast growth factors for triggering diabetic wound healing. Carbohydr. Polym. 287, 119336. https://doi.org/10.1016/J.CARBPOL.2022.119336.

Hasani, M., Abdouss, M., Shojaei, S., 2021. Nanocontainers for drug delivery systems: a review of halloysite nanotubes and their properties. Int. J. Artif. Organs 44 (6), 426–433. https://doi.org/10.1177/0391398820968836.

Implantable Formulations - Foster Corporation. https://www.fostercomp.com/custom-compounds/implantable-formulations/?matchtype=e&network=g&device=c&keyword=bioresorbable polymer&campaign=14991849720&adgroup=125919745382&gclid=CjwKCAjwq-WgBhBMEiwAzKSH6JK8R8gq0K_X4s9wABtnLuAcZiWOlElFiWa8X6TPF7CLYaCMCFRiARoChjIQAvD_BwE. (Accessed 23 March 2022).

Khot, S., Rawal, S.U., Patel, M.M., 2021. Dissolvable-soluble or biodegradable polymers. In: Drug Delivery Devices and Therapeutic Systems, pp. 367–394. https://doi.org/10.1016/B978-0-12-819838-4.00024-9.

Khunova, V., Kristof, J., Kelnar, I., Dybal, J., 2013. The effect of halloysite modification combined with in situ matrix modifications on the structure and properties of polypropylene/halloysite nanocomposites. Express Polym. Lett. 7 (5), 471–479. https://doi.org/10.3144/expresspolymlett.2013.43.

Khunová, V., Kováčová, M., Olejniková, P., Ondreáš, F., Špitalský, Z., Ghosal, K., et al., 2022. Antibacterial electrospun polycaprolactone nanofibers reinforced by halloysite

nanotubes for tissue engineering. Polymers 14 (4), 746. https://doi.org/10.3390/polym14040746.

Kim, H.S., Kang, J., Hwang, D., Han, J.K., Yang, H.M., Kang, H.J., et al., 2021. Durable polymer versus biodegradable polymer drug-eluting stents after percutaneous coronary intervention in patients with acute coronary syndrome. Circulation 143 (11), 1081–1091. https://doi.org/10.1161/CIRCULATIONAHA.120.051700.

Kurczewska, J., Pecyna, P., Ratajczak, M., Gajecka, M., Schroeder, G., 2017. Halloysite nanotubes as carriers of vancomycin in alginate-based wound dressing. Saudi Pharmaceut. J. 25 (6), 911–920. https://doi.org/10.1016/J.JSPS.2017.02.007.

Li, Y., Yuan, X., Jiang, L., Dai, H., Zhao, Y., Guan, X., et al., 2022. Manipulation of the halloysite clay nanotube lumen for environmental remediation: a review. Environ. Sci.: Nano 9 (3), 841–866. https://doi.org/10.1039/D1EN01032H.

Li, S., Jiang, M., Zhang, Y., Xie, X., Li, W., Ming, P.Y., et al., 2023. Multi-functional carboxymethyl chitosan/sericin protein/halloysite composite sponge with efficient antibacterial and hemostatic properties for accelerating wound healing. Int. J. Biol. Macromol. 234, 123357. https://doi.org/10.1016/J.IJBIOMAC.2023.123357.

Liang, Y., Li, Z., Huang, Y., Yu, R., Guo, B., 2021. Dual-dynamic-bond cross-linked antibacterial adhesive hydrogel sealants with on-demand removability for post-wound-closure and infected wound healing. ACS Nano 15 (4), 7078–7093. https://doi.org/10.1021/ACSNANO.1C00204.

Liu, M., Jia, Z., Jia, D., Zhou, C., 2014. Recent advance in research on halloysite nanotubes-polymer nanocomposite. Prog. Polym. Sci. 39 (8), 1498–1525. https://doi.org/10.1016/J.PROGPOLYMSCI.2014.04.004.

Lvov, Y., Abdullayev, E., 2013. Functional polymer-clay nanotube composites with sustained release of chemical agents. Prog. Polym. Sci. 38 (10–11), 1690–1719. https://doi.org/10.1016/J.PROGPOLYMSCI.2013.05.009.

Lvov, Y., Wang, W., Zhang, L., Fakhrullin, R., 2016a. Halloysite clay nanotubes for loading and sustained release of functional compounds. Adv. Mater. 28 (6), 1227–1250. https://doi.org/10.1002/ADMA.201502341.

Lvov, Y.M., DeVilliers, M.M., Fakhrullin, R.F., 2016b. The application of halloysite tubule nanoclay in drug delivery. Expert Opin. Drug Deliv. 13 (7), 977–986. https://doi.org/10.1517/17425247.2016.1169271.

Matoori, S., Veves, A., Mooney, D.J., 2021. Advanced bandages for diabetic wound healing. Sci. Transl. Med. 13 (585). https://doi.org/10.1126/SCITRANSLMED.ABE4839.

McKeen, L.W., 2014. Plastics used in medical devices. In: Handbook of Polymer Applications in Medicine and Medical Devices. Elsevier, pp. 21–53. https://doi.org/10.1016/B978-0-323-22805-3.00003-7.

Modesti, M., Lorenzetti, A., Bon, D., Besco, S., 2005. Effect of processing conditions on morphology and mechanical properties of compatibilized polypropylene nanocomposites. Polymer 46 (23), 10237–10245. https://doi.org/10.1016/J.POLYMER.2005.08.035.

Mohebali, A., Abdouss, M., Afshar Taromi, F., 2020. Fabrication of biocompatible antibacterial nanowafers based on HNT/PVA nanocomposites loaded with minocycline for burn wound dressing. Mater. Sci. Eng. C 110, 110685. https://doi.org/10.1016/J.MSEC.2020.110685.

Namathoti, S., Vakkalagadda, M.R.K., 2023. Mechanical and shape recovery characterization of MWCNTs/HNTs-reinforced thermal-responsive shape-memory polymer nanocomposites. Polymers 15 (3), 710. https://doi.org/10.3390/polym15030710.

Nanda, H.S., Yang, L., Hu, J., Mao, H., Jiang, S., 2022. Editorial: biodegradable polymers for biomedical applications. Front. Mater. 9, 414. https://doi.org/10.3389/FMATS.2022.944755.

Naser, A.Z., Deiab, I., Defersha, F., Yang, S., 2021. Expanding poly(lactic acid) (PLA) and polyhydroxyalkanoates (PHAs) applications: a review on modifications and effects. Polymers 13 (23), 4271. https://doi.org/10.3390/polym13234271.

Ndlovu, S.P., Ngece, K., Alven, S., Aderibigbe, B.A., 2021. Gelatin-based hybrid scaffolds: promising wound dressings. Polymers 13 (17), 2959. https://doi.org/10.3390/polym13172959.

Nedaipour, F., Bagheri, H., Mohammadi, S., 2020. "Polylactic acid-polyethylene glycol-hydroxyapatite composite" an efficient composition for interference screws. Nanocomposites 6 (3), 99–110. https://doi.org/10.1080/20550324.2020.1794688.

Nguyen, H.M., Ngoc Le, T.T., Nguyen, A.T., Thien Le, H.N., Pham, T.T., 2023. Biomedical materials for wound dressing: recent advances and applications. RSC Adv. 13 (8), 5509–5528. https://doi.org/10.1039/D2RA07673J.

O'Donnell, T.F., Lau, J., 2006. A systematic review of randomized controlled trials of wound dressings for chronic venous ulcer. J. Vasc. Surg. 44 (5), 1118–1125. https://doi.org/10.1016/J.JVS.2006.08.004.

Pappalardo, D., Mathisen, T., Finne-Wistrand, A., 2019. Biocompatibility of resorbable polymers: a historical perspective and framework for the future. Biomacromolecules 20 (4), 1465–1477. https://doi.org/10.1021/ACS.BIOMAC.9B00159.

Paul, A., Augustine, R., Hasan, A., Zahid, A.A., Thomas, S., Agatemor, C., et al., 2022. Halloysite nanotube and chitosan polymer composites: Physicochemical and drug delivery properties. J. Drug Deliv. Sci. Technol. 72, 103380. https://doi.org/10.1016/J.JDDST.2022.103380.

Pereira, I., Saleh, M., Nunes, C., Reis, S., Veiga, F., Paiva-Santos, A.C., 2021. Preclinical developments of natural-occurring halloysite clay nanotubes in cancer therapeutics. Adv. Colloid Interface Sci. 291, 102406. https://doi.org/10.1016/j.cis.2021.102406.

Pertici, G., 2017. Introduction to bioresorbable polymers for biomedical applications. In: Bioresorbable Polymers for Biomedical Applications. Elsevier, pp. 3–29. https://doi.org/10.1016/B978-0-08-100262-9.00001-X.

Ravichandran, G., Rathnakar, G., Santhosh, N., Chennakeshava, R., Hashmi, M.A., 2019. Enhancement of mechanical properties of epoxy/halloysite nanotube (HNT) nanocomposites. SN Appl. Sci. 1 (4), 1–8. https://doi.org/10.1007/S42452-019-0323-9.

Rust, T., Jung, D., Langer, K., Kuckling, D., 2023. Stimuli-accelerated polymeric drug delivery systems. Polym. Int. 72 (1), 5–19. https://doi.org/10.1002/PI.6474.

Samir, A., Ashour, F.H., Hakim, A.A.A., Bassyouni, M., 2022. Recent advances in biodegradable polymers for sustainable applications. Npj Mater. Degrad. 6 (1), 68. https://doi.org/10.1038/s41529-022-00277-7.

Santos, A.C., Ferreira, C., Veiga, F., Ribeiro, A.J., Panchal, A., Lvov, Y., et al., 2018. Halloysite clay nanotubes for life sciences applications: from drug encapsulation to bioscaffold. Adv. Colloid Interface Sci. 257, 58–70. https://doi.org/10.1016/J.CIS.2018.05.007.

Satish, S., Tharmavaram, M., Rawtani, D., 2019. Halloysite nanotubes as a nature's boon for biomedical applications. BJGP Open 6. https://doi.org/10.1177/1849543519863625.

Silva, A.C.Q., Silvestre, A.J.D., Vilela, C., Freire, C.S.R., 2021. Natural polymers-based materials: a contribution to a greener future. Molecules 27 (1), 94. https://doi.org/10.3390/molecules27010094.

Socci, M.C., Rodríguez, G., Oliva, E., Fushimi, S., Takabatake, K., Nagatsuka, H., et al., 2023. Polymeric materials, advances and applications in tissue engineering: a review. Bioengineering 10 (2), 218. https://doi.org/10.3390/bioengineering10020218.

Stoica, A.E., Chircov, C., Grumezescu, A.M., 2020. Nanomaterials for wound dressings: an up-to-date overview. Molecules 25 (11), 2699. https://doi.org/10.3390/molecules25112699.

Suh, Y.J., 2015. Use of natural halloysite as a functional cosmetics carrier. Econ. Environ. Geol. 48 (3), 247–253. https://doi.org/10.9719/EEG.2015.48.3.247.

The National Institutes of Health (NIH) Consensus Development Program: Clinical Applications of Biomaterials. https://consensus.nih.gov/1982/1982Biomaterials034html.htm. (Accessed 23 March 2022).

Udangawa, R.N., Mikael, P.E., Mancinelli, C., Chapman, C., Willard, C.F., Simmons, T.J., et al., 2019. Novel cellulose-halloysite hemostatic nanocomposite fibers with a dramatic reduction in human plasma coagulation time. ACS Appl. Mater. Interfaces 11 (17), 15447–15456. https://doi.org/10.1021/ACSAMI.9B04615.

Ulery, B.D., Nair, L.S., Laurencin, C.T., 2011. Biomedical applications of biodegradable polymers. J. Polym. Sci. B Polym. Phys. 49 (12), 832. https://doi.org/10.1002/POLB.22259.

Venkatesh, C., Clear, O., Major, I., Lyons, J.G., Devine, D.M., 2019. Faster release of lumen-loaded drugs than matrix-loaded equivalent in polylactic acid/halloysite nanotubes. Materials 12 (11), 1830. https://doi.org/10.3390/ma12111830.

Vuluga, Z., Corobea, M., Elizetxea, C., Ordonez, M., Ghiurea, M., Raditoiu, V., et al., 2018. Morphological and tribological properties of PMMA/halloysite nanocomposites. Polymers 10 (8), 816. https://doi.org/10.3390/polym10080816.

Wang, W., Wang, C., 2012. Polyurethane for biomedical applications: a review of recent developments. In: The Design and Manufacture of Medical Devices, pp. 115–151. https://doi.org/10.1533/9781908818188.115.

Wen, J., Weinhart, M., Lai, B., Kizhakkedathu, J., Brooks, D.E., 2016. Reversible hemostatic properties of sulfabetaine/quaternary ammonium modified hyperbranched polyglycerol. Biomaterials 86, 42–55. https://doi.org/10.1016/J.BIOMATERIALS.2016.01.067.

Wilkinson, H.N., Hardman, M.J., 2020. Wound healing: cellular mechanisms and pathological outcomes: Cellular mechanisms of wound repair. Open Biol. 10 (9). https://doi.org/10.1098/RSOB.200223/.

Wu, Y., Zhang, Y., Ju, J., Yan, H., Huang, X., Tan, Y., 2019. Advances in halloysite nanotubes–polysaccharide nanocomposite preparation and applications. Polymers 11 (6), 987. https://doi.org/10.3390/polym11060987.

Wu, M., Liu, W., Yao, J., Shao, Z., Chen, X., 2021. Silk microfibrous mats with long-lasting antimicrobial function. J. Mater. Sci. Technol. 63, 203–209. https://doi.org/10.1016/J.JMST.2020.02.060.

Yu, L., Shang, X., Chen, H., Xiao, L., Zhu, Y., Fan, J., 2019a. A tightly-bonded and flexible mesoporous zeolite-cotton hybrid hemostat. Nat. Commun. 10 (1), 1932. https://doi.org/10.1038/s41467-019-09849-9.

Yu, Y., Li, P., Zhu, C., Ning, N., Zhang, S., Julius Vancso, G., et al., 2019b. Multifunctional and recyclable photothermally responsive cryogels as efficient platforms for wound healing. Adv. Funct. Mater. 29 (35), 1904402. https://doi.org/10.1002/ADFM.201904402.

Zagni, C., Scamporrino, A.A., Riccobene, P.M., Floresta, G., Patamia, V., Rescifina, A., et al., 2023. Portable nanocomposite system for wound healing in space. Nanomaterials 13 (4), 741. https://doi.org/10.3390/nano13040741.

Zare, Y., Rhee, K.Y., 2022. Development of a model for modulus of polymer halloysite nanotube nanocomposites by the interphase zones around dispersed and networked nanotubes. Sci. Rep. 12 (1), 2443. https://doi.org/10.1038/s41598-022-06465-4.

Zhiraslanovna Ozkan, S., Petrovna Karpacheva, G., Aleksandrovich Chernavskii, P., Leont'evna Dzidziguri, E., Nikolaevna Bondarenko, G., Viktorovna Pankina, G., 2018. Hybrid materials based on poly-3-amine-7-methylamine-2-methylphenazine and magnetite nanoparticles immobilized on single-walled carbon nanotubes. Polymers 10 (5), 544. https://doi.org/10.3390/polym10050544.

This page intentionally left blank

CHAPTER 17

Biobehavioral structure, elastic, optical, and thermoluminescence properties of $Al_xCa_{y-x}Nd_{01}P_{70}$ bioglasses

Ravi Kumar Guntu
Department of Physics, Sreenidhi Institute of Science and Technology, JNT University, Hyderabad, Telangana, India

17.1 Introduction

Well-known calcio-phosphates and their derivatives, such as calcio-orthophosphates, $Ca(PO_2)_4$, are used for a variety of biomedical applications, including bio-bones and implants (Jeong et al., 2019). On the other hand, calcio-phosphate glass of Nd^{3+} ions has been widely recognized for various photonic or white LED semiconducting applications (Flórez et al., 2009). Researchers have been looking for highly effective radiative-capable, highly elastic optical, and biocompatible materials for the past 20 years, up until the present (Guntu, 2020). By using optical and biocompatible procedures, the $Al_xCa_{y-x}Nd_{01}P_{70}$ materials were created and described in this way (Wang et al., 2021). It is generally known that white light applications require Nd^{3+} ions to have a desirable wavelength of 1.06 μm. In this manner, Nd_2O_3 is selected to improve optical phenomena in calcio-phosphate glasses (Guntu, 2020). For many industrial and opto-biomedical applications, Nd_2O_3-doped calcio-phosphate glasses are the most important glassy matrices (Pugliese et al., 2020).

The best options for dental and optical replacements are made of phosphate glass, which is currently used extensively in biomedical technology (Islam et al., 2017). As a result of the solid-state (diode-pumped) laser technology's recent, quick advancement, advanced improvements in unique class laser resources have achieved considerable prominence (Brauch et al., 2022). Lasing evaluations owing to Nd^{3+} ions ($\lambda \sim 1.06$ μm) are

Bioresorbable Polymers and their Composites
ISBN 978-0-443-18915-9
https://doi.org/10.1016/B978-0-443-18915-9.00006-9
© 2024 Elsevier Ltd.
All rights reserved.

often helpful and meet practical needs. In order to achieve the desired properties for a successful implementation of high gain, the host material must be chosen appropriately. The prepared Nd_2O_3-doped P_2O_5 composite glasses are then thoroughly examined in the current work for their suitability for LED applications (Burtan-Gwizdala et al., 2023). Phosphate glasses usually have interdependent, amorphous structures and exhibit glass characteristics when heated to their melting point (Calahoo and Wondraczek, 2020). When it comes to opto-electronic and biomedical applications, P_2O_5 glasses are often dependable and known for their extensive creative and evolving use. Due to their strong optically stimulated luminescence, phosphate glasses with Al_2O_3 doping are typically utilized as dosimeters in radiation therapy and protection applications (Hirosawa et al., 2021). The development of a flexible, high-elastic bio-implant has drawn a great deal of interest due to its potential uses in areas including bio-bone, and also for uses that require its high elasticity and biocompatibility. $Al_xCa_{y-x}Nd_{01}P_{70}$ glasses may be most helpful in this area to create noncorrosive, flexible, highly efficient, and biocompatible materials that are radiative competent materials (Anil Kumar et al., 2021). Finding an appropriate glass matrix with excellent glass-forming ability, and optical and biocompatible qualities thus has become a research hotspot in the disciplines of optical and biomedical applications.

17.2 Methods and measurements

Glass samples were prepared using the melt quenching process. The quantified chemical composition, i.e., $Al_xCa_{y-x}Nd_{01}P_{70}$, was chosen for present synthesis, where "x" varies as 0, 3, 5, 8, and 10 mol%, and $y = 29$ mol%. The following is a list of the detailed chemical composition.

$$\mathbf{A_0}\ 00Al_2O_3 + 29\ CaF_2 + 01\ Nd_2O_3 + 70\ P_2O_5$$

$$\mathbf{A_3}\ 03Al_2O_3 + 26\ CaF_2 + 01\ Nd_2O_3 + 70\ P_2O_5$$

$$\mathbf{A_5}\ 05Al_2O_3 + 24\ CaF_2 + 01\ Nd_2O_3 + 70\ P_2O_5$$

$$\mathbf{A_8}\ 08Al_2O_3 + 21\ CaF_2 + 01\ Nd_2O_3 + 70\ P_2O_5$$

$$\mathbf{A_{10}}\ 10Al_2O_3 + 19\ CaF_2 + 01\ Nd_2O_3 + 70\ P_2O_5$$

Agate mortar is used to mix AR grade 99% (Sigma Aldrich) pure chemicals, such as Nd_2O_3, CaF_2, Al_2O_3, and P_2O_5, in the appropriate

mol%. The necessary chemical ratios were fully combined using an agate mortar and then liquefied over the course of 30 min at a temperature of 1265°C in a silica crucible using an automatic programmed furnace. The prepared melt was discharged into a brass cast, and the samples were annealed in a muffle furnace that ran at a temperature of around 415°C. Measurements of prepared glass are dimensionally improved for both structural (thickness $\geq$0.5 cm, both length and breadth $\geq$1 cm) and optical (thickness = 0.2 cm, both length and breadth = 1 cm) characterization. All of the existing characterizations were completed with the following tools. Both weight and density were measured using a Scale Tech digital weighing scale (weighing capacity: 0–250 g; precision: 10^{-4} gm/cm^3). The XRD measurements were conducted using a Shimadzu XRD-7000, X-ray diffractometer (range: 0–80°C; precision: 0.1°C). Surface morphology and chemical analysis studies were conducted using the Hitachi S 3700N (precision: ±1 μm; range: 1–200 μm). Elastic measurements were performed using a WT-311D ultrasonic flaw detector (precision: 0.1°C; range: 0–80°C). For pH measurements, a Manti MT-101 (pH range: 0–14; precision: 0.1 pH) was employed. For DTA measurements, a Hitachi DTG-60 H (range: 27–1200°C; precision: 1°C) was employed. TL measurements were performed using a 137 cesium irradiation source and a Nucleonix TL/OSL Reader (range: 27–550°C; precision: 1°C). MAC OS Version 10.15.1 based 2.3 MAT Laband 2019 MAC Office software was used to plot all the figures.

17.3 Results and discussion

17.3.1 Structural studies

Fig. 17.1 reports $Al_xCa_{y-x}Nd_{01}P_{70}$ materials. Fig. 17.2 reports X-ray diffraction analysis of $Al_xCa_{y-x}Nd_{01}P_{70}$ materials. Chemical analyses of

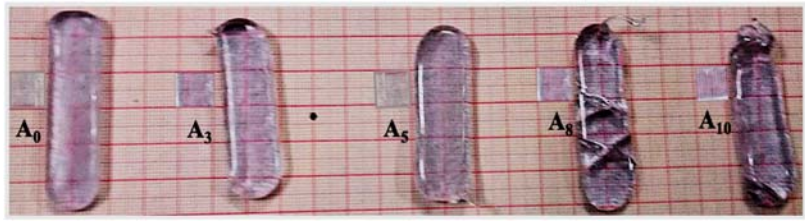

Figure 17.1 $Al_xCa_{y-x}Nd_{01}P_{70}$ glass materials, where, '*x*' varies as 0, 3, 5, 8 and 10 mol%; $y = 29$ mol%.

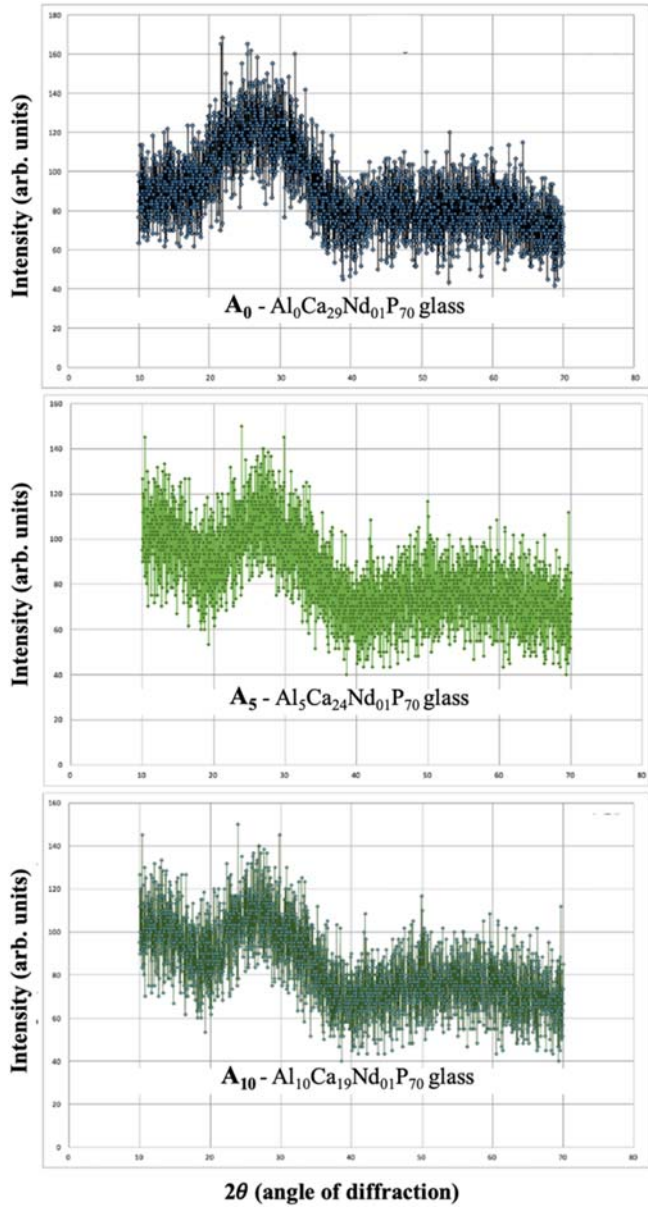

Figure 17.2 X-ray diffraction analysis of $Al_xCa_{y-x}Nd_{01}P_{70}$ glasses. The diffraction angles are taken up to an accuracy of ± 0.1 degree.

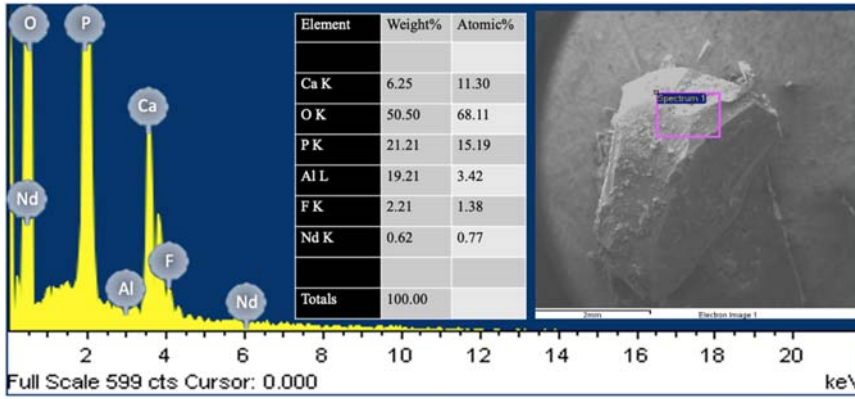

Figure 17.3 Chemical analysis of $Al_xCa_{y-x}Nd_{01}P_{70}$ glasses. Inset of the figure reports the surface morphology of sample A_5 recorded with 2 mm resolution.

$Al_xCa_{y-x}Nd_{01}P_{70}$ materials are shown in Fig. 17.3. The inset of the figure reports the surface morphology of sample code A_5. The results drawn from the X-ray diffraction reports reveal that the glass tests prepared are purely glassy (noncrystalline).

The evaluations of density and refractive index increase up to 5 mol% of Al_2O_3 concentration, however, the evaluations of molar volume follow an entirely different trend. Density was determined using the Archimedes method. Additional research was done on elastic characteristics including elastic modulus and microhardness of current glass testing. Microhardness (H) grades are ranked in the same order as Young's (Y) modulus assessments up to a concentration of 5 mol% Al_2O_3. Table 17.1 depicts both the physical and elastic parameter evolutions (Ravi Kumar, 2019). The evolution of the physical and elastic properties of the current glass series of tests were calculated using the following equations (Montoya-Quesada et al., 2020):

$$L = \rho V_L^2, \eta = \rho V_S^2, Y = (1+\sigma)2\eta, K = L - \frac{4}{3\eta}, \sigma = \frac{(L-2\eta)}{2(L-\eta)} \;\&$$

$$H = Y\frac{(1-2\sigma)}{6(1+\sigma)};$$

Fig. 17.4 illustrates the FT-IR spectra of $Al_xCa_{y-x}Nd_{01}P_{70}$ materials. All the absorbances at different wavenumber ranges suggest Ca-O (1410 cm^{-1}) units, phosphorus (1250, 1070 and 875 cm^{-1}) units, aluminum (710 and 440 cm^{-1}) octa- and tetrahedral units, and Nd-O (630 cm^{-1}) vibrations

Table 17.1 Summary of the elastic, thermal stability, optical, and thermoluminescence properties of $Al_xCa_{y-x}Nd_{01}P_{70}$ glasses.

Physical, elastic, and thermal stability analysis

Glass	Density (gm/cm^3)	Refractive index (μ)	Elastic modulus (Y) (GPa)	GTT T_g (°C)	GTC T_c (°C)	Thermal stability (ΔT)	Micro-hardness (H) (GPa)
$\mathbf{A_0}$	2.436	1.602	10.94	427	897	1.401	2.96
$\mathbf{A_3}$	2.503	1.615	10.82	423	895	1.435	2.87
$\mathbf{A_5}$	2.695	1.628	9.76	418	891	1.489	2.72
$\mathbf{A_8}$	2.612	1.624	9.82	419	892	1.475	2.88
$\mathbf{A_{10}}$	2.593	1.619	9.91	421	894	1.467	2.97

Optical properties

Glass	Oscillator strength ($\times 10^{-6}$)		λ_p (nm)	$\Delta\lambda$ (nm)	χ (Ω_4/Ω_6)	τ_R (μs)	A_t (s^{-1})	β (%)	σ (λ_p) (10^{-20} cm^2)	Judd–OFelt parameters ($\times 10^{-20}$ cm^2)		
	F_{exp}	f_{cal}								Ω_2	Ω_4	Ω_6
$\mathbf{A_0}$	2.11	1.71	1055	31	1.121	276	1612	51	3.45	9.25	4.56	4.37
$\mathbf{A_3}$	2.45	1.97	1059	33	1.025	270	1609	52	3.53	8.03	3.95	3.27
$\mathbf{A_5}$	2.54	2.09	1061	39	1.135	281	1635	56	3.65	9.31	4.71	4.31
$\mathbf{A_8}$	2.41	1.88	1063	37	1.084	284	1623	54	3.61	8.09	4.19	3.31
$\mathbf{A_{10}}$	2.21	1.62	1065	36	1.139	273	1629	53	3.64	9.54	4.98	4.42

δrms± 0.79									
Thermoluminescence properties									
Radiation dose	**Sample code**	**TM (K)**	**τ (K)**	**δ (K)**	**ω (K)**	***u***	**E_τ (eV)**	**E_δ (eV)**	**E_ω (eV)**
0 kGy	**A0**	526.1	24.1	15.9	40	0.397	3.509	2.652	2.685
	A3	529.1	24.1	14.9	39	0.382	3.325	2.596	2.586
	A5	536.1	28.1	12.9	41	0.314	3.081	2.467	2.380
	A8	534.1	27.1	12.9	40	0.322	3.224	3.029	2.485
	A10	532.1	28.1	13.9	42	0.330	3.405	3.131	2.528
15 kGy	**A0**	542	15.9	23	38.9	0.591	1.392	1.409	1.411
	A3	544	14.9	23	37.9	0.606	1.843	1.821	1.844
	A5	549	12.9	22	34.9	0.630	1.686	1.693	1.702
	A8	547	12.9	20	32.9	0.607	1.742	1.744	1.756
	A10	546	13.9	19	32.9	0.577	1.294	1.218	1.276
30 kGy	**A0**	553	26.9	22	48.9	0.449	1.269	1.132	1.229
	A3	556	26.9	21	47.9	0.438	0.948	0.397	0.781
	A5	559	22.9	22	44.9	0.489	0.997	0.503	0.846
	A8	558	23.9	21	44.9	0.467	0.969	0.572	0.845
	A10	555	22.9	20	42.9	0.466	1.294	1.218	1.276

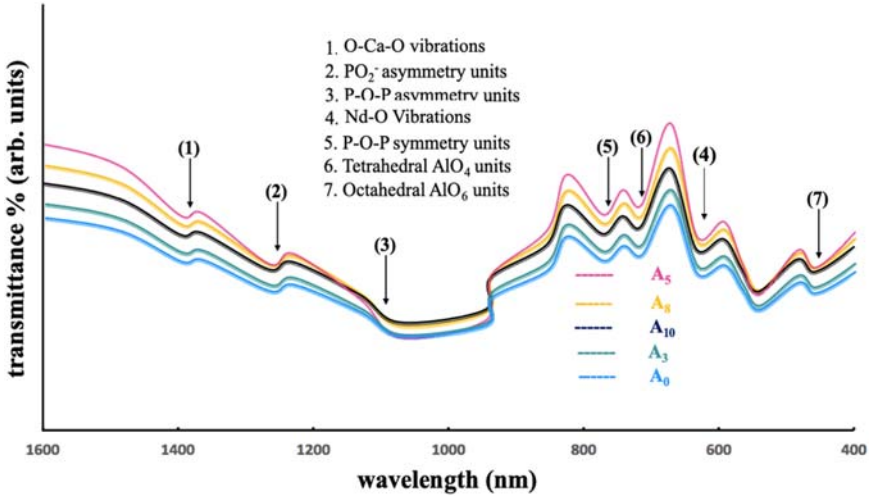

Figure 17.4 FT-IR spectra of $Al_xCa_{y-x}Nd_{01}P_{70}$ glasses. The wave numbers are taken up to an accuracy of $\pm 1\ cm^{-1}$.

(Gui et al., 2019; Guntu, 2019). DTA thermograms of existing glass materials are presented in Fig. 17.5. The evolutions of thermal stability are determined from DTA spectra and the values are observed to be decreasing with increasing concentration of Al_2O_3 up to 5 mol%. Phosphate glass nature of the present kind is quite different from the conduct of either pure phosphate or borate glass materials (Rajagukguk et al., 2019). Fig. 17.6 presents the structural analyses of existing glasses (Rama Krishna Chand et al., 2022). For the most part, the phosphate is a brief glass having PO_4 tetrahedron key units, and these units are interconnected through their corner sharing. The addition of Al_2O_3 to the phosphate cross-linkages and their tetrahedral units are made with Al_2O_3 chains supporting the P—O—Al linkages. Al_2O_3 is clearly not a straight glass at any rate in the case of a modernizer like CaF_2 as it gets into contact in the glass with both octahedral (AlO_6) and (AlO_4) tetrahedral units (Zhang and Liu, 2018).

The addition of calcium fluoride and alumina trioxide to existing phosphate glasses will liberate nonbridging oxygens. When Al_2O_3 is incorporated into phosphate glasses, the charge is exchanged for tetrahedral AlO_4 units. When the phosphate chains depolymerize and the pyramidal AlO_4 units withdraw, Al-O-Al connections are forced to form (Dimitriadis et al., 2020). The low magnitude of NBOs that were caused by variations in

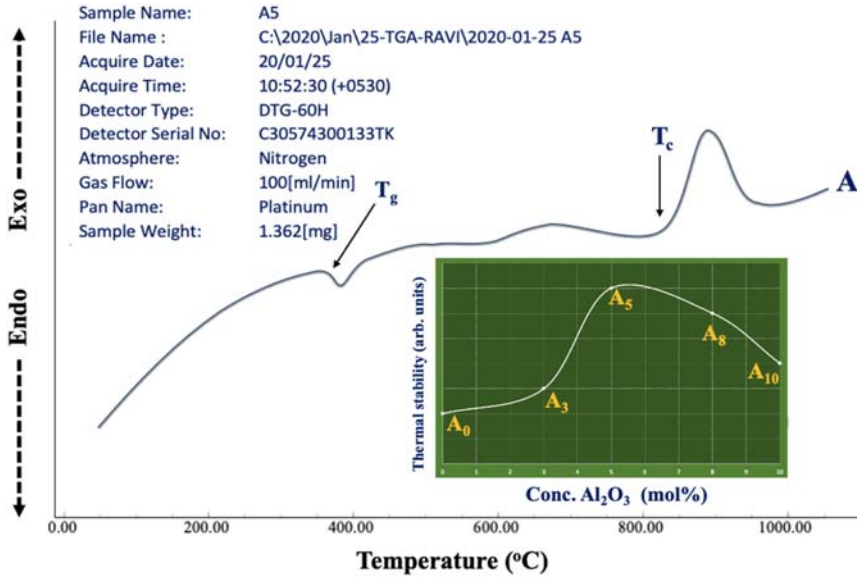

Figure 17.5 DTA spectrum of $Al_xCa_{y-x}Nd_{01}P_{70}$ glasses. Inset represents variation in thermal stability with Al_2O_3 concentration. The temperatures are taken up to an accuracy of ± 1°C.

the concentration of Al_2O_3 in the existing glass materials are affected by the addition of Nd_2O_3 to existing Al_2O_3 calcium phosphate glasses.

17.3.2 Thermoluminescence studies

Fig. 17.7 reports the thermoluminescence (TL) analysis (temperature ~ 27–375°C under 0, 15, and 30 min of γ-irradiation) of the present glasses. Existing glasses' TL glow curve intensities were shown to rise with increasing Al_2O_3 concentrations up to 5 mol%. The following are the formulae (Ravi Kumar, 2019; Guntu et al., 2020) that were utilized to determine the trap depth characteristics of preexisting glass samples:

$$E_\tau = C_\tau\left(\frac{KT_m^2}{\tau}\right) - b_\tau(2KT_m); E_\delta = C_\delta\left(\frac{KT_m^2}{\delta}\right) - b_\delta(2KT_m);$$

$$E_\omega = C_\omega\left(\frac{KT_m^2}{\omega}\right) - b_\omega(2KT_m);$$

where,

$$\tau = T_m - T_1; \delta = T_2 - T_m; \omega = T_2 - T_1;$$

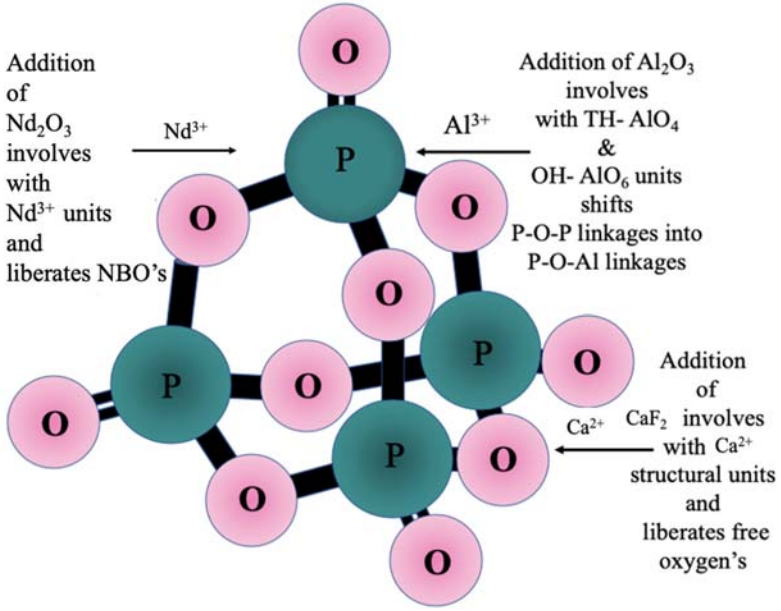

Figure 17.6 Molecular structure of $Al_xCa_{y-x}Nd_{01}P_{70}$ glasses. Mac-based Chem Draw Ultra version 12.0 was used to plot the figure.

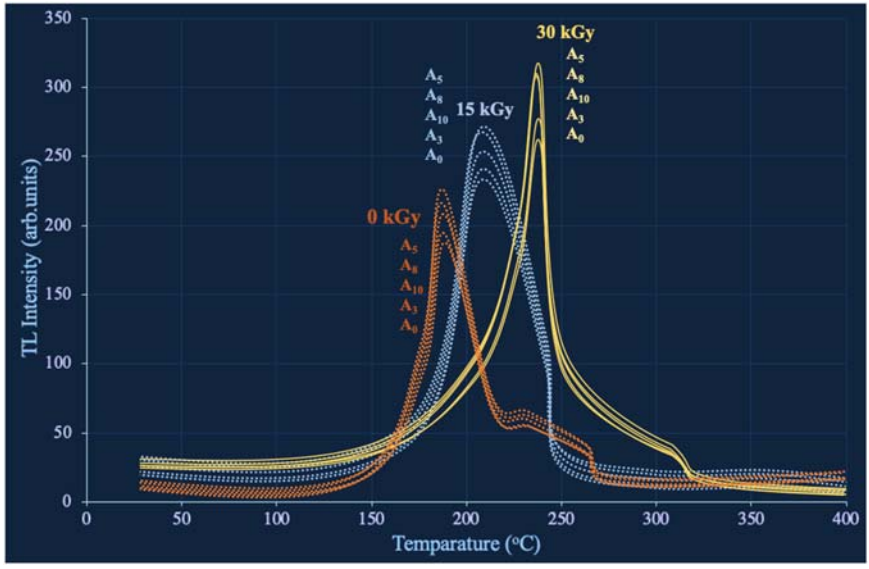

Figure 17.7 Thermoluminescence of $Al_xCa_{y-x}Nd_{01}P_{70}$ glasses recorded at various irradiation dose (0, 15, 30 kGy) range from room temperature to 400°C. The temperatures are taken up to an accuracy of ±0.1 C.

$$C_\tau = 1.510 + 3(\mu - 0.42);\ C_\delta = 0.976 + 7.3\ (\mu - 0.42);$$
$$C_\omega = 2.52 + 10.2(\mu - 0.42);$$
$$b_\tau = 1.510 + 3(\mu - 0.42);\ b_\delta = 0;\ b_\omega = 0;\ \mu = \frac{\delta}{\omega};$$

T_m—peak temperature maximum

μ_{sf}— shape symmetry factor

Table 17.1 presents the complete information regarding the TL measurements under 0, 15, and 30 kGy γ-irradiation doses. The results drawn from the TL measurements recommend that the induced electron and trap centers intensities both contribute to the unconventional referencing of TL output. Trap depth parameters such as A.E. (E_τ, E_δ, and E_ω) form symmetry ratios that are demonstrated to be ideal for the glass code with a concentration of 5 mol% Al_2O_3. The term "thermoluminescence" (TL) refers to the phenomena of light being produced by external heat energy. By adding the necessary irradiation, further traps were added. Analysis of TL investigations of existing materials was done under constant irradiation. Variations in the Ca^{2+} and Al^{3+} ion concentrations increase structural flaws such as interstitial areas or trap centers. Existing phosphate glasses include CaF_2, which along with all positive metal ions including Ca^{2+}, Al^{3+}, and Nd^{3+} ions, result in enhanced TL output when exposed to γ-irradiation. Under the proper γ-irradiation, Ca^{2+} ions of CaF_2 are oxidized into Ca^{3+} ions during this process. Additionally, this resulted in the release of electron mass, which can act as a trap and trigger enhanced thermoluminescence. Similarly, Nd^{3+} ions of Nd_2O_3 are oxidized to Nd^{4+} ions, which further results in trap centers that may be just below the conduction band of Nd^{3+}. The depth of the trap centers inside the existing materials was found to be ideal for the sample code "A5," which might work well with this TL mechanism. A higher number of produced Al-O-P connections along with an increase in the ratio of Al_2O_3 to CaF_2 might result in enhanced natural TL emission. The output intensities of the currently observed thermoluminescence may have increased the amount of Ca-O and Al-O bond connections and may be influenced by the site symmetry of both Ca^{2+} and Al^{3+} ions (Veerabhadra Rao et al., 2022). In this approach, the Ca atom with a larger surface area was oxidized first, followed by Nd, Ca, and Al atoms. In general, additional trap centers may be produced by atoms whose surface areas are totally exposed to the incoming radiation (Guntu, 2020). Asymmetry in glass is caused by the interionic interactions between the

Ca^{2+} and Nd^{3+} ions as well as the Al^{3+} ions, which affect minor orders of volume defects throughout the whole glass. The sample with a 5 mol% Al_2O_3 concentration exhibits the highest order of thermoluminescence and has the most surface area that can be exposed to Pb^{2+} and Nd^{3+} ions. According to all the observed TL experiments under the required gamma irradiation, the sample $\gamma\mathbf{A_5}$—is carried out most effectively for enhanced trap depth assessments and may be a helpful TL resource.

17.3.3 Optical studies

The variation in absorption strength as a function of frequency that happens when photonic energy is absorbed by the sample from the source is known as the absorption spectrum. With increasing Al_2O_3 content up to 5 mol%, the optical band edge (344.1 nm) of previous glass tests was shown to be growing. After that, the trend for OBE values is quite the opposite. Fig. 17.8 represents UV optical absorption spectra of existing glasses mixed with different concentrations of Al_2O_3 to reveal absorption bands such as $^4I_{9/2}$ (ground state) to the various excited states $^2G_{9/2} + {}^2D_{3/2} + {}^2K_{15/2}$, $^2G_{1/2} + {}^2G_{7/2}$, $^2H_{11/2}$,$^4G_{9/2}$, $^4G_{7/2}$, $^2P_{1/2} + {}^2D_{5/2}$, $^4F_{9/2}$, $^2F_{1/2} + {}^2H_{9/2}$ & $^4F_{3/2}$ (Rama Krishna Chand et al., 2022). All peak intensities were observed to be highest for the glass code $\mathbf{A_5}$. The deviation observed suggests that the most practical fit between theory and research represents

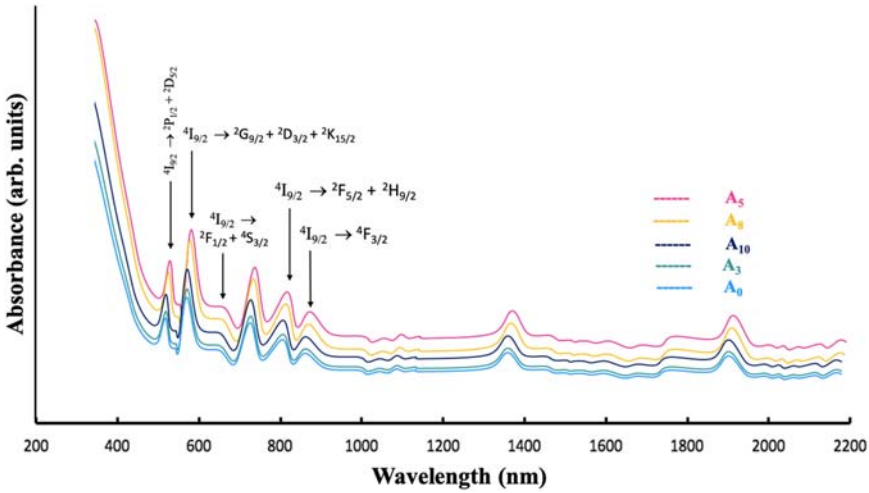

Figure 17.8 Optical absorption spectra of $Al_xCa_{y-x}Nd_{01}P_{70}$ glasses recorded at room temperature within the wavelength range of 200–2200 nm. The wavelengths are taken up to an accuracy of ±0.1 nm.

the applicability of J-O theory. JO parameter (Ω_λ) evaluation of existing glasses was found to be an increase $\Omega_2 > \Omega_4 > \Omega_6$ in the order. The following equivalence (Anil Kumar et al., 2021) was used to obtain f_{exp} (experimental oscillator strength), f_{cal} (calculated oscillator strength), and J-O intensity parameters of absorption transitions:

$$f_{exp} = 4.319 \times 10^{-9} \int \varepsilon(\nu) d\nu$$

$$f_{cal} = \frac{8\pi^2 mc\upsilon}{3h(2J+1)} \frac{(n^2+2)^2}{9n} \sum_{\lambda=2,4,6} \Omega_\lambda \langle \varphi J \| U^\lambda \| \varphi' J' \rangle^2$$

$$\delta_{rms} = \left[\frac{\sum \left(f_{exp} - f_{cal} \right)^2}{N-3} \right]^{\frac{1}{2}}$$

where, δ_{rms} is the root mean square deviation; ε (υ) is the molar absorptivity at frequency ν (in cm^{-1}); m is the mass of the electron; c is the velocity of light in a vacuum; ν is the wave number in cm^{-1}; h is Planck's constant; n is the refractive index; Ω_λ is the JO parameters; and $||U^\lambda||^2$ is the squared doubly reduced matrix elements of the unit tensor operator of the rank $\lambda = 2$, 4, and 6.

The overall number of transitions used in the fitting process is N. In most cases, a photon with energy "hv" interacts with electrons in the valence band and causes them to rise to the conduction band, spanning the band gap between the conduction and valance bands. Using the Mott and Davis hypothesis, one may calculate this band gap in materials. The absorption coefficient $\alpha(\nu)$ in terms of photon energy (h), as per the Mott and Davis theory, is given by

$$\alpha(\nu) = \frac{B(\mathrm{hv} - E_g)^n}{\mathrm{hv}}$$

where n is the index number depending on the kind of electronic transition, $n = 2$ and 1/2 corresponding to indirect and direct permitted transitions, respectively; B is the band tailing parameter; E_g is the optical band gap energy; and hv is the incident photon energy. The concentration of Nd_2O_3 dopant in the current study activity is set at 1 mol%. The Al_2O_3 concentration rises by 0, 3, 5, 8, and 10 mol%.

In the complete opposite direction, CaF_2 concentration dropped from 29 to 19 mol%. The optical absorption spectra of an $Al_xCa_{y-x}P_{70}$ glass host doped with 1 mol percent Nd_2O_3 were affected by different CaF_2 and

Al_2O_3 concentrations. Due of an imbalance in the interatomic interactions between the Ca^{2+} and Al^{3+} ions, the lattice of the current Nd_2O_3-doped phosphate glass host results in bonding defects. Additionally, this may cause tiny orders of gaps or fractures that, when they are opened, allow both Nd^{3+} and Ca^{2+} ions to be significantly influenced by gamma radiation, which would then improve the order of the trap centers. Similarly, more Nd^{3+} ions could be able to penetrate the second level of optical absorption if there was a greater surface area created by crystal defects in the phosphate glass lattice (Rama Krishna Chand et al., 2021). The incorporation of Nd_2O_3 into existing $Al_xCa_{y-x}P_{70}$ materials has an impact on the small size of trap centers and their dimensions, which were brought about by variations in Al_2O_3 and CaF_2 concentrations in the glass materials. Bonding defects and extra trapped centers created by gamma radiation improve all optical evolutions, suggesting the possibility of a second level of optical energy transformation. This happened on its own because photon energy from the provided optical energy filled the trap centers. The concentration of Nd_2O_3 dopant in the current study effort is set at 0.1 mol%. There is an increase in Al_2O_3 content from 0 to 10 mol%. Due of an imbalance in the interatomic interactions between the Ca^{2+} and Al^{3+} ions, the lattice of the current Nd_2O_3-doped $Al_xCa_{y-x}P_{70}$ glass host results in bonding defects. Additionally, this might result in tiny orders of gaps or fractures that, when opened, allow both Nd^{3+} and Ca^{2+} ions to be significantly influenced by gamma radiation, which would improve the order of trap centers. In a similar vein, more Nd^{3+} ions may be able to absorb light at the second level due to the phosphate lattice's increased surface area caused by crystal defects. And this is fairly high considering that the sample code has an Al_2O_3 content of 5 mol% (Guntu, 2019). These current glasses' luminescence spectra, which were captured at room temperature and stimulated at 350 and 850 nm, are shown in Fig. 17.9. The well-defined band $^4F_{3/2} \rightarrow {}^4I_{11/2}$ (1061 nm) was visible in the PL spectra. Peak intensities have been determined to be optimal for glass code A_5 out of all the available glass codes (Polymeris et al., 2017). It is suggested by the radiative evolutions, such as effective bandwidths of $\Delta\lambda \sim 39$ nm, stimulated emission cross-sections of $\sigma \sim 3.65 \times 10^{-20}\text{cm}^2$, transition probabilities of $A_t \sim 1635\ \text{s}^{-1}$, radiative lifetimes of $\tau_{rad} \sim 281\ \mu\text{s}$), and branching ratios of $\beta \sim 56\%$, that the sample code $\mathbf{A_5}$ is the useful 1.06 m emissive material (Swamy et al., 2014; Ivascu et al., 2011). The information on the luminous spectra of current glass testing is summarized in Table 17.1.

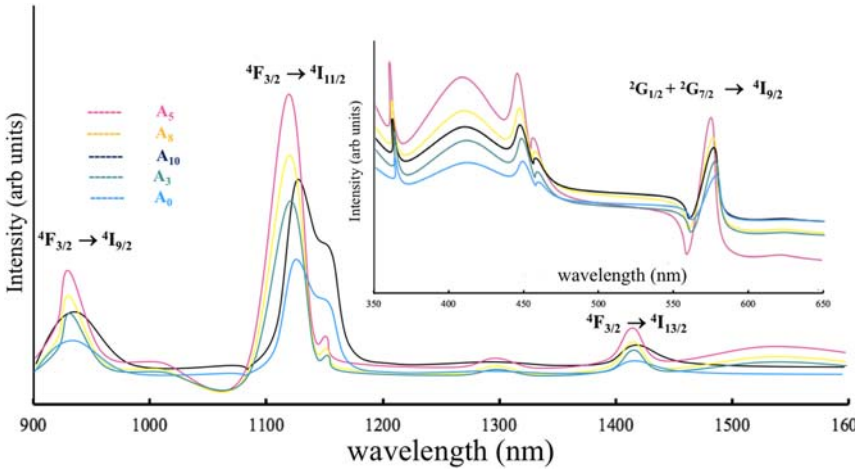

Figure 17.9 Photoluminescence spectra of $Al_xCa_{y-x}Nd_{01}P_{70}$ glasses recorded at room temperature within the wavelength range of 350–1600 nm and with excitation wavelengths of 300 and 850 nm. The wavelengths are taken up to an accuracy of ±0.1 nm.

17.3.4 Biocompatible studies

Figs. 17.10 and 17.11 address the X-ray diffraction, surface morphology, and chemical analyses of immersed existing glasses in simulated body fluid (SBF) for around 720 h (30 days) recorded at room temperature. The present study is about the results reported of vitro bioactive investigations, corresponding to the Al^{3+} ionic influence on $Al_xCa_{y-x}Nd_{01}P_{70}$ glasses. The structural observations from Figs. 17.10 and 17.11 and degradation nature in SBF advised of a very thin layer of crystalline hydroxyapatite grains on the surfaces of existing materials. Hydroxyapatite $Ca_5(PO_4)_3$ crystal grains were observed at 25.3 degrees (0 0 2), 33.1 degree (2 1 1), 49.8 degrees (2 1 3), and 54.6 degrees (0 0 4); average dimensions of the crystallites were evaluated to be ~117 nm (JCPDS no. 09-0432). Degraded content evolutions of existing glasses in simulated fluid are estimated by weight loss and pH (Figs. 17.12 and 17.13) of the simulated fluid remaining (Anil Kumar et al., 2021). The weight loss and pH data, together with the hydroxyapatite deposition on the surface of the samples that was found to be more prevalent in sample code "A_5," indicate that the degrading nature is a function of the Al_2O_3 concentration rising up to 5 mol%. Additionally, the in vitro bioactive investigations of Al_2O_3 mixed current materials has shown the deposition of crystalline hydroxyapatite grains under the effect of Al^{3+} ions

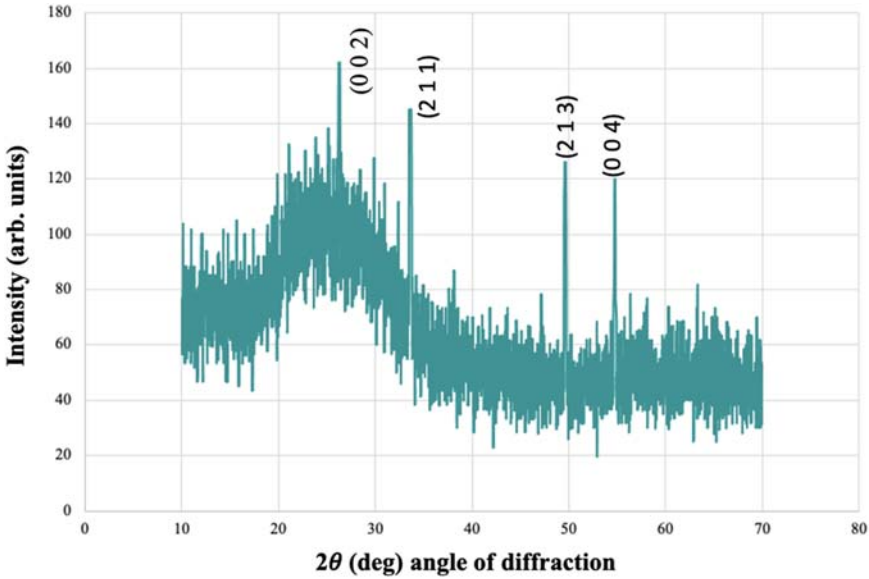

Figure 17.10 X-ray diffraction pattern of immersed sample code: A_5 in SBF of$Al_xCa_{y-x}Nd_{01}P_{70}$ glasses (JCPDS no. 09-0432). The diffraction angles are taken up to an accuracy of ±0.1°.

on the surfaces of the existing materials, which may be beneficial for a variety of advanced biomedical applications (Marghoub et al., 2019).

On the surface of glass materials, P_2O_5 often forms a layer of hydroxyapatite. The use of CaF_2 has the added benefit of speeding up the formation of the hydroxyapatite layer (Vijaya Kumari et al., 2019; Canillas et al., 2017). Together with P_2O_5, CaF_2 and CaO modify the structure of the glass network to create (calcium hydroxyapatite) $Ca_5(PO_4)_3(OH,F)$. The phosphate units' bonds are broken by oxygen from CaO, while Ca^{2+} ions are involved in SBF and create $Ca(OH)_2$. H_3PO_4 (phosphoric acid) deionizes H_2O in a simulated fluid by incorporating (Bai et al., 2017) P_2O_5.

$$5\ Ca\ (OH)_2 + 3\ H_3PO_4 \rightarrow Ca_5(PO_4)_3OH + 9\ H_2O$$

After soaking, neodymium ions, or Nd^{3+}, are quickly diffused from the glass and form apatite nucleation centers. Additionally, this accelerates the rate at which adjacent calcium and phosphate ions and trigonal neodymium ions interact. The supply of Ca^{2+} ions from the submerged glasses speeds up the development of apatite in the fluid. Al^{3+} ions interact with octahedral (AlO_6) and tetrahedral (AlO_4) units. It is anticipated that the tetrahedral

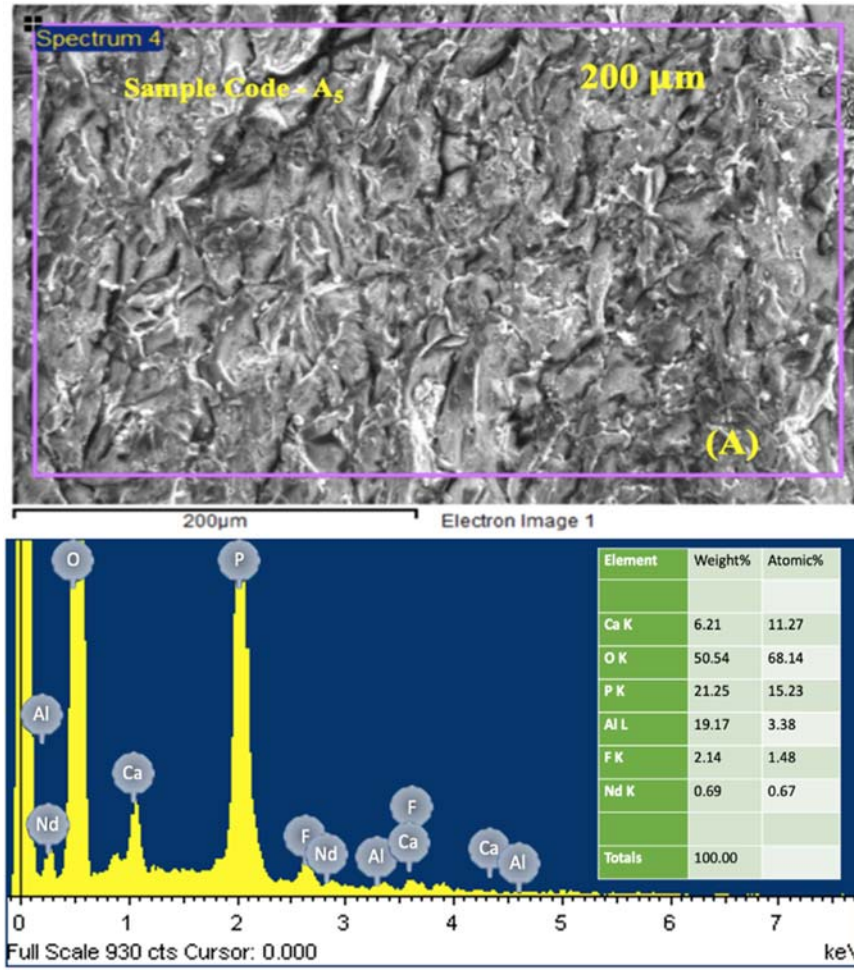

Figure 17.11 Chemical analysis of immersed sample code: A_5 in SBF of$Al_xCa_{y-x}Nd_{01}P_{70}$ glasses. Inset illustrates the surface morphology of sample A_5 recorded with 200 µm resolution.

AlO_4 ions will form a layer of Nd/Al by combining with Nd_2O_3 units (Liao et al., 2020; Perumal et al., 2019). Neodymium has a higher electronegativity than aluminum, therefore the Nd/Al layer can be considered to be in the form of Al^{3+}/Nd^{3+} to preserve the charge balance. Higher concentrations of OH- Al^{3+}ions would promote diffused Nd^{3+} ions, changing the tetrahedrally positioned locations of the aluminum ions (Asyikin et al., 2020; Gupta and Santhiya, 2017; Al-Bakhsh et al., 2019).

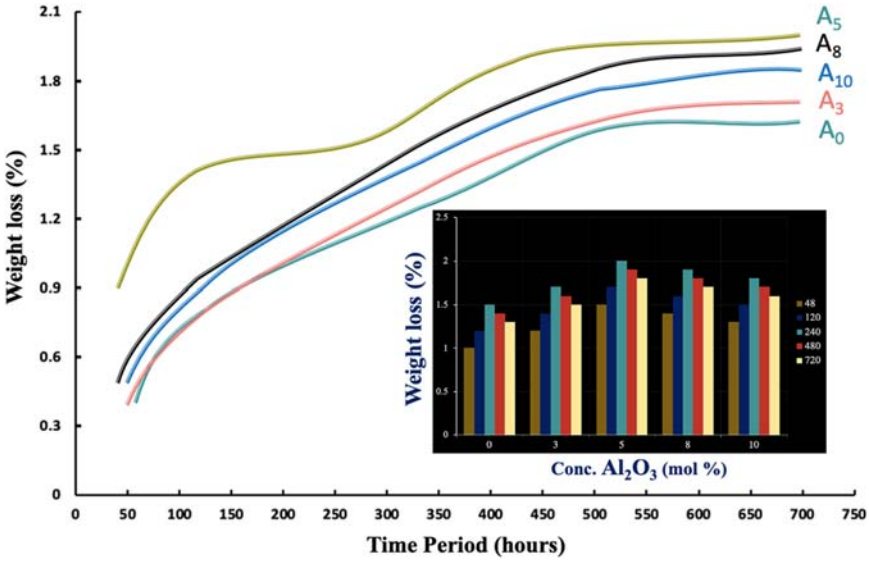

Figure 17.12 Variations in weight loss of immersed existing glasses in simulated body fluid with time in hours. Inset represents variations of weight loss of immersed samples in SBF with Al_2O_3 concentration at various intervals of time in hours.

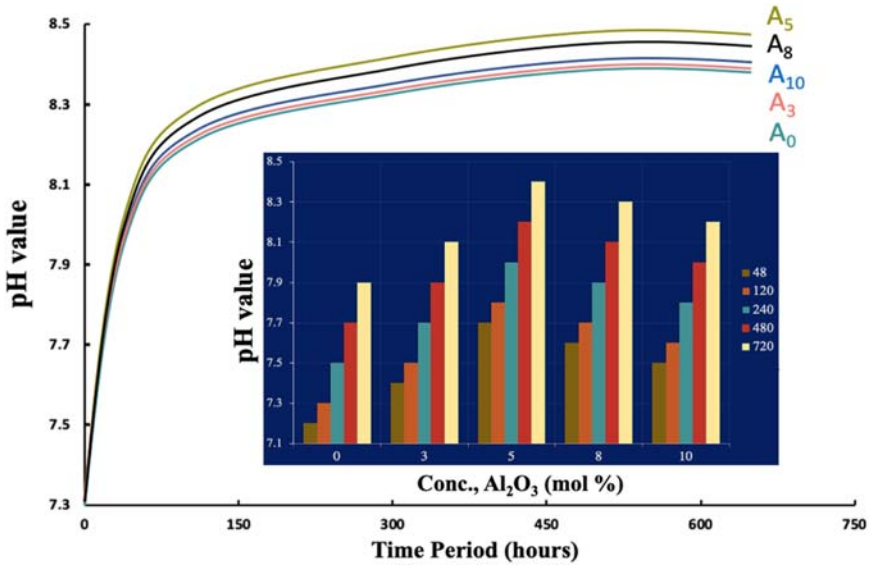

Figure 17.13 pH of SBF solution calculated at various time intervals of existing glasses. Inset represents the pH of residual solution calculated for each sample after immersion with Al_2O_3 concentration at various intervals of time in hours.

This causes a sample code "A5" to develop with the greatest concentration of hydroxyapatite. The changes in weight loss and pH of the leftover simulated fluid with Al_2O_3 concentration are strongly in favor of this hypothesis.

17.4 Summary and conclusion

We have selected $Al_xCa_{y-x}Nd_{01}P_{70}$ chemical make-up for standing analysis in order to prepare glass series. Bioactivity degradation and luminescent techniques are used to characterize existing samples.

- TL studies under different γ-irradiation dose ranges of $Al_xCa_{y-x}Nd_{01}P_{70}$ glasses are reported. The sample code "A_5" exhibiting good low AE ($E_{\tau} \sim 0.997$, $E_{\delta} \sim 0.503$, and $E_{\omega} \sim 0.846$ eV) and shape symmetry factor (~ 0.489) is advised to be a useful TL asset.
- JO parameters (~ 9.31, 4.71, and 4.31×10^{-20}cm^2), bandwidth (~ 39 nm), stimulated emission cross-section (3.65×10^{-20}cm^2), radiative lifetime (~ 281 μs), and branching ratio ($\sim 56\%$) assessed by optical studies indicated that the $Al_xCa_{y-x}Nd_{01}P_{70}$ glasses are a useful optical resource.
- The in vitro bioactivity behaviors of existing materials are reported, and the disintegration rate in SBF materials is calculated. The structural results of post-immersed glasses, such as pH and weight loss plots, indicated the growth of carbonated crystal grains of the hydroxyapatite layer and the highest degradability for the sample code $\mathbf{A_5}$. Conclusively, the bioactive degradation studies reveal that the thin layer of embedded crystalline hydroxyapatite deposition on the surface of existing glassy materials might be a useful biomedical resource.

According to all structural, biological activity, and optical evaluations of the available glass resources, sample code "A_5" is the most beneficial material for both luminous and biological medical applications.

Conflicts of Interest

The author has no conflicts of interest to declare.

References

Al-Bakhsh, B.A.J., Shafiei, F., Hashemian, A., Shekofteh, K., Bolhari, B., Behroozibakhsh, M., 2019. In-vitro bioactivity evaluation and physical properties of an epoxy-based dental sealer reinforced with synthesized fluorine-substituted

hydroxyapatite, hydroxyapatite and bioactive glass nanofillers. Bioact. Mater. 4, 322–333. https://doi.org/10.1016/j.bioactmat.2019.10.004.

Anil Kumar, G., Rambabu, Y., Guntu, R.K., Sivaram, K., Sreenath Reddy, M., SrinivasaRao, C., Venkatramu, V., Ravi Kumar, V., Sriman Narayana Iyengar, N.C., 2021. ZrxCa30-xP70 thermoluminescent bio glass, structure, and elasticity. J. Mech. Behav. Biomed. Mater. 119, 104517. https://doi.org/10.1016/j.jmbbm.2021.104517. ISSN 1751-6161.

Asyikin, A.S., Halimah, M.K., Latif, A.A., Faznny, M.F., Nazrin, S.N., 2020. Physical, structural and optical properties of bio-silica borotellurite glass system doped with samarium oxide nanoparticles. J. Non-Cryst. Solids 529, 119777. https://doi.org/10.1016/j.jnoncrysol.2019.119777.

Bai, X., Lü, S., Liu, H., Cao, Z., Ning, P., Wang, Z., Gao, C., Ni, B., Ma, D., Liu, M., 2017. Polysaccharides based injectable hydrogel compositing bio-glass for cranial bone repair. Carbohydr. Polym. 175, 557–564. https://doi.org/10.1016/j.carbpol.2017.08.020.

Brauch, U., Röcker, C., Graf, T., et al., 2022. High-power, high-brightness solid-state laser architectures and their characteristics. Appl. Phys. B 128, 58. https://doi.org/10.1007/s00340-021-07736-0.

Burtan-Gwizdala, B., Reben, M., Cisowski, J., Lisiecki, R., Jarzębąbek, B., Alshehri, A., Hussein, K.I., Yousef, E.S., 2023. Enhanced emission of tellurite glass doped with Pr^{3+}/Ho^{3+} and their applications. Materials 16, 925. https://doi.org/10.3390/ma16030925.

Calahoo, C., Wondraczek, L., 2020. Ionic glasses: structure, properties and classification. J. Non-Cryst. Solids X 8, 100054. https://doi.org/10.1016/j.nocx.2020.100054. ISSN 2590-1591.

Canillas, M., Pena, P., Antonio, H., Aza, de, Rodríguez, M.A., 2017. Calcium phosphates for biomedical applications. Bol. Soc. Espanola Ceram. Vidr. 56 3, 91–112. https://doi.org/10.1016/j.bsecv.2017.05.001.

Dimitriadis, K., Moschovas, D., Tulyaganov, D.U., Agathopoulos, S., 2020. Development of novel bioactive glass-ceramics in the Na_2O/K_2O-CaO-MgO-SiO_2-P_2O_5-CaF_2 system. J. Non-Cryst. Solids 533, 119936. https://doi.org/10.1016/j.jnoncrysol.2020.119936.

Flórez, A., Ulloa, E.M., Cabanzo, R., 2009. Optical properties of Nd^{3+} and Er^{3+} ions in fluoro-phosphate glasses: effects of P_2O_5 concentration and laser applications. J. Alloys Compd. 488 (2), 606–611. https://doi.org/10.1016/j.jallcom.2009.09.046. ISSN 0925-8388.

Gui, H., Cui, L., Lin, C., Zhang, Q., Luo, Z., Han, L., Liu, J., Liu, T., Lu, A., 2019. Glass forming, crystallization, and physical properties of MgO-Al_2O_3-SiO_2-B_2O_3 glass-ceramics modified by ZnO replacing MgO. J. Eur. Ceram. Soc. 39 (4), 1397–1410. https://doi.org/10.1016/j.jeurceramsoc.2018.10.002.

Guntu, R.K., 2019. Luminescence and dielectric properties of Ni^{2+} ions added to calcio yttria borophosphate glasses for optoelectronic uses. J. Lumin. 209, 258–266. https://doi.org/10.1016/j.jlumin.2019.01.051.

Guntu, R.K., 2020. Nd_2O_3 influenced Al_2O_3 & Sb_2O_3 functional PbO-SiO_2 glass materials, 1.06 μm photonic resource. Mater. Sci. Eng., B 262, 114784. https://doi.org/10.1016/j.mseb.2020.114784. ISSN 0921-5107.

Guntu, R. Kumar, Rambabu, Y., Srikumar, T., Rao, C.S., 2020. Thermo spectral advances of CoO doped alkali bismuth phospho silicate glasses for thermo and photo-luminescence applications. J. Non-Cryst. Solids 533, 119901. https://doi.org/10.1016/j.jnoncrysol.2020.119901.

Gupta, N., Santhiya, D., 2017. Role of cellulose functionality in bio-inspired synthesis of nano bioactive glass. Mater. Sci. Eng. C 75, 1206–1213. https://doi.org/10.1016/j.msec.2017.03.026.

Hirosawa, A., Matsubara, K., Morioka, Y., Kitagawa, M., Chusin, T., Takemura, A., December 2021. Use of optically stimulated luminescence dosimeter and radio photoluminescent glass dosimeter for dose measurement in dual-source dual-energy computed tomography. Phys. Eng. Sci. Med. 44 (4), 1311–1319. https://doi.org/10.1007/s13246-021-01063-6.

Islam, M.T., Felfel, R.M., Abou Neel, E.A., Grant, D.M., Ahmed, I., Hossain, K.M.Z., July 2017. Bioactive calcium phosphate-based glasses and ceramics and their biomedical applications: a review. J. Tissue Eng. 21 (8). https://doi.org/10.1177/2041731417719170.

Ivascu, C., Timar Gabor, A., Cozar, O., Daraban, L., Ardelean, I., 2011. FT-IR, Raman and thermoluminescence investigation of P_2O_5–BaO–Li_2O glass system. J. Mol. Struct. 993 (1–3), 249–253. https://doi.org/10.1016/j.molstruc.2010.11.047.

Jeong, J., Kim, J.H., Shim, J.H., et al., 2019. Bioactive calcium phosphate materials and applications in bone regeneration. Biomater. Res. 23, 4. https://doi.org/10.1186/s40824-018-0149-3.

Liao, Y.C., Song, S.M., Li, T.H., Li, J.B., Tsai, P.H., Jang, J.S.C., Huang, C.H., Huang, J.C., Huang, Y.S., Lin, C.H., Lin, Y.S., Chen, C.H., 2020. Synthesis and characterization of an open-pore toxic-element-free Ti-based bulk metallic glass foam for bio-implant application. J. Mater. Res. Technol. 9, 4518–4526. https://doi.org/10.1016/j.jmrt.2020.02.079 accepted article.

Marghoub, A., Libby, J., Babbs, C., Ventikos, Y., Fagan, M.J., Moazen, M., 2019. Characterizing and modeling bone formation during mouse calvarial development. Phys. Rev. Lett. 122 (4), 048103. https://link.aps.org/doi/10.1103/PhysRevLett.122.048103.

Montoya-Quesada, E., Villaquirán-Caicedo, M.A., Gutiérrez, R.M.de, Muñoz-Saldaña, J., 2020. Effect of ZnO content on the physical, mechanical and chemical properties of glass-ceramics in the CaO–SiO_2–Al_2O_3 system. Ceram. Int. 46 (4), 4322–4328. https://doi.org/10.1016/j.ceramint.2019.10.154.

Perumal, G., Singh Grewal, H., Ayyagari, A., Mukherjee, S., Arora, H.S., 2019. Enhancement in bio-corrosion resistance of metallic glass by severe surface deformation. Appl. Surf. Sci. 487, 1096–1103. https://doi.org/10.1016/j.apsusc.2019.05.158.

Polymeris, G.S., Giannoulatou, V., Kyriakidou, A., Sfampa, I.K., Theodorou, G.S., Sahiner, E., Meriç, N., Kitis, G., Paraskevopoulos, K.M., 2017. Bioactivity characterization of 45S5 bioglass using TL, OSL and EPR: Comparison with the case of 58S sol-gel bioactive glass. Mater. Sci. Eng. C 70 (1), 673–680. https://doi.org/10.1016/j.msec.2016.09.051.

Pugliese, D., Gobber, F.S., Forno, I., Milanese, D., Actis Grande, M., 2020. Design and manufacturing of a Nd-doped phosphate glass-based jewel. Materials 13, 2321. https://doi.org/10.3390/ma13102321.

Rajagukguk, J., Situmorang, R., Fitrilawati, Djamal, M., Rajaramakrishna, R., Kaewkhao, J., Minh, P.H., 2019. Structural, spectroscopic and optical gain of Nd^{3+} doped fluorophosphate glasses for solid state laser application. J. Lumin. 216, 116738. https://doi.org/10.1016/j.jlumin.2019.116738.

Rama Krishna Chand, N., Sudhakar, B.K., Ravikumar, G., Rao, G.S., Rao, C.S., 2021. Influence of manganese ions on elastic and spectroscopic properties of ZnO doped novel calcium fluorophosphate bio active glasses. Phys. Scripta 96 (12), 125020. https://doi.org/10.1088/1402-4896/abd202. ISSN 1402-4896.

Rama Krishna Chand, N., Sudhakar, B.K., Ravi kumar, G., Gayathri, V., Devika, P., Vennela, T., Srinivasa Rao, G., Srinivasa Rao, C., 2022. Influence of multi valent states of vanadium ions in ZnO doped novel calcium fluoro phosphate bio glasses. J. Mech. Behav. Biomed. Mater. 131, 105230. https://doi.org/10.1016/j.jmbbm.2022.105230. ISSN 1751-6161.

Ravi Kumar, G., 2019. Elastic, thermoluminescence, ionic and dielectric characterization of silicate doped by small concentrations of Cr2O3. Bull. Mater. Sci. 42, 214. https://doi.org/10.1007/s12034-019-1892-3.

Swamy, B.J.R.S., Sanyal, B., Vijay, R., Babu, P.R., Krishna Rao, D., Veeraiah, N., 2014. Influence of copper ions on thermoluminescence characteristics of $CaF_2-B_2O_3-P_2O_5$ glass system. Ceram. Int. 40 (2), 3707–3713. https://doi.org/10.1016/j.ceramint.2013.09.053.

Veerabhadra Rao, K., Ramesh, C., Shesha Devi, S., Ashok, P., Guntu, R.K., Bhikshamaiah, G., Appa Rao, B., 2022. Irradiative thermoluminescence, and defect center analysis in Ni^{2+} ionic $CaAl_2SiO_6$ glass lattice. J. Phys. Chem. Solid. 170, 110938. https://doi.org/10.1016/j.jpcs.2022.110938. ISSN 0022-3697.

Vijaya Kumari, C., Gandhi, Y., Sobhanachalam, P., Siva Sesha Reddy, A., Venkatramaiah, N., Venkateswara Rao, P., Ravi Kumar, V., 2019. Bioactive behaviour of NiO substituted $CaF_2-CaO-B_2O_3-BaO-P_2O_5$ glasses by means of spectroscopic studies. Opt. Mater. 97, 109394. https://doi.org/10.1016/j.optmat.2019.109394.

Wang, Y., Huang, Y., Bai, H., Wang, G., Hu, X., Kumar, S., Min, R., November 23, 2021. Biocompatible and biodegradable polymer optical fiber for biomedical application: a review. Biosensors 11 (12), 472. https://doi.org/10.3390/bios11120472.

Zhang, L., Liu, S., 2018. Influence of TiO_2 content on the structure and crystallization of $CuO\text{-}TiO_2\text{-}P_2O_5$ glasses and the derived porous glass-ceramics. J. Non-Cryst. Solids 500, 366–370. https://doi.org/10.1016/j.jnoncrysol.2018.08.023.

CHAPTER 18

A prospective utilization of biodegradable polymers for controlled drug-delivery applications

Dinesh Puri[1], Deepak Choudhary[2], Mohd Yasir[3], Rosaline Mishra[4], Sanjay Sharma[5], Radha Goel[6] and Praveen Kumar Gaur[4]

[1]School of Pharmacy, Graphic Era Hill University, Dehradun, Uttarakhand, India; [2]Department of Pharmaceutical Sciences, Mohanlal Sukhadia University, Udaipur, Rajasthan, India; [3]Department of Pharmacy, College of Health Sciences, Arsi University, Asella, Ethiopia; [4]Metro College of Health Sciences and Research, Greater Noida, Uttar Pradesh, India; [5]Shobhaben Pratapbhai Patel School of Pharmacy and Technology Management, SVKM's Narsee Monjee Institute of Management Studies, Mumbai, Maharashtra, India; [6]Lloyd Institute of Management and Technology, Greater Noida, Uttar Pradesh, India

18.1 Introduction

The approval of the first biodegradable suture in the 1960s opened a new vista of use of polymers in the medical world. Polymers play a very important role in the release of hydrophilic and hydrophobic drug substances.

Depending on the origin of biodegradable polymers, they can be divided into two categories: natural and synthetic polymers. There are several advantages to synthetic polymers over natural polymers in terms of mechanical and degradation properties. However, due to excellent biocompatibility and biodegradation, natural polymers remain the first choice of researchers (Piskin, 1995; Middleton and Tipton, 2000).

Biodegradation is a process in which polymers are decomposed by the action of enzymes and/or chemicals, through a living organism such as bacteria or fungi. Sometimes environmental factors including abiotic reactions such as oxidation, hydrolysis, and photodegradation, can also alter the polymer nature, which could affect the biocompatibiliy and biodegradation (Albertsson and Karlsson, 1996). Drug targeting without affect other sites in the body remains a challenge for researchers and these polymers play an important role in delivering drugs to a particular site in a

Bioresorbable Polymers and their Composites
ISBN 978-0-443-18915-9
https://doi.org/10.1016/B978-0-443-18915-9.00002-1
© 2024 Elsevier Ltd.
All rights reserved.

controlled manner (Kwon and Furgeson, 2007). Over a long period of time, biodegradable polymeric materials have been the choice of researchers for drug delivery due to their remarkable properties such as biocompatibility and biodegradability, with minimal toxicity or side effects (Heller, 1980). These polymers can be used in controlled drug delivery, implants, sutures, macroscopic drug depots, injectable micro- and nano-scale drug delivery. Over the last few years, biodegradable polymers with high molecular weight such as heparin, hyaluronic acid, dextran, pullulan, etc. have been utilized for designing controlled drug-delivery systems, especially for incorporating protein- or nucleic acid-based drugs, but these polymers display slow degradation in an in vivo system and hence may accumulate in the tissue site. To overcome this issue, low-molecular-weight biodegradable polymers have gained increased attention in controlled-release formulation development due to their greater permeability, solubility, and association efficiency because of their smaller particle size.

These polymers are utilized to design various polymeric nano drug-delivery systems, such as microspheres or microcapsules. In microspheres, the drug is encapsulated in a polymeric shell, while in nanocapsules, the drug is dispersed in a polymeric matrix (Idrees et al., 2020). Both types of nanomedicine carriers are presented in Fig. 18.1. Depending upon the target organ, a suitable biodegradable polymer can be selected as a drug-delivery carrier to deliver the drug to a specific site/organ in a controlled manner. Biodegradable polymers can be used in both topical and systemic delivery of drug release. Although these polymers are the choice of researchers, there may be a challenge for researchers to use biodegradable polymers in drug delivery due to compatibility issues of the polymer with

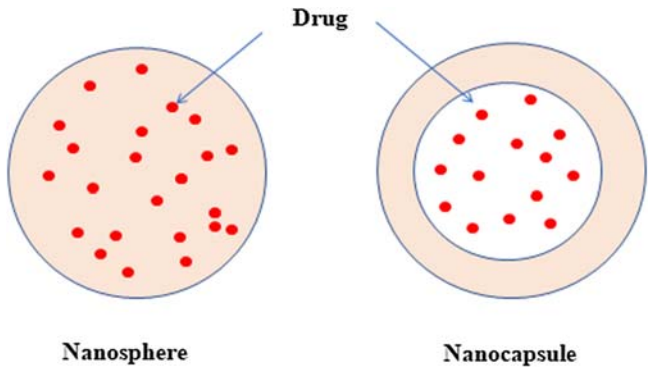

Figure 18.1 Types of nanomedicine.

body tissue (Kwon and Furgeson, 2007; Heller, 1980). Controlled drug-delivery systems are the area where biodegradable polymers are applied to control the release pattern of drugs (Brannon-Peppas, 1995; Gültekin and Değim, 2013). The FDA has also approved a number of polymers for use in controlled drug delivery and these mostly have amide, ester, and anhydride linkages that could be easily degraded (Osorno et al., 2021; Prajapati et al., 2019). Factors such as the mechanical properties, rate of degradation, biocompatibility, stability. and cost of polymers are among the criteria for the selection of polymers (Gunatillake et al., 2006).

18.2 Classification of biodegradable polymers for CDDS

There are many distinct types of biodegradable polymers used for drug delivery. Polymers can be divided into two groups according to their origin: natural and synthetic (Asghari et al., 2017; Deb et al., 2018; Dmour and Taha, 2018). A detailed classification of biodegradable polymers is provided in Fig. 18.2. Both natural and synthetic biodegradable polymers have various advantages such as biodegradability, compatibility, low toxicity, control, or/and sustained-release properties including specific targeted drug-delivery approaches (Doppalapudi et al., 2016). Some of the chemical structures of polymers are provided in Fig. 18.3.

Synthetic polymers are superior to natural polymers due to the contamination of microbes, batch-wise variation, and hydration of natural polymers in an uncontrolled manner (Gavasane, 2014). The side effects of drugs may be reduced by using biodegradable polymers in the formulation of nanomedicines. Biocompatible and harmless by-products are produced during the degradation of these polymers (Idrees et al., 2020).

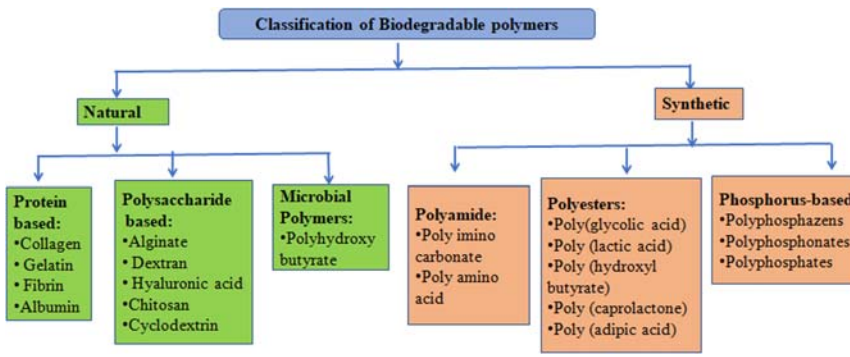

Figure 18.2 Classification of biodegradable polymers.

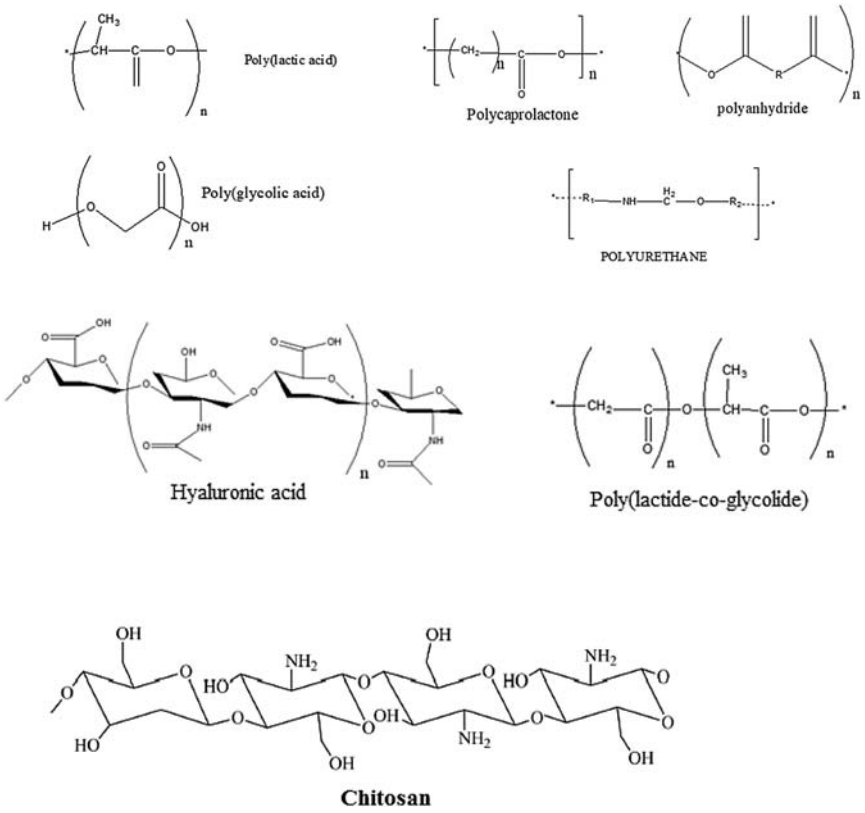

Figure 18.3 Examples of biodegradable polymers with chemical structures.

18.2.1 Collagen

Collagen has been widely applied in drug-delivery systems as well as in tissue engineering due to its excellent biocompatibility, moldability, mechanical properties, and easy modification with low antigenicity (Kwon and Furgeson, 2007; Lee et al., 2001; Wallace and Rosenblatt, 2003). It is practically insoluble in water, although its solubility can be increased by lowering the solutions' pH (Dmour and Taha, 2018). Rathore et al. fabricated collagen-based nanoparticles to increase the therapeutic effect of silymarin against cerebral neuronal injury. The results showed the remarkable effects on a group treated with nano-silymarin compared to a group treated with

silymarin (Rathore et al., 2020). Wallace et al. formulated collagen gel for the sustained release of therapeutic agents (Wallace and Rosenblatt, 2003). Nicklas et al. prepared hydrogel of collagen-loaded nanoparticles for prolonged release (up to 24 h) of estradiol (Nicklas et al., 2009). Nagarajan et al. fabricated solid collagen nanoparticles of theophylline through an electrospray deposition method. Cross-linking of collagen molecules helps in the controlled release of theophylline (Nagarajan et al., 2014).

18.2.2 Gelatin

Gelatin is a widely used polymer obtained by partial acid—base hydrolysis of animal collagen (Kumari et al., 2010). Due to its versatile features, it can be used to design various carrier systems such as microparticles, nanoparticles, fibers, and hydrogel (Foox and Zilberman, 2015). Its biodegradable, bioactive, and nontoxic properties makes it suitable for use in controlled release (Elzoghby, 2013). Mannan-coated gelatin nanoparticles showed sustained-release results of didanosine for up to 24 h, and, due to its sustained action, the frequency of administration was reduced which could lead to increased patient compliance (Kaur et al., 2008). The release of sulfamethoxazole was controlled by gelatin nanoparticles (100—300 nm) for up to 10 h (Bajpai and Choubey, 2005). Insulin release was controlled by the synthesis of gelatin-based nanoparticles (Goswami et al., 2009).

18.2.3 Chitosan

Chitosan is a biopolymer which shows potential application in drug-delivery systems (Kamaly et al., 2016). Chitin is changed to the natural polymer chitosan by an alkaline deacetylation process. Its non-toxic, biocompatible, and biodegradable properties make it a viable polymer for both established and cutting-edge drug delivery, gene delivery, and other medical applications (Foox and Zilberman, 2015; Elzoghby, 2013). It is used extensively in wound healing (Kim et al., 2007), oral drug delivery (Fonte et al., 2015), gene delivery (Molinaro et al., 2013), and pulmonary drug delivery (Benediktsdóttir et al., 2014). Membranes used in hemodialysis are a significant biomedical material of the 21st century due to their numerous uses, such as in artificial skin or bioactive wound dressings (Kaur et al., 2008). Chitosan that has undergone chemical modification can be

used to regulate the drug-release profile of bioactive compounds (Prabaharan, 2008). Lactic acid grafted chitosan nanoparticles showed high encapsulation efficiency with prolonged release of protein for up to 4 weeks (Bhattarai et al., 2006). Polyelectrolyte complex gel beads containing Ibuprofen were prepared by phosphorylated chitosan for controlled release through oral administration (Phyu Phyu et al., 2003). Phosphorous-containing chitosan-based beads were developed for the controlled release of indometacin (Jayakumar et al., 2006). Different chitosan polyelectrolyte complex-based microparticles of antibacterials for persistent and effective lung infection have been developed. A controlled drug device was developed using the graft copolymerization technique (Mishra et al., 2017). Drug release of up to 24 h was achieved by chitosan nanoparticles of cyclosporin A (De Campos et al., 2001). Chitosan-based nanoparticles of amiodarone completely released the drug in 14 days (Buyuk1 et al., 2020). Extended release of metronidazole was obtained through bionanocomposite beads of chitosan/graphene oxide (Kumar et al., 2021). Controlled release of Ketorolac tromethamine was obtained by cellulose nanofibrils/chitosan-based transdermal drug delivery (Sarkar et al., 2017). In vitro release of itraconazole was seen for 24 h using chitosan nanoparticles (Jafarinejad et al., 2012). Estradiol chitosan nanoparticles (Wang et al., 2008) and bioavailability and brain targeting of rivastigmine could be improved through the synthesis of nanoparticles using chitosan (Fazil et al., 2012). The hydrogel of a controlled drug-release system dependent on pH-sensitive chitosan and polyvinyl pyrrolidone for the administration of amoxicillin was created (De Campos et al., 2001). To regulate the release, chitosan and gum arabic were used to create insulin nanoparticles using the ionic gelation method (Buyuk1 et al., 2020). Chitosan-based mucoadhesive liposomes were created for localized sustained release of two model medicines of fluorescein isothiocyanate dextran with molecular weights of 4000 and 20,000 Da (Kumar et al., 2021).

18.2.4 Alginate

The polysaccharide known as alginate, which is derived from brown seaweeds, is made up of a series of two (1—4)-linked monomers called L-guluronate (G) and D-mannuronate (M) (Sarkar et al., 2017). Alginic acid is hydrated at low pH, resulting in the production of a high-viscosity acid gel that can be crucial in the creation of a formulation with controlled release

(Jafarinejad et al., 2012). The release of insulin for oral delivery was considerably delayed by a nanoemulsion coated with alginate/chitosan (Wang et al., 2008). Sustained drug delivery of indometacin was obtained through alginate-encapsulated mesoporous silica nanospheres (Hu et al., 2014). The release of vancomycin was controlled (22 μg per day for 14 days) by preparing lyophilized microparticles of chitosan−alginate polymers (Unagolla and Jayasuriya, 2018). An orally controlled release system of the macromolecular drug Blue Dextran was developed in the form of alginate gel beads (Kim and Lee, 1992). Hydrocortisone hemisuccinate-containing alginate microparticles were prepared for colonic drug delivery (Samak et al., 2017). Zn^{2+}-cross-linked alginate was used to prepare microparticles for delivery of bovine serum albumin through a spray-drying process (Karimi et al., 2016).

18.2.5 Albumin

Albumin protein plays a vital role as a biodegradable nanodrug carrier in the pharmaceutical field. Its versatile properties of targeted delivery capacity with nontoxicity and nonimmunogenicity make it attractive for researchers in treatments against tumor cells (Elzoghby, 2013; Karimi et al., 2016). A variety of albumins are used in various biomedical applications, including ovalbumin which is obtained from egg white, bovine serum albumin, human serum albumin, and rat serum album (Peters, 1985). Curcumin- (Kim et al., 2011) and doxorubicin-loaded (Dreis et al., 2007) human serum albumin nanoparticles were prepared which showed a greater therapeutic effect against cancer cells.

18.2.6 Polyhydroxybutyrate

Polyhydroxybutyrate is a bioderived polyester intracellular polymer which is synthesized for the source of carbon and energy in bacteria (Li et al., 2007; Suriyamongkol et al., 2007). Microspheres of rifampicin (Kassab et al., 1997), microspheres and microcapsules containing tetracycline (Gursel, 1999), and Tramadol-encapsulated microspheres showed drug release for more than 6 days (Salman et al., 2003), and curcumin nanoparticles (Aguilar-Rabiela et al., 2020) were prepared using polyhydroxybutyrate.

18.2.7 Polyamides

Polymers made up of repeating units that are linked by amide bonds are called polyamides. These may be natural like proteins or synthetic like

nylon (Boddu et al., 2021). Gachard et al. prepared a benzocaine controlled-release matrix using covalently linked N-protected poly(L-crystal-L-cystine) and poly(adipoyl-L-lysine) (Gachard et al., 1997). Nanoparticles for the controlled release of celecoxib were prepared using new s-triazine polyamides which contain glycine and thioglycolic acid (Khattab et al., 2016).

18.2.8 Polyesters

Due to the presence of a hydrolysable ester linkage in the backbone of the polyester family it is mostly used in controlled-release formulations. Poly-glycolic-acid, poly-lactic-acid, poly-hydroxyl-butyrate, poly-caprolactone, and poly-adipic acid are examples of polyesters which are used in formulations (Bhise et al., 2007; Jerbić, 2018; Christensen et al., 2007). Sustained-release microspheres of Nimesulide were prepared by polylactic acid (Freitas and Marchetti, 2005). Nanoparticles prepared by polylactic acid can retain the drug for at least 24 h in dermatotherapy (Rancan et al., 2009). Poly(lactic-co-glycolic acid) can also be used for controlled drug release (Hines and Kaplan, 2013), it is an FDA- and EMA-approved polymer for parenteral administration and is used for many hydrophilic and hydrophobic drugs (Danhier et al., 2012). Curcumin-loaded nanoparticles for prostate gland treatment were prepared by PLGA (Yallapu et al., 2012). Poly(caprolactone) can be used for the preparation of microspheres and nanospheres (Sinha et al., 2004) such as insulin-loaded particles for controlled drug release (Mukerjee et al., 2007), hollow nanoparticles (Park et al., 2019a), Holmium-165-loaded microspheres (Geraldes et al., 2011), theophylline nanoparticles (Jelvehgari et al. 2010), and repaglinide microspheres (Jagdish et al., 2009). Poly(glycerol adipate) was used for the preparation of nanoparticles of nonsteroidal antiinflammatory drugs (Wahab et al., 2012).

18.2.9 Phosphorus-based polymers

Phosphazenes and phosphoester are two major classes that contain phosphorus and are used for nanoformulations. Polyphosphazenes are a new class of biodegradable polymer because they can control deterioration and structural flexibility (Lakshmi et al., 2003; Ni et al., 2020; Ullah et al., 2017) and they have been tested and used as a controlled-release agent for several drugs (Schacht et al., 1996). Like the controlled release of polyphosphazene

microspheres of insulin (Caliceti et al., 2000), there are sustained-release polymeric nanocarriers of indometacin (Zhang et al., 2006) and indometacin micelle (Ni et al., 2020) for arthritis.

18.3 Application of biodegradable polymers in drug delivery

18.3.1 Mucoadhesive drug release

To increase the therapeutic action and medication plasma concentration, mucoadhesive dosage forms are employed to deliver a regulated rate of release through longer retention at the site of application (Ni et al., 2020; Ullah et al., 2017). Chitosan has been widely utilized as a mucoadhesive polymer because of its good biodegradability and biocompatibility (Schacht et al., 1996). For the treatment of bladder cancer, Moustafa et al. produced mucoadhesive nanodiamonds coated with chitosan (Caliceti et al., 2000). Modified boronated chitosan was created by Kolawole et al. and employed as a mucoadhesive polymer for intravesical medication delivery (Zhang et al., 2006). Dexamethasone–glycol chitosan (Dex-GCS) nanoparticles with mucoadhesive properties were created by Yu et al. for prolonged precorneal duration ocular medication administration (Alagha et al., 2020). Alagha et al. developed porous mucoadhesive biosponges of dexamethasone for oral mucositis by using collage, chitosan, and a blend of both. In vitro drug release has shown that a formulation based on a collagen–chitosan (1:1) blend can control release for up to 10 h (Alagha et al., 2020).

18.3.2 Controlled drug-delivery release

This type of system delivers the drug at a predetermined rate for a specific time and solves the problem related to conventional drug-delivery systems (Adepu and Ramakrishna, 2021). Buyuk et al. synthesized amiodarone-loaded chitosan nanoparticles which completely released the drug by the end of 14 days (Buyuk et al., 2020). Sorasitthiyanukarn et al. prepared chitosan/alginate nanoparticles for oral delivery of curcumin diglutaric acid (CG) for carcinogenic therapy. In their study, they found that CG-loaded chitosan/alginate nanoparticles showed sustained release after 24 h for all conditions (Sorasitthiyanukarn et al., 2018). Maghsoudi et al. prepared nanoparticles of curcumin using different polysaccharides including chitosan, alginate, and starch for anticarcinogenic activity.

Curcumin was released for 96 h from nanoparticles during an in vitro study (Maghsoudi et al., 2017). Agnohotri and Aminabhavi achieved controlled release of clozapine for up to 12 h through fabrication of nanoparticles based on chitosan (Agnihotri and Aminabhavi, 2004). Yang et al. formulated controlled-release steroidal saponins (SS)-loaded microspheres which showed retarded release of SS during an in vitro release study (Yang et al., 2019). Terzopoulou et al. prepared collagen-based curcumin patches for psoriasis topical therapy. Within the first burst, the release of curcumin continued and after 24 h, it had reached 55% (Terzopoulou et al., 2020). Poly 3-hydroxybutyrate biopolymer was used to produce films by Villegas et al., who achieved controlled release for the appropriate duration (about 14 days) (Fu and Kao, 2010). For the treatment of prostate cancer, Guo et al. created PLGA nanoparticles that were loaded with bicalutamide. The outcome demonstrated that the medication was released gradually, with 60% of the drug released by the end of 96 h at pH 7.4 (Alexis et al., 2004). Vancomycin was delivered under controlled conditions using poly(caprolactone) by Rai et al. to treat MSRA infection (Amkraut et al., 1989). Naproxen subcutaneous implants based on polyphosphazene were created by Conforti et al. for regulated release over a 28-day period (Conforti et al., 1996).

18.4 Mechanism involved in controlled release through polymers

Drug molecules are normally transported from the polymer matrix to the exterior before they eventually enter the surrounding environment (Uhrich et al., 1999).

To produce a steady-state drug concentration in the therapeutic range and maintain it for a longer length of time, a controlled/sustained drug delivery system is primarily desired (Dash et al. 2010; Mohamed Rizwan and Damodharan, 2020). These systems create an efficient and well-tolerated concentration release per unit time from carriers, and the drug behaves like zero-order kinetics (Ammala, 2013). The qualities of the drug, additives, and polymers, as well as their ratio in composition and interactions between components (physical and/or chemical), could all have an impact on the drug release profile (Langer and Peppas, 1983; Terzopoulou et al., 2020). Depending on how the drug molecules are released from the delivery system, multiple subcategories of the controlled drug-release mechanism may exist. These can be enumerated as follows: degradation-controlled release, diffusion-controlled release, erosion-controlled release, osmotic

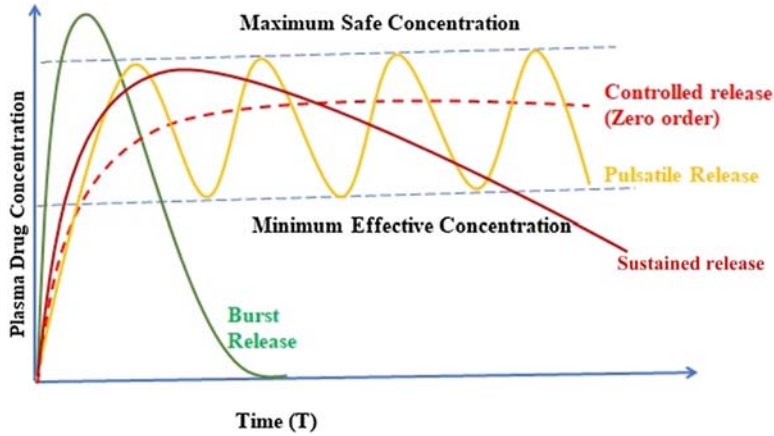

Figure 18.4 Plasma drug concentration—time curve for different release types.

pump-controlled release, and solvent-controlled release (Yun et al., 2015; Ammala, 2013; Blasi, 2019). Fig. 18.4 illustrates a plasma drug concentration versus time curve. Its shows the relation of release through burst of polymer, release in a controlled manner (zero order), sustained manner, and release in a pulsatile manner. Between the maximum safe concentration (MSC) and minimum effective concentration (MEC) there is the therapeutic range. A drug shows a toxic effect when the plasma concentration goes beyond the MSC and there is no therapeutic effect shown when the plasma concentration does not reach the MEC.

18.4.1 Dissolution controlled release

In dissolution controlled release, drugs are either coated or encapsulated within slowly dissolving polymers. These systems are mostly used in the production of enteric-coated dosage forms and drugs with high water solubility and dissolution rate. The steady-state dissolution process is described by the Noyes—Whitney equation. These formulations may be further divided into two types: matrix system (monolithic system) as in Fig. 18.5 and reservoir system (polymeric membrane) as in Fig. 18.6. In the matrix dissolution system, active pharmaceutical ingredients are uniformly distributed in the polymer matrix and molecules of API are released as the polymer matrix gets dissolved. In the reservoir system, drug molecules are coated or encapsulated by a rate-limiting polymer. The release of API molecules depends on the thickness and dissolution rate of the surrounding polymer membrane.

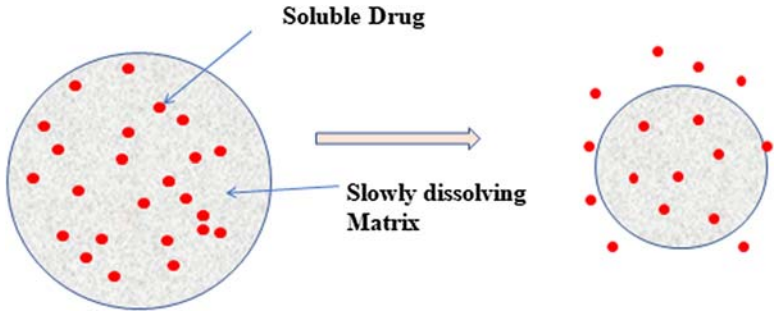

Figure 18.5 Drug release in the matrix system.

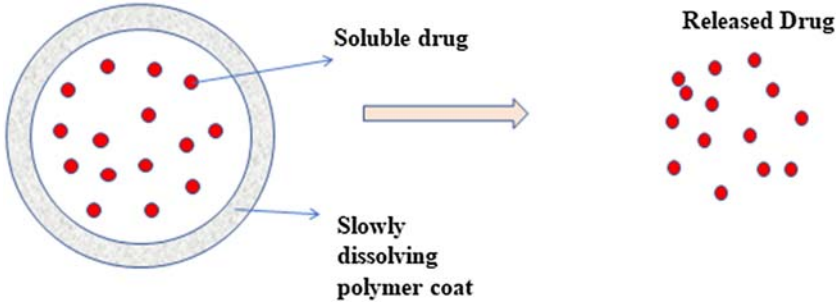

Figure 18.6 Drug release in the reservoir system.

18.4.2 Diffusion controlled-release

In a controlled-release system, drugs are mostly released through the diffusion method. In these systems, the drug is either dispersed within a polymeric matrix or encapsulated in it. Fig. 18.7 shows the release of drug through a diffusion mechanism where the drug is dissolved and dispersed in the polymer matrix. As per Fick's first law, the concentration gradient acts as a drive force for the movement of drug molecules through polymer matrices. Parameters including porosity, level of cross-linking, swelling behavior of polymers, and size of drug molecules play an important role in drug release (Alexis et al., 2004; Fu and Kao, 2010).

18.4.3 Degradation controlled release

This is the process by which polymers are broken down and the medicine is released at the needed location in the body. Polymer chains are split into oligomers and monomers during this process. Biodegradable polymers have linkages like ester and amide that may be broken down by enzymes or hydrolysis. Polymers are degraded to create physiologically acceptable

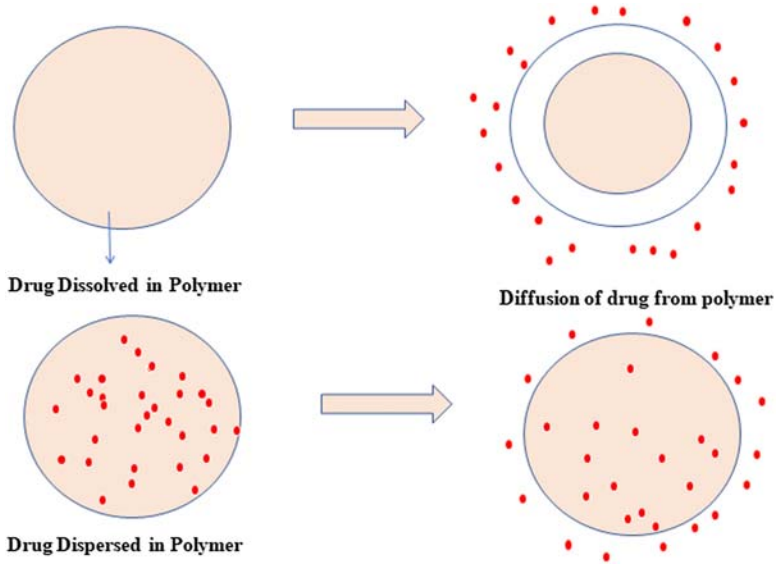

Figure 18.7 Release of drug through the diffusion mechanism.

agents, which are then eliminated from the body via a normal metabolic process. Surface and bulk degradation are the two types of deterioration (Fu and Kao, 2010).

18.4.4 Osmotic pumping release

Drug release can be controlled by application of one of the fundamental principles of biology: osmosis. A drug-delivery system which is based on osmosis can deliver drugs in an effective manner. In this system, osmotic pressure is created by the influx of water into a nonswelling system which is responsible for the transport of drug. Osmogens and semipermeable membranes are components in the design of an osmotically driven drug-delivery system (Amkraut et al., 1989; Conforti et al., 1996). A typical osmotic pump is shown in Fig. 18.8.

18.4.5 Erosion controlled release

The medicine is released in this sort of system as a result of the physical erosion/disintegration of polymers. Enzymes, hydrolysis, oxidation, or pH changes that lead to fragmentation can all contribute to polymer erosion. Polymers can experience either surface erosion (Fig. 18.9) or bulk erosion (Fig. 18.10), depending on the erosion mechanism (Hrkach and Langer, 2020). In surface erosion, polymers are degraded from the surface of the

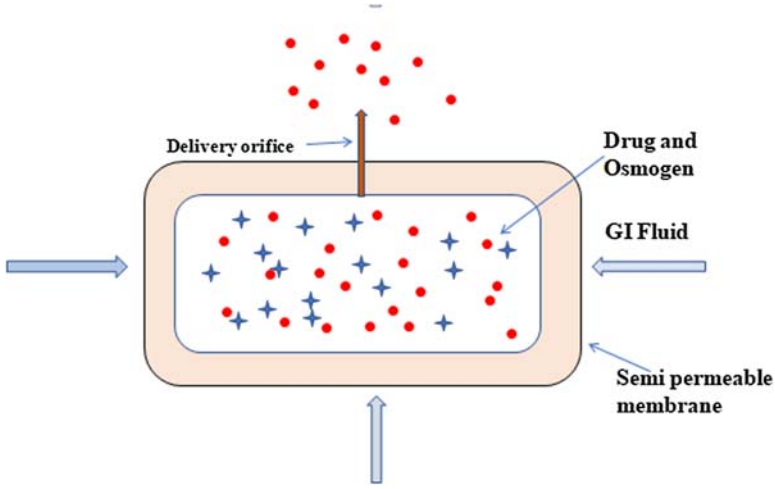

Figure 18.8 Release of drug through an osmotic pump.

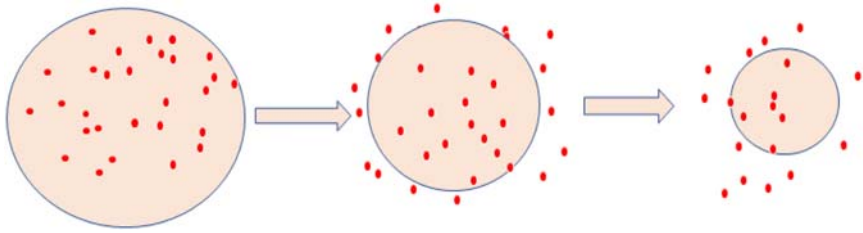

Figure 18.9 Release of drug through surface erosion polymer.

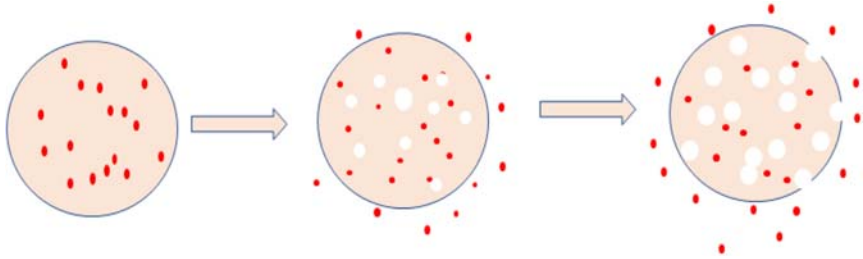

Figure 18.10 Release of drug through bulk erosion polymer.

matrix to the interior part, which occurs when the rate of erosion is greater than penetration of water in the system. When the rate of penetration of water is greater than the rate of erosion it results in bulk erosion where the whole matrix is starts to hydrolyze (Uhrich et al., 1999).

18.5 Release kinetic

Drug release kinetics depend upon the composition of the formulation, which includes the types of polymer, matrix system, method of preparation, and dissolution media. A kinetic model is further dependent upon the R^2 value. A zero-order kinetic model is used in controlled drug-delivery devices. Table 18.1 shows the release kinetic model with the respective equation which could be useful to evaluate the best-fitting model dependent upon the highest R^2 value.

18.6 Examples of commercially available biodegradable polymer base products

Several advantages over synthetic polymers make biodegradable polymers a choice for controlled drug delivery (Ammala, 2013). The theory of a drug-delivery system working in a controlled manner was introduced in 1952 as the sustained release formulation made by Smith Klein and during the first generation (1950–80) many oral and controlled releases were applied for clinical applications (Helfand and Cowen, 1983; Yun et al., 2015). Some of the commercial products available in the market are included in Table 18.2.

Table 18.1 Best-fitting models which are applied for kinetic release in drug delivery (Dash et al. 2010; Mohamed Rizwan and Damodharan, 2020).

S. no.	Kinetic model	Equation	Inference
1	Zero order	$WR = K0\ t \pm b$	Model with highest R^2 is consider as the best-fitting model
2	First order	$\ln (WL) = \ln W0 - K1\ t$	
3	Higuchi's model	$WR = K_H\ t^{1/2}$	
4	Korsmeyer–Peppas model	$\text{Log } (M_t/M\infty) = \log k + n \log t$	

Abbreviations: *WR*, quantity of drug released at the sampling time *t*; *WL*, quantity of drug remaining to be released at the sampling time *t*; *W0*, an initial quantity of drug; *K*, release rate constant of drug; *MT*, quantity of drug released up to time *t*; $M\infty$, total quantity of drug released up to time *t*.

Table 18.2 Examples of some commercially available products.

Regulatory approval year	Encapsulated drug	Product name	Controlled-release formulation/polymer	References
1986	Triptorelin	Decapeptyl SR	Microspheres/ poly(lactic-co-glycolic acid)	Blasi (2019)
1989	Leuprolide acetate	Lupron Depot®	Microspheres/ poly(lactide-co-glycolide)	Hrkach and Langer (2020)
1991	Bromocriptine	Parlodel® LAR	Microparticles/ poly-lactides (PLA) and poly lactide-co-glycolides (PLGA)	Schoubben et al. (2019)
1993	Risperidone	Risperdal®	Microparticles	Rawat et al. (2012)
1997	Octreotide	Sandonstatin® LAR	Microparticles/ poly(lactide-co-glycolide)	Park et al. (2019b)

1999	Cytarabine	Depocyt®	Microparticles/lipid	Bulbake et al. (2017)
2005	Paclitaxel	Abraxane®	Nanoparticles/ albumin	Martín (2015)
2010, 2000, 2001	Triptorelin-pamoate/ embonate	Pamorelin® LA, Trelstar ® depot, Trelstar ® LA	Microparticles/poly lactide-co-glycolides (PLGA)	Schoubben et al. (2019)
2006	Naltrexone	Vivitro®	Microspheres/poly-(lactide-co-glycolide)	Johnson (2007)
2009	Olanzapine pamoate	Zyprexa Relprevv®	Microcrystalline/poly lactide-co-glycolides	Sheehan et al. (2012)
2014	Lanreotide	Somatuline® Autogel	Microparticles/ poly(lactide-co-glycolide)	Wang et al. (2012)
2017	Exenatide	BydureonBCise®	Microparticles/PLA and PLGA	Abdul-Ghani et al. (2015) and Rentzepis et al. (2018)

18.7 Conclusion

Controlled medication may be delivered, by choosing the appropriate biodegradable polymers, to the target organ or other sites. Synthetic or natural biodegradable polymers can increase the therapeutic effectiveness of drug-delivery systems. The future application of biodegradable polymers in the development of regulated medication delivery. The most often utilized polymers in nanoformulation currently are collagen, PLGA, and PLA. Future advancements in science and technology may result in the creation of a variety of these molecules that could be used as potential medication carriers. A recent advancement in nanotechnology has also enabled stabilizing revolutionary molecular imprinting and drug-delivery system creation. Continuous research in the area of nano-technology may lead to the creation of new opportunities for regulated and targeted medication delivery.

References

Abdul-Ghani, M.A., et al., March 2015. Initial combination therapy with metformin, pioglitazone and exenatide is more effective than sequential add-on therapy in subjects with new-onset diabetes. Results from the Efficacy and Durability of Initial Combination Therapy for Type 2 Diabetes (EDICT): a randomized trial. Diabetes Obes. Metabol. 17 (3), 268–275. https://doi.org/10.1111/dom.12417.

Adepu, S., Ramakrishna, S., September 2021. Controlled drug delivery systems: current status and future directions. Molecules 26 (19), 5905. https://doi.org/10.3390/molecules26195905.

Agnihotri, S.A., Aminabhavi, T.M., April 2004. Controlled release of clozapine through chitosan microparticles prepared by a novel method. J. Contr. Release 96 (2), 245–259. https://doi.org/10.1016/j.jconrel.2004.01.025.

Aguilar-Rabiela, A.E., Hernández-Cooper, E.M., Otero, J.A., Vergara-Porras, B., February 2020. Modeling the release of curcumin from microparticles of poly(hydroxybutyrate) [PHB]. Int. J. Biol. Macromol. 144, 47–52. https://doi.org/10.1016/j.ijbiomac.2019.11.242.

Alagha, A., Nourallah, A., Hariri, S., February 2020. Characterization of dexamethasone loaded collagen-chitosan sponge and in vitro release study. J. Drug Deliv. Sci. Technol. 55, 101449. https://doi.org/10.1016/j.jddst.2019.101449.

Albertsson, S., Karlsson, A.-C., 1996. Chemistry and Technology of Biodegradable Polymers.

Alexis, F., Venkatraman, S.S., Rath, S.K., Boey, F., July 2004. In vitro study of release mechanisms of paclitaxel and rapamycin from drug-incorporated biodegradable stent matrices. J. Contr. Release 98 (1), 67–74. https://doi.org/10.1016/j.jconrel.2004.04.011.

Amkraut, A., Eckenhoff, J.B., Nichols, K., October 1989. Osmotic delivery of peptides and macromolecules. Adv. Drug Deliv. Rev. 4 (2), 255–276. https://doi.org/10.1016/0169-409X(89)90021-5.

Ammala, A., April 2013. Biodegradable polymers as encapsulation materials for cosmetics and personal care markets. Int. J. Cosmet. Sci. 35 (2), 113–124. https://doi.org/10.1111/ics.12017.

Asghari, F., Samiei, M., Adibkia, K., Akbarzadeh, A., Davaran, S., 2017. Biodegradable and biocompatible polymers for tissue engineering application: a review. Artif. Cells, Nanomed. Biotechnol. 45 (2), 185–192. https://doi.org/10.3109/21691401.2016.1146731.

Bajpai, A.K., Choubey, J., March 2005. Release study of sulphamethoxazole controlled by swelling of gelatin nanoparticles and drug-biopolymer interaction. J. Macromol. Sci. Part A 42 (3), 253–275. https://doi.org/10.1081/MA-200050357.

Benediktsdóttir, B.E., Baldursson, Ó., Másson, M., January 2014. Challenges in evaluation of chitosan and trimethylated chitosan (TMC) as mucosal permeation enhancers: from synthesis to in vitro application. J. Contr. Release 173, 18–31.

Bhattarai, N., Ramay, H.R., Chou, S.-H., Zhang, M., June 2006. Chitosan and lactic acid-grafted chitosan nanoparticles as carriers for prolonged drug delivery. Int. J. Nanomed. 1 (2), 181–187. Available: https://www.ncbi.nlm.nih.gov/pmc/articles/PMC2426789/. (Accessed 11 September 2022).

Bhise, K., Kotwal, V., Saifee, M., Inamdar, N., 2007. Biodegradable polymers: which, when and why? Indian J. Pharmaceut. Sci. 69 (5), 616. https://doi.org/10.4103/0250-474X.38465.

Blasi, P., July 2019. Poly(lactic acid)/poly(lactic-co-glycolic acid)-based microparticles: an overview. J. Pharm. Investig. 49 (4), 337–346. https://doi.org/10.1007/s40005-019-004953-z.

Boddu, S.H.S., et al., October 2021. Polyamide/Poly(Amino acid) polymers for drug delivery. J. Funct. Biomater. 12 (4), 58. https://doi.org/10.3390/jfb12040058.

Brannon-Peppas, L., 1995. Recent advances on the use of biodegradable microparticles and nanoparticles in controlled drug delivery. Int. J. Pharm. 116 (1), 1–9. https://doi.org/10.1016/0378-5173(94)00324-X.

Bulbake, U., Doppalapudi, S., Kommineni, N., Khan, W., March 2017. Liposomal formulations in clinical use: an updated review. Pharmaceutics 9 (2), E12. https://doi.org/10.3390/pharmaceutics9020012.

Buyuk1, N.I., Arayici, P.P., Derman, S., M., Z., Yucel, S., February 2020. Synthesis of chitosan nanoparticles for controlled release of amiodarone. Indian J. Pharmaceut. Sci. 82 (1), 131–138. https://doi.org/10.36468/pharmaceutical-sciences.630.

Caliceti, P., Veronese, F.M., Lora, S., December 2000. Polyphosphazene microspheres for insulin delivery. Int. J. Pharm. 211 (1–2), 57–65. https://doi.org/10.1016/s0378-5173(00)00588-3.

Christensen, D., Korsholm, K.S., Rosenkrands, I., Lindenstrøm, T., Andersen, P., Agger, E.M., October 2007. Cationic liposomes as vaccine adjuvants. Expert Rev. Vaccines 6 (5), 785–796. https://doi.org/10.1586/14760584.6.5.785.

Conforti, A., et al., 1996. Anti-inflammatory activity of polyphosphazene-based naproxen slow-release systems. J. Pharm. Pharmacol. 48. https://doi.org/10.1111/j.2042-7158.1996.tb05956.x.

Danhier, F., Ansorena, E., Silva, J.M., Coco, R., Le Breton, A., Préat, V., July 2012. PLGA-based nanoparticles: an overview of biomedical applications. J. Contr. Release 161 (2), 505–522. https://doi.org/10.1016/j.jconrel.2012.01.043.

Dash, S., Murthy, P.N., Nath, L., Chowdhury, P., 2010. Kinetic modeling on drug release from CONTROLLED drug delivery systems. Acta. Pol. Pharm. 67 (3), 217–223.

De Campos, A.M., Sánchez, A., Alonso, M.J., August 2001. Chitosan nanoparticles: a new vehicle for the improvement of the delivery of drugs to the ocular surface. Application to cyclosporin A. Int. J. Pharm. 224 (1–2), 159–168. https://doi.org/10.1016/s0378-5173(01)00760-8.

Deb, P.K., Kokaz, S.F., Abed, S.N., Paradkar, A., Tekade, R.K., 2018. Pharmaceutical and Biomedical Applications of Polymers. https://doi.org/10.1016/B978-0-12-817909-3.00006-6.

Dmour, I., Taha, M.O., 2018. Natural and Semisynthetic Polymers in Pharmaceutical Nanotechnology. Elsevier Inc. https://doi.org/10.1016/B978-0-12-813663-8.00002-6

Doppalapudi, S., Jain, A., Domb, A.J., Khan, W., 2016. Biodegradable polymers for targeted delivery of anti-cancer drugs. Expert Opin. Drug Deliv. 13 (6), 891–909. https://doi.org/10.1517/17425247.2016.1156671.

Dreis, S., Rothweiler, F., Michaelis, M., Cinatl, J., Kreuter, J., Langer, K., August 2007. Preparation, characterisation and maintenance of drug efficacy of doxorubicin-loaded human serum albumin (HSA) nanoparticles. Int. J. Pharm. 341 (1–2), 207–214. https://doi.org/10.1016/j.ijpharm.2007.03.036.

Elzoghby, A.O., December 2013. Gelatin-based nanoparticles as drug and gene delivery systems: reviewing three decades of research. J. Contr. Release 172 (3), 1075–1091. https://doi.org/10.1016/j.jconrel.2013.09.019.

Fazil, M., et al., August 2012. Development and evaluation of rivastigmine loaded chitosan nanoparticles for brain targeting. Eur. J. Pharm. Sci. 47 (1), 6–15. https://doi.org/10.1016/j.ejps.2012.04.013.

Fonte, P., et al., November 2015. Polymer-based nanoparticles for oral insulin delivery: revisited approaches. Biotechnol. Adv. 33 (6 Pt 3), 1342–1354. https://doi.org/10.1016/j.biotechadv.2015.02.010.

Foox, M., Zilberman, M., September 2015. Drug delivery from gelatin-based systems. Expert Opin. Drug Deliv. 12 (9), 1547–1563. https://doi.org/10.1517/17425247.2015.1037272.

Freitas, M.N., Marchetti, J.M., May 2005. Nimesulide PLA microspheres as a potential sustained release system for the treatment of inflammatory diseases. Int. J. Pharm. 295 (1–2), 201–211. https://doi.org/10.1016/j.ijpharm.2005.03.003.

Fu, Y., Kao, W.J., April 2010. Drug release kinetics and transport mechanisms of non-degradable and degradable polymeric delivery systems. Expert Opin. Drug Deliv. 7 (4), 429–444. https://doi.org/10.1517/17425241003602259.

Gachard, I., Bechaouch, S., Coutin, B., Sekiguchi, H., April 1997. Drug delivery from nonpeptidic α-amino acid containing polyamides. Polym. Bull. 38 (4), 427–431. https://doi.org/10.1007/s002890050069.

Gavasane, A.J., 2014. Synthetic biodegradable polymers used in controlled drug delivery system: an overview. Clin. Pharmacol. Biopharm. 3 (2). https://doi.org/10.4172/2167-065x.1000121.

Geraldes, A.N., Miyamoto, D.M., de Lira, R.A., 2011. Microspheres of Poly(ε-Caprolactone) Loaded Holium-165: Morphology and Thermal Degradation Behavior, p. 9.

Goswami, S., Bajpai, J., Bajpai, A.K., December 2009. Designing gelatin nanocarriers as a swellable system for controlled release of insulin: an in-vitro kinetic study. J. Macromol. Sci. Part A 47 (2), 119–130. https://doi.org/10.1080/10601320903458556.

Gültekin, H.E., Değim, Z., 2013. Biodegradable polymeric nanoparticles are effective systems for controlled drug delivery. Fabad J. Pharm. Sci. 38 (2), 107–118.

Gunatillake, P., Mayadunne, R., Adhikari, R., 2006. Recent developments in biodegradable synthetic polymers. Biotechnol. Annu. Rev. 12, 301–347. https://doi.org/10.1016/S1387-2656(06)12009-8.

Gursel, I., 1999. Antibiotic release from biodegradable PHBV microparticles. J. Contr. Release 59 (2), 207–217. Available: https://www.academia.edu/13959199/Antibiotic_release_from_biodegradable_PHBV_microparticles. (Accessed 19 October 2022).

Helfand, W.H., Cowen, D.L., 1983. Evolution of pharmaceutical oral dosage forms. Pharm. Hist. 25 (1), 3–18.

Heller, J., 1980. Controlled release of biologically active compounds from bioerodible polymers. Biomater. Silver Jubil. Compend. 1, 51–57. https://doi.org/10.1016/B978-008045154-1.50001-0.

Hines, D.J., Kaplan, D.L., 2013. Poly(lactic-co-glycolic) acid-controlled-release systems: experimental and modeling insights. Crit. Rev. Ther. Drug Carrier Syst. 30 (3), 257–276. https://doi.org/10.1615/critrevtherdrugcarriersyst.2013006475.

Hrkach, J., Langer, R., June 2020. From micro to nano: evolution and impact of drug delivery in treating disease. Drug Deliv. Transl. Res. 10 (3), 567–570. https://doi.org/10.1007/s13346-020-00769-6.

Hu, L., et al., August 2014. Alginate encapsulated mesoporous silica nanospheres as a sustained drug delivery system for the poorly water-soluble drug indomethacin. Asian J. Pharm. Sci. 9 (4), 183–190. https://doi.org/10.1016/j.ajps.2014.05.004.

Idrees, H., et al., October 2020. A review of biodegradable natural polymer-based nanoparticles for drug delivery applications. Nanomaterials 10, 1970. https://doi.org/10.3390/nano10101970.

Jafarinejad, S., Gilani, K., Moazeni, E., Ghazi-Khansari, M., Najafabadi, A.R., Mohajel, N., 2012. Development of chitosan-based nanoparticles for pulmonary delivery of itraconazole as dry powder formulation. Powder Technol. 222, 65–70. https://doi.org/10.1016/j.powtec.2012.01.045. Available: (Accessed 11 September 2022).

Jagdish, C., Vaishali, R., Tamizharasi, S., 2009. Preparation of biodegradable microspheres containing repaglinide. J. Young Pharm. 1 (2), 121. https://doi.org/10.4103/0975-1483.55743.

Jayakumar, R., Reis, R.L., Mano, J.F., July 2006. Phosphorous containing chitosan beads for controlled oral drug delivery. J. Bioact. Compat Polym. 21 (4), 327–340. https://doi.org/10.1177/0883911506066929.

Jelvehgari, M., Barar, J., Valizadeh, H., Heidari, N., 2010. Preparation and ealuation of poly (ε-caprolactone) nanoparticles-in- microparticles by W/O/W emulsion method. Iran. J. Basic Med. Sci. 13, 85–96.

Jerbić, I.Š., 2018. Biodegradable synthetic polymers and their application in advanced drug delivery systems (DDS). Nanotechnol. Appl. 1, 9.

Johnson, B.A., October 2007. Naltrexone long-acting formulation in the treatment of alcohol dependence. Ther. Clin. Risk Manag. 3 (5), 741–749. Available: https://www.ncbi.nlm.nih.gov/pmc/articles/PMC2376083/. (Accessed 19 November 2022).

Kamaly, N., Yameen, B., Wu, J., Farokhzad, O.C., February 2016. Degradable controlled-release polymers and polymeric nanoparticles: mechanisms of controlling drug release. Chem. Rev. 116 (4), 2602–2663. https://doi.org/10.1021/acs.chemrev.5b00346.

Karimi, M., et al., November 2016. Albumin nanostructures as advanced drug delivery systems. Expert Opin. Drug Deliv. 13 (11), 1609–1623. https://doi.org/10.1080/17425247.2016.1193149.

Kassab, A.C., Xu, K., Denkbas, E.B., Dou, Y., Zhao, S., Piskin, E., 1997. Rifampicin carrying polyhydroxybutyrate microspheres as a potential chemoembolization agent. J. Biomater. Sci. Polym. Ed. 8 (12). https://doi.org/10.1163/156856297x00119.

Kaur, A., Jain, S., Tiwary, A.K., March 2008. Mannan-coated gelatin nanoparticles for sustained and targeted delivery of didanosine: in vitro and in vivo evaluation. Acta Pharm. Zagreb Croat. 58 (1), 61–74. https://doi.org/10.2478/v10007-007-0045-1.

Khattab, S.N., et al., October 2016. Design and synthesis of new s-triazine polymers and their application as nanoparticulate drug delivery systems. New J. Chem. 40 (11), 9565–9578. https://doi.org/10.1039/C6NJ02539K.

Kim, C.-K., Lee, E.-J., February 1992. The controlled release of blue dextran from alginate beads. Int. J. Pharm. 79 (1), 11–19. https://doi.org/10.1016/0378-5173(92)90088-J.

Kim, I.Y., et al., August 2007. Evaluation of semi-interpenetrating polymer networks composed of chitosan and poloxamer for wound dressing application. Int. J. Pharm. 341 (1–2), 35–43. https://doi.org/10.1016/j.ijpharm.2007.03.042.

Kim, T.H., et al., January 2011. Preparation and characterization of water-soluble albumin-bound curcumin nanoparticles with improved antitumor activity. Int. J. Pharm. 403 (1–2), 285–291. https://doi.org/10.1016/j.ijpharm.2010.10.041.

Kumar, G., Chaudhary, K., Mogha, N.K., Kant, A., Masram, D.T., August 2021. Extended release of metronidazole drug using chitosan/graphene oxide bionanocomposite beads as the drug carrier. ACS Omega 6 (31), 20433–20444. https://doi.org/10.1021/acsomega.1c02422.

Kumari, A., Yadav, S.K., Yadav, S.C., January 2010. Biodegradable polymeric nanoparticles based drug delivery systems. Colloids Surf. B Biointerfaces 75 (1), 1–18. https://doi.org/10.1016/j.colsurfb.2009.09.001.

Kwon, G.S., Furgeson, D.Y., 2007. Biodegradable polymers for drug delivery systems. Biomed. Polym. 15, 83–110. https://doi.org/10.1533/9781845693640.83.

Lakshmi, S., Katti, D.S., Laurencin, C.T., April 2003. Biodegradable polyphosphazenes for drug delivery applications. Adv. Drug Deliv. Rev. 55 (4), 467–482. https://doi.org/10.1016/s0169-409x(03)00039-5.

Langer, R., Peppas, N., January 1983. Chemical and physical structure of polymers as carriers for controlled release of bioactive agents: a review. J. Macromol. Sci. Part C 23 (1), 61–126. https://doi.org/10.1080/07366578308079439.

Lee, C.H., Singla, A., Lee, Y., 2001. Biomedical applications of collagen. Int. J. Pharm. 221 (1–2), 1–22. https://doi.org/10.1016/S0378-5173(01)00691-3.

Li, R., Zhang, H., Qi, Q., September 2007. The production of polyhydroxyalkanoates in recombinant Escherichia coli. Bioresour. Technol. 98 (12), 2313–2320. https://doi.org/10.1016/j.biortech.2006.09.014.

Maghsoudi, A., Yazdian, F., Shahmoradi, S., Ghaderi, L., Hemati, M., Amoabediny, G., June 2017. Curcumin-loaded polysaccharide nanoparticles: optimization and anti-cariogenic activity against Streptococcus mutans. Mater. Sci. Eng. C 75, 1259–1267. https://doi.org/10.1016/j.msec.2017.03.032.

Martín, M., 2015. nab-Paclitaxel dose and schedule in breast cancer. Breast Cancer Res. 17 (1), 81. https://doi.org/10.1186/s13058-015-0587-y.

Middleton, J.C., Tipton, A.J., December 2000. Synthetic biodegradable polymers as orthopedic devices. Biomaterials 21 (23), 2335–2346. https://doi.org/10.1016/s0142-9612(00)00101-0.

Mishra, B., Mishra, M., Yadav, S.K., 2017. Antibacterial loaded spray dried chitosan polyelectrolyte complexes as dry powder aerosol for the treatment of lung infections. Iran. J. Pharm. Res. 16 (1), 74–92. Available: https://www.ncbi.nlm.nih.gov/pmc/articles/PMC5423235/. (Accessed 11 September 2022).

Mohamed Rizwan, I., Damodharan, N., 2020. Mathematical modelling of dissolution kinetics in dosage forms. Res. J. Pharm. Technol. 13 (3), 1339. https://doi.org/10.5958/0974-360X.2020.00247.4.

Molinaro, R., et al., December 2013. Polyethylenimine and chitosan carriers for the delivery of RNA interference effectors. Expert Opin. Drug Deliv. 10 (12), 1653–1668. https://doi.org/10.1517/17425247.2013.840286.

Mukerjee, A., Sinha, V.R., Pruthi, V., 2007. Preparation and Characterization of Poly-ε-Caprolactone Particles for Controlled Insulin Delivery, p. 5.

Nagarajan, U., Kawakami, K., Zhang, S., Chandrasekaran, B., Nair, B.U., May 2014. Fabrication of solid collagen nanoparticles using electrospray deposition. Chem. Pharm. Bull. (Tokyo) 62 (5), 422–428. https://doi.org/10.1248/cpb.c13-01004.

Ni, Z., et al., February 2020. Recent research progress on polyphosphazene-based drug delivery systems. J. Mater. Chem. B 8 (8), 1555–1575. https://doi.org/10.1039/C9TB02517K.

Nicklas, M., Schatton, W., Heinemann, S., Hanke, T., Kreuter, J., September 2009. Preparation and characterization of marine sponge collagen nanoparticles and employment for the transdermal delivery of 17β-estradiol-hemihydrate. Drug Dev. Ind. Pharm. 35 (9), 1035–1042. https://doi.org/10.1080/03639040902755213.

Osorno, L.L., Brandley, A.N., Maldonado, D.E., Yiantsos, A., Mosley, R.J., Byrne, M.E., 2021. Review of contemporary self-assembled systems for the controlled delivery of therapeutics in medicine. Nanomaterials 11 (2), 278. https://doi.org/10.3390/nano11020278.

Park, J.H., et al., 2019a. Poly(ε-caprolactone) (PCL) hollow nanoparticles with surface sealability and on-ddemand pore generability for easy loading and NIR light-triggered release of drug. Pharmaceutics 11 (10), 10. https://doi.org/10.3390/pharmaceutics11100528.

Park, K., et al., 2019b. Injectable, long-acting PLGA formulations: analyzing PLGA and understanding microparticle formation. J. Contr. Release 304, 125–134. https://doi.org/10.1016/j.jconrel.2019.05.003.

Peters, T., 1985. Serum albumin. Adv. Protein Chem. 37, 161–245. https://doi.org/10.1016/s0065-3233(08)60065-0.

Phyu Phyu, W., Shin-Ya, Y., Hong, K.-J., Kajiuchi, T., August 2003. Formulation and characterization of pH sensitive drug carrier based on phosphorylated chitosan (PCS). Carbohydr. Polym. 53, 305–310. https://doi.org/10.1016/S0144-8617(03)00068-7.

Piskin, E., 1995. Biodegradable polymers as biomaterials. J. Biomater. Sci. Polym. Ed. 6 (9), 775–795. https://doi.org/10.1163/156856295x00175.

Prabaharan, M., July 2008. Review paper: chitosan derivatives as promising materials for controlled drug delivery. J. Biomater. Appl. 23 (1), 5–36. https://doi.org/10.1177/0885328208091562.

Prajapati, S.K., Jain, A., Jain, A., Jain, S., 2019. Biodegradable polymers and constructs: a novel approach in drug delivery. Eur. Polym. J. 120. https://doi.org/10.1016/j.eurpolymj.2019.08.018.

Rancan, F., et al., August 2009. Investigation of polylactic acid (PLA) nanoparticles as drug delivery systems for local dermatotherapy. Pharm. Res. (N. Y.) 26 (8), 2027–2036. https://doi.org/10.1007/s11095-009-9919-x.

Rathore, P., Arora, I., Rastogi, S., Akhtar, M., Singh, S., Samim, M., 2020. Collagen nanoparticle-mediated brain silymarin delivery: an approach for treating cerebral ischemia and reperfusion-induced brain injury. Front. Neurosci. 14 (October), 1–21. https://doi.org/10.3389/fnins.2020.538404.

Rawat, A., Bhardwaj, U., Burgess, D.J., September 2012. Comparison of in vitro-in vivo release of Risperdal(®) Consta(®) microspheres. Int. J. Pharm. 434 (1–2), 115–121. https://doi.org/10.1016/j.ijpharm.2012.05.006.

Rentzepis, P.J., Kurian, M.J., Carracher, A.M., Close, K.L., December 2018. Practical ways to achieve targets in diabetes care. J. Diabetes 10 (12), 911–915. https://doi.org/10.1111/1753-0407.12842.

Salman, M.A., Sahin, A., Onur, M.A., Oge, K., Kassab, A., Aypar, U., September 2003. Tramadol encapsulated into polyhydroxybutyrate microspheres: in vitro release and epidural analgesic effect in rats. Acta Anaesthesiol. Scand. 47 (8), 1006–1012. https://doi.org/10.1034/j.1399-6576.2003.00180.x.

Samak, Y.O., El Massik, M., Coombes, A.G.A., January 2017. A comparison of aerosolization and homogenization techniques for production of alginate microparticles for delivery of corticosteroids to the colon. J. Pharmaceut. Sci. 106 (1), 208–216. https://doi.org/10.1016/j.xphs.2016.08.015.

Sarkar, G., et al., December 2017. Cellulose nanofibrils/chitosan based transdermal drug delivery vehicle for controlled release of ketorolac tromethamine. New J. Chem. 41 (24), 15312–15319. https://doi.org/10.1039/C7NJ02539D.

Schacht, E., Vandorpe, J., Dejardin, S., Lemmouchi, Y., Seymour, L., October 1996. Biomedical applications of degradable polyphosphazenes. Biotechnol. Bioeng. 52 (1), 102–108. https://doi.org/10.1002/(SICI)1097-0290(19961005)52:1<102::AID-BIT10>3.0.CO;2-Q.

Schoubben, A., Ricci, M., Giovagnoli, S., July 2019. Meeting the unmet: from traditional to cutting-edge techniques for poly lactide and poly lactide-co-glycolide microparticle manufacturing. J. Pharm. Investig. 49 (4), 381–404. https://doi.org/10.1007/s40005-019-00446-y.

Sheehan, J.J., Reilly, K.R., Fu, D.-J., Alphs, L., July 2012. Comparison of the peak-to-trough fluctuation in plasma concentration of long-acting injectable antipsychotics and their oral equivalents. Innov. Clin. Neurosci. 9 (7–8), 17–23.

Sinha, V.R., Bansal, K., Kaushik, R., Kumria, R., Trehan, A., June 2004. Poly-ε-caprolactone microspheres and nanospheres: an overview. Int. J. Pharm. 278 (1), 1–23. https://doi.org/10.1016/j.ijpharm.2004.01.044.

Sorasitthiyanukarn, F.N., Muangnoi, C., Na Bhuket, P.R., Rojsitthisak, P., Rojsitthisak, P., 2018. Chitosan/alginate nanoparticles as a promising approach for oral delivery of curcumin diglutaric acid for cancer treatment. Mater. Sci. Eng. C Mater. Biol. Appl. 93, 178–190. https://doi.org/10.1016/j.msec.2018.07.069.

Suriyamongkol, P., Weselake, R., Narine, S., Moloney, M., Shah, S., April 2007. Biotechnological approaches for the production of polyhydroxyalkanoates in microorganisms and plants – a review. Biotechnol. Adv. 25 (2), 148–175. https://doi.org/10.1016/j.biotechadv.2006.11.007.

Terzopoulou, Z., et al., October 2020. Preparation and evaluation of collagen-based patches as curcumin carriers. Polymers 12, 1–18. https://doi.org/10.3390/polym12102393.

Uhrich, K.E., Cannizzaro, S.M., Langer, R.S., Shakesheff, K.M., November 1999. Polymeric systems for controlled drug release. Chem. Rev. 99 (11), 3181–3198. https://doi.org/10.1021/cr940351u.

Ullah, R.S., et al., 2017. Synthesis of polyphosphazenes with different side groups and various tactics for drug delivery. RSC Adv. 7 (38), 23363–23391. https://doi.org/10.1039/C6RA27103K.

Unagolla, J.M., Jayasuriya, A.C., March 2018. Drug transport mechanisms and in vitro release kinetics of vancomycin encapsulated chitosan-alginate polyelectrolyte microparticles as a controlled drug delivery system. Eur. J. Pharm. Sci. 114, 199–209. https://doi.org/10.1016/j.ejps.2017.12.012.

Wahab, A., et al., August 2012. Development of poly(glycerol adipate) nanoparticles loaded with non-steroidal anti-inflammatory drugs. J. Microencapsul. 29 (5), 497–504. https://doi.org/10.3109/02652048.2012.665087.

Wallace, D.G., Rosenblatt, J., 2003. Collagen gel systems for sustained delivery and tissue engineering. Adv. Drug Deliv. Rev. 55 (12), 1631–1649. https://doi.org/10.1016/j.addr.2003.08.004.

Wang, X., Chi, N., Tang, X., November 2008. Preparation of estradiol chitosan nanoparticles for improving nasal absorption and brain targeting. Eur. J. Pharm. Biopharm 70 (3), 735–740. https://doi.org/10.1016/j.ejpb.2008.07.005.

Wang, S., et al., 2012. Preparation, characterization and related in vivo release, safety and toxicity studies of long acting lanreotide microspheres. Biol. Pharm. Bull. 35 (11), 1898–1906. https://doi.org/10.1248/bpb.b110726.

Yallapu, M.M., Dobberpuhl, M.R., Maher, D.M., Jaggi, M., Chauhan, S.C., January 2012. Design of curcumin loaded cellulose nanoparticles for prostate cancer. Curr. Drug

Metabol. 13 (1), 120–128. Available: https://www.ncbi.nlm.nih.gov/pmc/articles/PMC3632315/. (Accessed 29 October 2022).

Yang, C., Wu, H., Wang, J., July 2019. Formulation and evaluation of controlled-release of steroidal saponins-loaded collagen microspheres. Mater. Technol. 34 (9), 534–539. https://doi.org/10.1080/10667857.2019.1591727.

Yun, Y.H., Lee, B.K., Park, K., December 2015. Controlled drug delivery: Historical perspective for the next generation. J. Contr. Release 219, 2. https://doi.org/10.1016/j.jconrel.2015.10.005.

Zhang, J.X., et al., December 2006. Indomethacin-loaded polymeric nanocarriers based on amphiphilic polyphosphazenes with poly (N-isopropylacrylamide) and ethyl tryptophan as side groups: preparation, in vitro and in vivo evaluation. J. Contr. Release 116 (3), 322–329. https://doi.org/10.1016/j.jconrel.2006.09.013.

This page intentionally left blank

CHAPTER 19

Bioresorbable polymer-based sensors for medical applications

Thirumalaivasan Natesan[1], Senthilkumar Nangan[2] and Ramasubburayan Ramasamy[3]

[1]Department of Periodontics, Saveetha Dental College and Hospitals, Saveetha Institute of Medical and Technical Sciences (SIMATS), Saveetha University, Chennai, Tamil Nadu, India; [2]Department of Chemistry, Graphic Era (Deemed to be University), Dehradun, Uttarakhand, India; [3]Marine Biomedical Research Laboratory & Environmental Toxicology Unit, Department of Prosthodontics, Saveetha Dental College and Hospitals (SIMATS), Saveetha University, Chennai, Tamil Nadu, India

19.1 Introduction

The impact of bioresorbable polymer-based sensors on the medical technology landscape has been significant (Zhao et al., 2008; Arif et al., 2022; Ghaffari et al., 2021). These sensors offer real-time monitoring of physiological parameters, addressing issues with conventional sensors such as invasiveness and waste management. They are designed to be biocompatible and naturally degrade within the body, eliminating the need for secondary surgeries for removal (Kamrani and Fleck, 2019). Advancements in materials science, particularly bioresorbable polymers, drive their development. Bioresorbable polymers undergo a two-phase degradation process in the body, breaking down into fragments and then being metabolized by cellular mechanisms. This process is utilized to create sensors that can be implanted, function, and dissolve naturally, reducing complications (Sahandi Zangabad et al., 2023; Feng et al., 2022). These polymers enhance sensor functionalities and extend operational lifespan in the body. They offer benefits such as reduced infection risks, targeted treatment, and environmental sustainability.

Introduced in the 1970s, bioresorbable polymers have evolved in medical applications, including sutures made of materials like poly(glycolic acid), poly(lactic acid), and polydioxanone. Incorporating them into sensors presents challenges in biocompatibility and controlled degradation (Allizond et al., 2022). Customization requires knowledge of material science, sensor design, and biology. Bioresorbable sensors offer continuous

Bioresorbable Polymers and their Composites
ISBN 978-0-443-18915-9
https://doi.org/10.1016/B978-0-443-18915-9.00015-X
© 2024 Elsevier Ltd.
All rights reserved.

monitoring without surgical removal, improving patient experience (Ashammakhi et al., 2021; Nie et al., 2022). However, challenges like biocompatibility must be addressed for wider adoption. This chapter discusses bioresorbable polymer-based sensors, emphasizing their adaptability in healthcare. It explores their use in drug-delivery systems, with degradation rate influencing release kinetics. The sensors also address sustainability concerns by being biodegradable, offering an eco-friendly alternative to nonbiodegradable sensors (Won et al., 2021; Morsada et al., 2021; Islam et al., 2022).

The topics that are covered in this chapter include: (i) the essential principles of biodegradable polymers and their pertinent physiochemical attributes for medical utilization, (ii) a comprehensive review of current biodegradable sensing devices, classified according to their healthcare functionalities such as cardiac surveillance, glycemic level monitoring, and ophthalmic pressure assessment, (iii) a synopsis of the manufacturing methodologies employed in crafting sensors based on biodegradable polymers, (iv) mechanical sensing devices, and (v) analytical sensing devices.

19.2 The essential principles of biodegradable polymers and their pertinent physiochemical attributes for medical utilization

The medical technology sector is currently experiencing significant changes, largely attributable to the emergence of bioresorbable polymers. These materials are engineered to naturally disintegrate within the human body (Luzi et al., 2019). Their unique physiological and chemical traits make them essential for various medical uses. Therefore, gaining an in-depth comprehension of bioresorbable polymers and their physicochemical attributes is vital for both scholars in the field and healthcare professionals (Karade et al., 2021). To begin with the foundational concepts, bioresorbable polymers consist of extended molecular chains that the body can metabolize through its own physiological processes. These polymers often contain ester, ether, or anhydride linkages that are prone to hydrolytic breakdown (González et al., 2023; Xu et al., 2023). This hydrolysis leads to their eventual transformation into simpler compounds like water and carbon dioxide, which are then naturally eliminated from the body. This feature of being metabolizable distinguishes them sharply from nonbioresorbable materials such as metals, which persist within the body unless they are surgically extracted (Lin et al., 2023).

In contemporary healthcare applications, bioresorbable polymers have emerged as a focal point of interest, thanks in part to their distinct physicochemical attributes. This section offers a foundational understanding of these polymers and their significance in medical settings. Known for their ability to biologically decompose over a specific time frame, bioresorbable polymers negate the requirement for surgical extraction (Zielińska et al., 2023; Aguirre et al., 2023). This characteristic renders them highly applicable across various medical domains, such as controlled drug release, tissue scaffolding, and implantable medical equipment. A deeper understanding of their physicochemical traits, including degradation rates, mechanical stability, biocompatibility, and tissue interactions, is imperative to harness their full capabilities (Johansson et al., 2023). Through such insights, bioresorbable polymers hold the promise to transform the future of medical procedures and technologies. This section aims to offer an exhaustive exploration of the foundational elements and attributes of bioresorbable polymers, highlighting their potential utility and setting the stage for future innovations in medical science and engineering (Gandla et al., 2023).

Dissolvable sensors are emerging as critical tools in healthcare diagnostics and monitoring, showcasing advantages over their nondissolvable counterparts. These sensors are biologically safe, minimize environmental waste, and allow for distant tracking without requiring surgical removal (Ziesmer, 2023). This section organizes such sensors into categories based on their applications in healthcare, such as heart monitoring, glucose level assessment, and eye pressure tracking. The integration of these sensors is transformative for medical practices, enabling real-time data collection within the body and posing minimal environmental risks due to their biodegradable nature (Monge et al., 2023). This chapter outlines the various applications of dissolvable sensors, emphasizing their role in modern healthcare. These sensors are an innovative development, resolving issues related to implant removal and reducing medical waste. Their versatility makes them invaluable assets in healthcare, adaptable to specific needs, materials, and functionalities (Ramezani and Mohd Ripin, 2023; Tovar-Lopez, 2023).

The field of medical technology is undergoing significant changes, largely facilitated by the advent of bioresorbable polymers. These are materials engineered to naturally break down within the human body and exhibit characteristics that make them highly desirable for medical use (Aziz et al., 2023). A deep understanding of the core elements and physicochemical properties of these polymers is essential for both scholars in

the field and healthcare professionals. Bioresorbable polymers are complex molecular constructs that can be naturally processed by the body. They often contain bonds like esters, ethers, or anhydrides, which are prone to hydrolytic reactions (Sharma and Shankar, 2023). Through hydrolysis, these materials decompose into simpler compounds such as water and carbon dioxide, which are easily eliminated from the body. This is in stark contrast to nonbioresorbable materials like metals, which remain in the body unless they are physically removed. The physicochemical attributes of these bioresorbable polymers are influenced by various factors. For instance, molecular weight plays a significant role; polymers with higher molecular weights usually exhibit slower rates of degradation and greater stability. This makes them well-suited for long-term medical applications, such as bone implants. Additionally, the affinity of these polymers for water—whether they are hydrophilic or hydrophobic—also affects their rate of degradation. Hydrophilic polymers tend to break down more quickly due to increased water absorption, making them ideal for short-term uses such as drug-delivery systems. On the other hand, hydrophobic polymers are more suitable for applications requiring a slower degradation rate (Li et al., 2023; Giubilini et al., 2023).

The degree of crystallinity in polymers is a crucial factor; polymers with semicrystalline structures exhibit enhanced mechanical resilience, yet their rate of decomposition is slower due to the closely packed molecular formations. The glass transition temperature, which signifies the change from a glass-like to an elastic state, influences both the material's mechanical properties and its rate of degradation. Attributes like tensile strength, elasticity, and the ability to withstand compression are especially relevant in applications requiring load-bearing capacity, such as orthopedic implants. Various techniques like copolymerization, blending, or the introduction of additives allow for the fine-tuning of these features (Kim et al., 2023). Striking a balance between the material's mechanical capabilities and its rate of degradation is a complex, yet crucial, consideration in the development of polymers for medical usage.

In the realm of medication delivery, the dynamics governing how a healing compound is released from a polymer framework are critical. These dynamics are shaped by both how quickly the polymer breaks down and the diffusion characteristics of the drug. Certain polymers can be engineered to react to external signals such as temperature fluctuations or changes in acidity, facilitating precise regulation of medication release. In addition, the external attributes of the polymer play a significant role in its biocompatibility,

affecting how cells adhere and grow on it. Adjusting variables like surface texture, electrical charge, and chemical functionalities can either promote integration with bodily tissues or reduce bacterial attachment, depending on the medical objective (Pourmadadi et al., 2023; Princen et al., 2023). It is also crucial to ensure that any substances produced during the polymer's breakdown in the body are harmless and can be either metabolized or expelled easily. Understanding how these breakdown products are processed by the body is therefore a key consideration in selecting and designing polymers that are absorbed back into the body after serving their purpose. For example, polymers like polylactic acid (PLA) break down into lactic acid, a substance naturally found in the body, thus minimizing risks related to toxicity. Additionally, the method used to sterilize the polymer must be compatible; autoclaving may not be suitable for all such polymers, as it could alter their molecular structure and overall properties. On an ecological note, the ability of these polymers to biodegrade naturally helps to mitigate the issue of medical waste, setting them apart from traditional, nonbiodegradable materials (Lérida-Viso et al., 2023).

In essence, the various physical and chemical properties of biodegradable polymers, including factors like molecular mass, affinity for water, structural organization, mechanical features, rate of decomposition, and compatibility with biological systems, are crucial for their applications in healthcare. A deep grasp of these core attributes provides a foundation for improving both the effectiveness and the safety of medical devices, pharmaceutical delivery systems, and scaffolds for tissue regeneration (Priya et al., 2023; Sharma et al., 2023). As a result, in-depth scholarly research and stringent clinical evaluations are indispensable for unlocking the full potential of these innovative substances in the medical field.

19.3 A comprehensive review of current biodegradable sensing devices, classified according to their healthcare functionalities such as cardiac surveillance, glycemic level monitoring, and ophthalmic pressure assessment

The emergence of sensors that can be naturally absorbed by the body marks a transformative moment in medical diagnostic and surveillance technologies. Made from materials that are not only compatible with biological systems but also capable of breaking down naturally, these

devices offer the convenience of continuous data monitoring without necessitating additional surgeries for their removal (Munirathinam et al., 2023). This section offers an exhaustive review of these absorbable sensors, organizing them according to specific medical uses such as heart rate monitoring, blood sugar level tracking, and measuring pressure within the eye. For each category, detailed discussions are provided to explain the operational principles, constituent materials, and technologies that these sensors employ (Shen et al., 2023; Govindasamy and Thirumalaivasan). Furthermore, the chapter incorporates comparative assessments to outline the strengths and weaknesses of different kinds of sensors.

Advancements in medical technology have significantly elevated the standard of healthcare by facilitating early detection and continuous monitoring for optimized therapies. Sensors that are bioresorbable are particularly noteworthy, as they are both biocompatible and temporary, dissolving over a period of time to mitigate risks such as infections. This section provides a comprehensive examination of these sensors, organizing them based on their use-cases, such as monitoring heart activity, measuring blood sugar levels, and assessing intraocular pressure (Hosseini et al., 2021; Dash et al., 2019). This systematic categorization serves as a guide for healthcare practitioners to choose the most suitable sensors, while also highlighting existing obstacles and prospective advancements.

19.3.1 Cardiac monitoring

Innovations in bioresorbable sensors have led to a new era for heart monitoring, offering advantages not available with conventional implantable devices. Typically made from eco-friendly materials like polylactic acid (PLA) and polyglycolic acid (PGA), these sensors are constructed to decompose naturally within the human body, eliminating the necessity for surgical removal (Shanmugam et al., 2023). These sensors are adept at capturing crucial heart-related metrics such as electrical patterns and variations in heart rate, providing a holistic assessment of cardiovascular health. Additionally, they can be designed to deliver medications in a regulated fashion, thereby augmenting existing treatment methods. When placed in proximity to the heart, these devices track essential cardiovascular data such as heart rate and blood flow, eventually disintegrating naturally to avoid any further surgical procedures. Some of these cutting-edge sensors come with multifunctional capabilities, allowing for both the dispensation of medication and real-time tracking of cardiac functions, leading to a more cohesive treatment plan (Teijido et al., 2023). All in all, the emergence of

bioresorbable sensors has revolutionized the monitoring and treatment of heart-related disorders by providing real-time, minimally invasive options facilitated by materials that are biologically degradable, like PLA and PGA.

19.3.2 Blood glucose sensing

Implantable sensors made from materials that naturally degrade have revolutionized the field of diabetes management by offering a noninvasive, user-oriented solution for continuous blood sugar measurement. Unlike traditional glucose monitoring methods that require frequent finger pricking, these implantable sensors are placed beneath the skin and provide uninterrupted monitoring capabilities. Fabricated from materials like biodegradable polymers and soluble conductive materials, these sensors naturally disintegrate over time, eliminating the need for surgical removal. Constant monitoring of blood glucose levels is often challenging with existing technologies; however, these degradable sensors offer an appealing alternative (Zhu et al., 2023; Anand, 2023). They allow for subcutaneous implantation and wirelessly transmit data to external devices for immediate assessment. Some advanced models can even deliver insulin, acting as an artificial pancreas. The inherent biodegradability of these sensors circumvents the need for surgical extraction, providing a lasting solution for diabetes management. Moreover, these cutting-edge sensors address a key challenge in diabetes care: the discomfort and hassle associated with frequent blood tests. They employ enzyme-based electrochemical detection techniques, anchoring enzymes like glucose oxidase onto biodegradable platforms such as chitosan (Wang et al., 2023a; Bilal et al., 2023). This allows for accurate and targeted glucose detection, while the sensor naturally disintegrates after a set period. Consequently, these sensors enhance patient compliance and contribute to an overall improvement in their quality of life.

19.3.3 Intraocular pressure measurement

Consistent monitoring of intraocular pressure (IOP) is crucial for the effective management of glaucoma. Bioabsorbable sensors offer an advantageous means for such surveillance. In contrast to conventional techniques that often involve invasive procedures and yield periodic data, these sensors provide constant measurements and are designed to naturally break down after implantation. Created from biocompatible substances like polycaprolactone (PCL), the sensors are minimally intrusive while remaining highly compatible with biological tissues. Utilizing state-of-the-art materials such as bioabsorbable silicon and hydrogels, the sensors have appropriate

mechanical properties and undergo a regulated disintegration process (Liu et al., 2023a; Venkatesan et al., 2023). These devices offer a more convenient alternative to irregular and often uncomfortable hospital visits, as they can be embedded within the eye to enable continuous remote IOP tracking and timely clinical interventions. Capable of detecting pressure changes, these sensors ultimately disintegrate without inducing any adverse effects, allowing for more accurate modifications in the glaucoma treatment regimen (Molaei et al., 2018).

Dissolvable sensors represent a revolutionary step forward in medical diagnostic and monitoring technology, acting as an eco-friendly alternative to conventional sensors while also reducing electronic pollution. Utilized across a wide spectrum of healthcare uses from monitoring heart activity to measuring blood sugar levels and evaluating eye pressure, these sensors are integral to a more patient-centric model of healthcare. Benefiting from the latest developments in materials science, these sensors fulfill a range of medical necessities and simultaneously tackle environmental degradation through their ability to break down naturally. Although significant strides have been made, challenges persist in optimizing sensor longevity, data precision, and biological compatibility (Molaei et al., 2018; Nan et al., 2023; Nangan et al., 2023). By providing cutting-edge, eco-conscious, and patient-oriented solutions, dissolvable sensors are paving the way for advanced medical monitoring systems. This summary outlines the current range of uses and aspires to galvanize additional scholarly investigation into this burgeoning area.

19.4 An overview of the fabrication techniques for bioresorbable polymer-based sensors

Biodegradable sensors made from polymers are gaining attention for their applications in healthcare diagnostics, pharmaceutical delivery, and environmental monitoring. These sensors are environmentally responsible as they decompose naturally, thereby reducing electronic waste and providing a sustainable option. The effectiveness of these devices is closely tied to the manufacturing processes employed. This section aims to comprehensively assess the various production methods that are essential for improving the functionality and performance of such sensors (Yang et al., 2022). The field of sensors made from polymers that can be naturally broken down by the body has experienced significant expansion lately, paving the way for novel healthcare applications including drug delivery and ongoing monitoring of

vital signs. One distinctive advantage is that these materials degrade naturally, obviating the need for additional surgeries to remove them, which consequently reduces the long-term health implications. The cornerstone of their adaptability and efficacy is primarily rooted in the manufacturing processes used.

The increasing significance of sensors made from bioresorbable polymers in the medical field is paving the way for advanced scientific inquiries. These devices, compatible with biological systems, offer considerable advantages such as eliminating the requirement for subsequent surgeries and reducing risks commonly linked with implanted mechanisms. However, ample opportunities exist for ongoing research aimed at enhancing their performance features and diversifying their use-cases (La Mattina et al., 2020). The rapidly advancing field of sensors made from bioresorbable polymers has captured considerable attention in healthcare circles. These insertable instruments have a variety of functions, including continuous health surveillance and medication delivery, and they are organically metabolized by the body over a period of time. While they offer numerous inherent benefits such as a lower risk of infection and eliminating the necessity for surgical removal, there remain unexplored areas of research that could enhance their performance and extend their applications in healthcare settings (Boutry et al., 2012). This section seeks to explore these potential areas of study, focusing specifically on groundbreaking technological developments that could transform the domain of medical sensors.

19.4.1 Solvent casting

One of the earliest and simplest approaches is solvent casting, which finds frequent application in producing flat, film-like structures. In this method, an organic solvent is utilized to dissolve a polymer, followed by the introduction of active components such as therapeutic agents or sensing elements. After thorough mixing, the solution is poured onto a mold and allowed to undergo evaporation, resulting in the formation of a solidified film. Although straightforward in execution, solvent casting often gives rise to uneven component distribution, thereby restricting its utility in intricate devices (Beygisangchin et al., 2021). Solvent casting represents a direct and cost-effective strategy for manufacturing bioresorbable sensors. In this procedure, the polymer is initially dissolved within a suitable solvent to create a uniform solution. This liquid is subsequently cast into a mold resembling the desired sensor configuration, followed by solvent evaporation, culminating in the development of a solidified framework.

This method permits a notable level of customization; however, it may necessitate the use of harmful solvents that require complete evaporation (Revia et al., 2022; Lu et al., 2023).

Among the widely employed fabrication methodologies, solvent casting stands out as a prominent technique. This process involves dissolving the polymer in a suitable solvent and then casting it into a mold to achieve the desired shape. Once the solvent undergoes evaporation, the polymer solidifies and can be integrated with other sensor components (Borbolla-Jiménez et al., 2023). Solvent casting's popularity stems from its simplicity, although it does have limitations regarding the complexity of structures that can be effectively produced.

19.4.2 Electrospinning

Electrospinning stands as a widely employed method, particularly for the production of fibrous structures. This technique involves expelling a polymer solution through a syringe under the application of high voltage, resulting in the formation of micro- or nanofibers. These fibers can subsequently be manipulated or aligned into specific arrangements, offering significant benefits for sensing applications that necessitate ample surface area. The principle underlying electrospinning is rooted in harnessing electrical forces to generate fibers from a polymer solution or melt. By supplying a high voltage, the polymer solution becomes charged, forming what is known as a Taylor cone. As droplets emerge from this cone, they move toward a collector that is grounded, undergoing solidification in the process, thus transforming into fibers (Naveenkumar et al., 2023; Cao et al., 2023). This technique proves particularly proficient in crafting nanofibrous sensors, which exhibit a heightened surface area and expedited biodegradation. Electrospinning enables the creation of nanofibers, which boast remarkable surface-to-volume ratios, thereby enhancing the sensitivity of sensors. Through the application of an electric field, a polymer solution is expelled via a needle, yielding delicate fibers that accumulate on a grounded surface. Despite its advantages, electrospinning demands specialized equipment and can consume significant amounts of energy (Chakrapani et al., 2023). Nonetheless, it allows for the incorporation of diverse functional components into the polymer matrix, expanding its range of potential applications.

19.4.3 3D printing

The emergence of 3D printing technologies has facilitated the manufacturing of intricate shapes with a remarkable level of accuracy. The selection of 3D

printing method, whether it is fused deposition modeling (FDM) or stereolithography (SLA), dictates the compatibility with different types of polymer materials. This approach offers substantial customization options and is well-suited for swift prototyping, albeit with some constraints on material choices due to printer limitations. The utilization of additive manufacturing methods, such as 3D printing, has also been adapted for crafting bioresorbable sensors (Shilar et al., 2023). Leveraging meticulous precision and step-by-step assembly, 3D printing empowers the generation of intricate shapes and internal configurations. This technique proves particularly advantageous for tailoring designs to specific patients or customized applications. However, it requires advanced design software and can be time-intensive for large-scale production. Recent progressions in 3D printing technology have elevated its popularity as a means to produce bioresorbable sensors. This technique facilitates the creation of intricate three-dimensional structures that can be precisely customized for distinct purposes (Dew, 2023). Furthermore, 3D printing expedites prototype development, enabling faster cycles of iteration in the design process.

19.4.4 Photolithography

Photolithography, a fundamental process in microfabrication, utilizes ultraviolet (UV) light in conjunction with a photosensitive material to delineate intricate geometric configurations onto a substrate. In the realm of bioresorbable sensors, the utilization of photolithography enables the creation of complex structures possessing remarkable spatial resolution. This characteristic is indispensable for the production of diminutive implantable devices. Initially conceived as a technique for semiconductor manufacturing, photolithography has been ingeniously modified to cater to the demands of bioresorbable sensor fabrication (CS and Kandasubramanian, 2023). The methodology encompasses the deposition of a photosensitive polymer layer onto the substrate, which is subsequently subjected to UV exposure through a mask. Following this exposure, a development process ensues wherein the regions that were illuminated are selectively removed. This meticulous procedure culminates in the preservation of an exacting pattern on the substrate (Wang et al., 2023b). It is worth noting that the precision achieved through this approach is exceptional; however, its implementation can incur substantial costs. Consequently, its application is primarily tailored to scenarios demanding intricate patterns and uncompromising precision on a smaller scale.

Photolithography stands as a sophisticated technique that affords the capability to intricately pattern sensor constituents onto a polymer substrate. By utilizing UV light to induce chemical modifications in the photosensitive polymer layer, a template of intricate designs is rendered (Alowakennu et al., 2023). While this method is conventionally associated with the semiconductor industry, its adaptation to bioresorbable polymers underscores its versatility and pertinence in the context of emerging technologies.

19.4.5 Coating and layering techniques

This approach encompasses the sequential application of positively and negatively charged polymers onto a surface, achieved through electrostatic interactions. This process offers meticulous management over thickness and composition, enabling the integration of diverse functional materials into the sensor. Nonetheless, while effective, this method can require significant labor and is influenced by environmental factors such as pH and ionic strength. The procedure entails the successive deposition of polyelectrolytes with opposing charges onto a substrate (Kogularasu et al., 2023). This technique empowers precise manipulation of the sensor's thickness and accommodates multiple layers of distinct materials. This proves beneficial in intricate drug-delivery scenarios where varying release patterns are sought after. Coating methodologies often complement alternative fabrication techniques (Qureshi and Niazi, 2023). For instance, a sensor might undergo fabrication using photolithography, followed by a coating of biocompatible material through chemical vapor deposition. Layering approaches serve to introduce supplementary functionalities, such as coatings that respond selectively to particular biological markers.

The field of bioresorbable polymer-based sensor fabrication faces various challenges, including scalability, cost-effectiveness, and the integration of functional elements without compromising biocompatibility or performance. Advances in nanotechnology, material science, and computational modeling are expected to significantly impact future developments. Despite the advances in fabrication techniques, challenges remain in terms of scalability, reproducibility, and the integration of multiple functionalities within a single sensor (Pathak et al., 2023). Further research is needed to develop more efficient fabrication methods that can meet the growing demands for more sophisticated sensing capabilities.

The fabrication methods employed for bioresorbable polymer-based sensors encompass a diverse array, each offering distinct advantages and

limitations. Gaining a comprehensive grasp of these techniques stands as a pivotal factor in propelling the technology forward and broadening its applications within healthcare and other domains. As the field continues to mature, it is foreseeable that novel methodologies and hybrid approaches will come to the forefront, thereby paving the way for bioresorbable sensors that are more efficacious and versatile in nature. To summarize, the techniques used in fabricating bioresorbable polymer-based sensors exhibit diversity, with each method conferring unique benefits and challenges. The selection of a specific approach frequently hinges upon the intended application, material attributes, and the desired traits of the sensor (Ligon et al., 2017). The ongoing pursuit of research endeavors serves to continually innovate these techniques, aiming to enhance the functional aspects, scalability, and biocompatibility of these groundbreaking devices.

In conclusion, the potential harbored by bioresorbable polymer-based sensors for revolutionizing medical diagnostics and treatment is substantial. The trajectory of future research in this realm encompasses a multidimensional scope, necessitating an interdisciplinary approach that involves domains such as materials science, computer science, engineering, and ethical considerations. With the persistent advancement of technology, the outlook is promising for these transient, biocompatible devices to assume an increasingly pivotal role in healthcare, thereby significantly elevating patient outcomes and overall medical efficiency.

19.5 Physical sensors

Monitoring physiological conditions within the human body is significantly facilitated by the use of pressure and strain sensors. For healthcare surveillance, sensors with degradable materials and capacitive configurations have been engineered. These innovative sensors have uses in various domains, including electronic skin technology and malleable robotics. They employ a variety of structural designs that make use of disintegrable dielectric substances, as well as piezoelectric, piezocapacitive, and piezoresistive components. These monitoring devices are carefully positioned in specific body parts such as the brain, eyes, and muscles, primarily to mitigate the risks associated with elevated intracranial pressure following surgical interventions. As a case in point, a cordless sensor made of biodegradable materials was developed using principles of resonant frequency. This particular sensor featured zinc and iron bilayers, electrodeposited to function as conductive parallel plates. These conductive plates were distanced by

a layer of poly-L-lactic acid (PLLA) and sealed within a shell of polycaprolactone (PCL) (Banitaba et al., 2023). Air within the sensor interacted with a meticulously designed inductor coil. When external pressure impacted the sensor, the spacing within its capacitive assembly was reduced, causing a detectable alteration in the circuit's resonant frequency. This shift was remotely observed through an external coil situated outside the human body.

The transducer displayed a frequency reaction that corresponded linearly with the pressure exerted upon it. Sensitivity metrics were roughly gauged at 290 kHz/kPa over a span of 0–20 kPa. For assessing long-term reliability, the sensor was tested in an isotonic sodium chloride solution. Initial findings suggest that the sensor operated effectively for close to 107 h in this environment, eventually breaking down fully near the 170-hour mark. This pioneering technique in crafting biodegradable pressure-sensitive devices offers noteworthy advantages for noninvasive healthcare diagnostics and shows promise for future medical applications (Stewart et al., 2018). In a different but related vein, a pressure-sensitive device engineered for internal bodily placement has been introduced. This sensor is particularly designed for physiological pressure tracking in diverse body organs such as the brain, lungs, eyes, and heart. Its main constituent is piezoelectric poly(L-lactic acid) (PLLA), which gains its piezoelectric characteristics through thermal processing under mechanical stress to realign the polymer structures. Following this, the film undergoes precise sectioning to further optimize its piezoelectric characteristics. The architecture of the sensor includes dual layers of the piezoelectric PLLA material, sandwiched between miniature biodegradable Mo/Mg electrodes. These components are encased in layers of polylactic acid (PLA). The sensor's performance metrics are notable, capable of identifying minor variances in pressure in the range of 0–18 kPa. It manifests two separate sensitivity thresholds: the first is 75 mV/kPa for the 0–2 kPa pressure interval, and the second is 14 mV/kPa for the 3–18 kPa range. Importantly, the sensor's sensitivity can be calibrated by manipulating the number of PLLA layers used in its construction (Annese et al., 2014).

The sensor exhibits stable functionality by operating continuously for roughly 4 days in both regulated laboratory conditions with a 37°C phosphate-buffered saline (PBS) solution and a pH level of 7.4, as well as when it is surgically positioned in the back region of mice. Following this period, the sensor begins its process of deterioration, culminating in its complete dissolution. The entire disintegration process for the sensor takes

approximately 8 days, although full decomposition takes several weeks. In this context, the importance of the thickness of the sensor's casing made of polylactic acid (PLA) is highlighted as it plays a crucial role in affecting the speed of the sensor's breakdown (Lee et al., 2022). A separate example of a biodegradable pressure sensor is a single-use capacitive patch designed for heart rate monitoring. This particular sensor employs a dielectric layer made of poly(glycerol sebacate) (PGS) with a microstructured design, and this layer is sandwiched between two magnesium-based electrodes to form the capacitive system.

A novel methodology was used to create a biodegradable sensing device by leveraging POMaC and PHB/PHV materials, each with a 10 μm thickness, as well as a PLLA-based coiled spacer. The sensor was designed to wrap around a rat's femoral artery, situating the softer POMaC layer in contact with the vessel for a minimally invasive mechanical link to the arterial wall. The operational performance of the sensing device relied on changes in capacitance, which were detected in the picoFarad range. These changes were generated by the expansion and contraction of blood vessels. Such fluctuations led to alterations in the resonant frequency of an LCR electrical circuit, which could be remotely detected via a coupling mechanism with an external reading coil (Chen and Wang, 2002). Approximately 1 week after implantation, a noticeable reduction in the sensor's signal was recorded.

In a noteworthy development, Boutry and colleagues made substantial contributions to the field of biodegradable and implantable sensors with capacitive functionalities. The sensor is ingeniously engineered to enable real-time assessments of mechanical stresses on tendons as well as the deformation experienced by tissue post-surgery. The design of the sensor is versatile, allowing it to expand and thus simultaneously record both strain and pressure metrics during the healing of tendons. The device is built as a dual-layered system. The first layer features a specialized dielectric layer made of PGS, combined with magnesium (Mg) electrodes, which is focused on pressure measurement (Ruth and Bao, 2020). The second layer employs a different configuration, using interlocking Mg electrodes mounted on a PLLA base to capture strain data.

Evaluating the in vitro breakdown characteristics involved immersing the sensing apparatus in a saline solution buffered to a pH of 7.4, and maintained at a temperature of 37°C. In this setting, the apparatus exhibited consistent functionality over a 2–3-week period. When implanted into the dorsum of a rodent, the device continued to deliver reliable readings for

more than 3.5 weeks. Remarkably, the sensing mechanism displayed quick reaction times within the scope of milliseconds and excellent sensitivity, with the capability to sense as low as 0.4% strain and pressure comparable to the force generated by a single salt grain (12 Pa). A key feature of this sensing design is its ability to combine both pressure and strain metrics without the need for a separate interface (Guex et al., 2021). This innovation offers the possibility for tailored rehabilitation plans suited to individual needs.

A pressure sensor constructed from sustainable materials, namely a combination of glycine amino acid and chitosan polymer, has been designed for applications in wearables, such as for use beneath wound dressings to track pressure fluctuations. The creation process utilized electron-beam evaporation to apply gold electrodes to both surfaces of the glycine–chitosan film, adhering to a thickness standard of 10/90 nm (Hosseini et al., 2020). The sensor demonstrated a sensitivity of 2.82 ± 0.2 mV per kPa and was effective within a pressure range of 5–60 kPa. To evaluate its biodegradability, electrodes made of magnesium (Mg) were integrated into the sensor. These electrodes completely broke down when submerged in a phosphate-buffered saline solution with a pH level of 7.4, followed by the gradual dissolution of the remaining film material in subsequent days. The addition of chitosan to the composite not only improved the film's flexibility but also influenced the crystallization of glycine into its β-phase, a form known for its elevated piezoelectric constant.

In the realm of healthcare surveillance, thermal sensors are indispensable for both immediate and distance-based assessments of bodily heat levels. These instruments are especially effective for keeping track of temperatures within the brain and at wound sites, the latter of which is an indicator for potential infection. Generally, these sensors operate on the principle of piezoresistive compounds, leveraging the intrinsic relationship between electrical resistance and temperature. Two primary categories of sensor behavior exist: those with a positive temperature coefficient (PTC), where an uptick in temperature leads to higher resistance, and those with a negative temperature coefficient (NTC), where resistance dwindles as temperature ascends. PTC-based sensors are commonly employed in functions such as safeguarding against excess electrical current, self-adjusting heating systems, and miniature switch sensors (Liu et al., 2023b; Steinegger et al., 2020). On the other hand, NTC-based materials are apt for creating highly flexible thermistors that are incorporated into

wearable devices for thermal sensing, spatial temperature distribution, and thermal adjustments.

In a self-directed scientific investigation focusing on eco-friendly electronic devices, researchers employed the technique of femtosecond laser direct writing (FsLDW) to create unique graphene formations on organic materials such as leaves and wood. Using ultraviolet femtosecond lasers, they were able to concentrate heat production, which resulted in the carbonization of the components within the wood (Lee et al., 2023). Through repeated carbonization processes, distinctive laser-induced graphene patterns were successfully achieved. A prototype temperature sensor was constructed on a dried leaf that had an estimated thickness of 100 μm. This sensor exhibited a negative temperature coefficient of −0.08% per degree Celsius. In a similar manner, a related sensor was developed on a wooden surface, showing results comparable to the leaf-based sensor but with a longer response and recovery time.

In a novel scientific study, researchers engineered an eco-friendly photonic device capable of measuring factors such as tissue oxygen levels, temperature, and neuronal activity. The device was constructed with materials that are biologically absorbable, encompassing silicon-based unijunction light detectors, tricolor sensors with silicon P—N junctions, a layered optical filter, and optical fibers composed of poly(lactic-co-glycolic acid) (PLGA). To analyze the concentrations of silicon and zinc in various mouse tissues over a period of 7 days, analytical techniques such as inductively coupled plasma optical emission spectrometry (ICP-OES) and inductively coupled plasma mass spectrometry (ICP-MS) were employed (Hassan et al., 2023). The initial findings indicated an uptick in the levels of these elements in the kidneys, pointing toward renal elimination as the likely excretion pathway. Moreover, the device's light sensor, based on a silicon nanomembrane, was observed to fully break down within 2 weeks when immersed in a phosphate-buffered saline solution maintained at 37°C. The sensor's temperature-sensitive resistance allowed for precise monitoring of tissue temperature fluctuations, achieving a resolution nearly as accurate as 0.1°C.

Recent progress in optical sensor technology has concentrated on the continuous monitoring of pressure and temperature within the skull. The sensor is engineered to detect variations in the size of air pockets or alterations in the properties of photonic crystal arrays. These changes are triggered by the pressure-driven movements of the silicon nitride monolayer (Si-NM) diaphragm. Such movements cause a shift in the resonant

peak located in the reflection spectrum. The same sensor configuration is also capable of assessing temperature changes by observing alterations in the refractive index of silicon (Zhang et al., 2015). Notably, the sensor exhibited a temperature response rate of 0.090 nm per degree Celsius and a sensitivity to pressure changes at 3.8 nm per mmHg. When subjected to a PBS solution at a temperature of 37°C, the sensor was observed to completely disintegrate in approximately 195 days.

19.6 Chemical sensors

Chemical detection instruments are crucial for gathering information from biological markers in the human body, enabling the instantaneous and nonintrusive tracking of health metrics such as sugar concentration, acid–base equilibrium, levels of nitric oxide, and assorted ions. While studies have successfully shown that eco-friendly, biodegradable sensors can perform as well as their nonbiodegradable equivalents, there is a noticeable absence of exhaustive studies that focus on the creation and effectiveness of these biodegradable chemical sensors in ongoing healthcare monitoring scenarios. Addressing the obstacles in developing such sensors requires ensuring their operational integrity in physiological conditions without the need for protective casings, as well as their precise identification of targeted chemicals, even in the presence of other biologically active substances (Li and Wen, 2020).

Recent strides have been made in surmounting multiple obstacles in the field of sensor technology. One notable breakthrough has been the development of an electrochemical sensor strip composed of chitosan that is capable of dopamine detection. This device utilizes elements like chitosan, along with reduced graphene oxide and graphene, to enhance its sensitivity. This optimizes the sensor to identify dopamine concentrations as minimal as 10 ppm, making it well-suited for internal bodily applications. In another independent research endeavor, a humidity sensor was crafted using environmentally sustainable and biodegradable materials, particularly polysaccharides. The construction involved the layering of a chitosan–lignin blend in a 9:1 ratio onto a flexible PI substrate through spin-coating methods. This resulted in a sensor layer with an approximate thickness of 20 μm (Prabhu et al., 2022). Once Mg/Fe electrodes were integrated into this layer, the sensor displayed remarkable sensitivity toward humidity changes. This heightened sensitivity was linked to the formation of hydrogen bond networks between the water molecules and

the polysaccharides, which led to improved conductivity in humid environments. The sensor's compatibility with biological systems was verified through cytotoxicity tests that examined its interaction with human skin fibroblasts and human umbilical vein endothelial cells using the biocomposite film.

In a novel technique, experts harnessed the silk of spider egg sacs (SESS) to form an interference chamber inside a single-mode fiber (SMF). Variability in surrounding humidity led to shifts in the SESS diameter, which in turn modified the length of the interferometric cavity, resulting in a redshift in the spectral interference. This special quality made it possible to gauge humidity levels, with greater sensitivity emerging as the ambient humidity increased. Peak sensitivity reached 0.99 nm/%RH in the 90%–99% humidity range (Farahani et al., 2014). Within the arena of nanocomposite technology, investigators developed specialized composites consisting of zein, graphene oxide (Z-GO), Laponite, and carbon nanotubes (CNTs) using drop-casting methods. Created explicitly for detecting gliadin, a protein connected to autoimmune diseases, these composite structures showed a considerable improvement in detection performance compared to electrodes coated solely with pure zein (Martínez et al., 2017). Among the range of nanomaterials used, the composites that incorporated CNTs showed the strongest detection signals due to CNTs' innate ability to act as a binding agent for functional groups. These collective advantages led to superior sensor functionality, achieving an impressively low detection limit of as little as 0.5 ppm.

19.7 Conclusion

The advent of bioresorbable polymer-based sensors represents a groundbreaking shift in medical technology, specifically in the realms of minimally invasive procedures and personalized healthcare. Comprising naturally derived polymers like cellulose, chitosan, and alginates, as well as synthetic materials like polylactic acid (PLA) and polyglycolic acid (PGA), these sensors offer a multitude of clinical applications. They have particularly demonstrated their efficacy in orthopedics, where they can monitor stress and strain on implants and bones, and in cardiovascular care, where they assess parameters including blood flow, heart rate, and arterial conditions. The inherent capability of these materials to undergo bioresorption eliminates the need for additional surgical interventions to remove the sensors, thereby reducing medical costs and patient discomfort. Their biodegradable

nature not only alleviates the environmental burden but also contributes to a more cost-effective healthcare system. Ongoing research is geared toward fine-tuning the bioresorption rates and optimizing the longevity of these polymers, with the fields of miniaturization and materials science serving as catalysts for future advancements. In sum, bioresorbable polymer sensors are not merely a technological novelty but a substantive advancement that harmonizes with broader healthcare and environmental goals. They serve as a testament to the merging of medical innovation with ecological responsibility and patient-centric care. Their potential for further development and integration into mainstream medical practices holds promise for a future where medical monitoring is both efficient and less invasive.

References

Aguirre, M., Ballard, N., Gonzalez, E., Hamzehlou, S., Sardon, H., Calderon, M., Paulis, M., Tomovska, R., Dupin, D., Bean, R.H., Long, T.E., Leiza, J.R., Asua, J.M., 2023. Polymer colloids: current challenges, emerging applications, and new developments. Macromolecules 56 (7), 2579–2607. https://doi.org/10.1021/acs.macromol.3c00108.

Allizond, V., Comini, S., Cuffini, A.M., Banche, G., 2022. Current knowledge on biomaterials for orthopedic applications modified to reduce bacterial adhesive ability. Antibiotics (Basel) 11 (4), 529. https://doi.org/10.3390/antibiotics11040529.

Alowakennu, M., Omoniyi, A.O., Ejeromedoghene, O., Alli, Y.A., Akor, E., Nnyia, M.O., 2023. Harnessing photo-induced processes for the fabrication and application of functional conjugated and conducting polymer-based materials. J. Mol. Struct. 1292, 136149. https://doi.org/10.1016/j.molstruc.2023.136149.

Anand, T., 2023. Folate Receptor Beta as an Imaging Target in Myocardial Infarction.

Annese, V.F., De Venuto, D., Martin, C., Cumming, D.R.S., 2014. Biodegradable pressure sensor for health-care. In: Circuits Syst. (ICECS) 21st I.E.E.E. International Conference on Electronics, 2014. IEEE Publications, pp. 598–601. https://doi.org/10.1109/ICECS.2014.7050056.

Arif, Z.U., Khalid, M.Y., Sheikh, M.F., Zolfagharian, A., Bodaghi, M., 2022. Biopolymeric sustainable materials and their emerging applications. J. Environ. Chem. Eng. 10 (4), 108159. https://doi.org/10.1016/j.jece.2022.108159.

Ashammakhi, N., Hernandez, A.L., Unluturk, B.D., Quintero, S.A., de Barros, N.R., Hoque Apu, E., Bin Shams, A., Ostrovidov, S., Li, J., Contag, C., Gomes, A.S., Holgado, M., 2021. Biodegradable implantable sensors: materials design, fabrication, and applications. Adv. Funct. Mater. 31 (49), 2104149. https://doi.org/10.1002/adfm.202104149.

Aziz, T., Haq, F., Farid, A., Kiran, M., Faisal, S., Ullah, A., Ullah, N., Bokhari, A., Mubashir, M., Chuah, L.F., Show, P.L., 2023. Challenges associated with cellulose composite material: facet engineering and prospective. Environ. Res. 223, 115429. https://doi.org/10.1016/j.envres.2023.115429.

Banitaba, S.N., Khademolqorani, S., Jadhav, V.V., Chamanehpour, E., Mishra, Y.K., Mostafavi, E., Kaushik, A., 2023. Recent progress of bio-based smart wearable sensors for healthcare applications. Mater. Today Electr. 5, 100055. https://doi.org/10.1016/j.mtelec.2023.100055.

Beygisangchin, M., Abdul Rashid, S., Shafie, S., Sadrolhosseini, A.R., Lim, H.N., 2021. Preparations, properties, and applications of polyaniline and polyaniline thin films—a review. Polymers (12), 2003. https://doi.org/10.3390/polym13122003.

Bilal, M., Singh, A.K., Iqbal, H.M.N., Boczkaj, G., 2023. Enzyme-conjugated MXene nanocomposites for biosensing and biocatalysis acuities. Chem. Eng. J., 145020 https://doi.org/10.1016/j.cej.2023.145020.

Borbolla-Jiménez, F.V., Peña-Corona, S.I., Farah, S.J., Jiménez-Valdés, M.T., Pineda-Pérez, E., Romero-Montero, A., Del Prado-Audelo, M.L., Bernal-Chávez, S.A., Magaña, J.J., Leyva-Gómez, G., 2023. Films for wound healing fabricated using a solvent casting technique. Pharmaceutics 15 (7), 1914. https://doi.org/10.3390/pharmaceutics15071914.

Boutry, C.M., Chandrahalim, H., Streit, P., Schinhammer, M., Hänzi, A.C., Hierold, C., 2012. Towards biodegradable wireless implants. Phil. Trans. Roy. Soc. Lond. 370 (1967), 2418−2432.

Cao, W., Zhang, M., Ma, W., Huang, C., 2023. Multifunctional electrospun nanofibrous membrane: an effective method for water purification. Sep. Purif. Technol., 124952 https://doi.org/10.1016/j.seppur.2023.124952.

Chakrapani, G., Ramakrishna, S., Zare, M., 2023. Functionalization of electrospun nanofiber for biomedical application. J. Appl. Polym. Sci. 140 (23), e53906. https://doi.org/10.1002/app.53906.

Chen, L.J., Wang, M., 2002. Production and evaluation of biodegradable composites based on PHB−PHV copolymer. Biomaterials 23 (13), 2631−2639. https://doi.org/10.1016/s0142-9612(01)00394-5.

CS, A., Kandasubramanian, B., 2023. Hydrogel as an advanced energy material for flexible batteries. Polym. Plast. Technol. Mater. 62 (3), 359−383.

Dash, S., Shakyawar, S.K., Sharma, M., Kaushik, S., 2019. Big data in healthcare: management, analysis and future prospects. J. Big Data 6 (1), 1−25.

Dew, R., 2023. The Empathetic Algorithm Leveraging AI for Next-Level, Vol. CX.

Farahani, H., Wagiran, R., Hamidon, M.N., 2014. Humidity sensors principle, mechanism, and fabrication technologies: a comprehensive review. Sensors 14 (5), 7881−7939. https://doi.org/10.3390/s140507881.

Feng, Y., Liao, Z., Li, M., Zhang, H., Li, T., Qin, X., Li, S., Wu, C., You, F., Liao, X., 2022. Mesoporous silica nanoparticles-based nanoplatforms: basic construction, current state, and emerging applications in anticancer therapeutics. Adv. Healthcare Mater., 2201884

Gandla, K., Kumar, K.P., Rajasulochana, P., Charde, M.S., Rana, R., Singh, L.P., Haque, M.A., Bakshi, V., Siddiqui, F.A., Khan, S.L., Ganguly, S., 2023. Fluorescent-nanoparticle-impregnated nanocomposite polymeric gels for biosensing and drug delivery applications. Gels 9 (8), 669. https://doi.org/10.3390/gels9080669.

Ghaffari, R., Yang, D.S., Kim, J., Mansour, A., Wright Jr., J.A., Model, J.B., Wright, D.E., Rogers, J.A., Ray, T.R., 2021. State of sweat: emerging wearable systems for real-time, noninvasive sweat sensing and analytics. ACS Sens. 6 (8), 2787−2801. https://doi.org/10.1021/acssensors.1c01133.

Giubilini, A., Messori, M., Bondioli, F., Minetola, P., Iuliano, L., Nyström, G., Maniura-Weber, K., Rottmar, M., Siqueira, G., 2023. 3D-Printed poly(3-hydroxybutyrate-co-3-hydroxyhexanoate)-cellulose-based scaffolds for biomedical applications. Biomacromolecules. https://doi.org/10.1021/acs.biomac.3c00263.

González, S.C.E., Galindo, A.S., Herrera, R.R., Badillo, C.M.L., Palomo-Ligas, L., Fernandez, I.M., Valencia, V.D.J.S., 2023. Health applications of biodegradable polymers. In: Biodegradable Polymers. CRC Press, pp. 207−217.

Govindasamy, R., Thirumalaivasan, N., Heterogenous Copper(ii) schiff-base complex immobilized mesoporous silica catalyst for multicomponent Biginelli reaction. Available at: SSRN 4421779.

Guex, A.G., Poxson, D.J., Simon, D.T., Berggren, M., Fortunato, G., Rossi, R.M., Maniura-Weber, K., Rottmar, M., 2021. Controlling pH by electronic ion pumps to fight fibrosis. Appl. Mater. Today 22, 100936. https://doi.org/10.1016/j.apmt.2021.100936.

Hassan, J.Z., Raza, A., Babar, Z.U.D., Qumar, U., Kaner, N.T., Cassinese, A., 2023. 2D material-based sensing devices: an update. J. Mater. Chem. A 11, 6016–6063. https://doi.org/10.1039/D2TA07653E.

Hosseini, E.S., Manjakkal, L., Shakthivel, D., Dahiya, R., 2020. Glycine–Chitosan-based flexible biodegradable piezoelectric pressure sensor. ACS Appl. Mater. Interfaces 12 (8), 9008–9016. https://doi.org/10.1021/acsami.9b21052.

Hosseini, E.S., Dervin, S., Ganguly, P., Dahiya, R., 2021. Biodegradable materials for sustainable health monitoring devices. ACS Appl. Bio Mater. 4 (1), 163–194. https://doi.org/10.1021/acsabm.0c01139.

Islam, M., Lantada, A.D., Mager, D., Korvink, J.G., 2022. Carbon-based materials for articular tissue engineering: from innovative scaffolding materials toward engineered living carbon. Adv. Healthcare Mater. 11 (1), e2101834. https://doi.org/10.1002/adhm.202101834.

Johansson, Å., Andreassen, O.A., Brunak, S., Franks, P.W., Hedman, H., Loos, R.J.F., Meder, B., Melén, E., Wheelock, C.E., Jacobsson, B., 2023. Precision medicine in complex diseases—molecular subgrouping for improved prediction and treatment stratification. J. Intern. Med. https://doi.org/10.1111/joim.13640.

Kamrani, S., Fleck, C., 2019. Biodegradable magnesium alloys as temporary orthopaedic implants: a review. Biometals 32 (2), 185–193. https://doi.org/10.1007/s10534-019-00170-y.

Karade, V.C., Patil, R.B., Parit, S.B., Kim, J.H., Chougale, A.D., Dawkar, V.V., 2021. Insights into shape-based silver nanoparticles: a weapon to cope with pathogenic attacks. ACS Sust. Chem. Eng. 9 (37), 12476–12507. https://doi.org/10.1021/acssuschemeng.1c03797.

Kim, J.R., Thelusmond, J.R., Albright III, V.C., Chai, Y., 2023. Exploring structure-activity relationships for polymer biodegradability by microorganisms. Sci. Total Environ. 890, 164338. https://doi.org/10.1016/j.scitotenv.2023.164338.

Kogularasu, S., Lee, Y.-Y., Chang-Chien, G.-P., Govindasamy, M., Sheu, J.-K., 2023. Review—nanofibers: empowering electrochemical sensors for reliable detection of food and environmental toxins. J. Electrochem. Soc. 170 (7), 077514. https://doi.org/10.1149/1945-7111/ace8c2.

La Mattina, A.A., Mariani, S., Barillaro, G., 2020. Bioresorbable materials on the rise: from electronic components and physical sensors to in vivo monitoring systems. Adv. Sci. 7 (4), 1902872. https://doi.org/10.1002/advs.201902872.

Lee, G., Ray, E., Yoon, H.J., Genovese, S., Choi, Y.S., Lee, M.K., Sahin, S., Yan, Y., Ahn, H.Y., Bandodkar, A.J., Kim, J., Park, M., Ryu, H., Kwak, S.S., Jung, Y.H., Odabas, A., Khandpur, U., Ray, W.Z., MacEwan, M.R., Rogers, J.A., 2022. A bioresorbable peripheral nerve stimulator for electronic pain block. Sci. Adv. 8 (40), eabp9169. https://doi.org/10.1126/sciadv.abp9169.

Lee, Y., Low, M.J., Yang, D., Nam, H.K., Le, T.-S.D., Lee, S.E., Han, H., Kim, S., Vu, Q.H., Yoo, H., Yoon, H., Lee, J., Sandeep, S., Lee, K., Kim, S.W., Kim, Y.J., 2023. Ultra-thin light-weight laser-induced-graphene (LIG) diffractive optics. Light Sci. Appl. 12 (1), 146. https://doi.org/10.1038/s41377-023-01143-0.

Lérida-Viso, A., Estepa-Fernández, A., García-Fernández, A., Martí-Centelles, V., Martínez-Máñez, R., 2023. Biosafety of mesoporous silica nanoparticles; towards clinical

translation. Adv. Drug Deliv. Rev. 201, 115049. https://doi.org/10.1016/j.addr.2023.115049.

Li, G., Wen, D., 2020. Wearable biochemical sensors for human health monitoring: sensing materials and manufacturing technologies. J. Mater. Chem. B 8 (16), 3423–3436. https://doi.org/10.1039/c9tb02474c.

Li, J., Liu, J., Wu, Z., Shang, X., Li, Y., Huo, W., Huang, X., 2023. Fully printed and self-compensated bioresorbable electrochemical devices based on galvanic coupling for continuous glucose monitoring. Sci. Adv. 9 (29), eadi3839. https://doi.org/10.1126/sciadv.adi3839.

Ligon, S.C., Liska, R., Stampfl, J., Gurr, M., Mülhaupt, R., 2017. Polymers for 3D printing and customized additive manufacturing. Chem. Rev. 117 (15), 10212–10290.

Lin, J.-Y., Lee, I., Tzeng, J.-H., Li, W., Kim, H., Huang, C.-P., 2023. The surface acidity of freshly synthesized microplastics particles in simple electrolyte. Colloids Surf. A Physicochem. Eng. Aspects 675, 132000. https://doi.org/10.1016/j.colsurfa.2023.132000.

Liu, G., Lv, Z., Batool, S., Li, M.Z., Zhao, P., Guo, L., Wang, Y., Zhou, Y., Han, S.T., 2023a. Biocompatible material-based flexible biosensors: from materials design to wearable/implantable devices and integrated sensing systems. Small 19 (27), e2207879. https://doi.org/10.1002/smll.202207879.

Liu, T., Wang, Y., Hong, M., Venezuela, J., Shi, W., Dargusch, M., 2023b. Advances in biodegradable piezoelectrics for medical implants. Nano Today 52, 101945.

Lu, T., Ji, S., Jin, W., Yang, Q., Luo, Q., Ren, T.L., 2023. Biocompatible and long-term monitoring strategies of wearable, ingestible and implantable biosensors: reform the next generation healthcare. Sensors 23 (6), 2991. https://doi.org/10.3390/s23062991.

Luzi, F., Puglia, D., Torre, L., 2019. Natural fiber biodegradable composites and nanocomposites: a biomedical application. In: Biomass, Biopolymer-Based Materials, and Bioenergy. Elsevier, pp. 179–201.

Martínez, G.M., Newman, C.N., De Vicente-Retortillo, A., Fischer, E., Renno, N.O., Richardson, M.I., Fairén, A.G., Genzer, M., Guzewich, S.D., Haberle, R.M., Harri, A.-M., Kemppinen, O., Lemmon, M.T., Smith, M.D., de la Torre-Juárez, M., Vasavada, A.R., 2017. The modern near-surface martian climate: a review of in-situ meteorological data from viking to curiosity. Space Sci. Rev. 212 (1–2), 295–338. https://doi.org/10.1007/s11214-017-0360-x.

Molaei, A., Karamzadeh, V., Safi, S., Esfandiari, H., Dargahi, J., Khosravi, M.A., 2018. Upcoming methods and specifications of continuous intraocular pressure monitoring systems for glaucoma. J. Ophthalmic Vis. Res. 13 (1), 66–71. https://doi.org/10.4103/jovr.jovr_208_17.

Monge, J., Ribeiro, G., Raimundo, A., Postolache, O., Santos, J., 2023. AI-based smart sensing and AR for gait rehabilitation assessment. Information 14 (7), 355. https://doi.org/10.3390/info14070355.

Morsada, Z., Hossain, M.M., Islam, M.T., Mobin, M.A., Saha, S., 2021. Recent progress in biodegradable and bioresorbable materials: from passive implants to active electronics. Appl. Mater. Today 25, 101257. https://doi.org/10.1016/j.apmt.2021.101257.

Munirathinam, P., Anna Mathew, A.A., Shanmugasundaram, V., Vivekananthan, V., Purusothaman, Y., Kim, S.-J., Chandrasekhar, A., 2023. A comprehensive review on triboelectric nanogenerators based on real-time applications in energy harvesting and self-powered sensing. Mater. Sci. Eng. B 297, 116762. https://doi.org/10.1016/j.mseb.2023.116762.

Nan, X., Xu, Z., Cao, X., Hao, J., Wang, X., Duan, Q., Wu, G., Hu, L., Zhao, Y., Yang, Z., Gao, L., 2023. A review of epidermal flexible pressure sensing arrays. Biosensors 13 (6), 656. https://doi.org/10.3390/bios13060656.

Nangan, S., Kanagaraj, K., Kaarthikeyan, G., Kumar, A., Ubaidullah, M., Pandit, B., Govindasamy, R., Natesan, T., 2023. Sustainable preparation of luminescent carbon

dots from syringe waste and hyaluronic acid for cellular imaging and antimicrobial applications. Environ. Res. 237 (2), 116990. https://doi.org/10.1016/j.envres.2023.116990.

Naveenkumar, R., Senthilvelan, S., Karthikeyan, B., 2023. A review on the recent developments in electrospinned nanofibers for drug delivery. Biomed. Mater. Devices 1–23. https://doi.org/10.1007/s44174-023-00121-9.

Nie, Z., Kwak, J.W., Han, M., Rogers, J.A., 2022. Mechanically active materials and devices for bio-interfaced pressure sensors—a review. Adv. Mater., e2205609 https://doi.org/10.1002/adma.202205609.

Pathak, R., Punetha, V.D., Bhatt, S., Punetha, M., 2023. Carbon nanotube-based biocompatible polymer nanocomposites as an emerging tool for biomedical applications. Eur. Polym. J. 196, 112257. https://doi.org/10.1016/j.eurpolymj.2023.112257.

Pourmadadi, M., Yazdian, F., Koulivand, A., Rahmani, E., 2023. Green synthesized polyvinylpyrrolidone/titanium dioxide hydrogel nanocomposite modified with agarose macromolecules for sustained and pH-responsive release of anticancer drug. Int. J. Biol. Macromol. 240, 124345. https://doi.org/10.1016/j.ijbiomac.2023.124345.

Prabhu, A., Crapnell, R.D., Eersels, K., van Grinsven, B., Kunhiraman, A.K., Singla, P., McClements, J., Banks, C.E., Novakovic, K., Peeters, M., 2022. Reviewing the use of chitosan and polydopamine for electrochemical sensing. Curr. Opin. Electrochem. 32, 100885. https://doi.org/10.1016/j.coelec.2021.100885.

Princen, K., Marien, N., Guedens, W., Graulus, G.J., Adriaensens, P., 2023. Hydrogels with reversible cross-links for improved localised stem cell retention: a review. Chembiochem, e202300149. https://doi.org/10.1002/cbic.202300149.

Priya, A.K., Muruganandam, M., Imran, M., Gill, R., Vasudeva Reddy, M.R.V., Shkir, M., Sayed, M.A., AlAbdulaal, T.H., Algarni, H., Arif, M., Jha, N.K., Sehgal, S.S., 2023. A study on managing plastic waste to tackle the worldwide plastic contamination and environmental remediation. Chemosphere, 139979. https://doi.org/10.1016/j.chemosphere.2023.139979.

Qureshi, A., Niazi, J.H., 2023. Graphene-Interfaced flexible and stretchable micro–nano electrodes: from fabrication to sweat glucose detection. Mater. Horiz. 10 (5), 1580–1607. https://doi.org/10.1039/d2mh01517j.

Ramezani, M., Mohd Ripin, Z., 2023. 4D printing in biomedical engineering: advancements, challenges, and future directions. J. Funct. Biomater. 14 (7), 347. https://doi.org/10.3390/jfb14070347.

Revia, R.A., Wagner, B., James, M., Zhang, M., 2022. High-throughput dispensing of viscous solutions for biomedical applications. Micromachines 13 (10), 1730. https://doi.org/10.3390/mi13101730.

Ruth, S.R.A., Bao, Z., 2020. Designing tunable capacitive pressure sensors based on material properties and microstructure geometry. ACS Appl. Mater. Interfaces 12 (52), 58301–58316. https://doi.org/10.1021/acsami.0c19196.

Sahandi Zangabad, P., Abousalman Rezvani, Z., Tong, Z., Esser, L., Vasani, R.B., Voelcker, N.H., 2023. Recent advances in formulations for long-acting delivery of therapeutic peptides. ACS Appl. Bio Mater. https://doi.org/10.1021/acsabm.3c00193.

Shanmugam, D.K., Anitha, S.C., Souresh, V., Madhavan, Y., Sampath, S., Catakapatri Venugopal, D., Saravanan, M., 2023. Current advancements in the development of bionic organs using regenerative medicine and 3D tissue engineering. Mater. Technol. 38 (1), 2242732. https://doi.org/10.1080/10667857.2023.2242732.

Sharma, Y., Shankar, V., 2023. Technologies for the fabrication of crosslinked polysaccharide-based hydrogels and its role in microbial three-dimensional bioprinting—A review. Int. J. Biol. Macromol. 250, 126194. https://doi.org/10.1016/j.ijbiomac.2023.126194.

Sharma, S., Bhardwaj, A., Thakur, M., Saini, A., 2023. Understanding microplastic pollution of marine ecosystem: a review. Environ. Sci. Pollut. Res. Int. 1–44. https://doi.org/10.1007/s11356-023-28314-1.

Shen, X., Jiang, H., Liu, D., Yang, K., Deng, F., Zhang, T., Xiao, Z., Lui, J.C.S., Liu, J., Dustdar, S., Luo, J., 2023. PupilHeart: heart rate variability monitoring via pupillary fluctuations on mobile devices. IEEE Internet Things J. https://doi.org/10.1109/JIOT.2023.3277555, 1–1.

Shilar, F.A., Ganachari, S.V., Patil, V.B., Bhojaraja, B.E., Yunus Khan, T.M., Almakayeel, N., 2023. A review of 3D printing of geopolymer composites for structural and functional applications. Construct. Build. Mater. 400, 132869. https://doi.org/10.1016/j.conbuildmat.2023.132869.

Steinegger, A., Wolfbeis, O.S., Borisov, S.M., 2020. Optical sensing and imaging of pH values: spectroscopies, materials, and applications. Chem. Rev. 120 (22), 12357–12489. https://doi.org/10.1021/acs.chemrev.0c00451.

Stewart, M.P., Langer, R., Jensen, K.F., 2018. Intracellular delivery by membrane disruption: mechanisms, strategies, and concepts. Chem. Rev. 118 (16), 7409–7531. https://doi.org/10.1021/acs.chemrev.7b00678.

Teijido, R., Rubio, L.R., Zhang, Q., Lanceros, S., Vilela, J.L.V., 2023. Biopolymers and their application-oriented composites into a circular economy context. New Mater. Circ. Econ. 149, 105–141.

Tovar-Lopez, F.J., 2023. Recent progress in micro- and nanotechnology-enabled sensors for biomedical and environmental challenges. Sensors 23 (12), 5406. https://doi.org/10.3390/s23125406.

Venkatesan, P., Govindasamy, R., Periyasami, G., Rahaman, M., Pandiaraj, S., Thiruvengadam, M., Thirumalaivasan, N., Wu, S.-P., 2023. Eco-friendly, bright luminescent carbon dots and their potential applications for detecting hypochlorous acid in water and live cell imaging. J. Mater. Res. Technol. 24, 6522–6532. https://doi.org/10.1016/j.jmrt.2023.04.181.

Wang, S., Zhao, M., Yan, Y., Li, P., Huang, W., 2023a. Flexible monitoring, diagnosis, and therapy by microneedles with versatile materials and devices toward multifunction scope. Research 6, 0128. https://doi.org/10.34133/research.0128.

Wang, X., Liu, J., Zhang, Y., Kristiansen, P.M., Islam, A., Gilchrist, M., Zhang, N., 2023b. Advances in precision microfabrication through digital light processing: system development, material and applications. Virtual Phys. Prototyp. 18 (1), e2248101. https://doi.org/10.1080/17452759.2023.2248101.

Won, C., Kwon, C., Park, K., Seo, J., Lee, T., 2021. Electronic drugs: spatial and temporal medical treatment of human diseases. Adv. Mater. 33 (47), e2005930. https://doi.org/10.1002/adma.202005930.

Xu, S., Zhou, J., Pan, P., 2023. Strain-induced multiscale structural evolutions of crystallized polymers: from fundamental studies to recent progresses. Prog. Polym. Sci. 140, 101676. https://doi.org/10.1016/j.progpolymsci.2023.101676.

Yang, W.Y., Anusuyadevi, K., Lu, P.H., Thirumalaivasan, N., Hsuan Lin, W.-H., Velmathi, S., Wu, S.P., 2022. A two photon fluorescent probe for highly selective detection and endogenous imaging of hydrogen sulfide. Spectrochim. Acta Mol. Biomol. Spectrosc. 273, 121043. https://doi.org/10.1016/j.saa.2022.121043.

Zhang, Y.-n., Zhao, Y., Lv, R.-q., 2015. A review for optical sensors based on photonic crystal cavities. Sens. Actuators, A 233, 374–389. https://doi.org/10.1016/j.sna.2015.07.025.

Zhao, R., Torley, P., Halley, P.J., 2008. Emerging biodegradable materials: Starch- and protein-based bio-nanocomposites. J. Mater. Sci. 43 (9), 3058–3071. https://doi.org/10.1007/s10853-007-2434-8.

Zhu, Y., Li, J., Kim, J., Li, S., Zhao, Y., Bahari, J., Eliahoo, P., Li, G., Kawakita, S., Haghniaz, R., Gao, X., Falcone, N., Ermis, M., Kang, H., Liu, H., Kim, H., Tabish, T., Yu, H., Li, B., Akbari, M., Emaminejad, S., Khademhosseini, A., 2023. Skin-interfaced electronics: a promising and intelligent paradigm for personalized healthcare. Biomaterials 296, 122075. https://doi.org/10.1016/j.biomaterials.2023.122075.

Zielińska, A., Karczewski, J., Eder, P., Kolanowski, T., Szalata, M., Wielgus, K., Szalata, M., Kim, D., Shin, S.R., Słomski, R., Souto, E.B., 2023. Scaffolds for drug delivery and tissue engineering: the role of genetics. J. Contr. Release 359, 207–223. https://doi.org/10.1016/j.jconrel.2023.05.042.

Ziesmer, J., 2023. Hybrid Antibacterial Microneedle Patches against Skin Infections. Karolinska Institutet.

Index

'*Note:* Page numbers followed by "f" indicate figures and "t" indicate tables.'

A

ABA block copolymers, 283–284
Absorbable implant coating application in orthopedics, 269
Absorbable polymer, 386–387
Absorption
  bioresorbable polymers, 387
  spectrum, 432–433
Acrylated L-lactide-cotrimethylene carbonate (aPLA-co-TMC), 131–132
Activated monomer ring opening polymerizations (ROPs), 66
Active Pharmaceutical Ingredient (API), 170, 214
Additive manufacturing, 48, 90–91
Advanced Monte Carlo (MC) moves, 172
Aeromonas ichthiosmia, 108–109
Agar, 367
Agarose, 34–36, 367
Agate mortar, 422–423
Albumin, 449
Alcohol consumption, 361
Aldehydes, 8
Alginate(s), 6–7, 367, 448–449
  based wound dressing, 412
Alginic acid, 448–449
Alkaline polymers, 137–138
All-atom molecular dynamics (AAMD), 185
Alternating current (AC) electrospinning technology, 204–205
Alumina trioxide, 428–429
$Al_xCa_{y-x}Nd_{01}P_{70}$ bioglasses, 421
  methods and measurements, 422–423
  photoluminescence spectra, 435f
  results, 423–439
    biocompatible studies, 435–439
    optical studies, 432–434
    structural studies, 423–429
    thermoluminescence (TL) studies, 429–432
Alzheimer disease (AD), 56
Amide (NH_2), 152–153
  groups, 154–155, 187
Amines, 155
3-aminopropyl-trimethoxysilane-modified halloysite nanotube (HNT-APTS), 412
Analysis of variance (ANOVA), 240–242
Anionic ring opening polymerizations (ROPs), 65–66
Anterior cruciate ligament (ACL), 266
Antibacterial activity of halloysite nanotube (HNT)–polymer blends, 395–397, 399t
Antibacterial properties of halloysite nanotube (HNT), 395–397
Application(s)
  artificial skin, 268
  bioabsorbable polymers, 264–271
  bioresorbable tissue scaffold, 135–138
  bone tissue engineering, 270–271
  drug-delivery devices, 268–270
  implants for temporary fixation, 264–268
  ligament/tendon tissue engineering, 271
  neurosurgery, 266–267
  orthopedics, 264–266
  plastic surgery, 267–268
  tissue engineering, 270–271
Aqueous-soluble polymers, 154–155
Artificial bioabsorbable polymers, 261–262, 271
Artificial skin, application in, 268
Atomistic molecular dynamics simulations (aMDs), 174
Augmentation rhinoplasty, 267–268

Aureobasidium pullulans, 365
Azotobacter, 6–7

B

BAB block copolymers, 283–284
Bacillus
  B. cereus, 108–109
  B. pumilus, 108–109
Bacterial pigment prodigiosin (PG), 120
Baker and Lonsdale model, 235
Barium (Ba^{2+}), 151
Barrier membranes, 45
Basic fibroblast factor (bFGF), 261–262
Benzoic acid, 219–220
Best-fitting model, 242, 243t–247t
Beta-tricalcium phosphate (beta-TCP), 132–133
Bioabsorbable polymers, 259–260, 262–263, 265–266
  application, 264–271
    drug-delivery devices, 268–270
    implants for temporary fixation, 264–268
    tissue engineering, 270–271
  characteristics as implants, 262–263
    biocompatibility, 262
    degradability/absorbability, 263
    eliminable toxicity, 263
    sufficient mechanical strength, 262–263
  fixators, 264–265
Bioabsorbable sensors, 475–476
Bioabsorbable silicon, 475–476
Bioactive molecules, 366
Bio-based polymers, 63
Biocompatibility, 63, 71, 73, 109–110, 262, 386, 391, 443–444, 472–473
  of poly(lactic acid) (PLA) /poly(L-lactic acid) (PLLA) composites, 92
Biodegradability, 386–387, 443–444
  of poly(lactic acid) (PLA) /poly(L-lactic acid) (PLLA) composites, 92
Biodegradable polylactic-co-glycolic acid (PLGA) polymers, 299
Biodegradable polymers, 213–215, 386–387, 389, 443–445, 454–455
  application in drug delivery, 451–452
  classification for CDDS, 445–451
    albumin, 449
    alginate, 448–449
    chitosan, 447–448
    collagen, 446–447
    gelatin, 447
    phosphorus-based polymers, 450–451
    polyamides, 449–450
    polyesters, 450
    polyhydroxybutyrate, 449
  commercially available biodegradable polymer base products, 457
  materials, 85
Biodegradable sensing devices, 473–476
  blood glucose sensing, 475
  cardiac monitoring, 474–475
  intraocular pressure (IOP) measurement, 475–476
Biodegradable sensors, 476–477
Biodegradation process, 3–4, 443–444
Bioengineering, 24–28
Biofabrication, 101
Bio-fibers, 28–33
Bioglass 45S5, 294–295
Biological acceptability, 262
Biological adaptability, 262
Biological functionality, 67
Biological methods, 13
Biomaterials, 353, 386
Biomedical applications, 113–114
  filtration membranes, 208–209
  halloysite nanotube (HNT)–polymer blends, 413–414
Biomedical industries, 108
Biomedicine, 198–198
Bioplastics, 107–108
Biopolymer(s), 72–73
  composites, 63–64, 72–73
    polycaprolactone (PCL) structure, 64f
Bioprocessing, 184–185
Bioresorbable composites, 14–15, 24–28

of poly(lactic acid) (PLA)-poly(L-lactic acid) (PLLA), 48
Bioresorbable compounds, 353–354
Bioresorbable hydrogels, 148
Bioresorbable magnesium membrane, 45
Bioresorbable materials, 4–5, 23–24, 325
performance in medical interventions, 33–37
salient properties for biomedical application, 28–33
Bioresorbable microneedles (MNs), 56
Bioresorbable polymer scaffolds (BPSs), 126, 137–138
Bioresorbable polymers, 4, 12, 14, 126, 129, 135–138, 214–215, 270, 325, 385–389, 469, 471–472
applications, 387–389
based halloysite nanotube (HNT) composites, 393–394
biomedical applications, 14–17
bioresorbable materials
for biomedical application, 28–33
for medical applications, 29t
performance in medical interventions, 33–37
bioresorbable polymer-based sensors, 469, 480
chemical structures and behavioral properties, 32f
classifications, 5–10, 389–390
natural bioresorbable materials, 5–8
synthetic bioresorbable polymers, 8–10
drug-delivery systems, 326–330
degree of crystallinity, 327–328
hydrophobicity/hydrophilicity, 328–329
molecular weight, 329–330
medical devices, 330
physical properties of medically inclined polymers, 31t
polymer degradation, 10–11
properties, 363–364, 386–387
of polymers, 30t
resorption process, 11–13
in vitro methods of bioresorbability evaluation, 12–13
synthesis, 126–134
tissue engineering, 330–346
wound healing, 364–372
collagen, 369–371
glycolipids, 368
polysaccharides, 365–368
proteins and peptides, 368–371
proteoglycans, 368
synthetic polymers, 371–372
vegetal proteins, 368–369
Bioresorbable sensors, 469–470
Bioresorbable silicon electronic device, 47
Bioresorbable spectrometer, 47–48
Bioresorbable stent, 52–53
Bioresorbable tissue scaffold
applications of, 135–138
bone and cartilage tissue fixation, 137–138
vascular grafts and stents, 136–137
Bioresorbable-based polymer composites, 14–15
Biostability, 387
Biotronik's PK Papyrus coronary stent system, 206–207
Block-copolymer solutions, 151
Blood glucose, 475
sensing, 475
Bone
reconstruction method, 24–28
remodeling, 263
tissue engineering, 10
application, 270–271
tissue fixation, 137–138
Bovine serum albumin (BSA), 370
Brazel and Peppas model, 235–236

C

Calcification, 136
Calcioorthophosphates ($Ca(PO_2)_4$), 421
Calcio-phosphates glasses, 421
Calcium (Ca^{2+}), 151
Calcium fluoride, 428–429
Calcium phosphate ceramic, 293–294
Cancer therapy, 279–280

Carbon dioxide, 386–387, 470
Carbon nanotubes (CNTs), 487
Carboxylic acid, 152–153
Carboxymethyl benzalamide sulfonate dextran (CMDBS), 366
Carboxymethylcellulose/chitosan (CMC), 57, 152–154, 408–409, 411f
Cardiac monitoring, 474–475
Cardiac surveillance, 473–476
Carrageenan, 367–368
Carreau–Yasuda model, 88–90
Cartilage tissue fixation, 137–138
Catalysis, 392
Catalyst, 65
  initiator, 65
Cationic ring opening polymerizations (ROPs), 66
Cellulose, 7–8, 36–37, 271, 366
Cellulose acetate (CA), 44
Ceramics, 4, 67, 332
  nanoparticles, 374
Cerebrospinal fluid (CSF), 266–267
Cerium nanoparticle (CeNP) -loaded chitosan/polycaprolactone (PCL), 73
Cerium oxide (CeO_2), 373
Chain-absorbed conformation, 185
Chain-free state in solution, 184
Chameleon (simulation programs), 173
Characterization techniques, 14
Charge interactions, cross-linking by, 151
Chemical analysis studies, 422–423
Chemical cross-linking, 154–157, 338–339. *See* Physical cross-linking
  chemical reaction of complementary groups, 154–155
  cross-linking by photopolymerization, 155–156
  enzyme cross-linking, 157
  high-energy irradiation cross-linking, 156–157
  hydrogels, 154
  polymer–polymer cross-linking, 155
Chemical hydrolysis, 10
Chemical sensors, 486–487
Chemical stability, 392
Chemical structure of poly(lactic acid) (PLA) /poly-L-lactide (PLLA) polymers, 87
Chemotherapeutic drugs, 361
Chitin, 5–6, 6f, 366–367, 447–448
Chitosan (CS), 5–6, 6f, 154, 214, 260–261, 268, 270–271, 366–367, 375–376, 447–448, 451, 475
  based nanoparticles, 447–448
  polymer, 484
Chitosan-graft-polylactide copolymer (CS-g-PLA) hydrogels, 150–151
Chitosan–vanillin–bioglass (CVB), 270–271
Chlorhexidine (CHX), 98
Chronic wound dressings, 366
Ciprofloxacin hydrochloric acid (HCL)-loaded polyurethane, 372
Clinical applications of bioresorbable polymers, 4–5
Coarse grained molecular dynamics (CGMD), 185
Coating techniques, 480–481
Coaxial techniques, 71–72
Coefficient of determination, 242
Co-immobilization process, 366
Cold atmosphere plasma surface modification, 260
Collagen, 271, 369–371, 446–447
Combinational polylactic-co-glycolic acid (PLGA) polymeric composites, 304
Complementary groups, chemical reaction of, 154–155
Composite, 112–114
  materials, 113, 115
  scaffolds, 139
Compound addition, 11
Compound annual growth rate (CAGR), 107–108
Compression molding, 127–128
Computer modeling techniques, 170
Congenital heart defects (CHDs), 131–132

Conjugates, 368
Contact microscopy, 13
Controlled drug-delivery release, 451–452
Controlled drug delivery systems, 444–445
  biodegradable polymers
    application in drug delivery, 451–452
    classification for, 445–451
    commercially available, 457
  mechanism involved in controlled release through polymers, 452–457
  release kinetic, 457
Controlled radical polymerization techniques, 148–149
Controlled-release drug-delivery system (CRDDS), 213, 222
Controlled release through polymers
  degradation controlled release, 454–455
  diffusion controlled-release, 454
  dissolution controlled release, 453
  erosion controlled release, 455–457
  mechanism involved in, 452–457
  osmotic pumping release, 455
Conventional methods, 159–161
Conventional radical polymerization techniques, 148–149
Conventional stereocomplex process, 149–150
Conventional techniques, 51, 343
Conventional treatment approaches, 125
Coordination-insertion ring opening polymerizations (ROPs), 66
Copolymers
  of hydroxybutyric and hydroxyhexanoic acids (PHB/PHHx), 112
  of hydroxybutyric and hydroxyvaleric acids (PHB/PHV), 112
  of polylactic-co-glycolic acid (PLGA), 280–284
Copper nanoparticles (CuNPs), 373
Copper oxide nanoparticles (NPs) infused polycaprolactone (PCL), 73
Core–plasmonic nanoparticles, polylactic-co-glycolic acid (PLGA) composites applications with, 304, 305t–306t
Correlation coefficient (R), 242
Corrosion process, 114–115
Cosmetics development, 392
Covalent bonds, 154
COVID-19 pandemic, 205–206, 208–209
Cross-linking
  albumin microparticles, 232
  charge interactions, 151
  crystallization, 152
  hydrogels, 148–157
    chemical cross-linking, 154–157
    cross-linking strategies in hydrogel forming, 149f
    physical cross-linking, 149–153
  hydrogen bonding (H-bonding), 152–153
  photopolymerization, 155–156
Cross-WLF model, 88–90
Crystallinity of poly(L-lactic acid) (PLLA), 93
Crystallization, cross-linking by, 152
Cumulative drug release (CDR), 223–228
Curcumin diglutaric acid (CG), 451–452

D

Davis theory, 433
Degradability of polyhydroxyalkanoates (PHAs), 110
Degradation
  controlled release, 454–455
  factors influencing degradation of poly(lactic-co-glycolic acid) (PLGA), 291
  process, 11–12, 28–33, 325
  rate of bioresorbable polymers, 387
Degree of crystallinity, 327–328
  in polymers, 472
Demineralized bone matrix (DBM), 294–295
Density, 425

Dental materials, 98
Dental tissue engineering, 75
Dexamethasone–glycol chitosan (Dex-GCS), 451
Dextrans, 366
  electrospun nanofiber, 372
Diabetes, 360
Diabetic foot ulcers (DFUs), 360
Differential scanning calorimetry (DSC), 12–13, 114
Diffusion
  controlled-release, 454
  drug molecules, 326
  law, 217–219
    Fick's first law, 217–218
    Fick's second law, 218–219
  layer concept, 220
  rate, 218
Diffusional Deborah number, 235–236
Diffusional mechanisms, 238
Dimethyl sulfone ($DMSO_2$), 77
Dip-coating process, 54
Direct condensation polymerization, 87
Direct current (DC) electrospinning technique, 204–205
Dissimilarity factors, 241–242
Dissipative particle dynamics (DPD), 173
Dissolution controlled release, 453
Dissolvable sensors, 471, 476
Divinyl sulfone, 154–155
D-mannuronate (M), 448–449
Docetaxel nanoparticles (NPs), 230–231
Double bridging (DB), 172
Double emulsion process, 343
Droplet bioprinting, 161
Drug, 443–444
  molecules, 327–328, 452
  release, 150–151, 455
    factors affecting drug release from polymers, 216–217
    fundamentals, 219–221
    kinetics, 457
    mechanisms, 150–151
    patterns, 219
Drug delivery, 183, 387, 392, 444–445
  application, 71–72
    biodegradable polymers, 451–452
    controlled drug-delivery release, 451–452
    mucoadhesive drug release, 451
  capacity of halloysite nanotube (HNT)–polymer blends, 397–400, 401t–404t
  carrier, 67
  devices application, 268–270
    absorbable implant coating application in orthopedics, 269
    novel bioabsorbable drug-eluting scaffold, 269–270
  methods, 213
Drug-delivery systems (DDSs), 96–97, 176–177, 221, 229, 299, 300t, 397, 446–447, 455
  bioresorbable polymers, 326–330
Drug-eluting stent (DES), 269–270
Dual-response triblock copolymers, 177
Dual-responsive polymers, 188

E

Electrical currents, 183
Electron
  donor groups, 152–153
  electro-responsive polymers, 188
  mass, 431–432
Electron spray injection mass spectroscopy (ESI–MS), 13
Electrospinning, 116, 126–128, 131–132, 332–333, 337–338, 387, 478
  electrospun nanofiber membranes application in medical protective equipment, 205–209
  fundamentals, 198–205
    environmental parameters, 203–204
    principles of, 199–200
  improvement and development, 204–205
  parameters effects, 200–204
    processing parameters, 202–203
    solution parameters, 200–202
  technique, 295, 372, 197–198
Electro-spraying process, 76–77
Electrospun nanofiber(s), 198–198

membranes application in medical protective equipment, 205–209
filtration membranes for biomedical applications and wearables, 208–209
in-vitro three-dimension (3D) cancer models, 207–208
medical device and implant coating, 206–207
networks, 208–208
Electrospun polycaprolactone (PCL) /gel scaffold, 132
Electrospun poly-4-hydroxybutyrate (P4HB), 131–132
Electrospun scaffolds, 132
Emulsions, 343–344
Endocytosis process, 11–12
Energy irradiations, 156–157
Engineered natural substances, 363–364
Engineered tissue products, 363
Environment, 28
Environmental remediation, 392
Environmental scanning electron microscope (ESEM), 12
Enzymes, 370–371
cross-linking, 157
Epoxidized palm oil (EPO), 91
Epoxidized soybean oil (ESO), 91
Erosion, 326
controlled release, 455–457
Erythromycin (ERY), 395–397
Escherichia coli, 395–397, 408–409
analysis of Mueller–Hinton broth against, 400f
disk diffusion-based examination of, 398f
European Medicines Agency (EMA), 277
Explanatory data analysis approach, 222
Extracellular matrix (ECM), 33–34, 138–139, 207–207
Extrusion, 126, 129, 161–162

F

Fabricated scaffolds, 127
Fabrication technique, 44, 51, 284–291
biomaterials, 36–37
bioresorbable polymer-based sensors, 476–481
coating and layering techniques, 480–481
electrospinning, 478
photolithography, 479–480
solvent casting, 477–478
three-dimensional (3D) printing, 478–479
Femtosecond laser direct writing (FsLDW), 484–485
Fiber-reinforced materials, 34–36
Fibrin, 271
Fick's first law of diffusion, 217–218
Fick's second law, 220
diffusion, 218–219
outcomes, 219
Fickian process, 235–236
Fickian type drug transport mechanisms, 234
Field emission scanning electron microscopy (FE-SEM), 75, 406–408
Filtration membranes for biomedical applications and wearables, 208–209
First-order model, 228–229
polynomial equation, 239–240
Flow curves, 165
Fluoride substituted-hydroxyapatite (FHA), 75
Food and Drug Administration (FDA), 241–242
approved polylactic-co-glycolic acid (PLGA), 277
Forcespinning, 116
4D printing, 101, 126
Fracture electrostimulation device (FED), 41
Freeze casting, 157–159
Freeze-drying, 332–336
5-FU liposomes, 230–231
Fused deposition modeling (FDM), 49, 55, 90–91, 478–479

G

GalaFLEX-AlloDerm reconstruction, 267
Gamma radiation, 433–434
Gas foaming process, 130–131, 332–333, 336
Gelatin, 268, 369, 447
  nanofibers (NF), 73
Gelatin-methacryloyl (GelMA), 56, 147–148
Genipin (GP), 154
Glass, 4
  materials, 436
  samples, 422
  transition temperature, 472
α-Glucans, 365
β-Glucans, 365–366
Glucocorticoid steroids, 360–361
Glutaraldehyde (GA), 157–159
Glycemic level monitoring, 473–476
Glycine amino acid, 484
Glycolic acid (GA), 325
Glycolipids, 368
Glycosaminoglycans (GAGs), 24–28
Gold nanoparticles (AuNPs), 373
Gompertz model, 238–239
Grafted chains on surface, 185
Grafting of bone, 76–77
Graphene oxide (GO), 71–72, 152–153, 159, 487
Graphite nanoplatelets (GNP), 51–52
Guided bone regeneration (GBR), 45

H

Halloysite nanotube (HNT), 385–386, 391–392, 408–409
  antibacterial activity, 395–397
  applications, 392
    biomedical, 413–414
  bioresorbable polymer-based, 393–394
  challenges and limitations, 412–413
  drug-delivery capacity, 397–400
  properties, 391–392
    reinforced polymer blends mechanical, 394–395
  wound dressings based on, 405–412
Healing compounds, 72–73
Healthcare surveillance, 481–482
Heart disease, 55
Heparin, 206–207
Heteroglycans, 367–368
Hexamethylene diisocyanate (HMDI), 336–337
1,6-Hexamethylene diisocyanate, 154–155
1,6-Hexane dibromide, 154–155
High aspect ratio, 391
High-energy irradiation crosslinking technique, 156–157
High-intensity, 156–157
High-modulus composite scaffold, 127
Higuchi's model, 229–231
Hixson and Crowell's cube root law, 231–232
Hopfenburg model, 236–237
Hot pressing method, 14
Human dental pulp stem cells (hDPSCs), 75
Human mesenchymal stem cells (hMSCs), 94–95
Hyaluronan bioresorbable composite, 57
Hyaluronic acid methacrylate (HAMA), 147–148
Hyaluronic acid-modified hydrogels, 34–36
Hybrid polymers, 390
Hybrid techniques, 134
Hydrazides, 8
Hydrochloric acid-activated halloysite nanotube (HNT-HCL), 412
Hydrogel(s), 147–148, 164, 338–339, 376, 475–476
  applications, 340t
  cross-linking, 148–157
  drying method, 159
  fabrication techniques, 157–165
    mold casting, 157–159
    nanoparticle-templated nanogel fabrication, 159–161
    physically and chemically cross-linked hydrogels, 158t
    prilling or laminar jet break-up, 159
    rheological toolbox, 164–165
    three-dimensional printing (3DP), 161–164
  networks, 147–148
  preparation methods, 339

chemical cross-linking, 341t
physical cross-linking, 342t
Hydrogen bonding (H-bonding), cross-linking by, 152–153
Hydrolysis, 386–387
Hydrophilic compounds, 343
Hydrophilic polymers, 471–472
Hydrophilic synthetic polymer, 371
Hydrophilicity, 328–329
Hydrophobic polymers, 471–472
Hydrophobicity/hydrophilicity, 328–329
Hydroxyapatite (HA), 55, 74–75, 112–113, 117, 133
Hydroxyapatite poly-L-lactide (HPLLA), 265
3-Hydroxybutyrate (3-HB), 119
3-Hydroxyhexanoate (3-HHx), 119
Hydroxyl (OH) groups, 152–155
Hydroxyl propyl methyl cellulose (HPMC), 216–217
3-Hydroxyvalerate (3-HV), 119
Hypoxia-inducible factor-1 (HIF-1), 360–361

I

Ibuprofen (IBP), 127
Illicium verum polymeric nanoparticles, 215
Immuno-fluorescence (IF), 408–409
Implantable medical devices, 74–77
Implantable sensors, 475
Implants, 389
application for temporary fixation, 264–268
In situ polymerization, 14–15
In vitro methods of bioresorbability evaluation, 12–13
biological methods, 13
physico-chemical methods, 12–13
In-vitro three-dimension (3D) cancer models, 207–208
Inductively coupled plasma mass spectrometry (ICP-MS), 485
Inductively coupled plasma optical emission spectrometry (ICP-OES), 485
Inferior vena cava (IVC), 136–137
Inflammation, 355, 357–358
Initiator, 65
Injection molding, 126–128, 387
Inorganic nanoparticles, 304
based composites, 304–312
Inorganic polymers, 390
Inorganic salts, 200–201
Integrated biomedical devices, 47
Integrated stretchable gold-doped graphene microneedles, 57
Interdigitated dressing electrodes, 41
Interleukin-6 (IL-6), 408–409
Intramolecular double rebridging (IDR), 172
Intraocular pressure (IOP) measurement, 475–476
Iodixanol, 54–55
Isopropyl groups, 187

K

Kappa carrageenan (KC), 367–368
Kef-based hybrid scaffolds, 94
Keratin, 370
Korea Advanced Institute of Science and Technology (KAIST), 208–209
Korsmeyer–Peppas model, 233–235

L

L-guluronate (G), 448–449
L-lactide/trimethylene carbonate copolymer (PLLA-TMC), 134
L-lysine-coated magnetite (Lys@Fe_3O_4), 70
Laboratory-scale tools, 204–204
Lactic acid (LA), 9, 325, 447–448
monomers, 87
Lactide, 86
Lactide-ethanol ester-1myr3-trimethylene carbonate (LA-GA-TMC), 260
Laminar jet break-up, 159
Laminate stacking process, 14–15
Laponite, 487
Large-amplitude oscillatory shear flow (LAOS), 164–165
Laser cutting technology, 43

Layering techniques, 480–481
Lead chloride, 219–220
Levonorgestrel (LNG) -loaded microspheres, 228
Ligament tissue engineering application, 271
Linear models, polynomial equation for, 239–240
Lipid nanoparticles, 373–374
Lipophilic planar matrix system, 229–230
Liquid photosensitive resin, 50
Lithography, 41–43, 126, 134
Lower critical solution temperature (LCST), 184, 187
Lyophilization, 333–336
Lysostaphin, 370–371

M

Macro-molecular modeling methodologies, 171
Magnesium (Mg), 137–138, 151, 483–484
  based polylactic acid bioresorbable membranes, 14
  iodine encapsulated with polyanhydride composites, 48
Magnetic nanoparticles (MNPs), 117, 304
Magnetic resonance imaging (MRI), 117–119
Magnetite nanoparticles, 117–119
Mannan-coated gelatin nanoparticles, 447
Manufacturing technology, 260–261
Mathematical models, need for and objectives of, 221
Matrix composition, 11
Matrix-derived factor-1 α (SDF-1 α), 261–262
Maxillofacial surgery, 263
Maximum safe concentration (MSC), 452–453
Mechanical properties of bioresorbable polymers, 387
Mechanical strength, 76–77
Medical applications, 87–88, 92, 107, 109, 116
  biodegradable sensing devices, 473–476
  bioresorbable polymer-based sensors
    fabrication techniques, 476–481
    pertinent physiochemical attributes for medical utilization, 470–473
  chemical sensors, 486–487
  physical sensors, 481–486
Medical devices, 55–56
  bioresorbable polymers, 330, 331t
Medical field, 23–24, 28
Medical interventions, performance of bioresorbable materials in, 33–37
Medical protective equipment, application of electrospun nanofiber membranes in, 205–209
Medical sector
  poly(lactic acid) (PLA)/poly-L-lactide (PLLA) composites applications, 92–98
  polycaprolactone (PCL)
    applications in different, 68–77
    based composites advantages, 67
    challenges and future of, 77
Medical technology, 471–472
Medical utilization, biodegradable polymers and pertinent physiochemical attributes for, 470–473
Medications, 360–361
  delivery, 472–473
Melt compounding, 91
Melt extrusion, 129
Melt processing methods, 91
Membranes, 200–201
Meshes developments, 98
Meso scale (MS) modeling method, 171, 186–187
Metal oxides, 137–138
Metallic nanoparticles, 373
Metallic stents, 95–96
Metals, 332, 363–364
  based NPs, 373
  nanoparticles, 373
Methacrylates, 8
Methacrylic acid, 371
Methotrexate (MTX), 229

Metropolis Monte Carlo (MC), 173
Michael addition, 155
Microcontact printing, 134
Microelectromechanical systems-based implants, 4–5
Microhardness (H) grades, 425
Micro-molding, 55–57
Microneedles (MNs), 55–56
Microparticles (MP), 284, 341–346
Microspheres, 444–445
Minimum effective concentration (MEC), 452–453
Minitab (software), 239
Model–dependent approach, 223–239
  Baker and Lonsdale model, 235
  Brazel and Peppas model, 235–236
  first-order model, 228–229
  Gompertz model, 238–239
  Higuchi's model, 229–231
  Hixson and Crowell's cube root law, 231–232
  Hopfenburg model, 236–237
  kinetic release models, 224t–227t
  Korsmeyer–Peppas model, 233–235
  Peppas–Sahlin model, 238
  Weibull model, 237–238
  zero-order model, 223–228
Model–independent approach, 241–242
Modified Higuchi's model, 235
Mold casting, 157–159
Molding process, 127–128
Molecular dynamics (MD), 171, 174–175
Molecular mechanics (MM), 171
Molecular modeling, 169
  polymers
    molecular simulation methods for designing polymers, 171–175
    polymer-based smart nanocarriers applications, 175–188
Molecular simulation for designing polymers methods, 171–175
  molecular dynamics, 174–175
  Monte Carlo (MC)
    computer software, 173
    simulation with, 172
Molecular weight, 11, 329–330
Molybdenum (Mo), 46
Molybdenum disulfide (MoS_2) bioresorbable sensor, 48
Monte Carlo (MC), 171
  computer software, 173
  moves, 172
  simulation with, 172
Mott theory, 433
Mucoadhesive drug release, 451
Multifunctional poly(lactic acid) (PLA) polymers, 101
Multifunctional polymeric nanocarriers, 177
Multiple scale simulations of sensitive polymers, 186–188
  polymers
    with pH response in simulations, 186–188
    with photo-response in simulations, 187–188
    with temperature response in simulations, 187
  simulations of responsive polymers, 188
Multivariate analysis of variance (MANOVA), 223, 242
Multivariate approach, 223
Multiwalled carbon nanotubes (MWCNTs), 114

N

N,N -ethylenebis (stearamide), 393–394
Nano-bioactive glass, 137–138
Nanocarriers, 450–451
Nanocomposites for wound healing, 372–377
  nonpolymeric nanoparticles, 372–374
  polymeric nanoparticles, 374–376
Nano-drug-delivery systems (NDDSs), 213
Nanofibers (NFs), 295, 376–377, 198–198, 198–198, 203–204, 206–207
Nano-glycosaminoglycan, 368
Nano-hydroxyapatite (n-HA), 94
Nanomaterials (NMs), 372
Nanomedicine, 444–445

Nanometer-sized hydrogels or nanogels, 159–161
Nano/microparticles, 57–58
Nanoparticles (NP), 67, 284, 341–346, 372, 449–450
  Ag-chitosan/polycaprolactone (PCL) composite, 71–72
  nanoparticle-templated nanogel fabrication, 159–161
Nanoprecipitation, 344
Nanostructured lipid carriers (NLCs), 373
Nanotechnology, 101
National Institutes of Health (NIH), 386
Natural bioabsorbable polymers, 214, 260–262, 271
Natural bioresorbable materials, 5–8
  alginates, 6–7
  cellulose, 7–8
  chitin and chitosan, 5–6
Natural fibers, 24–28
Natural polymeric nanoparticles, 375–376
Natural polymers, 24–28, 116, 268, 364–365, 389, 443
Natural substances, 363–364
Needle-free technology, 204–205
Negative temperature coefficient (NTC), 484–485
Neodymium ions, 436–439
Neoproteoglycans, 368
Neural stem cells (NSCs), 295
Neural tissue engineering, 14
Neurosurgery, application in, 266–267
Nonconventional techniques, 134
Non-Fickian type drug transport mechanisms, 234
Nonlinear regression models, 240–241
Nonpolymeric nanoparticles, 372–374. *See also* Polymeric nanoparticles
  ceramic nanoparticles, 374
  lipid nanoparticles, 373–374
  metal and metallic nanoparticles, 373
Nonsteroidal antiinflammatory drugs (NSAIDs), 361
Norfoxacin (NOR), 98
Novel bioabsorbable drug-eluting scaffold, 269–270
Nucleophilic addition reaction (nGTMH), 95
Nutrition, 362

O

Oil-in-water (O/W) emulsion, 149–150
One-pot process, 336–337
Ophthalmic pressure assessment, 473–476
Oral diseases, 75
Oregano essential oil (OEO), 72
Organic solvent, 477–478
Organism degradation, 10
Orthopedics
  application, 264–266
  implants, 96–97
    absorbable implant coating application, 269
Osmotic pumping release, 455
Oxygenation, 356–357

P

Particle leaching, 129–130
Particulate structures, 57–58
Peppas–Sahlin model, 238
Peptides, 368–371
Pertinent physiochemical attributes for medical utilization, 470–473
Phosphate buffer solution (PBS), 16–17, 482–483
Phosphate glass fibers (PGFs), 93, 421–422, 425–428
Phosphazenes, 450–451
Phosphoester, 450–451
Phosphorus-based polymers, 450–451
Photo-response in simulations, polymers with, 187–188
Photo-responsive polymers, 187–188
Photoinitiators, 155–156
Photolithography, 479–480
Photoluminescence spectra of $Al_xCa_{y-x}Nd_{01}P_{70}$, 435f
Photopolymerization, cross-linking by, 155–156
pH-responsive polymers, 186

Physical cross-linkers, 149–153. *See* Chemical cross-linking
cross-linking
charge interactions, 151
crystallization, 152
hydrogen bonding (H-bonding), 152–153
stereocomplexation, 149–151
Physical sensors, 481–486
Physically cross-linked hydrogels, 149
Physico-chemical methods, 12–13
Plastic surgery, application in, 267–268
Pluronic F127, 161–162
Poly(acrylamide) (PAM), 147–148
Polyacrylic acid (PAA), 147–148, 156–157, 186
Poly(α-esters), 63, 215
Polyamides, 449–450
Polyanhydride (PA), 46, 85, 215
Polycaprolactone (PCL), 10, 47, 54, 63, 74–75, 85, 115, 131–132, 138, 261–262, 267–268, 371, 375, 390, 395–397, 475–476, 481–482
advantages in medical sector, 67
biological functionality, 67
drug-delivery carrier, 67
mechanical properties, 67
based composites, 67
biopolymer composites, 63–64
challenges and future in medical sector, 77
development and synthesis of, 64–66
polycondensation, 64–65
ring-opening polymerization, 65–66
different medical sectors applications, 68–77
application fields of copolymers and, 68f
drug-delivery application, 71–72
implantable medical devices, 74–77
tissue engineering, 68–70
wound healing/dressing, 72–74
ibuprofen (IBP), 127
oregano oil/gelatin scaffolds, 72
PCL-sulfated chitosan, 53
polymers, 71
Polycondensation, 64–65
reaction for polycaprolactone (PCL) synthesis, 65f
Polydimethylsiloxane (PDMS), 395–397, 399t
Polydioxanone (PDS), 215
Poly(D-lactide) (PDLLA), 149–150, 269
Polydopamine (PDA), 54
Polyelectrolyte composite nanoparticles (PCNs), 261–262
Polyesters, 450
Poly(ester anhydride) polymeric nanoparticles, 215
Polyethylene (PE), 28–33, 173
Polyethylene glycol (PEG), 9, 71–73, 114, 134, 147–148, 156–157, 371, 395
Poly(ethylene glycol-*b*-caprolactone-*b*-ethylene glycol) (PECL), 155
Poly(ethylene glycol)diacrylate (PEGDA), 56
Poly(ethylene oxide) (PEO), 131–132, 338
Poly(ethyleneterephthalate) (PET), 88–90
Poly(glutamic acid)(PGA), 85
Poly(glycerol adipate), 450
Poly glycerol secabate (PGS), 47, 85, 482–483
Polyglycolic acid (PGA), 131–132, 215, 268, 277, 325, 385, 474–475
Polyglycolide. *See* Polyglycolic acid (PGA)
Poly(glycolide-co-ϵ-caprolactone) (PGCL), 68
Polyhydroxyalkanoates (PHAs), 107–112
Poly-3-hydroxybutyrate (P(3HB)), 134, 451–452
Poly(4-hydroxybutyrate) (P4HB), 268
Polyhydroxybutyrate (PHB), 108–114, 449
Poly(hydroxybutyrate-co-hydroxyvalerate) (PHBV), 115–120
based nanofibrous materials, 117
compounds, 119
PLA multifilament fibers, 119

Polyhydroxybutyrate-polyhydroxyvalerate (PHB-PHV), 47
Poly(3-hydroxybutyric acid-co-3-hydroxyvaleric acid), 115
Poly-3-hydroxybutyrate-co-poly-3-hydroxyvalerate (PHBV), 109
Poly[(hydroxymethyl glycolide)-co-(ecaprolactone)] (pHMGCL), 131–132
Poly(2-hydroxyethyl methacrylate) (PHEMA), 184–185, 408
Polylactic acid (PLA), 9, 24–28, 46–47, 55, 97–98, 131–132, 268, 325, 371, 385, 472–475, 482–483
  applications in medical sector, 92–98
    drug-delivery systems and orthopedic implants, 96–97
    scaffolds for tissue reengineering, 93–95
    stent development, 95–96
    surgical tools/meshes developments and dental materials, 98, 99t–100t
  based composites, 86f, 96–98
  based hybrid scaffolds, 94
  based polylactic-co-glycolic acid nanocomposites, 277
  bioactive glass-based composite scaffolds, 16
  biocompatibility and biodegradability, 92
  chemical structure and synthesis, 87
  fabrication methods, 90–91
    additive manufacturing, 90–91
    melt compounding, 91
    solvent-based methods, 91
  future perspectives, 101
  monomer, 277
  multifilament fibers, 119
  physical and thermal characteristics, 88–90
Poly(lactic-co-ϵ-caprolactone) (PLCL), 55, 68, 206–207
Polylactic–co–glycolic acid (PLGA), 46, 55, 97, 215, 268, 277, 328–329, 450, 485
  carbon nanotubes (CNT) scaffolds, 312
  copolymer, 279
  future prospects, 312–313
  hydroxyapatite (HA) composite, 133
  microparticles/nanoparticles (MP/NP), 284
  nanocomposite
    applications, 293–312
    carriers, 284–291, 290t
    composites applications with core–plasmonic nanoparticles, 304
    drug-delivery system, 299
    factors influencing degradation of, 291
    and implant preparation techniques, 285t–289t
    inorganic-NP-based composites applications, 304–312
    nano/magnetic nanocomposites applications, 304
    synthetic bone substitute and repair, 293–295
    therapy and theranostic agents, 299
    tissue engineering, 295–299
  nanocomposites, 277
  polymer solution, 43
  properties, 280–284
    copolymers, 280–284
    physiochemical and biological properties, 281t–282t
Poly(L-lactide), 149–150
Poly-L-lactide acid (PLLA), 85, 149–150, 265, 371, 481–482
  applications in medical sector, 92–98
  biocompatibility and biodegradability of, 92
  chemical structure and synthesis, 87
  fabrication methods, 90–91
    additive manufacturing, 90–91
    melt compounding, 91
    solvent-based methods, 91
  physical and thermal characteristics, 88–90
Poly(lactide-co-glycolide) (PLCG), 329–330
Poly(p-dioxanone) (PPDO), 52
Poly(-propylene carbonate) (PPC), 114, 336
Polymeric biomaterials, 109

Polymeric materials, 184–185
Polymeric nanoparticles (PNs), 215, 374–376. *See also* Nonpolymeric nanoparticles
  hydrogels, 376
  nanofibers (NFs), 376–377
  natural, 375–376
  synthetic, 375
Polymeric scaffolds, 332
Polymerization, 65–66
Polymers, 4, 24–33, 126, 353, 364, 395, 443, 449–450, 455–457, 472
  based scaffolds, 332–333
  based smart nanocarriers applications, 175–188
    multiple scale simulations of sensitive polymers, 186–188
    smart polymer revolution, 180–185
  degradation, 10–11
  factors affecting drug release from, 216–217
  glycosaminoglycan complexes, 368
  matrix, 395
  methods for molecular simulation for designing, 171–175
  nanocomposites, 277–278
  particles, 175
  with pH response in simulations, 186–188
  with photo-response in simulations, 187–188
  polymer cross-linking, 155
  simulations, 169–170
  solution concentration, 200–201
  with temperature response in simulations, 187
Poly(methacrylic acid) (PMAA), 371
Polymethyl methacrylate (PMMA), 205–206
Poly(N-isopropylacrylamide) (PNIPAAM), 162–163, 187
Polynomial equation for linear, first-order, and quadratic models, 239–240
Poly(N-vinyl-2-pyrrolidone), 367–368
Poly(octamethylene maleate (anhydride) citrate) (POMac), 47
Polyphosphazenes, 450–451
Polypropylene (PP), 28–33, 112
Polysaccharides, 24–28, 365–368, 448–449
  based hydrogel microparticles, 159
  heteroglycans, 367–368
  homoglycans, 365–367
Polystyrene (PS), 112, 173
Polytetrafluoroethylene (PTFE), 28–33
Poly(trimethylene carbonate) (PLLA-PTMC), 46–47, 215
Polyurethane (PU), 85, 215, 333, 375
Polyvinyl alcohol (PVA), 8, 57, 147–148, 156–157, 326, 371
Polyvinyl chloride (PVC), 173
Polyvinylpyrrolidone (PVP), 57, 77, 371
Porogen leaching, 94–95
Positive temperature coefficient (PTC), 484–485
Post-processing, 51
Potassium chloride, 367–368
Pretreated polylactic acid (P-PLA), 94
Prilling process, 159
Processing techniques
  bioresorbable-based composites
    micro-molding, 55–57
    particulate structures, 57–58
    three-dimensional (3D) structure, 48–55
    two-dimensional (2D) structure, 41–48
  bioresorbable polymers, 387
  parameters, 127–128
Prodigiosin (PG), 119
Profilometry, 13
Proliferation, 355
Properties of bioresorbable materials for biomedical application, 28–33
Proteins, 24–28, 368–371
  based polymers, 390
  glycosaminoglycan, 368
Proteoglycans, 368
Proton nuclear magnetic resonance (^{1}H NMR), 13
Pseudomonas, 6–7
  P. huttiensis, 108–109
  P. putida, 108–109

Q

Quadratic models, polynomial equation for, 239–240
Quantum ATK polymer simulator software, 175
Quantum mechanics (QM), 171
Quercetin (Q), 71–72

R

Radiopaque bioresorbable stents, 54–55
Reaction ion etching (RIE) process, 44–45
Reepithelialization, 355
Regenerated silk fibroin (RSF), 412
Regenerative medicine, 34–36
Regenerative silk (RS), 51–52
RegJoint insertiz (RJ), 265
Regression model analysis, 239–240
  polynomial equation for linear, first-order, and quadratic models, 239–240
Reinforcement material, 392
Relaxational mechanisms, 238
Release kinetic model, 222–242, 457
  model-dependent approach, 223–239
  model-independent approach, 241–242
  nonlinear regression models, 240–241
  regression model analysis, 239–240
  statistical approach, 222–223
Remodeling, 355–356
Resins, 180
Resorption process, 11–12
Responsive polymers, simulations of, 188
Rheological models, 88–90
Rheological toolbox, 164–165
Rifampicin, 449
Ring-like inculcated device, 75
Ring opening polymerization (ROP), 10, 63, 65–66, 86

S

Salt
  leaching, 129–130
  responsive polymers, 188
Salting out, 344
Scaffolds, 125–126, 138, 261–262, 332–338
  based strategies, 34–36
  fabrication, 138–139
    advantages and limitations, 334t–335t
  tissue reengineering, 93–95
Scanning electron microscopy (SEM), 13, 406–408, 410f
Scanning probe microscopy, 13
Segmented poly(ester-urethanes) (SPEU) -glass ceramic scaffolds, 52
Selective laser sintering (SLS), 49, 54, 90–91
Self-reinforced poly-L, D-lactide copolymer (SR-PLA 96), 96
Semisolid lipid nanoparticles (SLNs), 228
Sensitive polymers, multiple scale simulations of, 186–188
Sensors, 473–474
Sericin–silver nanoparticles (Ser-Ag), 408–409
Sex hormones in aged individuals, 358
Shape-memory polymers (SMPs), 97
Silicon nanomembrane, 47
Silicon nitride monolayer (Si-NM), 485–486
Silk fibroin (SF), 48, 337, 370
Silk of spider egg sacs (SESS), 487
Silver nanoparticles (AgNPs), 373
Silver (Ag) particles, 205–206
Similarity factors, 241–242
Simple Monte Carlo moves, 172
Simulated body fluid (SBF), 435–436
Simulated nasal electrolyte solution (SNES), 234–235
Simulation(s)
  with Monte Carlo (MC), 172
  polymers with
    pH response, 186–188
    temperature response, 187
  of responsive polymers, 188
Single-chain Metropolis Monte Carlo (MC) simulations, 173
Single emulsion method, 343
Single-mode fiber (SMF), 487
Size-exclusion chromatography (SEC), 12

Skin tissues, 355
Smart brushes. *See* Chain-absorbed conformation
Smart polymers (SPs), 170, 180
  categorization based on structural conformation, 184–185
  classification, 184–185
  revolution, 180–185
Smart scaffolds, 139
Smart stimuli-responsive nano DDSs, 178–180
Smart surfaces. *See* Chain-absorbed conformation
Smart transportation methods, 170
Smoking, 362
Sodium alginate (SA), 268, 337
  polyvinyl alcohol (PVA) –polyvinylpyrrolidone (PVP) bioresorbable composite, 57
Sodium hyaluronic acid–sodium alginate –gelatin composite, 57
Solid lipid nanoparticles (SLNs), 373
Solution blending, 149–150
Solvent-based methods, 91
Solvent casting method, 48, 113, 129–130, 387, 477–478
Solvent casting/particulate leaching (SCPL), 332–333
Solvent-free nanofibers, 129
Sorting of "smart" polymers based on activating stimuli, 185
Sphingopyxis terrae, 108–109
Spray drying, 344
Staphylococcus aureus, 68–70, 366, 395–397, 408–409
  analysis of Mueller–Hinton broth against, 400f
  disk diffusion-based examination of, 398f
Starch-polycaprolactone (SPCL), 74
Statistical approach, 222–223
  explanatory data analysis approach, 222
  multivariate approach, 223
Stents, 95–96, 136–137, 389
Stereocomplex formation, 149–150
Stereocomplexation, 149–151
Stereo-lithography (SLA), 49–50, 90–91, 161, 478–479
Stimuli-responsive nanocarriers (SRNs), 176–177
Stimuli-responsive polymers, 185–186
Stress, 358–359
Styrene-butadiene-styrene (SBS), 97
Sublimation process, 333–336
Supercritical fluid technique, 346
Superparamagnetism, 117–119
Surface-modified magnesium hydroxide nanoparticles (nMH), 95
Surface morphology, 422–423
Surgical sutures, 389
Surgical tools, 98
Suspension arthroplasty (SA), 265
Sustained-release drug-delivery system (SRDDS), 213
Swelling interface number, 235–236
Synthesis
  approaches, 346
  bioresorbable polymers, 126–134
    electrospinning, 131–132
    gas foaming, 130–131
    hybrid techniques, 134
    melt extrusion, 129
    molding, 127–128
    solvent casting and particle leaching, 129–130
    three-dimensional (3D) printing, 132–134
  polycaprolactone (PCL), 64–66
  polylactic acid (PLA) /poly-L-lactide (PLLA) polymers, 87
Synthetic biopolymers, 8
Synthetic bioresorbable polymers, 8–10
  polycaprolactone (PCL), 10
  polyethylene glycol (PEG), 9
  polylactic acid (PLA), 9
  polyvinyl alcohol (PVA), 8
Synthetic bone substitute and repair, 293–295
Synthetic polymeric nanoparticles, 375
Synthetic polymers, 215, 268, 338–339, 371–372, 385–386, 389, 443, 445
Synthetic reinforced polymers, 24–28

T

Taylor cone, 478, 199–200
Temperature response in simulations, polymers with, 187
Temporary fixation
  application
    artificial skin, 268
    implants, 264–268
    neurosurgery, 266–267
    orthopedics, 264–266
    plastic surgery, 267–268
Tendon tissue engineering, application in, 271
Tetracycline hydrochloride (TCH), 412
Theranostic agents, 299, 301t–303t
Therapy, 299, 301t–303t
Thermal stability, 392
Thermally induced phase separation (TIPS), 94–95, 134, 332–333, 337
Thermoluminescence (TL) studies, 429–432
Thermoplastic gelatin (TG), 336
Thickness, 11
Thin film, 41, 46–47
Three-dimension (3D)
  advantages, 51
    fast design and production, 51
    flexible design, 51
    minimizing waste, 51
  biological printing, 260–261
  disadvantages, 51–55
    large volumes, 51–55
    limited materials, 51
    post-processing, 51
  fused deposition modeling (FDM), 49
  models, 207–207
  printed scaffolds, 133
  selective laser sintering (SLS), 49
  stereolithography apparatus (SLA), 49–50
  structure, 48–55
Three-dimensional printing (3DP), 48, 51, 126, 132–134, 161–164, 260, 478–479
Thromboembolic complications, 136
Thymol (Thy), 408
Tissue engineering (TE), 68–70, 116–117, 125–126, 295–299, 296t–298t
  application, 270–271
    bone tissue engineering, 270–271
    ligament/tendon tissue engineering, 271
  bioresorbable polymers, 330–346
    hydrogels, 338–339
    micro-and nanoparticles applications in tissue engineering, 345t
    micro/nanoparticle, 341–346
    scaffolds, 332–338
  polycaprolactone (PCL) composite applications, 69t–70t
  scaffolds
    bioresorbable polymers synthesis, 126–134
    bioresorbable tissue scaffold applications, 135–138
    future trends, 138–139
Tissue reengineering, 387–389
  scaffolds, 93–95
Titanium, 98
Titanium dioxide (TiO_2), 117, 312, 373
Trans-anethole (TA), 77
Trans-linked hydrogels, 184–185
Transmission electron microscopy (TEM), 13
Triboelectric nanogenerator (TENG), 41
Two dimension (2D)
  cancer models, 207–207
  structure, 41–48
    casting method, 47
    configuration and characterization of device, 42f
    insertion protocol of magnesium (Mg) barrier membrane, 45f
    production of parylene-silk probes, 44f
    schematic of fracture electrostimulation device (FED), 43f
Two-photon polymerization, 161

U

Ultraviolet (UV) light, 479
Unconventional methods, 101
Upper critical solution temperature (UCST), 187
Ureidopyrimidinone (UPy), 152–153

V

Vacuum heating-press sintering, 134
Vancomycin, 451–452
Vascular endothelial growth factors, 206–207
Vascular grafts, 136–137
Vegetal proteins, 368–369

W

Wall fractures, 76
Water, 386–387, 470
Wearables, filtration membranes for biomedical applications and, 208–209
Weibull model, 237–238
Weight loss, 13
Whey protein isolate (WPI), 154
Wound-healing process, 72–74, 74t, 355–356
  bioresorbable polymers, 364–372
    properties, 363–364
  factors affecting, 356–362, 356f
  future perspectives, 377–378
  local factors influence, 356–358
    infection and foreign bodies, 357–358
    oxygenation, 356–357
  nanocomposites, 372–377
  systemic factors influence, 358–362
    age, 358
    alcohol consumption, 361
    diabetes, 360
    medications, 360–361
    nutrition, 362
    obesity, 360–361
    sex hormones in aged individuals, 358
    smoking, 362
    stress, 358–359
Wounds, 354
  dressing, 72–74, 74t, 116–117, 389
    based on halloysite nanotube (HNT)–polymer blends, 405–412

X

X-ray diffraction (XRD), 12, 406–408, 423–425, 435–436

Y

Yersinia frederiksenii, 108–109
Young's (Y) modulus, 425
Yttrium oxide (Y_2O_3), 373

Z

Zein, graphene oxide (Z-GO), 487
Zero-order
  model, 223–228
    kinetic, 457
  release approach, 228
Zinc oxide nanoparticles (ZnO NPs), 373

This page intentionally left blank

WOODHEAD PUBLISHING SERIES IN BIOMATERIALS

Bioresorbable Polymers and their Composites provides a holistic view of these unique materials and their application in a range of biomedical applications. This book is evenly divided between fundamentals, processing methods and modeling approaches, and detailed coverage of a variety of applications, such as drug delivery, medical devices, and wound healing.

Key aspects including biocompatibility, biodegradability, and toxicology are also thoroughly covered, enabling the reader to be fully informed when fabricating and utilizing their selected bioresorbable polymer.

This book is an interdisciplinary and important reference for researchers in the fields of materials science, biomedical engineering, pharmaceutical science, and regenerative medicine, as well as R&D groups in the development of medical devices.

Key Features

- Introduces the reader to various processing and modeling techniques for bioresorbable polymers, including electrospinning, molecular, and finite element modeling.
- Covers a range of key bioresorbable composites, such as PCL, PLA/PLLA, and PHA/PHB/PHBV.
- Explores a wide selection of biomedical applications of bioresorbable polymers, from tissue engineering and stents to biosensors and medical devices/implants.

About the Editors

Deepak Verma, Research Assistant, Nano-science and Technology, Graduate School, Chulalongkorn University, Bangkok, Thailand. He also served as an Assistant Professor, Department of Mechanical Engineering, Graphic Era Hill University, Dehradun, India.

Manunya Okhawilai, Researcher, Metallurgy and Materials Science Research Institute (MMRI), Chulalongkorn University, Bangkok, Thailand.

Kheng Lim Goh, Director of Research and Associate Professor (Reader) in Materials Technology, Newcastle University, Singapore.

Seeram Ramakrishna, FREng, Everest Chair is a Professor of Materials Engineering at the National University of Singapore (NUS), Singapore.

Pooria Pasbakhsh, Adjunct Associate Professor at the School of Engineering, Monash University, Malaysia.

Mohit Sharma, Principal Scientist at the Institute of Materials Research and Engineering (IMRE), Agency for Science, Technology and Research (A*STAR), Singapore.

ELSEVIER

WP
WOODHEAD PUBLISHING
An imprint of Elsevier
elsevier.com/books-and-journals

ISBN 978-0-443-18915-9

9 780443 189159

ADVANCES IN BIOTECHNOLOGY and BIOSCIENCE

Volume - 12

Chief Editor

Dr. Harshada Joshi
Associate Professor in Department of Biotechnology, Mohanlal Sukhadia University, Udaipur, Rajasthan, India

AkiNik Publications ®
New Delhi

Published By: AkiNik Publications

AkiNik Publications
169, C-11, Sector - 3,
Rohini, Delhi-110085, India
Toll Free (India) – 18001234070
Phone No.: 9711224068, 9911215212
Website: www.akinik.com
Email: akinikbooks@gmail.com

Chief Editor: Dr. Harshada Joshi

The author/publisher has attempted to trace and acknowledge the materials reproduced in this publication and apologize if permission and acknowledgements to publish in this form have not been given. If any material has not been acknowledged please write and let us know so that we may rectify it.

© AkiNik Publications ™

Publication Year: 2022

Pages: 119

ISBN: 978-93-5570-501-3

Book DOI: https://doi.org/10.22271/ed.book.2009

Price: ₹ 731/-

Registration Details

- Printing Press License No.: F.1 (A-4) press 2016
- Trade Mark Registered Under
  - Class 16 (Regd. No.: 5070429)
  - Class 35 (Regd. No.: 5070426)
  - Class 41 (Regd. No.: 5070427)
  - Class 42 (Regd. No.: 5070428)

Contents

Chapters	Page No.
1. Silkworm Biotechnology *(Priyanka and Poonam Kumari Yadav)*	01-14
2. ESBL Genes Mediated Antimicrobial Resistance: A Mini-Review *(Sonakshi Gehlot)*	15-27
3. Polyphenols: Biosynthesis, Classification and Their Antioxidant Potential *(Jyoti Duhan, Nisha Kumari, Ram Avtar and Bharat Garg)*	29-53
4. MAGIC Population in Crop Improvement *(Abhay Kumar Pandey, Ruchi Singh, Sharad Singh and Atul Kumar Patel)*	55-63
5. An Overview of Bioremediation of Xenobiotics *(Satabdi Saikia)*	65-78
6. Green Synthesis of Iron Nanoparticles and Its Application towards Drug Development *(G. Yazhini S, Rajakumari K, R Thiruchelvi, P Vivek and S Ivo Romauld)*	79-92
7. Pharmacology Properties of *Cissus quadrangularis*: Review *(Mohammed Habibullah, S. Abishek Raj, R. Thiruchelvi, K. Rajakumari, Dr. P. Vivek and Dr. Ivo Romauld)*	93-105
8. A Review on Antimicrobial Activity of Marine Actinomycetes *(Ashwin K., S. Ivo Romauld, Meenambiga Setti Sudharsan, Sakthiselvan P and Satish Mohabe)*	107-119

Chapter - 1
Silkworm Biotechnology

Authors

Priyanka
Sri Karan Narender Agriculture University, Jobner, Jaipur, Rajasthan, India

Poonam Kumari Yadav
Sri Karan Narender Agriculture University, Jobner, Jaipur, Rajasthan, India

Chapter - 1

Silkworm Biotechnology

Priyanka and Poonam Kumari Yadav

Abstract

Silkworms have been used for generations to meet human requirements. The silk produced by the silkworm has a high economic value. Genetic engineering may result in improved silkworm species that produce more silk and are more resistant to illnesses and environmental variations. The silkworm is also a useful model for studying the molecular basis of development and gene expression utilising molecular biology methods.

Keywords: Biology genetic engineering, silkworm

Introduction

Today's biotechnology-based industry faces a bottleneck towards further advancement owing to the lack of proper gene expression systems. Despite the tremendous advancement of bioscience, there are still many proteins whose structures remain unknown. Scientists working in the field of life science needed a technique that could rapidly express protein in huge quantities and purify protein in a biologically active form. Thus said, with the completion of Human Genome Project, we have come across a herculean task of trying to understand the function of the proteins being coded by the genes. Many researchers proved silkworm biotechnology is one of solutions. Furthermore, recent reports showed that the recombinant baculovirus containing mammalian cell-active promoter can exhibit efficient gene transfer of potential vaccines into mammalian cells. This would be a great breakthrough in production of recombinant eukaryotic proteins and viruses, which will be a powerful tool in a new proteome It is a lepidopteran insect. The rearing of silkworm for production of silk is called as sericulture. Silk is secreted by silk gland of the silk worm and it is a fibrous protein of insect origin. Silk is known as the queen of textiles and BIOSTEEL because of its strength. Silk fiber consists of two types protein namely fibroin (75%) and sericin (25%). China ranks first in the production of silk. India is the second largest producer of silk after china. It is also the largest consumer of silk in

ADVANCES IN

BIOTECHNOLOGY

and

BIOSCIENCE

Volume - 13

Chief Editor

Dr. Harshada Joshi

Associate Professor in Department of Biotechnology, Mohanlal Sukhadia University, Udaipur, Rajasthan, India

AkiNik Publications ®

New Delhi

Published By: AkiNik Publications

AkiNik Publications
169, C-11, Sector - 3,
Rohini, Delhi-110085, India
Toll Free (India) – 18001234070
Phone No.: 9711224068, 9911215212
Website: www.akinik.com
Email: akinikbooks@gmail.com

Chief Editor: Dr. Harshada Joshi

The author/publisher has attempted to trace and acknowledge the materials reproduced in this publication and apologize if permission and acknowledgements to publish in this form have not been given. If any material has not been acknowledged please write and let us know so that we may rectify it.

The responsibility for facts stated, opinion expressed or conclusions reached and plagiarism, if any, in this book is entirely that of the author. So, the views and research findings provided in this publication are those of the author/s only. The Editor & Publishers are in no way responsible for its contents.

© AkiNik Publications ™

Publication Year: 2023

Pages: 165

ISBN: 978-93-5570-664-5

Book DOI: https://doi.org/10.22271/ed.book.2187

Price: ` 775/-

Registration Details

- Printing Press License No.: F.1 (A-4) press 2016
- Trade Mark Registered Under
  - Class 16 (Regd. No.: 5070429)
  - Class 35 (Regd. No.: 5070426)
  - Class 41 (Regd. No.: 5070427)
  - Class 42 (Regd. No.: 5070428)

Contents

Chapters	Page No.
1. Salinity Tolerance Mechanism and Responses of Plants *(Hidayah Faisal H. and Adajani Alotaibi)*	01-19
2. Advances in Breeding Strategies: Sesame (*Sesamum indicum* L.) *(Sruba Saha, Ranjana Chattopadhyay and Sushil Kumar Kothari)*	21-41
3. Bacterial Leaf Blight Disease, One of the Deadliest Disease of Rice Caused by *Xanthomonas oryzae* *(Ariba Khan and Tamil Selvan C)*	43-54
4. Tumor Cell Cycle Progression for a Potent Anticancer Plant *(Dr. Arun Kumar G)*	55-72
5. Fractional Analysis of Ethanol Extract of *Santalum album* in Search for a Potent Anticancer Agent *(Dr. Arun Kumar G)*	73-84
6. Recent Technology in Nano-fluids and Nanotechnology using in Biomedical Engineering *(Dr. A. Kalaiyarasan and K. Sankar)*	85-115
7. Role of Natural Nutraceuticals in Management of Oxidative Stress Related Diseases *(Pranabesh Ghosh, Abhishek Konar, Sirshendu Chatterjee, Abhishek Roy, Dip Das Dalal and Sanchali Mukherjee)*	117-145
8. A Practical Approach to Genome and Genomics using Bioinformatics *(Saroj Rani, Deepshikha Kaushik and Aanchal Gupta)*	147-165

Chapter - 1
Salinity Tolerance Mechanism and Responses of Plants

Authors

Hidayah Faisal H.
Ph.D., Life Science, Warwick University, Coventry, England

Adajani Alotaibi
Lecturer, College of Science, Princess Nourah Bint Abdulrahman University, Riyadh, Saudi Arabia

Chapter - 1

Salinity Tolerance Mechanism and Responses of Plants

Hidayah Faisal H. and Adajani Alotaibi

Abstract

Salt stress is a significant issue that impacts agriculture worldwide. Salinity negatively affects several physiological processes, and causes alterations on growth, development, and reproduction. To cope with such stressful conditions, plants have developed effective strategies to response to stressful conditions in fast and efficient manne. This chapter reviews our current understanding of salt stress impacts on plants. Recent research on salt mechanisms to tolerate a high salt level, including hormone regulation and metabolism modifications, has been summarized. The involvement of transcriptional and post-transcriptional gene regulation in plants' responses toward salinity has been briefly discussed. This knowledge will improve our understanding of salt stress in plants and how plants respond and alter their expression to develop salt-tolerant plants using bioengineering approaches. Finally, we highlighted some aspects that should be clarified in future research to understand salt tolerance well.

Keywords: salt stress, transcription factor, DREB2A, salt tolerance, epigenetic modification, hormone, DNA methylation, histone modification, metabolic modification, hormone regulation

Introduction

XXXXXXXXXXXXXXXXXXXXXXXXXXXXXXXXXXXXXXXXXXXXXX

1. Salinity: A Global and Cellular stress factor

The agricultural world faces serious challenges to enhance food production by 70 percent by 2050 to meet the global rising population's demands [1]. However, expanding the stress factor in the environment limits the growth of agricultural areas. According to the Food and Agriculture Organization of the United Nations, 800 million hectares are under hyperosmotic stress, representing 7 percent of the land, 20 percent of arable land, and 40 percent of the total irrigated land [1]. As a consequence of poor irrigation or other typical causes of soil salinity, such as fertilizer use [2].

ADVANCES IN

BIOTECHNOLOGY

and

BIOSCIENCE

Volume - 14

Chief Editor

Dr. Harshada Joshi

Associate Professor in Department of Biotechnology, Mohanlal Sukhadia University, Udaipur, Rajasthan, India

AkiNik Publications ®

New Delhi

Published By: AkiNik Publications

AkiNik Publications
169, C-11, Sector - 3,
Rohini, Delhi-110085, India
Toll Free (India) – 18001234070
Phone No.: 9711224068, 9911215212
Website: www.akinik.com
Email: akinikbooks@gmail.com

Chief Editor: Dr. Harshada Joshi

The author/publisher has attempted to trace and acknowledge the materials reproduced in this publication and apologize if permission and acknowledgements to publish in this form have not been given. If any material has not been acknowledged please write and let us know so that we may rectify it.

The responsibility for facts stated, opinion expressed or conclusions reached and plagiarism, if any, in this book is entirely that of the author. So, the views and research findings provided in this publication are those of the author/s only. The Editor & Publishers are in no way responsible for its contents.

© AkiNik Publications ™

Publication Year: 2023

Pages: 179

ISBN: 978-93-5570-714-7

Book DOI: https://doi.org/10.22271/ed.book.2292

Price: ` 789/-

Registration Details

- Printing Press License No.: F.1 (A-4) press 2016
- Trade Mark Registered Under
  - Class 16 (Regd. No.: 5070429)
  - Class 35 (Regd. No.: 5070426)
  - Class 41 (Regd. No.: 5070427)
  - Class 42 (Regd. No.: 5070428)

Contents

Chapters	Page No.
1. microRNA and its Regulation *(Pooja SK and Thota Joseph Raju)*	01-28
2. DNA Repair Mechanism *(Pooja SK and Thota Joseph Raju)*	29-57
3. Plasmid-Origins of Replication, Copy Number Control and Incompatibility Classes *(Gowhar Iqbal, Ad Viral Kumar Ganpatbhai and Lukram Sushil Singh)*	59-70
4. Purification of Recombinant Proteins *(Sumedha S Bobade)*	71-87
5. Discovery and Annotation of Long Non-Coding RNAs (lncRNAs) from Transcriptome Data *(Kishor U. Tribhuvan, Twinkle Mishra, Ankit Raj, Shivakumaraswamy M and Binay K. Singh)*	89-112
6. Cisgenesis: A One-Step Gene Transfer Technique Integrating Modern and Traditional Breeding for Sustainable Agriculture Growth *(Rhitisha Sood, Shailja Sharma and Ajay Chauhan)*	113-147
7. Beta-Galactosidase Overview: Its Properties, Sources and Applications in Biotechnology *(Rasheka Yousaf and Dr. Farheen Aslam)*	149-164
8. Pectinase Classification, its Sources and its Application in Today's Industrial Sector *(Dr. Farheen Aslam, Dr. Faiza Saleem and Sabahat Kulsoom)*	165-179

Chapter - 1
microRNA and its Regulation

Authors

Pooja SK
Assistant Professor, Division of Agricultural Biotechnology, COA, Hassan, UAS, Bangalore, Karnataka, India

Thota Joseph Raju
Assistant Professor, Department of Seed Science and Technology, COA, Hassan, UAS, Bangalore, Karnataka, India

Chapter - 1

microRNA and its Regulation

Pooja SK and Thota Joseph Raju

Abstract

Post-transcriptional gene expression is regulated by 18-22-nucleotide microRNAs (miRs, MiRNAs). MiRNAs regulate gene expression by interacting with the 3′- and occasionally 5′-ends of target gene mRNA. MiRs influence up to 60% of plant/animal protein-coding genes. miRNA regulate most biological processes. MiRNA misexpression changes cellular function, differentiation, apoptosis, and survival signalling, linking miRNA to disease pathophysiology. MiRNAs must be properly managed. Multiple processes in miRNA processing influence miRNA levels. MiRNA is regulated at various levels, including transcriptional (promoter methylation and transcription factors) and post-transcriptional (Drosha and Dicer in the nucleus and cytoplasm). RNA methylation, uridylation, adenylation, and editing affect miRNA stability. Also oestrogen and hypoxia effects. Human malignancies affect miRNA expression by abnormal DNA methylation. DNA hypomethylation upregulates onco-miRs and downregulates tumor-suppressor miRNAs. DNA hypermethylation downregulated tumour suppressor miR-132, which binds to paxillin's 3′-UTR posttranscriptionally in colorectal cancer cells. After 5-Aza-CdR therapy, miR was dramatically upregulated, suggesting that DNA hypermethylation downregulates miR-132 in CRC. Thus, cancer gene therapy now uses DNA methyltransferase inhibitors to restore miR-132 expression. CRC targeted therapy may use miR-132 methylation. Lin28 suppressed tumor-suppressing miR Let-7. Lin28 inhibited pre-miRNA processing via a conserved sequence with the terminal loop region. Lin28 recruits the terminal uridyl transferase TUT4 complex to cytoplasmically uridylate pre-let-7 to inhibit let-7. Uridylation hinders Dicer processing and degrades pre-let-7. Further characterization of regulatory elements of miRNA biosynthesis and function will shed light on the complex gene regulatory network governed by miRNA in various pathological mechanisms and the mutual regulation of DNA methylation and miRNA, providing a molecular basis and biomarkers for therapeutic strategies.

ADVANCED STUDIES IN MULTIDISCIPLINARY RESEARCH

Volume - 1

Chief Editor

Dr. Suprita Jha
Associate Professor, Department of English, Mata Sundri College,
University of Delhi, Delhi, India

Bright Sky
Publications

Published By: Bright Sky Publications

Bright Sky Publications
Office No 3, 1st Floor,
Pocket - H34, SEC-3,
Rohini, Delhi, 110085, India
Phone: +91-9911215212, +91-9999779515
Email: brightskypublications@gmail.com

Chief Editor: Dr. Suprita Jha

The author/publisher has attempted to trace and acknowledge the materials reproduced in this publication and apologize if permission and acknowledgements to publish in this form have not been given. If any material has not been acknowledged please write and let us know so that we may rectify it.

© Bright Sky Publications

Publication Year: 2022

Pages: 115

ISBN: 978-93-92804-13-7

Book DOI: https://doi.org/10.22271/bs.book.31

Price: ₹ 678/-

Contents

Chapters **Page No.**

1. The Stepping Stone to Formal Education: Early Childhood Care and Education in India in the Light of New Education Policy 2020 01-09
   (Bhagyashree Das)
2. Attitude of Headmasters of Government and Private High Schools towards Physical Education 11-26
   (Basavaraj Kumasi and Ravindra Gouda SM)
3. Emotional Dysregulation and Post Covid-19 Recovery: Issues and Explorations 27-37
   (Sunil Kumar, Deepak Malik, Yogita Sharma)*
4. Biotechnology Based Green Energy: A Solution towards Sustainable Development 39-59
   (Kailash Chandra and Harshada Joshi)
5. Complete Soft Graphs 61-70
   (Bobin George and Jinta Jose)
6. An Introduction to The Microalgae, *Spirulina* 71-92
   (Lesny Jacob, Arya P. Mohan and Lizzy Mathew)
7. Review of Nanotechnology Applications in Science and Engineering 93-115
   (Sayantan Ganguly)

Chapter - 4

Biotechnology Based Green Energy: A Solution towards Sustainable Development

Authors

Kailash Chandra
Department of Biotechnology, Vigyan Bhawan, Block B, Mohanlal Sukhadia University, Udaipur, Rajasthan, India

Harshada Joshi
Department of Biotechnology, Vigyan Bhawan, Block B, Mohanlal Sukhadia University, Udaipur, Rajasthan, India

Chapter - 4

Biotechnology Based Green Energy: A Solution towards Sustainable Development

Kailash Chandra and Harshada Joshi

Abstract

The energy resulting from nonrenewable resources such as natural gas, crude oil and coal, has encouraged technological progress and maintained advances in a wide variety of productive sectors. The demand for crude oil and natural gas has increased in the past years, which is responsible for global warming, the production of smog and water pollution. Therefore, high reliance on fossil fuels is observed. This overview can have risk from an energy security point of view owing to the continuous fluctuation in crude oil prices. In this sense, to develop a sustainable economy in the near future there will be a need of research on alternative energy sources. The use of renewable energy, its production and research have added importance in transportation, building and, industrial sectors, in response to grasp sustainable development.

Biotechnology plays a crucial role in biofuel production. It helps in decreasing agronomic inputs, optimizing process characteristics and engineering the plants to produce high yield and hence high energy. It helps in decreasing agronomic inputs, optimizing process characteristics and engineering the plants to produce high yield and hence high energy. Improvements in the synthesis of biofuels could be expected, as progress takes place in the field of biotechnology. The chapter comprises of various sources of green energy and role of biotechnology in exploring the alternative method for production of biofuels.

Keywords: Green energy, biofuel, biodiesel, biogas, bioethanol

1. Introduction

Energy does have an important role in modern life. Demand for energy is increasing exponentially day by day due to the exponential growth of the world population. The world has presently twin crises of fossil fuel depletion and environmental degradation. These problems can be overcome by green

Multifunctional Hypoxia Imaging Nanoparticles



Preeti Sharma, Pooja Kumari, Tikam Chand Dakal, Jyotsana Singh, and Narendra Kumar Sharma

Abstract Hypoxia is a condition in which there is a scarcity of oxygen. It is mainly associated with diseased circumstances, although it can also be a trait of healthy physiology. It is a pathophysiological condition linked to numerous ailments such as hyperglycemia and hypoglycemia inflammation, wounds, tumors, and so on. These conditions are all among the most detrimental to human health. Presently Rapid acknowledgment of this condition becomes essential. In the course of the evolution of clinical and preclinical investigation for the diagnosis of multiple diseases, molecular imaging has become a potent technique. A promising way to solve this drawback is the development of multifunctional hypoxia imaging nanoparticles that enhance the efficiency, specificity, and sensitivity of molecular imaging by providing molecular and functional information in an invasive manner under in vivo conditions. The most significant feature of Nanoparticles throughout the hypoxia imaging procedure is their higher penetration and retention implication with lengthy circulation capacity and easy encapsulation capability, generating them the most influential target for utilization in the biomedical application as a hypoxia imaging technique. Here, we concentrate on a recently generated nanoparticle that has been adopted as a tissue-level molecular imaging probe for numerous diseases.

Keywords Hypoxia · Nanoparticles · Hypoxia imaging · Specificity · Sensitivity

P. Sharma · P. Kumari · N. K. Sharma (✉)
Department of Bioscience and Biotechnology, Banasthali Vidyapith (Deemed University), P.O. Banasthali Vidyapith Distt., Tonk 304022, Rajasthan, India
e-mail: snarendrakumar@banasthali.ac.in; drnarendraks@gmail.com

J. Singh
Genome and Computational Biology Lab, Department of Biotechnology, Mohanlal Sukhadia University, Udaipur, Rajasthan, India

T. C. Dakal
University of Texas, MD Anderson Cancer Center, Houson, TX, 77030, USA

© The Author(s), under exclusive license to Springer Nature Singapore Pte Ltd. 2023

S. Chawla et al. (eds.), *Smart Nanomaterials Targeting Pathological Hypoxia*,
Smart Nanomaterials Technology, https://doi.org/10.1007/978-981-99-1718-1_12

Abbreviations

HIF	Hypoxia Inducible Factor
PH	Potential of Hydrogen,
MRI	Magnetic Resonance Imaging
UCNP	Up Conversion Nanoparticle Core
ROS	Reactive Oxygen Species
PDT	Photodynamic Therapy
O_2	Oxygen
MTT	(3.(4,5-Demethylthiazolyl-2)-2,5-diphenyltetrazolium bromide
MMC	Mitomycin c
AZQ	Aziquone
DNA	Deoxy Ribo Nucleic Acid
Np	Nanoparticle
NADPH	Nicotinamide adenine dinucleotide Phosphate
NOS	Nitric Oxide Synthase
HyP-1	Hypoxia Probe 1
PET	Positron emission tomography
PEGylated	Polyethylene Gylated

1 Introduction

Oxygen is a key determinant of standard aerobic metabolism in mammals. When cells suffer from lower-than-usual oxygen levels and pressure, it is called a hypoxic condition. Hypoxia is caused by poor oxygen transport, low blood oxygen levels, and decreased cellular oxygen uptake (Eltzschig and Carmeliet 2011).

Mammals have their mechanism of adaptation to hypoxia by increasing respiration, blood flow, and survival response. If in any situation oxygenation is disrupted, this adaptive mechanism assists them in restoring oxygenation and helping the body adapt to hypoxia. This cellular modification mechanism is dependent on the transcription factor HIF, which is active when there is a lack of oxygen and is dormant when oxygen is present. HIF (hypoxia-inducible factor) controls other immune responses in inflammatory bowel disease, certain cancers, and infections (Lee et al. 2019). Various studies show that hypoxia signals control human organ systems such as the lungs, liver, kidneys, and heart. So we can use this hypoxic state as a therapeutic board and also as a biomarker for imaging certain health problems. Recent studies show that hypoxia emerges as a hallmark for the early detection of tumors. This interdisciplinary research should focus on the development of nanomaterials that can be used for effective and non-invasive early detection of cancer (Lledos et al. 2018). In the case of a cancer study, the hypoxia-responsive nanoparticles act vigorously in the existence of a hypoxic tumor microenvironment. The various researchers' results suggest that its activity improves the effectiveness of radiotherapy, chemotherapy, and

other imaging and therapeutic strategies. Hypoxia is associated with many infections such as cancer, neurological disorders, and kidney disease. Numerous researches have been conducted to illustrate the benefit of hypoxia-activated nanoparticles and pro-drugs in tumor-directed cure. Hypoxia-responsive nanoparticles are dormant throughout perfusion and under standard physiological circumstances but become activated during hypoxia when they enter the hypoxic tumor microenvironment (Wang et al. 2021). Overcoming hypoxia is therefore a significant strategy used for the cure of dense tumors. For that purpose, researchers have attempted to enhance useful chemicals and nanoparticles that could be utilized for scanning and indulge hypoxic tumors noninvasively and efficiently. The aim is to retreat hypoxia by creating oxygen and activating nanomolecules/medicines into the hypoxic tumor microenvironment, as well as targeting tumor hypoxia biomarkers to enhance treatment efficacy.

In addition, so many studies are being conducted for non-invasive imaging using nanomaterial. In recent years, these suggesting approaches get more attention in which the formation of the multifunctional platform occurs including lanthano crystals, iron oxide, polymers, and gold. These are the active Nanoprobes that can respond to the nearby environment and serve as biomarkers to enhance the effectiveness, specificity, and sensitivity of molecular imagining. During this imaging, the physiological limits that come under will be redox state, presence of enzyme, pH, and hypoxia that can be designed as stimuli for the activated probes (Liu et al. 2019). At the moment, all researchers are looking for non-invasive imaging approaches. Non-invasive hypoxia imaging technologies that are commonly used include calculated tomography and positron emission tomography, MRI, photoacoustic imaging, and optical imaging. Optical hypoxia imaging is the most economical, sensitive, and high-output imaging technology in all of them. This is due to the design of the probe, which is mostly composed of a metal complex and organic dye. The metal complex has several properties, including high oxygen sensitivity, a lengthy phosphorescent for a lifetime, and the ability to penetrate within the cell membranes. It is applied in cell culture and it can also add to animal tissue samples of tumors. To improve the precision and stop the blocking of tissue, researchers develop a ratiometric hypoxia sensor that uses the hypoxia-insensitive dye with a hypoxia sensor and uses its percentage for describing the absorption of oxygen (Ma and Xia 2021).

Meanwhile, other investigators are concentrating on organelle structural hypoxia conditions like the distribution of mitochondrial hypoxia. It is essentially a sensor-based system in which the hypoxia sensor accomplished mitochondrial targeting, allowing us to detect the concentration of oxygen inside the cell. These probes and sensors could also be used in preclinical cancer diagnostics. Here, Fig. 1 depicted the basic design of nanoparticles with their vast applications.

To accommodate all scanning modalities through optical hypoxia imaging, the technologies require a transporter onto which entirely agents are inserted. The nanoparticle technique would be extremely suggested for this particular reason. Nanomaterials have unique properties that make them suitable for this purpose, such as lengthy circulation and facile endocytosis. These characteristics aid the hypoxic imaging sensor in reaching a specific location. Furthermore, the diverse basic designs of nanomaterials allocate each modality and purpose to act collectively (Das et al.

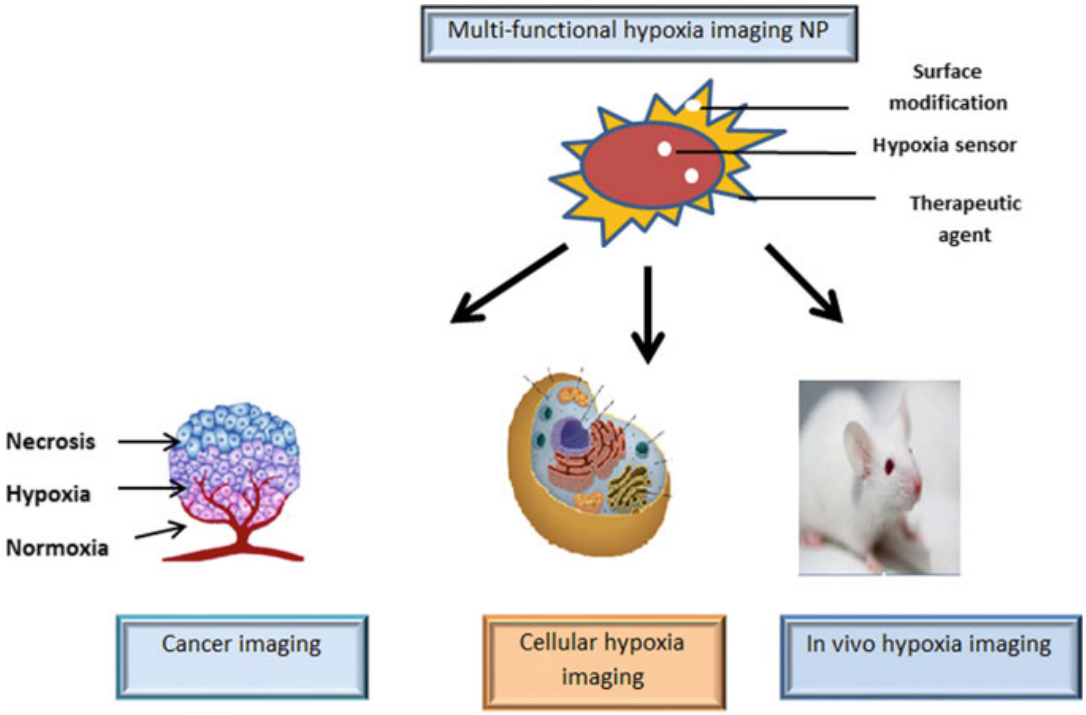

Fig. 1 Applications of multifunctional hypoxia imaging nanoparticles

2020). In this case, the nanoparticle can also apply active aiming and immune leak functional group by the surface alteration. Meanwhile numerous confront and drawbacks remain in the application of multifunctional hypoxia imaging nanomaterials. Here, we are focusing on recent advancements and various kinds of multifunctional hypoxia imaging nanoparticles.

2 Types of Nanoparticles

The complex architectures of multifunctional hypoxia imaging nanoparticles vary. Nanoparticles are characterized according to their structure as self-assembled nanoparticles, core–shell structure nanoparticles, micelle-liposome-like nanoparticles, and matrix dispersion nanoparticles.

2.1 Self-assembled Nanoparticles

The inner core–shell of these particles is inherently hydrophobic, making bioavailability much better than any other nanoparticle. Some researchers fabricate such particles using porphyrin Pt (II) and polyfluorene-based hyperbranched complexed polyelectrolytes. Substances that adhere to these particles are with a size of about

10 nm. They do not have much greater encapsulation or loading capacity compared to nanocarriers. Hydrophobicity and polarity play key roles in drug development and as a hypoxia sensor. These particles exhibit van der Walls binding between molecules, giving them a relatively loose structure. Some other related data also show that strength can be increased through crosslinking activity. This makes it much stronger (Park et al 2015; Shi et al. 2014; Zhou et al. 2015).

2.2 Core–Shell Nanoparticles

As the name suggests, these nanoparticles have a center and a shell. In most cases, the principal is formulated as a hydrophobic treatment and metal compound. Some nanoparticles are also formulated in the core part. They are hydrophilic in nature, making them inherently water soluble and biocompatible. It consists of biomaterials such as hyaluronic acid and many others. In one study, it was found that a researcher formed an up-conversion nanoparticle core (UCNP), the core of which interacts with hypoxia sensors in the shell. This modification ability of nanoparticles allows them to target hypoxia imaging therapy (Li et al. 2018a, b, c; Wang et al. 2016; Xu et al. 2016).

2.3 Micelle-Liposome-Like Nanoparticle

Micelles and liposomes work together to form an emulsion and deliver a drug. This is one of the best nanocarriers used in optical hypoxia sensors and drug delivery. Micelles have a monolayer and liposomes have bilayers. The lipophilic agent is layered in a single phase and the hydrophilic water phase can be loaded into the bilayer liposome. According to several types of research, it has been found that the cancer cell membrane shows binding with metal ions and they further show immune evasion ability for tumor targeting. A researcher attaches a cancer cell membrane to an organometallic porphyrin scaffold that exhibits a distinctive tumor-targeting feature. Apart from this, membrane-targeting phospholipid and amphiphilic polymers can also be used in the manufacture of these particles. There show biocompatibility and much better results than other nanoparticles (Feng et al. 2017a, b; Huang et al. 2018; Luo et al. 2016; Yu et al. 2017).

2.4 Matrix-Dispersed Nanoparticles

The matrix area of these particles consists exclusively of polymer. Wherein the sensors of hypoxia and the imaging agent are evenly distributed. These nanoparticles and sensors would be small by nature. A researcher fabricated polymer-based

Table 1 The general disruption of the general dispersed nanoparticles is summarized in the form of a table

Nanoparticles	Structure	Diagrammatic view	References
Self-assembled nanoparticles	Have a relatively loose structure	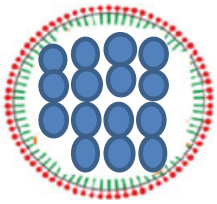	Zhou et al. (2015), Park et al. (2015), Shi et al. (2014)
Core–shell nanoparticles	High loading capacity	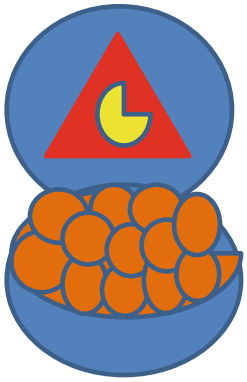	Xu et al. (2016), Wang et al. (2016), Li et al. (2018a, b, c)
Matrix-dispersed nanoparticles	Small molecules distributed evenly		Luo et al. (2016), Huang et al. (2018), Yu et al. (2017), Feng et al. (2017a, b)
Micelle-liposome-like nanoparticle	Better Biocompatibility	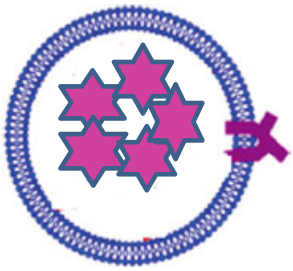	Li et al. (2018a, b, c), Qian et al. (2016), Liu et al. (2017), Liu et al. (2014), Papkovsky (2013)

supramolecular nanoparticles used for ratiometric hypoxia imaging. In some places, small nanoparticles can be encapsulated with a matrix to grow larger. These small particles are metal clusters, dots of quantum, and UCNP, which can serve as the fluorescent functional causes. These particles protect themselves by self-extinction (Li et al. 2018a, b, c; Liu et al. 2014, 2017; Papkovsky 2013; Qian et al. 2016). The general disruption of these particles is summarized in form of a table (Table 1).

3 Hypoxia Imaging Tumor-Directed Nanoparticles

Several multifunctional image-guided nanoparticles for the Therapy of cancer were evolved to construct a theranostic platform for the treatment of cancer. Hypoxia plays a debilitating role in cancer for physicians and patients. This state rendered the solid tumor resilient to radiotherapy and chemotherapy. Cancer cell mutations and

tumor metastasis can be caused by hypoxia. Hypoxia imaging can help localize the tumor area. Various techniques have been created by researchers to further exploit optical imaging of hypoxia to guide cancer therapy and observe therapeutic efficacy (Weissleder 2001).

3.1 Hypoxia Imaging by Phosphorescent Hypoxia Probe

In this procedure, phosphorescent hypoxia probes produce ROS that eliminates cancer cells. ROS can be generated by an agent known as a photosensitizer. This technique is also known as the PDT technique and shows a better therapeutic effect than chemotherapy. It has been widely recognized that chemotherapy can also produce some side effects such as drug resistance, and toxicity at the cellular and organ levels. Compared to PDT, it is a non-invasive method that is highly accurate. It is an image-directed therapy method. In this process, triplet O_2 particles respond through photosensitizer and thereafter convert to singlet form. These singlet species and reactive oxygen species are used to cure tumor cells. When the light source is applied to cancer cells, due to radiation, the photosensitizer switches oxygen into single free radical oxygen that helps kill cancer cells. Here, oxygen detection is built on the linear relationship between oxygen concentration and phosphorescence intensity. The three main factors that fall under this are oxygen, phosphorescence, and light. Hypoxia-based tumor microenvironment leads to tumor PDT resistance. This method shows high effectiveness for the diagnosis of early-stage tumor cells and also killed the cell by light irradiation. These in situ hypoxia images guide PDT techniques and results can be analyzed by confocal microscopy and MTT assay. Some more complicated ones also employ phosphorescent metals such as ruthenium, platinum, porphyrins, and iridium. This complex is used to detect the image and o_2 levels in existing organisms and hence can work as a real-time monitor for o_2 levels (Lv et al. 2018; Zhao et al. 2015; Zhou et al. 2015).

Ruthenium

HIF inhibition was utilized specifically to treat hypoxia-related illness in this manner. Some researchers created a hypoxia imaging agent based on ruthenium (II) anthraquinone complexes and HIF-1 alpha suppression. This particle shows a 40-fold change in phosphorescence intensity from 20 to 1% oxygen content, so we can say that this Ru has excellent intracellular hypoxia imaging ability. It presents effective liquid solubility and a potent phosphorescence emission in hypoxia. The binding capacity of ruthenium makes it favorable to use as a complex for particle formation. One researcher designed a UCNP mesoporous silica shell structure nanomolecules with an O_2 indicator for ruthenium dichloride. This form is used as a quenchable indicator to sense oxygen. Since the oxygen concentration can be reproduced through the luminescence at 613 nm and the excitation at 980 nm, by using this, we can do a deep tissue study (Lv et al. 2015).

Platinum (II) and porphyrin

Scientists have created Pt (II) porphyrin with luminous properties of photo physical like high photostability, and large stoke shift. It shows brilliant radiometric luminescence reaction to the o_2 level with great consistency and full reversibility. It was also observed in other studies for the identification of early phase and therapy system porphyrin illustrate a high PDT efficacy and extended lifetime and a high signal-to-noise ratio in fluorescence recognition (Lv et al. 2016).

Iridium (III) complex

This complex is reduced by intracellular oxygen which is repaired during a two-electron reduction in a hypoxic environment. A group of scientists designed an oxygen-sensing complex and covalently attach this to iridium to monitor oxygen concentration. One more scientist designed two iridium complexes that specially mark mitochondria and lysosomes in existing cells. These mitochondria are further targeted for the improvement of the PDT effect. This type of experiment and their data demonstrate that such alteration of complexes allows better imaging for hypoxia (Feng et al. 2017a, b).

4 Hypoxia Active Nanoparticles for Chemotherapy

Quinones

Pro-drugs are made up of quinones which could be employed as hypoxia-responsive nanoparticles. The structure of quinone could be triggered through the presence of a hypoxic situation in the cells of a tumor where it produces semiquinones radicals or some other two electron-reducing enzymes such as hydroquinones and DT diaphoresis (Zhu et al. 2012).

The class of natural compounds having quinone as their core structure becomes a highly active class for biologically active agents such as vitamin K, doxorubicin (anticancer compound), and coenzyme Q. In this quinone, some more compounds also included such as MMC (mitomycin C), porfiromycin, EO9, and AZQ. The MMC was isolated from Streptomyces caespitosus. This compound showed high solubility, and it was the first used quinone-based medication documented as bioreductive hypoxia selective alkylating agent. After the uptake of cellular or intracellular, it is distributed within the nuclei. Through a reductive metabolism, the MMC and its analogs show their cytotoxic effect. It binds with the DNA through great competence and specificity at the sequence CpG while MMC is related to acute or chronic toxicities. One researcher developed an MMC-soybean- phosphatidylcholine nanoparticle. That enhances the chemical activity of MMC NP in a hypoxia environment. One more nanoparticle was developed by the same researcher with improved characteristics that show lesser size dispersal and high zeta potential with improved stability (Caramés Masana and Reijke 2017; Erdogar et al. 2014). One

more nanoparticle was designed by researchers in which the first two-photon fluorescent probe combining luminescent ruthenium (II) complex by a redox-active form of anthraquinone moiety was further used for the in vivo imaging of hypoxia with high-resolution spatial imaging (Pierce et al. 2010).

Nitroimidazoles

It is a double responsive Nanotransporter that comes as the principal method which is used to enhance the traditional efficacy of PDT ability. This composition is made up of two components one is a 2 nitroimidazole grafting conjugated polymer and the other one is doxorubicin. This Nanocarrier complex generates reactive oxygen species after a light-triggered stimulus to release a hypoxia stimulus. This complete process starts with irradiation of light, and it generates ROS that successively induces hypoxia at the tumor site by converting 2- nitroimidazole into 2 amino imidazoles. This series of reactions occurs by the release of single electron reduction catalysis through a series of nitrocellulose reductase with bio-reducing agents like NADPH that disassembles the drug transporter. This doxorubicin induces cytotoxicity via the damaging of DNA. This strategy gives an innovative pattern for the drug release system (Hou et al. 2009, 2013).

Aliphatic N oxide

The AQ4N drug shows a Bis N oxide Quinone structure that experiences bioreduction in the hypoxic cell. This drug has been undergoing phase I and II clinical trials. In this process, the reduction by hem proteins including cytochrome (P 450) and nitric oxide synthase (NOS) occurs, and the final product AQ4 form. This reduction product AQ4 shows high DNA affinity by targeting topoisomerase II and this topoisomerase II stops the hypoxic cell to reenter the cell cycle. The AQ4N drug considers an ideal bioreductive drug that can enter intensely into the tumor and it shows very less tissue toxicity. Scientists designed hypoxia probe 1(HyP-1) a hypoxia-responsive agent that is used for photoacoustic imaging. In vitro, it can be used as a hypoxic activator, and in cultured cells or multiple diseases model, it is used in vivo. It is used for three-dimensional visualization of intertumoral hypoxia with the best resolution (McCarthy et al. 2003; Qian et al 2016; Zhang et al. 2015). The comparative studies of before and after administration of Hyp1 were done for understanding the clear role of these particles during hypoxia imaging. Knox et al. establish a hind limb ischemia model to understand the response of Hyp1 in a hypoxic environment during in vivo conditions. Additionally, regarding the use of AQ4N in diagnosis, Feng et al. designed an AQ4N liposome-based nanodrug that relies on a commercial hydrophilic particle as a hypoxia-activated prodrug by a modified hydrophobic Ce6 as a photosensitizer which shows encapsulation with PEGylated liposomes. This liposome can use a probe for positron emission tomography (PET) after chelation with a Cu isotope. That can be used in in vivo imaging of PET, PDT, and hypoxia-dependent cytotoxicity. Based on these results, Feng et al. composed AQ4N through glucose oxidase to obtain a hypoxia-activated therapy. In this process, the glucose oxidase stops the supply of glucose to the tumor and exhausts the tumor's oxygen to produce a hypoxic enrichment. Additional treatment with AQ4N loaded with

liposome enhanced activation of hypoxia and strong synergistic antitumor properties (Feng 2017a, b; Knox et al. 2017; Mehibel et al. 2009; Nishida et al. 2008; Paoni et al. 2002).

5 Conclusion and Future Scope

Even though nanotechnology has been studied for ages, while their therapeutic application has yet to be proven. The cause of this can be related to two parts: the tumor part and the nanomaterial part, with tumor heterogeneity being one of the most important. Tumor heterogeneity is defined by diverse genetic alterations and phenotypic appearance profiles at the genetic level, and by complex cells inside the tumor-like fibroblasts, other stromal cells, and inflammatory cells at the cellular level. Although the hypoxia-active nanoparticles play an important strategy to overcome tumor heterogeneity, they can also be employed to develop analytic and medicinal approaches for a wide range of tumor cells. And the nanomolecule has various disadvantages, including limited tumor retention due to its enormous size and rapid renal clearance due to its comparatively small size. Due to their positive charge, the nanoparticles have a short perfusion time, which allows them to easily pass through membranes. Scientists have created a nanoparticle with zero potential during its perfusion period that can become positively charged after being activated by a hypoxic microenvironment.

Here, we summarize recent advances in improving radiation efficiency by focusing on hypoxia. Built on the relationship between hypoxia and radiation resistance, numerous new substances have been developed for the treatment of hypoxic tumors.

Radioactively labeled NP is suitable for further research in this direction due to their consistent half-life and efficacy.

When compared to minor molecular imaging probes, nanoprobes are reflected as a suggesting stage for designing responsive mechanisms to various stimuli such as hypoxia, acidic conditions, various enzyme redox status, and so on, because their well-built particular area provides a large room to alter their functional moieties. Despite numerous accomplishments in this field, significant obstacles remain in the construction of activated nanoprobes for in vivo imaging.

Hypoxia is increasingly recognized as a significant factor in the pathophysiology of additional important causes of death, such as myocardial ischemia, metabolic disorders, reproductive disease, and cardiac disease. For this reason, more imaging-related nanoprobes must be created, as they will provide a wide field for imaging different diseases at the molecular level.

References

Caramés Masana F, de Reijke TM (2017) The efficacy of Apaziquone in the treatment of bladder cancer. Expert Opin Pharmacother 18(16):1781–1788. https://doi.org/10.1080/14656566.2017.1392510

Das SS, Bharadwaj P, Bilal M, Barani M, Rahdar A, Taboada P, Bungau S, Kyzas GZ (2020) Stimuli-responsive polymeric Nanocarriers for drug delivery, imaging, and Theragnosis. Polymers 12(6):1397. https://doi.org/10.3390/polym12061397

Eltzschig HK, Carmeliet P (2011) Hypoxia and inflammation. N Engl J Med 364(7):656–665. https://doi.org/10.1056/NEJMra0910283

Erdogar N, İskit AB, Eroglu H, Sargon MF, Mungan NA, Bilensoy E (2014) Cationic core-shell nanoparticles for intravesical chemotherapy in tumor-induced rat model: safety and efficacy. Int J Pharm 471(1–2):1–9. https://doi.org/10.1016/j.ijpharm.2014.05.014

Feng L, Cheng L, Dong Z, Tao D, Barnhart TE, Cai W, Chen M, Liu Z (2017a) Theranostic liposomes with hypoxia-activated prodrug to effectively destruct hypoxic Tumors post-photodynamic therapy. ACS Nano 11(1):927–937. https://doi.org/10.1021/acsnano.6b07525

Feng Z, Tao P, Zou L, Gao P, Liu Y, Liu X, Wang H, Liu S, Dong Q, Li J, Xu B, Huang W, Wong WY, Zhao Q (2017b) Hyperbranched phosphorescent conjugated polymer dots with iridium(III) complex as the core for hypoxia imaging and photodynamic therapy. ACS Appl Mater Interfaces 9(34):28319–28330. https://doi.org/10.1021/acsami.7b09721

Hou Z, Li Y, Huang Y, Zhou C, Lin J, Wang Y, Cui F, Zhou S, Jia M, Ye S, Zhang Q (2013) Phytosomes loaded with mitomycin C-soybean phosphatidylcholine complex developed for drug delivery. Mol Pharm 10(1):90–101. https://doi.org/10.1021/mp300489p

Hou Z, Wei H, Wang Q, Sun Q, Zhou C, Zhan C, Tang X, Zhang Q (2009) New method to prepare mitomycin C loaded PLA-nanoparticles with high drug entrapment efficiency. Nanoscale Res Lett 4(7):732–737. https://doi.org/10.1007/s11671-009-9312-z

Huang YY, Tian Y, Liu XQ, Niu Z, Yang QZ, Ramamurthy V, ... Wu LZ (2018) Luminescent supramolecular polymer nanoparticles for ratiometric hypoxia sensing, imaging and therapy. Mater Chem Front 2(10):1893–1899.https://doi.org/10.1039/C8QM00309B

Knox HJ, Hedhli J, Kim TW, Khalili K, Dobrucki LW, Chan J (2017) A bioreducible N-oxide-based probe for photoacoustic imaging of hypoxia. Nat Commun 8(1):1794. https://doi.org/10.1038/s41467-017-01951-0

Lee JW, Ko J, Ju C, Eltzschig HK (2019) Hypoxia signalling in human diseases and therapeutic targets. Exp Mol Med 51(6):1–13. https://doi.org/10.1038/s12276-019-0235-1

Li H, Lei W, Wu J, Li S, Zhou G, Liu D, Yang X, Wang S, Li Z, Zhang J (2018a) An upconverting nanotheranostic agent activated by hypoxia combined with NIR irradiation for selective hypoxia imaging and tumour therapy. J Mater Chem B 6(18):2747–2757. https://doi.org/10.1039/c8tb00637g

Li J, Shang W, Li Y, Fu S, Tian J, Lu L (2018b) Advanced nanomaterials targeting hypoxia to enhance radiotherapy. Int J Nanomed 13:5925. https://doi.org/10.2147/2FIJN.S173914

Li SY, Xie BR, Cheng H, Li CX, Zhang MK, Qiu WX, Liu WL, Wang XS, Zhang XZ (2018c) A biomimetic theranostic O_2-meter for cancer targeted photodynamic therapy and phosphorescence imaging. Biomaterials 151:1–12. https://doi.org/10.1016/j.biomaterials.2017.10.021

Liu H, Xie Y, Zhang Y, Cai Y, Li B, Mao H, Liu Y, Lu J, Zhang L, Yu R (2017) Development of a hypoxia-triggered and hypoxic radiosensitized liposome as a doxorubicin carrier to promote synergetic chemo-/radio-therapy for glioma. Biomaterials 121:130–143. https://doi.org/10.1016/j.biomaterials.2017.01.001

Liu J, Liu Y, Bu W, Bu J, Sun Y, Du J, Shi J (2014) Ultrasensitive nanosensors based on upconversion nanoparticles for selective hypoxia imaging in vivo upon near-infrared excitation. J Am Chem Soc 136(27):9701–9709. https://doi.org/10.1021/ja5042989

Liu J, Liu Z, Wu D (2019) Multifunctional hypoxia imaging nanoparticles: multifunctional tumor imaging and related guided tumor therapy. Int J Nanomed 14:707–719. https://doi.org/10.2147/IJN.S192048

Lledos M, Mirabello V, Sarpaki S, Ge H, Smugowski HJ, Carroll L, Aboagye EO, Aigbirhio FI, Botchway SW, Dilworth JR, Calatayud DG, Plucinski PK, Price GJ, Pascu SI (2018) Synthesis, radiolabelling and in vitro imaging of multifunctional nanoceramics. ChemNanoMat: Chem Nanomater Energy Biol More 4(4):361–372. https://doi.org/10.1002/cnma.201700378

Luo CH, Huang CT, Su CH, Yeh CS (2016) Bacteria-mediated hypoxia-specific delivery of nanoparticles for tumors imaging and therapy. Nano Lett 16(6):3493–3499. https://doi.org/10.1021/acs.nanolett.6b00262

Lv W, Yang T, Yu Q, Zhao Q, Zhang KY, Liang H, Liu S, Li F, Huang W (2015) A Phosphorescent Iridium(III) complex-modified nanoprobe for hypoxia bioimaging via time-resolved luminescence microscopy. Adv Sci (Weinheim, Baden-Wurttemberg, Germany) 2(10):1500107. https://doi.org/10.1002/advs.201500107

Lv W, Zhang Z, Zhang KY, Yang H, Liu S, Xu A, Guo S, Zhao Q, Huang W (2016) A mitochondria-targeted photosensitizer showing improved photodynamic therapy effects under hypoxia. Angewandte Chemie (International ed. in English) 55(34):9947–9951. https://doi.org/10.1002/anie.201604130

Lv Z, Zou L, Wei H, Liu S, Huang W, Zhao Q (2018) Phosphorescent starburst Pt(II) porphyrins as bifunctional therapeutic agents for tumor hypoxia imaging and photodynamic therapy. ACS Appl Mater Interfaces 10(23):19523–19533. https://doi.org/10.1021/acsami.8b05944

Ma T, Xia T (2021) Nanoparticle-based activatable probes for Bioimaging. Advanced Biology 5(1):e2000193. https://doi.org/10.1002/adbi.202000193

McCarthy HO, Yakkundi A, McErlane V, Hughes CM, Keilty G, Murray M, Patterson LH, Hirst DG, McKeown SR, Robson T (2003) Bioreductive GDEPT using cytochrome P450 3A4 in combination with AQ4N. Cancer Gene Ther 10(1):40–48. https://doi.org/10.1038/sj.cgt.7700522

Mehibel M, Singh S, Chinje EC, Cowen RL, Stratford IJ (2009) Effects of cytokine-induced macrophages on the response of tumor cells to banoxantrone (AQ4N). Mol Cancer Ther 8(5):1261–1269. https://doi.org/10.1158/1535-7163.MCT-08-0927

Nishida CR, Ortiz de Montellano PR (2008) Reductive heme-dependent activation of the n-oxide prodrug AQ4N by nitric oxide synthase. J Med Chem 51(16):5118–5120. https://doi.org/10.1021/jm800496s

Paoni NF, Peale F, Wang F, Errett-Baroncini C, Steinmetz H, Toy K, Bai W, Williams PM, Bunting S, Gerritsen ME, Powell-Braxton L (2002) Time course of skeletal muscle repair and gene expression following acute hind limb ischemia in mice. Physiol Genomics 11(3):263–272. https://doi.org/10.1152/physiolgenomics.00110.2002

Papkovsky DB, Dmitriev RI (2013) Biological detection by optical oxygen sensing. Chem Soc Rev 42(22):8700–8732. https://doi.org/10.1039/c3cs60131e

Park J, Lee J, Kwag J, Baek Y, Kim B, Yoon CJ, Bok S, Cho SH, Kim KH, Ahn GO, Kim S (2015) Quantum dots in an amphiphilic polyethyleneimine derivative platform for cellular labeling, targeting, gene delivery, and ratiometric oxygen sensing. ACS Nano 9(6):6511–6521. https://doi.org/10.1021/acsnano.5b02357

Pierce SE, Guziec LJ, Guziec FS, Brodbelt JS (2010) Characterization of aziridinylbenzoquinone DNA cross-links by liquid chromatography-infrared multiphoton dissociation-mass spectrometry. Chem Res Toxicol 23(6):1097–1104. https://doi.org/10.1021/tx1000738

Qian C, Yu J, Chen Y, Hu Q, Xiao X, Sun W, Wang C, Feng P, Shen QD, Gu Z (2016) Light-activated hypoxia-responsive nanocarriers for enhanced anticancer therapy. Adv Mater (Deerfield Beach, Fla.) 28(17):3313–3320. https://doi.org/10.1002/adma.201505869

Shi H, Ma X, Zhao Q, Liu B, Qu Q, An Z, ... Huang W (2014) Ultrasmall phosphorescent polymer dots for ratiometric oxygen sensing and photodynamic cancer therapy. Adv Funct Mater 24(30):4823–4830.https://doi.org/10.1002/adfm.201400647

Wang J, Huang J, Zhou W, Zhao J, Peng Q, Zhang L, Wang Z, Li P, Li R (2021) Hypoxia modulation by dual-drug nanoparticles for enhanced synergistic sonodynamic and starvation therapy. J Nanobiotechnol 19(1):87. https://doi.org/10.1186/s12951-021-00837-0

Wang XH, Peng HS, Yang W, Ren ZD, Liu YA (2016) Mitochondria-targeted theranostic nanoparticles for optical sensing of oxygen, photodynamic cancer therapy, and assessment of therapeutic efficacy. Microchim Acta 183(10):2723–2731. https://doi.org/10.1007/s00604-016-1917-1

Weissleder R (2001) A clearer vision for in vivo imaging. Nat Biotechnol 19(4):316–317. https://doi.org/10.1038/86684

Xu S, Zhang X, Xu H, Dong B, Qu X, Chen B, Zhang S, Zhang T, Cheng Y, Xu S, Song H (2016) Silane modified upconversion nanoparticles with multifunctions: imaging, therapy and hypoxia detection. Sci Rep 6:22350. https://doi.org/10.1038/srep22350

Yu Y, Wu Y, Liu J, Liu Y, Wu D (2017) Highly efficient dual-modal phosphorescence/computed tomography bioprobes based on an iridium complex and AuNP polyiohexol composite nanoparticles. Nanoscale 9(27):9447–9456. https://doi.org/10.1039/c7nr03185h

Zhang P, Huang H, Chen Y, Wang J, Ji L, Chao H (2015) Ruthenium(II) anthraquinone complexes as two-photon luminescent probes for cycling hypoxia imaging in vivo. Biomaterials 53:522–531. https://doi.org/10.1016/j.biomaterials.2015.02.126

Zhao Q, Zhou X, Cao T, Zhang KY, Yang L, Liu S, Liang H, Yang H, Li F, Huang W (2015) Fluorescent/phosphorescent dual-emissive conjugated polymer dots for hypoxia bioimaging. Chem Sci 6(3):1825–1831. https://doi.org/10.1039/c4sc03062a

Zhou X, Liang H, Jiang P, Zhang KY, Liu S, Yang T, Zhao Q, Yang L, Lv W, Yu Q, Huang W (2015) Multifunctional phosphorescent conjugated polymer dots for hypoxia imaging and photodynamic therapy of cancer cells. Adv Sci (Weinheim, Baden-Wurttemberg, Germany) 3(2):1500155. https://doi.org/10.1002/advs.201500155

Zhu C, Liu L, Yang Q, Lv F, Wang S (2012) Water-soluble conjugated polymers for imaging, diagnosis, and therapy. Chem Rev 112(8):4687–4735. https://doi.org/10.1021/cr200263w

Cardiovascular toxicity and therapeutic modalities targeting cardio-oncology:

From basic research to advanced study



Edited by
Dr. Imteyaz Qamar
Dr. Pawan Kumar Maurya

CHAPTER

12

Principles of cardiovascular rehabilitation

Preeti Sharma[a], *Poornima Pandey*[a], *Tikam Chand Dakal*[b], *and Narendra Kumar Sharma*[a]

[a]Department of Bioscience and Biotechnology, Banasthali Vidyapith, Banasthali Tonk, Rajasthan, India, [b]Genome & Computational Biology Lab, Department of Biotechnology, Mohanlal Sukhadia University, Udaipur, Rajasthan, India

1 Introduction

Cardiovascular disease is the leading cause of death in the world. According to the data, cardiovascular disease is responsible for an estimated 17 million deaths (30% of all deaths) each year around the world. Cardiac rehabilitation is an important factor in the prevention of cardiovascular disease and can help to minimize age-related cardiovascular mortality, which is a national health priority [1]. Cardiovascular rehabilitation recommends exercise, cardiac risk factors, therapy, and modification in educating people, according to the medical assessment. These services are explicitly designed to minimize the risk of premature death by limiting the physical and physiological effects of cardiac disease [2]. The overall principle is the identification of the patient first, then enrollment in cardiac rehabilitation programs. The ideas of family medicine are aligned with the modern concept of medical home, which includes complete risk factor reduction and longitudinal treatment [1].

Cardiovascular rehabilitation is a program that focuses on physical activity. It is a patient-specific program aimed at enhancing the patient's physical, behavioral, social, and occupational conditions. Via physical activity and educational techniques, cardiovascular rehabilitation services foster a number of advantages [3,4]. Although, the increased metabolic demand required for physical activity causes a number of adaptations in the

Cardiovascular Toxicity and Therapeutic Modalities Targeting Cardio-oncology
https://doi.org/10.1016/B978-0-323-90461-2.00011-0
Copyright © 2022 Elsevier Inc. All rights reserved.

cardiopulmonary and autonomic systems, which can be linked to the appearance of signs and symptoms. Cardiovascular rehabilitation comprises a multidisciplinary intercede, which includes psychological counseling, smoking cessation, patient education, exercise training risk factor control, and vocational reintegration [4].

2 Cardiopulmonary stress testing in prehabilitation, habilitation, and rehabilitation

Cardiopulmonary stress testing is a way to measure how well a person's heart and lungs are working during exercise. The measurements are made of the amount of oxygen taken by the body while riding a bicycle or walking on a treadmill. Cardiopulmonary exercise testing (CPET), also known as cardiopulmonary stress testing, has emerged as a valuable clinical method for evaluating exercise ability and projecting outcomes in patients with cardiac arrest and other cardiac issues. It demonstrates the importance of the integrative exercise response involving the pulmonary, cardiovascular, hematopoietic, neuropsychological, and skeletal muscle systems, which is not adequately expressed by individual organ system function measurements [5]. During a symptom-limited exercise test, CPET includes assessing respiratory oxygen absorption (VO_2), carbon dioxide emission (VCO_2), and ventilator steps.

3 Cardiopulmonary exercise testing

Several methods for calculating ventilation and respiratory gas parameters during exercise still exist in cardiopulmonary exercise testing. Breath-to-breath analysis methods are used in the most advanced clinical systems because they provide the most accurate indicator of metabolic response to exercise. A nonrebreathing valve is attached to a mouthpiece in the cardiopulmonary exercise testing system to avoid the mixing of inspired and expired air. A metabolic cart specifically designed for practical testing is normally built-in cart in the cardiopulmonary exercise testing machine for this oxygen, and carbon dioxide gas analyzers are usually built-in cart. The air flow signals are integrated over the time of inspiration and expiration to calculate respiratory volumes. The average minute volumes can be determined by multiplying the breath-to-breath data by the respiratory rate [6].

4 CPET protocol

Many different procedures are used for cardiopulmonary exercise testing. In addition, the procedure chosen is determined by the test's intent

TABLE 1 Comparative exercise equipment [5].

Variable	Cycle	Treadmill
(PVO_2) level	Low	High
Blood gas connection	Easier	More difficult
Noise	Comparatively less	Moderately high
In hand on safety	Safe	Moderately less safe
Load bearing in large subject	A lesser amount	Moderately high
Scale of leg strength exercise	A smaller amount	More
Suitable for	Patients	Energetic common subject

and the patient's functional ability. Both bicycle and treadmill procedures have been used in the treatment of patients with cardiopulmonary issues. Ergometry treadmill fitness testing has many benefits over cycling (Table 1), and for the majority of people, treadmill walking is a more familiar practice than cycling. It necessitates more muscle mass to function against gravity. As a result, PVO_2 on the treadmill is 5%–10% higher than on a cycle ergometer [5,6]. Treadmill walking with your hands on the handrails lowers the metabolic cost and should be avoided if at all necessary. With improved metabolic cost quantification, a cycle ergometer is less likely to cause noise. It is generally less expensive and takes up less space than a treadmill.

During exercise testing, patients with heart disease are subjected to constant ECG monitoring and repeated blood pressure tests. Since oral contact is typically difficult with the mouthpiece apparatus, the patient usually communicates with hand signals during exercise [5,6].

During an exercise-based stress test (CPET tests), respiratory oxygen uptake (VO_2), peak oxygen assimilation, respiratory switch ratio, carbon dioxide production (VCO_2), and ventilator aerobic ratio are measured for this state.

5 Oxygen assimilation

VO_2 (oxygen assimilation) is regulated by cellular oxygen demand up to a point where it equals the maximum rate of oxygen transport. As external work increases, one or more of the determinants of VO_2 approach limitation, and the relationship between VO_2 and work rate can begin to plateau. The strongest proof of VO_2max has traditionally been this VO_2 plateau. Genetic factors, age, sex, body size, and the amount of exercising muscle are the key determinants of PVO_2 [6]. The patient's preparation and encouragement may also have an effect on PVO_2. PVO_2 should be

expressed as a percentage of the expected value and in absolute values (1/min). PVO_2 values can range from 15 times the resting value (30–50 mL/kg/min) [6]. VO_2 can rise from a resting value of about 3.5 mL/kg/min to PVO_2 values of about 15 times the resting value (30–50 mL/kg/min).

6 Respiratory switch ratio

The gas exchange ratio, also known as the respiratory exchange ratio, is the ratio of carbon dioxide emission to oxygen absorption (VCO_2/VO_2) (RER). The RER equals the RQ (respiratory quotient) in a steady-state situation. The RQ value is determined by the fuels used in metabolic processes.

An RQ of 1 indicates metabolisms primarily of carbohydrates.

RQ < 1 indicates a mixture of carbohydrate with fat (an RQ of about 0.7) and protein (an RQ of about 0.8).

RER is a rough indicator of metabolic events. During exercise, the RER rises due to either buffered lactic acid or hyperventilation (usually at the end of the workout) [7].

7 Ventilator anaerobic ratio

The anaerobic ratio, formerly known as the ventilator anaerobic threshold, is used to estimate the exercise ability. Expired ventilation rises linearly with respect to VO_2 and represents aerobically generated CO_2 in the muscles during CPET, which lasts until 50%–60% VO_2max is reached. Since oxygen supply cannot keep up with the increased metabolic demands of exercising muscles, anaerobic metabolism occurs during the second half of the exercise. A substantial rise in blood lactate concentration and lactic acid production in the muscles occurs at this time. The lactate threshold corresponds to the VO_2 level at the start of blood accumulation. The VAR is a valuable metric since work at this stage covers the majority of everyday activities. Since patients who fatigue before hitting VAR are more likely to have a noncardiac problem, the ability to achieve the VAR may help distinguish between cardiac and noncardiac causes of exercise limitation. There are a number of strategies for addressing the VAR, which can be categorized as invasive or noninvasive. For the intrusive estimate of the VAR, direct blood sampling may be used. Since the function of the point of growing lactate necessitates multiple blood samples, it is rarely used in clinical applications. When this approach is used, the VAR is described as the VO_2 at which blood lactate levels begin to rise or, finally, when bicarbonate levels begin to fall. On the other hand, the exact meaning is still up for debate. The pattern of change in VCO_2 and

VE is measured using this noninvasive approach. As workout strength increases, this is proportional to VO_2.

While exercise-based intervention programs are recommended for cardiovascular prevention, different exercise parameters, such as intensity, duration, and frequency, may have a variety of effects on cardiovascular metabolic endpoints. Furthermore, there are interindividual differences in response to different forms or intensities of exercise, which may explain why some studies show similar findings with different types of exercise modalities. Exercise training research is being done now and in the future as well [6]. The effects of exercise-based CR on the progression of cardiovascular disease have been consistently positive. Recent research has shown that training impact varies greatly at the individual level, with up to a third of patients failing to display a substantial improvement in exercise ability despite sufficient compliance. An understanding of the variables and processes controlling the reaction to activity in bodies apart from the skeletal muscles, the heart, and the spinal cord, as well as their interaction at a systemic level, is required to enhance the effectiveness of fitness CR. Presently, cardiac recovery methods are used in cardiac prehabilitation, but they are used proactively rather than reactively. According to comprehensive evidence, such treatments before cardiac surgery may enhance result in a number of domains, including aerobic conditioning, respiratory muscle preparation, lifestyle improvements, diabetic regulation, sleep, and psychoeducation [6] (Table 2).

8 Positive outcomes of cardiac rehabilitation

Cardiac rehabilitation has been shown to have a number of positive results in properly chosen patients. Hypertension, hypotension, and nausea are all signs that have been diminished. Both fitness efficiency and physical activity engagement have increased. The standard of living has also improved. The number of people admitted to the hospital has decreased. About half of the decline in cardiac mortality is believed to be attributed to dietary improvements in stroke risk profiles. Exercise-only cardiac rehabilitation services resulted in a 27% decrease across all fatalities as compared to control program. The results of cardiac recovery in patients who have had a bypass and pericardial effusion surgery are poorly understood due to a lack of trial data. According to one study, cardiac recovery improves VO2max by 50% after a transplant. Following valve replacement surgery, patients who underwent cardiac rehabilitation showed a 25% improvement in VO2max and a 25% increase in functional ability. In the general population, it is unclear if cardiac recovery improves survival [9].

Prehabilitation is the process of improving an individual's functional ability so that he or she can survive a traumatic incident. Individuals are

TABLE 2 Measurement of performance from a cardiac rehabilitation program based on the following criteria: [1,8].

Performance measure	Goal	Intervention
Blood pressure control	< 140/90 mmHg or < 130 mmHg (diabetic patient)	Lifestyle moderation; drug
Diabetes control	AIC < 7%	Patient education, diet planning, BMI, and physical activity programming
Depression	Assess for the presence of depression	Use of a suitable screening method in combination with the required interference
Exercise capacity	Determine if you have a low patience for exercise	Each patient's exercise prescription is special
Lipid control	For patients with a heart condition LDL cholesterol level of 100 mg/dL	Lifestyle moderation; drug
Physical activity	30 min/day 5 days/week	Self-directed resistance training activity is customized to each person's unique needs and desires
Prevention medication	Taking preventive medications as prescribed	Preventive counseling and intervention for people of all ages and gender
Tobacco intervention	Cession of prohibition	Tobacco cession strategy
BMI	A BMI of 18.5–24.9 kg per m^2 and a waist circumference of 40 in. for men and 35 in. for women are recommended	Dietary modification, physical activity programming, and psychological support are all part of a multidisciplinary program

prepared to weather the storm of their activities and to stop or resolve applications by prehabilitation. The preparatory time is regarded as a teaching opportunity. Prehabilitation models should typically include three phases of screening, intervention, tracking, and postintervention evaluation for the benefit, as well as a high level of patient encouragement to improve behavior for preoperative benefits. All patients undergoing major surgery will benefit from prehabilitation, but the duration and severity may differ. To promote behavior change prior to surgery, the multidisciplinary team makes each touch count. Physical activity, inspiratory muscle conditioning, smoking, alcohol, diet, and psychological factors are all factors that are linked to prehabilitation strategies. The aim of inspiratory muscle training is to strengthen breathing muscles and lower the

risk of preoperative pulmonary complications. It is preoperative smoking cessation, preoperative alcohol-adjusted consumption of nonhazardous alcohol, preoperative management of anxiety and depression, and development of self-effectiveness for prehabilitation and surgery, and preoperative nutrition.

Physiological factor may affect rehabilitation as follows:

8.1 Aerobic capacity

In terms of physical activity, the purpose of prehabilitation is to increase aerobic ability. Increased frequency physical activity rehabilitation systems are used in patients with stable coronary artery disease and heart disease. Improved exercise efficiency and hemodynamic gain more than moderate-intensity exercise training, with no substantial increase in complications. This modality's exercise protocols differ. In one study, a 10-min warm-up at 50%–60% VO_2max was presented in the form of 4-min periods at 90%–95% maximum cardiac output (Rate of Perceived Exertion 171), with periods split by three-minute cycles of walking at 50%–70% peak cardiac output [8,10].

8.1.1 Expected outcomes

- A 5%–10% increase in cardiorespiratory fitness, flexibility, muscular endurance, and strength.
- Symptoms are lessened, and physiological responses are lessened.
- An increase in psychological well-being.

8.2 Nutrient

Prior to surgery, the main objectives of nutrient prehabilitation are to optimize nutrient stores and aerobic reserve, as well as to provide an enough reserve to substitute for the aerobic response of serious trauma or injury. Acutely replacing dietary deficiencies is not the same as nutritional prehabilitation. The nutritional intervention involves the timeline that begins with the consideration of surgery and continues through the preoperative and postoperative phases to ensure early patient involvement. The importance of moving away from reactive to proactive nutrition evaluations and action must be stressed. Nutritional therapies are less well studied, and when they are, it is usually in conjunction with exercise as part of a prehabilitation program. These promising preliminary findings warrant further investigation, with a focus on fine-tuning approaches, elucidating mechanisms, and assessing correlations between therapies and large-scale clinical efficacy trials [10].

8.2.1 Expected outcomes

Changes in risk factors are linked to an unhealthy or insufficient diet.

8.3 Smoking

Smoking status is strongly linked to how people use CR. Smokers seem to be less interested in attending even a regular CR training, and those that do participate are often more likely to break out. Addition to stopping smoking should be a priority. Priority is given to patients while they are in hospital. To provide extra assistance in the hospital, a variety of techniques may be used. For stop smoking, medications drugs and nicotine pharmacological intervention referrals to smoking cessation services may be given to patients. Smoking cessation assistance should be available during the prehabilitation program. This could be delivered in the form of community, consultations in learning, and focusing on cessation assistance, including specific targeting. In the case of a relapse, daily monitoring and deep obey and assistance is in place. Intensive ongoing counseling for smoking cessation should be available in the prehabilitation services. This could be achieved through group health teaching focused on cessation support, with personalized therapy available if appropriate, pharmacotherapy assistance if needed, and regular contact with long-term accept and assistance in the event of a repeat. The availability of an intensive cessation support network could entice more smokers to enroll in the program, and the increased support for cessation they receive could enable them to stay in the program longer [8].

8.3.1 Expected outcomes

It has the potential to improve smoking cessation for a long time.

8.4 Alcohol drinking

When compared to abstinence and heavy consumption, reasonable alcohol intake (1–2 drinks/day) is linked to lower cardiovascular and all-cause mortality. According to a collective estimation from approaching longitudinal studies of patients with coronary heart disease, patients who consumed the modest improvement quantities of alcohol daily had a 20% reduction in heart failure (relative risk 0.80, 95% confidence interval [CI] 0.78–0.83) compared to nondrinkers. When we look up the data regarding alcohol intake, it is represented by the J-shaped curve with a considerable added safety against cardiovascular mortality at approximately 25 g/d and significant maximum protection against all-cause mortality at 6–11 g/d. The quantity and pattern of alcohol consumption tends to be further significant than the form of alcohol consumed. HDL is enhanced by promoting the production of apo A-I and A-II in the liver, lowering

fibrinogen levels, increasing fibrinolysis, reducing inflammation, and suppressing platelet activation, which are all possible reasons for the benefits of moderate alcohol intake [11].

8.5 Behavioral and technical problems management

Personal and behavioral problems are common among heart patients, and they can have an effect on both morbidity and mortality. Following a myocardial infarction, up to 20% of patients experience depression, anxiety, and denial. Patients are routinely screened for nervousness, insomnia, and drug addiction, and family or other social justice issues are just some of the issues that people face during cardiac rehabilitation follow-up. In cardiac rehabilitation center, social workers and other experts on the multidisciplinary patients are given the tools and help they need in order to prepare for their workplace and daily routine. Clinical, behavioral, and cultural therapies tailored to the individual are available; they have been revealed to improve health.

The Interheart Research clearly showed that stress, after lipids and smoking, is one of the most significant risk factors for cardiac incidents. Social anxiety is responsible for 30% of the population's risk of myocardial infarction, which affects the progression of cardiovascular disease by increasing blood glucose, cholesterol, lipid profile, and body mass [11,12]. Atherosclerosis, inflammation, and endothelial dysfunction are all accelerated by it. Exercise training has been linked to lower stress levels and, as a result, lowers mortality rates. Several cardiac treatment services also have workshops on stress control to assist patients in recognizing, avoiding, and dealing with traumatic conditions. Cardiac rehabilitation is thus an effective therapeutic intervention for cardiac patients in distress. Numerous cardiac rehabilitation centers provide further anxiety control technique instructions, such as consideration, relaxation inhalation, and yoga, in addition to exercise [11].

8.5.1 Expected outcomes

The psychological sense of enough and a sense of well-being or the quality of life can be improved by reducing psychological difficulties or by acquiring stress management skills.

Prehabilitation aims to enhance these health metrics, such as endurance, in order to improve postoperative recovery and preserve physical function. During the preoperative screening cycle for elective procedures, it is the best time to create a prehabilitation program. At this stage, a multidisciplinary team composed of medicine, gerontology, anesthesia, surgery, dietetics, kinesiology/physiotherapy, and nursing will recommend a risk stratification model and determine the form and length of prehabilitation required to balance the potential benefit of such intervention against the potential harm of delaying surgery [13].

9 Risk factor for prehabilitation

All patients undergoing major surgery will benefit from prehabilitation, but the duration and severity may differ. A tiring system has been proposed [9]. Educational elements underpin cardiac and pulmonary recovery, with the aim of improving patient awareness of their conditions and the benefits of lifestyle changes. This is one way to improve a patient's self-efficacy. The transition from this to other major-surgery "surgery school" is now a key component of many prehabilitation programs. Patients are better equipped to participate in prehabilitation programs and improved recovery pathways if they are informed and perceptions of the preoperative period are managed [13].

10 Phases of cardiac rehabilitation

Cardiac recovery is divided into four stages. After your cardiac event, the first phase takes place in the hospital, and the remaining three stages take place in the home or in a cardiac treatment facility.

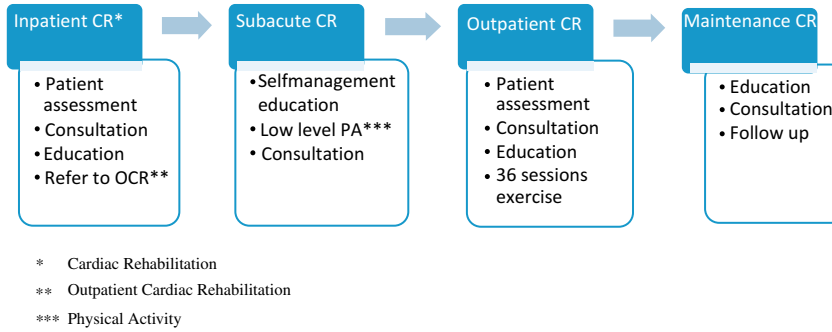

* Cardiac Rehabilitation
** Outpatient Cardiac Rehabilitation
*** Physical Activity

10.1 Phase 1

Acute phase Step 1 occurs when a patient is admitted to the hospital for an acute MI or another type of coronary incident. Throughout that time, the patient is subjected to appropriate regular exercise that is monitored and planned. However, hospitalization, clinical practice, potential risk adjustment, and treatment planning using close to zero multistage fitness tolerance testing are common. This is the first step that occurs during a cardiac incident. This process primarily aids at the beginning of mobility, determining the resilience and the effect of simple functional flexibility on the heart muscle, which are among the first targets of phase 1 cardiac rehabilitation. Prescribe healthy exercises to aid in the improvement of mobility and cardiac health. If an individual has had open-heart

surgery, medical personnel should be consulted. Trigger factors for heart events are being monitored. Patients and their families should be informed about their condition as well as the potential advantages and risks of a cardiac rehabilitation program. An individual may enter the second phase after a sufficient amount of time has passed and substantial healing has occurred.

10.2 Phase 2

The early outpatient phase of cardiac recovery is known as the subacute phase. The patient participates in a controlled regimen of physical exercise, diet therapy, behavioral support, and relative risk change during this period after being discharged from the hospital. To improve patient adherence, a program located in specialty clinic, a part of a hospital, or a cultural center can be constructed in the residential home. Cardiopulmonary recovery can take anywhere from 2 to 7 weeks and includes ongoing monitoring of the heart's reaction to exercise and activity. This step focuses on educating participants on correct workout techniques and how and when to consciously your heart rate and level of exertion when exercising. The individual ought to be able to start to do more individual research and operation at the end of phase 2.

10.3 Phase 3

Phase 3 of intensive outpatient therapy is aimed at maintaining lifestyle improvements made in phases 1 and 2. During step 3, the patient's symptoms, risk factor drug usage, and psychosocial support are all evaluated on a regular basis. The individual must be able to monitor his or her own pulse rate, simply a symptom stress response, and estimated exhaustion level (RPE). During this process of cardiac therapy, a personal trainer would be available to assist in improving exercise capacity and controlling any detrimental changes that might arise. The physical therapist helps customize a regimen of exercises, including agility, mobility, and strength training, as the individual becomes more confident during stage 3 of cardiovascular recovery.

10.4 Phase 4

Stage 4 is a self-governing upholding stage. Independent fitness and conditioning are critical for maintaining good health and avoiding any future heart complications. If a person has completed all three stages, he or she should have a thorough understanding of the disease, risk factors, and strategies for maintaining optimal health. Family physicians play an important role in all three stages of cardiac recovery by ensuring patient continuity; they also help to enhance the quality of life [14].

11 Is rehabilitation too late?

The effect on the result per day in CR remain time was determined using CR timing (i.e., the time among recommendation and begin of core CR) as a nonstop variable. A separate study looked at the effect of CR time as per the current guidelines for "early on" or "late" CR, which is described as starting within 4 weeks of recommendation.

For this, the following CR timing parameters were formed:

- early CR (0–27 days);
- late CR (27–365 days).

In certain circumstances, some patients began the CR in later age, mostly older persons tended to do so. Female, with a lower BMI, at minimum one comorbidity, high systolic blood pressure low diastolic blood pressure, and a low amount of exercise at the moment (less than 150 min per week), has a shorter baseline ISWT distance (all $p < 0.05$). Patients with MI-PCI (myocardial infarction-percutaneous coronary intervention) made up the majority of the participants in both the CR grades (early and late). In terms of patient improvement after CR, late CR attendees saw a smaller benefit for all fitness-related outcomes. Out of 100 people, 63% are identified as slow starter in CR; the average time it takes for a CR applicant to become a CR as per guidelines, it is 39 days. The percentage of MI, MI-PCI, PCI, and CABG patients who were delayed was 69% for MI, 64% for MI-PCI, 56% for PCI, and 63% for CABG patients.

The median wait times (days) for each patient group were compared with the recommended wait times (28 or 42 days for CABG). The median wait time exceeded the recommended maximum waiting time in each patient group; moreover, the post-MI population's median wait time exceeded the highest optional wait time, which was 12 days. Following several analyses, it was discovered that the duration of delayed cardiovascular recovery was a significant independent reason for lower fitness levels as compared to early CR. CR timing was also an important indicator when used as a variable. Latest cardiac care guidelines and articles suggest starting CR as early as possible whenever feasible. Comorbidity burden could be one reason because of the higher percentage of late comers. Compared to 69% of early CR attendees, 73% of late CR attendees had one comorbidity. The complexity of the case can cause a delay in the start of recovery. Difference in time interval among classes is concerning.

Post-MI patients belonged to another patient category. The median minimum wait time was well surpassed by the largest number of days (12 days). This may appear to be counterintuitive, given that post-MI patients do not undergo invasive revascularization operations, which may postpone the start of CR due to the recovery time. Pre-CR to post-CR changes in terms of fitness-linked outcomes were observed regardless of

CR timing. However, in late CR attendees, the level of change was limited. There are two methods used to investigate the effect of cardiovascular rehabilitation timing: for this continuous measure to investigate the connection between escalating wait time and outcome, and timing as a categorical measure (early/late) to investigate the relationship in the form of current guidelines. CR timing was found to be an important predictor of patient outcome in terms of fitness level in each strategy. According to these findings, delaying CR reduces the probability of reporting a positive physical activity level and health outcome. According to the recent study of CR patients, it is found that delayed enrolment is linked to improved patient outcomes [14].

The protection of early enrollment in CR was recently investigated in cardiovascular patients, with no significant difference in main incident rates between early and late enrolls. Aside from clinical results, additional research indicates that the timing of CR enrollment can have an effect on initial CR enrollment. A second study using routine patient records found a correlation between wait time and enrollment. The observed connection between CR timing and treatment outcomes in results of these findings supports the need for timely CR as prompted by current guidance. Since there is a clear correlation between exercise-based CR and lower mortality, avoiding any potential causes of suboptimal fitness shift is important. While it is understood that CR timing should be determined on a one-to-one basis, caution should be exercised to avoid unnecessary delays, such as long waiting lists [14].

12 A paradigm shift in cardiopulmonary rehabilitation

This will be linked to the patient, payer, physician, hospital, and societal health-care-financing preferences. Physical therapists and other rehabilitation providers will play an important role in the incorporation of health promotion in the changing paradigm change from illness and impairment prevention to secondary condition prevention in people with disabilities. Excess weight, as measured by body mass index, is linked to a higher risk of repeated coronary events after a heart attack, particularly in obese people. Jayawardena et al. describe how they used the "plate model" as a dietary intervention for cardiac rehabilitation [15,16]. The "plate model" is a practical way to defy the latest dietary pattern by through standard serving sizes of staple foods in daily courses while still having enough veggies and proteins. The intervention group lost substantially more weight than the control group ($P = 0.029$) over the 12-week follow-up period (intervention group: 1.27 3.58 kg; control group: 0.26 2.42 kg). Additionally, the intervention community saw a nonsignificant reduction in blood pressure and lipid levels. Just 15%–50% of CR patients continue to exercise 6 months

after CR, and even fewer do so after 12 months. About half of patients who smoked prior to a coronary incident continue to smoke 6 months later, and less than half of obese patients adhere to dietary guidelines. As a result, there are a few methods to obtaining the beneficial effects of healing. Patients will further integrate what else they have experienced throughout CR when they have a similar obey [15,16].

References

[1] M.B. Stephens, Cardiac rehabilitation, Am. Fam. Physician 80 (9) (2009) 955–959.
[2] C. Takahashi, F. Ribeiro, L.M. Vanzella, I.M. Lima, A.L. Ricci-Vitor, D.G.D. Christofaro, L.C.M. Vanderlei, Are signs and symptoms in cardiovascular rehabilitation correlated with heart rate variability? An observational longitudinal study, Geriatr. Gerontol. Int. 20 (10) (2020) 853–859.
[3] A.B. Gevaert, V. Adams, M. Bahls, T.S. Bowen, V. Cornelissen, M.D. Dorr, H.M.C. Kemps, P. Leeson, K. Craenenbroeck, Toward a personalized approach in exercise based cardiovascular rehabilitation: how can translation research help A call to action from the section on secondary prevention and cardiac rehabilitation of the European Association of Prevention Cardiology, Eur. J. Prev. Cardiol. 27 (13) (2019) 1369–1385.
[4] H.J.N. Bethell, R.J.P. Lewin, H.M. Dalal, Article on cardiac rehabilitation: so why it works so why is it not it done, Br. J. Gen. 58 (555) (2008) 677–679.
[5] R.M. Ross, ATS/ACCP statement on cardiopulmonary exercise testing, Am. J. Respir. Crit. Care Med. 167 (10) (2003) 1451.
[6] K. Albouaini, M. Egred, A. Alahmar, D.J. Wright, Cardiopulmonary exercise testing and its application, Postgrad. Med. J. 83 (985) (2007) 675–682.
[7] M. McCann, N. Stamp, A. Ngui, E. Litton, Cardiac prehabilitation, J. Cardiothorac. Vasc. Anesth. 33 (8) (2019) 2255–2265.
[8] G.J. Balady, M.A. Williams, P.A. Ades, et al., Core component of cardiac rehabilitation secondary prevention program updated: a scientific statement from American Heart Association Exercise, Cardiac Rehabilitation and Prevention Committee, the Counseling on Clinical Cardiology; the Councils on Cardiovascular Nursing, Epidemiology and Prevention and Nutrition Physical Activity and Metabolism; and the American Association of Cardiovascular Rehabilitation, Circulation 115 (20) (2007) 2675–2682.
[9] D. James, J.S. Sally, G. Dangous, Prehabilation, Clin. Med. (Lond.) 19 (6) (2019) 458–464.
[10] M.A. West, P.E. Wischmeyer, M.P.W. Grocott, Prehabilitation and nutritional support to improve perioperative outcomes, Anesthesiol. Rep. 7 (4) (2017) 340–349.
[11] M. Warner, Mampuya., Cardiac rehabilitation past, present and future: an overview, Cardiovasc. Diagn. Ther. 2 (1) (2012) 38–49.
[12] E. Diann, A.Y. Gaalema, S.T. Cutler, P.A. Higgins, Smoking and cardiac rehabilitation participation. Associations with referral, attendance and adherence, Prev. Med. 80 (2015) 67–74.
[13] F. Carli, C.S. Bergdahl, Prehabilitation to enhance perioperative care, Anesthesiol. Clin. 33 (1) (2015) 17–33.
[14] J. Fell, V. Dale, Does the timing of cardiac rehabilitation impact fitness outcomes? An observational analysis, Open Heart 3 (1) (2016), e000369.
[15] B. Barbara, L. Tina, G. Kathrin, R. Laura, R. Andres, The beneficial effects of cardiac rehabilitation, Cardiol. Ther. 9 (1) (2020) 35–44.
[16] D.W. Schopfer, E.F. Daniel, Cardiac rehabilitation in older adults, Can. J. Cardiol. 32 (9) (2016) 1088–1096.

Cardiovascular toxicity and therapeutic modalities targeting cardio-oncology: From basic research to advanced study

In view of the growing clinical and healthcare relevance of cancer survivors who are at an elevated risk of dying from cardiovascular diseases, *Cardiovascular Toxicity and Therapeutic Modalities Targeting Cardio-Oncology: From Basic Research to Advanced Study* analyzes the emerging field of cardio-oncology by reviewing the recent advancements in the field (how to monitor and treat cancer survivors for cardiotoxicity) and by identifying potential cardiac side effects in novel cancer therapies. By adopting a translational approach, the book first comprehensively covers the basic science, mechanisms, and concepts, followed by advanced state-of-art of cardio-oncology. This book begins with a brief introduction to cancer and cardiovascular diseases in cancer patients as well as the changes observed in the cardiovascular system, which serves to provide a deeper understanding of therapeutic approaches targeting cardio-oncology. The book then looks into the pathways and inhibitors involved in cancer immunology, as well as the biochemistry of tyrosine kinase inhibitors, anthracyclines, and biomarkers in cardiotoxicity induced by chemotherapeutic drugs. This book then concludes with clinical-focused chapters, including noninvasive cardiovascular imaging techniques, radiotherapy-induced cardiovascular risk, cardiovascular complication from cancer therapy, novel anticancer drugs related to cardiotoxicity, and principles of cardiovascular rehabilitation.

Written by leading researchers in various disciplines, the book serves as a valuable resource to those who are new to the field as well as to various other specialized scientists, researchers, oncologists, cardiologists, physicians, and ancillary staff.

Key Features

- Adopts a translational approach and comprehensively covers the basic science, mechanisms, and concepts, followed by advanced state-of-art of cardio-oncology
- Outlines the current knowledge of biomarkers in cancer therapy-related cardiotoxicity
- Provides improved understanding of the mechanisms of cardiovascular toxicity of various therapies that may lead to the identification of novel targets to reduce vascular complications while providing biological insights into cardiovascular pathophysiology and informing new platforms for drug discovery

About the Editors

Dr. Imteyaz Qamar is Assistant Professor at the School of Biotechnology, Gautam Buddha University, Greater Noida, India. His research focuses on stress biology and cancer genetics. He has written various manuscripts, grants, progress reports, pre-IND protocols, and animal protocols and published them in journals of international repute. He has also received various awards such as the Best Research Presenter Award (2007) from Brain Korea 21, Bharat Vikas Award (2016), Young Scientist Award (2017 and 2019), and STE Meritorious Award (2019). He serves as a member of editorial boards of various peer-reviewed journals. He is also a member of the Endocrinology Society, United States.

Dr. Pawan Kumar Maurya is Professor and Head in the Department of Biochemistry, Central University of Haryana, India. He has more than 13 years of teaching and research experience. His research focuses on biochemical diagnostics, nanomedicine, and clinical biochemistry. He has published more than 112 research articles in reputed journals. He has also edited of three books published by Elsevier, USA, and Springer-Nature, Singapore. He is the recipient of prestigious fellowships such as Science without Borders (Government of Brazil) and National Science Council, Taiwan.

ELSEVIER

ACADEMIC PRESS

An imprint of Elsevier

elsevier.com/books-and-journals

ISBN 978-0-323-90461-2

9 780323 904612

Please note, due to scheduled maintenance, eCommerce will be unavailable on 24th February 2024, between 03:30 to 10:00 BST. We regret any inconvenience this may cause.

Chapter

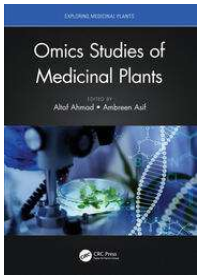

Translational Research for Medicinal Plants

Integrative Approaches, Trends and Perspectives

By Siva P. K. Chetri (/search?contributorName=Siva P. K. Chetri&contributorRole=author&redirectFromPDP=true&context=ubx), Lokesh Kumar Agarwal (/search?contributorName=Lokesh Kumar Agarwal&contributorRole=author&redirectFromPDP=true&context=ubx), Akanksha Vashishtha (/search?contributorName=Akanksha Vashishtha&contributorRole=author&redirectFromPDP=true&context=ubx), Vibhuti Singh (/search?contributorName=Vibhuti Singh&contributorRole=author&redirectFromPDP=true&context=ubx), Ratan Lal (/search?contributorName=Ratan Lal&contributorRole=author&redirectFromPDP=true&context=ubx), Amit Kumar Gupta (/search?contributorName=Amit Kumar Gupta&contributorRole=author&redirectFromPDP=true&context=ubx), Kuldeep Sharma (/search?contributorName=Kuldeep Sharma&contributorRole=author&redirectFromPDP=true&context=ubx)

Book Omics Studies of Medicinal Plants (https://www.taylorfrancis.com/books/mono/10.1201/9781003179139/omics-studies-medicinal-plants?refId=8c5144ed-8a90-4af6-9725-7358c8c882e0&context=ubx)

Edition	1st Edition
First Published	2023
Imprint	CRC Press
Pages	19
eBook ISBN	9781003179139

Share

Previous Chapter (chapters/edit/10.1201/9781003179139-1/medicinal-plants-health-care-neha-chaurasiya-altaf-ahmad?context=ubx)

Next Chapter (chapters/edit/10.1201/9781003179139-3/unraveling-medicinal-plant-chemical-diversity-novel-drug-discovery-biotechnological-interventions-mir-zahoor-gul-mohd-yasin-bhat-elizabeth-ryan-irfan-ghazi?context=ubx)

Policies

Journals

Corporate

Help & Contact

Connect with us

(https://www.linkedin.com/company/taylor-&-francis-group/) (https://twitter.com/tandfnewsroom?lang=en) (https://www.facebook.com/TaylorandFrancisGroup/) (https://www.youtube.com/user/Taylorar

Registered in England & Wales No. 3099067
5 Howick Place | London | SW1P 1WG

© 2024 Informa UK Limited

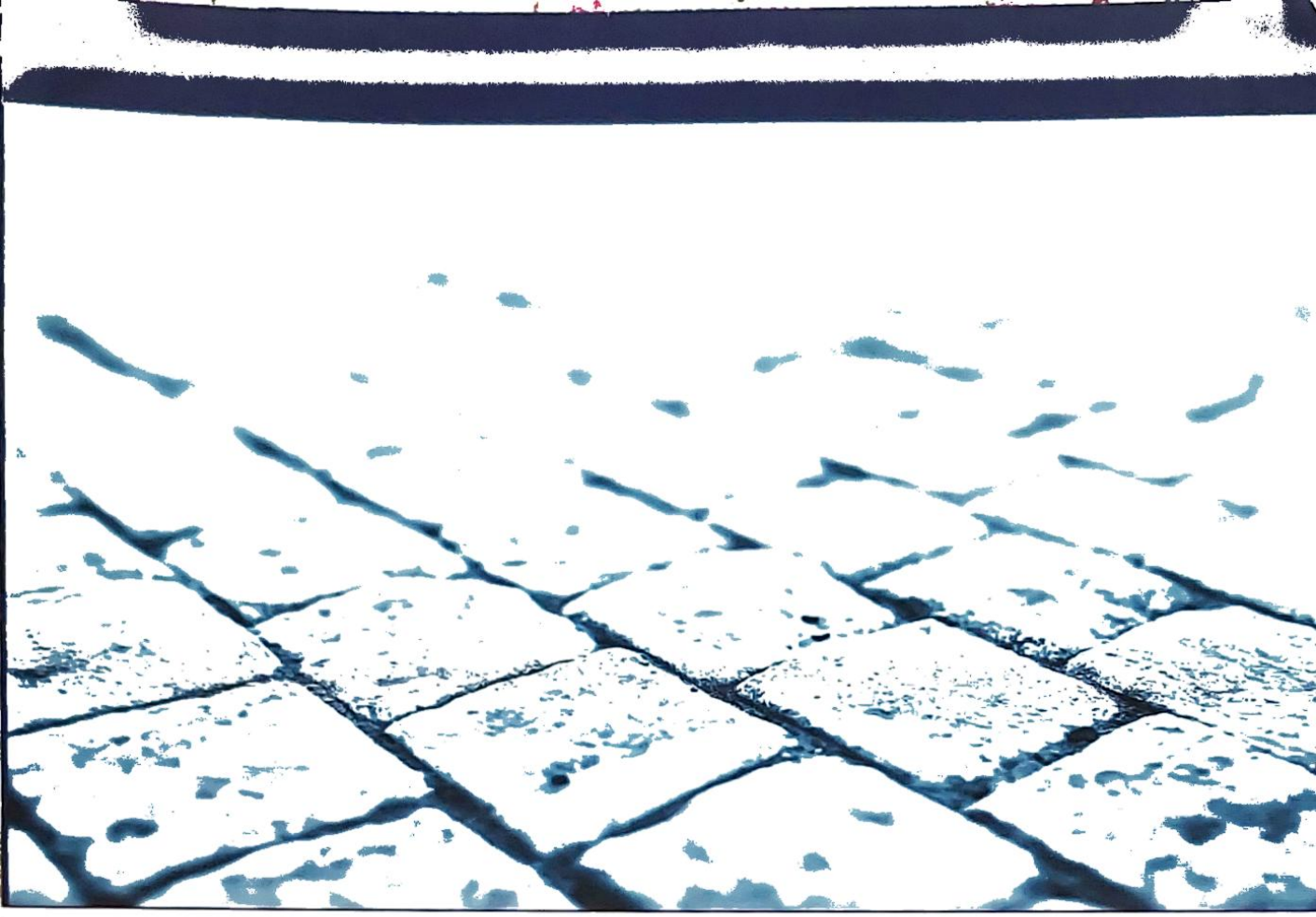

Sarita Jain
Kiran Rakibe

Trauma and Narrative

Navigating trauma through the power of narratives

LAP LAMBERT Academic Publishing

Imprint
Any brand names and product names mentioned in this book are subject to trademark, brand or patent protection and are trademarks or registered trademarks of their respective holders. The use of brand names, product names, common names, trade names, product descriptions etc. even without a particular marking in this work is in no way to be construed to mean that such names may be regarded as unrestricted in respect of trademark and brand protection legislation and could thus be used by anyone.

Cover image: www.ingimage.com

Publisher:
LAP LAMBERT Academic Publishing
is a trademark of
Dodo Books Indian Ocean Ltd. and OmniScriptum S.R.L publishing group

120 High Road, East Finchley, London, N2 9ED, United Kingdom
Str. Armeneasca 28/1, office 1, Chisinau MD-2012, Republic of Moldova, Europe
Printed at: see last page
ISBN: 978-620-6-78176-9

Copyright © Sarita Jain, Kiran Rakibe
Copyright © 2023 Dodo Books Indian Ocean Ltd. and OmniScriptum S.R.L publishing group

Contents

1. Trauma of negotiating between Language & Space in Postcolonial Literatures in English: Interpreting Shanta Acharya and Bharati Mukherjee.....5
Gargie Bhattacharya

2. From Conflict to Healing: An Analysis of the Trauma of Punjab Insurgency and the Indian Government's Restoration Initiatives.....18
Mayank Rohitashva Garg

3. Treating Psychological Trauma in the Female Character of Anita Desai's *Voices in the City* through Intrapersonal and Interpersonal Communication.....29
Dr. Anjana Tiwari and Dr. Kiran Haribhau Rakibe

4. Nazism as an Ideology.....43
Prof. Poornima Kaushik

5. Indian Partition narratives: An attempt of reinvestigating Trauma theory.....53
Dr. Tushar Chhabulal Patil

6. A Critical Study of Trauma Theory in William Golding's *Lord of the Flies*.....62
Prof.B.K.Patel and Dr.Pramod Kumar Shukla

7. A Study of Trauma in Bonnie Garmus's *Lessons in Chemistry*.....72
Dr. Sanju Choudhary

8. Surviving Through Trauma: An Emotional Death in Reference to Vera Brittain's Memoir *Testament of Youth*.....80
Dr. Sarla Singla

9. *The Glass Palace* by Amitav Ghosh: Eco-Grief Unveiled.....89
Prof. Dr. Veena Nare and Dr. Sharayu Sonawane

10. Holocaust – The Hollowness of humanity: An analysis of the works of the Survivors.....97
Ms. Ankita Verma

11. Derangement and Paranoia in "The Vietnam Project" from *Dusklands* by J. M. Coetzee.104
Dr.Snehlata Tailor

12. A Transactional Analytical Reading of Nagarkar's *God's Little Soldier*.....112
Dr.Susan Lawrencia Jackson V.J

13. The Study of Trauma as depicted in the Indian Regional Literature.....120

Munish Kumar Thakur

14. *The God of Small Things*: A Study of Trauma.....128
Dr. Bharati S. Rajebhosale and Dr. Narendra V. Deshmukh

15. The Scars of War and Migration: Understanding the Trauma Experienced by Displaced Populations.....139
Dr. Girija Joshi and Dr. Deepshikha Parashar

16. Exploring Trauma in the Hybrid Narrative of Doris Lessing's *Alfred and Emily*.....157
Dr. Kopal Vats

17. Critical and Feminist Perspective in the Study of Trauma Associated with War.....167
Dr. Karthiga S.V. and Dr. Manju Roy

18. Paradigms of Survival: Delineating the Quest for Identity and Survival Strategies of Migrants in Monica Ali's *Brick Lane*.....175
Dr. Anjana R B , Bhagya V J, Rukmini Sarma

19. Bhagvad Gita as Therapeutic Tool in Indian English Fiction: A case study of Arun Joshi's *The Foreigner*.....181
Dr. Anita Yadav

20. Trauma and its overwhelming effects in Alan Duff's *Once Were Warriors*.....194
Ms. Richa Tiwari

21. Theories of Cultural Trauma.....204
Dharmishtha Oza

22. Body, Violence and Trauma in the World of Toni Morrison: A Feminist Study.....216
Arunima Singh

23. A Re-reading of the Paradigm shift of Gendered Roles and Emotional Trauma in Mahasweta Devi's *The Hunt*.....224
Dr. Poonam Rani Gupta

24. War's psychological effects and post-survival.....231
Ms. Jayashree Khade

25. Traumatic Stress of Displacement in Bharti Mukherjee Select Works.....245
Dr. Isha Seegar

26. Reflection of Socio-Political Trauma in Fragmented Feminine Self in *I Am Malala* by Malala Yousafzai.....259
Dr. Yashoda Verma

POINTER

WHO DESERVES THE BOOKER?

Critiquing the Rich Legacy

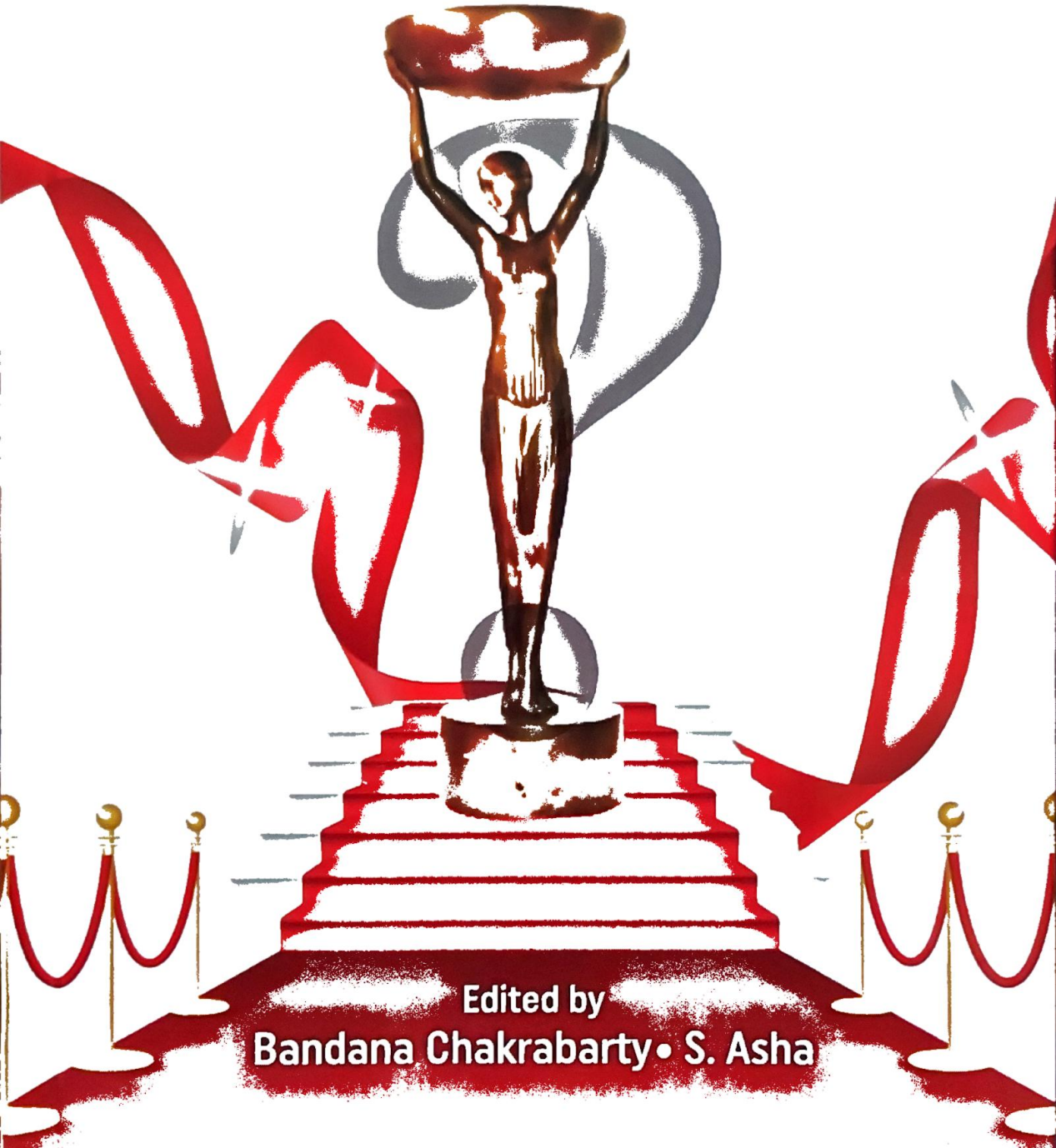

Edited by
Bandana Chakrabarty • S. Asha

Who Deserves the Booker?
Critiquing the Rich Legacy

Edited by
Bandana Chakrabarty | S. Asha

Pointer Publishers
Jaipur 302 003 (Raj.) India

Department of English
MLS University Udaipur- 313039

Dr. Minakshi Jain
Head

6376881743
english@mlsu.ac.in

No. UCSSH/Eng./2023/

Date: 7 Nov. 2023

Office Order

Mr Saurabh Meena is, hereby, allotted R.N. 116 and will shift from his room on the second floor. Dr Anjali Singh will continue to occupy her room no. 312. However, till she is allotted a separate room on the ground floor she may share Mr. Saurabh Meena's room as per her need.

Further, the three-seater sofa in room no. 116 will be moved to the room of Dr Kopal Vats and the two-seater sofa will be moved to Dr Bhanupriya Rohila's room.

The room no. 311 vacated by Mr Saurabh Meena will be for the Guest Faculty and Research Scholars of the Department.

7.11.2023

Head

Copy to all concerned

Distributed by
Prem C. Bakliwal
Aavishkar Publishers, Distributors
807, Vyas Building, Chaura Rasta
Jaipur 302 003 (Raj.) India
Phone : 0141-2578159
e-mail : aavishkarbooks@hotmail.com
website : aavishkarpublishers.com

© Editors

ISBN 978-81-19559-53-4

First Published in 2023 by
Mrs. Shashi Jain for
Pointer Publishers
Vyas Building, Chaura Rasta
Jaipur 302 003 (Raj.) India
Phones : 0141-2578159
e-mail : pointerpub@hotmail.com
website : www.pointerpublishers.com

Printed at
Trident Enterprises (UP)
Noida

CONTENTS

	Introduction	ix
1.	Iris Murdoch - A Novelist and Philosopher *—Santosh Gupta*	1
2.	The Quest for Identity in Naipaul's *In a Free State* : A Psychoanalytic Perspective *—Shalini Bhargava and Sunil Pathak*	13
3.	Re-reading *The Conservationist* in the Post-Apartheid Context *—Manila Kohli*	20
4.	Raj Nostalgia in *Heat and Dust*: Fiction and Film *—S. Asha*	27
5.	Multicultural Engagements in the Literary Works of J. M. Coetzee *—Snehlata Tailor*	38
6.	Magic Realism in the Works of Ben Okri and Arundhati Roy: An Experience of Disruption *—Vandana Beniwal*	46
7.	Refiguring Ecofeminist Concerns: Gender and Culture in Roy's *The God of Small Things* *—Kumkum Sharma and Shivangi Bhatt*	54

8. Gender Inequality in *The God of Small Things* 61
—*Priyanka Upadhyaya*

9. Reconfiguring the Self through Literary discourse: A Study of Atwood's *The Blind Assassin* 66
—*Sarita Jain*

10. Metamorphosis of the Protagonist in Margaret Atwood's *Surfacing* 82
—*Preeti*

11. Elucidating Reality in John Banville's *The Infinities* 89
—*Ritika*

12. Aspects of Immigration and Diasporic Sensibility in Kiran Desai's *The Inheritance of Loss* 98
—*Gunjan Sharma*

13. Divided Self: Identity Issues in *The Inheritance of Loss* and *The English Patient* 104
—*Pritam Singh*

14. Representations, Receptions and Rewards 112
—*Jyoti Sareen*

15. Master-Slave Dialectic: A Postcolonial Study of Adiga's *The White Tiger* 118
—*Smita Sharma*

16. From Script to Screen: Cinematic Representation of *The White Tiger* 123
—*Oorja Yadav*

17. What Gives Alice Munro's Stories Its Gothic Twist? 132
—*Bandana Chakrabarty*

18. *Wolf Hall*: Retelling of a Familiar Tale from an Unfamiliar Angle 143
—*Manju Shivran*

19. A Study of Distorted Memories and Delusional Self: Julian Barne's *The Sense of an Ending* 151
—*Sakshi Bharadwaj*

20. Introspection and Identity in David Grossman's *A Horse Walks into a Bar* 158

—*Kopal Vats*

21. Trauma and Gender Abuse: A Reading of Anna Burns' *Milkman* 167

—*Payal Dalal*

22. Dynamics of Womanhood : Bernardine Evaristo's *Girl, Woman, Other* 174

—*Ruchika Dahiya*

23. What It Truly Means to Feel Different: The Struggle against Societal Stigma in Evaristo's *Girl, Woman, Other* 182

—*Jyoti Meena*

24. Changing Notions of Home : Geetanjali Shree's *Tomb of Sand* 192

—*Shibali Kharbanda*

25. Finding their Voices: Translating the Essence of Oriental Womanhood in Geetanjali Shree's *Tomb of Sand* 199

—*Indresh Purohit*

Contributors 207

Who Deserves the Booker? Critiquing the Legacy is a comprehensive anthology on the coveted literary award the Booker Prize. Of the extensive list of the winners over six decades, six of them being Indians, including the latest awardee Geetanjali Shree, their works have become a subject of exploration. The essays in the present volume include awarded writings across the globe and make an honest attempt to critique these works. Today, literary awards provide a public platform for the appreciation of writers and their works, help them gain recognition and provide them with financial support to continue their work. The Booker Prize, previously known as the Man Booker Prize, is a literary award for the best English novel of the year published in the United Kingdom or Ireland. The winner of the Booker Prize is selected by a panel and receives £50,000. The present anthology comprises a collection of twenty-five articles contributed by eminent scholars as well as young and enthusiastic researchers who critique the rich legacy of the Booker Prize. The articles cover a span of six decades providing deep insight into varied themes which are subjects of universal concern. The book will open up doors to further study on such literary awards. It will be a valuable treasure house for further explorations both by researchers and scholars.



Bandana Chakrabarty, an independent scholar has an experience of over thirty seven years of teaching English in various Government Colleges of Rajasthan. Former Joint – Director(Academic) in the Commissionerate of College Education, Jaipur and as Principal of Rajasthan School of Art, Jaipur, she has been instrumental in organizing several Academic activities. Author of *Fictions of the Self: Alice Munro* she has co-edited several anthologies.



S. Asha has been Professor in Government College Tonk. She has a teaching experience of over thirty years in various Government Colleges of Rajasthan. She also has had administrative experience. Her research papers have been published in various journals and books. She has presented papers in International Conferences both in India and abroad. She has authored *Harold Pinter's Screenplays* and has co-edited an anthology titled *Embracing Glocal English*. She in the Vice-President of ELT@I Rajasthan Chapter. She has been a part of all the Conferences and workshops organized by the chapter and conducted several workshops.

₹ 1300.00

POINTER

POINTER PUBLISHERS
Vyas Building, Chaura Rasta
Jaipur-302 003 (Raj.) Ph.: 0141-2578159
e-mail : pointerpub@hotmail.com
Website : www.pointerpublishers.com

ISBN : 978-81-7132-953-4

Provided for non-commercial research and educational use.
Not for reproduction, distribution or commercial use.

This chapter was published in the book *Micro and Nano Technologies* published by Elsevier, and the attached copy is provided by Elsevier for the author's benefit and for the benefit of the author's institution, for non-commercial research and educational use including without limitation use in instruction at your institution, sending it to specific colleagues who you know, and providing a copy to your institution's administrator.

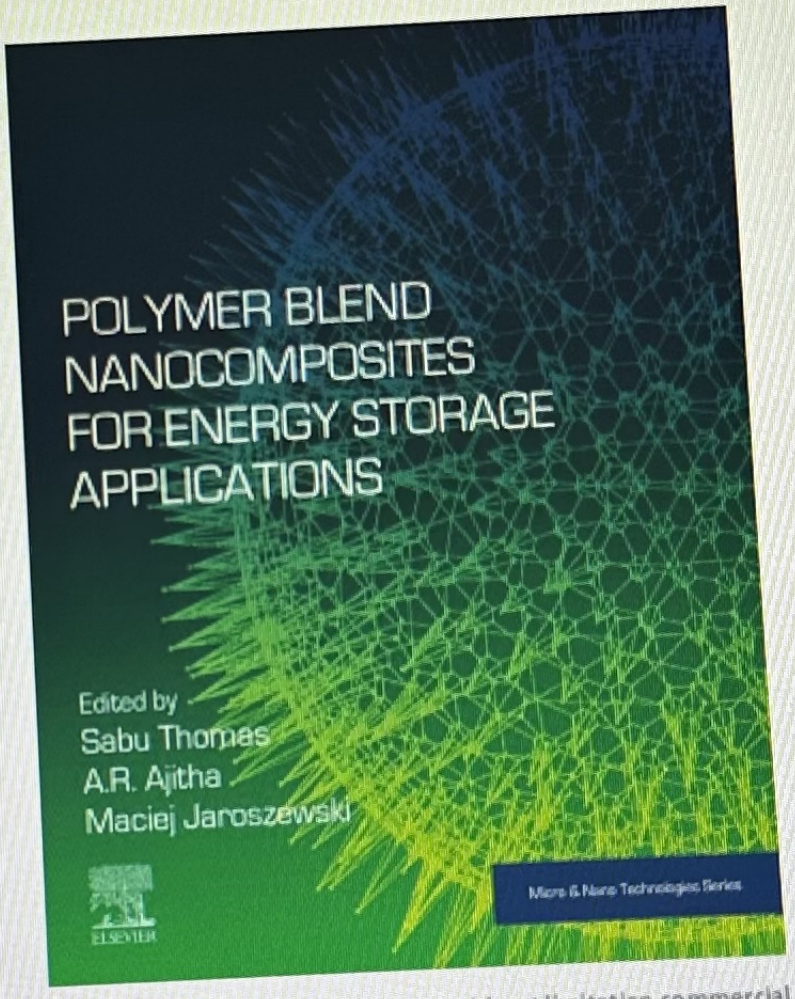

All other uses, reproduction and distribution, including without limitation commercial reprints, selling or licensing copies or access, or posting on open internet sites, your personal or institution's website or repository, are prohibited. For exceptions, permission may be sought for such use through Elsevier's permissions site at:

https://www.elsevier.com/about/our-business/policies/copyright/permissions

Rama Kanwar Khangarot, Ayushi Bhatnagar and Gangotri Pemawat, Polymer blend nanocomposites of fullerene for energy storage. In: Sabu Thomas, A.R. Ajitha and Maciej Jaroszewski (eds.) Micro and Nano Technologies. Burlington: Elsevier, 2023. pp. 293-310.
ISBN: 978-0-323-99549-8
© 2023 Elsevier Inc. All rights reserved.

GREEN TECHNOLOGY FOR THE SUSTAINABLE DEVELOPMENT

(DECONTAMINATION OF WATER AND ENVIRONMENT POLLUTION)

Dr. Azad Kumar
Dr. Ashok Kumar
Major Mukesh Kumar
Dr. Shiv Mahendra Singh





BlueRose ONE
Glorious Matter

INR 600

ACADEMIC

www.BlueRoseOne.com

GREEN TECHNOLOGY FOR THE SUSTAINABLE DEVELOPMENT

(DECONTAMINATION OF WATER AND ENVIRONMENT POLLUTION)

Dr. Azad Kumar
Dr. Ashok Kumar
Major Mukesh Kumar
Dr. Shiv Mahendra Singh





BlueRose ONE
Glorious Matter

INR 600

ACADEMIC

www.BlueRoseOne.com

GREEN TECHNOLOGY FOR THE SUSTAINABLE DEVELOPMENT

(DECONTAMINATION OF WATER AND ENVIRONMENT POLLUTION)

Dr. Azad Kumar
Dr. Ashok Kumar
Major Mukesh Kumar
Dr. Shiv Mahendra Singh





BlueRose ONE
Glorious Matter

INR 600

ACADEMIC

www.BlueRoseOne.com

GREEN TECHNOLOGY FOR THE SUSTAINABLE DEVELOPMENT

(DECONTAMINATION OF WATER AND ENVIRONMENT POLLUTION)

Dr. Azad Kumar
Dr. Ashok Kumar
Major Mukesh Kumar
Dr. Shiv Mahendra Singh





BlueRose ONE
Glorious Matter

INR 600

ACADEMIC

www.BlueRoseOne.com






Publishers:
Thanuj International Publishers,
8/173-B, Vengayapalayam, Rasipuram,
Namakkal, Tamil Nadu, India – 637406.
E-mail: thanujinternationalpublishers@gmail.com

Printers:
Dhazh Computers
No: 442- A, 10th East Cross Street,
Munthirithoppu, Annanagar,
Madurai – 20, Tamil Nadu, India.
E-mail: narennarayanasamy@gmail.com

ISBN: 978-93-94638-19-8
9 789394 638198

Copyright@Thanuj International Publishers, 2022.

Current and Future Perspectives of Environmental Pollution and it's Remediation

CURRENT AND FUTURE PERSPECTIVES OF ENVIRONMENTAL POLLUTION AND IT'S REMEDIATION

First Edition

Editors
Dr. Azad Kumar
Mr. Vinod Kumar Singh
Dr. Akhilesh Sharma



THANUJ INTERNATIONAL PUBLISHERS,
TAMIL NADU, INDIA.






Publishers:
Thanuj International Publishers,
8/173-B, Vengayapalayam, Rasipuram,
Namakkal, Tamil Nadu, India – 637406.
E-mail: thanujinternationalpublishers@gmail.com

Printers:
Dhazh Computers
No: 442- A, 10th East Cross Street,
Munthirithoppu, Annanagar,
Madurai – 20, Tamil Nadu, India.
E-mail: narennarayanasamy@gmail.com

ISBN: 978-93-94638-19-8
9 789394 638198

Copyright@Thanuj International Publishers, 2022.

Current and Future Perspectives of Environmental Pollution and it's Remediation

CURRENT AND FUTURE PERSPECTIVES OF ENVIRONMENTAL POLLUTION AND IT'S REMEDIATION

First Edition

Editors
Dr. Azad Kumar
Mr. Vinod Kumar Singh
Dr. Akhilesh Sharma



THANUJ INTERNATIONAL PUBLISHERS,
TAMIL NADU, INDIA.

छायावाद

एक पुनर्विचार

डॉ. नवीन नंदवाना

नेशनल पब्लिकेशन्स

जयपुर

CHHAYAVAD : EK PUNARVICHAR

by

Navin Nandwana

ISBN 978-93-92688-00-3

© लेखक

प्रथम संस्करण : 2022

❑

मूल्य : ₹ 595

❑

प्रकाशक

नेशनल पब्लिकेशन्स

श्याम फ्लैट्स, फतेहपुरियों का दरवाजा

चौड़ा रास्ता, जयपुर - 302 003

फोन : 0141-4914552

ई-मेल : natbooks337@gmail.com

❑

टाइपसैटिंग

नेशनल कम्प्यूटर्स, जयपुर

❑

मुद्रक

हरीश आर्ट प्रिंटर्स, जयपुर

भूमिका

छायावादी कवियों और उनके काव्य को लेकर कुछ गहन अध्ययन और उस पर लेखन की इच्छा लंबे समय से थी। वर्ष 2019 की फरवरी में जब सूर्यकांत त्रिपाठी 'निराला' की कविता पर संगोष्ठी आयोजित की, तब से यह इच्छा और बलवती होती गई किंतु प्रत्येक कार्य के होने या करने में हमारा वश कहाँ चल पाता है। राष्ट्रकवि दिनकर ने लिखा है—''यह सब उनकी कृपा, सृष्टि जिनकी निगूढ़ रचना है, झुके हुए हम धनुष मात्र हैं, तनी हुई ज्या पर से, किसी और की इच्छाओं के बाण चला करते हैं।'' अतः स्पष्ट है कि प्रत्येक कार्य का आरंभ और पूर्णता सभी कुछ नियत होते हैं और शायद उसी नियत के कारण इस पुस्तक का लेखन और प्रकाशन टलता रहा। वास्तव में इस विषय पर पुस्तक लेखन का विचार उस समय आया, जिस समय हम छायावाद का शताब्दी वर्ष मना रहे थे। पर वह केवल विचार मात्र ही रह गया। समय-समय पर संशोधन और परिवर्धन भी होते रहे और प्रकाशन तक आते-आते वर्ष 2022 आ गया। यह विचार अब इस पुस्तक का रूप ले पाया।

इस पुस्तक का लेखन-काल बड़ा ही कठिन और पीड़ादायी रहा है, मेरे व्यक्तिगत जीवन के लिए भी और संपूर्ण संसार के लिए भी। व्यक्तिगत वेदना ने मेरे हृदय के कितने टुकड़े किए होंगे, नहीं कह सकता। उन टुकड़ों को खोजना, एक साथ करना और पुनः एक सही आकार देना न मेरे वश का है और न ही संसार में किसी और के वश का। ऐसे में जब मैं अपने टूटे दिल से पीड़ा में डूबा था, तब वेदना एवं करुणा के भावों को और अधिक गहराई से समझा। तब यह विचार उमड़-घुमड़कर मेरे मन-मस्तिष्क में आता रहा कि 'पर शेष नहीं होगी मेरे प्राणों की पीड़ा'। पीड़ा के इसी सागर में जब संवेदनाओं की उथल-पुथल मची थी, इसी बीच कोरोना महामारी ने संपूर्ण विश्व को एक बड़े संकट में डाल दिया। अतः यह समय मेरे लिए व्यक्तिगत वेदना से विश्व वेदना की यात्रा का रहा है।

लॉकडाउन की अवधि ने हम सभी को घरों में कैद कर लिया था। छायावाद से जुड़ी कई किताबें पुस्तकालय से बहुत पहले निकलवा चुका था। घर की व्यक्तिगत लाइब्रेरी में भी बहुत पुस्तकें मिल गईं। ऑनलाइन सामग्री ने भी बहुत मदद की और ऐसे में वेदना से गुजरते हुए सबसे पहले महादेवी की रचनाओं को पढ़ा और धीरे-धीरे कुछ लिखने का प्रयास किया। पुस्तक लेखन जैसा विचार नहीं था किंतु लंबी लॉकडाउन की अवधी में धीरे-धीरे इस क्रम को जारी रखा जिससे यह पुस्तक अपना स्वरूप ले पाई।

इस पुस्तक में कुल पाँच अध्याय हैं। पहले अध्याय में छायावाद की सैद्धांतिकी पर विचार है। वहीं आगे के चार अध्यायों में छायावाद के चारों स्तंभ कवियों—प्रसाद, निराला, पंत एवं महादेवी के कृति-व्यक्तित्व की पहचान, पुनर्विचार एवं रचना वैशिष्ट्य की परख करने का प्रयास किया गया है। 'छायावाद' पर उपलब्ध चर्चित पुस्तकों के अध्ययन के बाद इस पुस्तक के लेखन में इस बात को विशेष रूप से ध्यान में रखा गया है कि पुस्तक में वर्णित विषयों का प्रतिपादन सहज और सरल भाषा में हो। साथ ही स्नातकोत्तर से लेकर प्रतियोगी परीक्षाओं के परीक्षार्थियों तक सभी के लिए यह पुस्तक सहायक सिद्ध हो। इसी कारण विद्यार्थियों से जुड़े सभी पाठ्यक्रमों, जैसे—विश्वविद्यालयी पाठ्यक्रम, लोकसेवा आयोग परीक्षाओं के पाठ्यक्रम और नेट-स्लेट आदि परीक्षाओं के पाठ्यक्रमों आदि को ध्यान में रखकर इस पुस्तक का लेखन किया गया है। आशा है यह पुस्तक सभी परीक्षार्थियों के लिए तो उपयोगी होगी ही, साथ ही रुचिवान पाठकों एवं शोधार्थियों के लिए भी सहायक सिद्ध होगी।

—डॉ. नवीन नंदवाना

अनुक्रम

1. छायावाद : अर्थ, अवधारणा और स्वरूप **1**

छायावाद : अर्थ, नामकरण एवं अवधारणा / 1 • छायावाद : प्रवर्तन, प्रवर्तक और समय सीमा / 3 • छायावाद : परिभाषाएँ / 4 • छायावाद : प्रवृत्तियाँ एवं स्वरूप / 5 • सौंदर्य चेतना / 5 • प्रेम निरूपण / 9 • वैयक्तिकता / 14 • रहस्यवाद / 16 • वेदनानुभूति / 18 • राष्ट्रीयता / 21 • मानवीकरण / 24 • प्रकृति वर्णन / 27 • मानवतावादी दृष्टि / 31 • काव्य भाषा / 33 • छंद योजना / 36 • अलंकार योजना / 40 • बिंब विधान / 44 • प्रतीक योजना / 46

2. जयशंकर प्रसाद **49**

जन्म एवं पारिवारिक जीवन / 49 • व्यक्तित्व वैशिष्ट्य / 51 • रचना संसार / 53 • छायावादी रचनाएँ / 57 • कामायनी : कथावस्तु / 66 • कामायनी : महाकाव्यत्व / 70 • कामायनी : रूपक तत्त्व / 73 • प्रसाद का काव्य : रचना-वैशिष्ट्य / 76 • सौंदर्य चेतना / 77 • प्रेम निरूपण / 78 • मानवीकरण / 79 • चित्रात्मकता / 80 • मानवतावादी दृष्टिकोण / 80 • राष्ट्रीयता / 81 • प्रकृति चित्रण / 82 • रस योजना / 83 • काव्य भाषा / 84 • छंद योजना / 84 • अलंकार योजना / 85 • लाक्षणिकता / 85 • बिंब योजना / 86 • प्रतीक योजना / 87

3. सूर्यकांत त्रिपाठी 'निराला' **88**

जन्म एवं पारिवारिक जीवन / 88 • शिक्षा-दीक्षा / 90 • संघर्ष और साहित्य / 90 • व्यक्तित्व वैशिष्ट्य / 91 • रचना संसार / 92 • रचना वैशिष्ट्य / 102 • प्रेम

निरूपण / 103 • आत्माभिव्यक्ति / 105 • मानवतावादी दृष्टिकोण / 106 • रहस्यवाद / 107 • प्रकृति चित्रण / 109 • राष्ट्रीयता / 110 • अभिव्यक्ति पक्ष / 111 • काव्य भाषा / 111 • छंद योजना / 112 • अलंकार योजना / 114 • बिंब विधान / 115 • प्रतीक योजना / 116

4. सुमित्रानंदन पंत 118

जन्म एवं पारिवारिक जीवन / 118 • शिक्षा-दीक्षा / 119 • व्यक्तित्व वैशिष्ट्य / 119 • काव्य प्रेरणा / 120 • पंत की काव्य यात्रा / 121 • रचना संसार / 122 • रचना वैशिष्ट्य / 133 • सौंदर्य चेतना / 133 • प्रेम वर्णन / 138 • पंत : प्रकृति चित्रण / 140 • काव्य भाषा / 146 • शब्द प्रयोग / 147 • अलंकार / 148 • बिंब विधान / 149

5. महादेवी वर्मा 150

जन्म एवं पारिवारिक जीवन / 150 • शिक्षा-दीक्षा / 151 • विराट व्यक्तित्व / 152 • रचना संसार / 154 • पुरस्कार, सम्मान और उपाधियाँ / 154 • अन्य उपलब्धियाँ / 155 • अवसान / 155 • यामा : चार याम / 155 • रचना वैशिष्ट्य / 159 • प्रेम निरूपण / 159 • सौंदर्य चेतना / 161 • वेदनानुभूति / 162 • रहस्यवाद / 164 • मानवतावादी दृष्टिकोण / 167 • स्वानुभूति की विवृत्ति / 169 • प्रकृति वर्णन / 171 • गीति योजना / 174 • काव्य भाषा / 179 • लाक्षणिकता / 180 • प्रतीकात्मकता / 180 • अलंकार योजना / 182

❑❑❑

21वीं सदी का हिंदी उपन्यास

संपादक
डॉ. नवीन नंदवाना

हिमांशु पब्लिकेशन्स
उदयपुर ☐ नई दिल्ली

मुद्रणाधिकार ©

इस पुस्तक के किसी भी अंश की किसी भी रूप में प्रतिकृति करना या किसी भी साधन-इलेक्ट्रॉनिक मैकेनिकल या अन्य प्रकार जैसे फोटोकॉपी, रिकॉर्डिंग या सूचना संचयन और पुनः प्राप्ति पद्धति द्वारा प्रसारित करना संपादक / प्रकाशक की लिखित अनुमति के बिना मना है।

HIMANSHU Publications

हिमांशु पब्लिकेशन्स

464, हिरण मगरी, सेक्टर 11, उदयपुर 313 002 (राज.), फोन: 0294-2421087

4379/4-B, प्रकाश हाऊस, अंसारी रोड़, दरियागंज, नई दिल्ली-2, मोबाईल: 96109-73739

Web : *himanshupublications.com;* email : *himanshupublications@gmail.com*

ISBN : 978-81-7906-962-2

संस्करण : 2022

मूल्य : ₹ 695.00

Distributor

ARYAS PUBLISHERS DISTRIBUTORS (P) LTD.

2-D, Hazareshwar Colony, Near Court Choraha, Udaipur (Raj.) - 313 001; Phone : 0294-2526160

E-mail : apdpl.2012@gmail.com

अनुक्रम

1. 'गिलिगडु' : वृद्धावस्था का यथार्थ — 1
प्रो. वृषाली मांद्रेकर

2. 'यहीं कहीं था घर' : स्त्री होने का दंश झेलती नारी — 6
डॉ. नामदेव एम. गौडा

3. 'शिगाफ' : विस्थापन, स्त्री और कश्मीर — 13
डॉ. कल्पना गवली

4. 'पोस्ट बॉक्स नं. 203 नाला सोपारा' : दृष्टिकोण की विकलांगता और बदलाव की अपेक्षा — 21
डॉ. संजय नवले

5. काटना शमी का वृक्ष पद्मपंखुड़ी की धार से : यह पथरीला दर्द काव्य का मुझ से सहा न जाता... — 26
प्रभात कुमार मिश्र

6. 'राग विराग' : जीवन की जटिलताओं से टकराहट — 44
डॉ. नवीन नंदवाना

7. 'कथा सतीसर' : आतंकवाद से जर्जर होती जिंदगी का अंकन — 55
डॉ. नयना डेलीवाला

8. 'सलाम आखिरी' : एक संवेदनशील 'कोलाज' — 61
डॉ. संगम वर्मा

9. 'अन्तर्वंशी' : बदलती नारी चेतना का अंकन — 68
डॉ. संदीप श्रीराम पाईकराव

10. 'ए.बी.सी.डी.' : प्रवासी भारतीयों का सांस्कृतिक संकट — 73
डॉ. निम्मी ए.ए.

11. 'कोहरे में कैद रंग' : जीवन के विभिन्न रंगों से साक्षात्कार 79
डॉ. शबाना हबीब

12. 'तिरोहित' : मनोवैज्ञानिकता की पड़ताल 85
डॉ. हिरल शादीजा

13. 'रेत' : देह से देह की मुक्ति का सफर 91
डॉ. नीतू परिहार

14. 'रेहन पर रग्घू' : मनुष्य के अकेलेपन का बेजोड़ आख्यान 104
डॉ. आदित्य कुमार गुप्त

15. 'प्रेम की भूतकथा' : प्रणय और मृत्यु की भूल-भुलैय्या 114
डॉ. लेखा. एम

16. 'दुक्खम : सुक्खम' : एक शास्त्रीय विवेचन 120
डॉ. जय राम त्रिपाठी

17. 'मिलजुल मन' : आत्म और पर का संयोग 125
डॉ. हेना

18. 'गाँव भीतर गाँव' : ग्रामीण यथार्थ की गहन पड़ताल 133
डॉ. शशिभूषण मिश्र

19. 'गुजरात पाकिस्तान से गुजरात हिंदुस्तान' : अतीत के झरोखे से 140
डॉ. रवीन्द्र अमीन

20. 'विनायक' : 21वीं सदी के हर असिद्ध नायक के जीवन का दस्तावेज 146
डॉ. अखिलेश चास्टा

21. 'तीसरी ताली' : हाशिए पर जीवन जीती तीसरी दुनिया का सच 153
डॉ. मनीषा शर्मा

22. 'दस द्वारे का पींजरा' : पिंजरे से मुक्ति का संघर्ष 162
डॉ. ईश्वर सिंह चौहान

23. 'पारिजात' : गंगा-जमुनी तहजीब का दस्तावेज 175
डॉ. संतोष विजय येरावार

24. 'फाँस' : उत्तर-आधुनिक समय में किसान जीवन का महाकाव्य 181
डॉ. विनोद कुमार विश्वकर्मा

25. 'सेज पर संस्कृत' के सकारात्मक सरोकार 194
डॉ. अनीता नायर

26. 'न भूतो न भविष्यति' : विवेकानंद और वर्तमान 205
डॉ. नीता त्रिवेदी

27. 'अधबुनी रस्सी : एक परिकथा' : इक्कीसवीं शताब्दी के वितान में बीसवीं सदी की दास्तान 216
डॉ. अश्विनी कुमार शुक्ल

28. 'कैसी आगी लगाई' : विविधताओं से भरे जीवन की कलात्मक अभिव्यक्ति 222
देवेन्द्र कुमार गुप्ता



कृष्ण साहित्य

(विविध संदर्भ)

सम्पादक
डॉ. नीतू परिहार

प्रतिलिप्याधिकार प्रकाशक व लेखक के अधीन सुरक्षित है। इनकी पूर्व लिखित अनुमति के बिना इस पुस्तक के किसी भी भाग का पुनः प्रकाशन वर्जित है। इस पुस्तक में व्यक्त विचार लेखकों के व्यक्तिगत हैं। इनसे किसी भी प्रकार की होने वाली हानि के लिए संपादक और प्रकाशक उत्तरदायी नहीं हैं। किसी भी विवादास्पद स्थिति में न्यायालय क्षेत्र उदयपुर मान्य होगा।

कृष्ण साहित्य : विविध संदर्भ

ISBN : *978-81-86064-98-6*

© : **संपादक**

मूल्य : **चार सौ रुपये**

संस्करण : **2023**

प्रकाशक : **अंकुर प्रकाशन**
1/1 कांजी का हाटा, गायत्री मार्ग
उदयपुर (राज.) 313001
फोन नं. : (0294) 2417094, 2417039
(मो.) 9413528299
ईमेल : ankurprakashan15@gmail.com

आवरण : डॉ. शंकर शर्मा, उदयपुर

टाईपसेटिंग : देवेन्द्र कम्प्यूटर, दिल्ली

मुद्रक : रिसर्च प्रेस इण्डिया, दिल्ली

Krishna Sahitya : Vividh Sandarbh *(Hindi Literature)*

Edited By : Neetu Parihar

₹ 400

अनुक्रम

1	आत्म प्रबंधन : कृष्ण और गीता—प्रो. बी.एल. चौधरी	13
2	कृष्णभक्ति-परंपरा में सखी-भाव : प्रेमलक्षणा भक्ति का उत्कर्ष—डॉ. कृष्णचंद्र गोस्वामी 'विभास'	16
3	संप्रदाय मुक्त कृष्ण काव्य: चिंतन और चेतना के संदर्भ—प्रो. श्रद्धा सिंह	30
4	भक्ति साहित्य में कृष्ण—प्रो. कृष्ण कुमार शर्मा	37
5	राजस्थान में पुष्टिमार्गीय परम्परा एवं वल्लभाचार्य के सिद्धान्तों की व्यावहारिकता—डॉ. चन्द्रशेखर शर्मा	50
6	कृष्णभक्ति सरोवर में तैरता हंस : रसखान—डॉ. नीतू परिहार	64
7	मध्यकालीनकृष्ण भक्ति काव्यधारा: प्रमुख कवि और काव्य वैशिष्ट्य—डॉ. नवीन नंदवाना	71
8	भक्ति का लोक मार्ग : पुष्टि भक्ति संदर्भ—सूरसागर एवं पुष्टिवर्धन—डॉ. नवनीतप्रिया शर्मा	83
9	श्रीमद्भगवद्गीता में प्रतिपादित कर्मयोग एवं पुष्टिमार्ग —डॉ. प्रीति भट्ट	97
10	जैन आगमों में श्रीकृष्ण —डॉ. आशीष सिसोदिया	103
11	राधा की अंतरंग अनुभूतियों का गायन : कनुप्रिया —डॉ. नीता त्रिवेदी	111
12	रीतिकाल में कृष्ण भक्ति काव्य स्वरूप (बिहारी एवं घनानंद के विशेष संदर्भ में)—डॉ. कैलाश गहलोत	127

7

मध्यकालीनकृष्ण भक्ति काव्यधाराः प्रमुख कवि और काव्य वैशिष्ट्य

—डॉ. नवीन नंदवाना

भक्ति भारतीय प्राणधारा की आधारभूमि है। सदियों से भारतीय लोकजीवन में भक्ति का शंखनाद सुनाई पड़ा है। अलग-अलग कालखंडों में विविध संतों और भक्तों ने अपने समय की माँग और साधना पद्धति के अनुरूप भक्ति चेतना का बिगुल बजाया। 'भक्ति' शब्द की व्युत्पत्ति 'भज्' धातु से मानी जाती है जिसका अर्थ होता है—भजना। आचार्य रामचंद्र शुक्ल अपने प्रसिद्ध निबंध 'श्रद्धा-भक्ति' में भक्ति को इस प्रकार स्पष्ट करते हैं कि—''श्रद्धा और प्रेम के योग का नाम ही भक्ति है। जब पूज्य भाव की वृद्धि के साथ श्रद्धा भाजन के सामीप्य लाभ की प्रवृत्ति हो, उसकी सत्ता के कई रूपों के साक्षात्कार की वासना हो, तब हृदय में भक्ति का प्रादुर्भाव समझना चाहिए।'' डॉ. धीरेन्द्र वर्मा अपने 'हिंदी साहित्य कोश' में भक्ति के स्वरूप को स्पष्ट करते हुए लिखते हैं कि—''नारद के अनुसार वह 'परमप्रेमरूपा' और 'अमृत स्वरूपा' है, जिसे प्राप्त कर मनुष्य सिद्ध, अमर और तृप्त हो जाता है। ...पाराशर पुत्र व्यास पूजादि में अनुराग तथा गर्ग कथादि में अनुरक्ति को भक्ति कहते हैं।''

हिंदी साहित्य के इतिहास के पूर्व मध्यकाल की प्रधान प्रवृत्ति भक्ति होने के कारण इस कालखंड को भक्तिकाल (1318-1643 ई.) की संज्ञा प्रदान की गई। यह युग अपनी साहित्यिक श्रेष्ठता के कारण स्वर्ण युग की संज्ञा से अभिहित किया गया। इस काल में कबीर, दादू, नानक और रैदास आदि संतों ने अपनी वाणियों के माध्यम से भक्ति के साथ-साथ समाज सुधार की चेतना फैलायी; वहीं दूसरी ओर

सूफी कवियों ने प्रेम तत्त्व के माध्यम से ईश्वर प्राप्ति का मार्ग दिखाया। राम भक्ति धारा के प्रमुख कवि गोस्वामी तुलसीदास ने समन्वय एवं लोकमंगल का संदेश दिया तो सूरदास की अनन्य कृष्ण भक्ति भी लोक प्रसिद्ध है। इस प्रकार इस कालखंड में विविध माध्यमों द्वारा भक्ति की प्रतिष्ठा के व्यापक प्रयास किए गए।

भक्ति-आंदोलन के सूत्रपात के विषय में आचार्य परशुराम चतुर्वेदी का मत है कि—''हिंदू धर्म इस्लाम के संपर्क से मात्र व्यक्तिगत साधना का केंद्र न रहकर सामूहिक साधना का रूप धारण करने लगा था और उसमें आंदोलनकारी प्रवृत्तियाँ उभरने लगी थीं। प्रायः सभी धर्मों में युगानुरूप परिस्थिति के अनुसार पंथों, संप्रदायों और उपसंप्रदायों की सृष्टि होने लगी, जिसका मुख्य उद्देश्य आत्म निरीक्षण और परिस्थिति परीक्षण द्वारा आवश्यक सुधार करके परंपरागत आचार-विचारों को किसी-न-किसी रूप में प्रश्रय दे कर उन्हें जीवित रखना था। इस प्रयास में वैष्णव धर्म ने भागवत संप्रदाय के रूप में नेतृत्व किया और व्यापक प्रभाव डाला, जिसके माध्यम से भक्ति-आंदोलन का सूत्रपात हुआ।''

इस दौर में भक्ति आंदोलन का अखिल भारतीय स्वरूप दिखाई पड़ा। भारतीय वैष्णव धर्म में भक्ति की प्रधानता थी। इनमें आत्मा-परमात्मा के संबंधों को लेकर द्वैत, अद्वैत, द्वैताद्वैत, शुद्धाद्वैत और विशिष्टाद्वैत आदि के आधार पर दार्शनिक चिंतन हुए। इसी प्रकार इस्लाम में शरा और बेशरा, श्रमण धर्मों में बौद्ध व जैन धर्मों में भी उप संप्रदाय जैसे मंत्रयान, वज्रयान, सहजयान आदि का जन्म हुआ। शैवों में भी कश्मीरी, लिंगायत, पाशुपत एवं वीर आदि तथा शाक्तों में वाममार्गी व दक्षिण मार्गी जैसे उप विभाजन हुए। यह सब कुछ भक्ति-आंदोलन के प्रभाव से हुआ। देश के अलग-अलग भागों में और कई संप्रदायों का जन्म हुआ। परशुराम चतुर्वेदी का मानना है कि—''केरल का शास्तापूजक संप्रदाय, बंगाल के धर्म-ठाकुर, सहजिया, बाउल, सत्यपीर और कर्त्ताभाजा आदि संप्रदाय, उड़ीसा का पंचसखा संप्रदाय महाराष्ट्र के वारकरी और महानुभाव-संप्रदाय भक्ति आंदोलन की ही उपज हैं।'' इनके अतिरिक्त गुजरात में नरसी मेहता और राजस्थान में मीरा बाई ने भक्ति का बिगुल बजाया। इस प्रकार भक्ति, आंदोलन का स्वरूप धारण कर देश भर में फैल गई।

विभिन्न परिस्थितियों ने भी भक्ति आंदोलन के उद्भव में सहायता की। आचार्य रामचंद्र शुक्ल अपने इतिहास ग्रंथ में लिखते हैं कि—''देश में मुसलमानों का राज्य प्रतिष्ठित हो जाने पर हिंदू जनता के हृदय में गौरव, गर्व और उत्साह के लिए अवकाश न रह गया। उसके सामने ही देवमंदिर गिराये जाते थे, देवमूर्तियाँ

तोड़ी जाती थीं और पूज्य पुरुषों का अपमान होता था और वे कुछ नहीं कर सकते थे। ऐसी दशा में अपनी वीरता के गीत न तो वे गा ही सकते थे और न बिना लज्जित हुए सुन ही सकते थे।...अपने पौरुष से हताश जाति के लिए भगवान् की शक्ति और करुणा की ओर ध्यान ले जाने के अतिरिक्त दूसरा मार्ग ही क्या था?''

आचार्य हजारीप्रसाद द्विवेदी का मत शुक्ल जी से भिन्न है। उन्हें शुक्ल जी की यह बात ठीक नहीं लगती कि भक्ति आंदोलन का उद्भव मुस्लिम आक्रमणों की प्रतिक्रिया स्वरूप हुआ। वे कहते हैं कि—''मुसलमानों के अत्याचार के कारण यदि भक्ति की भाव धारा को उमड़ना था तो पहले उसे सिंध में और फिर उत्तर भारत में प्रकट होना चाहिए था, पर हुई वह दक्षिण में।'' वे कहते हैं—''अगर इस्लाम नहीं आया होता तो भी इस साहित्य का बारह आना वैसा ही होता जैसा आज है।'' विभिन्न विद्वानों के मतों के अध्ययन के आधार पर कहा जा सकता है कि भक्ति भारतीय प्राणधारा का मूल तत्त्व है जो कि परंपरा से ही भारतीय जीवन का हिस्सा रही है। पूर्व मध्यकाल तक आते-आते यह प्राण धारा अधिक वेगवान और बलवती हुई और ऐसा होने के पीछे विविध सामाजिक, राजनीतिक और आर्थिक परिस्थितियों ने अपनी महती भूमिका निभाई। भक्ति आंदोलन के उदय के कारणों में हमें किसी एक विशिष्ट कारण को आधार न बनाकर समेकित प्रभाव को स्वीकारना होगा।

हिंदी साहित्य का भक्तिकाल विविधतापूर्ण रहा है। विविध संतों और भक्तों ने अपनी-अपनी साधना-पद्धति के अनुसार ईश्वर का स्मरण किया है। यदि संपूर्ण भक्तिकाल पर समग्रता से दृष्टि डालें तो पाते हैं कि ईश्वर आराधना के आधार पर इस काल की भक्ति चेतना को दो भागों निर्गुण भक्ति काव्यधारा और सगुण भक्ति काव्यधारा में बाँटा गया। पुनः इन दोनों काव्यधाराओं में उपभेद दिखाए पड़ते हैं। निर्गुण भक्ति शाखा को ज्ञानाश्रयी और प्रेमाश्रयी भक्तिधारा नाम दिया गया। जिसे संत काव्य और प्रेम काव्य या सूफी काव्य भी कहा जाता है। इसी प्रकार सगुण भक्तिधारा को भी अध्ययन की सुविधा और आराधना पद्धति के आधार पर दो भागों राम काव्यधारा और कृष्ण काव्यधारा में विभाजित किया गया है। आचार्य शुक्ल द्वारा प्रदत्त यह विभाजन हिंदी साहित्य में प्रतिष्ठा पा गया। आजकल इस विभाजन को लेकर विद्वानों के विरोध संबंधी स्वर यदाकदा सुनाई पड़ते हैं फिर भी यह विभाजन आज भी बहुजनमान्य है।

कृष्ण भक्तिधारा : प्रमुख कवि और उनका काव्य

हिंदी की कृष्ण काव्य परंपरा एक समृद्ध परंपरा रही है। इस काव्यधारा के कवियों ने कृष्ण और उनकी लीलाओं को आधार बनाकर विशेषत: ब्रजभाषा में काव्य रचना की। इस काव्यधारा के विविध संप्रदायों यथा- वल्लभ संप्रदाय, निम्बार्क संप्रदाय, हरिदासी संप्रदाय, चैतन्य संप्रदाय आदि के भक्त कवियों ने अपनी ईश्वर आराधना के पुष्प अर्पित किए। इस काव्यधारा के प्रमुख कवि इस प्रकार हैं–

सूरदास

हिंदी के ख्यातनाम कवि और कृष्ण भक्तिधारा के शिरमौर सूरदास का काव्य इस परंपरा की अमरनिधि है। कृष्ण काव्य कहते ही भारतीय लोकमानस में सूर की छवि उभरती हैं। सूर का जीवनकाल 1478 से 1583 ई. निर्धारित किया जाता है। जन्म स्थान को लेकर भी दो मत प्रचलित हैं। कुछ विद्वान आगरा के समीप रुनकता को तो कुछ दूसरे विद्वान दिल्ली के निकट सीही ग्राम को सूर का जन्म स्थल मानते हैं। सूर वल्लभाचार्य के शिष्य थे। उनका शिष्यत्व ग्रहण करने के बाद वे पारसौली ग्राम में चंद्रसरोवर के निकट रहने लगे थे। भक्तमाल के रचयिता नाभादास ने इनके विषय में कहा था कि–"सूर कवित्त सुनि कौन कवि, जो नाहिं सिर चालन करै।" वल्लभाचार्य का प्रभाव इनके साहित्य में परिवर्तन ले आया। उनसे भेंट होने से पूर्व ये विनय और दैन्य के पद लिखते थे किंतु बाद में उनकी प्रेरणा से सख्य, वात्सल्य और शृंगार रसों में पद रचना करने लगे। वात्सल्य वर्णन की दृष्टि से सूर का साहित्य अपना विशेष महत्त्व रखता है। आचार्य रामचंद्र शुक्ल ने इस विषय में कहा है कि–"सूर ही वात्सल्य है और वात्सल्य ही सूर है।"

सूरदास ने 'सूरसागर', 'साहित्य लहरी' और 'सूर सारावली' की रचना की। इनमें से अंतिम रचना की प्रामाणिता संदिग्ध है। 'सूरसागर' की रचना सूर ने भागवत की पद्धति पर द्वादश स्कंधों में की है। वहीं 'साहित्य लहरी' में सूरदास द्वारा रचित दृष्टकूट पद संगृहीत हैं। सूर के निधन पर वल्लभाचार्य के पुत्र विट्ठलनाथ ने कहा था कि–"पुष्टि मारग को जहाज जात है, सो जाकों कछु लेना होय सो लेऊ।"

सूरदास ने भागवत में आए भ्रमरगीत के संक्षिप्त प्रसंग को विस्तार के साथ अपने पदों में वर्णित किया है। भागवत के 10वें स्कंध के 47वें अध्याय में पद संख्या 12 से 21 तक वर्णित भ्रमर गीत का यह प्रसंग सूर की प्रतिभा से उनके पदों में लगभग 400 पदों का विस्तार पा गया। यह भ्रमरगीत प्रसंग हिंदी साहित्य की

अमरनिधि है। इन प्रसंगों में सूर ने निर्गुण का खंडन और सगुण का मंडन किया है–

निरगुन कौन देश कौ बासी।
मधुकर, कहि समुझाइ, सौंह दै बूझति सांच न हाँसी।।
को है जनक, जननि को कहियत, कौन नारि को दासी।
कैसो बरन, भेष है कैसो, केहि रस में अभिलाषी।।
पावैगो पुनि कियो आपुनो जो रे कहैगो गाँसी।
सुनत मौन ह्वै रह्यौ ठगो-सौ सूर सबै मति नासी।।

कुंभनदास

वल्लभ संप्रदाय के अष्टछाप के कृष्ण भक्त कवियों में कुंभनदास का नाम भी उल्लेखनीय है। ये गोवर्धन के समीप जमनावतौ ग्राम में रहकर कृष्ण आराधना करते थे। ये भी वल्लभचार्य के शिष्य थे। इनके रचे पद कांकरोली के विद्या विभाग और नाथद्वारा के पुस्तकालय से प्रकाशित हुए हैं। कहते हैं कि एक बार बादशाह अकबर ने इन्हें? फतेहपुर सीकरी बुलाया था। इनके पदों को सुनकर प्रसन्न होकर इन्हें कुछ माँगने के लिए कहा तो उन्होंने अपनी इच्छा इस प्रकार व्यक्त की–

संतन को कहा सीकरी सों काम?
आवत जात पनहियाँ टूटी, बिसरि गयो हरि नाम।।
जिनको मुख देखे दुख उपजत, तिनको करिबे परी सलाम।।
कुभंनदास लाल गिरिधर बिनु, और सबै बेकाम।।

नंददास

वल्लभ संप्रदाय के अष्टछाप के आठ कवियों में से एक नंददास वल्लभाचार्य के पुत्र विट्ठलनाथ के शिष्य थे। इनके पिता का नाम जीवनराम और चाचा का नाम आत्माराम था। ये ही आत्माराम तुलसी के पिता थे। इस प्रकार नंददास और तुलसीदास चचेरे भाई थे।

अनेकार्थमंजरी, मानमंजरी, रसमंजरी, रूपमंजरी, विरहमंजरी, प्रेम बारहखड़ी, श्यामसगाई, सुदामाचरित, रुक्मिणीमंगल, भंवरगीत, रासपंचाध्यायी, सिद्धांत-पंचाध्यायी, दशमस्कंधभाषा, गोवर्धनलीला और नंददास पदावली आपकी रचनाएँ हैं। हिंदी साहित्य जगत में ये जड़िया के नाम से प्रसिद्ध हैं। इनके विषय में उक्ति

चर्चित है कि—

''और कवि गढ़िया नंददास जड़िया।''

वल्लभ संप्रदाय के अन्य कवि

वल्लभ संप्रदाय के अष्टछाप कवियों में उपर्युक्त कवियों के अतिरिक्त परमानंददास, कृष्णदास, गोविंद स्वामी, छीतस्वामी और चतुर्भुजदास हैं। परमानंददास की रचनाएँ परमानंदसागर, और परमानंद के पद नाम से प्रकाशित हैं। कृष्णदास को अधिकारी के नाम से जाना जाता है। गोविंद स्वामी का पद चयन 'गोविंद स्वामी के पद' नाम से संकलित है।

निम्बार्क संप्रदाय के कृष्ण भक्त कवि

इस संप्रदाय के प्रवर्तक स्वामी निम्बार्काचार्य हैं। हिंदी कृष्ण काव्य परंपरा में निम्बार्क संप्रदाय के कृष्ण भक्त कवियों में इनके अलावा श्री भट्ट, हरिव्यास देव और परशुरामदेव हैं। इस संप्रदाय में राधा के युगल भाव की स्वीकृति है। यहाँ वृषभानुजा राधा के साथ श्रीकृष्ण की आराधना का विधान है। इस संप्रदाय की प्रधान पीठ सलेमाबाद (अजमेर) में है। वेदांतपरिजात सौरभ, दशश्लोकी और श्रीकृष्णस्तवराज जैसे ग्रंथों की रचना संप्रदाय के प्रवर्तक निम्बार्काचार्य ने की। श्री भट्ट जो कि इस संप्रदाय में हितू सखी के अवतार माने जाते हैं। इन्होंने युगल शतक नामक ग्रंथ की रचना की। हरिव्यास देव ने ब्रजभाषा में महावाणी लिखा। वहीं परशुराम देव का ग्रंथ परशुराम सागर है।

राधावल्लभ संप्रदाय के कृष्ण भक्त कवि

कृष्ण भक्ति परंपरा के इस संप्रदाय का प्रवर्तन सन 1534 में वृंदावन में हितहरिवंश ने किया। यहाँ रसोपासना का विधान है। इस संप्रदाय में राधा जी को कृष्ण से भी ऊँचा स्थान दिया जाता है। इस संप्रदाय के मंदिरों में कृष्ण के विग्रह के साथ राधा का विग्रह नहीं होता है बल्कि श्रीकृष्ण के वाम भाग में एक वस्त्र निर्मित गद्दी होती है जिस पर श्रीराधा अंकित किया हुआ एक स्वर्णपत्र रखा होता है। इसे इस संप्रदाय में गद्दी सेवा के नाम से जाना जाता है। इस संप्रदाय के भक्त कवियों में स्वामी हितहरिवंश ने हित चौरासी, स्फुटवाणी की रचना की। वहीं दामोदर दास जो इस संप्रदाय में सेवक जी के नाम से प्रसिद्ध हैं, ने सेवकवाणी लिखा। हरिराम व्यास ने व्यासवाणी और रागमाला ग्रंथों की रचना की। इस संप्रदाय के अन्य भक्त

कवियों में चतुर्भुजदास, ध्रुवदास और नेही नागरीदास के नाम उल्लेखनीय हैं।

हरिदासी संप्रदाय के कृष्ण भक्त कवि

हरिदासी संप्रदाय के कृष्ण भक्त कवियों में स्वामी हरिदास का नाम आदर के साथ लिया जाता है। ये इस संप्रदाय के प्रवर्तक हैं। इस संप्रदाय को सखी संप्रदाय और टट्टी संप्रदाय के नाम से भी जाना जाता है। हरिदास जी ने सिद्धांत के पद और केलिमाल नामक ग्रंथों की रचना की। अन्य भक्तों में जगन्नाथ गोस्वामी, बीठल बिपुल, बिहारिनदास, नागरीदास हैं।

ज्यौंहिं ज्यौंहिं तुम रखत हौं,त्योंहीं त्योंहीं रहियत हौं, हे हरि।
और अपरचौ पाय धरौं सुतौं कहौं कौन के पैंड भरि।
जदपि हौं अपनों भायो कियो चाहौं,
कैसे करि सकौं जो तुम राखौ पकरि।
कहै हरिदास पिंजरा के जानवर लौं
तरफाय रह्यौ उडिबे को कितोऊ करि।।

चैतन्य संप्रदाय के कृष्ण भक्त कवि

चैतन्य संप्रदाय के प्रवर्तक चैतन्य महाप्रभु हैं। जिन्हें गौर या गोरांग के नाम से भी जाना जाता है। इस संप्रदाय को गौड़ीय संप्रदाय भी कहा जाता है। इस संप्रदाय के अन्य भक्तों में रामराय, सूरदास मदनमोहन, गदाधर भट्ट, चंद्रगोपाल और माधवदास माधुरी हैं।

संप्रदाय निरपेक्ष कृष्ण भक्त कवि

अपनी-अपनी साधना पद्धतियों के अलावा हिंदी में मीरा और रसखान ऐसे कृष्ण भक्त हैं जिन्होंने किसी भी संप्रदाय की साधना पद्धति से बंधने के स्थान पर अपने मन की सहज अनुभूतियों को आधार बनाकर कृष्ण आराधना की। मीरा का जन्म 1504 ई. में रतनसिंह के घर मेड़ता के समीप कुड़की ग्राम में हुआ। इनका विवाह सन 1516 में भोजराज के साथ हुआ। मीरा बचपन से ही कृष्ण को अपना आराध्य मानती थीं। अतः उनकी भक्ति माधुर्य भाव की थी। मीरा द्वारा रचित कई ग्रंथों का उल्लेख विभिन्न विद्वान अपनी-अपनी पुस्तकों में करते हैं। किंतु स्फुट पद नामक रचना को मीरा की प्रामाणिक रचना माना जाता है। मीरा साफ घोषणा करती है कि—

मेरे तो गिरधर गोपाल दूसरो न कोई।।
जाके सिर है मोरपखा मेरो पति सोई।
तात मात भ्रात बंधु आपनो न कोई।।
छांड़ि दई कुलकी कानि कहा करिहै कोई।।
संतन ढिग बैठि बैठि लोकलाज खोई।।

अंसुवन जल सींचि-सींचि प्रेम-बेलि बोई।
अब तो बेल फैल गई आणंद फल होई।।

रसखान भी संप्रदाय निरपेक्ष कवियों में चर्चित नाम है। इनका मूल नाम सैयद इब्राहिम था। एक मुसलमान होते हुए जितनी श्रेष्ठता से कृष्ण भक्ति काव्य की रचना की है, वह वंदनीय है। सुजान रसखान, दानलीला, प्रेमवाटिका और अष्टयाम इनकी प्रसिद्ध रचनाएँ हैं। रसखान के पदों का प्रधान रस शृंगार और वात्सल्य है। सवैयों की रचना के लिए रसखान हिंदी जगत में अमर हैं—

मोरपखा सिर ऊपर राखिहौं, गुंज की माल गरे पहिरौंगी।
ओढ़ि पिताम्बर लै लकुटी, बन गोधन ग्वारन संग फिरौंगी।।
भावतो मोहि मेरो रसखान, सो तेरे कहे सब स्वाँग भरौंगी।
या मुरली मुरलीधर की, अधरान धरी अधरा न धरौंगी।।

कृष्ण भक्ति काव्य का वैशिष्ट्य

मध्यकालीन कृष्ण भक्त कवियों ने कृष्ण की लीलाओं का गान अपने काव्य के माध्यम से किया है। इन कवियों ने कृष्ण की माखन लीला, रास लीला, दान लीला, चीरहरण लीला और गोचारण आदि का हृदयग्राही वर्णन किया है। अपनी व्यक्तिगत अनुभूतियों को सरसता के साथ इन कवियों ने अभिव्यक्ति दी है।

मैया मैं नहिं माखन खायौ।
ख्याल परैं ये सखा सबै मिलि, मेरैं मुख लपटायौ।।
देखि तुही सींके पर भाजन, ऊँचौं धरि लटकायौ।
हौं जु कहत नान्हे कर अपनै मैं कैसैं करि पायौ।।
मुख दधि पोंछि, बुद्धि इक कीन्ही, दोना पीठि दुरायौ।
डारि साँटि, मुसुकाइ जसोदा, स्यामहि कंठ लगायौ।।

मध्यकालीन कृष्ण भक्त कवियों ने कृष्ण की लीलाओं के गान में अपनी ओर से मौलिक उद्भावनाएँ जोड़ दी हैं। कृष्ण की लीलाओं का गान हिंदी काव्य से पहले संस्कृत और प्राकृत आदि में हो चुका है। किंतु हिंदी में जो उनका रूप

उभर कर आया है, वह बहुत कुछ नूतन है। हिंदी कवियों ने कृष्ण की बाल लीलाओं को अधिक स्नेह के साथ वर्णित किया गया। ब्रजमंडल में कृष्ण के बीते समय की लीलाओं के साथ किशोर वय में उनके गोपियों और राधा के साथ प्रेम को भी इन कवियों ने मौलिक प्रस्तुति दी है। भागवत की कथा और प्रसंगों को आधार बनाकर भी ये कवि केवल उन प्रसंगों तक रुके नहीं रहे। हर कवि ने अपनी ओर से इन कथा प्रसंगों में कुछ नया जोड़ा है।

बूझत स्याम कौन तू गोरी।
कहाँ रहति काकी है बेटी देखी नहीं कहूँ ब्रज खोरी।।
काहे कों हम ब्रजतन आवतिं खेलति रहहिं आपनी पौरी।
सुनत रहति स्त्रवननि नंद ढोटा करत फिरत माखन दधि चोरी।।
तुह्मरो कहा चोरि हम लैहैं खेलन चलौ संग मिलि जोरी।
सूरदास प्रभु रसिक सिरोमनि बातनि भुरइ राधिका भोरी।।

कृष्ण भक्त कवियों ने कृष्ण की लीलाओं के गान में भगवद् रति का वर्णन प्रमुख रहा है। यहाँ कांता भाव के साथ-साथ वात्सल्य और सख्य भाव की भक्ति द्रष्टव्य होती है। यहाँ हमें रागानुरागा भक्ति के दर्शन होते हैं। वल्लभ संप्रदाय के भक्त कवि अपना सर्वस्व श्रीकृष्ण के भरोसे छोड़ देते हैं। यहाँ वे दीनानाथ की कृपा को ही सब कुछ मानते हैं—

जापर दीनानाथ ढरै।
सोई कुलीन, बड़ो सुन्दर सिइ, जिहिं पर कृपा करै।।
राजा कौन बड़ो रावन तें, गर्वहिं गर्व गरै।
कौन विभीषन रंक निसाचर, हरि हंसि छत्र धरै।।
रंकव कौन सुदामाहू तें, आपु समान करै।
अधम कौन है अजामील तें, जम तहं जात डरै।।

यह गति मति जानै नहिं कोऊ, किहिं रस रसिक ढरै।
सूरदास, भगवन्त भजन बिनु, फिरि-फिरि जठर जरै।।

कृष्ण काव्यधारा के कवियों ने विशेष रूप से शृंगार, वात्सल्य और शांत रस का निरूपण किया है। सूर के आरंभिक पदों में विनय और दैन्य भाव प्रधान था। जब वे वल्लभाचार्य के संपर्क में आए और शिष्यत्व ग्रहण किया तब से अपने गुरु की प्रेरणा से शृंगार, सख्य और वात्सल्य भाव के पदों की रचना करने लगे। विशेष रूप से कहा जा सकता है कि कृष्ण काव्य में ब्रजरस सर्वत्र व्याप्त है। ब्रज की गोपियों और कृष्ण का प्रेम सहज रूप से वर्णित है।

मैया! मैं माखन नहीं खायो।
ख्याल परै ये सखा सबै मिलि मेरै मुख लपटायो।।

उधो, मन न भए दस बीस।
एक हुतो सो गयौ स्याम संग, को आराधै ईस।।

मध्यकालीन कृष्ण काव्य में कवियों ने प्रकृति का भी सुंदर वर्णन किया है। कृष्ण की लीलाओं का अंकन करते समय इन कवियों की दृष्टि ब्रज क्षेत्र की प्रकृति जैसे-वन, उपवन, गोवर्धन पर्वत, यमुना नदी, गोचारण आदि पर भी रही और इन्होंने इनका प्रभावी अंकन किया है।

मधुबन तुम क्यौं रहत हरे।
बिरह बियोग स्याम सुंदर के ठाढ़े क्यौ न जरे।।

देखियति कालिंदी अति कारी।
अहो पथिक कहियौ उन हरि सौ, भई बिरह-जुर-जारी।।

कैसे कै भरिहैं री दिन सावन के।
हरित भूमि भरे सलिल सरोवर, मिटे मग मोहन आवन के।।
दादुर मोर सोर चातक पिक, सूनी निसा सिरावन के।।
गरज चहूँ घन घुमड़ दामिनी मदन धनुष धन धावन के।।

कृष्ण काव्य में वैसे तो संत कवियों और रामकाव्य परंपरा के समान वहाँ के समाज और संस्कृति का वर्णन नहीं आया है, किंतु यहाँ हम ब्रज संस्कृति की उपस्थिति देख सकते हैं। ब्रजमंडल के दैनिक जीवन का वर्णन यथा वहाँ के गोप-ग्वालों की दिनचर्या उभरकर आई है। स्वयं कृष्ण को कवियों ने गाय और प्रकृति से जोड़कर किसान वर्ग के साथ खड़ा किया है। गोवर्धन की पूजा का संदेश भी एक प्रकार से प्रकृति, पर्यावरण और किसान जीवन से जोड़ने वाला है। ब्रज के गीत और रास लीलाओं का वर्णन भी हमें वहाँ की संस्कृति से जोड़ता है। ब्रज मंडल की होली का दृश्य हम इस पद में देख सकते हैं—

खेलत फागु कुँवर गिरिधारी
अग्रज, अनुज, सुबाहु, श्रीदामा, ग्वाल, बाल, सब सखाऽनुसारी।
इत नागरि निकसी घर-घर ते दै आगे वृषभानु दुलारी।
नव सत सजि ब्रजराज द्वार मिलि प्रफुलित वदन भीर भई भारी।

ब्रज मंडल की चरवाहा संस्कृति भी इन कवियों के काव्य में वर्णित हुई है।

इस पद में हम इस संस्कृति की झलक देख सकते हैं—

आजु मैं गाई चरावन जैहों
वृंदावन के भाँति-भाँति फल अपने कर मैं खैहों।

कृष्ण काव्य परंपरा के कवियों पर रीति ग्रंथों के प्रणयन का प्रभाव भी द्रष्टव्य होता है। इन कवियों ने भक्ति चेतना से युक्त ग्रंथों की रचना के साथ-साथ रीति ग्रंथों की रचना में भी अपनी रुचि दिखाई है। सूरदास ने 'साहित्य लहरी' में रीति पद्धति को अपनाया है। इसी प्रकार नंददास की रसमंजरी और रूपमंजरी जैसी रचनाओं में भी रीति निरूपण देख सकते होता हैं।

कृष्ण काव्य परंपरा के कवियों ने कृष्ण की लीलाओं के गान को अपना लक्ष्य बनाया और इस लक्ष्य को आधार बनाकर लगभग सभी भक्त कवियों ने मुक्तक काव्य रूप में कृष्ण की लीलाओं और जीवन चरित का वर्णन किया है। यहाँ प्रबंधात्मक रचनाएँ लेखन की दिशा में इन कवियों ने अपनी रुचि नहीं दर्शायी। इन कवियों का रचना संयोजन और पद लेखन इस प्रकार का है कि यह मुक्तक होते हुए भी प्रबंध सा आनंद देता है। इन कवियों ने गेय मुक्तक शैली को अपनाकर कृष्ण आराधना में पदों की रचना की है।

इन कवियों ने कृष्ण के चरणों में अपने भक्ति पुष्प अर्पित करने के लिए ब्रज मंडल की भाषा ब्रजभाषा को चुना। सभी कवियों ने इसी भाषा में अपने हृदयोद्गारों को अभिव्यक्ति दी है। राम काव्य परंपरा में हमे ब्रज और अवधी दोनों ही भाषाओं में लेखन द्रष्टव्य होता है किंतु कृष्ण काव्य में ऐसा नहीं है। यहाँ सभी कवियों ने ब्रजभाषा में ही लेखन किया है। यह साहित्य इतनी श्रेष्ठता से रचा गया कि ब्रजभाषा भी इस साहित्य के कारण उच्च स्थान की अधिकारिणी हुई। वहीं ब्रजभाषा की सरसता और मधुरता ने इस साहित्य को भी जनप्रिय बनाने में महती भूमिका निभाई।

मध्यकालीन कृष्ण काव्य में कवियों ने अपनी भावनाओं के सुंदर और प्रभावी प्रस्तुतीकरण के लिए छंदों और अलंकारों के प्रयोग पर भी ध्यान दिया। इन कवियों ने अपने काव्य में चौपाई, चौबोला, सार और सरसी जैसे छंदों का प्रयोग किया है। वहीं दोहा, रोला, कवित्त, सवैया के प्रयोग भी किए हैं। रसखान तो हिंदी जगत में सवैया के लिए ख्यात हैं ही।

मानुस हौं तो वही रसखान, बसौं मिलि गोकुल गाँव के ग्वारन।
जो पसु हौं तो कहा बस मेरो, चरौं नित नंद की धेनु मँझारन।।
पाहन हौं तो वही गिरि को, जो धर्यो कर छत्र पुरंदर धारन।
जो खग हौं तो बसेरो करौं मिलि कालिंदीकूल कदम्ब की डारन।।

इस काव्य में उपमा, रूपक, उत्प्रेक्षा, श्लेष, वक्रोक्ति और यमक जैसे अलंकारों का प्रयोग किया है। सूरदास के यहाँ हम इस पद में सांगरूपक का सुंदर प्रयोग द्रष्टव्य होता है—

अब कै, माधव, मोहिं उधारि।
मगन, हौं भव, अम्बुनिधि, में, कृपासिन्धु मुरारि।।
नीर अति गंभीर माया, लोभ लहरि तरंग।
लियें जात अगाध जल में गहे ग्राह, अनंग।।
मीन इन्द्रिय अतिहि काटति, मोट, अघ सिर भार।
पग न इत उत धरन पावत, उरझि मोह सिबार।।

इस प्रकार कहा जा सकता है कि हिंदी का मध्यकालीन कृष्ण भक्तिकाव्य अपना विशेष महत्त्व रखता है। इन कवियों ने अपनी-अपनी साधना पद्धति और सिद्धांतों को अपनाते हुए भी कृष्ण की आराधन की। कृष्ण भक्ति की धारा में इन कवियों द्वारा रचित काव्य हिंदी साहित्य की अमरनिधि है।

सहायक ग्रंथ—

1. आचार्य रामचंद्र शुक्ल, चिंतामणि, भाग-1, हिंदी साहित्य सरोवर, आगरा, 2002
2. आचार्य रामचंद्र शुक्ल, हिंदी साहित्य का इतिहास, कमल प्रकाशन, नई दिल्ली, संवत् 1997
3. देशराज सिंह भाटी : सं. रसखान ग्रंथावली, नमन प्रकाशन, नई दिल्ली, 2009
4. डॉ. द्वारिका प्रसाद सक्सेना, हिंदी के प्राचीन प्रतिनिधि कवि, विनोद पुस्तक मंदिर, आगरा, 2006
5. डॉ. नगेन्द्र, सं. हिंदी साहित्य का इतिहास, मयूर पेपर बैक्स, नोएडा, 2012
6. माधव हाड़ा : मीरा : रचना संचयन, साहित्य अकादेमी, नई दिल्ली, 2017
7. मैनेजर पाण्डेय, भक्ति आंदोलन और सूरदास का काव्य, वाणी प्रकाशन, नई दिल्ली, 2012
8. योगेन्द्र प्रताप सिंह, कबीर-सूर-तुलसी, लोकभारती प्रकाशन, इलाहाबाद, 2012
9. रामस्वरूप चतुर्वेदी, भक्ति काव्य यात्रा, लोकभारती प्रकाशन, इलाहाबाद, 2003
10. डॉ. शिवकुमार शर्मा, हिंदी साहित्य : युग और प्रवृत्तियाँ, नवभारत प्रकाशन, जोधपुर, 2010
11. हजारीप्रसाद द्विवेदी, हिंदी साहित्य की भूमिका, राजकमल, प्रकाशन, नई दिल्ली, 2014
12. हजारीप्रसाद द्विवेदी, हिंदी साहित्य : उद्‌भव और विकास, राजकमल, प्रकाशन, नई दिल्ली, 2013
13. हरिचरण शर्मा : भ्रमरगीत सार, श्याम प्रकाशन, जयपुर, 2004

सह-आचार्य, हिंदी विभाग
मोहनलाल सुखाड़िया विश्वविद्यालय, उदयपुर
(राजस्थान) 313001

सबके राम



सम्पादक

माधव हाड़ा

ESTD.-1988

वाणी प्रकाशन

4695, 21-ए, दरियागंज, नयी दिल्ली 110 002

फ़ोन : +91 11 23273167 फ़ैक्स : +91 11 23275710

शाखाएँ

अशोक राजपथ, पटना 800 004, बिहार

कॉफ़ी हाउस कैम्पस, महात्मा गांधी मार्ग, इलाहाबाद 211 001, उत्तर प्रदेश

महात्मा गांधी अन्तरराष्ट्रीय हिन्दी विश्वविद्यालय, वर्धा 442 001, महाराष्ट्र

www.vaniprakashan.com
marketing@vaniprakashan.in
sales@vaniprakashan.in

In Association with

ESTD.-1986

Ayodhya Shodh Sansthan

presents

Sabke Ram

Edited by Madhav Hada

ISBN : 978-93-5518-573-0

Religion/Culture

© सम्पादक व लेखकगण

प्रथम संस्करण 2023

मूल्य : ₹ 695

इस पुस्तक के किसी भी अंश को किसी भी माध्यम में प्रयोग करने के लिए प्रकाशक से लिखित अनुमति लेना अनिवार्य है।

आर.के. ऑफ़सेट, शाहदरा, दिल्ली-110 032 में मुद्रित

वाणी प्रकाशन का लोगो मक़बूल फ़िदा हुसेन की कूची से

भरत के राम
—नवीन नन्दवाना 124

कैकेयी के राम
—कृष्णबिहारी पाठक 131

रावण के राम
—प्रवीण पण्ड्या 143

विभीषण के राम
—जीवन सिंह 154

सुग्रीव के राम
—ब्रजरतन जोशी 160

शबरी के राम
—इन्दुशेखर तत्पुरुष 162

अहल्या के राम
—अवन्तिका शुक्ला 171

निशाद के राम
—रेणु व्यास 175

जटायु के राम
—मुरलीधर पालीवाल 179

ब्रज के राम
—उमेश चन्द्र शर्मा 187

आदिवासी के राम
—अर्जुनदास केसरी 192

जनजाति के राम
—मोहन गुप्त 198

सबके राम
—विद्यानिवास मिश्र 214

भरत के राम

नवीन नन्दवाना

राम सृष्टा भी हैं और सृष्टि भी! राम द्रष्टा भी हैं और दृष्टि भी!
राम एकान्त भी हैं और महफिल भी! राम मार्ग भी हैं और मंजिल भी!
राम जीवन भी हैं और मुक्ति भी! राम युद्ध भी हैं और युक्ति भी!
राम मनहर भी हैं और मनस्वी भी! राम राजा भी हैं और तपस्वी भी!...
राम गृहस्थ भी हैं और सन्त भी! राम आदि भी हैं और अन्त भी![1]

हिन्दी के ख्यातनाम मंचीय कवि कुमार विश्वास की रचना 'अपने अपने राम' की इन पंक्तियों से हम राम की व्यापकता और भारतीय लोक जीवन में राम की उपस्थिति का सहज अनुमान लगा सकते हैं। भारतीय समाज में राम और रामकथा की धारा एक अजस्र स्रोतस्विनी के रूप में सदियों से प्रवाहमान है। इस रामकथा को भारतीय प्राणधारा में सहज स्थापित करने का श्रेय आदिकवि वाल्मीकि और गोस्वामी तुलसीदास को दिया जाता है। इन दोनों ही महत कवियों की रचनाओं ने भारतीय जनमानस में राम के एक श्रेष्ठ रूप की स्थापना की है। आज के दौर में हर व्यक्ति के अपने-अपने राम हैं। वह राम को अलग-अलग रूप में स्वीकार करता है।

वाल्मीकि कृत 'रामायण' से लेकर 'रघुवंश' (कालिदास) में, बौद्ध परंपरा में 'अनामर्क जातक', 'दशरथ जातक', 'दशरथ कथानक' आदि रचनाओं में, अपभ्रंश भाषा में स्वयंभू रचित 'पउमचरिउ' में तो विभिन्न आधुनिक भारतीय भाषाओं में भी रामकथा रचना की समृद्ध परंपरा मिलती है। गुजराती भाषा में 'रावण मंदोदरी संवाद' (श्रीधर), 'राम बालचरित' (भालण), 'रामायण' (नाकर), उड़िया भाषा में 'जगमोहन रामायण' या 'दाण्डि रामायण' या 'ओड़िआ रामायण', तेलुगु भाषा में 'भास्कर रामायण', 'रंगनाथ रामायण', 'रघुनाथ रामायण', कन्नड भाषा में 'कुमुदेन्दु रामायण', 'तोरवे रामायण', असमिया में 'कथा रामायण', वंगला भाषा में 'कृत्तिवास रामायण', पंजाबी भाषा में 'रामावतार' या 'गोविन्द रामायण', कश्मीरी में 'रामावतार चरित', मलयालम में 'रामचरितम्', तमिल में 'कंबरामायण' की रचना हुई। हिन्दी में गोस्वामी तुलसीदास की 'रामचरित मानस' और 'विनय पत्रिका' के साथ उनकी अन्य रचनाएँ अलग-अलग भूमिकाओं में राम की एक अलग छवि उपस्थित करती हैं।

रामकथाओं पर गहन विचार-मन्थन कर विविध विद्वानों ने राम की अलग-अलग छवियाँ उपस्थित की हैं। कौसल्या के अपने राम हैं, वहीं कैकेयी और सुमित्रा के भी अपने राम हैं। दशरथ के राम एक विशेष पहचान रखते हैं तो सीता, लक्ष्मण और भरत के भी अपने राम हैं।

ये सभी और इन सभी के साथ सदा से ही भारतीय समाज राम को अलग-अलग रूपों में देखता आया है। राम कभी आदर्श पुत्र के रूप में दिखायी पड़ते हैं तो कभी एक आदर्श भाई के रूप में, कभी एक आदर्श पति के रूप में तो कभी एक आदर्श सखा के रूप में। इस प्रकार राम का स्वरूप बड़ा ही व्यापक और वैविध्यमय है।

गोस्वामी तुलसीदास ने रामकथा की महत्ता का बखान करते हुए लिखा है कि 'मंगल करनि कलिमल हरनि तुलसी कथा रघुनाथ की।' इस मंगलकारी कथा को राम और भरत के सन्दर्भ में देखें तो पाते हैं कि 'रामचरितमानस' में राम और भरत के प्रसंग अनेक स्थानों पर आये हैं और भरत अपने ज्येष्ठ भ्राता राम के प्रति पूरी तरह समर्पित और निष्ठावान् हैं। मानस के अयोध्याकाण्ड में अनेक प्रसंग ऐसे हैं जो भरत के हृदय में बसी राम की छवि का उद्घाटन करते हैं। रामकथा के प्रसिद्ध आलोचक योगेन्द्र प्रताप सिंह लिखते हैं कि "अयोध्याकाण्ड का उत्तरांश अर्थात् भरत कथा इस पूर्वांश से कहीं अधिक महत्तम, कर्म तथा ज्ञान से भिन्न मात्र भक्ति की ऐकांतिक प्रतिष्ठा से परिपूर्ण आराध्य के ध्यान में विगलित तुलसी जैसे पिपासु भक्तों के लिए मानक आदर्श के रूप में है। अयोध्याकाण्ड के इस उत्तरांश के कथानायक भरत हैं और ये भरत दशरथ पुत्र ही नहीं, राम के अनुज भी नहीं, भक्तप्रवर गोस्वामी तुलसीदास की प्रतिमूर्ति हैं।"[2] यहाँ यह स्पष्ट हो जाता है कि दशरथ और भरत के मन में राम की अलग-अलग छवियाँ हैं। भरत जी के प्रयाग जाने और भरत-भारद्वाज संवाद के प्रसंग में गोस्वामी तुलसीदास भरत हृदस्थ भावों की जो सुन्दर अभिव्यक्ति देते हैं, उससे हम भरत के राम का एक परिचय प्राप्त कर सकते हैं–

अरथ न धरम न काम रुचि गति न चहउँ निरवान।
जनम जनम रुति राम पद यह बरदानु न आन।।
जानहुँ राम कुटिल करि मोही। लोग कहउ गुर साहिब द्रोही।
सीता राम चरन रति मोरें। अनुदिन बढ़उ अनुग्रह तोरें।"[3]

यहाँ भरत अपनी इच्छा को दर्शाते हुए यह स्पष्ट कर देते हैं कि उन्हें राम के अतिरिक्त धर्म, अर्थ, काम और मोक्ष आदि किसी प्रकार की कामना नहीं है। साथ ही सीताराम के चरणों में उनके प्रेम की दिनोंदिन वृद्धि की कामना रखते हैं। ऋषि भारद्वाज अपने कथनों के माध्यम से यह स्पष्ट कह देते हैं कि भरत तुम्हारा यश निर्मल है और लोक तथा वेद दोनों तुम्हारे निर्मल यश का गान करेंगे। भरत की माता कैकेयी के कारण मिले राम-वनवास पर भरत आत्मग्लानि महसूस करते हैं और यह सोचते हैं कि राम के मन में उनके प्रति क्या चल रहा होगा। इस पर मुनि का कथन राम के उदार स्वरूप और भरत के प्रति उनके प्रेम को दर्शाता है। मानस के अयोध्याकाण्ड में कथन है–

सुनहु भरत रघुबर मन माहीं। पेम पात्रु तुम्ह सम कोउ नाहीं।।
लखन राम सीतहि अति प्रीती। निसि सब तुम्हहि सराहत बीती।।
जाना मरमु नहात प्रयागा। मगन होहिं तुम्हरे अनुरागा।।
तुम्ह पर अस सनेह रघुबर कें। सुख जीवन जग जस जड़ नर कें।।[4]

राम के वनगमन और दशरथ के निधन के बाद के प्रसंग जब शत्रुघ्न सहित भरत अयोध्या लौटते हैं तो वे प्रसंग बड़े कारुणिक बन पड़े हैं। भरत अपनी माता कैकेयी को जब इन सबका कारण मानते हैं तो वे अपनी माता को बहुत भला-बुरा कहते हैं और राम के प्रति अपने

अनुराग को दर्शाते हैं। अपनी माता को उनके कृत्य पर धिक्कारते हुए वे राम और अपने परिवार के प्रति अपने अनुराग को कुछ इस प्रकार दर्शाते हैं–

भरतहि बिसरेउ पितु मरन सुनत राम बन गौनु।
हेतु अपनपउ जानि जियँ थकित रहे धरि मौनु।।

जौं पै कुरुचि रही अति तोही। जनमत काहे न मारे मोही।।
पेड़ काटि तैं पालउ सींचा। मीन जिअन निति बारि उलीचा।।
हंसबंसु दसरथु जनकु राम लखन से भाइ।
जननी तूँ जननी भई बिधि सन कछु न बसाइ।।[5]

इस पश्चात्ताप और दुःख की घड़ी में भी राम की माता कौसल्या भरत पर अपना स्नेह दर्शाती हैं और उनके मन में भरत के प्रति उनके प्यार में किसी प्रकार की कमी नहीं आती है। भरत इन सब अनर्थों का कारण स्वयं को स्वीकारते हैं।

मातु भरत के बचन सुनि साँचे सरल सुभायँ।
कहति राम प्रिय तात तुम्ह सदा बचन मन कायँ।।
राम प्रानहु तें प्रान तुम्हारे। तुम्ह रघुपतिहि प्रानहु तें प्यारे।।
बिधु बिष चवै स्रवै हिमु आगी। होइ बारिचर बारि बिरागी।।
भएँ ग्यानु बरु मिटै न मोहू। तुम्ह रामहि प्रतिकूल न होहू।।
मत तुम्हार यहु जो जग कहहीं। सो सपनेहुँ सुख सुगति न लहहीं।।[6]

यहाँ उपर्युक्त कथनों के माध्यम से कौसल्या माता यह आश्वस्त करती है कि हे भरत, राम को तुम अपने प्राणों से भी अधिक प्यार करते हो। अतः अपने मन में इस प्रकार का विषाद न लाओ। चित्रकूट के मार्ग पर भरत बहुत व्याकुल होकर बढ़ रहे होते हैं। वे मार्ग में मिलने वाले प्रत्येक जन से सीता-राम और लक्ष्मण की कुशल और स्थान के बारे में पूछते हैं। भरत जी के भाईपने, भक्ति और आचरण की प्रत्येक व्यक्ति सराहना करता है। स्वयं गोस्वामी तुलसीदास ने भी लिखा है कि "भायप भगति भरत आचरनू। कहज सुनत दुःख दूषन हरनू।।" जब चित्रकूट में भरत के आगमन से पूर्व लक्ष्मण राम के समक्ष यह शंका व्यक्त करते हैं कि भरत को राजमद हो गया है तो राम अपने भाई भरत के आचरण और व्यवहार के विषय में लक्ष्मण को जो कहते हैं उससे राम और भरत के परस्पर स्नेह-सम्बन्ध का ज्ञान होता है। राम कहते हैं–

भरतहि होइ न राजमदु बिधि हरि हर पद पाइ।
कबहुँ कि काँजी सीकरनि छीरसिंधु बिनसाइ।।
तिमिरु तरुन तरनिहि मकु गिलई। गगनु मगन मकु मेघहिं मिलई।।
गोपद जल बूड़हिं घटजोनी। सहज छमा बरु छाड़ै छोनी।।
मसक फूँक मकु मेरु उड़ाई। होइ न नृपमदु भरतहि भाई।।
लखन तुम्हार सपथ पितु आना। सुचि सुबंधु नहिं भरत समाना।।[7]

भरत के चित्रकूट आगमन पर सबके मिलाप के पश्चात राम-भरत संवाद में भी हम भरत के राम का स्वरूप जान सकते हैं।

मैं जानउँ निज नाथ सुभाऊ। अपराधिहु पर कोह न काऊ।।
मो पर कृपा सनेहु बिसेषी। खेलत खुनिस न कबहूँ देखी।।
सिसुपन तें परिहरेउँ न संगू। कबहुँ न कीन्ह मोर मन भंगू।।
मैं प्रभु कृपा रीति जियँ जोही। हारेहूँ खेल जितावहिं मोही।।
महूँ सनेह सकोच बस सनमुख कही न बैन।
दरसन तृपित न आजु लगि प्रेम पिआसे नैन।।[8]

यहाँ भरत जी के कथन सम्पूर्ण सभा पर अपना प्रभाव छोड़ते हैं और एक आदर्श भाई का स्वरूप सभी को यहाँ दृष्टिगत होता है। राम भी उन्हें स्पष्ट रूप से समझाते हैं कि जीवन की गति हमारे वश में नहीं है, ये सब ईश्वराधीन हैं। वे राम को तीनों कालों और तीनों लोकों में श्रेष्ठ होने की संज्ञा देते हैं। भरत के राम के प्रति इसी प्रेम के विषय में प्रसिद्ध आलोचक योगेन्द्र प्रताप सिंह लिखते हैं कि "हिन्दी साहित्य के विवेचकों ने भरत की भक्ति को भायप भक्ति के रूप में स्वीकार किया है। उनके अनुसार भरत में अपने अग्रज के लोकात्मक सम्बन्ध का एक ओर निर्वाह है तो दूसरी ओर उनमें आराधक की भाँति समर्पण निष्ठा भी है। इस प्रकार लोक सम्बन्ध तथा भक्ति निष्ठा का निर्वाह दोनों तत्त्व भरत के चरित्र द्वारा निर्दिष्ट किये जा सकते हैं। लोक सम्बन्ध मूलतः प्रसंग में नगण्य है। कथा सन्दर्भ है कि वे श्रीराम के लघु भ्राता हैं। कवि भायप भक्ति में भायप अर्थात् भातृत्व का धीरे-धीरे विलयन उनके भक्त व्यक्तित्व में करता है। राम के लिए सर्वस्व त्याग, उनके दर्शन की महती उत्कण्ठा एवं हर्षातिरेक, वहाँ तक पहुँचने के लिए सम्पूर्ण संकटों का वरण, अपने सम्पूर्ण जीवन को आराध्य राम की प्रियता के अनुकूल परिवर्तित करने का भाव और उनके लिए अगाध मोह–ये ऐसे तत्त्व हैं, जो उन्हें भाई की अपेक्षा भक्त अधिक स्वीकार कराते हैं।"[9]

भरत को राजपाट से कुछ भी स्नेह नहीं है। वह तो राम का साथ चाहते हैं, इसी कारण वे स्पष्ट शब्दों में कह उठते हैं कि राजतिलक ग्रहण करने की सभी सामग्री साथ लाई गयी है, आप इसे स्वीकार करें और मैं स्वयं वन जाकर पिता को दिया गया आपका वचन पूरा करूँगा। तुलसी इस प्रसंग को इस प्रकार वर्णित करते हैं–

जो सेवकु साहिबहि सँकोची। निज हित चहइ तासु मति पोची।।
सेवक हित साहिब सेवकाई। करै सकल सुख लोभ बिहाई।।
स्वारथु नाथ फिरें सबही का। किएँ रजाइ कोटि बिधि नीका।।
यह स्वारथ परमारथ सारू। सकल सुकृत फल सुगति सिंगारू।।
देव एक बिनती सुनि मोरी। उचित होइ तस करब बहोरी।।
तिलक समाजु साजि सबु आना। करिअ सुफल प्रभु जौं मनु माना।।
सानुज पठइअ मोहि बन कीजिअ सबहि सनाथ।
नतरु फेरिअहिं बंधु दोउ नाथ चलौं मैं साथ।।[10]

जनक-सुनयना संवाद में गोस्वामी जी ने भरत के गुणों और चरित्र का जो बखान किया है, वह अनुपम है। वे भरत को भरत के समान ही बताते हैं, उनकी दृष्टि में भरत के लिए कोई दूसरी उपमा उचित ही नहीं है। वे कहते हैं कि जैसे मछली का पृथ्वी पर विचरण असम्भव है वैसे ही भरत की महिमा का बखान असम्भव है। तुलसीदास जी लिखते हैं कि **"निरवधि गुन निरुपम पुरुषु भरतु भरत सम जानि। कहिअ सुमेरु कि सेर सम कबिकुल मति सकुचानि।।"**[11] राम के साथ संवाद करते समय भरत राम के शरणागत वत्सल स्वरूप का उद्घाटन करते हैं। अयोध्याकाण्ड की उत्तर कथा में हम इस प्रसंग के चरमबिन्दु को देख सकते हैं, जहाँ एक भाई के मन में वनगमन को लेकर कोई खेद नहीं है तो दूसरा भाई इतने बड़े राजपाट के मोह से बिल्कुल दूर है। एक आदर्श स्वरूप की रचना समाज को एक विशिष्ट सन्देश देती है। भरत का राम के साथ संवाद सुनकर उपस्थित साधुओं का समाज और अन्य परिवारजन सभी भरत जी की प्रशंसा करते नहीं थकते हैं।

रघुराउ सिथिल सनेहँ साधु समाज मुनि मिथिला धनी।
मन महुँ सराहत भरत भायप भगति की महिमा घनी।।
भरतहि प्रसंसत बिबुध बरषत सुमन मानस मलिन से।
तुलसी बिकल सब लोग सुनि सकुचे निसागम नलिन से।।[12]

राम और भरत के मिलन के विषय में योगेन्द्र प्रताप सिंह का कथन है कि "श्रीराम और भरत का यह सम्मिलन अयोध्याकाण्ड की कथा का कथाफल है। भरत की मानसिक संसक्ति एवं वासना के रूप में राम के वियोग की पीड़ा का मार्मिक चित्रांकन करके उसे भातृत्व वियोग से कहीं अधिक आराध्य राम के लिए भक्त की निरन्तर छटपटाहट के रूप में चित्रित करने के लिए कवि प्रयत्नशील है। एक योगी जिस प्रकार परासमाधि दशा में केवलाद्वैत भाव में प्रतिष्ठित रहता है, ब्रह्म के बिम्ब से प्रतिविम्बित उसका चित्त समाधि दशा में शून्य एवं जड़वत् हो उठता है वैसी ही दशा भरत एवं श्रीराम के गूढ़ स्नेह सम्मिलन की है।"[13]

राम की चरण पादुकाओं को ग्रहण कर अयोध्या लौटना और नन्दीग्राम में पर्णकुटी बनाकर उसमें निवास करते हुए रामाज्ञा मानते हुए राम के अयोध्या लौटने तक शासन सँभालने में भी भरत का व्यक्तित्व अधिक ऊँचाई ग्रहण करता है। राम के प्रति अगाध प्रेम के कारण ही भरत मुनि वेश ग्रहण कर उसी प्रकार का जीवन स्वीकार कर लेते हैं जिस प्रकार वनवासी राम का जीवन था। वे सिर पर जटा, वदन पर वल्कल वस्त्र धारण कर लेते हैं। वे भोजन, वस्त्र, व्रत और नियम आदि के पालन में ऋषियों की दिनचर्या को अपना कर राम के प्रति अपने एकनिष्ठ प्रेम को दर्शाते हैं। तुलसी लिखते हैं–

जटाजूट सिर मुनिपट धारी। महि खनि कुस साँथरी सँवारी।।
असन बसन बासन ब्रत नेमा। करत कठिन रिषिधरम सप्रेमा।।
भूषन बसन भोग सुख भूरी। मन तन बचन तजे तिन तूरी।।
अवध राजु सुर राजु सिहाई। दसरथ धनु सुनि धनदु लजाई।।
तेहिं पुर बसत भरत बिनु रागा। चंचरीक जिमि चंपक बागा।।
रमा बिलासु राम अनुरागी। तजत बमन जिमि जन बड़भागी।।[14]

लक्ष्मण मूर्च्छा के प्रसंग में हनुमान जी का संजीवनी लेकर लौटते समय भरत के बाण से आहत होने के प्रसंग में गोस्वामी जी ने भरत का अपने भाइयों के प्रति प्रेमभाव वर्णित किया है। हनुमान जी के मुख से रामनाम का उच्चारण सुनकर उन्हें भरत जी गले लगाते हैं और अपने किये पर पश्चात्ताप व्यक्त करते हैं। उन्हें यहाँ भी लगता है कि देव उनकी कठिन परीक्षा ले रहे हैं।

जेहिं बिधि राम बिमुख मोहि कीन्हा। तेहिं पुनि यह दारुन दुःख दीन्हा।।
जौं मोरें मन बच अरु काया। प्रीति राम पद कमल अमाया।।[15]

लंकाकाण्ड के उस प्रसंग में जब राम वनवास अवधि बीत जाने पर अयोध्या वापसी का कहते हैं तब वे विभीषण से अपने भाई भरत के विषय में जो कहते हैं उससे भरत के प्रति उनके अगाध प्रेम की अभिव्यक्ति मिलती है। तुलसीदास जी इस प्रसंग को इस प्रकार वर्णित करते हैं–

तोर कोस गृह मोर सब सत्य बचन सुनु भ्रात।
भरत दसा सुमिरत मोहि निमिष कल्प सम जात।।
तापस बेष गात कृस जपत निरन्तर मोहि।
देखौं बेगि सो जतनु करु सखा निहोरउँ तोहि।।
बीतें अवधि जाउँ जौं जिअत न पावउँ बीर।
सुमिरत अनुज प्रीति प्रभु पुनि पुनि पुलक सरीर।।[16]

राम को यहाँ स्पष्ट स्मरण है कि अवधि बीत जाने पर उन्हें तुरन्त अयोध्या पहुँचना है क्योंकि भरत वहाँ राम का वेसब्री से इन्तजार कर रहे हैं। अब राम का हर क्षण भरत के बिना एक कल्प के समान लग रहा है। यह इस बात को दर्शाता है कि जितना स्नेह भरत के हृदय में राम के प्रति है उतना ही स्नेह हमें राम के हृदय में भी भरत के प्रति दृष्टिगत होता है। उत्तरकाण्ड के प्रसंग में जब राम के वनवास की अवधि मात्र एक ही दिन शेष रह जाती है तब भरत के मन में पुनः शंका उठने के प्रसंगों का वर्णन गोस्वामी जी ने किया है। यहाँ यह भाव सहज ही द्रष्टव्य होता है कि जिनमें अटूट प्रेम होता है, वहाँ मन में कई बार विपरीत भाव भी संचरित हो जाते हैं। शायद इसी कारण भरत के मन में यह भाव आने लगा कि अवधि पूर्ण होने को है और राम के आगमन का समाचार नहीं मिला, कहीं राम ने मुझे भुला तो नहीं दिया। यहाँ भी राम के प्रति भरत का प्रेम दिखायी पड़ता है। गोस्वामी जी ने लिखा है–

रहेउ एक दिन अवधि अधारा। समुझत मन दुःख भयउ अपारा।।
कारन कवन नाथ नहिं आयउ। जानि कुटिल किधौं मोहि बिसरायउ।।
अहह धन्य लछिमन बड़भागी। राम पदारबिन्दु अनुरागी।।
कपटी कुटिल मोहि प्रभु चीन्हा। ताते नाथ संग नहिं लीन्हा।।
जौं करनी समुझै प्रभु मोरी। नहिं निस्तार कलप सत कोरी।।
जन अवगुन प्रभु मान न काऊ। दीन बन्धु अति मृदुल सुभाऊ।।[17]

स्वयं राम भी जब भरत से मिलते हैं तो हनुमान जी को सम्बोधित करते हुए यह बात स्पष्ट कर देते हैं कि "तुम्हु जानहु कपि मोर सुभाऊ। भरतहि मोहि कछु अन्तर काऊ।"[18] यह सब राम के हृदय की उदारता को दर्शाता है कि राम वनवास की लम्बी अवधि व्यतीत कर लौटे हैं,

किन्तु अपने भाई के प्रति उनके मन में कोई दुर्भाव नहीं अपितु और स्नेह संचरित है। अपनी इस रचना और विशेष रूप से अयोध्याकाण्ड की कथा नवधा भक्ति में भायप भक्ति को और जोड़ती है। भरत के माध्यम से तुलसीदास जी ने अपने हृदय के भक्तिभावों को सुन्दर अभिव्यक्ति दी है। भरत के माध्यम से गोस्वामी जी ने मध्यकालीन भक्ति के विशेष स्वरूप को रचा है जिसमें आराध्य आराधक से सम्पूर्णता से जुड़ता है। जिस प्रकार भरत चातक की भाँति अपने आराध्य राम के प्रति एकनिष्ठ हैं वैसे ही तुलसीदास जी ने भी अपने भटकाव को राम में केंद्रित कर स्थिरता दी है। वे अपनी रचना दोहावली में लिखते हैं–

एक भरोसो एक बल एक आस विश्वास।
एक राम घनस्याम हित चातक तुलसीदास।।[19]

सन्दर्भ सूची

1. https://99lyricstore-com/2019/11/apne-apne-ram-ram-katha-by-kumar.html
2. योगेंद्र प्रताप सिंह :, श्रीरामचरितमानस, अयोध्याकाण्ड, लोकभारती प्रकाशन, इलाहाबाद, दसवाँ संस्करण, 2019, पृ. 16
3. गोस्वामी तुलसीदास : श्रीरामचरितमानस, अयोध्याकाण्ड, गीता प्रेस, गोरखपुर, संवत् 2061, पृ. 467
4. गोस्वामी तुलसीदास : श्रीरामचरितमानस, अयोध्याकाण्ड, गीता प्रेस, गोरखपुर, संवत् 2061, पृ. 470
5. गोस्वामी तुलसीदास : श्रीरामचरितमानस, अयोध्याकाण्ड, गीता प्रेस, गोरखपुर, संवत् 2061, पृ. 433
6. गोस्वामी तुलसीदास : श्रीरामचरितमानस, अयोध्याकाण्ड, गीता प्रेस, गोरखपुर, संवत् 2061, पृ. 439
7. गोस्वामी तुलसीदास : श्रीरामचरितमानस, अयोध्याकाण्ड, गीता प्रेस, गोरखपुर, संवत् 2061, पृ. 411
8. गोस्वामी तुलसीदास : श्रीरामचरितमानस, अयोध्याकाण्ड, गीता प्रेस, गोरखपुर, संवत् 2061, पृ. 512
9. योगेंद्र प्रताप सिंह : श्रीरामचरितमानस, अयोध्याकाण्ड, लोकभारती प्रकाशन, इलाहाबाद, दसवाँ संस्करण, 2019, पृ. 18
10. गोस्वामी तुलसीदास : श्रीरामचरितमानस, अयोध्याकाण्ड, गीता प्रेस, गोरखपुर, संवत् 2061, पृ. 518
11. गोस्वामी तुलसीदास : श्रीरामचरितमानस, अयोध्याकाण्ड, गीता प्रेस, गोरखपुर, संवत् 2061, पृ. 534
12. गोस्वामी तुलसीदास : श्रीरामचरितमानस, अयोध्याकाण्ड, गीता प्रेस, गोरखपुर, संवत् 2061, पृ. 545
13. योगेंद्र प्रताप सिंह : श्रीरामचरितमानस, अयोध्याकाण्ड, लोकभारती प्रकाशन, इलाहाबाद, दसवाँ संस्करण, 2019, पृ. 19
14. गोस्वामी तुलसीदास : श्रीरामचरितमानस, अयोध्याकाण्ड, गीता प्रेस, गोरखपुर, संवत् 2061, पृ. 562
15. गोस्वामी तुलसीदास : श्रीरामचरितमानस, लंकाकाण्ड, गीता प्रेस, गोरखपुर, संवत् 2061, पृ. 758
16. गोस्वामी तुलसीदास : श्रीरामचरितमानस, लंकाकाण्ड, गीता प्रेस, गोरखपुर, संवत् 2061, पृ. 822
17. गोस्वामी तुलसीदास : श्रीरामचरितमानस, उत्तरकाण्ड, गीता प्रेस, गोरखपुर, संवत् 2061, पृ. 830
18. गोस्वामी तुलसीदास : श्रीरामचरितमानस, उत्तरकाण्ड, गीता प्रेस, गोरखपुर, संवत् 2061, पृ. 867
19. http://kavitakosh.org/kk/nksgkoyh_/_rqylhnkl_/_pृ._28

68th ANNUAL ILA CONFERENCE PROCEEDINGS

International Conference on

Re-engineering of Libraries in the Context of Emerging Technologies: Myth or Reality

Chief Editors

Dr. O. N. Chaubey & Dr. Pardeep Rai

Editors

Dr. Dharam Kumar

Dr. Abhijeet Sinha

Mr. Qumar Abbas

Organised by

Indian Library Association, Delhi

and

J. L. N. Medical College, Ajmer (Rajasthan)

in association with

Rajasthan Technical Library Association, Jaipur

2023

Editorial Advisory Board

Chairperson

Dr. Mohan R. Kherde

President, Indian Library Association,
Director, Knowledge Resource Centre
Sant Gadge Baba Amravati University
Amravati, Maharashtra

Members

Prof. B. D Kumbar
Vice Chancellor
Davangere University, Karnataka

Prof. Jagtar Singh
Former Professor DLIS,
Punjabi University, Patiala, Punjab

Dr. S.S. Dhaka
Former Director, Library Services
Ministry of External Affairs, New Delhi

Prof. Shailendra Kumar
HOD & Professor, DLIS
University of Delhi, Delhi

Prof. M. Koganuramath
Former Head, DLIS,
Central University, Gujarat

Prof. Ashu Shokeen
Former Professor, DLIS
Kurukshetra University,
Kurukshetra

Dr. D.V. Singh
Professor, SRM University, Sonepat
& Former University Librarian,
University of Delhi, Delhi

Prof. A. P. Singh
DG, RRRLF, Ministry of Culture,
Kolkata

©Indian Library Association, Delhi, 2023.

All rights reserved. No part of this publication can be reproduced, stored or transmitted in any form or by any means, electronic or mechanical, including photocopying, microfilming and recording or by any information storage and retrieval system, without the prior permission in writing of the Indian Library Association and the copyright owners.

The opinions expressed in the articles by the authors and contributors are their own and the Editorial Advisory Board, Chief Editors and Editors assume no responsibility for the same.

ISBN: 978-81-956643-1-3

Price: India: ₹ 3500/-; Overseas: US$ 175; Printed at: Anand Sons, Delhi-92

94.	Rudiments of Professional skills and Competencies for LIS Professionals in the Context of Re-Engineering of the Medical College Libraries Services	1027
	Upender Kumar, Dr. Bhaw Nath Pandey	

Theme 9: Digital Open Data – Open Science – Big Data – Data Mining

95.	Open data challenges and Benefits and its Resources	1042
	Dr. Aditi Joshi, Dr. Kirti Jachak , Dr. Purnima Kumari	
96.	*Syzygium aromaticum* (Medicinal Plant) Research: A Scientometric Analysis of Global Publications Output during 2011-2021	1053
	Satish Kumar, Dr. P. S. Rajput	
97.	Bibliometric Review of Big Data and Cloud Computing Publications in Library and Information Science: A Comparative Analysis	1070
	Md Safiqur Rahaman, Dr. Khatik Rashid, Dr. Md Rafiqur Rahman	
98.	Impact of ICT in the Delhi Public Library – A Study	1104
	Nirmala Boella, Dr. Dharam Kumar	

Syzygium aromaticum (Medicinal Plant) Research: A Scientometric Analysis of Global Publications Output during 2011-2021

Satish Kumar*
Faculty & Head, Dept. of Library and Information Science, Sophia Girls' College (Autonomous), Ajmer, Rajasthan, India, E-mail: satish@sophiacollegeajmer.in

Dr. P. S. Rajput
Assistant Professor & In-charge Head, Dept. of Library and Information Science, Mohanlal Sukhadia University Udaipur

ABSTRACT: Scientometrics is a branch of library Science which is used for analysing and calculating different parameters which specify researcher's quantitative research output. This study examines scientometric analysis on *Syzygium aromaticum* (Medicinal Plant) of Global Publications Output during 2011-2021. By measuring and analysing the distribution of articles, year-wise, annual growth rate, authorship pattern, author productivity, relative growth rates, doubling time, degree of collaboration, ranked list of authors, Collaborative Co-efficient and Modified Collaborative Co-efficient during this period. In this period of 11 years only 1569 publications were found. Publication of research in this field was steady and didn't was too productive. In the year 2017 has the highest and positive AGR (40.00 %). The total number of publications is 1569, in which 56 single author publications and all others are multiauthored. In years 2018 and 2020, the AAPP of publications as well as authors are highest and APA is lowest. The degree of collaboration, in 2018 is maximum (0.98).The Collaborative Co-efficient and MCC was 0.756 and 0.757 successively. After analysing above parameters it has been concluded that research work on this field, require further research.

KEYWORDS: *Syzygium aromaticum*, Relative Growth Rate, Authorship pattern. Coefficient Collaboration, Modified Coefficient Collaboration, Medicinal plant

1. Introduction

Medicinal plants have multifunctional applications and in this series *Syzygium aromaticum* (Medicinal Plant) (clove)has widely used in treatment of various diseases. Traditional Medicine are using by the all classes of people. Herbal medicinal products play a significant role for discovering new pharmaceutical molecules to treat serious diseases. According to El-SaberBatihaetal, (2020) "*Syzygium aromaticum*is have various pathogenic parasites and microorganisms, including pathogenic bacteria, Plasmodium, Babesia, Theileria parasites, Herpes simplex, and hepatitis C viruses. Several reports documented the analgesic, antioxidant, anticancer, antiseptic, anti-depressant, antispasmodic, anti-inflammatory, antiviral, antifungal, and antibacterial activity of eugenol against

several pathogenic bacteria including methicillin-resistant *Staphylococcus epidermidis* and *S. Aureus".*

Syzygium aromaticum (clove) is a traditional spice that has been used for food preservation and possesses various pharmacological activities. *Syzygium aromaticum* (clove) is an ingredient which has been employed for centuries as food preservative and various medicinal purposes including its antimicrobial and antioxidant properties (Kumar et al., 2021).

Scientometricsis a part of Library and Information Science in which data of researchers is collected and analysed with the help of scientometric tools. Merton and Garfield,1963 stated that scientometric as 'the field of enquiry given over to the quantitative analysis of science and scientific field'. According to the Glossary of Thompson Scientific Terminology, scientometric is the quantitative study of the disciplines of science based on published literature and communication.

2. Review of Literature

Literature review covers an assessment of works related to several aspects of Scientometric studies. Literature in any field always has an important role towards identification, formalization of research problem and orients the researcher to carry further research in a right direction with clear perception.

Sivasekaran (2021) assessed scientometrics on the Global Publication output on *Curcuma Longa* (Medicinal plant). The study covers 6087records of 2000 to 2019 with reference to Web of Science data. Global citation score distribution of publications by Journals, h- Index and citation profile are analysed. India is at top position followed by USA,China and Iran are contributing in this field. The Journal 'Food Chemistry' is at top in this field. In 2019 maximum research articles were published and lowest in 2001. Total 24 Journals contributed 13.49 percent contributions and they had 16.01 percent Citations.

Tabatabaei-Malazy et al. (2016) assessed scientometric analysis of research efficiency in pasture of Ant oxidative hypoglycaemic herbal medicine on diabetes. 468 documents were downloaded from Scopus database till 2015 related to human. Using VOS Viewer and SPSS the data was analyzed. US is the top most contributing county in this research

Massarrat & Kolahdoozan (2011) studied the contributions of the Iranand Turkey on medical journals which were indexed by WOS from 2007 to 2010. Six citations by the author and IF on the clinical research published from 60 international journals were contributions by the Iran and Turkey. 21 journals

from Iranian were indexed with ISI. Turkey,4,876 articles were published with 1,331 citations per author noticed. The average citations of the foreign authors per authors noticed that 0.19 was from Iranian researchers and 0.3 was gained by the Turkish researchers. Turkey had produced more articles, citations and citations per authors on international collaborations.

Ali & Kumari (2018) conducted a scientometric study on the biodiversity publications from 1989 to 2016. A total 1,54,654 records retrieved from WOS. BibExcel and MSExcel. Gastone, KJ is the most prolific author in biodiversity research with 257 publications. 90% of the article contributed buy multi-authors. Among the institutional contributions, Chinese Academy of Sciences got ranked first with 2,305 publications. It is identified 15.6% of the Articles did not receive any citations on biodiversity research.

Gupta et al. (2016) examined a study on the research contributions on Migraine,from the period 2006-2915 from Scopus. The study noticed that 9.80% was international collaboration 18 and 2.56 as share of global level publications. 75.3% of the publications was contributed by top most 10 countries. Numerous journals published the migraine research from Indian, among them top most 15 journals was rated as one third. The citation per article was rated as 149.57 among 1087 citations. The study concluded with requirement of national level policy to undertake the R&D policy for improving the migraine research for the common cause.

3. Objectives of the Study

This study has the following objectives:

1. To study year -wise distribution of the articles published during 2011 to 2021.
2. To find annual growth rate of Publications.
3. To reveal authorship pattern and author productivity.
4. To examine Relative Growth Rates and Doubling Time of Publications.
5. To recognize Degree of collaboration, Co-authorship and Collaboration Index.
6. To recognize Collaborative co-efficient and Modified co-efficient.
7. To study country wise distribution of publications.

4. Research Methodology

The required data was collected from Scopus database for the period 2011 to2021. It can be seen that 1569 research publication retrieved from this database on *Syzygium aromaticum* medicinal plant. The researcher downloads data and then further analysed the data with the help of MS Excel software as per the objectives ofthe study. The aim of the study to tabulate and to analyse thrust areas of *Syzygium aromaticum* medicinal plant.

5. Result and Discussions

5.1 (a) Year-Wise Distribution of Publications

Table 1: Year-Wise Distribution of Publications & Annual Growth Rate

S. No.	Year	No. of Publications	%	Cumulative No. of Publications	AGR (%)
1	2011	163	10.38	163	-
2	2012	158	10.07	321	-3.06
3	2013	125	7.96	446	-20.88
4	2014	126	8.03	572	0.80
5	2015	128	8.17	700	1.58
6	2016	98	6.24	798	-23.00
7	2017	138	8.79	1036	40.00
8	2018	117	7.45	1053	-15.21
9	2019	159	10.14	1212	26.41
10	2020	174	11.08	1386	8.62
11	2021	183	11.66	1569	6.32
Total		1569	100		

Table-1 shows total 1569 publications have been published in these eleven years. Maximum 183 publications are published in 2021. On this plant research was steady and shows oscillatory trends in this period of eleven years' publications becomes 183 from 163.

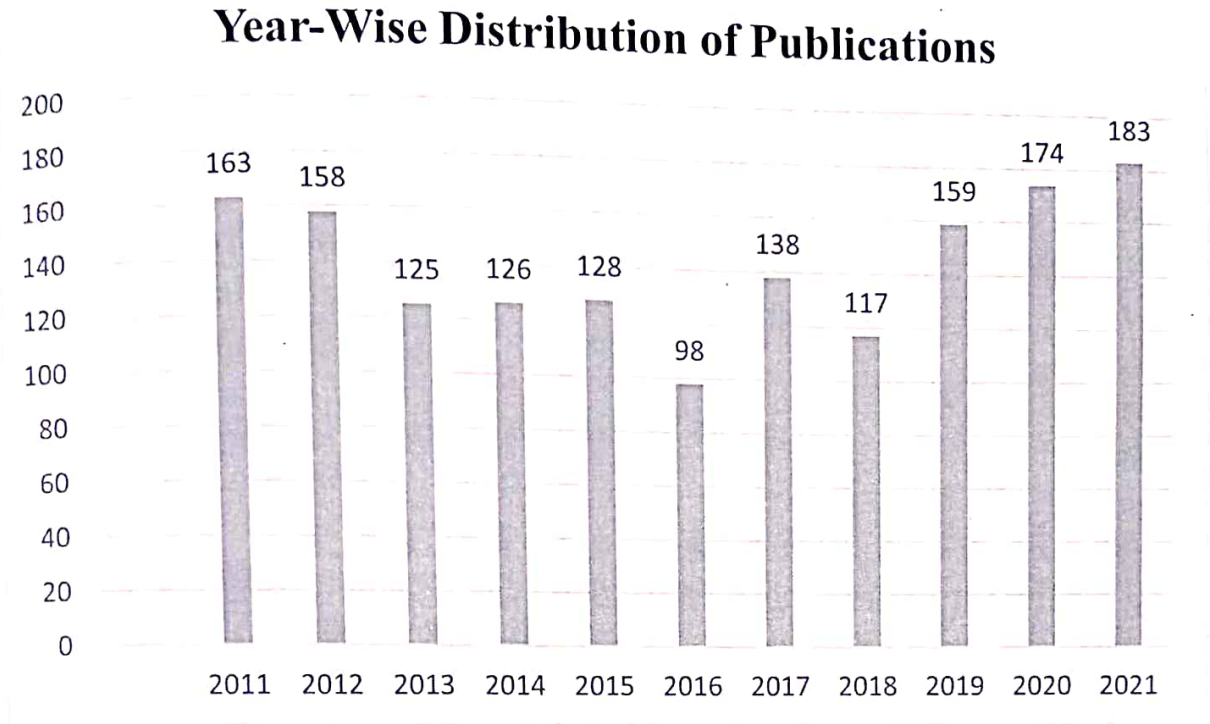

Fig. 1: Year-Wise Distribution of Articles

The year-wise distribution of Articles is displayed in Figure-1. The Figure is drawn between two parameters *No. of Articles* and *Year-wise growth* and shows the growth of Articles with respect to the Year. It is clear from the Figure that in 2021 maximum number of articles were published.

5.1 (b) Annual Growth Rate

The *Annual Growth Rate* (AGR) reflects the rate of growth over a single year.

$$\text{Annual Growth Rate} = \frac{(\text{Suceeding Value} - \text{Previous Value})}{\text{Previous Value}}$$

The following Figure-2 demonstrates the growth of publications with AGR. From this figure, it is observed that the year 2017 has the highest and positive AGR (40.00 %) among others. The year 2012, 2013, 2016 and 2018 have negative AGR (in %).

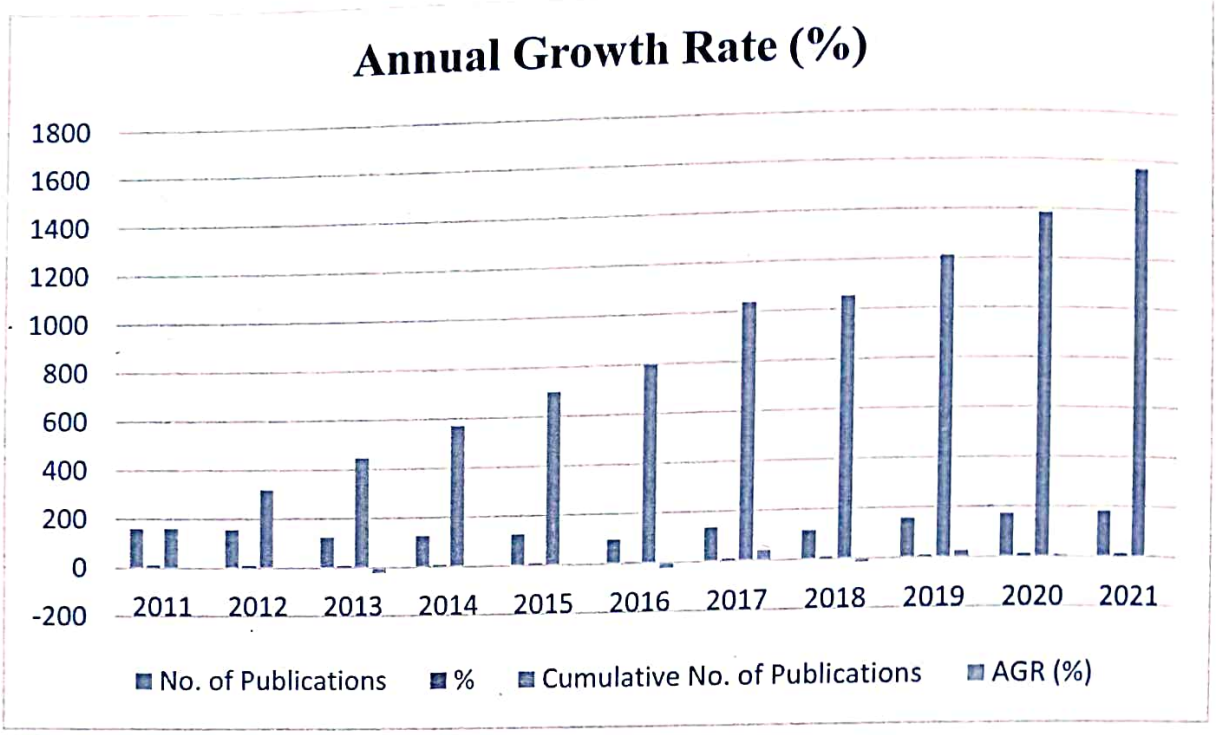

Fig. 2: Annual Growth Rate

5.2 Authorship Pattern

Table 2: Authorship Pattern

Year	Single Author	Two Authors	Three Authors	Four Authors	Five Authors	Six Authors	More than Six Authors	No. of Publications
2011	8	27	36	26	25	15	26	**163**
2012	5	28	36	32	21	19	17	**158**
2013	5	24	31	17	20	11	17	**125**
2014	8	13	21	25	27	9	23	**126**
2015	6	23	22	30	19	11	17	**128**
2016	3	13	15	23	20	10	14	**98**
2017	4	12	21	27	24	19	31	**138**
2018	2	12	13	31	16	20	23	**117**
2019	6	16	25	29	28	20	35	**159**
2020	4	9	30	37	25	23	46	**174**
2021	5	16	29	37	34	22	40	**183**
Total	56	**193**	**279**	**314**	**259**	**179**	**289**	**1569**
%	**3.56**	**12.30**	**17.78**	**20.01**	**16.50**	**11.40**	**18.41**	**100**

Table - 2 describes the authorship pattern of articles during the period 2011 to 2021.The total number of publications are 1569, in which 56 single author publications, 193 two authors publications, 279 three authors publications, 314 four authors publications, and so on. It shows that article publication trend was towards the multiple author approach.

The following Figure -3 demonstrates the authorship pattern between the No. of publication and years. From this figure, it is found that the category of four authors has the largest community that is 20.01%.



Fig. 3: Authorship Pattern

5.3 Author Productivity

Table 3: Author Productivity

Year	Number of Authors	Number of Publications	APA	AAPP
2011	204	163	0.79	1.26
2012	250	158	0.63	1.58
2013	175	125	0.71	1.40
2014	285	126	0.44	2.27
2015	363	128	0.35	2.85
2016	368	98	0.26	3.84
2017	399	138	0.34	2.94
2018	558	117	0.20	5.00

Year	Number of Authors	Number of Publications	APA	AAPP
2019	611	159	0.26	3.84
2020	859	174	0.20	5.00
2021	805	183	0.22	4.54
Total	7346	1569	0.21	4.76

Table 3 reveals the data which deals with author productivity.1569 publications are retrieved. The *Productivity per author* and *Average Authors Per Paper* are calculated by the following formulae

$$\text{Productivity per author} = \frac{\text{Number of Articles}}{\text{Number of Authors}} = 0.238 = 0.21$$

The *Productivity per author*is less than one which means on an average *Productivity per author* is only **21%**.

$$\text{Average Authors Per Paper} = \frac{\text{Number of Authors}}{\text{Number of Articles}} = \mathbf{4.76}$$

The *average number of authors per paper (publication)* is obtained by dividing the total number of publicationsby the total number of authors. This may be a very useful indicator for determining a journal's or author's average effect.

The following figure represents the year wise production between the no. of publication no. of authors, Productivity per author and average author per paper. From the Figure 4, it is clear that in years2018 and 2020, the AAPP of publicationsas well as authors are highest and APA is lowest.

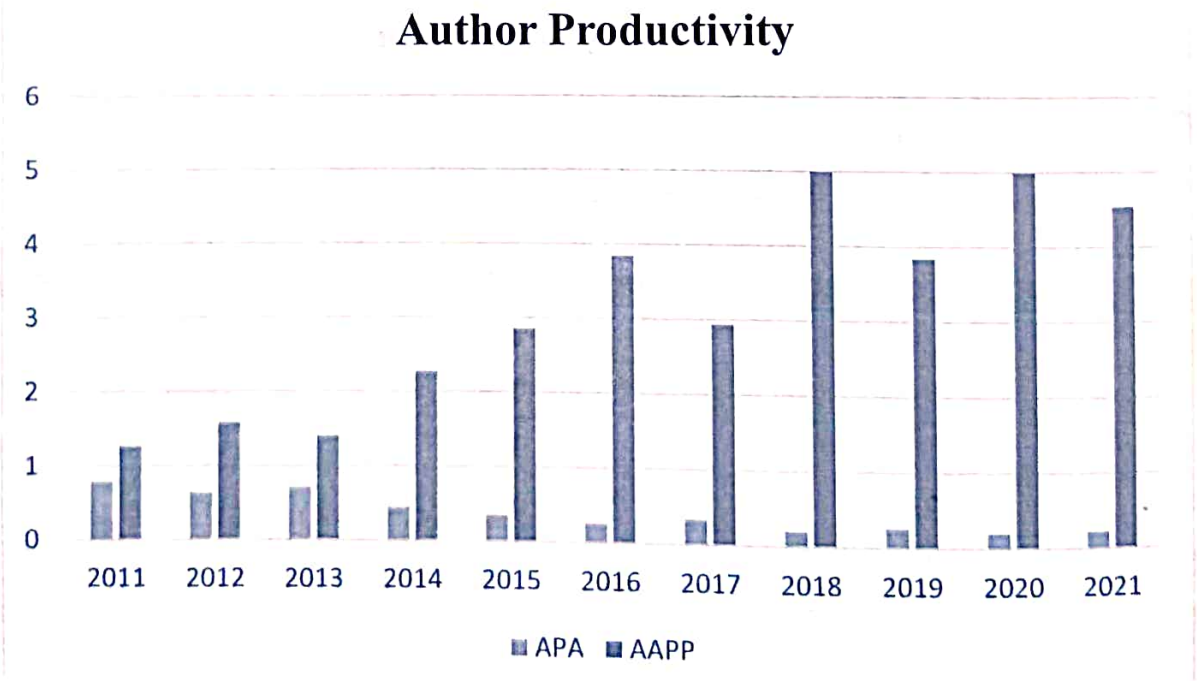

Fig. 4: Author Productivity

5.4 Relative Growth Rate of Publications & Doubling Time

Relative Growth Rate (RGR) is a measure to study the growth of number of articles over the period whereas Doubling Time (DT) is defined as the time when records become doubles values. The *Relative Growth Rate of Publications and Doubling Time* statics are mentioned in the following Table 4.

Table 4: Relative Growth Rate of Publications& Doubling Time

S. No	Year	No. of Publications	Cumulative Total	$LogW_1$	$LogW_2$	RGR	Doubling Time (DT=0.693/ RGR)	Mean RGR = ΣR/N	Mean ΣDt/N
1	2011	163	163	2.21	2.21	-	-		
2	2012	158	321	2.19	2.50	0.31	2.23		
3	2013	125	446	2.09	2.64	0.55	1.26		
4	2014	126	572	2.10	2.75	0.65	1.06		
5	2015	128	700	2.10	2.84	0.74	0.93	**0.710**	**0.908**
6	2016	98	798	1.99	2.90	0.91	0.76		
7	2017	138	1036	2.13	3.01	0.88	0.78		
8	2018	117	1053	2.06	3.02	0.96	0.72		
9	2019	159	1212	2.20	3.08	0.78	0.88		
10	2020	174	1386	2.24	3.14	0.90	0.77		
11	2021	183	1569	2.26	3.19	1.14	0.60		
Total		**1569**				**7.82**	**9.99**		

The RGR and DT model developed by Mahapatra (1985) and calculated by the following formula.

$$RGR = \frac{\log W_1 - \log W_1}{(T_2 - T_1)} = \mathbf{0.710}$$

where, T_1 and T_2 represent initial and final Time, respectively. $T_2 - T_1$ shows the time interval.

$$\text{Doubling Time} = \frac{0.693}{R} = \mathbf{0.908}$$

The following Figure 5 represents the graph of RGR and DT.

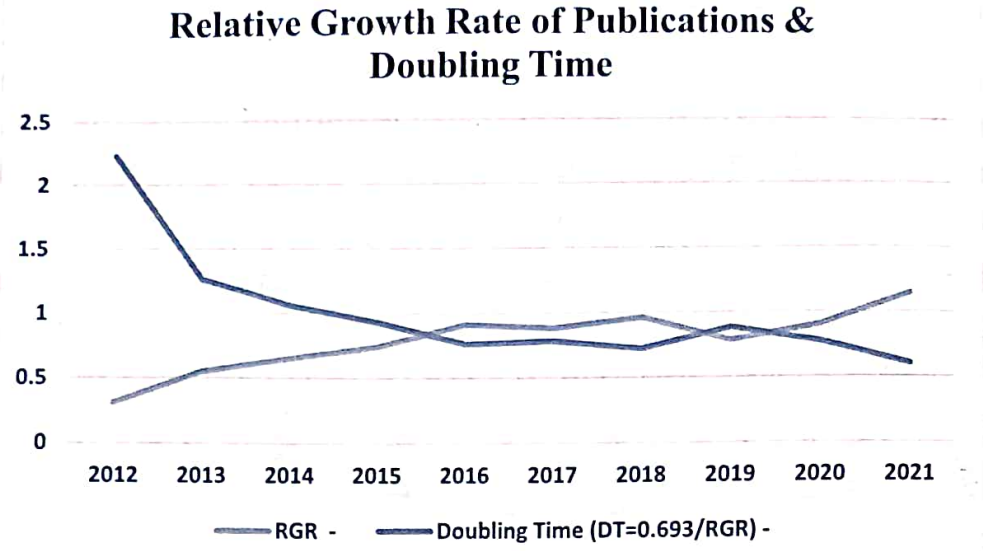

Fig. 5: AGR Growth and DT of Articles

5.5 Degree of Collaboration

The degree of collaboration is defined as the ratio of collaborative research publications to total research papers in the subject during a certain time period. Subramanyam (1983) proposed a formula for the degree of collaboration.

$$\text{Degree of Collaboration (DC)} = \frac{N_m}{(N_m + N_s)}$$

Where C represents the degree of collaboration. N_m and N_s represent the Multiple Author Publications and Single Author Publications respectively.

The Table 5 figures out the degree of collaboration. From this table, it is observed that in 2018 degree of collaboration is maximum (0.98). in years 2017, 2020 and 2021 have the 0.97 degree of collaboration. This implies that multiple authors contributed more than single authors.

Table 5: Degree of Collaboration

Year	Single Author Publications (Ns)	Multiple Author Publications (Nm)	Nm+Ns	Degree of Collaboration DC=Nm/(Nm+Ns)
2011	8	155	163	0.95
2012	5	153	158	0.96
2013	5	120	125	0.96
2014	8	118	126	0.93
2015	6	122	128	0.95

Year	Single Author Publications (Ns)	Multiple Author Publications (Nm)	Nm+Ns	Degree of Collaboration DC=Nm/(Nm+Ns)
2016	3	95	98	0.96
2017	4	134	138	0.97
2018	2	115	117	0.98
2019	6	153	159	0.96
2020	4	170	174	0.97
2021	5	178	183	0.97
Total	**56**	**1513**	**1569**	**0.964**

The following Figure 6 represents the graph of Degree of Collaboration.

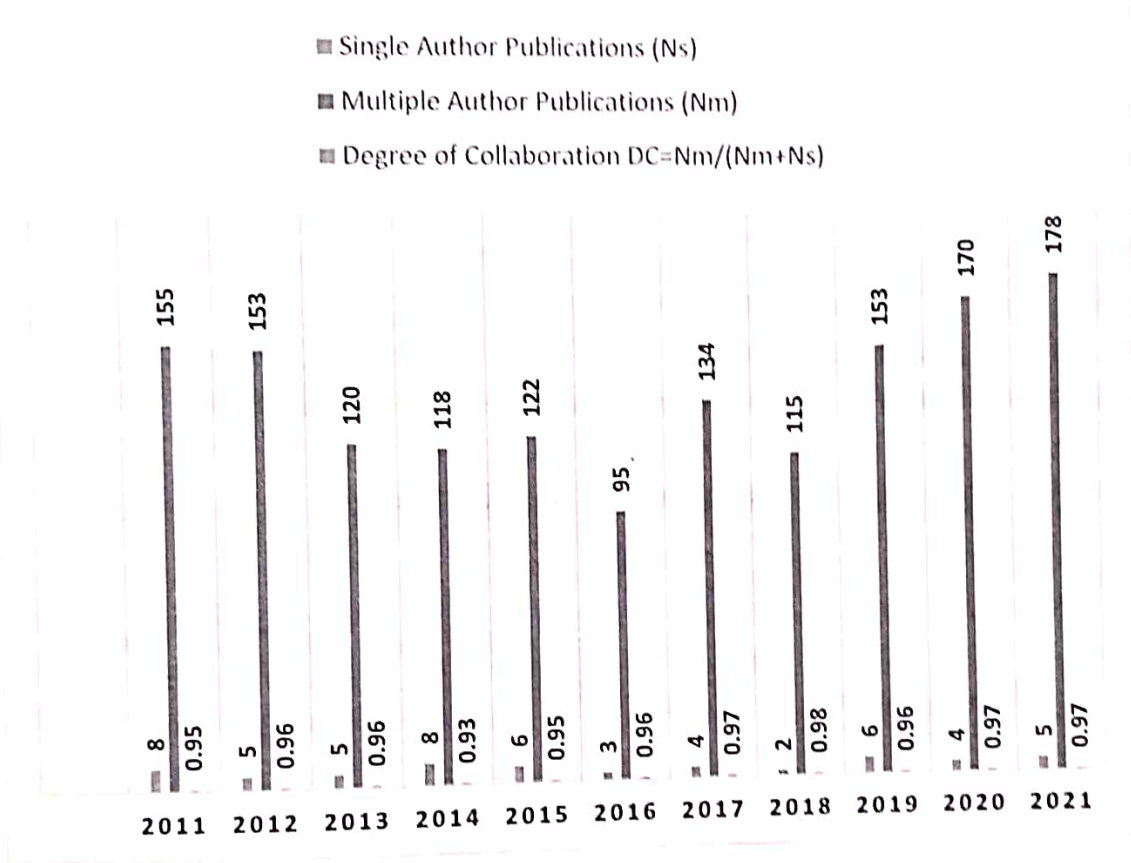

Fig 6: Degree of Collaboration

5.6 Collaborative Index (CI)

This index means number of authors per paper. To calculated collaborative Index formula is given by Elango and Rajendran.

$$CI = \frac{\text{Number of Authors}}{\text{Number of Joint Papers}}$$

Table 6: Collaborative Index (CI)

Years	Multi-author Papers	Total Authors of Multi-author Papers	Collaborative Index
2011	155	688	4.43
2012	153	645	4.21
2013	120	523	4.35
2014	118	568	4.81
2015	122	533	4.36
2016	95	431	4.53
2017	134	689	5.14
2018	115	583	5.08
2019	153	785	5.13
2020	170	928	5.45
2021	178	917	5.15
Total	**1513**	**7290**	**4.81**

Table 6 and figure 7 provide the year wise mean number of authors per joint authored paper. CI ranges from 4.43 (2011) to 5.15 (2021) were recorded, the highest CI (5.45) was recorded in 2020 and average CI was 4.81 for per Joint authored paper which indicates the researcher team trip between 4 and 6.

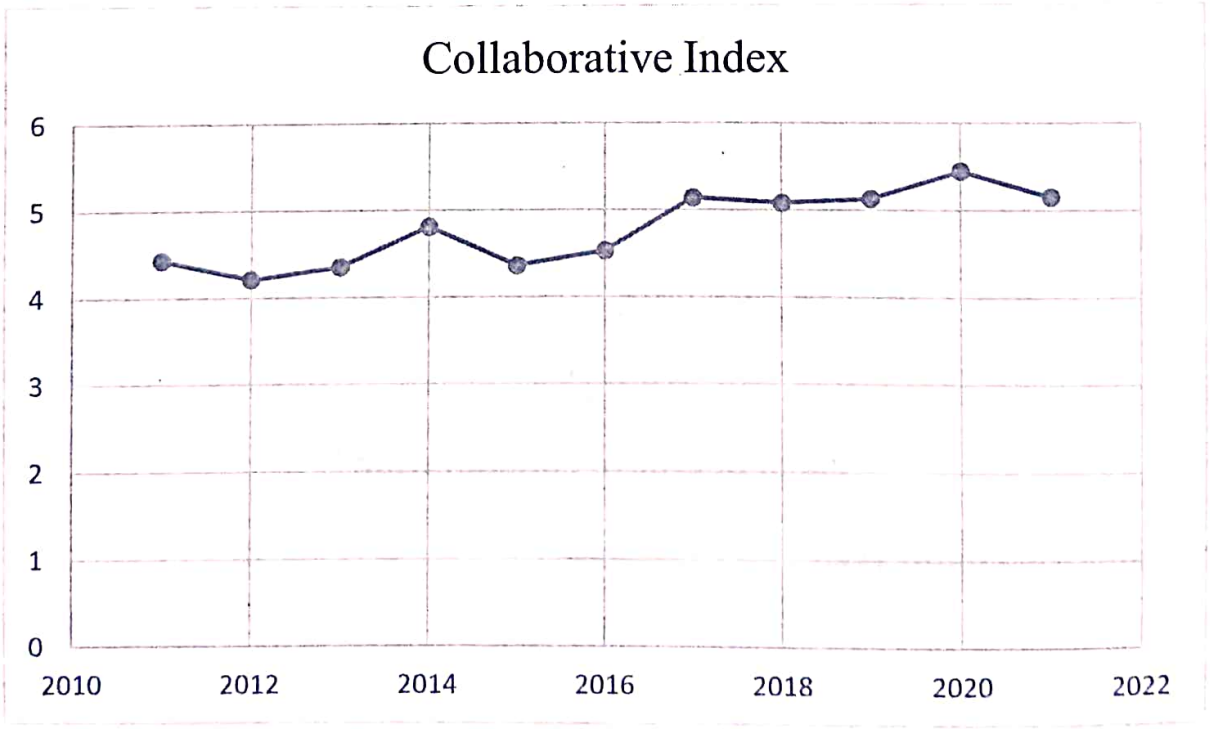

Fig. 7: Collaborative Index (CI)

5.7 Collaboration Coefficient and Modified Collaboration Coefficient

Ajiferuke, Burell and Tague have shown the mean number of authors per publications. According to them the part of multi authorship, as measures of degree of collaboration in a discipline, is inadequate. In this way; they proposed a measure combining some of the benefits of both measures into a term known as Collaborative Coefficient (CC).

The formula for Collaborative Coefficient (CC) is given by Ajiferuke et.al.

$$CC = 1 - \frac{1}{N}\sum_{j=1}^{k}\frac{1}{j}f(j)$$

Where,

fj= number of j-authors research publications published in a discipline during a certain period.

N = total number of research papers published in a discipline during a certain period

k = greatest number of authors per paper in a discipline.

$$\text{Calculation of Collaborative Coefficent} = 1 - \frac{f(1) + \frac{1}{2}f(2) + \frac{1}{3}f(3) + \frac{1}{4}f(4) + \cdots \frac{1}{n}f(n)}{N}$$

Based on the data in table 7Collaborative Coefficient for the year 2019 has been calculated as

$$CC = 1 - \frac{8 + \frac{1}{2}(27) + \frac{1}{3}(36) + \frac{1}{4}(26) + \frac{1}{5}(25) + \frac{1}{6}(15) + \frac{1}{7}(13) + \frac{1}{8}(18) + \frac{1}{9}(2) + \frac{1}{11}(2) + \frac{1}{12}(1)}{163}$$

$$CC = 1 - \frac{50.83}{163}$$

$$CC = 0.689$$

Similarly, all the data for CC calculated by this formula.

Modified collaboration coefficient (MCC)

The formula for calculation of MCC is given by Sarvanur and Srikanth.

$$MCC = \frac{A}{A-1}\{1 - \frac{1}{N}\sum_{j=1}^{k}\frac{1}{j}f(j)\}$$

$$MCC = 1 - \frac{8 + \frac{1}{2}(27) + \frac{1}{3}(36) + \frac{1}{4}(26) + \frac{1}{5}(25) + \frac{1}{6}(15) + \frac{1}{7}(13) + \frac{1}{8}(18) + \frac{1}{9}(2) + \frac{1}{11}(2) + \frac{1}{12}(1)}{163}$$

$$MCC = \frac{163}{162} X\ 0.689$$

MCC = 1.006 X 0.689 = 0.693

Similarly, the value of MCC for all the years can be calculated by using above formula.

Table 7: Collaboration Coefficient and Modified Collaboration Coefficient

Year	Single Authors	Two Authors	Three Authors	Four Authors	Five Authors	Six Authors	More than Six Authors	Total	CC	MCC
2011	8	27	36	26	25	15	26	163	0.689	0.693
2012	5	28	36	32	21	19	17	158	0.693	0.697
2013	5	24	31	17	20	11	17	125	0.687	0.691
2014	8	13	21	25	27	9	23	126	0.698	0.699
2015	6	23	22	30	19	11	17	128	0.688	0.689
2016	3	13	15	23	20	10	14	98	0.718	0.719
2017	4	12	21	27	24	19	31	138	0.750	0.751
2018	2	12	13	31	16	20	23	117	0.733	0.734
2019	6	16	25	29	28	20	35	159	0.741	0.742
2020	4	9	30	37	25	23	46	174	0.756	0.757
2021	5	16	29	37	34	22	40	183	0.745	0.746
Total	**56**	**193**	**279**	**314**	**259**	**179**	**289**	**1569**	**0.785**	**0.786**

Table 7 and figure 8 shows the Collaboration coefficient and Modified collaboration coefficient from the study. Highest CC and MCC was 0.756 and 0.757 successively listed in the year 2020. The total Collaboration coefficient (CC) was 0.785 and Modified collaboration coefficient (MCC) was 0.786.

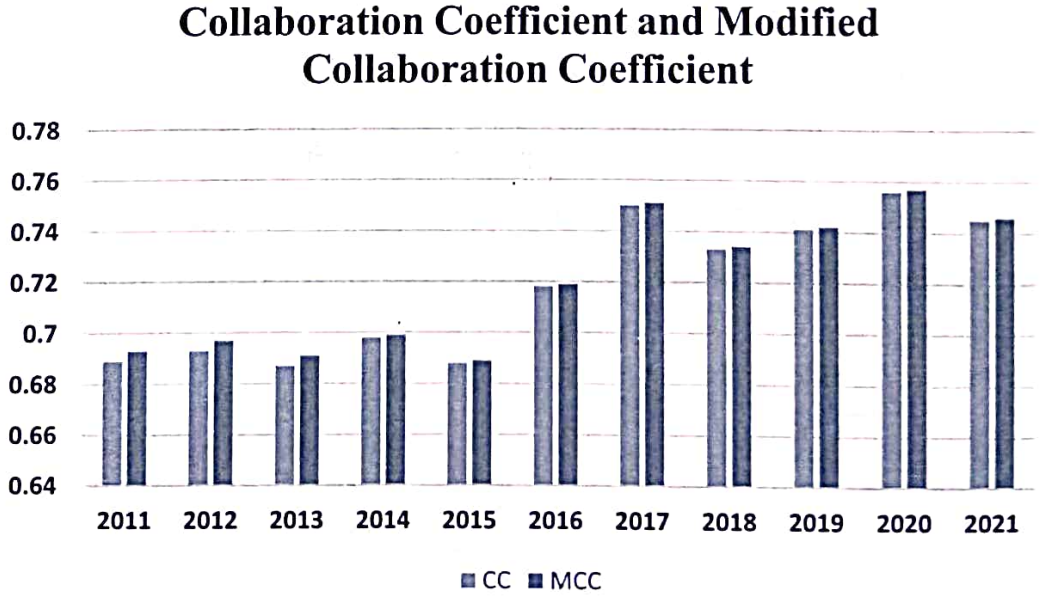

Fig. 8:Collaboration Coefficient and Modified Collaboration Coefficient

5.8 Countries–Wise Distribution of Articles (Top 10)

Table 8 and figure 9 shows displays the country-wise contribution of 1569 publication from different countries. It is found that the highest number of publications are from India (304), followed by the Brazil (167), China (100), Egypt (96), Indonesia (91), Iran (90), and so on.

Table 7: Country-Wise Distribution of Articles (Top 10)

Rank	Name of Country	Number of Publications
1	India	304
2	Brazil	167
3	China	100
4	Egypt	96
5	Indonesia	91
6	Iran	90
7	United States	85
8	Saudi Arabia	64
9	Thailand	64
10	Pakistan	59

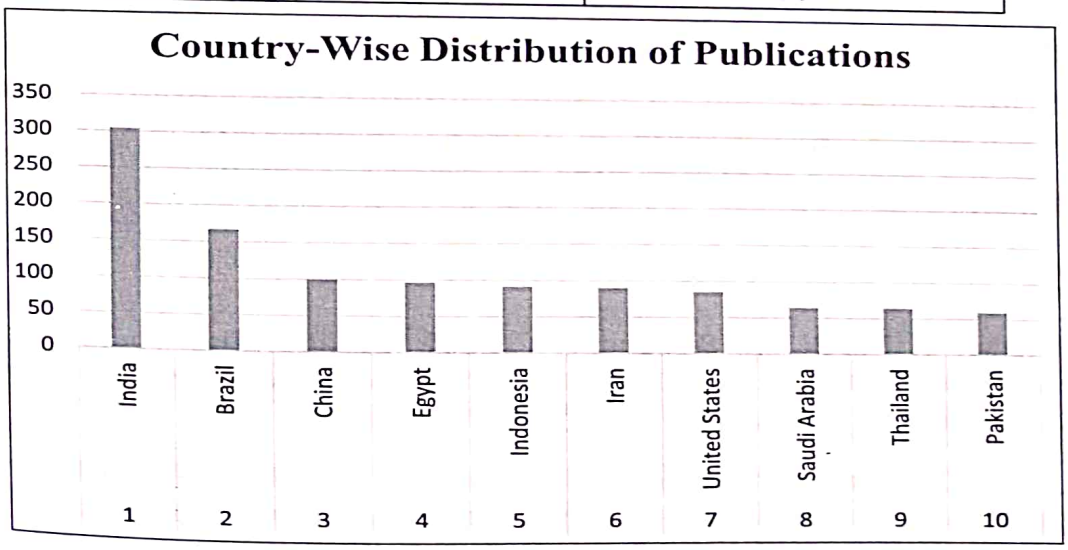

Fig. 9: Country-Wise Distribution of Publications

6. Findings and Conclusions

For studying ***Syzygium aromaticum*** **(Medicinal Plant) have 1569 publications** from the year of 2011 to 2021 using the Scopus database were retrieved. We have

examined such articles based on different scientometric parameters and their tools. We have demonstrated and discussed the observation using different Tables and Figure. The summary of the results are as follows.

- It has been found that in year 2020 maximum no. of articles 183 were published
- The total number of publications are 1569, in which 56 single author publications, 193 two authors publications, 279 three authors publications, 314 four authors publications, and so on. It shows that article publication trend was towards the multiple author approach.
- The *Productivity per author* and *Average Authors Per Paper* are 0.238 and 4.20.
- Relative Growth Rate (RGR) of publication of articles related to this field is 0.710 and average of Doubling time is 0.908.
- CI ranges from 4.43 (2011) to 5.15 (2021) were recorded, the highest CI (5.45) was recorded in 2020 and average CI was 4.81 for per Joint authored paper which indicates the researcher team trip between 4 and 6.
- The total Collaboration coefficient (CC) was 0.785 and Modified collaboration coefficient (MCC) was 0.786.
- It is found that the highest number of publications are from India (304), followed by the Brazil (167), China (100), Egypt (96), Indonesia (91), Iran (90), and so on.

References

1. Ajiferuke, I., Burell, Q., &Tague, J. (1988). Collaborative coefficient: A single measure of the degree of collaboration in research. *Scientometrics, 14*(5-6), 421-433.DOI: https://doi.org/10.1007/bf02017100

2. Ali, H., &Kumari, A. (2018). Scientometric Analysis of World Biodiversity Literature. International Journal of Library and Information Studies, 8(1), 261-271.

3. Elango, B., & Rajendran, P. (2012). Authorship trends and collaboration pattern in the marine sciences literature: a scientometric study. *International Journal of Information Dissemination and Technology, 2*(3), 166-169.

4. El-SaberBatiha, G., Alkazmi, L. M., Wasef, L. G., Beshbishy, A. M., Nadwa, E. H., &Rashwan, E. K. (2020). Syzygiumaromaticum L.(Myrtaceae): Traditional

uses, bioactive chemical constituents, pharmacological and toxicological activities. *Biomolecules, 10*(2), 202. DOI:10.3390/biom10020202

5. Gupta, R., Gupta, B. M., Bansal, J., & Kumar, A. (2016). Scientometric assessment of India's migraine research publications during 2006-15. *Journal of Young Pharmacists, 8*(4),294-301. https://www.jyoungpharm.org/sites/default/files/10.5530jyp.2016.4.2.pdf

6. Kumar, V., Mishra, D., Joshi, M. C., Mishra, P., &Tanwar, M. (2021). Herbs and Spices—New Processing Technologies. Syzygiumaromaticum: Medicinal Properties and Phytochemical Screening. In *Herbs and Spices-New Processing Technologies.* IntechOpen, 121-135.

7. Mahapatra, M. (1985, July). On the validity of the theory of exponential growth of scientific literature. In *Proceedings of the 15th IASLIC conference, Bangalore* (Vol. 6170).

8. Massarrat, S., &Kolahdoozan, S. (2011). Critical assessment of progress of medical sciences in Iran and Turkey: the way developing countries with limited resources should make effective contributions to the production of science. *Archives of Iranian medicine, 14*(6), 370-377.

9. Merton, R. K. & Garfield, E. (1963). Forward to Little Science, Bigscience and Beyond by DJ de solla Price. 1963. ColumbiaUniversity Press; New York.

10. Savanur, K., &Srikanth, R. (2010). Modified collaborative coefficient: A new measure for quantifying the degree of research collaboration. *Scientometrics, 84*(2), 365-371.DOI: https://doi.org/10.1007/s11192-009-0100-4

11. Scientometrics (2008). Glossary of Thompson Scientific Terminology online. Retrieved from http://science.thomsonreuters.com/support/patents/patinf/terms/>

12. Sivasekaran, K. (2021). *Curcuma Longa* (Medicinal Plant) Research: A Scientometric Assessment of Global Publications Output with Reference to Web of Science. *Turkish Journal of Computer and Mathematics Education (TURCOMAT), 12*(5), 1477-1496. DOI: https://doi.org/10.17762/turcomat.v12i5.2115

13. Subramanyam, K. (1983). Bibliometric studies of research collaboration: A review. *Journal of information Science, 6*(1), 33-38.

14. Tabatabaei-Malazy, O., Ramezani, A., Atlasi, R., Larijani, B., &Abdollahi, M. (2016). Scientometric study of academic publications on antioxidative herbal medicines in type 2 diabetes mellitus. *Journal of diabetes & metabolic disorders, 15*(1), 1-8. DOI: https://doi.org/10.1186/s40200-016-0273-3

प्राकृत-समय

डॉ. ज्योतिबाबू जैन



मूर्तिदेवी ग्रन्थमाला : हिन्दी ग्रन्थांक 95

ISBN978-93-90659-49-4

प्राकृत-समय

(प्राकृत विद्या : आधुनिक संदर्भ में)

(शोध)

संपादक : डॉ. ज्योतिबाबू जैन

प्रकाशक : **भारतीय ज्ञानपीठ**
18, इन्स्टीट्यूशनल एरिया, लोदी रोड, नयी दिल्ली-110 003

मुद्रक : भारतीय ज्ञानपीठ, नयी दिल्ली-110003

© डॉ. ज्योतिबाबू जैन

PRAKRIT-SAMAYA
(Reserach)
By Dr. Jyotibabu Jain

Published by
Bharatiya Jnanpith
18, Institutional Area, Lodi Road, New Delhi-110 003
Ph. : 011-24626467; 23241619 (Daryaganj)
Mob. : 9350536020; e-mail : bjnanpith@gmail.com
sales@jnanpith.net; website : www.jnanpith.net

First Edition : 2022
Price Rs. 600

अनुक्रम

संपादकीय -डॉ ज्योतिबाबू जैन
प्ररोचना- प्रो.सुदीप कुमार जैन

1. प्राकृत-काव्यों की मौलिक रमणीयता - प्रो.दामोदर शास्त्री/ 27
2. प्राकृत साहित्य में योग और ध्यान की परंपरा
- प्रो.भागचंद जैन भास्कर/ 34
3. प्राकृत-अध्ययन की उपयोगिता - प्रो.प्रेम सुमन जैन/47
4. प्राकृत साहित्य की परंपरा और उसकी विधाएं - प्रो.उदयचंद्र जैन/57
5. Importance of prakrit scriptures in modern times for our happiness - Dr.P.M Agrawal/ 66
6. प्राकृत पालि गाथाओं में साम्य - प्रो.धर्म चन्द्र जैन/ 76
7. आयुर्वेद में प्राकृत और संस्कृत की उपयोगिता - प्रो.ऋषभचंद जैन/ 85
8. प्राकृत आगमों में विज्ञान - प्रो. एन.एल.कछारा / 103
9. प्राकृत वाङ्मय में समत्व दृष्टि - प्रो.अशोक कुमार जैन/ 110
10. प्राकृत परम्परा के आचार्यो की समकालीन -युगचेतना
- प्रो.वीर सागर जैन/ 118
11. प्राकृत-सूक्तियों में लोकमंगल भावना - डॉ.रांका जैन/ 124
12. भारतीय साहित्य को प्राकृत का योगदान - डॉ.कमल कुमार जैन/ 130
13. प्राकृत शिलालेखों में समसामयिकता - डॉ.दिलीपधींग/ 145
14. प्राकृत आगमों के शैक्षिक संदर्भ - प्रो.जिनेंद्र कुमार जैन / 149
15. प्राकृतभाषा और आधुनिक संचार-माध्यम - प्रो.अनेकांत जैन/158
16. प्राकृत-काव्यों की समरसता - प्रो.जयकुमार उपाध्ये/ 166
17. आगमों में अंकित आचार-संहिता और पर्यावरण सुरक्षा - डॉ.अनिल कुमार जैन/174

18. प्राकृत आगमों में कषाय-विजय के उपाय - डॉ.ज्योति बाबू जैन/ 188
19. जैन आगम और वर्तमान कृषि-पद्धति - डॉ.श्याम लाल गोदावत/ 194
20. प्राकृतभाषा जनकल्याणी - डॉ.सुमत कुमार जैन/ 202
21. प्राकृत भाषा का जैन-पत्रकारिता के विकास में योगदान
- डॉ.धर्मेंद्र कुमार जैन/ 217
22. प्राकृत-साहित्य में शैक्षिक निहितार्थ - डॉ.शुद्धात्मप्रकाश जैन/ 221
23. प्राकृत-वाङ्मय में आध्यात्मिक-विकास के सोपान
- प्रो.डॉ. अनिल कुमार जैन/ 231
24. प्राकृत-सूक्तियों की समसामयिकता - प्रो.कल्पना जैन/ 245
25. प्राकृत-साहित्य में ध्यान और उसकी उपयोगिता - डॉ. सत्यनारायण शर्मा/251
26. प्राकृत के आधुनिक-चिंतक - डॉ.आशीष जैन/ 268
27. प्राकृत मंत्रों एवं स्तोत्रों का जीवन पर प्रभाव - प्रो.महावीर शास्त्री/ 290
28. प्राकृत में सट्टक-परंपरा एवं उसकी प्रासंगिकता - डॉ.पत्रिका जैन/ 305
29. विज्जावसुसावयायारो में अतिचारों की सामाजिक-स्थिति- डॉ.आनंद कुमार जैन / 313
30. प्राकृत-साहित्य में अंकित अचौर्यव्रत की महत्ता
- डॉ.आलोक कुमार/ 319
31. प्राकृत चरित-ग्रंथों का वैभव एवं उपयोगिता - डॉ. माधुरी शास्त्री/ 325
32. गुजराती मध्यकालीन साहित्य पर प्राकृत का प्रभाव
- प्रो. सलोनी जोशी/ 340
33. नम्मयासुंदरी कहा में स्त्री शिक्षा- डॉ. वंदना चौधरी/ 344
34. कर्म-सिद्धांत और मानसिक-शांति - डॉ.वीरचन्द्र जैन/ 350

प्राकृत भाषा से अनुप्राणित भारतीय भाषाएँ



डॉ. ज्योतिबाबू जैन

प्राकृत भाषा से अनुप्राणित भारतीय भाषाएँ

सम्पादक
डॉ. ज्योति बाबू जैन

भारतीय ज्ञानपीठ

मूर्तिदेवी ग्रन्थमाला : हिन्दी ग्रन्थांक 96

ISBN 978-93-90659-48-7

प्राकृत भाषा से अनुप्राणित भारतीय भाषाएँ

(शोध)

संपादक : डॉ. ज्योतिबाबू जैन

प्रकाशक : भारतीय ज्ञानपीठ
18, इन्स्टीट्यूशनल एरिया, लोदी रोड, नयी दिल्ली-110 003

मुद्रक : भारतीय ज्ञानपीठ, नयी दिल्ली-110003

© डॉ. ज्योतिबाबू जैन

PRAKRIT BHASHA SE ANUPRANIT BHARATIYA BHASHANE
(Reserach)
By Dr. Jyotibabu Jain

Published by
Bharatiya Jnanpith
18, Institutional Area, Lodi Road, New Delhi-110 003
Ph. : 011-24626467; 23241619 (Daryaganj)
Mob. : 9350536020; e-mail : bjnanpith@gmail.com
sales@jnanpith.net; website : www.jnanpith.net

First Edition : 2022
Price Rs. 550

विषयानुक्रमणिका

क्र.	विषय	पृ.क्र.
1.	भारतीय भाषाओं के विकास में प्राकृत का योगदान - डॉ ज्योति बाबू जैन	29
2.	प्राकृत भाषा महत्त्व एवं आधुनिक युग में इसके अध्ययन अध्यापन की दशा और दिशा - प्रो. फूलचंद जैन प्रेमी	39
3.	वैदिक संस्कृत पर प्राकृत प्रभाव - प्रो. दामोदर शास्त्री	51
4.	प्राकृत और संस्कृत का तुलनात्मक विवेचन -प्रो सुदर्शन लाल जैन	59
5.	प्राकृत अपभ्रंश एवं अन्य भारतीय भाषाएँ -प्रो. प्रेम सुमन जैन	70
6.	प्राकृत एवं बौद्ध संस्कृत - प्रो. विजय कुमार जैन	86
7.	प्राकृत भाषा के संरक्षण में संस्कृत साहित्य का योगदान -डॉ. सुदर्शन मिश्र	98
8.	पाली एवं प्राकृतों का परस्परिक संबंध - प्रो. धर्मचंद जैन	119
9.	प्राकृत का हिंदी को योगदान - डॉ दिलीप धींग	128
10.	बिहार की भाषाओं के विकास में प्राकृतों का योगदान -प्रो. ऋषभचंद जैन	133
11.	प्राकृत और पंजाबी भाषा सम्बन्ध - प्रो. प्रद्युम्नशाह सिंह	157

12. मागधी प्राकृत की उत्पत्ति और विकास
- डॉ. सुदर्शन मिश्र 165
13. प्राकृत संस्कृत मैत्री
- प्रो. वीरसागर जैन 180
14. प्राकृत और सिंधी भाषा संबंध
- डॉ. यशोधरा वाधवाणी 183
15. संस्कृत साहित्य में प्राकृत की उपादेयता
- डॉ. गिरीश कुमार शर्मा 197
16. प्राकृत एवं गुजराती भाषा संबंध
- डॉ. कुणाल एम कपासी 206
17. प्राकृत तमिल संबंध और प्रभाव
- डॉ. दिलीप धींग 218
18. कन्नड़ भाषा में प्राकृत व्याकरण
-डॉ. शांतिसागर शिरहट्टि 224
19. महाराष्ट्री प्राकृत एवं मराठी भाषा का अंत:संबंध -
प्रो. महावीर शास्त्री 241
20. प्राकृत का राजस्थानी पर प्रभाव
- डॉ. देव कोठारी 256
21. प्राकृत और बुंदेली भाषा का संबंध -
प्रो. कल्पना जैन 276
22. प्राकृत भाषा विकास और संरक्षण के उपाय
-डॉ. धर्मेन्द्र कुमार जैन 284
23. प्राकृत संस्कृत विभक्तियों की तुलना
-डॉ. ज्योति बाबू जैन 289
24. प्राकृत भाषा और ब्राह्मी लिपि
- डॉ. शुद्धात्मप्रकाश जैन 295
25. Influence of prakrit on Bengali phonology -
Pro. Jagat Ram Bhattacharya, Santiniketan 300

सम्पादकीय

विद्वद्वरेण्य पाइयविण्णो प्रो. जिनेन्द्र कुमार जैन, उदयपुर के सम्मानार्थ ग्रन्थ "णव-सिजणं" का प्रकाशन किया जा रहा है। यह हमारा परम सौभाग्य है कि हमें इस ग्रन्थ के सम्पादन का उत्तरदायित्व प्राप्त हुआ है। सभी सनेही मित्रों एवं गुरुओं की सतत प्रेरणा से ही इस ग्रन्थ का प्रकाशन सम्भव हो पा रहा है। ग्रन्थ के निर्माण हेतु पावन आशीर्वाद परमपूज्य प्राकृतशिरोमणी आचार्यश्री सुनीलसागरजी महाराज, परमपूज्य प्रज्ञाश्रमण अमितसागरजी महाराज एवं परमपूज्य मुनिश्री प्रणम्यसागरजी महाराज और परम-संरक्षक के रूप में परमपूज्य जगद्गुरु कर्मयोगी स्वस्तिश्री चारुकीर्ति भट्टारक महास्वामीजी, श्रवणबेलगोला का आशीर्वाद प्राप्त हुआ है, साथ ही संरक्षक एवं परामर्श प्रदानकर्त्ता के रूप में प्रो. प्रेम सुमन जैन, उदयपुर, प्रो. ऋषभचंद जैन, वैशाली एवं प्रो. जय कुमार जैन, मुजफ्फनगर तथा देश के ख्यातिलब्ध वरिष्ठ विद्वानों से निरन्तर मार्गदर्शन प्राप्त हुआ है।

प्रस्तुत कृति 'णव-सिजणं' का नामकरण सार्थक और उद्देश्यपूर्ण है। जहाँ एक ओर इस नामकरण में नूतनता का संचार है वहीं दूसरी ओर प्राच्यविद्यानुरागी हमारे गुरुवर का सम्मान है।

इस ग्रन्थ के सम्पादन में उत्तरदायित्व का निर्वहन गुरुवर्य प्रो. जिनेन्द्र कुमार जी के आशीर्वाद से ही सम्भव हुआ है। अभिनन्दनीय गुरुजी के विराट् व्यक्तित्व और कृतित्व को 'णव-सिजणं" ग्रन्थ की सीमित परिधि में निबद्ध करना असंभव था। गुरुजी ने महती कृपा करके अपने शोधलेखों में से कुछ विशिष्ट आलेखों को 'णव-सिजणं' ग्रन्थ में प्रकाशित करने की अनुमति प्रदान की है। हमारा निवेदन स्वीकार करके गुरुजी ने अपना जीवन-वृत्त तथा साहित्यिक अवदान प्रदान कर भी हमें उपकृत किया है। यह कार्य उनके द्वारा ही संभव था। उन्होंने अपने इस कार्य को पूरा करने में बड़ा श्रम किया है। ग्रन्थ की प्रूफ रीडिंग का कार्य भी अत्यन्त कठिन था। यह कार्य भी गुरुजी के सहयोग से ही पूर्ण कर पाए हैं। गुरूजी के घर पर मुझे गुरुजी और गुरुमाता श्रीमती मीना जी का असीम वात्सल्य प्राप्त हुआ है।

गुरुजी प्राकृत भाषा, साहित्य एवं जैनविद्या के अनुरागी एवं विश्रुत मनीषी है। आपकी जैन विद्वानों के साथ-साथ जैनेतर विद्वानों में आपके कार्यशैली की बड़ी प्रतिष्ठा है। यही कारण है कि इस ग्रन्थ हेतु जैन विद्वानों के साथ-साथ अनेक जैनेतर विद्वानों ने भी शुभकामनाएँ प्रेषित की हैं। सम्माननीय गुरुजी की निःस्वार्थ श्रुतसेवा और सारस्वत साधना का ही फल है कि उन्हें आचार्य, मुनि एवं भट्टारकजी ने आशीर्वाद प्रदान किया है। इसमें वरिष्ठ मनीषियों ने अपनी शुभकामनाएँ प्रदान की हैं। हम परमपूज्य आचार्य, मुनिश्री, भट्टारकजी एवं वरिष्ठ मनीषियों को सादर नमन करते हुए कृतज्ञता ज्ञापित करते हैं। जिन विद्वानों, साधर्मियों एवं स्नेही साथियों ने अपनी शुभाशंसाएँ प्रेषित की हैं, उनका भी हृदय से आभार व्यक्त करते हैं। विशेषरूपेण हम हमारे कनिष्ठ एवं वरिष्ठ शोधार्थी साथियों का हृदय से आभार व्यक्त करते हैं, जिनके सहयोग एवं प्रेरणा से यह दुरूहकार्य परिपूर्ण हो सका है। हमने णव-सिजणं ग्रन्थ का सम्पादन यथासंभव मनोयोग से पूर्ण किया है, फिर भी इसमें यदि कुछ त्रुटियाँ शेष रह जाना स्वाभाविक है, तो उनके लिए हम क्षमाप्रार्थी हैं।

डॉ. वीर चंद्र जैन
सहायक आचार्य
जैनदर्शन एवं प्राकृत विभाग
महारानी महेश्वर लता संस्कृत
विद्यापीठ, लोहना कामेश्वर सिंह
दरभंगा संस्कृत विश्वविद्यालय, दरभंगा

डॉ. दिनेश कुमार मिश्र
सह-आचार्य,
जैनविद्या
राजकीय बांगड़ स्नातकोत्तर
महाविद्यालय, पाली (राजस्थान)

डॉ सुमत कुमार जैन
सहायक आचार्य
जैनविद्या एवं प्राकृत विभाग
मोहनलाल सुखाड़िया विश्वविद्यालय,
उदयपुर (राजस्थान)

Scanned with OKEN Scanner

Contemporary Issues in Accounting

(Including Blockchain Technology)

Prof. Shurveer S. Bhanawat
Dr. Shilpa Vardia | Dr. Shilpa Lodha



Bharti Publications

About the Editors



Prof. Shurveer S. Bhanawat has been working as a Professor and Head, Department of Accountancy and Business Statistics, at Mohanlal Sukhadia University, Udaipur. He is director of MFC and M.Voc (ATA). Having twenty-six years of teaching experience. He possesses degrees of M.Com (gold Medal), M. Phil, Ph.D. and C.S. (1) with all through first-class academic records. Sixty-eight research articles have been published so far in international and national journals. Out of these ten research papers had been awarded 'Best research paper" and two "Quality Papers" in Indian Accounting Conferences and International seminars. He has been awarded Silver Shield for Second Best Research Paper in 2021 and Certificate of appreciation in 2022 under ICAI International Research Award in taxation category by the ICAI, New Delhi. He is also author of textbooks entitled 'Business Statistics and Cost Accounting published in Hindi and English versions. Three edited books are on his credit. He has completed two research projects on 'Socio-Economic Implication of Carbon Taxation: An Exploratory Research and "Determination of Shareholders wealth: A quantitative Analysis". He got president scout's award (1985) from President of India.



Dr. Shilpa Vardia has been working as an Assistant Professor in the Department of Accountancy and Business Statistics, Mohanlal Sukhadia University, Udaipur. She is having eighteen years of teaching experience at the graduate and postgraduate levels. She is the convener of the MFC and PGDIT Programme. She is an executive member of the Indian Accounting Association. She possesses degrees of M.Com and Ph.D. with a thorough meritorious academic record. Twenty-five research articles have been published so far in the journal of international and national repute. Six research papers have been awarded as Best Research Paper at Indian Accounting Conferences and other conferences. She also got the Certificate of appreciation under ICAI International Research award, 2020 from the ICAI, New Delhi. She is also the co-author of a textbook entitled "Business Statistics" published in Hindi version.



Dr. Shilpa Lodha is Assistant Professor at Department of Accountancy and Statistics, Mohanlal Sukhadia University, Udaipur. Having more than twelve years of teaching experience at graduate and post graduate levels, she is a UGC NET (2010) & UGC NET-JRF (2012) qualified faculty actively involved in teaching, research and consultancy. She has also been UCC-PDF. She possesses degrees of M.Com. (Gold Medal), M.Phil. (Gold Medal), and Ph.D., with all through meritorious academic record. She has got the Best Research Paper award three times in International Conferences. Her 20 research papers have been published in journals of national and international repute. She is also a co-author of books entitled "Cost Accounting" published in Hindi version and "Corporate Accounting" published in Hindi and English.

Presently three authors have been working as PI and Co-PIs under RUSA- sponsored departmental project entitled "Block Chain Accounting: An Exploratory Research.

Bharti Publications, New Delhi
Email-info@bartipublications.com | bhartipublication@gmail.com
www.bhartipublications.com

ISBN 978-81-19079-03-2

Price- Rs. 795/-

Contemporary Issues in Accounting

(Including Blockchain Technology)

Prof. Shurveer S. Bhanawat
Dr. Shilpa Vardia | Dr. Shilpa Lodha



Bharti Publications

About the Editors



Prof. Shurveer S. Bhanawat has been working as a Professor and Head, Department of Accountancy and Business Statistics, at Mohanlal Sukhadia University, Udaipur. He is director of MFC and M.Voc (ATA). Having twenty-six years of teaching experience. He possesses degrees of M.Com (gold Medal), M. Phil, Ph.D. and C.S. (1) with all through first-class academic records. Sixty-eight research articles have been published so far in international and national journals. Out of these ten research papers had been awarded 'Best research paper" and two "Quality Papers" in Indian Accounting Conferences and International seminars. He has been awarded Silver Shield for Second Best Research Paper in 2021 and Certificate of appreciation in 2022 under ICAI International Research Award in taxation category by the ICAI, New Delhi. He is also author of textbooks entitled 'Business Statistics and Cost Accounting published in Hindi and English versions. Three edited books are on his credit. He has completed two research projects on 'Socio-Economic Implication of Carbon Taxation: An Exploratory Research and "Determination of Shareholders wealth: A quantitative Analysis". He got president scout's award (1985) from President of India.



Dr. Shilpa Vardia has been working as an Assistant Professor in the Department of Accountancy and Business Statistics, Mohanlal Sukhadia University, Udaipur. She is having eighteen years of teaching experience at the graduate and postgraduate levels. She is the convener of the MFC and PGDIT Programme. She is an executive member of the Indian Accounting Association. She possesses degrees of M.Com and Ph.D. with a thorough meritorious academic record. Twenty-five research articles have been published so far in the journal of international and national repute. Six research papers have been awarded as Best Research Paper at Indian Accounting Conferences and other conferences. She also got the Certificate of appreciation under ICAI International Research award, 2020 from the ICAI, New Delhi. She is also the co-author of a textbook entitled "Business Statistics" published in Hindi version.



Dr. Shilpa Lodha is Assistant Professor at Department of Accountancy and Statistics, Mohanlal Sukhadia University, Udaipur. Having more than twelve years of teaching experience at graduate and post graduate levels, she is a UGC NET (2010) & UGC NET-JRF (2012) qualified faculty actively involved in teaching, research and consultancy. She has also been UCC-PDF. She possesses degrees of M.Com. (Gold Medal), M.Phil. (Gold Medal), and Ph.D., with all through meritorious academic record. She has got the Best Research Paper award three times in International Conferences. Her 20 research papers have been published in journals of national and international repute. She is also a co-author of books entitled "Cost Accounting" published in Hindi version and "Corporate Accounting" published in Hindi and English.

Presently three authors have been working as PI and Co-PIs under RUSA- sponsored departmental project entitled "Block Chain Accounting: An Exploratory Research.

Bharti Publications, New Delhi
Email-info@bartipublications.com | bhartipublication@gmail.com
www.bhartipublications.com

ISBN 978-81-19079-03-2

Price- Rs. 795/-

प्राकृत-समय

डॉ. ज्योतिबाबू जैन



Scanned with OKEN Scanner

प्राकृत-समय

(प्राकृत विद्या : आधुनिक संदर्भ में)

सम्पादक

डॉ. ज्योतिबाबू जैन

भारतीय ज्ञानपीठ

Scanned with OKEN Scanner

मूर्तिदेवी ग्रन्थमाला : हिन्दी ग्रन्थांक 95

ISBN978-93-90658-43-4

प्राकृत-समय

(प्राकृत विद्या : आधुनिक संदर्भ में)

(शोध)

संपादक : डॉ. ज्योतिबाबू जैन

प्रकाशक : भारतीय ज्ञानपीठ
18, इन्स्टीट्यूशनल एरिया, लोदी रोड, नयी दिल्ली-110 003

मुद्रक : भारतीय ज्ञानपीठ, नयी दिल्ली-110003

© डॉ. ज्योतिबाबू जैन

PRAKRIT-SAMAYA
(Reserach)
By Dr. Jyotibabu Jain

Published by
Bharatiya Jnanpith
18, Institutional Area, Lodi Road, New Delhi-110 003
Ph. : 011-24626467; 23241619 (Daryaganj)
Mob. : 9350538020; e-mail : bjnanpith@gmail.com
sales@jnanpith.net; website : www.jnanpith.net

First Edition : 2022
Price Rs. 600

Scanned with OKEN Scanner

अनुक्रम

संपादकीय –डॉ ज्योतिबाबू जैन
प्ररोचना– प्रो.सुदीप कुमार जैन

1. प्राकृत–काव्यों की मौलिक रमणीयता – प्रो.दामोदर शास्त्री/ 27
2. प्राकृत साहित्य में योग और ध्यान की परंपरा
– प्रो.भागचंद जैन भास्कर/ 34
3. प्राकृत–अध्ययन की उपयोगिता – प्रो.प्रेम सुमन जैन/47
4. प्राकृत साहित्य की परंपरा और उसकी विधाएं – प्रो.उदयचंद्र जैन/57
5. Importance of prakrit scriptures in modern times for our happiness - Dr.P.M Agrawal/ 66
6. प्राकृत पालि गाथाओं में साम्य – प्रो.धर्म चन्द्र जैन/ 76
7. आयुर्वेद में प्राकृत और संस्कृत की उपयोगिता – प्रो.ऋषभचंद जैन/ 85
8. प्राकृत आगमों में विज्ञान – प्रो. एन.एल.कछारा / 103
9. प्राकृत वाङ्मय में समत्व दृष्टि – प्रो.अशोक कुमार जैन/ 110
10. प्राकृत परम्परा के आचार्यो की समकालीन –युगचेतना
– प्रो.वीर सागर जैन/ 118
11. प्राकृत–सूक्तियों में लोकमंगल भावना – डॉ.रांका जैन/ 124
12. भारतीय साहित्य को प्राकृत का योगदान – डॉ.कमल कुमार जैन/ 130
13. प्राकृत शिलालेखों में समसामयिकता – डॉ.दिलीपधींग/ 145
14. प्राकृत आगमों के शैक्षिक संदर्भ – प्रो.जिनेंद्र कुमार जैन / 149
15. प्राकृतभाषा और आधुनिक संचार–माध्यम – प्रो.अनेकांत जैन/158
16. प्राकृत–काव्यों की समरसता – प्रो.जयकुमार उपाध्ये/ 166
17. आगमों में अंकित आचार–संहिता और पर्यावरण सुरक्षा – डॉ.अनिल कुमार जैन/174

Scanned with OKEN Scanner

18. प्राकृत आगमों में कषाय-विजय के उपाय - डॉ.ज्योति बाबू जैन/ 188
19. जैन आगम और वर्तमान कृषि-पद्धति - डॉ.श्याम लाल गोदावत/ 194
20. प्राकृतभाषा जनकल्याणी - डॉ.सुमत कुमार जैन/ 202
21. प्राकृत भाषा का जैन-पत्रकारिता के विकास में योगदान
- डॉ.धर्मेंद्र कुमार जैन/ 217
22. प्राकृत-साहित्य में शैक्षिक निहितार्थ - डॉ.शुद्धात्मप्रकाश जैन/ 221
23. प्राकृत-वाङ्मय में आध्यात्मिक-विकास के सोपान
- प्रो.डॉ. अनिल कुमार जैन/ 231
24. प्राकृत-सूक्तियों की समसामयिकता - प्रो.कल्पना जैन/ 245
25. प्राकृत-साहित्य में ध्यान और उसकी उपयोगिता - डॉ. सत्यनारायण शर्मा/251
26. प्राकृत के आधुनिक-चिंतक - डॉ.आशीष जैन/ 268
27. प्राकृत मंत्रों एवं स्तोत्रों का जीवन पर प्रभाव - प्रो.महावीर शास्त्री/ 290
28. प्राकृत में सट्टक-परंपरा एवं उसकी प्रासंगिकता - डॉ.पत्रिका जैन/ 305
29. विज्जावसुसावयायारो में अतिचारों की सामाजिक-स्थिति- डॉ.आनंद कुमार जैन / 313
30. प्राकृत-साहित्य में अंकित अचौर्यव्रत की महत्ता
- डॉ.आलोक कुमार/ 319
31. प्राकृत चरित-ग्रंथों का वैभव एवं उपयोगिता - डॉ. माधुरी शास्त्री/ 325
32. गुजराती मध्यकालीन साहित्य पर प्राकृत का प्रभाव
- प्रो. सलोनी जोशी/ 340
33. नम्मयासुंदरी कहा में स्त्री शिक्षा- डॉ. वंदना चौधरी/ 344
34. कर्म-सिद्धांत और मानसिक-शांति - डॉ.वीरचन्द्र जैन/ 350

Scanned with OKEN Scanner

प्राकृत भाषा जनकल्याणी

डॉ. सुमत कुमार जैन

भारतीय भाषा परम्परा में 'प्राकृत' एक प्राचीन भाषा मानी जाती है। प्राकृत भाषा जनसामान्य की भाषा रही है। जनमानस या लोक का शिष्ट या नागरिक समाज से अपना एक विशिष्ट सम्बन्ध एवं महत्त्व रहा है। बिना शास्त्रीय चर्चा, अनुशीलन और मनन के लोकजीवन से उद्भूत अनुभव की बातें अपनी अद्भुत सटीकता रखती हैं। उनके देश की सीमा तो की जा सकती है, पर वे काल की सीमा से मुक्त सदाबहार होती हैं।

जैनधर्म के अन्तिम तीर्थंकर महावीर और महात्मा बुद्ध ने अपने धर्म के उपदेश जनमानस के लिए जनसामान्य की प्राकृत भाषा में दिया था, क्योंकि उस समय जन-जन के मानस-पटल पर कथ्य-भाषा के रूप में प्राकृत विद्यमान थी। श्रमण परम्परा के इन महापुरुषों के ज्ञान का संदेश सहजता, सरलता और सुबोधता से जनसामान्य तक पहुँच सके और वे अपना हित सम्पादन कर सकें, इस मुख्य प्रयोजन की सिद्धि हेतु प्राकृत भाषा में उपदेश दिया गया। इसीलिए जैनधर्म के आगम-ग्रन्थ और बौद्धों के त्रिपिटक प्राकृत भाषा में लिपिबद्ध किये गये। यह जनसाधारण के लिए उदारवृत्ति से सृजित कल्याणकारी साहित्य था, किसी वर्ग या जातिविशेष के लिए निर्धारित नहीं था। साहित्य सृजन का प्रधान उद्देश्य लोक-मंगल है। लोकमंगल लोकभाषा में अपेक्षाकृत अधिक लोकोपयोगी होता है।

भगवान् महावीर के द्वारा उपदेशित जनकल्याणी कार्य कौन से हैं? जो जीव मात्र के कल्याणार्थ प्राकृत भाषा में निहित हैं, मेरा प्रतिपाद्य विषय है। प्राकृत भाषा का माहात्म्य निम्न प्रकार से द्रष्टव्य है-

सव्वजीव-हिदकरा कहदु हो! का वट्टदि जणभासा।
तित्थयरा वि जं आसेज्ज, सा का अत्थि सुभासा।।
अणादिकालदो णारीणं वि, का हिदयमणुहरेदि।
का सा भासा, जा इह भरहे, मादुभासा वि वट्टदि।।

Scanned with OKEN Scanner

सव्वजीव-हिदकरा सुणदु हो! पाइअभासा लोए।
तित्थयराणं दिव्वझुणीए, भासेसा हि सोहदि।।
णिय-सुहदोच्चारणदो एसा, णारीण मणाणं हरदि।
सव्वा मादुसत्तिओ वयणे, पाइयभासा धरदि।।[1]

डॉ. देवेन्द्र कुमार शास्त्री के अनुसार "प्रत्येक देश और जाति के मूल संस्कार, उसकी अपनी भाषा, साहित्य तथा संस्कृति में निहित रहते हैं। जातीय-जीवन, लोक-परम्परा एवं सामाजिक नीति-रीतियों के अध्ययन से हमें उनकी पूरी जानकारी मिलती है, अतएव भाषा और साहित्य का प्रत्येक अंग लोक-मानस की अभिव्यक्ति का ही लिपिबद्ध स्वर होता है। मौखिक रूप में आज भी हमें गुणाढ्य की ही बृहत्कथा तथा प्राकृत और अपभ्रंश में लिखित कथाएँ, सूक्तियाँ, सुभाषित एवं अन्य उक्तियाँ गांवों में प्रचलित सुनाई देती हैं। वस्तुतः युग-युगों से साहित्यिक तथा सामाजिक परम्परा परस्पर विचारों का विनिमय करती आयी है, इसीलिए परम्परा में केवल इतिहास तथा पौराणिकता का लेखा-जोखा न होकर लोकजीवन में परिव्याप्त यथार्थ और आदर्श रूप-कुरूप, नीति और उपदेश तथा वृत्ति एवं रीति का भी समाहार हो जाता है"।[2]

भारतीय भाषा का विकास वैदिक काल में ही प्रारम्भ हो गया था। ऋग्वेद के वाक्सूक्त तथा अथर्ववेद के पृथ्वीसूक्त में स्पष्ट कहा गया है कि लोग देश के नाना क्षेत्रों में भिन्न-भिन्न प्रकार की बोलियाँ बोलते हैं। अशोक के शिलालेखों से भी प्रमाणित होता है कि एक ही प्राकृत भाषा उत्तर-पश्चिम और पूर्व के प्रदेशों में भिन्न-भिन्न प्रकार से बोली समझी जाती थी।[3]

प्राकृत भाषा को विशेष प्रोत्साहन तब मिला जब ई. पू. छठी सदी में भगवान् महावीर और महात्मा बुद्ध जैसे महापुरुषों का अवतरण हुआ और उन्होंने अपने-अपने धर्म सम्बन्धी उपदेशों के लिए उस समय उनकी विहारभूमि में प्रचलित जनभाषा को अपनाया और उन्होंने अपने शिष्यों को भी आदेश दिया कि वे उसी भाषा में उनके उपदेशों की ग्रन्थ रचना करें। यह भाषा मगध देश की होने से 'मागधी' तथा उसके सीमा से लगे हुए शूरसेनादि प्रदेशों के सीमावर्ती क्षेत्रों में प्रचलित बोलियों से भी प्रभावित होने के कारण अर्द्धमागधी कहलायी। दुर्भाग्यतः जिस रूप में उक्त उपदेशों की प्रथम ग्रन्थ रचना हुई होगी, वह रूप हमें अब उपलब्ध नहीं है। बुद्ध के उपदेशों पर आधारित पालि-साहित्य का वर्तमान स्वरूप उसे बुद्ध से सदियों पश्चात् लंका में प्राप्त हुआ था। महावीर के उपदेशों पर आधारित 'द्वादशांग' आगम आज जिस रूप में उपलब्ध है, वह रूप ईसा की पाँचवीं सदी में हुई वल्लभीपुर वाचना का है।

Scanned with OKEN Scanner

प्राकृत भाषा का जो स्वरूप प्राप्त होता है वह प्राकृत का आदिकाल तथा भारतीय आर्यभाषा का द्वितीय या मध्यम स्तर माना जाता है। यह मध्यम स्तर अपने आदि रूप में यद्यपि व्याकरण की दृष्टि से संस्कृत भाषा की अपेक्षा बहुत भिन्न और सुगम है, तथापि उसमें संस्कृत की ध्वनियाँ बहुत कुछ समान पायी जाती हैं। यह स्तर हमें ई. की द्वितीय-तृतीय सदी तक रचे गये ग्रंथों, जैसे-पालित्रिपिटक, अश्वघोष के नाटक तथा राजा अशोक, खारवेल, आंध्रनरेशों के शिलालेखों में प्राप्त होता है।[4]

तत्पश्चात् मध्ययुगीन भाषा का द्वितीय स्तर प्रारम्भ हुआ। इसकी क्रान्तिकालीन परिस्थिति महाकवि भास के नाटकों में देखी जा सकती है। इसका विशेष लक्षण यह है कि शब्दों के क, ग, त, द आदि अल्पप्राण वर्णों का लोप होकर उनके स्थान में मात्र अ, इ आदि स्वर शुद्ध अथवा उच्चारण सौकर्य हेतु य से मिश्रित पाये जाते हैं तथा ख, घ, थ, ध आदि महाप्राणों के स्थान में 'ह' का आदेश कर दिया जाता है। इस प्रवृत्ति से प्रभावित वह समस्त प्राकृत साहित्य है जो विशेष रूप से तीसरी-चौथी सदी से लेकर छठी-सातवीं सदी तक रचा गया। यह मध्य व्यंजनों के लोप की प्रक्रिया महाराष्ट्री प्राकृत का विशेष लक्षण है और उसकी प्रतिनिधि रचनाएँ कालिदास कृत नाटकों के प्राकृत अंश, सेतुबंध, गाथासप्तशती, गउडवहो आदि हैं।[5]

हिन्दी आर्य भाषा के मध्यकाल का तृतीय स्तर का प्रतिनिधित्व करने वाली अपभ्रंश भाषा और उसका साहित्य है।

जनकल्याणी कार्य से तात्पर्य है, जिन कार्यों के निष्पादन से लोककल्याण सम्भव होता है। जो व्यक्ति के आत्मिक विकास में सहायक होते हैं तथा जिनसे समाज का नैतिक-आधार दृढ़ होता है। आगम-ग्रन्थों में प्रायः ऐसे कार्यों को अंकित करने का प्रयत्न किया गया है जो मानव मात्र को सद्भाव में प्रेरित करते हैं, मानव मात्र के लिए कल्याण का साधन बनकर पृथ्वीतल को सुखसम्पन्न एवं शान्ति-भूषित स्वर्ग के रूप में परिणत करने की क्षमता रखते हैं तथा जिनका अनुसरण लोकस्तर को ऊँचा उठाता है। इन्हीं उद्देश्यों के पूर्ति के लिए मुनि, आचार्य मनीषी लोक-वाणी प्राकृत में ग्रन्थों का प्रणयन करते हैं।

आगमों का प्रयोजन भी लोककल्याण से ओतप्रोत आदर्श तथ्यों की स्थापना करना ही रहा है। इसके अन्तर्गत अहिंसा की प्रतिष्ठा, आत्मशुद्धिपरक आध्यात्मिक-चिंतन, नैतिकजागरण, ग्राम्यजीवन की झांकी, आहारशुद्धि, सांस्कृतिक सौहार्द, सद्भाव एवं समन्वय, शिक्षा का महत्त्वपूर्ण घटक अनुशासन एवं विनय, सहनशीलता की मिशाल परिषहजय, मानवता, सद्धर्म श्रवण, जागरुकता का संदेश, परोपकारवृत्ति, संतोषवृत्ति- लोभ की अभिवृद्धि पर रोक, आहारशुद्धि, कर्म-प्रधान समाज, ब्रह्मचर्य व्रतों का राजा, अनुशासनहीनता का प्रतीक अविनय, उत्कृष्ट नारी-चरित्र, जातिवाद

व्यवसाय(पुरुषार्थ) में रहती है। यथा-

अप्पाणं अणुमन्ता जे आरंभन्ति दुग्गमं।
कज्जं परमुहपलोइयाणं, ताण कह होइ जयलच्छी।
न महुमहणस्स वच्छे मज्झे कमलाण नेय खीरहरे।
ववसायसायरे सुपुरिसाण लच्छी फुडं वसइ।।

परोपकारवृत्ति- परोपकार से अभिप्राय है- दूसरों का उपकार, दूसरे पर अनुग्रहबुद्धि, अन्य के प्रति भलाई का भाव।[9]

प्रो. सोगानी जी के अनुसार जनता में आस्था या विश्वास उत्पन्न होने से व्यक्ति में जो मूल्य-वृत्ति सबसे पहिले उत्पन्न होती है, वह है, पर उपकार वृत्ति।[10]

जनकल्याण के कार्यों का उल्लेख प्राकृत भाषा में सम्राट अशोक ने अपने शिलालेखों में किया है।[11] परोपकार के सम्बन्ध में मनुष्यों एवं पशुओं के बीच कोई भेद-भाव नहीं रखा गया है। कल्याण कार्यों में औषधियों और फल-वृक्ष के रोपे जाने, सड़कों पर मनुष्यों और पशुओं के लिए छायादार वृक्ष, आम्रवृक्षों की वाटिकाएँ, कुएँ, तालाब एवं जलासय का निर्माण, विश्रामगृह के निर्माण आदि के उल्लेख प्राप्त होते हैं।[12] उपकार वृत्ति के माहात्म्य बताते हुए कहा गया है कि दो प्रकार के पुरुषों ही पृथ्वी को धारण करते हैं, एक तो वह जिनकी बुद्धि उपकार में लगी रहती है तथा दूसरे वे जो किये गये उपकार को नहीं भूलते हैं। यथा-

वे पुरिसा धरइ धरा अहवा दोहि पि धारिया धरणी।
उवयारे जस्स मइ उवयरियं जो न पम्हुसई।।

समत्वदृष्टि- राग-द्वेष में समत्वदृष्टि। किसी को मत मारो, चोट मत पहुँचाओ, परिताप मत करो, क्लेश मत दो। आचारांग में कहा है-'हे मनीषियों! आपको दुःख प्रिय है या अप्रिय? यदि आप कहें कि दुःख प्रिय नहीं है, तब आपके इस सम्यक् उत्तर पर कहना चाहेंगे कि जैसे आपको दुःख प्रिय नहीं है, वैसे ही सब प्राणी, भूत, जीव और सत्त्वों के लिए दुःख अप्रिय, अशांतिजनक और महाभयंकर है।[13]

अन्यत्र यह भी कहा गया है कि व्यक्ति को विपत्ति और दुर्भाग्य के समय शान्ति और धैर्यपूर्वक जीवन-यापन करने का निर्देश दिया गया है, क्योंकि विपत्ति में ही सम्पत्ति और दुर्भाग्य में ही सौभाग्य का निवास रहता है। गाहासत्तसई में कहा गया है कि सज्जन पुरुष विपत्ति में उद्वेग रहित, सम्पत्ति में गर्व रहित, भय में धैर्य तथा समता-विषमता में अपरिवर्तित स्वभावी होते हैं। यथा-

वसणम्मि अणुव्विग्गा विहवम्मि अगव्विआ भए धीरा।
होन्ति अहिण्णसहावा समेसु विसमेसु सप्पुरिसा।।

Scanned with OKEN Scanner

विवेकसहित ज्ञान की जागृति- 'विवेक' व्यक्ति को हेय-उपादेय की पहचान कराने वाला चक्षु है। इस चक्षु के माध्यम से अच्छे और बुरे की पहचान की जा सकती है। विवेक ही मनुष्य को पशु से भिन्न करता है। विवेकमंजरी के मंगलाचरण में उन वीर प्रभु को नमस्कार किया है जो विवेकरूप दीपक से युक्त है और प्राणीमात्र को परमार्थ का ज्ञान कराते हैं-

सिद्धपुर सत्थवाहं वीरं णमिऊण वरं जिणनाहं।
सवण सुहारससरिअं वुच्चामि विवेकमंजरी अं।।1।।
दुट्ठकम्मवसगा भमंति भीम भवंमि निस्सीमं।
भद्द विवेकपईवो जीवाणं मुणंति परमत्थं।।2।।

विवेक की महिमा बताते हुए कहा है कि विवेकपूर्ण आचरण से मन की शुद्धि होती है।[14] इस शुद्धि के चार कारण निरूपित किये गये हैं - 1.चार शरणों (चत्तारिसरणं) की स्वीकृति 2.गुणों की सच्ची अनुमोदना 3.पापों की निन्दा और 4.बारह भावनाएँ। विवेक सहित ज्ञान शिक्षित करता है, ज्ञान गुणी बनाता है, ज्ञान पर को उपदेश देता है, ज्ञान से न्याय किया जाता है और ज्ञान से ही विनयी होता है। पद्मनंदि-पंचविंशति[15] ग्रन्थ में कहा है कि जो जन उत्तम गुरु के द्वारा प्ररूपित शास्त्र को नहीं पढ़ते हैं, उन्हें बुद्धिमान मनुष्य दोनों नेत्रों से युक्त होने पर भी अन्धा समझते हैं। जिनके अन्दर ज्ञान रूपी ज्योति जल जाती है, उनकी बुद्धि कभी मैली नहीं होती है।[16] यह भी कहा है कि ज्ञान के समान संसार में दूसरा कोई सुख का कारण नहीं है, क्योंकि यह ज्ञान ही जन्म, जरा और मृत्यु रूपी रोग दूर करने के लिए अमृत के समान है।[17] ज्ञान के बिना मोक्षमार्ग की प्राप्ति नहीं हो सकती है।[18] इस प्रकार ज्ञान की अद्वितीय महिमा बतायी गयी है।

शिक्षा का महत्त्वपूर्ण घटक अनुशासन एवं विनय-विनय का जीवन में अत्यन्त महत्त्व है। विद्या से विनय आती है। विनशीलता व्यक्तित्व की पहचान है। उत्तराध्ययनसूत्र के विनय नामक अध्ययन में विनय और अविनय के स्वरूप का विवेचन करते हुए कहा है कि अविनीत शिष्य सूकर और कुतिया की तरह होता है, वह सभी के लिए हेय होता है, जबकि विनीत शिष्य मेधावी होता है और वह गुरु एवं सभी के लिए उपादेय होता है।[19] विनीत का कथन करते हुए कहा गया है कि वह गुरु की आज्ञा और निर्देश का पालन करता, गुरु की शुश्रुषा करता है, गुरु के इंगित और आकार को जानता है। बिना पूछे कुछ नहीं बोलता, पूछने पर असत्य नहीं बोलता, क्रोध आ जाए तो उसे जीत लेता है, प्रिय और अप्रिय को अंगीकार करता है अर्थात् गुरु जैसा कहे उसे शिरोधार्य करता है।[20]

वर्तमान में विपरीत मार्ग पर चल रहे शिक्षार्थियों के सम्यक् बोध हेतु उत्तराध्ययन में वर्णित है कि विद्यार्थी की योग्यता एवं अयोग्यता क्या हो? इस हेतु बहुत ही मर्मस्पर्शी वर्णन किया गया है। यहाँ विद्यार्थी की योग्यता के लिए कहा है कि उसका आचार्यकुल में रहना, उत्साही, विद्या-प्रेमी, मधुरभाषी तथा शुभकर्मा होना आवश्यक माना गया है।[21] विद्यार्थी की योग्यताओं का विवेचन करते हुए उसमें इन आठ[22] गुणों का रहना आवश्यक बताया गया है- सहनशीलता, इन्द्रियनिग्रही, मधुर भाषी, शीलवान, रसों में अलोलुपता, अक्रोधी, शीलवृत्ति की दृढ़ता और सत्यभाषी। आदिपुराण के अनुसार विद्यार्थी में जिन मौलिक गुणों का होना अनिवार्य है, वे ये हैं[23] - जिज्ञासावृत्ति, श्रद्धा (अध्ययन और अध्यापक दोनों के प्रति आस्था), विनयशीलता, शुश्रूषा, श्रवण (पाठ-श्रवण के प्रति सतर्कता एवं जागरूकता), ग्रहण (गुरु द्वारा अध्यापन किए गए विषय को ग्रहण करने की अर्हता), धारणा (पठित विषय को सदैव स्मरण रक्षने की क्षमता), स्मृति (कालान्तर में नहीं भूलना), ऊह (तर्कणा-शक्ति), अपोह (पठित ज्ञान के आधार पर विचार-शक्ति का प्राबल्य एवं अकरणीय त्याग), निर्णीति (विचार करने की क्षमता), संयम, प्रमाद का अभाव, सहज प्रतिभा (विशेष क्षयोपशम शक्ति) और अध्यवसाय।

उक्त तथ्यों के आलोक में यह कहा जा सकता है कि आज जनजीवन में अशान्ति और अनुशासनहीनता के काले बादल मँडरा रहे हैं। उसका मूल कारण जीवन में विनय का अभाव है और अहंकार की वृद्धि है तथा विनय का अभाव परिवारिक, सामाजिक, राष्ट्रिय जीवनशैतान की आँत की तरह बढ़ रहा है, जिससे न परिवार सुखी है, न समाज सुखी है और न राष्ट्र के अधिनायक ही शान्ति में है।

आत्मतुला-प्राकृतिक पदार्थों तथा जिनमें जीवन का अस्तित्व है, चेतना है, ऐसे सजीव पदार्थों का मानव-जीवन के साथ गहरा सम्बन्ध है। तत्त्वार्थसूत्र में कहा गया- 'परस्परोपग्रहो जीवानाम्'[24] अर्थात् जीवों का स्वभाव परस्पर उपकार करना होना चाहिए। यही कारण है कि जैनधर्म के अन्तिम तीर्थंकर भगवान् महावीर ने कहा- धम्मं चरणस्स पंच निस्सा ठाणा तं जहा- छक्काए गणे राया सरीर अर्थात् जो व्यक्ति आध्यात्मिक धर्म का आचरण(साधना) करना चाहता है, उसके लिए निम्न पाँच स्थानों पर आलम्बन लेना बताया है। जैसे कि षट्कायिक जीव, गण, शासक, गृहपति और शरीर। इस सूत्र में छह काय (एकेन्द्रिय से लेकर पंचेन्द्रिय तक) के जीवों के आश्रय को प्राथमिकता दी गई है। अतएव जैनागमों में पृथ्वी, जल, अग्नि, वायु और वनस्पति में जीवन का अस्तित्व स्वीकार किया है एवं इन सभी का विस्तार से निरूपण प्राप्त होता है। ये जीव कहाँ-कहाँ रहते हैं? उनका शरीर किस-किस प्रकार का है, वे कैसे-कैसे श्वासोच्छवास, आहार आदि ग्रहण करते हैं? उनका विकास-

ह्रास कैसे-कैसे होता है? उनकी उत्कृष्ट आयु कितनी है? उनमें कितनी इन्द्रियाँ हैं, कितने प्राण है?- इन सभी प्रश्नों पर बहुत गहराई से विचार प्रस्तुत किया गया है।

क्षमा- क्षमा का अर्थ सहनशीलता है। बारस अणुवेक्खा के अनुसार क्रोध के उत्पन्न होने के साक्षात् बाहरी कारण मिलने पर भी जो थोड़ा भी क्रोध नहीं करता है, उसे उत्तम क्षमा धर्म होता है।[25] कार्तिकेयानुप्रेक्षा में कथन है कि देव, मनुष्य और तिर्यंचों द्वारा घोर व भयानक उपसर्ग पहुँचाने पर भी जो क्रोध से तप्त नहीं होता, उसे निर्मल क्षमाधर्म साधित होता है-

कोहेण जो ण तप्पदि, सुर-णर-तिरिएहि कीरमाणे वि।
उवसग्गे वि रउद्दे, तस्स खमा णिम्मला होदि।।

व्यक्ति को जहाँ तक सम्भव हो, वहाँ तक क्षमा धारण करना चाहिए। सभी प्राणियों के प्रति सुरक्षा, संयम, समुचित व्यवहार और मृदुता की भावना होनी चाहिए। यहाँ तक कहा गया है कि जो क्षमा करने में समर्थ हैं जो धनवान गर्व नहीं करते और विद्वान् विनम्र होते हैं- इन्हीं तीनों से पृथ्वी अलंकृत है। यथा-

जे जि खमेइ समत्थो, धणवन्तो जं न गव्वं उव्वहइ।
जं च सविज्जो नमिओ, तिसु तेसु अलंकिया पुहवी।।-

कार्तिकेयानुप्रेक्षा, गाथा-150

संयम-सम्यक् रूप से यम अर्थात् नियंत्रण संयम है[26] और आत्मा की रुचि का नाम भाव है जो सम्यक्त्व का कारण होता है।[27] शुद्ध चैतन्य शुद्धभाव है।[28] राजवार्तिक (9.6.16.596.1) के अनुसार भावशुद्धि संयम की आठ शुद्धियों में से एक है।

प्राकृत-मनीषियों ने जीवकायसंजमे अजीवकायसंजमे य अर्थात् जैसे जीवकाय के प्रति संयम रखने की प्रेरणा दी है, वैसे ही अजीवकाय (जड़, प्रकृतिजन्य वस्तुएँ या पुद्गलों) के प्रति भी संयम रखने की प्रेरणा दी है, किन्तु, आधुनिक समय में मानव इस तथ्य का नजरअंदाज करके जीवकाय और अजीव-काय दोनों प्रकार के पर्यावरण-संतुलन के लिए उपयोगी सजीव-निर्जीव पदार्थों के प्रति अधिकाधिक असंयम करके अंधाधुंध रूप से संतुलन बिगाड़ने का पराक्रम करके प्रदूषण फैला रहा है। षट्खण्डागम एवं समवायांगसूत्र के सत्रहवें समवाय में संयम का विस्तार से वर्णन उपलब्ध होता है- पृथ्वीकायिक-संयम, अप्कायिक-संयम, तेजस्काय-संयम, वायुकाय-संयम, वनस्पतिकाय-संयम, द्वीन्द्रिय-संयम, त्रीन्द्रिय-संयम, चतुरिन्द्रिय-संयम, पंचेन्द्रिय-संयम, अजीवकाय-संयम, प्रेक्षा-संयम, उपेक्षा-संयम, अपहृत्य-संयम, प्रमार्जना-संयम, मन:संयम, वचन-संयम, और काय-संयम। इन संयम के प्रकारों में पृथ्वीकायिक आदि नौ प्रकारों के जीवों के प्रति संयम रखना, उन जीवों

को कष्ट हो, त्रास हो, ऐसी प्रवृत्ति नहीं करना है। अजीवकाय संयम में प्रकृतिजन्य सभी निर्जीव पदार्थों के प्रति संयम की प्रेरणा है। प्रेक्षा, उपेक्षा, अपहृत्य एवं प्रमार्जना रूप संयम में प्रत्येक प्रवृत्ति करते समय देखें, पूर्वापर का, परिणाम का विचार करें, जिस स्थान पर या प्रवृत्ति में जीवहिंसा अधिक हो, जिससे अपने स्वास्थ्य परिवार एवं समाज की हानि हो, उस प्रवृत्ति के प्रति उपेक्षा करें। जहाँ सींचना, खोदना आदि हो वहाँ भी संयम रखें, ताकि किसी जीव को पीड़ा न हो, क्रोधादि में संयम रखें।

जीवन का सर्वांगीण विकास करना संयम का परम उद्देश्य है। समस्त प्राणियों में संयमभाव ही अहिंसा है- "अहिंसा निउणं दिट्ठा सव्वभूयेसु संजमा"[29] उसके सुख संयम में प्रतिष्ठित है। मन, वचन, काय से संयमी व्यक्ति स्व-पर का रक्षक तथा मानवीय गुणों का आगार होता है। शील संयमादि गुणों से भरपूर व्यक्ति ही सत्पुरुष है और ऐसे सत्पुरुष ही पर्यावरण का रक्षक होते हैं।

सदाचार- सामान्य सदाचार को धर्म का आधार बताते हुए वर्णित है कि "माता-पिता की शुश्रुषा, वृद्धों की शुश्रुषा, गुरुओं की शुश्रुषा, जीवों के प्रति दया, सत्यभाषण, शिष्यों द्वारा आचार्य का आदर और सम्बन्धियों के प्रति समुचित बर्ताव- ये सभी धर्म के तत्त्व हैं।[30] ये सभी आधार धर्म को पूर्णतया व्यवहारिक रूप में प्रस्तुत करते हैं। अशोक के अभिलेखों में धर्म के निम्नलिखित लक्षण उल्लिखित हैं।[31] -

अपासिनवे (पापों से दूर रहना), बहुकयाने (अनेक कल्याणकारी कार्य करना), दया (दीन-दु:खी प्राणियों पर दया करना), दान (आवश्यकतानुसार यथाशक्ति सभी को दान देना), सचे (सत्य बोलना) और सोचये (शरीर, वचन और विचार की शुद्धता)।

उत्कृष्ट नारी-चरित्र- भारतीय संस्कृति में नर की अपेक्षा नारी की विशेषता सिद्ध करने का प्रयास किया है। नारियों की प्रशंसा में कहा गया है कि "नार्यस्तु यत्र पूज्यन्ते रमन्ते तत्र देवता" जिस घर में स्त्रियों का सम्मान होता है, वहाँ देवता भी आनन्दपूर्वक निवास करते हैं। वस्तुत: घर को सुख-समृद्धि से परिपूर्ण बनाने में नारियों का ही प्रथम हाथ होता है। पुरुष तो हमेशा एक रूप में ही दिखाई पड़ता है, जबकि स्त्रियाँ अपने विविध रूप में होकर अपने उत्तरदायित्व को पूर्ण करती हैं। मुख्यत: नारियों के कन्या, पत्नी और माता रूप होते हैं। इन सभी रूपों की अभिव्यक्ति कण्हचरियं में उपलब्ध होती है। कण्हचरियं में राजीमती का कन्या के रूप में उत्कृष्ट आदर्श वर्णित है, जो अनुकरणीय की श्रेणी में रखे जाने योग्य है।

शीलवती स्त्री के रूप में राजीमती का जैसा वर्णन उत्तराध्ययन में वर्णित है, वह अन्यत्र दुर्लभ है। नेमिनाथ के लघुभ्राता रथनेमि राजीमती से विवाह का प्रस्ताव रखता है, तो वह स्पष्ट ही मना कर देती है, क्योंकि उसने मन से नेमिकुमार को अपना

Scanned with OKEN Scanner

जीवन-साथी स्वीकार कर लिया था। पुनः जब साध्वी के रूप में पवित्र राजीमती को रथनेमि विषयभोग के लिए प्रेरित करता है, तब वह उन्हें फटकारती है और प्रतिबोधित करती है। जैसे कहा है-

धिरत्थु ते जसोकामी! जो तं जीवियकारणा।
वंतं इच्छसि आवेउं सेयं ते मरणं भवे।।[22]

अर्थात् हे यशःकामिन! धिक्कार है तुझे जो तू भोगी जीवन के लिए वमी हुई वस्तु को पीने की इच्छा करता है। इससे तो तेरा मरण श्रेष्ठ है। इन बोधवचनों से राजीमती संयम से भटके रथनेमि को प्रतिबोधित कर सन्मार्ग पर लाती है। यहाँ राजीमती के रूप में नारी के उदात्तता का चित्रण किया गया है।

महाकवि हाल ने गाहासत्तसई में नारी के उत्कृष्ट-नारी चरित्र को उद्घाटित कर लोकजीवन के मूल्यों की स्थापना की है। कुछ उदाहरण इस प्रकार हैं:-

साहीणे विपिअअमे पत्ते वि खणे ण मंडिओ अप्पा।
दुग्गअ-पउत्थ-वइअं सअज्जिअं संठवंती ए।।- 1/39

अर्थात् अपने पति के प्रवास से वापस आ जाने पर भी नायिका कुसुंबी चीर इसलिए धारण नहीं करती है कि पड़ोसन एक तो गरीब है और दूसरे प्रोषितपतिका भी, अतः उसके मन को दुःख न पहुँचे। ऐसी परदुःखकातरता यदि आज नायिकाओं में आ जाए तो क्या बात है?

दिअरस्स असुद्धमणस्स कुलवहू णिअअ कुड्डु लिहिआइं।
दिअहं कहेइ रामाणु लग्गा सोमित्त-चरिआइं।।-1/35

अर्थात् अपनी भाभी पर बुरी नजर रखने वाले बिगडैल देवर को नायिका दिन-रात लक्ष्मण का चरित्र सुनाती है। ताकि वह देवर-भाभी के संबंधों की मर्यादा व पवित्रता को पहिचाने। वह सीधे डॉट सकती थी या पति से देवर की शिकायत कर सकती थी, परन्तु इससे संयुक्त परिवार की निश्चित ही हानि होती। इसलिए स्वयं व्यथा सही, परन्तु देवर को लक्ष्मण कथा कही।

अइकोवणा वि सासू रुआविआ गअवईअ सोण्हाए।
पाअपडणोण्ण आए दोसु वि गलिएसु वलएसु।।-5/93

अर्थात् सास के पैर छूने के लिए झुकने पर बहु के दोनों वलय(कंगन) गिर पड़े- बहु की ऐसी कृश-दशा देखकर गुस्सैल सास भी करुणा से रो पड़ी। यह आदर्श हाल के अतिरिक्त कौन प्रस्तुत कर सकता है?

सदगृहस्थ नारी के लक्षण वज्जालग्गं में वर्णित है कि जो नारी परिवार के समस्त सदस्यों के भोजन कर लेने के उपरान्त भोजन करती है, सभी परिजनों के सोने

Scanned with OKEN Scanner

के पश्चात् सोती है और प्रातःकाल सर्वप्रथम जाग उठती है, वह सामान्य गृहिणी नहीं, घर की लक्ष्मी है-

भुंजइ भुंजियसेसं, सुप्पइ सुत्तम्मि परियण सयले।
पढमं चेय विबुज्झइ, घरस्स लच्छी न सा घरिणी।।

-वज्जालग्गं, गाथा

इस प्रकार नारियाँ जहाँ भोग्योपभोग, ऐहिकसुख एवं सन्तानोत्पत्ति की साधन मानी जाती हैं, वहाँ अपने शील और संस्कृति की रक्षा करना अत्यन्त अनुकरणीय है।

आहारशुद्धि

प्राकृत साहित्य में स्वस्थ जीवन के लिए आहार-विज्ञान की उपयोगिता दृष्टिगत होती है। हमारा आहार कैसा हो? इस प्रश्न पर प्राचीन समय से ही निरन्तर चिंतन-मनन किया जाता रहा है। साधना और स्वास्थ्य, आहार-विज्ञान के मुख्य केन्द्र बिन्दु हैं।

स्वास्थ्य की दृष्टि से आहार का बहुत बड़ा महत्त्व है। आहार का सामान्य अर्थ है कि भोजन व पेय। आहार-विज्ञान का अर्थ है- वह विज्ञान जिसमें खाद्य पदार्थों के गुण-दोषों, पोषक तत्त्वों आदि का वर्गीकरण किया जाता है। प्राकृत साहित्य में आहार के चार प्रकार बतलाये हैं- अशन, पान, खाद्य और स्वाद्य। आवश्यक निर्युक्ति में विवेचित है-

असणं पाणगं चेव, खाइमं साइमं तहा।
एसो आहारविही, चउव्विहो होइ नायव्वो।।
आसुं खुहं समेई, असणं पाणाणुवग्गहे पाणं।
खे माइ खाइमं ति य, सएइ गुणे तओ साई।।-गाथा,1587-1588

अर्थात् अशन-जो क्षुधा का शीघ्र शमन करता है, भूखे व्यक्ति द्वारा जिसे खाया जाता है, उसे अशन कहते हैं। जैसे चावल आदि। पान- जो प्राणों का उपग्रह करता है, जिसे पीया जाता है, उसे पान कहते हैं। जैसे द्राक्षा का पानक आदि। खाद्य-जो मुखविवर में समा जाता है, जिसे खाया जाता है, उसे खादिम या खाद्य कहते हैं। जैसे मोदक, खजूर आदि। स्वाद्य- जिसका स्वाद लिया जाये जो मुखवास के रूप में काम आए, उसे स्वादिम अथवा स्वाद्य कहते हैं। जैसे ताम्बूल, सोंठ आदि।

प्राकृत साहित्य में आहार-विज्ञान से सम्बन्धित चर्चा माँस, मधु और पंच उदुम्बरफल का त्याग, रात्रिभोजनत्याग, जलगालन आदि के माध्यम से की गई है और अनशन, अवमौदर्य, वृत्तिपरिसंख्यान, रसपरित्याग आदि के माध्यम से आहार-शुद्धि को बताया गया है।

बहुत से लोग सही और गलत आहार से अनभिज्ञ हैं, वे इन दोनों के अन्तर को समझने में असमर्थ हैं। प्राकृत साहित्य में आहार-शुद्धि पर गहराई से चिन्तन-मनन किया गया है। इस साहित्य में वर्णित है कि अनशन, अवमौदर्य, रसपरित्याग आदि आहार शुद्धि के कारण हैं। इन तथ्यों को आज का विज्ञान भी स्वीकार करता है। यहाँ गाथा में द्रष्टव्य है-

अप्पाहारस्स न इंदियाई विसएसु संपत्तंति।
नेव किलम्मइ तवसा रसेसु न सज्जए यावि।।
थोवाहारी थोवभणियो य, जो होइ थोवनिद्दो य।

अर्थात् अल्पाहारी की इन्द्रियाँ विषयभोगों की ओर नहीं दौड़ती, तप करने पर भी क्लांत नहीं होती और न स्वादिष्ट भोजन में आसक्त होती हैं। जो साधक कम खाता है, कम बोलता है, कम नींद लेता है और धर्मोपकरण की सामग्री कम रखता है, उसे देवता भी नमन करते हैं।

वर्तमान में पाश्चात्य संस्कृति ने हमारी प्राचीन संस्कृति पर चारों ओर से आक्रमण किया है। परिस्थितियों ने भी करवट ली है। जंकफूड, फास्टफूड, पिज्जा आदि जैसे आधुनिक आहार प्रकारों ने एक ओर हमारे स्वास्थ्य पर आघात किया है, मधुमेह, ब्लड प्रेशर, हृदय रोग जैसी अनेक बीमारियों को आमन्त्रित किया है तो दूसरी ओर होटल संस्कृति ने हमारे आहार को अशुद्ध बना दिया है। जिसका असर हमारी मन-वचन-काय की क्रियाओं पर पड़ा है। निश्चित ही हमारे आहार से हमारे भाव प्रभावित होते हैं। भावों की शुद्धता के लिए आहार-शुद्धि एक आवश्यक और अपरिहार्य तत्त्व है, इसलिए कहा गया है-जैसा खाओ अन्न, वैसा होवे मन, जैसा पियो पानी, वैसी होवे वाणी।

संतोषवृत्ति

संतोष शब्द की व्युत्पत्ति है-समतुघज। संतोषवृत्ति का अर्थ है कि जो मिले उसी में प्रसन्न रहने की वृत्ति, संतोषवृत्ति है। संतोष के अन्य अर्थ है- तृप्ति, प्रसन्नता और धैर्य। जीवन में जिस मानव में संतोषवृत्ति होती है, उसका जीवन संयमित एवं सुखद होता है। स्वयं के प्रति उनकी श्रद्धा-आस्था होती है, वे जीवन में दुःखों के क्षणों का धैर्य और साहसपूर्वक मुकाबला करते हैं। संतोष के विपरीत तृष्णा को वर्णित करते हुए कहा है कि जिस प्रकार पाताल की गहराई और सागर की लहरों से उस वडवानल की तृष्णा बुझती नहीं है ,[33] उसी प्रकार मानव का तृष्णा रूपी गड्ढा भी कभी भरता नहीं है। अतः इच्छाओं को सीमित कर संतोषवृत्ति को अपनाना चाहिए। संतोष वृत्ति को धारण करने से ही मानव सुखी होती है।

Scanned with OKEN Scanner

द्वादशानुप्रेक्षा में सहिष्णुता के सम्बन्ध में कहा गया है कि व्रती पुरुष उपसर्ग तथा तीव्र परिषह को ऋणमोचन-कर्ज चुकाने की तरह मानता है। वह जानता है कि ये तो मेरे द्वारा पूर्वजन्म में संचित किये गये कर्मों का ही फल है।[64] दशवैकालिक सूत्र में सहिष्णुता के सम्बन्ध में कहा है कि क्षुधा, प्यास व दुःशैय्या, विषमभूमि-युत वासस्थान, सर्दी, गर्मी, अरति, भय- इन कष्टों को मुमुक्षु अव्यथित चित्त से सहन करे। समभाव से सहन किये गये, दैहिक कष्ट महाफल के हेतु होते हैं।[65]

निष्कर्षतः संक्षेप में कहा जा सकता है कि उपरोक्त अहिंसा, अनुशासन, विनय, सहनशीलता परोपकारवृत्ति, संतोषवृत्ति, आहारशुद्धि, उत्कृष्ट नारी-चरित्र, सम्यक्-आजीविका आदि विषयक जनकल्याणी तथ्यों को सम्यक् विधि से अपनाता है तो अपना जीवन सुखी, समृद्ध और आनंदमय बना सकता है। अपने परिवार में माता-पिता तथा वृद्धों की सेवा एवं आदर भाव, गुरुजनों के प्रति सेवा एवं आदर भाव, सम्बन्धियों के प्रति उचित व्यवहार, दास तथा भृत्यों के प्रति उचित व्यवहार, मित्र, स्वामी, परिचित, सहायक तथा परिवार के प्रति उचित व्यवहार, प्राणियों की हिंसा न करना तथा उन पर दया करना, दरिद्र एवं पीडित व्यक्तियों के साथ उचित व्यवहार और नम्रता, यथाशक्य क्षमा-भाव रखना आदि महत्त्वपूर्ण तथ्यों द्वारा पारिवारिक एवं सामाजिक गुणों के प्रति अपने उत्तरदायित्व को भलिभांति निभा सकता है। इन सभी पर आदर्श घर-परिवार, समाज तथा राष्ट्र का अस्तित्व निर्भर करता है। प्राकृत साहित्य में वर्णित कल्याणपरक तथ्यों को अपनाकर व्यक्ति, समाज, राष्ट्र और विश्व के कल्याण की कामना की जा सकती है।

सन्दर्भ सूची-

1. का पुण पाइयभासा, गीति- लेखक- प्रो. सुदीप कुमार जैन,संलेहणा (प्रवेशांक, जुलाई से दिसम्बर, 2018), षाण्मासिकी सन्दर्भित शोधपत्रिका में उद्धृत, महावीर परमार्थ फाउण्डेशन, नईदिल्ली, 2018ई.
2. भविसयत्तकहा तथा अपभ्रंश कथाकाव्य, देवेन्द्र कुमार शास्त्री, अ. 1, पृ. 15
3. णायकुमारचरिउ, कविपुष्पदंत, हीरालाल जैन, प्रस्तावना, पृ. 22, 23
4. णायकुमारचरिउ, पुष्पदंत, हीरालाल जैन, प्रस्तावना, पृ. 23
5. णायकुमारचरिउ, प्रस्तावना, पृ. 23
6. सूत्राकृतांगसूत्र- 1.2.3.163, श्री आगमप्रकाशन समिति, व्यावर (राज.), 1999 ई., पृ.161.
7. आवश्यकसूत्र-प्रतिज्ञासूत्र, 1.1, श्री आगमप्रकाशन समिति, व्यावर(राज.) 2001 ई., पृ.8.

Scanned with OKEN Scanner

8. कुलजोणिजीवमग्गणठाणाइसु जाणउफण जीवाणं।
तस्सारंभणियत्तणपरिणामो होइ पढमवदं।।- नियमसार: -56, अनेकान्त ज्ञान मंदिर शोध संस्थान, बीना(सागर) से 2010ई. में प्रकाशित।
9. परेषां सर्वसाधारणामनामुकारो हितसाधनं तस्यैक:।-जयोदय वृत्ति, 1/86, परेषां प्राणिनामनुग्रह एवं।-जयोदय वृत्ति, 1/12, परस्यायनुग्रहबुद्धि:। वीरोदय, 1/33, परोपकारेण सुरश्रिय: स। वीरोदय, 14/27
10. चेतना के आयाम और मूल्यात्मक अनुभूति, लेख- वज्जालग्गं= सामाजिक मूल्य, पृष्ठ 115, प्राकृत भारती अकादमी, जयपुर 2000 ई.
11. पाँचवे शिलालेऽ में लोक-कल्याण(कलाणं दुकरं) की बात कही गयी है और उसे दुष्कर बताया गया है। छठे शिलालेऽ (कतव्यमते हि मे लोकहित) के अनुसार प्रशासक का कर्त्तव्य लोकहित और पराक्रम होना चाहिए।
12. द्वे चिकिछ कता मनुसचिकीछा च पसुचिकीछा च ओसुढानि च यानि मनुसोपगानि च पसोपगानि च यत यत नास्ति सर्वत हारापितानि च रोपापितानि च- मूलानि च फलानि च यत यत नास्ति सर्वत हारापितानि च रोपापितानि च पंथेसु कूपा च खानापिता र्वछा च रोपापिता परिभोगोय पसुमनुसानं।- द्वितीय शिलालेख एवं सप्तम स्तम्भलेख में वर्णन है।
13. आचारांग-1.4.2.139, श्री आगम प्रकाशन समिति, ब्यावर, 2010ई.।
14. तस्स विभूसणमेअं, मणसुद्धी मंजरी वररुक्खस्स।
तीए समिच्छो एसो, सुहं फलरिद्धि पयच्छेइ।।-विवेकमंजरी, गाथा,4
15. ये पठन्ति न सच्छास्त्रं सद्गुरुप्रकटीकृतम्।
तेऽन्धा: स चक्षुषोऽपीह संभाव्यन्ते मनीषिभि:।।-पद्मनंदिपंचविंषति (6 उपासक संस्कार, श्लोक-20), मुनि पद्मनंदि, सम्पा. अनु.- पं. बालचन्द्र सिद्धान्तशास्त्री, जैन संस्कृति संरक्षण संघ, सोलापुर, 2000ई.
16. ज्ञान उदै जिनके घट अन्तर ज्योति जगी, मति होति न मैली।-भव्यप्रमोद, कविवर, पं. मक्खनलाल जैन, भारतवर्षीय दिग. जैन साहित्य प्रकाषन एवं प्रचार समिति, जयपुर, 2004ई. पृष्ठ 193
17. ज्ञान समान न आन, जगत में सुख को कारण।
इह परमामृत जन्म जरा मृतु रोग निवारण।-छहढाला, चौथी ढाल, पद्य-4, प्रकाशन- श्री दिग. जैन युवक संघ, इन्दौर, 2001ई.
18. ज्ञान विना शिवपन्थ न सूझै।-भव्यप्रमोद, कविवर, पं. मक्खनलाल जैन, पृष्ठ 193
19. जहा सुणी पूइकण्णी निक्कसिज्जइ सव्वसो।
एवं दुस्सील पडिणीए मुहरी निक्कसिज्जई।।

Scanned with OKEN Scanner

कणकुण्डगं चइत्ताणं विट्ठं भुंजइ सूयरे।
एवंसीलं चइत्ताणं दुस्सीले रमई मिए।।-उत्तराध्ययन,1/4 से लेकर 14 तक
20. उत्तराध्ययन, गाथा-1/2 एवं 14
21. वसे गुरुकुले निच्चं जोगवं उवहाणवं।
पियंकरे पियंवाई से सिक्खं लद्धुमरिहई।। - उत्तराध्ययन,11.14.
22. उत्तराध्ययनसूत्र (लाडनूं संस्करण), 11.4-5, पृ.438-39.
23. आदिपुराण (भाग-1) - 1.68, 1.140-48 एवं महापुराण (भाग-2) 38.109-118, भारतीय ज्ञानपीठ प्रकाशन।
24. तत्त्वार्थसूत्र, 5/21
25. कोहुप्पत्तिस्स पुणो बहिरंग जदि हवेदि सक्खादं।
ण कुणदि किंचिवि कोहं तस्स खमा होदि धम्मोत्ति।।- बारह अणुवेक्खा- गाथा 71
26. सम्यक् यमो वा संयमः- धवला, 7/2.1.3/7/3
27. भाव आत्मरुचिः जिनसम्यक्त्वकारणभूतो हेतुभूतः- भावपाहुड़ टीका, गाथा 66
28. शुद्धचैतन्यं भावः- प्रवचनसार (तात्पर्य वृत्ति) 115.161.14
29. दशवैकालिक सूत्रा- 6/9
30. चतुर्थ, नवम, ग्यारह और त्रयोदश शिलालेख।
31. द्वितीय स्तम्भलेख।
32. उत्तराध्ययन,22 अध्ययन गाथा 42
33. पायालुयरगहरीहिं सायरलहरीहिं जा न उल्हविया।
सा वडवानलतण्हा कह फिट्टइ सरिझलक्केहिं।।-गाहारयणकोस, गाथा-49
34. रिणमोयणं व मण्णइ, जो उवसग्गं परिसहं तिव्वं।
पावफलं मे एदं, मया वि जं संचिदं पुव्वं।।-द्वादशानुप्रेक्षा, गाथा 110
35. खुहं पिवासं दुस्सेज्जं, सीउण्हं, अरइ भयं।
अहियासे अव्वहिओ, देह-दुक्खं महाफलं।।

पता- सहायक आचार्य
जैनविद्या एवं प्राकृत विभाग
मोहनलाल सुखाडिया विश्वविद्यालय,
उदयपुर-313001(राज.)
मो. 9024764343,

Scanned with OKEN Scanner



Sustainable Development and Biodiversity 31

K.G. Ramawat
Jean-Michel Mérillon
Jaya Arora *Editors*

Agricultural Waste: Environmental Impact, Useful Metabolites and Energy Production

Springer

Sustainable Development and Biodiversity

Volume 31

Series Editor

Kishan Gopal Ramawat, Botany Department, Mohanlal Sukhadia University, Udaipur, India



Sustainable Development and Biodiversity 31

K.G. Ramawat
Jean-Michel Mérillon
Jaya Arora *Editors*

Agricultural Waste: Environmental Impact, Useful Metabolites and Energy Production

Springer

Sustainable Development and Biodiversity

Volume 31

Series Editor

Kishan Gopal Ramawat, Botany Department, Mohanlal Sukhadia University, Udaipur, India

ART PSYCHOLOGY & CREATIVITY

Selected Essays

Edited by
DR. LOVENEESH SHARMA
DR. IBADAT KHAN

Art, Psychology & Creativity

Editors
Dr. Loveneesh Sharma
Dr. Ibadat Khan

Scholar Publications
Karimganj, Assam, 788711

Art, Psychology & Creativity

ISBN: 978-81-955705-4-6
First Publication: September 2022
Cover Page Design by: Prof. Deepak Goswami

'Art, Psychology & Creativity', edited by **Dr. Loveneesh Sharma & Dr. Ibadat Khan** Published by **Biplab Bhattacharjee,** Scholar Publications, Karimganj, Assam, India.

Type Setting: Bedopriya Bhattacharjee

Printed at:
Scholar Publications, Karimganj, Assam, India
Website: http://www.scholarpublications.in
Email: pub@scholarpublications.in

©Scholar Publications

₹ 600.00

The views and contents of this book are solely of the authors. This book is being sold on the condition and understanding that its contents are merely for information and reference and that neither the author nor the publishers, Printers or Sellers of this book are engaged in rendering legal, accounting or other professional service.
The publishers believe that the contents of this book do not violate any existing copyright/intellectual property of others in any manner whatsoever. However, in the event the author has been unable to track any source and if any copyright has been inadvertently infringed, please notify the publisher in writing for corrective action.
All rights reserved. No part of the publication may be reproduced or transmitted in any form or by any means, electronics, mechanical, photocopying, recording or otherwise without the prior written permission of the copyright owner.

Contents

- **Art and Creativity: Psychological and Cognitive Perspectives** — 11-24
  Susmita Halder, Akash Kumar Mahato, Shinjini Samajdar
- **Art Therapy's Spiritual Implication and its Significance in Indian Context** — 25-36
  Miss Adelina Peter, Monika Rikhi
- **Visual Arts, Psychology and Creativity: The Socio-Literary Perspective** — 37-52
  Dhiraj Ambade
- **Art therapy as a Treatment Modality for Substance Abusers** — 53-60
  Ibadat Khan, Vandana Sharma
- **Abstract Art and Psychology** — 61-70
  Rashmi Singh, Deepika Mali
- **Effectiveness of Art Therapy and Sandtray Therapy in the Treatment of Autism Spectrum Disorders** — 71-83
  Ishita Aggarwal, Yusra Asif, Anchita Kumar, Shivangini Uberoi
- **Evolution and impact of Mehndi Art: A Study of its Continuity as Tradition and Fashion among the women of Delhi- NCR** — 84-107
  Suranjan Lahiri
- **Artist's Psychology** — 108-121
  Sandeep Singh
- **An Introduction to Art Therapy** — 122-135
  Puja Singh
- **Aesthetical Experience and its Psychological Impact on Human Mind** — 136-143
  Rishi Raj Tomar
- **Color Psychology in Creativity, Art & Fashion** — 144-162
  Shramana Mullick

understand. If only they would realize above all that an artist works of necessity, that he himself is only a trifling bit of the world, and that no more importance should be attached to him than to plenty of other things which please us in the world, though we can't explain them. Picasso clearly explained that art can't be mentioned in the verbal words, but it can only be experienced because its influence in every individual is so personal that it can't be generalized.

Abstract Art:

Visual art is also called as a metaphorical art. Art is reality, but it is situated on the boundaries of dream and reality where we can see it from memory. It can be said in this manner like, the things or events which are left behind from our observation or experiences; we can discover that through art. Art is the manifestation of lost sight, thought, memory and the mystery of our difference. The concept of abstraction has been prevalent in our life since ancient times. These elements have been seen in some form or the other in ancient, classical, folk arts. The concept of abstract art is nothing new. Rather, in the society we live in and the traditions, beliefs and religious beliefs we have, these abstract feelings and beauty have permeated for centuries. From the very beginning, artists started realizing that the beauty of the artwork comes from its abstract nature. Whether that art is made of any style or period, its success depends only on its intangible aesthetic qualities, that is, an artwork is formed by the coordination of many basic elements like line, colour, space, texture, rhythm, tone etc. Not by its morphological representation. Plato said about abstract beauty that "circles, imports are such shapes which are not beautiful because of any external reason or

suitability, but aesthetic. Similarly, there is beauty in the pure use of colours. If seen, abstract art is a visual combination of our feelings and emotions, which the artist does not want to name, but his excitement begins to appear in the picture space by castings images or shapes, in which the shape is clear and vague than the ever recognized.



Figure 1 Ankuran, S H Raza, , Acrylic on canvas, 1992
Source: https://www.architecturaldigest.in/content/art-trust-reveals-retrospective-sh-razas-works-spanning-six-decades/

Many artists have associated this concept of abstraction with its own special contexts and meanings. Raza sees the "point" of his paintings in the context of his own life and experiences. If we understand the concept of abstraction in a limited sense, then it is possible that we will be unable to present its detailed concept. The existence of a figure in abstract art is inspired by its special contextual touch and extremely abstract emotions. Beauty, joy and rasa are closely related in artwork which cannot be separated from each other. Rabindranath Tagore describes beauty, joy and rasa

etc. as abstract expressions of the artwork, which can only be felt. The intense desire to express the inner beauty in abstract forms revealed its inner form and quality through abstraction by banishing the external substance and resemblance to the object. Inspired by this line of thought, Kadiski stunned the then audience by composing the first abstract painting in 1910. Kandisky has repeatedly stated in his views that only the language of abstract forms.

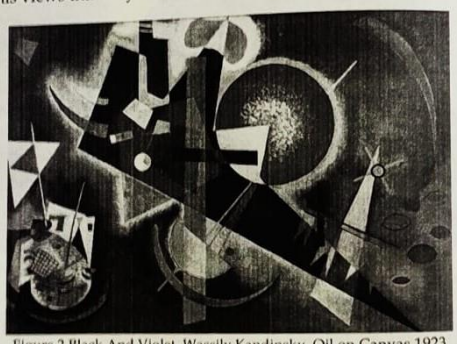

Figure 2 Black And Violet, Wassily Kandinsky, Oil on Canvas,1923
Source: https://www.wassilykandinsky.net/work-234.php

When abstract art was born in the 19th century, the argument was made to present it with a perspective of the illusion of visual reality. Its definition states that when an artist creates a combination in visual language consisting of shape, form, line, color, in which his freedom and perception acquire a visual context, then it, is called abstract art. The path of abstract art is different, it does not try to present the known truth. for the painter shape is just his sense with whi

he creates the abstract art, but the nectar painting would probably take this argument to its climax. If the form of the unknown is not fixed, then it is not possible to explore it with the help of known shapes.

Psychology of the Art:

It is the scientific study of various cognitive and emotional processes which is accelerated by seeing the aesthetic artefacts like watching painting or touching a sculpture. This focus on the experimental methods to measure qualitatively about the psychological responses to art and it includes the neuro-imaging techniques. Abstract art gives us no boundaries of right and wrong. It is open to the viewer's interpretation. It provides the observer the freedom to explore the art with his or her own cognition. It does not contain recognizable objects or themed so sometimes it makes the observer uncomfortable as sometimes he or she faces the difficulties in interpreting the artwork. Abstract paintings do not directly picture anything which is in real physical world.

Brain and Abstract Art:

Our brain is the most complex thing in the whole universe. It uses the top down and bottom-up processing for all analysis. Brain is always finding the familiarity and meaning to the patters as to make it a sense. Art is obviously free from the restrictions which are imposed by the visual system during our daily life. In an FMRI imaging study according to Kawabata and Zeki (2004) various activity evoked at localized and specific brain regions when they demonstrated the different categories of painting like landscape, portrait and still life. When abstract art was shown it did not activate a unique localized brain region. Instead, it activated the entire brain regions which are

related to other categories also. In fact, it can be assumed that there would be neural correlated for the specific cognitive category recognition of abstract art. Kawabata and Zeki (2004) and Vartanian and Goel (2004) found that it should not be expected a unique brain activity related to abstract art. Abstract art viewed does not belong to any other specific category. Lengger et al. (2007) founded that abstract stimuli evoked more positive emotions. This study was done in combination of behavioural and low resolution electromagnetic tomography analysis. He studied that representational artworks were found to be more interesting and were also better understood and also observers felt more association with it. In representation art there was higher activation in the left frontal lobe and bilaterally in the temporal, frontal and parietal lobe, limbic system. The increased brain activities for the representation art consist of the process of object recognition, memory and association system. Solso (2000) studied brain activity by comparing the brain activity of portrait artist and non- artist while drawing face. Brain activity of artist showed less activity in face processing areas (posterior parietal) than that of the non-artist. The lower level of activation of the artist face recognition area indicates that he may be more efficient in the processing of facial feature. While looking at a painting or a beautiful sculpture or any other artwork it increases the blood flow to the brain by 10 percent which is as much equal to the looking to someone whom we love. There is a process named embodied cognition which starts when we look at a piece of art. The more we watch, the more we analyse and we place ourselves to the scene and can actually feel the quality of art. In embodied cognition the mirror neurons in the brain turn things into the actions, movement and energy

which we seen in art into the actual emotions we can feel. The studies related to neuro-anatomical which used FMRI scans showed that representational paintings were more preferred over the abstract paintings. FMRI results revealed that activity in the right caudate nucleus decreased in response to decreasing preference for paintings, whereas the activity in left cingulated gyrus, bilateral occipital gyri, bilateral cerebellum increase in response to increasing preference for paintings. EEG brain scans revealed that there was less arousal was showed by the non- artist as compared to artist while watching the abstract arts whereas in figurative art both artist and non- artist had comparable arousal and the focused attention and evaluation of the art. From all these studies it may be concluded that abstract art seem to reduce the brain activity as compared with representational art which represent to the relevant control. These results indicate that the analysis of abstract art evokes less focal brain activation.

Abstract Art and Personality, Thinking Style:

Various studies have done in relation to the personality, thinking style and their art preferences. The person's choice of art can be useful to measure the type of personality. NEO Five factor inventory which is used to measure big five factors of personality after viewing abstract arts and representational arts. The personality which seeks to thrill and adventure, and Conscientiousness was positively correlated with the choice of representational art and disinhibition and neuroticism was related positively with abstract arts. Openness to experience was linked with both types of arts. Utmost abstract art is preferred by the individual who wants something new, they are open minded and are field independent thinkers. The abstract

thinking type individuals who have very low desire of orders are the viewer who loves to watch abstract art as they enjoy the task of exploring their capacities of organizing the disorganized content. It is clear that when a viewer sees a representational or realistic art it is the actual thing he is seeing like a human, nature, animal as the things we are familiar with. But when the abstract art is watched the brain faces difficulty in finding familiar objects. And then eyes move more on whole of the painting and not focusing on the specific objects. In a study held in 2011, it was observed that in response to the paintings of Jackson Pollock's fractal paintings the people used to move their eyes more uniformly across the whole canvas. The study published in Proceedings of the National academy of sciences points that how the viewing of abstract art is related to the psychologically closely or distantly they viewed it. In this study the researchers gathered eight hundred and forty subjects and was asked to view the artworks which was defined as purely abstract, having a clearly defined object, or partly abstract with a definable object. The subjects were asked to imagine that they were going to decide where to place the paintings on display. They could place the art according to their preferences either in gallery around the corner or in another state and also, they can show the date according to their timeline (in future, or tomorrow). The subject chose to place the abstract works in a distant gallery in the future than to do the same with the more grounded works. This shows the tendency of the association of abstract art with faraway places, and it indicates that we tend to place psychological distance between ourselves and abstract art. According to the psychological concepts abstract notions are seen as a very distant concept. Psychological distance is

the mental distance between self and other paces, events, and things.

Conclusions:

Abstract art free us from the boundaries of reality and watching the abstract art is to explore within oneself which is the reinforcement also. It enables us to flow in the inner states, create new emotional associations and activate the brain states that are harder to access. Abstract artist puts his/her inner self in his/her creative art whereas viewer of that art puts his/her emotions and feelings in the artist artwork. So it can be said the abstract art allows us to represent our inner conflicts, complexes, emotions, cognitions in the means of a beautiful artwork.

References:

1. Aviv V. (2014). What does the brain tell us about abstract art?. *Frontiers in human neuroscience, 8,* 85. Retrieved from https://doi.org/10.3389/fnhum.2014.00085
2. Furnham, Adrian; Walker, John (2001). Personality and judgements of abstract, pop art, and representational paintings. *European Journal of Personality,15* (1):57-72
3. Emma Betuel. One type of art can help you see the bigger picture in life- study. Mind and body retrieved from https://www.inverse.com/mind-body/abstract-art-mindset-study
4. Gridley, Mark. (2013). Preference for abstract art according to thinking styles & personality. *North American Journal of Psychology, 15,*463-481.

5. How looking at art can help your brain (The university of Arizona global campus) retrieved from https://www.uagc.edu/blog/how-looking-at-art-can-help-your-brain
6. Kawabata, H., and Zeki, S. (2004). Neural correlates of beauty. *J. Neurophysiol.* 91, 1699–1705. doi: 10.1152/jn.00696.2003
7. Solso, R. L. (2000). The cognitive neuroscience of art: a preliminary fMRI observation. *J. Conscious. Stud.*, *7*, 75–85.
8. Vartanian, O., and Goel, V. (2004). Neuroanatomical correlates of aesthetic preference for paintings. *Neuroreport, 15,* 893–897. doi: 10.1097/00001756-200404090-00032
9. Vartanian, Oshin; Goel, Vinod (2004). "Neuroanatomical correlates of aesthetic preference for paintings". *Cognitive Neuroscience and Neuropsychology, 15* (5), 893–897. doi:10.1097/00001756-200404090-00032. PMID 15073538. S2CID 7892067.
10. Bhaaratee, Meenaakshee (June 1993) *Samakaaleen Kala: Moort Amoort ke Beech Mein,* Lalit Kala Akaadamee, p. 61.
11. Raam, Tyauhaar & Sinha, Manohar, (June 1993), *Samakaaleen Kala: Amoortan Kuchh Sandarbh aur Sanket,* Lalit Kala Akaadamee, p.07.
12. Joshee, Jyotish (2019) Kala Addhati Haarateey Chintan, Bhaag 3 Yash Publication, Delhi.
13. *Kala Deergha,* Issue-13 October 2012, Archana Advertising Pvt. Ltd. Delhi.

Effectiveness of Art therapy and Sandtray Therapy in the treatment of Autism Spectrum Disorders

Ishita Aggarwa
Yusra Asif
Anchita kumar
Shvangini Uberoi
Daulat Ram College, University of Delhi, Affiliated to Amity University, Noida

Abstract

Symbolism is one of the primary sources for exploring one's psyche. Expressive art therapies are based upon this idea. They utilize the therapeutic nature of expressing itself as the art becomes the medium for one's healing. With growing attention on benefits of various expressive arts modalities, empirical evidence demonstrates how efficient and effective they are for diagnosing and treatment of the clinical population, including neurodevelopmental disorders like Autism Spectrum Disorders, ADHD, and many more. Moreover, to develop a deeper understanding, specific implications of Art therapy and Sandtray therapy in autism spectrum disorders are emphasized.

Keywords: *Autism, Art, Play, Therapy, Psychology*

Introduction:

Autism Spectrum Disorders (ASD) are a group of phenotypically heterogeneous neurodevelopmental syndromes characterized by impairments in social communication and behavioral flexibility (Sadock, 2007), often accompanied by cognitive underpinnings directly impacting human behavior (Lord et al., 2020). The DSM-5 criteria for ASD includes persistent deficits in social

Dr. Lovineesh Sharma
Assistant Professor
School of Fine Arts
Amity University Kolkata

Dr. Lovineesh Sharma has completed his MA and PhD in History of Art from Panjab University, Chandigarh. He has more than ten years of teaching and research experience at college and University level in the field of History of Arts and Aesthetics. He has an experience of serving both private and government education sectors. He has published ten research papers in national and international reputed journals along with two book chapters in national level books. He as an artist and has exhibited his artwork in national and international exhibitions. He has been invited as a visiting faculty for delivering lectures in several institutions in India. He is an advisory board member of reputed art organizations and publications in India and abroad.

Dr. Ibadat Khan
Assistant Professor
Department of Psychology, Vishwakarma University, Pune

Dr. Ibadat Khan has completed his MA and PhD in Psychology from Panjab University, Chandigarh. He has more than 7 years of teaching experience at the College and University level in the field of Psychology and Behavioral Sciences. He has more than 4 year's experience of serving Government and Private hospitals as a psychological counselor and psychologist dealing with Psychological problems and Substance use disorders. He has also served in PGIMER, Chandigarh in Drug De-addiction and Treatment Centre (DDTC) as a Counselor under Tobacco Cessation Centre. He is trained in Career Guidance and Counseling, Psychological Counseling, Meditative Techniques, and psychotherapies.

Cover image by Birmingham Museum Trust on Unsplash
Cover design by Deepak Goswami

9 788195 570546

SCHOLAR PUBLICATIONS SP

Scholar Publications
Karimganj, Assam, India

21st Century Business Management

RESHAPING THE BUSINESS WORLD POST-COVID-19

Management Strategies for Sustainable Behavior Change

Edited by

Arvind K. Birdie, PhD

Ruchi Joshi, PhD

APP APPLE ACADEMIC PRESS

First edition published 2024

Apple Academic Press Inc.
1265 Goldenrod Circle, NE,
Palm Bay, FL 32905 USA

760 Laurentian Drive, Unit 19,
Burlington, ON L7N 0A4, CANADA

CRC Press
2385 NW Executive Center Drive,
Suite 320, Boca Raton FL 33431

4 Park Square, Milton Park,
Abingdon, Oxon, OX14 4RN UK

© 2024 by Apple Academic Press, Inc.

Apple Academic Press exclusively co-publishes with CRC Press, an imprint of Taylor & Francis Group, LLC

Reasonable efforts have been made to publish reliable data and information, but the authors, editors, and publisher cannot assume responsibility for the validity of all materials or the consequences of their use. The authors, editors, and publishers have attempted to trace the copyright holders of all material reproduced in this publication and apologize to copyright holders if permission to publish in this form has not been obtained. If any copyright material has not been acknowledged, please write and let us know so we may rectify in any future reprint.

Except as permitted under U.S. Copyright Law, no part of this book may be reprinted, reproduced, transmitted, or utilized in any form by any electronic, mechanical, or other means, now known or hereafter invented, including photocopying, microfilming, and recording, or in any information storage or retrieval system, without written permission from the publishers.

For permission to photocopy or use material electronically from this work, access www.copyright.com or contact the Copyright Clearance Center, Inc. (CCC), 222 Rosewood Drive, Danvers, MA 01923, 978-750-8400. For works that are not available on CCC please contact mpkbookspermissions@tandf.co.uk

Trademark notice: Product or corporate names may be trademarks or registered trademarks and are used only for identification and explanation without intent to infringe.

Library and Archives Canada Cataloguing in Publication

Title: Reshaping the business world post-COVID-19 : management strategies for sustainable behavior change / edited by Arvind K. Birdie, PhD, Ruchi Joshi, PhD.
Names: Birdie, Arvind K., editor. | Joshi, Ruchi (Lecturer in psychology), editor.
Description: First edition. | Series statement: 21st century business management book series | Includes bibliographical references and index.
Identifiers: Canadiana (print) 20230445683 | Canadiana (ebook) 20230445802 | ISBN 9781774913406 (hardcover) | ISBN 9781774913413 (softcover) | ISBN 9781003372424 (ebook)
Subjects: LCSH: Organizational behavior. | LCSH: Personnel management. | LCSH: COVID-19 Pandemic, 2020.
Classification: LCC HD58.7 .R47 2024 | DDC 658.3—dc23

Library of Congress Cataloging-in-Publication Data

Names: Birdie, Arvind K., editor. | Joshi, Ruchi, editor.

Title: Reshaping the business world post-COVID-19 : management strategies for sustainable behavior change / edited by Arvind K. Birdie, PhD, Ruchi Joshi, PhD.

Description: Palm Bay, FL : Apple Academic Press, 2024. | Series: 21st century business management | Includes bibliographical references and index. | Summary: "The COVID-19 pandemic dramatically changed our normal-both in life and in business. The timely volume provides a map of how the world has been significantly changed by the post-COVID-19 pandemic, not only in terms of work and business life but also linking other areas of personal life as well. The volume explores the diverse impacts of the pandemic on businesses and workplaces, addressing topics such as changes in organizational structures, operations, and marketing and consumer behavior. Sharing their rich insights and perspectives on today's business world, the authors also look at personal psychological well-being, the role of spirituality, employee satisfaction, an organization's future competitiveness, and quality of life have been affected and changed by the COVID-19 pandemic. Chapters discuss the challenges and complications of flexible and hybrid working styles and digital collaboration platforms such as Microsoft teams. Other topics include changed consumer choices and shopping psychology, internet addiction, mental health challenges, new psychological aspects of the art and culture industry, and more. The authors also share effective strategies for creating work-life balance and improving psychological well-being and for navigating the "new normal." Reshaping the Business World Post-COVID-19: Management Strategies for Sustainable Behavior Change will be valuable for both industry and academia as it covers concepts of business from various perspectives. The book is sure to help managers of all types navigate the new normal"-- Provided by publisher.

Identifiers: LCCN 2023021318 (print) | LCCN 2023021319 (ebook) | ISBN 9781774913406 (hardback) | ISBN 9781774913413 (paperback) | ISBN 9781003372424 (ebook)

Subjects: LCSH: Management. | Organizational change. | Strategic planning. | COVID-19 Pandemic, 2020---Economic aspects.

Classification: LCC HD31.2 .R475 2024 (print) | LCC HD31.2 (ebook) | DDC 658--dc23/eng/20230512

LC record available at https://lccn.loc.gov/2023021318

LC ebook record available at https://lccn.loc.gov/2023021319

ISBN: 978-1-77491-340-6 (hbk)
ISBN: 978-1-77491-341-3 (pbk)
ISBN: 978-1-00337-242-4 (ebk)

Contents

Contributors ..... *xiii*

Abbreviations ..... *xv*

Preface ..... *xvii*

1. **COVID-19 and Employee Satisfaction with Leadership Influencing the Future Competitiveness of Organizations** **1**
   Maja Rožman, Anita Peša, Mladen Rajko, and Tjaša Štrukelj

2. **Hybrid Working: The Future of Organizations** **41**
   Tarun Kumar Sharma

3. **Mapping the Nature of Workplace Incivility in Post-COVID Work Culture** **69**
   Suyesha Singh and Rimjhim

4. **Changes of Collaboration Platforms' Use Perceived by Users Because of COVID: A Research Study of Changes in User Experience of Microsoft Teams Platform** **93**
   Zdenko Deželak, Simona Sternad Zabukovšek, and Samo Bobek

5. **The Culture Shock of COVID-19: A Study to Understand the Effects of Pandemic on the Art and Culture Industry** **127**
   Chirmi Acharya

6. **Is Resilience a Predictor of Psychological Well-Being Among Employees Amid Lockdown? A Literature Review-Based Study** **151**
   Monika Gwalani

7. **Impact of the Pandemic on Street Food Vendors Globally: Challenges and Coping Strategies** **175**
   Vismita Paliwal, Ruchi Joshi, and Nida Nafees

8. **Work and Life Allies or Enemies: A COVID Pandemic Perspective** **191**
   Varsha Sharma

Contributors

Chirmi Acharya
Assistant Professor, Department of Psychology, Manipal University Jaipur, Rajasthan, India

Samo Bobek
University of Maribor, Faculty of Economics and Business, Slovenia

Zdenko Deželak
University of Maribor, Faculty of Economics and Business, Slovenia

Neeta Gupta
Associate Professor, DAVPG College, Dehradun, Uttarakhand, India

Monika Gwalani
Assistant Professor, Amity University, Jaipur, Rajasthan, India

Ruchi Joshi
Assistant Professor, Department of Psychology, Manipal University Jaipur, India

Kashish Kakra
IND Analyst II-HCS, Aon Consulting Pvt. Ltd., Gurgaon, India

Attin Kumar
Cluster Manager, Reliance Trends, Gurgaon, India

Nida Nafees
Assistant Professor, Amity Institute of Behavioral and Allied Sciences, Amity University, Rajasthan, India

Vismita Paliwal
Associate Professor and Coordinator, Amity Institute of Behavioral and Allied Sciences, Amity University, Rajasthan, India

Anita Peša
University of Zadar, Department of Economics, Croatia

Mladen Rajko
University of Zadar, Department of Economics, Croatia

Rimjhim
Mphil Clinical Psychology, Department of Psychiatry, Government Medical College and Hospital, Chandigarh

Maja Rožman
University of Maribor, Faculty of Economics and Business, Slovenia

Tarun Kumar Sharma
Assistant Professor, Department of Psychology, Mohanlal Sukhadia University, Udaipur, Rajasthan, India

CHAPTER 2

Hybrid Working: The Future of Organizations

TARUN KUMAR SHARMA

Assistant Professor, Department of Psychology, Mohanlal Sukhadia University, Udaipur, Rajasthan, India

ABSTRACT

COVID-19 pandemic is considered a massive unplanned experiment in the world of work. The organizations were able to sustain its functioning by adopting work-from-home (WFH) policy. The experiences of remote working led us to understand that work can be performed with optimum productivity in WFH mode as well. The organizations like Microsoft and others have done extensive surveys to understand hybrid working perceptions among the employees. Hybrid working, its models and how different occupations/organizations differ in the possibility of adopting hybrid work arrangements is discussed.

Surveys such as Work Trend Index 2021 by Microsoft have revealed that the future of organizations is Hybrid work. The other surveys Riverbed/Aternity Hybrid Work Global Survey 2021, KPMG CEO 2021 outlook survey, NASSCOM have also reported the similar findings. The perspectives of Satya Nadella, Sunder Pichai, Mark Zuckerberg, Mark Dixon, and organizational perspectives by TCS, Goldman Sachs, and JP Morgan on Hybrid working are discussed.

However, hybrid work arrangements come with certain challenges and complications to be dealt with. The organizations would have to develop norms and policies to maintain optimum productivity and tracking the

Reshaping the Business World Post-COVID-19: Management Strategies for Sustainable Behavior Change. Arvind K. Birdie & Ruchi Joshi, (Eds.)
© 2024 Apple Academic Press, Inc. Co-published with CRC Press (Taylor & Francis)

Certificate of Publication

This is to certify that

Dr. (Ar.) Apoorva Ajmera and Er. Prafull Kothari

has authored and got published the book entitled

Geometry in Architecture

with ISBN No.: 978-93-94954-72-4 on dated 11-05-2023

HIMANSHU PUBLICATIONS

First Floor, 2-D, Hajareshwar Colony, Near Krishna Complex, Udaipur (Raj.); Phone : 0294-2421087
4379/4-B, Prakash House, Ansari Road, Daryaganj, New Delhi - 2; Phone : +91-96109-73739
e-mail : himanshupublications@gmail.com; web: www.himanshupublications.com

Harish Arya
Publishers